TRANSACTIONS

OF THE

AMERICAN SOCIETY

OF

MECHANICAL ENGINEERS

1944

VOLUME 66

PUBLISHED BY
THE AMERICAN SOCIETY OF MECHANICAL ENGINEERS
29 WEST THIRTY-NINTH STREET, NEW YORK, N. Y.

Copyright, 1945, by
THE AMERICAN SOCIETY OF MECHANICAL ENGINEERS

Printed in the United States of America by
The Mack Printing Co., Easton, Pa.

Foreword

VOLUM66 of the Transactions of The American Society of Mechanical Engine contains the individual papers published during 1944 under the sponsors of the Society's professional divisions and technical committees, incln the contributions of the Applied Mechanics Division, issued originally in uarterly known as *Journal of Applied Mechanics*, and the 1944 Society Rec and Index. The technical papers and reports that make up this volume resent the Society's annual contribution to the permanent record of manical-engineering achievement. Most of these papers and reports were sented at meetings of the Society and its professional divisions and local secns and were published in monthly issues, eight being distributed as the Trantions of The American Society of Mechanical Engineers and four as the *rnal of Applied Mechanics*. Indexes to other A.S.M.E. papers and publicats will be found on page RI-51 at the end of this volume.

In view of e fact that the material of which this volume is composed was originally iss periodically as the Transactions, *Journal of Applied Mechanics*, and Society ecords, three sets of page numbers will be found. Numbers without lett ymbols are those of the eight issues of Transactions, those with letter symbA preceding the number refer to the pages of the *Journal of Applied Mnics*, which follow, and those with letter symbol RI to the Society Recs and Index section, which concludes the volume.

All sectiof the Transactions are bound together at the end of the year for the conv ence of libraries and of engineers who wish all of the papers in permanent fn. Copies of the bound Transactions will be found in depositories locate selected engineering, university, and public libraries throughout the wor A complete list of these depositories will be found on pages RI-49 and -50 of the Society Records and Index. Copies of the Transactions hav so been set aside for sale.

The Soci Records of the A.S.M.E. for 1944, which form a part of these Transactio are the permanent records of the Society's activities for the year, includ lists of committees. The Index provides a means of locating special A.S.E. publications and articles in *Mechanical Engineering*, as well as in the Tran tions.

THE COMMITTEE ON PUBLICATIONS

Requirements for Relief of Overpressure in Vessels Exposed to Fire

By J. J. DUGGAN,[1] C. H. GILMOUR,[1] and P. F. FISHER[1]

Pressure-vessel codes and regulations prescribe pressure-relief equipment but do not completely specify the necessary relief capacity to insure safety. Investigations show that the most effective cause of pressure increase is fire exposure as encountered in accidental conflagrations, and tests of the effects of such fire exposure on pressure vessels have been made and analyzed. Part 1 of the paper details these tests and analyzes the results. Parts 2 and 3 develop the necessary formulas to determine the sizes and capacities of the relief connections and apparatus and also present detailed statements of the applications of these formulas to pressure vessels and atmospheric tanks.

PART 1 OBSERVED RATE OF HEAT ABSORPTION

Introduction

FROM the standpoint of protection from excessive internal pressure, probably the severest hazard to which a vessel may be subjected is that which accompanies exposure to external conflagration. (Internal reaction will be discussed in Part 2.)

Some 12 to 14 years ago, the American Petroleum Institute Committee on Fire Prevention, after study and deliberation, proposed the basis of 100 Btu per min per sq ft of surface wetted by the contents as a practical basis for determining the necessary relief area to limit the rise of pressure. In connection therewith a theoretical analysis of "The Rates of Vaporization in Gasoline in Storage Tanks Exposed to Fire,"[2] and a chart from which to determine the capacity and size of relief were made. This chart was drawn so that heat-input rates varying from 6000 Btu to 24,000 Btu per sq ft of wetted surface per hr might be selected. So far as is known, there was no practical basis for the choice of a heat rate, nor was any suggested.

The National Fire Protection Association and the National Board of Fire Underwriters, as well as other regulatory bodies, were given the benefit of these studies. They performed a valuable service in this matter of emergency relief and related considerations by providing the best generally known criterion for the "Safe Handling and Storage of Flammable Liquids."[3] The relief standards proposed were based upon 6000 Btu per hr per sq ft of wetted surface and are still generally recognized.

Some interest appeared later among the associations and concerns promulgating and using this information to inaugurate a variable heat-input rate. It is believed the suggestion which received widest acceptance was that which proposed a heat rate varying from 24,000 Btu per hr per sq ft for small tanks having 10 sq ft of surface to 3000 Btu per hr per sq ft for large vessels having 10,000 sq ft of surface. On this basis, a 6000-Btu rate held for vessels having a wetted surface of 1000 sq ft. So far as is known, no official action was taken on this variable rate, nor was it published for general use.

It was the unfortunate experience of the authors to learn that, while the 6000-Btu rate on tank surfaces of the order of 1000 sq ft was satisfactory for all ordinary circumstances, it was totally inadequate for severe exposures of even less than 15 min duration. Some of these cases are a matter of private record, and it may be stated that the materials contained were more stable than gasoline upon which existing standards are based. From information reviewed, it is believed that other organizations have encountered similar experiences.

Accordingly, known available literature on the subject was analyzed and a series of tests was conducted which follows:

Summary

It is concluded that pressure-relief areas should be designed on a basis of 20,000 Btu per hr per sq ft of wetted surface exposed to fire.

Exception is proposed to this heat-input rate for atmospheric-working-pressure tanks, as outlined in Part 3 of this paper.

So far as can be learned, there is no substantial theory or evidence to support the limiting of heat-input rates to any particular height. There are some indications to the contrary; that is, high gas temperatures apparently exist at relatively great heights above the fuel during large fires.

Analysis of Fetterly's Formula and Test

In order to specify safety valves for the protection of containers charged with liquefied gas, a formula was derived and a test conducted by John F. Fetterly, inspector, Bureau of Explosives, Association of American Railroads. His report[4] furnishes data of considerable interest on heat-input rates for tanks exposed to fire.

It will be seen that it is possible for the contents of a 300-gal tank exposed to fire to absorb heat at about 20,000 to 23,000 Btu per sq ft of wetted surface per hr during vaporization.

Probably the factor in the formula which might arouse criticism is that represented by C, namely, the over-all heat-transfer coefficient. The coefficient used was obtained from an empirical formula which was based on tests made before the film theory of heat transfer was recognized. However, having been based on actual test data, it is not surprising that the numerical value of C is of the order of magnitude that would be predicted by present-day theory.

For example, the heat-transfer coefficient from a flame to a surface would be calculated today approximately as follows

$$U = h_c + h_r = \text{Fetterly's } C \text{ or heat-transfer coefficient} \quad \ldots [1]$$

$$h_c = 0.27\,(T_f - T_s)^{1/4} \quad \ldots [2][5]$$

---

[1] Carbide and Carbon Chemicals Corporation, South Charleston, West Va., unit of Union Carbide and Carbon Corporation.

[2] Engineering Office of American Petroleum Institute, New York, N. Y.

[3] National Fire Protection Association Flammable Liquids Ordinance, National Board of Fire Underwriters, Pamphlet No. 30 of Standards.

Contributed by the Petroleum Division and presented at the Semi-Annual Meeting, Los Angeles, Calif., June 14–17, 1943, of The American Society of Mechanical Engineers.

Note: Statements and opinions advanced in papers are to be understood as individual expressions of their authors and not those of the Society.

[4] "The Determination of the Relief Dimensions for Safety Valves on Containers in Which Liquefied Gas Is Charged and When the Exterior Surface of the Container Is Exposed to a Temperature of 1200 Deg F," by J. F. Fetterly, Bureau of Explosives, 1928.

[5] "Heat Transmission," by W. H. McAdams, McGraw-Hill Book Company, Inc., New York, N. Y., 1942, second edition, Equation [16], p. 240.

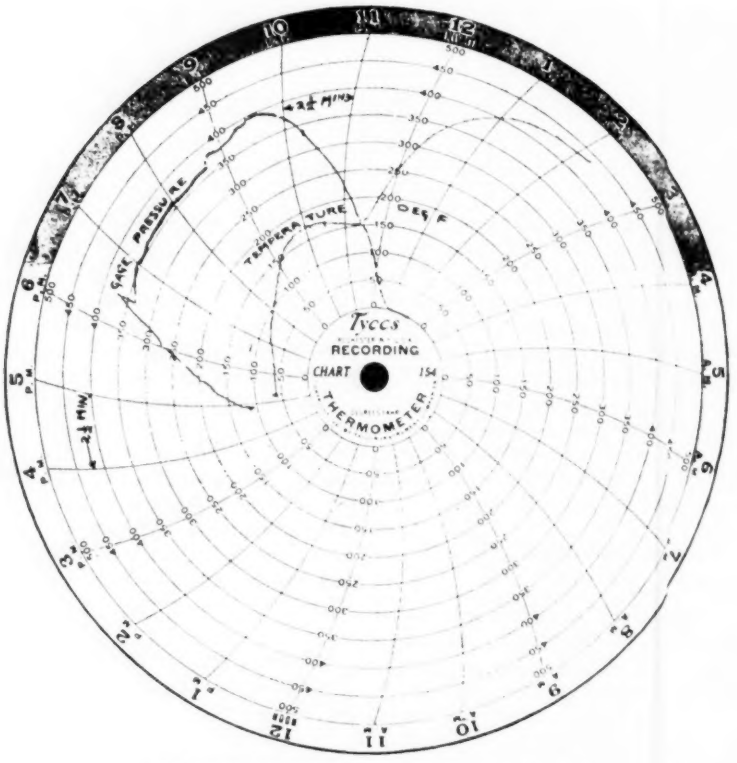


FIG. 1 FETTERLY'S TANK FIRE-EXPOSURE TEST[4]

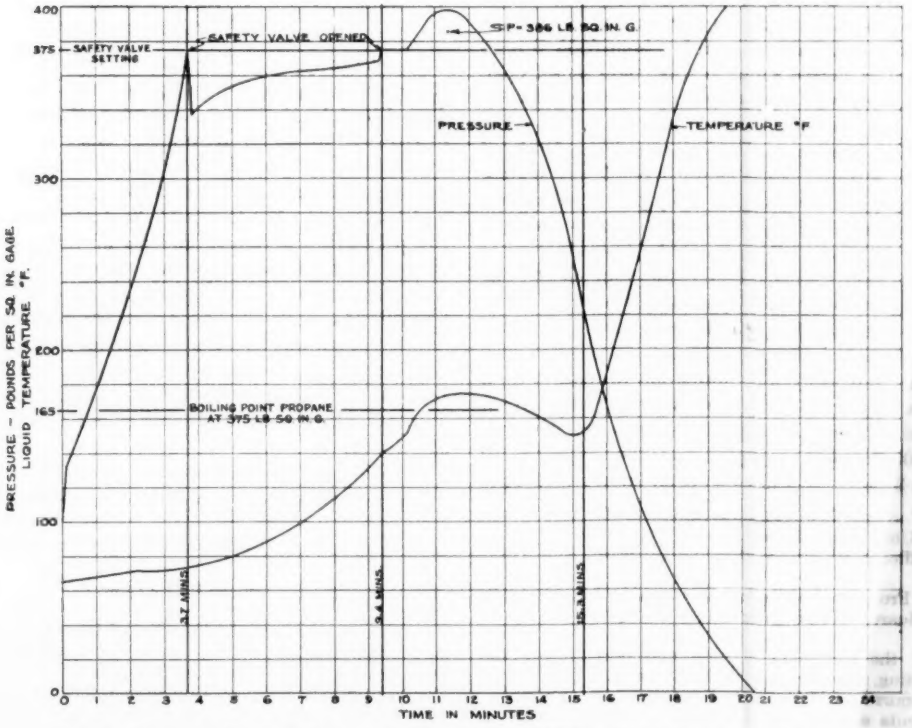


FIG. 2 OBSERVED DATA IN FETTERLY'S FIRE TEST OF 300-GAL TANK CONTAINING PROPANE
(Replotted from recording chart, Fig. 1.)

$$h_r = \frac{0.173\left[\left(\frac{T_f}{100}\right)^4 - \left(\frac{T_s}{100}\right)^4\right]}{(T_f - T_s)} \quad \ldots\ldots\ldots [3][6]$$

(Assuming the hot gas and tank surface are black, i.e., have a black-body coefficient of 1, the shape factor is unity, and that the heat resistance of the retaining wall and boiling liquid is negligible compared with the resistance of the film in contact with the flame.) Then if the flame is 1200 F and tank surface is 165 which are the temperatures used by Fetterly, the value of U would be

$$U = 0.27\,(1660 - 625)^{1/4} + \frac{0.173[(16.6)^4 - (6.25)^4]}{(1660 - 625)}$$

$$= 0.27 \times 5.67 + \frac{0.173\,(75{,}940 - 1540)}{1035}$$

$$= 1.53 + 12.44 = 13.97 \text{ Btu per hr per sq ft per deg F}$$

This is more than 95 per cent of the value obtained by Fetterly, specifically 14.68 Btu. It should be noted that this is equivalent to [13.97 (1200 — 165)] 14,500 Btu per hr per sq ft of wetted surface for a flame temperature of 1200 F, and a 23,000-Btu rate for a T_f of the order of 1400 F, as calculated from the test data to be given. It will be seen later that flame temperatures of this magnitude are conservative for industrial fires, particularly those involving flammable liquids.

Of particular interest and value are the test data obtained by Fetterly which consist of continuous pressure and temperature measurements taken while a wood fire burned around a tank containing 1000 lb of propane. From this record, it is possible to calculate the heat input to the tank and contents during the various phases of the test. The charts of pressure and temperature versus time are reproduced in Figs. 1 and 2 of this paper; the former is the actual instrument record and the latter is a replot of the same data to clarify the analysis. In order to give a better picture of the nature of the fire surrounding the tank, a diagram of the test setup, as interpreted from the description contained in Fetterly's paper, is shown in Fig. 3.

The safety valve was set to open at 375 psig. Note that the relief valve opened and closed again long before the liquid approached the boiling point (about 165 F), which is evidence that the vapor was superheated to a temperature sufficient to cause the pressure to rise to 375 psi. By reference to Fig. 3, it is obvious that the vapor space was subjected to intense fire for the first few minutes of the test, during which time the vapor was heated from 65 F to an estimated temperature of 1000 F, at the time the safety valve first opened after 3.7 min of exposure. This temperature was estimated from the best available physical characteristics[7] for propane. In this same period the liquid was heated from only 65 to 74 F.

The second phase of the test consists of the period in which part of the liquid was heated to the boiling point and the safety valve opened for the second time. This is the interval observed from 3.7 to 9.4 min in Fig. 2. During this time the fire level probably lowered, the intensity of the flame on the unwetted surface decreased, and the vapor did not expand as rapidly as before, as observed from the pressure curve.

The final phase of the test consists of the period of the vaporization and discharge of the contents. As shown in Fig. 2, this appears to have occurred in about 5.9 min. At the end of this period, the pressure had fallen rapidly to 245 psi (probably the safety valve stuck open), and the liquid temperature began to rise sharply as it would when the thermocouple was exposed to the hot vapor and tank walls. On the basis of 5.9 min, the heat absorbed by the contents may be calculated as follows:

Heating Liquid to Boiling

$$1000 \times 0.68\,(165 - 140) \times \frac{60}{3.2} = 318{,}800 \text{ Btu per hr}$$

Vaporizing Liquid

$$1000 \times 101 \times \frac{60}{5.9} = \frac{1{,}027{,}000 \text{ Btu per hr}}{1{,}345{,}800 \text{ Btu per hr}}$$

Heat Intensity

$$\frac{1{,}345{,}800}{57.82} = 23{,}300 \text{ Btu per hr per sq ft of wetted surface}$$

Vaporization Rate

$$1000 \times \frac{60}{5.9} = 10{,}170 \text{ lb per hr}$$

Safety-Valve Capacity

$$W = 306\,aP\sqrt{\frac{M}{T}} = 306 \times 0.312 \times 386\sqrt{\frac{44}{625}}$$

$$= 9800 \text{ lb per hr} \quad \ldots\ldots\ldots\ldots [4][5]$$

The vaporization rate is then 3.8 per cent greater than the calculated valve capacity, but some of the contents may have been discharged as droplets of liquid. However, if the vaporization rate had been as low as the safety-valve capacity, the heat intensity would still have remained as high as 22,600 Btu per hr per sq ft of wetted surface.

If it is assumed that the steel temperature is about 100 deg F higher than that of the boiling liquid, the effective flame temperature necessary to transmit the foregoing heat input may be calculated as follows:

(1) $U\Delta T = Q/A\theta = U(T_f - T_s) = 23{,}300$ Btu per hr per sq ft ..... [5]

(2) $$U = 0.27(T_f - T_s)^{1/4} + \frac{0.173\left[\left(\frac{T_f}{100}\right)^4 - \left(\frac{T_s}{100}\right)^4\right]}{(T_f - T_s)}$$ ..... [1]

[6] "Heat Transmission," Equation [17], p. 63.

[7] Pressure-volume-temperature relation.

[5] "API-ASME Code for Unfired Pressure Vessels," New York, N. Y., 1938 edition, p. 74.

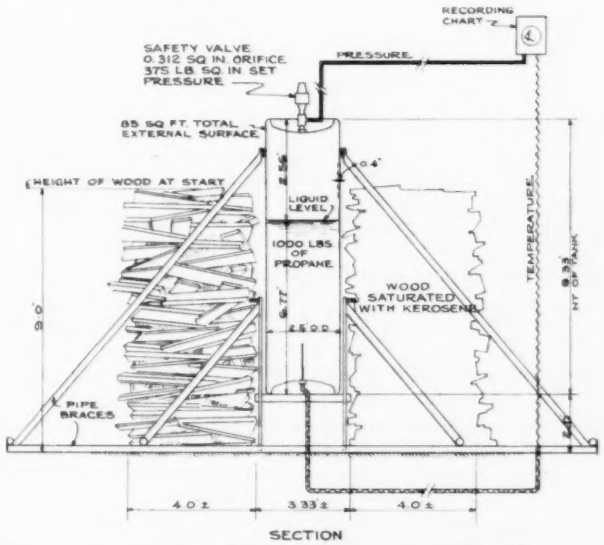


FIG. 3 DIAGRAMMATIC REPRESENTATION OF THE FIRE-EXPOSURE TEST OF A 300-GAL TANK CONTAINING PROPANE
(As described in ref. 4.)



FIG. 4 FIRE CONDITIONS 9 MIN AFTER IGNITION
(Appears to be height of fire, but note limited surface exposure.)

(3) $$U(T_f - T_s) = 0.27\,(T_f - T_s)^{5/4} + 0.173\left[\left(\frac{T_f}{100}\right)^4 - \left(\frac{T_s}{100}\right)^4\right]$$

$$= 23{,}300 \text{ Btu per hr}$$

(4) $T_s = 165 + 100 = 265$ deg F $= 725$ deg R

(5) $0.27(1888 - 725)^{5/4} + 0.173[(18.88)^4 - (7.25)^4]$

$$= 23{,}300 \text{ Btu per hr}$$

$1834 + 21{,}503 = 23{,}337$ compared to 23,300 Btu

$T_f = 1888$ deg R, or 1428 deg F, approximately

This is a reasonable mean effective temperature for a kerosene-soaked open wood fire. The National Bureau of Standards in co-operation with the National Fire Protection Association observed temperatures of 2000 F within 20 min from burning wood within a large brick building.[9]

NOMENCLATURE USED IN FETTERLY TEST ANALYSIS

The nomenclature used in analysis of Fetterly's test is as follows:

C = heat-transfer coefficient, Btu per hr per sq ft per deg F; Fetterly's
U = heat-transfer coefficient, Btu per hr per sq ft per deg F; over-all
h_c = heat-transfer coefficient, Btu per hr per sq ft per deg F; convection
h_r = heat-transfer coefficient, Btu per hr per sq ft per deg F; radiation
T_f = effective flame temperature, deg F absolute
T_s = temperature of tank surface, deg F absolute
ΔT = temperature difference, deg F
Q = total heat transferred, Btu
A = surface heated, sq ft
θ = time, hr
W = vapor rate of safety valve, lb per hr
a = orifice area of safety valve, sq in.
P = absolute pressure at inlet of safety valve, psi
M = molecular weight of vapor
T = vapor temperature, deg F absolute

ANALYSIS OF UNDERWRITERS' LABORATORIES, INC., TEST

In January, 1938, there appeared the results of some tests to show the effect of a film of water running over a plate exposed to fire.[10] The results of the tests were reported in terms of temperature or per cent of total heat input. The data are comprehensive enough to be used to calculate the heat absorbed from the flame.

The test apparatus consisted of a vertical plate 8 ft high by 3 ft wide by 1/8 in. thick suspended from one of its 3-ft edges. A fire was produced by burning gasoline in a pan 3 ft sq, placed directly in front of the plate. Tests were conducted both with and without a water film flowing down the plate.

After equilibrium had been established during the run, in which there was a protective water film, the following data were observed:

Water rate, 45 gpm; water temperature off, 97.5 F; water temperature on, 63 F; water temperature rise, 34.5 F.

From these data, the heat-absorption rate is calculated as follows:

$$45 \times 8.337 \times 60 \times 1 \times 34.5 = 776{,}000 \text{ Btu per hr}$$

[9] "Handbook of Fire Protection," by Crosby, Fiske, Forster, National Fire Protection Association, Boston, Mass., 1941, ninth edition, p. 384.

[10] "Opacity of Water to Radiant Heat Energy," Underwriters' Laboratories, Inc., Bulletin of Research No. 3, Chicago, Ill., Jan., 1938.



FIG. 5 CONDITIONS INTERPRETED TO BE ABOUT 25 MIN AFTER IGNITION
(Note no fire visible in pan under tanks.)

The intensity of heat absorption is

$$\frac{776{,}000}{24} = 32{,}300 \text{ Btu per hr per sq ft}$$

The average temperature of the water was 80 F, when flowed over the plate during the fire. The effective gas temperature required to transmit this quantity of heat would be approximately 1580 F, as calculated by the same procedure as given for the analysis of the Fetterly tests. A maximum flame temperature, a point temperature, of 3000 F was read with an optical pyrometer.

The results of this test show that the intensity of heat absorbed from a fire under these conditions is of the order of magnitude of 30,000 Btu per hr per sq ft.

Fire Tests on Truck Tanks

During 1930, the Aluminum Company of America, under supervision of committees from the American Petroleum Institute and the National Fire Protection Association, conducted fire-exposure tests[11] on two 150-gal tank-truck compartments made of aluminum (refer to Figs. 4 and 5). The data were taken to establish the suitability of the metal for truck-tank construction and are not sufficiently broad to record directly information essential to the calculation of heat-input rates. As will be explained, sufficient data were interpreted to estimate maximum and minimum heat-input rates for tank B in the report.

The time-temperature curves of thermocouples 9, 10, 11, and 12 were transposed from the original data[11] to Fig. 6 of this paper. This indicates by the abrupt temperature rises that the gasoline between three fourths and one fourth of the tank height vaporized in 10 min. By using the dimensions in the report, this was calculated to have been 90 gal. It appeared from the illustrations in the report that probably an area equivalent to not more than the lower half of the tank less one head was exposed to the flame during the period. This is about 15 sq ft of area. The gasoline weighed 6.3 lb per gal at normal conditions. Its latent heat of vaporization was about 130 Btu per lb. Then the heat absorbed would be calculated as follows:

$$\frac{90 \times 6.3 \times 130}{15} \times \frac{60}{10} = 29{,}500 \text{ Btu per hr per sq ft}$$

The data indicate that the exposure fire lasted in all about 25 min, during which time the tank metal was heated, the gasoline raised to the boiling point, and 129 gal were vaporized. On this over-all basis, the intensity of the fire to the tank may be calculated, as follows:

To Heat Metal

$$113 \text{ lb} \times 0.23 \times 325 \text{ deg avg } dt = 8{,}450 \text{ Btu}$$

To Heat Liquid to Boiling Point

$$147 \text{ gal} \times 6.3 \text{ lb} \times 0.57 \times 207 \text{ deg avg } dt = 109{,}200 \text{ Btu}$$

Latent Heat of Vaporization

$$129 \text{ gal} \times 6.3 \text{ lb} \times 130 = 105{,}700 \text{ Btu}$$

$$223{,}350 \text{ Btu}$$

Intensity

$$\frac{223{,}350}{31.5 \text{ sq ft total exposed}} \times \frac{60}{25} = 17{,}000 \text{ Btu per hr per sq ft}$$

The time-pressure curves show that rapid ebullition started at about 4 min after ignition. The vaporization period for 129 gal was then about 21 min, and a heat-input rate to the contents may be approximated:

$$\frac{105{,}700}{15} \times \frac{60}{21} = 20{,}100 \text{ Btu per hr per sq ft.}$$

It is concluded that the actual maximum heat-input rate lies between 20,000 and 29,000 Btu per hr per sq ft of wetted surface exposed.

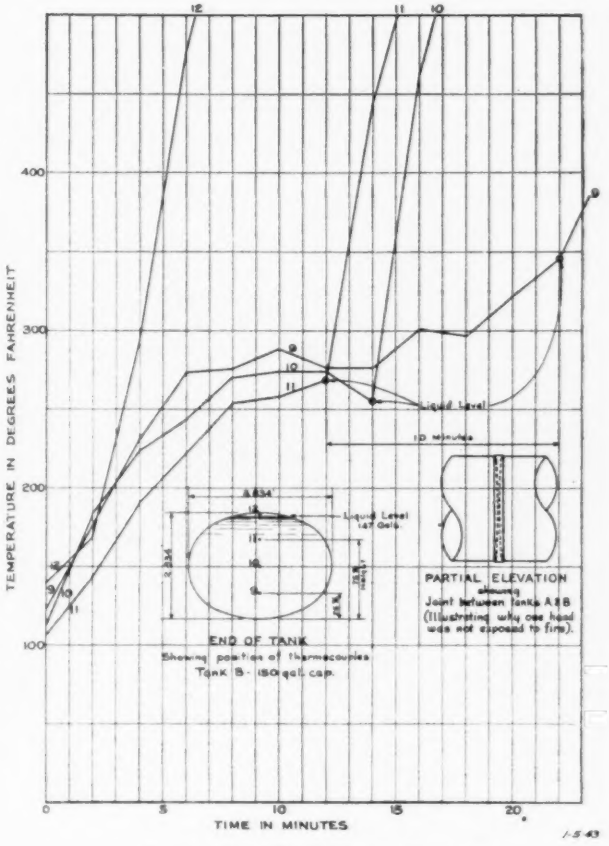


Fig. 6 Time-Temperature Curves
(Transposed from Fig. 4 of ref. 11.)

Tank Fire-Exposure Tests by the Authors

Introduction. Since existing information on the subject seemed inadequate, a series of exposure tests was conducted by the authors' company, in which a 3000-gal nominal-capacity tank containing 2300 gal of water was surrounded by an intense fire. These were begun in the fall of the year 1938 and were concluded in April, 1940. Herein are described and analyzed the last four tests, since the results obtained during these are considered the more accurate and comprehensive.

The tests were conducted (1) to establish a safe minimum heat-input rate for the basis of requirements for emergency relief, (2) to determine the necessary rate of application of external cooling-water film both to maintain a specified temperature within the contents and to approximate the amount required to preserve such vessels when involved in a conflagration. The latter consideration is the subject of a separate discussion, the present purpose being to determine a heat-input rate.

Summary. When a tank is surrounded by an intense fire having an effective temperature of about 1400 F, heat is absorbed from the flame at a rate of the order of 20,000 Btu per hr per sq ft of wetted surface exposed.

[11] Report on "Impact, Hydrostatic, and Fire Tests—Aluminum Alloy Compartments for Tank Trucks," Aluminum Company of America, New Kensington, Pa., 1930.

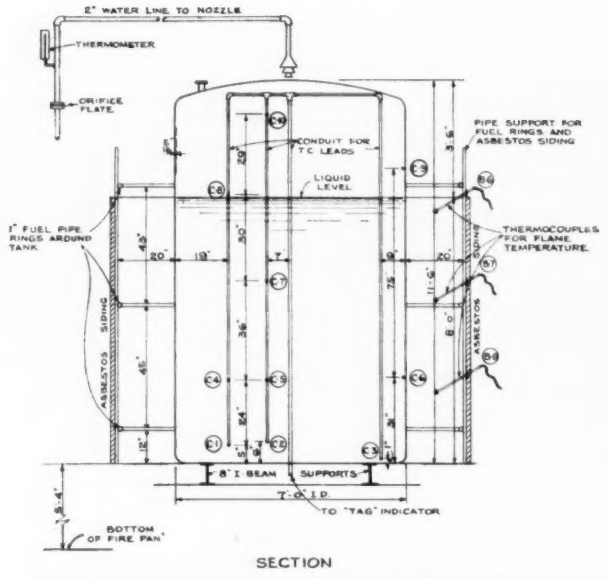


FIG. 7 EQUIPMENT ASSEMBLY TANK FIRE-EXPOSURE TESTS
(Carbide & Carbon Chemicals Corporation, South Charleston, W. Va.)

Test Setup. The general assembly of the equipment used is shown in Fig. 7. The tank used for the test was 7 ft in diam × 11 ft 6 in. high. It was found necessary to surround the equipment with a corrugated asbestos cylinder 10 ft, 4 in. in diam, in order to prevent wind from blowing the flame away from the tank, as may be observed in Figs. 8 and 9. For convenience and safety, the tank was set on steel beams at 5 ft 4 in. above the bottom of an existing fire pan.

The temperatures were measured with thermocouples placed inside the tank, on the tank wall, and in the flame. A direct-reading "Celectray" potentiometer was used for converting the electromotive-force readings to deg C. Mercury-in-glass thermometers were used to measure the cooling water and atmospheric temperatures.

The cooling water was measured with an orifice and was released on top of the tank through a funnel-type nozzle. It flowed over the head and wall in a uniform film and was collected in a trough. The cooling water was not only a part of the experiment but preserved the vessel as intended.

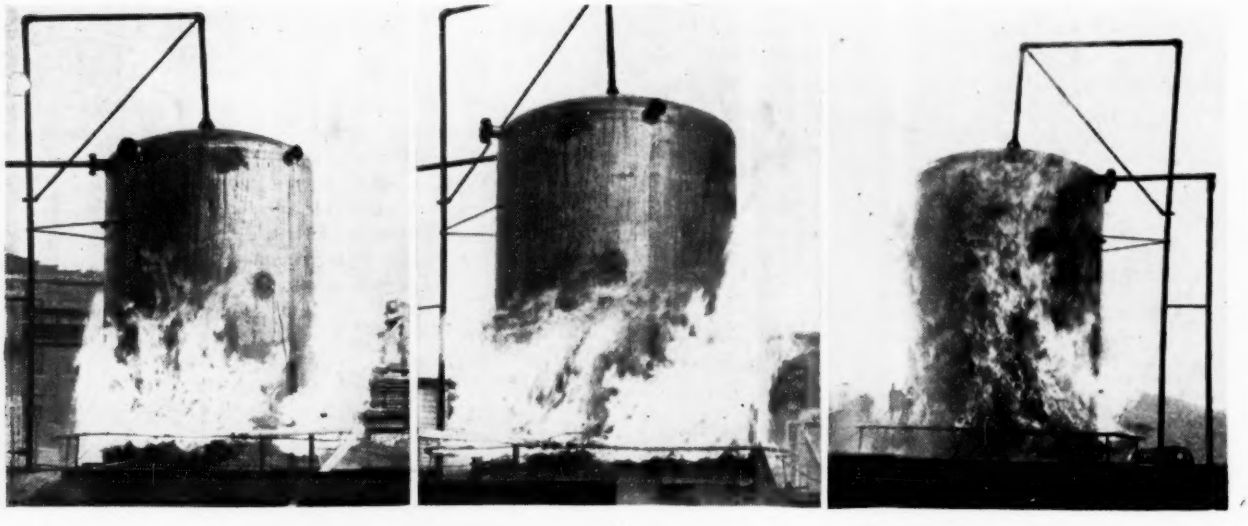
The fire was made by burning hydrocarbons in atmospheric air. The fuel was released through three 1-in. standard-pipe perforated rings, concentric with the tank. The fuel rings were about 4 ft apart vertically, as shown in Fig. 9, and from inspection produced a flame which surrounded the tank thoroughly. The liquid fuel was measured by observed difference in level, as indicated by calibrated tank gages.

Test Procedure. At the start of the tests, the tank contained 2300 gal of water. After making zero readings of the temperatures, the cooling water was started and the fuel was ignited. The fuel rate was kept relatively constant throughout a test run. The temperatures of the flame, cooling water, atmosphere, and contents (water) were recorded at approximately 15-min intervals. The cooling-water rate was adjusted to three values, 143 gpm, 71 gpm, and 37 gpm. No cooling water was used during run No. 4 and partial boiling occurred. During this last test, the fuel rate was reduced to less than one third that of the previous runs, but the flame temperature at the points read was maintained.

Data Obtained. When the temperature of the contained water remained constant, a condition of equilibrium existed, and the data shown in Table 1 correspond to that phase of the first three runs. During test No. 4 in which no cooling water was used, the experiment was stopped before stabilized conditions were reached (contents averaged 73.5 C), in order to avoid possible rupture of the vessel.

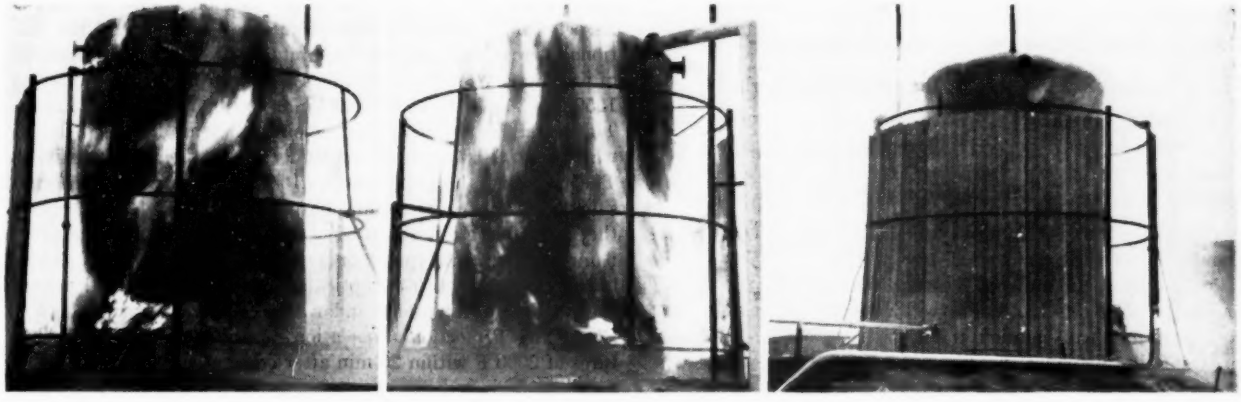
Discussion of Data. Surrounding the equipment with a cylinder to control windage no doubt increased radiation to the tank, but it is believed conditions are equally as severe where a vessel is surrounded by flame of considerable depth. As a counteractant to this effect, there occurred a strong updraft between the cylinder and tank. This was partly due to the 5-ft clearance under the tank as described.

The flame temperatures read are not believed to be maximum since the unshielded thermocouples could "see" the cooling-water film. The lower flame temperatures shown in runs Nos. 2 and 3 were apparently due to wind and rain. This resulted in lowered heat-input rates during these runs.



(*a*) (*b*) (*c*)

FIG. 8 TRIAL RUNS ON 3000-GAL WATER TANK EXPOSED TO INTENSE FIRE
(*a* and *b*, Trial run 10-18-38; H_2 and CH_4 gas fuel; larger quantity of fire needed. *c*, Trial run 10-19-38; liquefied hydrocarbons fuel; denser fire needed.)



(*a*) (*b*) (*c*)

FIG. 9 FURTHER RUNS ON TANK FIRE-EXPOSURE TESTS

(Test runs 11-2-38; liquefied hydrocarbon fuel released through three rings of pipe; windshield in place.)

TABLE 1 OBSERVED AND CALCULATED DATA PERTAINING TO A 3000-GAL STEEL TANK CONTAINING 2300 GAL OF WATER AND EXPOSED TO A FIRE

	Run No. 1	Run No. 2	Run No. 3	Run No. 4
Total cylindrical surface exposed to fire, sq ft	242	242	242	242
Cylindrical surface in contact with contained liquid, and exposed to fire, sq ft	176	176	176	132[a]
Rate of cooling water on external surface of tank, gpm	143	71	37	0
Temperatures, average, deg C:				
Cooling water off	61.2	61.3	58.0	...
Cooling water on	12.5	12.2	11.5	...
Cooling water rise	48.7	49.1	46.5	...
Cooling water average	37.0	37.0	35.0	...
Flame temperature	820	690	714	721
Water inside tank	58	84	92	9 to 73.5 per hr
Surface of tank, external	58	84	92	12 to 100 per hr
Surface of tank, internal	58	84	92	10 to 95 per hr
Surface of tank not in contact with contained water	36	58	66	10 to 190 per hr
Surface of tank, log mean average	46	70	78	10 to 140 per hr
Fuel vapor rate, cfh	40,857	40,857	40,857	12,200
Total available heat in fuel, Btu per hr	106,000,000	106,000,000	106,000,000	29,900,000
Heat absorbed by tank, contents, and cooling water, Btu per hr	6,270,000	4,186,000	4,522,000	2,311,100
Heat absorbed by radiation, Btu per hr	5,760,000	3,737,000	4,050,000	2,100,000
Heat absorbed by convection, Btu per hr	510,000	449,000	472,000	211,100
Sensible heat absorbed by cooling water, Btu per hr	6,270,000	3,137,000	1,550,000	0
Latent heat absorbed by partial evaporation of cooling water, Btu per hr	0	1,049,000	2,972,000	0
Heat absorbed by tank contents, Btu per hr	0	0	0	2,225,000
Rate of heat absorption (heat density), Btu per hr per sq ft	25,900	17,300	18,700	16,850 by contents

[a] See section "Discussion of Data."

During run No. 4 in which no cooling water was used and the fuel rate was reduced to less than one third by using only the lower fuel-pipe ring, it was estimated that 2 ft of the wetted height of the tank was not exposed to flame. Conditions were similar to those shown in Fig. 8 (*a* and *b*). This reduced the wetted surface exposed to 132 sq ft.

The experiment covered three conditions of a tank exposed to fire: namely,

1 Contents maintained at a certain maximum temperature as in run No. 1. The vent rate was kept low and the absorbed heat appeared as sensible heat in the cooling water film.

2 Contents heated to higher maximum temperatures as in runs Nos. 2 and 3. The absorbed heat appeared as both sensible heat and heat of vaporization in the cooling-water.

3 Contents allowed to heat up as under actual conditions where a tank is unprotected and exposed to fire. The vent rate became high and the absorbed heat appeared as sensible heat in the contained water.

Observed Heat Absorbed Compared With Theoretical Calculations. The data indicate that the flame transmits heat to the tank by radiation and that the heat thus transmitted is again transferred by convection to the water film flowing over the tank surface. As a result, no heat is transmitted to the contents after equilibrium conditions are established. The film of water flowing over the surface of the tank also absorbed heat directly from the flame by convection, and under conditions of low water flow, as in runs Nos. 2 and 3, some water is vaporized from the flowing film. Calculations for this apparent mechanism of heat transfer compare well with the observed heat absorbed in runs Nos. 1, 2, and 3 and are submitted as further evidence to support the heat-input rates tabulated for these runs. The sensible heat absorbed during run No. 4 is direct evidence and, of course, not affected by this theory since no cooling water was used.

Calculated values for run No. 1 follow:

The sensible heat absorbed by the water film is

$$143 \times 8.337 \times 60 \times 1.0 \times 1.8 \times 48.7 = 6{,}270{,}000 \text{ Btu per hr}$$

or 25,900 Btu per hr per sq ft

Theoretically, the heat transmitted to the tank surface by radiation using the data in Table 1 is

h_r = 18.5 Btu per hr per sq ft per deg F by Equation [3]

$$18.5 \times 242 \times (1508 - 114.8) = 6{,}240{,}000 \text{ Btu per hr}$$

The heat absorbed by the water film by convection using the data in Table 1 is

h_c = 1.65 Btu per hr per sq ft per deg F by Equation [2]

$1.65 \times 242 \times (1508 - 98.6) = 563{,}000$ Btu per hr

Then by the proposed theory, the total heat absorbed by the water film is

$$6{,}240{,}000 + 563{,}000 = 6{,}803{,}000 \text{ Btu per hr}$$

or 28,100 Btu per hr per sq ft

This theoretical, total heat absorption is only 8.5 per cent greater than the observed heat absorbed.

By the theory, the radiated heat absorbed by the tank surface is again transferred to the cooling-water film by convection. For this type of heat transmission, the transfer coefficient is obtained from the following equation

$$h_w = \frac{1}{2} \cdot \frac{f^{2/3}}{(CZ/h)^{2/3}} C(2g\rho^2\Gamma)^{1/3} \quad \ldots\ldots [6][12]$$

Using this and the observed data in Table 1, the heat absorbed from the tank surface by the water film is

h_w = 1490 Btu per hr per sq ft per deg F, by Equation [6]

$1490 \times 242 \times (114.8 - 98.6) = 5{,}840{,}000$ Btu per hr

This is only 6.41 per cent less than the calculated heat absorbed by the tank surface by radiation as given (6,240,000) and apparently establishes the heat-transfer theory.

Further, according to theory $\left(\frac{18.5}{(18.5 + 1.65)} \times 100\right)$, 91.8 per cent of the heat absorbed by the cooling water was taken by convection from that radiated to the tank surface, so

$$6{,}270{,}000 \text{ (observed)} \times 0.918 = 5{,}760{,}000 \text{ Btu per hr}$$

This compares well with the 5,840,000 Btu per hr calculated with the theoretical heat-transfer coefficient (1490).

Calculations for run No. 4 are as follows:

The sensible heat absorbed by the contents water is

$$2300 \times 8.337 \times 1.0 \times 1.8\ (64.5) = 2{,}225{,}000 \text{ Btu per hr}$$

or 16,850 Btu per hr per sq ft

The observed heat absorbed by the tank is

$$242 \times \frac{0.3125}{12} \times 487 \times 0.12 \times 1.8\ (130) = 86{,}100 \text{ Btu per hr}$$

Total heat absorbed ..... 2,311,100 Btu per hr

This observed heat absorbed is only 8.45 per cent less than the theoretical heat input when calculated as for run No. 1. The calculations indicate the heat absorbed by radiation to be 90.8 per cent of the total heat absorbed by the tank.

Flame Temperatures and Effective Height

Since the heat-input rate to a vessel exposed to fire is sensitive to the mean effective flame temperature, as previously noted under the discussion of Fetterly's work, it is well to emphasize the fact that high temperatures are common during fires. It has been shown that effective flame temperatures of about 1400 F produce heat-input rates of the order of 20,000 Btu per hr per sq ft of wetted surface exposed.

The standard time-temperature curve,[13] used by the American Society for Testing Materials, the National Fire Protection Association, the Underwriters' Laboratories, Inc., and the National Bureau of Standards for a "standard scale of measurement of fire severity" rises to 1000 F in 5 min, to 1300 F in 10 min, to 1550 F in 30 min, to 1700 F in 1 hr, and so on up to 2300 F, in 8 hr. These are effective temperatures since they are furnace heats to which materials are subjected to determine their fire resistivity. The authors of this paper observed 1600 F temperatures with unshielded thermocouples while burning liquefied hydrocarbons in the open. The Underwriters' Laboratories, Inc., read 3000 F flame temperatures (point or maximum) from an open pan of burning gasoline with an optical pyrometer. As stated before, the National Bureau of Standards in co-operation with the National Fire Protection Association observed wood-fire temperatures of 2000 F within 20 min after ignition within a large brick building.

The authors are unable to learn of a substantial theory or to find convincing evidence to support the limiting of heat inputs into vessels exposed, to any particular height above the fuel. Insurance underwriters' recommendations of fireproofing supporting columns within 20 ft of a source of fire, as well as the practice by reliable organizations to limit heat inputs to 20 ft elevation, have been noted, but these do not seem adequate. Aluminum (1125 F to 1490 F melting point), glass (1400 F to 1600 F melting point), and brass (1575 F to 1800 F melting point) have been observed melted more than 20 ft above grade after flammable-liquid-spillage fires in open areas. These fires were of less than 1 hr duration. Examination of the analysis of fires by the National Fire Protection Association and the Factory Mutual Fire Insurance Companies, particularly those involving storage-tank farms and elevated tanks, discloses that high heats do prevail at comparatively great heights above the fuel during severe fires.

The foregoing evidence and experience support the following suggestion:

Where vessels are in confined areas, buildings, or enclosures, and an intense fire could occur, no reduction from the maximum height of the surface to be wetted by the contents should be used when designing emergency pressure-relief or other fire protection. Where such equipment is in open areas, properly spaced, diked, and otherwise installed in accordance with the insurance inspection organization having jurisdiction, it is considered not economical to design for a heat-input height of less than 40 ft, and unsafe under average conditions to use less than 30 ft. Further, no reduction of heat input is proposed (except for atmospheric tanks as outlined in Part 3) to allow for the possibility that vessels may not be completely surrounded with flame during a general fire.

Conclusion

A rate of heat absorption for vessels exposed to fire as a basis of requirements for relief of overpressure is concluded as outlined under Summary from the foregoing experiments, theory, and experience.

The employment of this basis follows in Parts 2 and 3 of this paper.

The authors are cognizant that the observed absorption rate (20,000 Btu per sq ft per hr) appears high when compared to overall heat-absorption rates of boilers, tube stills, etc. It is reasonable, however, when compared to those rates[14] for waterwall sec-

[12] "Principles of Chemical Engineering," by Walker, Lewis, McAdams, and Gilliland, McGraw-Hill Book Company, Inc., New York, N. Y., 1937, Equation [11c], p. 114.

[13] "Handbook of Fire Protection," p. 380.

[14] For further information on absorption rates in boilers, refer to "Kent's Mechanical Engineers' Handbook," vol. 2, "Power," John Wiley and Sons, Inc., New York, N. Y., eleventh edition, 1937, pp. 6–17, 6–18, and 6–36; "The Trend of Boiler Design," Bulletin 3-180, The Babcock and Wilcox Company, New York, N. Y., 1935, pp. 3 and 4; "The Simple and Direct Answer to All Problems of Heat Transfer in Boilers," by L. R. Stowe, Wilmette, Ill., 1937, chapters 12 and 13.

tions and tubes adjoining combustion chambers which may absorb heat at rates from 50,000 to 150,000 Btu per sq ft per hr, based upon the projected area.

PART 2 REQUIREMENTS FOR RELIEF OF PRESSURE VESSELS[15]

Introduction

One of the fundamental considerations in all codes and regulations applying to boilers and unfired pressure vessels has been that of preventing overpressure and its attendant hazards. In all boiler codes and regulations, it has been almost universal practice to base the size and capacity requirements for safety valves on the potential heat input, which is computed from the total area of the heat-absorbing surfaces of a boiler. In codes and regulations applying to unfired pressure vessels, however, while pressure-relief devices are required and an overpressure limit is specified, there is no measurable basis upon which to compute the capacity of such relief devices. In Paragraph U-2 of the A.S.M.E. Unfired Pressure Vessel Code,[16] the question of relieving capacity is referred to by specifying that the relief devices shall be of such capacity as to prevent a rise of more than 10 per cent above the maximum allowable working pressure, but the user of a pressure vessel receives no directions from that code as to how to proceed to compute that capacity.

Actual operating experiences in industrial plants tend to give the general impression that an appreciable number of "code pressure vessels," if investigated, would be found to be under-equipped with pressure-relief capacity. It is often contended that pressure vessels equipped with automatic controls are inherently more safe than those not so equipped; yet it is a matter of record that when such automatic controls fail or become inoperative (as will happen occasionally) an accident often follows. The very natural relaxation of vigilance, which comes from depending upon automatic controls, causes neglect of the pressure-relief devices; and if they will operate, they are likely to be found inadequate in capacity. When pressure vessels do fail in service, it is always found that some one of the important safety considerations has been overlooked or neglected, and in many of such cases, it is found that the pressure-relief devices are inadequate in capacity.

Our experience during the past 8 years, in inspecting thousands of pressure vessels and testing thousands of relief valves and safety devices, has indicated a very definite need for more information on the subject of pressure relief, and the authors have undertaken an investigation to obtain additional data. The results to date appear to warrant presentation of a statement in order to learn whether the data will be useful to the A.S.M.E. Code Committee and other code-making bodies. The authors have in the past found the Unfired Pressure Vessel Code a most valuable aid in their work and, in appreciation thereof, desire to offer their co-operation in every way possible. If the data obtained appear likely to prove helpful to the code committees, they will be placed at the disposal of such committees, and if necessary, additional information will be gathered.

In any comprehensive study of this broad question of protection against overpressure, it is advantageous to consider the sources from which pressure is induced in vessels. In a large percentage of cases, the source of the pressure is mechanical pumping or compression with pressure regulation possible at the source, as is exemplified in air compressing and refrigerating systems; in these, overpressure is likely only on the rare occasions when control apparatus fails. In the large number of cases where pressure is transmitted from the source through systems of piping, as in chemical and petroleum processes, there is no such simplified control possible; and the pressure may be increased from overfilling, overheating, chemical action, or improper operation. Of these several causes, probably the most serious is overheating. In chemical and petroleum plants, where the condition of volatile contents in vessels is inherent and in cases where pressure vessels with relatively nonvolatile contents have been subjected to exposure fires, disastrous explosions have occurred. This class of equipment (chemical and petroleum) is probably representative of those most difficult to control from a safety viewpoint.

It is the observed tendency of codes and regulations to call for safety protection to meet the worst possible hazard which may be encountered and which, in pressure-vessel operation, is probably the overheating that may result from exterior fire exposure. In the past, it has been customary (with few exceptions) to treat such disasters as acts of the elements which are beyond human control, but our investigations tend to show that this conclusion is not warranted. During the past 4 years, the authors have been devoting study to this phase of relief of overpressure and are now of the belief that even such extreme conditions as fire exposure can be foreseen and provided for. Our studies have covered the effects of exterior heating by small fires and conflagrations, the heat-absorbing capacity of pressure vessels with differing contents, and the capacity necessary in the form of pressure-relief devices; and it is now our desire to present the results for general consideration.

From the observation that pressure vessels surrounded by fire, as in conflagrations, represent what is probably the most hazardous condition to which they may be subjected, the primary objective in the investigation mentioned has been to determine the resulting rise in pressure and the extent of relief capacities necessary to limit pressure rises to safe values. It is believed that, if we thus provide adequately for the worst possible condition, more complete safety can be assured, and that some judicial body, such as the A.S.M.E. Code Committee, will be able to determine what measures are necessary for intermediate cases. It will thus be evident that the primary condition to be studied was that of a pressure vessel filled or partly filled with a volatile liquid and completely surrounded by flame. With this object in view, the foregoing tests (summarized in Part 1) were carried out.

A heat-input rate having been concluded in Part 1, it now becomes necessary to correlate the several variables of container dimensions, working pressures, and properties of contents into useful expressions whereby the necessary relief capacity can be calculated in terms of relief area. This will be done in this section for vessels to operate at pressures above 15 psig.

Summary

Developments herein are based upon the premise that the liquid contents of vessels involved in fire will absorb heat at the rate of 20,000 Btu per hr per sq ft of wetted surface exposed, as developed in Part 1 of this paper.

It was concluded that two formulas, which are derived in the appendix, if properly applied to any vessel to operate at pressures above 15 psig, will specify the relief capacity in terms of area of opening required to limit the pressure rise within 10 per cent above the maximum allowable working pressure. These are as follows:

The diameter of a relief connection (a short tube) necessary to relieve a pressure vessel adequately, when the volatile-liquid contents are vaporized by the heat of the external fire, is determined by the following formula

$$d = \sqrt{\frac{97.3\,S_w}{(P + 14.7)}} \left(\frac{P + 448}{3333.3}\right) \quad \text{[7]}$$

[15] Above 15 psig.

[16] "A.S.M.E. Code for Unfired Pressure Vessels," New York, N. Y., 1940 edition, p. 2.

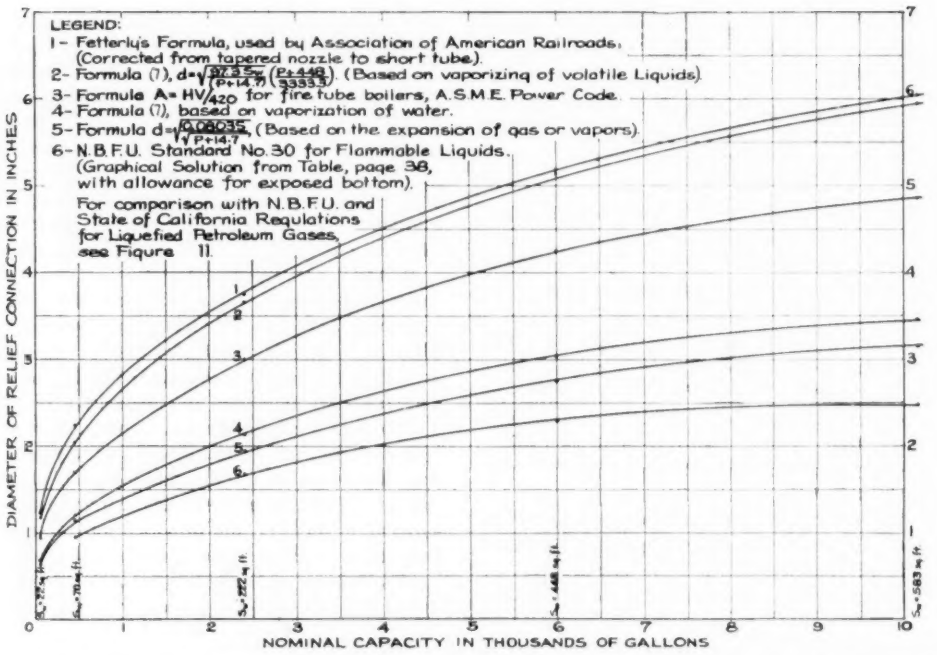


FIG. 10 COMPARISON OF REQUIRED DIAMETER OF CONNECTION TO RELIEVE PRESSURE VESSELS OF 15 PSIG WORKING PRESSURE WHEN EXPOSED TO FIRE

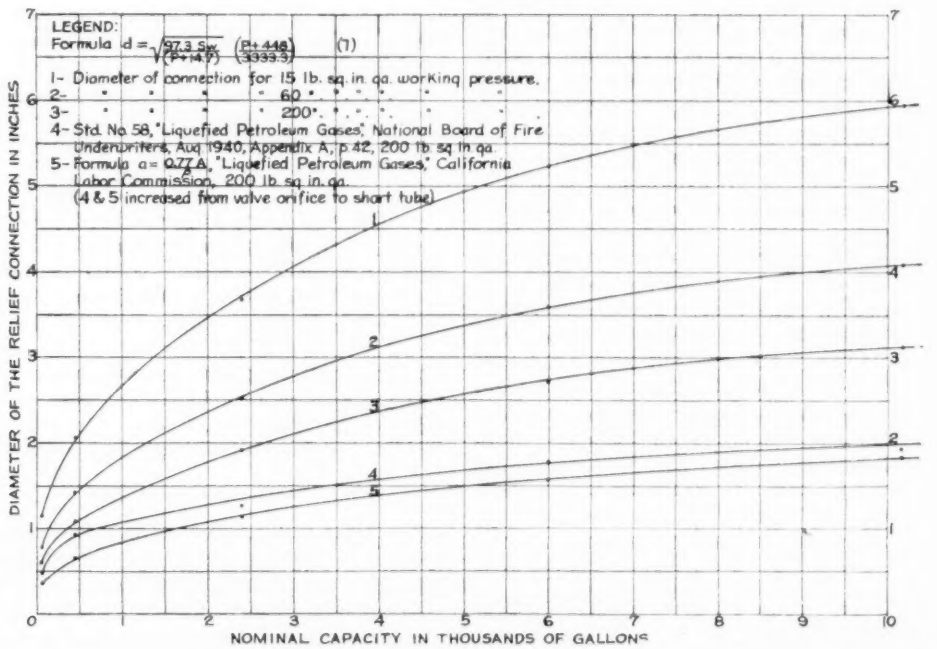


FIG. 11 COMPARISON OF REQUIRED DIAMETER OF RELIEF CONNECTION AT DIFFERENT WORKING PRESSURES FOR VESSELS EXPOSED TO FIRE

The diameter of a relief connection (a short tube) necessary to relieve a pressure vessel adequately when a gas or vapor (the only contents) is expanded by the heat of external fire is determined by the following formula

$$d = \sqrt{\frac{0.0803\,S}{\sqrt{(P + 14.7)}}} \qquad [8]$$

in which d is in inches, S_w under Equation [7] is wetted surface exposed in square feet, S under Equation [8] is total surface exposed in square feet, and P in either case is maximum allowable working pressure in pounds per square inch gage plus 10 per cent or the safety-device opening pressure, whichever is the lowest. The P in the second term of Equation [7] is not to exceed the numerical value of the critical pressure in pounds per square inch gage of the contents regardless of the working pressure.

In order that the results of these formulas may be compared with other known proposals or standards, Fig. 10 has been in-

cluded. In this it may be noted that the specifications for tank cars of the Association of American Railroads[17] (Fetterly's formula analyzed in Part 1) give relief areas (average over the range) about 10 per cent in excess of Equation [7]; that Equation [7] for volatile liquids gives relief areas about 50 per cent (in larger sizes) greater than those specified by the A.S.M.E. Code[18] for steam; and Equation [7] when modified by the properties of water, gives relief areas about 50 per cent less than the regulations for steam boilers. Although comparison of pressure vessels with boilers is hardly justified (wetted surface exposed to fire compared with boiler heating surface), it does show that the developed formulas give results in the logical direction. (About 6 times as much heat is required to vaporize water as to vaporize an equivalent weight of the volatile liquid considered.)

For comparison of Equation [7] with the National Board of Fire Underwriters' Regulations[19] and the Safety Orders by the Industrial Accident Commission of the State of California[20] for liquefied petroleum gases, see Fig. 11.

Analysis and Method

The reasoning in arriving at Equations [7] and [8] is as follows.

When a vessel is enveloped with flame, heat is absorbed by the contents and temperature within rises. If the contents be liquid, vapors are formed and boiling eventually occurs. The relief capacity must then be at least equal to the vaporization rate, or internal pressure will continue to rise and rupture may follow. If the weight rate of the relief connection is equated to the weight rate vaporized, Equation [9] results which is the origin of Equation [7]

$$d = \sqrt{\frac{IS_w}{205.5P}} \left(\frac{T}{Mr^2}\right)^{1/4} \quad \ldots\ldots\ldots\ldots [9]$$

in which I is the heat-input rate in Btu per hour per square foot, S_w is surface as in Equation [7], P is absolute pressure; and the last term is the contents factor F, in which T is the boiling point at the pressure P in deg F absolute, r is the latent heat of vaporization in Btu per pound at temperature T, and M is the molecular weight. The simplification of this factor is outlined under the heading *Contents Factor*, to be discussed later.

If a vessel contains gas or vapor and is exposed to fire, rapid expansion of the contents takes place (refer to the pressure curve, Fig. 2, Part 1). The relief capacity must then be at least equal to the rate of volume increase, or uncontrolled pressure rise results. If the weight rate of the relief connection is equated to the weight rate of expansion, the following equation results, which is the origin of Equation [8]

$$d = 0.02615 \frac{S^{1/2}}{P^{1/4}} \cdot \frac{(T_w - T)^{5/8}}{T^{0.325}} \quad \ldots\ldots\ldots [10]$$

in which S is surface as in Equation [8], P is absolute pressure, and the last term is the gas-expansion variable, in which T_w is the temperature to which the tank shell is heated, and T is the initial gas or vapor temperature both in deg F absolute. This term is reduced to a constant by inserting temperature limits, as described under *Gas Expansion Variable*, to be discussed. The rate of volume increase of a gas is always less (other conditions being equal) than the vaporization rate of liquids as will be seen.

For derivations of Equations [9] and [10] refer to the Appendix.

The relief capacity is proposed in terms of area of the relief connection (or connections) because the designer is primarily interested in selecting an adequate fitting of standard size for the vessel to be constructed, and because of the great variation in the capacity of commercial relief apparatus. This connection is ordinarily an inserted short tube with a square inner edge, somewhat rough from the standpoint of fluid flow. The relief device may afterwards be selected of a capacity (based on approved flow test) to pass the vapor rate of flow computed from relief area, as will be explained later. Although the vapors and gases to be contained and discharged have been assumed as perfect gases, the formulas give results in the direction of safety when there is deviation from the gas law.[21]

Weight Rate of a Short Tube. The formula[8] $W = 306\ aP \times \sqrt{M/T}$, which is generally known, is used in this development. It is universally employed and of proved accuracy. This expression is incorporated in the "API-ASME Code for Unfired Pressure Vessels," as the calculated capacity of relief devices of nozzle design. It was derived from the adiabatic flow of an ideal gas through an orifice, modified for flow above the critical-pressure ratio, and holds for this class of equipment having working pressures above 15 psig.

As written, the formula incorporates an orifice coefficient of 0.97 for a tapered nozzle. Generally, 0.83 is used for a short tube, such as the relief connection described (at pressures of this magnitude). Thus the constant has been multiplied by 0.83/0.97 so that the formula reads

$$W = 262\ aP \sqrt{\frac{M}{T}} \quad \ldots\ldots\ldots\ldots [11]$$

for the vapor weight rate of a short tube in pounds per hour. Refer to the Appendix for nomenclature.

The Contents Factor F, $\left(\frac{T}{Mr^2}\right)^{1/4}$. To use Equation [9], $d = \sqrt{\frac{IS_w}{205.5P}} \left(\frac{T}{Mr^2}\right)^{1/4}$, it is necessary to find values of temperature and latent heat of vaporization for the compounds contained, compatible with the set pressure of the device, P. For many liquids (at various pressures) common to industry, these are not available; and if they were, their use in individual cases would result in numerous vent sizes adequate only for materials of like properties at the same condition. In an effort to facilitate the use of the expression, several studies were undertaken.

Finally, it appeared possible that, if the properties of the known hazardous liquids were graphed, a value of the factor F might be chosen which would be satisfactory for the many compounds to be contained. Accordingly, Fig. 12 was prepared. This is a plot of the numerical value of the contents factor versus the vapor pressure of 36 compounds so far as latent-heat data are available. In so far as possible, a cross section was shown of the many types of liquids and gases commonly found in industry. If the graph were enlarged, additional curves at low pressures could be made intelligible in the more congested area for materials such as hexane, ethylene oxide, styrene, ordinary motor gasoline, isobutylene, vinyl chloride, and "Tetralin." Although of limited number, those shown are sufficient for the development of the discussion.

[17] "Specifications for Tank Cars," Standard, Association of American Railroads, Chicago, Ill., 1941 edition, p. 163.

[18] Minimum Total Areas in Fire Tube Boilers for Safety Valve Connection, "A.S.M.E. Code for Power Boilers," New York, N. Y., 1940 edition, p. 108.

[19] Standards of the National Board of Fire Underwriters, No. 58, "Liquefied Petroleum Gases," New York, N. Y., August, 1940, Appendix A, p. 42.

[20] "Handbook of Butane and Propane Gases," by George H. Finley, editor, Western Business Papers, Inc., Los Angeles, Calif., second edition., 1935, p. 297.

[21] "Discharge Capacity of Relief Valves for Oil Stills," by K. S. M. Davidson and D. W. MacArdle, reprinted from *Oil and Gas Journal*, by Crosby Steam Gauge and Valve Company, Boston, Mass., August, 1929.

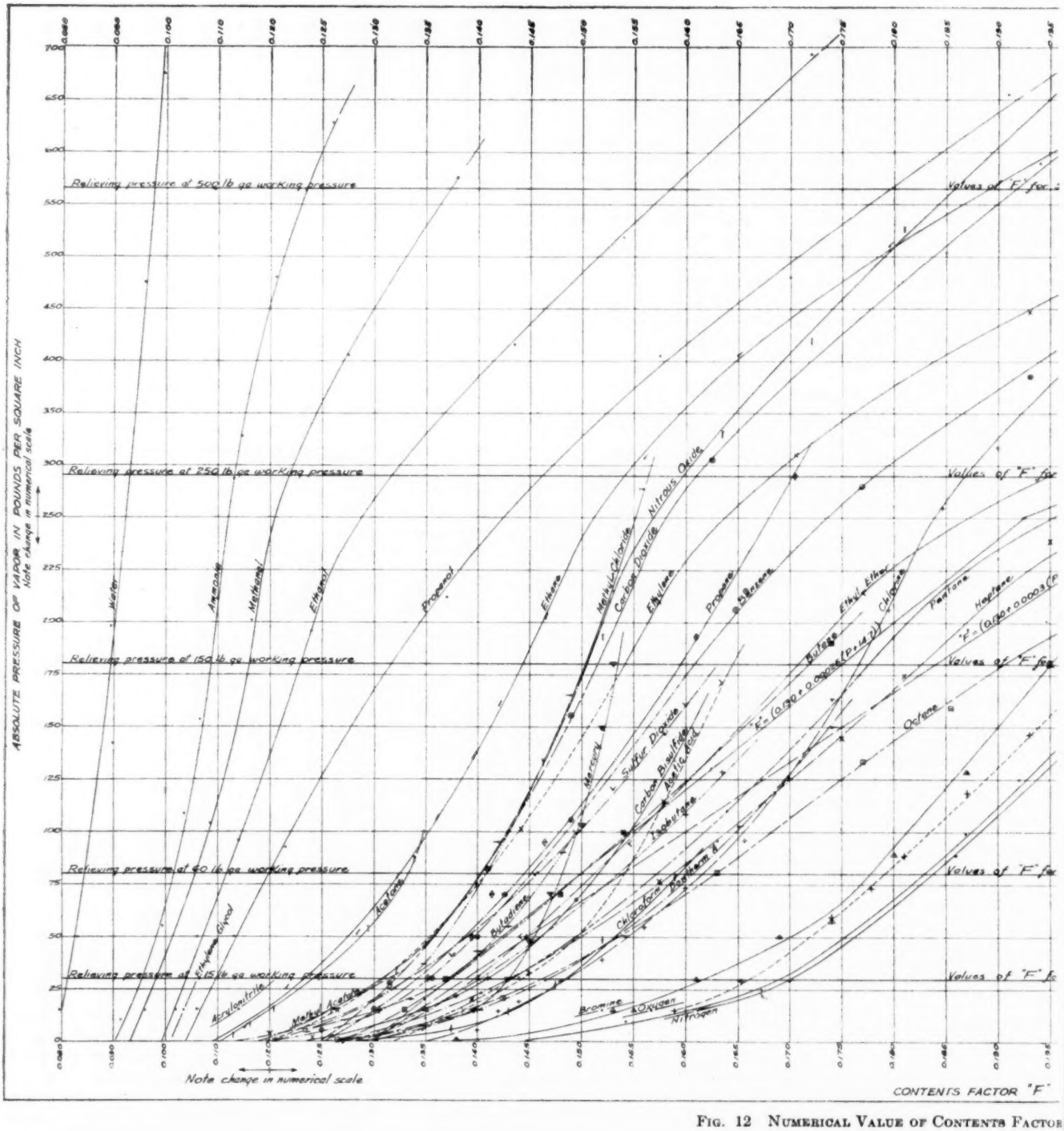


FIG. 12 NUMERICAL VALUE OF CONTENTS FACTOR F VARIO

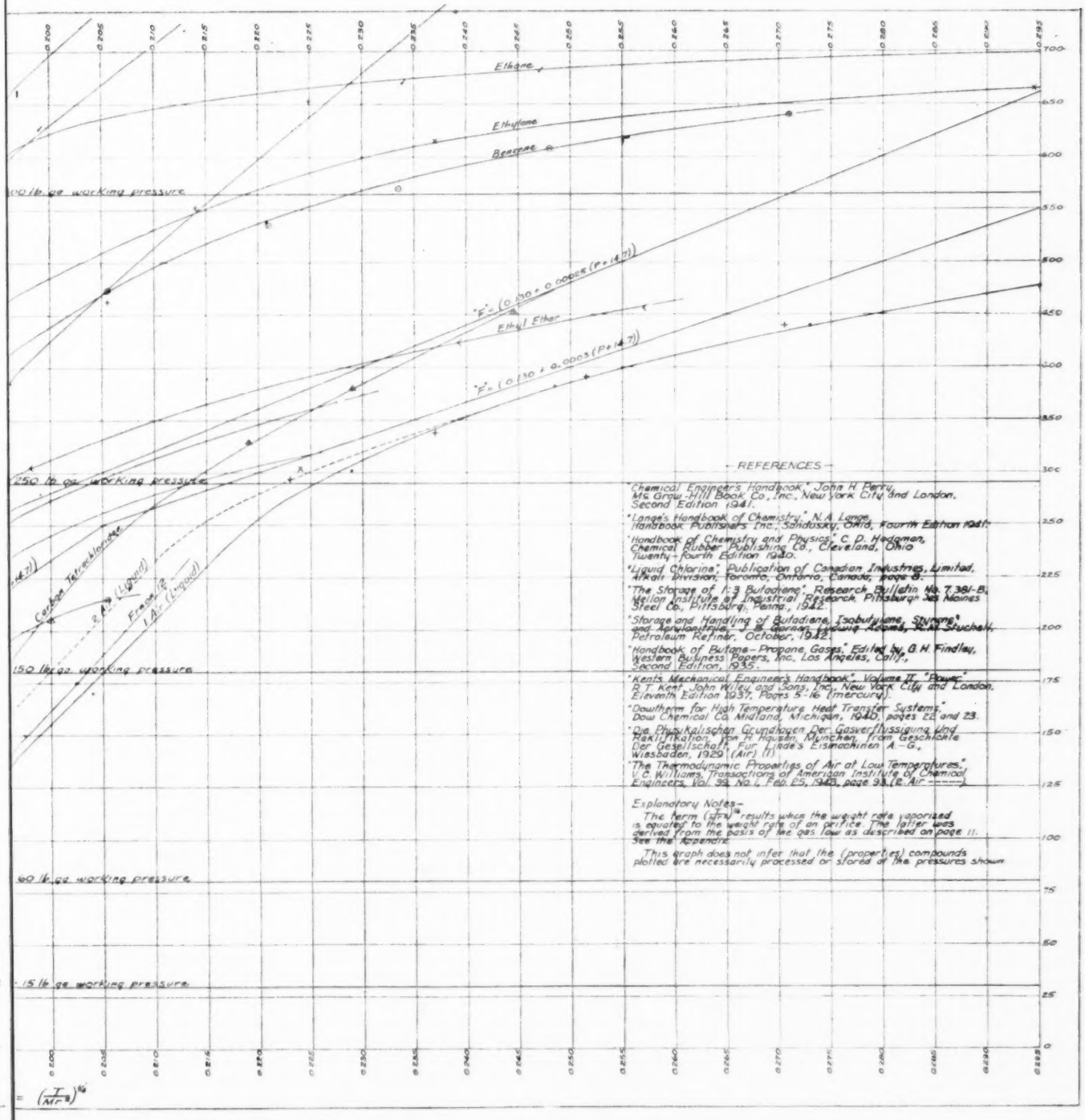
Latent-heat data may be calculated with satisfactory accuracy for other liquids of particular interest by any of several methods found in recent literature. Those provided by H. P. Meissner[22] and Donald F. Othmer[23] are recommended.

Further, the value of F for any compound at 15 psia may be quickly estimated by Trouton's rule, under which conditions F is equal to $(M/T\ 484)^{1/4}$, in which M is the molecular weight and T is the normal boiling point in deg F absolute. It would then be expected from the similarities in the curves in Fig. 12 that the loci of values for the compound considered would approximately parallel those of the compound shown on the graph which is most like that considered in chemical structure and properties.

Where two or more compounds are contained in a vessel, the value of the contents factor should be based on that which will produce the greatest vaporization rate when the volatility and weight per cent of the several components are considered.

[22] "Latent Heats of Vaporization," by H. P. Meissner, *Industrial and Engineering Chemistry*, vol. 33, 1941, p. 1440.

[23] "Correlating Vapor Pressure and Latent Heat Data," by D. F. Othmer, *Industrial and Engineering Chemistry*, vol. 34, 1942, p. 1072.



Various Liquids at Absolute Pressures

To illustrate the relative effect of type of contents and magnitude of pressure on the required relief area, Table 2 is given. The diameters were calculated for a large pressure vessel by Equation [9], using values of the contents factor from the graph. The multiplicity of the sizes resulting, the increase of relief diameter with ratio of M/T of the compounds, and the decrease of relief diameter with pressure in the ordinary ranges are then readily apparent. (The decrease in relief diameters above 200 psi working pressure is slight.)

To simplify the use of these data, it has been suggested that similar tables for various sizes of vessels be made, or that the properties of a liquid such as benzene be employed as a standard for values of the contents factor. However, these do not promote what appears to be the more practical manner of assuring adequate relief area for the contingency of fire exposure. The authors suggest that an arbitrary value of F be used which would specify minimum relief-connection size for vessels of any given capacity within certain ranges of pressure. This will also provide an adequate relief connection (within the limits shown in Table 2) for that class of equipment which undergoes changes in service

TABLE 2 ILLUSTRATING EFFECT OF DIFFERENT CONTENTS AND WORKING PRESSURES ON CALCULATED SIZE OF RELIEF CONNECTIONS FOR A 10,000-GAL PRESSURE VESSEL[a]

Contents	Working pressure, psig: 15	60	150	250	500	Critical temperature, deg F	Critical pressure, psia
	Std. I.P.S., in.			X.S. I.P.S., in			
Water	3.5	2.5	1.5	1.25	1.0	705.2	3198
Ammonia	4.0	3.0	2.0	1.5	1.25	270.3	1640
Methanol	5.0	3.0	2.0	2.0	1.5	464.0	1155
Ethanol	5.0	3.0	2.5	2.0	1.5	469.6	925
Ethylene glycol	5.0	...	...	...	...	806.0[b]	...
Propanol	5.0	3.5	2.5	2.0	2.0	506.7	733
Ethylene oxide	5.0	...	...	...	...	377.6	...
Acrylonitrile	6.0	...	...	...	...	...	...
Ethane	6.0	4.0	3.0	2.5	2.0	89.8	717
Acetone	6.0	4.0	...	...	...	455.0	690
Ethylene	6.0	4.0	3.0	2.5	2.5	49.5	746
Methyl acetate	6.0	...	...	...	...	452.7	678
Carbon dioxide	6.0	4.0	3.0	2.5	2.0	88.0	1070
Methyl chloride	6.0	4.0	3.0	2.5	...	289.6	965
Sulphur dioxide	6.0	4.0	3.0	...	...	315.0	1140
Propane	6.0	4.0	3.0	2.5	...	206.2	617
Nitrous oxide	6.0	4.0	3.0	2.5	...	97.7	1052
Benzene	6.0	4.0	3.0	3.0	2.5	551.3	701
Isobutylene	6.0	...	...	...	...	...	...
Butadiene	6.0	4.0	...	...	...	325.7	...
Butane	6.0	4.0	3.0	...	...	307.4	529
Styrene	6.0	...	...	...	...	671.0[b]	...
Ethyl ether	6.0	4.0	3.0	3.0	...	380.8	521
"Tetralin"	6.0	...	...	...	...	833.0[b]	...
Isobutane	6.0	4.0	...	...	...	273.2	544
Carbon bisulphide	6.0	4.0	...	...	...	523.4	1116
Mercury	6.0	4.0	3.0	...	...	>2822.0	>2940
Heptane	6.0	4.0	3.5	3.0	...	512.2	394
Pentane	6.0	4.0	3.5	3.0	...	387.0	485
Hexane	6.0	...	...	...	...	454.6	434
Acetic acid	6.0	4.0	3.0	...	...	610.9	839
Octane	6.0 and 2.0	5.0	3.5	...	...	564.8	361.5
"Dowtherm A"	6.0 and 2.0	5.0	...	...	...	968.0	...
Chloroform	6.0 and 2.0	5.0	...	...	...	505.4	...
Gasoline (ordinary)	6.0 and 2.0	...	...	...	...	...	...
Chlorine	6.0 and 2.0	5.0	3.5	3.0	2.5	291.2	1118
Bromine	6.0 and 3.5	...	...	...	...	576.0	...
Carbon tetrachloride	6.0 and 3.5	5.0	3.5	3.0	...	541.6	660
"Freon 12"	6.0 and 4.0	5.0	3.5	...	...	...	...
Air (liquid)	6.0 and 4.0	5.0	3.5	3.5	3.5	−253.2	547
When $F = 0.130 + 0.0003\ (P + 14.7)$	6.0	4.0	3.5	3.0	3.0	...	...
When $F = 0.130 + 0.00025\ (P + 14.7)$	6.0	4.0	3.0	3.0	3.0	...	...

[a] Dimensions of pressure vessel, 10 ft 6 in., diam; 18 ft 10 in., height.
[b] Approximate.
NOTE: This table does not infer that the compounds shown are necessarily processed or stored at the pressures listed. Calculations are based on the set pressure of the relief device being 10 per cent in excess of the working pressure.

and which would be desirable from the standpoint of maintenance and operation.

Values of F which might be used to specify the relief-connection size are represented by the designated straight lines in Fig. 12. Reference to Table 2 will show that practical values of d are obtained when F equals $0.130 + 0.00025\ (P + 14.7)$ or $0.130 + 0.0003\ (P + 14.7)$, and when relief devices are applied as suggested in the section, Summary for Use. For purposes of facilitating this development, it is the latter value of F which has been employed in simplifying Equation [9] to Equation [7], since it not only appears adequate, as will be explained, but is not exceeded (except by liquid air),[24] within the limits of available data at higher pressures by the individual contents-factor curves. Very probably, the relief area for pressure vessels larger than 10,000 gal nominal capacity should be computed by Equation [9] for the individual contents when the necessary latent heat - vaporpressure data are obtainable.

It is to be noted that the suggested value [0.130 + $0.0003\ (P + 14.7)$] of F gives diameters consistent with the large majority of the compounds, but less than for some of those tabulated which have high ratios of M/T. Calculations show that this inadequacy holds only at pressures below 100 psig when the next larger pipe size is used as the relief connection. Inasmuch as pressure vessels usually incorporate a strength safety factor of 5, the relief diameters are based upon a pressure increase limited to 10 per cent of the working pressure, and the vessels are assumed to be 90 per cent full of volatile material when exposed to fire, no doubt the straight-line value of F would prove adequate at any pressure. Such a value would also afford the benefits of standardization. It is understood, however, that such standardization will not be wholly agreeable to all concerned, and further improvement in regard to simplifying the contents factor appears warranted. Nevertheless, the suggested value of F in no degree nullifies the value of Equation [9] in calculating the required relief diameter directly for any contents.

Further, it should be noted that the individual curves of the contents factor flatten as the critical pressures of the compounds are approached. It is in this region that the latent heat of vaporization of the liquid approaches zero; and consequently, the individual value of F increases more rapidly so that the relief diameter increases slowly after having decreased rapidly with pressure below 200 lb working pressure. Such increase is in conformance with the trend of accelerated vaporization. However, the value of F should not be increased beyond the point of critical temperature and pressure in those exceptional cases where processes operate at pressures such that the relieving pressure exceeds the critical pressure of the material being processed. Critical pressures and temperatures of representative compounds are listed in Table 2. (Processes which operate altogether above the critical pressure and temperature are in gas service and Equation [10] applies.)

The Gas Expansion Variable, $\dfrac{(T_w - T)^{5/8}}{T^{0.325}}$.

The rate of volume increase just discussed is dependent upon

[24] This is as might be expected; since in the evaluation of the contents factor for gases, $(T/MC_p)^{1/2}$, the numerical value of the factor for air was found to be larger than that for any other gas whose properties were available in the reference literature (refer to the Appendix).

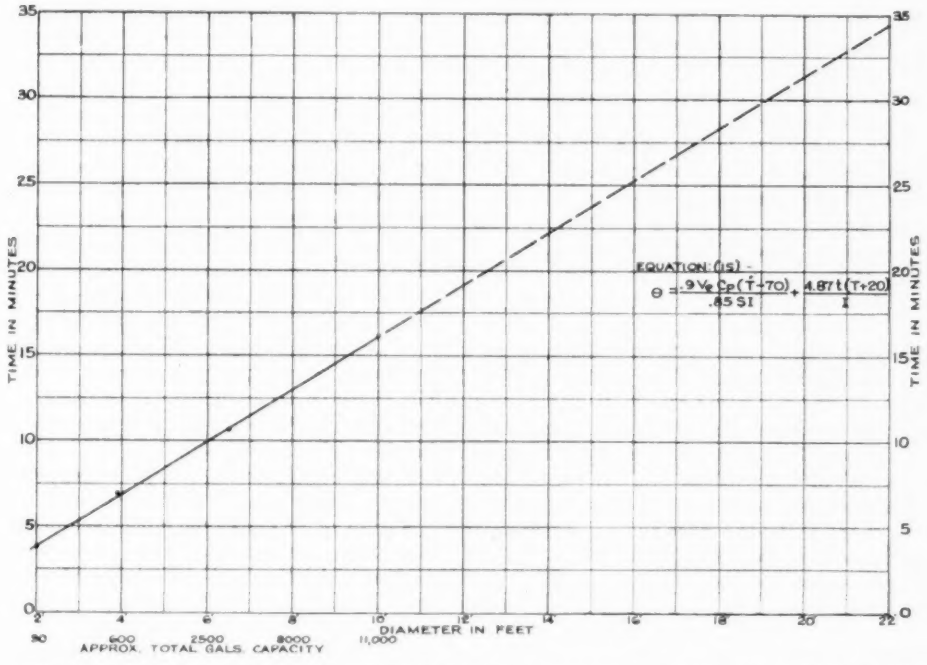


FIG. 13 ESTIMATED TIME FOR VOLATILE LIQUID CONTENTS OF PRESSURE VESSELS TO REACH 158 F WHEN ABSORBING HEAT AT 20,000 BTU PER SQ FT PER HR

(Contents of properties of F equals 0.142, T = 158 F; M = 74; r = 143 Btu; C_p = 0.447; ρ = 54.7 lb, at 15 psig.)

the rate of temperature rise in the contents (gas or vapor). This reduces mathematically (see derivation in Appendix) to the term shown. The probable maximum temperature difference is considered to be 1100 F; that is, $(T_w - T)$ = (1560 — 460) F abs, initial vapor temperature being zero F, and tank-wall temperature rising to 1100 F. Conceivably, this temperature difference may be greater, but distortion and possible failure of steel plate above 1100 F may be expected, even though the internal pressure is limited to a 10 per cent rise. When these temperature limits, typifying severest conditions, are inserted, the variable reduces to the constant 10.85.

The variable was derived using the properties of air in order to obtain maximum values and so provide adequate relief for any gas or vapor. Refer to the Appendix for comparison of values obtained with properties of other gases.

Flow Capacity in Terms of Area

If the relief area (not the next larger pipe size) as just determined, the molecular weight of the contents, and the absolute vapor temperature at the relieving pressure are inserted in weight rate Equation [11] of a short tube (a relief connection), the necessary capacity of the relief device may be computed. The apparatus may then be selected of a capacity (based on approved flow test) to pass the calculated rate which is as follows:

$$W = 262\ aP\ \sqrt{\frac{M}{T}}\ \text{lb per hr of vapor} \quad \ldots\ldots [11]$$

$$Q = \frac{1682\ aP}{\sqrt{MT}}\ \text{cfm at 68 F of free vapor} \quad \ldots\ldots [12]$$

$$Q = \frac{353.0\ aP}{\sqrt{T}}\ \text{cfm of free air at 68 F} \quad \ldots\ldots [13]$$

$$W = 42.7\ aP\ \text{lb per hr of saturated steam} \quad \ldots [14]$$

In all these cases, a is in square inches, P is the opening pressure of the relief device in pounds per square inch absolute, M is the molecular weight of the contents, and T is the contents vapor temperature in deg F absolute at the pressure P.

For conditions of fire exposure, T is approximately the temperature of the liquid contents when P is the vapor pressure, which may be obtained from temperature-vaporpressure data. For vessels in gas or vapor service only, T is approximately the temperature necessary to raise the pressure in the vessel from the absolute working pressure and temperature to the absolute set pressure of the relief device, as computed by the gas law, $T/P = T'/P'$.

The source of Equations [11], [12], [13], and [14] will be found in the Appendix.

It is in this determination of the capacity of the relief device (or devices) that allowance is made for the individual contents and immediate service, it being proposed, as already inferred, that the relief connection be the same size on all vessels of given capacity and range of working pressure. When equipment is so provided with adequate relief area for volatile compounds in the form of relief connections, the relief devices may be replaced to provide for any change in contents or more severe working conditions from the standpoint of relief requirements.

The procedure in determining the size of connections, capacity of devices, and selection of relief apparatus will be outlined in the Summary for Use.

The Time Element

If a vessel exposed to fire is large and the contents are of such properties that there would be a long delay before boiling and maximum efflux would occur, it would be desirable to select the relief device to provide for the vaporization rate which would take place within a certain safe period. The time required for the liquid contents of a steel vessel to reach a given average temperature during fire exposure may be approximated by use of the following formula

$$\theta = \frac{V\rho C_p(T - 70)}{S_w I} + \frac{4.87t(T + 20)}{I} \quad \ldots\ldots [15]$$

in which θ is the time in hours, V is volume of liquid contents in cubic feet, ρ is the density of the liquid in pounds per cubic foot, C_p is the specific heat of the liquid, T is the boiling point at the opening pressure of the relief device or temperature reached in a period θ in deg F, S_w is the wetted surface exposed to fire in square feet, I is the heat-input rate (20,000 Btu per hr per sq ft), and t is the thickness of the tank shell (steel) in inches. Derivation of this expression will be found in the Appendix.

The time required for volatile contents to reach the boiling point during fire exposure is very short. To illustrate, Fig. 13 has been included. It was assumed that the vessels were 90 per cent full with 85 per cent of the total surface wetted and exposed—a quite normal condition. Properties of the contents were taken as those having an F value of 0.142, and as otherwise noted in the caption of Fig. 13. Under these conditions, a short time element and a maximum venting rate may be expected. It will be seen that the time element is very largely a function of the diameter of the vessel. The calculations indicate that most (those under 20 ft diam) pressure vessels with volatile contents at 15 psi will boil when exposed to intense fire in less than $^1/_2$ hr.

When vessels are in gas or vapor service and become exposed to fire, the maximum venting rate will be reached within such a short period as to permit no reduction of the relief capacity as calculated by Equation [8]. Fig. 2, Part 1, shows this very clearly.

Effect of "Outage"

The term "outage" is used in the literature pertaining to containers to indicate the proportion of a tank which contains vapor rather than liquid. Thus, a tank which is only 40 per cent filled would have an "outage" of 60 per cent. Although this term does not appear in the developed formula, it has been considered. If the wetted height of the tank shell is used rather than the nominally full wetted height, the effect of "outage" is provided for. It is true that as the "outage" increases, the unwetted wall temperature will rise; but heat will be lost by conduction and radiation to the colder portions of the tank, and the hot wall temperature (steel) will probably not rise above the "critical" point of about 1100 F. When the "outage" is large, the wetted height is small, and the rate of vaporization is low; and although the vapor temperature will be higher than the temperature corresponding to the boiling point, it can be shown that the highest venting rate will occur when a tank is full of liquid.

The time required for a completely empty steel tank to reach 1100 F in a fire of intensity I would be approximately

$$\theta = \frac{5144\ t}{0.8\ I} \text{ or } 0.320\ t \text{ for 20,000 Btu input rate} \ldots . [16]$$

in which θ is time in hours for the tank wall to reach 1100 F, t is thickness of tank in inches, and I is intensity of fire in Btu per hr per sq ft. Thus in a fire of the intensity of 20,000 Btu per hr per sq ft, a tank made of $^1/_4$-in. steel would reach 1100 F in about 5 min.

$$\theta = 0.320 \times 0.25 = 0.080 \text{ hr} = 4.8 \text{ minutes}$$

This agrees very closely with time-temperature observations made by the Underwriters' Laboratories, Inc., in their tests previously referred to.[10] The source of this formula will be found in the Appendix.

Effect of Ranges of Pressure on Relief Areas

As mentioned previously, the internal diameters of the required relief connections vary rapidly with changes in working pressure up to about 200 psig. To show this clearly, Equation [7]

$$d = \sqrt{\frac{97.3\ S_w}{(P + 14.7)}} \left(\frac{P + 448.0}{3333.3}\right)$$

for vessels in volatile-liquid service has been graphed at 15, 60, and 200 psig working pressure, Fig. 11. Above 200 psi, a very gradual change in the required relief diameter continues, but the pipe size will not be affected for vessels of 10,000 gal nominal capacity or less until pressures above 700 psig are reached.

It is seen from Fig. 11 that it would be practical and economical to use different size relief connections for different ranges of working pressure on vessels of the same capacities. Further examination of the graph will disclose that the curves at the pressures indicated conform largely (more so than at other pressures when trial calculations are made) to pipe sizes. To take advantage of this effect, relief-connection formulas for ranges of working pressure will be provided in the Summary for Use.

In order to complete the comparison described under the Summary, of Part 2, the relief sizes of the National Board of Fire Underwriters and the State of California for liquefied petroleum gases at 200-psig working pressure have been added to Fig. 11. The difference between these and Equation [7] is principally due to the higher heat-absorption rate, although a somewhat larger contents factor is used in Equation [7].

A study of the shapes and proportions of vessels will disclose, as mentioned previously, that when calculating relief areas for connections, it is always adequate to use 85 per cent of the total exterior surface as the wetted area, provided the normal filling is not more than 90 per cent of the total volume. This has been employed in providing formulas for sizes of connections.

Emergency and Normal Relief

It is to be recognized that the requirement for relief of overpressure due to fire exposure represents an abnormal condition, and that this requirement, in most cases, is greatly in excess of that required to provide for operation fluctuations or disturbances. This latter requirement is considered by the authors to be "normal" relief and the former "emergency" relief. More specifically, normal relief is that required by process overheating, overfilling, improper operation, failure of control apparatus, the human element, plugging or mechanical failure within the system, etc. Emergency or abnormal relief is considered that due to fire exposure or uncontrolled, internal, chemical reaction.

The two present separate problems. Required normal relief can be determined from analysis of physical conditions within the system and calculation of the possible maximum "through-put." Relief required, due to fire exposure, may be provided for as outlined in this paper. As stated, the two requirements are widely separated in most cases, and it is practical to provide separate devices for the purposes as will be proposed.

Internal reaction is an emergency requirement not easily determined. The multiplicity and range of chemical reactions or rapid decompositions defy classification of rates of volume increase. Where likelihood of such expansion exists, special analysis and provisions are necessary to safeguard the individual installation.

On the other hand, there are special installations and processes in which the normal relief is the larger requirement. Some of these may be (depending upon analysis) vessels covered with substantial, fire-resistive insulation, those partly so insulated, vessels protected with reliable cooling systems, vessels processing nonhazardous plastics and semi-solids, etc. In some such cases, it will be apparent after analysis that no supplemental relief capacity need be provided for fire exposure as long as the immediate service is not made more severe from the standpoint of fire contingency; but these allowances in relief-device capacity should not effect a reduction in the area of the relief connection for fire exposure as previously specified. When vessels are partly protected with nonflammable insulation, the formulas may be correctly applied to the exposed surface in determining the necessary capacity of the relief device.

Relief due to fire exposure is assumed to be the release of vapor only. Liquid expansion due to the increased temperature is relatively negligible.

Proposed Summary for Use

1 Minimum sizes of relief connections for vessels not exceeding 10,000 gal nominal capacity (585 sq ft of wetted surface exposed): All pressure vessels should be provided with an emergency relief area (or areas) in the form of nozzles or connections. This area should be that computed by the following formulas or that required to limit the rise in working pressure to 10 per cent (as based on maximum possible "through-put" due to operation fluctuations or disturbances as defined), whichever of the two is the larger:

For vessels to have a working pressure from 15 to 60 psig, use

$$a = 0.0405\,S \text{ or } d = \sqrt{0.0515\,S} \quad \ldots\ldots\ldots [1]'$$

For vessels to have a working pressure from 60 to 200 psig, use

$$a = 0.0192\,S \text{ or } d = \sqrt{0.0244\,S} \quad \ldots\ldots\ldots [2]'$$

For vessels to have a working pressure from 200 to 700 psig use

$$a = 0.01112\,S \text{ or } d = \sqrt{0.01415\,S} \quad \ldots\ldots\ldots [3]'$$

In Equations [1]', [2]', and [3]', a is the relief area (or total areas) in square inches, S is the total external surface of the vessel in square feet, and d is the internal diameter of the circular relief opening in inches.

For vessels to have a working pressure above 700 psig, use

$$d = \sqrt{\frac{97.3\,S_w}{(P + 14.7)}} \left(\frac{P + 448}{3333.3}\right) \quad \ldots\ldots\ldots [4]'$$

in which d is as just given, P is the set pressure of the relief device (normally 1.1 the working pressure) in pounds per square inch gage, and S_w is the surface in square feet wetted by the contents and exposed to fire, P in the second term is limited to the critical pressure of the compound in process.

For vessels larger than 10,000 gal nominal capacity (585 sq ft of wetted surface exposed), use

$$d = \sqrt{\frac{97.3\,S_w}{(P + 14.7)}} \left(\frac{T}{Mr^2}\right)^{1/4} \quad \ldots\ldots\ldots [5]'$$

in which the symbols are as in the preceding paragraph except those in the last term which is the contents factor. It should be evaluated directly from Fig. 12, or calculated as recommended under the heading *Contents Factor*. In all cases, the nearest suitable pipe size (or sizes) of adequate area should be used.

2 Relief capacity in terms of area required at any pressure; liquid service: All pressure vessels in liquid service, or if used in systems which contain liquids, should have a relief flow capacity equivalent to the internal cross-sectional area (not the nearest pipe size) of a short tube, as calculated by the following formula, or that area required for "normal" relief, as described in paragraph 1, whichever is the larger

$$d = \sqrt{\frac{97.3\,S_w}{(P + 14.7)}} \left(\frac{T}{Mr^2}\right)^{1/4} \text{ and } a = 0.7854\,d^2 \quad \ldots\ldots [6]'$$

In Equation [6]', a is the relief area (or total of areas) in square inches, S_w is the wetted (wetted by the liquid contents when nominally full) surface exposed in square feet, d is the inside diameter of the free circular opening in inches, and P is the maximum allowable working pressure plus 10 per cent in pounds per square inch gage. The term $\left(\frac{T}{Mr^2}\right)^{1/4}$ is the contents factor and is evaluated as described in the preceding paragraph under Equation [5]'. (This is the emergency relief capacity required for vaporization of liquids due to fire exposure.)

Exceptions: In those exceptional cases where a, as determined by Equation [6]', exceeds the area of the relief connection, as set forth in paragraph 1, the relief connection will have to be increased or allowance permitted as suggested near the end of the section *The Contents Factors F*, $\left(\frac{T}{Mr^2}\right)^{1/4}$. If the relief capacity in terms of area approaches that of the relief connection, multiple relief devices will be required and should be applied as described in paragraph 5.

3 Relief capacity in terms of area required at any pressure; gas or vapor service only: All pressure vessels in gas or vapor service and in gas systems where no liquid can accumulate should have a relief flow capacity equivalent to the internal cross-sectional area of a short tube, as determined by the following formula, or that area required for "normal" relief, as described in paragraph 1, whichever is the larger

$$a = \frac{0.0631\,S}{\sqrt{(P + 14.7)}} \quad \text{or} \quad d = \sqrt{\frac{0.0803\,S}{\sqrt{(P + 14.7)}}} \quad \ldots\ldots [7]'$$

In Equations [7]', a is the relief area in square inches, S is the external exposed surface in square feet, d is the inside diameter of the relief connection in inches, and P is the maximum allowable working pressure plus 10 per cent in lb per sq in. gage. This is the emergency relief capacity required for gas or vapor expansion due to fire exposure.

4 Relief capacity of the required areas in terms of fluid flow: To select a relief device (or devices) of adequate capacity (based on approved flow test), use the area a, as determined in paragraph 2 or 3, in any one of the following formulas as the case may require:

$$W = 262.0\,aP\,\sqrt{M/T} \text{ lb of contents vapor per hr} \quad \ldots\ldots\ldots [8]'$$

$$Q = \frac{1682\,aP}{\sqrt{MT}} \text{ cfm of vapor at 68 F and atmospheric pressure} [9]'$$

$$Q = \frac{353.0\,aP}{\sqrt{T}} \text{ cfm of air at 68 F and atmospheric pressure} [10]'$$

$$W = 42.7aP \text{ lb per hr of saturated steam} \quad \ldots\ldots\ldots [11]'$$

In Equations [8]', [9]', [10]', and [11]', a is in square inches, and P is the opening pressure of the relief device in pounds per square inch absolute; M is the molecular weight of the contents, and T is the contents vapor temperature in deg F absolute at the pressure P. For conditions of fire exposure, T is approximately equal to the temperature of the liquid contents when P is the vapor pressure, which temperature may be obtained from temperature-vapor pressure data. For vessels in gas or vapor service only, T is approximately the temperature necessary to raise the pressure in the vessel from the absolute working pressure and temperature to the absolute set pressure of the relief device, as computed by the gas law, $T/P = T'/P'$.

5 Normal and emergency relief devices: It is preferable that separate spring- or weight-loaded safety devices be used for the "normal" relief requirement as described under that heading. The additional devices necessary to provide for fire exposure or internal reaction may supplement those required for operation fluctuations or disturbances. These may be in the form of rupture disks, safety heads, pilot-operated valves, or other apparatus and should be installed as specified in the recognized codes. If

rupturing devices are used, they should be calibrated to release at a pressure 50 to 100 per cent above the working pressure but not to exceed the test pressure of the vessel. In the exceptional cases where the "normal" and "emergency" relief are so nearly equivalent as to make the installation of multiple devices not economical, the one device should be of the capacity of the larger of the two requirements and set to relieve 10 per cent above the working pressure.

In those cases where the relief for operation fluctuations may be the larger requirement because of substantial fire-resistive insulation, nonhazardous contents or surroundings, etc., Equations [6]′ and [7]′ may be applied on the basis of the part of the surface not covered, or the part possible to be exposed when arriving at the relief capacity.

6 Back pressure: The pressure on the downstream side of the relief device should be limited to a maximum of from 10 to 25 per cent of the set pressure which must be adjusted to counteract the back pressure. If this limit is exceeded the capacity of the relief device may be reduced and redesign become necessary.[21]

7 Lower limit of size: For reasons of mechanical strength, it is recommended that no relief connection or safety device for manufacturing or service equipment be smaller than $^1/_2$ in. pipe size, regardless of the size of vessel to be protected.

8 Time element: To estimate the time for volatile liquids in a vessel exposed to fire to reach a given average temperature, apply the following formula

$$\theta = \frac{V\rho C_p(T - 70)}{S_w\, 20{,}000} + \frac{4.87\, t(T + 20)}{20{,}000} \quad \ldots\ldots [12]'$$

In Equation [12]′, θ is the time in hours, V is the volume of the liquid in cubic feet, ρ is the density of the liquid in pounds per cubic foot, C_p is the specific heat of the liquid, T is the boiling point at the opening pressure of the relief device, or temperature reached in a period θ in deg F, S_w is the wetted surface exposed in square feet and t is the thickness of the steel shell in inches.

If θ is $^1/_2$ hr or more (approximate time element for 20-ft-diam vessels containing volatile liquids at just above 15-psig working pressure) and there is assurance that effective cooling or fire-extinguishing equipment will come into operation during the half-hour period, the emergency-relief capacity may be reduced to the vaporization rate produced by the temperature rise within the half hour. For vessels exposed to fire in gas service, the maximum venting rate will occur within such a short time as to permit no modification of the calculated emergency relief.

Conclusion

The conclusions as outlined under Summary and detailed under Summary for Use are based upon the foregoing theory which is mathematically expressed in the Appendix.

The formulas proposed give relief capacities much greater than are at present employed and which are not adequate for the abnormal condition of fire exposure.

For example of use of the formulas refer to the Appendix.

Proposals herein hold only for pressures above 15 psig. For vessels operating at pressures not exceeding 0.50 psig, Part 3 will give details. Part 4 will appear at a later date covering vessels operating from 0.50 through 15 psig.

In addition to the lack of complete specifications in the recognized codes for the pressure-relief requirements of vessels, and the general statement that present relief areas as proposed by regulatory bodies were found to be inadequate for fire exposure, it has been suggested that further information be given to justify this study which shows a method of computing relief capacities for the contingency of fire exposure.

In its present form, the paper is based upon the mathematical development of the observations of vessels exposed to seven man-made fires by four separate organizations, as described in Part 1 of this paper. Since its preparation, two other similar tests by another company have been received, which support the tests herein analyzed.

Also in evidence are the reports of four equipment failures from accidental fire. These were vessels constructed in accordance with the A.S.M.E. Unfired Code and provided with relief areas compatible with a heat-absorption rate when exposed to fire of 7000 Btu per sq ft of wetted surface per hr. Three contained stable compounds, and the contents of the fourth probably underwent partial dissociation above the boiling point. All of the several contents had low-vapor pressures, boiling at much higher temperatures than water. No exact data on the fire intensity were obtained, but trial calculations by the developed formulas, using what data were available, gave results favorable to the test observations.

Further, the authors have reports of 31 failures of equipment (not due to fire exposure) other than those which may be obtained from several recording associations. Of these, 20 were due to excessive external pressure and 10 from excessive internal pressure. The overpressures occurred from miscellaneous causes for which the "normal" relief capacity should have been adequate, and it is not doubted that many of the failures would have been prevented had relief capacity for fire exposure also been incorporated in the installations.

Since it is not possible to specify a "normal" relief requirement for pressure vessels except by individual analysis of physical conditions within the process, and since it is possible to determine and provide relief capacity for fire exposure in a practical and relatively inexpensive manner, it is felt that this paper may provide a beginning for discussion, compilation of experience, and study which might eventually lead to more specific and safe specifications for minimum pressure-relief requirements.

Appendix to Part 2

Derivation of General Equations [9] or [3]*, and [10] or [15]″

Vapor weight rate of a short tube (above 15 psig)

$$W = 306\, aP\sqrt{\frac{M}{T}}$$

API-ASME Code: Weight rate of tapered nozzle

$$W = 306 \times \frac{0.83}{0.97}\, aP\sqrt{\frac{M}{T}}$$

$$W = 262\, aP\sqrt{\frac{M}{T}}$$

or

$$W = 262 \times 0.7854\, d^2P\sqrt{\frac{M}{T}}$$

$$W = 205.5\, d^2P\sqrt{\frac{M}{T}} \quad \ldots\ldots [1]''$$

in which

(Coefficient of flow of a short tube = 0.83)

W = rate, lb per hr
a = orifice area, sq in.
P = inlet pressure, psia
M = molecular weight of vapor
T = vapor temperature, deg F abs
d = orifice diameter, in.

Weight rate vaporized

$$\frac{Q}{S_w} = \frac{Wr}{S_w} = I$$

$$W = \frac{IS_w}{r} \quad \text{[2]''}$$

in which

Q = total heat input, Btu per hr
S_w = wetted surface heated, sq ft
r = latent heat of vaporization, Btu per lb
I = unit heat input, Btu per hr per sq ft
W = liquid vaporized, lb per hr

Required diameter of a short tube to pass the weight rate vaporized: Equate [1]'' and [2]''

$$\frac{IS_w}{r} = 205.5\, d^2 P \sqrt{\frac{M}{T}}$$

$$d^2 = \frac{IS_w}{r}\left(\frac{T}{M}\right)^{1/2}\left(\frac{1}{205.5\,P}\right)$$

$$d = \sqrt{\frac{IS_w}{205.5(P + 14.7)}}\left(\frac{T}{Mr^2}\right)^{1/4} \quad \text{[3]'' or [9]}$$

To apply Equation [3]''

d = diameter of relief connection, in.
I = 20,000 Btu per hr per sq ft
S_w = wetted surface heated, sq ft
P = set pressure of device, 1.1 working pressure, psig
T = boiling point at P, deg F abs
M = molecular weight of contents
r = latent heat of vaporization at T

Weight rate of expansion of gas or vapor due to heat transferred to a tank:

$$wC_p \frac{dT}{d\theta} = \frac{Q}{\theta} \quad \text{[4]''}$$

$$hS\,\Delta T = \frac{Q}{\theta} \quad \text{[5]''}$$

$$w = V\rho = V\frac{MP}{RT} \quad \text{[6]''}$$

From Equations [4]'' and [6]''

$$V\rho C_p \frac{dT}{d\theta} = \frac{Q}{\theta} \quad \text{[7]''}$$

$h = F\Delta T^{1/4}$ (ref. 5, Equation [16], p. 240)

From Equation [5]''

$$F\overline{\Delta T}^{1/4} S\,\Delta T = \frac{Q}{\theta} \quad \text{[8]''}$$

Equate [7]'' to [8]''

$$V\rho C_p \frac{dT}{d\theta} = FS\Delta T^{5/4}$$

$$\frac{dT}{d\theta} = \frac{FS\overline{\Delta T}^{5/4}}{V\rho C_p} \quad \text{[9]''}$$

From Equation [6]''

$$dw = \frac{-VMP}{R}\cdot\frac{dT}{T^2} \quad \text{[10]''}$$

$$-dw = \frac{w}{\theta}\,d\theta \quad \text{[11]''}$$

Equate [10]'' to [11]''

$$\frac{VMP}{R}\cdot\frac{dT}{T^2} = \frac{w}{\theta}\,d\theta \quad \text{[12]''}$$

$$\frac{dT}{d\theta} = \frac{w}{\theta}\cdot\frac{RT^2}{VMP} \quad \text{[13]''}$$

Equate [9]'' to [13]''

$$\frac{FS\overline{\Delta T}^{5/4}}{V\rho C_p} = \frac{w}{\theta}\,\frac{RT^2}{VMP} \quad \text{[14]''}$$

in which

w = weight of contained gas or vapor, lb
C_p = specific heat of gas or vapor
dT = change in temperature
$d\theta$ = change in time
Q = total heat transferred, Btu
θ = time, unit hr
h = heat-transfer coefficient, Btu per hr per sq ft per deg F
S = tank surface heated, sq ft
ΔT = difference between tank wall and contained gas, deg F
V = volume of contents gas or vapor, cu ft
ρ = density of contents gas, lb per cu ft
M = molecular weight of gas or vapor
P = pressure, psia
R = gas constant, 10.72
T = temperature of gas or vapor, deg F abs
F = function of physical properties of a gas
dw = change in weight
$W = \frac{w}{\theta}$ = venting rate, lb per hr

Required diameter of a short tube to pass the weight rate of gas expanded due to heat transferred to a tank (the same nomenclature is used as in the preceding group):

Insert Equation [1]'' in [14]''

$$205.5\, d^2 P\sqrt{\frac{M}{T}}\cdot\frac{RT^2}{VMP} = \frac{FS\overline{\Delta T}^{5/4}}{V\rho C_p}$$

$$d^2 = \frac{FS\overline{\Delta T}^{5/4} VMP}{V\rho C_p RT^2\, 205.5\, P}\left(\frac{T}{M}\right)^{1/2}$$

$$d^2 = \left(\frac{F}{C_p M^{1/2}}\right)\frac{S}{205.5}\cdot\frac{M\overline{\Delta T}^{5/4}}{RT^{3/2}\rho}$$

in which $\left(\rho = \frac{MP}{RT}\right)$

$$d = \left(\frac{F}{C_p M^{1/2}}\right)^{1/2}\cdot\frac{S^{1/2}}{14.33\,P^{1/2}}\cdot\frac{\Delta T^{5/8}}{T^{1/4}}$$

$$d = \left(0.375\,\frac{P^{1/4}}{T^{0.0753}}\right)\cdot\frac{S^{1/2}}{14.33\,P^{1/2}}\cdot\frac{\Delta T^{5/8}}{T^{1/4}}$$

Refer to following paragraph for $0.375\,\frac{P^{1/4}}{T^{0.0753}}$

$$d = 0.02615\,\frac{S^{1/2}}{P^{1/4}}\cdot\frac{\Delta T^{5/8}}{T^{0.325}} \quad \text{[15]'' or [10]}$$

To apply Equation [15]''

d = diameter of relief connection, in.
S = surface exposed, sq ft

P = set pressure of relief, 1.1 gage working pressure plus 14.7
$\Delta T = (T_w - T)$
T_w = temperature to which tank wall is heated, deg F abs
T = initial temperature of tank vapor, deg F abs

The term $\left(\frac{F}{C_pM^{1/2}}\right)^{1/2}$ in the foregoing, relating the properties of the contents fluid, was replaced by its maximum value $0.375\,\frac{P^{1/4}}{T^{0.0753}}$. This is justified in the following manner: The value of F, a function of the physical properties of a gas, varies with both temperature and pressure as will be seen. The value C_p, specific heat at constant pressure, varies with temperature. Inasmuch as pressure and temperature are working conditions to remain in the relief diameter Equation [15]', it is desirable to express the subject variable in terms of P and T. Now

$$F = D\left(\frac{\rho^2BC_pk^3}{Z}\right)^{1/4} \text{ (ref. 5, Equation [20], p. 242)}$$

$$\left(\frac{F}{C_pM^{1/2}}\right)^{1/2} = D\left(\frac{\rho^2BC_pk^3}{C_p{}^4M^2Z}\right)^{1/8}$$

$$= D\left[\rho^2Z^2\cdot\frac{B}{M^2}\cdot\left(\frac{k^3}{C_p{}^3Z^3}\right)\right]^{1/8}$$

in which

F = 0.27 for air at 68 F and atmospheric pressure
D = proportionality constant
k = thermal conductivity
C_p = specific heat
ρ = density
B = coefficient of thermal expansion
Z = viscosity
M = molecular weight
R = gas constant

Since B, M, and the ratio C_pZ/k (ref. 5, p. 417) are independent of P and T, we may write

$$\left(\frac{F}{C_pM^{1/2}}\right)^{1/2} = D'(\rho^2Z^2)^{1/8}$$

and ρ for a gas is MP/RT, then

$$\left(\frac{F}{C_pM^{1/2}}\right)^{1/2} = D'\left(\frac{M^2P^2}{R^2T^2}\cdot Z^2\right)^{1/8}$$

Again M and R are independent of P and T, so

$$\left(\frac{F}{C_pM^{1/2}}\right)^{1/2} = D''\left(\frac{P^2Z^2}{T^2}\right)^{1/8}$$

$$= D''\left(\frac{P^2T^{1.398}}{T^2}\right)^{1/8}$$

$$= D''\left(\frac{P^2}{T^{0.602}}\right)^{1/8}$$

$$\left(\frac{F}{C_pM^{1/2}}\right)^{1/2} = D''\left(\frac{P^{1/4}}{T^{0.0753}}\right)$$

Z^2 Varies with T for air as follows:

T	Z	Z^2
460 deg R	0.0162	0.0002625
528	0.018	0.000323
660	0.021	0.000440
860	0.025	0.000625
1060	0.029	0.000840
1260	0.032	0.001050
1460	0.036	0.001295
1560	0.038	0.001444

$$\left(\frac{1560}{460}\right)^n = (3.39)^n = \frac{1.444}{0.2625} = 5.50$$

$$n = 1.398$$

When P = 14.7 psia, and T = 528 deg R, C_p = 0.24 and F = 0.27 for air

$$\therefore D'' = \left(\frac{0.27}{0.24\times 29^{1/2}}\right)^{1/2}\times\frac{(528)^{0.0753}}{(14.7)^{1/4}}$$

$$D'' = 0.375$$

and

$$\left(\frac{F}{C_pM^{1/2}}\right)^{1/2} = 0.375\,\frac{P^{1/4}}{T^{0.0753}}$$

Now, it is also necessary to show that $\left(\frac{F}{C_pM^{1/2}}\right)^{1/2}$ gives higher values for air than for any other gases whose properties are available in the reference literature. To do this we use McAdams Equation [20],[25] again which is

$$F = D\left(\frac{\rho^2BC_pk^3}{Z}\right)^{1/4}$$

and in which the nomenclature is as before. Again, $\rho = MP/RT$ and $B = 1/492$. Then, at a constant pressure and temperature it would be expected that F would vary for different gases as follows:

$$F = D'\left(\frac{M^2C_pk^3}{Z}\right)^{1/4}$$

At 1 atm pressure and 20 C, F = 0.27 and $\left(\frac{M^2C_pk^3}{Z}\right)^{1/4}$ = 0.465 for air, so that the F value for any other gas, whose molecular weight, specific heat, thermal conductivity, and viscosity are known, may be determined from the relation

$$F_g = \frac{0.27}{0.465}\left(\frac{k^3C_pM^2}{Z}\right)_g^{1/4}$$

in which the subscript g applies to the gas other than air. On this basis, the F value for a number of representative gases has

[25] Ref. 5, p. 242.

TABLE 3 VALUE OF F FOR REPRESENTATIVE GASES

Gas	k[a]	C_p[a]	Z[a]	M[a]	$\frac{k^3C_pM^2}{Z}$	$\left(\frac{k^3C_pM^2}{Z}\right)^{1/4}$	F	$\frac{F}{C_pM^{1/2}}$
Air	0.0161	0.24	0.018	29	0.0468	0.465	0.270	0.209
Hydrogen	0.1075	3.50	0.009	2	1.9324	1.181	0.685	0.138
Acetone	0.0065	0.34	0.0077	58	0.0408	0.448	0.260	0.100
Acetylene	0.0124	0.43	0.010	26	0.0554	0.485	0.281	0.128
Benzene	0.0062	0.26	0.0075	78	0.0502	0.472	0.273	0.135
Ethyl alcohol	0.0089	0.40	0.0094	46	0.0634	0.501	0.290	0.107
Ethyl ether	0.0088	0.46	0.0077	74	0.222	0.687	0.398	0.100
Water	0.0110	0.48	0.0097	18	0.0213	0.382	0.221	0.108
Pentane	0.0083	0.34	0.0063	72	0.1599	0.632	0.366	0.127
Carbon dioxide	0.0109	0.21	0.0146	44	0.0360	0.436	0.252	0.181
"Freon 113"	0.0054	0.16	0.0103	187	0.0855	0.542	0.313	0.143

[a] Ref. 5, various pages.

been calculated as shown in Table 3, and it will be noted that the value of $\left(\frac{F}{C_p M^{1/2}}\right)^{1/2}$ for air is greater than for any of those values so obtained; and for many others, such as ammonia, nitrogen, and oxygen, whose properties were considered but not listed in the table.

Use of General Equations [9] or [3]', and [10] or [15]'

The following example is given of the use of Equation [3]' for a 10 ft 6 in. diam (D) × 18 ft 10 in. high over-all vertical tank with dished heads, nominally full of ethyl ether, operating at 15 psig, and surrounded with intense fire

$$d = \sqrt{\frac{IS_w}{205.5(P + 14.7)}} \left(\frac{T}{Mr^2}\right)^{1/4}$$

$$d = \sqrt{\frac{20{,}000 \times 583}{205.5 \times 31.2}} \times 0.140$$

$$d = 5.96 \text{ in.}$$

in which

$S_w = \pi D(0.266\ D + L)$
L = height of straight shell to filling level, ft
$S_w = \pi\ 10.5(0.266 \times 10.5 + 14.9)$
$S_w = 583$ sq ft
$P = (16.5 + 14.7) = 31.2$
$\left(\frac{T}{Mr^2}\right)^{1/4} = 0.140$ (see Fig. 12)

An example of the use of Equation [15]' for a 10 ft 6 in. diam (D) by 18 ft 10 in. high over-all air tank with dished heads, operating at 15 psig and surrounded by intense fire, is as follows

$$d = 0.02615 \frac{S^{1/2}}{P^{1/4}} \cdot \frac{(T_w - T)^{5/8}}{T^{0.325}}$$

$$d = \frac{0.02615 \times 26.45 \times 10.85}{2.363}$$

$$d = 3.17 \text{ in.}$$

in which

$S = \pi D(0.532\ D + L)$
L = length of straight shell between heads, ft
$S = \pi\ 10.5(0.532 \times 10.5 + 15.67)$
$S = 700$ sq ft, $S^{1/2} = 26.45$
$T = (0 + 460) = 460$ F abs
$T_w = (460 + 1100) = 1560$ F abs
$(T_w - T)^{5/8} = (1100)^{5/8} = 79.5$

$$T^{0.325} = (460)^{0.325} = 7.33$$

$$(T_w - T)^{5/8}/T^{0.325} = 10.85$$

$$P = (16.5 + 14.7) = 31.2$$

$$P^{1/4} = 2.363$$

Simplification of General Expressions to Equations [7] or [16]', and [8] or [17]'

The diameter of a connection necessary to relieve a pressure vessel in liquid service when involved with conflagration is as follows:

$$d = \sqrt{\frac{IS_w}{205.5\ P}} \left(\frac{T}{Mr^2}\right)^{1/4} \quad \text{[3]'}$$

$$d = \sqrt{\frac{20{,}000\ S_w}{205.5\ (P + 14.7)}} \times [0.130 + 0.0003\ (P + 14.7)]$$

$$d = \sqrt{\frac{97.3\ S_w}{(P + 14.7)}} \left(\frac{P + 448.0}{3333.3}\right) \quad \text{[16]'}$$

in which

I = 20,000 Btu per hr per sq ft
$\left(\frac{T}{Mr^2}\right)^{1/4}$ = contents factor, Fig. 12
S_w = wetted surface exposed, sq ft
P = 1.1 working pressure, psig

The diameter of a connection necessary to relieve a pressure vessel in gas or vapor (only) service when involved with conflagration is as follows

$$d = 0.02615 \frac{S^{1/2}}{P^{1/4}} \cdot \frac{(T_w - T)^{5/8}}{T^{0.325}} \quad \text{[15]'}$$

$$d = 0.02615 \left(\frac{S^{1/2}}{P^{1/4}}\right) \times 10.85$$

$$d = \sqrt{\frac{0.0803\ S}{\sqrt{(P + 14.7)}}} \quad \text{[17]'}$$

in which

S = surface exposed, sq ft
$\frac{(T_w - T)^{5/8}}{T^{0.325}}$ = *gas expansion variable*, as described under that heading, and as reduced to maximum constant (10.85) in preceding example
P = 1.1 working pressure, psig

Use of Equations [7] or [16]', and [8] or [17]'

An example of the use of Equation [16]' for a 10 ft 6 in. diam by 18 ft 10 in. high over-all vertical tank with dished heads, nominally full of volatile liquid, operating at 15 psig, and surrounded by intense fire is as follows

$$d = \sqrt{\frac{97.3\ S_w}{(P + 14.7)}} \left(\frac{P + 448.0}{3333.3}\right) = \sqrt{\frac{97.3 \times 583}{(16.5 + 14.7)}} \left(\frac{464.5}{3333.3}\right)$$

$d = 5.94$ in.

The following example gives the use of Equation [17]' for a 10 ft 6 in. diameter by 18 ft 10 in. high over-all tank with dished heads in gas (only) service, operating at 15 psig, and surrounded by intense fire

$$d = \sqrt{\frac{0.0803\ S}{\sqrt{(P + 14.7)}}} = \sqrt{\frac{0.0803 \times 700}{\sqrt{(16.5 + 14.7)}}}$$

$d = 3.17$ in.

Simplification of Weight Rate to Vapor Flow Capacity in Terms of Area

Weight rate of flow

$$W = 262\ aP \sqrt{\frac{M}{T}} \text{ lb per hr} \quad \text{[1]'}$$

Flow capacity in terms of cubic feet of vapor per minute

$$Q \text{ cu ft} = \frac{W \text{ lb}}{\rho \text{ lb per cu ft}}$$

$$Q = \frac{262}{60}\ aP \left(\frac{M}{T}\right)^{1/2} \frac{10.72(528)}{M(14.7)}$$

$$Q = \frac{1682\ aP}{\sqrt{MT}} \text{ cfm of free contents vapor at 68 F} \quad \text{[18]'}$$

where

$$\rho = \frac{MP}{RT} = \frac{M(0 + 14.7)}{R(68 + 460)} = \frac{M(14.7)}{10.72(528)}$$

at 68 F and atmospheric pressure

Flow capacity in terms of cubic feet of air per minute:

$$W = \frac{0.533\,CAP}{\sqrt{T}} \text{ lb per sec of air}^{26}$$

$$Q \text{ cu ft} = \frac{W \text{ lb}}{\rho \text{ lb per cu ft}}$$

$$Q = \frac{0.533 \times 0.83 \times aP \times 60}{0.0752\sqrt{T}}$$

$$Q = \frac{353.0\,aP}{\sqrt{T}} \text{ cfm free air at 68 F} \ldots\ldots [19]''$$

where

C = orifice coefficient, 0.83

$$\rho = \frac{MP}{RT} = \frac{29(14.7)}{10.72(528)}$$

$\rho = 0.0752$ at 68 F and atmospheric pressure

Flow capacity in terms of pounds of saturated steam per hour:
Napier's formula

$$W = \frac{aP}{70} \text{ lb per sec}$$

$$W = \frac{aP}{70} \times 3600 \times 0.83$$

(0.83 coefficient of flow for a short tube)

$$W = 42.7\,aP \text{ lb per hr of saturated steam} \ldots\ldots [20]''$$

Derivation and Use of Time Element Formulas

The estimated time required for the liquid contents of a vessel to reach a given temperature is derived as follows:

IS_w = total heat input, in Btu per hr

$\frac{V\rho C_p \Delta T}{\theta}$ = heat absorbed by liquid contents, Btu per unit time

$S \cdot \frac{t\rho C_p \Delta T}{12\,\theta}$ = heat absorbed by tank, Btu per unit time

$$IS_w = \frac{V\rho C_p(T - 70)}{\theta}^{*} + S \cdot \frac{t}{12} \cdot \frac{487 \times 0.12(T + 20)}{\theta}^{*}$$

$$(S_w \leq 0.85\,S)$$

$$\theta = \frac{V\rho C_p(T - 70)}{IS_w} + \frac{4.87\,t(T + 20)}{I} \ldots\ldots [21]''$$

In which

I = unit heat input rate, 20,000 Btu per hr per sq ft
S_w = wetted surface exposed to fire, sq ft
V = volume of liquid contents, cu ft
ρ = density, lb per cu ft (487 for steel)
C_p = specific heat (0.12 for steel)
ΔT = temperature difference, deg F
θ = time, hr
S = tank surface heated, sq ft
t = thickness of tank shell, in.
T = temperature of contents, deg F

The following example is given of the estimated time, Equation [21]'', required for the contents to reach the boiling point in a 10 ft 6 in. diam by 18 ft 10 in. high over-all tank with dished heads, nominally full of ethyl ether, operating at 15 psig, and surrounded by intense fire (the same nomenclature is used as for the preceding group):

$$\theta = \frac{V\rho C_p(T - 70)}{IS_w} + \frac{4.87\,t(T + 20)}{I}$$

$$\theta = \frac{(10{,}200 \text{ gal}/7.48) \times 44.5 \times 0.552\,(134.6 - 70)}{20{,}000 \times 583} + \frac{4.87 \times 0.375\,(134.6 + 20)}{20{,}000}$$

$\theta = 0.186 + 0.0141 = 0.2001$ hr or 12.0 min

Estimated time required for an empty steel tank to reach the "critical" temperature of 1100 F (the same nomenclature is used as before)

$$IS = S \cdot \frac{t}{12} \cdot \frac{487 \times 0.12(T - 50)}{\theta}$$

$$I = \frac{4.87\,t(1100 - 50)}{\theta}$$

$$\theta = \frac{5114\,t}{0.8I} = 0.320\,t \ldots\ldots [22]''$$

During the period of heating to 1100 F, the input I will be found only about 80 per cent effective due largely to reradiation losses.

Origin of Formulas for Ranges of Pressure

From 15 to 60 psig working pressure

$$d = \sqrt{\frac{97.3\,S_w}{(P + 14.7)}}\left(\frac{P + 448.0}{3333.3}\right) \ldots\ldots [16]''$$

in which

$$d = \sqrt{\frac{a}{0.7854}}$$

$$S_w \leq 0.85\,S$$

$$d = \sqrt{\frac{97.3 \times 0.85\,S}{(16.5 + 14.7)}}\left(\frac{16.5 + 448.0}{3333.3}\right)$$

$$d = \sqrt{0.0515\,S}\,; \quad \frac{a}{0.7854} = 0.0515\,S$$

$$a = 0.0405\,S \ldots\ldots [23]''$$

From 60 to 200 psig working pressure:

$$d = \sqrt{\frac{97.3 \times 0.85\,S}{(66 + 14.7)}}\left(\frac{66 + 448.0}{3333.3}\right)$$

[26] "Chemical Engineer's Handbook," by J. H. Perry, McGraw-Hill Book Company, Inc., New York, N. Y., 1934, Equation [21a], p. 710.

* Liquid contents are considered to have an average temperature of 70 F, and tank steel an average of 60 F, before exposure. The tank shell after heating is considered to be an average of 100 F hotter than the liquid contents, although this will vary somewhat with the compound contained.

$$d = \sqrt{0.0244S}; \qquad \frac{a}{0.7854} = 0.0244S$$

$$a = 0.0192\ S \ldots\ldots [24]''$$

From 200 to 700 psig working pressure

$$d = \sqrt{\frac{97.3 \times 0.85S}{220 + 14.7}\left(\frac{220 + 448.0}{3333.3}\right)}$$

$$d = \sqrt{0.01415\ S}; \qquad \frac{a}{0.7854} = 0.01415\ S$$

$$a = 0.0112\ S \ldots\ldots [25]''$$

EXAMPLE OF USE OF FINAL FORMULAS FOR RELIEF REQUIREMENTS

Relief requirements for a 10 ft 6 in. diam (D) by 18 ft 10 in. high over-all tank with dished heads, in gas service, operating at 150 psig are determined as follows (equation numbers refer to Summary for Use):

Relief-connection size

$$a = 0.0192\ S \text{ or } d = \sqrt{0.0244\ S} \ldots\ldots [2]'$$

$$a = 0.0192 \times 700 \text{ or } d = \sqrt{0.0244 \times 700}$$

$$a = 13.44 \text{ sq in. or } d = 4.13 \text{ in. (use 4 in. ASA150)}$$

where

S = tank surface, sq ft
$S = \pi D(0.532\ D + L)$
L = length straight shell, ft
$S = \pi\ 10.5(0.532 \times 10.5 + 15.67)$
$S = 700$ sq ft

Relief capacity in terms of area:

$$a = \frac{0.0631\ S}{\sqrt{(P + 14.7)}} \text{ or } d = \sqrt{\frac{0.0803\ S}{\sqrt{(P + 14.7)}}} \ldots\ldots [5]'$$

$$a = \frac{0.0631 \times 700}{\sqrt{(165 + 14.7)}} \text{ or } d = \sqrt{\frac{0.0803 \times 700}{\sqrt{(165 + 14.7)}}}$$

$$a = 3.30 \text{ sq in. or } d = 2.047 \text{ in.}$$

Relief capacity of the device in terms of fluid flow

$$Q = \frac{353.0a\ P}{\sqrt{T}} \ldots\ldots [10]'$$

$$Q = \frac{353 \times 3.30\ (165 + 14.7)}{\sqrt{666}}$$

$Q = 8100$ cfm of air at 68 F, and atmospheric pressure

in which the temperature required to open valve, air having initial temperature of 150 F, is

$$T/P = T'/P'$$

$$T = \frac{179.7 \times (150 + 460)}{164.7}$$

$$T = 666 \text{ F abs}$$

[Provided the relief capacity required for operation fluctuations and disturbances (capacity of the compressor at 165 lb discharge) is not greater. Three and four-inch valves of this capacity are commercially available.]

PART 3 REQUIREMENTS FOR RELIEF OF ATMOSPHERIC VESSELS[27]

INTRODUCTION

A considerable number of references in the literature specifying the relief requirements of atmospheric storage tanks have been available for many years. Various methods have been developed to establish the normal venting requirements, and at least three nationally known, reliable organizations have agreed upon and proposed venting capacities necessary to limit internal pressure safely in event of exposure to fire. The fire records of the National Fire Protection Association and similar bodies clearly indicate the need and value of emergency vent areas for this contingency and emphasize the inadequacy of normal relief apparatus when a vessel is involved with intense fire. The inadequacy of the latter will be very apparent in this presentation.

In this section a recent investigation of the normal requirement made by the authors will be set forth and compared with previous methods. By the procedure used in Part 2 for pressure vessels, the emergency requirement will be developed, compared, and discussed. Thereafter, a summary for the suggested employment of this information will be given.

SUMMARY

To summarize briefly the principal results of Part 3, Fig. 14 has been included, which shows the relation and suggested combination of normal and emergency vent sizes as determined for vertical cylindrical atmospheric storage tanks.

Study of Fig. 14, practical experience with present-day venting apparatus, and consideration for economy led to the venting requirements given in Table 7, which are considered adequate for both normal (1 in. water external, 3 in. water internal, pressure) venting and vaporization (at 0.5 psi at 50 gal, proportionally reduced to 3 in. water pressure at 70,000 gal) of contents due to fire exposure. The formulas from which the foregoing were calculated appear under the descriptive headings for which they apply. Other formulas which provide relief specifications for all vessels in liquid or gas service at working pressures not to exceed 0.50 psig are also given.

The suggested application of the information herein will be found under the heading, Proposed Summary for Use.

THERMAL BREATHING OR NORMAL VENTING OF UNINSULATED, ABOVE GROUND, ATMOSPHERIC STORAGE TANKS WHEN EXPOSED TO EXTREME ATMOSPHERIC CHANGES

Introduction During the years 1939 and 1940, for a period of 14 months, a continuous record of breathing characteristics was kept on a 440,000-gal (nominal capacity) gasoline storage tank at South Charleston, West Va., (38 deg north latitude, 600 ft elevation). Rates of venting, specific gravities of the vapors, vapor pressures, liquid levels, liquid temperatures, vapor temperatures, and atmospheric temperatures were measured and recorded. The data obtained furnished information for vapor-conservation analysis (the subject of a separate discussion) and the determination of normal breathing requirements.

Summary. Maximum thermal breathing was found to be that due to contraction during a hailstorm. A temperature drop of 41 deg F (average) in 20 min was observed within the tank vapor. The inhaling rate resulted in vent-size requirements larger than those determined by a number of well-known methods, except those sizes proposed by the National Board of Fire Underwriters[28] (up to 800,000 gal capacity).

[27] Conditions: 1 in. water external, 0.50 psi internal, pressure.

[28] "Containers for Storing and Handling Flammable Liquids," National Board of Fire Underwriters, Pamphlet No. 30, New York, N. Y., 1941, p. 37.

It was concluded that the maximum rate of thermal breathing of an atmospheric (1 in. water external, 3 in. water internal, pressure) storage tank is

$$Q = (S/0.290) + \text{emptying rate} \quad [16]$$

where Q and emptying rate are in cubic feet of air per hour at 68 F and atmospheric pressure, and S is the area of the tank roof and shell in square feet.

The diameter of the relief connection required for this venting rate is

$$d = \sqrt{Q/921} \quad [17]$$

where d is in inches and Q is in cubic feet of air per hour at the conditions given. Derivation of these formulas will be found in the Appendix of this section.

In order that the vent sizes determined by Equations [16]

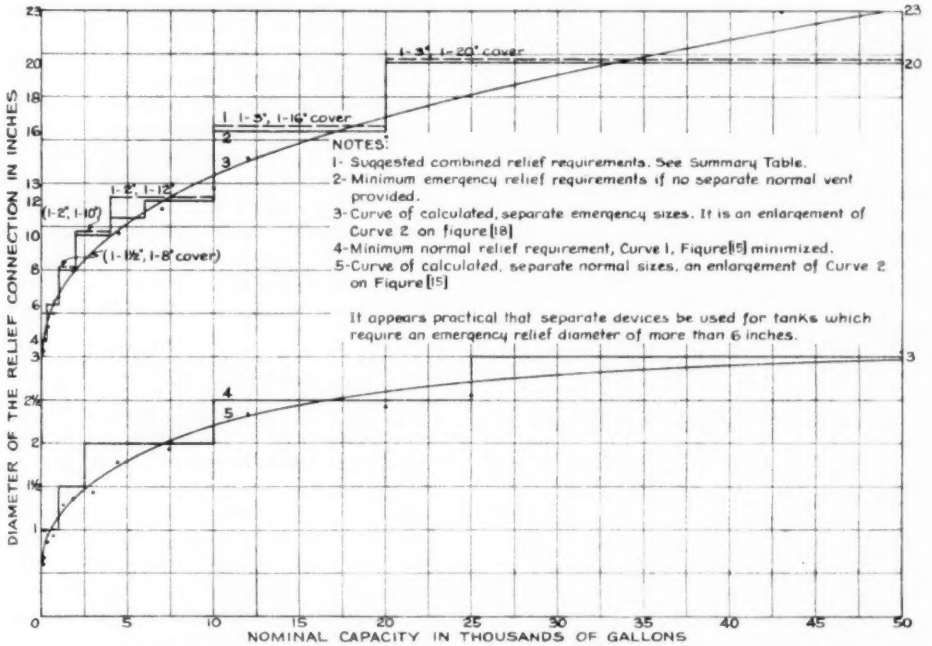


FIG. 14 COMPARISON OF NORMAL AND EMERGENCY RELIEF AREAS FOR ATMOSPHERIC TANKS TO FACILITATE SELECTION OF PRACTICAL AND ECONOMICAL COMBINATIONS OF THE TWO

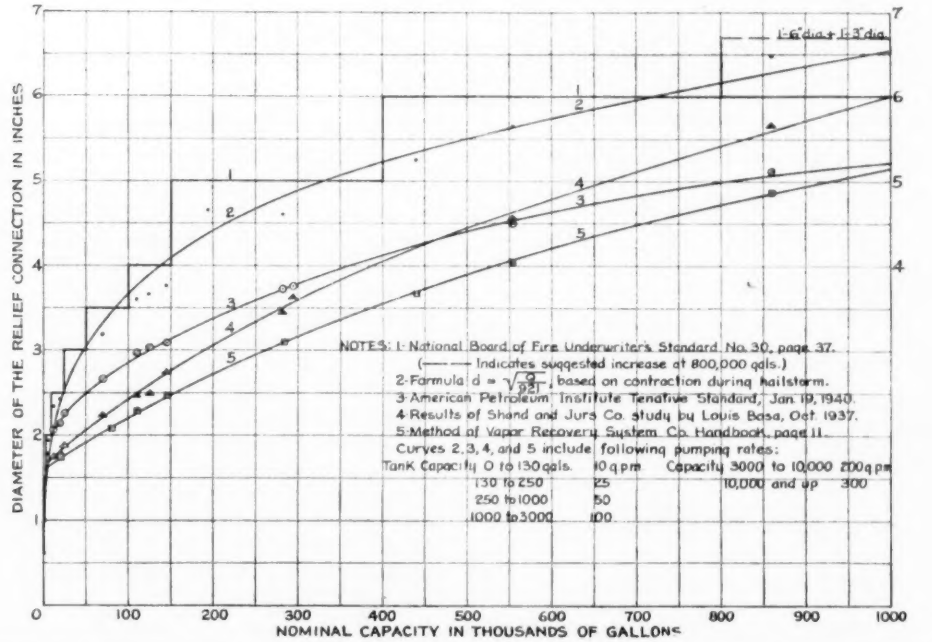


FIG. 15 COMPARISON OF REQUIRED DIAMETER OF RELIEF CONNECTION FOR ATMOSPHERIC PRESSURE STORAGE TANKS EXPOSED TO EXTREME ATMOSPHERIC CHANGES
(1 in. water external, 3 in. water internal, pressure.)

and [17] may be compared with those specified by other methods, Fig. 15 is given.

Equipment Arrangement. The tank on which a continuous record was kept was 50 ft diam × 30 ft 3 in. high (cylindrical shell), with an umbrella-type roof, and was painted with aluminum paint. The vessel was in active storage of finished gasoline.

An existing 8-in. standard pipe header about 600 ft long was used as a vent line. Two recording orifice meters were installed near the end of the line to measure both high and low flows in either direction. Also in connection therewith, a continuous-recording gravitometer was used to provide data for the vapor-density correction. A three-pen recording thermometer furnished atmospheric, tank vapor, and liquid-contents temperatures.

At the same time, other data were collected pertinent to related studies. Periods when the contained vapors were flammable were recorded by a combustible-gas instrument and recording potentiometer. While the effects of external water spray on vapor losses were being observed, a third orifice meter was used to measure the cooling-water rate. Frequent periodic analyses of the discharge vapors were made to determine the percentage of product contained at the indicated specific gravities.

Procedure. The experiment was given continuous attention and maintenance by operation and investigation personnel while the tank was being operated normally. A daily log was kept on all observations including weather, liquid level, vapor pressure, and pertinent comment. The data were transposed to a graph, a sample of which is included as Fig. 16. On this will be noted both ordinary and extreme breathing action during three representative periods.

Vapor and liquid temperatures and flammability of vapors were observed at various levels to obtain mean temperatures and to get indication of the location, frequency, and extent of combustible zones. Flash-arrester and emergency vacuum and pressure-relief protection, were maintained on the tank throughout the observations.

Data Obtained. The maximum breathing rates and corresponding information observed during the 14 months under various conditions are shown in Table 4. The contraction rate due to sudden cooling will be seen to be about 4 times as great as that for emptying, filling, solar heating, or combinations of conditions causing venting. No worth-while data on the efflux produced by mixing (by cycling contents) could be obtained other than that breathing rates so caused are not comparable to the maximum shown in Table 4.

Although not directly related to the subject, the data collected on the flammability of the vapor-air mixture were of interest. To show the relation between combustible contents and breathing action, Fig. 17 has been included.

For the most part (except for 3 months) the combustible-gas recorder operated in connection with the vent header at a point near its outlet. Flammable mixtures were present there at frequent intervals in an irregular pattern which was no doubt due to the lag in and large volume of the 600-ft long header. The interval from February 15, through February 26, 1940, Fig. 17, illustrates flammability within the header.

During June, July, and August, 1940, the combustible-vapor recorder operated directly in connection with the tank. It was found that explosive mixtures were present less frequently but for longer periods ranging up to 30 hr. In all, the tank vapors were within the flammable range 5 per cent of the time and "too rich to burn" 95 per cent of the time. The vapor-air mixtures when combustible were never in the lower limits, the gasoline content ranging from 2 to 53 per cent by volume, as based on laboratory analyses. Flammable limits of gasoline vapor-air mixtures are 1 to 6½ per cent by volume.[29]

All the recorded periods (seven in number) when the vapors within the tank were flammable are shown on the remainder of Fig. 17. It will be observed that in every case (except one of 45 min on June 17) the combustible mixture was produced by a combination of emptying and falling temperature. The exception was caused by a momentary in-breathing when a shower occurred while the vapors were warm (between 9 and 10 a.m.).

The use of flash arresters or inert-gas systems with atmospheric storage tanks containing volatile flammable liquids appears warranted by these observations.

Analysis. The data indicated that the maximum normal breathing requirement is that due to rapid contraction of the contained vapors. The quantity rate of contraction of a gas due to heat transferred to a colder tank wall is

$$Q = \frac{10.72FS(T - T_w)^{5/4}}{C_pMP} \quad \ldots\ldots\ldots\ldots [18]$$

in which Q is in cubic feet per hour, F is a function of the physical properties of the vapor (0.27 for air at atmospheric conditions),[30] S is the surface of the tank roof and shell enclosing the tank vapor in square feet, T is the initial vapor temperature in deg F, T_w is the final tank wall temperature (average) in deg F, C_p is the specific heat of the vapor, M is the molecular weight, and P is the average absolute pressure during contraction in pounds per square inch (14.736 internal for atmospheric tanks).

If the properties of air which constituted the greater percentage of the mixture ordinarily, and nearly the whole occasionally (air ranged 47 to 98 per cent by volume), and the observed temperatures from Table 4, Case 1, are used in Equation [18], maximum values of Q will be obtained. (For comparison with values for other vapors, see the evaluation of $\left(\frac{F}{C_pM^{1/2}}\right)^{1/2}$ in the Appendix of this section.) This value (cubic feet per hour) is then very nearly equal to $S/0.290$ as in Equation [16].

The capacity of the relief connection (a short tube) at pressures in this range is

$$Q = 4340d^2\sqrt{\frac{\Delta PT}{MP}} \quad \ldots\ldots\ldots\ldots [19]$$

in which Q and M are the same as in Equation [18], d is in inches, ΔP is pounds per square inch gage, P is pounds per square inch absolute, and T is the temperature of the vapor flowing in deg F absolute.

During the cooling process, the capacity of the relief connection must be equivalent to the rate of contraction at the permissible working pressure (1 in. water external). So, if Equation [18] is equated to Equation [19] at the observed conditions (Case 1), the required diameter will result as in Equation [17] $d = \sqrt{Q/921}$.

Derivation of Equations [18] and [19] will be found in the Appendix of this section.

Discussion. Although the contained vapors are not perfect gases and some condensation does take place during cooling, the comparison between observed breathing rates and those computed as for a gas on the basis of the rate of change of absolute temperatures is favorable and indicates results in the direction of safety.

The venting rate, $Q = S/0.290$, is based on a difference between initial vapor and final average tank-wall temperatures of 47 deg F and is equivalent to a fall in the vapor temperature of

[29] Ref. 9, p. 152.

[30] "Heat Transmission," p. 242.

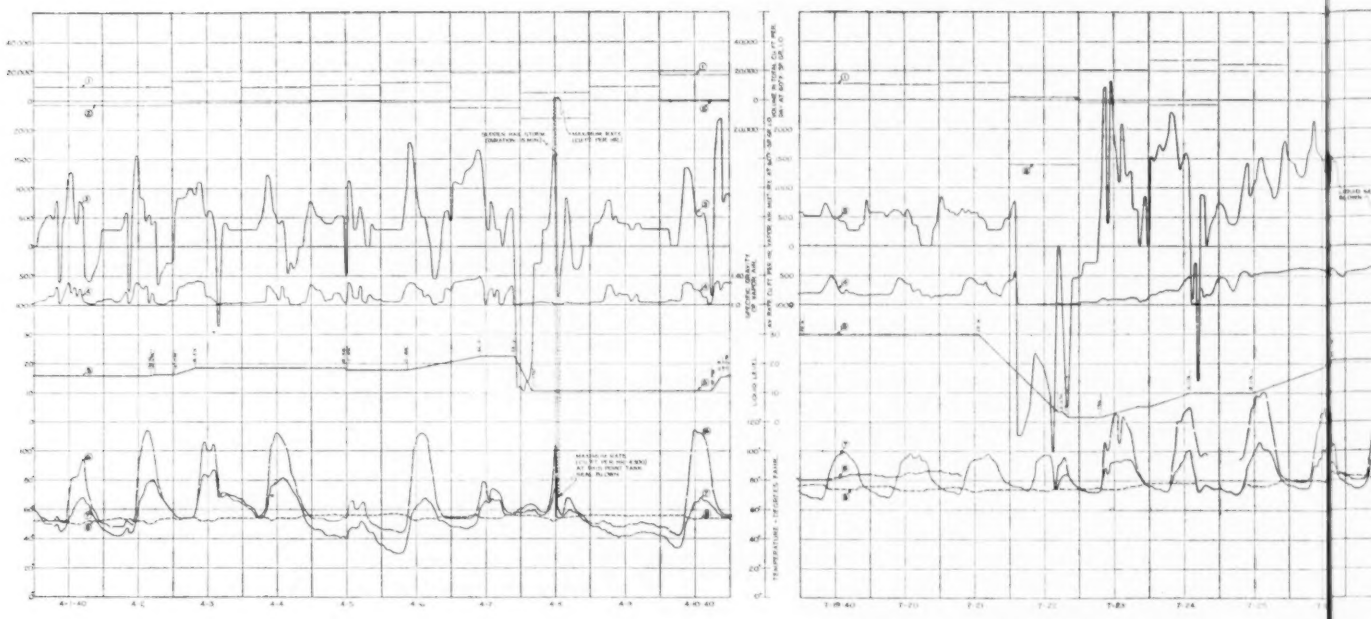


FIG. 16 BREATHING CHARACTERISTICS OF 10,000-BB TORA
(Significant periods of 14 months' continuous record sho

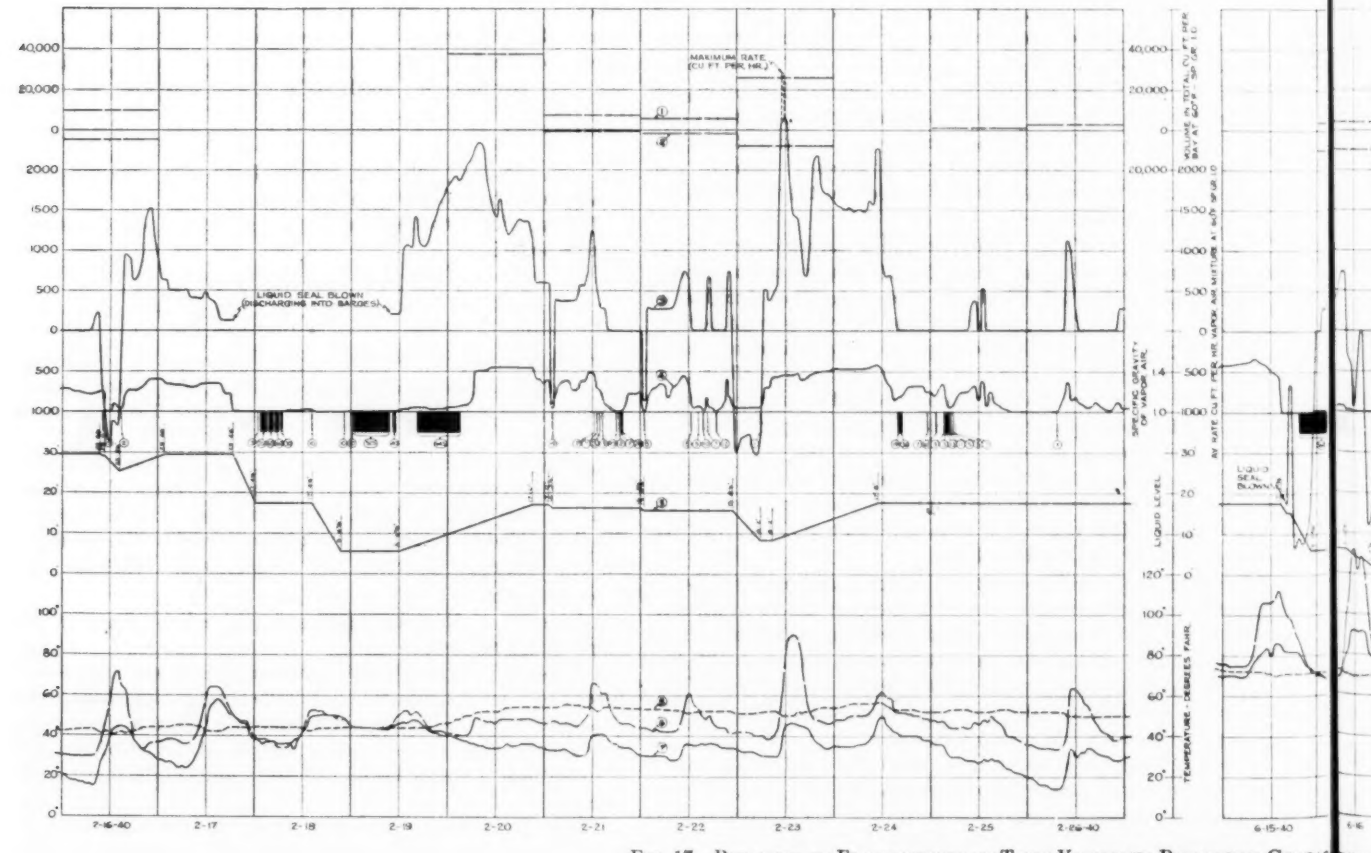
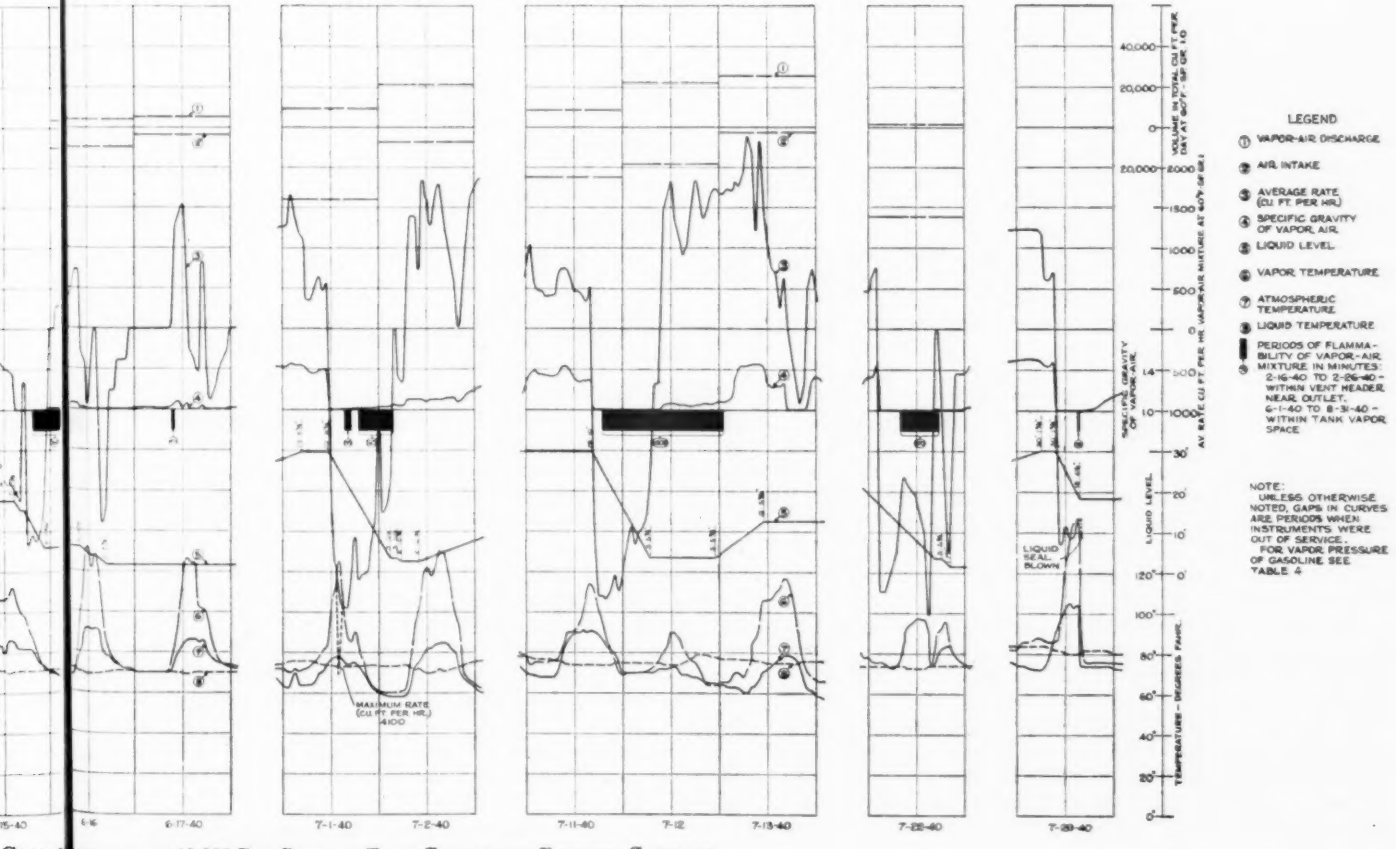


FIG. 17 RELATION OF FLAMMABILITY OF TANK VAPORS TO BREATHING CHARAC ERIS
(Representative periods 2 mo



000-Bbl Storage Tank Containing Finished Gasoline
as recorded shown in Table 4, Part 3 of this paper.)



Characteristics of 10,000-Bbl Storage Tank Containing Finished Gasoline
periods of 2 months' observation.)

TABLE 4 OBSERVED AND CALCULATED DATA ON MAXIMUM AGE TANK WHEN EXPOSED TO

Conditions	Hail Storm	Sudden Showers	
Temperatures:	April 8, 1940 11:50 a.m. to 12:10 p.m. Case 1	July 29, 1940 3:40 p.m. Case 2	May 31, 1940 2:05 p.m. Case 3
Atmospheric	73° to 54°F. in 20 min.	104° to 74°F. in 45 min.	78° to 65°F. in 30 min.
Vapor Contents	103° to 62°F. in 20 min.	146° to 84°F. in 1 hr.	95° to 67°F. in 30 min.
Maximum rate of change (vapor)	98° to 70°F. in 7 min.	119° to 111°F. in 2 min.	92° to 74°F. in 15 min.
Liquid Contents	52° to 56°F. in 20 min.	80° to 82°F. in 1 hr.	58°F. constant
Final Tank Wall about Vapor Space	56.0°F. (estimated average)		
Recorded Vapor Flow Rate (Max.)	4300 cu.ft. per hr. when 1 1/2 oz. per sq. in. vacuum seal blown	2650 cu.ft. per hr., when seal blown	*4450 cu.ft. per hr.
Liquid Level	10'-7 5/8" (constant)	19'-0" (constant)	0'-9" (constant)
Vapor Space Quantities	Volume 45,200 cu. ft. Surface (S) 5170 sq. ft.	Volume 28,800 cu.ft. Surface(S) 3860 sq.ft.	Volume 64,600 cu.ft. Surface(S) 6720 sq.ft.
Rate of Volume Change (Proportional to maximum abs. temp. rate as a gas).	18,850 cu. ft. per hr.	12,000 cu.ft. per hr.	*8400 cu.ft. per hr.
Proposed Breathing Rate (Based on S/0.290 as derived. Pump rate to be added).	17,830 cu. ft. per hr.	13,300 cu.ft. per hr.	23,200 cu.ft. per hr.
Reid Vapor Pressure (lb. per sq. in. at 100°F.)	8.3 lb. per sq. in.	8.3 lb. per sq. in.	5.6 lb. per sq. in.
Weather	Bright sun preceding storm, cloudy thereafter.	Hot sun shining before & after heavy rain storm.	Cloudy with intermittent sun before shower; bright sun thereafter.
Remarks:	Maximum condition (largest temperature drop in appreciable period found) used as basis of S/0.290.		

* Discrepancy between observed breathing rates and proportional rates of volume change is considered largely due to the pressure drop and lag in the recorded vapor flows were corrected to 60 F, the maxima at flowing

98 F to 70 F, in 7.86 min, when the vapor is assumed to be a gas. No additional temperature differential is considered necessary for a margin of safety. The vent sizes resulting are shown in Fig. 15, curve 2, which have a satisfactory service record of a number of years over a broad section of the country. As a matter of fact, a large number of comparable atmospheric tanks so vented were exposed to the same hailstorm cited, without giving any evidence of having been subjected to pressure above 1 in. of water external.

The capacity of a short tube, Equation [19], was derived from the adiabatic flow of an ideal gas through an orifice. It incorporates an orifice coefficient of 0.70 for flows where the ratio of upstream to downstream absolute pressure is less than 1.05.[31] Also, this is the coefficient used by the National Fire Protection Association under these conditions.[32] Tests were run on a typical tank and connection as a check on the formula derived. Actual flows were found to be 99 per cent of the theoretical within the atmospheric tank pressure range (0 to 3 in. water) and to be 100 per cent at a pressure of 5 in. of water (see Fig. 20 in the Appendix of this section).

[31] "Kent's Mechanical Engineers' Handbook," ref. 14, pp. 1–11.
[32] "Handbook of Fire Protection,"[9] p. 108.

Conclusion. The conclusions as outlined under *Summary* are adequate for the conditions specified and conform to the proposals of the National Board of Fire Underwriters up to 800,000 gal capacity, above which increased vent sizes as shown are suggested. Apparently, the average practice is to use vent sizes considerably smaller than this service-proved proposal (refer to Fig. 15).

Proposed sizes of connections with minimum capacities (based on 1 in. water external pressure) for the normal relief requirement for atmospheric tanks are listed in Table 5.

Relief capacities, concluded in Table 5, are not adequate for the condition of fire exposure now to be discussed and under which the relation of normal and emergency venting will be clarified.

To avoid excessive internal pressure due to accidental overfilling, the normal relief area should not be less than that of the fill pipe.

Requirements for Emergency Relief Due to Fire Exposure

Introduction. From the standpoint of emergency venting, atmospheric tanks (usually large) present a separate problem because of the very low safe working pressure (about 3 in. water

BREATHING RATES OF 10,000-BBL FINISHED GASOLINE STOR-
EXTREME ATMOSPHERIC CHANGES

Solar Heating May 5, 1940 - 7 hrs. Case 4	Emptying May 1, 1940 - 6-1/3 hrs. Case 5	Emptying April 19, 1940 - 5 hrs. Case 6	Filling Jan. 2, 1940 - 7 hrs. Case 7	Filling Jan. 9, 1940 - 23 hrs. Case 8
39° to 74°F. in 7 hrs.	73° to 61°F. in 30 min.	58° to 57°F. in 1 hr.	28°F. constant	31° to 26°F. in 5 hrs.
32° to 112°F. in 6 hrs.	78° to 62°F. in 45 min.	60° to 58°F. in 1 hr.	56°F. constant	33° to 32°F. in 4 hrs.
48° to 82°F. in 1 hr. (9 to 10 a.m.)	78° to 64°F. in 30 min.	As above	None	As above
50°F. constant	55° to 57°F. in 10 min.	55°F. constant	42°F. constant	40°F. constant
*2800 cu.ft. per hr.	*4275 cu.ft. per hr.	*4050 cu. ft. per hr.	4220 cu. ft. per hr.	3930 cu. ft. per hr.
1'-6 3/8" (constant)	11'-7 3/4" to 3'-10 3/4" in 6 1/3 hrs. Avg. 1.225 ft./hr.	29'-5" to 17'-4" in 5 hrs. Avg. 2.42 ft. per hr.	1'-9 3/4" to 4'-8 1/2" in 7 hrs. Avg. 0.414 ft. per hr.	3'-6 1/2" to 12'-2 1/2" in 23 hrs. Avg. 0.380 ft. per hr.
Volume 63,100 cu.ft. Surface(S) 6600 sq.ft.	Volume 44,400 cu.ft. Surface(S) 5110 sq.ft.			
*4200 cu.ft. per hr.	2200 contraction 2400 liq. discharge *4600 cu.ft. per hr.	Liquid Discharge Rate *4750 cu. ft. per hr.	Liquid Charging Rate 813 cu. ft. per hr.	Liquid Charging Rate 740 cu. ft. per hr.
22,750 cu.ft. per hr.	17,600 cu.ft. per hr.			
9.5 lb. per sq. in.	9.5 lb. per sq. in.	8.7 lb. per sq. in.	11.3 lb. per sq. in.	12.6 lb. per sq. in.
Clear & sunny all day.	Cloudy with intermittent rain all day.	Light rain all day.	Weak sun all day.	Blanket of snow on tank partly melted by a weak sun.
	Contraction was due to a sudden shower during first 30 min.	Contraction due to temperature drop is small enough to be neglected.	Vaporization promoted by turbulence and contained air caused larger discharge.	Out breathing is again about five times greater than displacement.

vent line, 600 ft in length, 8 in. diam. (It is also possible that the liquid seal may have been giving partial relief.) Furthermore, although the maximum conditions were not materially larger than the corrected flows.

TABLE 5 PROPOSED SIZES OF VENT CONNECTIONS FOR ATMOSPHERIC TANK NORMAL RELIEF REQUIREMENTS

Tank capacity, gal	Relief size, in. I.P. size	Minimum capacity, cu ft of air, per hr at 60 F, and atmospheric pressure
0 to 500	1[a]	708
500 to 2000	1 1/2[a]	1920
2000 to 10,000	2	3660
10000 to 50000	3	8230
50000 to 150000	4	14620
150000 to 400000	1–4, 1–3[b]	22820
400000 to 800000	6	32900
800000 to 1100000	1–6,1–3	41100
1100000 to 1300000	1–6, 1–4[c]	47500
1300000 to 1800000	8	58450
1800000 to 2000000	2–6	65800

[a] Units of 2-in. vent size for tanks are usually the smallest standard manufacture.
[b] One 6-in. vent unit may be cheaper than the two small units, but they have the mechanical advantage of multiple devices.
[c] Similarly, one 8-in. vent unit may be cheaper than one 6-in. and one 4-in. size.

internal), the relatively large vapor space, the lessened possibility of complete envelopment in flame, and the lengthened (time) exposure required to produce maximum vaporization. The effect of the first two of the factors mentioned is such as to result in calculated relief areas which are impractical. The latter two are the basis of reasonable assumptions to be made which result in more economical designs.

Summary. The required diameter of a relief connection to limit internal pressure (not to exceed 0.50 psig) within vessels when the volatile contents are absorbing heat at 20,000 Btu per sq ft per hr of wetted surface exposed is

$$d = \sqrt{\frac{0.913\, S_w}{\sqrt{P(P + 14.7)}}} \quad [20]$$

If the pressure limit be 3 in. of water, as for atmospheric storage tanks, Equation [20] becomes

$$d = \sqrt{0.721 S_w} \quad [21]$$

and if the atmospheric tank be vertical cylindrical with bottom resting on pad or foundation, Equation [21] becomes

$$d = \sqrt{2.265\, DH} \quad [22]$$

in which (Equations [20], [21], and [22]) d is the internal diameter of the connection in inches, S_w is wetted surface exposed to fire in square feet when nominally full, P is the pressure limit

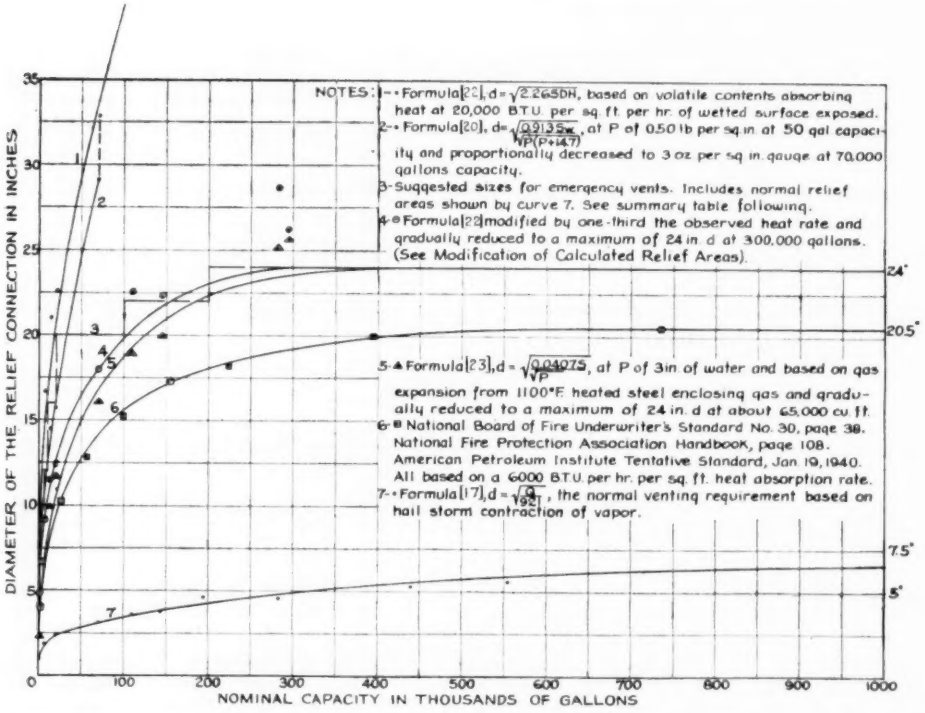


FIG. 18 COMPARISON OF REQUIRED DIAMETER OF RELIEF CONNECTION FOR ATMOSPHERIC STORAGE TANKS WHEN EXPOSED TO FIRE (1 in. water external, 3 in. water internal, pressure.)

in pounds per square inch gage (0.1083 for 3 in. water), D is the diameter of the tank in feet, and H is the height in feet of the contents on the exposed tank wall when it is nominally full.

For vessels in gas service only at pressures not to exceed 0.50 psig, the required diameter of the relief connection to limit internal pressure to a specified maximum is

$$d = \sqrt{\frac{0.0407\,S}{\sqrt{P}}} \quad \ldots\ldots\ldots\ldots\ldots\ldots [23]$$

in which d is the internal diameter of the connection in inches, S is the square feet of surface which may be exposed including unprotected roofs, and P is the maximum pressure permitted in pounds per square inch gage.

The origin of these formulas will be found in the Appendix of this section.

The formulas for liquid service, Equations [20], [21], and [22], should be applied to all vessels in the pressure range below 0.50 psig up to and including 15 ft diam; it then appears expedient for practical reasons to reduce the calculated relief sizes and to limit them to a maximum of 24 in. diam. These modifications are clarified as the discussion proceeds and are summarized under the heading, *Modification of the Calculated Relief Areas.*

Relief diameters for atmospheric tanks have been graphed in Fig. 18. The curve of Equation [22] is shown in relation to the same equation when modified by a heat rate one third of that concluded in Part 1. Between the two will be noted the suggested choice of vent size. For comparison, the proposal of the National Board of Fire Underwriters, the National Fire Protection Association, and the American Petroleum Institute is shown. Also appearing is the required size for normal venting which, though provided for in the emergency area, is not large enough to reduce it one pipe size over the entire range of tank capacity. Also observe that a contained gas or vapor will expand when in relatively large proportions, as in empty atmospheric tanks and when exposed to tank walls heated to 1100 F by external fire, at a rate nearly equivalent to the vaporization rate of volatiles.

Analysis and Method. The requirements for emergency relief of atmospheric tanks and low-pressure gasholders are based on the same reasoning as that for unfired pressure vessels as detailed in Part 2 of this paper. The physical conditions (pressure, temperature, and relative size) are merely different, necessitating the use of a different fluid-flow formula, a different value for the contents factor, and modification of calculated relief sizes as graphically suggested in Fig. 18.

As previously described, a vessel surrounded by fire absorbs heat and the temperature of its contents rises. If the content is liquid, its vapor pressure steadily increases and eventually boiling will occur; if a vapor or gas, progressive expansion takes place. (So-called empty tanks, equipped with adequate normal venting apparatus, have been observed to fail when involved with sudden, intense fire, although ignition of contents did not occur until after rupture.) Now, in either case, the relief apparatus must be of capacity equivalent to the rate of vaporization or the rate of volume increase. When the weight rate of the relief connection (at these low pressures) is equated to the weight rate of vaporization, the following Equation [24] results, which is the origin of Equations [20], [21], and [22]:

$$d = \sqrt{\frac{IS_w}{405\sqrt{P(P+14.7)}}}\left(\frac{T}{Mr^2}\right)^{1/4} \quad \ldots\ldots\ldots [24]$$

When the weight rate of expansion of a gas or vapor is equated to the weight rate of the relief connection, a second expression, Equation [25], results, which is the origin of Equation [23], namely

$$d = 0.0186 \cdot \frac{S^{1/2}}{\Delta P^{1/4}} \cdot \frac{(T_w - T)^{5/8}}{T^{0.325}} \quad \ldots\ldots\ldots [25]$$

In these equations, d is the internal diameter of the connection in inches, I is the heat-absorption rate in Btu per square foot per hour, S_w is wetted surface exposed in square feet, ΔP is the maximum pressure in pounds per square inch gage (0.1083 for 3 in. water), and S is total surface exposed in square feet. The terms $\left(\frac{T}{Mr^2}\right)^{1/4}$ and $\frac{(T_w - T)^{5/8}}{T^{0.325}}$ are the contents factor and gas expansion variable, which are reduced to constants, as described under subsequent headings. Equations [24] and [25], which are similar to Equations [8] and [9] in Part 2, are derived and simplified in the Appendix of this section to the useful Equations [20], [21], [22], and [23].

As in Part 2, the relief capacity is proposed in terms of area of the relief connection, because the designer is primarily interested in selecting an adequate fitting of standard size for the vessel to be constructed, and because of the variation in capacities of commercial relief apparatus. The vent apparatus may then be selected of a capacity, based on approved flow test, to pass the flow capacity of the calculated area, as will be shown.

Weight Rate of a Relief Connection. The vapor capacity of a short tube in pounds per hour at pressures not exceeding 0 5 psig is

$$W = 405\, d^2 \sqrt{\frac{MP(P + 14.7)}{T}} \quad \ldots\ldots\ldots\ldots [26]$$

in which W is the weight rate in pounds per hour, d is the internal diameter of the connection in inches, M is the molecular weight of the fluid, P is the inlet pressure in pounds per square inch gage, and T is the temperature of the fluid in deg F absolute.

This is the same formula used previously in this section for the determination of the normal breathing requirement, except that it was there given in cubic feet per hour. As stated before, it was shown to be accurate, and its derivation found in the Appendix of this section will be seen to conform to the procedure outlined by the American Gas Association.[33]

Contents Factor F, $\left(\frac{T}{Mr^2}\right)^{1/4}$. This term is identical with that derived and fully explained in Part 2 of this paper under the same heading. It is, as before, that which relates the properties of liquid contents. Since the developments in this section are limited to the pressure range of atmospheric to 0.50 psig, a single numerical value of the factor may be selected which would be adequate for any compound to be contained at these pressures.

For the present development, the value $F = 0.136$ has been used, for which reference is made to Fig. 12, Part 2. This value is considered adequate for any liquid which may be contained at these pressures, other than carbon tetrachloride. For this compound, use 0.155 for the contents factor in Equation [24].

Gas Expansion Variable, $\frac{(T_w - T)^{5/8}}{T^{0.325}}$. The rate of volume increase is dependent upon the rate of temperature rise within the vapor contents. Again, this is proportional to the value of the gas-expansion variable. If the formerly assumed maximum temperature difference of 1100 deg F, between initial vapor and final tank-wall temperatures is considered reasonable and adequate, the term reduces to the constant 10.85 (refer to Part 2, under the same heading as in this section).

As will be seen in the Appendix of this section, the variable was based upon the properties of air which apparently gives maximum values as therein demonstrated.

Flow Capacity in Terms of Area. If the relief diameters (not the next larger pipe size) as determined above, the molecular weight of contents, the relieving pressure, and the vapor temperature, are inserted in the weight rate of flow, Equation [26], of a short tube, the necessary capacity of the relief device may be computed. The apparatus may then be selected of a capacity (based on approved flow test) to pass the calculated rate which is as follows:

$$W = 405\, d^2 \sqrt{\frac{MP(P + 14.7)}{T}} \text{ lb per hr of vapor} \ldots [26]$$

$$Q = 156{,}000\, d^2 \sqrt{\frac{P(P + 14.7)}{MT}} \text{ cfh of free vapor at 68 F} \ldots [27]$$

$$Q = 29{,}000\, d^2 \sqrt{\frac{P(P + 14.7)}{T}} \text{ cfh of free air at 68 F} \ldots [28]$$

In Equations [26], [27], and [28], d is in inches, P is in pounds per square inch gage, and T is in deg F absolute.

For conditions of fire exposure, T is approximately the normal boiling point of the liquid contents. For vessels in gas service, T is about the temperature necessary to raise the pressure in the vessel from the absolute working pressure and temperature to the absolute set pressure of the relief device, as computed by the gas law, $T/P = T'/P'$.

A mathematical clarification of these equations is given in the Appendix of this section.

Time Element. The time required when exposed to intense fire for the liquid contents of a steel vessel to reach a specified average temperature may be estimated by applying the formula

$$\theta = \frac{V\rho C_p(T - 70)}{IS_w} + \frac{4.87t(T + 20)}{I} \quad \ldots\ldots\ldots [29]$$

in which θ is time in hours, V is the volume of contents in cubic feet, ρ is the density in pounds per cubic foot, C_p is the specific heat, T is the specified temperature in deg F, I is the heat-absorption rate in Btu per square foot per hour, S_w is the surface wetted by the product and exposed to fire in square feet, and t is the thickness in inches of the (steel) tank wall. This was introduced and derived in Part 2 of this paper. If this Equation is applied to vertical cylindrical flat-bottom tanks, it becomes (see Appendix of this section)

$$\theta = \frac{D\rho C_p(T - 70)}{4I} + \frac{4.87\, t(T + 20)}{I} \quad \ldots\ldots\ldots [30]$$

in which D is the diameter of the tank in feet. Results calculated by Equation [30] compare favorably with time-temperature observations in Part 1, Table 1.

From Equation [30], it is seen that the time required for the contents to absorb heat at any given rate is principally dependent upon the diameter of the tank. For illustration of the approximate time required to reach 100 F at the observed heat rate, Fig. 19 is shown. The tanks were assumed to be nominally full and of dimensions conforming to many tanks being used at this time. Calculations were made employing properties of compounds having a contents-factor value of 0.136, as shown in Fig. 19. Products having such properties are about as volatile as any stored at atmospheric pressure. Under the assumed conditions, a minimum time element and a maximum venting rate may be expected.

When vessels are in gas or vapor service and exposed to intense fire, the maximum venting rate will be reached in an even shorter time. Fig. 2, Part 1, illustrates the rapid expansion of tank vapors due to fire exposure.

Effect of "Outage." The term "outage" is used in literature pertaining to containers to indicate the proportion of a tank which contains vapor rather than liquid. Thus a tank which is only 40

[33] "American Gas Association Standards," New York, N. Y.

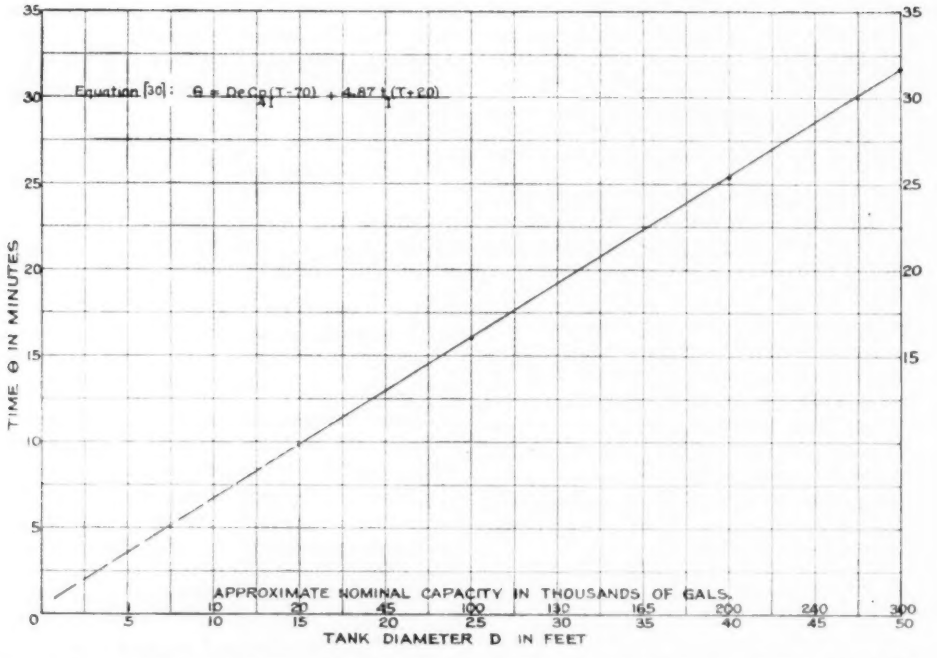


FIG. 19 ESTIMATED TIME FOR VOLATILE-LIQUID CONTENTS OF ATMOSPHERIC STORAGE TANKS TO REACH 100 F WHEN ABSORBING HEAT AT 20,000 BTU PER SQ FT PER HR

(Products of properties of $F = 0.136$; $T = 104$ F; $M = 74$; $r = 149.5$ Btu; $C_p = 0.447$; $\rho = 54.7$ lb.)

per cent filled would have an "outage" of 60 per cent. Although this term does not appear in the developed formula, it has been considered. If the wetted height of the tank is used rather than the nominally full wetted height, the effect of outage is taken care of. It is true that as the outage increases, the unwetted wall temperature will rise, but heat will be lost by conduction and radiation to the colder portions of the tank, and the temperature of the hot wall will probably not rise above the "critical" point of about 1100 F. When the outage is large, the wetted height is small, and the rate of vaporization is low; and, although the vapor temperature will be higher than the temperature corresponding to the boiling point, it can be shown that the highest venting rate will occur when a tank is full of liquid.

The time required for a completely empty steel tank to reach 1100 F in a fire of intensity I would be approximately

$$\theta = \frac{5114\,t}{0.8\,I} \text{ or } 0.320\,t \text{ for 20,000 Btu input rate} \ldots\ [31]$$

in which θ is time in hours for tank wall to reach 1100 F; t is thickness of tank wall in inches; I is intensity of fire in Btu per hour per square foot. Thus, in a fire of observed intensity of 20,000 Btu per hr per sq ft, a tank made of 1/4-in. steel would reach 1100 F in about 5 min.

$$\theta = 0.320 \times 0.25 = 0.080 \text{ hr} = 4.8 \text{ min}$$

This agrees very closely with time-temperature observations made by the Underwriters' Laboratories, Inc., in their tests described in Part 1. The source of this formula will be found in the Appendix of this section.

Emergency and Normal Relief. The requirements for relief of overpressure due to fire exposure represent an abnormal condition and are greatly in excess of those set forth for normal breathing and displacement. The emergency requirement is adequate for both conditions, and it appears both practical and economical to combine them into one device on the smaller vessels, as tabulated in the Summary for Use.

However, a separate apparatus for the normal requirement has the advantage of greater mechanical dependability over the much larger sizes needed for the combined requirement. Where flash arresters are needed, a further objection arises to large combined units. Efficiently designed arresters, as generally known today, would become huge and expensive, whereas the emergency requirement may be fulfilled separately by merely installing a vaportight hinged cover which may also be used as a manway. (These are available commercially.) If this cover be set to open above 3 in. water pressure, say 2 oz to 4 oz per sq in., no flash arrester would seem needed on this connection. When the emergency valve operated at such pressures, vaporization would already be considerable, and also the vapor would be "too rich to burn," until mixed with external air. Further, flows at 4 oz pressure for compounds having properties of $F = 0.136$ through ordinary vent connections, are of velocities ranging above 25 fps, which is more than the propagation rate of flame in a gas-air mixture at atmospheric pressure.

Modification of the Calculated Relief Areas. The discussion has now progressed so that the suggested reduction of the calculated relief sizes, as shown in Fig. 18, may be clarified.

It will be seen in Fig. 19 that the volatile contents of a 15-ft-diam tank (20,000 gal) may reach 100 F, in a matter of 10 min after being surrounded by intense fire. For this reason, the emergency-vent capacities should be compatible with the 20,000 Btu heat-absorption rate for all tanks from zero through at least 15 ft diam. For tanks above this diameter at these low pressures, the calculated relief areas become rapidly unreasonable (refer to Curve 1, Fig 18), but the likelihood of complete envelopment with fire of sufficient depth (probably about equal to the tank radius) to maintain the heat-input rate, observed in Part 1, becomes less and the time element larger. With these considerations in mind, the suggested vent size (Curve 3, Fig. 18) has been permitted to approach (at 100,000-gal capacity) the curve based on a 6000-Btu heat rate, which curve (the latter) has been gradually flattened to a maximum of 24-in. diam relief size at 300,000 gal capacity. If tanks of this capacity are of 40 to 50 ft diam, as is common, the time element for 100 F is in the neighborhood of

½ hr for severe conditions, which is perhaps sufficient time to employ protective (cooling or extinguishing) equipment reducing the exposure, or abandonment of the vessels.

Conclusion. The conclusions as outlined under *Summary* of this section apply only for the conditions specified.

Equations [20], [21], and [22] are not considered adequate for carbon tetrachloride, are not adequate to vent internal explosion, and are not intended to provide for internal reaction. No reduction in the area of the relief connections is considered for vessels covered with substantial noncombustible insulation, although allowance may be made for this protection in the capacity of the relief devices, which may be changed if the service becomes more severe from the viewpoint of fire exposure, see Proposed Summary for Use.

Equation [23] is not intended to apply to floating-type water-seal gasholders which have, by inherent design, adequate relief for fire exposure.

Suggested sizes of relief connections with necessary capacities for the emergency requirement for atmospheric tanks are given in Table 6 (based on 0.5 psi at 50 gal, proportionally reduced to 3 in. water pressure at 70,000 gal).

TABLE 6 SUGGESTED SIZES OF RELIEF CORRECTIONS FOR EMERGENCY REQUIREMENTS OF ATMOSPHERIC TANKS

Tank capacity, gal	Relief size, in. I.P. size	Minimum capacity, cu ft per hr of air at 60 F. and atmospheric pressure
50	2	13380
50 to 100	3	30100
100 to 300	4	54500
300 to 1000	6	120500
1000 to 2000	8	212000
2000 to 4000	10	326500
4000 to 10000	12	453000
10000 to 20000	16	753000
20000 to 100000	20	1048000
100000 to 200000	22[a]	744000
200000 and up	24	886000

[a] Not a standard pipe size.

Proposed Summary for Use

1 Minimum sizes of relief connections for vessels at pressures not to exceed 1 in. water external, or 0.50 psig internal: All vessels should be provided with relief area (or areas) in the form of connections or hatches. This area should be adequate for both normal breathing and emergency venting generated by exposure to fire.

(*a*) For the normal (based on contraction due to cooling and limited to 1 in. of water internal) requirement for vessels in volatile-liquid service use

$$a = \frac{Q}{1172} \text{ or } d = \sqrt{\frac{Q}{921}} \quad \ldots\ldots\ldots\ldots [1]'''$$

in which a is the relief area in square inches, d is the internal diameter of the relief connection in inches, and

$$Q = \frac{S}{0.290} + \text{emptying rate} \quad \ldots\ldots\ldots\ldots [2]'''$$

In Equation [2]''' Q and the emptying rate are in cubic feet of air per hour at 68 F, and atmospheric pressure, and S is the area of the tank roof and shell in square feet.

(*b*) For the emergency requirement (based on 0.50 psi at 50 gal proportionally reduced to 3 in. water internal pressure at 70,000 gal) for vessels not to exceed 15 ft diam in liquid service use

$$a = \frac{0.717\,S_w}{\sqrt{P(P+14.7)}} \text{ or } d = \sqrt{\frac{0.913\,S_w}{\sqrt{P(P+14.7)}}} \quad \ldots [3]'''$$

If the pressure limit be 3 in. of water as for atmospheric tanks, Equation [3]''' becomes

$$a = 0.566\,S_w \text{ or } d = \sqrt{0.721\,S_w} \quad \ldots\ldots\ldots [4]'''$$

and if the atmospheric tank be vertical cylindrical with bottom resting on pad or foundation, Equation [4]''' becomes

$$a = 1.78DH \text{ or } d = \sqrt{2.265\,DH} \quad \ldots\ldots\ldots [5]'''$$

in all of which a is the internal area and d the internal diameter of the relief connection in inches, S_w is the surface in square feet wetted by the contents when nominally full and exposed to fire, P is the relieving pressure in pounds per square inch gage (0.1083 for 3 in. water), D is the diameter of the tank in feet, and H is the height in feet of the contents on the exposed tank wall when nominally full.

For practical reasons, the emergency-vent sizes for all vessels in liquid service above 15 ft diam and, as calculated by Equations [3]''', [4]''', and [5]''' should be modified to conform to a lowered (below 20,000 Btu per sq ft per hr) heat-absorption rate, as proportionally represented by curve 2, Fig. 14, or curve 3, Fig. 18. The ultimate size should be limited to 24 in. diam.

The vent sizes and relief capacities for the normal and emergency requirements (basis as just given) for vertical, cylindrical, above ground (bottom resting on pad), atmospheric storage tanks are given in Table 7.

TABLE 7 VENTING REQUIREMENTS FOR ATMOSPHERIC STORAGE TANKS EXPOSED TO FIRE

Tank capacity, gal	Relief size (I.P. size) Normal; vent, in.	Relief size (I.P. size) Emergency; cover, in.	Minimum capacity, cu ft air per hr at 60 F and atmospheric pressure: Normal[d] (at 1 in. water flowing pressure)	Minimum capacity, cu ft air per hr at 60 F and atmospheric pressure: Emergency (at 3 in. water flowing pressure)
50	...	2[a]	...	6150
50 to 100	...	3[a]	...	13400
100 to 300	...	4[a]	...	24600
300 to 1000	...	6[a]	...	55400
1000 to 2000	1–1½	1–8	1920	98500
2000 to 4000	1–2	1–10	2805	153800
4000 to 10000	1–2	1–12	3660	221500
10000 to 20000	1–3	1–16	6180	344000
20000 to 50000	1–3	1–20	8230	615500
50000 to 100000	1–4	1–20	12500	615500
100000 to 150000	1–4	1–22[e]	14620	744000
150000 to 200000	1–4, [b] 1–3	1–22[e]	18100	744000
200000 to 400000	1–4, [b] 1–3	1–24	22820	886000
400000 to 800000	1–6	1–24	32900	886000
800000 to 1100000	1–6, 1–3	1–24	41100	886000
1100000 to 1300000	1–6, [c] 1–4	1–24	47500	886000
1300000 to 1800000	1–8	1–24	58450	886000
1800000 to 2000000	2–6	1–24	65800	886000

[a] The first four items of "Emergency relief size" are given in terms of "in. vent," all others in terms of "cover, in."
[b] Although one 6 in. may be cheaper, the two units have the advantage of multiple devices.
[c] Although one 8 in. may be cheaper, the two units have the advantage of multiple devices.
[d] To be used for selection of the normal relief devices. This capacity is included in that for the emergency requirement.
[e] Not a standard pipe size.

(*c*) For the emergency relief requirement for vessels in gas service not to exceed 40 ft diam use

$$a = \frac{0.03195\,S}{\sqrt{P}} \text{ or } d = \sqrt{\frac{0.0407\,S}{\sqrt{P}}} \quad \ldots\ldots\ldots [6]'''$$

in which a is the relief area in square inches, and d is the internal diameter of the relief connection in inches, S is the surface of the tank in square feet which may be exposed including the roof, and P is the relieving pressure in pounds per square inch gage.

Emergency relief connections for vessels in gas service above 40 ft diam should be modified to conform to a lowered heating rate as proportionally represented by curve 5 in Fig. 18, and limited to a maximum of 24 in. diam at 65,000 cu ft capacity.

(*d*) *General.* The relief area should be at least equivalent to

the area of the inlet connection to avoid excessive internal pressure due to accidental overfilling.

In all cases cited, the next larger pipe size should be used as the vent connection, which preferably should be located at the top of the tank vapor space.

No reduction in the size of the relief connection should be made for vessels covered with substantial noncombustible insulation, or provided with reliable cooling systems, although allowance may be made for this protection in the capacity of the relief device. When vessels are so equipped with an adequate relief connection, the relief apparatus may be changed if the service becomes more severe from the standpoint of operation or fire exposure.

2 The relief capacity of the required areas in terms of rate of fluid flow; liquid or gas service: To select a relief device or devices of adequate capacity, based on approved flow test, other than those capacities previously listed for atmospheric tanks, use the area a (not the next larger pipe size), as determined in paragraph 1 in any of the following formulas as the case may require

$$W = 516\,a\sqrt{\frac{MP(P+14.7)}{T}} \text{ or } 405\,d^2\sqrt{\frac{MP(P+14.7)}{T}} \quad [7]'''$$

lb per hr of vapor contents

$$Q = 198{,}500\,a\sqrt{\frac{P(P+14.7)}{MT}} \text{ or } 156{,}000\,d^2\sqrt{\frac{P(P+14.7)}{MT}} \quad \ldots\ldots [8]'''$$

cu ft per hr of vapor at 68 F, and atmospheric pressure

$$Q = 36{,}900\,a\sqrt{\frac{P(P+14.7)}{T}} \text{ or } 29{,}000\,d^2\sqrt{\frac{P(P+14.7)}{T}} \quad \ldots\ldots [9]'''$$

cu ft per hr of air at 68 F, and atmospheric pressure

In all of which a is the internal area in square inches, d is the diameter of the relief area in inches, P is the relieving pressure in pounds per square inch (not to exceed 0.50 lb), M is the molecular weight and T is the vapor temperature of the contents in deg F absolute.

For conditions of fire exposure, T is approximately the normal boiling point of the liquid contents. For vessels in gas service, T is about the temperature necessary to raise the pressure in the vessel from the absolute working pressure and temperature to the absolute set pressure of the relief device, as computed by the gas law, $T/P = T'/P'$.

Allowance may be made in the capacity of the relief device for vessels covered with substantial noncombustible insulation or provided with reliable cooling systems proportional to the reduction effected in the heat-transfer rate through the tank wall, if it is deemed advisable from a practical and economical standpoint.

3 Normal and emergency relief devices: It is preferable, as explained in the section, *Emergency and Normal Relief* that separate relief devices, when needed, be used for the venting requirement for normal operation for all vessels above 1000 gal capacity. The additional relief area required for fire exposure may be in the form of a vaportight hinged cover, hatch, or simple valve, each of which is considered more practical than a weak head seam.

Uncontrolled internal reaction and explosion in vessels of the subject category are emergency relief requirements to which this development does not apply. However, weak seams have been advantageous under such circumstances. The hazard of internal explosion may be minimized by the use of inert gas, grounding the vessel, or provision of flash arresters.

4 If relief capacity is inadequate for the contingency of fire exposure, additional protective features should be provided for the vessel and exposures. These may consist of fire-protective or extinguishment equipment, process-cooling systems, construction of dikes or walls, provision of drains, or fireproofing supports, etc.

5 Back pressure: In this low-pressure range, any back pressure on the downstream side of the relief device will reduce its flow capacity, as calculated by Equations [7]''', [8]''', and [9]''' proportional to the $\sqrt{P\,(P+14.7) - P'\,(P'+14.7)/P(P+14.7)}$ in which P' is the back pressure. Also, the opening pressure of the relief device must be adjusted to counteract the back pressure or the intended maximum pressure in the vessel will be exceeded.

6 Time element: The time required for the liquid contents of a vessel when exposed to fire to reach the boiling point (or any given average temperature) may be estimated by the following formula

$$\theta = \frac{V\rho C_p(T-70)}{IS_w} + \frac{4.87t(T+20)}{I} \quad \ldots\ldots [10]'''$$

in which θ is the time in hours, V is the volume of the contents in cubic feet, ρ is the density of contents in pounds per cubic foot, C_p is the specific heat of contents, T is the temperature reached in deg F, I is the heat-absorption rate in Btu per hour per square foot, and t is the thickness of the steel tank wall in inches. If Equation [10]''' is to apply to vertical, cylindrical, flat-bottom tanks, it becomes

$$\theta = \frac{D\rho C_p(T-70)}{4I} + \frac{4.87\,t(T+20)}{I} \quad \ldots\ldots [11]'''$$

in which D is the diameter of the tank in feet.

If θ is $^1/_2$ hr or more (approximate time for very volatile materials to reach 100 F, when contained in 40 to 50-ft-diam atmospheric tanks surrounded by intense fire) and there is assurance that effective cooling or fire-extinguishing equipment will come into play during the $^1/_2$-hr period, the emergency-relief (device) capacity may be reduced to the vaporization rate produced by the calculated temperature rise within the $^1/_2$ hr. For vessels exposed to fire in gas service, the maximum venting rate will occur within such a short time as to permit no modification of the calculated emergency relief.

Conclusion

The conclusions as outlined under *Summary* in the first of this section of the paper and as detailed under Summary for Use are based upon the foregoing theory which is mathematically expressed in the Appendix of this section.

The formulas proposed provide relief capacities greater than those provided by present average practice which capacities are not adequate for the abnormal condition of fire exposure.

For examples of use of the formulas see the Appendix.

Proposals herein presented hold only for pressures not to exceed 0.50 psig. For vessels to operate at pressures from 0.50 to include 15 psig, Part 4 of this paper will be presented at a later date. For pressures above that refer to Part 2.

Appendix for Part 3

Derivation of General Equations [24] or [3]^{iv}, and [25] or [15]^{iv}

1 Vapor weight rate of a short tube (at pressures not to exceed 0.50 psig), Equation [26]

$$V = C\sqrt{2g\Delta H}$$

$$Va = Ca\sqrt{2g\Delta H}$$

$$Va\rho = Ca\rho\sqrt{2g\Delta H}$$

$$3600Va\rho = 3600Ca\rho\sqrt{2g\Delta H}$$

$$W = 3600Ca\rho\sqrt{2g\Delta H}$$

When differential is pounds per square inch

$$\Delta H = \frac{\Delta P\ 144}{\rho^*}$$

$$\Delta H = \frac{\Delta P \times 10.72 \times T \times 144}{MP^*}$$

$$W = 3600 \times 0.70 \times \frac{0.7854d^2}{144} \times \frac{MP}{10.72T}\sqrt{\frac{64.35 \times \Delta P \times 10.72 \times T \times 144}{MP^*}}$$

$$W = 405\,\frac{d^2\,MP}{T}\sqrt{\frac{\Delta PT}{MP^*}}$$

$$W = 405\,d^2\sqrt{\frac{\Delta PMP}{T}} \quad \ldots\ldots\ldots\ldots [1]^{\text{I-V}}$$

In the development of Equation $[1]^{\text{I-V}}$ the following nomenclature was used:

V = velocity, fps
g = gravitational constant, 32.17
ΔH = differential head in ft of fluid*
C = coefficient of discharge
C = 0.70 when $p_1/p_2 < 1.05$ (see footnote 31)
a = area of short tube, sq ft
ρ = density of fluid, lb per cu ft
ρ = MP/RT for a gas
R = gas constant, 10.72
W = weight rate, lb per hr
M = molecular weight
P = absolute pressure, psi
T = absolute temperature, deg F
ΔP = differential pressure, psi
d = diameter of a short tube, in.

2 Weight rate vaporized

$$\frac{Q}{S_w} = \frac{Wr}{S_w} = I$$

$$W = \frac{IS_w}{r} \quad \ldots\ldots\ldots\ldots [2]^{\text{I-V}}$$

in which

Q = total heat input, Btu per hr
S_w = wetted surface heated, sq ft
r = latent heat of vaporization, Btu per lb
I = unit heat input, Btu per hr per sq ft
W = liquid vaporized, lb per hr

* It is theoretically correct to express the differential head ΔH in terms of the downstream density and so the P in the denominator in downstream pressure. Cancelling this P into the upstream pressure simplifies the equation, avoids confusion, and yet maintains theoretical accuracy within 0.36 per cent at 3 in. water pressure (1.7 per cent at 0.50 lb per sq in. gage). Note the comparison between calculated and actual flows in Fig. 20.

3 Required diameter of a short tube to pass the weight rate vaporized, Equation [24] or $[3]^{\text{I-V}}$:

Equate $[1]^{\text{I-V}}$ to $[2]^{\text{I-V}}$

$$405\,d^2\sqrt{\frac{\Delta PMP}{T}} = \frac{IS_w}{r}$$

$$d^2 = \frac{IS_w}{r \times 405}\sqrt{\frac{T}{M\Delta PP}}$$

$$d = \sqrt{\frac{IS_w}{405\sqrt{\Delta PP}}}\left(\frac{T}{Mr^2}\right)^{1/4} \quad \ldots\ldots [3]^{\text{I-V}} \text{ or } [24]$$

To apply Equation $[3]^{\text{I-V}}$

d = diameter of relief connection, in.
I = 20,000 Btu per sq ft per hr
S_w = wetted surface exposed, sq ft
ΔP = relieving pressure, psig
P = relieving pressure, psia
T = boiling point of contents at P, deg F abs
M = molecular weight of contents
r = latent heat of vaporization at T, Btu per lb

4 Weight rate of expansion or contraction of gas or vapor due to heat transferred to or from the tank wall:

$$wC_p\frac{dT}{d\theta} = \frac{Q}{\theta} \quad \ldots\ldots\ldots\ldots [4]^{\text{I-V}}$$

$$hS\Delta T = \frac{Q}{\theta} \quad \ldots\ldots\ldots\ldots [5]^{\text{I-V}}$$

$$w = V\rho = V\frac{MP}{RT} \quad \ldots\ldots\ldots\ldots [6]^{\text{I-V}}$$

From Equations $[4]^{\text{I-V}}$ and $[6]^{\text{I-V}}$

$$V\rho C_p\frac{dT}{d\theta} = \frac{Q}{\theta} \quad \ldots\ldots\ldots\ldots [7]^{\text{I-V}}$$

$h = F\overline{\Delta T}^{1/4}$ (see Part 1, ref 5)

From Equation $[5]^{\text{I-V}}$

$$F\overline{\Delta T}^{1/4}\,S\Delta T = \frac{Q}{\theta} \quad \ldots\ldots\ldots\ldots [8]^{\text{I-V}}$$

Equate $[7]^{\text{I-V}}$ to $[8]^{\text{I-V}}$

$$V\rho C_p\frac{dT}{d\theta} = FS\overline{\Delta T}^{5/4}$$

$$\frac{dT}{d\theta} = \frac{FS\overline{\Delta T}^{5/4}}{V\rho C_p} \quad \ldots\ldots\ldots\ldots [9]^{\text{I-V}}$$

From Equation $[6]^{\text{I-V}}$

$$dw = \frac{-VMP}{R}\cdot\frac{dT}{T^2} \quad \ldots\ldots\ldots\ldots [10]^{\text{I-V}}$$

$$-dw = \frac{w}{\theta}\cdot d\theta \quad \ldots\ldots\ldots\ldots [11]^{\text{I-V}}$$

Equate $[10]^{\text{I-V}}$ to $[11]^{\text{I-V}}$

$$\frac{VMP}{R}\cdot\frac{dT}{T^2} = \frac{w}{\theta}\cdot d\theta \quad \ldots\ldots\ldots\ldots [12]^{\text{I-V}}$$

$$\frac{dT}{d\theta} = \frac{w}{\theta}\cdot\frac{RT^2}{VMP} \quad \ldots\ldots\ldots\ldots [13]^{\text{I-V}}$$

Equate $[9]^{iv}$ to $[13]^{iv}$

$$\frac{FS\overline{\Delta T}^{5/4}}{V\rho C_p} = \frac{w}{\theta} \cdot \frac{RT^2}{VMP} \quad \ldots\ldots\ldots\ldots [14]^{iv}$$

In the development of Equations $[4]^{iv}$ to $[14]^{iv}$ the following nomenclature was used:

w = weight of contained gas or vapor, lb
C_p = specific heat of gas or vapor
dT = change in temperature
$d\theta$ = change in time
Q = total heat transferred, Btu
θ = time, unit hr
h = heat-transfer coefficient Btu per hr per sq ft per deg F
S = tank surface exposed, sq ft
ΔT = difference between tank wall and contained gas, deg F
V = volume of contents gas or vapor, cu ft
ρ = density of contents gas, lb per cu ft
M = molecular weight of gas or vapor
P = pressure, psia
R = gas constant, 10.72
T = temperature of gas or vapor, deg F abs
F = function of physical properties of gas
dw = change in weight
$W = \frac{w}{\theta}$ = weight rate, lb per hr

5 Required diameter of a short tube to pass the weight rate of a gas expanded or contracted due to heat transferred to or from the tank wall; Equation [25] or $[15]^{iv}$ (same nomenclature used as in section 4 preceding; also $\rho = MP/RT$):

Insert Equation $[1]^{iv}$ in $[14]^{iv}$

$$405\, d^2 \sqrt{\frac{\Delta PMP}{T}} \cdot \frac{RT^2}{VMP} = \frac{FS\overline{\Delta T}^{5/4}}{V\rho C_p}$$

$$d^2 = \frac{FS\overline{\Delta T}^{5/4}}{V\rho C_p} \cdot \frac{VMP}{RT^2\, 405} \sqrt{\frac{T}{\Delta PMP}}$$

$$d^2 = \frac{F}{C_p M^{1/2}} \cdot \frac{S}{405} \cdot \frac{\overline{\Delta T}^{5/4}}{T} \sqrt{\frac{T}{\Delta PP}}$$

$$d = \left(\frac{F}{C_p M^{1/2}}\right)^{1/2} \cdot \frac{S^{1/2}}{\sqrt{405}} \cdot \frac{\overline{\Delta T}^{5/8}}{T^{1/4}} \cdot \frac{1}{\Delta P^{1/4} P^{1/4}}$$

$$d = \frac{0.375 P^{1/4}}{T^{0.783}} \cdot \frac{S^{1/2}}{\sqrt{405}} \cdot \frac{\overline{\Delta T}^{5/8}}{T^{1/4}} \cdot \frac{1}{\Delta P^{1/4} P^{1/4}}$$

$$\left(\text{Refer to the following paragraph for } \frac{0.375\, P^{1/4}}{T^{0.0783}}\right)$$

$$d = 0.0186 \cdot \frac{S^{1/2}}{\Delta P^{1/4}} \cdot \frac{(T_w - T)^{5/8}}{T^{0.325}} \quad \ldots\ldots\ldots [15]^{iv} \text{ or } [25]$$

To apply equation $[15]^{iv}$

d = diameter of relief connection, in.
S = tank surface heated, sq ft
ΔP = relieving pressure, psig
T_w = temperature to which tank wall is heated or cooled, deg F abs
T = initial temperature of contents vapor, deg F abs; if T_w is less than T, reverse the signs

The term $\left(\frac{F}{C_p M^{1/2}}\right)^{1/2}$ in this section, relating the properties of the vapor contents, was replaced by its maximum value $0.375 \cdot \frac{P^{1/4}}{T^{0.0783}}$. This is justified in the following manner: The value of F, a function of the physical properties of a gas, varies with both temperature and pressure as will be seen. The value C_p specific heat at constant pressure varies with temperature. Inasmuch as pressure and temperature are working conditions to remain in the relief diameter Equation $[15]^{iv}$, it is desirable to express the subject variable in terms of P and T. Now

$$F = D\left(\frac{\rho^2 B C_p k^3}{Z}\right)^{1/4} \quad \text{(Part 1, ref. 5, Equation [20], p. 242)}$$

$$\left(\frac{F}{C_p M^{1/2}}\right)^{1/2} = D\left(\frac{\rho^2 B C_p k^3}{C_p{}^4 M^2 Z}\right)^{1/8} = D\left[\rho^2 Z^2 \cdot \frac{B}{M^2}\left(\frac{k^3}{C_p{}^3 Z^3}\right)\right]^{1/8}$$

Since B, M, and the ratio $C_p Z/k$ (Part 1, ref. 5, p. 417) are independent of P and T, we may write

$$\left(\frac{F}{C_p M^{1/2}}\right)^{1/2} = D'(\rho^2 Z^2)^{1/8}$$

and ρ for a gas is MP/RT, then

$$\left(\frac{F}{C_p M^{1/2}}\right)^{1/2} = D'\left(\frac{M^2 P^2}{R^2 T^2} \cdot Z^2\right)^{1/8}$$

Again M and R are independent of P and T, so

$$\left(\frac{F}{C_p M^{1/2}}\right)^{1/2} = D''\left(\frac{P^2}{T^2} \cdot Z^2\right)^{1/8}$$

$$= D''\left(\frac{P^2}{T^2} \cdot T^{1.398}\right)^{1/8}$$

$$= D''\left(\frac{P^2}{T^{0.602}}\right)^{1/8}$$

$$\left(\frac{F}{C_p M^{1/2}}\right)^{1/2} = D''\left(\frac{P^{1/4}}{T^{0.0753}}\right)$$

When $P = 14.7$ psia, and $T = 528$ deg R, $C_p = 0.24$, and $F = 0.27$ for air

$$\therefore D'' = \left(\frac{0.27}{0.24 \times 29^{1/2}}\right)^{1/2} \times \frac{(528)^{0.0753}}{14.7^{1/4}}$$

$D'' = 0.375$ and $\left(\frac{F}{C_p M^{1/2}}\right)^{1/2} = 0.375\, \frac{P^{1/4}}{T^{0.0753}}$

The nomenclature used in the foregoing derivations follows:

F = 0.27 for air at 68 F, and atmospheric pressure
D = proportionality constant
k = thermal conductivity
C_p = specific heat
ρ = density
B = coefficient of thermal expansion
Z = viscosity
M = molecular weight
R = gas constant

Z^2 varies with T for air as follows:

T, deg R	Z	Z^2
460	0.0162	0.000262
528	0.018	0.000323
660	0.021	0.000440
860	0.025	0.000625
1060	0.029	0.000840
1260	0.032	0.001050
1460	0.036	0.001295
1560	0.038	0.001444

$$\left(\frac{1560}{460}\right)^n = (3.39)^n = \frac{1.444}{0.2625} = 5.50$$

$$n = 1.398$$

TABLE 8 VALUES OF F FOR SEVERAL GASES

Gas	k[a]	C_p[a]	Z[a]	M[a]	$\frac{k^3C_pM^3}{Z}$	$\left(\frac{k^3C_pM^3}{Z}\right)^{1/4}$	F	$\frac{F}{C_pM^{1/2}}$
Air	0 0161	0.24	0.018	29	0.0468	0.465	0 270	0.209
Hydrogen	0 1075	3 50	0 009	2	1.9324	1.181	0 685	0.138
Acetone	0 0065	0.34	0 0077	58	0 0408	0.448	0.260	0.100
Acetylene	0 0124	0.43	0 010	26	0 0554	0.485	0.281	0.128
Benzene	0 0062	0.26	0 0075	78	0 0502	0.472	0 273	0.135
Ethyl alcohol	0 0089	0.40	0 0094	46	0 0634	0 501	0.290	0.107
Ethyl ether	0 0088	0.46	0 0077	74	0 2220	0 687	0.398	0.100
Water	0 0110	0.48	0 0097	18	0 0213	0.382	0.221	0.108
Pentane	0 0083	0.34	0 0063	72	0 1599	0 632	0 366	0.127
Carbon dioxide	0 0109	0.21	0 0146	44	0.0360	0.436	0.252	0.181
"Freon 113"	0.0054	0.16	0.0103	187	0.0855	0.542	0.313	0.143

[a] "Heat Transmission," by W. H. McAdams,[1] various pages.

Now it is also necessary to show that $\left(\frac{F}{C_pM^{1/2}}\right)^{1/2}$ gives higher values for air than for any other gases whose properties were available in the reference literature. To do this, we use McAdam's Equation [20][14] again which is

$$F = D\left(\frac{\rho^2BC_pk^3}{Z}\right)^{1/4}$$

and in which the nomenclature is as before. Again, $\rho = MP/RT$ and $B = 1/492$. Then, at a constant pressure and temperature it would be expected that F would vary for different gases as follows.

$$F = D'\left(\frac{M^2C_pk^3}{Z}\right)^{1/4}$$

At 1 atm pressure and 20 C, $F = 0.27$ and $\left(\frac{M^2C_pk^3}{Z}\right)^{1/4} = 0.465$ for air, so that the F value for any other gas, whose molecular weight, specific heat, thermal conductivity, and viscosity are known, may be determined from the relation.

$$F_g = \frac{0.27}{0.465}\left(\frac{k^3C_pM^3}{Z}\right)_g^{1/4}$$

in which the subscript g applies to the gas other than air. On this basis the F value for a number of representative gases has been calculated as shown in Table 8. It will be noted that the value of $\left(\frac{F}{C_pM^{1/2}}\right)^{1/2}$ for air is greater than for any of those so obtained, and for many others such as ammonia, nitrogen, and oxygen whose properties were considered but not listed in the table.

Simplification of General Expressions to Formulas For Use

1 The diameter of a short tube to limit internal pressure (not to exceed 0.50 psig) within vessels when the volatile-liquid contents are absorbing heat at 20,000 Btu per sq ft per hr of wetted surface exposed, Equations [20], [21], and [22], is derived as follows, the nomenclature being the same as used previously

$$d = \sqrt{\frac{IS_w}{405\sqrt{\Delta PP}}}\left(\frac{T}{Mr^2}\right)^{1/4} \quad \ldots\ldots [3]^{1/2} \text{ or } [24]$$

in which $\left(\frac{T}{Mr^2}\right)^{1/4}$ = contents factor, evaluated from Fig. 12, Part 2.

$$d = \sqrt{\frac{20{,}000\,S_w}{405\sqrt{P(P+14.7)}}} \times 0.136$$

$$d = \sqrt{\frac{0.913S_w}{\sqrt{P(P+14.7)}}} \quad \ldots\ldots [16]^{1/2}$$

If P be 3 in. water, 0.1083 lb

$$d = \sqrt{\frac{0.913S_w}{\sqrt{0.1083 \times 14.8083}}} = \sqrt{0.721S_w} \ldots\ldots [17]^{1/2}$$

If the tank be vertical cylindrical with bottom on pad

$$d = \sqrt{0.721\pi DH} = \sqrt{2.265DH} \ldots\ldots [18]^{1/2}$$

2 The diameter of a short tube to limit internal pressure to a specified maximum (not to exceed 0.50 psig) within vessels when the vapor contents absorb heat from the enclosing shell heated to 1100 F, Equation [23], is derived as follows, the nomenclature being the same as previously used:

$$d = 0.0186\,\frac{S^{1/2}}{\Delta P^{1/4}} \cdot \frac{(T_w - T)^{5/8}}{T^{0.325}} \ldots [15]^{1/2} \text{ or } [25]$$

in which $\frac{(T_w - T)^{5/8}}{T^{0.325}}$ = gas expansion variable. Then substituting the following values:

$T_w = 1100 + 460 = 1560$ deg F abs

$T = 0 + 460 = 460$ deg F abs

$(T_w - T)^{5/8} = 79.5$

$T^{0.325} = 7.33$

$(T_w - T)^{5/8}/T^{0.325} = 10.85$

$$d = 0.0186 \times \frac{S^{1/2}}{\Delta P^{1/4}} \times 10.85$$

$$d = \sqrt{\frac{0\,0407\,S}{\sqrt{P}}} \ldots\ldots [19]^{1/2}$$

when P is gage pressure.

3 The diameter of a short tube to limit external pressure on a tank to 1 in. of water when the vapor contents are contracted from the loss of heat to a colder tank wall, Equations [16], [17], [18], and [19], is derived as follows, the nomenclature being the same as previously used.

The weight rate of contraction is

$$W = \frac{FS\Delta T^{5/4}}{V\rho C_p}\,\frac{VMP}{RT^2} \ldots\ldots [14]^{1/2}$$

$$Q = \frac{FS\Delta T^{5/4}}{C_p} \cdot \frac{MP}{RT^2} \cdot \frac{R^2T^2}{M^2P^2}$$

$$Q = \frac{10.72\,FS(T - T_w)^{5/4}}{C_pMP} \text{ cu ft per hr}$$

in which

[14] Part 1, ref. 5, equation [20], p. 242.

$$\frac{\text{Weight rate, } W}{\text{Unit weight, } \rho} = \text{quantity rate, } Q$$

$$\rho = MP/RT$$

Applying the temperatures from Case 1, Table 4, and the properties of air

$$Q = \frac{10.72 \times 0.27 \times S(563 - 516)^{5/4}}{0.24 \times 29 \times 14.736}$$

(14.736 = average pressure during contraction)

$$Q = S/0.291 \text{ cu ft per hr} \ldots\ldots\ldots\ldots [20]^{\text{IV}}$$

When Equation $[20]^{\text{IV}}$ is used, the emptying rate must be added to provide for maximum in-breathing.

The weight rate of a relief connection (nomenclature as previously used) is

$$W = 405\, d^2 \sqrt{\frac{\Delta PMP}{T}} \ldots\ldots\ldots\ldots [1]^{\text{IV}}$$

$$Q = 405\, d^2 \sqrt{\frac{\Delta PMP}{T}} \cdot \frac{RT}{MP}$$

again $Q = \dfrac{W}{\rho}$

$$Q = 4340\, d^2 \sqrt{\frac{\Delta PT}{MP}} \text{ cu ft per hr} \ldots\ldots\ldots [21]^{\text{IV}}$$

(see Fig. 20).

Then the quantity rate of air at 68 F is

$$Q = 4340\, d^2 \sqrt{\frac{0.0361 \times 528}{29 \times 14.736^*}} = 918\, d^2 \text{ at 1 in. water pressure}$$

$$d = \sqrt{\frac{Q \times 14.7}{918 \times 14.736}} = \sqrt{Q/921} \text{ at atmospheric pressure } [22]^{\text{IV}}$$

Applying the surface from Case 1, Table 4, to Equations $[20]^{\text{IV}}$ and $[22]^{\text{IV}}$

$$Q = S/0.290 = 5170/0.290 = 17{,}830 \text{ cu ft of air}$$

$$d = \sqrt{Q/921} = \sqrt{17{,}830/921} = 4.40 \text{ in.}$$

Check by applying Equation $[15]^{\text{IV}}$ to Case 1, Table 4

$$d = 0.0186 \times \frac{S^{1/2}}{\Delta P^{1/4}} \times \frac{(T - T_w)^{5/8}}{T^{0.325}} \ldots\ldots [15]^{\text{IV}}$$

the following values being used:

$$S^{1/2} = \sqrt{5170} = 71.9$$

$$\Delta P^{1/4} = \sqrt[4]{0.0361} = 0.436$$

$$T^{0.325} = (563)^{0.325} = 7.82$$

$$T_w = 516 \text{ F abs}$$

$$(T - T_w)^{5/8} = (47)^{5/8} = 11.1$$

$$(T - T_w)^{5/8}/T^{0.325} = 1.425$$

then

$$d = \frac{0.0186 \times 71.9 \times 1.425}{0.436}$$

$$d = 4.37 \text{ in.}$$

A discrepancy exists of 3 parts in 438.5 between results by Equations $[15]^{\text{IV}}$ and $[22]^{\text{IV}}$. This is considered due to the average temperature difference between the tank vapor and external air during in-breathing for which Equation $[15]^{\text{IV}}$ does not provide.

4 The capacity of the relief areas in terms of fluid flow, Equations [26], [27], [28], [7]‴, [8]‴, and [9]‴.

The weight rate of vapor flow of a short tube is

$$W = 405\, d^2 \sqrt{\frac{MP(P + 14.7)}{T}} \text{ lb per hr} \ldots\ldots [1]^{\text{IV}}$$

The quantity rate is

$$Q = \frac{W \times 10.72 \times 528}{M \times 14.7}$$

where

$$Q = W/\rho$$

$$\rho = MP/RT$$

$$\rho = M\ (14.7)/10.72\ (528)$$

$$Q = 156{,}000\, d^2 \sqrt{\frac{P(P + 14.7)}{MT}} \ldots\ldots [23]^{\text{IV}}$$

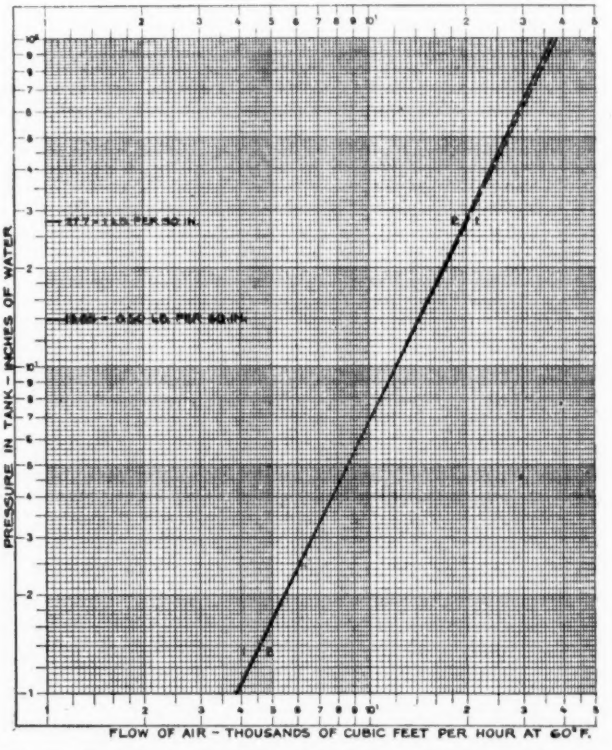


FIG. 20 COMPARISON OF THEORETICAL FLOW CAPACITY OF SHORT TUBE WITH THAT OF TYPICAL TANK CONNECTION AT LOW PRESSURES

NOTES: 1 Actual flows through a calibrated orifice to the tank.

2 Theoretical flow capacity equation $Q = 4340\, d^2 \sqrt{\dfrac{\Delta PT}{MP}}$ (coefficient of flow 0.70).

Refer to Part 3, "Relief of Vessels Exposed to Fire."

Capacity of a standard 2-in. nipple 6 in. long located in top head of 4 ft diameter by 5 ft high vertical cylindrical tank with inlet in lower shell. Actual flows were 99 per cent of theoretical at 1 in. water pressure.

* Actually, the external pressure during contraction cannot rise above 14.7 lb per sq in. absolute. Flows computed using 14.736 as P are within the accuracy illustrated by Fig. 20. Use of the P (14.736) is more than compensated for by using $Q = S/0.290$ instead of $S/0.291$.

cu ft per hr at 68 F and atmospheric pressure

The quantity rate of air is

$$Q = 156{,}000\, d^2 \sqrt{\frac{P(P + 14.7)}{29\, T}}$$

$$Q = 29{,}000\, d^2 \sqrt{\frac{P(P + 14.7)}{T}} \quad \text{.....[24]}^{\text{IV}}$$

cu ft per hr at 68 F and atmospheric pressure

At a flowing temperature of 104 F such as for compounds of $F = 0.136$

$$Q = 29{,}000\, d^2 \sqrt{\frac{P(P + 14.7)}{564}}$$

$$Q = 1222\, d^2 \sqrt{P(P + 14.7)} \quad \text{.....[25]}^{\text{IV}}$$

cu ft air per hr at 68 F and atmospheric pressure

When $P = 0.1083$ lb, 3 in. water

$$Q = 1550\, d^2 = 1972a \quad \text{.....[26]}^{\text{IV}}$$

cu ft air per hr at 68 F and atmospheric pressure

Derivation of Time-Element Formulas

1 Estimated time for the liquid contents of a vessel to reach a given temperature, Equations [29] and [30]

IS_w = total heat input, Btu per hr

$\frac{V\rho C_p \Delta T}{\theta}$ = heat absorbed by liquid contents, Btu per unit time

$\frac{St\rho C_p \Delta T}{12\,\theta}$ = heat absorbed by tank, Btu per unit time

$$IS_w = \frac{V\rho C_p (T - 70)}{\theta} + \frac{St\, 487 \times 0.12\, (T + 20)}{12\,\theta}$$

$$(S_w \leq 0.85\, S)$$

$$\theta = \frac{V\rho C_p\, (T - 70)}{IS_w} + \frac{4.87\, t(T + 20)}{I} \quad \text{.....[27]}^{\text{IV}}$$

(Liquid contents of an average temperature of 70 F and tank steel of an average of 60 F before exposure. Tank shell after heating of an average of 100 F hotter than liquid, although this will vary with the contents.)

If tank is vertical cylindrical with bottom on pad, $S_w = \pi DH$

$$\theta = \frac{D\rho C_p (T - 70)}{4\, I} + \frac{4.87\, t\,(T + 20)}{I} \quad \text{.....[28]}^{\text{IV}}$$

in which

I = heat absorption rate, Btu per sq ft per hr
S_w = surface wetted by contents exposed to fire, sq ft
V = volume of liquid contents, cu ft
ρ = density, lb per cu ft (487 for steel)
C_p = specific heat, 0.12 for steel
ΔT = temperature difference, deg F
θ = time, hr
S = surface of vessel heated, sq ft
t = thickness of tank shell in inches
T = temperature of contents, deg F
D = diameter of vessel, ft
H = height of contents on exposed wall, ft

2 Estimated time for an empty steel tank to reach the "critical" temperature of 1100 F, Equation [31], the foregoing nomenclature being used

$$IS_w = \frac{St}{12} \times \frac{487 \times 0.12\, (T - 50)}{\theta}$$

$$I = \frac{4.87\, t(1100 - 50)}{\theta}$$

$$\theta = \frac{5114\, t}{0.8\, I} = 0.320\, t \quad \text{.....[29]}^{\text{IV}}$$

(During the period of heating to 1100 F, the input I will be only about 80 per cent effective due principally to reradiation losses.)

Examples of Use of the Formulas

1 Assume an acetone tank (110,000 gal nominal capacity) 30 ft diam by 24 ft high, cylindrical shell with umbrella-type roof and flat bottom. The relief devices are to operate at 1 in. water external and 0.50 psi internal pressure.

(*a*) The normal breathing requirement (based on in-breathing) was determined as explained and tabulated in the Summary for Use in this section of the paper. This was done as follows

$Q = (S/0.290)$ + emptying rate ..... [2]'''

$Q = (3013/0.290) + 300$ gal per min
$Q = 10{,}400 + 2408$ cu ft per hr
$Q = 12{,}808$ cu ft air per hr at 68 F

$$Q = 12{,}808 \sqrt{\frac{520}{528}} = 12{,}710 \text{ at } 60 \text{ F}$$

$d = \sqrt{Q/921}$ .....[1]'''

$d = \sqrt{12{,}808/921} = 3.73$ in. (specify 4-in. standard I.P. size)

In this

$S = \pi D(H + 0.266D)$
H = height of straight shell
$S = \pi\, 30\, (24 + 0.266 \times 30)$
$S = 3013$ sq ft

The 4-in. size indicated is that recommended for this tank since it may be used at atmospheric pressure. However, the requirement may be figured more exactly (provide for the difference between 3 in. water and 0.50 psi internal pressure) as follows:

$$Q = \frac{S}{0.291 \times \frac{14.932}{14.736}} = S/0.295$$

See Equation [20]IV

$Q = (3013/0.295) + 2408$
$Q = 12{,}623$ cu ft air per hr at 68 F
$d = \sqrt{Q/921}$ ..... [1]'''
$d = \sqrt{12{,}623/921} = 3.70$ in. (use 4 in. as before)

(*b*) The emergency vent size at 3 in. water pressure is also tabulated in the Summary for Use of this section of this paper and is that recommended. Considerations involved in its selection are as follows

$$d = \sqrt{\frac{0.913 S_w}{\sqrt{P(P + 14.7)}}} \quad \text{.....[3]}'''$$

$$d = \sqrt{\frac{0.913 \times 2260}{\sqrt{0.50(15.2)}}} = 27.37 \text{ in.}$$

where

$S = \pi\, DH$
$S = \pi \times 30 \times 24$
$S = 2260$ sq ft

This is seen to be larger than the 24 in. maximum diam recommended (based on the lengthened time element and lessened pos-

sibilities of completely effective total heat absorption) for any vessel. It incorporates the observed 20,000 Btu per sq ft per hr heat-absorption rate.

The size (22 in.) recommended was based on a modified rate at 3 in. water pressure which rate may be obtained as follows

$$d = \sqrt{\frac{IS_w}{405\sqrt{P(P+14.7)}}}\left(\frac{T}{Mr^2}\right)^{1/4} \quad \ldots\ldots [24]$$

$$\sqrt{484} = \sqrt{\frac{I \times 2260}{405\sqrt{0.1083(14.808)}}} \times 0.136$$

$$I = \frac{484 \times 405 \times 1.268}{2260 \times 0.0185} = 5{,}950 \text{ Btu}$$

On the same modified rate basis, d for 0.50 psi relief pressure would become

$$d = 27.37\sqrt{\frac{5950}{20{,}000}} = 14.92 \text{ in.}$$

If this is used and the tank becomes involved with fire, the possibilities of rupture are greater.

If the recommended 22 in. be provided, the designed heat-absorption rate at 0.50-psi relief pressure is

$$I = 5950\sqrt{\frac{0.50(15.2)}{0.1083(14.808)}} = 12{,}950 \text{ Btu per sq ft per hr}$$

The relief capacity of the 22-in. connection at 3 in. water flowing pressure is

$$Q = 1222\, d^2\sqrt{P(P+14.7)} \quad \ldots\ldots [25]^{IV}$$

$$Q = 1222 \times 484\sqrt{0.1083 \times 14.808}$$

Q = 750,000 cu ft of free air per hr at 68 F (based on 104 F flowing temperature)

Compared with acetone vapor

$$Q = 4340\, d^2\sqrt{\frac{\Delta PT}{MP}} \quad \ldots\ldots [19]$$

$$Q = 4340 \times 484\sqrt{\frac{0.1083 \times 593}{58 \times 14.808}}$$

Q = 575,000 cu ft of acetone per hr at 3 in. water and 133 F

$$Q = 575{,}000\sqrt{\frac{528 \times 14.808}{593 \times 14.7}} = 544{,}000 \text{ cu ft of free vapor per hr at 68 F}$$

(*c*) Estimated time required to reach the boiling point at the observed (20,000 Btu) heat-absorption rate is

$$\theta = \frac{D\rho C_p(T-70)}{4I} + \frac{4.87\, l(T+20)}{I} \quad \ldots\ldots [11]'''$$

$$\theta = \frac{30 \times 49.5 \times 0.51(133-70)}{4 \times 20{,}000} + \frac{4.87 \times 0.375(133+20)}{20{,}000}$$

$$\theta = 0.5965 + 0.0140$$

$$\theta = 0.6105 \text{ hr} = 36.6 \text{ min}$$

2 Assume that the same vessel has been emptied and is then surrounded with intense fire:

(*a*) The shell metal would reach 1100 F in about

$$\theta = 0.320\, t = 0.320 \times 0.375 \quad \ldots\ldots [31]$$

$$\theta = 0.12 \text{ hr} = 7.2 \text{ min}$$

(*b*) After the heating period, the required size of vent to discharge the expanding vapor at 3 in. water pressure would be

$$d = \sqrt{\frac{0.0407\, S}{\sqrt{P}}} \quad \ldots\ldots [6]'''$$

in which

S = 3013 sq ft

$$d = \sqrt{\frac{0.0407 \times 3013}{\sqrt{0.1083}}} = 19.3 \text{ in.}$$

The necessary capacity of the relief device would be

$$Q = 1550\, d^2 \quad \ldots\ldots [26]^{IV}$$

Q = 578,000 cu ft of free air per hr at 68 F

Q = 9620 cu ft of free air per min at 68 F

Discussion

T. A. Gadwa.[35] The proposed constant heat-input rate of 20,000 Btu per sq ft per hr is considerably higher than the "Wartime Recommendations of Safety Valve Standardization Conference," which also considers a variable rate, depending upon the total surface of the vessel. The concept of wetted surface is a logical basis for calculation of exposed surface. Since the heat rate and wetted surface are the major factors affecting the relief-valve size, it would be desirable to have the conference review their recommendations with respect to these latest data.

The suggestion in the paper of considering the relief-valve connection as a short tube orifice is questionable. In order to obtain a 0.97 coefficient, a tapered nozzle is necessary, so that the inlet connection is always larger than the orifice, and both are established by the manufacturer. It is important always to connect the relief valve directly to a nozzle on the vessel rather than by means of a length of pipe, otherwise the pressure drop in the line will limit the capacity of the safety valve.

It is interesting to note that the code equation does not hold for pressures below approximately 15 psig and a different equation is necessary. When a relief valve operates at sufficiently high pressure, application of the gas-law deviation factor to the gas density will reduce the required orifice area. The code equation does not include this factor, although its use is suggested by the conference. Here again, possibly as a wartime measure, the API-ASME code could be revised to include the gas-deviation factor.

The heat rate for a vessel with insulation would be very useful since most fractionating towers would be in this category. Inasmuch as the recommended procedure requires orifice sizes larger than present methods, the question of whether test conditions duplicate the actual conditions must be considered before revisions are in order.

A. B. Guise.[36] The writer was especially interested in Part 1 of this paper, Observed Rate of Heat Absorption, because this is not only the key to the entire problem of adequate relief vents, but the subject of greatest controversy. When a member of the Flammable Liquid Committee of the NFPA, the writer became interested in the derivation of the tables of emergency-relief vents for tanks of various sizes and examined into the origins of these tables. As the authors mentioned, it was found that the only heat-absorption rate given was that of 6000 Btu per sq ft per hr, which applied only to large vertical tanks. In the course

[35] The Lummus Company, New York, N. Y.

[36] Vice-President, in Charge of Development, DuGas Engineering Corporation, Marinette, Wis.

of this committee's work, information was obtained from the Standard Oil Company of New Jersey on exposure fires around 1000-gal tanks in which heat-absorption rates of 24,000 Btu per sq ft per hr were obtained. These tests were not mentioned in the paper, so the assumption is that the authors were unaware of them. However, the figures check excellently with those found in the tests described in the paper.

Subsequently, the writer became curious as to the accuracy of the emergency-relief-vent tables when applied to pure compounds, such as benzol, alcohol, and acetone, and derived an equation similar to Equation [9] of the paper. However, simplification of this equation was never undertaken by the use a "contents factor," with which the authors have done such an excellent job of making this equation more readily usable.

It is noted that the vessels are assumed to be 90 per cent full of material when exposed to fire. In the writer's calculations, the same assumption was made, and he agrees thoroughly that this is the best condition to use for computations.

All of us who have struggled under the necessity of using our "best judgment," in place of the authoritative information and thoroughgoing analysis of the subject as given in this paper, will be pleased to have a logical basis upon which the fire protection engineer can attack his problems.

About 2 years ago such information would have been invaluable to the writer, when he was informed that a certain organization recommended the use of 3000 Btu per sq ft per hr as the heat input to a 38-ft-diam butadiene sphere. In his calculations, the value 12,000 Btu per sq ft per hr was used and fortunately his advice was followed in this case.

F. L. MAKER.[37] The authors have evidently done a very great amount of work in preparing this paper. Usually the results of so much labor should entitle the authors to some amount of grateful commendation from those whose future labors would be eased by the presentation of fundamentals completely worked out. In this case, however, it would appear that they brought most of the work on themselves by the fact that an essentially simple problem has been unbelievably complicated. The resulting recommendations, which do not necessarily follow from the facts presented, are in a form that is unsatisfactory from several points of view.

Time has not permitted preparation of a complete discussion of the entire paper, and the following remarks are concerned with the first two parts of the paper only, i.e., relief for vessels under pressure over 15 psi.

The test data presented in the first part include a description of tests run by Fetterly, the Underwriters Laboratory, by the Aluminum Company of America, and by the authors, in regard to maximum rates of heat absorption. As conclusions from these results, the authors recommend that the heat-absorption rate of 20,000 Btu per sq ft of wetted surface be adopted as the criterion for determining the relief capacity.

The authors recognize that this heat-absorption rate appears high when compared to over-all absorption rates on boilers and tube stills and point out that much higher rates are experienced in combustion chambers of radiant absorption sections of boilers. They are correct in regard to the much higher radiant-absorption rates in boilers; and even in oil stills rates in excess of 20,000 Btu per sq ft per hr on the surface most directly exposed to the fire are not uncommon. A point that was overlooked is that in oil stills the absorbing surface is deliberately arranged to limit the maximum heat-absorption rate to avoid coking or overheating of the oil on the inside of the tubes.

That such rates of heat absorption are possible is not new. The authors make reference to the Liquefied Petroleum Gas Safety Orders of the California Industrial Accident Commission. These were prepared about 9 or 10 years ago, and the writer suggested the particular form of the provision for safety valves that was adopted. A memorandum discussing the particular provision was presented at the time. This included the following:

"One of the most common emergency situations, particularly in the oil industry, is concerned with the possible exposure of a volatile fluid to fire. Tanks containing gasoline, casing head gasoline, butane, etc., may develop rather high vapor pressures at fairly moderate temperatures. In the case of a fire surrounding the vessels, which may occur due to breakage of lines, or perhaps from broken connections or leaks in the container itself, heat may be absorbed through the walls of the container that will cause vaporization of the volatile contents. In order to determine what amounts of vaporization might have to be taken care of, tests were run by the General Engineering Department of the Standard Oil Company of California some years ago (about 1925), in which a horizontal tank of water was surrounded by a fire in a pool of gasoline inside a dike and the quantity of vapor generated was measured. Heat-absorption rates were found as high as 25,000 Btu per sq ft of wetted surface; the tank being approximately half full of water."

The authors' 20,000 Btu per sq ft per hr would not be out of line for vessels completely exposed to fire. However, it does not appear reasonable to apply this same rate in all situations. The tests cited by the authors were in some cases run under conditions where the tank was pretty well enclosed. This condition might easily occur in a building, and for such cases the suggested rate would appear reasonable. The authors are apparently also interested primarily in vertical tanks. Most of the storage of products of high volatility in refinery and natural-gasoline processing plants, where the storage is within the plot limits of the plant, is usually in long horizontal tanks, running from 6 to 14 ft in diam, and lengths up to 100 ft. For such tanks the probability of the entire surface being exposed to maximum heat-absorption rates is small, particularly where they are installed in the open air and not inside of a building. Consequently, some deduction in average heat-absorption rate would appear to be reasonable. The suggestion made in connection with the California Liquefied Petroleum Gas Safety Orders was based on the following:

"For small containers, which are much more likely to be surrounded by fire, this maximum rate would probably be used as a basis for relief capacity. For larger containers it is unlikely that the entire surface will be surrounded by fire, so that lower rates appear reasonable. For butane tanks of sizes in the neighborhood of 1000 gallons capacity a rate of 20,000 Btu per sq ft per hour on 60 per cent of the total area of the tank (equivalent to 12,000 Btu per sq ft per hour on the entire surface of the tank) has been proposed. On very large tanks, and on those in which exposure on the entire tank might appear impossible, smaller rates yet may be used. In the case of butane tanks installed away from a source of fuel, except for a leak in piping, a rate of 25 per cent of the foregoing amounts was recommended. This amounts to 3000 Btu on the entire surface of the tank. D. V. Stroop, secretary of the API Fire Protection Committee, has proposed a somewhat similar condition in the form of a curve, which when plotted on logarithmic paper became almost a straight line. Making the substitution of a straight line leads to a formula of the following form

$$\frac{Q}{A} = \frac{48{,}000}{A^{1/4}}$$

where

Q = total amount of heat absorbed by vessel per hour
A = total area of vessel

[37] Designing Engineer for Refinery Plants, Standard Oil Company of California, San Francisco, Calif. Mem. A.S.M.E.

"The total heat absorbed by the vessel is therefore
$Q = 48{,}000\ A^{1}/_{1}$ Btu per hr"

This formula is admittedly arbitrary. On the other hand, it would appear more reasonable for large storage vessels than using the same rate of heat absorption regardless of size. If the vessel is so enclosed that it is possible for it to be entirely surrounded by fire, which implies a limited size, the use of a maximum absorption rate of 20,000 Btu per sq ft does not appear unreasonable.

In the case of the California Liquefied Gas Safety Orders, the formula was further simplified, because only two commercial products, namely, commercial butane and propane fuel, were being considered, and the corresponding pressure conditions for vessels constructed under the safety order were limited.

From this point on, the paper becomes more difficult to follow. The objective of the authors is not quite clear, nor is it clear just what provision they are finally recommending. They suggest that their recommendations be embodied in official codes. Before this could be done, however, the presentation would have to be considerably simplified and clarified, and the various suggestions involved separated, so that they could be evaluated on their own merits.

After considerable study of the text and the derivation of formulas in the Appendix to Part 2, it appears that what the authors are proposing is to determine the size of a nozzle to put on a vessel. They also seem to be concerned with the fact that after a pressure vessel is built, it is frequently found later to contain other than the product it was originally designed for, and they apparently have in mind that the so-called, "contents factor F," will in some way give them a nozzle that would be large enough for a number of different products.

In addition they superpose a further suggestion that these nozzles be designed in sizes only for a limited number of pressures, namely, 15, 60, 150, 250, and 500 psi.

The entire problem involved would appear to be much simpler than the amount of mathematics presented in this paper seems to indicate. It seems to involve only the following steps:

1 Determine the amount of heat absorption to be provided for.

2 Determine the maximum pressure at which the discharge through the emergency relief device is to be computed, and the corresponding temperature.

3 Determine, for the particular product concerned, the number of pounds per hour that would be vaporized for this total heat absorption.

4 Choose a suitable emergency-relief device having a capacity sufficient to discharge the amount of vapor thus computed.

There is no advantage in attempting to accumulate all these steps into one all-embracing formula, and particularly to do this only for a limited number of pressure ranges. Rather, such an over-all formula tends to hide the results of the individual steps and renders any check of their reasonableness difficult.

In regard to the total amount of heat to be absorbed, the rate of 20,000 Btu per sq ft per hr on a wetted surface appears reasonable for small containers that can be entirely surrounded by flame, or even for fairly large vertical containers that may be so enclosed that they are likely to be entirely surrounded by flame in case of fire. For containers installed outdoors, some reduction is reasonable to take care of the unlikelihood of an entire vessel of large size being surrounded by an intense fire. The relation previously given, as used by the API, appears reasonable. It is admittedly arbitrary and might be improved upon. It is, however, convenient to use, it is qualitatively in the right direction, and in view of lack of evidence to the contrary, it is suggested that it continue to be used.

The next step is to determine the pressure at which the relief should be computed. This, of course, depends indirectly upon the product concerned, in that the pressure vessels presumably are made strong enough to hold the contents under normal conditions, with some leeway above the vapor pressure that would be reached in normal operation to prevent frequent poppings. Actually the vessel will be stronger than required to maintain the product at the vapor pressure corresponding to its normal temperature. The vessel will usually have some additional thickness, due to the use of commercial thicknesses of plate, and while relatively new, to the provision of some corrosion allowances. In the case of vessels for fluids of low vapor pressures, such as less than 50 psi at ordinary operating temperature, it will generally be found that the minimum thickness for which it is desirable to make the vessel will give a safe working pressure that may be considerably higher than the normal vapor pressure of the contents. In this case economy will be achieved by taking advantage of the maximum working pressure of the vessel and designing the emergency relief for this pressure. The corresponding temperature can be obtained from a vapor pressure-temperature curve of the product, which will either be available or can be approximated by general rules, such as a line drawn on a Cox chart from a given boiling point at atmospheric pressure. A safety valve should be set at this maximum allowable pressure, and if this is the only provision for emergency relief, its capacity should be computed on the basis of whatever "accumulation" or increase above the initial popping pressure is permissible for the maximum discharge rate. The A.S.M.E. Unfired Pressure Vessel Code allows 10 per cent accumulation. However, it should not be overlooked that the emergency condition being provided for is hoped to be very unusual, and that there appears no good reason why a maximum accumulation up to the pressure at which the vessel has been hydrostatically tested (generally at least 50 per cent above the design pressure) should not be permitted. Even above this pressure the safety factor of the vessel provides further leeway before the vessel might be expected to explode.

If a safety valve is provided of such size that it can take care of only normally expected conditions, further emergency fire relief can be provided by some form of bursting disk. Bursting disks have the disadvantage, however, that they cannot be designed to have bursting pressures very close to the normal operating pressures and have a reasonable life. A bursting disk that will burst at a pressure twice or 1.5 times the normal maximum pressure can be expected, however, to have a reasonable life. If the normal operating pressure is close to the design pressure of the vessel, it is suggested that bursting disks added for emergency fire exposure, in addition to a safety valve set at the design pressure, be arranged to have their bursting pressure at 150 per cent of the design pressure of the vessel.

For bursting disks, which are relatively cheap compared to safety valves, it is usually simple to provide plenty of capacity.

The purpose of the "contents factor F," used the the authors, is not at all clear. Partly, it seems to be introduced in order to reduce the determination of relief provision size to a single formula. The advantage of this is doubtful, as it succeeds admirably in hiding the reasonableness of each step in the process. Partly also, an impression is gathered that the authors proposed this factor because of some doubt that data on latent heat of vaporization would be readily available, and that by use of Fig. 12 it would be easier to guess the value of the "contents factor F" than it would be to guess the latent heat of vaporization. It is much more accurate to estimate the value of the latent heat than to choose the correct value of the more complicated value F.

Time has not permitted checking the curves of Fig. 12 to see what provision the authors have included for variation of the

latent heat of vaporization with temperature, nor is any table given showing how the various points were computed. This is one of the disadvantages of the use of an all-embracing formula, in that there is no ready way of checking the reasonableness of an important value used in the formula. The authors mention the use of Trouton's rule. Actually a curve based on Hildebrand's rule, that covers vaporization at other than atmospheric boiling points, should be used. Such a chart has been published.[38]

With the heat absorption, the discharge pressure, the temperature, and the latent heat of vaporization fixed, the quantity to be handled can be easily computed and the necessary size of the safety device chosen.

The dimensions of the relief device will depend upon what kind it is. The formula used in the API-ASME Code, due to Davidson and MacArdle, is devised primarily for hydrocarbons having a considerable number of atoms in the molecule. It will be on the safe side by about 10 per cent for a simpler molecule, such as ethane and propane, and other gases having few atoms in the molecule; these have higher values of the ratio of specific heats. The formula includes a coefficient of 0.97 for a tapered nozzle, because the originators of the formula worked for a company making a safety valve of the nozzle type, for which this coefficient applied. This same coefficient might not apply for other types of safety valves, particularly the low-lift type, previously in common use on boilers and air tanks.

The authors modify this formula to apply to a short tube having a coefficient of 0.83 instead of 0.97. At this point again, the reasoning becomes vague. It is not quite clear from here on what the authors mean to do with the diameter thus found. They talk about using the diameter thus determined for the "relief connection size," implying that they mean the actual nozzle attached to the vessel and not the nozzle that may be part of the safety valve, nor the diameter of any bursting-disk device. If this is what they have in mind, the nozzle so determined will be too small. The actual connection to the vessel in the safety valve or other relief device should be considerably larger in diameter than the limiting discharge orifice. If this is not the case, the entrance to the nozzle constitutes in effect a second orifice in series with the principal relief orifice, and when the flow starts, the pressure drop will not be almost entirely concentrated at the relief orifice, but will be divided between the relief orifice and entrance losses and friction in the connecting pipe between the vessel and the safety valve. This may cause the pressure at the safety valve to drop below the pressure at which it reseats, causing the valve to chatter. When a safety valve is used, the normal procedure is to choose the size of the safety valve from tables, furnished by the manufacturers, or to take the size a manufacturer recommends for the conditions, and then make the pipe connection correspond to the inlet flange on the safety valve. This will be usually several times the diameter of the actual nozzle in the safety valve. The discharge connection will be even larger.

The authors apparently also have the idea of making such computations only for a limited number of pressures. Their Fig. 12, for example, indicates pressures of 15, 60, 150, 250, and 500 psig, and they give four formulas, Equations [1]′, [2]′, [3]′, and [4]′, for particular pressures. Presumably they are trying to make it easy for an inspector or a designer to pick the nozzle sizes. Actually deciding upon safety-valve sizes by steps in this manner will cause considerable trouble. For example, Equation [2]′ is suggested for working pressures from 60 to 200 psig. Presumably, therefore, it is based on 60 psig. If it is used to determine the area of a safety valve operating at 100 psig, it will require a larger-size safety valve than is actually needed. This may increase the expense very considerably in the case of the original installation, and even more if the rule is applied to an existing installation. A safety valve might be entirely adequate for the actual discharge pressure and yet not be large enough for the assumed lower pressure arbitrarily used for convenience. Such a provision is quite objectionable. The amount of time saved over computing the requirements for the actual operating conditions is inconsiderable, and the amount of extra expense in the installation may be of large magnitude.

As a general conclusion, the authors' suggestion that their recommendations be used as a basis for official codes probably will be emphatically disagreed with by most designers who have been using the API-ASME Code, because of its failure to allow for the less likelihood of exposure to fire of an entire area of a large tank, because of the lack of clarity of just what the authors are actually computing in their relief-device size, and because of the complicated way in which the result is arrived at, with the steps so combined that the implied values are not immediately evident for check as to their reasonableness.

T. McLean Jasper.[39] While the writer does not feel competent to discuss this paper so as to add constructive information or criticism, it is easily recognized that this type of information has positive value in analyzing a very important problem. It supplies data which will tend to reduce the danger. The particular tribute the writer wishes to pay to the authors is the resort to a practical approach to the problem, and this after all is the superior method for any intricate matter.

The next step is to devise a simple workable plan for placing safety valves or disks and connections which will evacuate inflammable liquids from fires when they occur, thus rendering them less hazardous and thereby safeguarding working personnel and property.

F. L. Newcomb.[40] On January 4 and 5, 1943, a meeting of safety-valve manufacturers and users in the petroleum industry was called by the Petroleum Administration for War to draw up recommendations for wartime standardized petroleum safety valves, including their application. At that time, a heat-input curve was submitted to the Petroleum Administration and adopted for the duration. This heat-input curve was prepared by the Standard Oil Development Company and was a modification of the curve proposed by D. V. Stroop of the American Petroleum Institute. Both this curve and the one proposed by Mr. Stroop have been referred to previously. The Standard Oil Development Company curve was the result of recommendations from process engineers concerned with the design of furnaces and other heat-transfer equipment and was the result of long and careful consideration.

Through membership on the API Subcommittee on Relief Valve Capacities, there was available to the writer some data on actual fires which had occurred in the petroleum industry where the safety valves had prevented overpressure during a fire. By assuming that the safety valves blew to capacity and knowing the characteristics of the contents of the container, it was possible to figure the maximum heat input per square foot of exposed area. If the safety valves were not discharging at full capacity, the heat input would have been less than computed, and therefore the assumption was on the safe side. When these calculations were made and plotted against the curve submitted to the Petroleum Administration for War, in every case the maximum heat input was less than required by the curve. The matter of heat input and numerous other features are under consideration

[38] Ref. (12) of authors' paper, p. 13.

[39] Engineer, A. O. Smith Corporation, Milwaukee, Wis. Mem. A.S.M.E.

[40] Senior Specialist, Standard Oil Development Company, Elisabeth, N. J. Mem. A.S.M.E.

by the API Subcommittee, and this curve has also been submitted to them as a proposal for a starting point in their work. It is possible that when time permits this committee to become more active and more data are obtainable, it may be advisable to modify the curve. It has, however, been in use for a number of years and there has never been any evidence that it has not been adequate. The lack of failures due to fire exposure of vessels reasonably protected with safety valves in the petroleum industry indicates that the present practices are adequate. It is felt that the recommendations contained in the paper under discussion would require unreasonably high safety-valve relieving capacity and place an entirely unnecessary burden on pressure-vessel users.

It is not felt, however, that the work done by the authors preparing this paper should, in any way, be overlooked in further studying the matter of safety-valve relieving capacity, but should be given due consideration along with all other data and experience which may be available.

R. C. Werner[41] and S. T. Russell.[41] This discussion has been limited to Part 1 on "Observed Rate of Heat Absorption." Each of the four groups of experiments was studied in turn and certain points were noted which were thought to have a vital bearing on the acceptance of a 20,000 Btu per hr per sq ft heat-absorption rate as a basis for sizing relief valves for vessels exposed to fire.

In regard to the test reported by J. F. Fetterly, Bureau of Explosives, 1929, the authors' use of 5.9 min as the time factor in calculating the rate of heat absorption of 23,300 Btu per hr per sq ft of wetted surface may be open to question.

It is reported by Fetterly: "It was intended that the safety valve should open to the full extent of its relief area, and when once opened to that area it should remain open until the contents of the container were discharged without exceeding 375 pounds per square inch gage pressure."

The irregularities in the pressure curve in Fetterly's publication may be explained entirely by Venturi effect, if the piping was arranged as in Fig. 3 of the paper under discussion, and the piping was of certain sizes. Fetterly's paper does not give details of the arrangement of the equipment. If it were assumed that the relief valve, once open, did not shut, the heat-absorption rate would have been 11,850 instead of 23,300 Btu.

It is plausible to reason that the temperature curve reported by Fetterly represents the condition at the bottom of the cylinder, and that vaporization might be taking place at the surface in spite of the temperature at the bottom being less than the theoretical boiling point of propane. If the propane contained some lower boiling material this effect would be more marked.

If one assumes that the mechanism outlined by the authors is correct the rate of heat absorption would vary as follows:

Time, min	Rate, Btu per sq ft per hr
0 to 3.7	1530
3.7 to 9.4	8410
9.4 to 15.3	23300

Fetterly's report does not indicate any physical basis for such a wide variation in rate of heat absorption.

In general, it may be said that it appears difficult to arrive at a correct value of the rate of heat absorption on the basis of the test data in Fetterly's publication.

In regard to the test made by the Underwriters' Laboratories, Inc., as reported in N.B.F.U. Bulletin of Research No. 3, 1938, the following three points are noted:

1 The introduction of a water film on the surface of a plate on the fire side increases the heat absorbed from the fire. A second test was performed with identical conditions except that no water film was present. From the dimensions of the vertical plate and the rate of the average temperature rise, the maximum rate at which heat was absorbed by the plate without the water film was calculated to be 461,000 Btu per hr, as compared to 776,000 Btu per hr with the water film. These results bring out the fact that if the quantity of heat absorbed is measured by a water film on the outside of the tank a considerably higher result will be obtained than for the case where no water film exists. This should be taken into account when applying other test data.

2 A considerable error may be introduced if one applies the results obtained from a small-scale test to commercial installations. As the oxygen supplied to burning fuel is increased to the theoretical quantity, the flame temperature increases rapidly. Therefore a fire with excess oxygen will generally be hotter than where a deficiency of oxygen exists. A small fire may well be the hotter because of its size, since an excess of oxygen over that needed for complete combustion can be easily obtained, but in the case of a fire of large area, it is difficult for the center portion to obtain any oxygen at all.

3 The size of the tank should also be considered. Although the actual initial flame temperature in two different cases may be identical, the larger tank will absorb a greater portion of the total heat in the flame and thus have a lower average flame temperature adjacent to the tank than for the other case. Small tanks and areas will, therefore, receive heat at a greater rate than large tanks or areas.

In regard to the report of the 1930 tests of the A.P.I. on aluminum-alloy tanks for tank trucks, the following points are noted:

1 To assume that a measure of the total heat supplied to the gasoline is the amount of heat needed to vaporize completely the gasoline may result in considerable error, particularly in the case of small tanks. Gasoline may leave the tank in the form of a liquid as entrainment. This can be gathered from the original data on this test. The vapors from the tank ignited at 4 min 20 sec after the start of the fire. At 6 min the fusible plug in the fill cap melted and atomized gasoline was observed to issue from the opening for several seconds. Since both openings are in the same cap it is possible that gasoline was atomized (leaving as a liquid) for the full period of 1 min 47 sec through the vent and probably longer but at a reduced rate.

2 To assume that the liquid level in the tank can be measured by the abrupt temperature rise as recorded by the thermocouples located at different elevations may result in error. The thermocouples were located on lugs on the outside surface. The temperature of the liquid on the inside of the tank would differ by the temperature gradient needed to transfer the heat from the outside surface through the metal walls and inside film to the liquid. This temperature gradient would vary from 30 to 200 F. With such a temperature gradient the inside temperature may be related to the thermocouple readings, but it would be difficult to determine the exact relationship.

On checking the original data, a difference was discovered between the recorded temperatures in the table and a plot of the temperatures. The value for the thermocouple No. 10 at 14 min is recorded as 355 F but plotted as 255 F. Replotting the temperature curve for thermocouple No. 10 with the correction given, it would appear that the abrupt temperature rise for both the No. 10 thermocouple (at 50 per cent level in the tank) and No. 11 thermocouple (at 75 per cent level in the tank) occurred at approximately the same time, i.e., 12 min from the start of the fire. Since both thermocouples rose abruptly at the same time, they do not seem to have given a very good indication of the liquid level.

[41] Blaw-Knox Construction Company, Pittsburgh, Pa.

A reasonable explanation may be obtained for this abrupt rise in temperature from the photographic record of the test in the original report. The photographs as a rule were taken every 3 min. At 9 min there was only a slight indication of any wind blowing. This could be observed from the burning vent gases. At 12 min a slight breeze was blowing the flame from the burning vent gases toward the end of the tank on which the thermocouples were mounted, which were those reported in this paper. The thermocouples on the second tank on the opposite side at no time indicated such a sharp rise although the tank was only one half full to start and was exposed to the same fire. It will be noted from the photographs that the flame was blown away from the second tank by the wind. The abrupt temperature rise, therefore, seems to be dependent upon whether or not the thermocouples were exposed to the radiation from the burning vent gases, and not primarily to the liquid level in the tank.

3 To assume, after rapid ebullition is started, that the only heat needed is for evaporation seems to be an error. From the properties of the gasoline used in the test the initial distillation point is 95 F, and the 51 per cent distillation point is 284 F. The heat needed to evaporate the gasoline is that heat required for the latent heat of evaporation plus that needed as sensible heat to raise the temperature of the remaining gasoline to a rising boiling point.

4 The data on the other 150 gal tank should have been considered. This second tank was directly attached to the first and was exposed to the same fire. The charge consisted of only 75 gal of which 30 gal remained after the test. In all, only 45 gal were vented as compared to 129 gal for the tank reported in the paper under discussion. This marked difference cannot be explained by the difference in exposed area only. Additional explanation may result in the consideration of entrainment. The half-full tank would have on an average a lower liquid level thus resulting in less entrainment.

5 In applying the results of these tests to the design of a relief valve to be attached to a storage tank located in the open, a correction factor should be used with the test data since a windshield was used. Theoretically the radiation from the shield to the tank may be almost as great as from the flame alone. Windshields also help the natural convection of the fire and increase the per cent air to a possible excess. In the case of burning gasoline spread over a large area, there would be a deficiency of air, and therefore a much lower flame temperature.

In regard to the test made by the authors of the paper under discussion, the following points are noted:

1 It is questionable whether the asbestos shield around the tank approaches the condition of a flame of considerable depth. The emissivity of asbestos is higher than can be reached in a flame, and a flame of considerable depth probably would be of a much lower temperature, due to the difficulty of oxygen reaching all parts of the flame. Therefore the heat-transfer rate with the asbestos shield would be higher than could be obtained by a tank surrounded by a large-area fire. The authors were aware of this fact, but believed that the strong updraft between the cylinder and the tank tended to offset the increased radiation.

2 However, it seems questionable whether the strong updraft between the cylinder shield and the tank has the indicated effect. This strong updraft increases the natural convection to the tank and probably causes an increase in the air supply giving a more theoretical mixture and thus a higher flame temperature, as compared to a large-area fire which would have a deficiency of oxygen in many places.

3 On checking the information presented for runs Nos. 2 and 3, it appears that the heat which the authors designate as latent heat absorbed is not a measured quantity but rather the difference between the actual measured sensible heat absorbed and the calculated theoretical possible heat absorbed. Therefore, the calculated rate of heat absorption is actually a theoretical value and should not be confused with the values reported in runs Nos. 1 and 4, which are actual measured rates.

4 The results obtained in run No. 4 are questionable due to the reduction in area used in the calculation by the assumption that a band of the wetted surface 2 ft wide is not exposed to the flame. By using the full wetted area a value of 12,630 Btu per sq ft per hr is calculated. If the authors' assumption is used, a value of 16,850 Btu per sq ft per hr is obtained which is 33.4 per cent higher. Since the actual measured flame temperature is higher than for runs Nos. 2 and 3, it is questionable whether such an assumption which results in a 33.4 per cent increase should be made without at least more test data.

5 As was pointed out in regard to the test made by the Underwriters' Laboratories, Inc., and which is observed when comparing runs Nos. 1 and 4 (25,900 as against 16,850 Btu per sq ft per hr) the tank or plate with water flowing on the surface facing the flame will absorb heat at a considerably higher rate than if the water film is omitted. This would indicate, as mentioned before, that a water film increased the absorption rate and therefore such test data cannot be applied to a dry tank.

6 In calculating the results of run No. 1, the authors have assumed a mechanism whereby the tank metal receives the radiation and then transfers the heat to the water film. This assumption is open to question. The measure of absorptivity of a material to radiation is its emissivity. McAdams reports the maximum emissivity of iron and steel at around 0.75, whereas for water a value of 0.96 is reported. This would indicate that the water film is more absorptive to heat radiation than steel.

Underwriters' Laboratories, Inc., reports in its test; "A simple experiment to gage the properties of water film may be performed by viewing a flame through a thin sheet of glass. The difference in heat energy sensed by the face or hand with or without the glass is not appreciable; but when an unbroken film of water is caused to pass over the glass surface the difference in the heat transmitted through the combination is quite perceptible, although translucency is not materially altered." However, in the authors' test the tank metal became hotter than the water film. This appears to be in contradiction to Underwriters' Laboratories, Inc., observation and to theory. More data along this line are therefore needed.

In summarizing there seem to be three experimental procedures of major importance which should first be evaluated before the results obtained by using such procedures are adapted to a relatively large storage tank located in the open and heated by flame such as a large-area open fire.

1 The use of a water film on the outside of a tank to measure the quantity of heat absorbed. The water film in two of the reported cases greatly increased the amount of heat absorbed.

2 The use of the quantity of material which is vented from the tank as a measure of the quantity of heat absorbed when it is assumed that the material was vented as a vapor. In one particular case, atomized gasoline was observed to issue from the tank.

3 The use of a windshield to control the fire. The emissivity of the shield is generally higher than the possible flame emissivity and thus greatly increases the radiation to the tank. In all the reported cases some type of windshield was used.

In conclusion, the authors of this paper should be congratulated for their contribution to the field of design and safety. It is good to see that even during a period of accelerated production the field of safety has not altogether been forgotten.

WALTER SAMANS.[42] Because of lack of time for adequate study of this paper, it would be an unwarranted presumption on the writer's part to make any off-hand comments on the authors' findings. However, their correlation of formerly existing test data with theory indicates that more tests were very much needed to confirm the theories. The chemical industries particularly will appreciate this report, and the authors' employers, who fostered the tests, in absorbing the costs for the equipment and personnel engaged, are entitled to commendation jointly with the authors themselves. The data thereby presented should prove the best possible source for the formulation of a more standardized practice in determining the required safety valves supplemented by relief disks or cups, and similar devices.

The writer's comments will apply principally to large vertical storage tanks. The authors have recognized a difference between test fires around small pressure vessels and fires in commercial plants where the hindrance offered to complete envelopment by flame will materially cut down the total heat absorbed. They have acknowledged this difference in Part 1 of their paper for the test reported by Fetterly, and those conducted for the A.P.I. and N.F.P.A. They have acknowledged the justification for a reduced heat input on vertical storage tanks over 15 ft diam, approaching a rate of 6000 Btu per sq ft per hr for a 100,000-gal-capacity tank, and reaching the maximum 24-in. size of relief vent for tanks of 300,000 gal (7000 bbl approximately) and arger, in Part 3, Fig. 18.

Although this appears to be a concession to the experience in actual tank fires, and purports to be a reasonable interpretation of test results, this may not prove a sound reason for discarding the present practices for petroleum storage tanks, as shown by curve 6 of Fig. 18. This stand is taken both because of the character of the hydrocarbon flame encountered when pools of petroleum, as crude, reduced crude, intermediates, or gasoline are on fire in a tank pit, and because vertical storage tanks do rupture at the edge of the roof without destructive explosion.

Assume that burning oil on the ground is a heavy petroleum product and that there is no appreciable wind (rain is not a consideration); there will be lots of smoke which screens the tank from radiant heat, except where the inrushing air enters the vapor. Inside of that boundary there is incomplete combustion, because of insufficient air, and consequently a lower temperature. Above the top of a tank 30 ft or more in height, the radiant heat has little effect on the roof. It is quite possible that the equivalent of only 1/6 of the wetted shell surface need be computed at a heat input of 20,000 Btu per sq ft per hr. In the case of burning gasoline, the flame may be almost free of smoke, or at least will appear so on the outer boundary of the burning cloud of vapor. There could not be a sea of fire over an area having an annular width equal to the radius of a large tank that could be "seen" by the wetted tank surface as the interior of the burning vapor cloud is not clear. Smoke does form.

Because of the greater area on fire, the inrushing air will carry the flame higher, but by attenuation of the flame, the radiant-heat effect will be reduced with height, radiating less total heat per average square foot on higher tanks, and to the tank roof. Intermediate oils, between heavy fuel and gasoline, will show "in-between" effects.

When there is a wind blowing, there is no great difference in rate of heat input until its velocity is higher than the air drawn to the fire by the draft. There can never be the chimney effect produced by the authors' tests, because there the gasoline was sprayed into the rising current of air to produce a hot continuous flame with resulting excess air, as far as the photographic cuts indicate.

To simulate a storage-tank fire, tests might be made by burning gasoline poured on top of a pool of water around the tank The screen or shield should be placed outside of the basin that holds or receives the cooling water, and air admitted through a sufficiently large clearance under the screen. The effect should be similar to that obtained in the trial runs using gas fuel, shown in Fig. 8, except that, gasoline vapor having a higher molecular weight, and the flame being screened, a higher rate of heat input may be expected.

In this connection the authors' "unfortunate experiences" with small tanks should not affect conclusions based upon good experience with large vertical oil-storage tanks. To evaluate the screening effect of the width (i.e., horizontal depth) of flame on the heat radiated to the surface of the tank, the Underwriters' Laboratory test made on a flat plate might be reproduced, but shielding the boundaries of the plate from flame contact so that the air-vapor mixture will not take place near the test plate. Obviously, the results should give a low rate of heat input, when a heavy fuel oil is burned and not as high a rate as on the authors' test recorded in the paper, when burning gasoline.

The statements just given are also intended to verify the authors' conclusion that open-air combustion cannot be compared with controlled combustion in a boiler furnace. In the latter, only the wall tubes and radiant-heat surface are comparable, but the type of furnace flame, with little obstruction, and that due to haze, is seldom reproduced in industrial fires. It is expected that the subject of vertical storage-tank fires, covered by this contribution to the discussion, will be amplified by the actual experience of some of the many oil men in California who have combated fires in oil refineries and field storage tanks. The record so obtained should be combined with the results of the authors' studies and tests and formulated into the best possible procedure for determining the protective venting needed for large tanks.

Another point which appears to need clarification is the statement in the Summary at the beginning of the paper: "So far as can be learned, there is no substantial theory or evidence to support the limiting of heat-input rates to any particular height. There are some indications to the contrary, that is, high flame temperatures apparently exist at relatively great heights above the fuel during large fires."

There appears no reason for this reversal of published "Fire Fighter" opinion, i.e., not by the text of the authors' paper, and there being no other publication referred to in this thesis, possibly the authors will say why this statement was made in the Summary of Part 1, where reported tests did not develop "relatively great heights," unless other records made and cited in the original reports were not herein reproduced. The wording of the statement referred to may be unintentionally misleading. "High gas" temperatures will exist wherever they are found, and what was no doubt meant was that high temperatures are radiated to relatively great heights, provided the fire is intense and large enough. As mentioned in this discussion on fires around oil tanks inrushing air over an annular flaming oil area surrounding a tank, "attentuates" the flames and, for the case herein considered, will hasten the completion of vapor combustion. Obviously, the larger the area covered by fire, the higher the flame will reach, and the greater the intensity of radiation in the most favorable directions. Reverting to the original statement on "the limiting of heat-input rates to any particular height," the authors' tests did not simulate an open-air fire and on such fires the radiation effect of flames above a pool of oil on the ground will diminish rapidly upward as the intensity decreases.

[42] Sun Oil Company, Philadelphia, Pa.; member of the A.S.M.E. Boiler Code Committee; Chairman of the API-ASME Committee on Unfired Pressure Vessels; Vice-Chairman, API-Oil Storage Tank Committee. Mem. A.S.M.E.

The authors' theories are presented in a usable manner by the formulas, and the derivations are of practical form. They seem well substantiated by the tests. The authors have also recognized the varied degree of exposure encountered with special protection that may be provided in the construction. It now remains for interested authorities, as represented by state inspectors, insurance engineers, and recognized technical committees to formulate reasonable assumptions of departure from test conditions, to which the authors' correlation between tests and theories may be properly applied to give adequate protection for each type and size of vessel or tank.

The authors' work was well worth while. The resulting forward steps have anticipated similar work by other organizations that was no doubt postponed because of the existing war emergency. The authors' continued work for the furtherance of their ideas should be aided and encouraged in all ways possible.

H. R. ZEIGLER.[43] The derivation of the fundamental equation is very simple and logical. The authors start with the formula given in the API-ASME Code which is used for determination of capacities of pressure-relieving safety devices. They claim that this formula is universally employed and is of proved accuracy. By substitution, factors for heat input, wetted surface, and latent heat are introduced to complete the formula.

A novel feature of the paper is a chart which shows "contents factors" for many compounds. This chart may be read and the reading substituted in place of one expression in the formula which involves temperature of the substance, molecular weight, and latent heat of vaporization of the substance.

In addition to the basic equation, the authors offer a few other equations, the purpose of which is not particularly clear. However, all of these equations are extremely easy of solution, whereas the well-known Fetterly formula is quite difficult of solution and offers many possibilities of error.

One novel suggestion is that relief valves be made the same size on all vessels of the same capacity and pressure range. This is to promote interchangeability of use of such vessels and, consequently, a high "content factor" is used.

The authors concede indirectly that the size of the tank has an influence, if the writer interprets the paper correctly. This statement is based on the fact that they treat of four pressure ranges for vessels not exceeding 10,000-gal capacity, and one formula only for vessels above that size. However, another way of looking at this is that they may consider it uneconomical to bother with different relief areas for vessels of many differ nt working pressures. The four pressure ranges are 15–60, 60–200, 200–700 psig and finally, pressures above 700 psig. Incidentally, in O. M. Setrum's study of the subject of relief valves, he suggested that the external temperature of tanks of 10,000 gal and larger should be 1000 F, instead of the 1200 F used for smaller tanks.

In leading up to the equation recommended, the authors exert all their efforts to establish a heat-input rate of 20,000 Btu per hr per sq ft of wetted surface. In reviewing previous work they point out that the API Committee on Fire Prevention prepared a chart 12 or 14 years ago for gasoline tanks exposed to fire. This chart shows capacity and size of relief devices for heat-input rates of 21,000 to 6000 Btu per hr per sq ft, but there was no practical basis presented for this choice of a heat rate. The relief standards contained in N.B.F.U. pamphlet 30 are based on heat input of 6000 Btu per hr per sq ft of wetted surface. They regard the work of Fetterly as outstanding and, therefore, discuss it at some length.

In discussing Fetterly's formula, the authors show that judged by modern methods of calculation, his coefficient of heat input was remarkably accurate. They then show that, since his estimate of surrounding temperature was 1200 F, the heat-input rate was about 14,000 Btu per hr per sq ft of wetted surface. However, they advance the idea that 1400 F is a more probable surrounding temperature and, therefore, according to Fetterly's coefficient the heat-input rate would be 23,000 Btu per hr per sq ft of wetted surface. The writer believes this disregards the fact that Fetterly's coefficient must have been obtained empirically from a calculated input rate and, therefore, the premise is untenable. It is also felt there were some other distortions of Fetterly's test data in the authors' analysis. Finally, the authors proved to their satisfaction that vaporization was in excess of relief-valve capacity in spite of the fact that the fire test on which Fetterly based his paper was satisfactorily performed.

The authors summarize their tests as follows: "When a tank is surrounded by an intense fire having an effective temperature of about 1400 F, heat is absorbed from the flames at a rate of the order of 20,000 Btu per hr per sq ft of wetted surface exposed."

The tests do not make out a very good case for either heat input of 20,000 Btu per hr per sq ft of wetted surface, or for the effective temperature of 1400 F. The tabulated results for three runs out of four were 25,900, 17,300, and 18,700 Btu and 1510, 1270, and 1315 F. These effective temperatures were measured at the center of the flame region under well-shielded conditions, and it is the writer's opinion that, unless a tank were installed within a building, windage would discount the effective temperature and, consequently, the heat-input rate very considerably.

The formula recommended by the authors seems to have only one weakness, namely, the heat-input rate which they have tried so hard to establish at 20,000 Btu per hr per sq ft of wetted surface.

The writer has worked out the following relief-valve areas for an 82.5-in-ID (7-ft-OD) × 42-ft T.L. tank. This tank was chosen because it has a nominal capacity of 10,000 gal and a total surface of 1000 sq ft. The working pressure is 200 psig, and this is chosen because it is a pressure very commonly used by the writer's company. This size and working pressure give an opportunity to show several different solutions for relief area.

Equation [2]′ covers vessels between 60 and 200 psig and is developed from Equation [4]′, being simplified by the insertion of 66 psia, and the wetted surface is expressed as 85 per cent of the total surface.

Equation [3]′ covers vessels between 200 and 700 psig and is developed in the same manner except that 220 psia is used.

Although Equation [4]′ will not be used, it is necessary to point out that this is based on the assumption that tanks should be equipped with relieving devices of sufficient capacity to promote interchangeability.

Equation [5]′ covers vessels larger than 10,000 gal. By inference the preceding equations are for vessels less than 10,000-gal capacity.

Equation [2]′ $a = 0.0192S = 19.2$ sq in.

Equation [3]′ $a = 0.01112S = 11.12$ sq in.

Equation [5]′ $d = \sqrt{\frac{97.3S_w}{(P+14.7)}} \left(\frac{T}{Mr^2}\right)^{1/4} = 2.715$ in...

.....$a = 6.15$ sq in.

Fetterly's formula using 1400 F.....$a = 4.91$ sq in.

Fetterly's formula using 1200 F.....$a = 3.52$ sq in.

$D \times U$ table where $D = 7$ and $U = 45$; $D \times U = 315$ and $a = 3.10$ sq in.

In Equation [5]′ S_w = wetted surface, sq ft

T = temperature F absolute of vapor

P = gage pressure (R.V. setting pressure)

[43] Phillips Petroleum Company, Bartlesville, Okla.

M = molecular weight of vapor
r = latent heat, Btu per lb

The writer feels that the authors have not proved their constants sufficiently for adoption, in view of the success of the present practices recommended by the National Board of Fire Underwriters in Pamphlet 58.

The authors have not proved the inadequacy of Fetterly's formula.

In general, the authors offer a very intelligent basic formula for the solution of relief-valve-area problems and, if their constants for heat input and surrounding temperatures can be adjusted downward to produce more reasonable results, the writer would like very much to see this basic formula adopted.

T. C. Smith.[44] The authors of this paper are to be congratulated for this excellent paper with its summary of fire tests conducted by themselves and others. Particular attention should be directed to the method used for cooling the test tank and recognition given to this type of protecting against overpressure or overheating of the tank surface in the vapor space.

It has been difficult to understand why the authors have chosen to determine the pipe size required for the relief-valve connection rather than the orifice area of the valve. Commercial spring-loaded relief valves have an orifice area ranging from 25 to 30 per cent of the connecting-pipe area, hence it would appear that the orifice should be of primary concern and the inlet-pipe connection of secondary interest.

Also, consideration should be given to replotting the curves of "content factors" with the term "pressure" incorporated in the equation. This will permit a series of charts, each consisting of a family of curves for various groups of contents.

The authors present heat-input rates ranging from 20,000 to 30,000 Btu per sq ft per hr, as obtained from three different sets of tests. These values are not questioned. Next, they compare these results with established venting rules and create doubt as to their safety. Lastly, they call attention to the absence of specified heat-input rates in two well-known pressure-vessel codes, thereby inferring that this matter has been given scant attention by bodies interested in the formulation of safety standards.

The writer hastens to correct any doubts, on the deficiency of these venting rules, or impressions that this subject has been or is being neglected by groups engaged in the initial drafting of safety standards. These existing rules, although differing in form, employ definite heat-input values which have been established by experience. Also, these sponsoring groups receive many reports of tank and vessel failure which are studied to determine whether revisions in their standards are necessary. The heat-input rates and some of the current work being done is reported herewith as a matter of record.

The first venting rules, for the protection of equipment from overpressure when exposed to external fire, appear to be for oil-storage tanks operating at atmospheric pressure. The American Petroleum Institute was asked to suggest some kind of a venting schedule, and after reviewing the records of their industry where tanks were involved in fires, arbitrarily selected a unit-heat-input rule which was represented by their experience. This rule expressed mathematically is

$$Q/A = \frac{48{,}000}{A^{1/3}}$$

where

Q = total heat absorbed by tank per hour
A = wetted surface exposed to heat

[44] General Petroleum Corporation, Los Angeles, Calif.

The development of liquefied petroleum gases for commercial use brought out two venting rules intended for small- and moderate-size pressure tanks. The California Safety Orders for Liquefied Petroleum Gases gave a rule which was based on 20,000 Btu input on 60 per cent of the surface, or an average of 12,000 Btu per sq ft on the gross surface. The National Board of Fire Underwriter's rule was based upon a modification of Fetterly's formula, using a flame temperature of 1200 F for tanks having a capacity of 10,000 gal or less, and 1000 F for tanks of 30,000 gal capacity or more, with adjusted temperatures for tanks of intermediate capacity. The heat input by this rule will vary between 23,000 and 13,000 Btu per sq ft per hr.

The application of either the California or NBFU rule to extremely large vessels resulted in relieving areas that appeared to be excessive and caused them to be questioned. The American Petroleum Institute, because of its interest in pressure-vessel safety and fire prevention, became interested in the problem and referred the matter to a subcommittee for further study. This subcommittee was instructed to confine its initial efforts to large pressure storage tanks and determine if the previous A.P.I. rule for heat input to atmospheric tanks was satisfactory for pressure tanks, also what modifications might be necessary for other factors involved.

The assignment has been divided into three parts for study, namely, (*a*) the correlation of test data to actual fire conditions; (*b*) further tests, if necessary, to determine the scale effect for both horizontal and vertical vessels; and (*c*) a survey of fires involving pressure vessels to determine the maximum average heat input.

Some progress has been made on the last item. A questionnaire was issued to the petroleum industry for histories of external fires on pressure vessels. Cases have been selected where the vessel was full or nearly full of liquid hydrocarbons and both incoming and outgoing lines were closed. Such cases with pertinent detail data permit the estimation of the average heat input by assuming that the open relief valve is an orifice. This survey has produced heat-input data for two extreme cases as follows:

(*c*-1) More than 11,000, but less then 17,000 Btu per sq ft per hr, for small propane cylinders having a wetted surface of 16 sq ft. Approximately twenty-five cylinders exposed in ten or twelve fires failed from insufficient relief-valve area (0.062 sq in.). This experience prompted a program for changing the type of relief valve to one having a larger orifice (0.100 in.), and the results to date show that some twelve cylinders have successfully withstood severe fires. In at least two cases there were, in the same fire, cylinders with each type of valve, and some of those with the small orifice failed from excessive pressure while all of those with the large orifice came through without damage.

(*c*-2) Approximately 2300 Btu per sq ft per hr on a sphere having a wetted surface of 4363 sq ft. This was a 48-ft-diam sphere subjected to a severe fire for 1 hr 7 min. At times the vessel was completely enveloped in flame. The relief valves were adequate and prevented failure of the sphere.

(*c*-3) In addition to the foregoing, three intermediate cases can be cited as follows:

3600 Btu on a natural-gasoline tank; wetted surface = 319 sq ft
2050 Btu on a natural-gasoline tank; wetted surface = 900 sq ft
1350 Btu on a natural-gasoline tank; wetted surface = 990 sq ft

In all of these fires, the average heat input is estimated to be less than the value obtained by the previously mentioned API heat-input rule for oil-storage tanks.

Reports have been received on many other vessels, but unfortunately, the data do not permit an estimation of heat input because of open lines discharging liquid or vapor, or flame impingement on a surface in the vapor space which resulted in

overheating and failure of the metal. Such failures cannot be prevented by relieving devices which maintain, regardless of the size of the device, a fixed pressure on the tank.

Previously, it would be both improper and premature to predict the final recommendations of this subcommittee.

As noted previously, there are existing rules for venting in use in the petroleum industry, and so far as is known, there is no evidence that these rules where properly applied have been inadequate to maintain safe conditions. The authors of the paper under discussion propose that these rules be superseded on the basis of the evidence and conclusions which they have submitted. In the writer's opinion, this is not justified by their data.

The experimental accuracy of their data is not being questioned, but the interpretation and extrapolation thereof on which their recommendations are based is open to criticism. They have employed results from a very limited number of tests run on a narrow range of vessel sizes under conditions which do not duplicate, nor in some cases resemble, actual service conditions. They have used these as a basis for a proposal that a satisfactory experience record be discounted and supplanted. This is unsound.

The data that they have derived justify conclusions only within the range of exposure conditions covered by the reported tests. However, if correlated with other accumulated data they can aid in reaching a reasonable solution for the over-all problem and for this purpose they are of full value. It is recommended that they be considered at this time only as a contribution to the study being made by the API subcommittee mentioned previously.

Authors' Closure

Reply to Discussion by T. A. Gadwa

Herewith are the authors' comments on the questions raised by Dr. Gadwa in his discussion of their paper.

Effective Height of Flame. Dr. Gadwa's reference to 50 ft for a minimum height for protection against fire exposures is the highest about which we have learned and with which we are in agreement to this extent: We have experienced heat failures (1000 to 1200F) of unprotected structural steel at a 50-ft elevation in the open. However, under such circumstances, a good part of the fire fuel was about 20 ft above grade. We have had such failures in the open at 30-to-40-ft above-ground spillage fires, and this was a part of the basis for the suggestions near the end of Part 1 of the paper. We are convinced that the more generally used height of 20 ft is inadequate.

Input Rate of 20,000 Btu per Sq Ft per Hr. At this time, we have a record of ten tests by six separate concerns, and five analyses of actual fires which indicate that the constant rate of 20,000 Btu per sq ft per hr of surface wetted by the contents is a safe minimum for vessels enveloped with intense fire. We do, however, suggest a reduction of this rate for atmospheric tanks above 20,000 gal nominal capacity, as proportionately represented by curve 2, Fig. 14, or curve 3, Fig. 18, of the paper. The authors interpret the "Wartime Recommendations . . ." to specify heat rates of 10,700 Btu for 10 sq ft of surface downward to 4800 Btu for 1000 sq ft per hr of wetted surface. In the light of our fire experience, this is inadequate, and no attempt will be made to co-ordinate our results with these recommendations.

Effect of Insulation. We suggest allowance for insulation in the capacity of the relieving apparatus but not in the area of the relieving connection. This would depend upon the reduction effected in the flow of heat by the insulation when exposed to hot gas temperatures of 1400F. No data have been prepared on this as it is expected that only in rare cases will allowances prove economical and practical.

Conversion of API-ASME Code Equation. To clarify the reason for the conversion of the API-ASME orifice equation, reference is suggested to its derivation. This will be found in "Discharge Capacity of Relief Valves for Oil Stills," by K. S. M. Davidson and D. W. MacArdle.[21]

It will be seen in this reference that the equation was derived using a ratio of specific heats of 1.001, a critical pressure ratio of 0.6064, and a coefficient of discharge of 0.97. These superficial or ideal values (the first two) were employed to assure adequate relief capacities for any of the heavier hydrocarbons. Since the formula is so universally employed, well known, and of proved accuracy, it was considered wise to incorporate it in the paper rather than those which we had derived for synthetic organics, even though there was little difference.

Further, it is our method to compute all relief capacities in terms of free area and then select the relief device of a capacity based upon approved flow test to pass the calculated rate. Since we use valves having capacities which range from 14 to 60 per cent of the capacity of the relief connection of the same size, it is frequently necessary to choose a larger relief connection than the calculated free area. We do not figure the relief capacity of the valve orifice itself because only those capacities for valves which are essentially free-blowing orifices (top guided, high lift, full bore) can be calculated readily with practical accuracy.

Also, it will be found expedient for most cases that the necessary relief device for fire exposure be supplemental to the usual spring-loaded safety valve, and that this device be simple, inexpensive, and of relatively large capacity. Such apparatus is available with free areas practically equivalent to the pipe-size connection. Reference is suggested to paragraph 5, Proposed Summary for Use, Part 2 of the paper.

Reply to Discussion by F. L. Maker

In order to simplify the authors' reply to Mr. Maker's lengthy discussion, a summary of his comments is given as follows:

1 Mr. Maker's comments refer to Parts 1 and 2 of the paper.

2 He states that heat-input rates of the order of 20,000 Btu per sq ft per hr are not new.

3 He suggests continued use of $\frac{Q}{A} = \frac{48{,}000}{A^{1/2}}$.

4 He wonders why we refer to nozzle size rather than relief-device size.

5 He is confused by the "contents factor."

6 He suggests how the problem should be solved.

All of Mr. Maker's comments in which relief devices are mentioned should be ignored because our paper is concerned with the free-relief area rather than the relief device itself.

The following reply is more to the points summarized:

1 Although Mr. Maker's comments refer to Parts 1 and 2, the authors wish to point out that a fire is no respecter of the working pressure of a vessel. Therefore, although the fire experience to which the authors refer consists of observed failure of low-pressure vessels up to 10,000-gal capacity exposed to fire out in the open. the intensity of a fire around similar high-pressure vessels would be the same. Reference is made by Mr. Maker to the difference between vessels in refineries and those in other plants. The codes do not recognize this differentiation and the authors are of the opinion that the code should be specific about the size and shape of a vessel in relation to heat input in an exposure fire, or else vessels should be designed for the worst condition. The formulas given apply to any shape and working pressure.

2 The authors are aware that possible heat-input rates of 20,000 Btu per sq ft per hr are not new but they desire to point out that very little information has been given to the public to this effect in the 18 years since heat-absorption rates of this

magnitude were observed by Mr. Maker. Furthermore, because of the use of recommended values of from one sixth to one third of the observed heat-input rates many a tank has probably suffered damage during this period.

3 Mr. Maker suggests continued use of the arbitrary expression $Q/A = \frac{48{,}000}{A^{1/3}}$ as a relation between heat input and surface area of a vessel. This is an example of arbitrary rule which the authors feel can and should be replaced by a more practical and accurate expression. The absurdity of this expression may be brought out by equating the right-hand side to 20,000 Btu per sq ft per hr and solving for A, the area of a vessel for which a heat-input rate of 20,000 Btu per sq ft per hr would be recommended; thus

$$\frac{48{,}000}{A^{1/3}} = 20{,}000$$
$$A^{1/3} = 2.4$$
$$A = (2.4)^3 = 13.8 \text{ sq ft}$$

This is equivalent to a vessel about 18 in. in diameter and 36 in. long. Our tests and fire experience indicate that 20,000 Btu per sq ft per hr may be expected up to areas of approximately 200 sq ft and 600 sq ft respectively. We, therefore, emphatically deny that this expression is reasonable.

4 The reasons for basing relieving capacity on the free-discharge area of relief connections are detailed in the reply to the comments by Turner C. Smith.

5 Mr. Maker is confused by the "contents factor." The authors feel that they have been quite clear in stating that this factor may be calculated for each individual liquid to be stored or processed and have suggested two excellent methods of estimating latent heats of vaporization. However, we also feel that by use of the recommended general expression for the "contents factor" in terms of pressure, one need not be concerned with the nature of material to be stored; and that not only is a factor of safety provided for, but also the cost of resulting vent nozzle is negligible compared to the cost of one which would be required for some particular liquid.

6 Finally Mr. Maker suggests the procedure to follow in determining relief areas, namely:

1 Determine the amount of heat input.
2 Determine maximum pressure of discharge.
3 Determine the vaporization rate.
4 Choose relief device to discharge vapor.

This is precisely the method used by the authors as shown in the paper.

Under item 1, we suggest 20,000 Btu per sq ft per hr, except for atmospheric tanks, as outlined in Part 3 of the paper.

Under item 2, we use the code rule in the paper of 10 per cent greater than the working pressure for maximum discharge pressure.

Under item 3, we determine the vaporization rate by use of the "contents factor."

Under item 4, we show a relation from which the minimum diameter of a circular relief area to discharge the vapor may be calculated.

We still feel that an "all-embracing" formula simplifies the problem for the host of equipment manufacturers and regulatory bodies who would need to go through these four steps, and that we are not trying to cover up any steps or introduce any irrelevant factors which would give unreasonable relief connections.

In answer to Mr. Maker's general conclusion, which of course refers to pressure vessels, the authors wish to point out that, whereas the information supplied by the paper may lack in application to large-size vessels, the existing available information is seriously lacking in application to small-size vessels.

Reply to Discussion by F. L. Newcomb

All of the actual fires used as a basis for the test of the curve described may not have been fires of great intensity. This committee should have asked for information from other industries besides the petroleum industry. A number of cases were cited by the authors in which the existing design rate of 6000 Btu was found to be inadequate, to which cases reference is suggested.

The only instance of a large tank being exposed, which supported the recommended curve, was that given by Turner C. Smith as example *c*-2. The apparent fallacy in its application is described under the reply to Mr. Smith's discussion to which attention is invited.

Reply to Discussion by R. C. Werner and S. T. Russell

The authors disagree with the tabulation of paragraph 6 and the statement of paragraph 7 in the comments by Mr. R. C. Werner and Mr. S. T. Russell, for the following reasons:

1 The very physical construction of the fuel around the propane cylinder would account for a variable heating rate on the wetted surface of the tank. As the wood is consumed and the fire bed lowers, the flame in the vicinity of the wetted surface would be more intense.

2 Up to the time of vaporization, the heat-transfer process is in an unsteady state. Thus, the steel vessel which weighs about 1000 lb and the propane vapor in the vapor space absorb heat, but as the temperature of the steel shell rises the rate of heat absorption decreases. However, as the fire level drops, then a relatively steady state is reached in the transfer of heat to the boiling liquid and practically all of the heat absorbed by the wetted surface goes into vaporization of the liquid. The values 1530 and 8410 Btu per hr per sq ft in the tabulation are evidently based upon the rise in liquid temperature only, and this low rate of sensible heat absorbed would be expected because of the mass of wood which surrounds the tank during the first few minutes of the fire.

Since these critics doubt the accuracy of Fetterly's test setup, as shown in Fig. 3 of the paper, the authors will be glad to display further information on request, including photographs and the results of two other tests conducted by Mr. Fetterly, or the critics may refer to files of the Bureau of Explosives in New York, N. Y.

In regard to the first point raised on the Underwriters' Laboratory tests, note that 461,000 Btu per hr (the heating rate at 1-min exposure) is still equivalent to 19,200 Btu per hr per sq ft. The chart shows that the plate heated from 65 F to 340 F in $^1/_2$ min, which is a heating rate of about $122 \times 0.12 \times 275 \times \frac{60}{0.5} =$ 483,000 Btu per hr. The maximum heating rate must be higher than this and exists at the first instant when the plate is at its lowest temperature. When the plate is at 600F (the temperature at 1-min exposure), it is losing heat from the rear and absorbs heat at a slower rate because of its high temperature.

The second point is rather abstract but actual observations of fires and the damage therefrom leave little doubt that air does exist in large areas so that combustion is complete enough to result in high temperatures. Reference may be made to the NFPA Handbook[9] on fire severity. Note also that a 3000-gal tank is not a small-scale tank but rather a commercial-process installation.

The third point is provided for in Part 3 of the paper. We agree that large-size tanks will not receive heat at the same rates as small-size tanks.

The comments on the Aluminum Company tests although lengthy are merely opinions of Messrs. Werner and Russell, and the authors of the paper do not grant that these opinions are superior to their own on these tests.

In regard to Items 4, 5, and 6, under the test made by the authors, note that the heat available in the fuel for test No. 4 is only 28 per cent of the quantity available in test No. 1. The two tests are, therefore, not comparable as far as determination of effect of water film is concerned. The emissivities for oxidized iron and steel, painted surfaces, and so on, are also reported as 0.95 to 0.98. The figure of 0.96 for water is calculated. Very few commercial surfaces will maintain a low emissivity for a long period of time.

In the summarization paragraph, Messrs. Werner and Russell refer to a large-area oil fire. We wish to point out that such a fire would not be as intense as a large-area butadiene or acetone fire. Large storage tank and large-area fire are not defined. The authors have given consideration to various sizes of tanks in using the observed heating rates.

It is the opinion of the authors that the summary statements of Messrs. Werner and Russell do not in any way detract from the observed heat-input rate of 20,000 Btu per hr per sq ft because:

1 They have calculated the input rate to a dry plate of 19,200 Btu per hr per sq ft (Underwriters' Laboratory tests); and if they are correct in their emissivities of iron and water, run No. 1 of the authors' tests would yield $25{,}900 \times 75/96 = 20{,}200$ Btu per hr per sq ft.

2 Damage to tanks and equipment in actual fires shows that vent sizes are too small whether they are venting air, vapor, or a combination of vapor and liquid.

3 A tank surrounded by other tanks and equipment would present the same windshield effect in an actual fire.

The authors would also point out that when human life is a consideration, it is customary to provide a factor of safety in the transposition of observed data to actual practice. For instance, in the design of pressure vessels a factor of safety of 4 or 5 is used. In view of the evidence of test data and the many cases of destruction of equipment in actual fires it is difficult to understand why anyone would desire to interpret data on the low side, or to design for any but the worst conditions that can be conceived.

Reply to Discussion by Walter Samans

The type of constructive criticism received from Mr. Samans is appreciated. The authors are in agreement with most of his comments. The following reply is made to several questions which he raised:

Mr. Samans feels that a heating rate of the order of one sixth of the observed rate (20,000 Btu) should apply to large atmospheric vessels. Solution of curve 3 in Fig. 18 of the paper will show that a rate, ranging from 5000 Btu at 300,000-gal capacity to 2300 Btu at 1,000,000-gal capacity, has been applied.

It was said that the authors' tests did not simulate fires in the open. This is true, as acknowledged, to an extent not great enough to affect materially the rate of heat absorption. The authors would point out that the test results were confirmed by five other independent organizations.

The reasons for stating, "So far as can be learned, there is no substantial theory or evidence to support the limiting of heat-input rates to any particular height. There are some indications to the contrary, that is, high gas temperatures apparently exist at relatively great heights above the fuel during large fires," will be found under the heading Flame Temperatures and Effective Height, near the end of Part 1 of the paper. In addition to the evidence there given, the authors have recently observed structural steel destroyed 30 to 40 ft above the liquid fuel. This was in the open and the structure was carrying only its own weight. The failures were the drooping type necessitating temperatures of at least 1000 to 1200 F.

Reply to Discussion by T. C. Smith

The following reply is made to specific quotations from Mr. Smith's discussion:

Mr. Smith's Comment. "It has been difficult to understand why the authors have chosen to determine the pipe size required for the relief-valve connection rather than the orifice area of the valve. Commercial spring-loaded relief valves have an orifice area ranging from 25 to 30 per cent of the connecting-pipe area, hence it would appear that the orifice should be of primary concern and the inlet-pipe connection of secondary interest."

Quotation Pertaining From Authors' Paper. "The relief capacity is proposed in terms of area of the relief connection (or connections) because the designer is primarily interested in selecting an adequate fitting of standard size for the vessel to be constructed, and because of the great variation in the capacity of commercial relief apparatus. This connection is ordinarily an inserted short tube with a square inner edge, somewhat rough from the standpoint of fluid flow. The relief device may afterwards be selected of a capacity (based on approved flow test) to pass the vapor rate of flow computed from relief area, as will be explained later."

Authors' Additional Comment. To elaborate further, the authors point out that of many popular types of safety valves studied, capacities were found to vary from 14 to 60 per cent of the capacities of tank connections of the same pipe size. It is generally recognized that only those capacities for valves which are essentially free-blowing orifices (top guided, high lift) can be calculated readily with practical accuracy. Such valves are in the minority of the many types manufactured. To repeat, the necessary relief capacity can always be calculated in terms of free area of the relief connection, and the apparatus chosen of a capacity (based on approved flow test) to pass the calculated rate.

The wide variation in the capacities of commercial relief devices and the questionable value of calculated capacities of valves which are not essentially free-blowing orifices will be obvious if reference is made to recent literature[15] on this matter.

It is further believed that the relief apparatus necessary for fire exposure, in most cases, would be supplemental to the usual spring-loaded safety devices and would also be a more simple, inexpensive device of relatively large capacity. Reference is suggested to paragraph 5, Proposed Summary for Use, Part 2, of the paper.

The method of specifying relief capacities in terms of free area is that shown in the "Proposed Tentative Standards: API Venting Guide" (May, 1940, p. 4). After Table 2, which gives the diameters of free areas with capacities, will be found the following statement in paragraph 7.1: "Certified capacity curves of venting equipment shall be based on flow tests conducted by commercial testing laboratories of institutions of recognized technical standing." Further, in the "A.S.M.E. Code for Power Boilers" (1940 edition, p. 108), will be found Table P-14 giving minimum total areas of openings (square inches) in fire-tube boilers for safety-valve connections.

The authors, therefore, feel that they have followed a recognized and rational method in expressing relief capacities in terms of free area.

Mr. Smith's Comment. "Also, consideration should be given to replotting the curves of 'contents factors' with the term 'pressure' incorporated in the equation. This will permit a series

[15] "Safety Valve Capacity Tests" (in accordance with the rules formulated by the A.S.M.E. Boiler Code Committee), National Board of Boiler and Pressure Vessel Inspectors, Columbus, Ohio, 1940; "Steam Flow Through Safety Valves," by E. K. Falls, Ohio State University, Columbus, Ohio, 1942; and "Safety and Relief Valves for Refrigerants," by E. K. Falls, *Refrigeration Engineering*, April, 1943, p. 257.

of charts, each consisting of a family of curves for various groups of contents."

Authors' Reply. This comment is not fully understood. It will be seen, in Fig. 12 of the paper, that the contents-factor values were plotted against pressure. No attempt was made to plot values for a substantial percentage of the numerous compounds but only for those considered representative and for which latent-heat data were directly available in the literature referred to in conjunction with Fig. 12. It is believed these are sufficient for the purpose of showing the method of solution and illustrating the value of simplification.

If a series of charts, consisting of values for families of compounds, were made, the present worth of Fig. 12 would be further enhanced. When trial solutions were made for numerous other compounds, the contents-factor values were found to be within the range of those now shown on the graph. "Their use in individual cases would result in numerous vent sizes adequate only for materials of like properties at the same condition." No different pipe-size relief connections other than those shown in Table 2 would result.

To emphasize again; the suggestion of a simplified value of the contents factor varying with pressure "in no degree nullifies the value of Equation [9] in calculating the required relief diameter directly for any contents."

Mr. Smith's Comment. "The authors present heat-input rates ranging from 20,000 to 30,000 Btu per hr as obtained from three different sets of tests."

Authors' Reply. Described and analyzed in Part 1 of the paper are tests by four (not three) separate organizations; seven tests in all. In the "Conclusion" of Part 2, further confirming tests by another company are referred to; while, in addition, four accidental fire exposures are pointed out as having supported the test data.

In the supplementary remarks to this paper made at Los Angeles on June 17, 1943, the authors cited one further test and one further actual example. The paper thus had for its practical basis the analysis and development of 10 man-made fire-exposure tests by six separate organizations and 5 actual cases confirming the test data. At this time, 6 additional failures due to fire exposure are being studied for further data.

Mr. Smith's Comment. "The speaker hastens to correct any doubts, on the deficiency of these venting rules, or impressions that this subject has been or is being neglected by groups engaged in the initial drafting of safety standards."

Authors' Reply. Early in Part 1, and again near the end of Part 2, the authors explained that the existing proposals for emergency venting were found to be inadequate. We believe this evidence to be convincing and will not repeat or elaborate on it here, but further explanation will be given in supplementary remarks. No inference was made that the subject was being neglected, but it was stated that the necessary information could not be obtained from the regulatory bodies. The following are quotations from a letter dated November 7, 1942, from the engineering office of one of the regulatory bodies in reply to our inquiry for information on the subject of rates of heat absorption during fire exposure:

> The subject of emergency relief of internal pressure was headed up some twelve to fourteen years ago in the NFP A Committee on Flammable Liquids when the API Committee on Fire Prevention undertook to make studies and recommendations for inclusion in the NFPA Suggested Ordinance.
>
> One of the first steps was a theoretical study along the lines of the enclosed, 'The Rates of Vaporization in Gasoline in Storage Tanks Exposed to Fire,' which was ultimately used as the basis for the typical bulk marketing tank of approximately 20,000 gallons capacity. There was a consensus among our fire prevention engineers that for such a tank we might reasonably expect absorption of heat energy at the rate of 100 Btu per minute per square foot of wetted surface.
>
> More recently there have been fragmentary data which indicated much higher heating rates than 6,000 Btu per square foot per hour for the entire wetted surface of smaller tanks such as tank truck compartments. These data encouraged me to suggest a variable heating rate such as that represented by the red line on the chart. One oil company has recommended the use of this assumption in the form of the equation
>
> $$h = \frac{48{,}000}{A^{0.5}}$$
>
> where h = heat absorbed to cause evaporation—Btu per hour per sq ft.
>
> A = external area of vessel.
>
> We are lacking in data on larger tanks but there seems to be a general feeling among fire protection engineers that this assumption is reasonably safe, particularly for the larger sized tanks.

This letter is typical of the replies of other authorities on the subject, and this lack of data led to the independent study in an attempt to solve our own problem.

Mr. Smith's Comment. "The National Board of Fire Underwriter's rule was based upon a modification of Fetterly's formula, using a flame temperature of 1200 F for tanks having a capacity of 10,000 gal or less, and 1000 F for tanks of 30,000 gal capacity or more, with adjusted temperatures for tanks of intermediate capacity. The heat input by this rule will vary between 23,000 and 13,000 Btu per sq ft per hr."

Authors' Reply. If this reference (the last sentence quoted) is intended to apply to Fetterly's formula, it is not in agreement with the figures ("these values are not questioned") to be found under the heading Analysis of Fetterly's Formula and Test, in Part 1 of the paper, where Fetterly's work is analyzed and compared with present-day theory. There is shown the figure of 14,500 Btu per hr per sq ft of wetted surface for an effective flame temperature of 1200 F, and for 1000 F temperature, 8100 Btu will result.

Mr. Smith's Comment. The authors' paper was severely criticized for proposing a solution for large vessels without giving actual data on large-scale fire exposures. It should be noted that Mr. Smith cites only one large-scale analysis, which is as follows:

Example: "(c-2) Approximately 2300 Btu per hr per sq ft on a sphere having a wetted surface of 4363 sq ft. This was a 48-ft-diam sphere subjected to a severe fire for 1 hr 7 min. At times the vessel was completely enveloped in flame. The relief valves were adequate and prevented failure of the sphere."

Authors' Reply. The report of this same case, dated June 5, 1941, was received from one of the eastern refiners on November 6, 1942. In it will be found that the vessel was surrounded by fire for only 10 min. The result of 2300 Btu per hr per sq ft was the average for 1-hr exposure. Maximum rates of heat absorption may, therefore, have been 6 times as great (13,800 Btu) for which the relief devices should be adequate in order to limit the pressure rise. This is an excellent example but its maximum and not average values should be used as guidance toward safety.

As explained in Part 3 of the paper, it is expedient for practical reasons to lower the design heat-absorption rates for large atmospheric vessels. The vessel described contained 6000 bbl. When a solution is made of Equation [24] from curve 3, Fig. 18, of the paper, for a tank of this capacity, a heat-absorption rate of 3670 Btu per hr per sq ft of wetted surface results. This compares favorably with 2300 Btu average when it is considered that both are arbitrary assumptions, but the authors would use a much higher rate for the hazardous and expensive sphere under consideration in accordance with Part 2 of the paper.

For further evidence to support this reasoning, the authors have observed 17-ft-diam × 19-ft 4 1/2-in-high aluminum tanks

completely surrouned by fire and melted down in a matter of a few minutes. This metal had a melting point of 1216 F. An effective temperature of this magnitude is commensurate with a heat-absorption rate of 15,000 Btu per hr per sq ft. Actual effective hot gas temperatures were probably higher than 1216 F.

Reply to Discussion by H. R. Zeigler

In the paper we tried to avoid the discussion of relief devices, their relative merits, etc. Suggestions were, therefore, confined to relief areas or relief connections, and their calculated capacities. Mr. Zeigler's statements, "One novel suggestion is that relief valves be made the same size on all vessels of the same capacity and pressure," and ". . . it is necessary to point out that this is based on the assumption that tanks should be equipped with relieving devices of sufficient capacity to promote interchangeability," are misinterpretations. We did say: "It being proposed, as already inferred, that the relief connection be the same size on all vessels of given capacity and range of working pressure. When equipment is so provided with adequate relief area for volatile compounds in the form of relief connections, the relief devices may be replaced to provide for any change in contents or more severe working conditions from the standpoint of relief requirements." We feel that the relief apparatus should be selected to pass the calculated vent rate at the same conditions, and this choice will govern its size. This procedure is given in the section Proposed Summary for Use, of Part 2.

We were not aware that the National Board of Fire Underwriters' Pamphlet No. 58 applied to processing and storage equipment other than that for liquefied petroleum gases. We have used specifications for relief requirements from Pamphlet No. 30 but not from No. 58. For that reason we do not know and did not say that the relief areas in No. 58 are inadequate. We merely plotted specifications from the latter for comparison.

It is unfortunate that it appeared we were trying to prove the inadequacy of Fetterly's formula. As a matter of fact, the evidence indicates that his method has given more accurate results than any other. With a given latent heat (not calculated by $L = 0.185\ T\ (V1 - V2)\ dP/dT$ as he proposed) and for low pressures, our formula gives relief areas only 10 per cent less than Fetterly's. This comparison will be found plotted in Fig. 10. Fetterly's heat-absorption rate of 22,600 Btu per hr per sq ft is based on the vaporization of 1000 lb of propane taking place in the observed time of 5.9 min. The other figures are merely cited to support this rate, and it will be noted that there is reasonable agreement among them. This analysis was mailed to Fetterly for criticism but no reply was received.

Finally, the magnitude of the observed rate (20,000 Btu) of heat absorption is the principal contention. This is a long story about which we and our critics have written many pages. It may be pointed out that rates as high as 20,000 Btu have been confirmed by five other organizations besides ourselves. A number of critics are in agreement on this figure except for large vessels. A summary of the tests and experience on which the 20,000 Btu rate and 1400 F effective temperature are based has been published.[46] Further, it may be noted that the average rate for our four tests was 19,688 Btu per hr per sq ft at an average temperature for the flame of 1357 F (820 C being 1508 F).

We are confident that future tests and analyses of vessels exposed to accidental fire will prove the proposed heat rate to be of the correct magnitude.

[46] "Venting of Tanks Exposed to Fire," by J. J. Duggan, C. H. Gilmour, and P. F. Fisher, *National Fire Protection Association Quarterly*, October, 1943.

Wood-Cloth and Wood-Paper Laminates

By JOHN DELMONTE,[1] LOS ANGELES, CALIF.

A growing tendency exists for the use of wood and resin-impregnated cloth or paper, which is an outgrowth of laminated - plywood developments. Combinations of cloth and paper with wood, in addition to serving as vehicles for the bonding glue in the manufacture of the laminates, also help stabilize the wood assemblies and provide structural advantages, as demonstrated by test data given in the paper. For example, when a reasonably large number of paper laminates are used, there is an apparent increase in the tensile properties of wood, attributable to prestressing of the wood resulting from differences in coefficients of thermal contraction as parts are cooled upon removal from the press. Dimensional stability in plywood faced with phenolic-resin-treated cloth and paper is found to be far superior to unprotected plywood.

A NATURAL consequence of laminated-plywood developments and laminated-plastic-material developments is a trend toward intermediate products combining wood and resin-impregnated cloth or paper. While it will be acknowledged that there are applications best served by wood alone or other applications best fulfilled by plastics materials, there are various properties developed by their combination that are not possessed fully by either material itself. There are not many evidences as yet of extensive adaptation of resin-impregnated cloths or papers with wood although a few are in the process of development for aircraft applications.

Examining the fundamental properties of wood, one will admit its superior advantages of low cost, light weight, and high strength although he will also recognize its anisotropic tendencies and susceptibility to moisture. Plywood developments were a logical evolution in that they balanced physical properties more evenly and reduced the effects of swelling. However, while resin-bonded plywoods were a step in the right direction, even these have not always possessed the necessary dimensional stability required of aircraft materials, in spite of synthetic-resin bonding agents, such as phenol formaldehyde, urea formaldehyde, and melamine formaldehyde. Elaborate finishing schedules offer some measure of protection to the plywood, but even these are beset by numerous practical problems (1).[2]

The most noteworthy developments for stabilizing plywood have been suggested by the Forest Products Laboratory (2, 3) in their publications upon resin-impregnated wood. This well-known technique involves a procedure of impregnating thin wood veneers with a water-soluble phenolic resin and curing the resin in the veneer by heat alone (Impreg), or by combination of heat and pressure (Compreg). Approximately 30 per cent resin diffused into the cell walls of the wood fibers has resulted in a decided improvement in wood-stabilizing characteristics, particularly against swelling effects of moisture. What few objections have been raised against these techniques include the following:

1 Increase in density without a substantial gain in strength.

2 Added difficulties in performing secondary gluing operations in aircraft as compared with unimpregnated plywood.

3 Problems of obtaining proper impregnation and its determination.

Also to be noted are the developments of superpressed plywood and multiple-phenolic-resin films which increase the ratio of resin to wood (4). High laminating pressures above 1000 psi have been employed to increase the penetration of resin into the wood. The cardinal advantage of this process is the development of superior shear strength in the plywood, which greatly increases for a slight increase in density. On the other hand, the rate of increase of tensile strength and compressive strength over density is only slight. This development is also significant in the technique of increasing resin content by adding multiple layers of phenolic-resin film, a procedure which would be unnecessarily prolonged if spraying were resorted to.

Both of these fairly recent developments in stabilizing plywood have taken into account the advantages of increasing the ratio of synthetic resin to wood in order to stabilize the wood. Ordinary synthetic-resin-bonded aircraft plywood contains anywhere from 10 to 25 lb per 1000 sq ft of dry-glue spread sufficient for good bonding, high shear strength, and good water resistance at the glue lines only.

The combinations of resin-impregnated cloth and papers with wood fulfill more than the function of vehicles for the glue; they also help to stabilize the wood assembly as well as make possible structural advantages as various test data disclosed in this paper will reveal. In addition, the wood-cloth and wood-paper laminates make possible more complicated assemblies and constructions, difficult with plywood alone.

Physical Test Conditions

Unless stated otherwise the various physical tests reported upon in this paper were performed upon wood-cloth or wood-paper laminates which had been conditioned at 50 per cent relative humidity for at least 48 hours in order to realize approximately 10 per cent moisture in the wood. Tests were performed under prevailing atmospheric conditions which, for the most part, were at room temperatures of 70 to 80 F, and relative humidities of 35 to 45 per cent. All tensile tests and flexural tests followed A.S.T.M. Standards for flat sheets of plastics materials (5). Specific-gravity determinations were made by measuring the volume of accurately machined samples and dividing this value into the weight. The moduli of elasticity reported were obtained by the simple cantilever-beam technique. This method is described elsewhere in its adaptation to plastics materials (6).

Test Laminates

The following laminates were prepared for physical tests and tests of dimensional stability under extremes of moisture condition. In Groups I and II the base material was standard-aircraft-grade 3-ply vertical-grain plywood with two birch faces and poplar core.

Group I:

(*A*) Plywood base, two birch faces, poplar core; over-all thickness 0.106 in.

(*B*) Resin-impregnated paper,[3] 2 layers on each face of plywood-base core (*A*)

(*C*) Resin-impregnated paper,[3] 5 layers on each face of plywood-base core (*A*)

---

[1] Technical Director, Plastics Industries Technical Institute. Mem. A.S.M.E.

[2] Numbers in parentheses refer to the Bibliography at end of paper.

Contributed jointly by the Rubber and Plastics Group and Aviation Division and presented at the Semi-Annual Meeting, Los Angeles, Calif., June 14–17, 1943, of The American Society of Mechanical Engineers.

Note: Statements and opinions advanced in papers are to be understood as individual expressions of their authors and not those of the Society.

(*D*) Resin-impregnated paper,[a] 10 layers on each face of plywood-base core (*A*)

[a] Consolidated Water Power & Paper Company; phenolic-resin content, 35 per cent.

NOTE: Group I samples were laminated at 250 psi for 10, 15, and 20 min at 310 to 320 F, for increasing layers of paper.

Group II:

(*A*) Plywood base, two birch faces, poplar core; over-all thickness 0.106 in.
(*B*) Phenolic-resin-impregnated canvas,[b] 1 layer on either face of plywood-base core (*A*)
(*C*) Phenolic-resin-impregnated canvas,[b] 2 layers on either face of plywood-base core (*A*)
(*D*) Phenolic-resin-impregnated canvas,[b] 5 layers on either face of plywood-base core (*A*)

[b] 9-oz canvas duck, phenol-formaldehyde impregnating resin varnish (BV-1115), 38 per cent resin content.

NOTE: Group II samples were laminated at 250 psi for 20, 25, and 30 min at 310 to 320 F for increasing layers of cloth.

Group III:

(*A*) Three-ply birch veneer, 0.032 in. thick, core cross-grain; phenolic-resin bonding agent, PR-14 (Amberlite)
(*B*) Similar to (*A*) except 2 phenolic-resin-impregnated papers added between each ply
(*C*) Similar to (*A*) except 5 phenolic-resin-impregnated papers added between each ply

NOTE: Group III samples were laminated at 250 psi, and 325 F for 15 min. Plywood shear tests were performed in accordance with AN-NN-P-511b Army-Navy Specification for Plywood and Veneer, dated October 28, 1942.

Group IV:

Two parallel-grained birch veneers, 1/16 in. thick, between which are laminated:

(*A*) 1 phenolic-resin-impregnated paper
(*B*) 5 phenolic-resin-impregnated papers
(*C*) 10 phenolic-resin-impregnated papers
(*D*) 20 phenolic-resin-impregnated papers

Group V:

Two cross-grained birch veneers, 1/16 in. thick, between which are laminated:

(*A*) 1 phenolic-resin-impregnated paper
(*B*) 5 phenolic-resin-impregnated papers
(*C*) 10 phenolic-resin-impregnated papers
(*D*) 20 phenolic-resin-impregnated papers

NOTE: Groups IV and V were laminated at 250 psi and temperature of 320 F for 20 min (*A* and *B*), 25 min (*C*), and 30 min (*D*).

RESULTS OF TESTS ON PHYSICAL PROPERTIES

The results of tests on the laminated assemblies may be divided into two groups, i.e., physical properties and dimensional stability under extremes of moisture conditions. The physical properties are presented first.

Results of physical tests upon Group I and Group II laminates are shown in Table 1. In order to keep variables to a minimum, laminating pressures of 250 psi are employed for these laminates as well as the others. This pressure likewise is not too far removed from those employed in rubber-bag-molding operations. Data reported for the straight plywood (10 per cent moisture) compare favorably with those reported in other publications (7). The most obvious improvement in physical properties is apparent in the wood-paper laminates (Group I). Not only are values of the tensile strength and modulus of elasticity decidedly improved but also the specific tensile strength, which is equal to the ultimate tensile value divided by the specific gravity. These improvements are due largely to the excellent properties of the phenolic-resin-impregnated paper employed in conjunction with the plywood.

Manufacturers' specifications for laminates of paper alone at 250 psi are as follows:

Ultimate tensile strength (with grain) 36,000 psi
Modulus of elasticity (with grain) 3,000,000 psi
Specific gravity, 1.38
Water absorption, 6 per cent (24 hr)

Unless indicated otherwise the test data of this report were obtained in a direction parallel to the grain of the impregnated paper. It was further observed that properties for the straight laminated paper decreased somewhat (tensile strength at 33,000 psi, for example), when the material was conditioned for several days at 50 per cent relative humidity. It was pointed out earlier that all the wood laminates were conditioned in this manner.

Table 1 also reports the stiffness factors ($E \times I$) for the various laminates assuming, for purposes of comparison, a constant panel weight of 0.5 lb per sq ft and then estimating moments of inertia from

$$I = \frac{bh^3}{12}$$

where b = 1 in.
h = thickness which at specific gravity indicated in Table 1 will give 0.5 lb per sq ft
I = moment of inertia.

Plywood faced with a few sheets of impregnated paper shows slight gains in the stiffness factor. While plywood faced with resin-impregnated canvas does not register the gains shown for the wood-paper laminates, the data nevertheless demonstrate the versatility of plastic materials in securing moduli of elasticity at very much lower values than with plywood alone. To the stress engineer this suggests decreased stiffness factors, but to the fabricator of compound curvatures it suggests an easier material to fabricate plus the added advantage of better dimensional stability under adverse weather conditions.

The load distribution within the various components of wood-cloth and wood-paper laminates are basically dependent upon the moduli of elasticity of the different components. For pure tension and pure compression it is obvious that

$$\delta = \frac{S_1}{E_1} = \frac{S_2}{E_2}$$

TABLE 1 PHYSICAL PROPERTIES OF SOME CLOTH-WOOD AND PAPER-WOOD LAMINATES[a]

	A	*B*	*B/A*			
Laminated assembly	Specific gravity	Ultimate tensile strength, psi	Specific tensile strength, psi	Modulus of elasticity, psi	Stiffness factor,[b] $E \times I$	Ratio of resin to inert material,[c] per cent
Laminated phenolic (canvas)	1.33	17500	13200	1080000	34	38
Plywood (birch faces, poplar core)	0.74	13680	18500	1780000	326	0
Plywood, faced with 2 layers phenolic-resin-treated paper	0.76	13250	17500	2250000	381	4.1
Plywood, faced with 5 layers phenolic-resin-treated paper	0.86	15270	17700	2250000	264	8.1
Plywood, faced with 10 layers phenolic-resin-treated paper	0.93	19000	20400	2320000	211	15.2
Plywood, faced with 1 layer phenolic-resin-treated canvas	0.82	11800	14400	1225000	163	6.3
Plywood, faced with 2 layers phenolic-resin-treated canvas	0.92	11600	12600	1228000	115	15.6
Plywood, faced with 5 layers phenolic-resin-treated canvas	1.08	11500	10600	1040000	61	24.7

[a] Prepared at 250 psi.
[b] Based on weight of 0.5 lb per sq ft.
[c] 35 per cent phenolic resin in paper; 38 per cent phenolic resin in canvas.

TABLE 2 RESULTS OF SHEAR TESTS ON PLYWOOD[a]

Plywood combination	Dry shear tests (average of 5 tests), psi	Results
3-ply birch, resin alone as bond	637	95–100 Per cent wood failure
3-ply birch, resin plus two layers of impregnated paper in each glue line	577	Approximately 70 per cent failure in paper
3-ply birch, resin plus five layers of impregnated paper in each glue line	542	Approximately 70 per cent failure in paper
Specification allowance	400	

[a] 3-ply, all birch, 1/32-in-thick veneers.
NOTE: Adhesive, phenol-formaldehyde resin (Amberlite PR-14). Additions to adhesive, phenolic-resin-impregnated paper (Consolidated Water Power & Paper Company). Test specification, AN-NN-P-511b (Army-Navy Aeronautical Specification Plywood and Veneer).

TABLE 3 PHYSICAL PROPERTIES OF GROUPS IV AND V LAMINATES

Laminate	Ultimate tensile strength, Psi	Modulus of elasticity, Psi
Parallel-grain birch:		
Faces 1, impreg; paper core	20100	1600000
Faces 5, impreg; paper core	22970	1850000
Faces 10, impreg; paper core	24490	2050000
Faces 20, impreg; paper core	29400	2400000
Cross-grain birch:		
Faces 1, impreg; paper core	3220	137000
Faces 5, impreg; paper core	7640	170000
Faces 10, impreg; paper core	12200	250000
Faces 20, impreg; paper core	17670	491000

where δ = unit deformation in composite assembly of material No. 1 and material No. 2
S_1 and S_2 = unit stresses in No. 1 and No. 2
E_1 and E_2 = moduli of elasticity in No. 1 and No. 2

Likewise, for calculating stress at any point within the plywood panel, the formula developed for straight plywoods (8) may be applied to cloth-wood and paper-wood laminates, considering the layers of paper or cloth in the same category as a layer of wood veneer

$$S_L = \frac{E_L}{E_P} \cdot \frac{M_P C}{I_P}$$

where S_L = stress in layer or laminate in question
E_L = modulus of elasticity of that laminate alone
M_P = bending moment at point in question
C = distance from neutral axis to layer or laminate in question
E_P = apparent modulus of entire plywood panel (see Table 1)
I_P = moment of inertia of entire plywood panel

Group III laminates were prepared largely with the idea of observing the effects of impregnated paper upon the shear strength of plywood. Samples were cut in accordance with the Army-Navy Aeronautical Specification for plywood and veneer (9) and tests performed as required. Results of these tests, disclosed in Table 2, demonstrate that all the plywood samples with and without impregnated papers at the glue line, passed the minimum requirements of the specification. However, there was a small, but definite decrease, in shear strength with an increase in paper content. This was occasioned by the appearance of paper failure which was marked by a separation of the fibers of the paper. Dry shear tests were performed upon five samples for each reading record in Table 2, after 48 hr conditioning at 50 per cent relative humidity.

Groups IV and V laminates serve the purpose of revealing further fundamental data on the co-relationship of paper and wood. While the plywood-paper samples prepared are unbalanced in the sense of uniform grain direction for the wood, without the benefit of cross-plies, results on the load distribution within the wood and impregnated paper are interesting. In Fig. 1, the marked increase in tensile strength, for example, is to be expected from the excellent properties of the paper employed. As indicated earlier, the ultimate tensile strength of this particular laminated paper alone is 36,000 psi, after dry conditioning, and about 33,000 psi after 50 per cent relative-humidity conditioning. It is significant, however, that the increase in tensile strength of the wood is greater than would be expected upon the addition of the paper. This is illustrated on the right-hand side of Fig. 1. In other words, assuming constant tensile strength for the laminated paper, the apparent strength of the wood increases with greater amounts of impregnated paper. These data were obtained, for pure tension, as follows:

$$P_1 + P_2 = P = A_1S_1 + A_2S_2$$

where P_1 = portion of load carried by impregnated paper
P_2 = portion of load carried by wood veneer
A_1 = cross-sectional area of paper laminate
A_2 = cross-sectional area of wood veneer
S_1 = stress intensity in paper laminate
S_2 = stress intensity in wood veneer
P = total load

Using the foregoing formula and calculating load distribution for increasing amounts of paper laminate, the increase in P could not be accounted for solely by the increase in high-strength-paper content. However, it is possible that thermal-expansion coefficients vary and upon removal of the laminate from the hot plates of the press, the wood veneers were under initial stress due to greater shrinkage of the laminated phenolic-paper layer upon cooling. Then

$$P = A_1S_1 + A_2S_2 + KE_2A_2$$

where K = unit deformation due to thermal-expansion difference during manufacture
E_2 = modulus of elasticity of wood veneer

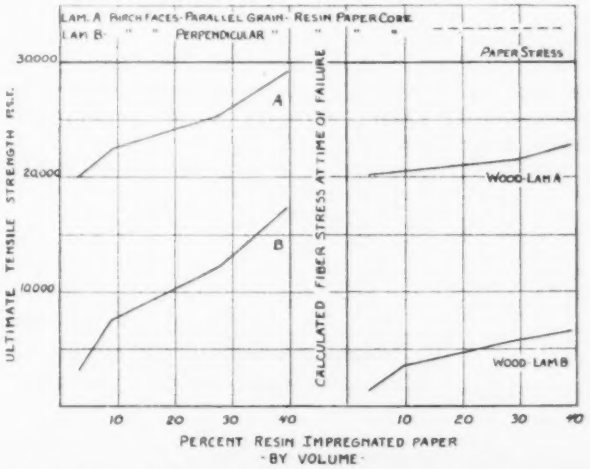


FIG. 1 ULTIMATE TENSILE STRENGTH OF WOOD-PAPER LAMINATES

In Table 3, are reported physical properties of Groups IV and V laminates after conditioning at 50 per cent relative humidity.

Results of Tests on Dimensional Stability

The effects of moisture gradients upon wood laminates are to bring about severe dimensional distortion. While the developments of synthetic-resin adhesives for the glue lines have created the so-called "waterproof" plywood, in the sense that shear failures would no longer be due to deterioration of the glue line the resin adhesives will not protect the wood structure itself. Faced with very large tangential and radial shrinkage in all wood veneers, plywood manufacturers are ever concerned with the avoidance of warping and distortion in plywood panels. Much care is necessary in preconditioning the wood veneers to uniform moisture content, and then in afterconditioning to compensate for loss of moisture in hot-pressing or the introduction of moisture from the glue.

As pointed out earlier, synthetic-resin impregnants have stabilized wood by greatly reducing the effects of moisture. Some stabilization is achieved by facings of impregnated canvas and impregnated paper on the outside of the plywood core (Groups I and II laminates) by creating a moisture barrier. The effectiveness of phenolic-resin-impregnated paper and cloth in stabilizing plywood may be determined by means of a test designed to measure distortion in plywood upon exposure to severe moisture gradients.

As shown in Fig. 2, one side of a plywood test sample was coated with a metal face, 1 mil in thickness, which extended up the sides of the test sample, excluding moisture from all surfaces except the top surface. Upon placing the plywood sample in a pan of water, immediate deformations are apparent as the plywood fibers in direct contact with the water begin to swell. This swelling or distortion in the 5-in. test length is measured with a depth gage, as shown in Fig. 2. Results are clear-cut and comparisons may be made in a short period of time, without any delay being necessitated for the less-significant percentage of water absorbed.

All test samples were conditioned at 50 per cent relative humidity for at least 48 hours prior to test, and distortion is less than would have occurred if the materials were started from a perfectly dry condition. However, the interest lies largely in the comparative results.

Data shown in Figs. 3 and 4 illustrate the distortion in plywood as a function of time. It is quite obvious that resin-treated papers and cloth greatly improve the dimensional stability of plywood by retarding the effects of moisture. The distortion curve for plywood alone demonstrates a peak value, indicative that moisture has diffused through the plywood and that the fibers nearest the protective metal foil have begun to swell counteracting the swelling on the exposed side. When the test is carried out for a long period of time the distortion in the plywood is largely recovered.

For purposes of comparison, the more conventional A.S.T.M.

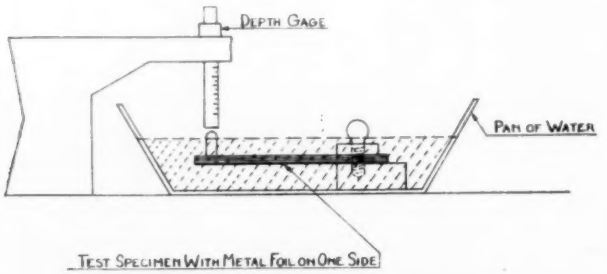


Fig. 2 Test for Dimensional Stability

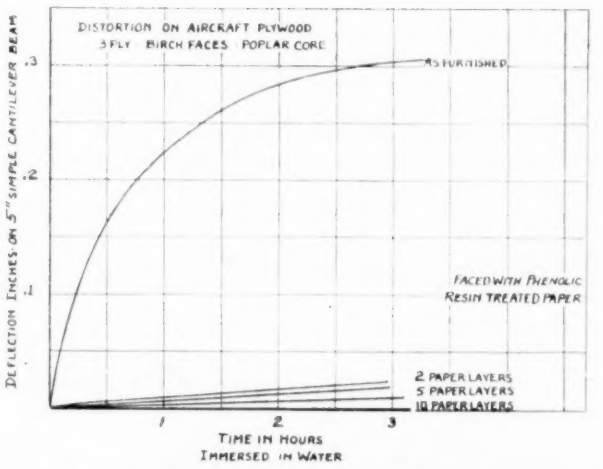


Fig. 3 Distortion in Plywood Faced With Phenolic-Resin-Treated Paper

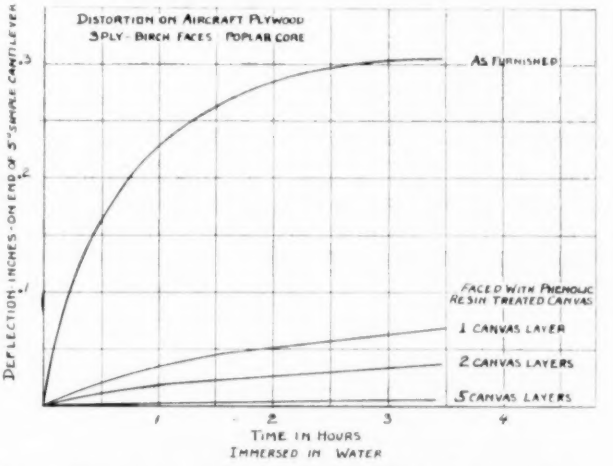


Fig. 4 Distortion in Plywood Faced With Phenolic-Resin-Treated Canvas

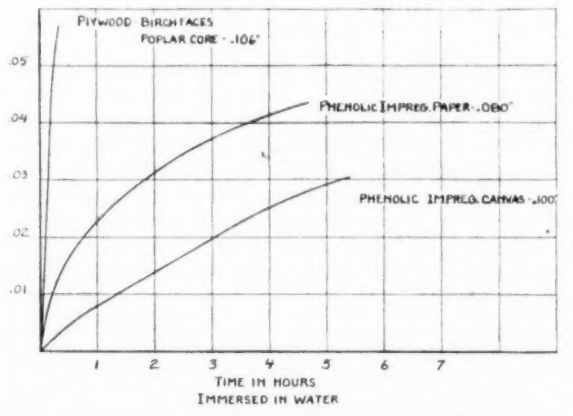


Fig. 5 Distortion of Laminated Canvas and Laminated Paper in Contact With Water

tests were performed upon plywood faced with one and two layers of phenolic-resin-treated canvas. Pieces which were dry-conditioned measured 1 in. × 3 in., the sides being protected against moisture by metal foils. The results follow:

Material	Water absorbed (in 24 hr), per cent
Plywood faced with one phenolic-resin-treated canvas	8.4
Plywood-faced with two phenolic-resin-treated canvas	3.1

As may be suspected, the plywood distortion in moisture may not be attributed to the plywood alone, but also to the resin-impregnated canvas and paper. This is borne out by the disclosures in Fig. 5 which show distortion of laminated canvas and laminated paper when they are brought in contact with water as shown in Fig. 2.

That some of the combinations with plywood show even lower distortions is explained by the greater over-all thicknesses of these assemblies.

Conclusions

It is apparent that there are physical advantages to be realized from the combinations of resin-impregnated paper and cloth with plywood; particularly for the high-strength paper employed in these tests. There is some evidence that when a reasonably large number of paper laminates are present there is an apparent increase in the tensile properties of the wood attributable to prestressing of the wood brought on by differences in coefficients of thermal contraction as parts are cooled upon removal from the press.

While resin-impregnated canvas did not add greatly to the physical properties of the plywood, the molders and fabricators of plywood parts would do well to recognize the benefits of canvas in its stretchability, allowing the attainment of smaller radii of curvature and a certain amount of drawing impractical in wood alone. This would suggest the usefulness of phenolic-resin-impregnated canvas in fulfilling discontinuities in a cloth-wood combination.

Dimensional stability in plywood faced with phenolic-resin treated cloth and paper is far superior to unprotected plywood. This advantage alone should suggest to manufacturers of aircraft plywood that a few facings of impregnated paper or cloth would improve the qualities of their products.

Acknowledgment

Acknowledgment is given to Mr. Foster Luce, Mr. E. Watkins, and Mr. W. F. Lusk of the Plastics Industries Technical Institute staff for assistance in preparation of some of the samples and performance of some of the physical tests, data for which are given in this paper.

BIBLIOGRAPHY

1 "Variations in Plywood Aircraft Finish," by W. Smith, *Wood Products*, Feb., 1943, p. 22.

2 "Anti-Shrink Treatment of Wood With Synthetic-Resin Forming Materials," A. J. Stamm, R. M. Seborg—R-1213, Forest Products Laboratories, December 15, 1938.

3 "Contributions of Synthetic Resins to Improvement of Plywood Properties," by D. Brouse, R-1212, Forest Products Laboratories, January, 1939.

4 "Superpressed Plywood," by R. K. Bernard, T. D. Perry, and E. G. Stern, *Mechanical Engineering*, vol. 62, 1940, pp. 189–195.

5 "Standard Methods of Testing Sheet and Plate Materials Used in Electrical Insulation," A.S.T.M. Standard D229–42, A.S.T.M. Standards, 1942, Part III, pp. 336–344.

6 "Permanence of Physical Properties of Plastics," by J. Delmonte, Trans. A.S.M.E., vol. 62, 1940, pp. 513–524.

7 "Data on Design of Plywood for Aircraft," Forest Products Laboratory, report 1302, Dec., 1941.

8 "Strength Characteristics of Plastic Bonded Plywood," by C. Parsons, *Aero Digest*, vol. 41, July, 1942, pp. 160, 162, 165, and 273–274; August, 1942, pp. 140 and 218.

9 Army-Navy Aeronautical Specification for Plywood and Veneer, AN-NN-P-511b (October 28, 1942.)

Superchargers for Aircraft Engines

By R. G. STANDERWICK[1] AND W. J. KING,[1] WEST LYNN, MASS.

This is a comprehensive treatment covering the development of turbosuperchargers, which today are making possible the outstanding performance at high altitudes of United States military aircraft. The basic function of supercharging is to increase the intake-manifold air pressure in an engine, as a result of which the primary objectives are attained of (*a*) maintaining full (rated) power at altitude; (*b*) increasing power at sea level; (*c*) improving fuel economy for cruising. Fundamental design considerations cover the means for accomplishing these ends, with some indication of the power requirements, temperature effects, and the like. Types of superchargers are discussed, and their systems of drives, and then particular attention is devoted to the General Electric turbosupercharger, as used on the Boeing Flying Fortress, Consolidated Liberator bomber, and Lockheed Lightning, and Republic Thunderbolt pursuit ships. Final sections of the paper are concerned with a comparison of various types of superchargers, and the present and future prospects for this most important aircraft-engine auxiliary.

Fundamentals of Supercharging

THE basic function of supercharging is to increase the intake-manifold air pressure in an engine. This has two immediate results; (*a*) the density of the charge forced into each cylinder is increased, and (*b*) a favorable excess or differential is maintained in the intake manifold pressure with respect to the exhaust back pressure. These two effects are utilized to accomplish the primary objectives of supercharging aircraft engines, as follows:

1 To maintain full (rated) power at altitude.
2 To increase power at sea level ("ground boosting").
3 To improve fuel economy for cruising.

A further effect of supercharging, which is beneficial in each of these respects, is to promote fuel vaporization and uniform distribution of mixture to the individual cylinders.

In order to appreciate the nature of the problem, in reference to these objectives, it is first necessary to take account of a few of the elementary relationships underlying the performance of present-day aircraft engines.

Other things being constant, the indicated horsepower developed in an engine is directly proportional to the mass rate of air consumption (as pounds per minute). For a given speed this means that the power is proportional to the density of the air, which is a function of its pressure and temperature. As a fairly close approximation (1),[2] the brake horsepower of an engine varies directly with the absolute pressure, p, and inversely as the square root of the absolute temperature, T, of the carburetor inlet air, as expressed in the formula

$$\frac{\text{Bhp}_0}{\text{Bhp}_1} = \frac{p_0\sqrt{T_1}}{p_1\sqrt{T_0}} \quad \ldots\ldots\ldots\ldots\ldots\ldots\ldots\ldots [1]$$

where the subscripts 0 and 1 refer to standard sea-level and altitude conditions, respectively.

Altitude Effects. Fig. 1 shows how these factors vary with altitude in a representative modern aircraft engine, except unsupercharged, using standard N.A.C.A. atmospheric data (2). A glance at this should suffice to indicate the occasion for supercharging military-airplane engines, where it is so vitally important for the engine to be capable of developing its full power at any level within its altitude range.

The significant fact here is that by the application of a suitable supercharger the same engine which gave less than 30 per cent

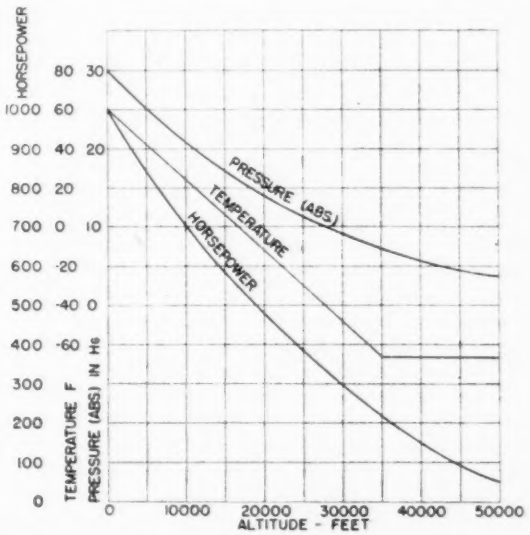


FIG. 1 VARIATION IN ATMOSPHERIC PRESSURE AND TEMPERATURE WITH ALTITUDE AND EFFECT UPON ENGINE POWER

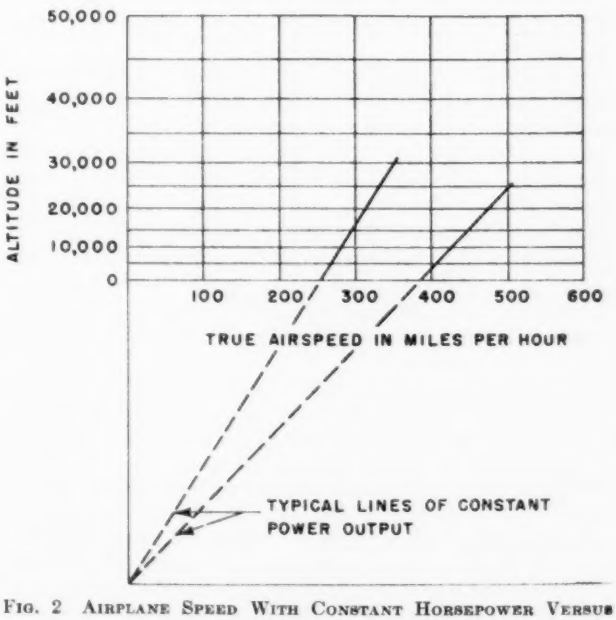


FIG. 2 AIRPLANE SPEED WITH CONSTANT HORSEPOWER VERSUS ALTITUDE

[1] Supercharger Engineering Division, General Electric Company.

[2] Numbers in parentheses refer to the Bibliography at the end of the paper.

Contributed by the Aviation Division and presented at the Semi-Annual Meeting, Los Angeles, Calif., June 14–17, 1943, of THE AMERICAN SOCIETY OF MECHANICAL ENGINEERS.

NOTE: Statements and opinions advanced in papers are to be understood as individual expressions of their authors and not those of the Society.

of its full power at 30,000 ft can be made to deliver 100 per cent power all the way from sea level to that altitude, and beyond. With proper attention to such factors as propeller design, propeller and engine speeds, and type of supercharger, it is further possible to maintain substantially the same fuel-consumption rate (pounds per horsepower-hour) at altitude as at sea level.

These two facts have a direct bearing upon the curves in Fig. 2, which shows the variation in the speed of a given airplane with altitude, if the engine power output can be held constant. This chart is calculated from theory and assumes constant propeller and airplane efficiency. Under these conditions, it may be seen that a plane having a speed of 250 mph at sea level may attain a speed of 350 mph at 30,000 ft, for the same power and time rate of fuel consumption. Of course actual airplanes will not follow this chart exactly, but Kendall Perkins of Curtiss Wright states that, on the average, the speed of a plane will increase by 1 per cent for each 1000 ft of altitude (3). Very likely a higher figure can be realized in a suitably designed plane. At all events it is clear that the ability to maintain power at high altitudes results in marked improvements in peak performance of the plane, saving valuable time in military or commercial operations, and increasing the speed at which satisfactory over-all economy can be maintained.

Ground Boosting. Superchargers can also be used very effectively for ground boosting, i.e., increasing the sea-level power of the engine, since the indicated mean effective pressure (imep) and horsepower are proportional to the intake-manifold air pressure (map). With a moderate allowance for friction and accessory power loss in the engine, the brake-mean-effective-pressure values, (bmep) and brake horsepower (bhp) likewise increase very nearly linearly with the manifold air pressure. Of course, the power output of an engine can also be increased by increasing the compression ratio, but the interesting fact here is that a given increase in bmep and bhp can be obtained with a considerably smaller rise in maximum cycle pressure and temperature by means of supercharging. The result is that the manifold pressure can be boosted to yield a substantially greater power output before the allowable limit is imposed by stresses, temperatures, or detonation. It is entirely practicable, for example, to increase the output of an unsupercharged engine from 500 to 800 hp by boosting the manifold air pressure from 29 to 40 in. Hg abs, without changing the speed. This extra power is frequently of great value in facilitating take-off.

In all of the foregoing comparisons, the engine speed has been assumed to remain constant. The variation of power with speed is expressed by the formula

$$\text{Bhp} = \text{const} \times \text{bmep} \times \text{rpm} \quad [2]$$

High power is therefore commonly obtained by a combination of high speed and high bmep. High speed is attained by setting the variable-pitch-propeller governor to hold the desired revolutions by appropriate adjustment of the propeller-blade angle, and high bmep is secured by boosting the manifold pressure either by opening the throttle or increasing the speed of the supercharger (if the latter is controllable).

Cruising Power. For cruising, the power can be reduced either by reducing the speed or the bmep, or both. If the propeller efficiency is not impaired, it is definitely more economical to reduce power by reducing the speed, keeping the bmep as high as practicable. This is a consequence of the reduction in engine friction losses at the lower speeds. When the speed is reduced for this purpose at cruising altitudes, it is frequently found that the most economical values of map and bmep cannot be attained even with full opening of the throttle without a considerable amount of boosting from the supercharger. As an example to help make this clear, the following figures are cited for a hypothetical engine for which the value of the constant in Equation [2] is 0.0025:

Power	Cruising (maximum economy)	Full
Manifold air pressure, in. Hg	30	47
Brake mean effective pressure, psi	140	220
Speed, rpm	1200	2700
Power, bhp	420	1485

At 15,000 ft, the manifold pressure could not be more than about 16.5 in. Hg without supercharging. This would yield a bmep of approximately 77 in. Hg, which would require a speed of 2180 rpm to produce the 420 bhp for cruising. The fuel consumption at this speed would normally be appreciably greater than at 1200 rpm. To maintain 420 bhp at still lower speeds would probably require richening of the fuel-air mixture to avoid detonation, and the propeller efficiency might be considerably reduced.

Supercharger Operating Range. Another serious obstacle to the maintenance of high manifold pressures for cruising is the limited range of satisfactory operation of superchargers now in common use, as indicated in Fig. 3. In this figure, Q represents

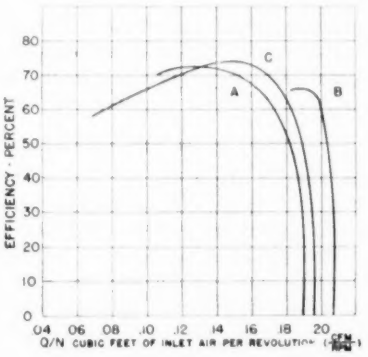


FIG. 3 TYPICAL RANGE CURVES OF SUPERCHARGERS

the volume flow of air supplied to the engine cfm, and is proportional to the engine power, at any given altitude; N is the supercharger speed, rpm, which is the chief factor in determining the pressure (map) supplied to the intake manifold. The useful operating range of a supercharger refers to the spread between the lower value of Q/N, usually established by the incidence of violent surging or instability, and the upper value beyond which the efficiency falls off very rapidly. Curve A is representative of the modern centrifugal supercharger. The significance of these curves will be discussed further. For the present purpose it will suffice to observe that curve A indicates the difficulty of attempting to reduce Q for very low power outputs while maintaining N at a relatively high level, in order to employ high manifold pressures. In addition to the fact that this tends to push the value of Q/N into the unstable region beyond the left end of the curve, a very flexible speed control is required to allow N to be maintained when the engine speed is reduced to less than one half of its maximum rating.

Differential-Pressure Effects in the Engine. Apart from its prime function of increasing the density of the charging air forced into the engine cylinders, supercharging has a further beneficial effect in promoting the scavenging of spent gases from the clearance volume, at the end of the exhaust stroke. Since the intake-manifold pressure is higher than the back pressure some of the hot residual gas is forced out during the "overlap" interval between the opening of the intake valve and the closing of the exhaust. This improves the volumetric efficiency, lowers the initial temperature of compression, and reduces the tendency to backfire with lean fuel-air mixtures.

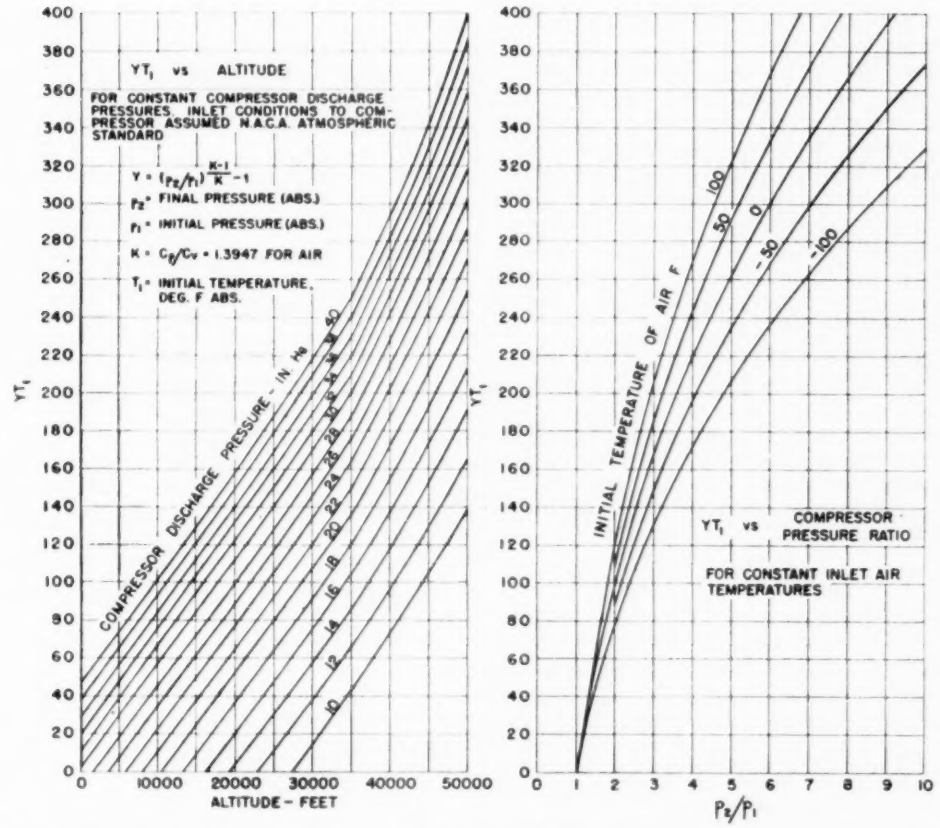


FIG. 4 VARIATION OF FUNCTION YT_1 WITH ALTITUDE, PRESSURE RATIO, AND INITIAL TEMPERATURE

The excess of the intake pressure over the exhaust must be taken into account in computing the effect upon the net engine power of the power required to drive the supercharger. A substantial portion of the latter, roughly 40 per cent, is returned to the engine in the form of "steam-engine power," which is the excess of the work done on the pistons during the intake stroke over the work done on the spent gas during the exhaust stroke.

Power Required for Driving Supercharger. Present-day aircraft engines consume about 0.12 lb of air per min per hp delivered. The power required to compress this air is determined chiefly by the ratio of the final to the initial absolute pressures, p_2/p_1, and the absolute temperature, T_1, of the inlet air. The theoretical power for isentropic compression is given by the formula (reference 4)

$$\text{Hp} = 0.00573\ YT_1 \text{ per lb air per min} \quad [3]$$

where

$$Y = (p_2/p_1)^{0.283} - 1$$

and T_1 is in deg F abs.

Values of the function YT_1 are given in Fig. 4. The curves on the left are based on the assumption that p_1 and T_1 correspond to the standard N.A.C.A. atmospheric values of Fig. 1, for each altitude. The curves on the right give the same function for the particular pressure ratio and inlet temperature involved in any case. To obtain the compressor-shaft-input power, the values obtained from Equation [3] must be divided by the efficiency.

In many practical cases p_1 may be assumed to be equal to the prevailing atmospheric pressure in flight, since the pressure drop in the upstream induction system is roughly balanced by the "ram" or kinetic pressure of the slipstream impinging upon the air scoop. For the typical internal-geared supercharger p_2 is the manifold pressure. Assuming a compressor efficiency of 70 per cent, the power required to develop 1000 hp at 10,000 ft with a manifold pressure of 32 in. Hg can then be obtained from Fig. 4 and Equation [3] as follows

$$YT_1 = 65$$

$$\text{Hp} = \frac{0.00573 \times 65 \times 120}{0.7} = 63.8$$

(This must again be divided by the mechanical efficiency of the drive train to obtain the power taken from the engine crankshaft.) The pressure ratio in this case is 1.55. For comparison, a supercharger to maintain 40 in. Hg of manifold pressure at 25,000 ft would have to develop a pressure ratio of 3.6, which would require an input of about 185 hp per 1000 hp of engine power.

The newcomer to this field sometimes finds it difficult to understand how a device which extracts such sizable blocks of power from the engine can be applied to sustain, or even increase, the net engine output. Perhaps this can be appreciated more readily from the analogy which it bears to the forced-draft blower of a stoker-fired furnace of a steam power plant, where a few hundred horsepower input to the blower enables the furnace to burn enough additional coal to generate several times the initial investment in power. Moreover, as mentioned, the supercharger compressor actually pumps a substantial portion of its shaft power back into the engine (5). For the electrical engineer the supercharger may be compared with the grid of an electronic tube, when the grid system is used to control the relatively large plate-circuit power in a regenerative hookup. The fact is that the supercharger is being employed to an increasing degree as the

primary means of controlling the power of an airplane engine, in place of the carburetor throttle.

Temperature Effects. Unfortunately, air cannot be compressed even with the perfect efficiency of an isentropic process, without a significant rise in temperature, unless the heat of compression is removed by cooling during the process. In aircraft superchargers it is not practicable to effect any appreciable amount of cooling in the compressor itself; in fact, the surface area is so small relative to the mass flow of air that the process is substantially adiabatic (and polytropic).

For an adiabatic process, the minimum temperature rise occurs in the case of reversible, isentropic compression, i.e., when the compressor efficiency is 100 per cent. In this case, the ideal temperature rise is numerically equal to the function YT_1 of Fig. 4

$$T_2 - T_1 = YT_1 \quad [4]$$

and the actual temperature rise in any case is this value divided by the compressor efficiency. This is the source of the very convenient and commonly used expression for compressor efficiency, otherwise known as the "temperature-rise ratio"

$$e_t = \frac{YT_1}{T_2 - T_1} \quad [5]$$

which should be equal to the actual shaft efficiency if there is no heat transfer to or from the surroundings.

Equation [4] and Fig. 4 can now be used to determine the temperature rise of the air in the foregoing examples of supercharger power. For the 32-in. manifold pressure at 10,000 ft

$$T_2 - T_1 = YT_1/0.7 = 65/0.7 = 93 \text{ F}$$

and for the 40-in. pressure at 25,000 ft

$$T_2 - T_1 = 188/0.7 = 269 \text{ F}$$

With an inlet-air temperature of —30 F, the manifold temperature in the latter case would be 239 F. This would be intolerably high, according to present standards, for reasons which will be discussed later. In practice, the total pressure ratio of 3.6 involved in this case would be divided between two stages of compression with an intercooler between them, as indicated in Fig. 5. With the conditions assumed in this illustration the manifold temperature would be reduced to 134 F.

Referring further to Fig. 5, the first-stage discharge pressure is commonly set at 31.67 in., in order to maintain standard sea-level pressure, 29.92 in., at the carburetor inlet, allowing for a drop of 1¾ in. Hg in the intercooler and ducting. The temperature rise in each stage was obtained from Equation [4], allowing for a compressor efficiency of 70 per cent. It will be observed that the first-stage pressure ratio, p_2/p_1, is 31.67/11.1 = 2.85, whereas the second-stage ratio is 40/28.6 = 1.4, in order to make

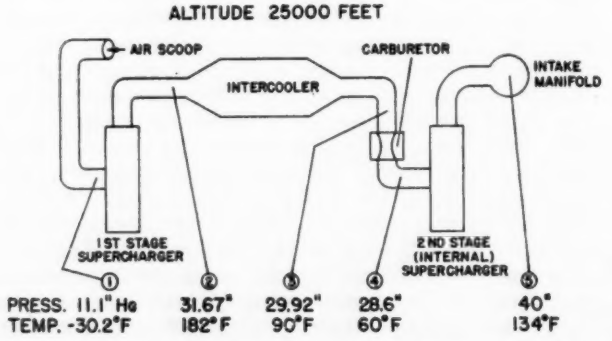


FIG. 5 PRESSURES AND TEMPERATURES IN A TYPICAL TWO-STAGE INDUCTION SYSTEM

more effective use of the intercooler. (Occasionally an aftercooler is used between the final stage and the manifold, but this is not convenient in radial engines.) The so-called "intercooler effectiveness" is the ratio of the drop in temperature of the compressed air to the initial temperature difference with respect to the ambient, or

$$\frac{t_2 - t_3}{t_2 - t_1} = \frac{182 - 90}{182 - (-30)} = 43.4 \text{ per cent}$$

which represents a compromise in performance to reduce cooler weight. The drop of 30 F in the carburetor is due to the absorption of latent heat by the evaporating gasoline. In some cases, most of this occurs in the passages of the internal supercharger, but the effect is about the same.

There are at least three reasons for limiting the manifold temperature to the lowest practicable level:

1 To avoid detonation or "knocking" in the engine, which has such a serious effect upon engine life as to constitute a major limitation to the allowable power rating. As the mixture temperature increases, fuel of higher-octane rating must be employed to maintain constant intensity of detonation.

2 To increase the density of the charge supplied to each cylinder, thereby increasing the power developed, as per Equation [1].

3 To reduce the combustion and exhaust temperatures of the engine.

These three results are promoted by improving the efficiency of the supercharger, which reduces the temperature rise during compression. In addition, any improvement in first-stage efficiency reduces the work of compression in a second stage by reducing the value of T_1 in Equation [3].

On the other hand, these same results can be promoted by increasing the effectiveness of the intercooler. In either case higher efficiency or effectiveness inevitably results in greater size and weight, at a given stage of the art. Optimum installation design therefore calls for a careful compromise of these factors to obtain best over-all performance, with due regard for total drag, power, and supercharger operating speed.

TYPES OF SUPERCHARGERS

Two basic types of compressors have been used to supercharge internal-combustion engines:

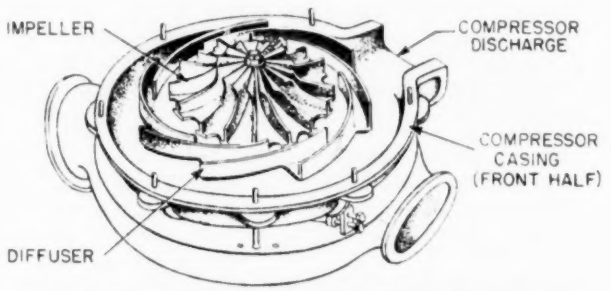


FIG. 6 CENTRIFUGAL COMPRESSOR IN TURBOSUPERCHARGER

1 The "positive-displacement" type, of which the Roots blower is a prominent example. This has two rotors carrying lobes which mesh with each other as do gear teeth, and which during their rotation open and close a displacement space between the dumbbell-shaped lobes. An excellent description of this blower was given by John L. Ryde in a recent S.A.E. paper (6). It has not been applied to the supercharging of airplane engines to any appreciable extent since the N.A.C.A. tests of 1930, reported by Oscar Schey (7). Other positive-displacement pumps,

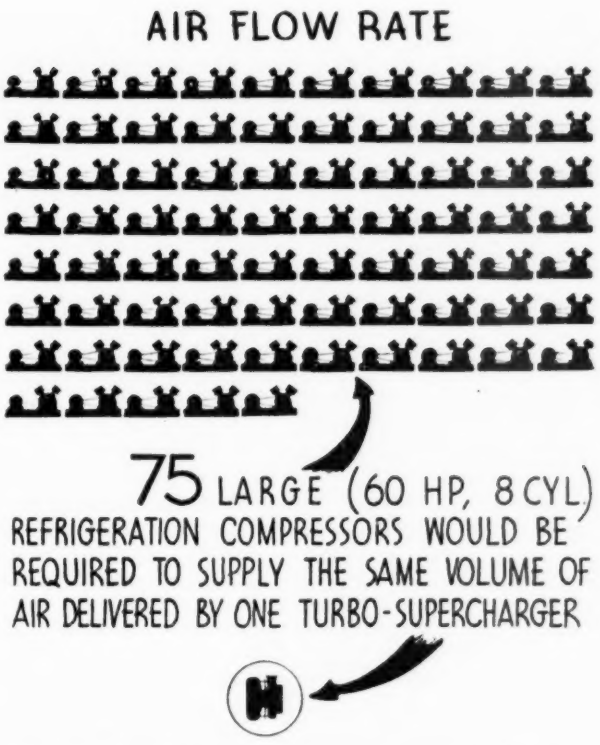


FIG. 7 CONTRAST BETWEEN SUPERCHARGER AND EQUIVALENT RECIPROCATING COMPRESSORS

such as the rotary-vane and reciprocating-piston types, have not been well adapted for use in aircraft, principally because of their relatively large size and weight for a given capacity.

2 The "centrifugal" type, the principal elements of which are a multivaned impeller and an annular diffuser, Fig. 6, enclosed in a suitable casing, which includes a collector or scroll surrounding the diffuser. The impeller is driven at speeds of the order of 20,000 to 30,000 rpm, with peripheral velocities or "tip speeds" commonly reaching 1100 or 1200 fps. The impeller imparts energy to the air principally by giving it violent peripheral and angular acceleration, roughly one half of this energy appearing as static pressure rise and half as kinetic energy at the exit (8). The function of the diffuser is to convert as much as possible of the velocity of the high-speed air streams into further increase in the static pressure, by a process of efficient deceleration. Because of its high speed of operation, the centrifugal supercharger has an exceptionally high volumetric capacity, which makes it especially well adapted for use in aircraft. By way of contrast, Fig. 7 shows graphically the relative size of a centrifugal supercharger (turbine-driven) as compared with the 75 conventional electrically driven reciprocating compressors which would be required to furnish the air for a 2000-hp engine.

The "axial-flow" compressor should be mentioned as another basic type, which has frequently been considered for supercharging engines (9). It is essentially a series of propeller-type fans, as many as 16 or 20, mounted on the same shaft, with a set of fixed turning vanes between stages, not unlike a multistage steam turbine. One of its limitations is its relatively narrow operating range, which has the character of curve *B* in Fig. 3, except that its peak efficiency may be appreciably higher. Its chief disadvantage is its large size, principally in axial length, due to the many stages required to produce a substantial pressure ratio. Mainly for these reasons, it has not been applied to aircraft engines, although it has been used commercially in gas-turbine power plants (10, 11).

CENTRIFUGAL-COMPRESSOR DESIGN FACTORS

In selecting a centrifugal compressor for a given supercharger application, the following factors must be taken into account: (*a*) Capacity, (*b*) maximum pressure ratio, (*c*) efficiency, (*d*) range, (*e*) impeller speed, (*f*) mechanical ruggedness, (*g*) size, (*h*) weight.

It is, of course, impracticable to discuss all of these factors exhaustively in a paper of this kind, but a brief survey of some of the major effects may be helpful to the uninitiated. More detailed discussions of the basic theory and practice will be found in references (8) and (12) of the Bibliography.

Capacity, usually expressed in pounds of air per minute, is governed primarily by impeller diameter, D, and revolutions per minute, N. For a series of "similar" machines, the volumetric flow Q (cfm) is proportional to ND^3, so that all sizes of such a series should have the same value of Q/ND^3. The basic capacity of the design, or "characteristic flow," which Q/ND^3 represents, can be increased by increasing the depth of the impeller passages or the "relative" area of the inlet. Any considerable departure from optimum proportions, however, will impair the efficiency.

As previously indicated, a supercharger must deliver 0.12 lb of air per min per engine hp. The volume flow at any altitude is obtained by dividing the mass flow by the density, to obtain the value of Q. The machine must then be selected or adjusted to bring the rated value of Q/N to the appropriate point near the peak of the characteristic curve, Fig. 3. In practice, the final adjustment of the capacity of the compressor is accomplished by changing the angle and the flow area of the diffusers suitably. (This is done by changing the entire diffuser, which is nonadjustable.) The volume flow required to maintain a given capacity increases rapidly with altitude, becoming 6.6 times as great at 50,000 ft as at sea level.

The maximum pressure ratio is an important criterion of the excellence of a given design, as it fixes the useful ceiling of the machine. The pressure-producing capacity of a centrifugal compressor is measured by the so-called "pressure coefficient"

$$\psi = \frac{6083 Y T_1}{V^2} \qquad [6]$$

where V is the impeller tip speed in feet per second. This coefficient compares the energy of isentropic compression of the air between the actual pressures involved in Y, with the energy theoretically imparted to the air by the impeller (which is proportional to V^2). From Equation [6], the necessary operating speed to deliver the required pressure ratio can be obtained as

$$V = \sqrt{\frac{6083 Y T_1}{\psi}} \qquad [7]$$

the value of YT_1 being taken from Fig. 4.

In general, pressure coefficients for impellers with straight radial blades vary with Q/N in about the same manner as the efficiency (e_i), as shown by the curves in Fig. 3. Although Equations [6] and [7] do not apply rigorously to impellers having curved blades, it may nevertheless be said that forwardly curved blades produce relatively high pressure coefficients, in that a lower tip speed is required for the same pressure ratio. This is secured, however, at the expense of a considerable reduction in stability and range of operation. Conversely, impellers with backwardly curved blades commonly show higher efficiencies but

lower pressure ratios for the same tip speed than the straight-bladed type.

Altitude performance depends upon the ability to develop pressure ratio with a minimum temperature rise over a wide range of stable operation, and therefore different types of superchargers should be compared on this basis, rather than at the same tip speed, as has sometimes been the practice in the past.

Substituting the value of Y in Equation [6], it can be shown that

$$p_2/p_1 = \left(1 + \frac{\eta V^2}{6083 T_1}\right)^{3.534} \quad \ldots\ldots\ldots\ldots [8]$$

The maximum pressure ratio which a given machine can develop is usually limited by the allowable stresses due to centrifugal force, which is proportional to the square of the speed. But, if this is not the limiting factor, there is a general tendency for the pressure coefficient and range to decrease at high speeds, as indicated by the change from curve A to curve B in Fig. 3. The ultimate ceiling may be reached at the point where the value of η collapses so that there is no further increase in pressure with speed.

The efficiency of a centrifugal compressor depends almost entirely upon how successfully the air is introduced into the impeller and conducted through the passages of the machine without shock, flow separation, or turbulence. This sounds much simpler than it actually is. The air entering the impeller is given a sudden terrific acceleration, sometimes reaching a figure of 6,000,000 fpsps, or 186,000 g. The internal air velocities are commonly of the order of 1000 to 1200 fps at the diffuser entrance. The latter figure would exceed the velocity of sound (about 1088 fps at 32 F) except for the fact that this velocity increases in proportion with the square root of the absolute temperature, which increases very considerably with the speed. At these speeds, the air particles tend to travel through the flow passages like rifle bullets, so that it is very difficult to make them turn corners and fill the varying flow sections without separation.

At the higher air velocities associated with relatively high-volume flow and tip speeds the performance of the compressor is usually limited by the occurrence of "shock waves" manifested by very sudden changes in pressure with high energy losses, as the velocity at the diffuser entrance approaches the sonic or acoustic value. The tendency of these shock losses to occur is measured by the so-called "Mach number," which is simply the ratio of the air velocity, u, to the velocity of sound, C, at the local temperature (or any convenient reference temperature). Since the critical value of u is determined by and is very nearly equal to the tip speed, V, and since $C = 49\sqrt{T}$ it is convenient to express the local Mach number as

$$M = \frac{V}{49\sqrt{T}} \quad \ldots\ldots\ldots\ldots [9]$$

Unfortunately, the local value of T at the diffuser inlet is usually not known, but for a given value of V it is determined by the inlet-air temperature, T_1, so that it is still more convenient to use a distorted Mach number

$$M_1 = \frac{V}{49\sqrt{T_1}} \quad \ldots\ldots\ldots\ldots [10]$$

in comparing the basic efficiencies of different compressors. This means that all of the values of efficiency versus Q/N should fall on the same curve, as A in Fig. 3, for a constant value of M_1 no matter how the speed and inlet temperature may be varied. A higher value of M_1 would tend to reduce the performance in the direction of curve B.

Since efficiency, pressure coefficient, and range are thus impaired by the high speeds and low temperatures required for high-altitude operation it is customary to employ two stages of compression when the total pressure ratio is greater than about 2 or 3 to 1. However, there is always a strong incentive to develop single-stage designs to yield the utmost in pressure ratio without too great sacrifices in performance, for reasons of mechanical simplicity, weight, and size.

The significance of the problem of operating range has already been indicated. The problem is becoming progressively more acute as the spread between maximum and minimum engine power increases, and as higher altitudes call for higher supercharger speeds. One expedient for increasing range is the use of a ring-type or vaneless diffuser, which gives the type of performance represented by curve C of Fig. 3. However, the penalty is usually a substantial increase in size (12), or else a loss in efficiency and pressure coefficient (13).

Speed, mechanical ruggedness, and weight are closely interrelated factors. The high speeds at which centrifugal superchargers operate not only set up high centrifugal stresses in the impeller but also generate vigorous vibrations in all parts of the machine, due to resonance effects and the impulses caused by the passage of impeller blades past the diffuser vanes. The energy and destructive power of these vibrations is sometimes surprising, and it requires very special care and experience to determine the necessary massiveness and structure to prevent premature fatigue failures.

For aerodynamic reasons, to preserve the proper proportions of the flow passages, the capacity of a given type of supercharger should not be increased faster than the square of the characteristic dimension, which is usually the diameter, i.e.

$$Q \propto D^2$$

In any series of similar machines, the weight increases with the cube of the characteristic dimension, or

$$W \propto D^3$$

Hence

$$W \propto Q^{3/2}$$

which indicates that the larger-capacity machines tend to become relatively heavy. This aspect of the problem becomes so serious that there is a strong incentive to cramp and compromise the design in order to maintain more nearly proportionate weights as the horsepower rating is increased. For this reason, the impression is sometimes given that the art is not progressing, since very real gains in basic merit are required to stand still with respect to efficiency while constantly progressing in capacity and altitude rating.

Types of Drives

The commonest type of supercharger, embodied in practically every major commercial and military aircraft engine today, is the radial centrifugal gear-driven from the rear end of the engine crankshaft. The speed is usually stepped up through two sets of gears to give impeller speeds of from 6 to 10 times the crankshaft speed.

For conservative performance at moderate altitudes, as in typical air-line service, a single-stage single-speed drive is adequate, but for high-performance military planes, it has been found expedient to employ some form of multispeed drive, for the following reasons:

If a centrifugal supercharger is operated at constant speed the pressure ratio and volumetric capacity are substantially independent of the initial pressure and density of the air. But the power is proportional to the weight flow, and hence to the density, and of course the final pressure increases in proportion with

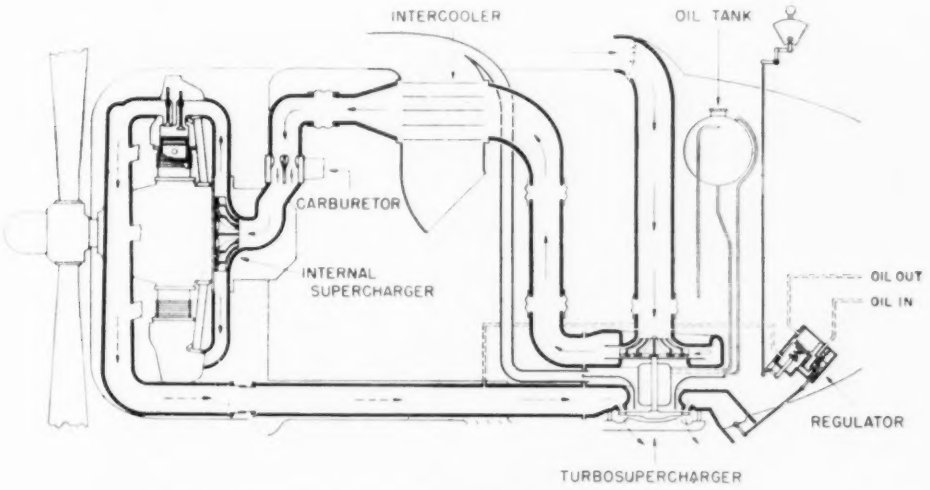


FIG. 8 SCHEMATIC DIAGRAM OF TURBOSUPERCHARGED POWER PLANT

the initial pressure. A supercharger designed to give a full-power manifold pressure of 45 in. Hg at 25,000 ft, where the pressure is 11.1 in. and the density is 0.0343 lb per cu ft, would therefore give a manifold pressure of 121 in. at sea level, and the power required to drive it would be 2.23 times normal. To avoid wrecking the engine immediately, the throttle would have to be closed to drop the manifold air pressure from 121 in. to 45 in. But the supercharger would still extract an unnecessarily large block of power from the engine, and the heat of compression, starting with a relatively high initial air temperature, would tend to cause heavy detonation unless the manifold air pressure and engine power were reduced still further. In order to maintain the maximum net engine power or economy at low altitudes it is therefore necessary to regulate the supercharger speed so that no more than the required pressure is generated at each level. In fact, it is one of the axioms of good flight engineering that the throttle should be kept open as far as practicable under all operating conditions.

Gear-driven superchargers, either single or two-stage, are now frequently provided with a two-speed drive having a mechanical clutch for shifting from low- to high-gear ratio. More recently, fluid couplings have been introduced, particularly in German engines, to provide continuously variable-speed control. An excellent description of the details of these drives is contained in a recent article by F. M. Kincaid of the Wright Aeronautical Corporation (14). All of them are characterized by a relatively high degree of mechanical complexity, especially when fully automatic control is provided to maintain the desired manifold air pressure independently of altitude. The variable-speed feature of the fluid couplings is achieved at the expense of considerable waste power, which must be dissipated in the form of heat in the oil coolers.

The exhaust-gas-driven turbosupercharger represents a very practical solution to the drive problem in terms of mechanical simplicity, flexibility, and power economy. As may be seen from the schematic diagram, Fig. 8, the impeller of the turbosupercharger is direct-connected to a single-stage turbine driven by the engine exhaust gas. The speed is controlled in a very simple manner by allowing excess gas, not required for turbine operation, to escape through the wastegate instead of through the turbine nozzles and wheel. This makes it possible to hold constant manifold pressure, with no throttling and no extraction of engine crankshaft power, from sea level to critical altitude. No more than the minimum required power is drawn from the turbine at any time, so that the excess back pressure which it imposes upon the engine is likewise never more than sufficient to supply the desired manifold air pressure. The significant fact here is that the reduction in engine power caused by this increased back-pressure is usually much less than the crankshaft power required to drive an equivalent geared supercharger (15).

As indicated in Fig. 8, it is common practice to employ an internal-geared supercharger in conjunction with the turbosupercharger, with an intermediate intercooler. With a relatively low pressure ratio, as in the system, Fig. 5, the internal stage has no speed control, since it will not generate excessive manifold pressures with open throttle at sea level if the turbo is cut out.

THE GENERAL ELECTRIC TURBOSUPERCHARGER

Figs. 9 to 12 show various views of the General Electric turbosupercharger of the type used in the Boeing Flying Fortress, Consolidated Liberator bomber, and the Lockheed Lightning and Republic Thunderbolt pursuits. Although military necessity prevents the disclosure of complete technical details, the major features may be indicated as follows:

Referring to the cutaway view, Fig. 9, the engine-exhaust stack connects to the nozzlebox *A*, which is directly above the turbine wheel *B*. The hot exhaust gases expand through the nozzles *C* and impinge upon the turbine buckets *D*. The pressure in the nozzlebox is regulated by means of the waste gage *E*, which vents excess gas to the atmosphere.

The power developed is transmitted through the shaft *F* to the impeller *G* (which is also shown in Fig. 6). The diffuser passages *H* discharge into a scroll-type collector in the outer portion of the compressor casing *J*, which has a radial outlet. The rotor assembly is carried in a ball bearing *K* at the impeller end to take the thrust load, and a roller bearing *L* at the turbine end to allow for expansion of the shaft.

The baffle ring *M* serves to shield the compressor casing from the heat of the nozzlebox, and its inner portion supports the nozzle ring.

The lubricating-oil pump *N* is driven by a worm gear from a worm sleeve keyed to the shaft. The pump is of the gear type, and actually consists of two separate pumps within a single casing. One element supplies oil under pressure to the gears and bearings. The other element is a scavenging pump which removes oil from the lower part of the bearing housing *P* and returns it to the supply tank.

The external appearance of the turbosupercharger is shown

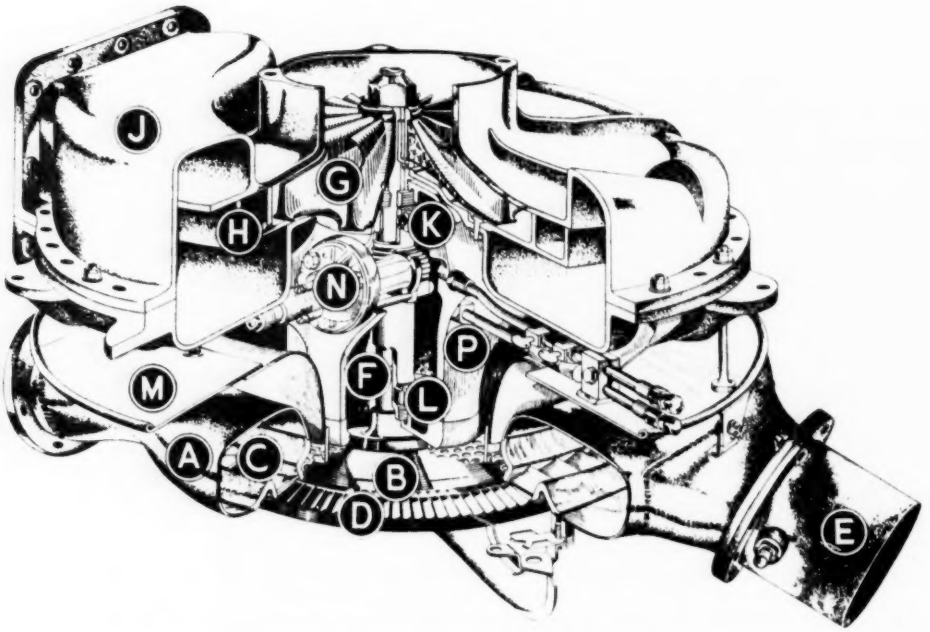


FIG. 9 CUTAWAY VIEW OF TURBOSUPERCHARGER

in Figs. 10, 11, and 12. In Fig. 10, the cooling cap has been removed to expose the turbine wheel.

The impeller is machined out of an aluminum-alloy forging. The compressor casing, diffuser, and bearing are aluminum-alloy castings. Turbine parts are made of alloy steels especially developed to withstand the high stresses, elevated temperatures, and corrosive action of the exhaust gases. Data on various materials of this latter class are given in reference (16).

As indicated in Fig. 8, regulation of the turbine waste gate is effected by means of a hydraulic servomotor containing a pressure-sensitive element connected to the engine exhaust stack ahead of the turbine. By adjusting the boost-control lever, the pilot sets the regulator to hold a constant nozzlebox pressure which will maintain the desired engine-intake-manifold pressure.

THERMODYNAMIC FEATURES OF TURBODRIVE

The development of the gas-turbine drive is described in references (16, 17, 18), and in a companion paper by Dr. Sanford A. Moss (19). The underlying thermodynamic principles are essentially the same as those applying to the conventional single-stage impulse-type steam turbine. The success of the turbosupercharger is based upon the development of an adequate mechanical design to enable the turbine to utilize the energy of the high-

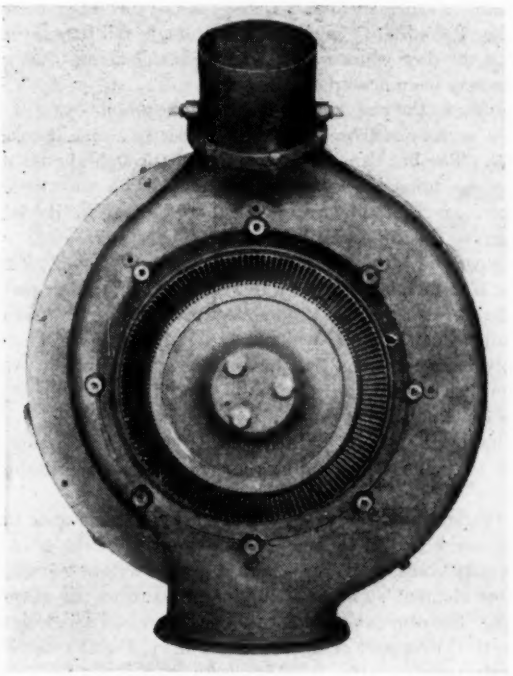


FIG. 10 WHEEL-END VIEW OF TURBOSUPERCHARGER

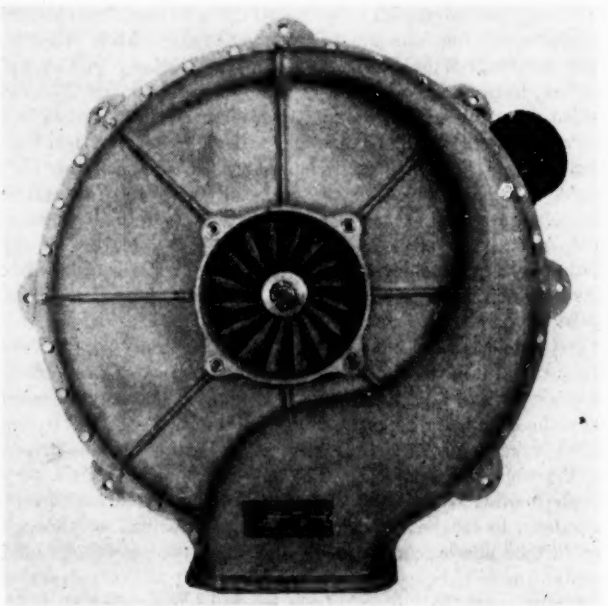


FIG. 11 COMPRESSOR-END VIEW OF TURBOSUPERCHARGER

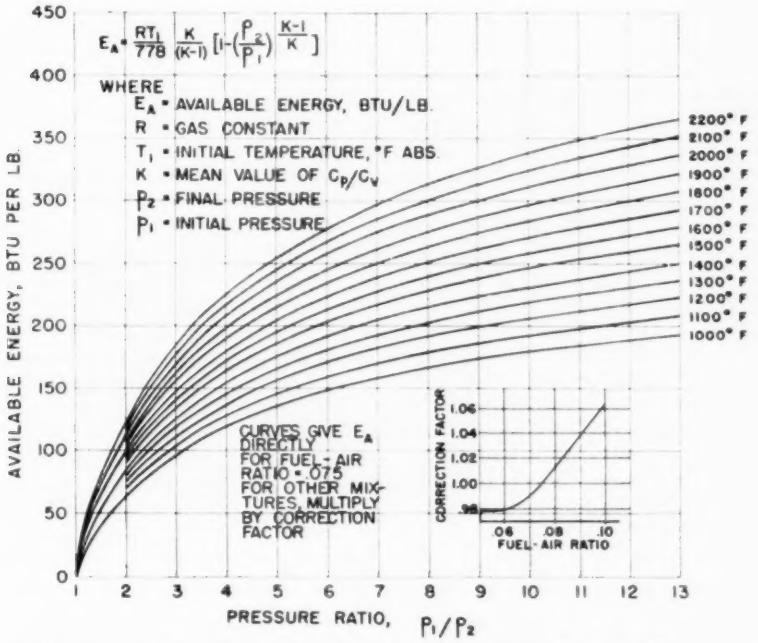


Fig. 13 Available Energy of Hot Exhaust Gas Versus Temperature, Pressure Ratio, and Fuel-Air Ratio
(Figures on curves are ordinary degrees F.)

temperature engine exhaust gases with satisfactory reliability and life and without undue penalties in weight or size.

Fig. 13 gives the available energy, in Btu per pound, of engine-exhaust gas for various temperatures, pressure ratios, and fuel-air ratios. The data are based upon recent information on the specific heat of gases reported by Heck (20), and Ellenwood, Kulik, and Gay (21), and are believed to be considerably more accurate for this purpose than the energy values based upon the properties of ordinary air. (To convert the available energy to hp per lb of gas per min, divide Btu per lb by 42.4.) It should be noted that this is primarily thermal energy, representing the waste heat of the exhaust gases and that the pressure ratio required to release a given amount of power decreases rapidly as the initial gas temperature increases.

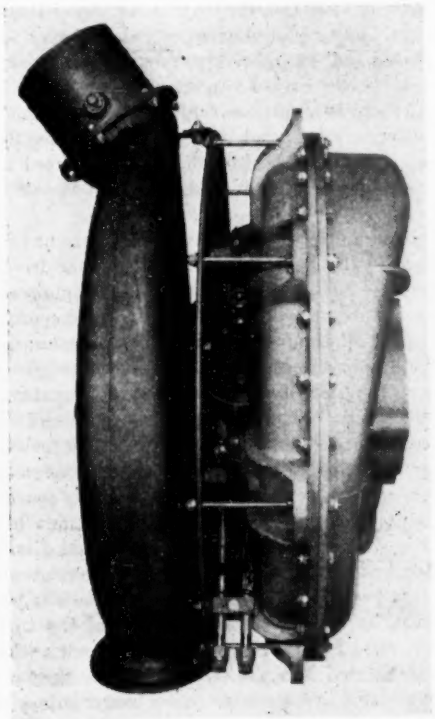


Fig. 12 Side View of Turbosupercharger

Actual exhaust-gas temperatures, in the case of high-powered military engines, vary from about 1200 to 1700 F, the higher figures being associated with higher outputs and leaner fuel-air ratios. Assuming a representative temperature of 1500 F, it is of interest to determine the available energy per pound of gas for a pressure ratio of 2.69, which corresponds to sea-level back pressure (p_1 = 29.92 in.) in the engine-exhaust stack at 25,000 ft (p_2 = 11.1 in.). The conservative "cruising lean" value of 0.075 will be used for the fuel-air ratio, although richer mixtures would be used for full power.

From Fig. 13, for p_1/p_2 = 2.69 and T_1 = 1500 F, the available energy is 122 Btu per lb, or 2.88 hp per lb per min. This figure must be multiplied by the turbine efficiency to obtain the actual shaft output.

The engine requires slightly less than 1 lb of air per lb of exhaust gas. It will be assumed that the turbocompressor delivers this air at sea-level pressure at the carburetor under the conditions of Fig. 5 (p_2 = 31.67) with a compressor efficiency of 70 per cent. From Equation [3] and Fig. 4, the required power input to the compressor will be

$$0.00573 \times 148/0.7 = 1.21 \text{ hp per lb per min}$$

This means that the turbosupercharger can maintain sea-level pressures at both ends of the engine at 25,000 ft so long as the turbine efficiency is greater than 1.21/2.88 = 42 per cent. This is entirely practicable, even after allowing for losses due to gas leakage, etc., and is the basis of most turbosupercharger applications.

As the altitude increases, the compressor must develop a greater pressure ratio, which requires more power. But with constant engine inlet and exhaust pressures, the pressure ratio across the turbine also increases with altitude, so that the power available

continues to balance the power required. The ultimate level above which this balance can no longer be maintained is determined either by the attainment of the maximum allowable "turbo" speed, or else by loss of efficiency at excessively high pressure ratios. Beyond this critical altitude, the carburetor pressure and engine power begin to decline in the normal manner.

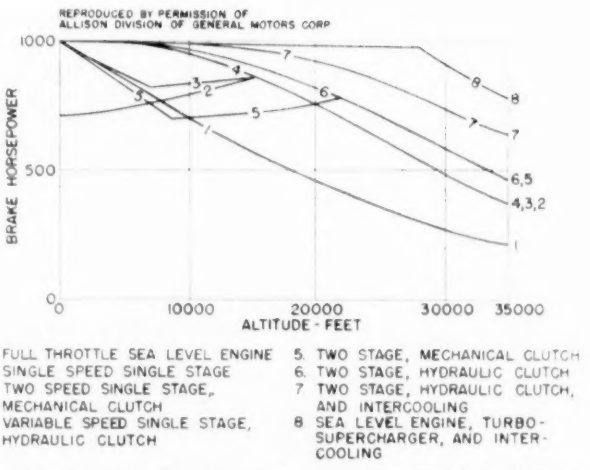
From the energy standpoint, it might be said that the turbo thrives on high exhaust-gas temperatures, as indicated by the curves in Fig. 13. However, at temperatures in the vicinity of 1700 F the cooling problem becomes very serious; to such an extent that it has been thought in many quarters, particularly abroad, that turbine operation at such temperatures was impracticable. The fact is that the ability of the turbine materials to withstand these high temperatures is due largely to the fact that no parts of the machine actually reach the full temperature of the gas. Practically all parts are cooled by intense radiation to the surroundings, and the nozzlebox is cooled about 400 deg below the gas temperature by the additional effect of a stream of "rammed" air. The effective temperature of the gas impinging upon the buckets is reduced several hundred degrees by virtue of the conversion of thermal energy into kinetic energy in the high-velocity jets (see reference 22). It appears, therefore, that present engine-exhaust temperatures are very nearly at the optimum level for turbo operation; if they were much higher the necessary reduction in turbine speed or life would be serious, and if they were much lower the performance would be impaired by the reduction in available power.

The problem of "afterburning" may be mentioned in this connection. Since aircraft engines are always operated with rich fuel-air mixtures at high powers, the exhaust gases contain considerable quantities of carbon monoxide and hydrogen; up to 14 per cent CO and 7 per cent H_2 (23). These highly inflammable gases will burst into flame if they come into contact with air before cooling below their ignition temperature (roughly 1100 to 1200 F). Because of their visibility at night, these flames must be suppressed in the case of bombers, many of which are provided with bulky quenching devices for this purpose. In turbosupercharger installations afterburning can cause local overheating if the gases come in contact with sufficient air, by entrainment or otherwise, before passing completely through and away from the turbine. But with suitable precautions to avoid this, the turbosupercharger has a salutary effect in helping to suppress visible flames by cooling the gas several hundred degrees, due to the conversion of heat into work.

Comparative Performance of Superchargers

The first criterion of supercharger performance is the ability to maintain full engine brake horsepower at all altitudes in the operating range of the airplane. The final measure is, of course, the actual performance of the plane, including rate of climb and maneuverability as well as speed in level flight.

The effect upon engine power can be determined or predicted a great deal more readily and accurately. Fig. 14 gives the results of a very interesting study of the performance of an engine equipped with various types of superchargers, recently published by the Allison Division of General Motors Corporation (24). Curve 1 represents a "sea-level engine" which has a small low-speed internal supercharger provided to produce full power by ground boosting the manifold pressure at sea level with full throttle. With a fixed impeller speed, the engine power is the same as that of the unsupercharged engine shown in Fig. 1. Curve 2 shows the result of speeding up the internal supercharger so as to produce maximum power at a rated critical altitude of 15,000 ft. This engine must be partly throttled at sea level to avoid excessive manifold pressure and detonation. The net output is reduced by the extra compressor power and temperature rise due to the higher impeller speed, as discussed in the section "Types of Drives." As the plane rises, the engine power increases, due to the reduced back pressure plus the favorable effects of the lower inlet-air temperatures, until the throttle is fully open at 15,000 ft.



1. FULL THROTTLE SEA LEVEL ENGINE
2. SINGLE SPEED SINGLE STAGE
3. TWO SPEED SINGLE STAGE, MECHANICAL CLUTCH
4. VARIABLE SPEED SINGLE STAGE, HYDRAULIC CLUTCH
5. TWO STAGE, MECHANICAL CLUTCH
6. TWO STAGE, HYDRAULIC CLUTCH
7. TWO STAGE, HYDRAULIC CLUTCH, AND INTERCOOLING
8. SEA LEVEL ENGINE, TURBO-SUPERCHARGER, AND INTER-COOLING

Fig. 14 Altitude Performance of an Engine With Various Types of Superchargers

The remaining curves are determined by similar considerations of the shaft power required to drive the compressor, and the effects of manifold air temperature upon detonation and charge density. As just mentioned, the outstanding performance of the turbosupercharger (curve 8) is due to its ability to supply exactly the required pressure with no extraction of crankshaft power. The principal adverse effect of the turbosupercharger is to prevent the engine back pressure from following the normal decline of ambient pressure at altitude. Although curve 8 shows a slight loss of power with altitude, it has been demonstrated by flight tests that it is entirely practicable and convenient to hold 100 per cent sea-level power or more all the way up to the critical altitude with a conventional turbosupercharger installation.

On the other hand, the gear-driven supercharger, particularly the simpler single-speed types, are considerably lighter and more compact. If there is no intercooler, the drag will be less. If a turbosupercharger is not used it is possible to convert more of the exhaust energy into thrust by the use of rearwardly directed ejector-type exhaust manifolds (25), although the efficiency of this process is low.

It is extremely difficult to make valid comparisons of the relative performance of a given airplane with a gear-driven supercharger or with a turbosupercharger for the simple reason that, for optimum results, the plane must be designed specifically for the particular installation used. This is especially true in pursuit ships, where the supercharger has a marked effect upon fuselage shape and weight distribution. Moreover, the requirements of a light "hedge-hopping" plane are apt to be quite different from those of a heavy, high-altitude design. The performance of any supercharger, and particularly the turbo, depends so greatly upon the excellence of the installation that it is entirely possible to reverse the results of any such comparison by suitably butchering the job. It is significant, however, that the gear-driven superchargers have had the benefit of much more intensive work on the installation problem, so that some account should be taken of the potential as well as the actual merit of the turbo type. Even the latest and best turbo installations are not as closely and completely integrated into the power plant as they might be. But the fact remains that the turbosupercharger enjoys an initial and basic thermodynamic advantage, as indicated in Fig. 14, which becomes even more marked at higher altitudes. Finally,

it is still more significant that four of the outstanding planes that this country has contributed in the present war, the B-17, B-24, P-38, and P-47 are turboequipped.

Present Status of Turbosupercharger

The question is sometimes asked: Why is it that no foreign country has used the turbosupercharger in military airplanes during the present war? The answer is that, although a considerable amount of experimental work has been carried on abroad as described by von der Nüll (16), the practical difficulties of design and production have discouraged any large-scale application to high-performance Otto-cycle engines. The Germans have succeeded in applying a turbo to their Junkers Jumo 207 Diesel on a small scale, but since the exhaust-gas temperature entering the turbine is about 1000 F, the performance is correspondingly low. The outstanding success of the turbo development in this country has resulted from the sustained effort and continuous experience with the manufacture and application of this type of supercharger since 1917 which has been made possible by the support and cooperation of the United States Army Air Forces. Consequently, at the outbreak of the war this country alone had both the technical "know-how" and the facilities for producing these machines in the necessary quantity and quality. It was in recognition of this achievement that the Collier trophy was awarded jointly to the Army Air Corps and Dr. Sanford A. Moss, of the General Electric Company, by the National Aeronautic Association in 1941.

For several years the turbosupercharger has been in mass production, at a rapidly increasing rate. At the present time it is being produced at the rate of thousands a month in five large plants, two of them especially built for this purpose. The Ford Motor Company and the Allis-Chalmers Manufacturing Company are contributing in a substantial degree to the production of the General Electric design.

Since the start of the war large numbers of turboequipped planes have seen active service in the battle areas all over the world. All have given an excellent account of themselves. The turbo itself has achieved a remarkable record of reliability and outstanding performance under an extreme range of operating conditions. Many favorable reports have also been received in respect to the relative ease with which it has been serviced and maintained in the field. The most enthusiastic tributes, however, have come from pilots and crews who have repeatedly been able to outclimb and outdistance enemy planes whose engines weaken and falter in higher altitudes.

Future Prospects of Supercharging

As in many other branches of aviation, the war has given a tremendous impetus to the development of all forms and applications of supercharging. All known areas of theory and practice are being explored searchingly and extensively and new fields are being opened up under the incentive to improve the performance and extend the capacity of existing machines. Unfortunately, it is obviously impossible to discuss the results that are being accomplished. About all that can be said is that the general direction is up, and that "the sky's the limit." It might be added that superchargers are definitely ahead of engines, planes, and propellers in this direction, at the present time.

With reference to postwar supercharger applications, it is confidently anticipated that turbos will be applied to commercial transport planes, particularly for the longer, high-altitude runs with definite advantage in operating economy. Although there is a lack of adequate flight data to support this point there are a number of sound reasons, some of which have been cited herein, upon which to base the expectation. Von der Nüll (16) mentions some prewar German tests with "modern high-altitude engines," showing specific fuel consumptions of 0.441 lb per hphr with a turbosupercharger, as compared with 0.584 lb per hphr with a gear-driven supercharger, but the details are not given.

The advantages of high-altitude flight (3) which led to the development of the famous Boeing Stratoliners will doubtless encourage the development of pressure-cabin planes for operation in the higher levels of the stratosphere. Very much more adequate cabin-supercharging systems will then be available. Here again the basic economy and flexibility of the turbocompressor can be utilized effectively. Since it delivers pure air at about the desired pressure and temperature, the engine turboinstallation can be used to pressurize and ventilate the cabin by bleeding off a small fraction of the air leaving the intercooler. The internal-type supercharger cannot be so employed because it discharges a mixture of fuel and air.

But whatever the future may bring, it can be stated with assurance that the supercharger in its various forms will be ready and adequate for the demands of new advances in high-altitude flight, for without it such flight as we know it today would have been impossible.

BIBLIOGRAPHY

1 "The Correction of Engine Output to Standard Conditions," by D. S. Hersey, *Journal of the Aeronautical Sciences*, vol. 9, Aug., 1942, pp. 355–377.

2 "Standard Atmosphere—Tables and Data," by W. S. Diehl, N.A.C.A. Report No. 218, U. S. Government Printing Office, Washington, D. C., 1940.

3 "Advantages of Substratosphere Flight" (excerpt from paper on "High Flight Engineering," by Kendall Perkins), *S.A.E. Journal*, (Trans.), vol. 43, 1938, p. 402.

4 "Engineering Computations for Air and Gases," by S. A. Moss and C. W. Smith, Trans. A.S.M.E., vol. 52, 1930, paper APM-52-8, pp. 93–102.

5 "Mechanically Driven Superchargers," by R. S. Buck, *Journal of the Aeronautical Sciences*, vol. 7, June, 1940, pp. 334–339.

6 "The Positive Displacement Supercharger," by J. L. Ryde, *S.A.E. Journal* (Trans.), vol. 50, 1942, pp. 304–313.

7 "Superchargers and Supercharging," by O. W. Schey, S.A.E. Trans., vol. 26, 1931, pp. 581–591.

8 "Energy Transfer Between a Fluid and a Rotor for Pump and Turbine Machinery," by S. A. Moss, C. W. Smith, and W. R. Foote, Trans. A.S.M.E., vol. 64, 1942, pp. 567–597.

9 "Problems Relating to the Control of Flow in Superchargers," by N. C. Price, *S.A.E. Journal* (Trans.), vol. 48, 1941, pp. 118–124.

10 "Gas-Turbine Locomotive With Electrical Transmission," by P. R. Sidler, *Mechanical Engineering*, vol. 65, 1943, pp. 261–266.

11 "The Combustion-Gas Turbine," by J. T. Rettaliata, Trans. A.S.M.E., vol. 63, 1941, pp. 115–123.

12 "Aircraft Engine Design," by Joseph Liston, McGraw-Hill Book Co., Inc., New York, N. Y., 1942.

13 "Mercedes-Benz DB-601A Aircraft Engine," by R. W. Young, *S.A.E. Journal* (Trans.), vol. 49, 1941, pp. 409–431.

14 "Two-Speed Supercharger Drives," by F. M. Kincaid, Jr., *S.A.E. Journal* (Trans.), vol. 50, 1942, pp. 80–96.

15 "Supercharger Installation Problems," by A. L. Berger and Opie Chenoweth, *S.A.E. Journal* (Trans.), vol. 43, 1938, pp. 472–484

16 "Exhaust-Turbine Superchargers: Part I—'Theoretical Considerations,' by A. Meldahl; Part II—'A German Survey,' by Werner von der Nüll; Part III—'American Experience,' by S. A. Moss; Part IV—'Properties of Materials Available,' " by H. Zschokke, *Aircraft Engineering* (British), vol. 14, 1942, pp. 182–195.

17 "Superchargers for Aviation," by S. A. Moss, (Booklet) National Aeronautics Council, Inc., New York, N. Y., 1942.

18 "The Turbo Supercharger," by A. L. Berger and Opie Chenoweth, S.A.E. (Trans.), vol. 26, 1931, pp. 592–607.

19 "Gas Turbines and Turbosuperchargers," by S. A. Moss, paper presented at the Annual Meeting, New York, N. Y., Nov. 29–Dec. 3, 1943, of The American Society of Mechanical Engineers.

20 "The New Specific Heats," by R. C. H. Heck, *Mechanical Engineering*, vol. 62, 1940, pp. 9–12; and vol. 63, 1941, pp. 126–135.

21 "The Specific Heats of Certain Gases Over Wide Ranges of Pressures and Temperatures," by F. O. Ellenwood, N. Kulik, and N. R. Gay, Cornell University Engineering Experiment Station, Bulletin No. 30, Oct., 1942.

22 "Measurement of High Temperatures in High-Velocity Gas Streams," by W. J. King, Trans. A.S.M.E., vol. 65, 1943, pp. 421–431.

23 "Interrelation of Exhaust-Gas Constituents," by H. C. Gerrish and F. Voss, N.A.C.A. Technichal Report 616, 1938, pp. 139–146.

24 "Some Fundamentals of Aircraft Engine Design," pamphlet published by Allison Division of General Motors Corp., 1943.

25 "High-Output Aircraft Engines," by E. W. Hives and F. L. Smith, *S.A.E. Journal* (Trans.), vol. 46, 1940, pp. 106–117.

26 "Aircraft Engines," by A. W. Judge, 2 vols. (vol. 1 discusses superchargers in detail); D. Van Nostrand Co., New York, N. Y., 1940–1941.

27 "The Internal Combustion Engine," by C. F. Taylor and E. S. Taylor; International Textbook Co., Scranton, Pa., 1938.

28 "Altitude Performance of Aircraft Engines Equipped With Gear-Driven Superchargers," by R. F. Gagg and E. V. Farrar, *S.A.E. Journal* (Trans.), vol. 34, 1934, pp. 217–225.

29 "Geared Centrifugal Superchargers for Airplane Engines," by S. A. Moss, *S.A.E. Journal* (Trans.), vol. 27, 1930, pp. 148–153, and 160.

Discussion

KENNETH CAMPBELL.[3] The paper constitutes a technical exposition of the basic principles, characteristics, and functioning of superchargers as applied to aircraft engines. It is clearly and comprehensively expressed, and the authors are to be congratulated on setting forth this condensed explanation of the subject as a whole. It is needed by the thousands of engineers in aeronautics whose assignments are nearly always concerned in some respect at least with the subject of supercharging and its many ramifications.

Without doubt, the authors would be the first to agree that the material of this paper is necessarily largely not new, measured by the very short time standards of aeronautical development, since everything in the field of aeronautics which is new, judged by these standards, is of use to the enemy and must therefore be left unsaid. The writer is privileged to be familiar, however, with the large amount of manpower and expenditure being devoted to physical research in the field of supercharging by the authors' organization, as well as with some of the results being obtained, and the reader can rest assured that the information given in the paper rightly comes from the oldest and one of the most active centers of supercharger development.

The paper is fundamentally sound, and we have little worthy comment to make taking issue with it technically. The authors recognize the existence of some exhaust energy from rearwardly ejected exhaust manifolds. It might be pointed out, however, that the thrust horsepower gain to the airplane from simple, rearwardly pointed exhaust stacks from each cylinder has for some years been calculated by many investigators to equal the mechanical power robbed from the crankshaft by the mechanically driven first stage, even in climbing flight. On the other hand, gain from directing the turboexhaust to the rear is necessarily slight. If these calculations be true, the comparison of curve 8 in Fig. 14 of the paper, representing the turbo performance, with the other performance curves of this figure will be very misleading to the uninitiated.

We enjoy and approve highly the statement made in the paper that the impression is sometimes given that the art of supercharging is not progressing, since very real gains in basic merit are required to stand still with respect to efficiency, while progress is constantly being made in altitude and capacity rating. During the period of supercharger knowledge covered by this paper, superchargers have increased from 500-engine-horsepower capacity to 5 or 6 times that capacity. As the authors indicate, in order to have maintained the efficiencies of the small superchargers in the larger models without further performance research, impeller diameters and other corresponding dimensions should have more than doubled; yet no such maintenance of dynamic similarity has had to take place. The fact that the efficiencies of superchargers of engines of 2000 hp are slightly better, and in some cases substantially better, today than the efficiencies obtained originally with superchargers for engines of 500 hp is the result of very extensive research work which has been going on in various localities in this country in supercharger development, without which the superchargers of large engines today would be failures. This is a point seldom appreciated in the past and one which the authors do well to express so clearly.

J. M. HELDACK.[4] It is extremely fortunate that the military authorities have allowed the presentation of such a timely subject, especially now when the nation's newspapers are full of the successes of our military airplanes, due especially to their superior high-altitude performance.

The authors have mentioned the problem of covering adequately the increased operating range of modern military-aircraft engines. Military operation requires both high-power and cruising-power operation at all altitudes up to and including the critical altitude of the installation. At present, the turbosupercharger is the only means of supercharging which allows this flexibility. It can be reasonably expected that postwar application on long-range transoceanic and transcontinental passenger and cargo airplanes will be predicated on turbosuperchargers designed to operate at their maximum efficiency while covering the cruising-power range of the engine. Such a combination allows the attainment of optimum conditions from the standpoint both of performance and weight saving.

It is not generally realized that the most economical engine revolutions (rpm) do not necessarily result in the most economical cruising speed for the airplane. The airfoil characteristics of the plane must also be considered. Normally, under given conditions of altitude and weight, there is a definite optimum point where increasing power slightly, even though it increases fuel consumption, results in a greater increase in aerodynamic efficiency to the extent that the over-all result is an increase in the ratio of miles per gallon.

Basically it becomes a problem of matching the plane speed, endurance, and economy to result in optimum performance. The flexibility of the turbo, and its resultant beneficial effect on economy, makes it an important factor to be considered in designing the aircraft power plant for postwar commercial airplanes.

AUTHORS' CLOSURE

The authors greatly appreciate Mr. Kenneth Campbell's generous comments, coming as they do from such a well-qualified source.

Mr. Campbell raises a controversial question of long standing as regards the extent to which the extra thrust from individual exhaust jets can be made to compensate for the extra power required from the crankshaft to drive the internal supercharger when a turbo is not used. The issue has remained controversial for so long chiefly because the actual result depends upon the conditions assumed in the comparison. The exhaust jets show up to best advantage in the case of high-speed pursuit planes at moderate altitudes, especially when fuel economy is of secondary importance, whereas the turbo is better adapted to heavy long-range bombers and transports or to any type of plane in the altitude levels above 30,000 ft. Even in the fighter class, the high-altitude performance of the P-38 and P-47 demonstrates

[3] Wright Aeronautical Corporation, Paterson, N. J.

[4] General Electric Company, San Diego, Calif. Jun. A.S.M.E.

the fact that the initial advantage of the turbo in respect to actual brake horsepower, as shown in Fig. 14, can be realized in practice, quite apart from calculations. It is freely conceded, however, that the excellent results lately obtained with two-stage gear-driven installations in pursuits will help to avoid any complacency in the turbo camp.

Mr. Heldack's comments are very pertinent and are especially welcomed in view of his close contact with the practical problems of aircraft design and performance. In reference to his remarks on the most economical engine speed, perhaps the matter might be stated this way: For a given airplane, total weight, and altitude there is an optimum "thrust horsepower," determined by the aerodynamics of the plane, which will give the best ratio of airplane speed to power. For a given thrust horsepower there is an optimum engine speed, determined by the characteristics of the engine and propeller, that will give the minimum fuel consumption. Optimum over-all economy, as measured by miles per gallon, can be obtained only by the proper selection of both power and engine revolutions (rpm).

The point is that the turbosupercharger makes it possible to realize this objective over a wide range of operating conditions, since the compressor speed, and hence the intake-manifold pressure, can be controlled independently of the engine speed without the loss due to throttling.



Test and Predicted Oil-Cooler Performance

By A. L. LONDON[1] and J. I. BREWSTER[2]

Air-side heat-transfer and pressure-drop laboratory test data are presented for a shell-and-tube-type oil cooler, employing steam as the shell-heating medium (1).[3] These data are compared with the information existing in the literature. The chief discrepancy observed is the surprisingly high Reynolds number obtained for transition between laminar and turbulent flow; the dip region being in the Reynolds number range 10,000 to 4000 instead of the usually expected range of 4000 to 2000. The test results, together with available oil-side conductance data, are employed to predict oil-cooling performance of the exchanger as a function of air-flow pressure drop.

Nomenclature

THE following nomenclature is used in the paper:

A_c = tube air-flow cross section for core
c, c_a = unit heat capacity of air stream, Btu/(lb °F)
c_0 = unit heat capacity of oil stream, Btu/(lb °F)
D = tube inside diameter (air side), $D = 4r_H$, ft
e = base of natural logarithms
f = over-all friction factor, including entrance and exit losses (dimensionless)
f' = tube skin-friction factor (dimensionless)
G = tube air-mass velocity, lb/(sec ft²), lb/(hr ft²)
g = 32.2 lb mass/slug mass (proportionality factor in Newton's second law, when employing both pound-force and pound-mass units)
h = unit conductance for thermal convection, air side, Btu/(hr ft² °F)
k = unit thermal conductivity of air, Btu/(hr ft² °F/ft)
K_f = constant relating β_f and β_q (Equation [1]) (dimensionless)
K_c = contraction-loss friction coefficient (dimensionless)
L = effective tube length, air side, ft
Δp = air-pressure drop, lb per sq ft, in. water
r_H = tube hydraulic radius, air side, equals flow cross section/wetted perimeter, $r_H = D/4$ (right circular cylinder), ft
t = temperature, F
t_{a1}, t_{a2} = air temperatures at tube entrance and exit, respectively, F
t_s = saturation temperature of core heating steam, °F
t_{o1}, t_{o2} = oil temperature at core entrance and exit, respectively, °F
T_{a1} = absolute temperature of entering air, $T_{a1} = t_{a1} + 460$, °R
Δt_1 = temperature difference, $(t_s - t_{a1})$, or average oil temperature to entering air, °F
U = over-all unit thermal conductance oil to air, Btu/(hr ft² °F)
V = air velocity, fps
w = oil flow rate, lb per hr
β = dimensionless moduli (see following group)
Δ = denotes pressure or temperature difference
ϵ = heat-transfer effectiveness (see following group)
σ = ratio of air-flow cross section to core cross section (dimensionless)
μ = air viscosity, lb/(hr ft), (centipoises)
ρ = air density, $\rho_0 = 0.075$ lb per cu ft, standard air density

Dimensionless Moduli:

$\beta_q = \frac{h}{Gc}\frac{L}{r_H}$ air-side number of transfer units
$\beta_a = \frac{U}{Gc}\frac{L}{r_H}$ over-all number of transfer units
$\beta_0 = \frac{\epsilon_a G c_a A_c}{w c_0}$ heat-transfer modulus employed in oil-cooling effectiveness expression, Equation [7]
$\beta_f = \frac{f}{2}\frac{L}{r_H}$ friction modulus analogous to β_q
ϵ_a = "air-heating effectiveness," $(1 - e^{-\beta_q})$, $(1 - e^{-\beta_a})$
ϵ_0 = "oil-cooling effectiveness," Equation [7]
f, f' = air-flow friction factors (see preceding group)
$\frac{L}{r_H}$ = modulus expressing air-side tube geometry
$N_{Nu} = hD/k$, Nusselt number, air side
$N_{Pr} = \mu c/k$, Prandtl number, air side
$N_{Re} = DG/\mu$, Reynolds number, air side

Description of Test Apparatus

The physical characteristics of the core tested are given in Table 1.

TABLE 1 PHYSICAL CHARACTERISTICS OF CORE

Tube material	Copper
Number of tubes	637
Tube pitch, in.	0.325
Tube layout, deg	60
Tube diameter, air side, ID, in.	0.256
Tube diameter, shell side, OD, in.	0.268
Effective heat-transfer length, air side, in.	9.0
Effective heat-transfer length, shell side, in.	8.0
Heat-transfer area, air side, sq ft	32.0
Frontal area (8.9 in. diam), sq in.	62.2
Tube-flow area, A_c, sq in.	32.8
Shell-side volume, cu in.	190
Number of shell-side passes along tubes	7
Length/hydraulic radius, air side, L/r_H	140
Tube-flow area/frontal area, σ	0.53
Tube-flow area/duct area	0.52

The core unit was installed in a 9-in-diam test duct connected to the suction side of a centrifugal blower. Air-flow control was provided by a variation of the blower speed afforded by the direct-current-motor drive. Details of the test duct-blower arrangement, together with the air-flow and pressure-drop-measuring instruments, are indicated in Fig. 1.

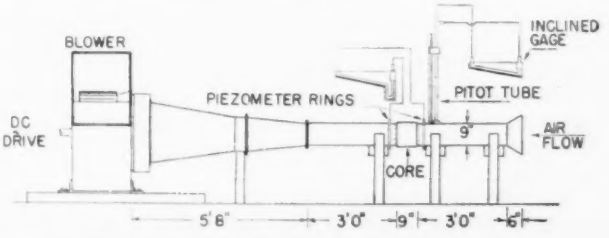


Fig. 1 Test Duct and Core Arrangement

[1] Assistant Professor of Mechanical Engineering, Stanford University, Calif. Jun. A.S.M.E.
[2] C. F. Braun Company, Alhambra, Calif. Jun. A.S.M.E.
[3] Numbers in parentheses refer to the Bibliography at the end of the paper.

Contributed by the Heat Transfer Division and presented at the Semi-Annual Meeting, Los Angeles, Calif., June 14–17, 1943, of The American Society of Mechanical Engineers.

Note: Statements and opinions advanced in papers are to be understood as individual expressions of their authors and not those of the Society.

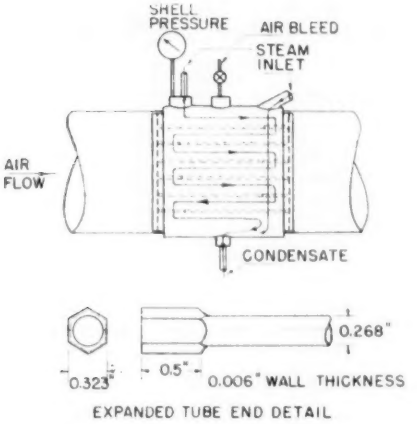


FIG. 2 SHELL-SIDE STEAM FLOW AND EXPANDED-TUBE-END DETAIL

The steam employed as the heating medium in the shell was delivered to a separator at about 30 psig pressure. After liquid separation, the steam was throttled to about 3 psig to provide some superheat at the entrance to the core. The condensate from the core drained to a standpipe and then to an aftercooler where some subcooling was provided to minimize flashing. The condensate was metered gravimetrically.

The energy state of the superheated steam entering the core was established by pressure-temperature measurements and the steam tables. The condensate state was determined by temperature measurement upstream from the standpipe. Steam and condensate temperatures were measured by mercury-in-glass thermometers with the bulbs extending 3 in. in the fluid streams through glands.

Air-state measurements were taken as follows: Air humidity, by wet- and dry-bulb readings in the room; air stream entering the core; by a mercury-in-glass thermometer located 2 ft upstream from the core; air heating, by a calibrated shielded difference thermocouple (copper-constantan). The upstream junction had a stationary location at the previously mentioned mercury-in-glass thermometer. The hot junction was located 8 in. downstream from the core and was arranged to provide an 8-point vertical traverse of the air stream, with the traverse points located at the centers of equal annular areas. The arithmetic average of the temperature readings served to approximate closely the bulk air temperature inasmuch as the velocity distribution was quite uniform.

Air flow was metered by a central location of the pitot tube after an 8-point traverse calibration established the relation between the center-line velocity and the average velocity with respect to flow area, Fig. 3(*a*).

Fig. 2 reveals schematically the 7-pass baffle arrangement and the steam-flow path in the shell. Also shown is a detail of the expanded hexagonal ends of the round tubes.

TEST RESULTS

Typical approach-velocity-head distributions are presented in Fig. 3 together with the calibration for average to center-line velocity. Also shown are typical temperature distributions downstream from the core as measured by the air-heating difference couple. The arithmetic average of the 8-point temperature traverse readings was used to evaluate the bulk air temperature rise.

Table 2 summarizes the cold-core pressure-drop data. In this table the Reynolds number is evaluated employing a viscosity of 0.018 centipoises (air at 80 °F)

TABLE 2 COLD-CORE PRESSURE-DROP DATA

Air density ρ, lb/ft³	Tube-air mass velocity, G lb/(sec ft²)	Δp, in. H_2O	Friction modulus, $(f/2)(L/r_H)$	Tube Reynolds number[a] $N_{Re} = DG/\mu$
0.0740	1.19	0.105	0.90	2060
0.0740	1.54	0.153	0.80	2710
0.0740	2.28	0.290	0.69	4020
0.0740	2.94	0.430	0.62	5090
0.0743	3.52	0.585	0.59	6210
0.0740	3.40	0.550	0.59	6000
0.0745	3.87	0.685	0.57	6830
0.0740	3.72	0.635	0.57	6580
0.0742	4.38	0.89	0.575	7750
0.0741	4.23	0.83	0.575	7480
0.0741	4.98	1.15	0.575	8800
0.0745	5.66	1.465	0.57	10000
0.0740	6.32	1.85	0.575	11200
0.0745	6.38	1.855	0.57	11300
0.0737	7.75	2.75	0.57	13700
0.0735	12.7	7.05	0.54	22400

[a] Based on viscosity $\mu = 0.018$ centipoises (80 F).

$$N_{Re} = \frac{DG}{\mu} \text{(dimensionless)}$$

which reduces to $N_{Re} = 1760G$ for G lb/(sec ft²). The friction-factor modulus is derived from the Fanning equation for the pressure drop

$$\frac{\Delta p}{\rho} = f \frac{L}{r_H} \cdot \frac{V^2}{2g} \text{ ft of air}$$

With G expressed in lb/(sec ft²) and p in in. of water this expression reduces to

$$\beta_f = \frac{f}{2} \cdot \frac{L}{r_H} = 167 \frac{\Delta p}{G^2} \cdot \rho$$

The foregoing calculation assumes negligible air-density change in passage through the tubes, which is a valid idealization providing the pressure drop does not exceed 4 per cent of the total pressure and the air is not heated in the core.

Mechanical-energy dissipation, as expressed by the modulus given, includes entrance-shock loss, skin friction in the tubes, and exit-shock loss.

Heat-transfer and pressure-drop data, obtained with steam heating of the core, are summarized in Table 3. Energy balances for the greater part of the runs are within 5 per cent, attesting to the general accuracy of the temperature and flow measurements.

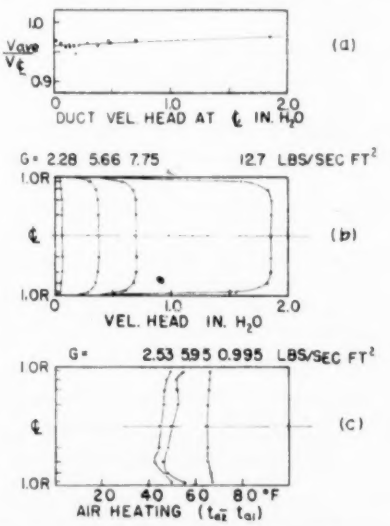


FIG. 3 AIR-TEMPERATURE-TRAVERSE DATA

(*a* Relation between bulk-average and center-line duct velocities upstream from core. *b* Velocity-head distribution upstream from core. *c* Temperature distribution downstream from core.)

TABLE 3 HOT-CORE HEAT-TRANSFER AND PRESSURE-DROP DATA

Air density, ρ, lb per cu ft	0.0725	0.0725	0.0724	0.0720	0.0720	0.0720	0.0730	0.0725	0.0726	0.0720	0.0718
Tube-air mass velocity, G, lb/ft² per sec	0.995	1.57	2.53	4.15	4.48	4.67	5.38	5.95	7.62	10.1	13.5
Pressure drop, Δp, in. H_2O	....	0.220	0.435	0.945	0.98	1.19	1.47	1.78	3.1	5.3	9.5
Entering-air temperature, t_{a1}, F	87	86	85.5	88	89	88	84	86	83.5	91	84.5
Inlet temperature difference, $(t_s - t_{a1})$, F	133	134	134.5	130	131	132	136	134	136.5	129	136.5
Air heating $(t_{a2} - t_{a1})$, F	66.0	55.7	46.5	45.0	45.5	46.8	50.7	51.0	53.0	49.0	50.1
Number of transfer units, $\beta_q = (h/Gc)/(L/r_H)$	0.685	0.537	0.425	0.425	0.426	0.438	0.467	0.481	0.492	0.477	0.457
[a] Unit conductance, h, Btu/(hr ft² F)	4.2	5.3	6.8	11.0	11.9	12.8	15.8	17.9	23.4	30.0	38.4
[b] Reynolds number, $DG/\mu = N_{Re}$	1670	2620	4220	6920	7480	7800	8970	9930	12800	16900	22600
[c] Energy balance per cent difference	....	....	8	7	4.3	....	2.6	2.4	2.9	0.6	0.9

[a] Based on $\frac{L}{r_H} = 140$, $c = 0.242$ Btu/(lb °F)

[b] Viscosity μ for average air temperature $\frac{t_{a1} + t_{a2}}{2} = 110$ F, $\mu = 0.019$ centipoises.

[c] Expresses per cent difference between heat transfer to the air and heat transfer from heating steam, based on steam-energy rate.

The number of heat-transfer units $\beta_q = (h/Gc)(L/r_H)$ were evaluated from the test data employing the relation

$$\epsilon_a = \frac{(t_{a2} - t_{a1})}{(t_s - t_{a1})} = 1 - e^{-\beta_q}$$

The unit conductance h was then determined as

$$h = (\beta_q Gc)/(L/r_H)$$

This procedure is equivalent to employing the log-mean rate equation with a heat-transfer rate evaluated from the air-heating data.

Examination of the air-temperature-traverse data shown in Fig. 3 indicates that the air from the lower half of the core was not heated as much as the air from the upper half. Conductances based on the upper-half temperature data were about 5 per cent ($N_{Re} > 7000$) higher than the average conductances listed in Table 3. This condition suggests the presence of a scale resistance on the shell side. An attempt to clean the core with commercial solvents and acid was not entirely successful. The data reported in Table 3 are for the core after cleaning was attempted. If the conductance, based on the upper-half temperature data are typical for the clean core, the magnitude of the scale resistance included in the h and β_q data of Table 3, amounts to about $^1/_{500}$ (hr ft² deg F)/Btu.

The friction modulus $\beta_f = \frac{f}{2}\frac{L}{r_H}$ (as obtained from the cold-core runs) and the number of heat-transfer units β_q are related by the Reynolds analogy (2). The similarity of these two moduli is revealed in Fig. 4, where β_f and β_q are plotted versus N_{Re}. A consideration of this graph indicates that

$$\beta_f \cong K_f \beta_q \text{ for } 8000 < N_{Re} < 20{,}500 \quad \ldots\ldots [1]$$

where

$$K_f = 1.2$$

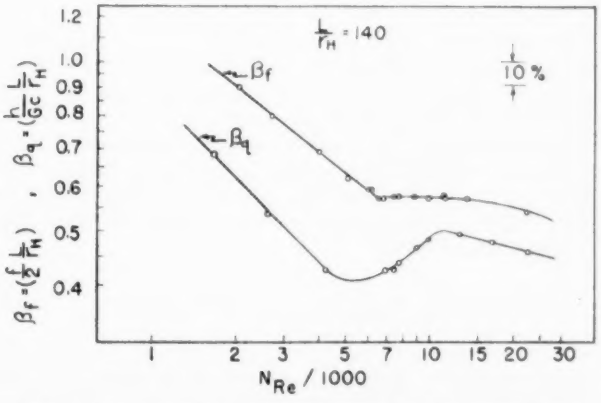


FIG. 4 EXPERIMENTAL HEAT-TRANSFER AND FRICTION DATA

The Reynolds analogy predicts a coefficient of 1 instead of 1.2 This increase can, in part, be attributed to shock at entrance and exit which contributes to the pressure drop, but is not associated with the skin-friction momentum and heat-transfer mechanism. Weise (3) reports a magnitude of 1.1 for the coefficient K_f.

An interesting revelation of these results (Fig. 4) is the definite dip in the characteristics starting at a Reynolds number of 10,000 for the β_q curve and 7000 for the friction-modulus characteristic. Normally, air flow with $N_{Re} > 4000$ is definitely turbulent in character, but for the core and test arrangement reported here fully turbulent flow obtained only for $N_{Re} > 10{,}000$. The reasons for this surprising result are not clear. Tentatively, it may be partially attributed to the following characteristics of the core- and test-duct arrangement:

1 Although the duct Reynolds number is 18 times that of the tubes (180,000 for a tube $N_{Re} = 10{,}000$), turbulence characteristic of this high Reynolds number was not established for the air entering the tubes because of the short approach section of the duct (4 diam), and the fact that the air was induced into the duct through a conical approach section from the relatively quiescent room conditions (Fig. 1).

2 The ends of the core tubes are expanded into hexagonals (Fig. 2) and thus provide a relatively smooth convergence from duct to tube flow. This minimization of shock at entrance may serve to perpetuate the duct-turbulence characteristic which is apparently considerably closer to laminar flow than the duct or even the tube Reynolds number alone would suggest, for the reasons first mentioned.

This rationalization is in part supported by the data of Washington and Marks (4) for flow through rectangular ducts having hydraulic radii of magnitudes comparable to that of the oil-cooler tubes. Their test arrangement provided for flow of compressed air into a relatively large inlet chamber, then through a rounded approach section into the duct of relatively small cross-sectional area. The turbulence of the air in the inlet chamber probably corresponded to quiescent air conditions and the smooth convergence approach section would tend to perpetuate this condition well into the duct. As a consequence the heat-transfer grouping h/Gc for the $^1/_8$-in. duct ($r_H = 0.0625$ in., as compared to the oil-cooler tube $r_H = 0.0640$ in.) departs markedly from the turbulent-flow characteristic in the neighborhood of Reynolds number = 10,000 (Bibliography reference 4, Fig. 8), which confirms the effect noted for the oil-cooler tubes.

This nonturbulent character of the flow at high Reynolds number is of more than academic interest in that turbulence conditions of the cold-air flow into an aircraft heat exchanger may correspond more closely to laminar conditions than to the turbulence characterized by the Reynolds number of the tubes. Therefore, predictions of heat transfer and pressure drop on the basis of turbulent flow may depart significantly from actuality.

For the core tested (ID = 0.256 in.) a $N_{Re} = 10{,}000$ corresponds to a 2 in. of water hot-core pressure drop, but for

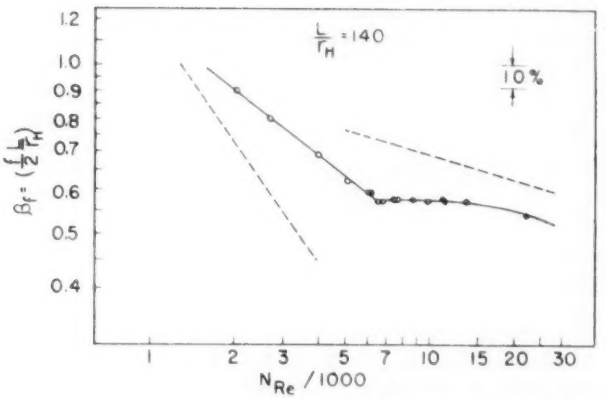


FIG. 5 COMPARISON OF PREDICTED AND EXPERIMENTAL FRICTION DATA

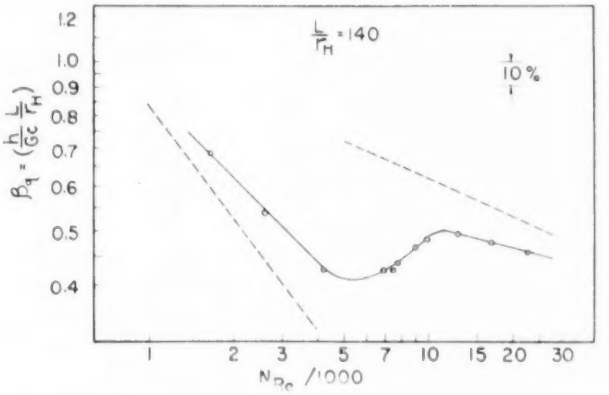


FIG. 6 COMPARISON OF PREDICTED AND EXPERIMENTAL HEAT-TRANSFER DATA

0.20-in-ID tubes of the same length at the same N_{Re} magnitude the pressure drop would be approximately 4 in. of water. Therefore this transition may occur in the design operating range of the oil cooler especially for the smaller tube sizes.

Fig. 5 compares the cold-core friction data with those predicted from available sources. The predicted curve is from the following equation given by McAdams (2)

$$\beta_f = \frac{f}{2}\cdot\frac{L}{r_H} = \frac{1}{2}\left[f'\frac{L}{r_H} + K_c + (1-\sigma)^2\right] \quad [2]$$

The first term in brackets $f'\dfrac{L}{r_H}$ is the contribution of tube skin friction; the second term K_c accounts for the contraction shock at entrance; while the third term $(1-\sigma)^2$ is the contribution of the sudden expansion at exit from the tubes.

For $5000 < N_{Re} < 25{,}000$ (ref. 2)

$$f' = 0.046\, N_{Re}^{-0.2} \quad [3]$$

and for purely viscous flow, $N_{Re} < 3000$

$$f' = 16/N_{Re} \quad [3a]$$

A sudden contraction at entrance would introduce a K_c magnitude of 0.27 for the area ratio $\sigma = 0.53$. However, the contraction is not sudden as the expanded hexagonal tube ends produce a converging section 1/2 in. long (Fig. 2). As a consequence $K_c \cong 0.27/2 \cong 0.135$ was assumed for this calculation.

These considerations introduced into Equation [1] result in the following relations used for the predicted curves in Fig. 5:

$$\beta_f = \frac{1}{2}\left(6.45\, N_{Re}^{-0.2} + 0.356\right) \quad [2a]$$

for

$$5000 < N_{Re} < 25{,}000$$

and

$$\beta_f = \frac{1}{2}\left(\frac{2240}{N_{Re}} + 0.356\right) \quad [2b]$$

for

$$N_{Re} < 3000$$

The exit and entrance losses contribute 20 to 30 per cent of the total friction.

Consideration of Fig. 5 reveals that the available friction-factor data adequately predict (within 15 per cent) the core behavior only for $10{,}000 < N_{Re} < 25{,}000$. For $N_{Re} < 3000$ the prediction based on viscous flow is not satisfactory since the entrance flow is not purely viscous and a parabolic velocity distribution does not obtain.

The comparison of experimental and predicted number of transfer-units data $\beta_q = (h/Gc)(L/r_H)$ is revealed in Fig. 6. The predicted characteristic for $N_{Re} > 5000$ was derived from the Dittus and Boelter correlation (2)

$$\frac{hD}{k} = 0.023\, N_{Re}^{0.8} N_{Pr}^{0.4} \quad [4]$$

which for air $N_{Pr} = 0.74$ reduces to

$$\frac{h}{Gc} = 0.0275\, N_{Re}^{-0.2} \quad [4a]$$

Tests by Brown and Barlow (5) performed on radiators having hexagonal tubes are in substantial agreement with Equation [4a], the magnitude of the conductances being only 4 per cent higher (coefficient of 0.0285 instead of 0.0275 in Equation [4a]).

For the laminar-flow region $N_{Re} < 4000$ the prediction of Norris and Stried (6) was employed

$$\frac{h}{Gc}\cdot\frac{L}{r_H} = 1.615\left(\frac{r_H}{L} N_{Pr} N_{Re}\right)^{-1/3} \quad [5]$$

or for $N_{Pr} = 0.74$

$$\frac{h}{Gc}\cdot\frac{L}{r_H} = 1.97\left(\frac{r_H}{L} N_{Re}\right)^{-1/3} \quad [5a]$$

Examination of Fig. 6 reveals that the predicted characteristic is within 20 per cent of the test performance for $10{,}000 < N_{Re} < 25{,}000$ and for $N_{Re} < 3000$. For the dip region, however ($3000 < N_{Re} < 10{,}000$) the agreement is poor.

Cold-core friction data together with the hot-core conductance data may be employed to predict accurately the hot-core pressure drop by use of the following approximate expression derived from Bernoulli's equation by assuming air density to be a function of temperature only.

$$\Delta p\,\frac{\rho}{\rho_0} = \frac{G^2}{g\rho_0}\left[\beta_f + \frac{\epsilon_a \Delta t_1}{2T_{a1}}(2 + \beta_f)\right] \quad [6]$$

In this expression $\Delta p\,\dfrac{\rho}{\rho_0}$ is the pressure drop (lb per sq ft) corrected to standard air-density conditions ($\rho_0 = 0.0750$ lb per cu

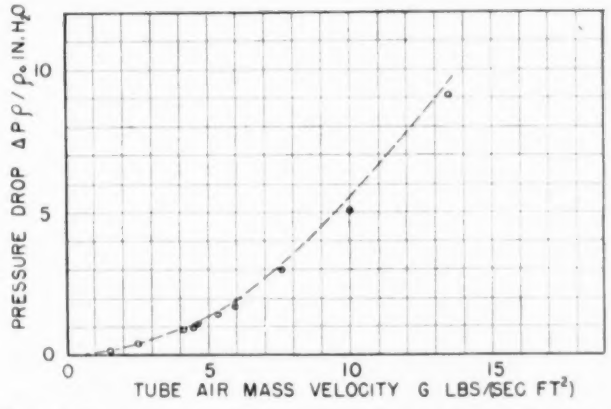


FIG. 7 COMPARISON OF PREDICTED AND EXPERIMENTAL HOT-CORE PRESSURE DROP

ft). To convert to $\Delta p \frac{\rho}{\rho_0}$ in inches of water, divide by 5.20 (lb per sq ft)/(in. H_2O).

Hot-core pressure drop exceeds that of the cold core, for a given mass rate of flow, for the two following reasons:

1 Increased skin friction and exit-shock loss as a result of higher air velocity.

2 A pressure drop necessary to produce the flow acceleration.

In Equation [6] the term $\left(\frac{G^2}{g\rho_0}\right) \beta_f$ is the "cold-core" pressure drop while the term $\left(\frac{G^2}{g\rho_0}\right) \frac{\epsilon_a \Delta t_1}{2T_{a1}} \cdot \beta_f$ is the additional skin friction and exit loss arising from the higher velocity flow. The remaining term $\left(\frac{G^2}{g\rho_0}\right) \epsilon_a \frac{\Delta t_1}{T_{a1}}$ is the pressure-drop requirement for the accelerated flow. The hot-core pressure drop will exceed that of the cold-core drop, by 14 to 18 per cent.

Comparison of predicted and experimental hot-core pressure drop is illustrative of the applicability of Equation [6]. For this calculation, the hot-core temperature difference Δt_1 is the temperature difference, saturated steam to entering air ($t_s - t_{a1}$). Magnitudes of β_f and β_q were obtained from Fig. 4. Term ϵ_a is evaluated as $\epsilon_a = 1 - e^{-\beta_q}$ The curve, Fig. 7, summarizes the results of these calculations and the data points of Table 3, corrected to standard density conditions, are superimposed for comparison. The agreement is within 5 per cent for most of the test points.

OIL-COOLER PERFORMANCE

The basic air-side thermal-conductance and friction data may be employed to predict oil-cooler performance provided oil-side conductance data are available. Oil-cooling performance can be conveniently related to core pressure drop by plotting "oil-cooling effectiveness," ϵ_0 versus core pressure drop, $\Delta p \frac{\rho}{\rho_0}$ for a given oil rate, as in Fig. 8.

In terms of temperature conditions

$$\epsilon_0 = \frac{(t_{01} - t_{02})}{(t_{01} - t_{a1})}$$

That is, ϵ_0 compares the actual oil cooling $(t_{01} - t_{02})$ to the maximum possible cooling $(t_{01} - t_{a1})$, which would obtain were the core cross section very large. "Oil-cooling effectiveness" may also be expressed in terms of the over-all conductance, air-flow rate, and oil-flow rate by integration of the basic heat-transfer-rate relations and energy-balance expressions, assuming constant U along the tube. The resulting equation is

$$\epsilon_0 = 1 - e^{-\beta_0} \quad \ldots\ldots\ldots\ldots\ldots\ldots\ldots\ldots [7]$$

where

$$\beta_0 = \frac{\epsilon_a G c_a A_c}{w c_0}, \quad \epsilon_a = 1 - e^{-\beta_a}, \quad \beta_a = \frac{U}{G c_a} \frac{L}{r_H}$$

Over-all unit resistance $1/U$ may be established from the resistance concept as consisting of the summation of air-side, tube-wall, scale, and oil-film unit resistances. For this illustrative calculation, the tube-wall unit resistance is neglected as being small. An estimated scale resistance of $^1/_{500}$ (hr ft² °F)/Btu is included in the test magnitude of h (Fig. 4). Oil-film resistance for an oil-flow rate of 4000 lb per hr (at an average temperature of 200°F) is estimated as $^1/_{130}$ (hr ft² °F)/Btu (7). Thus, $\frac{1}{U} = \frac{1}{h} + \frac{1}{130}$. From this expression and Fig. 4, U was evaluated as a function of G (for an average $\mu = 0.019$ centipoises). This information together with the assumed oil-capacity rate

$$w c_0 = 4000 \frac{\text{lb}}{\text{hr}} \times 0.49 \frac{\text{Btu}}{\text{lb °F}}$$

substituted into Equation [7] permitted the evaluation of "oil-cooling effectiveness" as a function of air-mass velocity G.

The prediction of pressure drop was accomplished employing Equation [6], together with an assumed inlet-air temperature $T_{a1} = 460 + 60 = 520$ °R, and an average oil temperature of 200° F. Thus $\Delta t_1 = 200 - 60 = 140$ °F. Departures of 20 °F from these assumed temperatures will not materially effect the evaluation of $\Delta p \frac{\rho}{\rho_0}$. Air-friction-factor modulus β_f, for the core was determined as a function of G from Fig. 4 (for an average μ

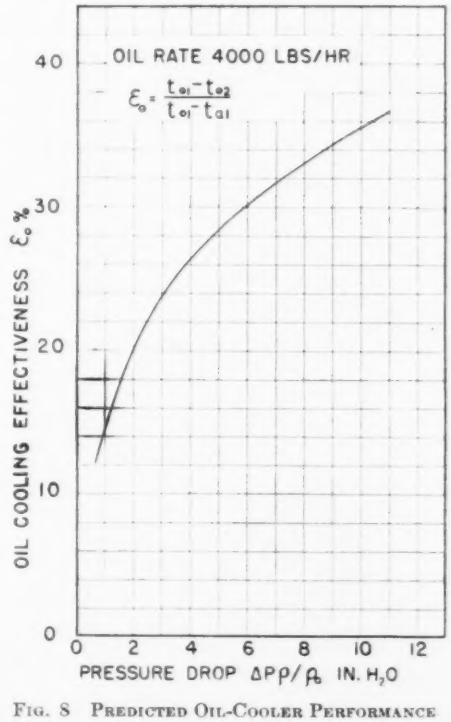


FIG. 8 PREDICTED OIL-COOLER PERFORMANCE

= 0.019 centipoises). The foregoing procedure allows the determination of $\Delta p \frac{\rho}{\rho_0}$ as a function of air-mass velocity G. The results of the prediction calculation for the particular 9-in. core employed in the test work, are revealed in Fig. 8. A family of similar curves could be plotted employing oil rate as a parameter. Such curves, together with oil-side pressure-drop data, would provide a complete expression of the performance of an oil cooler.

Summary and Conclusions

1 Air-side thermal conductance and friction-factor data are presented for a particular 9-in. shell-and-tube-type oil-cooler core.

2 The estimated magnitude of the scale resistance (shell side) which is included in the reported magnitudes of the air-side film conductance amounts to about 1 per cent at $N_{Re} = 1000$ and 8 per cent at $N_{Re} = 25{,}000$. This effect, in part, accounts for the discrepancy between the predicted and experimental conductance data. It also suggests the necessity for allowing for this significant scale resistance in design calculations.

3 An unexpectedly early transition from turbulent to semi-viscous flow is observed as starting at $N_{Re} = 10{,}000$ for both friction and heat transfer. This behavior may possibly be a characteristic of the core-duct test system, but data are lacking to confirm this suggestion.

4 Because of this early transition, predictions from published heat-transfer and friction data are not adequate for $N_{Re} < 10{,}000$.

5 The cold-core friction data may be employed to predict hot-core pressure drop with adequate accuracy.

6 Air-side thermal conductance and friction data, together with oil-side conductance and friction data may be employed to evaluate oil-cooler performance with respect to oil-cooling and pressure-drop requirements.

Acknowledgments

The authors express their appreciation to Prof. R. A. Seban of Stanford University and to Mr. R. H. Norris of the General Electric Company for their criticisms; to the Ethyl Gasoline Corporation for the graduate fellowship under which this work has been accomplished; and to Pratt and Whitney Aircraft for the loan of the oil cooler employed in the test work.

Bibliography

1 "Heat Transfer and Drag Characteristics of a Cowled Radiator System," by J. I. Brewster, Engineer's Thesis, Stanford University, 1941.

2 "Heat Transmission," by W. H. McAdams, McGraw-Hill Book Company, Inc., New York, N. Y., 1942, pp. 119–122, 162, 163, 168–171.

3 "The Conversion of Energy in a Radiator," by A. Weise, Technical Memorandum 869, National Advisory Committee for Aeronautics, 1938.

4 "Heat Transfer and Pressure Drop in Rectangular Air Passages," by L. Washington and W. M. Marks, *Industrial and Engineering Chemistry*, vol. 29, 1937, p. 337.

5 "Heat Dissipation of Ethylene Glycol Radiators and Comparison with Water Radiators," by C. A. Brown and F. C. Barlow, Technical Report of the Aeronautical Research Committee (Great Britain), R. and M. No. 1696, vol. 2, 1935.

6 "Laminar-Flow Heat-Transfer Coefficients for Ducts," by R. H. Norris and D. D. Stried, Trans. A.S.M.E., vol. 62, 1940, p. 525.

7 "Theory of Heat Transfer and Hydraulic Resistance of Oil Radiators," by N. B. Mariamov, Technical Memorandum 1020, National Advisory Committee for Aeronautics, 1942.

Boiler Embrittlement

By C. A. ZAPFFE,[1] BALTIMORE, MARYLAND

In the introductory section of this paper, boiler embrittlement as a field of study is traced back toward the very invention and genesis of steam boilers. The study is traced through the miscellaneous researches of several countries up to the establishment of unified research in three institutions: Britain's National Physical Laboratory in 1917, America's University of Illinois in 1917, and Germany's Vereinigung der Grosskesselbesitzern in 1920.

In the second part of the paper, the chronological study is extended to date, but with emphasis on a critical evaluation of all published work which can be found from America, England, Germany, France, Sweden, Italy, and Russia. The roles of stress, caustic, chemical attack, "aging," and hydrogen are given especial attention along with all other possible factors in boiler embrittlement. These factors are then shown to be identical with those observed in the attack of steel by hydrogen at elevated temperatures, a subject given peculiar neglect in the literature on boiler embrittlement.

In the concluding section, the various factors involved in boiler embrittlement are interpreted from the viewpoint that "boiler embrittlement" is nothing other than an intermediate stage in a naturally occurring hydrogen-purification process. The arguments which have revolved around intercrystalline and transcrystalline paths of the fracture, the behavior of inhibitors and accelerators, the prerequisition of stress and of caustic, and the role played by the steel are discussed to show how logically all observations resolve themselves in the light of this new conception. This interpretation for boiler embrittlement is then corroborated visually by simple experiments made directly upon specimens from boiler plate which exhibited "boiler embrittlement." Plans for future research along entirely new lines are suggested.

SINCE the imperial Russian yacht *Livadia*, built by the British for the Czar in 1879, suffered a mishap with the steam boilers employed in its radical design, the study of embrittlement in boiler plate has commanded international attention. Yet, subsequent decades of investigation have succeeded principally in defining the defect known as "boiler embrittlement," while its nature and underlying cause remain essentially unsolved.

Indeed a glance at even recent literature on boiler embrittlement reveals disagreement on nearly all points. The use of sodium sulphate, for example, was adopted many years ago into the A.S.M.E. Boiler Code (185)[2] as a prerequisite for preventing embrittlement; yet the Symposium on Boiler Embrittlement held by the Society just recently found most of the contributors refuting everything previously claimed for Na_2SO_4 (405, 406, 410). Parr and Straub patented the use of phosphate as an inhibitor of boiler embrittlement (266); but Schroeder and Partridge report a case in which commercial trisodium phosphate apparently caused cracking (319). Similarly, embrittlement from NaOH depends upon the presence of Na_2SiO_3, according to Schroeder and Berk (315), and Straub and Bradbury (320); whereas Desch refutes that claim by embrittling steel with pure NaOH (361); and Rice mentions that Na_2SiO_3 may even inhibit embrittlement (397). Within one publication, Schroeder and Berk prove that nitrates are excellent inhibitors of caustic attack, and then proceed to reproduce the phenomenon of boiler embrittlement, in their opinion, with nitrate attack (398). The steel itself plays no role in boiler embrittlement, according to Parr and Straub (211); yet the entire boilermaking industry in Germany has been based upon metallurgical studies of the steel. Even the descriptions of the defect are at variance, principally in regard to the path which the failure follows, until Perry has ventured to remark that transcrystalline or intercrystalline characteristics can be selected at the will of the operator (311).

Careful study of the mass of literature on the subject appears to reveal the basis for this disagreement. Indeed, half a dozen industries comparable to boilermaking long ago met and solved what undoubtedly is the identical problem, as will be shown.

At this late date, the annual cost of "boiler embrittlement" to the railroads alone is $500,000 according to a recent estimate (375). Besides that value in dollars and cents, one must reckon the loss in steel replacements, disruption of war production, and danger to lives and property—important factors in the present emergency.

1 EARLY HISTORICAL REVIEW OF INVESTIGATIONS LEADING TO STUDY OF BOILER EMBRITTLEMENT

Genesis of Boilers

Hero of Alexandria, in his book "Pneumatica," written about 130 B.C. (1), describes what were probably the world's first steam boilers. One, an "aeolipile," was a primitive steam-reaction turbine; the other was a hollow altar containing air which, when heated by a fire kindled underneath, allowed the expanding air to force water from a vessel below into a suspended bucket, which in turn then descended, opening the doors of a shrine. When the fire was extinguished, the air contracted, the bucket emptied, and the doors closed.

Except for such primitive nonsense, credit for the first commercial employment of steam as a medium of making heat do work belongs to Capt. Thomas Savery in England in 1698. His boiler was simply a hollow oval vessel made of metal (12). Among subsequent names of historic stature stands Newcomen in 1705, and Watt in the latter part of the same century. Of historical interest to many a locomotive engineer is the name "Rocket," which was the first successful steam locomotive, built in 1829.

Usually made of cast iron, early boilers often had flat surfaces and leaden, or even wooden, tops. Hoboken's great engineer, Stevens, who, in 1805, invented the water-tube boiler (12) which is essentially the progenitor of the modern boiler, constructed a boiler with its upper part shaped like a truncated cone and made of wooden staves held together with iron hoops. Copper was sometimes used, especially for parts in contact with the fire. About 1720, a boiler in Cornwall supplying steam for a Newcomen engine was actually constructed of large granite slabs

[1] Assistant Technical Director, Rustless Iron and Steel Corporation. Formerly Research Metallurgist, Battelle Memorial Institute, Columbus, Ohio.

[2] Numbers in parentheses refer to Bibliography at end of paper.

Contributed by the Joint Research Committee on Boiler Feedwater Studies and presented at the Annual Meeting, New York, N. Y., Nov. 30–Dec. 4, 1942, of The American Society of Mechanical Engineers.

Note: Statements and opinions in papers are to be understood as individual expressions of their authors and not those of the Society.

(12). Little wonder that records from those days mention nothing of embrittlement!

Watt's "Wagon Boiler," so named because of its resemblance to the principal covered vehicle of that great era, introduced wrought iron as a structural material for steam boilers.

In 1857, steel was first used by the English Admiralty for the construction of marine boilers, but the results were far from satisfactory (7). To the *Bellerophon* goes the distinction of having the first inboard steel boiler. The commercial marine reported conflicting results, although land boilers made of Bessemer steel gave good service. Steelmakers were challenged to provide a more satisfactory material (3), which resulted in successful steam trials by the *Iris* and, in 1876, adoption of steel for steam boilers by the English Navy.

The use of steel then became generally adopted, although Parker (4), in 1878, stated that only two "of the modern form" were in existence in England at that time. Parker went on to give the first published comparison of advantages of steel over iron as a structural material for boilers, stressing the saving in thickness for any given pressure. In 1881, the same author noted that 1100 steel boilers were then in marine service (6).

Early Investigations of Explosions

In London, in 1815, a disastrous boiler explosion led to the appointment of a Parliamentary Committee, in 1817, to investigate the cause of that explosion and others which occurred about the same time. The recommendation of that learned body was that boilers thereafter should be made of wrought iron instead of cast iron or copper. Thereafter, boilers were periodically inspected by the Manchester Company, the pioneer inspection company of the world, from whom that practice subsequently spread to other countries (10).

Until 1830, boilers worked at about 7 psi, rarely over 10. The principle of high-pressure steam, then in its infancy, soon boosted the pressure to 30 or 40 psi, without bringing a simultaneous redesigning of the boilers. As a result, 288 explosions were reported in England between 1865 and 1870 (10).

In America, a parallel situation developed when the United States Treasury Department, in 1872, requested Thurston, President of this Society in 1881, to prepare a report on the causes and conditions of boiler explosions. Congress magnanimously appropriated $100,000 and the President was authorized to appoint a board to investigate "the singular mystery that has been supposed to surround their causes" (11). Thurston's comment then bridges the 60 years which have elapsed: "They (the Board) at once proceeded to spend money very freely—laid quite large plans; but for causes that need not be mentioned here, the expenditure of money was not as wisely made as it might have been!" His description of the futile efforts made to get various groups to co-operate in tracking down boiler failures casts a complimentary glow upon the contrasting success of the present Joint Research Committee on Boiler Feedwater Studies.

No report of that proposed investigation was ever published, though printing costs could hardly have exceeded the appropriation. Thurston discusses it, however (9, 11), and his hair-raising case histories of a dozen explosions, in which houses were demolished, locomotives turned into scrap, and bodies blown to hilltops a quarter mile away are quite sufficient to impress one that no effort made to solve and prevent boiler failures is unwarranted.

Thurston's conception, incidentally, was that a steam boiler is comparable to an explosive ordnance magazine, and he sought the answer to the explosion in the "expansive power common at the moment to the steam and to the water," which typified the general unawareness in that day of insidious processes within the steel, now called "boiler embrittlement." Most explosions, he concluded, were attributable to three causes; ignorance, carelessness, and utter recklessness.

Recognition of Brittleness in Boiler Steel During Fabrication

The Livadia. Prior to the *Livadia*, mentioned in the introduction, the study of boiler failures was primitive and largely nontechnical, resulting in conclusions to be compared with those of Thurston. Suspicions of the steel went no further than corrosion (6), and those failures wherein overheating, caused by local accumulation of dirt or sludge within the boiler, led to a craterlike eruption through the plastic metal (16).

The *Livadia* was an epochal event in yacht building, as well as in boiler making (5, 6, 8, 38, 59, 101). With a length of 230 ft, a beam of 150 ft, a double bottom, and triple sides forming two cell-layers each 6 ft through, this odd craft was to be fitted with ten boilers 14 ft 3 in. in diam; eight of them double-ended, 16 ft long, and two single-ended, $8\frac{1}{2}$ ft long. The boiler shells comprised three strakes of acid open-hearth $\frac{3}{4}$-in. steel plate with the lap joints treble-riveted, holes punched $\frac{11}{16}$ in. and reamed to $\frac{3}{4}$ in. The steel had passed Lloyd's tests, but one of the plates, after being punched, slipped out of the slings and developed cracks around the rivet holes (6, 101). It was assumed that punching had made the metal brittle, whereupon it was returned for annealing.

After completion of the boilers, they were tested hydrostatically. The first failed longitudinally at the joints of all three strakes. Another cracked before water ever entered it. Upon dismantling, the plates were found to be so brittle that pieces could be knocked off with a hammer.

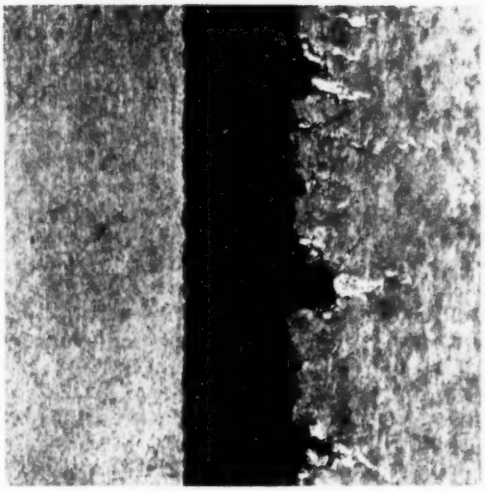
This event, then, turned the eyes of metallurgists toward the study of the steel itself; but only toward the type of brittleness which manifests itself during fabrication. Regardless of the possible relationship between this early trouble and the modern problem of "boiler embrittlement," it is important, for the present, to distinguish the two by pointing out that the cracking which concerns us today develops only after the steel has been exposed to service conditions.

At this date, but little finality can be read into the many explanations advanced then for this fabricational brittleness. On the other hand, our improved position in the science of metallurgy permits two rather significant conclusions to be drawn: (*a*) The steel of half a century ago contained excesses of impurities now known to lead to "aging," or loss of notch-impact toughness after cold-working; (*b*) brittleness from hydrogen was likely.

Because hydrogen is to be discussed in relation to contemporary troubles, the second conclusion warrants some expansion. In his extensive discussion of the *Livadia's* boilers, Parker (6) concludes that (*a*) ordinary chemical analyses of the steel reveal nothing; (*b*) further working to 50 per cent reduction before punching eliminates the trouble; and (*c*) the steel is sound until punched, when cracks develop for some distance around the holes.

When "ordinary chemical analyses reveal nothing," in relation to brittleness in steel, hydrogen is a prime wager even today. The second point argues against a role of "aging," which is *aggravated* by cold-working, and points directly to hydrogen; for hydrogen, and no other element, can be removed in critical quantities by cold-work (384, 387). His last point, although applicable to other types of brittleness, certainly applies to hydrogen brittleness, as demonstrated in Fig. 1. Two specimens of ordinary boiler steel were annealed in a laboratory furnace $\frac{1}{2}$ hr at 950 C (1742 F), one in H_2, and the other in air. When these plates were cold-deformed in a manner analogous to punching, severe cracking developed all along the edge of the hydrogen-treated specimen.

Belief that the *Livadia's* steel was similarly steeped in hydrogen



(*a*) (*b*)

FIG. 1 EDGES OF TWO SPECIMENS OF ORDINARY BOILER STEEL, CUT FROM SAME SHEET, HEATED 1/2 HR AT 950 C, AND COLD-ROLLED TO 50 PER CENT REDUCTION; ×3
(*a*, Annealed in air; *b*, annealed in hydrogen.)

during annealing can be based upon the known effect of a hydrogen anneal in removing nonmetallic impurities from the steel. Parker reports P and S diminished by one half near the surface; and C, which is most readily removed, was reduced to a trace. As Siemens, a famous metallurgist of that day, remarked in the discussion, such a condition cannot possibly be traced back to segregation in the ingot, but must have resulted from some subsequent treatment. One need not assume the annealing treatment was quite as severe as that in the experiment just cited; for, as Barnaby points out in the discussion, the failure was only one out of 1100 cases, a second set of plates causing no trouble at all. Treatment that severe would have caused 1100 failures out of 1100. Parker's remark that "absorption of gases in the annealing furnace" may have caused the embrittlement suggests that even they regarded hydrogen embrittlement as a serious prospect, although the defect was unknown then. He "intended to pursue the question of the possible absorption of gases" as "a fruitful source of inquiry;" and his observation that the embrittlement reduced the ductility without affecting the tensile strength is typical of hydrogen.

Incidentally, these "preservice failures," typified in Fig 1, are transcrystalline, i.e., through the grain, which distinguishes them again from the "service failures," or "boiler embrittlement," which are predominantly intercrystalline.

RECOGNITION OF BRITTLENESS IN BOILER STEEL DURING SERVICE: "BOILER EMBRITTLEMENT"

In England. This transitional study of brittleness lasted for some years (37, 38, 39, 101), the discussion settling around brittleness observed during hydraulic-testing. Inconclusive comparisons of acid and basic open-hearth steels were made (38, 39). Annealing came under close scrutiny, because the opening of a crack indicated a role of internal stress (38). Steels which passed all tests of the British Board of Trade Surveyor and the Surveyor to Lloyd's Register would fail unexpectedly. Again, it is interesting to note that the fracture types discussed by Milton (38), and Arnold (37) are typical of those caused by hydrogen (404, 423).

According to Houghton (84), Milton wrote the first paper (38) on "boiler embrittlement" in 1905, wherein he noted that flanged steel plates in boiler service may crack, but that tensile and bend tests of the adjacent metal are entirely satisfactory. This fact stands as basic today (233, 398). The recognition of the fact that cracking might develop in service, rather than failure through the obvious means of corrosion or overheating, was the turning point in this field.

A growing pain of historic consequence in that regard was the famous case of the Dutch steamship, *Pahud*, an unclassed coasting vessel employed around Java, whose boiler exploded so violently that the boat sank (101). The boiler had been made in 1908, by a Dutch firm using basic open-hearth plates from a large German steelworks. German law required all plates to be annealed but, in this case, the plates were so large that the furnace equipment was not well suited. The boiler was of the triple-riveted, double-butt-strap type, and the rupture occurred along a row of rivets on a longitudinal joint. Butt straps were then removed from several similar boilers on other ships, and cracks between the rivets were found.

Wolff (97) blamed the failure upon fatigue, reporting an elaborate series of tests on the elastic movements of plates. He felt that short coastal service, i.e., "boiler-working," was responsible in developing intermittent and unequal expansions in the boiler shell, and cited the case of a Clyde-built vessel employed on the Yangtze. At the sudden approach of a typhoon, steam was raised rapidly; the shell plate split longitudinally, but was patched and thereafter served for 40 years.

Wolff also stated that the worst failures were from basic open-hearth steel, although acid steel fails, too. The fact that only in a few isolated cases did boilers fail, he felt, pointed to the steel as the source of the trouble. Houghton (101), however, thought the answer lay in the work of Ridsdale (24, 27), who had demonstrated that steel worked at blue heat develops cracks between the crystals near the surface. Service (108) remarked on the evident harmfulness of shearing; Bryden (100) blamed rolling, finishing at too low a temperature, and pointed out that the failures discussed by Houghton all occurred at the edges of the plates; Marquand (102) blamed overheating, or finishing at too high a temperature, as evidenced by the large grain size at the failure; McCance (103) showed that steel plate hardens to one half its thickness, during shearing whether sheared cold or at blue heat; Houghton (101) and Marquand (102) both hint at the bogy of "oxidized steel;" and Ridsdale (106) blames the weather, remarking that a cold floor on Monday morning, or snow and rain, if the plate is cooled outdoors, may lead to local brittleness. Houghton (101) quotes Colville as opining that the *Pahud's* boilers had been made from a "wild charge of steel dosed with silicon," which may be said to complete this shotgun pattern of logic.

Finally, Stead (109), who agreed with Wolff in his opinion on fatigue, obtained a "good" and a "bad" piece of steel, each passing specifications; but the "bad" steel, as a specimen 1 in. wide, would crack during one bend, whereas the "good" steel required numerous bends for breaking. The method of bending as a test for boiler plate was thereafter generally adopted.

In Germany. In Germany, these events were more or less paralleled, although the importance of annealing was recognized long before it was adopted elsewhere. Meunier, in his Report of the Chief Engineer to the Elsässischen Vereines von Dampfkesselbesitzern (28) for 1902, discussed the explosion of a boiler built in 1869, and proposed that the ductility loss occurs during service, in opposition to the general picture of that time. Meunier, therefore, antedates Milton in recognizing "boiler embrittlement." All boilers having 35 years of service should be replaced, in his opinion (35). Principally as a result of his work, the Reichs Chancellor issued a decree, known as the Würzburg and Hamburg Code (40) of 1905, which standardized boiler inspection both during fabrication and during service (41, 44).

Bach (33, 41, 42, 48, 49, 60, 65, 70) and Baumann (50, 70, 77, 157) were the authorities in Germany on boiler failures. It is an amusing commentary on the elusive nature of "boiler embrittlement" to find Baumann writing a monumental article 35 years ago on "The Present Status of the Question of Cracking in Boiler Plate" (50), in which he presumes to have the answer to boiler embrittlement. The same title was used almost verbatim only 3 years ago in Germany, and in substance composed recent papers in England (396) and America (297), as well as the present one, each one still claiming an answer.

From the start, German investigators suspected the steel. Sulzer (54) attempted to relate cracking to thermal strain by various physical tests. Bach (48) used specimens from a fractured boiler dome and tested them at various temperatures, emphasizing the necessity for designing boilers on the basis of the properties of the steel at the operating temperature (33). Bach (60, 70), Bauer (99), and Baumann (77) then showed that incipient cracks developed during riveting when too severe pressures were used, a line followed by recent investigators in this country (311). Boiler explosions (71) in Germany, in 1912, were blamed on improper heat-treatment of the steel (67, 167), and hot-working at too low temperatures (73). Bauer (99) and Baumann (77) also investigated segregations and inclusions as causes of cracking. Starck (184) blamed the brittle nature of ferrite crystals. Finally, the problem still unsolved, a disastrous boiler explosion in 1920, in Germany (283, 361), provoked the formation of the Vereinigung der Grosskesselbesitzern.

In America. Corresponding concerted study of boiler embrittlement began in England at the National Physical Laboratory (251, 265, 296, 361), in 1917, the first results of which were published by Rosenhain and Hanson (128), in 1920. In America, Parr pioneered present studies with a publication (94), also in 1917, which covered his work begun in 1912, as a result of boiler failures occurring around Urbana, Ill. (220, 233), and concluded with a research by Merica (92) on caustic embrittlement. Boilers had been installed in a building at the University of Illinois in 1874. Surface water was used until 1888, when a 160-ft well was dug. In 1898, operating pressures were increased and embrittlement began shortly, although the first official record occurred in 1910. First attempts, in 1912, to neutralize the alkalinity ended in 1915 with Parr's suggesting that sulphuric acid be added to the feedwater. Today, the work at the University of Illinois Engineering Experiment Station (92, 94, 181, 197, 200, 211, 223–226, 232–234, 243, 244, 254, 266, 320, 352, 353, 369, 416), at the United States Bureau of Mines (297, 300, 315–319, 331, 348–351, 380, 381, 398, 399, 411–413), and that of the Joint Research Committee on Boiler Feedwater Studies, represents America's principal contribution to the international problem of boiler embrittlement.

Everything prior to the authoritative investigations of these great international organizations for the study of boiler embrittlement, just named, may be considered as having historical interest only, although it serves well to orient the student of this subject. The following discussion, while also chronological and stepwise, will subordinate historical features to a critical examination of the manifold, and often divergent, data provided principally by those international organizations over the past 25 years.

2 CRITICAL STUDY OF PUBLISHED DATA ON BOILER EMBRITTLEMENT

Caustic Embrittlement

Today, the defect known as "boiler embrittlement," the subject of this paper, is still often called "caustic embrittlement" (326, 256, 259, 371, 378, 390), and perhaps correctly. In any event, the roots of present research certainly extend from the observation that caustic solutions develop a brittleness in steel which is characteristic of the defect which is now being considered.

Thomson (19), in 1894, and Stromeyer (59), in 1909, appear to be the first to discuss that action of caustic when they cited cases of boilers containing caustic in which embrittlement had proceeded to a degree where the rivet heads flew off. Stromeyer's explanation was that, in the presence of caustic, water reacts with the iron and forms iron oxide and hydrogen, "which leads to hydrogen embrittlement." In 1914, Andrew (81) enlarged upon the argument; but 1917 stands as the epochal year.

In that year, Desch, discussing Wolff's paper (97), described the embrittlement of caustic tanks and ventured the explanation that hydrogen entered the grain boundaries and "gradually opened up the metal until the crystals were distinct." To Desch, one of Britain's ablest scientists, therefore, goes the credit for anticipating by a quarter of a century the recent results of the National Physical Laboratory (396). Stromeyer (95, 96), in a classic experiment, proved that caustic embrittles steel only when stressed in tension. Two concentric, tapered rings were forced together, placing one under tension, the other under compression. Regardless of previous working or annealing, the compressed ring would not embrittle in caustic, whereas the ring in tension did. Stromeyer assumed that sodium carbonate in the boiler water breaks down to form NaOH under operating conditions of temperature and pressure, and that the NaOH caused the embrittlement (59, 95, 96, 150, 171). Furthermore, he noticed a "penetrating influence" of the caustic, which seemed to operate upon metal removed from the solution by $^1/_4$ in. of steel.

In the same year, Merica (92) and Parr (94) initiated the series of publications from the University of Illinois. Parr pointed out that normal feedwater has no NaOH and far too little carbonate to act on boiler plate, but that concentration is likely. Furthermore, depending upon temperature and the removal of CO_2, hydrolysis of the carbonate yields NaOH. Tests with steel, immersed in 13.6-normal NaOH at temperatures up to 280 C, clearly established the role of caustic in developing the hydrogen necessary for the hydrogen theory, whereupon Parr concluded, "the evidence seems to show that the embrittling effect of NaOH on steel is due to the evolution of hydrogen, and the absorption by the steel of the hydrogen in the nascent state." This statement, though similar to Desch's, missed similar fruitfulness for reasons soon to be disclosed. On the basis of the hydrogen theory, he suggested adding an oxidizing agent, such as $Na_2Cr_4O_7$, to depolarize the iron electrode. Sulphates, he added, might also be useful, at least as diluents. These ideas remain more or less secure today.

Certain basic facts regarding boiler embrittlement, recorded by these same investigators, are worthy of mention, namely, that embrittlement (*a*) always occurs below the water line; (*b*) is associated with waters having high alkalinity; (*c*) usually occurs in conjunction with a leak or seam where concentration of the soluble material to its saturation point is promoted; and (*d*) is accompanied by an exterior accumulation of a strongly alkaline incrustation.

In attempting to elucidate the role of hydrogen in causing boiler embrittlement, which is a phenomenon characterized by grain-boundary reactions at elevated temperatures, Parr and Merica drew an unfortunate comparison with the hydrogen-caused phenomenon of "pickling brittleness," widely discussed since the time of Ledebur (14, 15), and relating only to short-time tests and temperatures usually well below the boiling point of water. Discussion of that error will be reserved until its importance is established in succeeding paragraphs.

The Role of Stress

In the Intercrystalline Failure of Metals. As an alternative to the hydrogen theory, Parr (94) and Merica (92) had also suggested that the caustic ate out the "amorphous intercrystalline cement," a primitive metallurgical conception of grain-boundary material which is probably less stable than the body of the crystal. Andrew (81) had previously suggested such a thing, and Schroeder and Berk (398) base their entire argument upon essentially the same conception. Let us examine the broad aspects of intercrystalline failure from direct chemical attack to detect relevancy to boiler embrittlement, if any.

Since Roberts-Austen (13), in 1886, touched an Au-Cu-Ag alloy with $FeCl_3$ solution and found it breaking within a few seconds along several inches of the metal, many similar observations have been reported which may strongly influence one toward such an explanation for boiler embrittlement. Amagat (17), in 1893, forced mercury through 3 in. of cast steel at 3000 atm pressure, with indications of a selective and highly penetrative amalgamation. No previous flaw could be detected in the steel with a microscope. Cailletet, Colardeau, and Riviere (25) observed the same phenomenon at higher temperatures proceeding under relatively low pressures. Bridgman (66) finally discovered the role of stress, demonstrating that pressures exceeding the elastic limit would force mercury through the strongest steel.

Similarly, Desch found beta brass containing Al to granulate within a few seconds when placed in a solution containing a salt of mercury (82, 133); although cast Zn, Sn, and Pb corroded gradually without granulation (112). Copper cathodes in molten NaOH developed intercrystalline brittleness (127). Rawdon reports that mercury solutions for testing crack sensitivity of manganese bronze were adopted into the New York Board of Water Supply Specifications in 1915, and that the Aircraft Board adopted an immersion test of 15 min in mercurous-nitrate solution (105). Phosphor-bronze bars, immersed in mercurous-nitrate solution, cracked in 3 min, according to Arnott (131). LeChatelier complains of the disintegration of military canteens in the first world war (116). Made of an aluminum alloy, containing 3 per cent copper, the canteens disintegrated in service, showing oxidation around the grain boundaries. Again, copper develops intercrystalline brittleness when heated in Zn vapor (151); and Desch and White showed that electrolytic corrosion of beta brass is so pronounced at the grain boundaries that the zinc is removed, leaving an enrichment of copper, which may oxidize (79). Similarly, nickel steel has been reported to oxidize granularly, leaving an enrichment of nickel in the grain boundary (89).

Nitrate solutions are particularly effective, lead disintegrating into crystals when placed in dilute HNO_3 (119), or when used as an anode in nitric acid (86). Lead acetate has a similar effect on lead (129), although a single crystal is relatively immune. Porter reports $NaNO_3$ causing cracks within a few hours running the entire diameter of a 100-ft NaCl evaporating pan (146), an observation also made by Malcolm for smaller pans (141). Smialowski (288) and Andrews (335) have demonstrated the intercrystalline attack of steel by ammonium nitrate, Andrews proposing that grain-boundary carbide is the cause of the attack. The work on boiler embrittlement at the Bureau of Mines leans heavily upon this action of nitrates (398).

Among the first to discover the critical role of stress in these failures was Rogers, who claimed to have developed, in 1905, a mercuric-salt method for revealing internal stress in brasses (118). Smith (121) thought that Roberts-Austen's experiment with the gold alloy (13) confirmed the presence of a highly stressed surface film which led to fracture when fissured. Jones (140), in a paper much quoted in work from the Bureau of Mines, stated that service failures of steel from caustic clearly required stress. He proceeded to develop intercrystalline cracking in steel at temperatures up to 250 C, using $Ca(NO_3)_2$, NH_4NO_3, $NaNO_3$, $NaNO_3$ plus 5 and 10 per cent $NaHCO_3$, and KOH solutions, although neither $NaHCO_3$ alone, $(NH_3)_2SO_4$, $CaCl_2$, fused $NaNO_3$ + KNO_3 mixture, nor air would cause cracking. Around rivet holes, $Ca(NO_3)_2$ produced cracks in 28 days. In spite of the fact that some students of boiler embrittlement have attached great importance to this nitrate cracking, Jones admitted that the action of the KOH, which was the only nitrate-free solution with which he produced cracking, was unique; and he actually concluded that the caustic produces hydrogen which selectively weakens the grain boundaries. The nitrate, he thought, might supply an analogous agent, possibly nitrogen. Subsequent investigators, who have referred to Jones's work, never mention his own evaluation of his results, but emphasize the nitrate cracking, which is irrelevant to boiler embrittlement, as will soon appear.

In further proof of the importance of stress, Jonson found that brass immersed in ammonia and stressed in tension was unaffected until the elastic limit was reached, whereupon the metal fractured (85). Dickenson showed that molten tin and solder penetrate the grain boundaries of stressed brass (123); Merica found a difference in potential to exist between stressed and unstressed wires (87); Austin obtained intercrystalline embrittlement by stressing various metals in tension in solder (302); van Ewijk demonstrated the penetration of high-strength alloy steels by solders at 400 C (301), similar to Schuster's experiments with liquid brass on steel (269); Hodge and Miller showed intracrystalline penetration of austenitic "stainless" steel by the chlorides of iron and mercury (373). However, the most thorough research on the penetration of stressed steel by molten metals and alloys was reported by Schottky, Schichtel, and Stolle (242), who concluded that intercrystalline failure will result only if the stress is above some minimum, and only for those systems exhibiting solubility.

In "season cracking" of brass is found the widest discussion of intergranular cracking. "Season cracking" is one of those hapless terms which have no technical significance and simply pinch-hit until the phenomenon to which they refer is understood. In this case, the term comes from the resemblance of the defect to the cracks developing in timber upon seasoning.

With copper-zinc alloys, the defect is thought to be limited to metal having less than 80 per cent copper (98). Strain is essential, which lends a serious aspect to the problem because brass is principally valuable in the hard worked condition. Diegel, in 1906, appears to have been the first to discuss season cracking (43). Merica and Woodward reviewed the literature (93), up to 1917. Masterful papers on the subject include those of Hatfield and Thirkell (115), and Moore, Beckinsale, and Mallinson (144), both written more than 20 years ago. Both show the role of stress, the latter demonstrating the intercrystalline cracking produced by salts of Hg and NH_3 in brasses sufficiently stressed. Pure copper was not cracked by those salts, and only those brasses cracked in which Zn was greater than 6 per cent. Bassett (98), writing in an era not yet adapted to the automobile, cites instances of spun- or drawn-brass lamps on carriages breaking during winter storage in stables. Condensation of moisture during temperature changes plus absorption of ammonia from the stable atmosphere was indicated.

On the role of stress in causing cracking, Heyn's 1914 lecture before the Institute of Metals remains a classic (83). Heyn was the first to set forth clearly the underlying principles and to measure the stress. Incidentally, his method of measuring stress by cutting concentric rings from the specimen, although independently conceived, had been used 20 years previously by Howard at the Watertown Arsenal (18).

These examples have been cited because today there are those who attach great, but ambiguous, importance to the similarities with boiler embrittlement, probably following a suggestion made in 1919 by Rosenhain and Archbutt that boiler embrittlement was nothing other than the defect known as season cracking in brass, and as granular disintegration in lead (120). Such an opinion simply reverses the adage about the trees obscuring the forest, for the phenomenon of intercrystalline embrittlement in metal springs from a multitude of causes, none of the foregoing having any real resemblance to boiler embrittlement except that under the microscope the failure is intercrystalline in both cases. If comparison is valuable, and it certainly can be when correctly made, why not compare boiler embrittlement with the mass of untouched information on intercrystalline embrittlement and granular deterioration from hydrogen? Since the active presence of hydrogen in boiler embrittlement has been so amply proved, why not select for comparison the intergranular failure occurring in chambers for ammonia synthesis, hydrogenation autoclaves, in decarburizing steels with hydrogen, in general purification treatments using hydrogen, in the well-known "hydrogen sickness" of copper and its alloys; rather than with aqueous solutions containing chemicals having but little relationship to boiler feedwater? Why do investigators of boiler embrittlement continue to cite cases of intercrystalline-cracking from nitrates (398) when the NO_3^- ion is deliberately added because it is a good "inhibitor" of boiler embrittlement (319, 405)?

In "Boiler Embrittlement." Similarly, stress has been found to be essential to the intercrystalline-cracking known as boiler embrittlement (226), even to the extreme of Hatfield's suggestion (193) that the question of boiler-cracking was settled in 1898 when Stead showed fissures in the steel caused by machining and working (21, 22). Bauer early noticed that boiler-cracking was always preceded by cold-working, a condition difficult to avoid in processing boilers (90). Heyn and Bauer made an elaborate study of the stresses in boiler plate (68) and decided that tensile tests were poor indicators of suitability for boiler service (74). Impact tests were advised. A great deal of work in Germany followed that general line of thought as a result of Fry's development of an etching technique which brought out the strain lines in steel (149, 169, 179, 180, 183, 187, 196, 219). Hanson (136) and Rosenhain (148) noted that the outer plate and rivets of a 4-strake boiler embrittled worse than the inner plate and suggested that stress was consequently a more likely cause of boiler embrittlement than chemical attack. Sufficient reason for cracking could be found in internal stresses and cold-working, according to Whiteley (110, 204), Bolsover (216), Strauss and Fry (149), and Ness and MacCallum (210), although Houghton demurred (138). That corrosion only started at loci already initiated by excessive strain during cold-working was Fletcher's viewpoint (134). As a matter of fact, the argument at the 1921 session of the Faraday Society centered around the relative importance of stress and chemical attack in causing embrittlement, as did the 1925 meeting of the Vereinigung der Grosskesselbessitzern in Germany (183). McAdam concluded that boiler embrittlement was simply a pitting form of stress corrosion wherein hydrogen played no part and NaOH was unnecessary (240). Such a conclusion, of course, is ill-advised, for no traces of pitting are ever found (240, 319), NaOH is essential (181, 211, 233), and the defect depends upon hydrogen, as will be shown.

At the National Physical Laboratory, Rosenhain and Murphy (241) and Jenkins (280, 293) performed experiments in which specimens were stressed in various ways in various solutions at various temperatures, but no intercrystalline failure could be produced even in tests lasting 5 years. Tests in air at 300 C for 5 years also failed to reproduce boiler embrittlement (199), whereupon the safe assumption could then be made that stress alone is not the cause of that defect. Since that temperature lies in the range of "blue brittleness," the tests also eliminated the analogy originally proposed by Ridsdale (20).

To accentuate the specific nature of "boiler embrittlement," White and Schneidewind (245) outlined and illustrated the various types of cracking which follow from stress alone, stress in conjunction with corrosion, and from caustic attack. Of course, it must be recognized that all boiler failures are not caused by caustic embrittlement (23, 175, 261, 299). Surface cracks may even carry over from hot-working (239); and true corrosion and fatigue cracks are quite possible under boiler-operating conditions (181, 195, 220, 240, 312, 313). Nevertheless, the defect known as "boiler embrittlement" (135, 186, 213, 218, 255, 367, 368, 383, 397) is a specific phenomenon, whose cause clearly depends upon both stress and chemical attack.

Interestingly, research in Germany followed steadfastly the role of stress as it related to the properties of the steel (270, 272, 286, 354, 392), whereas Americans have emphasized the chemical aspect (198). In England, besides the researches already mentioned, some considered embrittlement to result simply from pre-existent intercrystalline spaces (124, 249), the so-called "Rose' Canals," which were proved to exist by the clever research of Tammann and Bredemeier (172), or from fissures developed during riveting (21, 22, 191, 193). Rosenhain and Hanson, noting carbonless bands and grain growth from critical amounts of cold-working, argued heatedly that they had at last found the answer to boiler embrittlement in large, brittle ferrite crystals (107).

Finally, Münzinger took a trip to America to examine our practice and wrote upon it at length in 1925, after returning to Germany. His message to the folks back home was that interesting results were being obtained in America from feedwater studies, the opinion being that the caustic concentrated in leaky seams (163, 165, 166). The fall meeting of the Vereinigung der Grosskesselbesitzern in that year concerned itself largely with Münzinger's report (183), whereupon that date may be said to mark the beginning of concerted international attention being paid to the combined effects of stress and chemical attack from NaOH.

The Role of Chemical Attack

Chemical attack, of course, must relate to chemicals in the feedwater. That is a principal weakness in the argument based upon nitrate-cracking when much more significant comparisons can be so readily found. In fact, Schroeder and his colleagues have frequently pointed out the well-known characteristics of boiler embrittlement which distinguish it from ordinary chemical attack, but provide, as their best answer, a theory based upon direct chemical attack. As mentioned by Parr and Straub (181), nitrates, chlorides, and sulphates may lead to corrosion because corrosion is associated with the H^+ ion; but the OH^- ion, which characterizes the feedwater of embrittled boilers, should inhibit such attack in boilers. That it does is borne out by fact, except for some extraordinary conditions in high-capacity boilers (365).

There is another well-established fact: namely, that boiler embrittlement is founded upon the reaction of iron with water to form hydrogen and black magnetic oxide

$$3\ Fe + 4\ H_2O = Fe_3O_4 + 8\ H$$

The oxide characteristically occurs as a smooth, adherent, black scale to be distinguished sharply from the highly localized accumulations one must expect from selective corrosion, as required by the theory of Schroeder and his colleagues. The rusting of iron in general, which they admit is the basis of the phenomenon, is notoriously undiscriminating in its attack; that is, it is non-

selective (137). Other objections to their argument will be treated as they develop in the discussion.

Because the role of feedwater and chemical attack has been so frequently discussed in this country, only a skeletonized review of essential points will be made here. In the monumental publication by Hall and his colleagues (192), and in the papers of Straub (223, 225), Chapman (236), and others (207, 231), the subject is considered in detail.

Briefly, caustic is kept in the water as a necessary prevention of dissolution of metal at any anodes which may develop, 100 ppm effectively inhibiting corrosion. If carbon dioxide escapes, the caustic may concentrate

$$Na_2CO_3 + H_2O = CO_2 + 2\ \underline{NaOH}$$

Even with this increase in NaOH, however, the solution is still harmless to steel. Further concentration is necessary, as early pointed out by Parr (94). In 1910, Stromeyer had reported iron tubes cracking in caustic evaporators when NaOH exceeded 40 per cent (63). In 1917, Parr had shown that iron did not react with NaOH solutions from $^1/_2$ to 2 normal, but that, at higher concentrations, 5 to 10 normal, the passivity vanished and the anodic reaction proceeded (94)

$$Fe + x\ OH = FeO_x + x\ H$$

At 150 to 200 C, however, H was generated in a 1-normal solution, a fact shown by Krassa (58) in 1909. Still, such concentrations never occur in boiler water; whereupon the assumption was made that the solution concentrated around rivets and in leaky seams to a point where the steel was attacked (181). That was the viewpoint taken back to Germany by Münzinger and discussed by Thiel, Kriegsheim, Ries, Rösing, and Baumann at the meeting of the Vereinigung der Grosskesselbesitzern (183), and elsewhere by Baumann (188), and by Splittgerber (170).

Demonstration of such concentration soon followed. Berl (189), in 1927, used glass capillaries to show that evaporation and the slow diffusibility of substances in such confined spaces quite readily led to concentration. His observation (190) is today generally accepted as factual (233), especially because the alkaline incrustation always noted around failed parts is virtual proof of the mechanism (233).

For the prevention of embrittlement, Parr's early ideas were based upon the hydrogen theory and concerned adding salts that would react with the NaOH or with the H to make it harmless. Such an argument is still valid today, although the studies have been advanced to include many other additions. Endless argument over the results which have been obtained are principally due to causes that will be considered after the discussion of another phase of the problem has provided a basis for an understanding.

The Role of "Aging"

No adequate discussion of boiler embrittlement can fail to mention the energetic figure of Stromeyer who, as early as 1905, made bending tests after successive intervals of time and found that the ductility of boiler steel decreased upon standing at room temperature (39). Although admitting that the brittleness may begin at sheared edges, Stromeyer nevertheless felt that the defect was more generally located and proposed that P was to blame when its content exceeded 0.05 per cent. The same thing is observed today (200). In 1907, Stromeyer (52, 53) proposed his famous "aging" theory for boiler embrittlement, which threw steelmakers into consternation because he effectively showed them that steel may be harmed by boiling in water. Tests made at temperatures from a wintry —16 F to that of boiling water and for periods up to 16 years showed that steel became brittle with age, and that increasing the temperature accelerated the process. In 1909, Stromeyer introduced N into the question of aging (59), along with impurities in general, although he was never able to provide an explanation for the effect that was either logical or decisive.

About 20 years later, Fry (178, 209) brought the "aging" argument to practical fruition with the development of a "nonaging" steel, "Izett" steel, so named from the initials of the German words "*immer zäh*," meaning "always tough." Fry believed, as did Stromeyer, that boiler steel aged into brittleness upon heating at 200 C. Subsequent to the time of Stromeyer, oxygen was identified as a likely cause of aging; consequently, Izett was a steel to which sufficient Al had been added so that the oxygen was stabilized as Al_2O_3.

Because oxygen may not be the only element responsible for aging, Izett steel need not be the final answer. Pfeil (212), for example, blames C; and N was considered along with P by Stromeyer (59). However, it is possible to coalesce these seemingly contradictory opinions and to show that each nonmetallic impurity may play a part.

Unfortunately, the valuable lesson to be learned from these investigations on aging was obscured by the research of Parr and Straub (211), in 1928. Although Parr and Straub themselves state that cracking will not occur if the steel is not stressed above the range of the yield point (181), a fact widely recognized, they tested a group of steels without regard to load/strength ratios, and concluded by comparing a flange steel, tested at its yield point, with a specimen of Izett having a 25 per cent overload. Even under these conditions, the Izett specimen was 200 to 300 per cent more durable than most of the fifteen specimens tested, and had a life exceeded only by two S.A.E. 1112 steels and the flange steel just mentioned. Neuendorff (252) also remarks that Parr and Straub's results are valueless because, "for reasons unknown to the reviewer," the flange steel had less load than the Izett. Those tests were made exceedingly critical to the problem of boiler embrittlement by the authors emphasizing the erroneous conclusion (211): "The embrittling effect occurs without regard to impurities or composition of the plate and that any defense of the embrittling distress attempting to charge it against the faulty iron is without basis in fact" (181), and "any ideas that embrittling distress may be due to faulty iron is without basis in fact" (200). Again, Straub remarks (200), "Pure iron was embrittled in the same manner as boiler plate." Obtaining "pure" iron is an accomplishment but few metallurgists yet dare boast; none would in 1927. In the same article, on the other hand, he observes that S and P accelerate embrittlement.

Along the same line, Parr and Straub (181) tested 3.5 per cent Ni steels, again without regard for load/strength ratios, and concluded that Ni exerts "no effect other than raising the yield point and, consequently, the initial stress necessary to cause embrittlement." On the contrary, examination of their data shows that the 3.5 Ni steel had 1000 per cent longer life than the best plain-carbon steel; that the best Ni steel had a yield point of only 40,000 psi and lasted $8^1/_2$ days, whereas six of the eight carbon steels had yield points above 40,000 psi and failed before 1 day had elapsed, one with a yield point of 49,000 psi failing in $3^1/_2$ hr. In the same vein, these investigators later (211) discounted the effect of sorbitic heat-treatment because it doesn't "stop" embrittlement, thereby losing for the science the fact that the finer dispersion of the carbide is definitely favorable.

Such work has been aptly categorized by Gillett (395) as "metallurgical naïveness," who with numerous instances reminds investigators of boiler embrittlement that they err when assuming that "steel is steel." Perry (311) is essentially in agreement with Gillett, and with metallurgists in general, when he states that the railroads find it "impossible to accept the prevailing ideas

regarding the relation of . . . boiler water to the failures," and that "factors other than boiler-water conditions contribute to boiler failures, and until such factors are corrected, failures are bound to occur regardless of the water used."

Izett steel, in spite of this, has been amply defended, though American investigators of boiler embrittlement seem poorly informed of it. Ulrich (227, 235) deliberately repeated Parr and Straub's tests, but with careful arrangement of the ratio of load-to-tensile strength so that an acceptable basis for comparison resulted. In addition, his values were corrected for the variation of the tensile strength between room temperature and 250 C (154, 201), which apparently was overlooked in the work of Parr and Straub. The Izett showed a marked superiority over flange steel in respect to embrittlement in caustic solution, a result also reached by the German Official Testing Laboratory (194). Finally, American investigators likewise reported recently that aluminum-killed steels are more resistant to cracking (398).

Comparing Bessemer, open-hearth Duplex, and Izett steel with respect to embrittlement from cold-working and from heating, Epstein (248) found that Izett suffered no increase in tensile strength and but little decrease in ductility upon heating to the blue-brittle range, so that it was considerably more ductile than boiler steel; and that aging around rivet holes was so shallow that the notch toughness was unaffected. Fry (238) pointed out that boiler steels, if nonaging, would promote welding practice for boilers. Studying boiler plate at room temperature after cold-working, Bauer found a progressive decrease from 6.3 to 2 in notch-impact values over a period of 1 year, with no end point indicated (132, 252). In a similar study, Goerens reported a great improvement from an addition of 3 per cent Ni (160). Lastly, Herzog and Portevin (342) demonstrated that nitrate solutions, generally so destructive to steels, do not readily fissure killed steels, which shows the necessity of considering the metallurgical quality of the steel in such problems.

The Role of Hydrogen

The Fe-H_2O Reaction as a Source of Hydrogen. Since Ledebur (15), in 1889, discussed rusting brittleness in iron along with pickling brittleness, the hydrogen produced by the reaction of Fe and H_2O has received universal attention. In 1903, Whitney (32) originated the electrochemical theory for the corrosion of iron by water, wherein H^+ ions are replaced by metal ions, according to the theory of Nernst

$$Fe + 2\,H^+ = Fe^{++} + \underline{2\,H}$$

Walker and his colleagues (55, 56) extended the theory in 1907, and 2 years later Friend (57) measured the hydrogen produced by steam acting on iron foils and powders at temperatures up to 350 C. Friend showed that magnetic iron oxide resulted from the action, an observation substantiated by every case of boiler embrittlement (181), and presented curves showing that at the lower temperatures the reaction undoubtedly still proceeded, but more slowly.

In 1919, Fuller (114) published a research proving that tap water reacts with iron to produce hydrogen which diffuses through the iron, and that steam greatly aggravates the action. His observations are notable, because some have raised the question whether the nascent condition of the hydrogen in rusting really compares with the hydrogen developed during pickling, which is known to penetrate iron. It does, though the reaction is considerably slower.

Schikorr (221, 222) developed 18 atm pressure of hydrogen by reacting iron turnings with deaerated water without any limit being indicated. The evolution was doubled between 25 and 35 C, which is consistent with the logarithmic nature of chemical reactions. When an iron plate was used, a coating of Fe_3O_4 developed in 2 hr, but no measurable hydrogen was produced. This suggests that the gas may have been absorbed by the steel, as shown by Fuller (114). Powder has such a large ratio of surface to volume that reaction, rather than occlusion, would be favored. Baylis (176), and Berl and his co-workers (190, 206, 215, 229, 246), made similar observations, the latter reporting that NaOH added to the water in quantities above a certain minimum greatly increased the evolution of hydrogen.

In actual tests on boilers, Fellows found hydrogen both in saturated and in superheated steam, and in the water both as it entered and as it left the economizers (217). Fellows made the significant remark that a commercial process for producing H_2 is the steam-iron reaction. His attention, however, was centered upon the oxidizing phase of the reaction, and he did not note that his curve, showing increasing oxidation of the steel with increasing temperature, likewise represents increasing hydrogenizing, by virtue of the decomposition of H_2O, and the standard reaction

$$3\,Fe + 4\,H_2O = Fe_3O_4 + \underline{8\,H}$$

That H_2 may be a predominating noncondensable gas in steam was demonstrated by Hall and his co-workers (192) with a laboratory boiler. Straub and Nelson (369) collected great amounts of H_2 from water and caustic solutions allowed to react with steel. In the same line come the researches of Potter, Solberg, and Hawkins (330, 414, 415), which were prompted by the fact that modern boiler installations are using temperatures as high as 1200 F, and pressures of the order of 1400 psi, truly simulating in severity the commerical process for making hydrogen, mentioned by Fellows. Again, however, those investigators began with their attention turned to the oxygen rather than the hydrogen, principally because they were studying scaling. That gas finally forced their attention by diffusing through the steel and vitiating their results, and again by unexpected quantities suddenly evolving from the steel. Their method of measuring oxidation was to employ measurement of the hydrogen which was produced, since it would be a chemical equivalent. As a result, those investigators provide some interesting facts attesting the prominence of hydrogen in steam boilers.

In another field, Dällenbach (277) reports that the penetration of hydrogen through the steel walls of mercury-arc rectifiers from the cooling water upsets their service (298).

Finally, Norton (377) reports a research establishing further the penetration of iron by hydrogen from tap water. What is of special significance to investigators of boiler embrittlement is the fact that sodium chromate, an inhibitor known since the days of Parr (94), stopped the diffusion of H; and that a sand-blasted steel tube coated with Na_2SiO_3, a great accelerator of embrittlement, developed so much hydrogen on the opposite surface during 15 min of heating at 200 C that the experiment had to be discontinued.

These researches can leave no doubt that in steam boilers an unlimited supply of hydrogen is available; furthermore, that that hydrogen develops under conditions favoring its diffusion into the steel.

Action of Hydrogen on Steel at Ordinary Temperatures—Transcrystalline Brittleness. One of the prolonged arguments in the literature on boiler embrittlement is that concerning the path taken by the fracture, i.e., is it around grains or through grains?

When steel is exposed to nascent hydrogen at ordinary temperatures, as in acid-pickling, cathodic electrolysis, and the rusting reaction, the hydrogen atoms enter the iron lattice and diffuse through the body of the grain; not through the grain boundaries

(321). Consequently, the deleterious effect of the gas at ordinary temperatures is *intra*granular (186), rather than intergranular. The gas may enter grain boundaries, of course, but its pressure there cannot exceed the pressure within the grain unless secondary reactions with impurities set in. Although Pfeil (182) and Williams and Homerberg (162) appear to have recorded such an instance at ordinary temperatures, such reactions are unlikely over a short period of time.

In previous publications from Battelle Memorial Institute, the action of hydrogen within the grain at ordinary temperatures has been sufficiently discussed (384, 386–389, 404, 418–420),[3] so that anything more than a summary statement here is unwarranted. Briefly, each grain of the steel is intrapenetrated with a vast, geometric system of ultramicroscopic imperfections. These are commonly observed when the metal is cold-deformed or etched. They may also be observed when the metal is stressed internally by precipitations such as the Widmannstätten action, or during nitriding, or carburizing, when the supersaturated phase may be seen to collect along the crystallographic planes that once contained minute voids. Those same imperfections collect hydrogen when it is a supersaturated phase; and it always is, practically speaking.

Now, hydrogen can only enter the iron lattice when H_2 is dissociated into atomic H. That is why pickling, cathodic electrolysis, and rusting are prolific sources of absorbable H, for the H atom actually meets the iron lattice before it meets another H atom with which to combine to form stable, insoluble H_2. In a gaseous-hydrogen atmosphere, only one out of approximately 10^{30} of the gas particles is an atom. Consequently, gaseous hydrogen can be stored in steel containers without measurable loss. Conversely, no one has yet conducted a pickling experiment under such great pressures of H_2 that the pickling action was reversed. Nor has any investigator of boiler embrittlement ever carried the bomb test to a point where the pressure of H_2 was sufficient to reverse the oxide-forming reaction.

By the same token, it must be conceded that the hydrogen atoms within the steel, when encountering the crystal imperfections just discussed, or any other discontinuity, will recombine in the direction of equilibrium, which, at room temperature lies far toward the side of tremendous pressures of the insoluble, molecular gas. Actual measurement of the pressures which may develop in that manner is not difficult. Bardenheuer and Thanheiser (205) obtained nearly 5000 psi, using a dilute NaOH solution and found no more indication of an end point than in a similar test at Battelle Memorial Institute wherein hydrogen penetrated 1/4 in. of solid steel and became trapped under a pressure which ruptured the gasket at 500 psi (387). Secondary observations of blistering and swelling of heavy plate confirm the theory in indicating that that gas can rupture the strongest steel (387, 404).

[3] References (287, 340, 358, 384–389, 400–404, 417–427) constitute a complete bibliography of published work from Battelle Memorial Institute on hydrogen in iron and steel.

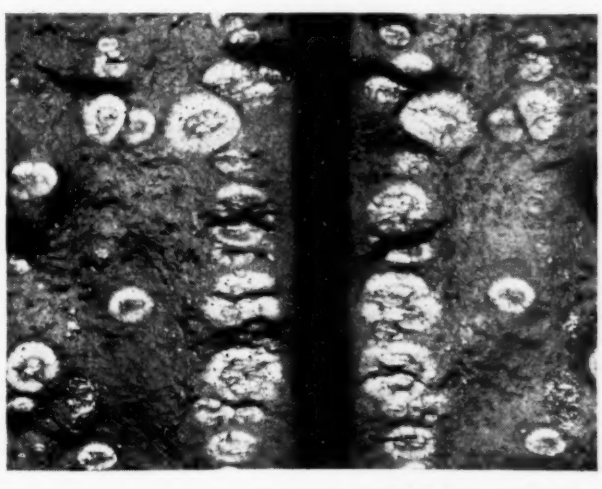


FIG. 2 LOCALIZED TRANSCRYSTALLINE HYDROGEN EMBRITTLEMENT CALLED "FISH EYES," OBSERVED ON FRACTURE OF A TENSILE SPECIMEN OF WELD METAL; ×3

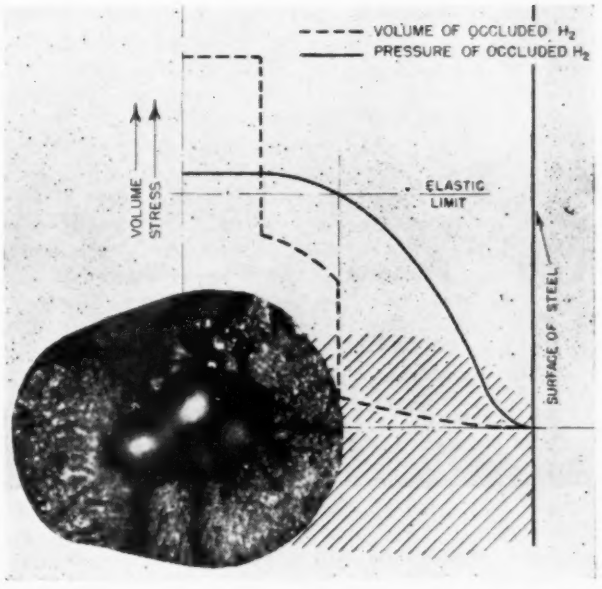


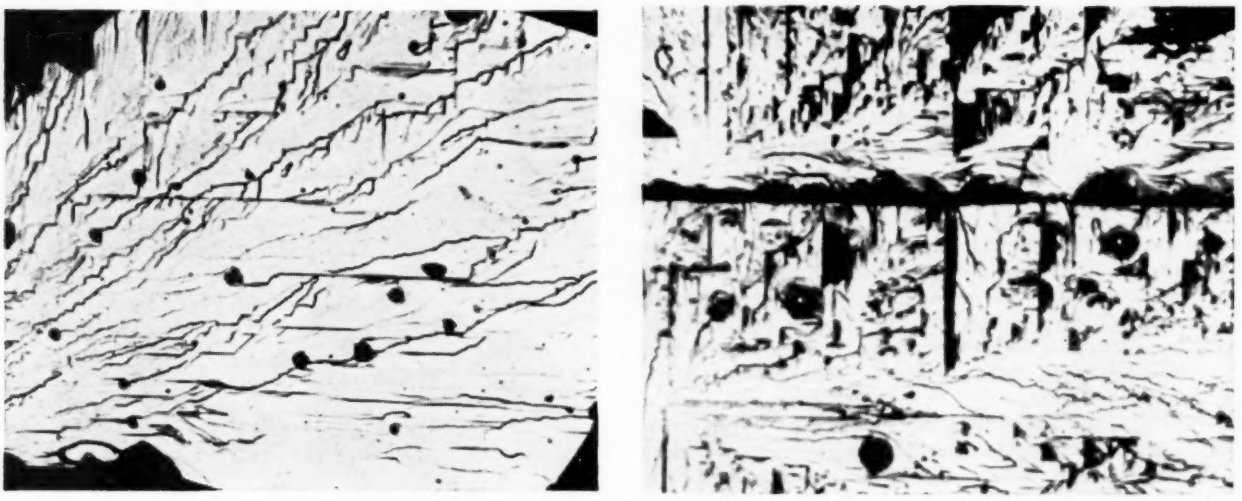
FIG. 3 ENLARGEMENT OF "FISH EYE," SUPERIMPOSED ON SKETCH DESIGNATING PROBABLE PRESSURE-VOLUME RELATIONSHIPS OF OCCLUDED HYDROGEN

(Note shiny interior suggesting presence of reducing gas such as hydrogen.)

When steel absorbs sufficient hydrogen to congest those slip discontinuities, "*intra*granular embrittlement" results.

In the following illustrations, this type of embrittlement, which is caused by hydrogen alone, is clearly illustrated. "Fish eyes," a welder's nuisance, appear in Fig. 2. In this case, the hydrogen has been obtained through dissociation of the gas at high temperatures, rather than through the energy of an aqueous reaction, as in pickling or rusting (26, 388). The shiny appearance of the embrittled zones is characteristic of hydrogen embrittlement and expresses the fact that the fracture in these zones lies along flat, transgranular imperfection planes which have been distended and extended by the trapped gas. Reflection of light from those flat, extensive facets is the cause of the brightness. One of the "fish eyes" is enlarged and superimposed upon a sketch in Fig. 3, which designates the probable pressure-volume relationships of the occluded gas. Note that, throughout the brittle zone, the gas is under pressure which exceeds the elastic, or cohesive, strength of the steel.

The two views in Fig. 4 were made possible by the fact that the fracture is transgranular across flat, crystallographic planes. Single facets under high magnification were observed by a technique recently developed at Battelle Memorial Institute (423). Note the system of "imperfection planes" which intersect the main cleavage plane being examined and reveal the crystallography of the metal. Certainly these illustrations give striking proof that the temporary brittleness from hydrogen at ordinary temperatures, variously called "pickling britteness," "acid brittleness," "hydrogen embrittlement," and so forth, is definitely and in-



(*a*) (*b*)

FIG. 4 DIRECT VIEW AT HIGH MAGNIFICATION OF SINGLE CLEAVAGE FACETS OF HYDROGEN-EMBRITTLED IRON BROKEN IN IMPACT
(*a*, Armco iron, purified in hydrogen and cooled at a sufficiently rapid rate to be embrittled by remnant gas; ×200. *b*, Purified Armco iron, embrittled cathodically; ×500.)

herently transcrystalline. Incidentally, specimen (*b*) in Fig. 4, though identical with "fish-eye" brittleness, is a steel embrittled cathodically, and therefore applies directly to the present argument.

Curiously enough, White and Schneidewind (245), and later Schroeder and Straub and their colleagues, used a research by Pfeil (182), in 1926, as illustrative of the type of fracture caused by hydrogen during pickling or cathodic electrolysis (385); yet Pfeil stands almost alone in reporting intercrystalline failure from pickling brittleness. This selection, it is interesting to note, actually counteracted their own unfortunate choice of pickling brittleness as a parallel case of boiler embrittlement, and probably sustained interest in hydrogen for a few years. Closer examination of Pfeil's work, however, shows that he actually obtained transcrystalline fracture, just as everyone else has, when ordinary specimens are used, and he discusses it at some length. However, when he went to the great trouble of growing crystals 1 in. or so in diam, the specimen broke through the grain boundaries, which is hardly surprising and is too far-fetched a case to be used excusably for comparison with boiler steel. Unhappily, Pfeil elected to display this unusual specimen upon the first page of his work, whereupon a great deal of misapprehension has resulted.

What investigators of boiler embrittlement have done, then, is to compare boiler embrittlement, which is predominantly intercrystalline, with ordinary pickling brittleness, which is distinctly transcrystalline; but they selected a misleading example purporting to show that pickling brittleness was intercrystalline, while the fact that, *under the conditions of boiler service, hydrogen attacks steel in a manner differing distinctly from pickling brittleness and which is truly intercrystalline is scarcely mentioned in the entire literature on boiler embrittlement.*

Action of Hydrogen on Steel at Elevated Temperatures—Intercrystalline Brittleness and "Boiler Embrittlement." Knowledge of intercrystalline attack of steels by hydrogen at elevated temperatures has stood in the literature at least since the invention of the Haber-Bosch process for ammonia synthesis (257, 267, 268) in 1908. In his Nobel Prize lecture in Stockholm (257), Bosch points out that one of the first problems which had to be faced was intercrystalline hydrogen embrittlement.

True, ammonia synthesis, such as the Haber-Bosch (257), or the Claude (289) process, utilizes pressures up to 1000 atm and temperatures from 400 to 600 C (752 to 1112 F); and hydrogenation processes, such as the Fischer-Tropsch, have conditions of temperature and pressure but little less severe at about 700 atm and 450 to 550 C (842 to 1022 F)(329); whereas only extraordinary steam units attain that temperature range, and never those pressures. Nevertheless, the difference is only of degree, for all processes supply H to the steel, although the rate varies. Boilers, accordingly, require months or years to fail in most cases, whereas the attack of boiler-type steel under the conditions of ammonia synthesis is so severe that its use is positively precluded. For example, Barber and Taylor (275) report steel actually pulverizing in 1000 hr from grain-boundary hydrogen attack in the hydrogenation of heavy liquid hydrocarbons. Investigators in that field have so little occasion to observe ordinary pickling brittleness that the following type of statement (275) abounds in their literature: "In all cases of hydrogen brittleness, the fracture takes place along the crystal boundaries." Compare this with the conclusion of Schroeder and Berk in their recent publication (398) on boiler embrittlement: "No intercrystalline cracking was found in any of the specimens," the "specimens" being steels loaded cathodically with hydrogen at room temperature, or for only short periods of time at elevated temperatures, in an attempt to reproduce boiler embrittlement under conditions which could not possibly result in anything but the irrelevant "pickling brittleness," if they became embrittled at all.

Among the major contributions in the literature on intercrystalline hydrogen attack are the researches of Vanick in America (156, 158, 161, 202, 203); Inglis and Andrews (262), and Sarjant and Middleham (314) in England; Naumann (329, 346) in Germany; Jacqué (334, 344, 345) in France; Giacomo (362) in Italy. Vanick began in 1922 with a steam-boiler failure which he associated with gases in the steel (156), but unfortunately did not blend that research with his subsequent conclusive studies on the behavior of steel under conditions of ammonia synthesis.

In 1923, Vanick (158) tested plain-carbon steel and wrought iron in NH_3. Below 300 C, reactions were slow, but at higher temperatures intergranular disintegration set in rapidly. De-

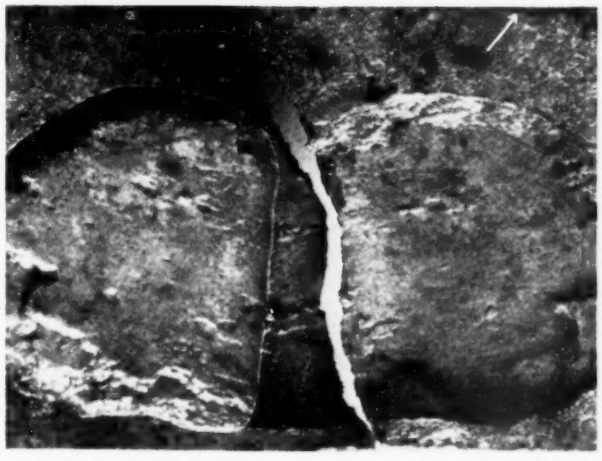


FIG. 5 PLAIN-CARBON-STEEL PLATE AFTER EXPOSURE TO NH_3 AT 500 C AND 12,000 PSI; ×3

(Note large, deep-seated blister which is peeled back, and smaller blister showing as a fissure, indicated by white arrow. The fracture through this zone illustrates a second hydrogen activity, i.e., intergranular embrittlement.)

carburization leading to fissuring was the principal reaction he observed, in exact agreement with the latest English research on boiler embrittlement (396). The deterioration, i.e., "internal decay," he so aptly called it, progressed evenly from the cool to the hot end of the tube, which is a significant demonstration that the intergranular hydrogen attack of steam boilers and ammonia chambers would differ in degree, or rate, as would be expected from the difference in operating temperatures. The fact that boiler embrittlement seems restricted to temperatures below 250 C should not confuse the present argument, since boiler embrittlement depends rather precariously in its fulfillment upon such factors as seam concentration and boiler-water impurities. How such factors change at temperatures above 250 C is but little known.

Vanick also observed that inclusions were definitely reduced in these tests, some being completely removed, by the infiltering H. When situated suitably with regard to the surface of the plate, these inclusions led to blisters from the accumulation of gaseous reaction products (275).

An example appears in Fig. 5. The specimen is carbon steel after exposure to NH_3 at 500 C and 12,000 psi. Note the large deep-seated blister which is folded back, and the smaller one showing as a fissure. The fracture through that zone reveals the simultaneous hydrogen embrittlement. In the micrograph, Fig. 6, may be seen the only remaining islands of pearlite which could be found in the entire section, and those appear nearly completely decomposed. The straight crystallographic lines are "needles" of iron nitride. In other words, the equilibrium with the external gas has demanded that both nitrogen and hydrogen penetrate the steel. At any discontinuity within the steel, those gases will tend, of course, to re-establish their relationships at 12,000 psi. Secondary reactions with carbon and other nonmetallics to form products such as insoluble CH_4 are likewise driven toward their respective equilibria, which lie sufficiently far to the right to cause effective removal of a visible precipitate such as iron carbide.

Williams and Homerberg (162), in 1924, likewise stated that hydrogen reduced inclusions in their tests on the role of hydrogen in boiler embrittlement (168). They recognized the two distinct forms of hydrogen embrittlement being discussed in this paper and concluded that water as a reaction product distends the grain boundaries and leads to subsequent failure of boiler plate. Unfortunately, they had used electrolytic methods and did not defend themselves when subsequent confusion over hydrogen embrittlement obscured the importance of their results. Their tests lasted about 30 days, which was apparently just long enough for sufficient reaction products to accumulate to cause some grain-boundary weakness. Many years before, Law (45, 51) discovered that hydrogen caused "pickling blisters" on steel sheet (31), but insisted they were formed from H_2O produced by H reacting with the oxide inclusion usually found there. Neither Law nor Williams and Homerberg modified that statement; whereupon Law lost the value of his argument, because water is not found in blisters, nor is oxide always present (46); and Homerberg and Williams became discredited by similar observations. At the ordinary temperatures of pickling and electrolysis, H reacts but slowly with impurities in the steel (153), and blisters, as well as the brittleness, are simply caused by molecular hydrogen. Higher temperature favors those reactions.

By the subsequent work of Vanick (161, 202); Vanick, de Sveshnikoff, and Thompson (203); Barber and Taylor (275); Maxwell (294, 310); Giacomo (362); Puchner (379); Jacqué (334, 344, 345); Wright and Habart (355); Kosting (281); Bosch (257, 267, 268); Naumann (329, 346); Sarjant and Middleham (314); Nowitt (376); and others (328, 336, 343, 363, 382, 391); the following general facts for hydrogen attack at elevated temperatures became clearly established:

1 H from the gas phase dissolves atomically within the lattice of the steel, leading to temporary brittleness.

2 H inside the steel then reacts with nonmetallic impurities, especially C, next with O, but depending entirely upon the stability of the oxide. S, N, and P may be attacked to varying extent, depending upon the stability of their respective phases. The insoluble gaseous products congest in grain boundaries, since they are insoluble in the grain.

3 When the pressure of these insoluble products exceeds the cohesive strength of the grains, the gas forces intercommunication and separation which manifests itself in loss of mechanical properties, cracking, swelling, blistering, or subsequent penetration of a corroding chemical.

4 The attack is favored by increasing temperature, pressure, and stress, is strongly influenced by the constitution of the steel and possibly by its heat-treatment.

Discussion of these facts has been available in textbooks for years (289, 372); yet, scarcely mention of it can be found in the entire literature of this country on boiler embrittlement.

Perhaps some actual cases of intercrystalline hydrogen at-



FIG. 6 MICROGRAPH OF SPECIMEN IN FIG. 5 SHOWING NITRIDE NEEDLES AND ADVANCED DECARBURIZATION; ×500



FIG. 7 SECTION OF CARBON-MOLYBDENUM STEEL FROM CATALYST BASKET, OR CONTAINER, SHOWING BLISTERS FROM HYDROGEN AND A FRACTURE FROM HYDROGEN EMBRITTLEMENT; ×3

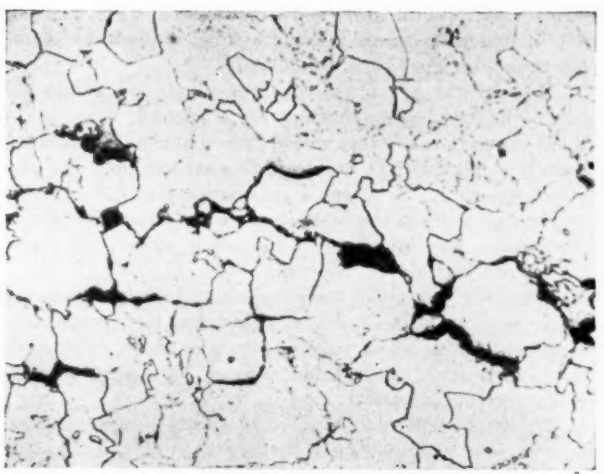


FIG. 9 MICROGRAPH OF SPECIMEN IN FIG. 8, SHOWING DISTINCTLY INTERGRANULAR NATURE OF HYDROGEN ATTACK; ×500

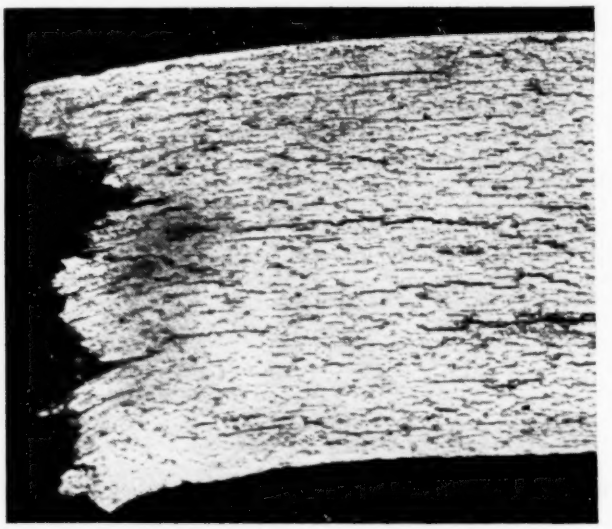


FIG. 8 CROSS SECTION OF FRACTURE IN FIG. 7, SHOWING DETERIORATION FROM HYDROGEN; ×3



FIG. 10 SECTION OF CARBON-STEEL TUBE AFTER 1 YEAR IN HYDROGEN AT 400 C AND 400 PSI, BENT WITH INTERIOR WALL IN TENSION TO SHOW DETERIORATION FROM HYDROGEN; ×3

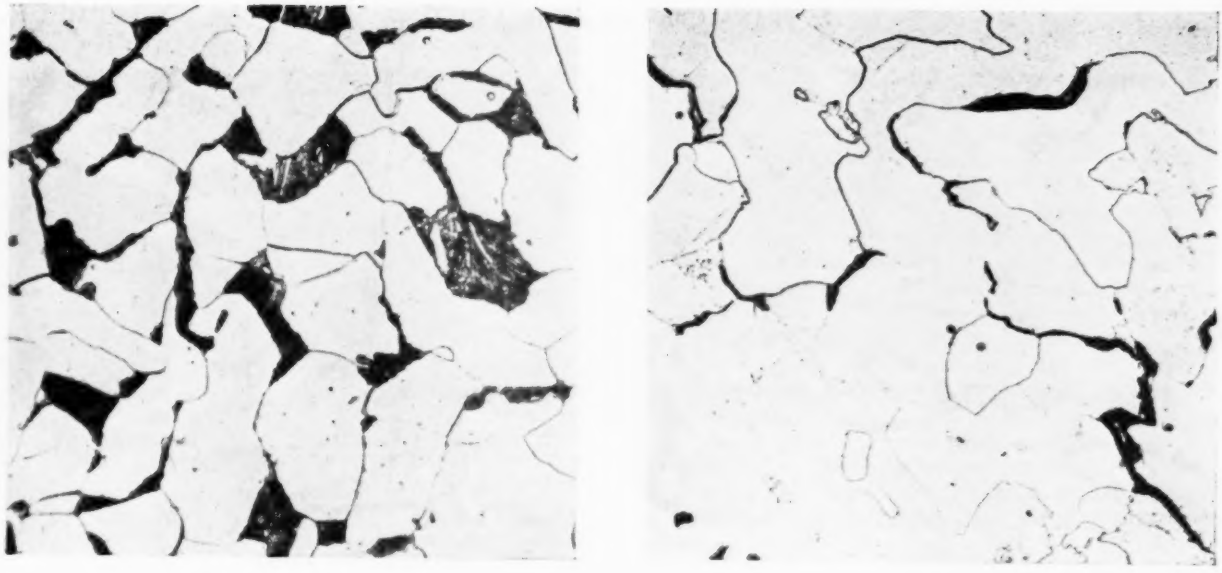
tack under conditions differing from steam boilers only in degree will be of value. In Fig. 7 is a macrograph of the surface of a carbon-molybdenum steel which served as a catalyst basket in an ammonia-synthesizing unit. Note the blisters in surface layers and the fracture occurring through embrittled metal, both defects being caused by hydrogen reacting with impurities in the steel. In Fig. 8, a section through that specimen shows the savage deterioration caused by the hydrogen. The micrograph, Fig. 9, shows intercrystalline attack with much greater definiteness than is obtained in cases of boiler embrittlement, if a distinction is to be drawn. Note the complete decarburization. The general absence of visible decarburization in boiler embrittlement in no way reduces the significance of these observations, as will appear later.

After 1 year of service in hydrogen at 400 C and 400 psi, a carbon-steel tube showed the deterioration evident in Fig. 10, where a section of the tube has been bent outward. In Fig. 11, micrograph (*a*) shows the condition of outer layers of that steel—carbide in the grain boundaries, but still largely unattacked; and micrograph (*b*) shows complete decarburization and marked intercrystalline fissuring in the inner layers.

The next two illustrations demonstrate a point that is vital to an understanding of boiler embrittlement, for it largely bridges the gulf that seems to stand between the operating conditions of steam boilers and the hydrogen-attacked units under discussion. Fig. 12 shows a section of a carbon-steel tube from service in high-purity hydrogen at 400 psi similar to that in Fig. 10. But, in this case, the temperature was 100 deg lower, i.e., 300 C, whereas the time of service was doubled to 2 years. Correspondingly, deterioration is practically identical for each case. A macro-etch shows the depth of the decarburized zone. In Fig. 13, micrograph (*a*) again shows pearlite between the grains, attacked but not destroyed; while micrograph (*b*), taken in the decarburized zone, again shows the complete removal of carbide and the marked intergranular fissuring. Though it cannot be stated with certainty, the accumulation of pearlite toward the grain boundaries of the ferrite seems to be a preliminary action in the removal of carbon from steel by hydrogen.

Correspondingly, K. G. Jones[4] points out: "At pressures above 400 psi, with temperatures above 200 C, we know that hydrogen will cause decarburization over a long period of time. Carbon steel would not be satisfactory in ammonia over 200 C at

[4] Personal correspondence; see acknowledgment.



(*a*) (*b*)

FIG. 11 MICROGRAPHS OF SPECIMEN IN FIG. 10

(*a*, Outer surface, showing carbide in grain boundary, but still largely unattacked; *b*, inner surface, showing complete decarburization and marked intergranular fissuring; ×500.)

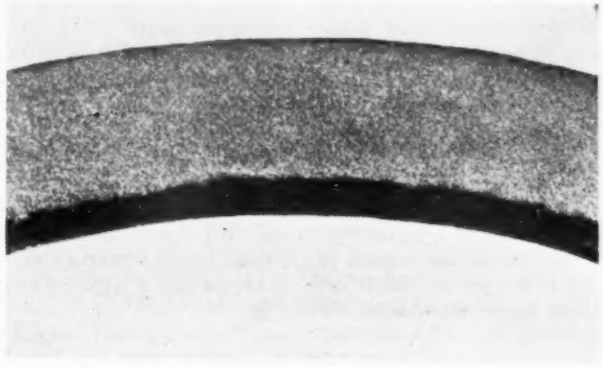
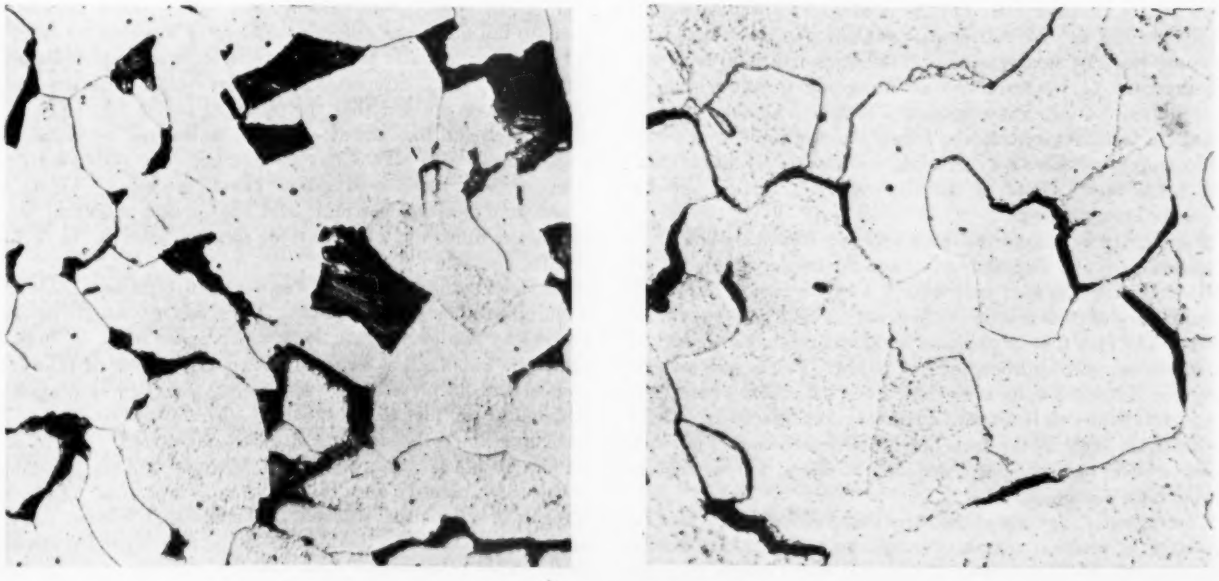


FIG. 12 CARBON-STEEL-TUBE SECTION SIMILAR TO THAT IN FIG. 10, BUT AFTER 2 YEARS AT 300 C IN HIGH-PURITY HYDROGEN AT 400 PSI

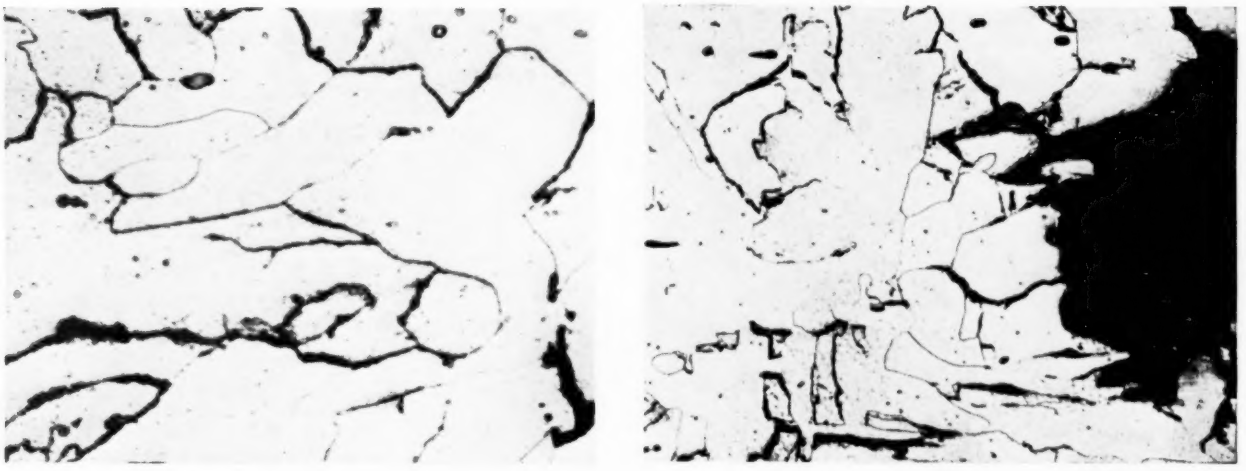
(Macro-etch delineates depth of decarburization; ×3.)



(*a*) (*b*)

FIG. 13 MICROGRAPHS OF SPECIMEN IN FIG. 12

(*a*, Toward external surface, showing pearlite between ferrite grains, but only slightly attacked; *b*, decarburized zone showing complete removal of carbon and distinct intergranular failure; ×500.)



(*a*) (*b*)

FIG. 14 MICROGRAPHS OF CARBON STEEL AFTER EXPOSURE TO AMMONIA AT 12,000 PSI AND 500 C; ×500
(Note (*a*) complete decarburization, marked intercrystalline fissuring, and, in micrograph (*b*) the adjoining corrosion which is obviously secondary to the hydrogen attack.)

our plant pressure of 12,000 psi." Compare this with the recent monumental report from the National Physical Laboratory on boiler embrittlement (396), wherein it is reported that boiler plate, embrittled in caustic solutions at temperatures slightly above 400 C, analyzed up to 10 volumes of gas per volume of metal, that the gas was predominantly methane, and that, upon reheating the steel to 625 C, internal fissures actually became recarburized on their surfaces.

Hydrogen attack in high-pressure plants is influenced markedly by pressure (289, 372). For example, Tongue (289) reports that H_2 at 1 atm pressure caused no decarburization of a high-carbon steel in 1 week at 500 C, but at 200 atm the carbon content of the surface layers decreased from 1.4 to 0.1 per cent in 16 hr. Autoclaves in hydrogenation processes never reach even the lowest H_2 equilibrium pressure shown in Fig. 17, which will be described shortly. At those lower pressures, Newitt (376) reports that H attack can be observed at temperatures as low as 200 C, even in their comparatively short-time tests. Inglis and Andrews report slight attack at 150 C, over a period of 2 years (262).

In Fig. 14 are shown two micrographs from a specimen similar to that in Fig. 6. No nitrides are evident, but decarburization is complete. In micrograph (*a*), intergranular failure is outstanding; in (*b*), the same type of intergranular failure is shown near a locus of outright corrosion. Is it not obvious that the corrosion is subsequent to the actual deterioration of the steel by hydrogen? "Selective corrosion" in this case is quite evident, but it has been *enabled* by the embrittling factor; it did not *cause* the embrittlement.

Plainly, the principal difference between the two fields of investigation, boiler embrittlement and hydrogen attack of reaction chambers, is that with boilers a longer period of time is required to complete reactions which are rapid at higher temperatures. The fact that in one case ammonia produces the soluble H, in another case hydrocarbons, or pure H_2, and in another case steam or NaOH, is quite irrelevant, since the ability of steam to cause steel to absorb H requires no further demonstration. Other distinctions, such as the lack of visible decarbonation in most cases of boiler embrittlement, are superficial and will be resolved during later discussion.

Consequently, a glance at the cures that have been provided for H attack in reaction chambers should be well repaid. Briefly, the industry developed both mechanical and metallurgical devices. Double-walled units were used with the nitrogen passing through the interspace to prevent hydrogen from penetrating the outer mantle (267). Another double-walled unit used an outer mantle built to withstand stress and drilled with holes to permit the escape of hydrogen that penetrated the inner wall, which was "gastight" and grooved on the outside to aid the gas in reaching the holes in the outer plate (267). Vanick (161), and later Lewkonja and Baukloh (263), tested an Al coat on iron and found good resistance, except that such a coating is impracticable because of its imperfections. Pier (284) patented a shell of 1–6 per cent Cr steel with a lining of Zn or Zn alloy. A British patent concerns a lining of Ta or Ta alloy (314).

Liquid steel was treated with H to remove O, C, S, P, and other impurities which might later react with H during service. Such steel, it is reported, actually did withstand H attack (289). An English patent suggested similar treatment of the plant parts with H while red-hot before the final forging or rolling. In test, such steel remained unchanged after 300 hr, whereas ordinary steel embrittled in 24 hr (289).

Most of the research, however, has had to do with the composition of the steel. Plain-carbon steel, which takes months or years to fail under the milder conditions of steam-boiler service, fails in a few hours in the more severe service of ammonia synthesis (274, 307). Consequently, alloy steels must be used. Research soon showed that the principal attack was on carbon in the steel, and that the attack could be lessened by stabilizing that element with alloy elements forming more stable carbides than does iron, much as oxygen is "killed" in steels by adding Al. Chromium received the most and the earliest attention, and, thereafter, numerous other carbide formers, such as Ti, V, Zr, Cb, Ta, and W.

On these additions, Krupp steelworks in Germany holds the most interesting patents (282). Their subject matter is well covered by Naumann (329, 346), whose paper (346), in 1938, is easily the outstanding contribution on the subject of H attack of steel and its prevention. His findings are largely contained in the diagram, Fig. 15, in which the effect of various alloy additions upon the resistance to H attack is illustrated. Si, Ni, and Cu had no effect. Mn, Cr, W, and Mo increased the resistance in the order named; and Ti, V, Zr, and Cb showed no special effect until a limit was reached, beyond which a sudden and astonishing resistance to the highest temperatures studied showed itself. This phenomenal action clearly depends upon carbide

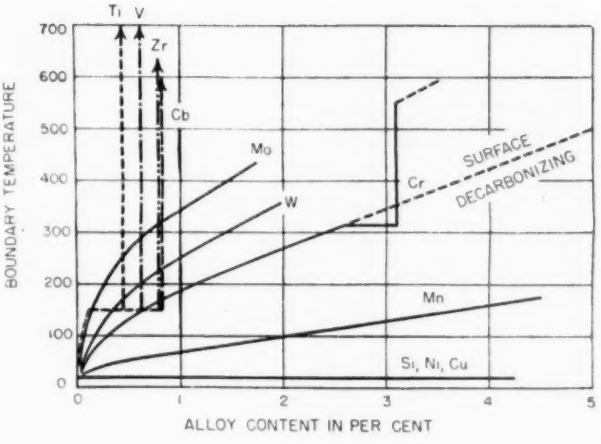


FIG. 15 EFFECT OF ALLOYING ELEMENTS ON RESISTANCE OF STEEL TO HYDROGEN ATTACK AT ELEVATED TEMPERATURES; NAUMANN

formation, and hence upon carbon content; but for ordinary mild steels, such as boiler plate, less than 1 per cent of any one of these elements is all that is required. The maximum effect occurs when the vanadium content, for example, is greater than 5.6 times the C content, the formation of V_4C_3 then being assured. In any event, the patents state, C should be kept below 0.30 to 0.35 per cent.

Again, it is interesting to compare a statement from the recent publication on boiler embrittlement by Schroeder and Berk (398), who finally demonstrate for the first time in this country that killed steels show "distinctly better resistance" to embrittlement, but who conclude that that effect cannot be due to deoxidation because vanadium "which is also considered an efficient deoxidizer" doesn't show that improvement. They refer to tests of their own on steels having a vanadium content of only 0.25 to 0.30 per cent; and, referring to the curves in Fig. 15, one can readily understand why such steels would not reveal the stellar role of that element. Also, metallurgists now regard vanadium as a weaker deoxidizer than aluminum.

In another field, intercrystalline attack by hydrogen is also sufficiently prominent to warrant some attention, i.e., the so-called hydrogen embrittlement of copper, or "copper sickness." Vanick had tested copper in an ammonia-cracking unit in 1924, and found, after 4 months at 400 C, that it had expanded by 30 per cent of its diameter and fissured to its core (161). In the catalyst well, where the hydrogen is expectedly more nascent, a copper tube fissured in 6 days along a temperature gradient from 200 C to 600 C. If the copper had been deoxidized with boron, only slight fissuring resulted; and an oxygen analysis of that copper showed a content only 10 per cent of the ordinary. Bosch also points out that the failure of Fe and Cu in H_2 is identical (257).

Forty years ago, Heyn showed that copper heated in hydrogen at temperatures above 600 C increased in volume and developed fine fissures from H reducing cuprous oxide to form steam which became trapped within the metal (34). Also, tin oxide in bronze led to the same result. Archbutt, about the same time, removed the oxygen from copper by heating it in hydrogen, and found similar fissuring and bloating (36). Bengough and Hill found that CO, as well as H, diffused into the copper and formed insoluble compound gases (61); although Sieverts and Krumbhaar, studying the solubility of N_2, CO_2, H_2, and CO in copper found only the hydrogen soluble (62).

Embrittlement from H_2, CO, and steam was established by Ruder, who showed that temperature controlled the reactions to a large extent (88), and that hydrogen at elevated temperatures causes intercrystalline attack (91). Dry H_2 incepted embrittlement at 400 C, moist H_2 at 600, steam at 700, and CO above 800 C. Copper, deoxidized with boron, was not affected at all. Similarly, Johnson found that copper, deoxidized with ferrosilicon, was not affected by H even at 780 C (80); and Bengough and Hill had reported an analogous role for arsenic (61), on the argument that the arsenic stabilizes the oxygen in copper. Because carbon does not dissolve appreciably in copper, H attack principally concerns oxygen. Al, P, Mg, and numerous other oxide stabilizers came into use (80), all on the basis of the assumption that the hydrogen-oxygen reaction led to intergranular failure just as in boiler embrittlement. Redding noticed embrittlement of copper sheets simply from remanent machining oil left on the surface during annealing (147), and Ellis reported a 70 per cent loss in strength and a 90 per cent loss in ductility when vaseline was smeared on copper plates before annealing in a closed furnace (143). Pilling noticed embrittlement during brazing copper in a gas flame (145). In all cases, the source of hydrogen is evident.

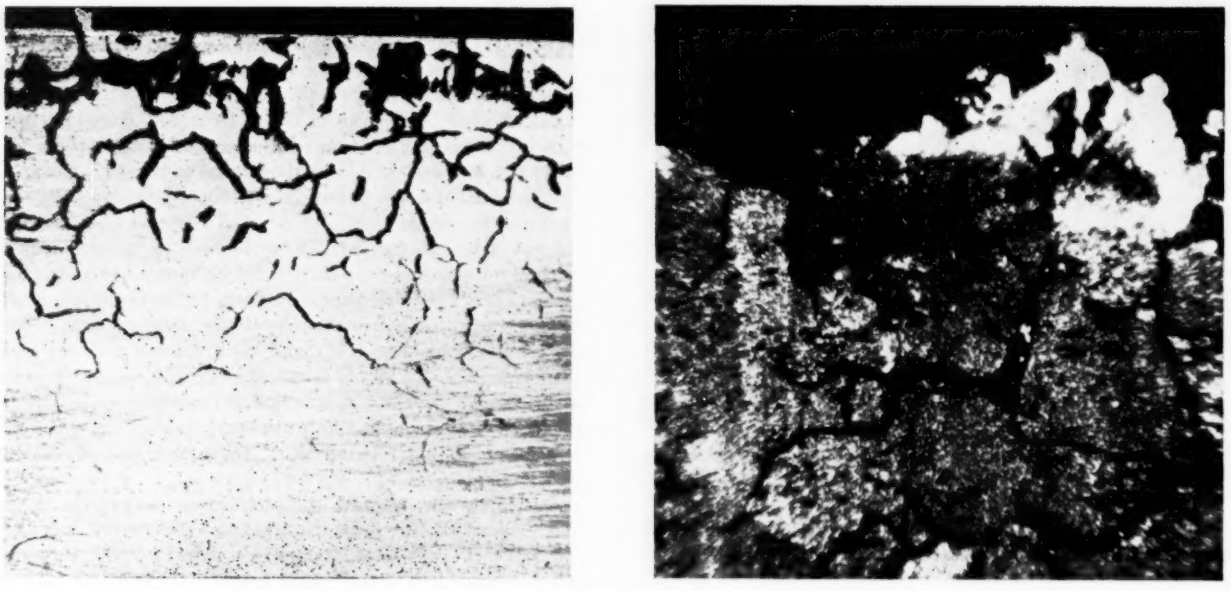
Determining the relative diffusion rates of various gases through copper, Pilling (104) lists H_2O at 65, CO at 17, and CO_2 at 0.6, when H is taken at 1000. If Cu is treated with H_2 while liquid, corresponding to the patent recently discussed for steel, a sound ingot results and embrittlement is prevented. However, if oxygen is absorbed, even during casting, the hydrogen-oxygen reaction is enabled (125). Sulphur in the grain boundaries also leads to intercrystalline failure (125); so oxygen is not alone, just as it is probably not alone in permitting boiler embrittlement, as evidenced by the incompleteness of "killed" steel. Moore and Beckinsale, in an outstanding paper (143), determined that as the oxygen content of copper became less, H attack began at higher temperatures. Bamford and Ballard (122) likewise discussed similar behaviorisms of hydrogen in brasses.

Finally, in purifying steel, especially in decarburizing, a hydrogen treatment at elevated temperatures is not only well known, but stands almost as the only means by which nonmetallics may be removed from solid steel. And, again, the grain boundaries are the path for occlusion and migration of the gaseous phase. The same Andrew whose work on caustic embrittlement (81) is quoted so widely in the literature, several years earlier had written on decarburizing steel with hydrogen (64, 69). Other investigators soon showed that H diffusing through the steel is attracted to impurity atoms, such as C, N, O, etc. (325, 347), and that insoluble reaction products develop whose removal constitutes the purification treatment (78, 111, 116, 117, 130, 152, 250, 253, 256, 263, 264, 279, 290–292, 303–305, 322–325, 338, 339, 347). The H removes not only C and O, for practicable desulphurization with H has been demonstrated (303, 304), at temperatures above that of boiler service, of course.

Other metals than steel and copper suffer similarly from these deleterious equilibria of hydrogen and nonmetallic impurities (237); and the scope of those reactions even extends into welding (337, 370).

During the hydrogen purification treatment, intergranular weakness is exhibited (263), as would be expected, because the seat of the reaction with the nonmetallics is in the grain boundary. In Fig. 16 are shown two typical examples of intergranular weakness in steels treated in hydrogen, but removed before the reaction products have escaped. Consequently, the grain boundaries are congested with the expansive gases, and the steel suffers from intergranular hydrogen embrittlement. If the treatment is allowed to go to completion, those insoluble gases escape, the grains weld together again, and the steel becomes ductile iron.

By now it should be firmly established that steel, when ex-



(*a*) (*b*)

FIG. 16 MICROGRAPHS OF FREE-MACHINING STEEL INTERRUPTED DURING A PURIFYING TREATMENT IN HYDROGEN AT ELEVATED TEMPERATURES

(*a*, Unetched, lightly polished; ×10; *b*, etched; ×30. Note distinctly intergranular fissuring.)

posed to hydrogen at sufficient temperature and for a sufficient period of time, suffers the following action:

1 Hydrogen enters the steel atomically.
2 Hydrogen reacts with the nonmetallic impurities.
3 Gaseous reaction products congest the grain boundaries to disruption, which is embrittlement.
4 Disruption permits escape of the gaseous products to the atmosphere.
5 Ductility returns.
6 The steel has become purified iron.

Because it is universally agreed that hydrogen does enter boiler plate, this progressive action positively must be an entity in "boiler embrittlement," whatever its degree of importance. Obviously, the action never even approaches completion; but only the first three steps are necessary for embrittlement.

Beginning with this firmly established background, let us now attempt to determine the ranking of hydrogen attack as the cause of "boiler embrittlement."

3 THE STATUS OF "BOILER EMBRITTLEMENT"

STEAM-IRON EQUILIBRIA: THE CASE OF THE CLOSED BOILER

In view of the consideration just paid intercrystalline hydrogen attack, an interesting comparison is afforded with recent statements of Schroeder and Berk (398), regarding the possible role of hydrogen in causing intercrystalline embrittlement in boilers. Those investigators succinctly dismiss hydrogen from all consideration by subjecting the hydrogen "theory" to two peculiar tests. They state that the theory "may be tested, first, by determining whether or not hydrogen will produce intercrystalline cracks," whereupon they conduct room-temperature and short-time tests at 250 C, which of course produce only transcrystalline brittleness, or none at all. Not a word of recognition is given in their report to any of the references just reviewed, in which intercrystalline failure from hydrogen attack is the only consideration.

Upon drawing the astonishing conclusion that hydrogen does not cause intergranular weakening, Schroeder and Berk proceed with a second and, in their opinion, a decisive test. They state: "The action of hydrogen might also be tested in a second way, namely, by determining whether or not intercrystalline cracks can be produced in its absence;" whereupon they resort to an "anodic" treatment, whose complete irrelevancy can be established in numerous ways. The simplest is probably to point out that boiler embrittlement has none of the visual evidence necessary for a selective anodic attack. There is the common observation that "embrittled specimens are not corroded but are covered with a thin shiny . . . layer of black iron oxide" (181); as well as Schroeder's own observation that boiler embrittlement is not corrosion or corrosion pitting (240). What can anodic attack, which almost by definition is direct attack beginning at the surface and working inward, possibly have to do with such a phenomenon? To a metallurgist, who is aware that the intercrystalline failure of metals covers a vast field of individual conditions and causes, it is inadequate to test a specific case like boiler embrittlement with a nonspecific test.

The hydrogen mechanism, on the other hand, is an indirect attack, and therefore provides an immediate and a simple answer, since the gas does not deteriorate the metal until after it has passed through a finite surface layer of solid metal, so that its reaction products may become trapped. Once inside the iron in atomic solution, the gas then may react with impurities to produce retained gases with resultant deterioration of the plate. Or, the deterioration may later breach the surface, of course, as demonstrated in Fig. 14.

From their inadequate tests, Schroeder and Berk draw a conclusion which threatens to suspend an understanding of boiler embrittlement for many more years. They state: "At present there seems little reason to believe that hydrogen causes boiler cracking or that it plays an essential part in such failures" (398). Similarly, the University of Illinois Engineering Experiment Station states: ". . . we should divorce the idea of hydrogen embrittlement from the phenomenon of caustic embrittlement . . . that type of embrittlement due to hydrogen . . . is not the effect that we get in the so-called embrittlement caused by caustic"

(181). Rech regards Parr and Straub's work, in which they compare boiler embrittlement with pickling brittleness, as "eliminating the hydrogen theory" (220).

On the other hand, the 1941 Report on "Intercrystalline Cracking in Boiler Plate" by the National Physical Laboratory in England, names hydrogen as the fundamental cause of boiler embrittlement. The English investigators studied the defect by analyzing the gases in boiler plate after laboratory tests under somewhat exaggerated conditions. They do refer to Naumann's research on hydrogen attack, just discussed, and conclude that ". . . cracking produced by the action of sodium hydroxide was almost identical with that produced by gaseous hydrogen under high pressure."

Reversibility of the Steam-Iron Equilibrium. Besides the reasons already given for the present misunderstanding of the role of hydrogen in boiler embrittlement, there is another which is almost more surprising because it concerns elementary chemical principles, and the work on embrittlement in this country has been dominated by chemists. For example, Partridge and Schroeder state: "That oxides would be reduced by hydrogen passing through the steel, as postulated by Williams and Homerberg, seems unlikely . . . in view of the evidence . . . that the reaction proceeds rapidly in the opposite direction, iron removing oxygen from water and forming a coating of oxide with the simultaneous liberation of hydrogen."

Surely the error in such a statement is evident. In the chemical reaction

$$A + B = C + D$$

one side of the equation represents reactants, the other products, and the direction of the reaction depends only upon the concentration of the various components in respect to their concentrations when at equilibrium. Consequently, the most avid reaction going from left to right that one can conceive can be made to go in the opposite direction by reducing the concentration of the reactants sufficiently. Thus hydrogen and oxygen explode to form water, but the water in turn can be broken down into hydrogen and oxygen again if means are available for removing the tiny amount of dissociation product which must always be in equilibrium with the compound. Electrolysis, for example, is an accelerated means for removing the 10^{-7} mols of hydrogen ion present in 1 liter of water, which shifts that strong reaction into reverse and the water disappears.

Within a steam boiler the reaction[5]

$$3\ Fe + 4\ H_2O = Fe_3O_4 + 4(2H = H_2)$$

visibly always goes to the right because one of the products escapes as a gas. The equilibrium concentration of H_2 never becomes realized, and the entities on the right are continuously generated so long as free iron remains in contact with steam. Researches already discussed have amply demonstrated the continuous presence of hydrogen in the steam coming from steel boilers. The *rate* of generation, of course, depends upon the many factors which influence that contact, and must not be confused with the *equilibrium* now to be considered.

On the other hand, the reduction of Fe_3O_4 by hydrogen to produce water vapor and metallic iron is well known in metallurgy. That is the reverse of the action in the steam boiler and gives practical proof of the well-established fact that the equation just given is truly reversible. In fact, the chemical relationships for that equilibrium over a great temperature range have been so well developed both in this country (260) and abroad (253) that it is difficult to reconcile the complete lack of recognition paid it in literature on boiler embrittlement.

Briefly, when both Fe and Fe_3O_4 are present in excess, as they are in the steam boiler, their chemical activities remain constant for any given temperature and may be conveniently placed at unity. The equilibrium constant for the reaction

$$K = \frac{(Fe_3O_4)(H_2)^4}{(Fe)^3(H_2O)^4}$$

may then be greatly simplified

$$K' = H_2/H_2O$$

in which the two gases may be expressed in terms of their partial pressures

$$K' = P_{H_2}/P_{H_2O}$$

This expression reveals the highly significant fact that, at any fixed temperature, the ratio of hydrogen to steam is fixed whenever iron and its oxide are present together. In terms of the "phase rule"

$$F = C - P + 2$$

there are three components and four phases when water and steam are both present; then

$$F = 3 - 4 + 2 = 1$$

and the system is seen to be univariant, having but one degree of freedom. That is, when temperature, for example, is specified, all other entities become fixed. Thus, for a boiler operating at 200 C, the steam-gage pressure automically becomes established at 211 psi, as is well known. What is not so well known, were one to judge from the published researches on boiler embrittlement, is that the potential pressure of hydrogen becomes fixed for exactly the same reason.

Notice the following interesting features of this system:

1 The *ratio* of H_2 to steam for any given temperature is fixed at some constant value by the thermodynamics of the Fe–Fe_3O_4–H_2–H_2O system.

2 The actual steam pressure, P_{H_2O}, for any given temperature is fixed at some constant value according to a similar thermodynamic law for saturated steam, as every boiler operator knows.

3 Consequently, the hydrogen pressure, P_{H_2}, becomes fixed at some constant value easily determined from the equilibrium constant $K' = P_{H_2}/P_{H_2O}$

In other words, the operator fixes the temperature of his boiler, which in turn fixes the pressure of the steam, which in turn fixes the potential pressure of hydrogen—a pressure which the boiler will always strive to attain, but in vain, unless the boiler is sealed to permit that gaseous product to accumulate.

That immediately suggests the question: *What maximum pressure of hydrogen could theoretically develop in a closed boiler?*

As already mentioned, the data for $K' = P_{H_2}/P_{H_2O}$ are readily available in the literature (253, 260). Because Fe_3O_4 is the stable form of iron oxide below 560 C (394), the system is unique, and its data are therefore applicable to the steam-iron equilibria wherever they occur. The universal agreement on the form of the Fe-H_2O equation underlying boiler embrittlement is especially fortunate, and should remove the last doubt about the validity and applicability of the values which are plotted in Fig. 17.

The lower curve represents the variation of steam pressure with temperature, and is more or less familiar to all boiler operators.

[5] In the reaction, the double designation of the hydrogen (2 H = H_2) is used to avoid a common, futile argument over the form the hydrogen actually takes, and to remind one that both the atomic and molecular forms do exist in keeping with their own equilibrium and that of the whole chemical system.

The upper curve represents the equilibrium pressures of hydrogen, P_{H_2}, corresponding to the saturated steam pressure for each temperature.

Those curves are undoubtedly surprising to many. Observe that the ordinate is logarithmic to allow encompassing the tremendous span of pressure involved. Even at 350 C, where the ratio nears a minimum, 10 lb of hydrogen pressure are required for every pound of steam; at 250 C, the ratio has risen to 100 to 1; and at 100 C, nearly 1,000,000 psi of H_2 must dilute the mere 15 psi of steam if equilibrium is to be reached.

The bewildering magnitude of such figures should not be allowed to confuse their significance. They simply show that the steam-iron equilibrium in a steam boiler at 100 C lies so far toward the right that for all practical purposes it is irreversible. Hydrogen could never accumulate under sufficient pressure to reduce the iron-oxide scale as rapidly as it was being formed, since the boiler obviously would explode before 1,000,000 psi could be reached.

The Grain Boundary as a Tiny, Theoretical Boiler. Within the body of the steel there is no steam, of course, but there may be hydrogen and nonmetallic impurities, such as the same iron oxide found within the boiler. The equation

$$3\,Fe + 4\,H_2O = Fe_3O_4 + 4(2H = H_2)$$

then must proceed *toward the left*, which is the reverse of the over-all boiler reaction.

In other words, hydrogen diffusing through the steel *must* tend to reduce each particle of iron oxide it encounters, just as iron ore is reduced by hydrogen in metallurgical practice. The reduction, of course, is governed by the same thermochemistry which governs the boiler reaction. Consequently, we can determine the potential, or limiting, pressures of H_2 and H_2O within the steel just as they were determined for the boiler. In fact, the locus of the oxide constitutes a tiny, theoretical boiler itself, wherein steam must be formed as a product of the hydrogen-oxide reaction. Because this is simply the reverse of the boiler reaction, the ultimate equilibrium is shown by the curves in Fig. 17, with an exception soon to be noted.

As a result, it now appears that cumulative gases within the steel could lead to congestion and disruption of the grain structure just as the cumulative gases could explode a sealed boiler if the steam-iron reaction were able to go to completion.

This, then, would seem to be the fundamental nature of the phenomenon of boiler embrittlement.

The same action is demonstrated in the hydrogen attack of catalyst chambers and hydrogenation units, as previously discussed. There, however, products besides H_2O are plainly involved, just as they undoubtedly are involved in boiler embrittlement (396). Parr and Straub (211), for example, found that high S and P led to more rapid failure, whereas, the general conclusion of work already reviewed is that O, C, and possibly S, N, and P are affected by the hydrogen (262). Straub, discussing White and Schneidewind's paper (245), mentions an instance of cracking being associated with nitrogen.

All nonmetallics with which hydrogen reacts, such as C, S, P, and N, must be expected to contribute to the total accumulation of gaseous products. Because P_{H_2} is fixed, these simultaneous equilibria are obviously similarly fixed. No calculations will be made here other than to point out that, for the equilibrium involving iron carbide and methane (253)

$$Fe_3C + 2\,H_2 = 3\,Fe + CH_4$$

$$K = (P_{H_2})^2/P_{CH_4}$$

$$\log K = -7990/T + 8.75$$

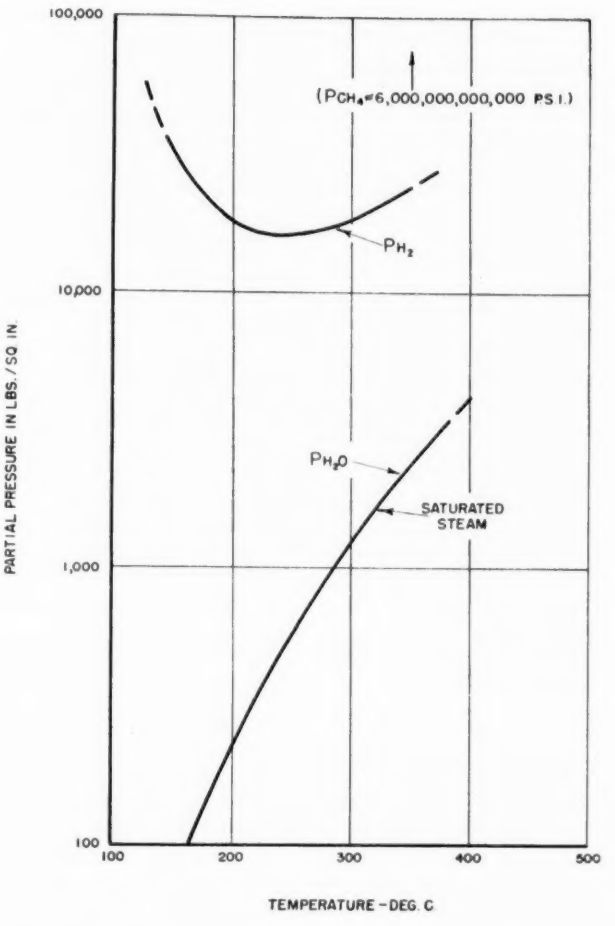


FIG. 17 CURVES SHOWING EQUILIBRIUM PRESSURES OF STEAM AND HYDROGEN OVER IRON AND ITS OXIDE FOR BOILERS OPERATING WITH SATURATED STEAM

whereupon, even at 350 C, the partial pressure of methane necessary for equilibrium with the steam and hydrogen prescribed for that temperature is approximately 5,760,000,000,000 psi! And at lower temperatures that figure rapidly increases! An arrow in Fig. 17, indicates that the methane pressures lie far off the graph.

Here again, the fantastic magnitude of these figures must not be allowed to contribute an impression of unreality. That monstrous value for P_{CH_4}, within its admittedly wide limits of accuracy, contributes the thoroughly sound information that iron, under the prescribed hydrogen pressure (see Fig. 17) of approximately 20,000 psi, could never be *carburized* by methane superimposed under any pressure available to us mortals. Or, from a more practical standpoint, the reaction to form methane under those conditions is irreversible. So long as carbon and hydrogen encounter one another within the steel, they will tend to add to the accumulation of insoluble gases. The concept is borne out by the fact that carbon may be removed from steel by hydrogen even at temperatures so high that methane is largely decomposed.

In this preliminary study, no conclusions will be drawn regarding the relative importance of the gaseous products in causing the grain disruption recognized as boiler embrittlement. Obviously, that is an important consideration, since it would indicate which nonmetallics in steel should be avoided. The beneficiation provided by deoxidizing steel with Al is undoubtedly

significant, as is the fact that such steel still ultimately fails in Schroeder's embrittlement detector. The literature on hydrogen attack concerns itself largely with carbon and methane, whereas decarburization is rarely noticed in boiler embrittlement. High-pressure boilers nowadays approach the service of hydrogenation units (365, 393); then decarburization is clearly indicated (365). Similarly, the English report marked decarburization from caustic embrittlement in tests on boiler plate at supernormal temperatures (396). Each of the gas reactions, of course, has its own equilibria and distribution of products and reactants over a temperature range. The same reaction need not be expected to predominate in these different services. The matter is best left temporarily simply as granular disruption by gases whose pressure can be expressed as

$$\Sigma P = P_{H_2} + P_{H_2O} + P_{CH_4} + P_{H_2S} + P_{NH_3} + \ldots\ldots\ldots$$

Equilibrium Versus Actual Boiler Conditions. Let it be understood that the foregoing calculations are based upon the ideal conditions of chemical equilibrium, but that they cannot be classed as being "only theoretical," since those equilibria have been determined and redetermined from actual experiment and have been made practicable. Of course, the values at high pressures are extrapolations and are subject to a consequent inaccuracy whose consideration is irrelevant at this time.

However, the question very naturally arises: *How closely are these calculated gas pressures likely to be approached in actual boiler service?*

Consider a unit, such as a boiler, separated into two compartments by a diaphragm of steel. In compartment *A*, the diaphragm has a clean fresh surface. In compartment *B*, the surface has such a heavy layer of Fe_3O_4 that for the present experiment it is inexhaustible. Compartment *B* is evacuated, leaving nothing but the Fe_3O_4, which is a product of the boiler reaction. Into compartment *A* saturated steam at 200 C is introduced, which is a reactant in the boiler reaction.

Immediately the steam reacts with the fresh iron surface of the diaphragm in the typical boiler reaction

$$3\ Fe + 4\ H_2O \longrightarrow Fe_3O_4 + 4(2H = H_2)$$

Now, regardless of the actual amount of the hydrogen which enters the steel, some quantity enters which is *that particular quantity injected by steam at 211 psi.*

In due time, some of the hydrogen will reach the Fe_3O_4 layer on the opposite surface of the diaphragm. There the well-established reaction for the reduction of iron oxide by hydrogen will occur

$$Fe_3O_4 + 4(2H = H_2) \longrightarrow 3\ Fe + 4\ H_2O$$

which is the reverse of the boiler reaction and has already been amply discussed, as have the pressures of the gases which must result.

Nevertheless, to recapitulate: H_2O will be produced in compartment *B* until enough steam is generated to reoxidize the iron and send H back into compartment *A* just as rapidly as the H_2O in that compartment is doing the same thing in the opposite direction. Obviously, the steam pressure in compartment *B* must then become 211 psi, since that is the steam pressure in compartment *A*.

At the same time that P_{H_2O} is increasing in compartment *B* enough H must precipitate from the iron without reacting with the oxide, of course, so that P_{H_2} is allowed to increase with P_{H_2O} n accordance with the curves in Fig. 17. Likewise, in compartment *A*, the portion of hydrogen which does not enter the steel will form molecular hydrogen until the steam is diluted with that same P_{H_2} that is ultimately attained in both compartments. The unit is then at equilibrium.

This fictitious experiment, of course, is simply a convenient means for representing the relationship between the steam boiler and the grain boundaries and inclusions within the steel which contain impurities reducible by hydrogen.

Reconsidering the "phase rule," an interesting thing will be noticed; within the grain boundary, or compartment *B*, there are only three phases, since water cannot exist at 200 C, until P_{H_2O} becomes 211 psi; then

$$F = 3 - 3 + 2 = 2$$

and the system is bivariant; whereas within the boiler, or compartment *A*, the system remains monovariant.

Thus the system is not completely described when the temperature alone is fixed. One more variable must also be stabilized. Ultimately, P_{H_2O} is that second variable which becomes fixed in the ideal unit when the steam therein reaches saturation and the fourth phase forms. But until the pressure of one of these gases is fixed, only the ratio of P_{H_2}/P_{H_2O} can be known, without any restriction as to the actual pressures of either gas. The total pressure may then be a matter of thousands of atmospheres, or only a few millimeters, so far as the chemical laws are concerned.

Without doubt, that brings us to the critical point in the phenomenon of boiler embrittlement, since the injection of hydrogen by the steam in the boiler cannot continue at the same rapid rate it had at that first instant when the surface of the iron was fresh and exposed. A covering of oxide immediately develops, which retards subsequent oxidation.

Without fear of confusion, we should now shift our attention from thermodynamics to kinetics; from ideal computations of equilibrium to actual rates of reaction, and how those rates may interfere with and upset the equilibrium. Plainly, the rate at which H is injected into the steel determines the concentration of the H within the steel, and that concentration in turn determines P_{H_2} within the grain boundary, or compartment *B*. This linking of rate with concentration is entirely valid, since the steel represents a reservoir for hydrogen through which the gas must obey the law of diffusion, in which rate and concentration are interdependent.

In other words, the gas ratio, and then the total pressure of $P_{H_2} + P_{H_2O}$ within the grain boundary, can become established by the fixing of P_{H_2}. Thus if H were supplied to the diaphragm in compartment *A* by some device, permitting a much greater rate of infusion than from steam at 211 psi, a superficial equilibrium could be imposed. The concentration of H within the metal would become abnormally high and the pressures of H_2 and H_2O in compartment *B* would adjust themselves to some supernormal values.

In the same way, if Fe_3O_4 in effect covers a part of the surface of the diaphragm in compartment *A* so that less H per unit time is injected into the steel, the gases in compartment *B* will adjust themselves to an equilibrium corresponding to steam in compartment *A* at something less than the actual pressure.

This, then, seems to be the explanation for the fact that boiler embrittlement depends upon agents like caustic and stress which will counteract the natural protection against hydrogen injection afforded by Fe_3O_4. Similarly, "accelerators," such as sodium silicate, counteract the depression of hydrogen absorption. Without these counteracting agents, all agree, boiler embrittlement will not occur; conversely, it is possible that every steam unit would suffer embrittlement if it were not for the retarding and protecting effect of this cumulative reaction product, Fe_3O_4.

Is Failure Intercrystalline or Transcrystalline?

Since time immemorial for this subject, an argument has raged over the path followed by cracking in embrittled boiler

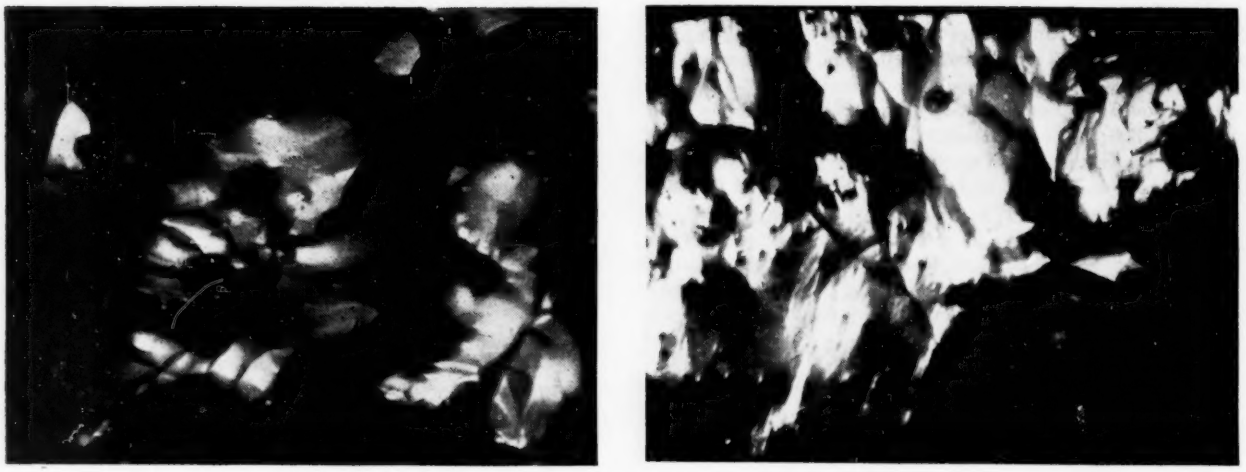


FIG. 18 DIRECT MICROGRAPHIC STUDY OF GRAIN BOUNDARIES ON A FRACTURED FACE OF INGOT IRON, EMBRITTLED INTERCRYSTALLINELY BY HYDROGEN

(Specimens fractured after interrupting a purification treatment in hydrogen; ×200.)

steel (97, 139). Many have given positive assertion to the fact that the cracks are exclusively intercrystalline (181, 220, 232); but others have noted that the cracks sometimes pass directly through the grain (137, 183, 406, 410), Perry (311) mentioning that either type may be shown "at the will of the operator." One case is even reported of cracking along twinning planes (133)! Numerous reasons have been advanced (128, 136), most of them superficial, none satisfying.

Now it should be clear why the cracks do exactly what they are observed to do. Let us refer again to Fig. 17. Only steam and hydrogen are shown there; but it is evident that at lower temperatures, the ratio of H_2/H_2O acquires such a predominance of H_2 that hydrogen must rely upon itself to embrittle steel. Its habitat is within the grain; consequently failure, when it occurs, is through the grain—transcrystalline. At higher temperatures, the ratio decreases until the sum of $P_{H_2} + P_{H_2O}$ is measurably greater than P_{H_2} alone; consequently failure, when it occurs, selects the habitat of the mixed gases, which is the grain boundary, since the gaseous product, H_2O, is insoluble in the grain.

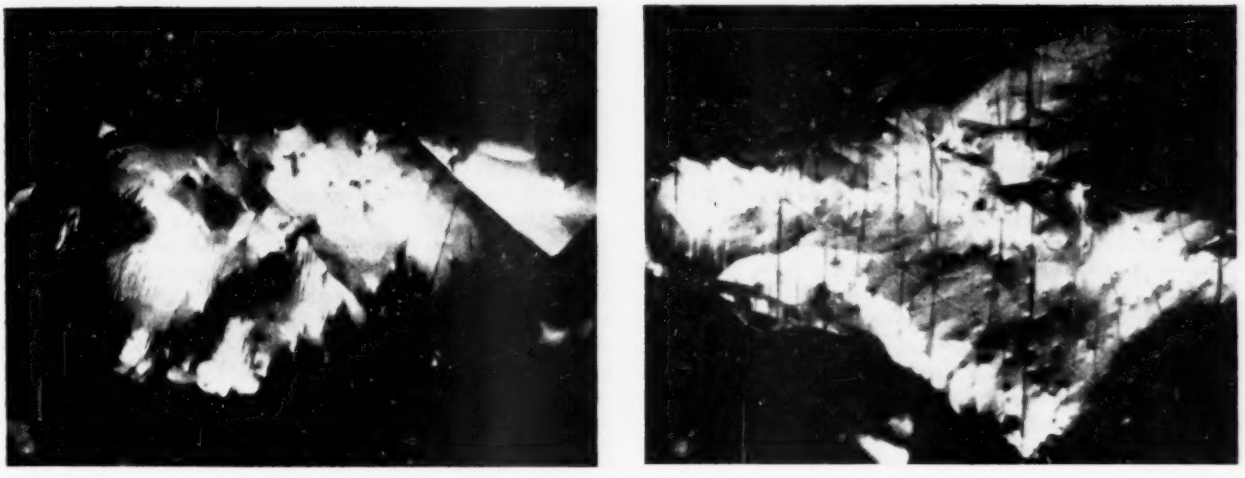
The gaseous products which are not shown, viz., CH_4, H_2S, NH_3, etc., have a role similar to that of steam with but one important distinction. That is, at lower temperatures some of their equilibria lie far toward the gaseous product, as is the case with methane, but without effect because the rate of reaction is so slow at ordinary temperatures. Consequently, grain-boundary failure, which depends upon an accumulation of those gaseous reaction products, tends to be suppressed at lower temperatures. Williams and Homerberg (162) found some reduction of oxide inclusions during cathodic electrolysis, as did Law years before (51). In fact, Pfeil's case of intergranular failure which has caused so much misunderstanding was unquestionably real.

In ammonia synthesis, then, intergranular attack is the rule; in acid-pickling and cathodic electrolysis, including short tests in caustic solutions at temperatures up to 250 C, or so, reaction products are seldom allowed to accumulate, and simple transcrystalline hydrogen brittleness is the rule. In boiler service, the tendency is definitely toward intergranular attack, because the extended period of service compensates for the low temperature; but the condition is sometimes intermediate. Some grains then break transgranularly, expressing the fact that the total gas pressure in the boundary may not always exceed that of pure hydrogen alone within the grain. The fact that sudden shock in the cracking process may also drive a fracture through a grain should not confuse this explanation, which applies to run-of-mill embrittlement.

Fortunately, this explanation need not rest upon theory alone, for the action can be directly followed through a micrographic technique recently developed at Battelle Memorial Institute (423). Samples of iron and steel showing various types of embrittlement by hydrogen have been fractured and studied at high magnification directly upon the untouched fractured face, as in Fig. 4. Micrographs showing both end stages and intermediate stages of embrittlement are presented in Figs. 18 to 20, inclusive. Fig. 18 is a view of a grain boundary as a surface instead of the customary line in sectioned specimens. Ingot iron, containing oxygen as its principal impurity, was heated in hydrogen at 1000 C for some days and was then withdrawn and fractured in impact. The specimen corresponds to those in Fig. 16, which were embrittled by accumulation of hydrogen reaction products in the grain boundary. Note the rough surface in the second view, suggesting that some impurities were still in place.

Fig. 19 represents the intermediate stage, wherein the pressure of grain-boundary gases is but little greater than the pressure of elemental hydrogen within the grain. The fracture, consequently, is intergranular, but transgranular planes of weakness have opened to accept the path of the fracture should a grain boundary hesitate. The first micrograph shows just a few crystallographic traces, and represents the specimen as it was removed from the hydrogen treatment. The second micrograph shows another specimen subsequently charged with hydrogen electrolytically, whereupon transcrystalline weakness was greatly developed. Nevertheless, that piece still chose to fracture predominantly through the grain boundaries in spite of the cathodic treatment. Evidently the pressure of residual gases in the grain boundary remained predominating—which may explain Pfeil's test, incidentally, since he may have occluded such products during his treatment for grain growth.

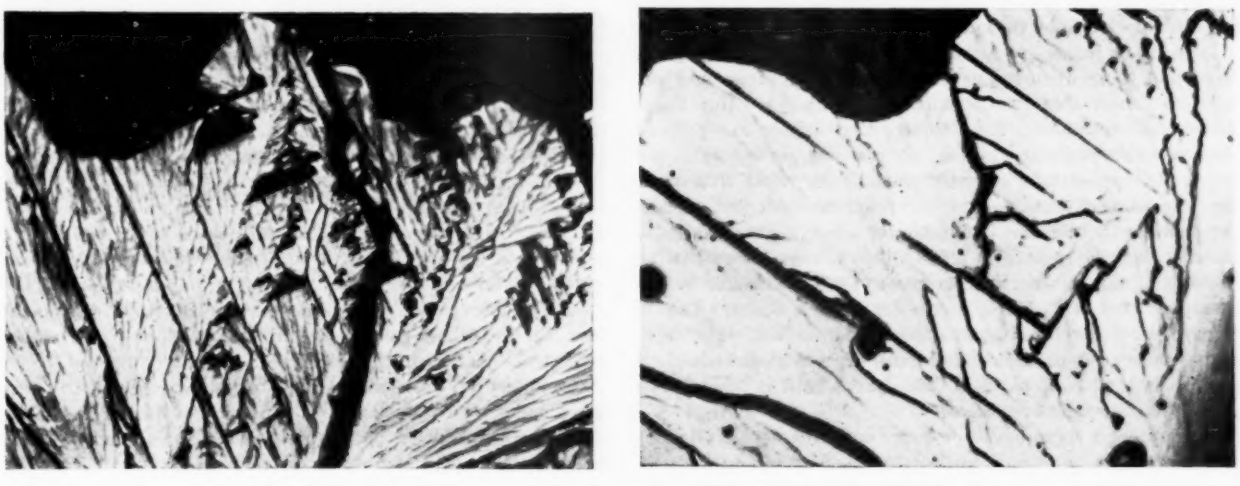
In any event, Fig. 19 verifies the discussion concerning the curves in Fig. 17, and explains why in certain cases the fracture of embrittled boiler plate occasionally chooses to pass through a grain. Fig. 20 is comparable to Fig. 4, and shows the other extreme. These specimens were purified in hydrogen, too, but the treatment was carried to completion. The grain boundaries were relieved of their burden during a subsequent treatment in vacuo, the metal healed, and cathodic electrolysis developed a strictly transgranular weakness.



(*a*) (*b*)

FIG. 19 MICROGRAPHIC STUDY SIMILAR TO FIG. 18, BUT SHOWING CRYSTALLOGRAPHIC MARKINGS DEVELOPED BY ELEMENTAL HYDROGEN WITHIN GRAIN

(*a*, As removed from hydrogen treatment; *b*, additional cathodic treatment to emphasize transcrystalline weakness; ×200.)



(*a*) (*b*)

FIG. 20 SAME TECHNIQUE USED AS IN FIGS. 18 AND 19, EXCEPT THAT NOW THE FRACTURE IS ENTIRELY TRANSCRYSTALLINE, AS IN FIG. 4

(Micrograph *a*, ×350; micrograph *b*, ×1000.)

Fig. 18 therefore may be said to represent hydrogen attack under conditions of ammonia synthesis; Fig. 20 pickling-brittleness; and Fig. 19 boiler embrittlement.

The key to another puzzling observation in boiler embrittlement may be contained in this same explanation. The fact that the metal adjoining a crack is not brittle (38 has been held by some to disprove the hydrogen theory (233). On the contrary, that observation is in exact accord with the present argument, since escape of the gas through the surface of the fracture will permit ductility to return in the surrounding metal, just as it is known that boiler steel will recover its ductility if allowed to lie around awhile at temperatures well below those for annealing (155, 177). Although the compound gases are highly insoluble, they do ultimately lose at least their high compression, just as hydrogen does in a shorter period of time in the case of pickling brittleness. How could a theory of selective corrosion possibly fit these facts?

On the other hand, Straub's broad statement (233) that the adjacent metal retains its original properties may be going too far. In spite of the tendency to recover upon standing, more careful examination would very likely show deterioration of the proportional limit, if not the tensile strength and ductility, in agreement with well-established characteristics of intercrystalline H attack (262, 314).

EFFECT OF STRESS

Stress is doubtless important to cracking in boilers, for it plays a similar role in all other forms of hydrogen activity. Certainly the crack itself is caused by superimposed stress since hydrogen itself only embrittles—never cracks—sound steel (404, 418–420, 423). There is, however, an outstanding paradox in existing conceptions on boiler embrittlement which has received no attention and yet is critical to the entire subject.

Long ago there was established as a fundamental in metallurgy that, at temperatures where steel is elastic, the grain boundaries appear to be stronger than the grain itself (47, 113, 137). As Humfrey, an English metallurgist examining a boiler failure 30 years ago (75), observed: "It is a well-marked fact that the joints

between . . . the individual crystals . . . are considerably stronger than the gliding or cleavage planes within them." A moment's reflection recalls the fact that "cold-work," almost by definition, causes plastic deformation of the metal along slip planes within the crystal. In other words, stresses "beyond the yield point," which are so necessary to attaining boiler embrittlement, can scarcely be conceived to weaken the grain boundary, because those stresses are relieved by the imperfections called slip planes operating within the grain. As a matter of fact, even at the ultimate breaking load, after the stress necessary to start slip has been greatly exceeded and failure finally takes place, that failure is still through the grain, taking place along major planes of imperfection within the crystal commonly called cleavage planes. If the grain boundary is weakened at all, stress must disrupt the grain itself even more. How, then, can one adopt a theory of selective corrosion, a theory which depends upon the preferential weakening of grain boundaries by strain, and find it at all congruous with the facts? Furthermore, cold-working increases the solubility of steel in aqueous solutions, it is well known; but the increased rate of solution involves the grain itself in most cases, because cold-working makes the metal anodic, and because the effect of the cold-work is upon the grain itself. The selective-corrosion theory would seem to require the grain boundary to become electropositive from cold-working, when the exact opposite appears to be the case.

True, other forms of cracking, such as "season-cracking" in brass, and those discussed earlier, depend upon stress and yet have no conceivable relationship with hydrogen. But those cases remain unsolved. Even though they appear to represent selective grain-boundary attack, no one has yet provided an acceptable explanation for the phenomena. And if anyone wishes to take advantage of this exception, he must first explain why boiler embrittlement is notable for occurring underneath a smooth, black layer of iron oxide which always attests its inception and source; whereas every case of intercrystalline failure from plain chemical attack, to the best of the author's knowledge, shows the expected granulation on the surface. The present gas theory is tenable in that regard, since hydrogen dissolves into the iron without physical disturbance until it reaches the scene of its subsequent reactions.

In the present specific case of boiler embrittlement, hydrogen affords a simple and ready answer to this seeming paradox of stress. Any stress which exceeds the yield point likewise opens the imperfection or slip planes which house hydrogen in the elastic range (refer to Figs. 4, 20). Two factors then come into play: (*a*) More hydrogen is produced by the steam-iron reaction, because the iron is made more active chemically and because infiltration of the liquid into those imperfection planes permits a greater reactive area; (*b*) more hydrogen is absorbed because of the greater chemical activity and because the opened rifts afford sites for occlusion. In other words, in cold-worked steel, a greater movement or flow of reactive hydrogen gas occurs through the metallic membrane of surface grains, permitting a sufficient supply to reach inner grain boundaries where resultant gaseous products accumulate until they disrupt the grain-to-grain contacts, and the matrix is brittle.

Although stress is admittedly vitally important to embrittlement of steam boilers, it must not be classed as a truly fundamental factor, except in actual cracking. The fundamental factor in the destruction of ductility is the equilibrium between infusing hydrogen and the impurities within the steel. Stress aids in the attainment of, or the approach to, that equilibrium. Whether it simply breaks off the protective Fe_3O_4 layer, or whether its action is more subtle, cannot now be determined. It is plainly an accelerating factor which increases the rate of hydrogen infusion beyond some value that is probably critical for boiler conditions, below which the gases either diffuse from the steel faster than they can develop embrittling pressures, or embrittling pressures are not attained in the lifetime of ordinary boilers. The actual cracking does depend upon superimposed stress, and should not be confused with embrittlement, which is simply a condition of the metal wherein it is unable to respond to stress except by rupturing.

Such a conception of stress can be strengthened by numerous observations. Even in "pickling-brittleness," Langdon and Grossman long ago observed that cold-working accelerated embrittlement (126); and that cold-worked steel occludes inordinate quantities of hydrogen is common knowledge (384–389). At temperatures of the hydrogenation plant, where stresses are likely to fade rather quickly, previous cold-working greatly increases the intercrystalline failure caused by hydrogen (332), as it does in ammonia synthesis (372). Körber noted a similar effect with regard to decarburization in hydrogen (327); and, at Battelle Memorial Institute, specimens of carbon steel heated in hydrogen showed a tremendous increase in decarburization when the steel was simultaneously deformed in tension. In conditions of ammonia synthesis, stress is exceedingly important in accelerating deterioration; but with longer periods of time quite the same results are obtained without stress.

Effect of Caustic

Similarly, the effect of caustic, as important as it is, must be regarded simply as an accelerating, or catalyzing factor. A great many reasons have been advanced to explain the admitted fact that boiler embrittlement, as it is observed, depends upon NaOH; and there is no reason to doubt that that chemical concentrating in seams and crevices leads directly to the trouble. But again, the ultimate gas pressure obtainable in the grain boundaries, which is the basis for embrittlement, is the same whether Fe_3O_4 is produced by caustic or by pure distilled water. The gases which can form are dependent only upon impurities within the steel, and their partial pressures are controlled only by temperature, for the whole gaseous system is proscribed by involving saturated steam, as already explained.

Consequently, caustic must be placed in a category with stress as an agent which accelerates the infusion of hydrogen so that the gases will occlude more rapidly than they disperse, leading to embrittlement in an observable period of time. Whether the caustic itself reacts with the iron (229), whether it increases the electromotive force of the solution with respect to the iron (211), or whether its function is to dissolve the oxide reaction product, which would otherwise seal off the steel for further attack by H_2O (360, 365), is at present immaterial. Tajc even suggests that NaOH is "neither an active ingredient of the corrosion process, nor a factor in determining the stability of the resulting iron oxide" (333). He concludes that NaOH peptizes the oxide to form a colloid, which befits the third suggestion just listed.

Be that as it may, the important feature is that caustic is the agent in boilers which provides hydrogen infusion at a rate sufficiently rapid to surpass that critical value above which embrittling pressures of gas develop and below which the gases dissipate rapidly enough to make harmless the reactions which have been discussed.

There can be little doubt that gaseous hydrogen under 20,000 psi, the pressure corresponding to the potential pressure of the hydrogen produced on the boiler wall, would produce embrittlement in boiler steel at 250 C in the absence of the steam-iron reaction, since intercrystalline H attack from less pressures and at lower temperatures has already received discussion.

Of course, the attack would depend upon the impurities in the boiler steel, for that pressure of hydrogen alone is insufficient to

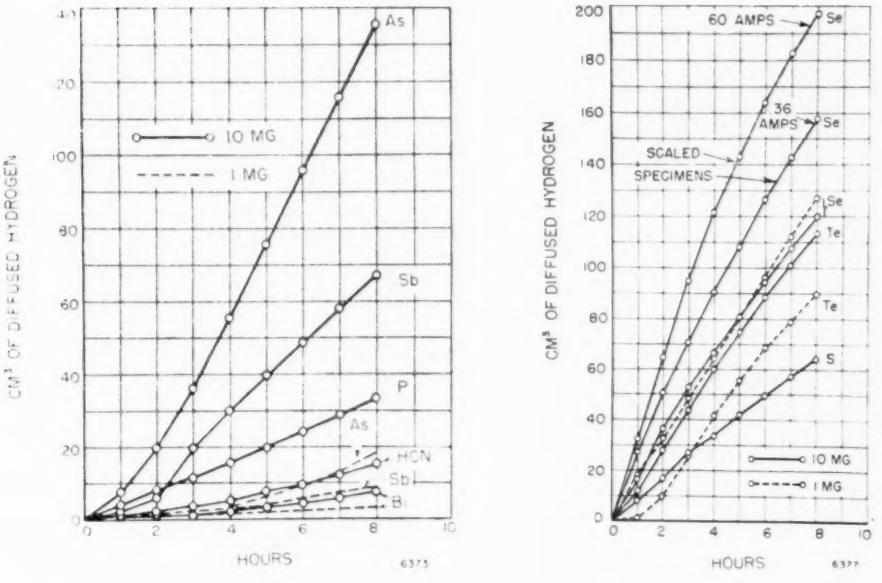


FIG. 21 HYDROGEN ABSORPTION FROM 10 PER CENT H_2SO_4 ELECTROLYTE
(*a*, Traces of elements from Group V of the Periodic Table added to the electrolyte. *b*, Same for Group VI. Steel surface = 10 sq in., T = 25 C. Baukloh and Zimmermann.)

cause embrittlement (refer back to Fig. 3). That, then, leads to conclusions regarding the role of the steel.

EFFECT OF COMPOSITION AND HEAT-TREATMENT OF THE STEEL

The foregoing suggests an important point, that boiler embrittlement is a metallurgical study as well as a chemical one. In fact, the work of Schroeder and of Straub, and their respective collaborators, has advanced the chemical aspects of the problem so far beyond the metallurgical aspects that the rest of the problem is now almost purely metallurgical. Their tests, however, also demonstrate that "killed" steel, i.e., steel whose oxygen is stabilized or removed, is superior in its resistance (398), a fact discovered 15 years earlier by the German investigator who invented Izett steel. Aluminum oxide, of course, is much more resistant to chemical attack than is iron oxide; and the ultimate equilibrium pressure of H_2O over Al and Al_2O_3 is so negligible that that oxide effectively precludes grain-boundary congestion from steam. In other words, iron containing no impurities other than Al and oxygen probably would never show hydrogen embrittlement until the pressure of the hydrogen itself became great enough to cause the transcrystalline type of brittleness.

Likewise, the general role of "aging," first mentioned by Stromeyer many years ago, should now be clear, since "aging" is nothing other than the precipitation of certain impurities from the mother lattice. As separate, precipitated phases, most of those impurities are amenable to H attack. A truly "non-aging" steel, such as is approached by Izett, would simply have no important quantities of nonmetallics with which the hydrogen could react.

In tests reported by Solberg, et al (414, 415), steel alloyed with Cr showed increased resistance to attack by steam, which now assumes significance in the light of the analogous results already discussed on H attack. Boilermen often decry the use of alloy steels because of expense; but in industries where the effects of hydrogen are recognized, nothing but alloy steels receive consideration. Pilling and Straub (409), it is interesting to note, just last year obtained a patent for alloy steels containing Ni, Cu, Al, Be, and Ti in amounts up to 3 and 5 per cent to resist caustic-cracking. Even the ammonia-synthesis industry seldom resorts to such alloys. According to Krupp's experience, a low-carbon steel with 1 per cent or less of vanadium may do the job. That would certainly bear investigating.

The problem is to obtain steel as low in nonmetallics as possible, while retaining necessary mechanical properties, and rendering those impurities which are present as harmless as possible both by alloying and by heat-treatment. No improvement need result from removing oxygen, if C, S, or N, for example, are left in harmful quantities. Stromeyer many years ago, discussing Houghton's paper (84), blamed embrittlement principally on N and P, and stated that when $P + 5\,N > 0.08$ per cent, failure results.

By heat-treatment, some nonmetallics can be put in solution. Rapid cooling from the anneal then tends to prevent their precipitation. At least, their migration to grain boundaries can be prevented, which acts to prevent accumulation of gaseous products in the grain boundary. Obviously, heat-treatment can only be a palliative. In carbon steels, a "sorbitic" heat-treatment is advised, because a finely disseminated pearlite results. Grain-boundary carbides seem especially harmful.

INHIBITORS AND ACCELERATORS

When hydrogen is accepted as the underlying cause of boiler embrittlement, an understanding of several hotly argued points on the action of so-called inhibitors and accelerators is possible. At the outset, Parr (94) concluded that oxidizing agents should inhibit embrittlement if hydrogen were its cause. In 1926, Parr and Straub stated that "NaOH is the only salt in the boiler which will embrittle steel" (181), and showed that Na_2SO_4 stops embrittlement when present in amounts approximately 3 times the total alkalinity as Na_2CO_3 (197). Then, in 1936, Straub and Bradbury (320) and Schroeder and Berk (315) simultaneously revealed a powerful role played by minute impurities in the caustic solutions that had been used in test (364). Principal among these was Na_2SiO_3, although the presence of Ca, Mg, and Al (320) and TiO_2, GeO_2, Sb_2O_3, and $SbCl_3$ (331) exerted an effect, too. Phosphates, chromates, tannates, acetates, besides

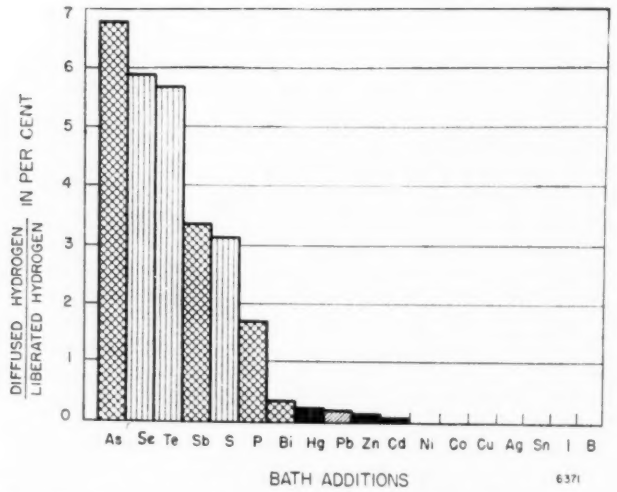


FIG. 22 DIAGRAM OF RATIO ABSORBED/LIBERATED HYDROGEN AS AFFECTED BY ACCELERATING ELEMENTS ADDED TO THE 10 PER CENT H_2SO_4 ELECTROLYTE IN 10-MG ADDITIONS PER LITER
(Current density 10 amp per sq ft, T = 25 C. Baukloh and Zimmermann.)

sulphates, were found to retard embrittlement by Parr and Straub (211), though a paper by Schroeder and Partridge (319) raises some question about Na_3PO_4. Schroeder, Berk, and O'Brien then state that dilute HNO_3 can be substituted for NaOH (331), although the year before Schroeder, Berk, and Partridge (317) found that sufficient quantities of oxidizing agents inhibit embrittlement; whereas in the recent A.S.M.E. Symposium on Boiler Embrittlement (405–408, 410, 412, 416) Bardwell and Laudemann (405) claim that their dilute addition of $NaNO_3$ has eliminated embrittlement in detector specimens on the whole Chesapeake and Ohio Railroad to date.

Finally, Na_2SO_4, the old stand-by written into the Boiler Code (185), itself failed to stop embrittlement (206, 311, 341, 397, 405, 406, 410), although Straub pointed out that the sulphate is ineffective unless a certain minimum of NaCl is also present (416). In the meantime, the National Physical Laboratory in England refuted Schroeder's silicate theory by obtaining embrittlement in pure NaOH, thereby proving that silicate can only be an accelerator. Rice even points out that the silicate may hinder embrittlement (397).

Desch undoubtedly comes closest to providing rhyme and reason when he observes that an inhibitor often acts as an accelerator under different conditions of temperature and pressure (361), similar to Straub and Bradbury's observation that sulphate protection disappears as the steam pressure increases, but that then another type of inhibitor fortunately becomes effective (352, 353).

In 1926, two Russian investigators, Alekseev and Polukarov (173, 174), discovered that a trace of As or Hg in an aqueous electrolyte led to rapid embrittlement of the steel cathode. Later, other elements were added to the list (250, 273), until Baukloh and Zimmermann (306), in 1936, provided the astonishing results shown in Figs. 21 and 22. The curves, in Fig. 21, show the tremendous increase in hydrogen absorption during cathodic electrolysis caused by seemingly negligible amounts of elements from groups V and VI of the Periodic Table. Arsenic present almost as a trace, for example, may increase the hydrogen absorption 100 times over that from a "pure" solution. As a matter of fact, in greater quantities these elements may act as inhibitors, which is significant in view of the analogous observations just recounted for boiler embrittlement (211, 361, 397). Körber and Ploum (250) even go so far as to suggest that iron containing none of these impurities will not dissolve in acid which contains none of them. In any event, these results offer significant comparison with the seemingly discordant findings of investigators on boiler embrittlement, for inhibitors and accelerators in hydrogen-caused boiler embrittlement would very reasonably be those inhibitors and accelerators here discussed. A diagrammatic illustration of the effect of these accelerators in aiding infusion at the expense of liberated portions of the gas stands in Fig. 22.

In the canning industry, the presence of sulphur and such elements has also been found to increase hydrogen evolution so greatly that the cans may swell and burst (247, 309).

In regard to inhibitors,[6] there is another interesting factor in boiler embrittlement which warrants study. Bardenheuer and Thanheiser (205), for instance, show very clearly that any inhibitor has its optimum range of temperature, and perhaps other conditions. When that range is exceeded, its inhibiting nature may disappear. One such instance is illustrated in Fig. 23, in which a plot of the ratio of absorbed to liberated hydrogen indicates that the absorbed fraction, which is the important fraction, of course, may increase without any evidence of a change in the visible evolution of gas.

The point to be made is that this type of action could operate at the steel-steam interface to promote or to inhibit the absorption of hydrogen, giving rise to the terms "inhibitors" and "accelerators." The suggestion simply amounts to an elaboration of Parr's original ideas. Christmann (258), for example, found that H from the steam-iron reaction reduces Na_2SO_4 in boiler water to form H_2S. Perhaps the inhibiting action of the sulphate is such a chemical one, removing a portion of the H before it can penetrate the iron. On the other hand, the argument over sulphate, i.e., whether its effect depends upon precipitation of a solid phase (181, 197, 297), may be explained by assuming that its precipitation on the steel would be a better barrier to hydrogen in spite of the fact that its chemical activity is then identical with that of the saturated solution (297). Na_2SO_4 is anhydrous above 33 C, whereupon a precipitated coating would protect the steel from steam attack. Na_2SiO_3, an accelerator, is strongly hydrated. Thus, Norton (377) observed a tremendous diffusion of hydrogen through an iron tube when it was coated with Na_2SiO_3, the accelerator, and heated to the boiler temperature of 200 C.

In further agreement, Norton found that sodium chromate, an inhibitor, completely stopped the diffusion through steel of hydrogen from tap water.

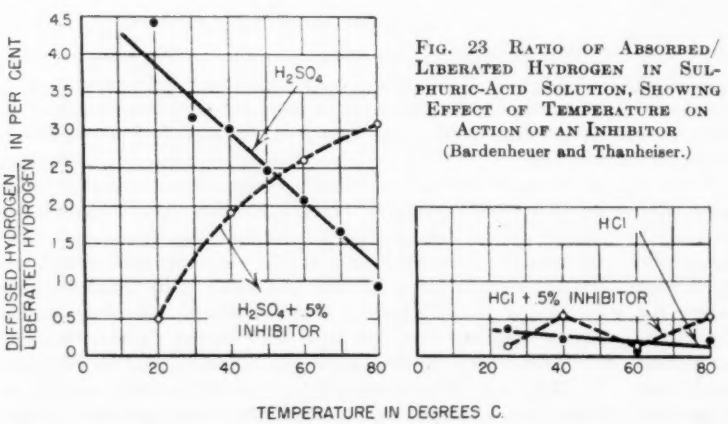
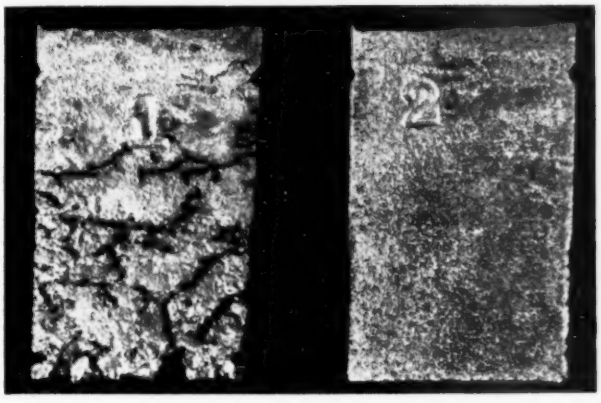


FIG. 23 RATIO OF ABSORBED/LIBERATED HYDROGEN IN SULPHURIC-ACID SOLUTION, SHOWING EFFECT OF TEMPERATURE ON ACTION OF AN INHIBITOR
(Bardenheuer and Thanheiser.)

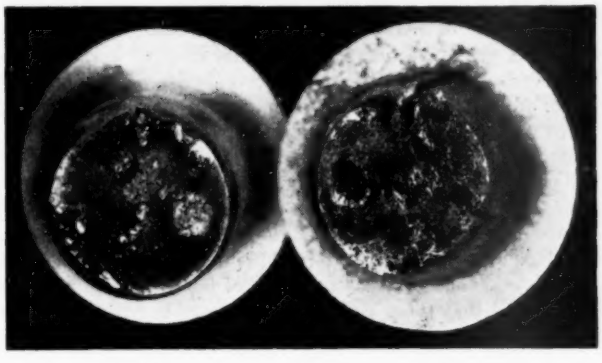
[6] For a more detailed discussion of inhibitors and accelerators, see reference 384.



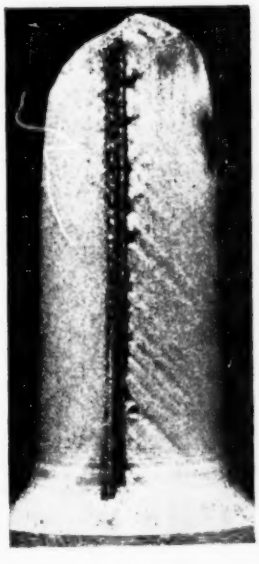
(*a*) (*b*)

FIG. 24 CLIPPINGS FROM SHEETS SHOWN IN FIG. 1, AFTER DEEP-ETCHING IN HCl

(*a*, Annealed in hydrogen; *b*, annealed in air.)



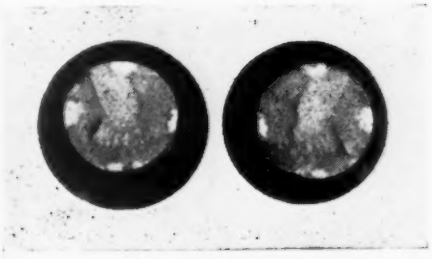
(*a*) (*b*)



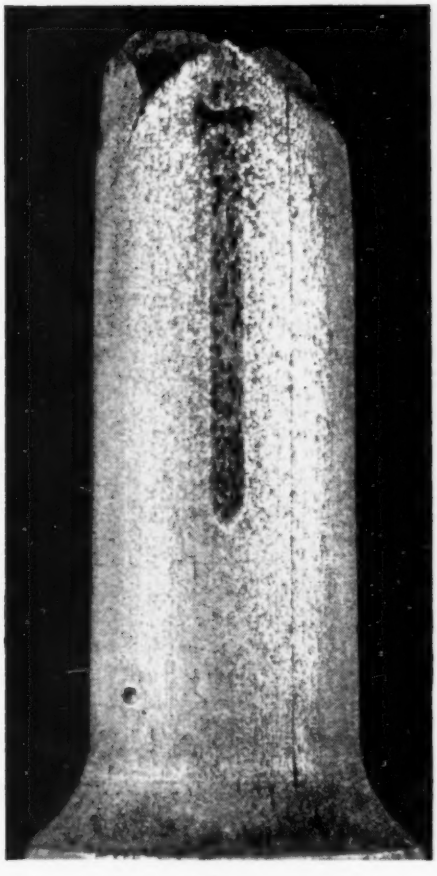
(*c*)

FIG. 25 TENSILE SPECIMEN OF WELD METAL CONTAINING HYDROGEN-EMBRITTLED ZONES, OR "FISH EYES," SHOWING PREFERENTIAL CHEMICAL ATTACK FROM CONCENTRATED HCl

(Fractured faces, etched and unetched; *a*, original fracture, *b*, after deep-etching; *c*, side view.)



(*a*)



(*b*)

FIG. 26 PHENOMENON IN FIG. 25, ARTIFICIALLY REPRODUCED BY EMBRITTLING ORDINARY STEEL TENSILE SPECIMEN ONLY ALONG FOUR THIN STRIPES AT QUADRANT POSITIONS

(*a*, Tensile fracture showing synthetic "fish eyes." *b*, Side view of half the specimen after deep-etching in HCl.)

Also, Langdon and Grossman long ago observed that Na_2SO_4 inhibited cathodic embrittlement from hydrogen (126). And Hill points out that Na_2SiO_3 is widely used in flotation, possibly because it has an interfacial effect on gas absorption (308).

Such observations suggest returning to the original opinions of Parr (94) on adding agents from the standpoint of frustrating hydrogen absorption. Simple tests at proper temperatures, using boiler steel as a diaphragm, with the various solutions on one side and a means of collecting transfusing hydrogen on the other side, might soon provide an empirical basis, at least, for selecting inhibitors suitable for any particular operating condition. Though Schroeder's embrittlement detector is a clever qualitative test, these diffusion experiments would provide quantitative information, and rapidly. Furthermore, that information would be so fundamental that running individual destructive experiments upon new boiler installations might become unnecessary, since the results could be predicted.

Why these substances affect hydrogen absorption as they do is

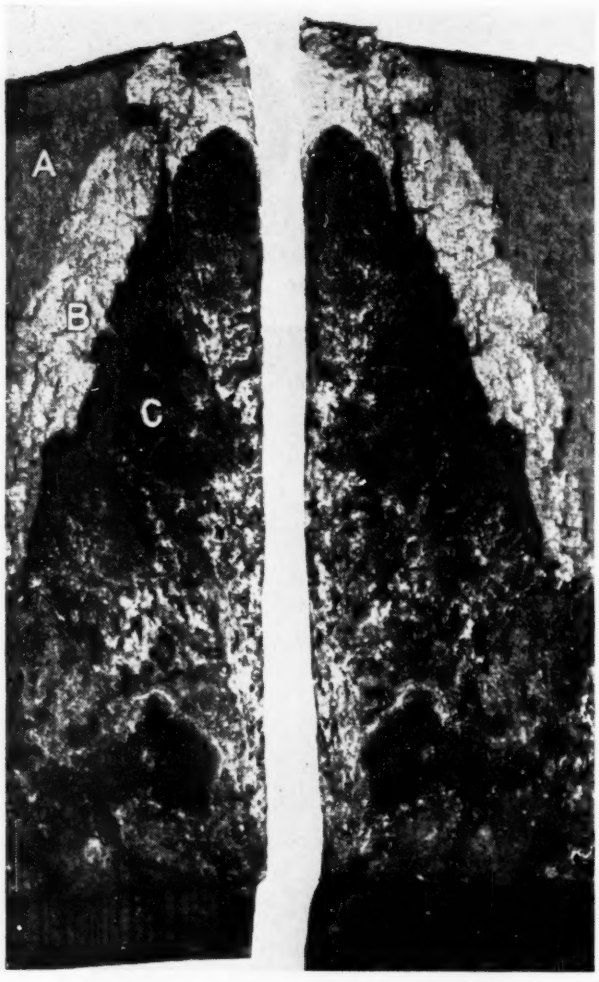


FIG. 27 FRACTURED FACES OF A PARTLY CRACKED BOILER PLATE
(*A* shows a zone of seemingly normal, ductile metal farthest removed from the source of attack; *B* is a zone of hydrogen-embrittled metal preceding *C*, which is a zone of direct chemical attack, progressing into the original crack and into the intergranular voids opened by the hydrogen attack. ×2.)

as yet unknown. That they do is sufficient basis for prosecuting such an investigation.

VISUAL PROOF OF THE HYDROGEN THEORY

In earlier sections of the paper, transcrystalline brittleness from elemental hydrogen was described as a function of pressure within crystallographic planes of the grain; and micrographs actually showed these planes opened by the gas during embrittlement. That they truly are opened, and with some permanent set, is shown in the illustrations which follow. In Fig. 24 are two clippings from the respective edges of the two sheets shown in Fig. 1. It will be recalled that one was embrittled by hydrogen and the other was not. Deep-etching in HCl developed severe fissuring in the embrittled specimen, as may be seen. In other words, the solution was able to penetrate more rapidly into metal that had been embrittled by hydrogen.

In Fig. 25, a similar instance is shown in regard to the "fish eyes" discussed earlier. The fractured faces of a tensile specimen of weld metal are shown as (*a*) and (*b*), the former being an original face; the latter the corresponding face after deep-etching in HCl; (*c*) is a side view of specimen (*b*). Note the savage attack of hydrogen-embrittled portions, attesting the distending and weakening forces of that trapped gas. In Fig. 26 the explanation is put to a more severe test. A tensile specimen of ordinary steel akin to boiler plate was coated with Glyptal except along four longitudinal stripes at quadrant positions. Cathodic electrolysis developed four synthetic "fish eyes," as may be seen in the fractures at (*a*). After 1 year of standing at room temperature, during which time all brittleness must have vanished, the specimen developed the marked preferential chemical attack shown in Fig. 26 (*b*). Thus hydrogen embrittlement truly distends and weakens the body of the grain. It must be remembered that these three figures pertain to transcrystalline brittleness, but also that they illustrate how hydrogen paves the way for subsequent chemical attack, a question which may have some significance in boiler embrittlement.

In intercrystalline H attack, such as boiler embrittlement, the compressed gas in the grain boundaries must have a similar effect, the only difference being that it opens the grain boundaries to subsequent chemical attack instead of the planes within the grain.

Accordingly, the whole story of boiler embrittlement seems to

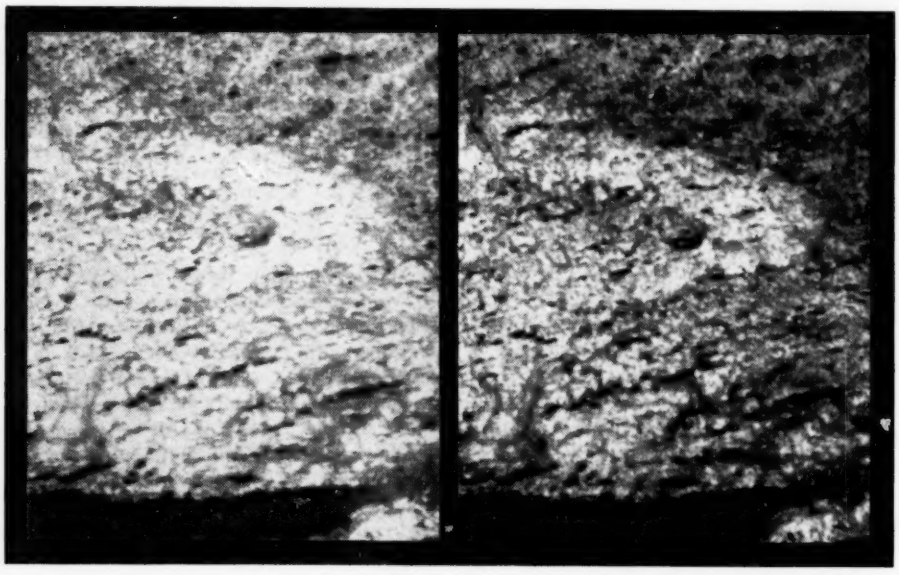


FIG. 28 STEREOMACROGRAPH OF ZONE *B* IN FIG. 27, SHOWING POROSITY FROM HYDROGEN ATTACK AND PROGRESSION OF BOILER EMBRITTLEMENT; ×10

lie within the single illustration, Fig. 27. Several samples of embrittled boiler plate were kindly furnished by Dr. Schroeder and Mr. Berk. Among other tests, these plates were broken open along visible cracks. A typical fracture through a crack beginning at a rivet hole in the outer plate of a double-plate boiler shell is shown in Fig. 27.

There are three obvious zones on the fractured faces; *A* is the gray fracture typical of normal, ductile metal and composes the zone furthest removed from the concentrated caustic solution in the leak around the rivet hole toward the inside of the boiler. Adjacent to that leaky seam and rivet hole is a zone of badly corroded metal, namely, zone *C*, obviously caused by penetration of the corrodant into the actual crack. In between these two is zone *B*.

Zone *B* is bright and clean, macroscopically and microscopically typical of metal reduced and purified in hydrogen. Zone *B* appears brittle, which is also typical of hydrogen attack. Zone *B* is intermediate between seemingly normal metal and cracked corroded metal; and that zone therefore represents an "advancing front" for this phenomenon of boiler embrittlement. The question: "Does the caustic enter the steel by creating fissures, i.e., selective corrosion, or are fissures created by another agent, such as hydrogen, which then permit the caustic to enter the steel?" seems to be answered clearly in Fig. 27.

Such an order of events is neither untoward nor unique. Long ago it was shown in the case of copper that granular deterioration from oxidation depended upon the grain boundaries first being opened by hydrogen embrittlement (142). Fig. 14 demonstrates the same thing for steel.

To convey the full significance of Fig. 27 as clearly as possible, a stereomacrograph[7] is included in Fig. 28. With the depth afforded by that type of illustration, one can more clearly see the marked porosity of the embrittled zone where nonmetallics have been removed from grain boundaries, seams, and inclusions, though photographic reproduction does this test an injustice. Into that porous mass, the corroding chemical can be seen advancing on one side; and on the other side one may observe that cavities also exist, but that the action is incomplete. Consequently, the metal there still appears ductile, although

[7] This stereograph may be examined with a pocket viewer of the Keystone type from which the back has been removed, or with a matched pair of low-power magnifying glasses. Many people can obtain fusion by holding the prints squarely before the eyes at the shortest possible focal distance and "staring through" them at an imaginary distant object.

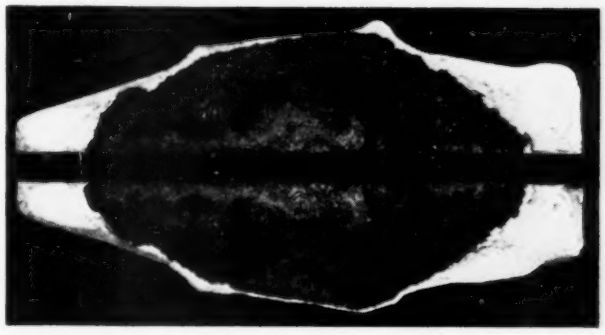


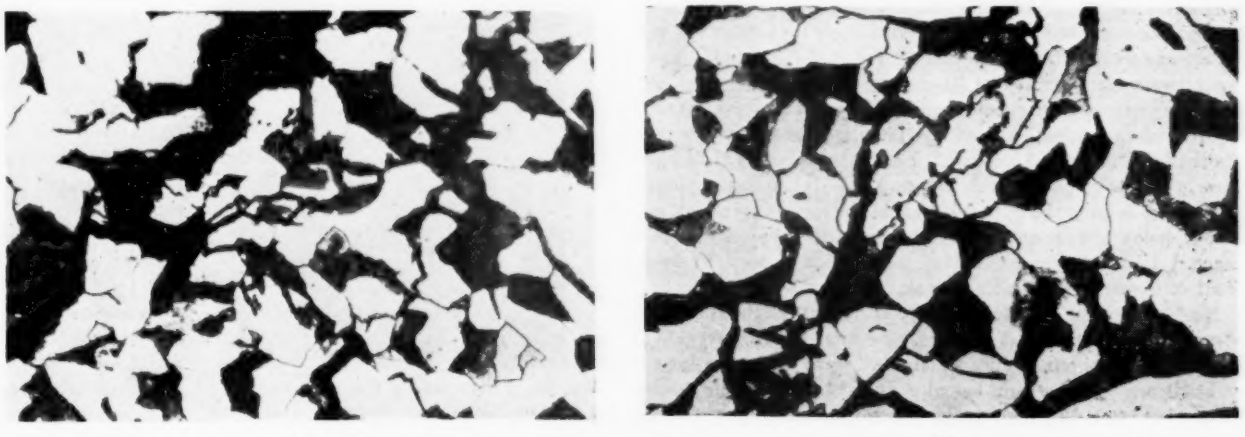
FIG. 29 SECTION OF RAILROAD RAIL FRACTURED THROUGH A CRACK SHOWING DUCTILE METAL, HYDROGEN EMBRITTLEMENT, AND CHEMICAL ATTACK SIMILAR TO BOILER PLATE IN FIG. 27

it must have contained grain-boundary gases under pressures which only lacked attaining that critical pressure at which the grains are forced apart and the metal is embrittled.

The whole appearance is in such exact accord with the present discussion that its importance can hardly be overestimated. The brightness of the brittle zone attests the strong reducing action of hydrogen; and the absence of flat cleavage facets in that zone shows that the attack is predominantly intercrsytalline, and that that fracture type was therefore imposed by the hydrogen function, since the fracture would normally be transcrystalline. The obvious and destructive porosity pervading the entire advance zone is sufficient testimonial *that boiler embrittlement and intercrystalline hydrogen attack are certainly identical.*

Actual cracking, it is well to repeat, is enabled—not caused—by the embrittlement. Use of the term "boiler embrittlement" for cracking is indiscriminate, since "embrittlement" only indicates a susceptibility to cracking, without further implication. Cracking first occurs when embrittled metal is subjected to stress. In boilers, that stress may be operational, or it may possibly arise from volume changes in the metal caused by the gas reactions, or both. The present study does not concern those stresses.

An observation with *trans*crystalline brittleness, directly analogous with that in Fig. 27, is shown in Fig. 29. A railroad rail, annealed in hydrogen for a short period at 1200 C, absorbed so much of the gas that it developed a large transverse crack from its own cooling stresses upon removing it from the furnace.



(*a*) (*b*)

FIG. 30 MICROGRAPHS OF SPECIMEN IN FIG. 27, TAKEN IN CORRODED ZONE *C*; ×500

(Note the thin fingers of gray material in and around the ferrite, which probably represent iron oxide formed from water vapor penetrating fissures opened by hydrogen attack.)

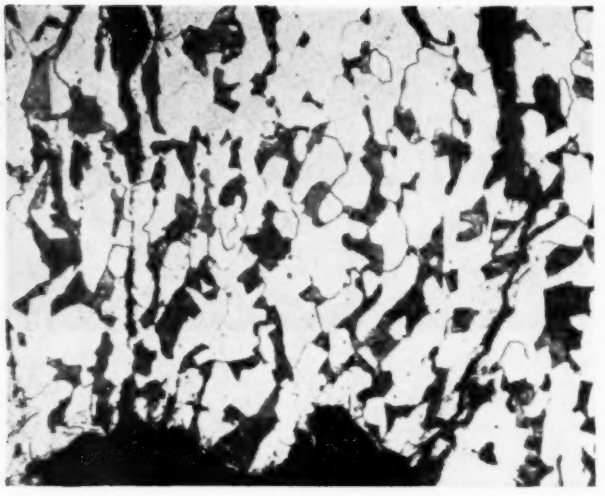


FIG. 31 MICROGRAPH TAKEN CLOSE TO BOUNDARY OF ZONES *A* AND *B* IN SPECIMEN OF FIG. 27, SHOWING ATTACK AND REMOVAL OF NON-METALLICS BY THE GAS REACTION; ×250

After reheating in air to a temperature which confers ductility upon normal rail steel, the specimen was fractured through the crack, just as the boiler plate was fractured. The same three zones were visible, as may be seen in Fig. 29, though their disposition is considerably different, in accordance with the different conditions. Note the thin fibrous rim around the specimen, which is always present in hydrogen-embrittled specimens because the hydrogen cannot be held under embrittling pressure so near to the surface for any appreciable period of time. Then there is the shiny, brittle zone, and next the zone of chemical attack, this time from oxidation during the heating in air. The hydrogen embrittlement, then, enabled both the cracking from the superimposed thermal stress and the subsequent chemical attack.

Micrographic study of the boiler plate in Fig. 27 further confirms the statements which have been made. In the corroded zone *C*, penetration principally along grain boundaries is easy to find. Near the crack, all fissures lead plainly to the surface, and all are filled with corrosion product. Deeper in the metal, the cracks cannot be followed to the surface. Because they are likewise filled with corrosion product, the surmise is well made that they do connect with the surface but that the two-dimensional section does not reveal it. Also, deeper in the metal under zone *C*, the corrosion product is neater, taking on a smooth, gray appearance resembling iron oxide. It is likely that water vapor—steam—penetrates these finer fissures ahead of the liquid. These features may be seen in Fig. 30.

In the hydrogen-embrittled zone *B*, the removal of nonmetallics is everywhere evident, just as was plainly observed in a macro-study of the untouched fracture. Empty holes betray the former presence of inclusions; but there is no trace of chemical corrosion. The action is quite the opposite, in that the metal is purified, and empty holes remain empty. The corrodant definitely has not reached the hydrogen-embrittled zone which is seen to lie in front of the zone of chemical attack.

No attack of the carbide is visible, in contrast to the specimens attacked by hydrogen at higher temperatures. However, C is only one of the nonmetallics which may serve as a basis for gas embrittlement, and reason has already been given for suspecting O in preference to C for boiler embrittlement. The English investigators found visible decarburization in boiler plate subjected to caustic embrittlement at temperatures above those of usual boiler service; and decarburization in high-pressure boilers has already been mentioned. At the temperatures of ordinary

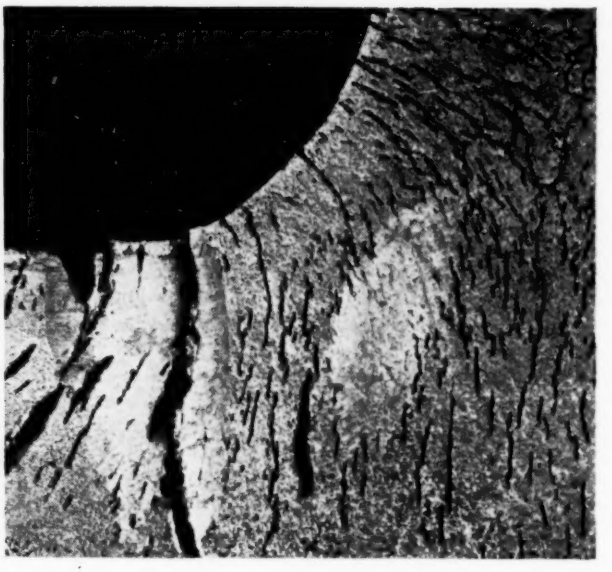


FIG. 32 APPARENTLY SOUND BOILER PLATE AFTER DEEP-ETCHING; COMPARE WITH FIGS. 24 TO 26

boiler service, another equilibrium than that of C-Fe-H may well predominate. Again, the embrittlement is likely due to an accumulation of several gases.

On the other hand, one must recognize that outright visible removal of carbon need not be a prerequisite for embrittlement. The conversion of a gas, such as methane, from a solid state, such as iron containing carbide and dissolved hydrogen, demands a volume increase of roughly 5000 times for 1 atm pressure and at boiler temperatures. If the reaction takes place within the solid, in the absence of a fortuitous cavity, its formation immediately imposes upon the surrounding metal a compression of approximately 75,000 psi, which can account for embrittlement without further ado. The equations already discussed, with their monstrous values for potential methane pressures, clearly indicate that a mere 75,000 psi will do nothing to reverse or discourage the reaction.



FIG. 33 FRACTURE OF CENTRAL PLATE IN A THREE-PLY BOILER SHOWING A BRITTLE ZONE ADVANCING FROM BOTH SIDES WITH A DUCTILE ZONE IN BETWEEN

(The central position of this plate has allowed solutions to concentrate on both sides, with resultant hydrogen attack proceeding from two directions toward the center.)

Nor would the amount of carbide lost by this efficacious reaction necessarily be visible under the microscope. Visible decarburization represents removal of the carbon from the steel, which *follows* embrittlement and,



FIG. 34 MICROGRAPH OF BOILER STEEL EMBRITTLED IN SCHROEDER'S EMBRITTLEMENT TEST
(Note definite presence of both inter- and transcrystalline fissures; ×300.)

consequently is in no way necessary for embrittlement. The higher temperatures of hydrogenation favor removal of the trapped gas, and decarburization becomes visible.

In ductile zone *A*, inclusions are only partly attacked, in agreement with earlier conclusions. In Fig. 31, a single micrograph shows two inclusions lying as close to the boundary of zones *A* and *B* as can be determined. Although it is almost too much to expect, the inclusion on the brittle side is completely removed, and the one on the ductile side is only partly removed. Each is typical of the zone on its side, and no point will be made over the surprising proximity of these two cases. The important thing to note is that the inclusions, and material in the rolling seams, have been attacked and largely removed by the gas reaction, as was surmised from macroscopic observation in the stereograph. The absence of visible decarburization again points to oxygen and oxides as being particularly vulnerable to the conditions for boiler embrittlement. The nature of the crack running from each inclusion out to the fractured face is not clearly understood, but may indicate either brittleness at the time of fracture, or previous rupture caused by the trapped gases. The specimen, incidentally, was polished with care to retain all nonmetallics, though it was perfectly clear from macroscopic observation of the freshly fractured face that zone *B*, and zone *A* to some extent, contained only vacuous pores where nonmetallics formerly were.

In Figs. 24 to 26, the accelerated attack of hydrogen-embrittled metal was demonstrated, and the opinion was advanced that grain-boundary gases should do the same. A section of the boiler plate submitted by Schroeder and Berk was accordingly deep-etched, with the result shown in Fig. 32. The mass of fissures was visible only after the etch treatment, which certainly suggests a close analogy with the action shown in Figs. 24 to 26.

That plate, which happened to be the center strake of a three-ply boiler, was fractured through a visible crack, with the interesting results shown in Fig. 33. In its central position, concentration of the solution could occur on both sides. Consequently, there are two brittle *B* zones, one proceeding from each side of the plate. In between is the ductile *A* zone not yet overrun. The action is plainly stronger on one side than on the other, corrosion being rather limited to the side having the principal concentration of chemicals.

Micrographic study revealed similar conditions to those in the other specimen.

Schroeder and Berk also submitted some boiler plate which had been cracked in synthetic solutions containing 500 ppm of NaOH. Micrographic examination of those specimens revealed a typical example of combined intercrystalline and transcrystalline failure. An example is shown in Fig. 34. In their rigorous, short-time tests does it not now seem reasonable that the compound gases causing intergranular failure should lag and transgranular failure from elemental hydrogen should correspondingly be favored? No further comment should be necessary regarding the balance of gas reactions and its relationship to the failure shown in Fig. 34.

CONCLUSION

A Concise Definition of "Boiler Embrittlement." This preliminary study now affords a new conception of the phenomenon known as "boiler embrittlement," a conception which can be simply stated as follows:

"*Boiler embrittlement is nothing other than an intermediate stage in a naturally occurring hydrogen purification treatment.*"

Thus, one begins with a boiler made of steel, which is the element iron containing certain nonmetallic impurities then:

1 The steam-iron reaction, which is enabled to progress more or less continuously, depending upon various factors, at loci where a caustic solution has concentrated, provides a more or less continuous infiltration of hydrogen through that steel.

2 The hydrogen reacts with the nonmetallics to form gaseous products within the steel.

3 These gases accumulate under pressure within the grain boundaries and at other seats of the nonmetallics until their pressure exceeds the cohesive strength of the grains and the granular structure is stressed to disruption.

That condition is recognized as "boiler embrittlement," and a stress applied to such metal may cause it to crack. The process, if allowed to continue, would then follow these well-established steps in the purification of steel by hydrogen at elevated temperatures:

4 Disruption of the grains extends communication of the gaseous accumulations until a portion escapes into the atmosphere, constituting the first actual removal of nonmetallics and incepting actual purification.

5 That degassing continues until the reactions are complete and insufficient gas remains to force itself through the structure out to the surface.

The material is then no longer steel, but is purified iron containing a small amount of residual gases. Embrittlement has vanished.

Direction and Aims of Future Research. As stated in the introduction as an opening premise, the present paper does not purport to provide a preventative of boiler embrittlement. Instead, it has attempted to interpret the work that has been done to date to show that a rational picture can be developed upon the new basis. With such an understanding, however, the battle is half won.

Simply stated, future research need have only two phases, one concerning a metallurgical study of steel to find an inexpensive

boiler plate for future boilers that will be relatively immune to hydrogen embrittlement from caustic attack, and the other concerning a chemico-metallurgical study of the role of inhibitors and accelerators in controlling hydrogen absorption so that the life of present boilers may be extended.

Both studies would be comparatively simple; and both promise extravagant results, because so little has as yet been done in direct relation to boilers, and yet from related fields a wealth of information is available.

Acknowledgment

Acknowledgment is made to Battelle Memorial Institute for the support of this work as part of its program for fundamental research; to K. G. Jones and H. L. Maxwell of E. I. du Pont de Nemours and Company, and to J. S. Vanick and the Chemical Construction Company of New York City, for their generous cooperation in submitting samples of deteriorated steel from chambers for hydrogenation and ammonia synthesis; to W. C. Schroeder and A. A. Berk for their kindness in supplying embrittled boiler plate; to G. A. Moore, J. L. Yarne, J. A. Finley, and R. W. Tindula, for their co-operation in preparing the metallographic specimens; and to C. E. Sims, under whose valuable supervision this work was conducted.

BIBLIOGRAPHY

1 Encyclopedia Brittanica: Steam Engines: Historical; see also Boilers.

2 British Patent no. 2855, by J. Stevens, 1805; see ref. no. 11.

3 "On Iron and Steel for Shipbuilding," by N. Barnaby, Trans. Institution of Naval Architects, vol. 16, 1875, pp. 131–136; discussion, ibid., pp. 136–146.

4 "Use of Steel for Marine Boilers and Some Recent Improvements in Their Construction," by W. Parker, Trans. Institution of Naval Architects, vol. 19, 1878, pp. 172–181; discussion, ibid., pp. 182–192.

5 "On the Russian Imperial Yacht *Livadia*," by E. E. Goulaeff, ibid., vol. 22, 1881, pp. 256–264.

6 "On the Peculiarities of Behavior of Steel Plates Supplied for the Boilers of the Imperial Russian Yacht *Livadia*," by W. Parker, ibid., vol. 22, 1881, pp. 12–25; discussion, ibid., pp. 25–37.

7 "Twenty Minutes on the Increased Use of Steel in Shipbuilding and Marine Engineering," by J. R. Ravenhill; ibid., vol. 22, 1881, pp. 38–51; discussion, ibid., pp. 51–53.

8 "On the Injuries Sustained by the *Livadia* in the Bay of Biscay," by E. J. Reed, ibid., vol. 22, 1881, pp. 265–270; discussion, ibid., pp., 271–283.

9 "Experimental Mechanics," by R. H. Thurston, Trans. A.S.M.E., vol. 2, 1881, pp. 55–58; discussion of O. Smith, pp. 58–69.

10 "The Protective Value of Boiler Inspection," by F. B. Allen, ibid., vol. 4, 1883, pp. 142–149.

11 "Steam Boilers as Magazines of Explosive Energy," by R. H. Thurston, ibid., vol. 6, 1885, pp. 199–223.

12 "Shell and Water-Tube Boilers," by A. Stirling, ibid., vol. 6, 1885, pp. 566–578; discussion, ibid., pp. 579–618.

13 "On Certain Properties Common to Fluids and Solids Metals," by W. C. Roberts-Austen, Proceedings Royal Institution of Great Britain, vol. 11, 1884–1886, pp. 395–412.

14 "On the Pickling Brittleness of Iron," by A. Ledebur, *Stahl und Eisen*, vol. 7, 1887, pp. 681–694.

15 "New Experiments on Pickling and Rusting Brittleness of Iron," by A. Ledebur, ibid., vol. 9, 1889, pp. 745–755.

16 "An Interesting Boiler Explosion," by F. H. Daniels, Trans. A.S.M.E., vol. 14, 1892–1893, pp. 118–125; discussion, ibid., pp. 125–146.

17 "Memoirs on the Elasticity and Dilation of Fluids at Very High Pressures," by E. H. Amagat, *Annales de Chimie et de Physique* vol. 29, 1893, pp. 68–136.

18 "Internal Strains in Section of Harveyized Steel Bar," by J. E. Howard, Watertown Arsenal, Tests of Metals, 1893, p. 285.

19 "Note on the Oxidation and Corrosion of Iron and Steel," by W. Thomson, *Journal*, Society of Chemical Industry, vol. 13, 1894, pp. 118–120.

20 "Brittleness in Soft Steel," by C. H. Ridsdale, *Journal*, Iron and Steel Institute, vol. 53, 1898, pp. 220–234.

21 "The Crystalline Structure of Iron and Steel," by J. E. Stead, ibid., vol. 53, 1898, pp. 145–189; discussion, ibid., pp. 190–205.

22 "Brittleness Produced in Soft Steel by Annealing," by J. E. Stead, ibid., vol. 54, 1898, pp. 137–154; discussion, ibid., pp. 155–184.

23 "Investigations of Boiler Explosions," by G. C. Henning, Trans. A.S.M.E., vol. 20, 1899, pp. 649–654; discussion, ibid., pp. 654–662.

24 "Practical Microscopic Analysis for Use in the Steel Industries, With an Introduction to a Systematic Study of Soft and Dead Soft Steel," by C. H. Ridsdale, *Journal*, Iron and Steel Institute, vol. 56, 1899, pp. 102–147; discussion, ibid., pp. 148–159.

25 "Tension of Saturated Mercury Vapor," by L. Cailletet, Colardeau, and Riviere, Comptes Rendus, vol. 130, 1900, pp. 1585–1591.

26 "Iron and Hydrogen," by E. Heyn, *Stahl und Eisen*, vol. 20, 1900, pp. 837–844.

27 "The Correct Treatment of Steel," by C. H. Ridsdale, *Journal*, Iron and Steel Institute, vol. 60, 1901, pp. 52–97; discussion, ibid., pp. 98–103.

28 "Physical Tests on an Old Boiler," by Walther Meunier, Report of Chief Engineer to Elsässischen Vereines von Dampfkesselbesitzern; *Zeitschrift, V.D.I.*, cf. vol. 46, 1902, p. 903.

29 "The Effect of Magnesium Chloride in theBoiler," by H. Ost, *Chemische Zeitschrift*, vol. 26, 1902, pp. 819–822.

30 "Copper and Hydrogen," by E. Heyn, *Metallographist*, vol. 6, 1903, p. 48.

31 "Diseases of Steel," by C. H. Ridsdale, *Journal*, Iron and Steel Institute, vol. 64, 1903, pp. 232–282; discussion, ibid., pp. 283–288.

32 "Corrosion of Iron," by W. R. Whitney, *Journal*, American Chemical Society, vol. 25, 1903, pp. 394–406.

33 "Investigation of the Mechanical Properties of Mild Steel Plate at Ordinary and Elevated Temperatures," by C. Bach, *Zeitschrift V.D.I.*, cf. vol. 48, 1904, pp. 1300–1308, 1342–1349.

34 "Copper and Oxygen," by E. Heyn, *Zeitschrift für anorg. Chemie*, vol. 39, 1904, pp. 1–23.

35 "Researches on Plate From Old Steam Boilers," *Zeitschrift V.D.I.*, vol. 48, 1904, pp. 217–219.

36 "Estimation of Oxygen in Copper," by L. Archbutt, *The Analyst*, vol. 30, 1905, pp. 385–394.

37 Several Reports Included in Appendix, by J. O. Arnold, ref. 38, pp. 368–383.

38 "Fractures in Large Steel Boiler Plates," by J. T. Milton, Trans. Institution of Naval Architects, vol. 47, part II, 1905, pp. 359–383; discussion, ibid., pp. 384–391.

39 See discussion, ref. 38, by C. E. Stromeyer, pp. 386–387.

40 Würzburg and Hamburg Code 1905, *Zeitschrift V.D.I.*, vol. 49, 1905, pp. 1958–1962.

41 "Formation of Cracks in Boiler Plate," by C. Bach, *Zeitschrift V.D.I.*, vol. 50, 1906, pp. 1–13.

42 "Formation of Cracks in Boiler Plate," by C. Bach, ibid., vol. 50, 1906, pp. 258–259.

43 "Delayed Cracking of Coldworked CopperAlloys," by Diegel, Verhandlungen d. Vereins zur Beförderung d. Gewerbefleisses, vol. 85, 1906, pp. 177.

44 "The Alleged Need of Flexibility in the Würzburg Standards," by R. Eichhoff, *Stahl und Eisen*, vol. 26, 1906, pp. 129–134.

45 "Brittleness and Blisters in Thin Steel Sheets," by E. F. Law, *Journal*, Iron and Steel Institute, vol. 69, 1906, pp. 134–144; discussion, ibid., pp. 145–160.

46 See ref. no. 45, R. L. Leffler, discussion, pp. 153–156.

47 "Deformation and Fracture in Iron and Steel," by W. Rosenhain, *Journal*, Iron and Steel Institute, vol. 70, 1906, pp. 189–228.

48 "Cracking of a Boiler Head During Pressure Testing," by C. Bach, *Zeitschrift V.D.I.*, vol. 51, 1907, pp. 465–468.

49 "Results of the Investigation of a Boiler Plate Ruptured in Pressure Testing," by C. Bach, ibid., vol. 51, 1907, pp. 747–751.

50 "The Present Status of the Question of Cracking in Boiler Plate," by R. Baumann, ibid., vol. 51, 1907, pp. 1982–1989.

51 "The Non-Metallic Impurities in Steel," by E. F. Law, *Journal*, Iron and Steel Institute, vol. 74, 1907, pp. 94–105.

52 "The Aging of Mild Steel," by C. E. Stromeyer, ibid., vol. 73, 1907, pp. 200–254; discussion, ibid., pp. 255–260.

53 "Further Experiments on the Aging of Mild Steel," by C. E. Stromeyer, ibid., vol. 75, 1907, pp. 86–107; discussion, ibid., pp. 108–113.

54 "Thermal Stresses and Cracking," by C. Sulzer, *Zeitschrift V.D.I.*, vol. 51, 1907, pp. 1165–1168

55 "Function of Oxygen in the Corrosion of Metals," by W. H. Walker, Trans. American Electrochemical Society, vol. 14, 1908, pp. 175–187.

56 "Corrosion of Iron and Steel," by W. H. Walker and A. M. Cederholm, *Journal*, American Chemical Society, vol. 29, 1907, pp. 1251–1264.

57 "The Action of Steam on Iron," by J. N. Friend, *Journal*, West Scotland Iron and Steel Institute, vol. 17, 1909–1910, pp. 66–79.

58 "The Passivity of Iron," by P. Krassa, *Zeitschrift für Elektrochem.*, vol. 15, 1909, pp. 490–500.

59 "The Aging of Mild Steel and the Influence of Nitrogen," by C. E. Stromeyer, *Journal*, Iron and Steel Institute, vol. 79, 1909, pp. 404–420; discussion, ibid., pp. 421–425.

60 "The Question of the Superiority of Machine Riveting," by C. Bach, *Zeitschrift V.D.I.*, vol. 54, 1910, p. 362.

61 "The Properties and Constitution of Copper-Arsenic Alloys," by G. D. Bengough and B. P. Hill, *Journal*, Metals Institute, vol. 3, 1910, pp. 34–79; discussion, ibid., pp. 80–97.

62 "The Behavior of Solid and Liquid Copper Toward Gases," by A. Sieverts and W. Krumbhaar, *Zeitschrift physikalische Chemie*, vol. 74, 1910, pp. 277–307.

63 "The Influence of Caustic Soda on Mild Steel," by C. E. Stromeyer, Memorandum by the Chief Engineer, Manchester Steam Users' Association, 1910, pp. 5–6.

64 "The Influence of Gases Upon the Critical Ranges of the Iron-Carbon Alloys," by J. H. Andrew, Iron and Steel Institute, Carnegie Scholarship Memoirs, vol. 3, 1911, pp. 236–248.

65 "On the Question of Crack Formation in Boiler Plates," by C. Bach, *Zeitschrift V.D.I.*, vol. 55, 1911, pp. 1296–1297.

66 "The Action of Mercury on Steel at High Pressures," by P. W. Bridgman, Proceedings American Academy of Arts and Sciences, vol. 46, 1911, pp. 325–341.

67 "Investigation of a Fractured Boiler Tube," by E. Heyn and O. Bauer, *Mitt. Kgl. Materialprüfungsamt*, Berlin, vol. 28, 1910, pp. 302–307.

68 "Stresses in Boiler Plate," by E. Heyn and O. Bauer, *Stahl und Eisen*, vol. 31, 1911, pp. 760–765.

69 "Iron and Nitrogen," by J. H. Andrew, *Journal*, Iron and Steel Institute, vol. 86, 1912, pp. 210–235.

70 "Investigation for Clarifying the Effect of Stresses, Which Develop in the Steel During Riveting and Lead to Rivet-Hole Cracking," by C. Bach and R. Baumann, *Zeitschrift V.D.I.*, vol. 56, 1912, pp. 1890–1895.

71 "Boiler Explosions in the Chemical and Allied Industries in Germany in 1912," *Chemische Zeitschrift*, vol. 37, 1913, pp. 1456–1457.

72 "On the Permeability of Iron for Hydrogen," by G. Charpy and S. Bonnerot, Comptes Rendus, vol. 154, 1912, pp. 592–594.

73 "Investigation of the Fractured End of a Marine Boiler," by E. Heyn and O. Bauer, *Stahl und Eisen*, vol. 32, 1912, pp. 1169–1174.

74 "Investigation of an Exploded Drum," by E. Heyn and O. Bauer, *Mitt. Kgl. Materialprufüngsamt*, Berlin, vol. 31, 1913, pp. 92–116.

75 "The Intercrystalline Fracture of Iron and Steel," by J. C. W. Humfrey, Iron and Steel Institute, Carnegie Scholarship Memoirs, vol. 4, 1912, pp. 80–107.

76 "Water Treatment and Boiler Troubles," by W. A. Pownall, Proceedings Western Railway Club, vol. 24, 1912, pp. 217–238.

77 "Thirty Boiler Plates With Cracks," by R. Baumann, *Stahl und Eisen*, vol. 33, 1913, pp. 1554–1561.

78 "On the Reactions Which Accompany the Diffusion of Hydrogen Through Iron," by G. Charpy and S. Bonnerot, Comptes Rendus, vol. 156, 1913, pp. 394–396.

79 "The Micro-Chemistry of Corrosion, Part I. Some Copper-Zinc Alloys," by C. H. Desch and S. White, *Journal*, Metals Institute, vol. 10, 1913, pp. 304–328.

80 "A Method of Improving the Quality of Arsenical Copper," by F. Johnson, ibid., vol. 10, 1913, pp. 275–293; discussion, ibid., pp. 294–303.

81 "The Embrittling of Iron by Caustic Soda," by J. H. Andrew, Trans., Faraday Society, vol. 9, 1914, pp. 316–329.

82 "The Solidification of Metals From the Liquid State," by C. H. Desch, *Journal*, Metals Institute, vol. 11, 1914, pp. 57–118.

83 "Initial Strains in Cold-Wrought Metals and Some Troubles Caused Thereby," by E. Heyn, ibid., vol. 12, 1914, pp. 3–37.

84 "Failures of Heavy Boiler Shell Plates," by S. A. Houghton, *Journal*, Iron and Steel Institute, vol. 89, 1914, pp. 266–292; discussion, ibid., pp. 293–316.

85 "Discussion on Failures of Forgeable Bars," by E. Jonson and others, *Journal*, American Institute of Metals, vol. 8, 1914, pp. 135–138.

86 "An Allotropic Modification of Lead," by H. J. M. Creighton, *Journal*, American Chemical Society, vol. 37, 1915, pp. 2064–2065.

87 "Failure of Brass. 2.—Effect of Corrosion on the Ductility and Strength of Brass," by Paul D. Merica, U. S. Bureau of Standards, Technical Paper 83, 1916, 7 pp.

88 "The Brittleness of Annealed Copper," by W. E. Ruder, *Journal*, The Franklin Institute, vol. 181, 1916, p. 859.

89 "Notes on Nickel Steel Scale and on the Reduction of Solid Nickel and Copper Oxides by Solid Iron," by J. E. Stead, *Journal*, Iron and Steel Institute, vol. 94, 1916, pp. 243–248.

90 "Studies on a Cracked Marine-Boiler Plate; Faulty Calking of Rivets," by O. Bauer, *Mitt. und Königl. Materialprüfungsamt zu Berlin*, vol. 35, 1917, pp. 194–203.

91 "Electrolytic Pickling Process and Its Effect on the Physical Properties of Iron and Steel," by J. Coulson, Trans. American Electrochemical Society, vol. 32, 1917, pp. 237–243.

92 "The Embrittling Action of Sodium Hydroxide on Mild Steel and Its Possible Relation to Seam Failures of Boiler Plate," by P. D. Merica, *Chemical & Metallurgical Engineering*, vol. 16, 1917, pp. 496–503.

93 "The Failure of Brass. 1.—Microstructure and Initial Stresses in Wrought Brasses of the Type 60 Per Cent Copper and 40 Per Cent Zinc," by P. D. Merica and R. W. Woodward, U. S. Bureau of Standards, Technical Paper 82, 1917, 72 pp.

94 "The Embrittling Action of Sodium Hydroxide on Soft Steel," by S. W. Parr, University of Illinois, Engineering Experiment Station, Bulletin 94, 1917, 57 pp.

95 "Memorandum by the Chief Engineer," Manchester Steam Users' Association, 1917; Abridged: "The Action of Caustic Liquors on Steel Plates," by C. E. Stromeyer, *Engineering*, vol. 104, 1917, pp. 645–646; also *Chemical Trade Journal*, vol. 61, 1917, p. 533; also, *Engineer*, vol. 124, 1917, p. 496; also, *Chemical & Metallurgical Engineering*, vol. 18, 1918, pp. 372–373.

96 See discussion, ref. 97, pp. 159–163, C. E. Stromeyer.

97 "The Failure of Boiler Plates in Service, and Investigations of the Stresses That Occur in Riveted Joints," by E. B. Wolff, *Journal*, Iron and Steel Institute, vol. 96, 1917, pp. 137–158; discussion, ibid., pp. 159–179; abstract, *Engineer*, vol. 124, 1917, p. 456.

98 "Causes and Prevention of Corrosion Cracking," by W. H. Bassett, Proceedings American Society for Testing Materials, vol. 18, 1918, part 2, pp. 153–162.

99 "Investigation on a Fractured Marine-Boiler Plate," by O. Bauer, *Stahl und Eisen*, vol. 38, 1918, pp. 457–463.

100 J. Bryden, see discussion, ref. 101, pp. 172–174.

101 "On Certain Failures of Steel Boiler Plates Under Pressure," by S. A. Houghton, *Journal*, West of Scotland, Iron and Steel Institute, vol. 25, 1917–1918, pp. 153–171; discussion, ibid., pp. 172–190.

102 A. B. Marquand, see discussion, ref. 101, pp. 174–175.

103 A. McCance, see discussion, ref. 101, pp. 175–178.

104 "The Action of Reducing Gases on Hot Solid Copper," by N. B. Pilling, *Journal*, The Franklin Institute, vol. 186, 1918, pp. 373–374; also, Trans. American Institute of Mining and Metallurgical Engineers, vol. 60, 1919, pp. 322–335; discussion, ibid, pp. 336–341.

105 "The Use of Mercury Solutions for Predicting Season Cracking in Brass," by H. S. Rawdon, Proceedings American Society for Testing Materials, vol. 18, 1918, part 2, pp. 189–200.

106 C. H. Ridsdale, see discussion, ref. 101, pp. 180–182.

107 "A Cause of Failure in Boiler Plates," by W. Rosenhain and D. Hanson, *Journal*, Iron and Steel Institute, vol. 97, 1918, pp. 313–324; also discussion, ibid., pp. 325–332.

108 T. M. Service, see discussion, ref. 101, pp. 178–179.

109 T. E. Stead, see discussion, ref. 101, pp. 182–186.

110 "Note on the Warping of Steel Through Repeated Quenching," by J. H. Whiteley, *Journal*, Iron and Steel Institute, vol. 98, 1918, pp. 211–214; discussion, ibid., p. 215.

111 "On the Decarburization of Steel With Hydrogen," by E. D. Campbell, ibid., vol. 100, 1919, pp. 407–415.

112 "Second Report to the Beilby Prize Committee of the Institute of Metals on the Solidification of Metals From the Liquid State," C. H. Desch, *Journal*, Metals Institute, vol. 22, 1919, pp. 241–263; discussion, ibid., pp. 264–276.

113 J. H. S. Dickenson, see discussion, ref. 112, pp. 274–275.

114 "The Penetration of Iron by Hydrogen," by T. S. Fuller, Trans. American Electrochemical Society, vol. 36, 1919, pp. 113–129; discussion, ibid., pp. 129–138.

115 "Season Cracking," by W. H. Hatfield and G. L. Thirkell, *Journal*, Metals Institute, vol. 22, 1919, pp. 67–91; discussion, ibid., pp. 92–126.

116 H. LeChatelier, see discussion, ref. 115, pp. 107–108.

117 H. LeChatelier, see discussion, ref. 111, p. 415.

118 F. Rogers, see discussion, ref. 115, pp. 114–115.

119 W. Rosenhain, see discussion, ref. 115, pp. 92–97.

120 "On the Inter-Crystalline Fracture of Metals Under Prolonged Application of Stress," by W. Rosenhain and S. L. Archbutt, Proceedings of the Royal Society of London, vol. 96, series A, 119–120, 1919, pp. 55–68.

121 E. A. Smith, see discussion, ref. 115, pp. 117–118.

122 "The Influence of Gases on High-Grade Brass," by T. G. Bamford and W. E. Ballard, *Journal*, Metals Institute, vol. 24, 1920, pp. 155–200.

123 "Note on a Failure of 'Manganese Bronze,'" by J. H. S. Dickenson, ibid., vol. 24, 1920, pp. 315–332.

124 "The Phenomena of Rupture and Flow in Solids," by A. A. Griffith, Philosophical Trans. Royal Society, vol. 221, series A, 1920–1921, pp. 163–198.

125 "Some Notes on the Effects of Hydrogen on Copper," by W. C. Hothersall and E. L. Rhead, *Journal*, Metals Institute, vol. 23, 1920, pp. 367–376; discussion, ibid., pp. 377–380.

126 "The Embrittling Effects of Cleaning and Pickling Upon Carbon Steels," by S. C. Langdon and M. A. Grossman, Trans. American Electrochemical Society, vol. 37, 1920, pp. 543–576; discussion, ibid., pp. 576–578.

127 "Peculiar Type of Intercrystalline Brittleness of Copper," by H. S. Rawdon and S. C. Langdon, U. S. Bureau of Standards, Technical Paper, 158, 1920, 5 pp.

128 "Intercrystalline Fracture in Mild Steel," by W. Rosenhain and D. Hanson, *Journal*, Iron and Steel Institute, vol. 102, 1920, pp. 23–30; discussion, ibid., pp. 31–37.

129 "On the Supposed Allotropy of Lead," by A. Thiel, *Berichte deutscher chemische Gesellschaft*, vol. 53, 1920, pp. 1052–1066.

130 "Experiments on the Deoxidation of Steel With Hydrogen," by J. H. Whiteley, *Journal*, Iron and Steel Institute, vol. 102, 1920, pp. 143–157.

131 "Note on Phosphor Bronze Bars," by J. Arnott, Trans. Faraday Society, vol. 17, 1921–1922, pp. 209–210.

132 "Contribution to the Knowledge of 'Aging' in Cold-Worked Iron," by O. Baurer, *Mitteilungen Materialsprüfungsamt*, Berlin-Dahlem, vol. 39, 1921, pp. 251–255.

133 "Chemical Influences in the Failure of Metals Under Stress," by C. H. Desch, Trans. Faraday Society, vol. 17, 1921–1922, pp. 17–21; abstract, *Engineering*, vol. 3, 1921, p. 418.

134 J. E. Fletcher, see general discussion, ibid., vol. 17, 1921–1922, pp. 156–159.

135 "Notes on Fractures in Locomotive Boiler Tubes," by H. Fowler, ibid., vol. 17, 1921–1922, pp. 82–90.

136 "Intercrystalline Fracture in Steel," by D. Hanson, ibid., vol. 17, 1921–1922, pp. 91–101; discussion, ibid., p. 146.

137 "The Mechanism of Failure of Metals From Internal Stress," by W. H. Hatfield; ibid., vol. 17, 1921–1922, pp. 36–46; discussion, ibid., pp. 147–148.

138 S. A. Houghton; see general discussion; ibid., vol. 17, 1921–1922, pp. 154–156.

139 C. F. Jenkin, see general discussion; ibid., vol. 17, 1921–1922, p. 148.

140 "Intercrystalline Cracking of Mild Steel in Salt Solutions," by J. A. Jones, ibid., vol. 17, 1921–1922, pp. 102–109; discussion, ibid., p. 154.

141 G. W. Malcolm, see general discussion; ibid., vol. 17, 1921–1922, pp. 159–160.

142 H. Moore; see Section III, general discussion; ibid., vol. 17, 1921–1922, pp. 58–61.

143 "The Action of Reducing Gases on Heated Copper," by H. Moore and S. Beckinsale, *Journal*, Metals Institute, vol. 25, 1921, pp. 219–240; discussion, ibid., pp. 241–258.

144 "The Season-Cracking of Brass and Other Copper Alloys," by H. Moore, S. Beckinsale, and C. E. Mallinson; ibid., vol. 25, 1921, pp. 35–125; discussion, ibid., pp. 126–152.

145 N. B. Pilling, see discussion, ref. 143, pp. 251–256.

146 A. W. Porter, see general discussion, Trans. Faraday Society, vol. 17, 1921–1922, pp. 150–151.

147 R. J. Redding, see discussion, ref. 143, pp. 244–246.

148 W. Rosenhain, see general discussion, Trans. Faraday Society, vol. 17, 1921–1922, pp. 149–150.

149 "Crack Formation in Boiler Plate," by B. Strauss and A. Fry, *Stahl und Eisen*, vol. 41, 1921, pp. 1133–1137.

150 C. E. Stromeyer; see Section III, general discussion, Trans. Faraday Society, vol. 17, 1921–1922, pp. 67–68.

151 F. Tomlinson, see discussion, ref. 143, p. 247.

152 "Hydrogen Decarburization of Carbon Steels With Considerations on Related Phenomena," by C. R. Austin, *Journal*, Iron and Steel Institute, vol. 105, 1922, pp. 93–142; discussion, ibid., pp. 143–155.

153 "Diffusion of Cathodic Hydrogen Through Iron and Platinum," by M. Bodenstein, *Zeitschrift Elektrochem.*, vol. 28, 1922, pp. 517–526.

154 "Strength and Elasticity of Boiler Plate at Elevated Temperatures," by H. J. French, *Chemical & Metallurgical Engineering*, vol. 26, 1922, pp. 1207–1209.

155 "Treatment of Feed Water," Report of the Prime Movers Committee, Proceedings National Electric Light Association, 1922, pp. 737–771.

156 "Occurrence of Oxides and Nitrides in Boiler Tube Steel," by A. E. White and J. S. Vanick, Trans. American Society for Steel Treatment, vol. 2, 1921–1922, pp. 323–330.

157 "Boiler Defects," by R. Baumann, *Zeitschrift V.D.I.*, vol. 67, 1923, pp. 1109–1113.

158 "Deterioration of Steel and Wrought Iron Tubes in Hot Gaseous Ammonia," by J. S. Vanick, Trans. American Society for Steel Treatment, vol. 4, 1923, pp. 62–78.

159 "The Compressibility of Five Gases to High Pressures," by P. W. Bridgman, Proceedings American Academy of Arts and Sciences, vol. 59, 1923–1925, pp. 173–211.

160 "Boiler Materials," by P. Goerens, *Zeitschrift V.D.I.*, vol. 68, 1924, pp. 41–47.

161 "Deterioration of Some Metals in Hot, Reducing Ammonia Gases," by J. S. Vanick, Proceedings American Society for Testing Material, vol. 24, part 2, 1924, pp. 348–372.

162 "Intercrystalline Fracture in Steel," by R. S. Williams and V. O. Homerberg, Trans. American Society for Steel Treatment, vol. 5, 1924, pp. 399–412; also, "Why Caustic Solutions Make Steel Brittle," *Chemical & Metallurgical Engineering*, vol. 30, 1924, pp. 589–591.

163 "Effects of Caustic and Caustic-Containing Feed Water on Boilers," *Stahl und Eisen*, vol. 45, 1925, pp. 393–394.

164 "Pitting and Corrosion of Boiler Tubes and Sheets," by M. E. McDonnell, Proceedings American Railway Engineering Association, vol. 25, 1925, pp. 164–166.

165 "Rivet-Hole Cracking in Water-Tube Steam Boilers," by F. Münzinger, *Zeitschrift V.D.I.*, vol. 69, 1925, p. 166.

166 "Steam Boiler Industry in the United States of America," by F. Münzinger, ibid., vol. 69, 1925, pp. 653–658, 773–778, 807–813, 840–844, 894–898, and 961–963; discussion, ibid., pp. 1088–1093, 1160–1164, and 1257.

167 "Boiler Explosion Due to Fatigue Fracture," by W. Quack, *Wärme*, vol. 48, 1925, pp. 369–372.

168 "Feed Water and Safety of the Steam Boiler," by F. Rapatz, *Stahl und Eisen*, vol. 45, 1925, pp. 722–723.

169 "Boiler Plate Failure," by E. Schulz, *Elektro-Journal*, vol. 5, 1925, pp. 1–8.

170 "Is an Alkaline Reaction of Boiler Water Injurious to Boiler Plate?" by A. Splittgerber, *Zeitschrift V.D.I.*, vol. 69, 1925, p. 939.

171 "Memorandum by Chief Engineer C. E. Stromeyer," Manchester Steam Users' Association, 1925.

172 "Channels in Metal, Which Communicate With the Surface," by G. Tammann and H. Bredemeier, *Zeitschrift für anorganische und allgemeine Chemie*, vol. 142, 1925, pp. 54–60.

173 "The Influence of Certain Elements on the Entrance of Electrolytic Hydrogen Into Steel and Consequent Change in Its Elastic Properties," by D. V. Alekseev and M. N. Polukarov, *Journal*, Russian Physical-Chemical Society, vol. 58, 1926, pp. 511–517.

174 "The Influence of Cathodic Hydrogen on the Strength of Steel," by D. Alekseev and M. N. Polukarov, *Zeitschrift Elektrochem.*, vol. 32, 1926, pp. 248–252.

175 Applebaum, see discussion, ref. 181, pp. 82–85.

176 "Effect of Temperature on Liberation of Hydrogen Gas by Corrosion of Iron and Zinc," by John R. Baylis, *Mechanical Engineering*, vol. 48, 1926, pp. 1133–1134.

177 "Embrittlement of Steel," by A. G. Christie, ibid., vol. 48, 1926, pp. 1368–1372; also *Journal*, American Waterworks Association, vol. 17, 1927, pp. 174–189.

178 "The Behavior of Materials Used in Boiler Construction When Subjected to Service Conditions," by A. Fry, *Kruppsche Monatshefte*, vol. 7, 1926, pp. 185–196.

179 "Cracking and Corrosion of Boiler Tubes," by F. Körber and A. Pomp, *Mitteilungen K. W. Institut Eisenforschung*, vol. 8, 1926, pp. 135–147; also, *Zeitschrift bayerischen Revisionsverein*, vol. 30, 1926, pp. 279–285, 295–301.

180 "Yield Point, Cold and Blue Brittleness," by P. Ludwik, *Zeitschrift V.D.I.*, vol. 70, 1926, pp. 379–386.

181 "The Cause and Prevention of Embrittlement of Boiler Plate," by S. W. Parr and F. G. Straub, University of Illinois, Engineering Experiment Station, Bulletin 155, 1926, 60 pp.; also Proceedings American Society for Testing Materials, vol. 26, 1926, part 2, pp. 52–79; discussion, ibid., pp. 80–91.

182 "Effect of Occluded Hydrogen on the Tensile Strength of Iron," by L. B. Pfeil, Proceedings of the Royal Society of London, vol. 112, series A, 1926, pp. 182–195.

183 "Speisewasserpflege (Feed Water Treatment)," Vereinigung der Grosskesselbesitzern E. V., Berlin, 1928 (Darmstadt Meeting, September, 1925).

184 "Formation of Cracks in Boiler Plate—Causes and Prevention," by E. Starck, *Archiv Wärmewirtschaft*, vol. 7, 1926, pp. 181–188, 292–296, 321–323.

185 "Suggested Rules for the Care of Boilers," A.S.M.E. Boiler Construction Code, 1926, sec. 7, par. CA-5, pp. 80–81.

186 "Treatment of Feed Water," Report of the Prime Movers Committee, Proceeding National Electric Light Association, 1926, pp. 1366–1395.

187 "Examples of Corrosion in Industry," by W. Werner, *Korrosion und Metallschutz*, vol. 2, 1926, pp. 63–70.

188 "On Safety in the Boiler Industry," by R. Baumann (Zur Sicherheit des Dampfkesselbetriebes), Vereinigung der Grosskesselbesitzern E. V., Julius Springer, Berlin, 1927.

189 "Investigations on the Effect of Caustic and Various Salts on Iron," by E. Berl, *Forschungsarbeiten auf dem Gebiete des Ingenieurwesens*, part 295, 1927, pp. 1–7.

190 "Investigations on the Effect of Caustic and Various Salts on Iron," by E. Berl, H. Staudinger, and K. Plagge, ibid., pp. 7–17.

191 "Embrittlement of Boiler Steel," *Engineering*, vol. 123, 1927, pp. 675–676.

192 "A Physico-Chemical Study of Scale Formation and Boiler-Water Conditioning," by R. E. Hall, et al, Mining and Metallurgical Investigation, Carnegie Institute of Technology, U. S. Bureau of Mines, Bulletin 24, 1927, 239 pp.

193 W. H. Hatfield, see discussion, ref. 199, pp. 125–126.

194 "Investigation on Boiler Tubes of Izett-Material," Test Report, Materialprüfungsamt Berlin-Dahlem, reprint no. 15, 1927, *Mitteilungen der Vereinigung der Grosskesselbesitzern*.

195 "Corrosion and Cracking of Boiler Plates and Tubes," by J. Jicinsky, *Glückauf*, vol. 63, 1927, pp. 1373–1380.

196 "Explosion of a Cellulose Cooker," by F. Müller, *Zeitschrift bayerischen Revisionsvereins*, vol. 31, 1927, pp. 195–197, 209–213.

197 "Embrittlement of Boiler Plate," by S. W. Parr and F. G. Straub, *Industrial & Engineering Chemistry*, vol. 19, 1927, pp. 620–622.

198 "The Intercrystalline Corrosion of Metals," by H. S. Rawdon, ibid., vol. 19, 1927, pp. 613–619.

199 "The Behavior of Mild Steel Under Prolonged Stress at 300° C," by W. Rosenhain and D. Hanson, *Journal*, Iron and Steel Institute, vol. 116, 1927, pp. 117–122; discussion, ibid., pp. 123–127.

200 "The Embrittlement of Boiler Plate," by F. G. Straub, *Blast Furnace Steel Plant*, vol. 15, 1927, pp. 94–99, 107.

201 "Physical Properties of Boiler Plate at Temperatures from 20° to 600° C," by G. Urbanczyk, *Stahl und Eisen*, vol. 47, 1927, pp. 1128–1135.

202 "Deterioration of Alloy Steels in Ammonia Synthesis," by J. S. Vanick, *Chemical & Metallurgical Engineering*, vol. 34, 1927, pp. 489–492.

203 "Deterioration of Steels in the Synthesis of Ammonia," by J. S. Vanick, W. W. de Sveshnikoff, and J. G. Thompson, U. S. Bureau of Standards, Technical Paper 361, vol. 22, 1927–1928, pp. 199–233.

204 "Hair Cracks in Steel Rails," by J. H. Whiteley, Trans. American Society for Steel Treatment, vol. 12, 1927, pp. 208–220, 234.

205 "Investigations on Pickling Low Carbon Steel Sheet," by P. Bardenheuer and G. Thanheiser, *Mitteilungen aus dem K. W. Institut für Eisenforschung*, vol. 10, 1928, pp. 323–342.

206 "The Protective Action of Sodium Sulphate on the Attack of Ingot Iron by Alkalies and Salts Under High Pressure," by E. Berl and F. van Taack, *Archiv für Wärmewirtschaft*, vol. 9, 1928, pp. 165–169.

207 J. J. Brennan, *Byllesby Management*, vol. 3, no. 5, 1928, p. 8.

208 "Embrittlement of Boiler Plates by Chemical Agency," *Iron and Coal Trades Review*, vol. 117, 1928, p. 367.

209 "Izett-Eisen," by A. Fry, *Zeitschrift bayerischen Revisionsvereins*, vol. 32, 1928, pp. 137–140, 150–153, 183–184.

210 "Notes Concerning Fractured Boiler Plates," by G. Ness and D. A. MacCallum, *Journal*, West Scotland Iron and Steel Institute, vol. 35, 1928, pp. 101–109.

211 "Embrittlement of Boiler Plate," by S. W. Parr and F. G. Straub, University of Illinois, Engineering Experiment Station, Bulletin 177, 1928. 67 pp.

212 "The Change in Tensile Strength Due to Aging of Cold-Drawn Iron and Steel," by L. B. Pfeil, *Journal*, Iron and Steel Institute, vol. 118, 1928, pp. 167–181.

213 "Treatment of Feed Water," Report of the Prime Movers Committee, Proceedings National Electric Light Association, 1928, pp. 1347–1403.

214 "Investigation of Boiler Plate of Izett-Material in Strength Classes I to IV," by M. Ulrich, *Zeitschrift bayerischen Revisionsvereins*, vol. 32, 1928, pp. 53–57, 68–72.

215 "Reasons for Sulfate Protection Against Attack of Boiler Plate in Salt Solutions," by E. Berl and F. van Taack, *Archiv für Wärmewirtschaft*, vol. 10, 1929, pp. 337–339.

216 "Brittleness in Mild Steel," by G. R. Bolsover, *Journal*, Iron and Steel Institute, vol. 119, 1929, pp. 473–487; discussion, ibid., pp. 488–500.

217 "The Dissociation of Water in Steel Tubes at High Temperatures and Pressures," by C. H. Fellows, *Journal*, American Waterworks Association, vol. 21, 1929, pp. 1373–1387.

218 "Boiler Metal Cracking—A Case Study," by M. Hecht and D. S. McKinney, *Power*, vol. 70, 1929, pp. 633–636.

219 "Failures in Steam Boiler Parts," by A. Pomp and P. Bardenheuer, *Mitteilungen aus dem K. W. Institut für Eisenforschung*, vol. 11, 1929, pp. 185–191.

220 "Recent Developments in Boiler-Metal Embrittlement," by H. F. Rech, *Mechanical Engineering*, vol. 51, 1929, pp. 589–593.

221 "On the System Iron-Water," by G. Schikorr, *Zeitschrift Elektrochem*, vol. 35, 1929, pp. 62–65.

222 "On the Reactions Among Iron, Its Hydroxides, and Water," by G. Schikorr, ibid., vol. 35, 1929, pp. 65–70.

223 "Water Treatment to Prevent Embrittlement," by F. G. Straub, *Journal*, American Waterworks Association, vol. 21, 1929, pp. 511–523.

224 "Embrittlement Prevention in Steam Boilers," by F. G. Straub, *Power Plant Engineering*, vol. 33, 1929, pp. 173–174.

225 "Control of Boiler-Water Treatment to Prevent Embrittlement," by F. G. Straub, *Mechanical Engineering*, vol. 51, 1929, pp. 366–367.

226 "The Effect of Cold Working on Boiler Drums," by F. G. Straub, R. K. Hopkins, and H. L. Whitney, *Power*, vol. 69, 1929, pp. 998–1002.

227 "Riveting of 35 mm. Izett Plate," by M. Ulrich, *Mitteilungen der Grosskesselbesitzern*, 1929, no. 22.

228 "Deterioration and Life of Steam Boilers in Relation to the Load and the Rigidity of the Unit," by M. Ulrich, *Die Wärme*, vol. 52, 1929, pp. 567–574.

229 "The Action of Caustic and Salts on Steel Under Conditions of High Pressure and the Protective Effect of Sodium Sulphate Against Attack by Sodium Hydroxide and Magnesium Chloride," by E. Berl and F. van Taack, *Forschungsarbeiten auf dem Gebiete des Ingenieurwesens*, vol. 330, 1930, pp. 14–17.

230 "Endurance Properties of Steel in Steam," by T. S. Fuller, Trans. American Institute of Mining and Metallurgical Engineering, vol. 90, 1930, pp. 280–290; discussion, ibid., pp. 290–292.

231 "Report of the Prime Movers Committee on Treatment of Feedwater," by R. E. Hall, National Electric Light Association, Publication 051, 1930, pp. 5–12.

232 "Intercrystalline Cracking in Steam Boilers," by F. G. Straub, Trans. Second World Power Conference, Berlin, vol. 7, 1930, pp. 363–366.

233 "Embrittlement in Boilers," by F. G. Straub, University of Illinois, Engineering Experiment Station, Bulletin 216, 1930, 125 pp.

234 "Recent Instances of Embrittlement in Steam Boilers," by F. G. Straub, Trans. A.S.M.E., vol. 52, 1930, FSP-52-39, pp. 339–340; discussion, ibid., pp. 340–345.

235 "American Experimentation on 'Embrittlement of Boiler Plate,' and Comparable German Investigations," by M. Ulrich, *Zeitschrift bayerischen Revisionsvereins*, vol. 34, 1930, pp. 13–17, 34–37, 49–51, 64–67, 88–89, 98–100, 129–130.

236 "Boiler Feed Water Treatment in Great Britain," by A. W. Chapman, *Journal*, American Waterworks Association, vol. 23, 1931, pp. 547–550.

237 "Nickel and Nickel Alloys Other Than the Nickel-Chromium-Iron Group," by C. A. Crawford and R. Worthington, Symposium on Effect of Temperature on Properties of Metals, American Society of Mechanical Engineers-American Society for Testing Materials, 1931, pp. 557–558.

238 "On the Metallurgy of Welding of Steel, With Special Consideration of Boiler Construction," by A. Fry, *Kruppsche Monatshefte*, vol. 12, 1931, pp. 201–214.

239 "Hair-Line Cracks in Boiler Plate Manufactured at the Vitkovitz Plant," G. A. Kashchenko, *Soobshcheniya Vsesoyuznogo Inst. Metal.*, 1931, no. 5–6, pp. 20–28.

240 "Influence of Water Composition on Stress Corrosion," by D. J. McAdam, Jr., Proceedings American Society for Testing Materials, vol. 31, 1931, part 2, pp. 259–278.

241 "Accelerated Cracking of Mild Steel (Boiler Plate) Under Repeated Bending," by W. Rosenhain and A. J. Murphy, *Journal*, Iron and Steel Institute, vol. 123, 1931, pp. 259–278; discussion, ibid., pp. 279–284.

242 "Red Shortness of Steel from Metals," by H. Schottky, K. Schichtel, and R. Stolle, *Archiv für das Eisenhüttenwesen*, vol. 4, 1930–1931, pp. 541–547.

243 "Embrittlement and Protection of Steam Boilres," by F. G. Straub, *Power Plant Engineering*, vol. 35, 1931, pp. 190–193.

244 "Identifying Causes of Boiler-Metal Cracking," by F. G. Straub, *Power*, vol. 73, 1931, pp. 809–812.

245 "Fractures in Boiler Metal," by A. E. White and E. Schneidewind, Trans. A.S.M.E., vol. 53, 1931, pp. 193–211; discussion, ibid., pp. 211–214.

246 "The Influence of Caustic and Salt Solutions on Boiler Plate," by E. Berl and H. Hinkel, *Archiv für Wärmewirtschaft*, vol. 13, 1932, pp. 298–300.

247 "The Effect of Hydrogen Sulfide on the Corrosion of Iron by Salt Solutions," by S. C. Britton, T. P. Hoar, and U. R. Evans, *Journal*, Iron and Steel Institute, vol. 126, 1932, pp. 365–373; discussion, ibid., pp. 374–377.

248 "Embrittlement of Hot-Galvanized Structured Steel," by S. Epstein, Proceedings American Society for Testing Materials, vol. 32, 1932, part 2, pp. 293–374; discussion, ibid., pp. 375–379.

249 "Caustic Embrittlement of Steel," by F. Hundeshagen, *Chemiker-Zeitschrift*, vol. 56, 1932, pp. 4–5, 17–18, 39–40.

250 "Diffusion of Hydrogen Through Iron During Treatment With Acid and the Hydrogen Content of This Metal," by F. Körber and H. Ploum, *Mitteilungen aus dem K. W. Institut für Eisenforschung*, vol. 14, 1932, pp. 229–248.

251 "Cracking of Boiler Plates," National Physical Laboratory Annual Report, 1932, pp. 247–248.

252 "Izett Steel: What It Is and What It Is Used For," by G. G. Neuendorff, *Metals and Alloys*, vol. 3, 1932, pp. 61–68.

253 "Physical Chemistry of Steel-Making," by H. Schenck, Julius Springer, Berlin, vol. 1, 1932, 306 pp.; vol. 2, 1934, 274 pp.

254 "Determination of Alkalinity in Boiler Waters," by F. G. Straub, *Industrial & Engineering Chemistry*, analytical edition, vol. 4, 1932, pp. 290–294.

255 "Treatment of Feed Water," Report of the Prime Movers Committee, Proceedings National Electric Light Association, 1932, pp. 1034–1057.

256 "The Influence of Hydrogen on Steel at Elevated Temperatures and Pressures," by D. V. Alekseev and V. V. Ostroumov, *Journal of Applied Chemistry*, U.S.S.R., vol. 6, 1933, pp. 621–629.

257 "Development of Chemical High-Pressure Technique in the Construction of the New Ammonia Industry," by C. Bosch (Nobel Lecture). *Zeitschrift V.D.I.*, vol. 77, 1933, pp. 305–317; also, *Chemische Fabrik*, vol. 6, 1933, pp. 127–142.

258 "Effect of Water and Steam on Boiler Materials," by N. Christmann, *Stahl und Eisen*, vol. 53, 1933, pp. 1353–1357.

259 "Development of Chemical High Pressure Technique in the Construction of the New Ammonia Industry," by C. Bosch, *Chemische Fabrik*, vol. 6, 1933.

260 "Gaseous Thermal Diffusion—The Principal Cause of Discrepancies Among Equilibrium Measurements on the Systems Fe_3O_4-H_2-Fe-H_2O, Fe_3O_4-H_2-FeO-H_2O, and FeO-H_2-Fe-H_2O," by P. H. Emmett and J. F. Shultz, *Journal*, American Chemical Society, vol. 55, 1933, pp. 1376–1389.

261 "Fatigue Strength of Boiler Steel and Its Response to Chemical Attack," by C. Holzhauer, *Mitteilungen der Materialprüfungsanstalt*, Technische Hochschule, Darmstadt, Berlin, no. 3, 1933, pp. 39–55.

262 "The Effect on Various Steels of Hydrogen at High Pressures and Temperatures," by N. P. Inglis and W. Andrews, *Journal*, Iron and Steel Institute, vol. 128, 1933, pp. 383–397; discussion, ibid., pp. 398–408; abridged: *Engineering*, vol. 136, 1933, pp. 613–614.

263 "Hydrogen Permeability of Armco-Iron and Iron with Various Carbon Contents at Temperatures from 700° to 1000° C," by G. Lewkonja and W. Baukloh, *Zeitschrift für Metallkunde*, vol. 25, 1933, pp. 309–310.

264 "Hydrogen Permeability of Steel from 700° to 1000° C," by G. Lewkonja, and W. Baukloh, *Archiv für das Eisenhüttenwesen*, vol. 6, 1932–1933, pp. 453–457.

265 National Physical Laboratory, Annual Report, 1933, pp. 154, 178.

266 "Preventing Embrittlement of Boiler Metal," by S. W. Parr and F. G. Straub, U. S. Patent no. 1,910,403, May 23, 1933.

267 H. Schottky; discussion of Bosch, ref. 257, *Stahl und Eisen*, vol. 53, 1933, pp. 1187–1189.

268 E. H. Schulz; discussion of Bosch, ref. 257; ibid., vol. 53, 1933, pp. 1313–1314.

269 "Investigation of the Mechanical Break-Down of Prime Movers and Boiler Plant," by L. W. Schuster, Proceedings of the Institution of Mechanical Engineers, vol. 124, 1933, pp. 337–435.

270 "The Evaluation of Boiler Plates by the Impact Test," by A. Thum and H. Holdt, *Stahl und Eisen*, vol. 53, 1933, pp. 505–50S.

271 "Strength Tests of Notched Bars and Fatigue Resistanec of Boiler Plate," by A. Thum and C. Holzhauer, *Wärme*, vol. 56, 1933, pp. 640–642.

272 "Corrosive Action on Constantly Stressed Boiler Steels," by A. Thum and C. Holzhauer, *Archiv Wärmewirtschaft*, vol. 14, 1933, pp. 319–321.

273 "The Influence of Cathodic Hydrogen on the Strength of Steel," by D. Alekseev, P. Afanasev, and V. Ostroumov, *Zeitschrift Elektrochem.*, vol. 40, 1934, pp. 92–98.

274 "The Construction of Cylindrical Casings Operating Under Pressure," by E. Audibert and A. Raineau, *Ann. de l'Office National des Combustibles Liquides*, vol. 9, 1934, pp. 203–277.

275 "High-Pressure Plant for Experimental Hydrogenation Processes," by A. T. Barber and A. H. Taylor, *Engineering*, vol. 138, 1934, pp. 576–578, 635–636; discussion, ibid., pp. 568–569.

276 "Penetration of Brass Solder Into Steel as a Result of Hydrogen Absorption During Pickling," by P. Bardenheuer and H. Ploum, *Mitteilungen aus dem K. W. Institut für Eisenforschung*, vol. 16, 1934, pp. 137–140.

277 "Large Rectifiers Without Vacuum Pumping," by W. Dällenbach, *Elektrotechnische Zeitschrift*, vol. 55, 1934, pp. 85–89.

278 "Problems in the Arc-Welding of Steel," by A. Fry, *Technische Mitteillungen Krupp*, vol. 2, 1934, pp. 33–42.

279 "Blistering in Hydrogen of Metals and Alloys Containing a Small Amount of Oxide," by Guichard, Clausman, Billon, *Chimie et Industrie*, vol. 31, April, 1934, p. 588.

280 "Accelerated Cracking of Mild Steel (Boiler Plate) Under Repeated Bending. Part II, Further Tests," by C. H. M. Jenkins and W. J. West, *Journal*, Iron and Steel Institute, vol. 130, 1934, pp. 279–291.

281 "Deterioration of Chromium-Tungsten Steels in Ammonia Gases," by P. R. Kosting, *Metals and Alloys*, vol. 5, 1934, pp. 54–56.

282 "Improvements in the Manufacture of Articles From Steel Alloys," by A. G. Krupp, British Patent 420,567, March 19, 1934; also British Patents 419,009, 425,073, and 427,585.

283 "Steam Boiler Damage," by E. Pfleiderer, Julius Springer, Berlin, 1934.

284 "Treatment of Coals, Tars, Mineral Oils, and the Like," by M. Pier, U. S. Patent 1,969,482, Aug. 7, 1934.

285 "Water as an Engineering and Industrial Material," by S. T. Powell, Proceedings American Society for Testing Materials, vol. 34, part 2, 1934, pp. 3–47.

286 "Comparative Investigations of Injuries to Boiler Parts—Study of the Influence of Hydraulic Testing on Their Occurrence," by R. Rist, *Zeitschrift bayerischen Revisionsverein*, vol. 38, 1934, pp. 137–141; also *Zeitschrift V.D.I.*, vol. 79, 1935, pp. 812–813; also, *Stahl und Eisen*, vol. 56, 1936, pp. 665–666.

287 "Preparation of Steel to Avoid Porosity in Castings," by C. E. Sims, Trans. American Foundrymen's Association, vol. 42, 1934, pp. 323–338; discussion, ibid., pp. 394–406.

288 "Intercrystalline Corrosion of Soft Iron in Ammonia Nitrate Solution," by M. Smialowski, *Korrosion und Metallschutz*, vol. 14, 1938, pp. 111–113.

289 "The Design and Construction of High Pressure Chemical Plant," by H. Tongue, D. Van Nostrand Company, Inc., New York, N. Y., 1934.

290 "On the Effect of Hydrogen on Cast Iron," by W. Baukloh, *Giesserei*, vol. 22, 1935, pp. 406–409.

291 "Decarburization of Several Alloy Steels by Hydrogen," by W. Baukloh and H. Guthmann, *Archiv für das Eisenhüttenwesen*, vol. 9, 1935–1936, pp. 201–202.

292 "Hydrogen Permeability of Copper, Iron, Nickel, Aluminum, and Several Alloys," by W. Baukloh and H. Kayser, *Zeitschrift für Metallkunde*, vol. 27, 1935, pp. 281–285.

293 "The Behavior of Mild Steel Under Prolonged Stress at 300° C. Part II, Experiments on Concentrated Stress in Notched and Drilled Specimens," by C. H. M. Jenkins, *Journal*, Iron and Steel Institute, vol. 132, 1935, pp. 281–289.

294 "The Effect of Gases on Ferrous Materials at High Temperatures and High Pressures," by H. L. Maxwell, Pennsylvania State College, Mineral Industries Experiment Station, Bulletin 18, 1935, pp. 128–136.

295 "Diffusion of Hydrogen Through Mild Steel Sheet During Acid Corrosion," by T. N. Morris, *Journal*, Society of Chemical Industry, vol. 54, 1935, pp. 7T–13T.

296 National Physical Laboratory; Annual Report, 1935, p. 164.

297 "The Embrittlement of Boiler Steel," by E. P. Partridge and W. C. Schroeder, *Metals and Alloys*, vol. 6, 1935, pp. 145–149, 187–191, 253–258, 311–316, and 355–360.

298 "Permeability of Steel Tubes to Hydrogen," *Brown Boveri Review*, Jan./Feb., 1935, p. 64.

299 "Possible Explanation for Brittle Fracture in Boiler Parts," by W. Ruttmann, *Mitteilungen der Vereinigung der Grosskesselbesitzern*, no. 53, August, 1935, pp. 168–176.

300 "Solubility Equilibria of Sodium Sulphate at Temperatures of 150 to 350° C. I.—The Effect of Sodium Hydroxide and Sodium Chloride," by W. C. Schroeder, A. Gabriel, and E. P. Partridge, *Journal*, American Chemical Society, vol. 57, 1935, pp. 1539–1546.

301 "Penetration of Steel by Soft Solder and Other Molten Metals at Temperatures up to 400° C," by L. J. G. van Ewijk, *Journal*, Institute of Metals, vol. 56, 1935, pp. 241–248; discussion, ibid., pp. 248–256.

302 "Effect of Molten Solder on Some Stressed Materials," by G. W. Austin, ibid., vol. 58, no. 1, 1936, pp. 173–185; discussion, ibid., pp. 185–192.

303 "Effect on Steel of Hydrogen Absorbed During Melting," by P. Bardenheuer and E. H. Keller, *Mitteilungen aus dem K. W. Institut für Eisenforschung*, vol. 18, 1936, pp. 227–237.

304 "Desulphurization of Iron by Hydrogen," by W. Baukloh, *Metallwirtschaft*, vol. 15, 1936, pp. 1193–1196; also, *Metallurgist*, vol. 11, 1937, pp. 28–29.

305 "Hydrogen Permeability and Hydrogen Decarburization of Steels, Armco-Iron, Copper, Nickel, and Aluminum at High Pressures," by W. Baukloh and H. Guthmann, *Zeitschrift für Metallkund*, vol. 28, 1936, pp. 34–40.

306 "Hydrogen Permeability of Steel by Electrolytic Pickling," by W. Baukloh and G. Zimmermann, *Archiv für das Eisenhüttenwesen*, vol. 9, 1936, pp. 459–465.

307 "Metallurgical Problems Arising in the Construction of Hydrogenation Tubes and Cracking Chambers," by C. Berthelot, *Revue de Metallurgie*, vol. 33, 1936, pp. 566–573, 619–626, 677–690, and 727–746.

308 E. G. Hill, see discussion, ref. 315, p. 401.

309 "Factors Influencing the Rate of Attack of Mild Steels by Typical Weak Acid Media," by T. P. Hoar and D. Havenhand, *Journal*, Iron and Steel Institute, vol. 133, 1936, pp. 239–265; discussion, ibid., pp. 266–291.

310 "Physical Properties of Metals as Affected by Conditions of Ammonia Synthesis," by H. L. Maxwell, Trans. American Society for Metals, vol. 24, 1936, pp. 213–224.

311 "Effect of Concentrated Sodium Hydroxide on Boiler Steel Under Tension," by A. S. Perry, Trans. A.S.M.E., vol. 58, 1936, pp. 211–216; discussion, ibid., pp. 493–494.

312 "Reasons for Injurious Cracking in Riveted Boiler Drums," by R. Rist, *Stahl und Eisen*, vol. 56, 1936, pp. 665–666.

313 "Deformationless Fractures in Boiler Parts," by W. Ruttmann, *Technische Mitteillungen Krupp*, vol. 4, 1936, pp. 23–29.

314 "Steels for Autoclaves," by R. J. Sarjant and T. H. Middleham, Trans. Chemical Engineering Congress, World Power Conference, London, vol. 1, 1936, pp. 66–110.

315 "Action of Solutions of Sodium Silicate and Sodium Hydroxide at 250° C. on Steel Under Stress," by W. C. Schroeder and A. A. Berk, Trans. American Institute of Mining and Metallurgical Engineers, vol. 120, 1936, pp. 387–400; discussion, ibid., pp. 400–403.

316 "Solubility Equilibria of Sodium Sulphate at Temperatures From 150 to 350° C. II. Effect of Sodium Hydroxide and Sodium Carbonate," by W. C. Schroeder, A. A. Berk, and A. Gabriel, *Journal*, American Chemical Society, vol. 58, 1936, pp. 843–849.

317 "Effect of Solution Composition on the Failure of Boiler Steel Under Static Stress at 250° C," by W. C. Schroeder, A. A. Berk, and E. P. Partridge, Proceedings American Society for Testing Materials, vol. 36, part 2, 1936, pp. 721–750; discussion, ibid., pp. 751–754.

318 "The Use of Solubility Data to Control the Deposition of Sodium Sulphate or Its Complex Salts in Boiler Waters," by W. C. Schroeder, A. A. Berk, and E. P. Partridge, ibid., vol. 36, part 2, 1936, pp. 755–769.

319 "Effect of Solutions on the Endurance of Low-Carbon Steel Under Repeated Torsion at 482° F (250° C)," by W. C. Schroeder and E. P. Partridge, Trans. A.S.M.E., vol. 58, 1936, pp. 223–231; discussion, ibid., pp. 494–496.

320 "New Laboratory Data Relative to Embrittlement in Steam Boilers," by F. G. Straub and T. A. Bradbury, ibid., vol. 58, 1936, pp. 389–390; also, *Power Plant Engineering*, vol. 40, 1936, pp. 104–105.

321 "Diffusion of Hydrogen Through Steel During Electrolytic Pickling," by W. Baukloh and W. Retzlaff, *Archiv für das Eisenhüttenwesen*, vol. 11, 1937–1938, pp. 97–99.

322 "Hydrogen Permeability and Decarburization of Cast Iron," by W. Baukloh and F. Springorum, *Metallwirtschaft*, vol. 16, 1937, pp. 446–449.

323 "Hydrogen Sickness of Several Metals," by W. Baukloh and W. Stromburg, *Zeitschrift Metallkunde*, vol. 29, 1937, pp. 427–433.

324 "Diffusion of Hydrogen Through Metals," by W. Baukloh and W. Wenzel, *Archiv für das Eisenhüttenwesen*, vol. 11, 1937, pp. 273–278.

325 "The Diffusion of Hydrogen Through Nickel and Iron," by W. R. Ham, Trans. American Society for Metals, vol. 25, 1937, pp. 536–570.

326 "Caustic Embrittlement in Boilers," by P. Hamer, *Engine and Boiler House Review*, vol. 51, 1937–1938, pp. 314–317.

327 F. Körber, see discussion, ref. 329, p. 898.

328 "Embrittlement of Steels at High Steam Temperatures," by J. H. G. Monypenny, *Metal Progress*, vol. 32, 1937, pp. 67–68.

329 "Effect of Hydrogen Under High Pressure on Unalloyed Steel," by F. K. Naumann, *Stahl und Eisen*, vol. 57, 1937, pp. 889–898; discussion, ibid., pp. 898–899.

330 "Investigation of the Oxidation of Metals by High-Temperature Steam," by A. A. Potter, H. L. Solberg, and G. A. Hawkins, Trans. A.S.M.E., vol. 59, 1937, pp. 725–732; addendum and discussion, vol. 60, 1938, pp. 610–615.

331 "Intercrystalline Cracking of Steel in Aqueous Solutions," by W. C. Schroeder, A. A. Berk, and R. A. O'Brien, *Metals and Alloys*, vol. 8, 1937, pp. 320–330.

332 "Steel for Pressure Vessels in Hydrogenation Plant," *Metallurgist*, vol. 11, 1937–1938, p. 23.

333 "A Thermodynamic and Colloidal Interpretation of Published Studies on the Corrosion Cracking of Stressed Mild Steel in Water Solutions," by J. A. Tajc, Proceedings American Society for Testing Materials, vol. 37, 1937, part 2, pp. 588–597; discussion, ibid., pp. 598–599.

334 "Action of Hydrogen on Carbides of Iron and Chromium," *Metallurgist*, vol. 11, 1937–1938, pp. 156–157.

335 "Cracking of Steel in Ammonium Nitrate Solutions," ibid., vol. 11, 1937–1938, p. 160.

336 "Attack of Superheated Steam on Steels," ibid., vol. 11, 1937–1938, pp. 99–101.

337 "Weld Sensitivity of Chrome-Molybdenum Steels," by P. Bardenheuer and W. Bottenberg, *Mitteilungen aus dem K. W. Institut für Eisenforschung*, vol. 20, 1938, pp. 77–86.

338 "Effect of Hydrogen on Metals," by W. Baukloh, *Chemische Fabrik*, vol. 11, 1938, pp. 449–455.

339 "The Mechanism of the Reaction Between Hydrogen and Carbon in Iron," by W. Baukloh and B. Knapp, *Iron and Steel Institute*, Carnegie Scholarship Memoirs, vol. 27, 1938, pp. 149–164.

340 "The Formation of Graphite in Gray Iron," by A. Boyles, Trans. American Foundrymen's Association, vol. 46, 1938, pp. 297–334; discussion, ibid., pp. 334–340.

341 "Cause of and Remedy for Pitting and Corrosion of Locomotive Boiler Tubes and Sheets With Special reference to Status of Embrittlement Investigation," by R. E. Coughlan, et al, Bulletin, American Railway Engineering Association, no. 404, 1938, pp. 73–76; also ibid., bulletin 400, 1938, pp. 194–196.

342 "Actual State of the Problem of Corrosion of Mild Steel by Nitrates," by E. Herzog and A. Portevin, *Métaux et Corrosion*, vol. 13, 1938, pp. 171–176.

343 "Hydrogen Attack of Steel," *Metallurgist*, vol. 11, 1937–1938, pp. 108–110.

344 "Action of Hydrogen on the Carbides of Iron and Chromium," by L. Jacqué, Comptes Rendus, vol. 206, 1938, pp. 1900–1902 also, *Metallurgist*, vol. 11, 1937–1938, pp. 156–157.

345 "Action of Hydrogen on Steel and Their Constituents," by L. Jacqué, *Chimie et Industrie*, vol. 40, 1938, pp. 850–862.

346 "The Effect of Alloy Additions on the Resistance of Steel to Hydrogen Under High Pressure," by F. K. Naumann, *Stahl und Eisen*, vol. 58, 1938, pp. 1239–1249; discussion, ibid., pp. 1249–1250.

347 "Diffusion of Hydrogen Through Nickel," by C. B. Post and W. R. Ham, *Journal of Chemical Physics*, vol. 6, 1938, pp. 598–605.

348 "Intercrystalline Cracking in Boiler Steel," by W. C. Schroeder and A. A. Berk, *Journal*, American Waterworks Association, vol. 30, 1938, pp. 679–694.

349 "Protecting Steel Against Intercrystalline Attack in Aqueous Solution," by W. C. Schroeder, A. A. Berk, and R. A. O'Brien, Trans. A.S.M.E., vol. 60, 1938, pp. 35–42.

350 "Bureau of Mines Investigation of the Intercrystalline Cracking of Boiler Steel," by W. C. Schroeder, A. A. Berk, and R. A. O'Brien, Bulletin, American Railway Engineering Association, no. 404, June-July, 1938, pp. 76–96.

351 "Cracking of Boiler Steel," by W. C. Schroeder, A. A. Berk, and R. A. O'Brien, *Railway Mechanical Engineer*, vol. 112, 1938, pp. 331–336, and 339.

352 "Boiler-Water Treatment: New Methods for Preventing Embrittlement," by F. G. Straub and T. A. Bradbury, *Mechanical Engineering*, vol. 60, 1938, pp. 371–376.

353 "A Method for the Embrittlement Testing of Boiler Waters,"

by F. G. Straub and T. A. Bradbury, Proc. American Society for Testing Materials, vol. 38, 1938, part 2, pp. 602–615.

354 "Question of Cracking in Boilers," by A. Thum and W. Mielentz, *Archiv Wärmewirtschaft*, vol. 19, 1938, pp. 33–37.

355 "Typical Failures of Still Tubes in Refineries," by E. C. Wright and H. Habart, *Metal Progress*, vol. 34, 1938, pp. 573–578, 685–688.

356 "Cracks in Boilers With Special Reference to Caustic Embrittlement," by W. O. Andrews, *Journal*, South African Institution of Engineers, vol. 38, 1939–1940, pp. 58–73.

357 "Present Status of the Understanding of Caustic Embrittlement in Boiler Plate," by G. T. Athavale, *Korrosion und Metallschutz*, vol. 15, 1939, pp. 73–81.

358 "Influence of Atmosphere and Pressure on Structure of Iron-Carbon-Silicon Alloys," by A. Boyles, Trans. A.I.M.E., vol. 135, 1939, pp. 376–395; also *Metals Technology*, T. P. 1046, vol. 6, April, 1939, 20 pp.

359 "Caustic Embrittlement of Boiler Plate," *Metallurgist*, vol. 12, 1939, pp. 17–18.

360 "Industrial Power," by C. W. E. Clarke, Trans. A.S.M.E., vol. 61, 1939, pp. 273–290.

361 "Intercrystalline Cracking in Boiler Plates," by C. H. Desch, *Iron and Steel Industry*, vol. 12, 1938–1939, pp. 304–307; also, *Engineer*, vol. 167, 1939, pp. 418–419.

362 "Investigation of the Action of Hydrogen on Steel," by E. Di Giacomo, *Calore*, vol. 12, 1939, pp. 248–260; also *Chem. Zentr.*, 1940, part I, p. 461.

363 "A Steam-Pressure Autoclave Injured by the Action of Caustic Liquors," by M. Gonni, *Calore*, vol. 12, 1939, pp. 145–149; also *Chem. Zentr.*, vol. II, 1939, p. 941.

364 "What About Embrittlement?" by E. P. Partridge, *Blast Furnace Steel Plant*, vol. 27, 1939, pp. 1056–1060, 1076, and 1080.

365 "Attack on Steel in High-Capacity Boilers as a Result of Overheating Due to Steam Blanketing," by E. P. Partridge and R. E. Hall, Trans. A.S.M.E., vol. 61, 1939, pp. 597–621; also discussion, ibid., pp. 621–622; vol. 62, 1940, pp. 711–717.

366 "Development of Water Treatment on the Alton Railroad," by R. W. Seniff, Proceedings Master Boiler Makers' Association, 1939, pp. 42–53.

367 "Welded Boilers Versus Caustic Embrittlement," by E. F. Spanner, *Welder*, vol. 11, 1939, pp. 306–308.

368 "Some Observations Concerning Metal Cracking in Naval Boilers," by W. C. Stewart, *Journal*, American Society of Naval Engineers, vol. 51, 1939, pp. 348–366.

369 "Corrosion in Partially Dry Steam-Generating Tubes," by F. G. Straub and E. E. Nelson, *Mechanical Engineering*, vol. 61, 1939, pp. 199–202.

370 "The Cause of Weld Sensitivity in Aircraft Steels," by O. Werner, *Archiv für das Eisenhüttenwesen*, vol. 12, 1938–1939, pp. 449–455; also discussion, ibid., pp. 456–458, and 517.

371 "Caustic Embrittlement of Steam Boilers," by W. S. Cazort, Jr., *Refiner and Natural Gasoline Manufacturer*, vol. 19, 1940, pp. 156–158.

372 "Metals and Alloys for High Temperatures," by W. Hessenbruch, Julius Springer, Berlin, 1940.

373 "Stress Corrosion Cracking of the Austenitic Chromium-Nickel Steels and Its Industrial Implications," by J. C. Hodge and J. L. Miller, Trans. American Society for Metals, vol. 28, 1940, pp. 25–67; also discussion, ibid., pp. 67–82; also; *Metal Treatment*, vol. 5, 1939–1940, pp. 175–176, 185.

374 "Investigating and Combating Intercrystalline Corrosion of Unalloyed Steels," by E. Houdremont, H. Bennek, and H. Wentrup, *Stahl und Eisen*, vol. 60, 1940, pp. 757–763, 791–797; also discussion, ibid., pp. 797–801.

375 "Intercrystalline Corrosion—How Can It Be Eliminated?" *Railway Age*, vol. 108, 1940, pp. 855–856, and 860.

376 "The Design of High-Pressure Plant and the Properties of Fluids at High Pressures," by D. M. Newitt, Clarendon Press, Oxford. 1940.

377 "Diffusion of Hydrogen From Water Through Steel," by F. J. Norton, *Journal of Applied Physics*, vol. 11, 1940, pp. 262–267.

378 "Caustic Embrittlement in Steam Boiler Material," by F. Odqvist, *Teknisk Tidskrift*, vol. 70, Oct. 19, 1940, Mekanik, pp. 103–109; abstract *Iron and Steel Industry*, vol. 14, 1940–1941, p. 246.

379 "Consideration of the Theory for Impairment of Steels by Hydrogen Under High Pressure," by O. Puchner, *Skoda Mitteilungen*, vol. 2, 1940, no. 5, pp. 155–160; vol. 3, 1941, no. 1, pp. 23–26; abstract, *Stahl und Eisen*, vol. 61, 1941, p. 435; abstract *Chemische Fabrik*, vol. 14, 1941, pp. 199–200.

380 "Intercrystalline Cracks in Locomotive Boilers," by W. C. Schroeder, A. A. Berk, and R. A. O'Brien, *Railway Age*, vol. 109, 1940, pp. 25–28; also, Association of American Railroads, Circulars DV-989, 1940.

381 "Embrittlement Detector," by W. C. Schroeder, A. A. Berk, and R. A. O'Brien, *Combustion*, vol. 12, Aug., 1940, pp. 19–21.

382 "From Materials to Construction," by H. Stäger, *Schweizer Archiv*, vol. 6, 1940, pp. 121–146.

383 "On Crack Formation in Steam Boiler Material," by G. Wallgren, *Teknisk Tidskrift*, vol. 70, Oct. 19, 1940, pp. 109–113; abstract *Iron and Steel Industry*, vol. 14, 1940–1941, p. 246.

384 "Metallurgical Aspects of Hydrogen in Electroplating," by C. A. Zapffe and C. L. Faust, Proceedings Educational Session, American Electroplaters Society, vol. 28, 1940, pp. 1–20; also discussion, ibid., pp. 20–25.

385 "Selected Bibliography of 500 References on Hydrogen in Steel," by C. A. Zapffe and C. E. Sims; obtainable as film or photoprint from Bibliofilm Service, U. S. Department of Agriculture Library, Washington, D. C., Document 1255.

386 "Relation of Defects in Enamel Coatings to Hydrogen in Steel," by C. A. Zapffe and C. E. Sims, *Journal*, American Ceramic Society, vol. 23, 1940, pp. 187–219; also discussion, ibid., pp. 291–300; also, *Foundry Trade Journal*, vol. 63, 1940, pp. 225–226, 228, 305–306, 308, 368 and 370; ibid., vol. 64, 1941, pp. 11–13, 92, 94, 96, 98, 164, 166, and 168.

387 "Hydrogen, Flakes, and Shatter Cracks," by C. A. Zapffe and C. E. Sims, *Metals and Alloys*, vol. 11, 1940, pp. 145–151, 177–184; also, ibid., vol. 12, 1940, pp. 44–51, 145–148.

388 "Defects in Weld Metal and Hydrogen in Steel," by C. A. Zapffe and C. E. Sims, *Welding Journal*, vol. 19, 1940, Welding Research Suppl., pp. 377s to 395s; also *Sheet Metal Industries*, vol. 14, 1941, pp. 791–796, 927–932, 1045–1051.

389 "Hydrogen in Steel," by C. A. Zapffe and C. E. Sims, *Blast Furnace Steel Plant*, vol. 28, 1940, pp. 1163–1166.

390 "Caustic Embrittlement," *Metal Progress*, vol. 39, 1941, pp. 696, 780, and 784.

391 "Corrosion of Metals by Gases," *Oberflächentechnik*, vol. 18, no. 2, 1941, p. 14.

392 "Embrittlement and Intercrystalline Cracking of Boiler Steels," by J. W. Donaldson, *Metal Treatment*, vol. 7, 1941, pp. 45–49.

393 "Review of Progress in Feedwater Treatment," by C. H. Fellows, *Journal*, Institute of Fuel, vol. 14, 1941, pp. 85–89.

394 "The Effect of the Physical State of the Solid Reactants on the Equilibrium Fe/Fe_3O_4 with H_2O/H_2," by R. Fricke, K. Walter, and W. Lohrer, *Zeitschrift Elektrochem.*, vol. 47, 1941, pp. 487–500, and 811; also *Chemical Abstracts*, vol. 36, 1942, cols. 4010–4011.

395 "Precipitation Hardening Effects in 'Plain' Ferritic Steels," by H. W. Gillett, *Metals and Alloys*, vol. 14, 1941, pp. 161–165.

396 Report from, National Physical Laboratory; "Intercrystalline Cracking in Boiler Plates," *Journal*, Iron and Steel Institute, vol. 143, 1941, pp. 93–158; also discussion, ibid., pp. 159–162.

397 "Boiler Embrittlement Protection," by C. W. Rice, *Combustion*, vol. 12, Jan., 1941, pp. 37–39.

398 "Intercrystalline Cracking of Boiler Steel and Its Prevention," by W. C. Schroeder and A. A. Berk, U. S. Bureau of Mines, Bulletin 443, 1941; abridged: "New Facts About Embrittlement," *Power*, vol. 86, Aug., 1942, pp. 103–105.

399 "Embrittlement Detector Testing on Boilers," by W. C. Schroeder, A. A. Berk, and C. K. Stoddard, *Power Plant Engineering*, vol. 45, Aug., 1941, pp. 76–79.

400 "Mechanism of Pin-Hole Formation," by C. E. Sims and C. A. Zapffe, Trans. American Foundrymen's Association, vol. 49, 1941, pp. 255–270; also discussion, ibid., pp. 270–281.

401 "Steel Defects Caused by Hydrogen," by C. A. Zapffe, *The Progress of Science*, Grolier Society, Inc., New York, N. Y., 1941, pp. 387–388.

402 "Cause of Pin-Holes and Some Related Defects in Enamel Coatings on Cast Iron," by C. A. Zapffe and C. E. Sims, *Journal*, American Ceramic Society, vol. 24, 1941, pp. 249–253; also discussion, ibid., pp. 254–256; abstract: "The Causes of Pin-Holes in Cast Iron Enamels," by C. A. Zapffe and C. E. Sims, *Ceramic Industry*, vol. 36, 1941, pp. 45–46.

403 "Hydrogen in Steel and Cast Iron and Defects in Applied Coatings," by C. A. Zapffe and C. E. Sims, *Metals and Alloys*, vol. 13, 1941, pp. 444–447, 584–589, and 737–742; also, ibid., vol. 14, 1941, pp. 56–60.

404 "Hydrogen Embrittlement, Internal Stress and Defects in Steel," by C. A. Zapffe and C. E. Sims, Trans. American Institute of Mining and Metallurgical Engineers, vol. 145, 1941, pp. 225–261; also discussion, ibid., pp. 261–271; also *Metals Technology*, vol. 8, Aug., 1941, T.P. no. 1307.

405 "Experience With Intercrystalline Cracking on Railroads," by R. C. Bardwell and H. M. Laudemann, Trans. A.S.M.E., vol. 64, 1942, pp. 403–407.

406 "Studies on the Cracking of Boiler Plate," by P. G. Bird and E. G. Johnson, ibid., vol. 64, 1942, pp. 409–416.

407 Discussion—"Symposium on Embrittlement;" ibid., vol. 64, 1942, pp. 431–444.

408 "Field Data From the Embrittlement Detector," by E. P. Partridge, C. E. Kaufman, and R. E. Hall; ibid., vol. 64, 1942, pp. 417–425.

409 "Steam-Pressure Vessel Resistant to Caustic Cracking," by N. B. Pilling and F. G. Straub, U. S. Patent 2,275,464, March 10, 1942.

410 "Embrittlement of Boiler Steel—Experiences With the Schroeder Detector," by T. E. Purcell and S. F. Whirl, Trans. A.S.M.E., vol. 64, 1942, pp. 397–402.

411 "Means for and Method of Testing Embrittlement Cracking Characteristic of Solutions," by W. C. Schroeder, U. S. Patent 2,283,955, May 26 1942.

412 "Summary of Papers Composing the Symposium on Em brittlement," by W. C. Schroeder and A. A. Berk, Trans. A.S.M.E. vol. 64, 1942, pp. 427–430.

413 "Apparatus for Testing the Embrittlement Cracking Characteristics of Solutions," by W. C. Schroeder and A. A. Berk, U. S. Patent 2,283,954, May 26, 1942.

414 "Corrosion of Unstressed Steel Specimens and Various Alloys by High-Temperature Steam," by H. L. Solberg, G. A. Hawkins, and A. A. Potter, Trans. A.S.M.E., vol. 64, 1942, pp. 303–313; also discussion, ibid., pp. 313–316.

415 "Corrosion of Carbon and Alloy Steel by High Temperature Steam," by H. L. Solberg, G. A. Hawkins, A. A. Potter, and J. T Agnew, *Valve World*, vol. 39, 1942, pp. 47–50.

416 "Results of Laboratory Embrittlement Testing of Boiler Waters," by F. G. Straub, Trans. A.S.M.E., vol. 64, 1942, pp. 393–396.

417 "Constitution of Iron-Hydrogen Alloys," by C. A. Zapffe; to be published in American Society for Metals "Metals Handbook."

418 "Fish-Eyes in Steel Welds Caused by Hydrogen," by C. A. Zapffe, *Metal Progress*, vol. 42, 1942, pp. 201–206.

419 "Defects in Cast and Wrought Steel Caused by Hydrogen," by C. A. Zapffe; ibid., pp. 1051–1056.

420 "Sources of Hydrogen in Steel and Means for Its Elimination," by C. A. Zapffe, *Metal Progress*, vol. 43, 1943, pp. 397–401.

421 "The Cause of Bleeding in Ferrous Castings," by C. A. Zapffe, *Metals Technology*, vol. 9, no. 7, Oct., 1942, T.P. no. 1515.

422 "Cause of Defects in Enamel Fired on Cast Iron at Temperatures above 725° C," by C. A. Zapffe, *Journal*, American Ceramic Society, vol. 25, 1942, pp. 175–180; abstract: "The Causes of Pin-Holes in Cast Iron Enamels," by C. A. Zapffe and C. E. Sims, *Ceramic Industry*, vol. 36, May, 1941, pp. 45–46.

423 "A Micrographic Study of the Cleavage of Hydrogenized Ferrite," by C. A. Zapffe and G. A. Moore, *Metals Technology*, vol. 10, no. 2, Feb., 1943, T.P. No. 1553.

424 "Further Considerations of Hydrogen as a Cause of Enamel Defects," by C. A. Zapffe and C. E. Sims, *Journal*, American Ceramic Society, vol. 25, 1942, pp. 205–215.

425 "Scratch Blisters," by C. A. Zapffe and J. L. Yarne, ibid., vol. 25, 1942, pp. 180–190; abstract: "Relation of Oxidation to Enamel Defects," by C. A. Zapffe and J. L. Yarne, *Ceramic Industry*, vol. 36, May, 1941, p. 44.

426 "Relation of Surface Oxidation to Certain Defects in Enamel Coatings on Steel," by C. A. Zapffe and J. L. Yarne, ibid., vol. 25, 1942, pp. 191–194; abstract: "Relation of Oxidation to Enamel Defects," by C. A. Zapffe and J. L. Yarne, *Ceramic Industry*, vol. 36, May, 1941, p. 44.

427 "Chips, Fish Scales, and Shiners," by C. A. Zapffe and J. L. Yarne, ibid., vol. 25, 1942, pp. 194–203; also discussion, ibid., pp. 203–205; abstract: "Fish Scales, Shiners, Chips in Enamel," by C. A. Zapffe and J. L. Yarne, *Ceramic Industry*, vol. 36, May, 1942, pp. 43–44.

Discussion

W. C. SCHROEDER[8] AND A. A. BERK.[9] The author is to be congratulated on the very large amount of data he has accumulated for his paper. Part of this information describes the two known effects of hydrogen on steel. Stated briefly these are as follows:

1 Hydrogen may enter or be trapped in steel at temperatures below the atmospheric boiling point of water to cause serious losses of impact strength. Fractures resulting from this brittleness are transcrystalline.

2 Hydrogen, under high pressure, at temperatures considerably above those at which riveted boilers operate will enter and decarburize steel, causing intergranular fissures to develop. At higher temperatures (1000 F), and a hydrogen pressure of 5000 psi, there is also a tendency for the inclusions in the steel to be reduced.

In contrast to the action of hydrogen at room temperatures and at very high temperatures, no intergranular fissure due to this gas has ever been reported to take place at temperatures from 250 to 460 F (15 to 480 psi), which includes the entire range in which embrittlement failures have occurred in boilers. This is particularly evident in the paper under discussion; for despite the very extensive bibliography, there are no illustrations or discussion of failures produced by hydrogen gas in the temperature range in which boiler embrittlement occurs. The author, nevertheless, postulates that such failures could occur by the following mechanism:

1 Boiler water concentrates by extreme evaporation in the boiler seams.

2 The strongly caustic solutions then react with boiler steel to form iron oxide and hydrogen.

3 The hydrogen enters the steel and reacts with carbides, oxides, sulphides, phosphides, and nitrides to form the corresponding hydrogen compounds.

4 The hydrides are not soluble in the grains, so that they congest in the grain boundaries, causing internal stress and fissures.

5 If the metal is externally stressed at the same time, it will crack when the load-carrying ability is sufficiently reduced by the fissures.

6 The crack allows the caustic solutions to penetrate and further corrosion and cracking follow.

Discussion of Proposed Mechanism. Let us examine and critically review each of the major items upon which this postulated mechanism is based. Step 1 relates to the accepted concept of formation of aggressive solutions from dilute boiler water and forms the basis of all modern thought concerning the incidence of intercrystalline cracking. The manner in which concentration occurs is not treated by the author.

Step 2 indicates that steel is attacked by the concentrated caustic solution. However, the author has misinterpreted Stromeyer's experiments to imply that caustic must act indirectly through hydrogen, because it seemed to operate on metal removed from the solution by $^1/_4$ in. of steel. Actually, in all of the embrittlement cracking that has been reported (including Stromeyer's tests) or that the discussers have examined, the failure can be shown to have been started at a metal surface in direct contact with a concentrated solution. This is true both of failures in boiler seams and the failure of specimens in embrittlement detectors. There is therefore no necessity to postulate an agency that can start cracks or fissures from within the metal.

If the postulated agency does tend to produce cracks or fissures from within the metal, it acts in a manner not in accord with known facts. Numerous sections of embrittled boiler seams have been examined microscopically and no such fissures have been found. Cracks that appeared to start and end in the heart of a two-dimensional plane were always traceable in the third dimension to the surface in contact with concentrated solution.

Step 3 demands the reaction of hydrogen in the steel with oxides, carbides, sulphides, phosphides, and nitrides to form corresponding hydrogen compounds. The experimental work cited to support this statement has been reviewed by the discussers. The original papers disclose that Whiteley (130),*

[8] Bureau of Mines, Washington, D. C. Mem. A.S.M.E.

[9] Bureau of Mines, Washington, D. C.

* Numbers in parentheses refer to the Bibliography at the end of the author's paper.

working at 1600 F, checked the results of Le Chatelier and found that hydrogen reduced iron oxide to only a slight depth in solid iron. Baukloh (304) found that while iron sulphide is affected by hydrogen above 750 F, manganese sulphide (the principal sulphur compound present in steel) is stable to 1800 F. Naumann (329) found that under circumstances producing decarburization (4000 psi hydrogen and 650–750 F), hydrogen is not able to remove phosphorus, sulphur, and oxygen. Zapffe and Moore (423), attempting to purify samples of steel with hydrogen at 1800 F found that carbon was readily removed but that oxygen, sulphur, nitrogen, and phosphorus were not removed even after 16-day treatments. This evidence does not support a belief that hydrogen will reduce the impurities in boiler-seam steel to form hydrides, for the temperatures at which these reactions proceed are far above those found in boilers.

The author, in an attempt to show through extrapolated equilibrium data that hydrogen would readily react with inclusions of magnetic oxide at boiler temperatures, made the error of confusing chemical kinetics with chemical equilibrium. What he has shown is that there is slight possibility for oxide to be reduced with the simultaneous formation of water vapor in the temperature range (250–480 F) in which boiler embrittlement occurs.

That the attainment of high pressures of hydrogen in steel at boiler temperatures is most improbable can be shown through calculations based on known diffusion constants. If the boiler steel were being corroded at the very rapid rate of $^1/_{32}$ in. per year, 130 cu in. of hydrogen (measured at standard conditions of temperature and pressure) would be generated per square inch of surface affected. If all of the gas were to enter and be trapped in the steel at 390 F, the rate at which hydrogen was being supplied would be 0.015 cu in. per sq in. of surface per hr. Possibly hydrogen can collect in a rift, cavity, or boundary at this rate. The pressure that would force the gas to leave the cavity by diffusion at the same rate can be calculated from data supplied by many investigators. The experiments of Smithells and Ransley[10] show that molecular hydrogen will diffuse from a cavity at the rate of 0.015 cu in. per sq in. per hr when the pressure is less than 400 psi. The results of experiments by Borelius and Lindblom,[11] by Ham (325), and by Ryder[12] provide figures of the same magnitude. A series of experiments by Naumann[13] also show that a pressure of 500 psi of molecular hydrogen will not only cause the gas to diffuse from a cavity quite rapidly but will cause 0.015 cu in. per sq in. per hr to diffuse through 0.2 in. of standard mild steel. Therefore the hydrogen pressure that may result in the steel of a boiler seam at 390 F cannot be very great.

The fact that boiler material embrittles without evidence of decarburization is shown by Fig. 35 of this discussion. This figure shows a crack in a boiler operated for a period of 9 years at 450 F. There is no evidence of decarburization or hydrogen purification. In contrast, the hydrogen attack that results in intercrystalline cracking is always preceded by decarburization.

Step 4 of the mechanism provides that the hydrides formed during the reduction of inclusions be rejected to the boundaries of the grain because they are insoluble in the grain. If they are not soluble and cannot diffuse in the grain it is difficult to understand why they do not remain in the cavity in which they are supposedly formed. Of course, if they happened to be formed between the grains they would presumably remain there.

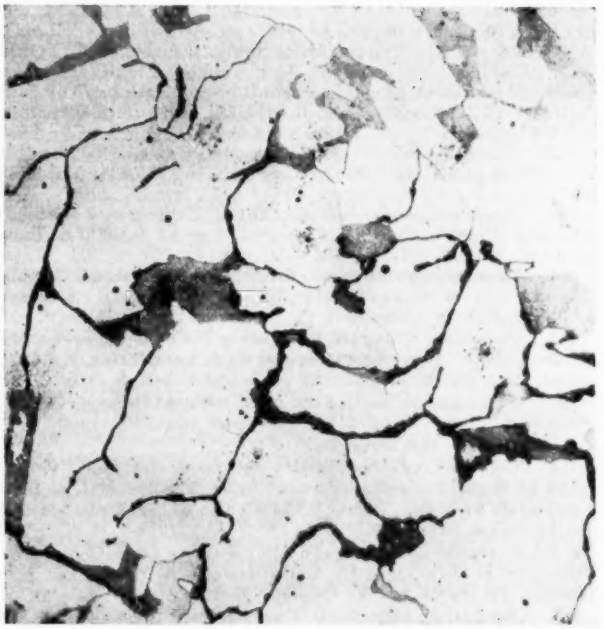


FIG. 35 NO DECARBURIZATION SHOWN IN CRACK IN SEAM OF BOILER OPERATED AT 480 F FOR 9 YEARS
(Surface etched with nital; ×300.)

Step 5 of the theory of cracking as developed in the paper makes it necessary to have not only high temperatures but high pressures of hydrogen or other insoluble gaseous products as well. The combined conditions of high temperature and pressure are believed to cause fissures and loss of load-carrying ability in the steel. The evidence to support this belief is drawn from experiments at much higher temperatures than those at which embrittlement has been encountered in boilers. For example, Naumann (329), working with a hydrogen pressure of 13,000 psi, did not attain fissures or cracking during a test of 2000 hr at temperatures below 480 F. Vanick (203) did not find fissuring below 570 F. Desch (396) still obtained intercrystalline cracks when the temperature was lowered to 570 F, but no cracks were found even after a month at 435 F. Inglis and Andrews (262) found that over 2 years of hydrogen service at 3500 psi and 410 F did not greatly affect the strength of a coarse-grained mild-steel tubing, although all the pearlite areas were slightly decarburized. A fine-grained tube of the same composition was not even decarburized by a year of service at 480 F and 3500 psi of hydrogen.

In contrast with the lack of effect of hydrogen at temperatures below 450 F even over very long periods, repeated experiments have shown that embrittlement can be produced in a few hours at 230 F by concentrated caustic solutions boiling under atmospheric pressure. This difference between the action of hydrogen and the action of caustic is supported by the paper; for, in spite of the search of the literature, there is no evidence of hydrogen cracking at the temperatures in which boiler embrittlement occurs, although a great many industries use hydrogen, or obtain the gas as a by-product, in steel containers at temperatures corresponding to those in boiler operation.

Fig. 27 of the paper is advanced as visual proof of the hydrogen theory of cracking. The gray fracture of normal ductile metal comprises the zone farthest removed from the concentrated caustic solution. The corroded zone was obviously affected by penetration of the solution. In between is a bright, clean, brittle

[10] "Diffusion of Gases Through Metals," by C. J. Smithells and C. E. Ransley, Proceedings of the Royal Society, London, England, series A, vol. 150, 1935, pp. 172–197.

[11] "Diffusion of Hydrogen Through Metals," G. Borelius and S. Lindblom, *Annalen der*, vol. 82, 1927, pp. 201–226.

[12] "Relations Between Gases and Steel," by H. M. Ryder, *Electrical Journal*, vol. 17, 1920, pp. 161–165.

[13] "Influence of Alloy Elements in Steel Upon Resistance to Hydrogen Under High Pressure," by F. K. Naumann, *Technische Mitteilungen Krupp, Forschungsberichte*, vol. 1, 1938, pp. 223–234.

area. It is inferred that this latter zone is affected by hydrogen, but the corroding liquors had not penetrated to it. Photomicrographs of the three areas are described as proving that hydrogen preceded the corroding agent and did most of the damage. However, no decarburization and no fissuring are evident in any zone although Fig. 31 shows that cracking had penetrated even the gray area. There is no apparent reduction of inclusions in the corroded zone, which indicates either that not enough hydrogen was present to produce any appreciable results on the metal or that the temperature itself was too low to allow it to produce any effect.

If the three distinct areas were not formed by hydrogen, how were they formed? Fig. 36 of this discussion shows a section of boiler plate, which was cut to produce a line of concentrated stress on the surface and was finally broken by impact with a hammer. Again there are three zones in the metal. Obviously none of them is corroded by a caustic solution since neither solution nor hydrogen was present. The example simply shows that three zones can be produced by impact and that any long discussion of what they mean is apt to lead to false conclusions. The characteristics of the surface are more likely to be determined by the way and the rate at which the steel is fractured than by any illusory internal conditions.

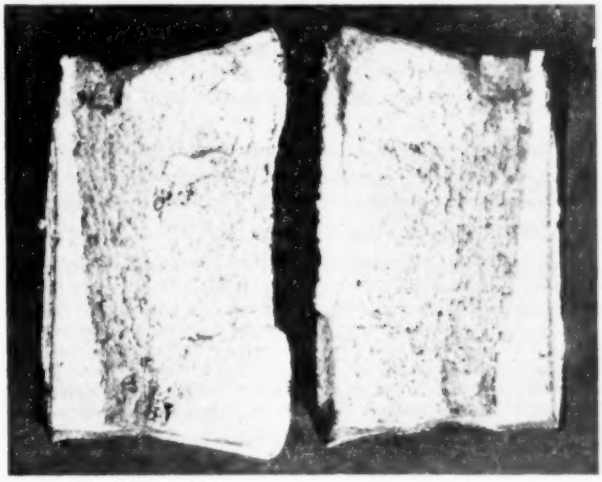


FIG. 36 BOILER PLATE, MILLED AND CRACKED BY SUCCESSIVE IMPACTS

Step 6 completes the author's theory, providing for propagation of the crack through the action of sodium-hydroxide solutions on the newly exposed surfaces. Again the supposition is that a series of fissures are formed through the action of hydrogen on inclusions in the steel and that the fissures are joined to the surface by a crack when the stress exceeds the load-carrying ability of the remaining metal. No such fissure has ever been observed in embrittled boiler seams. It is also interesting to observe that propagation is supposed to take place along grain boundaries, although a piece of steel broken in tension at these temperatures will always break along slip lines in the grains. At the higher temperatures of the ammonia-synthesis and hydrogenation processes from which the author draws his parallel, it is well known that the tensile strength at the boundaries tends to approach that within the grains, permitting the familiar pattern by which the fissures are joined.

This paper points out that certain steels have been developed which will resist the reducing and fissuring action of hydrogen gas. If there is any relationship between hydrogen attack and boiler embrittlement, it would then be expected that these same steels would also be resistant to boiler embrittlement. In the past few months, the discussers have had the opportunity to test steels containing manganese, chromium, and molybdenum of alloy contents which, according to Naumann (346) would greatly increase their resistance to attack by hydrogen. All of these steels were rapidly cracked in the embrittlement detector, and some were found to be particularly susceptible to the action of the caustic solutions. For example, Fig. 37 of this discussion shows a crack in a badly shattered specimen of alloy steel containing 5 per cent chromium and 1.5 per cent silicon. These results do not support the belief that hydrogen is a major factor in the cause of boiler embrittlement. At the same time, they indicate that results from testing with hydrogen gas cannot be interpreted in terms of boiler embrittlement without danger of reaching erroneous conclusions.

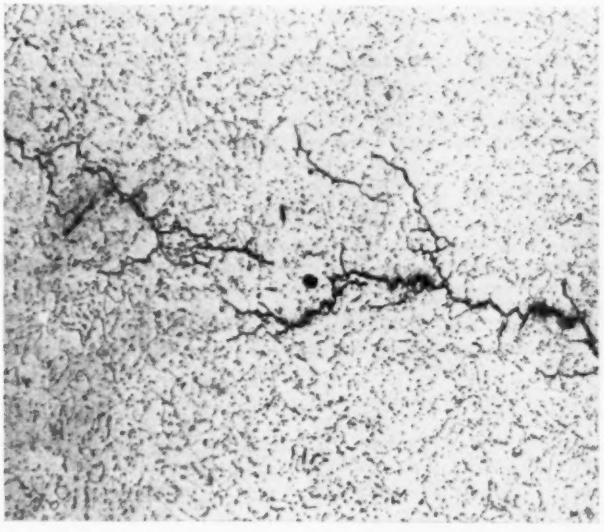


FIG. 37 INTERCRYSTALLINE CRACK IN EMBRITTLEMENT-DETECTOR-TEST SPECIMEN OF ALLOY STEEL CONTAINING 5 PER CENT CHROMIUM AND 1.5 PER CENT SILICON
(Surface etched with nital; ×300.)

Work of Other Investigators. In some instances, important references in the paper seem to have been interpreted improperly. Norton's experiments (377), for example, are cited to prove that sodium silicate, which sometimes accelerates boiler embrittlement, also accelerates hydrogen absorption.

Norton painted the outer surface of a steel radio tube with sodium silicate and measured the quantity of hydrogen penetrating to the interior when the tube was heated. He found that silicate-retained water reacted with the steel tube surface at the comparatively high temperature of 390 F. The experiment in no way measured the action of silicate on hydrogen penetration but instead measured its effect in retaining water at a high enough temperature so that a fairly rapid release of hydrogen could take place.

It is also noted that the work at the Bureau of Mines proved that sodium silicate was an accelerator of embrittlement while the work by Desch (396) in England stated that intercrystalline cracking could be produced in the absence of this salt. If the work at the Bureau of Mines is fully examined, it will be found that it does not disagree with the work in England. In the bulletin (398), cited by the author, appear the following statements:[14]

1 Under certain conditions sodium hydroxide alone can produce

[14] Reference (398), p. 45.

intercrystalline cracking. (See last two U-bend tests in Table 1, and detector tests 51, 29, and 45 in Table 9.)

2 Sodium silicate, especially the crystalline metasilicate, may accelerate cracking in some instances or broaden the range of conditions under which it occurs in others.

3 The effect of the silica in accelerating cracking appears to be more pronounced at 225 C and above than at lower temperatures.

4 The effect of the silica in accelerating cracking depends on the concentration of sodium hydroxide in contact with the steel. At high concentrations (especially at the higher temperatures) this latter material may attack so vigorously that general over-all corrosion proceeds as rapidly as grain-boundary corrosion. The addition of sodium silicate can suppress the over-all corrosion but still allow penetration at the boundaries. The influence of this salt in repressing over-all corrosion has already been illustrated.

5 The effect of silica on intercrystalline cracking depends on the applied or internal stress acting during the test. At the higher stresses any influence of the silica may be difficult to detect.

6 The influence of the silica depends on the physical and chemical characteristics of the steel being tested. On steels very susceptible to embrittlement (especially certain low-alloy steels) it is unnecessary to use this compound to produce cracking. On steels difficult to embrittle the silicate often appears to exert an accelerating effect.

7 At the lower boiler temperatures, certain types of sodium silicate may sometimes retard instead of accelerate intercrystalline cracking.

Particular attention should be directed to items 1 and 7 in this list since these show that Desch and the conditions of his test agree with those of the discussers. It is apparent that the action of the silicate is complex and that any attempt to treat it in too simple terms may lead to false conclusions.

The author's paper calls particular attention to the fact that tests with sodium nitrate are irrelevant in relationship to boiler embrittlement. He also feels that this salt ordinarily is not present in boiler water. It is now known that this belief is in error and simply existed because determinations of nitrate seldom are made in boiler-water analyses. Recent work has shown that high concentrations of sodium nitrate are present in a considerable number of boiler waters.

An interesting side light, concerning the comparison of cracking produced in sodium-nitrate solutions and caustic solutions is the development of the somewhat embrittlement-resisting Izett steel. The tests by which this steel was shown to be more resistant to intercrystalline cracking depended on the use of concentrated sodium-nitrate solutions. It is peculiar that this steel also exhibits increased resistance to caustic embrittlement if there is no relationship between action of the nitrate and the caustic solutions as postulated by the author.

The author in discussing the smooth, adherent, black-oxide scale that generally coats embrittled boiler seams states that these must "be distinguished sharply from the highly localized accumulations one must expect from selective corrosion, as required by the theory of Schroeder and his colleagues." The following quotations from the Bureau of Mines bulletin (398) may perhaps help to explain the term "selective corrosion:"

> If the solutions indicated in Table 2 produce intercrystalline penetration without extensive over-all corrosion of the crystal faces, it should be possible to observe the progress of this selective activity. For this purpose, a specimen was polished for microscopic examination and bent over a bar in the center by means of bolts at the ends, as shown in figure 15. When the specimen was immersed in a boiling sodium hydroxide-lead oxide solution for 1 or 2 days a deep crack developed, as shown in figure 16. If, however, it was removed from the boiling solution after 2 or 3 hours it was found covered with a thin film of oxide. Under the microscope this film, which was blue to the naked eye, appeared gray, as illustrated in figure 17. The fine slip lines apparent in most of the crystals result, of course, from bending of the specimen to create stress. After this blue or gray film has formed, if the specimen is again immersed in the boiling solution for several hours rather broad white lines appear that outline the approximate position of the grain boundaries. These can be seen in figure 17. With further boiling, short, black lines appear in the broader white ones, which ultimately merge to form distinct cracks, as shown in the figure.
>
> These experiments illustrate that development of the initial intercrystalline fissure is not a sudden or instantaneous process. Its growth can be followed over a considerable period. This type of initial attack would be expected from a selective corrosion process.
>
> The silica, under certain conditions at high temperatures, and the oxidizing agents, in the U-bend tests at lower temperatures, probably function in a similar manner to accelerate the cracking: that is, they protect the crystal faces and prevent over-all corrosion while leaving the grain boundaries open to attack. The films they establish on the crystals may also create electrochemical forces that intensify action at the boundaries.

It is also of interest to note that corrosion in solutions starts at grain boundaries[15] but generally quickly spreads so that the over-all corrosion obscures the selective action.

Course of Embrittlement Investigations in the United States. A careful study of the literature, both with respect to boiler embrittlement and hydrogen embrittlement, has often led to the belief that the actions are related or may be identical. This was true in the studies undertaken by Parr and Straub, for their first paper expressed the belief that hydrogen gas was the primary factor in boiler embrittlement. It was not until they had completed many years of study on the subject that they abandoned this concept.

At the start of their investigation, Partridge and Schroeder made a survey of the literature which covered much of the ground now reviewed by the author. Their conclusions contained the following statement:

> A thoroughly logical picture of the way in which the failure of boiler steel may be caused by hydrogen embrittlement may be built up on the basis of the information discussed in this report. When a boiler goes into operation its internal surfaces are immediately covered with a layer of magnetic oxide. This layer under ordinary conditions forms an almost impassable barrier between the boiler water and the steel. As the concentration of hydroxide increases, however, the layer becomes progressively less protective, and the reaction between the water and the steel increases its rate.
>
> This chemical reaction produces hydrogen under condition equivalent to an extremely high gas pressure. The hydrogen diffuses into the steel and causes a definitely brittle condition, probably by setting up internal stresses at grain boundaries and cleavage planes.
>
> Although the steel may be rendered very brittle by the absorption of hydrogen, no serious permanent damage is done until a localized stress at some point reaches a very high value, probably well up toward the ultimate strength of the metal. A piece of normally ductile steel subjected to a high local stress of this sort would yield slightly, automatically reducing the local stress by distributing it over a large section of metal. The embrittled steel, however, instead of gliding along slip planes in the manner of ductile metal, will ultimately crack at the point of high local stress. Although the initial failure may be only the boundary between two grains in the outermost surface layer, it represents a permanent damage to the steel. The high local stress, instead of being reduced in intensity, may then be transmitted to the next layer, with the result that the failure is eventually repeated here. As long as the concentration of hydrogen in the steel is sufficient to cause failure, the process of cracking will continue.

With this belief as a background, experiments were specifically designed to show that hydrogen was one of the primary factors in boiler embrittlement. Each of these experiments gave results in disagreement with preconceived ideas until, after an investigation of about 6 years, the conclusion was inescapable that the theory based on the action of hydrogen gas and developed through a study of the literature was incorrect. In fact, as the experiments were carried further, it was evident that some of the early interpretations of the work in the literature must necessarily be revised to quite different conclusions.

A brief description of one series of such experiments may be of interest. Fig. 38 of this discussion illustrates a piece of equip-

[15] "The Topochemistry of Corrosion and Passivity. III," by E. Pietsch, E. Josephy, B. Gross-Eggebrecht, and W. I. Roman, *Korrosion und Metallschutz*, vol. 8, 1932, pp. 57–68.

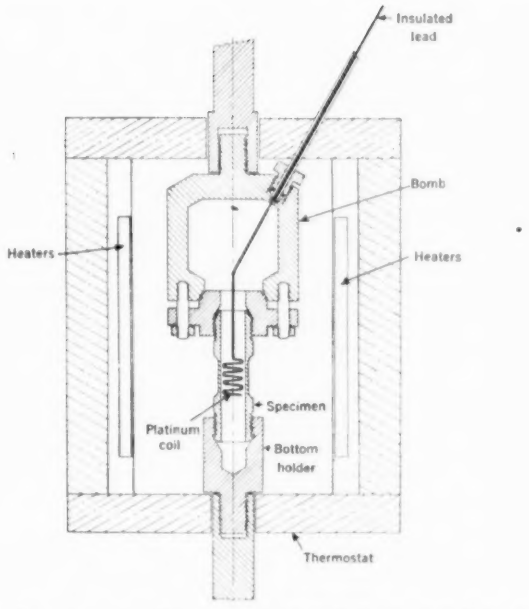


FIG. 38 EQUIPMENT FOR TESTING ACTION OF HYDROGEN AT ROOM OR ELEVATED TEMPERATURE

ment that was used at the Bureau of Mines to study the action of hydrogen gas on stressed steel. Hydrogen was released electrolytically at the surface of the specimen. When the apparatus was tested at room temperature it was found that the gas pressure rose to 1200 psi in 48 hr. The test specimen was then stressed to failure. The very brittle fracture that resulted indicated that the electrode was located satisfactorily with respect to the reduced section of the specimen.

Five specimens were then exposed to hydrogen attack at 250 C (482 F) for periods up to 122 hr. All specimens were stressed at about 50,000 psi during the tests, but no failures resulted. Each specimen was stressed to failure to complete the tests; in no case was any loss of load-carrying ability noted. There was some brittleness in the metal as would be expected from exposure under stress in the blue-brittle temperature region, but the fractures were much less brittle than that produced during the low-temperature test. A caustic solution in the same equipment produced failure in the specimen in 4 to 12 hr. The temperature for the latter tests was 250 C; the load on the test specimen was 50,000 psi; and no hydrogen was generated.

The author may now be in much the same position as were the investigators of the University of Illinois and the Bureau of Mines when they started their studies. Possibly through prolonged experimentation he, too, would revise his ideas and reach the conclusion that hydrogen was not as important as he now thinks it to be. His evident interest in the study of embrittlement, as shown by the large amount of work in the compilation of his bibliography, would certainly justify support for such work as he may wish to undertake. It is, of course, unfortunate that his bibliography does not refer to the important work on selective corrosion of Ulick Evans[16] in England, and Dix,[17] and Mears and Brown[18] at the research laboratory of the Aluminum Company of America.

Since previous investigators have been forced to discard the hydrogen-embrittlement theory, it might be best to undertake further investigation along this line without attempting to justify or prove preconceived ideas developed through literature study. A thoroughgoing investigation which gave equal credence, at least at the beginning, to all of the theories developed to explain boiler embrittlement would be very desirable. Careful experimental study of each of these would allow the investigators to reach conclusions that would be sound. The conclusions would be backed by a set of unprejudiced observations and would carry conviction to the people responsible for boiler operation.

In conclusion, it should be noted that boiler operators in the United States, working in close co-operation with research engineers, have found practical methods of preventing embrittlement cracking of boiler seams. These solutions of the problem have been achieved principally by tests with the embrittlement detector, which directly determines whether a boiler water can or cannot cause cracking. Although theoretical explanations are of considerable interest with relation to complete understanding of causes and effects, practical answers fortunately do not have to await their elucidation. For example, the sodium-nitrate treatment on the Chesapeake & Ohio Railway has effected a decrease in locomotive-boiler cracking, corresponding to a saving of more than 90 per cent of the engine time lost and the material and man-hours required for repair work. Under the present war conditions of transportation, this is indeed fortunate.

THOMAS DE VRIES.[19] There is additional evidence to substantiate the argument of the author that the diffusion of atomic hydrogen into steel is at the basis of the embrittlement phenomena. As early as 1864, Cailletet found that iron absorbed some hydrogen liberated by electrolysis. It has been known for a long time that iron is embrittled in pickling solutions by the hydrogen liberated in the reaction. The work of Bodenstein (153) and others has shown that atomic hydrogen permeates into the steel since the rate of permeation was proportional to the square root of the current density.

Borelius and Lindblom[20] have found a similar result for hydrogen produced by electrolysis. They also studied the permeation of molecular hydrogen into steel at different temperatures and pressures. The rate increased markedly with temperature, approximately as the fifth power of the absolute temperature. The rate also increased with the square root of the pressure thus proving definitely that the hydrogen must be in the atomic state before diffusion can occur.

Post and Ham,[21] investigating the permeation rate-pressure isotherms for hydrogen into nickel, found deviations from the square-root-of-pressure law, which they ascribed to the fact that some of the hydrogen was reacting with impurities in the nickel.

The author refers to Schenck for equilibrium constants for the reaction $Fe_3C + 2H_2 = 3Fe + CH_4$. Since Schenck's data were scattered and did not permit of very definite calculations, reference should be made to Watase,[22] whose data were critically examined by Kelley.[23] From his data for the interval 600–800 deg

[16] (*a*) "Metallic Corrosion, Passivity and Protection," by U. R. Evans, Edward Arnold & Company, London, England, 1937.

(*b*) "Velocity of Corrosion From the Electrochemical Standpoint," by U. R. Evans and T. P. Hoar, Proceedings of the Royal Society of London, England, vol. A137, 1932, pp. 343–365.

(*c*) U. R. Evans' discussion of "Intercrystalline Cracking in Boiler Plates," by C. H. Desch, Trans. North East Coast Institution of Engineers and Shipbuilders, vol. 55, 1938–1939, pp. D35–36.

[17] "Acceleration of the Rate of Corrosion by High Constant Stresses," by E. H. Dix, Jr., *Metals Technology*, T.P. 1204, vol. 7, 1940.

[18] "Causes of Corrosion Currents," by R. B. Mears and R. H. Brown, *Industrial and Engineering Chemistry*, vol. 33, 1941, p. 1001.

[19] Professor of Chemistry, Purdue University, Lafayette, Ind.

[20] "Durchdang von Wasserstoff durch Metalle," by G. Borelius and Sven Lindblom, *Annalen Physik*, vol. 82, 1927, pp. 201–226.

[21] Ref. (347), p. 599.

[22] "Studies on the Equilibrium: $Fe_3C + 2H_2 \rightleftarrows 3Fe + CH_4$," by Takeo Watase, *Journal of the Chemical Society of Japan*, vol. 54, 1933, pp. 110–132.

[23] "Contributions to Data of Theoretical Metallurgy. XIII. Thermodynamic Properties of Metal Carbides and Nitrides," by K. K. Kelley, Bureau of Mines Bulletin 407, 1933, p. 13.

K, the equilibrium constant is given by $\log K = -5937/T + 6.836$, whereas the author used the equation $\log K = -7990/T + 8.75$. Fortunately, the difference in the logarithm of the equilibrium constants (—2.69 and —4.07, respectively, at 350 C) calculated by the two equations is not sufficient to modify the author's argument.

However, it should be realized that the simple equation of Schenck is not suitable for extrapolation to higher temperatures and that this should be considered in any argument concerning decarburization. From the equation given by Kelley it can be calculated that the equilibrium constant, $K = (P_{H_2})^2/P_{CH_4}$, is 1.3×10^{-6} at 375 F (190 C), but 1.15 at 1100 F (600 C). Thus intercrystalline decarburization can definitely occur better at lower temperatures than at very high temperatures. This has been the experience of Potter, Solberg, and Hawkins (330).

R. B. MEARS.[24] This paper on boiler embrittlement is a valuable contribution to our knowledge on this subject.

In the paper, several theories of boiler embrittlement and other forms of stress corrosion cracking are described. However, we do not believe that the author has discussed one of the most probable explanations for stress corrosion cracking. As was pointed out by Dix,[25] stress corrosion cracking is often the result of selective attack caused by local potential differences between different portions of the metal or alloy surface. In many cases such potential differences exist between material adjacent to the grain boundaries and the matrix of the grain. In other cases potential differences can exist between slip planes or other metallurgical characteristics of the material and a grain matrix. As a result of these potential differences, the anodic areas suffer electrolytic corrosion and, if the material is under stress, selective attack can cause cracking of the material in a relatively short period of exposure. It has been well established that this is the mechanism of the stress corrosion cracking of the aluminum-base alloys containing copper (Duralumin-type alloys), and it appears to be responsible for the season cracking of brass also.[26]

Furthermore, there is a good indication that the same mechanism applies to the stress corrosion cracking of 18–8 stainless steel.[27] It seems quite possible that the mechanism of boiler embrittlement is also an electrochemical phenomenon of this same type, local differences in potential causing selective attack at certain planes in the metal. Cracking will then occur along these planes.

It has been found in the case of nonferrous alloys that stress corrosion cracking may, in the early stages, follow an intergranular path and then later the metal may fracture transgranularly. Thus, there often exists some confusion of the path of the fracture, since it may start out following grain boundaries and then later on cut through grains themselves. Evidently this same confusion has existed in the case of boiler embrittlement. In any event, whether or not the mechanism of boiler embrittlement is indeed electrochemical, as is the case with many other types of stress corrosion cracking, the electrochemical mechanism of stress corrosion cracking should be mentioned in an extensive review, such as this one by the author.

The stress corrosion cracking of many types of nonferrous materials can be prevented by cathodic protection. The article to be protected is made the cathode, and current is passed to it through the electrolyte from a sacrificial anode. It would seem that a test involving cathodic protection could well be used to examine the hydrogen mechanism of boiler embrittlement. If a boiler steel which cracks readily in the absence of cathodic protection does not crack under the same conditions when it is being cathodically protected, there would appear to be no justification for the hydrogen theory, since during cathodic protection atomic hydrogen is being deposited on the surface of the steel and so should actually accelerate cracking, if the hydrogen theory is correct. We suggest that this experiment should be performed as soon as possible in order to test out the hydrogen mechanism.

The author mentions that the season cracking of brass remains unsolved. We do not believe this statement is correct. Instead there is very conclusive evidence that the season cracking of brass is an electrochemical phenomenon, and actual potential differences between grains and grain boundaries in brass have been measured in solutions which cause season cracking.

The author discusses at some length the results of other workers where occasionally one chemical is found to be an inhibitor of boiler embrittlement under some conditions but a stimulator under others. This type of action is not at all unusual for corrosion inhibitors. In fact, it is the general rule. Most corrosion inhibitors with which this writer is familiar accelerate corrosion under some conditions and retard it under others. In general, inhibitors can localize attack and therefore very often stimulate selective attack which causes intergranular corrosion or stress corrosion cracking. In many cases, very small or very large amounts of an inhibitor will be distinctly beneficial while intermediate amounts will be harmful. An explanation for this behavior can often be obtained from electrochemical measurements, and the mechanism of inhibitor action appears to line up with its effect on the anode and cathode reactions.

In studying the stress corrosion cracking of nonferrous materials, it has been found necessary to investigate the matter on a statistical basis. If a large number of "identical" specimens are exposed to a given corroding environment while under stress, a certain percentage of them only may be found to develop stress corrosion cracking. This percentage is often rather reproducible and may be used to express the probability of stress corrosion cracking of that particular alloy under those particular conditions. Slight changes in the composition of this alloy will affect the percentage of specimens which crack in the test.[28] A change in the nature of the corroding environment will shift the probability of stress-corrosion-cracking figures in one direction or another, so that they may approach either 0 or 100 per cent.

We suggest that in boiler-embrittlement studies it would be desirable to use a statistical picture also, since it seems probable that it will apply in this case as it has in the case of stress corrosion cracking of nonferrous materials.

E. P. PARTRIDGE.[29] Much that might have been presented as hypothesis or opinion by a less enthusiastic protagonist appears in this paper in the guise of indubitable fact. While a point-by-point debate would be as lengthy and as barren of result as the medieval argument over how many devils could dance on the point of a needle, the writer cannot forbear a token challenge on two representative passages.

In Part 3, the author refers to the 1941 Report on "Intercrystalline Cracking in Boiler Plate," by the National Physical Laboratory, England. As is natural, he has mentioned the emphasis placed by the British investigators upon hydrogen as the cause of embrittlement, even though the experiments were conducted at 420 and 470 C, far above the highest temperature, about 250 C, at which intergranular cracking has ever been observed in riveted boiler seams, and were characterized by de-

[24] Chief, Chemical Metallurgy Division, Aluminum Research Laboratories, Aluminum Company of America, New Kensington, Pa.

[25] "Acceleration of Rate of Corrosion by High Constant Stresses," by E. H. Dix, Jr., Trans. A.I.M.E., Institute of Metals Division, vol. 137, 1940, pp. 11–40.

[26] "Causes of Corrosion Currents," by R. B. Mears and R. H. Brown, *Industrial and Engineering Chemistry*, vol. 33, 1941, p. 1002.

[27] Ibid., p. 1003.

[28] See for example, ref. 25, Fig. 16, p. 34.

[29] Director of Research, Hall Laboratories, Inc., Pittsburgh, Pa.

carburization of the steel, which has never been found in actual cases. What the author neglected, in his zeal for the hydrogen theory, was what might be called the "minority report" from the National Physical Laboratory, which described the "oxidizing" type of cracking produced by very concentrated caustic solutions at temperatures more nearly representative of boiler conditions. The following statement appears in the British report: "Cracks of the hydrogen type were often found throughout the whole mass of a cold-worked specimen, while those of the oxidizing type existed in patches always in communication with the outer oxide coat." This latter condition more nearly resembles what is observed in actual cracked boiler plate than does the former.

The second item to be challenged is the discussion, also in Part 3 of the paper, relative to the development of high gas pressures in grain boundaries. The author calculates from the steam-iron equilibrium that very high pressures of hydrogen and fantastically high pressures of methane could develop in a closed boiler by reaction of the boiler water with the steel. He then postulates, however, that a grain boundary may be regarded as a "tiny theoretical boiler" in which the same high pressures previously calculated could develop as hydrogen, diffusing through the steel reduced magnetic iron oxide to produce water vapor.

Actually, the operating boiler is not a closed system, and the partial pressure of hydrogen both inside and outside of it is extremely low. Considering the steel for the moment simply as a solid permeable to hydrogen, the pressure of hydrogen at any point within the metal could scarcely exceed the very small pressure of hydrogen within the boiler, something of the order of 0.1 to 0.001 psi. According to the fundamental equilibrium indicated in Fig. 17, the pressure of water vapor developed in the grain boundary would then be almost vanishingly small.

To the extent that molecular H_2 diffuses less readily through the steel than does atomic H at any temperature, the development of higher gas pressures within the grain boundaries is possible. For example, it has been suggested by others that atomic hydrogen diffusing through steel may combine into molecular hydrogen at the discontinuity created by a grain boundary. Even so, the possible localized pressure, based upon data for the diffusion of molecular hydrogen through steel at boiler temperatures is very low in comparison with those suggested in the present paper.

The author should be given credit for a monumental bibliography, for some exceptional photomicrographs, and for his stimulating insistence that we re-examine our previous concepts concerning embrittlement. The importance of this paper really resides, however, in two suggestions which may be subjected to experiment. These are the predictions (*a*) that an inexpensive steel resistant to hydrogen embrittlement will likewise not be subject to cracking in boiler tube ends or riveted seams and (*b*) that inhibitors which will minimize the absorption of hydrogen by ordinary low-carbon steel will at least prolong its service life under embrittling conditions.

Fig. 15 of the paper, representing the work of Naumann, indicates that the addition of no more than 1 per cent of Ti, V, Zr, or Cb to low-carbon steel confers phenomenal stability against damage by hydrogen up to temperatures far beyond any attained in a boiler. If the author's thesis is correct, such low-alloy steels should not crack in the embrittlement detector devised by Schroeder and his associates when tested under conditions which cause rapid failure of low-carbon steel. Experiments in the detector seem to offer an obvious direct test which may forestall endless bickering over the minutiae of mechanisms by which embrittlement is produced.

P. B. Place.[30] The author presents a very interesting and persuasive argument for the role of hydrogen in boiler embrittlement, together with a rather disturbing vision of ultimate failure of all boiler steel. This paper will undoubtedly revive interest in a problem that has been solved several times but which refuses to stay solved.

Although there may be considerable evidence to indicate that a zone of hydrogen attack precedes chemical attack in many cases of intercrystalline failure, practical experience supports the conclusion of other investigators, that initial chemical attack is necessary. The progress toward failure after this initial attack is of more academic than practical interest.

There does not appear to be any appreciable danger due to attack of normal boiler water on the oxide-coated drum and tube surfaces. Boiler embrittlement has been significantly absent in boilers having welded seams and is usually associated with leaky riveted seams and cracks where chemical can concentrate to sufficient strength to attack the metal and its protective oxide film.

It would be pertinent to determine if excessive amounts of hydrogen accumulate in boilers held on bank for long periods, and particularly in boilers that use colloidal iron as an oxygen scavenger. If dangerous amounts of hydrogen are being generated in boilers, passing through drum shells, and reacting with nonmetallic inclusions to form high-pressure pockets in the steel, it seems logical to expect that the outer surfaces of the drum shells of old boilers would show evidence of blisters caused by rupture of pockets close to the outside surface.

The true mechanism of intercrystalline failure in boiler steel must be left in the hands of students of chemistry and metallurgy. In time, a mutually satisfactory explanation will be forthcoming. In the meantime, progress in welded construction, improvement in rolled joints, elimination of riveted seams, and further experience with inhibitors seem likely to reduce the embrittlement hazard to a minimum and eventually eliminate it as a boiler-operating problem.

D. H. Rowland.[31] In the writer's opinion, the author has made some rather positive statements in his paper considering the fact that he has offered very little irrefutable evidence to substantiate his claims.

Since the writer's knowledge of the subject of boiler embrittlement is general rather than specific, he hardly feels qualified to offer a discussion of the paper as a whole. Yet, from a purely metallurgical standpoint, which includes thermodynamic considerations, it would seem that the author has left himself open to criticism in attempting to draw an analogy between what happens to steel in the ammonia-synthesis process and in the ordinary steam boiler, where temperatures and pressures are not comparable.

On the basis of the author's explanations, it is difficult to understand what relationship, if any, exists between boiler embrittlement and hydrogen embrittlement due to pickling or cathodic treatment. It seems likely, and there has been considerable evidence by various experimenters to support the view, that nascent hydrogen may fill voids in steel, and by becoming molecular exert considerable localized pressure, but the role of hydrogen as a decarburizer at boiler temperatures and pressures has not, to my knowledge, been established. On the basis of decarburization experiments with wet hydrogen at elevated temperatures[32] it appears that hydrogen is a rather weak decarburizer at atmospheric pressure. From a thermodynamic standpoint, the decar-

[30] Research and Development Department, Combustion Engineering Company, Inc., New York, N. Y. Mem. A.S.M.E.

[31] Senior Metallurgist, Research Laboratory, Carnegie Illinois Steel Corporation, Pittsburgh, Pa.

[32] "Grain-Size and Its Influence on Surface Decarburization of Steel," by D. H. Rowland and Clair Upthegrove, Trans. A.S.M., vol. 24, 1936, p. 96.

burizing power of hydrogen should and does become more pronounced as temperature and pressure are increased, but in so far as steam boilers are concerned, it is doubtful if there is a sufficient combination of temperature and pressure materially to increase the decarburizing tendency of hydrogen over that at atmospheric pressure. Certainly there is no apparent evidence of decarburization in Figs. 30 and 31 of the paper, notwithstanding the fact that one would expect to see some indication of decarburization where such a condition exists.

The author's statement, "Accordingly, the whole study of boiler embrittlement seems to lie within the single illustration, Fig. 27," is certainly open to criticism. No "story" as complex as boiler embrittlement can be summed up in one photograph, or in a dozen photographs for that matter. If the mechanism of boiler embrittlement were as simple as the author has inferred, it is astonishing why so many boilers could have been in service for years without failure.

On reading this paper, one gets the distinct impression that the author is indirectly advocating the use of certain low-alloy steels for boiler construction on the basis that their carbides are relatively stable in the presence of hydrogen. Such a conclusion, in the absence of considerable supporting evidence, does not appear to be warranted.

Author's Closure

For several years the author has tried by oral argument to point out, with little apparent success, one principal fact regarding previous studies of boiler embrittlement: That, *whether hydrogen is the cause of boiler embrittlement or not, the hydrogen theory has not as yet been tested by valid means.*

Where the paper seems to overemphasize the hydrogen aspect, it does so purposefully for the reason that other theories have been similarly overemphasized when they eliminated the principal competing theory without full cognizance of the record. By this, reference is made specifically to the complete disregard of the many established cases in which hydrogen does cause intercrystalline failure of a type highly resembling boiler embrittlement, and generally to the many other points made in the paper which need no repetition here.

Which theory is ultimately to be proved is of little consequence; the important thing is to prove one or the other. That depends upon a correct diagnosis, which did not stand in the literature. Admittedly, the present paper may likewise contain errors; but if it does nothing other than to cause the correct answer to be developed, and to bring chemists and metallurgists into agreement on certain basic facts, it is well worth the time and effort spent preparing it.

Consequently, Schroeder and Berk's extended criticism of this paper constitutes a valuable contribution, in that respect, to the study of boiler embrittlement. They are among the foremost chemists in this field; and their careful study of this metallurgical approach promises real advancement.

However, some weaknesses still stand in their argument and warrant mention to prevent continued confusion. Because they present their argument stepwise, let us consider it in turn by its steps.

Step 1. There was no need to review in this paper the manner in which concentration occurs, since that matter is satisfactory to everyone as it stands.

Step 2. This paper does not ". . . postulate an agency that can start cracks or fissures from within the metal." It is plainly stated throughout the paper that hydrogen does not cause observable cracking, but simply renders the metal brittle, preventing a ductile response to stress. The subtle fissures through which the gaseous molecules escape to the surface should not be confused with visible cracking. The crack leading to the surface, which we all see and agree upon, first develops from the operating stresses applied to this brittle metal, and not from chemical leaching of grain-boundary material, which is a secondary, not a primary, reaction, according to the argument.

Consequently, Schroeder and Berk's criticism up to Step 3 is inconsequential.

Step 3. As for Step 3, Schroeder and Berk, who suggest that the author confounded kinetics with equilibrium, persist in overlooking all aspects of equilibrium, especially its relationship to kinetics.

Quoting Lewis and Randall's standard text on "Thermodynamics," we find that ". . . in all thermodynamics there is no concept more fundamental than this [equilibrium]," and that ". . . every system which has not reached a state of equilibrium is changing continuously toward such a state with greater or less speed." This "speed" is the rate of the reaction under consideration, and its study constitutes "kinetics."

Although the equilibrium of a system tells us nothing about the "rate" of the individual reactions comprising it, the equilibrium rigorously dictates the *only possible direction* of each reaction, and the *ultimate goal* toward which those reactions strive. Consequently, because we know little of the reaction rates concerned in boiler embrittlement, our first step should be to determine where those reactions are trying to lead us. That information, fortunately, is available and is discussed in the paper.

For example, let us pursue Schroeder and Berk's own calculations to their logical conclusion. First, however, we find them a bit mystifying, since the diffusion equation

$$D = K/d[p^{1/2} \cdot e^{-E_t/(2kT)}]$$

is expressed in terms of volume of gas per area of surface per period of time per "thickness of plate." Their only mention of plate thickness occurs later in remarking on Naumann's experiment. A check of their calculations, however, shows that the figure they obtain applies to steel about $^1/_5$ in. thick, which is somewhat thin for boiler plate. Increasing thickness as shown by d in the equation decreases the gas loss linearly.

Nevertheless, let us accept the figure of 400 psi of H_2 that they give as a maximum value for the infiltrating gas and study its passage through the steel. The work of Ham (325), which they cite, went on to prove quite conclusively our basic assumption that the dissolved H reacts to some extent with the nonmetallics in the steel in the temperature range of 435 down to 260 F—boiler temperatures.

From the corrected methane equilibrium kindly supplied in the foregoing discussion by De Vries

$$\log K = -5937/T + 6.836$$

for the reaction

$$Fe_3C + 2H_2 = 3Fe + CH_4$$

$$K = (H_2)^2/CH_4$$

we find that 400 psi of H_2 in the steel at 390 F will engage carbon kinetically in an effort to reach the equilibrium pressure of *5,625,000,000 psi of CH_4!*

As for its reaction with iron oxide, we cannot expect such a large contribution. The equilibrium

$$Fe_3O_4 + 4H_2 = 3Fe + 4H_2O$$

$$K = H_2/H_2O$$

lies toward lower H_2O values as the temperature is lowered. The contribution from H_2O would not exceed 50 psi.

But let us re-examine this C-H reaction. The figure of nearly

6,000,000,000 psi wastes itself on the ordinary reader. Whereas Schroeder and Berk selected the H_2 pressure of 400 psi as a maximum value and tried to show its inefficacy, let us calculate what the *minimum* H_2 pressure actually need be to create embrittling stresses from methane alone.

Pressures greater than approximately 45,000 psi will deform ordinary boiler steel. If we use the equation supplied by De Vries and insert 45,000 psi for P_{CH_4} and calculate P_{H_2}, we obtain the enlightening result that $P_{H_2} = 1.1$ psi.

This value actually lies so close to the measured range of hydrogen pressures in boilers that it nearly eliminates the necessity for discussing atomic surface conditions, although the author still believes they may differ considerably from the distant atmosphere and will greatly increase that figure.

At the steel surface underneath concentrated alkali, however, any gaseous H_2 showing as bubbles would have a pressure of at least 1 atm, or 15 psi, still disregarding surface phenomena. Because of the quadratic relationship between H_2 and CH_4, the potential CH_4 pressure within the underlying metal would then be over 200 times 45,000 psi. That added factor may be the one which bridges the kinetic inefficiencies of the various reactions and allows embrittlement only at seats of such alkaline concentration. In any event, that figure is a "safety factor" of 200 in favor of the present argument.

As for the lack of visible decarburization in embrittled boiler steel, that point similarly disintegrates as a proof against the gas mechanism. At higher temperatures, actual escape of the gas from the steel permits decarburization to progress until it is visible at the time of failure. But that is an action which can be subsequent to embrittlement, especially at the lower temperatures of boiler operation where gaseous congestion within the metal is less readily relieved. There the gas necessary to cause the embrittlement may be obtained from a lesser quantity of C than is visible as a solid phase change.

For example, when the C as Fe_3C in pearlite reacts with H to form CH_4 and Fe, the density of the solid phase increases from 7.73 to 7.87 g per cc. That allows 0.0162 per cent of the original volume for the gas phase, which represents a compression of 80,000 atm, or 1,150,000 psi at 390 F. Once again we are faced with the fact that fantastic possible pressures of gas trapped within steel are a commonplace.

Obviously, there are vacuities available within the metal other than the one that might result from the phase transformation. However, under the highest magnification of the light microscope, grain boundaries still appear reasonably sound. If we make the large allowance of 0.1 micron, a figure just beyond microscopic resolution, as the thickness of a flat vacuity in a grain boundary, and consider the decarburization of an adjoining lamella of Fe_3C, then we find that 45,000 psi of CH_4 would develop at 390 F when that single cementite lamella was decarburized to a depth of only 0.25 micron. Such a feature would be entirely unrecognizable with the highest possible magnification of the light microscope. Perhaps with the electron microscope, decarburization can be detected. The matter should be investigated.

Step 4. Here the worry about diffusion is groundless. Carbon *is* removed from steel by hydrogen, and the path *is* intergranular. Whether the C diffuses to the grain boundary to react with H there, or whether it reacts within the grain and then diffuses along the internal surfaces depicted in Figs. 4 and 20 of the paper, is academic.

Step 5. The most unfortunate fallacy in all of Schroeder and Berk's discussion concerns their Fig. 36 and is representative of the severe handicap a chemist is under when studying purely metallurgical problems. The fracture they show is simply a typical metal fracture, as they point out in which the concentration of stress set up by the cut caused a typical fracture type. A metallurgist would not have bothered making that test, since its behavior is rudimentary knowledge.

That is why Fig. 33 of the paper was also presented, because these boiler fractures are not ordinary. It is no news to reproduce their Fig. 36, with its commonplace fracture type; but it is news when the same type of hammer blow reveals a ductile zone *between* two brittle zones, as shown in Fig. 33, especially when the concentration of alkali coincidentally was on two sides of this plate, in contrast to the single-sided attack of the plate in Fig. 27 of the paper.

That was also why the trouble was taken to include a stereographic projection and several micrographs, since the character of the metal was as different as day and night from the normal boiler steel shown in their Fig. 36. It would pay each reader well to "fuse" the stereographs in Fig. 28, and see for himself how ridiculous it is to compare that deteriorated metal with the normal steel of their specimen.

Fig. 39 is added here to explain this zoning phenomenon caused

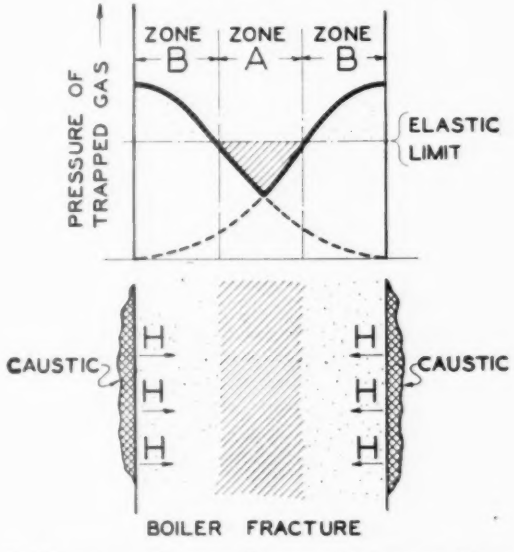


FIG. 39 SCHEMATIC DIAGRAM SHOWING FRACTURED SECTION OF BOILER PLATE (BELOW) ATTACKED FROM BOTH SIDES BY CAUSTIC WITH A DEPICTION (ABOVE) OF THE INTERNAL GAS PRESSURES SET UP BY TRANSFUSING HYDROGEN

(When gas pressures exceed the elastic limit of the steel, brittle zone B results. Ductile zone A includes the metal which is not so stressed.)

by gaseous congestion. Hydrogen, fed into the steel by the alkali, sets up internal gaseous congestion which is a maximum nearest to the source of the hydrogen and tapers off in pressure as it progresses into the steel (refer back to Fig. 3 of the paper). If the pressure exceeds the elastic limit of the steel near the surface of entrance, embrittling that section (zone B), a boundary will later be reached along the line of diffusion beyond which the gas pressure no longer exceeds the elastic limit of the steel and the ductility remains unimpaired. That boundary marks the beginning of the gray zone A. In that zone some cleansing action might be evident, but the gaseous products are not under sufficient pressure to cause embrittlement.

With unilateral diffusion, the gray zone always extends to the opposite surface. The bilaterally attacked specimen in Fig. 33 of the paper pertains to the diagram in full, showing a central ductile zone; whereas the specimen in Fig. 27 pertains only to one half of the diagram, the ductile zone extending to the far surface.

Step 6. Once again Schroeder and Berk are under a misconception concerning the role of hydrogen in causing cracking.

Since this was corrected in discussing Step 2, no further comments will be made.

As for their tests to check Naumann's work, the only alloying elements they used were the ones shown by Naumann to be least effective. Cr, one of the best of this minority group, was not designated by Naumann to contain the unusual silicon content of 1.5 per cent. As for Mo, what alloying content did they use? A misjudgment in similar early tests with vanadium was pointed out in the paper.

Also, if they tested these steels sufficiently to warrant their conclusions, a table of actual results would be valuable. Until satisfactory and systematic tests have been run on Ti and Cb steels, judgment should be withheld.

In closing the discussion of Schroeder and Berk's critique, several items might be mentioned.

1 The disagreement expressed between their work and that of the British was the opinion of the British (361), not the author's.

2 It is *not* peculiar that Al-killed steel should show improvement both to caustic and to nitrate attack. Each is basically intergranular corrosion; but for caustic, the corrosion may be indircet and gaseous, according to the present argument, thereby involving a mechanism distinct from that in nitrate cracking.

3 It is surprising to find these writers referring to the path they followed in testing the hydrogen theory and suggesting that the present paper parallels their first step taken in 1935, a step which finally led to their unfortunate conclusion in 1941 that intergranular failure cannot be caused by hydrogen. Where would the hydrogenation and ammonia-synthesis industries be today if they had proceeded on the basis of such an erroneous conclusion?

If these earlier writers had attempted to prove that boiler embrittlement is not intercrystalline hydrogen attack, the material in the present paper would then more or less represent one man's viewpoint; but they apparently failed completely to recognize that such a thing as intercrystalline H attack even existed. In addition, they were confused on the whole general behavior of gas-metal systems, drawing the numerous wrong conclusions which are discussed throughout the paper.

The author agrees with their decision expressed long ago that a thoroughgoing and sound investigation of the H mechanism be made, and suggests it at last be undertaken, since the subject has never received that treatment. Whether the hydrogen mechanism be proved unimportant or not, it remains to be so proved; and until then the author will hold the conclusion of the paper that by far the most likely mechanism for boiler embrittlement is the gas mechanism.

On the other hand, the present paper does not exclude the fact that caustic, when it does attack steel, may do so preferentially, especially when the grain boundaries are under great stress from trapped gases. Electrochemical corrosion may be a contributing factor to boiler embrittlement.

De Vries, Place, and Mears are to be thanked for their contributions to the discussion. Mears' assumption that boiler embrittlement is synonymous with stress-corrosion cracking is all right, but the present paper is based on the probability that the mechanism is of another type. The electrochemical theory is of little use in explaining the cracking of metals by other liquid metals and has nothing to do with intercrystalline gaseous attack, whether by O, H, S, or other gases. Consequently, every intergranular failure need not be lumped under an electrochemical subheading. If boiler embrittlement does belong there, the matter has already received ample discussion by others.

Mears' proposal for cathodic protection of the steel is very interesting, although the results of such a test might not be so simply interpreted as he suggests.

In Rowland's and De Vries' discussions, we find the interesting situation wherein one says H is a better decarburizer as the temperature goes up, and the other says it's better as the temperature goes down! A quick glance at the methane equilibrium shows that De Vries is the more correct in so far as the driving power or free energy of the reaction is concerned; but consideration of thermal energy shows that at lower temperatures the reaction may become so sluggish that it is quantitatively unimportant in *removing* carbon. Loose usage of the word "decarburization" both for the reaction and for the removal of CH_4 is to blame.

Correspondingly, Rowland is further confused when he speaks of hydrogen as a ". . . rather weak decarburizer at atmospheric pressure," on the basis of experiments he conducted at temperatures where CH_4 is almost nonexistent. And that ". . . from a thermodynamic standpoint, the decarburizing power of hydrogen should and does become more pronounced as temperature and pressure are increased." The *reaction* or the *removal*, and in what temperature range? The reacting power of H should *not* increase with increasing temperature. The free energy of methane formation decreases with increasing temperature. True, the *removal* is favored by heating; but even then that beneficial effect is soon counteracted by the sharp loss in the free energy of the reaction. In boiler embrittlement, the removal of the reaction product is only of secondary interest.

Rowland's objection to the present picture of boiler embrittlement because it is too simple takes the author so unawares, as does his worry about all the boilers which did not fail, that on answer will be made!

Partridge's criticisms, excepting his delightfully diversionary comments on devils and needle points, duplicate the remarks of others and therefore stand answered in the foregoing discussion.

A Sampling Inspection Plan for Continuous Production

By H. F. DODGE,[1] NEW YORK, N. Y.

The plan of sampling inspection, described for individual parts, subassemblies, finished articles, and the like, is intended primarily for use in process inspection where there must be assurance that the percentage of defective units is kept down to a low prescribed figure. The system is particularly applicable to products manufactured by conveyer or similar straight-line continuous processes. The object of the plan is to establish a limiting value of "average outgoing quality," expressed as a percentage of defective units, which will not be exceeded no matter what quality may be submitted to the inspector.

1 INTRODUCTION

THIS paper presents a plan of sampling inspection for a product consisting of individual units (parts, subassemblies, finished articles, etc.) manufactured in quantity by an essentially continuous process.

The plan, applicable only to characteristics subject to nondestructive inspection on a "Go - No Go" basis, is intended primarily for use in process inspection of parts or final inspection of finished articles within a manufacturing plant, where it is desired to have assurance that the percentage of defective units in accepted product will be held down to some prescribed low figure. It differs from others which have been published[2,3] in that it presumes a *continuous flow of consecutive articles or consecutive lots* of articles offered to the inspector for acceptance in the order of their production. It is accordingly of particular interest for products manufactured by conveyer or other straight-line continuous processes.

In operation, the plan provides a corrective inspection, serving as a partial screen for defective[4] units. Normally, a chosen percentage or fraction f of the units are inspected, but, when a defective unit is disclosed by the inspection it is required that an additional number of units be inspected, the additional number depending upon how many more defective units are found. The result of such inspections is to remove some of the defective units, and the poorer the quality submitted to the inspector, as measured in terms of per cent defective, the greater will be the corrective or screening effect. The object of the plan is the same as that incorporated in some of the sampling tables already published,[5] namely, to establish a limiting value of "average outgoing quality" expressed in per cent defective which will not be exceeded no matter what quality is submitted to the inspector. This limiting value of per cent defective is termed the "average outgoing quality limit (AOQL)."

The theoretical solution treats the case of inspecting a continuous flow of individual units and is based on the distribution of *random-order* spacing of defective units in product whose quality is statistically controlled.[6] Part 3 of the paper extends the application of the method to a continuous flow of individual lots or sublots of articles.

2 INSPECTION OF A FLOW OF INDIVIDUAL UNITS

Inspection of One Characteristic. Consider first the inspection of a flow of individual units, offered consecutively in the order of their production. Assume that inspection is to be made for only one quality characteristic, so that interest will be centered on one kind of defect. Subsequently, consideration will be given to the procedures when inspection is made simultaneously for several kinds of defects.

Procedure A. The procedure is as follows:

(*a*) At the outset, inspect 100 per cent of the units consecutively as produced and continue such inspection until i units in succession are found clear of defects.

(*b*) When i units in succession are found clear of defects, discontinue 100 per cent inspection, and inspect only a fraction f of the units, selecting individual sample units one at a time from the flow of product, in such a manner as to assure an unbiased sample.

(*c*) If a sample unit is found defective, revert immediately to a 100 per cent inspection of succeeding units and continue until again i units in succession are found clear of defects, as in paragraph (*a*).

(*d*) Correct or replace with good units, all defective units found.

Protection Provided by Plan. The inspection plan is defined by the two constants, f and i, which can be altered at will. For given values of f, i, and p (incoming fraction defective), there will result for product of statistically controlled quality a definite average outgoing fraction defective (average outgoing quality, AOQ). For given values of f and i, the AOQ will have a maximum for some particular fraction defective p_1 of incoming quality. As already noted, this maximum is referred to as the average outgoing quality limit (AOQL). For all other values of incoming fraction defective p greater or less than p_1, the AOQ will be less than AOQL. Many combinations of f and i will result in the same AOQL.

The protection offered by the plan discussed here can thus be expressed in terms of the AOQL, in per cent defective.

Theoretical Framework. We are concerned with the spacing between defective units when the individual units are arrayed in the order of their production, as shown in Fig. 1. If the manufacturing process is statistically controlled so that the

---

[1] Quality Results Engineer, Bell Telephone Laboratories.

[2] "Single Sampling and Double Sampling Inspection Tables," by H. F. Dodge and H. G. Romig, *Bell System Technical Journal*, vol. 20, 1941, pp. 1–61. An unpublished paper by Prof. Walter Bartky, (developed when he was associated with the Western Electric Company, 1927), provides a continuous multiple sampling plan involving two factors: f, as used here, and i, the number of units in a "compensating sample" required to be inspected for each defective unit found.

[3] "Standardized Inspection," by Lieut. R. J. Saunders, *Army Ordnance*, vol. 24, 1943, pp. 290–292; "Quality Through Inspection," by G. Rupert Gause, *Army Ordnance*, vol. 24, 1943, pp. 117–120.

[4] A unit of product that fails to meet the requirement for a characteristic is classed as nonconforming with respect to that characteristic, and for convenience is referred to as "defective." Thus, a deviation from a specified requirement or from accepted standards of good workmanship is termed a "defect."

Contributed by the Management Division and presented at a Joint Meeting of The American Society of Mechanical Engineers, and the Institute of Mathematical Statistics, New York, N. Y., May 29, 1943.

Note: Statements and opinions advanced in papers are to be understood as individual expressions of their authors and not those of the Society.

[5] Loc. cit., H. F. Dodge and H. G. Romig.

[6] "Statistical Control," as defined in the literature; see "Statistical Method From the Viewpoint of Quality Control," by W. A. Shewhart, The Graduate School, U. S. Department of Agriculture, 1939.

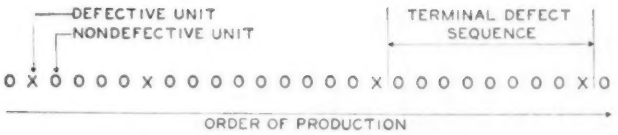


FIG. 1 SPACING OF DEFECTIVE UNITS

probability of producing a defective unit is constant and equal to p, then defective units will have an order spacing of a random character which is expressible in terms of certain probability laws. Product turned out by such a process will be referred to as having a process average fraction defective p. The "event" of particular interest is a "terminal-defect sequence" of $i + 1$ successive units following the observance of a defect, comprising a succession of i nondefective units followed by a defective unit, as shown in Fig. 1. The totality of all possible such sequences, where i varies from 0 to ∞, constitutes the universe of events under consideration.

Each such sequence of $i + 1$ units, comprising i successive nondefective units followed by a defective one, has a definite probability of occurrence, for a process average fraction defective, p. The complete set of such probabilities for all possible sequences, having respectively $i = 0, 1, 2, 3, \ldots \infty$, defines a probability distribution[7] of random-order spacing of defects in uniform product. This is shown in Table 1 in which 0 represents a nondefective unit, X represents a defective one, p is the fraction defective, and $q = 1 - p$.

TABLE 1 PROBABILITIES OF OCCURRENCE OF DEFECT SPACING

Sequence	Defect spacing (No. of units in sequence)	No. of nondefective units before finding the next defect	Probability of occurrence	No. of term in the power series
X	1	0	p	1st
$0X$	2	1	pq	2nd
$00X$	3	2	pq^2	3rd
$000X$	4	3	pq^3	4th
$0000X$	5	4	pq^4	5th
	.	.	.	.
	.	.	.	.
	.	.	.	.
$000\ldots.0X$	$i + 1$	i	pq^i	$(i + 1)$st
.	.	.	.	.
.	.	.	.	.
.	.	.	.	.

These probabilities are the successive terms in the infinite power series

$$\left.\begin{array}{l} p + pq + pq^2 + pq^3 + \ldots \\ \text{or} \\ p(1 + q + q^2 + q^3 + \ldots). \end{array}\right\} \quad \ldots\ldots\ldots\ldots [1]$$

The sum of this series is $p\left(\dfrac{1}{1-q}\right) = 1$; i.e., the total probability for all possible sequences is unity (as it should be).

The sum of the first $i + 1$ terms of the series is the probability of occurrence of a "terminal-defect sequence" (defect spacing) of $i + 1$ units or less. The sum of the first i terms is the probability, P_1, of failing to find the next i units clear of defects, which is

$$P_1 = \sum_{j=}^{j=i-1} pq^j = 1 - q^i \quad \ldots\ldots\ldots\ldots [2]$$

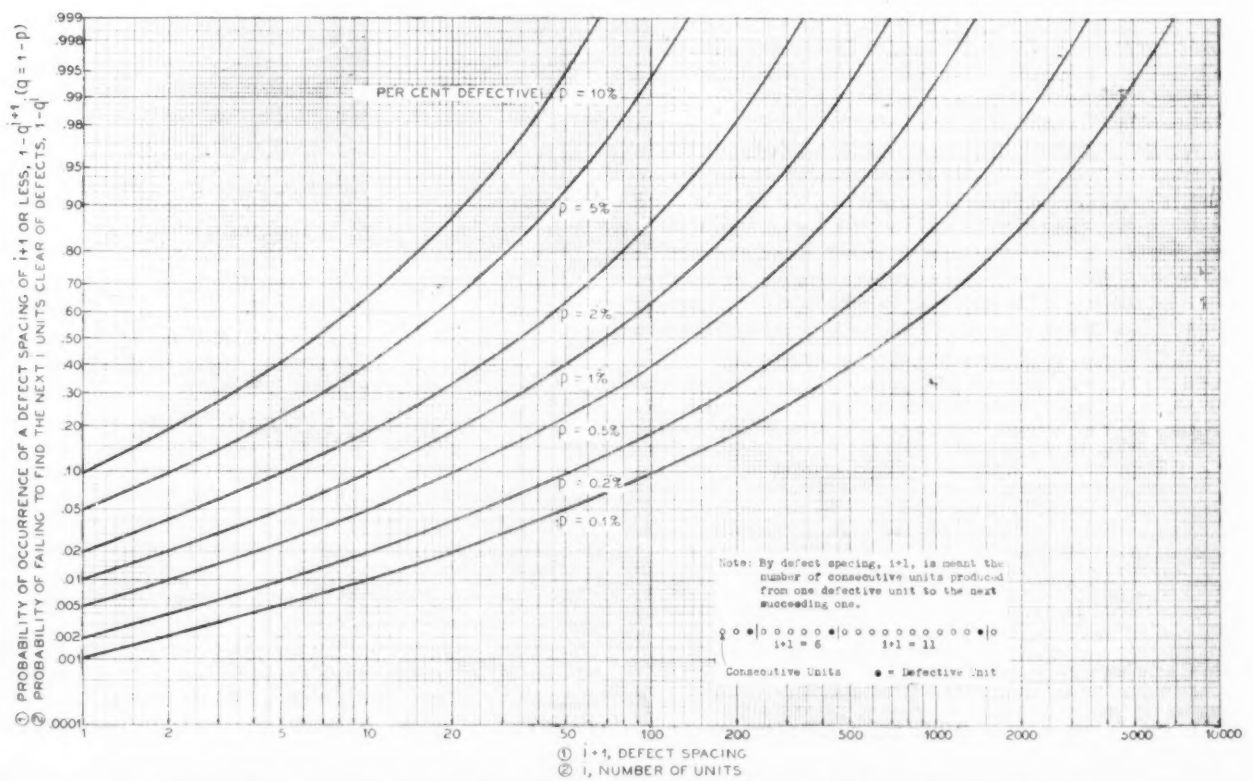


FIG. 2 CURVES DEFINING DISTRIBUTION OF RANDOM-ORDER SPACING OF DEFECTS IN UNIFORM PRODUCT

[7] "Due Nuovi Criteri di Controllo Sull 'andamento Casuale di Una Successione di Valori," by V. Romanovsky, *Giornale dell'Instituto Italiano degli Attuari*, 1932, discusses this probability distribution of spacing of events, referring to the spacing as the "length of a partial series." Our term "terminal-defect sequence" has the same significance as his term "partial series." See also "Note on Theoretical and Observed Distributions of Repetitive Occurrences," by P. S. Olmstead, *Annals of Mathematical Statistics*, vol. 11, 1940, pp. 363–366; "The Distribution Theory of Runs," by A. M. Mood, *Annals of Mathematical Statistics*, vol. 11, 1940, pp. 367–392.

In turn, the sum of all terms beyond the ith term is the probability of finding 0 defects in the next i units, which is

$$Q_1 = 1 - P_1 = q^i \quad [3]$$

These results and the power series [1] enter into subsequent portions of the discussion. The curves of Fig. 2 give values of $1 - q^i$.

Average Outgoing Quality. Suppose a plan is selected, choosing specific values of f and i. For given values of i and p, there will be an expected average number of units, u, inspected following the finding of a defect. Likewise, for given values of f and p, there will be an expected average number of units, v, that will be passed under the sampling procedure before a defect is found. The latter average number includes the sampling units actually inspected as well as the uninspected units produced between successive sample units.

The average fraction of the total product units inspected in the long run is

$$F = \frac{u + fv}{u + v} \quad [4]$$

It is now assumed for purposes of solution that the inspection operation itself never overlooks a defect and that all defective units found during the inspection of f and i will be corrected or replaced by good units.[8]

As a result of the screening effect of the inspection, the average outgoing quality, AOQ, designated p_A, is related as follows to the incoming quality p

$$p_A = p(1 - F) = p\left(1 - \frac{u + fv}{u + v}\right) \quad [5]$$

Determination of u. The average number of units, u, inspected on a 100 per cent inspection basis, following the finding of a defect, is a function of i and p, and may be determined from a consideration of two power series, one limited and the other infinite.

Once the 100 per cent inspection starts, there are several things that can happen before i units are found clear of defects. The first i may be found clear; or 1, 2, 3, or more defects may be found before finally a run of i units is found clear.

One of the quantities to be determined is the *average number of units* inspected in a "failure sequence;" that is, one terminating in a defect and comprising i or less units. This average number, designated as h, is the average of the distribution made up of the first i terms of the power series [1]. The average is

$$h = \frac{p}{1 - q^i}(1 + 2q + 3q^2 + 4q^3 + \ldots + iq^{i-1}) \quad [6]$$

where the denominator is the sum of the probabilities for the first i terms. This may be evaluated as follows

$$h = \frac{p}{1 - q^i} \frac{d}{dq}(1 + q + q^2 + q^3 + \ldots + q^i)$$

$$h = \frac{p}{1 - q^i} \frac{d}{dq}\left[\frac{1 - q^{i+1}}{1 - q}\right]$$

$$= \frac{1}{p(1 - q^i)}[1 - q^i(1 + pi)] \quad [7]$$

Note that if pi is small compared with unity, h is approximately $1/p$.

The next step is to determine the *average number of failure sequences* that will be encountered before finding i units clear of defects. This average number, designated as G, may be found from the probability distribution of all possible numbers of failure sequences, expressed by the infinite series

$$Q_1(1 + P_1 + P_1^2 + P_1^3 + \ldots) \quad [8]$$

where P_1 is given by Equation [2], $Q_1 = 1 - P_1$, as given by Equation [3], and the successive terms are the probabilities of occurrence of 0, 1, 2, 3, etc., failure sequences before finding i units clear of defects. The average number of failure sequences, G, is given by the sum of the infinite series

$$G = Q_1(0 + 1P_1 + 2P_1^2 + 3P_1^3 + \ldots)$$
$$= Q_1P_1(1 + 2P_1 + 3P_1^2 + 4P_1^3 + \ldots) \quad [9]$$

Summing the series, we have

$$G = Q_1P_1 \frac{1}{(1 - P_1)^2} = \frac{P_1}{Q_1} = \frac{1 - q^i}{q^i} \quad [10]$$

Now u, the average number of pieces inspected following the finding of a defect, is made up of a number of failure sequences followed by a run of i units clear of defects. Using the average values of G and h just found, we have

$$u = Gh + i = \frac{1 - q^i}{pq^i} \quad [11]$$

Determination of v. The average number of units, v, that will be passed in a period of sampling inspection will be $1/f$ times the average number of individual sample units inspected in such periods. Here again the solution will depend upon the random-order spacing of defects in uniform product. Whether the individual units selected during the sampling inspection procedure are selected by a random-spacing device, or by any other means which will prevent known bias in the sample, we may assume that defects will be found to occur in accordance with the distribution of random-order spacing, defined by the terms of the power series [1]. The average number of sample units inspected in a period of sampling inspection will thus be the average defect spacing for a product having fraction defective, p, which is given by the infinite series.

$$H = p(1 + 2q + 3q^2 + 4q^3 + \ldots) \quad [12]$$

Summing the series, we have

$$H = \frac{p}{(1 - q)^2} = \frac{1}{p} \quad [13]$$

and the value of v is found to be

$$v = \frac{H}{f} = \frac{1}{fp} \quad [14]$$

Determination of f and i for a Given Value of AOQL. From the considerations previously given, the average fraction of the product inspected, F, and the value of average outgoing quality, p_A, can be determined for any given values of p, f, and i. Substituting in Equation [5], the values of u and v given in Equations [11] and [14], we have

[8] The assumption that the inspection operation is perfect cannot be made without reservation. Machine inspection devices have their margins of error. Also, inspection fatigue prevents 100 per cent manual and visual inspections from insuring perfection, particularly if such inspections continue over a considerable period of time. But the efficiency of the latter inspections is generally higher when an interest incentive is provided as is usually the case in sampling inspection plans where the extent of such inspections hinges on their findings.

The solution given assumes correction or replacement of defective units. Where it is expedient to reject such units and not replace them Equations [19] to [22], inclusive, should be modified by replacing i by $(i - 1)$.

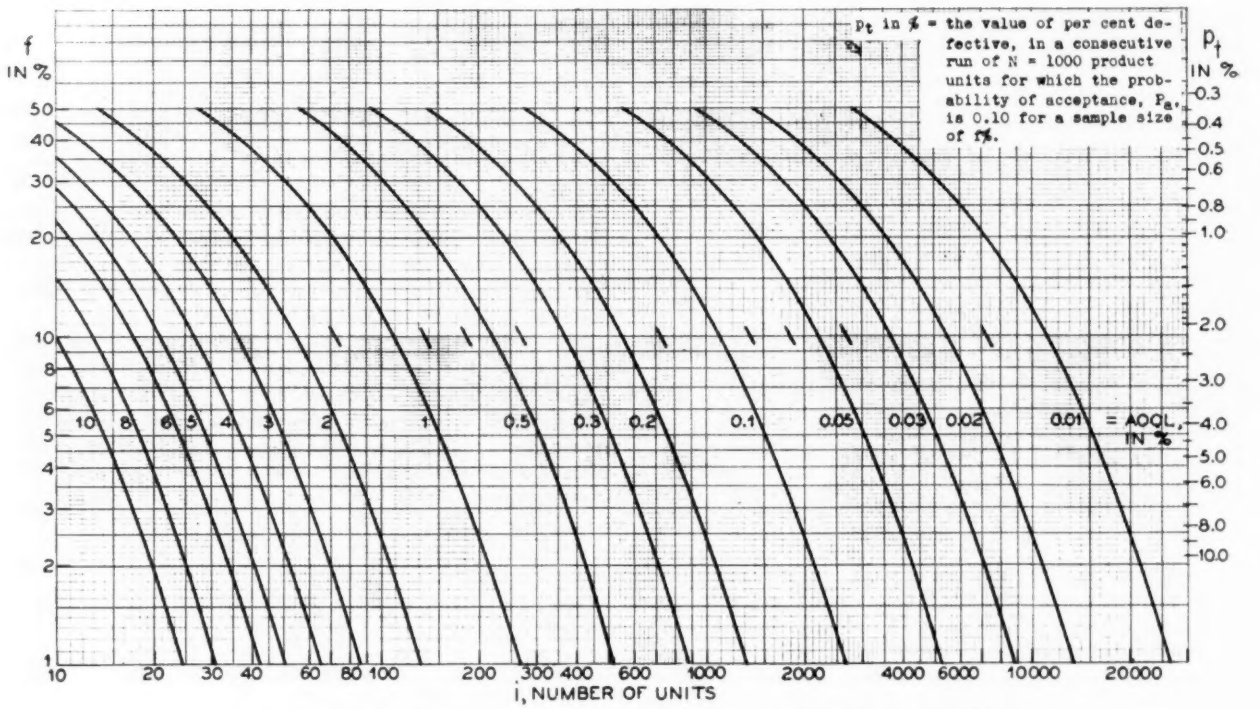


FIG. 3 CURVES FOR DETERMINING VALUES OF f AND i FOR A GIVEN VALUE OF AOQL

$$p_A = p\left[1 - \frac{f}{f + (1-f)(1-p)^i}\right] \quad \ldots\ldots [15]$$

The average outgoing quality limit, AOQL, (p_L) is the maximum value of p_A that will result for any given values of f and i, considering all possible values of p in the submitted product. The value of p for which this maximum value of p_A occurs is designated by p_1, hence

$$p_L = p_1\left[1 - \frac{f}{f + (1-f)(1-p)^i}\right] \quad \ldots\ldots [16]$$

The value of p_1 for which $p_A = p_L$ is determined by differentiating Equation [15] with respect to p, equating to 0, and solving for p, that is

$$\frac{dp_A}{dp} = 1 - \frac{f^2 + f(1-f)(1-p)^i + pfi(1-f)(1-p)^{i-1}}{[f + (1-f)(1-p)^i]^2} \quad \ldots\ldots [17]$$

Simplifying, and using the designation p_1 for the maximizing value of p, gives

$$(i+1)p_1 - 1 = \frac{1-f}{f}(1-p_1)^{i+1}$$

or

$$(1-p_1)^i = \frac{f[(i+1)p_1 - 1]}{(1-f)(1-p_1)} \quad \ldots\ldots [18]$$

Substituting in Equation [16] this value of $(1-p_1)^i$, we have

$$p_L = \frac{(i+1)p_1 - 1}{i} \quad \ldots\ldots [19]$$

hence

$$p_1 = \frac{1 + ip_L}{i+1} \quad \ldots\ldots [20]$$

From Equations [18] and [19], we have

$$p_L = \frac{1-f}{fi}(1-p_1)^{i+1} \quad \ldots\ldots [21]$$

hence

$$f = \frac{(1-p_1)^{i+1}}{ip_L + (1-p_1)^{i+1}} \quad \ldots\ldots [22]$$

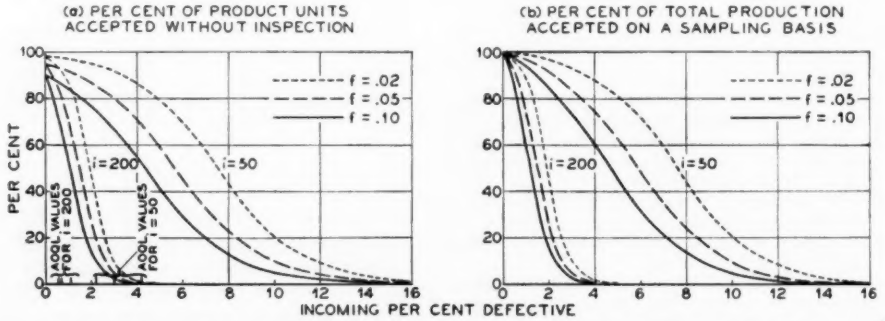


FIG. 4 CURVES SHOWING EFFECT OF f AND i ON OPERATING CHARACTERISTICS OF PLAN

The curves given in Fig. 3 were calculated by choosing values of i for given values of AOQL (p_L) and calculating p_t from Equation [20], and f from Equation [22]. Thus, for a given AOQL value, an i value may be found for a chosen f value and vice versa. It will be noted that for a given value of f, i varies inversely with the AOQL value, to a close degree of approximation.

Operating Characteristics of Plan. Figs. 4(*a*) and 4(*b*) give a picture of the operating characteristics of the general plan as f and i are varied. They indicate, for example, that for a moderate range of f values the factor i has a stronger influence than f in determining the discrimination that the method affords between high and low levels of incoming per cent defective. For the values of f and i shown, Fig. 4(*b*) indicates just what level of incoming per cent defective would force a correction of the manufacturing process, if the percentage of total production that would be accepted on a sampling basis falls below a critical value; often, a value of the order of 80 to 90 per cent.

Fig. 5 gives a comparison of the characteristics of several plans having the same AOQL value, 1 per cent. It indicates, for example, that when the normal level of incoming per cent defective is well below the AOQL, the AOQL value can be assured with less

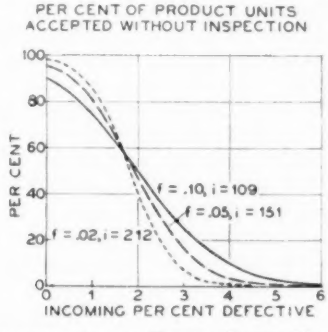


FIG. 5 CHARACTERISTICS OF THREE PLANS HAVING THE SAME AOQL OF 1 PER CENT

inspection by choosing f small and i large. But since, for a given AOQL value, the average amount of inspection approaches a minimum as f approaches 0, factors other than the minimum amount of inspection have a more important influence upon the choice of the most advantageous combination of f and i values for a given set of circumstances. For example, when the inspector is located at the end of the production line, it may be desirable to use a value of i not greater than some small multiple of the number of product units on the line at any one time. Or again, the value of f is often influenced by the normal work loads of the inspector and the operators on the line. Protection against "spotty" quality, such as may arise from temporary irregularities in workmanship or materials, should receive special consideration in connection with the choice of f.

Protection Against Spotty Quality. The p_t scale, at the right in Fig. 3 provides a guide concerning the protection afforded against spotty quality in a continuous run of product. The value of p_t is the per cent defective in a run of 1000 consecutive product units, for which the probability of acceptance by sample is 0.10 for a percentage sample equal to the corresponding f value shown on the chart.

This scale indicates that the protection against spotty quality falls off very rapidly with f and that the protection, considering runs of product of 1000 consecutive units each, becomes quite poor if f is less than 2 per cent.

Effect of Selecting Group Samples. The foregoing development assumes selection of individual sample units one at a time from the flow of product and immediate examination of a unit to determine whether or not it is defective. Deviations from this procedure will in general result in giving values of AOQL higher than those shown in Fig. 3.

For example, the actual AOQL may be higher than the theoretical value (*a*) if the inspector delays looking at the individual units immediately when they are withdrawn from the line, or (*b*) if he selects a group of units at one time from the production line. The effect of either of these two deviations, both constituting a delay, may be quite large if i is small, or if large group samples are taken.

Although the modification of the theoretical AOQL value resulting from the selection of group samples has not been thoroughly explored, this should not be excessive, (*a*) if group samples of $n = 10$ or less are drawn from the line, and (*b*) if $i = 50$ or more, provided there is no delay in examining the group samples drawn from the line.

It should be noted, however, that the effect of these delay factors on the AOQL may be compensated for in part if, when a defect is found, the 100 per cent inspection includes some of the units that have already passed the inspection point.

Where appreciable delays are unavoidable, an alternative is to withhold from acceptance a stipulated number of units pending the examination of the sample units that have been selected to represent this quantity of product. Such a procedure provides in effect a lot acceptance plan, the treatment for which is covered in Part 3.

Administration of Inspection Operations. The inspection plan is most effective in practice if it is administrated in such a way as to provide an incentive to clear up causes of trouble promptly. Such an incentive may be had by imposing a penalty on the operating or manufacturing department when defects are encountered. Normally, no such penalty is imposed if both the sampling inspection and the 100 per cent inspection are performed by the same person or group of persons and the two costs merged; the inspector then merely serves as an agency for screening defects when quality goes bad. It is accordingly recommended that the sampling inspection and the 100 per cent inspection operations be treated as two separate functions.

With this in mind, the inspection work can be performed by two different inspectors, designated inspector C and inspector M. Inspector C may be considered as the *consumer's* representative in that his work is performed as a function independent of the manufacturing group. The term "consumer" is used in the general sense of the recipient of the product after the inspection has been completed. Inspector M is responsible to the manufacturing department and the cost of his work is borne by that department. His work must, however, be subject to the surveillance and approval of inspector C.

The following method of administering the inspection plan can then be used:

1 Inspector C inspects the required fraction f. So long as no defects are found, product is considered acceptable and is passed.

2 When inspector C finds a defect, he proceeds as follows:

(*a*) Continues inspecting the fraction f.

(*b*) Places some identification on the succeeding flow of product to indicate nonacceptance (or diverts it from the regular production line if the design of the line permits), such designation to apply until clearance is obtained in accordance with paragraph (3).

(*c*) Calls inspector M to inspect the succeeding flow of product in accordance with paragraph (3).

3 Inspector M (one or more inspectors as needed) inspects all succeeding units, except those inspected by inspector C in the fraction f, until the required number of units, i, are found clear of defects. Inspector M reports immediately to inspector C all

defects found in the course of his 100 per cent inspection and notifies him when a run of i units has been found clear of defects.

4 When notified that a run of i units has been found clear of defects, inspector C, if satisfied with the work of inspector M, releases inspector M.

5 To facilitate speedy correction of causes of trouble, inspector C, on finding a defect, should promptly notify the production foreman or other designated authority and furnish the latter with detailed information regarding the character of the defect found.

It will be noted that the foregoing procedure requires calling inspector M whenever inspector C finds a defect. To avoid taking such action on the occurrence of a single defect, the procedure can be modified so that inspector M is called into the picture only when two defects in succession are observed by inspector C. Where this feature is desired, paragraph (2) may be modified to read as follows:

2 When inspector C finds a defect, he proceeds as follows:

(a) Immediately inspects all succeeding units up to a total of i units, and if no defects are found therein, he again limits his inspection to the fraction f. If, on the other hand, during the course of inspecting the next i units, inspector C finds a second defect, he immediately discontinues his 100 per cent inspection.

(b) He then places some identification on the succeeding flow of product . . . etc.

While this procedure carries the disadvantage of placing a varying work load on inspector C, it is often preferred since a single defect tends to be regarded as an isolated occurrence, whereas two defects in quick succession (like a first and second offense) are normally accepted as sufficient evidence to justify special action.

Inspection for Several Kinds of Defects Simultaneously. The procedure just given may be applied directly to an inspection covering two or more kinds of defects, provided that the chosen AOQL value applies to all defects collectively and each unit inspected is always inspected for all of the defects under consideration.

It is sometimes desired, however, when a defect of one kind is observed, to confine the 100 per cent inspection to this one kind of defect alone. This requires a modification of the general procedure and the establishment of a separate AOQL for each kind of defect. A similar modification is required, for example, where the inspection is to cover several kinds of defects, but where the defects are grouped into two or more classes, according to their seriousness, and the defects in each class treated collectively.

The following paragraphs outline for illustrative purposes a procedure for use where the defects under consideration are to be classified into two groups, "major" and "minor," and where all major defects are to be treated collectively and all minor defects likewise. By analogy, the procedure to be followed when each kind of defect is to be treated separately will be obvious. In any event, the fraction f is made the same for all classes or all kinds of defects.

Procedure:

Several kinds of defects are grouped into two classes with respect to seriousness; designated "major" and "minor."

All defects of the same class (major or minor) are treated collectively.

Preliminary:

1 Establish an over-all AOQL value for major defects and an over-all AOQL value for minor defects. Select a suitable value for f, applicable to both major and minor defects. From Fig. 3 determine a value of i for major defects, designated i_A, and a value of i for minor defects, designated i_B.

2 At the outset, inspect 100 per cent of the units consecutively for both major and minor defects until i_{max} units in succession are found clear of defects ($i_{max} = i_A$ or i_B, whichever is the larger).

Routine:

3 When i_{max} units in succession are found clear of defects, discontinue 100 per cent inspection and inspect only a fraction f of the units *for both major and minor defects*, selecting individual sample units one at a time from the flow of product.

4 If a major (or minor) defect is observed during sampling inspection, inspect 100 per cent of the succeeding units *only for defects of the class in question* until i_A (or i_B) units in succession are found clear of defects of this class.

(a) During the 100 per cent inspection referred to in paragraph 4, inspect a portion f *for both major and minor defects.*

(b) If during the 100 per cent inspection for a particular class of defect (major or minor), a defect of the other class is observed on an individual unit of product, start 100 per cent inspection for defects of the new class *only* if the new defect is observed on one of the f units that has been inspected for both major and minor defects, and continue such 100 per cent inspection for defects of the new class until i (as determined in paragraph 1 for the new class) units in succession are found clear of defects of the new class. Do not take such action, however, if the new defect happens to be observed on one of the non-f units.

5 When the proper number of successive units are found clear of defects as in paragraphs 4 or 4(b) reinstate sampling inspection as in paragraph (3).

From the foregoing, it may be appreciated that difficulties of administration are introduced in treating a large number of classes of defects or a large number of individual defects separately. How best to group defects together for collective treatment can generally be determined from the nature of the inspection operations, whether visual or gaging, and the expectancy of defects as determined from the quality history. Items involving visual inspection can often be treated collectively to advantage.

As is generally true, the layout of an inspection plan depends to a considerable extent upon the nature of inspection operations to be performed. Simplicity of administration is always to be desired. From the standpoint of minimizing over-all inspection costs, it is often preferable, where several quality characteristics are to be inspected, to break down the inspection work into two or more separate inspection steps, each covering a relatively small number of characteristics.

3 INSPECTION OF A FLOW OF INDIVIDUAL LOTS OR SUBLOTS

Purposes of Inspection. A manufacturer's inspection of his own product serves two purposes:[9]

1 "Process control" providing a basis for action with regard to the production process, with a view to better future product.

2 "Product acceptance" providing a basis for action with regard to the product already at hand.

The plan outlined in Part 2 has both of these purposes in mind, but the provision for selecting sample units continuously from the production line places special emphasis on control. It aids, for example, in the prompt detection of defects and location of causes of trouble in the manufacturing process.

The problem of acceptance of product is often eased, though at some sacrifice to the control aspects of the inspection work, if the product is submitted to the inspector in lots or sublots and a sample taken from each.

[9] See A.S.A. War Standard, Z1.3, "Control Chart Method of Controlling Quality During Production," American Standards Association, New York, N. Y., 1942, pp. 5–6.

Inspection Procedure for Sublots. With minor modifications, the plan and procedure of Part 2 can be extended to the case where material is offered as a *flow of consecutive sublots* of articles. In the inspection of parts, for example, the material may be offered in panloads or trays, each containing a collection of parts produced under essentially the same conditions. Or again, the product from a common source for a given short period of time, such as a $\frac{1}{2}$ hr, 1 hr, etc., may often be treated as a sublot and offered to the inspector as such for his acceptance. In what follows, however, it is essential that such sublots be kept in the *order of their production.*

The theoretical development given in Part 2 makes use of random-order spacing of defects in a statistically controlled product, with the specific provision that the units inspected be selected in the order of their production. In applying the general plan to the inspection of a *flow of consecutive sublots,* we no longer have individual units available in the order of their production. But we can use the same theoretical framework if we consider the random spacing of defects as their spacing in the chain of inspected units arranged in the *order of their inspection.* The probability distribution of the spacing of defects in inspected units will be the same regardless of the manner of selecting the units to be inspected, so long as we hold to the concept of statistical control in our solution.

The "i units in succession to be found clear of defects," discussed in Part 2, will now be defined as "i consecutively inspected units." During sampling inspection, a group sample of units will be selected from each sublot, and the fraction f will relate to the ratio of the number of units in the sample to the total number of units in the sublot. The fraction f will be held constant for all sublots. Furthermore, when it is required under the general plan to find i inspected units in succession clear of defects, the 100 per cent inspection must be allowed to extend into immediately succeeding sublots if i units in succession are not found clear in the current sublot.

Procedure B. The procedure is as follows:

1 At the outset, start inspecting 100 per cent of the units in a sublot and continue such inspection until i inspected units in succession are found clear of defects. Extend the 100 per cent inspection, if necessary, into one or more succeeding sublots in the order of their production.

2 When i inspected units in succession are found clear of defects, discontinue 100 per cent inspection and inspect only a fraction f of the units from each of the sublots, selecting the sample units in such a way as to fairly represent the sublot.

3 If a sample unit is found defective, start a 100 per cent inspection of the remainder of the sublot, and continue the 100 per cent inspection until again i inspected units in succession are found clear of defects, as in paragraph (1), extending such inspection into succeeding sublots, if necessary.

4 In the event the 100 per cent inspection extends into one or more succeeding sublots, if the number of units inspected in the last of such succeeding sublots exceeds a fraction f of the number of units in the sublot, accept this last sublot without further inspection. If on the other hand, the number of units inspected in this last sublot is less than the fraction f, inspect additional units from this same sublot to make up a sample equal to a fraction f of the number of units in the sublot.

5 Correct or replace with good units all defective units found.

As was the case in Part 2, the inspection plan is defined by two constants, f and i, and the protection offered is expressed in terms of AOQL. This sublot inspection plan differs from those already published in that the screening action is not confined to a single sublot but may extend over a succession of sublots, the entire production being regarded as a train of sublots that are linked together for purposes of inspection in the order of their production.

4 REMARKS

It will have been noted that the plan here outlined should be regarded as a "special-purpose" plan applicable under the conditions which have been enumerated: where production is practically continuous, where inspection is to be made during production or immediately thereafter and is to serve not only as a screening *acceptance* agency if necessary, but as an aid to *process control* by disclosing promptly any substandard quality conditions in the product. It is believed that the general plan provides a structure, which with possible variations in procedure to serve particular circumstances, may be found useful in designing additional sampling inspection techniques.

Physical Properties of a Structural Plastic Material

By CECIL W. ARMSTRONG[1]

THE aviation industry is vitally interested in high-strength low-density materials which show promise of utilization in airplane structures. This interest exists because of the following reasons:

1 The need for the further reduction in weight of all types of airplanes in order to obtain better performance characteristics.

2 The need for increasing the rigidity of all thin-gage sections to reduce local failures resulting from vibration and to maintain contours under all flight conditions.

3 The need for reducing the number of man-hours required for the tooling, fabrication, and final assembly of airframes.

4 The need for improvement in the over-all smoothness of all aerodynamic surfaces.

It is generally agreed among aeronautical engineers that the development of a low-density structural plastic material, capable of being molded in large assemblies with inexpensive molds, would help to satisfy the needs listed. The word "structural" necessarily implies that the plastic material will possess certain minimum mechanical properties. For structural use in airplanes, the strength-weight ratios and other mechanical properties must compare favorably with corresponding values of the commonly used aluminum alloys.

Many new resins have recently been developed and without doubt countless others will emerge from the numerous chemical laboratories. These resins are being copolymerized and interpolymerized. They are being cast, molded, and laminated with a large variety of organic and inorganic fibrous fillers, woven fabrics, macerated fabrics, and the like. It has become exceedingly difficult for the engineer to choose from among these thousands of combinations any one material for a specific application. The need exists for reliable engineering data on plastic materials so that an intelligent selection of a material for a specific application can be accomplished. Considerable progress is being made in this direction by the joint efforts of the Army, Navy, and the plastics industry, but much remains to be done.

Among the new resins which have become commercially available (military requirements first, of course), there are several thermohardening resins which are unique in that no external pressure is required during the process of molding a plastic part. These new resins may be used in combination with high-strength filler materials to produce low-density high-strength laminated plastics which soon may fulfill some of the needs which have been enumerated.

Methods of Laminating "No-Pressure" Resins

To produce a laminated-plastic article from one of these "no-pressure" resins, one or more layers of the filler material may be wrapped around or draped over a mold. The filler material may be saturated with the liquid resin either before or after placing in contact with the mold. The laminate then is cured (hardened) by application of heat. Curing temperatures seldom exceed 240 F. The curing period may require from thirty minutes to eight hours, depending upon the requirements of the particular resin, the thickness of the laminate, and the heat conductivity of the mold. If a smooth glossy surface is desired, nonporous cover sheets, such as Cellophane, may be used.

Parts having intricate shapes and double contours may necessitate the use of some pressure (0.1 to 10 psi) to keep the impregnated-fabric filler material in intimate contact with all surfaces of the mold and to prevent free resin from accumulating in localized spots. For application of these pressures, the use of thin transparent films of inexpensive thermoplastic materials has been found to be more suitable than the use of expensive synthetic-rubber bags. Many novel and ingenious techniques already have been developed for the fabrication of complete assemblies, which if made of metal would require the forming and assembly of several contoured parts. Because of the fact that pressures are low, molds may be simple, light in weight, and inexpensive. The primary requirement of molds for fabrication of parts from these new resins is that they be made to correct dimensions and contours.

Physical Test Program

A preliminary study of the limited amount of available data, supplemented by various laboratory tests, indicated that the MR-1A resin,[2] when laminated with certain of the Fiberglas fabrics, possessed better mechanical properties than any of the commercially available "no-pressure" resins. Accordingly, a modest test program was undertaken by the Lockheed Structures Research Laboratory. Results which are reported in this paper are typical of data thus far obtained.

Materials Tested and Methods of Testing

Data presented herewith were obtained from MR-1A resin laminated with Fiberglas-fabric fillers. A brief description of the Fiberglas-filler materials which were used in the preparation of flat sheet laminates, from which test specimens were machined, is given in Table 1.

TABLE 1 FIBERGLAS CONTINUOUS-FILAMENT CLOTHS USED FOR MR-1A LAMINATED TEST SPECIMENS[a]

CLOTH DESIGNATION	NOMINAL THICKNESS IN	WT-OUNCES PER SQ YD	WARP		FILLING	
			ENDS PER INCH	APPROX STRENGTH LBS/IN WIDTH	PICKS PER INCH	APPROX STRENGTH LBS/IN WIDTH
OC-63	.0115	9 12	46	675	12(Cotton)	3
ECC-11-127	.007	6 36	42	412	32	334
ECC-11-148	.012	10 95	30	625	19	459
ECC-11-161	.015	14 11	28	839	16	562

[a] Data supplied by Owens-Corning Fiberglas Corporation.

Tension- and bend-test specimens were prepared and tested in accordance with the General Federal Specification[3] for Organic

[1] Senior Research Engineer, Lockheed Aircraft Corp., Burbank, Calif.

Contributed jointly by the Rubber and Plastic Groups and the Aviation Division and presented at the Semi-Annual Meeting, Los Angeles, Calif., June 14–17, 1943, of The American Society of Mechanical Engineers.

[2] Manufactured by Marco Chemicals, Inc., Sewaren, N. J., laminated and distributed by Swedlow Aeroplastics Corporation, Glendale, Calif.

[3] Section IV (Part 5) of Federal Standard Stock Catalog, Superintendent of Documents, Washington, D. C.

TABLE 2 PHYSICAL TEST RESULTS MR-1A FIBERGLAS LAMINATES

LAMINATE DESIGNATION	223	224	309	236	221	241
FILLER, FIBERGLAS NO.	OC-63	OC-63	OC-63	ECC-11-127	ECC-11-148	ECC-11-161
NUMBER OF LAMINAE	12	12	8	18	10	8
STACK ARRANGEMENT	PARALLEL	CROSSED 90°	CROSSED 90°	CROSSED 90°	PARALLEL	CROSSED 90°
NOMINAL THICKNESS, INCHES	.104	.107	.107	.128	.124	.121
SPECIFIC GRAVITY	1.96	1.93	1.69	1.81	1.80	1.79
TENSION						
DIRECTION OF LOAD	WITH WARP	—	—	—	WITH FILL	—
ULTIMATE LOAD, LBS.	6,390	3,140	2,095	2,840	2,070	2,210
SPECIMEN WIDTH, IN.	.604	.502	.502	.502	.482	.505
ULT. LOAD PER INCH OF WIDTH PER LAMINA	880	520	520	315	430	550
TANGENT PROPORTIONAL LIMIT P.S.I.	50,000	32,000	21,000	26,000	13,000	13,500
.01% OFFSET PROPORTIONAL LIMIT	58,000	41,000	25,000	27,500	15,000	15,500
.2% OFFSET YIELD STRESS	—	58,000	—	38,700	30,800	24,300
ULTIMATE TENSILE STRESS	105,000	58,500	39,000	44,200	34,600	36,200
YOUNG'S MODULUS OF ELASTICITY P.S.I.	5,960,000	2,800,000	1,900,000	2,100,000	1,500,000	1,900,000
ELONGATION AT FAILURE (% OVER 2 INCH LENGTH)	1.8	2.3	2.1	2.6	2.6	2.9
COMPRESSION (EDGEWISE)						
DIRECTION OF LOAD	WITH WARP	—	—	—	WITH FILL	—
ULTIMATE LOAD, LBS.	1,340	1,380	1,580	1,393	1,000	1,200
SPECIMEN WIDTH, IN.	.496	.500	.495	.500	.500	.500
ULT. LOAD PER INCH OF WIDTH PER LAMINA	225	230	400	155	200	300
TANGENT PROPORTIONAL LIMIT P.S.I.	26,100	25,950	21,500	14,000	11,000	10,000
.01% OFFSET PROPORTIONAL LIMIT	—	—	23,700	15,000	14,000	12,000
ULTIMATE COMPRESSIVE STRESS	26,100	26,000	29,000	22,500	16,900	19,600
YOUNGS MODULUS OF ELASTICITY P.S.I.	5,500,000	3,000,000	2,260,000	2,800,000	2,200,000	2,300,000
DEFORMATION (% OVER 2 INCH LENGTH)	.47	.86	1.38	.86	.75	.93
MANNER OF FAILURE	DIAGONAL SHEAR	DIAGONAL SHEAR	DIAGONAL SHEAR	DIAGONAL SHEAR	DIAGONAL SHEAR	DIAGONAL SHEAR
BENDING (FLATWISE)						
LENGTH, WIDTH, THICKNESS, INCHES	5×1.02×.102	5×.745×.106	5×.749×.109	5×.751×.128	5×.751×.126	5×.746×.116
SPAN, INCHES	3	3	3	3	3	3
ULTIMATE LOAD AT CENTER OF SPAN, LBS.	138	90	128	105	94	78
TANGENT PROPORTIONAL LIMIT P.S.I.	55,000	41,000	45,000	17,000	19,000	19,000
MODULUS OF RUPTURE, P.S.I.	59,300	48,200	64,800	38,400	35,500	34,900
MODULUS OF ELASTICITY, P.S.I.	5,950,000	3,000,000	2,100,000	2,300,000	1,630,000	2,080,000
BEARING						
HOLE DIAMETER	—	.124	.124	.124	.124	.124
NOMINAL BEARING STRENGTH (4% HOLE DEFORMATION)	—	28,000	23,500	20,000	29,500	23,300
ULTIMATE BEARING STRENGTH, P.S.I.	—	32,100	31,300	38,500	34,800	34,600

TABLE 3 SPECIFIC STRENGTH VALUES MR-1A FIBERGLAS LAMINATES

MATERIAL	① SPECIFIC TENSILE STRENGTH P.S.I.	② SPECIFIC TENSILE MODULUS P.S.I.	③ SPECIFIC BUCKLING STABILITY P.S.I.	④ SPECIFIC MODULUS OF RUPTURE P.S.I.	⑤ SPECIFIC ULT BEARING STRENGTH P.S.I.
MR-1A FIBERGLAS-223	53,500	3,040,000	790,000	15,400	—
MR-1A FIBERGLAS-224	30,300	1,450,000	416,000	12,900	16,600
MR-1A FIBERGLAS-309	23,000	1,120,000	435,000	22,600	18,500
MR-1A FIBERGLAS-236	24,400	1,160,000	388,000	11,700	21,300
MR-1A FIBERGLAS-221	19,200	833,000	280,000	10,900	19,300
MR-1A FIBERGLAS-241	20,200	1,060,000	362,000	10,900	19,300
24S-T ALCLAD ALUMINUM ALLOY	20,200	3,800,000	495,000	7,300	29,600
24S-RT ALCLAD ALUMINUM ALLOY	22,400	3,800,000	495,000	8,100	32,400

① Specific Tensile Strength = Ult tensile strength divided by specific gravity.
② Specific Tensile Modulus = Tension modulus divided by specific gravity.
③ Specific Buckling Stability = Flexural modulus divided by (specific gravity)^3
④ Specific Modulus of Rupture = Modulus of rupture divided by (specific gravity)^2
⑤ Specific Ult Bearing Strength = Ult bearing strength divided by specific gravity.

Plastics, L-P-406, dated December 9, 1942. Bearing-stress-deformation data, Fig. 4, were obtained by use of a fixture similar to one developed at the University of Kansas.[4] Ultimate bearing-stress values were obtained from test specimens 2.50 in. wide, with 0.124-in-diam holes centrally located at an edge distance of 0.375 in. The small compression-test specimens were supported and tested in a jig, Fig. 5, designed by L. F. Bonza[5] and made in the Lockheed Structures Research Laboratory. Similar compression jigs have been widely used for some time.

Test Results

Typical test results are given in Table 2 and in Figs. 1 to 4.

[4] "Bearing Strength of Plastics and Plywood," by James Bond, Trans. A.S.M.E., vol. 65, 1943, pp. 9–14.

[5] Jun. Research Engineer, Lockheed Aircraft Corp., Burbank, Calif.

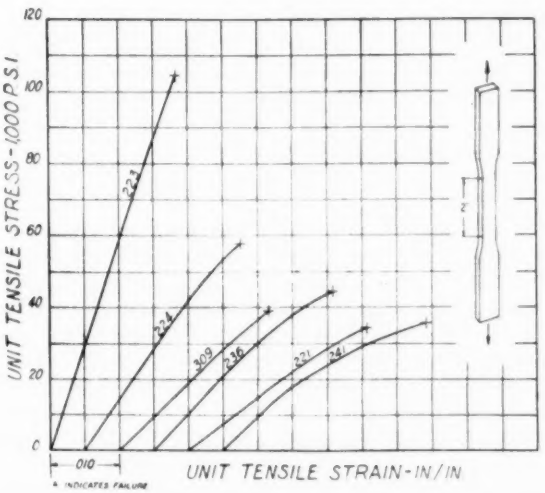


FIG. 1 TENSILE STRESS-STRAIN CURVES OF MR-1A FIBERGLAS LAMINATES

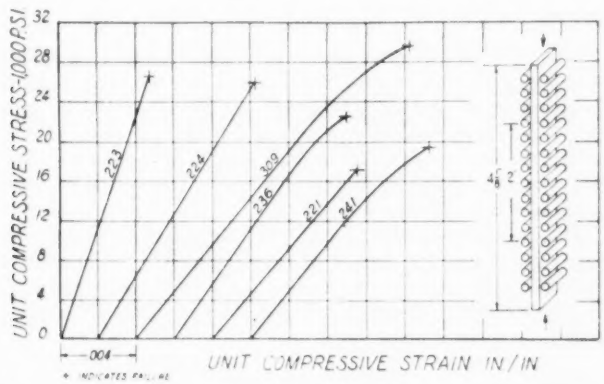


FIG. 2 COMPRESSIVE STRESS-STRAIN CURVES OF MR-1A FIBERGLAS LAMINATES

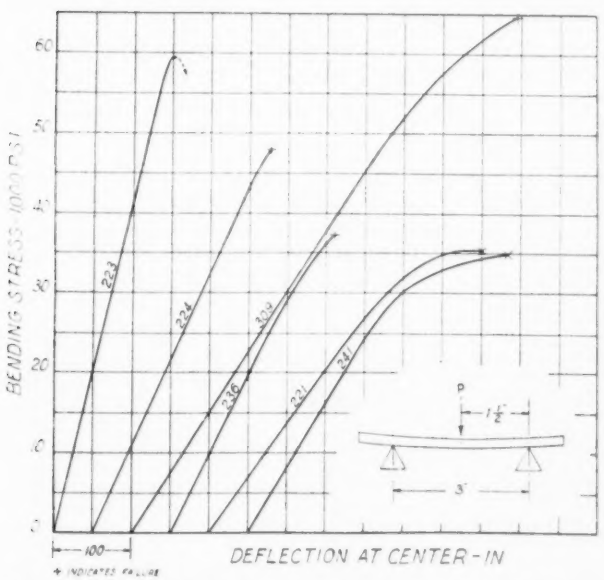


FIG. 3 FLEXURAL STRESS-STRAIN CURVES OF MR-1A FIBERGLAS LAMINATES

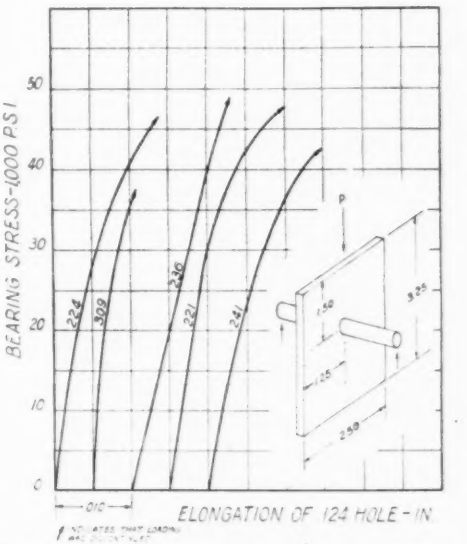


FIG. 4 BEARING-STRESS-DEFORMATION CURVES FOR MR-1A FIBERGLAS LAMINATES

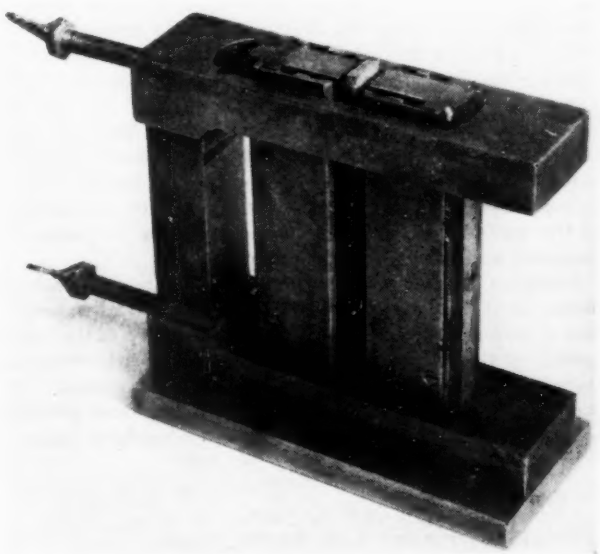


FIG. 5 JIG FOR TESTING SPECIMENS IN COMPRESSION

Certain of these values, adjusted to an equivalent-weight base, are compared with corresponding values of two aluminum alloys in Table 3. The specific-strength properties of the aluminum alloys were computed from previously published values.[6]

Attention is directed to the fact that these laminates are anisotropic, resulting from parallel stacking or cross-stacking (alternate laminae oriented at right angles) of unidirectional materials, such as OC-63 Fiberglas or bidirectional materials, such as are listed in Table 1. Results which are shown in Table 2 were obtained from specimens cut parallel to one of the two principal directions of the laminates.

Preliminary tensile tests made from specimens cut at 45 deg with the principal directions of the cross-stacked MR-1A Fiberglas laminates exhibited ultimate tensile-strength and tensile-modulus values thirty to forty per cent lower than corresponding "with-grain" values.

[6] "Strength of Aircraft Elements," U. S. Army-Navy-Civil Committee on Aircraft Requirements, Publication ANC-5, Dec., 1942.

Tensile tests made at room temperature from unfilled cast MR-1A resin (specific gravity = 1.2) indicated an average ultimate tensile strength of 6200 psi and an average tensile modulus of 370,000 psi.

The following data on other properties of the MR-1A Fiberglas laminates were supplied by the Swedlow Aeroplastics Corporation. Methods of testing were stated to have been in accordance with A.S.T.M. specifications:

Impact strength, notched Izod, ft-lb per in. of notch	25 - 100
Ultimate shear strength, psi	14000–33000
Ultimate compressive strength, flatwise, psi	41000–75000
Moisture absorption, per cent	0.2 - 0.4
Gasoline absorption, per cent	0.01 - 0.15
Burning rate, in. per min	0 - 0.4
Hardness, Rockwell M	71 - 107
Hardness, Barcol impressor	40 - 65
Heat distortion, deg F	300 - 350
Coefficient of linear expansion, 10^{-5} per deg F	2.7 - 5.2

Fatigue- and creep-test data and other physical properties which are not listed have not as yet been determined.

Discussion of Results Obtained

It is interesting to compare test results on a basis of pounds load per inch of width per lamina with corresponding values of the Fiberglas cloth. Note that for the unidirectional laminate (see Table 2, laminate No. 223) the ultimate tensile load per inch of width per lamina is 880 lb; also from Table 1, that the nominal breaking strength of the OC-63 Fiberglas is 875 lb. For cross-stacked laminates of the same material (No. 224 and No. 309) corresponding values of 520 lb were obtained; however, since only one half of the laminae were oriented parallel to the direction of the load, these values could be expressed as 1040 lb per in. of width for each lamina oriented in the direction of the applied load. Similar comparisons may be made with laminates made from the woven fabrics.

Attention is directed to the fact that both the thickness and density of the laminate are dependent upon the relative proportion of resin and filler materials. In tension, most of the load is carried by the filler material. Two laminates, each containing the same number of laminae but varying in resin content might carry equal tensile loads, but because of the greater thickness would have different ultimate unit-stress and modulus values.

Examination of the data will show that the resin content (low resin content results in high specific-gravity values) for optimum tensile properties will not result in optimum bend and compression properties. This fact may be demonstrated by comparing data obtained on laminate No. 224 with corresponding data obtained on laminate No. 309.

Costs of the Processed Materials

The present high prices of Fiberglas cloths impose serious limitations on the use of these materials for simple structural applications. Many high-strength organic and inorganic fibrous materials which recently have been developed, or ones known to be in the developmental stage, may offset this limitation.

For contoured structural shapes which generally begin with flat metal sheets and which require the forming of several parts with expensive dies by drop hammers or hydropress, followed by manual assembly of these parts, the use of a suitable plastic material can save cost and valuable man-hours of production time. Comparative totals of man-hours required for the tooling and fabrication of actual contoured metal parts and corresponding man-hours required for the tooling of the same "no-pressure" plastic parts should be very enlightening.

Conclusions

The MR-1A Fiberglas laminates possess physical properties which enable this material to be used to good advantage in many airplane structural applications. The ability to mold large contoured assemblies with substantially no pressure will, without doubt, result in substantial savings in cost and in man-hours of time required for the tooling and fabrication of many assemblies now made of metal.

Known disadvantages include the anisotropic properties of fabric laminates, the length of time required to complete the curing of each part, the low values of the modulus of elasticity, the low bearing strength, and the present incompleteness of important physical data.

Acknowledgment

The author is indebted to Mr. L. F. Bonza for his assistance in the conduct of certain of the physical tests and in the compilation of test data which are included in this paper.

Isothermal Pressure Drop for Two-Phase Two-Component Flow in a Horizontal Pipe

By R. C. MARTINELLI,[1] L. M. K. BOELTER,[2] T. H. M. TAYLOR,[3] E. G. THOMSEN,[4] AND E. H. MORRIN,[5] BERKELEY, CALIF.

The static pressure drop accompanying the isothermal two-phase two-component flow of air and eight various liquids, including benzene, water, and S.A.E. 40 oil, was measured for flow conditions varying from all air to all liquid in a 1-in. glass pipe and a ½-in. galvanized-iron pipe. The flow patterns existing at the various flow rates were studied visually and photographically. A macroscopic analysis of the flow phenomenon is presented, which allows the prediction of two-phase two-component static pressure drop under certain flow conditions. The application of the proposed method to the prediction of pressure drop along a pipe in which a fluid is evaporating is tentatively outlined.

Nomenclature

THE following nomenclature is used in the paper:

A_p = cross-sectional area of pipe of diameter D_p, sq ft
A_l = cross-sectional area of liquid flow, sq ft
A_g = cross-sectional area of gas flow, sq ft
D_H = hydraulic diameter, ft
D_g = hydraulic diameter for gas flow, ft
D_l = hydraulic diameter for liquid flow, ft
D_p = inside diameter of pipe, ft
f_c = unit thermal convective conductance, Btu/hr sq ft deg F
F_1, F_2, F_3, F_4 = functions utilized in Appendix 1
g = gravitational force per unit mass

$$= 32.2 \frac{\text{lb}}{\left(\frac{\text{lb sec}^2}{\text{ft}}\right)}$$

L = length of pipe, ft
m = exponent of Reynolds modulus in the Blasius expression for friction factor for the gas phase
n = exponent of Reynolds modulus in the Blasius expression for friction factor for the liquid phase
p = average static pressure in pipe, psi
P = average static pressure in pipe, psf
r = latent heat of vaporization of liquid, Btu per lb
t = average fluid temperature, deg F
T = average fluid temperature, deg R
v_g = velocity of gas, fps
v_l = velocity of liquid, fps
W_g = weight rate of gas, lb per sec
W_l = weight rate of liquid, lb per sec
W_T = total weight rate (vapor + liquid), lb per sec
Z = co-ordinate measured along pipe axis, ft
γ_g = weight density of gas, lb per cu ft
γ_l = weight density of liquid, lb per cu ft
ΔL = finite difference of length, ft
ΔP = finite difference of static pressure in length ΔL psf
$\left(\frac{\Delta P}{\Delta L}\right)_g$ = pressure drop per unit length due to gas flowing at a rate W_g, with density γ_g in a pipe of diameter D_p (lb per sq ft) per ft
$\left(\frac{\Delta P}{\Delta L}\right)_{T\text{-}P}$ = pressure drop per unit length for two-phase flow, (lb per sq ft) per ft
Δt = difference in temperature between tube wall and fluid being evaporated, deg F
μ_g = absolute viscosity of gas, lb sec per sq ft
μ_l = absolute viscosity of liquid, lb sec per sq ft

Dimensionless Moduli

α = flow-type modulus for liquid $= \dfrac{A_l}{\frac{\pi}{4} D_l^2}$

β = flow-type modulus for gas $= \dfrac{A_g}{\frac{\pi}{4} D_g^2}$

$\chi_{tt} = \left(\frac{\mu_l}{\mu_g}\right)^{0.111} \left(\frac{\gamma_g}{\gamma_l}\right)^{0.555} \left(\frac{W_l}{W_g}\right)$ = two-phase flow modulus for mechanism in which flow of both liquid and gas is turbulent

$\chi_{vt} = \dfrac{C_l}{C_g} (Re_g)^{-0.8} \dfrac{\gamma_g}{\gamma_l} \cdot \dfrac{\mu_l}{\mu_g} \cdot \dfrac{W_l}{W_g}$ = two-phase flow modulus for mechanism in which flow of liquid is viscous and that of gas is turbulent

$\chi_{vv} = \dfrac{\mu_l}{\mu_g} \cdot \dfrac{\gamma_g}{\gamma_l} \cdot \dfrac{W_l}{W_g}$ = two-phase flow modulus for mechanism in which flow of both phases is viscous

ζ_g = friction factor for gas (see Equation [2])
ζ_l = friction factor for the liquid (see Equation [1])
Φ_{tt} = function of χ_{tt} utilized in calculation of two-phase pressure drop
Φ_{vt} = function of χ_{vt} utilized in calculation of two-phase pressure drop
C_g = constant in empirical equation for friction factor for gas. Note that for turbulent flow $C_g = 0.184$ for smooth pipes
C_l = constant in empirical equations for friction factor for liquid. Note that $C_l = 64$ for viscous flow

Re = Reynolds modulus $= \dfrac{4}{\pi} \cdot \dfrac{W}{D\mu g} = \dfrac{vD\gamma}{\mu g}$

$Re_g = \dfrac{4}{\pi} \cdot \dfrac{W_g}{D_p \mu_g g}$ = Reynolds modulus for gas phase

[1] Assistant Professor of Mechanical Engineering, University of California. Jun. A.S.M.E.
[2] Professor of Mechanical Engineering, University of California. Mem. A.S.M.E.
[3] Mechanical Engineer, Research Department, Cutter Laboratories.
[4] Instructor in Mechanical Engineering, University of California.
[5] Research Engineer, Department of Mechanical Engineering, University of California. Jun. A.S.M.E.

Contributed by the Heat Transfer Division and presented at the Semi-Annual Meeting, Los Angeles, Calif., June 14–17, 1943, of THE AMERICAN SOCIETY OF MECHANICAL ENGINEERS.

NOTE: Statements and opinions advanced in papers are to be understood as individual expressions of their authors and not those of the Society.

TABLE 1 RANGE OF VARIABLES

	Fluids: Liquid	Fluids: Gas	Liquid viscosity,[a] lb-sec/ft²	Liquid, specific gravity[a]	Liquid surface tension,[a] lb per ft	Average pressure p, psia	Average temperature, t, deg F	Liquid rate: Minimum lb per sec	Liquid rate: Maximum lb per sec	Air rate: Minimum lb per sec	Air rate: Maximum lb per sec
Taylor tests, glass pipe 1.017 in. ID	Water	Air	2.34×10^{-5}	1.00	4.89×10^{-3}	18	60	0.015	4.68	0.00074	0.063
	Water + Nekal	Air	1.81×10^{-5}	1.00	3.12×10^{-3}	18	80	0.050	4.66	0.00063	0.069
	Kerosene	Air	4.35×10^{-5}	0.830	2.13×10^{-3}	18	78	0.029	3.70	0.00060	0.068
	Diesel fuel	Air	10.35×10^{-5}	0.867	2.03×10^{-3}	18	80	0.030	3.83	0.00088	0.071
	Blend no. 1 of Diesel fuel + oil B	Air	87.5×10^{-5}	0.901	2.16×10^{-3}	18	83	0.050	2.90	0.00087	0.068
	Blend No. 2 of Diesel fuel + oil B	Air	257×10^{-5}	0.913	2.23×10^{-3}	18	85	0.040	1.64	0.00091	0.060
	Oil B (S.A.E. 40)	Air	558×10^{-5}	0.912	2.31×10^{-3}	18	85	0.050	0.810	0.00089	0.054
Thomsen tests, ½-in. standard galvanized pipe	Benzene	Air	1.29×10^{-5}	0.876	1.93×10^{-3}	52	75	0.0141	0.0758	0.0052	0.0361
	Water	Air	2.05×10^{-5}	1.00	4.96×10^{-3}	52	70	0.0194	0.0832	0.0109	0.0304
	Water + Kemenol	Air	2.05×10^{-5}	1.00	3.30×10^{-3}	52	70	0.0226	0.0874	0.0081	0.0320
	Kerosene	Air	3.38×10^{-5}	0.910	2.08×10^{-3}	52	70	0.0172	0.0773	0.0051	0.0273

[a] Properties at temperature of test t, deg F.

based on W_g and pipe diameter D_p

$Re_l = \frac{4}{\pi} \cdot \frac{W_l}{D_p \mu_l g}$ = Reynolds modulus for liquid phase based on W_l and pipe diameter, D_p

Subscripts

c = cross-sectional, convective
g = gas
l = liquid
H = hydraulic
p = pipe
$T\text{-}P$ = two phase
tt = turbulent liquid, turbulent gas
vt = viscous liquid, turbulent gas
vv = viscous liquid, viscous gas

Introduction

Many flow systems in engineering design involve the simultaneous transport in pipes of a gaseous (or vapor) phase and a liquid phase. Examples of such systems are numerous; among them are water-steam mixtures in boiler tubes, petroleum liquids and their vapors in tube stills, liquid-vapor mixtures in refrigeration systems, oil-laden compressed air, condensate-return lines, gasoline-engine manifolds, and partial condensers in fractionation equipment. Air flow in cooling towers and steam flow in the low-pressure stages of turbines are more complex examples of this type of hydrodynamic problem. A considerable amount of experimental work in the field of two-phase flow has been reported in the literature but no satisfactory analyses of the data have been accomplished. This paper presents further data on the subject of static pressure drop in two-phase flow and outlines a macroscopic analysis of the test data, which allows prediction of the pressure drop under certain flow conditions.

Previous experimental work had indicated that the variables affecting the pressure drop per unit length for two-phase flow were the pipe diameter, the rate of liquid flow, the rate of gas (or vapor) flow, the liquid viscosity, and perhaps the surface tension of the liquid. A preliminary analytical analysis indicated that the liquid density and the gas density and viscosity were also pertinent variables.

To note the effect of these variables, a series of tests was performed in which the pressure drop along a 1-in. glass tube (1)[6] and a ½-in. galvanized-iron pipe (2), resulting from the two-phase two-component flow of air and various liquids, was measured. The range of variables covered by the tests is shown in Table 1. The data on the 1-in. glass tube include the greater range of variables, and the major portion of the discussion will be concerned with these results. The tests on the ½-in. pipe were found to substantiate the data obtained on the glass pipe.

The test arrangement for the 1-in. glass tube is shown in Fig. 1. The liquid and the air were mixed several feet before the test

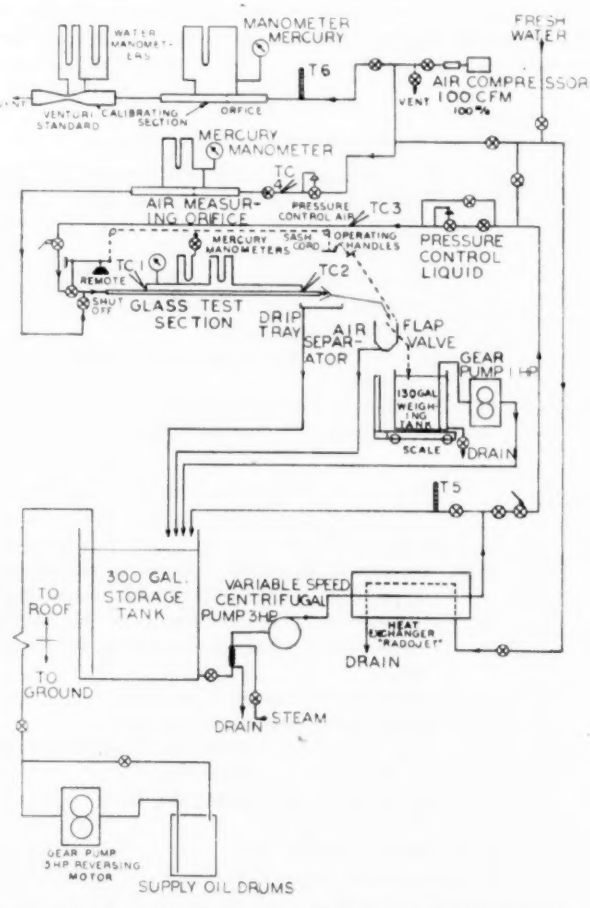


FIG. 1 SCHEMATIC DIAGRAM OF EXPERIMENTAL EQUIPMENT

[6] Numbers in parentheses apply to references at the end of the paper. A comprehensive Bibliography is also included.

section proper. The method used for mixing the two phases was chosen as a result of considerable experimentation. Trials were made with both air injected into the liquid and liquid injected into the air. These different modes of injection were tried to minimize "slugging," which is the name given a stream of alternate plugs of liquid and air. Such plugs were from a few inches to several feet long, depending upon the rates of flow. The arrangement necessary for minimum "slugging" required the introduction of the air into the upper surface of the liquid and perpendicular to it. Furthermore, any bends, valves, or other obstructions between the injection point and the measuring section must be avoided.

After being mixed, the fluids passed through a glass test section in which the flow pattern could be observed and the static pressure drop measured across the taps[7] shown in Fig. 1. The mixture of liquid and air exhausted into a separator, the liquid returning to the reservoir and the air exhausting to the atmosphere. Air rates were measured by means of calibrated orifices, and liquid rates were determined by gravimetric means. The average temperature and static pressure in the pipe were also recorded. The static pressure drops due to the flow of the two pure components, i.e., all air or all liquid, were carefully measured at intervals throughout the two-phase test runs.

The equipment utilized for the tests on the smaller pipe was practically identical to that just described.[7]

Data and Results

The experimental results obtained on the 1-in. glass tube are shown in graphical form in Figs. 2 to 8,[8] inclusive. Inspection of the data indicates the effect of the variables mentioned previously. Figs. 2 to 7, inclusive, reveal the pressure drop as a function of the gas and liquid rates for air and water, kerosene, Diesel fuel oil, two blends of Diesel fuel oil and S.A.E. 40 oil, and S.A.E. 40 oil. The data for water with a surface-tension-reducing additive are shown in Fig. 8 and indicate that the change of surface tension had no apparent effect on the pressure drop, although it influenced the flow pattern appreciably, as will be discussed later. The decrease in the surface tension of the water due to the additive was, however, only 36 per cent and it is possible that a greater change would influence the results.

The following general trends are evident in Figs. 2 to 7, inclusive:

1 The static pressure drop for two-phase flow is always greater than the pressure drop for each phase flowing alone at the weight rates which obtain in the two-phase flow.

2 For a given gas rate, adding liquid increases the pressure drop, the pressure drop becoming greater as more liquid is added.

3 When the air flow approaches zero for any constant liquid rate, the static pressure drop due to the flow of the pure liquid is approached. Thus the lines of constant liquid rate become horizontal as the gas rate is decreased.

4 As the gas flow is increased, for any constant liquid rate, the static pressure drop increases and approaches the 100 per cent gas line as an asymptote.

5 The flow for both the air and the liquid may be turbulent. Figs. 2, 3, 4, and 8 indicate this type of flow mechanism, for both the 100 per cent liquid and 100 per cent air data reveal a variation of pressure drop with the 1.8 power of the rate of flow.

6 The flow may be turbulent for the air and viscous for the liquid. Curves 5, 6, and 7 reveal this type of flow, for the pressure drop due to the liquid alone is seen to vary directly with the weight rate, while the pressure drop for the air alone varies with the 1.8 power of the air rate. The case in which both the air and the liquid flow was viscous was not observed in these tests.

7 The greater the viscosity of the liquid, the greater is its effect on the pressure drops for two-phase flow. This effect is particularly evident when the liquid is flowing viscously, Figs. 5, 6, and 7.

Simultaneously with the static pressure drop measurements, visual and photographic observations of the flow mechanism were made. These are of considerable interest because they reveal the complexity of the microscopic phenomena occurring during two-phase flow. As would be expected, two distinct types of flow phenomena were observed, one when the flow of both fluids was turbulent, the other when the flow of the liquid was viscous and the flow of the gas was turbulent.

The results of the observations are given in Table 2 and the flow types are illustrated in Fig. 9. In this figure, flow type 1 indicates air alone, and flow type 9, liquid alone. Type 2 is a frothy mixture of liquid and air and did not exist when the liquid flow was viscous. In type 3 the fluid moved along the bottom of the pipe, with the air above, waves of definite wavelength moving at the gas-liquid interface.[9] In the case of viscous flow of the liquid phase, the wavelengths were somewhat greater than in the case of turbulent flow of the liquid. Type 4 followed type 2 at medium air rates as the liquid rate was reduced, and consisted of definite liquid waves on both the bottom and top of the pipe traveling at different velocities. As the liquid rate was decreased further, the upper waves disappeared and type 6 appeared. In this interesting flow type, the crests of the waves point, as shown, in the direction opposite to the direction of fluid flow. When the air rate was very low and the liquid rate was reduced, type 2 flow was followed by type 7 in which small air bubbles collected in the upper half of the pipe. As the liquid rate was further reduced (at low air rates) type 5 appeared in which long bubbles, occupying almost one half the pipe cross-sectional area, moved along the pipe. At very low liquid rates and high air rates, "annular" flow occurred (type 8). The liquid flowed in the form of an annulus, even though the pipe was horizontal, and the liquid surface was covered with small capillary waves. When the surface tension of the water was lowered by adding Nekal BX, much foaming was observed, type 2 being prominent in the results.

It is then evident that the microscopic behavior of the two-phase flow system is extremely complex. Since, however, the static pressure drops for the water and the water-Nekal blend were almost identical, although the detailed flow patterns were quite different, it appears that it should be possible to analyze the problem from a macroscopic point of view and obtain results which are of utility from an engineering standpoint, even though the details of the flow mechanism are not clarified. This method of attack is of course the one employed whenever the "friction factor" is utilized, i.e., the "friction factor" allows prediction of static pressure drops in turbulent flow without the need for consideration of the complex details of turbulence.

Analysis of Results

The analysis of the static pressure drop accompanying two-phase flow results from the application of two basic postulates. The first postulate is that the static pressure drop for the liquid

[7] The static pressure taps for the 1-in. glass pipe were 21.6 ft apart and those for the 1/2-in. galvanized-iron pipe 50 ft apart. The pressure in many cases fluctuated severely due to the unavoidable "slugging" of the fluid. During these runs the differential manometer deflection was recorded at the estimated mid-point of the oscillation. The static pressure manometer was "throttled" to reduce oscillations.

[8] The pressure drops shown in Figs. 2 to 8, inclusive, have been corrected to atmospheric pressure conditions by the approximate method outlined in Appendix 2. Points for zero gas flow (100 per cent liquid) are plotted on the 0.0001 lb/sec gas rate abscissa for convenience.

[9] Such waves form at the interface of two fluids moving with different velocities (4).

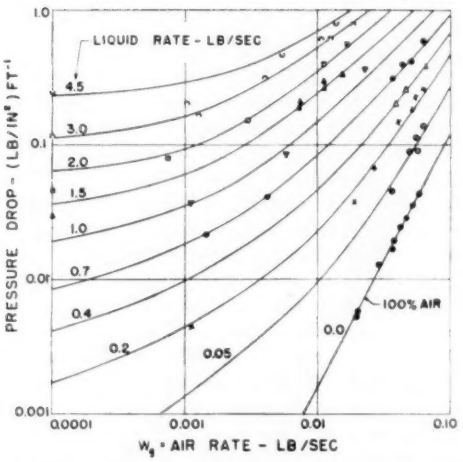


FIG. 2 PRESSURE DROP FOR FLOW OF AIR AND WATER IN 1-IN. GLASS PIPE
(Viscosity of liquid = 2.34×10^{-5}, lb sec/ft².)

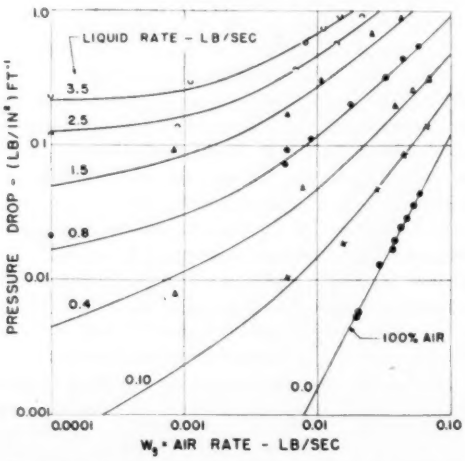


FIG. 3 PRESSURE DROP FOR FLOW OF AIR AND KEROSENE IN 1-IN. GLASS PIPE
(Viscosity of liquid = 4.35×10^{-5}, lb sec/ft².)

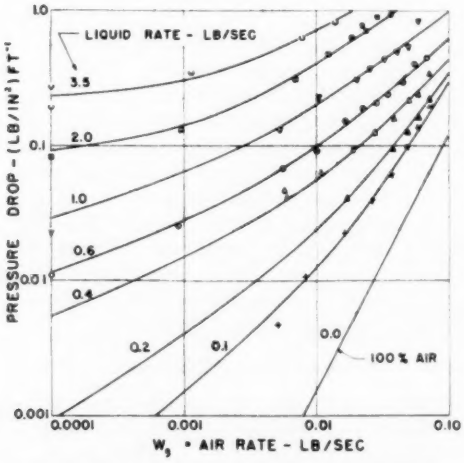


FIG. 4 PRESSURE DROP FOR FLOW OF AIR AND DIESEL FUEL OIL IN 1-IN. GLASS PIPE
(Viscosity of liquid = 10.35×10^{-5}, lb sec/ft².)

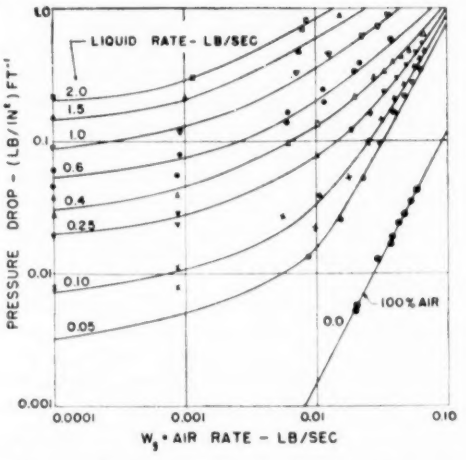


FIG. 5 PRESSURE DROP FOR FLOW OF AIR AND BLEND NO. 1 OF DIESEL OIL AND OIL B IN 1-IN. GLASS PIPE
(Viscosity of liquid = 87.5×10^{-5}, lb sec/ft².)

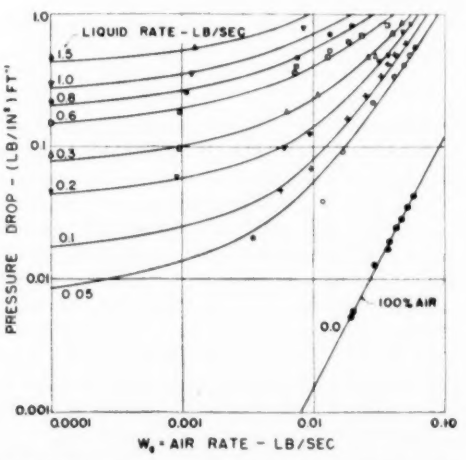


FIG. 6 PRESSURE DROP FOR FLOW OF AIR AND BLEND NO. 2 OF DIESEL OIL AND OIL B IN 1-IN. GLASS PIPE
(Viscosity of liquid = 257×10^{-5}, lb sec/ft².)

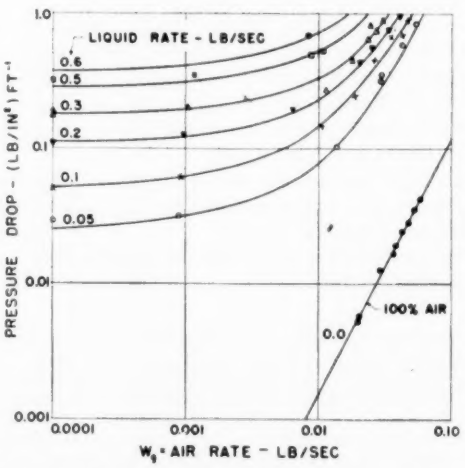


FIG. 7 PRESSURE DROP FOR FLOW OF AIR AND OIL B (S.A.E. 40) IN 1-IN. GLASS PIPE
(Viscosity of liquid = 588×10^{-5}, lb sec/ft².)

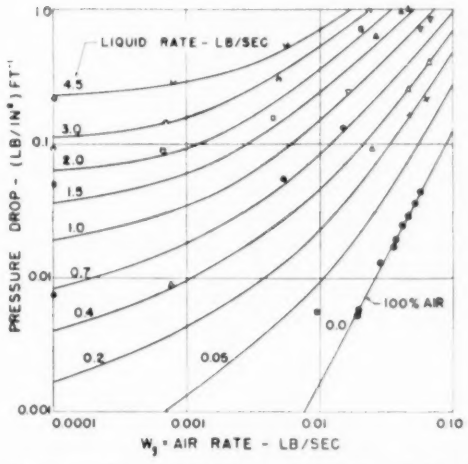


FIG. 8 PRESSURE DROP FOR FLOW OF AIR AND WATER PLUS NEKAL-BX IN 1-IN. GLASS PIPE

(The lines for constant liquid rates are the same as those shown in Fig. 2.)

TABLE 2 OBSERVATIONS OF FLOW MECHANISMS[a]

	Low air rate		Medium air rate		High air rate	
	Liq. turb.	Liq. visc.	Liq. turb.	Liq. visc.	Liq. turb.	Liq. visc.
Very low liquid rate..	3	3	3	3	8	8
Low liquid rate.....	5	3	6	3	8	8
Medium liquid rate...	7	7	4	4	4	4
High liquid rate.....	2	–	2	–	2	–

[a] See Fig. 9 for sketch of flow types.

phase must equal the static pressure drop for the gaseous phase regardless of the details of the flow, as long as appreciable static pressure differences do not exist along any pipe diameter. The second postulate is that the volume occupied by the liquid plus the volume occupied by the gas at any instant must equal the total volume of the pipe. The expression of these two propositions in algebraic form leads to the following equations for the prediction of two-phase-flow static pressure drop:

The static pressure drop due to the liquid flow may be written by the usual Weisbach equation as

$$\left(\frac{\Delta P}{\Delta L}\right)_{T-P} = \zeta_l \frac{\gamma_l}{D_l} \cdot \frac{v_l^2}{2g} \quad \ldots\ldots\ldots\ldots\ldots [1]$$

where D_l is the unknown "hydraulic diameter" of the liquid flow pattern. Similarly, for the gas flow

$$\left(\frac{\Delta P}{\Delta L}\right)_{T-P} = \zeta_g \frac{\gamma_g}{D_g} \cdot \frac{v_g^2}{2g} \quad \ldots\ldots\ldots\ldots\ldots [2]$$

The pressure drop in two-phase flow is greater than that for the flow of either single phase alone for various reasons, among which are the irreversible work done by the gas on the liquid and the fact that the presence of the second fluid reduces the cross-sectional area of flow for the first fluid. Thus, during two-phase flow the hydraulic diameters D_l and D_g will always be less than the pipe diameter D_p, and as noted in Equations [1] and [2], this reduction of hydraulic diameter will increase the pressure drop greatly. It should be observed that for a given weight rate of fluid the pressure drop varies inversely as the fourth or fifth power of the hydraulic diameter, depending upon the type of flow.

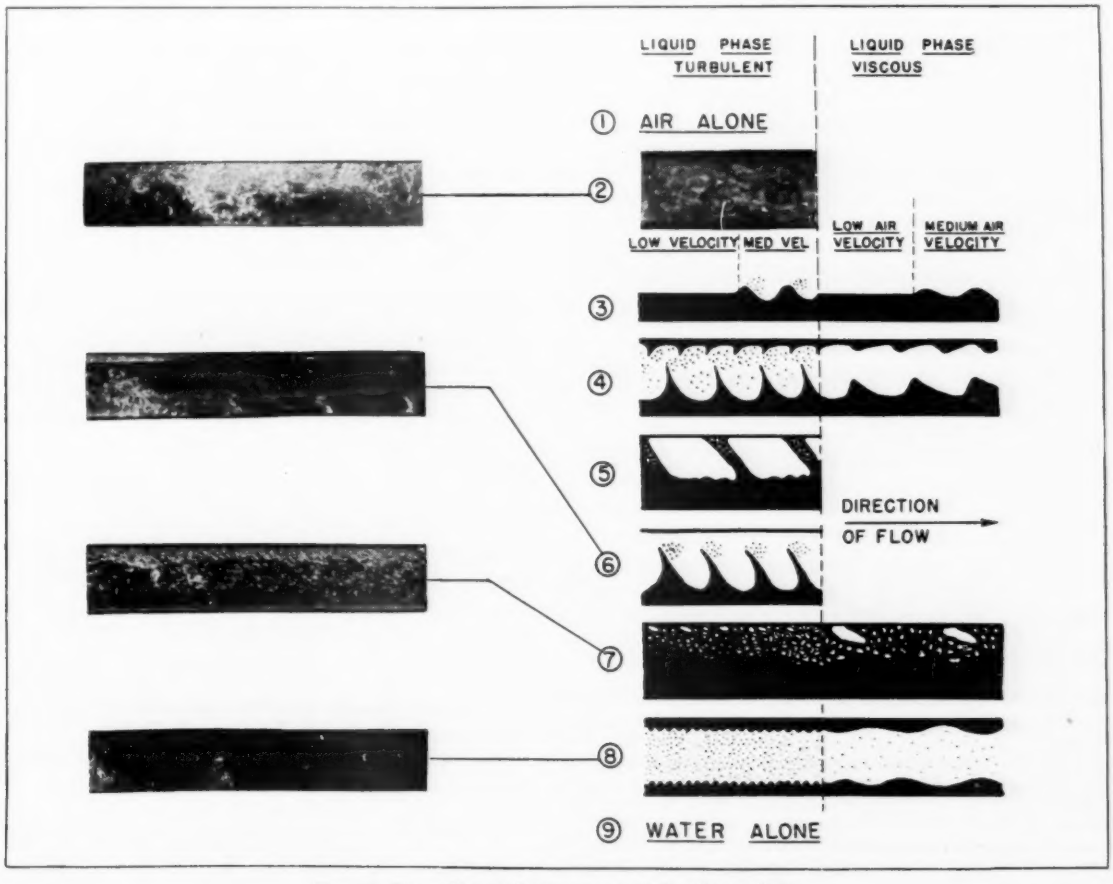


FIG. 9 FLOW TYPES OCCURRING IN 1-IN. GLASS PIPE

The hydraulic diameter of the flow pattern is related to the cross-sectional area through which the fluid is flowing at any instant. For a cylindrical flow pattern the simple relation

$$\frac{\pi}{4} D^2_H = A_c \quad [3]$$

applies. For a more complex cross-sectional area, such as that possessed by the fluids in the pipe, the following relations may be written

$$A_l = \alpha \left(\frac{\pi}{4} D^2_l \right) \quad [4]$$

$$A_g = \beta \left(\frac{\pi}{4} D^2_g \right) \quad [5]$$

where α and β are, in effect, the ratio of the actual cross-sectional area of flow to the area of a circle of diameter D_l and D_g, respectively. A consideration of the air flow indicates that as a first approximation, the cross-sectional shape of the air flow is approximately circular at all times, so that β can be considered as 1. On the other hand, at high rates of gas flow and low rates of liquid flow, the liquid can assume a thin annular shape, and thus, for this case, α is much greater than unity. As a reasonable approximation, therefore, α will be left as an unknown in Equation [4] while β is taken as unity.[10]

Equations [4] and [5] may be utilized to evaluate the respective velocities v_l and v_g: thus

$$v_l = \frac{W_l}{\alpha \left(\frac{\pi}{4} D_l^2 \right) \gamma_l} \quad [6]$$

$$v_g = \frac{W_g}{\left(\frac{\pi}{4} D_g^2 \right) \gamma_g} \quad [7]$$

The velocities, v_l and v_g, calculated from Equations [6] and [7], are the mean absolute velocities of the two fluids. The velocities v_l and v_g in Equations [1] and [2] involve the "relative" velocities between the fluids, and thus substitution of the magnitudes of the velocities from Equations [6] and [7] into Equations [1] and [2] is not exact.[11] This difficulty is not as serious as it first appears, for the ratio α is evaluated from experimental data and thus includes the effect of relative motion as well as the fluid geometry. A more precise analysis of the problem of two-phase pressure drop should include a consideration of the matter of relative motion in greater detail.

The friction factors ζ_l and ζ_g may be expressed in the generalized Blasius form

$$\zeta_l = \frac{\left(\frac{\pi}{4} \right)^n C_l}{\left(\frac{W_l}{\alpha D_l \mu_l g} \right)^n} \quad [8]$$

and similarly

$$\zeta_g = \frac{\left(\frac{\pi}{4} \right)^m C_g}{\left(\frac{W_g}{D_g \mu_g g} \right)^m} \quad [9]$$

For viscous flow, the constants C_g, C_l are equal to 64 and the exponents n and m are both unity. For turbulent flow C_l and C_g and n and m vary with the Reynolds modulus, but an average magnitude (3) for C_g and $C_l = 0.184$, and n and $m = 0.20$ may be utilized for smooth tubes for a range of the Reynolds modulus from 5000 to 200,000.

The proper choice of C_l, C_g and n, m depends upon the type of flow occurring in the pipe. Four distinct flow mechanisms are possible, as follows:

1 The flow of both the liquid and gas may be turbulent ($C_l = C_g = 0.184$ and $n = m = 0.2$).

2 The flow of the gas may be turbulent, and the flow of the liquid viscous ($C_l = 64$, $C_g = 0.184$, $n = 1$, $m = 0.2$).

3 The flow of both the liquid and gas may be viscous ($C_l = C_g = 64$ and $n = m = 1$).

4 The flow of the gas may be viscous and that of the liquid turbulent ($C_l = 0.184$, $C_g = 64$, $m = 1$, $n = 0.2$).

Of these four possible cases, the fourth is very improbable and thus has not been analyzed in detail, although the analysis would be almost identical to that of the second flow mechanism. The third case was not observed experimentally but has been analyzed since this mechanism may arise in practice (viz., flow in porous media). As discussed previously, both the first and second flow combinations were observed experimentally and are analyzed in the following sections of the paper.

Flow Mechanism 1. Liquid Turbulent, Gas Turbulent

In flow mechanism 1, in which both fluids are in turbulent motion, the magnitudes of C_l and C_g are equal to 0.184 for smooth pipes, and the exponents m and n are both equal to 0.2. Substitution of these magnitudes in Equations [8] and [9], and a further substitution of Equations [8], [9], [6], [7] into Equations [1] and [2] results in the equation

$$\left(\frac{D_l}{D_g} \right)^2 = \left(\frac{\gamma_g}{\gamma_l} \right)^{\frac{2}{5-n}} \left(\frac{\mu_l}{\mu_g} \right)^{\frac{2n}{5-n}} \left(\frac{W_l}{W_g} \right)^{\frac{2(2-n)}{5-n}} (\alpha)^{\frac{2(n-2)}{5-n}} \quad [10]$$

It is noted that, since the constants C_l and C_g are equal for both fluid phases, they cancel in the derivation of Equation [10], while the exponent n remains. In Equation [10], the three unknowns are D_l, D_g, and α. Equation [10] is the result of the first basic postulate previously discussed, i.e., the equality of the pressure drops for the two phase of flow. Substitution of $n = 0.2$ yields

$$\left(\frac{D_l}{D_g} \right)^2 = \left(\frac{\gamma_g}{\gamma_l} \right)^{0.416} \left(\frac{\mu_l}{\mu_g} \right)^{0.083} \left(\frac{W_l}{W_g} \right)^{0.75} \alpha^{-0.75} \quad [11]$$

Application of the second basic postulate, equating the sum of the liquid and gas volumes to the pipe volume yields

$$\alpha \left(\frac{\pi}{4} D_l^2 L \right) + \left(\frac{\pi}{4} D_g^2 L \right) = \frac{\pi}{4} D_p^2 L$$

$$\alpha D_l^2 + D_g^2 = D_p^2 \quad [12]$$

In Equation [12], the variables D_g and D_l are unknown. One of the unknown "hydraulic diameters," D_l, may be eliminated between Equations [11] and [12]. The resulting expression for D_g is

$$D_g = \frac{D_p}{\sqrt{1 + \alpha^{1/4} \left(\frac{\gamma_g}{\gamma} \right)^{0.416} \left(\frac{\mu_l}{\mu} \right)^{0.083} \left(\frac{W_l}{W} \right)^{0.75}}} \quad [13]$$

[10] A more precise analysis can be performed in which both α and β are left as unknowns. The modulus β can be assumed equal to unity and α estimated. By rearranging the equations, β can then be solved for approximately, utilizing the approximate magnitudes of α. A repetition of this trial-and-error procedure will finally yield magnitudes of both α and β. The present analysis, in effect, includes any variations of β in the modulus α. This may be one explanation of the scattering of the experimental points observed in Figs. 10 and 14.

[11] Noted by V. Skoglund in a verbal discussion of this paper at the 1943 Semi-Annual Meeting in Los Angeles, Calif.

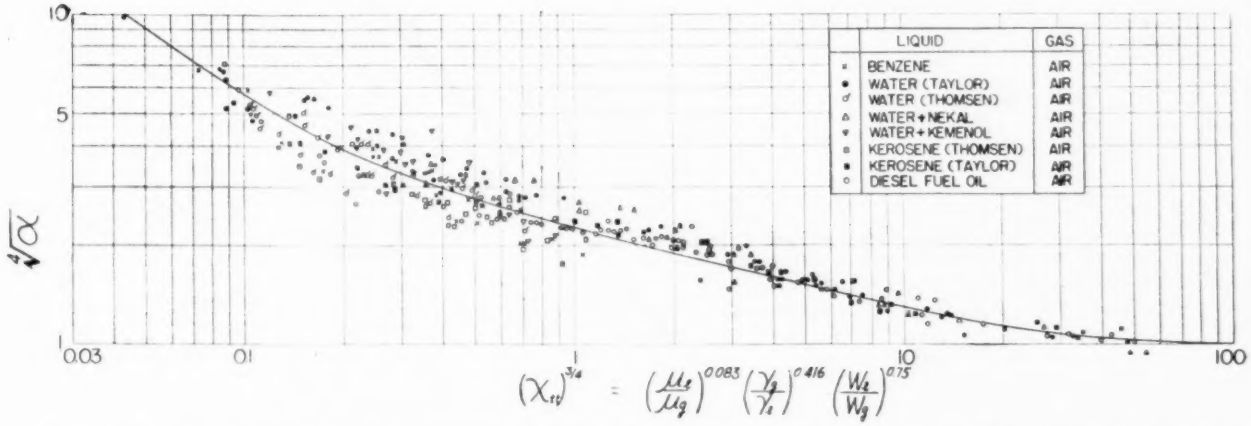


FIG. 10 FLOW TYPE MODULUS $\alpha^{1/4}$ AS A FUNCTION OF THE TWO-PHASE FLOW MODULUS $(\chi_{tt})^{3/4}$. FLOW MECHANISM IN WHICH BOTH LIQUID AND GAS ARE IN TURBULENT MOTION

It may be shown by reference to Equation [2] that the static pressure drop for the gas phase during the two-phase flow is:

$$\left(\frac{\Delta P}{\Delta L}\right)_{T-P} = \frac{\left(\frac{4}{\pi}\right)^{2-m} C_g}{\left(\frac{W_g}{D_g \mu_g g}\right)^m} \cdot \frac{1}{D_g} \cdot \frac{W_g^2}{2gD_g^4\gamma_g} \quad \ldots\ldots [14]$$

$$= \left[\frac{1}{2}\left(\frac{4}{\pi}\right)^{2-m} \frac{C_g \mu_g{}^m}{g^{1-m}\gamma_g} \cdot \frac{W_g{}^{2-m}}{D_p{}^{5-m}}\right]\left(\frac{D_p}{D_g}\right)^{5-m} \quad \ldots [14]$$

$$= \left(\frac{\Delta P}{\Delta L}\right)_g \left(\frac{D_p}{D_g}\right)^{5-m} \quad \ldots\ldots [15]$$

For the case under consideration $m = 0.2$, thus

$$\left(\frac{\Delta P}{\Delta L}\right)_{T-P} = \left(\frac{\Delta P}{\Delta L}\right)_g \left(\frac{D_p}{D_g}\right)^{4.8} \quad \ldots\ldots [16]$$

The term in brackets in Equation [14] may be demonstrated to be the pressure drop for the gas phase alone flowing with a weight rate W_g and density γ_g, in a pipe of diameter D_p. Thus, the pressure drop for two-phase flow is obtained by multiplying the static pressure drop for the gas phase alone (corresponding to W_g, γ_g, and D_p) by the ratio $(D_p/D_g)^{5-m}$. When both fluids are in turbulent motion, this ratio can be obtained from Equation [13] and substituted in Equation [16].

The final equation for the static pressure drop per unit length, when both the fluids are flowing in the turbulent regime, is then

$$\left(\frac{\Delta P}{\Delta L}\right)_{T-P} = \left(\frac{\Delta P}{\Delta L}\right)_g \left[1 + \alpha^{1/4}\left(\frac{\mu_l}{\mu_g}\right)^{0.083}\left(\frac{\gamma_g}{\gamma_l}\right)^{0.416}\left(\frac{W_l}{W_g}\right)^{0.75}\right]^{3.4} \quad \ldots [17]$$

Inspection of Equations [17] and [14] reveals that, as W_g approaches zero, the equation reduces to the expression for the pressure drop of the liquid flowing alone with a weight rate W_l through a pipe of diameter D_p.

In order to establish the cases for which Equation [17] is applicable, the Reynolds modulus for each fluid is calculated utilizing the rates W_g and W_l, the fluid viscosities, and the pipe diameter D_p. If the magnitude of both of these Reynolds moduli is greater than 2000, Equation [17] is applicable. An example of the method of calculation is shown in Appendix 1.

Evaluation of α for Flow Mechanism 1. In Equation [17] the function α is still unknown. This function, as mentioned earlier, represents the ratio of the actual cross-sectional area of liquid flow to the area calculated by the product $\frac{\pi}{4} D_l^2$ and should equal unity when the liquid completely fills the pipe and be greater than unity when the liquid flows along the pipe in a thin annulus. The function α was calculated from experimental data by substituting known magnitudes of the variables into Equation [17] and then solving for $\alpha^{1/4}$. The magnitudes of $\alpha^{1/4}$ varied from unity when the pipe was filled with liquid to about 10 when the liquid was flowing in an annulus.

In order to generalize the test results, a parameter was sought which would allow the correlation of the magnitudes of $\alpha^{1/4}$ for the various fluids and pipe diameters for which data were available. Many dimensionless groups were tried, but the best correlation of the data was obtained when the multiplier of $\alpha^{1/4}$ in Equation [17] was utilized. This parameter represents the ratio of shearing forces in the two fluid phases, and thus is a logical basis for the correlation of the magnitudes of α.

For simplicity in calculation, the dimensionless group

$$\chi_{tt} = \left(\frac{\mu_l}{\mu_g}\right)^{0.111}\left(\frac{\gamma_g}{\gamma_l}\right)^{0.555}\left(\frac{W_l}{W_g}\right) \quad \ldots\ldots [18]$$

was defined. The multiplier of $\alpha^{1/4}$ in Equation [17] is thus $(\chi_{tt})^{3/4}$. The subscript *tt* refers to the turbulent flow of the liquid and gas.

In Fig. 10 is shown the plot of $\alpha^{1/4}$ as a function of $(\chi_{tt})^{3/4}$. The scattering of the experimental points is rather severe at low magnitudes of the parameter χ_{tt}, but when it is observed that five different liquids, and data from two experimenters are plotted, the correlation is, on the whole, satisfactory. The scattering of the points is in part due to the use of a constant exponent of 0.20 in the empirical equation for the friction factor; the actual exponent varies with the Reynolds modulus. Further, due to the "slugging" flow of the liquid during certain runs, the pressure drop varied periodically with time, and the recorded mean pressure drop may not represent a true time average. Finally, the fact that $\alpha^{1/4}$ includes the effect of relative motion between the fluids, as well as the flow geometry, may cause some scattering. There seems to be some slight evidence that a third parameter may enter the correlation since the points for water are on the average somewhat higher than the points for the hydrocarbon liquids. The variation of surface tension obtained in these tests seems to be of little importance in the evaluation of $\alpha^{1/4}$, since the points for water, and the water-Kemenol, and water-Nekal mixtures are almost coincident.

From the point of view of ease in calculation, an interesting

point is to be noted; since $\alpha^{1/4}$ is a function of χ_{tt}, inspection of Equation [17] reveals that

$$\left(\frac{\Delta P}{\Delta L}\right)_{T-P} = \left(\frac{\Delta P}{\Delta L}\right)_g [1 + \alpha^{1/4}\chi_{tt}^{3/4}]^{2.4}$$

$$= \left(\frac{\Delta P}{\Delta L}\right)_g [1 + f(\chi_{tt})(\chi_{tt})^{3/4}]^{2.4} \quad \ldots\ldots\ldots\ldots [19]$$

Thus the pressure drop in two-phase flow depends only upon the product of the pressure drop of the gaseous component flowing alone, and a function of χ_{tt}. The latter function may be readily evaluated. A curve was faired through the experimental points

TABLE 3 MAGNITUDES OF THE FUNCTION Φ_{tt}

$\sqrt{\chi_{tt}}$	Φ_{tt}
0	1.00
0.10	1.50
0.20	1.68
0.40	2.13
0.70	3.03
1.00	4.08
2.00	8.30
4.00	19.6
7.00	42.3
10.0	71.0
20.0	222
40.0	770
46.2	1000

For $\sqrt{\chi_{tt}} > 46$ $\quad \Phi_{tt} = (\sqrt{\chi_{tt}})^{1.8}$

of Fig. 10. For each magnitude of χ_{tt} a value of $\alpha^{1/4}$ was established. Then

$$\left(\frac{\Delta P}{\Delta L}\right)_{T-P} = \left(\frac{\Delta P}{\Delta L}\right)_g [1 + \alpha^{1/4}\chi_{tt}^{3/4}]^{2.4} = \Phi_{tt}^2 \left(\frac{\Delta P}{\Delta L}\right)_g \quad [20]$$

where

$$\Phi_{tt} = [1 + \alpha^{1/4}\chi_{tt}^{3/4}]^{1.2}$$

Table 3 presents magnitudes of Φ_{tt} versus $\sqrt{\chi_{tt}}$. The square-root form was utilized in order to reduce the range of the variables to facilitate plotting. Fig. 11 presents Φ_{tt} versus $\sqrt{\chi_{tt}}$ and may be utilized directly for the calculation of two-phase pressure drop.

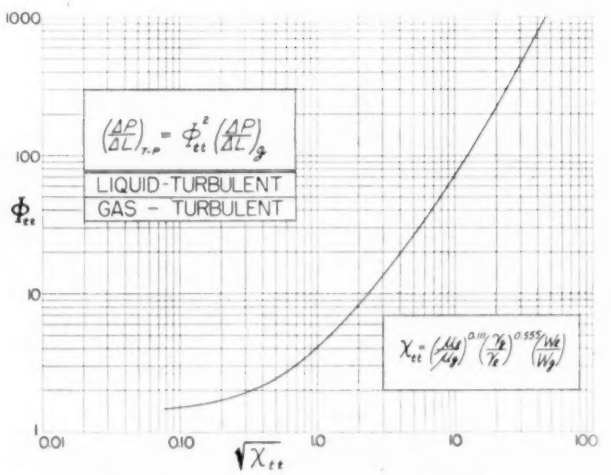


FIG. 11 MODULUS Φ_{tt} AS A FUNCTION OF TWO-PHASE FLOW MODULUS $\sqrt{\chi_{tt}}$ FOR FLOW MECHANISM IN WHICH BOTH LIQUID AND GAS ARE IN TURBULENT MOTION. THE MODULUS Φ_{tt} MAY BE UTILIZED DIRECTLY TO CALCULATE THE PRESSURE DROP OCCURRING IN TWO-PHASE FLOW

Fig. 11 reveals that, as χ_{tt} approaches zero, Φ_{tt} approaches unity very slowly due to the rapid increase of $\alpha^{1/4}$ at low magnitudes of χ_{tt}. It follows that, even if the fluid just wets the pipe wall (low values of χ_{tt}) the two-phase pressure drop is increased appreciably over that due to the gaseous components alone. For $\sqrt{\chi_{tt}}$ equal to 0.10 which corresponds to a reasonable liquid flow, the two-phase pressure drop is 2.25 times that of the gas alone. At high magnitudes of $\sqrt{\chi_{tt}}$ the curve of Φ_{tt} approaches an asymptote with a slope of 1.8.

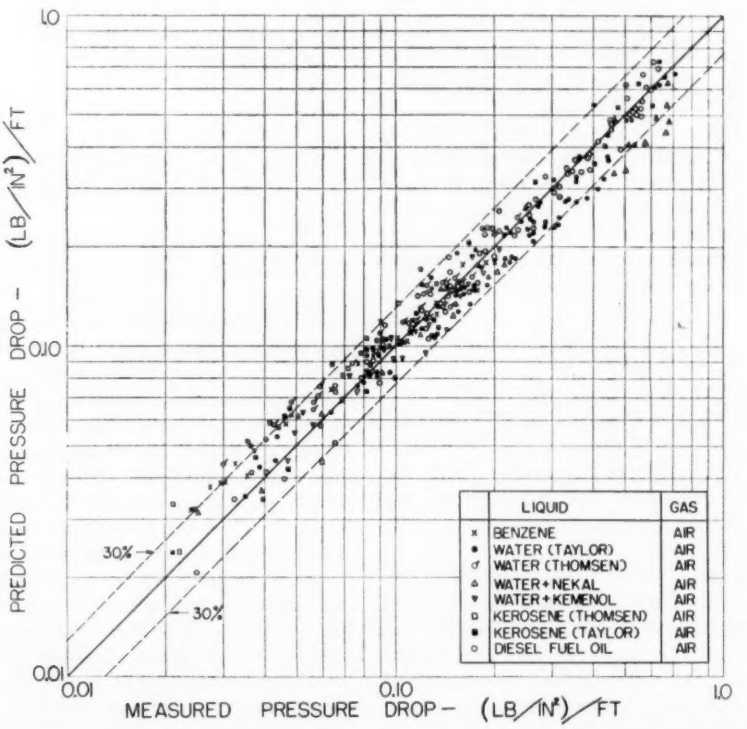


FIG. 12 COMPARISON OF PREDICTED AND MEASURED PRESSURE DROP FOR TWO-PHASE TWO-COMPONENT FLOW. FLOW MECHANISM IN WHICH BOTH LIQUID AND GAS ARE IN TURBULENT MOTION. PREDICTION BY MEANS OF FIG. 11

Fig. 11 was utilized to predict the pressure drops observed in the laboratory by calculating χ_{tt} based on experimental values of μ_g, μ_l, γ_g, γ_l, W_g, and W_l. The results of these calculations are shown in Fig. 12. The prediction is seen to be well within ±30 per cent for a large majority of the points. Thus, within the range of the experimental variables which are listed in Table 1, Equation [17], or its equivalent Fig. 11, may be utilized to predict the pressure drop accompanying two-phase two-component flow when both phases are in turbulent motion. Extrapolation of Equation [17] to magnitudes of the variables greatly different from those utilized in the tests should be made with caution until the general applicability of the parameter χ_{tt} is tested by further research.

In order to determine how well Equation [17] could predict the curve shapes obtained experimentally, Fig. 11 was utilized to predict the pressure drop along a 1-in. glass pipe in which air and water were flowing at an average pressure of 14.7 psia and a temperature of 66 F. The resulting predicted curves of pressure drop versus air rate for several constant liquid rates are shown in Fig. 13. The agreement between these curves and the experimental points shown in Fig. 2 is satisfactory. Lack of agreement at some points is no doubt due in part to the rather arbitrary method utilized to correct the experimental data shown in Fig. 2 to standard conditions (see Appendix 2).

Flow Mechanism 2. Liquid Viscous, Gas Turbulent

The equation for the two-phase pressure drop for the second flow mechanism is derived by substituting $m = 0.2$ and $n = 1$ in Equations [8] and [9]. Further substitution of Equations [8], [9], [6], [7] into Equation [1] and [2] yields

$$\frac{D_l^4}{D_g^{4.8}} = \left(\frac{\pi}{4}\right)^{0.8} g^{0.8} \frac{C_l}{C_g} \cdot \frac{\gamma_g}{\gamma_l} \cdot \frac{\mu_l}{\mu_g^{0.2}} \cdot \frac{W_l}{W_g^{1.8}} \cdot \frac{1}{\alpha} \quad \ldots\ldots [21]$$

or

$$\left(\frac{D_l}{D_g}\right)^4 = \left(\frac{\frac{\pi}{4} g \mu_g D_p}{W_g}\right)^{0.8} \frac{C_l}{C_g} \cdot \frac{\gamma_g}{\gamma_l} \cdot \frac{\mu_l}{\mu_g} \cdot \frac{W_l}{W_g} \left(\frac{D_g}{D_p}\right)^{0.8} \frac{1}{\alpha} \quad [22]$$

$$\left(\frac{D_l}{D_g}\right)^2 = (Re_g)^{-0.4} \sqrt{\frac{C_l}{C_g} \cdot \frac{\gamma_g}{\gamma_l} \cdot \frac{\mu_l}{\mu_g} \cdot \frac{W_l}{W_g}} \left(\frac{D_g}{D_p}\right)^{0.4} \alpha^{-1/2} \quad [23]$$

Both C_l and C_g appear in Equation [23] in contrast to Equation [10], in which neither constant appeared. For smooth pipes, magnitudes of $C_l = 64$ and $C_g = 0.184$ may be utilized as a good approximation.

It is convenient at this point to define a variable χ_{vt} which will be utilized to correlate the magnitudes of $\alpha^{1/2}$ for the second flow mechanism.

$$\chi_{vt} = (Re_g)^{-0.8} \left(\frac{C_l}{C_g} \cdot \frac{\gamma_g}{\gamma_l} \cdot \frac{\mu_l}{\mu_g} \cdot \frac{W_l}{W_g}\right) \quad \ldots\ldots [24]$$

Then Equation [23] may be written as

$$\left(\frac{D_l}{D_g}\right)^2 = \sqrt{\chi_{vt}} \left(\frac{D_g}{D_p}\right)^{0.4} \alpha^{-1/2} \quad \ldots\ldots [25]$$

The second fundamental relation, equating the sum of the gas and liquid volumes to the pipe volume yields, as before

$$\alpha D_l^2 + D_g^2 = D_p^2 \quad \ldots\ldots [26]$$

Eliminating D_l between Equations [25] and [26] results in the equation

$$\left(\frac{D_p}{D_g}\right) = \left[\left(\frac{D_p}{D_g}\right)^{0.4} + \alpha^{1/2} \sqrt{\chi_{vt}}\right]^{1/2.4} \quad \ldots\ldots [27]$$

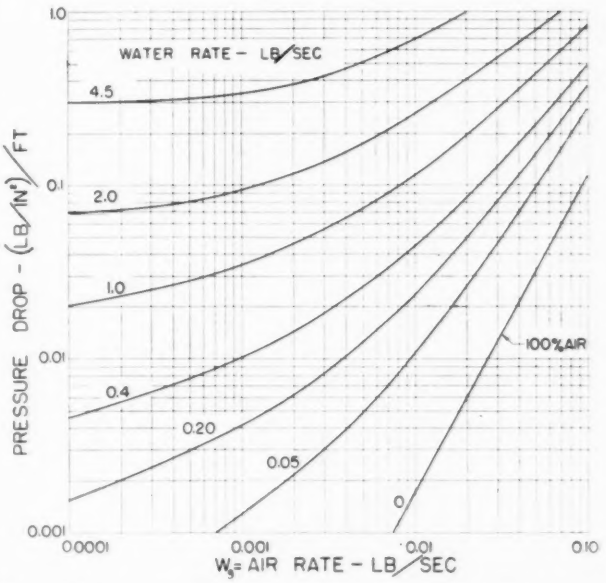


Fig. 13 Predicted Pressure Drop in Two-Phase Flow as a Function of Fluid Rates. Air-Water Flow in a 1-In. Glass Pipe, p = 14.7 Psia, t = 66 F. Both Fluids in Turbulent Motion. Prediction by Means of Fig. 11
(Compare with experimental curves in Fig. 2.)

Equation [15] is again applicable; thus

$$\left(\frac{\Delta P}{\Delta L}\right)_{T-P} = \left(\frac{\Delta P}{\Delta L}\right)_g \left(\frac{D_p}{D_g}\right)^{5-m} \quad \ldots\ldots [28]$$

The exponent $m = 0.2$, since the gas is flowing with turbulent motion. Substituting Equation [27] into Equation [28] yields

$$\left(\frac{\Delta P}{\Delta L}\right)_{T-P} = \left(\frac{\Delta P}{\Delta L}\right)_g \left[\left(\frac{D_p}{D_g}\right)^{0.4} + \alpha^{1/2} \sqrt{\chi_{vt}}\right]^2 \quad \ldots [29]$$

When the term $\left(\frac{D_p}{D_g}\right)^{0.4}$ is important in Equation [29], χ_{vt} is small. This occurs when W_g is large and W_l small, i.e., when the pipe is filled with gas. Thus, it is permissible, with little error, to replace $\left(\frac{D_p}{D_g}\right)^{0.4}$ by unity. The equation for two-phase pressure drop, for the case when the liquid is flowing viscously and the gas is in turbulent motion, then becomes

$$\left(\frac{\Delta P}{\Delta L}\right)_{T-P} = \left(\frac{\Delta P}{\Delta L}\right)_g \left[1 + \alpha^{1/2} (Re_g)^{-0.4} \sqrt{\frac{C_l}{C_g} \cdot \frac{\gamma_g}{\gamma_l} \cdot \frac{\mu_l}{\mu_g} \frac{W_l}{W_g}}\right]^2 \quad [30]$$

In order to establish the applicability of Equation [30] the Reynolds modulus for each fluid phase must be calculated, utilizing the rates W_g and W_l, the fluid viscosities, and the pipe diameter. If the Reynolds modulus for the liquid (Re_l) is less than 2000, and if the Reynolds modulus for the gas (Re_g) is greater than 2000, Equation [30] is applicable. An example of the method of calculation is shown in Appendix 1.

Evaluation of α for Flow Mechanism 2. Equation [30] was utilized to evaluate $\alpha^{1/2}$ from experimental data. The function $\alpha^{1/2}$ was found to vary from 1 at high liquid rates and low gas rates to about 5 at low liquid rates and high gas rates. The magnitudes of $\alpha^{1/2}$ for the three fluids employed in the test were correlated by means of χ_{tt}, as defined by Equation [24]. The

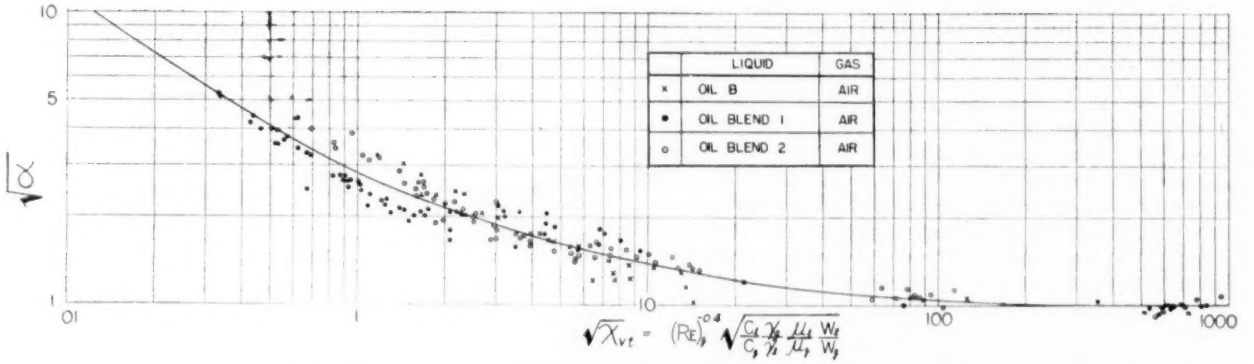


FIG. 14 FLOW TYPE MODULUS $\alpha^{1/2}$ AS A FUNCTION OF TWO-PHASE FLOW MODULUS $\sqrt{\chi_{vt}}$. FLOW MECHANISM IN WHICH THE LIQUID FLOWS VISCOUSLY AND THE GAS IS IN TURBULENT MOTION

TABLE 4 MAGNITUDES OF THE FUNCTION Φ_{vt}

$\sqrt{\chi_{vt}}$	Φ_{vt}
0	1.00
0.07	2.00
0.10	2.14
0.20	2.46
0.40	2.92
0.70	3.42
1.00	3.85
2.00	5.30
4.00	7.87
7.00	11.3
10.0	14.8
20.0	25.4
40.0	46.0
70.0	75.8
100	105
200	203
400	400
1000	1000
For $\sqrt{\chi_{vt}} > 1000$	$\Phi_{vt} = \sqrt{\chi_{vt}}$

resulting plot of $\alpha^{1/2}$ versus $\sqrt{\chi_{vt}}$ is shown in Fig. 14. The scattering of the data is about the same as in Fig. 10, evidence of a third parameter again being present, but the trend is not conclusive. A single curve was faired through the experimental points, and Φ_{vt} defined by

$$\Phi_{vt} = [1 + \alpha^{1/2}\sqrt{\chi_{vt}}] \quad [31]$$

was calculated. The resulting curve is shown in Fig. 15 and the data are tabulated in Table 4.

Fig. 15 reveals that, again, due to the rapid rise of $\alpha^{1/2}$ at low magnitudes of χ_{vt}, the curve of Φ_{vt} approaches unity slowly. Thus, even at very low liquid rates and high gas rates (walls just wetted) the two-phase pressure drop is increased greatly over that due to the gas phase alone. A small amount of viscous oil flowing along the walls of a pipe ($\sqrt{\chi_{vt}} = 0.10$) may quadruple the pressure drop. The curve of Φ_{vt} versus $\sqrt{\chi_{vt}}$ reaches an asymptote with a slope of unity at high magnitudes of $\sqrt{\chi_{vt}}$.

A plot of the predicted pressure drops versus the measured pressure drops is shown in Fig. 16. The prediction was accomplished by calculating χ_{vt} for the experimental conditions, obtaining Φ_{vt}, and calculating

$$\left(\frac{\Delta P}{\Delta L}\right)_{T-P} = \Phi_{vt}^2\left(\frac{\Delta P}{\Delta L}\right)_g \quad [32]$$

The shape of the experimental curves, shown in Fig. 7, are well predicted by Equation [30]. Fig. 15 was used to calculate the pressure drop along a 1-in. glass pipe in which air and oil *B* were flowing at an average pressure of 14.7 psia and a temperature of 66 F. The predicted curves of pressure drop versus air rate at constant oil rates are shown in Fig. 17 and agree very well with the experimental data of Fig. 7.

It may be concluded that Equation [30], or its equivalent Fig. 15, can be utilized to predict pressure drop in two-phase flow when the gas is flowing with turbulent motion and the liquid with viscous motion. Extrapolation to magnitudes of the variables very much different from those covered by the tests are to be made with caution until the general applicability of the parameter χ_{vt} is tested by further research.

FLOW MECHANISM 3. LIQUID VISCOUS, GAS VISCOUS

Although the type of two-phase flow in which both phases are flowing with viscous motion was not observed in the tests on the 1-in. and $^1/_2$-in. pipe, the analysis of this phenomenon will be presented. Flow of two phases in porous media is of this viscous character, and perhaps an application of the equations which have been developed to this type of problem is possible.

It will be readily seen that Equation [10] is directly applicable to this problem, with the exponent $n = 1$. This substitution yields

$$\left(\frac{D_p}{D_g}\right)^2 = \left(\frac{\gamma_g}{\gamma_l}\right)^{1/2}\left(\frac{\mu_l}{\mu_g}\right)^{1/2}\left(\frac{W_l}{W_g}\right)^{1/2}\frac{1}{\alpha^{1/2}} \quad [33]$$

Substitution of Equation [33] into Equations [12] and [15] results in the equation for pressure drop in two-phase flow when both phases are flowing with viscous motion

$$\left(\frac{\Delta P}{\Delta L}\right)_{T-P} = \left(\frac{\Delta P}{\Delta L}\right)_g\left[1 + \alpha^{1/2}\left(\frac{\mu_l}{\mu_g}\right)^{1/2}\left(\frac{\gamma_g}{\gamma_l}\right)^{1/2}\left(\frac{W_l}{W_g}\right)^{1/2}\right]^2 \quad [34]$$

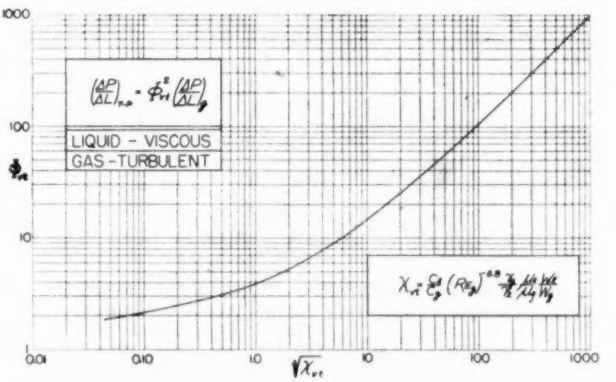


FIG. 15 MODULUS Φ_{vt} AS A FUNCTION OF TWO-PHASE-FLOW MODULUS $\sqrt{\chi_{vt}}$, FOR FLOW MECHANISM IN WHICH THE LIQUID FLOWS VISCOUSLY AND THE GAS IS IN TURBULENT MOTION. THE MODULUS Φ_{vt} MAY BE UTILIZED DIRECTLY TO CALCULATE THE PRESSURE DROP OCCURRING IN TWO-PHASE FLOW

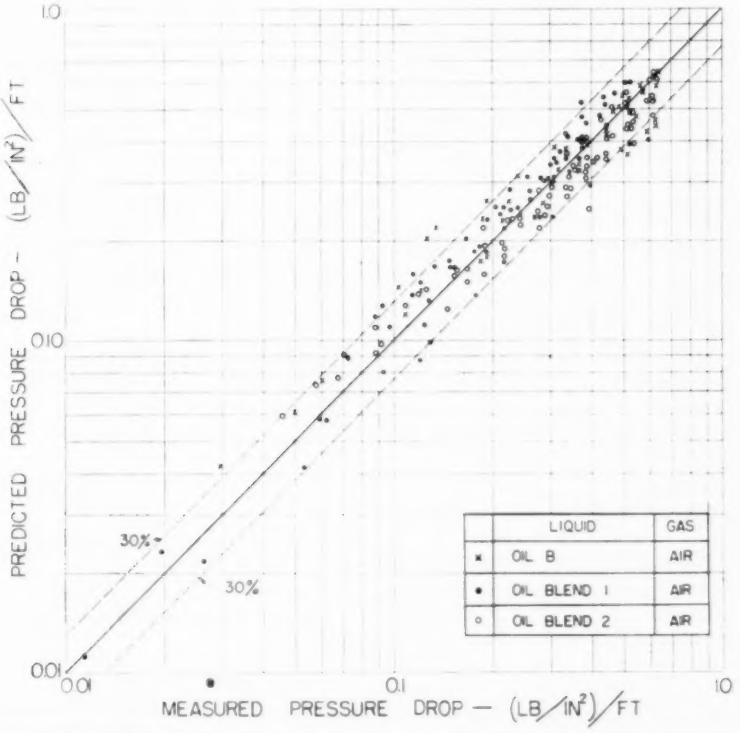


FIG. 16 COMPARISON OF PREDICTED AND MEASURED DROP FOR TWO-PHASE, TWO-COMPONENT FLOW. THE LIQUID FLOWS VISCOUSLY AND THE GAS IS IN TURBULENT MOTION. PREDICTION BY MEANS OF FIG. 15

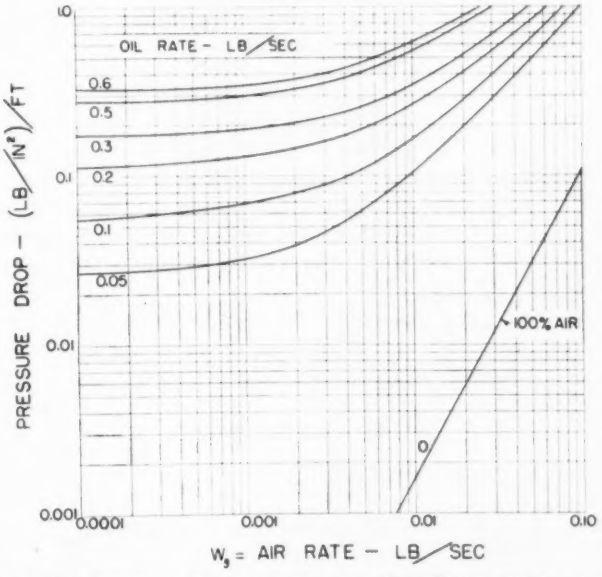


FIG. 17 PREDICTED PRESSURE DROP IN TWO-PHASE FLOW AS A FUNCTION OF FLUID RATES. AIR-OIL B FLOW IN A 1-IN. GLASS PIPE p = 14.7 PSIA, t = 66 F. OIL FLOWING VISCOUSLY, AIR IN TURBULENT MOTION. PREDICTION BY MEANS OF FIG. 15
(Compare with experimental curves in Fig. 7.)

Again $\left(\frac{\Delta P}{\Delta L}\right)_g$ is the pressure drop which would exist if the gas alone were flowing through the pipe of diameter D_p with weight rate W_g and density γ_g. In the case of flow through porous media $\left(\frac{\Delta P}{\Delta L}\right)_g$ would probably be the pressure drop through a given medium for the gas phase flowing alone with a rate W_g.

The function $\alpha^{1/2}$ will probably be correlated by means of the parameter $\chi_{tt} = \left(\frac{\mu_l}{\mu_g} \cdot \frac{\gamma_g}{\gamma_l} \cdot \frac{W_l}{W_g}\right)$.

FLOW MECHANISM 4. GAS VISCOUS, LIQUID TURBULENT

The fourth flow mechanism, in which the gas is flowing viscously and the liquid has turbulent motion, is very unlikely to exist in practice. The solution of this problem would, however, follow in detail the solution for the second flow mechanism, by merely interchanging the exponents of the gas and liquid phases.

CONCLUSIONS

1 There are four flow mechanisms possible in two-phase flow, as follows:

(*a*) Both gas and liquid may flow in turbulent motion.
(*b*) Gas may flow turbulently, liquid viscously.
(*c*) Both gas and liquid may flow viscously.
(*d*) Gas may flow viscously, liquid turbulently.

2 The first two mechanisms have been noted experimentally and have been analyzed macroscopically in this paper. The third type has been analyzed but has not been observed by the authors, although this mechanism undoubtedly exists in practice.

3 Equation [17], or Fig. 11, allows the prediction of two-phase pressure drop for the flow mechanism in which both phases flow with turbulent motion. Equation [17] predicts the experimental pressure drop with a maximum error of about ± 30 per cent.

4 Equation [30], or Fig. 15, allows the prediction of two-phase pressure drop for the flow mechanism in which the liquid is flowing viscously and the gas turbulently. Equation [30] predicts the experimental pressure drop with a maximum error of about ± 30 per cent.

5 Extrapolation of the equations to variables with magni-

tudes which are much different from those tested must be made with caution until the general applicability of the parameters X_{tt} and X_{vt} has been tested by further research.

6 Equation [34] is suggested as the equation to be utilized to predict two-phase pressure drop for the flow mechanism in which both phases are flowing viscously. The relation between α and χ_{vv} is still to be established.

Acknowledgments

The authors wish to thank E. A. Martinelli for many pertinent suggestions on experimental techniques, R. W. Ravenscroft, M. L. Taylor, and R. Guillou for experimental assistance, W. J. Cummings, H. L. Eagles, and J. DeCosta for aid in the construction of the equipment, and J. Rademacher, L. M. Grossman, and G. Young for assistance in computations. The authors also express their gratitude to the Shell Oil Company, Inc., for its 1941 Shell Fellowship, under which some of this work was done, and for the donation of the oils used in the tests.

Appendix 1

In order to illustrate the application of the method outlined in the paper, three examples will be presented. The first is an example of the prediction of the pressure drop in a 2-in. horizontal pipe in which both air and water are flowing at known rates. The second is an example of the calculation of the pressure drop along a 2-in. pipe in which air and an oil are flowing simultaneously. The third example presents a tentative outline for the application of the proposed method to the prediction of the pressure drop along a horizontal tube in which a liquid is being evaporated.

Example 1

It is desired to estimate the pressure drop in 100 ft of 2-in. pipe, in which air is flowing at a rate of 0.50 lb per sec, and water is flowing at a rate of 6 lb per sec. The temperature of the fluids is 77 F and the average pressure in the line is 100 psia.

(*a*) *Determination of properties and type of flow:*

W_g = 0.50 lb per sec
γ_g = 0.502 lb per cu ft at 100 psia and 77 F
μ_g = 0.388×10^{-6} lb-sec per sq ft at 100 psia and 77 F

Reynolds modulus for gas considered as a single phase (Re_g) = 295,000

W_l = 6.0 lb per sec
γ_l = 62.2 lb per cu ft at 77 F
μ_l = 1.87×10^{-5} lb-sec per sq ft at 77 F

Reynolds modulus for liquid considered as a single phase (Re_l) = 73,500

Equation [17] may be utilized since both phases are flowing turbulently.

(*b*) *Calculation of pressure drop due to air alone* = $(\Delta P/\Delta L)_g$:

The usual calculation reveals that the pressure drop resulting from the flow of 0.50 lb per sec of air at 77 F, 100 psia, in a 2-in. pipe is 1.03 psi per 100 ft of pipe. (For the flow of the gas in commercial pipe at Re_g = 295,000 the friction factor (3) is equal to 0.018).

(*c*) *Calculation of* X_{tt}:

$$X_{tt} = \left(\frac{\mu_l}{\mu_g}\right)^{0.111} \left(\frac{\gamma_g}{\gamma_l}\right)^{0.555} \left(\frac{W_l}{W_g}\right) = 1.28$$

(*d*) *Calculation of* Φ_{tt}:

$$\sqrt{\chi_{tt}} = 1.13$$

thus

$$\Phi_{tt} = 4.6 \text{ (Fig. 11)}$$

(*e*) *Calculation of* $(\Delta P/\Delta L)_{T-P}$:

$\left(\frac{\Delta P}{\Delta L}\right)_{T-P}$ = $(4.6)^2$ (1.03) = 21.8 psi per 100 ft of pipe, which is about 21 times the pressure drop for the air alone and 14 times the pressure drop for the water alone. (For the flow of the liquid in commercial pipe at Re_l = 73,500, the friction factor, reference 3, is equal to 0.0232.)

Example 2

It is desired to estimate the pressure drop in 100 ft of 2-in. pipe in which air is flowing at a rate of 0.50 lb per sec, and an oil (whose properties will be given) is flowing with a rate of 0.30 lb per sec. The temperature of the fluids is 77 F and the average line pressure is 100 psia.

(*a*) *Determination of properties and type of flow:*

W_g = 0.50 lb per sec
γ_g = 0.502 lb per cu ft (at 100 psia and 77 F)
μ_g = 0.388×10^{-6} lb-sec per sq ft (at 100 psia and 77 F)

Reynolds modulus for gas considered as a single phase (Re_g) = 295,000

W_l = 0.30 lb per sec
γ_l = 55 lb per cu ft (77 F)
μ_l = 600×10^{-5} lb-sec per sq ft (77 F)

Reynolds modulus for oil considered as a single phase filling the pipe (Re_l) = 11.5.

Since the liquid is in viscous motion and the gas in turbulent motion, Equation [30] must be utilized.

(*b*) *Calculation of* X_{vt}:

$$X_{vt} = \frac{C_l}{C_g} (Re_g)^{-0.8} \frac{\mu_l}{\mu_g} \cdot \frac{\gamma_g}{\gamma_l} \cdot \frac{W_l}{W_g}$$

Take C_l = 64 (see text for discussion)
C_g = 0.216 (for commercial pipe (3), the constant C_g is greater than 0.184 which applies only to smooth pipes)

Then χ_{vt} = 1.07

(*c*) *Evaluation of* Φ_{vt}:

$$\sqrt{\chi_{vt}} = 1.03$$

Thus

$$\Phi_{vt} = 3.9 \text{ (Fig. 15)}$$

(*d*) *Calculation of* $(\Delta P/\Delta L)_{T-P}$:

$$\left(\frac{\Delta P}{\Delta L}\right)_{T-P} = (3.9)^2 (1.03) = 15.7 \text{ psi per 100 ft}$$

Thus, the pressure drop for the two-phase case is about 15 times the pressure drop of the air alone and 15 times the pressure drop due to the oil flowing alone. Comparison of examples 1 and 2 reveals that 0.30 lb per sec of the oil had almost as much effect on the pressure drop as 6 lb per sec of water.

Example 3

It is desired to predict the pressure as a function of distance along a horizontal tube in which evaporation is occurring. If it is assumed that at each section of the tube, the steady-state results discussed in the paper are applicable, the method of procedure is as follows:

(*a*) *Determination of amount of vapor present at any point in tube:*

From a heat balance on an element of tube of length dZ

$$f_c(\pi D_p dZ)\,\Delta t = 3600r\,dW_g \quad \ldots\ldots [1a]$$

Thus

$$W_g = \int_0^Z \frac{\pi f_c D_p \Delta t}{3600r}\,dZ = F_1(Z) \quad \ldots\ldots [1b]$$

Where $F_1(Z)$ represents the pounds of vapor per second flowing at any point Z feet from the entrance to the heating section.

(*b*) *Ratio of W_l/W_g:*

Since the total fluid rate is constant at any point along the tube

$$W_T = W_l + W_g$$

Thus

$$\frac{W_l}{W_g} = \left(\frac{W_T}{F_1(Z)} - 1\right) \quad \ldots\ldots [1c]$$

(*c*) *Pressure gradient of any point Z due to vapor flow alone:*

$$\left(\frac{dP}{dZ}\right)_g = \frac{1}{2}\left(\frac{\pi}{4}\right)^{-1.8} \frac{C_g \mu_g^{0.2} W_g^{1.8}}{g^{0.8}\gamma_g D_p^{4.8}} \quad \ldots\ldots [1d]$$

$$= F_2(Z) W_g^{1.8} = F_2(Z)[F_1(Z)]^{1.8} = F_3(Z) \quad \ldots\ldots [1e]$$

(*d*) *Pressure gradient with two-phase flow:*

From Equation [17] (assuming turbulent flow of both phases)

$$\left(\frac{dP}{dZ}\right)_{T-P} = F_3(Z)\left[1 + \alpha^{1/4}\left(\frac{\mu_l}{\mu_g}\right)^{0.082}\left(\frac{\gamma_g}{\gamma_l}\right)^{0.416}\left(\frac{W_T}{F_1(Z)} - 1\right)^{0.75}\right]^{2.4}$$

$$= F_3(Z)\left[1 + F_4(Z)\left(\frac{W_T}{F_1(Z)} - 1\right)^{0.75}\right]^{2.4} \quad \ldots\ldots [1f]$$

(*e*) *Pressure at any point:*

Integrating Equation [1*f*]

$$P = \int_0^Z F_3(Z)\left[1 + F_4(Z)\left(\frac{W_T}{F_1(Z)} - 1\right)^{0.75}\right]^{2.4} dZ \quad \ldots [1g]$$

The graphical evaluation of Equation [1*g*] is tedious, but not difficult.

Appendix 2

The measured pressure drops for two-phase flow were corrected approximately to standard conditions by the following equation

$$\left(\frac{\Delta P}{\Delta L}\right)_{corr} = \left(\frac{\Delta P}{\Delta L}\right)_{meas}\left[1 + \frac{\left(\frac{\Delta P}{\Delta L}\right)_{meas} - \left(\frac{\Delta P}{\Delta L}\right)_l}{\left(\frac{\Delta P}{\Delta L}\right)_{meas}}\left(\frac{\gamma_m}{\gamma_{std}} - 1\right)\right]$$

where

$\left(\frac{\Delta P}{\Delta L}\right)_{meas}$ = measured two-phase pressure drop for W_l lb per sec liquid, and W_g lb per sec gas

$\left(\frac{\Delta P}{\Delta L}\right)_{corr}$ = two-phase pressure drop corrected to "standard" conditions

$\left(\frac{\Delta P}{\Delta L}\right)_l$ = pressure drop due to W_l lb per sec of liquid flowing alone

γ_m = density of air at conditions of test

γ_{std} = "Standard" air density (66 F and 1 atm)

The points shown on Figs. 2 to 8, inclusive, were corrected to standard conditions by this approximate method.

REFERENCES

1 "Pressure Drop Accompanying Isothermal, Two-Component, Two-Phase Flow in a Horizontal Glass Pipe," by T. H. M. Taylor, M.S. Thesis, University of California, 1942.

2 "Pressure Drop Accompanying Two-Component Flow in a Closed Conduit With Various Liquids and Air," by E. G. Thomsen, M.S. Thesis, University of California, 1941.

3 "Heat Transmission," by W. H. McAdams, McGraw-Hill Book Company, Inc., New York, N. Y., second edition, 1942, p. 119.

4 "Modern Developments in Fluid Dynamics," by Fluid Motion Panel of the Aeronautical Research Committee, edited by S. Goldstein, Oxford Clarendon Press, London, England, vol. 1, 1938, p. 30.

BIBLIOGRAPHY

1 "Pressure Drop Accompanying Two-Component Flow Through Pipes," by L. M. K. Boelter and R. H. Kepner, *Industrial and Engineering Chemistry*, vol. 31, 1939, pp. 426–434.

2 "Vaporization Inside Horizontal Tubes," by W. H. McAdams, W. K. Woods, and R. L. Bryan, Trans. A.S.M.E., vol. 63, 1941, pp. 545–552.

3 "Vaporization Inside Horizontal Tubes—II Benzene-Oil Mixtures," by W. H. McAdams, W. K. Woods, and L. C. Heroman, Jr., Trans. A.S.M.E., vol. 64, 1942, pp. 193–200.

4 "Studies of Heat Transmission Through Boiler Tubing at Pressures From 500 to 3300 Psi," by W. F. Davidson, P. H. Hardie, C. G. P. Humphreys, A. A. Markson, A. R. Mumford, and T. Ravese, presented before A.S.M.E. at the Annual Meeting, New York, N. Y., December 1941 (A.S.M.E. Miscellaneous Papers, no. 45, 1941).

5 "A Method of Determining the Pressure Drop for Oil-Vapor Mixtures Flowing Through Furnace Coils," by F. W. Dittus and A. Hildebrand, Trans. A.S.M.E., vol. 64, 1942, pp. 185–192.

6 "Flow of Steam and Condensation as Affected by High Pressures, Horizontal Offsets and Valves," by L. Ebin and R. L. Lincoln, Trans. A.S.H.V.E., vol. 30, 1924, pp. 323–338.

7 "Supersaturation and the Flow of Wet Steam," by G. A. Goodenough, *Power*, vol. 66, 1927, pp. 466–469 and 511–514.

8 "Supersaturated Steam," by J. I. Yellott, Jr., Trans. A.S.M.E., vol. 56, 1934, FSP-56-7, pp. 411–430.

9 "Critical Velocity of Steam and Condensate Mixtures in Horizontal, Vertical, and Inclined Pipes," by F. C. Houghten, L. Ebin, and R. L. Lincoln, Trans. A.S.H.V.E., vol. 30, 1924, pp. 139–156.

10 "The Co-Current Flow of Liquids and Gases in Pipes," by R. L. Hershey, of E. I. du Pont de Nemours and Co.; paper presented before the Fifth Chemical Engineering Symposium, Division of Industrial and Engineering Chemistry, American Chemical Society at Carnegie Institute of Technology, December 27–28, 1938.

11 "Two-Phase Flow of Fluids Through a Horizontal Pipe," by M. G. Kelakos and A. H. Crowley, Chemical Engineering, S.B. Thesis, Massachusetts Institute of Technology, 1935.

12 "Simultaneous Flow of Water and Air in Pipes," by L. S. O'Bannon, Trans. A.S.H.V.E., vol. 30, 1924, pp. 157–166.

13 "The Flow of Fluids in Two Phases Through a Horizontal Pipe," by H. L. Reichart, Jr., S.B. Thesis, Massachusetts Institute of Technology, 1934.

14 "Flow Resistance of Gas-Oil Mixtures," by L. C. Uren, P. P. Gregory, R. A. Hancock, and G. V. Feskov, *Oil and Gas Journal*, vol. 28, Oct. 3, 1929, pp. 148 and 152.

15 "Hydraulics in Flowing Wells," by J. Versluys, Trans. A.I.M.E., Petroleum Division, vol. 86, pp. 192–204, 1930.

The Differential Shrinkage of Wood

By W. L. GREENHILL,[1] SOUTH MELBOURNE, AUSTRALIA

This paper was prepared originally as discussion of a paper by A. J. Stamm and W. K. Loughborough (1),[2] but because of war conditions was not received until some months after publication of that paper and discussion. The results of shrinkage measurements made with the aid of the microscope on wood samples, consisting of thin radial sections cut entirely from rays, are of such interest that the Wood Industries Division considered their publication advisable. A discussion of the subject paper is also presented by A. J. Stamm and W. K. Loughborough.

THE fact that wood shrinks less in the radial than in the tangential direction is normally attributed to the restraining effect of the medullary rays. However, Stamm and Loughborough (1), mainly from the results of investigations by Ritter and Mitchell (2), state: "There can be no restraining action on the shrinking and swelling of wood in the radial direction by the ray cells." The work referred to consisted of a study of single cells of basswood holocellulose by polarized light, when it was found that the ray cells behaved differently from the fibers. The ray cells showed the same coloration as the fibers when their axes were perpendicular to the fibers, whereas when parallel one type of cell showed blue and the other yellow. It was concluded from these observations and from actual shrinkage measurements on isolated ray cells that rays have a large axial and small transverse shrinkage.

This explanation has already been challenged by Barkas (3), who points out that, in the examination of cells with polarized light, the preponderance of thickness determines the color in the microscope, whereas the strength of the fibrils in the different directions determines the swelling. In other words, the spirally wound fibrils in the primary walls of the ray cells may consist of a very thin layer which does not show in the microscope but which may exert considerable restraint on the lateral expansion of the secondary fibrils.

The use of shrinkage measurements on isolated fibers would in itself appear of doubtful value when applying the results to groups of fibers. To overcome this objection, shrinkage measurements have recently been made by the author on thin radial sections cut entirely from rays. In size these were up to 1/2 in. square and measurements were made with a microscope. Normal tangential and radial shrinkage values were determined for the same wood samples from thin cross sections. The results obtained are given in Table 1.

These results completely substantiate those of Clarke (4), and justify his conclusion that the axial shrinkage of the rays is less than the radial shrinkage of the wood as a whole, but that their transverse shrinkage is much greater than the longitudinal shrinkage of the wood as a whole. The evidence available thus appears to throw considerable doubt on Ritter's and Mitchell's conclusions. On the other hand, although the shrinkage of the rays axially is almost certainly less than the radial shrinkage of the wood as a whole, and therefore that the rays exert a restraining effect is indisputable, there is also some indication that, even without the restraining effect of the rays, radial shrinkage would still be less than tangential. To demonstrate this experimentally, shrinkage measurements have been made on small samples of three *Casuarina* species, some samples containing a normal proportion of the prominent rays in these species and some being prepared free from all but uniseriate rays. The results obtained, which are given in Table 2 show that by eliminating the large rays there is a definite increase in the radial shrinkage, but on the other hand an even greater increase would have been expected had the rays been solely responsible for the difference between the normal tangential and radial shrinkages.

TABLE 1 SHRINKAGE MEASUREMENTS ON THIN RADIAL SECTIONS

(Soaked to oven-dry; per cent soaked dimensions)

Species	Tangential[a]	Radial[a]	Longitudinal[a]
Casuarina luehmanni:			
Normal cross section	11.9	3.3	0.14
Rays	...	1.2	4.8
Grevillea robusta:			
Normal cross section	9.5	3.7	0.08
Rays	...	1.2	5.7
Xylomelum pyriforme:			
Normal cross section	8.0	2.0	0.17
Rays	...	0.7	1.8
Quercus sp:			
Normal cross section	9.2	4.9	0.32
Rays	...	3.2	3.5

[a] Actual directions in tree in all cases.

TABLE 2 SHRINKAGE MEASUREMENT ON CASUARINA SPECIES

(Soaked to oven-dry; per cent soaked dimensions)

Species	Tangential	Radial
Casuarina cunninghamii:		
Normal	10.6	2.6
Free from large rays	10.8	3.9
Casuarina torulosa:		
Normal	9.0	2.0
Free from large rays	9.1	5.0
Casuarina luehmanni:		
Normal	11.9	3.3
Free from large rays	12.0	4.3

Possible factors in addition to the ray cells which may be responsible for the differential shrinkage are as follows:

1 The presence of a greater number of pits on the radial than the tangential faces of the fibers, resulting in the fibrils on the radial faces being less perfectly oriented than on the tangential faces. This explanation, according to Stamm and Loughborough (1) is due to Ritter and Mitchell (2), although nothing to this effect can be found in the reference given.

2 The effect of bands of wood of varying density, such as early and late wood or wide bands of parenchyma adjacent to bands of normal wood fibers. This explanation is suggested by Frey-Wyssling (5).

Collapse

An explanation of the excessive and irregular shrinkage known as collapse was first given by Tiemann (6). His "liquid-tension" theory has been generally accepted and satisfactorily explains the phenomenon and its effects, although some criticism of the theory has been made from time to time. The alternative "stress" theory propounded by Stamm and Loughborough certainly cannot be accepted without question as the main cause of collapse, but on the other hand it is quite probable that drying stresses assist in producing collapse. Some of the evidence which

[1] Officer in Charge, Physics Section, Division of Forest Products' Council for Scientific and Industrial Research, Commonwealth of Australia.

[2] Numbers in parentheses refer to the Bibliography at the end of the paper.

Contributed by the Wood Industries Division for presentation in the Transactions of The American Society of Mechanical Engineers.

Note: Statements and opinions advanced in papers are to be understood as individual expressions of their authors and not those of the Society.

favors the liquid-tension theory and which appears to have been overlooked by Stamm and Loughborough is as follows:

1 The fact that the presence of air prevents the occurrence of collapse, according to the tension theory, can be used to demonstrate the validity of this theory. Using two matched samples of green timber of a species subject to collapse, such as mountain ash (*Eucalyptus regnans*), carefully air-dry one of the samples so that the "free" water is removed from the cells. This sample should then be thoroughly soaked until its moisture content is at least as high as that of the green sample which, incidentally, should be kept green meanwhile. Both samples should now be dried at a temperature of about 140 F and a relative humidity of 80 per cent, conditions which favor collapse. It will be found that collapse occurs to a much greater extent in the green than in the resoaked piece. The reason for this is that in the soaking after drying, the entrapped air in the cell cavities is removed completely only with great difficulty so that very few of the cells become liable to collapse. In the original green condition a considerable number of the cells may, quite conceivably, be completely filled with water. Furthermore, it is found that any trees of such species as mountain ash, with an unusually high green-moisture content are particularly liable to collapse.

2 The statement by Stamm and Loughborough (1) that collapse is not randomly distributed throughout the wood but is located in the central zone under compression shows a lack of knowledge of even the appearance of timbers which collapse. Indeed one of the most usual features of collapse is its extremely irregular nature. The effect of the collapse of a cell is not, of course, shown in an isolated cell, as it is not possible without disruption of the fibers, for one cell to collapse without distorting those cells surrounding it. However, the most logical explanation of the variation in the degree of collapse in different portions of a board is surely the random distribution of areas of collapse-producing cells.

3 By cutting successive cross sections of a piece of wood of a species such as mountain ash, starting with sections about $^1/_4$ in. thick and gradually reducing the thickness it will be found that on drying the sections the tangential and radial shrinkages gradually decrease with decrease in thickness. However, this does not continue indefinitely and for thicknesses below about 0.05 in., the shrinkage is constant. Tests of this nature, made on various species, have been reported previously (7), and it has been shown that the thickness at which the shrinkage becomes constant bears a fairly constant ratio (1.6–1.8) to the fiber length. At such a thickness the great majority of the fibers would be cut at one end, evaporation of the free water could then proceed from this end, and internal tensions would not be possible.

A similar effect suggested by Tiemann can be observed by cutting a wedge-shaped sample of green wood tapering from a fine edge to 5 or 6 times a fiber length in the grain direction. On drying such a sample under conditions producing collapse, it will be found that the thin end shrinks uniformly, but where the thickness has increased to about $1^1/_2$ fiber lengths, the shrinkage becomes much greater and irregular in nature. No convincing explanation of this behavior seems possible from a consideration merely of simple drying stresses.

BIBLIOGRAPHY

1 "Variation in Shrinking and Swelling of Wood," by A. J. Stamm and W. K. Loughborough, Trans. A.S.M.E., vol. 64, 1942, pp. 379–386.

2 "Crystal Arrangement and Swelling Properties of Fibers and Ray Cells in Basswood Holocellulose," by G. J. Ritter and R. L. Mitchell, *Paper Trade Journal*, vol. 108, Feb. 9, 1939, pp. 33–37.

3 "Wood Water Relationships-VI the Influence of Ray Cells on the Shrinkage of Wood," by W. W. Barkas, Trans. Faraday Society, no. 246, vol. 37, 1941, pt. 10, pp. 535–547.

4 "The Differential Shrinkage of Wood," by S. H. Clarke. *Forestry*, vol. 4, part 2, Dec., 1930, pp. 93–104.

5 "Die Anistropie des Schwindmasses aus der Holzquerschnitt," by A. Frey-Wyssling, *Holz als Roh und Werkstoff*, vol. 3 (2), 1940 pp. 43–45.

6 "Principles of Kiln Drying," by H. D. Tiemann, part 1, *Lumber World Review*, January 25, 1915.

7 "The Shrinkage of Australian Timbers, Part I—A New Method Determining Shrinkages and Shrinkage Figures for a Number of Australian Timbers," by W. L. Greenhill, Australian Council for Scientific and Industrial Research, pamphlet no. 67, 1936.

Discussion

A. J. Stamm[3] and W. K. Loughborough.[4] Ritter and Mitchell (2),[5] as a result of their optical and swelling measurements, concluded that "they (the ray cells) at least have a less restraining effect on radial swelling of wood than was previously believed." The author's data lead to the same conclusion. The matter of controversy thus rests on the degree to which ray cells can restrain radial swelling.

The author's data for the swelling of sections made up entirely of rays, show a swelling in the radial direction of the tree ranging from one third to two thirds of the swelling of the wood as a whole in the same direction. Ritter's and Mitchell's data (2), on the other hand, show a smaller difference between the swelling of individual ray cells and the wood as a whole in the same direction. These differences may be due to species differences, differences between measurements on single ray-cell fibers and ray-cell bundles, or differences in technique. In any case, the author's data indicate that the ray cells swell quite differently in their longitudinal direction (radial direction in the tree) from the longitudinal swelling of tracheids (10 times as much). This difference is explained by Ritter's and Mitchell's optical measurements.

Ritter and Mitchell recognize the fact that thickness of section in their optical measurements does affect the color to some extent. They have, however, taken this into consideration in drawing their conclusions. Their explanation of the retardation of radial swelling of wood by the pits did not, as the author states, appear in the article referred to. It appears elsewhere.[6]

The effect of pits on the swelling and shrinking will explain the differences obtained by the author between the radial swelling of normal wood and wood free from large rays. It is known that tracheids tend to end chiefly at junctions with ray cells and that the pits are more highly concentrated near the ends of tracheids. The tracheids of sections relatively free from ray cells will thus tend to have less pits on their surfaces and, as a result, will show a smaller swelling restraint along their radial walls.

Hence the writers feel that, on the basis of both the author's data and those of Ritter and Mitchell, the old concept of the ray cells furnishing the major restraint to radial swelling is not substantiated.

Collapse. Here again the controversy rests on a matter of differences in the extent to which two different mechanisms are effective in causing a certain phenomenon, rather than a complete difference in the mechanism. We believe that collapse in some cases is due to liquid tension, but in the case of North American

---

[3] Principal Chemist, Forest Products Laboratory, Forest Service, U. S. Department of Agriculture, Madison, Wis.

[4] Senior Engineer, Forest Products Laboratory, Forest Service, U. S. Department of Agriculture, Madison, Wis.

[5] Numbers in parentheses refer to the Bibliography at the end of the paper.

[6] "Structural Factors Contributing to the Directional Shrinking and Swelling of Wood," by G. J. Ritter and R. L. Mitchell, unpublished report of the Forest Products Laboratory, U. S Department of Agriculture, March, 1941.

woods, with which we are familiar, we feel that collapse is more frequently due to stresses than to a liquid tension. We include in our definition of collapse all cases where the shrinkage is abnormally high in contrast to some who consider that collapse has taken place only when groups of fiber cavities have completely caved in. Part of the difference of opinion as to the importance of the two forms of collapse rests on these two different definitions.

The author cites an experiment in which wood subject to collapse is carefully air-dried to remove free water and let air into the structure. Free water, however, cannot be removed from fibers which meet the requirements for liquid-tension collapse without causing the fibers to collapse. If air is admitted without collapse occurring, it is due to the fact that some air existed in the fiber cavities. In either case, stresses are set up during the initial drying. Decreased shrinkage after resoaking and again drying could be due either to a decrease in liquid-tension collapse, as maintained by the author, or to a decrease in stress collapse, as described in the writer's paper (1).

Experiments have been made at the Forest Products Laboratory in which sodium carbonate is allowed to diffuse into green blocks of wood, followed by the diffusion of acid into the structure to liberate carbon dioxide. This pretreatment did not reduce collapse when the block was dried under collapsing conditions. On the basis of the liquid-tension theory, the presence of gas in the cells should have eliminated collapse.

The writers have also made measurements on thin cross sections of wood. Under favorable drying conditions, it is true that collapse is decreased, but it is not eliminated as it would be if it were entirely due to liquid tension. The fact that the amount of collapse occurring in such sections can be varied appreciably under different drying conditions, makes us feel that it is largely due to stresses even in such sections. The existence of stresses in these thin sections can be observed by the way free water is first removed around the edges, giving a circular wet zone on the surface of each of the faces.

Collapse of the readily visible extreme type, we appreciate, may be somewhat randomly distributed, due to conditions for liquid-tension collapse, or due to groups of cell walls which have abnormally low compressive strengths. From our experience, however, the general decrease in fiber-cavity sizes seems to be chiefly concentrated in compression zones.

The writers wish to emphasize that the chief object of the latter part of their paper (1) was to point out that all collapse is not due to liquid tension, as so many believe, and that it can be logically explained on the basis of stresses. It is believed that the stress theory is more generally applicable than the liquid-tension theory.



ADVANCED-TRAINING PLANE, THE FAIRCHILD AT-21

Problems of Construction and Alternate Substitutions in Wood Aircraft

BY J. M. STEVENS,[1] HAGERSTOWN, MD.

Some of the problems coincident with the greatly expanded use of wood and plywood in aircraft construction are discussed in this paper. A greater use of certain approved alternate wood species in place of spruce and other critical aircraft materials is advocated. Several specific examples of what can be accomplished in the way of simplifying and standardizing the construction of flat and molded plywood constructions are presented.

WITH the advent of the present world conflict the demands made upon wood and plywood for use in aircraft manufacture have increased tremendously. As a result, these materials, first considered as noncritical, can now be considered only as less critical. In some instances they cannot be obtained at all in the quality and quantity required for our strategic offensive effort.

The magnitude of the demands that are being made upon the aircraft industry can be more readily understood when we recall President Roosevelt's speech made in the spring of 1940, in which he announced that the United States was going to produce 50,000 airplanes a year. This figure was subsequently boosted to 125,000 a year. It was soon apparent that our aluminum supply was not adequate to meet these requirements, so immediate plans were made for the expansion of our aluminum-producing facilities. In the meantime, manufacturers of light aircraft were requested to use nonstrategic materials wherever possible. As a result wood, in either laminated or plywood form rapidly gained a position of paramount importance in aircraft manufacture.

WOOD APPLIED SUCCESSFULLY TO TRAINING PLANES

One of the outstanding examples of the successful use of wood in aircraft construction is in the primary-training field, a typical example of which is the Fairchild designed PT-19.

The wings are constructed of two built-up spars with thin face-plating, and the ribs are constructed of square spruce capstrips reinforced by three-ply mahogany plywood gussets at all corners and joints. The outer wing covering is made of two sections of $^3/_{32}$-in. mahogany plywood with poplar core. This three-ply plywood is preformed to conform with the shape of the leading edge, and the bottom is flat, the two sections being joined at the trailing edge.

At present the rear cowling deck, formerly made of metal, is constructed of light veneers bonded by the Duramold process. Covers for the gas tanks on the underside of the center section formerly of aluminum alloy are also now made of wood. The

[1] Wood Technologist, Engineering Dept., Fairchild Aircraft.

Contributed by the Wood Industries Division and presented at the Spring Meeting, Davenport, Iowa, April 26–28, 1943, of THE AMERICAN SOCIETY OF MECHANICAL ENGINEERS.

NOTE: Statements and opinions advanced in papers are to be understood as individual expressions of their authors and not those of the Society.

flaps which on the first production models were made of aluminum alloy, are now constructed of plywood.

These PT-19's, have withstood hundreds of thousands of hours of grueling flight-training work under many climatic conditions. In most cases hangar facilities are not sufficient to house all these aircraft every night, and a large percentage must be left to the mercy of the elements. Even under such extreme conditions, very encouraging service reports have been obtained.

The Fairchild AT-21, a two-engined trainer announced recently, is another example of how wood is being used successfully to meet the expanding training requirements of the AAF. The Beech AT-10 is similar in size while the Curtiss C-76 cargo plane, contract now canceled, was to have been many times larger.

It can be readily seen that as the size of wooden airplanes is increased the quantities of wood required to construct them is also proportionately increased. For example, 220 fbm of spruce lumber are required to construct the PT-19 airplane, whereas 1260 fbm are required to construct the AT-21 airplane. On the plywood side of the bill of material, a comparison shows 850 sq ft of plywood used for the PT-19, 3000 sq ft for the AT-21, while an estimated 12,000 sq ft would have been required for the C-76 cargo. When volume is taken into consideration, these plywood differences may become even greater. In 1942, the aircraft industry used 6,000,000,000 fbm of aircraft plywood. In view of the trend to more and larger types of wood aircraft, it can be expected that in 1943 the production of aircraft-grade wood and plywood will have been doubled in order to meet production schedules.

Coincident with this rapid expansion in number and size of wooden airplanes has been the problem of procuring material in sufficient quantity that would meet AN specifications. Supposedly inexhaustible supplies of aircraft woods simply were not available. The chief contributing factor to this situation is that only the very best quality of wood can be used in aircraft construction. This limits the quantity suitable for aircraft use to a very small percentage of actual production. In addition, there is a shortage of precision milling equipment that can cut to the varied and peculiar demands of the aircraft industry; service demands plus the lure of better paying defense jobs have created a shortage of skilled woods labor; there are not sufficient lumber kilns and veneer driers to maintain rapid delivery schedules. Aircraft grades are practically always cut to special order and rarely, if ever, are carried in stock by producing sawmills. This is due to the highly specialized nature of such grades and the wide ranges of sizes and lengths required by various aircraft manufacturers. Also, there has been a lack of specific information on potential sources of supply for these aircraft grades of lumber and veneer.

Wood Fabrication Problems

In 1941, the production of Douglas fir lumber was 8,000,000,000 ft or a weekly average production of 150,000,000 ft; 1942 production was the same. In contrast, the 1941 production of Sitka spruce lumber was only 1,300,000,000 or a weekly average of 25,000,000 ft which by 1942, had dropped to 7,000,000 ft, a decrease of over 350 per cent. Further, according to the West Coast Lumberman's Association, not over 1 per cent of fir is going into aircraft production at the present time, but probably another 3 or 4 per cent now going into pontoon lumber, ship decking, and so on, would meet aircraft specifications. The Forest Product's Laboratory estimates that only 2 per cent of fir lumber and 5 to 6 per cent of spruce will meet aircraft specifications.

TABLE 1 FIR AND SPRUCE AVAILABLE FOR AIRCRAFT PRODUCTION

	Average weekly production fbm	Aircraft grade per cent	Average weekly amount available aircraft fbm	Rating (spruce 100)
Spruce.....	7,000,000	5	350,000	100
Douglas fir.....	150,000,000	2	3,000,000	860

Taking 2 per cent of the present production of fir and 5 per cent of the present production of spruce as representative averages of the foregoing data, the amounts available for aircraft use are given in Table 1.

Because spruce combines the qualities of lightness, great strength, and stiffness per unit of weight, and also a considerable degree of toughness, it has always been of great value in the manufacture of wood airplanes where just such qualities are demanded. It is now chiefly used in the construction of spars for wings, bulkheads and stringers for fuselages, and so on, which parts are usually made of solid or laminated spruce in preference to other species.

Faced with a declining spruce production, it became apparent as early as 1940 that there would not be sufficient high-quality aircraft spruce to meet the requirements of an expanding aircraft industry. At that time three possible solutions to the problem were investigated by the Civil Aeronautics Authority, as follows:

1 A possible broadening of the interpretation of current spruce specifications by establishing a mechanical method of judging the quality of the basic material and a more intelligent judging of the weakening effects of surface defects.

2 The use of varying thickness and short-length material through laminating and splicing.

3 The use of substitute material.

That the first method is still a subject of much controversy is evidenced from the report of a meeting held at Longview, Wash., February 26, 1943, and at Chicago, Ill., October 13, 1943, to discuss the problems involved in the inspection of aircraft lumber. At this meeting were representatives of the War Production Board, West Coast Lumberman's Association, West Coast Bureau of Lumber Grades and Inspection, Pacific Lumber Inspection Bureau, Army Air Force, U. S. Dept. of Agriculture, manufacturers of aircraft lumber, and interested aircraft manufacturers. (A discussion of their findings is not considered pertinent at this time since this paper is chiefly concerned with the last method.)

The second method, permitting the use of short lengths and narrow widths, has been in effect with most companies for some time; for example, laminations are being made of pieces edge-glued together to obtain a given width with the restriction that edge joints in adjacent laminations shall be not closer than the thickness of the lamination. Short lengths are joined by scarf joints provided that the slope is not steeper than 1 in 15 for softwoods or 1 in 15 for hardwoods.

Authority Given to Use Alternate Woods for Spruce

By so doing, the available supply of aircraft-grade spruce was greatly increased. However, a critical shortage still appeared imminent, so in June, 1942, wood-aircraft manufacturers were advised that certain alternate woods could be used in place of spruce without change in design. The alternate woods suggested were western hemlock, noble fir, and yellow poplar.

It was soon discovered that the lumber industry was not prepared to supply these alternate woods in the quality called for in AN specifications. Some of the reasons for this situation have already been outlined. The following month (July, 1942) Port Orford cedar, Douglas fir, Southern cypress, Alaska cedar, and Norway pine were also given approval as direct substitutes for spruce without change in design. However, spruce continued to be available, whereas the alternates were not.

In September, 1942, the use of Douglas fir was again recommended specifying normal Douglas fir with a specific gravity range of not less than 0.45. This was followed by an announce-



THE FUSELAGE SHELL, WINGS, TAIL SURFACES, AND MANY OTHER PARTS OF THE AT-21 ARE OF PLYWOOD CONSTRUCTION

ment, made in January, 1943, of a new classification of Douglas fir known as light Douglas fir, having a specific gravity of 0.38 to 0.47. As this latter class requires special selection and is therefore limited in quantity, its use has been restricted to certain types of wood aircraft. Latest information indicates that sufficient quantities of aircraft spruce, noble fir, western hemlock, and yellow poplar will be available to meet scheduled production requirements.

Thus it can be seen that, with the decline in the supply of aircraft spruce, the problem of what woods can or cannot be used as alternate materials has assumed ever greater importance. This is particularly true in the case of subcontractors, most of whom are having their first experience in aircraft construction and are frequently experiencing considerable difficulty in obtaining specified materials. In an attempt to clarify this somewhat confused situation a "Wood and Glue Alternate and Substitution Chart" was prepared by the author's company.

On this chart are listed all woods commonly used in aircraft construction. In one section are listed all alternates that may, without specific engineering approval, be used as replacements for the material specified on the drawing. In the second section is another group, classed as "substitutes," no one of which may be used as a replacement for the material specified on the drawing without specific engineering approval. Similar procedure has been adopted to aid in the proper selection and use of synthetic-resin adhesives. The current specifications are listed in order to provide an exact means of quality control.

In the preparation of this chart weight or specific gravity was the most important controlling factor in making each choice. Ease of working was also given consideration. As the availability of a given material cannot readily be determined and may change from day to day, this aspect was not considered pertinent in the analysis.

Weight is extremely important in all aircraft construction. For example, a complete change from spruce to western hemlock without any change in design would increase the weight of the PT-19 airplane by approximately 21 lb and the AT-21 airplane by approximately 92 lb. This is not overly serious. However, a complete change to Douglas fir (normal type) would increase the weights of these two airplanes by 70 and 294 lb, respectively. For this reason, Douglas fir cannot be considered as a desirable substitute for spruce without changes in design. Once an airplane is in production, any change in design is costly and time-consuming and should be avoided wherever possible.

PLYWOOD CONSTRUCTION PROBLEMS

Until quite recently, only a few woods, notably mahogany and poplar, were considered to be entirely satisfactory for flat and molded aircraft plywood constructions. Birch veneer has been used extensively for highly stressed plywood parts and for parts subject to excessive abrasion or wear. Other woods commonly but not extensively used for aircraft veneer are spruce, sweet gum, walnut, Douglas fir, and basswood.

The problems of veneer procurement and large molded-shell manufacture have long been complicated by the use of veneers under $^1/_{32}$ in. in thickness. Very flat veneers are required in the molding processes to permit accurate edge-fitting and fast laying of the veneer strips that are used to make up the large fuselage shells. Both gapping and overlapping which result from poor fitting subject these shells to extensive rework and occasionally to rejection. When veneers intended for layup into shells of simple curvature become buckled they cannot be joined and spliced successfully in the Diehl machines made for this purpose.

When veneer is cut and dried to $^1/_{48}$-in. thickness, only approximately 10 per cent of the total mahogany aircraft-veneer output, 7 per cent of the sliced-poplar aircraft-veneer output, and 3 per cent of the birch aircraft-veneer output are of suitable flatness for Duramold work. Use of any veneer other than flat stock results, as noted, in rework and rejection coupled with an increase in layup time ranging from 50 to 100 per cent. By increasing the cut thickness to $^1/_{32}$ in., it was found that approximately 25 per cent of the dried aircraft mahogany veneer, 20 per cent of the sliced-poplar veneer, and 10 per cent of the birch veneer could be efficiently utilized for Duramold work. This increase results from the following: (1) the thicker veneer, being stiffer, will remain flat when subjected to internal stresses developed during cutting and drying that would buckle a thinner veneer; (2) most modern veneer driers are so constructed that

they will flat-dry good veneer down to $^1/_{32}$ in. thick at a reasonable percentage of full capacity; full capacity being achieved when handling $^1/_{28}$-in. or thicker veneers. In order to get comparable results with $^1/_{48}$ in.-thick veneer, it is necessary to cut the drier capacity to 25 to 30 per cent of its total. In these times, veneer companies are unwilling to do this for even a 50 per cent premium.

Another factor, apart from that of thickness and flatness, complicating the present veneer situation, is the rapidity with which the various kinds of veneer fluctuate from noncritical to critical and back again. Several months ago mahogany appeared to be scarce, poplar and birch abundant. Today mahogany appears to be relatively plentiful, birch seems practically nonexistent, and poplar is very scarce. All veneer and plywood manufacturers are experiencing these difficulties, so these shortages can in no sense be considered as merely local.

Douglas fir and red gum provide two specific examples of procurement difficulties coincident with the manufacture of aircraft plywood. Douglas fir is only acceptable when quarter-sliced because vertical-grain fir veneer has more uniform strength properties than does rotary-cut veneer. Also, $^1/_{16}$ in. is about the usual minimum thickness that can be rotary-cut. As only three mills in the Pacific Northwest are equipped with slicing equipment, logs intended for aircraft veneer have to be shipped to the Midwest for processing. Red-gum veneer can be either sliced or rotary-cut but here again the rotary lathes located at the source of supply cannot cut aircraft veneers in quantity to the tolerances allowed, so it also becomes necessary to process these logs in the Midwest.

A third problem in the use of plywood has been, in the past, the lack of standardization of specifications. An example in point was the original Army and Navy plywood specification AN-NN-P-511 which did not specify the exact thicknesses of veneers that should be used in any given flat-plywood construction. This has since been corrected by revision "b" of this specification which calls out the exact thickness of faces, cross-bands, and cores for all standard aircraft plywood. These sizes are shown as decimal equivalents based on the kiln-dry-veneer thickness and will run slightly less than those given in the Wood Aircraft Fabrication Manual which are based on the green-veneer thickness.

Advantages of Standardization

To comply with a recent request of the Army Air Forces, who are attempting to increase production of plywood an estimated 80 per cent by standardization of veneer thicknesses and plywood constructions, and also to satisfy numerous and repeated requests from production departments, a detailed study was made of the plywood requirements of the AT-21 airplane with a view toward simplification of construction and species requirements wherever structurally possible. Such a study was made and the data prepared in chart form. Similar plywood charts have been prepared for other airplanes manufactured by the author's company.

In this chart, the plywood-construction preferences listed are based upon the following factors:

1 Minimum use of veneers under $^1/_{32}$ in. thick.
2 Adherence to standard veneer thicknesses.
3 Proper balance of finished plywood.
4 Availability of material.
5 Application to which material is put.
6 The use of over-all thicknesses and constructions that would give approximately the same strength as the original.

All-mahogany constructions have been given first preference in this chart. This reflects the relative ease of working and, apparently, of procuring this kind of veneer at this time as contrasted with the present scarcity of poplar. To offset to some extent the fluctuating supply of poplar, and to supplement the approved list of substitutes for poplar, it was recommended, wherever feasible, that the all-mahogany constructions be given preference over the mahogany-poplar constructions.

A detailed study, substantiated by test data on the fuselage assemblies, indicated that these simplified plywood constructions would offer the following advantages:

1 A net over-all decrease in weight on the airplane ranging from 9 to 19 lb, without any sacrifice in strength at highly stressed areas.

2 The procurement of satisfactory veneer would be simplified and use of critical material substantially reduced.

3. The time of layup and amount of glue (Tego film) used per unit would be materially reduced.

4 Production time per unit would be correspondingly decreased, thereby permitting the manufacture of more units than is now possible.

On this chart, in addition to the simplified plywood constructions, there is also an alternate and substitution chart for veneers. This is made up in the same manner as the wood chart previously described.

To check the comparative strengths of all the recommended alternate constructions, a series of tests was conducted of the various plywoods considered.

The results which follow are based upon comparative tests made from sample test panels constructed on a flat die by the bag-molding method. Process conditions were identical with those used in the manufacture of full-size shells. All veneers of a given thickness were taken from the same flitch in order that the variables inherent in tests of a nonhomogeneous material such as wood might be reduced as much as possible. It can be assumed therefore that the test results shown are reasonably indicative of what could be expected from any given Duramold shell.

Scope and Method of Testing Plywood

Tension Tests. Tests were made to determine the tensile strength of each plywood construction both parallel and perpendicular to the grain of the faces. Specimens 1 × 5 in. were used, with the center portion trimmed down to $^1/_2$ in. diam (radius $4^3/_4$ in.). The specimens were held by ordinary flat grips and tested in direct tension to rupture in a Riehle plywood-testing machine.

Shear Tests. Shear tests were made in the standard picture-frame-type shear-test fixture used by the Forest Products Laboratory. In all tests, face grain direction was either parallel (0 deg) or perpendicular (90 deg) to the direction of load.

Bending Tests. Bending tests, using strips of plywood 1 × 12 in. long, were used to obtain the modulus of rupture and the modulus of elasticity. Each plywood construction was tested in cross-bending as a simple beam. Bolts of $^1/_4$ in. diam mounted in roller bearings were used as end supports. This eliminated the effect of friction as the specimen bowed under load. Loads were applied by adding shot, in $2^1/_2$-lb increments, to a small container suspended from the center of the test specimen. Deflections at each increment of load were obtained from a Starrett gage, mounted directly over the point of application of load. Face-grain direction was either parallel (0 deg) or perpendicular (90 deg) to the long axis of the test specimen.

Summary of Test Data

Tables 2 and 3 summarize details of the test results. In these tables strengths have been averaged on both a pounds-per-square-inch and a total-load basis. The percentage comparison

TABLE 2 FRONT FUSELAGE; STRENGTH AND ELASTIC PROPERTIES

Plywood construction	M.C. at test, per cent	Ultimate strength in tension 0°	Ultimate strength in tension 90°	Ultimate strength in shear 0°	Ultimate strength in shear 90°	Static bending M R 0°	Static bending M R 90°	Static bending M E (× 1000) 0°	Static bending M E (× 1000) 90°
(a) Comparison on Basis of Strength, psi									
Present 9 ply.....	3.4	6850 (11)	6960 (12)	3560 (1)	2915 (1)	8520 (3)	4750 (3)	980 (3)	580 (3)
Revision (1) 7 ply...	5.0	6770 (10)	6380 (10)	3415 (1)	3070 (1)	8870 (3)	5800 (3)	1042 (3)	537 (3)
Revision (2) 7 ply...	3.5	6300 (11)	6350 (11)	3310 (1)	2880 (1)	8490 (3)	6430 (3)	1050 (3)	611 (3)
(b) Comparison of Actual Test Values,[a] lb									
Present 9 ply.....	3.4	740	740	8250	6750	29.61#	18.63#	...	..
Revision (1) 7 ply...	5.0	760–103%	720–97%	8500–103%	7650–113%	35.89–121%	23.43–140%	...	..
Revision (2) 7 ply...	3.5	722–97%	720–97%	8575–104%	7470–111%	36.15–122%	27.38–162%	...	..

TABLE 3 REAR FUSELAGE; STRENGTH AND ELASTIC PROPERTIES

Plywood construction	M.C. at test, per cent	Ultimate strength in tension 0°	Ultimate strength in tension 90°	Ultimate strength in shear 0°	Ultimate strength in shear 90°	Static bending M R 0°	Static bending M R 90°	Static bending M E (× 1000) 0°	Static bending M E (× 1000) 90°
(a) Comparison on Basis of Strength, psi									
Present 8 ply.....	3.4	6490 (13)	4650 (11)	2605 (1)	2515 (1)	8480 (3)	7580 (3)	976 (3)	602 (3)
Revision (1) 5 ply...	5.6	6590 (22)	6340 (34)	3010 (1)	2460 (2)	7680 (3)	5910 (6)	1059 (3)	480 (6)
(b) Comparison of Actual Test Values,[a] lb									
Present 8 ply.....	3.4	590	425	5190	5000	22.02 #	18.93#	...	..
Revision (1) 5 ply...	5.6	620–105%	610–143%	5610–108%	4970–99%	20.75–94%	15.64–83%	...	..

[a] Specimens identical except for differences in thickness.
NOTE: Numbers in parenthesis indicate numbers of tests made.

made on the basis of total load is more applicable to this type of analysis since the thicknesses of the alternates are not always the same as those of the original constructions.

The alternate plywood constructions shown in Tables 2 and 3 were found to be acceptable from the standpoints of balance and strength. A proposed revision (2) for the rear uselage, also a 5-ply construction, and several proposed revisions for the outer wing panel, substituting 3-ply for 5-ply, were tested but were not considered acceptable, and were therefore not given further consideration.

Analysis of Strength Data

(*a*) *Front Fuselage.* Tests at 45 deg grain direction were not considered necessary in tension, compression, and shear, because in a balanced plywood construction these results would be directly proportional to those obtained at 0 deg and 90 deg. Inspection of test results for revisions (1) and (2) show that both alternate constructions are balanced in tension parallel and perpendicular to the grain and are equivalent in actual tensile strength to the original. Shear and bending strengths are higher as are the moduli of elasticity (based upon pounds per square inch) except for revision (1), an all-mahogany construction which at 90 deg, is 7 per cent lower. It was concluded that both revisions could be considered as entirely satisfactory replacements for the present construction.

(*b*) *Rear Fuselage.* A comparison of actual test values between the present construction and proposed revision (1) shows that the 5-ply construction is better balanced in tensile strength parallel and perpendicular to the grain and considerably stronger, particularly perpendicular to the face grain. Shear strength at 0 deg and 90 deg, and modulus of rupture at 0 deg are equivalent to the present constructions. The modulus of elasticity at 0 deg is somewhat higher owing to the thicker face plies.

Both modulus-of-rupture and modulus-of-elasticity values at 90 deg are lower than those obtained from the construction now in use. However, this difference is not too pronounced and is to be expected when fewer plies are used, because, in the 5-ply construction, the cross-bands which provide most of the stiffness perpendicular to the face grain, are closer to the core or neutral axis. From a structural standpoint, this 5-ply construction can also be considered as a satisfactory replacement for the 8-ply construction.

(*c*) *Wings.* Tests were not made to substantiate the proposed revisions to the wing-shell constructions. While it is true that the proposed revisions in the outer panel shells will introduce plywood of lower strength than the originally used birch-face constructions, these shells are not critically stressed, and the consequent reduction in strength, in part offset by using a $^1/_{32}$-in. instead of $^1/_{48}$-in. core, can be safely taken. The same is true of the center-section leading edge. In the highly stressed center-section top panels, however, the birch faces have been maintained and thickened. The additional thickness of the birch faces will adequately offset the slight reduction in over-all thickness. Also, at the highly stressed points, the alternate reinforcement construction is thicker than was the original. This will additionally offset the decrease in thickness of the outer plywood.

(*d*) *Fin.* The proposed substitution of mahogany-core material for the present poplar will increase the strength slightly.

(*e*) *Secondary Structures.* The proposed alternate constructions for the nose-wheel door, bomb-bay doors, wing tip, gun-turret fairing and tail cone are all on the side of increased strength.

Conclusions

In conclusion, it is felt that most of the difficulties being experienced by plywood-aircraft manufacturers can be traced directly to a lack of specific information on the part of the lumber manufacturer, the veneer and plywood manufacturer, and the subcontractor on the exact requirements of the aircraft industry.

To prevent further unnecessary delays in production of wood aircraft, the following recommendations are made:

1 That suppliers of basic materials give more consideration to the production of larger quantities of aircraft grades in conformance with current AN Specifications.

2 That the use of acceptable alternate materials to replace critical species be more widely adopted by the industry.

3 That aircraft manufacturers, wherever it is structurally possible, simplify and standardize the design and construction of flat- and molded-plywood parts.

Analysis of Stretch-Forming Double-Curved Sheet-Metal Parts

By R. B. GLASSCO[1] and N. O. MYKLESTAD[2]

Double-curved surfaces, typical in airplane design, are classified according to direction of curvature. A qualitative stress analysis is made of stretch-forming (process of clamping metal sheet at two opposite edges and forcing a punch into the taut sheet) each class of surface, with special reference to the stress transverse to the direction of restraint. It is shown that there are two distinctly different sources of transverse stress during stretching. The resultant stress may be tension or compression, depending upon the direction and amount of curvature. When the resultant transverse stress is compression, undesirable wrinkling of the sheet may occur.

Introduction

STRETCH-FORMING is a process of forming sheet metal into a curved surface by clamping the sheet at two opposite edges and forcing a punch of the desired shape into the taut sheet. A typical application of the process is the forming of the skin or outer surface of the modern metal airplane.

There are two limiting conditions in the application of the stretch-forming process. These limitations depend upon the amount of curvature in the desired surface. The first and more obvious limitation is tearing or rupturing of the sheet before it has been stretched over the entire surface of the punch. This limitation of tearing is a function of the ductility properties of the particular metal being formed. Some work has already been done to determine and improve the limit of stretch-forming with regard to tearing (1, 2).[3]

The second limitation in the application of the stretch-forming process is buckling of the sheet. This buckling results from compressive stresses transverse to the direction of restraint and leaves the formed sheet with undesirable permanent wrinkles. The factors determining whether a particular curved surface is subject to wrinkling or not are more obscure than they are for the limitation of tearing. In order to understand and, in some cases, eliminate wrinkling, it is desirable to make a qualitative stress analysis of a sheet subjected to the stretch-forming process. This is done by determining the effect of the surface shape upon the deformations and loads in the stretched sheet.

Classification of Shapes

Double-curved surfaces may be classified by considering variations in the two principal curvatures which define the shape, that is, a surface may be convex, concave, or flat in one direction for a particular curvature in the other direction. In this report the curvature will refer to the top side of the sheet being stretch-formed, so that in the schematic illustration at the top of Fig. 1, both the curvatures $1/R_1$ and $1/R_2$ are concave as shown. The curvature $1/R_1$ will be called the transverse curvature, and $1/R_2$ the longitudinal curvature. In Fig. 1 (*a* to *i*) are shown the different combinations of curvature, defined in the foregoing manner. The longitudinal direction is the direction of restraint as determined by the location of the clamps. This location is the same for all sketches in Fig. 1 and is indicated by the schematic illustration at the top of the figure.

It is not possible to form all of the shapes shown in Fig. 1 with a punch approaching from above. Shapes with longitudinal convex curvature, illustrated in (*c*), (*f*), and (*i*) of Fig. 1 cannot be formed this way, as the area of the formed part of the sheet will be above the ends of the punch. However, the elimination of these three types does not limit the number of shapes which can be stretch-formed, since they are merely the inverted images of the three types (*g*), (*d*), and (*a*), diametrically opposite in Fig. 1. In addition, type (*e*) in the center of Fig. 1 may be disregarded since it is a flat sheet that requires no forming.

There remain only five cases, namely, (*a*), (*b*), (*d*), (*g*), and (*h*), to be considered in this analytical study of stretch-forming of curved parts. Of these five cases, (*b*), (*d*), and (*h*) have only single curvature and are considered special cases having zero curvature in one of the two principal directions. The other two types, (*a*) and (*g*), the real double-curved shapes, may be considered as combinations of these three, that is, (*a*) is a combination of (*b*) and (*d*), while (*g*) is a combination of (*d*) and (*h*). Thus, if a study is made of the three simple types,[4] (*b*), (*d*), and (*h*), first, and then of the effect of combining them, all simple types of double-curved surfaces will be covered.

Qualitative Analysis

The following qualitative analyses explain how wrinkles may occur during stretch-forming of the shapes shown in Fig. 1:

Case 1—Concave Cylindrical Part. Take as the first case the stretching of the concave cylindrical part shown in Fig. 1 (*b*). This would be a difficult part to form by stretching in the direction indicated because of the variation of longitudinal strain across the width. When the punch descends, it first touches the sheet along the longitudinal line *AB*, as shown in Fig. 2. If the sheet is flat, there is no punch pressure exerted in this position because a flat horizontal sheet can have no vertical reaction at its clamps.

As the punch descends farther, the part of the sheet that is in contact with it will be forced down below the clamps, as shown in Fig. 3. Since the longitudinal center line of the sheet now slopes down at the clamps, the restraining force will have a vertical component the total amount of which is the punch load *P*.

The longitudinal center line of the sheet has now been stretched a small amount which gives rise to a longitudinal stress determined by the stress-strain diagram of the material. As stretching of the sheet progresses, this stress is soon brought above the yield point at the middle of the sheet while it is still zero at the sides

---

[1] Stress Analyst, Lockheed Aircraft Corporation, Burbank, Calif. Jun. A.S.M.E.

[2] Research Associate in Aeronautics, Guggenheim Aeronautical Laboratory, California Institute of Technology, Pasadena, Calif.

[3] Numbers in parentheses refer to the Bibliography at the end of the paper.

Contributed by the Aviation Division and presented at the Annual Meeting, New York, N. Y., Nov. 29–Dec. 3, 1943, of The American Society of Mechanical Engineers.

Note: Statements and opinions advanced in papers are to be understood as individual expressions of their authors and not those of the Society.

[4] The cylindrical surfaces (*b*), (*d*), and (*h*) would not actually be formed by stretching in practice but probably would be bent by rolling; however, it is the analysis of the cylindrical parts which forms the basis for the analysis of double-curved parts.

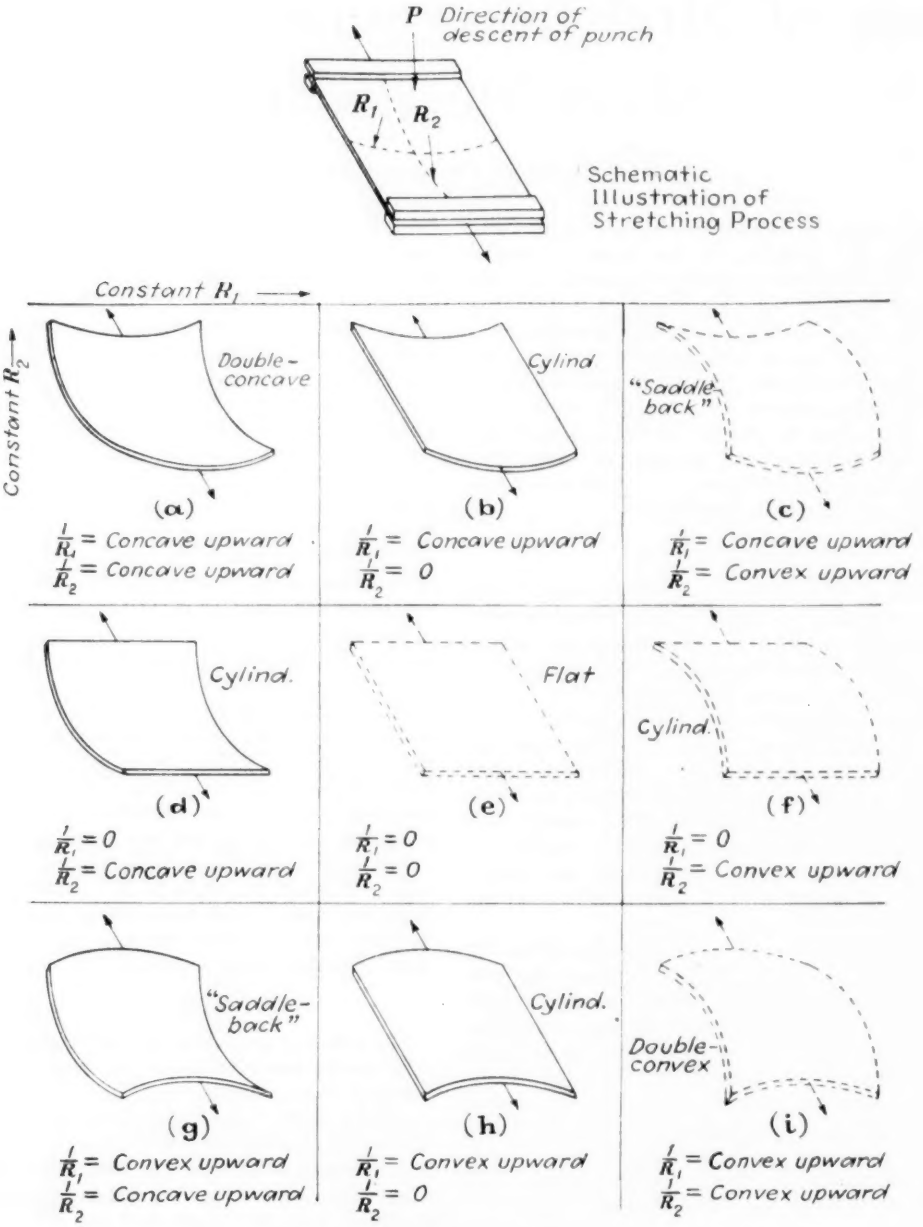


FIG. 1 COMBINATIONS OF CURVATURE

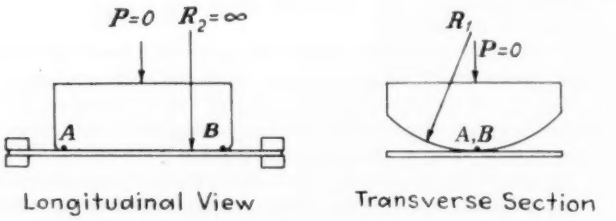


FIG. 2 FORMING OF CONCAVE CYLINDRICAL PART
(Condition just before stretching begins.)

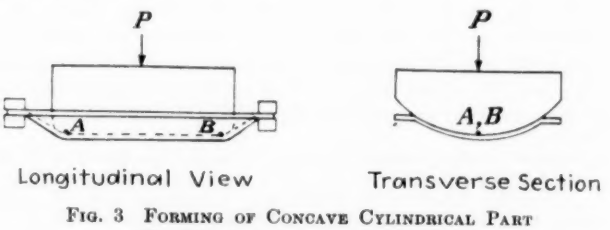


FIG. 3 FORMING OF CONCAVE CYLINDRICAL PART
(Condition just after stretching begins.)

where the punch has not yet contacted the sheet. This variation of strain across the width of the sheet is the cause of the tendency to wrinkle as explained later. Between points *A* and *B* there will be no pressure between the punch and the sheet, as such pressure could be only brought about by a tendency on the part of the sheet to bend up and press against the punch. Such a tendency is of course not present. This lack of pressure between the sheet and the punch means that the sheet has no support against wrinkling in this central portion between points *A* and *B*.

Transverse Stress Due to Uneven Stretching. How a transverse

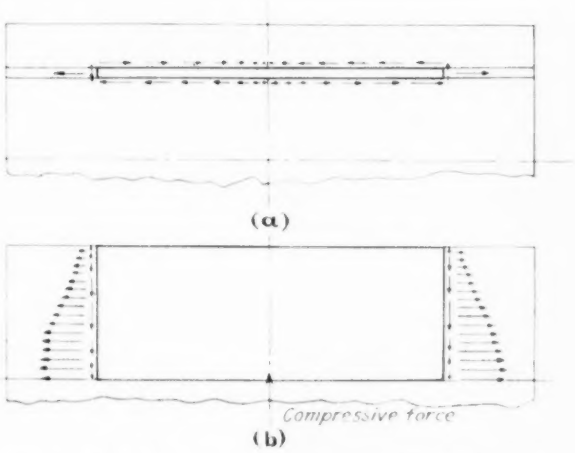


FIG. 4 FREE BODY SKETCHES, ILLUSTRATING TRANSVERSE COMPRESSION

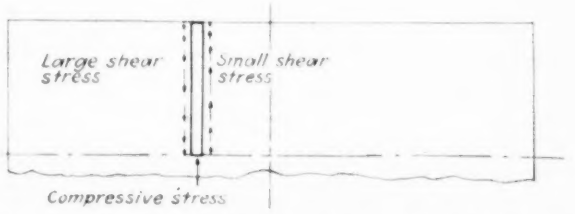


FIG. 5 TRANSVERSE HALF-STRIP, ILLUSTRATING HOW TRANSVERSE STRESS DEPENDS ON CHANGE IN SHEAR STRESS

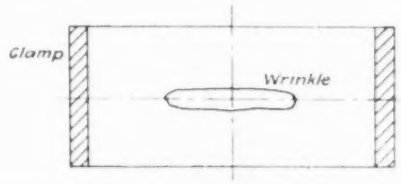


FIG. 6 LENGTHWISE WRINKLE CAUSED BY UNEVEN LONGITUDINAL STRETCHING

compressive stress can result from the uneven longitudinal stretching may be seen as follows: Consider the middle part of a narrow longitudinal strip of the sheet as a free body; it will have shear stresses along its sides as shown in Fig. 4 (*a*) in order to make its sides conform to the adjacent strips which were stretched different amounts. At the end of the strip there will be a transverse shear stress equal to the longitudinal one. When all adjacent strips are considered, from the edge of the sheet to the middle, a free body such as shown in Fig. 4 (*b*) will be obtained. It is seen from this that there must be a transverse compressive force on the sheet balancing the transverse shear forces.

The distribution of this transverse compression depends upon the longitudinal rate of change of shear stress. This is illustrated by the transverse half-strip shown in Fig. 5. The increase in the shear stress from the right side to the left side of the strip determines the magnitude of the transverse compression on this strip.

From symmetry the shear stress must be zero halfway between the clamps. It increases toward the ends of the punch, as shown in Fig. 4. This produces transverse compression over this region, resulting in a tendency to develop lengthwise wrinkling, as shown in Fig. 6.

Transverse Stress Due to Slope of Punch. At the ends of the punch, where the sheet bends up toward the clamps, the stretching force on a longitudinal strip will have a vertical component as shown by force S in Fig. 7. Since the side of the punch slopes, the normal pressure N between the punch and the strip will not be vertical but at an angle. To balance these forces S and N on the strip, there will have to be a third force which in this case must be a transverse tension T in the sheet.

The force T will be tangent to the punch and will be diminished by the friction force μN, where μ is the coefficient of friction. It is seen that as long as the slope of the strip is less than μ, the transverse stress remains zero. It must be remembered also that for a cylindrical punch this transverse tension is confined entirely to the part of the sheet which is pressed against the end edges of the punch, as there is no pressure between the punch and the sheet along the straight middle part. For a long cylindrical punch, then, this transverse tension will have little effect at the middle of the sheet and its influence on the wrinkling due to unequal tension, Fig. 6, will be but slight.

Case 2—Double Concave Part. Consider now the type of part which has a concave curvature in the longitudinal direction as well as in the transverse direction as shown in Fig. 1 (*a*). The longitudinal view, corresponding to Fig. 3, will now be as shown in Fig. 8. Due to the longitudinal curvature there will be normal pressure between the punch and the sheet all along its length, and the condition shown in Fig. 7 will hold true all along the length of the punch. The resulting transverse tension will, therefore, be effective in opposing the wrinkling shown in Fig. 6. The friction resulting from the normal pressure will also help to prevent wrinkling as it resists any relative motion between the punch and the sheet. Finally, the normal pressure also affords support to the middle of the sheet, which greatly increases its resistance to wrinkling.

The magnitude of the normal pressure between the punch and the sheet at any point is directly proportional to the longitudinal curvature at that point. How sharp this longitudinal curvature must be in order to avoid the wrinkling due to nonuniform stretching can best be determined by experiment. The minimum longitudinal curvature will be a function of the transverse curvature and the sheet thickness, as well as the dimensions of the punch, the method of support of the sheet, and the coefficient of friction.

For a longitudinal curvature too small to prevent wrinkling, it has been found that rubber pads stacked under the sheet give enough support to prevent wrinkling in many cases. This is illustrated by the two aluminum-alloy parts shown in Fig. 15.

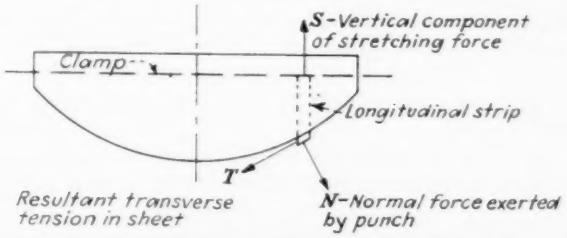


FIG. 7 TRANSVERSE SECTION AT END OF PUNCH SHOWING FORCES ON LONGITUDINAL STRIP OF SHEET



FIG. 8 FORMING OF DOUBLE CONCAVE PART
(Condition just after stretching begins.)

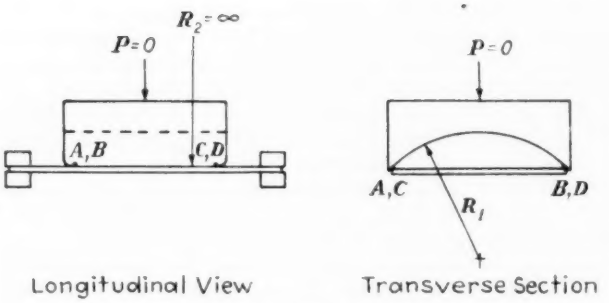


FIG. 9 FORMING OF CONVEX CYLINDRICAL PART
(Condition just before stretching begins.)

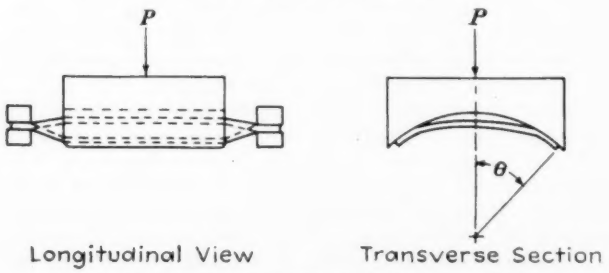


FIG. 10 FORMING OF CONVEX CYLINDRICAL PART
(Condition just after stretching begins.)

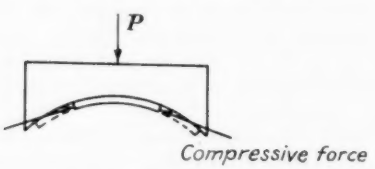


FIG. 11 TRANSVERSE SECTION ILLUSTRATING HOW TRANSVERSE COMPRESSION PUSHES SHEET AGAINST PUNCH

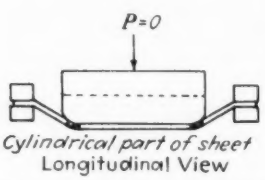


FIG. 12 FORMING OF CONVEX CYLINDRICAL PART (SHADED PORTION) FROM SAGGING SHEET
(Condition just before stretching begins.)

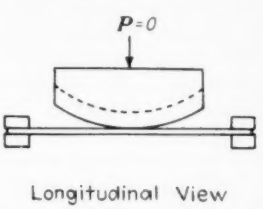


FIG. 13 FORMING OF SADDLEBACK PART
(Condition just before stretching begins.)

This expedient can be used in certain types of stretching machines only.

Case 3—Convex Cylindrical Part. Consider now the stretch-forming of a convex cylindrical part with the direction of restraint parallel to the axis of the cylinder as shown in Fig. 1 (*h*). Such a part would not be formed in this manner in actual production but is important as the limiting case of saddleback parts.

This case of the convex cylindrical part is entirely different from Case 1, the concave part. The uneven tension now varies in the opposite manner across the width of the sheet and consequently produces transverse tension where Case 1 produced compression. Similarly, the transverse stress in the sheet due to the slope of the punch now becomes compression, rather than tension as in Case 1.

Assume first that the sheet is clamped perfectly flat before stretching begins. Then the picture will look like Fig. 9, just as the punch touches the sheet.

As the punch descends farther, it puts pressure on the four points, *A*, *B*, *C*, and *D*, of the sheet. No pressure is exerted between points *A* and *C* nor between points *B* and *D* for the same reason as explained in Case 1. The descent of the punch now stretches the sheet along the sides, rather than along the center line, and in the transverse section there will be two arcs of contact as shown in Fig. 10. The bending moments due to the curvature of these arcs will have a tendency to bend the center of the sheet also and actually raise the center of the sheet an infinitesimal amount above the clamps, as shown exaggerated in Fig. 10.

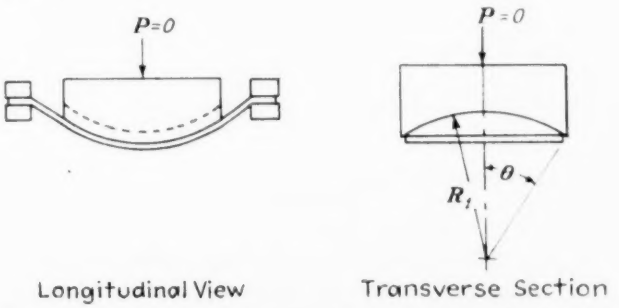


FIG. 14 FORMING OF SADDLEBACK PART FROM SAGGING SHEET
(Condition just before stretching begins.)

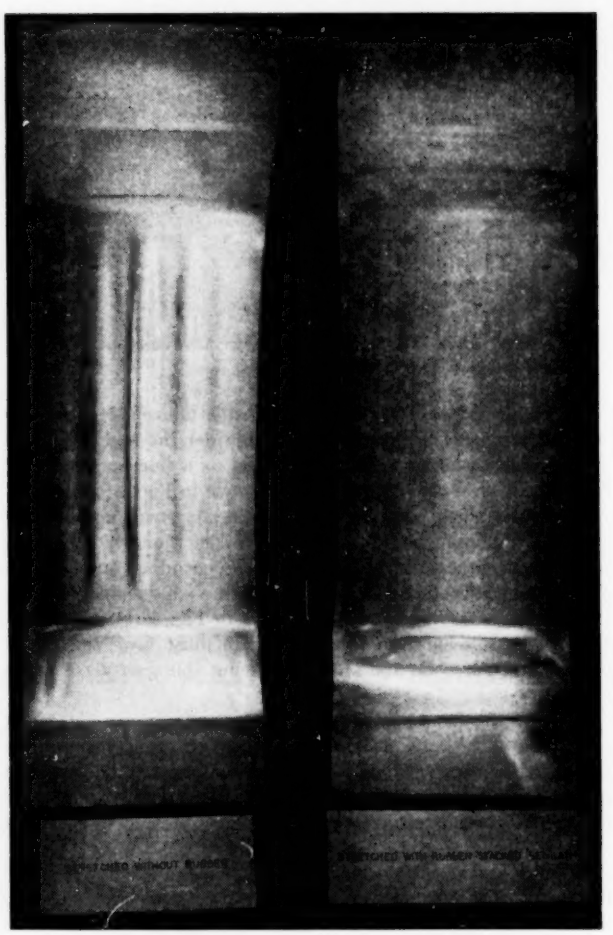


FIG. 15 CONCAVE CYLINDRICAL PARTS
(Material, 0.010 24S-T Alclad. Stretched with and without rubber stacked beneath.)

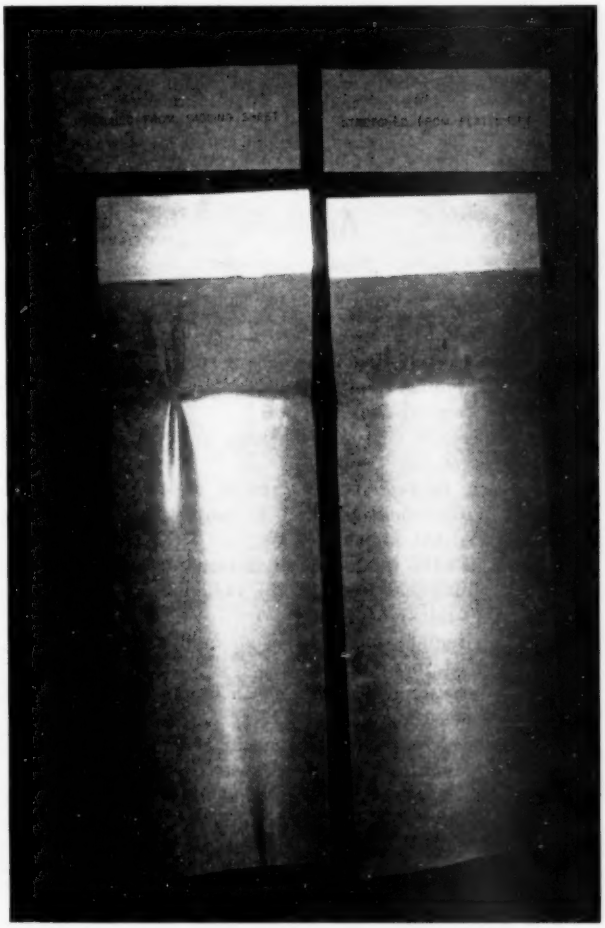


FIG. 16 CONVEX CYLINDRICAL PARTS
(Material, 0.010 24S-T Alclad. Stretched from sagging and flat sheets.)

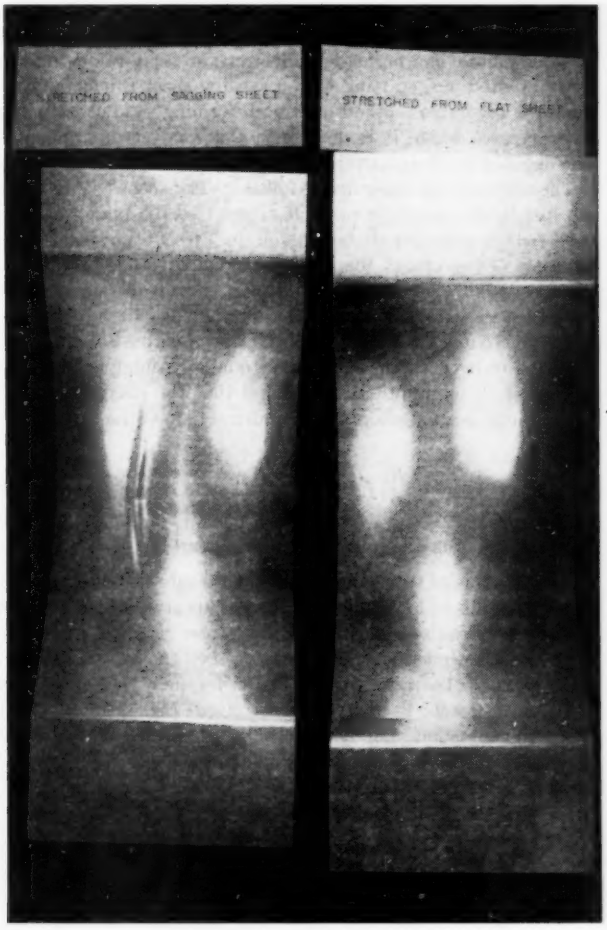


FIG. 17 SADDLEBACK PARTS
(Material, 0.010 24S-T Alclad. Stretched from sagging and flat sheets.)

Because of the fact that the sheet first comes in contact with the part of the punch that has the steepest slope, as indicated by the angle θ in Fig. 10, the transverse compressive stress due to this slope will be predominant over the transverse tension resulting from unequal stretching. This transverse compressive force will tend to push the center of the sheet farther in against the punch, as shown in Fig. 11. This represents buckling of the sheet, but in such a way that the buckle conforms to the transverse curvature of the punch. Additional buckles of smaller wave length (wrinkles) cannot occur before the sheet rests firmly against the center of the punch. Then this firm support of the sheet by the punch will help to prevent such wrinkles as the transverse compressive stress increases to its maximum value.

On the other hand, a slight variation in the method of clamping the sheet will alter considerably the possibility of wrinkles forming. If the sheet is placed in the press in such a way that it is allowed to sag between the clamps so that just before stretching begins it has a shape such as shown in Fig. 12, the case will be entirely different. In this case the sheet will be bent into a cylindrical shape at each end of the punch, as shown in Fig. 12. This longitudinal curvature at each end of the punch will offer a considerable resistance to transverse buckling of the sheet and will also prevent the sheet from bending easily to conform to the curvature of the punch. However, if the transverse compressive forces become large enough to cause buckling, these buckles will be of small wave length and will be likely to remain as permanent wrinkles when the stretching operation is completed. This is illustrated by the aluminum-alloy parts shown in Figs. 16 and 17.

Case 4—Convex-Concave Part (Saddleback). Consider that the part in Case 3 has in addition to the transverse convex curvature a longitudinal concave curvature. This results in a saddleback shape, such as shown in Fig. 1 (*g*). The same reasoning as in Case 3 also applies here regarding the transverse stresses due to uneven stretching and transverse slope of punch. The difference is, however, that in this case the transverse compressive stress is distributed over the entire part of the sheet in contact with the punch instead of being confined to the ends of the punch.

If a flat sheet is used (see Fig. 13), it will have a tendency to conform easily to the transverse curvature of the punch just as in Case 3, and the resulting support by the punch will help to prevent wrinkles as the transverse compressive stress increases. If the sheet is allowed to sag, however, it will conform to the longitudinal curvature of the punch just before stretching begins (see Fig. 14). This cylindrical part of the sheet will offer a considerable resistance to buckling just as for the sagging sheet in Case 3 (see Fig. 12). When buckling finally does occur, however, the resulting short waves are likely to remain in the sheet as wrinkles. It has been found that even a small amount of sag is often enough to cause wrinkling.

Quantitative Analysis of Saddleback Stretch-Forming. If a

saddleback part is stretch-formed from a sagging sheet, an analysis of the transverse compressive stress due to the transverse slope of the die can be made under certain assumptions. As already pointed out, starting with a sagging sheet is generally not the most favorable method of stretch-forming saddleback parts, but for cases where it is necessary, this analysis is applicable. The detailed analysis for this case may be found in the Appendix.

The assumptions made are as follows: The sheet has an initial sag just large enough to make it tangent to the punch near its ends (which corresponds fairly well to present methods); the influence of bending of the sheet is negligible; the width of the sheet does not change during stretching; and, in regions being stretched, the strain is in the plastic range, and hence the stress is approximately constant across the stretched part of the sheet. Also, the transverse stress due to unequal stretching is neglected.

With these assumptions it is found that the maximum transverse compressive stress in the cylindrical part of the sheet would be

$$(f_c)_{max} = \frac{R_1}{R_2} f_p[1 - e^{-\mu\theta}(2\mu \sin\theta + \cos\theta)] \quad [1]$$

in which equation the following notations are used:

R_1 = radius of transverse convex curvature of the part, in.
R_2 = radius of longitudinal concave curvature of the part, in.
f_p = longitudinal plastic tensile stress due to stretching (assumed constant), psi
θ = angle between vertical axis of punch and normal to stretched edge of sheet (see Fig. 14) (assumed constant, but does actually diminish slightly as the stretching progresses), radians
μ = coefficient of friction
e = 2.718, base of natural logarithms

The resistance to transverse buckling of a cylindrical sheet of radius R_2 and thickness t may be given by the following formula (3)

$$f_{cr} = E \frac{0.6\frac{t}{R_2} - 10^{-7}\frac{R_2}{t}}{1 + 0.004\frac{E}{f_{cy}}} \quad [2]$$

In this equation

E = modulus of elasticity in elastic range, psi
f_{cy} = compressive yield stress, psi

If $(f_c)_{max}$ according to Equation [1] is larger than f_{cr} according to Equation [2], buckling of the unstretched cylindrical center part of the sheet is likely to occur.

Conclusions

The conclusions to be drawn from the qualitative analyses and verifying tests made are:

1 There are two distinctly different sources of transverse stress during stretching. One is due to the variation of longitudinal tensile strain across the width of the sheet, and the other is due to the slope of a transverse cross section of the punch. These two effects are often opposed to each other so that if one causes compression, the other causes tension in the transverse direction. If the compressive effect predominates, a tendency to form longitudinal wrinkles will result.

2 The methods of stretch-forming may be so improved that, in some cases, the compressive forces causing wrinkling may be avoided, and in other cases enough support may be given to the sheet to prevent wrinkles even though the compressive forces are present. The only limit to stretch-forming in these cases is then the tearing of the sheet due to excessive elongation.

Bibliography

1 "Stretch-Forming Contoured Sheet Metal Aircraft Parts," by T. H. Hazlett and M. M. Rockwell, *Iron Age*, vol. 149, June 4, 1942, pp. 49–53.

2 "Technical Developments in High-Production Sheet-Metal Forming," by Wm. Schroeder and T. H. Hazlett, *S.A.E. Journal* (Transactions), vol. 51, May, 1943, pp. 170–192.

3 "Theory of Elastic Stability," by S. Timoshenko, McGraw-Hill Book Company, Inc., New York, N. Y., 1936, p. 463.

Appendix

Nomenclature

The following nomenclature is used in the Appendix:

R_1 = radius of transverse convex curvature of part, in.
R_2 = radius of longitudinal concave curvature of part, in.
f_p = longitudinal plastic tensile stress due to stretching (assumed constant), psi
f_c = transverse compressive stress on cylindrical part of sheet, psi
ϕ = angle between vertical axis of punch and normal to any element in sheet in contact with punch (see Fig. 18), radians
β = value of ϕ for innermost element of sheet in contact with punch (see Fig. 18), radians
t = sheet thickness, in.
dl = longitudinal dimension of an infinitesimal element of sheet, in.
N = normal force of punch on an infinitesimal element of sheet (see Fig. 20), lb
V = vertical resultant of longitudinal tensile forces on an infinitesimal element of sheet (see Fig. 20), lb
F = transverse compressive force on an infinitesimal element of sheet (see Fig. 20), lb
dF = change in F across infinitesimal element of sheet (see Fig. 20), lb
μ = coefficient of friction
e = 2.718, base of natural logarithms
E = modulus of elasticity, psi
f_{cy} = compressive yield stress, psi

Quantitative Analysis of Saddleback Stretch-Forming

Saddleback parts often wrinkle because the transverse curvature causes a transverse compression during the stretch-forming operation. The wrinkles are more apt to occur if the sheet is clamped with an initial sag. A quantitative analysis for the buckling stress in a saddleback part formed from a sheet with an initial sag will be given.

The following assumptions are made:

1 The initial sag in the sheet is enough to make the sheet tangent to the punch near its ends (Fig. 14).
2 The influence of bending is negligible.
3 The width of the sheet does not change during stretching.
4 The strain is in the plastic range, and hence the tensile

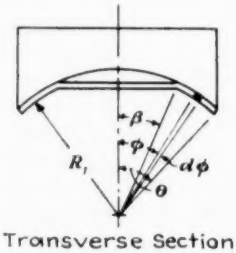


Fig. 18 Forming of Saddleback Part From Sagging Sheet (Condition after stretching begins.)

stress is approximately constant across the stretched part of the sheet.

5 The transverse stress due to unequal stretching is negligible.

Just before stretching begins the sheet has a cylindrical shape with the radius R_2 and touches the punch all along its circular edges, as shown in Fig. 14. After the forming is partially completed, the sheet will be stretched into contact with the punch for some distance in from the edges, and the center portion will still be cylindrical, as shown in Fig. 18.

Consider now an element of the stretched part of the sheet located at an angle ϕ from the vertical axis of the punch, as shown in Fig. 18. The width of this strip is $R_1 d\phi$, and the length is taken as dl as shown in Figs. 19 and 20. Due to the stretching

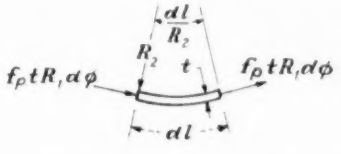


FIG. 19 LONGITUDINAL VIEW OF ELEMENT IN STRETCHED PART OF SHEET

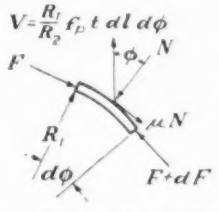


FIG. 20 TRANSVERSE VIEW OF ELEMENT IN STRETCHED PART OF SHEET

stress, the longitudinal forces acting on this strip are $f_p t R_1 d\phi$ (Fig. 19). The vertical resultant V of these forces is then

$$V = 2(f_p t R_1 d\phi) \sin \frac{dl}{2R_2} = \frac{R_1}{R_2} f_p t\, dl\, d\phi$$

which is shown in Fig. 20. Then in the transverse plane, Fig. 20, the condition for equilibrium in the tangential direction is satisfied if

$$\mu N = (F + dF) - F + V \sin \phi$$
$$= dF + \frac{R_1}{R_2} f_p t\, dl\, d\phi \sin \phi \quad \ldots\ldots\ldots\ldots\ldots [3]$$

The condition for equilibrium in the normal direction is satisfied if

$$N = 2F \sin \frac{d\phi}{2} + V \cos \phi$$

Since

$$\lim_{d\phi \to 0} \sin \frac{d\phi}{2} = \frac{d\phi}{2},$$

the foregoing equation becomes

$$N = F d\phi + \frac{R_1}{R_2} f_p t\, dl\, d\phi \cos \phi \quad \ldots\ldots\ldots\ldots [4]$$

Eliminating N from Equations [3] and [4] gives

$$\frac{dF}{d\phi} - \mu F = \frac{R_1}{R_2} f_p t\, dl\, (\mu \cos \phi - \sin \phi) \quad \ldots\ldots\ldots [5]$$

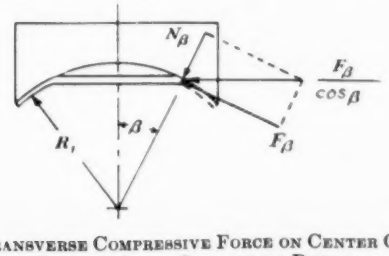


FIG. 21 TRANSVERSE COMPRESSIVE FORCE ON CENTER CYLINDRICAL SECTION AFTER STRETCHING BEGINS

Solving Equation [5] for the boundary condition that $F = 0$ when $\phi = \theta$ gives

$$F = \frac{R_1}{R_2} \cdot \frac{f_p t\, dl}{1 + \mu^2} \left\{ 2\mu \sin \phi + (1 - \mu^2) \cos \phi - e^{-\mu(\theta - \phi)} [2\mu \sin \theta + (1 - \mu^2) \cos \theta] \right\} \quad \ldots\ldots [6]$$

Equation [6] gives the value of F for any angle ϕ between β and θ, but the particular value of interest is F_β, the one for $\phi = \beta$ where the cylindrical part of the sheet meets the punch.

The compressive force on the cylindrical part of the sheet will be $\frac{F_\beta}{\cos \beta}$ as shown in Fig. 21, where N_β is the punch reaction at that point. (The friction force μN_β is neglected here for simplicity.) The compressive stress f_c on the cylindrical part of the sheet is then

$$f_c = \frac{F_\beta}{t\, dl \cos \beta}$$
$$= \frac{R_1}{R_2} \cdot \frac{f_p}{1 + \mu^2} \left\{ 2\mu \tan \beta + (1 - \mu^2) - \frac{e^{-\mu(\theta - \beta)}}{\cos \beta} [2\mu \sin \theta + (1 - \mu^2) \cos \theta] \right\} \quad \ldots\ldots\ldots [7]$$

Since the buckling load of a thin-walled cylinder is independent of its length, it is only the maximum compressive stress $(f_c)_{max}$ that is important in determining whether or not buckling will take place. The value of β at which $(f_c)_{max}$ occurs is found by setting the first derivative of f_c with respect to β equal to zero

$$\frac{df_c}{d\beta} = 0 \quad \ldots\ldots\ldots\ldots\ldots\ldots [8]$$

By differentiating Equation [7], it is found that

$$\frac{df_c}{d\beta} = \frac{R_1}{R_2} \frac{f_p}{(1 + \mu^2) \cos^2 \beta} \left\{ 2\mu - (\sin \beta + \mu \cos \beta) e^{-\mu(\theta - \beta)} [2\mu \sin \theta + (1 - \mu^2) \cos \theta] \right\}$$

To satisfy the condition of Equation [8], the expression within the braces must be zero

$$2\mu - (\sin \beta' + \mu \cos \beta') e^{-\mu(\theta - \beta')} [2\mu \sin \theta + (1 - \mu^2) \cos \theta] = 0$$

where β' is the particular value of β giving the maximum value of f_c. Placing all terms containing the variable β' on the left gives

$$(\sin \beta' + \mu \cos \beta') e^{-\mu(\theta - \beta')} = \frac{2\mu}{2\mu \sin \theta + (1 - \mu^2) \cos \theta} \quad \ldots [9]$$

This value of β', found from Equation [9] and substituted into Equation [7] for the compressive stress, gives $(f_c)_{max}$. Thus

$$(f_c)_{max} = \frac{R_1}{R_2} \cdot \frac{f_p}{1 + \mu^2} \left\{ 2\mu \tan \beta' + (1 - \mu^2) - \frac{e^{-\mu(\theta - \beta')}}{\cos \beta'} [2\mu \sin \theta + (1 - \mu^2) \cos \theta] \right\} \quad \ldots\ldots [7a]$$

However, no simple explicit expression for β' can be obtained from Equation [9] to substitute into Equation [7a], but the following study of Equation [9] indicates that an accurate approximate formula for $(f_c)_{max}$ can be obtained which does not contain β'.

Take a representative case such as that wherein $\theta = 60$ deg. Solving Equation [9] for β' for this case, it is found that

$$\begin{aligned} \beta' &= 21.6 \text{ deg when } \mu = 0.20 \\ \beta' &= 13.1 \text{ deg when } \mu = 0.10 \\ \beta' &= 1.7 \text{ deg when } \mu = 0.01 \\ \beta' &= 0 \text{ deg when } \mu = 0.00 \end{aligned}$$

Thus, when the coefficient of friction μ is very small, as would be the case for a lubricated punch, the value of β' is also very small, that is, the maximum compressive stress occurs when almost the entire sheet is in contact with the punch. An approximate form of Equation [7*a*] may be obtained for small values of μ and β' by considering that

$$\begin{aligned} \mu^2 &\leqq 0 \\ \mu \tan \beta' &\leqq 0 \\ e^{\mu\beta'} &\leqq 1 \\ \cos \beta' &\leqq 1 \end{aligned}$$

The approximate equation for $(f_c)_{max}$ then becomes

$$(f_c)_{max} \leqq \frac{R_1}{R_2} f_p \left[1 - e^{-\mu\theta}(2\mu \sin \theta + \cos \theta)\right] \quad [7b]$$

This is the equation given as Equation [1] in the main report.

The resistance to transverse buckling of the cylindrical portion of the sheet is given by the following formula (3)

$$f_{cr} = E \frac{0.6 \frac{t}{R_2} - 10^{-7} \frac{R_2}{t}}{1 + 0.004 \frac{E}{f_{cy}}} \quad [10]$$

This is the equation given as Equation [2] of the main report. If $(f_c)_{max}$ according to Equation [7*b*] is larger than f_{cr} according to Equation [10], buckling of the unstretched cylindrical center part of the sheet is likely to occur.

Plastic Plywoods in Aircraft Construction

By R. D. HISCOCKS,[1] OTTAWA, CANADA

Using a typical fuselage fabricated from plastic plywood and veneer as an example, the author indicates the general procedure followed in building wood aircraft. Basic design problems were solved by extensive investigations and tests conducted by the National Research Council. A method is described for fabricating disposable fuel tanks for fighter planes from veneer and plywood, as representing the wide range of possiblities of wood in war and postwar industry.

AT the beginning of the war it was felt in the National Research Council that the possibilities of the wooden airplane were not fully appreciated. It was considered that the factors which govern the speed with which a prototype machine might be developed and placed in full-scale production weighed heavily in favor of wood, especially when the question is examined in the light of Canadian facilities.

As a result, we undertook in the Structures Section to set up a small pilot plant in order to test and develop these ideas and, in particular, with the object of demonstrating that recent advances in materials and techniques can be applied rapidly to produce an airplane which is not merely a metal substitute but a machine of technical merit.

Strength Properties of Wood

Although wood is one of the oldest structural materials in the world there has accumulated surprisingly little information as to its strength properties. Admittedly far from the isotropic ideal dear to the elastician, the elastic properties of the material are specified by at least 12 constants or rather parameters which vary with moisture content, specific gravity, and even from the heartwood to the sapwood of the same tree. Time effects are important and, particularly when shear loads are involved, both deflections and loads at failure will vary with the time the load has been applied.

This may sound like a rather vague proposition for an engineering material but if the experimental data on the external loading condition of an airframe is critically examined, it is apparent that the only logical assessment should be on a statistical basis; and therefore, providing the probable variations fall within reasonable limits, there is no inconsistency in employing a material the strength properties of which are not uniquely determined. Moreover, since the leading dimensions of an airplane are defined chiefly by aerodynamical and operational requirements, few compact structural sections can be employed without an excessive penalty in weight. Stiffness, therefore, rather than ultimate strength considerations usually govern the design. In elastic-stability problems, it can be shown that the ratio of Young's modulus to density, to density squared, or even to density cubed is the figure of merit for any material and that, under such conditions, an expanded material such as wood is supreme. Finally, with the present insistence on perfectly smooth surfaces, it is not difficult to see that contemporary metal construction is considerably handicapped.

[1] Aeronautical Division, National Research Council of Canada.

Presented at a joint meeting of The American Society of Mechanical Engineers and The Engineering Institute of Canada, Toronto, Canada, Sept. 30–Oct. 2, 1943.

Note: Statements and opinions advanced in papers are to be understood as individual expressions of their authors and not those of the Society.

Tests on Basic Design Problems

In view of the broad scope of the problem, we felt at the Research Council that useful results could most quickly be obtained by concentrating on one or two design problems, performing such basic tests as from time to time appeared desirable and acquiring in the same process a good deal of useful experience in shop technique.

One cannot proceed very far with the design of shell structures without some basic data, and a few of our early tests were conducted on cylinders in compression, Fig. 1. Some of these

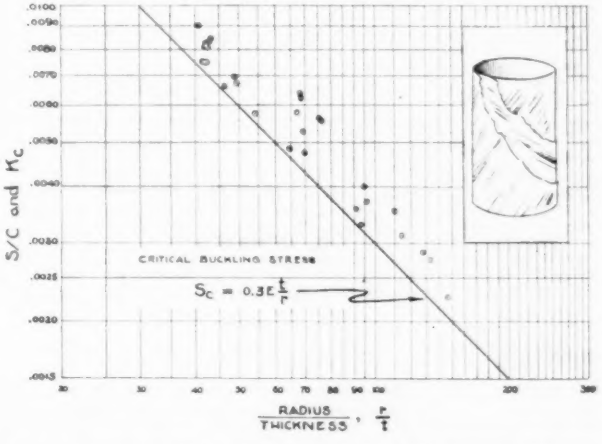


Fig. 1 Buckling Tests on 45-Deg Birch and Spruce Plywood Cylinders

cylinders were hot-press-molded with a rubber bag in the autoclave, others were formed with two-ply veneer and cold-press resin on a wrapping machine. The grain of the wood was in all cases at 45 deg to a generator, with inner and outer plies parallel and the grain of the core plies at right angles. The diameter of the cylinders ranged from 6 to 24 in. We have been able to detect a slight length effect with matched specimens but consider that it is negligible for all practical purposes.

It is interesting to observe that the critical compressive buckling stress can be expressed in the familiar form $F_{crit} = KE\frac{t}{R}$, where K is an experimental constant, E is the modulus of elasticity of the material, in our case parallel to the direction of the load, t is the wall thickness, and R the radius of curvature. A conservative value for design purposes is obtained by taking $K = 0.3$, a value which has enjoyed considerable popularity in the design of metal structures for years.

We have conducted few bending tests on cylinders to date and, in most applications, the problem is complicated by the addition of shear loads. The results of a few pure bending tests indicate that the critical stress again, as in the case of metal cylinders, is some 25 to 40 per cent higher than the critical value in compression.

The curves shown in Fig. 2 are based on the results of a fair number of compression tests on plywood blocks. With compact section, the elastic modulus and ultimate strength vary rapidly with changes in the grain angle.

The low bearing strength of wood perpendicular to the grain

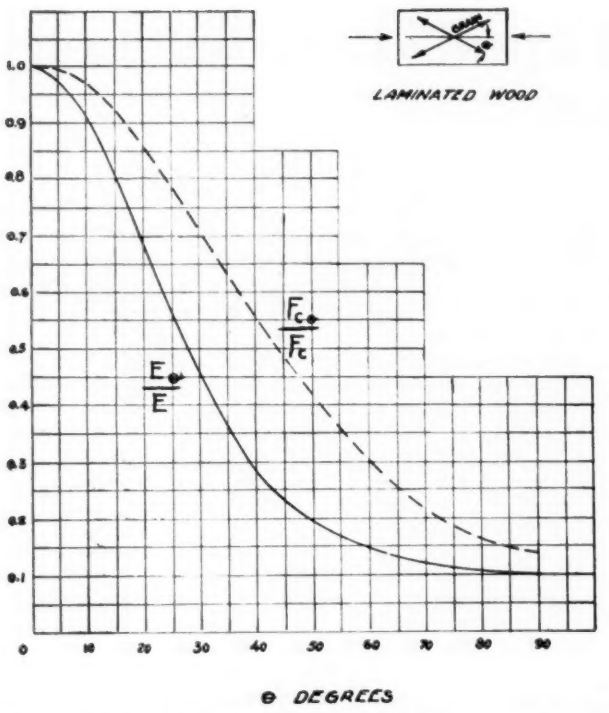


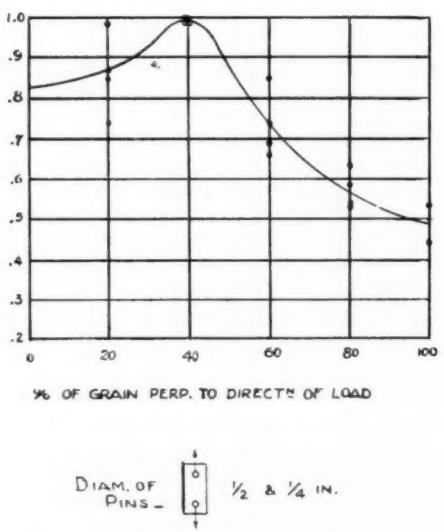
FIG. 2 RELATIVE ULTIMATE COMPRESSIVE STRENGTH AND YOUNG'S MODULUS VERSUS GRAIN ANGLE

is a shortcoming which can be avoided by the use of plywood. The values given in Fig. 3 have been found useful in the design of joints employing rivets or short bolts. With concentrated loads of any magnitude, the size and number of pins required to transmit the forces directly to the plywood structure usually become formidable, and the need arises for an intermediate material having a high bearing strength, reasonable tensile and shear values, and a moderate density. We have found phenolic-fabric-base laminates satisfactory for this purpose. These are available with a bearing strength of the order of 30,000 psi. Form factors are apt to be unpredictable, however, and it is good practice to conduct a few simple tests in order to determine safe loads for any specific condition.

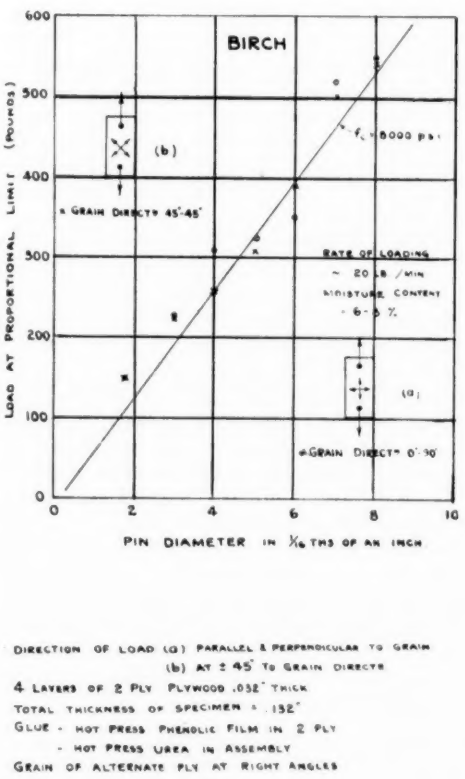
ADHESIVES AN IMPORTANT FACTOR IN PLYWOOD STRUCTURES

The phenolics usually will bond to wood effectively only with hot-press resins. Since the temperature coefficients of linear expansion for the plastics usually differ substantially from that of wood, it is important to avoid excessive temperature stresses. We consider that the most satisfactory expedient is first to glue a thin layer of veneer to the laminate with hot-press adhesive and then to bond the wood face to the remainder of the structure with a cold-setting adhesive. The same considerations apply in bonding metal to wood.

The problem of diffusing a concentrated load into a shell structure is always troublesome and particular care should be taken with plywood structures because wood has no elastic limit in tension. Highly localized tensile stresses may cause failure even if the average stress in a member is quite moderate, be-



(a)



(b)

FIG. 3 BEARING STRENGTH OF PLYWOOD
(a, Variation with percentage of end grain. b, Variation with pin diameter.)

cause the material cannot yield plastically and distribute the local stresses.

Many of the weathering difficulties which have arisen with wooden airplanes in the past can be attributed to the use of primitive glues, and it is safe to say that recent advances in the art largely are the outcome of improvements which have occurred in glues. Many synthetic-resin adhesives are now available which have a high resistance to water, ample shear strength, and are proof against mold and extremes of temperature. Quite a number will even survive the boiling-water test still cherished by some specifications, although it has never been explained why anyone should want to boil an airplane.

Contrary to popular opinion, high pressures are not required in gluing, and it is quite possible to construct satisfactory joints with a pressure of less than 1 psi if the viscosity of the glue is not excessive. The pressure requirements are determined solely by the forces necessary to obtain a thin glue line and, if the veneers are thin and the pressure uniformly distributed, then the forces required are small. With more rigid sections, high pressures are essential only if the faces of the wood do not match reasonably well. On thin members, nails or screws will provide ample pressure but it should not be assumed that the nails or screws will be effective after the glue has set because large shear deflections, sufficient to cause the glue to fail, are necessary for these elements to assume any load.

It is not unduly difficult to produce a bond with a shear strength equal to that of the wood, but it does not follow that every joint can transmit a load corresponding to the block shear strength of the wood. For example, in the standard three-ply test specimen, the stresses in the joint are far from pure shear, and it is not surprising that the failing load, for a thin specimen and with the grain in the core parallel to the face grain, is of the order of 25 per cent of the strength of the wood in pure shear. A further reduction results when the grain of the intermediate ply is not parallel to the load; at 90 deg, for example, there is a further decrement of 30 to 50 per cent due to the rolling effect of the wood fibers.

The rolling-shear type of failure has always to be guarded against. Fig. 4 is a very convenient spar section which behaved rather badly until we provided sufficient glue area in the flange-web joint. The bond between the parallel fibers in the flange and the web was entirely satisfactory but trouble arose where the veneers crossed at right angles further in the web.

Sometimes failures in box beams are unfairly charged to the glue. A thin web will buckle at very moderate shear stresses and continue to carry the load in diagonal tension. As a result the maximum shear stresses in the flange-web joint are more than double the values calculated from simple shear considerations.

It relieves the load on glued joints considerably if the ends of stiffeners are tapered. In flooring, decking, and the like, where local distortion may be large, we find rivets extremely effective in discouraging peeling in the glue joint.

In gluing it is of the utmost importance to match the moisture content of the pieces which are to be glued together. If a thin strip of veneer is coated with liberal quantities of a water-soluble glue and bonded to a heavier piece which is perfectly dry, it is obvious that the wet member will contract in drying and the result will be a badly warped component. Moreover, wood is a hygroscopic material and no amount of finishing will prevent it from shrinking and swelling with changes in the moisture content of the air. Most of the dimensional change occurs in a direction perpendicular to the grain and, if two pieces of veneer are glued together with the grain at right angles, then at only one value of the relative humidity will the panel remain flat.

For a stable material, it follows that three plies of veneer

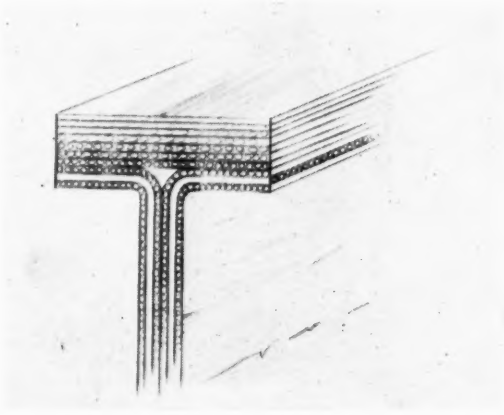


FIG. 4 SPAR SECTION SHOWING CONSTRUCTION TO AVOID ROLLING-SHEAR FAILURE

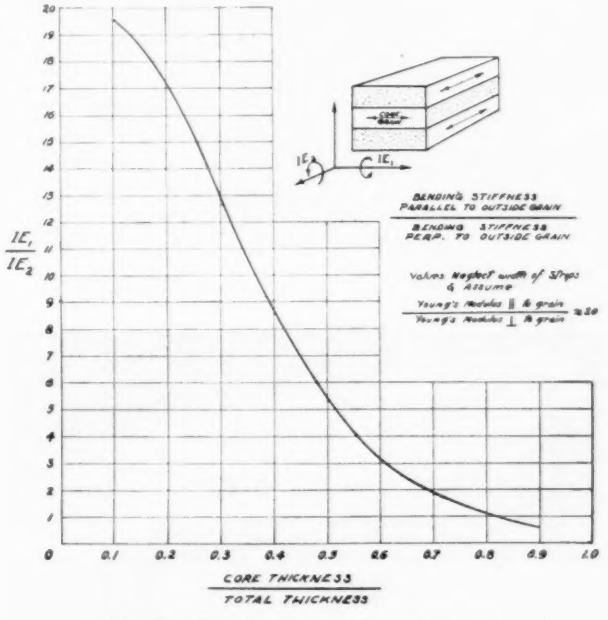


FIG. 5 THREE-PLY PLYWOOD IN FLEXURE

are the minimum. Unfortunately, conventional three-ply is composed of veneers of equal thickness and the bending stiffness parallel to the face grain is some 12 times the stiffness at right angles. Therefore, unless special design considerations demand a much superior strength in one direction, from the standpoint of general stiffness and dimensional stability, it is preferable to employ a construction which gives a more comparable stiffness in both directions (Fig. 5).

TESTS ON MOLDED FUSELAGE

Turning our attention to more ambitious experiments, Fig. 6 indicates the general structure of a rear fuselage which we designed and constructed in molded plywood. It did not appear desirable to redesign the forward portion of the structure because the existing steel-tube framework with detachable side panels permitted access to a large amount of equipment which could not readily be moved. Hence the detail design of this portion was predicated somewhat by the original metal layout, but every attempt has been made to approach the true monocoque form. The skin is sufficiently thick to carry all loads ex-

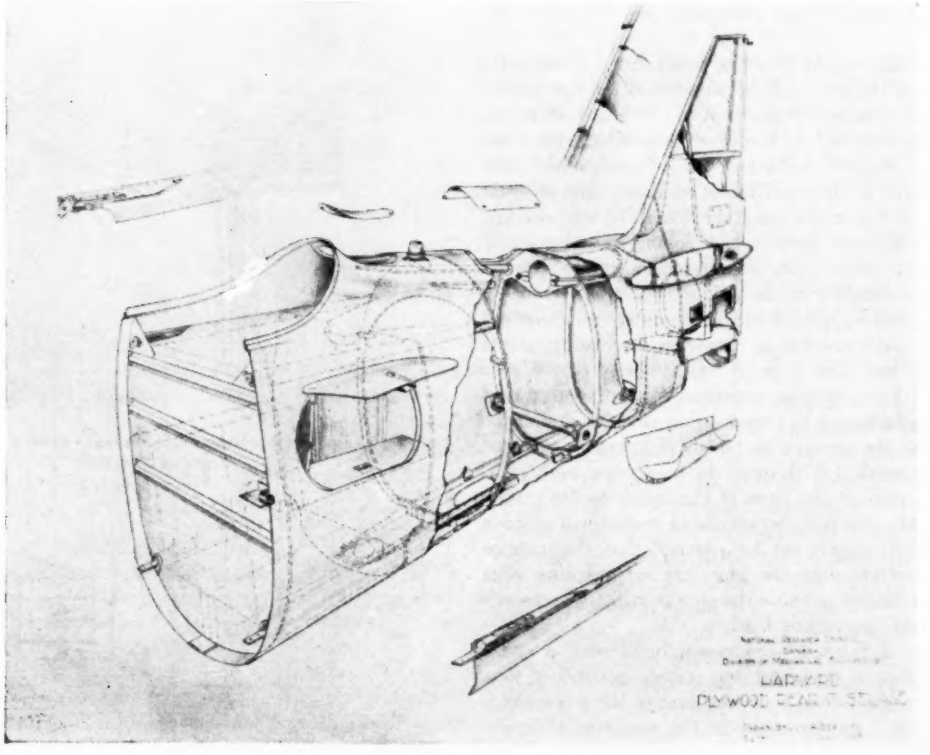


FIG. 6 REAR FUSELAGE STRUCTURE OF MOLDED PLYWOOD

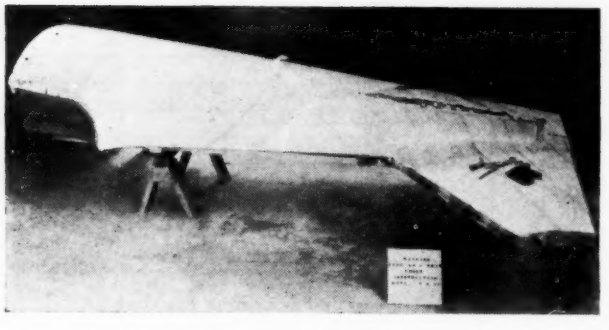


FIG. 7 FOUR LAYERS OF SPRUCE VENEER BONDED WITH THERMOSETTING UREA GLUE FORM THE FUSELAGE SKIN WHICH IS MOLDED IN HALVES

cept in the vicinity of cutouts and in the forward portion where the loads from the four attachment points are distributed by stub longerons. Light wooden frames maintain the correct shape. Plastic pads transmit the axial loads from the attachment fittings to the longerons. It is interesting to note that the problem of stress diffusion is frequently less difficult with a plywood than with a metal structure. With the longerons, for example, we have endeavored to taper the cross-sectional area and to graduate the elastic properties by varying the construction so that the glue joint between the longeron and the skin is uniformly stressed.

The skin, Fig. 7, which is molded in two halves, is composed of four layers of spruce veneer bonded with thermosetting urea glue. The veneers are trimmed to shape and stapled in place on a wooden mold with the inner and outer layers at right angles to the middle layers and at an angle of 45 deg to the fuselage center line. Successive layers are coated with adhesive, the

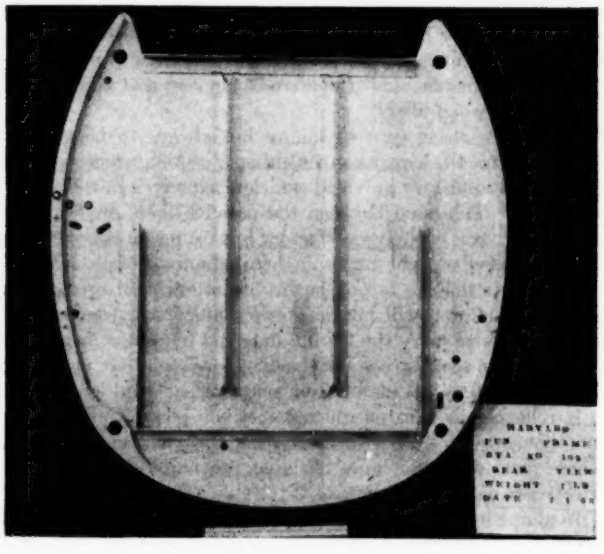


FIG. 8 VIEW OF FRONT BULKHEAD

assembly is sealed in a rubber bag and cooked with steam in the autoclave for about 35 min at a temperature of 240 F and a pressure of 30 psi.

Fig. 8 is a view of the front bulkhead. Plastic pads again transmit shear loads from the fittings to the frame. It will be observed that we have borrowed a leaf from metal practice in using molded top-hat sections to stiffen the flat panels. We prefer to fabricate the frames separately, mounting these in a jig to glue the half-skin to the frames with cold-setting glue. Woodscrews at a liberal pitch are supplemented with webbing

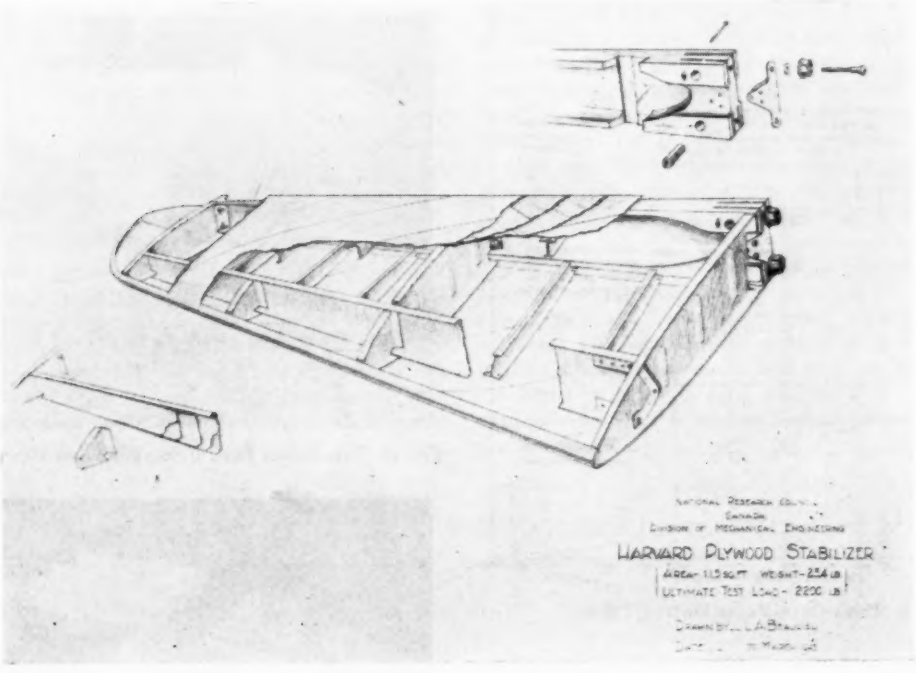


FIG. 10 STABILIZER STRUCTURE

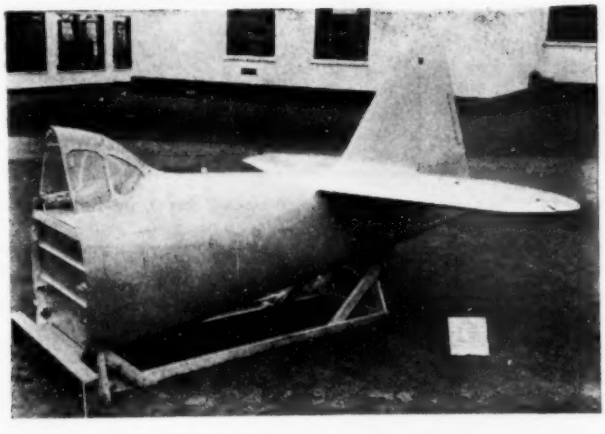


FIG. 9 COMPLETED REAR FUSELAGE

at appropriate sections to apply the pressure and, with the drying accelerated by infrared lamps, the entire operation is completed in less than 1 hr.

The fuselage, Fig. 9, was static-tested in six different flight and landing conditions and proved well up to design requirements. Weighing 154 lb, as tested, it has carried a down load on the tail equal to the design breaking load for a Spitfire fighter aircraft. In the landing attitude it has sustained a tailwheel reaction slightly in excess of 2.5 tons.

Fig. 10 is a view of the stabilizer structure. The skin is hot-press-molded and stiffened with channel-section molded stiffeners. The ribs are also flanged and bonded in a rubber bag. For the rear spar we chose an I-beam section with the grain in the plywood web running diagonally. The root fitting consists of a pair of ball-and-socket joints attached to trunnions. These trunnions transmit the loads to a phenolic laminate inserted in the spar flanges. The total stabilizer weight is 23 lb. On test it carried 2200 lb without evidence of distress.

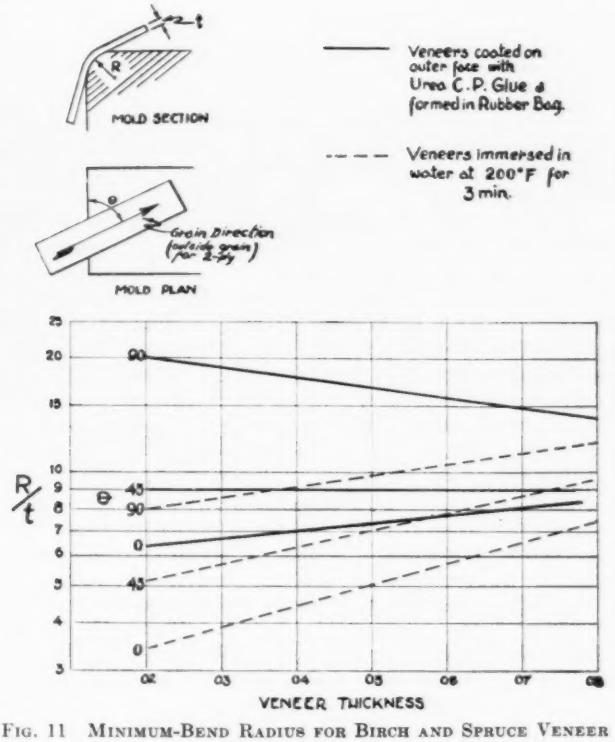


FIG. 11 MINIMUM-BEND RADIUS FOR BIRCH AND SPRUCE VENEER AND TWO-PLY PLYWOOD

The elevator is similar in construction to the stabilizer shown in Fig. 10. The skins and stiffeners are assembled on the bench and then glued to the channel-section spar and end ribs in one operation. Finally the molded leading edge is glued in place. The complete weight less mass balance is 13 lb. The structure failed at a test load of 1040 lb or 140 per cent of the design load.

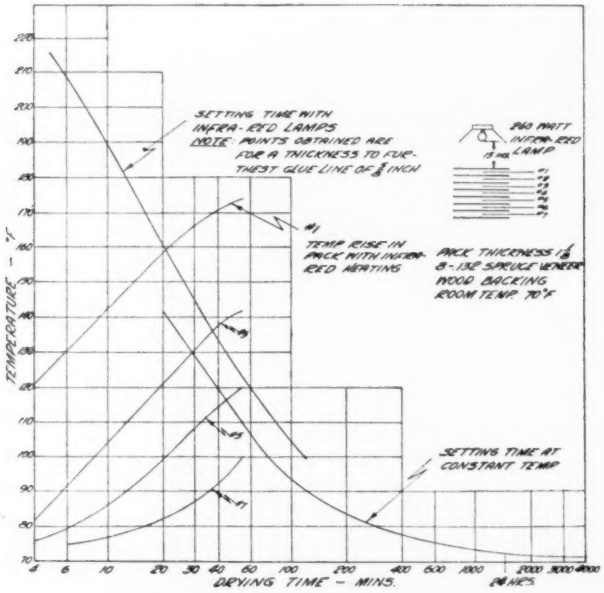


FIG. 12 UREA COLD-PRESS DRYING TIME

With the rudder, as in the foregoing components, we endeavored to make the skin the major structural element. The bottom fairing which is detachable is composed of fabric impregnated with urea-formaldehyde resin, and molded in the autoclave. Weighing 18 lb complete with mass balance, it was tested to 150 per cent of the design load without any evidence of failure.

One of the first things one needs to know in designing these structures is a safe bend radius to use with the various veneer thicknesses. Fig. 11 gives values which we consider to be a practical minimum.

Infrared lamps will greatly accelerate the drying of cold-setting resin adhesives. Fig. 12 indicates the time required to achieve a reasonable shear strength at a constant temperature. The time is very considerable at the temperatures which frequently prevail in workshops. Referring to Fig. 12, the time-temperature curves for a thick pack of veneers exposed to an infrared lamp are given. As a simple example, consider a glue line $^1/_8$ in. below the surface. During the first 8-min interval, the average temperature is roughly 120 F. At that temperature, we see from this curve the total time required would be 40 min for the glue to set. Therefore, in 8 min we obtain 20 per cent of the required cooking. During the next interval, the average temperature is about 145 F, and the total time required would be 20 min. Therefore, in 8 min, we obtain an additional 40 per cent of the required cooking. Adding the percentages to a total of 100 per cent, we obtain the required time with this lamp and distance to set a glue line $^1/_8$ in. below the surface. This curve is based on experimental results with a $^5/_8$-in. panel and shows the considerable time saving which can be realized.

THE TECHNIQUE OF BAG MOLDING

No description of the bag-molding art is necessary, as it has received a good deal of attention in the literature lately. Lockheed employed the fluid-pressure idea 15 years ago to produce a number of extremely refined plywood airplanes, but the production possibilities of the method have only recently received attention. The wooden mold, rubber bag, and autoclave, as currently used, form a convenient arrangement for experimental work but suffer numerous drawbacks for large-scale production.

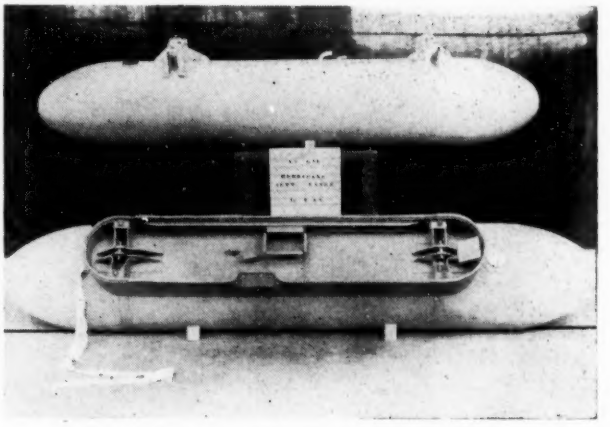


FIG. 13 DISPOSABLE FUEL TANKS FOR LONG-RANGE FIGHTER PLANES

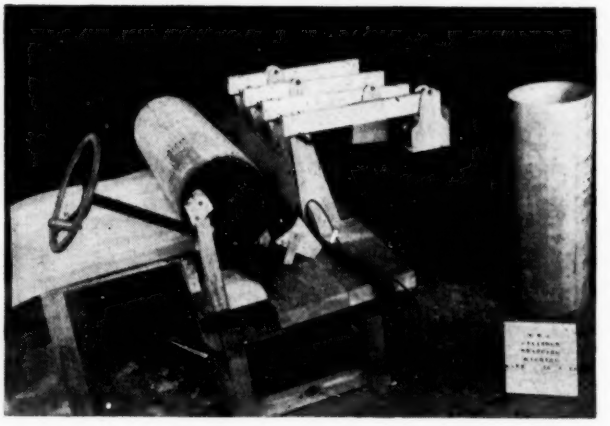


FIG. 14 COLLAPSIBLE DRUM FOR WINDING SHELL OF FUEL TANK

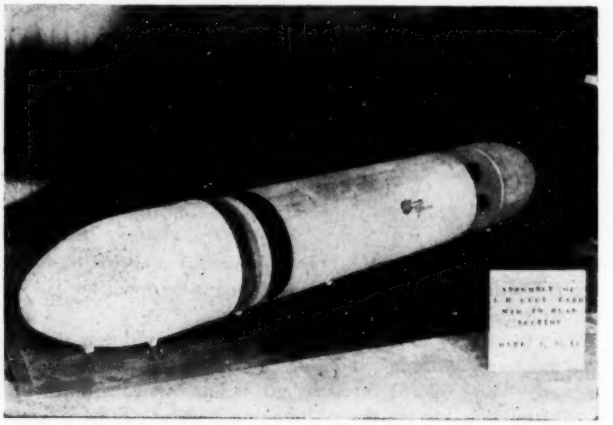


FIG. 15 ASSEMBLY OF CENTER SECTION, DOUBLER RINGS, AND LAMINATED END SECTIONS OF FUEL TANK

Wooden molds are woefully impermanent when subjected to frequent heating and cooling cycles, a great deal of time and heat are wasted in cooking the great bulk of the mold, and its size and general awkwardness present a considerable handling problem not to mention the wear and tear on rubber bags. Alternative methods are in use with varying degrees of success, but we believe that a metal mold in the majority of production applications will quickly pay for itself. The form is metal, and internally

heated, preferably with steam. The veneer-and-glue assembly is placed on the form and stapled to wooden inserts at the edges. Over this assembly is placed a reasonably airtight blanket; it does not need to be rubber and even a few leaks do not matter. Finally a light outer shell is dropped in place and sealed. Compressed air can therefore provide the pressure independently of the temperature. We have performed a number of cookings on a unit of this type; the temperature rise is extremely rapid and the results uniformly satisfactory.

Forming Fuel Tanks to Be Jettisoned

Another plywood enterprise in which we have been engaged is a jettisonable or disposable fuel tank for a long-range fighter aircraft, Fig. 13. The machines carry two of these tanks, one under each wing, and when the fuel is consumed the tanks are dropped. Therefore cheapness and simplicity of construction are essential.

We start with a two-ply veneer which is wound on a collapsible drum, shown in Fig. 14. Metal bands are loaded with a lever weight arrangement to apply pressure. Infrared lamps supply the heat necessary to set the cold-press resin as the two-ply ribbon is wound on the drum. The nose and tail are of the same shape and are composed of 5 layers of two-ply hot-press-molded wood. Laminated rings, which also carry the loads from the attachment fittings, serve as doublers between the ends and the cylindrical portion, Fig. 15. Pipe and attachment fittings are riveted in place first, then the ends are glued on and a fairing added. The tanks are flushed with a gasoline-resistant sealing compound, pressure-tested, and with a coat of paint are ready for service.

We have performed a number of tests on these tanks but none so drastic as that which recently occurred when one laden with 100-octane fuel was accidently released from an aircraft about to land. The tank dropped a distance of 4 or 5 ft and commenced a journey across the field at some 100 mph. Although enveloped in spray, it did not ignite and despite considerable damage was still a complete unit when retrieved by the somewhat shaken ground crew.

Pressure Loss in Elbows and Duct Branches

By ANDREW VAZSONYI,[1] CAMBRIDGE, MASS.

The pressure loss in a duct branch is a function of at least six independent variables, and there is no complete set of data available for correlation. Equations [II] and [III] of this paper are derived on a theoretical and experimental basis. These equations correlate all available data with fair accuracy with the aid of four experimental curves (Figs. 2, 3, and 5). Furthermore, they permit prediction of probable pressure losses for ducts heretofore untested. Similar formulas can be derived for elbows, diffusers, contracting passages, and other configurations, e.g., Equation (1) presents losses for elbows.

Nomenclature

The following nomenclature is used in the paper:

A = area of cross section
d = diameter of pipe
f = friction factor
h = mixing loss = total loss — friction loss (given in Equation [9])
H = total loss = $(p_1 + {}^1/_2 \rho V_1^2) - (p_2 + {}^1/_2 \rho V_2^2)$
l = length of pipe
p = pressure
P = circumference of pipe
Q = mass rate of flow
V = velocity
$\bar{V}$ = mean velocity based on mass rate of flow
α, β, γ = angle of deflection in elbow or branch pipe
α', β', γ' = effective angle of deflection of stream
ρ = density
τ = shear force on wall of duct
λ = new loss coefficient
η = diffuser efficiency
ζ = standard loss coefficient

Introduction

When the practicing engineer is confronted with the problem of predicting pressure losses in ducts, he can find little help from the available literature. There are so many different types of ducts that one could hardly expect to chance upon the one desired. However, it is somehow expected that a duct system can be separated into different types of "elementary" ducts, and one hopes that knowing pressure losses for these elementary ducts, the total pressure loss in a duct system can be predicted by summation. Therefore it is very desirable to know pressure losses for a great variety of ducts, and indeed a vast number of experiments have been run for this purpose. Unfortunately, nothing like a convenient and practical summary of data exists. Furthermore, often the available material is somehow confused, even contradictory.

The subject of this paper is the presentation of losses for duct branches, and so let us examine this configuration in detail. What does the pressure loss depend upon in this duct system? In order to obtain any answer, we have first to specify completely the configuration considered. Let us assume that we have three circular pipes "meeting" at a point. In order to avoid flow disturbances by the entrance and exit, let us assume that all the pipes are very long. Now we have a well-defined elementary duct, and we can ask for the pressure loss in this duct. The pressure loss will obviously depend (at least) upon the following quantities: The diameters of the pipes; the respective fluid velocities; the angles of inclination of the branching pipes; roughness of the wall; and the kinematic viscosity of the fluid—altogether ten variables.

Using the continuity equation and similarity considerations, four of these variables can be eliminated and the remaining six can be listed as follows: Ratios of exit areas to inlet area; ratio of velocities in two of the pipes; the branching angles; friction factor. No more reduction in the number of variables is possible and experiments have shown that all these variables are of major importance. Hence we see that to obtain a complete survey of the losses would necessitate an enormous number of experiments. But even if all these data were known, how could they be put into a useful form for the designing engineer? The situation is somehow similar to that of the friction-factor data at the time when the Reynolds number was not yet used.

Investigators of the Hydraulic Institute of the Technical University of Münich have run extensive tests on duct branches (13, 28, 30, 35).[2] Nine different configurations were selected. In all of them there is a main pipe continuing ahead; the duct branch forms an angle of 30, 45, or 90 deg with the main pipe; the ratio of the diameter of the branch pipe to that of the main pipe is $\frac{15}{43}, \frac{25}{43}, \frac{43}{43}$.

The pressure loss is expressed as a fraction of the kinetic energy (per unit of mass) of the fluid in the main pipe, as is customary for friction-factor data. For the independent variable the ratio $\frac{Q_1}{Q_0}$ is used. We have replotted these curves, using the velocity ratio $\frac{V_1}{V_0}$ for the independent variable, as this appears to suit better the nature of the problem, e.g., Fig. 10 shows losses for three different duct branches, each of them having an angle of deflection of 45 deg. The data lie fairly well on one and the same curve, and so one curve replaces the three different curves given in the original papers. Figs. 11 and 12 show two further curves of the many presented by the German investigators. It can be seen that the pressure-loss coefficient varies between —10 and +45. (Negative pressure-loss coefficients indicate pressure rises.) Similar curves can be found in the original papers for the nine configurations, and also for some slightly different ducts. But let us suppose we do not have a duct with an angle of 30, 45, or 90 deg, or the area ratios do not check with those tested. The coefficients vary so much, that interpolation can be of little help.

The pressure-loss-data presentation as a fraction of the kinetic energy of the main pipe is a fully arbitrary one, and its only justification is that it works well for straight pipes. As it is certainly not satisfactory in the duct-branch case, why not use some combination of the kinetic energies of the different pipes of the duct system? The difficulty now is how to select suitable formulas.

[1] Teaching Fellow in Mechanical Engineering, Graduate School of Engineering, Harvard University.

Contributed by the Heat Transfer Division and presented at the Annual Meeting, New York, N. Y., Nov. 29–Dec. 3, 1943, of The American Society of Mechanical Engineers.

Note: Statements and opinions advanced in papers are to be understood as individual expressions of their authors and not those of the Society.

[2] Numbers in parentheses refer to the Bibliography at the end of the paper.

In this paper a trial is made in this direction. First of all the pressure loss is divided into two parts, i.e., friction loss and mixing loss. The former can be determined by the knowledge of the friction factor; the latter is supposed to be (approximately) independent of the wall roughness. After some theoretical investigation, formulas are derived for the mixing loss. There are experimental coefficients in these formulas which are determined to fit the available test data. The main results are as follows:

Elbow Losses:

$$2h_{12} = V_1^2 + (2\lambda - 1)V_2^2 - 2\lambda V_1 V_2 \cos \alpha \ldots\ldots [I]$$

where for circular elbow $\lambda = 0.6$, for rectangular elbow $\lambda = 0.75$.

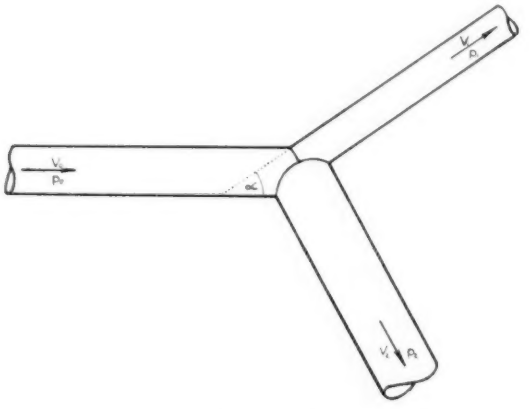


FIG. 1 DUCT BRANCH WITH SEPARATING FLOW

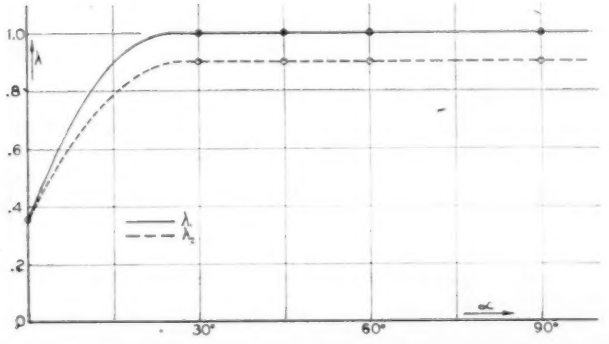


FIG. 2 PRESSURE LOSS IN DUCT BRANCH WITH SEPARATING FLOW
(λ_1 and λ_2 of Equation [II], as functions of angle of deflection α.)

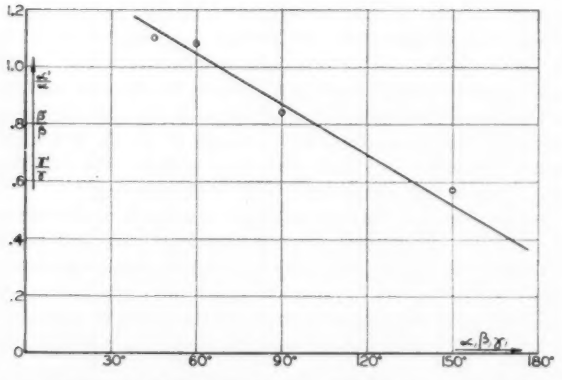


FIG. 3 EFFECTIVE ANGLE OF DEFLECTION AS FUNCTION OF ANGLE OF DEFLECTION; EQUATIONS [II] AND [III]

Straight Pipe Branching Into Two Pipes:

$$2h_{01} = \lambda_1 V_0^2 + (2\lambda_1 - \lambda_2)V_1^2 - 2\lambda_2 V_0 V_1 \cos \alpha' \ldots\ldots [II]$$

where λ_1, λ_2, α' are functions of α given in Figs. 2 and 3.

Two Straight Pipes Discharging Into One Pipe:

$$2h_{10} = \lambda_3 V_1^2 + V_0^2 - 2V_0\left(\frac{V_1 Q_1}{Q_0}\cos\beta' + \frac{V_2 Q_2}{Q_0}\cos\gamma'\right). [III]$$

where λ_3 is a function of β given in Fig. 5, β' and γ' are functions of β and γ in Fig. 3.

THE ENERGY LOSS

Consider some kind of duct system. The law of conservation of energy states that

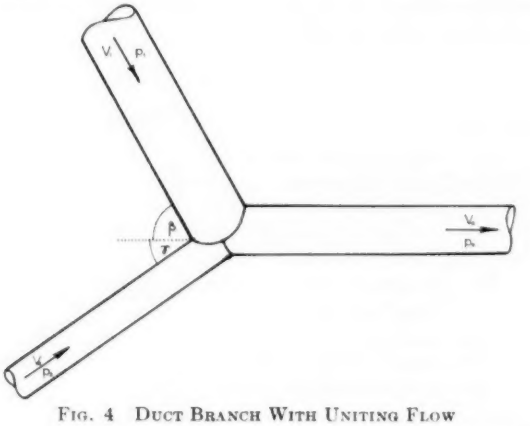


FIG. 4 DUCT BRANCH WITH UNITING FLOW

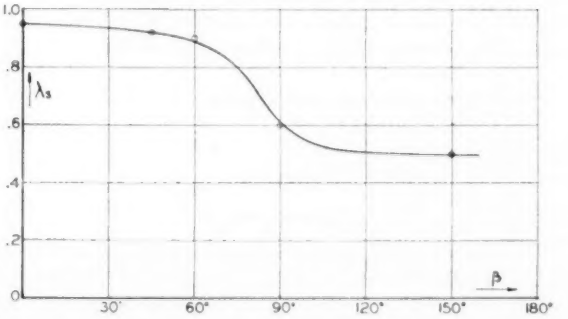


FIG. 5 PRESSURE LOSS IN DUCT BRANCH WITH UNITING FLOW
(λ_3 of Equation [III] as function of β the angle of deflection.)

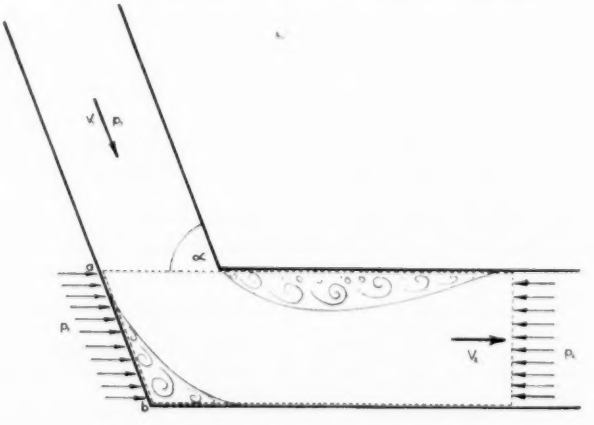


FIG. 6 PRESSURE LOSS IN A MITER ELBOW
(Dotted lines enclose section to which momentum equation is applied.)

$$\int_{A_1}\left(p+\frac{1}{2}\rho V^2\right)VdA = \int_{A_2}\left(p+\frac{1}{2}\rho V^2\right)VdA + \rho HQ \ldots [1]$$

where Q is the mass rate of flow and H is the work done by the fluid per unit of mass flow. By definition, H is the loss through the duct system. In what follows, we will consider only incompressible fluids, and so we can assume that ρ is constant.

Straight Pipe

Consider the case of a straight pipe and assume that p is constant across the pipe. Then Equation [1] can be written in the form

$$\frac{p_1}{\rho}+\frac{1}{Q}\int_{A_1}\frac{1}{2}V^3dA = \frac{p_2}{\rho}+\frac{1}{Q}\int\frac{1}{2}V^3dA + H \ldots [2]$$

Now, if we further assume that we are dealing with a steady-state case, i.e., the velocity profile is everywhere the same, we get

$$\frac{p_1-p_2}{\rho} = H \ldots [3]$$

Writing the momentum equation for the case considered, we get

$$A(p_1-p_2) = Pl\tau \ldots [4]$$

where P is the circumference of the pipe and τ is the shear force on the wall. Introducing the friction factor

$$f = \frac{\tau}{\frac{1}{2}\rho V^2} \ldots [5]$$

we get

$$\frac{p_1-p_2}{\frac{1}{2}\rho V^2} = f\frac{lP}{A} \ldots [6]$$

and for the loss

$$\frac{H}{\frac{1}{2}V^2} = f\frac{lP}{A} \ldots [7]$$

Equations [6] and [7] show that the pressure drop along the pipe measures the energy dissipation. It is important to emphasize that this is true only in the case of a straight pipe, and under the assumption made that the velocity profiles are the same along the pipe.

More General Ducts

Let us now consider Equation [1] in a more general case, e.g., a diffuser or elbow. In order to determine the loss, it is necessary to measure the pressure and the velocity across the entrance and exit areas and to integrate Equation [1]. This is a much too elaborate procedure, and so it is usually assumed that both p and V are constant across the cross sections. This condition is sufficiently well approximated for turbulent flows by inserting a long straight pipe before and after the duct. Then Equation [1] becomes

$$p_1+\frac{1}{2}\rho V_1^2 = p_2+\frac{1}{2}\rho V_2^2 + H \ldots [8]$$

or the loss is given by the difference of the total pressures. It is to be emphasized that Equation [8] holds true only when both p and V are constant across the entrance and exit areas. Some investigators have used the total pressure difference as the loss for cases where these conditions did not hold, and obtained contradic-

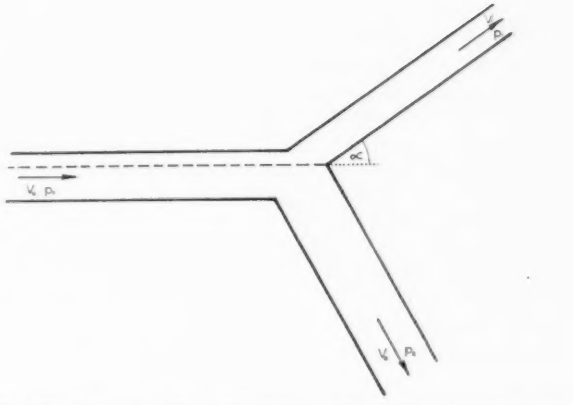


Fig. 7 Duct Branch With Separating Flow Decomposed Into Two Miter Elbows

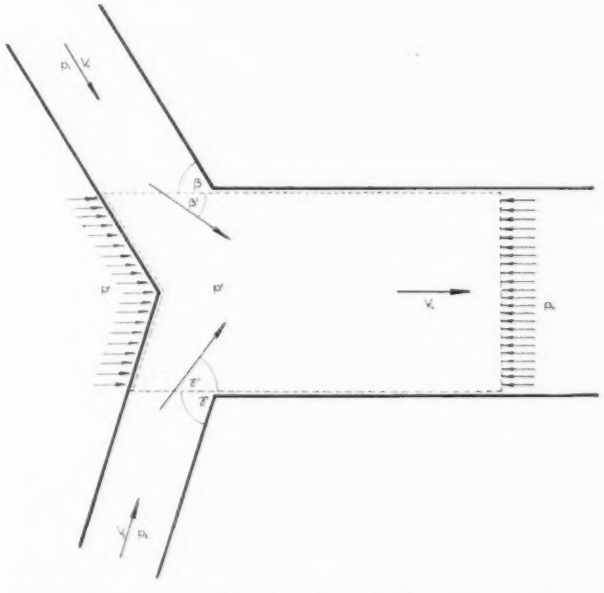


Fig. 8 Pressure Loss in Duct Branch With Uniting Flow
(Dotted lines enclose section to which momentum equation is applied.)

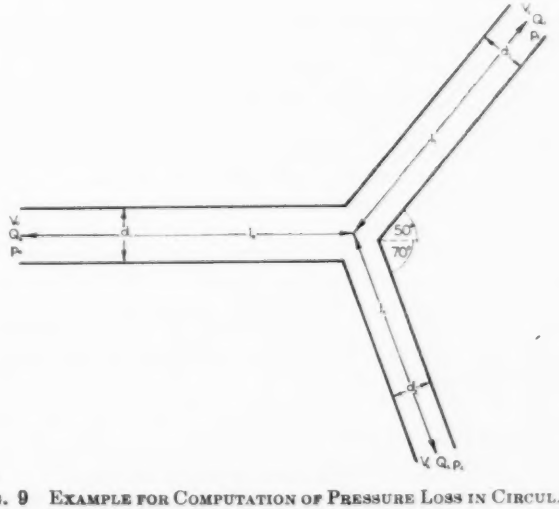


Fig. 9 Example for Computation of Pressure Loss in Circular Duct Branch With Separating Flow

tory loss coefficients. It makes considerable difference whether an elbow discharges into open air or into another pipe. In the latter case there is a recovery in the static pressure, while in the former case the losses are much higher. From now on it will be assumed that we are considering ducts for which Equation [8] can be used.

Obviously, the lengths of the inserted pipes before and after the duct are of extreme importance for the tests. Probably a pipe 50 diam in length is long enough to dissipate disturbances. However, there are examples where disturbances prevail for a distance of over 100 diam. It appears that a rotation of the flow (as for instance after a double elbow) persists for a particularly long distance.

Friction and Mixing Loss

The loss in a duct will obviously depend upon the wall roughness, besides the geometry of the duct, the velocities, etc. How-

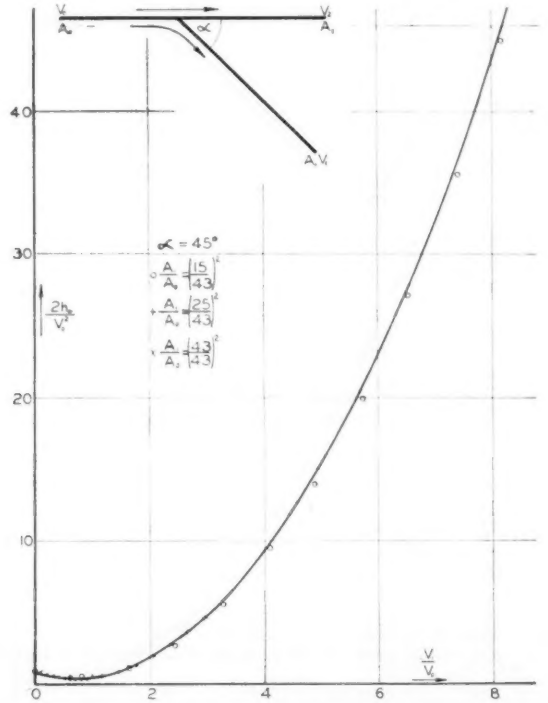


Fig. 10 Pressure Loss in Circular Duct Branch With Separating Flow, Expressed as Fraction of Kinetic Energy of Entering Fluid

(Angle of deflection 45 deg; diameter ratio d_1/d_0 = 15/43, 25/43, 43/43. Data from Bibliography (28), pp. 106, 107, 108.)

ever, it is possible to divide the losses into two groups "the friction loss" and the "mixing loss." Consider the duct "straightened out" in such a way that the center line becomes straight but its length is unchanged. This is a rather indeterminate procedure in general but rather well defined for elbows or a system of long pipes. The loss due to wall friction in the straightened-out duct of the same center-line length is the so-called friction loss of the original duct. The remaining part will be called the mixing loss. Consider, for example, an elbow; then Equation [8] can be written in the form

$$p_1 + \frac{1}{2}\rho V_1^2 = p_2 + \frac{1}{2}\rho V_2^2 + \frac{f_1 l_1 P_1}{A_1} \cdot \frac{1}{2}\rho V_1^2 + \frac{f_2 l_2 P_2}{A_2} \cdot \frac{1}{2}\rho V_2^2 + h\rho \quad \ldots\ldots [9]$$

where h is now the mixing loss by definition. Experiments have shown that h does not vary too much when the wall roughness varies while, obviously, the total loss varies considerably with the roughness, both entrance and exit pipes being necessarily

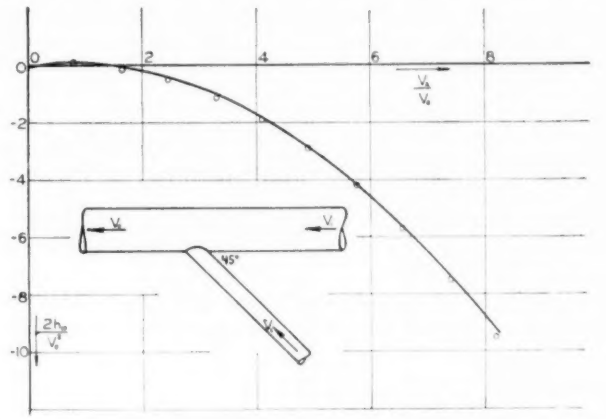


Fig. 11 Pressure Loss in Circular Duct Branch With Uniting Flow Expressed as Fraction of Kinetic Energy of Leaving Fluid

(Angle of deflection 45 deg; diameter ratio d_2/d_0 = 15/43. Data from Bibliography (28), p. 106.)

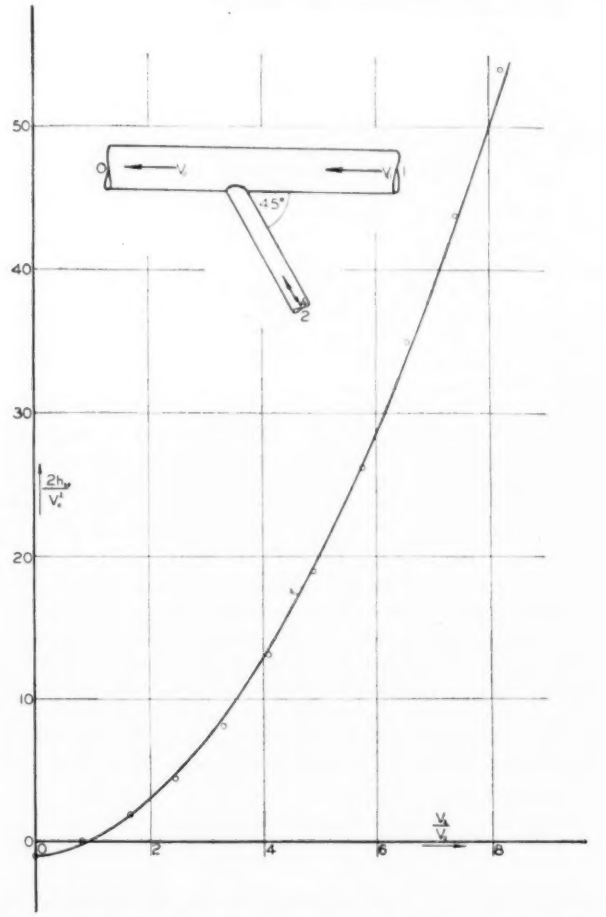


Fig. 12 Pressure Loss in Circular Duct Branch With Uniting Flow, Expressed as Fraction of Kinetic Energy of Leaving Fluid

(Angle of deflection 45 deg; diameter ratio d_2/d_0 = 15/43. Data from Bibliography (28), p. 107.)

long. Furthermore, the total loss depends also upon the lengths of the exit and entrance pipes.

Miter Elbow

In order to develop an appropriate formula for this duct, let us consider first qualitatively what happens to the fluid in this passage.

Let us assume that the angle of deflection is small. The elbow acts as a diffuser and little turbulence occurs in the passage. Diffuser losses have been successfully correlated with the expression

$$2h = (1 - \eta)(V_2^2 - V_1^2) \quad [10]$$

where η is the efficiency of the diffuser, and it might be expected that elbows with a small angle of turn can be correlated with the same formula.

On the other hand, let us consider the case when the angle of turn is large. In this case, considerable turbulence occurs in the fluid and we have a situation similar to that of the suddenly enlarging pipe. But it is known that for this case the so-called Carnot formula, which is based on the momentum equation, works very well (33). So we are going to try to use the momentum equation for an elbow. The pressure in the dead-water region is unknown, and so we write the momentum equation in the direction of the leaving fluid, eliminating thereby this unknown pressure. We assume, furthermore, that the pressure on the wall $a - b$ (Fig. 6) equals p_1, the initial pressure. The momentum equation yields

$$p_1 A_2 + \rho V_1^2 A_1 \cos \alpha = p_2 A_2 + \rho V_2^2 A_2 \quad [11]$$

where it is assumed that the fluid enters under an average angle α and that the effect of wall friction is negligible. Combining

$$p_1 + \frac{1}{2}\rho V_1^2 = p_2 + \frac{1}{2}\rho V_2^2 + h\rho \quad [12]$$

with Equation [11], we get for the mixing loss

$$2h = V_1^2 + V_2^2 - 2V_1 V_2 \cos \alpha \quad [13]$$

This equation is not to be expected to be exact because of our assumptions. So we complete it with an experimental coefficient

$$2h = \xi(V_1^2 + V_2^2 - 2V_1 V_2 \cos \alpha) \quad [14]$$

Now we have two different expressions for the elbow loss, Equations [10] and [14], and we combine the two expressions to get

$$2h = \xi(V_1^2 + V_2^2 - 2V_1 V_2 \cos \alpha) + (1 - \eta)(V_2^2 - V_1^2) \quad [15]$$

or

$$2h = \lambda_4 V_1^2 - 2\lambda V_1 V_2 \cos \alpha + (2\lambda - \lambda_4) V_2^2 \quad [16]$$

Now let us consider an elbow with an extremely narrow inlet pipe, where $V_2 = 0$. Obviously, all the entering kinetic energy will be dissipated and so we get $\lambda_4 = 1$. Hence the final formula is

$$2h_{12} = V_1^2 - 2\lambda V_1 V_2 \cos \alpha + (2\lambda - 1) V_2^2 \quad [17]$$

Fig. 13 shows losses for a circular miter elbow with equal entrance and exit cross sections. Putting $\lambda = 0.6$ in the formula, a curve results which fits the data well. Fig. 14 shows losses for rectangular elbows. The experimental points are too badly scattered to get a reliable estimate of λ. But by considering the limiting case when fluid is discharged from a large container into a pipe, it appears that $\lambda = 0.75$ is a good value.

Pipe Branches With Separating Flow

Consider the branch pipe composed of two elbows, as shown in Fig. 7. Then we can apply our elbow formula, Equation [16], to each of these elbows. We get for the mixing loss in the branch pipe

$$2h_{01} = \lambda_1 V_0^2 + (2\lambda_1 - \lambda_3) V_1^2 - 2\lambda_0 V_0 V_1 \cos \alpha' \quad [18]$$

where we assume that the fluid leaves the branch pipe through opening 1 at an average angle of α'. This angle will be called the effective angle of turn. In order to determine λ_1 we consider experiments when all the fluid is discharged through opening 2. Then $V_1 = 0$ and an experimental curve for λ_1 can be drawn. This curve is plotted in Fig. 2. Then by drawing best fitting

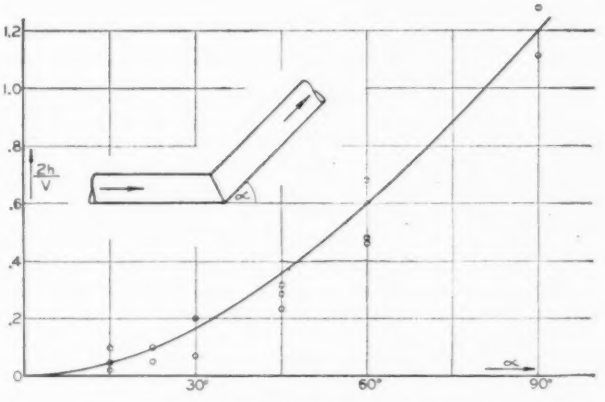


Fig. 13 Pressure Loss in Circular Elbow, Expressed as Fraction of Kinetic Energy of Fluid
(Inlet diameter equals exit diameter. Data from Bibliography (34).)

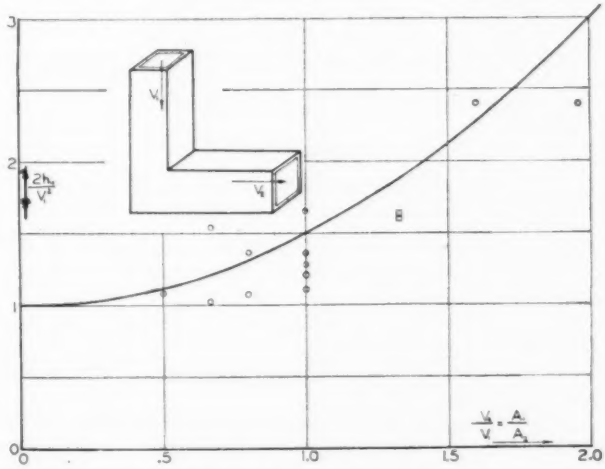


Fig. 14 Pressure Loss in Various Rectangular Elbows With 90-deg Angle of Deflection, Expressed as Fraction of Kinetic Energy of Entering Fluid
(Data from Bibliography (10), (25), (34).)

curves, λ_3 and the effective angle of turn are determined as functions of α (Figs. 2 and 3).

Pipe Branch With Uniting Flow

The derivation of the loss formula for this case will be briefly indicated. Let p' be the "average" pressure in the section of the duct where the two entering fluid streams meet (see Fig. 8). The inlet pipes act as diffusers, and so it is to be expected that the values of p' can be correlated with a formula similar to Equation [10]. This is indeed the case, and the unknown coefficients can be determined from the special experimental cases when $V_1 = 0$ or $V_2 = 0$. After p' has been determined in this fashion,

the momentum equation can be used in the direction of the leaving flow as indicated in Fig. 8. The final result is Equation [III] of the introduction.

Example

Problem. Determine the pressure loss with uniting flow through the duct in Fig. 9, assuming that the rate of flow through pipes 1 and 2 is given as Q_1 and Q_2.

Solution. First we determine the velocities in the pipes

$$V_0 = \frac{4(Q_1 + Q_2)}{\pi {d_0}^2}, \quad V_1 = \frac{4Q_1}{\pi {d_1}^2}, \quad V_2 = \frac{4Q_2}{\pi {d_2}^2} \ldots\ldots [19]$$

Now, knowing the velocities, we can compute the Reynolds number and look up the friction factors corresponding to the given wall roughness, and determine the friction loss as follows

$$\text{Friction loss from 0 to 1} = \frac{4f_0 l_0}{d_0} + \frac{4f_1 l_1}{d_1} \ldots\ldots [20a]$$

$$\text{Friction loss from 0 to 2} = \frac{4f_0 l_0}{d_0} + \frac{4f_2 l_2}{d_2} \ldots\ldots [20b]$$

In order to get the mixing loss, we have to find the effective angle of turn and the λ_1, λ_2 values corresponding to the angles 50 and 70 deg. We find from Figs. 2 and 3

when $\alpha = 50$ deg, then $\alpha' = 55$ deg, $\lambda_1 = 1, \lambda_2 = 0.9, 2\lambda_1 - \lambda_2 = .2$

when $\alpha = 70$ deg, then $\alpha' = 68.5$ deg, $\lambda_1 = 1, \lambda_2 = 0.9, 2\lambda_1 - \lambda_2 = .2$

Putting these values into Equation [II], we get for the mixing loss

$$2h_{01} = V_0^2 + 0.2V_1^2 - 1.8V_0V_1 \cos 55 \text{ deg} \ldots\ldots [21a]$$

$$2h_{02} = V_0^2 + 0.2V_2^2 - 1.8V_0V_2 \cos 68.5 \text{ deg} \ldots\ldots [21b]$$

From Equations [20] and [21], we get the total loss by addition.

Conclusions

The results and methods of this paper are believed useful in the following respects:

1 The formulas presented permit the calculation of losses in many duct branches by reasonably accurate correlation of sparse test data.

2 The number of curves required to present experimental data can be greatly reduced.

3 The method is applicable to many other configurations, including diffusers.

4 The formulas obtained by the method presented point the way to necessary tests in future test programs.

Acknowledgment

The author wishes to expresses his appreciation to Prof. H. W. Emmons of Harvard University for the suggestion of the subject and for his invaluable aid in the work.

BIBLIOGRAPHY

1 "Hydraulics, With Working Tables," by E. S. Bellasis, fifth edition E. & F. N. Spon, Ltd., London, England; Spon & Chamberlain, New York, N. Y., 1931.

2 "Plötzliche Umlenkung (Stoss) von Wasser in geschlossenen unter Druck durchströmten Kanälen," by R. Bambach, FAGI, Bulletin 327, 1930.

3 "Versuche über die Strömungsvorgänge in erweiterten und verengten Kanälen," by H. Hochschild, FAGI[3], Bulletin 114, 1912.

4 "Handbuch der Experimentalphysik," Akademische Verlagsgesellschaft M.B.H., Leipzig, vol. 4, 1932, sect. 4, Pipes.

5 "Handbuch der Physik," J. Springer, Berlin, vol. 7, 1927, chapt. 2, sect. IV, p. 139.

6 "Der Verlust in 90° Rohrkrümmern mit gleichbleibendem Kreisquerschnitt," by A. Hofmann, MHIM,[4] Bulletin 3, 1929, pp. 45–67.

7 "Die Energieumsetzung in saugrohrähnlich-erweiterten Düsen," by A. Hofmann, MHIM,[4] Bulletin 4, 1931, pp. 44–69.

8 "Hydraulik," by P. Forcheimer, third edition, B. G. Teubner, Leipzig, 1930.

9 "Verminderung des Strömungswiderstandes von Körpern durch Leitflachen," by K. Frey, FGI,[5] vol. 4, 1933, pp. 67–74.

10 "Verminderung des Strömungsverlustes in Kanälen durch Leitflächen," by K. Frey, FGI,[5] vol. 5, 1934, pp. 105–117.

11 "Angewandte Hydromechanik," by W. Kaufmann, Julius Springer, Berlin, 1934.

12 "Study of Data on Flow of Fluids in Pipes," by E. Kemler, Trans. A.S.M.E., vol. 55, 1933, HYD-55-2, pp. 7–22.

13 "Beitrage zur Kenntnis der hydraulischen Verluste in Abzweigstücken," by E. Kinne, MHIM,[4] Bulletin 4, 1931, pp. 70–93.

14 "Der Energieverlust in Kniestücken," by H. Kirchbach, MHIM,[4] Bulletin 3, 1929, pp. 68–97.

15 "Experimentelle Untersuchung der Entwicklung der Geschwindigkeitsverteilung bei der turbulenten Rohrströmung," by H. Kirsten, Leipziger Diss. Weidai. Thur. 1927.

16 "Die Entwicklung der Geschwindigkeitsverteilung bei der turbulenten Rohrströmung," by L. Schiller and H. Kirsten, *Zeit. für Technische Physik*, vol. 10, 1929, pp. 268–274.

17 "Strömungsform und Durchflusszahl der Messdrosseln," by F. Kretschmer, FGI,[5] vol. 7, 1936, p. 312; also FAGI,[3] Bulletin 381, 1936.

18 "Versuche über Strömungen in stark erweiterten Kanälen," by R. Kroner, FAGI,[3] Bulletin 222, 1920.

19 "Strömungserscheinungen in rotierenden Rohren," by F. Levy, FAGI,[3] Bulletin 322, 1929, pp. 18–45.

20 "Pressure Losses in Rectangular Elbows," by R. D. Madison, and J. R. Parker, Trans. A.S.M.E., vol. 58, 1936, pp. 167–176.

21 "Einfluss der Querschnittsverformung auf die Entwicklung der Geschwindigkeits und Druckverteilung bei turbulenten Strömungen in Rohren," by E. Mayer, FGI,[5] vol. 9, 1938, p. 108; also FAGI,[3] Bulletin 389, 1938.

22 "Über turbulente Wasserströmungen in geraden Rohren bei sehr grossen Reynoldsschen Zahlen," by J. Nikuradse, Vorträge aus dem Gebiete der Aerodynamik und verwandter Gebiete, Aachen 1929; edited by A. Gilles, L. Hopf, and Th. v. Kármán, J. Springer, Berlin, 1930, p. 63.

23 "Widerstandsgesetz und Geschwindigkeitsverteilung von turbulenten Wasserströmungen in glatten und rauhen Rohren," by J. Nikuradse, Proceedings of the 3rd International Congress for Applied Mechanics, vol. 1, 1930, pp. 239–248.

24 "Gesetzmässigkeiten der turbulenten Strömung in glatten Rohren," by J. Nikuradse, FGI,[5] vol. 3, 1932, p. 260; also FAGI,[3] Bulletin 356, 1932.

25 "Über den Strömungsverlust in Gekrümmten Kanälen," by H. Nippert, FAGI,[3] Bulletin 320, 1929.

26 "Modern Diffuser Design," by G. N. Patterson, *Aircraft Engineering*, vol. 10, 1938, pp. 267–273.

27 "The Design of Aeroplane Ducts," by G. N. Patterson, *Aircraft Engineering*, vol. 11, 1939, pp. 263–268.

28 "Der Verlust in schiefwinkligen Rohrverzweigungen," by F. Petermann, MHIM,[4] Bulletin 3, 1929, pp. 98–117.

29 "Der Reibungsverlust in Rohrleitungen, die aus überlappten Schüssen hergestellt sind," by O. Poebing and J. Spangler, MHIM,[4] Bulletin 3, 1929, pp. 118–120.

30 "Der hydraulische Verlust in Formstücken," by D. Thoma, Trans. of the Tokyo Sectional Meeting, World Power Conference, Tokyo, vol. 2, 1929, pp. 446–472.

31 "Der Druckabfall in gekrümmten glatten Rohrleitungen," by H. Richter, FAGI,[3] Bulletin 338, 1930.

32 "Curve Resistance in Water Pipes," by E. W. Schoder, Trans. A.S.C.E., vol. 62, 1909, pp. 67–96.

33 "Losses of Pressure Head Due to Sudden Enlargement of a Flow Cross Section," by H. C. Schutt, Trans. A.S.M.E., vol. 51, 1929, HYD-51-10, pp. 83–87.

34 "Der Energieverlust in Kniestücken bei glatten und rauher Wandung," by W. Schubart, MHIM,[4] Bulletin 3, 1929, p. 121.

35 "Untersuchungen über den Verlust in rechtwinkligen Rohrverzweigungen," by G. Vogel, MHIM,[4] Bulletin 1, 1926, pp. 75–90; and Bulletin 2, 1928, pp. 61–64.

[3] *Forschungsarbeiten auf dem Gebiete des Ingenieurwesens*, vom Verein deutscher Ingenieure.

[4] *Mitteilungen des Hydraulischen Institut der Technische Hochschule, Munich.*

[5] *Forschung* auf dem Gebiete des Ingenieurwesens.

36 "Verluste in glatten Rohrkrümmern mit kreisrundem Querschnitt bei weniger als 90° Ablenkung," by R. Wasielewski, MHIM,[4] Bulletin 5, 1932, pp. 53–67.

37 "Experiments at Detroit, Mich., on the Effect of Curvature Upon the Flow of Water in Pipes," by G. S. Williams, C. W. Hubbell, and G. H. Fenkell, Trans. A.S.C.E., vol. 47, 1902, pp. 1–196.

38 "New Data for Design of Elbows in Duct Systems," by L. Wirt, *General Electric Review*, vol. 30, 1927, pp. 286–296.

39 "Versuche an der hydraulischen Rückstromdrossel," by R. Zobel, MHIM,[4] Bulletin 8, 1936, pp. 3–47.

Discussion

MAURICE MARTIN.[6] The author should be commended for attempting to correlate the results of previous experiments. One of the outstanding features of previous work in this field has been the divergence of test results. This is due, of course, to the many unknown variables mentioned by the author. The writer has found that the best method for determining losses is to make and test typical duct layouts utilizing workmanship and material available to the engineer in actual construction. If this proves too cumbersome a method, the writer has found remarkable agreements in present literature on the losses in elbows and branches, i.e., "Fan Engineering" of the Buffalo Forge Company.

The writer has found that in Dr. Vazsonyi's attempt to apply the equation developed for elbows to losses in branches, he has failed to take into account the fact that the amount of air that will turn from the main and enter the branch will depend almost entirely on the resistance or back pressure set up by the entire length of branch as compared to the resistance of the remaining portion of main duct. One cannot, therefore, consider an imaginary splitter n the main to take off a definite portion of air. This is especially true in consideration of the two branches at the end of the main.

[6] Assistant Naval Architect, Navy Yard, Brooklyn, N. Y. Jun. A.S.M.E.

Most modern experiments on the subject agree that the losses in both elbows and branches can be expressed best in terms of the velocity or velocity pressure in the duct and, workmanship and other things being equal, for geometrically similar elbows and branches will depend directly on this pressure. When approached from this viewpoint I think that the author will find little disagreement in the more recent experiments.

E. O. BERGMAN.[7] Several tests of branching pipes have been made by the U. S. Bureau of Reclamation to check and extend the work of Professor Thoma. These have been published in Boulder Canyon Projects Final Reports; Part VI, Hydraulic Investigations; Bulletin 2, Model Studies of Penstocks and Outlet Works.

AUTHOR'S CLOSURE

Mr. Martin is right in stating that in certain cases "the amount of air that will turn from the main and enter the branch will depend almost entirely on the resistance or back pressure set up by the entire length of branch, etc." However, Equation [9] of the paper takes care of the resistance of the branch pipe, whereas the "mixing-loss" formulas take care only of the additional "nonfrictional" losses. This is exactly the reason why it was necessary to separate the friction loss from the mixing loss.

Mr. Martin is also right in stating that many experimenters did not pay due attention to the great number of variables and thus received contradictory results. However, it is difficult to see how such experiments could be made satisfactory by introducing new variables.

The reports quoted by Mr. Bergman were not known to the author.

[7] Technical Advisor, C. F. Braun & Co., Alhambra, Calif. Mem. A.S.M.E.

Laboratory and Field Tests on Coal-in-Oil Fuels[1]

By J. F. BARKLEY,[2] A. B. HERSBERGER,[3] and L. R. BURDICK[4]

It has been determined from extensive laboratory and field tests on the stability of coal suspensions in fuel oil that each installation must be given individual consideration if satisfactory results are to be obtained. However, no particular difficulty in devising equipment or operating routine for efficient use need be experienced. A sufficiently stable suspension of coal in oil for practical purposes can be prepared by dispersing 40 per cent coal by weight ground from 98 to 99 per cent through a 230-mesh screen in heavy fuel oil. Careful control of storage and handling temperatures is required for most successful operation. Combustion efficiency is likely to be slightly less than that of fuel oil. The best opportunity for the successful use of coal-in-oil suspension is in the larger plants with better operating personnel and more readily accessible equipment.

Introduction

THE following report covers laboratory studies on the stability of coal suspensions in oil, the mixing of pulverized coal and oil, and field tests on these mixtures in typical oil-burning equipment. This work was undertaken to obtain needed practicable information not found in technical literature, a review of which was given by Schroeder[5] in 1942. The work is the result of a joint effort by the Federal Bureau of Mines and The Atlantic Refining Company of Philadelphia, Pa. The laboratory work and preparation of the fuels were done by The Atlantic Refining Company. The main series of field tests made at The Atlantic Refining Company's Philadelphia Plant and additional tests made at the Cambria Silk Hosiery Company and the National Airoil Burner Company, both in Philadelphia, were conducted by the Bureau of Mines.

Laboratory Studies

In the laboratory, stabilities of coal-in-oil suspensions were studied by measuring the change in the center of gravity of the suspensions by means of a pendulum arrangement. This method was first used by Manning and Taylor.[6] The results are reported as the percentage of the coal settled, based on 100 per cent settled, as determined in an alcohol-water mixture. Other methods were also used to check the results obtained in this manner. Details of the procedures are given in the Appendix.

The majority of the samples were mixed by vigorous stirring under about 10-mm vacuum. This was done to avoid including air in the samples which would eventually interfere with the pendulum readings.

The absolute viscosities, reported in Figs. 1 and 2, were obtained by means of a Brookfield Synchro-lectric viscometer which had been calibrated for average rates of shear and shearing stresses. The coal used in most of the experimental work was

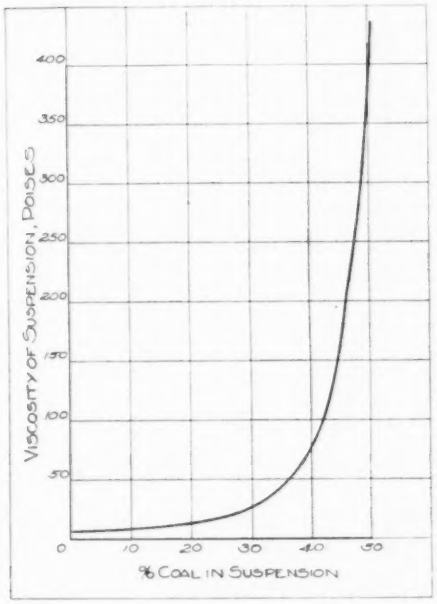


FIG. 1 VISCOSITY OF SUSPENSIONS: CURVE SHOWING EFFECT OF PERCENTAGE OF COAL IN MIXTURE ON VISCOSITY AT 77 F
(Coal No. SC-2, minus 230 mesh; No. 6 fuel oil.)

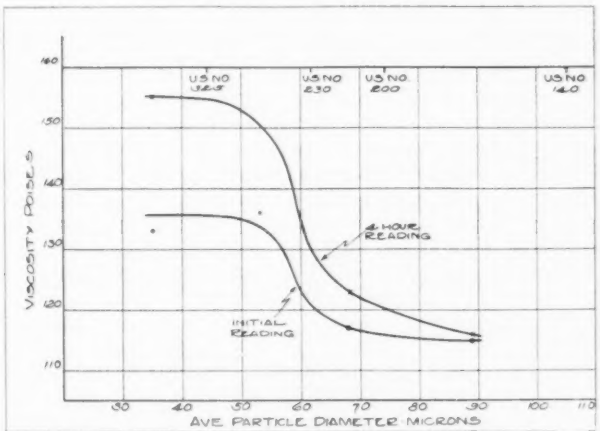


FIG. 2 VISCOSITY OF SUSPENSIONS: CURVES SHOWING EFFECT OF PARTICLE SIZE OF COAL IN MIXTURE ON VISCOSITY AT 77 F
(Coal No. SC-1, 40 per cent by weight; No. 6 fuel oil, 60 per cent by weight.)

[1] Published by permission of the Director, Bureau of Mines, U. S. Department of the Interior.

[2] Chief, Division of Solid Fuels Utilization for War, Bureau of Mines, Washington, D. C. Mem. A.S.M.E.

[3] Research and Development Department, The Atlantic Refining Company, Philadelphia, Pa.

[4] Senior Fuel Engineer, Division of Solid Fuels Utilization for War, Bureau of Mines, Washington, D. C. Mem. A. S. M. E.

[5] "Use of Mixtures of Oil and Coal in Boiler Furnaces," by W. C. Schroeder, *Mechanical Engineering*, vol. 64, 1942, pp. 793–798, 804.

[6] "Colloidal Fuel," by A. B. Manning and R. A. A. Taylor, Trans. Institution of Chemical Engineers (London, England), vol. 14, 1936, pp. 45–59.

Presented at a Joint Meeting of THE AMERICAN SOCIETY OF MECHANICAL ENGINEERS and the American Institute of Mining and Metallurgical Engineers, Fuels and Coal Divisions, Pittsburgh, Pa., Oct. 28–29, 1943.

NOTE: Statements and opinions advanced in papers are to be understood as individual expressions of their authors and not those of the Society.

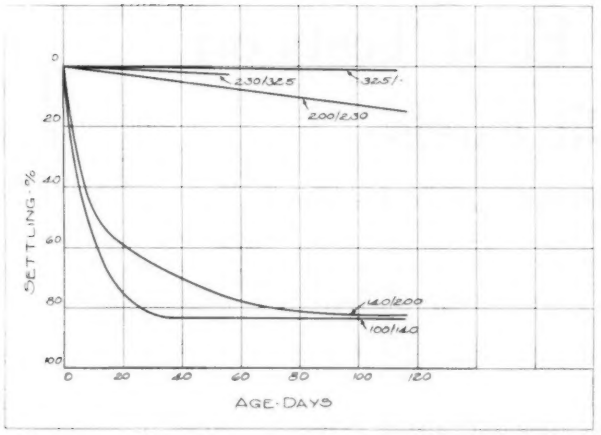


FIG. 3 STABILITY OF SUSPENSIONS: CURVES SHOWING EFFECT OF PARTICLE SIZE OF COAL IN MIXTURE ON STABILITY AT 77 F
(Coal No. SC-1, 40 per cent by weight; No. 6 fuel oil, 60 per cent by weight.)

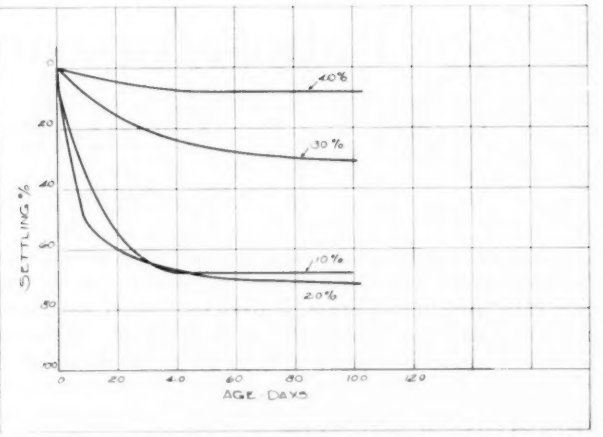


FIG. 6 STABILITY OF SUSPENSIONS: CURVES SHOWING EFFECT OF PERCENTAGE OF COAL IN MIXTURE ON STABILITY AT 77 F
(Coal No. SC-2, minus 230 mesh; No. 6 fuel oil.)

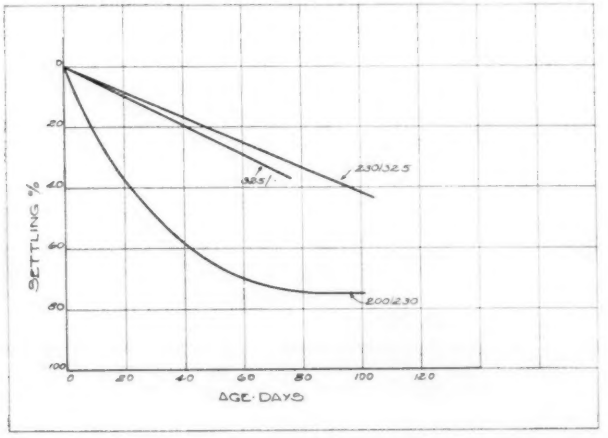


FIG. 4 STABILITY OF SUSPENSIONS: CURVES SHOWING EFFECT OF PARTICLE SIZE OF COAL IN MIXTURE ON STABILITY AT 120 F
(Coal No. SC-1, 40 per cent by weight; No. 6 fuel oil, 60 per cent by weight.)

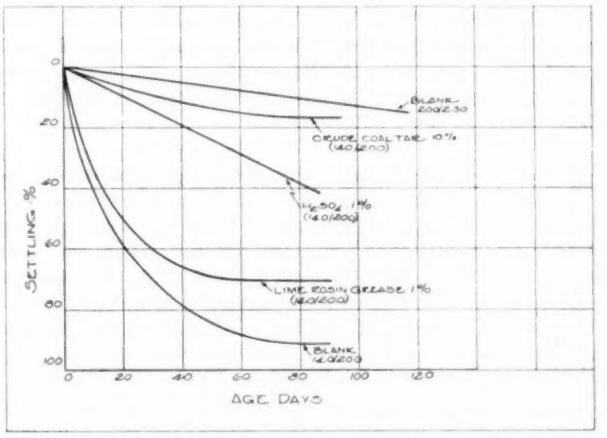


FIG. 7 STABILITY OF SUSPENSIONS: CURVES SHOWING COMPARISONS AS TO STABILITY AT 77 F, WHEN VARIOUS STABILIZING MATERIALS WERE ADDED TO COAL-IN-OIL MIXTURES
(Coal No. SC-2, 40 per cent by weight; No. 6 fuel oil, 60 per cent by weight.)

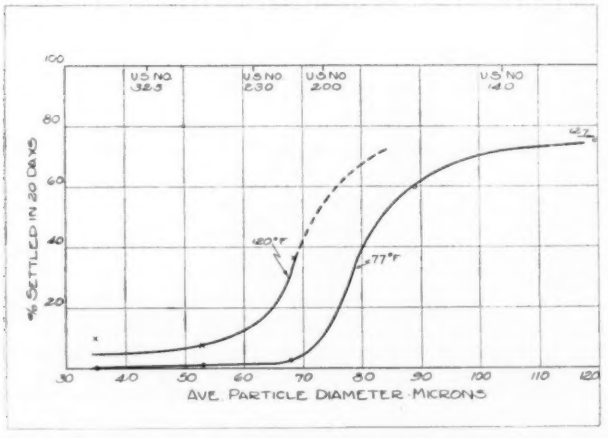


FIG. 5 STABILITY OF SUSPENSIONS: CURVES SHOWING EFFECT OF PARTICLE SIZE OF COAL IN MIXTURE ON AMOUNT OF SETTLING IN 20 DAYS
(Coal No. SC-1, 40 per cent by weight; No. 6 fuel oil, 60 per cent by weight.)

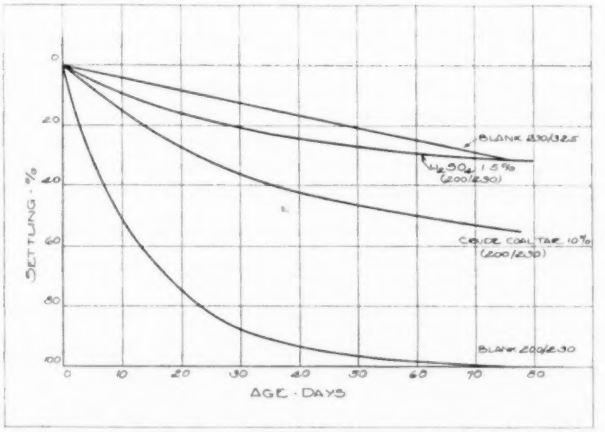


FIG. 8 STABILITY OF SUSPENSIONS: CURVES SHOWING COMPARISONS AS TO STABILITY AT 120 F, WHEN VARIOUS STABILIZING MATERIALS WERE ADDED TO COAL-IN-OIL MIXTURES
(Coal No. SC-2, 40 per cent by weight; No. 6 fuel oil, 60 per cent by weight.)

screened to narrow size ranges. The data presented in Figs. 1 to 8, inclusive, are representative of a large number of experiments. The properties of the bituminous coal and the oil used in this particular set of experiments are given in Table 1. The oil was a typical refinery product containing both straight-run and cracked components.

From consideration of elementary formulas, relating settling

TABLE 1 PHYSICAL PROPERTIES OF COALS AND OIL USED IN LABORATORY EXPERIMENTAL STABILITY STUDIES

Coal	No. SC-1	No. SC-2	No. 6 Fuel oil	
Specific gravity at 60 F	1.29	1.34	A.P.I. gravity at 60 F	14.6
Volatile, per cent	33.1	22.1	Viscosity at 122 F	56 Furol
Ash, per cent	3.5	4.5	Viscosity at 210 F	86 Saybolt
Moisture, per cent	0.7	0.4		
Fixed carbon, per cent	62.7	73.4		
Sulphur, per cent	0.78	1.19		

velocities to particle size, gravity differential between the particles, and the liquid medium and its viscosity, it was evident that the best results would be obtained by using bituminous coals (low specific gravity), and oils of high specific gravity and high viscosity. It was also evident that suspensions of high coal content would be more stable than those of low content because of hindered settling.

The actual conditions for settling in concentrated suspensions are complex. Such suspensions develop rigidity for high solids content. Coal-in-oil suspensions have been shown to develop this rigidity[7] in the neighborhood of 38 volume per cent of coal.

A number of experiments were run to determine the effect of coal concentration on the viscosity of the coal-in-oil suspension. For finely divided coals in heavy fuel oils, the viscosities of the suspension were found to rise markedly in the region of 40 to 50 per cent of coal by weight, such results being in general agreement with those reported by others. This rapid rise in viscosity in the range of 40 to 50 per cent of coal was found to be relatively independent of the viscosity of the oil and the temperature of the measurement. These suspensions were also found to be non-Newtonian, i.e., the viscosity varied with the rate of shear, this deviation from viscous flow resulting from the development of structure in the suspension. Fig. 1 shows a typical viscosity-per cent coal curve.

If it is assumed that the rigidity in concentrated coal-in-oil suspensions results from the particles touching each other, it would appear that the smaller the diameter of the particle, i.e., the larger the surface area per unit concentration of coal, the greater the interference between particles. This should be evidenced by the effect of particle size on viscosity for concentrated suspensions, other variables being constant. Fig. 2 shows the effect of particle size of the coal on the viscosity of a 40 per cent by weight suspension of coal in oil. It is seen that a rapid increase in viscosity occurs between the coal sizes of 200/230 and 230/325 mesh (U. S. Standard screen). This rapid rise in viscosity and then a flattening out may be regarded as the result of a critical increase in surface area where the interference between particles has become large. The viscosity of these suspensions was measured fresh and after aging. The positions of the two curves show that the suspensions are thixotropic, i.e., the viscosities decrease with agitation. This property is more pronounced with the smaller-size particles.

Determinations of the stability of 40 per cent by weight suspensions of bituminous coal in oil were made in which the particle size of the coal and the temperature were varied. The effect of these variables is shown graphically in Figs. 3 and 4. The suspensions are relatively stable at 77 F when the maximum particle size is not larger than 200 mesh. At 120 F a satisfactory degree of stability is obtained if the maximum particle size does not exceed 230 mesh. Fig. 5 is a plot of percentage settled in 20 days against average particle size.

It is to be noted that the marked improvement in stability occurring with decreasing particle size falls in approximately the same particle-size range as the rapid rise in viscosity occurs, as shown in Fig. 2.

[7] "Laminar Flow of Oil-Coal Suspensions," by F. J. Gradishar, W. L. Faith, and J. E. Hedrick, Trans. American Institute of Chemical Engineers, vol. 39, April 25, 1943, pp. 201–222.

The relation of the stability of the suspension to the coal concentration was determined for minus-230-mesh bituminous coal. These results are shown in Fig. 6. No worth-while degree of stability is obtained until a coal concentration of approximately 40 per cent by weight is used.

The effect of physical properties of the oil and coal on stability of suspensions was also found to be important. Oils with either low viscosity or low specific gravity, in general, gave less stable suspensions. No marked differences in the stability of suspension of bituminous coals of slightly different properties were observed, although the range of bituminous coals studied was narrow. One experiment was run on a sample of anthracite which proved to be considerably less stable than a similar suspension containing a bituminous coal. Data illustrating these facts appear in Table 2.

TABLE 2 EFFECT OF PHYSICAL PROPERTIES OF COAL AND OIL ON STABILITY OF SUSPENSION[a]

Coal			Oil		
Type	Specific gravity at 60 F	Mesh	A.P.I. gravity at 60 F	Furol viscosity at 122 F	Stability, 10 per cent settled at 120 F, days
Bituminous	1.29	230/325	14.6	56	23
Bituminous	1.29	230/325	..	29	3
Anthracite	1.56	minus 230	12.7	64	5
Bituminous	1.32	99 per cent minus 230	14.4	66	12
Bituminous	1.32	99 per cent minus 230	17.5	89	6

[a] Coal by weight, 40 per cent.

TABLE 3 EFFECT OF OVERSIZE PARTICLES ON STABILITY OF 40 PER CENT SUSPENSION OF COAL IN OIL BY WEIGHT

Size of oversize coal	Oversize coal, per cent (based on coal)	Stability 10 per cent settled at 120 F, days
Blank—230/325-mesh bituminous coal in No. 6 fuel oil	..	23
100/140	5	14
6/100	5	5

Laboratory samples were mixed by vigorous stirring under about 10-mm vacuum; other methods of mixing were also tried, such as passing the mixture through a homogenizer and ball-milling. Neither of these methods gave suspensions of better stability than those obtained by vigorous agitation of the mixture.

The coal used in the laboratory experiments was screened to a narrow range of sizes. From a practical point of view the effect of the maximum-size coal particles on the stability of the suspensions is important. The presence of small quantities of oversize particles was found to decrease the stability of the suspensions; data are shown in Table 3.

Figs. 7 and 8 show some stability tests on coal-in-oil suspensions containing stabilizers. Tests were conducted on 140/200 U. S. Standard-mesh coal at 77 F, and on 200/230-mesh coal at 120 F. Lime-resin soap (1 per cent), claimed to be an excellent stabilizer, was found to be very poor. Of all the stabilizers studied, the addition of 1 to 1.5 per cent of sulphuric acid to the coal surfaces before mixing with the oil was found to give the best results. Coal tar when used as 10 per cent of the oil mixture showed a stabilizing action. However, even these two materials, which were considerably better than any others of a large number tried, were not as effective as additional grinding of the coal, say, from minus-200 to minus-230 mesh. Also, both sulphuric acid and 10 per cent coal tar have practical disadvantages—sulphuric acid because of its probable corrosive action and coal tar because of the large quantity required.

If the criteria, from a stability and handling viewpoint, of a satisfactory coal-in-oil fuel are (1) high degree of stability at normal temperature, (2) sufficient stability at elevated temperatures to permit handling in conventional oil-burning equipment and (3) reasonable viscosity, the results of this work point

toward a 40 per cent by weight suspension of minus-230-mesh bituminous coal dispersed in No. 6 fuel oil. For practical purposes, the coal-specification size could be set at 98–99 per cent passing a 230-mesh screen and the limiting oil properties at 12 to 14.8 A.P.I. gravity at 60 F, and 55–70 Furol viscosity at 122 F. The laboratory results also indicate that the coal can be dispersed in the oil by relatively simple methods.

Tests in Typical Oil-Burning Plants

To obtain information on the operating problems involved in handling and burning coal-in-oil mixtures in typical oil-burning plants, tests were made at three different plants. From the laboratory information, it was decided to experiment with fuel of about 40 per cent coal by weight. Four batches of fuel were prepared, one batch having coal of a fineness of about 88 per cent through a 230-mesh A.S.T.M. (U. S.) Standard screen, one of about 95 per cent, and two of about 99 per cent. Coal could be ground to this fineness in present standard commercial equipment. As far as the authors know, no equipment is available at present that will, from a practical standpoint, continuously and satisfactorily produce coal of, say, the extreme fineness of minus 325 mesh. Table 4 gives data on the coal and oil used in the mixtures. In addition, the Appendix gives the distillation results, Bureau of Mines, Hempel method, obtained with the oil used in batch 3.

TABLE 4 DATA ON COAL, OIL, AND RESULTING COAL-IN-OIL FUELS

Batch no.	1	2	3	4
Coal, approximate percentage by weight in mixture	39.4	39.7	39.5	40.7
Proximate analysis:				
Moisture, per cent	1.7	1.5	1.3	1.4
Volatile, dry basis, per cent	35.5	35.9	37.0	36.6
Fixed carbon, dry basis, per cent	58.4	56.3	58.6	58.9
Ash, dry basis, per cent	6.1	7.8	4.4	4.5
Sulphur, dry basis, per cent	0.8	0.8	0.7	0.8
Btu, dry basis	14310	13990	14540	14520
Ash, initial deformation, deg F	2300	2230	2540	2570
Ash, softening temperature, deg F	2410	2300	2660	2690
Ash, fluid temperature, deg F	2720	2770	2910	2850
Ultimate analysis, dry basis:				
Carbon, per cent	79.9	78.0	81.5	81.1
Hydrogen, per cent	5.3	5.1	5.4	5.4
Oxygen, per cent	6.3	6.9	6.5	6.7
Nitrogen, per cent	1.6	1.4	1.5	1.5
Sulphur, per cent	0.8	0.8	0.7	0.8
Ash, per cent	6.1	7.8	4.4	4.5
Fineness, approximate, U. S. Std sieves:				
Retained on No. 100 sieve, per cent	0.3	0.02	0	0
Retained on No. 200 sieve, passing No. 100 sieve, per cent	6.5	2.68	0.3	0.2
Retained on No. 230 sieve, passing No. 200 sieve, per cent	5.7	2.8	0.3	0.2
Retained on No. 325 sieve, passing No. 230 sieve, per cent	12.1	8.4	6.4	6.4
Passing No. 325 sieve, per cent	75.4	86.1	93.0	93.2
Total, per cent	100.0	100.00	100.0	100.0
Oil, approximate percentage by weight in mixture	60.6	60.3	60.5	59.3
Ultimate analysis:				
Carbon, per cent	86.6	86.4	86.9	87.0
Hydrogen, per cent	10.6	10.6	10.7	10.8
Oxygen, per cent	1.0	0.9	0.5	0.4
Nitrogen, per cent	0.2	0.2	0.2	0.3
Sulphur, per cent	1.5	1.8	1.6	1.2
Ash, per cent	0.1	0.1	0.1	0.3
Btu	18320	18290	18440	18360
Specific gravity	0.980	0.980	0.979	0.977
Water content, per cent	0.20	0.18	Trace	0.2
Sediment by extraction, per cent	0.60	0.12	0.21	2.3
Pour point, deg F	30	40	35	50
Flash point,[a] deg F	270	265	275	275
Aniline point	Too dark	Too dark	Too dark	Too dark
Viscosity:				
Saybolt Furol at 70 F, sec	585.4	760.5	580.2	1119.0
Saybolt Furol at 100 F, sec	128.7	154.3	121.1	189.3
Saybolt Furol at 130 F, sec	46.0	51.9	44.7	56.7
Saybolt Universal at 170 F, sec	165.2 (17)	173.5 (17)	151.4 (15)	189.7 (19)
Saybolt Universal at 210 F, sec	82.6 (8)	88.3 (9)	81.3 (8)	93.1 (9)
Coal-in-oil:				
Viscosity				
Saybolt Furol at 70 F, sec	3368	5854		7181
Saybolt Furol at 100 F, sec	642	1015		867
Saybolt Furol at 130 F, sec	211	343		273
Saybolt Universal at 170 F, sec	734 (73)	1074 (107)		934 (93)
Saybolt Universal at 210 F, sec	327 (33)	477 (48)		426 (43)
Pour point, deg F				60

[a] Cleveland open cup.

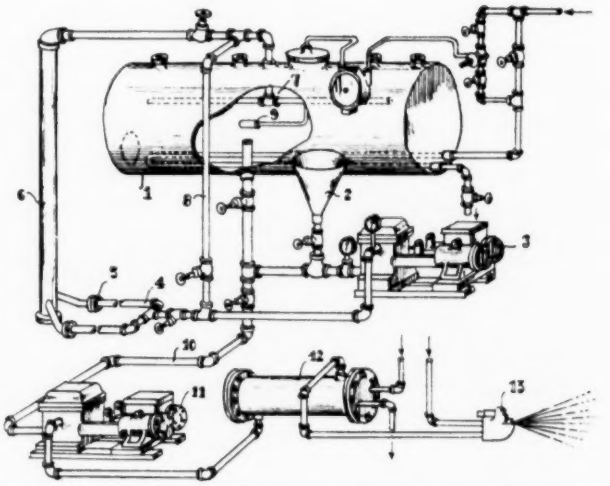


FIG. 9 TEST ASSEMBLY SHOWING GENERAL ARRANGEMENT OF MIXING DEVICE AND OIL-BURNING EQUIPMENT

1 Steam coil
2 Hopper, powdered-coal intake (approx 2.5 ft diam)
3 Duplex double-acting pump: Steam end, 7.5 in. ID Liquid end, 7.5 in. ID Stroke, 10 in.
4 Split flow
5 Knothole mixer (1 in.)
6 Riser
7 Spreader
8 By-pass
9 Temperature controller
10 Feed line to burner system
11 Reciprocating feed pump
12 Preheater
13 Steam-atomizing burner (1/2 in. Best)

As indicated by the laboratory results, it was found in the field that the mixing of the coal and oil needed for the tests did not present much difficulty. A simple batch-mixing device shown in the upper part of Fig. 9 was used. The fuel oil required for a batch, (about 5000 to 7000 gal), was put in the storage tank and then pumped from the tank suction line by an ordinary reciprocating pump. The oil temperatures used varied from about 75 to 120 F, the chosen temperature being maintained by steam coils in the tank. In the suction line, mounted on a tee and valve, was a funnel kept filled with pulverized coal. The coal under hand valve control was allowed to flow slowly into the stream of oil on its way to the pump. The mixture was discharged by the pump through two horizontal pipes, each having an orifice near the end. After passing the orifices, the two streams of fuel met at the base of a vertical pipe and then passed on to the storage tank. The fuel was spilled into the tank from two outlets, one at each end of the tank. The coal was fed into the oil at the rate of about 1500 lb per hr, and the fuel was continually circulated at a rate of about 9000 gph.

After the required amount of coal was fed for the batch, the fuel was circulated for about 12 hr. Laboratory tests of samples of fuel taken at various places throughout the tank showed that the mixture was uniform. No further recirculating of the fuel was done during burning tests, the mixing device being valved off from the suction line.

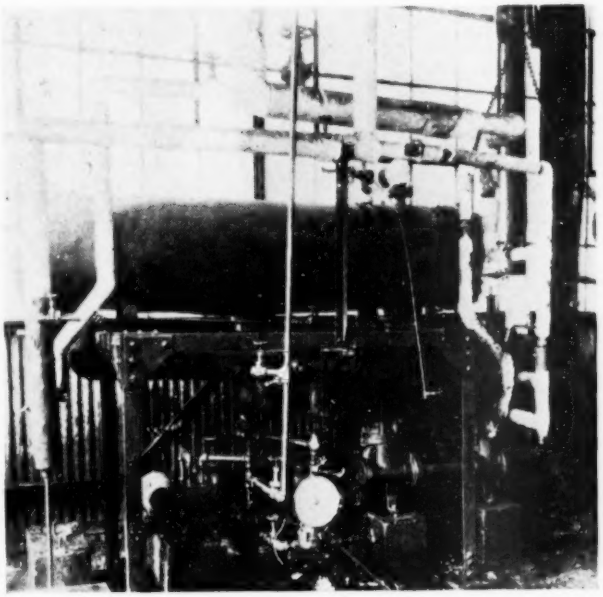


FIG. 10 HEATER-PUMP SET USED

Putting coal into oil produces a fuel having characteristics different from those of oil. The mixture used was about 10 per cent heavier in weight per unit volume than oil; it was about 4 to 8 times as viscous depending upon the temperature; it was much more abrasive; any settling out of the coal resulted in paste-like accumulations in various parts of the equipment, such as tanks, heaters, and valves; the ash from the coal was set free in the furnace.

TESTS AT ATLANTIC REFINING COMPANY BOILER PLANT

The first and main series of tests was made at one of the boiler plants of the Atlantic Refining Company. The boiler-plant equipment was typical of that of many oil-burning plants. The suction line from the outside above-ground oil storage tank ran underground about 100 ft to the heater-pump set. A steam line, that helped maintain fuel temperatures to the pump, paralleled the oil suction line. Fig. 10 shows the heater-pump set. One pump was a reciprocating and the other a rotary. The fuel was heated to about 160 to 200 F at the set and was pumped about 110 ft to the boiler. A standard Best steam-atomizing burner was used, as shown in Fig. 11. The fuel reaches a horizontal slot at the burner tip through the lower pipe; the steam reaches a vertical slot through the upper pipe and sweeps the fuel into the furnace. The fuel and steam were under hand control.

The boiler was a 151-hp, long-drum, straight water-tube Babcock & Wilcox boiler, 8 tubes wide and 9 tubes high. Fig. 12 shows the boiler layout. The boiler was first operated on oil to establish normal operating characteristics. It was then operated continuously on coal-in-oil fuel. Table 5 shows the average results when fuel oil and coal-in-oil fuels were used. These tests were not specially run by test operators but were run as part of the regular plant steam production with the usual company plant operators. As shown in the tabulation, these operators obtained slightly lower boiler efficiencies with the coal-in-oil fuels than with the oil; about 79.5 to 80.5 per cent was obtained with the coal-in-oil fuels against 81.2 per cent with the oil; the difference is small enough to be within test errors. There was a small loss, item 69, of unburned combustible in the fly ash for the coal-in-oil fuels that was measurable.

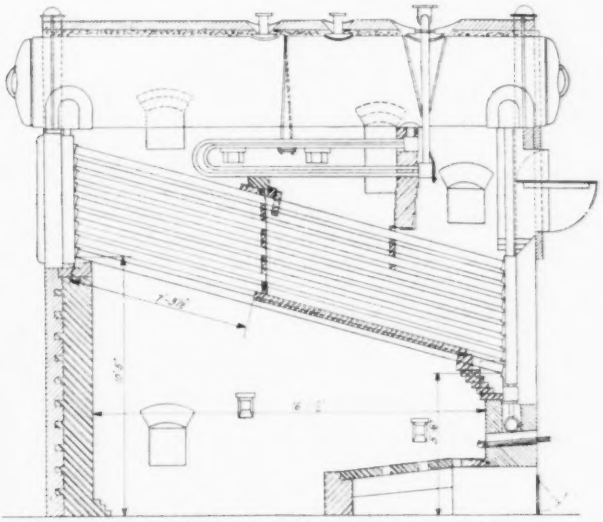


FIG. 12 GENERAL LAYOUT OF BOILER AND FURNACE

No difficulties arose in burning the coal-in-oil fuels in the furnace with the steam-atomizing burner used. The flame responded smoothly to changes of boiler load and to variations of the quantity of air used for combustion. It could be controlled with the same ease as fuel oil. The CO_2 content of the products of combustion could be carried as chosen up to about 16 per cent with no CO. During operation no difficulties were experienced in the production of smoke; smoke could be controlled the same as with oil. However, in starting up a cold furnace with a coal-in-oil fuel, considerable smoke was produced. Fig. 13 shows conditions when starting. The boiler was operated at about rating during most of the testing, this load fitting best into the plant steam requirements from this boilerhouse. However, ratings from about 40 per cent to over 200 per cent were carried for several hours without difficulty.

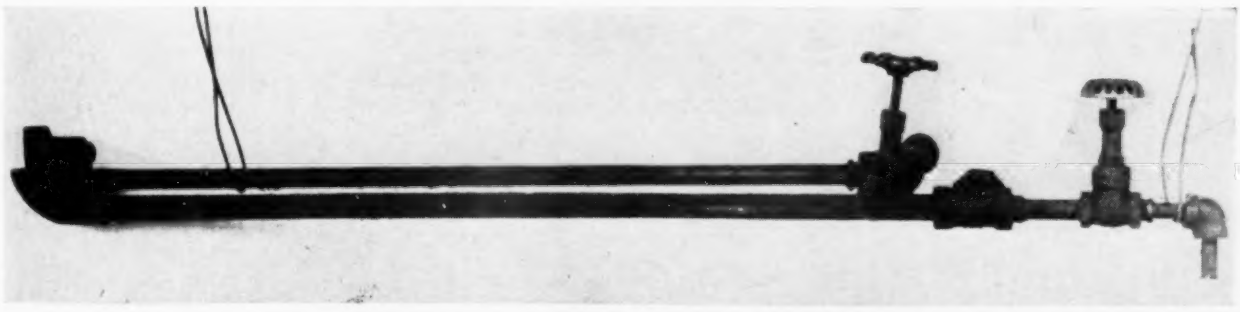


FIG. 11 STANDARD BEST STEAM-ATOMIZING BURNER USED
(Fuel reaches a horizontal slot at burner tip through lower pipe; steam reaches a vertical slot through upper pipe and sweeps fuel into furnace.)

TABLE 5 TESTS OF OIL AND COAL-IN-OIL FUELS, ATLANTIC REFINING COMPANY BOILER UNIT

		1	2	3	4
1	Test no.				
2	Date of test, 1943	March 3–11	April 1–7	March 22–27	April 14–21
3	Maker and type of boiler	The Babcock & Wilcox Company; longitudinal drum			
4	Maker and type of superheater	The Babcock & Wilcox Company; convection type			
5	Maker and type of fuel-burning equipment	Best outside-mix steam-atomizing burner			
6	Boiler heating surface, sq ft	1510			
7	Superheater surface, sq ft	282			
8	Total heating surface, sq ft	1792			
9	Number of burners	One			
10	Method of producing draft	Natural-draft chimney			
11	Fuel: Type	No. 6 fuel oil	Coal-in-oil		
	Batch no.		Batch No. 1	Batch No. 2	Batch No. 3
	Coal through 230 U. S. Std mesh screen, per cent		87.5	94.5	99.4
12	Area of furnace floor, 5′-0″ wide × 16′ 1½″ deep, sq ft		80.6		
13	Height of furnace, mean, floor to nearest boiler heating surface, ft		8.0		
14	Total furnace volume (approximate), cu ft		550		
15	Furnace volume per sq ft boiler heating surface, cu ft		0.36		
	Fuel (Moisture-Free)				
16	Moisture (as fired), per cent	0.1–	0.9	1.5	0.9
17	Heating value per lb, Btu	18380	16820	16670	16960
18	Flash point (open cup), deg F				260
19	Carbon, per cent	87.4	84.5	83.8	85.5
20	Hydrogen, per cent	10.6	8.6	8.4	8.6
21	Oxygen, per cent	0.5	2.5	2.6	2.2
22	Nitrogen, per cent	0.2	0.7	0.7	0.7
23	Specific gravity at 60/60 F	0.982	1.082	1.094	1.083
24	Sulphur, per cent	1.3	1.3	1.4	1.2
25	Ash, per cent		2.4	3.1	1.8
	Products of Combustion				
26	Gas analysis, boiler outlet:				
	CO_2, per cent	12.8	12.2	13.9	14.7
	O_2, per cent	4.5	5.8	3.6	2.7
	CO, per cent	0.0	0.0	0.0	0.0
	N_2, per cent	82.7	82.0	82.5	82.6
27	Dry gas per lb dry fuel, boiler outlet, lb	17.2	17.3	15.1	14.7
28	Dry gas per lb dry fuel (no excess oxygen), lb	13.8	12.9	12.8	13.1
	Pressures and Drafts				
29	Steam pressure by gage, superheater outlet, psi	122	125	124	126
30	Pressure of fuel at burners, psi	0.3	1.5	3.0	2.0
31	Pressure of fuel at pump inlet, psi	+1.3 to +1.8	−2.2 to +0.1	−3.1 to +0.5	−3.7 to −0.4
32	Draft in furnace, in. of water	−0.01	−0.04	−0.04	−0.02
33	Draft at boiler outlet, in. of water	+0.04	+0.01	+0.02	+0.03
	Temperatures				
34	Steam temperature at superheater outlet, deg F	435	457	451	438
35	Superheat, deg F	84	104	99	85
36	Temperature of air for combustion, deg F	59	62	69	64
37	Temperature of gases leaving boiler, deg F	457	480	476	455
38	Temperature of feedwater entering boiler, deg F	222	192	215	212
39	Temperature of fuel in storage tank, deg F	75	81	88	84
40	Temperature of fuel at pump, deg F	60 to 70	85 to 125	75 to 110	70 to 95
41	Temperature of fuel leaving heater, deg F	180 to 200	160 to 180	180 to 195	150 to 170
42	Temperature of fuel at burner, deg F	163	154	163	142

		1	2	3	4
	Hourly Quantities				
43	Duration of test, hr	192	144	120	120
44	Fuel per hour (as fired), lb	347	383	395	387
45	Fuel per hour (moisture-free), lb	347	380	389	384
46	Fuel per cu ft furnace volume per hour (as fired), lb	0.63	0.70	0.72	0.70
47	Fuel per burner per hour (as fired), lb	347	383	395	387
48	Actual water per hour, lb	4930	4670	4870	4950
49	Atomizing steam per hour, lb	90	150	130	160
50	Atomizing steam per lb of fuel (as fired), lb	0.26	0.39	0.33	0.41
51	Atomizing steam per cent of steam produced, per cent	1.8	3.2	2.7	3.2
	Unit Quantities				
52	Heat absorbed by water and steam, Btu per lb	1050	1092	1066	1061
	Refuse				
53	Dust in breeching, per cent of fuel (moisture-free), per cent		0.8	0.9	0.8
54	Refuse in furnace, per cent of fuel (moisture-free), per cent		0.4	0.8	0.3
55	Dust entering stack, per cent of fuel (moisture-free) (estimated), per cent		1.9	2.3	1.2
56	Percentage of combustible in breeching dust, per cent		32	36	28
57	Percentage of combustible in furnace refuse, per cent		0	0	0
58	Ash in furnace and breeching, per cent of ash in fuel, per cent		40	45	50
	Evaporation				
59	Rate of heat absorption per lb fuel (moisture-free), kB	14.93	13.42	13.34	13.67
60	Rate of heat absorption per sq ft of heating surface per hour, kB	2.89	2.85	2.90	2.93
61	Rating developed based on boiler heating surface only (10 sq ft per boiler horsepower), per cent	103	101	103	104
	Efficiency				
62	Efficiency, per cent	81.2	79.8	80.0	80.6

		Test No. 1		Test No. 2		Test No. 3		Test No. 4	
	Heat Balance, Based on Dry Fuel	Btu	Per cent	Btu	Per cent	Btu	Per cent	Btu	Per cent
63	Heating value of fuel, Btu per lb	18380	100.0	16820	100.0	16670	100.0	16960	100.0
64	Heat absorbed by boiler and superheater	14930	81.2	13420	79.8	13340	80.0	13670	80.6
65	Heat loss due to moisture in fuel	0	0.0	11	0.1	19	0.1	11	0.1
66	Heat loss due to water from combustion of hydrogen	1183	6.4	966	5.7	937	5.6	955	5.6
67	Heat loss due to dry chimney gases	1643	9.0	1736	10.3	1475	8.9	1379	8.1
68	Heat loss due to carbon monoxide	0	0.0	0	0.0	0	0.0	0	0.0
69	Heat loss due to combustible in dust leaving furnace (estimated)			105	0.6	131	0.8	67	0.4
70	Heat loss due to unconsumed hydrogen and hydrocarbons, radiation, and unaccounted for	624	3.4	582	3.5	768	4.6	878	5.2

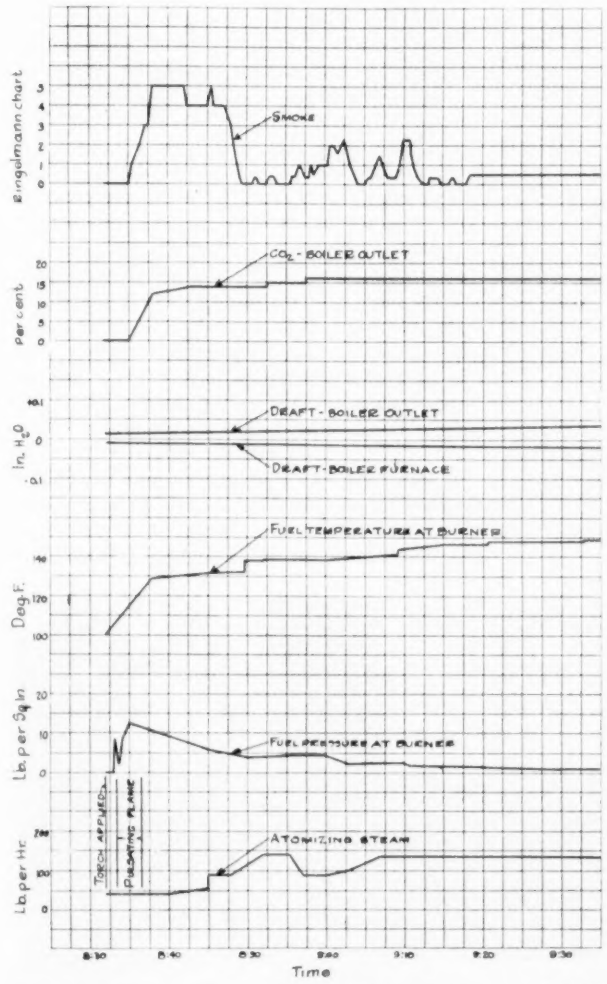


FIG. 13 CURVES SHOWING OPERATING CONDITIONS WHEN STARTING WITH COAL-IN-OIL FUEL IN COLD BOILER FURNACE

As shown in Table 5, about two-thirds more atomizing steam was required for the coal-in-oil fuels than for the oil. Both saturated steam and superheated steam were tried. Essentially the same amount of each was required to produce the same combustion results, as far as could be measured. It was found, however, that superheated steam gave a little less difficulty from pulsations and blowing of flame from the burner when higher amounts of steam per pound of fuel were used.

Troubles from the ash of the coal in the furnace were less than had been anticipated. The use of pulverized coal has supplied a vast amount of information on the action of ash in boiler furnaces and passes. In general, much less ash troubles should be expected with coal-in-oil fuels. It is not desirable to re-explore this field to any great extent in connection with an emergency fuel.

Fig. 14 is a view of the furnace with the ash accumulation after one week of operation. There was no dripping or slagging. The fly ash on the tubes was cleaned without difficulty every 8 hr during the test by the boiler soot blowers. Fig. 15 shows the effects of soot-blowing on the flue-gas temperatures when running at about rating with a CO_2 range from about 14.7 to 15.9 per cent. As shown in Table 5, about 45 per cent of the ash in the fuel accumulated in the furnace and breeching of the boiler.

It was found that with batch No. 1, for which coal had been ground to a fineness of about 88 per cent through a 230-mesh screen, there was considerable sludge accumulation at the bottom of the tank after about 7 days. The average temperature maintained in the tank was 81 F; no movement was given the fuel. With batch No. 2, for which coal had been ground to 95 per cent through a 230-mesh screen, only a small amount of sludge had accumulated at the end of 5 days. The average temperature in this case was 85 F. With batch No. 3, for which coal had been ground to 99 per cent through a 230-mesh screen, no discernible settling occurred after 9 days with the temperature in the tank at about 82 F. When the temperature was raised to 120 F, however, sludge accumulation was definitely discernible at the end of a few days. About 1500 gal of batch No. 4, for which coal had been ground to 99 per cent through a 230-mesh screen, was loaded in a typical delivery tank truck at about 115 F. The truck was then driven on the highway for about 9 hr covering about 150 miles; it was then allowed to stand for 32 hr. No settling occurred. The fuel was allowed to stay in the standing truck about 8 weeks. No settling was found at the end of this period. These field findings check with the laboratory findings.

No settling or clogging was experienced in the pipe lines from tank to pump to burner, although the lines were relatively long and the fuel was at elevated temperatures. For a given temperature, the coal in a coal-in-oil fuel separates much more readily when quiet than when the fuel is in motion.

There was appreciable accumulation of coal-oil paste in the heater when both batch No. 1 and batch No. 2 were used. It was unnecessary, however, to clean the heater during either test run. With the 88 per cent coal, there was an accumulation of 113 lb of paste after about 7 days; with the 95 per cent coal, 84 lb of paste after about 6 days. With the 99 per cent coal, the accumulation after about 9 days was practically negligible, being so

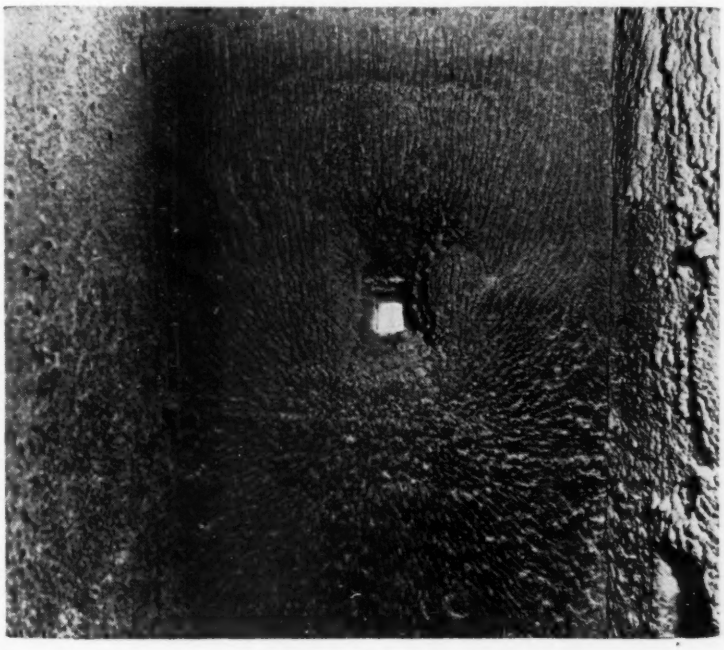


FIG. 14 INTERIOR OF BOILER FURNACE SHOWING ASH ACCUMULATION AFTER ONE WEEK OF OPERATION

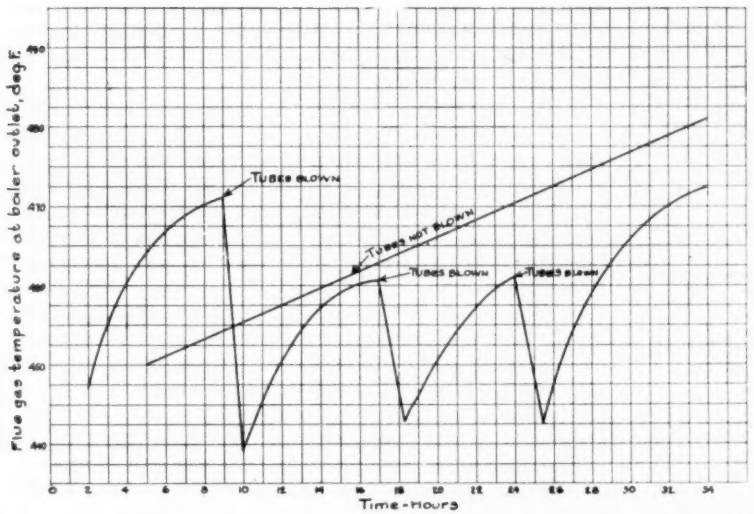


FIG. 15 CURVES SHOWING EFFECT OF USE OF BOILER SOOT BLOWERS ON EXIT TEMPERATURES OF FLUE GASES

somewhat higher amount of steam, which could readily be done when superheated steam was used, appeared to help prevent this trouble.

Coal-in-oil fuels with their higher specific gravity and viscosity present new pumping problems when used in oil equipment. Studies of the flow of oil-coal suspensions have been reported by Gradishar, Faith, and Hedrick;[7] they supply formulas for determining pressure differentials. Table 1 gives viscosity comparisons of the coal-in-oil fuels, and the oil from which they were made.

The main pumping problem was from the storage tank to the pump; after the fuel was heated in the heater it was not so hard to pump. Coal-in-oil suspensions would have to be heated to temperatures of 140 to 170 F to give about the same viscosity as that of oil at about 100 F. These higher temperatures were avoided in the storage tank in order to eliminate settling of coal-oil paste. At The Atlantic Refining Company boiler plant, the storage tank was above ground, and when oil was pumped at about 70

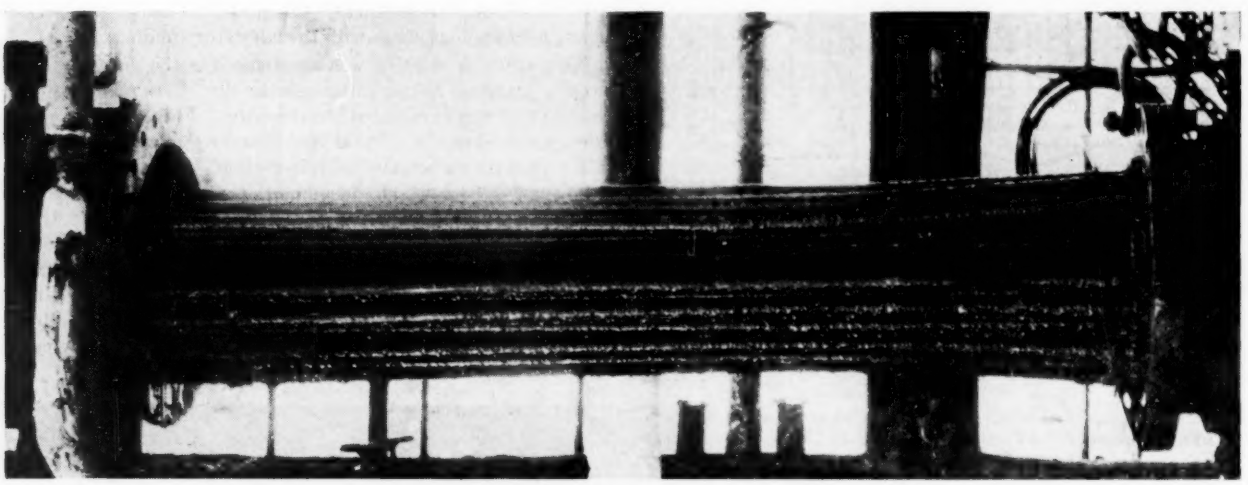


FIG. 16 VIEW OF HEATER COILS AFTER ABOUT 9 DAYS OF USE IN HEATING TO ABOUT 150 TO 170 F COAL-IN-OIL FUEL HAVING 99 PER CENT OF COAL GROUND TO MINUS 230 MESH
(Accumulation was so slight as not to warrant cleaning for the next run.)

slight as not to warrant cleaning the heater. Fig. 16 shows the heater coils after the 99 per cent coal was used. In a steam heater of this type, some of the fuel is heated much hotter than the average temperature shown at the heater outlet. Fuel in contact with the steam coil approaches the temperature of the steam which was of the order of 350 F entering the coil. An offsetting factor, however, is the movement of the fuel which helps keep the coal in suspension. When coal-in-oil fuel is used, it is best not to heat it any hotter than necessary at any point in the system up to the furnace. Operating routine can be arranged to clean the heater when found necessary. If there are two heaters, they could be used alternately.

There was some clogging in the meters and screens with all of the coal-in-oil fuels. By-passes prevented loss of load during cleaning. Occasionally throughout the day the fuel control valve tended to clog, but it could be readily cleared by opening it wide quickly. Control-valve clogging would be apt to create some difficulties under automatic control. The burner tip occasionally clogged a little and had to be blown clear with a shot of steam piped to blow through the oil slot. Carrying continuously a F at the pump the pressure at the oil-pump inlet was about 1.5 psi; when coal-in-oil fuels were pumped at about that temperature the inlet pressure was about 7 in. of vacuum or —3.4 psi. In starting up on coal-in-oil fuel, with no fuel in the lines about 1 hr pumping with the reciprocating pump was required to bring the fuel, at a temperature of about 80 F, from the tank to the burner; the rotary pump was not successful in starting the fuel but was quite satisfactory after the flow was established. When the fuel in the tank was 120 F, about $^1/_4$ hr of pumping was required to start.

About 30 lb pressure was in general maintained ahead of the burner oil-control valve for both oil and coal-in-oil fuels. Table 5 shows the pressures at the burner; much higher relative pressures were required for the coal-in-oil fuels. The electric inputs to pump motors were increased. Under one set of operating conditions this input was about doubled. The increase in motor input depends upon the percentage of the total pump load which comes from moving the fuel itself.

For the rotary pump used the capacity dropped about 20 per cent. No satisfactory measurement was obtained in the loss of capacity of the reciprocating pump. The higher-viscosity fuel

DIMENSIONS OF COLLOIDAL FUEL PUMP AT No. 14 BOILER HOUSE

	DATE INSPECTED	5-3-43	5-30-43	6-8-43	6-21-43	5-4-43
A	O.D. OF ROTOR	2.4995"	2.4985"	2.496"	2.496	2.496"
B	WIDTH OF ROTOR	.9985"	.9965"	.992"	.990"	.994"
C	O.D. OF SHAFT	.628"	.622"	.620"	.620"	.619"
D	THICKNESS OF ROTOR WALL	.534"	.538"	.532"	.532"	.530"
E	THICKNESS OF ROTOR TEETH	.2765"	.276"	.275"	.275"	.274"
F	I.D. OF CASING	2.513"	2.518"	2.513"	2.514"	2.513"
G	O.D. OF IDLER	1.929"	1.929"	1.924"	1.929"	1.924"
H	THICKNESS OF IDLER	.660"	.6585"	.655"	.655"	.654"
I	I.D. OF IDLER BUSHING	.627"	.634"	.648"	.647"	.654"
J	DIAMETER OF PIN	.625"	.618"	.616"	.610"	.606"
K	THICKNESS OF CRESCENT	.281"	.271"	.268"	.267"	.266"
	HRS.	75	75	159	105	73

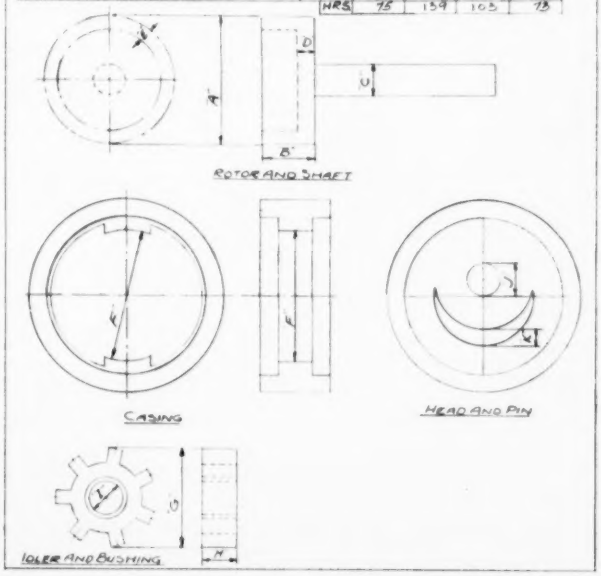


FIG. 17 TABLE AND SKETCH SHOWING WEAR ON ROTARY PUMP FROM PUMPING COAL-IN-OIL FUEL

causes the valves of reciprocating pumps to seat at a slower speed; stiffer valve springs helped to overcome this difficulty.

Coal-in-oil fuel was found to be rather abrasive. It acted something like a lapping powder. Fig. 17 gives a record of the wear on the rotary pump shown in Fig. 18. Appreciable wear occurred at the spindle; no repairing, however, was found necessary during the entire series of tests. There was also some cutting of the burner tip. Fig. 19 shows this erosion at both outer edges of the tiptable. It was unnecessary, however, to change the tip during the tests, good combustion being obtained. It is doubtful if this abrasive characteristic would necessarily be a serious handicap to successful operation. Equipment affected would have to be watched and repaired as found necessary.

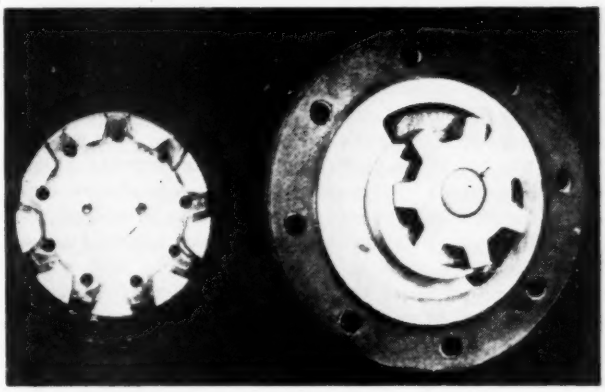


FIG. 18 ROTARY TYPE OF OIL PUMP USED AS PART OF HEATER-PUMP SET
(Most of the wear was at spindle.)

TESTS AT CAMBRIA SILK HOSIERY COMPANY BOILER PLANT

A part of the batch No. 4 coal-in-oil fuel was burned in the boiler plant of the Cambria Silk Hosiery Company, Philadelphia, Pa. This plant was typical of the smaller industrial plant burning No. 6 fuel oil. The boiler used on the trial was a typical brickset 72-in. × 18-ft 150-hp H.R.T. boiler, equipped with one burner. The burner was a standard Johnson type 30-H automatic on-and-off rotary-cup burner having a maximum capacity of about 90 gph of oil. The oil pump, rated at 150 gph, an integral part of the burner assembly, drew oil from an underground storage tank through a 16-wire-mesh strainer and discharged it to a steam heater; from the heater the oil took two paths, one through a manually set relief valve back to the storage tank, and one to a 24-wire-mesh strainer to an electric heater, through a control orifice, and then to the burner cup. Primary air was supplied by a fan on the burner; additional air was dampered through a checkered furnace floor. Automatic ignition was effected by electric spark and gas pilot which were cut off after ignition.

In switching this plant from oil, the coal-in-oil fuel was not put into the underground storage tank. It was supplied to the pump through an auxiliary suction line of the same size as the main suction line direct from the delivery tank truck stationed about over the underground tank. This eliminated the suction lift. With the fuel at about 85 F in the truck, it was found that insufficient fuel could be pumped to maintain an even fire—perhaps

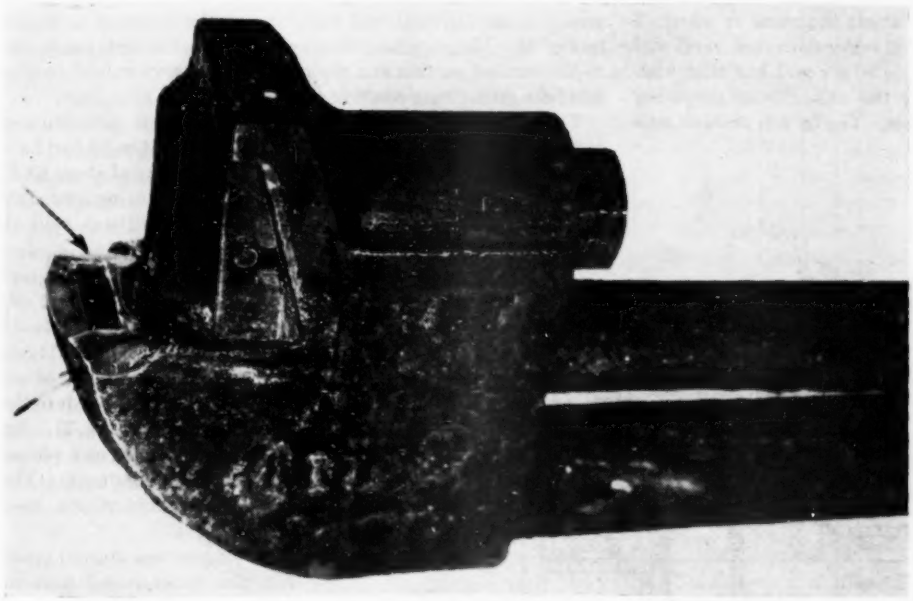


FIG. 19 VIEW SHOWING EROSION AT OUTER EDGES OF THE TIP-TABLE OF STEAM-ATOMIZING BURNER FROM USE OF COAL-IN-OIL FUEL

30 per cent of burner capacity—although 18 in. of vacuum was registered at the strainer just ahead of the pump. Under normal operation with No. 6 fuel oil at about 90 F from the underground tank, only 6 in. vacuum was required. A special heater was installed near the suction outlet in the tank and the relief hot-oil return flow was also piped closer to this outlet. This was done to heat the fuel at the suction outlet, where there was considerable movement; it was considered that the main body of fuel in the tank should be kept cool to avoid settling of coal-oil paste. When the fuel temperature at the suction was increased to about 95 F, the burner could be fired near capacity with a small amount of return oil to the tank. At 120 F very satisfactory pumping conditions resulted, a vacuum of 7 in. being carried.

On the delivery side of the pump it was found necessary to change the size of the orifice from 0.0935 in. diam as regularly used, to a larger orifice 0.161 in. diam to lessen restriction of flow. Under normal operating conditions with oil and with the smaller orifice, an oil pressure of about 15 to 18 lb was carried; with coal-in-oil fuel and with the larger orifice, a pressure of about 20 to 23 lb was required for the same load. The 24-mesh screen ahead of the electric heater became clogged after about 3 hr; a larger-mesh screen would be desirable for coal-in-oil fuels. The final temperature of the fuel to the burner ranged in general from about 140 to 160 F.

When starting with a comparatively cold furnace, it was found that the automatic ignition would not ignite coal-in-oil fuel; a hand torch had to be used. A larger gas pilot was needed. With a hot furnace, however, the automatic ignition operated quite satisfactorily.

The revolving cup of the burner for use with oil fuel was tapered outward somewhat. The flame of the heavier coal-in-oil fuel flared out from the cup more than the flame of the oil. This caused carbon masses to accumulate on the circular brickwork throat of the burner, which had to be cleaned about every 15 min. The tapered cup of the burner was changed to a straight-line cup; the brickwork of the throat was flared out a little farther. These changes resulted in satisfactory operation. The burner was readily adjusted and the CO_2 could be carried as chosen. Somewhat improved operation could be had by heating the fuel to about 160 to 170 F ahead of the burner. The efficiency when coal-in-oil fuel was used was about the same as when oil was used. The maximum load on the boiler with coal-in-oil fuel on this installation was approximately 10 per cent less than with oil. This was caused primarily by the difficulty of supplying enough secondary air in the right spots. The fly-ash problem was of little moment.

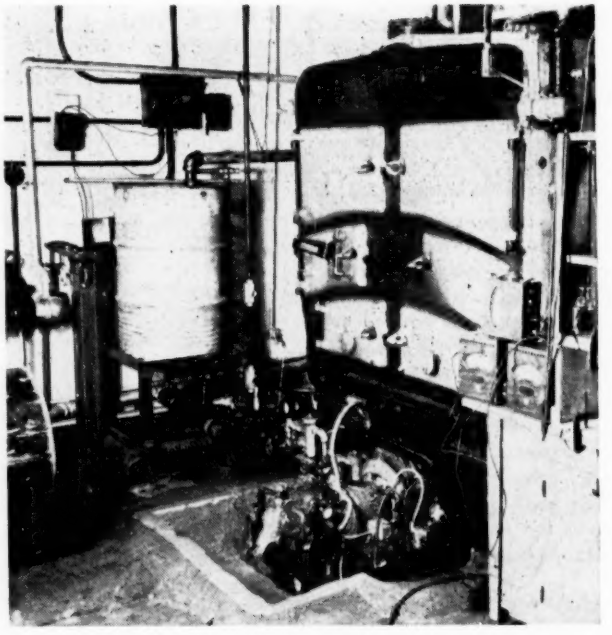


FIG. 21 VIEW OF BOILER FRONT AND BURNER AT HEATING PLANT OF NATIONAL AIROIL BURNER COMPANY

TESTS AT NATIONAL AIROIL BURNER COMPANY HEATING PLANT

In co-operation with the National Airoil Burner Company of Philadelphia, Pa., part of batch No. 4 of coal-in-oil fuel was tried in its office headquarters' heating boiler. This boiler was a cast-iron sectional boiler having an output of about 3,060,000 Btu (approximately 90 hp). It was equipped with a small rotary-cup burner of a capacity of 20 gph of oil. Figs. 20 and 21 show the general layout. This plant was typical of the small heavy-oil-burning heating plant.

Normally the plant uses No. 6 oil pumped from an underground storage tank. Since it was believed that the regular burner setup would not be able to pump coal-in-oil fuel from the underground tank, a 275-gal tank was installed above ground as shown in Fig. 21. The suction and return lines, *A* and *B*, were connected to the existing suction and return piping properly valved so that fuel from either tank could be used.

The oil burner was started with oil, and normal operation was established. The equipment was switched to coal-in-oil fuel having a temperature of about 68 F. The pump suction registered 20 in. of vacuum and was held at this point for 1 hr, but no fuel reached the burner. The equipment was switched back to oil, and the vacuum dropped to 15 in., giving a good oil flow. It was then decided to install a 52-gal tank above and to the side of the burner, as shown in Fig. 21. An electric fuel heater was placed directly under the tank. The usual suction and return lines were installed.

The burner was started on oil from the underground tank at 65 F, and a burner pressure of about 26 lb was used. The pump suction was about 13 in. of

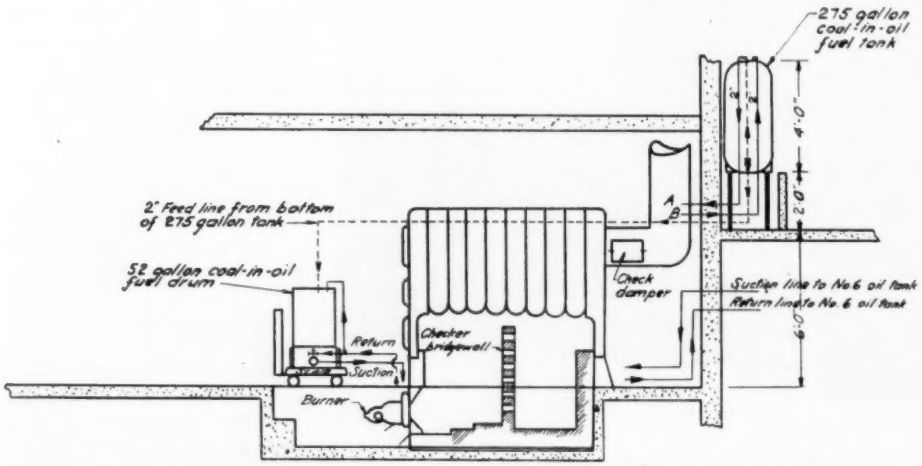


FIG. 20 GENERAL LAYOUT OF TEST SETUP AT HEATING PLANT OF NATIONAL AIROIL BURNER COMPANY

vacuum; the CO_2 ranged from about 11.5 to 13.5 per cent; the stack temperature was about 570 F. The equipment was switched to coal-in-oil fuel ranging in temperature at the tank from about 85 to 110 F. The pump pressure was about 26 lb; the pump suction was about 0; the CO_2 ranged from about 10.5 to 13.5 per cent; the stack temperature was about 625 F. The combustion was not satisfactory, as the flame was smoky at the outer edges. Carbon deposits accumulated on the side walls.

The equipment was shut down and allowed to cool to determine possibilities of cold starting with this type of equipment. After the fuel cooled in the pipe lines, it was very difficult to pump. The burner pressure was raised to about 40 lb to move it. The gas pilot would not ignite it. Ignition was finally obtained with a hand torch, and after furnace and fuel had reached higher temperatures, the flame was fairly well established. The carbon deposits continued to build up on the brickwork around the burner and in front of the cup until the opening was choked and it was necessary to shut down after about 20 min. The wider angle of the flame of the coal-in-oil fuel was the main cause of this difficulty.

Conclusions

Coal-in-oil fuel has its own peculiar characteristics which must be given thorough consideration for each job if satisfaction is to be obtained. However, this fuel does not present a particularly difficult problem in devising equipment and operating routine for efficient use. It appears that in some instances premixing of the fuel might be eliminated. The direct introduction of the coal into the flowing stream of oil to the heater-pump set offers possibilities. The information obtained from this work on bituminous coal-in-oil fuels leads to the following conclusions:

1 A sufficiently stable suspension of coal in oil for practical purposes can be prepared by dispersing 40 per cent coal by weight, ground from 98 to 99 per cent through a 230-mesh screen, in heavy fuel oil. The coal must be ground to this fineness to avoid most of the difficulty arising from unstable suspensions.

2 Mixing the coal into the oil does not present a particularly difficult problem.

3 Careful control of storage and handling temperatures is required for most successful operation.

4 Careful attention must be given the pumping of coal-in-oil-fuels, particularly in cases where underground storage tanks are used.

5 The combustion efficiency of coal-in-oil suspensions is apt to be slightly less than that of oil.

6 The load-carrying flexibilities of oil and coal-in-oil fuels are about the same.

7 The best opportunity for the successful use of coal-in-oil suspension is in the larger plants with the better operating personnel and more readily accessible equipment.

Acknowledgments

Acknowledgment should be given to the following persons for their part in carrying out this work: of The Atlantic Refining Company, C. J. Cutting, W. A. Myers, S. W. Ferris, W. A. Schmidheiser (for his part in getting the first large-scale test under way), J. C. Reid, and K. M. Thompson (the last two for performing most of the laboratory work); of the Bureau of Mines, Dr. W. C. Schroeder, R. Wiggers, and J. G. Mingle (the last two for their general field-testing work).

Appendix

Description of Pendulum Apparatus and Procedure for Its Use in Studying Stability of Coal-in-Oil Suspensions

Since the opacity of the oil used in coal-in-oil suspensions precludes visual observation of settling phenomena, the evaluation of stability presents a problem. A modification of a method, described by Manning and Taylor[6] and again by McMillen, Stutzman, and Hedrick,[8] has proved satisfactory for this study. The apparatus used, Fig. 22, consists of a carriage which is supported on knife-edges and is so designed that a tube containing a suspension of coal in oil may be fitted into it and held rigidly in place. The periods of this system (acting as a compound pendulum, observed first with the tube in its normal position in the carriage, and then with the tube raised through a known distance referred to its support by the insertion of a block of known dimensions), provide a means of calculating the location of the center of gravity of any tube and its contained suspension.

Period T of a compound pendulum may be expressed

$$T^2 = \frac{4\pi^2 I}{Mg\bar{r}}$$

where I is the moment of inertia of the pendulum about the axis of support, M is the mass of the pendulum, g is the acceleration due to gravity and $\bar{r}$ is the radius of the center of gravity. Combining this equation with the theorem of mechanics relating the moment of inertia I about any axis to the moment of inertia I_0 about an axis through the center of gravity

$$I = I_0 + M\bar{r}^2$$

and separating the various parts of the system, the location of the center of gravity of the tube and its contained suspension is given by

$$\bar{r}_t = \frac{\bar{r}_c M_c g T_1^2 + [gdM_t - (\bar{r}_c M_c g + \bar{r}_b M_b g)]\, T_2^2 + 4\pi^2 I_b + 4\pi^2 M_t d^2}{gM_t\,(T_2^2 - T_1^2) + 8\pi^2 M_t d}$$

[8] "A Pendulum Method for Measuring Settling Velocities," by J. H. McMillen, L. F. Stutzman, and J. E. Hedrick, *Industrial and Engineering Chemistry*, Analytical Edition, vol. 13, 1941, pp. 475–478.

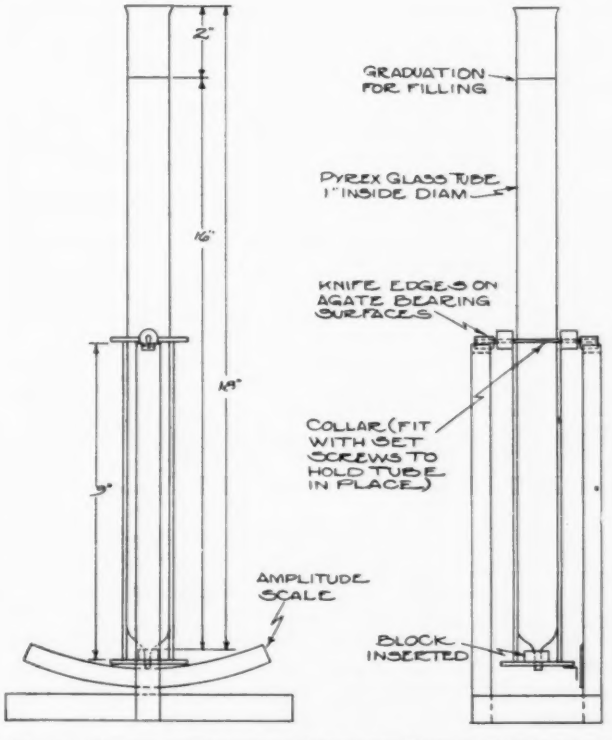


Fig. 22 Sketch of Pendulum Apparatus Used in Determining Settling in Coal-in-Oil Suspensions

where

$\bar{r}_t$ = radius of center of gravity of tube and contained suspension in its initial position, cm
$\bar{r}_c$ = radius of center of gravity of carriage, cm
M_c = mass of carriage, g
g = acceleration due to gravity, cm per sec per sec
d = distance through which tube is raised, cm
M_t = mass of tube and contained suspension, g
$\bar{r}_b$ = radius of center of gravity of inserted block, cm
M_b = mass of inserted block, g
I_b = moment of inertia of inserted block about axis of support, g × cm²
T_1 = period of compound pendulum without block, sec
T_2 = period of compound pendulum with block inserted, sec

Experimental results for the pendulum used in these experiments indicate an average deviation of ±0.025 cm in $\bar{r}_t$ calculated by this equation. For the best accuracy the carriage should be as light as possible and the axis of support should be only a short distance above the center of gravity of the pendulum. Temperature fluctuations affect the accuracy of this work and must be compensated for unless the tests are run at constant temperature. Suitable compensation may be effected by plotting the period against the age of the sample, thereby deriving an average curve from which corrected values may be taken.

The change in the position of the center of gravity may be correlated with the percentage of settling that has occurred. For example, complete settling, determined for a 40 per cent suspension of coal in an ethanol-water solution of the same specific gravity as the oil, results in a net change of 0.48 cm (±0.02 cm) in the position of the center of gravity of a tube and its contained suspension. Assuming that the net effect of the sedimentation is a gradual concentration of the slurry, a linear relationship between the change in the center of gravity and percentage of settling may be used. Thus with the sensitivity of the pendulum method previously noted, a single determination of the percentage settled is accurate to within about 5 per cent. Through the use of the compensation method described, large errors may be detected readily and the accuracy of the determinations considerably improved.

As a check on the pendulum test, samples that had shown no change in the position of the center of gravity on long standing were analyzed top and bottom by quantitative methods. The results obtained showed the same concentration of coal at top and bottom. The stability was checked further by visual examination of beaker mixes; a removable disk was placed at the bottom of the beaker and the material adhering to the disk was examined periodically. Tests in such studies confirmed the findings of the pendulum tests. Visual results were proved by quantitative methods.

TABLE 6 OIL USED IN BATCH NO. 3[a]

Distillation at atmospheric pressure, 742 mm. First drop, 185 C (365 F):

Fraction number	Cut at deg C	Cut at deg F	Per cent	Sum, per cent	Specific gravity, 60/60 F	Deg A.P.I., 60 F	C.I.	S.U. viscosity at 100 F., sec	Cloud test, deg F	Aniline point, deg C
1	50	122								
2	75	167								
3	100	212								
4	125	257								
5	150	302								
6	175	347								
7	200	392								
8	225	437								
9	250	482	4.0	4.0	0.868	31.5	..			28.1
10	275	527	5.8	9.8	0.909	24.2	66			29.0
Distillation continued at 40 mm:										
11	200	392	1.7	11.5	0.921	22.1	67	41	5	..
12	225	437	5.8	17.3	0.928	21.0	67	47	25	46.5
13	250	482	8.6	25.9	0.935	19.8	67	64	50	53.2
14	275	527	9.3	35.2	0.942	18.7	67	110	70	59.9
15	300	572	9.5	44.7	0.946	18.1	66	230	85	65.7
Residuum			55.2	99.9	1.016	7.8				

Carbon residue of residuum, 19.3 per cent; carbon residue of crude, 10.9 per cent.

[a] Distillation, Bureau of Mines, Hempel method.

Extreme care is required in the preparation of mixes for the evaluation of stability by pendulum test. Air carried into the mixture by the coal is lost very slowly, and by resulting in reduced volume, changes the period of the pendulum in a manner that may easily be misinterpreted as settling. This difficulty may be overcome by heating the mixture to 160 F with hand mixing and then stirring the warm mixture for 15 min at an absolute pressure of 10 mm Hg.

The coal used throughout the laboratory tests was ground in a hammer mill as received. Various sizes were separated carefully by screening. No effort was made to dry the pulverized coal beyond its equilibrium value with the atmosphere.

Discussion

E. G. Bailey.[9] This paper gives some interesting data covering important factors in relation to the burning of mixtures of pulverized coal and oil. The physical factors are one thing, the economic factors quite another.

It is the writer's opinion that with respect to the so-called emergencies we have already had, and those which we may yet expect, it is still better to continue the use of oil in those plants, which are not readily convertible 100 per cent to coal, and make those conversions which should be made to balance the fuel supply, by converting the installations which can readily be operated 100 per cent with coal.

It would seem to take substantially as much pulverizing and special classifying equipment to prepare 40 per cent coal for the mixture, as it would for 100 per cent coal with proper fineness, to be burned in those places where it can be done. Therefore, more oil could be saved with the same equipment or the same saving with less equipment if conversion to 100 per cent coal were the chosen method.

A higher degree of fineness in burning pulverized coal enables its use in many places where it is considered unadaptable with the coarser coals which many people have tried with unsatisfactory results. Many so-called expert opinions on this subject are hand-me-downs from experiences with coarser coal and poor burners of by-gone days, and such opinions and decisions should not prevail over the later experience with finer pulverization and modern equipment.

W. C. Schroeder.[10] The tests reported in this paper give a complete picture of the preparation and burning of colloidal fuel in a relatively small boiler which is typical of a number of oil-burning installations. The authors' work parallels, in several respects, an investigation that has been carried out by W. I. Jones of Powell Duffryn Associated Collieries in Wales.[11] This discussion will show that the results from the two studies are in substantial agreement and will also present additional information available from the work abroad.

Stability of Oil-Coal Suspensions. From the tests which were made in

[9] Vice-President, The Babcock & Wilcox Company, New York, N. Y. Fellow A.S.M.E.

[10] Assistant Chief, Fuels and Explosives Service, Bureau of Mines, Washington, D. C. Mem. A.S.M.E. This discussion is published by permission of the Director, Bureau of Mines, U. S. Department of the Interior.

[11] The information for this discussion was provided by W. Idris Jones, of Powell Duffryn Associated Collieries. The writer is indebted to him for this material and for permission to publish it.

Wales the following statements were made concerning stability:

"This is a relative term and no coal-in-oil suspension is perfectly stable. The stability decreases with a decrease in coal content or fineness and with increasing temperature. Stability also depends on the nature of the oil. Cracked residual fuels of the Bunker C type have adequate inherent stabilising characteristics to yield a stable suspension with 99% through 200-I.M.M. (230-U. S. Standard) mesh, coal in concentrations preferably of 40–45%. Regular laboratory tests and careful inspection of tanks and pipe lines have shown that these suspensions are adequately stable for all normal commercial requirements, provided there is no intense local overheating. In this connection, our storage tank at Aberaman was fitted with hot-water coils instead of steam coils. Coal-in-oil suspensions should not be kept in a static condition in the presence of steam coils more than is strictly necessary to ensure the mobility of the fuel. Turning full steam pressure on the coils is to be avoided unless the fuel is being circulated.

"Reduced stability at elevated temperatures is not accompanied by the precipitation of coal as such. What actually occurs is a gradation in coal concentration increasing from the top layer to a maximum of about 58% in the bottom 20% layer.

"In the case of 40% suspensions of 200-I.M.M. dry steam coal in Bunker C oil numerous stability tests since 1933 have enabled us to draw up the following table (Table 7) which sets out the various times taken to attain a concentration of 45% and 58% of coal in the bottom 20% layer of the "Hurrelled"[12] fuels at various temperatures:

TABLE 7

Temperature,	Deg	Time to reach a coal concentration in the bottom layer of—	
C	F	45%	58%
15	59	More than 150 days	More than 500 days
30	86	Approximately 65–70 days	Approximately 240 days
50	122	Approximately 28 days	Approximately 85–90 days
70	158	Approximately 5 days	Approximately 17 days

"The figures in column 3 show the approximate maximum time for which it is safe to allow a 40% suspension (Hurrell) in Bunker C oil to stand at various temperatures to permit of its direct use from a heated tank. The figures in column 4 indicate the approximate times in which the mixture will break down completely at various temperatures, leaving a top layer of fuel oil.

"Summing up, it may be claimed that if due precautions are taken against overheating, the fuel suspensions containing 40–45% of coal in Bunker C oil are stable enough for all practical commercial requirements and can be handled by the normal oil-handling equipment. The coal, however, must be ground and classified to yield not less than 98.5% through a 200-I.M.M. mesh screen and then thoroughly wetted with the oil, first in a primary mixer and then in a final mixer of the Hurrell Homogeniser type, normally used for making emulsions."

The effect found for temperature, time, coal fineness, and coal concentration on stability are in good agreement with those reported by the authors of this paper. Jones, however, went to somewhat greater length to insure thorough mixing of the finely pulverized coal and oil.

TABLE 8

Coal in mixture, per cent	Viscosity, Saybolt Furol sec. at—			
	100 F	150 F	200 F	250 F
55	...	14000	6000	3000
50	1800	570	250	140
45	660	190	79	37
40	380	110	46	24
35	290	88	42	19
30	190	46	17	....

[12] Run through Hurrell homogeniser (G. C. Hurrell, Limited, Old School Works, Woolwich Road, Charlton, England). In all of this work the coal was ground to the desired fineness, mixed with the oil, and then passed through the homogeniser.

Effect of Coal Concentration and Temperature on Viscosity. The data in Table 8 give the results Jones secured for the effect of coal concentration and temperature on viscosity. These data carry the viscosity values to higher temperatures than reported in the paper.

The figures were secured from logarithmic graphs compounded from a very large number of mixtures examined during the course of the work. In general the coal was about 98–99 per cent through 200-I.M.M. (230-U. S. Standard) sieve, while the Bunker C oils showed the following characteristics:

Specific gravity at 60 C	0.98–0.99
Flash point, deg C	156–208
Viscosity, Saybolt Furol, sec	
122 F	99–499
175 F	27–33
225 F	14–17
Pour point (A.S.T.M.), deg F	10–15

Combustion Tests. Jones carried out over 150 combustion tests with colloidal fuel on a boiler having the following characteristics:

Type	3 drum
Heating surface, sq ft	3947
Working pressure, psi	175
Furnace volume, cu ft	795
Evaporation rate, lb per hr	18000–20000
Preheated air, deg F (mean)	335
Air pressure at burners, in.	2–3
Fuel pressure at burners, psi, avg	120
Fuel temperatures at burners, deg F	260–280

He reported as a result of this work that the boiler furnace, when using coal-in-oil suspensions, even when viewed by a skilled observer, was not different in appearance from the oil-fired furnace. The efficiency depended upon the fineness of the coal, the volatile content of the coal, the nature of the oil, and the type of burner used.

Tests were run with coals containing 12 to 40 per cent volatile matter. The mixtures containing high-volatile coal gave a somewhat higher efficiency than those containing low-volatile coal. Under the worst conditions, efficiencies dropped about 5 per cent below those for oil alone. Under the best they were within 1 per cent of oil.

Jones states, "One of the most pleasing features of the boiler tests was the almost complete freedom from burner stoppages. Ignition was hardly ever lost in the tests due to the burners going out. In fact, the whole equipment, comprising pumps, filters, heaters, and atomizers, gave a performance which was quite indistinguishable from that obtained when using fuel oil in the same plant." This seems in essential agreement with the work reported in the paper.

Jones ran his tests with a variety of pressure, pressure and air, or pressure and steam burners and he states, "The Babcock and Wilcox pressure oil burners were adopted for convenience for most of the tests, but other burners of this type would be equally suitable."

Manufacturing. During the period in which this work was carried out in Wales, a small plant was erected to make about 0.75 ton per hr of oil-coal suspension. From this pilot plant, estimates were made of capital and manufacturing costs. On this basis, the writer has estimated that the cost of preparing 60 per cent oil - 40 per cent coal suspensions in the United States today would be about $0.80 to $1 per ton for a plant of about 100 tons per day.

This does not, of course, include the cost of the coal or oil but it does include all preparation costs, i.e., services, power, manage-

ment and supervision, labor, maintenance, rent, interest on investment, taxes, depreciation at 10 per cent, and insurance. It must be recognized, however, that there is considerable chance for error in translating costs in one country to another, which could not be avoided with the data available.

Summary. From the work done in this country and abroad, sufficient technical information is now available to contemplate the erection of colloidal-fuel plants of considerable size with reasonable assurance that the product could be used in certain oil-burning installations with little modification of existing equipment. This procedure provides a means for saving oil without the large equipment alterations necessary to convert plants and furnaces completely from oil to coal. It might therefore be of value during the war period with the prevailing critical equipment shortages. In general, the Bureau of Mines has not looked on the oil-coal mixtures as having a permanent place as an industrial fuel. Under normal conditions, with the necessary equipment available for handling any fuel, a plant will use oil or solid fuel alone, according to the dictates of cost, convenience, or other demands of a particular installation. From the long-range point of view, it is difficult to visualize a large field for colloidal fuel.

During the period in which this work was carried out, even the short-range viewpoint has altered greatly. The shortage of coal in both the United States and Great Britain becomes steadily more acute, and the saving of oil at the expense of coal looks much less attractive than it did a year ago. Unless this situation changes, it is doubtful if there will be any extensive use of colloidal fuel during this war.

C. C. WRIGHT.[13] The authors are to be congratulated for their presentation of a timely and much needed clarification of the technical factors concerning the production and use of coal-in oil fuels. From the viewpoint of the fuel technologist, a small amount of additional data on specific gravities would be most helpful in settling questions regarding the volume of fuel produced upon admixture of coal and oil. Specifically, the writer would like to see data included on the specific gravity of the coal-in-oil fuels reported in Table 2 of the paper, the specific gravity of the coal used in the preparation of the fuels reported in Table 4; also whether or not any change in specific gravity of the coal-in-oil fuel was observed with aging.

[13] Professor of Fuel Technology, The Pennsylvania State College, State College, Pa.

AUTHORS' CLOSURE

The authors agree thoroughly with the statement in Mr. Bailey's discussion that "the physical factors are one thing, the economic factors quite another." In this paper, attempt was made to supply new and needed information of a physical nature; such facts are required before economic factors can be soundly considered. Economic studies have been made both by The Atlantic Refining Company and the Bureau of Mines. Publication of these studies has not been made but they are available.

Dr. Schroeder supplies interesting information from unpublished work recently done in England which adds to the value of the paper.

In answer to Mr. Wright's inquiries, the following is submitted:

The specific gravities of the coal-in-oil fuels of Table 2 were not determined. The specific gravity of the coal of batches 1 and 2 of Table 4 was 1.30 and of batch 3 and 4, 1.32.

The following table gives typical specific gravities and viscosities of a coal-in-oil fuel over a period of eight days; other stable suspensions examined for gravity after much longer periods of storage showed no significant changes in gravity as the result of storage:

TABULATION OF SPECIFIC GRAVITIES

Batch No. 3

	Initial tank	Daily analysis of fuel April, 1943							
Per cent coal in mixture	inspection	14	15	16	17	18	19	20	21
		40.0	40.2	40.1	39.6	40.6	39.0	39.0	39.0
Sp. Gr. @ 80 F	1.085	1.089	1.079	1.090	1.085	Sample	1.077	1.078	1.087
Vis. @ 122 F (Furol)	331	412	380	397	368	lost	361	324	328
Vis. @ 210 F (Furol)	40	52	48	49	47		46	42	44

Wear-Resisting Materials for Lathe Construction

By R. W. DAYTON,[1] C. H. LORIG,[1] AND R. E. ADAMS,[1] COLUMBUS, OHIO

It was found, from tests of all the materials now in general use as the bearing surfaces of lathes, that the combination of hardened steel and alloy cast iron was far more wear-resistant than others and was adequately scoring-resistant.

A process referred to as "flame refining" was developed for improving the wear resistance of cast iron. An iron treated by this process and used with hardened steel formed the best combination tested, having greatly improved wear resistance and scoring resistance.

A wear test in simulated lathe service confirmed the earlier work and also showed that for minimum wear of a combination containing cast iron and hardened steel, the steel should form the carriage surface and the cast iron the bed surface.

GENERAL-purpose machine tools change but little in design from year to year and would remain useful almost indefinitely if they retained their initial accuracy. However, they do not, largely because of wear on the friction surfaces of the bed and the carriage which causes a gradual but eventually fatal loss of accuracy.

Machine tools vary in ability to resist deterioration of their ways. The ways of grinders, for example, remain true for many years because the conditions of service and the possibilities of design are such that the causes of wear are avoided. Thus materials of great wear resistance are not essential, so the original and most readily used material for machine-tool construction, plain cast iron, is still in use for all rubbing surfaces.

Other types of machine tools such as lathes operate under adverse, almost abusive, conditions. Since design can do little to make these conditions tolerable, wear-resistant materials must be used if the lathe is to have a long useful life. Accordingly, plain cast iron is being used less, and hardened steel and cast iron more, for the beds and carriages of lathes.

The number of materials which can be used for lathe-bed and carriage construction is limited. The body of both bed and carriage must be made of cast iron for economic reasons, so if different types of bearing surfaces are desired, they must be applied on the surfaces. Two methods of altering the bearing surfaces are now in use, flame-hardening the cast iron itself or fastening hardened-steel strips to the surface.

One other limitation in the choice of materials must be observed, namely, that either the carriage or the bed must be soft enough to be scraped to a fit by hand, for machine tools cannot economically machine the bed and carriage surfaces to a satisfactory fit. This prevents the use of fully hardened surfaces on both bed and carriage, a combination which might be the most wear-resistant of all.

As a result of the limitations of choice, only four combinations of materials for the wearing surfaces of lathe beds and carriages are in general use. These are the following:

1 Cast-iron bed, cast-iron carriage
2 Flame-hardened cast-iron bed, cast-iron carriage
3 Hardened-steel-faced bed, cast-iron carriage
4 Cast-iron bed, hardened-steel-faced carriage.

The manufacturing advantages and disadvantages of each of these types of construction are thoroughly understood, but the serviceability of each is not. The purpose of the study being reported was to appraise the serviceability of each of the combinations and then, if possible, to develop one better than any. The problem proved so complex that nearly four years of study were required to achieve the desired result.

Testing Methods

Lathe beds and carriages may experience two distinctly different types of damage. Either they may wear, losing material gradually from their rubbing surfaces until the accuracy of the lathe is lost, or they may gall, material being torn out of one surface in small pieces and welding to the other causing deep gouging and scratching. It can be expected that proper materials for the ways of lathes will not gall and will wear only slowly.

Wear of lathes is generally due to either abrasive or lack of lubrication. With adequate lubrication and abrasive-free conditions, no wear occurs as shown both by laboratory tests and by long-time running of a full-sized lathe under these conditions. If lubrication is lacking because of carelessness, very rapid wear will occur; so unlubricated wear was studied. However, since only a minute amount of oil suffices to prevent unlubricated wear, and since the necessary amount is likely to be present on the bed in all but rare instances, the results for unlubricated wear are considered less significant than those for abrasive wear.

Practically all lathe-bed wear is abrasive in character. If abrasive could be prevented from working between the rubbing surfaces, lathe beds would be as long-lived as grinder beds. Unfortunately, design considerations do not permit adequate protection of beds as long as those of some lathes.

Two types of abrasive cause most lathe-bed wear; scale from heat-treated steel and dust from cast iron. Both of these are brittle enough to crush small particles that get trapped between the rubbing surfaces, and hard enough to cause wear. Tests for abrasive wear were made in both of these abrasives. Some description of the wear tests is given in the caption of Fig. 1.

The galling, or scoring, which infrequently occurs between bed and carriage, is an acute form of failure. It is induced by "short-stroke" work in which the carriage moves back and forth many times over a short distance on the bed. The action appears somewhat similar to the wringing together of gage blocks, the continued slight reciprocation bringing the surfaces closer and closer together until molecular attraction causes welding. The only certain method of resisting this form of failure is to lift the surfaces out of contact at intervals, as by an oiling system which forces oil between the surfaces periodically.

No metals seem capable of resisting this type of failure indefinitely, even at minute loads, when the stroke is short. However, metals vary in their ability to resist scoring for a longer

[1] Battelle Memorial Institute, Columbus, Ohio.

Contributed by the Production Engineering Division and presented at the Annual Meeting, New York, N. Y., Nov. 29–Dec. 3, 1943, of THE AMERICAN SOCIETY OF MECHANICAL ENGINEERS.

NOTE: Statements and opinions advanced in papers are to be understood as individual expressions of their authors and not those of the Society.

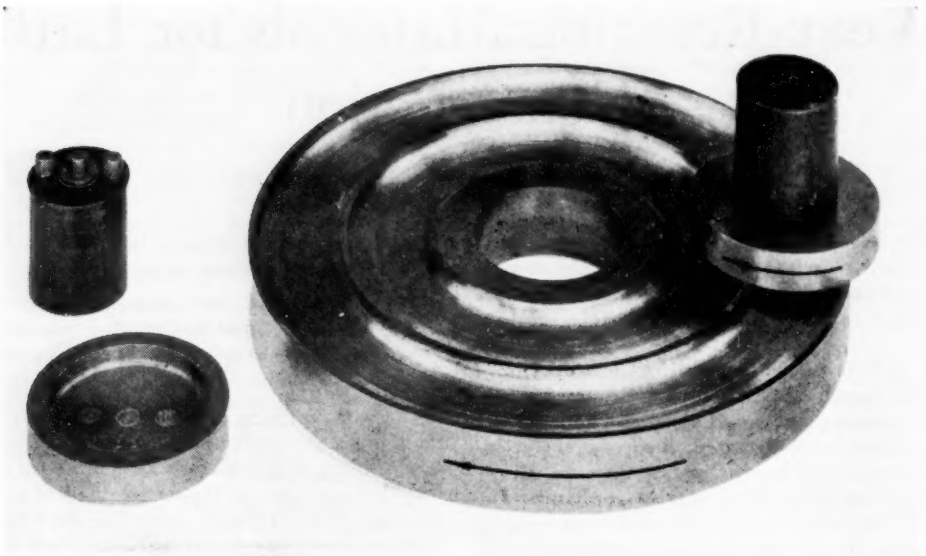


FIG. 1 THE WEAR-TEST SPECIMENS USED IN THE EARLY INVESTIGATION

(The large plate is made of one of the materials under test; the two small specimens like the one inverted in the lower left hand of the photograph are made of the other. The holder behind the small specimen centers and drives it, allowing rocking for alignment. During a test, both small specimens rest on the plate, one in the position shown, the other diametrically opposite. All three specimens are driven at the same angular speed in the direction indicated by the arrows. Unlubricated tests were made in both dry and humid air, for humidity was found to affect wear. The conditions under which each type of test listed in Table 1 is run are as follows:

Scale. The specimens are submerged in an agitated mixture of 25 per cent of —200 mesh heat-treating scale and oil. They are run at 148 ft per min and 210 psi of pressure. Three successive two-hour tests are run and an average taken.

Modified Scale. This test is used to distinguish between slow-wearing combinations. The conditions are the same as for the test in scale, except that the three two-hour tests are preceded by a 16-hour wearing-in period, during which the specimens are roughened and charged with abrasive so that rapid wear occurs.

Cast Iron. The same as the test in scale, except that the specimens are submerged in a mixture of 25 per cent of —200-mesh cast-iron dust and oil.

Dry Air. The specimens are surrounded with thoroughly dried air and run unlubricated, at a speed of 16 ft per min and a load of 75 psi. Four two-hour tests are run.

Moist Air. The same conditions as the test in dry air, except that the air is brought to about 100 per cent humidity and the load is 510 psi.)

stroke, and it is desirable that the best be selected for lathe-bed service. For sorting out the various materials, a scoring test was used which oscillated two specimens together, as discussed in the caption of Fig. 2.

PRELIMINARY TEST RESULTS

The results of the preliminary wear and scoring tests are summarized in Table 1. Each of the values reported is an average of three or more tests of each sample, generally of at least three samples and occasionally of seven or eight. In the cases where only a single material of a type was tested, the hardness is listed as a single number instead of a range.

A "relative-wear index" appears in next to the last column of Table 1. It was introduced to facilitate rough comparisons between the various combinations. The index was obtained by taking a weighted average of all the tests which were first reduced to a ratio, using combination IV-*a* as standard. A relative weight of 4 was assigned to the abrasive tests and of 1 to the unlubricated tests. This weighting takes cognizance of the fact that most lathe-bed wear is of the abrasive type and assumes that four times as much wear results from abrasive as from lack of lubrication.

Groups I, II, III-*a*, and IV-*a* of Table 1 are the combinations of materials in use in lathes at the present time. A study of the data for these four combinations shows that the two combinations in which cast-iron forms, both rubbing surfaces wear far faster, particularly in abrasive, than the two combinations in which fully hardened steel is one component. This is attributed to the fact that a cast-iron surface embeds abrasive in its pores which causes wear of the opposing surface. When both surfaces are cast iron, both will wear rapidly because the hardness of the abrasives exceeds even that of flame-hardened cast iron. When fully hardened steel is one component, there is little wear because it does not embed abrasive to wear the opposing cast-iron surface and is too hard to be worn much by the abrasive embedded in the cast iron. Thus if cast iron were run against softer steel, which could be worn by the abrasive embedded in the cast iron, rapid wear, particularly of the steel, would be expected to occur. The data for groups IV-*c* and IV-*d* show that this does happen.

The unlubricated wear of the two cast iron - cast iron combinations was also appreciably higher than that of the two hardened steel - cast iron combinations, though this fact is considered less serious.

The scoring resistance of the flame-hardened cast iron - plain cast iron combination was the highest. It was not, however, so

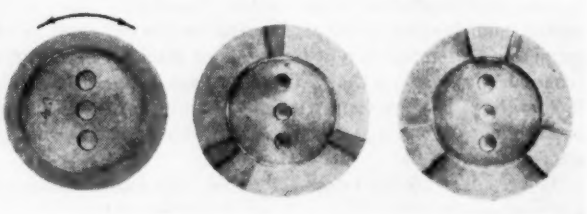


FIG. 2 THE SPECIMENS USED IN THE SCORING TESTS

(The one on the left oscillates as indicated by the arrow, with the annular face in contact with the three narrow (10 deg and 30 deg) raised segments of either of the two specimens on the right. The bearing faces are lapped optically flat for test. For the tests reported in Table 1, the angular motion was 25 deg, and the segmental specimen was like the one on the right with three 30-deg segments. Tests were run in an oil bath at 100 F for 15 min at 570 cycles per min. No scoring starts after this time.)



FIG. 3 THE TYPICAL MICROSTRUCTURE OF A CHILLED-CAST-IRON BED; ×100
(The matrix is fully pearlitic and the graphite is in spidery clusters. This iron is neither as wear-resistant nor as scoring-resistant as the alloy iron in Fig. 4.)

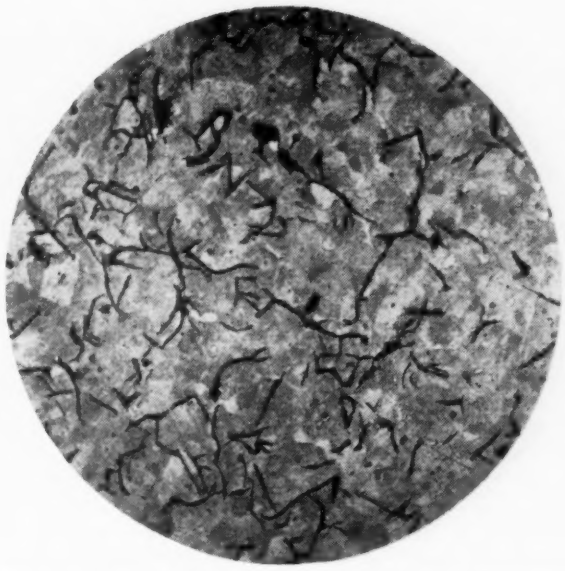


FIG. 4 THE TYPICAL STRUCTURE OF AN ALLOY-CAST-IRON BED
(The graphite is in small flakes randomly distributed. This iron is quite wear- and scoring-resistant.)

much higher than the scoring load of combination IV-*a* as the data would indicate at first glance, for the plain-cast-iron sample tested against all the flame-hardened irons was highly scoring-resistant, and when it was tested against hardened steel, scored at the highest load of all the iron tested in combination IV-*a*, 360 lb. Thus it seems that the combination of flame-hardened cast iron and plain cast iron is inherently only about 50 per cent

TABLE 1 AVERAGE RESULTS OF WEAR AND SCORING TESTS ON VARIOUS LATHE BED-CARRIAGE COMBINATIONS

			Average wear rate —0.001″ per hour						
			Abrasive wear			Unlubricated wear			
Combination no.	Combination of materials	Vickers hardness	Scale	Mod. scale	Cast iron	Dry air	Moist air	Relative wear index	Scoring load, lb
I	Cast iron	200–230	0.640		0.060	0.025	0.009		
	Cast iron	217	1.13		0.064	0.033	0.013		
			1.77		0.124	0.058	0.022	44.6	
II	Flame-hardened cast iron	450–610	0.049		0.009	0.008	0.007		
	Cast iron	198–217	0.234		0.029	0.044	0.019		
			0.283		0.038	0.052	0.026	8.9	490–590*
III-*a*	Chilled cast iron	225–230	0.013		0.005	0.005	0.035		
	Fully hardened steel	765–820	0.009		0.003	0.001	0.005		
			0.022		0.008	0.006	0.040	1.4	170–210
III-*b*	Ferritic chilled cast iron	195	0.028		0.018	0.046	0.072		
	Fully hardened steel	800	0.012		0.006	0.018	0.002		
			0.040		0.024	0.064	0.074	3.8	70–100
IV-*a*	Alloy cast iron	205–280	0.011	0.080	0.004	0.004	0.005		
	Fully hardened steel	765–820	0.008	0.072	0.004	0.003	0.004		
			0.019	0.152	0.008	0.007	0.009	1.0	216–360
IV-*b*	Ferritic alloy cast iron	140	0.027		0.017	0.022	0.066		
	Fully hardened steel	800	0.014		0.016	0.049	0.002		
			0.041		0.033	0.071	0.068	4.3	
IV-*c*	Alloy cast iron	270	0.115		0.005	0.032	0.002		
	Tempered steel	600	0.20		0.009	0.033	0.012		
			0.315		0.014	0.065	0.014	8.4	
IV-*d*	Alloy cast iron	270	0.222		0.016	0.026	0.005		
	Tempered steel	435	0.72		0.013	0.053	0.004		
			0.942		0.029	0.079	0.009	22.5	
V-*a*	Flame-refined cast iron	230–300	0.007	0.056	0.002	0.004	0.004		
	Fully hardened steel	765–820	0.006	0.052	0.007	0.002	0.007		
			0.013	0.108	0.009	0.006	0.011	0.8	316–440**
V-*b*	Flame-refined ferritic irons	240–260	0.012		0.006	0.004	0.009		
	Fully hardened steel	765–820	0.006		0.004	0.002	0.002		
			0.018		0.010	0.006	0.011	1.1	

* Fifty per cent higher scoring load than the same piece of plain cast iron against hardened steel.
** Each of the hardened irons scored at a 50 per cent higher load than the same iron not flame-treated.

more resistant to scoring than hardened steel and plain cast iron, instead of 100 per cent better as the data of Table 1 would indicate.

These results indicated that combinations of hardened steel and cast iron were inherently more wear-resistant than combinations of cast iron and cast iron, so the former were investigated more thoroughly. A comparison was made between two types of beds, chilled and alloy iron, being made for the manufacturer sponsoring this work. The former is an iron containing approximately 3.3 per cent carbon, 0.40 per cent chromium, and up to 0.50 per cent copper cast against chills on the wearing surface to produce a fine-grained iron; the latter contains approximately 3.0 per cent carbon, 0.20 per cent chromium, 0.75 per cent copper, and 0.30 per cent molybdenum, cast without chills but just as fine-grained as the chilled iron because of its composition. The photomicrographs of Figs. 3 and 4 show that there is far more difference in microstructure than the slight composition differences would indicate. The chilled iron has what is called a "modified" graphite flake, the alloy iron a normal graphite flake.

Wear and scoring tests showed that chilled beds wore faster and scored at lower loads than unchilled beds. Chilled beds have another disadvantage in that foundries making chilled beds are more likely to produce an occasional ferritic bed than a foundry making alloy-iron beds, and as a comparison of combinations III-*b* and IV-*b* with III-*a* and IV-*a* will show, ferritic irons are extremely poor bearing surfaces. The manufacturer discontinued the use of chilled beds when this information was available and has obtained the indicated improvement in performance.

Investigation of the effect of composition of the cast iron on the performance of combination IV-*a* showed that the composition given was as good as any. Increase of the carbon content or small changes in the alloy content do not greatly change the rate of wear or the scoring load, so long as the iron is fully pearlitic. Ferritic irons like combinations III-*b* or IV-*b* must be avoided or rapid wear and scoring will be experienced. Low-carbon irons too must be avoided, for one fully pearlitic iron with only 2.53 per cent carbon scored at an extremely low load, 140 lb. High-alloy irons, containing considerable amounts of free carbide, wore a little more slowly and scored at somewhat higher loads, but they were expensive and extremely difficult to scrape because the many carbide particles dulled scrapers with extreme rapidity.

Effects of Heat-Treatment

The results of the composition study provided little hope that any considerable improvements could be obtained from modifications of composition alone. Heat-treatment was then tried as a means of obtaining the desired improvement. From furnace heat-treating experiments, it was found that better results were



Fig. 6 The Microstructure of the Unaffected Zone of the Bar of Iron, Fig. 5; ×500
(The iron is comparatively soft, 190 Brinell, as the coarseness of the pearlite would indicate.)

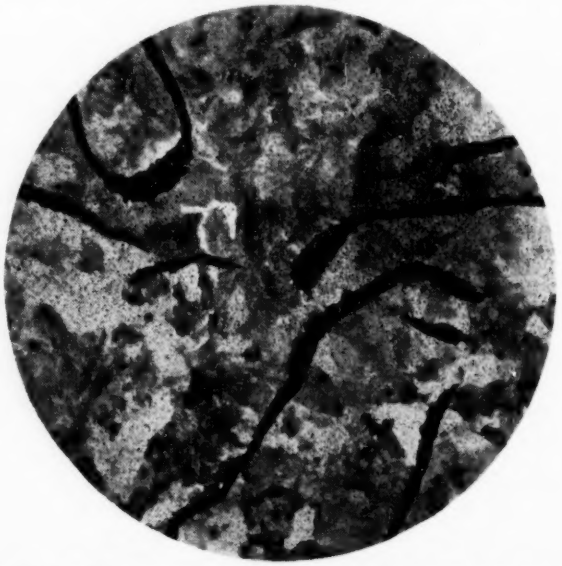


Fig. 7 The Microstructure of the Flame-Refined Part of the Bar of Iron, Fig. 5; ×500
(The pearlite lamellae are much finer, the hardness has been increased to 280 Brinell, and the iron is more wear- and scoring-resistant.)

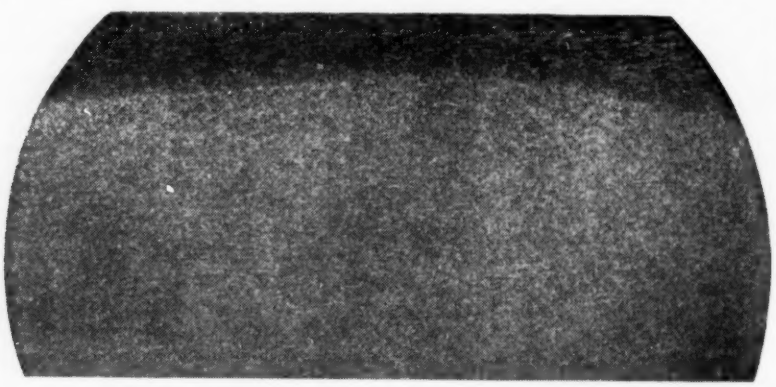


Fig. 5 The Cross Section of a Flame-Refined Bar of Cast Iron, Showing the Depth of the Hardened Zone; ×2

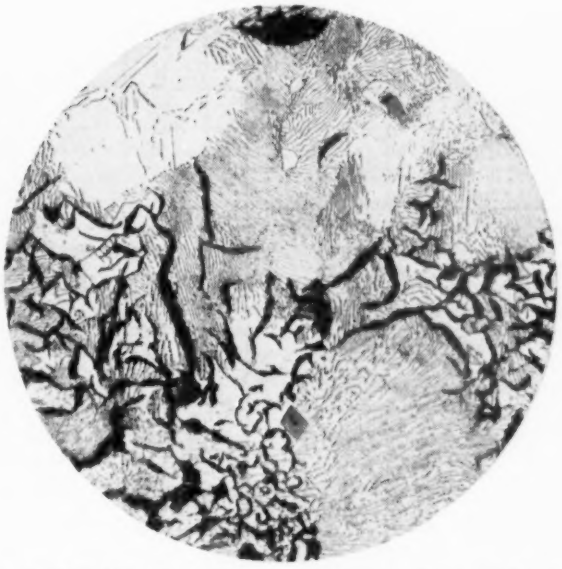


FIG. 8 THE MICROSTRUCTURE OF A MODIFIED FERRITIC TYPE OF IRON; ×500

(The white patches of free ferrite in dispersed grains and between the clusters of graphite flakes form approximately 25 per cent of the structure. This type of iron scores readily and wears rapidly.)

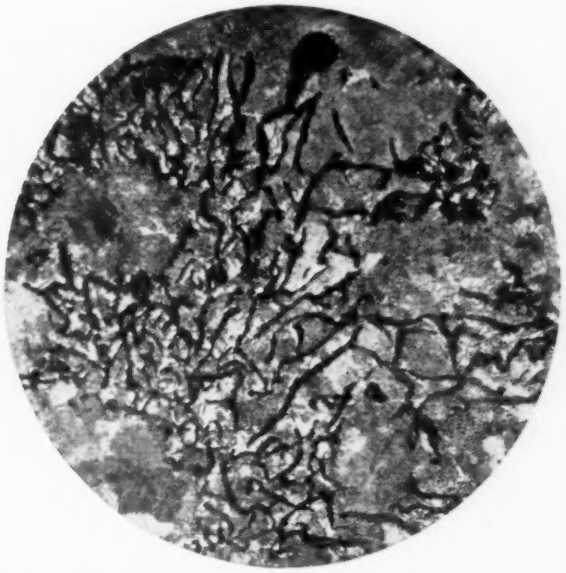


FIG. 9 THE SAME IRON AS IN FIG. 8 AFTER FLAME-REFINING; ×500

(The ferrite has been almost entirely converted to pearlite, and the pearlite has a finer grain size. The hardness of the iron has been increased from 180 to 225 Brinell. The wear and scoring resistance is almost as good as for a flame-refined originally pearlitic iron.)

obtained by cooling comparatively rapidly from above the critical temperature, to produce an extremely fine pearlitic structure, than by quenching and drawing to the same hardness to produce a sorbitic structure.

The experiments were extended to sections of beds, and it was found that the desired structure and wear resistance could be obtained by heating the surface with a flame-hardening torch to above the critical temperature and depending on the heat drain from the cooler interior of the bed to produce the proper rate of cooling. It was found that the temperatures of the underlying bed must be somewhat elevated, by making a preheating run with the torches, to prevent too rapid cooling and excessive hardness. This process is called "flame refining"[2] to distinguish it from flame hardening where a quench is essential and full hardness is desired. By experiment, it was found that these heat-treated irons could be scraped at hardnesses up to 30–35 Rockwell C if carbide-tipped scrapers were used. The structure of an iron before and after treatment is shown in Figs. 6 and 7 where it is evident that the pearlite is greatly refined by the process. The depth of hardening is apparent in the cross section illustrated in Fig. 5.

Wear and scoring tests of these heat-treated irons showed that wear in abrasive was only 70 per cent as great as that of the same irons before heat-treatment, and that the scoring load was 50 per cent greater than for the same irons not hardened. The data for the tests are given under combination V-*a* in Table 1. The heat-treating process performs even more strikingly on ferritic irons, as a comparison of the data for combination V-*b* with III-*b* and IV-*b* shows. It is to be expected that the flame-refining process would have such an effect, for it eliminates free ferrite from the structure, as a comparison of Figs. 8 and 9 shows.

SIMULATED SERVICE TESTS

The results up to this point indicated that a combination of fully hardened steel and flame-refined cast iron was the most wear-

[2] Patent applied for.

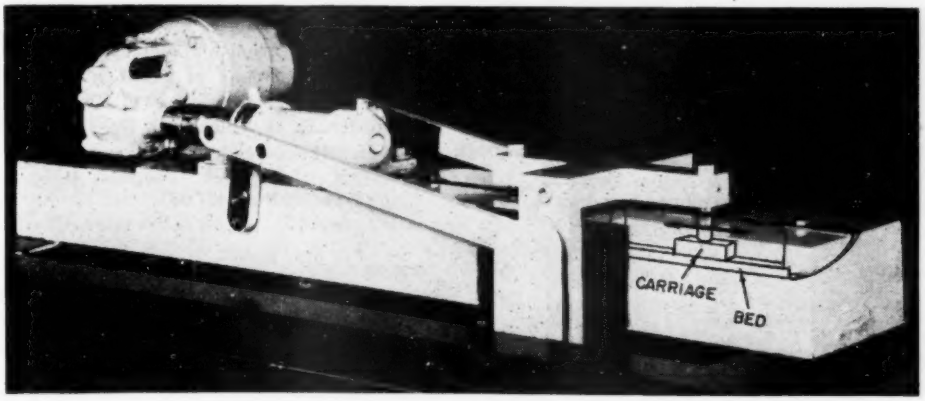


FIG. 10 A RECIPROCATING WEAR-TESTING MACHINE USED FOR SIMULATED LATHE-BED SERVICE WEAR TESTS

(The form of the specimens is shown in phantom outline. The specimens were run in the same slurry of heat-treating scale as the preliminary wear tests. The machine operated at 11½ cycles per min with a 4-in. stroke. The bearing load was 15 psi.)

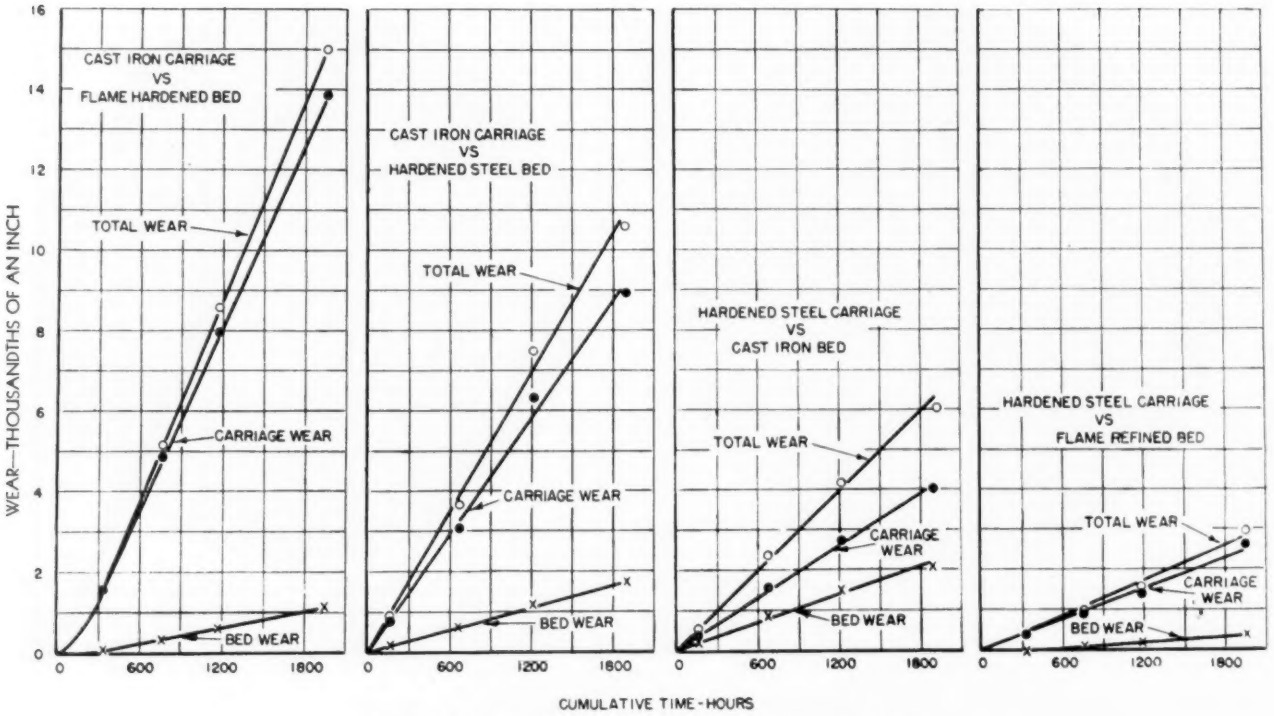


FIG. 11 WEAR OF MATERIALS IN SIMULATED SERVICE TESTS

resistant, but did not show which of the two materials should be the carriage and which the bed. To determine this, as well as to obtain additional confirmation of the results up to this point, long-time abrasive wear tests were made in an apparatus which simulated the wearing action of a lathe. The apparatus is illustrated and described in Fig. 10. The results for four combinations of materials are given in Fig. 11. The materials used in this test were those which had been proved by the earlier work to be the best of their types.

The first combination of a cast-iron carriage and a flame-hardened bed shows little wear of the bed, but relatively enormous wear of the carriage. After test, the originally square ends of the carriage were rounded off, indicating that they had acted as wedges, permitting a great deal of abrasive to work between the surfaces.

The second combination, again of a cast-iron carriage but with a fully-hardened-steel bed, showed slightly more bed wear but considerably less carriage wear. However, the carriage wore at the ends the same as against a flame-hardened bed.

The third combination of an alloy-cast-iron bed and a fully-hardened-steel carriage showed slightly more wear of the bed but far less wear of the carriage than the other two. The carriage remained square at the ends.

The fourth combination of a flame-refined cast-iron bed and a fully-hardened-steel carriage was superior in every respect. Carriage wear was only 60 per cent as great, bed wear only 25 per cent as great, and total wear only 45 per cent as great as on the best of the other combinations in these individual respects.

CONCLUSIONS

The results indicate that the combination of a carriage faced with fully-hardened-steel strips[3] and a cast-iron bed flame-refined to the maximum allowable hardness for scraping will wear far less than any other combination. The combination appears to be about as scoring-resistant as any other, and 50 per cent better than unhardened cast iron against hardened steel. Since service records show no scoring difficulties with this latter combination, except for infrequent ferritic beds, the scoring resistance appears more than adequate.

ACKNOWLEDGMENT

This investigation was made for the Lodge and Shipley Machine Tool Company of Cincinnati, Ohio. The assistance of Mr. W. L. Dolle and Mr. Fred Schoeffler of that organization, and of Dr. H. W. Gillett and Dr. H. W. Russell of Battelle has been greatly appreciated.

[3] U. S. Patent No. 2,167,609.

Porous Chromium in Engine Cylinders

By RUSSELL PYLES,[1] OLEAN, N. Y.

In recent years it has been possible to deposit thick coatings of chromium electrolytically on machined parts, where lubrication is a vital factor. Diesel-engine cylinders and piston rings may be included among the most critical engine parts from a wear standpoint, and in this application, porous chromium has demonstrated its ability to increase the life span of an engine. The author outlines the properties inherent in porous chromium which contribute to its low wear rate in engine cylinders, i.e., hardness, exceeding that of any other cylinder-lining material; high thermal conductivity; low friction coefficient, and low affinity for other metals; corrosion resistance, preventing surface deterioration.

THE element chromium was discovered in 1798, but not until 1859 was it isolated by F. Wohler who obtained small quantities by reduction of the trichloride. As early as 1848–1854 (1)[2] efforts were being made to electrodeposit chromium. Decorative chromium as thin coatings of 0.00001–0.00002 in. became a commercial fact about 1924 (2). It is interesting to note, too, that the metallurgical advantage of chromium as a steel-alloying agent was put to use in 1870, when Midvale produced 2400 tons of 1 per cent chrome steel for the Eads Bridge over the Mississippi River at St. Louis (3).

Only in the last few years, however, have thick coatings of porous chromium been developed for machine applications where lubrication is a vital factor (4). Cylinders and piston rings are among the most critical engine parts from a wear standpoint. Here porous chromium has demonstrated that it will increase the life span of an engine.

Properties of Electrodeposited Chromium

Hardness. Hardness alone is not accepted as being a criterion for low wear but it is true, that for the same material, wear is lessened when hardness is increased. This has been indicated by many tests on cast-iron engine cylinders and heat-treated steels. Hardness, though, may be a dominant factor where erosion is a problem. Chromium is hard but some variations in hardness are obtainable by control of plating factors, such as bath composition, current density, and temperature. However, within the usual limits of these plating factors the hardness variation is slight.

TABLE 1 HARDNESS TABLE

	Brinell hardness (load 3000 kg; 10-mm ball) or equivalent
Chromium	800–1000
Cast-iron cylinder compositions	150–275
Cast-iron cylinder compositions, heat-treated	Max 400
Steel 4140 heat-treated	250–375
Steel, carburized	625
Nitralloy in cylinders after removal of surface stock	650–750

Chromium is harder than any other of the metals in general use for engine cylinders, and this hardness is maintained throughout the thickness of the case while the hardness of nitralloy or carburized steels decreases with depth. The hardness of the base metal under the chromium is not such an important factor in cylinders, although it may be in other special applications. Crushing loads, due to piston-ring and gas pressures, are relatively light in engine cylinders and porous chromium performs just as well on soft steels and cast irons as it does on nitralloy. Thus, the engine designer may choose his basic cylinder material without any regard for its wear characteristics. Alloy irons are not necessary, except as determined by structural-strength requirements. Cylinders may be of low-carbon steel for good welding where the cylinder assemblies are fabricated for lightness. These economic features are important in normal times and even more so now, when alloys are so difficult to obtain.

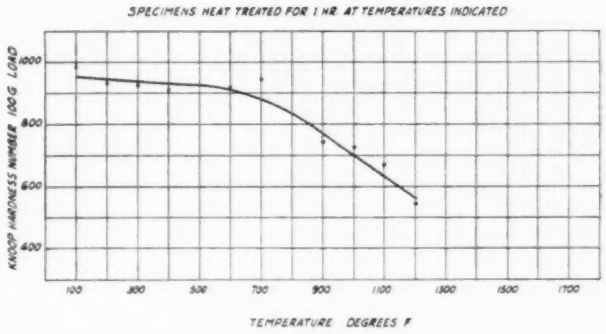


FIG. 1 KNOOP HARDNESS, POROUS-CHROME CYLINDER
(0.0045 in. chromium on cast iron.)

The hardness numbers in Table 1 are given for comparison in Brinell numbers, but it should be noted that the Brinell test is not used for the higher hardnesses and particularly for determining hardness of thin coatings. Because usual hardness tests, such as Rockwell, Shore, and Brinell, cover relatively large areas and are influenced by an appreciable depth of the underlying metal, they do not give a true picture where thin hard coatings are to be tested. The Knoop indentor (5) overcomes this difficulty by using a small diamond pyramid with shallow indentation. This machine is well adapted to use on porous chrome because the short length of the impression (approximately 0.004 in.) readily fits into the plane areas between the pores.

Contrary to many metals, chromium maintains its hardness very well within the range of cylinder-wall operating temperatures, Fig. 1.

TABLE 2 EXPANSION COEFFICIENTS AND THERMAL CONDUCTIVITY

Metal	Linear thermal expansion at 68 F × 10^{-6}	Thermal conductivity, cal/cm²/cm/deg C/sec at 20 C	Melting point, deg F
Chromium, electrolytic	4.5	0.165	3325+
Cast iron	6.6	0.12	2500
Steels	6.2–6.6	0.11	2700–2800
Aluminum	12–13	0.52	1216
Copper	9.1	0.92	1981

The linear-expansion coefficient of chromium is lower than that of cast iron or steel, yet no cases of bond failure due to this have been noted. The surface temperature in a cylinder is higher than that of the underlying metal, there being a steep

[1] Chief Engineer, Van der Horst Corporation of America.

[2] Numbers in parentheses refer to the Bibliography at the end of the paper.

Presented at the National Meeting of the Oil and Gas Power Division, Baltimore, Md., June 14–16, 1943, of THE AMERICAN SOCIETY OF MECHANICAL ENGINEERS.

NOTE: Statements and opinions advanced in papers are to be understood as individual expressions of their authors and not those of the Society.

temperature gradient through the cylinder wall. This condition, for minimum heat stresses, theoretically calls for an expansion coefficient varying from a lower value at the inner wall to a higher value at the outer cylinder wall. An inside layer of chromium partially fulfills this ideal requirement. Chromium has been plated on the aluminum piston crown of a Lauson engine $1^3/_4$ in. bore $\times$ $1^7/_8$ in. stroke and run for 54 hr without any signs of bond failure or change in surface appearance under the microscope. Many cases of record in high-output air-cooled airplane engines, with 700 to 1000 hr, show no tendency of the chromium to loosen due to differential expansion between the chromium and the steel. These engines are running with cylinder-wall temperatures much higher than those encountered in stationary-engine service. This evidence indicates that the low expansion of chromium may be a desirable feature for cylinder walls.

It should be noted that the thermal conductivity of chromium is approximately 40 per cent higher than for steel or cast iron. Maximum metal temperatures of the cylinder are at the inner cylinder surface particularly in the combustion zone. Any improvement in heat transfer results in a lower wall temperature and will improve piston and ring lubrication. Heat actually gets away faster through chromium. Tests on air-cooled porous-chrome cylinders have shown that more heat passes to the barrel fins because a greater quantity of cooling air on the barrel is required to maintain a standard thermocouple temperature. Other tests have shown a higher than normal temperature at the cylinder flange, indicating greater heat transfer to the barrel. Specific fuel consumption was normal so there is no reason to believe that there was any increase in total heat loss. This additional cylinder heat then must have been subtracted from heat loss to the cylinder head, piston, and lubricating oil. It is a fact that in some engine types the bottleneck for heat dissipation lies in the cylinder head. The heat distribution for an air-cooled airplane-cylinder assembly is of the order of 60 per cent to the head and 40 per cent to the barrel. Any diversion of heat to the barrel is evidently very desirable and chromium seems to accomplish this.

The question naturally arises concerning heat transfer through the bond where two dissimilar metals are joined. Inspection of photomicrographs of porous chromium applied directly to iron or steel shows no space or void between the two metals. Of course, the basic metal must be absolutely clean before plating but this is readily accomplished by a short electrolytic etch, which, at the same time, produces some mechanical keying and interlocking on the basic-metal surface.

In some plating the metal is transferred from the anode to the cathode, but in chromium plating, the chromium comes directly out of the bath solution which is essentially chromic acid (CrO_3 H_2O). It is deposited as molecular chromium on the cathode, the molecules being of insignificant size dimensionally. Thus the chromium fills in the smallest irregularities of the surface being plated and a bond approaching fusion such as in welding is obtained. Chromium under the microscope even at high magnification exhibits no crystalline structure such as we see in steels, but the crystalline structure has been indicated by X-ray diffraction. Because of the fineness and intimacy of this bonding good heat transfer results. Mechanical failure at the bond is the least of our worries, calling only for meticulous care in the cleaning of the basic-metal surface.

Friction. Chromium is conceded to have the lowest coefficient of friction of any of the generally used structural metals. The value of the sliding coefficient for chromium on chromium has been given as 0.12 and for chromium on steel as 0.16, while steel on steel is 0.20 (6). It should be pointed out here that our experience with chromium running on chromium under boundary lubrication has been unsatisfactory.

For rotating shafts chromium was found to have the lowest friction of any of the metals tested (7). Friction in an engine cylinder can hardly be estimated from any simple friction tests, and no actual engine tests have yet been run by the author's company to check comparative friction losses with porous-chrome cylinders.

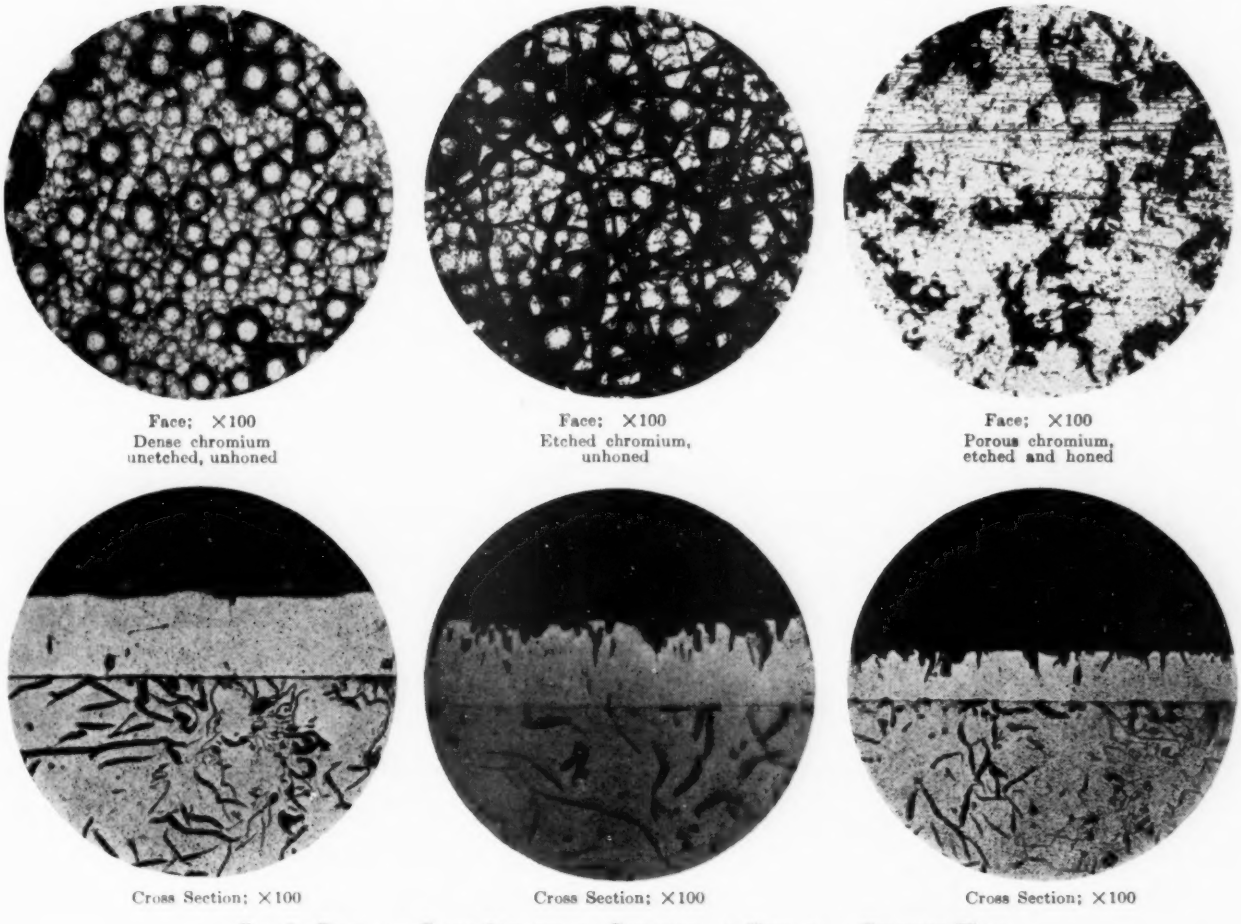
Corrosion Resistance. The corrosion resistance of chromium is high and is an important contributor to its low wear rate in engines. Sulphur is always present to some degree in Diesel fuels ranging from $^1/_2$ to 3 per cent by weight. At the high temperature and pressure existing in the cylinder, sulphur may combine with oxygen to form sulphur trioxide (SO_3) which, with water as a product of combustion, forms dilute sulphuric acid. Chromium is only very slightly attacked by sulphuric acid but ferrous metals are quickly and vigorously attacked. Another sulphur compound, hydrogen sulphide, may be encountered as a corrosive agent, particularly in gas engines running on sour gas.

A steel rod plated over a part of its length was subjected to moist hydrogen sulphide at temperatures ranging from 120 F to 220 F for 252 hr. After this exposure the unplated portion of the rod was blackened and badly corroded, but the chromium-covered portion was unattacked. This resistance to hydrogen-sulphide corrosion has been confirmed in service by excellent performance in gas engines operating on natural gas with an H_2S content as high as 1 per cent by volume. In spite of the resistance of chromium to corrosion from sulphur compounds they should always, in so far as possible, be removed from gaseous fuels because their tendency to increase fuel knock adversely affects combustion. Chromium is unaffected by nitric acid and saturated solutions of ammonia, but it is dissolved by hydrochloric and bromic acid.

Chromium resistance to atmospheric corrosion is well recognized. Porous-chrome cylinders may be stored indefinitely with little or no protection to the chromium surface and no detrimental effect results.

Having mentioned some of the good characteristics of chromium, it is well to note also some of the deficiencies so that its limitations may be recognized. Its tensile strength seems to be negligible. We have made rather crude tests for tensile strength of electrodeposited chromium and obtained a value of around 2000 psi. Chromium was deposited on a copper strip to a thickness of 0.005 in. and the copper was then dissolved by nitric acid, leaving 0.005 in. of chromium. This was very fragile and brittle but with care was clamped and pulled. Search of existing literature fails to reveal any values for tensile, shear, or compressive strength, yet this information is desirable when chromium is used as an engine material. However, chromium, in common with other brittle materials such as cast iron, must have appreciable compressive and shear strength as evidenced by its performance in engine cylinders and on piston rings.

Porous Chromium. Porous chromium has all of the characteristics peculiar to chromium but differs principally in its surface condition. This is responsible for its ease of lubrication and ability to carry high bearing loads. Fig. 2 shows face and cross sections of chromium as used on a cylinder wall. When chromium is electrodeposited to a thickness of 0.004 to 0.015 in., it becomes nodular and exhibits a network of cracks. Thin deposits of the order of 0.00001 to 0.00005 in., as used in decorative work also invariably show checking, except that they may be smeared over by cold working in buffing or polishing operations. These cracks are due to tensile stresses beyond the ultimate tensile strength of the chromium. They are shrinkage cracks probably resulting from the evolution of hydrogen (8). In the plating process, hydrogen is generated at the cathode (cylinder wall), and the chromium as deposited may contain large volumes of occluded hydrogen.



Face; ×100
Dense chromium
unetched, unhoned

Face; ×100
Etched chromium,
unhoned

Face; ×100
Porous chromium,
etched and honed

Cross Section; ×100

Cross Section; ×100

Cross Section; ×100

FIG. 2 FACE AND CROSS SECTIONS OF CHROMIUM AS USED ON A CYLINDER WALL

When this hydrogen diffuses out, a change in volume occurs, the result being, for analogy, a condition similar to dried mud from which water has evaporated. These cracks are not the grain boundaries as commonly seen in etched steel. Because tensile failure has occurred along these lines it cannot be assumed that the chromium is stress-relieved. Appreciable stresses still exist throughout the plate, but they are below the ultimate strength. Electrolytic action preferentially attacks along stress lines or planes and the current-reversing process, which is the treatment for producing porous chromium, does exactly this (9). As the reversing process proceeds, the existing cracks become wider and deeper at the same time they tree or sprout branches until the whole surface is completely cut up, appearing under the microscope like a coal pile. Fig. 3 shows well the effect of progressive electrolytic etching or reversal. This porosity treatment effects a great reduction in residual stresses and may be responsible for the slight reduction in endurance limit found on porous-chrome-plated steel specimens (10–15 per cent, while dense unetched chromium may show a reduction of as much as 50 per cent).

Strips of 0.005-in-thick shim stock were plated with the results shown in Fig. 4. Upon plating the strip (*a*) on one side only, it assumed the curvature shown at (*b*), yet the chromium surface on microscopic inspection showed no cracks. Shrinkage of the chromium occurred, but due to the thinness of the steel base strip, it conformed, and the stresses in the chromium did not exceed its ultimate strength. However, the application of reverse current (*c*) produced a reduction in curvature and also many surface cracks, demonstrating that residual stresses were relieved. Strip (*d*) was plated on both sides with the same thickness of chromium. It remained substantially straight, but the chromium surface on each side was cracked exhibiting tensile surface failures because the stresses of deposition were not relieved by conformation or current reversal.

The current-reversing process may be carried to the point of complete removal or stripping of all of the deposited chromium, but in the production of cylinders it is stopped short of any appreciable dimensional change in the bore diameter. Honing of the bore then results in a smooth surface containing microscopic indentations, recesses, or pits.

Wettability. The term "wettability" has been applied to surfaces and oils to define that property of either which affects the rate of oil dispersion. It is a function of both the oil and the surface. Oils vary in wetting characteristics. Surface geometry and profile also play a major part. The porous-chromium surface after honing, with its flats dotted with microscopic pits, depressions, or crevices is readily wetted with oil, which spreads quickly and covers. It has the further advantage of oil retention. Oil may be scraped from the flat surfaces but some remains in the pores, and this will creep up and rewet.

The mechanism of wettability, which has been ably discussed by J. T. Burwell (10), is such that an oil drop on a plane smooth surface will reach a state of equilibrium, where it will neither spread nor recede. At this condition the dome-shaped drop makes a definite contact angle with the plane surface, this contact angle depending upon inherent characteristics of the oil.

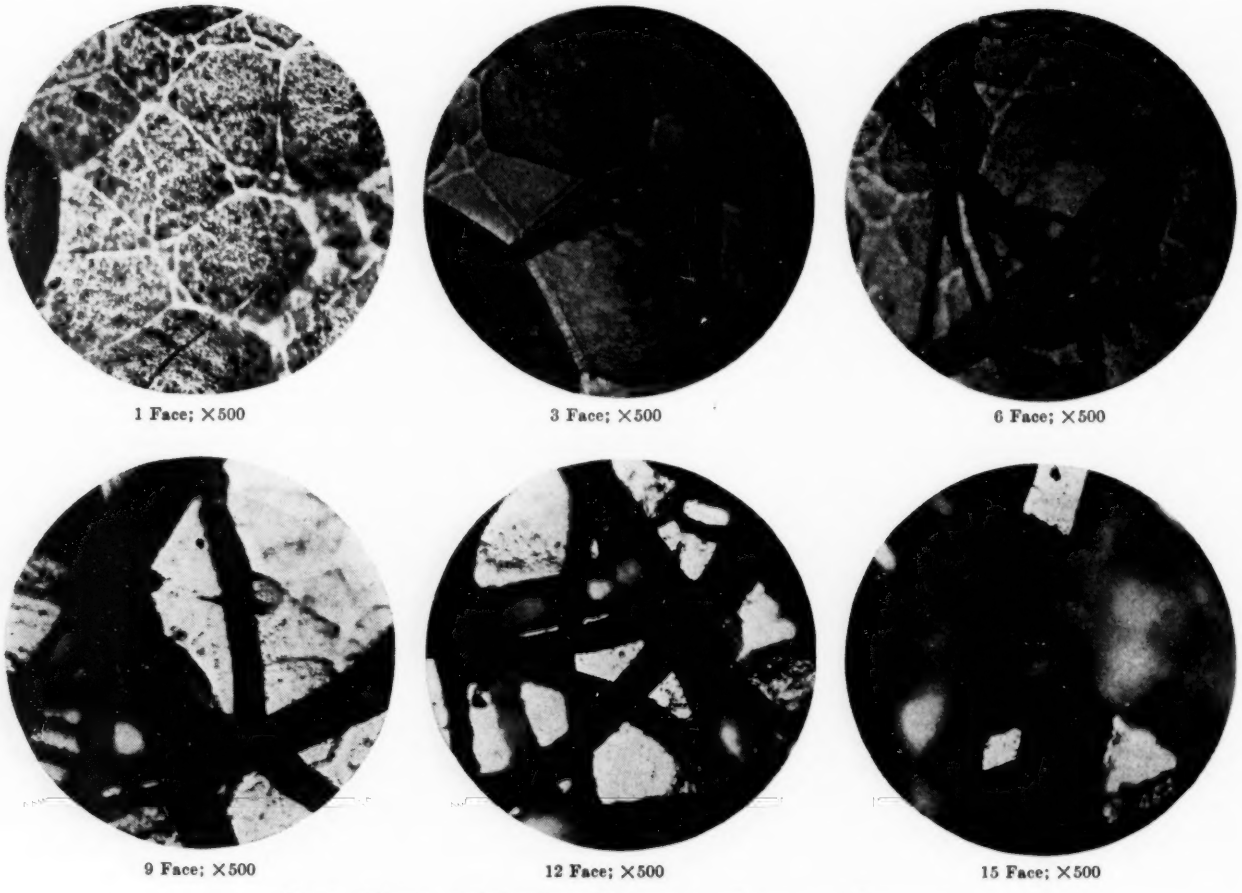


FIG. 3 EFFECT OF PROGRESSIVE ELECTROLYTIC ETCHING ON CHROMIUM

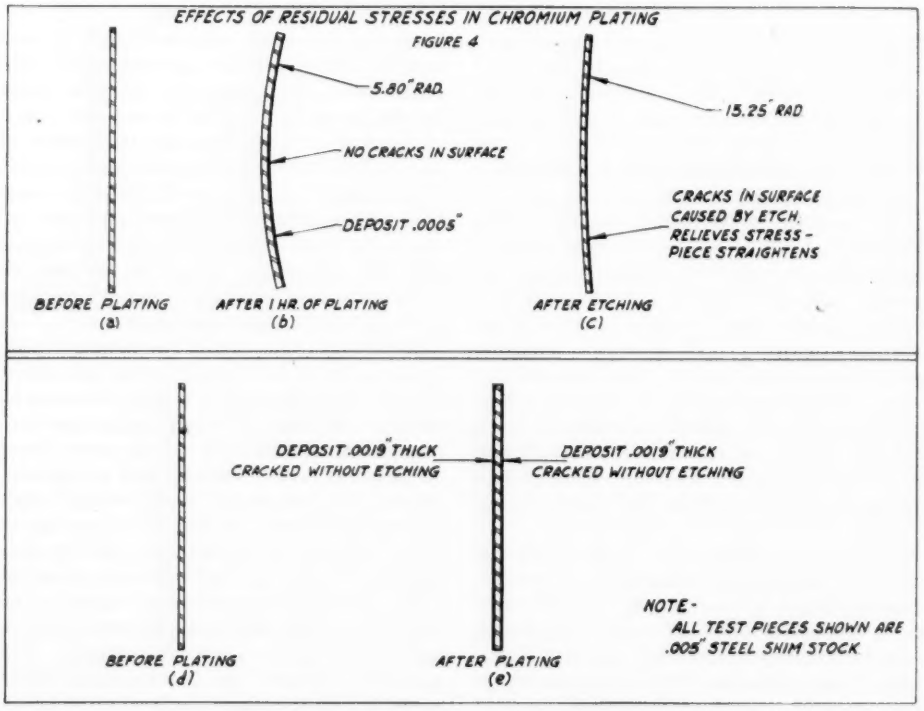


FIG. 4 EFFECTS OF RESIDUAL STRESSES IN CHROMIUM PLATING

itself. The energy of adhesion of the oil W is given by $W = \alpha (1 + \cos \theta)$ (10), where α is the surface tension and $\cos \theta$ is the contact angle.

A $^1/_4$-in-diam area on porous chromium may contain fifty to several hundred pores or crevices depending upon the "porosity." Taking a section through the diameter of such a surface with an oil drop on it, we will find the edge of the drop may be on a flat surface and at this point it will stop spreading when the equilibrium contact angle is reached. However, there is an infinite number of diameters that may be taken through the oil drop and every one will show a different geometrical condition of the porous-chrome surface at the edge of the drop. Circumscribing a circle on a photomicrograph of the porous-chrome surface, it will cut through flats, the downslope of pores, and the upsloping sides. As a result, the condition at the periphery of drop is unstable, because the contact angle of equilibrium can never be reached at all points. The oil thus proceeds to execute enveloping tactics around the flat areas, and to spread over the whole surface.

Our experience indicates that on any metal surface which has roughness, for instance, scratches running in all directions, oil will spread faster than when the surface is smooth. On a specimen polished in one direction, the oil will also spread faster in the direction of the polish scratches than it will at 90 deg to them. In this case the drop becomes elliptical, the major axis being in line with the scratches. This action is explainable by the variation of the contact angle at the edge of the oil drop.

Load Capacity of Porous Surfaces

With full oil-film lubrication the capacity of a bearing is a function of bearing area if other factors such as viscosity and speed are constant. Crankshaft bearings operate, at least during a large part of the cycle, under conditions approaching full film lubrication. An increase of bearing area here results in an increase in load capacity generally. Under conditions of boundary-layer lubrication such as exists between piston rings, piston, and cylinder wall, the case is reversed and load capacity increases with a decrease in bearing area. This is entirely at variance with accepted theories of hydrodynamic lubrication, but this type of lubrication cannot be maintained on cylinder walls. Oil control requires removal of oil from the cylinder wall, what remains being subjected to high temperature and combustion flame as well as dilution from fuel or condensation of combustion products. The dynamic factor of velocity is a requisite for hydrodynamic oil-film maintenance, yet at the top center position of the piston, where all of the adverse conditions accumulate, the piston-ring velocity is zero. Boundary-layer lubrication is the best that can be expected in the upper ring travel.

Notable investigations of boundary-layer conditions have been made by F. P. Bowden (11) and collaborators. Macy O. Teetor (12) has analyzed and experimented on these conditions for the specific case of piston rings and cylinders. The results are startling and establish some novel concepts of factors involved in boundary-layer lubrication. Evidence seems to indicate that scuffing or scoring results when the surface temperatures of the metals in contact reach the melting points, then fusion or welding occurs. These surface temperatures, even under conditions of smooth running and low friction, have been found to exceed 1100 F, yet the body of the test specimen remained at room temperature (11 *b*).

That these temperatures can sometimes exceed the melting point of cast iron is evidenced by inspection of seized cast-iron pistons where we may find some of the cylinder-wall material welded on the piston or the reverse condition of piston surface welded on the cylinder wall. The factors producing heat at the surface are speed, load, and frictional characteristics of the metals in contact, but friction depends to a large degree upon the surface geometry (rough or smooth), and the actual net area of contact. The larger the contact area the greater will be the amount of heat generated. Cooling of the surface is accomplished partially by oil but mainly by heat transfer into the base material. Teetor's work (12) demonstrates that reducing contact area by interrupting the surface results in a smaller amount of generated heat because by so doing he was able to carry higher bearing loads. The low limit for contact area may be dependent upon the physical characteristics of the contacting metals, particularly their shear and compressive strength at operating temperature. The amount of heat that can be carried away from the surface depends upon the thermal conductivity, and the limiting operating surface temperature is fixed by the melting points of the contacting materials. Briefly, the following steps are indicated for increasing load capacity under boundary-lubrication conditions:

1 Reduce the net actual contact area.
2 Choose materials with high thermal conductivity.
3 Choose materials with high melting points.

It is interesting to note how porous chromium fits into these requirements:

1 Inspection of face and cross sections of Fig. 2 shows that contact area is reduced by the pores or crevices. This we call porosity and have come to speak of it on a percentage basis; thus 30 per cent porosity signifies 30 per cent of the total area in depressions and 70 per cent of the area as flats, plateaus, or contact surface. This percentage porosity is to some extent controllable in the electrolytic processing and in the finish-honing.

2 The thermal conductivity of chromium is 40 per cent higher than steel or cast iron, permitting rapid heat flow for the maintenance of lower surface temperature.

3 The melting point of electrolytic chromium is approximately 800 F higher than cast iron and 500 F higher than steel, thus raising the limit for operating-surface temperature.

The exceptional performance of porous-chromium cylinders and piston rings in severe service is a fact and lends credence to these explanations of why it works.

Processing. Before applying porous chromium to a cylinder it should be ground or bored oversize and then honed to a smooth finish of 10 μ in. rms or less. A fine finish is desirable for the following reasons:

1 It gives a more definite calculable actual surface area for plating. Control must be maintained over the thickness of deposited chromium and with a given plating solution this depends upon area, current density, and time. The latter two are controllable but the actual net area is inherent in the part to be plated.

2 Deposition of chromium tends to exaggerate initial surface irregularities; a rough surface becomes rougher as the thickness of deposition builds up. As a finished cylinder must always come within both dimensional and surface-finish tolerances, it is desirable to have a uniform thickness of chromium throughout the bore.

Cracks, inclusions, and spongy spots in the cylinder wall are accentuated by plating; in fact the process displaces the necessity for magnaflux checking. Cracks which are invisible to the eye are clearly shown up after plating.

The cylinders are then assembled in fixtures with accurately centered anodes, given a short anodic treatment, immersed in a plating tank, and plated with the required thickness of chromium. The fixture-and-cylinder assembly is then removed as a unit to an etch tank where it receives a porosity treatment. Upon

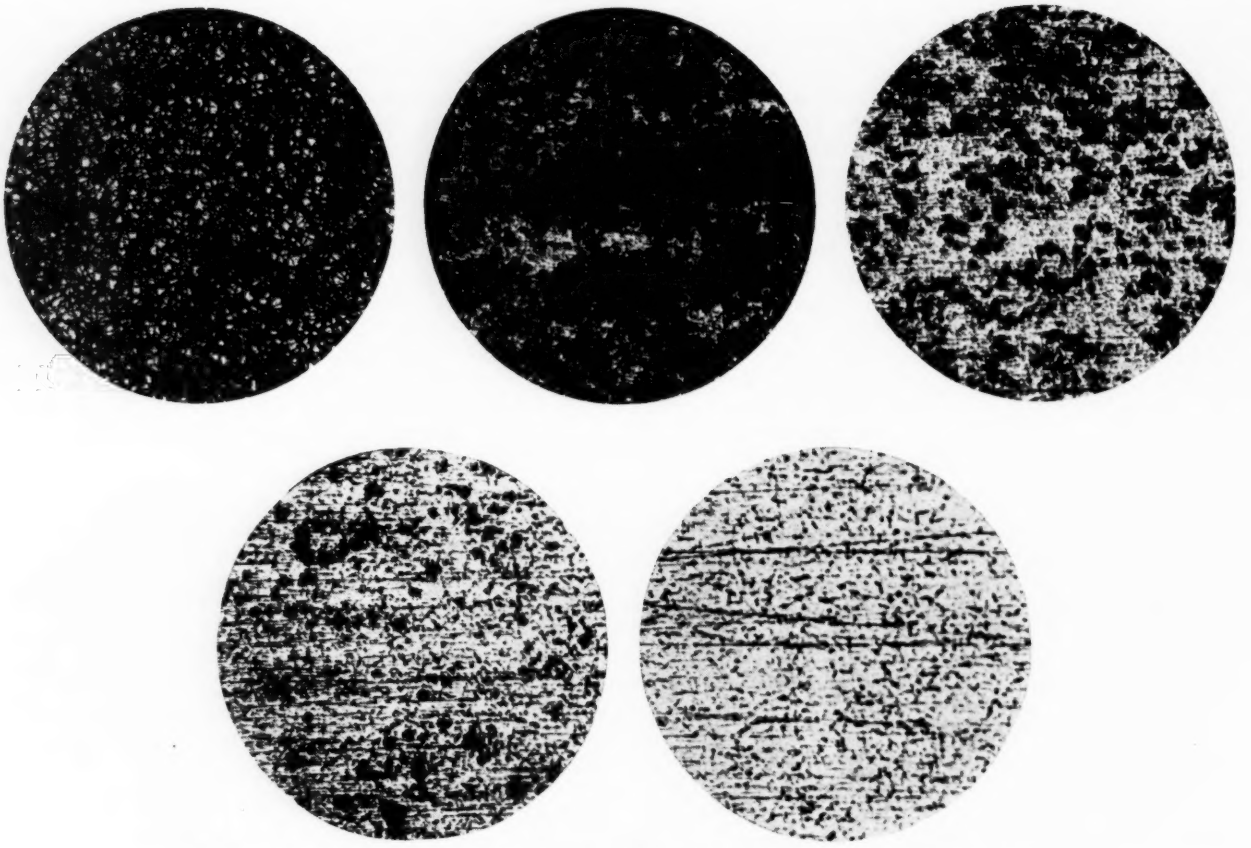


FIG. 5 EFFECT OF PROGRESSIVE REMOVAL OF METAL ON THE POROSITY OF CHROMIUM; ×50
(No. 0 emery paper used.)

disassembly the cylinders are ready for finishing. The porous chromium is readily honed with proper abrasives, but here finishing differs from the usual procedure of honing to a bore dimension only. Surface finish or porosity must also come within limits, because porosity has an influence on oil wettability. Fig. 5 shows the influence of surface stock removal on porosity. The factors affecting the finished cylinder bore are as follows:

1 Initial bore dimensions: the bore should be straight and round, as the ideal plating can do no better than deposit chromium to a uniform thickness throughout the cylinder.

2 Plating control of solution, composition, and temperature, current density, and time to obtain exactly the desired thickness of chromium.

3 Removal of correct amount of stock in finishing to obtain the desired surface finish.

Because of these additional requirements final dimensional tolerances on cylinder bores must be wider than those usually held where the only limiting factor is diameter.

For some time the profilometer was used as an inspection instrument in checking porous chromium for surface finish. However, the profilometer fails to give a true indication of surface condition in this case. Fig. 6 shows clearly that the standard profilometer needle does not trace the surface of porous chromium. Engine tests have subsequently established that surface porosity is an important characteristic and accordingly this property is considered in final inspection. While there is a reasonable correlation between the μ in. reading rms and percentage porosity, Fig. 7, it has been found more accurate and expedient to check porosity directly by microscopic inspection. Photomicrographs of various degrees of surface finishing have been planimetered to determine the percentage of flat and below-surface areas. Inspectors using a 50-power right-angle microscope can then search the bore and by comparison with the calibrated photomicrographs, make a reasonably accurate estimate of porosity.

In order to speed up inspection and minimize human errors of judgment we are now adapting the photoelectric cell to this work. The pores, depressions, or pits in the surface will reflect very little light with vertical illumination, while the smooth flats will have high reflectivity. Thus with a constant light source a photoelectric cell can be made to measure reflected light quantity. This, with a properly calibrated meter, can be a measure of the percentage of flat area or, inversely, of porosity. Such a "porosity meter" is shown diagrammatically in Fig. 8. Experiments to date indicate that this may be a satisfactory shop-inspection instrument, but more actual experience with it will be necessary to establish its utility definitely.

A wealth of experience under service conditions is being accumulated with porous-chrome cylinders on all types of engines, but for military reasons no details can now be given. However, other test data of interest are available, particularly accelerated wear tests on $^3/_4$-hp Lauson engines. This is a $1^3/_4$-in. bore × $1^7/_8$-in. stroke air-cooled 4-cycle gasoline engine. Two engines were run for 9 hr under load, one with the standard cast-iron cylinder and one with a porous-chrome cylinder. Allis-Chalmers type B dust (86 per cent below 5 microns, 100 per cent below 15 microns) was added to the initial charge of crankcase oil, the proportion of dust being 8.6 per cent by weight to accelerate wear. Tables 3 and 4, and Fig. 9, show the cylinder, piston, and ring wear.

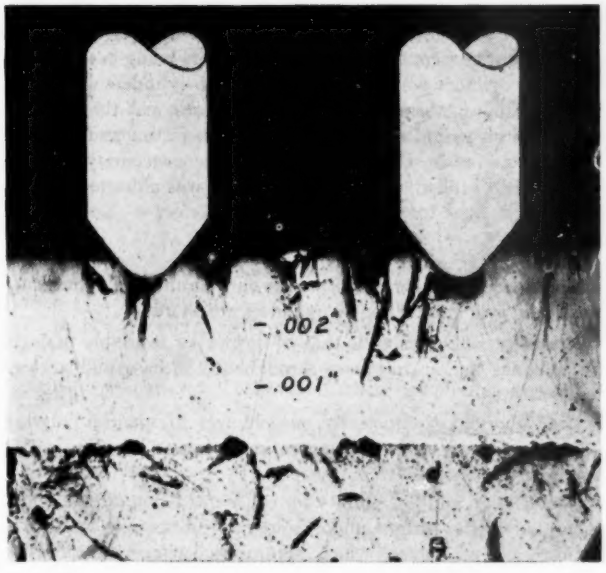


FIG. 6 SHOWING RELATION OF STANDARD 0.0005-IN-RADIUS PROFILOMETER NEEDLE TO PORES
(Honed porous chromium; ×500.)

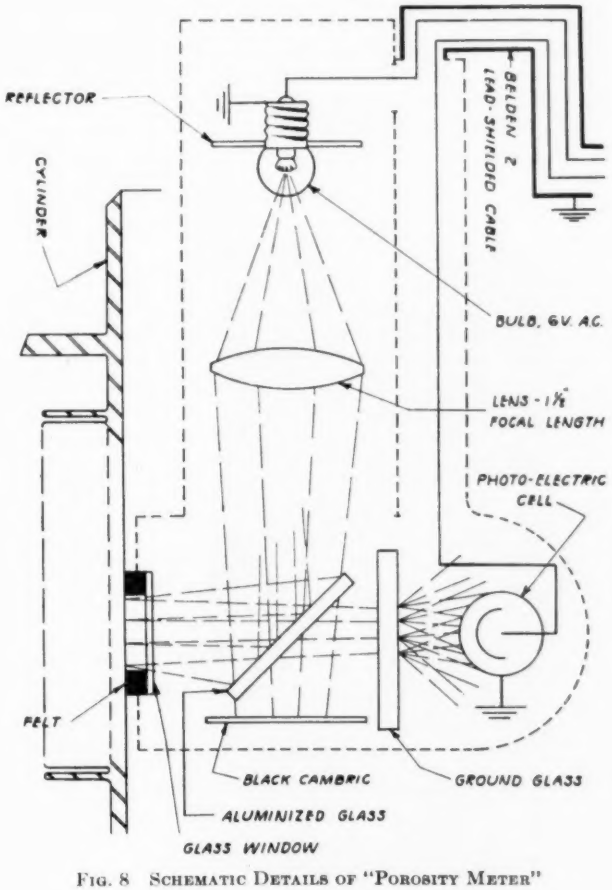


FIG. 8 SCHEMATIC DETAILS OF "POROSITY METER"

The relative wear of the rings is illustrated graphically in Fig. 10 which shows the sections of the worn rings compared with new rings. This test under such severe abrasive conditions, while not quantitatively applicable to full-scale engines,

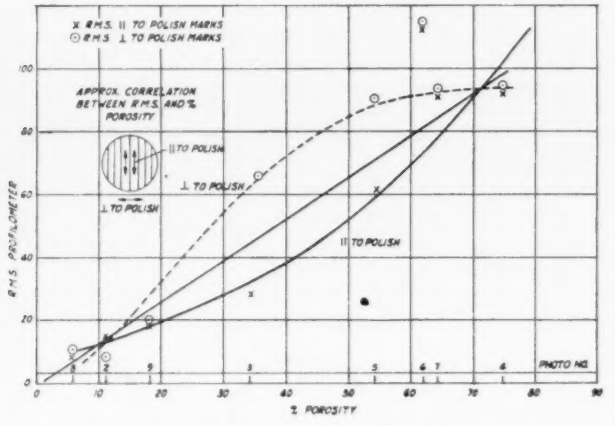


FIG. 7 APPROXIMATE CORRELATION BETWEEN RMS AND PERCENTAGE OF POROSITY

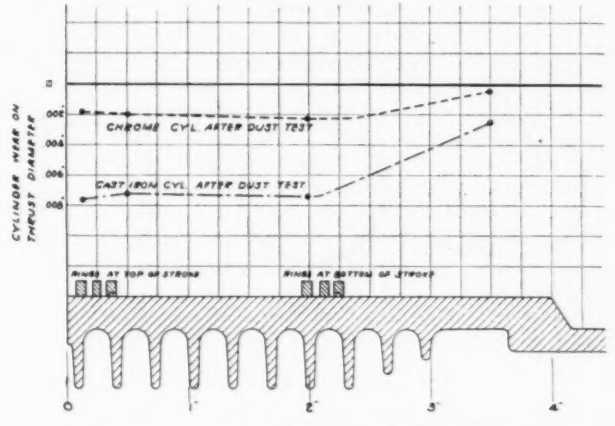


FIG. 9 CYLINDER WEAR ON CHROME AND CAST-IRON CYLINDERS

does indicate greatly lower cylinder wear with porous chromium and at the same time a great reduction in ring wear. Both results have been confirmed in service engines where records have been established of $^1/_{24}$ normal cylinder wear and $^1/_8$ normal

TABLE 3 CYLINDER WEAR

Location	Diametral wear, in. Cast-iron cylinder	Porous-chrome cylinder	Wear ratio, cast-iron cyl., porous-chrome cyl.
$^1/_8$ in. below head end....	0.0077	0.0018	4.3–1
$^1/_2$ in. below head end....	0.0071	0.0021	3.4–1
2 in. below head end.....	0.0083	0.0022	3.8–1

TABLE 4 PISTON AND RING WEAR

	In cast-iron cylinder		In porous chrome cylinder		
	Grams	Per cent of original weight	Grams	Per cent of original weight	Wear ratio, cast-iron cyl., porous-chrome cyl.
Aluminum piston loss in weight.....	0.589	0.90	0.316	0.45	1.9:1
Top ring loss in weight.....	2.506	56.	0.849	18.9	3.0:1
Second ring loss in weight....	2.586	57.8	0.972	21.8	2.6:1
Oil ring loss in weight.....	1.260	46.5	0.865	31.9	1.5:1

ring wear. Of course engines differ, and the improvement resulting from the use of porous chromium will vary with the particular engine.

Another manner in which porous chromium in cylinders immediately shows up to advantage is in the initial test or green

run of an engine. Because of its relative immunity to scuffing and ability to take abuse, ring scuffing and piston seizure are eliminated, and engine production is accelerated. Fig. 11 illustrates two identical pistons from a 10-in. × 12-in. two-cylinder gas test engine, one of the cylinders being cast iron and the other cylinder porous chromium. Both cylinders were carrying the same load and exhaust temperatures, yet the piston in the cast-iron cylinder seized, ruining both piston and cylinder. The piston in the porous-chrome cylinder was only polished where it had rubbed hard and the cylinder was unharmed.

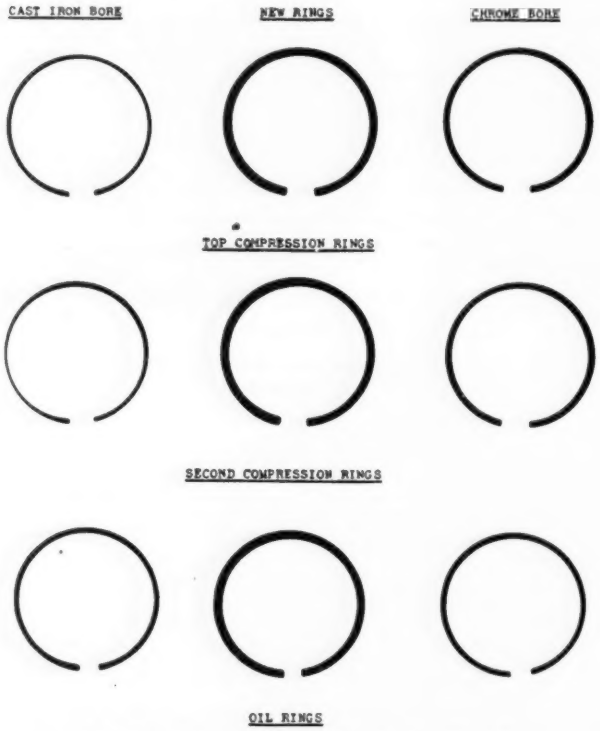


FIG. 10 COMPARISON OF WORN RINGS WITH NEW RINGS

SUMMARY

The inherent properties of porous chromium which contribute to its low wear rate in engine cylinders are as follows:

Hardness, which exceeds that of any other available material for cylinder liners; hardness throughout the case and at high temperatures.

High thermal conductivity, which aids in maintaining low internal cylinder-surface temperatures, improving lubrication and heat transfer.

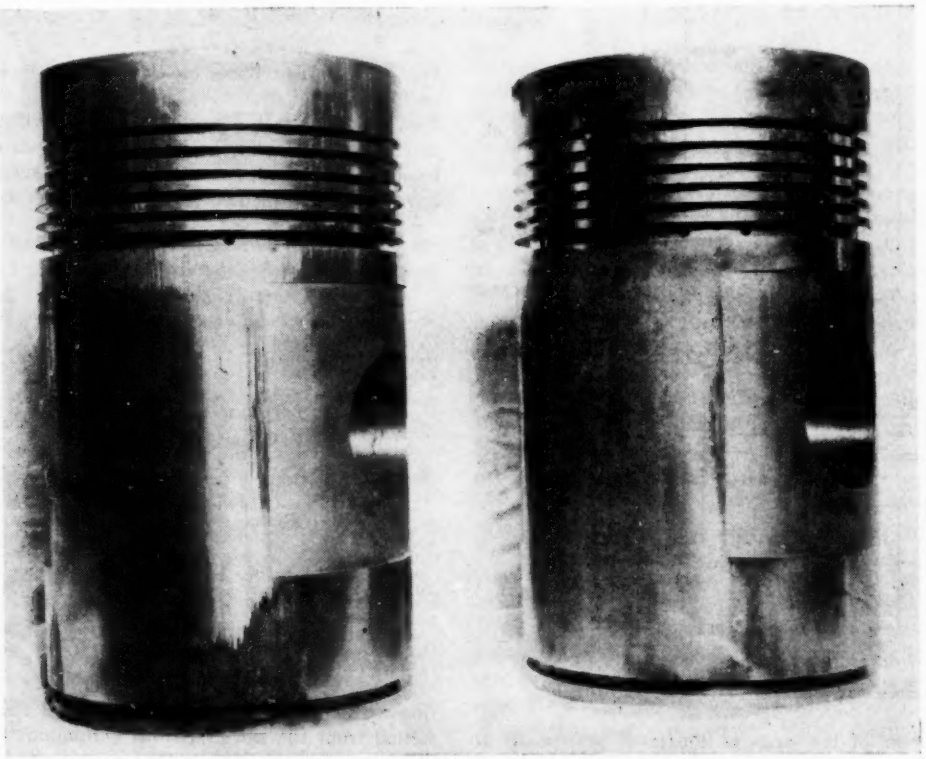
Low friction and low affinity for other metals, minimizing heat generated at the surface under boundary-lubrication conditions.

Corrosion resistance, which eliminates surface deterioration from action of the products of combustion.

In the light of recent theories concerning boundary lubrication an attempt has been made to explain how and why the peculiar surface geometry of porous chromium fits into the theories resulting in high load capacity and wettability.

The processing, finishing, and inspection procedures have been briefly described. The most important factors here are control of solutions, current density, temperature, and time, as well as a final surface finish.

Much has yet to be learned, but the need for intensive re-



(a) (b)

FIG. 11 RESULTS OF SEIZURE TESTS ON PISTONS IN CAST-IRON CYLINDER (*a*), AND IN POROUS-CHROME CYLINDER (*b*)

search on the potential possibilities of porous chromium is recognized and such a program is under way.

ACKNOWLEDGMENTS

The author wishes to express his appreciation to Mr. H. Van der Horst for the continuous assistance and encouragement he has given to this work. Thanks are also due the author's co-workers, particularly Messrs. A. Baum, R. H. Howard, and F. M. McNall for their help in the preparation of data.

BIBLIOGRAPHY

1 *Annalen der physik*, R. Bunsen, vol. 91, 1854, pp. 619–625. Junot de Bussy, French patent 3564, Nov. 17, 1848; Junot de Bussy, certificate of addition to French patent 3564, Nov. 12, 1849. Chaudron-Junot, French patent 13,902, Oct. 8, 1855; C. J. E. Junot, British patent 1183, Dec. 28, 1852.

2 Bibliographies on Chromium Plating are given by G. Dubpernell, Trans. of the Electrochemical Society, vol. 80, 1941, p. 589; also H. E. Haring and W. P. Barrows, Technologic paper No. 346, U. S. Bureau of Standards, 1926–1927.

3 *Nickel Steel Topics*, March, 1943, p. 4 (one paragraph), International Nickel Company, New York, N. Y. (deals with description of Eads Bridge over the Mississippi using chrome steel, about 1870).

4 "The Chrome-Hardening of Cylinder Bores," by H. Van der Horst, *Mechanical Engineering*, vol. 63, 1941, pp. 536–539 and 542; also "Chromium Plating of Engine Cylinders," by H. Van der Horst, *S.A.E. Journal*, vol. 46, June, 1940, pp. 30–32.

5 "Metals in Thin Layers—Their Microhardness," by C. G. Peters and F. Knoop, *Metals and Alloys*, vol. 12, Sept. 1940, pp. 292–297.

6 "Industrial Chromium Plating," Bulletin S-200, 1A, Worthington Pump & Machinery Corp., 1931. F. E. Allen, *Worthington News* 2, nos. 6, 2, 6, Oct., 1930; nos. 7, 1, 4, Nov., 1930; nos. 8, 1, 4, Dec., 1930; nos. 9, 1, 8, Jan., 1931; nos. 10, 2, Feb., 1931; nos. 11, 1, 4, Mar., 1931.

7 "Boundary Friction in Bearings at Low Loads," by L. M. Tichvinsky and E. G. Fischer, Trans. A.S.M.E., vol. 61, 1939, p. A-109.

8 "Thermal Expansion of Electrolytic Chromium," by Peter Hidnert, National Bureau of Standards, *Journal of Research*, vol. 26, R.P. 1361, 1941, pp. 81–91.

9 "Method of Producing Chromium Wearing Surfaces," by H. Van der Horst, U. S. Patent No. 2,314,604, March 23, 1943; and "Method of and Means for Providing a Hard Wearing Surface in the Cylinder Bores of Internal-Combustion Engines," by H. Van der Horst, U. S. Patent No. 2,048,578, July 21, 1936.

10 "The Role of Surface Chemistry and Profile in Boundary Lubrication," by J. T. Burwell, *S.A.E. Journal*, vol. 47, Oct., 1942, pp. 450–457.

11 (*a*) "Physical Properties of Surfaces—II. Viscous Flow of Liquid Films. The Range of Action of Surface Forces," by S. H. Bastow and F. P. Bowden, Proceedings of the Royal Society of London, series A, vol. 151, 1935, pp. 220–233.

(*b*) "Physical Properties of Surfaces—III. The Surface Temperature of Sliding Metals. The Temperature of Lubricated Surfaces," by F. P. Bowden and K. E. W. Ridler, Proceedings of the Royal Society of London, series A, vol. 154, 1936, pp. 640–656.

(*c*) "Physical Properties of Surfaces—IV. Polishing, Surface Flow, and the Formation of the Beilby Layer," by F. P. Bowden and T. P. Hughes, Proceedings of the Royal Society of London, series A, vol. 160, 1937, pp. 575–587 .

(*d*) "The Nature of Sliding and the Analysis of Friction," by F. P. Bowden and L. Leben, Proceedings of the Royal Society of London, series A, vol. 169, 1938–1939, pp. 371–391.

(*e*) "The Area of Contact Between Stationary and Between Moving Surfaces," by F. P. Bowden and D. Tabor, Proceedings of the Royal Society of London, series A, vol. 169, 1938–1939, pp. 391–413.

12 "Load-Carrying Capacity Phenomena of Bearing Surfaces," by Macy O. Teetor, *S.A.E. Journal*, vol. 47, Trans. section, 1940, pp. 497–503.

Discussion

K. W. SCHWARTZ.[3] Our laboratory measurements on the hardness of chromium indicate that all bright chromium deposits from a chromic-acid bath have about the same hardness, and that holds regardless of the bath composition, temperature, current density, or other plating conditions. However, if the deposit obtained is dull in appearance, the hardness is considerably lower than that of a bright deposit. Our figures indicate a hardness of about 1000 Bhn for bright chromium and a hardness of about 650 Bhn for dull chromium. So-called "milky" chromium has a hardness intermediate between these values, that is, about 800.

As to methods of determining hardness, we have found that practically all of the methods referred to in the literature involve crushing of the chromium deposit to get a reading. This may not be entirely reliable, particularly when the indentation that is made might be influenced by the hardness of the underlying base.

We experimented some years ago with methods of determining so-called hardness of chromium and found that we could get quite consistent results by means of a scratch hardness test. The apparatus which we used was a Bierbaum microcharacter, and the principle on which the apparatus functioned was quite simple. It merely uses a diamond point of definite shape, to which is applied a given weight. The diamond point is drawn across the surface of the chromium to be tested at a regulated speed. The width of the scratch is then measured under the microscope at a magnification of 1000. The results obtained are quite consistent and reproducible. We found that by means of this method the hardness measurements made on chromium deposits, even as thin as 0.001 in., were entirely independent of the base metal on which the chromium was plated.

In connection with comments on the plating operations, it should be stated that pure chromic acid alone, when dissolved in water, will not give a plating bath. The current can be passed through such a solution indefinitely, but no metallic chromium will be plated out. It is quite interesting, and rather unique as an electrochemical phenomenon, that by adding a catalyst to the chromic-acid solution a plating bath results. The catalysts that can achieve this result, interestingly enough, are acid radicals and, as we electrochemists refer to them, they are anions. They have a negative charge and are attracted to the anode, yet they perform their function at the cathode where the metal is deposited.

It is essential that any chromic-acid solution have present in it a certain amount of acid-radical catalyst to enable it to plate; commercially that acid radical is usually sulphate. Whether we add it as sulphuric acid, sodium sulphate, or any other soluble sulphate makes no difference. The point is that the sulphate radical or an equivalent radical must be present in the solution to enable it to plate.

The author states that chromium fills in the smallest irregularities of the surface being plated. From experience, we have found that chromium deposits tend to follow the irregularities in the underlying surface and to reproduce them. For example, let us take the surface of a cylinder liner that had been honed. The reader will be familiar with the honing marks or scratches that are present on the surface. A thickness of chromium as high as 0.008 in. on the radius can be deposited, for example, and the honing marks will tend to be reproduced in the deposit. Furthermore, and this is quite an important precaution, pits in the base metal do not tend to be bridged over by the chromium deposits. Such other things as nonmetallic inclusions in the base metal will not be covered by the chromium deposit, because quite obviously they are not conductors of current, and as such do not take the deposit. Therefore it is quite important that the surface on which we plate the chromium be as free from nonmetallic inclusions as possible.

Incidentally, any uncombined carbon or graphite in cast iron should be kept at the lowest possible minimum, because the con-

[3] United Chromium, Incorporated, New York, N. Y.

ductivity of carbon is very much lower than that of iron, and that will tend to produce undesirable irregularities in the plate.

In connection with chromium deposits on the bore of cylinders, in addition to the degree of porosity, that is to say, the relationship between the so-called table tops or plateaus and depressions, the depth of these depressions is quite important. While we know that electrodeposited chromium is extremely hard and that it functions very well on the bores of liners, it nevertheless does wear after long service. In order to get the maximum serviceable life out of the chromium deposit, these depressions or pores should be as deep as it is practicable to make them. In plating so-called "porous" or oil-retaining deposits of chromium, careful control of the plating conditions and final finishing operations is necessary. This should be performed so that the plated liner when ready to install in the engine has a maximum depth of porosity in addition to the other properties required for satisfactory results.

HANS BOHUSLAV.[4] We have made a few applications of chrome-plated steel liners in high-speed gasoline engines, and one of the drawbacks has been the length of time of break-in of such liners. In our first tests, it took 25 to 30 hr break-in time which, on engines of this type, is too long for efficient production. Even after that, our oil consumption was erratic. So we tried different methods such as match-lapping and individual honing, and found that apparently it was not practical at least on steel liners. Recently we have had some hope of overcoming the difficulty by using taper-face rings. We have found that such rings allow for more irregularities in the liner, at least in plain-steel liners. To try this, we used some of the liners which had been tested some months previously and which had been somewhat misused. Despite the fact that these liners were quite irregular, having been put in a new block which did not allow the same position for the surfaces, the oil consumption came down very rapidly. In about 2 hr running, we were within the normal oil consumption; in another 2 hr, we were considerably below our average.

The author's comments on the following questions would be appreciated: With all the cracks and porosity in the plating, it is the writer's understanding that considerable honing is done after the plating. What happens to the fine particles left during and after the honing operation?

The second question relates to the control of the areas of the metal so they will not fall out. In other words, if two cracks are too close together, or are not exactly perpendicular to the surface, there would normally be some areas in which the cracks finally merged on the steel or on the base surface.

H. VAN DER HORST.[5] It has been shown by tests on porous-chromium cylinders, conducted at the Naval Experiment Station at Annapolis, that the use of chromium plating in a well-known high-speed high-output Diesel engine which had been run for 6000 hr resulted in a reduction in wear of 1 to 14. That is a large figure, and what is more surprising, a reduction of ring wear to 22 per cent was made, which means only 22 per cent of what is known to occur when running-in cast-iron cylinders.

AUTHOR'S CLOSURE

The catalytic effect of the sulphate radical in chromium deposition is known to all concerned in plating, but the author did not wish to burden mechanical engineers with the electrochemical phase of the work. It is true, in general, that chromium deposition tends to follow the base-metal surface. However, the author has observed photomicrographs of edge sections where the base metal has been selectively etched, and the chromium has deposited into the pits and recesses.

Concerning Mr. Bohuslav's question about excessive oil consumption, the only comment is that every engine is a separate personality and often requires some special treatment of its own. As he says, very fortunately now, the taper-faced rings have done the job. The abrasives in the finishing or honing operation, of course, are washed down to some extent by the copious flow of coolant in the honing. It is easily conceivable that some abrasive may lodge in the pores and crevices. However, in the normal procedure, these are thoroughly washed before they ever go into service, and it is doubtful if there has ever been any failure which could be attributed to retaining the abrasive from the honing operation itself.

Regarding the cracks and their proximity, it may be explained by the fact that edge sections through the porous chromium show the table top and the sides coming down from the table top at an angle. The table top has a good firm base. It is not as though it were undercut and standing up like a column. It is rather a truncated cone, if we want to think of it that way, so that the structure is pretty well cantilevered. We have had no breakage or failure of the chromium due to the geometry of the metal structure.

[4] Sterling Engine Company, Buffalo, N. Y.

[5] Van der Horst Corp. of America, Olean, N. Y.

High-Pressure Pipe-Line Research

By F. W. LAVERTY and F. M. McNALL,[1] OLEAN, N. Y.

In estimating gas-pipe-line costs prior to undertaking the detailed design, it has been the practice generally to utilize graphical determinations of such variables as pipe-line diameter, compressor-station spacing, operating pressures, and the like. The graphical method is a time-consuming process, however, entailing the preparation and consideration of a large number of curves. The purpose of this paper is to show the derivation of an empirical equation containing all of the design variables, to which the methods of the differential calculus may be applied to yield a general series of expressions for the most economical design of any pipe line.

Nomenclature

The following nomenclature is used in the paper:

a = compressor brake horsepower per million cubic feet per day of gas compressed, 18.5 for curve data
A = cross-sectional area of pipe, sq ft
avg = average condition
B = fixed charge on pipe, fraction of investment (taken as 0.12 for curve data)
$C = \left(1 - \frac{1}{C_r^2}\right)$
C_I = total investment, dollars per mile
Cy = total yearly cost, dollars per year per mile
Cf = fuel cost, dollars per 1000 standard cu ft (taken as 0.10 for curve data)
Cr = compression ratio
d = inside diameter of pipe, ft
D = inside diameter of pipe, in.
E = experience or efficiency factor for flow equation
f = friction factor, defined by Fanning's equation
F = friction, feet of gas; load factor expressed as a decimal
g = acceleration due to gravity, fpsps (taken as 32.2 for illustrative data)
G = constant in pipe-laying cost, dollars per ton per mile, 12 in data for curves
H = constant in pipe-laying cost, dollars per mile, 3000 in data for curves
K = constant = $(\alpha X + 86.4Cf + 6.79)$ = 19.43 for curves
K_1 = constant = $(B)\ (Y + G)\ (28.2)$ = 328.3 for curves
K_2 = constant = $\frac{80.8}{\rho_0 \mu^{0.0814}} \left[\frac{M}{T}\right]^{0.541}$ = 765.3 for curves
l = distance, interval of pipe between compressor stations, ft
L = distance interval of pipe between stations, miles
m, n = coefficients of optimum diameter equation
M = molecular weight, lb (16 for methane)
N = constant in pipe-laying cost, dollars per in. of diam per mile (270 for illustrative data)
P = absolute pressure, psi
p = absolute pressure, psf
P_0 = base pressure, absolute
P_1 = compressor discharge pressure, psia
P_2 = compression suction pressure, psia
q = quantity of gas transported, cfs, measured at P_0 and T_0
Q = quantity of gas transported, cu ft per day, measured at P_0 and T_0
R = gas constant = 1546 for illustrative data
S = allowable hoop stress, psi (20,000 psi for illustrative data)
T = flowing temperature deg R (520-deg R for illustrative data)
T_0 = base temperature, deg R
t = thickness of pipe wall, in.
u = linear velocity, fps
V = specific volume, cu ft per lb
W = weight of pipe, tons per mile
X = cost of compressors, dollars per bhp, installed (80 for illustrative data)
Y = cost of pipe, dollars per ton (85 for illustrative data)
Z = constant in gas equation, "supercompressibility," dimensionless
α = fixed charge on compressors, fraction (0.05 for illustrative data)
ρ_0 = density of gas, lb per cu ft at T_0 and P_0 (0.0422 for illustrative data)
ρ = density of gas, lb per cu ft at T and P
μ = absolute viscosity of gas, lb per ft-sec (7×10^{-6} for methane)
d = symbol for differential, e.g. ($\bar{d}p$ differential of pressure)

General Considerations for Pipe-Line Cost Estimates

The detailed design of a gas pipe line is so laborious and time-consuming that it is generally desirable first to estimate rather closely the optimum values of the design variables for the case at hand. In general, these include pipe-line diameter, compressor-station spacing and operating pressures as functions of material cost, labor cost, and the character and quantity of gas to be handled.

Previous methods for estimations of this type (1, 3, 4, 6, 7)[2] have for the most part been graphical in nature, entailing the preparation and consideration of a large number of curves. In addition, the effects of deviations from the perfect-gas laws have been in some cases neglected.

If the total cost of a gas pipe line can be represented by an empirical equation containing all of the design variables, the methods of the differential calculus may be applied to yield a general series of expressions for the most economical design of any pipe line.

The first requirement for the development of a generalized cost equation is a gas-flow equation which will be dependable over a wide pressure and composition range. An equation which corresponds fairly well with known pipe-line conditions may be developed from Bernoulli's theorem combined with the Fanning equation. Based on the assumption that the flow is isothermal and at constant elevation, the differential form of Bernoulli's theorem

$$-V\bar{d}p = \frac{\mu}{g}\bar{d}u + \bar{d}F \qquad [1]$$

---

[1] Clark Brothers Company.

Contributed by the Petroleum Division and presented at the Semi-Annual Meeting, Los Angeles, Calif., June 14–17, 1943, of The American Society of Mechanical Engineers.

Note: Statements and opinions advanced in papers are to be understood as individual expressions of their authors and not those of the Society.

[2] Numbers in parentheses refer to the Bibliography at the end of the paper.

may be combined with the differential form of the Fanning equation

$$\bar{d}F = 2f\left(\frac{\mu^2}{g}\right)\frac{dl}{d} \quad \ldots\ldots [2]$$

to yield the expression

$$-V\bar{d}p = \frac{\mu}{g}\bar{d}u + 2f\left(\frac{\mu^2}{g}\right)\frac{dl}{d} \quad \ldots\ldots [3]$$

Now

$$u = \frac{q\rho_0 V}{A} \quad \ldots\ldots [4]$$

and

$$V = \frac{ZRT}{pM} \quad \ldots\ldots [5]$$

hence the differential form of the flow equation becomes

$$\frac{-M}{ZRT}p\bar{d}p = \frac{q^2\rho^2}{gA^2}\left(2f\frac{\bar{d}l}{d} - \frac{\bar{d}p}{p}\right) \quad \ldots\ldots [6]$$

Integrating between limits leads to

$$q = \frac{A}{\rho_0}\left[\frac{\frac{gM}{2Z_{avg}RT}(P_1^2 - P_2^2)}{\frac{2fl}{d} + \ln p_1/p_2}\right]^{1/2} \quad \ldots\ldots [7]$$

and neglecting ($\ln p_1/p_2$) in comparison to $\frac{2fl}{d}$, it simplifies to

$$q = \frac{A}{\rho_0}\left[\frac{gMd(p_1^2 - p_2^2)}{4flZ_{avg}RT}\right]^{1/2} \quad \ldots\ldots [8]$$

For the Reynolds numbers between 5×10^4 and 5×10^7, which covers practically all gas-transmission practice, an average straight line can be drawn through the logarithmic plot of the Drew and Genereaux data (2)

$$f = 0.03015\left(\frac{du\rho}{\mu}\right)^{-0.1505} \quad \ldots\ldots [9]$$

Substituting the value of f in Equation [9] in Equation [8], and replacing A by $\pi d^2/4$

$$q = \frac{2.467}{\rho_0}\left[\frac{d^{4.85}gM(p_1^2 - p_2^2)}{lZ_{avg}RT\mu^{0.1505}}\right]^{0.541} \quad \ldots\ldots [10]$$

Using the common engineering units and introducing the necessary conversion constants, Equation [10] takes the form

$$Q = \frac{(2.467)(144)^{1.081}(24)(3600)(32.2)^{0.541}}{(12)^{2.622}(5280)^{0.541}(1546)^{0.541}} \frac{1}{\rho_0}\left[\frac{D^{4.85}M(P_1^2 - P_2^2)}{LZ_{avg}T\mu^{0.1505}}\right]^{0.541} \quad \ldots\ldots [11]$$

$$Q = \frac{80.8}{\rho_0\mu^{0.0814}}\left[\frac{D^{4.85}M(P_1^2 - P_2^2)}{LZ_{avg}T}\right]^{0.541}E \quad \ldots\ldots [12]$$

where E is an experience factor ordinarily having a value of from 1 to 1.03 for natural gas.

For simplicity, let

$$K_2 = \frac{80.8}{\rho_0\mu^{0.0814}}\left[\frac{M}{T}\right]^{0.541}E \quad \ldots\ldots [13]$$

a constant for any particular case, then

$$Q = K_2\left[\frac{D^{4.85}(P_1^2 - P_2^2)}{LZ_{avg}}\right]^{0.541} \quad \ldots\ldots [14]$$

Cost on a Minimum Yearly Basis

One of the possible cost bases for pipe-line computation is minimum yearly cost, or that which gives the most economical gas transportation. The total yearly cost may be divided into fixed charges and operating expense.

Compressor Cost. The fixed charges on gas compressors may be formulated as follows: The initial installed cost of compressors is X dollars per horsepower. To pump Q cubic feet of gas per day for a distance of L miles requires aZ_2 brake horsepower per million cubic feet per day, where Z_2 is the deviation of the gas from the perfect-gas laws at the suction pressure, and a is the reference brake horsepower per million cubic feet of gas per day, dependent only upon the nature of the gas and the ratio of compression. The investment in compressors is then

$$X\left(\frac{Q_0Z_2}{L10^6}\right) \text{ dollars per mile}$$

The fixed charge on the compressors α includes interest on the capital investment, depreciation, taxes, insurance, etc. The yearly fixed charge on the compressors is then

$$\left(\frac{\alpha XQ_0Z_2}{L10^6}\right) \text{ dollars per year-mile}$$

Pipe Cost. The fixed charges on the pipe may be found from the pipe cost, Y dollars per ton, and the necessary W tons of pipe per mile. For steel pipe, $W = 28.2\,(D + t)t$, where D is the inside diameter of the pipe in inches, and t is the pipe-wall thickness in inches. The Barlow expression for wall thickness of pipe in terms of maximum pressure P, pounds per square inch, and maximum allowable stress, S pounds per square inch, is $t = \frac{P_1D}{2(S - P_1)}$. The direct pipe investment is then

$$YW = Y28.2\left[D + \frac{P_1D}{2(S - P_1)}\right]\left[\frac{P_1D}{2(S - P_1)}\right] \quad \ldots\ldots [15]$$

dollars per mile.

According to the A. O. Smith report (4), a good division of pipe-laying cost is H dollars per mile for right of way, surveying, clearing, supervision engineering, undistributed costs, and a part of ditching, painting, and cleaning expenses; G dollars per ton-mile for unloading, hauling, aligning, placing, and welding or coupling; and N dollars per mile per inch of diameter for ditching, painting, backfilling, and laying equipment.

The total pipe cost is then ($YW + H + GW + ND$) dollars per mile. At $B \times 100$ per cent fixed charges on the installed pipe (depreciation, taxes, insurance, interest on capital, salaries of pipe-line personnel, and all operating expenses chargeable to line maintenance), the fixed yearly charges on the installed pipe are

$$B(Y + G)(28.2)\left[D + \frac{P_1D}{2(S - P_1)}\right]\left[\frac{P_1D}{2(S - P_1)}\right] + BND + BH \quad \ldots\ldots [16]$$

Operating Expenses

The pipe-line operating expenses may be expressed as functions of the amount of gas transported, if average values of the individual items are considered. Labor, supervision, salaries, etc. amount to about $1750 per month for a 4000-hp compressor

station. Assuming direct proportionality for other stations of approximately the same size, this expense is

$$\frac{1750 \times 12}{4000}\left(\frac{QaZ^2}{L10^6}\right) = 5.25\left(\frac{QaZ_2}{L10^6}\right) \text{ dollars per year per mile.}$$

The average value of maintenance is \$0.50 per hp per year; lift water approximately \$0.20 per hp per year; and oil about \$0.84 per hp per year. The yearly cost of these items is then \$1.54 per hp per year per mile. About 10 standard cu ft of 1000 Btu fuel gas per bhp-hr are required by the gas compressors at a cost of Cf dollars per 1000 standard cu ft. The yearly fuel cost is then

$$\frac{10 \times 24 \times 360}{1000} Cf \frac{QaZ_2}{L10^6}$$

or

$$86.4\, Cf \frac{QaZ_2}{L10^6} \text{ dollars per year per mile.}$$

An allowance for gas lost from the pipe line may also be made, and for present purposes it will be taken as \$100 per year per mile. Taken in this manner, the loss figure has no effect on the design variables.

Upon adding all of the fixed and operating costs, the total yearly cost per mile

$$Cy = (\alpha X + 86.4Cf + 6.79)\frac{QaZ_2}{L10^6} + B(Y + G)(28.2)D^2 \left[\frac{P_1}{2(S - P_1)} + \frac{P_1^2}{4(S - P_1)^2}\right] + BND + BH + 100 \quad [17]$$

For convenience in manipulating any specific problem, let

$$K = (\alpha X + 86.4Cf + 6.79) \quad [18]$$

and

$$K_1 = 28.2B(Y + G) \quad [19]$$

Then

$$Cy = \frac{KQaZ_2}{L10^6} + K_1D^2\left[\frac{P_1}{2(S - P_1)} + \frac{P_1^2}{4(S - P_1)^2}\right] + BND + BH + 100 \quad [20]$$

A set of values of compressor suction pressure P_2, compressor discharge pressure P_1, pipe diameter D, and compressor-station spacing L, which makes the total yearly cost a minimum, must satisfy the requirement that the partial derivatives of the total yearly cost with respect to each of these variables must simultaneously equal zero. Proof that a set of values so found corresponds to minimum-cost conditions may be found by substitution of the set in the cost equation, comparing the total yearly cost with that resulting from any other set.

The term L may be eliminated from the yearly cost equation on replacing it by its value determined from the flow Equation [14]

$$\left(\frac{K_2}{Q}\right)^{1.85}\frac{D^{4.85}(P_1^2 - P_2^2)}{Z_{avg}} = L \quad [21]$$

The yearly cost equation then becomes

$$Cy = \frac{KQ^{2.85}Z_2aZ_{avg}}{10^6K_2^{1.85}D^{4.85}(P_1^2 - P_2^2)} + K_1D^2\left[\frac{P_1}{2(S - P_1)} + \frac{P_1^2}{4(S - P_1)^2}\right] + BND + BH + 100 \quad [22]$$

The partial derivatives of Cy with respect to D, P_2, and P_1 are

$$\frac{\partial Cy}{\partial D} = \frac{-KQ^{2.85}Z_2aZ_{avg}\,4.85}{10^6K_2^{1.85}D^{5.85}(P_1^2 - P_2^2)} + 2K_1D\left[\frac{P_1}{2(S - P_1)} + \frac{P_1^2}{2(S - P_1)^2}\right] + BN \quad [23]$$

$$\frac{\partial Cy}{\partial P_2} = \frac{2KQ^{2.85}Z_2aZ_{avg}P_2}{10^6K_2^{1.85}D^{4.85}(P_1^2 - P_2^2)^2} + \frac{KQ^{2.85}Z_2a}{10^6K_2^{1.85}D^{4.85}(P_1^2 - P_2^2)}\frac{\partial Z_{avg}}{\partial P_2} + \frac{KQ^{2.85}Z_2Z_{avg}}{10^6K_2^{1.85}D^{4.85}(P_1^2 - P_2^2)}\cdot\frac{\partial a}{\partial P_2} + \frac{KQ^{2.85}aZ_{avg}}{10^6K_2^{1.85}D^{4.85}(P_1^2 - P_2^2)}\cdot\frac{\partial Z_2}{\partial P_2} \quad [24]$$

and

$$\frac{\partial Cy}{\partial P_1} = \frac{-2KQ^{2.85}Z_2aZ_{avg}P_1}{10^6K_2^{1.85}D^{4.85}(P_1^2 - P_2^2)^2} + \frac{KQ^{2.85}Z_2Z_{avg}}{10^6K_2^{1.85}D^{4.85}(P_1^2 - P_2^2)}\cdot\frac{\partial a}{\partial P_1} + \frac{KQ^{2.85}Z_2a}{10^6K_2^{1.85}D^{4.85}(P_1^2 - P_2^2)}\frac{\partial Z_{avg}}{\partial P_1} + \frac{K_1D^2S^2}{2(S - P_1)^3} \quad [25]$$

Setting $\frac{\partial Cy}{\partial D}$ equal to zero, and multiplying all terms of the resulting equation by $\frac{D^{5.85}}{K_1\left[\frac{P_1}{S - P_1} + \frac{P_1^2}{2(S - P_1)^2}\right]}$ the first expression for minimum value of Cy is

$$D^{6.85} + \frac{BN}{K_1\left[\frac{P_1}{S - P_1} + \frac{P_1^2}{2(S - P_1)^2}\right]}D^{5.85} = \frac{4.85KQ^{2.85}Z_2aZ_{avg}}{10^6K_2^{1.85}(P_1^2 - P_2^2)K_1\left[\frac{P_1}{S - P_1} + \frac{P_1^2}{2(S - P_1)^2}\right]} \quad [26]$$

Equating $\frac{\partial Cy}{\partial P_2}$ to zero, and multiplying all terms of the resulting equation by $\frac{10^6K_2^{1.85}D^{4.85}(P_1^2 - P_2^2)}{KQ^{2.85}Z_2aZ_{avg}}$, the second expression for the minimum value of Cy is

$$\frac{2P_2}{P_1^2 - P_2^2} + \frac{\partial \ln Z_{avg}}{\partial P_2} + \frac{\partial \ln a}{\partial P_2} + \frac{\partial \ln Z_2}{\partial P_2} = 0 \quad [27]$$

Using the empirical relationship for methane gas

$$a = 56.8 \ln P_1/P_2 + 5.1 \quad [28]$$

and finding that $\frac{\partial \ln Z_{avg}}{\partial P_2}$ and $\frac{\partial \ln Z_2}{\partial P_2}$ are very small numbers from $P_2 = 0$ to $P_2 = 2000$ psi, Equation [24] reduces to

$$\ln [P_1/P_2] = \frac{1}{2}(P_1^2/P_2^2) - 0.5898, \text{ or } P_1/P_2 = 1.33 = Cr \quad [29]$$

Following the same method of approach, Equation [25] reduces to

$$\frac{-2}{P_1C} + \frac{56.8}{P_1a} + \frac{10^6K_2^{1.85}D^{6.85}S^2P_1^2CK_1}{2(S - P_1)^3KQ^{2.85}Z_2aZ_{avg}} = 0 \quad [30]$$

from which

$$P_1 = \frac{S}{1 + D^{2.283}\left(\frac{K_2^{1.85}S^2K_1}{KQ^{2.85}Z_2Z_{avg}}\right)^{1/3}} \quad (17.40) \quad \ldots\ldots [31]$$

Equations [26] and [31] may be solved simultaneously for P_1 and D by plotting P_1 versus D for both equations. The intersection of the two curves in the positive quadrant then yields the desired values of P_1 and D. As a convenience in evaluating D in Equation [20] for trial values of P_1 it may be considered to be of the form

$$D^{4.85} + mD^{4.85} = n$$

or preferably

$$D^{4.85} = \frac{n}{m + D}$$

Two or three trial values of D should then be sufficient to obtain the proper value of D.

The station spacing L may then be found from Equation [21], and the minimum total yearly cost then computed from the cost Equation [17].

It is obvious that there is but one such set of positive values of P_1, P_2, and D. The total cost Cy is either a maximum or minimum, and that this set corresponds to a minimum value of Cy may be seen from the total yearly cost Equation [20]. The value of Cy can be made larger than any previously assigned value by increasing suitably the numerical values for P_1 and D. Obviously, the maximum value of Cy is infinite, and the values

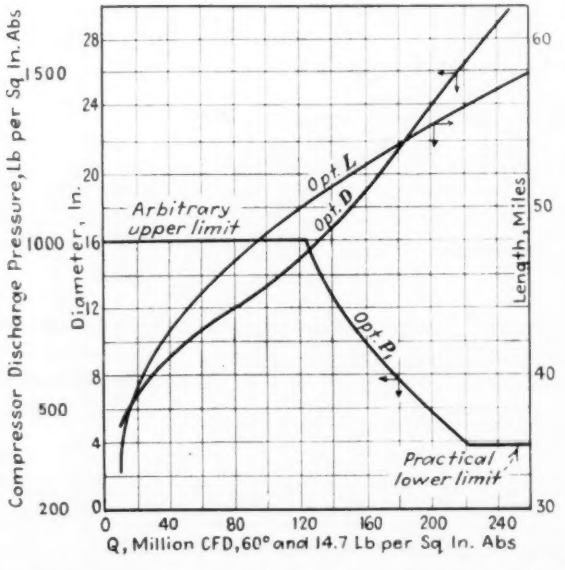


FIG. 1 OPTIMUM VALUES OF P, L, AND D FOR VALUES OF Q, BASED ON OPTIMUM COMPRESSION RATIO, Cr = 1.33 AND MINIMUM YEARLY COST

found from the partial derivatives must represent a minimum. The solution of Equation [26] for a range of values of P_1 and subsequent determination of Cy by means of Equation [22] as a function of P_1 is in many cases a more rapid and convenient method for determining the optimum operating conditions.

Using hypothetical values for material and labor costs which are approximately averaged over the country, but which do not represent any particular case, a set of optimum design conditions for the transportation of several different amounts of methane have been computed and plotted in Fig. 1. It may be seen that for quantities of methane up to approximately 100,000,000 cu ft per day, the optimum compressor-discharge pressure is over 1000 psi which was taken as an arbitrary limit. For greater gas quantities, the optimum compressor-discharge pressure decreases until, at approximately 220,000,000 cu ft per day, it is about 400 psi which was taken as an arbitrary lower limit. Both the optimum pipe diameter and compressor-station spacing increase with increasing gas quantities.

For methane at ordinary temperatures, the optimum compression ratio is not affected appreciably by deviation from the ideal gas laws, but for hydrocarbon gases which show greater deviations, the optimum compression ratio increases, the optimum operating pressures increase, and the optimum pipe diameter decreases.

COSTS ON A MINIMUM INITIAL BASIS

If minimum initial investment is taken as the goal for gas-pipeline design, the total investment may be computed from the yearly cost Equation [17] by omitting the yearly charges and the estimated loss figure. Thus

$$C_1 = \frac{XQZ_2a}{L10^6} + (Y + G)(28.2)D^2\left[\frac{P_1}{S - P_1} + \frac{P_1^2}{2(S - P_1)^2}\right] + ND + H \quad \ldots\ldots [32]$$

On setting $\frac{\partial C_1}{\partial P_2}$ equal to zero, the optimum compression ratio is found to be 1.33, identical with the first case considered when methane or an ideal gas is considered.

On setting $\frac{\partial C_1}{\partial D}$ equal to zero, the form of this equation is similar to that found before

$$D^{4.85} + \frac{N}{(Y + G)(28.2)\left[\frac{P_1}{S - P_1} + \frac{P_1^2}{2(S - P_1)^2}\right]} D^{4.85} = \frac{4.85 \times Q^{2.85}Z_2aZ_{avg}}{10^6K_2^{1.85}(P_1^2 - P_2^2)(Y + G)\left[\frac{P_1}{S - P_1} + \frac{P_1^2}{2(S - P_1)^2}\right](28.2)} \quad \ldots\ldots [33]$$

and may be solved in the same manner.

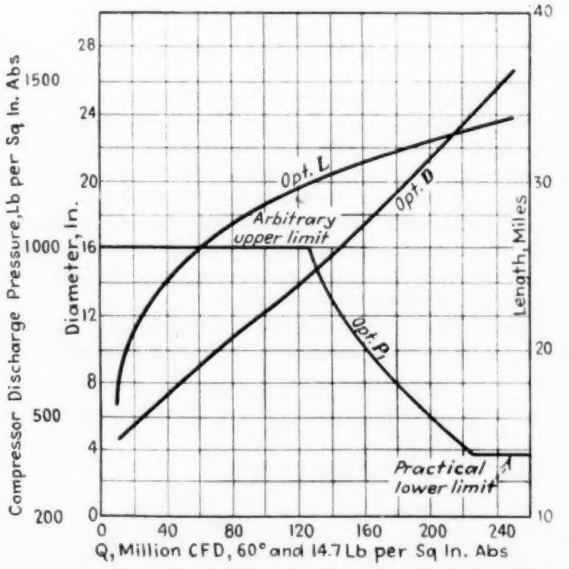


FIG. 2 OPTIMUM VALUES OF P, L, AND D FOR VALUES OF Q, BASED ON OPTIMUM COMPRESSION RATIO, Cr = 1.33, AND MINIMUM INITIAL COST

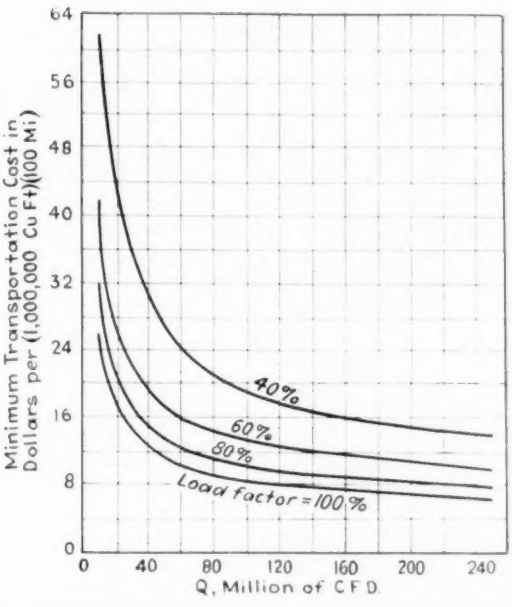


FIG. 3 MINIMUM TRANSPORTATION COST VERSUS DAILY QUANTITY TRANSPORTED, BASED UPON OPTIMUM CONDITIONS FOR MINIMUM YEARLY COST

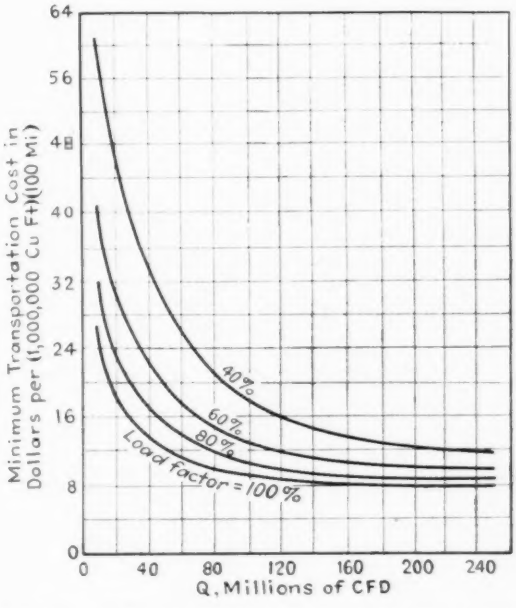


FIG. 4 MINIMUM TRANSPORTATION COST VERSUS DAILY QUANTITY TRANSPORTED, BASED UPON OPTIMUM CONDITIONS FOR MINIMUM INITIAL COST

The third defining equation for minimum initial investment, found by setting

$$\partial C_T/\partial P_1 = 0$$

becomes

$$P_1 = \frac{S}{1 + D^{3.283}\left(\frac{K_2^{1.85}S^2(Y+G)(28.2)}{XQ^{2.85}Z_1Z_{avg}}\right)^{1/3}(17.40)} \quad \ldots\ [34]$$

Simultaneously, Equations [33] and [34] may now be solved graphically for any value of Q. In most cases of practical interest, however, it is more practical and instructive to solve Equation [33] for a range of pressures, and to plot C_I from Equation [32] as a function of P_1 for the gas flow under consideration. The results of a series of such solutions are shown in Fig. 2, wherein L is computed from the flow equation as before. It may readily be seen that, although the optimum operating pressures have not changed appreciably, the best pipe diameters and station spacings are smaller than for the case when minimum yearly cost was the goal. Actually, the percentage of total capital invested in compressor stations has increased, and the portion of total capital invested in pipe has decreased compared to the first case. Obviously, the cost of transporting a given quantity of gas per year is greater than that in the first case studied.

The effect of load factor on transportation cost may readily be computed from the yearly cost Equation [17] by segregating the fixed and variable operating expenses, and introducing the term F, load factor, expressed as a decimal. The new total operating cost is equal to F (operating expense) + (fixed charges), and the cost of transporting any given quantity of gas in dollars per cubic foot is given by the equation

$$\text{Cost} = \frac{F\,(\text{Operating expense}) + (\text{fixed charges})}{FQ \times 365} \times \text{miles} \ldots [35]$$

The effect of load factor on the minimum transportation cost is shown in Fig. 3, and on the transportation cost for minimum initial investment in Fig. 4 for the cases already discussed.

GENERAL CONCLUSIONS

While no specific conclusions may be reached without the substitution of actual cost figures in the equations advanced, some generalizations may be made. The optimum compression ratio is entirely dependent upon the nature of the gas handled. This dependence is threefold, based upon the power necessary to compress a given standard volume of the gas, the manner in which the power changes with compression ratio, and, to a lesser extent, on the change in compressibility of the gas with suction pressure. The best operating pressure for the system is increased as the quantity of gas to be transported decreases, as the allowable pipe stress increases, and as the compressibility of the gas increases. Pipe diameter and station spacing are rather complex functions of all of the design conditions, increasing with an increase in the quantity of gas to be handled.

It must be emphasized that the numerical data represented by the curves in this paper are derived from purely hypothetical cost figures and do not necessarily represent conditions for any actual gas pipe line.

BIBLIOGRAPHY

1 "Gas Flow Computations," by P. M. Biddison, Proceedings, American Gas Association, Natural Gas Section, 1941, pp. 51–83.

2 "Fluid Flow in Clean Round Straight Pipe," by T. B. Drew and R. P. Genereaux, Trans. American Institute of Chemical Engineers, vol. 32, 1936, pp. 17–19.

3 "Flow of Natural Gas Through High-Pressure Transmission Lines," by T. W. Johnson and W. B. Berwald, U. S. Bureau of Mines, Monograph 6, 1935. Can be obtained only from American Gas Association, 420 Lexington Ave., New York, N. Y.

4 "Gas Pipe Line Factors Effecting a Minimum Cost," by W. R. Kepler, Proceedings, American Gas Association, 1930, pp. 797–819; also Bulletin No. 510, A. O. Smith Corp., Milwaukee, Wis., 1930.

5 "The Compressibility of Methane at Pressures to 1000 Atmospheres and at Temperatures From —70 to 200°," by H. M. Kvalnes and V. L. Gaddy, *Journal of the American Chemical Society*, vol. 53, 1931, pp. 394–399.

6 "The Economic Design of Gas Transmission Lines," by S. J. Pirson, *Oil Weekly*, vol. 94, July 10, 1939, pp. 22, 24, 26, 28, 30, 32, 34, and 36.

7 "Problems in Natural-Gas Engineering," by T. R. Weymouth, Trans. A.S.M.E., vol. 34, 1912, pp. 185–231; discussion pp. 231–234.

Limiting Isothermal Flow in Pipes

By R. C. BINDER,[1] LAFAYETTE, IND.

An explicit formulation is given for the limiting isothermal flow of a gas in a horizontal pipe. For isothermal flow, the ratio of critical pressure to initial pressure equals the initial Mach number times the square root of the ratio of specific heats. The critical-pressure ratio for isothermal flow is higher than that for adiabatic flow. Some comparisons are drawn between isothermal, adiabatic, and incompressible flow.

IN dealing with the general problem of the flow of gases through pipes, it is common to consider separately two cases, i.e., (1) adiabatic flow and (2) isothermal flow. Adiabatic flow has been detailed in the literature. Complete solutions, for example, can be found in the works of Stodola,[2] and Schüle.[3]

These solutions bring out some important differences between incompressible and compressible adiabatic flow. For one thing, expanding adiabatic flow is characterized by a limiting condition at which the fluid velocity equals the velocity of pressure propagation. The simple relations for incompressible flow do not indicate any limiting conditions. Limiting isothermal flow apparently has not received due and full recognition in the literature. The purpose of the present paper is to give a similar explicit formulation for isothermal flow, to detail limiting conditions, and to draw some comparisons between isothermal, adiabatic, and incompressible flow.

The following discussion will be confined to the flow in horizontal, constant-diameter pipes. It will be necessary to examine some basic relations first before investigating limiting conditions.

Basic Relations

The following nomenclature will be used:

- c = velocity of pressure propagation
- D = internal diameter of pipe
- f = pipe friction coefficient
- g = gravitational acceleration
- k = ratio of specific heat at constant pressure to specific heat at constant volume
- l = pipe length
- M = Mach's number, V/c
- p = absolute pressure at any point in pipe
- v = specific volume
- V = velocity of fluid

Let dl represent the length along a pipe of an infinitesimal element of fluid. The specific volume of the fluid in this element is v. The pressure drop across the element is dp and the velocity change is dV. The general energy equation, in differential form, can be written as

$$v\,dp + \frac{d}{2g}(V^2) + dh = 0$$

where dh is the lost head. The usual practice will be followed, in expressing the lost head in the form

$$dh = f\frac{V^2}{2gD}\,dl$$

The general energy equation can then be written as

$$\frac{2gv}{V^2}\,dp + \frac{2dV}{V} + \frac{f\,dl}{D} = 0 \quad \ldots\ldots\ldots\ldots [1]$$

For isothermal flow, the Reynolds number is constant along the pipe, and hence the friction factor is also constant. The equation of state gives the relation

$$\frac{dp}{p} = -\frac{dv}{v} \quad \ldots\ldots\ldots\ldots\ldots\ldots [2]$$

The equation of continuity gives the relation

$$\frac{dV}{V} = \frac{dv}{v} \quad \ldots\ldots\ldots\ldots\ldots\ldots [3]$$

Limiting Conditions

The velocity of pressure propagation c is given by the relation

$$c = \sqrt{kgRT} = \sqrt{kgpv}$$

where R is the gas constant, and T is the absolute temperature. For isothermal flow c is constant along the pipe.

Let the subscript 1 refer to inlet conditions, and the subscript 0 refer to limiting or critical conditions. For example, p_0 is the limiting pressure. As gas flows along the pipe, the pressure decreases below the inlet pressure p_1, and the velocity increases above V_1. The pressure in the constant-diameter pipe cannot drop below p_0.

Equations [1], [2], and [3] can be combined to give the form

$$\frac{gpv}{V^2}\left(\frac{dp}{p}\right) - \frac{dp}{p} + \frac{f\,dl}{2D} = 0 \quad \ldots\ldots\ldots\ldots [4]$$

Limiting conditions are reached at the end of the pipe when $f\,dl = 0$. For these conditions, Equation [4] shows that

$$\frac{gpv}{V_0^2} = 1$$

$$V_0 = \sqrt{gpv} = \sqrt{gRT} = \frac{c}{\sqrt{k}} \quad \ldots\ldots\ldots\ldots [5]$$

The maximum velocity that can be developed in the pipe is V_0; this velocity is less than the acoustic velocity.

Mach's number is a convenient parameter for studying compressible flow. Mach's number M is defined as the dimensionless ratio V/c. The ratio of inertia to elastic force is directly proportional to the square of Mach's number. Let M_1 represent the inlet Mach number.

The critical pressure ratio p_0/p_1 can be determined by using the equation of state, equation of continuity, and Equation [5] to give

---

[1] Associate Professor of Mechanical Engineering, School of Mechanical, Aeronautical Engineering, Purdue University. Mem. A.S.M.E.

[2] "Steam and Gas Turbines," by A. Stodola, McGraw-Hill Book Company, Inc., New York, N. Y., 1937, vol. 1, p. 62.

[3] "Technical Thermodynamics," by W. Schüle, Pitman and Sons, London, 1933.

Contributed by the Main Research Committee and presented at the Annual Meeting, New York, N. Y., Nov. 29–Dec. 3, 1943, of The American Society of Mechanical Engineers.

Note: Statements and opinions advanced in papers are to be understood as individual expressions of their authors and not those of the Society.

$$\frac{p_0}{p_1} = \frac{v_1}{v_0} = \frac{V_1}{V_s} = \frac{V_1\sqrt{k}}{c} = \sqrt{k}\ M_1 \quad \ldots\ldots\ldots [6]$$

For isothermal flow the ratio of critical pressure to initial pressure equals the initial Mach's number times the square root of k.

Various investigators have shown that the critical-pressure ratio for adiabatic flow can be expressed in the form

$$\frac{p_0}{p_1} = M_1^2 \left\{ \left(\frac{k-1}{k+1} \right) \left[1 + \frac{2}{(k-1)M_1^2} \right] \right\}^{1/2} \quad \ldots\ldots\ldots [7]$$

The solid line in Fig. 1 is for isothermal flow, whereas the dotted line is for adiabatic flow. Fig. 1 and subsequent plots in this paper were drawn for a value of $k = 1.40$; $k = 1.40$ for air, carbon monoxide, hydrogen, and oxygen. Fig. 1 shows that the critical-pressure ratio for isothermal flow is higher than that for adiabatic flow.

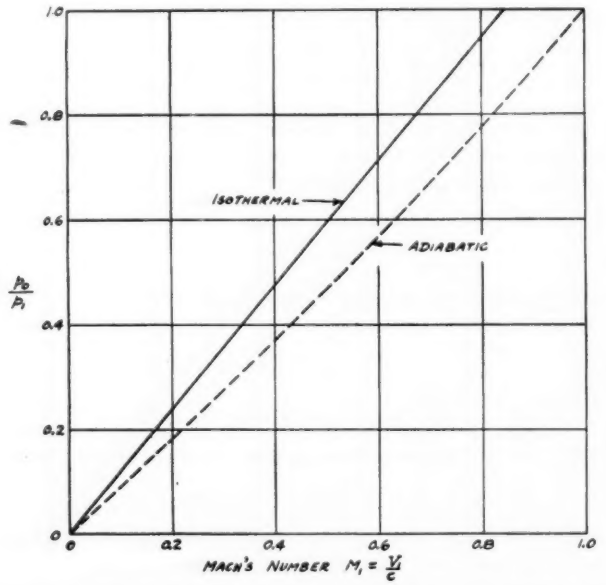


FIG. 1 LIMITING VALUES OF PRESSURE RATIO AS A FUNCTION OF MACH'S NUMBER, FOR GASES WITH $k = 1.40$

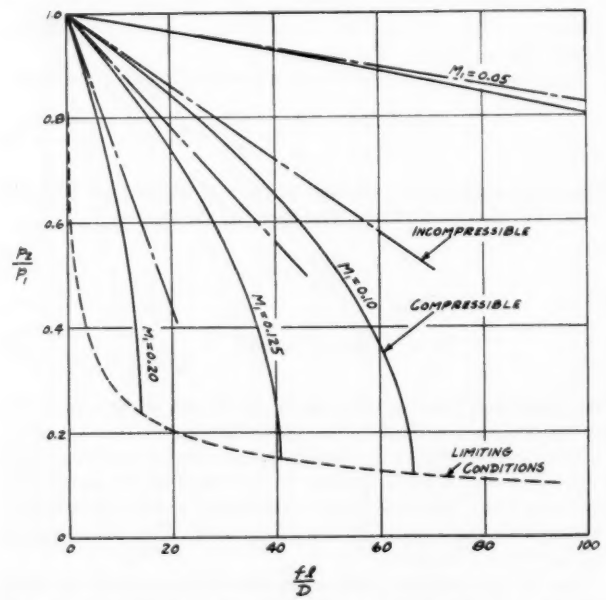


FIG. 2 VARIATION OF PRESSURE RATIO WITH fl/D AND MACH'S NUMBER FOR ISOTHERMAL FLOW, FOR GASES WITH $k = 1.40$

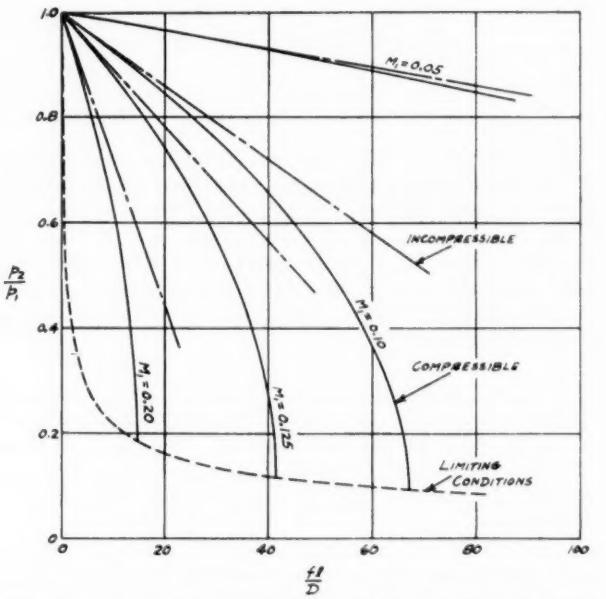


FIG. 3 VARIATION OF PRESSURE RATIO WITH fl/D AND MACH'S NUMBER FOR ADIABATIC FLOW, FOR GASES WITH $k = 1.40$

The continuity equation and the equation of state can be combined to put the first term of Equation [1] into a form convenient for integrating. The final result, after integrating, is

$$p_1^2 - p_2^2 = \frac{V_1^2 p_1}{g v_1} \left[2 \log_e \frac{V_2}{V_1} + \frac{fl}{D} \right] \quad \ldots\ldots\ldots [8]$$

where the subscript 2 refers to a condition for any length.

It is convenient to rearrange Equation [8] such that the dimensionless ratio fl/D is a function of k, the initial Mach number, and the pressure ratio. A regrouping of terms gives the form

$$\frac{fl}{D} = \frac{1}{kM_1^2} \left[1 - \left(\frac{p_2}{p_1} \right)^2 \right] - 2 \log_e \frac{p_1}{p_2} \quad \ldots\ldots\ldots [9]$$

Fig. 2 shows a plot of p_2/p_1 versus fl/D at several initial Mach numbers for isothermal flow. The dotted line in Fig. 2 represents limiting conditions. Fig. 3 shows the same type of plot for adiabatic flow. Except for a region close to limiting lengths, the solid curves in Fig. 2 are somewhat similar to those in Fig. 3.

COMPARISON BETWEEN INCOMPRESSIBLE FLOW AND COMPRESSIBLE FLOW

The relation for the flow of an incompressible fluid in a pipe is simpler than the relations for the flow of a compressible fluid. The question is frequently raised as to the limits of application of the incompressible-flow relations, and the possibility of using the incompressible-flow relation for studies of compressible flow. The question of application frequently depends upon the accuracy desired.

The pressure drop for the flow of an incompressible fluid in a horizontal pipe can be written as

$$p_1 - p_2 = \frac{flV_1^2}{2gDv_1}$$

$$\frac{p_2}{p_1} = 1 - \frac{k}{2} (M_1^2) \frac{fl}{D} \quad \ldots\ldots\ldots [10]$$

Equation [10] was employed to plot the straight dot-dash lines in Figs. 2 and 3. A comparison of a dot-dash line and a solid line, for the same M_1, brings out the differences between compressible and incompressible flow. Figs. 2 and 3 show that the difference between the incompressible and the compressible relations is not very great at low Mach numbers and short lengths. The difference becomes appreciable, however, at high Mach numbers and long lengths.

A more direct comparison between the two types of flow can be given by the type of plot shown in Fig. 4. Equations [9] and [10] were employed to plot the curves for the three initial Mach numbers. The difference between compressible and incompressible flow may be large. For example, the compressible-flow relation gives a pressure drop of $p_1 - p_2 = 0.6p_1$ for certain conditions with an initial Mach number of 0.30. The incompressible-flow relation for the same pipe length and same initial conditions gives a pressure drop of about $p_1 - p_2 = 0.305p_1$.

In some discussions of isothermal flow, the change in kinetic energy is considered negligible. The statement is sometimes made that, if the pipe is "long," the term $2 \log_e V_2/V_1$ is negligible in comparison with the term fl/D. If the change in kinetic energy is neglected, then Equation [8] takes the form

$$p_1^2 - p_2^2 = \frac{V_1^2 p_1}{g v_1} \frac{fl}{D} \quad \ldots\ldots\ldots\ldots\ldots\ldots [11]$$

Equations [10] and [11] can be written as

$$\text{Compressible flow} \left\{ \frac{p_1 - p_2}{p_1} = 1 - \sqrt{1 - \frac{flV_1^2}{gDp_1v_1}} \right.$$

$$= 1 - \sqrt{1 - 2B} \quad \ldots\ldots\ldots [12]$$

$$\text{Incompressible flow} \left\{ \frac{p_1 - p_2}{p_1} = \frac{flV_1^2}{2gDp_1v_1} = B \right. \quad \ldots\ldots [13]$$

where B represents the dimensionless ratio given in Equation [13]. Equations [12] and [13] can be compared for identical values of B. A graphical comparison is shown by the curve A in Fig. 4.

Sometimes the rule is given that the incompressible-flow relation can be used for isothermal compressible-flow problems if the pressure drop $p_1 - p_2$ is less than 10 per cent of the initial pressure p_1. Curve A illustrates the accuracy of this rule.

A comparison of curve A with the other solid curves in Fig. 4 shows the effect of the change in kinetic energy. There is a considerable difference between curve A and the curve for $M_1 = 0.20$, for example, at long lengths. For long lengths, it appears that the change in kinetic energy can be neglected only for low Mach numbers.

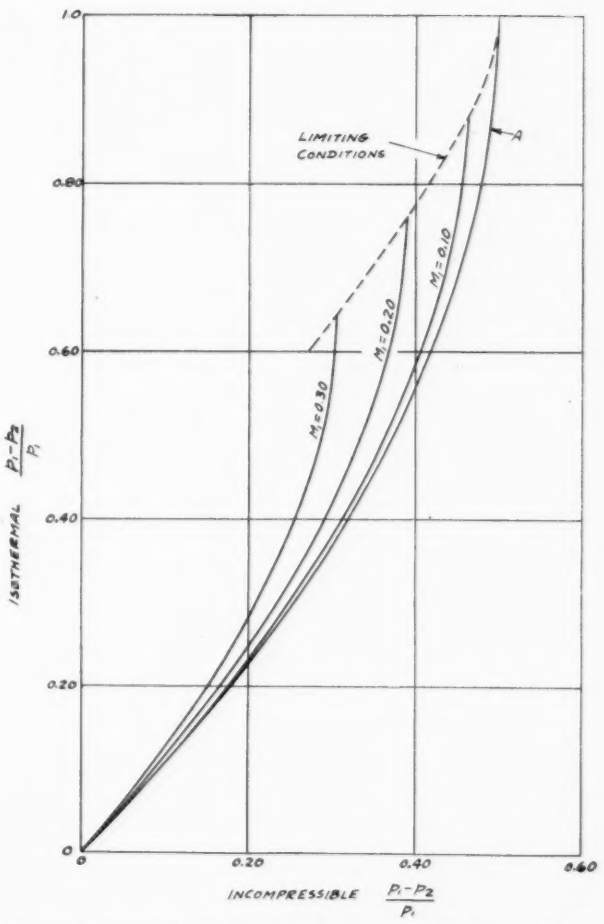


FIG. 4 PRESSURE-DROP RATIO FOR ISOTHERMAL FLOW AS A FUNCTION OF PRESSURE-DROP RATIO FOR INCOMPRESSIBLE FLOW

Application and Design of Package Conveyers

By H. C. KELLER,[1] SYRACUSE, N. Y.

Conveyers used for material handling are divided into two groups, namely, for bulk materials like ore, gravel, coal, ash, sand, and so on, and for unit loads such as cartons, boxes, barrels, sacked goods, tote boxes, etc. This paper will discuss the latter group, dealing with application and design. In giving the various formulas on design, certain liberties with theory are taken and short cuts are used, but all formulas have been checked and proved by actual performance.

Roller Conveyers

ROLLER conveyers, Figs. 1 and 2, consist of side rails in which rollers are mounted. The load then travels by gravity on the rollers or is propelled along the line of conveyer.

Application. The load to be conveyed must have a rigid riding surface in order to span the space between the rollers. Fragile loads should not be permitted to travel by gravity. The best results are obtained when the loads are constructed of similar materials and are approximately uniform in weight. Heavy loads (in excess of 100 lb) should not be allowed to travel by gravity, without first making a careful investigation of all conditions to be certain that no damage will result. Loads up to 40,000 lb have been handled on roller conveyers, but such loads should not be allowed to operate by gravity.

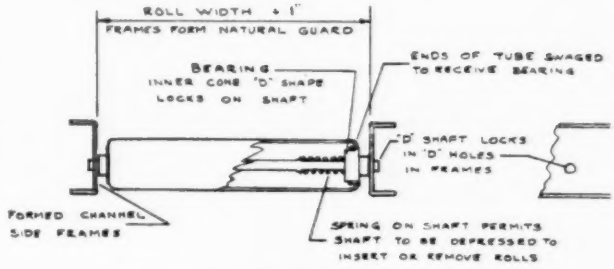


Fig. 1 Section Through Roller Conveyer

Design. The side rails are structural-steel members (usually angle or channel shapes), designed for maximum deflection of 0.33 in. in a 10-ft span.

The rollers are constructed of tubing with ball bearings adapted to the ends of the tubing. A shaft extends through the hubs of the bearings into the side rails. The tubing should be of sufficiently heavy gage to withstand damage due to impact of loads on the conveyer. The amount of impact is not always known,

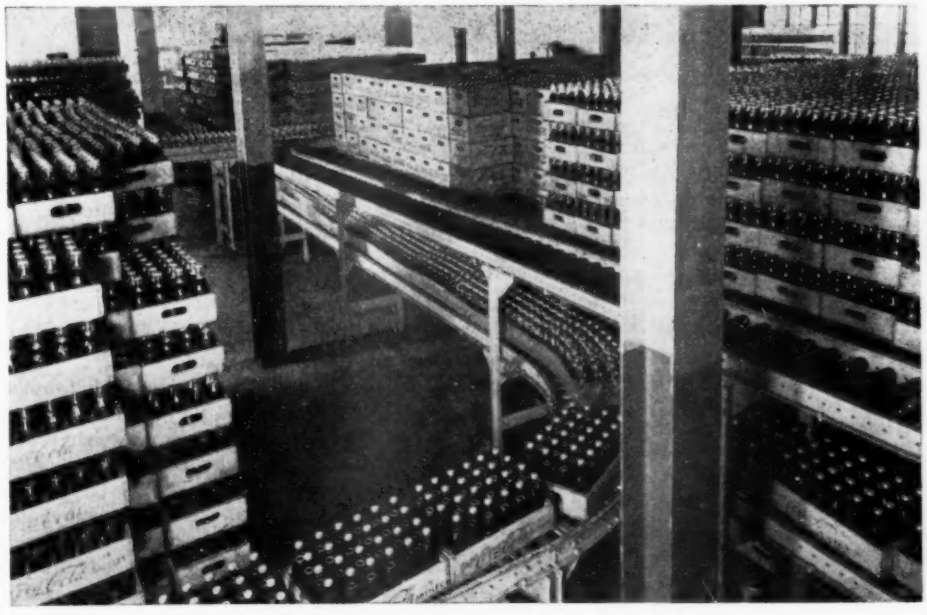


Fig. 2 Typical Roller Conveyer in Bottling House
(The Coca-Cola Company, Syracuse, N. Y.)

TABLE 1 DETAILS AND CAPACITIES OF ROLLER CONVEYERS

Roll diameter, in.	Load capacity of roll lb	Wall thickness
1 to 2	50 to 200	18 gage to 12 gage
$2^1/_8$ to $2^9/_{16}$	150 to 1000	16 gage to 7 gage
$2^3/_4$ to 4	500 to 5000	10 gage to $^1/_2$ in.
over 4	7500	$^3/_4$ in.

[1] Lamson Corporation.

Contributed by the Special Design Committee and presented at the Annual Meeting, New York, N. Y., Nov. 29–Dec. 3, 1943, of The American Society of Mechanical Engineers.

Note: Statements and opinions advanced in papers are to be understood as individual expressions of their authors and not those of the Society.

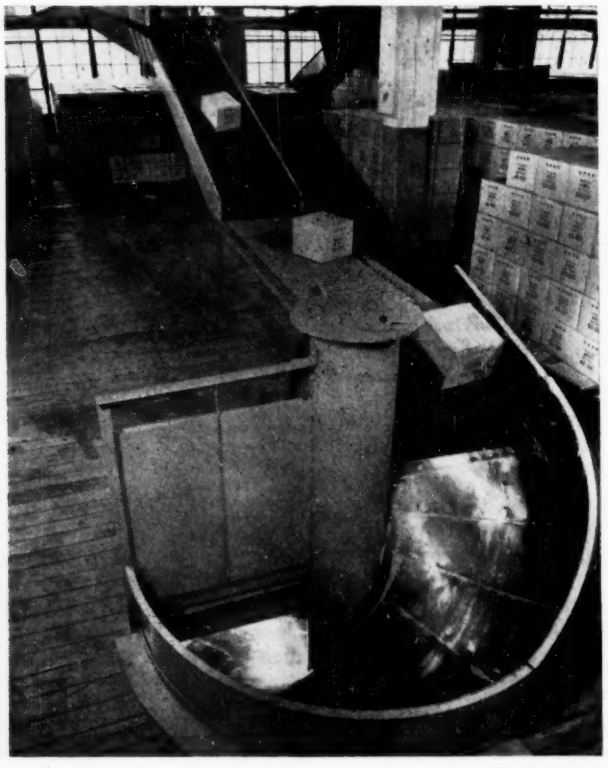


FIG. 3 STRAIGHT CHUTE RECEIVING LOADS FROM BELT CONVEYER AND LEADING TO A SPIRAL CHUTE
(S. C. Johnson & Son, Racine, Wis.)

and we must depend on past experience. The wall thicknesses, indicated in Table 1, have proved satisfactory.

In almost every case, the wall thickness is greater than required to make the tubing structurally as strong as the bearings and shaft.

The shafts are designed so that they lock in the side rails, and the inner races of the bearings are in turn locked to the shaft. This prevents the bearing from turning on the shaft, and the shaft from turning in the side rails.

Generally the ball bearings are of the open free-running type, but frequently wet, dirty, or acid conditions require a grease-packed ball bearing. These latter bearings are sometimes equipped with grease fittings so that the grease can be replenished.

As the bearings are mounted in the ends of the rolls and the bearings are always adjacent to side rails, the capacity of the roll is not materially decreased as the length increases.

There should always be at least three rolls under the load, and the spacing of rolls in the frame is determined by the formula

$$\text{Maximum spacing} = \frac{\text{Minimum length of load}}{3}$$

The grade at which the conveyer is set depends upon the weight of the load and the type of riding surface. The type of bearing used in the roll also affects the grade. As each manufacturer has his own standard diameter of roll, thickness of tubing wall (affecting the dead weight), type of bearing, and so on, it is impossible to establish gradients for the entire line of roller conveyers. Generally, a grade of $^1/_2$ in. per ft will be satisfactory for cartons; $^3/_8$ in. per ft for steel tote boxes or hardwood boxes weighing between 15 and 75 lb. On hard-bottom loads, the grade is reduced as the weight increases, and this is also true for some cartons, but in the latter case only to the point where the weight does not cause the bottom of the carton to drape over the rolls.

STEEL CHUTES

Description. These chutes, Fig. 3, are made straight, curved, and helical (better known as "spiral chutes").

The straight chute consists of a bedplate and two side plates or guards.

The curved chute consists of a bedplate with outer and inner guard plates.

The spiral chute is usually built around a center core with a bedplate and outer guard plate.

Application. As all chutes are used only to guide loads from an upper level to a lower point, they should not be used when there is great variation in weight; when the weight is over 300 lb, or for fragile loads. The spiral chute offers some opportunity for control of speed by varying the shape of the bed and the pitch and is therefore preferred in most cases to straight chutes.

Atmospheric conditions also affect the operation of chutes, especially when cartons or sacked goods are being conveyed. This type of conveyer very seldom gives satisfactory service where there is likely to be great variation in the humidity of the surrounding air.

Design. Table 2 gives the gages of metal usually used in chutes. Straight chutes are frequently made by bending up side guards from the bedplate, in which case the gage specified for the bed is the one to use.

TABLE 2 METAL GAGES FOR CHUTES

Type of load	Straight chute		Curved chute		Spiral chute	
	Bed	Guard	Bed	Guard	Bed	Guard
Cartons or sacks..	14	16	14	14	14	14
Wood boxes.....	14	14	14 to 12	14 to 12	12	12
Wire-bound boxes or steel pans....	12	14	12	12	10	10

Under average conditions, straight chutes are declined at a 20-deg angle for cartons, 18 deg for wood boxes, and 15 to 17 deg

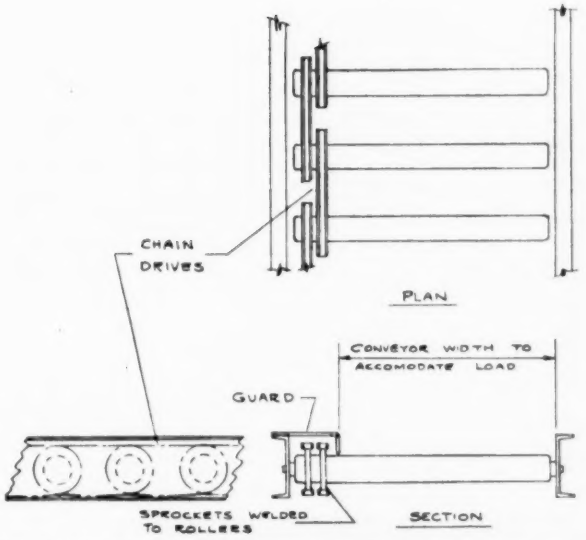


FIG. 4 MULTIPLE-STRAND, CHAIN-DRIVEN, LIVE-ROLL CONVEYER

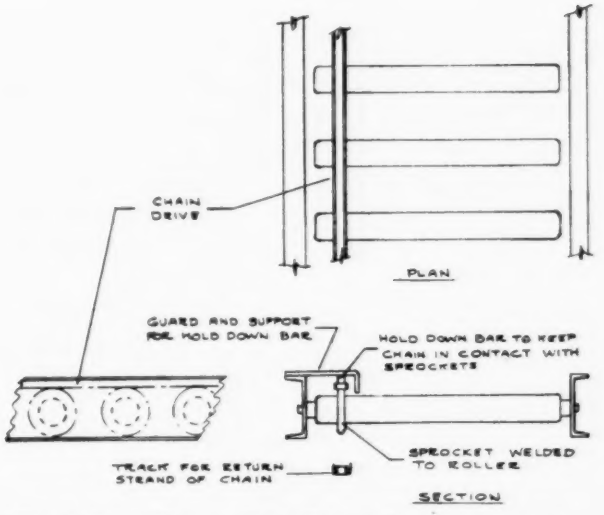


FIG. 5 SINGLE-STRAND, CHAIN-DRIVEN, LIVE-ROLL CONVEYER

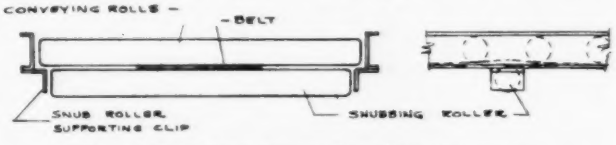


FIG. 6 FLAT-BELT-DRIVEN LIVE-ROLL CONVEYER

for steel pans. On curved and spiral chutes the angle at the outer guard rail is the same as the angle of decline specified for straight chutes. The height of the side guards on straight chutes should be no less than one third the height of the highest load. On curved and spiral chutes, the outer guard rail should be somewhat higher than the greatest height of the load. The height of the guard is measured at right angles to the bed.

LIVE-ROLL CONVEYERS

Description. This type of conveyer, Figs. 4 to 7, employs the use of roller-conveyer sections with various means used to power the rolls. Flat belts or round belts are snubbed against the underside of the rolls by means of snubbing rolls or sheaves, placed between the carrying rolls. The flat-belt type is used when the conveyer is straight and the round belt when there are curves in the conveyer. Another type of live-roll conveyer employs roller-chain drives over sprockets fitted to the roll shafts. In this case the roll and shaft are made integral and the shaft operates in bearings built into or mounted on the side rails. In other types of chain-driven conveyers, the sprockets are welded to the roll tubes, and the conventional roll with bearings adapted to the ends of tubing are used.

Application. As in the case of roller conveyers, the load must have a rigid riding surface but unlike the roller conveyer any variation in weight of the various loads is not important. Fragile loads should not be conveyed if the conveyer is to be used for storage, as blocking these loads will damage them.

Design. In addition to the features given for the roller conveyer, we must consider the matter of power required to operate the conveyer.

To determine the horsepower required to operate horizontal live-roll conveyers, the percentages of friction, given in Table 3, should be used.

TABLE 3 PERCENTAGE OF FRICTION IN LIVE-ROLL CONVEYERS

Type of conveyer	Weight of load, lb	Friction, per cent
Belt-driven.....	Up to 75	6
Belt-driven.....	Over 75	10
Chain-driven.....	Unlimited	5

The percentages, given in Table 3, are based on antifriction bearings. Also, it may be advisable to explain why different frictions are given for belt-driven live-roll conveyers. The belting on this type of conveyer should never be snubbed more than just enough to propel the loads. It naturally follows that greater snubbing action is necessary as the weight of the load increases.



FIG. 7 LIVE-ROLL CONVEYER DRIVEN BY ROUND BELT SHOWN OVER ROLLER CONVEYERS
(Norwich Pharmacal Company, Norwich, N. Y.)

The horsepower required at the head shaft of belt-driven conveyers is

$$\text{Hp} = \frac{(W + w) \cdot f \cdot S}{33{,}000}$$

where W = weight of live load on conveyer, lb
w = weight of all rolls and belting, lb
f = friction given in Table 3
S = speed of conveyer, fpm

In the chain-driven type of conveyer, one design consists of a

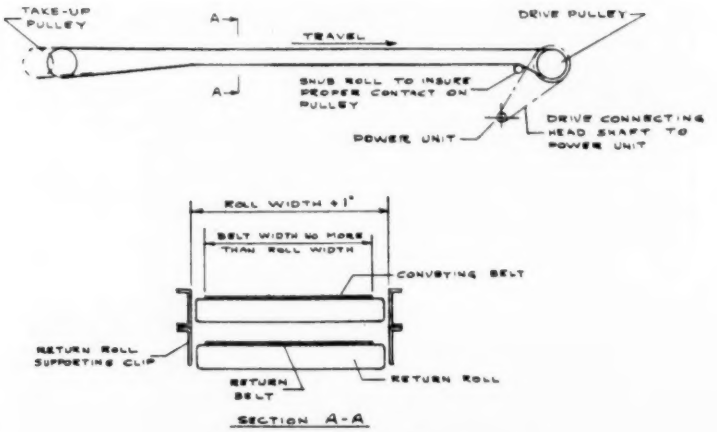


FIG. 8 TYPICAL BELT CONVEYER

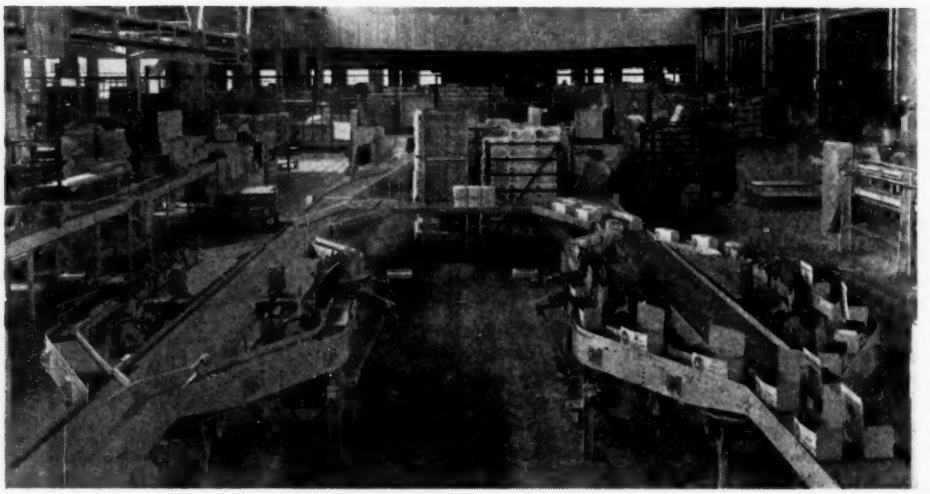


FIG. 9 TYPICAL BELT-CONVEYER INSTALLATION

(This shows two main-line belts bringing filled cartons from a packing table. Each belt carries a double line of cartons which are deflected to spur sidings where the cartons pass through closers and convey back into one line; the cartons now deflect to a table as shown for loading to trucks, or they may pass the deflector and deliver to the bundling conveyer.)

single strand of chain, while in another, multiple strands of chain are used. In the latter case two sprockets are employed on each roll and a complete drive is used from one roll to the next roll. The single strand of chain allows only a tangential contact with the sprocket and should only be used on light-duty conveyers. The multiple-strand design permits full 180-deg contact on each sprocket.

On single-straight-chain conveyers, the horsepower formula given for belt-driven conveyers can be used by changing the value of w. In this case, w = weight of rolls, sprockets, and chain.

On multiple-strand-chain-driven conveyers, the effective pull on each drive must be figured progressively, allowing 98 per cent efficiency for each chain drive.

BELT CONVEYERS

Description. Belt conveyers, Figs. 8 to 10, also employ roller-conveyer sections with belting supported by the rolls. In another type, the belting is supported by a steel or wood bed over which the belting slides.

Application. As the load is supported directly on the belting, almost any type of unit load can be conveyed on this conveyer. Unit loads weighing in excess of 50 lb per sq ft should not be con-

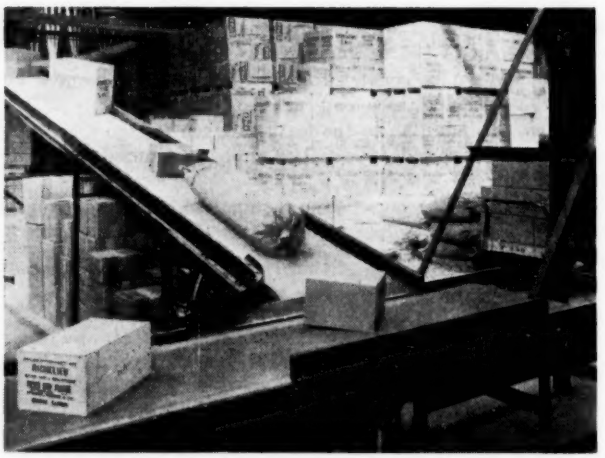


FIG. 10 HORIZONTAL AND DECLINED BELT CONVEYERS
(Sprague Warner)

veyed on the slider-bed type of construction, as excess weight causes the belting to seize to the bed of the conveyer.

Design. When the roller type of intermediate support is used, the spacing of the rolls on the load-carrying bed is determined by the length and weight of the load. When extremely light loads are to be conveyed rolls can be spaced 24 in. and in some cases 36 in. on centers. Heavier unit loads such as cartons, boxes, and so on, require roll spacing no greater than $^1/_2$ the length of the shortest load. The return belt on either type of conveyer is supported by rolls usually spaced no more than 10 ft on centers.

The horsepower required at the head shaft of horizontal belt conveyers is

$$\text{Hp} = \frac{(W + w) \cdot f \cdot S}{33{,}000}$$

where W = weight of live load on conveyer, lb
w = weight of rolls and belting, lb
f = friction given in Table 4
S = speed of conveyer, fpm

TABLE 4 PERCENTAGE OF FRICTION OF BELTING ON ROLLER AND SLIDER BEDS

Type of bed	Cotton or untreated-canvas belting, per cent	Rubber-impregnated canvas belting, per cent
Roller	3 to 5	3 to 5
Steel slider	20	21
Wood slider	22	30

There are numerous types of belting, each best suited for specific operating conditions. A complete study and analysis is impossible in this paper, but, generally, the cotton and untreated-canvas belt should be used where atmospheric conditions are fairly constant, as is the case in most indoor installations. The rubber-impregnated belt is used where there is great variation in humidity, and, in many cases where the belting is exposed directly to the elements, completely rubber-covered belting should be used. The latter belting is never used on slider-bed types of conveyers.

Belt conveyers can be inclined to elevate or to lower loads. Correction for the horsepower due to the incline must be made, and the conveying run of belting must be calculated independently of the return run. In elevating conveyers, the horsepower at the head shaft is

$$\text{Hp} = \frac{[0.05\ r + L \sin\theta + fL \cos\theta + 0.05\ l \cos\theta - l \sin\theta] \cdot S}{33{,}000}$$

where r = weight of all rollers, lb
L = weight of upper run of belting and live load, lb
l = weight of return run of belting, lb
θ = angle of incline, deg
f = friction given in Table 4
S = speed of conveyer, fpm

When the conveyer is used to lower loads the formula becomes

$$\text{Hp} = \frac{[0.05\ r + l \sin\theta + fL \cos\theta + 0.05\ l \cos\theta - L \sin\theta] \cdot S}{33{,}000}$$

It is frequently found that this formula gives a minus value, but it must be considered the same as a plus value in order to obtain the required strength in the drive gearing to hold back the load and prevent the conveyer from running away.

Another way of expressing the head-shaft horsepower is to substitute the term "effective pull" for all load factors in the preceding formulas

$$\text{Hp} = \frac{\text{Effective pull} \times \text{speed}}{33{,}000}$$

The effective pull permits us to determine other factors, such as total load on the head shaft, and the stress in the belting. The tension in the tight side of the belting at the head pulley is expressed as T_1 while the tension in the slack side is expressed as T_2. Table 5 gives the values of T_1 and T_2 for the most common conditions.

TABLE 5 TENSION IN BELTING AT HEAD PULLEY

Amount of wrap on pulley, deg	T_1	T_2
180	1.64	0.638
200	1.54	0.541
210	1.50	0.500
220	1.46	0.462
230	1.43	0.428

To obtain the maximum stress in the belting, multiply the effective pull by the proper factor for T_1. The maximum load on the head shaft is the sum of the effective pull multiplied by the factor T_1 plus the effective pull multiplied by factor T_2.

A take-up pulley is provided in the conveyer to compensate for stretch in the belting. The take-up is usually made by screw adjustment. The amount of adjustment varies with the type of belting. Canvas belting requires a take-up adjustment of 1 per cent of the length of the conveyer. Rubber belting requires approximately one half the adjustment provided for canvas belting.

Automatic weighted take-up pulleys are used on long conveyers and sometimes on shorter conveyers when there is a wide range in surrounding air temperature and humidity. The weight required to operate this type of take-up is twice the value of T_2 or

$$\text{Weight} = 2 \times \text{effective pull} \times \text{factor } T_2$$

If the conveyer is to be reversed to convey loads in opposite direction at different times, the weight should be twice T_1 or

$$\text{Weight} = 2 \times \text{effective pull} \times \text{factor } T_1$$

Slat Conveyers

Description. Slat conveyers, Figs. 11 to 13, are constructed with wood or steel slats (pallets) fastened to attachments on two strands of roller chain, which in turn travel in or on structural-steel tracks.

Application. This type of conveyer is used when the character of the load is such that it would damage the belting on belt conveyers or does not have a riding surface adaptable to travel on live-roll conveyers.

Design. The slats, Fig. 12, are designed as a simple beam supported at either end. The width of each slat is somewhat less than the pitch of the chain, i.e., about $3^1/_2$ in. wide for a 4-in-pitch chain, $5^1/_2$ in. wide for a 6-in-pitch chain, etc.

Wood slats are usually standard commercial sizes, as 2 in. × 4 in., 2 in. × 6 in., etc., dressed on all four sides.

Steel slats may be flat bar, with or without reinforcing members, formed or rolled channel shapes, etc.

When plain rollers are used in the chain, the tracks are structural angles or channels. On heavy-duty conveyers, a flanged roller is used in the chain, and standard rail sections are then used for the tracks.

The horsepower required at the head shaft of a horizontal slat conveyer is

$$\text{Hp} = \frac{(W + w) \cdot f \cdot S}{33{,}000}$$

where W = weight of live load on conveyer, lb
w = weight of chains and slats, lb
f = friction as given in Table 6
S = speed of conveyer, fpm

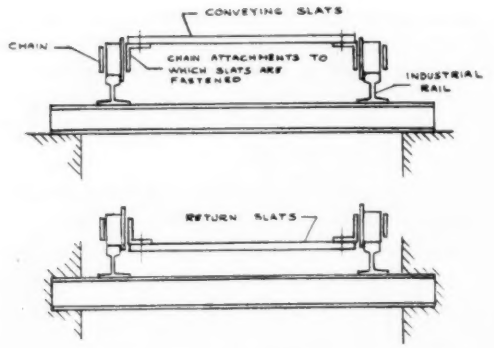


FIG. 11 SECTION THROUGH SLAT CONVEYER
(Showing construction using flanged rollers in chain.)

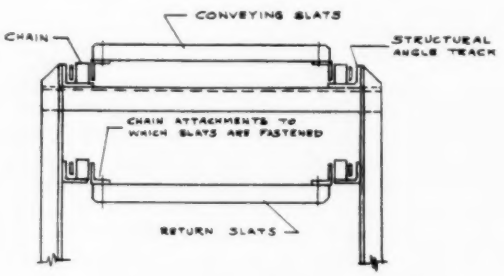


FIG. 12 SECTION THROUGH SLAT CONVEYER
(Showing construction using plain or straight rollers in chain.

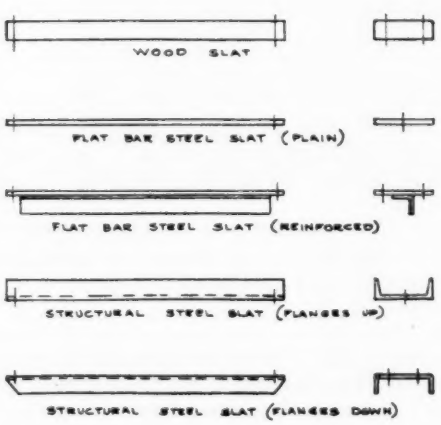


FIG 13 SOME OF THE MORE POPULAR FORMS OF SLATS

where L = weight of upper run of chains, slats and live load, lb
l = weight of return run of chains, and slats, lb
θ = angle of incline, deg
f = friction given in Table 6
S = speed of conveyer, fpm

and when loads are to be lowered

$$\text{Hp} = \frac{[l \sin \theta + f(L + l) \cos \theta - L \sin \theta] \cdot S}{33{,}000}$$

In the latter case, any minus value must be treated as a plus value as explained for belt conveyers.

Take-ups are provided to compensate for stretch in the chains. On this type of conveyer, the adjustment is of the screw type. The amount of adjustment is only enough to permit a chain link to be readily removed and has no relation to the length of the conveyer.

APRON CONVEYERS

Description. The apron conveyer, Fig. 14, is a modification of the slat conveyer in which the aprons or slats form a continuous bed. The aprons overlap one another and in some cases sides are provided so that the bed of the conveyer presents a continuous trough.

Application. This conveyer is seldom used in package conveying. It is employed only when small loads are to be conveyed and where the spaces between the slats on a slat conveyer would be objectionable.

Design. Refer to "Slat Conveyers," substituting the weight of aprons for slats in the horsepower formulas.

DRAG-CHAIN CONVEYERS

Description. In this type of conveyer, Figs. 15 and 16, single or multiple strands of chain slide in steel tracks conveying the load directly on the chain.

Application. Single-strand chains are employed successfully when a uniform-size load is to be conveyed, and multiple strands when loads vary in size. This type of conveyer can negotiate 90-deg corners very readily with most loads. It is particularly adaptable to bottling houses, dairies, and breweries where the loads generally are uniform in size and weight.

Design. Refer to "Slat Conveyers," substituting the weight of the chain only for chains and slats in the horsepower formulas, and use a sliding friction of 30 per cent for the chain on the steel track.

When horizontal turns are employed, the effective pull of each section must be figured progressively.

The turns are usually designed so that the chain is guided in a steel track. Wheels or rollers may be used to reduce the friction loss at the turns, but it is very difficult to make an economical design because of the necessity of clearing the load resting directly on the chain.



FIG. 14 DETAIL OF APRON CONVEYER

TABLE 6 PERCENTAGE FRICTION OF CHAINS ON STEEL TRACKS

Diameter of roller in chain, in.	1 1/2	2	2 1/2	3
Friction, per cent	20	20	15	12

The horsepower for inclined conveyers elevating loads is

$$\text{Hp} = \frac{[L \sin \theta + f(L + l) \cos \theta - l \sin \theta]S}{33{,}000}$$

OVERHEAD CHAIN CONVEYERS

Description. Overhead chain conveyers, Figs. 17 to 19, consist of a two-plane flexible chain supported from an overhead track by means of trolleys. Various types of attachments, from which the loads are suspended, are spaced on the chain. Frequently, cars or carriers are suspended from the attachments and the loads are then placed directly on the cars.

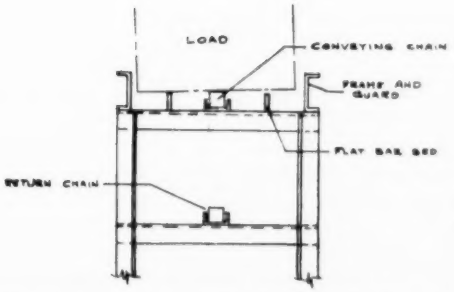


FIG. 15 SECTION THROUGH DRAG-CHAIN CONVEYER



FIG. 16 DRAG-CHAIN CONVEYER WITH PUSHERS AUTOMATICALLY CONVERGING LOADS FROM TWO LINES TO A SINGLE LINE OF ROLLER CONVEYER
(Pepsi-Cola, Long Island City, N. Y.)

Application. Almost any type of load can be conveyed by this conveyer. The conveyer is extremely flexible; loads may be deposited on the cars or hooked to the chain attachments at any working height, the load then being elevated to the ceiling or floors above for transportation and again brought down to a working height for unloading at the next operation. The conveyer makes an ideal storage unit or traveling stock pile as any load not removed at a station will recirculate and keep returning to that station until the operator is ready to take it off and perform his work. The floor between operations is kept clear for other work and the otherwise wasted space at the ceiling is utilized to good purpose.

Design. The most common types of conveyer are the 3-in. and 4-in. sizes. These sizes indicate the size of I-beam track used. Two-wheel trolleys, operating in the I-beam, support the chain, and the load attachments are usually arranged directly below the trolley so that the pull is on the trolley, the chain then becoming the propelling means for advancing the trolleys and loads along the path of the track.

Horizontal turns are made in two types, the multiple-roller curve and the traction wheel. The roller type is more generally



FIG. 17 OVERHEAD CHAIN CONVEYER TOWING TRUCKS



FIG. 18 TYPICAL LOADING-STATION DIP ON OVERHEAD CHAIN CONVEYER
(Glen L. Martin, Baltimore, Md.)

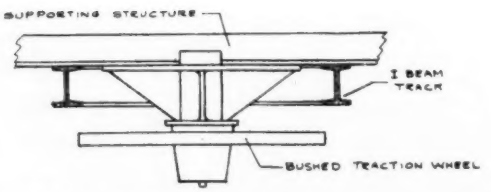


FIG. 19 TRACTION WHEEL FOR OVERHEAD CHAIN CONVEYER

used because of its lower frictional resistance and its adaptability to large radii. When the turn is to operate in high temperatures (over 400 F), the traction wheel should be used, as it is provided with a special bushing and a large oil reservoir supplying ample lubrication.

The drives are made in two types, the corner-sprocket drive and the caterpillar drive. The corner-sprocket drive is used when conditions permit, and the caterpillar drive where the radius of the corner is too large for sprocket drives. The drive should be placed at the point of maximum pull and, preferably, near a down curve so that any slack in the chain will automatically be taken away from the drive. Drives should never be placed inside oven or spray-booth enclosures.

Take-ups are usually provided to permit removal of links when slack in chain becomes excessive. Take-ups may be omitted on long conveyers or those with several dips where links may be removed from the chain without the necessity of adjusting a sprocket or corner. Take-ups should always be provided on conveyers subjected to great temperature changes. In this latter case, the track should also be provided with expansion joints based upon a coefficient of 0.0000065 per unit length per deg F.

Radii of vertical bends or dips should be as large as practical for smooth operation.

The technical data, given in Table 7, will be helpful in designing the conveyer.

TABLE 7 DESIGN DATA FOR OVERHEAD CHAIN CONVEYERS

	Size of system	
	3 in.	4 in.
Chain:		
Pitch	3.031	4.031
Weight per foot, lb	2.25	3.125
Ultimate strength, lb	18,000	30,000
Allowable working load in lb (level)	1800	3000
Allowable working load in lb (dips)	1000	2000
Minimum amount of take-up, in	7	9
Trolleys:		
Weight, lb	3.5	7.5
Multiple of spacing, in	6	8
Maximum spacing, in	30	32
Maximum load, lb	80 to 150	200 to 400
Average friction, ball bearings, per cent	2	2
Average friction, bronze bearings, per cent	3	3
Track:		
Size of I-beam, in	3	4
Weight per foot, lb	5.7	7.7
Vertical Bends:		
Trolley spacing, minimum radius	30 in.–10 ft	32 in.–12 ft
Trolley spacing, minimum radius	24 in.– 8 ft	24 in.–10 ft
Trolley spacing, minimum radius	18 in.– 6 ft	16 in.– 8 ft
Trolley spacing, minimum radius	12 in.– 5 ft	...

To determine the horsepower at the head shaft, the formula is

$$\text{Hp} = \frac{W \cdot f \cdot S}{33{,}000}$$

where W = weight of chain, trolleys, cars, and live load, lb
f = friction, depending upon type of bearing in trolley
S = speed of conveyer, fpm

When the conveyer has small dips or vertical bends, they usually balance, and there is no appreciable extra pull in the chain. If, however, the inclines are long, the extra pull must be added to the calculation, and the horsepower formula then becomes

$$\text{Hp} = \frac{(W \cdot f + L \sin \theta) \cdot S}{33{,}000}$$

where L = live load on incline, lb
θ = angle of incline, deg

When the conveyer has more than four horizontal turns, the pull on the chain must be calculated for each section progressively, adding 5 per cent friction loss for each turn.

VERTICAL CONVEYERS

There are numerous types of vertical conveyers (Fig. 20 is an example). There are special applications of vertical belt conveyers and vertical slat conveyers. In both cases, cars or shelves are attached to the belt or slats and the loads then placed on these shelves.

Other continuous-operating vertical conveyers employ single or double strands of chain, attached to which are rigid or pendant cars. The loads sometimes are placed on and taken off the cars manually. The cars can be designed with fingers or arms that pass through corresponding fingers on stations so that loads are deposited automatically on and off the cars. The fingers of the stations may be constructed of rollers so that loads travel automatically into or out of the path of the cars. The station fingers may also be narrow belt conveyers, slat conveyers, drag chains; in fact any type of powered conveyer.

Vertical conveyers may also be of the reciprocating type where a single car delivers the load to another station and then returns to the sending station to receive another load.

There are unlimited combinations and designs of vertical conveyers, and it would be impossible to describe in detail even a few of the more popular types in this paper.

SPECIAL CONVEYERS

There are a great many special conveyers which are really modifications of the more standardized types of conveyers discussed in

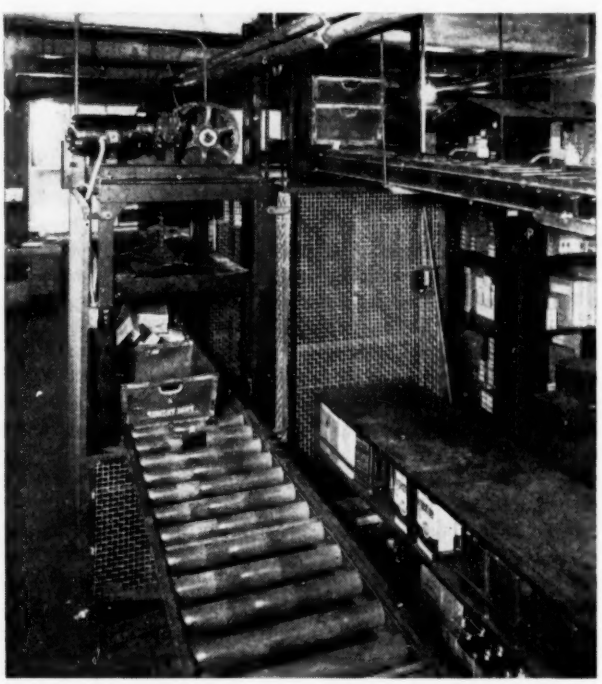


FIG. 20 RECIPROCATING-TYPE VERTICAL CONVEYERS, ILLUSTRATING TYPICAL AUTOMATIC LOADING AND UNLOADING STATIONS
(W. T. Gilmore Drug Company, Pittsburgh, Pa.)

this paper. There is one possible exception and that is the pusher-bar conveyers. This conveyer consists of two strands of chain with a bar extending between the chains. These bars push the load over a steel slider bed, a wood slider bed, or a roller bed. The pusher-bar conveyer at one time was very popular (it is still used extensively in bottling houses), but inclined belt conveyers are rapidly replacing the pusher-bar type of booster.

Automatic conveyers are frequently designed to pick up loads and discharge them at predetermined points. One design of fully automatic conveyer consists of a vertical conveyer with automatic loading and unloading stations. In this installation, an operator places a load on the loading-station platform and sets a dial indicating the station to which the load is dispatched. When an empty car approaches, it operates the loading station which places the load onto the car and sets a mechanism on the car. When that car reaches the designated unloading station (and that station is empty and ready to receive a load), the station picks the load off the car and deposits it on the unloading-station platform.

Another example of fully automatic conveyer consists of an overhead chain conveyer with reciprocating type of vertical conveyers, loading and unloading the cars on the overhead conveyer. In this installation, the loads are placed on the vertical-conveyer car near the floor level. When an empty car on the overhead conveyer approaches, the vertical conveyer elevates the load and deposits it on the car on the overhead conveyer. The overhead conveyer then delivers the load to another part of the building, or to another building, where a vertical conveyer removes the load and lowers it to a station near the floor level.

Pneumatic tubes are also used to convey unit loads, but the application and design features are too complex to be discussed in this paper.

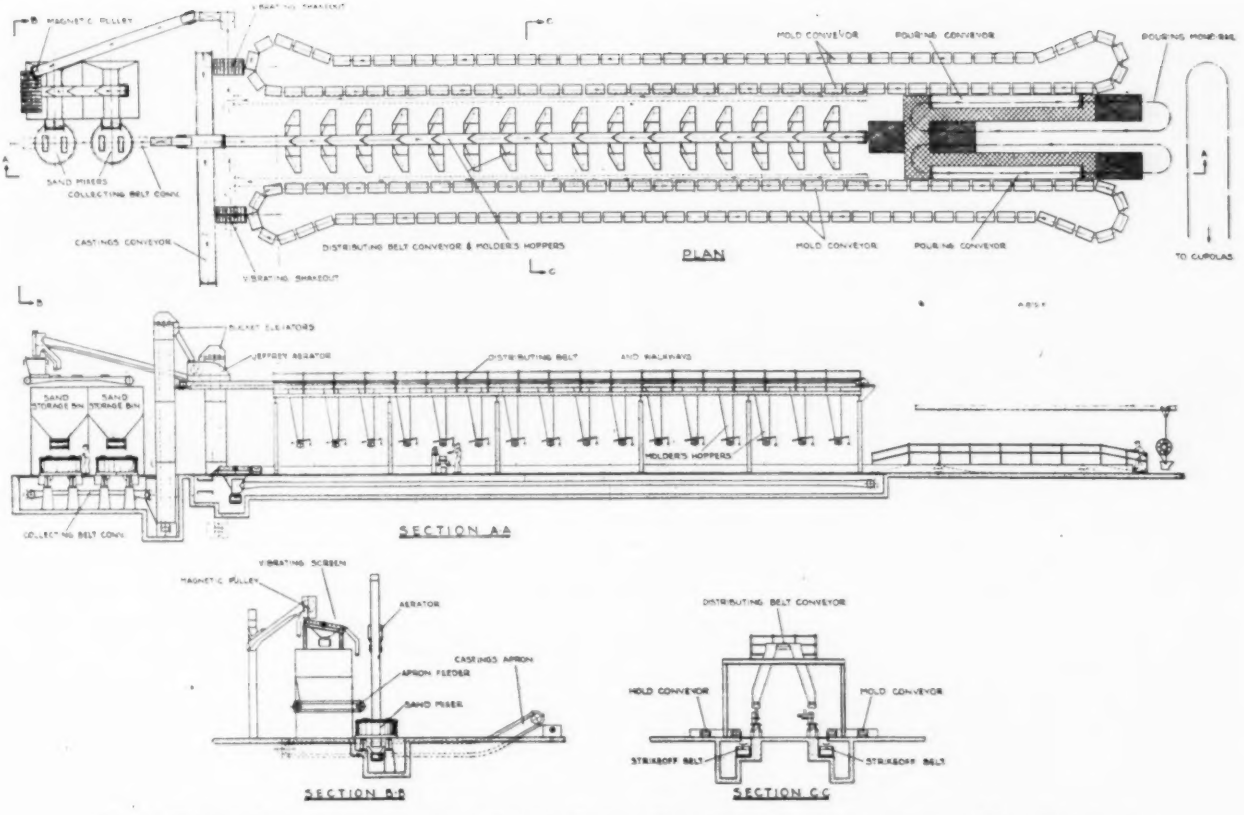


FIG. 1 TYPICAL LAYOUT OF A CONTINUOUS POURING SYSTEM, USING CONTINUOUS-POWER-DRIVEN MOLD CONVEYERS

Design Features of Conveying Equipment for the Foundry Industry

BY F. B. HENRY AND G. N. WILEMAN,[1] COLUMBUS, OHIO

The design of conveying equipment used in the foundry industry is covered in its general applications, with consideration given to the design of some of the more important details. Emphasis has been placed on equipment used in the handling of sand, molds, and castings, since they offer the major opportunities for economies and savings in manufacturing costs.

CONVEYING equipment for the foundry industry embodies conveyers and elevators handling practically all materials in the foundry, from raw materials to finished product. Raw materials, such as limestone, coke, sand, clay, pig iron, and so on, are handled mechanically from railroad cars to the point of usage.

Sand used in the molding process is handled mechanically from the shakeout through the reconditioning process back to the molding stations.

Molds, after being made (except in the case of very large castings) are handled mechanically from the pouring and cooling stations to the shakeout. Flasks are commonly returned from the shakeout to molders by means of conveyers.

Cores used in making the molds are handled on conveyers from coremakers through the baking process, and frequently distributed to the molders.

Castings from the shakeout are often handled by conveyer through the cooling step to the cleaning room, and, in the case of production castings, are handled through the cleaning process on conveyers. Remelt at times is also returned to the melting operation by means of conveyers.

From the foregoing, it can be seen that conveying equipment plays a vital part in the operation of a modern foundry, and a conveying system often represents the largest equipment investment in the plant.

A few general rules should be kept in mind when designing equipment for any foundry. These are as follows:

1 Due to the extremely abrasive nature of foundry sand

[1] The Jeffrey Manufacturing Company.

Contributed by the Special Design Committee and presented at the Annual Meeting, New York, N. Y., Nov. 29–Dec. 3, 1943, of THE AMERICAN SOCIETY OF MECHANICAL ENGINEERS.

NOTE: Statements and opinions advanced in papers are to be understood as individual expressions of their authors and not those of the Society.

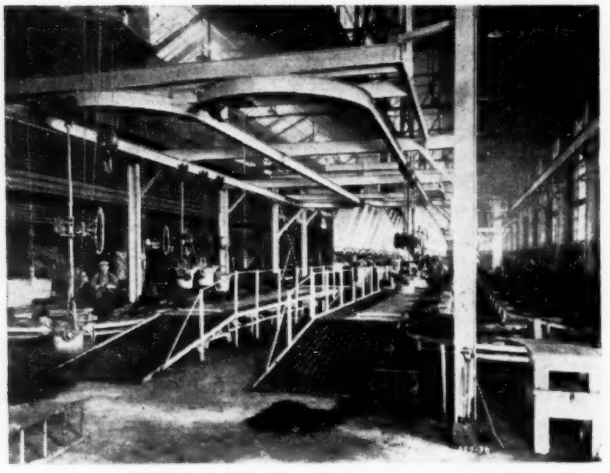


FIG. 2 PRODUCTION FOUNDRY MAKING GRAY IRON

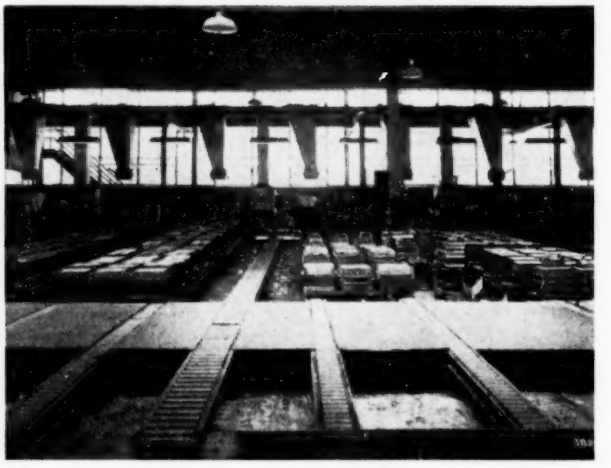


FIG. 4 SEMICONTINUOUS FOUNDRY MAKING SMALL STEEL CASTINGS

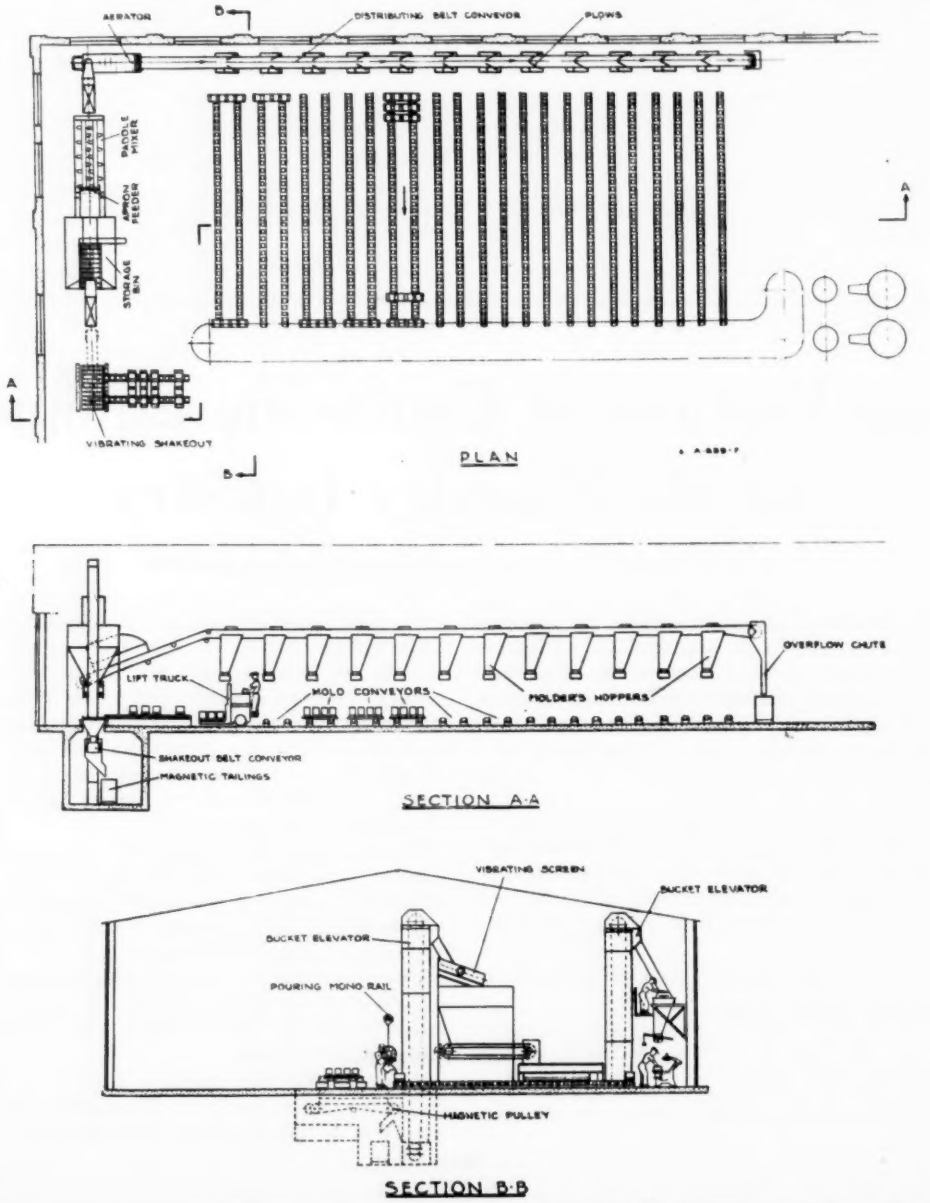


FIG. 3 TYPICAL LAYOUT OF FOUNDRY USING ROLLER-TYPE CONVEYER, MOLD STORAGE, AND CENTRAL SHAKEOUT

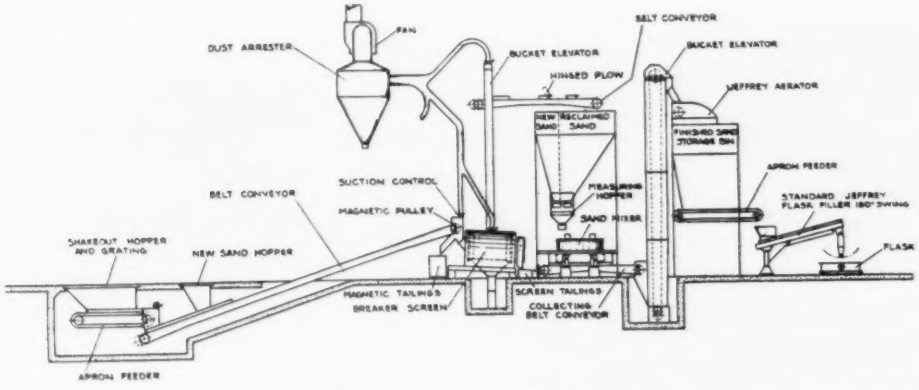


FIG. 5 TYPICAL LAYOUT OF STEEL FOUNDRY

and dust, friction parts should be entirely enclosed if possible, particularly those parts having high loads. This practically eliminates, or keeps to a minimum, all sliding types of conveyers.

2 Generous space should be provided in pits and walkways for proper maintenance and inspection.

3 Points in the system where dry sand is transferred from one conveyer to another, or from conveyer to bins, should have properly designed chutes and hoods for removal of dust, steam, smoke, and gases. Individual installations should be designed to meet state law requirements.

4 Chutes and hoppers handling prepared or damp sand should have angles of at least 60 deg, rounded corners, and generous cleanout doors.

TYPICAL ARRANGEMENTS FOR MECHANIZED FOUNDRIES

Before considering the individual types of conveyers used in the various applications, and their design features, it may be well to consider some typical layouts used in different types of mechanized foundries.

Layout of Typical High-Production, Continuous, Gray-Iron Foundry (Figs. 1 and 2). This arrangement lends itself to any foundry—steel, gray iron, malleable iron, aluminum, or magnesium—having high production of duplicate castings, with continuous hot metal available. Sand is prepared in the mixers, aerated, and distributed to the molders' hoppers at each molding station. After the mold is completed, it is placed on the mold conveyer for pouring, cooling, and conveying to the shakeout station. Sand passes through the shakeout machines, is screened, and conveyed to the storage bin for another cycle. The castings are collected from the ends of the shakeout machines and conveyed to the cleaning room.

Layout of Typical Gray-Iron or Brass Foundry; Noncontinuous (Figs. 3 and 4). This arrangement is applicable to any type of foundry having relatively small work and allows sufficient storage of molds to take care of intermittent metal supply. While this layout shows a paddle mixer in the sand plant, the muller type could be substituted if the sand required it. After mixing, the sand is distributed to the molders. Finished molds are stored on a roller conveyer for pouring and cooling. A car or conveyer will transfer the molds to the shakeout station, from which the sand is returned to the storage bin, while the castings may be put into boxes or conveyed directly to the cleaning room.

Layout of Typical Steel-Foundry System (Figs. 5 and 6). Steel foundries may use conveyers for handling molds from the molder to the shakeout, depending upon the class of work. Sand from the shakeout passes over a magnetic pulley, through a breaker screen to reduce lumps and remove refuse, then to the sand bins

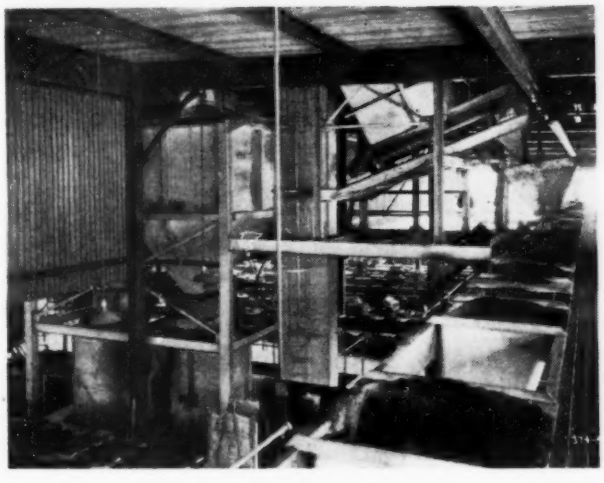


FIG. 6 STEEL FOUNDRY WITH TRAMRAIL DISTRIBUTING SYSTEM

and mixers. Prepared sand is distributed by conveyer or bucket to the molding stations. In the case of large molds these are frequently hoppers fitted with feeders for filling the flasks.

TYPES OF CONVEYERS USED

Following is a detailed discussion of various types of conveyers used in the typical systems described:

Shakeout (Figs. 7 and 8). The mechanical shakeout is now very widely used in all types of foundries and is available for molds from small snap molds, weighing possibly 100 lb, to very large molds weighing as much as 50 tons. They consist fundamentally of a vibrating perforated deck or grid on which the mold is placed, the sand falling through the grid to the conveying means underneath, with the flask and casting remaining on the grid or being discharged from one end. Large molds are frequently stripped before being shaken out. Supports for shakeout machines must be extremely heavy and rugged.

Feeder Under Shakeout. Means must be provided for conveying the sand from the hopper underneath the shakeout machine. This hopper is always designed to contain at least the total amount of sand in the largest mold being handled. This sand frequently is very hot and may contain considerable metallic refuse, such as gaggers and rods, as well as fins, sprues, and so on, which may be broken from the casting in the shakeout process. There are three types of conveyers used for feeding the sand from the shakeout:

(*a*) A belt feeder, Fig. 9, is sometimes used in cases where the castings are very light and the sand does not contain any ma-

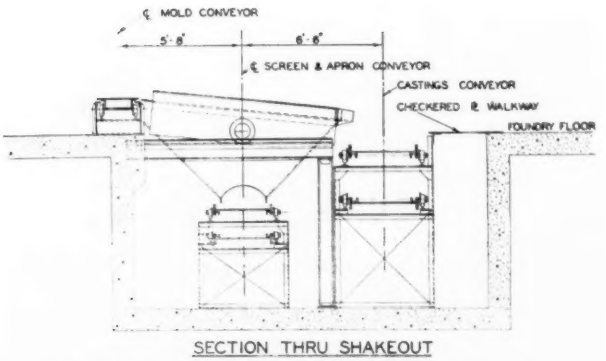


FIG. 7 SHAKEOUT FOR SMALL GRAY-IRON CASTINGS



FIG. 8 STEEL-FOUNDRY SHAKEOUT

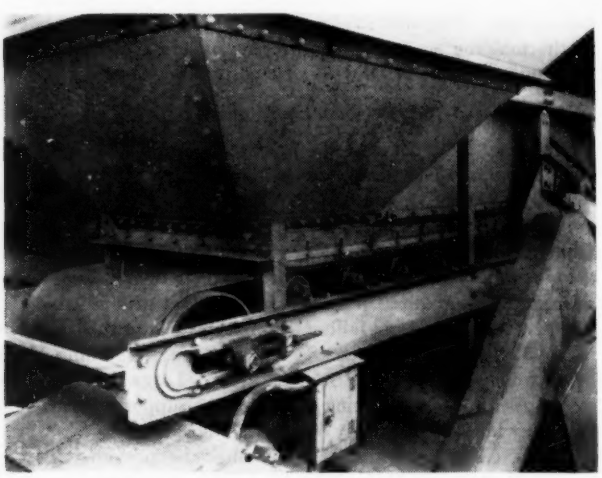


FIG. 9 BELT FEEDER UNDER SHAKEOUT

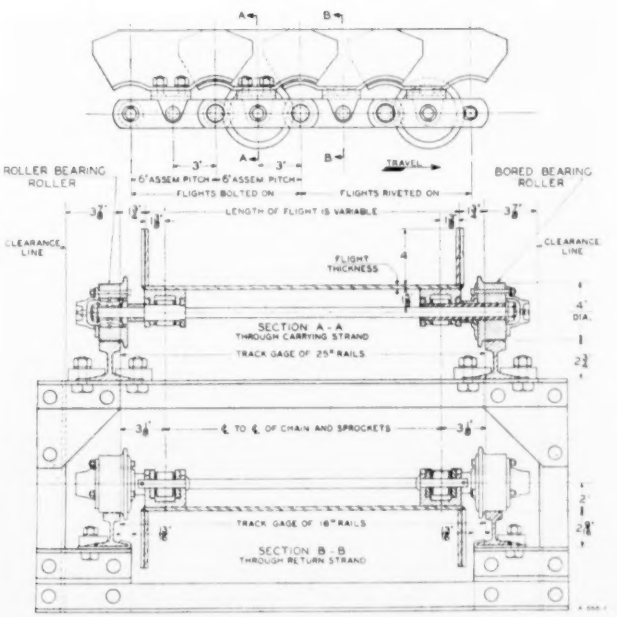


FIG. 10 CROSS SECTION OF APRON FEEDER

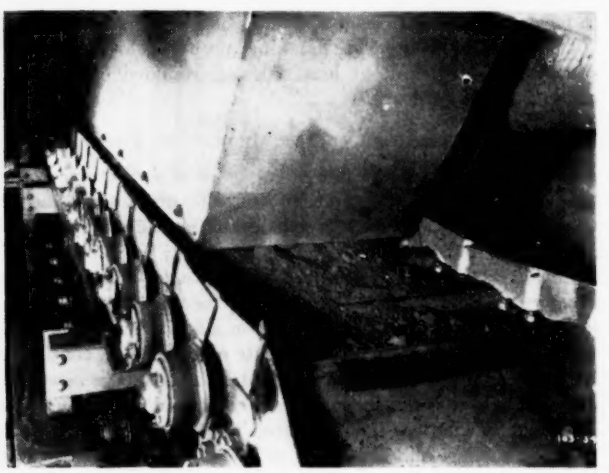


FIG. 11 APRON FEEDER UNDER SHAKEOUT

terial amount of metallic refuse such as in a foundry making very light iron or brass castings. Closely spaced idlers or flat steel plate are required under the load.

(*b*) Apron feeders, Figs. 10 and 11, are commonly used for this service and where used should be of the leakproof type, with a tight-fitting enclosed outboard roller. Pans have welded ends to prevent leakage of dry sand and are removable from the conveyer without dismantling the chain. The drive should be protected by a shear pin or similar device. While the apron will stand heat in a satisfactory manner, damage frequently results to the pans from gaggers or rods which get through the shakeout grating.

(*c*) During the last few years, the electric vibrating feeder, Fig. 12, has come into wide usage in this application. It offers a perfectly smooth deck with no obstructions for rods or gaggers; it can stand the heat without injury, and is free from dribble since it has no return run.

Belt Conveyer Having Magnetic Pulley (Fig. 13). In the usual installation, sand is fed from the shakeout hopper to a belt conveyer equipped with a magnetic head pulley, for removal of magnetic refuse such as gaggers, rods, nails, sprues, shot, and so on. This is important for various reasons. It is essential that foreign material be removed to prevent injury to some of the other parts of the equipment. Gaggers and rods are salvaged for re-use. Sprues, shot, and other parts of the casting metal

are returned for remelt. Rubber belt is used when the sand is comparatively cool, with heat-resisting, impregnated-fabric belts for hot sands. Belt-conveyer idlers should have a high-pressure type of lubrication which forces out the old grease. Closely spaced idlers or a plate should be placed under the loading point of the conveyer to take the load.

A short belt with a magnetic pulley may be applied over the main belt for picking off large pieces of metallic material.

Screens (Figs. 14 to 16). Screens may be either of the rotary type or of the vibrating type and are used principally to get rid of nonmagnetic refuse such as wood wedges, tiles and rags, etc. Rotary-type screens are ordinarily used where heavy work is encountered, as they have a very definite lump-breaking and sand-cooling action. Vibrating screens are used where very fine sand is required, such as, in foundries making small castings. It is the usual practice to provide hoods and air suction on these screens for the removal of dust, fines, steam, etc.

Bucket Elevators. Bucket elevators used in the foundry industry are almost always of the centrifugal-discharge belt-and-bucket type, although chain elevators are used infrequently. Malleable buckets are universally used. Foot pulleys are of the slatted type with internal cones so that sand falling inside the belt will not build up on the foot pulley. Boots should have large and readily accessible cleanout doors.

Main Storage Bins (Figs. 17 and 18). Design of the storage bins depends upon the particular application and the method of feeding the sand from them to the mixers. The tendency in modern installations is to make them relatively large in capacity. In continuous systems, a minimum of 2 hr supply of sand is ordinarily used. Storage bins are often designed to include, in addition to the main compartment for old sand, one or more compartments for new sand or binders. Bins having apron feeders should be fitted with regulating baffles to insure a uniform sand withdrawal along the entire length of the bin.

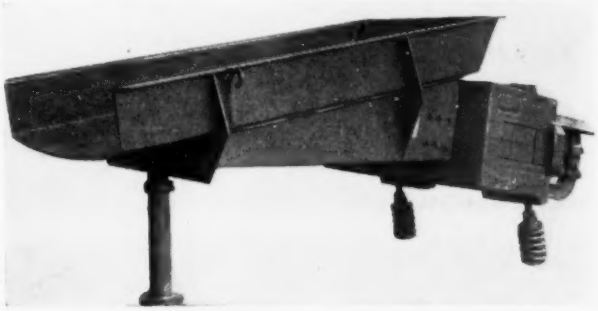


FIG. 12 VIBRATING FEEDER FOR USE UNDER SHAKEOUT

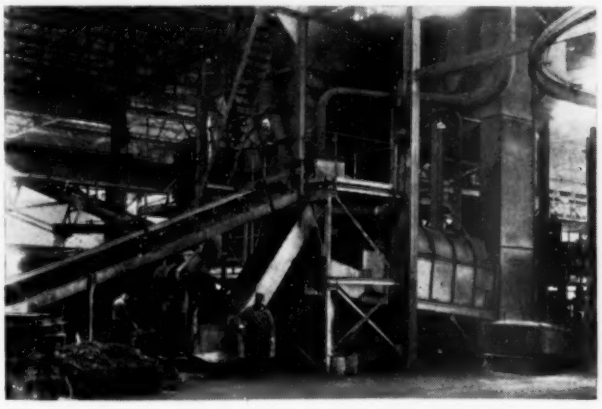


FIG. 13 SHAKEOUT BELT CONVEYER HAVING MAGNETIC HEAD PULLEY

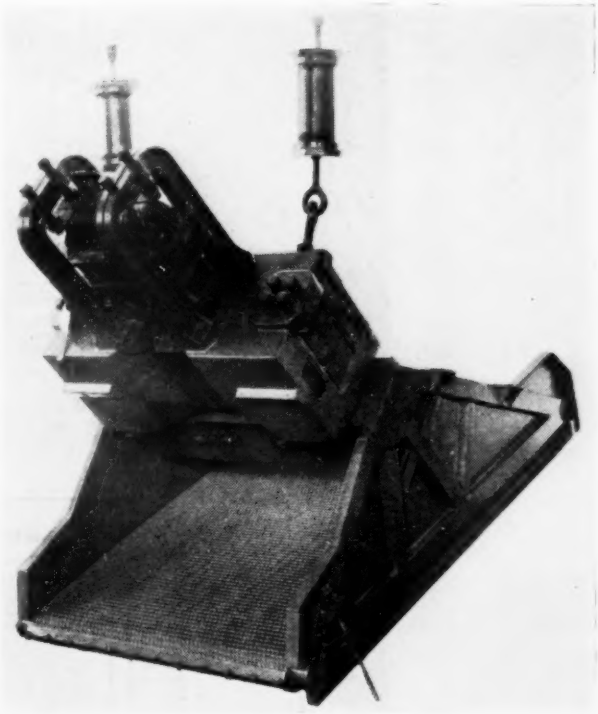


FIG. 14 VIBRATING SCREEN

Feeders From Storage Bins to Sand Mixers. There are two common methods of feeding the sand from the main storage bin to the sand mixers, either with gates and measuring hoppers, or apron feeders.

If muller-type mixers are used, the sand must be batched in suitable quantities. One method is the use of volumetric batch hoppers or of weigh hoppers, the batch hopper or weigh hopper containing the proper charge for the mixer. Weigh hoppers have the advantage of being able to properly proportion shakeout sand and new sand. The storage bins used with this type of batch method are gravity-type bins, provided with clamshell valves for feeding the batch hoppers which, in turn, are discharged by clamshell valves into the mills. With this type of bin it is best practice to divide the bin into two compartments, with two discharge valves, to prevent piping of the sand down through the center of the bin, Fig. 19.

The other method frequently employed uses apron-type feeders for charging the batch-type mixers. The feeders are arranged with either a limit switch, or timer so as to operate for a certain number of seconds to give the proper charge. This feeding arrangement will allow for more economical design of bin and one which is much lower in height, Fig. 20.

Paddle mixers use the continuous-moving-apron feeder almost exclusively. Vibrating feeders or small screw conveyers are used for feeding binders to the mixers, Fig. 21.

Sand Mixers. Sand mixers used are either of the paddle-mixer type or of the muller type. Paddle mixers are continuous mixers which give satisfactory results on natural sands. The muller-type mixers are batch mixers and are always used when synthetic sands are being made.

Aerators (Figs. 22 and 23). Aerators are used between the mixers and the distribution system on practically all installations.

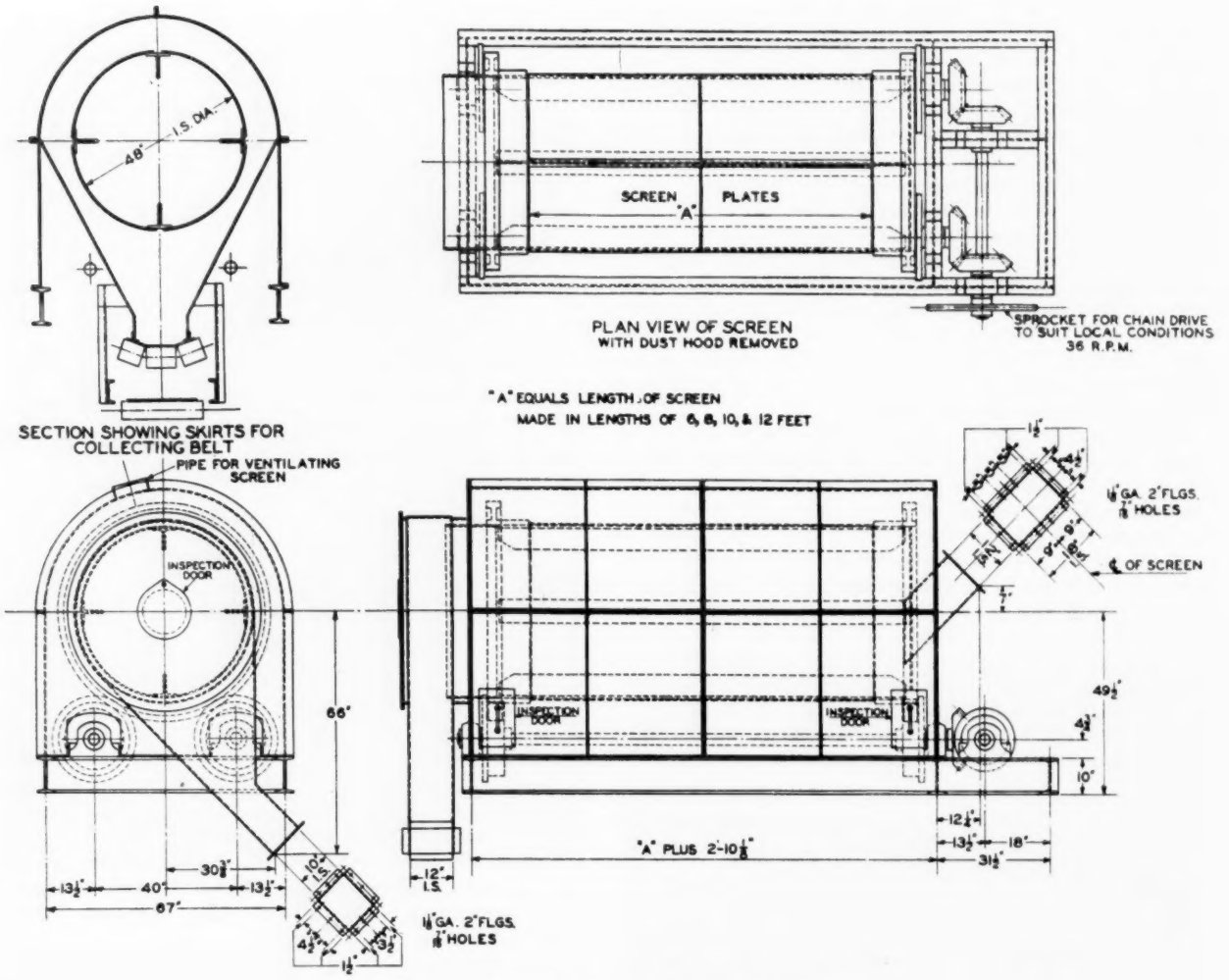


FIG. 16 DETAILS OF ROTARY BREAKER SCREEN

They are used for the final mixing and aeration of the prepared sand, before it is delivered to the molders.

Distributing System. Flat-belt conveyers with plows are most commonly used for distributing the prepared sand to the molders' hoppers. The belt is supported on flat idlers between the plows and on a flat plate directly under the plows. Plows are usually hinged, employing some simple mechanism for raising or lowering by hand. The part riding the belt should be edged with rubber to prevent injury. Belt cleaners should be installed at the head of this as well as any other belt handling prepared sand, Fig. 24.

In occasional installations, scraper-type conveyers are used. These scraper-type conveyers have the advantage that they will continuously and automatically fill the molders' hoppers. When one becomes full sand is scraped into next hopper, Fig. 25.

Hoppers for Molders. Hoppers and bins at the molding stations should be as small as practical. They usually contain from $1^1/_2$ to 2 tons of sand for smaller-size molds. They are designed with two vertical sides and with corners rounded to at least 3 in. radius. Clamshell valves are used for discharging the sand from the hopper to the mold. Quite frequently air cylniders are used for operating the valves, Fig. 26.

Where large molds are being made, it is necessary to provide a larger hopper, and in such cases the bottom of the hopper is fitted with an apron feeder for dragging the sand from the hopper into the flask, Fig. 27. Occasionally a swivel belt is employed between the end of the apron and the molding station. This allows the one hopper and feeder to service several molders, Fig. 28.

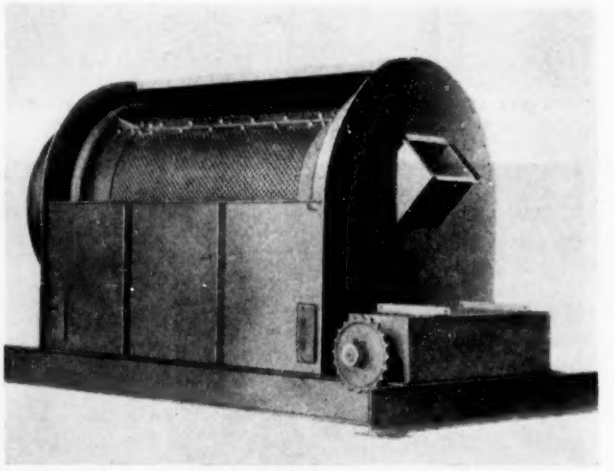


FIG. 15 VIEW OF ROTARY BREAKER SCREEN

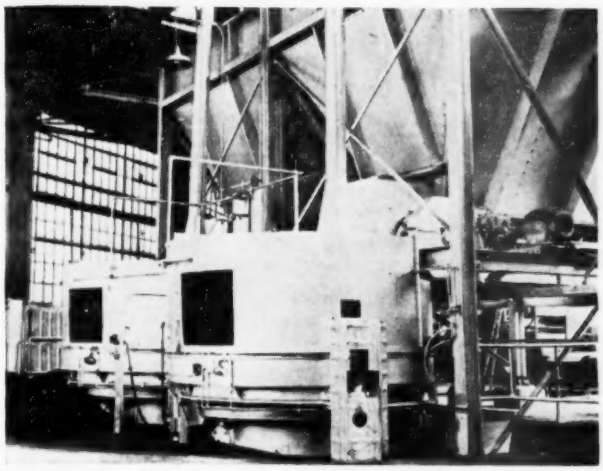


FIG. 17 STORAGE BINS WITH APRON FEEDERS AND BATCH MIXERS

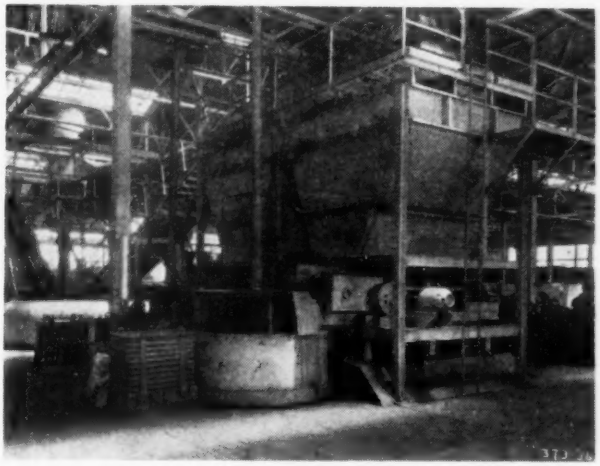


FIG. 20 APRON FEEDERS FOR BATCH MIXING

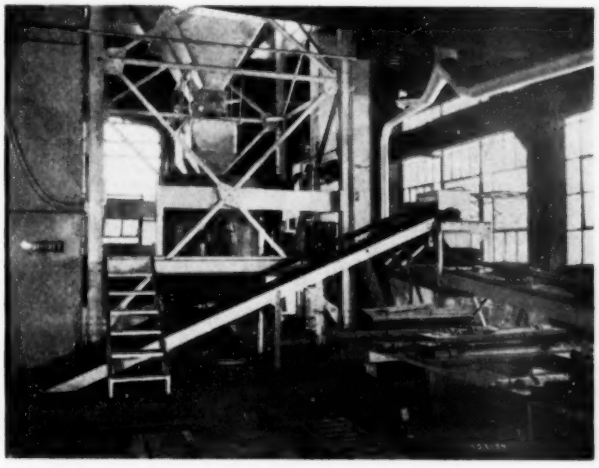


FIG. 18 STORAGE BIN WITH MEASURING HOPPER AND BATCH MIXER

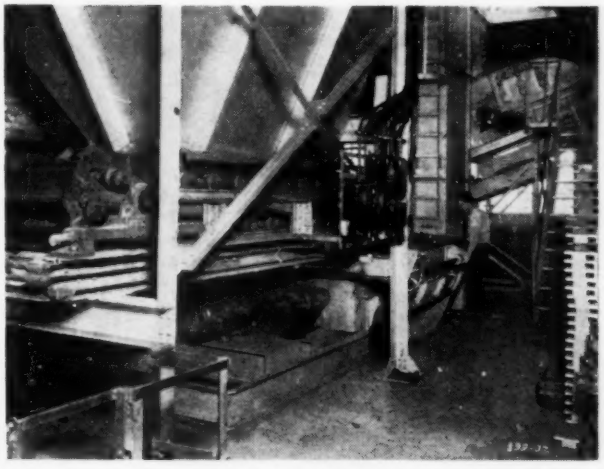


FIG. 21 APRON FEEDER FOR CONTINUOUS-TYPE PADDLE MIXER

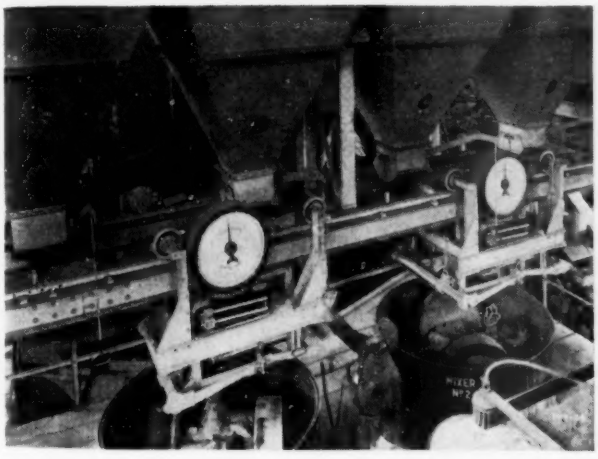


FIG. 19 TRAVELING WEIGH HOPPERS FOR BATCHING

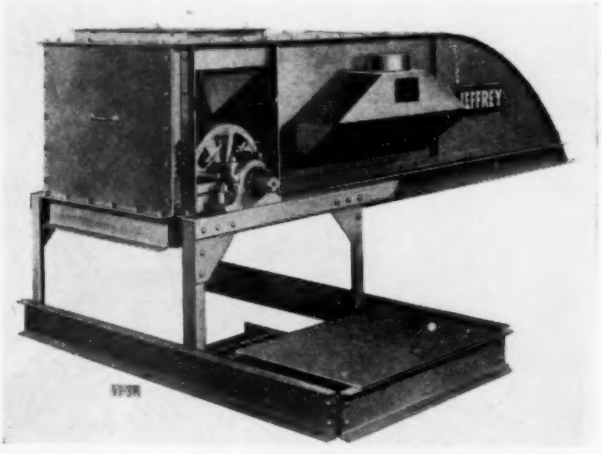


FIG. 22 BAR-TYPE SAND AERATOR

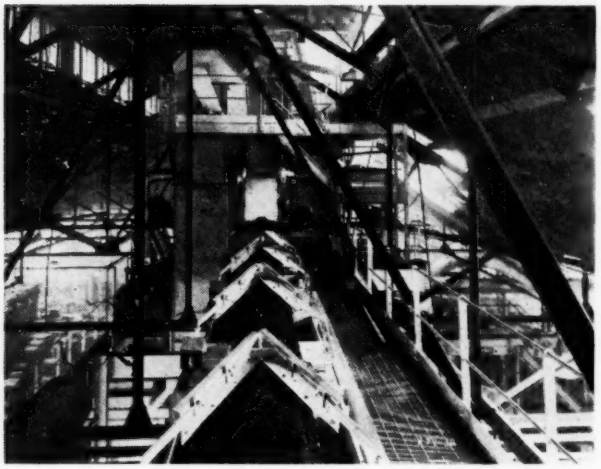


FIG. 23 AERATOR INSTALLED BETWEEN PREPARED-SAND ELEVATOR AND DISTRIBUTING BELT CONVEYER

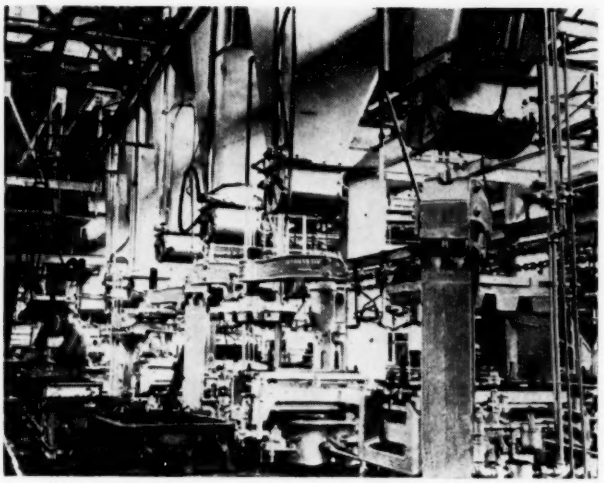


FIG. 26 MOLDERS' HOPPERS WITH AIR-OPERATED VALVES



FIG. 24 FLAT-BELT DISTRIBUTING CONVEYER



FIG. 27 MOLDERS' HOPPER WITH APRON FEEDER AND CHUTE TO FLASKS ON LARGE MOLDING MACHINE



FIG. 25 SCRAPER-TYPE DISTRIBUTING CONVEYER



FIG. 28 MOLDERS' HOPPER WITH APRON FEEDER AND SWIVEL BELT FOR FLOOR MOLDING

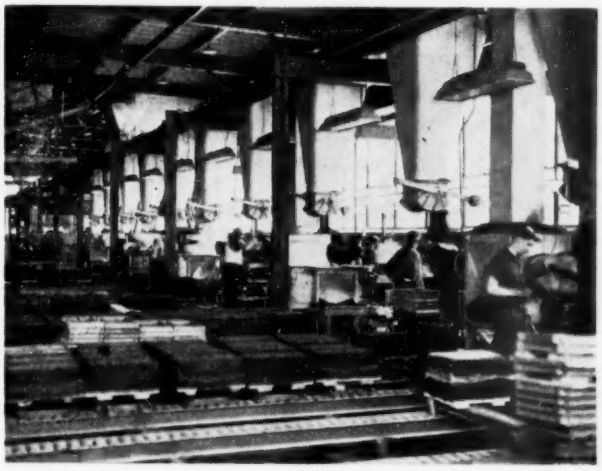


FIG. 29 SHOVEL-OUT HOPPERS FOR FACING SAND SERVING MOLDER ON EITHER SIDE

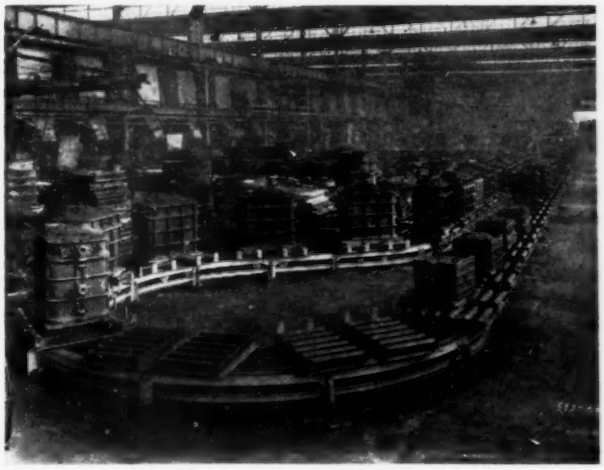


FIG. 31 CONTINUOUS-TYPE MOLD CONVEYER USING ROLLER CONVEYER TOPS

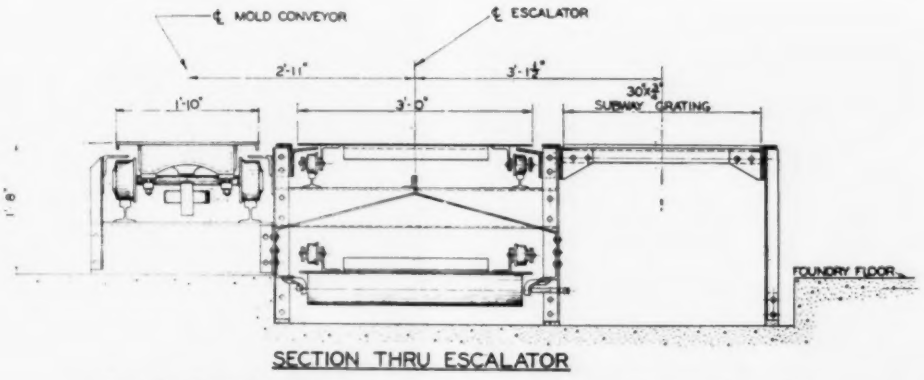


FIG. 30 CROSS SECTION THROUGH MOLD CONVEYER AND POURING PLATFORM

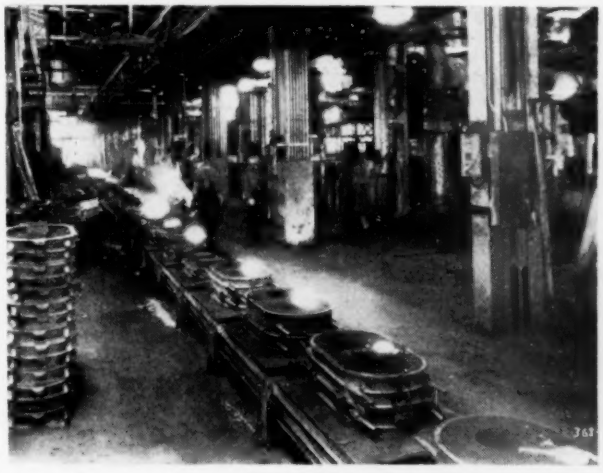


FIG. 32 CONTINUOUS-TYPE MOLD CONVEYER AT POURING STATION



FIG. 33 MOLD STORAGE USING ROLLER CONVEYERS

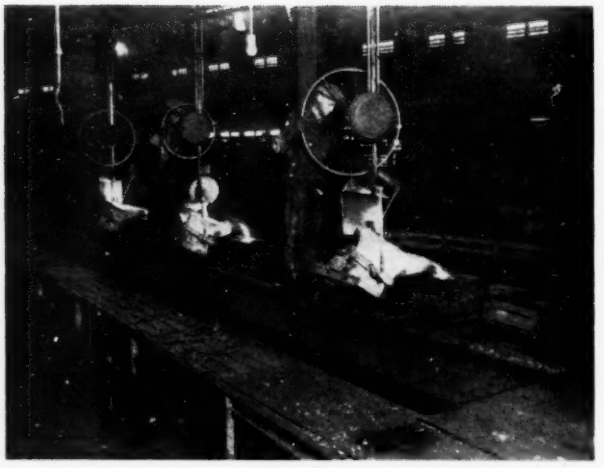


FIG. 34 POURING CONVEYER FOR CONTINUOUS-TYPE MOLD CONVEYER

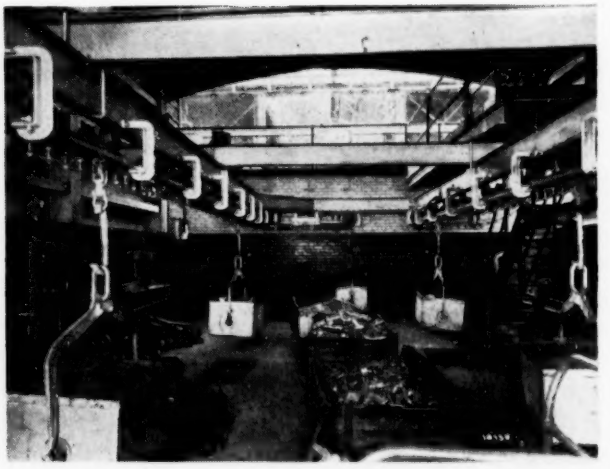


FIG. 36 TROLLEY-TYPE CASTINGS CONVEYER

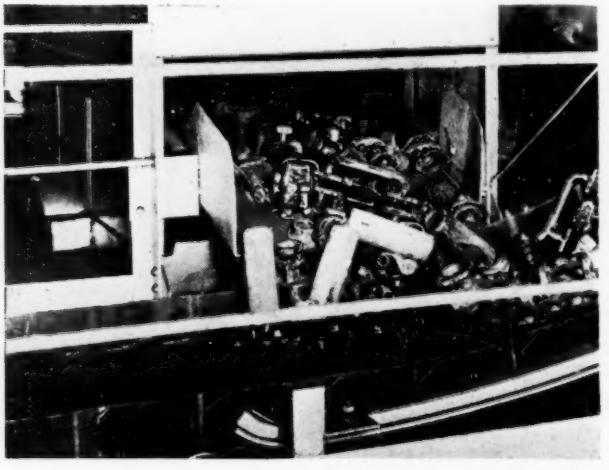


FIG. 35 CASTINGS DISCHARGING FROM SHAKEOUT TO APRON-TYPE CASTINGS CONVEYER

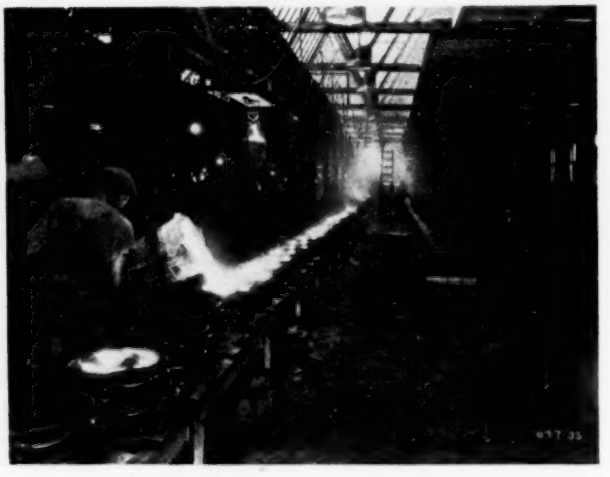


FIG. 37 ROLLER CONVEYER USED FOR FLASK RETURN

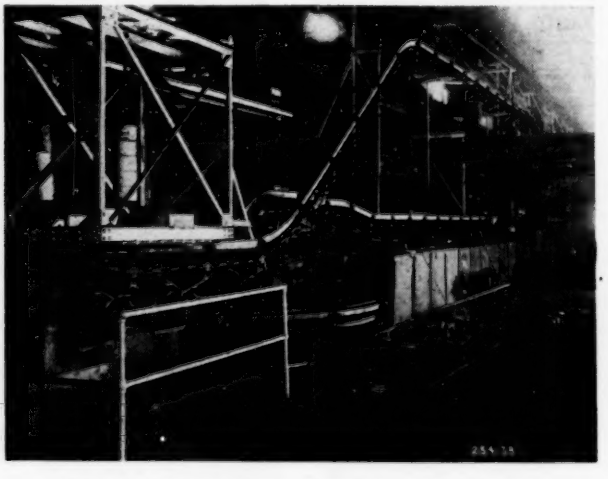


FIG. 38 TROLLEY-TYPE FLASK-RETURN CONVEYER

When facing sand is handled over the conveyer system, hoppers are provided on the floor, with shovelout openings. These hoppers are filled by separate plows and chutes from the distributing belt. In some few cases facing sand is stored in hoppers with feeders adjacent to the backing sand hopper, Fig. 29.

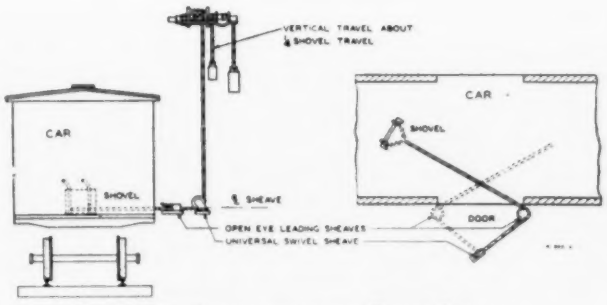


FIG. 39 ARRANGEMENT FOR POWER SHOVEL



FIG. 40 UNLOADING SAND FROM BOXCAR WITH POWER SHOVEL

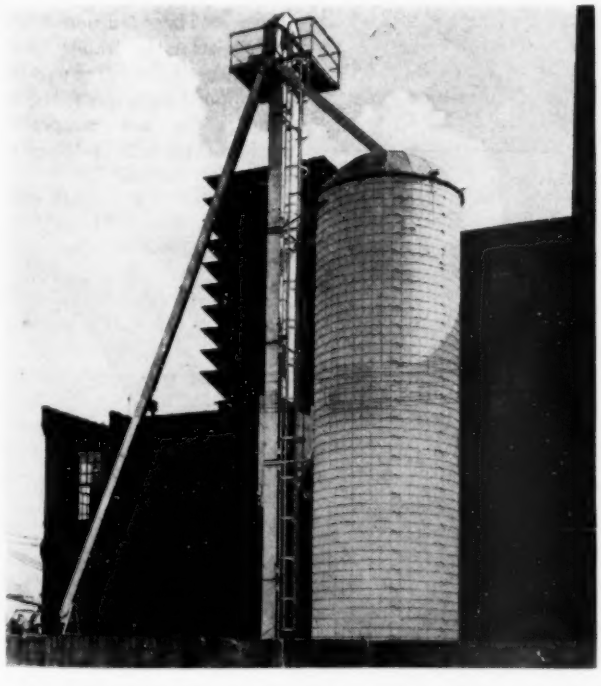


FIG. 41 CONCRETE STAVE-TYPE SILO FOR BULK STORAGE

Mold Conveyers. Layouts for continuous pouring will ordinarily utilize continuous-type mold conveyers for receiving the molds at the molding stations and conveying them through the pouring stations to the shakeout. They must be designed so that sufficient cooling time is available from the pouring station to the shakeout. This may vary from as little as 5 min. for very light castings to ½ to 1 hr for larger molds. Air-cylinder pushers are frequently used to push the mold onto the shakeout. The use of a mold conveyer permits the molder to devote practically all of his time to molding, instead of using part of it for carrying out molds to the floor, Figs. 30, 31, and 32.

Where the pouring is not continuous, roller-type-conveyer layouts are used for handling the molds from the molders to the pouring station. This type of layout is also used where large numbers of alloys are encountered, so that the various types can be segregated for pouring, Fig. 33.

Pouring Conveyers. When continuous-mold conveyers are used and the speed exceeds about 15 fpm, moving pouring platforms are used. These operate in time with the mold conveyer so that the men pouring the metal can stand on this moving platform without any relative motion between the mold being poured and the ladle. These are apron-type conveyers with flat tops, Fig. 34.

Hot-Castings Conveyers. From the shakeout, it is necessary to take away the castings, and, in the case of smaller castings, this is frequently done with an apron-type hot-castings conveyer, Fig. 35. When used for this service, the apron should be of the leakproof type so that sand from the cores, etc., will not be spilled, but will discharge over the head with the castings, at one point. For heavier castings, such as cylinder blocks, the overhead-trolley-type conveyer is frequently used, Fig. 36, the castings being hooked on the trolley conveyer at the shakeout and frequently carried a considerable distance for cooling purposes.

Flask-Return Conveyers. Flasks must also be returned from the shakeout to the molders, and, in the case of smaller work, either the roller-type conveyer, Fig. 37, or the overhead-trolley conveyer, Fig. 38, may be used.

Sand Reclamation. Sand-reclamation systems have been introduced quite recently, and at the present time are occupying a prominent place in the plans for foundry improvements. As the name implies, they are systems for reclaiming sand which has outlived its usefulness and by special cleaning methods is returned to the foundry. The finished product compares very favorably with new sand, at considerably less cost. It also eliminates one of the present foundry problems, i.e., what to do with the spent sand.

Miscellaneous Conveyers. In modern installations, there is an increasing use of mechanical sand-unloading equipment. When dry sand is used, coming into the plant in boxcars, the power shovel has frequent application, Figs. 39 and 40. This power shovel may discharge into the bucket elevator, which will elevate the sand to the raw-storage bins. When the sand comes in hopper-bottom cars, it is common to use a track hopper with apron feeder to the elevating unit.

Concrete silos, either of the stave or monolithic type, are coming into wide usage for the storing of foundry sands, Fig. 41.

Several types of skip hoists have been used successfully for charging the cupolas in iron foundries.

Some of the larger steel foundries have used car hauls for handling the charging buggies to and from the open-hearth furnaces.

Coke and limestone have been handled from railroad car through track hopper, feeder, elevator, and belt conveyers to bulk storage.

The handling of bonding materials covers a wide range, going

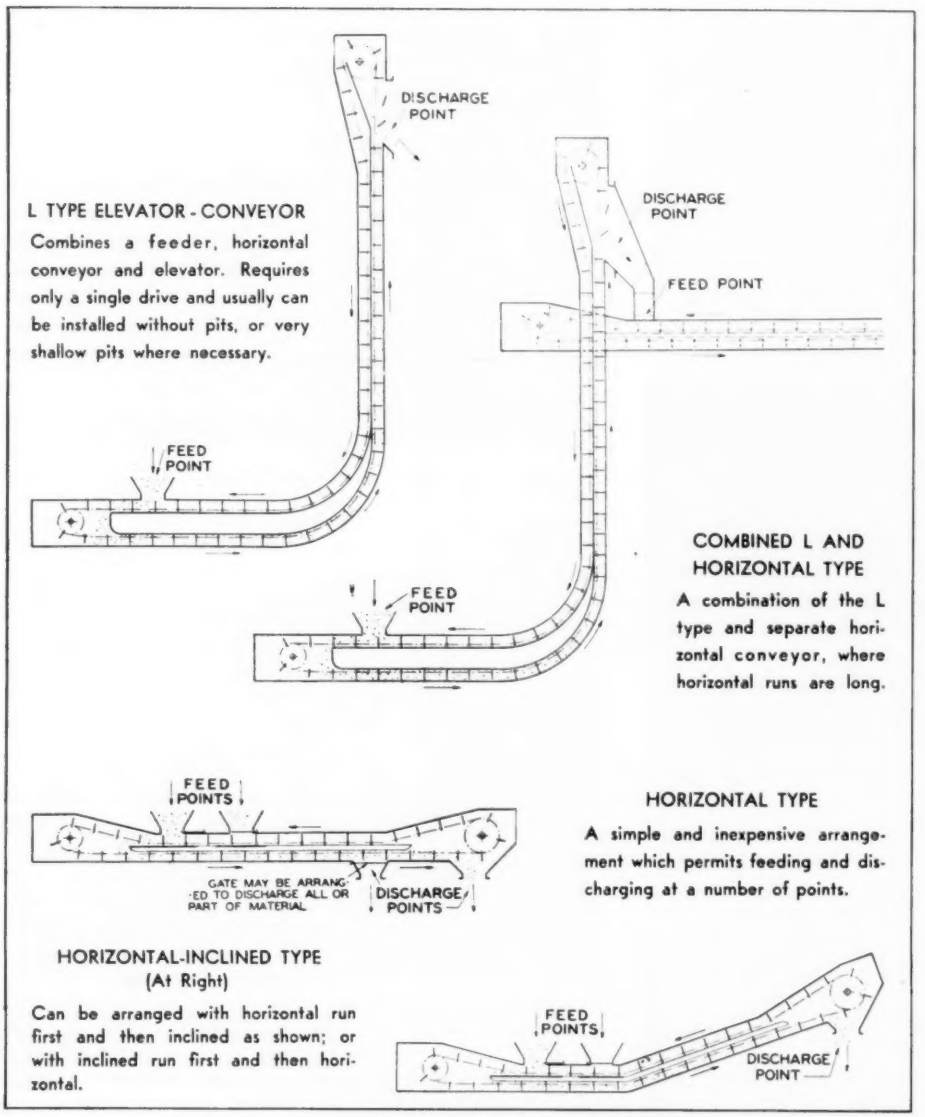


FIG. 42 BULK-HANDLING CONVEYERS FOR BONDING MATERIAL

from entirely manual operations to complete mechanization. They can be successfully handled from railroad cars through small track hoppers and bulk-handling conveyers, Fig. 42, to storage silos. From the silos, they are handled through the same type conveyer or screw conveyers to storage hoppers at the mixing stations. Small screw or electric-vibrating feeders can be

(*Continued at top of right-hand column*)

timed to feed out prearranged proportions direct to the mixers on continuous types, or into weigh hoppers on batching types of mixers.

Several types of pig-mold conveyers have been developed for the nonferrous foundries for pigging the virgin metal and also the remelt, Fig. 43.

CONCLUSION

In conclusion, it is quite evident that conveying equipment for the foundry, regardless of the type, has been developed to a high degree, with individual units designed for particular requirements. The proper layout and selection of equipment results in material reduction in the pound price of castings produced. This is accomplished in several ways, i.e., by increasing the output of the molders, reduction of labor, greatly increasing production with no increase in building space, reduction of scrap losses through better control of sand characteristics, and providing better working conditions for employees. Conditions caused by the war have influenced the installations in recent years. A manpower shortage has required that machinery be employed to the greatest possible degree. This has resulted in better working conditions, which have reacted favorably to the mechanized foundry. Foundries so equipped have a material advantage in the competitive market which will probably develop after the war.



FIG. 43 PIG-MOLD CONVEYER FOR MAGNESIUM, USING APRON CONVEYER TO ELEVATE PIGS TO BOXES

Discussion

W. S. Giele.[2] Materials handling in foundry operations is characterized, first, by its relative magnitude. Conditions of foundry operation vary so widely that exact data on any particular operation would have little application in other operations.

It may be said, however, that the total weight of material passing over the shakeout may easily be 20 times the net weight of castings finally shipped. In other words, the shipment of each 100 lb of castings may involve the handling of a ton of material at the shakeout, and every pound of that ton will have been handled several times before it gets to the shakeout.

Materials handling in foundry operations is further characterized by the abrasive nature of the materials handled and by the high temperatures frequently encountered.

The authors have referred to the application of high-pressure-type lubrication to belt-conveyer idlers in order that new lubricant may force out the old and the abrasive grit with it. Where feasible, it is believed to be desirable to go a step further by installing a centralized lubrication system, piped to the various bearings, in order to eliminate the introduction of the abrasive dirt that accumulates on the high-pressure fittings.

It is, of course, advantageous to keep speeds low and to operate with a minimum of lubrication. Ball and roller bearings in conveyer rolls often last longer when run dry than when lubricated, in foundry applications. Impregnated bushings of wood or of metal often give good service in the foundry. Powdered graphite carried into a bearing by some volatile liquid like kerosene gives good service in the wheel bearings of mold-oven cars and in car-hearth annealing furnaces. Where plain bearings are used it is often advantageous to use a wear sleeve on the shaft.

Materials handling in foundry operations is characterized also by wide load surges and by the frequent introduction of foreign material; and equipment must be designed with ample overload protection and surge capacity at every point.

The authors refer specifically to the use of shear-pin hubs on apron-feeder drives. The use of this device or its equivalent is recommended on all drives where an overload might cause serious damage to equipment. It is desirable, also, so to connect the drive that the motor stops automatically when the pin shears.

In any system including a number of units, each feeding the next in sequence, it is important to interlock the electrical controls so that the units will start or stop only in the proper sequence. Pilot lights, to indicate whether or not units not visible from the operating station are running, are desirable.

It is well, also, in a system of this sort to make each unit of a capacity slightly larger than the capacity of the unit which feeds it to make sure that there will be no flooding.

Bucket elevators should have provision to prevent backtracking in the event of power failure. Self-energizing friction brakes are often used. Positive ratchets are better. They may be of the silent type. Bucket elevators are not well adapted to handling facing sands. An inclined belt conveyer or a skip hoist is preferable for this service.

The authors make a good point in recommending storage bins of large capacity. While the 2-hr supply mentioned in the paper is adequate for continuous systems, as there stated, a much larger capacity is required to absorb the wide surges common in intermittent operation. A 10-hr supply is none too much for a foundry which pours and shakes out all its molds on a Saturday night and resumes operation on the following Monday morning.

[2] Walter Giele Company, Lebanon, Pa.

The authors develop some very good points on bin design. The writer would add only that, if molding sand did not have the property of bridging over an opening, it would never be possible to lift a cope. Vibrators will often relieve a bridging bin. Volumetric or gravimetric hoppers will deliver more nearly uniform batches if provided with vibrators to insure complete discharge at each cycle.

Vibrators are frequently of advantage on molders' hoppers, particularly on facing sand in steel foundries. Where facing hoppers are supplied with shovelout openings, it is possible to make them larger at the bottom than at the top to minimize the tendency to bridge.

Bins with downwardly converging sides opposite each other, particularly when in the shape of inverted cones or pyramids, have a marked tendency to bridge when used for prepared or other damp sand. A vertical partition will often reduce this tendency.

Roller conveyers work to good advantage wherever it is desirable to transfer loads from one conveyer system to another by means of cranes or tramrails. Roller-conveyer systems also work well with high-lift fork trucks. Roller-conveyer lines may be double-checked to segregate finished work from unfinished or to permit return of empty containers, as between a molding station and a pouring station.

Trolley conveyers are adaptable to intermittent operation on miscellaneous jobbing work as well as to continuous mass production.

Among their peculiar advantages are the following:

1 They can be made to travel in any path and will follow vertical as well as horizontal curves. They can be made to go around or over or under obstructions and to serve one or more floor levels.

2 They do not obstruct the floor.

3 The wheel bearings and track surfaces are above the dirt level.

4 They consume very little power.

5 They are endless and will return empty containers.

6 They will assemble components from a series of stations to a single assembly point or distribute to a series of stations. For illustration, they will collect cores from a series of core-making stations, bring them all to one spray station, and then distribute them to racks according to size.

7 They will carry work through process as through a spray booth, a dipping tank, or a drying oven.

8 They will accommodate any time interval between operations by changing length while keeping speed constant, as is done in castings-cooling conveyers.

Authors' Closure

Mr. Giele has brought out several interesting points in his discussion.

Regarding the use of centralized lubrication systems in connection with sand-handling machinery, while this may be desirable, it is hardly practical in the case of belt conveyers, elevators, etc., as this would involve piping the grease over very great distances. In many cases belt conveyers may be several hundred feet long.

We are very much interested in his comments on the running of ball and roller bearings dry. In foundry mold conveyers, which run at a very slow rate of speed, we have found that by running the roller bearings in the wheels dry their life is considerably lengthened. Only a small amount of light oil is added, to prevent the bearings from corroding.

On the subject of bucket elevators, back-stops are certainly desirable. We use the self-energized band brake type. Inclined belt conveyers are certainly preferable in handling facing sands, but in many instances bucket elevators are used successfully when

space limitations are such that inclined belts cannot be used.

Regarding the use of vibrators on storage bins, these are sometimes necessary to relieve bridging. However, if the opening or gate at the discharge point of the bin is not open, the vibrator may tend to pack the sand. The vibrators should be operated only when the discharge of the bin is open.

Air jets have been used in large storage bins for the purpose of relieving sticky and bridging action.

The Theory and Design of Electronic-Control Apparatus

By W. D. COCKRELL,[1] SCHENECTADY, N. Y.

Since the mechanical engineer is vitally concerned with control mechanisms involving electronics in some form, the author believes the explanation of theory involved and design of electronic apparatus given in this paper should be helpful. The almost infinitely fast and inertialess electronic tube can supplement mechanical control to produce many results hitherto considered impossible. After outlining the fundamental conceptions of the electronic tube, describing the types of tubes used, and explaining something of the operation of individual control circuits, the author indicates practical applications of electronics to standard control circuits. Examples of such controls are the photoelectric relay, electronic timer, motor control, resistance welding, photoelectric register control, and others.

Introduction

THE mechanical engineer has a larger stake in electronic control, particularly in photoelectric control, than many realize. In this new tool he has a means of supplementing his own mechanical operations in many ways. The almost infinitely fast and inertialess electronic tubes can supplement his mechanical control to produce many results hitherto considered impossible. The beam of light, or the small voltage, or change in magnetic or electrostatic field, produced by mechanical or chemical means, may act as a lever, pushrod, cam follower, or trip latch. On the other hand, since most electronic control must eventually end in mechanical motion, the electronic engineer must depend upon the mechanical engineer for assistance in solving problems of vibration, high-speed operation, and hunting or stabilization problems. No complete apparatus can be considered satisfactory unless it is correct both electronically and mechanically.

Electronics

Electronics has been defined as the art of working with an electric charge or current in the form of a stream of electrons or ions, free from the restraint of conventional conductors. As such, electronics includes the high-frequency phenomena of radio and television. However, in this paper we will simplify considerably the theoretical background to be covered. The theory required for industrial electronics, for instance, compares with that required for short-wave radio as the gravitational theory of Isaac Newton compares with that of Dr. Einstein.

Speed of Electrons and Electronic Radiation. It is sometimes difficult for one accustomed to dealing with mechanical things to realize the terrific speed at which electronic equipment can function. Airplane designers worry when the speed of their plane approaches that of sound, about 1100 fps. The propagation of electronic radiation is that of light, 186,000 mps. In a vacuum, an electron is accelerated by a difference of potential of 1 volt to a speed of 386 mps. Compare this with the pull of gravity which produces a speed of only 32 fps in the first second.

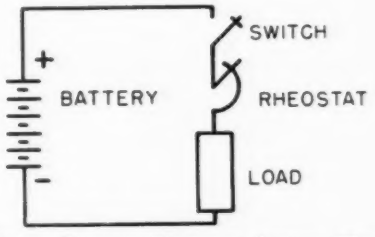


Fig. 1 A Direct-Current Electric Circuit With Rheostat Control
(Conventional current flow is clockwise; electron flow is counterclockwise.)

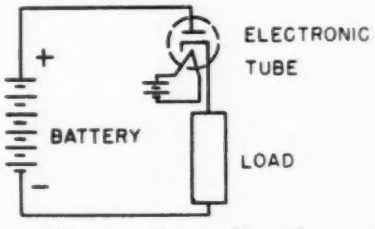


Fig. 2 A Direct-Current Circuit With Electron-Tube Control
(Electron flow is counterclockwise.)

Nature of the Electric Current. Modern electrical theory considers the current as a flow of electrons through the circuit. These electrons, the ultimate particles of negative electricity, are drawn to a potential more positive, just as a ball rolls down hill under the pull of gravity. To control a current is to control this flow of electrons. Those materials which permit a free flow of electrons are called "conductors," and those which resist the electron movement are called "insulators" or "dielectrics."

Control of Electric Current. The usual method of controlling an electric current is to change the resistance of a part of the circuit, or to replace part of the conducting path by an insulator, such as by opening a switch, Fig. 1. Another way is to control the electron flow by means requiring no mechanical movement; this is the electronic way, Fig. 2.

The Electronic Tube. The electronic switch consists of a device which may be inserted in the conductor path, and through which we may control the flow of electrons at will. Fundamentally it must consist of two parts, i.e., a source of electrons or emitter, called the "cathode," and an element to receive the electrons, called an "anode." To permit the best movement of the electrons, these elements are enclosed in an evacuated envelope.

Types of Emission. Electrons may be made available at the surface of the cathode in one of three ways. The electrons may be drawn out of the cold cathode by a positive charge placed very close to the surface. This method of obtaining electrons is used in cold-cathode voltage-regulator tubes and in ignitrons. A second method is the application of heat to special cathode

---

[1] Electronics Application Engineer, General Electric Company.

Contributed by the Special Design Committee and presented at the Annual Meeting, New York, N. Y., Nov. 29–Dec. 3, 1943, of The American Society of Mechanical Engineers.

Note: Statements and opinions advanced in papers are to be understood as individual expressions of their authors and not those of the Society.



FIG. 3 METHODS OF OBTAINING ELECTRON EMISSION FROM A CATHODE



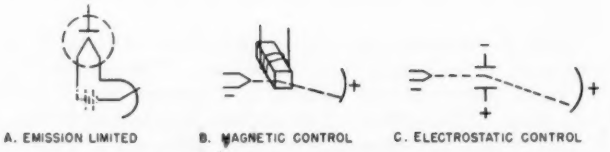


FIG. 4 METHODS OF CONTROL OF ELECTRON STREAM

materials so that the electrons are literally boiled free from the cathode surface. This is the customary method. Finally, some cathode surfaces are sensitive to the action of light and liberate electrons when struck by light of various colors. This includes both visible light, that beyond the red (the infrared), and the waves too short to be seen by the human eye (the ultraviolet). By these three methods electrons are liberated, which may be drawn by a positive potential in a steady stream of negative electric current to the anode, Fig. 3.

Control of Electron Stream. The control of the electron stream may be accomplished in three different ways, or by a combination of them. The most obvious way is to change the amount of energy for liberating the electrons. Thus if we remove the light from a photoelectric surface, or if we decrease or stop the heat from the thermionic cathode, we will reduce or stop the number of electrons available for the stream. These methods are shown in Fig. 4.

Since the stream of electrons represents an electric current, it may be acted upon by a magnetic field just as the current in a motor armature reacts to the magnetic field of the motor. This magnetic control of the stream has been used to a certain extent for television picture tubes, for the generation of high-frequency oscillations, and for a few other purposes, but has not been utilized to the extent to which the third form of control has been exploited.

The third, and most important, form of control is that of electrostatic deflection. This means simply that, if we insert a third element in the tube between the anode and cathode, and if this element is made negative, it will repel or deflect the electron stream away from it, and if positive, will assist in accelerating the electrons. This control element may consist simply of a plate, which will bend the stream of electrons toward or away from itself and thus change the point at which they strike the anode. This has a limited use in the cathode-ray oscillograph and in indicator tubes. A much more important effect, however, is obained by making this element a grid, or series of parallel wires, through which the electron stream must pass on its way to the anode. If this grid is made sufficiently negative, the electron stream is throttled down or even stopped entirely, and no current can flow between the cathode and anode, Fig. 5. A very important item to be noted in this form of control is that the grid, being negative, attracts no electrons, and hence there is no current flowing to the grid. Electric power consists of the product of current and voltage. Since there is no current there is, theoretically, no work done here so that the electron stream can be controlled with the expenditure of a minimum of power.

Sometimes more than one grid is used in a tube, Fig. 6. If positive with respect to the cathode, these other grids will assist in speeding up the electrons past the first grid. If negative, they will reduce or stop the flow of electrons in the same manner as a series of valves in a pipe.

We have now done two things. We have reduced the electric current to a stream of pure electrons, and we have found means

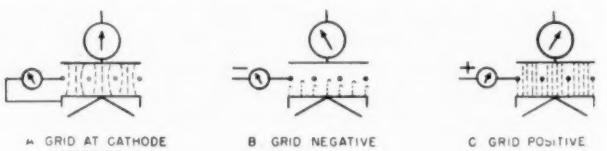


FIG. 5 GRID CONTROL OF ELECTRON STREAM

(The grid is placed in the electron stream between the cathode and anode. When the grid is at the same potential as the cathode, it affects the flow of electrons very little. When the grid is made more negative than the cathode, it repulses the electrons, and thus decreases the flow from cathode to anode. When the grid is positive with respect to the cathode, it increases the flow of electrons, but also attracts a flow of electrons to it.)

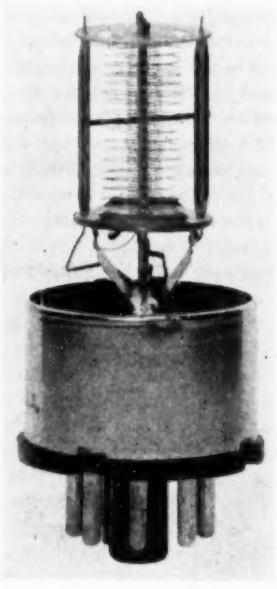


FIG. 6 A PENTODE, 3-GRID, AMPLIFIER VACUUM TUBE WITH GLASS ENVELOPE REMOVED

to control this stream with a minimum amount of power. Finally, since the speed of the electrons between cathode and anode is so great, we can, by changing potential of the grid fast enough, start, stop, and control the flow of electrons at a much more rapid rate than would ever be required for use with mechanical devices.

USES OF HIGH-VACUUM ELECTRON TUBES

We have described the electron tube as a valve, but since we have made only one of the elements capable of emitting the electrons, current can flow in but one direction, so it is a one-way valve. Some functions make use of the one-way effect, others use the throttling effect, while a few use both effects.

Rectifiers. The one-way action may be used like a mechanical pawl-and-ratchet action or, if preferable, like a crank-and-piston action, to change the alternating current normally supplied by the power companies to direct current which is more useful for such things as operating variable-speed motors, charging batteries, and for many chemical processes. The usual alternating voltage supplied to a transformer reverses its potential 120 times per sec. If we connect our two-element electron tube in such a circuit, it will permit the electrons to flow only when the anode potential is positive. This will permit the current to flow through the load in only one direction; but, since the power supply is reversed half the time, this load current will be intermittent. This is similar in action to a one-cylinder gasoline engine and, like the gasoline engine, a large electrical flywheel is necessary to provide continuous power to the load, Fig. 7. To secure a more even flow of power, we may use a reverse transformer winding to supply a positive potential to a second rectifier during the half-cycle that the first is inoperative, Fig. 8. This, of course, provides better direct-current output with a smaller electrical flywheel. Finally, by using a number of tubes, 3, 6, or 12, and a multiphase alternating-current supply, we may produce a smooth direct-current power, just as a multicylinder gasoline engine produces a smooth flow of power with a minimum-sized flywheel, Fig. 9.

The Electronic Amplifier. A second most important use of electronic tubes is to amplify, or step up, a weak input signal to a strong output signal. This input signal must be applied to the

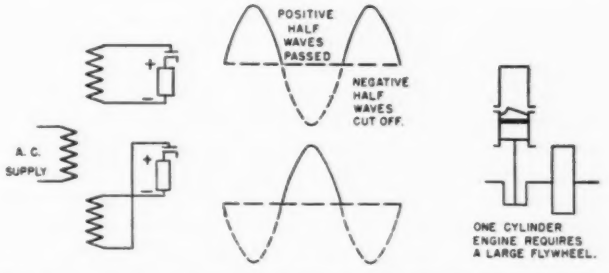


FIG. 7 HALF-WAVE RECTIFIERS COMPARED WITH A ONE-CYLINDER GASOLINE ENGINE
(The cathode heater circuit has been omitted for simplicity. Curves are graphs of power output against time.)



FIG. 8 A FULL-WAVE OR BIPHASE, HALF-WAVE RECTIFIER
(It will be noted that this is a combination of the two half-wave rectifiers of Fig. 7. Curves are graphs of power output against time.)

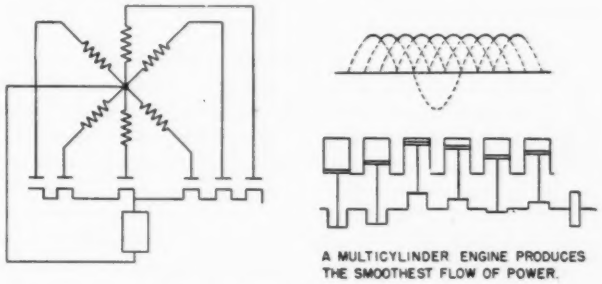


FIG. 9 A MULTIPHASE RECTIFIER PRODUCES A SMOOTH DIRECT-CURRENT OUTPUT

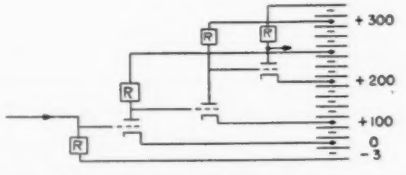


FIG. 10 A 3-STAGE VACUUM-TUBE AMPLIFIER CIRCUIT
(The current through each tube flows through the resistor R to produce a potential, which is applied to the grid of the next tube. The power is taken from a battery of 303 v, off which are tapped the required potentials for the individual tubes. Such an amplifier can step up the incoming signal many thousand times.)

grid of the amplifier tube as a voltage or potential change. If the weak signal is in the form of a small current, it must be transformed to a voltage by forcing the current through a high resistance to obtain a large potential difference across it. It is similar to obtaining a high-pressure reading from a small flow of water by forcing the water through a small pipe. This resistance may be many millions of ohms, so that even should the input signal consist of currents expressed in millionths, or even billionths, of an ampere, the voltage produced will be usable. It will be remembered that no power was required on the grid of the tube, but some power is required in this input resistor.

The change in potential on the tube grid will cause a change

in the current or electron flow between cathode and anode. If, we place in series with the anode another resistor, or impedance, through which the tube current must be forced, the potential change in this impedance will be much greater than that of the grid potential change. If this, in turn, is transferred to the grid of a second tube, and its anode current is again passed through an impedance to control the grid of a third tube, it is evident that immense amplification or magnification of the first potential change will be available at the anode of this final tube, Fig. 10. Most amplifier circuits transfer their signal between an anode and following grid through a capacitor or transformer, but the principle remains the same.

Let us pause to note that no power has been produced by the tubes. They have simply acted as valves to release a larger amount of power from some external power source, such as a battery which forces current through the tubes and their connected impedance.

Theoretically we can amplify signals thousands of times in a single tube, and, in standard industrial applications, a voltage amplification of hundreds of times, and power amplification between input and output of millions of times, is quite common.

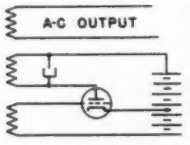


FIG. 11 A VACUUM-TUBE OSCILLATOR TO CONVERT DIRECT-CURRENT POWER TO ALTERNATING CURRENT

(The transformer at the left feeds the alternating-current power to the load and supplies a small amount of alternating-current power to control the electron-tube action. This is similar to the action of the valves and mechanism of a steam engine, which takes the constant pressure from the boiler and from it produces the necessary reciprocating action.)

Oscillators. Since the power required at the grid of the tube is only a very small part of the output-controlled power, we may take a very small amount of this output power and feed it back to control the grid at the proper frequency thus obtaining a controlled alternating-current output from the direct current supplied to the tube, Fig. 11.

Rotating equipment can generate frequencies up to 5000 or 10,000 cycles per sec. Because of the immense speed of the electrons, electronic equipment can generate frequencies up to many millions of cycles per second.

Oscillator tubes provide the type of power necessary for radio broadcasting, dielectric heating of plastics, and induction heating of small pieces of metal. However, it must be remembered that to control, by the use of high-vacuum tubes, any large amount of power, such as needed for industrial purposes, is extremely expensive, so that most electronic control of industrial power is ultimately obtained from the gas-filled tube which will now be discussed.

GAS-FILLED TUBES

When in a simple two-element vacuum tube, the electrons are being drawn from cathode to anode, an interesting thing happens. Electrons move across the space because they are negative charges, being attracted by the positive anode. However, since they themselves are negative, they will tend to shield all electrons between themselves and the cathode from the action of the anode in the same manner that the negative grid does. This effect is so great that, in order to obtain the 1 amp current necessary to light a 100-w lamp, it might be necessary to apply 1000 v between anode and cathode. This means that high-vacuum tubes are most useful at low currents or with high-voltage loads.

However, if we introduce into our vacuum-tube envelope a small amount of gas, about 0.0001 of atmospheric pressure, a remarkable change in this space charge takes place. The gas may be one of the inert gases, such as Argon or Xenon, or the mercury vapor above a small drop of mercury at normal room temperature.

Ionization. If the positive potential on the anode is less than 8 v, the electrons leaving the cathode bump into the many gas molecules on its path to the anode so that their progress is slowed down very much and the current flowing is very small. However, somewhere between 8 and 12 v, depending upon the type of gas and the pressure, some electrons attain sufficient velocity so that, in striking these gas atoms, they knock an electron or two from them. Then, for each original electron, we have two free electrons moving toward the anode, and the atom, losing an electron, becomes a positive ion which drifts toward the cathode. The glancing electron may hit other atoms and knock out other electrons on its erratic course to the anode, until finally almost the whole area between cathode and anode, no matter what its shape or length, is filled with flying electrons and positive ions. Of course many atoms recombine with electrons giving up their energy in the form of the familiar glow seen in gas-filled tubes. Yet, on the whole, this so-called "plasma" is composed of approximately equal numbers of positive ions and negative electrons. Electrons are always arriving at this plasma from the cathode and are leaving at the anodes, but the plasma maintains always a potential of about 10 or 15 v positive with respect to the cathode for, if more electrons should leave than arrive, the average potential of the plasma will rise, accelerating the electrons to a higher speed and thus knocking more electrons from the neutral atoms within the plasma. If more electrons arrive than leave, the potential of the plasma will be lowered and the average potential of the arriving electrons from the cathode will be less. Thus, no matter what the current from the cathode, even though it be thousands of amperes, the potential of the plasma will change very little. Fig. 12 gives an idea of the potential gradient or voltage distribution in a vacuum tube and in a gas-filled tube.

Cathode Abuse. It must be noted that this low voltage potential of the anode for high current depends upon having a sufficient number of electrons available at the cathode for the ionization. If for any reason there are not sufficient electrons available, the plasma potential may rise above 22 v. At about this potential, the heavy positive ions are drawn toward the cathode with sufficient velocity to damage the cathode surface, and may even chip off flakes of the active material, ruining the surface within a very short time. Thus it will be understood why it is so necessary that hot-cathode tubes be permitted to warm up to obtain an efficient emitting temperature before the anode circuit is closed.

Mercury-Pool Rectifier and the Ignitron. In the mercury-pool or tank rectifier, and in the ignitron, the cathode consists of a pool of mercury. Once ionization has taken place in these tubes, the positive ion, drifting near the cathode, draws out the electron by the potential gradient effect. In this manner, a plentiful supply of electrons is assured at a potential drop between 15 and 20 v. These, then, are the tubes which are used for the high currents required for resistance welding, railroad electrification,

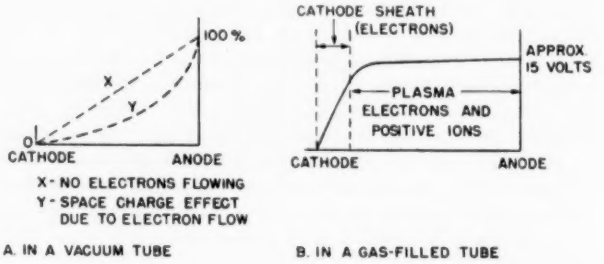


FIG. 12 ELECTRICAL POTENTIAL GRADIENT BETWEEN THE CATHODE AND ANODE OF A VACUUM TUBE AND A GAS-FILLED TUBE

(In the vacuum tube, the anode potential may be many hundred volts. In the gas-filled tube it should never be more than 20 v.)

and electrochemical processes. Fig. 13 shows the construction of an ignitron.

Before the ionization action can take place, however, the plasma must be established. In the tank rectifier, this is done

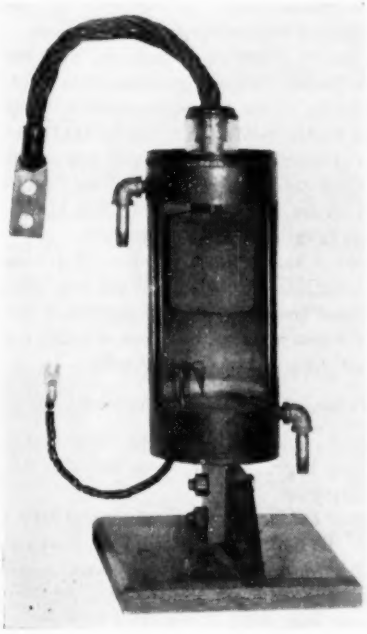
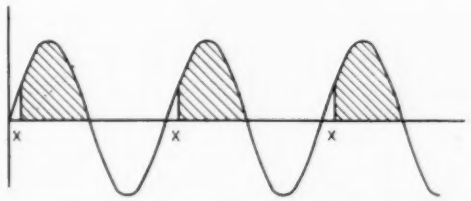


FIG. 13 CUTAWAY VIEW OF AN IGNITRON

(Normally there is a pool of mercury in the bottom of the tube, into which the igniter, shown at lower left, projects. The anode in the top of the tube is a large block of graphite, which, with its heavy stranded lead projecting from the top of the tube, is designed for the heavy current conducted by this tube. The cathode connection is the copper lug by which the tube is mounted. Inlet and outlet pipes are shown for the water, which circulates within the hollow shell of the tube for cooling.)

by mechanical means, and in the ignitron by the action of a small piece of crystal dipping into the mercury, which is called an igniter. For most precise applications the igniter is controlled by a hot-cathode thyratron.



a. THYRATRON (OR IGNITRON) STARTS CONDUCTION AT X, EARLY IN THE POSITIVE HALF CYCLE. THE AVERAGE CURRENT, SHOWN IN THE SHADED AREAS, IS ALMOST MAXIMUM.



b. THYRATRON (OR IGNITRON) STARTS CONDUCTION AT Y, LATE IN THE CYCLE. THE AVERAGE CURRENT, SHOWN IN THE SHADED AREAS, IS LOW

FIG. 13(a) OPERATION OF A THYRATRON

(The average current of a thyratron or ignitron is changed by retarding the time of beginning conduction in each cycle. These tubes may be connected in multiphase circuits also to permit a smoother flow of output power.)

Gas-Filled Tubes With Grids. Since the gas filling in the tube makes possible its use with low losses when conducting high currents, it is the one which we must use for the usual applications requiring power, such as driving motors or operating a solenoid. We wish to control these gas-filled tubes also by some form of grid, as in the case of the high-vacuum tubes. Unfortunately, however, the control cannot be attained in the same manner so that a slightly different method of control must be obtained from the grids in the gas-filled tubes.

The Hot-Cathode Thyratron. It should be fairly evident that the conventional grid, inserted in the gas-filled tube in the plasma between cathode and anode, would have little effect on the erratic and random motion of the electrons and ions filling the space. It is true that, when the grid is made quite negative before a positive potential is applied to the anode, it may keep

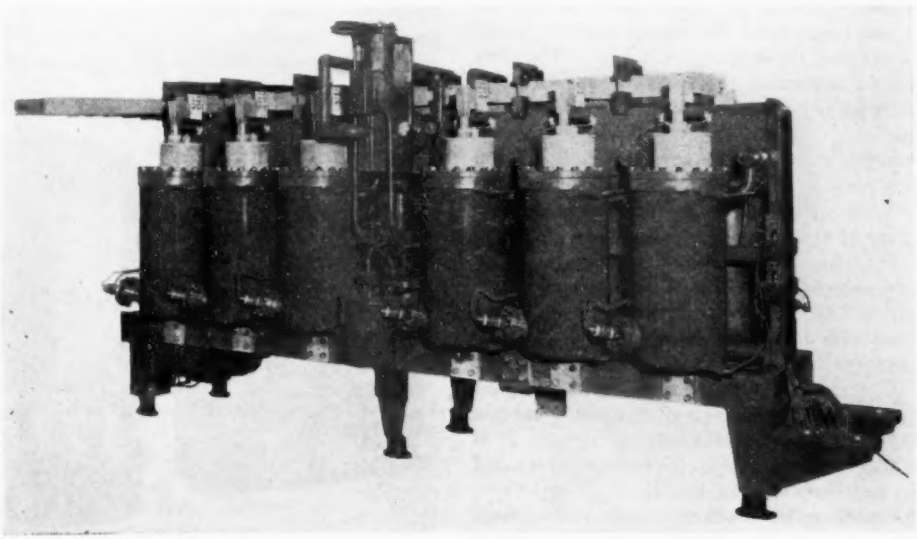


FIG. 14 A LARGE MULTIPHASE IGNITRON RECTIFIER

(Six large ignitrons are shown. They are connected in a circuit similar to that of Fig. 9, to convert alternating current into the direct current required in a large aluminum plant.)

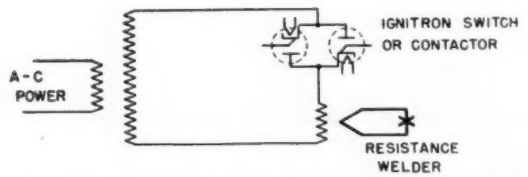


FIG. 15 INVERSE-PARALLEL IGNITRON CONNECTION, ACTING AS AN ALTERNATING-CURRENT SWITCH TO CONTROL A LOAD SUCH AS A RESISTANCE WELDER

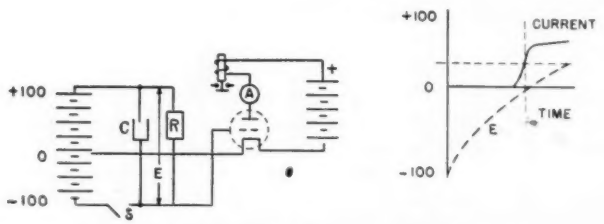


FIG. 16 ELEMENTARY ELECTRONIC-TIMER CIRCUIT

(The battery at the left charges the capicator C to a potential of 200 v. The grid of the electron tube is connected to the negative end of the capacitor, and hence is 100 v negative with respect to its cathode. Therefore no electron flow takes place in the tube. When the starting switch S is opened, the capacitor charge leaks off through the resistor R, and the grid potential gradually rises until the grid approaches the cathode potential, and electrons begin to flow in the tube, sufficient to pick up the relay and close the control circuit.)

all electrons from flowing from the cathode and thus prevent the formation of the plasma. But once the plasma has formed, the grid is powerless to stop the electron flow.

Since the grids can only prevent the conduction through the thyratron, but cannot stop it once it has begun, a question may arise as to the usefulness of this type of tube. The answer lies in its use on alternating-current power. It will be remembered from the discussion on rectifiers that, when alternating-current power is applied to the tubes, the anodes become positive one half of the time and negative for the other half. During the time that the anode is negative, no electrons will flow, and the positive ions may recombine with the electrons, or deionize, thus permitting the grid to regain control. If the grid is negative when the next half cycle begins, the electron flow cannot begin until the grid becomes positive, and thus it can determine the point in the positive half cycle where conduction starts. By retarding the grid firing angle to the desired point within this positive half cycle, one may control the *average* current passed by the thyratron and, thus, the output to the load. The same reasoning may be used concerning the action of the igniter in the ignitron, to decrease the maximum current which may be passed by that tube.

Thyratron and Ignitron Circuit. The thyratron and ignitron may be used in the rectifier circuits discussed previously, but with much higher efficiency for larger loads. In fact, multiphase ignitron rectifiers have become the basic means of obtaining direct current from alternating current in many industries. Thyratrons, so connected, supply variable power for the control of direct-current motors and similar uses, Fig. 14.

Although electronic tubes are inherently rectifiers, two of them may be connected in the "inverse-parallel" circuit, to permit passing both halves of the alternating-current wave and thus become an effective alternating-current switch which combines both high-speed switching action and throttling action. It is this type of circuit that is used to supply the precisely measured amount of power for resistance welding, Fig. 15.

Miscellaneous Control Circuits. Both thyratrons and vacuum tubes may be used in connection with the more conventional electrical components, such as capacitors and inductances, to produce a variety of functions.

If the energy is stored in a capacitor and then is permitted to be dissipated through a resistor, the capacitor potential will be reduced at a well-known and easily calculable rate. If this potential is applied to the grid of an electron tube, the anode current will be varied, or the thyratron grid will reach the firing potential in a definite time. In this way, an accurate and unvarying timing relay is developed, Fig. 16.

Combinations of resistors, capacitors, and inductances are used to obtain the grid and anode phase relations required for the proper functioning of the thyratron control circuit. Electronic tubes are used for the excitation of the fields of electric generators in many jobs in both the industrial and military fields. Thyratrons supply the direct-current power for the large saturable reactors such as used for the Radio City Music Hall lighting and for critical electric-furnace applications.

Needless to say these are only a few of the functions of the tubes and the methods by which they are controlled. There are many others, and the number will continue to grow, as long as man exercises ingenuity and the types of tubes are improved or modified to suit the new uses and demands.

STANDARD ELECTRONIC-CONTROL CIRCUITS

Now that we have the tubes and the individual control circuits available, let us begin to put them together to obtain some practical applications.

A Photoelectric Relay. Suppose we start with a simple photoelectric relay. To make this, we will take first a simple rectifier to obtain direct current from the alternating-current supply (which is usually the only kind available). At the output end of the rectifier, we will place a capacitor to store up energy between the positive pulses of the alternating-current circuit, and across this output we will also place a series of resistors which will act as a voltage divider to permit obtaining both anode and grid potential from the one direct-current source.

Next, we will add the necessary phototube to convert the change in light into a change in electric current. The drop across the phototube resistor is then applied to the grid of an amplifier tube, in order to step up the signal sufficiently to operate a small contactor placed in the amplifier-anode circuit.

As a finishing touch, we may add a rheostat so that we may vary the amount of direct current which is normally applied to the grid, in order to select the amount of light which must fall on the phototube before the grid is made sufficiently less negative to operate the contactor. As further refinements, we may add a very small capacitor between grid and plate of the amplifier tube

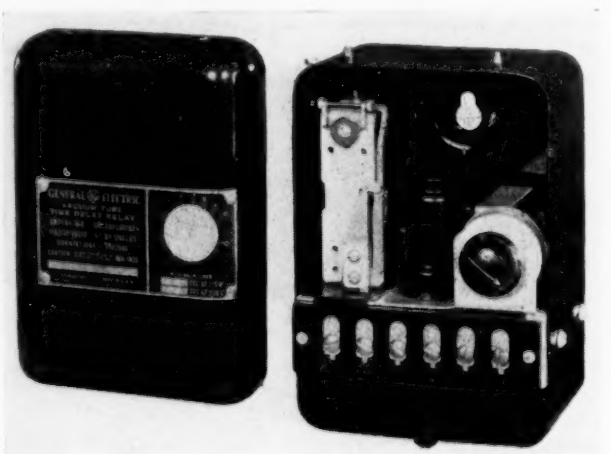


FIG. 17 COMMERCIAL FORM OF ELECTRONIC TIMER

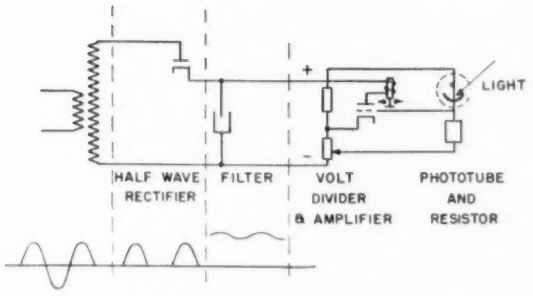


FIG. 18 PHOTOELECTRIC-RELAY CIRCUIT

(This combines the half-wave rectifier of Fig. 7 and a capacitor filter which acts as a flywheel to produce a steady direct current. Next, a tapped resistor voltage divider provides the necessary potential for the electronic amplifier tube and the phototube. When the phototube is dark, no electrons flow through it or its resistor, and the electron-tube grid is far negative, so that no electrons flow in the amplifier tube. When light strikes the phototube, the phototube electrons, forced through the phototube resistor, raise the grid of the amplifier tube sufficiently to permit it to conduct and pick up its relay.)

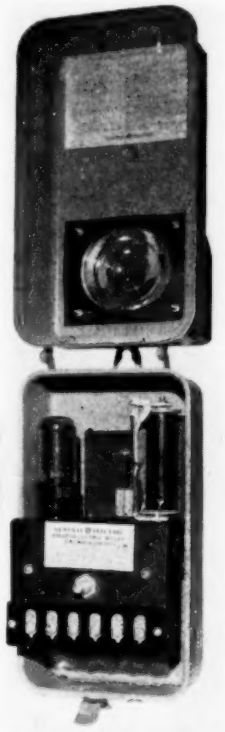


FIG. 19 COMMERCIAL PHOTOELECTRIC RELAY USING CIRCUIT OF FIG. 18; COVER THROWN UP

to prevent operation on slight light flickers and another capacitor between the direct-current potential and ground to prevent action due to slight changes in the alternating-current power supply.

The circuit is shown in Fig. 18, and the relay in Fig. 19. Hundreds of these relays have been sold and are now doing all sorts of useful jobs, such as counting people or autos, packages and cabbages, and cartons freshly painted.

An Electronic Timer. In a similar manner, we may build up an electronic timer by combining the capacitor-resistor fundamental timing circuit with an amplifier and a contactor operated by the amplifier, Fig. 17.

Tube Control of Motors. A motor control, Fig. 20, which will regulate the speed of the motor quite accurately may be made by a pair of rectifiers, one or both of which may be controllable, to supply the motor armature and field of a direct-current motor. Then we may obtain an indication of the motor speed, either by connecting a tachometer generator to it which will produce a voltage proportional to speed, or take the back-induced voltage from the motor. This is compared to a reference voltage, and the difference is amplified and applied to the control of the armature or field to hold the motor speed constant. If we wish, we can add other circuits which operate from the motor current to limit this current to a safe value for motor and tube in spite of the demand for speed. A control can even be added to compensate for the resistance of the motor armature to obtain a flat compounding which is superior to that which can be obtained from a direct-current compound motor.

Resistance Welding. The electronic control of resistance welding has played a major part in the fabrication of equipment used to fight this war. The principle of resistance welding is old, that of squeezing two pieces of metal together and then passing current through the resistance of their junction sufficient to melt the material and thus cause it to fuse together. This method of fabrication is extremely fast and, in some cases, the cost is only one tenth that of riveting. However, satisfactory welding of such materials as stainless steel, which must be melted at the junction point, but must heat and cool through the critical temperature quickly to prevent loss of its stainless properties, and aluminum, which is a very good conductor of both heat and electricity and is so soft that a little too much heat will quickly ruin the weld, is made possible only by the precise timing and heat control of the electronic device. To obtain the most effective control, we start with the electronic timer, Fig. 21 (*a*), or if this is to be a seam welder which produces a series of pulses rather than a single hot spot, with two timers, one to control the heating period and the other the cooling period between the heat pulses. We may then add a heat control which determines the phase angle at which the control thryratron and ignitron will fire to produce the desired amount of heat at each pulse, Fig. 21 (*b*). Finally, we have the large ignitrons themselves which pass

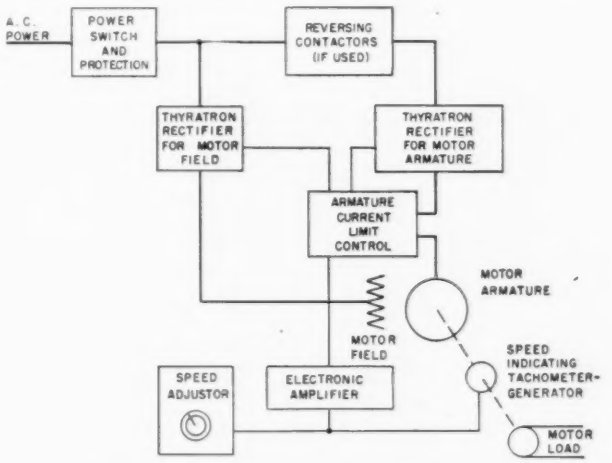


FIG. 20 ELECTRONIC MOTOR CONTROL

(The indication of motor speed, taken from the tachometer-generator, is compared with the speed-adjustment setting, and the resulting signal is amplified to control the power applied to the armature and field of the motor. The current-limit feature prevents overloading motor or tubes. Speeds constant to 1 per cent from no load to full load over a speed range of better than 20 to 1 are possible.)

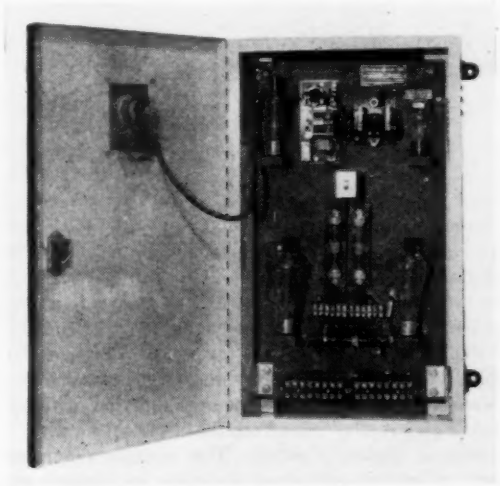


FIG. 21(*a*) ELECTRONIC TIMER CONTROLS DURATION OF HEAT PULSE, FOR RESISTANCE WELDER

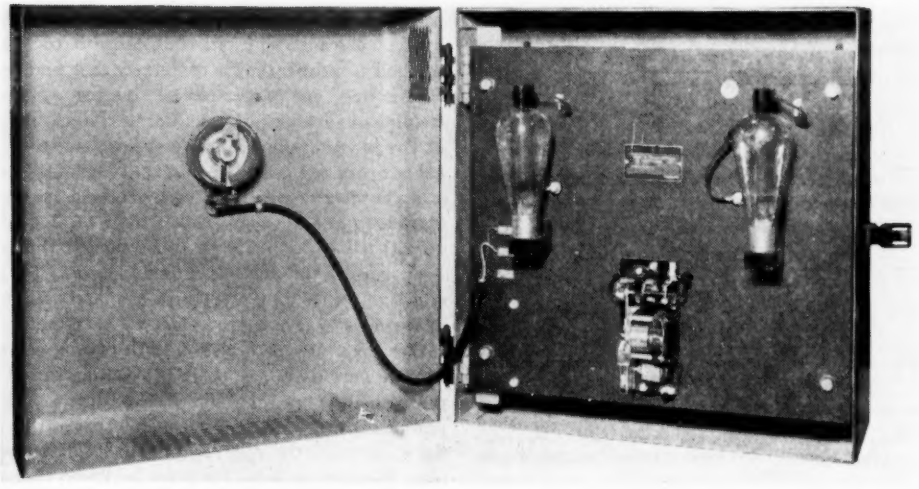


FIG. 21(*b*) THYRATRON GRID-PHASE CONTROL PANEL TO CONTROL RATE OF HEATING (WATTS) DURING HEAT CYCLE OF RESISTANCE WELDER

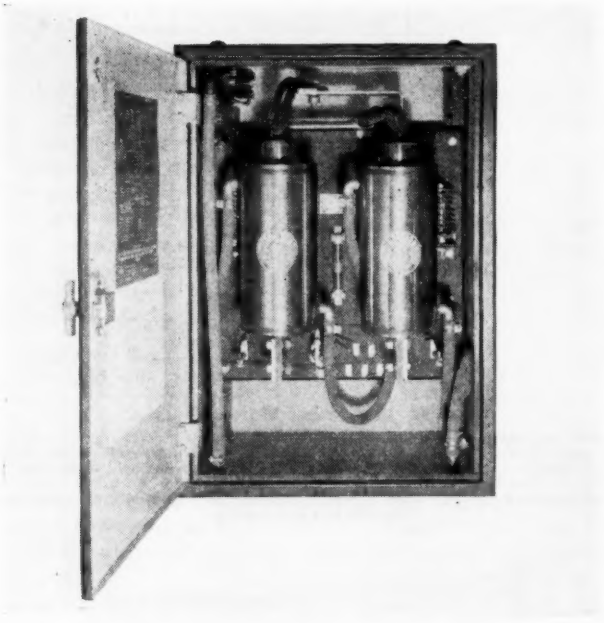


FIG. 21(*c*) IGNITRON CONTACTOR SWITCHES ON AND OFF RESISTANCE WELDER POWER

(This is the type of panel used in the circuit of Fig. 15.)

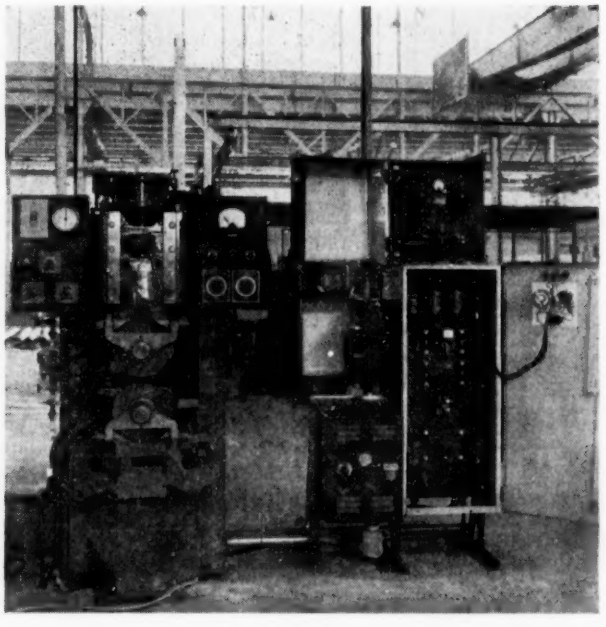


FIG. 21(*d*) THIS EQUIPMENT, SHOWN IN AN ACTUAL INSTALLATION, IS THE MORE USUAL FORM OF PANEL COMBINING FUNCTIONS OF THE THREE PANELS SHOWN IN FIGS. 21(*a*, *b*, *c*)

the actual power current required by the welder, Fig. 21 (*c*). These large tubes are capable of handling tens of thousands of amperes for the short time required to make the weld. They are cooled by a flow of water which circulates in their double shell.

Other types of welders use rectifiers to store up the energy in a large bank of capacitors, or in an inductance, and then discharge this energy suddenly into the weld. They are thus able to supply a large amount of energy in a very short time by storing up this energy from the power line over a period of time, rather than demanding it all at once from the electrical supply.

Photoelectric Register Control. The circuits described have been more or less self-contained electronic equipments operating a particular device. In the case of the photoelectric register control, that is, the registering of printing with some mechanical operation such as cutting or folding the printed paper, there is allowed much more freedom of engineering in the over-all application. For instance, for the simplest type, say that of a candy-wrapping machine where the paper moves very slowly and may be stopped each time that a bar is to be wrapped, an index mark may be printed along the edge of the sheet so that, when it intercepts the light to the phototube, either by transmitted or reflected light, the paper will be stopped in order that the required operation may take place before the paper is permitted to move forward again. Fig. 22 shows a typical wrapping machine.

On the other hand, when the paper moves somewhat more rapidly, it may be drawn forward slightly too much, each time, and then, when the register mark reaches the limit of the permitted tolerance (as determined by the position of a

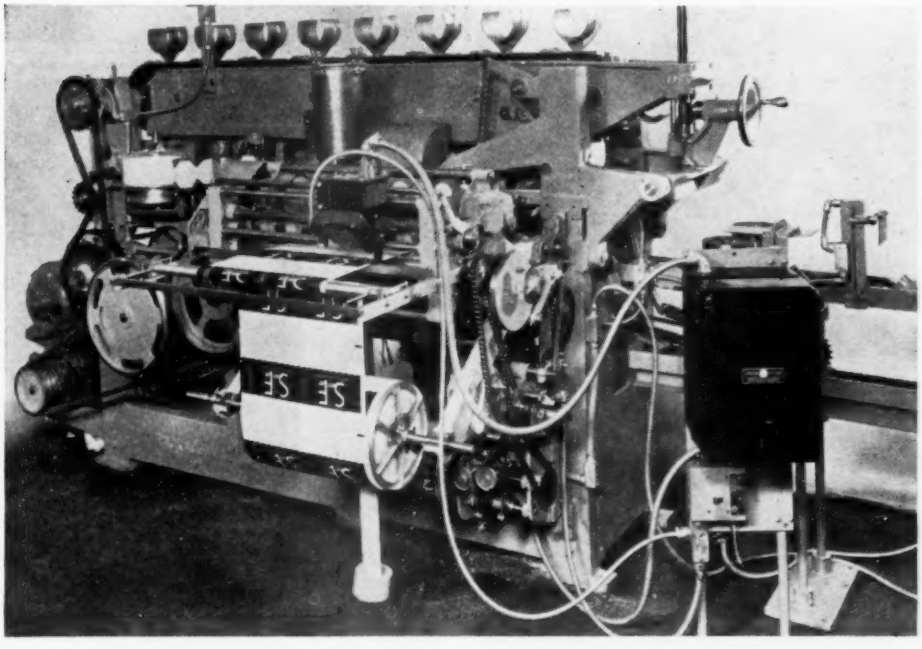


FIG. 22 PHOTOELECTRIC REGISTER CONTROL OF LABEL POSITION ON WRAPPING MACHINE

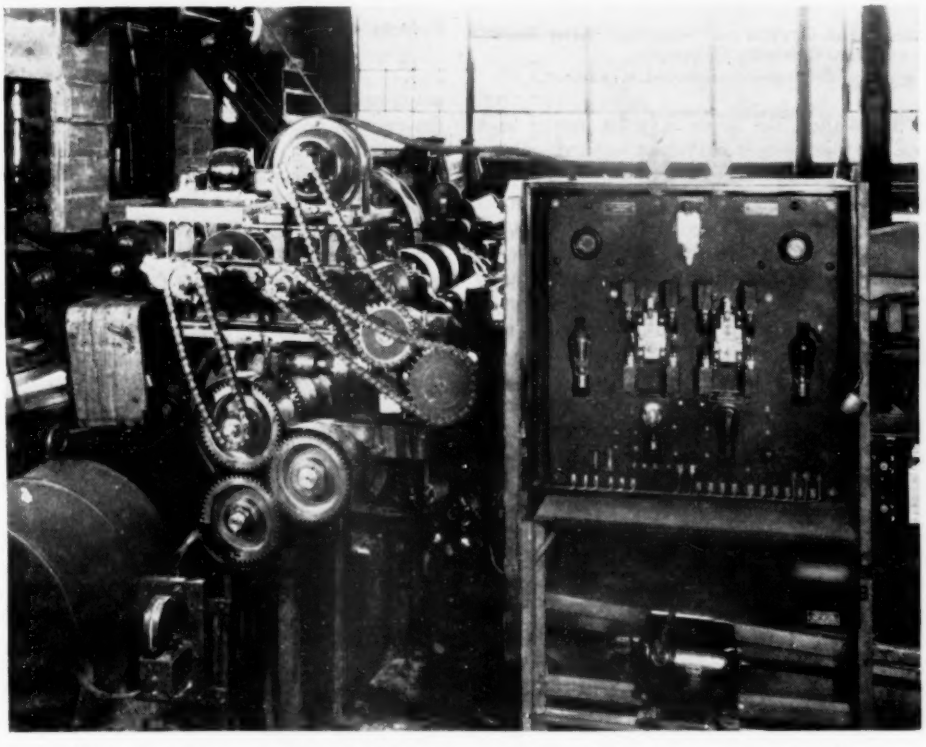


FIG. 23 ONE OF THE FIRST PHOTOELECTRIC REGISTER-CONTROL EQUIPMENTS, 1932
(Note mass of chain and gearing.)

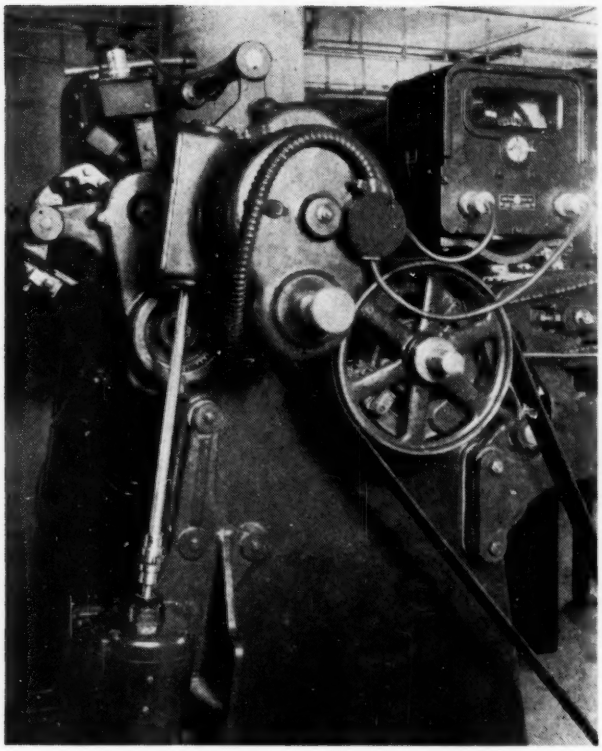


FIG. 24 (*a*) MODERN PAPER CUTTER OR "SHEETER" WITH PHOTOELECTRIC REGISTER CONTROL
(One correcting motor, electronically controlled, is sufficient.)

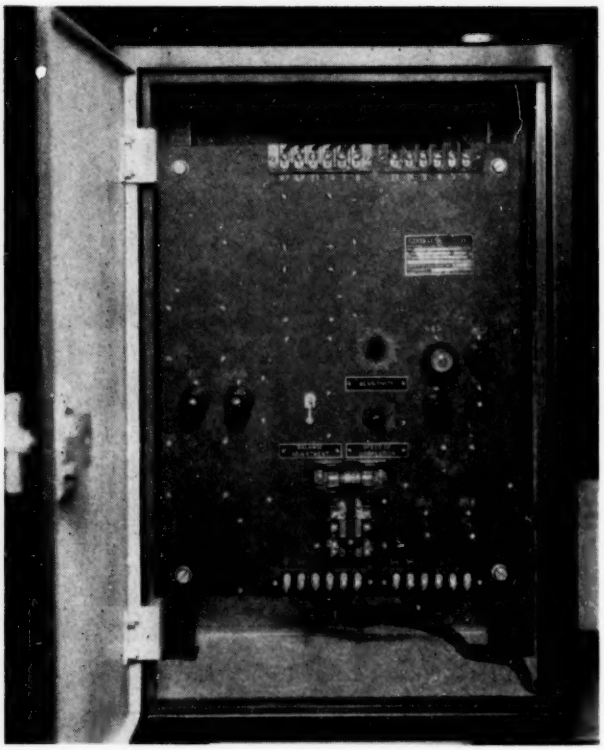


FIG. 24 (*b*) ELECTRONIC PANEL FOR CONTROL OF CORRECTING MOTOR ON MACHINE SHOWN IN FIG. 24 (*a*)

contact geared to the knife), the paper may be moved back by a notching action and then permitted to creep forward again.

As speed is increased, it becomes necessary to control the speed of the web accurately so that it will always be cut near the proper point. This can be done completely by electronic means, all the way from the phototube to the thyratrons supplying power to the correcting motor driving a differential to synchronize exactly the speed of the web and cutter. For most precise action at high speeds, a combination of phototubes and a slotted disk may be used to indicate the position of the knife.

However, at any point in this complete system from the first amplifier tube and its small contactor to the end, mechanical devices may be used to replace electrical devices. It is here that the ingenuity of the mechanical engineer is necessary to determine the best combination of electrical and mechanical equipment for that particular application.

It is interesting to note that through the years sound judgment, as shown by results, has dictated the ever-increasing part to be taken by the electronic components. Fig. 23 shows one of the first installations (1932) and is typical of the large part that mechanical operation played in the older equipment. Fig. 24 (*a*) and (*b*) shows a modern equipment in which tubes do many things formerly done by mechanical means.

Application of Electronic Control

By E. H. VEDDER,[1] EAST PITTSBURGH, PA.

This paper describes typical applications of electronic control. Motor control including an adjustable-speed drive for direct-current motors and a speed-regulator system are shown. The importance of resistance welding in production of sheet-metal assemblies and the use of ignitron equipment for control of time and current are discussed. Many uses for control using light, including loop, tin-flow, and paper-cutting regulation are described, as well as pinhole detection in steel strip, and general-purpose photoelectric relays. The importance of close co-ordination of design of the electrical and mechanical elements of a complete system is emphasized.

ELECTRONIC control is now used in a variety of ways as a component part of systems which are usually partly mechanical and partly electrical. Inasmuch as many functions may be done either electrically or mechanically, careful consideration must be given to co-ordination of the two elements to produce the best system.

The first principle we need to establish is that electronics will live up to its publicity only if it is really put to work as an accepted workaday tool. If electronics is allowed to become a gadget business, we have failed to utilize the tool properly. The gadget angle can be avoided only by critical survey of every application. Electronic control has been developed which will do many things better, less expensively, faster, or more precisely, as well as many things previously impossible. But electronics is not a cure-all for every trouble. It is merely a new tool which must be properly used within its limitations. To illustrate the type of things for which electronics is suited, a few applications will be described.

Motor Control

Many motor-drive problems, particularly those connected with machine tools, are best solved by the characteristics inherent in a shunt-wound direct-current motor. The almost universal availability of alternating-current power and relative unavailability of direct-current power has made it much more difficult to use the desirable direct-current motor for these drive applications. There has also been a growing desire for a greater nicety of control than can be readily obtained even if a direct-current system is available. An electronic control has now been developed which operates a direct-current motor from an alternating-current line and has additional desirable features not previously available. The electronic adjustable-speed drive shown in Fig. 1 consists of a direct-current shunt-wound motor whose field and armature are energized by separate thyratron rectifier circuits. These rectifiers are so controlled as to vary the input to the motor, regulate the motor speed to a preset value, and limit the maximum current furnished the motor during acceleration and reversal.

The control permits smooth stepless adjustment of motor speed over a range of at least 20:1 below the base speed of the motor, and over an additional field-control range of as much as 4:1 above the base speed of the motor. This speed control is readily obtained over the full range below and above basic speed by means of a small potentiometer located in the push-button station convenient to the operator.

Combined with the wide range of speed control are the very flat speed-torque characteristics over the whole range. This is obtained by speed-regulating circuits which insure that the motor will be held to the preset speed chosen by the operator. In a properly adjusted system, the speed over a 10:1 range below basic speed will not vary more than 4 per cent from a preset value, with torque varying from no load to full load, nor will it vary more than 8 per cent for any speed within the speed range of 20:1. Normal variations in alternating-current voltage have only a small effect on the speed regulation.

It is necessary that capacitors made of foil and paper be wound with uniform tension to insure good insulation. The electronic motor-speed control is used for this purpose. The operator controls speed in this application with a foot-operated speed adjuster consisting of a variable reactor with foot treadle. Continuous speed adjustment is available from zero to maximum winding speed. Greatly increased production resulted because of the smoother speed control by the operator.

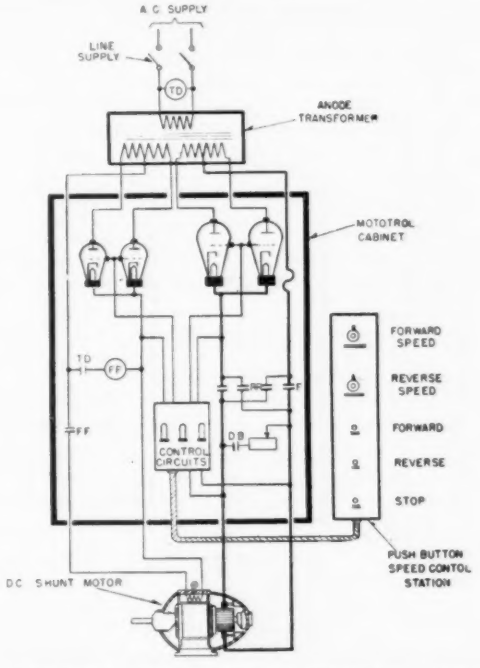


Fig. 1 Schematic Arrangement of Electronic Adjustable-Speed Motor Drive

⊣	Relay contact which is open when relay is de-energized
—○—	Relay magnet coil
—□—	Dynamic braking resistor
TD	Time delay protective relay to prevent operation until the cathodes are heated
FF	Field failure relay to prevent operation of motor if field is not energized
R, F	Reverse and forward contacts on contactor for reversing motor rotation
DB	Dynamic braking relay contact. Used to brake motor when stopping or reversing

[1] Manager, Resistance-Welding Engineering, Westinghouse Electric & Manufacturing Company.

Contributed by the Special Design Committee and presented at the Annual Meeting, New York, N. Y., Nov. 29–Dec. 3, 1943, of The American Society of Mechanical Engineers.

Note: Statements and opinions advanced in papers are to be understood as individual expressions of their authors and not those of the Society.



FIG. 2 ELECTRONIC ADJUSTABLE-SPEED MOTOR DRIVE ON CAPACITOR WINDING MACHINE

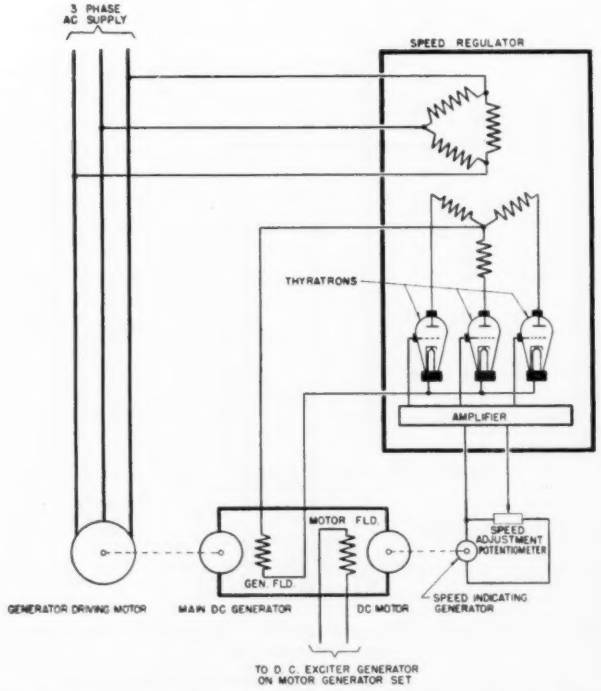


FIG. 3 SCHEMATIC DIAGRAM OF A VARIABLE-VOLTAGE SPEED CONTROL WITH ELECTRONIC SPEED REGULATOR

There are many motor-control systems where speed regulation is desired, but there is no advantage in full electronic control. For this purpose, a speed-regulator system has been developed as shown in Fig. 3. In this particular system, the direct-current motor is furnished with power by a motor generator set. The motor-generator-set field is energized from the electronic regulator. The motor speed is indicated by the speed-indicating generator whose output voltage is proportional to speed. The indicating voltage is applied through an amplifier and regulating circuit to the grids of the rectifying tubes which furnish the generator field. This device has found ready acceptance in paper mills for regulating the speed of a single-motor paper-machine drive. It maintains the speed to an accuracy of approximately 0.5 per cent and may be adjusted over a speed range of 10:1. A similar regulator is used to hold constant speed on the Wright Field 40,000-hp wind-tunnel drive.

RESISTANCE-WELDING CONTROL

Resistance welding is being extended rapidly to speed production of fabricated assemblies. It is particularly adaptable to manufacturing processes involving large quantities of repetitive assemblies. It is most commonly used on sheet metal, although heavier parts including heavy plate and premachined pieces are also being welded.

Resistance welding is accomplished by passing a heavy current through two or more pieces of metal. The resistance of the metal to current flow develops heat, which fuses the pieces together. The material is clamped between copper or copper-alloy electrodes which apply pressure and conduct the heavy current to the junction point. The welding machine itself consists essentially of a heavy framework supporting a special transformer, electrodes, and pressure head for the electrodes.

For many years, the use of resistance welding was confined almost entirely to the coarser sheet-steel structures which could tolerate a considerable amount of electrode marking, warping, and discoloration. The process has become in recent years more of a precision process and has been extended to a variety of alloy

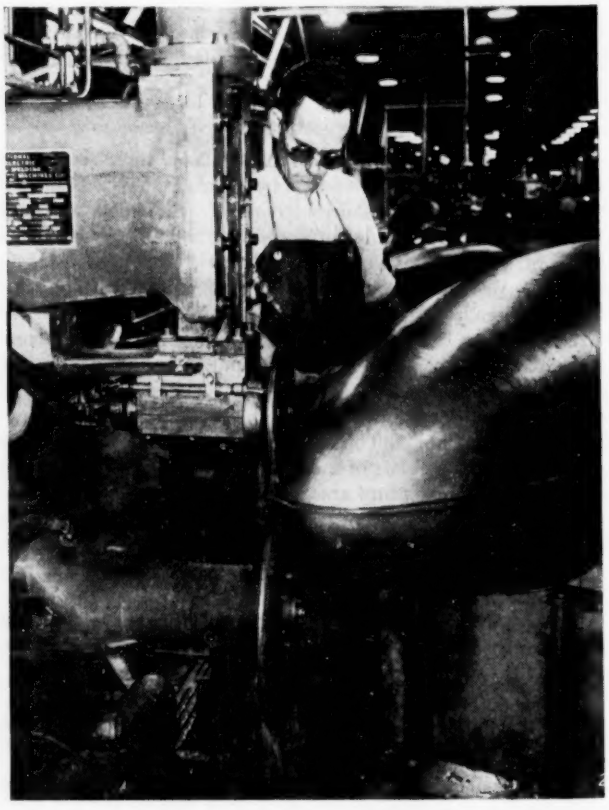


FIG. 4 SEAM-WELDING MACHINE

metals such as stainless steel, brasses, and bronzes, and to nonferrous metals of sharp fusion points such as aluminum. In wartime industries, welding has rapidly found its place in the manufacture of airplanes, trucks, shells, gasoline drums, airplane drop tanks, and other similar assemblies.

Resistance welding is divided into several different general types, the more distinct classes being spot, projection, butt, and seam welding. Spot, projection, and butt welding differ only in the type of electrodes and method of holding the materials during welding and use the same control unit. The control measures out one or more pulses of current to make an individual weld. Seam welding uses roller electrodes, and the control is quite different from that for spot welding. The control causes the current to flow in individual pulses of a few cycles' duration each and with a few cycles time between each pulse for as long as welding is proceeding.

Fig. 5 is a typical resistance-welding system, showing in this particular case spot-welding electrodes, although the diagram applies equally well to seam welding when roller electrodes are substituted for the pointed tips. The resistance-welding system consists of the welding machine with the welding transformer mounted in it, together with control equipment including an ignitron power assembly for controlling the energy fed to the welding transformer, a timing control, and the current or heat control. When the operator's foot switch is depressed, the welding electrodes are lowered to the work and when pressure has been fully applied, the timing unit causes the ignitron unit to conduct current to the welding machine. The timing control determines the length of time that welding current will flow and, after the predetermined length of time, causes the current to stop. The timing is usually between 1 and 30 cycles. For various work, it is necessary to have different values of current, and therefore the current input to the welder must be adjusted when setting up. The heat-control unit serves this purpose. For some special applications the current is modified automatically during the progress of the weld. Electronic control has proved valuable for resistance welding because of reduced maintenance at high operating speeds and also because of the precision obtainable.

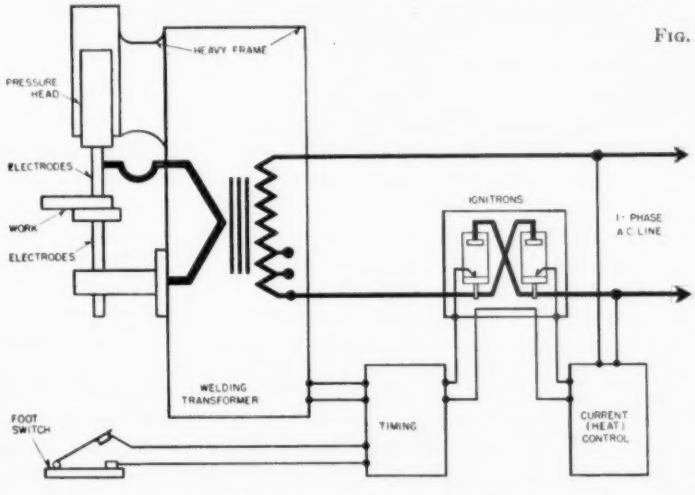


FIG. 5 SCHEMATIC ARRANGEMENT OF A SPOT WELDER AND ITS CONTROL

(The timing and current controls shown as blocks operate in the control circuit of the ignitron power tubes to time the duration of the flow of current and determine its magnitude. The proper time and current values are selected by experience and preset manually for the material being welded.)

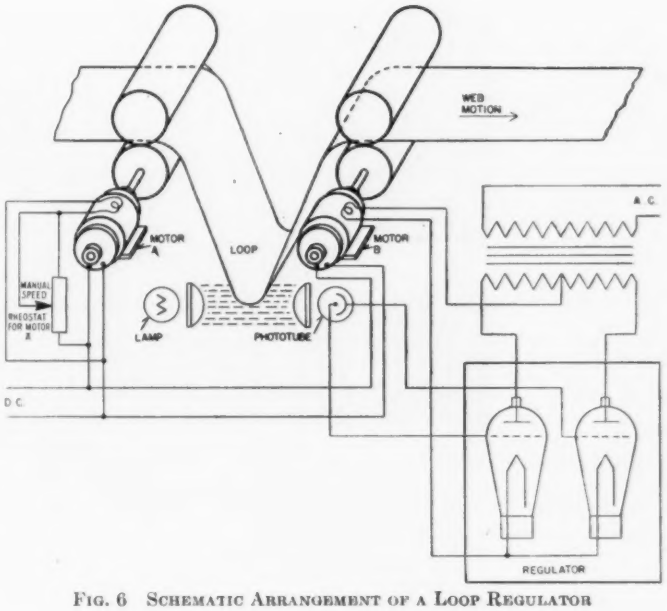


FIG. 6 SCHEMATIC ARRANGEMENT OF A LOOP REGULATOR

The ratings of welding control are based upon the current-carrying capacity of the control and the duty cycle primarily, the ignitron tubes being rated at currents up to 10,000 amp during the weld at low-duty cycle. Inasmuch as the welding transformer steps current up several times, this value of primary current would correspond to perhaps 80,000 or 100,000 amp in the weld itself. Most equipment operates from industrial voltages of 220 or 440 v, although control is now available for 2300-v operation. The high voltage operation is particularly desirable for large welding machines to minimize the effect of the high current demand on the line voltage and in many cases to save on the amount of bus required for feeding the power to the machine.

CONTROL USING LIGHT

Control utilizing light is called "photoelectric" because it is actuated by the response of a light-sensitive element called a "phototube." Photoelectric control is useful for actuating a system in response to a change of color, shade, density, shape, or position without mechanically touching the controlling object.

Many of the more important photoelectric applications may be classed as process regulators. Thus a loop regulator on a paper-coating machine or on a steel strip mill watches the loop position and calls for slowing down or speeding up one of the sections of the mill to maintain a constant loop. The system in Fig. 6 is a simplified arrangement used where the speed range is not more than about 4 to 1. The web is driven by motor *A* into the loop and taken out of it by motor *B*. Motor *A* and motor *B* can, for instance, operate two different sections of a conveyer or two separate stands of a mill. The speed of motor *A* is adjusted as desired, and the regulator then keeps the speed of motor *B* at the proper value to maintain a constant loop between the two sections. An increase of loop length reduces the amount of light reaching the phototube from the light source and modifies the field excitation of motor *B*, adjusts its speed, and brings the loop back to the proper position.

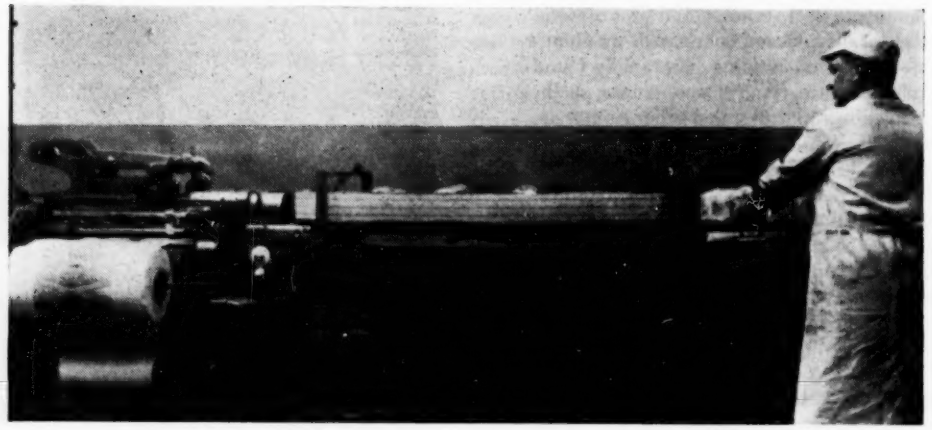


FIG. 7 BREAD-WRAPPING MACHINE WITH PHOTOELECTRIC CONTROL OF CUTTING TO PLACE TRADE-MARK AT SAME SPOT ON EACH LOAF

A regulator used frequently in the paper, cellophane, and glassine processing industry is that for maintaining the position of cut when taking from a roll of preprinted stock for making bags or packages. Although the machine feeds paper at a rate approximately correct to match the speed of the rotating knife, the cut will never remain registered perfectly without either manual or automatic supervision. A register regulator corrects for changes of paper slippage, stretch, and speed relative to the cutter speed. The position of the printed material is indicated by a rectangular register mark in the design or margin which is scanned by a phototube. The position of the mark with respect to the cutter is checked and the speed of paper feed modified if necessary. A typical installation of this type is shown in Fig. 7, for packaging bread.

When slitting strip material, it is often necessary to regulate the sideways position of the web to insure cutting at the proper point relative to a trade-mark or printed design. The slitter regulator in Fig. 8 scans the edge of the paper web or a line in the printed design. The proper web position is obtained by moving the roll of material to the position called for by the phototube in the scanning device. The same device is used to scan the edge of a web and correct the roll position to insure smooth roll windup when rewinding mill rolls. An installation of this device on a printing press is shown in Fig. 9.

The wartime shortage of tin brought about the necessity for thinner coating of tin on strip steel for cans. This has been accomplished by the electrolytic tinning process. The electroplating process leaves the tin surface with a silvery appearance and somewhat porous structure. It is necessary to heat the strip enough to melt and flow the tin and thus obtain a more perfect coating. Not only does an electronic high-frequency oscillator supply power for flowing the tin after electroplating, but it is also necessary to regulate the flowing of the tin so that exactly the right amount of high-frequency power is furnished, thereby avoiding spoilage. If too much power is furnished to the high-frequency induction heating coil, the flow line will occur much earlier in the heating coil than it would at lower power levels. It is therefore desired to maintain the power input to the heating coil at a level which will cause the tin to flow at a certain predetermined position in the coil. The flow line is readily distinguished because the tin coming directly from the plating tank has a very diffusing surface whereas that tin which has been flowed has a mirror surface. The regulating system is shown in Fig. 10 with a light source and phototube scanning the plated strip. The scanner detects the exact line at which this change of condition occurs. If the speed of the tinning line changes, it is necessary to modify the power input accordingly. This is accomplished through the scanner which observes that the position of flow line has changed, and which energizes through the thyratrons either relay F or R to start the induction-regulator motor. This adjusts the regulator so as to increase or decrease the power furnished to the oscillator and to bring the flow line back to the proper position.

DETECTING HOLES IN STRIP STEEL

Not all photoelectric applications are for regulation purposes. An important steel-mill application of another type is that for detecting holes in strip steel. This application is particularly desirable on steel which will be used for the canning industry. Prior to the use of pinhole detectors, it was difficult to inspect visually the strip effectively and food spoilage resulted. The pinhole detector, Fig. 11, will inspect steel strip at speeds up to 1500 fpm and detect $^1/_{64}$-in. or smaller holes. The detector operates a marker which places a visible mark on the strip at the location of the hole so that it can be readily located later on. In many installations, the detector also operates a classifier to reject defective sheets automatically, after they have gone through the shear which usually immediately follows the pinhole detector.

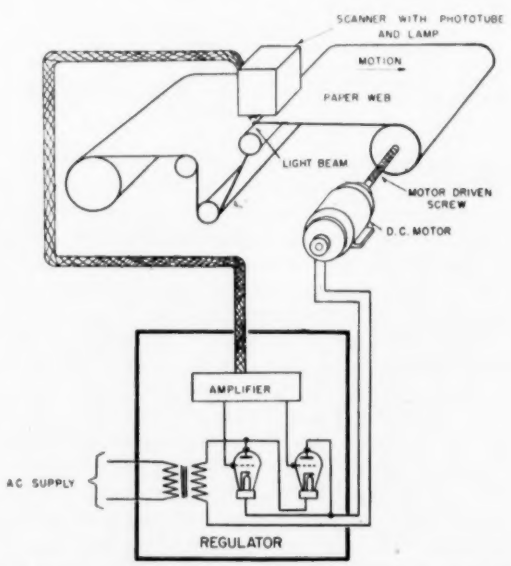


FIG. 8 SCHEMATIC ARRANGEMENT OF REGULATOR FOR CONTROLLING SLITTING OR REWINDING OF PAPER, GLASSINE, OR CELLOPHANE

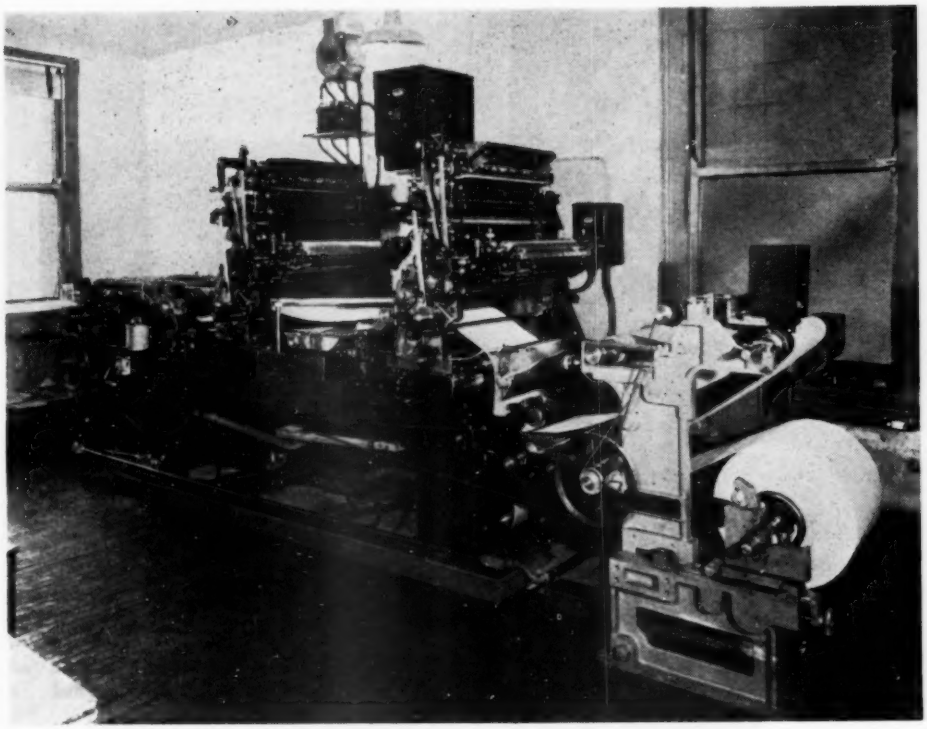


FIG. 9 SLITTER REGULATOR USED ON A PRINTING PRESS TO MAINTAIN POSITION OF PAPER WEB

The pinhole detector is probably one of the more prominent commercial applications of sorting.

Much loose publicity has been given to the use of phototubes for sorting applications. It should be realized that the phototube responds only to a difference of light energy reaching it and also in some degree to changes of the color of the light. The phototube does not have any intelligence and therefore cannot duplicate the performance of the human eye for the great majority of sorting problems. The only way in which a phototube can be made to appear to have judgment or intelligence is to design the optical system so that the phototube will receive a varying amount of light depending upon a particular characteristic of the material which it is desired to detect. The application of phototubes to sorting problems is usually very expensive because of the considerable development involved and many times cannot be justified for that reason alone. This development expense can be absorbed if the commercial possibilities for the finished design are sufficiently enticing, but if they are not, the individual user is not ordinarily willing to pay the development charges.

Many applications for photoelectric control can be taken care of by general-purpose devices called photoelectric relays which may be considered as light-sensitive limit switches. These are available in varying forms and at varying prices, depending upon the desired sensitivity and functions to be performed, and can be adapted by the purchaser to his own application. These include counting, drinking-fountain control, door control, and conveyer control as shown in Fig. 12, and numerous others known only to the many users.

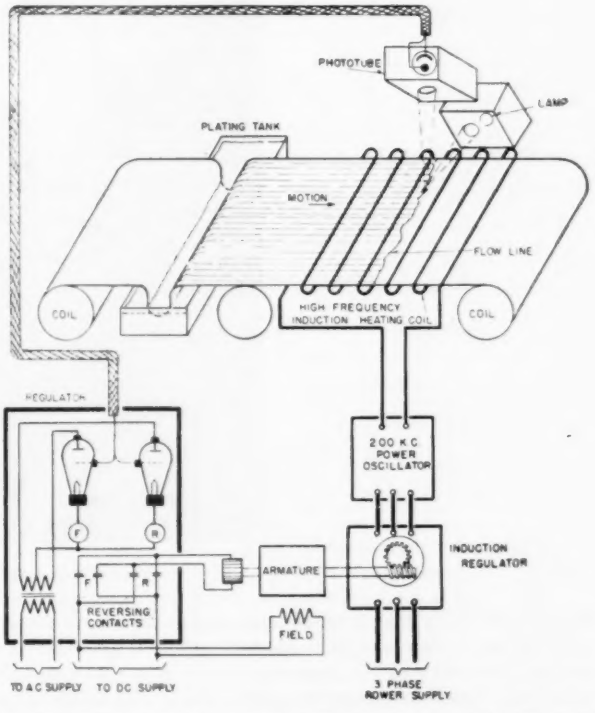


FIG. 10 SYSTEM FOR REGULATING POWER INPUT IN TIN-FLOWING PROCESS

—O— Relay coil F Forward relay
⊣⊢ Relay contact R Reverse relay

CONCLUSION

The applications described show a typical variety for electronic control. These have come about through close co-ordination of the electrical and mechanical design. Only by this co-operation has it been possible to insure that the electrical and mechanical equipment will match each other in precision and reliability. If they do not match, a regulator with $^1/_{64}$-in. accuracy may be attempting vainly to control a machine with $^1/_8$-in. backlash, or a

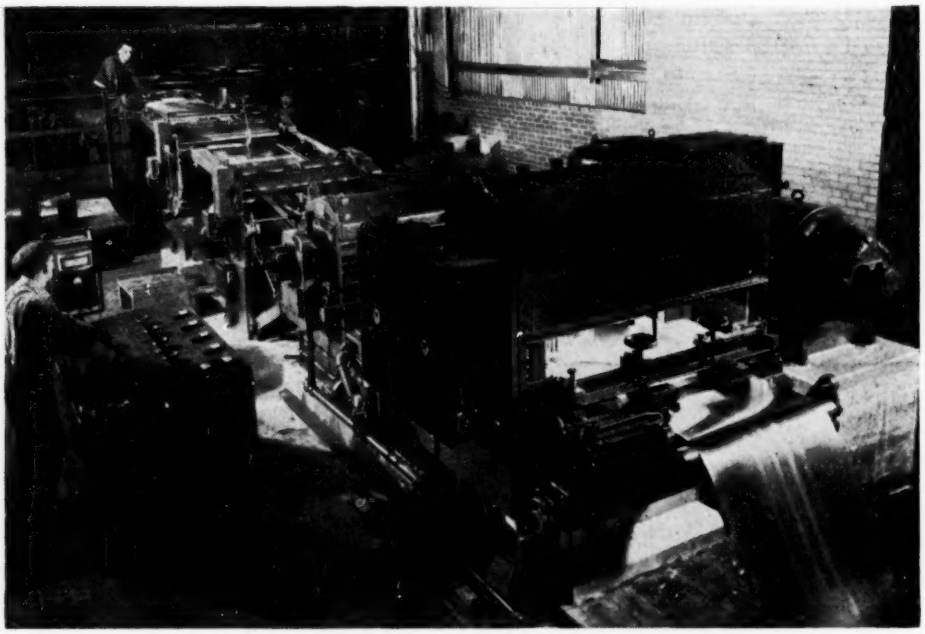


FIG. 11 PINHOLE DETECTOR IN A STEEL-STRIP SHEARING LINE



FIG. 12 COUNTING OR CONVEYER CONTROL

precision machine may lose its value because of coarse control.

Electronic control, properly selected for applications where it can perform better or less expensively, will do what seems to be miracles. This is so because new tools with incredible speed and versatility have been added to the designer's kit. His vision is thus broadened beyond the pure mechanical or the electromechanical device to the electronic tube which is purely electrical and has incredible speed and versatility. Through proper combination of all three of these tools designers are unfolding new engineering accomplishments with amazing possibilities.

Radiation Pyrometry in Turbosupercharger Testing

By V. P. HEAD,[1] WEST LYNN, MASS.

With increase in operating temperatures and speeds of turbines such as are used in turbosuperchargers, the demands for turbine-wheel and bucket temperature measurement have become increasingly exacting. Requests appear for such measurements under operating conditions with measurement tolerances varying from ±50 F in flight test to ±5 F in certain ground tests. This paper outlines the procedures used for measurements ranging from as low as 300 F up.

THE following alternate procedures have found limited application in measuring turbosupercharger turbine-wheel and bucket temperatures:

1 *Optical Pyrometry.* Bucket hot-spot temperatures have been determined with a monochromatic optical pyrometer of the disappearing-filament type. Above about 1400 F such readings have been accepted with an allowance of about ±30 F.

2 *Fusible Alloys.* Temperature versus radius curves on the wheel have been obtained with fusible-alloy plugs with accuracy limited by the interval between consecutive melting points of the alloys available. Maximum temperatures during the tests, rather than instantaneous values, were obtained and have been valuable in determining wheel operating temperatures with various cooling methods.

3 *Fusible Compounds.* Fusible compounds commercially available as pellets, with melting points at 50 F intervals, have been used to give wheel temperature versus radius curves with a probable error of 1 or 2 per cent of the absolute temperature. Again indications represent maximum values, but the pellets are made to indicate approximate instantaneous values by approaching desired test temperatures gradually with no overshoot.

4 *Contact Thermocouples.* Base-metal thermocouples, peened into the wheel at various radii, have been used successfully with slip rings to give instantaneous readings in comparing cooling methods, but speed limitations and complexity of rotating parts have prevented the more general application of this procedure.

General Methods and Applications of Thermoelectric Radiation Pyrometry

Thermoelectric radiation pyrometers commercially available have been applied to give the local temperatures at wheel-rim and bucket surfaces within about ±50 F at 1000 F, and with increase in accuracy at higher temperatures, by mounting and cooling appropriately. The area of the spot observed has been varied arbitrarily by the proximity of the pyrometer to the "target" (wheel or bucket surface), by the size of aperture, or by the use of lenses. A knowledge of the pyrometer-jacket temperature as well as the pyrometer output has been required, and the use of a cooled shutter for determining the magnitude of the "zero drift" (described in the section entitled "Theory") has helped to facilitate the readings. In flight tests, conducted by the General Electric Company and Boeing Aircraft Company in 1941, adequate results were obtained by scooping atmospheric air to cool the pyrometer mounting and prevent soot accumulation, where a spread of 50 F in the observed temperatures was permissible. The pyrometers used were of the glass-bulb vacuum thermocouple type.[2]

Such thermoelectric radiation pyrometers have been adapted to meet recent exacting demands for greater accuracy at lower temperatures. Calibration repeatability within ±5 deg over a range of temperatures from 600 F up has been obtained. The inherent error of base-metal thermocouples used to measure the calibrating-target temperatures has limited the absolute accuracy obtained.

The experimental miniature pyrometer described herein has provided instantaneous readings of wheel and bucket temperature during test and is now being employed as a guide for the control of test conditions when arbitrary temperature versus radius curves are desired.

The arrangement may be applied to the temperature measurement of gases and vapors by sighting into the end of a long "honeycomb"[3] in a well-lagged duct through which the gas may be passed.

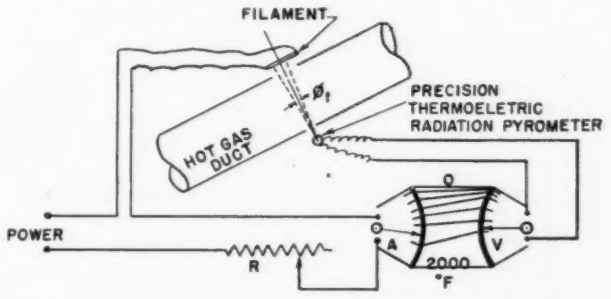


Fig. 1 Proposed Adaptation of Kurlbaum's Flame Method to Static Temperature of High-Velocity High-Temperature Gases Not Completely Transparent

(A: Ammeter calibrated for filament temperature. V: Galvanometer indicating filament temperature by thermoelectric radiation-pyrometer output, calibrated with clean, dry cold air in duct. R: Manual filament-temperature-control resistor. ϕ = pyrometer sight angle, completely subtended by filament surface.)

The static temperature of hot gases at high velocity may be measured by replacing the optical pyrometer of Kurlbaum's flame method[4] with a precision thermoelectric radiation pyrometer. One possible arrangement is suggested in Fig. 1, in which the manual adjustment of a single resistor permits variation of a background temperature until the actual and indicated background temperatures are equal, when the indicated tempera-

---

[1] Supercharger Engineering Division, General Electric Company.

Contributed by the Aviation Division and Industrial Instruments and Regulators Division and presented at the Annual Meeting, New York, N. Y., Nov. 29–Dec. 3, 1943, of The American Society of Mechanical Engineers.

Note: Statements and opinions advanced in papers are to be understood as individual expressions of their authors and not those of the Society.

[2] "Vacuum Thermocouples of the Radiation Type," by S. S. Stack, *General Electric Review*, vol. 42, 1939, pp. 365-366.

[3] "Measurement of High Temperatures in High-Velocity Gas Streams," by W. J. King, Trans. A.S.M.E., vol. 65, 1943, pp. 421–431.

[4] "The Measurement of Flame Temperature," by G. Ribaud. Y. Lauri, and H. Gaudry, *Journal of the Institute of Fuel*, vol. 12, 1939, pp. S-18–S-30.

ture will be actual gas-static temperature, regardless of gas emissivity.

It is proposed that the arrangement may be used as a secondary standard in the calibration of base-metal thermocouples, thermometers, and the like, for temperatures above 1000 F.

It is conceivable that rigorous application of thermoelectric radiation-pyrometry theory may permit sharper definition in the "International Centigrade Temperature" scale at elevated temperatures, reducing the spread entailed by the brightness-comparison methods of optical pyrometry, since the "readability" of the output increases with approximately the third power of the measured temperature.

An interesting application is the measurement of pressure at high vacuum, using a target of constant temperature such as a lamp with controlled voltage, and connecting the pyrometer chamber to the vacuum to be measured, as described further under "Tests."

Arrangements. Fig. 2 shows the arrangement of a mounting used in a high-velocity hot-gas stream. The commercial pyrometer, an evacuated-glass-bulb type, was wrapped in aluminum

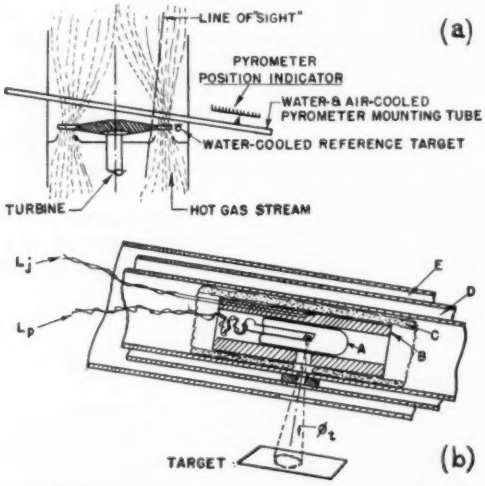


FIG. 2 (*a*) TYPICAL INSTALLATION OF PYROMETER MOUNTING FOR TURBINE-WHEEL TRAVERSE. (*b*) MOUNTING ARRANGEMENT FOR A COMMERCIAL VACUUM-TYPE PYROMETER

A — Pyrometer
B — "Heat mass" (extra heavy pipe)
C — Thermal insulation
D — Cooling-water passage
E — Air Passage
L_p — Pyrometer leads
L_j — Pyrometer-jacket thermocouple leads
ϕ_t = Solid angle of sight

foil and encased in a heavy-walled tube of high thermal conductivity and high specific heat, which acted as a heat "flywheel" to prevent sudden changes in pyrometer temperature. A thin layer of thermal insulating material supported the massive tube within a cylindrical water-cooled outer jacket. An additional jacket carrying air prevented soot accumulation at the sighting aperture. A water-cooled reference target permitted zero-drift observation, and even with the best combination of heat capacity and thermal insulation, corrections amounting to several times the full-scale reading of the galvanometer were frequently required. For this purpose a zero-drift compensator was inserted in the pyrometer circuit, Fig. 3, so that by introducing the proper electromotive force, the galvanometer could be rapidly set to zero. The reflection of extraneous radiation from the surface of the reference target left this adjustment open to some question, and the necessity for the elimination of zero drift, together with the need for reduced bulk in the pyrometer mounting led to the development of the miniature radiation pyrometer, Fig. 4.

Fig. 4 shows the essential features of a thermoelectric radiation pyrometer embodying the theoretical requirements for precision. Tests conducted on a model of this type show that its repeatability is well within the limits of error of the base-metal thermocouples employed in calibrating. It has the further advantage of small size and self-contained "heat capacity," so that the jacket required for mounting in a high-velocity hot-gas stream may be kept to a minimum bulk. The necessity for a cold reference target and zero-drift compensator has been eliminated.

Attempts to seal this model to hold a vacuum permanently have been unsuccessful to date and the device is employed at atmospheric pressure. The sacrifice of high output has been largely offset by the relative freedom from changes in calibration

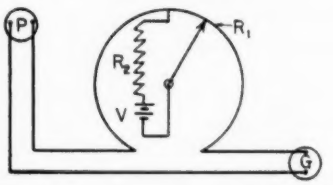


FIG. 3 RAPID ZERO-DRIFT COMPENSATOR FOR PRECISION THERMOELECTRIC RADIATION PYROMETER CIRCUIT

P — Pyrometer
G — Galvanometer or potentiometer
R_1 — Low-resistance slide-wire
R_2 — High resistance
V — Dry cell

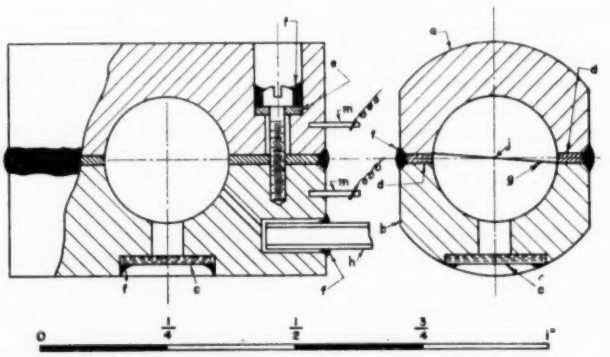


FIG. 4 MINIATURE RADIATION PYROMETER EMBODYING PRECISION REQUIREMENTS

a, b: Upper and lower half-jackets, serving also as thermal capacitance and electric conductors; commercially pure copper
c: Window: glass, rock salt, etc.
d, e: Electric insulation
f: Sealing compound
g: Thermoelectric element with receiver and hot junction at center (*j*), and cold junctions at pyrometer walls
h: Glass evacuating and sealing tube
m: Pyrometer leads
Not shown: Thermal insulation, outer cooled mounting, and sight-limiting aperture

with small changes in jacket temperature, a characteristic which is highly desirable. The output is read on a light-beam-type galvanometer of portable construction having a full-scale deflection (100 mm) at about 50 μv. The characteristics of the pyrometer are such that a relatively small target temperature range is conveniently spread over the upper 90 per cent of the scale range, Fig. 7(*b*). The use of a direct-reading galvanometer requires that there be no change in lead resistance between calibration and application, but no attempts to use a potentiometer have been successful. The time required to balance a potentiometer permitted inestimable zero drift with the commercial high-output-type pyrometer, and the readability of the potentiometers available has been inadequate for the miniature type.

NOMENCLATURE

The following nomenclature is used in discussing the theory of thermoelectric radiation pyrometry:

T_t = target absolute temperature
T_j = absolute temperature of pyrometer jacket
T_r = absolute temperature of pyrometer receiver
K_0 = constant governing radiation between target and receiver
K_1, U_1 = constants governing radiation between receiver and jacket
K_2, U_2 = constants governing convection between receiver and jacket
U_3 = constant governing conduction between receiver and jacket
ϕ_t = solid angle of radiant influx from target to pyrometer receiver
y = exponent of temperature difference applicable to convection between receiver and jacket

Theory of Thermoelectric Radiation Pyrometry

Fig. 5 shows an idealized radiation pyrometer: a small receiver of low heat capacity, a spherical jacket of high heat capacity and temperature T_j, and a transparent window through

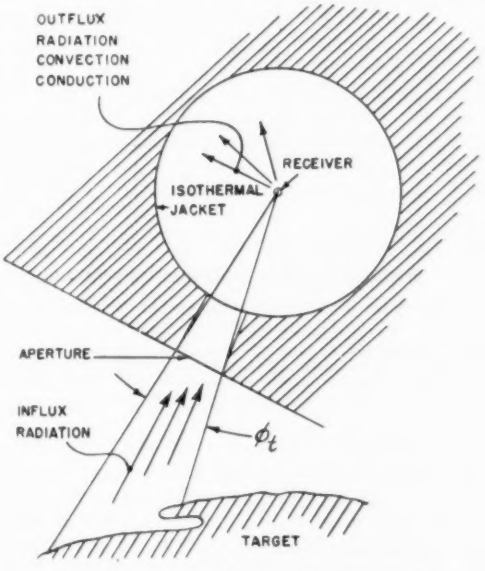


Fig. 5 Idealized Radiation Pyrometer

which a target of temperature T_t may be "seen" by the receiver through a solid angle of ϕ_t steradians. We may write the steady-state energy-flow equation governing the receiver temperature T_r

$$K_0(T_t^4 - T_r^4) = K_1(T_r^4 - T_j^4) + K_2(T_r - T_j)^y + U_3(T_r - T_j) \quad [1]$$

or in words, the influx radiant energy to the receiver is equal to the net energy transfer from receiver to jacket by radiation, convection, and conduction.

We may introduce a gross approximation for the convection term without seriously jeopardizing our qualitative conclusions

$$K_2(T_r - T_j)^y = U_2(T_r - T_j) \quad [2]$$

If the difference between T_r and T_j is less than, say, 1 per cent of either, the receiver-to-jacket radiation term may be written with fair precision

$$K_1(T_r^4 - T_j^4) = U_1 T_j^3(T_r - T_j) \quad [3]$$

On the left side of Equation [1], T_r may be replaced by T_j, since compared to T_t their difference is in general negligible.

We may now rewrite Equation [1] to give a function which is more readily scanned by eye, if slightly less precise

$$K_0T_t^4 = (U_1T_j^3 + U_2 + U_3)(T_r - T_j) + K_0T_j^4 \quad [4]$$

Then in order to measure T_t with precision, we must measure precisely a quantity proportional to $(T_r - T_j)$ and we must know T_j itself at least approximately.

Many forms of radiation pyrometers have been built in which radiation from a hot target is intercepted by a receiver to produce a temperature difference between the receiver's "hot" junctions and "cold" junctions located vaguely somewhere else. It must here be recognized that the criterion temperature difference is that between the receiver and the jacket walls. Failure to locate the thermoelectric cold junctions at the walls leads to a time lag between the walls and the cold junctions when the slightest drift in jacket temperature occurs. This will produce the "zero drift," previously referred to, which in low-temperature applications may frequently amount to *several hundred per cent* of the criterion temperature difference $T_r - T_j$, and render the output of the pyrometer meaningless. This random location of cold junctions "somewhere else" may be largely responsible for the prevalent notion that radiation pyrometry is impractical at temperatures appreciably below 1400 F.

Let us therefore locate in our ideal pyrometer a thermoelectric element with hot junction at the receiver and with cold junctions at the walls, and since we will require a knowledge of $T_r - T_j$ to within a few thousandths of a degree, let us use a massive high-conductivity jacket to assure that its temperature will be *uniform* throughout.

The term $K_0T_j^4$, Equation [4], will be found negligible for 0.1 per cent accuracy in target temperature measurement, when T_t is more than 4 times T_j, while a 4 per cent variation of T_j from that at which calibration was made will be negligible when T_t is only about 2.5 times T_j. Thus at normal room temperature, T_j may vary ± 20 deg with no effect when T_t is above about 800 F, so far as the influx of radiant energy from the target is concerned.

A more troublesome effect of jacket temperature deviation lies in the variation of radiant energy transfer within the pyrometer, indicated by the factor $U_1T_j^3$, Equation [4]. When we strive for high output by evacuating the pyrometer jacket and making the thermoelectric elements as slender as possible (decreasing U_2 and U_3), we make the effect of jacket temperature change more and more critical. By retaining a high convection rate at a sacrifice of output, and by polishing the inner jacket wall to reduce U_1, we may render the effects of small deviations of jacket temperature negligible.

The coefficient K_0, Equation [4], is dependent upon the geometry of the arrangement and the "blackness" of the target surface. It may be increased by increasing the value of ϕ_t by the change of aperture size, usually entailing an undesirable increase in area of the target portion viewed, or by the use of a lens. A lens or window is never perfectly transparent, and contributes to the effective jacket temperature. A large lens external to the heavy jacket proper is therefore apt to present difficult temperature-control problems and is to be avoided. Constant K_0 may be further increased by pretreatment of the target surface as described under "Tests." Here repeatability of calibration is even more important than the increase in output.

The radiation transmission within the pyrometer may be reduced for increased output by polishing the inner-jacket-wall surface. The conduction factor U_2 has been commonly reduced by using extremely thin thermocouple wires or ribbons.

The convection factor U_3 is a function of the shape, size, and pressure of the jacket interior. In general, evacuating a pyrometer will increase its output by a ratio of 7 or 10 to 1. The

transition of sensitivity occurs rather suddenly over a limited range of pressures, through which the mean free path of the molecules of gas in the jacket appear to be of comparable order to the linear dimensions of the inner jacket chamber. It must be remembered that the tempting increase in output will demand much closer control and measurement of the pyrometer jacket temperature, unless the radiation factor $U_1T_j^3$ can be reduced proportionately. A more detailed analysis of the constants involved and their bearing upon the problem of jacket temperature deviation has been given elsewhere.[5]

A rigorous analysis of pyrometer performance will yield an equation very different from Equation [4], involving among other things an integration of a function of "monochromatic" radiation "density" in a differential spectral band at varying temperature with respect to the spectral distribution of a non-black surface, further modified by the selective transmission of the particular window or lens material; hardly a feasible project in wartime. It is sufficient to say that the result is not a fourth-power function, nor is the pyrometer in any sense a "total radiation" pyrometer. Empirical formulas, involving a temperature exponent between 4 and 5, have been found to fit portions of the calibration curves, but they have contributed nothing to the usefulness of the project. Attempts to use Equation [4] for any but qualitative considerations should be avoided.

Tests of Commercial and Experimental Pyrometers

1 Tests of zero drift in a commercial vacuum-type pyrometer were conducted to determine the optimum arrangement of thermal resistance and capacitance between a water-cooled housing of fixed diameter and the pyrometer. No aperture or target was used. The criterion for zero drift was the pyrometer-output versus time curve of each arrangement, produced by a sudden drop of 30 deg F in water temperature. Fig. 6 shows the results obtained with seven such arrangements, which are numbered in order of increase of "heat-mass" concentration. The dashed line through the peaks of these curves shows the trend from high drift of short duration to low prolonged drift. Curve 7 was obtained with an arrangement similar to Fig. 2(*b*), which in service permitted zero-drift adjustment, a target observation, and a good zero check after observation.

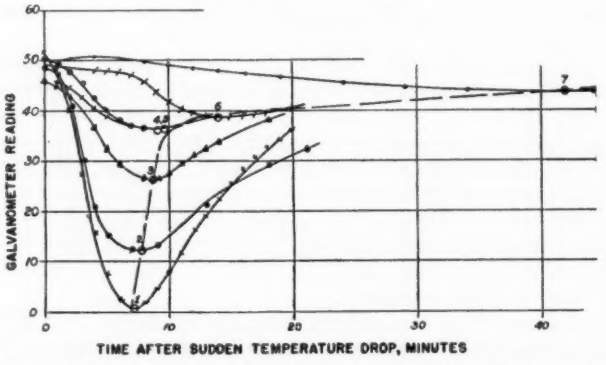


Fig. 6 Zero Drift in a Commercial Vacuum-Type Pyrometer
(Solid lines: zero-drift versus time curves produced by a sudden 30 F drop in cooling-water temperature with seven combinations of thermal resistance and capacitance confined in outer jackets of equal size. Dashed line: trend of magnitude and duration of zero drift with variation in jacket construction, indicated by the peaks, i.e., numbered points, of the solid lines. Point numbers go up with increase in "heat-mass" concentration of the jacket arrangements tested.)

Zero drift in the experimental pyrometer, Fig. 4, was determined by a sudden increase of 37 deg in the jacket temperature. The zero drift persisted for about 7 min, and its maximum value was about four galvanometer divisions at the end of 3 min. The effect of this zero drift is shown in Fig. 9 (*b*). Since no such sudden jacket transients occurred in service, the use of a zero adjuster and cold reference target was discontinued, eliminating the reference-target reflection error previously described.

2 Repeat calibrations at several jacket temperatures indicated the significance of jacket deviations in service. The commercial pyrometer required a correction of a little over 1 deg per deg deviation of jacket temperature at a target temperature of 1200 F, and an increase in the correction as the target temperature rose. The corresponding correction for the experimental pyrometer without vacuum was less than $^1/_4$ deg per deg, with a tendency to decrease with an increase in target temperature. This tendency is not apparent from Equation [4] and is best explained by the fact that the convection exponent y, Equation [1], is appreciably greater than unity, so that the value of U_2, Equation [4], increases with $(T_r - T_j)$. In words, the rate of heat transfer between the receiver and jacket by convection increases with target temperature faster than does the transfer by radiation. The effect upon the required correction is a real trouble saver.

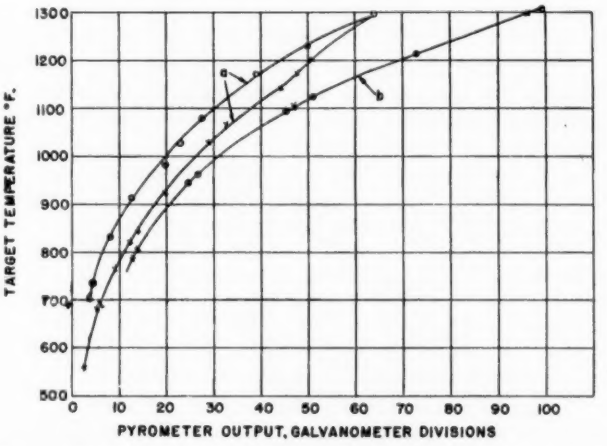


Fig. 7 Effects of Target Pretreatment on Thermoelectric Radiation Pyrometry
(*a*, Target polished before test. *b*, Target lightly sandblasted and preheated to 1400 F. Encircled test points indicate increasing temperature. Crossed test points indicate decreasing temperature. Point scatter, curve *b*, is typical of pyrometer repeatability.)

3 Tests on the effects of target emissivity drift were conducted by using a calibrating target of test-target material, initially bright, which was gradually heated and cooled. Readings of pyrometer output with increasing and decreasing target temperature were observed. Fig. 7 shows the results obtained with two initial surface conditions. It was found that a light sandblast of the calibrating target rendered the emissivity drift negligible, Fig. 7(*b*), though in subsequent tests where turbine-wheel temperatures were to be observed, both wheel and calibrating target were preheated to the highest contemplated test temperature (or as closely as possible without metallurgical damage) after a light surface sandblast.

4 The "calibration-repeatability" tests were identical with the target emissivity variation tests where no visible effect of emissivity variation occurred, Fig. 7 (*b*). In addition, a series of closely spaced calibration points was obtained and plotted on a highly expanded scale. The scatter of the test points about a smooth curve drawn through them is shown in Fig. 9 (*a*) and (*c*), where the greatest deviation noted is $3^1/_2$ deg, or a spread of

[5] "An Improved Radiation Pyrometer," by T. R. Harrison and W. H. Wannamaker; "Temperature—Its Measurement and Control in Science and Industry," American Institute of Physics, Reinhold Publishing Corporation, New York, N. Y. 1941, pp. 1206–1224.

7 deg. It was expected that the point scatter would decrease at elevated target temperatures because of the decrease in slope of the calibration curve. In practice, it was found that at temperatures above 1000 F, target-temperature versus time curves taken with the radiation pyrometer were much smoother than those taken with the base-metal contact thermocouple peened into the surface of the target. It is justifiable, therefore, to blame the persistent scatter at elevated temperatures on the poor adaptability of the contact thermocouple to precise measurement of surface temperatures when air or gases at different temperatures are present.

In early wheel tests, vibration produced occasional shift between pyrometer and jacket, changing the solid angle of sight. Another source of difficulty was sooting of the pyrometer aperture, which was eliminated by the use of an air jacket outside the water jacket. This also eliminated the water film formed occasionally by condensation on the aperture. Water is extremely opaque to infrared radiation. All of these possibilities must be carefully guarded against in any application.

5 Tests on the effect of varying internal pyrometer pressure were conducted on the experimental pyrometer, Fig. 4, by sighting on an electric lamp of controlled voltage and connecting the evacuating tube to a good vacuum pump. Fig. 8 shows the result and is comparable to the characteristic curve of a thermocouple-type vacuum gage. Note that rough evacuation produces no appreciable change in sensitivity and that there is a point, presumably where conduction and radiation transfer swamp out the remaining convection transfer, where further refinement of the vacuum is useless. It is interesting to note that the inflection point of the curve in Fig. 8 occurred at a pressure corresponding to a mean-free-path for air molecules of approximately 0.1 in., while the actual distance from receiver to inner jacket wall was about 1/8 in.

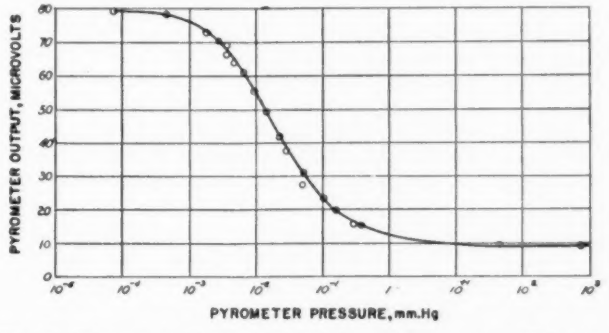


FIG. 8 EFFECTS OF INTERNAL PRESSURE VARIATION ON THERMOELECTRIC-RADIATION-PYROMETER OUTPUT WITH CONSTANT TARGET TEMPERATURE

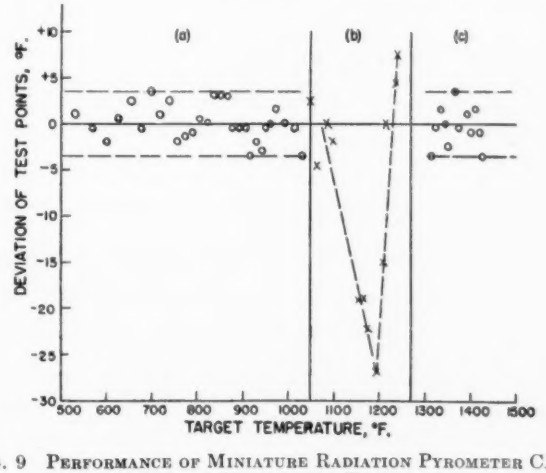


FIG. 9 PERFORMANCE OF MINIATURE RADIATION PYROMETER CALIBRATED AT ATMOSPHERIC PRESSURE

(*a*, *c*, Point scatter about a smooth curve. Pyrometer jacket held at 66 ± 2 F. *b*, Zero drift introduced by a sudden increase of 37 F in jacket temperature.)

To date, the device in Fig. 4 has presented sealing difficulties and has been applied in turbine-wheel temperature measurement at atmospheric pressure in mountings similar to that shown in Fig. 2, with considerable reduction of bulk. The resulting reduced sensitivity has been offset at low temperatures by the use of certain crystalline salt apertures, transparent to infrared, in place of glass. The relative freedom of this arrangement from the effects of small jacket-temperature deviation has reduced personal supervision of tests to a minimum.

CONCLUSIONS

The requirements for basically sound thermoelectric radiation pyrometry may be briefly stated as follows:

1 The target surface must be of constant "blackness" throughout calibration and application.

2 It is necessary to make a precise measurement of the difference in temperature between a receiver and its surrounding jacket, or the corresponding emf or galvanometer equivalent.

3 It is necessary to measure or know at least approximately, and in applications below about 800 F, precisely, the temperature of the jacket.

4 It is advantageous to sacrifice the high output associated with an evacuated pyrometer when freedom from the effects of small jacket-temperature variations is essential.

5 There must be interposed between the pyrometer cold junctions and a cooled outer jacket a high heat-capacity, high-conductivity jacket, surrounded by at least a thin layer of good thermal insulation.

Thermoelectric radiation pyrometers are normally free of the deteriorating influences to which high-temperature contact pyrometers of even the noble-metal thermocouple type are subject. A little regard for the thermodynamics governing their performance has lowered the minimum practical application temperature from 1500 F[6] to about 300 F, and there is no reason to state a minimum for further development. The field of application has been broadened from industrial-furnace applications, requiring about 1 sq in. of "target" area, to include local surface measurement with target diameters of 1/4 in. or less, with repeatability equal to or greater than that of the contact thermocouple. Procedures for improved hot-gas temperature measurement utilizing the thermoelectric radiation pyrometer are in sight. The integration of the laws of monochromatic radiation over the broad spectral band of a suitable window or lens material to create a reproducible high-temperature standard of long life is not beyond the realm of postwar probability.

ACKNOWLEDGMENTS

The pioneering in this project was made possible by the efforts and enthusiasm of Messrs. S. S. Stack, W. S. Thompson, N. F. Frischhertz, and R. H. Norris.

The author is also indebted for the valuable assistance of many other employees of the General Electric Company, and acknowledges particularly the efforts and suggestions of Dr. C. W. Hewlett, Messrs. S. I. Pearson, R. D. Ellis, F. O. MacFee, W. J. King, M. C. Hemsworth, W. MacRobbie, Jr., and G. W. Crosby toward the design, construction, and test of the experimental equipment described.

[6] A.S.M.E. Power Test Codes: "Instruments and Apparatus:" Part 3, "Temperature Measurement," chapt. 2, "Radiation Pyrometers."

High-Speed Multiple-Point Potentiometer Recorder for Measuring Thermocouple Temperatures During Test-Plane Flights

By I. M. STEIN,[1] A. J. WILLIAMS, JR.,[2] AND W. R. CLARK[3]

Measuring exhaust-gas temperatures in flight-testing large planes requires the use of thermocouples of special design and requires also an instrument capable of recording rapidly, accurately, and directly a large number of temperatures. This paper describes a multiple-point, null potentiometer for this purpose. It accommodates 140 thermocouples and records each temperature in 1.63 sec. Flexible arrangements are provided for switching the numerous thermocouples, and this switching may be operated manually by push-button control and also automatically by the recorder. Operating characteristics and performance in flight tests are discussed.

Introduction

IN the early part of December, 1940, representatives of the National Advisory Committee for Aeronautics (N.A.C.A.) Special Subcommittee on Exhaust Gas Turbines and Intercoolers approached the A.S.M.E. Committee on Industrial Instruments and Regulators with a request for assistance in solving certain problems involved in the measurement of high temperatures in high-velocity gas streams. On December 4, 1940, the A.S.M.E. Committee on Industrial Instruments and Regulators appointed a Subcommittee on Exhaust Gas Temperature Measurement to co-operate with the N.A.C.A. subcommittee in solving these problems. The general problem assigned to this special A.S.M.E. subcommittee was made up of two parts, the first one involving the design of the sensitive elements, that is, the thermocouples, and the second one involving the instrumentation. A paper reporting on the first part of the problem has been presented by W. J. King.[4] The present paper deals with the instrumentation part of the problem.

Among the first steps taken by the special A.S.M.E. subcommittee was the circularization of all well-known domestic suppliers of thermocouples and measuring instruments for use with thermocouples, in an attempt to find what, if anything, might be available to meet the particular requirements of the exhaust-gas-temperature problem. In this way some information was obtained on sensitive elements, but all answers to the inquiries with reference to the availability of instruments were negative. As a result of the negative returns to the circular letters, the members of the special subcommittee were urged to encourage developments that might lead to the solution of the instrumentation problem.

The type of instrument needed was a high-speed multiple-point recorder, preferably of the potentiometer type. Fortunately, certain elements essential in the design of such an instrument were either fully or partially developed at the time the request was received from the N.A.C.A. subcommittee, and the availability of these elements shortened considerably the time needed for the development of the complete high-speed multiple-point potentiometer recorder described in the present paper. The paper is limited to a general description of the recorder and its adaptability to the exhaust-gas-temperature problem. A detailed discussion of the electrical circuits involved is reserved for a later paper, as are the applications of the recorder to other problems.

Recorder Requirements in Exhaust-Gas-Temperature Measurements

Number of Points. In each test installation, many thermocouples are involved, and it was felt that one instrument should be capable of recording temperatures of at least 50 thermocouples and preferably of 100 or more.

Ranges and Accuracy Required. The temperatures involved range from those approaching —100 F to those approaching 2000 F. A limit of error of 5 F was desired.

Recording Speed. A relatively high speed of recording was sought because the temperature measurements were to be made during flight tests of planes, and it was desired to record as many temperatures as possible while the plane was gaining or losing altitude at a rapid rate. If possible, the objective was to obtain 20 or more readings in 10 sec, that is, a recording speed of $^1/_2$ sec or less per point. However, it was desired to have the record appear immediately on a printed chart or tape. In other words, the time required for photographic development of charts or tapes was to be avoided. It was recognized that without resorting to photographic recording, it might be necessary to allow more than $^1/_2$ sec per point for recording.

Push-Button Operation. One requirement of the switching facilities was that the arrangement should be such that by means of push-button operation, the recorder could be promptly connected to any one of the many thermocouples and allowed to record continuously the temperature of that thermocouple.

Flight Requirements. Because its principal use would be in connection with flight-testing of planes, it was necessary for the recorder to meet the general requirements of flight instruments; namely, it must operate from the d-c power supply available on planes, its accuracy and reliability must not be unduly influenced by changes in level, by vibration, or by the wide range of ambient temperatures encountered in aerial navigation. In addition, the instrument should not produce radio interference and, naturally, should be as small and light as practicable. Because the instrument was to be used primarily in large planes, it was not considered necessary to reduce the size and weight to the extent that would be essential for use in smaller planes.

---

[1] Director of Research, Leeds and Northrup Company, Philadelphia, Pa. Mem. A.S.M.E.

[2] Chief, Electrical Division, Research Department, Leeds and Northrup Company.

[3] Electrical Research Engineer, Leeds and Northrup Company.

[4] "Measurement of High Temperatures in High-Velocity Gas Streams," by W. J. King, Trans. A.S.M.E., vol. 65, 1943, pp. 421–431.

Contributed by the Instruments and Regulators and the Aviation Divisions and presented at the Annual Meeting, New York, N. Y., Nov. 29–Dec. 3, 1943, of THE AMERICAN SOCIETY OF MECHANICAL ENGINEERS.

NOTE: Statements and opinions advanced in papers are to be understood as individual expressions of their authors and not those of the Society.

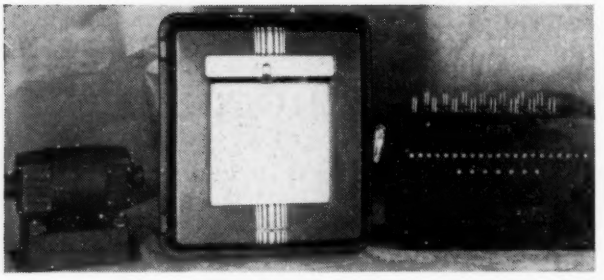


FIG. 1 FLIGHT-TEST RECORDER AND ACCESSORIES

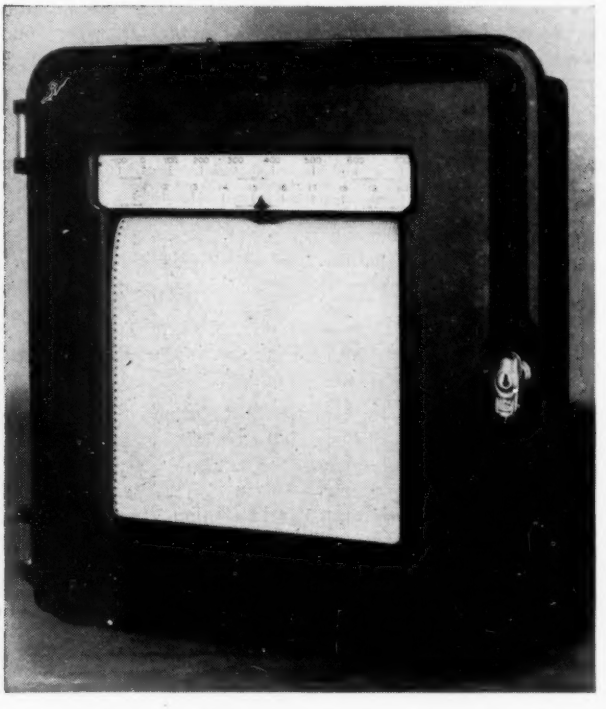


FIG. 2 FLIGHT-TEST RECORDER, SHOWING DETAILS OF SCALES

GENERAL DESCRIPTION

A general view of the recorder and its accessories is shown in Fig. 1. The accessories are a multiple-point switch box and a small rotary converter. The weight and dimensions of these items are as follows:

Recorder: Weight, 110 lb; size, $18^3/_8 \times 20^1/_8 \times 12^7/_8$ in. This weight is for a steel case. If aluminum were available, the weight would be 95 lb.

Switch box: Weight, 55 lb; size, $17^7/_8 \times 11^5/_{16} \times 9^{11}/_{16}$ in. This weight includes the 15 plug connectors which have a total weight of 4 lb.

Rotary converter: Weight 35 lb; size, $11^1/_2 \times 9^1/_4 \times {}_4{}^6$ in. This weight is for a 200 v-a unit. If available, a 150 v-a unit would be ample and the weight would be 26 lb.

Power Supply. The recorder proper is designed to operate from a 115-v, 60-cycle supply. The switch box and one or two auxiliary circuits in the recorder are designed to operate directly from the d-c supply available in the plane, usually 24 or 28.5 v. To provide for complete operation from the d-c supply in the plane, the small rotary converter is used to obtain the 115-v 60-cycle supply for the recorder proper. The total power requirement from the d-c supply is 220 w continuous, plus a maximum momentary requirement of 95 w when all stepping switches are being reset simultaneously.

Recorder. A large view of the recorder proper is shown in Fig. 2, and a block diagram of the circuits is shown in Fig. 3. From Fig. 2, it will be seen that the recorder is provided with two ranges, one spanning 800 F (—100 to +700 F) and the other spanning 950 F (1050 to 2000 F). The former is calibrated to correspond to the characteristics of copper-copnic thermocouples, and the latter to correspond to the characteristics of chromel-alumel thermocouples. These particular ranges and calibrations met the requirements of a particular problem. It will be noted that there is a gap of 350 F between the upper end of the lower scale and the lower end of the upper scale. If, in some other problem, temperatures were to be measured in the range where this gap exists, the matter could be handled in one of two ways: Either the two ranges could be expanded somewhat to close the gap, or a third range, closing the gap and overlapping the other two ranges, could be added. The former method would entail some sacrifice in accuracy whereas the latter would not. The range-changing is completely automatic in a

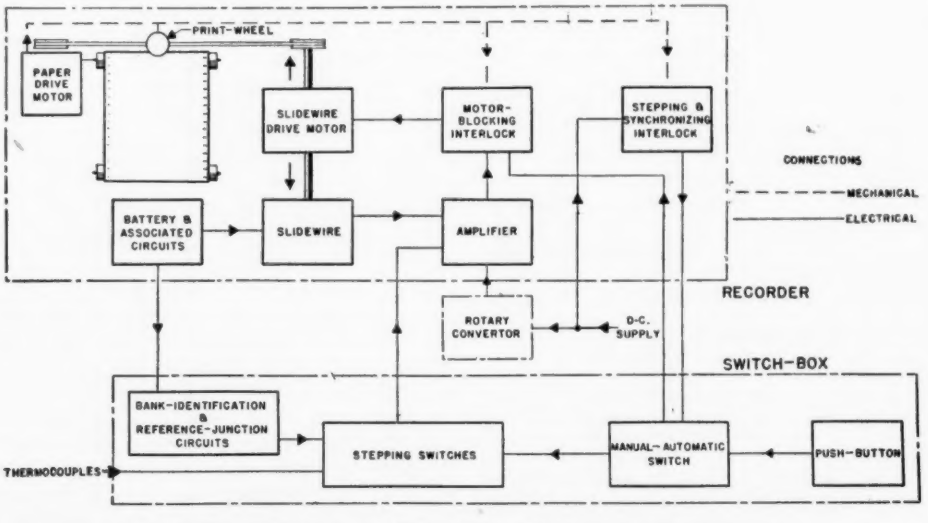


FIG. 3 BLOCK DIAGRAM OF FLIGHT-TEST RECORDER AND ACCESSORIES

manner which will be described more fully in connection with a discussion of the operating characteristics.

The recorder circuit is that of a null potentiometer. The recorder contains no galvanometer and is not affected by changes in level or by acceleration. It is built to withstand the vibrational effects encountered in plane service, provided only that it is mounted in the usual antivibration frame. The thermocouple voltage is modulated by a vibrating element and then passes through an electronic amplifier. The output of the amplifier is sufficiently powerful to operate a reversible motor, which moves the balancing contact on the slide wire of the potentiometer circuit. Associated with the potentiometer is a resistance-capacitance network, which provides appropriate damping. The vacuum tubes used in the amplifier are all of standard types, thus facilitating replacement should this be necessary. Life expectancy on these tubes is at least 1000 hr.

Switch Box. An enlarged view of the switch box is shown in Fig. 4. The seven telephone-type keys, shown at the center of the panel, control the circuits of 140 thermocouples arranged in banks of 20. As many of the seven banks as desired may be cut out of service by throwing down the respective keys. These may be cut out of service in any order, and even if all but one of the banks are cut out of service, the recorder will continue to recycle on the 20 thermocouples connected to the remaining bank. The bank on which the recorder is operating at any moment is indicated clearly by a signal lamp immediately above the bank key. The longer row of signal lamps above the bank signal lamps indicates the particular thermocouple, in any bank, that is being recorded at the moment. It will be noted that this row of signal lamps contains 21 lamps, although there are only 20 thermocouples in each bank. The additional point on each bank is used for "bank identification" on the recorder chart, as will be discussed under "Operating Characteristics."

The connections to the thermocouples are made by means of the plug connectors at the top of the switch box. Each plug connector handles 10 thermocouples so that there are two plug connectors for each of the seven banks. The "power" plug connector, at the extreme left in Fig. 4, handles the interconnections between the switch box and the recorder proper.

A quick-acting push button, shown below the fifth and sixth bank keys, provides push-button control of the bank switches, as mentioned in outlining the requirements. The telephone key, shown below the first and second bank keys, is a selector switch to give control of the switching to the recorder mechanism or to the push button.

The switch-box housing is lined completely with copper for the purpose of eliminating radio interference. The relays, switches, and other parts used in the switch box have been chosen to withstand satisfactorily the vibration and other conditions encountered in plane service.

The selector switches were chosen carefully to insure reliable operation and long life. They are of a type which has undergone exhaustive development for use in automatic-telephone circuits, and all sliding contact surfaces are heavily gold-plated, Fig. 5.

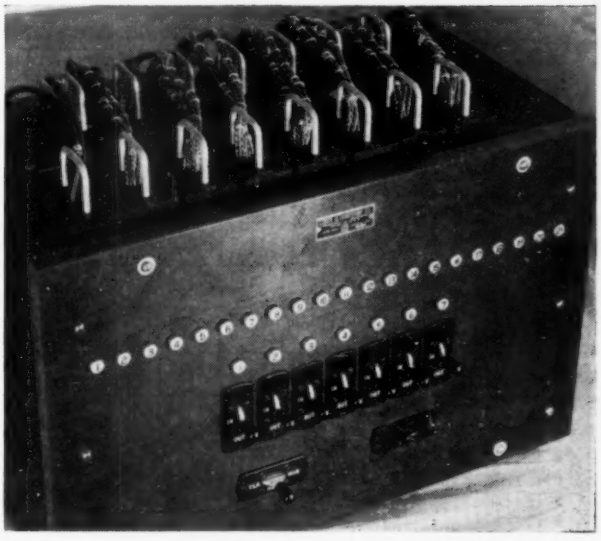


FIG. 4 SWITCH BOX, SHOWING PANEL DETAILS

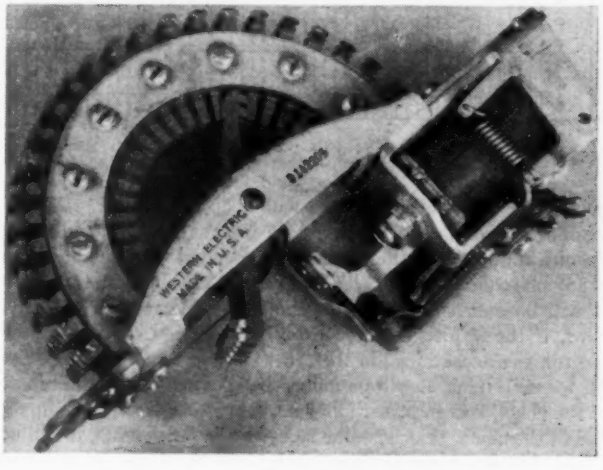


FIG. 5 SELECTOR SWITCH

OPERATING CHARACTERISTICS

Accuracy, Sensitivity, and Speed. The sensitivity of the recorder and the readability of the chart are better than ± 0.25 per cent of the scale range, and the limit of error is less than ±0.5 per cent of the scale range. In a range of 800 F, 0.25 per cent corresponds to 2 F and 0.5 per cent corresponds to 4 F. The time required for recording on each point is somewhat under 2 sec, specifically, 1.63 sec per point, so that all 147 points (140 thermocouples and 7 bank-identification points) are covered in a period of 4 min. The design of the recorder is such that the constant time-cycle of 1.63 sec is adequate to permit a complete null balance on each point regardless of whether successive points are at nearly the same temperature or are at the extreme ends of the 10-in. chart. The constant time-cycle makes it unnecessary to group the thermocouples according to their temperatures. Hence they may be grouped according to some other scheme as, for example, according to the units on which the temperature measurements are being made.

Fig. 6 is a reproduction of the recorder chart, showing a complete record of all 147 points. It will be seen that all 147 points are obtained without crowding on only an 8 in. length of chart. Because an 11 in. length of chart is always visible, at least one recording for each thermocouple is always visible. This is for a chart speed of 2 ipm. By throwing a lever, the speed of the chart may be reduced to 4 iph. This slower speed would be used in the event that it were desired to record continuously the temperature of one of the thermocouples. A careful examination of the chart will disclose a number of the operating features of the recorder. In examining the chart, it should be remembered that the normal motion is downward so that the record proceeds from the bottom to the top.

At the extreme left of the chart will be found, in order, the

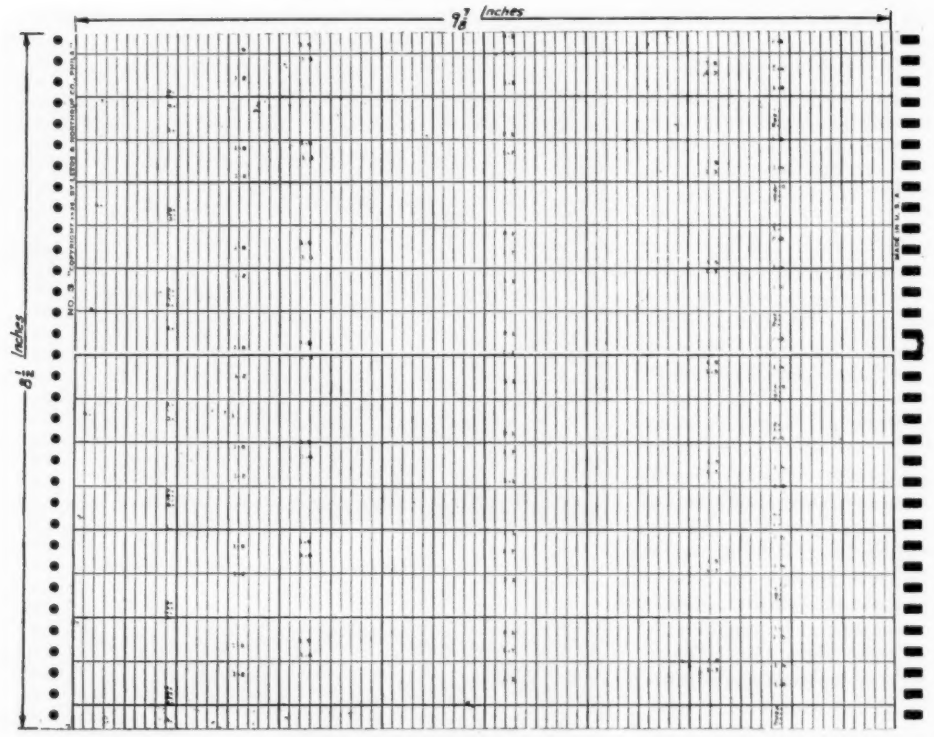


FIG. 6 REPRODUCTION OF RECORDER CHART

numerals 1 to 7, inclusive; these will be discussed later. The remaining six columns of numerals on the chart correspond to six definite voltages, and the small dots associated with each numeral in any one column should all fall at the same position on the chart. It will be seen that this condition is approached very closely. Now, if the sequence of recording is examined, that is, if the recordings are examined in the order of their numbers, from 1 to 21, for each bank, it will be found that point 21, near the center of the chart, was recorded following a printing toward the upper end of the chart, that is, point 20. On the other hand, it will be found that the recording for point 17 in the same column was made following a printing on point 16, which is much lower on the chart. Hence, the printwheel came in from a higher point on the scale to record point 21 and came in from a lower point on the scale to record point 17, and yet the two points are in nearly perfect alignment. This is a reliable index of the sensitivity and reproducibility of the recorder mechanism. If the first and the last of the six columns are examined, it will be found that, in a number of cases, series of successive numerals appear in the same column. For instance, near the upper part of the last column, points 7, 8, 9, and 10 were recorded successively. The recording for point 6 will be found to be near the other end of the chart. Hence point 7 was recorded after a large travel of the printwheel, whereas points 8, 9, and 10 were recorded without any occasion for travel of the printwheel, but the recording for point 7 is in perfect alignment with the recordings for points 8, 9, and 10. This is an indication that the 1.63 sec allowed for recording each point is ample to provide for complete balance, even when the temperatures to be recorded are widely spaced on the chart.

The balancing characteristic of the instrument may be recorded automatically by adding a pen to the printwheel carriage and by using an increased chart speed. The normal balancing characteristic obtained in this way is shown in Fig. 7, in the curve marked "damped." The balancing characteristic with the damping removed also is shown in Fig. 7. These curves are for a chart traverse approximating 40 per cent of the full width of the chart, and the chart speed was more than 20 times the normal chart speed of 2 ipm. Referring to the damped curve, it will be seen that about $^2/_{10}$ of the total cycle of 1.63 sec is required for the linear traverse (motor running at constant speed), and that about $^3/_{10}$ of the total cycle is required by the residual oscillations. The time for the linear portion of the traverse increases in proportion to the length of the traverse, and the time for the residual oscillation is a constant. Hence, for a full-scale traverse, one half of the full time-cycle would be required for the linear portion of the traverse. Adding $^3/_{10}$ for the residual oscillations gives a total time corresponding to $^5/_{10}$ of the complete cycle. As may be seen from Fig. 8, more than 92 per cent of the complete cycle is available for balancing. Similar analysis would show that, without damping, the oscillations would be sustained beyond the end of the cycle and would cause erratic operation.

Referring to Fig. 8, the diagram marked "automatic operation" shows the sequence of operations and the times available for them, when the switching is being done automatically by the recorder. It will be seen that 1.51 sec, or more than 92 per cent of the total cycle of 1.63 sec, are available for balancing.

Bank Identification. The numerals 1 to 7, inclusive, at the left of the chart, Fig. 8, are used for bank identification. It will be noted that each of these identification points occupies a specific position on the chart. The fact that each of these identification markings appears in its own particular position on the chart

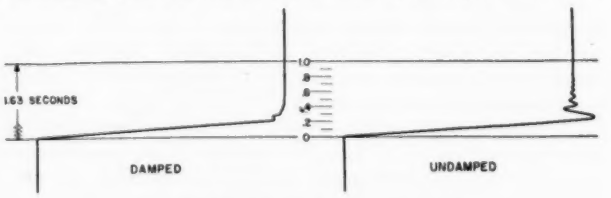


FIG. 7 BALANCING CHARACTERISTIC

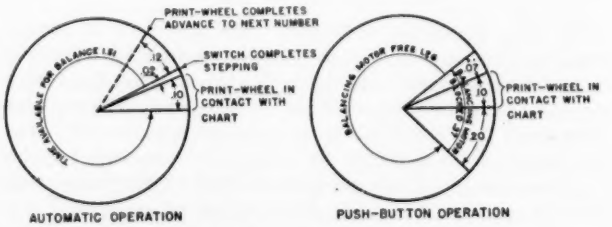


FIG. 8 SEQUENCE OF OPERATIONS
(Numbers on circle diagrams give time in seconds.)

indicates that there is complete synchronization between the switching mechanism and the printing mechanism. The bank identification is accomplished in the following manner: On bank No. 1 there is no thermocouple connected to the No. 1 switch point. Instead this switch point is connected to an electrical network so arranged that the recorder printwheel prints No. 1 at a specific location on the chart assigned for the identification of the No. 1 bank. Likewise, in bank No. 2 there is no thermocouple connected to the No. 2 point on the switch, the connections to the No. 2 point again being made to a network which causes the recorder printwheel to print the numeral 2 at a place on the chart specifically assigned for the identification of the No. 2 bank; and so on for all seven banks.

Automatic Range-Changing. In discussing the two or more ranges provided for the recorder, it was mentioned that range-changing is completely automatic. This is accomplished in the following manner: Each one of the seven banks of 20 thermocouples may be associated with a different network to provide a different recorder range for each bank, or several of the banks may be connected to provide the same range while the remaining bank or banks may be connected to provide another range. For instance, if most of the thermocouples were to be of the copper-copnic type for measuring temperatures in the range of —100 F to +700 F, the first six banks would be associated with that range on the recorder, and the seventh bank would be associated with the range of 1050 to 2000 F, calibrated for chromel-alumel couples. In that case, as part of the automatic cycling operation, the range remains unchanged when switching between banks, until bank No. 7 is reached and then is changed automatically. When bank No. 7 has been recorded and the recorder is switched to another bank, the range automatically changes back to the lower one. Automatic range-changing applies also to push-button operation.

Automatic Reference-Junction Compensation. The fourteen plug connectors, Fig. 4, which bring the thermocouple leads to the switch box connect to fourteen receptacles which are built into a "thermal-equilibrium" chamber, housed in the top of the switch box. This chamber is provided to keep all of the reference junctions at the same temperature regardless of what that temperature may be. This thermal-equilibrium chamber also houses one or more resistance-type compensators to provide automatic compensation for the temperature of the reference junctions.

Push-Button Operation. The push-button operation feature introduced certain problems that had to be met in a reliable way and without introducing undue complications. Obviously, when the switches are operated by push button, all synchronization between the switching and the recorder printing is lost so that, when the control of the switching is returned to the recorder mechanism, some provision must be made to resynchronize the switching and printing. This is accomplished by an electrical interlock between the printwheel and the automatic selector-switch advancing mechanism. Under automatic operation, the selector switches are always started from the No. 1 position and, by means of the interlock, the switching is not allowed to start until the printwheel is ready to print the numeral "1." By itself, this simple interlock feature is not entirely satisfactory because, even though the first active selector switch were thus synchronized, the remaining ones might be out of synchronism due to having been left in random positions as the result of push-button operation. Of course, after a full cycle, involving the automatic operation of all seven selector switches, the synchronization would be complete, but this might require an interval of 4 min, which is much too long. This delay is overcome by causing all selector switches to "clear" automatically at the time the switching control is transferred from "push button" to "automatic." The "clearing" operation sends all selector switches to their No. 1 positions in a maximum of 6 sec. The automatic synchronization of the printwheel, which follows immediately, requires a maximum of 34 sec, so that the total time for complete synchronization varies from a minimum of less than 1 sec to a maximum of 40 sec.

Although the constant-time printing cycle is advantageous in several respects, its use in combination with push-button operation introduced another problem. Under push-button operation, the selector switches are stepped quickly from one thermocouple to another without waiting for the recorder to balance and print. Hence the recorder might be attempting to rebalance at the instant the printwheel was in contact with the paper, thus causing damage to the chart, the printwheel, or both. This problem was met by interlocking the balancing motor with the printwheel, so that, at the moment the printwheel is in contact with the chart, the balancing motor is prevented from operating. This interlock is effective only when push-button operation is used. It is unnecessary during automatic operation from the recorder (see Fig. 8, diagram marked "push button").

"Grounding" of Thermocouples. In some applications, the thermocouples are not in direct contact with metallic structures and in other applications they are; that is, the thermocouples may be either "grounded" or "ungrounded." For this reason, it was necessary to arrange the measuring circuits so that satisfactory operation could be obtained under either condition. This is a matter of the detailed electric circuits, including their insulation and guarding, which is somewhat beyond the scope of the present paper.

Operating Experience—Availability

Operating experience with this recorder has necessarily been limited, but the observations so far made have been encouraging. During the many months involved in the development of the recorder, the selector switches were subjected to many thousands of operations and not a single failure was recorded. The automatic compensator for reference-junction temperature was subjected to ambient temperatures as low as 0 F, and no error outside the tolerance claimed for the instrument was observed. This test will be repeated with still lower ambient temperature, but the tests already made show a lag of 1 hr between the time a temperature change is made at the exterior and the time when one half of such change is effected in the interior of the "equilibrium chamber." This high degree of lagging is a fairly reliable indication that further lowering of the ambient temperature will not cause appreciable error, under expected service conditions.

The instrument has had approximately 12 hr of actual flight service at altitudes ranging up to 35,000 ft. The ambient temperature at the recorder was as low as —20 F, and this low ambient temperature did not appear to affect the instrument operation in any way. Accelerations caused no apparent effect on any part of the instrument. In fact, no difficulties attributable to the recorder or switch box were encountered during the whole flight-test period. During this flight test, the instrument was not provided with automatic compensation for the thermocouple reference junctions, the temperature of these being fixed by ice baths.

This new recorder is not now in commerical production and is available only in limited quantity for very urgent war problems.

Acknowledgment

Throughout the development work and the field testing, the authors have had the splendid co-operation of Messrs. W. J. King and S. F. Richardson, both of the General Electric Company, and their respective staffs, and wish to express their thanks for this assistance.

High-Temperature-Steam Corrosion Studies at Detroit

By I. A. ROHRIG,[1] R. M. VAN DUZER, JR.,[2] AND C. H. FELLOWS[1]

A program was undertaken by The Detroit Edison Company to determine the rate of corrosion and the relative corrosion resistance in an unstressed condition of various materials that could be used in the construction of steam generators, piping, and turbines. Specimens were exposed in a steam atmosphere at 380 psi and at temperatures of 925 F and 1100 F. The investigation required 5 years for completion; during that time 46 different materials were studied, including nickel, nickel-copper alloys, chromium and chromium-nickel stainless steels, medium- and low-alloy steels, carbon steels, and alloy cast iron. The tests were conducted under plant-operating conditions, and samples were exposed in superheated station steam for periods ranging from 4000 to 16,000 hr. Weight-loss, hardness, and metallographic data were obtained after successive exposure periods for many of the samples. Trends in the corrosion rate were plotted for some of the materials. The test results, reported in this paper, indicate that the weight loss of plain-carbon steel exposed to 1100 F steam continues at a high rate, whereas the rate of loss of the alloyed materials decreases with time. The high chromium-nickel and the 12-chromium stainless steels were the most corrosion-resistant. The corrosion rate of 0.50 molybdenum and 1.0 chromium steels compared favorably with that of steels containing 5 chromium. Nonferrous materials were not as corrosion-resistant in high-temperature steam as the high-alloy ferrous materials. Materials which corroded rapidly at 1100 F corroded only slightly at 925 F, and at this lower temperature there was little difference between the rate of corrosion of plain carbon and alloy steels.

Introduction

EXPERIENCE gained in the operation of two experimental installations utilizing steam at high temperatures located in plants of The Detroit Edison Company led to an investigation of the corrosion effects of high-temperature steam on a selected group of metals for superheaters, piping, and turbines (1, 2).[3] The results of an extended study of this subject are the basis for the present paper.

One of these experimental high-temperature installations was made at the Delray Plant in 1930; it comprised a turbogenerator and superheater. Materials in the superheater and piping were high-alloy stainless steels of high creep resistance that were known not to corrode significantly under the influence of high-temperature steam. In 1934, certain low-alloy steels were used in the tubing of the superheaters installed at the Connors Creek Plant to supply steam at 840 F. The alloys used at Delray, although highly corrosion-resistant, were too costly for this use. At Connors Creek, within the first 2 years of operation there were indications of corrosion resulting from the reaction between the high-temperature steam and the low-alloy steels used there. The experiences with both of these installations and concurrent development in high-creep-resistant low-alloy materials indicated that future installations for large-scale generation could be made with more economical and more suitable materials than those used in the original installations.

Several years earlier, in anticipation of the use of steam above 700 F, in the generation of electric power, some thought had been given to the reaction between steel and high-temperature steam. Laboratory-type studies were begun in 1927 that demonstrated the trend of the reaction between plain-carbon and high-alloy steel and steam at about 1100 F (3). These studies were not comprehensive enough to permit the data obtained to be used in engineering design, and moreover, by 1934, other alloys, especially low-alloy steels, were offered for high-temperature service. With the upward trend in the temperature of steam used in the generation of electricity, it became desirable, not only to examine the new alloys offered for high-temperature service and to evaluate them from a corrosion-resistance standpoint, but also to obtain data that would enable the usefulness of these alloys over long periods of time to be estimated.

Facilities were available for carrying out a comprehensive examination of this steel-steam reaction under what were practically power-plant operating conditions. Accordingly, a program of investigation was discussed with an interested steel manufacturer, the purpose of which was to determine what the effect of high-temperature steam would be on a group of low-alloy materials then being used or proposed for use in high-temperature equipment. The specific object was to determine the rate of weight loss over an approximately 2-year period and all materials would be tested in an unstressed condition.

Information then available gave only the total weight lost for samples exposed to furnace gases or air for short periods of time. Such data gave no indication of what rate of metal loss could be expected over a period of years, or was there any reason to believe that metal losses as the result of oxidation in furnace gases or air would be of the same order of magnitude as losses resulting from corrosion in a steam atmosphere.

At the time this program was being considered, A. A. Potter, H. L. Solberg, and G. A. Hawkins (4) started a similar investigation at Purdue University, utilizing high-temperature high-pressure steam equipment available in their laboratory, in which they planned to obtain fundamental engineering data related to the steel-steam reaction. The two investigations had as their objective the determination of the rate of weight loss of materials subjected to the action of high-temperature steam. They differed, however, in one important respect. The Detroit Edison Company's tests were to be conducted under average steam-power-plant conditions of fluctuating steam temperature and intermittent operation, whereas those at Purdue University were to be conducted under precise laboratory control for much shorter continuous-exposure periods.

The initial group of nine materials, with which the authors'

[1] The Detroit Edison Company, Research Department, Detroit, Mich.

[2] The Detroit Edison Company, Production Department, Detroit, Mich. Mem. A.S.M.E.

[3] Numbers in parentheses refer to the Bibliography at the end of the paper.

Contributed by the Research and Power Divisions and presented at the Annual Meeting, New York, N. Y., Nov. 29–Dec. 3, 1943, of THE AMERICAN SOCIETY OF MECHANICAL ENGINEERS.

NOTE: Statements and opinions advanced in papers are to be understood as individual expressions of their authors and not those of the Society.

tests were begun, comprised steels suitable for superheater and piping use and were subjected to 1100 F steam. Additional materials were added during the course of the investigation, which continued for 5 years, from 1937 to 1942; and the scope of the work was enlarged by subjecting some of the materials to 925 F steam. All materials are described elsewhere in this paper.

The corrosion results, some of which were obtained during exposure periods up to 16,000 hr at 1100 F, show that in the case of steels of low alloy content, there is a definite retardation in the rate of metal loss with increase in the exposure period. The behavior of the carbon steels is entirely different, however; with continued exposure, the loss due to corrosion approaches a straight-line function. The results of the 925 F exposure tests do not indicate the marked differences between the alloy steels and the carbon steels that were evident in the tests at 1100 F. In the case of most of the materials tested at 925 F the losses were so small that accurate weight-loss determinations could not be made.

The results of this work agree with those published by Solberg, Hawkins, and Potter (5) for 2000-hr exposure in that the same rate-of-loss trends are shown for similar materials tested at the same temperatures, although the magnitude of the weight losses does not correspond because of the difference in testing procedure. Moreover, these results assume added significance because of the further findings of Solberg, Potter, Hawkins, and Agnew (6) that stress does not influence the corrosion rate of steels in steam at high temperatures. The information should be of value in design problems, inasmuch as the materials were tested under actual operating conditions of temperature variations and for sufficiently long time periods to establish definitely the trend of corrosion of a number of the materials studied.

Materials Investigated

The material studied in this investigation covered a variety of alloys that could be used for power-plant service, such as in superheater tubing, turbine-shell castings, turbine buckets, valves, and miscellaneous high-temperature equipment, such as flow nozzles, thermometer wells, and so forth. Included were both rolled and cast products. All samples were installed inside an experimental high-temperature steam line. In all, 46 separate materials were tested, varying in composition from relatively pure nickel through nickel-copper alloys, chrome-nickel stainless steels, medium- and

TABLE 1 COMPOSITION OF MATERIALS TESTED IN 925 F AND 1100 F STEAM

Sample No.	General type	Chemical composition C	Si	Mn	P	S	Cr	Ni	Mo	Cu	Fe	Al	Sn	Cb	Pb	Structural condition	Heat-treatment[a]	Duration of test, hr At 925 F	At 1100 F
	Nonferrous alloys:																		
1	Low-carbon nickel	0.03	0.03	0.22		0.005		99.60		0.03	0.06					Cast	A		7461
2	High-carbon nickel	0.14	0.04	0.11		0.005		99.51		0.06	0.11					Cast	A		7471
3	Magnesium deoxidized nickel	0.11	0.08	0.08		0.005		99.62		0.03	0.05					Cast	A		7461
4	Inconel	0.05	0.14	0.09		0.005	12.86	80.97		0.08	5.78					Rolled	A		7461
5	"K" Monel	0.17	0.28	0.38		0.005		66.79		28.59	0.31	2.93				Rolled	A		7461
6	"S" Monel	0.14	4.14	0.81		0.003		63.91		29.31	1.64					Cast	A		7461
7	Nickel-copper-tin alloy	..	0.66	0.59	0.69			52.66		32.51	1.50		11.10		0.09	Cast	None	4351	
8	Copper-nickel alloy	..	2.47	2.39				47.70		46.38	0.61					Cast	OQ, D	4351	
9	Copper-nickel-iron alloy	..	..	0.43				31.12		64.44	3.81					Cast	None	4351	
	Stainless Steels:																		
10	35 Nickel-15 chrome	0.14	0.70	0.86			15.46	35.56								Cast	A		7461
11	20 Nickel-25 chrome-2 columbium	0.39	0.51	0.75			24.00	19.44						2.43		Cast	A		7461
12	20 Nickel-25 chrome, type 310	0.12	1.09	0.90			25.06	20.18								Cast	A		7461
13	12 Nickel-25 chrome, type 309	0.09	0.59	0.79			22.46	12.75								Cast	A		7461
14	18 Chrome-8 nickel-2 columbium, type 347	0.13	0.46	0.71			17.63	8.73						2.08		Cast	A		7461
15	18 Chrome-8 nickel, type 304	0.07	0.16	0.14			17.60	10.20								Rolled	WQ		15143
16	12 Chrome-2 molybdenum	0.05	0.30	0.13	0.024	0.011	12.18	0.10	2.01							Rolled	A		16526
17	12 Chrome, type 420	0.32	0.22	0.36	0.014	0.008	13.57									Rolled	OQ, D	13165	16526
18	12 Chrome, type 403	0.10	0.20	0.35	0.017	0.022	12.33	0.18								Rolled	A	13165	16526
19	12 Chrome, type 416	0.11	0.25	0.35	0.016	0.308	12.27									Rolled	A		16526
20	12 Chrome, type 410	0.08	..	..			12.23									Cast	OQ, D	4351	
21	12 Chrome, type 403	0.13	0.24	0.29		0.01	11.87	0.37		0.15						Cast	OQ, D		7461
	Alloy and Carbon Steels:																		
22	5 chrome-moly-silicon	0.10	1.55	0.30	0.010	0.016	4.83		0.51		Ti 0.46					Rolled	A		15143
23	5 Chrome-moly-titanium	0.06	0.41	0.36	0.010	0.008	5.18	0.19	0.58							Rolled	A		16526
24	5 Chrome-moly	0.13	0.32	0.45	0.010	0.016	4.96		0.52							Rolled	A	13165	15143
25	2.50 Chrome-moly-silicon	0.11	0.78	0.41	0.012	0.013	2.50		0.50							Rolled	A		15143
26	1.25 Chrome-moly-silicon	0.09	0.78	0.41	0.010	0.013	1.21		0.58							Rolled	A	13165	15143
27	1.25 Chrome-moly-silicon	0.10	1.40	0.41	0.010	0.013	1.24		0.58		V					Rolled	A		15143
28	1 Chrome - vanadium, S.A.E. 6120	0.24	0.28	0.65	0.020	0.021	0.94				0.18					Rolled	A		15143
29	1 Chrome-moly	0.10	0.25	0.36	0.011	0.014	0.97		0.55							Rolled	A	13165	
30	Nitrided nitralloy	0.35	0.25	0.40	0.020	0.020	1.25		0.20			1.20				..	..	13165	16526
31	3 Nickel-moly	0.37	0.17	0.65				3.03	0.49							Cast	A		7461
32	1.25 Nickel-chrome-moly	0.41	0.28	0.77			0.73	1.25	0.59							Cast	A		7461
33	1 Nickel-chrome-moly	0.21	0.26	0.55	0.029	...	0.61	1.04	0.39							Cast	N, D	4351	
34	Silicon-moly	0.11	1.35	0.19	0.010	0.012			0.50							Rolled	A		15143
35	Carbon-moly	0.15	0.34	0.40	0.023	0.015			0.49							Cast	A, D		16526
36	Carbon-moly	0.18	0.35	0.70					0.51							Cast	N, D		16526
37	Carbon-moly	0.17	0.15	..					0.56							Rolled	A	13165	
38	Carbon-moly	0.26	0.40	0.71	0.035				0.49							Cast	N, D	4351	
39	Low-carbon, S.A.E. 1010	0.11	..	..												As rolled	None	13165	15143
40	Low-carbon, aluminum-killed	0.18	0.15	0.51			0.01	0.05	0.01	0.04						Cast	A		7461
41	Low-carbon, high phosphorus	0.12	0.10	0.50	0.17											As rolled	None	4351	
42	Medium-carbon, S.A.E. 1035	0.34	..	..												As rolled	None	13165	16526
	Cast Iron:																		
43	NiResits cast iron	3.13	1.77	1.18			3.80	13.29		6.00						Cast	None		7461
44	NiResist cast iron	2.18	2.86	1.54			1.92	15.52		6.05						Cast	None		7461
45	NiResist cast iron	2.62	1.83	1.17			2.12	20.07		0.10						Cast	None		7461
46	Invar cast Iron	2.04	1.88	0.92			3.58	35.55		0.20						Cast	None		7461

[a] A, annealed; OQ, oil-quenched; D, drawn; WQ, water-quenched; N, normalized.

low-alloy steels to plain-carbon steels, and alloy cast irons. The materials included 9 nonferrous alloys, 12 stainless steels, 17 medium- and low-alloy steels, 4 carbon steels, and 4 alloy cast irons.

Table 1 gives a tabulation of the materials and their chemical composition. This table includes information concerning the structural condition of the materials, that is, whether cast or rolled, the heat-treatment, the temperature at which they were tested, and the total hours of exposure.

Test Apparatus

The test apparatus consisted of an experimental high-temperature steam line supplied with steam from a separately fired superheater of the radiant type, installed in 1929 as experimental equipment at the Trenton Channel Power House. Station steam was supplied to the superheater at 380 psi and 700 F, and it was capable of superheating to 1100 F 6000 lb per hr of steam which passed into a 65-ft experimental section of $5^1/_2$-in-OD tubing. A schematic view of the superheater and piping is shown in Fig. 1. Advantage was taken of the various flanged joints in this piping system to insert test cages holding the specimens where they were subjected to the action of high-temperature steam.

The temperature of steam leaving the superheater was so controlled that at joint *B* Fig. 1 its temperature was 1100 F ±50 F, as indicated by a thermocouple installed at that point. The specimens tested at 1100 F were placed in the steam line between the outlet joint *A* and joint *B*. At joint *C* the temperature was reduced so that the temperature of the steam, as measured by a thermocouple adjacent to joint *D* was 925 F ±20 F. The specimens for test at 925 F were placed in the steam line between joints *C* and *D*. The steam velocities in the two sections of the steam line were low, varying from approximately 8 fps in the 1100 F section to approximately 6 fps in the 925 F section. At joint *E* the steam temperature was further reduced to 700 F at which temperature the steam was used in a turbine.

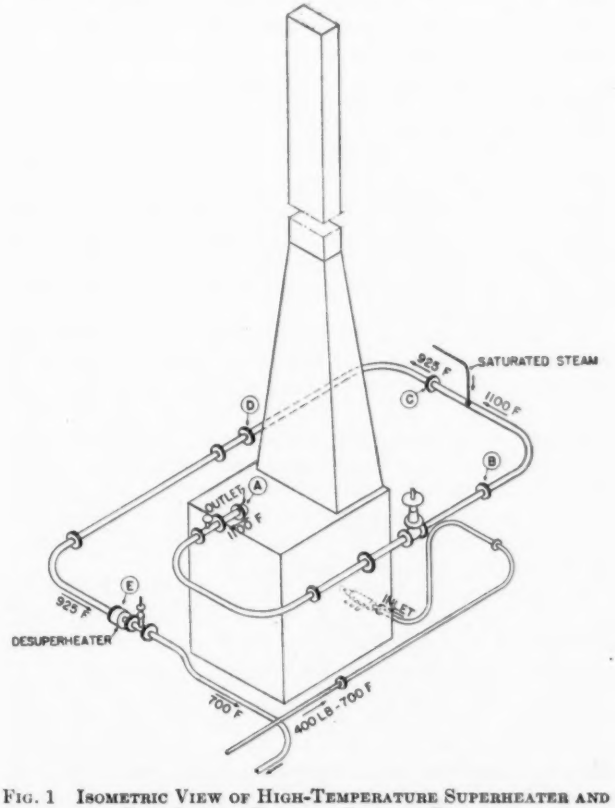


Fig. 1 Isometric View of High-Temperature Superheater and Pipe System, Trenton Channel Plant

Testing Procedure

Corrosion-test specimens and specimens used for initial-weight determinations were made from each material, according to the detail shown in Figs. 2 and 3, respectively. In the preparation of these specimens, each was given a ground finish and every precaution was taken to insure that the surfaces of all specimens were uniform and that the dimensional variations were small. These precautions were necessary since the weight loss of the specimens after exposure was determined by a comparison of the weight of a selected portion of each, after descaling, with the weight of an initial-weight specimen, 1 in. long, similar to that shown in Fig. 3. The diameter of each test specimen was carefully measured and its weight per unit length was determined by reference to the weight and diameter of the initial-weight specimens, which as noted was 1 in. in length.

The specimens were assembled into test cages made according to the detail shown in Figs. 4 and 5. The materials were tested in groups made up of individual cages welded together with short spacer rods. Each such group was placed in the steam line and held in place by tack-welding. At the conclusion of exposure periods of approximately 4000 hr, the group was withdrawn from the steam line, one cage detached, and the remaining cages replaced in the steam line for continued test.

When, at the conclusion of exposure periods, cages or assem-

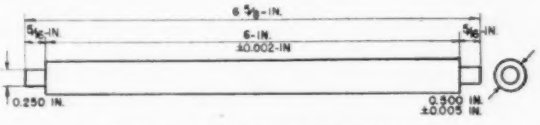


Fig. 2 Corrosion Test Specimen

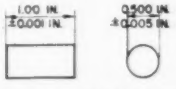


Fig. 3 Specimen for Initial-Weight Determination

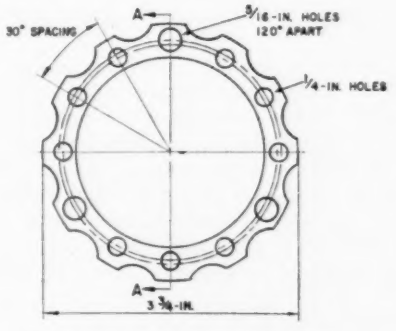


Fig. 4 Detail of Cage Ring

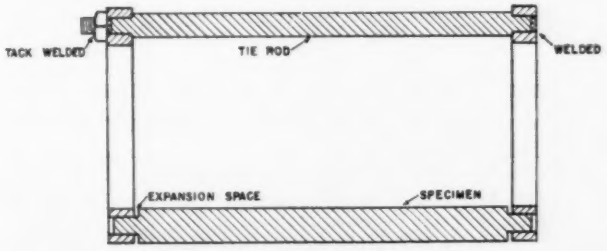


Fig. 5 Cage Assembly, Section A-A

blies of specimens were removed from the steam line, the assembly was taken apart, and the specimens prepared for examination. Two pieces, each approximately $^1/_2$ in. long, one for metallographic examination and the other for hardness determination, were cut from one end of each test specimen. The remaining portion of the specimen, that is, approximately a 5-in. length, was used for weight-loss determinations. In order to insure that the weight per unit length of the weight-loss specimens could be measured with extreme accuracy, the ends of these and of the initial-weight specimens were cut off exactly perpendicular to the longitudinal axis.

The specimens were treated in the following manner in order to determine the weight lost through corrosion.

The weight-loss specimens were first cleaned of corrosion products and then weighed. During the early stages of the investigation, the specimens were descaled with a solution of 100 parts by weight of concentrated hydrochloric acid, 5 parts by weight of stannous chloride, and 2 parts by weight of antimony oxide as inhibitors. Some of the stainless-steel specimens were descaled with concentrated hydrochloric acid containing 1 per cent by weight of quinoline ethiodide as an inhibitor. Later, most of the specimens were descaled electrolytically in a solution of 10 per cent by volume of sulphuric acid with 0.1 per cent by weight of quinoline ethiodide inhibitor. In the electrolytic method, the descaling was done in a lead container that served as the anode, the specimen acting as the cathode. The current was 6v d-c and the current density was about 0.5 amp per sq in. of specimen surface. The weight per unit length of these specimens, after removal of the corrosion products, was then compared with the original unit weights of the specimens.

Hardness readings were made on all the specimens after they were tested as well as on specimens representing the initial condition of all the materials before test. These readings were obtained with the appropriate Rockwell penetrator.

The station steam used in the tests contained no carbon dioxide and less than 0.01 ppm of oxygen. It was considered to be of high purity.

Losses Due to Corrosion

The losses due to corrosion are reported in Table 2, in terms of penetration and as per cent loss in weight, and as penetration only in Figs. 6 and 7.

In reviewing the data based upon the loss in weight, it should be remembered that rather small specimens and small values are being dealt with. In those cases where the materials scaled considerably no difficulty developed in determining the weight lost; but for such materials as did not scale, for example, the stainless steels, the weight losses were very slight and in some instances could not be measured. The relative weight losses of such materials were estimated by comparing the condition of the specimens after test with the condition of other materials of similar composition for which the weight losses resulting from longer exposure periods were known, Table 2 and Fig. 7.

For nine of the materials tested at 1100 F, weight-loss data were obtained after each of three successive exposure periods; for another set of nine materials, weight-loss data were obtained after four exposure periods; and for the last group, containing 19 materials, tested at 1100 F, data were obtained after one exposure period only. Data were obtained for the materials tested at 925 F, after three exposure periods for nine materials, and after one period only for seven materials.

Sufficient data were obtained over these relatively long exposure periods, approximately 4000 hr each, to establish the general trend of the corrosion losses, as is shown in Fig. 8, for 1100 F exposure. Although the curves included are for only 18 of the materials tested, the three general classes of materials investigated, namely, carbon, alloy, and stainless, are represented and their relative rates of corrosion, as established by these tests, are illustrated.

Corrosion at 1100 F. The curves are typical for the ferrous materials tested at 1100 F, in that the high-chromium alloys were the most corrosion resistant. In referring to the 12 per cent chromium steels, it is interesting to note that the free-machining grade sample 19 (type 416) had suffered little surface attack during 16,526 hr of exposure to steam at 1100 F, whereas the other steels in the same class, i.e., sample 17 (type 420) and sample 18 (type 403), had suffered considerable surface pitting. The 18 chromium-8 nickel steel, sample 15 (type 304) was pitted more than the straight-chromium steels.

The 12 per cent chromium-2 per cent molybdenum steel, sample 16, had a higher weight loss than the other samples of the general group in which it would normally be placed, that is, the stainless steels. The higher weight loss of this sample is also shown in Figs. 6 and 7. Improved corrosion resistance in air is reported (7) for 12 per cent chromium alloys containing 1 per cent of molybdenum over that of similar alloys without the molybdenum addition. The results of this test show, however, that in high-temperature steam a 12 per cent chromium alloy containing 2 per cent of molybdenum will scale considerably, whereas a straight 12 per cent chromium steel will exhibit only a slight tendency to scale. Pitting can be expected, however. The behavior of sample 19, which contained 0.30 per cent sulphur, indicates that an increase in the sulphur content of 12 per cent chromium alloys will further improve their corrosion resistance to the extent that pitting may be prevented in high-temperature-steam atmospheres. These tests, however, do not show conclusively that a high sulphur content will improve the corrosion resistance in steam of 12 per cent chromium steels.

Progressive weight losses were not obtained for the nonferrous alloys, samples 1 to 9, inclusive, since only two specimens of each were tested and both specimens were removed from the steam line at the same time. The relative weight losses of these samples in comparison with the ferrous materials tested at the same temperatures and for similar exposure periods are also shown in Fig. 7. The nickel samples 1, 2, and 3 had suffered intergranular attack and the two nonferrous alloys containing a high silicon content, samples 6 and 8, had scaled, sample 6 at 1100 F and sample 8 at 925 F. Furthermore, a layer of copper was found on the surface of both of these alloys after descaling. The high chromium-nickel-ferrous alloys, 10, 11, 12, 13, and 14, together with the chromium stainless steel, sample 19, had the lowest weight losses of the samples tested.

The corrosion losses of the medium- and low-alloy steels did not differ very much in that those steels containing 5 per cent chromium were not greatly superior to those containing 1 per cent chromium; in fact, the losses did not differ greatly from those for 0.50 per cent molybdenum steels. In general, those alloys having silicon contents higher than normal, 0.15 to 0.25 per cent by weight, had approximately the same, and in some cases higher, weight losses than similar alloys of low silicon content. This is contrary to the findings reported for air oxidation, where a high silicon content is beneficial (8).

The highest weight losses were obtained for the carbon steel, 39 (S.A.E. 1010) and 42 (S.A.E. 1035). Sample 40, which was approximately an S.A.E. 1020 steel that had been aluminum-killed had a much lower weight loss when exposed to steam at 1100 F than either the 1010 or the 1035 steels. At 925 F, however, the weight losses of the carbon steels were approximately the same as the weight losses of the low-alloy steels. Materials 5 and 30, which had relatively high aluminum contents, had better corrosion resistance in steam than similar alloys to which only small amounts of aluminum may have been added for deoxidization

TABLE 2 LOSSES RESULTING FROM EXPOSURE TO 925 F AND 1100 F STEAM

Sample No.	General type	Penetration during test periods, in. — 1100 F Test				925 F Test	Calculated penetration per 10,000 hr, inches at conclusion of test[d]		Per cent loss in weight at conclusion of test[d]	
		4000 hr	8000 hr	12000 hr	15000 hr	13000 hr	At 1100 F	At 925 F	At 1100 F	At 925 F
1	Low-carbon nickel		0.00348				0.00467		2.77	
2	High-carbon nickel		0.00257				0.00345		2.06	
3	Magnesium deoxidized nickel		0.01647				0.02208		13.09	
4	Inconel		0.00070				0.00094		0.57	
5	"K" Monel		0.0011				0.00148		0.88	
6	"S" Monel		0.00541				0.00725		4.32	
7	Nickel-copper-tin alloy	...[a]								
8	Copper-nickel alloy	...[a]								
9	Copper-nickel-iron alloy	...[a]								
10	35 Nickel-15 chrome		0.00006				0.00009		0.05	
11	20 Nickel-25 chrome-2 columbium		0.00034				0.00046		0.27	
12	20 Nickel-25 chrome, type 310		0.00008				0.00011		0.06	
13	12 Nickel-25 chrome, type 309		0.00006				0.00009		0.05	
14	18 Chrome-8 nickel-2 columbium, type 347		0.00006				0.00008		0.045	
15	18 Chrome-8 nickel, type 304	0.00074	0.0005	0.00002	0.0003		0.00020		0.20	
16	12 Chrome-2 molybdenum	0.00094	0.0011	0.00186			0.00152		1.50	
17	12 Chrome, type 420	...	0.00004	...		0.00004	0.00005	0.00003	0.32	0.0055
18	12 Chrome, type 403	...	...	0.00002		0.00002	0.00001	0.00002	0.13	0.0050
19	12 Chrome, type 416	...	0.00003	...			0.00003		0.21	
20	12 Chrome, type 410	...[a]								
21	12 Chrome, type 403		0.00047				0.00062		0.32	
22	5 Chrome-moly-silicon	0.0032	0.0035	0.0039	0.0044		0.0029		3.55	
23	5 Chrome-moly-titanium	0.0012	0.0028	0.0034			0.0028		2.74	
24	5 Chrome-moly	0.0022	0.0031	0.0038	0.0036	...[b]	0.0024		2.96	..[b]
25	2.50 Chrome-moly-silicon	0.0037	0.0042	0.0050	0.0051		0.0034		4.16	
26	1.25 Chrome-moly-silicon	0.0034	0.0034	0.0036	0.0041	0.00047	0.0027	0.00035	3.24	0.39
27	1.25 Chrome-moly-silicon	0.0045	0.0054	0.0059	0.0083		0.0055		6.71	
28	1 Chrome-vanadium, S.A.E. 6120	0.0034	0.0038	0.0043	0.0047		0.0031		3.77	
29	1 Chrome-moly	...[c]				0.00048		0.00036		0.38
30	Nitrided nitralloy	0.0017	0.0025	0.0031		0.00089	0.0025	0.00067	2.53	0.72
31	3 Nickel-moly		0.0028				0.0037		2.21	
32	1.25 Nickel-chrome-moly		0.0032				0.0045		2.59	
33	1 Nickel-chrome-moly	...[a]								
34	Silicon-moly	0.0037	0.0041	0.0045	0.0048		0.0032		3.86	
35	Carbon-moly	0.0021	0.0035	0.0041			0.0034		3.29	
36	Carbon-moly	0.0022	0.0033	0.0038			0.0031		3.03	
37	Carbon-moly	...[c]				0.00046		0.00035		0.37
38	Carbon-moly	...[a]								
39	Low-carbon, S.A.E. 1010	0.0107	0.0223	0.0274	0.025	0.00027	0.017	0.00021	20.04	0.22
40	Low-carbon, aluminum killed		0.0032				0.0042		2.51	
41	Low-carbon, high phosphorus	...[a]								
42	Medium-carbon, S.A.E. 1035	0.0041	0.0116	0.0156		0.00043	0.013	0.00033	12.46	0.35
43	NiResist cast iron		0.0033				0.0044		2.60	
44	NiResist cast iron		0.0035				0.0046		2.75	
45	NiResist cast iron		0.0028				0.0037		2.21	
46	Invar cast iron		0.0045				0.0060		3.58	

[a] Tested at 925 F only. Total exposure period was 4351 hr. Weight loss was not measured.
[b] Specimen damaged during cleaning, weight loss not determined.
[c] Tested at 925 F only.
[d] See Table 1 for total time of exposure.

purposes. This is in accord with the findings of Houdremont and Bandel (9) who pointed out that aluminum, like chromium, improves corrosion resistance in an atmosphere of high-temperature steam.

In the case of the chromium-molybdenum high-silicon, the chromium-molybdenum, the chromium-molybdenum-titanium, the silicon-molybdenum, and the carbon steels at 1100 F, the outer scale was brittle and tended to flake off, exposing new surfaces. In general the scale was more brittle on those steels having the higher silicon contents, which explains their relatively higher corrosion rates in steam than in air and indicates also that the mechanism of corrosion is different in steam from that in air. This has been reported also by Solberg, Hawkins, and Potter (5).

The 0.50 per cent molybdenum steels, at 1100 F, compared favorably with the 5 per cent chromium - 0.50 per cent molybdenum and the nitrided nitralloy steels. They were far superior to the plain-carbon steels.

At 1100 F, all of the cast-iron samples had approximately the same weight loss irrespective of their alloy content, Fig. 7.

Corrosion at 925 F. At 925 F, the 12 per cent chromium stainless steels were again the least affected. At this temperature there appeared to be no great difference between the 5 per cent chromium - 0.50 per cent molybdenum steel, the 0.50 per cent molybdenum steels, the plain-carbon steels, the high-phosphorus steel, the chromium-molybdenum-silicon steels, the chromium-nickel-molybdenum steel, and the nitrided nitralloy steel, as each had scaled only slightly, Fig. 11. Although the actual weight losses of the nonferrous materials, 7, 8, and 9, tested at 925 F, could only be estimated (see Fig. 7), metallographic examination indicated that they had corroded more than the 12 chromium steels tested at the same temperature.

Surface Characteristics. The weight losses were so slight, in the case of many of the materials tested, particularly at 925 F, that it is better to consider similar materials, for example, the high chromium-nickel stainless steels, as a group. In view of this, the results of the metallographic examinations are important. On that basis a distinction can be made between the samples when no such distinction can be made on the basis of weight-loss measurements. The photomicrographs, Fig. 9, show that sample 19, the free-machining grade of 12 per cent chromium stainless steel, had greater surface stability than the other steels of the same general type. The 18-8 stainless steel, sample 15, had pitted more than any of the 12 per cent chromium steels but the columbium-stabilized 18-8 stainless steel, sample 14, had not pitted. In general, the steels of this class had good surface stability and corrosion resistance in high-temperature steam.

A uniform and adherent scale formed on all the steels at 925 F except the chromium stainless steels, which had pitted slightly at this temperature. Fig. 12 illustrates the surface condition of representative steels at the conclusion of test exposure periods. The scale found on the specimens, exposed to 925 F steam, is shown to be adherent, Fig. 12 (*a*), whereas in the case of similar steels exposed to 1100 F steam, Fig. 12 (*b*), much of the scale, especially the outer layers, had flaked off. Fig. 12 (*c*) illustrates typical adherent scales formed at 1100 F.

This apparent greater adherence of the scale at 925 F than at 1100 F is one reason for less severe corrosion at the lower tempera-

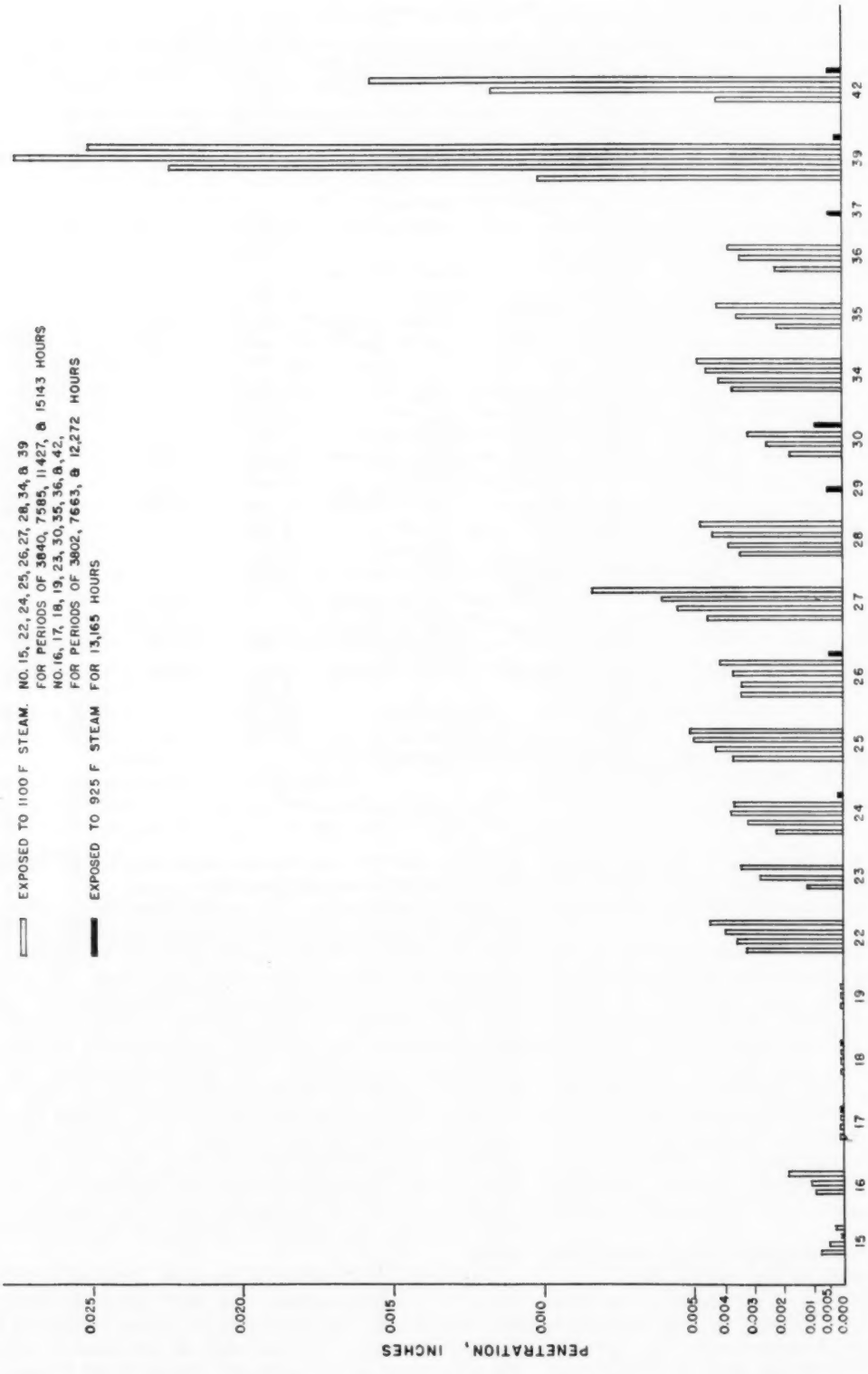


FIG. 6 PENETRATION DUE TO CORROSION OF METALS EXPOSED TO HIGH-TEMPERATURE STEAM FOR DIFFERENT EXPOSURE PERIODS

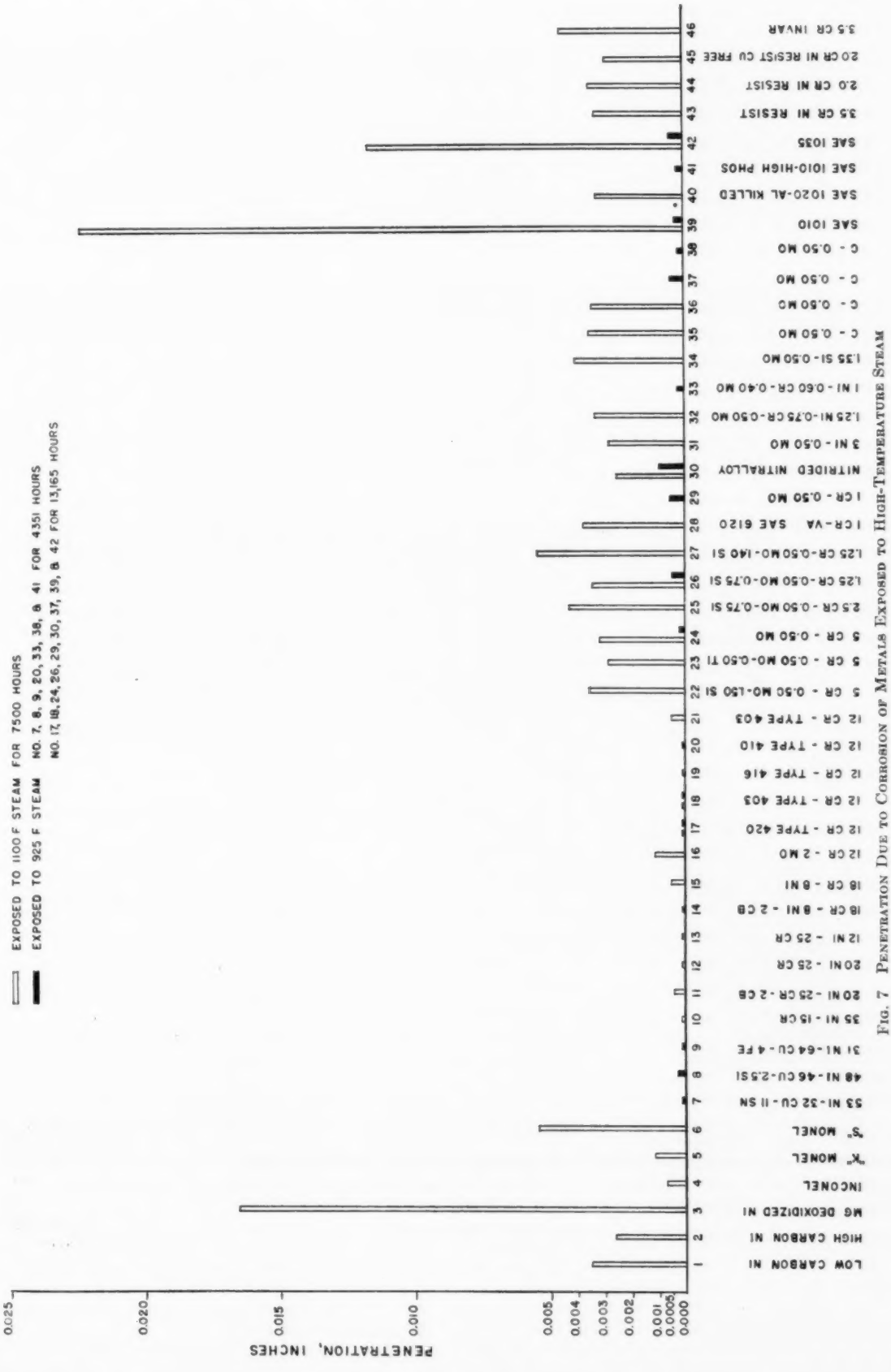


FIG. 7 PENETRATION DUE TO CORROSION OF METALS EXPOSED TO HIGH-TEMPERATURE STEAM

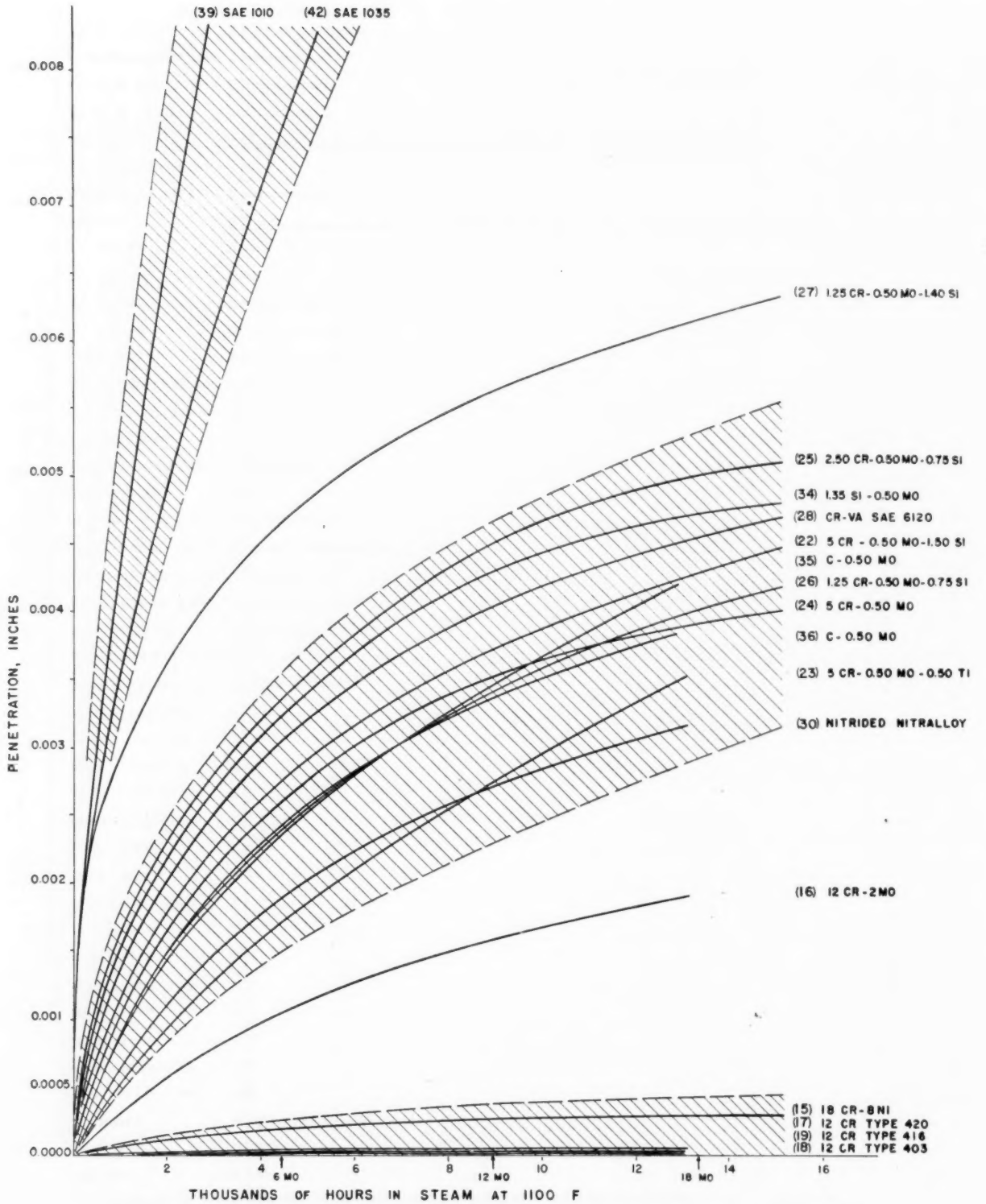


FIG. 8 EFFECT OF LONG-TIME EXPOSURE TO STEAM AT 1100 F UPON CARBON- AND ALLOY-STEEL BARS

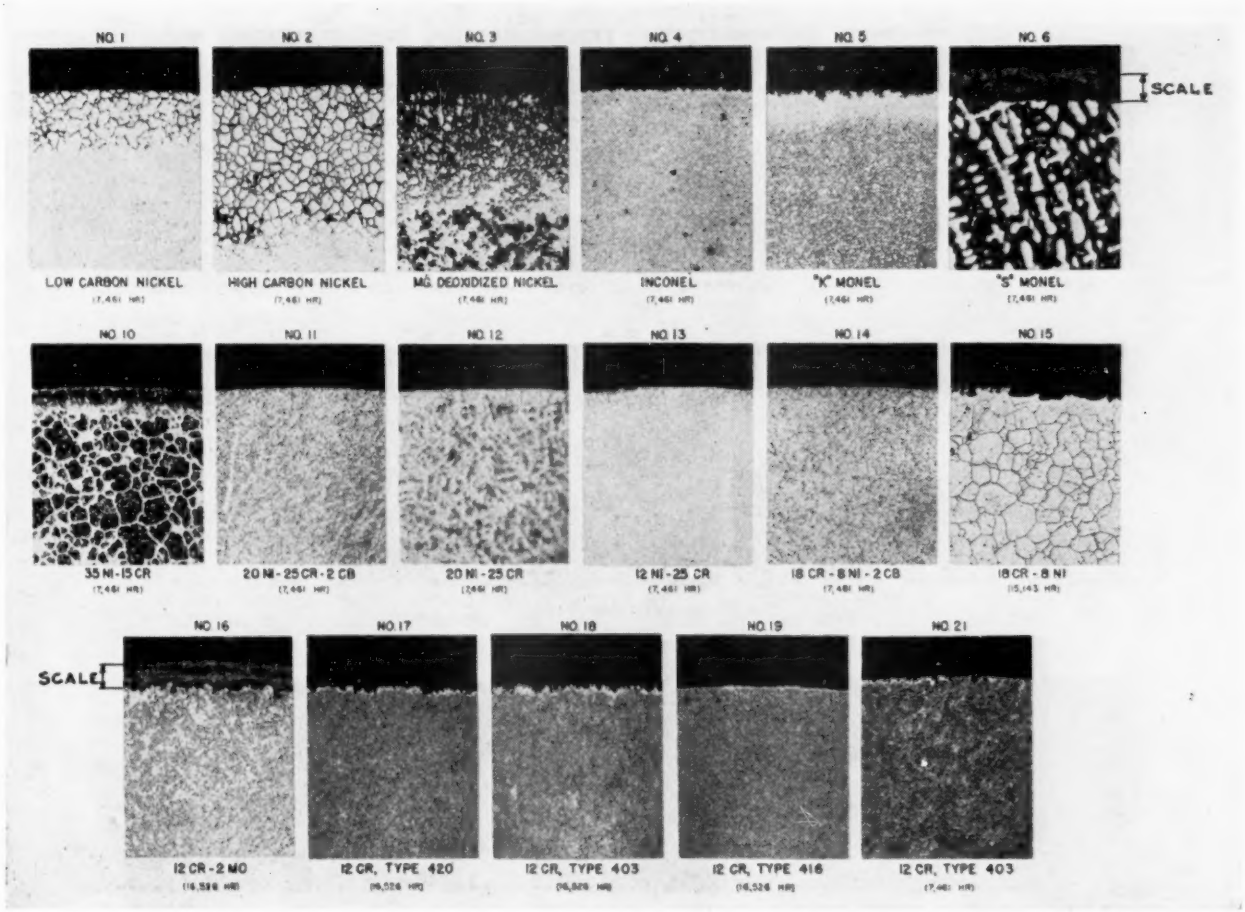


FIG. 9 PHOTOMICROGRAPHS SHOWING EFFECT OF 1100 F STEAM ON METALS

ture. The greater reaction rate between steam and the materials at 1100 F than at 925 F is a further reason for the difference in corrosion at the two temperatures.

For certain of the steels tested, the scale formed in distinct layers and tended to flake off as a result of temperature changes when the superheater was cooled to room temperature. This may offer an explanation for the relatively high weight loss of these samples in spite of their alloy content. The scale on the carbon steels, except sample 40, formed in thick layers. The scale on certain of the samples was tight and adherent at 1100 F, in spite of temperature variation.

The ability of a metal to maintain an adherent protective scale during high-temperature service is important and apparently can be controlled by using or limiting certain elements in an alloy; as, for example, 0.50 per cent of molybdenum added to a plain-carbon steel greatly improves the corrosion resistance in steam at 1100 F, but 2 per cent of molybdenum added to a 12 per cent chromium steel lowers the corrosion resistance of that steel. Silicon also can be considered in the same way, in that a high silicon content does not improve the corrosion resistance of steels in steam as it does in air.

Hardness. The hardness of all materials tested is given in Table 3. The hardness of most of the nonferrous alloys was reduced by exposure at 1100 F, but at 925 F two of the materials, 7 and 9, increased in hardness owing to the fact that they were precipitation-hardening alloys. Increases in hardness after 1100 F exposure also occurred in several of the stainless steels, namely, 10, 12, 13, 14, and 15.

In general the hardness of the low-alloy, medium alloy, and plain-carbon steels was reduced through exposure to the high-temperature-steam atmosphere. In some instances, however, as shown in Table 3, practically no change occurred. This may be attributed to the heat-treatment that the materials had received.

Indications of slight precipitation reactions were shown by the hardness changes of steels 22, 35, and 37, and hardness increases were found for three of the cast irons, 43, 44, and 46.

CONCLUDING COMMENT

Although this investigation has been comprehensive in that in it were included a fairly large number of different materials in the several classes of metals proposed for high-temperature service, the conclusions drawn from the results must be qualified by reason of the fact that in many instances only one specimen was examined for a given material at any one temperature and exposure period. To have done otherwise would have provided many more data, but would have required much larger quantities of material and an enormously greater expenditure of man-hours than it appeared could be justified at the time of the inception of the work.

In summarizing the results of this investigation, the following statements can be made:

1 In general, ferrous alloys containing high percentages of chromium alone are corrosion-resistant in steam at 1100 F.

2 Ferrous alloys containing high percentages of chromium and nickel are corrosion-resistant in steam at 1100 F.

3 Nonferrous alloys containing high percentages of nickel

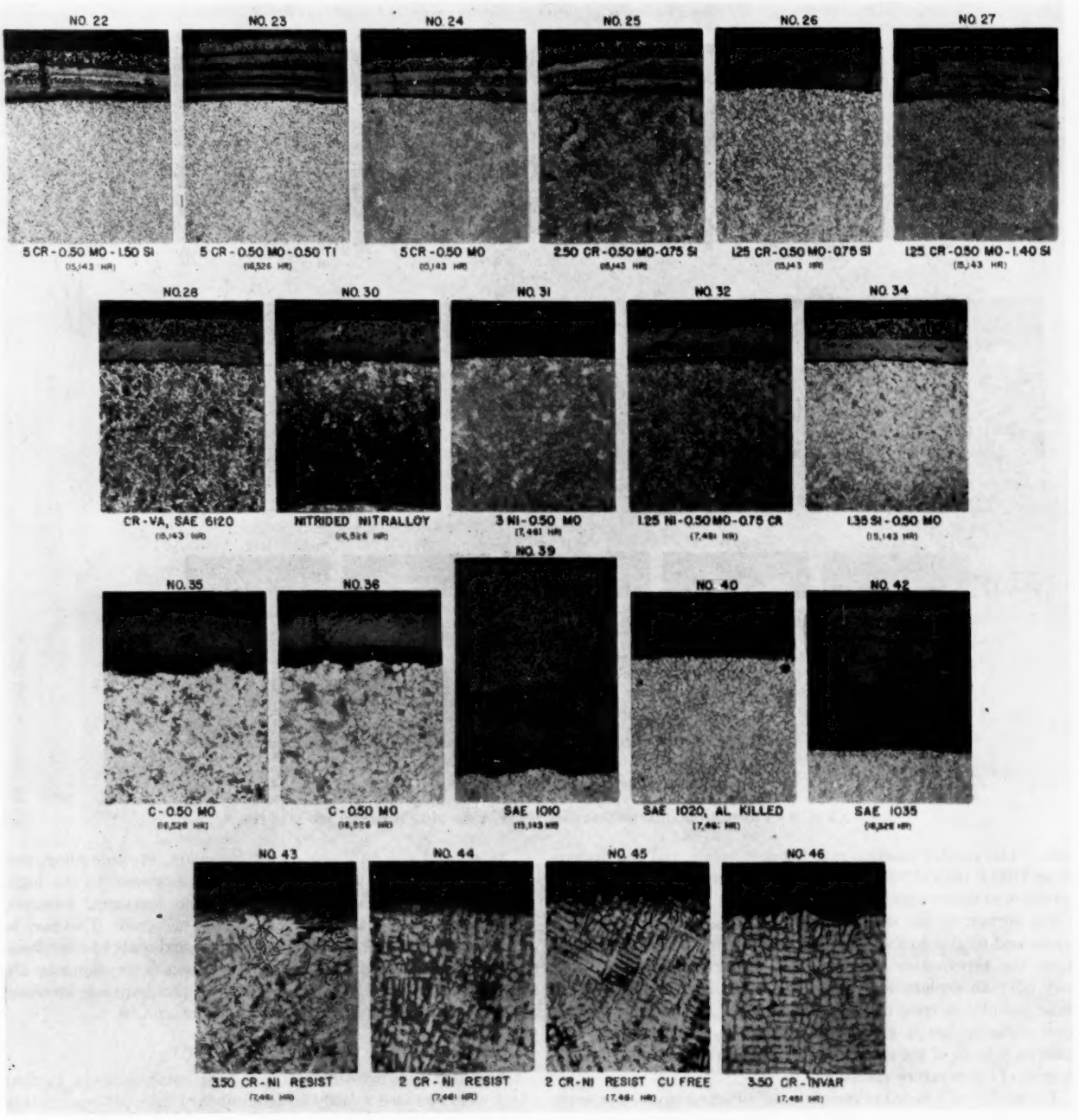


FIG. 10 PHOTOMICROGRAPHS SHOWING EFFECT OF 1100 F STEAM ON METALS

and copper that were tested in either 925 F or 1100 F steam can be expected to corrode in steam at those temperatures.

4 Although significant differences exist between the corrosion rates of carbon steels and medium- or low-alloy steels at 1100 F, at 925 F only a slight difference exists.

5 At both 925 and 1100 F, many steels that have a relatively low alloy content (0.5 molybdenum, samples 35, 36, 37, and 38) compare favorably in corrosion resistance with steels of medium alloy contents (5 chromium, samples 22, 23, and 24).

6 The formation and maintenance of an adherent scale materially increases the corrosion resistance of materials exposed to high-temperature steam.

7 The trends in the reaction between steam at high temperatures and the various steels for which weight-loss rates were determined, the authors believe, have been satisfactorily demonstrated, and on the basis of these trends the user of such steels may be assured that their rates of corrosion in steam atmospheres do not continue to increase. They flatten out and, as has been shown in the case of many of the low-alloy steels, the rates tend to be materially reduced after 15,000 to 16,000 hr at 1100 F. Some reasons for this have been suggested, but the exact mechanism which underlies these reasons has not been fully explored.

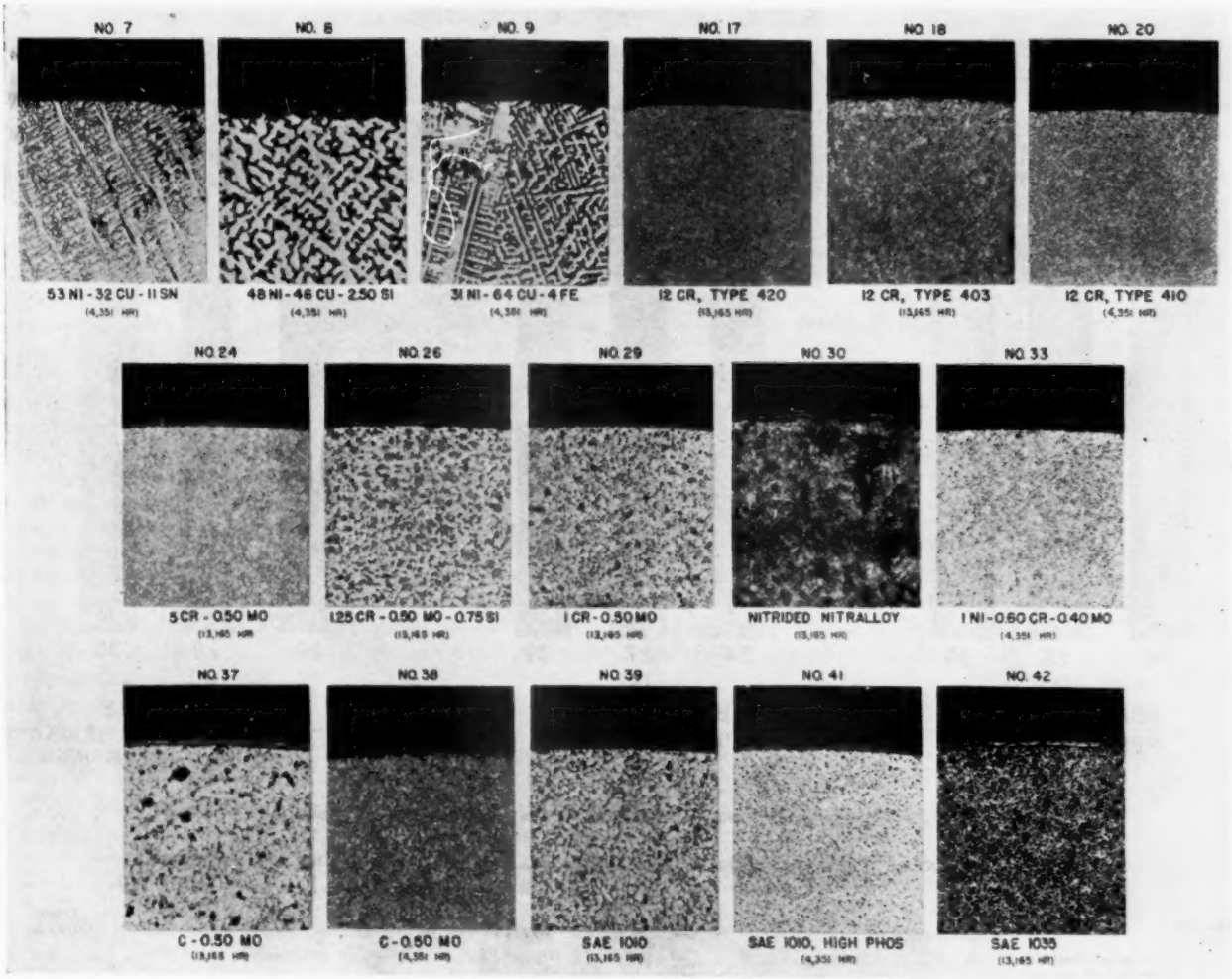


FIG. 11 PHOTOMICROGRAPHS SHOWING EFFECT OF 925 F STEAM ON METALS

ACKNOWLEDGMENT

The authors wish to acknowledge the co-operation from the Steel and Tube Division of the Timken Roller Bearing Company, the Lunkenheimer Company, the National Tube Company, the International Nickel Company, and the General Electric Company. These companies supplied most of the materials studied. Acknowledgment is made also of the co-operation of the Climax Molybdenum Company in permitting the use of its laboratory equipment for cutting the specimens after each exposure period.

The authors are indebted also to their associates in the company who worked on this study and assisted in the many activities incidental to its progress.

[Fig. 12 and Table 3 will be found on the following page.]

BIBLIOGRAPHY

1 "High-Temperature-Steam Experience at Detroit," by P. W. Thompson and R. M. Van Duzer, Jr., Trans. A.S.M.E., vol. 56, 1934, pp. 497–514.

2 "High-Temperature-Steam Experience at Detroit," by R. M. Van Duzer, Jr., and Arthur McCutchan, Trans. A.S.M.E., vol. 61, 1939, pp. 383–401.

3 "The Dissociation of Water in Steel Tubes at High Temperatures and Pressures," by C. H. Fellows, *Journal American Water Works Association*, vol. 21, 1929, pp. 1373–1387.

4 "Investigation of the Oxidation of Metals by High-Temperature Steam," by A. A. Potter, H. L. Solberg, and G. A. Hawkins, Trans. A.S.M.E., vol. 59, 1937, pp. 725–732.

5 "Corrosion of Unstressed Steel Specimens and Various Alloys by High-Temperature Steam," by H. L. Solberg, G. A. Hawkins, and A. A. Potter, Trans. A.S.M.E., vol. 64, 1942, pp. 303–316.

6 "The Corrosion of Stressed Alloy-Steel Bars by High-Temperature Steam," by H. L. Solberg, A. A. Potter, G. A. Hawkins, and J. T. Agnew, Trans. A.S.M.E., vol. 65, 1943, pp. 47–52.

7 "Improved 12 Per Cent Chromium Steel Containing Molybdenum," *Metals and Alloys*, vol. 18, July, 1943, pp. 55–62.

8 "Influence of Chromium, Silicon, and Aluminum on the Oxidation Resistance of Intermediate Alloy Steels," by A. E. White, C. L. Clark, and C. H. McCollam, Trans., American Society for Metals, vol. 27, 1939, pp. 125–148.

9 "The Reactions of Hot Gases With Heat-Resisting Steels," by E. Houdremont and Gerhard Bandel, *Archiv für das Eisenhüenwesen*, vol. 11, 1937–38, pp. 131–138.

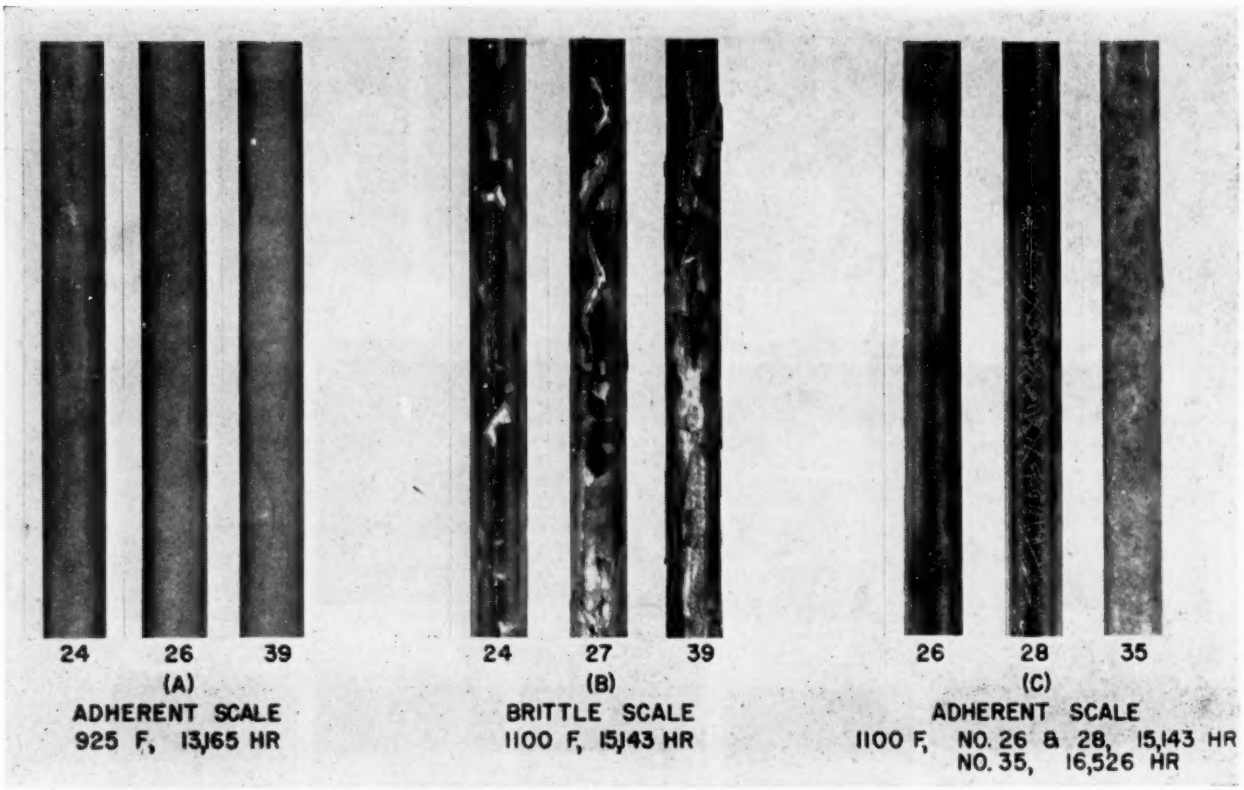


FIG. 12 SURFACE CONDITION OF TYPICAL SPECIMENS AFTER EXPOSURE TO 925 F AND 1100 F STEAM

TABLE 3 BRINELL HARDNESS BEFORE AND AFTER EXPOSURE TO 925 F AND 1100 F STEAM

Sample no.	General type	1100 F Tests: Before test	After 4000 hr	After 8000 hr		After 12000 hr	After 15000 hr	925 F Tests: Before test	After 4000 hr	After 8000 hr	After 13000 hr	
1	Low-carbon nickel	93		90	93							
2	High-carbon nickel	124		87	88							
3	Magnesium deoxidized nickel	157		130	95							
4	Inconel	152		152	155							
5	"K" Monel	326		247	248							
6	"S" Monel	316		274	292							
7	Nickel-copper-tin alloy							247	335			
8	Copper-nickel alloy							331	325			
9	Copper-nickel-iron alloy							97	158			
10	35 Nickel-15 chrome	133		190	190							
11	20 Nickel-25 chrome-2 columbium	171		169	176							
12	20 Nickel-25 chrome, type 310	142		185	186							
13	12 Nickel-25 chrome, type 309	159		183	184							
14	18 Chrome-8 nickel-2 columbium, type 347	149			162							
15	18 Chrome-8 nickel, type 304	121	143	143		147	144					
16	12 Chrome-2 molybdenum	240	194	185		181	174					
17	12 Chrome, type 420	482	207	199		199	193	321	257	234	248	251
18	12 Chrome, type 403	227	214	207		204	188	221	221	221	241	234
19	12 Chrome, type 416	239	207	203		204	204					
20	12 Chrome, type 410							263	217			
21	12 Chrome, type 403	212		220	219							
22	5 Chrome-moly-silicon	158	168	163		160	159					
23	5 Chrome-moly-titanium	123	122	123		119	117					
24	5 Chrome-moly	141	144	146		161	139	138	129	139	132	133
25	2.50 Chrome-moly-silicon	274	174	172		166	166					
26	1.25 Chrome-moly-silicon	161	146	148		143	144	161	174	176	181	186
27	1.25 Chrome-moly-silicon	174	165	158		158	159					
28	1 Chrome-vanadium, S.A.E. 6120	241	190	172		165	159					
29	1 Chrome-moly							129	133	126	126	130
30	Nitrided nitralloy[a]	573	432	415		377	372	534	524	515	472	496
31	3 Nickel-moly	270			187							
32	1.25 Nickel-chrome-moly	277		211	219							
33	1 Nickel-chrome-moly							192	188			
34	Silicon-moly	166	166	161		161	156					
35	Carbon-moly	120	133	135		121	122					
36	Carbon-moly	162	143	134		128	124					
37	Carbon-moly							95	101	102	102	101
38	Carbon-moly							174	179			
39	Low-carbon, S.A.E. 1010	148	78	83		77	68	139	136	124	124	125
40	Low-carbon, aluminum-killed	111		86	85							
41	Low-carbon, high-phosphorus							140	138			
42	Medium carbon—S.A.E. 1035	156	132	125		123	124	157	163	159	158	159
43	NiResist cast iron	174		224	226							
44	NiResist cast iron	145		199	184							
45	NiResist cast iron	133		128	134							
46	Invar cast iron	146		153	155							

[a] The values given are for the nitrided case.

Discussion

E. N. Skinner,[4] Jr., and J. T. Eash.[4] Through their extensive study of the corrosion of metals and alloys by high-temperature steam, the authors have obtained data undoubtedly of considerable practical worth to those concerned with power-plant design, as well as valuable information with respect to the little understood question of high-temperature corrosion.

With regard to their results on the three samples of malleable nickel, it may be useful to state here that experience has made it apparent that nickel which is used at temperatures between 750 and 1400 F should be low in carbon. In this temperature range, it has been found that, regardless of the atmosphere, nickel containing carbon may become embrittled with time due to an intergranular precipitation of graphite. In any application involving the use of wrought nickel at these temperatures, the commercial carbon-free nickel which contains a maximum of 0.02 per cent carbon should be specified.

The results of some laboratory tests that we have conducted on the oxidation of nickel in tap-water steam suggest that the presence of minor quantities of residual elements associated with the production of malleable nickel for widely diverse fields of application has a marked effect on its oxidation resistance in steam. Carbon is particularly harmful in promoting rapid intergranular corrosion such as found by the authors.

Our tests indicate, in addition, that a nickel which does not contain small amounts of residual elements has a low rate of oxidation in steam. Such a product is found in electroplated nickel. Specimens of this type of nickel exposed at 1100 F for 600 hr oxidized at approximately one seventh the rate of a wrought nickel containing about 0.08 per cent carbon; furthermore, this electroplated nickel was completely free from the intergranular attack noted by the authors.

The practical value of electro-nickel in steam applications is a matter which designers of equipment may wish to consider.

H. L. Solberg,[5] G. A. Hawkins,[6] and J. T. Agnew.[7] Through the courtesy of The Detroit Edison Company and the authors the Engineering Experiment Station of Purdue University has been provided with copies of progress reports covering the extensive high-temperature corrosion studies which have been carried on by the company over the past several years. The writers have greatly appreciated the fine spirit of co-operation which has made this information available to us, and wish to congratulate the authors on the excellent job they have done in condensing the contents of these numerous and extensive reports into this paper.

The writers reported[8] in an earlier paper upon certain tests which were carried on with steam at 1200 F, and with the specimens subjected to sharp fluctuations in temperature, in order to determine the resistance of the scales formed on the various alloy steels to spalling under fluctuating-temperature conditions. It was found that, in general, as the chromium content was increased to 4–6 per cent, the scale which was formed became more dense and brittle. The addition of either silicon or aluminum in more than normal amounts tended to aggravate the tendency of the scales to spall under temperature fluctuations. These results are confirmed by The Detroit Edison Company tests. Steels containing more than 7 per cent of chromium formed a tightly adherent thin scale which showed no tendency to spall under the test conditions.

Tests with specimens of various shapes indicated that the spalling action of low-chrome steels was severe on the outside of bars and on flat surfaces but was negligible on the inside surfaces of a tube section of 1-in-ID tubing. It is probable that the scale which is formed on a concave surface is in compression and, consequently, resists spalling caused by temperature fluctuation and furnishes better protection than does the scale which is formed on the outside of bar stock. It is, therefore, possible that the long-time corrosion rates determined in The Detroit Edison tests on $^1/_2$-in. round bars are higher than those which would be encountered in superheater tubing in which the shape of the tube might tend to hold the scale in place.

The Detroit Edison tests show a marked reduction in the corrosion rate of carbon-moly steel, as compared with that of low-carbon steel. The results obtained at Purdue University with a fairly large number of specimens of each type of steel do not indicate a very significant difference in the corrosion rates of these steels. Both cast and rolled specimens were tested at temperatures of 1100 F and higher, under conditions of steady as well as fluctuating temperatures for periods of time which were shorter than those employed by The Detroit Edison Company. Table 5 of this discussion has been compiled from previously published data[8] and summarizes some of these results. All specimens were given the heat-treatment recommended by the producers of the steels used in these tests.

TABLE 4 COMPARISON OF CORROSION OF LOW-CARBON AND CARBON-MOLY STEELS

Length of test, hr	Reference	Temperature, deg F	Low carbon: No. of specimens	Low carbon: Average penetration, in.	Carbon-moly: No. of specimens	Carbon-moly: Average penetration, in.	Ratio of penetration, carbon-moly to low carbon
500	Table 9[a]	1100	16	0.001317	16	0.00122	0.926
570	Table 10[a]	1200	2	0.0118	2	0.01252	1.06
570	Table 10[a]	1200	2	0.01139	2	0.01049	0.92
1300[b]	Table 12[a]	1200	4	0.0156	4	0.0152	0.975

[a] From reference (8) of this discussion.
[b] Constant temperature for 500 hr followed by intermittent operation for 800 hr.

F. N. Speller.[9] The experimental data from the 5-year period of testing by The Detroit Edison Company is a welcome addition to our limited knowledge of the corrosion of metals in steam at 925 and 1100 F. It would be useful to know whether the corrosion found is uniform or localized in the form of pitting. Considering the relative cost, the favorable corrosion rate of 0.50 molybdenum plus 1 per cent chromium steels is encouraging. In 1933, we published data showing the favorable physical and corrosion-resistant properties of 3 per cent Cr compared with 5 per cent Cr steels. For oil-cracking tubes at 1100 F, the 2-$^1/_4$ per cent Cr, 1 per cent molybdenum steel has since then shown

[4] Metallurgists, International Nickel Company, Research Laboratories, Bayonne, N. J.
[5] Head, School of Mechanical and Aeronautical Engineering, Purdue University, Lafayette, Ind. Mem. A.S.M.E.
[6] Professor, Mechanical Engineering, Purdue University, Lafayette, Ind. Mem. A.S.M.E.
[7] Assistant in Engineering Experiment Station, Purdue University, Lafayette, Ind.
[8] "Corrosion of Unstressed Steel Specimens and Various Alloys by High-Temperature Steam," by H. L. Solberg, G. A. Hawkins, and A. A. Potter, Trans. A.S.M.E., vol. 64, 1942, pp. 303–316.
[9] Metallurgical Consultant, Pittsburgh, Pa.

very promising results in practice. In fact, experience in high-temperature oil-cracking around 1100 F affords experience on the relative strength of these steels over long periods at elevated temperatures that should be quite useful in the design of high-pressure steam boilers.

Authors' Closure

Respecting the comments of Messrs. Skinner and Eash, we are glad to have an explanation of the intergranular deterioration that was observed in the three samples of malleable nickel. The explanation that this was due to intergranular precipitation of graphite agrees with the results of our tests in that the lesser amount of intergranular deterioration was found in the sample which had the lowest carbon content.

It is interesting also to learn that the corrosion rate of electroplated nickel exposed to 1100 F steam for 600 hr was approximately one seventh that of wrought nickel containing 0.08 per cent carbon. The weight loss for electroplated nickel, as calculated from the factor given by Skinner and Eash in their 600-hr test, i.e., one seventh the value for wrought nickel, would indicate that, although the corrosion rate appeared to compare favorably with that found for the chromium and chromium-nickel stainless steels, on the basis of a 7461-hr test, the corrosion rate of electroplated nickel might not be found to compare so favorably with that for these stainless steels.

The comment of Messrs. Solberg, Hawkins, and Agnew that scale on a concave surface is more protective than on a convex surface and, consequently, the results given in the paper may be somewhat high, as compared with corrosion rates that would be encountered in the inner surface of tubes in service, is probably true. With respect to the relative rates of corrosion instead of the actual rates under service conditions of the 46 different materials, it is felt that, since each material was tested by the same type of specimen, i.e., $\frac{1}{2}$-in-diam bar specimens, the comparative tendency of these materials to corrode and scale has been established. To interpret such data in terms of corrodibility of tube forms in service, will require more such studies as those carried on at Purdue University. There are many applications in power plants, such as turbine buckets, various sections of turbine shells, valve-trim materials, and other uses in which the service conditions would be similar to those under which our tests were made.

In contrast to the Purdue test results, our tests have shown a marked reduction in the corrosion rate of carbon-molybdenum steel as compared with that of carbon steel. Our finding is based upon consistent test results obtained over a period of approximately 16,000 hr of exposure to 1100 F steam, during which time four different specimens of each sample were examined. Our shortest exposure period was approximately 4000 hr, whereas the Purdue results are based upon exposure periods of only 500 hr in 1100 F steam. To compare the test results of the two separate investigations, the shape of the "rate-loss" curve would have to be determined between 0 and 4000 hr of exposure in steam at 1100 F. This point is significant. Furthermore, the metallographic examination made of our test specimens at the conclusion of each 4000-hr exposure period showed a marked difference in the thickness of the scale on carbon steel, as contrasted with carbon-molybdenum steel. The carbon-steel specimens consistently had a much thicker and less adherent scale than the carbon-molybdenum steels. Two different carbon steels and two different carbon-molybdenum steels were each tested at 1100 F. At 1200 F there may be very littly difference in the scaling resistance of carbon steel and carbon-molybdenum steel as shown in Table 4, given in the Purdue comments. At 925 F we found practically no difference between the scaling rate of carbon and carbon-molybdenum steels.

Our test results indicate that carbon content is a significant factor in the corrosion rate of carbon steels exposed to steam at 1100 F. Consistently higher weight losses and thicker scale were found for low-carbon steel than for medium-carbon steel. We did not study the effect of carbon content as related to the corrosion resistance of carbon-molybdenum steel in steam at 1100 F.

Mr. Speller's question concerning whether the corrosion found is uniform or localized in the form of pitting is answered as follows: In general the corrosion found on the carbon steels and the low-and medium-alloy steels was quite uniform. Whenever the surface of the specimens was completely covered with a scale of measurable thickness, which could be seen easily at a magnification of 100 diam in a cross-sectional specimen, we prefer to think of the corrosion as being of a uniform type provided that no intergranular attack has occurred. In the case of the cast materials, considerable surface roughness was observed beneath the scale which is believed to be due to segregation in the cast alloy. Similar materials when tested in the wrought condition did not show such roughening of the surface beneath the scale.

Pitting of the surface as a result of exposure to 1100 F steam was found in the stainless materials, particularly in the 18 Cr-8 Ni without columbium, and in the 12-Cr steels with the exception of Sample 19 which was a Type 416, 12-Cr steel and which had shown very little surface attack after 16,526 hr of exposure. Pitting of the surface was also found in Inconel and "K" monel after 7461 hr of exposure. Intergranular attack at the surface was found in the nickel samples and, as mentioned by Messrs. Skinner and Eash, this was caused by intergranular precipitation of graphite at the test temperature.

No tests were made of 1 per cent chromium, 0.50 per cent molybdenum steels in 1100 F steam. Two steels of that general type were tested but contained a high silicon content and are, therefore, not comparable to such steels with normal silicon. A 1 per cent chromium, 0.50 per cent molybdenum steel was tested in 925 F steam for 13,165 hr. At that temperature its corrosion rate appeared to be about the same as that of 0.50 per cent molybdenum steel and plain-carbon steel, all of which had scaled approximately the same amount. In steam at 1100 F, however, the beneficial effect of 1 per cent of chromium would probably enhance the corrosion resistance of 0.50 per cent molybdenum steels. No tests were made of steel containing $2\frac{1}{4}$ per cent chromium, 1 per cent molybdenum, but from its favorable showing in oil-cracking applications at 1100 F, as reported by Mr. Speller, it probably would be suitable for many steam-power-plant applications.

The Corrosion of Alloy Steels by High-Temperature Steam

By G. A. HAWKINS,[1] J. T. AGNEW,[2] AND H. L. SOLBERG[3]

This paper presents additional test results obtained at the Engineering Experiment Station of Purdue University dealing with the relative resistance to corrosion by steam of unstressed specimens of various alloy steels at temperatures between 1000 F to 1800 F. All of the steels tested, except for the very high chromium-nickel alloys, show rapid corrosion beyond a limiting temperature which increases with chromium content. Data are presented relative to the chemical composition of the scale layers formed during tests at 1500 F and 1800 F.

INASMUCH as steam temperatures in modern power plants and in some of the process industries are approaching and in some cases exceeding those which may be used for the production of hydrogen by reaction between steam and iron, an investigation was undertaken at Purdue University of the corrosion by steam of the various steels which are available for high-temperature service. Apparatus has been constructed and techniques developed for measuring the amount of corrosion on unstressed specimens due to steam temperatures up to approximately 1800 F.

Description of Apparatus

A complete description of the apparatus used in this investigation together with the temperature-control circuit has been published (1).[4] Briefly, steam was passed through a counterflow gas-fired steel-tube superheater, after which it flowed through an electrically heated superheater constructed from 25-20 stainless-steel pipe $^5/_8$ in. OD × $^3/_8$ in. ID. It was then admitted to a reaction chamber made from a piece of 2-in-OD double-extra-heavy 25-20 stainless-steel pipe 10 ft long. A plate was welded over one end of the reaction chamber and was drilled and tapped for the superheater-inlet pipe. The other end of the chamber was threaded and closed with a pipe cap made of 7-Cr steel to facilitate insertion and removal of the test specimens. The reaction chamber was heated externally to the same temperature as the steam by means of two main and two guard heaters constructed from chromel wire. The reaction chamber was suitably insulated. Pyod-type chromel-alumel thermocouples were used to measure the temperatures along the reaction chamber. The steam discharging from the reaction chamber was condensed in a coiled-copper-tube heat exchanger and weighed.

Test Specimens and Testing Procedure

The specimens were machined to a length of 6 in. and a diameter of $^1/_2$ in. After the specimens had been machined, the surfaces were sandblasted in order to obtain identical surface conditions. After sandblasting, the specimens were weighed and placed in small cages made of stainless-steel welding wire and inserted into the reaction chamber, which had been brought up to the desired operating temperature. After remaining in the reaction chamber in contact with flowing steam for the desired length of time, the samples were withdrawn. The outer scale layers were removed mechanically in order to preserve the scale for chemical analysis. All of the remaining scale was removed by making the specimen the cathode in an electrolytic cell containing a 10 per cent solution of sulphuric acid with 1 g per liter of quinoline ethiodide as an inhibitor and with a current density of approximately 1 ampere per sq in. (2). The stripped samples were reweighed and the loss in weight determined by difference was taken as the measure of the amount of corrosion.

Corrosion Results

Samples of S.A.E. 1010, 3 Cr-Moly, 4-6 Cr-Moly, 7 Cr-Moly, 9 Cr-Moly, 12 Cr, 18-8 Cb (Stabilized), 21 Cr, 27 Cr, 25-20, and 25-15-2W steels were subjected to steam temperatures ranging from 1400 F to approximately 1800 F for 500 hr. The results for the various tests are given in Table 1. These data are represented in Fig. 1 by smooth curves drawn through the average of the test points. These curves are based upon the data presented in this paper as well as the results which have been reported in earlier papers (1, 2, 3).

The S.A.E. 1010, 3 Cr-Moly, 4-6 Cr-Moly, 9 Cr-Moly, 12 Cr-Moly, and 18-8 steels show a definite breaking point at a particular temperature. This same fact would probably have been observed for the 21 Cr, 27 Cr, 25-20, and 25-15-2W if the tests had been carried out at high temperatures. Only two points are available for the 7 Cr-Moly steel at the higher temperatures; hence no general curve is presented. The available data on the 7 Cr-Moly steel lie close to the 9 Cr-Moly curve.

An attempt was made to establish a simple single equation which could be used to compute the loss in weight for the steels tested for 500 hr at the various test temperatures. This was not possible due to the fact that the high-chromium steels show little corrosion until a certain temperature is reached above which an abrupt increase in the corrosion rate occurs at higher temperatures, while the low-chromium steels show a gradual increase in the rate of corrosion with increasing temperature. In order to use one equation, it was necessary to employ a very complex relation which would not be satisfactory from an engineering standpoint. As a result, a family of equations was established of the form

$$C = a(x - b)^d \quad [1]$$

wherein the constants, a, b, and d differ for each steel and are given in Table 2. The symbol C is the corrosion or loss in weight as a percentage of the initial weight. The term x is equal to the following

$$x = \frac{t - 1000}{100} \quad [2]$$

where t is the temperature under consideration in degrees F. This family of equations represents the test results within the

[1] Professor of Thermodynamics, Purdue University, Lafayette, Ind. Mem. A.S.M.E.

[2] Assistant in Engineering Experiment Station, Purdue University, Lafayette, Ind.

[3] Head, School of Mechanical and Aeronautical Engineering, Purdue University, Lafayette, Ind. Mem. A.S.M.E.

[4] Numbers in parentheses refer to the Bibliography at the end of the paper.

Contributed by the Special Research Committee on Critical-Pressure Steam Boilers and the Power Division and presented at the Annual Meeting, New York, N. Y., Nov. 29–Dec. 3, 1943, of The American Society of Mechanical Engineers.

Note: Statements and opinions advanced in papers are to be understood as individual expressions of their authors and not those of the Society.

TABLE 1 CORROSION OF STEEL BARS IN CONTACT WITH STEAM FOR 500 HR

Steel	Chemical analysis, ladle, per cent												Steam temp, F	Loss in weight, per cent of original weight
	C	Mn	P	S	Si	Cr	Ni	Mo	Cb	W	Cu	N		
S.A.E. 1010	0.08	0.30	0.017	0.034	....	.....	.....	....	....	....	....	.....	1736	100.0
													1498	62.4
													1400	34.1
3 Cr-Moly	0.11	0.51	0.014	0.017	0.36	2.95	.....	0.98	....	....	....	.....	1736	74.8
													1501	44.3
													1400	21.7
4-6 Cr-Moly	0.11	0.33	0.020	0.027	0.28	5.66	0.22	0.50	....	....	....	.....	1772	77.7
													1736	70.0
													1501	28.8
													1400	19.1
7 Cr-Moly	0.11	0.43	0.012	0.011	0.92	7.33	.....	0.50	....	....	....	.....	1772	57.4
													1506	12.2
9 Cr-Moly	0.11	0.38	0.010	0.016	0.27	9.00	.....	1.22	....	....	....	.....	1772	62.7
													1728	60.1
													1680	41.3
													1550	28.3
													1506	14.6
													1475	1.9
12 Cr	0.10	0.52	0.014	0.015	0.32	12.92	0.12	....	....	....	....	.....	1680	23.6
													1550	0.0
													1508	0.0
													1475	0.0
18-8	0.06	0.50	0.03	0.03	0.61	17.75	9.25	....	....	....	....	.....	1675	0.0
													1560	0.0
													1470	0.0
18-8 Cb (Stabilized)	0.07	0.26	0.015	0.012	0.39	18.62	9.90	....	1.11	....	....	.....	1765	11.5
													1728	12.3
													1675	0.0
													1560	0.0
													1508	0.0
													1470	0.0
21 Cr	0.11	0.39	0.016	0.016	0.42	21.45	.....	....	....	....	1.18	.....	1670	0.0
													1570	0.0
													1480	0.0
27 Cr	0.11	0.48	0.014	0.014	0.38	26.02	0.20	....	....	....	....	0.101	1670	0.0
													1570	0.0
													1480	0.0
25-20	0.07	1.62	.....	.....	0.34	24.45	20.30	....	....	....	....	.....	1751	0.0
25-15-2W	0.10	1.75	.....	.....	0.56	24.18	14.34	....	....	2.06	....	.....	1751	0.0

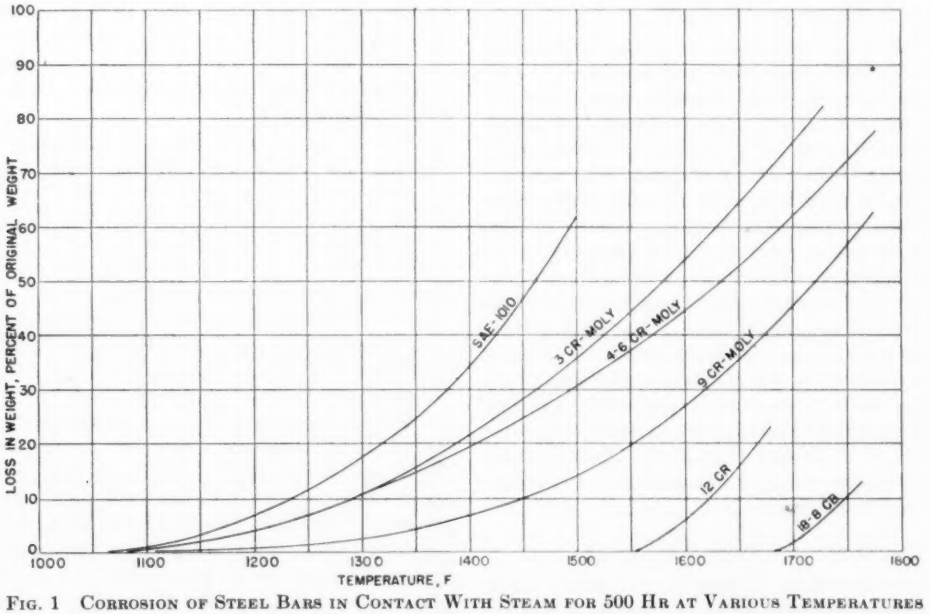


FIG. 1 CORROSION OF STEEL BARS IN CONTACT WITH STEAM FOR 500 HR AT VARIOUS TEMPERATURES

range of temperatures investigated and should not be used for temperatures in excess of the test limits.

TABLE 2 CONSTANTS FOR USE IN CORROSION EQUATION $C = a(x - b)^d$

Steel	Constants		
	a	b	d
S.A.E 1010	1.1	0	2.5
3 Cr-Moly	0.93	0	2.27
4-6 Cr-Moly	1.0	0	2.13
9 Cr-Moly	0.07	0	3.33
12 Cr	16.45	5.5	1.34
18-8 Cb (Stabilized)	15.40	6.75	1.33

CHEMICAL ANALYSIS OF SCALE LAYERS

The steels listed in Table 3 were tested at temperatures in excess of 1700 F for a period of 500 hr.

An extremely thin tightly adhering layer was found on all of the scales next to the parent metal. It was found impossible to remove enough of this inner layer to analyze it.

The scale formed on the 3 Cr-Moly steel consisted of a thick porous and brittle outer layer and a dense brittle middle layer The outer and middle layers were separated mechanically by using a sharp probe. In many cases sections of both layers stuck together. Although the color of the middle and outer layers was

TABLE 3 CHEMICAL COMPOSITION OF VARIOUS SCALE LAYERS FORMED ON STEEL SPECIMENS IN CONTACT WITH STEAM AT APPROXIMATELY 1700 F FOR 500 HR

	Chemical analysis, ladle, per cent								Chemical composition of scale layers, per cent						Steam temp,
									Middle layer			Outer layer			
Steel	C	Mn	P	S	Si	Cr	Ni	Mo	Cr	Si	Mo	Cr	Si	Mo	F
3 Cr-Moly	0.11	0.51	0.014	0.016	0.36	2.95	....	0.98	7.44	0.75	2.34	0.33	0.03	0.05	1736
4-6 Cr-Moly	0.11	0.33	0.020	0.027	0.28	5.66	0.22	0.50	11.61	0.57	1.12	0.40	0.03	0.03	1736
9 Cr-Moly	0.11	0.38	0.010	0.016	0.27	9.00	....	1.22	11.94	1.48	0.97	0.34	0.01	0.03	1728

TABLE 4 CHEMICAL COMPOSITION OF VARIOUS SCALE LAYERS FORMED ON STEEL SPECIMENS IN CONTACT WITH STEAM AT APPROXIMATELY 1500 F FOR 500 HR

	Chemical analysis, ladle, per cent								Chemical composition of scale layers, per cent						Steam temp,
									Middle layer			Outer layer			
Steel	C	Mn	P	S	Si	Cr	Ni	Mo	Cr	Si	Mo	Cr	Si	Mo	F
3 Cr-Moly	0.11	0.51	0.014	0.016	0.36	2.95	....	0.98	5.08	0.58	1.65	1.07	0.06	0.15	1501
4-6 Cr-Moly	0.11	0.33	0.020	0.027	0.28	5.66	0.22	0.50	9.38	0.49	0.84	0.32	0.03	0.025	1501
7 Cr-Moly	0.11	0.43	0.012	0.011	0.92	7.33	....	0.59	8.86	1.15	0.70	1.07	0.17	0.025	1506
9 Cr-Moly	0.11	0.38	0.010	0.016	0.27	9.00	....	1.22	12.35	0.26	1.54	2.06	0.09	0.29	1506

the same, it was very easy to distinguish between the two. The dividing plane between the layers was very sharp, due to the fact that the exposed surfaces of the particles which composed the middle layer reflected ordinary light differently from those contained in the outer layer. Samples of the outer and middle layers were analyzed for Cr, Mo, and Si. The results are given in Table 3.

The 4-6 Cr-Moly showed a scale-layer formation similar to the scales formed on the 3 Cr-Moly steel. The outer layer was very brittle and readily separated from the middle layer. The outer layer of scale formed on the 9 Cr-Moly steel was quite brittle and was easily separated from the adjacent layer. The middle layer was very dense and hard to remove. It was not possible to distinguish the middle layer from a layer next to the parent metal, if such a layer existed. The percentage of chromium in the outer scale layer for the 4-6 Cr-Moly and 9 Cr-Moly steel was larger than for the 3 Cr-Moly steel.

The steels listed in Table 4 were held in a steam atmosphere at 1500 F for 500 hr. From visual observations the scales formed on the 3 Cr-Moly, 4-6 Cr-Moly, and 9 Cr-Moly samples appeared to be quite similar to those formed in the same type of steel specimens tested at 1700 F for 500 hr. The 7 Cr-Moly and 9 Cr-Moly scales were quite similar. The results differ materially from those obtained on the 500-hr test at 1700 F.

The data presented in Tables 3 and 4 indicate that a concentration of chromium, silicon, and molybdenum has occurred in the middle scale layer. The increase in concentration for the middle layer may be clearly brought out by studying the ratio of the percentage of the alloying element in the scale layer to the percentage in the base steel. These data are presented in Tables 5 and 6. For the chromium the relative concentration increase ranged from 1.21 to 2.52, for silicon from 0.96 to 5.48, and for molybdenum from 0.79 to 2.39.

In every case the alloy content in the outer layer is lower than in the middle layer. This agrees with many of the oxidation theories which have been advanced, in that since the outer layer is composed chiefly of iron, the iron diffused through the alloy-rich middle layer.

These results tend to indicate that in all probability the steam-oxidation resistance of the alloy steels tested is due to thin and very dense tightly adhering inner layer of scale and a dense middle layer which contains a higher concentration of the alloying agents than is present in the base steel. An outward diffusion of the alloying agents from the base steel to and into the inner and middle layers must occur. In order to have a steam-corrosion-resisting steel there must be sufficient amounts of the alloying agents to combine with the oxygen diffusing inward to form the dense protective inner and middle layers. These general conclusions are in agreement with those found by White, Clark, and McCollam on air-oxidation tests (4).

It is thus possible that long-time tests would show less difference in the total amount of corrosion for medium- and high-alloy steels than has been found by conducting tests of from 500 to 2000 hr duration.

TABLE 5 RELATIVE CONCENTRATION OF ALLOYING ELEMENTS IN MIDDLE SCALE LAYER FOR SPECIMENS IN CONTACT WITH STEAM AT APPROXIMATELY 1700 F FOR 500 HR

	Ratio of percentage of alloying agent in middle layer and base steel		
Steel	Chromium	Silicon	Molybdenum
3 Cr-Moly	2.52	2.08	2.39
4-6 Cr-Moly	2.05	2.03	2.24
9 Cr-Moly	1.33	5.48	0.79

TABLE 6 RELATIVE CONCENTRATION OF ALLOYING ELEMENTS IN MIDDLE SCALE LAYER FOR SPECIMENS IN CONTACT WITH STEAM AT APPROXIMATELY 1500 F FOR 500 HR

	Ratio of percentage of alloying agent in middle layer and base steel		
Steel	Chromium	Silicon	Molybdenum
3 Cr-Moly	1.72	1.61	1.68
4-6 Cr-Moly	1.75	1.75	1.69
7 Cr-Moly	1.21	1.25	1.18
9 Cr-Moly	1.37	0.96	1.26

Conclusions

The data obtained on the steels tested together with previously reported data (1, 2, 3) which are graphically presented in Fig. 1 show the effect of temperature on corrosion by high-temperature steam. All of the steels tested except the 25-20, 25-15-2W, 21 Cr, and 27 Cr specimens start to corrode rapidly at some temperature less than 1675 F. After the break occurs the rise in corrosion rate is much more rapid for the steel containing 12 per cent chromium and the 18-8 stainless steel than for the steels containing less chromium. The 25-20 and 25-15-2W steels which were tested at temperatures of 1751 F show no corrosion at the end of 500 hr. The temperature at which rapid corrosion begins increases with the chromium content. The 18-8 Cb steel shows the same tendency toward rapid corrosion above some limiting temperature that the S.A.E. 1010 steel shows at a much lower temperature.

Relatively simple empirical equations have been established to aid in computing the amount of corrosion produced in 500 hr at temperatures within the test range for the various steels tested.

Chemical analysis of the various scale layers produced on the 3 Cr-Moly, 4-6 Cr-Moly, 7 Cr-Moly, and 9 Cr-Moly steels during 500-hr tests at temperatures of 1500 and 1730 F are presented. The chemical analysis of the inner scale layer indicated a build-up in concentration of chromium, silicon, and molybdenum. The diffusion of the alloying agents and the inward diffusing oxygen combine to form the dense protective inner layer.

From the results obtained, the chromium content of a steel is a major factor in controlling the amount of corrosion produced by high-temperature steam.

ACKNOWLEDGMENT

The authors wish to express their appreciation to the members of the A.S.M.E. Special Research Committee on Critical-Pressure Boilers for their valuable assistance during the course of the investigation.

Part of this investigation was made possible through the financial support of the Engineering Foundation, The Babcock & Wilcox Company, The Timken Roller Bearing Company, the General Electric Company, the National Tube Company, The Globe Steel Tubes Company, and The Combustion Engineering Company.

The authors are particularly indebted to Dr. C. L. Clark and The Timken Roller Bearing Company, Steel and Tube Division, for making the chemical analyses of the scales reported in this paper.

Appreciation is also expressed to the various alloy-steel manufacturers who have contributed steel samples from time to time for use in this investigation.

BIBLIOGRAPHY

1 "Corrosion of Unstressed Specimens of Alloy Steel by Steam at Temperatures up to 1800 F," by G. A. Hawkins, H. L. Solberg, J. T. Agnew, and A. A. Potter, Trans. A.S.M.E., vol. 65, 1943, pp. 301–308.

2 "Corrosion of Unstressed Steel Specimens and Various Alloys by High-Temperature Steam," by H. L. Solberg, G. A. Hawkins, and A. A. Potter, Trans. A.S.M.E., vol. 64, 1942, pp. 303–316.

3 "The Corrosion of Stressed Alloy-Steel Bars by High-Temperature Steam," by H. L. Solberg, A. A. Potter, G. A. Hawkins, and J. T. Agnew, Trans. A.S.M.E., vol. 65, 1943, pp. 47–52.

4 "Influence of Chromium, Silicon, and Aluminum on the Oxidation Resistance of Intermediate Alloy Steels," by A. E. White, C. L. Clark, and C. H. McCollam, Trans., American Society for Metals, vol. 27, 1939, p. 125.

Discussion

R. C. COREY.[5] Since its inception, the work at Purdue University on the corrosion of metals and alloys by high-temperature steam has been followed with considerable interest. No other laboratory studies of this important subject, either here or abroad, have been as comprehensive as the present series, and the authors are to be commended for the excellent data that they have obtained.

It is gratifying to note that the authors conducted their tests for 500 hr. All too frequently one finds data in the literature on the rate of corrosion, intended for general use, but which are based upon extremely short test periods. In a recent article,[6] it was shown that with everything else essentially equal, the corrosion rate varies markedly with the duration of test. It may be argued that regardless of the test period, the relative rate of corrosion of different metals and alloys studied simultaneously under the same conditions will remain the same. Considering, however, that the rate of corrosion of most metals and alloys is greatest initially (except in the unusual case where corrosion increases linearly with time), it is possible that an otherwise satisfactory metal will appear to be unfavorable if the test period is too short.

It is not clear why the authors changed the unit for expressing corrosion from that of penetration, as used in previous reports, to percentage loss of original weight. In order that data of this kind may be compared with those of other investigators, the rate of corrosion is expressed more rationally in terms of the amount of metal lost per unit area in unit time, or as the depth of penetration in unit time. The literature on high-temperature corrosion studies is confusing and difficult to correlate as the result of the use of units which cannot be reduced to a common basis.

If the authors have the data available, it might be of interest to plot the loss of metal against time and thereby determine the specific type of scaling that occurs. Such information would be valuable for interpreting the corrosion mechanism of the various alloys that were studied. Recent papers[7,8] on this subject indicate that scaling may occur linearly, parabolically, or logarithmically with time, depending upon the temperature, conditions, and the metal under study. Thus, the sharp break at a certain temperature noted by the authors for certain of the alloys studied may be the result of recrystallization[9] of the oxide above a certain temperature, which may lead to logarithmic scaling, a factor determined only by the type of plot just mentioned.

The chemical analyses of the scales are of great interest as such data are the first step toward developing a mechanism for corrosion. It is not apparent why the Si increased and the Mo and Cr decreased in amount in the middle oxide layer with increasing chromium content of the alloy at both 1500 F and 1700 F. It is suggested that if possible the authors should have an X-ray diffraction study made of these scales to determine how these elements are distributed, that is, as solid solutions, stoichiometric compounds, or spinels. Such information would afford them valuable supplementary data.

The data of Table 1 of the paper show that Cb-stabilized 18-8 steel loses about 12 per cent of its weight between 1728 F and 1765 F. It might be of interest to study plain 18-8 steel at the same temperature for 500 hr in order to determine if the Cb decreases the corrosion resistance of this alloy.

With reference to the remarks of the authors concerning diffusion of oxygen through the oxide, the following is offered as an alternate explanation: Assuming for the moment that the gas phase diffuses through the oxide to meet and react with metal ions, it is probable that steam and not oxygen, as the authors state, would be involved as it is not until oxidation takes place that oxygen is released, and then it probably combines immediately as an oxide. On the other hand, it is doubtful that a steam molecule could diffuse interstitially through a compact oxide lattice because of the large size of the gas molecule with respect to the interatomic spacing of the lattice. However, if the oxide was porous or fissured the gas could reach the metal ions readily. Also there are cases where a gas like oxygen may be taken into solid solution in an oxide which is deficient in oxygen atoms, i.e., an oxide that is not of stoichiometric composition. The oxide FeO and certain of the spinel type of oxides like $FeO{\cdot}Fe_2O_3$, $FeO{\cdot}Al_2O_3$, and $FeO{\cdot}Cr_2O_3$ are capable of taking a small amount of oxygen into solid solution, but the quantities involved are too small to be significant, thus the rate of scaling probably depends primarily upon the rate at which the iron ions reach the oxide-gas interface.

W. TRINKS.[10] On account of being a furnace engineer, the writer's interest in high temperature begins where the power engineer quits. In furnace work we have learned that water vapor scales iron and steel more rapidly than air does. The writer attributes this phenomenon to dissociation. The professors of thermodynamics tell us that dissociation at the temperature

[5] Research and Development Department, Combustion Engineering Company, New York, N. Y.

[6] "Corrosion by Hot Gases," by R. C. Corey, *Combustion*, vol. 15, 1943, pp. 34–39.

[7] "The Transition State Theory of the Formation of Thin Oxide Films on Metals," by E. A. Gulbransen, preprint 83–4, 1943, The Electrochemical Society.

[8] "Laws Governing the Growth of Films on Metals," by U. R. Evans, preprint 83–10, 1943, The Electrochemical Society.

[9] "Oxidation of Metals and the Formation of Protective Films," by N. F. Mott, *Nature*, vol. 145, 1940, pp. 996–1000.

[10] Professor of Mechanical Engineering (Emeritus), Carnegie Institute of Technology, Pittsburgh, Pa.

in question is negligible. They are right, if we limit ourselves to permanent dissociation. They are wrong if we consider instantaneous dissociation. Collision of the molecules causes some dissociation at all temperatures. Ordinarily, the atoms reassociate immediately without leaving any trace of their dissociation; but if a material is present for which oxygen has a greater affinity than it has for hydrogen, it goes after that material, because the oxygen is atomic (in the nascent state) and leaves the unwanted hydrogen to look out for itself.

Water vapor is triatomic and, for that reason is dissociated or cracked more easily than the diatomic oxygen molecule.

The variations in the composition of the scale are what we should expect. Iron oxide has a vapor pressure. Every steel-furnace engineer knows that fact. In a superheater tube the heat comes from the outside. The scale next to the tube is hotter than the scale next to the steam. For that reason the iron oxide gets away from the tube toward the cooler steam. It is a migration which some people call diffusion.

As regards cracking of the scale, we know from the sheet industry that a thin scale adheres and that a thick scale cracks. If we could chromium-plate the inside of the tubes and have the plating stick, then we should have a thin retentive greenish chromium scale which would not crack.

Authors' Closure

The authors are indebted to Messrs. Corey and Trinks for their written discussions and for their excellent comments concerning the mechanism of scale formation.

Mr. Corey has suggested that the data on corrosion be presented in terms of penetration rather than per cent loss in weight. In their earlier reports (1, 2, 3),[11] the authors presented the data in terms of inches of penetration. However, the high-temperature tests reported in this paper produced very thick layers of scale on some of the specimens which were originally 6 in. long and $^1/_2$ in. in diam. This resulted not only in a significant reduction in the diameter of the parent metal during the course of the tests but also produced a shortening of the specimens and a tapering of the parent metal at the ends of the specimens.

Mr. Corey has made some pertinent comments on the effect of time upon the usefulness of corrosion data. The tests which are reported in Table 1 are for 500 hr, and data for shorter periods of time are not available. However, the authors have published data showing the effect of time upon the corrosion of various steels for periods up to 2000 hr at a steam temperature of 1100 F (2).

In conclusion, the authors wish to thank all of those who presented discussions for their interest, comments, and constructive suggestions.

[11] Numbers in parentheses refer to Bibliography at end of original paper.

Surface Fatigue of Plastic Materials

Progress Report No. 16 of the A.S.M.E. Special Research Committee on Strength of Gear Teeth

By EARLE BUCKINGHAM,[1] CAMBRIDGE, MASS.

GREATER knowledge of the surface-fatigue characteristics of materials will serve many useful ends. Surface fatigue is a phenomenon largely responsible for one type of wear, commonly known as pitting. Definite information will permit the more intelligent and effective choice of materials for specific service conditions. Again, as noted in our preceding report,[2] if the surface-fatigue characteristics of the materials used are known and the surfaces of a mechanism are carefully watched, dynamic loads that cause surface failure can be detected before any harm is done to any other part of the mechanism, and a reasonably close measure of their intensity can be made from the condition and appearance of the surface failure of the specific part. Thus such information will give us a tool, or weighing scale, by which to measure the intensity of existing loads on all types of mechanisms in actual operation, and also to make possible more accurate comparisons between many laboratory test results and actual service conditions.

A special testing machine, shown in Fig. 1, has been built, and tests have been run almost continuously during the past 6 years. In brief, the testing machine consists of two shafts running in plain bearings, one mounted in a heavy fixed frame and the other mounted in a substantial swinging frame. The test rolls, with a maximum face width of one inch and from 2.200 in. to 4.00 in. in diameter, are mounted on the shafts. A load is set up between them by a calibrated spring acting against the swinging frame. Revolution counters are connected to each shaft. Gears may be mounted on the ends of the shafts in such a manner as to obtain any desired amount of slipping or rubbing between the two test rolls. Many of the tests under rolling conditions are run without gears, the rolls driving each other by friction. The majority of tests to date have been made under rolling conditions only.

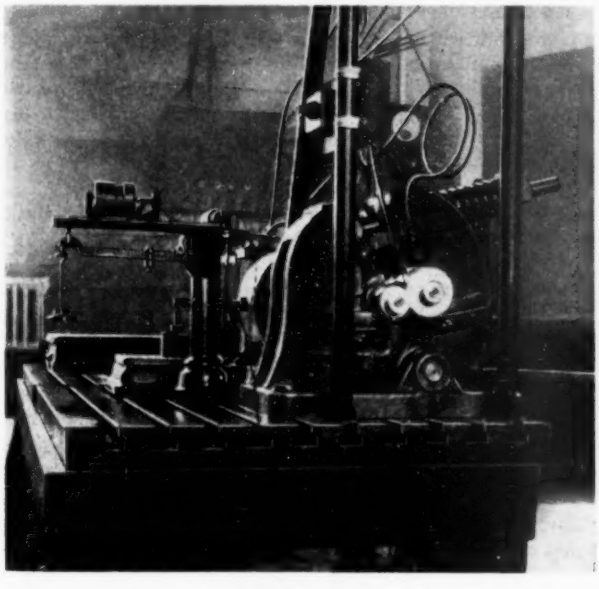


FIG. 1 TESTING MACHINE

Plain bearings were used to avoid the possible dynamic effects of ball or roller bearings. An oil pump provides oil for the bearings and the gears. The testing machine is driven by a small Sprague dynamometer, and records are kept of the torque input during the runs.

The physical properties and the structure of the materials under test appear to have a pronounced influence on the nature of the surface failure. The following is an attempt to put into words a detailed account of the several phenomena that occur concurrently under test conditions of rolling contact. Considering only the plastic materials, the following have been observed.

PLASTIC FLOW OF SURFACE LAMINA AND WORK-HARDENING

The action of one roll upon the other carries a plastic and elastic wave ahead of the contact area between them, setting up conditions quite similar in many respects to the conditions existing when cold-rolling metals. This action cold-works the surface lamina, increasing its hardness and raising the physical properties of the surface of the material. This action appears to be progressive, tests indicating that the depth of this cold-working (which might well be called "mechanical case-hardening") increases with the number of repetitions of stress up to a maximum depth, this maximum depth probably depending upon the pressure. The hardness also increases with the number of repetitions of stress, as well as with increase of load; but depth of penetration appears to depend mostly upon the number of repetitions of load.

This increase of surface hardness has been observed on practically all samples of plastic materials which have been tested. Special tests to study this phenomenon were made by E. L. Bartholomew, Jr., in 1937, using rolls of stainless steel (18–8 steel). The three following tests were run on rolls of 2.3 in. diam, 1 in. face width, against a hardened and ground steel roll of the same size.

Test no.	Load, lb	Number of repetitions of stress	Maximum specific compressive stress, psi	Maximum shear stress, psi
110	2362	500000	146000	44400
111	2362	2069000	146000	44400
112	3150	4940000	184000	56000

The stresses are computed as though loaded under static conditions. Photoelastic tests indicate that, under the combined stress conditions existing in rolling contact, the stress distribution is changed and that the stresses are greater than those existing under static conditions of simple radial loading. In the absence

[1] Professor of Mechanical Engineering, Massachusetts Institute of Technology, Cambridge, Mass.

[2] "Qualitative Analysis of Wear," by Earle Buckingham, 15th Progress Report of the A.S.M.E. Special Research Committee on Strength of Gear Teeth, *Mechanical Engineering*, vol. 59, 1937, pp. 576–578.

Contributed by the Special Research Committee on Strength of Gear Teeth, and the Production Engineering Division, and presented at the Annual Meeting, New York, N. Y., Nov. 29–Dec. 3, 1943, of THE AMERICAN SOCIETY OF MECHANICAL ENGINEERS.

NOTE: Statements and opinions advanced in papers are to be understood as individual expressions of their authors and not those of the Society.

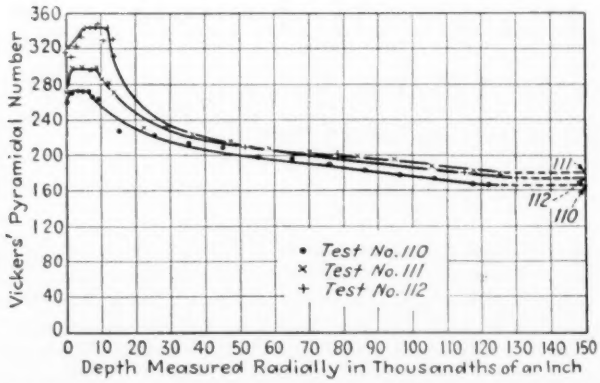


FIG. 2 RESULTS OF TESTS TO DETERMINE EFFECT OF MINIMUM TORQUE CONDITIONS

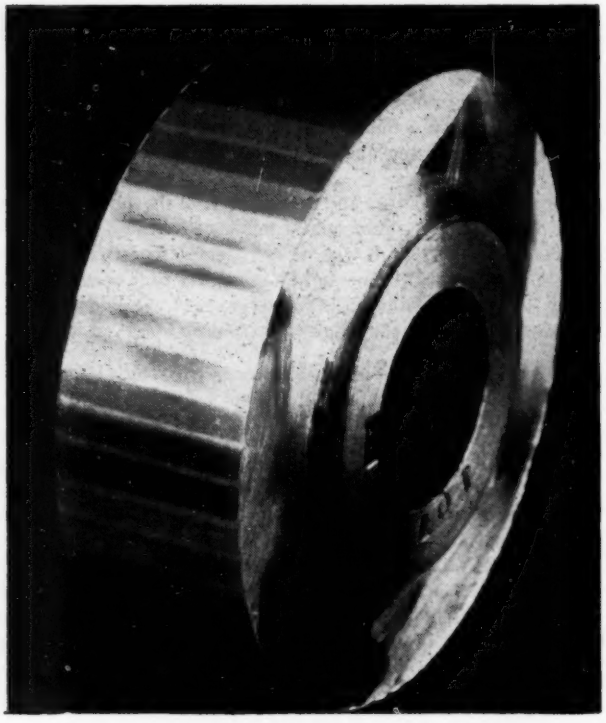


FIG. 3 TEST ROLL NO. 109, CARBON MACHINE STEEL
(3.30-in-diam roll, 0.50 carbon steel, with 8 per cent sliding, 1940-lb load, 67,800 cycles.)

of more exact methods, conditions are compared on the basis of static radial loading only.

On several tests, it has been noticed that the input torque tended to decrease to a minimum as the test progressed, and then to rise slightly after a long period of running under minimum torque conditions. This increase of torque takes place before any indication of destructive pitting can be detected by an examination of the unetched surface. Destructive pitting then occurs in from one or more million cycles after the increase of torque has been detected. Test No. 112 was run until the torque was observed to rise from a minimum of about 1.90 to 2.06 lb at a radius of 1 ft. The results of these tests are plotted in Fig. 2, showing the Vickers hardness numbers against the depth in thousandths of an inch below the surface. The dotted lines at the ends of the graphs show the hardness of the core.

It will be noted that the maximum-hardness reading is obtained at a distance of a few thousandths of an inch below the surface; also, that the depth of maximum hardness is greater for test No. 111 than for test No. 110. It is possible that there is a tendency for the surface material to start to disintegrate, perhaps because of the reversed bending action on the surface as the elastic wave travels ahead of the contact. Photomicrographs taken just below the surface show slip lines, indicative of cold-working. In that of test No. 112, the structure had a semblance of having been more severely worked than either of the other two samples. The grains had the appearance of having shattered in this case. The structure as a whole showed a general precipitation at the grain boundaries and many slip planes.

With very plastic materials, such as soft steel and brass, under heavy loads, this plastic flow of the surface material results in definite waves or corrugations on the surface, much the same as may be found on gravel roads, particularly on the uphill grades. One possible explanation is that when the plastic flow has hardened the material sufficiently, the plastic flow is stopped or reduced at that point; then the rolls ride over and start to build up another wave. Sliding accentuates this condition greatly. Similar waves or corrugations are often found on railroad rails, particularly on curves where sliding between the wheel and rail is greater than on straight stretches.

Fig. 3 shows a 3.3-in-diam test roll of 0.50 carbon machine steel (substantially S.A.E.-1050) which was run with a hardened-steel roll of 2.2 in. diam under a load of 1940 lb for 67,800 cycles. The hardness of the core material was 77 Rockwell B; that of the crest of the waves 89 Rockwell B, and that of the trough of the wave 86 Rockwell B. The pitch diameters of the gears used on the ends of the shafts were 3.20 in. and 2.30 in., thus introducing a relative sliding action between the rolls of slightly less than 8 per cent. Another sample of the same material, 3.5 in. diam, was run with a 2.3-in-diam roll of hardened steel, with rolling action only, under a test load of 3500 lb for 3,000,000 cycles without destructive pitting or waves becoming apparent on the surface.

It is believed that the change in torque observed as the test progresses is some measure of the work done in the plastic deformation of the test samples. For example, on test No. 112, the initial scale load (at a radius of one foot) shortly after the test was started was 3.5 lb. After about one hour, it had fallen to 2.30 lb. After 24 hours continuous running, it had fallen to 2.25 lb. Then it showed a continuous decrease to 1.9 lb at the end of about four million cycles before it started to rise again to 2.06 lb when the test was stopped for examination of the structure of the surface material. The first reduction of from 3.5 lb to 2.25 lb was largely the influence of the warming up of the testing machine. The further reduction of torque is believed to be a measure of the plastic working. When the torque has reached a minimum, and continues there without further change, it is felt that this is reliable evidence that the material has been cold-worked to its limit under the specific test conditions, and that any deformations, other than those resulting from failure of the material, are elastic ones only.

INFLUENCE OF ELASTIC DEFORMATION

At the same time that the surface lamina is being cold-worked by the plastic flow, and even after the surface has been cold-worked to the limit, the elastic wave traveling ahead of the contact imposes reversed bending conditions on this surface lamina. The result appears to be, in many cases, the development of microscopic cracks at right angles to the direction of rolling. Microscopic examination of the stainless-steel samples showed evidence, as already noted, of disintegration of the surface material at the grain boundaries.

Incidentally, the number of cycles of stress required to establish the surface-endurance limits is very much greater than the number of cycles required to establish the flexural or bend-

ing endurance limit. Where, in general, from one to five million cycles will establish the flexural endurance limit of the softer steels, from twenty to thirty million cycles appear to be necessary to establish the surface-endurance limit.

In some cases, tests have been run to twenty-five or thirty million cycles without any surface indications (without etching) of destructive pitting, and the test has then been stopped. To make sure that the material is still sound, a light lathe cut has been made on the surface. In some cases, the material has crumbled away in front of the cutting tool, showing the disintegration of the surface material, although it was not evident from a careful examination of the surface. In other cases, a clean chip was obtained, which indicated that the surface material was still sound, yet the appearance of the surfaces which gave either types of chip conditions appeared to be the same. In all cases where a chip has been taken on the surface of rolls which have failed by destructive pitting, the material crumbled away in front of the cutting tool.

In all cases where the loads are appreciable, whether the stresses are above or below the surface-endurance limits of the material, small pits are evident on the surface. These are shallow, possibly up to 0.005 in. deep at most, generally much less, and the shapes appear to depend upon the structure of the material. Some are microscopic, only a few thousandths of an inch across; others are one sixteenth of an inch or more, and of irregular shapes. This we have called "incipient pitting." Various explanations have been suggested to account for this phenomenon. Dr. Stewart Way[3] ascribes it to the formation of microscopic surface cracks followed by the penetration of oil which lifts these small sections out because of the hydrostatic pressure developed at the region of contact. It has also been called "corrective pitting" and ascribed to the high local pressures developed on the ridges or peaks of surface irregularities left by the cutting tool. It has also been suggested that the plastic flow of the surface lamina builds up local shearing stresses that shear these particles out after the surface cracks appear. Possibly any or all of these explanations may be true, depending upon the conditions and nature of the material. At all events, this incipient pitting does not appear to be the cause of any great concern. If the loads are below the surface-endurance limits, this incipient pitting appears to progress to a certain extent and then to cease. It is our belief that the elastic wave traveling ahead of the contact is a contributing factor to this phenomenon.

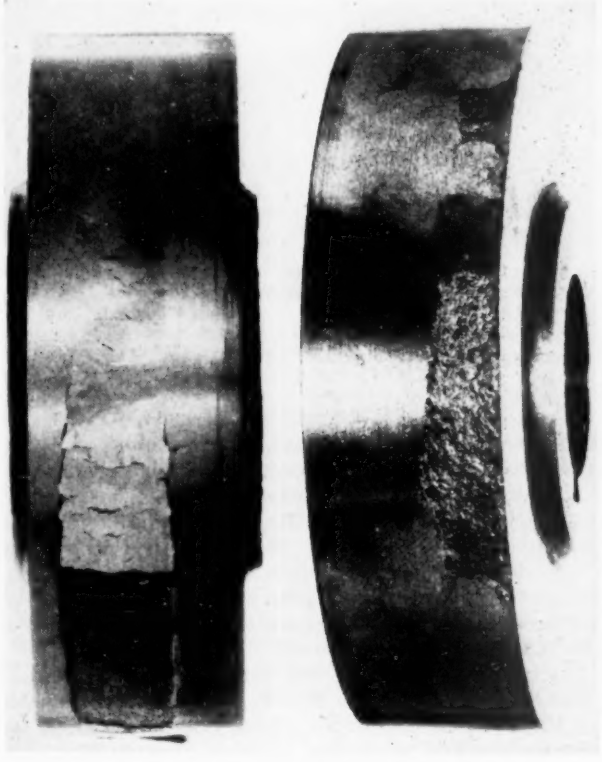


FIG. 4 BLISTER IN BRASS TEST ROLL RUNNING WITH HARDENED-STEEL ROLL
(Brass roll, 3.5 in. diam; 3500-lb load; 305,000 cycles. Thickness of flake, 0.018–0.021 in.)

FIG. 5 SURFACE FAILURE OF NICKEL-CAST-IRON TEST ROLL
(Test No. 23: 4.00-in-diam roll; 3500-lb load; 406,000 cycles.)

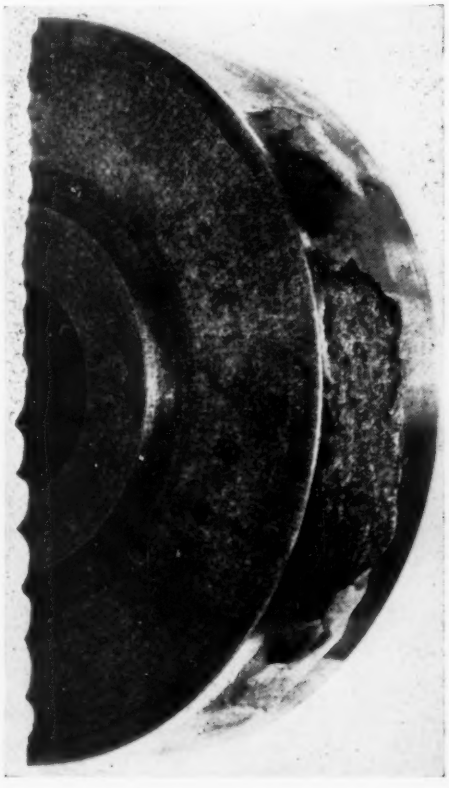


FIG. 6 HEAT-TREATED NICKEL-CAST-IRON ROLL AFTER RUN OF 400,000 CYCLES UNDER 3435-LB LOAD
(Test No. 34: 3.80-in-diam roll; thickness of flake, 0.033–0.036 in.)

DESTRUCTIVE PITTING

Simultaneously with the foregoing phenomena, and probably with many others not yet observed, shear stresses are repeatedly imposed upon the material below the surface. When the loads imposed develop stresses beyond the surface-endurance limits of the material, particles or flakes will be sheared out of the surface of the material; and thus far in these tests, with very few exceptions, the thickness of these flakes or the depth of the pits has been equal to or greater than the depth to the point of maximum shear.

In the case of a phenolic laminated test roll (bakelite) of 4 in. diam running with a 2.3-in-diam hardened-steel roll under a load of 1720 lb, both rolls of 1 in. face width, at the end of 107,000 cycles of the bakelite roll, a blister appeared on the surface with

[3] Research Engineer, Westinghouse Electric & Manufacturing Company, Research Laboratories, East Pittsburgh, Pa. Jun. A.S.M.E.

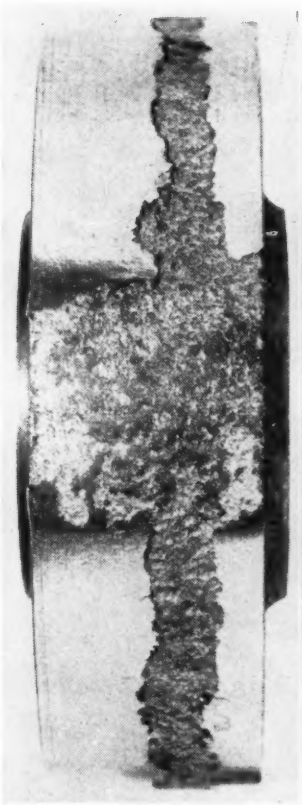


FIG. 7 CHROME-NICKEL-CAST-IRON ROLL AFTER RUN OF 661,000 CYCLES UNDER 2500 LB LOAD
(Test No. 25: 3.70-in-diam roll.)



FIG. 8 CHROME-NICKEL-CAST-IRON ROLL AFTER RUN OF 13,090,000 CYCLES AT 1500 LB LOAD
(Test No. 21: 3.70-in-diam roll.)

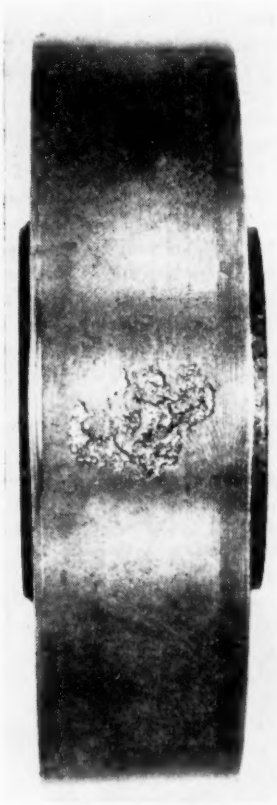


FIG. 9 PHOSPHOR-BRONZE ROLL AFTER RUN OF 1,125,000 CYCLES UNDER 3500 LB TEST LOAD
(Test No. 26: 4-in-diam roll.)

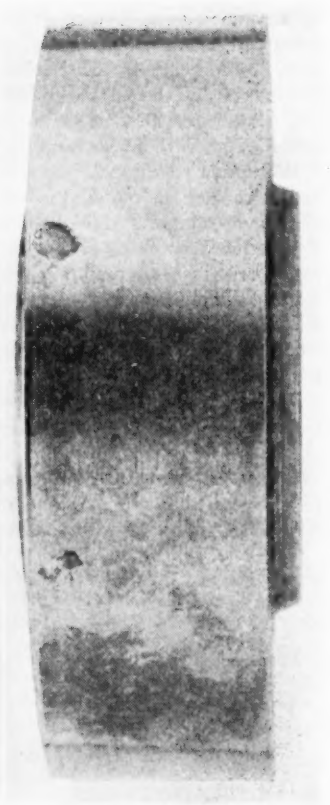


FIG. 10 MACHINE-STEEL ROLL AFTER RUN OF 808,000 CYCLES UNDER 4750 LB LOAD
(Test No. 103: 3.50-in-diam roll, 0.20 carbon steel, 4750-lb load, 808,000 cycles.)

no cracks or other signs of failure on the surface. When the sample was split to examine the blister, a crack about one quarter of an inch long about 0.15 in. below the surface was found to have developed under the blister. In addition, a circular band of the typical dark-brown color of overheated phenolic resins, about 0.030 in. wide and 0.150 in. below the surface, was present, running entirely around and concentric with the surface. A similar dark-brown band of about one half this width was also observed, extending from the surface to slightly below it. Here, the material itself made an automatic record of the heat concentration built up by the internal friction created by the stresses imposed. The testing of these materials is thus further complicated by these thermal conditions. The material has high internal friction, low heat conductivity, and appreciable loss of strength at higher temperatures. Thus in the case of a test roll of this material, 2.3 in. diam, running with a hardened-steel roll of the same diameter, under a test load of 1181 lb running at 950 rpm, the test roll blistered after 7000 cycles. Another roll of the same size and material, under the same test load, running at 350 rpm, blistered after 122,000 cycles.

As noted in Progress Report No. 15,[2] on a brass sample, a blister of similar character to that on the bakelite extended around nearly three quarters of the circumference. This roll is shown in Fig. 4. The brass roll was 3.50 in. diam running with a hardened-steel roll 2.30 in. diam under a load of 3500 lb. The failure occurred at the end of 305,000 cycles; the thickness of flake varied from 0.018 to 0.021 in. The surface hardness before test was 51 Rockwell B and after the test was 87 Rockwell B.

On the softer and more plastic cast-iron alloys, large flakes sheared out of the surface, some one quarter of an inch wide and as much as one inch in length. On the harder heat-treated cast-iron alloys, these flakes were sometimes as small as one eighth of an inch and of irregular shape. These flakes varied in thickness from about 0.010 in. to 0.035 in., depending largely upon the intensity of the load and the number of cycles. Fig. 5 shows the failure of the surface of a 4-in-diam test roll of nickel cast iron, running with a 2.30-in-diam hardened-steel roll under a load of 3500 lb, at the end of 406,000 cycles.

Unless otherwise noted, all tests were run against a hardened-steel roll of 2.3 in. diam. Fig. 6 shows a heat-treated nickel-cast-iron roll, 341 Bhn, 3.80 in. diam, after a run of 400,000 cycles under a load of 3435 lb. The flakes measured from 0.033 to 0.036 in. in thickness.

Fig. 7 shows a chrome-nickel-cast-iron roll, 3.7 in. diam, after a run of 661,000 cycles under a load of 2500 lb. Fig. 8 shows another roll of the same size and material after a run of 13,090,000 cycles under a load of 1500 lb.

Fig. 9 is a phosphor-bronze roll, 4 in. diam, after a run of 1,125,000 cycles under a load of 3500 lb.

Fig. 10 illustrates a machine-steel roll (substantially S.A.E. 1020), 3.5 in. diam, after a run of 808,000 cycles under a load of 4750 lb. The original hardness was 22 Rockwell C, and the surface hardness at the end of the test had increased to 32 Rockwell C.

These illustrations show some of the different types of destructive pitting; on some, the shallow cavities left by the incipient pitting may be seen. There does not appear to be any con-

nection between the incipient pitting and the destructive pitting.

The exact sequence of the different phenomena is a matter of question. Probably in some cases a crack may start under the surface in the region of high shear stresses before the disintegration of the surface material progresses far. This appears to be the case with the phenolic-laminated materials and brass. In other cases, the reverse may be true. Again, both types of failure may progress together. Probably the specific physical characteristics of the materials influence these conditions.

Tests on Cast-Iron Alloys

The most extensive series of tests to date has been on several cast-iron alloys. All of these tests were with rolls, 1 in. face width and running with a hardened-steel roll, 2.30 in. diam, unless otherwise noted. The first test rolls were 4 in. diam and were then turned down after one test and used again in a succeeding test. Here it was noted that the surface material crumbled away ahead of the cutting edge of the tool, so the diameter was reduced until the nature of the chip indicated sound material. The results of some of these tests indicated that the properties of the material might be changing as the diameter was reduced more and more from the original size. Therefore, on later tests, the rolls were cast to a size to finish 2.3 in. diameter. The smaller rolls were used to permit higher speeds of the test disks within the same range of surface velocities as before, to save time, particularly after it became evident that the tests must run to thirty million cycles or more to establish the surface-endurance limits of these materials.

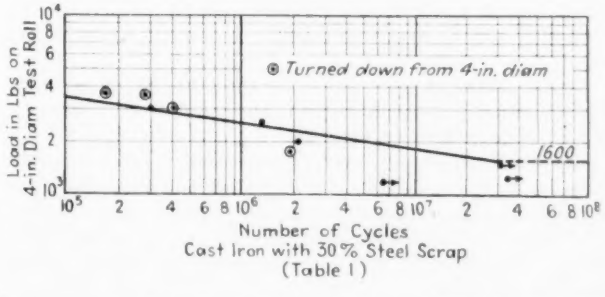
The following tables give representative test results. The actual test data are given first, followed by the equivalent load (based upon static stress conditions) on a 4-in-diam test roll, and the equivalent Brinell hardness number for purposes of comparison.

Semisteel. Table 1 gives the test results on gray iron with

TABLE 1
CAST IRON WITH STEEL SCRAP (SEMI-STEEL)

Test No.	Roll Dia.	Load in Lbs.	Hardness Core	Hardness Surface	Thickness of Flakes	Number of Cycles	Equiv Load 4 in Roll	Equivalent Brinell Core	Equivalent Brinell Surface
32	3.50*	3330	22-C	24-C	———	173,000	3620	240	248
47	3.80*	3435	96-B	102-B	.012-.014	279,000	3500	216	256
131	2.30	2362	190	209	.013	300,000	3000	190	209
48	3.80*	2940	95-B	98-B	———	400,000	3000	210	228
129	2.30	1968	180	190	.007	1,330,000	2500	180	190
128	2.30	1575	——	——	.010	2,093,000	2000	——	——
18	3.70*	1720	26-C	30-C	———	1,920,000	1770	260	283
126	2.30	1181	——	——	NO FAILURE	32,530,000	1500	——	——
125	2.30	1024	——	——	NO FAILURE	36,240,000	1300	——	——
17	3.70*	1210	94-B	97-B	NO FAILURE	6,499,000	1245	205	222

* TURNED DOWN FROM ORIGINAL 4" DIAMETER AFTER EARLIER TESTS



30 per cent steel scrap, sometimes known as "semisteel." The chemical analysis of a sample of this material is as follows: Silicon, 1.84; sulphur, 0.136; manganese, 0.65; phosphorus, 0.387; total carbon, 3.25; graphite, 2.80; combined carbon, 0.45.

The results of tests of the physical properties of this material were as follows:

	As cast	Heat-treated
Ultimate strength, psi	35200	45950
Elastic limit, psi	15000	35750
Brinell hardness number	223	255
Flexural endurance limit	21000	25000

The heat-treatment (tests Nos. 18 and 32) was as follows: Heat to 1500 F, and quench in oil; draw to 950–1000 F.

After some tests, the surface was so thoroughly destroyed that no reliable hardness measurements could be made. In many cases, the flakes were so broken that no measurement of their thickness could be made.

The surfaces were turned on the samples that did not fail, and the nature of the chips indicated sound material.

As none of the samples under rolling contact failed after 30,000,000 cycles, the intersection of the line representing the load against the number of cycles on a logarithmic chart with the 30,000,000-cycle point has been used to estimate the surface-endurance limit. Thus, the surface-endurance limit of this material has been estimated as between 1500 and 1600 lb load on a 4-in-diam test roll of 1 in. face width in rolling contact with a hardened-steel roll of 2.30 in. diam. The equivalent maximum specific compressive stress, on the basis of static-stress conditions of load, is equal to 87,500 psi.

Nickel Cast Iron. Table 2 A gives the test results on gray iron

TABLE 2A
NICKEL IRON - AS CAST

Test No	Roll Dia	Load in Lbs	Hardness Core	Hardness Surface	Thickness of Flakes	Number of Cycles	Equiv. Load 4 in Roll	Equivalent Brinell Core	Equivalent Brinell Surface
33	3.90*	3500	97-B	100-B	———	360,000	3530	222	242
93	2.30	2760	250	266	.010-.012	410,000	3500	250	266
50	4.00	3500	98-B	100-B	———	610,000	3500	228	242
39	3.50*	2900	99-B	99-B	———	275,600	3150	235	235
51	4.00	2500	98-B	100-B	———	1,670,000	2500	228	242
46	3.70*	2435	93-B	95-B	———	314,000	2500	200	210
44	3.80*	2450	94-B	98-B	———	243,000	2500	205	228
52	4.00	1500	98-B	98-B	———	2,663,000	1500	228	228
53	4.00	1100	101-B	101-B	NO FAILURE	15,651,000	1100	250	250

* TURNED DOWN FROM ORIGINAL 4" DIAMETER AFTER EARLIER TESTS

alloyed with nickel, with the rolls as cast. The chemical analysis of a sample of this material is as follows: Silicon, 1.42; sulphur, 0.117; manganese, 0.37; phosphorus, 0.448; total carbon, 3.36; graphite, 2.50; combined carbon, 0.86; nickel, 1.52.

The results of tests on physical properties tested were as follows:

Ultimate strength, psi	35400
Elastic limit, psi	12600
Brinell hardness number	217
Flexural endurance limit, psi	16000

The roll used for test No. 53 did not fail. The surface could be turned after test and the nature of the chips indicated sound material.

On the early tests, the rolls were turned down after previous tests. The results seemed to indicate a possible change in the material away from the original cast surface. Some of the tests were repeated with rolls cast to finish 4.00 in. and 2.300 in. diam. The results showed longer life. The tests were not continued further because heat-treated rolls appeared to give much better results. The surface-endurance limit under the rolling-test conditions

TABLE 2 B
NICKEL IRON - AS CAST WITH ABOUT 9% SLIDING ACTION

TEST No	ROLL DIA.	LOAD IN LBS.	HARDNESS CORE	HARDNESS SURFACE	THICKNESS OF FLAKES	NUMBER OF CYCLES	EQUIV. LOAD 4 IN. ROLL	EQUIVALENT BRINELL CORE	EQUIVALENT BRINELL SURFACE
140	2.20	1575	——	——	.013-.018	1,220,000	2000	——	——
141	2.20	860	——	——	NO FAILURE	32,250,000	1100	——	——

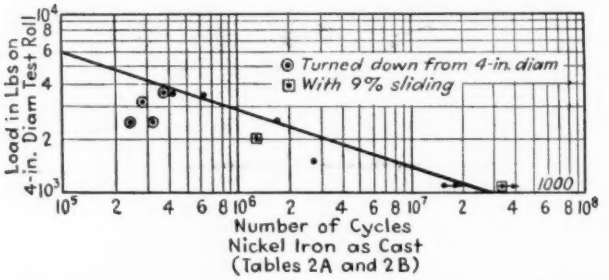
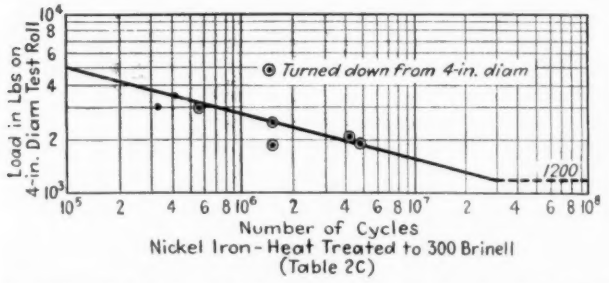


TABLE 2 C
HEAT TREATED NICKEL CAST IRON ABOUT 300 BRINELL

TEST No	ROLL DIA	LOAD IN LBS	HARDNESS CORE	HARDNESS SURFACE	THICKNESS OF FLAKES	NUMBER OF CYCLES	EQUIV. LOAD 4 IN. ROLL	EQUIVALENT BRINELL CORE	EQUIVALENT BRINELL SURFACE
23	4.00	3500	33-C	——	——	406,000	3500	305	——
34	3.80*	3435	341	——	.033-.036	400,000	3500	341	——
24A	4.00	3000	32-C	——	——	320,000	3000	296	——
36	3.80*	2940	32-C	——	.029-.031	558,000	3000	296	——
45	3.50*	2375	30-C	——	.025-.027	1,630,000	2580	283	——
63	3.80*	2058	32-C	32-C	.016-.020	4,070,000	2100	296	296
67	3.50*	1805	32-C	32-C	.013-.014	4,802,000	1960	296	296
66	3.20*	1740	29-C	——	.025-.033	1,650,000	1898	276	——

* TURNED DOWN FROM ORIGINAL 4" DIAMETER AFTER EARLIER TESTS.



was estimated at about 1000 lb load on the 4.0-in-diam roll. The equivalent maximum specific compressive stress was about 69,200 psi.

Two tests were conducted, introducing about 9 per cent sliding by using a 2.40-in-diam hardened-steel roll, and a 2.20-in-diam nickel-cast-iron roll with gears of 2.3 in. pitch diam on the end of each shaft. These results are given in Table 2B.

The roll used for test No. 141 did not fail. The turned surface indicated sound material. The surface endurance limit with about 9 per cent sliding appears to be about the same as for rolling action, although it appears to fail sooner with test loads greater than the endurance-limit loads.

Another series of tests was made with this nickel cast iron heat-treated as follows: Heat to 1500 F, and quench in oil; draw to 980 F.

The physical properties tested as follows:

Ultimate strength, psi	41700
Elastic limit, psi	24000
Brinell hardness number	246

Table 2C gives the results of rolling tests on this heat-treated material.

TABLE 2 D
HEAT TREATED NICKEL CAST IRON ABOUT 350 BRINELL

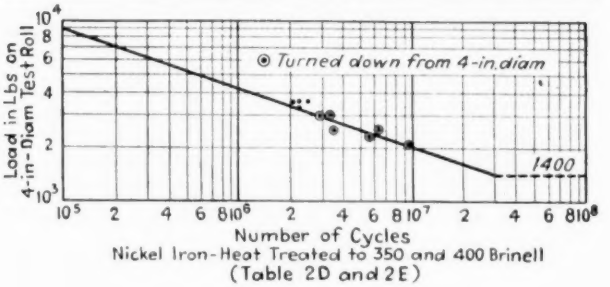
TEST No	ROLL DIA	LOAD IN LBS	HARDNESS CORE	HARDNESS SURFACE	THICKNESS OF FLAKES	NUMBER OF CYCLES	EQUIV. LOAD 4 IN. ROLL	EQUIVALENT BRINELL CORE	EQUIVALENT BRINELL SURFACE
22	4.00	3500	341	——	——	2,202,000	3500	341	——
24	4.00	3200	341	——	——	2,200,000	3200	341	——
35	3.80*	2940	38-C	——	——	2,940,000	2970	352	——
38	3.50*	2375	38-C	——	.024-.029	3,312,000	2580	352	——
49	3.20*	2108	36-C	——	.024-.029	5,600,000	2300	333	——
62	3.80*	2058	39-C	39C	.020-.025	9,192,000	2100	362	362

* TURNED DOWN FROM ORIGINAL 4" DIAMETER AFTER EARLIER TESTS

TABLE 2 E
HEAT TREATED NICKEL CAST IRON ABOUT 400 BRINELL

TEST No	ROLL DIA	LOAD IN LBS	HARDNESS CORE	HARDNESS SURFACE	THICKNESS OF FLAKES	NUMBER OF CYCLES	EQUIV. LOAD 4 IN. ROLL	EQUIVALENT BRINELL CORE	EQUIVALENT BRINELL SURFACE
27	4.00	3500	44-C	——	——	2,513,000	3500	415	——
29	4.00	3500	——	——	——	2,165,000	3500	——	——
42	3.80*	2940	44-C	——	.028-.032	3,177,000	2970	415	——
43	3.80*	2450	42-C	——	.023-.026	6,100,000	2500	393	——

* TURNED DOWN FROM ORIGINAL 4" DIAMETER AFTER EARLIER TESTS



The tests on these heat-treated rolls, which were turned down from earlier tests, seemed to indicate that the material nearer the original cast surface was better than that away from it, much the same as in the case of the materials as cast. These tests were not continued further because a more effective heat-treatment for this material had been developed. The surface-endurance limit of this heat-treated material under rolling action is estimated at about 1200 lb load on a 4-in-diam test roll. The equivalent maximum specific compressive stress is equal to about 75,800 psi.

Another series of tests were made with this nickel cast iron, heat-treated as before, but drawn to about 350 Bhn. The results of these tests are given in Table 2D.

These tests were not continued further because a more effective heat-treatment had been developed for this material. The surface endurance limit under rolling action was estimated to be about 1400 lb test load on a 4-in-diam test roll. The equivalent maximum specific compressive stress is equal to about 81,900 psi.

Another series of tests was made with this nickel cast iron, heat-treated as before, but drawn to about 400 Bhn. The results of these tests are given in Table 2E.

The surface endurance limit under rolling contact was estimated to be about 1400 lb test load on a 4-in-diam roll. The equivalent maximum specific compressive stress is equal to 81,900 psi. When the test points are plotted, they group together with those of the tests on this same material heat-treated to 350 Bhn.

While the foregoing tests on heat-treated nickel cast iron were being made, experiments were being conducted by the company

supplying the material on different heat-treatments. The following heat-treatment was developed which changed the structure of the material, particularly the form and dispersion of the graphite, which gave much higher physical properties to the material (patents have been applied for on this heat-treatment): Heat to 1500 F and hold until thoroughly heated; quench to 650 F and hold until heat is uniform; cool in boiling soda water. On the test rolls, the parts are held about 30 min.

This interrupted-quench treatment gave the following properties to a test sample:

Ultimate strength, psi	46500
Elastic limit, psi	25000
Brinell hardness number	287
Flexural endurance limit, psi	19000

The results of the tests for surface endurance are given in Table 2F.

Rolls used on tests Nos. 122 and 123 did not fail; the surface being turned after test showed sound material.

Test No. 121, being out of line with the others, led to suspicion of the material. A microscopic examination disclosed an improper structure, believed to be evidence of too short a time of heat-treatment. Untested rolls, later used on tests Nos. 122, 123, and 124 were also examined and found to be of the same improper structure. These rolls were heat-treated again, and test No. 124 gave results beyond the average, a possible indication that the double heat-treatment improved the material still further. The surface-endurance limit under rolling action is estimated to be about 2400 lb on a 4-in-diam test roll. The equivalent maximum specific compressive stress is equal to 107,300 psi.

Three additional tests were made, introducing about 9 per cent sliding by using a 2.4-in-diam hardened-steel roll and a 2.2-in-diam nickel-cast-iron roll, with gears of 2.30 in. diam on each shaft. The results of these tests are given in Table 2G.

With 9 per cent sliding action, the estimated surface-endurance limit appears to be about 1800 lb on a 4-in-diam test roll. This is about 75 per cent of the value under rolling conditions. The equivalent maximum specific compressive stress is equal to 92,900 psi.

Chrome-Nickel Cast Iron. Table 3 gives the test results on chrome-nickel cast iron. The chemical analysis of a sample of this material is as follows: Silicon, 1.24; sulphur, 0.130; manganese, 0.44; phosphorus, 0.297; total carbon, 3.39; graphite, 2.50; combined carbon, 0.89; nickel, 1.44; chrome, 0.50.

The physical properties of this material tested as follows:

	As cast	Heat-treated
Ultimate strength, psi	39000	44730
Elastic limit, psi	15100	31600
Brinell hardness, Bhn	234	243

The heat-treatment was as follows: Heat to 1500 F; quench in oil; draw to desired hardness.

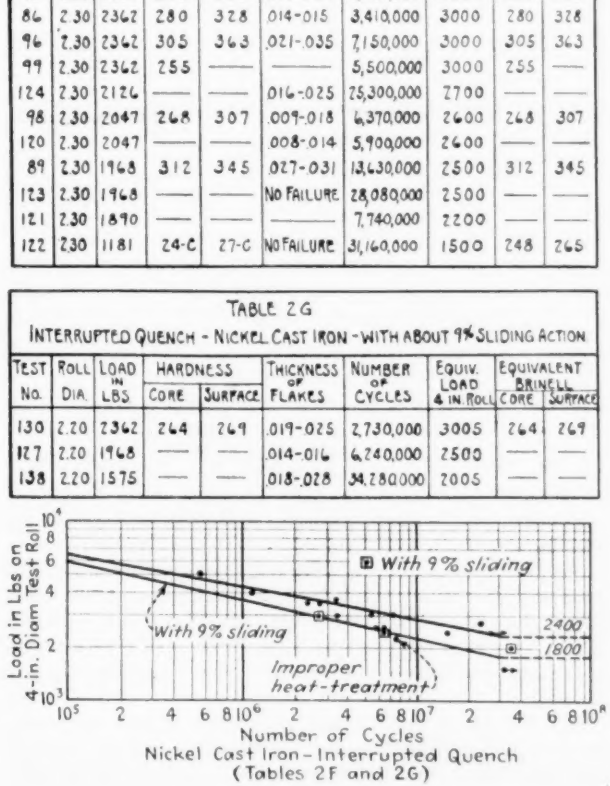
The heat-treatment employed did not appear to have very

TABLE 2F
INTERRUPTED QUENCH - NICKEL CAST IRON

Test No.	Roll Dia.	Load in Lbs	Hardness Core	Hardness Surface	Thickness of Flakes	Number of Cycles	Equiv. Load 4 in Roll	Equivalent Brinell Core	Equivalent Brinell Surface
71	3.20	4580	32-C	——	.025-.030	550,000	5000	296	——
97	2.30	3150	303	325	.015-.017	1,120,000	4000	303	325
68	3.50	3330	30-C	30-C	——	3,383,000	3620	283	283
91	2.30	2760	300	——	.021	2,731,000	3505	300	——
95	2.30	2760	302	363	.017-.025	2,480,000	3505	302	363
86	2.30	2362	280	328	.014-.015	3,410,000	3000	280	328
96	2.30	2362	305	363	.021-.035	7,150,000	3000	305	363
99	2.30	2362	255	——	——	5,500,000	3000	255	——
124	2.30	2126	——	——	.016-.025	25,300,000	2700	——	——
98	2.30	2047	268	307	.009-.018	6,370,000	2600	268	307
120	2.30	2047	——	——	.008-.014	5,900,000	2600	——	——
89	2.30	1968	312	345	.027-.031	13,630,000	2500	312	345
123	2.30	1968	——	——	NO FAILURE	28,080,000	2500	——	——
121	2.30	1890	——	——	——	7,740,000	2200	——	——
122	2.30	1181	24-C	27-C	NO FAILURE	31,160,000	1500	248	265

TABLE 2G
INTERRUPTED QUENCH - NICKEL CAST IRON - WITH ABOUT 9% SLIDING ACTION

Test No.	Roll Dia.	Load in Lbs	Hardness Core	Hardness Surface	Thickness of Flakes	Number of Cycles	Equiv. Load 4 in Roll	Equivalent Brinell Core	Equivalent Brinell Surface
130	2.20	2362	264	269	.019-.025	2,730,000	3005	264	269
127	2.20	1968	——	——	.014-.016	6,240,000	2500	——	——
138	2.20	1575	——	——	.018-.028	34,280,000	2005	——	——

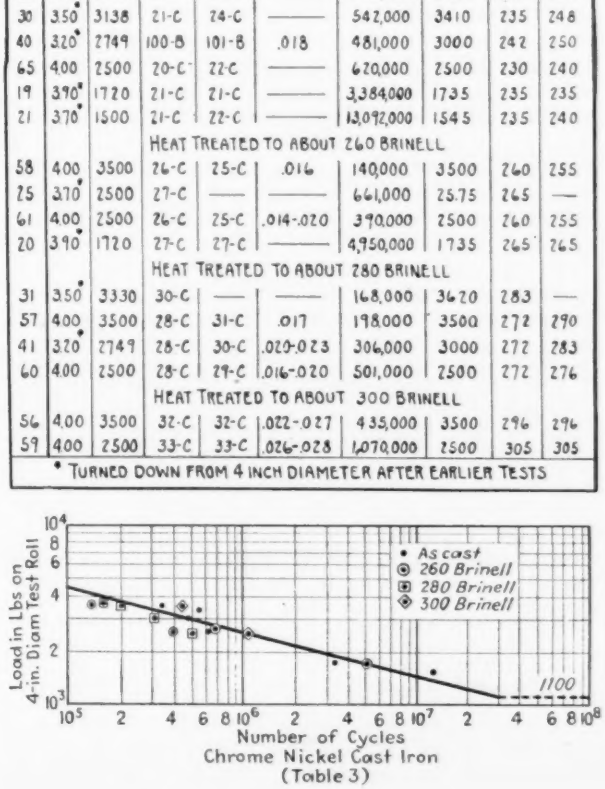


Nickel Cast Iron - Interrupted Quench
(Tables 2F and 2G)

TABLE 3
CHROME NICKEL CAST IRON

Test No	Roll Dia.	Load in Lbs.	Hardness Core	Hardness Surface	Thickness of Flakes	Number of Cycles	Equiv. Load 4 in Roll	Equivalent Brinell Core	Equivalent Brinell Surface
64	4.00	3500	21-C	23-C	——	334,000	3500	235	245
30	3.50*	3138	21-C	24-C	——	542,000	3410	235	248
40	3.20*	2749	100-B	101-B	.018	481,000	3000	242	250
65	4.00	2500	20-C	22-C	——	620,000	2500	230	240
19	3.90*	1720	21-C	21-C	——	3,384,000	1735	235	235
21	3.70*	1500	21-C	22-C	——	13,092,000	1545	235	240
			HEAT TREATED TO ABOUT 260 BRINELL						
58	4.00	3500	26-C	25-C	.016	140,000	3500	260	255
25	3.70*	2500	27-C	——	——	661,000	2575	265	——
61	4.00	2500	26-C	25-C	.014-.020	390,000	2500	260	255
20	3.90*	1720	27-C	27-C	——	4,950,000	1735	265	265
			HEAT TREATED TO ABOUT 280 BRINELL						
31	3.50*	3330	30-C	——	——	168,000	3620	283	——
57	4.00	3500	28-C	31-C	.017	198,000	3500	272	290
41	3.20*	2749	28-C	30-C	.020-.023	306,000	3000	272	283
60	4.00	2500	28-C	29-C	.016-.020	501,000	2500	272	276
			HEAT TREATED TO ABOUT 300 BRINELL						
56	4.00	3500	32-C	32-C	.022-.027	435,000	3500	296	296
59	4.00	2500	33-C	33-C	.026-.028	1,070,000	2500	305	305

* TURNED DOWN FROM 4 INCH DIAMETER AFTER EARLIER TESTS



Chrome Nickel Cast Iron
(Table 3)

TABLE 4
MOLYBDENUM CAST IRON

Test No.	Roll Dia.	Load in Lbs	Hardness Core	Hardness Surface	Thickness of Flakes	Number of Cycles	Equiv. Load 4 in Roll	Equivalent Brinell Core	Equivalent Brinell Surface
			AS CAST						
133	2.30	2760	215	240	———	2,750,000	3505	215	240
134	2.30	1968	213	240	———	3,200,000	2500	213	240
135	2.30	1575	212	247	———	4,700,000	2000	212	247
			HEAT TREATED - INTERRUPTED QUENCH						
136	2.30	2760	107-B	113-B	.014-.018	7,365,000	3505	291	333
132	2.30	2362	106-B	108-B	———	18,690,000	3000	284	298
137	2.30	2204	106-B	109-B	.010-.014	28,000,000	2800	284	305

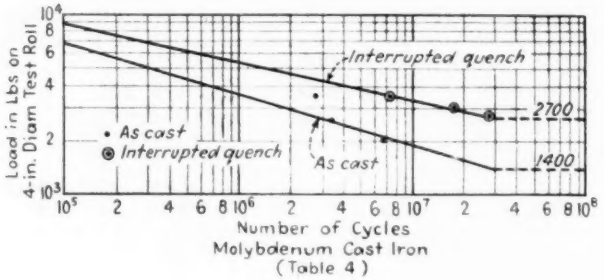
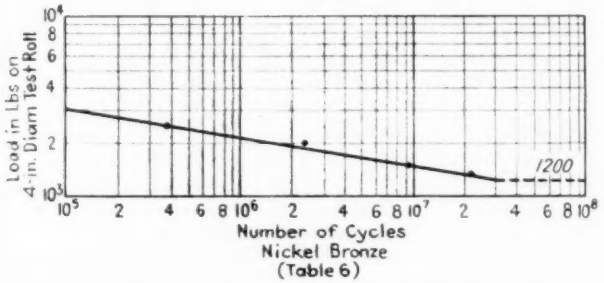


TABLE 6
NICKEL BRONZE

Test No.	Roll Dia.	Load in Lbs.	Hardness Core	Hardness Surface	Depth of Pits	Number of Cycles	Equiv. Load 4" Roll	Equivalent Brinell Core	Equivalent Brinell Surface
174	2.3	1968	43-B	46-B	.012-.014	381,000	2500	83	87
173	2.3	1575	44-B	53-B	.017-.018	2,320,000	2000	85	97
172	2.3	1181	39-B	46-B	.008	9,110,000	1500	79	87
175	2.3	1024	48-B	46-B	.006-.008	22,060,000	1300	90	87



much influence on the surface endurance, which was estimated at about 1100 lb on a 4-in-diam test roll under rolling action.

Molybdenum Cast Iron. Table 4 gives the test results on molybdenum cast iron. The heat-treatment used was the same interrupted quench as was used on the nickel cast iron and reported in Table 2F. The chemical analysis of a sample of this material is as follows: Silicon, 1.77; manganese, 0.59; total carbon, 3.12; molybdenum, 0.66.

The physical properties of this material, heat-treated, are as follows:

Ultimate strength, psi	49000
Elastic limit, psi	22400
Brinell hardness, Bhn	290
Flexural endurance limit, psi	22000

The estimated surface-endurance limit under rolling action on a 4-in-diam test roll was about 1400 lb for material as cast, and about 2700 lb for interrupted quenched material. The equivalent

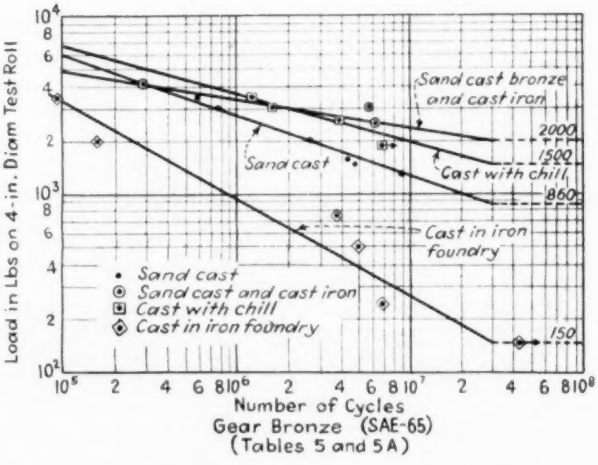
TABLE 5
PHOSPHOR GEAR BRONZE - SUBSTANTIALLY SAE 65

Test No.	Roll Dia.	Load in Lbs	Hardness Core	Hardness Surface	Thickness of Flakes	Number of Cycles	Equiv. Load 4 in Roll	Equivalent Brinell Core	Equivalent Brinell Surface
			CAST AGAINST A CHILL						
26	4.00	3500	48-B	92-B	———	1,125,000	3500	90	195
54	3.80*	2940	107-V	187-V	.023	1,696,000	3000	187	187
37	4.00	2500	48-B	92-B	———	3,842,000	2500	90	195
56A	3.70*	1845	———	———	No Failure	4,789,000	1900	———	———
			CAST IN SAND WITHOUT CHILL						
78	2.30	2756	43-B	85-B	.019-.028	570,000	3500	83	165
79	2.30	2362	45-B	84-B	———	760,000	3000	86	162
80	2.30	1575	47-B	72-B	———	2,600,000	2000	88	130
84	2.30	1332	68	———	———	4,100,000	1695	68	———
85	2.30	1175	62	———	———	4,750,000	1495	62	———
88	2.30	1023	82	———	.010-.015	8,550,000	1300	82	———
			TESTS WITH 2.30 DIA CAST IRON ROLLS - 341 BRINELL						
75	2.30	3214	42-B	92-B	BRONZE FAILED BRONZE FAILED	280,000	4080	82	195
77	2.30	2362	47-B	76-B		5,820,000	3000	88	139
76	2.30	1970	49-B	81-B	.028	4,016,000+	2500	92	153

* TURNED DOWN FROM 4 INCH DIAMETER AFTER EARLIER TESTS.
\+ BOTH ROLLS FAILED.

TABLE 5A
PHOSPHOR GEAR BRONZE — CAST IN IRON FOUNDARY

Test No.	Roll Dia.	Load in Lbs.	Hardness Core	Hardness Surface	Depth of Pits	Number of Cycles	Equiv. Load 4" Roll	Equivalent Brinell Core	Equivalent Brinell Surface
166	2.3	2760	51-B	86-B	.010-.014	99,000	3500	95	169
167	2.3	1575	30-B	79-B	.007-.010	168,000	2000	72	147
168	2.3	590	41-B	65-B	.009	3,841,000	750	81	116
169	2.3	394	43-B	51-B	.008-.011	4,936,000	500	83	95
170	2.3	197	30-B	44-B	.0035-.0045	6,849,000	250	72	85
171	2.3	118	23-B	36-B	Did Not Fail	42,842,000	150	66	76



maximum specific compressive stress for the heat-treated material is equal to 113,700 psi.

Phosphor Bronze. Tests were made on two lots of phosphor gear bronze, both of them being substantially the same as S.A.E. 65 bronze. One lot was cast against a chill, the other was not. Three tests were run with the bronze rolls against heat-treated nickel-cast-iron rolls. The results of these tests are given in Table 5.

The test roll on test No. 56A did not fail. When turned after test, the material crumbled ahead of the cutting tool, showing the disintegration of the surface material. The surface-endurance

limit of material cast against a chill was estimated to be about 1500 lb on the 4-in-diam test roll under rolling action. The equivalent maximum specific compressive stress was equal to 82,800 psi.

The estimated surface-endurance limit for sand-cast material under the same conditions is about 1000 lb; equivalent maximum specific compressive stress, 67,600 psi.

The estimated surface-endurance limit for sand-cast material, running with a cast-iron roll under the same conditions, is about 2000 lb; equivalent maximum specific compressive stress, 83,300 psi.

Another lot of similar material was tested, which was cast in a cast-iron foundry with little regard for the technique of handling bronze. The results are given in Table 5A.

This material was evidently badly overheated when it was melted before pouring. The alloy was obtained in pigs from a reliable bronze company. The differences in original hardness would indicate that the samples, identified by the test numbers, were poured in the following order from the ladle: Nos. 171, 167, 170, 168, 169, 166.

The samples from tests Nos. 166 and 167 were etched, and also broken to examine the fracture. Very large crystals were apparent in No. 167, while they were much smaller in No. 166. On the outside surface, where destructive pitting was present, no crystal structure could be seen, indicating amorphous material where the surface had started to disintegrate. The fractures were in keeping with the porous overheated material. When proper foundry practices are followed, this material should have a surface-endurance limit of over 800 lb on a 4-in-diam test roll under rolling action. The estimated surface-endurance limit on these overheated rolls is about 150 lb.

Summary

Although the complex behavior of plastic materials under the repeated surface stresses set up by rolling and sliding is still far from being understood, and also because the actual intensities of the several stresses, compressive, tensile, and shear, are thus far indeterminate, yet the actual test-load results may be applied safely to design. These tests were started in 1931, and the test results have been successfully applied in the design of cams and their roller followers, and in the design of gears since then. The comparative results between different materials as found in these tests are confirmed by the behavior of these materials in service as elements of automatic machines operating in production. The limiting loads, as determined from these tests, have thus far resulted in designs with no appreciable wear.

For the purpose of setting up a load-diameter-stress factor, we will start from the Hertz equation for the stresses set up between two loaded cylinders in contact. When

s = maximum specific compressive stress, psi
w = load on cylinders, lb per in. of length
r_1 and r_2 = radii of cylinders, in.
E_1 and E_2 = modulus of elasticity of materials

$$s^2 = \frac{0.35w(1/r_1 + 1/r_2)}{(1/E_1 + 1/E_2)}$$

We will now introduce an experimental factor of load and stress concentration, based upon the test values; whence K_1 = experimental load-stress factor for two cylinders

$$K_1 = w(1/r_1 + 1/r_2) \quad \text{(by definition)}$$

and

$$w = K_1/(1/r_1 + 1/r_2)$$

Referring now to Table 1, for the test results on a roll of 4.00 in. diam of semisteel running with a hardened-steel roll of 2.300 in. diam, both with a face of 1.00 in., we have an experimental surface-endurance-limit load of 1600 lb. This gives the following values for use in the foregoing equation:

$$w = 1600 \text{ lb}$$
$$r_1 = 1.150 \text{ in.}$$
$$r_2 = 2.000 \text{ in.}$$

$$K_1 = 1600\ (1/1.150 + 1/2.00) = 2191$$

These factors (K_1) are used to determine the limiting surface loads between two curved surfaces. These limiting loads are the ones which can be carried indefinitely without appreciable wear. (If abrasive particles are present, these values do not apply.) For example, if the minimum radius of curvature of a cam is 4 in., and the cam roll is 2.00 in. diam., the cam being made of semisteel and the roll of hardened steel, then

$$r_1 = 1, \qquad r_2 = 4.00$$

$$w = 2191\ (1/1 + 1/4.00) = 1.25 \times 2191 = 2738 \text{ lb}$$

For involute-spur-gear teeth, where

K = load-stress factor for gear teeth
ϕ = pressure angle
D_1 = pitch diameter of pinion, in.
D_2 = pitch diameter of gear, in.
N_1 = number of teeth in pinion
N_2 = number of teeth in gear
F = face width of gears, in.
W_w = limiting load for wear, lb
Q = ratio factor

$$r_1 = D_1 \sin \phi/2$$
$$r_2 = D_2 \sin \phi/2$$

$$(1/r_1 + 1/r_2) = (2/\sin \phi)\ (1/D_1 + 1/D_2)$$

Let

$$K = s^2 \sin \phi\ (1/E_1 + 1/E_2)/(4 \times 0.35)$$
$$Q = 2N_2/(N_1 + N_2) = 2D_2/(D_1 + D_2)$$
$$W_w = D_1FKQ$$

The value of (K_1) for cylinders is

$$K_1 = w(1/r_1 + 1/r_2) = s^2(1/E_1 + 1/E_2)/0.35$$
$$K/K_1 = \sin \phi/4$$
$$K = K_1 \sin \phi/4$$

Hence, for this combination of semisteel and hardened steel, we have the following:
For $14^1/_2$-deg gears

$$K = (2191 \times 0.25038)/4 = 137$$

For 20-deg gears

$$K = (2191 \times 0.34202)/4 = 187$$

As an example, we will use a pair of 6 DP gears, 20-deg pressure angle, 2 in. face, of 24 and 36 teeth. This gives the following values for the limiting wear-load equation:

$$N_1 = 24 \quad N_2 = 36 \quad D_1 = 4 \quad K = 187 \quad F = 2$$
$$Q = 72/60 = 1.2$$
$$W_w = 4 \times 2 \times 187 \times 1.20 = 1795 \text{ lb}$$

The following values of (K_1) and of (K) have been computed in this manner from the experimental values. Except where noted

Table no.	Material	Cylinder K_1	Gears $14^1/_2$ deg K	Gears 20 deg K
1	Semisteel	2191	137	187
2(*a* and *b*)	Nickel cast iron	1369	85	117
2(*c*)	Nickel iron, heat-treated, 300B	1643	102	140
2(*d* and *e*)	Nickel iron, heat-treated to 350–400	1917	120	163
2(*f* and *g*)	Nickel iron, interrupted quench	3286	205	280
2(*f* and *g*)	Nickel iron, interrupted quench, with 9 per cent sliding	2465	154	210
3	Chrome-nickel cast iron	1506	94	128
4	Molybdenum cast iron	1917	120	163
4	Molybdenum iron, interrupted quench	3697	231	316
5	Phosphor bronze, sand cast	1177	73	100
5	Phosphor bronze, chilled	2054	128	175
5	Phosphor bronze, overheated when cast	205	12	17
5	Phosphor bronze, sand cast and nickel iron, interrupted quench	2739	171	234

otherwise, a hardened-steel test roll has been used in contact with the material specified.

Discussion

G. B. WARREN.[4] Professor Buckingham is to be congratulated upon making another fundamental contribution to gear information. The writer hopes that the author will be able to extend the excellent data contained in this paper to a larger variety of steels with different hardness values, since hardened steels are the more common gear materials used in high-duty machines today. Fundamental data of this character are required in order to extend these designs still further, or to design with greater assurance of reliable performance.

Some of the tests reported in the paper were run with sliding between the rollers. A few of the tabulations indicate a significant increase in the tendency to pit with sliding when the member under consideration is running at a slower speed than its mating roller. There is considerable evidence in actual gear performance and in some tests which have been run by Brown-Boveri along similar lines to indicate that the pitting resistance of the higher-speed roller, of two rollers that are rolling and sliding on each other, is greatly increased. The writer would like to discuss this matter briefly and to draw certain conclusions which may have considerable significance in connection with gear design and performance.

While not posing as a gear expert, it so happened that some gear-pitting difficulties in connection with a gear-reduction job were brought to the writer's attention. In posting himself on the subject, some of the principal contributions to the literature which have been made in recent years were obtained from the company library. Four rather outstanding references were found which are to some extent extracted in the Appendix to this discussion.

After studying these, the writer has come to the following conclusions and hypotheses regarding pitting, some of which fit in with previously advanced theories and some are additions thereto, which, so far as he has been able to determine, have not been made before. These are being submitted herewith for critical consideration:

Referring to Fig. 11 of this discussion, based upon the information which the writer has been able to obtain, particularly from reference (1) in the Appendix, it would seem that there are two types of pitting as follows:

1 A large number of usually disconnected small pits as shown at *N* on the dedendum of the gear, that is, below the pitch line. It is understood this is sometimes called "benign" pitting which very frequently occurs on gears in their early stages of operation and which, although somewhat harmful and a source of annoyance to users, may be self-limiting, i.e., it will reach a stable point and not progress further, particularly on soft gears which are not too heavily loaded. It is not clear what is its end point on harder more heavily loaded gears. This is sometimes called "spalling" in the English literature.

2 Pitting, as shown at *O* between the arrows *P-P* directly on the pitch line, is a form of surface failure which, so far as can be ascertained, only occurs on extremely heavily loaded gears. The pits may form connected areas from which the entire surface may be removed, and this form probably leads to ultimate failure.

With respect to type 1 of pitting described, it seems to be the

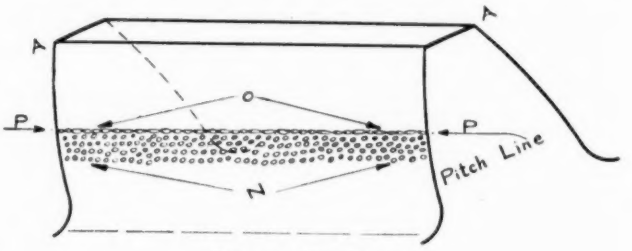


FIG. 11 GEAR PITTING

general consensus of opinion: (*a*) This is a difficulty associated with high pressure between two rolling surfaces; (*b*) it takes place only when sliding is in a direction opposite to the rolling; and (*c*) it will only take place in conjunction with and is due to the action of the lubricant.

As a result of the following analysis, and to the evidence of reference (1) the writer has concluded that this type of pitting is much less prevalent on case-hardened gears than on deep-hardened or unhardened gears, and that it might be entirely eliminated by a treatment which would put the surface of the gear tooth under compression, as is done on case-hardened, induction-hardened, or flame-hardened gears which are not ground subsequently.

Let us consider Figs. 12, 13, and 14, of this discussion, respectively, showing the action of two gear teeth along the line of action *a-b-c*, in successive stages of the tooth contact.

In Fig. 12 is shown the first stage of the contact with the motion from left to right and the lower gear driving the upper with the contact at b_1.

The rolling progresses between the two convex surfaces of the teeth upward as the gear turns. Looking at the point of contact in the case of Fig. 12, the tooth on the upper gear slides on the tooth of the lower gear so that the sliding of the upper gear tooth is downward on the lower gear tooth, away from the pitch line, and in such a way as to put the skin of the lower gear tooth, that is, the driver, in tension due to the frictional forces, and the corresponding section of the upper gear tooth, the driven tooth, in compression.

Considering Fig. 13, when the two teeth have progressed so that the contact is at the point where the line of action a_2-b_2-c_2 goes through the pitch line of the two gears, then we have pure rolling contact and theoretically no sliding.

Let us consider Fig. 14, where the contact is on the upper end of the driving tooth just before it leaves contact with the driven tooth at b_3 on the line of action a_3-b_3-c_3. At this point, the gear teeth are being pulled apart by the instantaneous motion, and the driving tooth is sliding downward along the dedendum surface of the driven surface as shown by the arrow *Z*.

[4] Designing Engineer, Turbine Engineering Division, General Electric Company, Schenectady, N. Y. Mem. A.S.M.E.

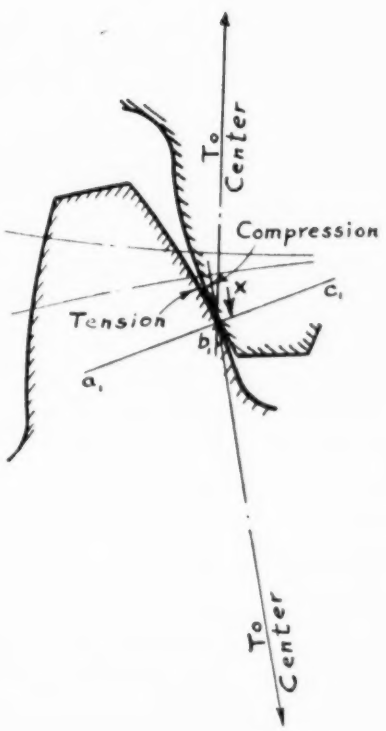


FIG. 12

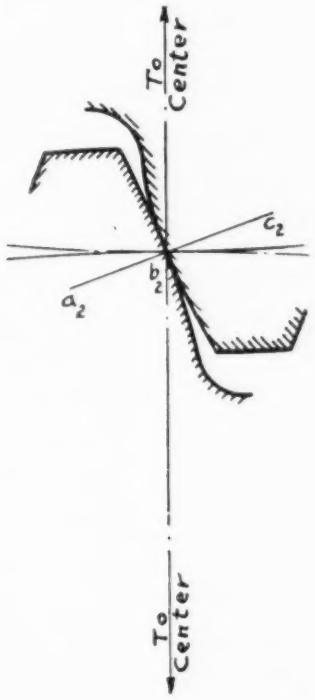


FIG. 13

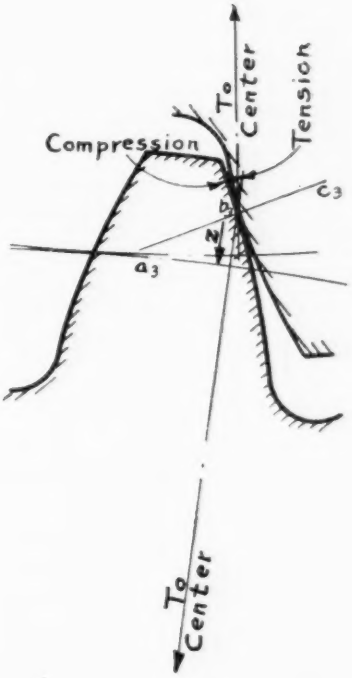


FIG. 14

As stated, the rolling action is progressing upward as the teeth move through the line of action. A careful examination of these three figures will indicate that the addendum, that is, the section of the tooth outside of the pitch line, in each case, is sliding radially on the dedendum portion of the opposite tooth in such a way as to stretch the material of the dedendum ahead of the rolling, and that the oil which has been fed onto the surfaces of the gears is being rolled into this point of contact by the progression of the point of rolling.

This action has been simulated between two rollers, as shown in Fig. 15, by numerous investigators, in which the rollers are

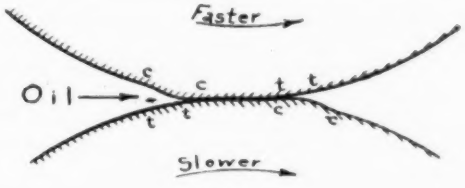


FIG. 15

rolling together in the direction as shown by the arrows but not at the same peripheral speed. If this is done, it can be seen that the traction of the friction parallel to the surface, when the surfaces are forced hard radially together, is such as to produce a tension in the surfaces marked *t-t* and a compression in the portion of the rollers marked *c-c*. The oil is also shown being fed in advance of the rolling point.

Fig. 16 shows an enlarged view of what might be considered as taking place on the surface in which any minute cracks or imperfections on the lower roller would be opened up and correspondingly closed up on the upper roller. The oil would, of course, then be forced into these cracks and raised to very high pressures by its passage under the point of contact, with resulting progressive fatigue failure which would finally lift small pieces of the surface out. This is apparently what happens. Observations show that invariably the pits form on the roller in which the friction of the sliding would produce tension and do not form on the roller in which the sliding would produce compression. This is so marked that even when the upper roller as shown, that is, in this case the higher speed one, is made one half the hardness of the lower roller, the upper roller develops no pits.

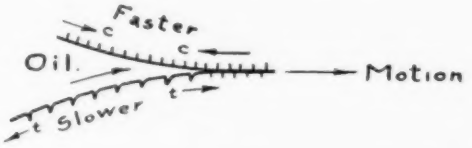


FIG. 16

It would seem that, if the surface could be put in compression to such an extent as to more than offset that which would be formed by the sliding friction, then it might be possible to preclude the formation of this type of pitting on either gear tooth. This is borne out to some extent by the observations that case-hardened gears do not form such pits so readily, although there is good reason to believe that if case-hardened gears are ground there would still be residual surface tension, as evidenced by frequent rejections due to grinding cracks (reference 4). Some tests on induction-hardened rollers which we have made seem to bear this out.

This hypothesis is further evidenced by the fact that on soft gears such pits on the dedendum inside or below the pitch lines, frequently formed during the initial stages of operation, sometimes seem to reach a stable point and do not increase or enlarge from that time on. It would seem as though the formation of a number of pits might permit the escape of the trapped oil, and hence result in a lesser building up of the hydraulic pressure. Also, on soft gears the initial running-in will produce cold work

on the surface and may result in a surface compression stress which would reduce the further formation of these pits.

With respect to type 2 pitting, as shown in Fig. 11 of this discussion, at *O* along the pitch line, the following hypothesis may explain this formation:

Consider the rolling in Figs. 17 and 18, which takes place at the pitch line of the gearing, as shown in Fig. 13. Theoretically, pure rolling is taking place with no sliding. Actually, up to the pitch line, the sliding had been as shown by the arrows in Fig. 17.

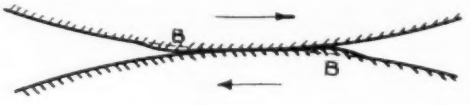


FIG. 17

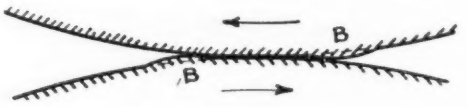


FIG. 18 GEAR PITTING

Immediately when the pitch line is reached and passed, the sliding reverses to the direction of the arrows as shown in Fig. 18. It is quite probable that some bulging of the surface, as shown exaggerated in *B-B* in Figs. 17 and 18, might take place. A more serious situation, however, might exist in the shear forces just below the surface but approximately parallel to the surface due to the tractional or frictional forces existing and to their sudden reversal.

At no other point on the tooth surfaces are these subsurface shear forces reversed through 180 deg in the same material. If the gears are heavy or if the gears and centers are rigid, then this sudden reversal probably takes place along one highly localized line immediately below the surface at the pitch line of both gears. This, it would seem, might easily account for the peculiar types of pits formed at this point, and for the fact that these pits when they are once started seem to progress and run into each other, because, unlike the formation of the other pits, the formation of a few pits would give no relief to the material and would actually increase the pressure on the remaining good surface of the gear.

It is not possible at this time to see any immediate means of remedying this situation.

The Appendix to this discussion contains excerpts from the four references which have been cited and which form the basis for the writer's conclusions.

It is to be hoped that the author or others will extend these roller tests in the near future, including such tests as will prove or disprove the hypotheses presented.

APPENDIX TO DISCUSSION

Reference 1. Excerpts from an article entitled, "Durability of Gears," by H. D. Mansion, which appeared in the *Automobile Engineer*, October, 1941:

Spalling denotes a type of mottled surface failure which appears to consist of a large number of tiny pits extending over a fairly large area, there being no lines in the direction of sliding such as are found in scoring. It has usually been observed on the dedendum of the driven gear teeth and sometimes on the addendum of the driving gear teeth, i.e., mainly during recess in conditions where the oil film is not broken down. Spalling might, in some instances, almost be described as pitting, but the latter term is reserved for the deeper failure to be described.

Pitting is the breaking out from the surface, usually on or near the pitch line, of large flakes, the resultant pits or holes being much deeper than any of the foregoing forms of surface failure. Pitting is generally considered to be a fatigue failure of the surface, though some difference of opinion exists as to the mechanism by which it occurs.

It was now found, in general, that this steel (Ni-Cr-Mo 100-ton oil-hardening steel, type F) would fail by pitting rather than by scuffing. With jet lubrication only, pitting occurred after short periods at loads of 2300 and 2460 lb per in., but with jet and bath lubrication, in a series of 1-hr tests, pitting did not occur until loads of 3830 and 4520 lb per in. were reached.

Of the surface failures which have occurred, two distinct types of pitting have been observed. The direct-hardening steels produce pits which are generally approximately circular and which do not, as a rule, join up with one another. The case-hardening steels, however, appear to become pitted right across the pitch line as though the case had flaked off over that area. It remains to be seen whether this will occur also on gears which are more deeply cased.

Referring in greater detail to the results shown in the tables and dealing first with the 8 D. P. design, it would appear from tables II and III, so far as the irregular nature of these first tentative tests permits of drawing conclusions, that the Ni-Cr-Mo 100-ton oil-hardening steel, when heat-treated in cyanide, in which condition it is virtually case-hardened, has greater resistance both to pitting and to fatigue failure than when simply oil-hardened without cyanide and can consequently carry a higher load without surface failure or breakage.

The incidence of pitting does not appear to be consistently affected by the grinding method used.

Reference 2. Excerpts from an article entitled, "Testing Gear-Wheel Material," which appeared in the *Brown-Boveri Review* for October, 1939:

A new apparatus developed by Brown-Boveri for the testing of gear-wheel material is described in this article. Some results of tests made are given. It is shown that direction of the sliding movement plays a preponderant part in the durability of the material.

Now, in order to reproduce faithfully the conditions pertaining to teeth faces, it is necessary to generate a sliding movement between the rollers. It is not desirable, to this end, simply to cause the shafts to rotate at different speeds. However, it is possible to create a sliding movement even when both shafts have the same number of revolutions, by making the test cylinders of different sizes or by coupling the shafts through eccentric involute gear wheels. The latter is the solution generally adopted in the present tests. It allows of the faithful reproduction on the periphery of one single test cylinder of all the movements occurring between two tooth faces, and thus of determining the behavior of the material by means of a few tests only.

If the sliding and rolling movements of the teeth of a gear wheel are studied, the following results are obtained: The rolling movement on a driving tooth is from root toward tip while on a driven tooth it is from tip toward root. The sliding on a driving tooth is always directed away from the rolling point and on a driven tooth it is directed toward the rolling point. Therefore, on the addendum, the rolling and sliding motions are in the same direction while being opposite on the dedendum.

Contrary to seizing, pitting only appears after a longer testing time. Small particles break out of the roller surface; the appearance of a typical pit is that of a sector of a circle with an angle of 90 to 120 deg. The fracture, being in the center of a sector in formation, penetrates from here at about 15 deg beneath the surface. On the surface, all that is to be seen at first are the two radii as very fine cracks, until finally the crack has advanced so far that the whole wedge now loosened—probably

under the pressure of the lubricating oil forced in—is lifted out of the surface and breaks off in circular shape.

The surface of the fracture is shell-like, and it can be seen that the fracture has advanced progressively as takes place in a fatigue fracture.

The tests show quite clearly that, contrary to seizing, pitting appears exclusively on one of the two test bodies. As is seen in all the illustrations, the pitting only appears on the dedendum arc *a* whereas the addendum arc *b* is always unaffected.

The limitation of pitting to the dedendum arc *a* is very sharply defined indeed. The pitting stops abruptly at rolling point *A*, the limit is sharply defined and coincides with the theoretically determined rolling point, to 0.01 in.

Thus the tests show that the pitting is furthered very much by sliding, but only when the sliding movement is counter to the direction of the rolling movement. The proclivity to pitting is increased to an astonishing degree and the illustrations show some exceptional examples. In one case with a roller of heat-treated chromium-nickel steel having a yield point of about 48 tons per sq in. much pitting appeared on the dedendum arc *a*, while on the other roller of carbon steel with a yield point of about 29 tons per sq in. no pitting occurred at all on the addendum arc *b*. On another roller, the width of the addendum arc *b* was reduced to less than half, and the linear pressure thus more than doubled. Despite this the addendum arc *b* remained intact while the dedendum arc *a* showed marked pitting.

The influence of the viscosity of the lubricating oil is also of interest; the more fluid the lubricating oil the bigger the pit. With transformer oil, big pits of 5 mm diam are formed, while with cylinder oil thep its are hardly bigger than a pinhead. This seems to confirm the view that the lubricating oil forced into the fatigue cracks helps pit formations and finally lifts the loose material from the surface. A heavy cylinder oil will be more likely to detach the material loosened from the lower layer and thus to complete the formation of a pit than a thin transformer oil which can easily escape from the narrowest cracks.

In order to investigate more completely the resistant character of the addendum arc, further tests were carried out with somewhat different apparatus. As said before, it is possible to generate a sliding movement of the two test rollers, one on the other, by imparting uniform running to the shafts but by using test rollers of different sizes. The sliding movement is then the same at every point. With the dimensions chosen here the specific sliding on the smaller test piece was minus 0.29 and on the bigger one plus 0.22. The result of these tests was as follows:

The smaller test pieces were made of carbon steel and of nickel steel with a yield point of 29 and 25 tons per sq in., respectively. The bigger test piece was of chromium-nickel steel with a yield point of 48 tons per sq in. After 3 to 6 hr, pits appeared on the smaller roller. The linear pressure was 1500 lb per in. on this test, the speed being 1000 rpm.

The contrary arrangement, that is, with smaller test pieces of chromium-nickel steel having a yield point of 48 tons per sq in., and the bigger ones of carbon steel and nickel steel having yield points of 29 and 25 tons per sq in., respectively, stood up to 100 running hours without any pitting at all. In order to force deterioration of the addendum arc, the surface of the bigger cylinder was turned down to about half its width and the load increased as much as the safety of the bearings would permit. The linear load was then 3500 lb per in., the stressing, according to the Hertz formula, 70 tons per sq in. After about 100 hr of running, in one case the smaller chromium-nickel roller broke down; in spite of having a yield point of 48 tons per sq in., it could not stand up to the bigger nickel-steel cylinder, having a yield point of only 25 tons per sq in.

We are at a loss, up until today, to furnish a plausible explanation of why the same material should support such exceptionally different stressings according to the direction of the sliding movement. Perhaps subsequent tests will give the answer to this problem.

Reference 3. Excerpts from a paper entitled, "Westinghouse Roller and Gear Pitting Tests," by Dr. Stewart Way, which was presented at the 24th Annual Meeting of the American Gear Manufacturers Association, May 1940:

The investigations being carried on at the Westinghouse Research Laboratories of surface fatigue failures (pitting) are of two types, roller tests and gear tests. Both are more or less indefinitely continuing activities, as new questions about pitting are always arising. Some of the results of the roller tests have been reported previously. (These roller tests were run at the same peripheral speed and were not sliding relatively. —G. B. Warren.)

As a result of these tests there are certain things which can now be put down as fairly definitely known about the formation of surface fatigue cracks on cylindrical surfaces.

We know they originate because of stresses due to surface irregularities rather than because of the theoretical Hertz stress system for smooth cylinders. The theoretical stresses for smooth cylinders do not depend on roughness; on the other hand, pitting strengths depend to a marked degree on roughness. Furthermore, if the pitting cracks were due to the theoretical stress system for smooth cylinders, they would be expected to start at a distance below the surface several times greater than the thickness of the surface layer in which the cracks are observed to start.

We know that it is possible to subject a piece of metal to a range of shearing stresses considerably larger than the shearing endurance range and yet have no failure. Thus the last pair of rollers listed in Table 3 was run 9.4 million cycles at a load of 202,000 psi theoretical compressive stress with no sign of pitting. This loading would give rise to a range of shearing stress plus or minus 50,500 psi on planes parallel to the surface at a depth of 0.0047 in. The shear endurance range of the material was only about plus or minus 30,000 psi, yet when one of these rollers was sectioned there was no evidence of cracks below the surface. The explanation of this is probably that high uniform compression, which exists in the metal below the loaded region, tends to prevent the formation of a fatigue crack at a range of shearing stress that would normally cause a crack.

We know that the growth of surface fatigue cracks to pits is made possible by the action of the oil in the cracks. Pitting cracks which develop in rollers run without oil will not grow to pits. By drilling a small hole (0.006 in. diam) in such a position as to relieve any oil pressure in a growing pitting crack, the growth of the crack can be arrested. The pitting cracks assume a direction that slopes obliquely into the metal; they are roughly in the form of a conical surface so that they meet the surface in the from of a parabola or V, with the vertex of the V being the part that is run over first. It is observed that reversing the direction of rotation after such sloping cracks have formed will stop the growth of the cracks.

When the fatigue cracks form, they may at first slope in various directions. However, there will most likely be some directions more probable than others. All cracks that have been observed in an early stage, both when viewed on the surface and in sections, are oriented in such a way that a perpendicular to the plane of the crack drawn in the outward direction leans in the direction of motion of the contact area. This means that any oil which enters such a crack will tend to be trapped as the crack passes under the loaded region, and a high pressure may be built up in it. A high oil pressure in a crack will produce high tensile stresses at the end of the crack, unless such tension is

canceled by the stresses due to external loads. It is quite possible that a crack, filled with oil, may come under the loaded area so that a high pressure is developed in the oil before the external loads can cause compression stress at the end of the crack to cancel the tension developed by the oil pressure. The crack might then easily be driven further into the metal. If this theory is accepted as a hypothetical picture of what goes on after a surface fatigue crack is formed, it accounts for the observations that oil is necessary for crack growth, that changing the direction of rotation stops crack growth, and that relief of oil pressure in the crack stops its growth.

To study the pitting resistance of gear teeth as influenced by various factors, and to determine what relations exist, if any, between the pitting limits of gear and pinion materials, as determined by roller tests and the pitting strengths of these materials when built into gear teeth, a gear-testing program has been undertaken.

We are here concerned only with the surface compressive stresses, not with the stresses due to tooth bending.

A synopsis of several gear tests shows the following:

The pitting of the gear was confined to the region between the pitch line and the end of one tooth contact.

It is significant that no pitting occurred above the pitch line, although the compressive stresses were slightly higher there.

There was no pitting above the pitch line on the pinion, and nine out of the ten pits were below the pitch line in the region of one-tooth contact.

In reviewing the Brown-Boveri results (2), Dr. Way goes on to say: It was found that negative specific sliding, as occurs in the dedendum region, diminishes pitting resistance, and positive specific sliding increases it (that is the resistance). A carbon steel that pitted at 92,000 psi compressive stress with negative specific sliding carried 140,000 psi without pitting, with positive specific sliding. This finding agrees well with the observation in our gear tests that pitting practically never occurred in the addendum region. It also indicates that negative specific sliding decreases the pitting resistance as compared to that for pure rolling contact.

Future rolling tests with rollers of different ratios and with various amounts of sliding will throw more light on the expected performance of gear teeth.

In a discussion of his article Dr. Way states the following:

On the sketch this is the pitch point and in this region the sliding is in the direction toward the pitch line. It was actually observed in gear tests that pitting was more or less entirely distributed over that whole region below the pitch line and in the region of one-tooth contact, rather than there being any particular tendency for pitting to occur at the pitch line. And since pitting occurred in the region of one-tooth contact where the contact pressure was even lower than it was just above the pitch line, it seems that the sliding, when it is in the direction opposite to the rolling, has the effect of promoting the pitting rather than retarding it, as might be expected, if this view of the oil-film formation is accepted.

You will observe in this region, just above the pitch line, where one pair of teeth was in contact that there was no pitting, while below the pitch line, even though the pitch line where the stresses were much lower than this, there was pitting.

Reference 4. Excerpt from an article entitled, "Peened Surfaces Improve Endurance of Machine Parts," by J. O. Almen, which appeared in *Metal Progress* for February, 1943:

When carburized parts such as bearing races, wrist pins, and gear teeth are ground, we may expect the surface to be stressed in tension.

The residual compressive stress in the carburized layer may be a hazard for members stressed in tension, because the tension stress in the core is equal to the working stress plus the tension stress due to the compressive preload of the case. For members stressed in bending and in torsion the internal compressive stress in the carburized case improves the fatigue strength of the part, except for the thin surface layer which, especially after grinding, is severely stressed in tension. It is, however, a simple matter to convert this thin tension-stressed layer into stress in compression by a suitable peening or rolling operation.

Author's Closure

The Research Committee accepts with thanks Mr. Warren's discussion as a valuable addition to the report. The only comment is in relation to his statement in his fifth paragraph: ".... it would seem that there are two types of pitting as follows:"

This could well be amended to read ".... there appears to be at least two types of *surface* pitting as follows:"

The breakdown of the surface is a very complex process; many different influences are acting and many types of pitting may be present. The author's presentation has been primarily of that type of pitting which results from the subsurface shear stresses. The many surface manifestations of distress deserve much more study, and it is hoped that continued tests, particularly with the harder materials, will shed more light on this phase of the problem.

Simplified Method of Analysis of Reactions Developed by Expansion in a Three-Anchor Piping System

By BORIS LOCHAK,[1] NEW YORK, N. Y.

Existing methods of stress analysis in a three-dimensional piping system fully restrained at three points involve the predetermination of 78 coefficients, and the solution of 12 simultaneous equations. The author proposes a method which reduces the complicated three-anchor problem virtually to a simple two-anchor problem, involving only 21 constant coefficients and the determination of 6 equations. Actually, only routine tabulated computations are required by this method.

THE determination of the reactions set up by expansion in a three-dimensional piping system fully restrained in three points, as illustrated in Fig. 1, is regarded as a complicated problem of pipe stress analysis. The total number of component reactions developed in such a system amounts to 18, as follows:

3 Component moments, and 3 component forces at point *A*
3 Component moments, and 3 component forces at point *B*
3 Component moments, and 3 component forces at point *C*

The 6 reactions at point *C* being equal, with opposite signs, to the sums of the respective reactions at the two other points *A* and *B*, 12 unknowns only remain to be found:

6 unknowns at point *A*
6 unknowns at point *B*

The determination of the 12 unknown reactions requires 12 simultaneous equations which are obtained from the following conditions of equilibrium:

1 There is no rotation in either direction at point *A;* i.e., the summation of the moment areas between the points *A* and *C* alongside the branches I and III is equal to zero. This condition supplies 3 equations.

2 There is no translatory movement of point *A* in either direction, i.e., the summation of the moments about the point *A* of the moment-areas between the points *A* and *C* is equal to zero. This condition supplies 3 more equations.

3 No rotation at point *B:* 3 equations analogous to 1.

4 No movement of point *B:* 3 equations analogous to 2.

The four groups, of 3 equations each, constitute the system of 12 simultaneous equations solving the problem.

Existing Methods. The existing methods of stress analysis, whether it is the slope-deflection method, the moment-area method, or column analogy, all lead to the formulation of 12 equations, and various procedures proposed for the solution of three-anchor problems actually use 12 equations in numerical applications. So does the method published by the M. W. Kellogg Company,[2] in which the constant coefficients appearing in the equations have been given definite, although dissimilar, mathematical expressions.

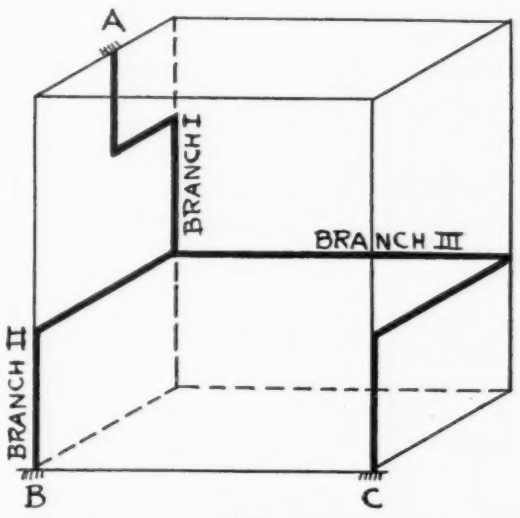


FIG. 1

All these methods involve the predetermination of 78 coefficients, which is exacting work, requiring thorough mathematical training and special skill. They require also the solution of 12 simultaneous equations.

PROPOSED METHOD

The proposed method to be described goes two steps further:

1 The 12 equations have been developed first by the moment-area method, and then reduced to 6 only by means of a quite extensive mathematical transformation which has to be omitted from this paper. In the 6 equations, the moments have been eliminated, and only the 6 unknown component forces appear. The number of constant coefficients has therefore been reduced from 78 to 21. The determinant of the 6 equations is symmetrical about the diagonal, offering therefore a simple solution by using the Kellogg method.[3]

2 By selection of the co-ordinate system, the 21 constant coefficients are given very simple mechanical meanings. These coefficients are either moments of inertia, or products of inertia, elementary notions with which every designer is quite familiar. No mathematics whatsoever is required for the understanding and the use of the method, only routine tabulated computations being necessary.

With these two transformations, the solution of the complicated three-anchor problem becomes practically as simple as the solution of the two-anchor problem by S. W. Spielvogel's well-known method.[3]

[1] Structural Engineer, Gibbs & Hill, Inc.

[2] "Design of Piping Systems," published by the M. W. Kellogg Company, New York, N. Y., 1941.

Contributed by the Power Division of THE AMERICAN SOCIETY OF MECHANICAL ENGINEERS.

NOTE: Statements and opinions advanced in papers are to be understood as individual expressions of their authors and not those of the Society.

[3] "Piping Stress Calculations Simplified," by S. W. Spielvogel, McGraw-Hill Book Company, Inc., New York, N. Y., 1943.

Procedure. (*a*) Refer the piping system to a system of axis of co-ordinates centered at point *O*, junction point of the three branches, Fig. 2. Designate the branch *OA*, branch I; branch *OB*, branch II; branch *OC*, branch III. Assume positive directions of co-ordinates, as shown by the arrows, Fig. 2.

(*b*) Project each branch of the piping system on the three co-ordinate planes X-Y, X-Z, Y-Z, Fig. 3.

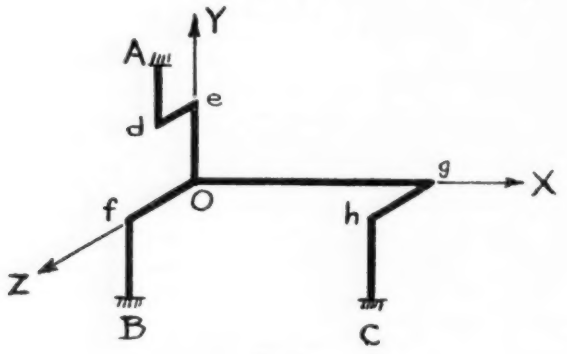


FIG. 2

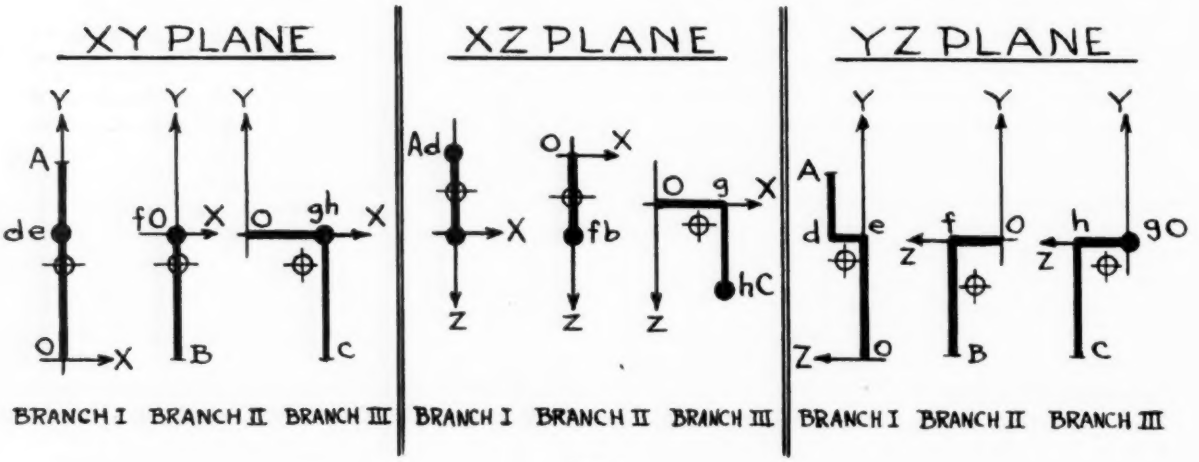


FIG. 3

(*c*) Compute in each projection the elastic centroid of each branch.[4] In doing this (as well as in all the computations hereafter), attribute a stiffness factor equal to 1 to each member projected in a line, and a stiffness factor equal to 1.3 to each branch projected in a point (ratio of EI in bending and GI_p in torsion). The elastic length of every member having a different size, or in general, a different value of EI, shall be corrected in the reversed ratio of the EI values; the stiffer, the shorter. Locate the computed centroids in each projection with reference to the origin (point *O*).

Designate by $(x_1y_1z_1)$ the co-ordinates of the centroid of branch I
Designate by $(x_2y_2z_2)$ the co-ordinates of the centroid of branch II
Designate by $(x_3y_3z_3)$ the co-ordinates of the centroid of branch III

(*d*) Designate also:

By (a, b, c), respectively, the (x, y, z) distances between the centroids of the branches I and III
By (d, e, f), respectively, the (x, y, z) distances between the centroids of the branches II and III

These distances shall be used with their signs as they come out, with reference to the co-ordinate axis centered at *O*. (Refer to their algebraical expressions in the general table of notations, Chart 1.)

(*e*) Compute in each projected plane the K constant[5]

$$K = \frac{1}{\frac{1}{L_1} + \frac{1}{L_2} + \frac{1}{L_3}}$$

where L_1, L_2, L_3 are the developed elastic lengths, respectively, of the branches I, II, and III.

(*f*) Compute the moments and the products of inertia of each branch about its own elastic centroid.[4]

The foregoing computations have to be carried out algebraically with signs as they come out with reference to the axis under consideration.

Setting Up the Equations. The six simultaneous equations are given in Chart 2 in the shape of a determinant. Each coefficient is an algebraical sum of the constants previously computed.

Example 1: The coefficient of X_1 in the first equation is equal to

$$+ [Ix_1 + Ix_3 + K(b^2 + c^2)]$$

(Refer to Chart 1, general table of notations.)

The moments of inertia Ix_1 and Ix_3 are computed in the X-Y and X-Z planes, i.e., about the OX direction.

The term Kb^2, which is also a moment of inertia, is computed in the X-Y plane. *Note:* y term and X axis.

The term Kc^2, also a moment of inertia, is computed in the X-Z plane. *Note:* z term and X axis.

Example 2: The coefficient of Y_1 in the first equation is equal to

$$-[Ixy_1 + Ixy_3 + Kab]$$

The three terms are products of inertia computed in the X-Y plane. *Note:* $a = x$ term, $b = y$ term

Following the numerical example given hereafter, the entire procedure will be clarified.

Computation of Expansion Constants. Release the anchors of branch I and branch II, and let the piping system, anchored at the point *C*, expand freely. Compute the expansion constants as usual with their signs as they come out with reference to the positive direction of the co-ordinate axis.

Computation of Moments. When the 6 equations have been

[4] This can be done in accordance with the basic rules of column analogy, or as explained by S. W. Spielvogel.[3]

[5] The K quantity is an equivalent length. Note the analogy with the expression of the equivalent resistance in electrical network.

solved and the 6 reactions obtained, the moments are easily computed by using the formulas given in Chart 2.

Single-Plane Three-Anchor Problems

Cancel all the z terms, z constants, and z equations. The determinant will be reduced to 4 equations only, and the computations to a surprising simplicity.

Charts 1 and 2 summarize the entire method of analysis of the three-anchor problem.

Numerical Example

The numerical example given in Charts 3, 4, 5, and 6 is taken from M. W. Kellogg's[2] work.

The reactions obtained by Kellogg's method involving the solution of twelve simultaneous equations are (in pounds):

$$X_1 = -4939,\ Y_1 = -6418,\ Z_1 = 2579,\ X_2 = -5515,\ Y_2 = 389,\ Z_2 = 1769$$

The reactions obtained by the method presented involving the solution of six simultaneous equations only are:

$$X_1 = -4937,\ Y_1 = -6468,\ Z_1 = 2600,\ X_2 = -5500,\ Y_2 = 429,\ Z_2 = 1755$$

Acknowledgment

Appreciation is expressed here to Mr. J. Rabinovitz, structural designer, Gibbs & Hill, Inc., for his valuable assistance in the preparation of this paper, especially in working out the charts and the numerical example.

THREE ANCHOR PROBLEM— NOTATIONS

$X_1\ Y_1\ Z_1$ Reactions applying to branch I

$X_2\ Y_2\ Z_2$ Reactions applying to branch II

$I_{x_1}\ I_{y_1}\ I_{z_1}$ Moments of Inertia of the branch I about its centroid.

$I_{x_2}\ I_{y_2}\ I_{z_2}$ " " " " " " II " " "

$I_{x_3}\ I_{y_3}\ I_{z_3}$ " " " " " " III " " "

$I_{x_1y_1}\ I_{x_1z_1}\ I_{y_1z_1}$ Products " " " " " I " " "

$I_{x_2y_2}\ I_{x_2z_2}\ I_{y_2z_2}$ " " " " " " II " " "

$I_{x_3y_3}\ I_{x_3z_3}\ I_{y_3z_3}$ " " " " " " III " " "

$\Delta x_1\ \Delta y_1\ \Delta z_1$ Component expansions of point "a" when released.

$\Delta x_2\ \Delta y_2\ \Delta z_2$ " " " " " "b" " "

$E\ I$ Modulus of elasticity and sectional moment of inertia of the pipe.

$S_{x_1}\ S_{y_1}\ S_{z_1}$ Static moments of branch I about the origin of coordinates.

$S_{x_2}\ S_{y_2}\ S_{z_2}$ " " " " II " " " " " "

$S_{x_3}\ S_{y_3}\ S_{z_3}$ " " " " III " " " " " "

L_1 Developed elastic length of branch I.

L_2 " " " " " II.

L_3 " " " " " III.

$$a = \frac{S_{x_1}}{L_1} - \frac{S_{x_3}}{L_3} \qquad b = \frac{S_{y_1}}{L_1} - \frac{S_{y_3}}{L_3} \qquad c = \frac{S_{z_1}}{L_1} - \frac{S_{z_3}}{L_3}$$

$$d = \frac{S_{x_2}}{L_2} - \frac{S_{x_3}}{L_3} \qquad e = \frac{S_{y_2}}{L_2} - \frac{S_{y_3}}{L_3} \qquad f = \frac{S_{z_2}}{L_2} - \frac{S_{z_3}}{L_3}$$

$$K = \frac{1}{\frac{1}{L_1} + \frac{1}{L_2} + \frac{1}{L_3}}$$

$$X_1 = \frac{S_{x_1}}{L_1} \qquad X_2 = \frac{S_{x_2}}{L_2} \qquad X_3 = \frac{S_{x_3}}{L_3}$$

$$Y_1 = \frac{S_{y_1}}{L_1} \qquad Y_2 = \frac{S_{y_2}}{L_2} \qquad Y_3 = \frac{S_{y_3}}{L_3}$$

$$Z_1 = \frac{S_{z_1}}{L_1} \qquad Z_2 = \frac{S_{z_2}}{L_2} \qquad Z_3 = \frac{S_{z_3}}{L_3}$$

} Coordinates of the centroids of the branches

$Mox_1\ Moy_1\ Moz_1$ Moments at the origin of coordinates applying to branch I.

$Mox_2\ Moy_2\ Moz_2$ " " " " " " " " " II.

$Mox_3\ Moy_3\ Moz_3$ " " " " " " " " " III.

$Max\ May\ Maz$ " " any point "a" of the system.

Chart 1

THREE ANCHOR PROBLEM

Determinant of the six (6) simultaneous equations solving the Reactions X_1 Y_1 Z_1 and X_2 Y_2 Z_2.

CONSTANTS	X_1	Y_1	Z_1	X_2	Y_2	Z_2
$\Delta x_1 EI$	$+\begin{cases} I_{x_1} \\ I_{x_3} \\ K(b^2+c^2) \end{cases}$	$-\begin{cases} I_{xy_1} \\ I_{xy_3} \\ Kab \end{cases}$	$-\begin{cases} I_{xz_1} \\ I_{xz_3} \\ Kac \end{cases}$	$+\begin{cases} I_{x_3} \\ K(be+cf) \end{cases}$	$-\begin{cases} I_{xy_3} \\ Kbd \end{cases}$	$-\begin{cases} I_{xz_3} \\ Kcd \end{cases}$
$\Delta y_1 EI$	$-\begin{cases} I_{xy_1} \\ I_{xy_3} \\ Kab \end{cases}$	$+\begin{cases} I_{y_1} \\ I_{y_3} \\ K(a^2+c^2) \end{cases}$	$-\begin{cases} I_{yz_1} \\ I_{yz_3} \\ Kbc \end{cases}$	$-\begin{cases} I_{xy_3} \\ Kae \end{cases}$	$+\begin{cases} I_{y_3} \\ K(ad+cf) \end{cases}$	$-\begin{cases} I_{yz_3} \\ Kce \end{cases}$
$\Delta z_1 EI$	$-\begin{cases} I_{xz_1} \\ I_{xz_3} \\ Kac \end{cases}$	$-\begin{cases} I_{yz_1} \\ I_{yz_3} \\ Kbc \end{cases}$	$+\begin{cases} I_{z_1} \\ I_{z_3} \\ K(a^2+b^2) \end{cases}$	$-\begin{cases} I_{xz_3} \\ Kaf \end{cases}$	$-\begin{cases} I_{yz_3} \\ Kbf \end{cases}$	$+\begin{cases} I_{z_3} \\ K(ad+be) \end{cases}$
$\Delta x_2 EI$	$+\begin{cases} I_{x_3} \\ K(be+cf) \end{cases}$	$-\begin{cases} I_{xy_3} \\ Kae \end{cases}$	$-\begin{cases} I_{xz_3} \\ Kaf \end{cases}$	$+\begin{cases} I_{x_2} \\ I_{x_3} \\ K(e^2+f^2) \end{cases}$	$-\begin{cases} I_{xy_2} \\ I_{xy_3} \\ Kde \end{cases}$	$-\begin{cases} I_{xz_2} \\ I_{xz_3} \\ Kdf \end{cases}$
$\Delta y_2 EI$	$-\begin{cases} I_{xy_3} \\ Kbd \end{cases}$	$+\begin{cases} I_{y_3} \\ K(ad+cf) \end{cases}$	$-\begin{cases} I_{yz_3} \\ Kbf \end{cases}$	$-\begin{cases} I_{xy_2} \\ I_{xy_3} \\ Kde \end{cases}$	$+\begin{cases} I_{y_2} \\ I_{y_3} \\ K(d^2+f^2) \end{cases}$	$-\begin{cases} I_{yz_2} \\ I_{yz_3} \\ Kef \end{cases}$
$\Delta z_2 EI$	$-\begin{cases} I_{xz_3} \\ Kcd \end{cases}$	$-\begin{cases} I_{yz_3} \\ Kce \end{cases}$	$+\begin{cases} I_{z_3} \\ K(ad+be) \end{cases}$	$-\begin{cases} I_{xz_2} \\ I_{xz_3} \\ Kdf \end{cases}$	$-\begin{cases} I_{yz_2} \\ I_{yz_3} \\ Kef \end{cases}$	$+\begin{cases} I_{z_2} \\ I_{z_3} \\ K(d^2+e^2) \end{cases}$

Moments at the origin of Coordinates

$$Mox_1 = K\left[Z_1\left(\frac{Y_1}{L_2}+\frac{Y_1}{L_3}+\frac{Y_3}{L_1}\right) - Y_1\left(\frac{Z_1}{L_2}+\frac{Z_1}{L_3}+\frac{Z_3}{L_1}\right) - \frac{1}{L_1}(Z_2e - Y_2f)\right] \quad (YZ\ Plane)$$

$$Moy_1 = K\left[X_1\left(\frac{Z_1}{L_2}+\frac{Z_1}{L_3}+\frac{Z_3}{L_1}\right) - Z_1\left(\frac{X_1}{L_2}+\frac{X_1}{L_3}+\frac{X_3}{L_1}\right) - \frac{1}{L_1}(X_2f - Z_2d)\right] \quad (XZ\ Plane)$$

$$Moz_1 = K\left[Y_1\left(\frac{X_1}{L_2}+\frac{X_1}{L_3}+\frac{X_3}{L_1}\right) - X_1\left(\frac{Y_1}{L_2}+\frac{Y_1}{L_3}+\frac{Y_3}{L_1}\right) - \frac{1}{L_1}(Y_2d - X_2e)\right] \quad (XY\ Plane)$$

$$Mox_2 = K\left[Z_2\left(\frac{Y_1}{L_1}+\frac{Y_1}{L_3}+\frac{Y_3}{L_2}\right) - Y_2\left(\frac{Z_1}{L_1}+\frac{Z_1}{L_3}+\frac{Z_3}{L_2}\right) - \frac{1}{L_2}(Z_1b - Y_1c)\right] \quad (YZ\ Plane)$$

$$Moy_2 = K\left[X_2\left(\frac{Z_1}{L_1}+\frac{Z_1}{L_3}+\frac{Z_3}{L_2}\right) - Z_2\left(\frac{X_1}{L_1}+\frac{X_1}{L_3}+\frac{X_3}{L_2}\right) - \frac{1}{L_2}(X_1c - Z_1a)\right] \quad (XZ\ Plane)$$

$$Moz_2 = K\left[Y_2\left(\frac{X_1}{L_1}+\frac{X_1}{L_3}+\frac{X_3}{L_2}\right) - X_2\left(\frac{Y_1}{L_1}+\frac{Y_1}{L_3}+\frac{Y_3}{L_2}\right) - \frac{1}{L_2}(Y_1a - X_1b)\right] \quad (XY\ Plane)$$

$$Mox_3 = +(Mox_1 + Mox_2)$$
$$Moy_3 = +(Moy_1 + Moy_2)$$
$$Moz_3 = +(Moz_1 + Moz_2)$$

Moments at any point of the system

Branch I
$$\begin{cases} M'x = Mox_1 - (yZ_1 - zY_1) \\ M'y = Moy_1 - (zX_1 - xZ_1) \\ M'z = Moz_1 - (xY_1 - yX_1) \end{cases}$$

Branch II
$$\begin{cases} M''x = Mox_2 - (yZ_2 - zY_2) \\ M''y = Moy_2 - (zX_2 - xZ_2) \\ M''z = Moz_2 - (xY_2 - yX_2) \end{cases}$$

Branch III
$$\begin{cases} M'''x = Mox_3 - (yZ_3 - zY_3) \\ M'''y = Moy_3 - (zX_3 - xZ_3) \\ M'''z = Moz_3 - (xY_3 - yX_3) \end{cases}$$

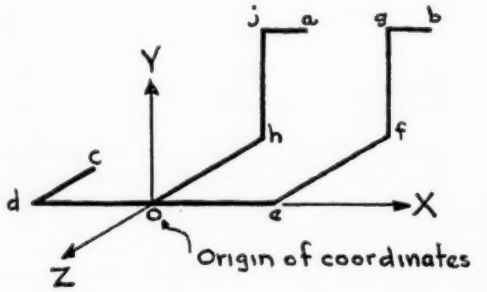
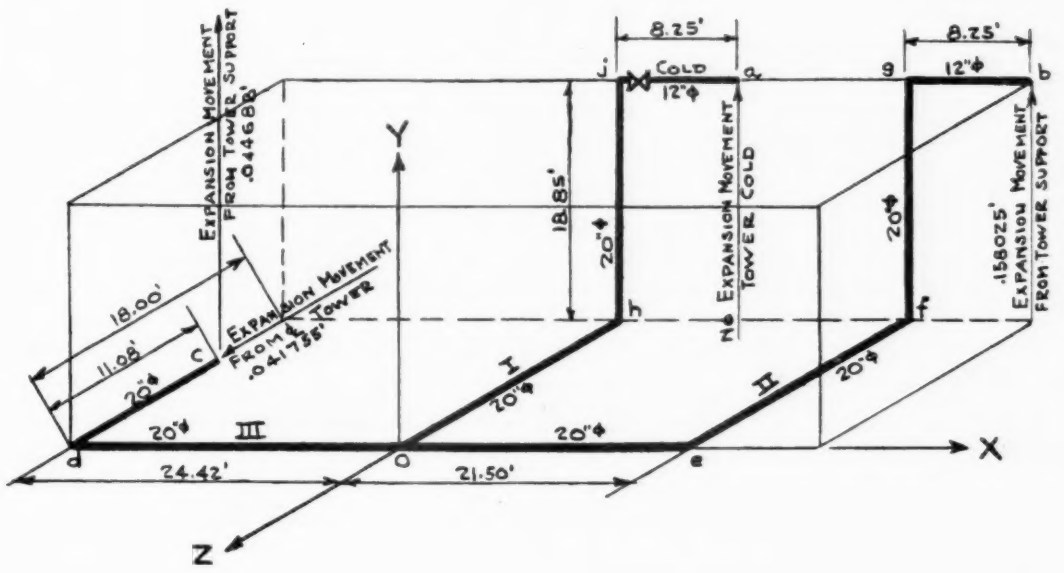


CHART 2

THREE ANCHOR PROBLEM



DATA :–

Carbon Steel
Line Temperature 825° F.
Room Temperature 70° F.
Temperature Diff. 755° F.
Expansion per ft. per 1° = 7.9×10^{-6}
Expansion per ft. per 755° = .005965 Ft.

$E = 29.0 \times 10^6$ for member (a j) only
$E = 23.1 \times 10^6$ for all other members
$I = 1457.0''^4$ for 20" ϕ
$I = 361.5''^4$ for 12" ϕ
$EI = 233,727\,000\ \#ft^2$
$EI = 57,991\,000\ \#ft^2$ (bg) only
$EI = 72,802\,000\ \#ft^2$ (a j) only

COMPUTATION OF CONSTANTS

$\Delta x_1 EI$ =	233 727 000	[(.005965	× 24.42)]	= + 34 046 000
$\Delta y_1 EI$ =	do	[(do	× 18.85) + .044688]	= + 36 725 000
$\Delta z_1 EI$ =	do	[(do	× 6.92) − .041755]	= + 111 000
$\Delta x_2 EI$ =	do	[(do	× 54.17)]	= + 75 522 000
$\Delta y_2 EI$ =	do	[(do	× 18.85) + .044688 − .158025]	= − 210 000
$\Delta z_2 EI$ =	do	[(do	× 6.92) − .041755]	= + 111 000

STIFFNESS CORRECTIONS

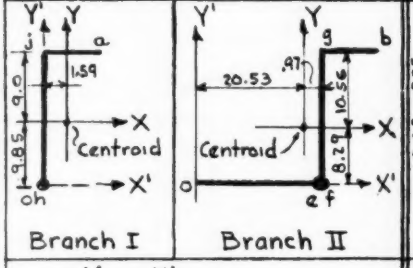
Member (a j) = $\frac{233\,727}{72\,802} = 3.21$

Member (b g) = $\frac{233\,727}{59991} = 4.03$

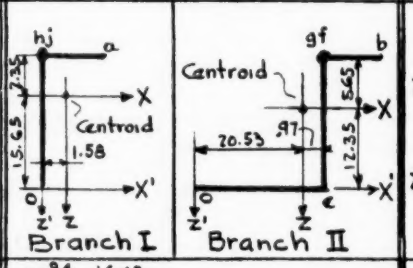
All other Members = 1.00

PROJECTION IN

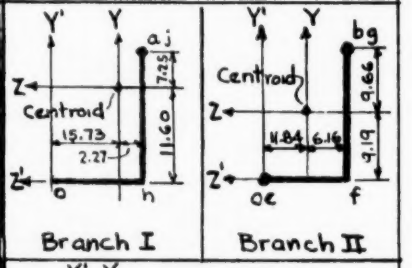
XY PLANE

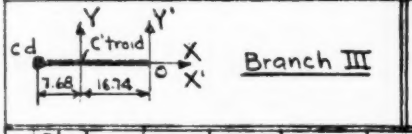


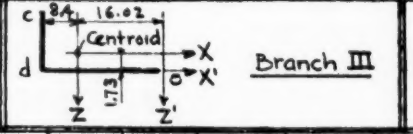
XZ PLANE

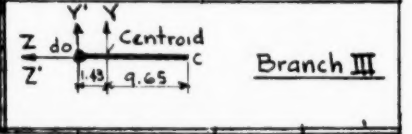


YZ PLANE









XY PLANE

Branch		L	X'	Y'	lx'	ly'	x	y	lxy	lx²	ly²	I own X	I own Y	Iy	Ix
I	aj	26.49	+4.125	+18.85	+109.27	+499.34	+2.535	+9.00	+604.37	170.23	2145.69	150.22	—	320.45	2145.69
	jh	18.85	0.0	+9.425	0.0	+177.66	- 1.59	-.425	+ 12.74	47.65	3.40	—	585.15	47.65	561.55
	ho	23.40	0.0	0.0	0.0	0.0	- 1.59	-9.85	+366.48	59.16	2270.33	—	—	59.16	2270.33
	Σ	68.74	+1.59	-9.85	+109.27	+677.00			+983.59					427.26	4977.57
		L1	X1	Y1	Sx1	Sy1			Ixy1					Iy1	Ix1
II	bg	33.25	+25.625	+18.85	+852.03	+626.76	+5.095	+10.56	+1788.96	863.14	3707.83	188.59		1051.73	3707.83
	gf	18.85	+21.50	+9.425	+405.28	+177.66	+0.97	+1.135	+ 20.75	17.74	24.28	—	558.15	17.74	582.43
	fa	23.40	+21.50	0.0	+503.10	0.0	+0.97	- 8.29	- 188.17	22.02	1608.14	—	—	22.02	1608.14
	eo	21.50	+10.75	0.0	+231.13	0.0	- 9.78	- 8.29	+1743.14	2056.44	1477.57	728.20	—	2384.64	1477.57
	Σ	97.00	+20.63	+8.29	+1991.54	+804.42			+3364.68					3976.13	7375.97
		L2	X2	Y2	Sx2	Sy2			Ixy2					Iy2	Ix2
III	od	24.42	-12.21	0.0	-298.17	0.0	+4.53	0.0	0.0	501.12	0.0	1213.54	—	1714.66	0.0
	dc	14.40	-24.42	0.0	-351.65	0.0	-7.68	0.0	0.0	849.35	0.0	—	—	849.35	0.0
	Σ	38.82	-16.74	+0.0	-649.82	0.0			0.0					2564.01	0.0
		L3	X3	Y3	Sx3	Sy3			Ixy3					Iy3	Ix3

XZ PLANE

Branch		L	X'	Z'	lx'	Lz'	x	z	lxz	lx²	lz²	I own X	I own Z	Iz	Ix
I	aj	26.49	4.125	-18.00	+109.27	-476.82	+2.545	-2.35	- 158.43	171.58	146.29	150.22	—	321.80	146.29
	jh	24.505	0.0	-18.00	0.0	-441.09	- 1.58	- 2.35	+ 90.99	61.17	135.33	—	—	61.17	135.33
	ho	18.00	0.0	- 9.00	0.0	-162.00	- 1.58	+6.65	- 189.13	44.94	796.01	—	486.0	44.94	1282.01
	Σ	69.00	+1.58	-15.65	+109.27	-1079.91			-256.57					427.91	1563.63
		L1	X1	Z1	Sx1	Sz1			Ixz1					Iz1	Ix1
II	bg	33.25	+25.625	-18.00	+852.03	-598.50	+6.095	- 5.65	- 957.16	863.14	1061.42	188.59	—	1051.73	1061.42
	gf	24.505	+21.50	-18.00	+526.86	- 441.09	+0.97	- 5.65	- 134.30	23.06	782.26	—	—	23.06	782.26
	fa	18.00	+21.50	- 9.00	+387.00	-162.00	+0.97	+3.35	+ 58.49	16.94	202.01	—	486.00	16.94	688.01
	eo	21.50	+10.75	0.0	+231.13	0.0	- 9.78	+12.35	-2596.83	2056.44	3279.23	728.20	—	2784.64	3279.23
	Σ	97.26	+20.53	-12.35	+1997.02	-1201.59			-3679.80					3876.37	5810.92
		L2	X2	Z2	Sx2	Sz2			Ixz2					Iz2	Ix2
III	od	24.42	-12.21	0.0	-298.17	0.0	+3.81	+1.73	+160.96	+354.48	73.09	1213.54		1568.02	73.09
	dc	11.08	-24.42	-5.54	-270.57	-61.38	- 8.40	- 3.81	+354.60	781.80	160.84		113.35	781.80	274.19
	Σ	35.50	-16.02	-1.73	-568.74	- 61.38			+515.56					2349.82	347.28
		L3	X3	Z3	Sx3	Sz3			Ixz3					Iz3	Ix3

YZ PLANE

Branch		L	Y'	Z'	ly'	lz'	y	z	lyz	ly²	lz²	I own Y	I own Z	Iz	Iy
I	aj	34.43	+18.85	-18.00	+649.01	-619.74	+7.25	-2.27	-566.63	1809.73	177.41	—	—	1809.73	177.41
	jh	18.85	+9.425	-18.00	+177.66	-339.30	-2.175	-2.27	+ 93.07	89.17	97.13	558.15		647.32	97.13
	ho	18.00	0.0	-9.00	0.0	-162.00	-11.60	+6.73	-1405.22	2422.08	815.27	—	486.00	2422.08	1301.27
	Σ	71.28	+11.60	-15.73	+826.67	-1121.04			-1878.78					4879.13	1575.81
		L1	Y1	Z1	Sy1	Sz1			Iyz1					Iz1	Iy1
II	bg	43.23	+18.85	-18.00	+814.89	-778.14	+9.66	- 6.16	-2572.43	4043.03	1640.39	—	—	4043.03	1640.39
	gf	18.85	+9.425	-18.00	+177.66	-339.30	+.235	- 6.16	- 27.29	1.04	715.27	558.15		559.19	715.27
	fa	18.00	0.0	-9.00	0.0	-162.00	- 9.19	+2.84	-469.79	1520.21	145.18	—	486.00	1520.21	631.18
	eo	27.95	0.0	0.0	0.0	0.0	- 9.19	+11.84	-3041.23	2360.55	3918.19	—	—	2360.55	3918.19
	Σ	108.03	+9.19	-11.84	+992.55	-1279.44			-6110.74					8473.98	6905.03
		L2	Y2	Z2	Sy2	Sz2			Iyz2					Iz2	Iy2
III	od	31.75	0.0	0.0	0.0	0.0	0.0	+1.43	0.0	0.0	64.93	—	—	0.0	64.93
	dc	11.08	0.0	-5.54	0.0	-61.38	0.0	- 4.11	0.0	0.0	187.16	—	113.35	0.0	300.51
	Σ	42.83	0.0	-1.43	0.0	-61.38			0.0					0.0	365.44
		L3	Y3	Z3	Sy3	Sz3			Iyz3					Iz3	Iy3

CHART 4

SUMMARY OF CONSTANTS FROM PRECEDING CALCULATIONS

$I_{x_1} = 4977.57 + 1563.63 = 6541.20$	$I_{y_1} = 427.26 + 1575.81 = 2003.07$	$I_{z_1} = 427.91 + 4879.13 = 5307.04$
$I_{x_2} = 7375.97 + 5810.92 = 13186.89$	$I_{y_2} = 3976.13 + 6905.03 = 10881.26$	$I_{z_2} = 3876.37 + 8473.98 = 12350.35$
$I_{x_3} = 0.0 + 347.28 = 347.28$	$I_{y_3} = 2564.01 + 365.44 = 2929.45$	$I_{z_3} = 2349.82 + 0.0 = 2349.82$
$I_{xy_1} = +983.59$	$I_{xz_1} = -256.57$	$I_{yz_1} = -1878.78$
$I_{xy_2} = +3364.68$	$I_{xz_2} = -3629.80$	$I_{yz_2} = -6110.74$
$I_{xy_3} = +0.00$	$I_{xz_3} = +515.56$	$I_{yz_3} = +0.00$

ADDITIONAL CONSTANTS

XY PLANE

K: $\frac{1}{\frac{1}{L_1}+\frac{1}{L_2}+\frac{1}{L_3}} = \frac{1}{\frac{1}{68.47}+\frac{1}{97.0}+\frac{1}{38.82}} = 19.755$

a	$\frac{S_{x_1}}{L_1} - \frac{S_{x_3}}{L_3} = 1.59 + 16.74 = +18.33$	
b	$\frac{S_{y_1}}{L_1} - \frac{S_{y_2}}{L_3} = 9.85 - 0.0 = +9.85$	
d	$\frac{S_{x_2}}{L_2} - \frac{S_{x_3}}{L_3} = 20.53 + 16.74 = +37.27$	
e	$\frac{S_{y_2}}{L_2} - \frac{S_{y_3}}{L_3} = 8.29 + 0.0 = +8.29$	

XZ PLANE

K: $\frac{1}{\frac{1}{L_1}+\frac{1}{L_2}+\frac{1}{L_3}} = \frac{1}{\frac{1}{69.0}+\frac{1}{97.26}+\frac{1}{35.5}} = 18.889$

a	$\frac{S_{x_1}}{L_1} - \frac{S_{x_3}}{L_3} = 1.58 + 16.02 = +17.60$	
c	$\frac{S_{z_1}}{L_1} - \frac{S_{z_3}}{L_3} = -15.65 + 1.73 = -13.92$	
d	$\frac{S_{x_2}}{L_2} - \frac{S_{x_3}}{L_3} = 20.53 + 16.02 = +36.55$	
f	$\frac{S_{z_2}}{L_2} - \frac{S_{z_3}}{L_3} = -12.35 + 1.73 = -10.62$	

YZ PLANE

K: $\frac{1}{\frac{1}{L_1}+\frac{1}{L_2}+\frac{1}{L_3}} = \frac{1}{\frac{1}{71.28}+\frac{1}{108.03}+\frac{1}{47.83}} = 21.441$

b	$\frac{S_{y_1}}{L_1} - \frac{S_{y_3}}{L_3} = 11.60 - 0.0 = +11.60$	
c	$\frac{S_{z_1}}{L_1} - \frac{S_{z_3}}{L_3} = -15.73 + 1.43 = -14.30$	
e	$\frac{S_{y_2}}{L_2} - \frac{S_{y_3}}{L_3} = 9.19 - 0.0 = +9.19$	
f	$\frac{S_{z_2}}{L_2} - \frac{S_{z_3}}{L_3} = -11.84 + 1.43 = -10.41$	

XY PLANE	K	a	b	d	e	a^2	b^2	d^2	e^2	ab	ad	ae	bd	be	de
	19.755	+18.83	+9.85	+37.27	+8.29	335.99	97.02	1389.05	68.72	180.55	683.16	151.96	367.11	81.66	308.97
	Multiplied by K →					6637.48	1916.63	27440.68	1357.56	3566.77	13495.83	3001.97	7252.26	1613.19	6103.70

XZ PLANE	K	a	c	d	f	a^2	c^2	d^2	f^2	ac	ad	af	cd	cf	df
	18.889	+17.60	-13.92	+36.55	-10.62	309.76	193.77	1335.90	112.78	−244.99	643.28	−186.91	−508.78	147.83	−388.16
	Multiplied by K →					5851.06	3660.12	25233.82	2130.30	−4627.62	12150.92	−3530.54	−9610.35	2792.36	−7331.95

YZ PLANE	K	b	c	e	f	b^2	c^2	e^2	f^2	bc	be	bf	ce	cf	ef
	21.441	+11.60	-14.30	+9.19	-10.41	134.56	204.49	84.46	108.37	−165.88	106.60	−120.76	−131.42	148.86	−95.67
	Multiplied by K →					2885.10	4384.47	1810.90	2323.56	−3556.63	2285.61	−2589.22	−2817.78	3191.71	−2051.26

Substituting the above constants into the Determinant we obtain the coefficients for the 6 equations

X_1	Y_1	Z_1	X_2	Y_2	Z_2
$I_{x_1} = 6541.20$	$I_{xy_1} = 983.59$	$I_{xz_1} = -256.57$	$I_{x_3} = 347.28$	$I_{xy_3} = 0.00$	$I_{xz_3} = +515.56$
$I_{x_3} = 347.28$	$I_{xy_3} = 0.00$	$I_{xz_3} = +515.56$	$kbe = 1613.19$	$kbd = 7252.26$	$kcd = -9610.35$
$kb^2 = 1916.63$	$kab = 3566.77$	$kac = -4627.62$	$kcf = 2792.36$		
$kc^2 = 3660.12$					
$+12468.23$	-4350.36	-4368.63	$+4752.83$	-7252.26	-9094.79
	$I_{y_1} = 2003.07$	$I_{yz_1} = -1878.78$	$I_{xy_3} = +0.00$	$I_{y_3} = 2929.45$	$I_{yz_3} = 0.00$
	$I_{y_3} = 2929.45$	$I_{yz_3} = -00.00$	$kae = +3001.97$	$kad = 13495.83$	$kce = -2817.78$
	$ka^2 = 6637.48$	$kbe = -3556.63$		$kcf = 3191.71$	
	$kc^2 = 4384.47$				
	$+15954.47$	-5435.41	$+3001.97$	$+19616.99$	-2817.78
		$I_{z_1} = 5307.04$	$I_{xz_3} = +515.56$	$I_{yz_3} = 0.00$	$I_{z_3} = 2349.82$
		$I_{z_3} = 2349.82$	$kaf = -3530.54$	$kbf = -2589.22$	$kad = 12150.92$
		$ka^2 = 5851.06$			$kbe = 2285.61$
		$kb^2 = 2886.10$			
		$+16393.12$	-3014.98	-2589.22	$+16786.35$
Symmetrical about diagonal ↘			$I_{x_2} = 13186.89$	$I_{xy_2} = 3364.68$	$I_{xz_2} = -3629.80$
			$I_{x_3} = 347.28$	$I_{xy_3} = 0.00$	$I_{xz_3} = +515.56$
			$ke^2 = 1357.56$	$kde = 6103.70$	$kdf = -7331.95$
			$kf^2 = 2130.30$		
			$+17022.03$	$+9468.38$	-10446.19
				$I_{y_2} = 10881.26$	$I_{yz_2} = -6110.74$
				$I_{y_3} = 2929.45$	$I_{yz_3} = 0.00$
				$kd^2 = 27440.68$	$kef = -2051.26$
				$kf^2 = 2323.56$	
				$+43574.95$	-8162.00
					$I_{z_2} = 12350.35$
					$I_{z_3} = 2349.82$
					$kd^2 = 25233.82$
					$ke^2 = 1810.90$
					$+41744.89$

CHART 5

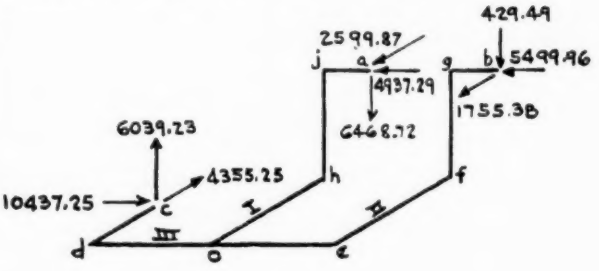
The 6 equations are as follows:

$$+12465X_1 - 4550Y_1 + 4369Z_1 + 4753X_2 - 7252Y_2 + 9095Z_2 + 34046000 = 0$$
$$-4550X_1 + 15954Y_1 + 5435Z_1 - 3002X_2 + 19617Y_2 + 2818Z_2 + 36725000 = 0$$
$$+4369X_1 + 5435Y_1 + 16398Z_1 + 3015X_2 + 2589Y_2 + 16786Z_2 + 111000 = 0$$
$$+4753X_1 - 3002Y_1 + 3015Z_1 + 17022X_2 - 9468Y_2 + 10446Z_2 + 75522000 = 0$$
$$-7252X_1 + 19617Y_1 + 2589Z_1 - 9468X_2 + 43575Y_2 + 8162Z_2 - 210000 = 0$$
$$+9095X_1 + 2818Y_1 + 16786Z_1 + 10446X_2 + 8162Y_2 + 41775Z_2 + 111000 = 0$$

Solving these equations:

$X_1 = -4937.29$; $Y_1 = -6468.72$; $Z_1 = +2599.87$
$X_2 = -5499.96$; $Y_2 = +429.49$; $Z_2 = +1755.38$
$X_3 = -(X_1 + X_2) = +10437.25$
$Y_3 = -(Y_1 + Y_2) = +6039.23$
$Z_3 = -(Z_1 + Z_2) = -4355.25$

ALL FORCES GIVEN IN POUNDS



COMPUTATION OF THE MOMENTS AT THE ORIGIN OF COORDINATES

$$Mox_1 = 21.441\left[2599.87\left(\frac{11.60}{108.03} + \frac{11.60}{42.83} + \frac{0.00}{71.28}\right) + 6468.72\left(\frac{-15.73}{108.03} + \frac{-15.73}{42.83} + \frac{-1.43}{71.28}\right) - \frac{1}{71.28}\left(1755.38 \times 9.19 - 429.49 \times -10.41\right)\right] = -59040^{\#}$$

$$Moy_1 = 18.889\left[-4937.29\left(\frac{-15.63}{47.26} + \frac{-15.65}{35.50} + \frac{-1.73}{69.0}\right) - 2599.87\left(\frac{1.58}{47.26} + \frac{1.58}{35.50} + \frac{-16.02}{69.0}\right) - \frac{1}{69.0}\left(-5499.96 \times -10.62 - 1755.33 \times 36.55\right)\right] = 68456^{\#}$$

$$Moz_1 = 19.755\left[-6468.72\left(\frac{1.59}{47.0} + \frac{1.59}{38.82} + \frac{-16.74}{68.74}\right) + 4937.29\left(\frac{9.85}{47.0} + \frac{9.85}{38.82} + \frac{0.0}{68.74}\right) - \frac{1}{68.74}\left(429.49 \times 37.27 - 5499.96 \times 8.29\right)\right] = 40870^{\#}$$

$$Mox_2 = 21.441\left[1755.38\left(\frac{9.19}{71.28} + \frac{9.19}{42.83} + \frac{0.00}{108.03}\right) - 429.49\left(\frac{-11.84}{71.28} + \frac{-11.84}{42.83} + \frac{-1.43}{108.03}\right) - \frac{1}{108.03}\left(2599.87 \times 11.60 + 6468.72 \times -14.30\right)\right] = 29627^{\#}$$

$$Moy_2 = 18.889\left[-5499.96\left(\frac{-12.35}{69.0} + \frac{-12.35}{35.50} + \frac{-1.73}{47.26}\right) - 1755.38\left(\frac{20.53}{69.0} + \frac{20.33}{35.50} + \frac{-16.02}{47.26}\right) - \frac{1}{47.26}\left(4937.29 \times -13.92 - 2599.87 \times 17.60\right)\right] = 28550^{\#}$$

$$Moz_2 = 19.755\left[429.49\left(\frac{20.53}{68.74} + \frac{20.33}{38.82} + \frac{-16.74}{47.0}\right) + 5499.96\left(\frac{8.29}{68.74} + \frac{8.29}{38.82} + \frac{0.00}{47.0}\right) - \frac{1}{47.0}\left(-6468.72 \times 18.33 + 4937.29 \times 9.85\right)\right] = 56114^{\#}$$

$Mox_3 = +(-59040 + 29627) = -29413^{\#}$
$Moy_3 = +(+68456 + 28550) = +97006^{\#}$
$Moz_3 = +(+40870 + 56114) = +96984^{\#}$

Moments at point "a":

$Max = -59040 - (18.85 \times 2599.87) + (-18.0 \times -6468.72) = +8389^{\#}$
$May = +68456 - (-18.0 \times -4937.29) + (8.25 \times 2599.87) = -1034^{\#}$
$Maz = +40870 - (8.25 \times -6468.72) + (18.85 \times -4937.29) = +1169^{\#}$

Moments at point "b":

$Mbx = +29627 - (18.85 \times 1755.38) + (-18.0 \times 429.49) = -11193^{\#}$
$Mby = +28550 - (-18.0 \times -5499.96) + (29.75 \times 1755.38) = -18226^{\#}$
$Mbz = +56114 - (29.75 \times 429.49) + (18.85 \times -5499.96) = -60337^{\#}$

CHART 6

Behavior of Synthetic Phenolic-Resin Adhesives in Plywood Under Alternating Stresses

By A. G. H. DIETZ[1] and HENRY GRINSFELDER[2]

Because plywood is being used in ever-increasing quantities in the construction of aircraft and boats of many types, it is essential to know the effect upon this material of vibrating loads. Hence whether failure occurs in the wood or in the adhesive under repeated stress, what allowable stresses may be applied, and what the fatigue limit may be, are questions which the engineer must be prepared to answer. The present paper gives the results of a research program covering the behavior of plywood and laminated wood bonded with synthetic phenolic-resin adhesives, undergoing alternating stress, in the unweathered and weathered conditions, and at high and low temperatures. This is a continuation of a previous report,[3] which presented some findings with respect to fatigue behavior of plywood and laminated wood under alternating stresses.

Introduction

PLYWOOD is being employed in increasing quantities in aircraft and seacraft, in both of which it is subjected to vibrating loads. It is important for engineers to know whether or not the wood or the adhesive is likely to fail under repeated stress, what behavior should be expected of both wood and adhesive, what allowable stresses can be employed, and what the fatigue limit may be. Should the bond show a tendency to weaken, it is desirable to know the extent of the loss in strength. It should be known whether or not there is any loss of stiffness under alternating stress. In this paper are contained the results of a program of research undertaken to determine

(*a*) The fatigue behavior of plywood and laminated wood under alternating stress.

(*b*) The behavior of the synthetic-resin adhesives used in plywood and laminated wood, under alternating stress.

(*c*) The effect, under alternating stresses, of weathering on the properties of the adhesives used in plywood.

(*d*) The effect, under alternating stresses, of high and low temperatures on the properties of the adhesives used in plywood.

A previous report[3] presented some of the findings with respect to the fatigue behavior of plywood and laminated wood under alternating stresses. In that paper, only item (*a*), that is, the fatigue behavior of plywood and laminated wood as a whole, was reported, but no attempt was made to analyze the effect of alternating shear stresses upon the strength of the glue line. In this paper, items (*b*), (*c*), and (*d*) are reported, that is, the results of investigations into the behavior of the adhesives in plywood under alternating shear stresses. For the sake of completeness, the earlier results are included in this report.

[1] Assistant Professor of Structural Design and Materials, Department of Building Engineering and Construction, The Massachusetts Institute of Technology, Cambridge, Mass.

[2] Senior Chemist, The Resinous Products and Chemical Company, Philadelphia, Pa.

[3] "Behavior of Plywood Under Repeated Stresses," by A. G. H. Dietz and H. Grinsfelder, Trans. A.S.M.E., vol. 65, 1943, pp. 187–191.

Contributed by the Wood Industries Division and presented at the Annual Meeting, New York, N. Y., Nov. 29–Dec. 3, 1943, of The American Society of Mechanical Engineers.

Note: Statements and opinions advanced in papers are to be understood as individual expressions of their authors and not those of the Society.

Previous Work

Of the fatigue behavior of plain wood, comparatively little is known, and still less is known about that of plywood. Stanton (1)[4] in 1916 concluded that the endurance limit of spruce was about 27 per cent of the tensile strength, which, in the material he employed, was low (6800 psi). Kommers (2) in 1927 reported tests made at the Forest Products Laboratory, on the basis of which values ranging from 26 to 30 per cent of the static bending strength were assigned Southern white oak, Sitka spruce, and Douglas fir. Schlyter (3) found that Sitka spruce, European spruce, and common European pine had endurance limits 22 to 25 per cent of the static bending strength. Kraemer (4), working with hardwoods (walnut and ash) and softwoods (pine and spruce), found endurance limits ranging from 25 to 33 per cent of the bending strength. He discovered, moreover, that the endurance limit of the heavier woods could in some instances be determined by as few as 20,000 cycles whereas the lighter specimens required several million cycles. Kollmann (5) evaluating the foregoing results, points out that although the endurance limits for wood are relatively low, the ratio of endurance limit to specific gravity may be relatively high compared to the metals used in aircraft. Kraemer (6) investigating plywood bonded with synthetic phenolic-resin film and with casein, found that if the grain of face plies was parallel to the axis of the test piece, the endurance limit was 26 per cent of the tensile strength for resin-bonded and 25 per cent for casein-bonded plywood. If the grain of the face plies was placed at an angle of 45 deg to the axis, the endurance limit for resin-bonded material rose to 52 per cent; for casein-bonded it remained practically the same, or 26 per cent. Failure of the casein-bonded plywood in this instance was caused by exfoliation of the veneers.

Tests on Unweathered Specimens

Materials

Aircraft-quality birch veneer was selected because of its strength and toughness and because it is moderately difficult to bond. The combination of strong wood and somewhat difficult bonding ability consequently was expected to reveal any tendency of the bond to fail under repeated stress.

Adhesives were as follows:

1 Thermosetting phenol-formaldehyde film.

2 Aqueous solution of thermosetting phenolformaldehyde.

3 The same as item 2, but extended with ground walnut shells (Glufil).

[4] Numbers in parentheses refer to the Bibliography at the end of the paper.

4 Aqueous solution of cold-setting urea-formaldehyde.

These were representative of the principal types of synthetic-resin adhesives commonly employed.

Veneers, $^1/_{16}$ in. thick, were laid up and bonded as follows:

1 Phenolic-resin film: Two-ply laminated; three-ply laminated; three-ply plywood.

2 Phenolic-resin, plain aqueous solution: Three-ply plywood.

3 Phenolic-resin, extended aqueous solution: Three-ply plywood.

4 Cold-setting urea resin, plain aqueous solution: Three-ply plywood.

Both laminated and regular plywood construction were investigated in the film-bonded material because differing stress conditions are set up in laminated wood and in plywood. Laminated wood behaves much the same as solid wood, but in plywood with the face grain parallel to the specimen axis, the bending stresses are almost entirely concentrated in the face plies and the shear-stress intensity practically reaches its maximum at the glue line. If the bond were weakened by repeated stress, the behavior of laminated wood and plywood might be expected to differ. Only three-ply plywood was investigated with the other three adhesives because experience with the film-bonded materials indicated that glue-line failure was more apt to occur, if at all, in plywood than in laminated wood.

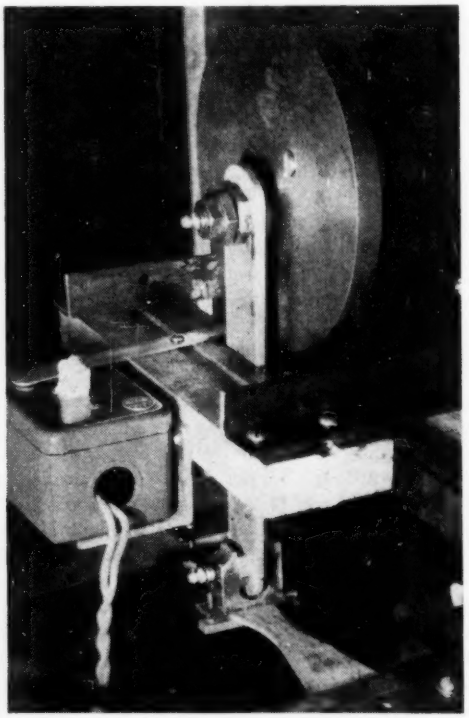


FIG. 1 CANTILEVER-TYPE MACHINE EMPLOYED WITH FATIGUE SPECIMENS

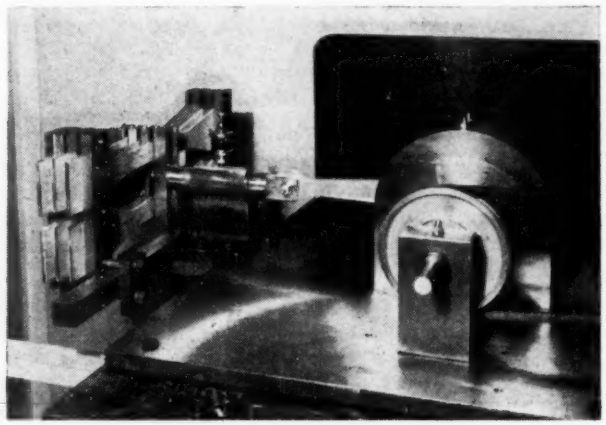


FIG. 2 CANTILEVER-TYPE MACHINE EQUIPPED TO HANDLE SEVERAL SPECIMENS SIMULTANEOUSLY

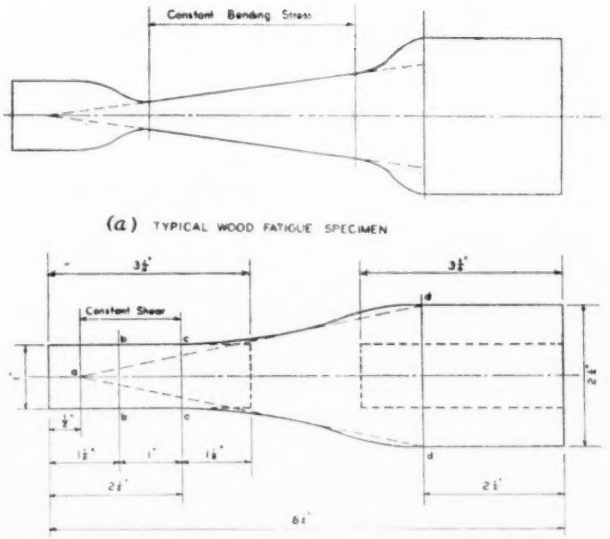


FIG. 3 TYPES OF SPECIMENS TESTED

MACHINES

Cantilever-type machines were employed because these were more adaptable to flat stock than rotating-beam machines, and because both bending and shear stresses are induced in cantilever specimens. In the earlier work, the machines, as shown in Fig. 1, handled one specimen at a time. Because of the large number of specimens involved, however, and because of the length of time required for some of the tests, a machine was constructed which could handle as many as twelve specimens at one time, as illustrated in Fig. 2.

In this apparatus the specimens, in groups of two or four, are clamped between upright pairs of cold-rolled steel plates which are in turn bolted to a heavy horizontal steel bar fastened to the steel base plate supporting the entire apparatus. The free ends of the specimens are forced back and forth by a pusher designed to hold the specimen firmly but to allow the end to deflect freely. The pusher is attached to a driving rod pinned to a connecting rod in turn mounted on an eccentric which forms part of a heavy steel driving wheel. The eccentric can be adjusted to give a throw ranging from zero to $1^1/_2$ in. The driving wheel is mounted in a heavy bronze bearing and is belt-driven by a 1-hp motor. The machine can be run at various speeds, but was generally operated at 1100 to 1300 rpm.

TYPES OF SPECIMENS

Alternating Stress. Two types of specimens were employed as shown in Fig. 3. To study the fatigue behavior of laminated wood and plywood, the shape shown in Fig. 3(*a*) was selected and found generally satisfactory. It provided a considerable

length over which the bending stresses were constant, and still allowed enough taper to prevent splitting in the outer veneers. Tests were run at uniform amplitude, and length was varied in accordance with the stresses desired. A specimen of this kind is shown in Fig. 1. It has failed in the tapered portion.

A different specimen was required to study the behavior of the adhesives under alternating shear stresses. In this instance, the specimen was also designed for flexing as a cantilever and was of such a shape as to provide a constant shear-stress area 1 in. sq at the loaded end while the strength at the supported end was sufficient to avoid overstressing the outermost fibers in bending.

The specimen is illustrated in Fig. 3(*b*). Load was applied at *a*. The specimen was 1 in. wide to point *c* where it was flared as shown to line *d-d*. From *d-d* to the end, the specimen was held in the grips during test. The distance *b-c* was 1 in. and the area *bbcc* was the 1-in-sq area over which uniform alternating shear was induced by the flexing of the specimen. After being run through a given cycle of stress, a glue-line shear test specimen was cut from this portion of the specimen as shown. The far end of the specimen was made long enough to provide sufficient area for rigid clamping and to provide a second glue-line shear test specimen with an unstressed central portion for comparison with the stress specimen.

Five alternating-stress test specimens were cut from each panel, as shown in Fig. 4. From the end of each specimen a third glue-line shear test specimen was cut to provide a second comparative test for the stressed sample. Each panel consequently yielded five "fatigue" specimens, five vibrated glue-line shear specimens, and ten unvibrated glue-line shear specimens.

Glue-Line Shear Test Specimens. As shown in Fig. 3(*a*), glue-line shear test specimens were the standard type commonly employed in the testing of plywood (7). They were tested in a briquette-testing machine equipped with a set of standard glue-line shear-testing jaws. Specimens were loaded at the rate of 600 to 800 lb per min.

Static Controls. To provide standards of comparison, simple static bending specimens 1 in. wide were cut from the panels and tested as center-loaded end-supported beams on spans 20 times the depth of the specimen. From these, modulus-of-rupture values were obtained. In addition, tension test specimens were cut from the same panels as the film-bonded-plywood fatigue specimens, but experience indicated that bending tests provided a better basis of comparison than did tension inasmuch as the alternating-stress tests were essentially bending tests.

Testing Procedure

Fatigue Tests. Each fatigue specimen was first calibrated by clamping the fixed end and loading the free end with dead weights to obtain the load-deflection curve. From this the stress for a given deflection could be calculated. The same procedure was employed for calibrating the alternating-shear test specimens and is illustrated in Fig. 5.

The specimen was clamped rigidly to a heavy table, a hook and pan were hung from the free end of the cantilever, and deflections were read to the nearest thousandth inch on the dial, whose stem rested on a small horizontal plane on top of the hook. The hook hung from the loading point of the specimen and dead weights were supported on the pan directly below the loading point.

After calibration, the fatigue specimen was subjected to alternating stress. In the preliminary runs the motor was stopped at rather frequent intervals and the specimen inspected for extent and type of incipient rupture. After a satisfactory shape and size of test piece had been found, specimens were in general permitted to remain in the machine until failure had occurred.

It was necessary to determine some criterion of failure because a piece which had cracked and was carrying no load might hang on for a considerable number of cycles before parting. Consequently, when a crack had formed completely across the width of the piece so that the cantilever to all intents and purposes was merely hinged at the line of the crack, failure was considered to have occurred. In general, it was found that failure, so defined, followed soon after the first appearance of a fatigue crack.

Fatigue stresses ranged from 90 to 20 per cent of the static moduli of rupture of the controls. Because of the variability of the material, four to six pieces of each length were tested and six to eight lengths were employed.

Alternating-Shear Tests. Alternating-shear test specimens were given the same preliminary calibration as the fatigue test specimens. Since these specimens were not vibrated to destruction, it was possible to recalibrate them after vibration to determine if repeated stress had any effect upon the load-deflection curve,

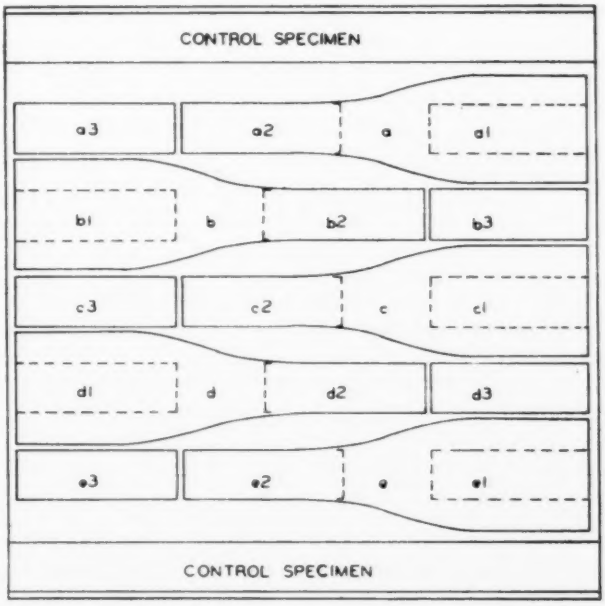


Fig. 4 Cutting Schedule for Alternating and Static Shear Specimens

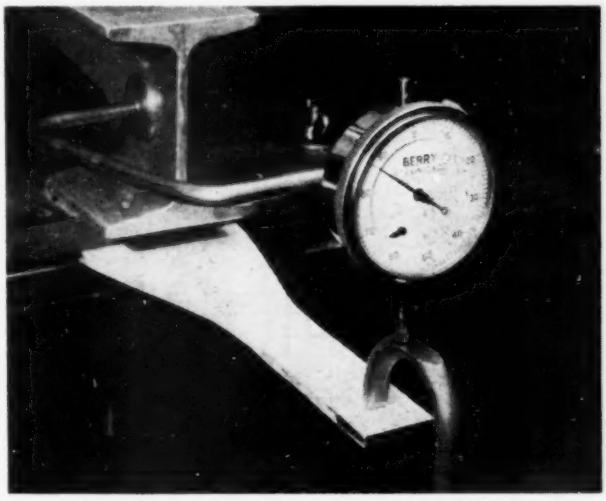


Fig. 5 Calibrating Specimens by Loading With Dead Weights

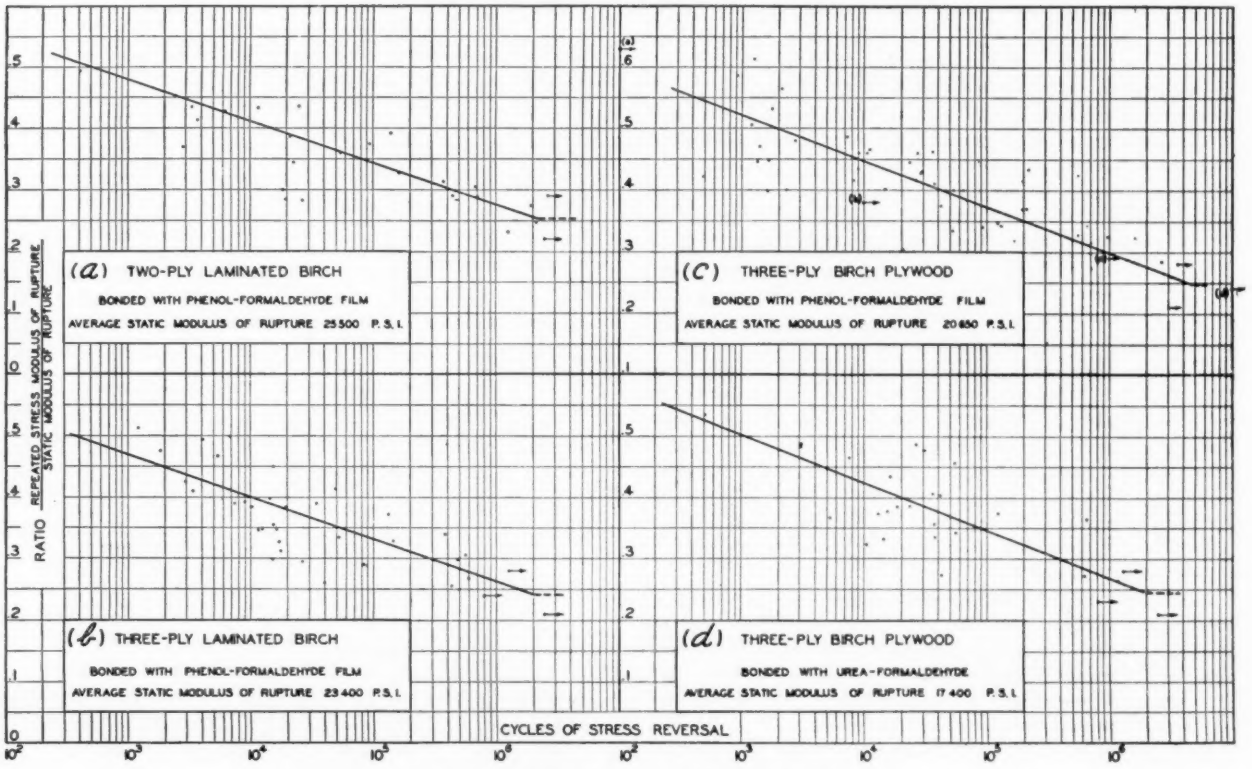


FIG. 6 SUMMARY OF RESULTS OF FATIGUE TESTS

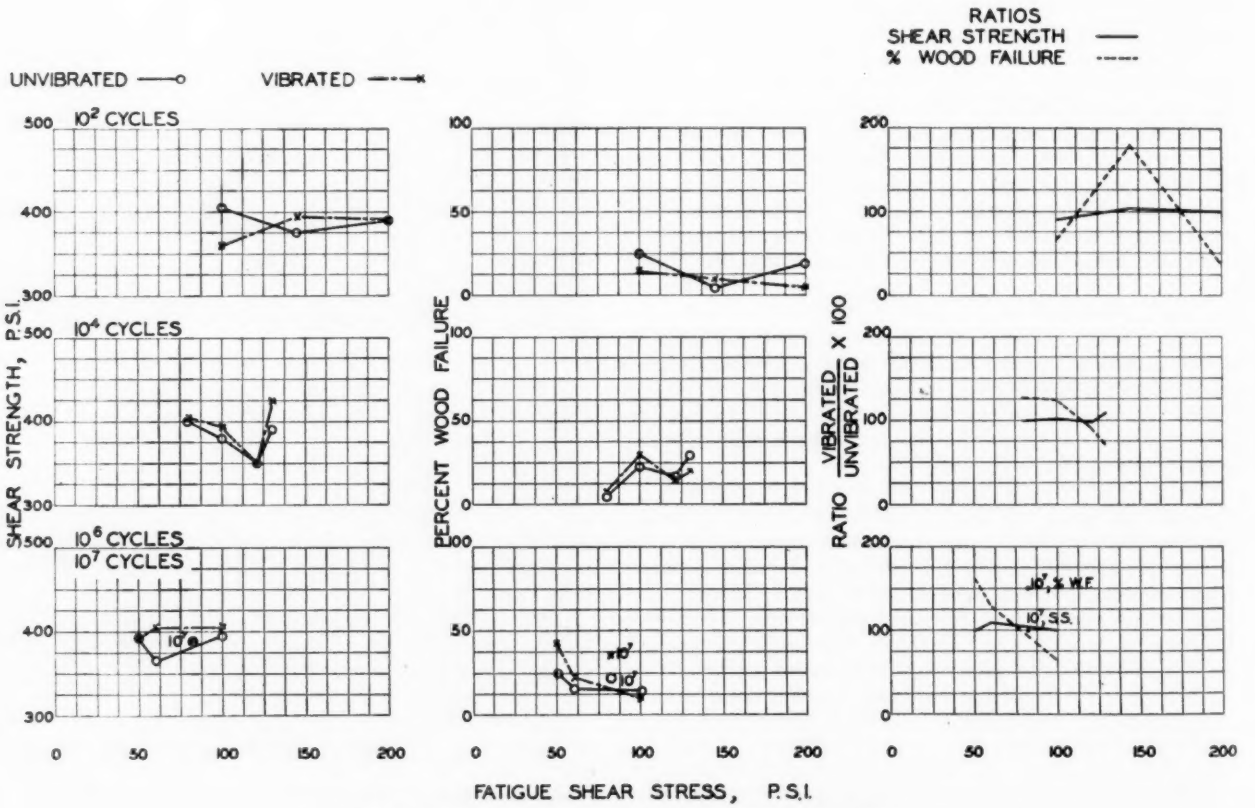


FIG. 7 RESULTS OF TESTS ON PHENOL-FORMALDEHYDE FILM

TABLE 1 CYCLES AND AVERAGE ALTERNATING SHEAR STRESS IN UNWEATHERED SPECIMENS

Number of cycles	Shear stress, psi: Phenol-formaldehyde film	Phenol-formaldehyde solution: Plain	Phenol-formaldehyde solution: Extended
100	200	200	207
	144	160	153
	101	127	124
		94	95
10000	131	126	126
	123	94	90
	101	79	78
	80	...	...
1,000,000	101	99	92
	62	80	64
	50	67	...
10,000,000	86	59	68

that is, if there had been any change in the modulus of elasticity of the plywood.

Tests were run at 100 cycles, 10,000 cycles, 1,000,000 cycles, and 10,000,000 cycles. At each of these cycles, loads were regulated to induce three or four different shear stresses in the glue lines, in order to ascertain if there was any progressive tendency to weaken the adhesive as the shear stress was increased. The highest load applied at any given number of cycles was the highest that could be employed without causing the specimen to fail in bending fatigue. Specimens were made as short as feasible in order to obtain the highest possible shear stresses. Five to fifteen specimens were tested at each combination of cycles, and shear stress to obtain a dependable average. Cycles and stresses are given in Table 1.

Test Results

Fatigue Tests. Fatigue results are summarized in Fig. 6 (*a* to *d*). Fatigue stresses are plotted as ratios of the static moduli of rupture, and numbers of cycles are plotted on a logarithmic scale to bring out the trend. As is to be expected, a considerable amount of scatter is found in spite of the care with which the material was selected and cut. The general trend is apparent, however, and the averages of the plotted points fall fairly close to the indicated straight lines.

The horizontal dotted lines, at approximately 25 per cent of modulus of rupture, represent averages of specimens which had not failed at 1,000,000 to 3,000,000 cycles of stress reversal. In Fig. 6(*c*), the points marked *a*, *b*, *c*, and *d* represent the averages of the most heavily loaded film-bonded specimens employed in the second phase of this research, that is, the alternating-shear specimens. Each of these points represents the average of five to fifteen tests, none of which resulted in failure. Points *c* and *d*, in particular, fall close to the straight line derived from the fatigue tests.

Periodic examination of specimens during the test runs revealed little tendency for the bond to fail or the veneers to separate. After the outer plies had cracked through to the glue line, that is, after failure as previously defined had occurred, delamination did in some instances take place. This tendency was somewhat more prevalent in the plywood than in the laminated material.

TABLE 2 RESULTS OF ALTERNATING-SHEAR TESTS ON UNWEATHERED SPECIMENS

Cycles of Stress Reversal	Static Controls: Glue-Line Shear Strength p.s.i.	Static Controls: Percent Wood Failure	Vibrated Specimens: Alternating Shear Stress p.s.i.	Vibrated Specimens: Glue-Line Shear Strength p.s.i.	Vibrated Specimens: Percent Wood Failure	Ratios Vibrated to Unvibrated: Shear Strength Percent	Ratios Vibrated to Unvibrated: Percent Wood Failure	Change in Modulus of Elasticity Percent
Phenol-Formaldehyde Film								
10^2	393	20	200	392	7	100	35	-3
	375	5	144	396	9	106	180	-2
	403	25	101	362	16	90	64	0
10^4	392	30	131	428	20	109	67	-2
	353	17	123	353	16	100	94	-2
	381	24	101	393	30	103	125	-5
	400	7	80	403	9	101	128	-1
10^6	397	14	101	405	9	102	64	-
	367	17	62	406	22	111	129	4
	397	26	50	397	43	100	165	0
10^7	380	23	86	385	35	101	152	-5
Phenol-Formaldehyde Solution, Plain								
10^2	380	14	200	365	18	96	129	0
	404	31	160	369	25	91	81	+1
	396	39	127	401	38	101	98	0
	431	25	94	333	2	77	8	0
10^4	398	39	126	344	35	86	90	0
	386	33	94	417	34	108	103	0
	441	32	79	407	7	92	22	0
10^6	412	14	99	368	10	89	71	0
	395	27	80	378	15	96	56	-1
	429	25	67	375	25	87	100	0
10^7	345	31	59	403	45	117	76	-1
Phenol-Formaldehyde Solution, Extended								
10^2	400	74	207	428	49	107	66	0
	447	85	153	450	76	101	89	+2
	446	76	124	436	60	98	79	+1
	461	83	95	414	69	90	84	1
10^4	500	60	126	465	50	93	83	0
	458	63	90	453	72	99	114	+2
	459	75	78	425	74	93	99	+2
10^6	461	82	92	425	69	92	84	0
	473	91	64	445	79	94	87	+2
10^7	500	68	79	422	67	84	98	+1

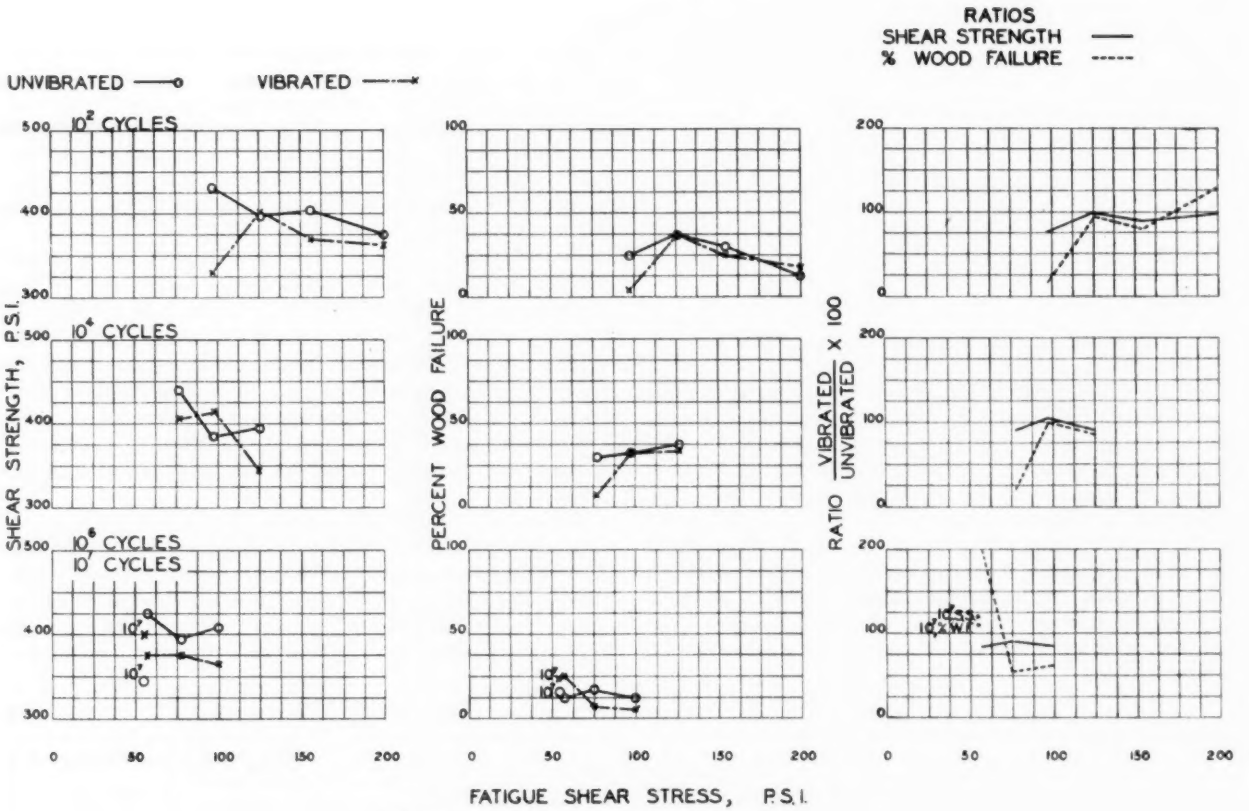


FIG. 8 PHENOL-FORMALDEHYDE SOLUTION, PLAIN

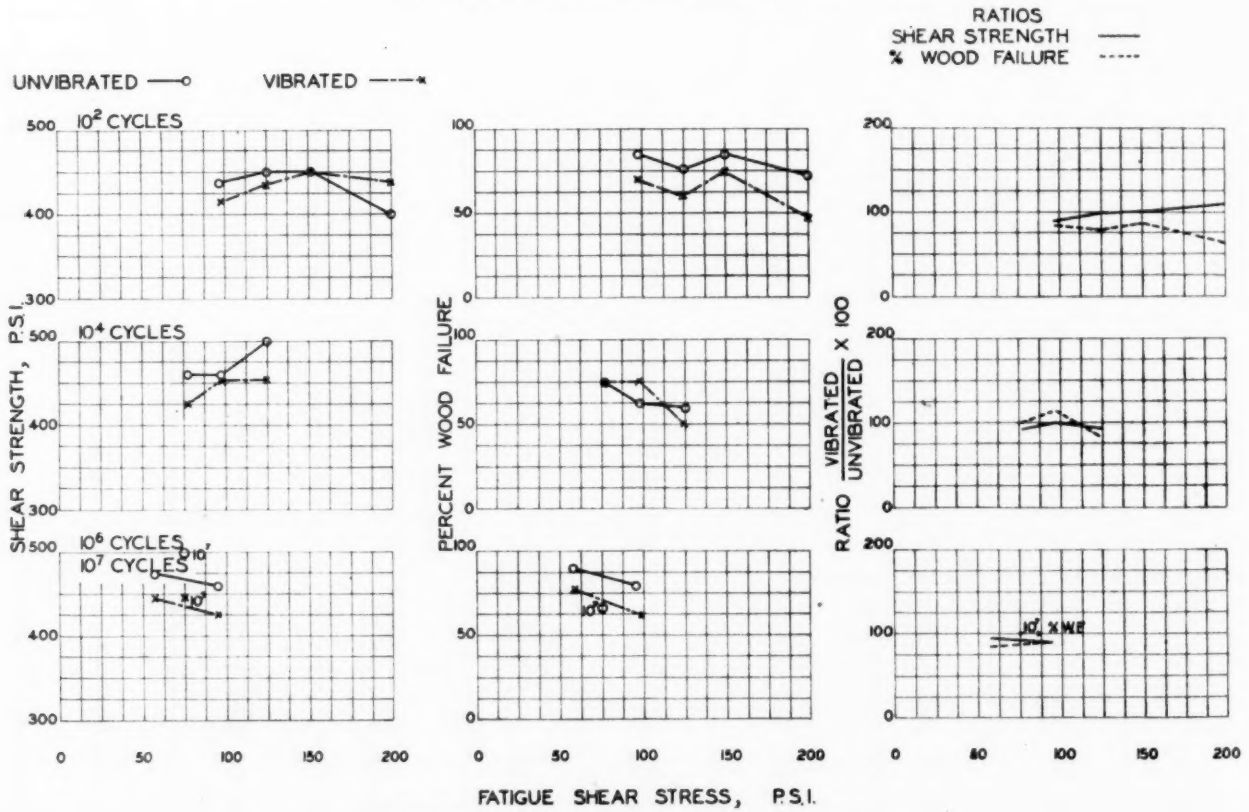


FIG. 9 PHENOL-FORMALDEHYDE SOLUTION, EXTENDED

Alternating-Shear Tests. Results are summarized in Table 2 and in Figs. 7 to 9, inclusive. For each type of adhesive and for each number of cycles of stress, values are given for the average glue-line shear strengths and percentages wood failure of the static controls, the average alternating shear stresses at the glue lines, the average glue-line shear strengths and percentages wood failure after vibration, and the percentage changes in modulus of elasticity.

1 Phenol-formaldehyde film (Table 2, Fig. 7): The most striking feature of the results is that there is no loss in glue-line shear strength after stressing in alternating shear. This is best shown by the ratios of glue-line strength of stressed to unstressed specimens in Fig. 7. The lines lie very close to the 100 per cent mark, in some instances even rising slightly above it. The ratios are strikingly constant in spite of the variation in the actual glue-line strengths of the individual panels. Equally striking is the manner in which the material holds its stiffness. The secondary calibrations show very little change in modulus of elasticity, the largest average for any panel being 6 per cent. A few recalibrations seem to indicate a small increase in stiffness but this is undoubtedly more apparent than real. For all practical purposes, it can be said that there is no significant change in modulus of elasticity under the conditions of alternating stress employed in this research.

No definite trend in percentages wood failure is discernible. At 10,000 cycles, the more heavily vibrated specimens exhibit lower percentages of wood failure relative to the unvibrated controls than do the more lightly vibrated. This is true of the specimens at 1,000,000 cycles. In both instances, however, the lightly vibrated pieces exhibit higher percentages wood failure than do the unvibrated. It does not seem probable that light stressing in alternating shear would actually increase the shear strength, and the trends seemingly indicated by these two sets of specimens are probably more apparent than real. Furthermore, at 100 cycles the material stressed at 146 psi exhibits much higher percentages of wood failure than do the unvibrated controls while that stressed at both 101 and 200 psi is lower, and by nearly the same amount. At 10,000,000 cycles, the vibrated material shows higher percentages wood failure than does the unvibrated. Finally, the variation in percentages wood failure from piece to piece is considerably greater than the variations in the averages from stress to stress or cycle to cycle.

2 Phenol-formaldehyde solution, plain and extended (Table 2, Figs. 8 and 9): In general, the results are similar to those for the film series, in that no great losses in glue-line strength are observed, as shown by the strength ratios of vibrated to unvibrated specimens. This is particularly true at 100 and 10,000 cycles, where the strength-ratio lines hug the 100 per cent line quite closely.

At 1,000,000 cycles both the plain and the extended materials show strength ratios for the vibrated specimens averaging consistently 7 to 9 per cent less than the strength of the unvibrated material. At 10,000,000 cycles, on the other hand, the "plain" vibrated material runs 17 per cent higher than the unvibrated, whereas the "extended" material runs 16 per cent lower. The unvibrated "extended" controls, however, are considerably stronger than the unvibrated "plain" controls.

Table 2 shows that approximately 75 to 80 per cent of the vibrated specimens run lower in glue-line strength than the unvibrated controls, but the diminutions in strength in no instance exceed 16 per cent, and in most instances are less than 10 per cent. This is less than the variation found within a single panel.

Like the strength ratios, the per cent wood-failure ratios are in 75 to 80 per cent of all instances less than 100 per cent, but here the scatter is more marked, as is to be expected. Generally speaking, however, the drops are small and are less than the variation to be found within a single panel.

Quite striking is the consistent behavior of the "extended" adhesive. In not one instance does the glue-line shear strength, either before or after "fatigue" stressing, fall below 400 psi. Percentages wood failure are correspondingly high. Consequently, although the vibrated specimens generally show a diminution of strength properties, the absolute strength values are higher.

Changes in modulus of elasticity are so small as to be insignificant. The majority of the specimens show no change in stiffness after being subjected to vibration, some show an apparent



FIG. 10 WEATHERED AND UNWEATHERED PLYWOOD PANELS
(Weathered material has turned color and shows surface checks but gives no indication of disintegration at the glue line.)

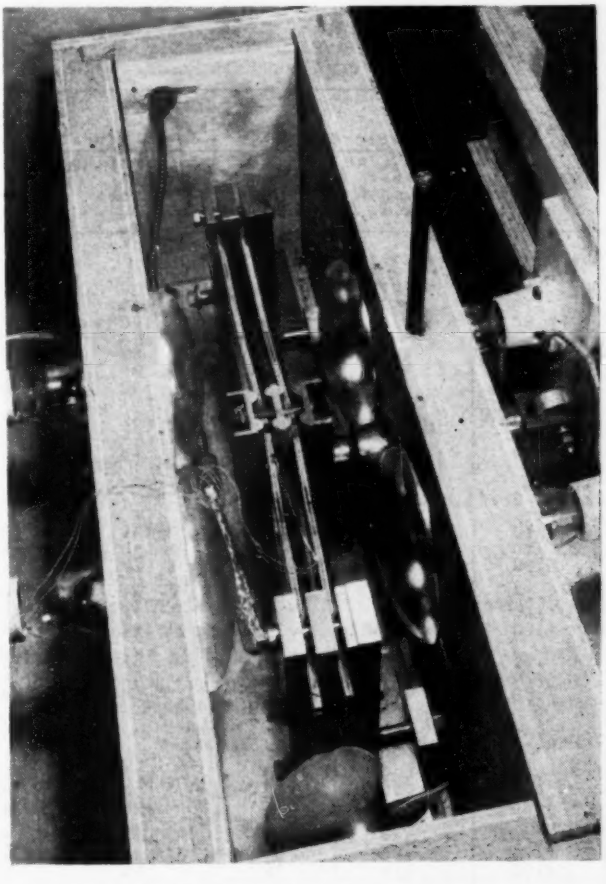


FIG. 11 VIBRATION TEST, HIGH TEMPERATURE
(Four 250-w infrared lamps supply power. Heat controlled in chamber by thermostat, and temperature checked inside specimens by thermocouple.)

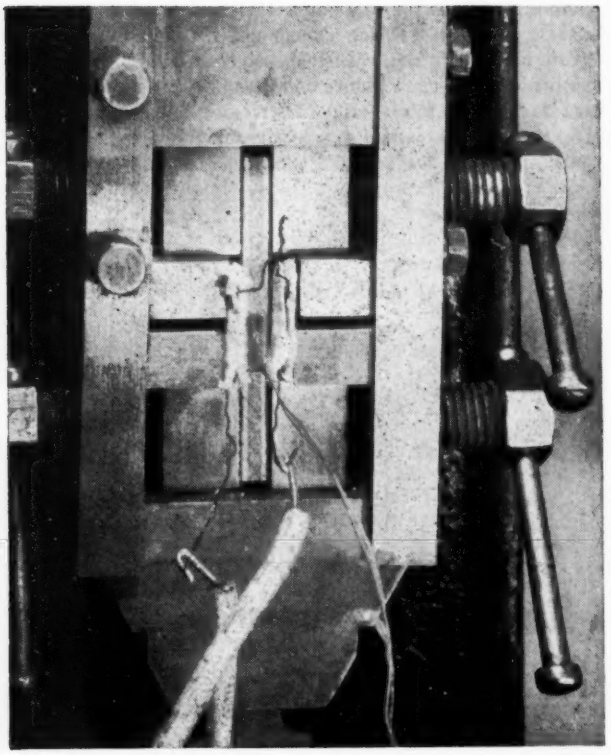


FIG. 12 PLYWOOD SHEAR TEST, HIGH TEMPERATURE; HEATING PADS AND THERMOCOUPLE IN PLACE

TABLE 3 AVERAGE ALTERNATING-SHEAR STRESS IN WEATHERED PLYWOOD

Temperature, deg F	Adhesive	Shear stress, psi — Number of cycles — 10,000	1,000,000	10,000,000
— 70	Film	127	83	57
	Solution:			
	Plain	125	81	65
	Extended	121	77	65
+ 70	Film	134	84	66
	Solution:			
	Plain	130	77	64
	Exended	133	78	65
+180	Film	140	100	58
	Solution:			
	Plain	128	95	58
	Extended	125	94	60

increase of 1 or 2 per cent, some a correspondingly small decrease. As a matter of fact, the "extended" adhesive shows more increases than decreases.

TESTS ON WEATHERED SPECIMENS

MATERIALS

Nine plywood panels, similar to those previously described, were exposed to the weather for 6 months, February–July, 1943, on the Florida coast. Three panels were bonded with phenolic-resin film, three with plain phenol-formaldehyde solution, and three with extended phenol-formaldehyde solution. These were fabricated into specimens and tested in alternating shear in the same manner as the unweathered plywood, except that tests were run at the following three temperatures: —70 F, + 70 F (room temperature), + 180 F. This series was designed to ascertain

TABLE 4 RESULTS OF TESTS ON WEATHERED PLYWOOD; 3-PLY, 1/10-IN., ROTARY-CUT BIRCH

Cycles of Stress Reversal Temperature	Static Controls: Glue-Line Shear Strength p.s.i.	Static Controls: Percent Wood Failure	Vibrated Specimens: Alternating Shear Stress p.s.i.	Vibrated Specimens: Glue-Line Shear Strength p.s.i.	Vibrated Specimens: Percent Wood Failure	Ratios Vibrated to Unvibrated: Shear Strength Percent	Ratios Vibrated to Unvibrated: Percent Wood Failure	Change in Modulus of Elasticity Percent
Phenol-Formaldehyde Film								
10^4 -70°F	297	50	127	288	65	97	130	-
+70	467	20	134	471	35	101	175	-5
+180	365	35	140	428	10	117	28	-1
10^6 -70	331	55	83	382	75	115	136	-5
+70	457	15	84	553	5	121	33	-2
+180	421	15	100	372	50	93	330	-
10^7 -70	301	5	57	322	15	107	300	-7
+70	447	25	66	533	25	117	100	+2
+180	404	15	58	452	5	112	33	-
Phenol-Formaldehyde Solution, Plain								
10^4 -70	361	65	125	347	45	96	69	-
+70	476	35	130	484	25	102	72	-2
+180	385	30	128	435	30	113	100	+1
10^6 -70	384	65	81	291	5	76	8	-3
+70	425	25	77	435	20	102	82	-1
+180	396	30	95	458	10	116	33	-
10^7 -70	338	45	65	345	25	102	56	-6
+70	429	45	64	411	15	96	33	-2
+180	448	15	58	465	10	104	67	-4
Phenol-Formaldehyde Solution, Extended								
10^4 -70	409	90	121	404	100	99	111	-
+70	560	70	133	528	80	94	114	-6
+180	431	75	125	450	90	104	120	-3
10^6 -70	442	85	77	365	70	83	83	0
+70	550	85	78	526	85	96	100	0
+180	514	75	94	547	65	106	87	-2
10^7 -70	379	85	65	367	95	97	112	-4
+70	524	85	65	552	70	105	83	-5
+180	487	95	60	552	95	113	100	-5

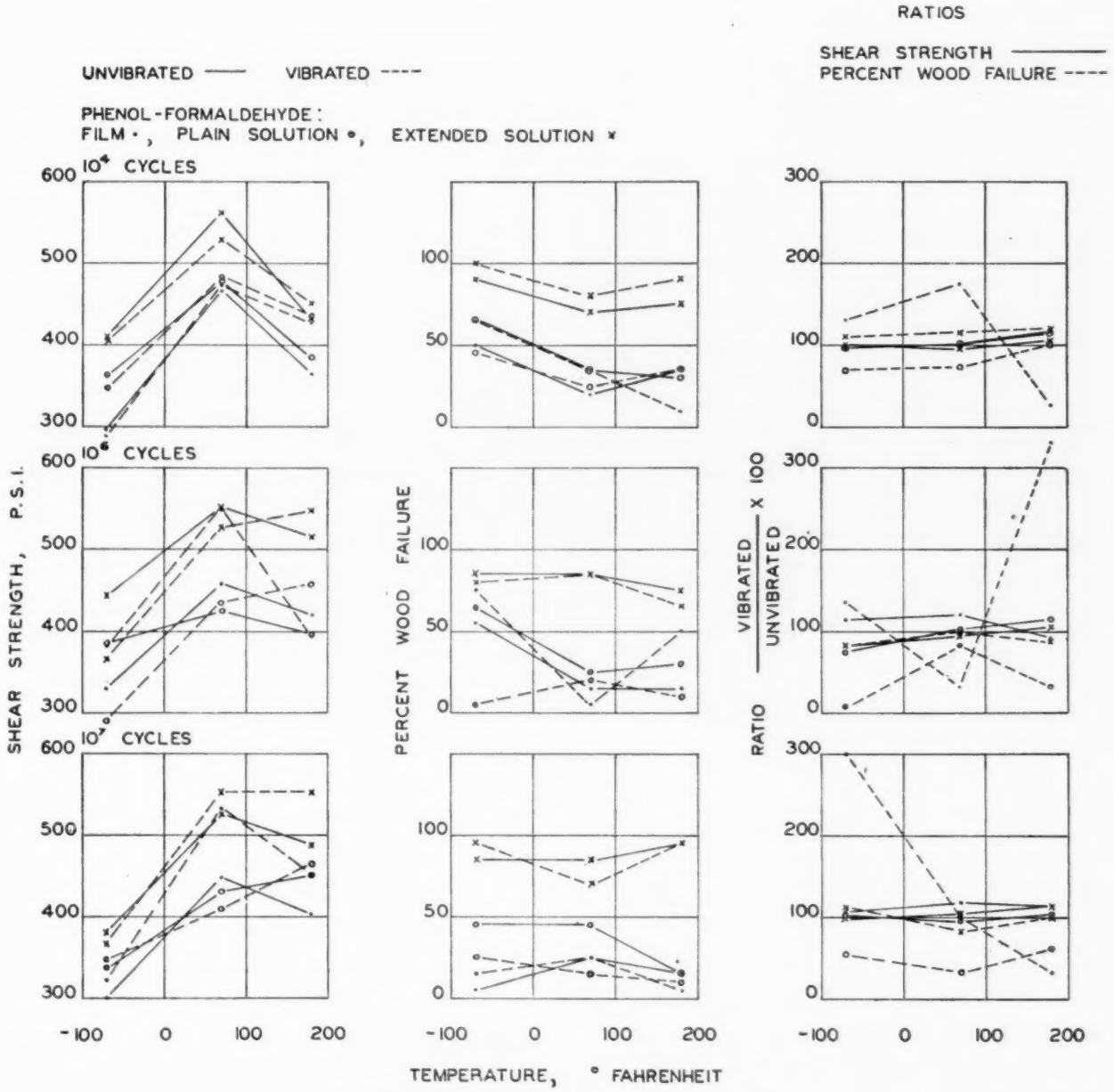


FIG. 13 RESULTS OF TESTS ON WEATHERED PLYWOOD

if weathering, high temperatures, and low temperatures have any effect upon the strength properties of phenolic-resin-bonded plywood. Typical weathered and unweathered panels are shown in Fig. 10.

HIGH-TEMPERATURE TESTS

Vibrating. The pusher and specimen holders of the fatigue machine were surrounded with an insulated cabinet, as shown in Fig. 11, equipped with four 250-w infrared lamps. Lamps were arranged in two parallel-series pairs, and connected to a 110-v a-c main. Power supplied was controlled by two rheostats, one permanently in the line, and another, in parallel with the first, automatically switched in and out by an aluminum-foil-coated thermostat, set to maintain 180 F. Temperature inside the specimens was checked by thermocouples, and the machine was not started until this temperature had risen to +180 F. A small fan maintained air circulation.

Plywood Shear Tests. Small electrical-resistance heating pads, as shown in Fig. 12, were made to be slipped into the standard plywood shear jaws adjacent to the center of the specimen. Pads were designed to heat and to hold the specimen at 180 F. Temperatures were checked by a thermocouple inserted into a small hole drilled in the center ply. Power was controlled by Variac.

LOW-TEMPERATURE TESTS

Vibrating. The fatigue machine was placed in a room maintained at —10 F to —20 F, and the insulated cabinet around the specimens was packed with dry ice. It was found by thermocouple readings that this arrangement permitted average temperatures of —70 F to be maintained in the specimens.

Plywood Shear Tests. Specimens were packed in dry ice, and the shear apparatus was placed in the —10 to —20 F room. Experiment showed that specimens removed from dry ice and placed in the shear tester rose to —70 F during the short time needed to make the tests.

Test Results

Because of the limited material available, tests were run at 10,000 cycles, 1,000,000 cycles, and 10,000,000 cycles only, and at only one shear stress for each number of cycles. Shear stresses were somewhat lower than the maximum values employed with the unweathered material, because weathering had worn away some of the surface plies and thereby reduced the maximum load which the plywood could sustain. Even with the reduced stresses, a few specimens showed incipient wood fatigue failures at the completion of the alternating stress cycles.

Cycles, stresses, and temperatures are summarized in Table 3. Results of all weathered plywood tests are presented in Table 4 and in Fig. 13.

Effect of Weathering. Comparison of Tables 2 and 4 reveals that weathering causes no glue-line strength to be lost at room temperatures. As a matter of fact, all three types of adhesives exhibit higher room-temperature strengths in the weathered than in the unweathered material. This is true of both vibrated and unvibrated specimens. Percentages wood failure in weathered and unweathered, vibrated and unvibrated, material are comparable.

Effect of Temperature. All three adhesives drop off in strength, as a rule, at both low and high temperatures, with the greater diminution occurring at —70 F. Again, this is true of both vibrated and unvibrated material. There is no definite trend in percentages wood failure; individual deviations are much more marked than any average trends.

At —70 F, the plywood shear strength of unvibrated phenolic film drops approximately one third, plain phenolic solution approximately one sixth, and extended phenolic solution approximately one tenth. At +180 F, all three drop approximately one tenth. Vibrated film and extended-resin solution both drop about one third at —70 F, and plain resin solution about one fifth. At +180 F, the vibrated film shows a drop of about one fifth, but the solutions maintain their strength at all but 10^4 cycles (heavy stress, large amplitude).

Effect of Vibration. As in the unweathered material, vibration does not affect the glue-line strength at any of the three temperatures. Generally speaking, the ratios of strengths do not deviate greatly from 100 per cent, with the vibrated material testing stronger, if anything, than the unvibrated. Variations in individual percentage wood failures are much larger than any average trends, so that no general conclusion can be drawn. Although vibration appears to cause a small decrease in modulus of elasticity, the apparent difference is too small to be of practical significance.

Conclusions

Fatigue Specimens. The fatigue tests indicate that, in birch plywood and laminated wood, bonded with thermosetting phenol-formaldehyde film, and in plywood bonded with an aqueous solution of cold-setting urea-formaldehyde resin, at room temperatures (70 to 80 F):

1 Fatigue failures are primarily wood failures.

2 Delamination of the veneers occurs very seldom before the outer plies have given way.

3 Laminated material may be expected to withstand at least 2 000,000 and film-bonded plywood at least 10,000,000 stress reversals without failing, when stressed to 25 per cent or less of the static modulus of rupture.

Alternating Shear Stress. It may be concluded that at room temperature (70 to 80 F):

1 Alternating bending stresses inducing alternating shear stresses up to 200 psi at 100 cycles, up to 125 psi at 10,000 cycles, up to 100 psi at 1,000,000 cycles, and up to 85 psi at 10,000,000 cycles may be expected to decrease the glue-line shear strength of birch plywood not more than an average of 7 to 9 per cent, and the percentages of wood failure by approximately the same amount.

2 Absolute values of strength of phenol-formaldehyde film-bonded plywood and plywood bonded with plain and extended aqueous solutions of phenol formaldehyde may be expected to run within approximately 10 per cent of each other.

3 Vibrations inducing the stresses just given have no discernible effect upon the stiffness (modulus of elasticity) of the material.

Weathering. Weathering has no adverse effect upon the glue-line strength of phenolic-resin-bonded plywood. This is true of percentage wood failure as well, and of both vibrated and unvibrated material.

Temperature. The following may be concluded concerning the effect of temperature:

1 Temperatures as low as —70 F cause a loss in glue-line shear strength in materials bonded with all three phenolic resins. Percentage wood failures do not indicate clearly whether the loss in strength is caused by the effect of cold upon wood or upon resin. Film-bonded material loses approximately one third of its strength; plain-phenolic-solution-bonded material approximately one tenth to one sixth and extended-phenolic-solution-bonded material approximately one tenth to one third in unvibrated and vibrated material, respectively.

2 Temperatures as high as +180 F cause losses in glue-line strength but these are less marked than at low temperatures. All three, unvibrated, drop approximately one tenth. Vibrated film-bonded drops about one fifth, the others show little or no loss in strength.

Acknowledgments

The authors acknowledge their indebtedness to the individuals who assisted in this program, particularly to Mr. Harry Majors, Jr., Instructor in the Department of Mechanical Engineering at the Massachusetts Institute of Technology, and Mr. John D. Barry, Research Assistant, who carried the brunt of the experimental work. Dr. Wm. F. Murray of the Department of Mechanical Engineering was instrumental in devising the testing equipment. Messrs. S. N. Tu, M. Becker, and F. Carroll assisted in the testing.

BIBLIOGRAPHY

1 T. E. Stanton, *Engineering*, vol. 101, 1916, p. 604.

2 "The Fatigue of Metals," by H. F. Moore and J. B. Kommers McGraw-Hill Book Company, Inc., New York, N. Y., 1927, p. 245.

3 "Researches Into Durability and Strength Properties of Swedish Coniferous Timbers," by R. Schlyter, Papers of the 1931 Congress, International Association for Testing Materials, Zürich, 1932, vol. 2, pp. 47–66.

4 "Dauerbiegeversüche mit Hölzern," by O. Kraemer, 190. Bericht, deutsche Versuchsanstalt für Luftfahrt Jahrbuch, 1930, pp. 411–420.

5 "Technologie des Holzes," by F. Kollmann, J. Springer, Berlin, 1936, p. 203.

6 "Aufbau und Verleimung von Flugzeugsperrholtz," by O. Kraemer, *Luftfahrtforschung*, vol. 11, 1934, p. 46.

7 "The Gluing of Wood," by T. R. Truax, U. S. Department of Agriculture, Bulletin 1500, Washington, D. C., 1929.

Maintenance of Hydroelectric Generating Units

By GEORGE H. BRAGG,[1] SAN FRANCISCO, CALIF.

This paper covers the complete overhaul of a 40,000-hp vertical Francis-type hydraulic turbine, operating under 454 ft head to drive a 35,000-kva generator at 257 rpm. Some of the work done was to repair normal wear due to operation over a 20-year period. Other work was of a corrective nature modifying the original design to include improvements found desirable after prolonged operation. Interesting problems were met and solved in some of the work, which involved the handling of heavy parts, and in the use of materials not originally included in the design of the unit.

MODERN hydroelectric generating units usually perform with such reliability that high praise should be given to the manufacturers' engineers who have progressively incorporated improvements in their design and produced machines which often operate continuously year after year without service interruption.

A typical case history usually records only minor annual maintenance work such as repairing the cavitated areas and cleaning the generator windings, etc., all of which may be done in a comparatively short time and without disassembling the unit. But of course there comes a time when a general overhauling is imperative, in which the parts are completely dismantled for careful examination. Then, unusual conditions may be discovered, some of which are due to "wear and tear" while others to "shortcomings" in manufacture.

A good illustration of this is a general overhaul job on a 40,000-hp Francis-turbine-driven unit which had been in continuous operation for almost 20 years. Of course minor repairs had been made on it from time to time but it had not been previously disassembled.

The items of work involving problems of interest were as follows:

(1) Pitting of runner due to cavitation; (2) damaged shaft bushing; (3) shaft packing; (4) worn guide vanes; (5) guide-vane lubrication; (6) runner tip; (7) cavitated liner plates; (8) shaft journals; (9) cavitated relief valve; (10) generator-stator winding.



FIG. 1 PITTED AREAS HAVE BEEN ARC-WELDED BUT NOT FINISHED

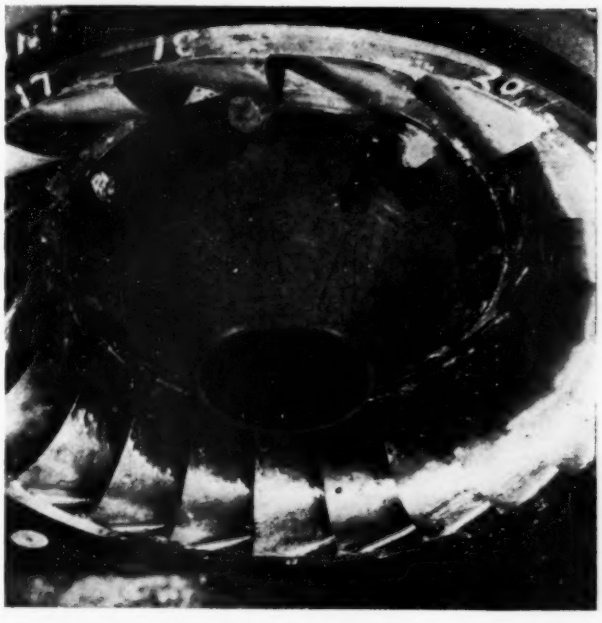


FIG. 2 RUNNER IN PLACE AFTER ALL REPAIRS HAVE BEEN COMPLETED

Pitting of Runner Due to Cavitation. It is rarely possible for a hydraulic-turbine runner to operate over an extended period without pitting of certain areas due to cavitation. The extent and length of time required for pitting to become serious varies greatly but, in general, it is possible to keep it under control by restoring the affected areas by welding at intervals of sufficient frequency to keep the amount of welding at a minimum.

The repair of the pitted areas on the runner vanes required no unusual technique, aside from the precaution to warm the entire casting to 100 C before applying the arc. As no normalizing oven was available to relieve internal strains resulting from localized excessive temperature, the welding was not done continuously in one place but was carried on by skipping from one part to another doing small patches at a time.

In preparing the surface for welding, the spongelike metal is chipped out of the pitted area. The chipping may be as much as $^1/_2$ in. deep in some spots and feather out to the edges of an area which may be 20 or 30 sq in. in extent. With a $^5/_{32}$-in. welding rod a single bead of metal is deposited on a section about $^1/_2$ in. × 2 in., after which the welding is shifted to another blade while the first section cools. When the entire area has been covered with a single bead, it is peened and any slag is chipped off, after which the second layer is added and so on until the required contour is built up. Rotary files applied to the welded surface remove the excess material faster than emery-wheel grinders.

[1] Engineer of Maintenance, Pacific Gas and Electric Company.

Contributed by the Hydraulic Division and presented at the Annual Meeting, New York, N. Y., Nov. 29–Dec. 3, 1943, of THE AMERICAN SOCIETY OF MECHANICAL ENGINEERS.

NOTE: Statements and opinions advanced in papers are to be understood as individual expressions of their authors and not those of the Society.



FIG. 3 SHAFT BUSHING WORN BY PACKING

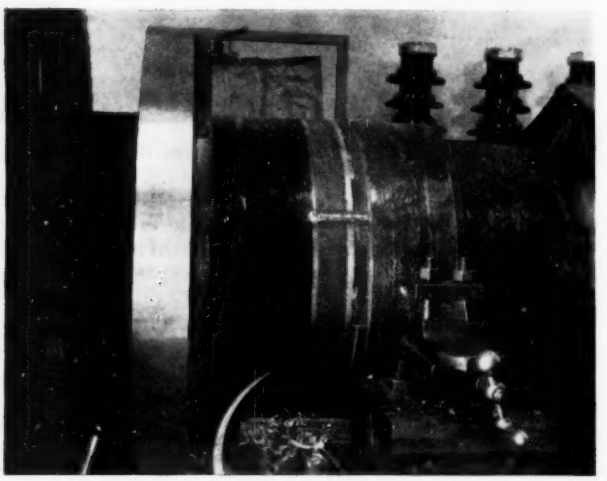


FIG. 5 STAINLESS-STEEL BAND WELDED IN PLACE

However, the surface was finished by emery-wheel grinding, Figs. 1 and 2.

Shaft Bushing. As originally constructed, the turbine shaft was provided with a bushing at the point where the shaft passes through the stuffing box in the turbine head cover. This bushing was about 15 in. long and made from carbon steel $1^1/_2$ in. thick. On account of the flanges on either end of the turbine shaft, it was necessary to make the bushing in halves and join them together by means of special keys having an H-section. Because of the fact that the bushing was made of carbon steel operating submerged in water, deep grooves were found worn into the surface of the metal against which the segmental lignum-vitae packing bore, Figs. 3 to 6, inclusive.

After considering an entirely new bushing made of noncorrosive metal, the cost of which would have been in excess of $800, it was decided not to disturb the worn bushing but to repair it in place.

Accordingly, the turbine shaft, with bushing in place, and weighing approximately 10 tons, was supported horizontally in its own guide bearings on the floor of the powerhouse. A motor-operated worm wheel was bolted to a flange, which revolved the shaft at a proper lathe cutting speed. A compound slide rest with tool post holder was then set in position on T-rail cribbing and a rectangular recess was turned in the bushing, removing all the irregular worn material. The dimensions of the recess are width 4 in., depth $^1/_2$ in.

The ring to fill the recess was made of bar nickel steel which measured 4 in. $\times$ $^5/_8$ in. It was rolled into a circular form of proper diameter, cut into halves, fitted into the recess and secured by welding it circumferentially to the bushing. Both longitudinal joints were then welded thus making a band inserted into the recess.

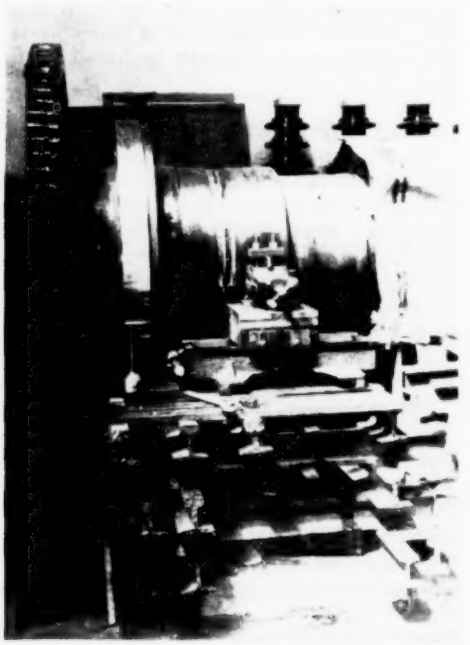


FIG. 4 MOTOR-OPERATED WORM DRIVE ATTACHED TO FLANGED END OF SHAFT, ALSO COMPOUND SLIDE REST SUPPORTED ON T-RAIL CRIB



FIG. 6 STAINLESS-STEEL SURFACE WAS GIVEN A MIRRORLIKE FINISH

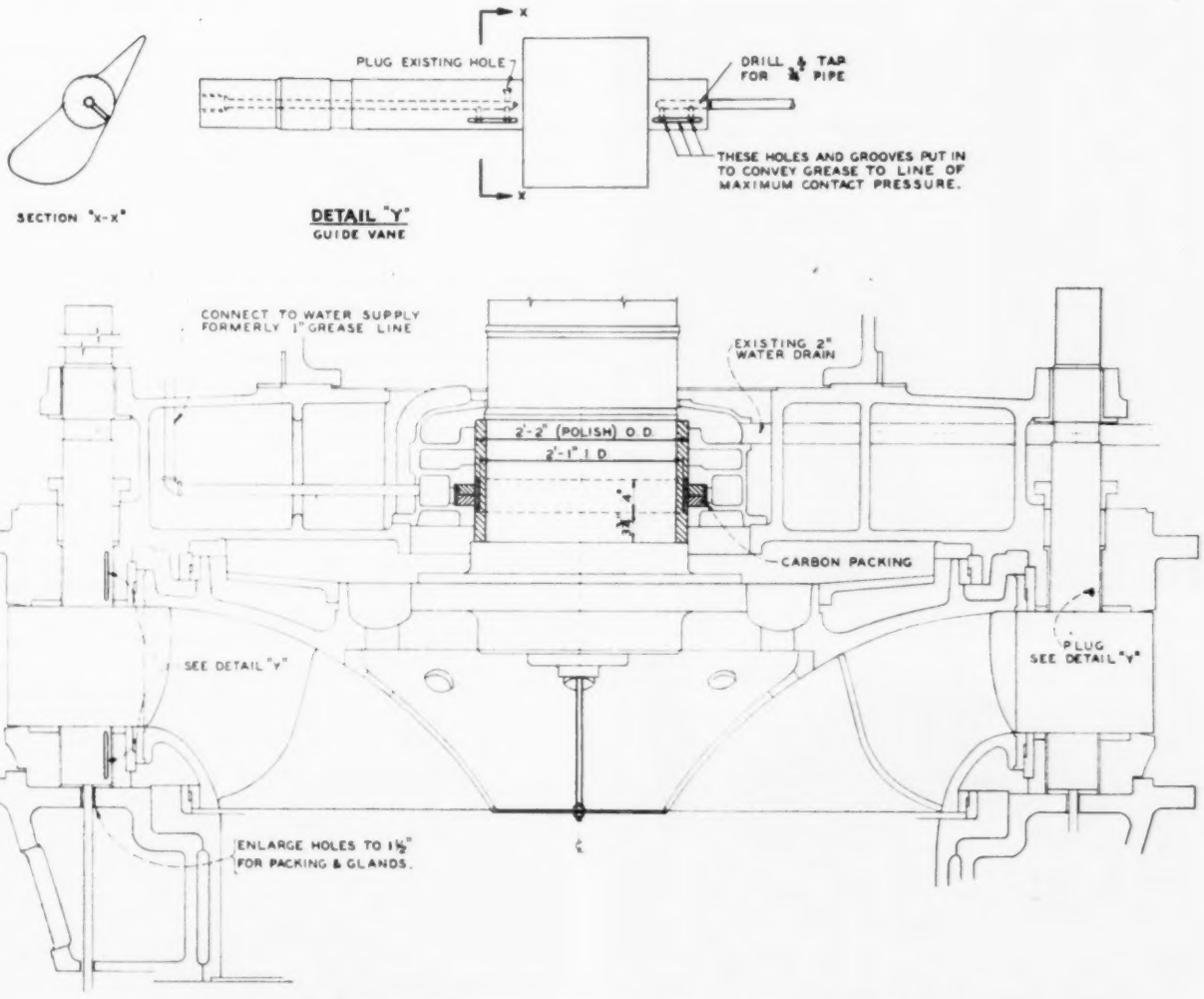


FIG. 7 REPAIR AND RECONSTRUCTION OF 40,000-HP FRANCIS TURBINE

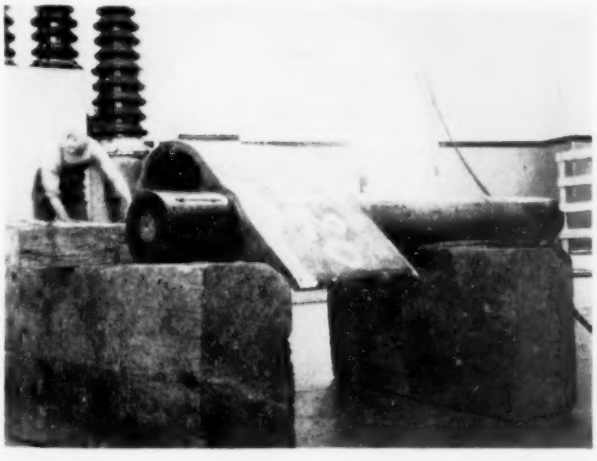


FIG. 8 GUIDE VANE REPAIRED BY ARC-WELDING STEEL TO WORN EDGES

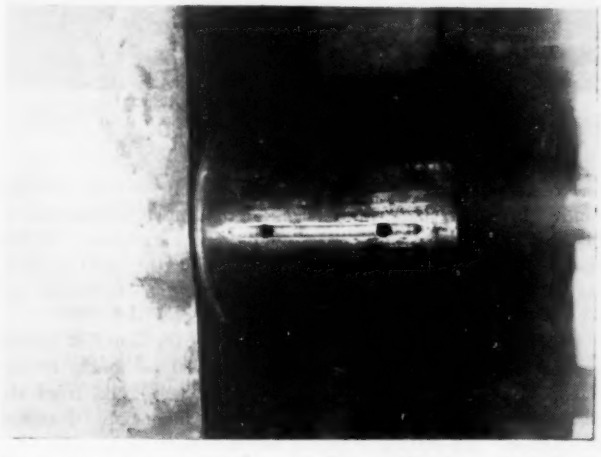


FIG. 9 GUIDE-VANE STEM SHOWING GREASE GROOVE TO LUBRICATE ALONG LINE OF MAXIMUM PRESSURE

The nickel-steel band was then turned, trued, ground, and polished to a mirrorlike finish to minimize the friction and wear on the carbon packing which was installed to replace the lignum-vitae packing.

Shaft Packing. Originally, the shaft packing, serving as a water seal in the turbine head cover, was made of two segmental rings of lignum vitae held in position by means of circular retaining springs. Lignum vitae has certain disadvantages but up to a

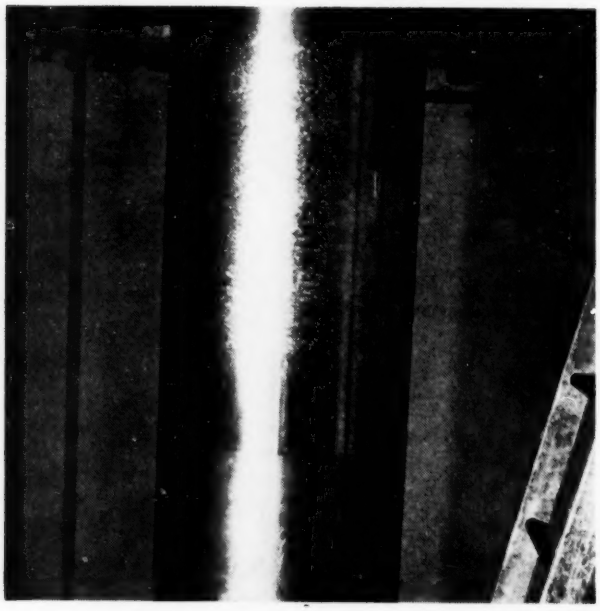


FIG. 10 SHAFT JOURNAL MARRED BY SHAFT CURRENT

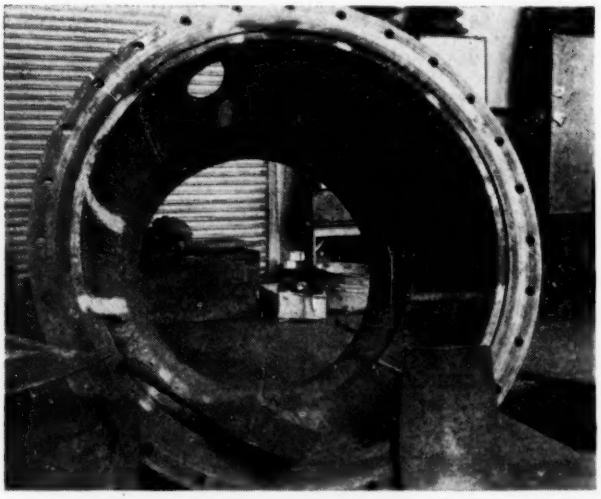


FIG. 12 STEEL PLATES 1/4 IN. THICK PREFORMED AND FITTED TO COVER PITTED SURFACE

few years ago was the best available material for such installations. In recent years, micarta and carbon have become available and offer many advantages over the lignum vitae. In this case, it was decided to use carbon as being the most durable material of the three and the least severe on the metal against which it is pressed, Fig. 7.

The carbon rings were each made of six segments of special carbon having a crushing strength of 20,000 psi and a Brinell hardness of 180 ±. The segments were purchased from the manufacturer in strict accordance with the dimensional drawings submitted. No cutting or fitting was necessary on the job.

Guide Vanes. Ordinarily the most wear on the guide vanes occurs on the edges which are in contact with the throat liner plates, but if some sand is carried by the water, erosion takes place on the streamlined surfaces. In either case, the missing metal may be replaced by arc-welding and the original shape restored by resorting to the manufacturer's methods in fabricating new ones from castings or forgings. Such work can be expertly done by the plant mechanics if a lathe of adequate size to swing the guide vanes is available in the shop, Fig. 8.

Guide-Vane Lubrication. In detailing the guide-vane lubricating system, designers sometimes overlook the fact that the place to exude the grease is between the bearing surfaces which are most intimately in contact for otherwise the lubricant flows in the path of least resistance where it does not serve its purpose.

When upon dismantling the guide vanes the stems are found to be dry and worn where the pressure has been the greatest, the greasing system should be reconstructed by providing a recess on the surface of the stem at top and bottom into which the grease may flow from the central duct to the contact surface between the stem and the bushed bearing. Then if the vanes are moved while the grease is being pumped, the surface will be "wiped" and lubricated without waste, Figs. 7 and 9.

Runner Tip. The runner tip is a separate hollow conical casting attached to the discharge side of the runner, forming a continuation of the upper shroud. The vent holes in the center of the runner were ported within the conical tip and the leakage water from the top side of the runner escaped to the draft tube from the center of the hollow cone.

Notwithstanding close running clearances and a minimum quantity of seal-ring water, a back pressure of 10 psi was built up on top of the runner at full load which subjected the thrust bearing to an additional load of about 75,000 lb.

After analyzing these facts, it was concluded that the rotating conical tip functioned as a centrifugal-pump runner and actually caused the back pressure which retarded the free discharge of the seal-ring water into the draft tube.

Although the thrust bearing had operated at normal tempera-

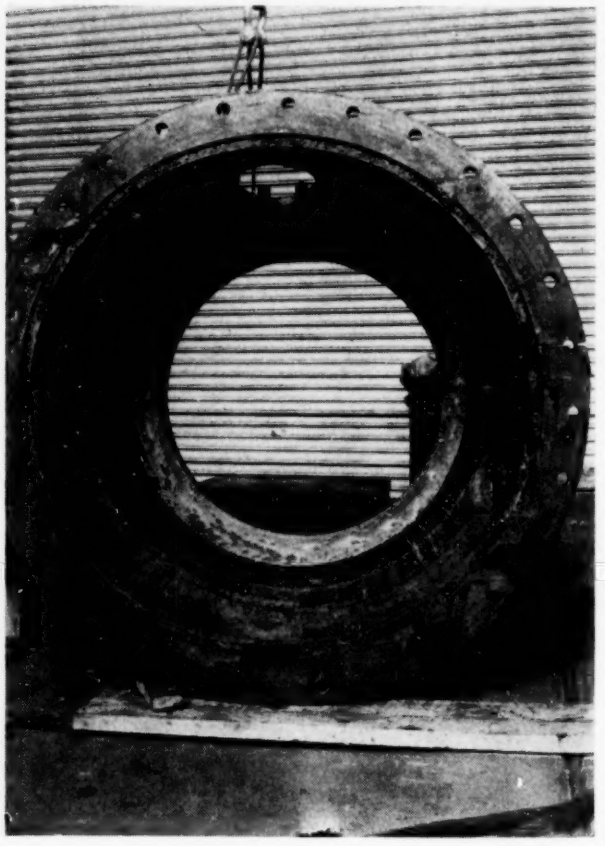


FIG. 11 PITTED BODY OF RELIEF VALVE OF 40,000-HP FRANCIS TURBINE

ture at all times, it was deemed advisable to relieve it of the extra load by providing holes in the tip opposite those in the runner and a plate which closed the center opening. After doing this, the seal-ring water escaped to the draft tube through the drilled holes in the conical tip, and thereafter the pressure above the runner was reduced from 10 psi at full load to a negative value at all loads, Fig. 7.

Liner Plates. Although, as previously stated, the turbine had been in continuous operation for almost 20 years, the seal-ring clearances, contrary to usual experience, had not enlarged appreciably.

When first installed, both upper and lower clearances were 0.030 in., and, when measured prior to taking the unit out of service, the upper one was 0.032 in. and the lower one 0.035 in. This is exceptional and may be explained by the fact that the water carries no sand. The seal rings therefore were not replaced, nor was it necessary to remove the throat liner plates. The slight cavitations in them were arc-welded and the surfaces were refinished by rotary files and emery wheels.

Shaft Journals. It is evident by the appearance of the shaft journal that shaft currents may flow without being detected by the operator. The upper guide bearing was insulated but probably had become short-circuited in some unaccountable manner. Such a condition in a vertical unit is not necessarily serious for the bearing temperature in this instance had not been abnormal at any time. The surface was polished by rubbing it with abrasive

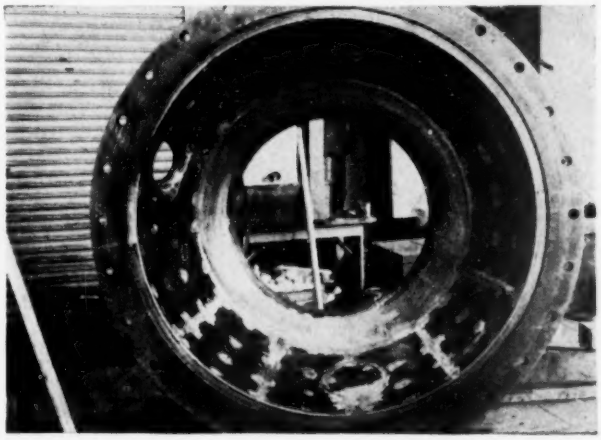


FIG. 13 STEEL PLATES COMPLETELY LINE INNER SURFACE
(Plates were welded along the joints and fastened with patch bolts.)

cloth which lined wooden blocks shaped to fit the journal. The blocks in turn were rotated manually by radial levers. This improved the surface, but of course did not remove the pits, Fig. 10.

Relief Valve. The turbine relief valve invariably pits near the seat rings and, if not allowed to progress too far, effective repairs may be made which will compare favorably with a substitution of new parts for the damaged ones. Irregularities in the bronze seat rings are filled by arc-depositing alloy from a rod having approximately the same composition as that of the parent metal. The contours of the surfaces are restored by filing and grinding according to a template.

The cast-iron body is lined inside by steel plates $^1/_4$ in. thick preformed to fit the curvature of the casting and attached by means of patch bolts. The joints between the plates are welded after all the plates have been attached, and when the surface has been made smooth by grinding, the completed steel surface will be more resistant to pitting than the original cast iron.

Upon reassembling the valve, the seat-ring surfaces are coated with grinding compound and the valve is pressed against the body

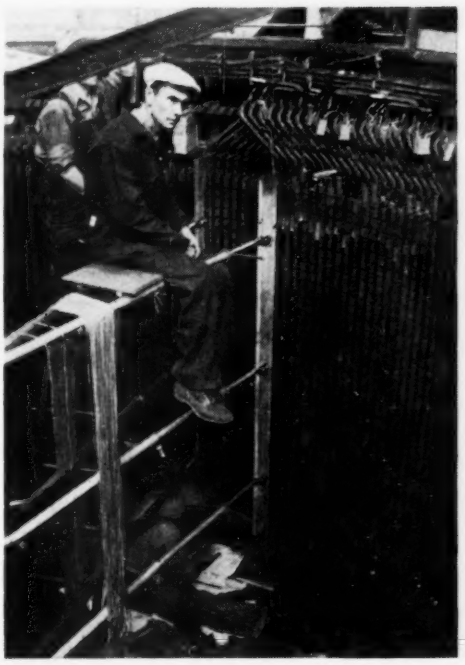


FIG. 14 STRONGBACKS ATTACHED TO SCREW JACKS FORCED COILS INTO SLOTS

seat as if it were in the closed position. It is then oscillated and rotated manually by radial levers, simulating the technique of grinding in automobile-engine valves. The contact eventually becomes perfect and there will be absolutely no leakage, Figs. 11 to 13, inclusive.

Generator Winding. While the turbine was being overhauled by one crew, all the generator-stator coils were removed and replaced with new coils by another crew. As the coils were too heavy to be handled and manipulated safely, mechanical devices for various operations were adopted. Of these a description of the screw jacks which forced the coils into the slots may be of interest. A vertical pipe was rigidly positioned in the center of the stator core. Four screw jacks were then fabricated into radial arms each of which was attached to the center pipe by a ring which allowed the arms to be rotated about the pipe center. A wooden strongback was then attached to the outer extremities of each pair of arms. As the coils were set in place in front of their slots, the strongback was rotated and the jacks adjusted so that pressure throughout the entire length of the straight portion of the coil was uniformly applied until the coil was finally seated in its slot. This device, Fig. 14, definitely avoided any possibility of applying a strain to the mica insulation which might produce a crack that later would break down when the generator was in service.

By restoring each worn part carefully and making improvements where necessary at stated intervals, generating units should maintain their records of continuity of service indefinitely and give reasonable assurance that failures will not occur at inopportune times.

Discussion

P. M. HESS.[2] This paper, dealing with the complete overhaul of a 40,000-hp vertical Francis-type hydraulic turbine operating

[2] Station Superintendent, Safe Harbor Water Power Corporation, Safe Harbor, Pa.

under a head of 454 ft, should be of interest to all companies having hydraulic generating stations. This is particularly true for stations which were built many years ago. During the last 25 years, however, much improvement of design features has been made, and the use of better materials has to a great extent eliminated the need for much of the repair work mentioned in this paper.

Pitting Repairs. Repairs to pitted areas due to cavitation, as described in this paper, are treated along the lines followed by most companies. However, it is of interest to note that rotary files have been used for the rough-grinding, thereby greatly reducing the grinding time which constitutes an appreciable item of expense.

Shaft Repairs. The work of repairing the worn part of the shaft at the packing gland is interesting, but it is believed that this job could have been done satisfactorily by the use of sprayed stainless steel. Recently, information has become available on the use of carbon packing to eliminate most of the wear at this point.

Wicket Gates. Leakage through the guide vanes or wicket gates is of concern to most companies, especially where corrosive or erosive waters are encountered. On the latest designs at Safe Harbor, the contact surfaces are prewelded with stainless steel which thus far is proving well worth the additional investment. On the extremely large units, where complete dismantling of the unit is a major job, it is desirable to weld these corroded contact areas of the gate in place. This job certainly will be a difficult one without warping the surface. It is believed, however, that some attempts should be made to coat these areas with a noncorrosive hard stainless material in place. There is a possibility of applying sprayed stainless steel to the heel part of the gate, but it is doubtful whether or not a sprayed material will adhere properly to the tip.

Shaft Currents. Much discussion is heard concerning damage to bearings from shaft currents, but it is believed that in vertical hydraulic units there are very few cases on record of guide-bearing failures from this cause. It is desirable to insulate at two points in order to provide additional protection and permit testing.

Correcting Pitting From Cavitation. This paper stresses the necessity of complete overhaul after a period of many years' operation but further states that minor repairs in place have been made from time to time. We are of the opinion that, when dealing with propeller-type units, where much damage can be done to the blades in a period of a year or less, very frequent inspections should be made during this early operating period. Local cavitation, which is due to improper shaping of the blades or poor surface conditions, will show its early presence, if not by actual pitting, by the disappearance of the paint or protective coating on the blades. These local conditions can be corrected by grinding ahead of the pitted section to relieve the high spot and reshaping if due to improper shape.

Fig. 15 of this discussion shows a condition of severe pitting resulting from improper shape of the entrance edge of a Kaplan blade after only 6 months of operation. This pitted area could have been corrected by welding with an 18-8 stainless material, but this would not have corrected cavitation. The cavitation or the cause of the pitting was eliminated by reshaping the entrance edge to eliminate the jump of the water. No welding was resorted to, and after 10 years of operation no more pitting has been discovered.

A similar condition is shown in Fig. 16, where the trailing edge was rounded. This rounded surface set up cavitation close enough to the metal so that pitting occurred and continued progressively. The pitting was corrected by making provision for a rectangular trailing edge so that the cavitation which did result existed in the water sufficiently far away from the metal to prevent attack.

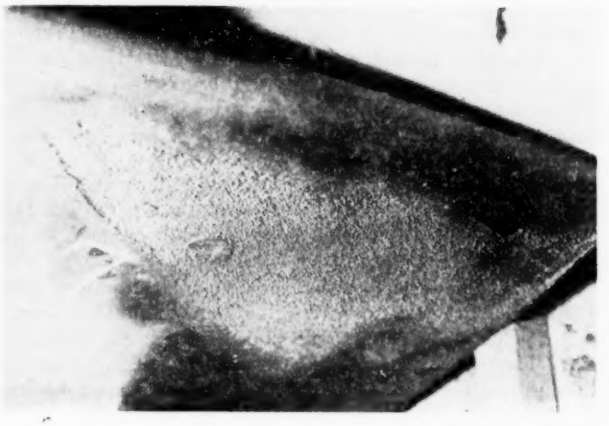


FIG. 15 PITTING ON BOTTOM OF BLADE

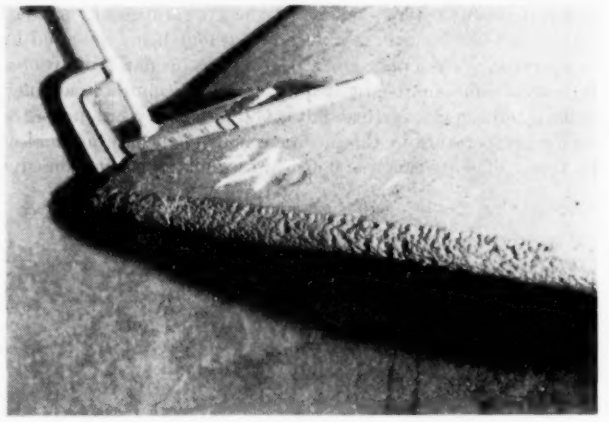


FIG. 16 PITTING ON TRAILING EDGE OF BLADE



FIG. 17 PITTED AREA ON BOTTOM TRAILING SIDE

Fig. 17 shows a condition of pitting at various points due to local cavitation. These areas were corrected by grinding the more or less high section ahead of the pitted area. Here again no weld was required to prevent further pitting.

Recently, one of our newer units showed considerable pitting on the pressure and suction side of the leading edge. Some of this area was prewelded with 18-8 stainless and withstood the attack, but the mild steel pitted rapidly. Investigation showed that a comparatively blunt section of the entrance edge existed,



FIG. 18 PITTING ON UNDER SIDE AND LEADING EDGE OF TURBINE BLADE

causing a tendency for the water to break away from the blade surface. Fig. 18 shows this condition on the suction side of a blade. Here again it would have been possible to combat this pitting by extending the stainless weld over the pitted area; instead, due to the scarcity of stainless welding rod at this time, it was decided to reshape the entrance edge properly. In order to do this, it would have been necessary to grind away practically all of the prewelded stainless steel. Nevertheless, this was done and has almost entirely eliminated the pitting. This is of interest, because pitting, which is shown in Fig. 18, occurred after approximately 1 year of operation, and, after more than a year's additional operation, the reshaped surfaces are still good.

It is therefore suggested that pitting resulting from cavitation should be corrected, if possible, by eliminating the cause, namely, cavitation.

Blade Packing. When the Kaplan units were installed in the Safe Harbor plant, they were many times larger in capacity and dimensions than any units previously built or installed in this country. One problem encountered in the early days was the sealing of the area around the blade journals or shanks to keep the lubricating oil in the hub from leaking outward and the water from leaking inward. A special design, Fig. 19 of this discussion, utilizing a leather packing, was provided for this area, but it never proved entirely satisfactory, growing progressively worse to the point that oil wastage was a considerable factor. Furthermore, it was necessary from time to time to shut the unit down to drain water, which entered at certain loads, from the hub. On the newer designs the water-removal problem has been simplified by the installation of a special pipe within the shaft; also the packing has been redesigned. However, in these units it was extremely difficult to redesign the packing area, and so it was necessary to experiment with different materials and shapes.

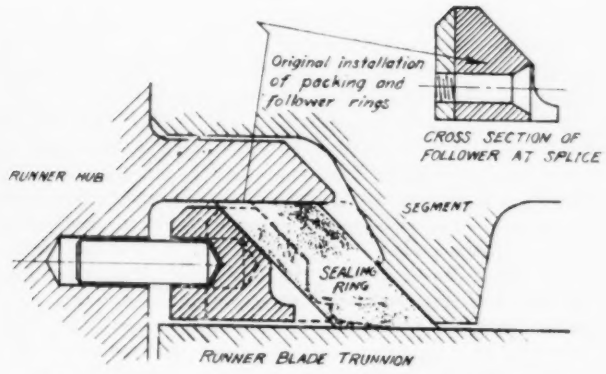


FIG. 19 ORIGINAL RUNNER-BLADE PACKING INSTALLATION

(The dotted lines show how neoprene packing is pressed out of shape and lifted from the trunnion with the original-type installation.)

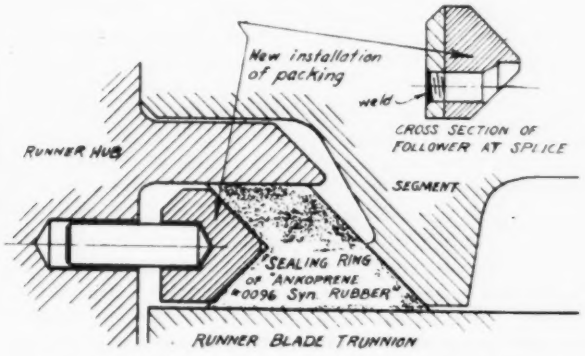


FIG. 20 NEW INSTALLATION OF RUNNER-BLADE PACKING

(Sketch shows how original follower rings were machined.)

After much experimentation, it was found that a neoprene rubber reshaped to the section, as shown in Fig. 20, has practically eliminated any leakage of oil out or water in. It was necessary to secure a neoprene of the proper hardness, because this material has a tendency to become quite hard at freezing temperature and, if made too soft, it will have a tendency to stretch, creep, or swell too much under oil pressure. The neoprene rings shaped similarly to the leather cross section, shown in Fig. 19, were more satisfactory than the leather but did not entirely eliminate all the leakage.

Some of the units have considerable pitting just outside of the sealing ring which caused increased leakage when using the leather. This pitted condition is not as serious when using the neoprene or more pliable material for packing. It has, however, been necessary in several cases to chip, weld, and grind these pitted areas.

The more frequent presentation of similar papers by operating men who are in contact with the equipment in the field is highly desirable, since such information, based upon actual operating experience, has much more value than that to be found in many of the papers which give only opinions without experience.

J. F. ROBERTS.[3] The writer has been greatly interested in the turbines dealt with in this paper, since he spent several months at the plant when it was first started up in 1923. Early in the operation of these units, it was found that there was an unusual vibration which caused a loud humming noise and considerable movement in the exposed parts of the penstocks. The turbines

[3] Manager, Hydraulic Department, Allis-Chalmers Manufacturing Company, Milwaukee, Wis. Mem. A.S.M.E.

themselves operated quite satisfactorily and there appeared to be no unusual vibrations around them.

The penstocks are housed in concrete-lined tunnels underneath the switch structure on the upstream side of the powerhouse, and while they are supported at intervals of 18 to 20 ft, the actual movement of the penstocks in this location and the noise which they produced were quite disturbing.

We feel sure that, in the ensuing 20 years, most other manufacturers have had similar occurrences, and we are not disclosing any professional secrets when we reveal that the cause of these disturbances was in the water wheel itself. We found that the space between the inlet edge of the runner blades and the guide vanes was too small so that, in effect, as each runner blade passed the guide vane, it tended to shut off the flow of water from that opening. This sent a small pressure wave back through the guide-vane opening into the spiral casing, and these pressure waves added together and were transmitted up the penstock. There were 19 runner blades operating at 257 rpm and the pressure waves corresponded exactly to this product, or 4880 vibrations per min. The actual pressure variation was in the neighborhood of $1^1/_2$ psi, or about 0.75 per cent variation on 195 lb static pressure. The difficulty was first eliminated by cutting down the diameter of the runner 5 in. by burning off the inlet edges of the blades. Subsequently, new runners were installed having a smaller inlet diameter and a different number of runner blades, and the results were very satisfactory.

We would be interested in knowing if the author has any records of the change in efficiency of this unit after about 20 years of operation. The original units, as tested by Professor Allen in April, 1925, showed about 90 per cent turbine efficiency. At that time the power company had some venturi connections in the penstock, and they expected to keep a continuous record of the performance of the units. Such records would be interesting to the profession, particularly in view of the rather unusual capacity of these units and the date on which they were installed.

The author mentions the matter of wear on the guide-vane bodies themselves but does not give any figures as to the wear on the guide-vane stems. Apparently the water in the Pit River is extremely clean, as he points out that the runner clearances had not increased appreciably in the 20 years of operation, but some figure on the amount of wear on the guide-vane stems and the bushings would be of interest. The writer has had considerable experience with mountain streams containing silt where the guide-vane stems were worn so badly that they had to be built up by welding and then turned to restore them to the original diameter.

The Pit River units are equipped with 9-ft-diam butterfly valves operating under 450 ft head, the valves having snap rings or piston rings on the disk, in order to give them a tight seal and take up any deflection which occurs in the valve housing under pressure. Originally the leakage on these valves was relatively small, possibly 5 to 10 gpm. It would be interesting if the author could supply information as to how these valves maintained their original tightness.

Illustrations are shown in the paper of the welding on the bottom side of the runner blades which was done to fill in the pitted areas. At the time of the installation of this plant, the question of suction head was not as thoroughly understood as at present, and to our knowledge cavitation tests on model runners had not then been conducted.

The throats of the Pit River No. 1 runners are set about $11^1/_2$ ft above normal tail water. Present practice would require that these units be set down within 4 to 5 ft of the tail water, in order to reduce the sigma value to a figure which is now considered good practice for units of this type.

This powerhouse is located at an altitude of nearly 2900 ft above sea level, and at this altitude perfect vacuum occurs at slightly under 30 ft of water vacuum. With the relatively high draft head which exists, it is not surprising that some pitting has taken place, but the amounts indicated in the paper do not appear excessive in view of the long life of these machines and the operating conditions.

The author's method of correcting the wear in the main-shaft sleeve is interesting and instructive. The use of a high-chrome steel with from12 to 15 per cent chrome is now common practice and appears to give the best results. It stands up considerably better than a nickel-chrome steel. The change in the method of draining the pressure from the upper side of the runner is interesting, and we hope that the results will be available at a later date.

F. H. Rogers.[4] The high-head turbine described in this paper had an excellent record of 20 years of continuous operation before major repairs were required.

The pitting of the runner, as described, occurred on the back of the runner vanes beyond the discharge orifice, which is the usual location for pitting on high-head Francis runners, as it is difficult to guide the water so that it will remain in contact with the back of the vane after the water leaves the orifice formed by the preceding vane.

In recent years, prewelding of the runner vanes has often been done during manufacture to protect the areas where pitting may occur, as determined by past experience. This is now quite general practice in the case of propeller-type runners and has been done in a few cases on high-head Francis runners. The surfaces to be prewelded are cast as depressions about $^1/_8$ in. below the final contour. The initial cost of this work is rather high, and its advisability may be questioned in the case of Francis runners as the actual pitting may not always occur at the protected surfaces.

The cause of pitting in a particular installation may be due to faulty operation as well as to faulty design. The runner is designed for operation under given conditions of horsepower output, total head, and minimum tail-water elevation, as specified by the purchaser. The designer allows some margin over the rated horsepower required to allow for speed regulation, ordinarily from 5 to 10 per cent.

To prevent cavitation, it is necessary that a reasonable absolute pressure exist at all points on the runner vanes. The absolute pressure available is dependent upon the water barometer pressure at the plant site (from 30 to 33 ft, depending upon elevation above sea level). This absolute pressure is reduced by (1) elevation of runner above tail water, (2) regained velocity head of the flowing water, and (3) local pressure drop due to curvature of the vanes, or to the pressure difference required to develop power. All these factors are taken into account by the designer, so that the actual remaining absolute pressure will be from 5 to 10 ft at all points on the vanes.

In actual operation, the turbine may develop a full-load capacity of from 5 to 10 per cent in excess of its rated capacity; the efficiency, however, at this load being somewhat reduced. If the unit is operated at this overload, the discharge will be considerably higher than at the rated output. Under such conditions, the absolute pressure on the runner vanes will be reduced below the value established by the designer and may fall so low as to result in a break in the continuity of the flow causing cavitation and pitting.

This condition is illustrated by the curves in Fig. 21 of this discussion, produced from the actual design of a 60,000-hp turbine operating under a head of 390 ft at a speed of 225 rpm. At the

[4] Manager, I. P. Morris Department, Baldwin-Southwark Division, The Baldwin Locomotive Works, Philadelphia, Pa. Mem. A.S.M.E.

normal rating, the discharge is 1500 cfs. At the elevation of this plant above sea level, the atmospheric pressure minus the water-vapor pressure at 80 F is 31.8 ft. This total absolute pressure at the runner discharge is reduced by the three factors previously mentioned, the values of which as shown are as follows:

		Feet
1	Elevation of tail water (static draft head)	= 5.2
2	Average velocity head regained	= 11.1
3	Local pressure drop	= 9.4
	Total pressure reduction	= 25.7
	Margin in pressure	= 6.1
	Total available pressure	= 31.8

If this unit is operated at full gate, developing 64,500 hp, or 7½ per cent excess power, the efficiency falls to 86 per cent, and

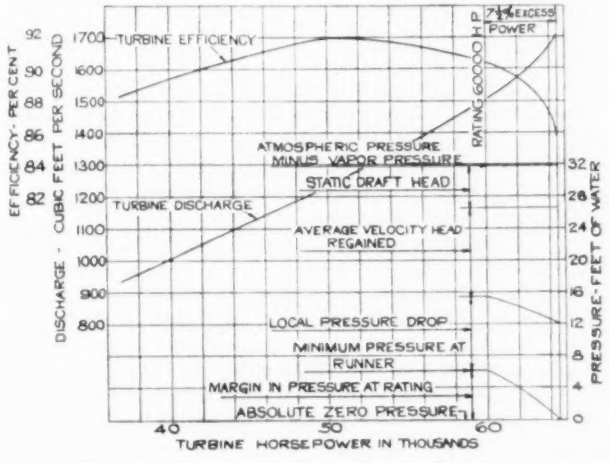


FIG. 21 CAVITATION EFFECT DUE TO OVERLOADS

the discharge increases to 1700 cfs. As both the velocity head regained and the local pressure drop vary as the velocity squared or the discharge squared, it will be noted that these two curves drop rapidly, so that at this output the pressure reduction is made up of the following:

		Feet
1	Elevation above tail water	= 5.2
2	Average velocity head regained	= 14.4
3	Local pressure drop	= 12.2
	Total pressure reduction	= 31.8

Under these conditions all the design margin is lost and only the water-vapor pressure occurs at the vanes, resulting in cavitation and pitting. To avoid this danger it is good practice to furnish the plant operators with charts showing the maximum allowable outputs at various heads and tail-water elevations, based on data furnished by the manufacturer. Under emergency conditions a unit may be operated beyond these limits for a short period of time, recognizing the fact that pitting may occur, the extent of which would be dependent upon the period of operation. The value of this additional output versus the cost of repairs and outage time should be studied carefully by the operating company before permitting such overloading of the unit.

The repair work on the guide vanes, described in the paper, is frequently found in high-head units where abrasive materials are carried by the water. It is now usual practice to preweld the guide vanes at the manufacturer's plant at certain locations for high-head plants where it is known that the water carries silt or other abrasive materials. This is done by welding with stainless steel on the vertical contact lines between the guide vanes, as this hard metal not only preserves the shape of the vanes at the point of highest velocity but also maintains the leakage at the original low value when the guide vanes are closed. This is of considerable value when shutting down a unit and applying the brakes, as it is frequently found that after the guide vanes are worn the leakage in the closed position is so great that the unit cannot be stopped with the brakes and it is necessary to close the main intake valve. Wear at the top and bottom of the guide vanes also increases the leakage at the distributor plates, resulting in loss in efficiency as well as difficulty in shutting down the unit. This portion of the vanes is sometimes protected by welding stainless-steel plates to the top and bottom of the vanes before final machining. This protective work can be done at lower cost in the manufacturer's shop than after wear has occurred in the plant.

Another method of reducing leakage above and below the guide vanes is the use of the so-called "disk guide vanes." In this type, disks are cast with the guide vanes, machined for a close fit in holes bored in the upper and lower distributor plates. These disks reduce the leakage area above and below the guide vanes by the difference between the diameter of the disk and the diameter of the vane shanks.

T. C. STABLEY.[5] The complete overhauling of the 40,000-hp turbine, as outlined in this paper, is more or less typical of Francis-type turbines. Generally, the most common maintenance problems are pitting of runner by cavitation, lack of grease lubrication at crucial points, water-lubricated bearings, wear of shaft or shaft sleeves at bearings and packing glands, and corrosion.

Another more serious condition, which has appeared in recent years and which is confined mainly to cast-iron runners, is that of cracking of blades at the runner crown, beginning at the outflow edge and progressing toward the inflow edge. On this condition very little has been published.

The California Unit. Repairs and modifications to the 40,000-hp turbine were carried out evidently under favorable conditions, in that it was possible to dismantle the entire unit completely. This method is undoubtedly the most satisfactory and should be used where time and costs permit, as it facilitates and insures a more dependable job, especially so when the runner can be positioned for flat welding instead of the usual difficult overhead method.

Considering the capacity and the extraordinarily high head, the runner evidently is made of cast steel, which lends itself readily to the production of a first-class and enduring welding job of the pitted areas with stainless steel.

The most difficult repair method of welding runners is in the overhead position when it is not convenient to dismantle, especially so with cast-iron runners which are the most common type. Great care must be exercised in these welding repairs to re-establish the original contours by grinding. Experience has proved that if only the general curvature of buckets is followed high spots remain, causing severe pitting to appear well beyond the welded section.

Stainless-Steel Welding. We pioneered with welding stainless steel (18-8 and 18 Cr) on cast-iron runners in the overhead position in 1929 and 1930. Since then we have welded ten large runners with excellent results, so that none of the welds indicates any trace of pitting. In some of our early jobs, insufficient attention had been given to contours, resulting in further expansion of pitting beyond the welds.

Shaft Repairs. Like runner repairs, work on shafts can be more readily carried out when dismantled and set up in a lathe, or in some improvised turning rig as described by the author. In recent years, several interesting articles have been published on

[5] Station Superintendent, Pennsylvania Water & Power Company, Holtwood, Pa.

truing or machining vertical shafts in position, because of corroded or worn sections. We have found it necessary to machine 24-in-diam shafts on two vertical 20,000-hp single-runner, 60-cycle units at the water-lubricated, lignum-vitae, guide-bearing section of the main shaft, where split bronze sleeves 62 in. long are attached. Water entered between the shaft and the sleeve, causing considerable corrosion and loss of metal, allowing some clearance between the shaft and the sleeve. With a locally fabricated tool-holding rig, mounted within the bearing barrel, the shaft was trued to clean metal at 13 rpm. In each case this was accomplished by driving the 60-cycle unit as a synchronous motor with a 13,500-hp 25-cycle unit as the generator, on hand control, running at approximately 38 rpm. The two generators were directly connected through temporary cables between the corresponding oil circuit breakers. To compensate for the slightly reduced shaft diameter, the contact ribs of the bronze sleeve were slightly enlarged in the bore, bronze rings fitted and bored to the reduced shaft diameter.

Inhibiting Shaft Corrosion. On previous fittings of shaft and sleeve, the former was liberally coated with thick white lead, which in time was dissolved by the entrance of water. A "No-Ox-Id" preparation was applied on the last fitting and this is expected to be more durable than white lead.

Restoration of Worn Runner Seals. The author states that the runner seals required no attention in 20 years of service, which is an excellent record. The unit surely must have been operating under very favorable conditions, such as the absence of sand, silt, or other abrasives common to rivers, during freshets and floods. We have seven vertical double-runner units (13,500 hp), and three vertical single-runner units (20,000 hp) in the Holtwood plant with from 19 to 33 years of service, in all of which the seals have become considerably enlarged. These enlargements are caused locally by operating conditions that generally do not apply to all hydrostations.

During the winter months, when frazil ice troubles occur, we are obliged to raise the intake screens which allows all trash, timbers, tree stumps, railroad ties, etc., to enter wheel pits for the duration of the ice run, which may last for several days at a time. Many of these obstructions do not pass through runners but become lodged between the buckets causing unbalancing and excessive shaft oscillations. The units frequently operate under these conditions for extended periods before unwatering and removal of obstructions, hence the seals become progressively larger yearly, owing to the runner band rubbing on the distributor ring.

Efficiency losses are a factor to be considered when a number of units are involved; accordingly this year we began reducing these losses on a 13,500-hp unit, by electrically welding a bronze seal band 1 in. wide on the inside of the lower cast-iron distributor ring, thereby restoring the original clearance of $^1/_{16}$ in.

Determining Normal Position of Runner. The inside diameter of the lower distributor of this unit was found to be worn eccentrically. To locate the normal running position of the runner, the unit was rotated as a motor and measurements taken at the seal of the varying clearances around the distributor. It was surprising to learn that the runner band rotated nearly concentric with the shaft. Owing to the great amount of work entailed in dismantling the entire unit, the job was simplified by removal of vanes, unbolting the distributor and raising it 8 in. for the welding job. After welding, the excess metal was ground off and a true circle established by means of a chart showing all dimensions from a circle drawn on the distributor plate through the fulcrum-pin holes.

The following unusual turbine troubles are cited:

Cracked Blades. Several years ago, we were confronted with a major repair problem in that cracks had developed close to the crown at the base of the fillet in two 20,000-hp (53-ft head) cast-iron runners. (Over-all dimensions: Throat diameter 14 ft, height 9 ft.) Fortunately the cracks were discovered in time to prevent disastrous results. Only a brief summary of the job will be given.

All fractures started at the outflow edges of the blades and progressed toward the inflow, varying in length from a minimum of 4 to a maximum of 32 in. and extending through the blades from the pressure to the suction side. The line of juncture at blade and crown is 57 in. long. A survey of the situation revealed that similar troubles had been experienced and corrected elsewhere by welding. After a thorough study of several methods of restoring the runner, it was decided to make repairs by electric welding without dismantling the unit. Briefly, the cast iron was chipped to a width of 3 in. on either side of the cracks, $^3/_8$ in. deep, and generously studded with $^5/_8$- and $^3/_4$-in. steel studs, carefully welded and ground to smooth contours. All upper sections of the outflow edges were chipped off. Steel inserts 16 in. long and 4 in. wide at the top, and tapering to zero at the lower end, were fitted between blades at crown and runner hub and securely welded. The hub, crown, and blades were liberally studded to make a secure bond so as to reinforce the blade and to reduce the likelihood of cracks starting at the outflow edges again.

Elaborate studies were made by means of seven strain gages fixed to the outflow edge of a blade and used in conjunction with an oscilloscope and oscillograph with the unit operating under varying loads, unloading and loading, to determine conditions which might overstress the blades. Since these analyses have involved pioneering work in the measurement field, as well as in the exploration of stresses in a blade under operating conditions, there is naturally some uncertainty in the results of the studies which remain to some extent in an inconclusive stage. Several theories have been advanced as to conditions overstressing blades, i.e., that of the transition period of the rising water column in the draft tube when changing from condenser operation to power generation, due to impact of water column striking rotating blades; another, fluttering of outflow edges of blades, owing to the long cantilever span between crown and shroud ring causing vibration fatigue of metal. Still another theory advanced is the "out-of-step" condition which occurred a number of times on these units and may have produced severe shocks and irregular rotation. It is thought possible that the thrust on the turbine could increase to such an extent as to cause failure between blades and crown.

Runners of the Francis type made of cast steel would be a marked improvement over cast iron owing to added strength, far less likelihood of failure, such as the development of fractures and broken out section of blades, and would have the added advantage of allowing welding repairs to be made readily on the pitted areas by the application of stainless steel on the vulnerable spots.

Runner-Blade Replacement. A year ago we were obliged to perform another unusual piece of mechanical surgery on a 33-year old 13,500-hp vertical double-runner turbine in which a blade had completely broken out of the lower runner between the crown fillet and the shroud ring. The over-all dimensions of the cast-iron runner are throat-ring diameter 10 ft 7 in., height 6 ft. The blade had been previously welded at what was considered a fatigue crack extending approximately one third of the way across the face of the blade slightly below the crown fillet. Fortunately, the broken-out blade was found intact directly outside the draft-tube discharge and was used as a pattern for casting a new steel blade. Forged-steel anchor plates were fitted to crown and shroud ring, and the new blade welded to these plates, making a secure job and restoring the capacity of unit to normal. In order to compensate for the added weight of the new anchor plates, counterweights were secured to the crown and band

on the opposite side to balance the runner. The fitted blade was 60 in. long, 27 in. to 32 in. wide, and weighed 580 lb.

In 1925, the writer presented a similar paper[6] outlining maintenance problems and procedure which mainly concerned early (1907) low-head types of vertical double-runner units, early welding procedure with high-carbon steel, rubber bearings, etc. The general overhauling periods of these old units have been extended by scheduled inspection periods and minor repairs from every 7 years to an average of 12 years. This was accomplished by providing better lubrication, grease retainers, fitting bronze bushings to unbushed moving mechanisms, and the substitution of stainless steel for ordinary steels to eliminate corrosion in the submerged operating mechanism. Reference was made in the present paper to the first use of rubber for bearing linings in vertical hydraulic turbines. The trial was made in the Holtwood Station in 1924, and since that date eight of the ten main, and two exciter, units have been fitted with rubber bearings; numerous similar installations have been made throughout the country. These bearings have given excellent results and long life; in fact, we have found them far superior to lignum vitae and other modern substitute materials.

In 1925, a rubber liner was fitted to a bearing housing for a 16,500-hp vertical unit and has been in continuous service to date. The only modification made was to enlarge the bore slightly to accommodate a new stainless-steel sleeve fitted on the shaft to replace a worn bronze sleeve. We have likewise found that stainless-steel sleeves on the main shaft at bearing locations are far more durable than bronze owing to its resistance to the abrasive actions of sand and silt in the river.

Vertical Thrust Bearings. It may be of interest to mention that Kingsbury thrust bearings for large vertical hydraulic units had their first trial and development in 1912 in the Holtwood Station, and since have had wide application.

E. B. Strowger.[7] The author has described an ingenious method of installing a split bushing on the shaft of a 40,000-hp Francis turbine after it had been in operation for almost 20 years. This record of performance seems to be very good, and the methods used show ingenuity in handling maintenance problems. The method now used in maintaining the shafts of the 5500-hp vertical turbines of The Niagara Falls Power Company, some of which are 40 years old, might be of interest for the record. The 11-in. nickel-steel shafts have worn in the guide bearings and to a greater extent in the stuffing boxes. No provision in the original design was made for a sleeve to take up this wear. Until recently, the shafts were repaired by truing them up at the guide-bearing section and at the packing-gland section by machining to the depth of the grooves worn by the packing and then fitting a split sleeve or band in the recess and welding it together and fastening it in place. The shaft was then finished to the proper dimensions. With this method, as repairs were made, the various shafts kept decreasing in diameter at the bearing and eventually no two shafts had exactly the same diameter at this point.

To overcome the difficulties resulting from this nonuniformity it was decided to try metallizing. In 1939, one of these shafts was built up by metal-spraying over a length of about 4 ft 4 in., which included the section at the lower packing gland, the bearing section, and the section at the upper packing gland. Fig. 22 of this discussion shows the spraying in progress. The diameter was increased from 1/4 in. to about 1 in. above the worn size using stainless steel. The shaft was then machined and placed in service and is still running. An impregnated flax packing was

[6] "Hydraulic Maintenance at Holtwood Plant," by T. C. Stabley, *Mechanical Engineering*, vol. 48, 1926, pp. 341–349.

[7] Hydraulic Engineer, The Niagara Falls Power Company, Niagara Falls, N. Y. Mem. A.S.M.E.



Fig. 22 Metal-Spraying Turbine Shaft

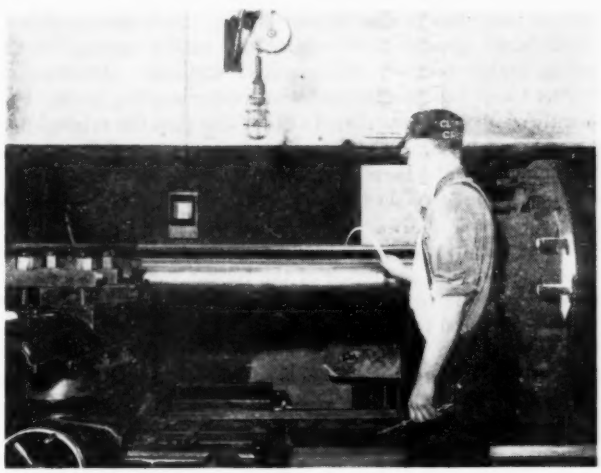


Fig. 23 Completed Shaft Built Up by Metal-Spraying Stainless Steel

used in the packing gland. Fig. 23 shows the completed job.

On this work it was found that while the flax packing was very satisfactory, some of the original U-shaped leather packing rings could not be used because particles of stainless steel would adhere to the leather and the resulting abrasive surface of the metal would quickly wear the leather away. It is therefore necessary in such repair work to make sure that the combination of materials chosen is suitable for the job.

I. M. White.[8] The maintenance time required in connection with the author's modification to the shaft sleeve and the relief-valve body clearly indicates the desirability of taking considerable care in initial purchasing in order to hold turbine outage time to a minimum. For instance, in modern turbine installations a spare split-shaft sleeve is normally ordered at the time of original manufacture. In such cases, the spare sleeve can be completely finished in the manufacturer's shop so as to eliminate any need of special fixtures that might be required should the spare sleeve only be ordered at a later date. Such spare sleeves can be held together with either H-section keys as noted by the author or by special machine screws. Normally, a small notch is

[8] Chief Engineer, The Pelton Water Wheel Company, San Francisco, Calif. Mem. A.S.M.E.

provided at the two joints to permit welding or brazing of the notch at final field assembly. After the welding, the metal can be ground and finished by hand to form a very smooth surface contour. In present-day designs, such sleeves are normally made of stainless steel in order to provide maximum wearing life.

The author has indicated that considerable work was required in the lining of the relief valve in order to overcome cavitation. This excessive repair work and consequent outage of the turbine could have been almost eliminated had the relief valve been made of cast steel at original manufacture. It is probable that the relatively small additional cost of providing initially a cast-steel body would have been offset by the outage time required for the extensive repair.

The change in head cover pressure by modification of the runner tip as discussed by the author has been found to exist on other installations. Several experiments have been conducted in order to determine the best place for venting the upper head cover through the runner. The results of these tests indicate that the author has selected a very desirable location.

Modern practice in connection with the replaceable seats of relief valves indicates a preference for the utilization of 18-8 layer weld on mild steel in place of cast bronze. Such seats cannot be satisfactorily ground as noted by the author because of the galling action between stainless-steel surfaces. However, an excellent seat can be obtained with proper cutting tools. Frequently spare seats are ordered at the same time the original unit is purchased. With such an arrangement, it is possible to install the spare seats and then to recondition the original seats in the machine shop so that they may be returned for use as spares when the need arises.

The author does not specifically mention the type of rod used in connection with the repair of the runner vanes and repair to other cast-steel surfaces. Experience indicates that an 18-8 stainless-steel rod is very satisfactory. This rod provides a surface which has proved of high quality in resistance to cavitation. Another factor that greatly influences the cavitation of the runner

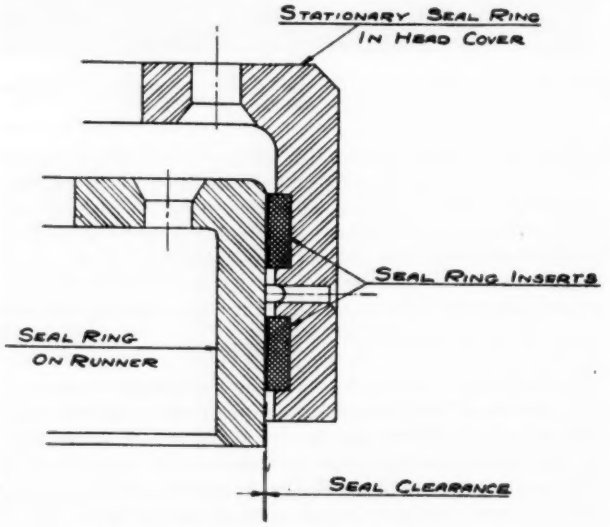


FIG. 24 TYPICAL SEAL-RING CONSTRUCTION

is the actual contour of the runner surfaces upstream from the area experiencing cavitation. It has been found that a very slight high spot upstream will have a tendency to start cavitation, which accelerates as the cavitation becomes more and more severe. It is advisable to take considerable care in inspecting the area upstream of a repaired cavitated area in order to insure that no high points exist which would make the stream of water leave the surface and thereby create cavitation.

The author has stated that the seal rings on the subject turbine showed practically no wear after the 20 years of service. This is indeed unusual and indicates that very clean water undoubtedly passed through the turbine. In many cases, excessive wear of the seals does develop. Consequently, the operating companies desire to make repairs with the minimum of difficulty. Fig. 24 of this discussion indicates a scheme which has proved very satisfactory in providing new seal rings with low outage time required.

The seal-ring inserts indicated are cast in segments and then individually peened into slightly dovetailed grooves. The ends of the segments are joined together by heating with a torch. Seal-ring segments are made of Parsons white brass which has proved to be very desirable from a wearing standpoint. Close clearances can be used without danger of galling between the stationary and moving seal ring, since the Parsons white-brass material has a tendency to wipe clear should contact develop.

The seal-ring inserts can be easily ground in the field to the exact diameter required to suit the runner wearing rings. In many instances, a spare set of rings is ordered with a turbine so that it becomes a very simple matter to make a complete replacement in the field. The worn rings can be repaired at the convenience of the operating personnel.

In addition to the foregoing maintenance points, wear is sometimes experienced in the butterfly-valve seats, guide vanes, liner plates, head cover, and runner throat. In modern turbines, these parts are either made replaceable or provided with replaceable liners so that maintenance work can be accomplished with the minimum of outage time. Special wear plates are sometimes provided in the head covers so that as wear, either from erosion or cavitation, takes place, the plates can be more easily repaired or replaced than the main part itself. Replaceable plate-steel liners are normally installed in the draft tube immediately below the runner. Cavitation frequently occurs at this point and, consequently, a replaceable steel liner is of considerable advantage in maintenance.

During the past several years considerable study has been undertaken by turbine manufacturers concerning cavitation problems. These studies have definitely disclosed that runner and draft-tube cavitation is a function of turbine setting, specific speed, and barometric pressure. As a result, proper operating conditions and unit setting can be established for a new installation so that cavitation and consequent maintenance problems are reduced greatly over what has been the case in the past. Such care in initial selection of units together with proper consideration for spare parts should greatly reduce maintenance problems of present-day turbines in contrast with older turbines.

AUTHOR'S CLOSURE

The discussions presented by various central-station engineers and manufacturers' representatives embrace the practice throughout the United States and contribute much to the scope of the subject.

By keeping the problems of maintenance before designing engineers, progress of improvement in performance of equipment must ensue.

Apparently, there is a gravitation toward the usage of 18-8 stainless steel as an "antidote" to cavitation, erosion, and corrosion. We have all tried various alloys from time to time, but thus far our experience indicates that none offer any advantage over the stainless steels.

Likewise, the metal-spray process has been employed with varying degrees of success. In general, it has been satisfactory on shafts and the like, but it has not done so well on flat surfaces

or shapes upon which the sprayed metal is in the form of a patch.

Packings of various materials and forms have also engaged the attention of maintenance men. No one type, however, is a "panacea" for all conditions. Metallic packings and rawhide seem to be less severe on the shaft or trunnion than others; especially the square-plaited flax.

Mr. J. F. Roberts is probably more intimately acquainted with the units at Pit River No. 1 powerhouse than any one else, for he "lived" with them when their service life was in its "infancy," and so his contribution supplies interesting information which otherwise would have been lacking in the paper.

Supplementing his comments, relating to the runner vibration, a complete revelation of this may be found in a paper by Roy Wilkins.[9] A unique device was employed to record graphically the magnitude and frequency of the vibrations. This is described and some of the records have been reproduced.

The efficiency tests on the Pit River No. 1 units, conducted by Prof. Charles M. Allen, in 1925, have not subsequently been repeated.

[9] "Study of Irregularity of Reaction Francis Turbines," by Roy Wilkins, *Journal of the American Institute of Electrical Engineers*, vol. 42, 1923, pp. 1141–1144.

With seal-ring clearance unchanged, and runner and guide-vane surfaces restored in 1942, the turbine efficiency should be about the same as it was in 1925. It may even be slightly higher, due to the reduction of the load on the Kingsbury thrust bearing, by virtue of the reduction of pressure on the top side of the runner brought about by the vent holes drilled in the runner cone.

The guide-vane stems of the Pit turbines were not worn sufficiently to warrant repairs. This is due to the absence of grit and foreign matter in the water and also to greasing at regular intervals, performed with the vanes in motion.

In answer to Mr. Roberts' inquiry concerning the seat rings of the Pit River No. 1 turbine butterfly valves, the only attention they have had in their 20 years of service is a dressing of the roughened areas by use of a drawfile. They were then readjusted to minimize the leakage.

We have more than twenty-four turbine butterfly valves in service at various hydroplants, varying in size from 36 in. to 9 ft, and operating under heads up to a maximum of 700 ft. Thus far, it has not been necessary to replace the seat rings in any of them. It is our practice to prevent the surfaces from becoming rough or cavitated by arc welding periodically or filing them, or both.

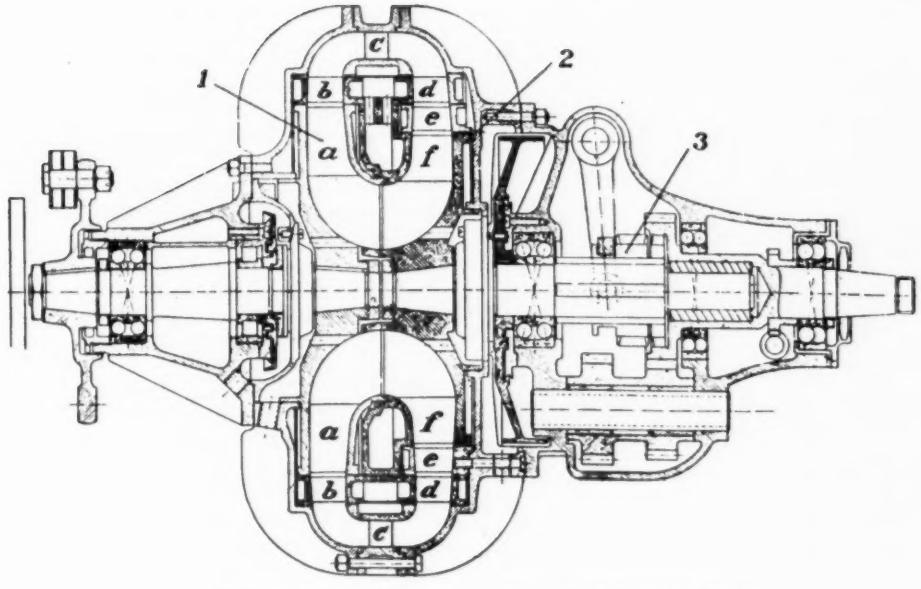


FIG. 1 LYSHOLM-SMITH CONVERTER WITH REVERSE GEAR
(*a*, pump; *b*, *d*, *f*, turbine; *c*, *e*, guide).

Development of the Lysholm-Smith Torque Converter

BY A. LYSHOLM,[1] STOCKHOLM, SWEDEN

The author's experience in the design and construction of hydraulic transmissions for automotive drives goes back over a 15-year period when the outstanding development was the Föttinger transformer, incorporating a coaxial pump impeller and turbine which was used as a speed reducer for ship propellers. Present-day designs of the Lysholm-Smith torque converter employ the Föttinger coaxial arrangement, but with improved multiple-stage turbine blading which enables the torque-speed range to become automatically variable within a wide range of high efficiency. The paper is concerned principally with the theory of the torque converter, details of early experiments in Sweden, and design features of hydraulic drives of various types as now widely applied in the automotive and railroad fields.

ABOUT fifteen years ago the author took up the problem of hydraulic transmission for automotive drives. At that time the Föttinger transformer which incorporates a coaxial pump-impeller and turbine had been used as a speed reducer for ship propellers. According to published information this converter had a very high efficiency at a certain speed ratio, but at other ratios the efficiency dropped off rather rapidly.

With the Lysholm-Smith torque converter which, like all modern hydrodynamic converters incorporates the Föttinger coaxial arrangement, it has been possible to obtain high efficiency as well as a flat efficiency curve, principally by means of improved multiple-stage turbine blading, which enables the torque-speed range to become automatically variable within a wide range of high efficiency. Fig. 1 shows the original test converter which has one pump impeller, three rotating turbine rings and two stationary guide-blade rings. An account will be given of some of the fundamental principles of the torque converter and the experimental work leading to the evolution of the present types, namely, the fixed-blade type, the adjustable-blade type, and the type with direct drive.

THEORY OF THE TORQUE CONVERTER

In a hydraulic gear of the turbine type, the following are the principal normal losses:

1 Friction loss in the pump wheel
2 Carry-over loss between pump and turbine
3 Friction loss in the turbine blading
4 Carry-over losses between the turbine stages
5 Carry-over loss between turbine and pump
6 Leakage losses
7 Rotational losses
8 Mechanical losses
9 Auxiliaries.

A summary of these losses is given in Table 1.

The friction losses in the pump wheel and turbine in the table include all losses due to the flow through the blading, together with the eddy-current losses at the inlet and outlet edges of the blades, but do not include leakage losses. When running at different torque-speed ratios, the blading losses due to varying inlet angles are the most important and account for nearly the total loss at the stalling point and racing speed. Therefore, only these losses will be considered in the following analysis, as this simpli-

[1] Chief Engineer, Ljungstrom Corp., Karlaplan II, Stockholm, Sweden.

Contributed by the Hydraulic Division and presented at the Annual Meeting, New York, N. Y., Nov. 30–Dec. 3, 1943, of THE AMERICAN SOCIETY OF MECHANICAL ENGINEERS.

NOTE: Statements and opinions advanced in papers are to be understood as individual expressions of their authors and not those of the Society.

TABLE 1 BALANCE OF LOSSES

Item	First test converter	Standard bus converter	Standard rail-car converter
1 Friction, pump wheel	3.5	4.5	4.5
3 Friction turbine	2.5	3.0	3.0
6 Leakage	2.5	3.5	3.5
7 Rotation	1.5	1.5	1.5
8 Mechanical	0.5	1.5	1.0
2, (4), (5), (9) Others	0.5	1.0	1.0
Efficiency, per cent	89	85	85.5

fied assumption gives a fairly good view of the operation of a torque converter at varying speeds.

If the turbine is provided with only one runner, and if the leaving energy cannot be utilized, its efficiency at different speeds of the turbine shaft and with a constant supply of energy will, according to the principles of hydrodynamics, vary in accordance with a parabola. Conditions will be entirely different, however, if the leaving energy from each wheel is fully utilized in the next wheel. In the subsequent calculation, it is shown how the turbine "frictional" efficiency will then vary. Strictly speaking, the calculation is only valid for an axial-flow turbine and an infinite number of stages.

If c is the velocity of discharge from a blade and w designates the inlet velocity, then the useful pressure drop in the blade will be

$$\Delta h_u = \frac{c^2 - w^2}{2g} \quad [1]$$

The pressure drop on account of the friction can be expressed by the following formula

$$\Delta h_f = \frac{f}{2} \cdot \frac{c^2 + w^2}{2g} \quad [2]$$

where f is the friction coefficient, which also includes eddy losess.

Thus the total pressure drop in the blade is

$$\Delta h = \Delta h_u + \Delta h_f = \frac{c^2 - w^2}{2g} + \frac{c^2 + w^2}{2g} \cdot \frac{f}{2} \quad [3]$$

The efficiency of each blade will evidently be obtained from the relation between Δh_u and Δh, or

$$\eta = \frac{\Delta h_u}{\Delta h} \quad [4]$$

The values of Δh_u and Δh are obtained from the foregoing equations.

In the description to be given, the pump will be considered as an energy producer, and the efficiency of the turbine at different speeds will be examined, assuming a constant energy supply, that is, a constant product of pressure drop and quantity to be produced by the pump and absorbed by the turbine. Thus the pressure drop in the turbine, multiplied by the circulating-fluid quantity Q, must be constant, or

$$Q\Delta h = \text{const}$$

Assuming for the moment that Q is constant, then if a triangle for c, w, and u is drawn, and the peripheral speed u is assumed to vary with constant flow, the value of w will be seen to decrease from c, when the turbine is stationary, to a minimum value when the direction of w is perpendicular to u (in the following called the optimum point or the optimum speed), and then to increase to c again at racing speed. From Equations [1], [2], and [3], it will be seen that the value of Δh_u will vary between zero and a maximum value, the value of Δh_f between $f/2 \cdot (c^2/g)$ and a minimum value, and the total pressure drop Δh between $f/2 \cdot (c^2/g)$ and a maximum value. Thus at maximum torque at the stalling point, and zero torque at racing speed, all the available energy is absorbed by friction.

To get a constant product of $Q \times \Delta h$, however, the flow of liquid must be increased at all speeds in relation to the flow at the optimum point. At increased flow, the pressure drop varies with the second power of the flow, and thus the energy consumption must vary with the third power of the velocity of flow. The increased flow at a pressure drop Δh in relation to the flow at the optimum point will thus be obtained from the following relation

$$\sqrt[3]{\frac{\Delta h_{max}}{\Delta h}}$$

where Δh_{max} denotes the pressure drop at the optimum point.

Hence it is clear that the velocity-ratio triangles must be enlarged in the same degree as shown in Fig. 2, where the triangles at starting and racing, as well as at a few intermediate speeds, are given. The triangles are drawn for different "relative speeds," that is, the speed of the turbine in relation to the speed of the turbine at the optimum point.

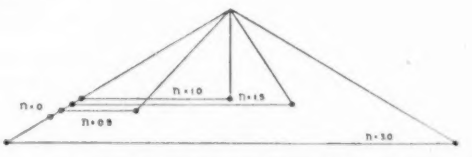


FIG. 2 VELOCITY TRIANGLES WITH $Q\Sigma\Delta h$ CONSTANT
(n = relative speed.)

It may be argued that the number of stages is of no importance for the efficiency of the converter, as the leaving loss always is utilized as inlet energy of the pump but that is not correct, since a certain percentage of the leaving velocity is always lost. Furthermore, it is possible with a multiple-stage converter to get a suitable stalling torque without using too large pump diameter and too much backward slinging of the pump blades which results in efficiency loss over the whole speed range.

Experience with converters, having similar types of blading, indicates that with turbines having one to three stages, the maximum efficiency may be about the same, but that with an increased number of stages, the stalling ratio as well as the over-all performance is improved. The three-stage converter is thus a good combination for most purposes.

When laying out the blading of a converter, the usual pump and turbine equations should be used; thus

$$H_p = \frac{y_p}{g} (U_2 C_{2u} - U_1 C_{1u})$$

$$H_t = \frac{1}{y_t \cdot g} \sum (U_1 C_{1u} - U_2 C_{2u})$$

where

H_p = pump head
H_t = turbine head
y_p = pump efficiency
y_t = turbine efficiency
C_{1u} = peripheral component of absolute inlet velocity
U_1 = peripheral velocity of inlet
C_{2u} = peripheral component of absolute outlet velocity
U_2 = peripheral velocity of outlet

Obviously the head of the pump and turbine must be equal and, further, the exhaust energy of the pump as well as of the last tur-

bine must be equal to the inlet energy of the turbine and pump, respectively, excepting of course carry-over losses.

Naturally due consideration must also be taken of the other losses mentioned in Table 1.

The foregoing equations are preferably solved by a cut-and-try method.

Early Experiments in Sweden

In order to investigate the blade friction at different speeds, some preliminary tests were made with a reaction balance, Fig. 3, by means of which the friction factors at different inlet angles could be studied. The results for two blade-section investigations (Nos. 3 and 2*b*) are given in Fig. 4. Blade section No. 3, Fig. 5, is a reaction blade of ordinary design and section 2*b* is especially suitable for varying inlet angles. However, the last-mentioned type of blade proved to be even better at ideal inlet angles of flow. In Fig. 4, a curve is drawn, calculated from later tests made on the complete hydraulic converter with blades principally of section No. 2*b*.

As will be seen, the results obtained with the converter followed closely the test values with the reaction balance for inlet angles between 50 and 145 deg. At angles smaller than 50 deg, the real values of f are, however, higher than those obtained with the reaction balance, and it is thought that this is due to the fact that the number of blade channels in the reaction balance was too small. However, this test gave sufficiently good results to enable construction of the blade system of the complete gear. It is interesting to note that the blade friction closely corresponds to the friction loss in a smooth tube, as determined by "Blasius" tests.

The blade system in the original Swedish test gear, Fig. 1, consisted of a pump wheel and three rotating blade rings, as well as two fixed guide-blade rings in the stator. Performance tests were made by measuring input torque and stator reaction, as well as primary and secondary speeds.

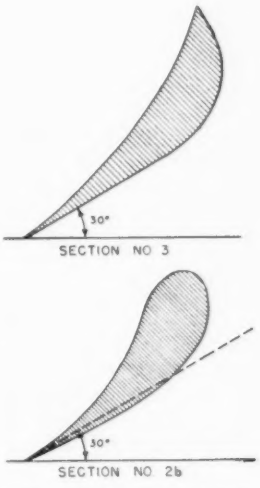


Fig. 5 Blade Sections

Fig. 6 shows the efficiency curve as a function of the turbine speed on the assumption that 50 hp is supplied on the primary side. This efficiency curve is very flat and attains a maximum value of 89 per cent. The corresponding turbine-torque curve is also shown. This curve has a hyberbolic shape which differs considerably from the straight line corresponding to a parabolic efficiency curve.

During the tests, the velocity of the circulating flow of liquid was also measured with a Pitot tube at 800 and 1000 rpm of the primary shaft. From these measurements it appeared that, at a constant primary input, the flow of liquid at stalling speed was 22 per cent, and at racing, 50 per cent higher than at the speed corresponding to the optimum point.

Fig. 7 shows the test results in another form. Here the efficiency curves are drawn for various constant primary speeds from 500 to 1600 rpm as a function of the secondary speed. The maximum efficiency for 500 primary rpm is 83 per cent, and at 1400 rpm the efficiency has increased to nearly 89 per cent.

Converter Input Characteristics. A normal three-stage converter with short third turbine blades absorbs more power at

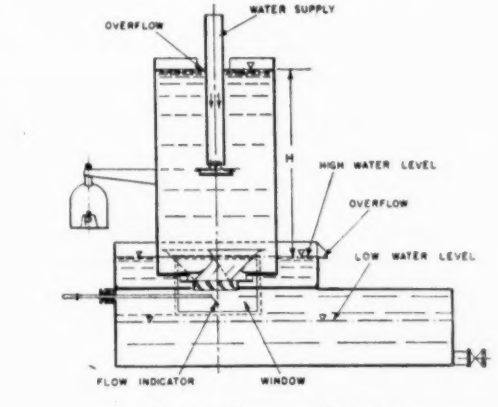
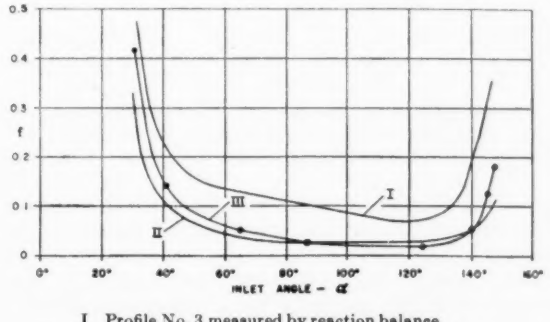


Fig. 3 Reaction Balance



I Profile No. 3 measured by reaction balance
II Profile No. 2b measured with reaction balance
III Profile No. 2b brake test with hydraulic gearing

Fig. 4 Test Values for Friction Factors

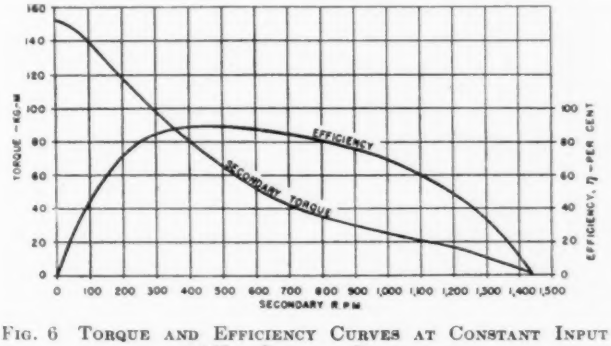
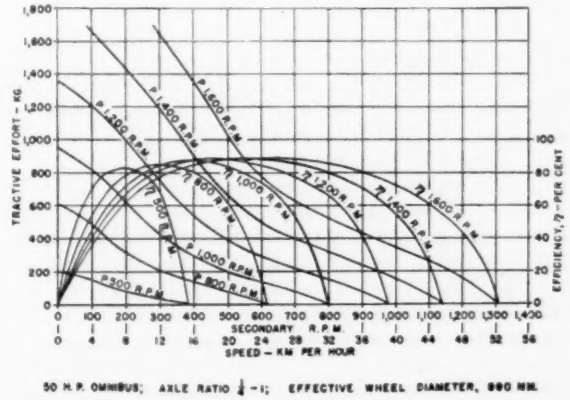


Fig. 6 Torque and Efficiency Curves at Constant Input of 50 Hp; Original Converter



50 H.P. OMNIBUS; AXLE RATIO $\frac{1}{4}$ – 1; EFFECTIVE WHEEL DIAMETER, 880 MM.

Fig. 7 Tractive Effort and Efficiency Curves; Original Converter

stalling through racing, and thus the engine speed at stalling decreased to about 70 per cent of racing speed. This is very important for automotive drives as it prevents overspeeding of the engine at stalling and flattens out the efficiency curve.

However, an increased stalling torque of about 15 to 20 per cent can be obtained by using long blades in the last turbine stage, reducing the ratio mentioned to 80 per cent. This is very useful for most industrial applications where engine speeds are generally lower. A further increase in stalling torque of 15 per cent is obtainable by using adjustable pump blades, which also permits control of the input power.

Range of Torque Converter. In order to obtain the correct performance from a torque converter, it must be used with an engine of suitable torque-speed characteristic, in the same way that a ship's propeller must be designed to suit the engine characteristic. Certain variations from the standard characteristic can, however, be made without material alteration of design, or efficiency. The easiest way to alter the torque-speed characteristic is as follows:

1 To reduce the external diameter of the pump wheel, if it is desired to use an engine of lower torque.

2 To increase the effective outlet angle of the pump blades by increasing the number of blades or the blade angle for an engine of higher torque.

3 To use third turbine blades, which increases the input power considerably at high speed ratios.

4 To incorporate a primary step-up or reduction gearing.

Some experiments showing the effect of altering the blade angle are illustrated in Fig. 8. The efficiency curves are shown

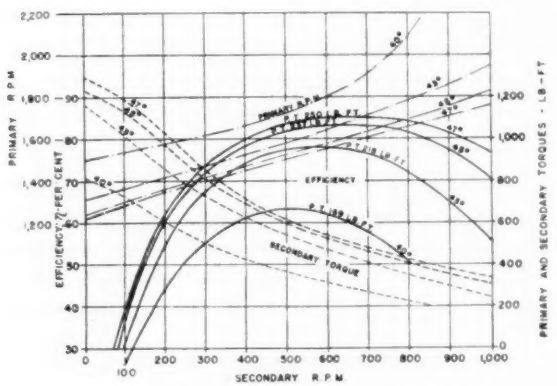


FIG. 8 EFFICIENCY TESTS ON HYDRAULIC TORQUE CONVERTER

for constant primary torques, and the decreased range of the converter and lower efficiency as the angle is decreased will be noted. The available primary-speed range is also shown on the curves for each angle. The curves show the very great importance of having a correct pump-blade angle.

The effect of reducing the pump wheel diameter is shown in the curves in Figs. 9 and 10. It will be noted that, as the diameter is reduced, the efficiency at the lower end of the curve is reduced, and is increased at the higher end. Reducing the diameter displaces the curves along the secondary speed axis owing to the increased input. Fig. 11 shows the alteration of the stalling characteristic produced by reduction of the pump diameter.

From these results a suitable pump wheel diameter to suit any particular engine characteristic or conditions can be determined. The efficiency curves in Fig. 9 are shown for only one constant primary torque and only represent one condition. It will be

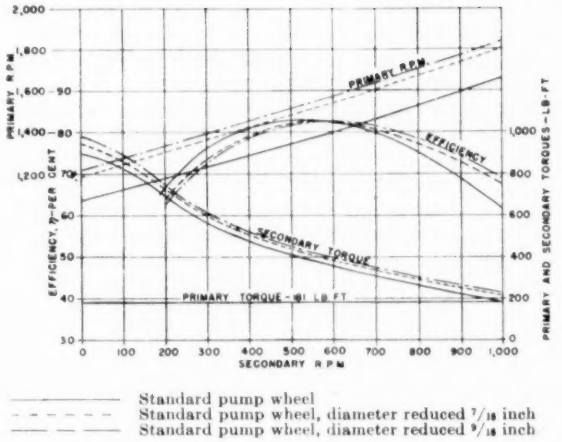


FIG. 9 SPEED-EFFICIENCY CURVES FOR VARIOUS DIAMETERS OF PUMP WHEEL

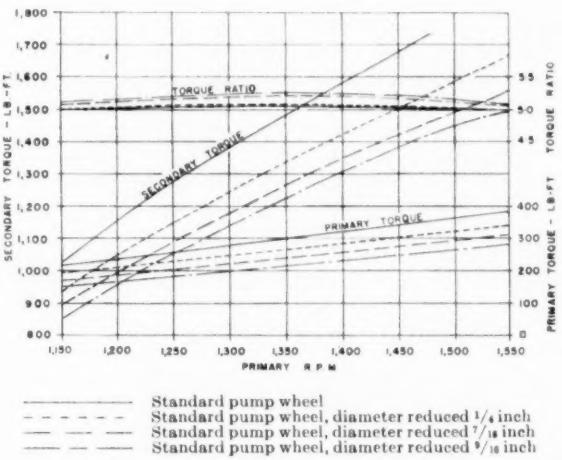


FIG. 10 STALLING TESTS ON PUMP WHEELS OF VARIOUS DIAMETERS

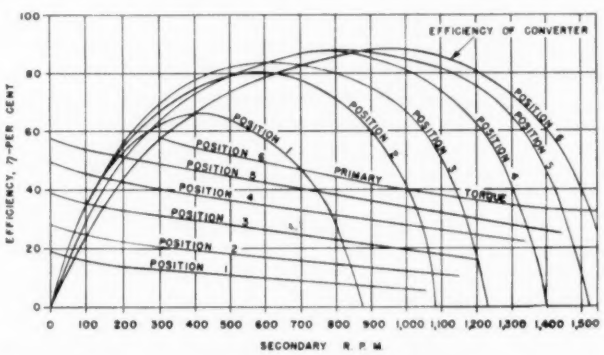


FIG. 11 EFFICIENCY AND PRIMARY TORQUE CURVES FOR HYDRAULIC TORQUE CONVERTER WITH ADJUSTABLE BLADES
(Constant primary speed, 1700 rpm.)

noted in Fig. 10, that the torque ratio at stall increases with decrease of wheel diameter, in about inverse proportion to the diameter.

Torque Converter With Adjustable Pump Blades. In Fig. 11, characteristic curves are given for a torque converter having adjustable pump blades. The numbers of the curves indicate different positions of the adjustable pump blades. It will be noted that the efficiency is less sensitive for different blade posi-

tions than in the case of the pump blades corresponding to Fig. 8. The advantages of the adjustable blades are:

1 Practically no secondary torque with closed blades.
2 Higher stalling torque ratio, up to 6:1.
3 Flatter efficiency curve.
4 Possibility of overloading the engine when desired.
5 Possibility of avoiding critical speeds of the engine crankshaft.

Effect of Turbine Variations. It is a very simple matter to alter a pump wheel on a production converter, as it may only have from 14 to 20 blades, but it is not so easy to make turbine-blade alterations, because of the large number of blades. However, as already mentioned, two different types of third-stage blades are used, a short blade and a long blade. It may be stated generally, however, that the calculations for the turbine are made for a speed which corresponds approximately to a flow perpendicular to the inlet of a blade ring. This "calculation" speed corresponds to the optimum speed previously mentioned. For the tested converters, the speed corresponding to the maximum efficiency is generally higher than the optimum speed owing to the type of blading used.

Maximum Efficiency Speed. The speed at the maximum efficiency point will depend upon (*a*) the number of stages, (*b*) the diameter of the blade rings, (*c*) the head to be utilized, and (*d*) other factors. Obviously, the optimum speed is increased by (*a*) a smaller number of stages, (*b*) a smaller diameter of stages, and (*c*) a larger head. This may also be expressed as a ratio which corresponds to the "Parsons figure" or "quality figure," as used for steam-turbine calculations, namely, $\Sigma u^2/h$, where Σu^2 is the sum of the squares of the turbine-blade velocities, and h is the head utilized in the turbine. For modern steam turbines, this ratio is generally about 2000 (metric units) for impulse turbines having some reaction, and up to 3500 for pure reaction turbines of the Ljungstrom double-rotation type, for instance. To get a direct comparison with these figures it is necessary to multiply the corresponding values for torque converters by the metric mechanical equivalent of heat, 427. The converters now made have a Parsons figure of 3200 to 3500 at "calculation" speed, and up to 50,000 at racing.

It is also possible to use the "specific speed" of the pump and turbine as a basis of comparison. For torque converters, the specific speed n_s will preferably be expressed by the following formula

$$n_s = 3.65 \frac{n\sqrt{Q}}{h^{3/4}}$$

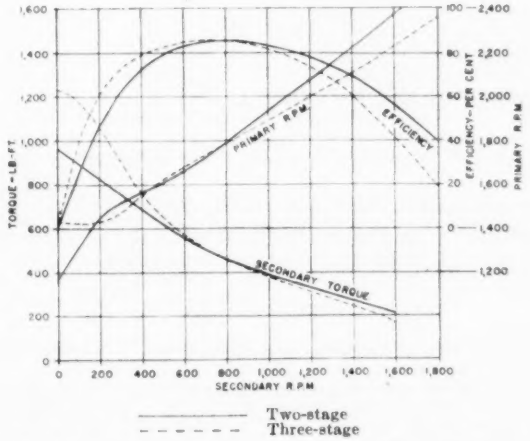


FIG. 12 COMPARISON OF TWO- AND THREE-STAGE TURBINES AT CONSTANT PRIMARY TORQUE OF 245 LB-FT

where n is the revolutions per minute of pump or turbine, Q is the quantity in cubic meters per second, and h is the total head in meters produced by the pump.

The average value of n_s for the pump in the present converters varies between 190 to 210, and for the turbine between 150 to 165 at "calculation" speed.

With a given diameter of converter, the number of stages can be reduced from three to two, but it is not easy to alter the diameter of the stages materially without altering the converter diameter.

Some of the results of changing from a three-stage to a two-stage converter in the same casing are shown in Fig. 12. From Fig. 12, it will be seen that the efficiency curve of the two-stage converter at constant torque is lower for the first 800 rpm of the secondary and, above this speed, is higher. There is also a considerable alteration in the stall ratio, that of the two-stage converter being constant at 4 to 1, and the three-stage varying from 4.5 to 1 to 5 to 1. These figures refer only to the two particular converters compared in the test. Higher stall ratios are available with different blade combinations. The effect of this on the secondary torque curve and engine speed at the commencement of converter operation is very marked. Both converters have the same maximum efficiency of 85 per cent.

DESIGN OF TORQUE CONVERTER

In the design of an efficient and mechanically satisfactory torque converter, the following considerations are important:

1 It is necessary to prevent the short-circuiting of the fluid between the revolving parts and the casing. This is done by a number of labyrinth seals as shown in Fig. 13.

2 Seals must be provided to prevent loss of fluid. These seals are normally of the axial-sealing type generally using a steel ring against a carbon ring for sealing the surfaces having difference in rotational speed. One of these rings has axial movement by means of a copper bellows or a synthetic-rubber diaphragm.

3 Evacuation of gas from the converter must be provided for. New fluid under certain conditions of circulation and temperature is liable to gasify to a slight degree. To insure the removal of this gas, it is drawn through a small pipe from the top of the converter.

4 It is very necessary, in order to prevent cavitation, that the converter be kept full of fluid under pressure. The automatic replacement of fresh fluid is insured by an injector or mechanically driven pump which draws it from a reserve tank as required and feeds it under pressure to the converter.

5 To provide for a temperature rise in the working fluid which may result from prolonged use of the converter, a small cooler is placed in the fluid circulation. This cooler circuit also includes a filter.

Converter Blading. The major component parts of a modern converter are shown in Fig. 13.

Direct-Drive Type. This type was first developed in Sweden by the Ljungstrom Company and in England by Leyland Motors. By using a double-acting clutch, converter drive or direct drive may be obtained at will. In the latter case the pump impeller is cut out by the clutch and the turbine by means of a free wheel and thus all hydraulic losses are eliminated.

A later variety of this type, fitted with an angle drive, is shown in Fig. 14. This unit was built by the Spicer Company for General Motors Truck & Coach Company's buses. The direct-drive type is also very suitable for rail cars and rail-car trains.

The horsepower of the direct-drive converter varies generally between 100 and 300 hp. Many thousands of buses and several hundreds of rail cars equipped with this converter type are in service in Europe, Africa, Australia, and the Americas.



FIG. 13 MAJOR COMPONENT PARTS OF MODERN CONVERTER

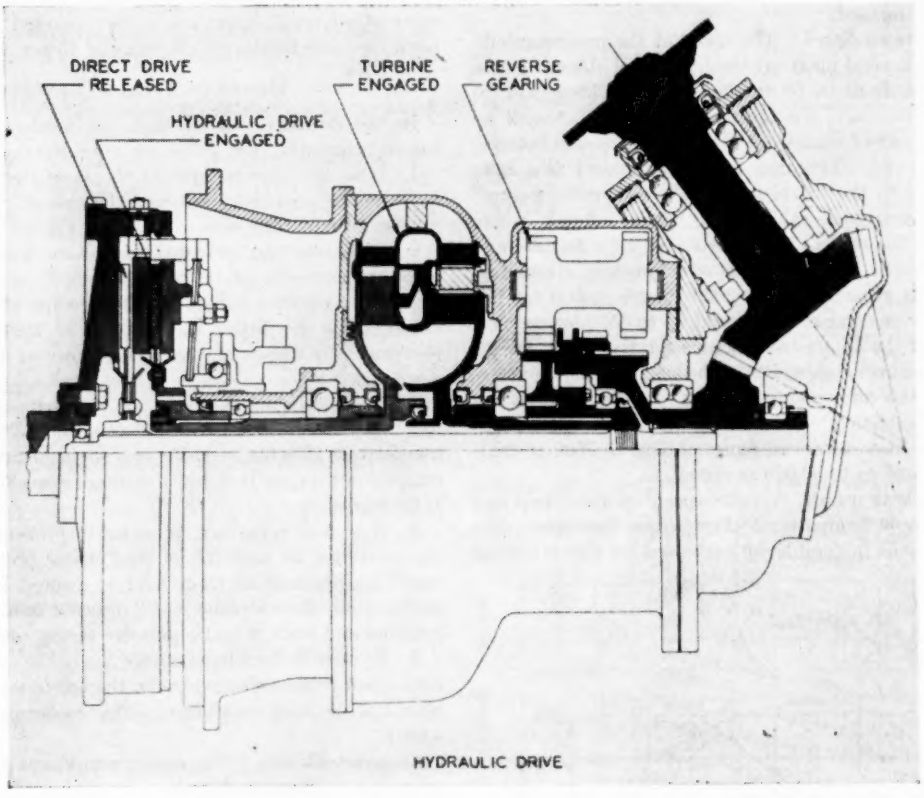


FIG. 14 DIRECT-DRIVE TYPE OF HYDRAULIC TRANSMISSION, FITTED WITH ANGLE GEARING FOR BUS OPERATION

Fixed-Blade Type. This type has been used extensively by the Twin Disc Clutch Company for tractors, for oil-drilling rigs, for logging, for locomotives, and for construction and locomotive cranes. The horsepower generally ranges between 100 and 300 hp.

Adjustable-Blade Type. Fig. 15 shows an installation of a twin-disk adjustable-blade converter for oil-field application.

The largest converter of this type so far has been built for a 1200-hp Diesel-driven locomotive for the Bergen-Oslo Railway in Norway.

New Developments. It is regrettable that, owing to war restrictions, the latest available test data and improvements cannot be included in this paper. It may be said, however, that it seems possible to raise the maximum efficiency as well as widen the range of high efficiency operation considerably.

BIBLIOGRAPHY

1 "En ny automatisk, hydraulisk växel," *Teknisk Tidskrift*, supplement, *Mekanik*, vol. 59, March 16, 1929, pp. 32–38.

2 "Possibilities of Oil Hydraulic Locomotives," by A. Lysholm World Power Conference, Stockholm, Sweden, vol. 6, 1933, paper 126, pp. 411–416.

3 "Use of a Hydraulic Torque Converter for Buses and Railcars," by A. André and G. Göransson, World Power Conference, Stockholm, Sweden, vol. 6, 1933, paper 123, pp. 668–678.

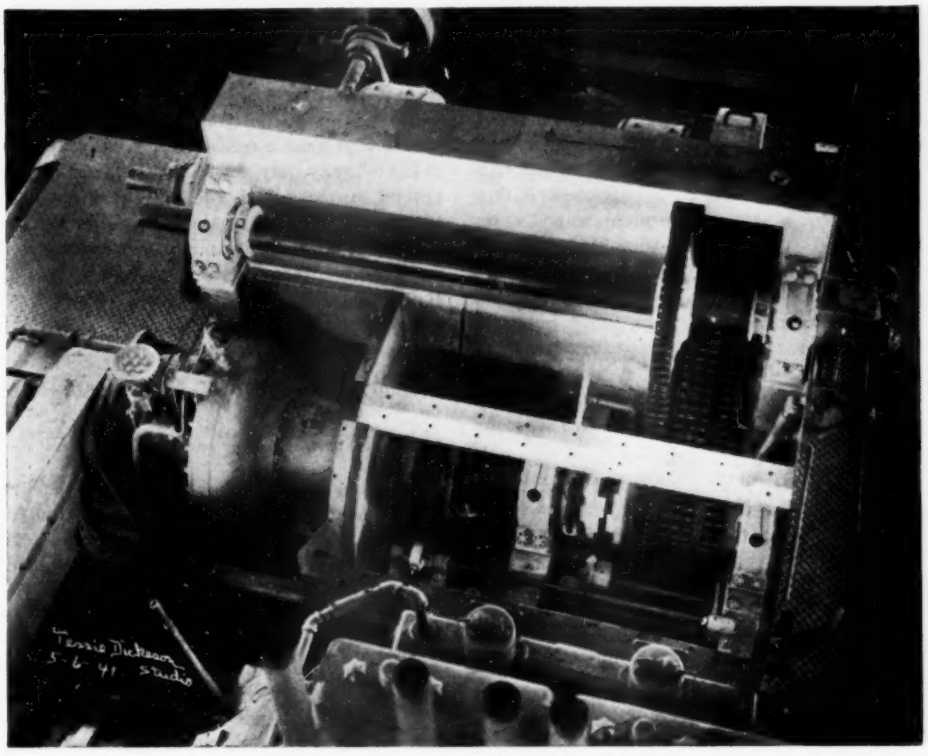


FIG. 15 SHOWS INSTALLATION OF TWIN-DISK ADJUSTABLE-BLADE CONVERTER FOR OIL-FIELD APPLICATION

4 "An Analysis of the Lysholm-Smith Hydraulic Torque Converter," by J. C. Marble, *S.A.E. Journal*, vol. 34, 1934, pp. 182–188.

5 "The Leyland Torque Converter," *Modern Transport*, May 19, 1934.

6 "An Accelerated Service in Northern Ireland," *Oil Engine*, vol. 2, 1934–1935, pp. 80–82.

7 "Torque Converter Buses on Hilly City Services," *Leyland Journal*, November, 1935.

8 "Torque Converter Buses in Service," *Modern Transport*, January 25, 1936.

9 "This Municipality Has Scrapped Its Trolley Buses," *Leyland Journal*, May, 1938.

10 "Main Line Diesel Hydraulic Railcars for New Zealand," *Railway Gazette*, vol. 69, 1938, pp. 424–429.

11 "Triple-Car Diesel Train for the L.M.S.R.," *Railway Gazette*, vol. 68, 1938, pp. 770–779.

12 "Yellow's New Hydraulic Drive," by G. A. Green, *Bus Transportation*, vol. 17, 1938, pp. 448A-448D.

13 "Hydraulic Transmission for Yellow Coach," *Automotive Industries*, vol. 79, 1938, pp. 438–440.

14 "Torque Converter Tractor Yarding Units," *West Coast Lumberman*, June, 1941.

15 "Hydraulic Torque Converter and Its Application to Logging, *West Coast Lumberman*, July, 1942.

16 "The Development of Power Drilling," *Drilling*, August, 1941

17 "Hydraulic Torque Converters, *The Iron Age*, vol. 145, May 16, 1940, pp. 44–46.

18 "Air Conditioned Railcars," *Railway Electrical Engineer*, vol. 31, 1940, pp. 176–179.

19 "Torque Converters in Logging Field," *The Timberman*, vol 41, May, 1940, pp. 48–50.

20 "What Is a Torque Converter?" by R. W. Wadman, *Diesel Progress*, vol. 5, November, 1939, pp. 20–33.

Discussion

R. EKSERGIAN.[2] The desirable characteristic of any torque converter is a high-efficiency curve through a long speed range. The early Föttinger transformer, when modified to a variable-speed torque converter, had roughly a parabolic efficiency curve, with a decreasing linear output torque against increase of secondary speed. Through his excellent researches, using multistages on the turbine end together with blunt blade sections, the author has greatly improved the efficiency over the entire speed ranges, resulting in a more nearly hyperbolic secondary torque.

It is known in turbine theory that the multistage reaction turbine tends toward increased flow rates at reduced speeds, resulting in increased torque amplification over that of the impulse type with only a single or a few stages. The decreased pressure drop per stage on the turbine end, for a given total head, also results in reduced losses due to the decreased velocities, so that multireaction stages tend toward improved efficiency.

The torque-speed characteristic of a turbine with constant flow rate is approximately linear, decreasing with speed. This implies a parabolic output curve against speed. With improved efficiency, particularly in the speed ranges either above or below the optimum speed at maximum efficiency, the flow rate itself increases, resulting in increased starting torque and an improved efficiency throughout the entire speed range. The effective head is the difference between the impeller head, corresponding to the mechanical input, and the counter head of the turbine, corresponding to the output power. The effective head is balanced by the friction head, corresponding to the shock and friction losses in the circuit. As the secondary speed either decreases below or increases above the rated speed, the turbine-output counter head decreases much more rapidly than the impeller head since the latter operates at more nearly constant speed, and at constant input. At optimum speed, the losses at best are small, and then the impeller head more nearly balances the counter turbine head. At other than optimum speed, particularly at the more extreme over- and under-speeds, if the unbalance effective head is considerable, so that the friction head is small, the flow rate would in-

[2] Chief Consulting Engineer, Edward G. Budd Manufacturing Company, Philadelphia, Pa. Fellow, A.S.M.E.

crease rapidly. Actually, the shock losses increase very rapidly at both lower and overspeeds, thus increasing the friction head and checking the growth of circulation to a much smaller value.

Now the torque on the turbine at any given speed depends upon the change in angular momentum of the fluid per unit time at the several reaction stages and thus directly on the flow rate. Increasing the flow rate therefore increases the torque and output at any given speed. On the other hand, the increase of flow rate results in an increase in torque on the pump impeller, increasing roughly as a quadratic function of the flow rate. But the impeller torque also increases linearly with the speed. For this reason, to maintain constant engine torque and to permit increased flow rate in the starting zone requires a lower pump or engine speed, that is, the primary speed must increase with secondary speed at constant primary torque, as shown in the author's Fig. 8. In some cases it appears that it is not always possible to absorb the full engine output at all turbine-shaft speeds.

In a previous paper, the writer established a compatibility equation $F(Q, \omega_p, \omega_s) = 0$, where Q is the flow rate, ω_p and ω_s are the primary and secondary speeds. This equation was established by expressing the primary torque as a function of the flow rate and primary speed, and the secondary torque as a function of the flow rate and both secondary and primary speeds. On combining with the energy equation of the entire circulating flow and expressing the losses in terms of the flow rate and speeds, the foregoing function was obtained.

Provided the losses can be estimated accurately through proper interpolation of test data, the characteristics of the performance of a torque converter can be arrived at for any given design. For this reason, the author's experimental studies, while interesting for over-all characteristics, would further prove very valuable if the data could be presented in a more detailed form for estimating component losses.

For instance, it would be desirable to express such losses between blade groups in terms of blade angles and relative speeds with different flow rates. It would also be helpful in the present paper to give actual dimensional data of the various proportions of the torque converter in connection with the curves presented.

G. F. Wislicenus.[3] It is a recognized fact that, while there have been various modifications of the original form of the Föttinger transformer, the Lysholm-Smith torque converter represents a significant advance in this field. In view of this situation, the present paper constitutes a valuable contribution to the technical literature on the subject of hydrodynamic transmissions and, as such, might have been presented more fully. It is to be regretted that the paper was not worked out in sufficient detail to offer the reader an adequate introduction into the theory and fundamental characteristics of this type of machinery. There seem to be some omissions in the text which make it difficult to follow the derivations. In order to substantiate this statement, the writer will point out but a few items which he considers to be either incompletely or incorrectly presented.

The difficulties of determining the losses in various parts of hydrodynamic machines are generally recognized. For this reason, it would be most instructive if the method whose results are given in Table 1 could be explained in some detail. It also seems desirable to explain more fully what is meant by "carry-over losses" between the various parts of the machine.

With reference to the following derivations, it is hoped that the author can supplement the paper by a list of notations without which these equations cannot be understood properly. While Equation [1], for instance, is easy to understand with respect to stationary-vane systems, the same equation does not appear to be correct with respect to the moving-vane systems which are in the present case responsible for the greatest part of the head drop through the secondary part of the machine. If, for instance, c and w are interpreted as designating the "relative" velocity, it is seen that what is called the "useful pressure drop" in Equation [1] is actually only the change in "static" pressure in the vane system, always adhering to the author's assumption that this system is considered as one with axial-through-flow direction. The total useful pressure drop in such a vane system, however, differs appreciably from the static pressure drop. In instances under the assumption of a relative entrance angle of 90 deg, measured against the peripheral direction of the system and zero absolute rotation of the fluid at the discharge side, the static head drop without losses is $\frac{u^2}{2g}$ which corresponds to Equation [1], while the total head drop is $\frac{u^2}{g}$, as could be calculated for instance from the equation for H_t, given below Fig. 2 of the paper. It is seen that in this case the total head drop differs from the static head drop by a factor of 2, so that Equation [1] can in general not be used for the total head change in the systems considered. The subsequent derivations, however, seem to indicate that c and w are absolute velocities. Also under the latter assumption, Equation [1] cannot be used for moving-vane systems. For the example just given, the actual head drop through the system would again be twice as great as that given by Equation [1].

Equation [2] for the friction head does not appear justified without further explanations. This equation gives one the impression that the friction losses are calculated as the sum of two friction losses, one being proportional to the velocity head at the entrance and the other to the velocity head at the discharge of the system. If this is true, it is not easy to understand why the same friction factor is applied in both cases. Furthermore, the friction factor must certainly be expected to change over wide limits as the flow conditions vary as a function of the secondary speed, so that the corresponding variations in the total pressure drop cannot even be approximated under the assumption that f is a constant.

From a theoretical point of view, the result that the rate of flow through the transformer reaches a minimum at the point of best efficiency appears to this writer highly improbable, chiefly because of the variations of the primary torque at constant primary speed, as described by the test results given. At constant primary speed, the primary torque appears to fall off as the secondary speed is increased. This fact, in connection with a primary or pump runner of the type used, seems to indicate a reduction in pump capacity. Even if the primary speed is then increased to obtain constant power input (as assumed by the author), the capacity cannot regain its original value, because the primary runner operates at another point of its head-capacity curve than that of best efficiency. In view of this apparent contradiction, it would be highly desirable if the author would give additional information on the method used in determining the rate of flow through the converter by Pitot tube. These test results, if substantiated, would seem to be of far-reaching significance with respect to the theory of this type of machinery.

As indicated in the beginning, the writer believes that most of the foregoing difficulties could be cleared up if the author would have the opportunity to explain his theoretical approach more fully than was apparently possible in this paper. In view of the great interest which exists throughout the industry in this kind of machinery, it is believed that a fuller presentation of the theory would be fully justified.

[Because of wartime conditions, we have been unable to obtain a closure from the author, Mr. Lysholm.—Editor.]

[3] Research Engineer, Worthington Pump & Machinery Corp., Harrison, N. J. Mem. A.S.M.E.

Gas Turbines and Turbosuperchargers

By SANFORD A. MOSS,[1] PH.D., LL.D., WEST LYNN, MASS.

Since his university days, the author has been associated with many of the developments relating to the gas turbine and particularly to the perfection of the airplane-engine turbosupercharger. It is from this intimate and interested viewpoint that he outlines the history of the gas turbine and its potential use as a prime mover. A comprehensive Bibliography of the art of gas-turbine design has been included in the paper to support the author's purpose of outlining the evolution of each component of the modern gas turbine from its earliest inception. United States and foreign gas-turbine research projects are referred to, and then details of advancements in such items as nozzles, compressors, and the like, are discussed. While the gas turbine as a prime mover has not been applied except in isolated cases, such as the Neuchâtel, Switzerland, 4000-kw emergency gas-turbine plant and the Swiss Federal Railway gas-turbine locomotive, partial gas-turbine cycles are in somewhat extensive commercial operation. Examples of these are the Diesel exhaust-gas turbine, the Diesel boiler cycle, the divided-manifold cycle, all of which are mentioned in some detail. The final part of the paper is devoted to consideration of the extremely vital development of the constant-pressure aviation turbosupercharger, which has been brought to its highest state of development by the author's company, in which work the author has taken a leading role, from its inception in the last war down to its present state of extensive application.

PRODUCTION of power by direct action of products of combustion on a turbine wheel has been an engineering dream for a century and a half. A number of approaches to the complete scheme now are in successful commercial operation, and it seems possible that these are paving the way for the long-sought accomplishment of the primary plan of the gas turbine as an efficient prime mover. So it would now seem opportune to give some history and reminiscence (without any thermodynamics), list the partial accomplishments now in commercial use, and speculate on the future. The author can do this from personal association with many of the items ever since he became, in 1895, one of the many who have had dreams in the matter.

This association with gas-turbine developments has occurred during an engineering career which began in San Francisco in 1889, with a machinist apprenticeship, following with work as draftsman, in the shop of Mr. Edward A. Rix (an early master in compressed-air engineering); and continuing as a draftsman in various gas-engine shops. This was before the days of electric transmission and there were several plans of compressed-air power and transmission in successful operation. One was use by Mr. Rix of the early impulse water wheel of Pelton to drive an air compressor, with a transmission pipe line some miles long, and then a reciprocating hoisting engine using the transmitted air after it had been reheated by coal or coke so as to increase its volume (1).[2] So this really was a combustion heat-engine cycle. Its thermodynamics, which is that of the "Brayton constant-pressure cycle," is an early item of the present subject. Mr. Rix and his associates also had a street railway in New York City operating on compressed air stored in steel cylinders. But the author remembers how these and similar schemes soon were replaced by the early electric transmissions.

Gas-Turbine Proposals

Beginning about 1889 both the steam turbine and the internal-combustion reciprocating engine began the competition which finally resulted in the elimination of the reciprocating steam engine as a prime mover, except for the steam locomotive, and some ship installations.

Ever since the beginning of this period it keeps occurring independently to students of thermodynamics that the steam turbine and internal-combustion engine might be combined, and so they "invent" the gas turbine. The usual form of this, shown in Fig. 1, has a chamber into which is forced compressed air and fuel, usually oil, so as to give combustion under pressure. The products pass through a nozzle so as to drive a turbine wheel, part of whose power drives the combustion-chamber compressor, and the remainder (if any) is the net power derived from the fuel burned.

The author was one of the many of these "inventors," while a student in the classes in thermodynamics and hydrodynamics of Prof. Frederick G. Hesse at the University of California in 1895. Since then, the author's engineering career, now drawing to a close, always has been directed toward the gas turbine. He also has tried to keep posted on the numerous advances in other fields which could help the gas turbine, as well as on the many gas-turbine publications, some of which are given in the references.

Like most of the other inventors, the author at first thought he was alone in the gas-turbine field. In 1900 an account was written as a Master's thesis (2) and filed in the University of California Library, which gives early proposals of some details.

Associated with Mr. Rix and the compressed-air street railway in New York City was a Chicago firm, "The Vimotum Company," engaged in promoting operation of railway cars by internal combustion. The author participated during 1898-1899 in the actual operation on the "Big 4" railway tracks between Columbus, Ind., and Indianapolis, Ind., and later on the Pennsylvania Railroad tracks between Chester and Darby, Pa., of full-sized railway passenger cars, self-propelled by gasoline engines, using the "variable-speed transmission" of the Reeves Pulley Company of Columbus, Ind. This probably was the predecessor of all modern internal-combustion locomotives. Plans were formulated in 1898 for replacing the gasoline engine by a gas turbine as was set forth in the Master's thesis (2) cited. This is the earliest proposal that the author knows of for a gas-turbine

[1] Consulting Engineer, Supercharger Engineering Division, General Electric Company. Fellow A.S.M.E.

Contributed by the Aviation Division and presented at the Annual Meeting, New York, N. Y., Nov. 29–Dec. 3, 1943, of The American Society of Mechanical Engineers.

Note: Statements and opinions advanced in papers are to be understood as individual expressions of their authors and not those of the Society.

[2] Numbers in parentheses are references contained in the Bibliography at the end of the paper. An attempt is made in the figures herein and the references to give the first published proposal of each item. Of course, this cannot be done with certainty, but at any rate the figures and references give early if not the original proposals. The author would appreciate references to earlier proposals of any items.

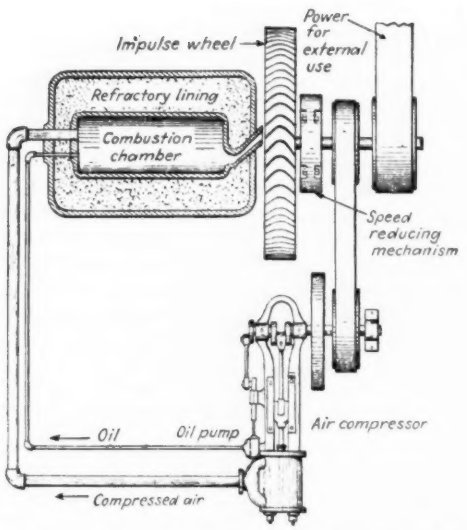


FIG. 1 DIAGRAMMATIC PLAN OF FUNDAMENTAL GAS TURBINE
Reproduced from the Doctor's Thesis, Ref. 9, of 1903. This diagram does not include "Heat Interchanger," of the Theses, Refs. 2, 9.)

locomotive. But the proposition never came to a head, which was just as well, because then it never could have been made operative.

During the planning for this proposed gas-turbine locomotive, patent searches were made, and unexpectedly there was found a British patent of November 30, 1791, to John Barber (3), giving probably for the first time the fundamental gas-turbine plan. There was a combustion chamber into which fuel and air were introduced, with a nozzle from which the products of combustion issued onto a turbine wheel. This supplied power to drive the compressor, as well as external power.

An early diagram of Barber's cycle is given in Fig. 1, from the Thesis (9). Many gas turbines proposed since differ in plan only by the addition of a heat interchanger for transferring the heat of the exhaust gases to the compressed air proceeding to the combustion chamber. An early mention of this is in the Doctor's Thesis (9) and an experimental model of 1905 is shown in Fig. 4. It is not probable that the apparatus shown in Barber's British patent ever was operated.

Davey (8) lists some partial approaches to the gas turbine and gives a list of British patents beginning in 1856. The earliest complete United States gas-turbine patent of which the author has personal knowledge is to Charles G. Curtis, June 24, 1895 (4). Mr. Curtis had extensive connections with regard to steam turbines, with the General Electric Company. The author has some knowledge of these, but none of any actual work on gas turbines by Mr. Curtis.

At this same time was a United States Patent to Læon LePontois (5) filed December 5, 1895, on an explosion combustion chamber for a gas turbine. This was the subject of a Doctor's Thesis at Cornell University by Walter O. Amsler in 1897 (6). Actual tests were made of LePontois' explosion apparatus, as well as a theoretical study, with unfavorable conclusions.

UNITED STATES GAS-TURBINE RESEARCH

The author always has had in mind continuous combustion, and after the gas-turbine-locomotive scheme, proposed in 1898, came to naught, he started gas-turbine research in 1901 in the Sibley College Laboratory, Cornell University. Laboratory time for a year was required to get a continuous-combustion chamber in stable operation. It frequently went out and then the oil on the red-hot firebrick lining filled the neighborhood with dense black smoke, so the Sibley College people well knew of the gas-turbine research.

The first De Laval steam turbine in the United States, Fig. 2, which had been exhibited at the World's Fair in Chicago in 1893, was used for the De Laval nozzle-patent demonstration mentioned

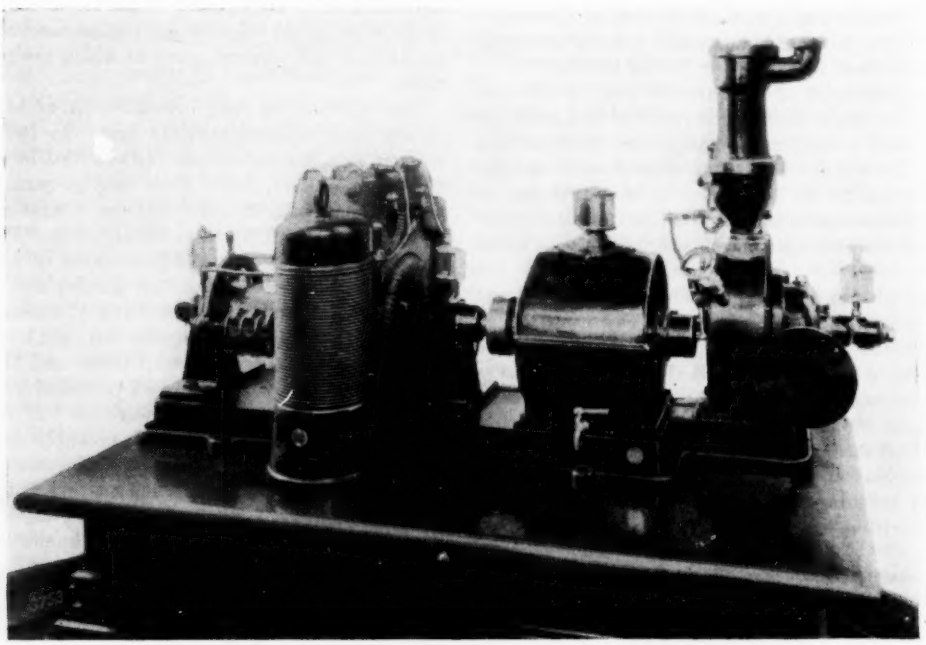


FIG. 2 FIRST DE LAVAL STEAM TURBINE IN THE UNITED STATES, 1893
(Exhibited in the Chicago World's Fair and then sent to Sibley College, Cornell University. The wheel of this turbine was used in 1902 in the gas-turbine research of the Doctor's Thesis, Ref. 9, and was the first turbine operated on products of combustion in the United States and possibly the first anywhere. Reproduced from De Laval pamphlet of Ref. 10.)



FIG. 3 COMBUSTION CHAMBER OF GENERAL ELECTRIC GAS-TURBINE RESEARCH, 1903

(This was made spherical to give minimum radiating surface. This research started in Schenectady in 1903 and was transferred to Factory K, General Electric Company, West Lynn Works, in 1904.)

later (10), and then went to Cornell. So the bucket wheel of this turbine was borrowed and operated with the combustion chamber, about the end of 1902. This probably was the first turbine wheel actually operated by products of combustion in the United States, and possibly was the first such turbine wheel ever operated. The entire power was absorbed by a prony brake, and the air for compression was furnished by a steam compressor, with computation of the power required.

But, as with many other experimental gas turbines, the power for compression was more than the turbine power. So except for the historical fact that the combustion chamber actually operated the turbine wheel, the experiment was a flat failure. A Doctor's Thesis (9) was prepared and presented to Charles P. Steinmetz and Ernest J. Berg of the General Electric Company. The author previously had been a draftsman on steam-turbine work with General Electric. In June, 1903, the connection was resumed and has continued ever since, with work on various items more or less connected with gas turbines.

A number of General Electric models of gas turbines successively were gotten into operation, first at Schenectady, and beginning in 1904 at Lynn, with consultation with Prof. Elihu Thomson and Richard H. Rice. There were combustion chamber, heat interchanger, nozzle, and single-stage impulse turbine wheel; but with power for compression from an independent air compressor and allowed for by computations. Some U. S. patents were obtained during this research (9½). Figs. 3, 4, and 5, respectively, show the combustion chamber, heat interchanger, and nozzle jet of 1903 and 1905. The results of this research will be given later in the paper. The patent drawings (9½) show fairly well the actual apparatus that was used.

FOREIGN GAS-TURBINE RESEARCH

A gas-turbine patent was applied for by Charles Lemale (8) about 1901 and he began association with Réné Armengaud in 1903 in actual operation in France of a continuous-combustion gas turbine (8, 21). This probably was the earliest elaborate gas-turbine experimental work. From then on, there have been many proposals and tests of various sorts of gas turbines.

Numerous publications have been made, a few of which are given herewith, i.e., references, (4, 5, 6, 7, 8, 12, 13, 21, 22, 23, 24, 25, 26, 27). Others are in the Engineering Index Annual and in references (7, 8). Some of these operate with a hydraulic column; operate below atmospheric pressure; have cooling by water injection; have hollow turbine buckets with cooling; have cooling by air excess; use pulverized coal; use reheating combustion; or have cooled compressors. But most of these have not led to any conclusive results. The cycle now receiving the most attention is that of Fig. 1 with the addition of the heat interchanger of the previously mentioned theses (2, 9).

NOZZLES FOR STEAM AND GAS TURBINES

Beginning about 1885 there were many arguments concerning the power that could be obtained by expansion in a nozzle of a jet

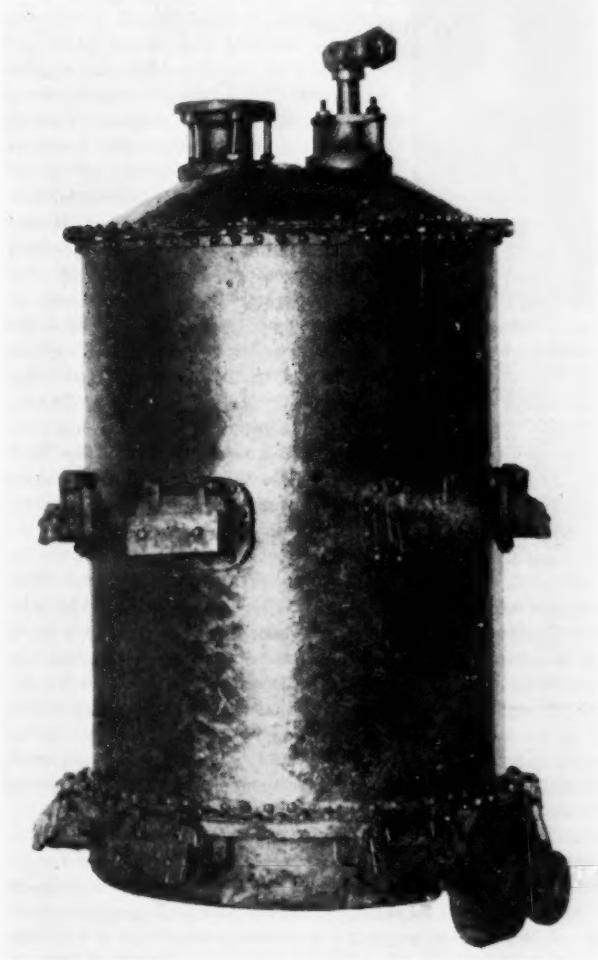


FIG. 4 HEAT INTERCHANGER OF GENERAL ELECTRIC GAS-TURBINE RESEARCH, 1905

(The air from the compressor passed through some tubular coils on its way to the combustion chamber. The turbine exhaust gases circulated outside of these coils.)

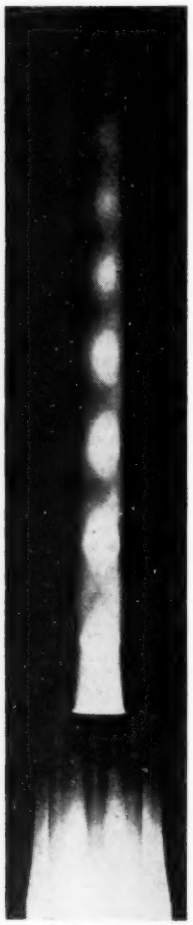


FIG. 5 NOZZLE JET OF GENERAL ELECTRIC GAS-TURBINE RESEARCH, 1905

(Curious white-hot nodes appeared in this jet of products of combustion, being of one type when the mouth of the convergent-divergent nozzle was too small for the pressure ratio; of another type when it was too large, and vanishing between when it was about the right size. Similar nodes later have been observed with steam nozzles.)

directed on a turbine wheel. Napier had shown experimentally that when steam was discharged from an opening in a vessel into a region of lower pressure, the flow increased as the pressure in the outer region decreased, until the outer pressure became about one half of the pressure in the vessel. For lower values of the outer pressure there was no increase in flow. Therefore, it was argued that full theoretical velocity of a steam-nozzle jet could not be obtained when the pressure ratio was less than 0.5. It seemed reasonable to assume that the theoretical power from a steam-turbine wheel was the same as from a reciprocating steam engine, for pressure ratios between 1.0 and 0.5. But Napier's law meant that for pressure ratios less than 0.5, a steam turbine would not theoretically give the same power as a steam engine.

Carl Gustaf Patrick De Laval was building single-stage steam turbines in Sweden with steam pressures of 115 psia or so, exhausting into atmospheric pressure of about 15 psi. He said he was avoiding the disability of Napier's law by using a nozzle first convergent and then divergent, popularly called an "expanding nozzle" because of the final divergent portion. De Laval tried to get a United States patent on this shape, and the official file shows that Napier's law was cited against him, with the support of scientific experts, including Gustave Zeuner, the famous German engineer. Finally, De Laval with his 1893 Chicago World's Fair turbine of Fig. 2 gave an actual demonstration that he was right (10).

The theoretical reasons for a nozzle first convergent and then divergent already had been given by Osborne Reynolds (11), with the first diagram of such a nozzle, reproduced as Fig. 6. But this was buried in a philosophical magazine and does not seem to have been appreciated by engineers. At a much later date it began to be understood that the theoretical available energy for a steam turbine with proper nozzles is the same as for the corresponding reciprocating engine. But there was a period within the memory of the author when engineering ignorance in this matter held back steam-turbine development.

Next it was argued (12, 13) that, while proper power could be developed by use of a steam nozzle, it was because of proximity of the fluid to condensation. But, so it was said, circumstances differed with gases far removed from condensation, such as products of combustion, so that a gas-turbine nozzle never could be efficient. Experimental measurements were published (12) of temperatures measured along a nozzle producing a jet of a nearly perfect gas, showing that the temperature did not fall with lowering of pressure as was predicted by the formulas for isentropic expansion. It was pointed out that with an expanding gas, mechanical energy only could be developed by conversion of internal energy, as manifested by temperature drop. Thus it was argued that proper conversion of pressure drop into velocity could not be accomplished by a gas-turbine nozzle.

To give further support to this contention, a test was published (13) in which a De Laval single-stage turbine was operated at full speed with compressed air. To avoid complication, no power was abstracted from the turbine shaft. There was measurement of temperature in the pipe preceding the nozzle, and in the exhaust pipe. The pressures in the inlet pipe varied in different tests from about 12 to 123 psi, with atmospheric pressure in the exhaust pipe. But in spite of these pressure drops, which corresponded to appreciable drops of isentropic temperature, the temperatures in the exhaust pipe always were nearly the same as in the inlet pipe. Since compressed air within the pressure limits used is nearly a perfect gas, the equality of temperature showed that in spite of passage through the nozzle no internal energy had been abstracted corresponding to an isentropic drop of temperature. Thus a nearly perfect gas such as air or products of combustion would not liberate its energy by isentropic drop in a turbine nozzle, and so a gas-turbine could not be efficient.

This experiment was published in all seriousness as a demonstration of the point made. But if a student of engineering has not by now detected the fallacy, he has fallen into a trap which often before has been set by the author for the unwary thermodynamist. As was mentioned with planned casualness, no energy was abstracted from the turbine shaft, so that all of the kinetic energy of the jet, which no doubt was nearly the theoretical isentropic value, was converted into heat by turbine-bucket and rotation-loss friction. With the nearly perfect gas used, this restored the original temperature, as could be expected.

The temperature-measurement experiment (12) was equally fallacious. The jet flowing along the nozzle no doubt had the full isentropic velocity and low temperature at each point corresponding to the pressure drop. But the temperature-measureing apparatus destroyed this velocity, converting it into heat, and so, with a perfect gas, restoring the initial temperature.

The theory of this, possibly for the first time, was published in

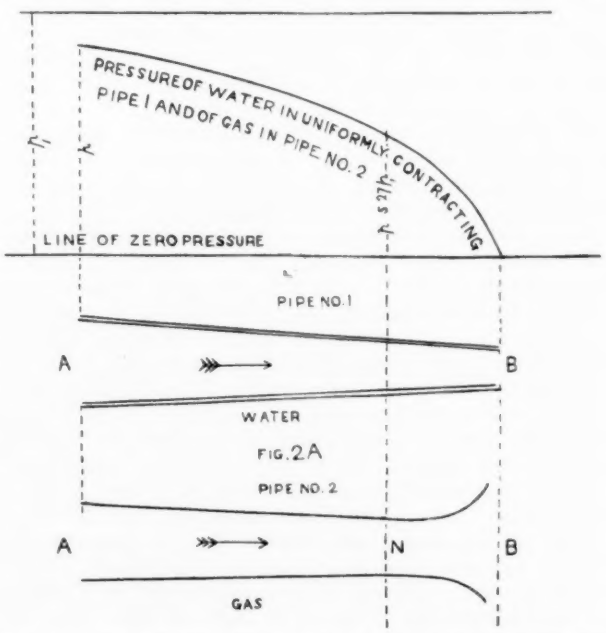


FIG. 6 FIRST PROPOSAL FOR A NOZZLE FOR ELASTIC FLUID TURBINES, WHICH WAS FIRST CONVERGENT AND THEN DIVERGENT (Reproduction of Fig. 2A of the 1885 paper of Osborne Reynolds, Ref. 11.)

1916 (14). This paper describes an experiment made by the author about 1905. Steam, initially slightly wet, and at an appreciable pressure, was discharged into the atmosphere through a properly shaped nozzle. As is well known, the initially wet steam became wetter as it expanded to atmospheric pressure, and so the jet leaving the nozzle had the "static" temperature of wet steam at atmospheric pressure, which is 212 F. But a thermometer inserted in the nozzle jet showed a much higher temperature, the result of conversion of some of the jet velocity into heat. Complete conversion would give a temperature called "impact temperature" in the 1916 reference (14), but now beginning to be called "total temperature." The situation nowadays is fairly well understood (14½), and it seems to be remembered that it was explained in the 1916 publication (14) of the 1905 experiment.

But although the fallacies of the two publications mentioned (12, 13) are very evident now, and cannot be cited against the ultimate success of the gas turbine, and were partially refuted at the time (12, 13), they were disturbing factors during the General Electric gas-turbine research and had to be argued against.

Compressors for Gas Turbines

A part of a gas-turbine plant is an air compressor to force air into the combustion chamber, which must be driven by part of the power from the turbine wheel. In the fall of 1903, the General Electric gas-turbine research began to include development of a "centrifugal compressor," with rotative speed suitable for direct connection to the gas-turbine wheel. High-speed wheels previously had been proposed for air compression (15, 16), with some sort of "reversed nozzle," since called a "diffuser," for converting into pressure the absolute velocity of air leaving the wheel periphery. Such diffusers had begun to be used for incompressible fluids. They probably first had been used in 1895 in a centrifugal pump of the famous English scientist Osborne Reynolds (17), which is shown in Fig. 7.

But De Laval's plan of a turbine nozzle, first convergent and then divergent, for a compressible fluid, now was firmly fixed. With this was the idea that a "reversed nozzle" for converting velocity into pressure with a compressible fluid such as air always should be the reverse of the De Laval expanding nozzle. Therefore the foregoing compressor references (15, 16) show such passages beyond the high-speed wheels, with the minimum section or throat of De Laval, and speak of "throat conversions of velocity into pressure." The famous French engineer August Rateau was working on high-speed centrifugal air compressors about this time (18), but the author never has been able to find out if he then used diffusers, and if so what his early ideas were about their shape. Rateau supplied centrifugal compressors for the Armengaud-Lamale gas-turbine work (7, 8, 18, 21).

In a patent applied for in 1904 (19), it was set forth correctly, probably for the first time, that with velocities below the velocity of sound, in the case of a diffuser for a compressible fluid, the velocity changes are the major items, so that passage areas change inversely as velocities, just as with an incompressible fluid. But with velocities greater than the velocity of sound, the change of volume with a compressible fluid, due to change of pressure, is the major item, so that increase of velocity in a nozzle requires increase of area, and decrease of velocity in a diffuser requires decrease of area. So with a centrifugal air compressor with impeller exit velocity less than the velocity of sound, the diffuser must be divergent, just as with a centrifugal pump. But for velocities greater than the velocity of sound, the theoretical diffuser first is convergent, has a throat, and then is divergent. All of this now is elementary knowledge, but in 1904 it was not evident.

The velocities of the General Electric centrifugal compressor for the proposed gas turbine always were such as to require theoretically a divergent diffuser, and development work on this basis was begun in 1904 under the supervision of Richard H. Rice, with the collaboration of the author and other General Electric engineers. When the primary gas-turbine research ceased in 1907, the centrifugal compressor had developed so that it became a commercial product of itself. One early result was the use of centrifugal compressors for blast furnaces for production of pig iron (20). This met early opposition from advocates of reciprocating "blowing tubs," and it was alleged that a centrifugal compressor, operated by a flow-metering device to deliver a constant weight flow of air, nevertheless was subject to a process called "churning" whereby the impellers would rotate without delivering any air, in spite of the indication of the flow meters. This was shown to be a fallacy. Also it was shown (20) that even though internal-combustion engines operated by blast-furnace gas might have somewhat better thermal efficiency, the small fixed and maintenance charges of the centrifugal compressor gave lower total cost of blast-furnace operation.

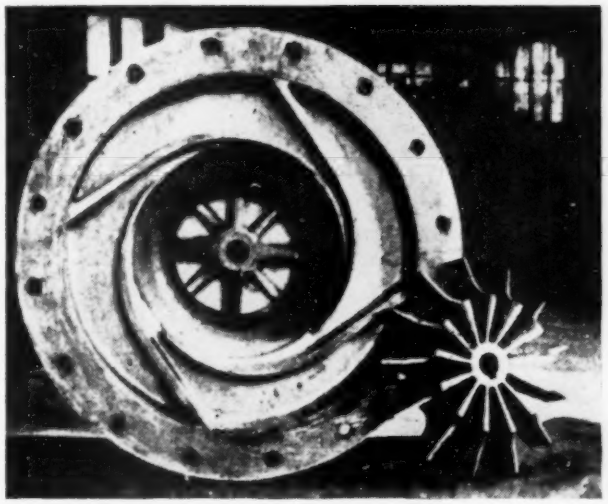


Fig. 7 First (or Very Early) Fluid Pump With Impeller Having Axial-Flow Inlet and Radial Vanes at Exit, and Diffuser for Converting Into Pressure the Impeller Exit Absolute Velocity

(Mather-Reynolds pump of 1895 from Ref. 17, p. 112.)

Rateau did some early centrifugal-compressor work already mentioned, a great deal of it for gas turbines (7, 8, 18, 21). Some work probably also was done elsewhere in Europe. The Ingersoll-Rand Company has continued the development in the United States. As one result, centrifugal compressors, started in the United States as a gas-turbine by-product, now are almost exclusively used throughout the world for blast-furnace blowing, as well as for many other purposes.

As another part of the General Electric development, geared centrifugal superchargers for United States aviation engines began about 1925 and now are in enormous production (28), using impellers based on the original Osborne Reynolds design (17), Fig. 7. But in spite of the fact that some of this centrifugal-compressor development was inspired by the gas turbine, there is present evidence that the centrifugal compressor may be exceeded in efficiency by a comparatively recent competitor, the "axial-flow blower." If so, this blower will be the one used in the ultimate gas turbine. These blowers are used in the Neuchatel gas-turbine power plant (34) and Swiss gas-turbine locomotive (35). But on the other hand they have a shorter operating range and many more stages than the centrifugal compressor, and progress is being made in improvement in effi-

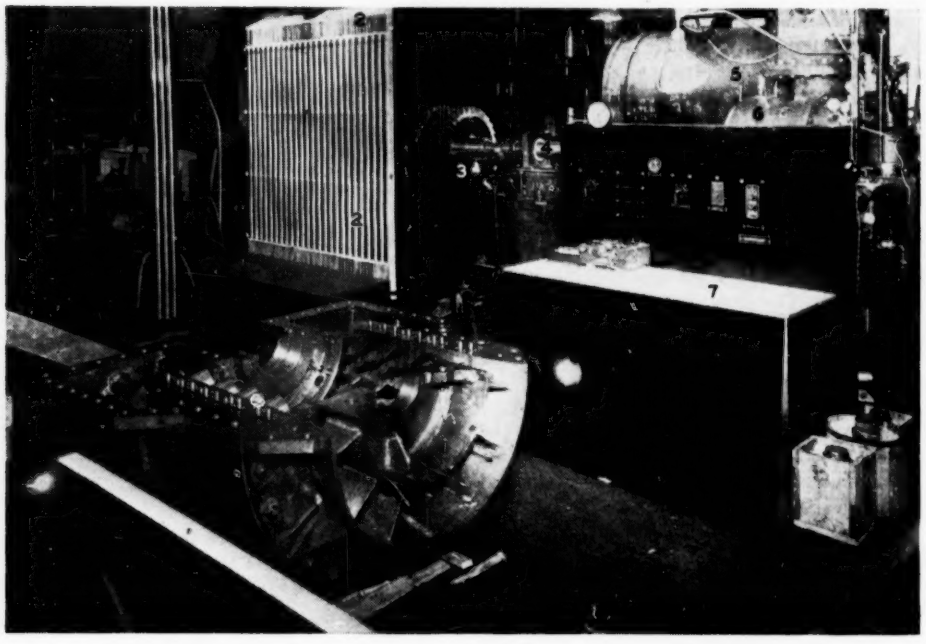


FIG. 8 GAS-TURBINE LABORATORY NOW IN OPERATION IN THE UNITED STATES

ciency of the latter. However, this is a matter for the future and cannot be settled here. At any rate, the gas turbine had its part in introducing centrifugal compressors for blast furnaces, many industrial purposes, and present geared and turbosuperchargers.

UNITED STATES GAS-TURBINE RESEARCH CONTINUED

The General Electric gas-turbine work, previously mentioned as beginning in June, 1903, continued until about 1907. At first the power for compression consumed all of the turbine power. Some approximate figures will show why. Suppose a gas-turbine wheel theoretically delivered 100 hp, and suppose the compressor theoretically required 49 hp. Then there would be theoretically 51 net hp. But the turbine wheel might have an efficiency of 70 per cent so that it actually would deliver 70 hp; and the compressor might have an efficiency of 70 per cent, so the net horsepower would come out $100 \times 0.70 - 49/0.70$. Before the reader is cruel enough to laugh at this result, let him put himself in the place of lots of us gas-turbine inventors who have sweated blood through years of research only to come out this way or worse. The reason is that with the 51 theoretical hp net, we have apparatus of 149 theoretical hp, with consequent losses, instead of the losses directly corresponding to 51 hp. A reciprocating internal-combustion engine deducts the power for compression from the gross power, before any power is delivered, and so the losses are based upon the net power output rather than upon the sum of powers of compression and expansion.

This paper purports to give items other than the vast number of gas-turbine thermodynamic computations which have been published by many persons, the author among them. But a simple approximate computation can be made which will show the other side of the foregoing picture of a gas turbine with a zero net power. This is on the basis that the products of combustion act as a perfect gas and have mass and properties of the same nature as those of the original air for combustion. Suppose the initial pressure for the compressor and the exhaust pressure of the turbine is 14.7 psia and suppose the final pressure of the compressor and the nozzle inlet pressure of the turbine is 49 psig or 63.7 psia. With such equality of initial and final pressures for turbine and compressor, the ratio of the theoretical power from the turbine to the theoretical power required for the compressor is equal to the ratio of the absolute temperature at nozzle inlet to the theoretical absolute temperature at the end of isentropic air compression.

A test of the Neuchatel gas turbine is cited later (34), and its figures should be before every gas-turbine student. The ratio of the theoretical powers in test No. 2 is 1.83 and the ratio of the absolute temperatures is 1.82 which shows the character of the approximation here being made. With 70 F inlet temperature the compressor isentropic final temperature is 802 F abs. Suppose the temperature at the turbine nozzle inlet is 1946 F. This is a high temperature, but within the bounds of possibility. The absolute temperature at the nozzle inlet then is 2406 F. The ratio of absolute temperatures, which is approximately the ratio of the theoretical powers, then is 3, that is, the theoretical power for the compressor is 33 per cent of the theoretical turbine power.

Using the efficiencies of the Neuchatel gas-turbine test (34), the compressor efficiency is about 85 per cent, so the actual power for the compressor is 0.33/0.85 or 39 per cent of the theoretical turbine power. With 88 per cent efficiency of the turbine, the actual power from the turbine is 88 per cent of the turbine theoretical power. That is to say, the net power is (0.88—0.39)/0.88 or 55 per cent of the turbine actual power. This figure is far beyond the 1907 possibility and is on the basis of all of the progress since that date, and then some. The Neuchatel gas-turbine test has a turbine temperature of about 1000 F, much lower than the 1946 F previously assumed, so that the net power only is about 27 per cent of the actual turbine power. But while in 1907 we hoped for everything that since has been shown by the Neuchatel test, the turbosupercharger, and all the other progress, the actual reality was far different.

So the General Electric gas-turbine research continued until a fuel consumption was in sight, of 4 lb of kerosene per net hphr. At that time good oil engines were using 1 lb of oil per net hphr. Even though it seemed certain that the clouds cast upon the operation of a gas-turbine nozzle (12, 13) had no basis in fact, it was thought desirable to measure actual spouting velocity of products of combustion. So the combustion chamber was flexibly mounted and nozzle reaction measured.

The work was difficult to conduct with accuracy, but enough was done to indicate that the only corrections needed were to take account of departures from the perfect gas laws of the products of combustion. Similar nozzle-reaction experiments later were conducted by Mr. Glenn B. Warren (30) with similar results. Recently, Dr. Chester W. Smith and other General Electric engineers have worked on tables of available energy of products of combustion for turbosuperchargers, with exact values of specific heat. But probably more work needs to be done to get exact available energies for gas turbines.

All early General Electric gas-turbine work was conducted with temperatures possible with materials then known, and no vision was had of the possibilities which the turbosupercharger work to be described later has developed. So the temperatures were kept low by air excess or water injection, both resulting in inefficiencies. No way then seemed open to do better, and so the gas-turbine part of the research was postponed, but with vigorous commercial work on centrifugal compressors, as already mentioned.

Among the many persons who long have had gas-turbine ideas are two with whom the author has had the pleasure of personal acquaintance, and who have made some publication, Dr. Harvey N. Davis (29), president of Stevens Institute of Technology, and Mr. Glenn B. Warren (30), designing engineer of the Steam Turbine Division of the General Electric Company.

Explosive and Continuous Combustion

The gas turbine had been expected to replace the reciprocating internal-combustion engine, and so there was an early idea that it was essential gas-turbine combustion should be similar. This led to a number of proposals for explosion gas turbines, as in the case of LePontois (5, 6) already cited. A German engineer, Hans Holzwarth, has made extensive publications on such apparatus through many years. But there seems doubt as to whether he ever reported performance of a complete machine which compressed its own air (27).

Opposed to these explosion gas turbines are those based on continuous combustion under pressure. The possibility of efficient operation once was doubted. Since then many continuous combustion chambers have been operated with complete success, so demonstration on this point no longer is needed.

An original, or at least an early continuous-combustion chamber, was that of the Doctor's Thesis (9). Such combustion in a chamber at a pressure of any amount above atmospheric proceeds exactly as it does in the open combustion chamber of a steam boiler, where the absolute pressure is about 14.7 psi; and the same heat of combustion is liberated. Because of constancy of conditions, the nozzle-spouting velocity is constant, which is a necessary condition for efficient operation of a turbine. On the other hand an explosion combustion chamber delivers a jet with variable velocity, which only can be proper for the turbine speed during a fraction of the time and so results in inefficiency. At any rate modern gas turbines are wholly on the continuous-combustion basis, and explosion outfits are not now attracting any attention.

Gas-Turbine Prime Movers

Thus the gas-turbine idea has been kept alive through many years, with some partial approaches, as will be discussed later, but always with the hope among enthusiasts that someday it will compete with such high-efficiency prime movers as the modern steam central station or the internal-combustion reciprocating engine. Prof. Lionel S. Marks, now professor emeritus of the Graduate School of Engineering of Harvard University, long has been a gas-turbine student (31), and on December 14, 1939, he gave a lecture (32) which presented a realistic view of immediate gas-turbine prime-mover probabilities. He pointed out that the successful use of the temperatures necessary to give high efficiency might be far off, but that there were many immediate prospects with lower temperatures. Among these were locomotives to compete with the modern steam locomotives of moderate efficiencies, plants where water is scarce, and stand-by plants where low first costs would give total charges competing with more efficient but expensive units. Similar ideas were expressed by Dr. Adolphe Meyer of Brown, Boveri & Company (33), in a paper which mentioned the starting in the Brown-Boveri shops of the Neuchatel 4000-kw gas turbine (34) and the Swiss Federal Railway gas-turbine locomotive (35), whose completion is described next.

The town of Neuchâtel, Switzerland, arranged for an emergency power plant, in a bombproof place, as a war protection, and a 4000-kw gas-turbine plant was constructed. An efficiency test of this in actual operation was published by the famous Swiss turbine authority, then in his old age, Dr. A. Stodola, and seems to be a worth-while operation of a gas-turbine prime mover (34).

Recently actual test results have been published of the gas-turbine locomotive mentioned by Dr. Meyer as being constructed by Brown-Boveri for the Swiss Federal Railway (35), which seems ready for actual use. This is another operation of the sort of gas-turbine prime mover which has been sought through many years. Both of these gas-turbine prime movers are of the sort that Professor Marks and Dr. Meyer mention, where useful purposes are served by temperatures of about 1000 F. But like the other cycles here mentioned, they pave the way for such higher temperatures as will make high gas-turbine efficiency a primary object. Admiral Mills recently has mentioned development by the United States Navy of gas turbines for ship propulsion (35½). Fig. 8 shows part of the laboratory in which gas-turbine research now is being conducted in the United States.

Partial Gas-Turbine Cycles

There are some gas turbines in extensive commercial operation, but not as complete prime movers. An early one is the gas turbine in extensive use by Brown, Boveri & Company and others, to supply compressed air to the supercharged combustion chambers of the steam boilers for the Brown Boveri Velox System (36) and other similar systems.

Many partial gas-turbine cycles have been in successful operation for years, for oil refineries, built by the Allis-Chalmers Company (37), which has some connection with Brown-Boveri. Outfits of a similar sort have been constructed or planned by the General Electric Company (38) and others. Fig. 9 shows an example.

All of the foregoing outfits are planned for the comparatively moderate temperature of about 1000 F. They use gases produced in the course of chemical and combustion operations, and drive air compressors. They do not have the obligation imposed on a gas-turbine prime mover, which has to produce net power as well as to compress the air which produces by combustion or otherwise the fluid which drives the turbine. But they are definite steps in gas-turbine progress.

In the meantime, temperatures used in steam turbines have been rising, and many are operating at temperatures around 900 to 1000 F and show present general use of such temperatures (39). But to a "red-hot" enthusiast who lathers himself into a white heat in trying to get white-hot gas turbines, a mere 900 F is almost a refrigerator temperature. But it is a step on the way.

Reciprocating Engines Exhausting Into Gas Turbines

A gas-turbine enthusiast dreams of complete prime movers such as the Neuchatel power plant (34) and the gas-turbine

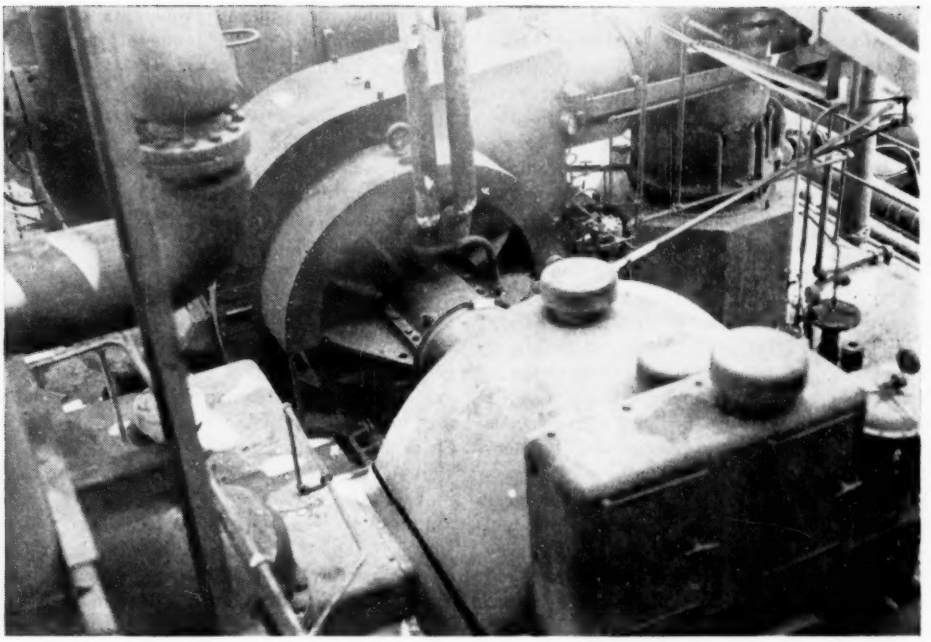


FIG. 9 GAS TURBINE OPERATING ON PRODUCTS OF COMBUSTION AT ABOUT 1000 F, AT UNION OIL COMPANY, OLEUM, CALIF. (Manufactured by General Electric Company.)

locomotive (35), but with such temperatures as will give efficiencies competitive with any other cycles. However, there are those who argue that for moderate powers, the upper part of the high-temperature range which is necessary for high prime-mover efficiencies, can best be handled in a reciprocating engine, with the gas turbine to take the gases at a reduced temperature and carry the expansion to the limit. But whether or not this is going to be the ultimate is a question. There are three sorts of such cycles in present use where reciprocating internal-combustion engines exhaust into gas turbines. These may be called (*a*) Diesel-boiler or Götaverken-Sulzer cycle, (*b*) Büchi divided-manifold cycle, and (*c*) constant-pressure-turbosupercharger cycle; and will be discussed in this order.

(*a*) *Diesel-Boiler Cycle.* An early system was proposed by the engineer Johannsen (40) of Götaverken, a prominent shipbuilding concern of Gothenburg, Sweden, of which Mr. Hugo Heyman has been managing-director. A two-cycle Diesel engine exhausts at the high back pressure of about 4 atm and drives only its scavenging reciprocating air compressor, which is mounted on its crankshaft. The exhaust, cooled by a large amount of scavenging air, proceeds to the turbine, all of whose power is net. Sulzer Brothers, Ltd., of Winterthur, Switzerland, has been working on various modifications of the same general plan (41), as shown in Fig. 10. Free pistons also have been used.

(*b*) *Divided-Manifold Cycle.* Dr. Alfred Büchi of Winterthur, Switzerland, long has worked on turbosuperchargers and, as discussed next (43), made a very early proposal for the modern type with constant pressure, since used by others. Büchi and his associates, Brown, Boveri & Company, also have used what may be called a divided manifold (42). This has a Diesel engine with the usual sort of turbosupercharger, next discussed, except that nozzle-box sections and exhaust-manifold passages are divided so that a given exhaust passage into which exhaust is proceeding from one cylinder is never connected to another cylinder which is at the end of exhaust and beginning of intake. Büchi says there never can be "blowback" of exhaust gas into the intake manifold during the overlap period when both exhaust and intake valves of a cylinder are open at the same time. This cycle also has been used by Rateau.

In most cases, the cycle is used with Diesel engines having low exhaust temperatures and low speeds, as compared with aviation engines. The divided-manifold sections are of such reduced area as to avoid sudden drop of exhaust pressure. Furthermore, each cylinder exhausts by itself until its exhaust pressure dies out.

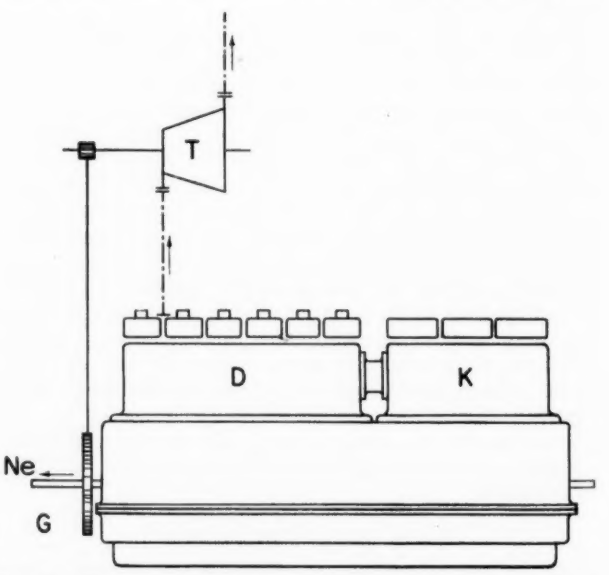


FIG. 10 HIGHLY SUPERCHARGED TWO-STROKE DIESEL ENGINE, WITH DIRECT-COUPLED RECIPROCATING COMPRESSOR AND MECHANICAL TRANSMISSION BETWEEN EXHAUST-GAS TURBINE AND DIESEL ENGINE

(The exhaust-gas turbine is coupled by gearing, represented diagrammatically as chain gear, to the crankshaft of the two-stroke engine; Ref. 41.)

D Two-stroke Diesel engine
K Compressor
T Exhaust-gas turbine
G Gear between Diesel engine and exhaust-gas turbine
Ne Effective output at the shaft

So there is a variable nozzle-spouting velocity, which does not match the turbine-wheel speed during the entire time and thus causes a loss. The system of interlocking sections of the exhaust manifold connected to the different cylinders causes appreciable complexity.

With a turbosupercharger system of such efficiency that the intake-manifold pressure is nearly equal to or less than the exhaust-manifold pressure, the divided-manifold-system advocates say that it avoids "blowback" and gives scavenging instead, and so maintains full engine power. But with the aviation turbosuperchargers next discussed, the efficiency is such that the intake-manifold pressure is higher than the exhaust-manifold pressure, and so there is proper scavenging with the constant-pressure-turbosupercharger cycle.

History of Aviation Turbosuperchargers

The constant-pressure-turbosupercharger cycle first began practical use with high-altitude aviation. The constant pressure started as that of sea-level atmosphere, 30 in. of mercury abs, and the expansion and compression are to and from the low pressure of altitude atmosphere. The part of this aviation turbosupercharger in the gas-turbine picture will be begun with its history, by taking a flashback to World War I. Military aviation was in its infancy, but already there was difficulty in the loss of engine power even at the moderate altitudes then possible. Hence efforts were made to attach, by gearing, air compressors of various sorts, to give airplane-engine supercharging, but none was successful. General Electric later supplied geared superchargers having the design of the centrifugal compressor developed during the gas-turbine research, but these did not come into use until 1925.

During World War I Dr. William F. Durand was chairman of the National Advisory Committee for Aeronautics, and in the course of one of his duties of examination of schemes for aviation improvement, there came to him in the fall of 1917 a plan of the French engineer, Rateau, for using a turbine wheel driven by the products of combustion of the engine exhaust, at constant pressure, to drive a centrifugal compressor to do the supercharging. Dr. Durand had been a professor at Sibley College, Cornell University, in 1901, and he remembered the black smoke from the gas-turbine research and knew of the extensive business that the General Electric Company then had in steam turbines and centrifugal compressors. So he asked General Electric (42½) to undertake turbosupercharger development in the United States. General Electric engineers had their own ideas about design details from their experience with gas turbines, steam turbines, and centrifugal compressors, and so started a development entirely independent of Rateau, which has continued to this day, with production successively increasing on account of the present war.

The first General Electric turbosupercharger was constructed with wartime speed and was assembled on one of the Liberty motors then being used, by the U. S. Army Air Corps, McCook Field, Dayton, Ohio, in May, 1918, as shown in Fig. 11. It was operated there so far as possible at sea level and then tested at the 14,000-ft summit of Pike's Peak, Col.

The airplane turbosupercharger is so arranged that as the plane ascends to the successively lower atmospheric pressures at altitude, there continues to be maintained in the exhaust manifold and turbine nozzle box the normal sea-level pressure. The difference between this and the low pressure of altitude gives the nozzle jet that drives the turbine wheel. This drives a centrifugal-compressor impeller on the same shaft, which compresses the low-pressure air of altitude and supplies it at sea-level pressure to the engine intake manifold. So, regardless of altitude, the engine exhausts at sea-level pressure and receives its charge at sea-level pressure. So it continues to deliver sea-level power at all altitudes, up to the critical one where the turbine wheel reaches its maximum safe speed. Due to the low resistance of the low-density air at altitude, sea-level engine power gives increased airplane speed.

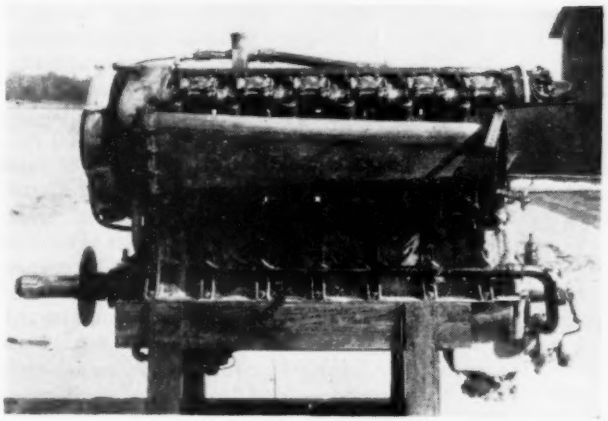


Fig. 11 First American Turbosupercharger on a Liberty Motor at McCook Field, Dayton, Ohio, May, 1918

The constant pressure of the engine-intake manifolds of the early airplane turbosupercharger was 30 in. of mercury. This is greatly exceeded nowadays. Values around 50 in. are usual for take off or short periods, and continuous operation is common with "boost" of intake-manifold pressure as discussed later.

Rateau's turbosupercharger development in France continued for a while after World War I and developments were started in England and Germany. But the resources devoted to the project abroad do not seem to have been sufficient to bring it to a state that warranted continuation. At any rate there is no evidence of any turbosuperchargers other than those of General Electric being used in the present conflict. Other differing American designs recently have begun to be developed.

It once was thought that the 1917 work in France was first mention of the modern turbosupercharger plan, but later searches show what seems to be an earlier publication by Büchi (43). Nevertheless, Rateau made important contributions (44).

In the United States, the development encountered the usual experience of the "glassy eye." But there were enough enthusiasts among the officers and engineers of the United States Army Air Forces, and enough help from them (44½), from engine and airplane manufacturers, and from metallurgists, and sufficient resources available to General Electric, to bring the project to its present originally undreamed of state (45).

The principal interest that the turbosupercharger has in connection with the gas-turbine problem is its development of a turbine to operate at high temperatures of products of combustion. It is true that the aviation turbosupercharger has only short-time operation at extreme conditions and does not have to meet the conditions of continuous operation in a power plant. Nevertheless, many problems have been solved, due to the impetus of World War II, which advance the prospects of a gas turbine as a prime mover. Thus the turbosupercharger, originally a gas-turbine by-product, has not only proved very useful of itself, but has accelerated gas-turbine development.

The turbosupercharger in the United States started in 1918 with a turbine wheel suited only for steam temperature, provided in a rush by the De Laval Steam Turbine Company. Since then there has been continuous progress in materials, fabrication, heat-treating, design, and cooling, of all of the parts, whether exposed to exhaust-gas temperatures or not.

Originally the nozzle area covered only a portion of the wheel

periphery, with cooling between, and this may be an item in the ultimate gas turbine. But for many years the turbosupercharger has had a 360-deg nozzle arc. For years, the rated temperature at the nozzle-box entrance was 1200 F. This meant that the entire nozzle box and the outer portion of the turbine buckets were visibly red-hot, at rotative speeds of about 22,000 rpm. Successive improvements have permitted much greater rated temperatures. Since about 1930 a part of the General Electric turbosupercharger research has been a "hot-gas test" where turbines were operated in the laboratory on products of combustion, with all conditions as when flying at altitude. By opening a peekhole in the altitude chamber in which the turbine wheel was running, there was seen for the first time operation with red-hot turbine buckets, and colored photographs were taken. Since the author always has considered the turbosupercharger as merely a step on the way to the gas turbine, he has often exhibited as gas-turbine propaganda this really inspiring sight of a turbine wheel operating at about 1200 fps with buckets red hot.

Fig. 12 is an accurate reproduction of a water color taken from life, showing a recent turbosupercharger undergoing a standard factory endurance test with products of combustion. In this test, and in actual service, the exhaust-gas conduit from engine to turbine is incipient white, and the nozzle box varies from white to red. A few inches away is the air inlet of the compressor, with a temperature at high altitude of about 50 F below zero, the reproduction of which in the test covers the pipe with frost. Similar conditions exist in the many turbosuperchargers which are reported as successfully flying at high altitude in the war in Europe, Asia, Africa, and the South Pacific, with the *Flying Fortress* B-17 made by Boeing, the *Lightning* P-38 made by Lockheed, the *Liberator* B-24 made by Consolidated, and the *Thunderbolt* P-47 made by Republic. Some of this is shown in the Army illustration, Fig. 13. This is not the place to give details of turbosuperchargers, as this has been done by Reginald G. Standerwick and W. J. King, engineers of the General Electric supercharger Division, in a paper read at the Semi-Annual Meeting of the A.S.M.E., in Los Angeles, Calif., June, 1943, and published in the Transactions of the A.S.M.E. for January, 1944.

(*c*) *Constant-Pressure-Turbosupercharger Cycle.* Turbosuperchargers on American airplanes are examples of the third of the cycles previously mentioned, where reciprocating engines exhaust into gas turbines. They are designed for pressure ratios which give absolute pressures above sea-level value, when flying at altitude. This means that absolute pressures in the engine-intake manifold appreciably above sea-level value are easily possible at moderate altitudes. Such pressures are used for take-off or for regular operation under special circumstances, which is called "boost." Pilots flying airplanes with turbosuperchargers have instruments showing airplane altitude, intake-manifold pressure, turbosupercharger speed, various temperatures, and so on. They have rules and technical orders which give values for the readings of the various instruments which give values for the boost of engine-intake-manifold pressures safe for the engine and turbosupercharger. The greater the boost, the greater the engine horsepower and the greater the airplane speed.

Thus when a pilot with a turbosupercharger is in battle, he has means of greatly increasing his plane speeds at most altitudes, by increased boost. So, when an enemy plane is on his tail, does the pilot take out his technical orders, look at his instruments, and figure out what he ought to do? He does *not*, but subjects the turbosupercharger to pressures far beyond its test rating.

Extension of such operation, which easily is possible independent of aviation, would give a four-stroke Otto- or Diesel-cycle engine with a constant-pressure turbosupercharger, which is this third one of the cycles where a reciprocating internal-combustion engine exhausts into a gas turbine. It has been called a "compound internal-combustion cycle."

As already mentioned, reports of operation of turbosuperchargers in war show that they are subjected to conditions far exceeding their test rating. Therefore the average of the conditions in war has some relation to conditions of long-time operation at sea level to which a gas-turbine prime mover would be subjected.

High-Temperature Progress

One major item in operation of turbine wheels at high temperature is "creep," which is continuous nonelastic elongation, finally resulting in rupture. Hence stresses for a gas turbine to be operated in a power plant for years are lower than for a turbosupercharger in war. Information about creep is rapidly accumulating in connection with turbosupercharger as well as with other turbine work (46).

Reference already has been made (42) to Büchi, Brown-Boveri, and Rateau work on turbosuperchargers with divided manifolds, probably always with low-exhaust-temperature, low-speed Diesel engines. Accounts also have been published (47) of Swiss, French, and German use of turbosuperchargers on aviation engines, with Diesel or Otto cycles and with divided or constant-pressure manifolds. None of the apparatus thus referred to is in use in World War II, the only known turbosuperchargers being those of the United States Army Air Forces, which as already mentioned are in very extensive use.

Nevertheless, some progress is being made abroad with turbine wheels operated by products of combustion. One example is a publication by Brown-Boveri (48), which includes a night picture of a turbosupercharger for an aviation engine (probably with a constant-pressure exhaust manifold) in a factory test at about 1800 F and 30,000 rpm. Glowing exhaust-gas conduit and nozzle box are shown with the remark, "The set presents an exceptional and fascinating appearance. It is surrounded by the glowing gas pipe and carries the mind back to some medieval machine."

Thus the thousands of turbosupercharger turbines, in operation by the United States Air Forces, and being investigated abroad, are adding to the other gas-turbine items already mentioned, in paving the way for temperatures much higher than those which have been used, and with a minimum of loss from cooling. No thermodynamic studies can be given here, but it is well understood that such higher temperatures mean higher gas-turbine efficiencies. So the long sought gas-turbine prime mover, with temperatures much beyond the 1000 F now in use, and consequent higher efficiency, seems to be getting nearer. Of course, this same progress is paving the way for higher temperatures and higher efficiencies with the regular steam cycle and with two fluid cycles. So we only can speculate as to whether the gas turbine with its compressor, combustion chamber, and heat interchanger is going to compete with the other cycles which instead have economizers, feedwater heaters, feed and air pumps, boilers, and condensers.

Acknowledgment

The author is greatly indebted to many individuals and companies who have been kind enough to furnish data, references, and illustrations which are used in this paper.

BIBLIOGRAPHY

1 "A Water Power and Compressed Air Transmission Plant for the North Star Mining Company, Grass Valley, California," by Arthur De Wint Foote, with Appendix by Edward A. Rix, etc., Trans American Society of Civil Engineers, vol. 36, 1896, pp. 171–190.

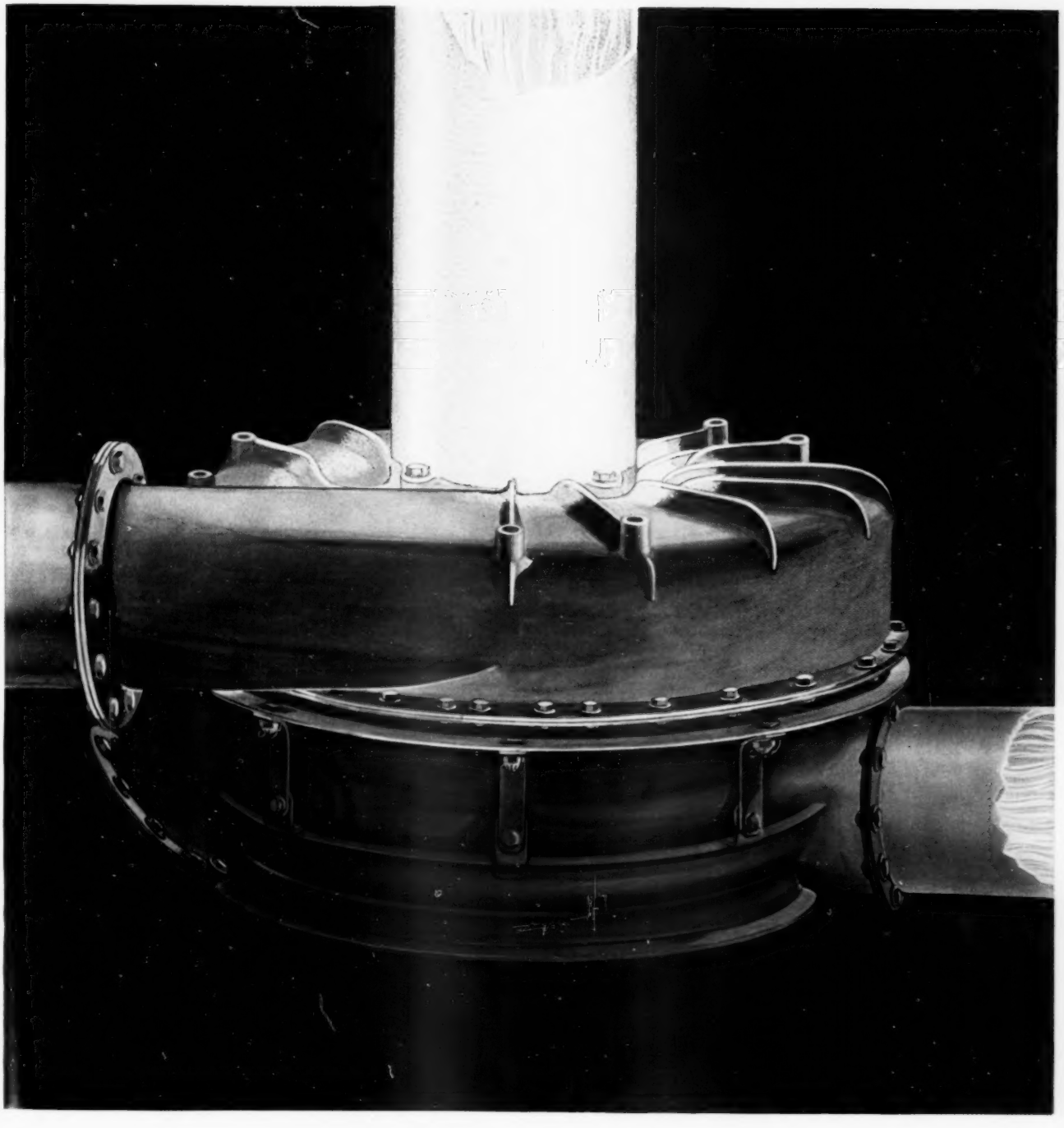


FIG. 12 GENERAL ELECTRIC TURBOSUPERCHARGER OPERATING UNDER STRATOSPHERE CONDITIONS
(Painting from laboratory test.)

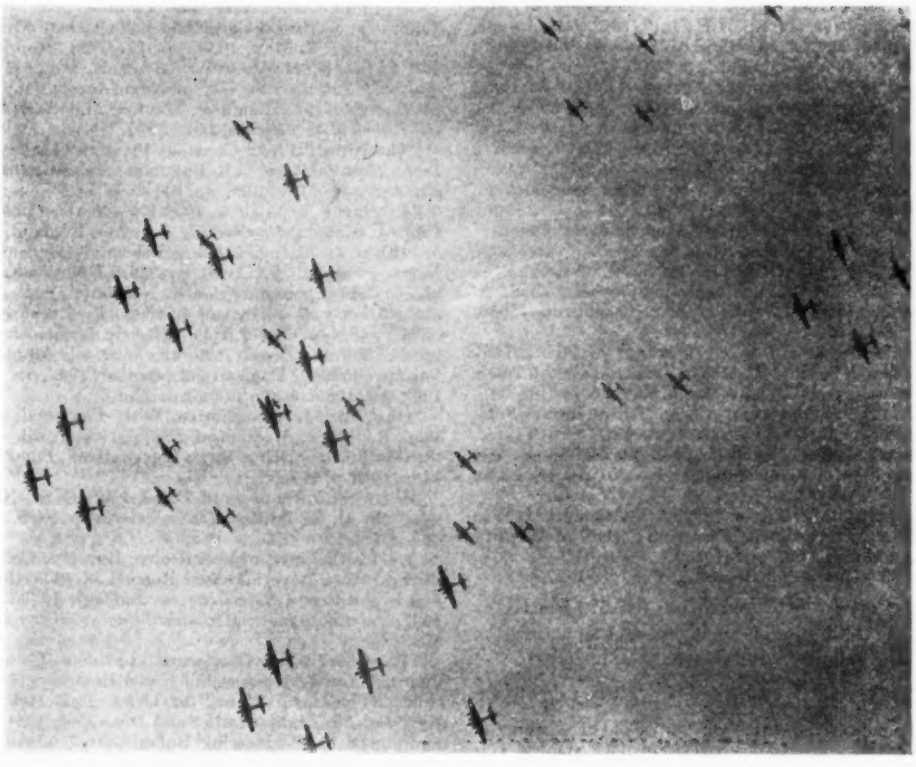


FIG. 13 SQUADRON OF BOEING FLYING FORTRESSES, EACH WITH FOUR TURBOSUPERCHARGERS
(Every one, in battle everywhere, as well as every Consolidated *Liberator*, Lockheed *Lightning*, and Republic *Thunderbolt*, has four, two, or one gas turbines receiving products of combustion from aviation engines.)

2 "Thermodynamics of the Gas Turbine," thesis for degree of Master of Science, by Sanford A. Moss, December, 1900, Library of University of California. The author's draft of this thesis includes thermodynamics of a regenerator or heat interchanger, but this first was published in the Doctor's Thesis (9).

3 "British Patent Reports," vol. XXIII, 1791–1792. Nov. 30, 1791, patent number 1833 to John Barber; shows a complete gas turbine. The illustration of this patent was reproduced in (9, 8, 7, 33, 37).

4 U. S. Patent 635919 to Charles G. Curtis. Filed June 24, 1895; issued Oct. 31, 1899.

5 U. S. Patent No. 617753 to Leon LePontois. Filed Dec. 5, 1895; issued Jan. 17, 1899. Shows an explosion combustion chamber for a gas turbine.

6 "An Investigation of the Gas Turbine," by Walter O. Amsler, thesis for degree of Doctor of Science, 1897; Cornell University Library. Published in Sibley *Journal of Engineering*, May, 1900. A theoretical and experimental study of LePontois explosion combustion chamber of (5); mentions (3).

7 "The Gas Turbine," by H. H. Supplee, published by Lippincott, Philadelphia, Pa., 1910.

8 "The Gas Turbine," by Norman Davey, published by Constable & Co., London, England, 1914.

9 "The Gas Turbine," thesis for degree of Doctor of Philosophy, by Sanford A. Moss, M.S., published in Ithaca, N. Y., May, 1903; Cornell University Library. This has gas-turbine mathematics and a brief account of a turbine wheel actually operated by products of combustion but with very poor performance. There was included the gas-turbine-cycle diagram reproduced in Fig. 1, which was an early representation of Barber's cycle in diagrammatic form. There also was included the "regenerator" or heat interchanger for transferring the heat of the turbine exhaust gases to the air proceeding from compressor to combustion chamber, which may be the first publication of this item. The drawing of Barber's British Patent (3) is reproduced probably for the first time since 1791. This was afterward reproduced in (8, 7, 33, 37). This thesis is referred to in (7), pp. 6 and 26.

9½ General Electric Gas-Turbine Patents (issued to the author, S. A. Moss), as follows:

	Filed	Issued
1064665 Gas Turbine	Dec. 31, 1904	June 10, 1913
891715 Combustion Chamber	April 4, 1906	June 23, 1908
969760 Gas Turbine	April 4, 1906	Sept. 6, 1910
1000968 Governor Mechanism for Gas Turbines	April 4, 1906	Aug. 15, 1911
1000969 Regenerator	April 4, 1906	Aug. 15, 1911

10 U. S. Patent 522066 to Carl Gustaf Patrick De Laval; filed May 1, 1889; issued June 24, 1894. British Patent 7143; filed April 29, 1889; issued March 1, 1890.

"A Pioneer in High Pressure Steam," by George H. Gibson, *Power*, Nov. 6, 1928; republished, with Fig. 2 herein, by De Laval Steam Turbine Company, pamphlet E1141A, 1936.

11 "On the Flow of Gases," by Osborne Reynolds, paper read before Manchester Literary and Philosophical Society, Nov. 17, 1885. Published in London, Edinborough, and Dublin *Philosophical Magazine*, fifth series, vol. 21, no. 130, March, 1886, p. 185, and "Scientific Papers of Osborne Reynolds," vol. 2, p. 311; source of Fig. 6 herein.

12 "Pressures and Temperatures in Free Expansion," by A. Borsody and R. C. Cairncross, presented by Prof. C. E. Lucke, Trans. A.S.M.E., vol. 26, 1905, pp. 114–158.

"Practical Investigations in the Gas Turbine Problem," by C. E. Lucke, *Engineering Magazine*, April, 1905, pp. 96–101.

Discussion by Charles E. Lucke of "Some Possibilities of the Gasoline Turbine," by Prof. Frank C. Wagner; *Journal A.S.M.E.*, vol. 31, no. 2, Febuary, 1909, pp. 241–242.

Partially refuted by Professor Wagner in the closure to his paper, Ibid., p. 244.

Also partially refuted by "The Question of the Gas Turbine," by Prof. Sidney A. Reeve, *Engineering Magazine*, vol. 29, 1905, p. 407.

13 "The Gas Turbine, Some Tests of Practical Efficiency," by Charles E. Lucke, *Engineering Magazine*, vol. 31, August, 1906, pp. 641–656.

Completely refuted by Prof. Frank C. Wagner in closure to his paper given in (12), and by Prof. Sidney A. Reeve in his paper (12).

14 "The Impact Tube," by Sanford A. Moss, Trans. A.S.M.E., vol. 38, 1916, pp. 766–769, section on "Impact Temperature." This since has been called "Total Temperature," to correspond to "Total Pressure."

14½ "Measurement of High Temperatures in High-Velocity Gas Streams," by W. J. King. Trans. A.S.M.F., July, 1943, pp. 421–428.

15 U. S. Patent 1086755, "Elastic-Fluid Compressor," to Charles G. Curtis; filed Aug. 4, 1896; issued Feb. 10, 1914.

16 U. S. Patent 1086754, "Rotary Compressor, Blower and Pump," to Charles G. Curtis; filed June 14, 1902; issued Feb. 10, 1914.

17 *Engineering* (London), Jan. 26, 1912, pp. 112–113, gives a description and illustration of a Mather-Reynolds centrifugal pump of 1895, showing a diffuser and an impeller with axial inlet buckets; here reproduced as Fig. 7.

18 "Ventilateaurs et Pompes centrifuges Pour hautes Pressions," by A. Rateau. Extrait du Bulletin de la Société de l'Industrie Minerale, 1902. Engineering Societies Library, New York, N . Y.

19 U. S. Patent 1075300, "Centrifugal Compressor," to S. A. Moss; filed Dec. 10, 1904; issued Oct. 7, 1913; reissued as Re 13665, Dec. 30, 1913.

20 "Turbo Blowers for Blast Furnace Blowing," by Richard H. Rice (with collaboration of Sanford A. Moss), Trans. American Institute of Mining and Metallurgical Engineers, vol. 50, 1915, pp. 104–142.

"Notes on Blast Furnace Operation With a Turbo Blower," by S. G. Valentine (with collaboration of Sanford A. Moss), Trans., American Institute of Mining Engineers, vol. 50, 1915, pp. 90–103. Details of operation of a machine, as given in the preceding paper.

"Blast Furnace and Steel Mill Power Plants," by Richard H. Rice and Sanford A. Moss. Proceedings, Engineers Society of Western Pennsylvania, vol. 33, March, 1917, pp. 81–130.

U. S. Patent 161733 to Moss and Robinson, Feb. 28, 1927.

Following is an effort to give a complete list of all early or epochal publications relating to gas turbines; but some may be missed. A list of later references is too large to be included.

21 "The Gas Turbine," by Réné Armengaud, *Cassier's Magazine*, vol. 31, no. 3, January, 1907, pp. 187–198.

22 "A Scientific Investigation Into Possibilities of Gas Turbines," by A. M. Neilson, Proceedings of The Institution of Mechanical Engineers (England), October, 1904, pp. 1061–1131.

23 "La Turbine a gaz-son rendement," by Alfred Barbezat, *Revue D'Électricité*, Nov. 12–19, 1904, and *Schweizerische Bauzeitung*, no. 9, vol. 44.

24 "The Gas Turbine," by M. L. Sekutowicz, Memoirs of the Society of Civil Engineers of France, February, 1906, pp. 195–300.

25 "The Gas Turbine," by Dr. A. Stodola, given as a section in his book, "Steam Turbines," with an Appendix on "Gas Turbines," in the second German edition, 1904; English translation, 1906, and probably in the original articles in *Zeitschrift des Vereines deutscher Ingenieure*, 1903, and the first German edition, 1903; also in later editions.

26 "The Lorenzen Gas Turbine and Supercharger for Gasoline and Diesel Engines," by Christian Lorenzen, *Mechanical Engineering*, vol. 52, 1930, pp. 665–672.

27 "The Internal-Combustion Turbine," by W. J. Stern, report No. 54 of Aeronautical Research Committee of British Air Ministry, September, 1920. Discusses a number of gas turbines, including the Holzwarth and Karavodine explosion turbines, and says: "Mr. Holzwarth's calculations are made in this slipshod manner, even when on non-controversial grounds; he makes errors and gets inconsistent results . . . . . the claimed horsepower results must be fallacious."

28 "Geared Centrifugal Superchargers for Airplane Engines," by Sanford A. Moss, *Journal*, Society of Automotiv Engineers, August, 1930, pp. 148–153, 160.

"Centrifugal Compressors for Diesel Engines," by Sanford A. Moss, *Mechanical Engineering*, vol. 47, 1925, pp. 1075–1084, and vol. 48, 1926, pp. 473–474.

29 "A PQ Plane for Thermodynamic Cyclic Analysis," by Dr. Harvey N. Davis, Proceedings of the American Academy of Arts and Sciences, April, 1905.

30 "An Experimental Study of Problems in Gas Turbine Design," by Glenn B. Warren and others; thesis for degree of Bachelor of Science, 1919, University of Wisconsin Library.

"Gas Turbine Combustion Chamber," by Glenn B. Warren, *Power*, June 28, 1921, pp. 1059–1060.

"An Experimental Study of Gas Turbine Chambers and Nozzles," by Glenn B. Warren, *Wisconsin Engineer*, vol. 26, October, 1921, pp. 1–5; also November, 1921, pp. 24–26.

31 "Gas Turbines," by Lionel S. Marks and M. Danilov, Trans. A.S.M.E., vol. 46, 1924, pp. 1095–1129.

32 "Recent Developments in Power Generation," by Lionel S. Marks, *American Scientist*, vol. 30, no. 3, summer issue, 1942, p. 171. Beginning p. 186 is an abstract of Professor Marks' 1939 lecture before the Harvard Engineering Society.

33 "The Combustion Gas Turbine," by Dr. Adolphe Meyer, Journal and Proceedings of The Institution of Mechanical Engineers, vol. 141, no. 3, May, 1939, pp. 197–222. Reprinted, with changes and additions, *Mechanical Engineering*, vol. 61, 1939, p. 645, and *Journal*, American Society of Naval Engineers, August, 1939, with discussion in *The Engineer*, London, March 31, 1939, p. 406. Also see *Brown Boveri Review*, June, 1939.

"The Brown Boveri Constant Pressure Gas Turbine, a Waterless Power Station," by Ad. Baumann and W. Broggi, *Brown Boveri Review*, April–May, 1939, pp. 103–106.

34 "Load Tests of a 4000-Kw Combustion-Turbine Set," by Prof. A. Stodola, *Engineering* (London, England), vol. 149, January 5, 1940, p. 1; reprinted, *Power*, February, 1940, pp. 62–63; *Mechanical Engineering*, vol. 62, 1940, p. 239. Describes a 4000-kw gas turbine stand-by power station in Neuchatel, Switzerland, with a thermal efficiency shown by test, of 16 to 17 per cent at about 1000 F.

35 "A New Gas Turbine Electric Locomotive in Switzerland," by F. Steiner, *Diesel Railway Traction*, Supplement of *Railway Gazette* (London, England), September, 1942, pp. 100–103; October, 1942, pp. 106–109 (with continuation).

"Gas Turbine Locomotive With Electrical Transmission," by Paul R. Sidler, *Mechanical Engineering*, April, 1943, pp. 261–264

"Gas Turbine Drives Swiss Locomotive," *Popular Science Monthly*, May, 1943, p. 114.

35½ "Some Aspects of Diesel Engines for Navy Main Propulsion," by E. W. Mills, *Mechanical Engineering*, vol. 65, 1943, pp. 625–627.

36 The Velox System of Brown, Boveri & Company is described in the Brown Boveri Annual Reports of 1935–1936 and 1936–1937, and in the *Brown Boveri Review*, January, 1932, January–February, 1937, and other issues; *Mechanical Engineering*, vol. 57, 1935, pp. 469–478.

"The Gas Turbine Challenges," by Lieut. Comdr. Warren Noble, *Journal*, American Society of Naval Engineers, May, 1939, p. 178.

37 "The Gas Turbine," by Dr. J. T. Rettaliata, *Allis-Chalmers Electrical Review*, September and December, 1941, and March, 1942, reproduced as Engineering Bulletin no. 7 of Allis-Chalmers. This gives a reference to (3) as well as to other early forms of partial gas turbines, some given in (7) and (8). See also other Allis-Chalmers Bulletins, and reference (45), "Energy Transfer Between a Fluid and a Rotor," Fig. 6*a*.

38 "Turbines for Power Generation From Industrial-Process Gases," by John Goldsbury and J. R. Henderson, of the Lynn Turbine Division of General Electric Company, Trans. A.S.M.E., vol. 64, 1942, pp. 287–298. This includes details, Figs. 1, 2, and 3, of the plant herein shown in actual operation as Fig. 9.

39 "Electrical Developments of 1942, Power Generation Transmission, Measurement," by Guy Bartlett, *General Electric Review*, vol. 46, January, 1943, pp. 8, 9, 10; see also *Power*, September, 1940, pp. 561–567; and September, 1941, pp. 655–663. Gives tables with details of many steam plants above 900 F.

40 "First Announcement of a New System of Ship Propulsion," by A. C. Hardy, *The Journal of Commerce and Shipping Telegraph*, Liverpool and London, England, July 13, 1933.

"A Diesel Boiler," by A. C. Hardy, *Diesel Railway Traction*, supplement to the *Railway Gazette*, London, England, Oct. 6, 1933. Describes the cycle as applied to ships, and also to the Gota locomotive.

41 "The Supercharging of Two-Stroke Diesel Engines," *Sulzer Technical Review*, Dec. 31, 1941. Sulzer Brothers, Limited, Winterthur, Switzerland. Source of Fig. 10 herein. *Mechanical Engineering*, vol. 64 1942, p. 779.

42 "Supercharging of Internal Combustion Engines With Blowers Driven by Exhaust Gas Turbines," by Dr. Alfred Büchi, Trans. A.S.M.E., vol. 49, 1937, pp. 85–96; vol. 60, 1938, pp. 430–456. See also many references in *Brown Boveri Review*.

42½ Copy of letter of 1917:

National Advisory Committee for Aeronautics
Washington, D. C., November 19, 1917

Mr. E. W. Rice
General Electric Company

Dear Sir:

At the present time in connection with the development of the airplane and the Liberty engine for driving same, there is not a problem which is perhaps more seriously before the Government officials than that of maintaining at high altitudes the power of the engine. In this connection we are especially desirous of developing the possibilities of a precompression of the air before going to the engine carburetor, thus maintaining as nearly as may be constant conditions regarding pressure at all altitudes.

In this connection we believe that your Dr. Sanford A. Moss could be of very great service in advising with us regarding the possibilities

of turbo-compression as applied to this problem, and I have written informally to Dr. Moss inviting his attention to the problem as outlined.

I desire, therefore, to ask your approval of this request, and that, if possible, you will authorize Dr. Moss to give to us the results of his experience in the study of such matters.

Thanking you in advance for your anticipated cooperation in this matter, I remain,

Very truly yours,
/s/ W. F. Durand
Vice-Chairman

43 "Über Vebrennungskraftmaschinen," by Dr. Alfred Büchi, *Zeitschrift fur das gesamte Turbeninwesen*, 1909, pp. 313–316, 322–332, 347–351. Clearly shows a turbine wheel driven by engine exhaust gases on a shaft separate from the engine shaft, and driving a "turbokompressor" which supplies air through a "kuhler" to the cylinders of a reciprocating internal engine of either what is now called the "Otto" or "Diesel" types. Mentions the use of the process on "aircraft, automobiles, motorboats, railway motors, stationary engines," etc. Refers to German patent 204, 630, filed Nov. 16, 1905, issued Nov. 28, 1908; but this shows turbine and compressor on the engine shaft.

"Supercharging in Internal Combustion Engines," by Alfred Büchi, *The Engineer*, London, England, Aug. 14, 1925, p. 171.

44 "Use of the Turbo Compressor for Attaining the Greatest Speed in Aviation," by Auguste C. E. Rateau; Proceedings of The Institution of Mechanical Engineers, London, England, 1922, pp. 795–831; abstract in *Engineering*, London, England, vol. 114, July 28, 1922. Discussion by Sanford A. Moss, *Engineering*, vol. 115, Jan. 19, 1923, p. 86.

"Flight at Very High Altitudes and the Use of Turbo-Compressor," by A. Rateau, "Comptes Rendus des Seances de L'Academie des Science," vol. 170, no. 13, March 29, 1920, pp. 782–788.

"Turbo-Compressors for High-Speed Aviation," by A. Rateau, *Engineering*, vol. 114, July 21, 28, 1922, nos. 2951–2952, pp. 91–94, pp. 123–135.

Summaries of A. Rateau, Alfred Barbezat, J. Rey, and A. Gouvy; Memoirs of Society of Civil Engineers of France, April, 1910, pp. 217–350. Paper by M. Gautier, *Genie Civil*, February, 1940.

The following are papers written by the staff of the United States Army Air Corps and National Advisory Committee for Aeronautics:

44½ "Superchargers and Supercharging Engines," by Major George E. A. Hallett (then of the U. S. Army Air Corps), January, 1920, meeting of Society of Automotive Engineers; Trans. S.A.E., vol. 15, part 1, p. 218. *General Electric Review*, June, 1920, pp. 468–473.

"Airplane Turbosupercharger Development in the United States," by David Gregg, *S.A.E. Journal*, May, 1924, pp. 533–538.

"America From the Air," work of Cols. A. W. Stevens and John A. Macready, *National Geographic Magazine*, July, 1924.

"Supercharged Engine Performance, Calculated and Actual," by Opie Chenowith, Trans. S.A.E., vol. 22, 1927, part II, pp. 256–268.

"Comparative Flight Performance With a N.A.C.A. Roots Supercharger, and a Turbo-Centrifugal Supercharger," by O. W. Schey and A. W. Young, N.A.C.A. Report 355, 1930.

"Superchargers and Supercharging," by O. W. Schey, *S.A.E. Journal*, May, 1931, pp. 524–534, and N.A.C.A. Report 384, 1931.

"The Turbosupercharger," by A. L. Berger and Opie Chenowith, *S.A.E. Journal*, October, 1931, pp. 280–295, and December, 1931, p. 476.

"Supercharger Installation Problems," by A. L. Berger and Opie Chenowith, Journal of the Society of Automotive Engineers, November, 1938, pp. 472–484.

Only a few of the many publications relating to Turbosuperchargers can be listed:

45 "Supercharging Internal Combustion Engines," by C. R. Short, *S.A.E. Journal*, February, 1926, pp. 185–194. Discussion by Sanford A. Moss, *S.A.E. Journal*, October, 1926, pp. 385–391.

"The General Electric Turbosupercharger for Airplanes," by Sanford A. Moss, *General Electric Review*, June, 1920, pp. 476–485.

"Engineering Computations for Air and Gases," by Sanford A. Moss and Chester W. Smith, Trans. A.S.M.E., vol. 52, 1930, paper APM-5-8, pp. 93–102.

"Energy Transfer Between A Fluid and a Rotor for Pump and Turbine Machinery," by Sanford A. Moss, Chester W. Smith, and William R. Foote, Trans. A.S.M.E., vol. 64, 1942, pp. 567–597.

"American Experience With Turbosuperchargers," by Sanford A. Moss, Aircraft Engineering (London, England), 1942, pp. 191–194.

"Air Compression With Temperatures Above Adiabatic, With Special Reference to Airplane Superchargers," by Sanford A. Moss, Trans. A.S.M.E., vol. 55, 1933, paper AER-5-5, pp. 35–43.

"Turbosuperchargers for Airplanes," by Sanford A. Moss, *Aeroplane*, London, October, 1941.

"Superchargers for Aviation," by Sanford A. Moss, magazine "Aeronautics" nos. 37 to 42, 1941. Published in book form, Wm. H. Wise Co., N. Y., second edition, 1944.

46 "100,000-Hour Creep Test," by Ernest L. Robinson, Turbine Engineering Dept., General Electric Company, *Mechanical Engineering*, vol. 65, 1943, pp. 166–168. Much better high temperature materials than mentioned in the paper now are known.

"Properties of Materials," by H. Zachokke, *Brown Boveri Review*, vol. 28, nos. 8–9, Aug.–Sept., 1941, pp. 209–210; also, *Aircraft Engineering* (London, England), July, 1942, pp. 194–195.

47 "A German Survey of Turbosuperchargers," by Werner von der Null, *Zeitschrift V.D.I.*, vol. 85, no. 43/44, November, 1941, pp. 847–857; and *Aircraft Engineering* (London, England), July, 1942, pp. 184–191.

48 "Theoretical Consideration of Altitude Supercharging of Aeroplane Engines by Means of Charging Blowers Driven by Exhaust Gas Turbines," by A. Meldahl, *Brown Boveri Review*, August–September, 1941, pp. 213–217, and *Aircraft Engineering*, July, 1942, pp. 182–183.

"The First Gas Turbine Locomotive," by Dr. Adolf Meyer, The Institution of Mechanical Engineers (London), Journal and Proceedings, November, 1943.

Discussion

A. G. CHRISTIE.[3] The author has presented an interesting history of the development of the gas turbine and turbosupercharger. He discusses his early experimental work at Cornell University using the DeLaval steam-turbine wheel of the unit that was shown at the Chicago World's Fair and which was said to be the first De Laval unit in this country.

The writer went to Cornell in October, 1904, as an instructor. When the late Prof. R. C. Carpenter, then in charge of the mechanical laboratories, learned that the writer had built steam turbines, he asked whether or not the old De Laval turbine could be fixed up and run. Professor Carpenter said that a former student had tried to use this rotor as a gas turbine and, as a result of overheating, the shaft had broken.

Balancing was not a refined art in those days. The De Laval designers provided a flexible shaft to care for wheel unbalance. This shaft was reduced to a small diameter (about $^3/_8$ in. as nearly as can be recalled) on either side of the disk. The fracture occurred in one of these small sections. The shaft was either repaired by a sleeve or replaced, for the turbine was in service the following winter for laboratory purposes.

The blading of the wheel showed no ill effects of its operation as a gas turbine. In view of our more extended knowledge of fatigue failures, it is quite certain that the shaft fracture was due to fatigue rather than to Dr. Moss's use of it as a gas turbine. The shaft was well away from the wheel, and the wheel itself showed no ill effects from the application of gas. The writer recalls that Professor Carpenter said the wheel had been "very hot," so his curiosity was aroused to see what had been the effect on the blades and disk. Apparently, the effect was not serious for the unit ran for some time afterward in regular laboratory service.

Later, about 1912, when the writer was at the University of Wisconsin, the late Prof. Carl C. Thomas had him fit up a small gasoline engine with a quick-opening valve on the indicator-cock connection. This valve was opened somewhat before the end of the power stroke and the gas was discharged through a nozzle onto a small turbine wheel. This ran satisfactorily and developed a small amount of power but the hot gases quickly de-

[3] Professor of Mechanical Engineering, The Johns Hopkins University, Baltimore, Md. Fellow, A.S.M.E.

stroyed the valve. The writer believes that Professor Thomas later filed an application for a patent on this device as a power-generating unit but no further construction or experimental work was done.

W. F. Durand.[4] In this paper, the author has presented a vast amount of historical information on the development of the gas turbine which will be of the greatest interest and value to all who are concerned with this new form of combustion engine. My own small part in this history goes little beyond the letter which I wrote in the fall of 1917, to Mr. Rice, president of the General Electric Company, asking him to detail Dr. Moss on the problem of the exhaust turbosupercharger, as an aid to the airplane in reaching higher atmospheric levels.

In 1917, the members of the National Advisory Committee for Aeronautics were becoming acutely impressed with the need of some means for the maintenance of sea-level power at high altitudes. We knew something of what Rateau in France had been doing in this line, and the salvaging of some of the power wasted in the exhaust seemed a promising means for achieving this end. As Dr. Moss has noted in his paper, I had been in contact with his work at Cornell in 1901 and knew of his connection with the General Electric Company in 1917; and hence it seemed to be a most natural approach to address the letter to Mr. Rice as he has noted. The response was prompt and generous and the work was started.

The growth, since that beginning in 1917, has far outrun anything that either Mr. Rice, Dr. Moss, or I could have possibly foreseen or even imagined at that time. The turbosupercharger is firmly established as an absolutely essential feature of aircraft motive equipment where navigation at high altitudes is contemplated, and the rate of production in recent months has reached figures which, 26 years ago, would have seemed nothing short of a fantastic dream.

The splendid record of achievement in this particular domain of power drive may well be an indication of continually improving adaptation of the gas turbine as a prime mover, to the requirements of engineering and industry broadly.

J. S. Haverstick.[5] The author has presented an interesting and instructive account of his work, and the work of others, in attempting to develop a commercial gas-turbine power plant. It is to be hoped that recent wartime developments, both in this country and abroad, may soon be published for the benefit of those who design this type of equipment.

This year is the fiftieth anniversary of the first De Laval steam turbine in the United States. We were interested to note that its bucket wheel was probably the first to operate on exhaust gas; and, further, that 25 years later De Laval was the source of supply for high-speed wheels.

Since mention has been made of the bucket wheel supplied to the author in 1918, we feel that we should add a few notes on the other development program which paralleled that of the author, and with which De Laval was connected more intimately.

Fig. 14 of this discussion is a copy made from the drawing by Rateau and is probably the starting point for turbosuperchargers in this country.

During 1918, tests were conducted at De Laval for the Fergus Motors of America, Inc., using the turbosupercharger developed the previous year by E. H. Sherbondy. Several changes in design were made as the tests progressed, for it was soon found that

[4] Chairman, Special Committee on Jet Propulsion, National Advisory Committee for Aeronautics, Washington, D. C. Past-President, and Honorary Member, A.S.M.E.

[5] Mechanical Engineer, De Laval Steam Turbine Company, Trenton, N. J.

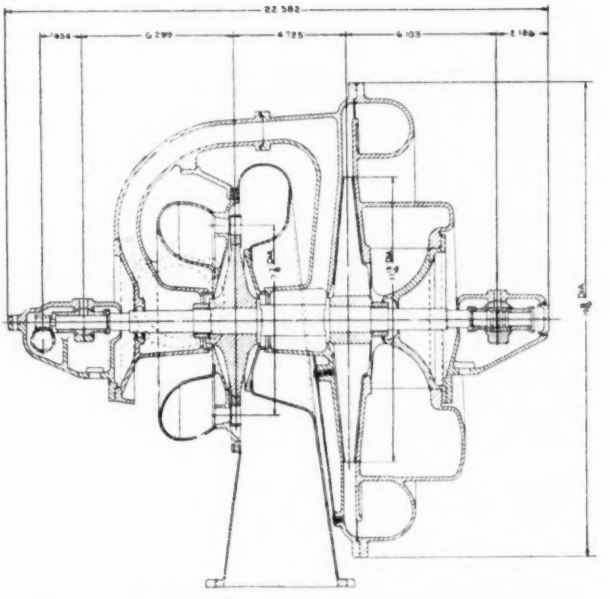


Fig. 14 Turbocompressor Operating at 20,000 Rpm for 330-Hp Motor
(Copy of French drawing from Rateau, dated November 3, 1917.)

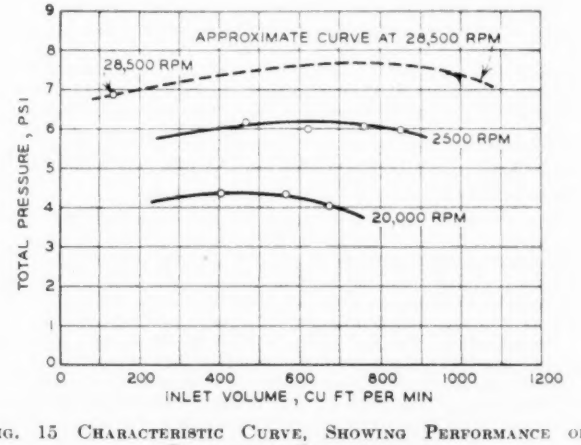


Fig. 15 Characteristic Curve, Showing Performance of Centrifugal Compressor

the unit could not be brought to its full speed of 30,000 rpm because of congestion in the flow passages. Fig. 15 is a characteristic curve of the compressor taken before completion of the tests.

Unfortunately, this program was discontinued after the last war. For a description of the machine one should refer to Stodola's text (25),[6] where it is shown in cross section alongside the General Electric turbosupercharger of that period.

Richard Herold.[7] This paper presents a valuable chronological history of the gas turbine with a quite natural emphasis on the work done in this country. Due no doubt to the imposition of wartime secrecy, the paper does not add anything to the facts already known; it does not submit any figures about present results, and it does not offer suggestions about the probable aspect of further gas-turbine development.

The writer feels therefore that while the paper is of great

[6] Numbers in parentheses in this discussion refer to the author's Bibliography.

[7] Sulzer Bros., Ltd., New York, N. Y. Jun. A.S.M.E.

value for all those interested in gas turbines, it does not offer material for discussion. It is regretted that the author has not mentioned the studies which he has surely made, with a view to using gas turbines for jet-propulsion high-altitude aircraft. This again, is unquestionably due to wartime secrecy.

W. J. KING.[8] One of the most remarkable aspects of this subject of gas turbines is the rapidity with which interest has developed within the very recent past, as manifested in the published literature and in the transactions of several of our engineering societies. Along with this, there seems to be a similar growth of interest in various combinations of the gas turbine with other types of heat engines, such as the Velox boiler and the "Diesel boiler" or Götaverken cycle which the author mentions.

After reading the article on the Diesel boiler, to which the author refers, the writer became interested in comparing the theoretical efficiency of the particular cycle described with that of the simple gas-turbine cycle. Of course the actual performance of either cycle will depend to a major degree upon the efficiencies of the component machines, but it was felt that the results of a basic thermodynamic analysis using idealized compression and expansion, with adiabatic or 100 per cent efficiency, would be of some interest.

The cycles assumed in this study are indicated in Fig. 16 of this

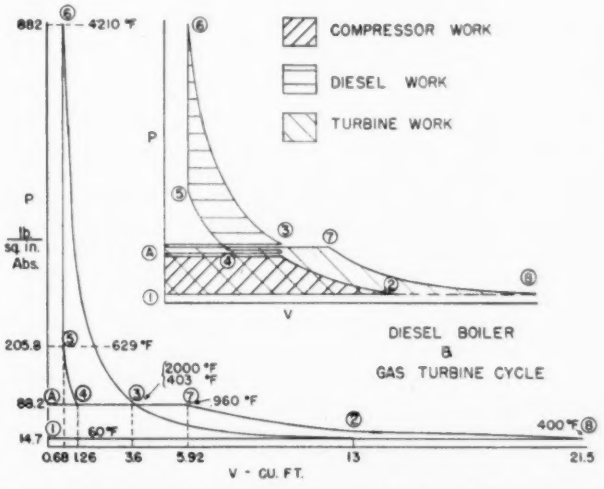


FIG. 16 THEORETICAL INDICATOR DIAGRAM FOR GAS TURBINE AND "DIESEL BOILER" OR GÖTAVERKEN CYCLES
(Lower diagram is to scale, upper diagram is schematic, to show sequence of operation.)

discussion, in which the "Diesel boiler" cycle is superposed upon the ordinary gas-turbine diagram. In either case, atmospheric air is initially compressed through a 6:1 ratio in a separate compressor, which discharges it at 88.2 psia and 403 F, at point 3. In the simple gas turbine, this air is heated in the combustion chamber to a temperature of 960 F, at constant pressure. It is then expanded down to atmospheric pressure in the turbine. The efficiency, defined as the difference between the turbine work and the compressor work divided by the heat input, is 40 per cent.

In the Götaverken cycle, all of the air discharged from the compressor is taken into the Diesel cylinder, point 3, but on the compression stroke the exhaust valve is not closed until 65 per cent of the charge has been expelled into the exhaust-receiver feeding the turbine. The remaining 35 per cent is compressed along line 4–5 to a pressure of 205.8 lb, where it is mixed with fuel, ignited, and heated to 4210 F at 882 lb, point 6. It is then expanded isentropically to point 3, where it is discharged into the receiver at 2000 F. The mixing of this hot gas with the 403-deg air, previously expelled into the receiver, results in the same temperature, pressure, and weight of gas at point 7 as before. The work done in the turbine is, therefore, exactly the same as in the previous case, but the cycle has been so chosen that the net output of the Diesel supplies the work done in the compressor. The efficiency is, therefore, equal to the total turbine output divided by the heat input between points 5 and 6, which turns out to be 49.2 per cent. This particular cycle is thus 23 per cent more efficient, on this idealized basis, than the simple gas turbine.

The advantage of the Diesel boiler cycle in this instance cannot be attributed to the fact that the maximum temperature of the cycle is much higher than in the simple gas turbine. With isentropic compression and expansion, as assumed herein, it is interesting to note that the over-all efficiency of the gas turbine is independent of the temperature of the gas entering the turbine. The superiority of the Diesel cycle lies in the fact that it supplies the compressor work more efficiently by virtue of the greater expansion ratio in the Diesel cylinder, 5.30, as compared with 3.63 in the gas turbine.

On the basis of actual compressor and turbine efficiencies, substituting the rather optimistic figure of 85 per cent for both units, the over-all gas-turbine efficiency drops from 40 to 16.4 per cent. If the Diesel output is likewise 85 per cent of the theoretical value, the actual efficiency of the Götaverken cycle would be reduced to about 30 per cent. With lower efficiencies of the components, it may be seen that the gas-turbine cycle rapidly collapses to zero output, at the specified inlet temperature of 960 F, unless the Diesel or some other engine is provided to drive the compressor. These considerations indicate that the addition of a relatively small piston engine in this manner may make it possible to utilize a gas turbine as the final drive under conditions where it would otherwise be impracticable.

R. C. MUIR.[9] The author's closing statement shows great restraint, when one considers the faith that he has in the ultimate successful development of the gas turbine, a faith supported by study, experiment, and research on the gas turbine throughout his entire engineering career of nearly 50 years; and those who know the author know that these were years of great activity.

It must be with great satisfaction that he has seen the gas turbine become such an important part of the gas-and-oil-engine cycle, more specifically in the form of the turbosupercharger which has given us superior airplanes.

However, he does speak encouragingly when he says the gas-turbine prime mover seems to be getting nearer, notwithstanding the equities and probable improvements in other heat cycles.

The gas-turbine prime mover has been slow in coming because its principal elements, the compressor and the turbine, had to be highly perfected before the gas turbine had any output. Other forms of prime movers gave some output even though each element was very inefficient. With efficiencies of turbines and compressors in the 80 to 90 per cent bracket, and with materials capable of high stress and low creep at temperatures of more than 1000 F, we have arrived at a point where the gas-turbine prime mover is a fact.

There are some applications where light weight, low space factor, and scarcity of water are necessary, and these are the applications for which the gas turbine should be studied today,

[8] Supercharger Engineering Division, General Electric Company, West Lynn, Mass. Mem. A.S.M.E.

[9] Vice-President in Charge of Engineering, General Electric Company, Schenectady, N. Y. Mem. A.S.M.E.

even though its thermal efficiency is less than that of some other heat cycles.

However, it is probable that higher efficiencies of turbine and compressor will be obtained, and that materials capable of higher temperatures under stress conditions in the turbine will come through metallurgical research, and with these the gas-turbine prime mover will become a legitimate competitor of other forms of prime movers in more extended fields of application.

FREDERICK NETTEL.[10] The story of the good old days of the gas turbine, when everybody was happy if it turned at all, as related by the Nestor of American gas-turbine engineers, is truly fascinating and will forever form a valuable contribution to the history of this oldest and, at the same time, newest, power machine.

The historic references may be rounded out by mentioning a few pioneer thinkers, whose contributions to the art, even though in the form of patent specifications only, seem important enough, or may become so, considering the more recent trend of developments in gas or air turbines. These are as follows:

1 U. S. Patent 18,435 to Philander Shaw of Boston, dated May 2, 1854: Reissue No. 1014, dated July 17, 1860, which discloses the principle of passing the air exhausted from a hot-air engine through the fire (in the furnace) for purposes of economizing heat. This is important in connection with efforts to realize coal-burning air-turbine plants.

2 British Patent 18,435, convention date Norway, Aug. 26, 1903, to J. W. A. Elling of Christiania (Oslo) showing an early example of gas-turbine plant with multiple-stage centrifugal compressor embodying precooling and intercooling of the air in two stages, in combination with one turbine and recuperator.

3 German Patent 216,191 of Sept. 12, 1906, to S. Z. de Ferranti of Sheffield, England, illustrating probably for the first time useful power turbine and compressor driving turbine on separate shafts. The turbines are arranged in series as regards the flow of the combustion gases, with the low-pressure turbine driving the compressor. Included is the first discussion of regulating problems in multishaft gas-turbine plants.

4 U. S. Patent 853,124 to E. L. Schaun of Baltimore, May 7, 1907, describes for the first time starting of a gas turbine by compressed air.

5 U. S. Patent 1,316,234 of Sept. 16, 1919, to J. O. Heinze of Springfield, Ohio, mentions most likely for the first time gas turbines with oppositely rotating runners used for neutralizing gyroscopic action on vehicles with particular reference to airplanes. (This was in the meantime reinvented several times!)

While the author quite logically omits detailed thermodynamic computations in his predominantly historical paper, he draws certain conclusions from a simple approximate calculation which at this date tempts the "red-hot" gas-turbine enthusiast to a few remarks:

Much has happened since the days when it was thought possible to dispose of the gas-turbine problems "comprehensively" or even "definitively" by thermodynamical calculations of probable efficiencies along textbook lines.

Without wishing to go into details in this discussion, it appears timely to take cognizance of the fact that during the last few years much fundamental work has been done all over the world on the thermodynamics of the gas and air turbine. This brought to the fore, among other things, the long underestimated value of intercooling and reheating of the working fluid. Due to the war, and other considerations, much of this work will have to remain unpublished for some time. However, it seems opportune here to emphasize in the interest of the healthy development of the gas turbine, that its future as a serious competitor of the steam turbine, and under certain circumstances even of the Diesel engine, is today no more predicated upon the employment of extraordinarily high temperatures.

[10] Manhasset, L. I., N. Y.

In short, a modern gas-turbine plant of about 4000 hp, or preferably more, working at a maximum gas temperature of 1050 F, consisting of two stage compressors with interposed intercooler, two turbines with interposed reheater, and a recuperator of acceptable size, can be designed and built to give a rated-load thermal over-all efficiency of 30 per cent, referred to the coupling of the useful power turbine. The efficiencies assumed in that plant for both turbines and compressors, as well as the parasitic losses (pressure drops, etc.) are well within the range of figures measured in actual plants (Neuchâtel, etc.)

Steam-turbine designers know only too well why they prefer not to go much above 1000 F at present, in spite of the fact that the steam turbine would also profit from a rise in superheat, particularly in high-pressure plants. If they thus avoid what they consider grave risks, evaluated from vast experience, there is little basis for crediting gas-tu bine designers, with much less to build upon, with greater ingenuity or wizardry in dealing with 1200 F, or even 1500 F.

Since, as mentioned, the gas turbine must be considered a potential thermal and—on account of savings in weight, space, and cooling water—economic rival of high-pressure steam plants, even when employing gas temperatures in the range of what has been accepted for some years for steam turbines, higher temperatures should be resorted to only with the greatest caution and gradually.

Setbacks due to gambling with higher temperatures are liable to be unjustly blamed on the gas turbine and are bound to retard rather than to assist its healthy development.

J. T. RETTALIATA.[11] The author, in devoting his efforts since the beginning of the century to the advancement of the gas turbine, deserves much credit for the recognition it is receiving at the present time. In his interesting paper, he rightly points out the antiquity associated with the gas-turbine art, thus correcting any erroneous beliefs, which may have arisen due to the recent attention being accorded it, that the gas turbine is a modern invention.

The author may well be proud of his contributions in the many years of development of the turbosupercharger, a device playing such a vital part in the present conflict. The modern turbosupercharger is exhibiting admirable performance in the type of installation now being employed. The efficiencies of its respective compressor and turbine elements are adequate in the present application where no additional power is required from the turbine beyond that needed to effect compression.

Since the aim of the aviation industry is ever to decrease the weight per horsepower of the power plant, the next logical modification of the turbosupercharger would be to achieve compressor and turbine efficiencies of the highest order so as to produce an excess of power. This additional power could be fed back into the engine or propeller shafts or utilized in the form of a jet-propulsion effect from the turbine exhaust gases.

The large-scale prime-mover type of combustion-gas turbine has benefited and will, undoubtedly benefit from turbosupercharger experience but it should be remembered that they are basically different types of units. The supercharger approaches a limit design in that minimum-weight requirements necessitate relatively high speeds and stresses resulting in a limited service life. Some of the high-temperature metallurgical problems of the supercharger therefore differ from those of the more conservatively designed, longer-life, prime-mover type of gas turbine. For the supercharger, materials having good stress-rupture properties are desirable, whereas, for longer-life units creep char-

[11] Chief Research Engineer, Steam Turbine Department, Allis-Chalmers Manufacturing Company, Milwaukee, Wis. Jun. A.S.M.E.

acteristics may be more important. Further, high-temperature alloy castings and forgings in sizes suitable for superchargers are easier to produce than those required for large-size gas-turbine units.

As a prime mover, the combustion-gas turbine is quite versatile owing to the many different kinds of cycles that can be employed; giving a wide range of thermal efficiencies. The basic cycle, embodying a single turbine, compressor, and combustion chamber, will represent the lowest part of the range. Fortunately, it can be modified so, when operated with temperatures permissible with materials now available, good thermal efficiencies are possible.

One such cycle modification, comprising intercooling in the compressor, reheating between the power and compressor turbines, and preheating of the compressor discharge air with the turbine-exhaust gas, is shown in Fig. 17 of this discussion. This cycle is capable of yielding a coupling thermal efficiency of 30 per cent when operated with turbine, inlet temperatures of 1200 F, a pressure ratio of 5, and 1500 and 5000 sq ft of surface in the intercooler and heat exchanger, respectively.

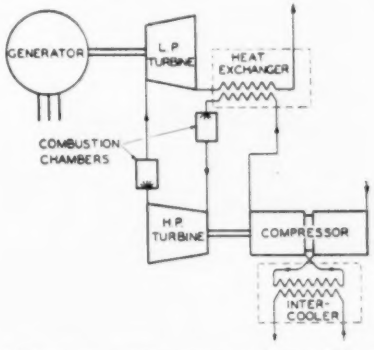


Fig. 17 Gas-Turbine Regenerative Cycle With Reheating and Intercooling

As has been pointed out previously on many occasions the gas turbine has progressed mainly through the development of better materials and more efficient compressors. As a further step, assuming thermal efficiencies of 30 per cent for the present, it will probably be necessary to adapt pulverized fuel to justify economically the general use of the gas turbine in central-station practice. Such a procedure appears to have merit considering the appreciable difference in cost between coal and oil and the possible future scarcity of the latter.

The major commercial application in this country of the combustion-gas turbine in prime-mover sizes has been in oil refineries employing the Houdry catalytic cracking process in the manufacture of high-octane gasoline. Figs. 21 and 22 of Mr. Sidler's discussion show the first of these machines supplied by Brown Boveri. Many other units of the same type have since been built by Allis-Chalmers under Brown Boveri license. To date Allis-Chalmers has supplied 27 such gas turbines to the oil industry and much valuable operating experience has been obtained with these units.

The well-recognized limitations of the gas turbine preclude the possibility of its being considered as the answer to all future power problems. It is believed, however, that its inherent characteristics make it an ideal aspirant for certain applications in land, heavy traction, aeronautical, and marine fields.

P. R. Sidler.[12] In the course of the last 3 or 4 years several papers on gas turbines have appeared in the technical literature; some also have been presented before meetings of this Society. It is perhaps more than a coincidence that quite a few of them, notably those covering the subject in greater detail, devote very considerable space to a historical survey. Possibly Dr. Meyer's paper (33)[13] before The Institution of Mechanical Engineers and before this Society in 1939 started this trend. At any rate, several of the early gas-turbine "inventors" mentioned there have since reappeared in a number of papers, only to be summarily dealt with, as having contributed rather little that could be of use today.

It is interesting to speculate on the purpose of such extensive backward glances, especially if it is admitted that most of the gas-turbine proposals advanced during the first decade of this century were impractical or not workable at all. One good reason may be the desire to establish priority of ideas; another to make a case for continuity of research and study undeterred by early failures or lack of appreciation; still another could be to show why there is as yet in many quarters only a modest beginning on the road toward real gas-turbine power machinery.

Whatever the reasons, such historical surveys do help to focus attention on the many difficulties that stood in the way of a practical gas turbine which actually delivers useful power. They also emphasize that modern technical accomplishments are not the invention of any individual but the result of a co-operative effort of many minds, a structure slowly built up on primitive and often rather unsafe foundations. Again, the gas-turbine development shows that even large numbers of patents, issued through the years to many corporations and individuals in various countries, do not necessarily insure success. What really counts is the slow but consistent accumulation through tests and research of data and experiences, the building-up of shop techniques, and of "know-how."

The present paper is a very interesting account of the author's struggle with gas-turbine problems for over 40 years and of his successes in the field of turbosuperchargers for airplanes. The very detailed Bibliography should also be of definite value to the student of gas-turbine matters.

The fundamental work done in this field by Prof. A. Stodola (25) would seem to merit greater emphasis. A large part of his life work as research scientist, teacher, and consultant had been devoted to the development of the gas turbine, and he had the satisfaction of seeing his dreams come true (34), before he died on Christmas Day, 1942.

In the author's discussion on compressors for gas turbines there are a few points where the picture might be rounded out on the basis of available records.

It is stated that Rateau supplied centrifugal compressors for the Armengaud-Lemale gas-turbine work carried out in France. It is known that Professor Rateau had some preliminary models of single-stage centrifugal compressors built for this experimental gas-turbine work, but when the definite gas-turbine design was evolved in 1906, and the need for a larger centrifugal compressor developed, Mr. Armengaud turned to Brown Boveri. Fig. 18 of this discussion shows this machine on the test floor of the Brown Boveri factory in Switzerland. This is a three-cylinder unit with 25 impellers, built for about 2150 cfm at 55 psig, 4000 rpm, and required about 328 hp. It showed an efficiency between 65 and 70 per cent, depending upon the load.

This was incidentally the first commercial centrifugal compressor in the world and it was so successful that Brown, Boveri & Company immediately launched a manufacturing program for this new machine. Between 1906 and the end of 1910, a total of nineteen centrifugal compressors or blowers for blast-furnace operation were installed, among them six in England, three each in France and Chile, two each in Belgium and in Canada, and single units in a few other countries. Their air

[12] Resident Engineer, Brown, Boveri & Co., Ltd., of Baden, Switzerland, 19 Rector St., New York, N. Y. Mem. A.S.M.E.

[13] Numbers in parenthesis in this and subsequent discussions refer to the author's Bibliography.

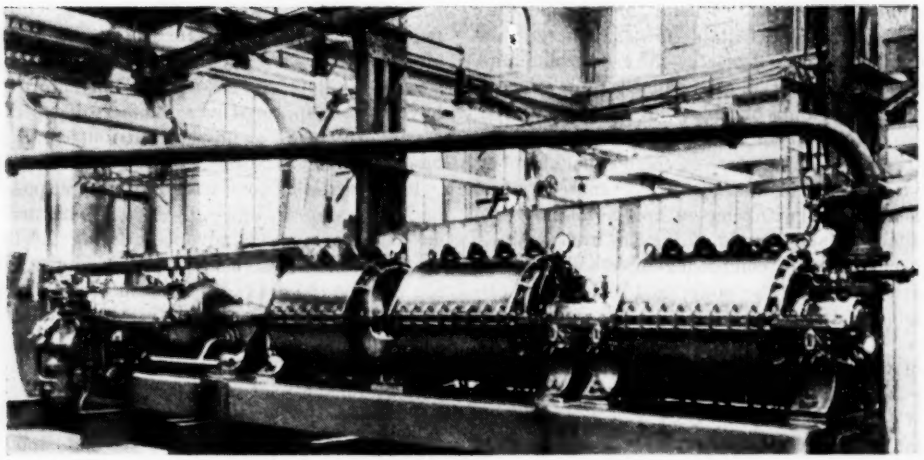


FIG. 18 THREE-CYLINDER TURBOCOMPRESSOR BUILT IN 1906 FOR ARMENGAUD-LEMALE GAS TURBINE

volume varied between 5000 and 32,500 cfm. During the same period Brown Boveri also completed eight turbocompressors for pressures between 62 and 103 psig and for installations in France, England, and other countries, besides about a dozen centrifugal blowers in various applications. It is interesting to note that this development finds a close parallel in the decisions of the General Electric Company, which installed the first two blast-furnace turbocompressors in this country in 1910.

With this background in centrifugal-compressor work and fully realizing its limitations, Brown Boveri worked on the development of a more efficient rotating machine and found the solution around 1931, in an improved axial-flow compressor, the principle of which had already been known for over 20 years. In fact Parsons had built several machines of this type in the period, 1905–1908, but had abandoned the design as it did not then show any advantage over the centrifugal compressor. It was only by applying newly developed data from the field of aerodynamics that a more efficient axial-flow compressor could be built. Since 1932, there have been put into commercial operation over seventy-five multistage axial-flow compressors in Velox plants, some forty units in gas-turbine applications, and about a dozen large machines up to 128,000 cfm in other fields, such as wind tunnels for airplane research, refrigerating plants, etc. Operating results on some of these plants have been published repeatedly and prove that the axial-flow compressor is indeed much more efficient than a centrifugal machine. Adiabatic efficiencies between 82 and 86 per cent have been consistently obtained (34).

Fig. 19 of this discussion shows the cylinder of an axial compressor built about 1933, for a Velox plant. The machine has 10 blade rows and produces a pressure of 36 psig. Fig. 20 shows the rotor for the same machine. To be sure, the pressure ratio of the axial-flow blower is at present somewhat lower than that of centrifugal compressors, but this is not considered a serious handicap for successful gas-turbine operation. Their greater number of stages on the other hand is no cause for apprehension either. There are many thousand steam turbines of the reaction type in service in the world today which have even more blade rows and work under more severe conditions of pressure and temperature.

This higher efficiency of the axial-flow compressor is one of the basic reasons for the existence of a practical gas turbine today, that is, a prime mover which actually delivers useful power and does not use up all its output for driving the air compressor.

Incidentally, the axial-flow compressor is a perfect illustration

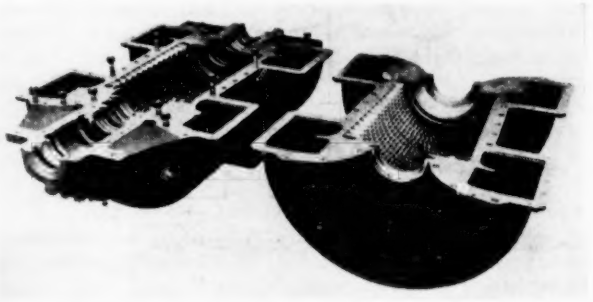


FIG. 19 UPPER AND LOWER HALVES OF AXIAL-COMPRESSOR CYLINDER FOR VELOX BOILER

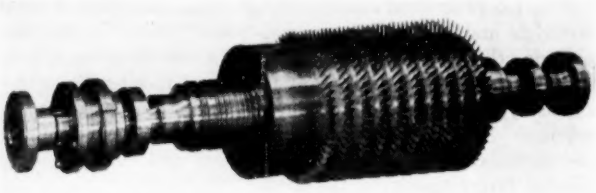


FIG. 20 ROTOR OF AXIAL COMPRESSOR AS PER FIG. 19, WITH ROLLER BEARINGS AND COUPLING FLANGES

for the statement that patents by themselves do not necessarily result in practical machinery. "It is rather the careful attention to details in manufacturing, rigid inspection, and thorough testing, in short, "know-how," which insures success. Even seemingly minor deviations from these rules may spell the difference between a machine that goes into service immediately after erection and another that requires perhaps several months of adjustment and partial rebuilding.

It is true that the application of such machines in the Houdry catalytic cracking process does not constitute a self-contained prime mover. Their main purpose in this process is the delivery of substantial air volumes. Nevertheless, all these units (nearly thirty machines are now in operation in the United States, the first eight being imported from Switzerland between 1936 and 1939) show a net surplus of power and are thus properly classified as gas turbines. In most cases this surplus is fed back into the electrical system, except where local conditions or contractual arrangements make it desirable to take it out in the form of heat.

Fig. 21 shows the rotating element of the first gas-turbine unit for the Houdry process, built in 1936, and in continuous operation since January, 1937, except for a few days of inspection and maintenance work on the whole plant, every 6 months. To the right is the five-stage gas turbine, to the left the 21-stage axial compressor, which is designed for 40,000 cfm at a delivery pressure of 45 psig and a speed of about 5100 rpm. The gear and the electric generator for the surplus power are not shown here, but may be seen in Fig. 22; at the extreme right is the starting motor for bringing the whole set up to speed, which can be uncoupled after the gas turbine takes over.

Beside the 4000-kw Neuchatel gas turbine and the 2200-hp unit powering the Swiss locomotive our company completed, during 1939 and 1940, four other self-contained gas turbines

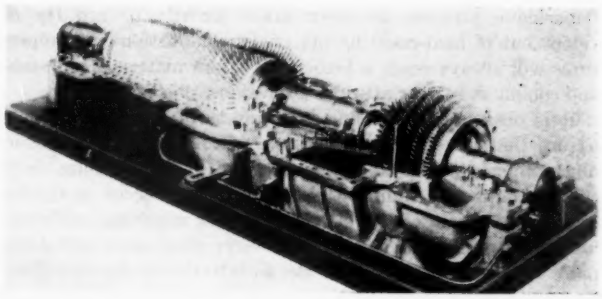


FIG. 21 GAS-TURBINE-DRIVEN COMPRESSOR SET FOR HOUDRY PROCESS WITH TOP CASING REMOVED

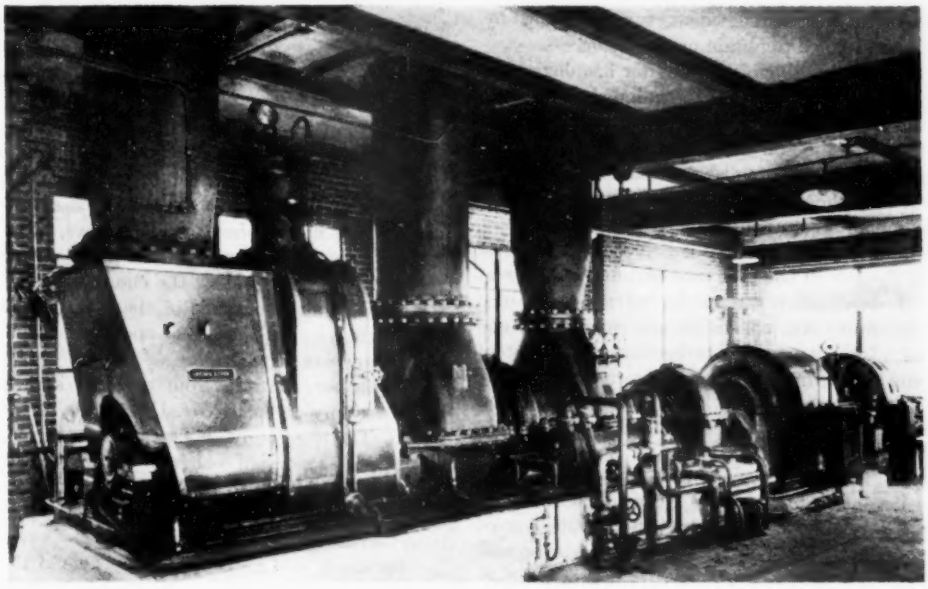


FIG. 22 FIRST GAS-TURBINE-DRIVEN COMPRESSOR SET FOR HOUDRY PROCESS, INSTALLED IN EASTERN REFINERY

which went into operation after extensive tests. Two of them are working in blast-furnace plants, delivering the blast air and burning furnace gas. Unfortunately, it has not been possible to publish any performance data on these units due to wartime restrictions, but there is room for the hope that such information will be available before long.

In the field of superchargers, the author indicates that the first gear-driven machines for United States aviation engines were built in 1925. It might be noted in passing that several hundred gear-driven centrifugal superchargers, following Rateau or Brown Boveri design, were in use in Europe during the first world war.

As to exhaust-turbine-driven superchargers, the writer has noted the statement that no turbosuperchargers other than those of General Electric are in use in the present conflict. He does know, however, of rather extensive developmental programs started several years prior to the outbreak of this war with well-known airplane-engine builders in England and France, following the Brown Boveri - Büchi system. It would seem likely that these efforts have produced some results, although no supporting evidence is available due to censorship restrictions.

Under the heading "High-Temperature Progress," the author mentions some tests made in the Brown Boveri shops with an airplane supercharger running at 30,000 rpm and about 1800 F. It should be added that the diameter of the turbine wheel is in the range of 10–12 in. This is considerably smaller than that of turbosuperchargers used in this country and running at substantially lower speeds and temperatures.

After discussing some controversial points, the writer is very glad to conclude with a note of entire accord, namely, in regard to the important contributions of the author's work on turbosuperchargers, especially in the line of high-temperature operation, for the advancement of the combustion-gas turbine. This experience will be particularly interesting for checks and comparison with the results of research work that has been going on in other quarters, all directed toward the development of alloys which will stand up in gas turbines for continuous service with gas temperatures of 1500 to 1700 F.

By using these results in conjunction with the other known and developed elements of the gas-turbine cycle, particularly the efficient axial-flow compressor, we shall surely construct in the coming peace years gas-turbine power plants of high thermal efficiency which will find ready acceptance in many fields that are now being regarded as the exclusive domain of the steam turbine or the Diesel engine.

W. E. TRUMPLER.[14] In this presentation, attention has been called to the importance of heat-resisting materials, high compressor and turbine efficiencies. It is felt that not enough emphasis has been placed on the problem of blade cooling. While

[14] Development Engineer, Carrier Corporation, Syracuse, N. Y Mem. A.S.M.E.

remarkable progress has been made recently toward the development of heat-resisting materials, combustion-gas temperatures will always reach a higher level than materials can stand, and cooling may offer attractive solutions.

It is obvious that cooling in a gas turbine is of a different nature that in combustion engines. Cooling by air circulation must supersede the cooling-water jacket. Air cooling to be effective must use similarly high velocities as occur in the turbine-blade channel. To do this without involving additional losses, the cooling circulation must serve some other useful purpose, such as compression of the air into the combustion chamber. The losses then are only slightly higher than with compression performed independently. Lorenzen (26) is to the writer's knowledge the first to have used passages in the turbine wheel and through hollow blades to produce centrifugal compression and cooling combined. His arrangement suffered from hydraulic imperfection and failed to obtain practical success.

Following the same basic principle, the writer has devised an arrangement wherein the turbine wheel is equipped with specially shaped blades suitable for both compression and expansion and partially admitted to the flow of each function. The blade in question is bound to be a compromise design and the blade efficiency will suffer, also the change from one operation to the other twice during one revolution involves additional losses. Very complex hydraulic problems must be solved to keep these losses to a tolerable figure. It has been proved, however, even at this early stage of development, that the advantage gained by cooling the blades more than offsets the additional hydraulic and thermal losses. It is impossible to predict the extent of future improvements in this direction, but it is certain that blade cooling will have an economic justification in the gas turbine of the future.

G. B. Warren.[15] The development of the gas turbine has been the grand passion of the author's life. His not inconsiderable participation in the development of the centrifugal compressor, then of the steam turbine, and finally of the airplane turbo and geared centrifugal supercharger, has, if the writer judges him correctly, been but a stepping stone in his quest for the ultimate development of the gas turbine itself. It is altogether fitting and proper that as a result to an appreciable extent of these efforts, combined, to be sure, with the achievements now of many other men, the author can begin to see the real possibilities of the development of several successful gas turbines on the part of numerous groups. This new but old form of prime mover is destined to play a very important role in our industrial life.

Another important achievement, for which it is believed the author is more responsible than any other one man and regarding which he says nothing in his paper, but which came as a by-product of his other work, was the development of the gear-driven centrifugal supercharger for airplane engines. This machine is now used on practically every military airplane engine in the world whether or not a turbosupercharger is used. A very large number of these have been produced from the designs of the division of the General Electric Company that the author organized.

It is, of course, unfortunate that the requirements of the national war effort limit the matters which the author could have discussed in this paper. Such will not always be so, and the sequel to this paper written by the author or others will make interesting reading when that time comes.

The very complete Bibliography will undoubtedly prove to be a particularly helpful tool to the many others now working in this field.

[15] Turbine Engineering Division, General Electric Company, Schenectady, N. Y. Mem. A.S.M.E.

Author's Closure

The author feels highly complimented by the discussions which have been contributed and wishes to express his thanks and appreciation. A number of the discussions are by eminent authorities who have had actual experience with the subject so that they add a great deal to the author's presentation. The author also is thankful for a number of new references which may increase the bibliographical value of the paper. Some of these are given in the discussions, and a few have been communicated to the author and are added to the list of references.

As several of the discussers have mentioned, some of the items presented in the paper already are known to some extent. However, correspondence which the author has received indicates that even though some items may be known to some of the older generation, it is desirable to include them all for the sake of completeness and for the benefit of the younger generation. They are the ones who are to have the task of bringing the gas turbine to the successful fruition which is foretold by the present situation.

In spite of some belief to the contrary, the author feels that the ultimate gas turbine will successfully and conservatively operate at very high temperatures. Fig. 12 of the paper, and colored photographs that have been taken, of nearly white-hot nozzle boxes and red-hot turbine wheels, are visual evidence of the purpose of the portion of the paper devoted to turbosuperchargers, which is to show the enormous contributions that the thousands upon thousands of these turbosuperchargers now in use are making to the art of operating turbines safely at very high temperatures.

The author can add from personal knowledge, to the discussion kindly given by Mr. Haverstick of the De Laval Company. The Sherbondy apparatus that Mr. Haverstick mentions started out as a design sent from France by Rateau to his American agents, the Rateau-Battu-Smoot Company, and no doubt shown in Mr. Haverstick's Fig. 14. But there was great change from this design of Rateau in the course of the development work by Sherbondy and Fergus Motors. One of the changed models is given in the 1927 New York edition of Stodola (25),[16] as Mr. Haverstick states. But the accompanying diagram (Fig. 1086) is not, as stated by Stodola, the General Electric apparatus, but is a general diagram of the cycle, probably first presented by Rateau. The General Electric details always differed materially from Rateau or Sherbondy. Major George E. A. Hallet had charge during this period of the Powerplant Division of the United States Army Air Corps, McCook Field, Dayton. He wrote at the time ($44^1/_2$,) which gives further details of this period, " . . . . . no way was seen to overcome the faults of the Sherbondy machine. Therefore, the latter was dropped and General Electric was given a contract to rebuild the old supercharger designed by Dr. Moss." Major Hallett recently gave similar details, which have been quoted by Frederick Neely.[17] The Rateau machine did operate in France and was given a test in England. But as the author and other General Electric engineers have learned the hard way, it is one thing to have apparatus that operates on paper or on test, and another to obtain actual service on many airplanes at high altitude. The "know-how" that Mr. Sidler of Brown Boveri appropriately mentions only is obtained through such experience.

There has been included the oft-repeated gas-turbine thermodynamics only by citation of references. But one thermodynamic item that probably is novel has been called to the author's attention by Mr. F. K. Fischer of the Westinghouse

[16] Bibliography (25), Fig. 1086a, p. 1252.

[17] "Conquest of the Stratosphere," by Frederick Neely, *Air Transport*, March, 1944.

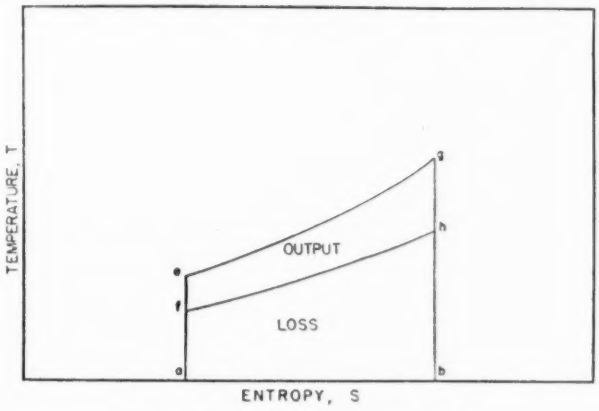


FIG. 23 SIMPLE GAS-TURBINE CYCLE

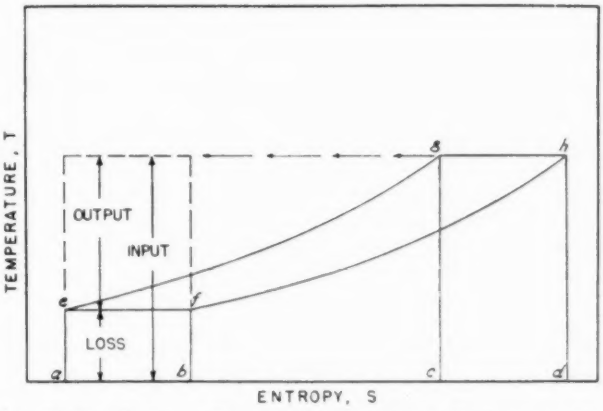


FIG. 24 GAS-TURBINE CYCLE WITH COMPLETE REHEATING, REGENERATION, AND INTERCOOLING

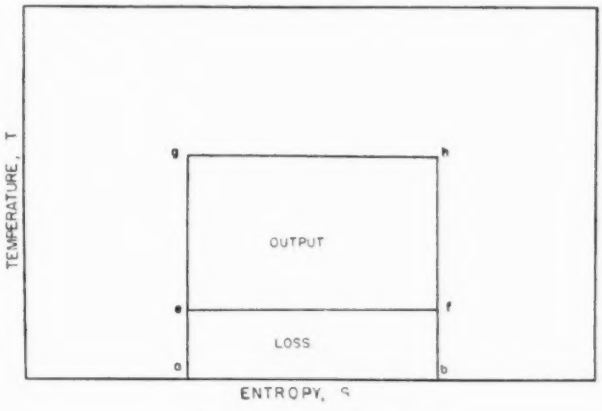


FIG. 25 CARNOT CYCLE

Company, Philadelphia, and Mr. Lee J. Fischer of the General Electric Supercharger Division, Lynn, Mass., and seems worthy of inclusion as follows:

Although the simple gas-turbine cycle, Fig. 23, has a lower efficiency than the Carnot cycle for given temperature limits, a plan with complete reheat, regeneration, and intercooling will give a theoretical cycle, Fig. 24, which has the full Carnot efficiency, which is the maximum of efficiency obtainable with given temperature limits Fig. 25. Dr. Rettaliata's Fig. 17 shows a well-known partial approach to this scheme.

The simple gas-turbine cycle, Fig. 23, consists ideally of an isentropic compression (*f* to *e*), a constant pressure heating (*e* to *g*), an isentropic expansion (*g* to *h*), and a rejection of the exhaust gases at constant pressure (*h* to *f*).

The improved cycle Fig. 24, has compression (*f* to *e*) in a compressor with sufficient intercooling to maintain practically constant temperature. The constant pressure heating (*e* to *g*) is completely accomplished through regeneration by a theoretically infinite heat exchanger, utilizing the heat of the exhaust gases (*h* to *f*, area *b-f-h-d* being essentially equal to area *a-e-g-c*). The gases are expanded (*g* to *h*), in a turbine having sufficient reheat to maintain constant temperature.

The only external heat added to the improved cycle is, therefore, that put in during the reheating process (area *c-g-h-d*). The heat rejected is that rejected to the compressor cooling medium (area *a-e-f-b*). The work done (area *e-g-h-f*), Fig. 24, practically is equivalent to a rectangular area of the same base and height. This assumes that expansion and compression through the same pressure ratio gives the same entropy increment, (which is the case with a perfect gas). Consequently, for the same temperatures, the efficiency of this improved cycle is the equal of the Carnot cycle, Fig. 25, in which the compression (*e* to *g*) practically is isentropic, the heating process (*g* to *h*) practically is isothermal, the expansion (*h* to *f*) is isentropic and the rejection of heat (*f* to *e*) also practically is isothermal.

In actual practice, therefore, if sufficient heat-exchanger surface and properly high efficiency of the various elements could be obtained, the gas-turbine cycle would be able to approach Carnot efficiency as a limit.

Of course, this only is a theoretical dream and there are a lot of limitations and practical difficulties to be overcome betore its realization even can be approached. But it is inspiring to realize that there is such a theoretical possibility even though it may take a long time to approach it.

The author has had many years of pleasant association with Mr. Glenn B. Warren and must admit the statement made in his discussion, that the development of the gas turbine has been the "grand passion" of the author's engineering career. This career no doubt now is drawing to a close; but nevertheless the author expects to see many power-plant-gas turbines commercially developed by the younger generation.

Bursting Tests of Steam-Turbine Disk Wheels

By ERNEST L. ROBINSON,[1] SCHENECTADY, N. Y.

Bursting tests on model disks of steam-turbine-rotor material both with and without a central hole show that the average hoop stress at bursting speed for a good alloy steel is likely to exceed the tensile strength of the material as determined in an ordinary tensile test whether or not the hole is present. With a good turbine-wheel material, the maximum stress at bursting speed in a flat disk, calculated on the basis of elastic theory, greatly exceeds the tensile strength of the material; and if there is a central hole, it is more than double the tensile strength. Thus a comparison of tensile strength with average hoop stress in a wheel gives a fairly reasonable estimate of the factor of safety against actual bursting. Test results are also given on low-carbon and on high-alloy materials.

DURING the past 10 years and especially since steam temperatures have increased to the level where materials suffer a gradual deformation called creep, it has become quite common to construct turbine rotors out of solid forgings instead of assembling a succession of wheels on a shaft and expecting them to stay tight by virtue of their elastic grip on the shaft. Such rotors are often quite large, and it has been thought good practice to bore an inspection hole through the geometrical center in order to be sure of the soundness of the material. Under such conditions a calculation of the elastic-stress distribution in the immediate vicinity of the central hole shows the tangential stress to rise at the edge of the hole to double the value in the center of the rotor without any hole.

There is no question as to the existence of this elastic-stress concentration, but only a limited amount of material which depends on the size of the hole is subjected to the extra stress. Thus with a ductile material it seems likely that no ill effects will be experienced in having such a local stress exceed ordinary rules of design. Thus it may be reasonable to be guided by the bore stress in a shrunk-on wheel, but it does not seem equally reasonable to count the local stress at the boundary of an inspection hole. Of course, this stress can be avoided by not boring such a hole. However, such a decision would tend to place too much reliance on the attainment of a perfect calculation and would blindly assume perfection of the material. It has therefore been deemed good practice to bore the hole and not count the local stress concentration.

The several series of tests described herewith were originally undertaken to make sure that this judgment was well founded, and this turned out to be the case.

Heat-Treated Nickel-Chrome-Molybdenum Steel, S.A.E. 4340

Chemical Composition: (Per cent) C—0.39, Ni—1.81, Cr—0.74, Mo—0.38, V—0.09, Mn—0.57, Si—0.18

Heat-Treatment: 950 C (1742 F) 8 hr furnace cool, 100 C (180 F) per hr, 650 C (1202 F) 4 hr furnace cool

The first series of wheels consisted of four flat disks 11 in. diam and $^{9}/_{16}$ in. thick, two without any center hole and two with a center hole 1.5 in. in diam. Fig. 1 shows the elastic-stress distribution in these wheels. It may be noted on the right-hand scale that the maximum stress at the center (without any hole), as given by the ordinary elastic theory, is 10,000 psi at 10,000 rpm, while the average bursting stress is 80 per cent of the maximum, or 8000 psi. The diagram also gives at the left the stresses at 40,000 rpm, the stress being greater in proportion to the square of the speed.

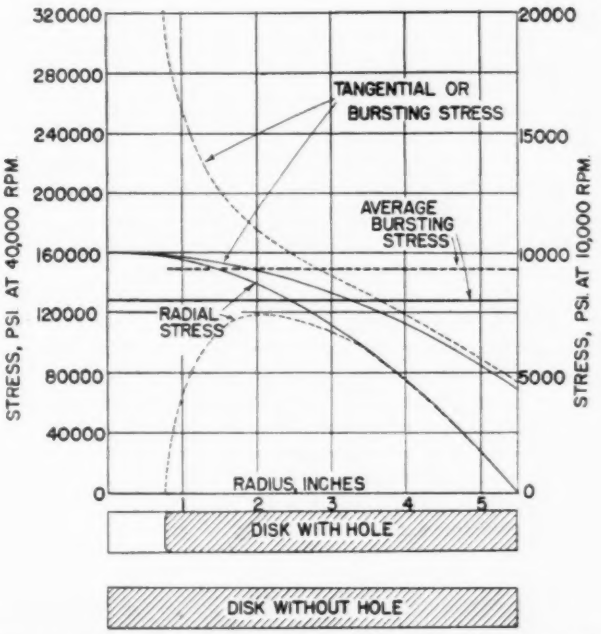


FIG. 1 ELASTIC STRESS DISTRIBUTION IN ROTATING DISKS WITH AND WITHOUT A CENTRAL HOLE

(The solid lines represent the stress distribution in the solid disk and the dotted lines the disk with hole.)

Table 1 gives the physical properties and the results of the bursting tests. Regardless of whether or not the central hole was present, these wheels burst with average stresses ranging from 121,600 psi to 131,000 psi, or 98.9 to 106.5 per cent of the tensile strength. The presence of the central hole thus reduced the actual bursting strength just about in proportion to the amount of material cut out.

The maximum center or bore stresses which would have existed at bursting speed if the wheels had remained elastic amounted to 130.1 and 131.3 per cent of tensile strength for the solid wheels and 229.3 and 213.0 per cent of tensile strength for the wheels with holes. Thus with this typical steam-turbine-rotor material the average bursting stress is an excellent measure of ultimate strength.

The measured deformation also given in Table 1 may or may not be significant. WB4 with center hole enlarged almost 4

[1] Turbine Engineering Division, General Electric Company. Mem. A.S.M.E.

Contributed by the Applied Mechanics and Power Divisions and presented at the Annual Meeting, New York, N. Y., Nov. 29–Dec. 3, 1943, of THE AMERICAN SOCIETY OF MECHANICAL ENGINEERS.

NOTE: Statements and opinions advanced in papers are to be understood as individual expressions of their authors and not those of the Society.

TABLE 1 PROPERTIES AND RESULTS OF BURSTING TESTS ON WHEELS OF HEAT-TREATED NICKEL-CHROME-MOLY STEEL, S.A.E. 4340

PHYSICAL PROPERTIES

Tensile strength, 123,000 psi — Elongation, 15.0 per cent
Elastic limit, 80,400 psi — Reduction in area, 39.1 per cent

STRESSES AT BURSTING SPEED

Disk no.	Speed, rpm	Average stress, psi	Per cent of T.S.	Elastic stress, psi	Per cent of T.S.
11-in-diam flat wheels without hole					
WB1	40000	129000	104.9	160000	130.1
WB3	40200	130400	106.0	161500	131.3
11-in-diam flat wheels with 1.5-in. center hole					
WB2	37500	131000	106.5	282000	229.3
WB4	36120	121600	98.9	262000	213.0

DEFORMATION IN DISK, PER CENT

	Rim diam	Rim thickness	Center thickness	Bore diam	Bore thickness
11-in-diam flat wheels without hole					
WB1	0.91[a]	—2.67	—10.9	...	...
WB3	2.28	—2.67	—16.3	...	...
11-in-diam flat wheels with 1.5-in. center hole					
WB2	2.0	—2.13		31.3	—11.4
WB4	3.72	—1.07		32.8	—10.7

[a] Based on diameter after last run before bursting.

per cent on the diameter; whereas, the solid wheel WB1 had enlarged less than 1 per cent on the last run before bursting. This wheel went into very small fragments, the largest "piece of pie" being just about 1/8 of the whole. Three of these fragments had radii smaller than the original wheel as if bursting had released a star- or spider-shaped void in the center and allowed the rim to go scallop-shaped. Undoubtedly it is necessary to take note of such behavior in order to understand the results and assign proper significance to them.

original 11 in. may be seen plainly on the foot rule. The thinning toward the center is also perceptible below the straight edge of the rule. The white paper sticking out of the center hole shows how much it has enlarged over the original 1.5 in.

LOW-CARBON STEEL, S.A.E. 1020

Chemical Composition: (Per cent) C—0.15 to 0.25, Mn—0.30 to 0.60

Heat-Treatment: 850 C (1562 F) oil quench, 650 C (1202 F) air cool

The second series of wheels consisted of four flat disks just like those of the first series. In addition, there were two more disks made with the bottle-shaped cross section necessary to give a uniform distribution of stress over the entire interior of the wheel as shown in Fig. 3. These two wheels were designed to get the maximum peripheral speed out of a given material. They are directly comparable with the flat wheels of 11-in. diam, since the elastic stress at 10,000 rpm is also 10,000 psi. This stress, as with the flat wheels, would rise to 160,000 psi at 40,000 rpm. However, whereas the stresses in the flat wheel fall off from the maximum at the center to much lower values toward the outside, both the radial and tangential stresses remain equal and of constant magnitude from the center to the inside of the small rim. In the rim there is a slight falling off of the hoop stress, and within the small increase of dimension the radial stress drops rapidly from its maximum value to zero at the outside.

Thus these six wheels of the same material all have strictly



FIG. 2 NICKEL-CHROME-MOLYBDENUM STEEL DISK, WB4, 11 IN. DIAM AFTER RUN AT 36,000 RPM
(Enlargement at rim, 2.2 per cent; at hole, 21.2 per cent; thinning at rim, 1 per cent; at hole, 9.7 per cent.)

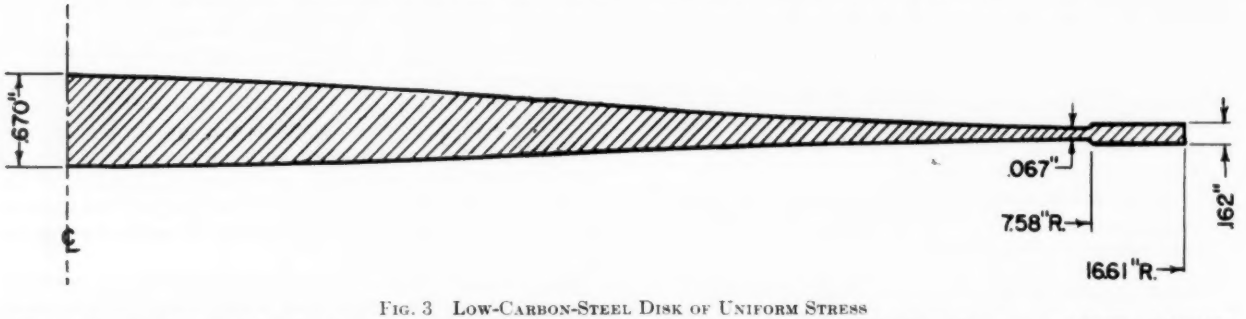


FIG. 3 LOW-CARBON-STEEL DISK OF UNIFORM STRESS
(The small rectangular rim takes the place of a bucket loading and is the only portion of the wheel in which the uniform stress of 10,000 psi at 10,000 rpm is not maintained. The thickness in inches, t, of this wheel at any radius r in inches is given by the formula $t = 0.670\ e^{-0.04r^2}$ where 0.670 in. is the center thickness.)

The solid wheel WB3 thinned 16.3 per cent at the center, an amount in excess of the elongation in the tensile test. The other wheels thinned about 2/3 as much. The center holes enlarged approximately one third from 1.5 in. diam to about 2 in. diam.

Fig. 2 shows one of these disks, WB4, with the central hole, after it had been run to 36,000 rpm, very close below the bursting speed of 36,120 rpm. The enlargement of diameter over the

comparable elastic-stress distributions at the same speed. In the two solid wheels the maximum elastic stresses are the same, but localized around the center of the flat wheel and of wide extent in the bottle-shaped wheel. In the flat wheel with the central hole the elastic-stress distribution in the outer half radius or 3/4 of the volume is very close to that in the flat wheel without any hole. However, in the inner half radius, comprising less than 1/4 of the volume of the wheel, the elastic stress rises

TABLE 2 PROPERTIES AND RESULTS OF BURSTING TESTS ON WHEELS OF LOW-CARBON STEEL, SAE 1020

PHYSICAL PROPERTIES

Tensile strength, 68,650 psi — Elongation, 37.5 per cent
Elastic limit, 47,150 psi — Reduction in area, 60 per cent

STRESSES AT BURSTING SPEED

Disk no.	Speed, rpm	Average stress, psi	Per cent of T.S.	Elastic stress, psi	Per cent of T.S.
11-in-diam flat wheels without hole					
WB5	29000	67800	98.8	84100	122.5
WB7	29400	69700	101.6	86500	126.0
11-in-diam flat wheels with 1.5-in. center hole					
WB6	24300	55000	80.1	118400	172.5
WB8	24400	55500	80.8	119400	174.0
16.6-in-diam wheels of uniform stress (no hole)					
WB9	25500	65000	94.7	65000	94.7
WB10	25200	63500	92.5	63500	92.5

DEFORMATION IN DISK, PER CENT

Disk no.	Rim diam	Rim thickness	Center thickness	Bore diam	Bore thickness
11-in-diam flat wheels without hole					
WB5	9.09	—4.97	—38.4	...	...
WB7	7.37	—4.80	—38.4	...	...
11-in-diam flat wheels with 1.5-in. center hole					
WB6	3.91	—3.2	...	46.0	—19.5
WB8	3.84	—3.55	...	42.8	—18.2
16.6-in-diam wheels of uniform stress (no hole)					
WB9	9.48[a]	—6.17	—18.9	...	...
WB10	2.83[a]	—8.63	—26.1	...	...

[a] Based on diameter after last run before bursting.

to a maximum value at the bore which is twice what it is in the other wheels. (Precisely speaking, this ratio is nearer 201 per cent than 200 per cent.)

This material was chosen as representative of very ductile materials, and it was heat-treated for maximum ductility. In examining the results, it is necessary to keep these facts in mind. The tensile test shows a real "yield point" where the material refuses to hold until it has stretched a considerable amount. After this stretching has occurred, it holds again, but this kind of ductility has its disadvantages.

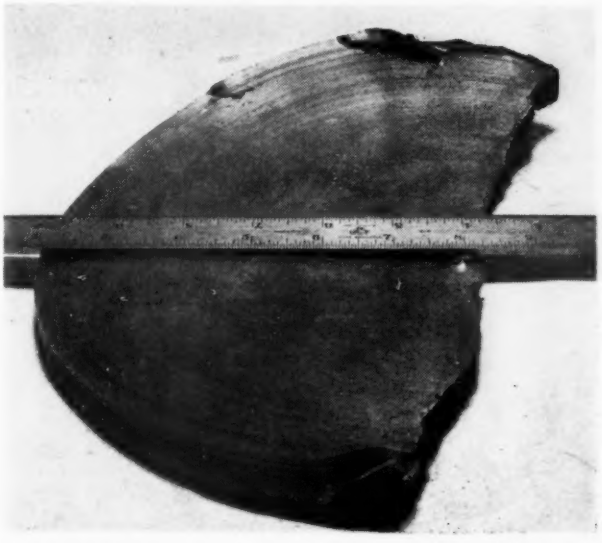


FIG. 5 LOW-CARBON-STEEL DISK WB5, 11 IN. DIAM AFTER BURSTING AT 29,000 RPM

(Enlargement at rim 9.1 per cent; thinning at rim, 5 per cent; at center, 38.4 per cent. Note that this is just about a full half wheel. The rupture is close to perpendicular to the plane of the disk.)

much as it got longer which is like a tensile bar. The wheel as a whole got thinner at the center, 38.4 per cent in each case, as compared to 37.5 per cent elongation in the tensile test. In each case this is the deformation in the direction of the axis of deformation, although the nature of the deformation is completely opposite. In the tensile test, the bar is pulled along its axis and goes in from all sides. The bursting disk is pulled out in all directions and goes in along its axis.

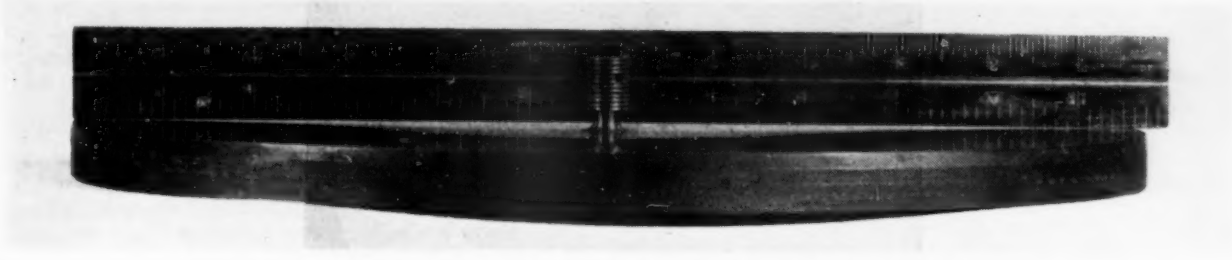


FIG. 4 LOW-CARBON-STEEL DISK WB7, 11 IN. DIAM AFTER RUN AT 28,320 RPM

(Enlargement at rim, 5.5 per cent; thinning at rim, 2.7 per cent; at center, 9.7 per cent.)

Table 2 gives the physical properties and the results of the bursting tests. The two solid wheels, WB5 and WB7, burst with average stresses based on the original dimensions of 98.8 per cent and 101.6 per cent of the tensile strength. However, the wheels enlarged 9.09 per cent and 7.37 per cent, respectively, with corresponding increases in the actual centrifugal bursting forces. Thus, going by the enlarged diameters, these wheels actually had average stresses at bursting of approximately 108 per cent of tensile strength. A pretty good case could be made out for basing the actual stress on the square of the enlarged diameter; but, since the centrifugal force itself goes only with the first power of the radius, such a procedure would correspond with the occasional practice of computing tensile strength on the basis of the reduced section instead of on the original dimensions. Analysis in terms of the original dimensions has the advantage that such dimensions are known in advance.

Note that the circumference got thinner about one half as

The two wheels with holes burst at too low speeds to develop average stresses equal to the tensile strength even if credit is allowed for the enlargement at the rim. (This has not been done in the table where all calculations are based on original dimensions.)

The rims got thinner almost as much as they got larger, but the center holes enlarged more than 40 per cent and only thinned less than 20 per cent.

The enlargement of these wheels was less than one half as much as the solid wheels. Apparently this material has a kind of ductility that does not allow all portions of these wheels to participate in the job of resisting the centrifugal force. The burst takes place at a time when the rim is not able to do its share in carrying the load or at least has not yet picked up its full share.

Fig. 4 illustrates WB7 after having been run at 28,320 rpm which is a little more than 1000 rpm below its bursting speed of 29,400 rpm. The foot rule in this picture shows plainly the

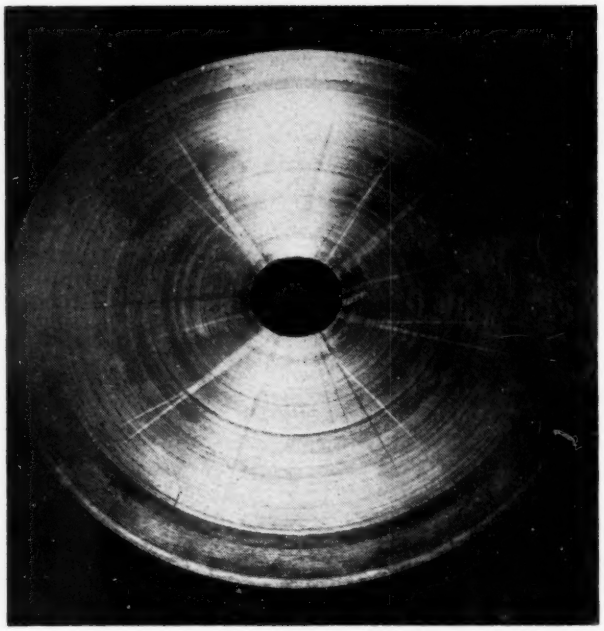


FIG. 6 STRAIN LINES SPREADING OUTWARD FROM EDGE OF HOLE AS THEY APPEARED ON SURFACE OF LOW-CARBON STEEL DISK WB8, 11 IN. DIAM, AFTER RUN AT 20,100 RPM

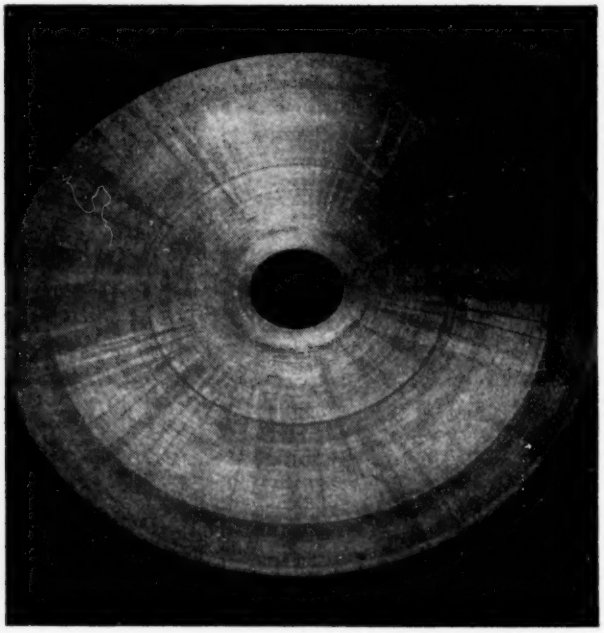


FIG. 7 STRAIN LINES REACHING TO RIM OF DISK WB8, AFTER RUN AT 21,300 RPM

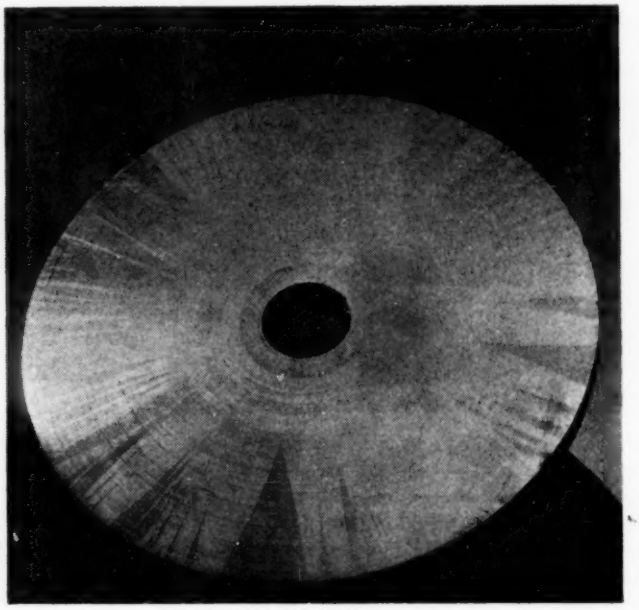


FIG. 8 STRAIN LINES DISAPPEARING OFF RIM OF LOW-CARBON STEEL DISK WB6, 11 IN. DIAM, AFTER RUN AT 22,380 RPM

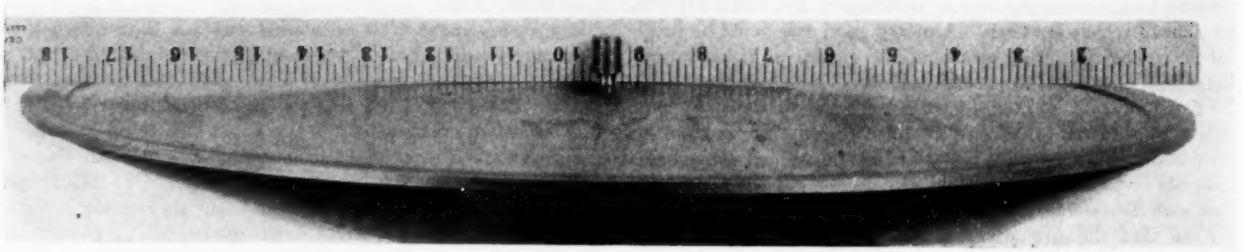


FIG. 9 LOW-CARBON STEEL DISK WB9, 16.606 IN. DIAM, PROPORTIONED FOR UNIFORM STRESS DISTRIBUTION, AFTER RUN AT 25,200 RPM
(Enlargement at rim, 9.5 per cent.)

enlargement of the diameter of the disk and its thinning toward the center.

Fig. 5 shows the fracture in the case of disk WB5. This appears to be a rather characteristic fracture. It seems necessary to conclude that, however instantaneous the burst, the fracture started at the center and finished up at the outside. There appears to be a tendency for these wheels in the final stages of enlargement to try to neck down on two perpendicular diameters, thus ever so slightly trying to make a square out of a circle.

Strain Lines. Fig. 6 shows the appearance of strain lines on the surface of disk WB8 after having been run to 20,100 rpm. The markings originate at the bore which is the first part of the wheel to attain a stress in excess of the yield point of the material. Fig. 7 shows the appearance of the same disk after having been run to 21,300 rpm. The markings have now reached the periphery of the disk while the region around the central hole has cleared up. Fig. 8 shows the appearance of the other identical disk WB6 after having been run to 22,380 rpm. The entire inner quarter of the surface out to the half radius of the disk has now cleared up.

Uniformly Stressed Wheels. The two wheels of uniform stress developed slightly less than full tensile strength on the basis of their original dimensions. However, it should be noted that WB9, shown in Fig. 9, enlarged from $16^{5}/_{8}$ to $18^{3}/_{16}$ in. diam or almost 10 per cent without bursting. Based on the actual centrifugal force with these enlarged dimensions, this wheel developed at least 105 per cent of tensile strength when it burst. While the flat wheels appear to have all burst from the center, these wheels of uniform stress both lost their rims, and neither gave way anywhere throughout the whole central web.

Peripheral Speeds. It is noteworthy that WB3 which was just a flat wheel with a tensile strength of 123,000 psi attained a peripheral speed of 1975 fps at bursting, and that WB9 with the theoretical shape and a tensile strength of only 68,650 psi attained a peripheral speed of 2025 fps at bursting. (In each case credit is here taken for the enlargement of diameter.) These figures give some indication as to the real value of design shape. Thus in this comparison the special contour of the wheel of uniform stress enabled a material 56 per cent as strong to attain fully as high a speed, or even a trifle higher.

Cyclops 17W

Chemical Composition: (Per cent). C—0.49, Mn—0.68, Si—0.60, Cr—13.30, S—0.012, P—0.020, Ni—19.31, Mo—0.68, W—2.30 (Allegheny Heat 34413).

Heat-Treatment: Preheat 5 hr at 1500 F; transfer to 2100 F and hold for 1 hr; forge to within 10 per cent of finished forging thickness; cold work at 1200 F to finished size; anneal 2 hr at 1200 F.

The third series of tests consisted of four 10-in-diam wheels of Cyclops 17W material $^{7}/_{16}$ in. thick, two without center holes and two with center holes 1.364 in. diam. This size of center hole bears the same relation to the over-all diameter as the 1.5-in-diam hole in the 11-in-diam disk. Thus all stresses are comparative with the first two series at a speed ratio of 11/10. In other words, the stresses in the 10-in. disks when running at 10 per cent higher speed are the same as in the 11-in. disks.

The results of the bursting tests are given in Table 3. The two solid wheels burst with average stresses of 77.4 and 81.3 per cent of the tensile strength. If perfectly elastic at bursting, the maximum stresses would have been 95.7 per cent and 100.6 per cent of tensile strength.

The two wheels with holes in them burst with average stresses 79.7 per cent and 81.2 per cent of the tensile strength. If they had remained elastic, the maximum stresses would have been 171.3 and 174.8 per cent of the tensile strength.

It is a noteworthy happenstance that the two wheels without holes in them burst when the maximum elastic stress reached 100 per cent of the tensile strength. This is not a reliable criterion for bursting, however, because the maximum elastic stress in the wheels with holes reached almost 75 per cent over the tensile strength.

For these wheels the best rule for bursting would be to say that they would develop an average stress equal to 80 per cent of the tensile strength, and this would be approximately true whether or not there is a center hole.

TABLE 3 PROPERTIES AND RESULTS OF BURSTING TESTS ON WHEELS OF CYCLOPS 17W MATERIAL

Physical Properties

(Standard 1/4-in-diam test specimen from rim)

Disk no.	Tensile strength, psi	Proportional limit, psi	Elongation, per cent	Reduction of area, per cent	Brinell No. Rim	Brinell No. Center
W1	131200	73400	18.0	22.6	255	269
W2	139500	89600	15.0	26.6	285	269
W3	135500	89600	15.0	26.6	277	255
W4	131200	77400	17.0	26.0	269	255

Stresses at Bursting Speed

Disk no.	Speed, rpm	Average stress, psi	Per cent of T.S.	Elastic stress, psi	Per cent of T.S.
10-in-diam flat wheels without hole					
W1	39000	101500	77.4	125500	95.7
W4	40000	106700	81.3	132000	100.6
10-in-diam flat wheels with 1.364-in-diam center hole					
W2	38000	111200	79.7	239000	171.3
W3	37800	110000	81.2	237000	174.8

Deformation in Disk, Per Cent

Disk no.	Rim diam	Rim thickness	Center thickness	Bore diam	Bore thickness
10-in-diam flat wheels without hole					
W1	2.65	—0.16	—6.25	...	...
W4	0.99	—0.80	—5.97	...	...
10-in-diam flat wheels with 1.364-in-diam center hole					
W2	1.20	—0.07	...	6.84	—2.76
W3	1.56	—0.16	...	5.09	—2.38

Gamma Columbium

Chemical Composition: (Per cent) C—0.34, Mn—0.45, Si—0.45, Cr—14.74, Si—0.010, P—0.013, Ni—25.06, Mo—4.32, Cb—1.88 (Allegheny Heat 34658)

Heat-Treatment: Same as for Cyclops 17W

The fourth series of tests consisted of four 10-in-diam wheels of "gamma columbium" material, $^{7}/_{16}$-in. thick, two without center holes and two with center holes, 1.364 in. diam. These four wheels were the same size as the third series.

The results of the bursting tests are given in Table 4. The

TABLE 4 PROPERTIES AND RESULTS OF BURSTING TESTS ON WHEELS OF GAMMA COLUMBIUM MATERIAL

Physical Properties

(Standard 1/4-in-diam test specimen from rim)

Disk no.	Tensile strength, psi	Proportional limit, psi	Elongation, per cent	Reduction of area, per cent	Brinell no. Rim	Brinell no. Center
G1	130200	81500	18.0	32.7	255	241
G2	127000	81500	18.0	25.5	255	255
G3	128200	79500	15.0	23.2	255	255
G4	130200	85500	18.0	31.4	262	248

Stresses at Bursting Speed

Disk no.	Speed, rpm	Average stress, psi	Per cent of T.S.	Elastic stress, psi	Per cent of T.S.
10-in-diam flat wheels without hole					
G2	39600	104700	82.8	129500	102.0
G3	40000	106700	83.2	132000	103.0
10-in-diam flat wheels with 1.364-in-diam center hole					
G1	36600	103000	79.2	222000	169.8
G4	37200	106500	81.8	229000	175.8

Deformation in Disk, Per Cent

Disk no.	Rim diam	Rim thickness	Center thickness	Bore diam	Bore thickness
10-in-diam flat wheels without hole					
G2	1.07	—0.78	—5.74	...	...
G3	2.45	—0.95	—7.75	...	..
10-in-diam flat wheels with 1.364-in-diam center hole					
G1	1.51	—0.66	...	5.46	—4.42
G4	1.44	—0.62	...	7.58	—4.00



FIG. 10 GAMMA COLUMBIUM DISK G4, 10 IN. DIAM, WITH 1.364-IN-DIAM HOLE AFTER BURSTING AT 37,200 RPM

(Note that the wheel has quartered itself. The rupture in the foreground approximates 45 deg to plane of disk, except near the center hole.)

two solid wheels burst with average stresses 82.8 per cent and 83.2 per cent of the tensile strength. Had they remained elastic, the maximum stresses at bursting would have been 102.0 per cent and 103.0 per cent.

The two wheels with holes in them burst with average stresses 79.2 per cent and 81.8 per cent of tensile strength. If they had remained elastic, they would have burst with maximum stresses of 169.8 per cent and 175.8 per cent of tensile strength.

The behavior of these wheels was remarkably similar to the behavior of those in the third series, and the same remarks might be made about them.

Fig. 10 shows typical fragments, illustrating the manner in which the wheels of the three high-alloy series burst. The sequence of the several types of rupture is not so clear as for the single type illustrated in Fig. 5. Certain interesting speculations might be indulged in as to what type of stress or strain reached a limiting value and constituted itself the trigger to release the burst. It seems certain that a variety of limitations can be observed among the various types of break so that the most useful conclusion is that no one theory of failure can be relied on to represent all conditions of stress or strain.

TIMKEN "25-16-6"

Chemical Composition: (Per cent) C—0.15, Mn—1.14, P—0.010, S—0.022, Si—0.84, Cr—16.75, Ni—25.26, Mo—6.29, N_2—0.175 (Heat No. 0213)

Heat-Treatment: Same as for Cyclops 17W

The fifth series of tests consisted of four wheels of Timken 25-16-6 material, $^7/_{16}$ in. thick, all 10 in. diam, except T1 which was 8.517 in. diam. As in the third and fourth series, two wheels were solid and two had center holes 1.364 in. diam.

The results of the bursting test are given in Table 5. The two solid wheels burst with average stresses 71.6 per cent and 61.5 per cent of tensile strength. If they had remained elastic, the stresses at bursting speed would have been 88.6 per cent and 76.2 per cent of tensile strength.

The two wheels with holes in them burst with average stresses 75.2 per cent and 72.5 per cent of tensile strength. If they had remained elastic, the stresses at bursting would have been 156.9 per cent and 156.4 per cent of tensile strength.

The behavior of these wheels differed somewhat from that of all the other series. The average stresses at bursting speed were lower relative to the tensile strength than for any of the other materials, being 71.6 and 75.2 per cent, respectively, except for T4 which developed only 61.5 per cent.

It is noteworthy that the wheels with center holes actually ran to practically the same bursting speeds as the solid wheels. The average stress at bursting was actually a higher percentage of the tensile strength in the wheels with holes than in the solid wheels.

TABLE 5 PROPERTIES AND RESULTS OF BURSTING TESTS ON WHEELS OF TIMKEN "25-16-6" MATERIAL

PHYSICAL PROPERTIES

(Standard $^1/_4$-in-diam test specimen from rim)

Disk no.	Tensile strength, psi	Proportional limit, psi	Elongation, per cent	Reduction of area, per cent	Brinell No.—Rim	Brinell No.—Center
T1	134500	87600	17.0	22.6	277	255
T2	137500	95600	17.0	16.3	285	269
T3	134500	93900	11.0	9.4	277	255
T4	140500	93900	16.0	22.6	285	269

STRESSES AT BURSTING SPEED

Disk no.	Speed, rpm	Average stress, psi	Per cent of T.S.	Elastic stress, psi	Per cent of T.S.
	10-in-diam flat wheels without hole				
T3	38000	96300	71.6	119200	88.6
T4	36000	86400	61.5	107000	76.2
	10-in-diam flat wheels with 1.364-in-diam center hole				
T1[a]	36200	101100	75.2	212000	156.9
T2	36000	99700	72.5	215000	156.4

DEFORMATION IN DISK, PER CENT

Disk no.	Rim diam	Rim thickness	Center thickness	Bore diam	Bore thickness
	10-in-diam flat wheels without hole				
T3	1.48	0.00	—2.98	...	...
T4	1.90	—0.23	—2.26	...	...
	10-in-diam flat wheels with 1.364-in-diam center hole				
T1[a]	4.76	0.57	...	22.8	—1.60
T2	0.71	0.23	...	1.87	—0.74

[a] Wheel T1 was actually only 8.517 in. diam and burst at 42,000 rpm; 36,200 rpm would give the same average stress with a 10-in-diam wheel. The elastic stress is based on the actual original dimensions.

THE HIGH-ALLOY MATERIALS

As a lot, the materials of the third, fourth, and fifth series differ in certain characteristics of performance from those of the first two series. They are like the first two series in that all the bursts on flat wheels appear to originate at the center where both the elastic stress and the measured strain are maximum. However, the three high alloys show a change of center thickness or bore diameter around one third of the percentage elongation in the tensile test while the carbon-steel and nickel-chrome-molybdenum wheels show corresponding deformations equal to or greater than those attained in the tensile test.

If there is a quality that might be called "biaxial ductility," the wheels of the first two series might be said to possess it while those of the last three series are not so ductile under biaxial stress regardless of the tensile-test results.

However, in spite of this condition, these high-alloy materials develop average bursting stresses of about the same level relative to their tensile strengths as the very ductile carbon steel. But none of them equals the nickel-chrome-molybdenum material in developing an average bursting stress equal to or greater than the tensile strength.

The nickel-chrome-molybdenum steel has both biaxial ductility and a continuously increasing strength with deformation. It has no region of weakness such as the carbon steel displays when "the beam drops" in the tensile test.

TABLE 6 PERCENTAGE ELONGATION IN TENSILE TEST AND SPEED REDUCTION DUE TO CENTER HOLE OF VARIOUS MATERIALS

	Elongation in tensile test, per cent	Speed reduction due to center hole, per cent
Low-carbon steel	37.5	16 to 17
Ni-Cr-Mo steel	15.0	6 to 10
Gamma Columbium	15 to 18	6 to 8
Cyclops 17W	15 to 18	3 to 5
Timken 25-16-6	11 to 17	0 to 5

The lower ductility of the high alloys would suggest that these materials might be more sensitive to the elastic-stress concentration near the center hole shown in Fig. 1. However, the results, collected in Table 6, appear to show these materials to be even less sensitive than the more ductile materials.

The actual bursting speeds of the various wheels were influenced by some variation in tensile strength for which it would be proper to make some correction. However, it is impossible to escape the conclusion that the most ductile material at the top of the list, the carbon steel, loses most due to the hole, while the least ductile material at the bottom of the list is very little affected by the center hole.

It is to be noted that the two carbon-steel wheels with center holes did not enlarge so much in over-all diameter as did the solid wheels with no center hole, although the center holes in the low-carbon steel had the greatest percentage enlargements measured in any of the wheels. It may be that the rims had not yet stretched enough to be carrying their fair share of load while the holes were working at the limit of what the material was good for.

At the bottom of Table 6, the high-alloy materials may have had the elastic-stress concentrations to some degree neutralized by the cold work during heat-treatment. Thus these disks may initially have been in a state of internal compression with the rim in tension like the tire on a wagon wheel. This would give the outer portions of the disk a head start toward carrying a fair share of the bursting load in contrast to the handicap in the case of the rims of the low-carbon steel disks.

These tests do not include any comparisons with small and highly localized concentrations such as would be caused by keyways, bolt holes, pinholes, or balance holes. It is, however, evident that the manufacture of a high-speed wheel is a complex art which involves much more than any mathematical analysis of stress distribution. Furthermore, these tests do not reflect any evaluation of the high-temperature qualities of the various materials. That would be quite another story.

Factors of Safety and Criterions of Failure: It would seem that a series of tests to complete destruction should offer some useful data relative to factors of safety and criterions of failure. In considering these questions, it is necessary to decide on a point of view as to what constitutes a failure.

It is no doubt legitimate to call a bad case of malfunctioning due to unbalance, with consequent vibration, a failure. Similarly, a gradual loss of clearances with resulting rubbing, injury to packings, and consequent deterioration of efficiency might be called failure. But failure is a rather strong word; and if easily repairable malfunctioning is to be called failure, what word is left for destructive rupture?

Many articles are written in which the incidence of any plastic distortion with consequent permanent set, however small, is called failure. It would be more accurate to say that elastic theory has failed to apply than that any real failure has occurred in the machine.

However, it is certainly true that there are few useful structures either among machines or buildings that do not exceed the elastic limit in many regions of local overstress. Certainly this does not constitute failure. Indeed, its occurrence is usually very difficult to detect.

On the other hand, there is usually no doubt about the complete destruction accompanying actual rupture. Largely for this reason, but also because it seems a fundamentally sound viewpoint, the wheel bursts here reported have been discussed in terms of bursting speed rather than in terms of the speed or local maximum stress at which some measurable permanent set was first detected.

Certainly elastic stresses should be computed and design proportions should take account of them, but when the question of a true ultimate factor of safety is concerned, it would seem better judgment to compare operating conditions with actual rupture rather than with some half-way point of less critical significance.

Conclusions

The fact that the average bursting stress frequently equals or exceeds the tensile strength throughout the first series of tests shows that in some locations there must be maximum stresses considerably in excess of the tensile strength, since it is hard to believe that the leveling effect of the plastic yielding can have completely reduced all stresses to the average value. Thus it is necessary to conclude at least for the nickel-chrome-molybdenum steel, that the biaxial-stress distribution has some strengthening value which would tend to justify the maximum-strain theory of ultimate failure. In other words, looking at the center of the solid wheels, the presence of two equal stresses at right angles to each other enables each to attain a higher value than it could if deformation were not in part restrained by the presence of the other stress.

It might be possible to study the redistribution of stress during the plastic enlargement of the disk by noting the change of thickness along the radius. However, the fact that carefully duplicated bars show widely varying plastic behavior under stress suggests that such a detailed analysis would not be fruitful of any useful information.

The most important item of information given by these tests is that with ductile materials such as here tested the real factor of safety against bursting may be more closely estimated by comparing the average bursting stress with the ordinary tensile strength than by trying to go by the maximum elastic stress. Thus, the weakening effect of an inspection hole is nowhere near the 50 per cent that elastic theory suggests. In fact, with the type of material most likely to be used, the weakening effect is no more than in proportion to the material removed.

Acknowledgments

The author wishes to acknowledge the generous co-operation of K. D. McMahan of the General Electric Research Laboratory in Schenectady, E. E. Stoeckly of the Supercharger Engineering Division, and W. L. Badger, Thomson Laboratory, both of River Works of the General Electric Company, West Lynn, Mass. together with their respective associates.

Appendix

The formulas for elastic stress distribution in flat disks with and without central hole are collected herewith for convenient reference. Note that the centrifugal force per cubic inch of steel is

$$8N^2r$$

where r is the radius in inches and N the speed of rotation in thousands of revolutions per minute. (The even figure 8 happens to be correct for the density of steel. For other metals, this figure should be multiplied by the density relative to steel.)

Elastic-Stress Distribution in a Flat Steel Disk

The elastic distribution of the stresses in a flat disk due to centrifugal force is described by the following formulas:

Hoop stress at any radius r in a solid flat disk of diameter $2R$ is

$$N^2[(3 + n)R^2 - (3n + 1)r^2]$$

where n is Poisson's ratio.

The radial stress is

$$N^2[(3 + n)(R^2 - r^2)]$$

The maximum value of each occurs at the center and is

$$N^2[(3 + n)R^2]$$

Hoop stress at any radius r in a flat disk of diameter $2R_2$ with a central hole of diameter $2R_1$ is

$$N^2\left[(3+n)\left(R_2^2+R_1^2+\frac{R_2^2R_1^2}{r^2}\right)-(3n+1)r^2\right]$$

The maximum value occurs at $r=R_1$

$$2N^2[(3+n)R_2^2+(1-n)R_1^2]$$

The radial stress is

$$N^2\left[(3+n)\left(R_2^2+R_1^2-\frac{R_2^2R_1^2}{r^2}-r^2\right)\right]$$

Average Bursting Stress in a Flat Steel Disk

Regardless of the stress distribution throughout the volume of the disk, the average bursting stress may be computed by dividing the total centrifugal bursting force by the total area of cross section.

The average bursting stress in a flat disk of diameter $2R_2$ with a central hole of diameter $2R_1$ is

$$\frac{8}{3}N^2\frac{R_2^3-R_1^3}{R_2-R_1}$$

If there is no central hole the average bursting stress in a flat disk of diameter R is

$$\frac{8}{3}N^2R^2$$

The ratio of the average bursting stress in the solid flat disk to the maximum stress at the center under elastic conditions is

$$\frac{8}{3}N^2R^2/N^2[(3+n)R^2]=\frac{8}{3(3+n)}$$

For various values of n this ratio is as follows:

n	$\frac{8}{3(3+n)}$
0.25	0.820
0.30	0.808
0.33	0.800
0.40	0.784
0.50	0.762

Computation of Centrifugal Bursting Stress for Special Steel Shapes

In any particular wheel, the average centrifugal bursting stress may be computed as follows where t is the thickness in inches:

$$\frac{8N^2\int tr^2dr+\frac{N^2}{2\pi}\times\text{total radial bucket load at 1000 rpm}}{\text{Cross-sectional area of disk profile from center out}}$$

For a section of uniform thickness

$$8N^2\int_{R_1}^{R_2}tr^2dr=8N^2t\frac{R_2^3-R_1^3}{3}$$

For a section of conical profile whose thickness is t_1 at R_1 and t_2 at R_2

$$8N^2\int_{R_1}^{R_2}tr^2dr=8N^2\left[(t_2+AR_2)\frac{R_2^3-R_1^3}{3}-A\frac{R_2^4-R_1^4}{4}\right]$$

where $A=(t_1-t_2)/(R_2-R_1)$

For a section of hyperbolic profile defined by the relationship

$$\frac{t}{t_2}=\left(\frac{R_2}{r}\right)^k$$

$$8N^2\int_{R_1}^{R_2}tr^2dr=8N^2\frac{t_2R_2^k}{3-k}(R_2^{3-k}-R_1^{3-k})$$

In the last case the corresponding area of cross section between R_1 and R_2 is

$$\int_{R_1}^{R_2}tdr=\frac{t_2R_2^k}{1-k}(R_2^{1-k}-R_1^{1-k})$$

The area for the first two profiles is easily computed without formulation.

Discussion

Hans Dahlstrand.[2] A short time ago the writer's company made similar tests to those of the paper on disks machined from a large forging which was scrapped because of flaws in one end of the forging. These flaws consisted of inclusions and pin-point cavities which occasionally occur in forgings. Normally, flaws of this type will cause the forging to be scrapped if they are located at a critical point or if the flaws cover a large area. There are at present no reliable means by which the extent of such flaws below the finished surface may be examined; consequently, the decision of whether or not the forging is suitable for use rests largely upon the judgment of the engineer. It is clear that any cracks or seams cannot be tolerated, as during operations flaws of that nature are likely to increase until bursting occurs.

The purpose of the tests was to determine the extent to which the inclusions and round cavities would affect the ductility and the strength of the steel. Several disks from this forging, both from the area showing the flaws and from areas showing sound metal, were machined for the tests. While the report of tests has not been fully completed, it is sufficient to mention that flaws of the nature described do not materially affect the strength or the ductility of the steel. It is therefore concluded that forgings having such flaws may be used with safety without any particular danger. Care nevertheless must be exercised in the examination of the flaws before approving the use of such forgings, as it is reasonable to assume that these flaws may be of such nature and cover such large areas at vital points that the forgings could not be safely used.

R. V. Kleinschmidt.[3] Perhaps the most interesting data presented in this paper, and material which would warrant very careful study, are the behavior of the disks at speeds lower than the rupturing speed. The study of distortion gives considerable insight into the actual phenomena occurring. It would be interesting to have more consideration of the phenomena of distortion, and some comments as to the practical possibilities of prestressing wheels by overspeeding to stabilize the deformations before final finishing and assembly.

The findings on the importance of ductility in relation to stress concentration around a central hole are somewhat surprising until we realize that all of the materials tested were sufficiently ductile to permit the necessary relief of stresses without

[2] Consulting Engineer, Steam Turbine Department, Allis-Chalmers Manufacturing Company, Milwaukee, Wis. Mem. A.S.M.E.

[3] Commander, U.S.N.R., Bureau of Ships, Navy Department, Washington, D. C. Mem. A.S.M.E.

rupture. An extension of the tests to materials having 2 to 5 per cent elongation would probably present another story. Also, it must be remembered that these remarks apply to a central hole with uniform stress conditions around it. It is doubtful if similar conclusions can be drawn with respect to holes eccentrically placed. Possibly the author could comment upon experience with such holes in disks.

Another item which has not been mentioned and which must be considered is that of temperature effects. There are three interesting conditions which come to mind: (1) Uniform high temperature or low temperature, will change the strength and ductility relationships of the materials. Atmospheric tests alone may be misleading at other temperatures. (2) Stresses due to nonuniform temperature distribution. In this connection one possible type of nonuniform temperature distribution would appear, from the data given, to be very serious, namely, a cooled disk with a hot rim. (3) Temperatures varying rapidly with time as in heating up and cooling down. One of the major problems in gas-turbine development may be the possibility of changes of several hundred degrees in the temperature of the working fluid in a fraction of a second.

R. P. Kroon.[4] It is a commonly accepted idea that when a ductile material is under steady load, a local stress concentration is not too serious. It is assumed that there will be some plastic flow, after which the stresses will be distributed more evenly. This presupposes that the amount of local deformation will not be sufficient to cause rupture.

On this basis the notion that average stress instead of local peak stresses should be a criterion for disk failure seems sound enough.

We are confronted, however, with the results shown in Table 6, indicating that "the most ductile material loses most due to a hole."

It would certainly be interesting to establish whether this behavior is due to some internal-stress condition of the disks or whether the type of stress-strain curve of the material might play a role. A mathematical analysis might prove helpful in the latter case.

The high-temperature alloy disks with holes, examined by the author, have elongations of at least 15 per cent and fail at stresses in the order of 120,000 psi at room temperature.

In high-temperature service these materials would be loaded with stresses of perhaps 30,000 psi, and their elongation, with a reasonable service life, would be only a few per cent.

It would be extremely interesting to know whether under high temperature, with creep as the dominant factor, the comparison of disks with and without holes would be similar to that established at room temperature. Can the author throw any light on this phase of the disk problem?

J. A. Maul.[5] This paper has positively answered a question which has been an open point for discussion in the dynamometer engineering section of our company for several years, i.e., the possibility of taking advantage of the fact that a solid wheel theoretically has only one half the maximum stress of a corresponding wheel with a small central hole. Cracks at the center of a forging or minute openings between the grains may be the equivalent of a central hole.

It is important to know that we can run a solid wheel to higher speed than the corresponding shrunk-on shaft construction. However, the writer would be interested in knowing how much faster the solid wheel could be run. Evidently the limiting feature in the case of the solid wheel would be the ductile expansion of the outer surface of the wheel. In the case of a shrunk-on wheel, the limiting feature would be the expansion of the bore to the point where the wheel loosened on the shaft.

D. J. McAdam, Jr.[6] The writer cannot agree that the evidence presented by the author gives a basis for conclusions as to criteria for "failure."

The combination of principal stresses affects all three strength indexes; yield stress, ultimate stress, and breaking stress.[7,8,9] In considering criteria for fracture, one should compare "true" breaking stresses under different stress systems, and allowance should be made (if possible) for differences in total plastic deformation under the two conditions. The author, however, compares the breaking stress, either average or "elastic," with the tensile strength of a specimen under unidirectional loading. The "true" breaking stress under unidirectional loading would be somewhat greater than the ultimate stress, and probably would be greater than the breaking stress under biaxial loading. The higher value under uniaxial loading, however, would be due to the greater total plastic deformation. The relative values of the two technical cohesion limits would be the resultant of two factors, total plastic deformation (ductility) and the stress system. As the ductility (measured by decrease in sectional area) was much less for biaxial than for uniaxial loading, the influence of the stress system cannot be determined from the experiments.

For a brittle metal, the technical cohesion limit probably would be greater under biaxial than under uniaxial loading. Such a relationship, however, would not necessarily mean that the criterion for fracture is the greatest principal strain. As illustrated in Fig. 17 of a paper by the writer,[7] the criterion for fracture possibly is a function of both the volume stress and the greatest principal stress; if not, the criterion must be expressed in terms of the three principal stresses.

Arthur McCutchan.[10] This paper is a straightforward account of tests made to verify engineering judgment regarding the significance of certain types of stress concentration. Such tests insure that results of stress analysis will be considered in their proper perspective.

The improvement in performance of the wheels made with a special contour giving a uniform stress throughout the wheel is noteworthy. An examination of the cross section of this special design, as shown in Fig. 3 of the paper, however, suggests that straight lines giving a trapezoidal shape would be simpler to produce than the double-curve bottle shape and should give practically identical results.

The means of fastening the solid disks onto the rotating device is evident from Fig. 4 of the paper, but how this was accomplished for the disks with center holes is not shown. It would seem that any clamping or expanding device applied at or around the hole might appreciably affect the results. It would be of interest to learn how the wheels with holes were attached in making these tests.

---

[4] Manager, Development Engineering, Steam Division, Westinghouse Electric & Manufacturing Company, Lester, Pa. Mem. A.S.M.E.

[5] Motor and Generator Engineering Division, General Electric Company, Fort Wayne, Ind.

[6] Metallurgist, National Bureau of Standards, Washington, D. C.

[7] "The Technical Cohesive Strength and Yield Strength of Metals," by D. J. McAdam, Jr., tech. pub. 1414, Trans. A.I.M.E., vol. 150, 1942, pp. 311–357.

[8] "An Investigation of the Technical Cohesive Strength of Metals," by D. J. McAdam, Jr., and R. W. Mebs, A.I.M.E. tech. pub. 1615, Metals Technology, August, 1943.

[9] "The Technical Cohesive Strength and Other Mechanical Properties of Metals at Low Temperatures," by D. J. McAdam, Jr., and R. W. Mebs, American Society for Testing Materials, preprint no. 40, 1943.

[10] Engineer, Engineering Division of The Detroit Edison Company, Detroit, Mich. Mem. A.S.M.E.

While, as stated by the author, the evaluation of high-temperature qualities of the various materials is another story, it occurs to the writer that if spinning tests of this kind could be made at high temperatures they might furnish quite different information than conventional creep and rupture tests. For one thing, it is possible that the ductility of the high-alloy materials under biaxial stress might be more nearly like that of the carbon and low-alloy steels than found from tests at room temperature.

K. D. McMahan[11] and E. E. Stoeckley.[12] This paper confirms the intuitive beliefs of most designers of high-speed rotors who lacked actual tests to prove them. The work signals the approach of a new method of specifying materials for high-speed rotors. Fortunately, most "good rotor materials" give a higher factor of safety than classical calculations indicate. However, rotors from certain aluminum alloys, usually having low elongation in tensile tests, are known to burst at speeds equal to or below that at which the bore stress, as calculated by classical methods, equals the tensile strength. Similarly other alloys having not too different tensile characteristics behave like the turbine-rotor materials and burst at speeds corresponding very nearly to average stresses. Thus the difference in bursting speeds of similar specimens may vary almost by a factor of 2:1 for materials having the same apparent tensile strengths as determined by the usual tensile tests.

A discussion of this paper seems incomplete without mentioning the rather unique apparatus that makes these bursting tests possible. As early as 1939, the G. E. Research Laboratory, noting the work of Beams[13] and others, undertook to develop apparatus for whirling aluminum-alloy rotors weighing from 10 to 25 lb up to 50,000 rpm. Subsequently, in March, 1940, a steel rotor weighing 25 lb was burst at just under 40,000 rpm. Since the early work in the laboratory, the art has progressed beyond all early expectations, and there now seems to be no limitation to the size of rotors that may be tested by this method.

An adequate description of this test apparatus is a subject for a paper in itself. Plans have been made for such a paper when the time permits. It must suffice at present to state that the specimens are driven by a small air turbine while suspended on a small vertical piano-wire shaft in an evacuated explosion chamber.[14] The turbine mounts atop the chamber with a special seal to prevent leakage around the wire shaft.

A. Nadai.[15] The distribution of the internal stresses in a rotating steam- or gas-turbine disk which has been stressed beyond the plastic limit of the material is an attractive mechanical problem which, however, is not new. Several investigation reports have been published dealing with the analysis of this case and some related cases of biaxial stresses with a rotational symmetry in the plastic state, to which no references could be found in the paper. The writer believes that a quantitative analysis of plastic distributions of stress of this kind can give and has already given valuable information to the designers of turbine wheels, even if some of these computations have been based upon idealized conditions with regard to the flow, and despite the fact (mentioned in the paper) that duplicate tests made with bars of some of the alloy steels showed widely varying plastic behavior under stress. Whether the opinion expressed by the author "that such detailed analysis would not be fruitful of any useful information" is sufficiently justifiable or can be based on facts, must be left an open question.

Engineers are accustomed to base the design of steam- and gas-turbine disks in the elastic range of strains on the analytical methods which have been developed for such computations. It is believed that there cannot be advanced any serious reasons against attempts why these well-established methods could not be utilized with success and furnish reliable information to designers also when the plastic state has been reached in revolving disks. It may even occur that the distributions of stress in this latter state are simpler to analyze due to certain simplifications which can be introduced in the assumptions, because, for certain ductile steels (such was the case for low-carbon steel S.A.E. 1020), the tangential stresses change much less rapidly with the radial distance from the disk center, as in the elastic state. This alone probably explains several facts concerning fracture which were recorded in the author's paper in an empirical fashion.

In artillery arsenals, a related problem was investigated long ago, namely, the plastic distribution of the stresses in gun barrels which have been cold-worked and overstressed by internal hydrostatic pressure. In A. Stodola's book on steam and gas turbines, the case of an overspeeded turbine disk has been treated.[16] F. Laszlo[17] dealt with the same problem, and particularly with the stability of the equilibrium of rotating disks in the plastic state. He showed that their equilibrium may become unstable under certain conditions which depend upon the shape of the stress-strain curve of the material.

L. H. Donnell and the writer in a joint paper[18] investigated the stress distribution in rotating disks of equal thickness of ductile materials after the yield point had been reached in them. In this paper, two or three typical cases of flow were considered in detail, namely, "progressive" yielding and "complete" yielding for a material having a well-defined yield stress. In the former case, the outer portion of the disk is stressed elastically, while in the inner portion the stresses were assumed at the plastic limit. In the third case which was considered, it was assumed that the material had a stress-strain curve in which strain-hardening would become more pronounced. A case was worked out as an example in which the true stress was a linear function of the conventional permanent strains. This curve had a definite yield point and a finite slope. Such examples show that the distributions of the radial and tangential stresses can be obtained in rotating disks in the plastic state, at least in a few characteristic simple cases, in a quantitative manner. The means which are available for an analysis of the stresses in overstressed or overspeeded disks are precisely of the same or an analogous nature as those which are in use by designers in the elastic range of the strains. Stress-strain relations have been studied in the plastic range under biaxial or combined stress conditions in a satisfactory manner for moderate strains. (Such were the fairly small permanent strains which were observed in the author's overspeed tests.)

It may perhaps interest readers of the paper to note that some

---

[11] Research Laboratory, General Electric Company, Schenectady, N. Y.

[12] Supercharger Engineering Division, General Electric Company, Lynn, Mass.

[13] "High Speed Centrifuging," by J. W. Beams, *Reviews of Modern Physics*, vol. 10, 1938, pp. 245–263.

[14] "High-Altitude Hot-Gas Standards for Testing Turbosuperchargers and Engines," by E. E. Stoeckley, presented at the Annual Meeting, New York, N. Y., Nov. 29–Dec. 3, 1943, of The American Society of Mechanical Engineers.

[15] Consulting Mechanical Engineer, Westinghouse Research Laboratories, East Pittsburgh, Pa. Mem. A.S.M.E.

[16] "Steam and Gas Turbines," by A. Stodola, McGraw-Hill Book Co., Inc., New York, N. Y., 1927, vol. 2, p. 1080. Reference is also made to an article, "Contribution au Calcul des Disques," *Brown-Boveri Review*, vol. 6, 1919, pp. 260–263.

[17] "Geschleuderte umdrehungskörper im Gebiet bleibender Deformation," by F. Laszlo, *Zeitschrift für angewandte Mathematik und Mechanik*, vol. 5, 1925, pp. 281–293.

[18] "Stress Distribution in Rotating Disks of Ductile Material After the Yield Point Has Been Reached," by L. H. Donnell and A. Nadai. Trans. A.S.M.E., vol. 51, 1929, paper APM-51-16.

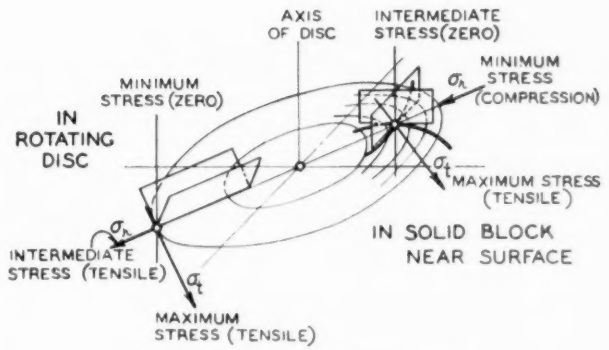


FIG. 11 ORIENTATION OF SLIP PLANES

of the author's observations, namely, those concerning the orientation of the flow figures which became visible on the flat sides of the low-carbon-steel disks, also conformed quite nicely with what was to be expected from the Mohr theory of the formation of the surfaces of slip in a ductile metal. It is characteristic that they appear usually in an orientation in which the two equivalent planes of slip in a point in a plastic metal intersect each other along the line of the intermediate principal stress. This is illustrated in Fig. 11 of this discussion, which refers to two characteristic cases of rotational symmetric plastic flow. On the right side of Fig. 11 is shown the orientation of the two slip planes in a point situated in the surface of a solid block near an impression in which high concentrated localized compression stresses are applied to the surface in the perpendicular directions to it. In this case one of the principal stresses is a high tensile stress (the peripheral stress σ_t) and the other is a compression stress (the radial stress σ_r). The direction of the intermediate stress (which in the surface is equal to zero) is therefore perpendicular to the free surface of the solid block. The two planes of slip must therefore be perpendicular to this plane and intersect the radii and concentric circles (shown in Fig. 11) under an angle of 45 deg. The flow figures should therefore consist of a series of logarithmic spirals, like the ones which are indicated in Fig. 12 of the discussion. Such flow lines are frequently observed around punched holes in heavy plates, Brinell impressions, etc., in mild steel.

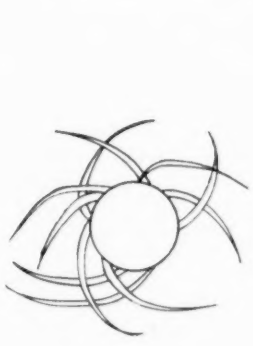


Fig. 12

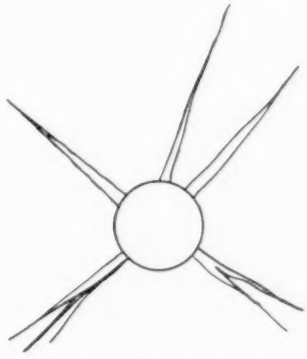


Fig. 13

FIG. 12 SURFACE OF A SOLID BLOCK NEAR AN IMPRESSION

FIG. 13 ROTATING DISK

In the case of the rotating disk, on the other hand, both principal stresses are tensile stresses. The radial (σ_r) is always smaller than the tangential (σ_t), the third one (σ_z) is again zero. The intermediate stress acts now in the radial directions. Consequently, the flow lines should appear along the radii of the revolving disks. This was the case in the Figs. 6, 7, and 8 of the paper for the overspeeded disks of low-carbon steel. The flow lines in them appeared in the directions shown in Fig. 13 of this discussion.

The tests described in the paper should throw some light on an important question, to which attention should be called also through these remarks. Suppose that a small circular hole is present in a disk which is stressed uniformly in its plane in all directions. What is the nature of the disturbance in the distribution of the stresses caused through the presence of the hole? More precisely, what is the distribution of the radial and tangential components of stress σ_r, σ_t around the hole? In an elastic material one expresses the result of such computations by stating the ratio k of the peripheral stress at the boundary of the hole to the stress in large distances of it. This is known as the factor of stress concentration. In this case it is $k = 2$. In our paper,[18] it was shown that in a rotating disk having a small hole the tangential-stress components are nearly uniformly distributed over the entire disk if the material yields under a constant stress. Since the periphery of the hole is in a state of pure tension the factor of stress concentration for a perfectly plastic disk must have been reduced to unity. From these considerations one should expect that the factor k should essentially depend upon the shape of the stress-strain curve or on the law of strain-hardening, according to which $\sigma = f(\epsilon)$, where ϵ is the plastic strain. Not much has yet become known quantitatively in this respect about values of k, the difficulty being that with the increasing stresses the dimensions of the plate near a hole must also be changing. In one case the writer has computed an exact expression for the factor of stress concentration in a plastic disk having a hole, which was uniformly stressed in its plane.[19] The strains were assumed to be small and for the material in the plastic state a stress-strain curve was assumed

$$\sigma = \sigma_0 \epsilon^m$$

or a power function (σ stress, ϵ permanent strain, σ_0, m material constants, $0 < m < 1$). Factor k for this strain-hardening law was found to equal

$$k = \left(\frac{2}{1 + 3m}\right)^{\frac{2m}{1 - 3m}}$$

which gives for

Exponent m	= 1	2/3	1/2	1/3	1/4	1/5	0
Factor of stress concentration k	= 2	1.72	1.56	1.40	1.31	1.25	1

As long as the maximum value of the peripheral stresses should occur in the boundary of the hole and not as it could in some special cases also occur, in the interior of the disk, one would expect that the material should break at the hole in pure tension. It would, however, not be permissible to base the design on the value of the tensile strength or of the true fracture stresses which were observed in ordinary tensile tests run with standard round bars, because necking in a plate around a hole or in a wide flat bar under tension must be restricted, compared to the usual mode of necking in the standard round-bar tensile test. This points to the need of studying fracture conditions in the ductile metals under special conditions which cannot be reproduced through the standard tensile test.

E. M. PHILLIPS.[20] The author's tests indicate the previously accepted theory of safety as dependent upon the maximum elas-

[19] "On the Creep of Solids at Elevated Temperatures," by A. Nadai, *Journal of Applied Physics*, vol. 8, 1937, p. 430.

[20] Turbine Engineering Division, General Electric Company, (Lynn) River Works, Lynn, Mass. Mem. A.S.M.E.

TABLE 7 BURSTING TESTS ON SHAPED TURBINE-WHEEL DISKS

		Physical Test Results			Bursting Test Results			
Material	Location	Tensile stress, psi	Elongation, per cent	Reduction, per cent	Bursting speed, rpm	Average tangential stress, psi	Ratio (7)/(3)	Ratio tensile strength (at center)/(at rim)
(1)	(2)	(3)	(4)	(5)	(6)	(7)		
Gamma cb.	Rim	147000	8	32.1	42000	79600	0.542	0.835
	Center	123000	4	6.9			0.648	
Gamma cb.	Rim	131100	10	23.1	46800	98800	0.743	0.936
	Center	124700	8	11.6			0.793	
Gamma cb.	Rim	122400	10	21.0	38700	67500	0.552	1.00
	Center	122400	5	18.2			0.552	
Gamma cb.	Rim	157400	11	17.5	43000	83400	0.530	0.90
	Center	141900	6	4.7			0.588	
Gamma cb.	Rim	149400	8	19.0	42000	79600	0.533	0.80
	Center	119300	2	3.1			0.667	
Gamma cb.	Rim	148600	8	14.5	41000	75700	0.510	0.835
	Center	124000	1	0.81			0.610	
								0.884 Avg
17W	Rim	138000	15	20.4	43000	81400	0.590	
17W	Rim	133700	15	40.4	49000	105500	0.791	
17W	Rim	142100	16	32.0	48600	104000	0.731	

TABLE 8 COMPARISON OF TEST RESULTS

Material	Ratio average tangential stress to tensile strength		Ratio	Based on tests at
	E. L. Robinson	Tests Table 7		
Gamma cb.	0.812 avg	0.510 to 0.743	0.628 to 0.915	Rim
		0.552 to 0.793	0.68 to 0.977	Center
17W	0.793 avg	0.590 to 0.791	0.745 to 0.998	Rim

tic stress to be in error. The evidence presented shows rather that safety is dependent either upon the average stress or upon the ductile properties at the point of maximum elongation or reduction in area.

These tests were made upon smooth wheel disks. Disks having points of stress concentration may be expected to show less favorable performance. Table 7 of this discussion shows fracture results on nine shaped turbine-wheel disks $9^9/_{16}$ in. diam, bolted to a shaft hub through three reamed holes $^7/_{16}$ in. diam on a radius of $2^3/_4$ in. These holes are rounded by $^1/_8$ in. radius at the disk faces. In addition, there is a male rabbet $1^9/_{16}$ in. diam joined to the disk face by a radius of $^5/_{32}$ in. Breaks in these disks pass through the attaching holes and are probably influenced by the concentrations at the holes and at the rabbet. The table also includes tensile-test properties taken from broken sections of the disk. The test elongation values may have been influenced by the cold work in bursting.

It is interesting to note that the tensile strength at the center varies from 80 per cent to 100 per cent of that at the rim, the average value being 88 per cent.

In comparison, Table 8 herewith indicates a reduction due to stress concentration as high as 32 per cent when based upon center properties and 37 per cent when based upon rim properties.

ARTHUR M. G. MOODY.[21] Mr. Robinson's valuable paper supplies us with a good deal of quantitative information in a field where we have been largely limited to conjecture. It also raises some questions, one of which the writer would like to discuss.

Mr. Robinson mentions that the word "failure" is not always clearly defined. It is often taken to mean the plastic yielding of some part of a machine as a result of the presence of a stress in excess of the elastic limit. He states that this is often not detrimental to the performance of a machine, and he therefore turns our attention to the bursting speed of a disk rather than the speed at which the elastic limit is reached.

Now it is probably perfectly true that designers, in dealing with stresses, do not consciously subscribe to the view that failure refers to the elastic limit. Nonetheless, it is probably also true that the rules by which designers are guided have this philosophy implicit in them.

Most disk stress criteria consist of a comparison between a stress (maximum or average) calculated on the basis of elastic theory, and some property found from a single tensile test, such as the yield point. But Mr. Robinson has made it clear that bursting speeds have practically no connection with elastic stresses. Should we not, therefore, have other criteria?

As a matter of fact, a good deal can be said against permitting extensive yielding in a disk, so that perhaps our design criteria should, after all, be kept on a basis similar to that now in general use. One important change might, however, be made, namely, the use of an effective elastic limit making allowance for the stiffening effect of the biaxial stress condition which exists in the disk. Such an elastic limit would be based on the simple tensile test but would be corrected, perhaps empirically, according to the degree of elongation and reduction of area.

It would be most interesting if Mr. Robinson could find the opportunity to conduct further tests relating to the incidence and progress of plastic yielding.

AUTHOR'S CLOSURE

The author concurs with Mr. Dahlstrand's remarks. However, the bursting test may show the general soundness of the material, but may not reveal a weakness in the matter of fatigue resistance.

Commander Kleinschmidt inquires about the distortion preceding rupture. The wheels were run at successively higher speeds, and, after the first appearance of plastic set, records were kept of dimensional changes. These records were rather voluminous, and the author feared that the paper might get too long for publication had they been included. Suffice it to say here that the different materials behaved quite differently.

As regards his inquiry about prestressing by overspeeding before assembly, the author has always felt that just as much good or even more would be done by such overstressing as occurs in ordinary service as by deliberate overspeeding in advance of assembly. Under actual service conditions, no more prestressing than necessary is applied. Overspeeding in advance is attended by the remote possibility of aggravating some hidden flaw or weakness that would not otherwise be serious. This is only a statistical possibility. If in any particular case the material is presumed to be perfectly sound, prestressing should be beneficial. Undoubtedly, this procedure helps keep a shrunk-on wheel tight on the shaft. However, evidence is accumulating that resistance to fatigue is improved by initial compression and reduced by initial tension. Bearing this in mind, the bore of the wheel would be

[21] Chief Research Engineer, DeLaval Steam Turbine Company, Trenton, N. J. Jun. A.S.M.E.

improved in fatigue strength by the localized initial compression induced by overspeeding; whereas the outer regions of the wheel would be very slightly weakened by the small initial tension. Thus overspeeding a wheel does nothing to improve the fatigue strength of the part of a wheel which may be subject to vibration but improves the part that does not need it. On the other hand, the dovetail connections of a fully assembled turbine bucket wheel might well be improved in fatigue strength by overspeeding the finished and bucketed wheel to a speed which would result in some residual compression in the local regions of maximum stress.

Commander Kleinschmidt also inquires about holes eccentrically placed. Such holes are very likely to be located in a region where the radial and tangential stresses are not greatly different in size. Under such conditions, the behavior should be much the same. Of course, if the radial and tangential stresses differ greatly, the behavior might be expected to differ. On the other hand, the author believes that a more important consideration may be the fact that such holes are likely to be of small size and that there may be a worst size for regions of stress concentration.

Mr. Phillips has kindly contributed in Table 7 the results of bursting tests on actual shaped wheels containing small-size eccentrically located holes, such as referred to by Commander Kleinschmidt. Table 8 shows that such wheels when made of the gamma columbium material develop average bursting stresses 0.628 to 0.915 of the author's average figure. (Rim physical properties are used because all the author's comparisons are with rim tests.) In the case of the Cyclops 17W material, the actual shaped wheels containing eccentric holes were 0.745 to 0.998 as strong as the author's wheels. In both cases there is evidence of a reduction of strength due to the local stress concentration, but this reduction is not as bad as one might be led to believe on the basis of elastic theory.

Commander Kleinschmidt asks three questions covering the importance of temperature effects. These are certainly very important considerations upon which the author can only speculate as follows, at the present time:

1 High temperature is likely to be accompanied by a loss of strength and an increase of ductility while low temperature would have the opposite result. There are variations from these relationships, and certain unexpected effects connected with the nature of the ductility. Certainly the atmospheric tests must not be assumed to give conclusions valid for other temperatures.

2 There are mitigating circumstances associated with the increase of stress at the center of a wheel with a hot rim so that this condition is, perhaps, not quite so serious as it might seem to be. The colder and more highly stressed center is usually stronger than the rim by virtue of its lower temperature. Furthermore, the volume of stressed material is usually very much larger toward the center, with the result that a larger thermal strain in a rim of small cross section cannot cause a very excessive opposite strain in the very large cross section of the central web or hub.

3 Certainly the effect of rapidly varying temperatures is a very real problem. In this matter, the author can only suggest that much similar effects exist at a lower temperature level in steam turbines using lower-alloy materials. It is to be hoped that the newer alloys will behave equally well at the higher levels.

The author shares with Mr. Kroon the desire for some rationalization of the paradoxical results given in Table 6. The author believes that both influences suggested by Mr. Kroon were present. In retrospect, it is only possible to speculate on the likelihood that initial internal stresses would go a long way toward explaining what happened. As regards Mr. Kroon's question about high-temperature behavior, the author is at present unable to give any answer.

In connection with Mr. Maul's problems, it is important, of course, to consider the difference in the physical properties of the material available for a solid rotor, as compared with what may be obtained in separate shrunk-on wheels.

The author has a good deal of sympathy with Dr. McAdam's disagreement as to criteria for "failure." The crux of the question seems to be the definition of "failure," but the point of view is just as important also. If one is investigating the ultimate nature of a material, certainly, "true" breaking stresses should be determined as Dr. McAdam suggests, allowing "(if possible) for differences in total plastic deformation." In the first draft of his paper the author started to do this. However, upon reflection, it occurred to him that plastic deformations are never, and by the nature of the materials cannot with certainty, be available to a designer. Therefore having the designer's viewpoint, it seemed better to base the figures on dimensions available to the designer, as is done in the tensile test under unidirectional loading. The artificiality of the results must be admitted, but there is a corresponding directness of utility to a designer that rests for its validity only on the systematic outcome of the results. The author regrets that complete data on the progressive deformation of the wheels were omitted in the interest of brevity, as Dr. McAdam's analysis of the "true" stresses, taking account of plastic deformation, would be valuable to have.

The author agrees with Mr. McCutchan that the trapezoidal cross section should be practically identical in result with the bottle shape. In fact, the weakest point in this design was the generous fillet uniting the very modest rim with the web. This detail was not generous enough.

How to float the disks with center hole while rotating at 40,000 rpm proved to be quite a real problem by itself and various devices were tried. Suffice it to say that the most successful device was shaped like a tulip blossom and about that size, with the wheel seated just below the petal tips and the pistil of the flower serving as drive shaft. The outward centrifugal pressure of the petals at the small central radius was practically inconsequential but sufficed to transmit the small torque required for acceleration.

The author agrees as to the importance of securing similar information at high temperature in order to find out how to apply conventional creep and rupture tests.

The author is completely indebted to Messrs. McMahan and Stoeckly for carrying out all his bursting tests in their high-speed stands and looks forward to the time when these most useful testing machines may be adequately described. Their remarks in passing about the different behavior of certain aluminum alloys should be noted.

Mr. Moody recalls a totally different implication in the use of the term "failure" from that suggested by Dr. McAdam. Designers must certainly always have in mind that their machines may be put out of business by a very little permanent deformation of an amount which may not suffice to permit bursting or stresses anywhere near bursting. Doubtless this is a legitimate use of the word "failure," but the author regrets the practice of basing a "factor of safety" on the attainment of the elastic limit, because usually no safety is in jeopardy when this occurs even though the type of failure mentioned may be imminent.

The author wishes to express his appreciation of Dr. Nadai's valuable and illuminating discussion. He makes a good case in favor of attempting to predict behavior after plastic action has set in with sufficient accuracy to be useful to designers. The author would regret having the skepticism expressed in his quoted remark taken to mean that a sound and useful analysis would not be welcome. Certainly it would be desirable if a satisfactory analysis could be agreed upon which would improve upon the simple average stress suggested by the author. However, such a setup for design purposes would have to be accompanied by data on the appropriate strength values. It is plain from both

Dr. McAdam's remarks and from Dr. Nadai's also that ordinary tensile-test results could not be used. The author believes that Dr. Nadai's last paragraph expresses opinions pretty much in agreement with his own and also with those of Dr. McAdam. The more common use of high-speed test stands may, in future, make it possible to determine the bursting strength of a test coupon having the size and shape of a baker's cookie instead of a stick of candy.

In answering one of Commander Kleinschmidt's questions, the author made use of some of the data contributed by Mr. Phillips. There is another lesson to be learned from these figures. Mr. Phillips gives physical tests from both rim and center of the gamma columbium wheels, showing the center usually to have lower tensile strength anywhere from 80 to 100 per cent of the rim tensile strength. All the tensile tests cited by the author were based upon coupons taken from the rims before the wheels were made. Since all the bursts except those of the wheels of uniform stress design apparently originated near the center or at the edge of the center hole, this variation of material strength may go a long way to explain the deviation from a uniform relationship between average bursting stress and ordinary tensile strength. The author does not, of course, claim that this relationship is other than fortuitous with so artificial a property as the conventional tensile test. It may, however, be nonetheless quite a real and useful relationship.

Fluid Flow Through Two Orifices in Series—II

By MILTON C. STUART[1] AND D. ROBERT YARNALL[2]

This is the second of a series of papers on the characteristics of fluid flow through two orifices in series. The first paper (1)[3] presented a theoretical analysis of the flow of water and steam through two orifices in series over a wide range of pressures and temperatures. This paper presents the results of experimental investigations on this subject using water at an initial pressure of 100 psia and over a range of temperatures from room temperature to saturation temperature. The principal data sought were the pressures established in the intermediate chamber between the two orifices, and especially the variations of this intermediate pressure with reference to the temperature of water supplied and the type of orifice. One of the most significant facts revealed by these researches is that under certain conditions of flow the fluid assumes a metastable state which greatly influences the characteristics of the process. Finally, a device responsive to the pressure variations obtained between two orifices in series constitutes a control element, useful, among other things, to control flow in response to the state of the fluid supplied.

Nomenclature

The following nomenclature is used in the paper:

M/A = mass rate of flow, lb per sec per sq ft
U = velocity, fps
V = specific volume, cu ft per lb
H = enthalpy, Btu per lb
P = absolute pressure, psf
p = absolute pressure, psi
F = temperature,

Subscript 1 refers to entrance to first orifice
Subscript x refers to intermediate chamber
Subscript 2 refers to downstream section following second orifice
Subscript s refers to constant entropy process
"Chamber pressure," (p_x), is absolute pressure in intermediate chamber between two orifices
"Cold water" is water which has a temperature lower than saturation temperature corresponding to lowest pressure attained by water during flow
"Compressed liquid," see "subsaturated" liquid
"Critical pressure" is lowest pressure which will exist for flow of expanding fluid in converging portion of nozzle
"Discharge pressure," (P_2), is pressure of liquid after passage through second orifice
"Flashing" is process of partial evaporation of liquid caused by adiabatic reduction of pressure
"Hot water" is water which has a temperature higher than saturation temperature corresponding to lowest pressure attained by water during flow
"Initial temperature" (t_1) is temperature of fluid at entrance to first orifice
"Initial pressure" (p_1) is absolute total pressure of liquid at entrance to first orifice
"Metastable" refers to a fluid condition in which pressure of fluid is less than saturation pressure of liquid corresponding to existing temperature, or, alternately, a fluid condition in which temperature of fluid is higher than saturation temperature of liquid at existing pressure
"Orifice" is a converging or parallel-sided passage provided for flow
"Quality" is percentage of vapor present in a liquid-vapor mixture
"Saturated liquid" refers to water having a temperature equal to temperature listed in Steam Tables corresponding to existing pressure
"Saturation pressure" refers to pressure listed in Steam Tables corresponding to existing temperature of water
"Saturation temperature" refers to temperature of water as listed in Steam Tables corresponding to existing pressure
"Stable" refers to a fluid condition in which pressure of fluid is equal to or greater than saturation pressure, or alternately, a fluid condition in which temperature of fluid is equal to or less than saturation temperature
"Subpressure" is reduction of pressure of metastable water below saturation pressure
"Subsaturated liquid" (compressed liquid) is a liquid having a temperature less than saturation temperature, or alternately, a liquid having a pressure higher than saturation pressure
"Superheated liquid," same as "metastable liquid"
"Superpressure" is excess of pressure of stable water over saturation pressure
"Supertemperature" is excess of temperature of metastable water over saturation temperature
"Total pressure" is measured absolute pressure of a fluid at any point
Vapor is used in this paper to designate vapor phase of water
Water is used in this paper to designate liquid phase of water

Introduction

In a previous paper (1) the authors presented a theoretical analysis of the flow of saturated and subsaturated water through two orifices in series over a wide range of pressures and temperatures. Since the presentation of that paper an extensive experimental investigation has been conducted in the high-pressure laboratory (2) of the Yarnall-Waring Company to determine the characteristics of flow of hot water through various types of orifices in series. The most significant facts revealed by these researches are that in many types of flow the fluid is in a metastable state and that in the metastable state the characteristics of the

[1] Professor of Mechanical Engineering, Lehigh University, Bethlehem, Pa. Mem. A. S. M. E.
[2] Yarnall-Waring Co., Chestnut Hill, Philadelphia, Pa. Fellow, A. S. M. E.
[3] Numbers in parentheses refer to the Bibliography at the end of the paper.
Contributed by the Research Committee on Fluid Meters and the Power Division and presented at the Annual Meeting, New York, N. Y., Nov. 29–Dec. 3, 1943, of The American Society of Mechanical Engineers.
Note: Statements and opinions advanced in papers are to be understood as individual expressions of their authors and not those of the Society.

flow of water through orifices differ greatly from the characteristics under stable conditions. This paper presents the experimentally determined characteristics and a thermodynamic analysis of the flow of saturated and subsaturated water through orifices in series with special consideration of the existing metastable state.

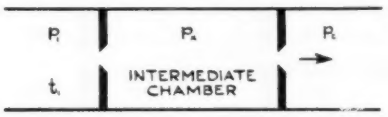
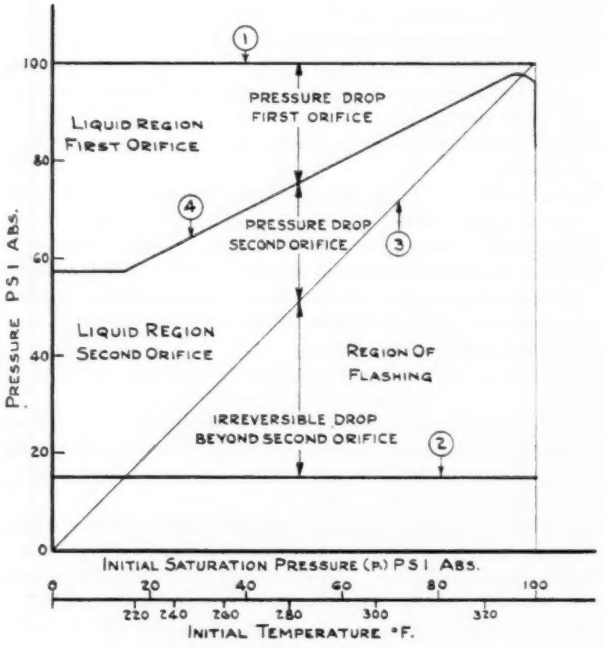


FIG. 1 ARRANGEMENT OF TWO ORIFICES IN SERIES



1 Constant initial total pressure
2 Constant discharge-region pressure
3 Initial saturation pressure
4 Intermediate pressure

FIG. 2 PRESSURE DIAGRAM FOR IDEAL STABLE FLOW OF WATER THROUGH TWO ORIFICES IN SERIES

FLOW OF HOT WATER UNDER STABLE CONDITIONS THROUGH TWO ORIFICES IN SERIES

In the paper presented by the authors in 1936 (1) on fluid flow through two orifices in series a thermodynamically stable condition of the fluid was predicated. It was assumed that when the pressure decreased to a point as low as the saturation pressure corresponding to the temperature of the liquid, vapor immediately started to form and the temperature of the resulting mixture of liquid and vapor was subsequently that corresponding to the saturation pressure. Following are some of the conclusions of the former paper which pertain to the present investigations:

(*a*) The flow of subsaturated water under stable conditions through an orifice or nozzle is characterized by a critical-pressure phenomenon just as is the flow of a gas or vapor. For subsaturated water this critical pressure is practically equal to the saturation pressure of the entering liquid.

(*b*) Because of this critical-pressure phenomenon, the rate of flow of hot water under stable condition through orifices is much lower than the rate of flow of cold water. In orifice flow, the energy available to cause flow is limited by the amount of energy rendered available by the change in state of the liquid from the initial pressure to the critical pressure.

(*c*) In flow of hot water under stable conditions through two identical sharp-edged or rounded-entrance orifices in series, critical pressure existed at the outlet of the second orifice and the intermediate pressure in the chamber between the two orifices automatically adjusted itself to be midway between the initial pressure at the entrance to the first orifice and the critical pressure. Flashing did not occur in the intermediate chamber until the saturation pressure of the liquid closely approached the initial pressure.

Pressures existing throughout the system for flow under stable conditions through two orifices in series, Fig. 1, are shown graphically in the pressure diagram, Fig. 2. In this diagram the abscissa is the initial saturation pressure of the water entering the first of two identical orifices with an initial total pressure 100 psia. The corresponding initial temperatures are also marked on the abscissa. Ordinates represent pressures existing throughout the system for flow under conditions of the various initial temperatures (and corresponding initial saturation pressures).

Line 1 represents the constant initial pressure; line 2 represents the constant pressure in the discharge region beyond the second orifice; line 3 represents the initial saturation pressure and is also the pressure which, under stable conditions, must necessarily exist at the throat of the second orifice. Line 4 represents the variation of the pressure in the intermediate chamber between the two orifices. It may be noted that for initial temperatures below 213 F the intermediate pressure is always 57.5 psi, being midway between the initial pressure, p_1, of 100 psi, line 1, and the discharge pressure, p_2, of 15 psi, line 2. For any initial temperature above 213 F the intermediate pressure increases linearly with initial saturation pressure and is midway between initial total pressure and initial saturation pressure. This feature, it was pointed out in the former paper, constitutes the factor in the utilization of two orifices in series for controlling the flow of hot water. For initial temperatures very near the saturation temperature, the critical pressure is only slightly less than the saturation pressure with a correspondingly slight effect on the intermediate pressure.

In Fig. 2 are also indicated the liquid region of the first orifice, the liquid region of the second orifice, the region of flashing which occurs after the second orifice, and the corresponding pressure drops in the first orifice, in the second orifice, and beyond the second orifice.

It should be recalled that the foregoing analysis of flow under stable conditions applies equally well to sharp-edged and rounded-entrance orifices.

DESCRIPTION OF APPARATUS AND EXPERIMENTAL METHODS

The apparatus used in this investigation, Fig. 3, consists essentially of a continuous hot-water supply leading to two identical orifices arranged in series and a means of measuring the following quantities: Pressure of water at the entrance to the first orifice; temperature of water at the entrance to the first orifice; intermediate pressure; intermediate temperature; downstream pressure beyond the second orifice; and the rate of flow.

Hot water and steam were obtained from blowoff and steam connections, respectively, of a gas-fired high-pressure boiler (2) supplied with distilled water. Initial temperature control of water entering the apparatus was obtained by maintaining the boiler pressure considerably above the desired pressure and by proportioning flow from a direct boiler connection and a parallel connection through a water-cooled coil. Valves with by-passes served further to throttle the water to the pressure maintained in

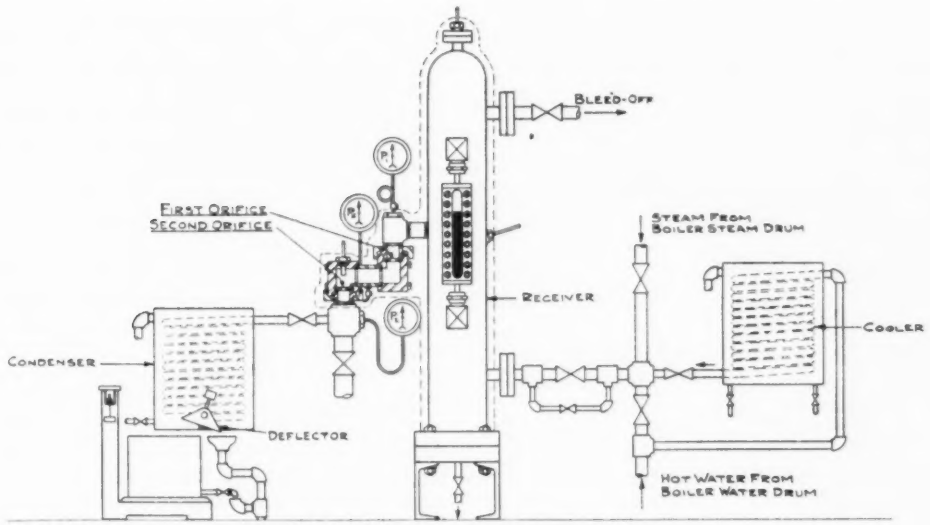


FIG. 3 ARRANGEMENT OF APPARATUS

the receiver. The column-type receiver was provided with water glass, thermometer well, upper and lower bleedoff connections, and an outlet leading to the orifices under investigation. Pressure gages served to indicate the initial, intermediate, and discharge pressures. The orifices, clamped between gaskets in union-type fittings, were purposely offset to eliminate velocity effects of the first orifice upon the second orifice and to return the enthalpy of the fluid in the intermediate chamber to its initial value.

The intermediate chamber between the orifices was provided with a thermometer well and a pressure gage. On the downstream side of the orifices a connection was provided through the gate valve to the water-cooled condenser which served to cool the discharged fluid preparatory to weighing. A deflector provided means of diverting the flow from the drain connection to the weighing tank on a platform scale, so that it was possible to measure accurately by a stop watch the rate of flow over a period of time.

The operating procedure consisted of establishing steady flow through the orifices at the desired initial temperature and pressure. The initial pressure was maintained at 100 psia for all experiments. The initial temperature was varied from 70 F to the saturation temperature of 327.8 F. Discharge pressure was maintained at approximately 15 psia.

Flow determinations were based upon time intervals ranging from 1 to 4 min. The stop watch was checked against a watch of known accuracy. The platform scale was sensitive to $^1/_2$ oz, approximately equivalent to 0.1 per cent of the average quantity of water weighed. At the beginning and end of each interval, observations were taken of initial pressure, initial temperature, intermediate-chamber pressure and temperature, and discharge pressure.

Pressure gages were of the standard Bourdon-tube type and were frequently checked by a dead-weight tester during the course of the investigation. Temperature readings were obtained by means of accurately calibrated mercury-in-glass thermometers inserted in mercury-filled thermometer wells.

THE METASTABLE CONDITION

Before presenting the results of this investigation, a word of explanation is given concerning stable and metastable conditions of water. By definition, "stable" refers to the condition in which the pressure of the liquid, or of the mixture of liquid and vapor, is not less than the saturation pressure corresponding to the existing temperature, or, conversely, that the temperature of the liquid or the mixture is never higher than the saturation temperature corresponding to the existing pressure. If a condition exists where the pressure of a liquid, or of a liquid-and-vapor mixture, is less than the saturation pressure corresponding to the existing temperature, the condition is said to be "metastable." The most important characteristic of the metastable state is the delay in an anticipated phase change. Metastable states are known to exist in many circumstances where a change of phase is about to occur (3). Examples are the cooling of liquid water below the freezing temperature and the cooling of steam below the condensation temperature; the latter condition occurs in the well-known supersaturation phenomenon which exists in steam flow through nozzles.

The metastable state of a liquid may be attained in several ways, all of which involve the phenomenon that bubbles of vapor do not form in the mass of liquid when temperatures exceed the saturation temperature corresponding to the existing pressure of the liquid, or, alternately stated, when pressures become lower than the saturation pressure corresponding to the existing temperature of the liquid. Some of the means of attaining a metastable state in a liquid are by the careful heating of water at constant pressure; by the sudden release of the pressure of a quiescent liquid; and by the flow of a liquid without turbulence through an orifice or nozzle to a discharge pressure less than the saturation pressure of the liquid. The retardation of the formation of bubbles has been attributed to the time necessary for the mass and heat transfers which are required for a bubble formation.

A more basic explanation of the metastable state depends upon the phenomenon of surface tension and the role of surface energy in delaying the initiation of very small steam bubbles in a mass of pure liquid (3). It is supposed that the formation of the initially minute bubbles is accelerated by impurities in the liquid, gases, or solids in solution, turbulence, ionization, or any other factor which will assist in creating an initially minute curved surface or nucleus about which the bubble may form.

In the flow of water through orifices it is known that the attainment of metastable states is favored by the purity of the water and by the smoothness of the passage, and also by a minimum of turbulence and friction. The existence of metastable states in the flow of water through orifices has been established by a number of investigators (4, 5, 7, 8).

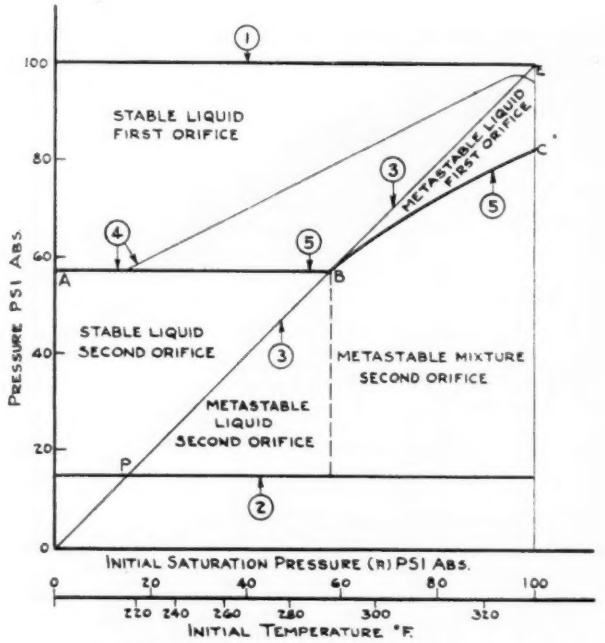


FIG. 4 PRESSURE DIAGRAM FOR FLOW THROUGH TWO SHARP-EDGED ORIFICES IN SERIES

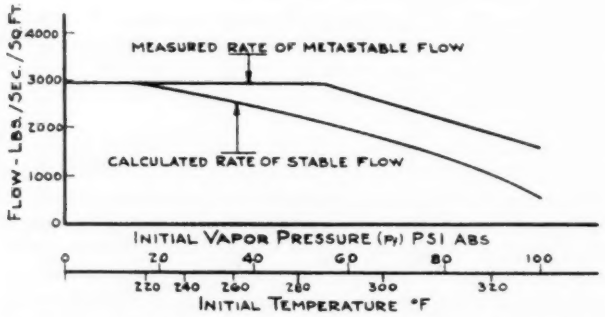


FIG. 5 RATES OF STABLE AND METASTABLE FLOW; SHARP-EDGED ORIFICES

FLOW OF HOT WATER UNDER METASTABLE CONDITIONS THROUGH TWO SHARP-EDGED ORIFICES IN SERIES

The characteristics of flow of hot water through orifices in series will vary greatly with the type of orifice used. The sharp-edged orifice was selected as a standard for determining the basic phenomena of the process. Two sharp-edged orifices $^1/_8$ in. diam, $^1/_8$ in. thick, and chamfered at 45 deg to a working edge of 0.020 in. were arranged in series in the apparatus shown in Fig. 3. The essential data yielded by a run consisted of the initial pressure, the initial temperature, the intermediate pressure, and the measured rate of flow through the orifices.

Results for runs over the entire range of initial temperatures are presented in Figs. 4 and 5. In the pressure diagram, Fig. 4, the abscissa is the initial saturation pressure. The measured temperatures of the inlet water are also marked along the abscissa. Ordinates represent pressures existing throughout the system for various inlet temperatures. As in Fig. 2, line 1 represents the constant initial pressure of 100 psi, line 2 represents the constant discharge-region pressure of 15 psi, and line 3 is the initial saturation pressure. The measured intermediate pressures are shown by line 5. Line 4, which represents intermediate pressures for flow under stable conditions, is redrawn from Fig. 2 for purposes of comparing characteristics. In Fig. 5 are plotted the rates of flow as measured and, for comparison, the rates as calculated for ideal stable fluid flow. The most significant results of this investigation, as disclosed by an examination of Figs. 4 and 5, are (*a*) that the intermediate-chamber pressure, as calculated for stable fluid flow, line 4, is much higher than the measured intermediate pressure, line 5, and (*b*) that the calculated rate of stable fluid flow is much lower than the actual measured rate of flow. These striking differences in the measured characteristics and the similar characteristics, as calculated for stable fluid flow, can be accounted for completely and uniquely by recognizing the existence of the metastable state of the fluid in certain regions during the passage of the hot water through the orifices.

In stable fluid flow, the lowest pressure which can exist at the end of the second orifice is the saturation pressure, as shown by line 3 in Fig. 4. In actual flow, under certain conditions, the water continues through an orifice as a liquid in the metastable condition, that is, at pressures lower than the saturation pressure, without flashing, and with temperatures higher than saturation temperatures. In order definitely to establish the regions in which metastable conditions exist, a thermodynamic analysis is made in the following paragraphs.

THERMODYNAMIC ANALYSIS OF METASTABLE FLOW

It may be established quite directly from the pressure diagram in Fig. 4 that the metastable condition must exist in the second orifice for initial temperatures of water at least up to the point *B* because equal pressure drops and equal flow in each orifice can be accounted for only by the maintenance of a liquid condition in the second orifice along the entire line *A-B*. If flashing occurred in the second orifice, as would be required for the stable condition, a greater pressure drop would be required in the second orifice than in the first orifice. However, in the region from *B* to *C* it is not immediately evident to what extent metastable conditions exist, since a greater pressure drop exists in the second orifice than in the first. In order to investigate the existence of the metastable state, a complete thermodynamic analysis was made of the flow of initially saturated water at 100 psi and 327.8 F by assuming in turn that the fluid was stable in both orifices, metastable in the first orifice only, and finally metastable in both orifices. By comparing the results of this analysis with the data obtained in the experiment in regard to intermediate pressure and rate of flow, it was definitely established that the metastable condition existed in the first orifice in the region bounded by *EBC* in Fig. 4. The metastable condition also existed in the second orifice in the entire region below the line *PBC*.

The results of this thermodynamic analysis of the flow of saturated water through two sharp-edged orifices in series under both stable and metastable conditions are shown graphically in Fig. 6. The intermediate pressure is the measured value of 84 psia. The calculations for stable conditions were made on the basis of constant entropy during flow. Calculations for flow through the first orifice were made for quality, specific volume, change of enthalpy, velocity, and mass rate of flow per unit area. All calculations were by usual methods, except that calculations for the change of enthalpy were made by numerical integration of $\int V dP$ (ref. 1). The state in the intermediate chamber was known because in the throttling process H_1 equals H_2.

Calculations for flow through the second orifice, assuming constant entropy and stable expansion, were made in the same manner as for the first orifice. These results, plotted in Fig. 6, disclosed the usual critical pressures and the corresponding possible maximum rates of flow through each orifice. The maximum

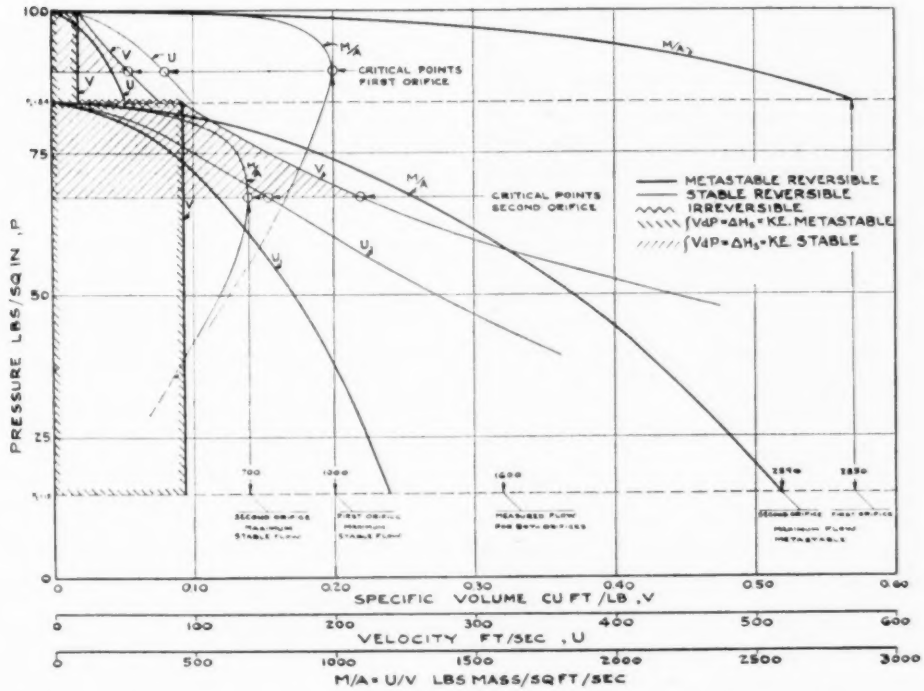


FIG. 6 THERMODYNAMIC ANALYSIS OF FLOW OF SATURATED WATER THROUGH TWO SHARP-EDGED ORIFICES IN SERIES

calculated rates of flow obtainable under stable conditions were each much lower than the actual measured rates of flow. This phenomenon of actual rates of flow in excess of ideal rates of flow is characteristic of the metastable state.

Calculations were next performed assuming the existence of metastable conditions. For these calculations it was assumed that the fluid passed through the first orifice as a liquid with no change in volume from the initial volume of the saturated liquid. Further assumptions were that in the intermediate chamber stable conditions were restored, flashing occurred, and the enthalpy, H_2, returned to the original enthalpy, H_1. For the metastable condition in the second orifice it was assumed that the fluid, consisting of liquid and vapor bubbles, passed completely through the second orifice with no change in volume, no further evaporation, and no decrease in temperature. Calculations of enthalpy change, velocity, and mass rate of flow were thus made for metastable conditions in each orifice. The calculated rates of flow for metastable conditions were 2850 lb per sec per sq ft for the first orifice, and 2590 lb per sec per sq ft for the second orifice. These calculated rates of flow exceeded the measured rate of flow for each orifice, which was 1600 lb per sec per sq ft. The flow coefficients for the first and second orifice were 0.562 and 0.618, respectively. These coefficients, although not equal, were both acceptable for fluid flow through sharp-edged orifices. This circumstance, contrasted with the similar circumstance for previously assumed stable condition, established the condition of the flow as metastable or nearly metastable, in both orifices.

Similar thermodynamic analyses showed that, as previously anticipated in Fig. 4, the metastable condition existed in the first orifice in the region bounded by *EBC* and in the second orifice in the entire region below the line *PBC* which extends completely down to the discharge pressure. Even with some vapor present at the entrance to the second orifice, further evaporation was suppressed by the persistence of the metastable state.

It is noted that in the second orifice the liquid-vapor mixture attained a supertemperature of 102.4 F, which is the excess of

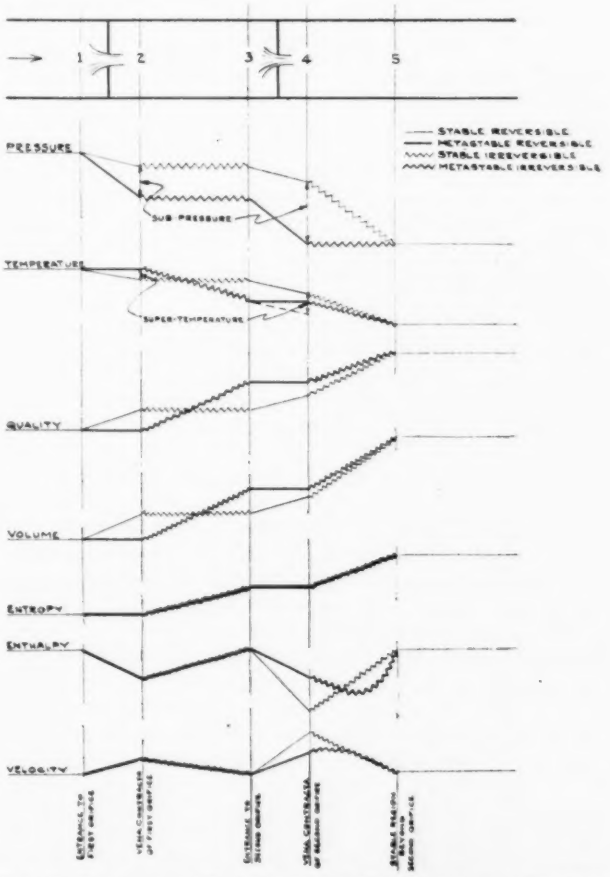


FIG. 7 CHANGES IN THERMODYNAMIC PROPERTIES FOR FLOW OF SATURATED WATER THROUGH TWO ORIFICES IN SERIES

the actual temperature of 315.4 F over the saturation temperature of 213.0 F.

Qualitative Changes in Properties of Fluid During Flow

Comparisons of progressive changes in the properties of the fluid as it passes through the two orifices in series under stable and metastable flow conditions are portrayed graphically, but not to scale, in Fig. 7. Pressure, temperature, quality, volume, entropy, enthalpy, and velocity changes of the fluid throughout the system for stable and metastable conditions of initially saturated water are indicated at five significant reference points, viz., 1, entrance to first orifice, 2, vena contracta of first orifice, 3, entrance to second orifice, 4, vena contracta of second orifice, and 5, stable discharge region beyond the second orifice. It should be noted that in the region from orifice entrance to vena contracta the metastable state persists, and that immediately beyond the vena contracta there is an irreversible turbulent return of the fluid to a stable condition.

Physical Appearance of Jet of Hot Water Discharging From Sharp-Edged Orifice Into Atmosphere

In order further to verify the existence of the metastable state during flow, photographs were taken of jets of hot water discharging vertically downward from a sharp-edged $^1/_8$-in-diam orifice into the atmosphere. The initial pressure of the water was 100 psia, and temperatures were varied from 155 F to saturation temperature of 327.8 F. The apparatus used to produce the jet is shown in Fig. 8. The views, Fig. 9, are arranged progressively with increasing initial temperatures from 155 F to 327.8 F.

With cool water supplied, the jet was clear and of constant area and shape to a distance of 10 in. or more from the orifice. This form of jet persisted with increasing temperature but vapor was emitted from the surface of the stream as the temperature approached the boiling point. Fig. 9(*a*) for a temperature of 155 F, is characteristic of the appearance of the jet at all temperatures below 212 F. At 212 F there was no indication of boiling within the observed length of jet, but vapor emission from the surface of the stream was more pronounced. This vapor emitted from the jet was hot to the touch, and at temperatures somewhat in excess of 212 F the vapor emission was of noticeable intensity although the jet remained clear, an indication that there was no boiling in the interior of the stream.

With increase in temperature to about 225 F, Fig. 9(*b*), the vapor emission increased and the jet started to stream into filaments at a point about 12 in. from the orifice. Further increase in temperature caused a greater degree of streaming and spreading of the jet closer to the orifice, as shown in Fig. 9(*c*), for a temperature of 260 F.

The spreading of the stream assumed the conical form at a temperature of 275 F, indicated in Fig. 9(*d*). As the temperature increased, a transition point was reached at about 280 F where the streaming previously referred to changed to droplet formation. In contrast to the rather smooth and uniformly increasing streaming action, droplet formation proceeded explosively from a clear jet at a point 2 or 3 in. beyond the end of the orifice. Fig. 9(*e*) shows the form of the jet at a temperature of 285 F, slightly above this transition point, in contrast to Fig. 9(*d*) taken at a temperature just below the transition point. At a temperature of 300 F, Fig. 9(*f*), the average distance from the throat section of the orifice to the point of jet expansion was about 1 in. The discharge cooled rapidly in the region beyond the point of jet expansion and was relatively cool to the touch beyond the region of full expansion. The point of jet expansion did not remain at a fixed distance from the orifice, but moved up and down the jet over a range of possibly $^3/_4$ in. with a crackling explosive sound.

Figs. 9(*g*) and 9(*h*) show the decreasing length of clear jet at temperatures of 310 F and 322 F, respectively. The transition point where marked jet expansion occurred was taken to be indicative of transition from the metastable to the stable state. If the region beyond the transition point assumed a conical form, it was presumed that the fluid consisted of a continuous liquid phase containing bubbles of vapor. If at the transition point the expansion was marked and explosive, it was presumed that the subsequent fluid consisted of a continuous vapor phase with entrained drops of liquid.

In the case of saturated water supplied to the orifice, Fig. 9(*i*), an explosive transition was definite, the change occurring quite near the orifice.

With steam flow, Fig. 9(*j*), the issuing jet assumed approximate conical form within a very short distance from the orifice. Because the jet was almost invisible for initially dry saturated steam a trace of moisture was introduced to outline the jet. The form of the jet did not appear to be visibly affected by this moisture addition.

These observations verify the existence of the metastable condition of hot water during flow through, and somewhat beyond, the sharp-edged orifice. The distance beyond the orifice marked by the existence of the metastable state appears to be an inverse function of the temperature of the water. For the jet of water at a temperature of 225 F (a supertemperature of 12 deg) the jet persists for a distance of 12 in. For the jet of water at a temperature of 322 F (a supertemperature of 107 deg) the metastable jet persists only for a fraction of an inch. Thus the time of existence of metastability is an inverse function of the supertemperature.

Flow Characteristics of Rounded-Entrance Orifices

The maintenance of the metastable condition in both sharp-edged orifices down to the vena contracta is attributed to the almost completely reversible (frictionless and nonturbulent) flow produced by the sharp-edged orifice. Anything which produces friction or turbulence will prevent the maintenance of the metastable state during flow. A rounded-entrance orifice introduces a much larger surface of contact than the sharp-edged orifice, and to this extent may produce conditions departing from the metastable. Investigations were conducted with various pairs of identical rounded-entrance orifices in series. The radius of entrance was $^1/_8$ in. and the minimum diameter about $^1/_8$ in. The lengths

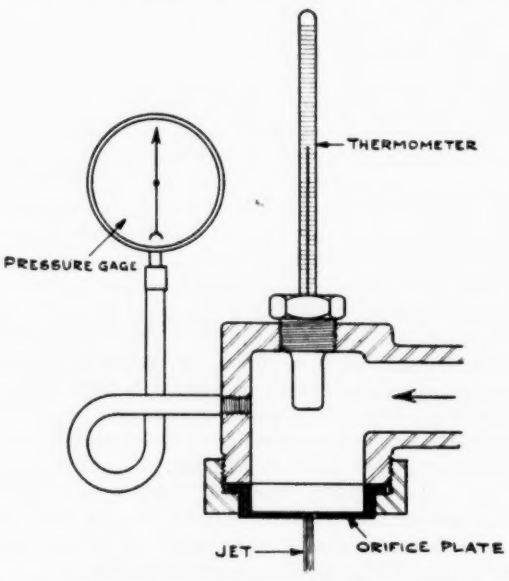
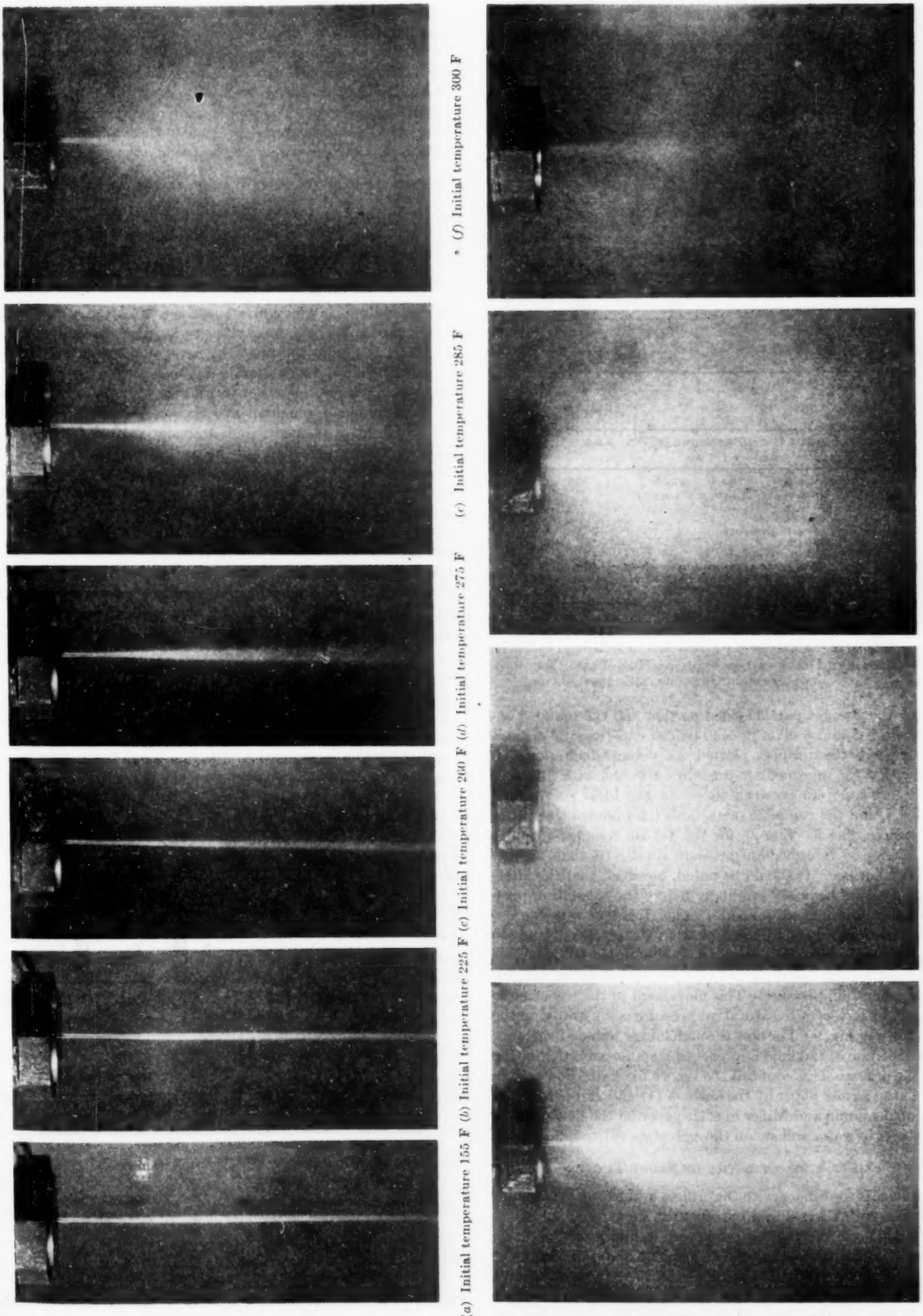


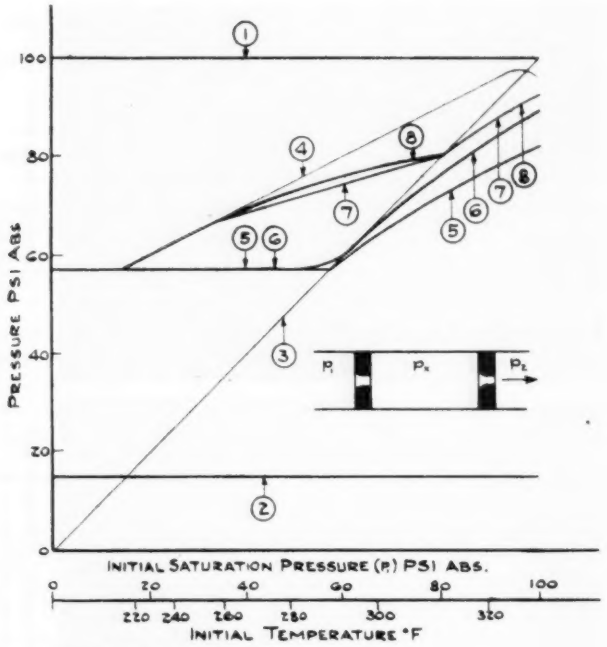
Fig. 8 Arrangement to Determine Physical Appearance of Jet of Hot Water Discharging From Orifice



(*a*) Initial temperature 155 F (*b*) Initial temperature 225 F (*c*) Initial temperature 260 F (*d*) Initial temperature 275 F (*e*) Initial temperature 285 F (*f*) Initial temperature 300 F

(*g*) Initial temperature 310 F (*h*) Initial temperature 322 F (*i*) Initial temperature 327.8 F (saturated) (*j*) Steam 327.8 F

FIG. 9 JET OF HOT WATER DISCHARGING THROUGH A SHARP-EDGED ORIFICE FROM INITIAL PRESSURES OF 100 PSIA INTO ATMOSPHERE



1 Constant initial total pressure
2 Constant discharge-region pressure
3 Initial saturation pressure
4 Stable flow intermediate pressure
5 Metastable flow intermediate pressure for sharp-edged orifices
6 Metastable flow intermediate pressure for rounded-entrance orifices, 1 diam long
7 Metastable flow intermediate pressure for rounded-entrance orifices, 5 diam long
8 Metastable flow intermediate pressure for rounded-entrance orifices, 8 diam long

FIG. 10 PRESSURE DIAGRAM FOR FLOW OF HOT WATER THROUGH ROUNDED-ENTRANCE ORIFICES IN SERIES

including the straight parallel-sided portion and the rounded entrance were 1, 5, and 8 diam in each pair of experimental orifices. The results with these orifices, plotted as a pressure diagram in Fig. 10, show that the intermediate pressures attained with rounded-entrance orifices were between those for the ideal stable fluid flow, line 4, and the complete metastable fluid flow of the sharp-edged orifices, line 5. Line 6, for the 1-diam rounded-entrance orifice, shows an intermediate pressure similar to that for the sharp-edged orifice. It should be noted, however, that the intermediate pressure increases gradually before the saturation pressure reaches intermediate pressure. This, together with the observed reduction in flow, is indication that the point marking the start of the transformation from metastable liquid to the stable mixture had moved upstream and into the second orifice with increasing saturation pressure. This movement of the transformation point with respect to saturation pressure is illustrated in the views shown in Fig. 9. For flow through longer rounded-entrance orifices the state of the fluid approached a stable condition at the end of the orifice. This confirms the theory for stable flow as presented in the former paper by the authors (1) and agrees with the results of Benjamin and Miller in their paper on the flow of flashing mixtures of water and steam through pipes (6).

FLOW CHARACTERISTICS OF SHORT TUBES

Experiments were made with the orifices in the form of standard short tubes with sharp-edged entrance, as shown in Fig. 11. A characteristic of a short tube, well known in hydraulics, is that a vena contracta forms in the tube and upon expansion causes the water to fill the tube at the exit. This fact introduces distinctive characteristics in the flow of hot water through short tubes. As shown in Fig. 11, the intermediate pressures for short tubes are somewhat similar to those for rounded-entrance orifices but differ in the important aspect that intermediate pressures obtained were higher than for orifices with rounded entrances and even higher than for stable flow with sharp-edged orifices.

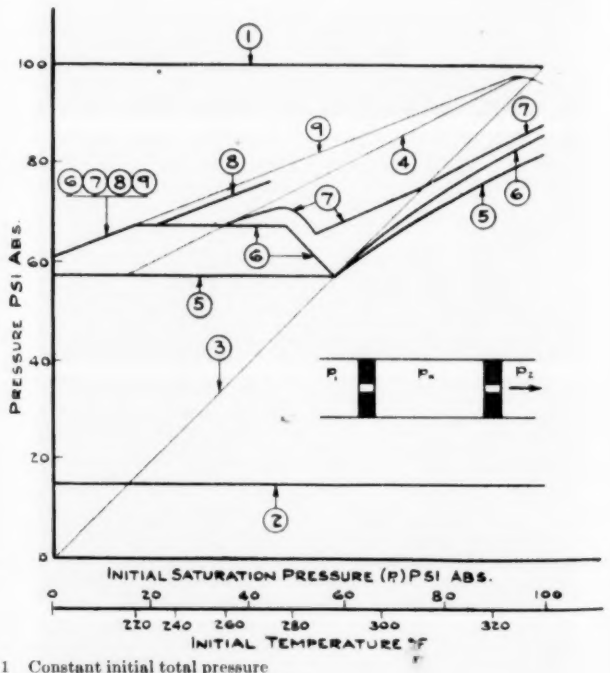
All of the data presented are based upon flow through two identical orifices in series. The combination of various types and differing sizes of orifices makes it possible to obtain desired intermediate-chamber pressure characteristics.

CONTROL OF FLOW OF HOT WATER BY MEANS OF ORIFICES IN SERIES

The characteristics of fluid flow through two orifices in series, as presented in this paper, may serve as a basis for the design of a control element. Such an element consists of an arrangement of two orifices in series, in which the state of the fluid supplied causes variations in pressure between the two orifices, these pressures being in turn communicated to a pressure-sensitive member. Fig. 12 shows the practical form of a two-orifice control element developed for automatic condensate drainage.

The piston valve, which constitutes the only moving part, fulfills the combined requirements of the series-control orifices, pressure-sensitive element, and drainage valve. The annular clearance between the disk on the piston valve and the wall of the cylinder forms the first orifice, the space in the cylinder above the disk constitutes the intermediate chamber, and a small rounded-entrance orifice at the top of the piston valve communicating with the discharge through the center of the valve constitutes the second orifice.

In order to obtain the required area relationship between the two orifices, the cylinder wall is tapered and the cylinder is made vertically adjustable to permit variation of the clearance between disk and cylinder wall.



1 Constant initial total pressure
2 Constant discharge-region pressure
3 Initial saturation pressure
4 Intermediate pressure for thin-plate orifices, stable state
5 Intermediate pressure for thin-plate orifices, metastable state
6 Intermediate pressure for short tube 1 diam long, metastable state
7 Intermediate pressure for short tube 4 diam long, metastable state
8 Intermediate pressure for short tube 8 diam long, metastable state
9 Intermediate pressure for short tube 1 diam long and over, stable state

FIG. 11 PRESSURE DIAGRAM FOR FLOW OF HOT WATER THROUGH SHORT TUBES IN SERIES

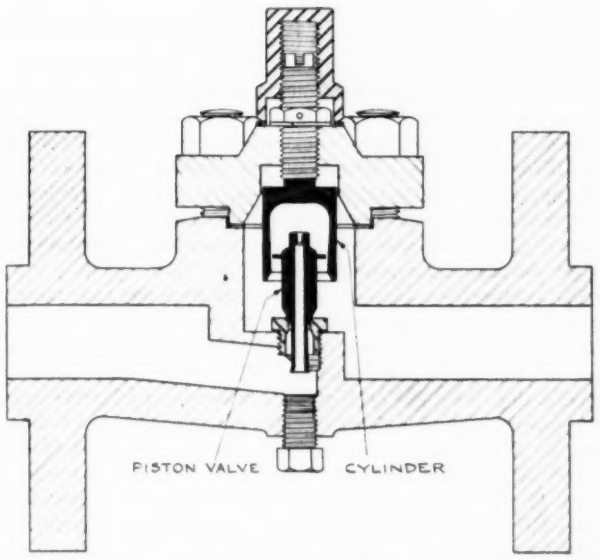


FIG. 12 PRACTICAL FORM OF CONTROL ELEMENT FOR CONDENSATE DRAINAGE

On proper adjustment, the relatively high intermediate pressure acting on the upper surface of the piston for steam and very hot condensate flow is sufficient to close the valve. With cooler condensate the correspondingly lower intermediate pressure permits the valve to lift and discharge the condensate.

The device is operative in like manner over a wide range of initial pressures without further adjustment. As suggested earlier in the paper, desired characteristics for the variation of the intermediate pressure with initial temperature may be obtained by suitable choice of types of orifices and by relative sizes of the orifices. Further, the existence of the metastable state, as disclosed in this paper, makes it possible to obtain a far wider range of control conditions than would be possible if the fluid remained in the stable state throughout the process.

ACKNOWLEDGMENTS

The authors acknowledge with appreciation the work of John F. McKee, engineer associated with the Yarnall-Waring Company, in the original development of the control element of fluid flow through two orifices in series.

The authors are indebted to W. J. Kinderman, of the Yarnall-Waring Company, for his invaluable aid in the design and construction of the apparatus, conduct of the research, and interpretation of the results. They also wish to acknowledge the assistance of J. A. Karas, of the mechanical-engineering department of Lehigh University, in the preparation of this paper.

BIBLIOGRAPHY

1 "Fluid Flow Through Two Orifices in Series," by Milton C. Stuart and D. Robert Yarnall, *Mechanical Engineering*, vol. 58, 1936, p. 479.

2 "2500-Lb Research Boiler," by D. Robert Yarnall, *Mechanical Engineering*, vol. 53, 1931, p. 883.

3 "Thermodynamics," by Joseph H. Keenan, John Wiley & Sons, Inc., New York, N. Y., chapt. 25, 1941.

4 "Flow of Boiling Water Through Orifices and Pipes," by W. T. Bottomley, Trans. North East Coast Institution of Engineers and Shipbuilders, vol. 53, 1936–1937, pp. 65–100.

5 "The Flow of Saturated Water Through Throttling Orifices," by M. W. Benjamin and J. G. Miller, Trans. A.S.M.E., vol. 63, 1941, pp. 419–429.

6 "The Flow of a Flashing Mixture of Water and Steam Through Pipes," by M. W. Benjamin and J. G. Miller, Trans. A.S.M.E., vol. 64, 1942, pp. 657–669.

7 "The Flow of Hot Water Through a Nozzle," by B. Hodkinson, *Engineering*, London, England, vol. 143, 1937, pp. 629–630.

8 "Discharge Capacity of Traps," by A. E. Kittredge and E. S. Dougherty, *Combustion*, vol. 6, Sept., 1934, pp. 114–119.

Discussion

E. BROWN.[4] Study of the metastable state of water will probably help toward a better understanding of pitting in water turbines of the pressure type. As the water passes from the scroll case to the draft tube its pressure is lowered, and high vacuum may occur in the draft tube near the discharge tips of the blades. It is probable that in certain localized zones the vacuum is much higher than the general average vacuum across the whole section of the draft tube. In such zones the pressure may fall below the saturation pressure corresponding to the temperature of the water, because the drop of pressure is fairly rapid. The time element is probably an important factor in determining the rate at which small pockets or bubbles of water vapor, or of gases held in solution, are formed. The rapid collapse of such bubbles or voids may cause local pressures of great intensity which destroy the metal with which the water comes in contact. This was first demonstrated by the late Sir Charles Parsons in connection with the corrosion or pitting of ships' propellers. Whether this theory, or the alternative one of chemical action, be accepted, the fundamental conception is the formation of bubbles of released gases or water vapor. In water turbines such gases or vapor tend to be reabsorbed as the pressure in the water rises during its passage to the tailrace. The gradual formation of such voids, and their subsequent gradual disappearance, has been proved by photographs, and the writer has found experimental evidence of distinct differences between the gas content of water drawn from the draft tube of a small turbine from a zone where erosion was occurring, and a zone where there was no erosion. In both cases the gas content was less than that of water at the intake.

The writer has tested many models of water turbines during the past 20 years in connection with water-power developments. His experiences of corrosion or pitting have been varied, and in many cases seemingly contradictory. He has long held the view however that more intensive pitting may develop in a large turbine than in a small model even when they are operated on the same head. Under such conditions, the velocity of the water will be the same in both cases. But if the model is to, say, one-twelfth scale, the water in the large turbine will take 12 times as long as the water in the model to flow between corresponding points above and below the runner, and the harmful bubbles will probably be created at a different rate. Questions of heat transfer and surface tension are involved, and impurities in water may have some definite influence. The problem of relating the behavior of models to that of water turbines of greatly increased size is fraught with many difficulties. The work of the authors, apart from its evident value in such processes as those discussed in their paper, should contribute toward a clearer scientific understanding of some of the troubles of the engineer engaged in the development of water power.

G. A. HORNE.[5] This paper suggests some interesting points to the refrigerating engineer. In the refrigeration cycle, the liquid refrigerant is generally assumed to be in a stable condition throughout.

The writer has two-stage ammonia compression systems in

[4] Professor of Applied Mechanics and Hydraulics, McGill University, Montreal, Canada.

[5] Consulting Engineer, Merchants Refrigerating Company, New York, N. Y. Mem. A.S.M.E.

which all the liquid passes from the condenser through Venturi meters for measurement. To insure any change of state from liquid to vapor at the throat of the meter, the liquid is sufficiently reduced below saturation temperature by means of a cooling coil placed between condenser and meter.

In these two-stage compression systems all of the liquid is passed through an expansion valve into an intermediate cooler at the intermediate pressure between the two stages of the compressor. In this operation, it is generally assumed that the refrigerant remains in a stable condition so that the amount of vapor formed is the anticipated quantity in accordance with the pressure drop. However, the liquid which accumulates in the intermediate cooler is in a quiescent state and is maintained at a certain level while the vapor mixes with the balance of the vapor from the low-pressure cylinder, thence to the high-pressure cylinder.

The liquid from the bottom of the intermediate receiver passes through an expansion valve into the low-temperature evaporator or brine cooler. A certain residual amount remains in the receiver to serve as a trap.

The question which is prompted by the authors' work on fluid flow is therefore: Under the operation just described, would a metastable condition of the liquid refrigerant be apt to exist in the intermediate receiver?

Obviously, if this were the case, the efficiency of the system would be lowered and would result in an increase in the horsepower to drive the compressors.

The authors refer to certain means of attaining a metastable state in a liquid. A few years ago the writer was interested to observe an example of this phenomenon in determining the freezing point of grapefruit juice. It had generally been assumed in the fruit trade that oranges and grapefruit should be carried in cold storage at temperatures varying from 34 to 38 F. It had been found that lower temperatures, as low as 30 F were of considerable advantage in lengthening the storage period and improving the quality of the products. Although certain authorities showed the freezing point of the juice to be around 29 F, we decided to check it.

A 1-in. test tube was filled with juice, inserted through a cork into a bottle, and the bottle immersed in a large vessel containing brine at —5 F. Through a cork in the test tube an accurate thermometer was placed. It was expected that crystals would appear when the temperature of the juice reached 28 or 29 F. However, nothing happened while the temperature gradually dropped to 19 F. At that point the writer stirred the juice a little and immediately the entire contents became a mass of grapefruit ice, the temperature rose to 28.6 F and stayed there for some time.

It seems probable that the greater subcooling of water and water solutions, as compared to other liquids, is partly due to the fact that the maximum density of water is several degrees above the freezing point. As the authors point out, the metastable state depends upon surface tension. The ice crystals must form at the surface instead of at the bottom.

J. H. KEENAN.[6] This paper is an important contribution to our knowledge of the flow of liquids in the neighborhood of the saturation state. The literature on this subject, as indicated by the Bibliography included in the paper, is indeed limited.

As pointed out by the authors, the expansion of a liquid across its saturation line, like the flow of a vapor across its saturation line, results in metastable states. Various investigators from Wilson to Yellott[7] have attempted with a degree of success to determine the extent to which the expansion of a vapor may be extended beyond the saturation line before the first evidence of condensation appears.

This paper sheds some light on the analogous problem in the liquid phase, namely, to determine the extent to which the expansion of the liquid may be extended beyond the saturation line before the first evidence of vaporization appears. The photographs of Fig. 9 suggest that expansion to atmospheric pressure may occur at a temperature as high as 285 F without vaporization. This corresponds to an expansion of about 40 psi below the saturation pressure.

These illustrations, however, are not conclusive in this regard, because they are of such small scale that it would be impossible to detect the presence of small bubbles of vapor where the stream first attains atmospheric pressure. Somewhat better evidence appears in curve 6 of Fig. 10, which indicates that for rounded-entrance nozzles no evidence of vaporization appears for expansion to atmospheric pressure until the temperature exceeds 280 F. In a rounded-entrance nozzle, the pressure in the exit plane of the nozzle approximates the pressure in the exhaust space for a radius of rounding equal, as in this case, to the diameter of the nozzle. It appears, therefore, that expansion to approximately atmospheric pressure occurred in the downstream rounded-entrance nozzle without vaporization.

The rough agreement between the indications of the views in Fig. 9 and curve 6 in Fig. 10 does not support the statement of the authors that "a rounded-entrance orifice introduces a much larger surface of contact than the sharp-edged orifice, and to this extent may produce conditions departing from the metastable." The statement may be true, nevertheless.

In this connection, it should be noted that curve 5 in Fig. 10, which represents the performance of sharp-edged orifices, offers no such conclusive evidence as curve 6. In flow through a sharp-edged orifice the pressure in the plane of the orifice does not even approximate the pressure in the exhaust space but exceeds it by a large fraction of the total pressure drop. It would be entirely possible, therefore, to have considerable vaporization in the stream at pressures in excess of the exhaust pressure without any effect on the flow through the orifice. Thus the calculated curve 4 is relevant to the rounded-entrance orifice but not to the sharp-edged orifice.

The curves in Fig. 11, for flow through short tubes, show many curious characteristics. Perhaps the authors could suggest some explanation of the reversal in the effect of rising temperature on the intermediate pressure which appears in curves 6 and 7.

If the heavy lines in Figs. 4, 10, and 11 represent experimental values, as they appear to, that fact is somewhat obscured by the label "metastable flow." Labeling of curves should be factual rather than interpretive.

It is a temptation not to be resisted to point out that the so-called metastable expansion assumed in Fig. 6 for the second orifice is an adiabatic process of decreasing entropy.

In the absence of experimental points, some indication should be given of the reproducibility and the precision of the data.

L. K. SPINK.[8] Referring to the diagrammatic arrangement of the apparatus, some of the pressure gages are shown connected with loops or syphons. The gage registering Px is connected with a self-draining connection. Bourdon-tube gages not only zero differently but also calibrate slightly differently when the tube is filled with a material of different density. The magnitude of the discrepancy is not sufficient to affect the reliability of this work, but is mentioned as a point of general interest.

The dimensions of the conduit between the two orifices are not

[6] Professor of Mechanical Engineering, Massachusetts Institute of Technology, Cambridge, Mass. Mem. A.S.M.E.

[7] For references see "Thermodynamics," Bibliography (3) of the paper.

[8] The Foxboro Company, Foxboro, Mass.

given but appear sufficient to reduce the velocity of approach to a negligible value. Only in that case would the location of the taps and the shape of the tap openings be of no importance. This low velocity of approach would also minimize the effect of the disturbed flow condition set up by the two right-angle turns in the conduit.

Although it is natural to expect a variation in the discharge coefficients of nearly identical orifices as small as $^1/_8$ in., the value 0.562 appears abnormally low. The orifice thickness is slightly in excess of that generally accepted for thin-plate orifices for flow measurement; but this, and the small diameter, would tend to increase the coefficient. If both values were true discharge coefficients, an intermediate pressure midway between the initial pressure and the discharge pressure, as shown by line *A-B* in Fig. 4, would be difficult to explain. The exact significance of the coefficient of the second orifice is obscured by the assumption that the vapor bubbles undergo a change in pressure without any change in volume.

Presumably the authors have a reason for assuming that the vapor does not expand in passing through the second orifice, and have additional data or a theory to explain the apparent inconsistency of the coefficients. Further elaboration on these points would be appreciated.

P. W. Swain.[9] This paper, like its predecessor, published in 1936, interests the writer chiefly because of the directness of its application to commercial power equipment.

In recent years American engineers have advanced notably in their ability and will to analyze phenomena in terms of the abstractions of mechanics and thermodynamics. Of this trend, this paper is a good example. However, it would seem that too many of the engineer researchers and analysts have been happy to stop with a published report and analysis. This the writer could never understand, for it would seem that the whole life of the true engineer is so wrapped up in the building and operation of machines that abstractions, even experiment and experimental data, could never satisfy him, except as a means to some practical end.

[9] Editor, *Power*, New York, N. Y. Mem. A.S.M.E.

The condensate drainer, pictured in Fig. 12, gives everyday meaning to the research and analysis of the authors. The writer sincerely hopes that it evidences an increasing interest of scientifically minded engineers in practical applications. It is possible that this interest in application largely explains the immense productivity of American engineering as compared, for example, with that of prewar France, a country gifted with many fine and highly trained technical minds, yet singularly sterile in engineering results.

Authors' Closure

The discussions pertain chiefly to metastable phenomena rather than directly to the characteristics of flow through series orifices. Most significant are the remarks of Professor Brown in regard to the influence of the metastable state in promoting cavitation in water turbines, and the instances cited by Mr. Horne where the possibility of metastable phenomena are encountered in refrigeration.

The authors accept the criticisms of both Professor Keenan and Mr. Spink that the assumption of a truly constant volume process in the second orifice is undoubtedly too dogmatic. An assumption more nearly in agreement with the facts is that the vapor bubbles in the mixture increase in volume adiabatically, with perhaps a slight increment due to evaporation from the metastable liquid portion of the mixture.

The reversal in the effect of the rising temperature on the intermediate pressure for flow through short tubes, referred to by Professor Keenan, is attributed to the limitation of the minimum pressures which may exist in the vena contracta as within the short tubes. When a short tube is flowing full at the exit, the pressure at the vena contracta within the tube does not become less than the saturation pressure.

Mr. Swain correctly surmises that it was the embodiment of a scientific principle in a practical commercial device which prompted the authors to undertake these experiments, intended both to explain the operation of the device and to reveal further basic information on the principles involved.

The Combustion of Barley Anthracite

By ALLEN J. JOHNSON,[1] PHILADELPHIA, PA.

Because of its availability, excellent combustion qualities, and low cost, "barley" or No. 3 buckwheat anthracite is one of the most economical of all industrial fuels. After giving the analyses and physical properties of this fuel, the author discusses the effect of utilizing barley upon boiler performance. Details of the equipment available for burning this fuel, either by hand or stoker firing, are outlined, as well as practical suggestions for actual operation of the various types.

Preparation, Quality, and Characteristics

THE 1942 production of "barley" or No. 3 buckwheat amounted to 5,800,000 tons which represented 10 per cent of the total production of anthracite. Interest in its industrial use centers around the combined facts that it is an excellent fuel for both hand and stoker firing, and that it is one of the most economical of all industrial fuels. At the present time, barley is one of the few fuels, if not actually the only one, of which there is a substantial surplus at the mines with adequate transportation facilities.

Adequate Supply Available. Because of the greatly increased demand for the larger or domestic sizes of coal without a corresponding industrial absorption, the production of barley now exceeds consumption by several thousand tons a week, thus creating substantial stock piles, available without fear of interruption to all plants having suitable utilization equipment. Sizing specifications, analyses, and physical properties of barley anthracite are given in Tables 1 and 2, respectively.

Quality of Barley. Like many other valuable commodities, barley originates as a by-product prepared from the breakage of the larger sizes of anthracite. With this accidental beginning, all resemblance to a by-product ceases, as the modern concentrator tables and other equipment upon which barley is cleaned are capable of preparing it to a high quality with any reasonable specifications of size and ash content. In fact, the fineness of the coal particles actually facilitates the removal of impurities. However, because of its small size and the consequent limitation of use to plants having specific combustion equipment, the price of barley is low, as shown in Table 3.

Effect of Coal Size and Quality Upon Boiler Performance

Several characteristics of coal affect the efficiency and capacity of boilers. However, in comparing the properties of coals, the terms efficiency, capacity, and economy are likely to be confused. Increased efficiency from a quality fuel may not overbalance its increased cost in one plant; while in another, increased capacity may be of sufficient importance to justify a sacrifice of efficiency and even of economy. The following factors should thus be carefully considered.

When to Use Barley. Barley anthracite is the smallest and cheapest size commonly used in all but the largest (traveling-grate) plants. Many plants now using rice (No. 2 buckwheat), or even No. 1 buckwheat would effect substantial savings by changing to this size, with the important advantage of assurance of supply.

Even where excessive loads in existing equipment preclude the continuous use of barley, substantial economies may be effected by burning it during off-peak seasons, as for example during mild weather in heating plants.

In general the following are requisite to the use of barley:

(*a*) Adequate forced draft or natural draft from unusually high stacks (preferably 300 ft or more as in large hotels or office buildings).

TABLE 1 STANDARD SIZING SPECIFICATIONS OF BARLEY ANTHRACITE AT BREAKER[a]

Through round-mesh screen, in.	3/16
Over round-mesh screen, in.	3/32
Oversize maximum, per cent	10
Undersize maximum, per cent	20
Undersize minimum, per cent	10

[a] A breaker is the preparation plant at the mines.

TABLE 2 ANALYSES AND PHYSICAL PROPERTIES OF BARLEY ANTHRACITE

	Approximate ranges	Average of 41 breakers[a]
Proximate analyses, per cent:		
Volatile matter	3.0 to 8.0	4.4
Fixed carbon	77 to 86	82.1
Ash	9.5 to 17.5	13.6
Sulphur	0.5 to 1.2	0.7
Fixed carbon dry mineral matter, free basis, per cent	92 to 98	...
Heat value Btu, dry basis	12000 to 13600	12890
Moisture (as received), per cent	5 to 7	7.2[b]
Softening temperature of ash, deg F	2400 to 3000	2800
Approximate ignition temperature, deg F	525 to 775	...
Weight and volume:		
Specific gravity	1.45 to 1.75	...
Pounds per cu ft	50 to 60	...
Cu ft occupied by 1 ton	33 to 40	...
Tendency to spontaneous combustion	None	None
Grates recommended:		
Proper type	Stationary or dumping	...
Max size of air opening	3/16 to 3/32	...
Free air space per cent	4 to 10	...
Combustion rate (lb per sq ft per hr):		
Hand-fired	15 to 20	...
Hand or "semi" stokers	18 to 23	...
Traveling-grate stokers	20 to 40	...
Availability:		
Tons mined in 1942	5,800,000	...
Percentage of total breaker production	10.0	...
Approximate f.o.b. mines:		
Cost (present O.P.A. ceiling)	$2.50	...

[a] Based upon U. S. Bureau of Mines Report R. I. 3283, 1935, analyzing 268 samples from 41 breakers mining 50 per cent of all anthracite.
[b] Measured at breaker.

TABLE 3 FREIGHT AND APPROXIMATE COST DATA ON BARLEY ANTHRACITE

	Typical f.o.b. mines cost	Freight rate[a]	Total carload cost on railroad sidings per net ton[b]
Harrisburg, Pa	$2.50	$1.45	$3.95
Lancaster, Pa	2.50	1.54	4.04
Philadelphia, Pa	2.50	2.05	4.55
Wilmington, Del	2.50	2.23	4.73
Albany, N. Y.	2.50	2.27	4.77
New York, N. Y.[b]	2.50	2.42	4.92
Rochester, N. Y.	2.50	2.50	5.00
Baltimore, Md.	2.50	2.50	5.00
Washington, D. C.	2.50	2.50	5.00
Buffalo, N. Y.	2.50	2.61	5.11
New Haven, Conn.	2.50	3.08	5.58
Springfield, Mass.	2.50	3.18	5.68
Boston, Mass.	2.50	3.18	5.68

[a] Calculated to net-ton basis, and also includes 4 cents per net ton Federal tax.
[b] Add 8 to 15 cents per ton for points outside harbor limits.

---

[1] Mechanical Engineer, Anthracite Industries, Inc. Mem. A.S.M.E.

Contributed by the Fuels Division and presented at the Annual Meeting, New York, N. Y., Nov. 29–Dec. 3, 1943, of The American Society of Mechanical Engineers.

Note: Statements and opinions advanced in papers are to be understood as individual expressions of their authors and not those of the Society.

(*b*) Stationary or dumping grates having a mesh of not over $^{3}/_{16}$ in.

(*c*) Semi- or hand stokers, with grates as described in (*b*).

(*d*) Traveling-grate stokers.

(*e*) Proper arch and furnace design when stokers or semi-stokers are used.

(*f*) Properly proportioned grate areas.

The use of straight barley anthracite upon underfeed stokers is not often recommended, unless the load is considerably below boiler and stoker rating, because of reduced effective grate areas available. However, mixtures of barley and bituminous are in use very successfully upon underfeed stokers.

Effect of Btu Value. The heat value or Btu content of coal is of course a direct measure of its value. In addition, since freight rates are on a per-ton basis, it costs more, per pound of useful combustible, to transport low Btu fuel. In considering this point, it is noteworthy that the further the plant is located from the mines the more significant coal quality becomes, because of the greater effect of freight rate.

Boiler ratings are also in direct proportion to Btu because, for any given number of pounds of coal per hour, fewer pounds of combustible will be consumed, as the percentage of inert material or ash increases. In plant design, however, this point can be overcome to permit the use of coal with practically any Btu content by adding grate surface. In this connection, the additional cost of the grates is usually insignificant, as compared with fuel savings over the life of the equipment.

Boiler efficiency is not always proportionately affected by heat value especially if the plant has been designed with the particular coal in mind. It is entirely possible to obtain "relatively" high efficiencies with low-grade coals even though the design problems are materially increased.

Effect of Ash. In anthracite, heat value is inversely proportional to ash content, Fig. 1. The effects of high ash upon economy, ratings, and efficiency are therefore as described for low heat content.

With respect to efficiency, Fig. 2 shows that, in a representative test over the entire range of ash contents, there was a drop of only 2 per cent in over-all boiler efficiency. Thus if the plant has been designed with sufficient grate surface to compensate for the lower outputs of high-ash coal it should operate satisfactorily, although never at the ratings obtainable with better fuel.

In all cases, the cost of handling and removing ash should be added to the price of coal plus the freight rate, in making cost comparisons. The best system consists of placing all fireroom labor, fuel and ash costs, and handling charges on a basis of cost per million Btu. Direct comparisons may then be made, which will place costs on a basis of the heat actually received rather than the relatively meaningless price of Btu at the mines.

Effect of Undersize. Fig. 3, based upon tests by L. A. Stenger (1),[2] shows the rate of air flow through coals having different percentages of dust content. The shape of this curve illustrates the well-known fact that uniformity of sizing is one of the most important points in connection with the combustion of barley. With more than 20 per cent undersize, the resistance of the fuel bed to the flow of air rises so rapidly as to change completely all combustion characteristics. It is thus significant that the Anthracite Institute Committee on Standards of Sizing selected 20 per cent as the maximum allowable undersize for barley. Conversely, however, 10 per cent was set as a minimum limit of undersize as it was not considered practical to prepare coal to finer standards.

With anthracite, the effect of dust is severalfold. It is difficult to maintain a uniform fuel bed because of a segregation of fines and the consequent blowing of holes; and the fines impede the flow of air to increase any tendency toward clinker and reduce combustion rates. In addition, fly ash and siftings are usually in proportion to the dust content.

In analyzing undersize content, one additional point is of particular importance, i.e., the character of the fines is as important as the percentage. Thus if a given percentage of undersize is almost all dust, serious difficulties may ensue; if, however, a large percentage of the fines is just slightly under the minimum screen size, considerably better results may be expected. It is thus suggested that sizing tests be reported on the following basis:

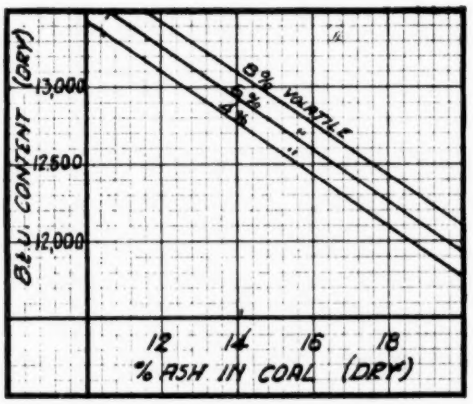


Fig. 1 Btu Versus Ash Content for Anthracite

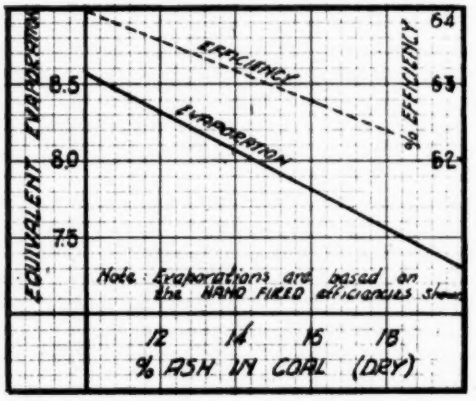


Fig. 2 Effect of Ash on Performance

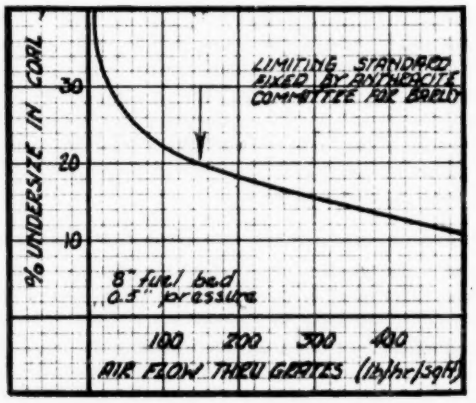


Fig. 3 Reduction of Air Flow to Undersize

[2] Numbers in parentheses refer to the Bibliography at the end of the paper.

(*a*) Per cent larger than No. 3 buckwheat (over $^3/_{16}$ in. screen)
(*b*) Per cent of No. 3 buckwheat through ($^3/_{16}$ in. over $^7/_{32}$ in.)
(*c*) Per cent of No. 4 buckwheat through ($^3/_{32}$ in. over $^3/_{64}$ in.)
(*d*) Per cent smaller than No. 4 buckwheat (through $^3/_{64}$ in.)

This method of analysis will show whether the undersize is really dust, or whether it is merely a mixture of No. 3 and No. 4 buckwheats, a much more desirable condition.

Effect of Moisture. As will be seen in Fig. 4, the boiler efficiency, calculated mathematically, is in direct relation to the moisture content of coal in that each 1 per cent of increase in moisture content will result in 0.4 per cent decrease in boiler efficiency. In actual practice, however, there is a reason to doubt the infallibility of this rule. A certain percentage of moisture (probably as high as 4 per cent) is credited by many engineers with being useful in tempering the fire to produce better combustion conditions. In many plants jets of steam are introduced into the ashpit to supply this moisture artificially. Properly controlled, they are believed helpful in reducing clinker formation. In addition Stenger (1), in reporting the effect of dust, remarked, "wetting dust-bearing coal practically doubles the air flow." It is thus probable that if Fig. 4 could be based upon actual tests instead of upon calculations it would be a flat curve, or even rise to show a maximum efficiency at about 4 per cent moisture. However, beyond 12 to 14 per cent moisture, much difficulty may be expected in obtaining either capacity, efficiency, or even ignition.

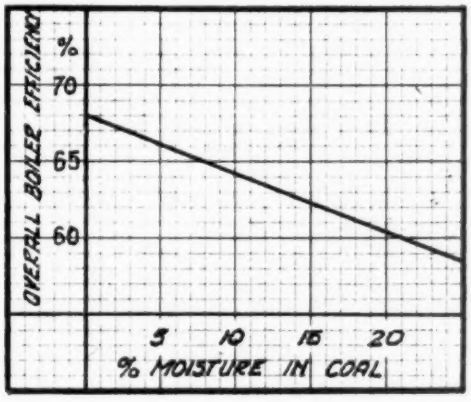


FIG. 4 EFFECT OF MOISTURE ON EFFICIENCY

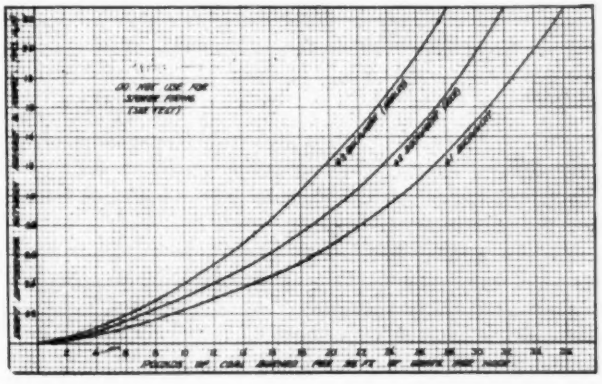


FIG. 5 DRAFT REQUIRED AT DIFFERENT COMBUSTION RATES WHEN BURNING COMMERCIAL SIZES OF ANTHRACITE

In a car or in a rectangular pile 8 ft deep, 1 in. of rain could produce only 1 per cent of moisture even if none drained off or evaporated. Furthermore, with anthracite, moisture is merely a surface condition which may be readily drained and dried. It is thus unlikely to become a significant factor especially if the storage pile is properly drained.

Effect of Volatile. Generally speaking, high fixed-carbon coals, such as anthracite, are the most efficient because the problem of a proper supply of secondary air is simplified. Within the anthracite industry, the entire range between the lowest- and highest-volatile coals mined is so small that this is a negligible factor, except when comparing anthracite with other fuels.

Furnace Volume. One other practical advantage of the relatively low volatile content of anthracite is the greatly increased permissible heat release per cubic foot of furnace volume. This results from the fact that, with anthracite, combustion is much more nearly complete at the surface of the fuel bed than with bituminous coal. However, it is the concensus of leading engineers that proper mixing of gases, turbulence, secondary combustion, and slag or fly-ash formation are directly and materially affected by furnace and arch design.

Air Requirements. The theoretical weight of air for the complete combustion of any fuel is practically a constant at an average of 7.65 lb of air per 10,000 Btu. With 12,900-Btu (dry) barley, 9.85 lb of air are thus required per lb of coal. With entering-air temperatures of 90 F, 13.85 cu ft equals 1 lb. Thus 137 cu ft of air will be required theoretically for the combustion of each pound at maximum CO_2 of 20.1 per cent (no excess air). Table 4 shows similar air requirements for other CO_2 values.

TABLE 4 AIR REQUIREMENTS FOR BARLEY ANTHRACITE

CO_2 in furnace, per cent	Excess air, per cent	Air required, lb[a]	Air at 90 deg F, cu ft[a]
6	225	32.0	445
8	150	24.6	342
10	100	19.7	274
12	65	16.2	226
14	43	14.1	196
16	25	12.3	172

[a] Total cubic feet per pound of coal burned.

Air and Draft Pressure. With barley as with other sizes, the combustion rate per square foot of grate varies in accordance with the differential pressure between the ashpit and the furnace. These rates, as shown in Fig. 5, will apply irrespective of the source of air supply (i.e., on either forced, induced, or natural draft, or any combination). Thus natural draft may be used for barley where it is adequate to produce the necessary combustion rate. However, where natural draft is used, it will produce such a high suction above the fire that extreme care should be exercised to keep all brickwork and openings extremely tight. For this reason many operators prefer a "balancing" forced-draft fan even though sufficient natural draft is available.

With both hand-firing and semistokers, it is necessary (on forced draft) to provide sufficient maximum air pressure in the ashpit to burn the coal properly when the fuel bed is at maximum thickness just before cleaning. A static pressure of $2^1/_2$ in. of water is suitable for fans when delivering the rated quantity of air for barley anthracite.

Air pressures, as shown in Fig. 5, will not apply with traveling-grate equipment because the continuous discharge of ash permits materially thinner fuel beds with correspondingly lower air requirements. The zoning of air on traveling grates also permits the admission of air in steps proportional to the actual rate of combustion. On traveling grates, maximum air pressures do not usually exceed $1^1/_2$ to 2 in. of water.

(As the exact air pressure required depends entirely upon such factors as fuel-bed thickness and rating, these rules refer to the maximum pressure that should be available to the operator rather than the pressures to be actually used.)

Furnace Draft. Where forced draft is available, it is customary to balance it against the pull of the stack or induced draft. However, in such cases, the furnace draft should not be below 0.05 in. of water since lower pressures will result in excessive gas and heat penetration into the brickwork with greatly increased maintenance costs. Conversely, drafts in excess of about 0.10 in. of water can be considered to carry an unnecessary amount of heat to the stack.

Furnace drafts of about 0.05 in. of water should be maintained under the nose of the rear arch of traveling- or chain-grate-stoker installations for best results.

Mechanical draft regulators, designed to hold furnace drafts between these limits, are very desirable. In their absence visual furnace draft gages are a "must" in every plant.

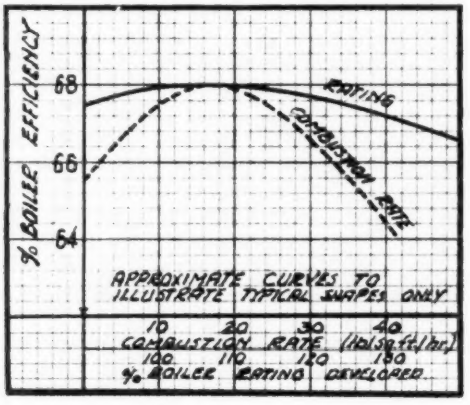


FIG. 6 BOILER EFFICIENCY VERSUS RATE AND OUTPUT

Proper Boiler Ratings. In many plants it is common practice to attempt to carry as much of the load as possible on a relatively few boilers, even though idle boilers are available. This is particularly noticeable in plants that have just recently converted from oil. From Fig. 6, it will be seen that this does not always result in the most efficient or economical operation. While boiler installations differ materially, they all have characteristics similar to those shown in the curves.

Peak test efficiencies usually occur somewhere between 100 and 150 per cent of rating on boilers without heat-recovery equipment, however, in actual daily operation, the best operating efficiency will be at a somewhat higher rating because of greater stability in the furnace and fuel bed. The addition of heat-recovery equipment may make the most economical point at some higher rating, and the efficiency will not fall off as rapidly with increased rating. The problem of whether or not to operate a sufficient number of boilers so that each will be as nearly as possible at its peak operating efficiency is a rather complex one requiring careful study for each individual case. This involves the shape of the daily load curve, maintenance and operating labor costs because of having extra equipment in service, etc. For example, in a plant with a flat load curve or a long-sustained peak, it may be advisable to operate a sufficient number of boilers to hold each boiler close to its maximum efficiency, whereas in a plant where the load is of shorter duration, the banking loss during light-load periods may offset any possible increase in efficiency. In some cases, operation of additional boilers requires additional operating labor, which nullifies the fuel savings possible.

On the other hand, attempts to operate barley fires at excessive rates of combustion frequently necessitate cleaning the fires before they are completely burned out with resultant high ashpit losses. The additional skill required for high ratings, and the strain on labor due to too frequent attention and cleaning periods are further factors.

In brief, the question of the number of boilers to be used is one of sufficient importance to warrant careful study, as based upon individual plant conditions.

EQUIPMENT AVAILABLE FOR BURNING BARLEY

In general three types of equipment are employed for burning barley:

1 Pinhole grates or grates with narrow slots (such as herringbone).
2 Semistokers with inclined grates.
3 Traveling-grate stokers.

A selection between these is usually made on a basis of size of installation and degree of automatic operation desired, as balanced against relative equipment costs. Approximate costs are shown in Table 5.

TABLE 5 APPROXIMATE COST OF BARLEY EQUIPMENT[a]

Pinhole grates (dumping), per sq ft	$10 to $12
Semistokers, per developed hp[b]	$12.50 to $13
Traveling-grate stokers per developed hp	$20 to $26

[a] All prices f.o.b. factories, not including installation.
[b] Includes forced-draft equipment.

HAND-FIRED BARLEY GRATES

Description and Design Data. Hand-fired grates for barley should be of the "pinhole" or slotted type. The latter are commonly known as herringbone grates when the adjacent rows of slots are set at an angle. A choice between the two types seems largely to be a matter of manufacturer and plant preference. The minimum practical limitation of size is about 10 sq ft; the maximum is a fuel-bed length of about 10 to 12 ft. Dumping-grate weights will usually be between 60 and 80 lb per sq ft.

Both dumping and stationary grates are available, but a substantial percentage of all grates now being sold is of the dumping type. Grates that dump to the center have the advantage of keeping hot ash away from the front of the ashpit and the rear ash closer to the point of removal.

The size of the pinholes ranges from $^3/_{16}$ to $^5/_{64}$ in., depending upon the manufacturer. They are flared or tapered underneath to make them self-cleaning and to secure a modified Venturi effect. The distance between individual pinholes is usually about $^3/_4$ in.; and the over-all metal thickness of the grates is also usually about the same.

Important points of design are the percentage of free air space and the uniformity of air delivery. If the free air space through the grates is less than 4 per cent, they are likely to restrict the flow of air unduly, and thus necessitate excessive velocities; if on the other hand the free air space exceeds 8 to 10 per cent of the grate area, the velocity will be so low for the required air delivery that much of the desired "jet" or blast effect will be lost.

Uniformity of air delivery is unusually important because of the "jet" type of operation. Either dead or unusually active areas of only a few inches will invariably produce unequal air distribution, resulting in ridges or patches of less or more active combustion with corresponding difficulty due to spotty fires.

Method of Hand-Firing. The primary rule in firing any size of anthracite is "let it alone." This applies with full force to barley. In addition, it should be fired lightly and often. It is also good practice to clean only one half of a boiler at a time, skipping every other door, going back to them only after the row has been completed. By this method, the output will be more nearly continuous, the CO_2 higher, and the gases more completely consumed.

In the case of all barley equipment, the drafts should be ad-

justed so that the surface of the fuel bed just begins to float without either being dormant or "boiling" too violently.

While the frequency of cleaning the fires is necessarily a function of design, boiler load, and quality of fuel, cleaning not oftener than once per 8-hr shift is recommended as being easier both on labor and equipment.

Spreading Method of Firing. In the spreading method, sometimes called "the alternate" method, a small amount of coal is fired at one time and spread evenly over the fuel bed from the front to the rear. The firing is done alternately through the fire doors, so that the entire fire is not blanketed with green coal. Hand-firing practice leans more and more to spread-firing.

The Bureau of Mines recommends burning coal rapidly and at high temperatures in order to secure the best available economy. Fire small quantities of coal at short intervals, so that thin places do not burn through and admit large excess of air. The quantity depends upon the grate area and draft. Firing and cleaning should be so co-ordinated as to produce a total fuel-bed depth of not over 6 to 8 in. just prior to cleaning.

Cleaning Hand Fires. Cleaning of the fire is necessitated by the fact that clinker and coarse ash will not pass through the grates. The intervals between cleanings depend upon the proportion of ash in the coal, the character of ash, and the type of the grate. If the coal contains much ash, or ash that is fusible, the fires have to be cleaned often; if light fires are carried, less clinker forms, and under such conditions the fire can often be run through a day shift without cleaning. The cleaning of the fires should be done thoroughly. All the clinker and ash should be removed, so that they cannot fuse to the side wall. They should be removed in such a way as to waste very little combustible. There are two methods of cleaning hand-fired furnaces.

In the side method one side of the fire is cleaned at a time. The good coal is scraped and pushed from one side to the other. The clinkers may have to be removed from the grates by the slice bar. When they have been loosened and broken up, they are dumped into the ashpit, or on stationary grates, and scraped out of the furnace with the hoe. The fireman should gather the clinker on the front part of the grate before pulling it out into the wheelbarrow, as this saves him from exposure to the heat. After the one side is cleaned, the burning coal from the other is moved and scraped to the clean side.

At this point, it is advisable first to spread a thin layer of coal on the grates so that the full heat of the live fire will not rest directly on the grates. A few shovelfuls of fresh coal are then added, in order to have enough burning coal to cover the entire grate when the cleaning is done. This adding of coal is important, especially when the cleaning must be done with the load on the boiler. The clinkers are then removed from the second half of the grate. In cases where the load is heavy, a time interval is recommended between cleaning the two halves of the grate, in order to allow the new fire to build up to its load-carrying capacity.

When cleaning is started, there should be so much burning coal in the furnace that enough will be left to start a hot fire quickly, when the cleaning is completed. If a light fire is carried, it may be necessary when starting to clean to put some fresh coal on the side to be cleaned last. During cleaning the damper should be partly closed. A fireman, after becoming familiar with the side method, should be able to clean a 200-hp boiler furnace in 10 to 12 min.

In the front-to-rear method of cleaning, the burning coal is pushed with the hoe against the bridge wall. It is usually preferable to clean one half of the grate at a time. The clinker is loosened and pulled out of the furnace and the burning coal is spread evenly over the bare grates. If the front-to-rear method must be used while the load is on the boiler, the side method should be employed after the day's run is over, so as to prevent

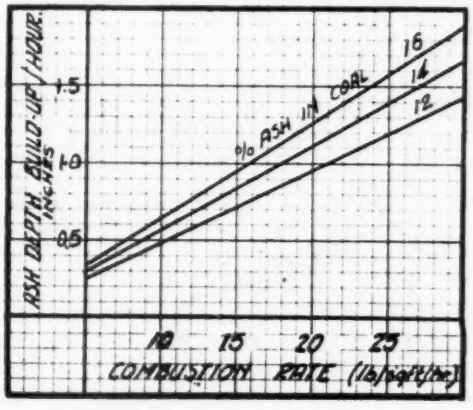


FIG. 7 ASH ACCUMULATED BETWEEN CLEANINGS

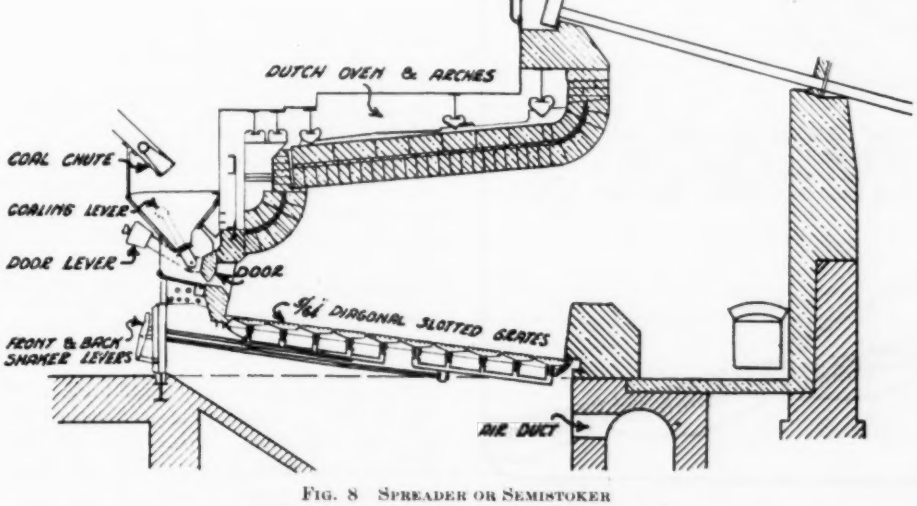


FIG. 8 SPREADER OR SEMISTOKER
(Courtesy of the McClave Company, Allentown, Pa)

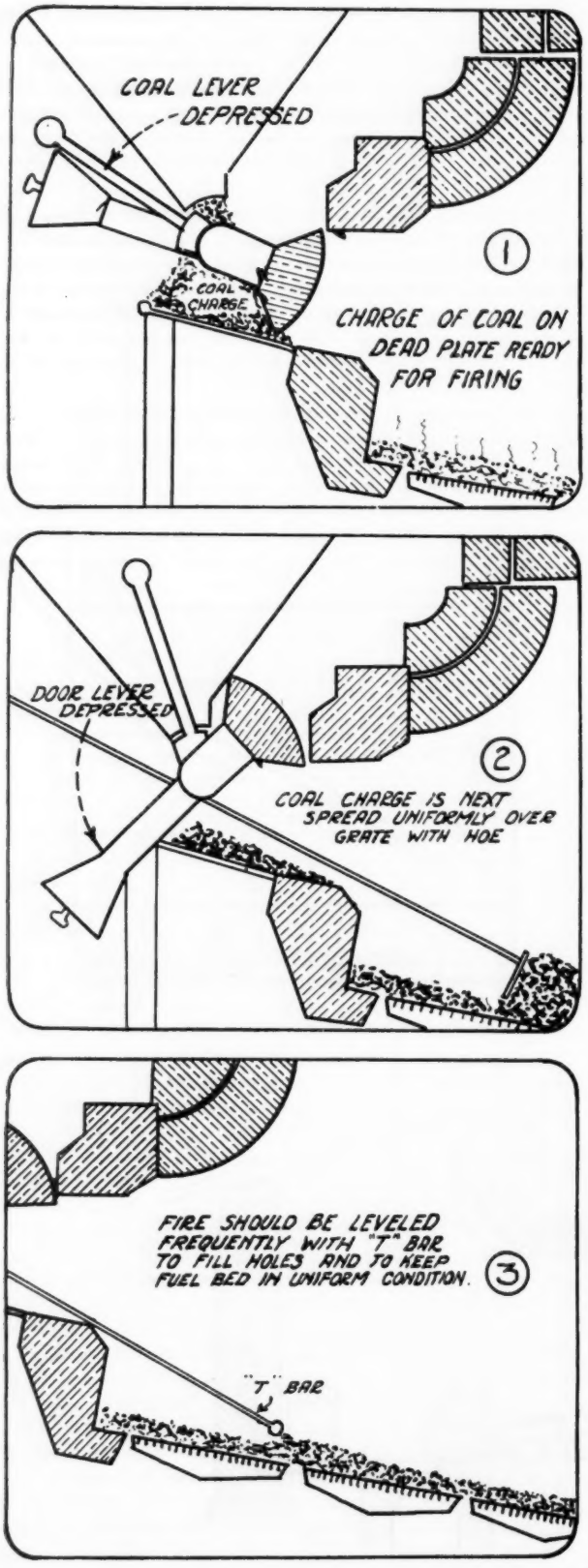


FIG. 9 PROPER METHOD OF OPERATING HAND STOKER

the large accumulation of thick and hard clinker at the bridge wall.

Some firemen have the habit of pulling the clinkers out of the furnace without scraping and pushing the burning coal against the bridge wall or to one side. This really is not a method of cleaning the fire. They run a slice bar under the clinker to lift it to the surface of the fuel. Then they take a hoe and pull the large pieces out. The small pieces are not easily detected and are left in the fire. These fuse in a few minutes, due to the high temperature near the surface of the fuel bed, and to the air deficiency under the clinker. Thus more masses of clinker are formed which are usually worse than those previously removed. This habit should be discouraged.

The cleaning of a banked fire should be done about 2 hr before steam is needed. It is advisable to bank the fire at the front of the grate near one of the doors. This exposes the clinkers which can be pulled out.

As cleaning intervals are largely determined by the ash accumulation, Fig. 7 shows the depth of pure ash produced in each hour under various conditions.

Operating Results. With good firing and cleaning, combustible in the ash will be as low as 12 to 18 per cent; and CO_2 of from 10 to 12 per cent can be carried continuously without danger of CO.

Light-Load Firing. As has been stated 6 to 8 in. is a proper "full-load" fuel-bed depth for hand-fired barley. However, in periods of light loads, the attention required may be considerably decreased by firing considerably heavier.

HAND OR SEMISTOKERS

A type of semiautomatic equipment especially suitable for barley coal is the semistoker, such as is shown in Fig. 8. These stokers consist of a suitably inclined dumping grate usually of the slotted type having openings approximately $^5/_{64}$ in. wide, and a total air space of approximately 8 per cent.

By means of an ingenious arrangement of gates, coal may be dropped onto a convenient hearth at the upper edge of the inclined grate. It is then spread over the live coals manually by means of a long-handled spreader bar.

While not a stoker in a sense of being motor-driven, this equipment does have the advantage of hopper storage of coal with manual attention reduced to the actual operation of spreading the coal, cleaning the fire, and dumping the ash or clinker. The amount of manual attention involved is thus comparable or even better than the removal of clinker from the familiar bituminous underfeed stoker. Installations of this nature have been made in outstanding schools, office buildings, and industrial plants with perfect success, and extremely satisfactory operation.

Sizes Available. Semi-stokers are available in a full range of sizes up to about 12 ft long and 14 ft wide, with capacities from 100 to 600 developed hp. Approximately 7 to 10 ft of setting height is required for their installation.

Operating Characteristics. The operating characteristics of the semistoker are similar to those on dumping grates. As has been stated, labor is less, and, because of the type of firing, operators feel that more uniform better conditioned fuel beds can be carried. Somewhat higher loads can thus be carried, as are reflected in the ratings given in Table 2. Typical operating methods for a semistoker are shown in Fig. 9.

CHAIN- AND TRAVELING-GRATE STOKERS

The ultimate in the mechanical-firing of barley and the No. 4 buckwheat sizes of anthracite is through the use of moving grates of the endless or "belt" type. There are two familiar versions of these, i.e., chain-grate stokers, and traveling-grate stokers. The latter type is shown in Fig. 10.

Chain-Grate Stokers. In principle, the chain of a chain grate

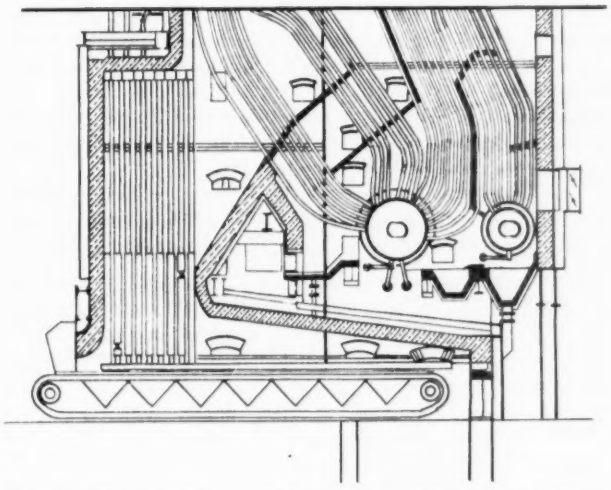


FIG. 10 MODERN TRAVELING GRATE WITH ARCHES FOR ANTHRACITE

consists of a series of individual links made up into the form of an endless chain. The edges of the links are usually serrated to provide from 7½ to 10 per cent free air space for the passage of combustion air.

Traveling-Grate Stokers. The traveling-grate stoker is similar to the chain-grate stoker, the difference being that in traveling grates the grate bars consist of small individual castings or keys carried forward in endless-belt fashion on chains but not being in themselves a part of the chain. The free-air openings are usually about the same as on the true chain-grate type.

A characteristic advantage of the traveling grate is the ability to replace and add burned keys without disassembling the chain.

As all other points of construction and operation are practically identical, the remainder of this section applies equally to chain and traveling grates, even though for the sake of simplicity the term "traveling grate" is used.

An outstanding advantage of these types of stokers lies in the fact that the air can be carefully regulated and zoned as combustion proceeds. As the coal burns progressively from its ignition at the front of the grate to ash at the rear, from three to seven (or even more) partitioned wind boxes are employed to divide the air supply into zones. In extremely large installations, the rear wind box is also subdivided longitudinally to equalize the burning-out of the tail end of the fire.

Size and Design Data. Traveling-grate stokers are manufactured in a wide range of sizes. The largest stoker of this type so far built is located at the Calco Chemical Company, Bound Brook, N. J. This stoker is 24 ft wide × 28 ft long with 672 sq ft of grate. Another outstanding traveling grate is at the Cedar Street Plant of the Pennsylvania Power and Light Company in Harrisburg, which is 23 ft wide × 25½ ft long with 586 sq ft of grate.

It has been authoritatively stated that, with No. 3 buckwheat (barley) of 12,900 Btu, it is possible to design and build a stoker to deliver 300,000 lb of steam per hr continuously. This is given as the present practical limit of size for stokers on anthracite.

At the other extreme, traveling grates are manufactured as small as 3 ft wide × 7 or 8 ft in length, but it is not usually economically feasible to install them for less than 100 developed hp.

The development of the traveling grate has seen many changes with material improvement in both flexibility and combustion. Grate speeds, originally 15 fph, now range from 40 to as high as 100 fph. Fuel-bed thicknesses have decreased from 6 to 8 in. to a present maximum of 4 to 4½ in. (with barley). Vastly improved arch design has stepped up combustion rates from 25 lb to a present practice of 35 to 40 lb, and on extremely large jobs where provision for the re-use of siftings and fly ash has been made, 45 to 50 lb per sq ft have been reported.

Performance Characteristics. With old-style front-arch furnaces, combustible in the ash of 25 to 30 per cent is considered good practice on traveling grates. With the new-type rear arches, the combustible in the ash will be as low as 10 per cent. CO_2 of 12 to 14 per cent can be consistently carried without CO.

CONCLUSIONS

In conclusion, with adherence to a very few fundamental rules, satisfactory economical performance may be expected from barley on several classes of equipment:

1 The coal should be as free from fine undersize or dust as practical.

2 Low ash content is preferable unless the plant has been specifically designed for high-ash fuel.

3 The fundamental rule of firing anthracite is "let it alone."

4 A selection of hand-firing, semi-hand-firing, or fully automatic stokers is available on a basis of initial equipment cost, cost of operating labor, capacity which can be developed in a given boiler, and maintenance cost.

5 Regardless of the firing method, anthracite is free from all smoke and soot and not subject to spontaneous combustion.

ACKNOWLEDGMENT

For assistance in preparing the material for this paper the author is grateful to C. H. Frick, Plant Betterment Engineer, Pennsylvania Power & Light Company, Allentown, Pa.; Roy Johnson, Carbondale Grate Bar Company, Scranton, Pa.; J. H. Kerrick, Fuel Engineer, Philadelphia & Reading Coal & Iron Company, Philadelphia, Pa.; Christian Schillinger, President, Coxe Stoker Engineering Company, Hazleton, Pa.; Charles Warg, Chief Engineer, The McClave Company, Allentown, Pa.; Harvey Rettew, Chief Mechanical Engineer, Philadelphia School Board; John Van Brunt, Vice-President, Combustion Engineering Company; Otto de Lorenzi, Combustion Engineering Company; A. C. Fieldner, Chief, Fuels Service, U. S. Bureau of Mines; Chas. Schantz, Weston Dodson & Company.

BIBLIOGRAPHY

1 "Finding and Stopping Waste in Modern Boiler Rooms," Cochrane Corporation, Philadelphia, Pa.

2 "Steam," The Babcock & Wilcox Company, New York, N. Y.

3 "Quality of Anthracite as Prepared at Breakers Operated by Members of the Anthracite Institute in 1935," Reports of Investigations, U. S. Bureau of Mines, 3283.

4 "Chart for Estimating Btu of Anthracites," by H. G. Turner and G. S. Scott, State College, Pa.

5 "The Performance of Anthracite on Traveling-Grate Stokers," by J. H. Kerrick, A.S.M.E. Miscellaneous Paper No. 15, 1941; on file at the Engineering Societies Library, 29 W. 39th St., New York, N. Y.

Discussion

A. A. BATO.[3] In the present fuel shortage, the author has rendered a most valuable service in directing attention to barley anthracite, a fuel available in large quantities, yet neglected even in cases in which it could be used with little or no difficulty. Every bit of information in connection with the use of this fuel is welcome, because, in the present emergency, plant managements cannot experiment with new fuels, unless they get full and

[3] Consulting Engineer, 227 Park Avenue, East Orange, N. J. Mem. A.S.M.E.

reliable data enabling them to use such fuels readily in an efficient manner. On the other hand, due warning should be given concerning cases in which the fuel cannot be used without creating disturbances in plant operation.

The writer can state from actual experience that the use of steam jets in the ashpit to avoid clinkering, concerning which the author says that it is believed to be helpful, is actually of great help, easy to install, and comparatively economical, as the amount of steam used does not exceed 2 to 3 per cent of the steam generated, even in extreme cases.

The importance of proper grates has been somewhat overemphasized. There are two points involved; (*a*) excessive sifting of coal into the ashpit, and (*b*) the danger of holes being blown into the fuel bed in the case of too large air openings. As to item (*a*), it must be remembered that on hand-fired grates the coal does not rest on the grate but on the ashes of the coal burned previously, except immediately after fire-cleaning. Accordingly, if grates with small openings are not readily available, the fireman may either cover the grates after fire-cleaning with a thin layer of ashes or preferably small-sized clinkers, or use a small quantity of larger-sized coal for this purpose. As for item (*b*), the danger of holes being blown into the fuel bed is somewhat more serious, but prevails only during the first half hour or so after fire-cleaning, and can be minimized with a little care and frequent checking of the fire. This settles also the question of the grates of various shapes claimed to direct the jets of air at various angles, crosscurrent, etc., into the fuel bed, usually illustrated with "trained arrows." As a matter of fact, the direction, shape, etc., of the air jets reaching the live coal are determined by the ashes immediately under the latter.

The statement concerning furnace draft, "drafts in excess of about 0.10 in. of water can be considered to carry an unnecessary amount of heat to the stack," can be accepted only for cases in which the boiler setting is not tight, or in which other features of the design permit the infiltration of outside air into the furnace or the passes. If the setting is practically airtight, the stack loss depends upon the amount of combustion air only, independent of whether the draft was produced by low forced-draft pressure and high furnace draft, or vice versa. In the case of a heating plant serving a very tall building, the height of the chimney is likely to be determined not by the draft requirements but by the height of the building, resulting in a very high furnace draft. In such a case, it might be more economical to provide the boiler setting with a steel casing to prevent air infiltration, or to install a barometeric damper to reduce the stack draft and thus to save on the power used to produce forced draft.

The low volatile content of barley anthracite, especially when combined with a high moisture content, results in a characteristic of slow and difficult ignition, as compared with the flashy, high-volatile soft coal. This may cause some difficulty, as in the case of traveling-grate stokers, where the ignition of the coal may proceed more slowly than the velocity of the grate, in which event the fire "runs away" from the hopper gate. When this occurs, the grate must be stopped for a short time or slowed down, resulting in reduced performance. Such a condition may be due to faulty arch design, etc., and is likely to prevail when the stoker designer had to adapt the stoker to a narrow and long boiler. It is not likely to happen to a wide and short grate traveling at a slower speed for the same performance.

Slow ignition naturally causes difficulties in picking up sudden peak loads; consequently the real field for the use of barley coal is in plants having uniform loads.

As to mixing barley with bituminous coals, the following procedure should be adopted to avoid difficulties: Suppose the minimum volatile content at which the equipment can operate was found to be, let us say, 22 per cent, this being the volatile content of the coal used in the past. Suppose also, that barley coal of 5 per cent volatile content and bituminous coal of 35 per cent volatile are available. In such a case, the proper mixture will be about 42 per cent anthracite to 58 per cent bituminous coal, giving a volatile content of 22 per cent. In addition to the volatile content, the texture of the coal may have an influence upon ignition characteristics.

The information concerning the importance of the undersized coal is especially interesting. The paper is quite comprehensive, covering the field in a full and practical manner.

J. F. Barkley.[4] For some months, the Bureau of Mines, in co-operation with the War Department, and Athracite Industries, Inc., has been experimenting with the use of mixtures of barley anthracite and slack-size bituminous coal on underfeed stokers. Successful results have been obtained at several plants now regularly using a mixture; trials at further plants are proceeding.

With the eastern caking coals on single-retort stokers, the addition of some 15 to 20 per cent of barley is usually sufficient to open up the fuel bed and give less trouble from caking. At one plant, where the bituminous coal was high in ash, the air-pressure drop through the fuel bed lessened with the increase of barley, making it possible to carry higher ratings than with straight bituminous slack. At this plant, as much as 80 per cent barley gave satisfactory operation and carried the required load. At another plant, 50 per cent of barley was decided upon as the best ratio. At this plant, the number of times the fireman resorted to hand-working the fuel bed was reduced as the percentage of anthracite increased.

The effect of the anthracite varies with the amount of ash in the bituminous coal with which it is mixed. For low-ash bituminous coals, lower percentages of anthracite give better results, the higher percentages giving less flexibility on load changes and lower ratings. For high-ash bituminous coals, higher percentages of anthracite can be used satisfactorily in obtaining similar loads.

The combustible in the ash and refuse from single-retort stokers varied from about 18 per cent for straight bituminous up to 35 for an 80 per cent anthracite mixture. Combustible in the flue ash also increased with the percentage of anthracite.

As a broad general statement, the efficiencies obtained on single-retort stokers with various percentages of anthracite were about the same as with straight bituminous, the gain in better fuel-bed conditions due to the anthracite being offset to some extent by the increase in combustible in the ash and refuse.

The amount of smoke produced lessened as the percentage of anthracite increased.

Author's Closure

Both Mr. Bato's and Mr. Barkley's discussions are appreciated as being valuable additions to this paper. With reference to Mr. Bato's comment with regard to the relatively slow ignition of anthracite, we believe that this can be largely offset by modern arch design to a point which will permit a sufficiently high degree of flexibility on chain-grate stokers for all practical purposes.

The writer is familiar with several installations in dyehouses and other plants having wide fluctuations in load, and in no instance has the lack of flexibility been cited as a disadvantage where arch and furnace design was at all modern.

Mr. Barkley's comments relative to the use of mixtures of barley and bituminous are particularly important since in view of current shortages of soft coal, this subject is receiving very serious attention from many plant owners at this time.

[4] Chief, Division of Solid Fuels Utilization for War, Bureau of Mines, Washington, D. C. Mem. A.S.M.E. This discussion is published by permission of the Director, Bureau of Mines, U. S. Department of the Interior.

New Combustion-Control Methods for All Standard Fuels

By ROBERT REED,[1] TULSA, OKLA.

As a result of extensive study and field experience with combustion problems, the author offers suggestions for increasing the accuracy of combustion control in all types of furnaces and with all types of standard fuels. This is accomplished by overcoming the existing limitations of flue-gas-analyzing methods either by recorded CO_2 concentrations, or by Orsat analysis. Curves are given which provide a simple means for determining "excess air by CO_2" and "excess air by O_2," by the use of which excess-air control can be quickly adjusted for any change in fuel to obtain unimpaired combustion. The importance of determining the presence of aldehydes in flue gases is recognized and a positive method for their indication has been developed in the form of a simple apparatus which is described. This check on combustion may save considerable fuel, and a great deal of mechanical difficulty with furnaces.

IT is the purpose of this paper to offer some new and perhaps revolutionary suggestions for obtaining genuinely accurate control of combustion in all types of furnaces and with all types of standard fuels. It is needless to say that very precise standards for such control have already been set up and within their limitations these standards have real value for the engineer.

The fact that existing control standards have limitations which are universally recognized justified further thought toward arriving at means of eliminating the limitations as far as possible. We have done considerable research on this problem and offer the results thereof.

It is to be recognized that in a furnace fired with fuel which has fixed characteristics as to analysis and heating value such suggestions as we make will have less bearing than in the case of a furnace fired with two or more different types of fuels. We find, however, that furnaces fired with but one fuel are comparatively rare except in the Gulf Coast area where an abundance of cheap natural gas relegates auxiliary fuels to emergency status. Many such furnaces operate for years without change of fuel.

In the average installation where two, three, or even more types of fuel must be used to maintain operating conditions, or where the analysis of a given type of fuel is subject to change without notice (such as is the case in all refineries), the engineer is confronted with a serious problem in maintaining control of combustion through all the fuel changes.

Limitations of Flue-Gas-Analyzing Methods

Again, as we all know, control is taken through either recorded concentration of CO_2 in the flue gases or by Orsat analysis. If the first is the case, the engineer must estimate the amount of excess air as represented by a given CO_2 indication based upon the ultimate CO_2 available from the fuel being fired. If two or more fuels are being fired in combination in the same furnace the recorded CO_2 will have almost no value at all unless the precise volume of each fuel is known, and it would be necessary to resort to Orsat analysis to find the true condition of excess air.

Orsat analysis, where time and trained technicians are available, is far more satisfactory; but even here we find much room for improvement. The principal fault with such procedure lies in the fact that the Orsat reveals conditions existing at the time the sample was taken and these are subject to change many times during the course of a day. Other sources of error lie in faulty technique with the Orsat; dilution of the sample by air and exhausted or contaminated reagents, or leveling water in the burette.

We hasten to say that through long association we have the greatest respect for the Orsat flue-gas-analyzing apparatus but we must recognize its limitations. It will, if properly operated, indicate the concentrations of CO_2, O_2, and CO in the sample being tested, but beyond that it is no longer valuable.

The engineer may wonder just what further information on the analysis of flue gas might be needed. In order to answer this question, the author will review a little of the theory of combustion and cite some experiences in the field pertaining to this matter.

Combustion Theory

It seems to us that combustion theory is just that, as we have encountered conditions which seem to refute most of it; but after having made such a qualifying statement we will say combustion of hydrocarbons proceeds as a race between hydroxylation and thermal decomposition according to the type of fuel being burned and the manner in which it is burned. A clear flame indicates hydroxylation and a luminous flame indicates thermal decomposition, but neither condition denies or makes impossible the presence of the other. In both cases the end products of complete combustion are CO_2 and H_2O.

In the case of thermal decomposition which produces a luminous flame, the luminosity comes from the presence of glowing free carbon which would, in complete combustion, burn to CO_2 in the normal manner. If this free carbon should, however, be chilled to a temperature below its kindling point before combustion is complete, it will appear as soot. It will also appear as soot if sufficient O_2 is not immediately available.

In the case of thermal decomposition in the course of hydroxylation caused by either a lack of turbulence to force mixture with O_2, lack of O_2, or chilling to a temperature slightly below the kindling point of the intermediate compound, aldehydes will appear in the flue gas. At times free H_2 in quite appreciable quantity has been found in flue-gas samples, but such conditions are rare.

We would point out, therefore, that if the true condition of combustion is to be found, means of indicating the presence of soot, aldehydes, and free H_2 might be necessary in addition to the classical CO_2, O_2, and CO. Soot, if present in appreciable quantity, may be seen emerging from the stack. The presence of free H_2 is rare, so for all practical purposes we need only consider the aldehydes as important.

Some fuels, such as blast-furnace gas, burn with a clear flame

[1] Engineer, John Zink Company.

Contributed by the Fuels Division and presented at the Annual Meeting, New York, N. Y., Nov. 29–Dec. 3, 1943, of The American Society of Mechanical Engineers.

Note: Statements and opinions advanced in papers are to be understood as individual expressions of their authors and not those of the Society.

in which no hydroxylation is involved because the nature of the burning of such combustible elements precludes possibility of luminosity in the flame. With such a fuel the Orsat is entirely sufficient. Coke also falls within this classification as long as its volatile content is very low.

Combustion Experiences in the Field

One of the author's most unusual experiences in connection with combustion problems related to the operation of an HRT boiler in a relatively small, but exceedingly well-managed plant in the Southwest where only one very closely controlled fuel was used.

In this particular plant the management had spent some $5000 improving conditions in the boiler room. New burners had been purchased; the furnaces had been rebuilt; steam leaks had been hunted down relentlessly, and in general no means of obtaining efficient operation of the boilers and the boiler plant had been overlooked. Hourly Orsat samples were taken from the breeching of the boilers and at no time was the excess-air factor as indicated by the Orsat analysis allowed to exceed 10 per cent.

Any engineer would say that with such operation the management could reasonably expect to make steam at a very low cost. Such was not the case, however, for immediately upon starting up the reconditioned plant the fuel costs rose 10 per cent for the same steam production. For 6 months the plant operated in this manner, despite frantic efforts on the part of the plant personnel and various other engineers.

The hourly Orsat checks showed, with minor variations, as follows: CO_2, 10.7 per cent; O_2, 2.0 per cent; CO, 0.0 per cent.

This analysis indicates an excess-air factor of 10 per cent when using a 0.55-specific-gravity natural gas which was the condition set as a standard. Since no CO was indicated, it was felt that satisfactory results were being obtained and the 10 per cent increase in fuel cost was due to some other factor in the plant.

It was at this point that the author entered the picture, merely as a person who had heard of an interesting condition and wanted to examine it firsthand. We found the burner making a beautiful clear fire with no haze. We found the furnace draft was being held at 0.02 in. w.c. and we checked the flue-gas condition with our own Orsat to get identically the same analysis as had been obtained by the plant personnel for some hours previous to the time of our visit. We noted the flue-gas analysis checked with the fuel H/C ratio by weight. We were prepared to agree that the trouble with the plant lay in some other condition, until we went to the back end of the furnace to look through a peephole at the burner in order the better to admire the beautiful fire it was making.

Remember that furnace draft of 0.02 in. at the burner level. The peephole was considerably above the level of the burner so a pressure existed at the peephole level to cause the furnace gases to pour out into the boiler room. The furnace gases were heavy with the odor of formaldehyde and at once we had a clue to the 10 per cent increase in fuel cost.

We suggested increasing the furnace draft and despite some opposition from the plant management, the draft was raised to 0.08 in. w.c. to see what would happen. The load on the boilers was very constant and the fuel flow remained exactly as it had been before the draft was increased; yet the boilers popped within a minute of the time the draft was increased.

The next hourly Orsat sample showed as follows: CO_2, 11.4 per cent; O_2, 2.0 per cent; CO, 0.0 per cent.

This, while it reflected a decidedly improved condition in the furnace, did not check with the H/C ratio of the fuel. A union in the flue-gas sampling line was found to be leaking and, after being tightened, the flue gas checked as follows: CO_2, 11.7 per cent; O_2, 0.0 per cent; CO, 0.0 per cent.

This analysis checked with the H/C ratio of the fuel and was presumed to be correct. The furnace draft was raised again until a true indication of 10 per cent excess air was obtained, and the fuel costs instantly dropped to a level which would justify the installation of the new equipment.

In this case tremendous fuel loss was suffered for more than 6 months despite very careful control according to accepted methods. The errors in this case were the inability of the Orsat to show the presence of aldehydes in the flue gas, and the fact that the leak in the flue-gas sampling line allowed sufficient O_2 to appear in the sample to check the sample against the H/C ratio-by-weight of the fuel.

Another incident, which is very much in point concerns the operation of a large boiler in an Eastern refinery. Fuels being burned were refinery gas and oil. Close control was being maintained according to accepted standards, yet this boiler operated for weeks in such a manner that numerous heat balances refused to check by about 10 per cent. No smoke appeared at the stack and the Orsat showed no CO in the flue gas.

A corps of engineers set about trying to discover the difficulty and failed completely to do so until a most fortunate mistake occurred. A fireman was instructed to raise the draft on an adjoining boiler but misunderstood his orders. He raised the draft on the boiler being checked, and the increased draft produced some startling results.

One of the results was an almost instant increase of about 10 per cent in the production of steam with the same fuel flow, and the other result was that the heat balance checked very closely.

In order to determine just what conditions existed in the furnace with the original furnace draft, the damper was returned to its original setting. Steam production fell off 10 per cent as had been the case before. Samples of flue gas were sent to a laboratory for analysis which revealed the presence of free H_2 along with other unburned hydrocarbons.

In this case, because two fuels were being burned in combination, it is evident that checking the H/C ratio of the fuel against the flue-gas analysis had been neglected and leakage of air into the samples was not detected. The leakage of air into the samples caused O_2 to show in the analysis while in the furnace there was actually a deficiency of O_2 for complete combustion.

Checking CO by Orsat Unnecessary

The author's experience in the field has been almost entirely with oil- and gas-fired furnaces of all types, forms, and sizes. In the course of a number of years of work with such furnaces, we are compelled in all honesty to admit that we have never found CO in detectable quantities with Orsat analysis of flue gas. We do not question its presence in very minute quantity but, without resorting to very painstaking analysis by the iodine-pentoxide method (which is far too exacting and expensive for ordinary use) we have found checking for CO a formality which has an almost inevitable answer of "zero per cent."

In order to avoid confusion, it must be said that, in the burning of coal or coke where carbon is burned directly and alone, following the evolution of such volatile elements as may be present in the fuel, CO in very appreciable quantities may by found. Our remarks do not, then, apply for the burning of such fuels.

We have discussed the issue of CO with many engineers in the field and the consensus is that the CO reagent in the Orsat unless coke or coal is being burned, is more or less useless. Many say frankly that they never use it in ordinary checking. We

recognize this statement as being highly revolutionary but we submit it is concurred in by a majority of operating engineers in the field. Even where coal is being burned, combustion deficiency is not fully indicated by the CO reagent since the volatile elements burn partly by hydroxylation and unburned substances other than CO can, therefore, readily appear in the flue gases.

Controversial as our statements have been, we hope it will be agreed that steps to correct for Orsat deficiencies should be taken in the operation of a majority of the furnaces in America, in order that high efficiencies may be maintained and precious fuel saved.

It has been indicated that by far the greater portion of the deficiency may be taken care of by obtaining suitable means for indicating the presence of aldehydes in the flue gases. It has also been pointed out that there is a very definite relationship between flue-gas analysis and the H/C ratio by weight of the fuel being burned. If the Orsat analysis does not check with this ratio, something is wrong in the operation of the furnace or the method of sampling.

Simple Means for Determining Excess-Air Factor of Fuels

In the course of poring over data on flue-gas analysis, we have also come across a most singular fact which, up to this time, seems to have escaped the notice of the profession at large. This concerns the fact that a certain concentration of O_2 in the flue gases indicates almost exactly the same excess-air factor for any fuel from natural gas to coke within the limits of accuracy of analysis and observation. This also is applicable for firing any of the fuels in the range previously noted in combinations of two or more.

It is our observation that the O_2-excess-air relationship is independent of the CO_2 concentration of the flue gases which would change with variations in the H/C ratios by weight of the fuels being burned. The CO_2 concentration of the flue gas is therefore relegated to the provision of a means of checking the flue-gas analysis against the H/C ratio of the fuel or fuels.

We have plotted two sets of curves on "Excess Air by CO_2" and "Excess Air by O_2" for consideration and use in the field. These curves, Figs. 1 and 2, are based upon data provided by various excess-air charts now in common use. These charts are very accurate as is proved by the fact that the data, shown on the curves as plotted, check calculation of excess air based on the N_2 content of the flue gases. This is true for the entire H/C ranges covered by the curves.

In the use of the curves it is to be presumed that there is no dilution or contamination of the flue-gas sample by air which would confuse results and make the sample useless.

As an example, consider the case of a power-plant boiler being fired with natural gas when, because of an emergency, it is necessary quickly to shift the firing to 75 per cent oil and 25 per cent gas. The use of oil would make it necessary to raise the excess-air factor from, say, 10 to 15 per cent. If excess-air control is being taken on the basis of the CO_2 concentration of the flue gases, only a mathematical wizard could tell the operator in anything like a reasonable time what CO_2 indication he should have and hold to maintain efficiency.

It is here that the "Excess Air by O_2" curves become genuinely valuable as a time and efficiency saver. The chief engineer could instruct his operator to hold the O_2 concentration of the flue gases at 2.9 per cent and let the CO_2 go where it will. If it is necessary later to go 100 per cent on oil, the operator may continue to disregard the CO_2 indicator and hold the O_2 at the same 2.9 per cent to remain with very close limits of the 15 per cent excess-air factor. The same conditions would prevail if the fuel

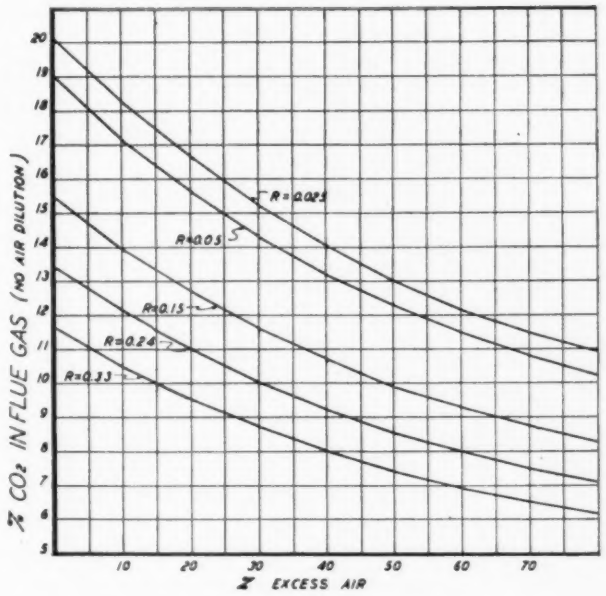


Fig. 1 Excess Air by CO_2

$R = H/C$ Ratio by Weight

Coke (mean)	$R = 0.025$
Anthracite coal (mean)	$R = 0.025$
Bituminous coal (mean)	$R = 0.05$
Oil (mean)	$R = 0.15$
Refinery gas (mean)	$R = 0.24$
Natural gas (mean)	$R = 0.33$

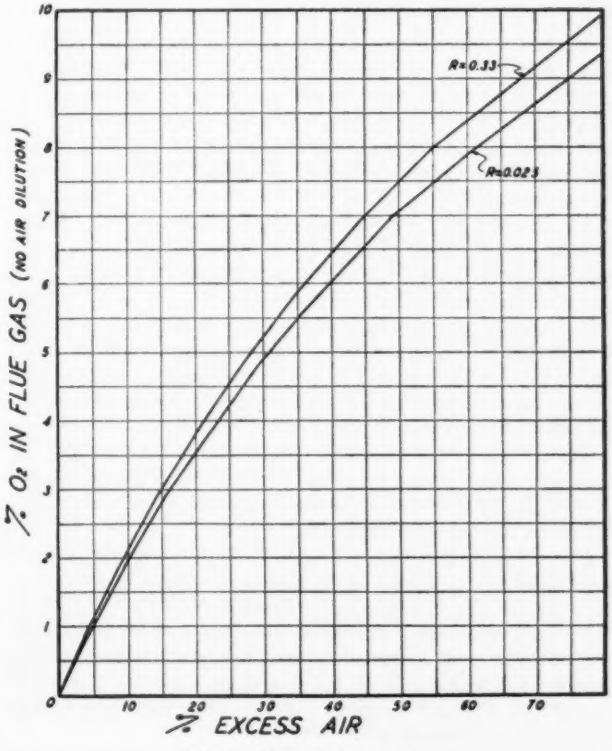


Fig. 2 Excess Air by O_2

$R = H/C$ Ratio by Weight

Coke	$R = 0.025$
Anthracite coal (mean)	$R = 0.025$
Bituminous coal (mean)	$R = 0.05$
Oil (mean)	$R = 0.15$
Refinery gas (mean)	$R = 0.24$
Natural gas (0.55 sp. gr.)	$R = 0.33$

change was from oil to coal or any other combination or combinations necessary to maintain operation.

The O_2 observation may be taken either by Orsat or by any one of a number of continuous recorders which are available. That these recorders are reliable is proved by the fact that they are being used in the control of very delicate catalytic operations in the refining industry with excellent results.

If CO is present in the flue gas, the amount of air necessary to burn it must be subtracted from the indicated excess air to arrive at a true condition. Fuels bearing high concentrations of N_2 will require additional calculation to arrive at true excess-air conditions.

The curves may also be used to check the flue-gas analysis against the H/C ratio by weight of the fuel. As an example, consider a furnace being fired with oil having an H/C ratio of 0.15. If the excess-air factor has been set at 30 per cent, the Orsat analysis should be as follows: CO_2, 11.75 per cent; O_2, 5.07 per cent; CO, 0.0 per cent. If the analysis is at variance something is wrong either by dilution of the sample, lack of sufficient air for combustion, poor mixture of fuel and air, or some other more obscure error. Checking should continue until the flue-gas analysis checks the conditions which should exist with the fuel being burned.

Determining the Presence of Aldehydes in Flue Gases

In considering the presence of aldehydes in the flue gases, we have pointed out that their presence should be indicated by failure of the Orsat analysis to check with the H/C ratio of the fuel being burned. At times, however, because of air dilution of the sample or for some other reasons, this check may become unreliable. Further and more positive means of indicating the presence of the aldehydes becomes necessary.

In collaboration with J. A. Hart and L. N. Hollis, chemists of a major oil company, we have arrived at what we think is a simple and most effective means of indicating the presence of aldehydes in flue gases through the use of a standard reagent in connection with some very simple apparatus. Fig. 3 is a more or less self-explanatory sketch of the apparatus. The reagent is prepared as follows:

Dissolve 0.2 g of certified basic fuchsin in 10 cc of a freshly prepared cold saturated aqueous solution of SO_2. Allow this solution to stand for several hours until all pink color disappears and the solution becomes either colorless or pale yellow. Dilute with distilled water to 200 cc and preserve in a tightly stoppered dark bottle. The reagent must be protected from both light and air. Particular attention is to be directed to the fact that acid fuchsin may not be used. The solution thus prepared is a standard aldehyde indicator.

About 15 cc of the reagent is poured into the flask of the test apparatus which is then connected to a tube leading to the source of flue gas. Before the connection is made, the tube must first have been thoroughly purged of air.

Flue gas is then caused to bubble through the reagent for not less than 2 min by means of the aspirator. The apparatus may then be disconnected from the sampling tube and allowed to stand for 2 min more. Any pink, red, purple or blue discoloration of the reagent indicates the presence of aldehydes, and the operator will know that all the fuel being introduced into the furnace is not being consumed. He may then take steps to find the trouble and correct it.

We think that since the test is so simple and easy to run, it would be well to check the flue gases thus at hourly intervals or (in boiler plants) at the time boiler-water samples are taken.

It should, perhaps, be pointed out that incomplete combustion may exist despite the presence of ample O_2 to burn all the fuel because of failure of the burners to provide a thorough mixture

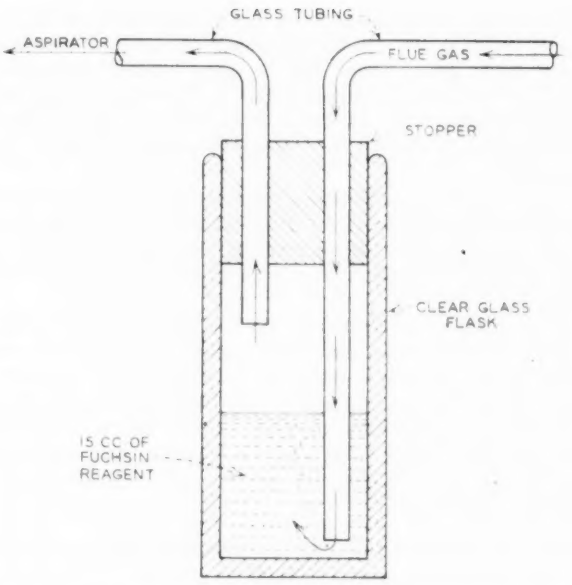


Fig. 3 Apparatus for Fuchsin Aldehyde Indicator as Suggested for Checking Flue Gas

of air and fuel. This failure may be due to plugging, clogging, or obstruction of portions of the burner. A radical change in fuel characteristics, which may not be noted by the plant personnel, may also result in incomplete combustion. The aldehyde test is really a double check which may save a great deal of fuel and mechanical difficulty with the furnace.

Perhaps the greatest source of error in flue-gas analysis lies in dilution of the samples by air. Chinks, cracks, and holes in the furnace, breeching, and stack are chief offenders, while leaks in sampling tubes come in for their share of condemnation. No pains should be spared to see that such sources of dilution are closed.

The best place from which to take a sample is from the furnace proper at a point where combustion has been completed some distance away and also at a point where minimum draft or subatmospheric pressure exists.

Such a point will be found near the arch of the furnace or, in the case of a boiler or generator, in or near the first pass. If the sample is to be taken from a zone of high temperature, it is necessary to use a water-cooled sampling tube to avoid loss of O_2 from the sample in oxidation of the tube metal. Means of obtaining an average sample should be considered important.

Discussion

A. A. Bato.[2] So far we have heard mostly of the presence of hydrocarbons only in the unburned flue gases, but this paper reports other cases involving aldehydes, that is, carbohydrates.

The importance of checking the flue-gas analysis against the H/C ratio, or, to be more exact, against the ratio of $H_2 - \frac{H_2}{8}$ to C, cannot be too strongly emphasized. In a previous paper,[3] the writer showed mathematically that a flue gas may contain CO and unburned H_2 in some form in such proportions that a check of the CO_2 and O_2 content against the H/C ratio may indicate the absence of CO, and therefore be misleading. A. H.

[2] Consulting Engineer, East Orange, N. J. Mem. A.S.M.E.

[3] "Flue Gas Computations," by A. A. Bato, *Mechanical Engineering*, vol. 48, 1926, pp. 330–336.

Senner[4] of the Bureau of Agricultural Engineering published the results of some tests made on domestic oil burners with a Bureau of Mines analyzer which involved such cases. Out of eight tests, about six check more or less closely in the manner mentioned, with the gases containing considerable quantities of hydrocarbons, also CO up to 5.1 per cent, with 1.2 per cent as the average.

They also indicate that the gases should be tested for CO with the Orsat, especially when burning light oils, notwithstanding the opinions of the many engineers quoted by the author as saying that the CO reagent in the Orsat is more or less useless. Their opinions may have had their origins in the assumption that, where there is no smoke in an oil- or gas-fired furnace, there is no CO either, consequently, it is enough to set the burner for smokeless combustion and test the gases for CO_2 and eventually for O_2 only. Senner's tests show heat balances with "unaccounted-for" losses up to 15 per cent, which, however, were explained with the aid of the complete gas analysis.

Concerning the effect of leaks in the gas-sampling pipe line, it must be emphasized that it can be misleading in one respect only, i.e., it may give the result that there is more excess air present in the gases than in reality. The analysis will be the same if some air got into the gases through the burner, crack in the brickwork, checkerwork, or any other opening, or a leak in the sampling pipe, and it will be impossible to tell the difference, unless there is some other instrument or control device connected to the furnace indicating the amount of excess air. It is impossible, however, that a gas analysis which does not check with the H/C ratio of the fuel with a leaking sampling tube should check when the leak was removed, as described by the author in connection with the first case mentioned in the paper. An analysis will check or not check with the H/C ratio independently of the amount of excess air, whichever way this air got into the sample, through a leak in the sampling tube, or with the combustion air into the furnace. Accordingly, there must have been an error in the second analysis of the first case given by the author which can be demonstrated mathematically as follows: This analysis gave 11.4 per cent CO_2, 2.0 per cent O_2, and 0.0 per cent CO, consequently, the N_2 content was 86.6 per cent. After the analysis was taken, a leak was discovered and removed in the gas-sampling pipe line, with the result that the gas analysis changed to 11.7 per cent CO_2, 0.0 per cent O_2, and 0.0 per cent CO. In the following it will be proved that this change could not have been the result of the stopping of the leak.

Before the leak was stopped 100 cc of gas contained 11.4 cc of CO_2, 2 cc of O_2, and 86.6 cc of N_2. If as a result of stopping the leak 2 cc of O_2 were removed from the sample, a corresponding amount of N_2 equaling 7.75 cc also was removed, leaving a total of 90.25 cc, while the amount of CO_2 remained the same, that is, 11.4 cc. The latter amount, however, equals 12.6 per cent of the 90.25 cc, and not 11.7 per cent as the analysis taken after the removal of the leakage showed, consequently, there must have been some other cause than the leakage for the 2 per cent O_2 in the second analysis. It seems to be certain, however, that the second analysis, made immediately before the discovery of the leak, was the erroneous one, whatever the cause might have been, as it did not check with the H/C ratio of the fuel, while the others did. These two analyses indicate an H/C ratio of 0.33, which in turn checks with the specific gravity of the fuel gas given as 0.55 of the air, indicating methane, more than 99 per cent pure. The H/C ratio corresponding to the second analysis would have been 0.28, or in order to check with the 0.33 value the O_2 content should have been 0.4 per cent.

A more thorough mathematical evaluation of the results may lead to an explanation of the first gas analysis combined with the 10 per cent loss in the following manner:

It is possible that aldehydes, for instance formaldehyde, is present in the gases, and yet the analysis checks with the H/C ratio, provided some unburned hydrogen is also present. The presence of formaldehyde decreases the percentage of CO_2 in the gases, while that of hydrogen increases it, if the carbon that formed the methane with this hydrogen burns to CO_2. The quantities of formaldehyde and hydrogen may be present in such proportion that they balance each other, with the result that the gas analysis checks with the H/C ratio. To this ratio corresponds a ratio of the two quantities of methane, of the one quantity that was hydroxylated to formaldehyde and water vapor, to the other quantity that was dissociated to hydrogen and carbon, with the latter burned to CO_2. A simple calculation shows that if for 100 parts of methane decomposed with the carbon burned to CO_2 and the hydrogen escaping unburned, there are 35.3 parts of methane hydroxylated to formaldehyde and water vapor, with the latter condensed, both without any excess air, the resulting gas mixture will have a CO_2 content of 11.7 per cent, which is the same as when methane is burned to CO_2 and water vapor without excess air, that is, it will check with the H/C ratio. Evidently, any amount of this mixture can be added to the products of a complete combustion of methane, with or without excess air, and the analysis of the gases will check with the H/C ratio as if there were no hydrogen and formaldehyde in the mixture. This requirement, that for every 100 parts of decomposed methane there shall be 35.3 parts of methane hydroxylated, can be put down in the form of one equation.

Another requirement, furnishing another equation, is that the hydrogen and the formaldehyde present in the proportion just described shall represent a loss of 10 per cent. The solution of the two equations shows that this requirement is fulfilled if 11.4 per cent of the methane burned is decomposed and 4.05 per cent hydroxylated. The loss through decomposition is equal to the heat value of the escaped hydrogen, in this case 7.46 per cent, while the loss due to hydroxylation is equal to the heat value of the escaped formaldehyde, in this case 2.54 per cent of the heat value of the total methane burned.

Under these conditions, the hydrogen content of the flue gases will be 2.76 per cent, which is not impossible, as for instance Senner,[4] in his tests mentioned, found 2.2 per cent. At the same time the formaldehyde content will be 0.515 per cent by volume.

This explains the results of the first test with the exception that it admits decomposition, while the flame is described as not "luminous," that is, indicating decomposition, but "clear." As both decomposition and hydroxylation might have taken place, this point may or may not be a sure indication of the phenomena which actually occurred.

Figs. 1 and 2 of the paper are slight but handy modifications and extensions of Figs. 2 and 3 in Ostwald's "Contributions to Graphic Combustion Engineering."[5] These curves can be used to check the accuracy of the analysis in the Orsat as to the presence or absence of CO, but not the accuracy of the sample-taking from the point of view of possible admixture of air.

The otherwise well-known fuchsin test for aldehydes comes certainly very handy in connection with flue-gas analysis, as it is very simple; still it must be emphasized that it is only qualitative and not quantitative, and that even if used in combination with the Orsat it does not settle the question of hydrocarbons and carbohydrates other than aldehydes. Although the author

[4] "Domestic Oil Burners," by A. H. Senner, *Mechanical Engineering*, vol. 58, 1936, p. 705.

[5] "Beiträge zur graphischen Feuerungstechnik," by Walter Ostwald, Otto Spamer, Leipzig, Germany, 1920. An instance in American literature, Heating, Ventilating, Air-Conditioning Guide, 1942, p. 162.

mentions the presence of aldehydes in connection with gaseous and liquid fuels only, it would be worth while to investigate the flue gases of solid fuels as well. The importance of volatile matter in solid fuels appears if we consider that such matter may be contained in a coal to the extent of 35 per cent by weight only and yet represent 41 per cent of the heat value at the same time. Thus, elusive as the hydrocarbons and carbohydrates are when flue gases are analyzed, they may represent considerable losses. That carbohydrates may be present in the products of combustion of solid fuels in some special cases is illustrated in the case of Highland Scotch whiskey, which gets its special flavor due to the fact that the malt used in preparing it is dried in kilns fired with peat. All this is also a warning that flue gases of anthracite and some other "smokeless" fuels should be tested for hydrocarbons.

Altogether, the paper represents a very good contribution to our knowledge of flue gases and their analysis and is excellent proof of the faculty of observation and resourcefulness of the author.

Author's Closure

It was the intention of the author to call the attention of the power industry to the fact that existing methods of combustion control were inadequate. The inadequacy exists through human error as much as in any other manner it is true but this in no wise mitigates the urgent need to save every possible heat unit in the fuel being burned.

It is probable that through weight of sheer numbers of Orsat tests made by him, the author may consider himself quite well trained in Orsat technique, yet as has been pointed out in the discussion it is entirely possible that Orsat data as presented in the paper were incorrect.

Mr. Bato has pointed out evidence of error in the first field test as reported. The author agrees with Mr. Bato with reservations.

If increased draft should cause air to enter the flue-gas passage at a point where the temperature was above the kindling point of such unburned products as might exist, the complete or partial burning of these products might be expected to change the Orsat data obtained. It is also entirely possible for the incomplete combustion to occur in such manner as to cause the Orsat data to check the H/C ratio of the fuel. If such a condition existed before the draft increase it is entirely possible for such burning as might result through leakage after the draft increase to upset the Orsat-H/C relationship.

The question of quantitative as well as qualitative analysis of flue gases for aldehydes has been raised. It is the author's thought that such analysis is hardly justified for two reasons. The first is that if combustion exists in a marked shortage of O_2, products other than aldehydes may easily appear in the flue gases along with the aldehydes, therefore quantitative analysis of the aldehydes alone would not necessarily indicate the true fuel loss. The second reason is that if aldehydes are found in the flue gases the operator should be concerned with means for burning his fuel completely rather than with the fuel loss due to their presence.

Particular care should be taken to check for the presence of aldehydes in the flue gases coming from a furnace in which haze, flame, or terminal combustion exists in the immediate vicinity of cold surfaces such as the pass from the furnace into the boiler tubes, etc. Chilling of the gases in contact with the relatively cold tubes is a very potent source of incomplete combustion. So-called "cold" furnaces such as those in water-wall furnaces, oil-processing furnaces, steel and cast-iron boiler furnaces, or any furnace in which heat is transferred with extreme rapidity from the flame directly to the absorbing surfaces should be checked closely.

Investigation of Blade Characteristics

Performance and Efficiency of Turbine and Axial-Flow Compressor Stages

By J. R. WESKE,[1] CLEVELAND, OHIO

The investigation reported in this paper deals with the flow through blade rows of turbine or axial-flow compressor stages on the basis of airfoil theory. Correlation was established by means of this theory between the aerodynamic characteristics of blade elements and the performance characteristics of the blade row. Test results from a rotating grid of sufficiently low solidity to eliminate interaction of neighboring blades are presented. It was found that the coefficients of lift of blade sections in rotating grids, especially near the hub of the wheel, are higher than might be expected from wind-tunnel tests. Methods of experimental aerodynamic investigation were adapted to the rotating-blade grid for the determination of the profile drag, in an attempt to broaden the basis for a rational determination of the efficiency of turbine and compressor stages.

Introduction

CONSIDERABLE progress has been made in the calculation of the performance of turbine and compressor stages through the development of mathematical theory of potential flow of the working fluid through the blade row. Solutions have been obtained for the lift forces on blades in axial-flow blade rows as related to the lift force on a similar airfoil in the wind tunnel, for the performance of a radial-flow impeller with a given number of blades as related to the corresponding hypothetical impeller with infinite number of blades. Furthermore, the potential theory gives numerical data, e.g., in regard to the effect of thickness of profiles in axial-flow grids upon performance. Thus the potential theory is justifying its value in design, since the results obtained with it are in closer correlation with actual performance data than those of earlier theories.

These advances in potential-flow theory, which strictly apply to perfect fluid, accentuate the need for a logical procedure of calculation relating the known basic laws of fluid flow of the real fluid, in particular the laws of fluid resistance to the performance of the turbine or compressor stage. Of particular interest are (*a*) the effect of skin friction and turbulent-energy dissipation upon efficiency, and (*b*) the effect of fluid resistance in causing deviation from the performance characteristics postulated by potential-flow theory and in limiting the performance of stages.

Review of Earlier Work

The theoretical treatment of the problem of fluid resistance in blade rows and of its effect upon stage efficiency of turbines and compressors has received attention in publications of the following authors: Keller (1),[2] Ruden (2), Amstutz (3), Kraft and Berry (4), New (5), Dozinsky (6), and Soerensen (7).

Amstutz (3) analyzed the losses in a Kaplan turbine and was able to calculate an efficiency curve closely corresponding to the actual curve obtained by test.

Methods of direct measurement of the losses in fixed-blade rows by means of the wake-traverse method were developed by Kraft and Berry (4), by New (5), and are currently used as an effective aid in the design of turbines.

There is justification for the assumption that the three-dimensional nature of the flow through blade rows, whether of the axial- or radial-flow type, has a greater effect upon the efficiency in the stage than it has upon other factors of performance. Under certain conditions, as in the case of very short blades (aspect ratio: $\frac{\text{span}}{\text{chord}} \approx$ unity), the treatment of the flow as a two-dimensional flow may lead to results in regard to losses which are utterly at variance with actual losses. This fact was recognized by Dozinsky (6), who derives relations for the flow through blade rows from analogies drawn with the flow in curved ducts. However, it seems that as long as the nature of flow in curved ducts is not more fully understood in its details than at present, it would appear to be more expedient to analyze the problem of losses in blade rows in first approximation as a two-dimensional problem as done by Keller and Ruden. The effect resulting from the three-dimensional nature of the flow in that case would find consideration in the choice of the numerical quantities involved, or through correction factors applied to the results obtained by the two-dimensional approach. It is obvious that three-dimensional effects are more prominent in blades of small span than in blades of long span.

It is known that the results obtained from measurements of the efficiency of fixed-blade rows cannot be applied directly to moving rows even in the case where the main flow of the working fluid takes place on concentric cylinders. Attempts to measure with fixed instruments the losses in moving rows, however, encounter disproportionately greater difficulties because of the kinematic transformation required when applying the measurements obtained in the absolute system to the determination of the drag of the moving blades.

In view of this, an investigation of the blade characteristics of a rotating-blade row and of their relation to the performance characteristics of the row seemed of timely importance.

Theoretical Analysis

The performance of turbine stages can be related to the interaction of the fluid and the immersed blades, which in the last analysis is a result of the stresses in the fluid working on the surface of the blades. Distinction is made between normal stress or the pressure and the tangential stress or the shear stress because of basic differences of these two types of stresses in regard to their origin and their nature.

The distribution of pressure over the surface of the blade is largely a function of the flow in the main body of the fluid outside of the thin boundary layer in the immediate vicinity of the solid surface. This flow may be regarded as potential flow and can be calculated by mathematical methods (8, 9), developed for its determination.

The distribution of tangential or shear stresses, i.e., skin friction, on the other hand is related to fluid friction, including turbu-

---

[1] Case School of Applied Science. Mem. A.S.M.E.

[2] Numbers in parentheses refer to the Bibliography at the end of the paper.

Contributed by the Power Division and presented at the Annual Meeting, New York, N. Y., Nov. 29–Dec. 3, 1943, of The American Society of Mechanical Engineers.

Note: Statements and opinions advanced in papers are to be understood as individual expressions of their authors and not those of the Society.

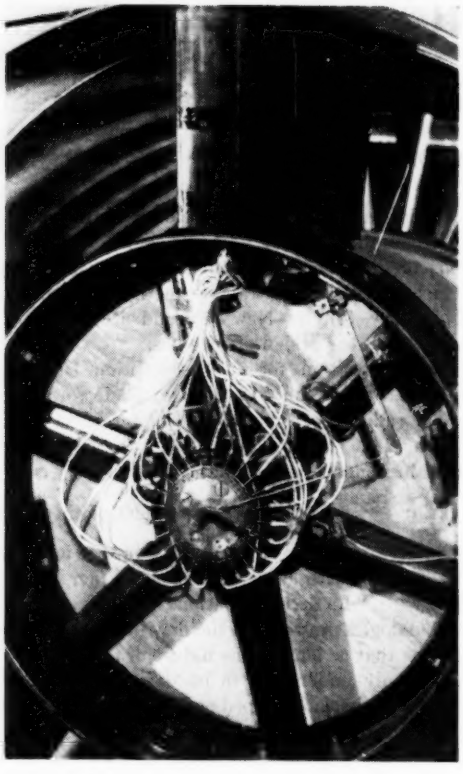


FIG. 1 MASTER AIRFOIL, SELECTOR DEVICE AND WAKE-TRAVERSE MECHANISM

lent momentum transfer. Shear stresses are a function largely of the flow in the boundary layer and depend to a lesser extent upon the pressure distribution over the surface of the blade. The tangential stresses are the source of losses in the blade row, and therefore affect the efficiency of the stage directly. It is seen that the division, originated by Prandtl, of the region of flow into a region in which the effect of viscosity can be neglected, in which the flow consequently may be regarded as potential flow, and into a boundary-layer region, is justified by the contrasting physical nature of the two flows. The present investigation is concerned primarily with the losses, and therefore with the flow, in the boundary layer.

It will be necessary to establish a relation between the factors influencing the interaction of the blades and the fluid resulting from motion of the two relative to each other and the performance data of the blade row. These relations are expressed in a number of equations which are conveniently presented in three groups, each group representing a distinctive link in the chain of the interrelation.

The three groups define the following functional relationships:

(*a*) Between the pressure and shear-stress distribution on the blade element and the resultant force and its direction.

(*b*) Between the force acting on the blade and the quantities of the velocity diagram.

(*c*) Between the quantities of the velocity diagram and the performance data.

NOMENCLATURE

Equations will be formulated embodying the foregoing relations, in which the following nomenclature will be used:

r = radius
z = number of blades
l = chord
$t = \frac{2\pi r}{z}$ = pitch
$\frac{l}{t}$ = solidity ratio
ω = angular velocity
c = absolute velocity
w = relative velocity
β = angles in relative system
β_p = angle of profile section
$\alpha = \beta_p - \beta'$ = angle of attack
$'$ refers to mean condition
Subscript 1 refers to inlet condition
Subscript 2 refers to outlet condition
Subscript u indicates component in circumferential direction
Subscript m indicates component in axial ("meridional") direction
R = resultant force per unit radial length
N = component normal to chord of blade section
M = component parallel to chord of blade section
L = lift component
D = drag component
D_p = pressure-drag component
D_f = friction-drag component
S = component normal to grid
T = component tangential to grid
$C_L = \frac{L}{lq'}$ = lift coefficient
$C_D = \frac{D}{lq'}$ = drag coefficient
ρ = mass density
p = static pressure
η_r = efficiency of blade element
Δh = total head
$q = \frac{\rho w^2}{2}$ = velocity pressure

(*a*) The pressure distribution about a blade section may be obtained theoretically by potential-flow theory or experimentally, e.g., by the method described hereafter. It may be presented as a plot against distance along the chord of the blade section and against distance normal to the chord. Integration of the area under these two curves leads to the component normal to the chord N, and the chordwise component M, of the resultant-pressure force per unit length of blade along the radius, R. Let the component of the resultant force parallel to the grid be denoted by T, normal to the grid by S. Before the lift component L, defined as the component normal to the direction of the mean relative velocity w' past the blade, and the drag component D parallel to w' may be found, this velocity is to be determined from the equation

$$w' = \sqrt{C'_m{}^2 + \left(r\omega - \frac{C_{u1} - C_{u2}}{2}\right)^2} \quad \ldots\ldots [1]$$

and its direction from

$$\tan \beta' = \frac{C'_m}{r\omega - \frac{C_{u1} - C_{u2}}{2}} \quad \ldots\ldots [2]$$

where

$$C'_m = \frac{C_{m1} + C_{m2}}{2}$$

These and the other quantities, defined in the nomenclature, may be identified in Fig. 3.

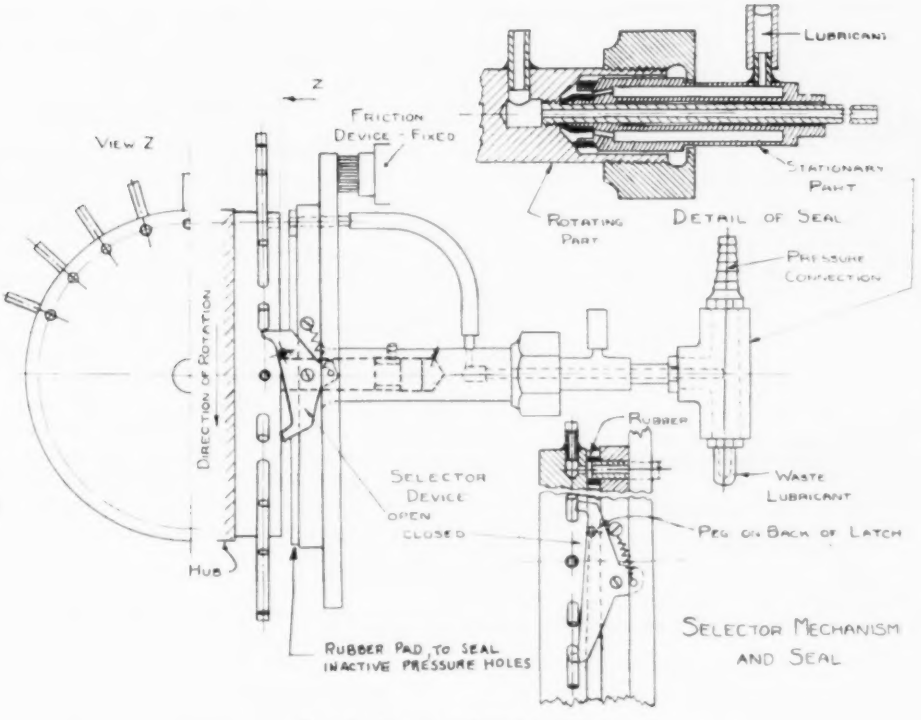


FIG. 2 SELECTOR VALVE AND SEAL

The drag component, obtained from pressure distribution, constitutes only a part of the drag of the blade section, namely, the pressure drag D_p. For conditions of operation of the grid sufficiently close to design conditions so that the circulation

$$\Gamma = (C_{u1} - C_{u2}) \frac{2\pi r}{z}$$

does not vary appreciably along the radius, the induced drag may be neglected, and the skin-friction drag D_f only need be considered, in addition to D_p, since in that case $D = D_p + D_f$. Methods of calculation (10) have been developed by which the skin friction may be calculated theoretically from local shear stresses for airfoils in indefinite flow. These calculations, however, are tedious and do not appear to be readily applicable to blade grids. Experimentally the most promising approach seems to be the measurement of wake traverses, discussed in a later section, which yields the profile-drag directly.

The following nondimensional forms have been used in calculations relating to blade forces

Lift coefficient $C_L = \dfrac{L}{lq'}$

Drag coefficient $C_D = \dfrac{D}{lq'}$

further

$$C_T = \frac{T}{lq'} = C_L \sin \beta' + C_D \cos \beta' \quad \ldots\ldots [3]$$

$$C_S = \frac{S}{lq'} = C_L \cos \beta' \pm C_D \sin \beta' \quad \ldots\ldots [4]$$

where the upper sign applies to turbine the lower to compressor operation.

(*b*) In calculating the velocity diagram of the moving row, it is assumed that the inlet conditions and the axial-velocity component at the outlet are known. The velocity diagram may then

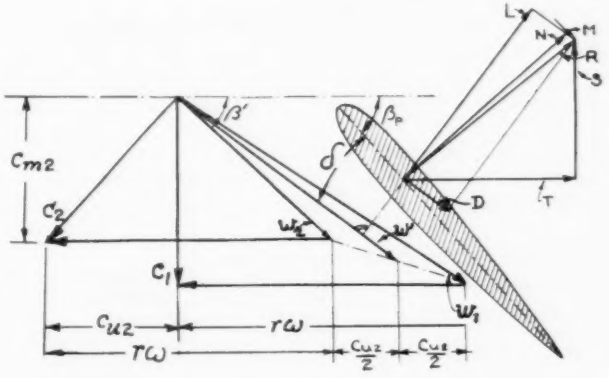


FIG. 3 VELOCITY AND FORCE DIAGRAM

be drawn after the change of circumferential-velocity component has been calculated from the momentum equation

$$2\pi r C'_m \rho' (C_{u1} - C_{u2}) = zT$$

which may be reduced to

$$C_{u1} - C_{u2} = \frac{l}{t} \cdot \frac{C_T}{2} \cdot \frac{C'_m}{\sin^2 \beta'} \quad \ldots\ldots [5]$$

(*c*) The total head Δh across the blade element is given by the energy equation

$$\Delta h = \frac{zSC'_m}{2\pi r C'_m \rho' g} = \frac{C_S}{\sin^2 \beta'} \cdot \frac{l}{t} \cdot \frac{\overline{C'_m}^2}{2g} \quad \ldots\ldots [6]$$

and the efficiency of the blade element

$$\eta_r = \frac{C_T r\omega}{C_S C'_m} \quad \ldots\ldots [7a]$$

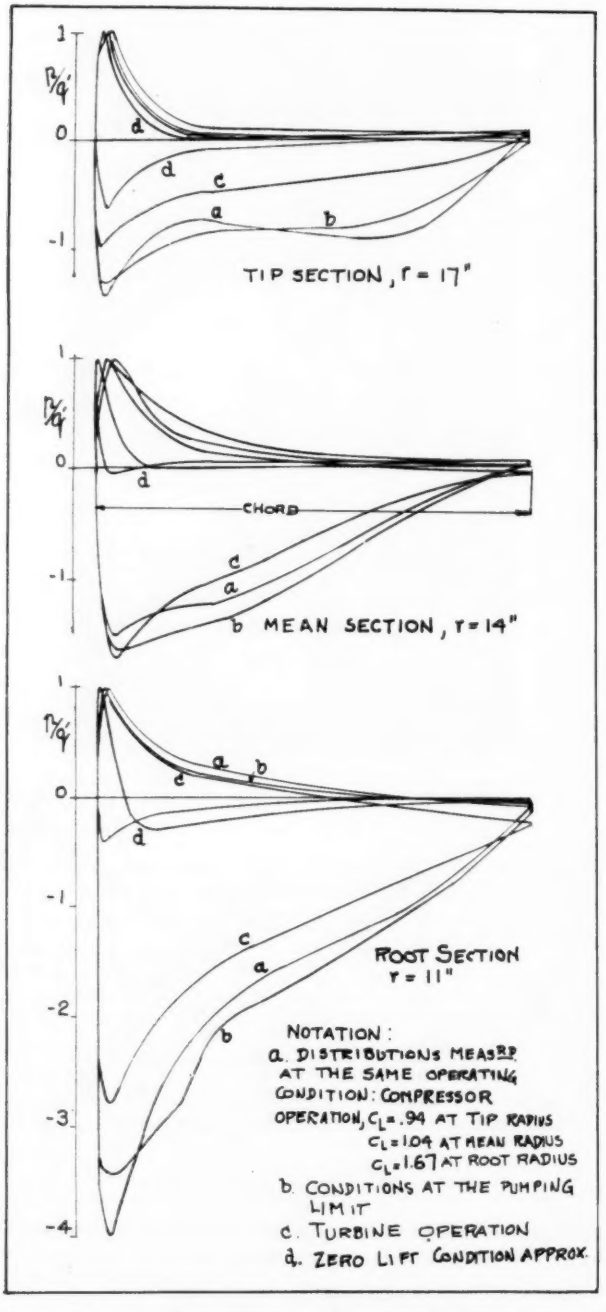


FIG. 4 (*a* to *c*) NONDIMENSIONAL PRESSURE DISTRIBUTION p/q FOR TIP, MEAN, AND ROOT SECTION OF THE BLADE
(Grid with a single airfoil; solidity $1/t$ = 0.09.)

for turbine operation and

$$\eta_r = \frac{C_S C'_m}{C_T r\omega} \quad \ldots\ldots\ldots\ldots\ldots\ldots [7b]$$

for compressor operation.

The efficiency, as formulated here, being based upon lift and profile drag of the blade element, does not take account of certain losses resulting from turbulent momentum transfer associated with the decay of the wake downstream of the row. These losses, however, are small compared with the profile drag in the case of two-dimensional flow for rows of conventional solidity ratios. The equations given in this section are applicable to both compressible and incompressible flow.

EXPERIMENTAL WORK

In developing an experimental program, it seemed important to reduce the test conditions to the greatest possible simplicity. To this end choice was made of a symmetrical profile for the blade section. The direction of flow upstream was chosen to be axial for turbine and compressor operation. Test results of the single-bladed grid only have been included in the analysis, in order to exclude problems of blade-to-blade interference.

Experimental investigations were conducted on a rotating axial-flow grid of 36 in. tip diam and 20 in. root diam, consisting of blades of symmetrical airfoil section N.A.C.A. 0010, twisted for constant geometric pitch when the angle at the root section is 45 deg. The rim was rigidly connected to the blades and rotated with the wheel, thus adding to the rigidity of the latter and eliminating tip leakage. The blades have a chord of 8 in. The number of blades in the grid may be varied and grids of 1, 2, 3, 4, 6, or 12 equally spaced blades may be tested giving a range of solidity ratios $= \frac{\text{chord}}{\text{pitch}}$ on mean diameter of from 0.09 to 1.09. Spacer bolts were provided through each blade, or in place of the blades to hold rim and hub together. One of the blades referred to as the master blade, Fig. 1, was made of lucite and provided with numerous pressure holes arranged in three cylindrical sections, namely, 23 each on the mean radius, 1 in. above the root radius and 1 in. below the tip radius.

The pressure holes in each cylindrical section can be connected successively to a stationary pressure manometer by means of a selector device and seal, shown in Figs. 1 and 2, the latter figure explaining its mechanism. An earlier design of the device was described in (10).

The grid was mounted on the shaft of an electric motor and made a part of a test setup, also described in (10), which was placed into the working section of the return-type wind tunnel of the aerodynamics laboratory of Case School of Applied Science.

Provisions were made to operate the grid both as a compressor and as a turbine. The grid was rotated at speeds ranging from 500 to 1000 rpm. Conditions of operation were varied (*a*) by varying the quantity of air circulated in the wind tunnel, and (*b*) by varying the passage area of an adjustable diaphragm located at the outlet of the cylindrical section, 4 ft downstream of the grid, shown in Fig. 1. This diaphram was found necessary to obtain operation at and beyond the pumping limit, for compressor operation of the grid.

Since the blades are twisted for constant geometrical pitch at the setting just indicated the condition of constancy of circulation, hence of flow on concentric cylinders, is fulfilled only at the point of operation which divides the regions of turbine and compressor operation. Deviations from the assumed condition of flow on concentric cylinders, while inappreciable at small lift coefficients, are presumed to become more severe as the lift coefficients become large. These deviations cause a variation of axial-velocity component between inlet and outlet for which reasons each of these quantities had to be determined separately.

The following measurements were taken:

1 Total- and static-pressure measurements both upstream and downstream of the grid.

2 Measurements of static pressures at the hub and at the casing, both upstream and downstream.

3 Pressure distribution measurements.

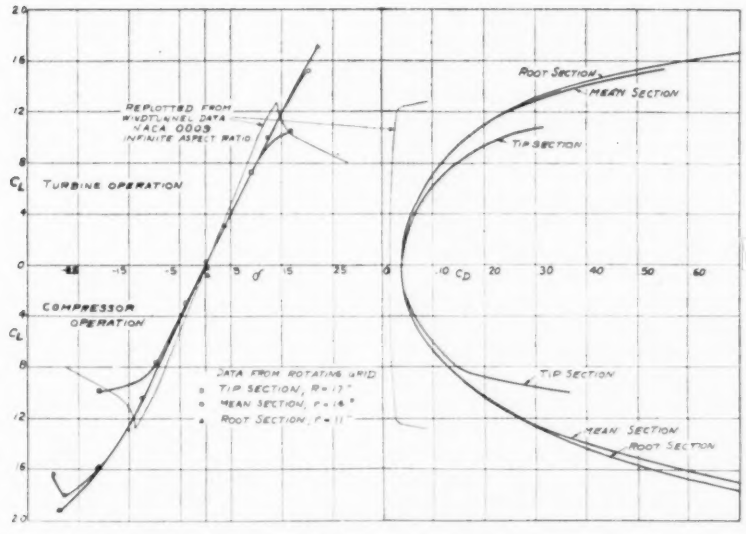
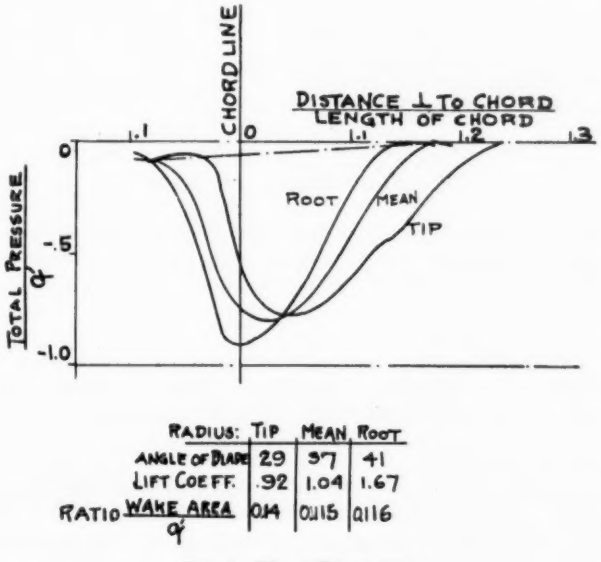


FIG. 5 LIFT AND PRESSURE-DRAG COEFFICIENTS, TIP, MEAN, AND ROOT SECTIONS (Solidity $1/t = 0.09$.)



RADIUS:	TIP	MEAN	ROOT
ANGLE OF BLADE	29	37	41
LIFT COEFF.	.92	1.04	1.67
RATIO WAKE AREA / q'	0114	0115	0116

FIG. 6 WAKE TRAVERSES

4 The rotative speeds were held constant at specified values by a stroboscopic device.

5 Special measurements were obtained of the profile drag of blade sections by means of wake traverses.

TEST RESULTS

Measured pressure was plotted along the chord of the blade section and normal to the cord. The force components per unit length of blade in a radial direction normal and tangential to the chord, respectively, were obtained from these pressure-distribution diagrams and the corresponding resultant force by vector addition, Fig. 3. Not included in the latter is the skin-friction drag which will be treated later.

The data of the velocity diagram, Fig. 3, were calculated directly from measured data, namely, C_{m1}, C_{m2}, and $r\omega$, or from pressure-distribution measurements, namely, C_{u2} from Equation [5], ω' and β' from Equations [1] and [2].

The lift coefficient $C_L = \dfrac{L}{lq'}$ and the pressure-drag coefficient $C_{Dp} = \dfrac{D_p}{lq'}$ were calculated from the respective components of the resultant force, Fig. 2.

The experimental data thus obtained are presented in the following figures:

Fig. 4 (*a* to *c*) shows nondimensional pressure distributions $\dfrac{p}{q'}$ for tip, mean, root radius, for one airfoil in the grid, solidity 0.09.

Fig. 5 shows lift and pressure-drag coefficients, solidity 0.09. For purpose of comparison, Fig. 5 also shows the corresponding coefficients from wind-tunnel tests, reduced to infinite aspect ratio, replotted from (12). The large increase of measured drag coefficients over corresponding wind-tunnel values may be ascribed partly to impairment of the aerodynamic properties of the airfoil surface by the pressure holes and partly to low effective aspect ratio.

It was of interest to ascertain experimentally the magnitude of the profile drag of the blade sections, only a part of which is represented by the pressure drag. To this purpose a total-pressure tube was mounted on the rotating hub placed at a distance of 1.2 in. in the chordwise direction downstream of the airfoil, as shown in Fig. 1. This tube was pointed upstream in the direction of the mean relative flow and connected through the seal to a stationary pressure gage. A simple mechanism was constructed by which the total-pressure tube could be moved between measurements a known small distance in the circumferential direction through operation of the selector device. In this manner, complete total-pressure traverses of the wake were obtained without requiring stoppage of the unit between individual measurements.

While in the present stage, the results of these tests fail to give all the information needed to determine the profile drag precisely, due to the fact that it was not possible to obtain static-pressure readings in the wake simultaneously and coincidently with the total-pressure readings, nevertheless they permit a qualitative insight.

Fig. 5 shows three typical wake traverses obtained from the grid with a single airfoil in place (solidity ratio 0.09) at the same condition of operation at three different radii, namely, at 1 in. above the hub, at the mean radius, and at 1 in. below the rim. Given are the lift coefficients obtained from pressure-distribution measurements, and the areas of the wake profiles. It is noted

that the wake area divided by the velocity pressure of mean relative velocity is smaller for the mean blade section than the corresponding quantity for the section near the tip, although the lift coefficient of the latter is smaller. If the ratio, wake area/velocity pressure of mean velocity, may be taken as proportional to the profile drag, it may be concluded that contrary to what might be expected from the two-dimensional theory, the profile drag near the tip is larger. Three possible explanations are:

1 It may be argued that, since the circulation is not constant along the radial extent of the blade, this result may have been caused by a displacement of the flow outside the wake.

2 The apparent increase of profile drag near the tip may be the result of losses from interference originating in the corners between the blade and the rim. That this latter cannot be the only cause is brought out by the fact that a correspondingly larger value of the ratio was not measured at the section near the hub.

3 The boundary layer of the airfoil and likewise the wake are displaced radially outward by centrifugal force. In order to substantiate the theory of radial displacement of the wake, unexposed Ozalid paper was glued on the surface of the blade around certain of the pressure holes. A mixture of air and ammonia vapor was then emitted by way of the pressure seal through these holes, and an indication of the direction of flow in the boundary layer was obtained by a darkened streak produced by the ammonia vapor on the Ozalid paper. Available photographs of these records are not suitable for reproduction but they indicate clearly that at all points there is an appreciable radial velocity in the boundary layer, particularly on the suction side of the airfoil.

It is concluded from the foregoing that, in determining the profile drag of a blade section of rotating axial-flow grids, account must be taken of the three-dimensional nature of the flow in the boundary layer and in the wake of the blade.

Performance Characteristics

The performance characteristics of the rotating-blade row were calculated from the results of the pressure-distribution measurements for the three blade sections investigated, namely, the total head from Equation [6], and the efficiency of the blade element η_r from Equations [7*a*] and [7*b*]. The results are plotted in Fig. 7. Also plotted on this figure for comparison are corresponding curves calculated from the wind-tunnel characteristics of the symmetrical airfoil profile N.A.C.A. 0009, for infinite aspect ratio. The experimental efficiency curves are based upon the pressure drag only, and no account has been taken of the friction drag of the blade sections.

Conclusions From Experimental Investigation

The following conclusions are derived from the results of the experimental investigation:

1 Tests of blades, placed at wide spacing in a rotating-blade row, show that the range of lift coefficients for the root and mean section exceed the range available for the fixed blade, and maximum-lift coefficients are higher than corresponding wind-tunnel data for compressor operation, as well as for turbine operation.

2 Stalling of the three blade sections investigated was found to occur at the same condition of operation. The stalling characteristics of the blade as far as could be discovered from pressure-distribution measurement, were much less critical than those of the same profile obtained in the wind tunnel.

3 Evidence is presented by the tests that the displacement of the boundary layer and of the wake of the blades radially outward by centrifugal force affects both the lift characteristics and the profile drag, in both cases to the advantage of the root sections of the blades.

4 Performance curves of blade sections, based upon experimental data calculated from pressure-distribution measurement

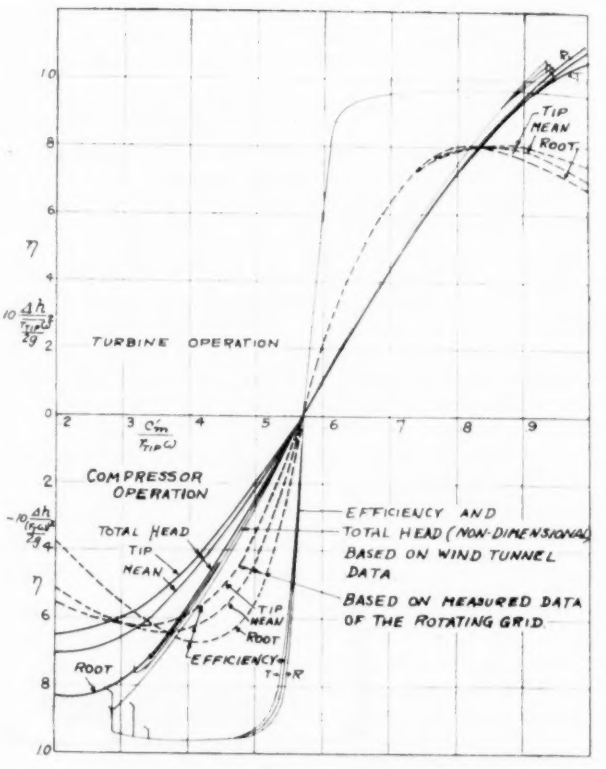


Fig. 7 Total Head and Efficiency

of a rotating-blade row, show lower efficiencies and a higher pumping or stalling limit than corresponding characteristics calculated from airfoil data obtained in the wind tunnel.

Acknowledgment

Acknowledgment is made to Messrs. Morris Sable, and Robert Christiansen, students of Case School of Applied Science, who constructed equipment and assisted in the experimental work.

BIBLIOGRAPHY

1 "The Theory and Performance of Axial-Flow Fans," by C. Keller and L. S. Marks, McGraw-Hill Book Company, Inc., New York, N. Y., 1937.

2 "Single Stage Axial Blowers," by P. Ruden, *Luftfahrtforschung*, vol. 14, 1937, pp. 325–346 and 458–473.

3 "Theoretical Calculation of the Characteristics of Axial-Flow Runners of High Specific Speed," by E. Amstutz, *Stodola Festschrift*, Orell Füssli Verlag, Zürich, Switzerland, 1929, pp. 8–15.

4 "Automatic Integrating Pressure-Traverse Recorder for Study of Flow Phenomena in Steam-Turbine Nozzles and Buckets," by H. Kraft and T. M. Berry, Trans. A.S.M.E., 1940, pp. 479–488.

5 "An Investigation of Energy Losses in Steam-Turbine Elements," by W. R. New, Trans. A.S.M.E., 1940, pp. 489–502.

6 "Losses in the Channels of Moving Blades 'Sov. Kotloturb,'" by G. E. Dozinsky, U.S.S.R. no. 3, 1940, pp. 90–94, RTP Translation No. 1395, British Ministry of Aircraft Production.

7 "The Effect of Wall Roughness on the Performance of Turbo Machinery," by E. Soerensen, *Forschung*, vol. 8, 1937, pp. 25–29.

8 "Die Strömung um die Schaufeln von Turbomaschinen," by F. Weinig, J. A. Barth, Leipsig, Germany, 1935.

9 "A Method for Calculating the Theoretical Characteristics of Rotating Blade Systems," by G. Klingemann, *Ingenieur Archiv*, vol. 11, no. 3, June, 1940, pp. 151–178, RTP Translation No. 1377, British Ministry of Aircraft Production.

10 "Characteristics of Airfoils in a Cylindric Axial-Flow Grid," by J. R. Weske and F. E. Marble, *Journal of the Aeronautical Sciences*, Oct., 1943, pp. 289–294.

11 "The Calculation of the Profile Drag of Airfoils," by H. B. Squire and A. D. Young, British Air Min. R.&M. No. 1838, 1937.

12 "United States N.A.C.A. Report No. 460," 1933, fig. 5, p. 7

Discussion

G. F. Wislicenus.[3] This paper is a most important contribution and one whose significance is obvious at this time, in view of current developments in the field of compressors and turbines. While investigations of a similar nature are being carried out in the industry, to the best knowledge of this writer no one particular study duplicates the author's work. At Worthington, for example, there has been in progress for some time a series of investigations on parallel-vane systems. As a consequence of detailed work in this line, the writer is only too familiar with the inherent difficulties of the problem. The author is to be congratulated on overcoming some of the more serious technical difficulties involved, particularly in the test arrangement.

Perhaps his most valuable single finding is the experimental confirmation of the important difference between the flow in a rotating-vane system, as compared with that in a parallel stationary-vane system, that difference being the "radial" motion of the fluid particles in the boundary layer. While this writer, and doubtless other engineers, had suspected this to be a fact, the experimental proof is of great significance. The author's findings are conclusively demonstrated by his comparison between vane characteristics obtained in the wind tunnel and measurements on the inside of the rotating vane. The writer is referring to the ingenious use of ammonia-vapor traces on Ozalid paper, as well as to the critical study of the change of the maximum lift coefficient. The verification of the idea of radial motion in the boundary layer would alone justify the paper.

As for the theoretical aspects, an explanation of the difference between the through-flow components C_{m2} and C_{m1} (Fig. 3) would be helpful. From the information given in the paper, it seems evident that both the hub and outside periphery are cylindrical; in that case wherein lies the difference between C_{m2} and C_{m1}? From the velocity diagram it is seen that C'_m is assumed to be the arithmetic mean between C_{m2} and C_{m1}. This cannot be explained by the contraction due to the thickness of the vanes, since this thickness would cause C'_m to be larger than either C_{m2} or C_{m1}. Use of the arithmetic mean seems to indicate that the variations in C_m refer to the compression of the fluid. However, for the dimensions and speed of rotation given, the compression of the air must have been practically negligible, particularly with a single-vane grid. The velocity diagram is stated to have been constructed on the basis of measured data. Perhaps some amplification of this statement would clarify the points just mentioned.

The writer assumes that the "pressure drag" is that drag which is caused by a change in the static pressure distribution due to surface friction, since obviously in an ideal fluid the pressures must necessarily be distributed in such a manner that there exists no component in the direction of the flow and, consequently, no pressure drag. The differentiation between pressure drag D_p and the skin-friction drag D_f is new to this writer and an explanation would be appreciated.

In Equation [6] of the paper, Δh is stated to be the total head across the blade element. As given in this equation, it represents rather the change in the static head only, since it expresses the work due to the axial motion under the influence of the axial component S of the vane forces; it does not take into account the change in kinetic energy due to the change in rotation. As a consequence of this fact, the turbine efficiency (Equation [7*a*]) is actually too high and the compressor efficiency (Equation [7*b*]) too low. (Equation [7*b*] is strictly valid for a ship or airplane propeller.) With the present test arrangement, using only a single vane, this discrepancy is quite small, but would be appreciable in actual turbine or compressor wheels.

The author's conclusions are of great interest. It would be helpful if he would explain further what is meant by the statement that the stalling characteristics of the blade were "much less critical." Fig. 5 seems to indicate that, with the exception of one of the curves, the change in lift coefficient during stalling appears to be less drastic than in wind-tunnel tests. Is this the correct interpretation of item 2 of the "Conclusions?"

Does the difference (Fig. 5) between the measured drag and wind-tunnel data hold true for current designs, or has this particular setup certain features which may be responsible for this difference as well as for the low efficiency of the compressor (Fig. 7)? It is of interest to note that the drag coefficients of the turbine and the compressor bear a close resemblance (Fig. 5) but the efficiencies are quite different.

With respect to results obtained with a single vane, the average pressure change through the system would be practically negligible. This is probably responsible for the fact that the maximum-lift coefficients (Fig. 5) are nearly the same for compressor and turbine operation. If the vanes were to be more closely spaced, the pressure increase or drop through the runner would become appreciable as compared with the local pressures on the vanes. Consequently, the vane characteristics in turbine and pumping operation could be expected to differ considerably, the compressor vane acting in a field of increasing static pressure, and vice versa.

The writer is wholeheartedly in agreement with the author's policy of starting his investigations under the simplest conditions possible. It would be most valuable if these experiments could be extended to include more closely spaced vanes. Provisions have evidently been made to increase the solidity ratio to about 1.09. An even higher ratio would yield profitable results, possibly in connection with slightly thinner and suitably curved vanes. It is particularly with such higher solidity ratios that results such as those given in this paper would be of the greatest practical value for compressor and turbine development. For this reason, continuation of this work would constitute a real help to the industry.

Additional details of the technique of pressure measurements in a rotating system and the derivation of the methods of evaluation would be of great interest to many engineers who have been working with similar mechanisms. For instance, Mr. Arthur Oschwald, Jr., of the writer's company brought up the questions: How is it possible to check the measuring system for leakage during rotation; and what steps have been taken to minimize the effect of any possible leakage on the readings? It is hoped that these and other questions can be covered by subsequent publication of information on this interesting and important line of research.

Author's Closure

Dr. Wislicenus' generous comments and constructive criticism are greatly appreciated. An attempt is made to answer the questions raised in the discussion in the following paragraphs.

The velocity and force diagram, Fig. 3, of the paper, was drawn to explain the general relations involved and does not represent any of the diagrams used for the calculation of a particular operating condition. The variation of axial-velocity component was intentionally assumed to be large to show the relation of the mean relative velocity to the relative velocities at inlet and outlet. As pointed out in the discussion, variations of axial velocity are, in the absence of compressibility effects, related to variations of the axial-flow area. A virtual decrease of the axial-flow area downstream of the grid is caused by the wakes of the blades which

[3] Research Engineer, Worthington Pump and Machinery Corporation, Harrison, N. J. Mem. A.S.M.E.

is of significance, however, only in grids of high solidity. No consideration has been given in the paper to the effect of blade thickness.

The designation "pressure drag" was used with reference to the drag calculated from the measured pressure distribution about the airfoil.

The equations for the efficiency, Equations [7*a*] and [7*b*], apply specifically only to the blade grid under investigation, namely, to a single rotating grid without stationary grid upstream or downstream.

As an expression for the efficiency generally applicable to an annular element of a stage consisting of two grids, indicated by subscripts I and II, respectively, either one moving or both moving (the latter case being that of a counter-rotating stage), the following equations, corresponding to Equations [7*a*] and [7*b*] are proposed:

$$\text{turbine} \qquad \eta_r = \frac{(C_T r\omega)_{\mathrm{I}} + (C_T r\omega)_{\mathrm{II}}}{(C_a C'_m)_{\mathrm{I}} + (C_a C'_m)_{\mathrm{II}}}$$

$$\text{pump} \qquad \eta_r = \frac{(C_a C'_m)_{\mathrm{I}} + (C_a C'_m)_{\mathrm{II}}}{(C_T r\omega)_{\mathrm{I}} + (C_T r\omega)_{\mathrm{II}}}$$

It is seen that, for the case of the experimental grid, these equations reduce to the form given in the paper. The form of the equation as just given should have merit in calculations relating stage performance directly to the basic airfoil characteristics. They are believed to apply without restriction to the ducted blade grid.

Available information is insufficient to analyze fully the measured efficiencies, Fig. 7. The low values may be explained partly by the absence of the fixed grid, further by the influence of particular features of the experimental equipment, such as the increase of effective roughness of the blade by the pressure holes, and the absence of fillets at the root and the tip of the blade. Losses in grids and their causes are receiving special attention in further investigations. An extensive investigation of these and other factors has been made by A. Meldahl.[4]

In regard to the experimental demonstration of the occurrence of radial velocities in the boundary layer of the blades of an axial-flow grid, it should be stated that the author, in 1934, presented photographic records of streamlines,[5] obtained by the same method as described in the paper. The same method was applied by P. Ruden to the investigation of an axial-flow fan.[6]

A simple method was developed for checking the experimental pressure-measuring apparatus for leaks. All pressure holes on the airfoil were closed off by a strip of Scotch tape, and a run was taken at which pressure measurements were obtained successively for all pressure connections. Leakage in the rotating portion of any of the pressure leads was then indicated by a negative pressure on the manometer, good connections giving zero reading. The magnitude of the suction pressure served as a clue for the location of the leak, as it is a rough indication of the radial distance of the leak from the axis of rotation.

[4] "The End Losses of Turbine Blades," by A. Meldahl, *The Brown Boveri Review*, vol. 28, 1941, pp. 356–361.

[5] "Experimental Investigation of the Flow of Air Through a Propeller Applied to the Design of an Axial Fan," by J. R. Weske, thesis for the D.S. Degree, Graduate School of Engineering, Harvard University, 1934.

[6] "Untersuchungen über Einstufige Axialgebläse," by P. Ruden, *Luftfahrtforschung*, vol. 14, 1937, pp. 325–346, 458–473.

Notch-Toughness Tests of Carbon-Molybdenum Pipe Material

By W. F. KINNEY,[1] I. A. ROHRIG,[2] AND H. S. WALKER[3]

The development of materials for high-temperature-steam piping is of considerable importance in view of the upward trend in power-plant operating temperatures. Chemical composition, steel-melting practice, and heat-treating procedure, and their effects upon physical properties and microstructure are important factors in appraising the probable behavior of a material in service. The metallurgist and power-plant engineer are particularly interested in the influence of these factors upon notch toughness of the material. Starting with the premise that there may be some correlation between notch toughnessand performance of high-temperature pipe and that significance should be attached to the interpretation of notch toughness with respect to the behavior of carbon-molybdenum pipe material in power-plant service, the authors give details of an investigation conducted in The Detroit Edison Company laboratory on notch-toughness testing. The specific problem studied was to determine the influence on the uniformity of test results and on the magnitude of average notch-toughness values, both at room temperature and at 925 F, of three variables, namely, (*a*) the type of specimen, (*b*) the heat of steel, and (*c*) the condition of the steel. In connection with this testing program, a survey of the literature was conducted and inquiries were directed to various authorities regarding their experience with this problem. The authors conclude that when the significance of notched-bar testing of carbon-molybdenum pipe material is fully understood, it may be possible to select material of the best quality for high-temperature service on the basis of notched-bar tests.

Introduction

As a result of the upward trend in steam-power-plant operating temperatures, considerable attention has been directed toward developing materials for high-temperature-steam piping. As a part of the development, much discussion has taken place regarding the application of carbon-molybdenum steel to superheated-steam piping service and the criteria by which its expected behavior in this service may be predicted. Chemical composition, steel-melting practice, and heat-treating procedure, each with its attendant effects upon physical properties and microstructure, are important factors in the appraisal of the probable behavior of a material in service. The influence of these factors upon one of the physical properties, namely, the notch toughness, is of interest to the metallurgist and the power-plant engineer, because it is believed that notch-toughness data reveal properties that cannot readily be evaluated on the basis of the usual hardness and tensile tests (1).[4]

It is recognized that the property of notch toughness is seldom used as a a measure of acceptability of carbon-molybdenum steel for high-temperature pipe, and notched-bar test failures generally have not been regarded as being analogous to pipe failures in the field. In this regard, McAdam and Clyne (2), in referring to impact tests using notched and unnotched specimens, stated: "An impact test should not be viewed as a simulation of shock in service, and should not be limited to metals that are to be subjected to impact in service." Further, Hoyt (3), in reviewing the likelihood of service failures, has stated: "We have another group of 'internal' notches which are less subject to control because they are not usually visible. Examples of these are . . . heat checks, grinding cracks, shrinkage cracks in castings and welds . . . To these may be added the fatigue crack which forms a very effective notch . . . Corrosion pits and corrosion cracks may also produce a serious notch effect."

Therefore it seems unwarranted to assume that there is no correlation between notch toughness and performance of high-temperature pipe; and a very real significance should be attached to the interpretation of notch-toughness data with respect to the behavior of carbon-molybdenum pipe material in power-plant service. However, information and test data of this nature are meager and controversial issues have been raised from time to time regarding notch toughness, particularly with reference to the apparent lack of uniformity of V-notch test results and the difference in magnitude of average V-notch values as compared with those of keyhole-notch or U-notch results.

In this regard, it might be well to consider for a moment the viewpoint expressed by Hoyt (4) in his statement: "Acceptance of the notched-bar test has not been at all unanimous. Perhaps the chief reason for this is that some experimenters report that the results are apt to be decidedly irregular among themselves and that they give one a feeling that the test lacks meaning and precision. On consecutive heats of steel the results are apt to vary considerably though they are made to the same specification and are otherwise replicas of each other. With such uncertainty and fluctuation it is difficult to correlate the results with other properties or with service records." With reference to tests upon groups of specimens from a material, Hoyt comments further (4): " . . . . . While the results are usually in satisfactory agreement one may and frequently does get quite wide variations . . . . . Does this lack of agreement reflect vagaries of the test itself or does it reveal actual variations in the material? . . . . . One frequently hears that the results are unreliable, by which is meant that, due to imperfections in the testing procedure, sometimes high results and sometimes low results will be secured from identical samples. The chance causes of the spread are assigned to the test procedure and not to the material itself." After further description of tests that were conducted to clarify this question, and in which satisfactory agreement among specimens of a homogeneous sample was obtained, Hoyt (4) concluded, "I could no longer ascribe real variations in test results to vagaries of the test and I believe the point is now seldom raised any more."

[1] Research Department, The Detroit Edison Company, Detroit, Mich. Mem. A.S.M.E.

[2] Research Department, The Detroit Edison Company.

[3] Director of Research, The Detroit Edison Company. Mem. A.S.M.E.

[4] Numbers in parentheses refer to the Bibliography at the end of the paper.

Contributed by the Power Division and presented at the Annual Meeting, New York, N. Y., Nov. 29–Dec. 4, 1943, of THE AMERICAN SOCIETY OF MECHANICAL ENGINEERS.

NOTE: Statements and opinions advanced in papers are to be understood as individual expressions of their authors and not those of the Society.

Carbon-molybdenum pipe material is subject to these uncertainties regarding notch-toughness testing. The present investigation in The Detroit Edison Company grew out of an attempt to account for discrepancies that were noticed between notch-toughness values obtained at an outside laboratory and at the Company's research laboratory on supposedly identical Charpy V-notch specimens, when only one or two specimens were tested at a time. Subsequent tests at both locations on a large number of specimens from the same carbon-molybdenum pipe sample in the "laboratory-normalized at 1725 F" condition revealed that the average values and range of values obtained on the two machines checked surprisingly well. It was thereupon concluded that, if a sufficient number of carefully prepared Charpy V-notch specimens were tested, a reasonably close check should be obtained on the material under consideration but that a wide variation in notch-toughness values among individual specimens in any group might be expected. However, this conclusion was predicated solely upon room-temperature tests of Charpy V-notch specimens of normalized pipe, and the question was immediately raised as to whether this conclusion were also warranted for tests both at room temperature and at operating temperature, on various types of standard specimens, on various heats of carbon-molybdenum pipe material, and in various heat-treated conditions encountered in the company's high-temperature piping investigations.

The specific problem therefore was to determine the influence on the uniformity of test results and on the magnitude of average notch-toughness values both at room temperature and at 925 F, of three variables, namely, (*a*) the type of specimen, (*b*) the heat of steel, and (*c*) the condition of the steel. In connection with this testing program, a survey of the literature was conducted and inquiries were directed to various authorities regarding their experience with this problem.

Test Procedure

The tests were conducted on specimens of 10 and 12 in-nps, schedule 100 carbon-molybdenum pipe material from a number of heats which have been furnished commercially during the past 5 years and which represent the more recent installations of this steel. The material tested was made according to the silicon-killed coarse-grained melting practice. The pipe sections were received in either the "hot-rolled and drawn at 1200 F" condition or the "shop-normalized[5] at 1725 F" condition;[6] the former provided the samples, approximately 4 × 6 in. in size, which were laboratory-normalized for 1 hr at the desired temperature in an electric muffle furnace. Specimens were cut longitudinally from the mid-section of each sample, following a pattern that distributed the various types of specimen at random throughout the sample. Notches were cut in that surface of the specimen nearest the outer surface of the pipe wall. Care was taken to see that test specimens were as nearly identical as possible and truly representative of the pipe section from which they were removed.

After a survey was made of the specimen dimensions recommended by A.S.M.E. (5), A.S.T.M. (6), A.S.M. (7), and in various technical articles, the dimensions shown in Fig. 1 were selected as corresponding to approved standards in the essential details.

The scope of the tests included the following:

[5] This term, as used in this paper, describes the normalizing treatment given to pipe in the fabricating shop and is intended to distinguish that procedure from laboratory normalizing of test samples. It is advisable to preserve such a distinction in all laboratory investigations of heat-treated material.

[6] In accordance with A.S.T.M. Designation A206-41T, except that the normalizing temperature specified by the authors' company was 1725 F rather than 1700 F.

TABLE 1 NOTCH TOUGHNESS AT ROOM TEMPERATURE OF A TYPICAL HEAT OF COARSE-GRAINED CARBON-MOLYBDENUM PIPE MATERIAL USING VARIOUS TYPES OF TEST SPECIMEN[a]

Type of specimen	Notch toughness, ft-lb		
Charpy V-notch	59, 82, 87, 78, 72, 80, 78	Avg	**77**
		Max 87	(+13%)[c]
		Min 59	(−23%)[c]
	82, 83, 79, 86, 87, 55, 77	Avg	**78**
		Max 87	(+12%)
		Min 55	(−30%)
	74, 83, 72, 86, 84	Avg	**80**
		Max 86	(+ 8%)
		Min 72	(−10%)
Charpy keyhole-notch	46, 47, 48, 45, 49, 48, 47	Avg	**47**
		Max 49	(+ 4%)
		Min 45	(− 4%)
Charpy U-notch	46, 47, 46, 47, 46, 47, 48	Avg	**47**
		Max 48	(+ 2%)
		Min 46	(− 2%)
Izod V-notch	68, 59, 61, 68, 70, 62, 66	Avg	**65**
		Max 70	(+ 8%)
		Min 58	(−11%)
Tensile impact	150, 150, 152, 181, 179, 182, 176, 160, 151, 181, 174, 197	Avg	**169**
		Max 197	(+17%)
		Min 150	(−11%)

[a] Heat 5085, laboratory-normalized at 1725 F for 1 hr.
[b] Tests conducted at an outside laboratory.
[c] Variation of maximum and minimum values from average value in each group.

1 Tests on 19 Charpy V-notch specimens from a typical heat in the "laboratory-normalized at 1725 F" condition, 7 of which were tested at an outside laboratory.

2 Tests of 7 each of Charpy V-notch, Charpy keyhole-notch, Charpy U-notch, Izod V-notch, and tensile impact specimens all from the same heat in the "laboratory-normalized at 1725 F" condition.

3 Tests at room temperature and at 925 F of 2 typical heats in the "hot-rolled and drawn at 1200 F" condition, using Charpy V-notch, Charpy keyhole-notch, and Charpy U-notch specimens.

4 Tests at room temperature and at 925 F of the same two typical heats in the "laboratory-normalized at 1650 F" condition.

5 Tests at room temperature and at 925 F of the same two heats and two additional typical heats, all in the "laboratory-normalized at 1725 F" condition.

These data were augmented by data on file from inspection tests on several heats that had been shop-normalized at 1725 F.

The V-notch and U-notch specimens were machined using milling cutters whose profiles had been checked and were known to be within the specified tolerances. The keyhole notch was prepared in the standard manner using a fixture to align the specimens and guide the drill. The dimensions of all specimens were checked by means of a sharp-pointed needle on the shaft of a dial gage which was rigidly mounted above a ground face

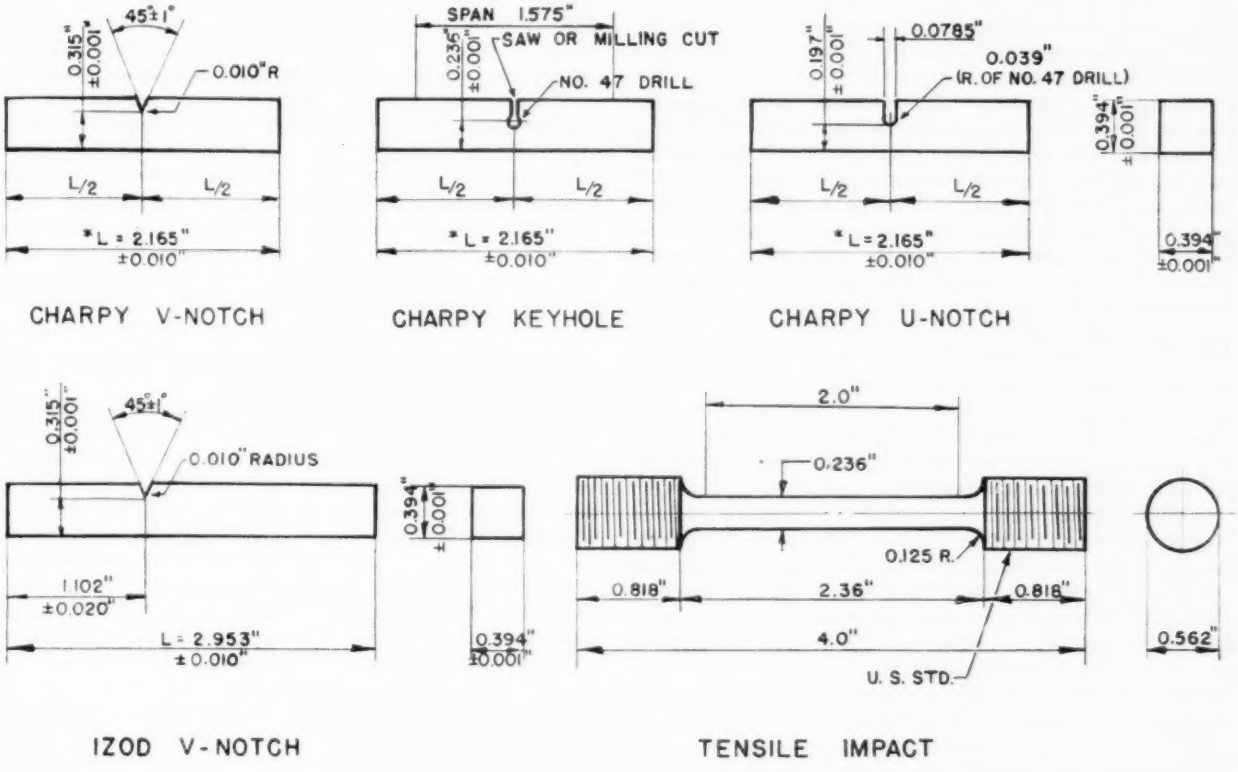


FIG. 1 DIMENSIONS AND PRESCRIBED TOLERANCES[7] OF TEST SPECIMENS

plate. The radius of each notch was checked by enlarging its profile 50 magnifications on a metallurgical microscope and comparing the curvature with the specified radius on the ground-glass viewing plate.

After machining, the specimens were heated at 160 F for about 16 hr to remove machining stresses.

All tests, except those that were made at the outside laboratory, were conducted on a Riehle universal impact-testing machine of 220 ft-lb capacity and of which the velocity of the striking head was about 18 fps. Inasmuch as the five different types of specimen under consideration were all tested on the same machine, this procedure obviously eliminated any variations that might be attributed to (*a*) differences among testing machines, i.e., whether of the Charpy or Izod type, or of different manufacture; (*b*) length of span; (*c*) velocity of the striking head; (*d*) shape and condition of the anvil, vise, and hammer.

The room-temperature tests were conducted at 70 to 75 F in all cases. The testing technique that was employed for the Charpy tests at 925 F was based upon similar tests that had been conducted a few years previously in which it was shown that, after soaking at 950 F for at least 1 hr, a specimen could be rapidly transferred with insulated tongs from the thermostatically controlled electric muffle furnace to the near-by testing machine in about 5 sec, in which time the temperature of the specimen would drop to about 925 F. Timing of the operation during the present tests indicated that there was only a very slight variation in the elapsed time, so the specimens were all at virtually the same temperature at the moment of impact, which is the significant factor in the technique.

The photomicrographs that were made for metallographic examination of each heat and condition of pipe material tested were taken of the V-notch specimen that broke at the value nearest the average for each respective group.

RESULTS OF TESTS

The results of the notch-toughness tests conducted at room temperature on a typical heat of carbon-molybdenum pipe material in the "laboratory-normalized at 1725 F" condition using various types of test specimens are shown in Table 1.[8]

The first two groups of data afford an interesting comparison among 14 supposedly identical Charpy V-notch specimens tested at two different laboratories. The agreement between the two groups is significant both with respect to the average values obtained and to the degree of variation among individual specimens. The average of the 5 extra Charpy V-notch specimens which were tested also agreed with the averages of these two groups. However, because of the wide variation observed, it was thenceforth considered necessary to test at least 7 Charpy V-notch specimens in any group, provided sufficient material were available, in order that the test results might be representative of the sample being studied.

Selection of Types of Specimen for Further Study. As shown in Table 1, the Charpy V-notch tests of this typical heat showed relatively high notch-toughness values, and the results covered a wide range among individual specimens, from 55 to 87 ft-lb in one case. Having established the reliability of the data obtained

[7] "The accuracy that is usually maintained is 0.001 in. although if it will lower the cost of preparing test bars this can be increased to 0.003 in. on harder steels and to 0.005 in. on softer steels without endangering the reliability of the results" (7).

[8] See Fig. 2(*f*) for photomicrograph of this normalized heat.

using Charpy V-notch specimens of this heat, on the basis of tests at two different laboratories, it was felt that the magnitude and variation of these results were typical of the particular heat of steel being tested.

A comparison of the test results on Charpy keyhole specimens with those on Charpy U-notch specimens reveals not only that the average notch toughness of 7 specimens of each type was the same but that the degree of uniformity among individual specimens was practically the same. Both sets of results were considered to be very uniform. In view of this conclusion, it was decided that tests of as few as 3 specimens of either type would suffice in most cases to represent the sample under consideration. For both types of specimen, the average value was considerably lower than that obtained with the Charpy V-notch specimen.

The Izod V-notch test results were somewhat more consistent than the Charpy V-notch results in that there was a smaller spread in the values for individual specimens, and the average value was lower. On the other hand, the Izod V-notch results were not as uniform as the Charpy keyhole and U-notch results, and the average value was much higher.

In the case of the tensile-impact tests, which were introduced to indicate the behavior of the material in the absence of a notch, the unexpected variation that was encountered in the results as the tests proceeded prompted the testing of 12 rather than 7 specimens. At least a part of the observed inconsistency in results has been attributed to improper alignment of the specimen owing to the lack of spherical seats[9] in the design of the testing machine. This prevented the application of the load at the correct angle and resulted in some instances in the bending of the reduced section of the specimen at the moment of impact. This difficulty with the tensile-impact specimens tended to mask differences which might have been present in the material and, for this reason, this type of specimen was dropped from further consideration.

Therefore in keeping with the general practice of most pipe manufacturers and fabricators, who prefer the Charpy keyhole type of specimen and because of the growing popularity of the Charpy U-notch specimen as evidenced by inclusion of it in the A.S.M.E. Boiler Construction Code (5), it was decided to subject these two types of specimen to further investigation along with the Charpy V-notch type of specimen, which had been found to give relatively high average notch-toughness values, and thus provide a significant comparison with the lower values obtained with the other two Charpy specimens.

The results of the subsequent notched-bar tests, conducted at room temperature and at 925 F on various heats of steel in different conditions, are given in Table 2. The photomicrographs in Fig. 2 show the representative microstructure of each group of specimens. An analysis of these data on Charpy V-notch, keyhole-notch, and U-notch specimens discloses the following:

Variations With Type of Specimen. In most cases the average V-notch results were higher than both the keyhole and U-notch values, but in a few cases they were lower. Therefore it cannot be taken for granted that the results obtained on V-notch specimens of carbon-molybdenum pipe material will be consistently higher or consistently lower than keyhole- and U-notch results.

In general, the keyhole- and U-notch results were more uniform among individual specimens than the V-notch results obtained at any test temperature on any heat in any condition in which specimens were tested. However, attention is called to the fact that, contrary to expectations, considerable variation, roughly ±20 per cent, was encountered in one group of keyhole-type specimens and in one group of U-notch type specimens, both from heat 6347 in the "hot-rolled and drawn at 1200 F" condition when tested at room temperature, as shown in (*a*), Table 2. A comparison of the test results on Charpy keyhole specimens with those on U-notch specimens reveals that there was very little difference between the two types as regards the variation among individual specimens or the magnitude of the average results obtained at any test temperature on any heat in any condition.

Variations With Heat of Steel. In the tests at room temperature, wide differences among average notch-toughness values were obtained for V-notch specimens from various heats in a given condition, ranging in one case from an average value of 56 to a value of 105 ft-lb, as shown by a comparison of (*e*), (*f*), (*g*), and (*h*) in Table 2. However, when tested at 925 F these differences ceased to exist and complete agreement among average notch-toughness values for V-notch specimens was obtained for different heats in a given condition.

In the tests at room temperature, it was generally true that the results obtained with the keyhole and U-notch specimens were alike for various heats in a given condition. The only exception was the difference noted in the case of heats 6347 and 5085 in the "laboratory-normalized at 1650 F" condition, shown in (*c*) and (*d*), Table 2, for which no explanation is apparent. However, as in the case of the V-notch tests, complete agreement was obtained when the tests were conducted at 925 F.

Although the average notch-toughness values varied among heats, no heat consistently gave a better degree of uniformity among individual specimens than another, irrespective of the type of specimen used or the test temperature.

Variations With Condition of Steel. For all three types of Charpy specimen, the average notch-toughness values obtained at room temperature for a given heat of steel increased as a result of normalizing at 1650 or 1725 F. Tests at 925 F showed no such improvement as a result of normalizing in that the average values were about the same for a given type of specimen, for all conditions of all heats. Further, good uniformity was obtained in the tests at 925 F for all three types of Charpy specimen, for all conditions of all heats. The greatest variation in any group of specimens tested at 925 F was +9 per cent and —15 per cent for the keyhole-notch specimens of heat 5085, hot-rolled and drawn at 1200 F, as shown in (*b*), Table 2.

It should be noted that tests of material in the "shop-normalized at 1725 F" condition, using both Charpy V-notch and keyhole-notch specimens, gave lower values than those on material in the "laboratory-normalized at 1725 F" condition, as shown in (*e*), (*f*), (*i*), and (*j*), Table 2. The values for individual specimens in each group varied about as much for the shop-normalized material as they did for the laboratory-normalized material.

Discussion of Results

There seem to be almost limitless avenues of approach to the interpretation of the results of the present notched-bar tests but for the sake of conciseness, the discussion will be confined to the factors involved in the practical problems at hand, namely, "how to conduct notched-bar tests on carbon-molybdenum pipe material," and "what is the significance of the results?"

Considering for a moment the broad aspects of the determination of notch toughness of materials, there are numerous variables that affect the magnitude and the uniformity of the results. Further, the relationship between the magnitude of notch-toughness values and the service behavior of the materials always enters into the interpretation of test results and is controversial. By means of correspondence and a review of the literature on the subject, some information but few specific and pertinent data were obtained relative to carbon-molybdenum pipe material. The articles contained in the Bibliography[4] have been reviewed, among others, and found to be the most pertinent to this subject.

[9] Discussed by S. W. Lyon (8).

Information from these sources forms the basis for much of the following discussion.

Variables. The influence of many variables on notch-toughness value has been stressed in the literature. It is acknowledged that these variables, such as the striking velocity, the temperature of the test, the type and dimensions of the specimen, the heat of the steel, and the condition of the steel, all contribute to some confusion in attempting to evaluate notch-toughness results.

Data presented in the literature revealed that striking velocities were commonly within the range of 12 to 20 fps, and that caution in the interpretation of results must be exercised if the striking velocity falls outside of this range. However, as long as all tests under the present investigation were conducted on the same machine, with a striking velocity of about 18 fps, the effect of this variable on the comparability of test results does not enter into the problem.

Temperatures at which notch-toughness tests have been conducted by various investigators range from about —300 to 1000 F. Within that range, the effect of the temperature variable on both the magnitude and uniformity of notch-toughness values is of extreme importance.

Many investigators have commented to the effect that "Temperature has a prominent effect on notch toughness . . . The standard test is made at room temperature and ignores the circumstances that the same notch might produce brittle failure and a low impact value at a temperature but slightly lower" (3). Further, a recent theory regarding the importance of the test temperature on the transition point in notched-bar testing is expressed in the following remarks by Gillett (9): "The transition temperature, at which the type of fracture of a notched-bar specimen of a steel shifts from tough to brittle, is plainly a criterion through which differences not otherwise obvious might be made evident, so low-temperature notched-bar testing might be a useful tool in the constant search for the underlying causes of the 'inherent individuality' of a particular heat of steel, even though that heat might not be destined for low-temperature work." In so far as the authors have been able to ascertain, notched-bar tests of carbon-molybdenum pipe material have not been conducted at lower than room temperature; if such data are available they would be a welcome part of the discussion on this paper. Such an investigation might well be undertaken in order to further this study.

The results of the present investigation have shown that tests at 925 F fail to reveal significant differences among various heats and conditions of steel, in contrast with the marked differences that were observed when testing at room temperature, particularly with the V-notch type of specimen. It may be, as suggested by those that have conducted studies of materials at low temperatures, that even greater differentiation might be possible among heats and conditions of carbon-molybdenum pipe material by means of tests at relatively low temperatures.

Type of Specimen. In order to arrive at a reasonable answer to the question of the correct procedure that should be followed in notched-bar testing of carbon-molybdenum pipe material, frequent reference must be made to the relative merits of the sharp V notch as contrasted with the blunt keyhole or U notch. This phase of the present study found its counterpart in work of other investigators who have commented as follows:

". . . the V-notch type of specimen is likely to be a more sensitive indicator of impact strength than the standard Charpy keyhole specimen" (10).

"The . . . (V) notch is used by some because it gives a larger numerical spread between notch tough and notch brittle materials than is obtained with the more generous radius of the Charpy (keyhole) notch" (7).

"Most commercial specifications are based on values secured from testing Charpy bars with keyhole notch . . . . . this type of notch is not so sensitive to differences in either composition or temperature as the Vee notch . . . . " (11).

The results obtained in the present investigation on carbon-molybdenum pipe material confirm these opinions of other investigators that better discrimination among various qualities of steel is afforded by the sharp V notch than by the blunt keyhole notch or U notch. It is likely that tests made using the keyhole notch or the U notch give a measure of the bend strength under conditions of sudden loading rather than of the true notch toughness of a material.

Heat of Steel. The following comments are probably the most significant that have been found pertaining to the variation that is attributable to differences among heats of steel. Armstrong and Gagnebin (11) stated, " . . . the present state of the art does not permit use of composition, grain size, and heat-treatment as criteria for resistance to impact, which indicates the advisability of subjecting each lot to test . . . "

In a discussion accompanying that paper, Rosenberg mentioned, " . . . impact tests secured on a single heat of steel are more or less peculiar to that individual heat, and will not necessarily be duplicated by another heat of the same kind of steel. Individual heats apparently have what may be termed 'inherent' resistance to impact within certain limits, and this is dependent upon factors not at present recognized . . . "

In the present investigation it is significant that although the chemical composition[10] was virtually the same for all the heats under consideration, and metallographic examination revealed only slight differences in microstructure among the heats in a given condition, the Charpy V-notch test results show marked differences among the average notch-toughness values for various heats; however, these differences are not revealed by either keyhole- or U-notch tests.

Condition of the Steel. The increase in the notch-toughness values as a result of normalizing at either 1650 or 1725 F, which was observed in the room-temperature tests using all three types of Charpy specimen, is consistent with the findings of Crocker and White (12) that normalizing of carbon-molybdenum pipe material improves the notch toughness.

The data shown in (*i*) and (*j*), Table 2, which were incorporated into this investigation from inspection test results on two heats of pipe material, shop-normalized at 1725 F, provide an interesting comparison between the practical aspects of notched-bar testing, as applied to material under consideration for installation, and the technical aspects of notched-bar testing in a laboratory investigation. It is readily apparent that, as judged by the results of Charpy V-notch and keyhole-notch tests on an adequate number of individual specimens, the laboratory-normalized material yielded higher notch-toughness values than the shop-normalized material. Examination of the microstructure reveals that these higher notch-toughness values were accompanied by relatively smaller grain size. These data appear to indicate that, on these two particular heats, the temperature might have been somewhat higher during the shop-normalizing than during the laboratory-normalizing treatment, or that the pipe had been held at normalizing temperature longer during shop-normalizing.

Summary of Discussion

The foregoing observations and discussion comprise the authors' interpretation of the test results that were obtained at

[10] Typical chemical analysis of carbon-molybdenum pipe material used in these tests: C = 0.18, Mo = 0.52, Si = 0.28, Mn = 0.45, S = 0.020, P = 0.017.

TABLE 2 CHARPY NOTCH TOUGHNESS OF TYPICAL HEATS OF COARSE-GRAINED CARBON-MOLYBDENUM PIPE MATERIAL

Hot-Rolled and Drawn at 1200 F — Laboratory Normalized at 1650 F

	(a) HEAT 6347 Notch toughness, ft-lb		(b) HEAT 5085 Notch toughness, ft-lb		(c) HEAT 6347 Notch toughness, ft-lb		(d) HEAT 5085 Notch toughness, ft-lb	
	Room temperature	925 F	Room temperature	925 F	Room temperature	925 F	Room temperature	925 F
V-NOTCH	20 21 Avg 23 21 26 Max 32 (+39%)* 32 22 Min 20 (-13%)* 20	56 60 Avg 55 55 54 Max 60 (+9%) 55 54 Min 54 (-2%) 54	50 39 Avg 42 63 34 Max 63 (+50%) 47 35 Min 26 (-38%) 36	47 48 Avg 50 52 49 Max 52 (+4%) 52 52 Min 47 (-6%) 51	25 33 Avg 48 28 28 Max 70 (+46%) 70 66 Min 28 (-42%) 62	57 57 Avg 58 59 58 Max 61 (+5%) 58 58 Min 57 (-2%) 61	94 81 Avg 71 77 70 Max 94 (+32%) 74 62 Min 41 (+40%) 41	55 54 Avg 57 55 58 Max 59 (+4%) 58 58 Min 54 (-5%) 59
KEYHOLE-NOTCH	26 36 Avg 36 39 33 Max 42 (+17%) 42 35 Min 26 (-28%) 38	36 33 Avg 35 35 35 Max 36 (+3%) 35 35 Min 33 (-6%) 34	39 36 Avg 35 38 33 Max 39 (+11%) 33 37 Min 32 (-9%) 32	32 36 Avg 33 35 34 Max 36 (+9%) 28 32 Min 26 (-15%) 31	46 Avg 45 41 Max 49 (+9%) 49 Min 41 (-9%)	39 Avg 39 39 Max 40 (+3%) 40 Min 39 (-0%)	37 Avg 37 39 Max 39 (+5%) 35 Min 35 (-5%)	37 Avg 37 37 Max 37 (+0%) 36 Min 36 (-3%)
U-NOTCH	30 34 Avg 37 38 41 Max 43 (+16%) 43 35 Min 30 (-19%) 40	33 34 Avg 34 34 35 Max 36 (+6%) 34 36 Min 33 (-3%) 35	29 32 Avg 32 33 32 Max 35 (+9%) 35 32 Min 29 (-9%) 32	30 32 Avg 32 31 31 Max 37 (+16%) 31 32 Min 30 (-6%) 37				

Note: * Variation of the maximum and minimum values from the average value in each group.

Laboratory Normalized at 1725 F — Shop Normalized at 1725 F

	(e) HEAT 6347 Notch toughness, ft-lb		(f) HEAT 5085 Notch toughness, ft-lb		(g) HEAT 3398 Notch toughness, ft-lb	(h) HEAT 24,440 Notch toughness, ft-lb	(i) HEAT 6347 Notch toughness, ft-lb	(j) HEAT 5085 Notch toughness, ft-lb
	Room temperature	925 F	Room temperature	925 F	Room temperature	Room temperature	Room temperature	Room temperature
V-NOTCH	54 Avg 63 66 Max 70 (+11%) 70 Min 54 (-14%)	58 58 Avg 58 57 59 Max 59 (+2%) 57 57 Min 57 (-2%) 58	82 83 Avg 78 72 86 Max 87 (+12%) 87 55 Min 55 (-29%) 77	57 55 Avg 55 55 56 Max 57 (+4%) 54 54 Min 54 (-2%) 55	62 51 Avg 56 48 63 Max 63 (+13%) 56 55 Min 48 (-14%) 54	102 106 Avg 105 109 108 Max 109 (+4%) 109 99 Min 99 (-6%) -	36 30 Avg 33 30 30 Max 36 (+9%) 32 30 Min 30 (-9%) 35	49 55 Avg 51 49 51 Max 58 (+14%) 58 49 Min 43 (-14%) 43
KEYHOLE-NOTCH	49 Avg 49 47 Max 51 (+4%) 51 Min 47 (-4%)	39 Avg 38 37 Max 39 (+3%) 37 Min 37 (-3%)	46 47 Avg 47 48 45 Max 49 (+4%) 49 48 Min 45 (-4%) 47	37 Avg 36 35 Max 37 (+3%) 35 Min 35 (-3%)	43 45 Avg 47 46 52 Max 52 (+11%) 48 47 Min 43 (-9%) 50	45 47 Avg 45 45 42 Max 47 (+4%) 46 46 Min 42 (-7%) 45	42 42 Avg 42 42 42 Max 42 (+0%) 42 39 Min 39 (-7%) 42	42 42 Avg 42 44 42 Max 44 (+5%) 44 40 Min 40 (-5%) 40
U-NOTCH		37 Avg 37 37 Max 37 (+0%) 36 Min 36 (-3%)	46 47 Avg 47 46 47 Max 48 (+2%) 46 47 Min 46 (-2%) 48	35 Avg 36 37 Max 37 (+3%) 35 Min 35 (-3%)	46 46 Avg 48 49 47 Max 50 (+4%) 49 46 Min 46 (-4%) 50	48 44 Avg 44 50 44 Max 50 (+14%) 44 41 Min 41 (-7%) 43		

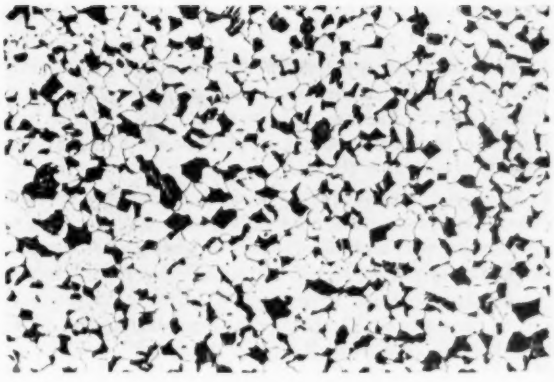
Hot-Rolled and Drawn at 1200 F



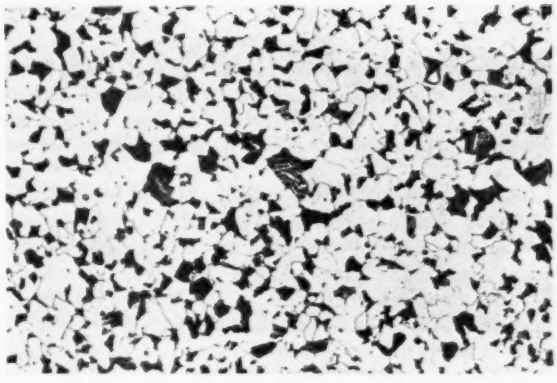
(a) Heat 6347; A.S.T.M. grain size 2–4 (b) Heat 5085; A.S.T.M. grain size 2–5

FIG. 2 TYPICAL MICROSTRUCTURE OF COARSE-GRAINED CARBON-MOLYBDENUM PIPE MATERIAL
(Etchant 3 per cent nital; ×100.)

Laboratory-Normalized at 1650 F

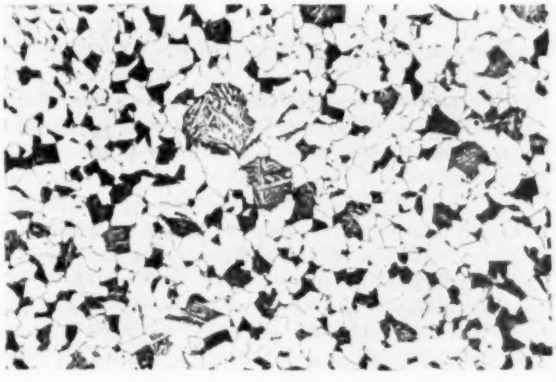


(*c*) Heat 6347; A.S.T.M. grain size 6

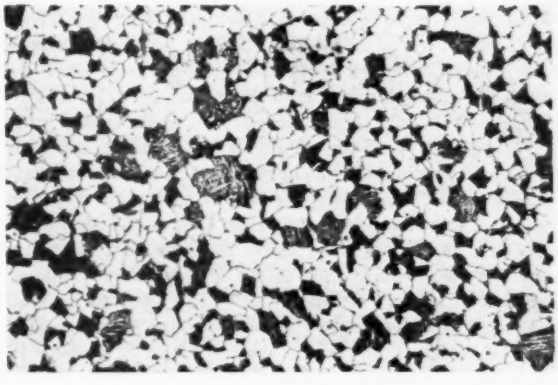


(*d*) Heat 5085; A.S.T.M. grain size 6

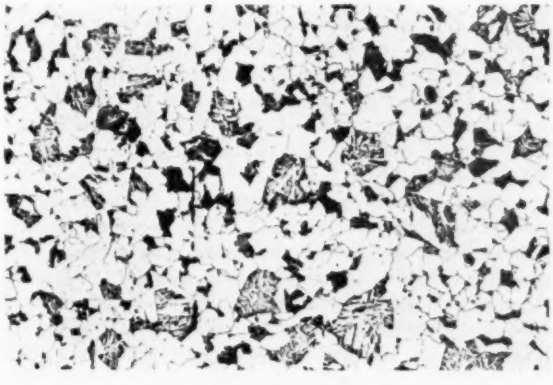
Laboratory-normalized at 1725 F



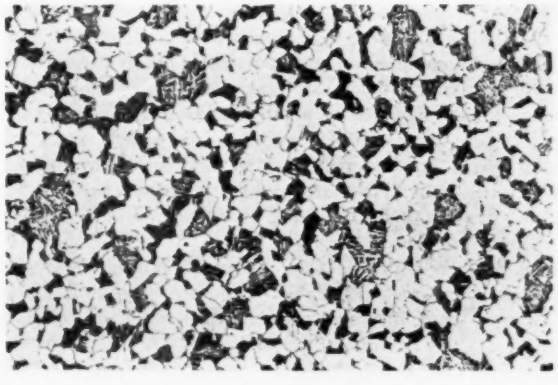
(*e*) Heat 6347; A.S.T.M. grain size 4–6



(*f*) Heat 5085; A.S.T.M. grain size 5–6

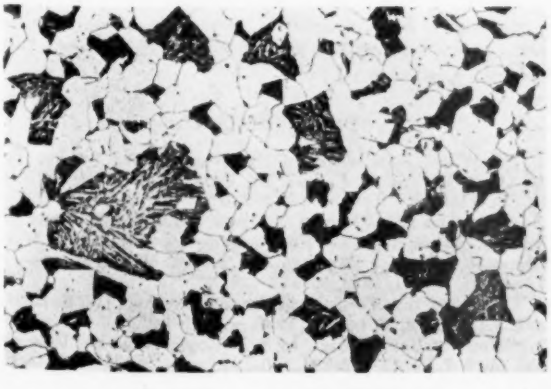


(*g*) Heat 3398; A.S.T.M. grain size 5–6

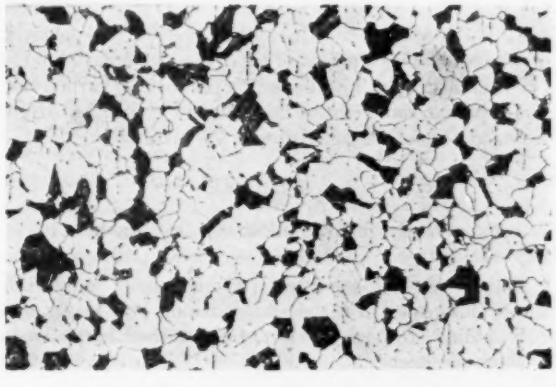


(*h*) Heat 24,440; A.S.T.M. grain size 5–6

Shop-normalized at 1725 F



(*i*) Heat 6347; A.S.T.M. grain size 2–6



(*j*) Heat 5085; A.S.T.M. grain size 5–6

FIG. 2 (*Continued*) TYPICAL MICROSTRUCTURE OF COARSE-GRAINED CARBON-MOLYBDENUM PIPE MATERIAL
(Etchant 3 per cent nital; ×100.)

room temperature and at 925 F, using various types of specimen from a number of heats of carbon-molybdenum pipe material in various conditions. This discussion has been augmented by frequent references that correlated with the findings in the present investigation.

In so far as the review of the literature is concerned, the present problem on carbon-molybdenum pipe material apparently has not been approached before from the viewpoint taken by the authors, namely, the determination of the influence on the magnitude and uniformity of results of the type of specimen, the heat of the steel, and the condition of the steel. However, this discussion would not be complete without some reference to other possible aspects of the problem that warrant further investigation. Of these, the influence of relatively low temperatures on notch-toughness values of carbon-molybdenum pipe material has already been mentioned. Also, the review of the literature reveals considerable interest in the use of double-width specimens as a source of additional information in debatable cases where tests of standard-width specimens indicate some peculiarity in the particular sample in question.

Riegel and Vaughn (1) mentioned " . . . when we find a heat of steel which is close to the minimum foot-pound value with our single-width specimen, we believe that a more critical examination of the steel is necessary by the use of the intensified notch effect of a specimen similar to that shown but of double the width. If, under this more severe test, the heat of steel gives double the foot-pound values of the single-width specimens, our suspicions on relative sensitivity to brittle cleavage are allayed. If the foot-pound values of the double-width specimens are less than double that of the single-width specimens, the heat is not accepted for the purpose intended."

Inasmuch as such instances occur from time to time in studies of carbon-molybdenum pipe material, it would be well to investigate the influence of double-width specimens on the behavior of various heats in order that some provision for possible tests of double-width specimens might be included in any inspection procedure involving notched-bar tests. Also, some search into the reasons for the inconsistent notch-toughness behavior of carbon-molybdenum pipe material would be in order. Data which might reveal possible relationships between notch-toughness characteristics of this material and microstructure, or steel-melting practice or heat-treating procedure would be a valuable contribution to the art.

Finally, there is the question of correlation of notch-toughness test data and expected behavior in service. While it has been possible in many instances, such as those cited by Riegel and Vaughn (1), for manufacturers to correlate notch-toughness requirements with field performance, and thereby gradually to improve their standards by better control of steel-melting and heat-treating practice, such a correlation, as it applies to carbon-molybdenum pipe material, is still vague. However, it is hoped that if, as those authors point out, wide differences in average notch-toughness values of successive mill heats have been minimized over a period of time, then a similar high standard of steel-melting and heat-treating practice for carbon-molybdenum pipe material might be maintained by continual attention to notch-toughness characteristics of the material.

Conclusions

To summarize the findings under this investigation, it can be concluded that:

1 Charpy V-notch specimens provide a more sensitive indication of differences in carbon-molybdenum pipe material than can be obtained through the use of either the Charpy keyhole- or U-notch specimens.

2 Tests made using the sharp V-notch give a more significant indication of notch toughness than either of the other two types of Charpy notch, inasmuch as the ability of a material to resist propagation of a crack under conditions of sudden loading is accurately revealed by the sharp notch.

3 In cases where the blunt type of notch is sufficiently sensitive for the intended purpose, Charpy keyhole- and U-notch specimens may be used interchangeably for testing carbon-molybdenum pipe material inasmuch as both types of specimen give substantially the same magnitude of average values for any group of specimens and about the same degree of uniformity among individual specimens in any group.

4 An adequate number of carefully selected specimens must be used to insure that the results are representative of the whole sample under consideration. This conclusion is based upon the degree of variation among individual specimens which was encountered with all three types of Charpy specimens. In general, more sharp-notched specimens should be used than blunt-notched specimens.

5 Tests at room temperature show significant differences among heats and conditions of steel, depending in degree upon the type of notch used, whereas tests at 925 F do not reveal such significant differences.

6 Results of notch-toughness tests and metallographic examination of material in the "shop-normalized at 1725 F" condition differed from those obtained on material in the "laboratory-normalized at 1725 F" condition.

Hence the ability of an investigator to determine and evaluate correctly the notch-toughness characteristics of various heats and conditions of carbon-molybdenum pipe material depends upon (*a*) selection of samples from each lot of steel in order to take into account the "inherent" resistance to notched-bar impact that is peculiar to each heat; (*b*) use of a type of notch that will reveal significant differences which may exist among heats and conditions of the steel; (*c*) careful preparation of an adequate number of test specimens to represent the whole sample under consideration; (*d*) proper selection of test conditions, and care in the conduct of the test, to include refinements in technique that will eliminate the testing variables commonly referred to in the literature.

In addition to the physical-strength tests commonly conducted on carbon-molybdenum pipe material at either room temperature or elevated temperatures, the notched-bar test should appeal to producers and consumers, not only because of the significance of the results obtained, but also from the standpoint of economy, simplicity, and expediency.

It can be ably argued by metallurgists that there are very definite influences present in every heat of steel which are directly related to the notch toughness of the material. Therefore it may not be entirely in the realm of speculation to assume that, when the significance of notch-bar testing of carbon-molybdenum pipe material is fully understood, it may be possible to select material of the best quality for high-temperature service on the basis of notched-bar tests.

Bibliography

1 "Practical Application of the Notched-Bar Impact Test," by G. C. Reigel and F. F. Vaughn, Proc. A.S.T.M., vol. 38, part II, 1938, pp. 60–70.

2 "The Theory of Impact Testing: Influence of Temperature, Velocity of Deformation, and Form and Size of Specimen on Work of Deformation," by D. J. McAdam, Jr., and R. W. Clyne, Proc. A.S T.M., vol. 38, part II, 1938, pp. 112–134.

3 "Notched Bar Testing and Impact Testing," by S. L. Hoyt, Proc. A.S.T.M., vol. 38, part II, 1938, pp. 141–156.

4 "Notched Bar Testing," by S. L. Hoyt, *Metals and Alloys*, vol. 7, 1936, pp. 5–7, 39–43, 102–106, 140–142.

5 A.S.M.E. Boiler Construction Code, Section VIII, Unfired Pressure Vessels, 1940.

6 "Tentative Methods of Impact Testing of Metallic Materials," A.S.T.M. Designation: E23-41T, A.S.T.M. Standards, 1941 Supplement, part I, Metals, pp. 572–585.

7 "Notched Bar Testing of Steel," American Society for Metals Handbook, Cleveland, 1940.

8 "The Effect of Hardness and of Temperature on the Strength, Ductility, and Toughness of a Heat-Treated Carbon Steel," by S. W. Lyon, Trans. A.S.M., vol. 28, 1940, pp. 128–142.

9 "Impact Resistance and Tensile Properties of Metals at Subatmospheric Temperatures," by H. W. Gillett, A.S.T.M. Project No. 13, Philadelphia, August, 1941.

10 Private Communication.

11 "Impact Properties of Some Low-Alloy Nickel Steels at Temperatures Down to —200 F," by T. N. Armstrong and A. P. Gagnebin, Trans. A.S.M., vol. 28, 1940, pp. 1–24.

12 "Effect of Grain Size and Structure on Carbon-Molybdenum Steel Pipe," by A. E. White and Sabin Crocker, Trans. A.S.M.E., vol. 63, 1941, pp. 749–764.

Discussion

G. F. Comstock.[11] Although we have not used the methods of testing on the type of steel to which this paper is restricted, our general experience with other kinds of steel has led us to agree with the authors in preferring the V notch to the keyhole notch for Charpy tests. Our reasons, however, are different from those of the authors, as we have found that results with the V notch seem to be more consistent so that fewer specimens are required for a reliable conclusion, and accuracy of machining is much more easily secured than with the keyhole notch.

Some strictly comparable results with the two types of notches, obtained in our laboratory from Charpy tests, at 30 deg below zero F, on standard specimens cut from practically the same locations in $^1/_2$-in. plates of commercially rolled low-alloy manganese-copper-phosphorus steel, might be cited to illustrate our experience. Two to four specimens were tested from each location, the results in foot-pounds being as reported in Table 3 of this discussion.

TABLE 3 CHARPY RESULTS ON TEST SPECIMENS

Sample designation	Location in plate	Charpy results, ft-lb at —30 F: V notch	Average	Keyhole notch	Average
4	Center	2.9	3.3	5.1	7.7
		3.6		3.6	
				14.5	
		7.2		26.0	
		7.2		30.4	
4	Near edge	5.1	6.9	26.8	27.8
		8.0		28.2	
		5.1		25.3	
		7.2		25.3	
5	Near edge	3.6	4.7	25.3	20.0
		2.9		4.3	
		2.9		3.6	
7	Center	3.6	3.1	2.9	3.4
		2.9		3.6	
		5.8			
		5.8		34.0	
7	Near edge	5.8	5.4	32.5	24.6
		4.3		7.2	
		2.9		13.7	
8	Near edge	2.2	2.7	18.8	11.6
		2.9		2.2	

The variation in results, leading to doubt as to the value of the averages, or as to the inconvenient necessity for considering all the individual results separately, seems much greater with the keyhole notches. Generally, except for tests at subnormal temperatures, we prefer to use the Izod method, since it is easier to secure concordant check results in that way, and more tests can be made with less machining expense from a limited amount of sample stock.

[11] Metallurgist, The Titanium Alloy Manufacturing Company, Niagara Falls, N. Y.

H. W. Hiemke.[12] This paper appears to be a contribution to the effort currently being made by power-plant engineers to gain a better understanding of toughness and tendencies for embrittlement of carbon-molybdenum steel at power-plant operating temperatures. From an examination of the data, it may be concluded that the materials examined by the authors demonstrated a relatively high degree of notch toughness at room temperature and at 925 F, in both the as-rolled and normalized conditions and for all conditions of test.

The authors quite properly conclude that the V-notch specimen is more sensitive than the U- or keyhole-type of notch. It is the opinion of the writer, however, that this extra sensitivity is obtained by sacrificing reproducibility of results. Also, in order to obtain reliable data with the V-notch type, it is necessary to make a larger number of tests than is the case with the keyhole- or U-type specimen. In this connection, it is desirable to quote the recommendations of the Advisory Committee of the War Metallurgy Committee regarding the advantages of using a Charpy keyhole-type specimen. The reasons for this recommendation were stated as follows:

1 Ease of reproducibility of an accurate radius of curvature of the notch.

2 Extraneous notches caused by drilling the hole are in the most desirable position with a drilled hole.

3 The area back of the notch in the standard Charpy bar is less than the simple beam Izod and a minimum amount of drag and bending occurs in tough specimens thus precluding fictitiously high values.

4 Permits correlation of the data with other results on low temperature impact as most engineering specifications require Charpy keyhole-notched specimens.

It is the opinion of the writer that the reasons advanced by the War Metallurgy Committee in favor of the keyhole-notch type far outweigh the added sensitivity found by the present authors in the use of the V-notch type.

J. L. Holmquist.[13] The authors suggest that the notched-bar impact test may be useful as a correlating device to help establish cause-and-effect relationship between obscure variables not evaluated or even detected by the common tests for chemical composition, tensile properties, and microstructure, and the performance of carbon-molybdenum pipe in high-temperature service.

It is believed to be a generally accepted fact that the notched-bar impact test is sensitive to obscure variables, which may be, for example, very small amounts of nitrogen, oxygen, or hydrogen, the presence or influence of which may not be detected by chemical analysis, tensile tests, or examination of microstructure.

It is to be noted that the notched-bar impact test does not identify such obscure variables, but merely identifies materials which may differ with respect to them although alike in all other respects. The notched-bar impact test can be used as a screening device to single out for the investigator suitable samples on which to pursue his investigations.

The "notch-sensitivity" of a metal depends upon a complex interworking of shear strength, cohesive strength, and the response of each to strain hardening. It is the writer's impression that a full understanding of these phenomena does not exist at present. But the concepts of shear and cohesive strength are more fundamental than notch sensitivity, as measured by the

[12] Senior Materials Engineer, Bureau of Ships, Navy Department, Washington, D. C.

[13] Director of Research, Spang-Chalfant, Division of the National Supply Company, Ambridge, Pa.

notched-bar impact test. A study of the manner in which shear and cohesive strength is influenced by minor constituents or heat-treatment, employing techniques already developed, might be more illuminating than a study of their effect on the notched-bar impact test.

It does not follow that the notched-bar impact tests or shear-cohesive strength studies are the only or necessarily the best means for distinguishing between materials with respect to the presence or absence of obscure variables. Such properties as electrical resistivity, the several magnetic properties, thermoelectric emf, the thermal and stress coefficients of these properties, single electrode potentials, rate of attack by chemical reagents, etc., might provide as good or better screening devices.

It would have added considerable interest to the paper if the authors had given from their experience some examples of differences in high-temperature performance of carbon-molybdenum steels which were considered acceptable for such service by current manufacturing and testing procedures. Only one example has come to the writer's attention. In this case, graphitization occurred adjacent to a weld in a carbon-molybdenum tube. On the other side of the weld, a carbon-molybdenum steel forging was not graphitized, although exposed to the same service conditions for the same length of time.

T. McLean Jasper.[14] The writer wishes to suggest that consideration of the broad subject of testing and correlation with service must be made in connection with notch-impact testing. This has been attempted several times without any marked success. A symposium on "Notched-Bar Impact Test" was presented at the Zurich meeting of the International Association for the Testing of Materials in 1931. The report on such tests covering about 80 pages of carefully considered results on various types of test specimens and on a considerable range of steels together with discussion and summaries should not be overlooked. For the record it is desired to quote from the summary report of Dr. W. Rossenhain, president of Group A, which is attached to the symposium.

"From the reports submitted and the discussion which took place, certain definite conclusions could be gathered:

"1 With one or two dissentients, it was the opinion of those present that the notched-bar impact test is of great practical value as a reception test provided that it is carried out on a test piece of satisfactory type and that the results are interpreted within the limitations which the nature of the test imposes.

"2 It was generally agreed that the results of notched-bar impact tests cannot be used for the quantitative comparison of different types of materials but that they can be used as a test of the quality (satisfactory heat-treatment) of different batches or specimens of similar types of steel. In this sense, the test is to be regarded as little more than qualitative so that only the larger differences between results are important."

While the writer has copied only two of the seven paragraphs in the summary, it is believed that they are sufficient to inject an atmosphere of caution in the use of notched-bar impact values. The experience of the writer in endeavoring to correlate notched-bar impact results with service has been baffling. The test values presented in this paper have not remedied this defect. It is believed that the notched-bar test has been in existence for over 40 years. We are at this time without any "put-your-finger-on-the-spot" correlative values that we may apply in service with a satisfied feeling. It might seem that it would help machinery designers to avoid steels that were most sensitive to sharp corners in designs. Curiously enough notched fatigue specimens do not correlate with the single-blow notched-bar impact.

[14] Engineer, A. O. Smith Corporation, Milwaukee, Wis. Mem. A.S.M.E.

In considering carbon-molybdenum steel and the values presented, the writer would state that the test values are all good. The V notch has a higher average but a greater spread in test-value percentage. This may well be expected since the section area under the V is considerably larger than that under the U or keyhole and also because the V is much harder to machine with the same degree or percentage of precision than the other two.

In saying that the values are all good, it is meant that the values are all above 20 ft-lb and, since no strength and ductility values are available, there is no other comparison to draw. Some of our very expensive high-strength alloy steels cannot meet the values shown nor even a minimum of 20 ft-lb with the Charpy keyhole notch, yet they are successfully used in the services where shock is very severe and where high service stresses are essential for the successful operation of the part.

G. C. Riegel.[15] The authors have taken a rather bold premise concerning the correlation of notch sensitivity of steel and its performance in high-temperature pipe service. After having diligently read the paper, the writer was disappointed in not finding any service data to correlate with the metallurgical investigations of the material. It is presumed that these data will have to await some months or years of application in service.

There remains no question that the more severe the state of stress set up by a notch, the more readily steel can be made to exhibit a brittle behavior. In other words, either the severity of the notch or some other factor such as a change in the geometry of the specimen which increases the state of stress, the influence of temperature, especially a reduction from normal, will bring about a transition of the steel from a tough fracture to a brittle fracture, or failure.

It remains for the technician and the engineer to determine how far from some norm a material may depart, either in its characteristic inheritance, its pretreatment, or application in service (design considered) before one may say this heat of steel is satisfactory or that heat of steel is unsatisfactory.

The pursuit of this plan as proposed by the authors will do much to increase our knowledge and judgment in the manufacture and use of steel.

Authors' Closure

The authors appreciate Mr. Comstock's comments and the supplementary data on a different type of steel, which tend to emphasize the distinction the authors have drawn for C-Mo pipe material between the V notch, as contrasted with the the keyhole or U notch.

Mr. Hiemke has contributed to a broader evaluation of the present problem by bringing to the reader's attention the recommendations of the Advisory Committee of the War Metallurgy Committee. The four points raised are widely recognized and are usually followed in connection with notched-bar testing of most types of steel. With regard to the question of reproducibility of test results, the authors feel that, if a material is reasonably homogeneous or uniform with respect to the factors which influence notch toughness, there is ample evidence that the keyhole and U notch are likely to be more satisfactory than the V notch from the standpoint of reproducibility of test results. However, it seems that the less sensitive blunt notches might be likely to impose a certain "reproducibility of results" on materials which might not be inherently uniform or homogeneous. The findings in the present investigation tend to show this likelihood, inasmuch as it is inconceivable that the great differences in notch-toughness values with the V notches are fictitious or nonexistent if judged by the uniformity of the keyhole-notch results.

[15] Chief Metallurgist, Caterpillar Tractor Company, Peoria, Ill.

When dealing with a coarse-grained C-Mo steel such as is used for high-temperature pipe, and a wide divergence of values for individual specimens in a given group is obtained, investigators cannot afford to overlook the possibility that such variations might be attributable to the absence of uniformity of the factors which influence notch toughness rather than always to deduce that such differences can be accounted for only by "inaccuracies" in the V notch and "lack of reproducibility of results" when using the V notch. Further, the opinion is widely held that scratches or other stress raisers in notches are more likely to affect the magnitude of results when the values are low rather than high; in the present tests, relatively high values were obtained in all cases, so the effect of possible inaccuracies or stress raisers in the V notches should not reasonably be considered as accounting for the variations obtained among individual V-notch specimens.

It should not be inferred that the authors are attempting to depreciate the merits of the keyhole notch for most types of steel, but when it is recalled that the more recent heats of C-Mo pipe material are among the very few coarse-grained types of steel in service, a different aspect of notched-bar testing is introduced that seems to provide an exception to the usual concepts of this test. In this case, test results show that blunt notches do not accurately reveal true relationships among heats and conditions of this steel. The authors have therefore attempted to show by means of these data that the V notch should be used for this particular material if correct evaluation of various heats and conditions of this steel is desired.

This viewpoint is confirmed to some extent by Mr. Holmquist's remarks regarding the ability of notched-bar tests as a "screening device" to identify materials which differ from one another with respect to obscure variables, even though it is acknowledged that the test does not identify those obscure variables. Mr. Holmquist suggests that a study of cohesive strength and shear strength may reveal more explicit information regarding the effect of minor variables in composition or heat-treatment. But since these properties influence notch sensitivity, the notched-bar test might be regarded as a simpler, more practical way of revealing a composite picture of certain differences among batches of material.

Although not usually specified, the notched-bar test has been used by some consumers of C-Mo pipe material as a source of added information and, when low notch-toughness values have been encountered in any particular piece of pipe more comprehensive investigations have been initiated to insure that the pipe will be acceptable. In this way, notched-bar tests have served as a so-called "red flag" in installations of C-Mo pipe, and values for minimum notch toughness have been set, mentally at least, relatively high (about 15 or 20 ft-lb), as compared to those encountered in many low-temperature tests (about 3 to 6 ft-lb).

In commenting on Mr. Jasper's discussion, the test findings are in keeping with point 2 of the Zurich Meeting of the International Association for Testing Materials, on the subject of notched-bar tests, namely, "that they can be used as a test of the quality (satisfactory heat-treatment) of different batches or specimens of similar types of steel. In this sense, the test is to be regarded as little more than qualitative so that only the larger differences between results are important."

The present tests, using the V notch, have revealed large differences among heats and different heat-treated conditions of a single type of steel. Mr. Jasper's word of caution is particularly applicable when making comparisons among various types of steel. Inasmuch as the present tests were limited to a single type of steel and only the test temperature, the heat number, and the condition of this steel were varied, it seems that direct comparison of notched-bar results should be admissible in this case.

The authors wish to reiterate that no attempt was made in this study to correlate, at this time, test results and performance in service. Such a correlation might be possible only after many more years of service data become available. This also applies to Mr. Riegel's comment, for it should be remembered that coarse-grained carbon-molybdenum pipe is a relatively new material, compared with many other types of steel for which test results and service data are abundant.

Firing High-Pressure Furnaces

By E. G. PETERSON,[1] NEW YORK, N. Y.

Developments in the oil-refining industry, particularly in the catalytic-cracking process, have created a need for furnaces capable of carrying high pressures and sustaining high loadings. Direct-fired air heaters are in service which operate at pressures of 45 to 55 psi or higher, with furnace loadings of 500,000 to 2,500,000 Btu per hr per cu ft of volume. The design requirements of such heaters, their details of construction, and operating characteristics are discussed in this paper. The subject is of great importance since the possibility of wide application for this combustion system already exists. One of the most important fields under consideration is that of ship propulsion with power generated by gas turbines and direct-fired air heaters. "Package power" units made up of similar equipment may be used for power generation in small plants.

IT has been fairly common practice for some years to fire boiler or process furnaces under moderate pressures, as, for instance, naval boilers, in which furnace pressures approximate 0.5 psig at high steaming rates. In this same application, heat release in the furnace will reach 250,000 to 300,000 Btu per hr per cu ft of volume. Limited space dictates these operating conditions. In certain industrial processes, furnace pressures have reached 5 psig but, as a rule, the firing is intermittent, occupying a relatively short period in the cycle.

Furnace pressures of 15 to 35 psig and heat liberation in the order of 900,000 Btu per hr per cu ft of furnace volume have been employed in connection with the Velox boiler, as well as in European installations of direct-fired air heaters and gas turbines for power generation. Such installations, however, have been very limited in their number and scope of application.

More recently, in this country, high furnace pressures and furnace loadings have become important in connection with catalytic refining processes in the oil industry. Many direct-fired air heaters are now in service with pressures of 45 to 55 psig or higher, and furnace loadings of 500,000 to 2,500,000 Btu per hr per cu ft of volume. Process requirement and operation of heat-recovery units (gas turbines) fix the system pressure, while economy in pressure-vessel design, rather than space limitation, is responsible for small furnace volume and consequent high rate of heat release per unit volume. In some cases the introduction of high-temperature combustion air (900 to 1000 F) during certain phases of the operation presents a problem in materials and operability. A large volume of relatively cool air, compactness of units consistent with reliability of service at high rates of combustion, and accessibility of parts requiring cleaning or repair demand the careful consideration of the designer of the burner and heater unit.

In the combustion system, Fig. 1, a large amount of compressed air is furnished by a high-efficiency axial compressor. During the process of catalytic cracking, heat is given off and the heated air returned to the inlet of the gas turbine in sufficient quantity to produce all the power required to drive the compressor. On starting up, however, none of this heat is available. Furthermore, the catalyst chambers, ducts, etc., must be brought to operating temperature. Two direct-fired air heaters are provided, one to supply heat to the process chambers, and the other to make up the balance of the energy to be transformed into mechanical power in the gas turbine for operating the compressor.

On starting up, the compressor is run at approximately one-quarter speed by means of a small motor or steam turbine. The air flows to heater No. 1, where its temperature is raised to 900 to 1000 F; the mixture of hot air and combustion gases passes through the catalytic chambers and is reheated in heater No. 2 before entering the gas turbine. The firing rate in heater No. 2 on starting is approximately 50 per cent greater than in No. 1 but, when equilibrium is reached, this burner may be shut off entirely. In some installations, however, heater No. 2 is kept in service continuously to provide additional power output from the gas turbine.

Direct-Fired Air-Heater Designs

The direct-fired air-heater unit, shown in Fig. 1, is one of the earlier designs having a capacity to heat 23,000 cfm of air from approximately 350 F to 900 F. The gas turbine is rated at 3650 hp, 2950 hp being used to compress the air; the additional 700-hp capacity is surplus power which may be used for the operation of the generator.

More recent installations utilize compressors of 40,000 cfm and 60,000 cfm capacity and 55 psi discharge pressure, with gas turbines of 7100 and 9500 hp, respectively, having correspondingly larger air heaters and burners.

Refractory-lined furnaces are largely used. All-metal furnaces have been employed with quite satisfactory results although original cost and maintenance are somewhat higher than the refractory type.

A direct-fired, air-heater burner-and-furnace unit of more recent design, operating at pressures of 3 to 25 psig and firing rates of 10,000,000 to 100,000,000 Btu per hr, is illustrated in Fig. 2. This unit was designed to heat 64,000 cfm of air from 50 to 1250 F outlet temperature, corresponding to a firing rate of 96,000,000 Btu per hr.

While there have been many improvements in the mechanical features of the burner and the heater since the first unit was designed, it is to be noted that the principles worked out for the original unit are employed in the most recent installations. The air stream is divided, and dampers are arranged to control the amount of combustion air to the burner, in order to maintain furnace temperatures sufficiently high to insure complete combustion of the fuel. The additional air to be heated, or "quench" air, passes through the annular space between the furnace and the outer shell and mixes with the hot gases after combustion of the fuel is completed. The burner is exactly the same in so far as mixture of fuels and air is concerned, but it is greatly improved mechanically over the original arrangement.

It is true that experimental units have been set up to operate at furnace loadings up to 10,000,000 Btu per cu ft per hr under conditions of furnace pressures and exit temperatures in excess of those encountered in the commercial applications mentioned, but the tendency in connection with these commercial units has been toward conservative loadings of 250,000 to 750,000 Btu per cu ft per hr, depending upon conditions of operation.

[1] Manager, Air Heater Department, Peabody Engineering Corporation.

Contributed by the Fuels Division and presented at the Annual Meeting, New York, N. Y., Nov. 29–Dec. 3, 1943, of The American Society of Mechanical Engineers.

Note: Statements and opinions advanced in papers are to be understood as individual expressions of their authors and not those of the Society.

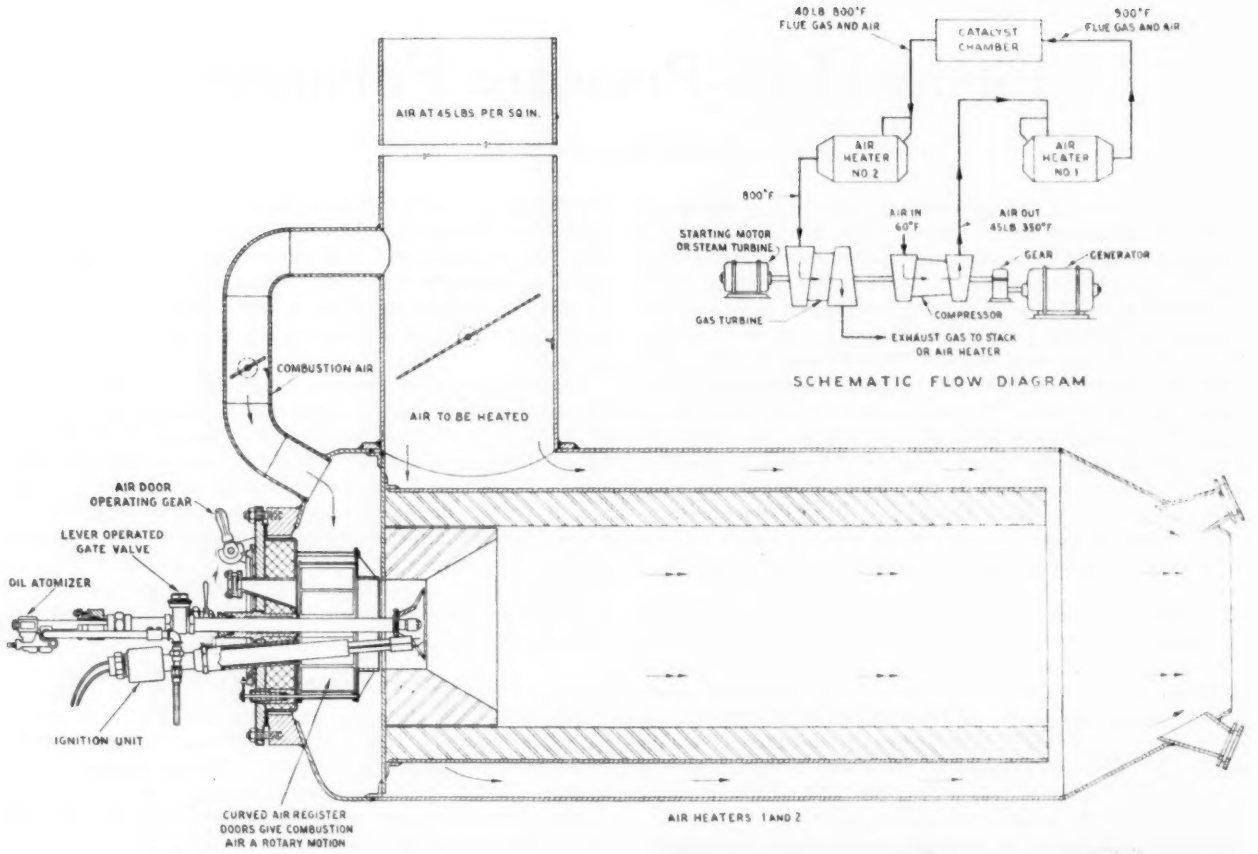


FIG. 1 BURNER ARRANGEMENT

However, in one case, space limitations required a furnace loading of 2,500,000 Btu per cu ft per hr, with 45 psi furnace pressure and 950 F exit temperature. This unit has functioned satisfactorily for several years.

The original burner used in this service is shown in Fig. 3. Only the atomizer was removable with the unit under pressure. The electric igniter was fixed in position, with the result that it was necessary to remove the entire burner in order to replace a cracked porcelain or burned electrode tip. The peephole was rectangular in shape, flared to give a wide vision; however, in bolting the glass between the two rectangular plates, severe mechanical strain could be set up causing rapid failure of the glass when the additional temperature strains were imposed during operation of the unit. The mechanism for the operation of the register louvers consisted of a rotatable ring, mounted on the outside of the register front, carrying pins which engaged in the slots of the cams attached to the driving rods of the louver doors. This necessitated extending individual driving rods through the burner-front plate and fitting them with stuffing boxes to prevent leakage of air from the plenum chamber. Aside from details such as those just enumerated, the general construction features and operating principles of this burner have been retained in later designs.

Fig. 4 illustrates the design of burner now used, subject to modification to fit operating conditions of individual installations. The air doors or louvers, which give the combustion air a rotary motion, are linked together and are operated simultaneously by the master air door whose hinged rod extends through a stuffing box in the register-front plate and is fitted with operating handle and quadrant. The air-register-front plate is designed to meet pressure conditions in accordance with

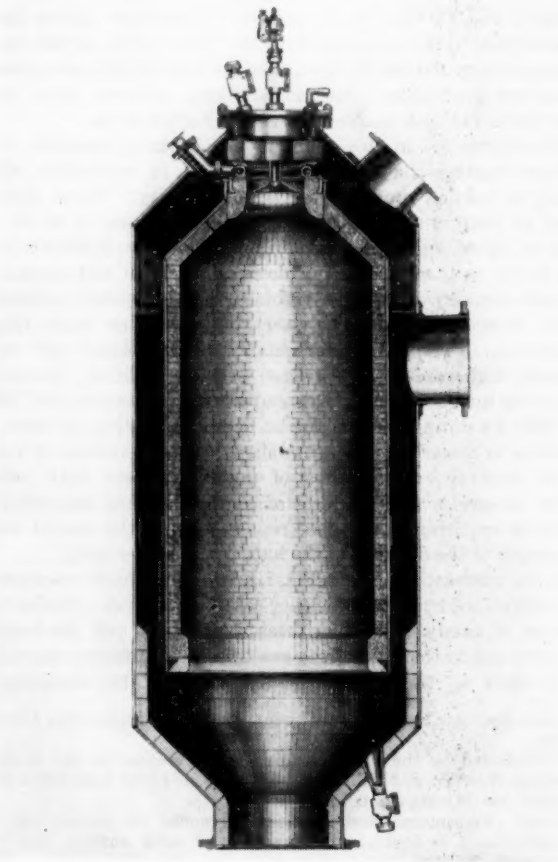


FIG. 2 COMBINED GAS-AND-OIL-FIRED AIR-HEATER UNIT

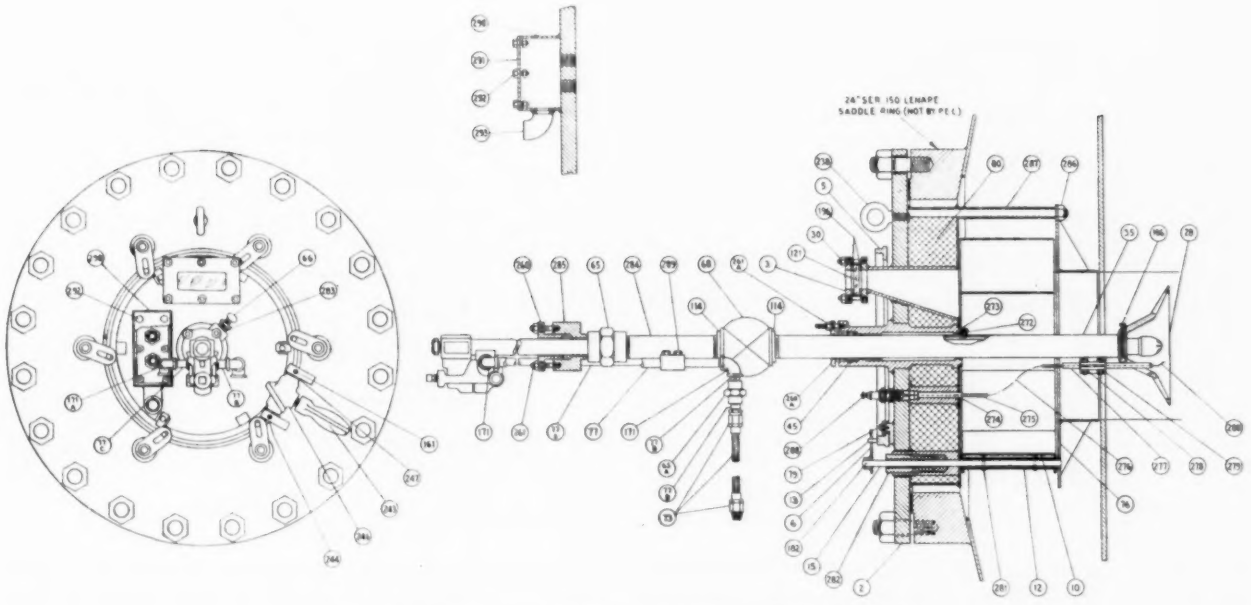


FIG. 3 ORIGINAL DESIGN OIL BURNER FOR HIGH-PRESSURE FIRING

the A.P.I.-A.S.M.E. Code for Unfired Pressure Vessels and is heavily insulated for protection against radiant heat or high-temperature combustion air. The louver doors are of heavy, flanged construction, designed to retain the proper shape under most severe air-temperature conditions. All parts of the burner in contact with highly preheated air are of stainless-steel material, and expansion provision is based upon the type of material and temperature of the combustion air.

The opening through the center of the front plate carries the oil-burner assembly consisting of the diffuser, diffuser pipe, quick-closing valve, union, atomizer stuffing box, atomizer yoke coupling with fittings, and the oil atomizer itself. The position of this assembly with reference to the burner throat may be adjusted with the unit under full pressure. Furthermore, the atomizer may be withdrawn from the assembly under the same condition. The type of atomizer may be either steam-atomizing, as shown, or wide-range mechanical-atomizing; both forms are operating successfully in this service.

Additional openings through the register front plate are provided for the peephole, electric or gas-electric igniter, flame-protection electrode, or other sensitive element, used in connection with the flame-failure shutoff controls. All of these openings are valved so they may be closed against furnace pressure; and, where the adjustment of position or withdrawal of the element is a requirement, stuffing boxes are fitted to prevent leakage of hot gases and possible injury to the operator. The valve in the peephole sleeve protects the glass from radiant heat; the glass is also covered by a wire gauze which assists in distributing heat strain and affords protection against flying glass if breakage from any cause should occur. In some installations, two igniters and flame protectors are used and openings in the register front plate must be provided for the additional unit.

In view of the fact the quick-closing valves are necessarily of steel, in order to conform to general refinery practice, the location of as many as six $2^1/_2$-in. valves on the burner front presents rather a problem when dealing with available commercial valves. In fact, there would not be room for one half that number, so it was found necessary for the company to design and manufacture valves for this special application. The same situation applied to the igniter, and to the small winch which is used for hauling it into position against furnace pressure.

DEVELOPMENT OF SUITABLE BURNERS

The gas burner consists of a tubular ring, correctly positioned to inject the gas fuel into the combustion-air stream, and protected from radiation. The port area is designed to meet operating conditions of capacity, fuel pressure, furnace pressure, fuel-heating value and density, etc. This type of gas burner is stable in operation over a wide range of capacities, pressures, and fuel characteristics.

The development of the burner for this type of service has followed a well-defined pattern. Certain essential standards were set up: (1) The burner must be efficient and capable of producing a flame to fit limited furnace dimensions; (2) it must be operable under all conditions of service; (3) it must provide for the safety of the operator and require a minimum of his time and attention.

High-combustion efficiency is a requirement which has to do not so much with economy in fuel consumption as with the ability to effect complete combustion of the fuel to avoid fouling of turbine blades or passing undesirable combustibles to the process chambers, and to confine the combustion to a relatively small volume without detriment to the furnace lining. This high efficiency is obtained through controlled turbulence resulting from correct shape and disposition of the fuel-distributing elements and baffle surfaces, and the ability to make adjustments from outside the burner with the furnace under pressure.

Under operability, we consider not only mechanical features as selection of materials of construction, allowance for expansion, one-hand control of louvers, etc., but also the fact that the burner must light off with the furnace under pressure and maintain ignition under varied conditions of load. The igniter can be adjusted for correct positioning with respect to the fuel element; adjustable baffle surfaces protect the flame from direct impingement of the air stream until combustion is well established.

Safety and ease in operation have been given careful consideration. The heavy steel register-front plate is adequately insulated against high-temperature combustion air and radiant

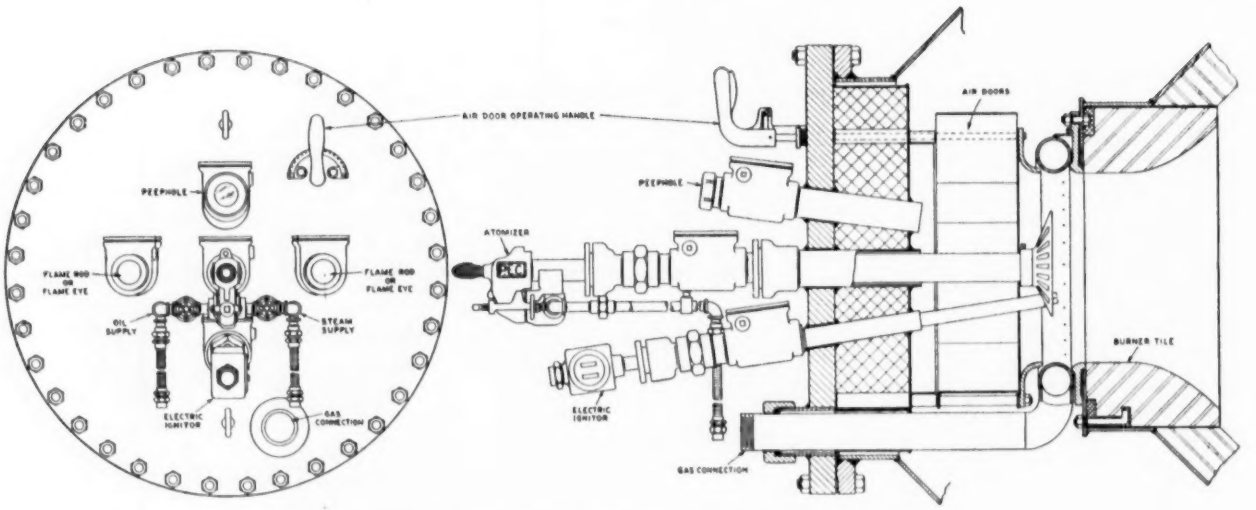


FIG. 4 COMBINED GAS AND OIL BURNER FOR HIGH-PRESSURE FURNACE FIRING

heat; the heat-resisting peephole glass is covered with wire gauze and protected against radiant heat by a quick-closing valve; adjustable or removable elements are positively locked; and flame-protection devices are built into the burner to insure closing of fuel valves in case of flame failure from any cause and to prevent reignition, except as controlled by the operator.

CONTROL AND PROTECTIVE DEVICES

The flame-protective system, Fig. 5, consists essentially of a relay which receives its impulse from a flame-contact rod or electrode when burning gas, or a photoelectric cell when burning oil, and in turn transmits this impulse to solenoid valves directly in the fuel lines or mounted on air-controlled, diaphragm-operated valves in the fuel line. The layout shown covers a dual system, consisting of two relays, two flame rods, two transformers, etc., which operate in parallel. The object of the dual system is to minimize the possibility of delays in starting or shutdowns due to short-circuit or ground in the various elements making up the control system.

In operation on oil fuel, the flame eye will be inserted in one of the flame-rod openings which are so arranged that this element can "see" the oil flame. The oil burner can be operated and adjusted by hand on starting up, by closing the key switch which by-passes the relays and opens the solenoid valves in the oil- and steam-supply lines. During the time the key switch is closed, an alarm sounds to warn the operator that the safety-control device is not in operation. Ignition of the oil flame is obtained on closing the push-button switch and, after the flame is adjusted for stable operation, the key is withdrawn from the key switch and the control takes over. During the time the burner is on oil, the gas-flame electrodes are withdrawn, at least out of the range of the oil flame, for their protection.

When starting up on gas fuel, the two flame electrodes are placed in position and the gas-supply valve in the main line is opened. Closing the push-button switch completes an electrical circuit through the transformers and opens a solenoid valve in the by-pass line to the gas-pilot burner. Ignition of the pilot burner takes place at a low rate which is increased when the pilot flame contacts the electrode. At the same time, the pilot flame is increased in size through the opening of the second valve in the pilot line, and the impulse from the relays is transmitted to the three-way magnetic valves controlling the diaphragm air supply to the main gas valve which opens and permits flow of gas to the main gas ring. When ignition is completed and the push button is released, the by-pass solenoid valve shuts, and both the center pilot burner and the main burner are under control of the relays.

Generally, the control systems are considerably simpler than that shown as they are designed for operation on only one fuel, either gas or oil. On certain gas-fired installations, where oil may be used simply as an emergency fuel, it is not considered essential to have the safety shutoff controls on both fuels. The complication in the system arises from the fact that no one as yet has devised a photoelectric device which will operate on gas fire without a dangerous time lag. It is therefore necessary to use the conductivity of the gas flame rather than radiation to a photoelectric cell which, if it were feasible, would necessitate only a change in filters to operate on either oil or gas flames.

Modifications to this control system are made to suit operating conditions, burner capacities, etc. However, the general features or principles apply to all installations. In any case, the most important consideration is the proper location of the elements which transmit the flame impulse to the relays.

DETAILS OF MODERN HEATER

From the beginning of our connection with this type of work, the essential form and dimensions of the direct-fired air heater have been considered from the viewpoint of the burner designer. To the best of our knowledge, the majority of, if not all, air heaters of this type, whether of our own or other manufacture, have followed the same basic principles developed for the first installation. On first approach to this problem, it was recognized from previous experience with furnace loadings up to 1,000,000 Btu per hr per cu ft of volume, that the high combustion rates involved required a high-efficiency turbulent-type burner, and that such a burner would give its best performance with a limited quantity of excess air through the burner proper. The first step, then, was to divide the air stream so that the quantity of combustion air could be properly controlled and the burner function within its efficient range. The remaining air was diverted to the annular space between the furnace and the outer shell, or allowed to enter the furnace for cooling purposes, outside of the combustion zone. Structurally, the heater shell is designed in accordance with the A.P.I.-A.S.M.E. Code for Unfired Pressure Vessels of materials and workmanship as specified by the Code, with the proper disposition of refractories and insulation to prevent metal parts attaining temperatures beyond those for which they are designed. Air passages must be so

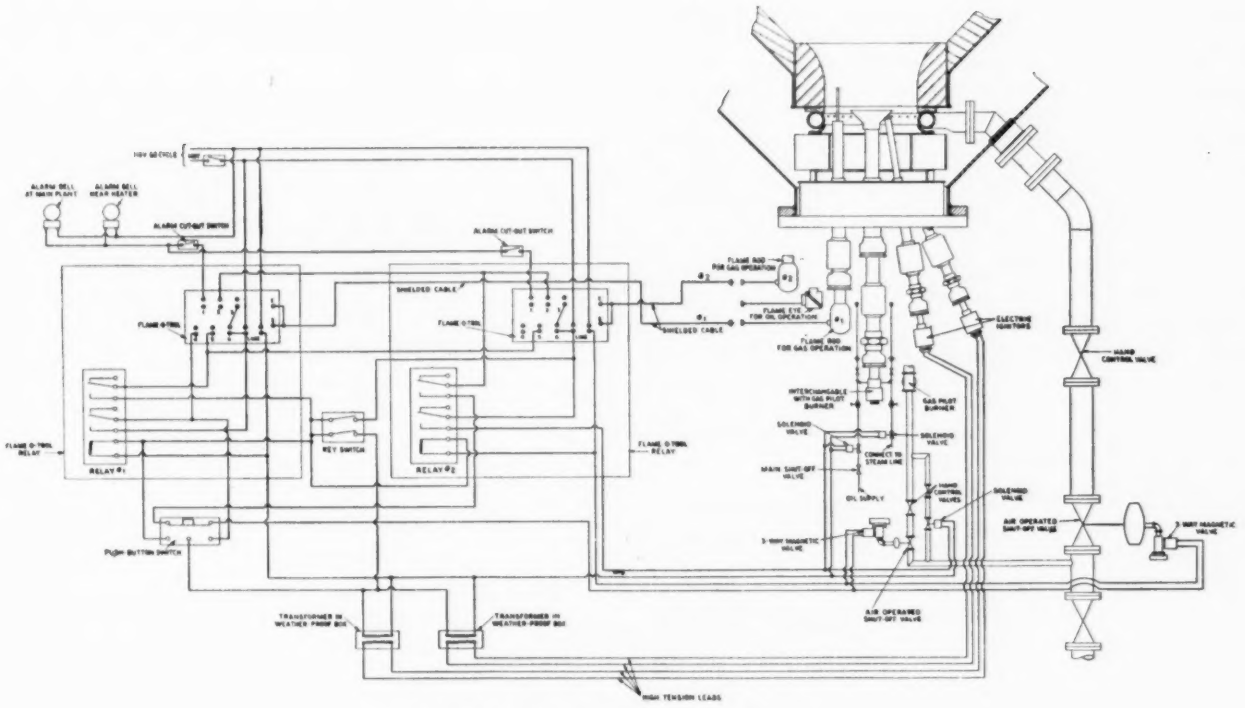


FIG. 5 DUAL-FLAME PROTECTIVE SYSTEM

designed as to keep down pressure loss, and dampers must be easily operated and their controls accessible to the operator, in order to insure that adjustments will be made when required for satisfactory operation.

The flow of heat through the furnace lining and through the outer-shell insulation must be considered in designing the air passages, selecting materials, and applying stiffening to the various members. When units are insulated externally, the thickness of such insulation must be proportioned to the type and thickness of the furnace lining, also to the velocity and quantity of air passing through the annular space between the furnace and outer shell, in order that metal temperatures in the furnace casing and shell are kept within reasonable limits. Convection transfer rates to the cooling air in the annular passage are relatively low, since velocities ordinarily do not exceed 20 fps. However, the area in contact with the air is quite large, as radiation of heat across the passage from the furnace casing to the shell makes the inner surface of the shell effective in the transfer of heat to the cooling air.

Toward the end of the annular passage some insulation should be provided on the inside surface of the shell as the cooling effect of the "quench" air diminishes. The air passage is thus restricted, velocity increased, and a somewhat higher heat-transfer rate obtained for a short distance.

In some cases, insulating firebrick, coated with a special cement to resist sloughing effect of high-velocity air, is used for protection of the shell; it is relatively inexpensive and easy to install. On other units, high-efficiency block-type or castable insulation is employed, requiring a cover of alloy steel for protection against erosion by the air and furnace gases. Where alloy steel is used in this manner, allowance must be made for its higher coefficient of expansion, also for its high temperature compared with the protected shell. Unless provision for this difference in expansion between shell and insulation cover plate is made, buckling of the light cover plate will take place.

When alloy steels are used in the construction of pressure parts of the vessel and are joined to carbon steel, the difference in expansion rate will set up severe strain unless the joint is properly located.

MANY APPLICATIONS POSSIBLE

While we have quite properly confined our discussion to applications in the catalytic refining field, in which we have had experience with upward of 100 installations, there are other applications outside of this field which are gaining in importance and which will demand more thought and consideration on the part of the engineering profession when the present demand on our energies for production of indispensable necessities, such as 100-octane gasoline, begins to abate somewhat. Of these other applications that of ship propulsion by power generated by gas turbines and direct-fired air heaters probably holds the greatest appeal, although we should not lose sight of the fact that there are many problems in other lines which are opening up to consideration. The possibility of applications of direct-fired air heaters to driers, incinerators, etc., and of the development of "package units" for power generation in small plants, requiring a minimum of technical skill for installation, operation, and maintenance, appears to be extensive.

The author realizes that only the high spots of this comparatively new subject have been covered and that he has dealt more in generalities than in specific data. However, the object of this paper has been to acquaint the prospective user of this type of equipment with what he should expect from the designer of the unit rather than to give instruction in the art; also to promote discussion on present applications, whether commercial or experimental, and to induce interest in the future broadening of the uses to which the equipment may be put.

Discussion

A. M. G. MOODY.[3] It would be interesting if the author

[3] Chief Research Engineer, DeLaval Steam Turbine Co., Trenton, N. J. Mem. A.S.M.E.

would add to his already valuable paper some information on the degree to which he has been able to get uniform flow across the exit from the combustion chamber. If the products of combustion are to be used in a turbine, it is imperative that the flow be at a fairly uniform temperature, having no local hot or cold spots. If this condition does not prevail, a smoothing-out section would have to be added, the weight and volume of which would be directly chargeable to the combustion chamber.

Author's Closure

It is recognized that in the refinery installations the volume of duct work connecting the air heater to the vessel in which the heated air is to be used may be many times the volume of the heater itself. Therefore temperature distribution at the heater outlet is not considered of primary importance and no provisions have been made in these installations for obtaining data on this condition.

Where the air heater discharges directly into the inlet of a combustion-gas turbine the distribution of temperature at the heater outlet must be such that local departures from the mean do not exceed 25 F, plus or minus. This has been accomplished satisfactorily by application of positioning control to the individual louvers of the burner air register. Control of the flow of combustion air can be obtained within the relatively small space of the burner air register where the velocity is at a maximum. This construction eliminates the necessity of providing adjustable dampers, vanes, etc., in the larger and less accessible quench air passages toward the hot end of the chamber.

"Temp-turb" Temperature-Control System

By J. R. CAMPBELL,[1] ONTARIO, CALIF.

The "Temp-turb" system of temperature control, described in this paper, consists basically of a means for utilizing the kinetic energy in a flowing fluid in a manner to control the temperature of the fluid. A turbine wheel, the blades of which change their position with temperature changes, has all, or a sample of the flowing fluid, passed through it. Direction of rotation, rate of rotation, and torque output are a function of temperature when fluid-flow rate is constant. Power available from the turbine wheel actuates the valves which determine the fluid temperature.

THE amount of work available from any basic temperature-sensitive element is relatively small and must be substantially amplified by some form of external energy before the response to temperature change can be made to register effectively on the control means. In aircraft, the control means might be an exit flap, such as on an intercooler; a butterfly valve, such as in a heating and ventilating duct; a mixing valve, such as in a heating and ventilating system; shutters or flaps for oil coolers; dump valve for thermal deicing system, etc.

The "Temp-turb" system of temperature control uses the kinetic energy of the flowing fluid being controlled to amplify the work done by the basic temperature-sensitive element. The kinetic energy available in fluid-flow systems in aircraft is generally substantial, and enough energy can be harnessed to operate control means without introducing a harmful pressure drop.

Fig. 1 shows a Temp-turb control unit, as used in the Douglas A-20 for controlling the temperature of air leaving a combustion heater. This air is for cabin heating, windshield defrosting, and turret heating. The Temp-turbs are set to maintain a control point of 200 F ± 15 deg and actually control to within ± 5 deg. As shown in Fig. 2, the control unit is furnished as an integral part of the modulating valve. Operation of the assembly is to allow more air to flow over the heater as temperature tends to increase, and to reduce the air flow as temperature tends to decrease. Heaters in this system are ram-operated.

Operation of Control Unit

Fig. 3 indicates the operation of the rotor or turbine wheel for the type of Temp-turb used on the Douglas A-20. Turbine blades are made of high-activity bimetal 0.005 in. thick and are calibrated to be straight at the control point. Any deviation from the control-point temperature results in a curvature of the turbine blade (the direction of curvature depending upon the direction of the temperature deviation). As the device is a radial-flow turbine, the curvature of the blade imparts a torque to the rotor which is transmitted through a gear reduction to the modulating valve.

After the turbine blades are formed and stabilized (to maintain calibration under all conditions to which control might be subjected), it is not feasible to vary the control point of the unit by varying the form of the blades. Therefore, the angle at which the fluid enters the rotor is varied. Referring to Fig. 1, the inlet guide vanes are mounted as cantilevers at the edge of the inlet nozzle, and their free ends engage a shift ring by means of small pins. Moving the shift ring in either direction from neutral varies the direction of fluid flow over the rotor to either side of pure radial flow. The amount of deviation from pure radial flow is determined by the amount the shift ring is moved. When the flow through the rotor is deviated from radial, the rotor assumes a new temperature-control point. This adjustment allows the control point to be varied about ± 40 F from the normal.

The assembly, shown in Fig. 2, operates on a sample of air which varies from about 5 to 10 per cent of rated flow for a full-open valve. Fig. 4 is a partial cutaway view of the assembly in Fig. 2 and shows the inlet scoop and exhaust outlet from the turbine back to the duct.

Numerous other applications of the Temp-turb principle of temperature control are in the developmental stage; however, the two examples mentioned should provide an adequate picture for an understanding of the system in general.

The work available in any Temp-turb unit is a function of the following:

1 Deviation from the control point.

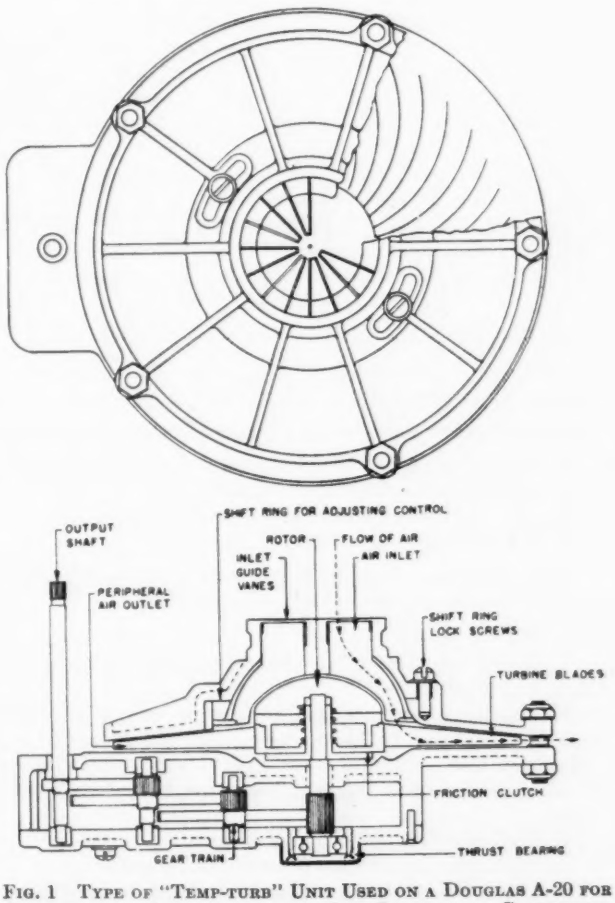


Fig. 1 Type of "Temp-turb" Unit Used on a Douglas A-20 for Controlling Temperature of Air Leaving a Combustion Heater

[1] General Electric Company. Mem. A.S.M.E.

Contributed by the Heat Transfer Division and presented at the Annual Meeting, New York, N. Y., Nov. 29–Dec. 3, 1943, of The American Society of Mechanical Engineers.

Note: Statements and opinions advanced in papers are to be understood as individual expressions of their authors and not those of the Society.

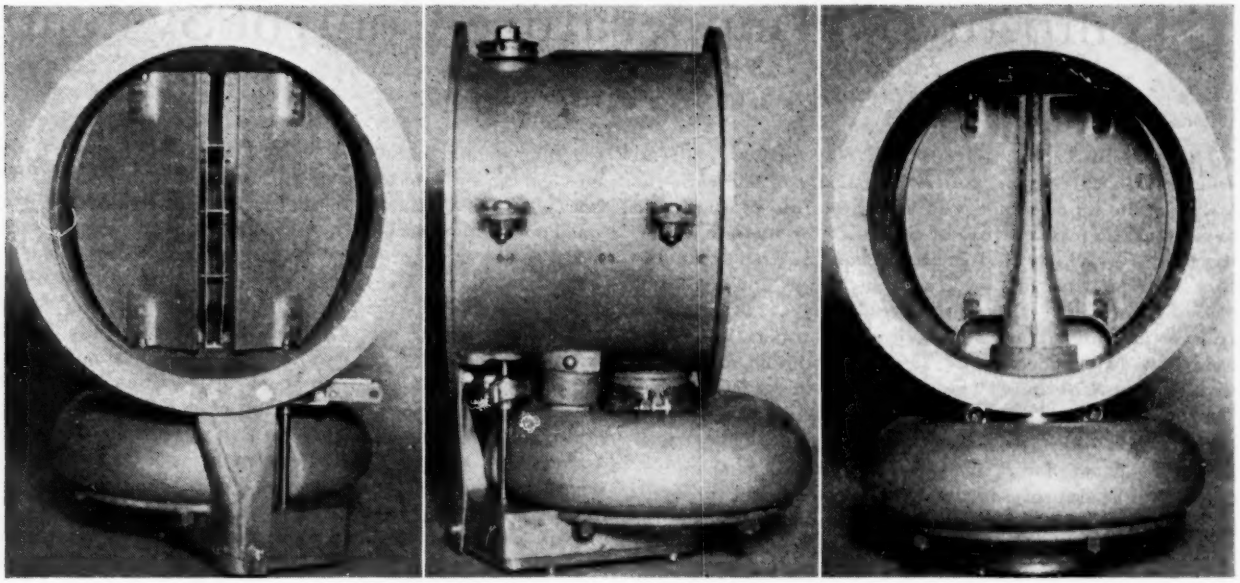


FIG. 2 CONTROL UNIT IS AN INTEGRAL PART OF THE MODULATING VALVE

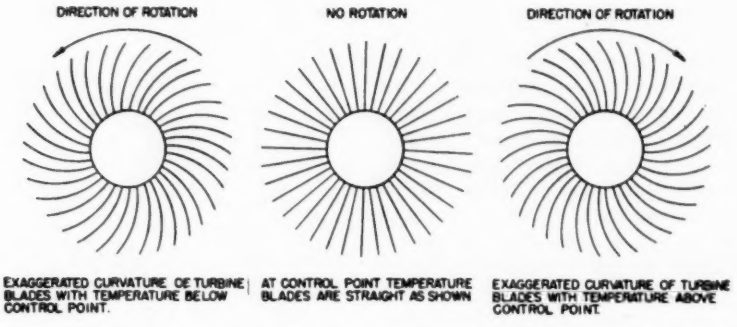


FIG. 3 OPERATION OF TURBINE WHEEL ON TYPICAL "TEMP-TURB" CONTROL UNIT

2 Mass flow of fluid, which for air has to be corrected for

(*a*) Temperature
(*b*) Altitude
} Density

The temperature sensitivity is a function of the following:

1 Massiveness of the basic temperature-sensitive elements.
2 Velocity of the fluid being controlled.
3 Gear ratio between rotor and control valving.
4 Thermal lag of the system.

When designing a Temp-turb unit for a specific application, it is first necessary to determine the following items:

1 Control point.
2 Degree of accuracy to which temperature must be controlled.
3 Maximum work required to operate valving or control means. This may be broken down into the following: (*a*) Maximum torque required. (*b*) Rate at which control means must be moved when operating under maximum-torque conditions.
4 Mass-flow rate of the fluid in system.
5 Allowable pressure drop (drop due to Temp-turb).
6 If system involves flow modulation, what is the minimum flow allowable. In this system, it is always necessary to have a sample of the fluid flowing over the Temp-turb rotor at all times. It is not practical to design for a minimum flow of less than the amount needed for a sample.
7 Allowable space.
8 Allowable weight.
9 Cross-sectional area of ducting or piping in the zone where Temp-turb is to be installed.
10 Whether or not the control point has to be adjustable: (*a*) As a service operation; (*b*) as an "in-use" operation.

PRINCIPAL CHARACTERISTICS OF SYSTEM

General characteristics of the Temp-turb system of temperature control are as follows:

1 Inherently nonhunting: The deflection of the blades, whether made of temperature-sensitive material or actuated by a temperature-sensitive element, is proportional to temperature changes; therefore, the output of the rotor is proportional to temperature changes. A large temperature deviation produces a large corrective force and a large rate of correction. A small deviation produces a small corrective force and a small rate of correction. As temperature error is being corrected, the correcting force and speed (produced by rotor) are reduced in proportion to the error until the control point is reached, at which time corrective force and speed of correction become zero.

Numerous tests under transient conditions have proved that

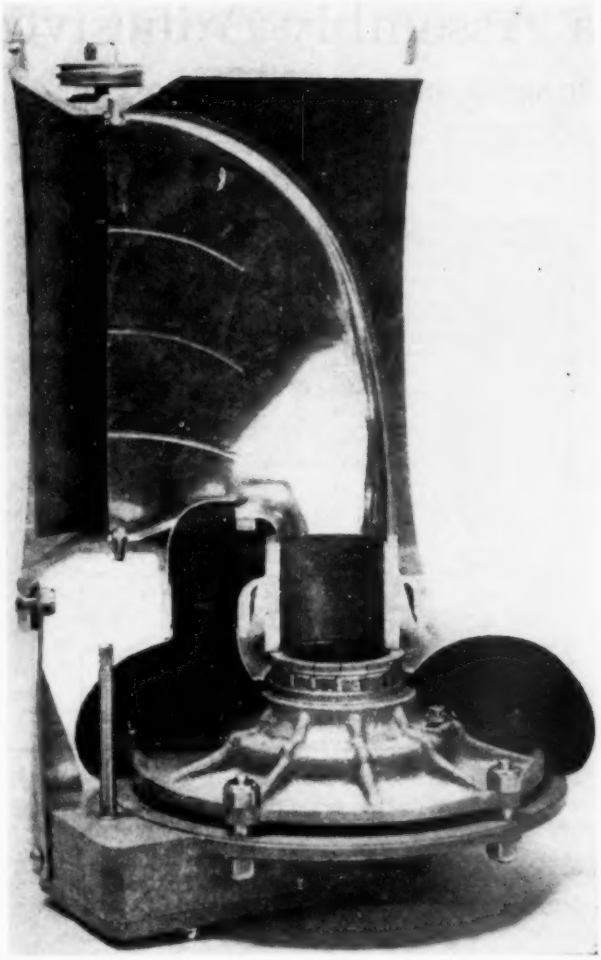


FIG. 4 PARTIAL CUTAWAY VIEW OF TEMP-TURB ASSEMBLY OF FIG. 2

the system is inherently stable. Of course, the thermal balance of the system must be within reasonable limits, and the gear ratio between rotor and control means also must be within reasonable limits.

2 Falling torque characteristics with velocity pressure increases above a certain value: The turbine blades, being operated by resilient thermoelements, are spring-loaded into proper position. This feature allows the blades to be blown into a neutral position under conditions where excessive velocity pressure might result in damaging loads or wear on the mechanism. This factor is of value on high-speed aircraft where ram pressures at times become quite high.

3 Adequate sampling of fluid being controlled: Temperature-sensitive elements have large area exposed to flowing fluid, which is particularly helpful under conditions wherein there is "temperature layering" in the duct. Also, the system is adaptable to special types of sampling scoops.

4 Low thermal lag: Bimetal temperature-sensitive elements are thin and subjected to relatively high-velocity fluid flow, resulting in almost instantaneous response to temperature changes.

5 Not affected by vibration: The torque produced by a vibrating turbine blade is the same as for a nonvibrating blade.

6 Output related to demand on unit: As flow rates increase, causing greater loads on control means, the rotor output increases accordingly.

7 The type of Temp-turb assembly as shown in Fig. 2 has the characteristic of not being affected by radiant heat from a glowing combustion chamber on a combustion heater. The sampling scoop and the location of the Temp-turb control unit make the device respond to air temperature only. This condition is of importance when the control is mounted immediately downstream from the combustion heater.

OPERATING EXPERIENCE

Experience to date indicates no unusual difficulties from a manufacturing standpoint. Any remarks on cost must be predicated on the somewhat limited manufacturing and commercial experience encountered to date. Based upon this experience, it may be said that Temp-turb type controls cost no more than competitive devices.

Concerning service life, Temp-turb controls on test have demonstrated that they have a trouble-free life of greater duration than other forms of controls used for the same operations. It is likely that this is due largely to freedom from complexity. Two units on life test actually worked better after 3000 hr than at the start of the test, due to "wearing-in" of bearings.

The temperature range, over which the Temp-turb principle could be applied, is approximately from —60 F to +600 F. This is on the basis of response and durability of the bimetal temperature-sensitive elements. Greater problems are offered in bearing design at extreme temperatures, and at this time the bearings and their lubrication actually determine the applicable range. On this latter basis, the range is about —60 F to + 350 F.

Fatigue Studies on Urea Assembly Adhesives

By A. G. H. DIETZ[1] and HENRY GRINSFELDER[2]

Assembly adhesives made of "cold-setting," urea-formaldehyde, synthetic resins, are employed in the fabrication of wooden aircraft such as gliders and motor-driven airplanes. Adhesives so used are frequently subjected to vibrating loads which induce alternating stresses in the glue; of these shear, in the plane of the glue, and direct tension, perpendicular to the glue line, are the two which are most likely to bring about failure. It is well known that most materials fail under alternating stresses smaller in magnitude than the static stresses required to cause failure, and synthetic-resin assembly adhesives are no exception. Little has been known quantitatively, however, respecting the behavior of such adhesives under alternating stresses.

In this paper are presented the results of researches into the failures to be expected in glue joints of this kind, particularly the nature of the failure, cycles of stress to failure at various amplitudes and stresses, and the probable "fatigue limit" of such an assembly. Tests were carried out at room temperatures on an assembly adhesive representative of those employed in aircraft fabrication.

Materials and Test Specimens

THE research on "cold-setting," urea-formaldehyde, synthetic resins, as representative of assembly adhesives used in wood aircraft fabrication, was carried out as follows:

Panels. Panels of overlapping 1/8-in. rotary-cut maple veneers were made up, as shown in Figs. 1 and 2. The two outer members *a* overlapped and were glued to the two inner members *b* over a distance approximately 1 1/2 in. The line *b-b* was glued throughout its length, so that the center member behaved as a single piece 1/4 in. thick. Maple was chosen because it is standard shear-block material, is relatively difficult to bond, and is moderately strong.

The panels were prepared according to the formulation: Urea-resin powder, 70 parts; water, 30 parts.

Spreading was by hand brushing and was on both surfaces being bonded. The assembly time ranged from 5 to 25 min, and in all cases the assemblies were closed immediately after spreading and kept closed until the pressure was applied. Bonding was for 16 hr at a temperature of 75 F, and the bonding pressure was 200 psi applied by means of a Black "compressometer."

Two sets of panels were made because difficulties encountered in obtaining satisfactory results with the first set necessitated the fabrication of more material. Panels were numbered as follows:

First	Second
A2	AA1
A3	AA2
A4	AA3
A5	AA4
A6	AA5
A7	AA6

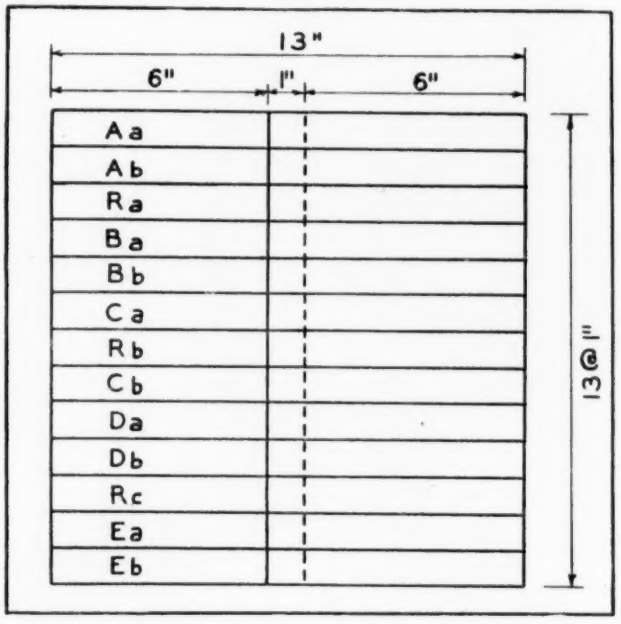


Fig. 1

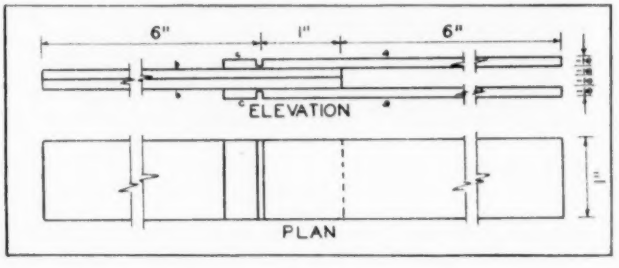


Fig. 2

Specimens. Specimens 1 in. wide were cut from the panels, as shown in Figs. 1 and 2. The overlap was cut to 1 in., as shown in Fig. 2, to provide 2 sq in. of glue line, although a few specimens were cut to 3/4 in. for experimental purposes. In some instances the remaining piece *c* was removed, but in the majority of the tests it was found better to leave it in place.

At the ends of glue lines *a-b*, Fig. 2, beads of glue had squeezed out into the internal corners. In some instances the bead was removed and in some it was notched with a saw, but it was found by test that the glue actually cracked after a few alternations of stress, so that is was unnecessary to pay any particular attention to the fillet caused by glue bead.

Specimens were marked as shown in Fig. 1. Those marked Ra, Rb, and Rc were intended for "modulus-of-rupture" tests, that is, to determine the breaking strength of the assemblages. Specimens Aa, Ba, . . . were intended for vibration, specimens Ab, Bb, . . . for static shear. It was not possible to adhere to this schedule rigidly for the first set of panels because of experimental difficulties to be described, but the specimens were in general so employed in the second set of panels. Moisture content of the material was approximately 9 per cent during the tests.

[1] Assistant Professor of Structural Engineering and Materials, Department of Building Engineering and Construction, Massachusetts Institute of Technology, Cambridge, Mass.

[2] Senior Engineer, Resinous Products and Chemical Company, Philadelphia, Pa.

Contributed by the Aviation Division, the Rubber and Plastics Group, and the Wood Industries Division and presented at the Annual Meeting, New York, N. Y., Nov. 29–Dec. 3, 1943, of The American Society of Mechanical Engineers.

Note: Statements and opinions advanced in papers are to be understood as individual expressions of their authors and not those of the Society.

TEST METHODS

Vibration

Machine. Because of the number of specimens involved and the length of time required for some of the tests, it was necessary to employ a machine which could handle several specimens at one time. The machine is shown in Fig. 3. In this apparatus the

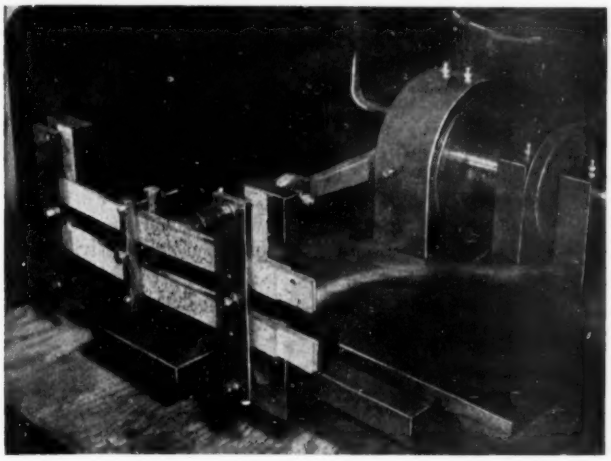


Fig. 3 Vibration Machine With Two Alternating Stress Specimens in Place; End Supports Are Semiclamped

specimens, in groups of two, are held between upright pairs of cold-rolled steel plates which in turn are bolted to a heavy horizontal steel bar fastened to the steel base plate supporting the entire apparatus. The centers of the specimens are forced back and forth by a pusher attached to a driving rod pinned to a connecting rod in turn mounted on an eccentric which forms part of a heavy steel driving wheel. The eccentric can be adjusted to give a throw ranging from zero to $1^1/_2$ in. The driving wheel is mounted in a heavy bronze bearing and is belt-driven by a 1-hp motor. The machine can be operated at various speeds, but in these tests was limited to 1100 to 1300 rpm.

End Supports. Three different methods of supporting the ends of specimens were tried. The first, rigid clamping, as shown in Fig. 4, resulted in fairly frequent fatigue failures in the wood at

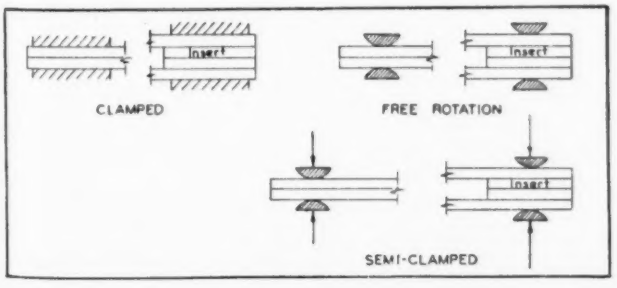


Fig. 4

the supports. Free rotation of the ends, the second method of support, required large deflections at the centers to yield appreciable stresses and caused numerous wood fatigue failures at the center. The end support finally adopted, and the one which yielded generally satisfactory results, consisted of rounded supports, between which the specimens were firmly held by bolts exerting pressure as shown. This allowed a little rotation at the ends, resulting in a semiclamped condition.

Pusher. Four different positions of the pusher were tried, as shown in Fig. 5. Position 2 was first employed, but resulted in fatigue failures in the wood rather than glue-line failures because even the slight compression applied by the pusher to the glue line prevented tensile stresses from building up to the point where

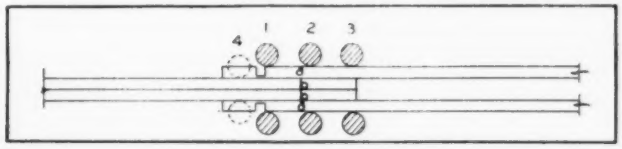


Fig. 5

failure could occur. Such a condition would not generally be found in actual practice. Position 3 was somewhat better, but position 4 resulted in rather quick wood failures. Position 1, finally adopted for the pusher, proved best from all standpoints. It allowed tensile stresses to develop freely. Fairly high percentages of glue-line failures resulted when the combination of pusher in this position was employed, and when saw cuts were held approximately $^1/_{32}$ in. short of glue line *a-b* to avoid local concentrations of stresses which would cause the wood to fail in fatigue. The pusher was not pressed firmly against the wood but was allowed to clear by a few thousandths of an inch or, at most, to come into light contact.

Tests were carried to failure or to 5,000,000 cycles. Two, four, or six specimens were tested at one time, depending upon the amplitude.

Static Shear

Static-shear control specimens were placed in the tension grips of a 10,000-lb Riehle beam-type universal testing machine and pulled apart, as shown diagrammatically in Fig. 6. Under

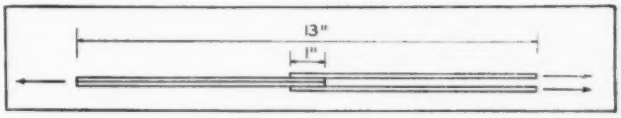


Fig. 6

this load, shear stresses are set up in the glue lines *a-b*, accompanied by some tension perpendicular to the glue line occasioned by the eccentricities in the joints.

Static Bending

Modulus of Rupture. Selected specimens, generally those marked Ra, Rb, Rc, were loaded statically to rupture to determine the breaking strengths and deflections so that the amplitudes to employ in the vibration tests could be decided. As shown diagrammatically in Fig. 7, specimens were supported at the ends

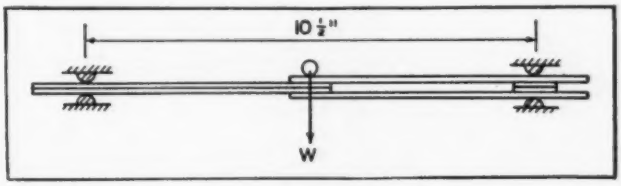


Fig. 7

in the same manner as the vibrated specimens and were loaded with dead weights at the center in the same manner as the vibrated specimens, except that loads were carried to failure. Loads and deflections to failure were both recorded.

Calibration. Each vibration specimen was calibrated by load-

ing in the same manner as the modulus-of-rupture specimens, except that loads were carried only to deflections corresponding to the amplitudes through which the specimens were to be vibrated.

In order to determine the end restraining moments at the supports induced by clamping and semiclamping, a number of specimens were tested twice, once as freely supported simple beams with no end restraint, and again as clamped or semiclamped specimens.

If d_f = deflection at center of a freely supported beam loaded at the center
d_c = deflection at center of a beam completely restrained at its ends and loaded at the center
W = concentrated load at center
L = length of beam
E = modulus of elasticity
I = moment of inertia
M_f = bending moment at center of a freely supported beam loaded at the center
M_c = bending moment at center of a beam completely restrained at its ends and loaded at the center
M_r = restraining moment at ends of a completely restrained beam

$$d_f = \frac{1}{48} \cdot \frac{WL^3}{EI} \quad \ldots\ldots [1]$$

$$d_c = \frac{1}{192} \cdot \frac{WL}{EI} = \frac{1}{4} d_f \quad \ldots\ldots [2]$$

$$M_f = \frac{WL}{4} \quad \ldots\ldots [3]$$

$$M_c = \frac{WL}{8} \quad \ldots\ldots [4]$$

$$M_r = -\frac{WL}{8} \quad \ldots\ldots [5]$$

For semiclamped specimens, the deflections are intermediate between Equations [1] and [2], and the corresponding center moments are intermediate between Equations [3] and [4]. By determining the deflections for Equation [1] and for the semiclamped condition, the center moments for the semiclamped condition can also be determined, and from these the maximum tensile stresses perpendicular to the glue line at the overlap. Shear stresses can be determined from the load, whose magnitude is known as a function of the amplitude (or deflection).

Fig. 8 shows the approximate relationship between the external

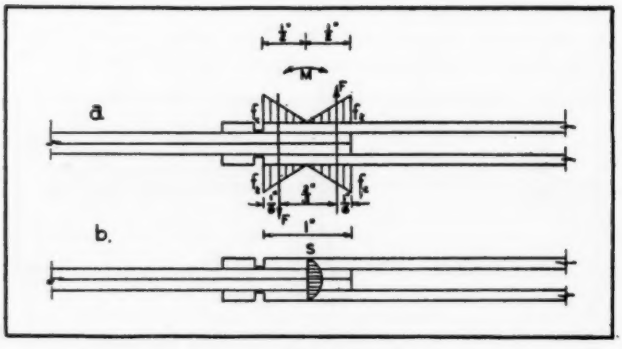


FIG. 8

center bending moment M and the internal resisting moment. With the pusher in position 1 (Fig. 5), tensile and compressive stresses are set up across the glue lines and are approximately triangular in distribution. The varying stresses f have resultants F, acting at the centers of gravity of the triangular stress volumes. The equal and opposite resultants F form a couple $F \times \frac{2}{3}^{\text{in.}}$ which resists the external moment M. The resultant F is equal to

$$F = \frac{2f}{2} \times \frac{1}{2}^{\text{in.}} \times 1^{\text{in.}}, \text{ and } F \times \frac{2}{3}^{\text{in.}} = \frac{f}{3} \quad \ldots\ldots [6]$$

or

$$M = \frac{f}{3} \text{ and } f = 3M \quad \ldots\ldots [7]$$

The actual stress distribution is somewhat different from the simplified diagram, here shown, inasmuch as M varies slightly from one end of the overlap to the other because of shear. This tends to increase f in some portions of the overlap and to decrease it in others. For practical purposes, the stress distribution is closely enough that shown.

Average shear stress in the plane of the glue lines is given by the familiar expression

$$s = \frac{VQ}{bI} \quad \ldots\ldots [8]$$

and is as shown as in Fig. 8(*b*). This is the average condition. It is probable that the true shear stress deviates from this at the ends of the overlap.

TEST RESULTS

General

Test results are summarized in Tables 1 to 3.

Considerable scatter in the results is found, although trends are clearly visible. Marked difficulty was encountered in obtaining satisfactory failures at the glue lines; failure was as apt to occur in the wood as in the glue line. This was particularly true of the vibration specimens.

Static Tests

Static Shear. Table 1 gives the average results of static shear tests for the various panels. In the first set, average strength is 1458 psi, accompanied by 80 per cent average wood failure. In the second set the corresponding figures are 1403 and 90, respectively.

TABLE 1 STATIC SHEAR

Panel	Average load, lb	Average shear stress, psi	Average per cent wood failure
A2	2857	1428	75
A3	2626	1313	83
A4	2842	1422	70
A5	2664	1332	99
A6	2788	1394	90
A7	2960	1458	95
Averages[a]	2916	1458	80
AA1	2864	1432	90
AA2	2851	1425	95
AA3	2929	1465	85
AA4	2700	1350	70
AA5	2706	1353	90
AA6	2792	1396	100
Averages[a]	2807	1403	90

[a] Averages of all individual tests, panel averages weighted in accordance with number of tests from each panel.

The shear-strength averages are less than are found in the standard shear block but are considerably higher than in the standard plywood shear specimens. The shape of the specimen and its general proportions, inducing variable amounts of tension because of eccentric loading, as well as nonuniform shear distribution in the joint, must account for the different values attained.

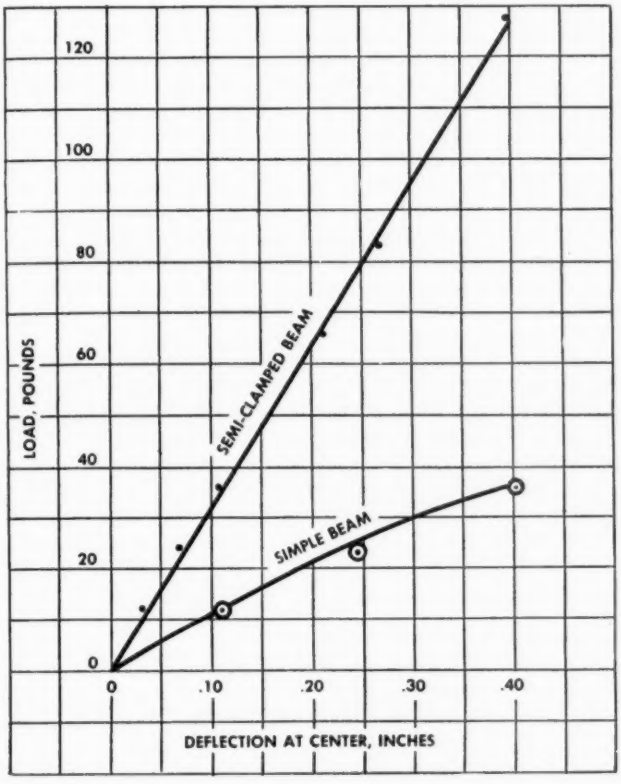


FIG. 9 TYPICAL LOAD-DEFLECTION DIAGRAMS; SIMPLE AND SEMI-CLAMPED BEAMS

Modulus of Rupture. Fig. 9 is a typical set of load-deflection curves for a modulus-of-rupture specimen. The lower curve is for the specimen simply supported, the upper for the semi-clamped end. In general, deflections for the semiclamped condition were approximately one third those for the simple beam, indicating a center moment of approximately $\frac{WL}{7}$. Center moments for the clamped and semiclamped tests ranged from slightly better than $\frac{WL}{6}$ to $\frac{WL}{8}$.

Average values of modulus of rupture for the various panels tested, averages for the two sets of panels, and over-all averages are given in Table 2. Shear stresses were calculated by Equation [8] and maximum tension across the glue line from center moments determined from Equations [6] and [7].

The first set of panels yielded somewhat higher results than the second, but over-all averages and limits were as follows:

Shear: average 190, low 120, high 230 psi
Tension: average 815, low 530, high 1015 psi
Wood failure: average 65, low 45, high 100 per cent

Alternating Stresses. Table 3 summarizes the tests in which glue-line failures occurred under alternating stresses at amplitudes of $^5/_{16}$, $^1/_4$, $^3/_{16}$, $^1/_8$, and $^1/_{16}$ in. Tests in which wood failed in fatigue are not included. Furthermore, the results are for clamped or semiclamped specimens, and for specimens in which failure was complete, except for those which ran to 5,000,000 cycles without failure. The same results are presented graphically on logarithmic paper in Fig. 10. The following appear to be the chief points of interest:

1 Maximum amplitude, $^5/_{16}$ in. induced maximum tensile stresses perpendicular to the glue line approximately two thirds of those found in the modulus-of-rupture tests. Minimum ampli-

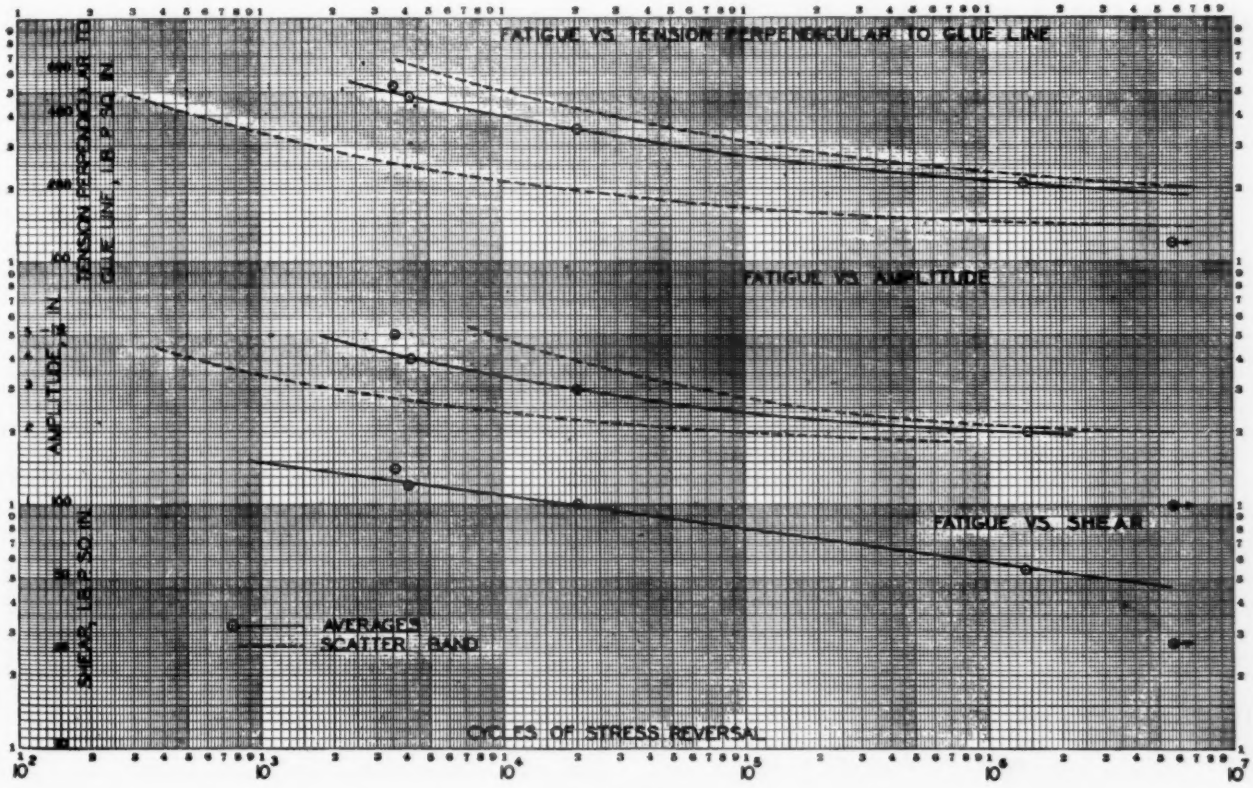


FIG. 10

TABLE 2 MODULUS OF RUPTURE

Panel	Load, lb	Shear stress, psi	Tension across glue line, psi	Per cent wood failure
A2	203	230	865	50
A3	132	150	695	75
A5	152	170	800	100
A6	148	165	775	90
Averages[a]	174	195	815	70
AA1	203	230	1015	50
AA2	187	210	935	90
AA3	170	190	850	95
AA4	167	190	835	45
AA5	172	195	860	70
AA6	106	120	530	45
Averages[a]	165	185	815	65
Total average	169	190	815	65

[a] Average of all specimens, not of averages.

TABLE 3 DEFLECTIONS, STRESSES, CYCLES

Specimen	Amplitude, in.	Shear stress, psi	Tensile stress, psi	Number of cycles	Per cent wood failure	Static shear: Stress, psi	Static shear: Wood failure
A3-Ea	5/16	135	510	8800	5	..	..
A4-Bb		135	515	500	50	..	..
A4-Ea		135	520	1100	60	..	..
A5-Ba		135	520	7700	85	..	..
A5-Ea		115	440	4400	40	..	..
A6-Ea		140	540	1100	60	..	..
AA1-Aa		175	660	2700	70	..	..
Averages		140	530	3600	55		
A3-Rc	1/4	115	440	500	40	..	..
A4-Rc		125	470	500	60	..	..
A6-Rc		115	440	6600	60	..	..
AA1-Ba		135	510	2200	15	..	..
AA3-Ba		115	510	11000	20	..	..
Averages		120	475	4200	40		
A3-Db	3/16	80	310	4400	10	..	..
A4-Db		95	360	49500	40	..	..
A5-Db		85	330	40700	50	..	..
AA1-Ca		90	350	600	0	..	..
AA3-Ca		145	420	7400	5	..	..
Averages		100	350	20500	30		
A3-Cb	1/8	40	130	570000	80	..	..
A4-Cb		50	190	220000	15	..	..
A6-Cb		50	190	5780000	85	..	..
AA2-Da		65	240	688000	30	..	..
AA3-Da		65	280	1040000	5	..	..
AA4-Da		50	230	149000	5	..	..
Averages		55	210	1408000	40		
AA4-Ea	1/16	27	120	5770000	None	1733	95
AA5-Da		27	120	5770000	None	1462	85
AA5-Ea		27	120	5770000	None	1862	90
AA6-Da		26	115	5770000	None	1347	45
AA6-Ea		26	115	5770000	None	1712	65
Averages		27	120	5770000	None	1603	75

tude, 1/16 in. induced tensile stresses approximately one seventh of those found in the modulus-of-rupture tests.

2 Shear stresses were quite low, compared with the static shear tests; the maximum at 5/16 in. amplitude was 5 per cent of the static shears.

3 Failures were primarily tension perpendicular to the glue line and were the kind that would be found in most actual structures.

4 At 1/8-in. amplitude, one specimen ran to better than 5,000,000 cycles. The others failed at approximately 150,000 to 1,000,000 cycles.

5 At 1/16-in. amplitude, all specimens ran to better than 5,000,000 cycles without any signs of failure.

6 When tested in static shear, the unbroken vibrated specimens yielded results which actually averaged a little higher than the static controls. This indicated that at least there was no loss in strength

7 In those vibration specimens which failed during test, lower percentages of wood failure were found than in the modulus-of-rupture controls. No definite trend with respect to numbers of cycles and stress could be discerned.

8 In Fig. 10, the numbers of cycles of stress reversal are plotted against amplitude, shear stress, and maximum tension perpendicular to the glue line. Curves are drawn for the arithmetical averages and for the approximate limits of the scatter bands in the graphs of cycles versus amplitude and cycles versus tension perpendicular to the glue line. Scatter for the shear results is not plotted, inasmuch as shear was a minor factor in causing failure. The curves of amplitude and maximum tension versus cycles to failure flatten to practically zero slope well above the 5,770,000-cycle point.

Conclusions

Conclusions must be drawn with some reservations from these tests, inasmuch as the scatter in the results renders generalizations somewhat difficult. It appears, however, that the following may be said with some assurance with respect to stresses at room temperatures:

1 A joint having the general proportions of those tested, and subjected to vibrations, is as apt to fail in fatigue in the wood as in rupture in the glue line.

2 Inasmuch as the sections tested were quite heavy and spans were short, so that higher shears were induced in the glue lines than would customarily be found, it seems safe to say that failures in glue lines of this type will occur primarily because of tension perpendicular to the glue line (and the grain of the wood) rather than by shear in the glue line.

3 If maximum tensile stresses perpendicular to the glue lines of these adhesives are kept below 120 psi, there should be no failures. As a matter of fact, extrapolation of the observed curves indicates that it is highly probable that stresses can be 150 to 160 psi, that is, 20 per cent of the "modulus of rupture," or static ultimate stresses. If stresses reach 200 psi, failure may be expected to occur at 5,000,000 cycles or less, and as the stresses go still higher, the number of cycles to failure becomes rapidly smaller, with highly variable results. The "fatigue limit," if that term may be employed here, appears to be 20 per cent of the ultimate.

The foregoing conclusions are based upon tests made at room temperature upon specimens at approximately 9 per cent moisture content.

Application of these results depends upon the ability to determine stresses in vibrating structures, by analysis or test. Wherever members cross each other, bending moments are apt to set up tensile stresses perpendicular to the glue line and the grain of the wood. Such stresses may be uniformly distributed or may vary from maximum to minimum approximately as in the tests here described. In such instances, the dimensions of the overlapping parts should be large enough to keep the tensile stresses from exceeding 20 per cent of the tensile strength of the wood perpendicular to the grain. For species such as maple and birch, alternating tensile stresses of 125 to 150 psi may be employed, for other species such as spruce or mahogany, the stresses will be less.

Acknowledgments

Acknowledgments are due particularly to John Barry, Research Assistant, who carried out the experimental work, and to Prof. W. M. Murray, of the Department of Mechanical Engineering at the Massachusetts Institute of Technology, who was instrumental in the design of the testing apparatus. The laboratory staff of the Resinous Products and Chemical Company made the test material.

Heat and Vapor Transfer in the Dehydration of Prunes

By R. L. PERRY,[1] DAVIS, CALIF.

Quality of prunes is known to be influenced by the temperature and relative humidity of the dehydrator air, and by the time required for drying, long exposures to high temperatures at high humidities resulting in excessive caramelization and cooked taste. To determine the actual temperatures of prunes during dehydration, readings were made by thermocouples inserted at different points in prunes for three test runs at about 166 F, and relative humidities of 15, 27, and 43 per cent. To permit adapting the data obtained to commercial dehydrators, surface thermal conductances were computed. The vapor conductance at the surface was estimated from the thermal conductance, by employing the heat-mass transfer analogy. From the vapor conductance and the evaporation rate, the difference in vapor concentration required to move vapor from the prune surface to the air stream was calculated. Moisture movement within the prune was investigated by cutting the flesh of samples, removed after 3, 6, 10, and 16 hr drying, into two parts, that near the surface, and that near the pit.

Nomenclature

The following nomenclature is used in this paper:

A = area of prune surface, sq ft
A_d = area of prune surface, per pound of dry matter, sq ft per lb
B = drying coefficient, slope of free-moisture line on semi-logarithmic paper, 1/hr
c = unit heat capacity, Btu/lb F
c_d = heat capacity of prune, per pound of dry matter, Btu/lb F
C = moisture concentration, lb per cu ft
D = diameter, ft
e = base of Naperian logarithms, 2.7183
E = equilibrium-moisture ratio, pounds of moisture per pound of dry matter
f = unit surface thermal conductance, Btu/hr ft² F
f' = unit surface vapor conductance, lb/hr ft² (lb/ft³) or ft/hr
F = free-moisture ratio, pounds of free moisture per pound of dry matter. ($F = M - E$)
H = relative humidity, per cent
k = thermal conductivity, Btu/hr ft² (F/ft)
k' = moisture conductivity within prune, lb/hr ft² (lb/ft⁴) or ft²/hr
M = total-moisture ratio, pounds of moisture per pound of dry matter
n = exponent of Prandtl modulus in forced-convection equations
N = prune count, number of dried prunes, of 0.2 moisture ratio, per lb
q_c = convective- and radiant-heat-exchange rate, between prune and its surroundings, Btu per hr
q_s = sensible-heat-gain rate of prune, Btu per hr
q_v = heat rate in evaporation, Btu per hr
r = latent heat of evaporation of water, Btu per lb
R = radius, ft
t = temperature, F
V = air velocity in free cross section of tunnel, fpm
w = evaporation rate, lb per hr
W = weight of prunes
α = diffusivity of water vapor through air, ft²/hr
γ = weight density, lb per cu ft
θ = time, hr
μ = weight viscosity, lb/hr ft

Subscripts:

i, for prune-air interface
0, for outside
∞, for remote air stream
1, initial

Dimensionless moduli:

fD/k = Nusselt modulus for convective heat transfer at a fluid boundary
$f'D/\alpha$ = Nusselt modulus for convective mass transfer at a fluid boundary
$c\mu/k$ = Prandtl modulus of fluid properties for convective heat transfer
$\mu/\alpha\gamma$ = Prandtl modulus of fluid properties for convective mass transfer
$k'\theta/R^2$ = Fourier modulus for mass conduction in solids
$f'R/k'$ = Biot modulus for mass transfer at a solid-fluid interface

Introduction

In this paper, data on the temperature and moisture distribution in prunes during dehydration are presented. Surface conductances for heat and vapor are computed from the data, and the vapor concentration and relative humidity at the prune surface are found. The deviation of moisture distribution within the prune from that which would occur with constant moisture diffusivity is disclosed.

Studies by Moses, Cruess, et al (1)[2] fixed the over-all limiting dehydrator conditions of temperature and humidity for production of prunes of high quality. Although it was known that prolonged high air temperature and high humidity gave a dark, caramelized, low-grade prune, the actual prune temperatures during drying were not observed. In order to extend the results of their dehydration tests made at constant air temperature and humidity to commercial practice, where counterflow, parallel-flow, center-exhaust, end-exhaust, and cross-flow dehydrators are used, the prune temperature itself was needed.

The empirical equations developed by Guillou (2) led to the first marked advance in prune-dehydrator design technique since

[1] Associate Professor of Agricultural Engineering, and Associate Agricultural Engineer in the Experiment Station, University of California. Mem. A.S.M.E.

Contributed by the Heat Transfer Division and presented at the Annual Meeting, New York, N. Y., Nov. 29–Dec. 3, 1943, of The American Society of Mechanical Engineers.

Note: Statements and opinions advanced in papers are to be understood as individual expressions of their authors and not those of the Society.

[2] Numbers in parentheses refer to Bibliography at the end of the paper.

the work of Christie and Ridley (3), but they left several questions unanswered. No explanation was available for the observation that variations in relative humidity did not influence drying rate unless the relative humidity exceeded 35 per cent. This was contrary to the observation that in some other materials the drying rate is proportional to wet-bulb depression. Another unanswered question was why the equilibrium-moisture content, determined by plotting drying rate against moisture ratio, differed from that observed by Guillou (4), Table 2, on prunes held in atmospheres of different humidities until constant weights were reached.

The investigations reported herein were planned to throw more light on the answers to these questions. No previous attempts to measure either temperature or moisture in fruit-drying dehydration had been noted in the literature.

The Dehydration Process

When a fresh prune is placed in a high-temperature air stream of a moisture concentration lower than that which represents equilibrium with the prune flesh at the air temperature, heat is transferred by convection and radiation to the prune surface; thus

$$q_c = fA(t_\infty - t_i) \quad [1]$$

At first this heat results principally in a rise in temperature

$$q_s = cW \frac{\partial t}{\partial \theta} \quad [2]$$

in which t represents the average temperature of the prune, the interior being warmed by conduction from the surface. However, as the surface layers rise in temperature, the vapor concentration at the surface rises. When it exceeds that in the adjacent air stream, vapor escapes through the resistance offered by the adjacent air-vapor mixture

$$w = f'A(C_i - C_\infty) \quad [3]$$

The vaporization absorbs heat

$$q_v = wr \quad [4]$$

or, combining Equations [3] and [4]

$$q_v = rf'A(C_i - C_\infty) \quad [5]$$

(An additional quantity of heat is necessary to warm the vapor from the temperature at which it escapes from the prune to that which it attains in the air stream. This is a minor item which can be neglected, especially since only part of it has to pass through the resistance of the adjacent air-vapor mixture.) The heat available from convection and radiation is utilized in temperature rise and evaporation

$$q_c = q_s + q_v \quad [6]$$

As the temperature rises, the heat available from convection and radiation decreases, but the evaporation rate increases, so that there is soon little heat available for further temperature rise. The prune temperature is then, combining Equations [1] and [5] and noting that q_s is negligible in Equation [6]

$$t_i = t_\infty - \frac{f'r}{f}(C_i - C_\infty) \quad [7]$$

Equation [7] is of limited utility because of inability to establish the value of the surface-moisture concentration C_i, except indirectly from test data. The surface concentration is related to the moisture ratio of the prune flesh, and to the temperature, but varies with the drying history of the prune. It is evident, of course, that as vapor escapes from the surface, a moisture-concentration gradient is established within the prune, so that moisture moves to the surface, but not rapidly enough to maintain the initial concentration. The evaporation rate thus decreases gradually, and the temperature approaches more closely that of the air. Even with the help of the data at hand, however, the formulation of an ideal system, which would describe adequately the dehydration of a prune, has not been realized. The continually changing balance between vapor and heat transfer which determines the drying rate and the prune temperature is not yet mathematically predictable, and reference must still be made to empirical relations such as are presented herewith.

Test Apparatus and Procedure

Two groups of tests were conducted. In the first group, simultaneous observations of weight of sample and of temperature at prune surface and prune pit were made during constant-condition dehydration runs. The initial and final dimensions, volume, and density were noted, and the final moisture content measured. In the second group, several prunes were removed at successive drying times, and the flesh was dissected into two sections, that near the skin and that near the pit, for moisture-content determination. Subsequently, the dried skin was planimetered to find its area, in order to learn the area and thickness of the segments which had been removed.

Temperature-Distribution Tests. In each run of the first group,

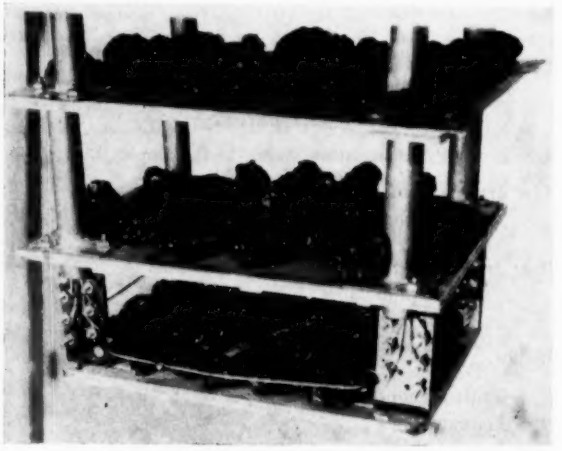


Fig. 1 Test Tray of Prunes, at End of Run

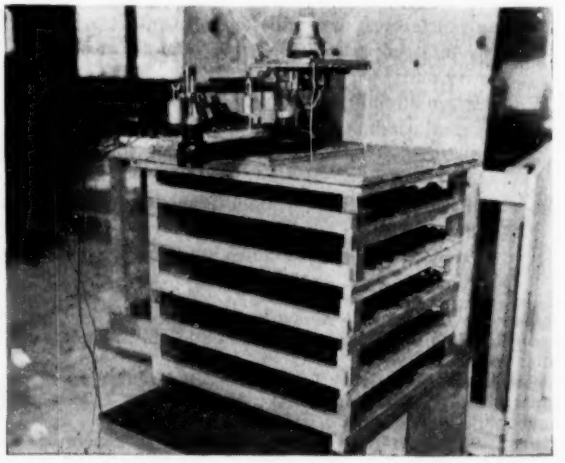


Fig. 2 Test Tray, Surrounded by Guard Trays

temperatures at three points in each of five prunes were taken by means of No. 36 gage copper-constantan thermocouples, read with a Leeds & Northrup No. 8662 portable semiprecision potentiometer. One thermocouple was inserted just under the skin at the top of each prune, the junction being so close to the surface that it could be seen through the translucent skin, and the leads continuing just under the skin for about $^{5}/_{8}$ in., to minimize conduction errors. One thermocouple was placed next to the pit. In three of the five prunes, the third point was just beneath the skin on the side which was to lie on the tray, while in the other two, the third point was just under the skin at the side.

These five test prunes were placed among twenty others of similar size and maturity on a tray of $^{1}/_{4}$-in. plywood, which could be weighed as drying proceeded, the thermocouple extension leads serving as suspensions from the scales. This tray, Fig. 1, was hung in the center of a larger guard tray which was included in the center of a stack of five, Fig. 2, placed in the dehydrator tunnel, 17 in. square in cross section. Only the lower tray in Fig. 1 was weighed, the two above it being access hatches which fitted into the two upper guard trays. Although the suspending leads were sheltered from the air stream by the tubular shields noticeable in Fig. 1, and the tray was restrained laterally by bridles, it was found necessary to close the air-control damper while weighing was being done.

Four runs were made, each at about 166 F air temperature, and at an air velocity of 600 fpm, in the free cross section of the tunnel. It was found during the first run that the thermostat was in need of repair, having a range of 7 F, so that, although the periodic heat exchange with the prune was of some interest, the data were of little direct value. Subsequent runs were made with manual control, an auxiliary heater being adjusted with a variac. General data for these runs are given in Table 1.

TABLE 1 GENERAL DATA ON PRUNE TEMPERATURE TESTS

Run number	2	3	4
Average air temperature, deg F	169	166.5	166
Average wet-bulb temperature, deg F	122	134	105
Average relative humidity, per cent	27	43	15
Tray loading, lb per sq ft	3.98	3.90	3.94
Duration of run, hr	16.1	18	17.2[a]
Final-moisture content,[b] 20 prunes per cent	20.3	21.0	19.3
Average weight, lb:			
Initial, 5 temp test prunes	0.0500	0.0511	0.0519
Initial, 20 additional prunes	0.0502	0.0485	0.0488
Final, 5 temp test prunes	0.0163	0.0168	0.0186
Final, 20 additional prunes	0.0169	0.0170	0.0168
Moisture ratio, pounds of moisture per pound of dry matter:			
Initial, average of 25 prunes	2.76	2.67	2.58
Final, average of 25 prunes	0.26	0.27	0.24
Average volume, cu ft:			
Initial, 5 temp test prunes	0.000713	0.000728	0.000757
Final, 5 temp test prunes	0.000205	0.000212	0.000233
Average density, lb per cu ft:			
Initial, 5 temp test prunes	70.2	70.2	68.7
Final, 5 temp test prunes	79.6	79.3	69.9
Axial dimensions, 5 temp test prunes, ft:			
Initial major axis	0.134	0.135	0.133
Initial horizontal minor axis	0.102	0.102	0.102
Initial vertical minor axis	0.100	0.101	0.101

[a] Tunnel air damper inadvertently shut at 1 hr, opened at 1.58 hr.
[b] Wet basis.

After completing each run, the final moisture content of the twenty companion prunes was determined with the electric-resistance moisture tester of the Dried Fruit Association. The thermocouples were examined to discover if they had inadvertently been misplaced in completing the lead connections or in installing trays in the tunnel. In general the top and side thermocouples influenced the wrinkling in such a way that the junction was on a ridge, as shown in prune *B*, Fig. 3, with the following exceptions:

Run 2, prune 3: Top thermocouple in a ridge, but not at apex, being about $^{1}/_{16}$ in. or $^{1}/_{3}$ of ridge height below apex, see *A*, Fig. 4.

Run 3, prune 4: Top thermocouple in valley, as *B*, Fig. 4.
Run 4, prune 2: Top thermocouple in valley, as *B*, Fig. 4.
Run 4, prune 2: Side thermocouple near ridge at edge of bottom, as *C*, Fig. 4.
Run 4, prune 5: Side thermocouple in double ridge, as *D*, Fig. 4.

As the prunes softened with rise in temperature and loss of moisture, the bottom began to flatten, so that at about 2 hr of drying, the flat spot was about $^{1}/_{4}$ as long and as wide as the prune. Wrinkling was just discernible at this time. After 6 to 8 hr, the flat spot was about $^{2}/_{3}$ as long and as wide as the prune.



FIG. 3 DRIED PRUNES CONTAINING THERMOCOUPLES

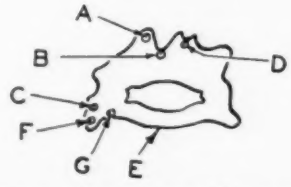


FIG. 4 CROSS SECTION OF DRIED PRUNES SHOWING THERMOCOUPLE LOCATIONS

As the end of drying was approached, the bottom shrank up toward the pit, Fig. 3, prunes *A* and *C*, so that it was cupped with a slight convexity at the middle, Fig. 4, *E*. The bottom junction was usually found just under the pit, in the bulge, with the following exceptions:

Run 3, prune 1: Bottom thermocouple at ridge at edge of bottom, as *F*, Fig. 4.
Run 3, prune 5: Bottom thermocouple near ridge at edge of bottom, as *G*, Fig. 4.

Moisture-Distribution Tests. Two runs were made for measuring moisture distribution, each at 166 F and 105 F wet-bulb temperature. In these runs, four lots of similar prunes were weighed and placed on the trays for drying. After 3 hours, samples from the first lot were removed, weighed, and the skin, with an adhering adjacent layer of flesh, was sliced off for a moisture determination. The flesh adhering to the pit was also removed, and moisture determinations were made on it and on the pit. A similar procedure was followed at 6, 10, and 16 hr. In the second run, the slices from the top, sides, and bottom of the outer layer were kept separate. Some loss, from 6 per cent in the 3-hr sample, to 2 per cent in the 16-hr sample, occurred in the dissecting, and this was allotted to the inner and outer layers on a proportional-weight basis.

The moisture determinations were made by drying to constant weight in an atmospheric oven at 65 C (149 F), for want of a vacuum oven. After the moisture was found, the skin sections of the second run were soaked, the flesh removed, and the skin was dried in small pieces for the purpose of measuring its area with a planimeter. This procedure permitted estimating the average thickness of the top, bottom, and side slices of the second run.

Test Results

Temperature Distribution. The temperatures of the prunes rose rapidly in the first half hour, until within about 20 F of the air temperature, as shown in Fig. 5. They then rose more slowly, until at the end of drying, the surface temperatures were only 2 to 3 deg below air temperature. Because of trouble in controlling the air temperature precisely (there was a periodic fluctuation of 1 to 2 deg in air temperature even with a steady heat input, noticeable in the air-temperature curve in Fig. 6) and of the rapidity with which the prunes tended to respond to a change in air temperature, the data were first plotted as broken lines from point to point, Fig. 6. From such preliminary graphs, smoothed curves were sketched by eye, with consideration of any air-temperature changes which were occurring simultaneously. The air temperature, the mean of the prune surface, and of the prune-center temperatures, and the weight of the 25 prunes are shown for Runs 2, 3, and 4, in Figs. 7, 8, and 9, respectively. The maximum and minimum prune temperatures are also shown in these figures, the curves overlapping at some points as one prune rose above or fell below the others.

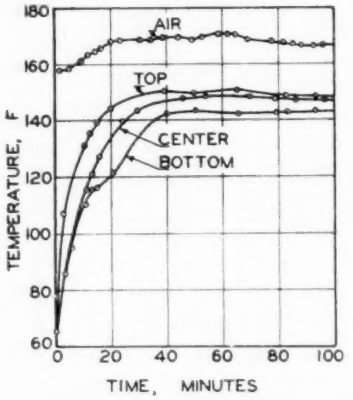


Fig. 5 Temperatures of Prune During Initial Warming; Run 2, Prune 5

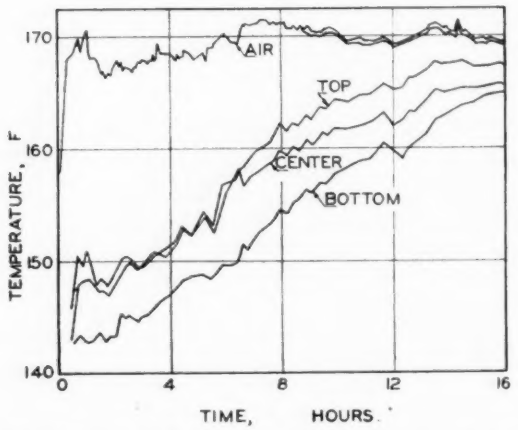


Fig. 6 Graph of Original Temperature Data; Run 2

The considerable variations in temperatures of prunes in the same runs are illustrated in Figs. 10, 11, and 12. Thus in Run 2, Fig. 10, center temperatures of two prunes differed as much as 13 F at one time, nearly as much as the difference of the mean of the five prunes from the air temperature. In Run 3, Fig. 11, however, there was much less variation. That the peculiar dip in the curve for the coldest prune at 12½ hr in Run 4, Fig. 9, is not an error is substantiated by the additional curves for this run, Fig. 12, where it can be seen that the temperature of several, but not all, of the points dropped temporarily at this time. The drop at 13½ hr was obviously due to a drop in air temperature. No explanation is available for this peculiar behavior, except possibly sticking and subsequent loosening from

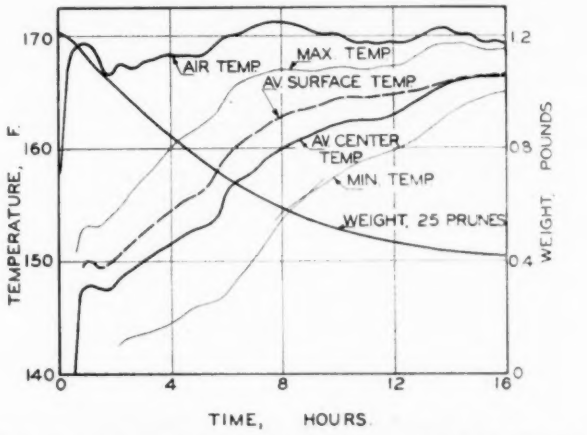


Fig. 7 Weight of 25 Prunes, Air Temperature, and Average Temperature of Prune Surface and Prune Center; Run 2

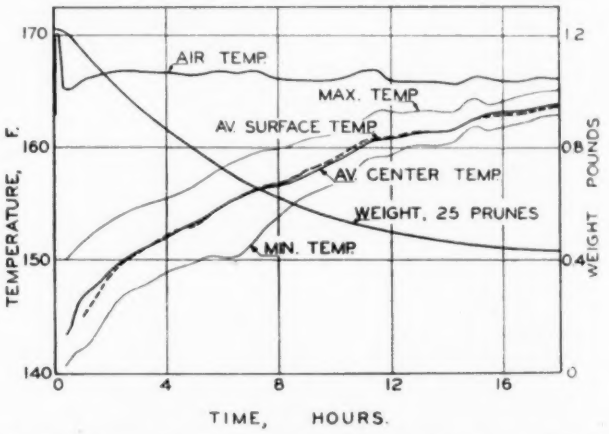


Fig. 8 Weight of 25 Prunes, Air Temperature, and Average Temperature of Prune Surface and Prune Center; Run 3

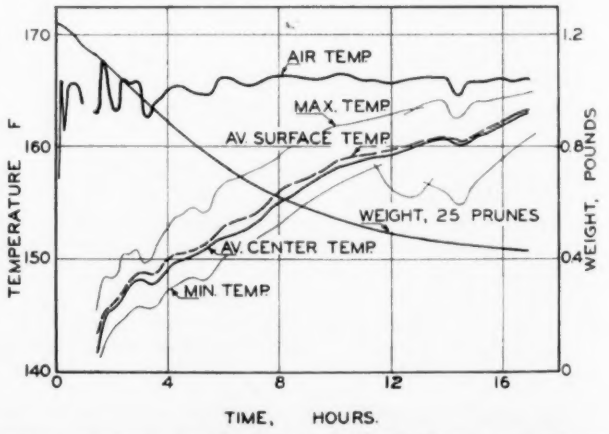


Fig. 9 Weight of 25 Prunes, Air Temperature, and Average Temperature of Prune Surface and Prune Center; Run 4

the tray caused by shrinking. This would permit part of the prune to dry slowly for a time, and then evaporate rapidly when it loosened, giving a temporary depression for a limited area.

The mean difference between the top-, side-, or bottom-surface temperature and the center temperature, was computed by giving the side point 4 times the weight accorded the top and bottom

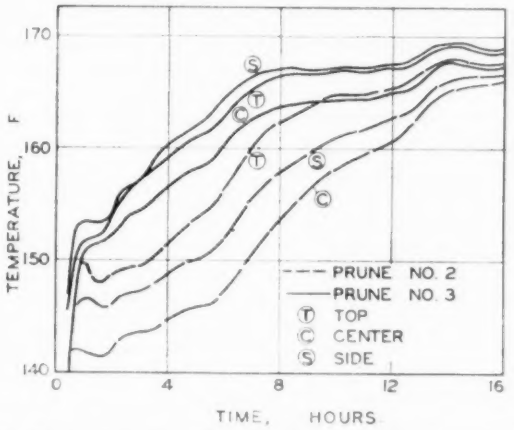


FIG. 10 TEMPERATURES OF TOP, SIDE, AND CENTER; PRUNES NOS. 2 AND 3, RUN 2

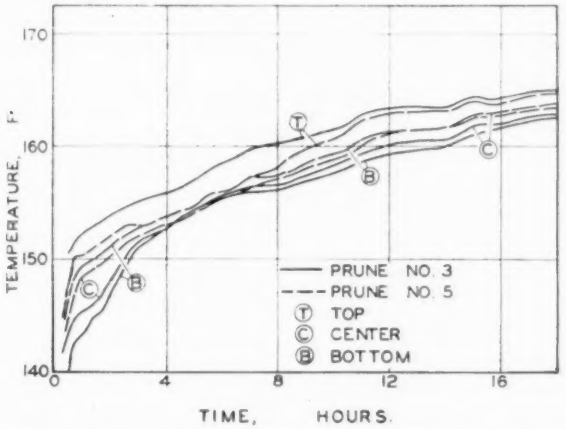


FIG. 11 TEMPERATURES OF TOP, CENTER, AND BOTTOM; PRUNES NOS. 3 AND 5, RUN 3

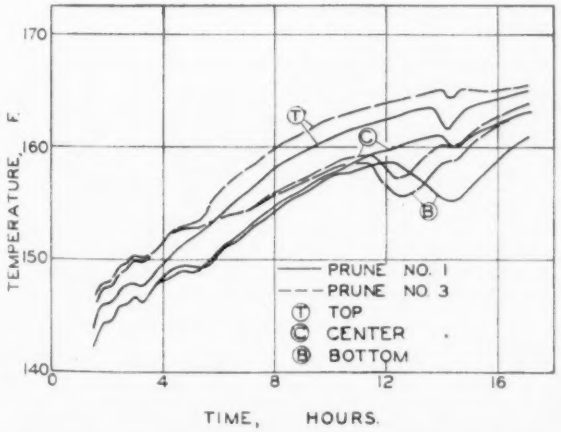


FIG. 12 TEMPERATURES OF TOP, CENTER, AND BOTTOM; PRUNES NOS. 1 AND 3, RUN 4

points, because the arrangement of the prunes on the tray suggests that about these proportions of its surface have similar exposures. Unfortunately, this was not realized when the tests were planned, so that the points were not placed in these proportions. From the mean center temperature of the five prunes, and the mean surface-to-center difference, the mean surface temperature was found. From the surface temperature and the

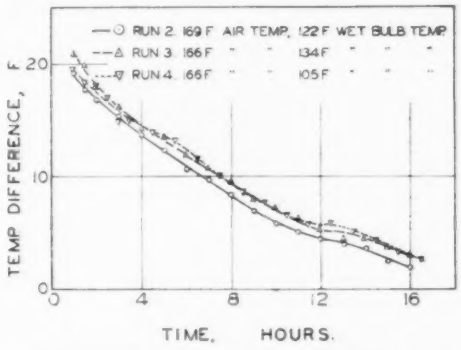


FIG. 13 DIFFERENCE BETWEEN AIR AND PRUNE AVERAGE SURFACE TEMPERATURE

air temperature, the differences between the air and the prune-surface temperatures were obtained, as shown in Fig. 13.

Evaporation Rate. The evaporation rate is indicated by graphs of free-moisture ratio (pounds of free moisture per pound of dry matter), plotted against time on semilogarithmic coordinates, Figs. 14, 15, and 16. The free-moisture ratios were calculated from the prune-weight data, the final-moisture content, and the equilibrium-moisture data, Table 2. The points on these curves did not fall on a single straight line, the slope becoming greater in the middle of the drying period and falling off at the end. For each straight section, the moisture ratio is

$$F = F_1 e^{-B\theta} \quad [8]$$

and the evaporation rate $$\frac{dF}{d\theta} = -BF_1 e^{-B\theta} = -BF \quad [9]$$

TABLE 2 EQUILIBRIUM-MOISTURE RATIOS FOR FRENCH PRUNES AT 150 F (4)

Relative humidity, per cent	Moisture ratio: Pounds moisture / Pounds dry matter
18	0.044
28	0.052
62	0.34
74	0.63
81	1.05
95	1.75

Heat Transfer. The rate of heat transfer to the prune was taken to be the sum of the sensible- and latent-heat rates. The sensible-heat rate per pound of dry matter is the product of the rate of temperature rise and the heat capacity per pound of dry matter. The unit heat capacity of cellulose and levulose being about 0.3 Btu/lb F, the heat capacity per pound of dry matter is

$$c_d = 0.3 + 1.0M \quad [10]$$

The latent-heat rate per pound of dry matter was taken to be the latent heat of water at the temperature of the surface, multiplied by the evaporation rate per pound of dry matter. This calculation neglects the heats of solution of dissolved components, which are not known, but which are probably small. Except during the first half hour, when the rate of temperature rise is high, and the rate of evaporation low or possibly negative, the sensible-heat rate is less than 1 per cent of the latent-heat rate.

In order to compute the unit surface conductances, it was first

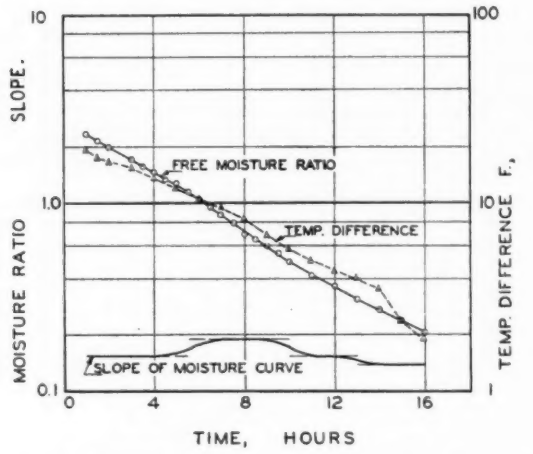


FIG. 14 FREE-MOISTURE RATIO AND TEMPERATURE DIFFERENCE; RUN 2

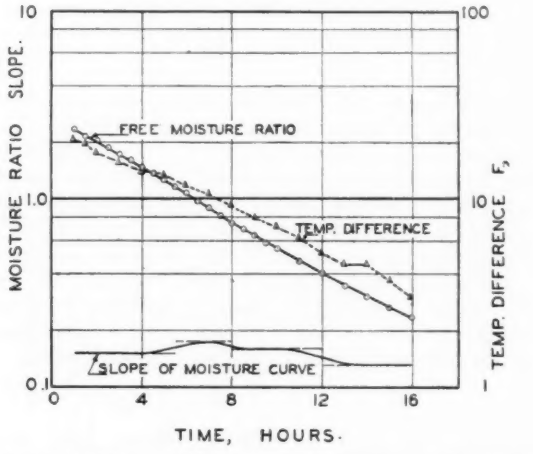


FIG. 15 FREE-MOISTURE RATIO AND TEMPERATURE DIFFERENCE; RUN 3

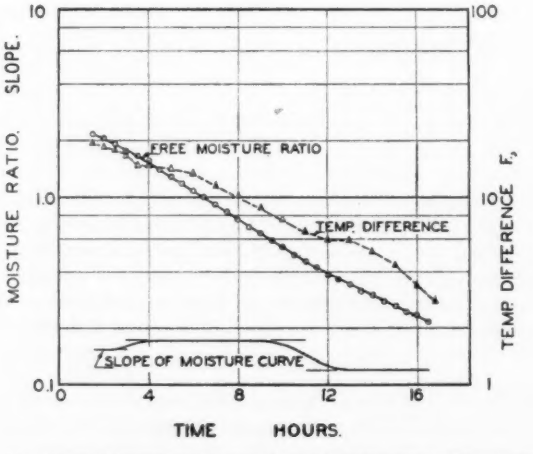


FIG. 16 FREE-MOISTURE RATIO AND TEMPERATURE DIFFERENCE; RUN 4

necessary to find the surface area of the prunes. The initial surface area was taken to be that of a spheroid with a major axis that of the prune, and a minor axis the mean of the two minor axes, which were nearly equal. The final surface area was found from the area data of the dried samples in the second group of tests. The 3, 6, 10 and 16-hr samples were found to have a dried-skin area of 70, 67, 74, and 62 per cent, respectively, of the initial spheroid surface, averaging 68 per cent. Lineal shrinkages of strips cut in two directions around a prune were 78 and 82 per cent, representing an area shrinkage of 64 per cent, but the figure of 68 per cent from the second group of tests was thought to be more reliable. In order to establish the surface area as a function of the moisture ratio, an additional point was obtained from the observation that the prunes were beginning to wrinkle at about 2-hr drying time, when the moisture ratio was about 2.05. At this time, the moisture loss has been primarily from the outer layers, and the volume shrinkage has corresponded to the skin-area shrinkage so that wrinkling has not occurred. After this, the skin does not dry or shrink as rapidly as the prune does, so that wrinkling results.

The relation between prune volume and moisture ratio was found by plotting average density, as found from the initial and final volume and weight data, against moisture content on a wet basis, giving nearly a straight line, Fig. 17. To facilitate calculations, this was converted to density as a function of moisture ratio, and is given with prune-volume and surface-area data in Fig. 18. The volume at a moisture ratio of 2.05 was then used to fix the surface area of the spheroid at this moisture ratio, wrinkling just having started as previously noted. The surface area-moisture ratio curve in Fig. 18 is strictly valid only for the dehydrator conditions of the tests. In counterflow, and other dehydrator arrangements, where the temperature and humidity change from point to point, the relation between the moisture

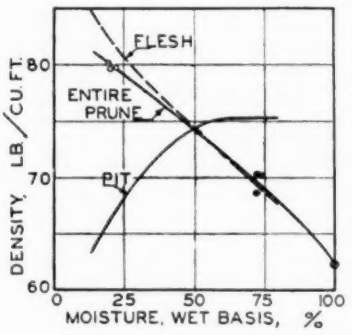


FIG. 17 PRUNE-MOISTURE CONTENT AND DENSITY

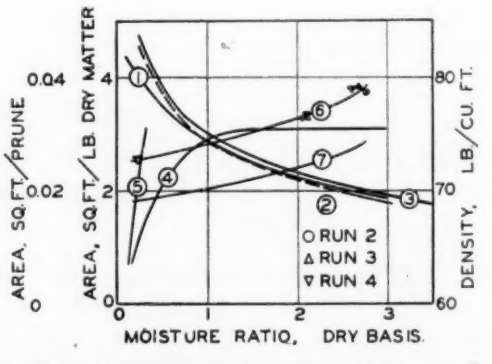


FIG. 18 PRUNE-MOISTURE RATIO, SURFACE AREA, AND DENSITY

Curve 1 Density of entire prune vs. moisture ratio of prune
Curve 2 Density of prune flesh vs. moisture ratio of prune
Curve 3 Density of prune flesh vs. moisture ratio of flesh
Curve 4 Density of pit vs. moisture ratio of prune
Curve 5 Density of pit vs. moisture ratio of pit
Curve 6 Surface area, sq ft per prune vs. moisture ratio of prune
Curve 7 Surface area, sq ft per lb of dry matter vs. moisture of prune

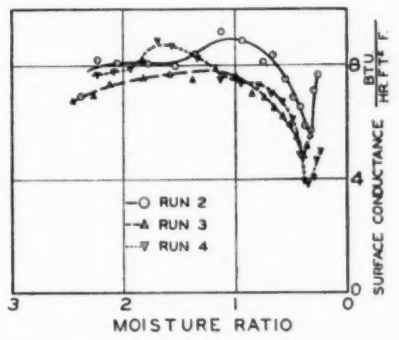


FIG. 19 SURFACE THERMAL CONDUCTANCE PER SQUARE FOOT

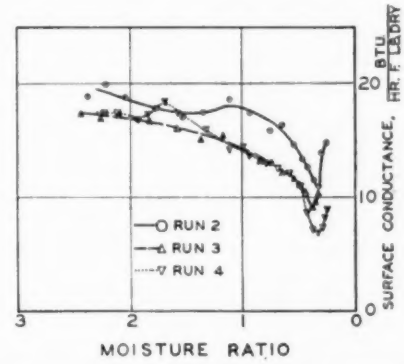


FIG. 20 SURFACE THERMAL CONDUCTANCE PER POUND DRY MATTER

content of the surface and interior will vary, and the surface area-moisture ratio curves will differ somewhat.

With the surface-area, temperature-difference, and heat-rate data in hand, the unit surface thermal conductances were calculated, both on a prune-surface area and a dry-weight basis, and are given in Figs. 19 and 20. The conductance on a surface-area basis is the conventional conductance, but that on a dry-weight basis is more readily usable and avoids the uncertainty of the actual prune-surface area. The conductance at first increases as drying proceeds, remains nearly constant for a time, drops appreciably near the end of drying, and then seems to rise again. The final drop and rise are puzzling, but were observed in all three runs.

Vapor Conductance and Concentration. In order to find the difference in vapor concentration at the prune surface and in the air stream, the unit surface vapor conductance is required. This is obtained from the observed thermal conductance, using the heat-mass-transfer analogy. According to Boelter, Cherry, and Johnson (5), the Nusselt modulus for mass transfer ($f'D/\alpha$) can be predicted from the Nusselt modulus for heat transfer (fD/k), and the Prandtl moduli for mass and heat transfer, ($\mu/\alpha\gamma$ and $c\mu/k$), as follows

$$\left(\frac{f'D/\alpha}{fD/k}\right) = \left(\frac{\mu/\alpha\gamma}{c\mu/k}\right)^n \quad \ldots\ldots\ldots\ldots\ldots\ldots [11]$$

where n is the experimentally determined exponent of the Prandtl modulus for the analogous heat-transfer system. McAdams (6) recommends a value of 0.3 for n for fluids flowing normal to tubes and banks of tubes. Canceling in Equation [11], and using 0.3 for n

$$f'/\alpha = f/k(k/c\gamma\alpha)^{0.3} \quad \ldots\ldots\ldots\ldots\ldots\ldots [12]$$

At 166 F, the value of k for dry air (International Critical Tables) is 0.0156 Btu/ft hr F, and from Hilpert's data, reported

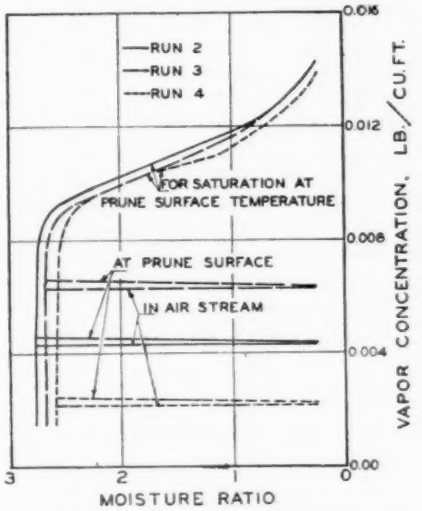


FIG. 21 VAPOR CONCENTRATION AT PRUNE SURFACE

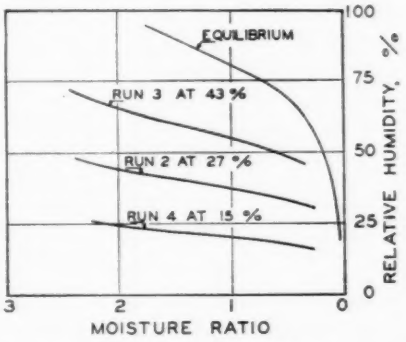


FIG. 22 RELATIVE HUMIDITY AT PRUNE SURFACE

by Boelter, Cherry, and Johnson (5), α is 1.28 sq ft per hr. The density of dry air at this temperature is 0.063 lb per cu ft and the unit heat capacity is 0.24 Btu/lb F. Substitution of these values in Equation [12] gives, for the conditions of these tests

$$f' = 77f \quad \ldots\ldots\ldots\ldots\ldots\ldots [13]$$

The air-vapor mixture adjacent to the prune has an appreciable humidity and a temperature below 166 F, particularly at early stages of drying, but corrections for temperature and humidity will not change the constant of 77 by more than 1 per cent. As shown in Equation [3], the vapor-concentration difference depends upon the evaporation rate and the surface conductance. Rearranging Equation [3], and introducing the equivalent of f' from Equation [13]

$$C_i - C_\infty = 0.013\, w/fA \quad \ldots\ldots\ldots\ldots\ldots\ldots [14]$$

It was more convenient to use, instead of the evaporation rate w, the rate per pound of dry matter from Equation [9], $-BF$, and the surface area per pound of dry matter, A_d, which gave

$$C_i - C_\infty = -0.013BF/fA_d \quad \ldots\ldots\ldots\ldots\ldots\ldots [15]$$

Vapor-concentration differences and vapor concentrations at the prune-air interface are given in Fig. 21. The vapor concentrations for saturation at the prune-surface temperatures, needed in finding the relative humidity at the prune-air interface, are also shown. These curves are based on a uniform air temperature of 166 F, using the data in Fig. 13, to give prune-surface temperatures, and adding the vapor-concentration differences to

TABLE 3 PRUNE MOISTURE-DISTRIBUTION DATA

Time of removing sample, hr	3	6	10	16
Weight, lb:				
Initial, top flesh	0.0053	0.0085	0.0075	0.0054
Initial, side flesh	0.0191	0.0185	0.0215	0.0232
Initial, bottom flesh	0.0057	0.0062	0.0059	0.0048
Initial, inner flesh	0.0121	0.0091	0.0095	0.0114
Initial, pit	0.0022	0.0024	0.0023	0.0024
Initial, entire prune	0.0443	0.0446	0.0467	0.0473
Final, top flesh	0.0036	0.0042	0.0027	0.0017
Final, side flesh	0.0137	0.0099	0.0079	0.0075
Final, bottom flesh	0.0042	0.0038	0.0026	0.0016
Final, inner flesh	0.0107	0.0061	0.0045	0.0041
Final, pit	0.0022	0.0024	0.0022	0.0022
Final, entire prune	0.0344	0.0264	0.0199	0.0170
Moisture ratio, pounds of moisture per pound of dry matter:				
Initial, all flesh	3.40	3.34	3.04	2.82
Initial, pit	0.34	0.34	0.34	0.34
Initial, entire prune	2.90	2.83	2.63	2.46
Final, top flesh	1.91	1.11	0.43	0.20
Final, side flesh	2.15	1.28	0.46	0.22
Final, bottom flesh	2.16	1.64	0.75	0.20
Final, inner flesh	2.82	1.85	0.87	0.36
Final, pit	0.34	0.33	0.27	0.17
Final entire prune	2.03	1.26	0.55	0.24
Density, lb per cu ft:				
Initial, all flesh	69.0	69.1	69.5	69.9
Initial, pit	75.5	75.5	75.5	75.5
Initial, entire prune	69.3	69.6	69.8	70.2
Final, top flesh	71.8	74.5	80.5	84.5
Final, side flesh	71.3	73.7	80.2	84.2
Final, bottom flesh	71.3	72.5	76.9	84.7
Final, inner flesh	69.9	72.0	76.0	81.6
Final, pit	75.5	75.1	71.5	66.0
Final, entire prune	70.9	73.3	77.2	80.2
Free-moisture concentration, lb per cu ft:				
Initial, all flesh	53.1	53.0	52.1	51.3
Final, outer flesh	48.1	41.1	25.4	12.4
Final, inner flesh	51.5	46.3	34.4	20.0
Free-moisture concentration ratio, final/initial:				
Outer flesh	0.91	0.78	0.49	0.24
Inner flesh	0.97	0.88	0.66	0.39
Volume, cu ft:				
Initial, outer flesh	0.000436	0.000481	0.000503	0.000477
Initial, inner flesh	0.000174	0.000132	0.000137	0.000163
Initial, pit, and 1/2 inner flesh	0.000117	0.000097	0.000099	0.000114
Initial, pit, inner, 1/2 outer flesh	0.000422	0.000414	0.000418	0.000434
Initial, entire prune	0.000639	0.000644	0.000671	0.000673
Final, top flesh	0.000050	0.000056	0.000034	0.000020
Final, side flesh	0.000192	0.000134	0.000098	0.000089
Final, bottom flesh	0.000058	0.000052	0.000034	0.000019
Final, inner flesh	0.000154	0.000085	0.000059	0.000050
Final, pit	0.000030	0.000031	0.000031	0.000032
Final, pit, and 1/2 inner flesh	0.000107	0.000074	0.000060	0.000057
Final, pit, inner, 1/2 outer flesh	0.000334	0.000238	0.000173	0.000146
Final, entire prune	0.000485	0.000358	0.000257	0.000211
Axis lengths, ft:				
Initial, major	0.132	0.133	0.135	0.136
Initial, average minor	0.102	0.102	0.104	0.104
Final, major, of equal spheriod	0.117	0.106	0.094	0.089
Final, minor, of equal spheriod	0.089	0.081	0.072	0.068
Surface areas, sq ft:				
Initial spheroid	0.0378	0.0381	0.0390	0.0396
Final spheroid of equal volume	0.0290	0.0239	0.0189	0.0169
Dried skin, top	0.0053	0.0054	0.0056	0.0054
Dried skin, side	0.0161	0.0152	0.0172	0.0137
Dried skin, bottom	0.0051	0.0048	0.0060	0.0055
Dried skin, total	0.0265	0.0254	0.0288	0.0246
Final, top of equal spheroid	0.0058	0.0051	0.0037	0.0037
Final, side of equal spheroid	0.0176	0.0143	0.0113	0.0094
Final, bottom of equal spheroid	0.0056	0.0045	0.0039	0.0038
Depth of slice, volume/area, ft:				
Final, top	0.0086	0.0110	0.0092	0.0054
Final, side	0.0109	0.0094	0.0087	0.0095
Final, bottom	0.0105	0.0116	0.0086	0.0050
Depth ratio, depth/minor semiaxis:				
Final, top	0.19	0.27	0.25	0.16
Final, side	0.24	0.23	0.24	0.28
Final, bottom	0.24	0.29	0.24	0.15
Mean radius of sphere of equal volume, during time increment, ft:				
Inner flesh	0.029	0.028	0.026	0.024
Outer flesh	0.045	0.041	0.036	0.033
Entire prune	0.052	0.047	0.041	0.038
Mean radius ratio, fraction of entire prune mean radius:				
Inner flesh	0.56	0.60	0.62	0.64
Outer flesh	0.87	0.88	0.88	0.88

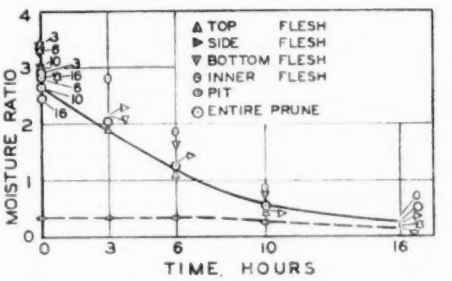


FIG. 23 MOISTURE RATIOS OF SUBDIVISIONS OF PRUNE FLESH

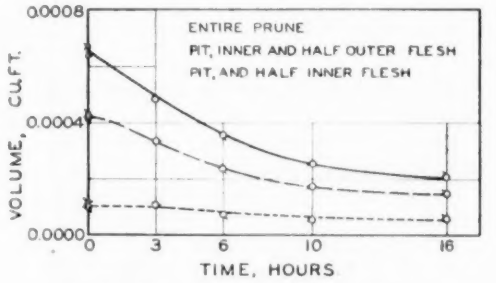


FIG. 24 PRUNE VOLUME DURING DRYING

the average vapor concentration for each run. This was done to avoid distraction by insignificant fluctuations which would result from plotting the data directly with its short-time irregularities in air temperature and humidity. The relative humidities at the prune-air interface, calculated from vapor concentration and vapor concentration for saturation, from Fig. 21, are given in Fig. 22.

Moisture Distribution. The first moisture-distribution test was of limited value because the depth of cut was not evaluated. The second run yielded the data in Table 3, upon which Fig. 23 is based. In comparing the moisture concentrations in top, side, and bottom slices, variations in depth of cut, noted in Table 3, must be borne in mind.

To determine the depth of cut, the volume and surface area of each section was needed, the weight of dry matter and moisture content being known. The area was given directly by planimetering the dried skin, as previously described. The density of the flesh, used in finding the volume, was obtained by subtracting weight and volume values for the pit from those for the whole prune, yielding separate density data for flesh and pit, given in Figs. 17 and 18.

The sets of original data for the 3, 6, 10, and 16-hr observations were necessarily on different lots of similar prunes, which as can be seen in Table 3 varied in initial dimensions and moisture content. In order to estimate what the condition of each sample would have been at the other times, the time-volume curves in Fig. 24 were prepared.

DISCUSSION OF RESULTS

Drying rates in these tests were a little slower than those indicated by Guillou's Equation [2] for drying in hardware cloth racks

$$B = 0.2(t/165)^{4}(V/600)^{0.2}\frac{(100-H)}{60}(N/50)^{0.67}\ldots[16]$$

The mean drying coefficients for a change of moisture ratio from 2 to 0.2 lb per lb were 93, 87, and 99 per cent, respectively, of the prediction of equation for Runs 2, 3, and 4 of the first group, and 93 per cent of the predicted value for the 16-hr sample of the second group.

Temperature of Drying Prunes. Temperature differences be-

tween air and prune were nearly the same for all three runs, Fig. 13, even though the wet-bulb depressions were 32.5, 47, and 61 deg for Runs 3, 2, and 4, respectively. This result is in accordance with the fact that the drying rate is not appreciably affected by changes in relative humidity of the dehydrator air below 35 per cent. The temperature difference depends primarily upon the drying rate and the surface conductance; thus, if the drying rates and surface conductances are the same, temperature differences will also be the same.

It does not seem worth while to develop an equation giving prune temperatures directly, because, in the usual commercial dehydrator, constant drying conditions do not occur. The air-to-prune temperature difference can be estimated from the drying rate and surface conductance. Then the prune temperature can be obtained by subtracting the temperature difference from the air temperature. The surface thermal conductance per pound of dry matter can be given roughly for these runs as

$$fA_d = 10 + 4M \quad \ldots\ldots\ldots\ldots\ldots\ldots [17]$$

At the start of drying, this can be expected to vary with the 0.8 power of the air velocity, the flow pattern being that in a channel, while near the end of drying it may vary with the 0.6 power, flow being around irregular shapes on the tray surface. It will be proportional to the prune count to the $^2/_3$ power, since it is expressed on a unit-weight basis, for which the surface is proportional to the $^2/_3$ power of the number of prunes per pound. It will be a little higher for tray loadings of less than 4 lb per sq ft, but will be materially reduced by heavier loadings which can be obtained only by piling prunes, obstructing air access to prune surface.

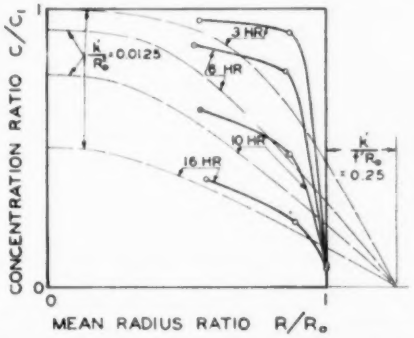


FIG. 25 MOISTURE DISTRIBUTION DURING DRYING

Vapor Concentration and Relative Humidity. The vapor-concentration difference between the prune surface and the air stream is small, so that it has a minor influence upon vapor concentration at the surface. The relative humidity at the prune surface is dependent primarily upon the vapor concentration in the air stream and the surface temperature of the prune. The evaporation rate is not greatly influenced by the relative humidity of the air stream until the relative humidity at the prune surface rises high enough to raise the equilibrium-moisture ratio appreciably. As shown in Table 2, the equilibrium-moisture content does not rise rapidly with relative humidity until humidities of over 50 per cent are reached. The free-moisture ratio (total- minus equilibrium-moisture ratio) was not greatly influenced by raising the air-stream relative humidity from 15 to 27 per cent, Fig. 22, but the further rise to 43 per cent reduced the free-moisture ratio materially at the start of drying.

As the end of drying is approached, the relative humidity at the prune surface drops because the prune-surface temperature approaches that of the air. A low relative humidity is important here if a low final-moisture ratio is required.

Moisture Distribution. A simple, but inadequate, ideal system with which to compare the moisture-distribution data, is that of a homogeneous sphere which dries without shrinking, with a constant moisture conductivity and a constant surface vapor conductance. The moisture distribution for this sphere can be found directly from its thermal analog. Assuming k'/R_0^2 to be constant at 0.0125 (1/hr) and $k'/f'R_0$ to be 0.25, the moisture-concentration ratios are given by the dashed curves in Fig. 25, using values for temperature distribution in a sphere from McAdams (6) or Boelter et al (5). These constants were arbitrarily selected to approximate the actual distribution at 16 hr.

From the volumetric data of Table 3, the mean radius with respect to volume was computed for the outer surface, outer layer of flesh, and inner layer of flesh, for each of the time intervals (viz., 0–3 hr, 3–6 hr, 6–10 hr, and 10–16 hr) of the moisture-distribution run. The free moisture concentration in pounds per cubic foot was then expressed as a fraction of the initial free moisture concentration, and plotted against the mean radius ratio in Fig. 25. The surface concentration was taken to be that in equilibrium with the prune-surface air-vapor mixture, at the relative-humidity values in Fig. 22. The departure of all the surface points, and the internal points at times other than 16 hr, from the ideal system is marked. The comparison is of course considerably qualified by the fact that the observed points are placed at the mean radius ratios of the sphere which was changing in volume with time. The result is similar to that noted for a slab of soap by Hougen, McCauley and Marshall (7).

The concentration gradients, represented by the observed points, indicate that the moisture conductivity within the prune decreases as the flesh becomes drier. As long as the thickness of the layer of decreased conductivity is not too great, the resistance is not greatly increased because the path is short and the cross section, nearly that of the prune surface, is large. Near the end of drying, however, the distance that moisture must travel through low-conductivity material is greater, and the path near the center is of smaller cross-sectional area, so that the drying rate tends to drop off. If prunes are to be dried only to 20 per cent moisture (16.7 per cent on a wet basis), the departure from a logarithmic curve is not pronounced, but for low terminal-moisture contents, a reduced drying rate can be expected.

SUMMARY AND CONCLUSIONS

1 The temperature difference, air stream to prune surface, dropped from 20 F at the end of the first hour, to 3 F at the end of drying, for prunes drying from a moisture content of 2.7 to 0.27 lb per lb of dry matter in 16 hr.

2 The unit surface thermal conductance rose from 7 Btu/hr ft² F at the start of drying to 8 at intermediate stages, and then dropped to 6, at an over-all air velocity of 600 fpm, measured in the free tunnel cross section.

3 Changes of air-stream relative humidity do not appreciably influence drying rates of prunes if the relative humidity is less than 35 per cent because:

(*a*) The equilibrium moisture content - relative humidity curve does not rise rapidly until relative humidities over 50 per cent are reached.

(*b*) The concentration difference between the prune surface and the air stream is small. The moisture conductivity of prune flesh is low, compared with the surface conductance, so that most of the resistance is within the prune.

(*c*) The prune-surface-temperature depression is only a fraction of the wet-bulb depression, so that the vapor concentration required for saturation at the prune-surface temperature is much higher than it would be at the wet-bulb temperature.

4 The moisture distribution within a prune during drying indicates a decrease in moisture conductivity with decrease in

moisture content, so that the differential equation for diffusion for a system with constant properties (the Poisson-Fourier equation) is not applicable.

5 Although the drying rate is nearly proportional to the free-moisture ratio in the usual drying range (down to 0.2 lb of moisture per lb of dry matter), it decreases for lower moisture contents, because of the decrease in moisture conductivity of prune flesh. Extrapolation of the evaporation rate moisture content curve beyond the usual drying range thus intersects the moisture-content axis at an abnormally high value which does not coincide with observed equilibrium-moisture-content values. This is of commercial importance only where very low final-moisture contents are required.

ACKNOWLEDGMENTS

The author wishes to thank Coby Lorenzen, Jr., for preparing and installing the thermocouples in the prunes; B. D. Moses, Rene Guillou, and Coby Lorenzen, Jr., who helped in conducting the tests; and L. M. K. Boelter who gave stimulating suggestions on technique and on the analysis of results.

BIBLIOGRAPHY

1 1941 Project Report, California Committee on the Relation of Electricity to Agriculture, by B. D. Moses, W. V. Cruess, et al., p. 727; on file in the Agricultural Engineering Division, University of California, Davis, Calif.

2 "Developments in Fruit Dehydrator Design," by Rene Guillou, *Agricultural Engineering*, vol. 23, 1942, pp. 313–316.

3 "Construction of Farm Dehydrators in California," by A. W. Christie and G. B. Ridley, *Journal*, A.S.H.V.E., vol. 29, 1923, pp. 687–716.

4 M.S. Thesis in Mechanical Engineering, by Rene Guillou, 1942; on file in the Engineering Library, University of California, Berkeley, Calif.

5 "Heat Transfer Notes," by L. M. K. Boelter, V. H. Cherry, and H. A. Johnson, University of California Syllabus Series, second edition, 1942, chapt. XVI, pp. 14, 15; chapt. V, p. 44.

6 "Heat Transmission," by W. H. McAdams, McGraw-Hill Book Company, Inc., New York, N. Y., second edition, 1942, p. 226.

7 "Limitations of Diffusion Equations in Drying," by O. A. Hougen, H. J. McCauley, and W. R. Marshall, Jr., Trans. American Institute of Chemical Engineers, vol. 36, 1940, p. 190.

A New Approach to the Problem of Conditioning Water for Steam Generation

By R. E. HALL,[1] PITTSBURGH, PA.

Modern boilers, because of their high operating pressures and ratings, and their high rates of heat adsorption, intensify the problems associated with the continuous operation which is of such critical importance in our vast productive program. For instance, actual consumption of the boiler tubes by the high-pressure boiler water must be continuously guarded against. Destructive boiler scale such as that composed of sodium silicate, sodium-aluminum and sodium-iron silicates, sodium sulphate and sodium phosphate, must not be permitted to form. The boilers must not fill up with sludge, and the turbines must be kept free of deposits on their intricate blading. Suspecting that sodium for a number of reasons is of destructive influence in the boiler water, the author has initiated building boiler waters on a potassium basis, with affirmative results that are set forth in this paper.

Starting with substitution in the boiler water of potassium for the universal sodium equilibrium, the author has been led to give consideration to the problems of "hide-out" of boiler-water salts, corrosion by the bonded oxygen of the boiler water, silica in boiler and turbine, equilibria developed in the superheater in any carry-over of boiler water, and under certain conditions, protection from embrittlement. In systematizing the results which must ensue from the complex network of interrelations of temperature, pressure, and concentration, under these conditions, he makes use of the conceptions of the concentrating-film boiler water, generalizes the temperature-pressure-concentration relations in the form of a Δt function, and points out how the relationship of incongruent solubility between water and the silicates must be controlled.

Introduction

SOME years ago, introduction of equilibrium-wise thinking into boiler-water chemistry brought into use maintenance of the phosphate equilibrium in the boiler water as the final step in its conditioning for elimination of the alkaline earth-metal scales. Inasmuch as engineers were demanding larger boiler units, higher pressures, higher ratings, and higher rates of heat absorption, but, particularly in the industrial field, felt well-nigh frustrated by the drastic restrictions (1)[2] on feedwater deemed necessary therefor, this innovation was timely in removing these restrictions, and thus contributing to the progress achieved in attainment of the objectives sought.

Scarcely were the alkaline earth-metal scales under control, however, when new difficulties arose in the form of siliceous deposits comprising silica and sodium silicate, sodium-aluminum and sodium-iron silicates. The phosphate equilibrium was not designed to, nor could it, prevent their formation. At about the same time, another phenomenon, the hiding-out of boiler-water salts in the boilers of high pressure and high rating, became well recognized. Purer water for the boiler was conceived to be an answer to this problem, but the purer boiler waters which resulted brought to light a problem of their own, namely, furrowing and channeling of tubes, with development of large amounts of magnetic iron oxide, and final failure; or, development of large quantities of magnetic iron-oxide sludge without channeling or furrowing in evidence at any special point. Since these cases of special corrosion have been attributed to dissolved oxygen entering the boiler in the feedwater, tremendous effort and expense have been brought to bear on removal of the last vestige of dissolved oxygen from the feedwater, but without remedying the condition. As a last straw, as boiler-water alkalinities have been lowered almost to the vanishing point in another move to combat such corrosion, there has arisen an epidemic of silica deposition in the lower pressure stages of turbines, not amenable to steam-washing, but requiring caustic-washing (26) or complete shutdown of the unit for cleaning. Elimination of the silica content in the boiler water would seem to be the obvious move to make; but soft boiler deposits, relatively high in magnesium content, and not removable by blowdown, then become another cause of irritation and distress.

Faced with deficiencies of circulation in hard-worked tubes that might very well function as planned if these other problems were solved, the engineers have come to the point of bluntly questioning the chemists whether further progress in conditioning boiler waters is possible.

Inauguration of Potassium Equilibrium in Boiler Water

During the summer of 1942, with the end in view of attempting to break the deadlock which existed relative to solving these different problems, we inaugurated the drastic change of maintaining the boiler water on a potassium equilibrium, in place of the sodium equilibrium which has characterized boiler waters from the beginning of steam generation. As illustrated in Table 1, boiler deposits in the evaporative sections, before the advent of phosphate equilibrium in the boiler water, consisted mainly of calcium and magnesium salts with variety provided at times by silica, sodium silicate, and magnetic oxide of iron. After the advent of phosphate equilibrium, the deposits as illustrated in Table 2, while containing minor amounts of calcium

[1] Director, Hall Laboratories, Inc. Mem. A.S.M.E.

[2] Numbers in parentheses refer to the Bibliography at the end of the paper.

Contributed by the Joint Research Committee on Boiler Feedwater Studies and presented at the Annual Meeting, New York, N. Y., Nov. 29–Dec. 3, 1943, of The American Society of Mechanical Engineers.

Note: Space does not permit publication as an appendix of the tabulated data which have been used, but a complete set of these tables is on file at the Engineering Societies Library, 29 West 39th Street, New York, N. Y., for reference. The original data are available in the references of the Bibliography.

Statements and opinions advanced in papers are to be understood as individual expressions of their authors and not those of the Society.

and magnesium salts, were dominated instead by sodium salts, i.e., sodium silicate, sodium-aluminum silicate, sodium-iron silicate, sodium phosphate, and sodium sulphate, along therewith, silica and magnetic oxide of iron.

It was decided to get rid of sodium in the boiler water and to substitute potassium therefor. Potassium and sodium are chemical equivalents, but are not always peers chemically, as is well illustrated by the simple examples of hard and soft soaps, and such differences as make potassium silicate a preferred binder in special flux coatings for welding rods, and a more successful vehicle than sodium silicate for pigments in some decorative paints (39). The problem to be studied was whether the substitution of potassium for sodium might demonstrate a difference at the temperatures and pressures of the boiler-water cycle which would eliminate alkali-metal deposits.

Messrs. L. E. Hankison and M. D. Baker of the West Penn Power Company expressed willingness that this experiment be put into practice at the Springdale Station of the company. It was Hankison, who at the same station had previously carried on the experimental work in practical operation for the phosphate equilibrium (2).

From the time it started, this work has continued at Springdale and, because results are remarkably definite, will continue. Meanwhile, in the early spring of 1943, with the results at Springdale as a background, we brought the system of potassium equilibrium to the attention of the engineers in a few plants which had specific problems to which the system pertained.

Fundamental Phenomena of the Boiler-Water Cycle

The troublesome problems, which have been noted, existed in mild form in the older lower-pressure boilers, but were considerably minimized by low ratings and by scale formation. The cleaner boilers that have resulted from phosphate-equilibrium treatment, along with higher pressures, temperatures, ratings, and higher rates of heat absorption, have magnified these trouble-making factors seriously.

Why?

To answer that question, we must bring clearly into focus what happens as the dilute over-all boiler water traverses those surfaces where steam is generated, where the boiler tubes are exposed on the heated side to furnace temperatures of 2000 to 2500 F, where they must rapidly absorb the furnace heats both of radiation and convection, and must transfer this heat to the water they contain at a rate such that their external surfaces will remain at 800 to 900 F, or thereabouts. In the boiler-tube raceway, unimpeded flow of boiler water and formation of myriad steam bubbles therefrom interest us most.

Whatever may be the mechanism by which the steam bubbles form, Fig. 1 will serve to illustrate, conventionally, a transient state of affairs with billions of recurrences. What happens on the tube surface *A* under the steam bubble? Partridge (3) a

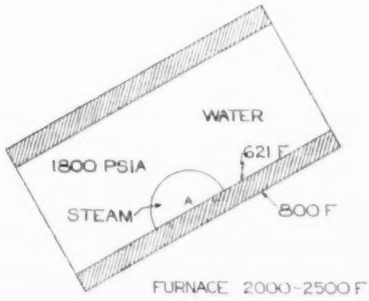


Fig. 1 Transient State of Affairs With Billions of Recurrences

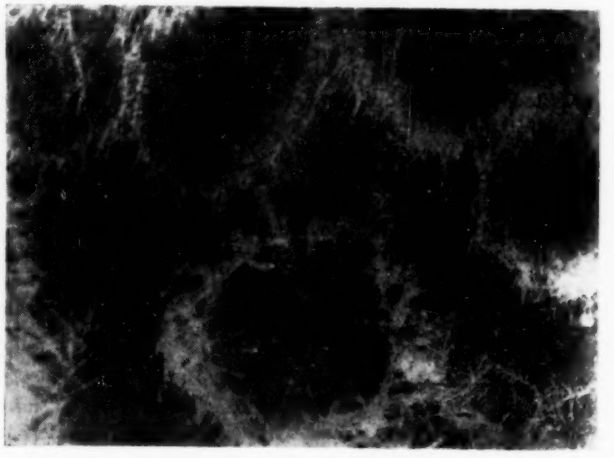


Fig. 2 Mechanism of Formation of Calcium-Sulphate Scale

number of years ago initiated the move to answer that question when he photographed the process of calcium-sulphate scale formation, as shown in Fig. 2. In explanation, he stated: "Due to the great increase in resistance to heat flow of the gas film over the resistance of the liquid film, the metal surface tended to overheat locally, in the area within the interface." Along therewith, the film of boiler water covering the surface under the bubble concentrated or evaporated, and deposited its content of calcium sulphate in the form of scale at the periphery of the contact of the bubble with the tube surface.

May we assume therefore that wherever a steam bubble forms, or where the more severe conditions of steam-blanketing,

TABLE 1 EXAMPLES OF BOILER (EVAPORATIVE SECTION) SCALES WITHOUT PHOSPHATE TREATMENT OF BOILER WATER

	Per cent			
	1	2	3	4
Calcium sulphate	74.8	3.4	1.2	33.3
Calcium carbonate	3.9	31.8	4.8	0.5
Calcium silicate	2.7	..	61.5	..
Magnesium carbonate	..	1.3	..	..
Magnesium silicate	11.5	28.7	4.1	4.6
Magnesium hydroxide	4.3	21.6	..	1.4
Magnetic iron oxide	0.4	7.5	6.7	54.8
Aluminum oxide	..	..	..	0.7
Moisture and organic	1.5	7.2	5.7	5.4
Sodium silicate	..	..	13.2	..
Silica	..	..	5.3	..

TABLE 2 EXAMPLES OF BOILER (EVAPORATIVE SECTION) SCALES WITH PHOSPHATE EQUILIBRIUM MAINTAINED IN BOILER WATER

	Per cent							
	1	2	3	4	5	6	7	8
Calcium phosphate	0.9	8.7	6.9	16.5	10.1	3.6	23.5	2.8
Magnesium phosphate	0.4	5.2	3.0	6.6	1.9	1.1	1.8	..
Magnesium silicate	..	..	4.6	..	2.8	2.5	0.9	..
Moisture and organic	0.8	3.0	0.7	3.3	5.7	8.6	2.4	..
Magnetic iron oxide	1.9	13.9	19.6	19.2	..	1.7	47.1	97.8
Copper	..	6.8	..	7.2	..	..	20.6	..
Sodium sulphate	..	5.0	8.5	..	..	..	0.9	..
Sodium phosphate	0.2	11.5	20.0	0.3	..	..	0.3	..
Sodium silicate	3.3	0.8	..	21.6	0.6	..	..	..
Sodium-aluminum silicate	86.7	45.0	37.6	24.2	35.0	..	..	..
Sodium-iron silicate	..	..	..	..	28.9	64.9	..	..
Silica	5.1	..	..	..	16.5	19.9	..	..

or film-boiling, as noted by Davidson and Associates (4, 5) occur, the film of boiler water on the surface will evaporate to dryness,[3] or so concentrate as to deposit its salt in solid form? To answer that question, let us consider the experiment illustrated in Fig. 3. In the flask, with its vapor-containing wall carefully insulated against loss of heat, a dilute solution of calcium chloride is boiling, at atmospheric pressure, freely discharging its steam to atmosphere through the side arm of the flask. The boiling temperature t_l, of the solution equals t_v, the temperature of the carefully heat-insulated vapor, which, however, issuing from the side arm immediately drops in temperature to 212 F. The difference between the temperature t_v of the steam in the flask and the temperature $t\mathrm{H_2O}$ of steam developed by pure water boiling at the same pressure is Δt. Concentration of the solution, constantly increasing because of loss of steam through the side arm, finally reaches 70.6 per cent or 0.28 mol fraction[4] which, at atmospheric pressure or 14.7 psia, is saturation concentration. The equal temperatures of solution and vapor, t_l and t_v, have likewise increased with the increasing concentration, and at saturation are designated t_s, and Δt becomes Δt_s. For the condition of saturation, t_s = 326 F, $t\mathrm{H_2O}$ = 212, and the steam in the flask is superheated 114 deg ($\Delta t_s = t_s - t\mathrm{H_2O}$). The initial concentration of the calcium chloride, whether a few parts per million, or a few per cent, is a matter of indifference. If the pressure is fixed at 14.7 psia, and heat is supplied at the requisite level, the conditions for saturation as noted will eventually obtain. With continuation of boiling and discharge of steam, t_s and Δt_s will not increase, but instead, separation of solid salt will begin and continue until only solid calcium chloride remains. On the other hand, if the heat level is not sufficient to raise Δt to Δt_s, boiling will cease and equilibrium will obtain at the maximum Δt corresponding to the heat level in question, saturation never being reached unless the heat level is increased to raise Δt to Δt_s.

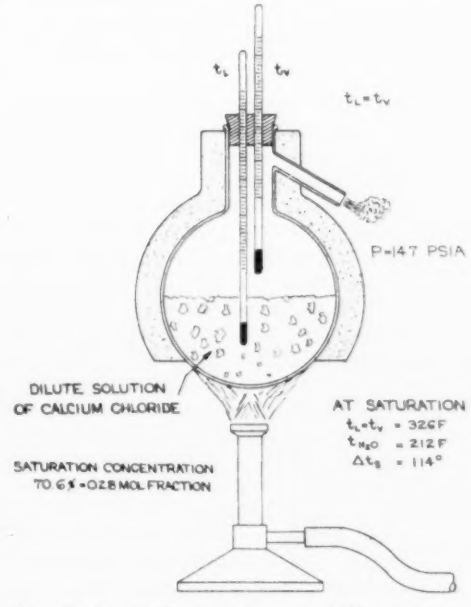


FIG. 3 SIMPLE ILLUSTRATION OF Δt FUNCTION

In the experiment, pressure is fixed at atmospheric, and if the flask contained pure water, boiling would occur at 212 F ($t\mathrm{H_2O}$). With solution in the flask, however, boiling does not occur at 212 F, a fact which signifies that the vapor pressure of the solution is less than that of pure water. In general, at any temperature t, decrease in vapor pressure of any solution becomes greater as its concentration increases, and thus is a function of the concentration of the solution, or equally, of the number of solute molecules in the solution. It was Raoult who pointed out that in dilute solutions of nonelectrolytes, the function is closely that of strict proportionality (A, II).[5]

When the temperature of a solution of any given concentration is increased, its vapor pressure is thereby increased. In the experiment, with pressure fixed at atmospheric, when the temperature t_l of the solution was raised sufficiently above 212 F, the increment of temperature (Δt) over 212 F sufficed to increase the vapor pressure of the solution to atmospheric, and boiling then occurred. As evaporation proceeded, and concentration of the solution accordingly increased, the increment of temperature Δt over 212 F, required to occasion boiling, likewise increased. The relationship thus established for pressure of 14.7 psia and $t\mathrm{H_2O}$ = 212 F, is applicable as well to all boiler pressures and the corresponding boiling temperatures or $t\mathrm{H_2O}$ values. It is thus obvious that Δt is a function of the concentration of the solution or, equally, of the number of solute molecules in the solution.

In the light of these conclusions, let us examine what happens to a film of boiler water on surface A, Fig. 1, if the temperature of the surface becomes heated above boiler-water temperature, 621 F, by an amount Δt. Pressure is fixed at 1800 psia. As the film begins to boil and concentrate at this fixed pressure, because of increased temperature Δt, its vapor pressure must attempt to decrease because its number of solute molecules is increasing. This attempt, however, is offset or compensated by the tendency of the vapor pressure of the solution to increase with rise in temperature. Meanwhile concentration of the film proceeds in its effort to establish the relationship among the different forces which represents equilibrium for the particular Δt value assumed. As concentration thus proceeds, some components of the solution may reach saturation, and be deposited, while others, more soluble, carry on the work of building the concentration to the degree required for equilibrium. If the Δt assumed happens to be greater than the Δt_s of saturation concentration of all components in the solution, evaporation to complete dryness must occur. This is what happened in the development of scale illustrated in Fig. 2, since calcium sulphate at saturation has a low value of Δt_s. But if the Δt_s value of some components at saturation is greater than the Δt assumed, they will remain dissolved and merely increase in concentration by the amount necessary to establish equilibrium.

These considerations illustrate the distinction between the customary conditions obtaining in measurements of vapor-pressure lowering and boiling-point rise, and those which obtain at the steam-water interfaces in a boiler. In the first, temperature and concentration are usually the independent variables with vapor pressure the dependent variable; in the second, vapor pressure and concentration are independent variables, temperature the dependent variable. But in the boiler, pressure, fixed by the boiler, and temperature, established by the degree of overheating Δt at a surface such as A, Fig. 1, are the independent variables, and the concentration of the concentrating-film boiler water is the dependent variable. Its value is commonly expressed as a mol fraction, and frequently indicated by X_2.

We shall designate as the Δt function relations of this type, occurring at the steam-water interfaces of the boiler-water and

[3] W. Otte has assumed evaporation to dryness in all cases (49), (50).

[4] The mol fraction of any constituent in any solution is the number of mols of that constituent divided by the total number of mols in the solution.

[5] References to the Appendix are thus indicated throughout the paper. See footnote on page 457.

steam cycle. Whenever we shall refer to the Δt function, we shall thereby signify the equilibrium that will be reached or approached on the basis of the variables pressure, temperature, and concentration, operating in accordance with the rules heretofore set down. Under the dynamic conditions that exist at a surface such as A, Fig. 1, or even areas where steam-blanketing or film-boiling exists, any well-defined equilibrium for any certain set of conditions may not be reached because of insufficiency of time. The film on surface A will continually struggle to establish equilibrium, however, and in so doing will at all times follow the pattern laid down by the principles of the Δt function.

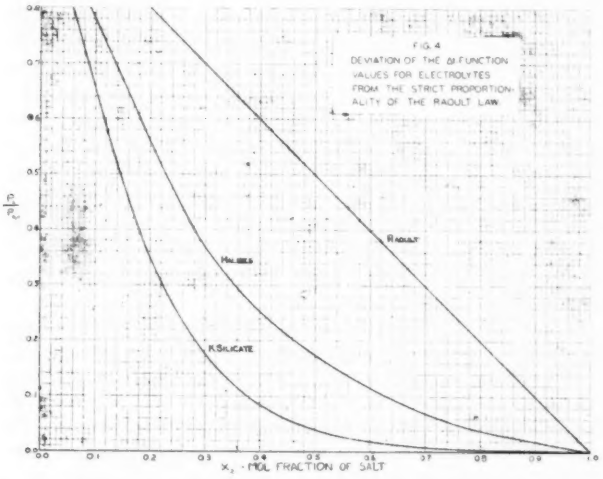


FIG. 4 DEVIATION OF THE Δt-FUNCTION VALUES FOR ELECTROLYTES FROM STRICT PROPORTIONALITY OF THE RAOULT LAW

This will be illustrated by examples. In the experiment, Fig. 3, if sodium chloride, potassium chloride, or sodium sulphate, respectively, were used in place of calcium chloride, the results would be as follows (A, III, 4, 5, 19; IV, 3, 4, 12):

Pressure = 14.7 psia	Saturation concentration X_2 = mol fraction	t_s deg F	Δt_s deg
Sodium chloride	0.109	228	16
Potassium chloride	0.123	227.5	15.5
Sodium sulphate	0.051	217.1	5.1

If the pressure were 1800 psia, as in Fig. 1, on the surface A under the steam bubble, the results would be thus:

Pressure = 1800 psia	Saturation concentration X_2 = mol fraction	t_s deg F	Δt_s deg
Sodium chloride	0.190	692	71
Potassium chloride	0.292	745	124
Sodium sulphate	0.0095	625	4

This means that if the solution of potassium chloride were evaporating on the surface A, Fig. 1, the overheating of that surface on the inner side of the tube to produce saturation in the solution would necessarily be 124 deg. For the sodium-chloride solution, overheating to the extent of 71 deg, and for that of sodium sulphate, only 4 deg, would produce saturation. If for instance the overheating at A were 35 deg, the solution of neither potassium nor sodium chloride would attain saturation, but that of sodium sulphate would evaporate to dryness.

In the generally strong solutions of electrolytes which result from the concentration of boiler water, the curves plotted on the basis of the Δt function variables provide a valuable guide in the study of these solutions. Fig. 4 illustrates the deviation of the halides (sodium and potassium chloride, bromide, and iodide) (6) and of the potassium silicates (7) in saturated solution, from the strict proportionality of Raoult's law. (P_s and P_{h_2o} are, respectively, the vapor pressures of the saturated solution and of pure water at t_s). Later sections will develop the use of these curves.

Suppose that the solution had contained two species of molecules, for instance, sodium sulphate and sodium chloride: According to the Δt function, the value of Δt is a function of the number of solute molecules present, and largely independent of their kind. Thus, in this mixture, both the sodium chloride and the sodium sulphate will each exert its influence toward increasing Δt, hence with less concentration of either one for a given Δt than if either were in solo solution. At the pressure of 1800 psia under consideration, the data of Schroeder, Gabriel, and Partridge (8), (A, VII, 2) show that with increasing concentration of sodium chloride, no marked increase occurs in the solubility of sodium sulphate. Hence if a solution containing these two components evaporated on surface A, Fig. 1, overheating of the surface of somewhat more than 4 deg, depending upon their relative concentrations, would cause saturation concentration of the sodium sulphate, and it would begin to precipitate as solid phase on the surface, while the sodium chloride would remain in solution and keep on concentrating, requiring a considerably higher temperature to effect its saturation. If in place of sodium sulphate, very soluble sodium or potassium nitrate (A, III, 10, 11; IV, 9) were the other component of the solution, the degree of overheating of the surface A which would be necessary in order to cause saturation concentration of either component would be largely increased over what it would be for either one. The significance of this is that once sufficient data have been acquired in relation to the Δt-function properties of the boiler-water salts, it will be possible to predetermine for any value of Δt, whether a boiler water upon concentration will finally become saturated with respect to one or all components, and by appropriate adjustment of their relative concentrations, to impose on the solution the desired condition of these components as Δt is reached.

Thus, in Fig. 1, we can readily picture what will happen at the surface A, if the boiler water contains constituents of limited solubility like sodium sulphate along with some caustic soda. As the temperature at A rises by some amount Δt, the film of boiler water must concentrate in accordance with its Δt-function value. Sodium sulphate will precipitate, and the caustic will concentrate. Deposition of sodium sulphate or attack of the surface by the concentrated caustic, either or both, will create resistance to the flow of boiler water. If, however, we condition the boiler water so that quite soluble salts are present to concentrate along with the caustic, then since the attainment of Δt rests mainly upon the number of molecules in solution, and not largely on their species, neither the caustic nor the soluble salts will concentrate excessively in developing the equilibrium corresponding to the rise in temperature Δt on the tube surface. By this preclusion of development in the boiler tubes of impediments to flow, maximum flow of boiler water is assured. Therewith the probability of steam-blanketing or film-boiling conditions is lessened, and the life span of the bubble, Fig. 1, and also the Δt value of the A surface are kept at a minimum.

Thus from this careful examination of events contingent upon bubble formation, or more broadly, occurring at interfaces of boiler water and steam, there evolves a pattern for molding them to the best advantage of boiler operation. Cognizance must be taken of the fact that in any boiler, there are in reality two different boiler waters to consider, namely, the dilute over-all and the concentrating-film boiler waters. In the boiler, wherever the dilute over-all boiler water governs conditions, we need consider only its isobaric-isothermal properties; but where concentration occurs, as in the concentrating-film boiler water under

the steam bubbles which are forming, or at points of steam-blanketing or film-boiling, we must give heed to its isobaric-polythermal properties as it concentrates in accordance with the Δt function. When any carry-over of the dilute boiler water enters the superheater, it is subjected to isobaric-polythermal conditions, and it will concentrate therein in accordance with the pressure and temperature relations which obtain. The concentrated magma thus formed upon passing into the turbine meets the falling pressure and temperature which characterize conditions therein, and we must consider its properties in relation to the polybaric-polythermal conditions to which it is subjected. In Table 3, these facts are briefly summarized.

TABLE 3 PRESSURE-TEMPERATURE RELATIONS AFFECTING BOILER WATER AND CARRY-OVER

		Isobaric isothermal	
		Over-all boiler water	
		Isobaric polythermal	Polybaric polythermal
A	*Boiler:* boiler water	Concentrating-film	*Turbine:* Gradual dilution of concentrated carry-over
B	*Superheater:*	Highly concentrated boiler-water carry-over	

Particularly, Table 3 emphasizes the need of a systematized procedure to take cognizance of the changes occurring in the isobaric-polythermal regions of the boiler or superheater, and the polybaric-polythermal region of the turbine, in addition to that which has been generally applied to the dilute over-all boiler water. Such systematic procedure means so balancing the proportional relationship and character of the components in the dilute over-all boiler water, which can be readily established as desired and checked by analysis, that changes of concentration occurring at interfaces of boiler water and vapor in accordance with the Δt function cannot result in development of high causticity, or in the separation of water-insoluble components, especially those siliceous in nature.

In order to arrive at the features which must be embodied in this inclusive procedure, we shall now subject the problems enumerated in the introduction, and, incidentally, factors relating to protection from caustic embrittlement also, to examination in the light of the potassium equilibrium and the application of the Δt function.

The Problems of Hide-Out of Boiler-Water Salts

The boiler-water salts which have been mainly recognized as guilty of hide-out are sodium sulphate and sodium phosphate. Some recent data, however, in which the silica concentration was followed closely, have shown that sodium silicate is equally guilty with the phosphate and sulphate.

In the range of boiler-water temperatures the solubilities of sodium phosphate and sodium sulphate (A, III, 13, 19) decrease rapidly with temperature increase. The fact that sodium silicate joins with the sodium sulphate and phosphate as a hide-out salt ties in well with the very limited solubility data on sodium silicate which are available (A, III, 15) and which show it to have a decreasing solubility curve in the range of boiler-water temperature. From the customary thinking in terms of retrograde solubility alone, however, it is difficult to see how hide-out would occur, since the sulphate and phosphate solubilities are a couple of thousand parts per million or more at operating pressures well above those in which hide-out has been characteristic. Neither is it likely that the double salts of sodium sulphate and sodium phosphate, which were recognized and discussed by Schroeder, Berk, and Gabriel (9), (A, VII, 7), are the reason for the hide-out of these two salts, as the solubilities of these double salts are appreciable.

In the illustration of overheating of surface *A*, Fig. 1, we must remember that Δt_s governs the number of molecules necessary for saturation and hence deposition, and that the apparently considerable solubility of sodium sulphate as viewed from the standpoint of parts per million shrinks to a relatively insignificant value when expressed as mol fraction. Reference to the values of Δt_s for sodium sulphate (A, IV, 12), over the range of boiler temperatures, discloses a maximum of 8 deg only and at the temperature of 600 F, of no more than 4. This means that if the water surface of a boiler tube is heated only a very few degrees above boiler-water temperature, where rapid evaporation is occurring or where there is a tendency to film-boiling or steam-blanketing, sodium sulphate will precipitate readily enough. Low Δt_s values are a characteristic of salts whose saturation concentration is given by small value of the mol fraction or, in other words, by a relatively small number of molecules in the solution. Thus sodium carbonate (A, IV, 2) is similar to sodium sulphate, its maximum Δt_s being 10 deg.

Sodium carbonate does not appear as one of the hide-out salts, presumably because of its ready decomposition into caustic soda, and because so little of it is present in the boiler waters at even medium boiler pressure. Reference to the solubility tables of sodium phosphate and sodium silicate discloses that their saturation concentrations are given by extremely small mol fractions, so that while their vapor pressures are unknown, and therefore likewise their values for Δt_s, yet doubtless these are very small and probably lower than Δt_s for sodium sulphate.

The question might be raised if the increased solubility of sodium sulphate in the presence of caustic soda at higher temperatures and pressures as found by Schroeder, Gabriel, and Partridge (8), (A, VII, 1), would not tend to minimize the hide-out tendency of sodium sulphate by considerably increasing its Δt_s value. While no values are available for the vapor pressure of such solutions, the mol fraction of sodium sulphate at saturation concentration is small even with its increased solubility in the caustic-soda solution, and the inference therefore is that deposition of sodium sulphate would occur with relatively low Δt_s. According to the work of Schroeder, Berk, and Gabriel (9), (A, VII, 7, 8), caustic soda has little influence on the solubility of sodium phosphate, and hence on the value of Δt_s, at which deposition would occur.

Plainly, the elimination of hide-out demands that the components in the boiler water shall be of much higher Δt_s than that characteristic of sodium sulphate. This viewpoint is supported by the high values of Δt_s for sodium hydroxide and sodium chloride (A, IV, 3, 5), since neither of these salts is guilty of hide-out propensities.

At one of the stations on which we initiated potassium-equilibrium conditioning during the spring of 1943, but while sodium-conditioning was still in effect, measurements on hide-out had shown the conditions to be as bad as, and probably worse than, any we had previously experienced. Both the sulphate and the phosphate skyrocketed when boiler load was reduced. With potassium-equilibrium treatment well established, successive tests have shown complete absence of sulphate hide-out, and elimination of all but the barest trace of phosphate hide-out. Why should this be the case? So little is known of the solubility of potassium phosphate (A, III, 14), that no help in answering this question is to be gotten from it. The solubility of potassium sulphate (A, III, 20) is of low mol fraction, however, about double that of sodium sulphate. Thus while the vapor pressure of saturated potassium-sulphate solutions at the temperature in question (625 F) is unknown, the Δt_s value is doubtless a little higher than that of sodium sulphate. But unless small differences in Δt_s values are of very critical influence in the occurrence or nonoccurrence of hide-out, it seems improbable that the only slightly larger Δt_s of potassium sulphate in itself could have been the major reason for its disappearance in this case. Comparison of potassium chloride and sodium chloride A, III, 4, 5; IV,

TABLE 4 COMPARISON OF Δt_s FOR SATURATED SOLUTIONS OF K_2SiO_3 AND NA_2SO_4

(Na_2SiO_3 is similar to Na_2SO_4)

Saturation concentration Mol fraction	Per cent	Boiling temperature at P_s t_s	$t_s - t_{H_2O}$	Vapor pressure P_s at t_s, psia	Δt_s $t_s - t_{H_2O}$
		K_2SiO_3			
0.30	78.7	446	264	38	182
0.35	82.3	542	294	62.4	248
0.40	85.0	621	311	79.4	310
0.50	89.6	815	366	164	449
0.60	92.8	995	360	153	635
		Na_2SO_4			
0.058	32.7	464	456	450	8
0.046	27.3	527	520	813	7
0.012	8.7	617	614	1710	3
0.003	2.3	662	661	2380	1
>0.0	>0.0	705	705—	3206—	>0

3, 4), for example, at boiler pressure of 1400 psia (Table 5) shows that saturation concentration for the former occurs at mol fraction of 0.274, and Δt_s of 104 deg; for the latter, at mol fraction of 0.182, and Δt_s of 65 deg. These values, while favoring potassium chloride, are high enough in either case to dispel any thought of their activity in hide-out. For either potassium metasicilate or disilicate (A, III, 17, 18; IV, 10, 11), Δt_s is extremely high, and the solubilities likewise are high, in very decided contrast to sodium silicate. What we consider to be the most feasible reason for disappearance of the hide-out is our establishment in the boiler water of an environment of soluble salts, which, together with the gain from the higher Δt_s value of potassium sulphate and perhaps phosphate, effected the result.

While all the data that we would like to have for their bearing on this problem of hide-out are not of record, yet enough are available to make it feasible to conclude that elimination of hide-out requires a Δt_s value for dissolved components in the boiler water which, as concentration occurs at any steam-water interface, is considerably greater than that of sodium sulphate. With sodium equilibrium maintained in the boiler water, this means that the concentrations of salts with low Δt_s value such as sodium sulphate, phosphate, and silicate must be carefully controlled and held as low as possible. On the basis of very limited observation, it appears that the substitution in the boiler water of potassium equilibrium for the customary sodium equilibrium increases markedly the permissible tolerance of sulphates, phosphates, and silicates. Because the methods used in obtaining the solubility data for potassium sulphate are not beyond question, and because solubility data on potassium phosphate are lacking, we are engaged at the present time in the determination of their solubilities at boiler-water temperatures. As more data of the kind become available, it will be possible to bring the details of this problem into sharper focus.

The Problem of Magnesium Deposits

An excellent example of this problem is a seaboard plant in which condenser leakage of salt water supplies magnesium to the boiler without simultaneously supplying sufficient silica to combine with it as serpentine or other magnesium silicate. A soft deposit, definitely characterized by magnesium phosphate, or at times, hydroxide, develops in the boiler. Though not forming hard scale, it clings to the surfaces and resists removal by blowdown. A similar condition may arise with the use as feedwater of a natural or treated water containing excess of magnesium over silica.

Magnesium silicate, which is the most, or at least one of the

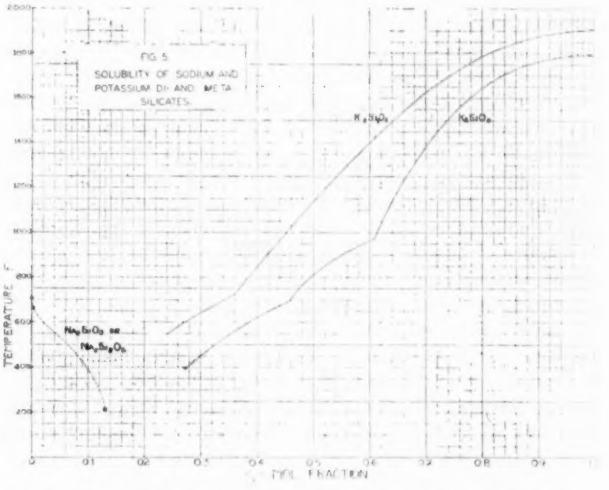


Fig. 5 Solubility of Sodium and Potassium Di- and Metasilicates

TABLE 5 CONDITIONS IN ISOBARIC-POLYTHERMAL REGION OF SUPERHEATER

Boiler pressure, psia	1400
Temperature of boiler water and saturated steam, deg F	587
Temperature at superheater outlet, deg F	1000
Degrees superheat	413

Properties of some boiler-water and other salt solutions under these conditions

Salt solution	Saturation temperature, deg F	Δt_s, deg	Saturation concentration, a per cent	Condition at 1000 F
Sodium sulphate	592	5	15	Complete evaporation
Sodium phosphate[a]	Similar to sodium sulphate			Complete evaporation
Sodium carbonate	594	7	6	Complete evaporation
Sodium di- or metasilicate[a]	Similar to sodium sulphate			Complete evaporation
Sodium chloride	652	65	42	Complete evaporation
Sodium bromide	753	166	74	Complete evaporation
Potassium chloride	691	104	61	Complete evaporation
Potassium chloride plus sodium bromide	874	287	84.6 (est.)	Complete evaporation
		Δt		
Potassium chloride plus sodium bromide	984	413[c]	Unsaturated in solution	
Potassium disilicate	b	413[c]	Unsaturated in solution	
Potassium metasilicate	b	413	Unsaturated in solution	
Sodium hydroxide	b	413	93[d] in solution	
Potassium hydroxide	a	Similar to sodium hydroxide		

a Vapor-pressure data not available.
b Saturation pressure never attains boiler pressure.
c Saturation pressure less than boiler pressure.
d Concentration of the unsaturated solution.

most insoluble of the silicates, forms in the boiler water as a sludge which remains dispersed therein and is removed from the boiler by blowdown. Very likely its high insolubility plays a major role in this, resulting in its complete precipitation in the body of the dilute over-all boiler water, and thus its avoidance of taking any part in the reactions which characterize the concentrating-film boiler water.

The fact stands out that if any magnesium is to gain entry into the boiler water, provision should be made therein of sufficient silica to insure its combination with the magnesium as one of the magnesium silicates, thus avoiding magnesium phosphate or hydroxide.

Add silica for the purpose if necessary? Yes, why not? To be sure, the finger of suspicion has been leveled at silica universally, and its constant companion, sodium, has remained unsuspected and been accepted as a matter of course. The case is one of mistaken identity, and the truth is that if the influence of sodium over silica is replaced by that of potassium—if the boiler water is maintained on the potassium equilibrium—silica, in the amount required, can be accepted safely as a member of the boiler-water salts, and be of real use. The logic of this conclusion is foreshadowed by the diametrically opposite solubility properties of the sodium and potassium silicates in the range of boiler-water temperatures (A, III, 15, 16, 17, 18), as demonstrated by the curves in Fig. 5, the former being of the same retrograde type as sodium sulphate and phosphate, and the latter being of the type of sodium and potassium chloride. As regards relationships in the turbine, further facts will develop as we proceed.

The Iron-Oxide Sludge Problem: Corrosion by the Bonded Oxygen of the Boiler Water

In any plant, with the excellent deaeration characteristic of present-day operation, dissolved oxygen entering the boiler in the feedwater is of the order of a millionth of a per cent, while the oxygen it contains, bonded to hydrogen, constitutes 88.9

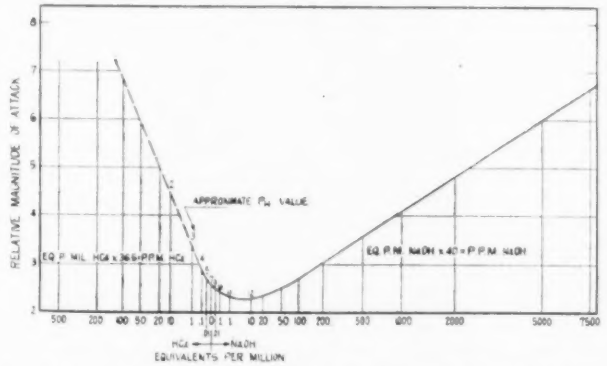


Fig. 6 Attack on Steel at 590 F by Water of Varying Degrees of Acidity and Alkalinity

per cent of its weight. If this bonded oxygen is in some way unleashed in quantity, the possibilities of damage to the boiler are better imagined than experienced. The pertinent questions are: May the bonded oxygen be readily unleashed, and if so, what measures may be taken to prevent it?

In answering the first question, we may well start with the curve in Fig. 6, developed by Partridge (10) on the basis of data obtained by Berl and van Taack (11). As demonstrated by the curve, susceptibility of boiler steel to dissolution in the contacting water increases with increase either of acidity or alkalinity. In conformity with the teaching of this curve, the over-all boiler water is in general held in the pH range of 8.3 to 12, the former being that naturally assumed by water boiled in an iron vessel (12). In this pH range the steel is only slightly susceptible to dissolution by the boiler water. Inasmuch as boiler waters are thus maintained alkaline, we shall confine our attention to the alkali side of the curve. Increasing of alkali concentration results in greater relative magnitude of attack on the steel, a result in conformity with the reaction involved

$$FeO + 2HONa = Fe(ONa)_2 + H_2O \quad [1]$$

Thereby the steel surface is deprived of its protective film of iron oxide and renews it by reacting with water thus

$$Fe + H_2O = FeO + H_2 \quad [2]$$

or, finally, probably, in the boiler with formation of magnetic oxide, Fe_3O_4 (10, 28). Simply, then, as recorded in Reaction [2], the bonded oxygen of the boiler water is unleashed from its hydrogen and combines with the boiler steel, thus providing the protective film so necessary therefor, and preventing or greatly retarding any further release of bonded oxygen, so long as the film remains intact. It is the entry of Reaction [1], and more specifically, the degree of alkali concentration in the reaction, which, in the end, destroys the film, and thereupon, with infinite recurrence of both Reactions [1] and [2], takes its toll of the boiler metal. It is the bonded oxygen of the boiler water which, uniting with the boiler steel, gives rise to the heavy deposits or sludges of magnetic iron oxide, sometimes with destructive furrowing and channeling, or more localized severe pitting; sometimes with merely general action on the surfaces as attested by the magnetic-oxide deposits.

Briefly, the problem of preventing this action involves the features of having alkalinity as required in the over-all boiler water, but at the same time making provision that in the concentrating-film boiler water, the concentration of alkali will be sufficiently restricted to nullify Reaction [1].

To get some idea of the alkali concentration at which Reaction [1] is sufficiently rapid to be damaging, Kaufman and Marcy in our laboratory, rotated 5 per cent solutions of caustic soda and potassium hydroxide in bombs of boiler-steel construction at approximately 470 F for a number of hours [see also (32)]. The solutions put into the bombs were clear and free of precipitate. In case the bombs were not pickled before the experiment, the solutions removed were heavily contaminated with iron-oxide sludge, presumably developed from the iron-oxide coating of the bomb walls by the mechanism of Reaction [1]. When sodium sulphite was added in sufficient quantity to account for any dissolved oxygen, similar results ensued. However, if the bombs were pickled just prior to the experiment, thus largely removing their iron-oxide coating, with or without sodium sulphite, very little iron-oxide sludge was apparent in the solution after a number of hours at the elevated temperature of the experiment. In other words, while the 5 per cent concentration of caustic was sufficient to carry through Reaction [1] with considerable speed, Reaction [2] was too sluggish to be damaging under the conditions and in the duration of the experiment. Longer duration would doubtless have occasioned formation of the iron-oxide sludge in larger amount, without segregation of the attack in any one spot. We believe these conditions parallel those in boilers which, on inspection, are found with considerable magnetic-oxide sludge distributed pretty well throughout the boiler, usually with some marked accumulation in drums or headers, but without evidence of intensified attack in any particular areas.

Are there, however, factors in the boiler which will speed up Reaction [2]? Further experiments by Kaufman and Marcy tested the effect of increasing the caustic concentration. At the same temperature previously noted, they found a 10 per cent caustic solution to attack the surface of the bomb very little in-

deed, if it was pickled prior to the experiment; when a 20 per cent solution of caustic was used, the attack, while not heavy, nevertheless was considerable, as indicated by the amount of magnetic-oxide sludge produced. In a parallel experiment with 10 per cent caustic solution, but with the surface of the bomb not pickled prior to the experiment, the attack produced a heavy sludge of magnetic oxide. As illustrated in Fig. 6, Berl and van Taack at 590 F similarly found magnitude of attack to increase with increased caustic concentration. Thus one very decided

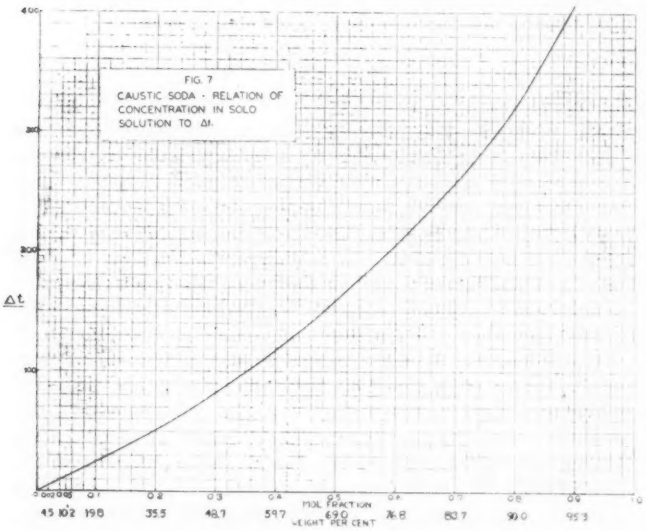


FIG. 7 CAUSTIC-SODA RELATION OF CONCENTRATION IN SOLO SOLUTION TO Δt

factor in speeding up Reaction [2] (and Reaction [1] as well) is an increase in caustic concentration. Another factor is increase of temperature, not illustrated by the foregoing experiments at fixed temperature, but undoubtedly of big influence (29).

With these factors in mind, let us consider what may happen in the concentrating-film boiler water, as formed for example on surface *A*, Fig. 1, under the steam bubble, where simultaneous increase both of temperature and concentration is brought to bear on a restricted area. Fig. 7 (A, V, VI) shows the result. If Δt is only 5 deg, a solo solution of caustic soda will attain concentration of approximately 4.5 per cent at equilibrium; if 50 deg, the caustic concentration will rise to 35.5 per cent; and to greater concentration if Δt is larger. At any steam-water interface, therefore, such as *A*, Fig. 1, and more markedly wherever steam-blanketing or film-boiling may occur, the factors of temperature and caustic concentration, increasing in unison, exercise on a restricted area their combined power of acceleration on both Reactions [1] and [2].[6]

[6] For illustrations of bonded-oxygen corrosion, see reference (10), both items. We believe Fig. 7(*a*) is an apt illustration of this type of corrosion, but with special circumstances leading to its development. As evident from the illustration, discrete pieces of deposit have been randomly stacked. Composed mainly of calcium phosphate and a little calcium carbonate, silica negligible, they were almost certainly formed in a part of the boiler remote from the evaporative section where they were found, and were transported in the circulating boiler water until an eddy or backwater resulted in their being gathered together as shown. Their relation to bonded-oxygen corrosion lies in their being firmly cemented together by a matrix of magnetic oxide of iron (little copper is present). The eddy or backwater indicates interruption of maximum boiler-water flow, a condition which favors steam-blanketing or film-boiling. The further impetus given to this condition by the overburden of stacked pieces of deposit quite evidently resulted in a concentrating-film boiler water of sufficient concentration to accelerate Reactions [1] and [2], and thus provide the magnetic-oxide matrix.

However vicious may be the attack on the boiler metal by the combined power of these two factors, it is made still more devastating by another factor. As shown by the vapor-pressure data of solutions of caustic soda (A, III, 6; IV, 5; V; VI), and the specific illustration of 1400 psia and 1000 F of Table 5, the concentrating-film boiler water will never go to dryness if it contains caustic soda (or, for that matter, caustic potash). On the contrary, the solution of caustic, instead of shriveling with increasing Δt on the surface, will spread instead in accord with its well-recognized characteristic of so doing (34), and thus broaden the area of attack. At the same time, the attack according to Reaction [2] by the water, held in liquid form frequently well above critical temperature of 705 F, will be maximum since the contacted surface cannot build a protective oxide covering because of the rapid dissolution thereof, according to Reaction [1] by the high caustic concentration of the contacting concentrating-film boiler water.

All factors considered, it is not surprising that attack on the metal is very rapid and devastating. Results thereof have been described by Drewry (30) and others (10, 31).

At such surfaces, concentration of caustic to the degree at which embrittlement readily occurs requires only a moderate value of Δt.

How, then, shall required alkalinity be provided in the over-all boiler water, and yet be adequately restricted in concentration in the concentrating-film boiler water?

One method consists in providing in the over-all boiler water a ratio of potassium or sodium chloride to alkalinity, such that as



FIG. 7(*a*) CORROSION BY BONDED OXYGEN

concentration in accordance with the Δt function occurs as required by the Δt of any steam-blanketed surface, the alkalinity will remain of small amount and innocuous. For instance, if the boiler water contains 1 molecule of alkalinity and 4 molecules of potassium chloride, then the concentration of caustic that will result will be only one fifth of what it would be if the potassium chloride were not present. In Reaction [2], the intensity factor of liquid water in contact with the metal surface will remain, but opposing this, by strict limitation of the caustic concentration, Reaction [1] can be held in check, and the iron-oxide film on the metal, not being dissolved off so rapidly, has the chance to be protective to the metal, at least in considerable degree. It is an

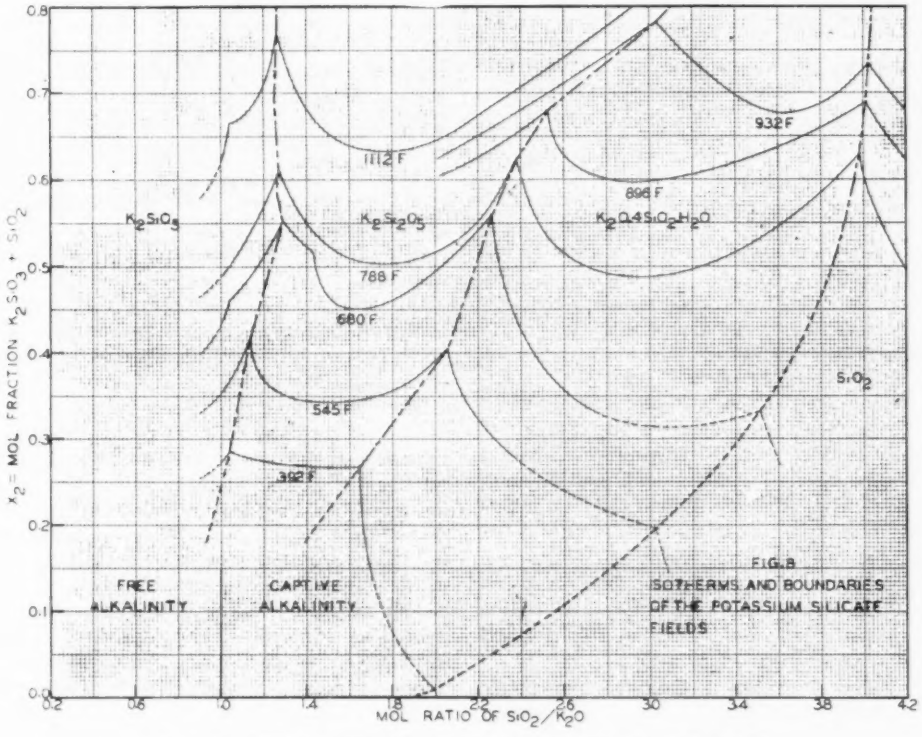


FIG. 8

FIG. 8 ISOTHERMS AND BOUNDARIES OF POTASSIUM-SILICATE FIELDS

interesting point that as a boiler water is purer, so is it more aggressive in the development of iron-oxide sludge, unless its alkalinity is practically nil. Further, it is evident that sodium sulphate can be only slightly effective in preventing concentration of alkalinity, because sodium sulphate reaches saturation concentration at very low value of Δt, thereupon merely precipitating, and leaving it up to the caustic molecule to provide a great share of the concentration demanded by Δt, the very thing that must be avoided.

Another method of approach is to have all boiler-water alkalinity that of hydrolysis (13, 35), so that when the over-all boiler water, concentrating at a surface, becomes concentrating-film boiler water, the hydrolytic alkalinity will return to the parent molecule and not accumulate excessively. The alkalinity of hydrolysis we term "captive alkalinity," as opposed to free alkalinity, which will concentrate highly at a surface. Such captive alkalinity in the boiler water can be given by the hydrolysis of the phosphates and, of especial interest to us, by that of di- and metasilicates. The hydrolysis of the phosphates is not of so much value for this use, because they, or at least the sodium phosphate, follow sodium sulphate in their solubility relationships. On the other hand, the potassium di- and metasilicates are very soluble, keep on increasing in solubility with temperature increase and therefore are particularly valuable in control of the boiler-water alkalinity in the form of captive alkalinity. At the present time, to take care of this problem of magnetic-oxide sludge, we are using the potassium-chloride method at one plant; at another, a combination of potassium chloride and captive alkalinity, supplied by potassium silicate; and the same also at a third plant in which the potassium silicate is of value not only for captive alkalinity but to provide the silicate in the boiler water to prevent soft magnesium deposits.

In some cases, efforts to eliminate corrosion by bonded oxygen have followed the course of maintaining extremely low alkalinities in the boiler water. In this case, Reaction [1] is made negligible, and the concentrating-film boiler water may most likely evaporate to dryness, changing the concentration of H_2O in Reaction [2] from that of liquid water when caustic maintains the film liquid, to the value corresponding to the density of steam at the temperature of the surface in question. The method is effective, but not infallible, if Δt is sufficiently large, as proved by a number of instances (36, 31, 25). In any event, however, the method provides optimum conditions for silica deposition in boiler and turbine, as will become apparent in the sections which follow.

The Problem of Silica in the Boiler

There are only two possible methods of procedure relative to silica, namely, remove it, or else live with it and make it behave. In fact, silica is a component in boiler waters that must be reckoned with whether or not steps are taken for its removal, since whatever may be left after treatment for its removal accumulates in the boiler water, and in lesser or greater degree the silica problem holds sway. But, as previously noted, it has virtue in combining with magnesium, and thus preventing the soft but troublesome high-magnesium boiler deposits. As shown in Fig. 5, both sodium metasilicate and disilicate (A, III, 15, 16) in the boiler-water temperature range show retrograde solubility, that is, decrease of solubility with temperature increase, and must therefore be classed in the group of salts such as sodium sulphate, carbonate, and phosphate, and hence at surprisingly low value of Δt in the Δt-function, reach saturation and deposition on evaporative surfaces. On the other hand, both potassium metasilicate and disilicate (A, III, 17, 18) show increasing solubility with temperature increase through the whole range to their melting point. In this respect, therefore, they may be classed with the group of materials, such as sodium chloride, potassium chloride, and sodium and potassium hydroxides, which behave similarly. In contrast to the sodium silicate, their Δt_s values (A, IV, 10, 11) are extremely high, and thus wherever a concentrating-film boiler

water develops, they will aid in the prevention of deposition rather than abet it.

Table 4 comprises a comparison of Δt_s of saturated solutions of potassium metasilicate and sodium sulphate, values for the latter being used, since the solubility of sodium sulphate and sodium metasilicate are similar in type, and since no vapor-pressure values for sodium-silicate solutions are available. For example, at 621 F, potassium metasilicate has a saturation concentration of 0.40 mol fraction or 85 per cent, the vapor pressure of the solution is 79.4 psia, water at this pressure boiling at 311 F. Thus Δt_s has the surprisingly high value of 310 deg. On the other hand, sodium sulphate and undoubtedly sodium silicate practically to the same extent at 617 F, or approximately the same temperature, has a saturation concentration of 0.012 mol fraction or 8.7 per cent, the vapor pressure of the solution is 1710 psia, and water at this pressure boils at 614 F. Thus Δt_s in the latter case is only 3 deg. What this means in the concentrating-film boiler water is clearly evident from the previous discussion of the Δt function: The potassium metasilicate will not hide out, and will not be scale-forming, while the sodium silicate will hide out, and will be scale-forming. Or stated in a different way, in the 1800-psia tube, illustrated in Fig. 1, potassium silicate can never reach saturation in the concentrating-film boiler water at surface A, since the vapor pressure of its solution at saturation never attains that pressure; while with sodium sulphate and sodium silicate, Δt of not over 3 deg brings about saturation.

Fig. 8 illustrates further properties of the potassium silicate that emphasize the value of maintaining the boiler on potassium equilibrium, thus avoiding the sodium silicates. The concentration as mol fraction is plotted as ordinate, and the abscissa is the mol ratio of SiO_2/K_2O. This brings out a fact concerning the silicates that does not pertain to other boiler-water salts. If, for instance, one started with a pure solution of potassium hydroxide, the ratio SiO_2/K_2O would be zero. If silica is now added, it dissolves, and the amount of silica added may be such that the mol ratio of SiO_2/K_2O becomes 0.6, 1.6, 2.0, or more, or any intermediate figure. Let us consider what happens to a solution of silica and potassium hydroxide with varying ratio of SiO_2/K_2O, and let us choose the isotherm of 680 F, which is one of those chosen by Morey (7) in the experiments in which he obtained the data plotted in this figure. With a ratio SiO_2/K_2O of 1.0, and concentration to saturation, the solid product that precipitates is potassium metasilicate. As the ratio SiO_2/K_2O is increased, and becomes almost 1.3, the solid product that precipitates is no longer potassium metasilicate, but potassium disilicate. Continuing along the 680 F isotherm, with silica concentration increasing until the ratio SiO_2/K_2O is a little greater than 2.2, the saturated solutions precipitate potassium disilicate as solid phase. Beyond this point, the solid phase becomes tetrasilicate ($K_2O \cdot 4SiO_2 \cdot H_2O$). Finally, only when the ratio SiO_2/K_2O is somewhat more than 3.4, is the field reached in which silica precipitates. Following the 392 F in place of the 680 F isotherm, we find that at a ratio SiO_2/K_2O of 2, the dotted line separating the field of silica from the field of potassium tetrasilicate intersects the experimental isotherm of 392 F, at practically zero concentration. Therefore if the boiler water contains silica and potassium hydroxide in the mol ratio of 2, and the operating pressure is 225 psia, corresponding to 392 F, precipitation of potassium tetrasilicate and silica might readily occur in the concentrating-film boiler water. But, if the ratio SiO_2/K_2O under that condition were 1.6 or lower, then this precipitation would not occur, and at the pressures above 225 psia, and at ratios of silica to alkali in the range of 2 or less there is practically no possibility of deposition of silica or the potassium-silicate compounds in the concentrating-film boiler water for any values of the Δt function within the range of reason. The interesting point is, that the higher the operating pressure of the boiler, the more certainly this is the fact.

Now contrast with this what happens in the case of sodium silicate. The exact data are not known, as they are being worked upon by Morey (14, 15) at the present time. But one can gain an idea of what they will be by reference to Fig. 5, depicting the enormous contrast in the solubilities of the sodium and the potassium silicates. As regards stability, also, the potassium silicates have the advantage (16), since, as far as known, no tetrasilicate of sodium comparable to the tetrasilicate of potassium exists, and any decomposition of sodium disilicate results directly in deposition of silica. The relationship of incongruent solubility (27) between water and the silicates, signifying their decomposition by water, may occur in the boiler as well as in the turbine, but will be discussed as a part of the role of silica in the turbine.

Our observations under actual operating conditions of the boilers at Springdale, and of test experiments carried out in bombs, agree fully with the conclusions which are reached by study of this diagram.

But, the question may arise, this is true for the potassium silicates as compared with the sodium silicates, but what of the potassium-aluminum silicates and the potassium-iron silicates as compared with the sodium-aluminum silicates and the sodium-iron silicates? Inasmuch as only very limited (33) experimental data are available, so far as we know, dealing with solubilities of the alkali-aluminum silicates, we must revert for our conclusions to our observations in operating boilers. In the Springdale boilers, in the generating tubes, where hard, flinty deposits of sodium-aluminum silicate, mixed with silica, magnetic iron oxide, and copper, prevailed during the maintenance of sodium equilibrium in these boilers, in spite of everything that we could do, with advent of the use of potassium equilibrium and the appropriate relationship between silica and alkali in the boiler water, these deposits have completely disappeared and the tube surfaces are clean. Very likely, the vastly different solubility of the potassium silicate as contrasted with the sodium silicate is the influential factor in producing this result.

Application of the Δt Function to the Isobaric-Polythermal Conditions in the Superheater

Thus far, in our discussion of the concentrating-film boiler water, and the conclusions that follow from application thereto of the Δt function, we have directed our attention mainly to problems involving the low Δt_s values of substances like sodium sulphate, sodium phosphate, and sodium silicate. But where conditions of steam-blanketing or film-boiling are severe, Δt of the tube surface may be quite high, as indicated by finding a spheroidized condition of cementite in, or even decarburization of, the metal when metallographic examination is made. In the superheater, too, any boiler water which carries over in the steam must concentrate and come to equilibrium therewith at a value of Δt equal to the superheat of the steam. Conditions are more severe, but the principles are the same as those illustrated in the experiment, Fig. 3. It will be sufficient for our purposes to consider the temperature range from 212 to 1400 F, and, therefore, maximum Δt of 1188 deg. This involves consideration of solutions well above the critical temperature of water.

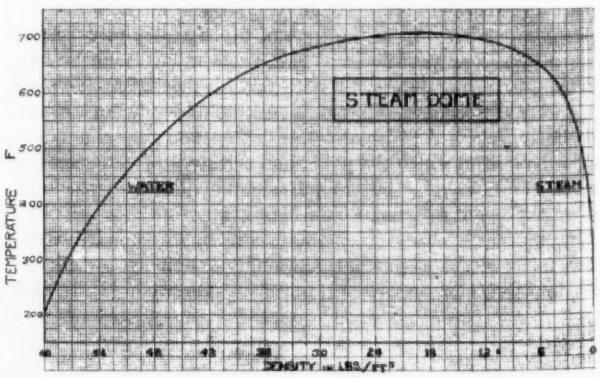


Fig. 9 The Steam Dome

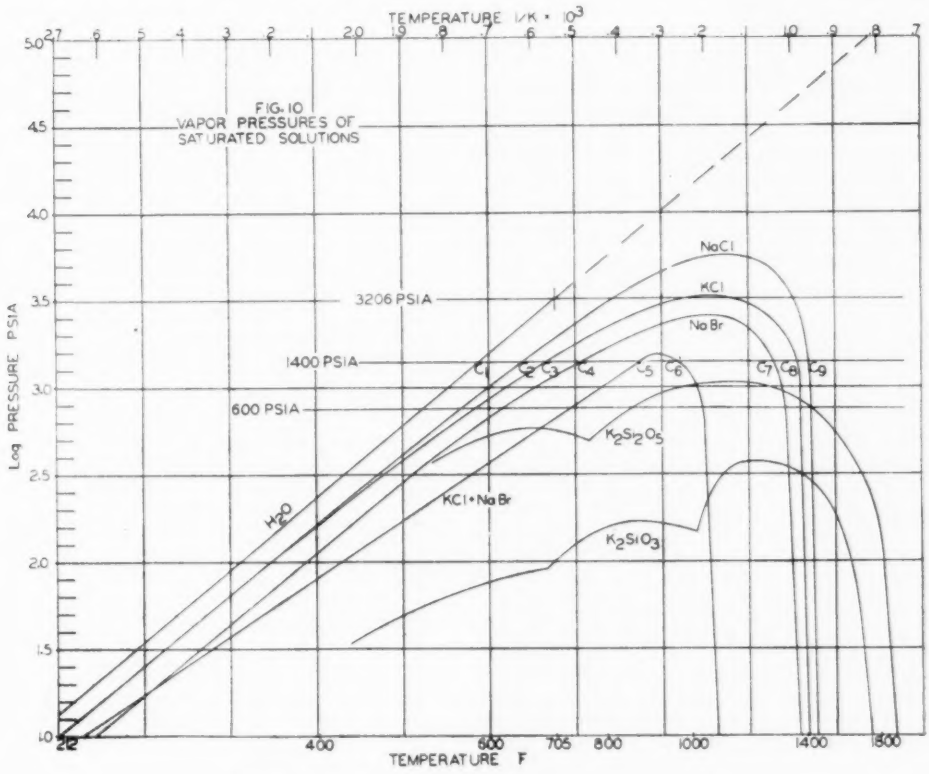


FIG. 10 VAPOR PRESSURES OF SATURATED SOLUTIONS

What is the significance of critical temperature of water in relation to solutions? Morey (14), calling attention to the steam dome as illustrated in Fig. 9, points out that the densities of water and steam gradually approach each other and become equal at critical temperature without discontinuity. Increase in density of steam is very rapid as critical temperature is approached. At and just below critical temperature, the steam dome is almost flat. He states:

"There is no discontinuous change at the critical temperature of water, and there is no reason to expect a change in the solvent power of water at critical temperature when the liquid and vapor phases merge continuously into each other.

"The critical temperature of water is a characteristic of pure water only. When a binary system consisting of water and a soluble compound such as potassium disilicate is considered, the critical temperature of water is without significance. A solution of salt in water raises the boiling point, that is, decreases the vapor pressure, and if the salt is sufficiently soluble, the vapor pressure of the saturated solution at the critical temperature of water is far less than the vapor pressure of pure water."

Fig. 10 shows the relationship for a few salts (A, III, IV) of vapor pressure to temperature of saturated solutions, the data for these curves being taken from papers by Morey (7) and Keevil (6), and from the International Critical Tables (17). These curves, representing the vapor pressure of saturated solutions at ascending temperatures, evidence no break at the critical point of water and show the course that such salt solutions would take in the concentrating-film boiler water or in the superheater, in their endeavor to reach equilibrium on the basis of the Δt function at any value of Δt under consideration.

Table 5 shows what happens when such solutions of one dissolved component or in one case of mixed components (potassium chloride and sodium bromide) are carried over in the steam of a boiler operating at 1400 psia and are raised in temperature to 1000 F in passing through the superheater. The data are obtained as follows:

The isobar of 1400 psia, Fig. 10, intersects the vapor-pressure curve of water at C_1, then successively on their ascending branches, those of NaCl at C_2, KCl at C_3, etc.; and on their descending branches, NaCl at C_5, KCl at C_6, etc. The isobar does not intersect the curves of $K_2Si_2O_5$ or K_2SiO_3, or those of NaOH or KOH, which are not shown because they lie below 10 psia, the base line of the diagram. To illustrate the significance of an intersection, let us consider C_3 of KCl. The temperature corresponding to C_3 is 691 F, which is the saturation temperature for a solution of KCl with vapor pressure of 1400 psia. The saturation concentration of 61 per cent is obtained from the solubility curve of KCl (see solubility data, A, III, 5). The difference of the temperatures corresponding, respectively, to C_3 and C_1, 691 and 587 F, or 104 deg is Δt_s. Since saturation occurs at 691 F, and 1400 psia, and since the temperature in the superheater rises to 1000 F, pressure remaining unchanged, the solution must evaporate to dryness, in a manner similar to the solution of calcium chloride, illustrated in Fig. 3.

The Δt_s values corresponding to the other intersections C_2, C_4, and C_5 also lying on the ascending branches of the curves, are less than the superheat, 413 deg, hence the solutions to which they correspond must evaporate to dryness. The huge difference that may exist between solo solutions and mixtures is well illustrated by the Δt_s values of only 104 and 166 deg, respectively, for KCl and NaBr, while that of their mixture is 287 deg, or more than the sum of their separate Δt_s values. Inasmuch as the 1400-psia isobar does not intersect the vapor-pressure curves of solutions of the potassium silicates, nor of those of caustic soda and caustic potash, these solutions will not attain saturation under the conditions we have assumed, and the salts will remain

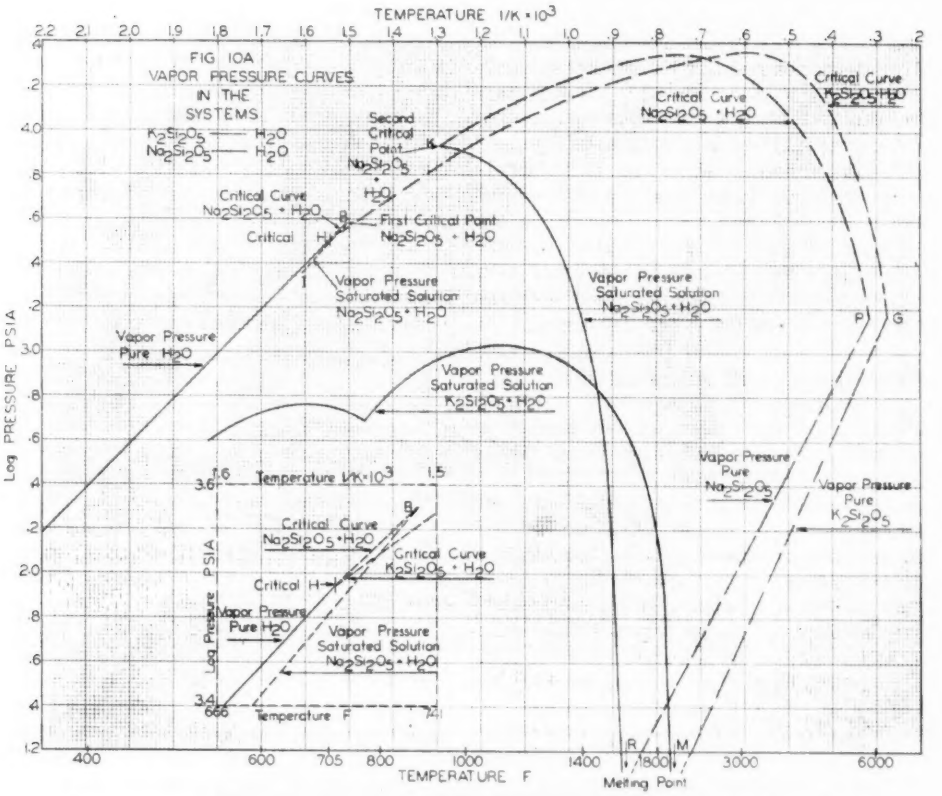


FIG. 10(*a*) VAPOR-PRESSURE CURVES IN THE SYSTEMS $NaSiO_5$-H_2O AND $K_2Si_2O_5$-H_2O

in solution even as they pass from the superheater at the full temperature of 1000 F.

The intersections of the 1400-psia isobar with the descending branches of the various saturation curves shown, occur well above the superheat temperature of 1000 F, except in the case of the mixture KCl + NaBr. In that case, the saturation curve reaches its maximum vapor-pressure value at approximately 914 F and, thereafter, as its equilibrium vapor pressure becomes lower with increasing temperature (also increasing concentration), intersects the 1400-psia isobar at C_6, 970 F, and at 1000 F lies well below it. This means that at 970 F, the potassium chloride and sodium bromide must redissolve, and at 1000 F, will pass from the superheater in solution. If the superheat temperature was a little above 1400 F, all solo salts noted in Fig. 10 would redissolve and pass from the superheater in solution. In case of mixtures, evaporation to dryness might never occur, but if it did, redissolution would be almost certain to occur, and very likely at temperatures considerably lower than 1400 F. The mixture of potassium chloride and sodium bromide is the only one on which data are available at present. On the descending, as well as on the ascending branch of its saturation curve, its marked difference in values from those of the saturated solo-solution curves of its components emphasizes the need of data of this sort for mixtures of salts which will be representative of those characterizing boiler waters. Experimental technique is extremely difficult, but Partridge and Kaufman of our laboratories are drawing plans for the work.

The vapor-pressure curves of saturated solutions thus far discussed, and presented in Fig. 10, are of salts whose solubilities continuously increase with rise of temperature. The descending branch of each of the vapor-pressure curves is approaching closely to the melting temperature of the dry salt as it intersects the base line (pressure = 10 psia) and attains that temperature somewhat below at a pressure which is the vapor pressure of the pure salt, and a concentration of 100 per cent dry salt.[7]

If, now, the temperature of the melted salt is raised, the pressure created by the pure vapor of the salt increases. In the case of potassium silicate, Fig. 10(*a*), this follows a line such as *MG*,[8] originating at the melting point and attaining critical state at *G* (assuming no decomposition of salt or vapor), just as water attains its critical state at *H*. The line connecting *G* and *H*, and representing the lowest vapor pressures of critical conditions for mixtures of water and potassium disilicate, is known as their critical, or plait-point curve. The critical curves of sodium chloride and potassium chloride for a short distance beyond *H* have been determined by Schröer (A, VIII). The significant point about this curve is that throughout its length, it lies well above the vapor-pressure curve of saturated solutions of potassium disilicate, no intersection of the saturation vapor-pressure curve and of the plait-point curve occurring. This is a general property of the plait-point curves of substances whose solubilities increase with increasing temperature in both branches of the saturation vapor-pressure curve. Between the saturation vapor-pressure curve and the plait-point curve of any substance lie the vapor-pressure curves of its unsaturated solutions, critical state

[7] The melting point under these conditions will be very slightly different from the melting point usually cited in the handbooks, a value obtained under ordinary atmospheric conditions.

[8] The broken-line curves *MG*, *RP*, *GH* and the two segments *PK* and *BH* are hypothetical only, definite points not having been established. *K* has been tentatively fixed by Morey. Definite location of *B* is not established other than that it lies slightly above the critical temperature of water. One point of *BI* has been established by Morey (private communication) at 662 F, but the general form of these curves of decreasing solubility along the ascending branch has been established by the data on Na_2CO_3 and Na_2SO_4 (A, III, 2, 19). The incongruent solubility relationship of $Na_2Si_2O_5$ probably begins shortly below *I*.

of the solutions occurring at their points of tangency to the plait-point curve (40). At or above the critical point of the solution, there is no discontinuity of solubility, the substance dissolved in the water remaining in solution in the gaseous phase, and solubility increasing with both temperature and pressure, but especially the latter (41, 20, 42).

Now let us consider the salts whose solubilities are retrograde in the range of boiler-water temperatures. In keeping with their low solubilities, their Δt_s values are low, and at 1400 psia (Table 5), evaporation to dryness will occur almost immediately upon entry into the superheater. The question of moment to anyone interested in boiler waters is: Will this same condition continue, as temperature is increased well above 705 F in the superheater, or will changes occur resulting eventually in a descending branch of the vapor-pressure curve, and therefore greater solubility?

In regard to critical characteristics, the data on sodium disilicate by Morey and Ingerson (14, 15) are alone available. Line IB represents the saturation vapor-pressure curve of sodium disilicate. It passes close to the critical point of water H and, slightly beyond at B intersects the critical or plait-point curve joining H with P, the critical point of sodium disilicate, and passes through points B and K, but with a break in the curve over the interval BK. Beginning at point B, the intersection with the critical curve, the sodium disilicate exists only in solid form, or dissolved in the fluid (gaseous) phase; the coexistence of liquid and vapor is impossible.

Morey and Ingerson (21) state: "When the critical curve is intersected in one point by the solubility curve (as at B), it must also be intersected in a second point."

In searching for this second point, they (15) started with sodium disilicate at its melting point just below R, Fig. 10(a), and by controlling as desired the pressure of steam with which they surrounded it, found vapor pressure to increase with falling temperature along the line RK. Finally near K (8500–8700 psia, 932 F), the second point of intersection of the saturation vapor-pressure curve with the critical curve has been located tentatively. From K, the descending branch of the vapor-pressure curve extends unbroken through R to the melting point of the salt, saturation concentration being high and increasing with temperature increase.

The break BK between the first and second intersections of the saturation vapor-pressure curve and the critical or plait-point curve is a little-explored region, of which Morey (14) states:

"Numerous experiments have been made at temperatures ranging from 375 to 500 C (707 to 932 F) and at pressures up to 16,500 psia and with mixtures ranging in composition from sodium metasilicate to the eutectic between sodium disilicate and quartz. These studies are not complete, but they all indicate that under the conditions of experiment the percentage of sodium oxide and silica in the vapor becomes large. Some results as yet unconfirmed indicate over 50 per cent by weight of solid material in solution in the vapor.

"The conditions of these experiments are more drastic than those encountered in steam boilers and superheaters, but, nevertheless, the very considerable power of steam under these more drastic conditions to transport ordinarily nonvolatile components will be paralleled by a smaller transport power per unit of steam at the lower pressures."

For the theory of these relationships, in the temperature range above critical for water, which characterize the salts of retrograde solubility, the reader is referred particularly to Morey and Ingerson (21) and to Schröer (20).

The very great difference in behavior in the region above 705 F of sodium disilicate, representative of the inorganic salts, with retrograde solubilities approaching zero at the critical temperature of water from those of steadily increasing solubility is apparent from Fig. 10(a). While no data on the former are available, other than those of Morey and Ingerson on sodium disilicate, it seems practically certain that they, like it, must have a descending branch to their saturation vapor-pressure curves, and along that branch must increase in solubility with rising temperature.[9] The physical characteristics of such solutions, for instance fluidity, are unknown. Where the curves of mixtures of salts, some with retrograde and some with continuously increasing solubilities, as boiler-water salts, would lie on the diagram, and whether their temperatures on the descending branches of the curves would be low enough to be significant as regards conditions in the superheater, we can only surmise until pertinent data have been obtained.

Once the essential data are available to establish Δt-function curves, such as those in Figs. 4, 10, and 10(a), for boiler-water compositions, an analysis of the dilute over-all boiler water, expressed in mol fractions of the components, will make feasible estimation of concentrations and of the condition of the components in the concentrating-film boiler water, or of carry-over in the superheater at different values of Δt, and likewise at any point in the turbine of which the temperature and pressure are known. We may illustrate the principle by the following example:

In Keevil's (6) work, from which the data of the KCl-NaBr mixture were obtained, the concentration of the saturated solutions was not measured. Kaufman and Morris in our laboratory made a saturated solution by agitating water with solid KCl and NaBr and found the boiling point at atmospheric pressure to be 245 F, the composition of the solution being expressed by 0.044 mol fraction of KCl, 0.029 of KBr, and 0.117 of NaBr, a total of 0.19 mol fraction or 56.4 per cent. At intersection C_s, Fig. 10, P_s = 1400 psia or boiler pressure; t_s = 874 F; and P_{H_2O}, the vapor pressure of pure water at t_s, read from the extension beyond critical of the H_2O vapor-pressure curve (hypothetical, but of use in the calculations) is 8040 psia. The ratio P_s/P_{H_2O} = 0.174. Now, let us assume, in the absence of data on mixtures, that the deviation curve of the Halides, Fig. 4, applies to their mixtures as well as to their solo solutions; this may or may not be true but is as near the truth as we can get until more data are available. The value of 0.174 on the ordinate P_s/P_{H_2O} corresponds to X_2 = 0.5 mol fraction on the abscissa. The evalua-

[9] The data of Goranson on albite, $NaAlSi_3O_8$, and orthoclase, $KAlSi_3O_8$, indicate that the complex silicates, such as analcite, $NaAlSi_2O_6.2H_2O$, and leucite, $KAlSi_2O_6$, belong in this class (44, 45).

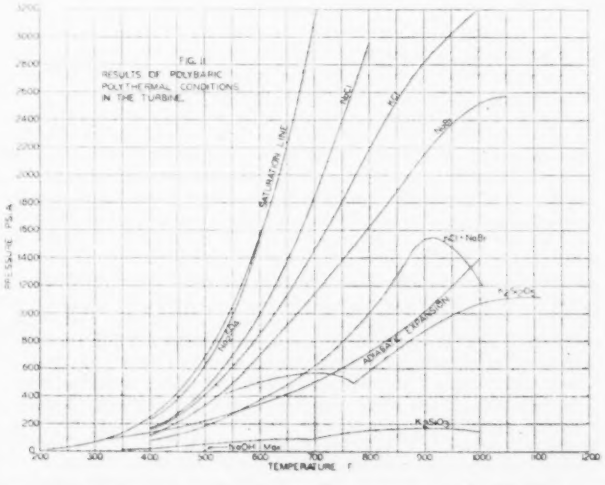


FIG. 11 RESULTS OF POLYBARIC-POLYTHERMAL CONDITIONS IN TURBINE

tion of mol fraction into per cent involves uncertainty because of lack of knowledge of the relative proportions of K, Na, Cl, and Br in the saturated solution at 874 F. However, as the solubility curves of the salts involved are similar in form and in so far as we know do not form double salts, we shall assume that their proportionate concentrations at 874 F, and 1400 psia, remain essentially what Kaufman and Morris found them at 245 F and 14.7 psia. On that basis, the molar concentration of the saturated solution at 874 F is estimated to be 0.116 of KCl, 0.076 of KBr, 0.308 of NaBr, 0.500 H_2O, which correspond to 14.8 per cent KCl, 15.5 per cent KBr, and 54.3 per cent NaBr, a total of 84.6 per cent. The outside limits of variation would be represented by 80.6 per cent if the solution contained only KCl, and 85.2 per cent, if only NaBr. When data become available to obviate the uncertainties involved in the assumptions necessarily made in this case, the method will give a clear picture of the condition of any salts transported as carry-over in the steam, if the temperature and pressure of the latter are known.

Returning to Fig. 10, we note that for a superheat temperature of 850 F, and a boiler pressure of 600 psia, only potassium metasilicate and the alkalies lie below the isobar, and would leave the superheater in solution.[10]

Presumably in a great majority of cases any carry-over of boiler water in the steam, attaining even a semblance of equilibrium at the temperature of the superheater, has become a magma (that is, a thin paste of solution with precipitated salts dispersed therein) by the time it enters the turbine. Once their Δt-function properties are known, it will be possible to prescribe and maintain in the over-all boiler water, proportional relationships among its components which, as concentration occurs, will result in magmas of least disadvantage both to superheater and turbine.

Role of Silica in the Turbine

The magmas, as they leave the superheater, are the product of equilibrium corresponding to its high temperature and boiler pressure. As they enter the turbine and experience lowering of temperature and pressure, they must change in seeking to maintain equilibrium under the new conditions. What happens to the magmas[11] of solo solutions, and of the one known mixture of potassium chloride and sodium bromide, is shown in Fig. 11, developed by Kaufman, for pressure of 1400 psia and total temperature of 1000 F. An ideal adiabatic expansion curve has been used for purposes of illustration, but the conclusions drawn will hold equally well for operating conditions. All curves falling within the area bounded by the saturation line and the adiabatic expansion curve represent undissolved or solid condition of the different substances concerned in this example; all curves falling below the adiabatic expansion curve represent a dissolved condition of the respective substances. Thus at all pressures and temperatures, potassium metasilicate and potassium or sodium hydroxide enter the turbine and continue on through in dissolved form. Sodium sulphate, chloride, and bromide, and potassium chloride, enter in solid form, and remain thus until the region of condensation or close thereto is reached, finally dissolving. The sodium di- and metasilicates, because of low solubility and consequent small Δt, values like sodium sulphate, almost certainly enter and remain in solid form until the lower-temperature region of the turbine is reached. Apparently potassium disilicate enters the turbine under consideration in dissolved form, begins crystallizing at about 730 F and 560 psia, and then at 536 F enters the region of its incongruent solubility relationship with any moisture, a relationship discussed fully later. The mixture of potassium chloride and sodium bromide enters in solution, then saturates and crystallizes at 984 F and 1330 psia, but redissolves at about 563 F and 300 psia, where its saturation curve crosses the adiabatic expansion curve, considerably above the region of condensation.[12]

With the establishment of Δt-function curves for boiler-water salt mixtures, it will be possible to relate the composition and condition of magmas entering the turbine to their tendency for adherence (47, 48), and hold this minimum by establishing appropriate relationships in the dilute over-all boiler water. However, because of certain intrinsic properties of the silicates, enough is already known to point the way toward rendering them least obnoxious in any carry-over.

In the turbine, above the temperature range approximately 500 F, silica found in any deposition is probably combined in the form of sodium silicate, and thus is water-soluble at the temperatures usual in washing turbines; below the 500 F range, it is uncombined and insoluble, usually being in the form of quartz down to perhaps 250 F, and in the amorphous form thereafter. This quite signal temperature boundary between sodium silicate on the high, and uncombined silica on the low side, leads to the conclusion that there must be definite chemical characteristics of the silicates which cause this condition to exist. What are these characteristics?

In studying the silicates to answer this question, we must perforce use the potassium salts as our examples, as sufficient data on the sodium salts are not of record. One conclusion, however, may be inferred, i.e., that the sodium silicates, because of their retrograde solubility, and consequent very small Δt, value, will at least equally, and perhaps more strongly, exemplify the characteristics brought out than will the potassium salts.

Morey (14, 27) states: "A large number of compounds become decomposed by, and are incongruently soluble in, water at elevated temperatures." In a solution in which the ratio of silica to potash is that of the disilicate ($2SiO_2$:$1K_2O$) and the temperature is lowered to below 536 F, "the disilicate becomes decom-

[10] As pointed out by Hall (43), the passage of superheated steam over solid sodium chloride in determinations of its solubility in the steam may result in dissolving the sodium chloride with formation of a strong solution, thus largely changing the conditions of the experiment. In Spillner's (18) work, for example, with total steam temperature of 765 F, below 2600 psia (183 kg per cm²) the sodium chloride would remain solid as long as it retained its purity; at 2600 psia, and 765 F, it would dissolve to form a solution of 0.214 mol fraction or 47 per cent, the solution becoming more dilute over the remaining range of experimental pressure terminating at 3980 psia (280 kg per cm²). In his experiments on potassium chloride, dissolution of pure solid salt would occur at 1930 psia (135 kg per cm²) and 765 F, the solution formed having a concentration of 0.302 mol fraction or 64.2 per cent, and dilution occurring with increased pressure. In Straub's (19) experiments at 1540 psia, the sodium chloride would be dissolved up to the temperature 667 F, and solid above that temperature; at 2200 psia, it would be dissolved up to 732 F, and solid above. It is apparent from the curve of KCl + NaBr (Fig. 10) that, if the sodium chloride should collect any impurity from its surroundings during the experiment, the maximum temperature at which it would remain in dissolved form at the pressure level of the experiment would be higher than for the pure salt.

[11] Perhaps better in this case, "equilibrium products" since the example deals only with solo solutions, and one mixture of two components only.

[12] What would happen in the case of a mixture such as that of sodium sulphate and sodium hydroxide? At high temperatures of the superheater, the solubility of sodium sulphate in sodium-hydroxide solutions is probably quite high (the data of Schroeder et al. (8) lead to this conclusion). With temperature falling rapidly in the turbine, solid sodium sulphate would almost certainly form in the magma. In this connection, it is notable that sodium sulphate readily crystallizes as deposit in high-pressure turbines (43). Sodium silicate in the magma would probably duplicate the performance of sodium sulphate (43). In the latter case, the separation of sodium silicate may result in a remanent magma with higher $Si:O_2/Na_2O$ ratio. Silica enrichment of this type has played a large part in the differentiation of molten magmas in nature, with granite, which is high in silica, forming in the latter stages (46).

posed by water, and crystallizes only from solutions which contain an excess of potassium oxide. If a solution containing potash and silica in the disilicate ratio is cooled and crystallized below 536 F, the compound separating is not potassium disilicate but potassium tetrasilicate ($K_2O.4SiO_2.H_2O$), and below this temperature potassium disilicate is incongruently soluble in water.... Potassium tetrasilicate becomes decomposed by water at temperatures below 680 F, with quartz becoming the stable phase."

In the light of these facts, we can visualize the chain of events started by the exceptional property of the disilicate of crystallizing from solution in the turbine beginning at about 730 F, as just noted, (Fig. 11). Farther on as the crystals thus formed redissolve at lower temperatures, it seems probable that the relationship of incongruent solubility between water and disilicate develops, with formation of tetrasilicate, which in turn and by the same mechanism splits off silica. The high solubility and high Δt, value of potassium metasilicate insure its presence in solution throughout the turbine, and by excess of alkali over silica development of the incongruent solubility relationship with water is avoided. The disilicate of sodium, with retrograde solubility curve and small Δt, value, is very likely to be already crystallized in the magmas entering the turbine from the superheater, but as a region of lower temperature is reached, at which its solubility is higher, decomposition by water presumably proceeds, thus directly forming silica without the interposition of any tetrasilicate. The course of sodium metasilicate in the turbine is probably similar, but more easily controlled than that of the disilicate.

Also significant is the abrupt ending of the solubility curves of potassium disilicate and metasilicate in Fig. 5, the cause thereof being the beginning at the temperature indicated of their incongruent solubility relationship with water, as evidenced by their decomposition thereby.

One may also read the story from the curves in Fig. 8. Starting for instance with a solution in which the ratio of SiO_2/K_2O is 2 (that of the disilicate), we find that the vertical co-ordinate representing this ratio crosses the saturation isotherm of 1112 F at 0.645 mol fraction, and well within the field of stability of $K_2Si_2O_5$, so that any crystals separating from solution will be potassium disilicate, which has high solubility. Following the same co-ordinate downward, we find it crossing the saturation isotherm of 680 F at 0.495 mol fraction, and still well within the field of disilicate stability. But a little lower, at a mol fraction value of 0.385, this co-ordinate crosses the boundary line separating the field of potassium-disilicate stability from that of potassium tetrasilicate. From that point on, down to the very small mol fraction or solubility value of the intersection of this co-ordinate with the 392 F saturation isotherm, any crystals separating will be potassium tetrasilicate, which in this temperature range has the property of decomposition by water with formation of silica. Thus, a ratio of silica to alkali of even a little less than 2 (Fig. 8), normally as one of its inherent properties, splits off silica in the lower temperature region of the turbine. As the ratio of silica to alkali increases, the effect becomes more pronounced.

How are these conclusions affected, if Spillner's work (18) on solvent action of steam is finally found correct? While there has been considerable discussion of the vaporization of boiler-water salts with the steam, and their transport in this form into the turbine, the point is not settled. Straub (19) has been working on it and has made an excellent report. Morey's work (14) indicates that any volatilization of the sodium silicates into the steam will occur as salts and not as silica, if the $SiO_2/(alkali)$ ratio in the boiler water is appropriately controlled by the boiler-water alkalinity. In any event, in the turbine, condensation from vapor phase to solid phase or solution must precede deposition as solid phase. As any silicates thus condense from the vapor phase, they will follow immediately the course of reaction just described, and will likewise equally respond to conditions directed toward controlling the course of reaction.

For the application of these facts to the control of silica deposition in the turbine, we can reduce them to the formula of appropriately controlling the ratio $SiO_2/(alkali)$ in the over-all boiler water, thus obviating conditions favoring any development of the relationship of incongruent solubility between water and the silicates in the turbine, and also thereby establishing conditions unfavorable to any separation of insoluble silica, and in fact favorable to the dissolution of silica already deposited.

With these facts in mind, it is not surprising that there has been an epidemic of silica deposition in turbines. Every step taken in the direction of very low alkalinities in the boiler water, usually as an aid in combating the ravages of corrosion by the bonded oxygen thereof, raised the ratio of SiO_2/Na_2O in the over-all boiler water, and thus abetted the certainty and extent of a relation of incongruent solubility between any silicate, and any moisture or any solution developing in the lower-temperature range of the turbine. Very likely boiler waters have been made too pure. The absence of other soluble salts to exercise their influence in the Δt function of the concentrating-film boiler water, thus restraining an otherwise exaggerated rise in caustic concentration, has led to the necessity of so far decreasing boiler-water alkalinity that the $SiO_2/(alkali)$ ratio has risen to values highly favorable to silica deposition in the turbine. It should be noted that it is not the absolute value of the silica in the boiler water, but the value of the ratio of silica to alkali that is the governing factor. Quite evidently, the practical answer in operation is to build the dilute over-all boiler water to meet the requirements, as expressed both by the Δt function and by the $SiO_2/(alkali)$ ratio, and so to maintain it.

Protection From Embrittlement in the Light of the Δt Function

If caustic embrittlement is caused by strong caustic-alkali solutions, resulting from strongly concentrating boiler water at vapor-water interfaces, application of the Δt function to the problem of protection therefrom leads to significant results. If the evaporation necessary to concentrate the boiler water to high causticity occurs at boiler pressures or thereabouts, and at a surface such as A, Fig. 1, subject to higher temperature than corresponds to the steam pressure, concentration of the boiler water will proceed according to the Δt relationship, and the rapid increase of caustic concentration with increase of Δt, unless restrained by other suitable salts in the boiler water, is illustrated by the curve in Fig. 7.

The type of embrittlement (25) produced by reaction of the boiler water on a tube surface such as A, Fig. 1, is illustrated in Fig. 13, in which the damage resulted, we believe, from a concentrating-film boiler water due to relatively large Δt value. Under such conditions of boiler pressure and Δt values, any protective action of sulphate must be that of scale formation or plugging action, since its solubility is of such small mol fraction even with its increment of solubility in caustic solution, that its aid in deterring concentration of caustic to meet the Δt requirement is negligible for all practical purposes, unless perchance Δt is enough so that the temperature environment is that corresponding to the descending branch of the vapor-pressure curve of sodium sulphate, or its mixtures with caustic soda and other salts (see sodium disilicate, Fig. 10(a), and the discussion concerning it). The usual absence of spheroidization of the cementite in embrittled metal disputes the existence of the necessary temperature, unless the descending branch of the curve is shifted to much lower temperature by reason of the mixture of salts. Sodium phosphate, as used by Schroeder and Berk (24) and by Whirl

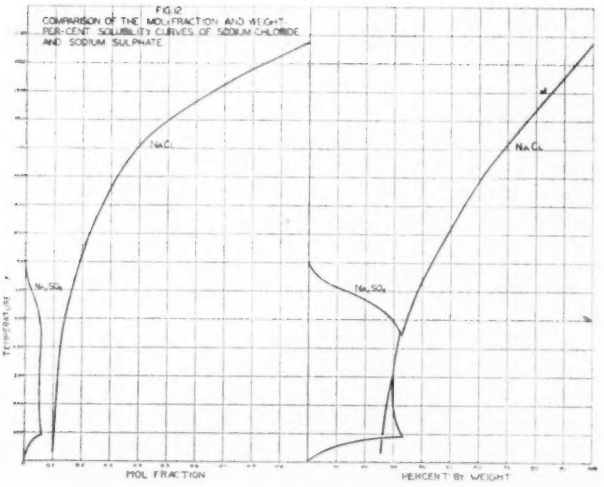


FIG. 12 COMPARISON OF MOL-FRACTION AND PER-CENT-BY-WEIGHT SOLUBILITY CURVES OF SODIUM CHLORIDE AND SODIUM SULPHATE

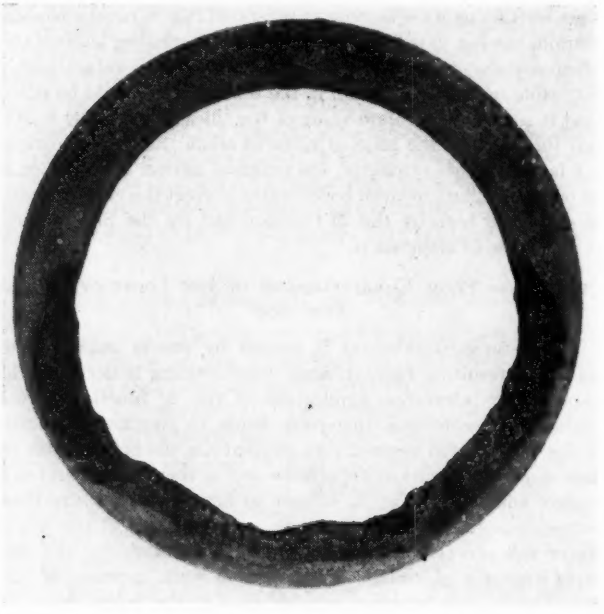


FIG. 13 EMBRITTLEMENT DUE TO Δt-FUNCTION CONDITIONS ON A GENERATING TUBE SURFACE

and Purcell (13), holds any concentration of alkalinity in check, because purposely the over-all boiler-water alkalinity is of captive type based on sodium phosphate.

On the other hand, sodium or potassium chloride, and the potassium silicates, with their relatively high mol-fraction solubilities, and correspondingly large values of Δt_s, if maintained in appropriate concentration in the over-all boiler water in relation to caustic, can thus be made to restrain the caustic concentrations within limits recognized as safe. Examples of protection thus obtained, though not purposely, are found in the boilers of ocean-going vessels, in which embrittlement has only infrequently been recognized (37, 38), and whose boiler waters contain considerable chloride, resulting mainly from condenser leakage. Tighter condensers on the newer ships may alter this record unless appropriate protective measures are taken. The ratio of chloride along with sulphate, recommended by Straub (22), falls in the same category of protective measures. The potassium silicates are not only of high Δt_s value, but combine as well with that part of the captive alkalinity which must be credited to them in the over-all boiler water.

If the evaporation of the boiler water in concentrating the caustic occurs at high temperature but with escape of the steam readily so that pressure at the water-vapor interface is low, then about the only salts that would help in the protection from embrittlement by curbing alkalinity are the phosphates and potassium silicates on the basis of captive alkalinity, and potassium metasilicate by reason of its high solubility. Any effect of the other salts is apparently a scale-forming or plugging action.

If the evaporation is at a cooler temperature, the results are practically the same as for the high-temperature low-pressure conditions. It is interesting to note from Fig. 12, that sodium chloride for all conditions of temperature and pressure has a higher mol-fraction solubility than sodium sulphate, and is thus of more value in curbing caustic concentration. The same is true of potassium chloride. Perhaps scale-forming or plugging action of the sodium sulphate enhances its protective action against embrittlement. In view of its very small Δt_s value, that seems to be the only logical reason for any advantage in the different levels of the ratios of sodium sulphate to alkalinity in relation to pressure which have been so widely used for the purpose of protection from embrittlement.

On the Technique of Substituting Potassium for Sodium

In condensing plants supplied with evaporated make-up water, the feedwater is practically devoid of sodium save for small amounts derived from condenser leakage and evaporator carry-over, up to the point at which treating chemicals in the form of sodium salts are added. Use of potassium chemicals in the treatment in place of sodium chemicals will thus result in a boiler water in which the ratio of potassium to sodium is quite high, and controlling.

In those plants in which the make-up is treated with zeolite softeners of various types, substitution of potassium chloride for sodium chloride in the process of regeneration of the zeolite effects the result that the softener may be run to substitute potassium for sodium, as well as for calcium and magnesium. Work done in our laboratories shows that this is readily feasible and economical. This applies to the zeolite softeners run on the sodium cycle. On the other hand, if the zeolite is run on the acid cycle, neutralization of the treated water with potassium hydroxide or other alkaline potassium salts will supply a feedwater which in many instances will contain the required amount of potassium to establish satisfactory potassium equilibrium in the boiler water. If the zeolitic operation includes use both of the sodium and the acid cycles, then regeneration with potassium chloride will change the sodium cycle to a potassium cycle, and the neutralization of the water from the acid cycle with potassium hydroxide or with the water from the potassium cycle will result in a feedwater of sufficient potassium concentration.

If the softening operation is of the lime-soda type, the substitution of potash for soda ash will increase considerably the ratio of potassium to sodium in the water. In coagulation processes, the substitution of potassium for sodium salts will also aid in building the potassium concentration in the water.

In general, the requisite supply of potassium salts in the boiler water for potassium equilibrium will be accomplished if throughout the treating processes, the sodium chemicals now in use are replaced by corresponding potassium salts. In the case of some raw waters relatively low in sodium content, it may be possible to build a sufficient potassium concentration in the boiler water for the potassium equilibrium, by the addition of potassium treating chemicals appropriately chosen, and supplied in amount to maintain in the boiler water, as determined by analysis thereof,

the essential preponderance of potassium over sodium in the ratio K/Na. In a great majority of the cases, however, it will be advantageous to effect substitution of potassium for sodium in the feedwater by one of the methods of treatment as indicated. For the boiler water itself, in order to establish the relationships demanded on the basis of the Δt function, and the required ratio of SiO_2/K_2O for the prevention of any incongruent-solubility relationship in the turbine, the potassium chemicals of required type may be added as direct treatment.

Tiger (23) has recently proposed that the anion-cation exchangers, which produce water well-nigh equivalent to distilled water in so far as most of the dissolved salts are concerned, could well be used for make-up purposes in condensing plants in place of evaporators. He states, however, that silica is not removed in the process and suggests, therefore, that silica-removal equipment be supplied for preliminary treatment to remove silica before the water goes to the exchanger. The vast difference that is wrought by maintenance of potassium equilibrium on the boiler water, and substitution of potassium for sodium therein, is well illustrated by the fact that retention of silica in the water from the anion-cation exchangers may very well be advantageous for the purpose it serves in the boiler water, and in any event can be readily taken care of in the boiler water merely by proper attention to the demands, according to the Δt function, and the appropriate SiO_2/K_2O ratio. If Tiger's proposal to use the anion-cation exchangers will provide practically the equivalent of distilled water, except for a little silica present, and if it will fit into the heat balance of the plant, we see no reason at all to shy away from the scheme.

Conclusion

Starting with substitution in the boiler water of the potassium equilibrium for the universal sodium equilibrium, we have been led to give consideration to a number of problems concerning the boiler-water and steam cycle. In this discussion, we have included those relating to magnesium deposits, hide-out of boiler-water salts, corrosion by the bonded oxygen of the boiler water, silica in boiler and turbine, equilibria developed in the superheater in any carry-over of boiler water, and protection from embrittlement.

The problem of magnesium deposits involves equilibrium under the isobaric-isothermal conditions of the over-all boiler water, and has been included because of the usefulness of boiler-water silica, and the potassium equilibrium in its solution.

There is nothing fortuitous in this grouping of the other problems. Each one derives its origin from that fundamental and ubiquitous phenomenon of the boiler-water and steam cycle, the steam-water interface, where the manifold variations of isobaric-polythermal and polybaric-polythermal conditions are spurred on by the mighty forces set free in the boiler furnace. In systematizing the results which must ensue from the complex network of interrelations of temperature, pressure, and concentration under these conditions, the concept of the concentrating-film boiler water and the application of the Δt function have proved most useful, likewise the relationship of incongruent solubility between water and the silicates. We believe that we would have been considerably dismayed by the conclusions to which we were inevitably led, had not the tools of potassium equilibrium and, in that environment, the utility of silica, been at hand. Many more data are still needed, but we feel confident that this logical approach to the problems of the steam-water interfaces will give to the engineers those cleaner surfaces for the boiler-tube raceway which will bring calculated and actual circulation into better agreement.

Acknowledgment

To Hankison and Baker, of the West Penn Power Company; to Morey, of the Geophysical Laboratory; and to his associates, particularly Kaufman, Cerna, and Partridge, the author expresses his sincere appreciation for their assistance.

Bibliography

1 "Value of Higher Steam Pressure in the Industrial Plant," by William F. Ryan, Trans. A.S.M.E., vol. 47, 1925, pp. 779–820.

2 "A Physico-Chemical Study of Scale Formation and Boiler-Water Conditioning," by R. E. Hall and Associates, Mining and Metallurgical Investigations, Carnegie Institute of Technology Bulletin 24, 1927, pp. 72-73; "Overcoming Boiler-Water Troubles With Tri-Sodium Phosphate," by B. C. Sprague, *Power*, vol. 65, 1927, pp. 321–322.

3 "Formation and Properties of Boiler Scale," by E. P. Partridge, University of Michigan, Engineering Research Bulletin No. 15, Ann Arbor, Mich., 1930, pp. 71–74.

4 "Studies of Heat Transmission Through Boiler Tubing at Pressures From 500 to 3300 Pounds," by W. F. Davidson and Associates, Trans. A.S.M.E., vol. 65, 1943, pp. 553–591.

5 "Natural Circulation Problems," by A. A. Markson, Proceedings of the Midwest Power Conference, vol. 5, 1942, pp. 188–195.

6 "Vapor Pressures of Aqueous Solutions at High Temperatures," by N. B. Keevil, *Journal of the American Chemical Society*, vol. 64, 1942, pp. 841–850.

7 "The Ternary System H_2O–K_2SiO_3–SiO_2," by George W. Morey, *Journal*, American Chemical Society, vol. 39, 1917, pp. 1173–1229.

8 "Solubility Equilibria of Sodium Sulfate at Temperatures of 150 to 350° C.," by W. C. Schroeder, A. Gabriel, and E. P. Partridge, *Journal of the American Chemical Society*, vol. 57, 1935, pp. 1539–1546.

9 "Solubility Equilibria of Sodium Sulfate at Temperatures of 150 to 350°, by W. C. Schroeder, A. A. Berk, and A. Gabriel, *Journal of the American Chemical Society*, vol. 59, 1937, pp. 1783–1790.

10 "Attack on Steel in High-Capacity Boilers as a Result of Overheating Due to Steam Blanketing," by E. P. Partridge and R. E. Hall, Trans. A.S.M.E., vol. 61, 1939, pp. 597–622; also see "Coordination of Water Conditioning With Operating Problems," by R. E. Hall and C. E. Kaufman, *Power Plant Engineering*, vol. 45, Sept., pp. 61–64, and Oct., 1941, pp. 59–61.

11 "The Action of Caustic and Salts on Steel at High Pressures," by E. Berl and F. van Taack, *Forschungsarbeiten auf dem Gebiete des Ingenieurwesens*, Berlin, 1930.

12 "The pH, Dissolved Iron Concentration and Solid Product Resulting From Iron and Pure Water," by R. C. Corey and T. J. Finnegan, Proceedings of the A.S.T.M., vol. 39, 1939, pp. 1242–1260.

13 "Protection Against Caustic Embrittlement by Coordinated Phosphate pH Control," by T. E. Purcell and S. F. Whirl, Proceedings of the Third Annual Water Conference, Engineering Society of Western Pennsylvania, Pittsburgh, Pa., 1942, pp. 45–60; Trans. Electrochemical Society, vol. 83, 1943, pp. 279–295.

14 "Solubility of Solids in Water Vapor," by George W. Morey, Proceedings of A.S.T.M., vol. 42, 1942, pp. 980–988.

15 "The System, Water-Sodium-Disilicate," by George W. Morey and E. Ingerson, *American Journal of Science*, vol. 35-A, 1938, pp. 217–225.

16 "New Crystalline Silicates of Potassium and Sodium, Their Preparation and General Properties," by George W. Morey, *Journal of the American Chemical Society*, vol. 36, 1914, pp. 215–230.

17 International Critical Tables, McGraw-Hill Book Company, Inc., New York, N. Y., 1930, vol. 3, pp. 368–375.

18 "High-Pressure Steam as a Solvent," by F. Spillner, *Die Chemische Fabrik*, vol. 13, 1940, pp. 405–416.

19 "Solubility of Salts in Steam at High Pressures," by F. J. Straub, Proceedings of Third Annual Water Conference, Engineering Society of Western Pennsylvania, Pittsburgh, Pa., 1942, pp. 31–38; also, "Turbine Blade Deposits," Proceedings of the Midwest Power Conference, vol. 6, 1943, pp. 50–55; *Blast Furnace and Steel Plant*, vol. 31, 1943, pp. 1166–1169.

20 "The Critical State of Water and Aqueous Solutions," by Erich Schröer, *Zeit. für Physikalische Chemie*, vol. 129, 1927, p. 79.

21 "The Pneumatolytic and Hydrothermal Alteration and Synthesis of Silicates," by G. W. Morey and E. Ingerson, *Economic Geology*, supplement to vol. 32, August, 1937, pp. 607–760.

22 "A Method for the Embrittlement Testing of Boiler Waters," by F. J. Straub and T. A. Bradbury, Proceedings of the A.S.T.M., vol. 38, 1938, pp. 602–630.

23 "Demineralizing Solutions by a Two-Step Ion Exchange Process," by H. L. Tiger and S. Suesman, *Industrial and Engineering Chemistry*, vol. 35, 1943, pp. 186–192.

24 "Intercrystalline Cracking of Boiler Steel and Its Preven-

tion," by W. C. Schroeder and A. A. Berk, U. S. Bureau of Mines Bulletin No. 443, 1941, pp. 64–66.

25 "Water Problems in Small Power Plants," by E. P. Partridge and A. L. Soderberg, *Blast Furnace and Steel Plant*, vol. 30, 1942, pp. 664–670; also Proceedings of the Midwest Power Conference, vol. 5, 1942, pp. 105–117.

26 "Removal of Water-Insoluble Turbine Deposits by Caustic Washing," by W. L. Webb, and R. G. Call, *Combustion*, vol. 14, June, 1943, pp. 37–39; Trans. A.S.M.E., vol. 65, 1943, pp. 713–717.

27 "The Properties of Glass," by G. W. Morey, Reinhold Publishing Company, New York, N. Y., 1938; pp. 104–107; also "Solubility and Decomposition in Complex Systems," *Journal*, Society of Glass Technology, vol. 6, 1922, pp. 20–29.

28 "Corrosion by Liquids," by R. C. Corey, *Combustion*, vol. 15, August, 1943, pp. 35–39.

29 "Investigation of the Oxidation of Metals by High-Temperature Steam," by A. A. Potter, H. L. Solberg, and G. A. Hawkins, Trans. A.S.M.E., vol. 59, 1937, pp. 725–732; also, vol. 60, 1938, pp. 610–615.

30 "Port Washington's Second Year," by M. K. Drewry, *Combustion*, vol. 9, February, 1938, pp. 18–24.

31 Discussions of "Attack on Steel in High-Capacity Boilers as a Result of Overheating Due to Steam Blanketing," by R. T. Hanlon, W. L. Webb, and L. E. Hankison, also, author's closure, Trans. A.S.M.E., vol. 62, 1940, pp. 712–717.

32 "Corrosion in Partially Dry Steam-Generating Tubes," by F. G. Straub and E. E. Nelson, *Mechanical Engineering*, vol. 61, 1939, pp. 199–202.

33 "Analcite. Preparation and Solubility Between 182° and 282° C," by F. G. Straub, *Industrial and Engineering Chemistry*, vol. 28, 1936, pp. 113–114.

34 "The Embrittling Action of Sodium Hydroxide on Mild Steel, and Its Possible Relation to Seam Failures of Boiler Plate," by P. D. Merica, *Chemical and Metallurgical Engineering*, vol. 16, 1917, pp. 496–503.

35 "Embrittlement Detector Testing on Boilers," by W. C. Schroeder, A. A. Berk, and C. K. Stoddard, *Power Plant Engineering*, vol. 45, 1941, pp. 76–79.

36 "Port Washington Station Sustains Its Economy," *Combustion*, vol. 11, 1940, pp. 33–34.

37 "Note on the Chemical Intercrystalline Fracture of Riveted Joints in Boilers," by S. F. Dorey, Trans. Inst. Naval Architects, vol. 79, 1937, pp. 50–56; discussion, pp. 57–76; digest in *Engineering*, vol. 143, 1937, pp. 392–393.

38 "Adams Discussion," ref. (13), p. 60.

39 "Soluble Silicates in Industry," by J. G. Vail, Chemical Catalog Company, Inc., New York, N. Y., 1928, pp. 191, 269; "Silicate P's and Q's," vol. 23, 1943.

40 "Verdampfung und Verflüssigung von Gemischen," by J. P. Kuener, Leipzig, 1906, pp. 78–80; also "Verflüssigung von Gasgemischen," by F. Caubet, *Zeitschrift für physikalische Chemie*, vol. 40, 1902, pp. 283–287.

41 "On the Solubility of Solids in Gases," by J. B. Hannay, Proceedings of the Royal Society of London, vol. 30, 1880, pp. 178–188 and 484–489; also "On the State of Fluids at Their Critical Temperatures," ibid., vol. 30, 1880, pp. 478–484.

42 "Untersuchungen über den kritischen Zustand. IV. Kritischer Zustand der Athylatherlosungen," by E. Schröer, *Zeitschrift für physikalische Chemie*, vol. 142, 1929, pp. 365–390.

43 "Solubility of Solids in Water Vapor," Discussion by R. E. Hall, Proceedings of the A.S.T.M., vol. 42, 1942, pp. 993–1000.

44 Handbook of Physical Constants, Geological Society of America, Special Papers No. 36, 1942, pp. 213–222.

45 "Solubility of Water in Granite Magmas," by R. W. Goranson, *American Journal of Science*, vol. 22, 1931, pp. 481–502. "Some Notes on the Melting of Granite," ibid., vol. 23, 1932, pp. 227–236. "Silicate-Water Systems: Phase Equilibria in the $NaAlSi_3O_8$–H_2O and $KAlSi_3O_8$–H_2O Systems at High Temperatures and Pressures," ibid., vol. 35A, 1938, pp. 71–91.

46 "Water in Geological Processes," by G. W. Morey, Carnegie Institution of Washington, Publication No. 501, 1938, pp. 49–58.

47 "Cause and Prevention of Turbine-Blade Deposits," by F. G. Straub, Trans. A.S.M.E., vol. 57, 1935, pp. 447–454.

48 "The Behavior of Boiler-Water Salts in Superheater and Turbine," by A. Splittgerber, *Vom Wasser*, vol. 12, 1937, pp. 375–380.

49 "Kesselbauform Speisewassereinflüsse," by W. Otte, *Mitt. Verein. Grosskesselbesitzer*, no. 17, 1928; *Zeitschrift des Bayerischen Revisionsverein*, vol. 31, 1927, pp. 241–245 and 254–256.

50 "Die Physikalische Chemie der Kesselsteinbildung und ihrer Verhüttung," by R. Stumper, *Sammlung Chemischer und Chemisch-Technischer Vorträge*, New Series, no. 3, second edition, F. Enke in Stuttgart, Germany, 1933, pp. 57–66.

Appendix References

The following references pertain to data in the Appendix:

51 International Critical Tables, McGraw-Hill Book Company, Inc., New York, N. Y., vol. 4, 1926–1930, pp. 230–240.

52 "Solubilities of Inorganic and Metal Organic Compounds," by A. Seidell, third edition, D. Van Nostrand Company, Inc., New York, N. Y., vol. 1, 1940.

53 "Gmelin's Handbuch der Anorganischen Chemie," eighth edition, System No. 22, Kalium, Lieferung 5, 1938, p. 992.

54 "Aqueous Solubility of Salts at High Temperatures. 1. Solubility of Sodium Carbonate from 50 to 348°," by W. F. Waldeck, G. Lynn, and A. E. Hill, *Journal*, American Chemical Society, vol. 54, 1932, pp. 928–936.

55 "Solubility Equilibria of Sodium Sulphate at Temperatures of 150–350°," by W. C. Schroeder, A. A. Berk, and A. Gabriel, *Journal*, American Chemical Society, vol. 58, 1936, pp. 843–849.

Discussion

R. C. Corey.[13] Sixteen years ago, with the completion of a co-operative investigation by the Hagan Corporation and the Bureau of Mines, the author and his associates published a research bulletin,[14] in which the physicochemical basis for scale formation and prevention in steam boilers was presented. To the present day this bulletin is a sound fundamental guide to the principles of water-conditioning.

In the intervening years, the intensity factors, temperature and pressure, and the unit-heat-absorption rate of boilers have increased considerably to provide greater over-all thermal efficiency. It was inevitable that, as the operating temperatures and pressures increased, the sequence of events within a steaming boiler, from the standpoint of chemical reactions, should approach those of a geological nature. Witness, for example, the occurrence in boilers of analcite, acmite, and a host of other complex solid phases that are found as natural constituents in the earth's crust where they were formed as the result of high temperatures and pressures. The tools of the petrographer and the mineralogist, the polarizing microscope, and the X-ray diffraction apparatus, now are familiar equipment in water-conditioning technology.

The new problems presented by modern boiler-operating practice have become manifold. Hide-out, turbine-blade deposits, excessive metal temperatures as the result of resistance to heat transfer offered by unusual solid deposits, and corrosion of steel surfaces by alkali have required that new ideas be developed of the events occurring at the metal-water and metal-vapor interfaces in the boiler. In an effort to find an answer to the questions presented by these phenomena, the author has taken the initiative and applied the logical reasoning of physical chemistry, not the classical concepts found in our physical-chemistry textbooks, but data that have heretofore been of interest to a relatively small group concerned with the study of phase equilibria at high temperatures and pressures; a field of investigation in which the experimental procedures are very difficult. The principles presented in the present paper are not contradictory to those expressed 16 years ago, as the latter still are valid for the isobaric-isothermal conditions of the over-all boiler water. Rather, they have been developed with the realization that isobaric-polythermal and polybaric-polythermal conditions between the steaming surfaces and the turbine discharge can

[13] Research and Development Department, Combustion Engineering Company, New York, N. Y.

[14] "A Physico-Chemical Study of Scale Formation and Boiler-Water Conditioning," by R. E. Hall, G. W. Smith, H. A. Jackson, J. A. Robb, H. S. Karch, and E. A. Hertzell, Bulletin No. 24, Carnegie Institute of Technology, 1927.

produce changes in the solid and liquid phases that are markedly different from those with which we have been familiar heretofore.

The writer was greatly interested in the author's statement that, when the potassium treatment was initiated at a station in which the sodium treatment still was in effect, the hide-out of salts became worse. The following may offer a possible explanation for this condition: Sodium and potassium sulphate will, either when fused together or when crystallized from an aqueous solution of the two salts, form a solid phase known as glaserite (or aphthitalite). The literature is not definite whether this phase is a double salt or a mixed crystal, i.e., a solid solution of limited range. The most recent view[15] is that at room temperature it is a solid solution of limited range of Na_2SO_4 in α-K_2SO_4 and is given the nominal formula $K_3Na(SO_4)_2$, indicating content of three mols of K_2SO_4 to one of Na_2SO_4. The factors applying most directly to the present case are its solubility and vapor pressure at high temperatures, and these data unfortunately are not available. Therefore the author may find it advisable to carry out such determinations in order to determine if excessive hide-out or other undesirable characteristics, associated with low solubility and Δt, values, are apt to occur when changing from sodium to potassium treatment or where condenser leakage introduces sodium ion.

With reference to the use of silica to precipitate magnesium silicate in lieu of magnesium hydroxide or phosphate, is this contradictory to the principles outlined in the previous bulletin?[14] The writer would guess that present-day practice results in a form of magnesium silicate, identified in high pressure boilers as serpentine, which differs in physical properties from that formed at lower temperatures.

Considering the extreme importance of the implications of Fig. 10 of the paper, in which the vapor pressure of saturated solutions of several salts is plotted against temperature, and the events at various isobars are described, it is believed that greater clarity of certain statements, particularly those referring to the descending branches of the vapor-pressure curves, would obtain if this material were introduced by a generalized statement of the characteristics of plots of this kind. Although vapor-pressure curves are familiar to many, it is not always evident that they are a special form of phase diagram.

With reference to Fig. 13 of the paper, described as an example of a tube embrittled by a relatively large Δt value in the presence of sodium sulphate and sodium hydroxide, it is not clear that the steel is embrittled in the usual sense of the word; rather it appears to resemble the type of attack which might occur as the result of contact with concentrated alkali at high temperature.

Data indicating the potential solubility of iron in caustic solutions at a concentration, that the author has shown may be easily attained on evaporative surfaces with sufficiently high Δt values, have been developed by Scholder and Weber,[16] who found a boiling 50 per cent NaOH solution to contain 5000 ppm of iron at equilibrium.

G. C. Daniels.[17] Most of the utilities treat their feedwater; some of them because of necessity, others through force of habit or fear of consequences if they did not follow the general practice.

The author admits that there is no problem with dissolved oxygen in the feedwater since it can readily be and is removed by various methods in practically all plants. Yet, the feeding of sodium sulphite is generally continued, and as it hides away in the boiler, more is added. When the boiler water is treated, the pH is maintained in the region of 10.5 to avoid corrosion which nevertheless takes place under steam bubbles where high concentrations and high causticity are reached, as pointed out by the author.

In contrast to the difficulties which have been encountered, when using boiler-water conditioning with its attendant high boiler concentrations, carry-over, and turbine-blade deposits, is the extreme simplicity of using no treatment whatsoever either to absorb any dissolved oxygen that might possibly be present or to maintain any predetermined pH. When pure water is fed into the boiler, the pH generally is found to be between 8 and 8.5. A very thin film of oxide is formed on the internal boiler surfaces which adequately protects the metal and is not dissolved, as is the case if caustic is present, and no concentrations of salts can form under the steam bubbles which are also very much smaller when no dissolved solids are present. The only tube failures that can result from the use of pure water will be those caused from inadequate boiler circulation or flame impingement.

When using no boiler-water conditioning, only three conditions must be observed, all external to the boiler, as follows:

1 The occluded oxygen in the feedwater must be kept below 0.05 ml per l.

2 The operation of the evaporator must be such as to keep the carry-over at a minimum.

3 Condenser leakage must be eliminated. This is not difficult to do with the instruments now available for detecting leaks immediately, and with the divided waterbox condenser, the leaks can readily be located and fixed without shutting down.

Our experience with no boiler-water treatment dates back to 1925 and covers many makes of boilers in the 400- and 900-psi-pressure class. Carry-over and turbine-blade deposits are practically nil or entirely absent. The total solids in the boiler water are frequently below 10 ppm after months of operation. No sludge or iron-oxide accumulations are found in these boilers, and the iron content in the boiler water is a very small fraction of one ppm.

Assuming that the author's theories are correct and that the potassium salts will ameliorate the conditions now encountered with sodium salts, would it not be better to determine in the individual plants whether it is at all necessary to condition the boiler water?

In referring to the experiment on the elevation of the boiling point of water by the addition of salts, the author gives the impression that the steam issuing from the flask is at 212 F instead of being superheated to the temperature of the liquid. The fact that the temperature of the vapor as shown by the thermometer immediately above the liquid is the same temperature as the boiling liquid might be accounted for by the radiation from the surface of the liquid in the flask, which is carefully insulated above the water line.

L. E. Hankison[18] and M. D. Baker.[19] Phosphate in the form of sodium phosphate was introduced for boiler-water conditioning into the 350-psi boilers at Springdale Station in 1923. Results obtained with this treatment have been satisfactory to the extent that some boilers erected in 1924 and 1925 have not been completely turbined since their installation. Clean internal surfaces were maintained by washing the boilers with a stream of water when they were down for overhauling. This type of cleaning did not require the removal of hand caps and,

[15] "A New Group of Isomorphous Compounds," by M. A. Bredig, *Journal of the American Chemical Society*, vol. 63, 1941, p. 2533.

[16] "Über anionisches Eisen," by R. Scholder and H. Weber, *Angewandte Chemie*, vol. 49, 1936, pp. 255–259.

[17] Mechanical Engineer, The Commonwealth & Southern Corp., Jackson, Mich. Mem. A.S.M.E.

[18] Superintendent Efficiency Department, West Penn Power Company, Pittsburgh, Pa. Mem. A.S.M.E.

[19] West Penn Power Company, Pittsburgh, Pa.

consequently, some tubes in the boilers have never been inspected.

After 12 or 15 years of operation there was some loss in capacity of these boilers but inspections of the lower tubes disclosed no adhering scale or deposit. Because these tubes where the greatest evaporation occurred were clean, no inspections were made of the upper bank of tubes. When the 1350-psi boilers were installed in 1937, six 350-psi boilers, erected prior to 1923, were removed. An inspection made of all tubes in one of these boilers disclosed considerable analcite scale (sodium-aluminum silicate) in the tubes of the upper bank. This scale was found in spots and was possibly 1/4 to 3/8 in. thick. While the scale was quite prevalent in the upper bank of tubes, it is questionable whether the entire loss in load on the boilers could be attributed to scale.

After the 1350-psi boilers had been placed in continuous service, analcite scale was found in the generating-section tubes. In an endeavor to eliminate this scale, a steel tank was substituted for the concrete make-up-water storage tank from which silica was being dissolved. Following the use of the steel tank, the amount of silica as SiO_2 in the high-pressure-boiler water was reduced from about 20 ppm to 10 ppm per 1000-ppm concentration of boiler water. While this reduction in silica appeared to be beneficial, it was still necessary to turbine the generating tubes periodically for the removal of silica scale. This scale would form under the loose deposits which accumulated in the tubes in the generating section of the boilers. It was on the bottom of the tubes in patches varying from 1 to 3 in. length and 1/8 to 3/8 in. thickness. The formation of this scale could not be predicted as there were periods of 2 or 3 months' operation, following which an inspection showed no scale formation. At another inspection of the same boiler, sometimes after only 14 days' operation, there would be scale in 50 per cent of the tubes. There have been times when it required 4 hr of turbining to remove a patch of scale from one tube. The boilers were never operated for more than 6 months without requiring turbining in some of the tubes. An analysis of the hard scale that was found is as follows:

	Per cent
Sulphur trioxide (SO_3)	2.5
Carbon dioxide (CO_2)	0.0
Phosphorus pentoxide (P_2O_5)	8.9
Silica (SiO_2)	13.3
Iron oxide (Fe_3O_4)	45.9
Aluminum oxide (Al_2O_3)	10.7
Calcium oxide (CaO)	5.2
Magnesium oxide (MgO)	1.5
Sodium oxide (Na_2)	9.2
Copper (Cu)	1.1
Net ignition loss (calculated)	2.9

Trouble with scale of this nature emphasized the need for some correction in treatment. The problem was discussed with the the author, and upon his recommendation on August 25, 1942, potassium salts were substituted for the sodium salts used for boiler-water treatment. All boilers in the Springdale Station, high and low pressure, were placed under the potassium treatment.

After about 2 months' of treatment, leakage occurred around several handhole plates and at tube rolls. Within the next 6 weeks, the leakage had become so pronounced that there was no question as to the immediate cause for such a large amount of trouble. The potassium treatment was dissolving any silica that had deposited around the gaskets and at the tube rolls where it had been serving as a seal. The gaskets used were monel-clad asbestos, and their failure was caused by the cracking of the metal due to expansion and contraction during the time they were in service. There was no chemical attack on the monel. The potassium-treated water would dissolve the silica scale that was sealing the cracks and permit leakage to occur. This type of trouble was eliminated after regasketing the entire boiler completely, and rerolling all leaking tubes. With potassium treatment, any "sweating" or leakage of a gasket or roll on a hydrostatic test will not take up when the boiler is in service. Gasket-failure leakage had started prior to the use of potassium treatment but the change precipitated the trouble. Within a period of 2 months gasket leakage occurred that might otherwise have been extended over a period of several years.

About the time that gasket leakage was being corrected, large amounts of loose scale were noticed in the boilers. The scale found was mostly magnetic iron oxide containing less than 2 per cent of silica as SiO_2. Scale loosened from the evaporating surfaces of the boiler was found in all the headers and was most abundant about the fifth or sixth month after starting the potassium treatment. In some headers, there was sufficient scale to stop circulation and to cause failure of one tube. Following this failure, all headers were thoroughly cleaned and the loose scale removed. Also, all tubes were turbined to remove any material that might still be adhering to their internal surfaces. An analysis of this scale is as follows:

	Per cent
Sulphur trioxide (SO_3)	Trace
Carbon dioxide (CO_2)	Negative
Phosphorus pentoxide (P_2O_5)	10.7
Silica (SiO_2)	1.8
Iron oxide (Fe_3O_4)	60.3
Aluminum oxide (Al_2O_3)	0.4
Calcium oxide (CaO)	7.3
Magnesium oxide (MgO)	6.2
Copper (Cu)	8.1
Total ignition gain	2.3
Net ignition loss	2.2

This iron-oxide scale could have been caused by either of the following reasons:

1 The silica being dissolved from the acmite (sodium-iron-silica) scale that was present in the boilers when the treatment was started.

2 The hydroxide alkalinity (50 to 100 ppm OH) was concentrating at points of high evaporation and attacking the metal.

It is doubtful if scale was formed by the caustic attack, but the presence of large amounts of loose magnetic iron oxide in sludge deposits could readily be attributed to the high alkalinity. The pH value of the boiler water before and after the use of potassium was maintained in excess of 11. The maintenance of this pH value with potassium produced no hard scale in the sludge or on he evaporating surfaces.

A change in treatment was made to reduce and possibly eliminate caustic attack on the metal. This change was the reduction of the hydroxide content to 10 ppm with a pH value maintained at 10.5 or lower. Potassium chloride was added so that at all times the chloride (Cl) was considerably in excess of the hydroxide (OH). Normally the ratio is 5 of Cl to 1 of OH. The effect of the reduction in alkalinity was soon noticed in the characteristics of the boilers deposits. The sludge in the boilers instead of being soft and fine contained many little scale-like particles. Also, the boiler tubes instead of being clean had the appearance of dried sludge adhering to the entire surface of the tubes. No attack could be detected on the evaporating surface and the color of the deposits changed from black to light gray. In an endeavor to stop the formation of the scale-like particles in the sludge and on the evaporating surfaces, the alkalinity was restored to its former values but the chloride-hydroxide ratio was maintained. Inspections made since the increase in alkalinities have shown no attack on the evaporating surfaces, light-gray deposits in the boilers, and no adhering scale.

In the 1350-psi boilers, the potassium treatment has changed

the characteristics of sludge deposits so that at the present time no sticky sludge is adhering to the drum or tube surfaces. The drums are clean and the tubes are coated with a thin film of light-gray deposit throughout their length. This coating can be easily and completely removed with a stream of water. No adhering scale is found after washing. This condition may result from a change in characteristics of the magnesium compounds present in the sludge. Previously, large amounts of magnesium phosphate and magnesium hydroxide were noted when making microscopic examination. Now magnesium silicate is present. When using sodium treatment, the cleaning schedule was that each third time a boiler was removed from service, regardless of the time interval between, or the first outage after 3 months of service, the tubes in the generating section had to be washed and those containing scale turbined. Recently, with potassium treatment, the boiler had seven outages, due to gasket and roll leakage, during a 4-month period without cleaning the internal surfaces. The tubes were then washed but their condition was such that the boiler could safely have been put in service without cleaning. After 15 months of potassium treatment, there has been no need for turbining tubes to remove silica scale that was being formed.

Following the discovery of silica-bearing scale in the 1350-psi boilers a complete inspection of all tubes in some of the 350-psi boilers was made. The inspections showed thin layers of scale under loose sludge deposits in the upper bank of tubes where there is little circulation, and sludge accumulates. Several of the boilers were turbined to remove this scale. No boilers have been turbined since the introduction of potassium treatment, and the scale has disappeared from the boilers that were not turbined.

Since potassium treatment was started, no turbines have been opened, so the condition of the blades is not known. The reduction in capacity now existing may be restored by water-washing or spindle adjustment.

MAX HECHT.[20] Within a span of some 40 years, high-pressure steam generation has increased tenfold since the initial operation at 250 psi at the old Fish Street Station. Throughout this period, the general trend in so far as it concerns the purity of the boiler water has been to generate steam from relatively dilute boiler waters. Credit for this trend should be accepted by the mechanical engineers who demonstrated that pure water could be produced by distillation, and that one of the gases contributing to corrosion, dissolved oxygen, could be removed mechanically by deaeration. Credit for the application of distilled water for make-up in stationary plants is given to the late Prof. C. F. Hirshfeld, The Detroit Edison Company, for his pioneering work at the old Delray Station, and for deaeration, to the researches of J. R. McDermet of the Elliott Company, which resulted in the commercial utilization of the vacuum-type deaerator. Both of these developments came in the period, 1910–1920.

The concept of generation of steam from relatively dilute boiler water has persisted, marked by design changes in the equipment to meet the demands of higher steam pressures and temperatures, and the availability of new chemical processes for conditioning the boiler feedwater. New chemical processes and apparatus have been made commercially available for the primary conditioning of boiler-feed make-up, and numerous chemical reagents are used for the secondary conditioning of the boiler water. In the early 20's, boiler manufacturers supplied equipment of liberal design, and such units were operated at not too excessive ratings. Steam pressures were relatively moderate and steam temperatures were not unduly high.

The problems and difficulties of deposits on boiler tubes, in superheaters, and on turbine blades, and of corrosion now being encountered, were present in the earlier operations, either entirely masked, or if observed were of less major significance than they are today.

During the past 25 years, the water technologist has drawn heavily from the knowledge of the physical chemist, and in the paper under discussion, from the studies of the geophysicist. An important and notable contribution was made by George W. Morey, geophysical laboratory, Carnegie Institution of Washington, Washington, D. C., in his paper, "The Solubility of Solids in Water Vapor." This formed the principal paper of the Round Table Discussion on Action of Water Vapor at High Temperatures and Pressures, presented at the 1942 meeting of the American Society for Testing Materials, Proceedings of the A.S.T.M., vol. 42, 1942, pages 980–988. The proper utilization of this knowledge has permitted the water technologist more accurately to analyze conditions brought to his attention, and so make the proper recommendations to ameliorate the troubles that the operator is encountering. It is apparent that in the past the thought in treatment has been directed toward the main body of the boiler water. The investigations of F. G. Straub, pointing toward improvements in ratios for embrittlement protection and turbine-blade deposits are, in direction, a departure from this concept. Lack of adequate solution of problems encountered in the steam-and-water cycle of the present-day high-pressure-and-temperature stations demands a new approach, and this, it is believed, has been made by considering the behavior of water at the steam-water interface.

It is apparent that the operator has been demanding a fluid for use in evaporative processes, which has had removed from it all of the deposit-forming and corrosive characteristics, both in the liquid and vapor state. This implies either the complete removal of the solid phases or their conversion to a form that is not troublesome throughout the steam-and-water cycle, as well as the total elimination of all of the gases contributing to corrosion. In spite of the stepwise progress on separate phases of the general problem made in the past, to meet this demand, new and unpredictable water problems have confronted the operators. Are the present concepts in this paper adequate to overcome these difficulties?

The author has made an impressive and convincing presentation, based upon scientific information now available. His analysis requires detailed study to appreciate the valid theoretical considerations advanced. The operators may find adequate proof of the theoretical applications proposed, presumably from the short experience presented in the operating discussions, and possibly by trial in their own plants. The writer is frank to admit that it will require some time to digest the author's valuable presentation. There come to mind some minor items which may be of interest.

In the writer's opinion, "hide-out" is a self-aggrevating condition. It is most likely to begin in tubes with poor circulation. The deposition of salt further impedes the already restricted flow. The composition of the water must therefore be such that t_s is never reached, even in the tubes having the poorest circulation.

It has been observed that, when boilers are initially put into service, with no preparation other than the customary boiling-out, a considerable amount of iron oxide is found in the drums. This has been attributed to the mechanical removal of mill scale from the drums and tubes during the shakedown operation. Kaufman and Marcy removed iron oxide from bombs containing 5 per cent caustic soda at 470 F but found no attack on the iron. It might be of interest that in the same temperature range, with low alkalinities (pH 8. to 9.5), hydrogen has been detected in steam from boilers even though iron-oxide sludge was not a problem. Oxygen was also found simultaneously with the hydrogen. It is therefore not necessary to have com-

[20] Pittsburgh 17, Pa.

plete absence of dissolved oxygen in order to secure hydrogen evolution or attack of the iron by water.

The values reported[21] are as follows:

	Oxygen, cc per l	Hydrogen, cc per l
Boiler feedwater	0.20	0.0380
Boiler water (drum)	0.05	Not detectable
Steam superheater outlet	0.22	0.0648

C. E. KAUFMAN.[22] In the intelligent application to boiler-water treatment of many of the principles enumerated by the

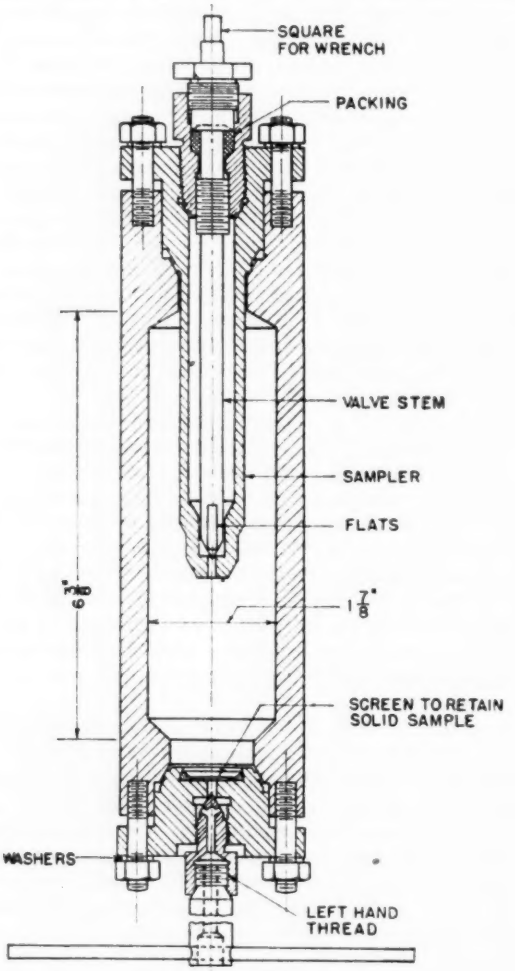


FIG. 14 SOLUBILITY BOMB

author, fundamental data on solubilities and vapor pressures at relatively high temperatures are required. The author has marshaled pertinent material available from the literature but gaps are evident, especially in the data relating to aqueous solutions of potassium compounds, and in the almost completely neglected field of salt mixtures in water.

We are endeavoring currently to fill in some of the missing facts. The experimental technique at elevated temperatures and pressures is somewhat involved, and fixing of quantitative values requires repeated trials. Therefore, at this time, we shall merely mention briefly qualitative behavior.

[21] "Corrosion, Its Causes and Prevention," by F. N. Speller, second edition, McGraw-Hill Book Company, Inc., New York, N. Y., 1935, Tables LXV and LXVI, pp. 424, 425.

[22] Research Engineer, Hall Laboratories, Inc., Pittsburgh, Pa.

The solubility bomb in Fig. 14 of this discussion, of the type used by Schroeder, Berk, Partridge, and Gabriel[23] at the U. S. Bureau of Mines, is being employed in a suitable thermostat. Saturated solution, representing the equilibrium existing at a fixed experimental temperature, is taken through the valved

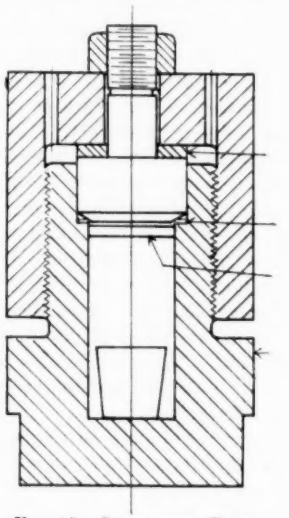


FIG. 15 QUENCHING BOMB

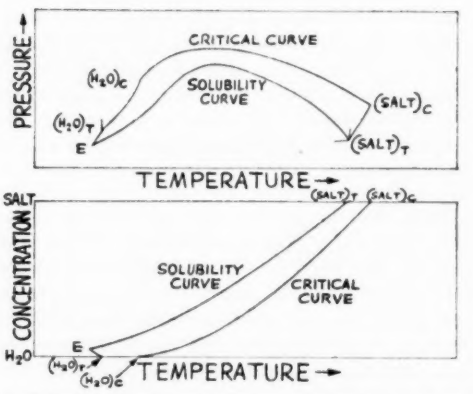


FIG. 16 NONINTERSECTING CRITICAL AND SOLUBILITY CURVES

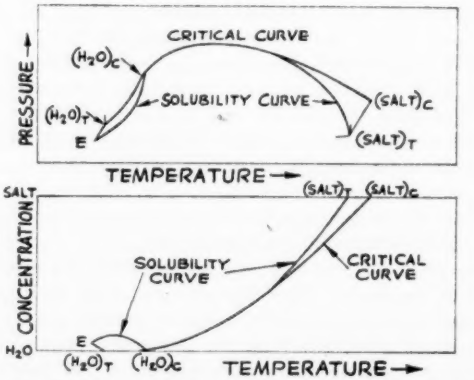


FIG. 17 INTERSECTING CRITICAL AND SOLUBILITY CURVES

sampler, while the solid phase can be isolated by blowing down excess liquid through the bottom valve. In other experiments,

[23] "Solubility Equilibria of Sodium Sulfate at Temperatures of 150 to 350°," by W. C. Schroeder, A. A. Berk, E. P. Partridge, and A. Gabriel, *Journal of the American Chemical Society*, vol. 57, 1935, p. 1539; vol. 58, 1936, p. 843; vol. 59, 1937, p. 1783.

the sampling head can be removed and connection made to a pressure gage. In a preliminary investigation with materials of glass-forming properties, the quenching bomb of Morey,[24] Fig. 15, is being utilized.

As the author has mentioned, aqueous solutions of individual salts, and perhaps mixtures, can be classified in two ways, subject to certain variations:

1 Those whose solubility or vapor-pressure curves do not intersect the critical curve.

2 Those with intersections.

Fig. 16 of this discussion illustrates the first type with continuous solubility extending up to the melting point of the pure salt. Sodium chloride, potassium chloride, and the potassium silicates behave in this manner. Fig. 17 shows typical plots for salts of the second type with the solubility curve interrupted by the critical curve. A number of substances of this class are normally found in boiler waters: sodium sulphate, sodium phosphate, and the sodium silicates, for example. Moreover, these salts show retrograde solubility in the temperature range before the first intersection with the critical curve and are assumed to have very low solubilities at the critical temperature of water.

The salts of constantly increasing solubility will naturally be of advantage in the boiler water, as explained in the paper, because their ΔT_s values are in general much greater than those of the retrograde type for the pressures corresponding to boiler operation.

We have then the following preliminary information: In confirmation of values in the literature, potassium sulphate appears to resemble sodium sulphate; solubility becomes retrograde well below the critical point of water, and ΔT_s is probably never very appreciable in any part of the range up to the intersection of the solubility curve with the critical curve at a point somewhat above the critical temperature of pure water.

On the other hand, tripotassium phosphate, from the evidence of both solubility and vapor-pressure measurements, has the properties of the salts shown in Fig. 16, a continuously increasing solubility curve which does not intersect the critical curve and large values of ΔT_s.

What does this mean in practice? For one thing, tripotassium phosphate is quite unlike trisodium phosphate, which follows the curves in Fig. 17. Trisodium phosphate is one of the worst offenders as far as hide-out is concerned in hard-pressed boilers. With tripotassium phosphate, any tendency to hide out should be entirely curbed or drastically minimized. Again, if a solution containing free alkali starts to concentrate on an overheated surface, trisodium phosphate cannot concentrate with the caustic to blunt in some measure the severity of attack, whereas tripotassium phosphate can do so. In brief, tripotassium phosphate is as advantageously unlike trisodium phosphate as the potassium silicates are advantageously unlike the sodium silicates.

Later on, it is expected that we shall have additional pressure-temperature-concentration data of a more comprehensive character, including information on the complex mixtures which represent the practical working media in all boilers.

N. B. KEEVIL.[25] Solubilities and vapor pressures of aqueous solutions at high temperatures are of considerable importance in interpreting the phenomena of boiler-water chemistry and in conditioning water for steam generation, as well as being essential to the understanding of hydrothermal processes responsible for ore-desposition in the earth's crust. Experimental data for soluble salts are meager, being limited to work by Morey at the geophysical laboratory, and the writer under the auspices of the

[24] "The Ternary System H_2O-K_2SiO_3-SiO_2," by G. W. Morey, *Journal of the American Chemical Society*, vol. 39, 1917, pp. 1173–1229.

[25] Professor, University of Toronto, Toronto, Canada.

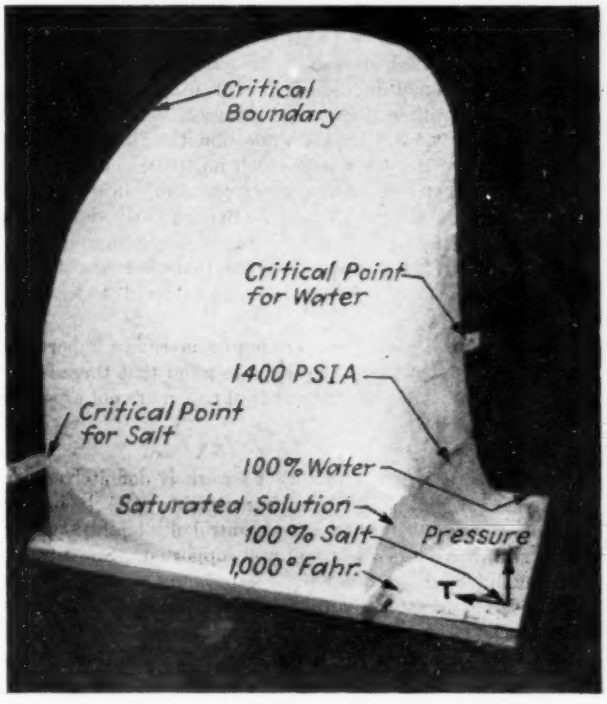


FIG. 18 PRESSURE-TEMPERATURE-COMPOSITION MODEL FOR AN AQUEOUS SOLUTION
(Data for NaI-H_2O; maximum is close to that of aqueous solutions of KCl-NaBr-H_2O and a little higher than $K_2Si_2O_5$-H_2O.)

Harvard Geophysics Committee. This work has revealed important differences in the properties of salts of potassium and sodium at the temperatures encountered industrially in boilers and in steam cycle, the halides and silicates of potassium being more soluble, and their solutions having lower vapor pressures than their sodium analogues.

The application of these differences to water-conditioning for steam generation has been developed by the author, by substituting potassium equilibria for convential sodium equilibria. Theoretically this should reduce many of the common difficulties of scale, hide-out, and sludge formation, and good practical results have been reported. The lowering of vapor pressure sufficiently to prevent precipitation is controlled largely by mol fraction, as well illustrated by the three-dimensional model for pressure P, temperature T, and composition X, shown in Fig. 18 of this discussion, and the results on various halides. This model, with pressure as the vertical axis, illustrates the remarkable effect of dissolved molecules in reducing the escaping tendency of water. In the two-component system shown in Fig. 18, the 1400-psia isobar intersects the P-T-X surface with resulting boiling and precipitation. Additional components in solution leading to a greater mol fraction would reduce the range of vapor pressure sufficiently to prevent precipitation and permit salts to remain in solution when they pass from the superheater at the full temperature of 1000 F.

The difficulty in predicting the exact conditions in the boiler and turbine is that experimental research has been of necessity, largely confined to solo solutions, while those met in practice are multicomponent systems. However, one result obtained by the writer for a two-component system has proved of considerable value in showing a marked lowering of vapor pressure below the equilibrium pressures exhibited by the pure saturated solutions of soluble salts.

There is some indication that in the competition for a place in

a complex solution, the most soluble component may be disproportionately high in the final solution, so that in the K^+, Na^+, Cl^-, Br^- solution studied by the writer the composition at 874 F might have mol fractions 0.23 KBr, 0.20 NaBr, 0.06 KCl, and 0.01 NaCl rather than those extrapolated by the author from the data at 245 F. In this connection, the use of potassium may be preferable to other ions which might be considered for their greater effect in reducing vapor pressure, since the solubilities of $K_2Si_2O_5$, KBr, KCl (and NaBr) are fairly close in the neighborhood of 900 F. Furthermore, in a system containing these components, it is reasonably certain that the range of vapor pressures would be lowered enough for the materials to leave the superheater in solution.

Although critical phenomena are not ordinarily of importance in boiler problems, it should be borne in mind that there is evidence that the phenomena in the critical region are not as simple as is generally believed.

I. G. McCHESNEY.[26] The author's work is definitely a forward step in methods of boiler-water treatment. His elaboration on the process of scale formation and control of solubilities within the concentrating film is clear and well supported. Substitution of a potassium equilibrium for the usual sodium equilibrium as a means of avoiding saturation in the concentrating film is a new and practical attack on analcite-scale formations.

The use of phosphates with sodium equilibrium, low boiler-water concentrations, and reduced alkalinities has brought trouble with analcite scales and turbine deposits.

High Boiler-Water Concentrations. The writer will cite an instance of successful water treatment in a modern high-pressure plant where the procedure closely follows an alternate method of water-conditioning suggested by the author. This plant uses from 40 to 60 per cent make-up. Lime-soda treatment of river water is followed with an aftertreatment of phosphate. Oxygen is efficiently removed by deaeration and an excess of sodium sulphite of approximately 5 ppm is used. Excess phosphates are in the order of 2 to 5 ppm.

Early in the operation of the plant, steam-washer tests were made with boiler-water concentrations up to 6800 ppm. In the final steam-washer design (tray type), priming was not appreciably increased until concentrations in excess of 5000 ppm were reached. Boiler operation at 3000 ppm was standardized after careful consideration of effect of concentration on priming over a range from 1800 ppm to 6800 ppm.

Operation with 3000 ppm total solids in the boiler water permitted an alkalinity of 11.5 without evidence of channeling corrosion. Over several years, corrosion and iron-oxide sludge have not been serious.

High concentrations and steam-washing have effectively prevented silica-scale formation on turbine blading. This is pointed to as experience in one of the makeshifts suggested by the author. His method is superior in many ways and shows good promise of overcoming many of the high-pressure feedwater problems.

Turbine Deposits. Deposition of quartz scales on the 3rd to 8th turbine stages indicates condensation of silicates. The powdery silica deposit in the 13th to 16th stages is likely formed from the repeated boiling to dryness which occurs near the dew point in the turbine expansion. In one Midwest plant this deposit in the later stages of the turbine was accompanied by embrittlement and failure of turbine blades. Maintaining the proper SiO_2/K_2O relation will likely prove effective in preventing both scale and embrittlement.

Messrs. L. E. Hankison and M. D. Baker should be commended for their task in pioneering and developing power-plant experience by the author's method.

D. S. McKINNEY.[27] The troubles that accompany steam generation in high-pressure boilers may logically be divided into two groups, as follows:

1 Those that arise due to faulty design of the boiler and can be eliminated by changing the design.

2 Those that arise primarily due to the chemical properties of the water and the materials dissolved in it.

In the writer's opinion, the problems of "hide-out," corrosion due to bonded oxygen in water, and, to a considerable extent, carry-over, belong to group 1. Proper design should eliminate "hide-out" and bonded-oxygen corrosion and should considerably reduce carry-over. Operators should insist upon and be willing to pay for properly designed boilers, in order that these difficulties may not plague them for the entire life of the boiler.

Chemical treatments to alleviate troubles falling in group 1 do not eliminate the cause of the trouble and should be resorted to only to make existing boilers usable; even in these cases the operator and the manufacturer should make every effort to correct the design in situ in order to eliminate the difficulty.

The problems of magnesium scale, silica in the boiler, and, to some extent, carry-over, belong to group 2. The use of potassium salts, as proposed by the author, is a logical solution of these problems. The advantageous properties of the potassium silicates over those of the corresponding sodium silicates should be especially valuable.

The reasons which the writer has for classifying "hide-out," corrosion due to bonded oxygen, and to a considerable extent, carry-over, as due to faulty design of the boiler, are as follows: The mechanism given by the author for explaining hide-out is undoubtedly correct. However, he does not go quite far enough. The conditions necessary for maintaining the hide-out are not explained.

Consider the hide-out of sodium sulphate. The author gives its solubility at a temperature corresponding to 1800 psi as 0.0095 mol fraction and at 1400 psi as 20 per cent. These figures, expressed in parts per million, are: at 1800 psi, 70,000 ppm, and at 1400 psi, 200,000 ppm. Assuming that the bulk boiler water contains 1000 ppm of Na_2SO_4, then 98.6 per cent of the water must evaporate to reach 70,000 ppm, and 99.5 per cent to reach 200,000 ppm. If evaporation proceeds beyond these figures (at the respective pressures and temperatures), solid Na_2SO_4 will deposit. However, if the evaporating steam bubble breaks away, and a new supply of fresh boiler water arrives, the solid Na_2SO_4 will immediately begin to redissolve. Hence in order that Na_2SO_4 form scale of appreciable thickness, the rate of supply of fresh water to the tube must not exceed the rate of evaporation by more than about 2 per cent at 1400 psi, and about 0.5 per cent at 1800 psi. In other words, nearly complete evaporation must occur in one pass through the tube. Such a state of affairs can be caused only by poor circulation, or by excessive rates of heat transfer; or by both, since excessive heat transfer may cause poor circulation.

It is very likely that such a state of affairs is confined to relatively few tubes or parts of tubes in the boiler. The solution to the problem is to reduce the heat transfer by relocation of the tubes or to provide sufficient circulation to allow them to handle the heat transfer demanded.

Regarding corrosion due to bonded oxygen, and assuming the author's mechanism to be correct, it is necessary that very high concentrations of caustic be produced by the same mechanism that causes hide-out, in order to dissolve or peptize the pro-

[26] Lieutenant, U.S.N.R., Barberton, Ohio. Jun. A.S.M.E.

[27] Assistant Professor of Chemistry, Carnegie Institute of Technology, Pittsburgh Pa.

tecting film of iron oxide from the tube wall. Obviously, the solution of the problem is the same as in the case of hide-out. If his mechanism is not correct, and the attack is due merely to steam-binding with attendant overheating of the tube, the solution is again one of improving circulation by allowing more ready release of steam.

Finally, turning to the problem of carry-over, it appears reasonable that if the tremendous concentrations previously mentioned are permitted in the steam-generating tubes, a portion of this very concentrated water will be carried along as a mist with the escaping steam. Hence an appreciable amount of boiler solids will be carried into the superheater, even though the amount of liquid water accompanying the solids is very low. This condition, too, can be improved by improving circulation or reducing the heat-transfer rate as just suggested. In addition, the modern high-pressure boiler still suffers from many of the same defects as older boilers. Provisions are poor for separating steam from water as it comes from the steam-generating tubes. Much splashing must occur in the drums. Redesign to secure smoother steam release from the water in the drums without splashing and droplet formation, together with adequate provision for release of droplets carried with the steam, should greatly reduce carry-over troubles.

A. C. Pasini.[28] This paper offers a theory for boiler treatment which throws some light on results that have puzzled and worried power-plant managers. In this field there has been confusion and misunderstanding.

A little over a year ago, we had occasion to discontinue sodium-sulphite treatment so that a study could be made to determine where the oxygen was entering the feedwater system. (This treatment was stopped because reducing agents such as sulphite affected the accuracy of the determination of dissolved oxygen.) We were told that if the proper sodium sulphate to sodium hydroxide ratio were maintained by the addition of sodium sulphate, no trouble from carry-over should result. In less than 2 months the first-stage pressure on our turbines increased more than 10 per cent, while the plant heat rate went up 200 Btu per kwhr. Considering that the plant output was in excess of 5,000,000 kwhr daily, the loss was substantial. Further inquiry disclosed that, in other plants where the proper ratio had been maintained and with very little carry-over, both sodium sulphite and sodium sulphate were used.

Another theory which gained prominence was and is known as "total phosphate control." It is stated that proper water-conditioning will result. But this means carrying high residuals. We feel that the lower the residuals carried in the boiler water, the less chance there is for carry-over.

We have silica and iron-oxide deposits amounting to an increase in turbine first-stage pressure of approximately 2 per cent per year. On 3-year inspections we remove the deposits by hand. It is a dirty and tedious job. We want to eliminate this work.

The author states that the silica deposits will be held to a minimum or eliminated, but the residuals to be carried will be higher than ever. Are we going to get into more trouble from some other source? The chemists will have to search diligently.

In the paper, it is stated that chloride concentrations for years prevented boiler troubles on ocean-going vessels. It is unfortunate that this significant fact was not recognized sooner and applied to land boilers. What was the drawback?

If tube temperatures are 200 to 300 F above the temperature of saturation and also above the temperature of superheat, what effect has this on Δt and on the action of the potassium salts?

Nevertheless, the theory now advanced at least gives to power-plant managers an engineering appraisal of the phenomena of boiler-water equilibrium. Dr. Hall is to be congratulated.

W. C. Schroeder[29] and A. A. Berk.[30,31] Over a period of several years, and particularly since the advent of the waterwall furnace with high rates of heat transfer, there has been a disquieting but rather vague feeling that boiler water was not always acting as a dilute solution. The hiding-out of boiler-water salts, the formation of silica scale, and the appearance of intercrystalline cracks in boiler tubes all indicated concentrations much greater than normal.

The author has made a frontal assault upon this problem, proposing (*a*) what appears to be a reasonable explanation of how the dilute solution can concentrate, at least momentarily, at tube surfaces, and (*b*) the beginning of a sound analysis of the effect of this concentration upon the deposition of salts from the boiler water.

Existence of dilute and concentrated boiler water makes it necessary to analyze the effect of the various salts under both conditions. For example, Fig. 6 of the paper shows that enough sodium hydroxide to give a pH of about 11.5 (measured at room temperature) corresponds to a minimum attack upon the steel. When this dilute solution concentrates, however, the caustic will soon reach proportions that will cause the solution to attack the steel more vigorously than it would if water alone were present. In brief, the caustic added to minimize corrosion in the dilute boiler water accelerates corrosion in the concentrated boiler water. Presumably then, if the maintenance of a pH above 7 in a boiler water with caustic is still believed to be desirable, it is because (1) the area of metal exposed to the concentrated solution may be reduced to zero by proper boiler design and operation, (2) the concentration reached is not high enough to cause corrosion at a rate appreciably greater than that caused by water alone, or (3) the time during which the concentrated solution can act at a given area may be too short to cause damage.

Considering only the chemicals added for feedwater treatment, two procedures are available to eliminate the action of the concentrated caustic. The first is to operate the boiler with distilled water alone. Theoretically, this would cause general corrosion over the entire boiler surface at a rate slightly in excess of that for a boiler water at a pH of 10 to 12, but it would cause less corrosion at points of concentration. This scheme has been tried and is reported to be successful in some boilers at present. It has been unsuccessful in others, and in any event it demands that evaporators and condensers must function especially well to prevent entrance of extraneous solids. Deaeration also must be very good, or oxygen corrosion will occur.

The alternative method would be to substitute an alkaline salt, such as sodium or potassium phosphate, for caustic. This makes it possible to control the pH at the desired level, but at points on the tube surfaces that are very hot the solution cannot attain a high concentration of caustic that will rapidly attack the metal. Instead, there will be only a deposit or concentrated solution of phosphate salt. There is strong reason to believe that iron or steel is much less soluble in these salts than in caustic and, consequently, less corrosion of the tube surface would be anticipated. Maintenance of alkalinity with sodium phosphate is now being tried in several boilers operating in the range from 400 to 2000 psi. So far, these tests appear to have been quite successful. On the other hand, the corrosivity of concentrated

[28] Technical Engineer, The Detroit Edison Company, Detroit, Mich. Mem. A.S.M.E.

[29] Assistant Chief, Fuels and Explosives Service, Bureau of Mines, Washington, D. C. Mem. A.S.M.E.

[30] Associate Chemist, Bureau of Mines, Washington, D. C.

[31] Discussion published by permission of the Director, Bureau of Mines, U. S. Dept. of Interior.

solutions of sodium or potassium silicates or chlorides on steel is as yet unknown.

The author states that the decreasing solubility of sodium silicate with increase in temperature will tend to promote the deposition of insoluble silica at relatively hot surfaces. On the other hand, if the salt is potassium silicate instead of sodium silicate, the solubility characteristics are reversed, and in contact with high-pressure steam it becomes difficult if not impossible to reach temperatures high enough to drive all the water out of the solid and to deposit potassium silicate in a form in which it cannot rapidly redissolve when the surface is again wet. If the effect of the other salts that may be present in a boiler water on the solubility characteristcs of the sodium and potassium silicates at high temperatures were known, a major tool for the solution of boiler-water problems would be available. The solubility and vapor-pressure data for the potassium and sodium salts should be extended as rapidly as possible, at least to the critical temperature of water. If sodium silicate is insoluble under conditions that may exist in steam-generating tubes and may incongruently form silica scale, it is also necessary to know the limiting ratio of sodium to potassium at which this effect no longer occurs.

On the basis of solubility and vapor-pressure data, the author offers a brief explanation of how chlorides can raise the boiling temperature of the solution on an overheated surface to such a degree that the concentration of caustic required to cause embrittlement-cracking could not be attained. How effective these salts are in preventing such concentrated caustic solutions will depend upon the temperature reached at the overheated surface. With respect to the embrittlement detector, where the difference between the operating temperature in the boiler and the atmospheric boiling temperature is available to concentrate the solution, it has been found that ratios of sodium chloride to caustic of 20 to 1 had no effect in preventing cracking. This statement applies to tests conducted at pressures as low as 210 psi.

In embrittlement-testing equipment developed by Straub, where concentration of the solution occurs by loss of water vapor toward the full steam pressure, the effect of this factor may be more important. It appears also to offer a partial explanation of the different results obtained with mixtures of chloride with sodium sulphate or R_2O_3 in this unit, as compared with the results obtained in the embrittlement detector. It would seem therefore that maintaining a high chloride concentration would tend to prevent intercrystalline cracking of tubes that overheat at high ratings rather than of boiler seams and tube ends which generally do not receive direct heat.

For protecting riveted seams, the author recommends "captive" alkalinity, in which the alkalinity of the water is captured in the form of phosphates and silicates as the water is concentrated. The embrittlement detector has shown this method to be successful with phosphate alkalinity, and it has been proved that concentrated solutions of trisodium phosphate in the absence of sodium hydroxide will not cause embrittlement cracking. It has not yet been shown that concentrated solutions of potassium or sodium silicate, which may be much more alkaline, will similarly not cause embrittlement. Embrittlement-detector tests with sodium or potassium silicates are now being carried out.

Turning from the boiler, the chemist is still awaiting enough data to determine how salts are carried from the boiler water to the superheater and then into the turbine. Carry-over from the boiler water undoubtedly is a major factor, but at the high steam pressures now employed some salts may be soluble in steam. The factors that influence carry-over are not clear, and a bare beginning has been made in studying solubility in steam. In the superheater, the higher temperatures would tend to increase solubility of some salts in steam, but at the same time the lower specific gravity of the steam would tend to decrease their solubility.[32] The effect of these factors doubtless will have to be determined for each salt involved. The situation in the turbine is equally as involved, and few data are available to help in analyzing it.

Since the specific gravity of steam, or, in other words, the close packing of the molecules, appears to be the largest factor in its ability to act as a solvent for salts, it may be possible to determine the conditions under which the boiler salts could dissolve and where they might deposit in the turbine. Spillner[33] compared observed volumes of vapors at their critical points with values calculated from pressure-temperature-volume relationships and concluded that to act as a solvent a vapor must show a certain minimum departure from the gas laws. The crowding of steam molecules at high pressures can be estimated from the specific gravity and the Maxwell distribution law. It is quite

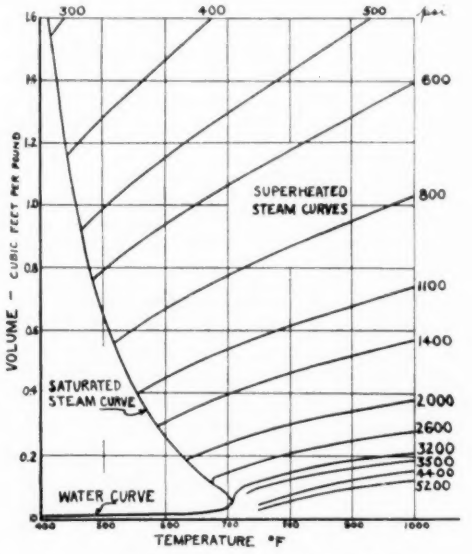


FIG. 19 VOLUME OF SUPERHEATED STEAM

probable that a mathematician could tell us at what special arrangement the molecules will be so far apart as to be able no longer to attract salt molecules sufficiently strongly to hold them in solution.

As a start in this direction, Fig. 19 of this discussion compares the volume occupied by 1 lb of steam at different temperatures and pressures with the volume occupied by 1 lb of water in equilibrium with saturated steam. Saturated steam expands as it is superheated, approaching a perfect gas at lower pressures and higher temperatures. Of special significance is the region around the critical point. At about 650 F, the specific gravity of water begins to decrease rapidly. Saturated steam formed at this temperature shows a similar unusually high coefficient of expansion for a very small region on the curve. At the critical point, this effect is much more pronounced, and the specific gravity of critical steam is reduced by half during a rise in temperature of about 15 deg F. This behavior may be very significant, as the attraction of steam molecules for each other has been shown to increase very rapidly as the distance between them is decreased.[34]

[32] "The Hydrothermal Solubility of Silica," by G. C. Kennedy, Economic Geology, vol. 34, no. 1, 1944, pp. 25–32.

[33] "High-Pressure Steam as a Solvent," by F. Spillner, *Die Chemische Fabrik*, vol. 13, 1940, pp. 405–424.

[34] "Steam Research Program, Part 3," by L. B. Smith and F. G. Keyes, Proceedings American Academy of Arts and Sciences, vol. 69, 1935, pp. 285–314.

It is believed that such attraction controls the degree of solubility of salts in steam.

The author has called attention to the possible marked effect substitution of potassium salts for sodium salts may have upon turbine deposits. As yet it is difficult to associate the separation of silica as an insoluble phase with the appearance of compact crystalline masses on turbine blades. How do they get there?

Also, what is the boiler operator to do while the chemist is unwinding this complex solubility-vapor-pressure-temperature equilibrium? He can rely upon chemical treatment to correct one set of difficulties, but this may accelerate others or move the trouble from the boiler to the superheater or turbine. At the same time, a method that has been applied successfully in one plant will not necessarily work equally well in another, for factors affecting the results may be overlooked owing to lack of data or failure to understand an involved but important chemical effect.

It must also be realized that the analysis of solubility and vapor-pressure equilibrium, as applied to boiler operation, has so far been tried for relatively simple solutions containing one or two compounds. Actually, most boiler waters contain half a dozen salts or compounds, each of which may alter drastically the relationships involved in the mixture. The treatment of so complex a solution to determine the conditions it can produce in a boiler, superheater, or turbine can be extremely involved, assuming that all the necessary data are available.

These statements are not intended to discourage the accumulation or full application of solubility and vapor-pressure data to the modern high-pressure boilers. Instead, they indicate that the work must be pursued vigorously and without delay to determine just how far valuable application can be made. While this is being done, there is also the chance that test methods or devices will appear or be developed that, together with a better understanding of the physical chemistry of the processes, will allow direct determination of the action of a given boiler water, or the steam from it, in boiler, superheater, and turbine. Such a development may furnish a shortcut that the boiler operator can readily interpret to test the effect of any specific set of conditions. It may also place a greater burden upon the manufacturers of boilers and auxiliary equipment to avoid trouble created primarily by design characteristics.

While the boiler operator is awaiting this further work, the one thing he can do to relieve difficulty is to reduce to a minimum the salts carried into the system through condenser leakage and evaporator carry-over. If they are at a minimum in the boiler water, it is reasonable to assume that this condition will favor the best operation of boiler, turbine, and superheater. The boiler operator who does not exercise the greatest care in this regard is missing the best opportunity for preventing trouble. Assuming that this does not overcome all his difficulties, he is then in a position to apply a minimum of chemical treatment to help solve any remaining problems.

F. G. Straub.[35] It is rather difficult to discuss this paper since the author attempts to cover the entire field of water treatment from steam-blanketed tubes, superheaters, and embrittlement through turbine-blade deposits, and offers one method of approach to solve all these difficulties experienced by the power-plant industry. As he points out, the data available are few and incomplete. Thus in Fig. 5 of the paper, he compares the solubility of sodium and potassium di- and metasilicates. The sodium salts have only two points on the curve over a range of 450 F. In a previous theory advanced by the author, he based his reasoning on the increase of solubility with increasing temperature curve of calcium carbonate, as compared to the decrease in solubility with increase in temperature of calcium sulphate. A short time later, Partridge showed that both salts decreased in solubility with increase in temperature. The writer would suggest that more data be made available before such definite conclusions can be drawn.

The real importance of the suggested potassium substitution for sodium will depend upon the results obtained in actual operation. Here again, caution should be the watchword in drawing conclusions. Often, several changes are made at one time and it becomes difficult to point out definitely which change actually caused the beneficial results obtained.

In 1936, the writer[36] called attention to the fact that sodium hydroxide would not produce a saturated solution in superheated steams, while sodium carbonate and sulphate would form saturated solutions and precipitate the dry salts under similar conditions. In 1939, we showed[37] that in steam-blanketed areas the corrosion (or as the author refers to it "embrittlement") could be controlled by chemical treatment. However, we found that if the metal temperature increased above a certain point, the chemical treatment was no longer effective. These results indicated that it would be possible to retard tube corrosion and resulting deposits as long as the tube temperature could be controlled and kept below a certain value. The author's recommended treatment should be beneficial in boilers where the steam-blanketing is such that the metal temperature is below this limiting temperature; however, if this temperature increases, the treatment will fail. It is believed that the ultimate solution of this type of trouble will involve proper circulation and wetting of the tube.

The author states that sodium hydroxide is not guilty of hide-out propensities due to its high Δt_s value. The writer knows of many boilers where sodium hydroxide is guilty of hide-out.

The statement is made to the effect that the silica deposition in the turbines is the result of the mechanical carrying of the silicates in the boiler water into the steam. A. Splittgerber[38] calls attention to the fact that dilute solutions of the silicates will hydrolyze at higher temperatures and liberate appreciable amounts of silicic acid. The silicic acid will be present in the steam even with the absence of mechanical carry-over. The deposition of the silica from the silicic acid at the lower temperatures and pressures in the turbine is a much more logical explanation of the silica deposition than that of the author.

W. L. Webb.[39] Regardless of whether the theories presented in this paper are borne out entirely in practice, this attack of the problem stimulates productive thinking and will lead the way to fundamental improvement in control technique.

Our experience with potassium treatment has been confined to its use in two boilers rated 750,000 lb per hr, 1350 psi, 950 F steam temperature at the Beech Bottom Power Company's Windsor Station since early in April, 1943. These 3-drum bent-tube tangentially-fired wet-bottom boilers are two of four boilers of approximately the same capacity which supply steam to two 60,000-kw topping turbines exhausting at 230 psi, 550 F to six 30,000-kw condensing units.

The two 1350-psi boilers under test present a number of problems considered susceptible of solution by potassium treatment. These include the following:

---

[35] University of Illinois, Urbana, Ill.

[36] "The Cause and Prevention of Steam Turbine Blade Deposits," by F. G. Straub, Bulletin 282, Engineering Experiment Station, University of Illinois, 1936.

[37] "Corrosion in Partially Dry Steam-Generating Tubes," by F. G. Straub and E. E. Nelson, *Mechanical Engineering*, vol. 61, 1939, pp. 199–202.

[38] "Die Flüchtigkeit der Kieselsäure," by A. Splittgerber, *Archiv. für Wärmewirtschaft*, vol. 22, 1941, p. 66.

[39] Engineering Department, American Gas and Electric Service Corporation, New York, N. Y.

1 Sludge accumulation on the steam scrubbers and driers and downtake and riser tubes.

2 Deposition of sodium-aluminum-silicate scale on heating surfaces.

3 Water-insoluble deposits in low-pressure turbines.

The sludge-and-scale problem comes about primarily from excessive condenser leakage, bringing into the system raw Ohio River water containing hardness, silica, and alumina.

Between late 1941, when the boilers were first put into service, and the time potassium treatment was started, much trouble was experienced with furnace-tube wastage. In the wastage zones, many tubes blistered, and a number developed leaks in longitudinal cracks usually located in slight bulges. On inspection these tubes showed thin hard deposits of sodium-aluminum-silicate scale. Several other tube failures occurred which were attributed to design faults.

Inasmuch as a number of new aspects developed during October and November, 1943, in the boilers under potassium treatment, the discussion of our experience is divided into two parts:

First Six Months of Experience With Potassium Treatment

Under potassium treatment from April to September, 1943, inclusive, only two boiler-tube failures occurred, both in the same boiler, on May 3. These failures were in wastage areas and were repaired by window-welding. What bearing, if any, potassium treatment may have on furnace-tube wastage rates is not known.

Contrary to expectations, no leakage of gaskets in contact with boiler water has occurred. Flexitallic hand-hole gaskets are used throughout.

Riser Tube Deposits. Typical analyses of the more important constituents of deposits turbined from wall bifurcated tubes under the two treatments are shown in columns 1, 2, 3, and 4, of Table 6 of this discussion.

It was concluded that sodium-aluminum-silicate deposits not only were not forming but also that previously formed deposits were being removed by the potassium chemicals. Furthermore, at least some of the silica was being precipitated as magnesium-silicate sludge.

TABLE 6 WALL-TUBE DEPOSITS

	Sodium treatment		Potassium treatment		
Column no.	1	2	3	4	5
Date of sampling	4/5/43	3/14/43	7/24/43	6/27/43	10/10/43
Boiler no.	84	82	84	82	82
Bifurcated-tube nos.	5–6 n. wall	117–118 w. wall	5–6 n. wall	117–118 w. wall	Hard scale at failure[a]
Deposit removed:					
Grams	344	209	73	168	...
Grams per linear foot	5.5	3.3	1.2	2.7	...
Analysis, per cent:					
Sulphur trioxide (SO_3)	Neg.	...	Neg.	0.5	1.8
Carbon dioxide (CO_2)	Neg.	...	Neg.	Neg.	Neg.
Phosphorus pentoxide (P_2O_5)	7.4	13.9	19.4	17.8	7.6
Silica (SiO_2)	11.6	11.6	2.8	4.1	29.5
Iron oxide (Fe_3O_4)	53.3	20.7	30.4	26.7	24.8
Aluminum oxide (Al_2O_3)	4.2	7.0	Neg.	2.4	12.6
Calcium oxide (CaO)	6.6	8.6	15.3	15.3	1.0
Magnesium oxide (MgO)	3.6	3.6	6.4	7.1	2.2
Sodium oxide (Na_2O)	3.8	6.3	...	...	7.6
Potassium oxide (K_2O)	...	...	Neg.	...	10.1
Copper (Cu)	3.5	15.2	22.1	18.2	Neg.
Net ignition loss (calc.)	4.2	11.3	3.8	8.9	1.6
Total	98.2	98.2	100.2	101.0	98.8

[a] Hard scale taken from area of failure of Boiler 82 north wall tube after removal of soft sludge.

Sludge Deposits. With substantially the same condenser leakage under the two treatments, the drum internal and visible tube surfaces were appreciably cleaner under the potassium treatment than under the sodium treatment, following operating periods of comparable steam output. This has been particularly true of the steam scrubbers and downcomer tubes, Table 7 indicating typical analyses of these sludge deposits.

TABLE 7 SLUDGE DEPOSITS

	Sodium treatment		Potassium treatment	
Date of sampling	4/2/43	4/2/43	6/27/43	6/27/43
Sample source	Turbulent drum	Steam washer	Turbulent drum	Steam washer
Analysis, per cent:				
Sulphur trioxide (SO_3)	Neg.	Neg.	0.5	0.5 to 1.0
Carbon dioxide (CO_2)	Neg.	Neg.	Neg.	Neg.
Phosphorus pentoxide (P_2O_5)	10 to 12	30	32.4	33.0
Silica (SiO_2)	1.4	0.3	0.1	0.5
Iron oxides (Fe_3O_4 & Fe_2O_3)	35.5	15	20.7	17.0
Aluminum oxide (Al_2O_3)	...	...	Nil	...
Calcium oxide (CaO)	10 to 12	40 or more	28.1	32.0
Magnesium oxide (MgO)	2 to 3	7–8	10.2	11.0
Ignition loss	3.2	2	6.7	6.0
Copper (Cu)	33.6	Slight	...	...

TABLE 8 TURBINE-WASHING SUMMARY

	Unit no. 2	Unit no. 4	Unit no. 6
	Under sodium treatment		
Date of wash	5/24/42	5/10/42	5/17/42
Capacity restored	3000 kw	4000 kw	3000 kw
Date of wash	6/27/42[a]	11/1/42	1/17/43
Capacity restored	1000 kw	4000 kw	1500 kw
	Under potassium treatment		
Date of wash	7/11/43[b]	5/30/43	[c]
Capacity restored	1500 kw	3000 kw	...

[a] Washed just before overhaul to determine effectiveness of cleaning method.

[b] Part of previously observed capacity loss was found due to faulty governor mechanism.

[c] Unit has lost about 2000 kw capacity and is shortly to be washed.

TABLE 9 BOILER-WATER ANALYSES AND TREATMENT

	Sodium treatment	Potassium treatment	
		First month	Subsequently
Boiler water conditions:			
OH, ppm	15	5 to 15	15
PO_4, ppm	40	25 to 50	40
SO_4, ppm	150	50 to 150	150
Cl, ppm	15	50 to 100	100
Na_2SO_3, ppm	5 to 10	0	0
SiO_2, ppm	10	7 to 40	8
Total Solids, ppm	400	350 to 700	600
pH	10.8	10.0 to 10.8	10.8
SiO_2/K_2O, epm	...	0.5 to 2.0	0.5
K/Na, epm	...	1 to 2	2
Average condenser leakage (per cent of feedwater)	0.1	0.1	0.1
Average blowdown (per cent of feedwater)	0.2	0.2	0.2
Treating chemicals (Average per million pounds of feedwater):			
NaOH, lb	0.15	...	...
Na_2HPO_4, lb	0.2	...	...
Na_2SO_3, lb	0.2	...	...
KOH, lb	...	0.2	0.5
KCl, lb	...	0.3	0.5
KH_2PO_4, lb	...	0.3	...
H_3PO_4 (75 per cent), lb	...	...	0.4
Average chemical cost (per million pounds of feedwater), cents	2.6	7.6	10.0

Turbine Deposits. The relative rates of build-up of deposits in low-pressure turbines under the two treatments are confused

somewhat by the fact that these units receive some steam from sodium-treated low-pressure boilers.

The deposits became troublesome during the first half of 1942, during which time condenser leakage was unusually high and the cooling water high in suspended matter. Caustic-washing of turbines was started soon thereafter. Condenser leakage was greatly reduced but deposits continued to build up.

The washing dates of the turbines receiving steam from the potassium-treated boilers and approximate capacities regained by washing are indicated in Table 8 of this discussion.

Since July, 1943, stage-pressure data of units Nos. 2, 4, and 6 have been obtained and plotted. The curves for unit No. 6 only show progressive increases in pressures with time. Further experience is needed to show definitely the effect of potassium versus sodium on deposit build-up especially since units Nos. 1, 3, and 5, receiving steam only from sodium-treated boilers, now show slower rates of accumulation of deposits.

Boiler-Water Conditions. Typical boiler-water conditions, and chemical feed rates and costs under the two treatments are shown in Table 9.

Governed principally by changing rates of condenser leakage, the boiler-water sampling and analysis schedules are normally the same under the two treatments. Determinations ordinarily are made for OH and PO_4 five times and the other usual constituents once per 24 hr per boiler.

Conclusions. Based upon the first 6 months of experience with potassium treatment in the two 1350-psi boilers, the following tentative conclusions are drawn:

1 Indications point to complete elimination of sodium-aluminum-silicate scale and presumably all silica scales from heating surfaces.

2 All surfaces of the boiler circuits and of the steam scrubber are freer of sludge deposits than when sodium treatment was used.

3 Indications point to a reduced rate of build-up of low-pressure-turbine deposits under potassium treatment than under sodium treatment.

Eighth and Ninth Month of Experience With Potassium Treatment

During an outage of boiler 82 on October 10, one tube in the furnace wastage area of the north wall was found to be leaking, the failure being in the form of a series of longitudinal cracks in a small bulge. The 12-ft section of this tube, removed for internal examination, revealed the presence of thin hard scale on the fire side and some slight internal corrosion in the scaled areas. About half a dozen small bulges in other tubes in the wastage area in this wall were found and about half that number were observed in the east wall, a condition not previously experienced under potassium treatment. To what extent the formation of bulges can be attributed to old scale laid down under sodium treatment is not known.

The study of the thin, hard scale in the failed tube is as yet incomplete but X-ray analyses show the absence of analcite. The scale appears to be some form of potassium-aluminum silicate. Its chemical analysis is indicated in column 5 of Table 6 of this discussion.

During the November 21 outage of boiler 84, no bulges were observed on any of the wall tubes. Sludge deposits, however, were somewhat heavier than usual, due perhaps to a greater than normal time interval between shutdown and draining. The following quantities of deposits were turbined from selected bifurcated tubes of the north wall:

Tubes Nos. 5 and 6—3 g (previously turbined 7/24/43)
Tubes Nos. 17 and 18—385 g
Tubes Nos. 43 and 44—333 g

Analyses of the foregoing deposits have not yet been made.

Lacking details concerning the October-November run with potassium treatment, no conclusions are being drawn. Consideration, however, is being given to the following:

(*a*) Raising the silica in the boiler water by feeding potassium silicate to assist in precipitating magnesium as magnesium silicate for the purpose of reducing the tendency of the sludge to adhere to boiler surfaces.

(*b*) Removal of existing deposits from one of the high-pressure boilers by acid-cleaning to determine whether scales containing alumina and silicon are formed under potassium treatment.

It is possible that the scales, recently observed, were initially deposited under sodium treatment as analcite, and under potassium treatment they are being converted to a potassium-sodium-aluminum-silicate complex through zeolitic action.

Potassium treatment like all other pioneering must be modified to fit new conditions as they arise in practice. That in some respects it should meet with apparent failure is no cause for discouragement. The writer is confident that as needed vapor-pressure and solubility data become available, and the theories derived thereform are tempered by field application, boiler deposits will cease to be the problem they are today.

S. F. Whirl.[40] A new mode of thinking in the field of boiler-water treatment has been born. In diagnosing the water-steam problems encountered in high-pressure high-temperature operation, the author has utilized sound physicochemical reasoning instead of trial-and-error methods. Substitution of potassium for sodium salts is an outgrowth of this innovation. The approach is so fundamental and logical that we naturally ask ourselves the question, why did not someone conceive and apply it years ago?

Perhaps the main reason for the delay in attacking these problems in the present scientific manner has been a lack of apparent data. The author is to be complimented for the compilation and utilization of the data presented in the paper, particularly Morey's data on the behavior of silicates at high temperatures and pressures, presumably of interest only to the geophysicist and the glass manufacturer. Too often in seeking a practical solution of troubles, we overlook the findings of chemists in other fields of endeavor.

As repeatedly pointed out in the paper, the data supporting many of his contentions are very meager, and considerable research will be necessary to attain a thorough understanding of the behavior of the solids in the boiler, superheater, and turbine.

The available data deal chiefly with "solo" solutions, those in which only one chemical is dissolved in water. As other substances are added to these solutions, as in the case of actual boiler waters, the original data no longer apply, and therefore theoretical consideration of such a complex system as boiler water may lead to erroneous conclusions. This is aptly illustrated by the behavior of KCl-NaBr mixtures as compared to the behavior of these salts individually, shown in Fig. 11 of the paper.

Iron-Oxide Sludge. Corrosion of boiler metal by water is a natural oxidation process whereby iron tends to seek its most stable form under the conditions of its environment. It will continue as long as metal and water are in contact. All we can hope for is to reduce the intensity of the reaction to a negligible value by chemical treatment which favors the development and maintenance of a protective iron-oxide film on the metal surface. In the absence of dissolved oxygen in the boiler water, the reaction is fundamentally the capture of oxygen from the H_2O molecule by the iron with an unleashing of a corresponding amount of hydrogen. In fact, the amount of molecular hydrogen

[40] Chief Chemist, Duquesne Light Company, Pittsburgh, Pa.

in the steam is an indication of the intensity of the corrosion. Since caustic indirectly promotes the corrosion process by destroying the protective barrier, any efforts to reduce its concentration at the evaporative surfaces will be a step in the right direction, whether it be by the addition of other salts having high Δt, values or by co-ordinated phosphate—pH control, as suggested by Purcell and Whirl.[41,42,43]

The presence of iron-oxide sludge in the boiler, however, does not necessarily indicate wastage of boiler metal. Iron oxide is continuously being formed throughout the entire system and is transported from the economizer, deaerator, heaters, condensers, pipe lines, etc., into the catch-all, the boiler. We must bear these facts in mind and not be misled on finding accumulations of iron oxide in the boiler at inspections, especially on starting up new units which are inclined to contain considerable iron oxide as a result of atmospheric rusting.

Boiler Water Carry-Over and Deposits in Steam System. In spite of improvements in steam quality in recent years, troubles

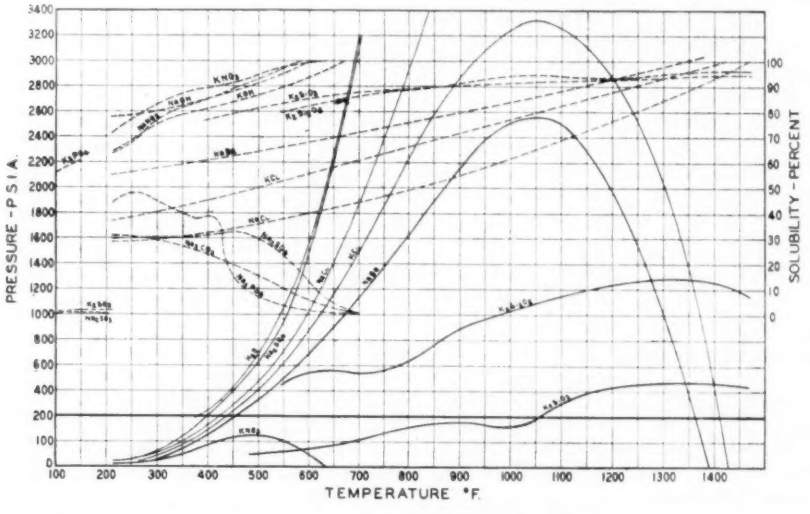


FIG. 20 SOLUBILITY-TEMPERATURE-VAPOR PRESSURE RELATIONS FOR WATER SOLUTIONS OF VARIOUS SALTS

with turbine deposits continue. This is not surprising, however, when one considers that even with steam containing less than 1 ppm of solids, the amount of chemicals entering a turbine over a period of a year is a matter of tons, not of pounds. The important item in turbine operation is whether or not these chemicals "stick and stay stuck." The extent to which operation is affected depends upon the amount of deposit and its location. Such factors as the nature of the solids carried over, temperature, pressure, velocity, pH of the steam, and turbine operation evidently all play a part. The author has supplied us with a very important piece of this complex jig-saw puzzle. Since silica is the chief offender in high-pressure operation, he suggests a method of boiler-water treatment designed to keep the silica in solution as it passes through the turbine. It must be recognized, however, that the supporting data deal only with solo solutions, and the effect of other salts may completely alter the behavior of the silica. This can be determined only by experimental investigation.

Is keeping the silica in solution the complete answer, though? Let us consider a droplet of boiler water carried over with the steam. By the time it has passed through the superheater and entered the turbine, certainly it will be a concentrated solution of some chemicals. Some salts will precipitate and their behavior is a matter of conjecture. Will they settle out, or will they remain with the concentrated droplet? Most important, however, will the final droplet be a liquid which will pass on through the turbine or will it be a viscous, pasty, wet mass which will adhere to the blading?

To give an idea of the extent of the solubility of different salts under superheater and turbine conditions, some of the solubility and pressure-temperature data in the appendix have been plotted in Fig. 20 of this discussion. By means of these curves the weight per cent of the salt in solution is given directly for various pressure-temperature conditions. It is interesting to note that at 1000 psi and 900 F, a number of the solutions are richer in chemicals than in water; for instance, 70 per cent KCl, 30 per cent H_2O; 100 per cent KOH; 91 per cent K_2SiO_3, 9 per cent H_2O. We would naturally expect a mixture of these to be quite viscous.

There are many questions concerning the behavior of silica which cannot be readily explained. The silica concentration in the saturated steam at one of our plants operating at 900 psi has been found, by careful evaporation studies, to be more than tenfold that which would be expected. Is this indicated selective carry-over due to the solubility of silica in the vapor or to mechanical carry-over, promoted by the tendency of silicates to concentrate at the steam-water interface?

Another question is prompted by the E.E.I. investigation of several years ago,[44] and the comprehensive study now under way. A number of cases are on record where no silica difficulties were encountered in the low-pressure turbines until after topping units were installed. In general, the quality of the steam has been improved. In some instances, the treatment in the high-pressure and the low-pressure boilers has been essentially the same. The tendency has been to carry lower alkalinities in the high-pressure boilers, but there are a few cases where the reverse is true. There is one principal difference, however, that is, the higher superheat temperature to which the droplets of boiler water are subjected in the high-pressure superheater. Would we expect this factor to have any particular influence on the behavior of silica in the turbine, using sodium treatment in the boiler water? A phase-rule study similar to that presented in Fig. 8 of the paper, but including all of the salts present, would most certainly determine the conditions under which the various constitutents would precipitate from solution. Whether or not and where they may "stick and stay stuck" are different problems.

The same phase-rule study would apply to deposition of solids in the boiler and might correlate many experiences which now seem contradictory. As an example, after several months'

[41] "Embrittlement of Boiler Steel—Experiences With the Schroeder Detector," by T. E. Purcell and S. F. Whirl, Trans. A.S.M.E., vol. 64, 1942, pp. 397–402.

[42] "Protection Against Caustic Embrittlement by Co-ordinated Phosphate-pH Control," by S. F. Whirl and T. E. Purcell, Third Annual Water Conference, Engineering Society of Western Pennsylvania, 1942, pp. 45–60.

[43] "Protection Against Caustic Embrittlement by Co-Ordinated Phosphate-pH Control," by T. E. Purcell and S. F. Whirl, Trans. Electrochemical Society, vol. 83, 1943, pp. 279–295.

[44] "Power Station Chemistry," Edison Electric Institute, Publication No. E 10, 1937

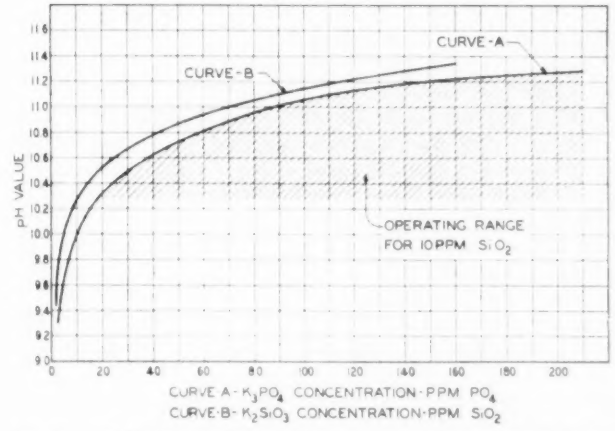


FIG. 21 pH VALUES OF WATER SOLUTIONS OF TRIPOTASSIUM PHOSPHATE AND POTASSIUM METASILICATE

operation with co-ordinated phosphate-pH control in two 300-psi B&W cross-drum boilers, the silica-rope scale, always found tightly adhering to the sides of the top rows of generating and upper steam-circulating tubes, was observed to be loosening, and many pieces, several inches in length, were flaked off and lying on the bottoms of the tubes. This observation is offered for what it may be worth and not as a recommendation of a method of treatment for removing silica.

Caustic Embrittlement. At the last two Annual Meetings of this Society, the corrective measures offered for the prevention of caustic embrittlement, when the boiler water was treated with sodium salts, included inhibitors and our co-ordinated phosphate-pH control of alkalinity,[41,42,43] the latter being especially suited to high-pressure operation. That the principle of our method might apply to other salts of weak acids and strong bases was fully recognized. The author terms this application "captive alkalinity." However, in utilizing the potassium silicates for this purpose, as suggested by the author, the question logically arises, can these salts in themselves promote embrittlement, especially the potassium metasilicate, because of its high solubility and high Δt_s value? The reason why pure trisodium phosphate will not cause embrittlement is evidently due to its low Δt_s value with consequent insufficient alkalinity in its saturated solution to promote this type of attack. We would expect much higher alkalinities from a saturated potassium-metasilicate solution.[45]

Since no two boilers have the same characteristics with respect to concentrating-film boiling at localized areas, and since the addition of other salts like KCl with high Δt_s values are not effective when the concentration is produced by evaporation to atmosphere, the only assured protection against caustic embrittlement is the elimination of caustic as such from the boiler water. The method of treatment to be described is offered as a practical means of protection against caustic embrittlement and, at the same time, a possible means of holding the silica in check.

Additional experimental data will be necessary to determine its effectiveness with respect to the latter. In Fig. 21 of this discussion are plotted separately the pH values of solutions of K_3PO_4 and K_2SiO_3. It is suggested that the pH of the boiler water be maintained below the phosphate-pH curve and above the pH value corresponding to the silica concentration in the boiler water, assuming the silica to be present as K_2SiO_3. The operating region for 10 ppm SiO_2 in the boiler water is indicated in Fig. 21 of this discussion.

[45] "Silicate of Soda in the Building Industry," by J. A. Vail, *Industrial and Engineering Chemistry*, vol. 27, 1935, pp. 888–893.

It is realized that, in the light of the data presented in Fig. 8 of the paper, this method may not appear logical with respect to preventing silica deposits. However, it should be pointed out that these data deal only with silicates and caustic potash; we do not know what effect the phosphates will exert on the equilibrium, especially when the pH is below that corresponding to the K_3PO_4 concentration. We would expect the Δt_s values of the phosphates to be higher with lower pH, and as the Δt of the solution increases and the vapor pressure decreases, what effects will the phosphates have on the silicate equilibrium? The nature of the phosphate salts which separate will also have a bearing on the ultimate behavior of the silica. For the complete picture, we must go still further and consider what happens to the concentrated boiler-water droplets as dilution occurs with lowering temperature in the turbine in an environment of various dry salts, having varying degrees of solubility at the different temperatures.

Potassium treatment was started in the 900-psi boilers of our Frank R. Phillips Station on August 1, 1943. The boiler-water condition is summarized in Table 10 of this discussion.

TABLE 10 AVERAGE ANALYSIS OF BOILER WATER; NO. 1 BOILER, F. R. PHILLIPS POWER STATION; AUGUST 1 TO NOVEMBER 20, 1943

pH: Determined	10.59
From phosphate-pH curve	10.86
Sp. Cond., micromhos	625
Dissolved salts, ppm	374
Phosphate, PO_4, ppm	87
Sulphate, SO_4, ppm	138
Sulphite, SO_3, ppm	11
Chloride, Cl, ppm	10
Hydroxide, OH, ppm[a]	0
Silica, SiO_2, ppm	8

[a] By modified Winkler method.[44]

Since inspections have not been made in the interim, no information can be offered concerning the effect of the treatment on boiler, superheater, and turbine deposits.

An embrittlement-detector test, however, was terminated at the end of 58 days instead of our usual 90 days, for the purpose of submitting the information in this discussion. Neither the hot- nor the cold-rolled specimen cracked. It is noteworthy that the deposit accumulations on the specimens were much softer and more readily dissolved in water than those of any previous test, using sodium treatment in the boiler water.

It is apparent that this paper opens a new and wide field of research in boiler-water treatment, and we may be certain that the method of approach will serve to guide others in future study.

AUTHOR'S CLOSURE

The constructive character of the discussion is outstanding. Only a few points need be given further consideration.

Mr. Corey's impression regarding higher hide-out by potassium than by sodium salts must be reversed. *Less* hide-out occurs with potassium than with sodium salts.

Mr. Daniels, who completely eschews any treatment of the boiler water, ably supports his position by the excellence of results in his plants. By maintaining his condensers tight, and avoiding carry-over from his evaporators, he is in position to say "Go thou and do likewise" to anyone objecting to his methods, because these sources may provide impurities in the boiler water. Many, however, conservatively sanction the added insurance embodied in a second defense line maintained in the boiler water, no matter how impregnable they may consider their primary defenses to be. As pointed out in the section on "The Iron Oxide Sludge Problem," the low pH value of untreated boiler water "provides optimum conditions for silica deposition in boiler and turbine." Also, where salt water is used in condensers, in addi-

tion to more severe problems of corrosion, the operator is confronted with a hundredfold or more increase of dissolved impurities over that derived from the same per cent of inleakage of typical fresh water.

Professor Keevil emphasizes the dearth of solubility and vapor-pressure data on multicomponent systems at temperatures and pressures such as those met in boilers and turbines. Continuance of the work discussed by Mr. Kaufman will in time result in obtaining such data, and probably with results as unexpected as the totally unlike solubilities of sodium and potassium phosphate.

It is pleasing to note that Dr. Schroeder and Mr. Berk, in their discussion, by use of the principles set forth in the section on "Protection From Embrittlement in the Light of the Δt Function" arrive at a logical explanation of the differences in results obtained by use of the embrittlement-testing equipment developed by Straub, on the one hand, and, on the other, by use of the embrittlement detector of Schroeder and Berk.

Professor Straub notes in relation to the tentative solubility curve of sodium meta- or disilicate (Fig. 5) that there are "only two points on the curve over a range of 450 F," and that he "would suggest that more data be made available before such definite conclusions can be drawn." Relative to this solubility, Dr. George W. Morey, of the Geophysical Laboratory, Carnegie Institution, Washington, D. C., states (14): "Experiments at comparatively low temperatures have shown that the solubility of sodium metasilicate is strongly retrograde. For example, at 100 C, the saturated solution of sodium metasilicate in water contains about 50 per cent of the anhydrous compound, but at 350 C, the solubility is measured only in tenths of a per cent." The broken curve of Fig. 5 for sodium metasilicate has been drawn in accordance with these data.

Professor Straub states, "The statement is made to the effect that the silica deposition in the turbines is the result of the mechanical carrying of the silicates in the boiler water into the steam." On the contrary, both in this paper (Section on "Role of Silica in the Turbine") and in the A.S.T.M. Round-Table Discussion of 1942 (43), the author has taken the position that the question of mechanical transfer, on the one hand, or transfer by vaporization, on the other, is an open one whose answer must await further data.

Professor Straub states, "We showed that in steam-blanketed areas the corrosion (or as the author refers to it 'embrittlement') could be controlled by chemical treatment." Reference to the section of the paper entitled, "The Iron Oxide Sludge Problem: Corrosion by the Bonded Oxygen of the Boiler Water," fails to disclose any mention of embrittlement in connection with this type of corrosion. However, in some cases, a type of embrittlement develops under such conditions, as noted in the section "Protection From Embrittlement, etc."

As brought out in Mr. Webb's discussion, and particularly by analysis No. 5, Table 6, potassium aluminum silicate, analogous to sodium aluminum silicate, will form under severe conditions. The conclusion is thus inescapable that with either sodium or potassium conditioning of the boiler water, the concentration of aluminum therein must be held to the minimum possible.

The author is very appreciative of the time and thought which has been given by the several contributors in the development of this discussion.

Theoretical Regenerative-Steam-Cycle Heat Rates

By A. M. SELVEY,[1] PITTSBURG, CALIF., AND P. H. KNOWLTON,[2] SCHENECTADY, N. Y.

The calculation of heat rates for a theoretical steam cycle with an infinite number of heaters regenerating feedwater to throttle saturation temperature is facilitated by the development of a simple tabular-integration method of computation which takes into account boiler-feed-pump work. A table of theoretical heat rates is presented for throttle-steam conditions, ranging from 300 to 3200 psia, and from saturation temperature to 1200 F, and for an absolute exhaust pressure of 1 in. of mercury. Means are provided for calculating heat rates at other exhaust pressures within the wet-steam region. These heat rates serve two purposes, i.e., (1) as a standard of power-plant performance; and (2), as a first step in estimating regenerative-cycle economy at unfamiliar steam conditions. The derivation of factors necessary to complete economic estimates, however, must await a more favorable opportunity. In the meantime, existing plant records can be made to provide approximate factors as substitutes for those it is hoped will be computed and published later. The economy of using superheated steam, integral moisture extraction, etc., are discussed briefly. An Appendix provides full directions for using or adapting the tabular-integration method for steam-cycle studies.

FOR several years a need has existed for a simple method of calculating theoretical regenerative-steam-cycle heat rates to serve as a standard of comparison for steam-power-plant performance. Such a standard has been set for the simple Rankine cycle by publication at various times of theoretical steam rates.[3] This paper presents a similar set of tables for a hypothetical regenerative cycle as described hereinafter.

Many expositions have been made by various writers of means for determining the performance of regenerative cycles, but it appears to the present authors that such performance is best obtained in two main steps, namely, (1) the determination of theoretical heat rates with zero engine and heat losses; and (2) the use of factors of "efficiency" for the various actual pieces of the working-cycle apparatus, to reduce the theoretical heat rates to practical cases. Information concerning step (1), namely, the production of the necessary tables of theoretical performance, is contained in this paper, with a description of the method and a set of tables showing the resulting heat rates, which are proposed as an acceptable standard, depending only upon the properties of steam, and therefore not subject to change unless, as appears unlikely, the basic steam tables are revised.

Step (2), the delineation of factors of actual performance, will be concerned with evaluating the effects of such losses as occur in actual apparatus—engines, boilers, feed heaters, pumps, etc., and in their arrangement. Work on step (2), however, has been postponed because of prior demands by the war effort. It is hoped that the work will be executed later. In the meantime, with the theoretical heat rates completed, there seemed good reason for making this material available for use in engineering studies. Estimating plant heat rates for higher steam conditions than are now in general use can be accomplished with reasonable accuracy by computing a series of proportionality factors or ratios from the performance of an actual plant and applying them in turn to the new conditions. This procedure should prove of some use until time is available for work on step (2).

Numerous interesting problems arose while work was proceeding on this study. Neither time nor space, however, will permit more than one or two of these secondary topics being introduced and discussed. Accordingly, this paper is confined to defining and describing the chosen theoretical regenerative cycle, discussing the mathematical procedure for computing heat rates, some brief mention of possible applications for the data, and some views on two recent proposals concerning the regenerative cycle. An Appendix demonstrates two computation forms, a short and a long, which may be adapted as desired to suit various modifications of the regenerative cycle.

The Theoretical Regenerative Cycle

A clear picture of the theoretical regenerative cycle considered in this paper is essential as several writers have proposed and discussed different modifications which also can be classified strictly as regenerative cycles. In addition, engineers still lack a universally acceptable steam-cycle terminology and, consequently, have resorted to naming cycles as they personally feel justified. Under such circumstances, definitions, descriptions, and diagrams need to be complete.

Definition. The theoretical regenerative steam cycle is viewed herein as one in which steam, expanded isentropically (at constant entropy) through a prime mover, in this case a turbine, is extracted (bled) for heating feedwater to throttle saturation temperature in an infinite number of progressive steps of zero terminal difference, each assisted by an attendant boiler feed pump of 100 per cent efficiency powered from the prime mover.

Other terms sometimes used instead of "theoretical," in speaking of such a cycle, are "ideal," "perfect," "hypothetical," etc. The term "ideal" is used often to indicate 100 per cent mechanical efficiency, reversibility, and possibly the idea of the cycle being "imaginary." The designation "ideal cycle," however, has been applied also to regenerative cycles of less than an infinite number of feedwater heaters and to a cycle in which only saturated steam and wet steam are bled for feedwater regeneration. Whatever the cycle is called, a more lengthy description is desirable.

Description. The heat rates provided by this paper are for a regenerative steam cycle of the following component parts:

1 A turbine, having no mechanical losses, through which steam is expanded at constant entropy (engine efficiency is 100 per cent).

2 A regenerative feedwater system having an infinite number

[1] Chief Engineer, Shell Point Plant, Shell Chemical Division, Shell Union Oil Corporation; formerly Engineer, Engineering Division, The Detroit Edison Company, Detroit, Mich. Mem. A.S.M.E.

[2] Engineer, Turbine Engineering Department, General Electric Company. Mem. A.S.M.E.

[3] See, for example, "Theoretical Steam-Rate Tables," by J. H. Keenan and F. G. Keyes, published by The American Society of Mechanical Engineers, New York, N. Y., 1938.

Contributed by the Power Division and presented at the Annual Meeting, New York, N. Y., Nov. 29–Dec. 3, 1943, of The American Society of Mechanical Engineers.

Note: Statements and opinions advanced in papers are to be understood as individual expressions of their authors and not those of the Society.

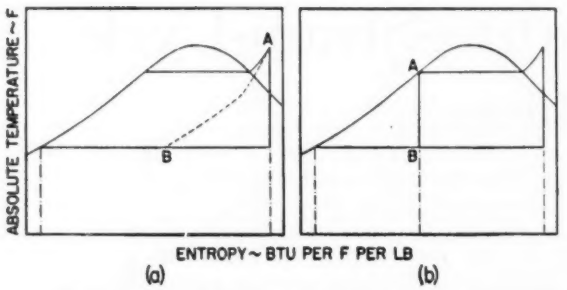


FIG. 1 TEMPERATURE-ENTROPY DIAGRAM FOR THEORETICAL REGENERATIVE STEAM CYCLE, OPERATING BETWEEN 1000 PSIA 700 F AND 1 IN. HG STEAM CONDITIONS

(*a*, Conventional diagram. *b*, Diagram based on construction method described in reference 5.)

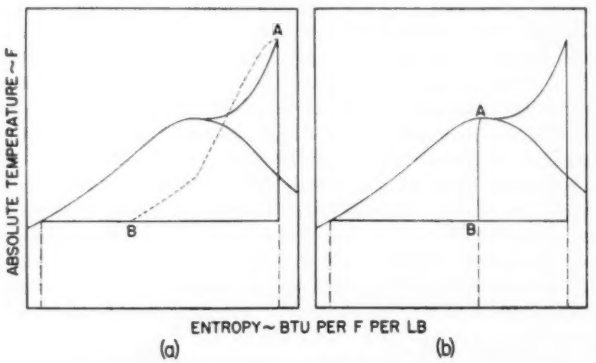


FIG. 2 TEMPERATURE-ENTROPY DIAGRAM FOR THEORETICAL REGENERATIVE STEAM CYCLE, OPERATING BETWEEN 3200 PSIA 1200 F AND 1 IN. HG STEAM CONDITIONS

(*a*, Conventional diagram. *b*, Diagram based on same construction method as used for Fig. 1*b*.)

of bled-steam heaters heating to the saturation temperature corresponding to the throttle-steam pressure, and with zero terminal difference between the saturation temperature of the bled steam and the temperature of the feedwater leaving the heater, even when superheat is present in bled steam,[4] and an attendant feed pump of 100 per cent efficiency with each heater to step up the feedwater pressure to the level of the next higher heater.

3 An electric generator of 100 per cent efficiency, which supplies, without line loss, the boiler feed pumps.

4 A steam generator of 100 per cent efficiency, in which blowdown, soot-blowing losses, etc., are zero.

Since energy required to drive fans, fuel equipment, general services, etc., is considered zero in a theoretical cycle, auxiliary-power usage other than that required for the boiler feed pumps, as described in item (2), is not included.

Diagrams. A conventional diagram for the theoretical regenerative cycle is shown in Fig. 1(*a*) for throttle-steam conditions of 1000 psia 700 F and 1 in. Hg exhaust pressure. The dotted line *AB*, representing the reduction in weight of steam passing through the turbine, is not an expansion line. The area below the dotted line is not significant. The chief advantage of the diagram is that it appears familiar.

In attempting to make a diagram in which areas are significant and bear the correct relationship of cycle efficiency, recourse was taken to a method of construction described fully by Barnard, Ellenwood, and Hirshfeld.[5] This method was used to produce Fig. 1(*b*) which is drawn for same steam conditions as Fig. 1(*a*). In Fig. 1(*b*) the area below the saturation line, bounded by condensate entropy and line *AB*, represents heat given up to feedwater.

With high-pressure and high-temperature throttle steam conditions, such as 3200 psia 1200 F, these diagrams, however, undergo unusual changes as are indicated in Figs. 2(*a*) and 2(*b*). Parallelism between line *AB* and the isentropic expansion line, the apparently meritorious feature of Fig. 1(*b*), no longer extends over the whole length of *AB*, in Fig. 2(*b*), but exists only up to the temperature level where the expansion line crosses the saturated-vapor line. Above that point, line *AB* shows to a more or less pronounced degree the effect of bleeding superheated steam. Curvature of line *AB* in Figs. 1(*b*) and 2(*b*) actually will exist whenever superheated steam is bled, but it is only noticeable on a small-scale diagram with throttle steam relatively highly superheated. Even then, curvature is apparently so slight that casual inspection of Fig. 2(*b*) might lead to the contention that a simple formula could be developed for calculating theoretical regenerative-cycle heat rates even for top throttle conditions. The significance of this curvature in line *AB* of Fig. 2(*b*) is not easily apparent, and it is hoped that the discussion will bring forth an explanation.

The closest approximation by "short-cut" formula would obtain if a straight line could be drawn vertically through point *B*. But the location of *B* cannot be found without recourse to the integration method to be described later. Accordingly, no labor can be saved in this case. The next approximation would be based on the assumption that the straight line passed vertically through known point, *A*. A short-cut formula for this case would be

$$\text{Theoretical heat rate}^{6}\ \text{(inaccurate)} = \frac{3412.75\ (H_t - h_f)}{H_t - h_f - T_s(S_t - S_f)}$$

[4] In actual practice, where a desuperheating zone is provided in a feedwater heater, a temperature crossover or negative terminal difference may exist where superheated steam is being bled. Since the number of degrees crossover varies with heater design and the degrees of superheat, an acceptable allowance for this effect feasibly cannot be included in a theoretical study.

[5] "Heat Power Engineering," by W. N. Barnard, F. O. Ellenwood, and C. F. Hirshfeld, John Wiley & Sons, Inc., New York, N. Y., third edition, part 1, sec. 217, 1926, pp. 353–356.

[6] An approximately similar incorrect equation will be found in connection with Fig. 712, of "Steam Power Plant Engineering," by F. G. Gebhardt, sixth edition, John Wiley & Sons, Inc., New York, N. Y., 1925.

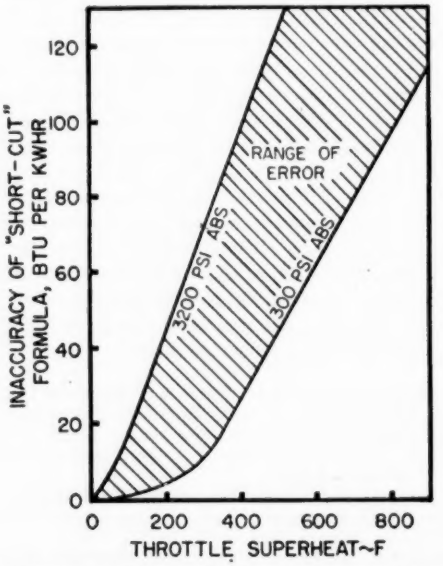


FIG. 3 A SIMPLE OR "SHORT-CUT" FORMULA FOR DETERMINING APPROXIMATE THEORETICAL REGENERATIVE-CYCLE HEAT RATES PRODUCES RESULTS WHICH ARE TOO LOW

(The diagram demonstrates how this inaccuracy increases with the amount of superheat in the throttle steam.)

where subscript t refers to throttle, f to saturated feedwater, and e to turbine-exhaust conditions. This formula is incorrect because it fails to take into account the sizable vertical strip bounded on one side by the line AB and on the other by a vertical through A. Heat rates computed by the short-cut formula are too low. The extent of the error is shown in Fig. 3.

The theoretical regenerative cycle, as defined and described, has been considered commonly as representing the best economy actually approachable in practice and, on this score, has been viewed by many as a standard of attainment. A recent suggestion, to be described later, of a novel but probably impractical regenerative cycle having Carnot efficiency does not seem to detract from the already established regenerative-cycle standard. The fact that a simple computation method, which will be described next, has been developed and heat rates calculated for a wide range of steam pressures and temperatures should minimize objections on the grounds of complication to the continued use of the theoretical regenerative cycle as an acceptable standard.

Development of Computation Methods

The Ernest L. Robinson equations for calculating the theoretical weight and energy value of bled steam appear in the Appendix of his 1923 paper.[7] The heat balance for an infinitesimal heater is

$$dw(H - h) = (1 + w)dh$$

which, when integrated, gives

$$1 + w = e^{\int_{h_2}^{h_1} \frac{dh}{H-h}}$$

where $(1 + w)$ is the pounds of steam at any point in the turbine. In the 1923 paper,[7] with a maximum steam condition of 1000 psia 800 F, integration was performed graphically. (The nomenclature used appears in the Appendix.)

Twenty years later, attention is focused on much higher steam conditions. There appears a definite need to provide theoretical regenerative-cycle heat rates for a wide range of throttle pressure and temperature up to 3200 psia and 1200 F. Because the effect of pump work on cycle efficiency is appreciable at high feedwater pressure, and because of the larger number of heat rates that would have to be computed to cover the greater range of steam conditions, Robinson's equation[7] had to be modified and adapted to a tabular method of computation.

Step-by-Step Integration. If $dh/(H - h)$ were to be integrated graphically, the quantity $1/(H - h)$ would be plotted against h as shown in Fig. 4. The product $dh/(H - h)$ is the area of an infinitesimal strip below the curve AB. The integral of $dh/(H - h)$, by the Robinson equation, is the whole area $ABCD$. Some energy, however, is added by the boiler feed pump. For each strip, dh, representing heat added by bled steam, there is an attendant strip, dF, representing the boiler-feed-pump work. Since the steam flow in the turbine depends upon the amount of steam bled, the enthalpy added by the pump in each step must be subtracted from the gross gain in enthalpy.[8]

In order to calculate accurately rather than to planimeter the area below the curve, it is necessary that sufficiently narrow strips be so chosen that the section of curve bounding the top of each strip is essentially a straight line. This provision permits determining the area of the strip by taking the equivalent height as the average of the two sides. About 35 steps from throttle to condenser for steam pressures of 2000 to 3200 psia have proved adequate. (An extra 20 steps were found unnecessary.) The steps, however, must be chosen so that the area of each strip, i.e., $dh/(H - h)$, is the same. An initial selection with constant increments of h may be proportioned to give constant values of $dh/(H - h)$ on a second or third trial. The method is described in the Appendix under "Short-Form Computation." With throttle pressure of 1000 psia or less, 25 steps may be chosen, and equal values of dh are satisfactory.

Checking the Method. Only one independent check on the method is available. A theoretical regenerative cycle supplied with saturated steam will have Carnot-cycle efficiency. Checks made on this basis have proved the method to be reliable.

[7] "The Margins of Possible Improvement in the Central-Station Steam Plant," by Ernest L Robinson, Trans. A.S.M.E., vol. 45, 1923, p. 644.

[8] The work done by the perfect boiler feed pump should be read from Fig. 3, p. 75, of the Keenan and Keyes "Thermodynamic Properties of Steam," John Wiley & Sons, Inc., N. Y., 1936. In the tabular-integration method, however, steps are so small that Fig. 3 cannot be read accurately enough. Since the change in specific volume of compressed water is insignificant on three scores, namely, (1) the change in feedwater temperature during compression is small, (2) the change in pressure is small, and (3) the effects of the foregoing oppose each other, the simple equation $F = Nv/5.4$ proved satisfactory. This form substitutes for the correction

$$-\frac{1}{J}\int_{r-1}^{r} v\,dP$$

recently suggested by Dr. W. J. Kearton; see *Journal* and Proceedings of The Institution of Mechanical Engineers, vol. 147, 1942, pp. 114–115, comment on paper by H. S. Horsman, reference 9.

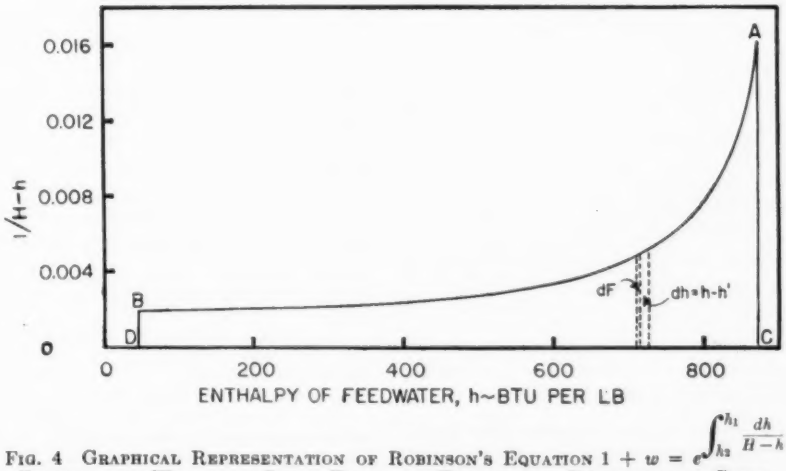


Fig. 4 Graphical Representation of Robinson's Equation $1 + w = e^{\int_{h_2}^{h_1} \frac{dh}{H-h}}$ Determining Weight of Steam Bled in a Theoretical Regenerative Cycle
(Example is for 3200 psia saturated steam.)

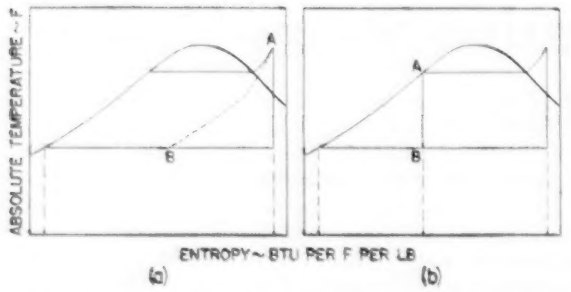


FIG. 1 TEMPERATURE-ENTROPY DIAGRAM FOR THEORETICAL REGENERATIVE STEAM CYCLE, OPERATING BETWEEN 1000 PSIA 700 F AND 1 IN. HG STEAM CONDITIONS

(*a*, Conventional diagram. *b*, Diagram based on construction method described in reference 5.)

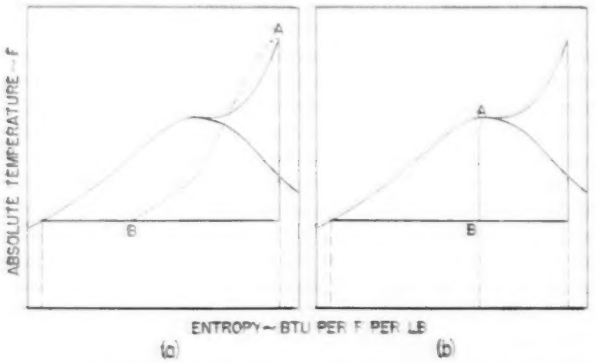


FIG. 2 TEMPERATURE-ENTROPY DIAGRAM FOR THEORETICAL REGENERATIVE STEAM CYCLE, OPERATING BETWEEN 3200 PSIA 1200 F AND 1 IN. HG STEAM CONDITIONS

(*a*, Conventional diagram. *b*, Diagram based on same construction method as used for Fig. 1*b*.)

of bled-steam heaters heating to the saturation temperature corresponding to the throttle-steam pressure, and with zero terminal difference between the saturation temperature of the bled steam and the temperature of the feedwater leaving the heater, even when superheat is present in bled steam,[4] and an attendant feed pump of 100 per cent efficiency with each heater to step up the feedwater pressure to the level of the next higher heater.

3 An electric generator of 100 per cent efficiency, which supplies, without line loss, the boiler feed pumps.

4 A steam generator of 100 per cent efficiency, in which blowdown, soot-blowing losses, etc., are zero.

Since energy required to drive fans, fuel equipment, general services, etc., is considered zero in a theoretical cycle, auxiliary-power usage other than that required for the boiler feed pumps, as described in item (2), is not included.

Diagrams. A conventional diagram for the theoretical regenerative cycle is shown in Fig. 1(*a*) for throttle-steam conditions of 1000 psia 700 F and 1 in. Hg exhaust pressure. The dotted line *AB*, representing the reduction in weight of steam passing through the turbine, is not an expansion line. The area below the dotted line is not significant. The chief advantage of the diagram is that it appears familiar.

In attempting to make a diagram in which areas are significant and bear the correct relationship of cycle efficiency, recourse was taken to a method of construction described fully by Barnard, Ellenwood, and Hirshfeld.[5] This method was used to produce Fig. 1(*b*) which is drawn for same steam conditions as Fig. 1(*a*). In Fig. 1(*b*) the area below the saturation line, bounded by condensate entropy and line *AB*, represents heat given up to feedwater.

With high-pressure and high-temperature throttle steam conditions, such as 3200 psia 1200 F, these diagrams, however, undergo unusual changes as are indicated in Figs. 2(*a*) and 2(*b*). Parallelism between line *AB* and the isentropic expansion line, the apparently meritorious feature of Fig. 1(*b*), no longer extends over the whole length of *AB*, in Fig. 2(*b*), but exists only up to the temperature level where the expansion line crosses the saturated-vapor line. Above that point, line *AB* shows to a more or less pronounced degree the effect of bleeding superheated steam. Curvature of line *AB* in Figs. 1(*b*) and 2(*b*) actually will exist whenever superheated steam is bled, but it is only noticeable on a small-scale diagram with throttle steam relatively highly superheated. Even then, curvature is apparently so slight that casual inspection of Fig. 2(*b*) might lead to the contention that a simple formula could be developed for calculating theoretical regenerative-cycle heat rates even for top throttle conditions. The significance of this curvature in line *AB* of Fig. 2(*b*) is not easily apparent, and it is hoped that the discussion will bring forth an explanation.

The closest approximation by "short-cut" formula would obtain if a straight line could be drawn vertically through point *B*. But the location of *B* cannot be found without recourse to the integration method to be described later. Accordingly, no labor can be saved in this case. The next approximation would be based on the assumption that the straight line passed vertically through known point, *A*. A short-cut formula for this case would be

$$\text{Theoretical heat rate}^6 \text{ (inaccurate)} = \frac{3412.75\ (H_t - h_f)}{H_t - h_f - T_e(S_t - S_f)}$$

[4] In actual practice, where a desuperheating zone is provided in a feedwater heater, a temperature crossover or negative terminal difference may exist where superheated steam is being bled. Since the number of degrees crossover varies with heater design and the degrees of superheat, an acceptable allowance for this effect feasibly cannot be included in a theoretical study.

[5] "Heat Power Engineering," by W. N. Barnard, F. O. Ellenwood, and C. F. Hirshfeld, John Wiley & Sons, Inc., New York, N. Y., third edition, part 1, sec. 217, 1926, pp. 353–356.

[6] An approximately similar incorrect equation will be found in connection with Fig. 712, of "Steam Power Plant Engineering," by F. G. Gebhardt, sixth edition, John Wiley & Sons, Inc., New York, N. Y., 1925.

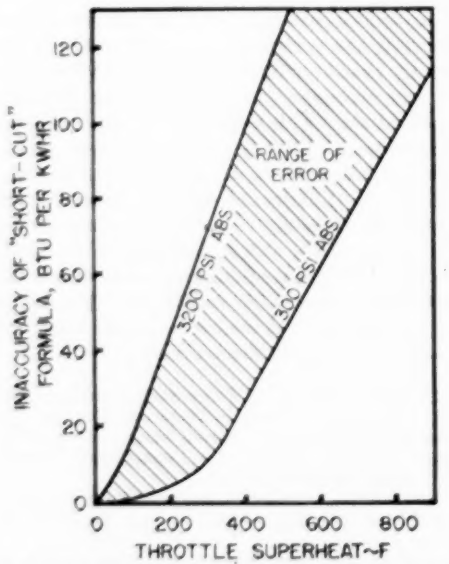


FIG. 3 A SIMPLE OR "SHORT-CUT" FORMULA FOR DETERMINING APPROXIMATE THEORETICAL REGENERATIVE-CYCLE HEAT RATES PRODUCES RESULTS WHICH ARE TOO LOW

(The diagram demonstrates how this inaccuracy increases with the amount of superheat in the throttle steam.)

where subscript t refers to throttle, f to saturated feedwater, and e to turbine-exhaust conditions. This formula is incorrect because it fails to take into account the sizable vertical strip bounded on one side by the line AB and on the other by a vertical through A. Heat rates computed by the short-cut formula are too low. The extent of the error is shown in Fig. 3.

The theoretical regenerative cycle, as defined and described, has been considered commonly as representing the best economy actually approachable in practice and, on this score, has been viewed by many as a standard of attainment. A recent suggestion, to be described later, of a novel but probably impractical regenerative cycle having Carnot efficiency does not seem to detract from the already established regenerative-cycle standard. The fact that a simple computation method, which will be described next, has been developed and heat rates calculated for a wide range of steam pressures and temperatures should minimize objections on the grounds of complication to the continued use of the theoretical regenerative cycle as an acceptable standard.

Development of Computation Methods

The Ernest L. Robinson equations for calculating the theoretical weight and energy value of bled steam appear in the Appendix of his 1923 paper.[7] The heat balance for an infinitesimal heater is

$$dw(H - h) = (1 + w)dh$$

which, when integrated, gives

$$1 + w = e^{\int_{h_2}^{h_1} \frac{dh}{H-h}}$$

where $(1 + w)$ is the pounds of steam at any point in the turbine. In the 1923 paper,[7] with a maximum steam condition of 1000 psia 800 F, integration was performed graphically. (The nomenclature used appears in the Appendix.)

Twenty years later, attention is focused on much higher steam conditions. There appears a definite need to provide theoretical regenerative-cycle heat rates for a wide range of throttle pressure and temperature up to 3200 psia and 1200 F. Because the effect of pump work on cycle efficiency is appreciable at high feedwater pressure, and because of the larger number of heat rates that would have to be computed to cover the greater range of steam conditions, Robinson's equation[7] had to be modified and adapted to a tabular method of computation.

Step-by-Step Integration. If $dh/(H - h)$ were to be integrated graphically, the quantity $1/(H - h)$ would be plotted against h as shown in Fig. 4. The product $dh/(H - h)$ is the area of an infinitesimal strip below the curve AB. The integral of $dh/(H - h)$, by the Robinson equation, is the whole area $ABCD$. Some energy, however, is added by the boiler feed pump. For each strip, dh, representing heat added by bled steam, there is an attendant strip, dF, representing the boiler-feed-pump work. Since the steam flow in the turbine depends upon the amount of steam bled, the enthalpy added by the pump in each step must be subtracted from the gross gain in enthalpy.[8]

In order to calculate accurately rather than to planimeter the area below the curve, it is necessary that sufficiently narrow strips be so chosen that the section of curve bounding the top of each strip is essentially a straight line. This provision permits determining the area of the strip by taking the equivalent height as the average of the two sides. About 35 steps from throttle to condenser for steam pressures of 2000 to 3200 psia have proved adequate. (An extra 20 steps were found unnecessary.) The steps, however, must be chosen so that the area of each strip, i.e., $dh/(H - h)$, is the same. An initial selection with constant increments of h may be proportioned to give constant values of $dh/(H - h)$ on a second or third trial. The method is described in the Appendix under "Short-Form Computation." With throttle pressure of 1000 psia or less, 25 steps may be chosen, and equal values of dh are satisfactory.

Checking the Method. Only one independent check on the method is available. A theoretical regenerative cycle supplied with saturated steam will have Carnot-cycle efficiency. Checks made on this basis have proved the method to be reliable.

[7] "The Margins of Possible Improvement in the Central-Station Steam Plant," by Ernest L. Robinson, Trans. A.S.M.E., vol. 45, 1923, p. 644.

[8] The work done by the perfect boiler feed pump should be read from Fig. 3, p. 75, of the Keenan and Keyes "Thermodynamic Properties of Steam," John Wiley & Sons, Inc., N. Y., 1936. In the tabular-integration method, however, steps are so small that Fig. 3 cannot be read accurately enough. Since the change in specific volume of compressed water is insignificant on three scores, namely, (1) the change in feedwater temperature during compression is small, (2) the change in pressure is small, and (3) the effects of the foregoing oppose each other, the simple equation $F = Ns/5.4$ proved satisfactory. This form substitutes for the correction

$$-\frac{1}{J}\int_{r-1}^{r} v_w dP$$

recently suggested by Dr. W. J. Kearton; see *Journal* and Proceedings of The Institution of Mechanical Engineers, vol. 147, 1942, pp. 114–115, comment on paper by H. S. Horsman, reference 9.

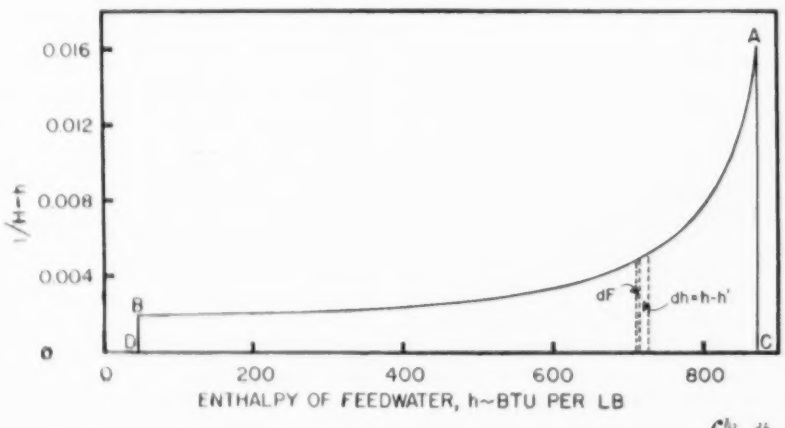


Fig. 4 Graphical Representation of Robinson's Equation $1 + w = e^{\int_{h_2}^{h_1} \frac{dh}{H-h}}$ Determining Weight of Steam Bled in a Theoretical Regenerative Cycle
(Example is for 3200 psia saturated steam.)

Application to Modified Regenerative Cycles. The step-by-step integration can be used to compute heat rates of other theoretical cycles such as the moisture-extraction cycle, the isothermal compression regenerative cycle, etc. It may be applied also to theoretical cycles where dry-stage efficiencies less than 100 per cent have been taken into account. In some cases, the second Robinson equation

$$E = \int_{h_2}^{h_1} \frac{H_1 - H}{H - h} (1 + w)dh$$

will have to be used. The method of handling this equation is explained in the Appendix under "Long-Form Computation."

To those interested in studying theoretical cycles, the tabular-integration method should prove a useful tool. The theoretical regenerative-steam-cycle heat-rate table, given in this paper, is a typical application of the method.

Theoretical Heat-Rate Tables

The production of a theoretical heat-rate table is a straightforward enough operation, although some ingenuity is required to minimize the necessary work to be done. Applying the short-form method, described in the foregoing discussion and illustrated in the Appendix, heat rates were calculated for a number of "key points," where throttle pressure and temperature are represented by round numbers. Temperature intervals were taken every 100 F; pressure intervals varied from 100 to 300 psia to suit circumstances.

Heat rates thus computed were plotted on a large curve sheet. A cross-plot also was used. The combination of the main and cross-plots established the principal connecting links between key points. Work sheets consisting of large skeleton tables were made up from the heat-rate readings given by the curve sheet. The skeleton was adjusted slightly where obviously necessary and eventually filled in mathematically by a system of uniform progressive differences. The application of this system to the data on the work sheets minimized errors of interpolation.

Table 1 gives theoretical regenerative-cycle heat rates at 1 in. Hg abs exhaust pressure for steam pressures from 300 to 3200 psia and from saturation temperature to 1200 F. The selection of pressures and temperatures for which heat rates are given was based (1) on the steps used in the 1936 steam tables and (2) on the need to insure that proportional interpolation between readings would be accurate. The table provides a means of determining quickly the heat rate of any theoretical regenerative-cycle power plant.[9] Theoretical heat rates at 1 in. Hg abs exhaust pressure are shown also in Fig. 5(*a*).

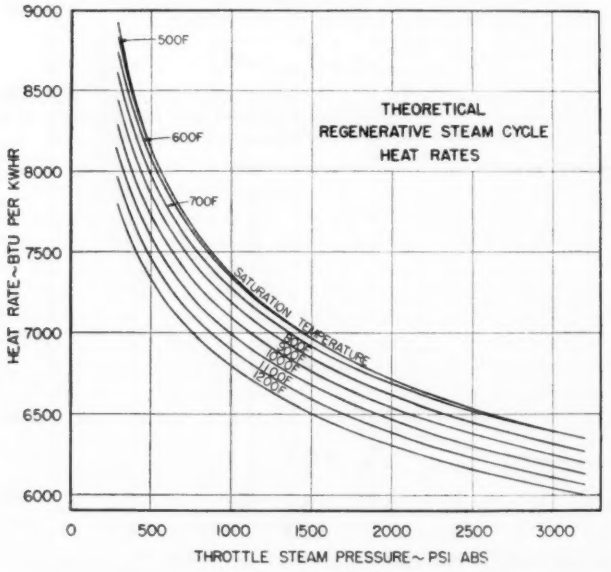


Fig. 5(*a*) Theoretical Regenerative-Steam-Cycle Heat Rates

(Throttle steam conditions as noted; exhaust pressure = 1 in. Hg abs. Infinite number of bled-steam feedwater heaters and attendant boiler feed pumps. Zero terminal difference. Feedwater heated to throttle saturation temperature.)

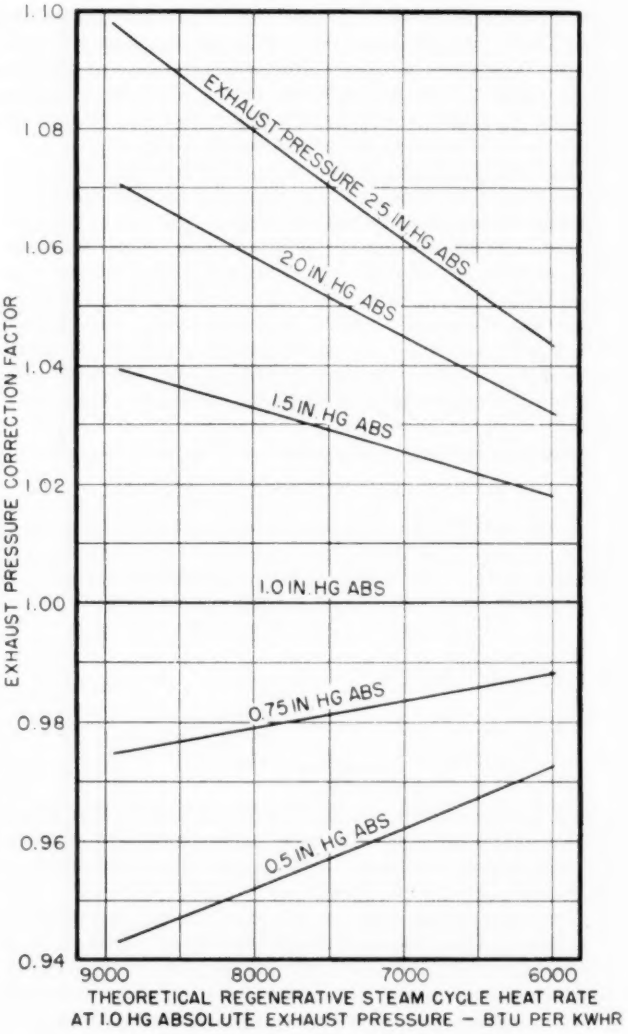


Fig. 5(*b*) Exhaust-Pressure Correction Factor

(To obtain the heat rate, HR_T, at a particular exhaust pressure within the wet-steam region: [1] Read the heat rate, HR_0, from Table 1 or Fig. 5*a* for 1 in. Hg abs exhaust pressure; [2] find the correction factor, F, from Fig. 5*b* corresponding to HR_0 and the new exhaust pressure; [3] multiply HR_0 by F to get HR_T. See revised Fig. 5(*b*) on page 511.)

Exhaust-pressure corrections are based upon the fact that, within the wet-steam region, the theoretical regenerative cycle has Carnot efficiency, from which it follows that, with constant throttle conditions, the heat rejected is proportional to the abso-

[9] A comprehensive paper titled, "The Regenerative Cycle: An Efficiency Basis Having Special Reference to the Number of Feedwater Heating Stages," by H. S. Horsman, was published in the *Journal* and Proceedings of The Institution of Mechanical Engineers, vol. 146, 1941, pp. 5–19. In the foregoing paper, however, feedwater temperature is limited to a maximum of 460 F, corresponding to 467 psia saturation pressure, and hence provides little opportunity to check data given here in Table 1, where final feedwater temperatures may be up to 705 F.

lute temperature of the exhaust. The generation of A Btu of useful work (say 1 kwhr or 3412.75 Btu) requires a heat input of HR_0 (the theoretical heat rate in Btu per kwhr given in Table 1), followed by the rejection of $(HR_0 - A)$ Btu at T_0 exhaust temperature. If the exhaust temperature is reduced by ΔT to T, then additional useful work for the same heat input is obtained, amounting to

$$\frac{\Delta T}{T_0}(HR_0 - A)$$

As the heat rates of the cycle at constant steam conditions, but varying exhaust temperatures, are inversely proportional to the amounts of useful work generated, a heat-rate correction factor F may be obtained from the equation

$$F = \frac{HR_T}{HR_0} = \frac{A}{A + \frac{\Delta T}{T_0}(HR_0 - A)} = \frac{1}{1 + \frac{\Delta T}{T_0}\left(\frac{HR_0}{A} - 1\right)}$$

$$= \frac{T_0}{T_0 + \Delta T\left(\frac{HR_0}{A} - 1\right)}$$

Substituting $T_0 - T$ for ΔT, cycle efficiency η for A/HR_0

$$F = \frac{\eta T_0}{T_0 - T(1 - \eta)} = \frac{538.72\eta}{538.72 - T(1 - \eta)}$$

Where T = new exhaust temperature in absolute degrees F, and $\eta = 3412.75/$(theoretical heat rate) from Table 1, or Fig. 5(*a*). The corrected heat rate, for exhaust pressure other than 1 in. Hg abs, is obtained from the equation

$$HR_T = F \times HR_0$$

Values of F for various exhaust pressures are given in Fig. 5(*b*). The alteration in heat rate, $D = HR_T - HR_0$, to be added to the heat rate found in Table 1, is obtained from the equation

$$D = \frac{HR_0(T - 538.72)(1 - \eta)}{538.72 - T(1 - \eta)}$$

When the value of D is negative, as is the case when the exhaust pressure is less than 1 in. Hg abs, D is to be subtracted from the heat rate given in Table 1.

Possible Application of Data

Two ways in which the heat-rate table might be used are (1) as a comparative standard of power-plant design and operation; and (2) as an aid in estimating plant performance with steam conditions somewhat above the current level.

In recent years, several technical papers have been written proposing this or that standard for use as a bogey for particular plant installations. The percentage ratio of actual to theoretical heat rate for any plant, however, combines inefficiencies both of design and operation. To gage plant operation alone, additional factors must be included in the standard.

These additional factors are required also where power-plant performance is to be estimated. For estimating purposes, modifying factors would be applied to the theoretical heat rate. For instance, turbine efficiency would change the heat rate so much. The use of four instead of an infinite number of heaters would result in an increase in heat rate. Similarly, modifying factors would be required for boiler efficiency, auxiliary power, exhaust pressure, etc. With these factors available, it would be possible to compute operating efficiency and estimate performance exactly.

These modifying factors, however, have not been computed yet, as prior demands on the authors' time by the war effort prevented any further extensive work being done on the study. In addition, it is felt that the factors will be extensive enough to warrant being the subject of a second or companion paper. The method of computing factors has not definitely crystallized but it is viewed as requiring about three steps, as follows:

1 Turbine engine efficiencies would be obtained from a paper by Warren and Knowlton.[10]

2 A number of heat-balance calculations would be made for typical feedwater-heater arrangements[11] using a range of terminal difference and final feedwater temperature, and taking into account condensate- and feedwater-pump efficiency.

3 Power-plant operating data for different steam conditions would be analyzed for as many stations as obtainable, to determine the effect on plant efficiency of boiler performance and auxiliary services.

Data would be tabulated ultimately as "efficiency" factors to show what increase in turbine and plant heat rate was due to each particular item of power-plant heat balance and operation. It is hoped that, with the publication of these theoretical cycle heat rates, others may be encouraged to take a hand in supplying needed performance data, in determining some of the factors, and in making them available to the engineering profession.

In the meantime, the data here presented can be helpful if a certain amount of ingenuity is used. In making estimates, existing plant and turbine-performance data usually will provide sufficient information for calculating approximate modifying factors which in turn may be applied directly or after adjustment to the theoretical heat rate at the steam conditions under investigation. Plant performance can be reported as a percentage of the theoretical figure. By so doing, the advantage one plant has over another through using higher steam pressure and temperature is eliminated from the performance comparison. Undoubtedly, other uses in addition to these two will come to mind.

An example of the relationship between theoretical-cycle and actual plant heat rates is shown in Table 2. Although in the cases cited, plants B and C differ in economy by 700 Btu per kwhr, they are operating almost equally effectively, as indicated by the similarity in plant-design and performance factors. To demonstrate roughly how modifying factors might be applied to theoretical heat rates, Table 2 shows a typical but incomplete breakdown of the over-all factors into a list of items and attendant factors which affect plant performance.

These factors were obtained from turbogenerator heat-balance data and actual plant performance of three different stations. In the normal course of events, the companion paper will contain tables of factors covering a complete pressure-temperature range of steam and feedwater conditions for typical power-plant design based upon available up-to-date information on turbine and station performance. Subsequently, if a marked change in power-plant design occurs, supplementary factors would be published to bring the series again up to date.

Lacking time now to make heat-balance computations and analyze plant records, the authors provide Table 2 solely to illustrate how factors might apply in the cases cited for three different power stations. A discussion of methods used to obtain factors will be incorporated in the companion paper. Items, it is hoped, will be subdivided eventually to indicate the effect on economy of the more detailed phases of plant design and operation. In the meantime, correlations between theoretical cycle and plant heat

[10] "Relative 'Engine Efficiencies' Realizable From Large Modern Steam-Turbine-Generator Units," by G. B. Warren and P. H. Knowlton, Trans. A.S.M.E., vol. 63, 1941, pp. 125–135.

[11] As, for instance, any "standardized" cycles which may be the outcome of the "Preferred Standards for Steam Turbine Generators," proposed Nov. 3, 1938, by the Subcommittee on Standardization of the National Defense Power Committee, and subsequent work thereon instigated by the A.S.M.E.

rates of existing power stations will help engineers in predicting heat rates for somewhat extended throttle conditions.

Other Regenerative Cycles

At least two modifications of the regenerative cycle proposed in recent years merit comment. One suggestion is for moisture extraction in the wet stages, and the other, for isothermal compression of superheated bled steam.

Moisture Extraction. Within the wet-steam region, the theoretical regenerative cycle has Carnot efficiency without requiring 100 per cent moisture withdrawal, as proposed by Dr. W. M. Meijer,[12] since expansion is assumed to take place isentropically. This thoughtful proposal of an integral moisture-withdrawal provision, however, merits serious attention on two practical scores, i.e., (1) moisture causes a definite loss of efficiency in an actual turbine attributable to bucket-impingement shock and supersaturation effect, and (2) the possibility of bucket erosion by moisture in the lower stages appreciably restricts turbine designers in the selection of turbine-throttle conditions.

Moisture withdrawal of 100 per cent might be difficult to attain without occasioning other serious thermodynamic losses. Fortunately, such effectiveness is not essential. For instance, if 12 per cent moisture were deemed the maximum permissible practical limit, and if in any stage not more than 2 to 3 per cent moisture were produced, then it would be necessary to withdraw only 2 to 3 per cent moisture to keep within the 12 per cent limit. Efficiency of withdrawal then need be only 15 to 25 per cent in each stage to permit steam expansion to continue to low exhaust conditions which otherwise might be equivalent to 20 per cent moisture or better. Hence provision for moisture withdrawal at even this low efficiency would be sufficient to overcome present objections on the score of bucket erosion to using high throttle steam pressures without attendant high superheated-steam temperatures. There remains, however, sufficient reason for the present high superheat temperatures, on the grounds of improved cycle efficiency as well as improved turbine efficiency, as compared to what is possible with the saturated-steam cycle.

With the application of superheat, the efficiency of the theoretical regenerative steam cycle does increase although not to the extent of the Carnot cycle. The use of superheat, however, is advantageous, and particularly so where superheated steam is bled for regeneration. Even where an arbitrary restriction is placed on the regenerative cycle that only dry-saturated and wet steam may be bled, the provision of superheated steam to the cycle is still advantageous. Fig. 6 shows the relation of theoretical heat rates versus throttle steam temperature for the two foregoing cycles, namely, regeneration only by saturated and wet steam,[13] and regeneration up to throttle saturation temperature using bled superheated steam. In either case, a reduction in heat rate with increased superheat is noticeable.

Isothermal Compression. While, with the use of superheated steam, the theoretical regenerative-cycle efficiency does increase, it falls below the corresponding Carnot efficiency because it is not a wholly reversible cycle. James F. Field[14] points out that "the ideal engine would therefore require additional elements to compress this superheated bled steam isothermally to the corresponding saturation temperature and pressure before actually mixing with feedwater." This cycle can be studied by means of the tabular-integration method. A typical example, taking into account all auxiliary power usage, showed the cycle to have Carnot efficiency.

The choice of a system for gaging power-plant performance cannot be made arbitrarily. At present, the economy of American power plants is reported in terms of British thermal units per kilowatthour. British plants use a scale of percentage efficiency. In both cases, a plant of high steam conditions would be recorded as having a better economy than one with lower steam conditions. The latter, however, may have been operated more creditably and deserves proper recognition. By relating plant performance to some standard, whether it be the theoretical regenerative-cycle heat rate, the Carnot cycle, or even the basic efficiency,[15] a somewhat better gage can be obtained of what advantage operating personnel is taking of the facilities at their command. Before a universal gage is established, however, engineers will have to agree among themselves as to what standard they will adopt, how closely such a standard needs to match the steam cycles for which it is established, and what allowance will be made for uncontrollable losses attendant on the number of feedwater heaters installed, load distribution, etc.

Conclusion

This paper has described a tabular-integration method for computing theoretical heat rates, and demonstrated its use by presenting a table of heat rates for a theoretical regenerative steam cycle. It is hoped that this table will prove helpful in at least three ways:

[12] "The Extraction of Condensate From Expanding Steam," by Dr. W. M. Meijer, Trans. Institution of Naval Architects, vol. 81, 1939, pp. 36–58; see also *Engineering*, vol. 147, April 7, 1939, p. 147.

[13] A Typical formula for computing the efficiency of wet-steam-regeneration cycle may be found in "High Pressure, Reheating, and Regenerating for Steam Power Plants," by C. F. Hirshfeld and F. O. Ellenwood, Trans. A.S.M.E., vol. 45, 1923, p. 663.

[14] "A Suggested Basis of Comparison for the Efficiency of Steam Turbo-Generators and Steam-Electric Generating Stations," *Journal* of The Institution of Civil Engineers, vol. 10, 1938, pp. 241–253.

[15] The use of basic efficiency was described by Sir Leonard Pearce, C.B.E., D.Sc., in his Thomas Hawksley Lecture on "A Review of Forty Years' Development in Mechanical Engineering Plant for Power Stations," *Journal* of The Institution of Mechanical Engineers, vol. 142, 1940, pp. 305–363. In an appendix under "Operating Efficiency," Sir Leonard discusses the use of some major factors modifying theoretical or basic plant efficiency.

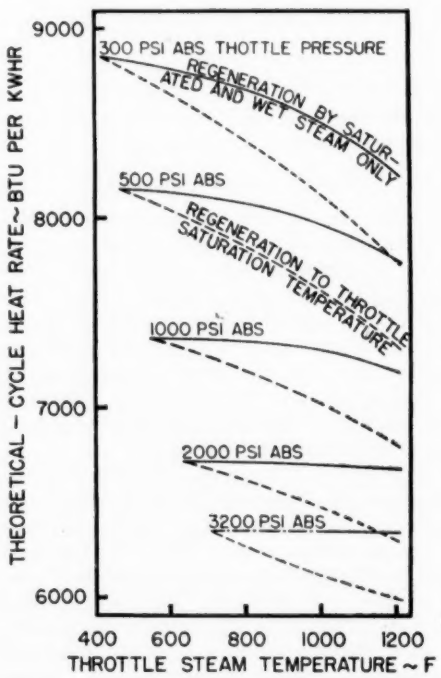


Fig. 6 Reduction in Theoretical Regenerative-Cycle Heat Rates With Increased Superheat in Throttle Steam

1 In comparing design and operation of different power plants operating at different steam conditions.

2 In estimating the approximate performance of power plants.

3 In stimulating others to undertake preparation of tables of modifying factors for use in making exact performance estimates.

Since the tabular-integration method of calculating heat rates can be adapted readily, it is thought that it will prove useful to others in studying new cycles.

Acknowledgment

The authors wish to express their appreciation for the assistance of everyone concerned with the preparation of this paper. We are indebted to Mr. Sabin Crocker whose stimulating interest and hearty encouragement helped on the work; to Mr. Max W. Benjamin and Mr. E. L. Robinson for timely and helpful suggestions; to the General Electric Company for providing the means for computing "key-point" heat rates; and to The Detroit Edison Company for making the study possible.

Appendix

Nomenclature

The following nomenclature is used in the first part of the paper and in the Appendix:

H_1 = enthalpy of throttle steam, Btu per lb
H = enthalpy of steam at any stage in the prime mover, Btu per lb
h = enthalpy of saturated feedwater, corresponding to the pressure in the selected stage of the prime mover, Btu per lb
$F = Nv/5.4$ = energy added by the perfect boiler feed pump, Btu per lb
N = increase in feedwater pressure in the pump, psi
v = specific volume of feedwater at pump suction, cu ft per lb
$h' = h + F$ = enthalpy of feedwater leaving the boiler feed pump after isentropic compression, and entering the next higher heater, Btu per lb
$dh = h - h'$ = heat added in heater by bled steam, Btu per lb of feedwater
$1 + w$ = weight of steam at any turbine stage, lb
= weight of feedwater returning at any stage, lb
dw = weight of steam bled at any turbine stage, lb
e = Naperian logarithmic base

Short Form for Computing Theoretical Regenerative-Cycle Heat Rates

In Table 3, an example is carried through according to the short form for computing theoretical regenerative-cycle heat rates. The conditions stated are throttle-steam pressure = 3200 psia; throttle-steam temperature = 1200 F; throttle-steam entropy = 1.5745.

To complete the computations of Table 3, by short form, the following steps must be taken:

(*a*)

$$1 + w = e^{\sum_{\text{avg}} \frac{dh}{(H-h)}}$$

Add up column (9) = 0.9773690
Convert to logarithmic base 10
$0.9773690 \times 0.43428 = 0.4244518$
Find antilog = 2.6574

(*b*) Heat input to cycle = heat supplied at throttle less heat returned to steam generator

$= (1 + w)(H_1 - h_1)$
$= 2.6574 \times 697.5$ from column (7)
= 1853.54 Btu per lb of steam at condenser

(*c*) Heat rejected to condenser

$= 1(H_e - h_e)$
$= 1 \times 799.14$ Btu from column (7)

(*d*) Heat converted to energy and delivered at electric-generator terminals = item (*b*) — item (*c*) = 1853.54 — 799.14 = 1054.40 Btu

(*e*) Cycle efficiency = output/input = 1054.40/1853.54 = 0.56886

(*f*) Theoretical heat rate = 3412.75/cycle efficiency = 5999 Btu per kwhr.

Computations by Long Form

For the same example, the long form for computing regenerative-cycle heat rates and boiler-feed-pump work is demonstrated in Table 4, which is a continuation of the short form.

To complete the computations by long form, the following steps must be taken:

(*a*) Rankine cycle output = heat at throttle minus heat at exhaust
= first minus last reading, column (2)
= 1569.9 — 846.19
= 723.71 Btu

(*b*) Extra output by regenerative cycle = E = 359.64 Btu

(*c*) Total prime-mover output (*a*) + (*b*) = 1083.35 Btu

(*d*) Less boiler-feed-pump work = 28.99 Btu from column (14)

(*e*) Net regenerative-cycle output = 1054.36 Btu

(*f*) Heat rejected = 799.14 Btu from column (7)

(*g*) Cycle input = 1853.50 Btu

(*h*) Cycle efficiency = 1054.36/1853.50 = 0.56885

(*i*) Theoretical cycle heat rate = 3412.75/0.56885 = 5999 Btu per kwhr

Note: Investigation of the isothermal-compression regenerative cycle, for example, would require the use of the long form of computation. Calculations of the work of compressing bled steam would be handled in a manner similar to that used for the boiler feed pump. Additional columns of calculations, however, would be required to suit the case being studied.

TABLE 1 THEORETICAL REGENERATIVE-STEAM-CYCLE HEAT RATES, BTU PER KWHR (1 IN. HG ABS EXHAUST PRESSURE)

Throttle pressure, psia	Saturation temperature, deg F	Throttle temperature																				
		Saturation	420F	440F	460F	480F	500F	520F	540F	560F	580F	600F	620F	640F	660F	680F	700F	720F	740F	760F	780F	800F
300	417.3	8850	8850	8846	8838	8828	8813	8796	8777	8756	8732	8708	8683	8657	8630	8602	8573	8543	8512	8481	8450	8418
310	420.4	8802		8799	8792	8783	8768	8751	8732	8711	8688	8664	8639	8614	8588	8561	8532	8502	8472	8442	8411	8379
320	423.3	8756		8753	8747	8739	8725	8709	8690	8669	8646	8622	8598	8573	8548	8521	8493	8464	8435	8405	8374	8342
330	426.2	8712		8710	8704	8696	8683	8667	8649	8628	8605	8582	8558	8534	8509	8483	8455	8427	8398	8368	8337	8306
340	429.0	8670		8668	8662	8654	8642	8626	8609	8589	8567	8544	8520	8496	8472	8446	8418	8390	8362	8333	8303	8272
350	431.7	8629		8628	8622	8615	8603	8588	8571	8551	8530	8507	8484	8460	8436	8410	8382	8355	8327	8299	8270	8239
360	434.4	8589		8588	8583	8576	8565	8550	8533	8514	8494	8472	8449	8425	8401	8375	8348	8321	8294	8266	8237	8207
370	437.0	8551		8550	8546	8539	8528	8514	8498	8479	8459	8438	8415	8391	8367	8341	8315	8288	8261	8234	8205	8176
380	439.6	8515		8515	8511	8504	8493	8479	8463	8445	8426	8405	8383	8359	8335	8309	8283	8257	8230	8203	8174	8145
390	442.1	8479			8476	8470	8460	8447	8431	8413	8394	8373	8351	8327	8303	8278	8252	8226	8199	8172	8144	8116
400	444.6	8445			8443	8438	8428	8416	8400	8382	8363	8342	8320	8297	8273	8248	8222	8196	8169	8142	8115	8088
410	447.0	8411			8409	8406	8397	8385	8370	8352	8333	8312	8290	8267	8244	8219	8193	8167	8141	8115	8088	8061
420	449.4	8379			8378	8376	8367	8355	8340	8322	8303	8282	8261	8238	8215	8190	8165	8140	8114	8088	8062	8035
430	451.7	8348			8347	8346	8338	8326	8311	8293	8274	8253	8232	8210	8187	8163	8138	8113	8088	8062	8036	8010
440	454.0	8318			8317	8316	8309	8297	8282	8265	8246	8225	8204	8182	8160	8136	8112	8087	8062	8037	8012	7986
450	456.3	8289			8289	8287	8281	8269	8255	8238	8219	8198	8177	8156	8134	8111	8087	8063	8038	8013	7988	7962
460	458.5	8260			8260	8259	8253	8242	8228	8212	8193	8172	8152	8131	8109	8086	8062	8038	8014	7990	7965	7939
470	460.7	8232				8231	8226	8215	8201	8186	8167	8147	8127	8106	8084	8061	8038	8015	7991	7967	7942	7916
480	462.8	8205				8205	8200	8189	8175	8160	8142	8123	8103	8082	8060	8038	8016	7992	7969	7945	7920	7894
490	464.9	8179				8179	8175	8164	8151	8136	8119	8100	8080	8059	8038	8016	7994	7970	7947	7923	7898	7873
500	467.0	8154				8154	8150	8141	8128	8114	8097	8078	8058	8037	8016	7994	7972	7949	7926	7902	7877	7852
520	471.1	8106				8106	8102	8094	8082	8069	8053	8035	8016	7995	7974	7952	7930	7907	7884	7861	7838	7812
540	475.0	8059				8059	8056	8048	8037	8024	8009	7992	7973	7953	7933	7912	7890	7868	7845	7822	7799	7775
560	478.8	8015				8015	8012	8005	7994	7981	7967	7951	7933	7914	7895	7874	7852	7830	7808	7785	7762	7738
580	482.6	7972					7971	7964	7954	7942	7928	7912	7894	7875	7856	7836	7815	7793	7771	7749	7726	7702
600	486.2	7931					7931	7925	7916	7904	7890	7875	7858	7839	7820	7800	7780	7759	7737	7715	7692	7669
620	489.8	7892					7892	7888	7880	7869	7855	7840	7823	7804	7785	7765	7745	7724	7703	7681	7659	7637
640	493.2	7855					7855	7851	7844	7833	7820	7806	7789	7771	7752	7732	7712	7691	7670	7649	7628	7606
660	496.6	7819					7819	7816	7809	7798	7786	7773	7757	7739	7720	7700	7680	7660	7640	7619	7598	7576
680	499.9	7784					7784	7782	7776	7766	7754	7740	7725	7708	7689	7670	7650	7630	7610	7590	7569	7546
700	503.1	7751						7749	7744	7735	7724	7711	7695	7678	7660	7641	7621	7601	7582	7562	7542	7521
720	506.2	7720						7718	7713	7705	7694	7681	7665	7649	7631	7612	7593	7574	7555	7535	7515	7494
740	509.3	7689						7688	7684	7676	7665	7652	7637	7621	7603	7585	7566	7547	7528	7509	7489	7468
760	512.4	7659						7659	7656	7648	7637	7624	7609	7593	7576	7558	7539	7520	7501	7482	7463	7443
780	515.3	7630						7630	7628	7621	7610	7597	7582	7566	7549	7531	7513	7495	7477	7458	7439	7419
800	518.2	7601						7601	7600	7594	7584	7571	7556	7540	7523	7506	7488	7470	7452	7434	7415	7395
820	521.1	7575							7574	7568	7558	7546	7532	7516	7499	7482	7464	7446	7428	7410	7391	7372
840	523.9	7549							7548	7543	7534	7522	7508	7492	7476	7459	7441	7423	7405	7387	7369	7350
860	526.6	7523							7522	7518	7509	7498	7484	7469	7453	7436	7418	7401	7383	7365	7347	7329
880	529.3	7498							7497	7494	7486	7475	7461	7446	7430	7413	7396	7379	7362	7344	7326	7308
900	532.0	7474							7474	7471	7463	7453	7439	7424	7408	7392	7375	7358	7341	7323	7305	7287
920	534.6	7450							7450	7448	7441	7431	7418	7403	7387	7371	7354	7337	7320	7303	7285	7267
940	537.2	7427							7427	7426	7419	7410	7397	7383	7367	7351	7334	7317	7300	7283	7266	7248
960	539.7	7405							7405	7404	7398	7389	7376	7362	7347	7331	7314	7298	7281	7264	7247	7229
980	542.2	7384								7383	7377	7368	7355	7341	7327	7311	7295	7279	7263	7246	7229	7211
1000	544.6	7364								7361	7355	7347	7334	7321	7307	7292	7276	7260	7244	7228	7211	7193
1025	547.6	7338								7336	7332	7324	7311	7298	7284	7269	7254	7239	7223	7207	7190	7172
1050	550.6	7314								7312	7309	7301	7288	7275	7261	7247	7232	7217	7201	7185	7168	7151
1075	553.3	7290								7288	7286	7279	7267	7254	7240	7226	7211	7196	7180	7164	7147	7130
1100	556.3	7267								7266	7264	7257	7245	7232	7219	7205	7190	7175	7159	7143	7126	7109
1125	559.1	7245								7245	7243	7236	7224	7212	7199	7185	7170	7155	7139	7123	7106	7089
1150	561.9	7223									7221	7215	7204	7192	7179	7165	7150	7135	7120	7104	7087	7070
1175	564.5	7202									7200	7194	7183	7171	7158	7145	7131	7117	7102	7086	7069	7052
1200	567.2	7181									7179	7174	7164	7152	7139	7126	7112	7098	7083	7067	7051	7034
1225	569.8	7161									7159	7154	7144	7133	7120	7107	7093	7079	7064	7048	7032	7016
1250	572.4	7141									7139	7134	7124	7113	7101	7088	7075	7061	7046	7031	7015	6999
1275	574.9	7122									7119	7115	7106	7096	7084	7071	7058	7044	7029	7014	6998	6982

TABLE 1 (*Cont.*) THEORETICAL REGENERATIVE-STEAM-CYCLE HEAT RATES, BTU PER KWHR (1 IN. HG ABS EXHAUST PRESSURE)

Throttle pressure, psia	Throttle temperature																			
	800F	820F	840F	860F	880F	900F	920F	940F	960F	980F	1000F	1020F	1040F	1060F	1080F	1100F	1120F	1140F	1160F	1180F	1200F
300	8418	8385	8352	8320	8288	8256	8224	8192	8160	8127	8094	8062	8029	7996	7963	7931	7898	7866	7834	7802	7771
310	8379	8347	8315	8283	8251	8219	8187	8156	8124	8092	8060	8028	7996	7963	7930	7898	7866	7834	7803	7772	7741
320	8342	8310	8278	8246	8215	8184	8153	8121	8089	8058	8027	7996	7964	7931	7899	7867	7836	7804	7773	7742	7712
330	8306	8275	8244	8213	8182	8151	8120	8088	8057	8026	7995	7964	7932	7900	7868	7837	7806	7775	7744	7714	7684
340	8272	8241	8210	8180	8149	8119	8088	8057	8026	7995	7964	7933	7901	7870	7839	7808	7777	7747	7717	7687	7657
350	8239	8208	8178	8148	8118	8088	8058	8027	7996	7965	7934	7903	7872	7841	7810	7780	7750	7720	7690	7661	7631
360	8207	8177	8147	8117	8087	8057	8027	7997	7966	7936	7905	7875	7844	7814	7784	7754	7724	7694	7664	7635	7606
370	8176	8147	8118	8088	8058	8028	7998	7968	7938	7908	7878	7848	7818	7788	7758	7729	7699	7669	7640	7611	7582
380	8145	8116	8087	8058	8029	8000	7971	7941	7911	7881	7852	7823	7793	7763	7734	7705	7676	7646	7617	7588	7559
390	8116	8088	8060	8031	8002	7973	7944	7914	7885	7856	7827	7798	7769	7739	7710	7681	7652	7623	7594	7565	7537
400	8088	8060	8032	8004	7976	7948	7919	7890	7861	7832	7803	7774	7745	7716	7687	7658	7629	7600	7572	7544	7516
410	8061	8033	8006	7979	7952	7924	7895	7866	7837	7808	7779	7750	7721	7692	7664	7636	7607	7579	7551	7523	7495
420	8035	8008	7982	7955	7928	7900	7872	7843	7814	7785	7756	7727	7698	7670	7642	7614	7586	7558	7530	7502	7475
430	8010	7983	7957	7931	7904	7877	7849	7820	7791	7763	7734	7706	7677	7649	7621	7593	7565	7537	7509	7482	7455
440	7986	7959	7933	7907	7881	7854	7826	7798	7769	7741	7713	7685	7657	7629	7601	7573	7545	7517	7490	7463	7436
450	7692	7936	7910	7884	7858	7831	7803	7775	7747	7719	7692	7664	7636	7608	7580	7553	7525	7498	7471	7444	7417
460	7939	7913	7887	7861	7835	7809	7782	7754	7726	7699	7672	7644	7617	7589	7561	7534	7507	7480	7453	7426	7399
470	7916	7891	7865	7839	7813	7787	7760	7733	7706	7679	7652	7624	7597	7569	7542	7515	7489	7462	7435	7408	7381
480	7894	7869	7844	7818	7792	7766	7740	7713	7686	7660	7633	7606	7579	7551	7524	7497	7471	7444	7417	7391	7364
490	7873	7848	7823	7798	7772	7746	7720	7693	7667	7641	7614	7587	7560	7533	7506	7479	7453	7426	7400	7374	7348
500	7852	7827	7802	7777	7752	7726	7700	7674	7648	7622	7595	7568	7542	7515	7489	7462	7436	7409	7383	7357	7332
520	7812	7788	7763	7738	7713	7688	7663	7637	7611	7585	7559	7532	7506	7480	7454	7428	7402	7376	7350	7324	7299
540	7775	7751	7727	7702	7677	7652	7627	7602	7576	7550	7524	7498	7472	7446	7421	7396	7370	7344	7319	7293	7268
560	7738	7714	7690	7666	7642	7617	7592	7567	7542	7517	7491	7466	7441	7415	7390	7365	7340	7315	7290	7265	7240
580	7702	7679	7655	7631	7607	7583	7559	7534	7509	7484	7459	7434	7409	7384	7359	7335	7311	7287	7262	7238	7213
600	7669	7646	7622	7598	7574	7550	7526	7502	7478	7453	7428	7403	7378	7354	7330	7306	7282	7258	7234	7210	7186
620	7637	7614	7591	7567	7543	7519	7495	7471	7447	7423	7398	7374	7350	7326	7302	7278	7254	7230	7207	7183	7160
640	7606	7583	7560	7537	7513	7489	7465	7441	7417	7393	7370	7346	7322	7298	7274	7251	7228	7205	7182	7159	7136
660	7576	7554	7531	7508	7484	7460	7436	7412	7389	7366	7343	7320	7296	7273	7249	7226	7203	7180	7157	7135	7112
680	7546	7526	7504	7480	7456	7433	7409	7386	7363	7340	7317	7294	7271	7248	7225	7202	7179	7156	7134	7111	7089
700	7521	7499	7476	7453	7429	7406	7383	7360	7337	7314	7291	7269	7246	7224	7202	7179	7157	7134	7112	7089	7067
720	7494	7472	7449	7426	7402	7379	7356	7333	7310	7288	7266	7244	7222	7200	7178	7156	7134	7112	7090	7068	7046
740	7468	7446	7423	7400	7376	7353	7330	7308	7286	7264	7242	7220	7198	7176	7154	7133	7112	7090	7068	7046	7025
760	7443	7422	7399	7376	7352	7329	7307	7285	7263	7241	7219	7197	7175	7153	7132	7111	7090	7069	7048	7026	7005
780	7419	7398	7376	7353	7329	7306	7284	7262	7240	7218	7197	7175	7154	7132	7111	7090	7069	7048	7027	7006	6986
800	7395	7374	7353	7330	7307	7284	7262	7240	7218	7197	7176	7154	7133	7112	7091	7070	7049	7028	7007	6987	6967
820	7372	7352	7331	7308	7286	7263	7241	7219	7197	7176	7155	7134	7113	7092	7071	7051	7030	7009	6988	6968	6948
840	7350	7330	7309	7287	7265	7242	7220	7198	7176	7155	7134	7113	7092	7072	7052	7032	7011	6990	6970	6950	6930
860	7329	7310	7289	7267	7245	7222	7200	7178	7157	7136	7115	7094	7074	7054	7034	7014	6993	6972	6952	6932	6912
880	7308	7289	7269	7247	7225	7202	7180	7159	7138	7117	7096	7076	7056	7036	7016	6996	6976	6955	6935	6915	6895
900	7287	7268	7248	7227	7205	7183	7161	7140	7119	7098	7077	7057	7037	7017	6997	6978	6958	6938	6918	6898	6878
920	7267	7248	7228	7207	7186	7164	7143	7122	7101	7080	7059	7039	7019	6999	6980	6961	6941	6921	6901	6881	6862
940	7248	7229	7209	7188	7167	7146	7125	7104	7083	7062	7041	7021	7001	6982	6963	6944	6924	6904	6884	6865	6846
960	7229	7210	7190	7170	7149	7129	7107	7086	7065	7045	7024	7004	6985	6966	6947	6928	6908	6888	6869	6850	6831
980	7211	7192	7173	7153	7132	7111	7090	7070	7049	7029	7008	6988	6969	6950	6931	6912	6892	6873	6854	6835	6816
1000	7193	7174	7155	7135	7115	7095	7075	7055	7034	7014	6993	6973	6953	6934	6915	6896	6877	6858	6840	6821	6802
1025	7172	7153	7134	7114	7094	7074	7054	7034	7014	6994	6973	6953	6934	6915	6896	6877	6858	6839	6820	6801	6782
1050	7151	7133	7114	7094	7074	7054	7034	7014	6994	6974	6954	6935	6916	6897	6878	6859	6839	6820	6801	6782	6763
1075	7130	7112	7093	7074	7054	7034	7015	6995	6976	6956	6936	6917	6898	6879	6860	6841	6821	6802	6783	6764	6745
1100	7109	7091	7073	7054	7035	7015	6996	6976	6957	6937	6918	6899	6880	6862	6843	6824	6804	6785	6766	6747	6728
1125	7089	7071	7053	7035	7016	6997	6978	6959	6940	6920	6901	6882	6863	6845	6826	6807	6788	6769	6750	6731	6712
1150	7070	7052	7034	7016	6998	6979	6960	6941	6922	6903	6884	6866	6847	6829	6810	6791	6772	6754	6735	6716	6697
1175	7052	7035	7017	6999	6981	6962	6944	6925	6906	6887	6868	6850	6831	6813	6794	6775	6756	6738	6719	6701	6682
1200	7034	7017	6999	6981	6963	6945	6927	6909	6890	6871	6852	6834	6815	6797	6778	6759	6741	6723	6704	6686	6667
1225	7016	6999	6982	6964	6946	6928	6910	6892	6874	6855	6836	6818	6800	6782	6763	6744	6726	6708	6689	6671	6652
1250	6999	6983	6966	6948	6930	6912	6894	6876	6858	6840	6821	6803	6785	6767	6748	6729	6711	6693	6674	6656	6637
1275	6982	6966	6949	6932	6914	6896	6878	6860	6842	6824	6806	6788	6770	6752	6734	6715	6697	6679	6660	6642	6623

TABLE 1 (*Cont.*) THEORETICAL REGENERATIVE-STEAM-CYCLE HEAT RATES, BTU PER KWHR (1 IN. HG ABS EXHAUST PRESSURE)

Throttle pressure, psia	Saturation temperature, deg F	Throttle temperature																	
		Saturation	580F	600F	620F	640F	660F	680F	700F	720F	740F	760F	780F	800F	820F	840F	860F	880F	900F
1300	577.6	7104	7100	7096	7087	7077	7066	7054	7041	7027	7012	6997	6982	6966	6950	6933	6916	6898	6880
1325	579.9	7085	7082	7078	7069	7059	7048	7036	7024	7010	6996	6981	6966	6950	6934	6917	6900	6882	6864
1350	582.4	7067		7060	7051	7041	7030	7019	7007	6994	6980	6965	6950	6934	6918	6901	6884	6867	6849
1375	584.8	7049		7043	7035	7025	7014	7003	6991	6978	6964	6949	6934	6919	6903	6886	6869	6852	6834
1400	587.1	7033		7027	7019	7009	6999	6988	6976	6963	6949	6934	6919	6904	6888	6871	6854	6837	6820
1425	589.4	7016		7012	7004	6994	6984	6973	6961	6948	6934	6919	6904	6889	6873	6857	6840	6823	6806
1450	591.7	7000		6997	6989	6980	6970	6959	6947	6934	6920	6905	6890	6875	6859	6843	6826	6809	6792
1475	594.0	6984		6982	6975	6966	6956	6945	6932	6920	6906	6891	6876	6861	6845	6829	6812	6796	6779
1500	596.2	6969		6968	6961	6952	6942	6931	6919	6906	6892	6877	6862	6847	6831	6815	6798	6782	6766
1525	598.4	6954		6954	6947	6938	6928	6917	6905	6892	6878	6864	6849	6833	6817	6801	6785	6769	6753
1550	600.6	6940			6933	6924	6914	6903	6892	6878	6864	6850	6835	6820	6804	6788	6772	6756	6740
1575	602.8	6925			6920	6911	6901	6890	6879	6865	6851	6837	6822	6807	6791	6775	6759	6743	6727
1600	604.9	6911			6907	6898	6888	6877	6866	6852	6838	6824	6809	6794	6778	6762	6746	6730	6714
1625	607.0	6896			6894	6886	6876	6865	6854	6840	6826	6811	6796	6781	6766	6750	6734	6718	6702
1650	609.0	6882			6881	6873	6864	6853	6842	6828	6814	6799	6784	6769	6754	6738	6722	6706	6690
1675	611.1	6869			6868	6861	6852	6841	6829	6816	6802	6787	6772	6757	6742	6726	6710	6694	6678
1700	613.1	6857			6856	6850	6841	6830	6818	6805	6791	6776	6761	6745	6730	6714	6698	6682	6666
1750	617.1	6832			6831	6825	6817	6806	6794	6782	6769	6754	6739	6723	6708	6692	6676	6660	6644
1800	621.0	6807				6800	6792	6782	6771	6759	6746	6732	6717	6701	6686	6670	6654	6638	6622
1850	624.8	6783				6778	6770	6760	6749	6737	6724	6710	6695	6679	6664	6649	6633	6617	6601
1900	628.6	6760				6757	6749	6739	6728	6716	6703	6689	6674	6658	6643	6628	6613	6597	6581
1950	632.3	6738				6736	6728	6718	6707	6695	6682	6668	6652	6637	6622	6607	6592	6577	6561
2000	635.8	6717				6716	6708	6698	6687	6675	6662	6648	6633	6617	6602	6587	6572	6557	6542
2050	639.2	6696				6696	6689	6679	6668	6656	6643	6629	6614	6598	6584	6569	6554	6539	6524
2100	642.8	6676					6671	6661	6650	6638	6625	6611	6596	6580	6566	6551	6536	6511	6506
2150	646.0	6657					6653	6643	6632	6620	6607	6593	6578	6563	6549	6534	6519	6494	6489
2200	649.5	6638					6636	6626	6614	6602	6589	6575	6561	6546	6532	6517	6502	6487	6472
2250	652.6	6620					6619	6609	6597	6585	6572	6558	6544	6529	6515	6500	6486	6471	6456
2300	655.9	6602					6602	6592	6580	6568	6555	6541	6527	6512	6498	6483	6469	6455	6440
2350	659.1	6585					6585	6575	6563	6551	6538	6524	6510	6495	6482	6467	6453	6439	6424
2400	662.1	6568						6559	6547	6535	6522	6508	6494	6480	6466	6451	6437	6423	6408
2450	665.1	6551						6544	6532	6520	6507	6493	6479	6465	6451	6436	6422	6408	6393
2500	668.1	6535						6530	6518	6506	6493	6479	6465	6450	6436	6421	6407	6393	6378
2550	671.0	6520						6516	6504	6492	6479	6465	6451	6436	6422	6407	6393	6379	6364
2600	673.9	6505						6502	6491	6478	6465	6451	6437	6422	6408	6393	6379	6365	6350
2650	676.7	6490						6488	6478	6464	6451	6437	6423	6408	6394	6379	6365	6351	6336
2700	679.5	6476						6475	6465	6451	6437	6423	6409	6394	6380	6365	6351	6337	6322
2750	682.2	6462							6452	6437	6423	6409	6395	6380	6366	6351	6337	6323	6308
2800	685.0	6449							6439	6424	6410	6395	6381	6367	6353	6338	6324	6310	6295
2850	687.7	6435							6427	6411	6397	6382	6368	6354	6340	6325	6311	6297	6282
2900	690.3	6422							6416	6400	6385	6370	6355	6341	6327	6313	6299	6285	6270
2950	692.8	6410							6405	6388	6373	6358	6343	6329	6315	6301	6287	6273	6258
3000	695.4	6398							6394	6377	6361	6346	6331	6317	6303	6289	6275	6261	6246
3050	697.9	6386							6384	6367	6350	6334	6319	6305	6291	6277	6263	6249	6234
3100	700.3	6374								6357	6340	6324	6308	6293	6279	6265	6251	6237	6223
3150	702.8	6362								6346	6329	6312	6296	6281	6267	6253	6239	6226	6212
3200	705.1	6351								6336	6318	6301	6285	6270	6256	6242	6228	6215	6201

TABLE 1 (*Cont.*) THEORETICAL REGENERATIVE-STEAM-CYCLE HEAT RATES, BTU PER KWHR (1 IN. HG ABS EXHAUST PRESSURE)

Throttle pressure, psia	Throttle temperature															
	900F	920F	940F	960F	980F	1000F	1020F	1040F	1060F	1080F	1100F	1120F	1140F	1160F	1180F	1200F
1300	6880	6863	6845	6827	6809	6791	6773	6755	6737	6719	6701	6683	6664	6645	6627	6608
1325	6864	6847	6829	6812	6794	6776	6759	6741	6723	6705	6687	6669	6650	6631	6613	6594
1350	6849	6832	6815	6798	6780	6762	6745	6727	6709	6691	6673	6655	6636	6617	6599	6580
1375	6834	6817	6800	6783	6766	6748	6731	6713	6695	6677	6659	6641	6623	6604	6586	6567
1400	6820	6803	6786	6769	6752	6734	6717	6699	6682	6664	6646	6628	6610	6591	6573	6554
1425	6806	6789	6772	6755	6738	6720	6703	6686	6669	6651	6633	6615	6597	6578	6560	6541
1450	6792	6776	6759	6742	6725	6707	6690	6673	6656	6638	6620	6602	6584	6565	6547	6529
1475	6779	6763	6746	6729	6712	6694	6677	6660	6643	6625	6607	6589	6571	6553	6535	6517
1500	6766	6750	6733	6716	6699	6681	6664	6647	6630	6612	6595	6577	6559	6541	6523	6505
1525	6753	6737	6720	6703	6686	6668	6651	6634	6617	6600	6583	6565	6547	6529	6511	6493
1550	6740	6724	6707	6690	6673	6656	6639	6622	6605	6588	6571	6553	6535	6517	6499	6481
1575	6727	6711	6695	6678	6661	6644	6627	6610	6593	6576	6559	6541	6523	6505	6487	6470
1600	6714	6698	6682	6666	6649	6632	6615	6598	6581	6564	6547	6529	6511	6493	6476	6459
1625	6702	6686	6670	6654	6637	6620	6603	6586	6569	6552	6535	6517	6499	6482	6465	6448
1650	6690	6674	6658	6642	6625	6608	6591	6574	6557	6540	6523	6505	6488	6471	6454	6437
1675	6678	6662	6646	6630	6614	6597	6580	6563	6546	6529	6511	6494	6477	6460	6443	6426
1700	6666	6650	6634	6618	6602	6586	6569	6552	6535	6518	6501	6484	6467	6450	6433	6416
1750	6644	6628	6612	6597	6581	6565	6548	6531	6514	6497	6480	6463	6446	6429	6413	6397
1800	6622	6606	6590	6575	6559	6544	6528	6511	6494	6477	6460	6443	6426	6410	6394	6378
1850	6601	6585	6569	6554	6538	6523	6507	6491	6474	6457	6440	6423	6407	6391	6375	6359
1900	6581	6565	6549	6534	6518	6503	6487	6471	6455	6438	6421	6405	6389	6373	6357	6341
1950	6561	6545	6529	6514	6498	6483	6467	6451	6435	6419	6402	6387	6371	6355	6339	6324
2000	6542	6526	6510	6495	6479	6464	6448	6432	6416	6400	6384	6369	6353	6337	6322	6307
2050	6524	6508	6492	6477	6461	6446	6430	6414	6398	6382	6366	6351	6335	6319	6304	6290
2100	6506	6491	6475	6460	6444	6429	6413	6397	6381	6365	6349	6334	6318	6303	6288	6274
2150	6489	6474	6458	6443	6427	6412	6396	6380	6364	6348	6333	6319	6303	6288	6273	6259
2200	6472	6457	6441	6426	6410	6395	6379	6364	6348	6333	6318	6303	6288	6273	6258	6244
2250	6456	6441	6425	6410	6394	6379	6363	6348	6332	6317	6302	6287	6272	6257	6243	6229
2300	6440	6425	6410	6395	6379	6364	6348	6333	6317	6302	6287	6272	6257	6242	6228	6214
2350	6424	6409	6394	6379	6364	6349	6334	6319	6303	6288	6273	6258	6243	6228	6214	6200
2400	6408	6393	6378	6364	6349	6334	6319	6304	6289	6274	6259	6244	6229	6215	6201	6187
2450	6393	6378	6363	6349	6335	6320	6305	6290	6275	6260	6245	6230	6216	6202	6188	6174
2500	6378	6363	6348	6334	6320	6306	6291	6276	6261	6246	6232	6217	6203	6189	6175	6161
2550	6364	6349	6334	6320	6306	6292	6277	6262	6247	6233	6219	6204	6190	6176	6162	6148
2600	6350	6335	6320	6306	6292	6278	6263	6248	6234	6220	6206	6191	6177	6163	6149	6135
2650	6336	6322	6307	6293	6279	6265	6250	6235	6221	6207	6193	6178	6164	6150	6136	6122
2700	6322	6308	6294	6280	6266	6252	6237	6222	6208	6194	6180	6166	6152	6138	6124	6110
2750	6308	6294	6280	6267	6253	6239	6224	6209	6195	6181	6167	6153	6139	6126	6112	6098
2800	6295	6281	6267	6254	6240	6226	6212	6197	6183	6169	6155	6141	6127	6114	6100	6086
2850	6282	6268	6254	6241	6227	6213	6199	6184	6170	6156	6143	6129	6115	6102	6088	6074
2900	6270	6256	6242	6228	6214	6200	6186	6172	6158	6144	6131	6117	6103	6090	6076	6063
2950	6258	6244	6230	6216	6202	6188	6174	6160	6147	6133	6120	6106	6092	6079	6065	6052
3000	6246	6232	6218	6204	6190	6176	6162	6149	6136	6122	6109	6095	6082	6069	6055	6042
3050	6234	6220	6207	6193	6179	6165	6151	6138	6125	6111	6098	6084	6071	6058	6044	6031
3100	6223	6209	6196	6182	6168	6154	6140	6126	6113	6100	6087	6073	6060	6047	6033	6020
3150	6212	6198	6185	6171	6157	6143	6129	6116	6103	6089	6076	6062	6049	6036	6022	6009
3200	6201	6187	6174	6160	6147	6133	6119	6106	6093	6079	6065	6052	6039	6026	6012	5999

TABLE 2 APPLICATION OF DESIGN AND PERFORMANCE FACTORS TO THEORETICAL REGENERATIVE-CYCLE HEAT RATES FOR THREE POWER PLANTS

		A		B		C	
	Power plant						
	Throttle pressure, psia	396		628		841	
	Throttle temperature, F	693		815		899	
	Exhaust pressure, in. hg	0.89		0.99		0.98	
		Performance factor	Heat rate, Btu per kwhr	Performance factor	Heat rate, Btu per kwhr	Performance factor	Heat rate, Btu per kwhr
1	Theoretical heat rate		8237		7612		7223
2	Engine-efficiency and exhaust-loss factor	0.8130		0.8328		0.8352	
3	Cycle-design factor[a]	0.9523		0.9592		0.9625	
4	Operating efficiency[b]	0.9756		0.9752		0.9668	
5	Mechanical and electrical efficiency	0.9580		0.9698		0.9740	
6	Turbine heat rate, gross output, Item 1 / (Item 2 × item 3 × item 4 × item 5)		11383		10075		9542
7	Auxiliary-power-usage factor	0.9270		0.9585		0.9707	
8	Evaporated make-up factor	0.9977		0.999		0.997	
9	Pipe-radiation-loss factor	0.9888		0.9929		0.993	
10	Soot-blowing and miscellaneous steam-usage factor	0.9918		0.9952		0.996	
11	Steam-generating efficiency	0.8869		0.885		0.881	
12	Plant heat rate, net output, Item 6 / (Item 7 × item 8 × item 9 × item 10 × item 11)		14150		12030		11317
13	Plant design and performance factor	0.582		0.6328		0.6382	

[a] If and when the second stage of this study is developed, Item 3 along with many of the other items undoubtedly will be subdivided into several smaller factors for significant plant losses.

[b] Includes influence on turbine heat rate of (*a*) operation off ME point; (*b*) dirtiness of turbine blading; (*c*) departure from designed heater-terminal difference, etc.

TABLE 3 SHORT FORM FOR COMPUTING THEORETICAL REGENERATIVE-CYCLE HEAT RATES

Example: Throttle-Steam Pressure = 3200 psia; Throttle-Steam Temperature = 1200 F; Throttle-Steam Entropy = 1.5745

Column no.	(1)	(2)	(3)	(4)	(5)	(6)	(7)	(8)	(9)
Heading	Throttle and stage pressures, psia P	Enthalpy of throttle and bled steam, Btu per lb H	Enthalpy of feedwater at saturation pressure and temperature, Btu per lb h	Boiler feed pump work, Btu per lb $F = Nv/5.4$	Enthalpy of feedwater at pump discharge, Btu per lb $h' = h + F$	Increase in feedwater enthalpy by bled-steam heating, Btu per lb $dh = h - h'$	Heat given up by bled steam in heating feedwater, Btu per lb $H - h$	Average of two adjacent readings of $(H - h)$	$\frac{dh}{\text{avg } (H - h)}$
Computation instructions	(a) Throttle pressure (b) Pressures corresponding to enthalpy shown in column (3) (c) Condenser pressure	(a) Throttle enthalpy (b) Enthalpy of steam at pressures given in column (1) and at throttle-steam entropy for isentropic expansion	(a) Enthalpy of saturated feedwater. Choose 25 to 35 steps so that the quantity $dh/\text{avg } (H - h)$ shown in column (9) will be constant[a]	N = throttle pressure minus first-stage pressure, also 1st–2nd, 2nd–3rd, etc. v = specific volume cu ft per lb at saturation temperature of lower of two pressures used to find N 5.4 is a constant $\left(\frac{778}{144}\right)$	(a) Add h for 1st to F for throttle minus 1st stage (b) Continue steps down column (c) Where F is less than 0.005 Btu, h' becomes h leaving next lower heater	Subtract data in column (5) from column (3) to determine heat added per lb of feedwater by bled steam	Column (2) minus column (3)	(a) Add first and second readings in column (7), divide by 2, and insert result in top position column (8) (b) Add second and third readings in column (7), divide by 2, and insert in second position column (8) (c) Continue down column	Divide column (6) by column (8)
Example	3200 3170 3099 2983 .... 2.5 1.16 1 in. Hg abs	1569.9 1568.4 1564.8 1558.9 .... 926.3 886.4 846.19[b]	872.4 849.3 824.9 799.6 .... 102.2 74.7 47.05	.... 0.23 0.49 0.74 .... 0.01	849.53 825.39 800.34 774.37 .... 74.70 47.05	22.87 23.91 24.56 25.23 .... 27.50 27.65	697.5 719.1 739.9 759.3 .... 824.1 811.7 799.14	708.3 729.5 749.6 767.9 .... 817.9 805.42	0.0322886 0.0327759 0.0327641 0.0328558 .... 0.0336227 0.0343299 ....

[a] For a first approximation, it is satisfactory to divide $h_1 - h_2$ into equal intervals. Having found $dh/\text{avg } (H - h)$ for the first approximation, h may be reoriented by proportion to result in obtaining approximately constant values of $dh/\text{avg } (H - h)$.

[b] Always compute end point to two decimal points using saturated-steam data in steam tables.

TABLE 4 LONG FORM FOR COMPUTING THEORETICAL REGENERATIVE-CYCLE HEAT RATES AND BOILER-FEED-PUMP WORK[a]

(10)	(11)	(12)	(13)	(14)	(15)	(16)	(17)	(18)	(19)	(20)
$\log_e (1 + w) = -\int_{h_2}^{h_1} \frac{dh}{\text{avg } (H - h)}$	$\log_{10} (1 + w)$	$(1 + w)$ See footnote[b]	Average feedwater flow avg $(1 + w)$	Boiler - feed-pump work, Btu $F(1 + w)$	Work done by steam in prime mover, Btu per lb $H_1 - H$	$\frac{H_1 - H}{H - h}$	$\frac{H_1 - H}{H - h}(1 + w)$	Average of $\frac{H_1 - H}{H - h}(1 + w)$	$\frac{H_1 - H}{H - h}(1 + w)dh$	$\int_{h_2}^{h_1} \frac{H_1 - H}{H - h}(1 + w)dh = E$ Energy added to Rankine cycle
Add up column (9) step by step starting from bottom and inserting progressive total in column (10)	Change logarithm to base 10 by multiplying column (10) by 0.4342945	Read antilog of column (11) and insert in column (12)	Add adjacent readings in column (12) and divide by 2	Column (4) multiplied by column (13)	Subtract column (2) from enthalpy of throttle steam	Column (15) divided by column 7	Column (16) multiplied by column (12)	Add adjacent readings in column (17) and divide by 2	Column (18) multiplied by column (6)	Add up column (19)
0.9773690 0.9450804 0.9123045 0.8795404 .... 0.0679526 0.0343299 0.0	0.4244518 0.4104295 0.3961956 0.3819668 .... 0.0295105 0.0149088 0.0	2.6574 2.5729 2.4900 2.4097 .... 1.0703 1.0349 1.0000	.... 2.6151 2.5315 2.4498 .... 1.0884 1.0526 1.0174	.... 0.601 1.240 1.813 .... 0.011 0.0 0.0 28.986 Total	0 1.5 5.1 11.0 .... 643.6 683.5 723.71	0 0.002086 0.006893 0.014487 .... 0.780973 0.842060 0.905611	0 0.005367 0.017164 0.034909 .... 0.835875 0.871448 0.905611	0.002683 0.011266 0.026036 0.047485 .... 0.853662 0.888529	0.0614 0.2694 0.6394 1.1980 .... 23.4757 24.5678	359.64

[a] Continuation of Short Form, Table 3.

[b] As calculated $(1 + w)$ is the theoretical flow of steam or feedwater past a chosen point in the infinite number of steps or stages of steam expansion and feedwater heating.

Discussion

THEODORE BAUMEISTER.[16] This paper is in many respects a companion piece to that offered by H. S. Horsman[9] before the British Institution in 1942, and cited by the authors. Both papers offer an ideal or theoretical standard of performance for regenerative steam-power-plant cycles.

The questions which the writer raised with reference to Mr. Horsman's paper can similarly be raised in discussion of the current paper. The criterion for judging the real worth of such a paper is in its practical utility. Will it facilitate or help in the solution of design and operating problems on actual steam power plants? If the answer is affirmative then the value of the current paper is demonstrated. If it does not give an affirmative answer then the paper is essentially an academic exercise. The authors imply, in Table 2 and its attendant paragraphs, that much additional work is necessary to accomplish this important affirmative step. Presumably it is the result of their experience that the theoretical heat rates of Table 1 can be used for the comparison of two proposed real alternate cycles. Or better, upon accumulation and correlation of further experience and data, Table 1 may then be used to answer the recurrent question of choice between two real alternate power-plant cycles.

Thus from detailed and accurate calculations the over-all heat rate may have been determined as 11,000 Btu per kwhr of net output, including all allowances for inefficiencies and auxiliaries. The appropriate theoretical heat rate of the idealized cycle might be read from Table 2, as 6945 Btu per kwhr. If the same arrangement of equipment and the same inefficiencies were applicable then some second cycle, which might have a threoretical heat rate of 6759 Btu per kwhr from Table 2, could then be estimated to give an actual over-all thermal performance of

$$11{,}000\,\frac{6759}{6845} = 10{,}860 \text{ Btu per kwhr net output}$$

This procedure, of course, would be a great convenience and reduce the tedium and errors of lengthy heat-balance calculations. Unfortunately, however, the mechanism or engine efficiencies will usually change along with the cyclic values, and the solution is not as convenient as may be anticipated.

In any event, high orders of accuracy are necessary because the power engineer is concerned with the evaluation of savings, i.e., differences in heat rates. These differences are small numbers and unless a high degree of accuracy is otained the answers, because of too few significant figures, cannot be used. The writer therefore would like to inquire if the authors believe that their paper can be so used to give reliable and convenient answers to the following typical questions which arise in the development of a plant cycle:

1 Proposed alternate use of drip pumps, drain coolers, or direct flashing for heater drains.

2 Terminal temperature differences to be used on closed feed heaters.

3 Proper disposition of turbine gland leakage.

4 Make-up evaporator location in the cycle.

5 Thermal advantages of alternate locations of feed pumps in the cycle.

6 Recovery or nonrecovery of heat supplied to generator coolers and lubricating-oil coolers in the feedwater.

7 Electrically driven, steam-driven or internal-combustion-engine-driven plant auxiliaries.

8 Pressure drop between turbine shell and heater.

If the authors believe that the solution of these and similar problems can be expedited by the methods outlined in their paper, then it is the writer's opinion that they should be encouraged to collect and correlate the necessary data for the preparation of the supplementary paper which they recommend.

M. W. BENJAMIN.[17] This contribution to steam-power engineering provides, in Table 1, data which are just as fundamental to the regenerative cycle as are the tables of theoretical steam rates to the Rankine cycle. The practical usefulness of the theoretical heat rates will depend to a large extent upon the successful working out of a second paper to provide the factors necessary for bridging the gap between the hypothetical and the practical. In years past the existence of such information could have saved unknown man-hours of calculation in the planning of new plants and rehabilitation projects.

As applied to the design of new plants, the value of this paper and its proposed companion may be limited henceforth to the investigation of projects outside the range of the standardized turbines now being considered by the industry. Performance figures for standard units will be well known, and calculations will be unnecessary except for minor changes in the cycle. It is doubtful whether the companion paper could provide factors for all such possible refinements. It would be a mistake to assume, however, that the present paper had come too late merely because turbine standardization is now being considered seriously. Until some radically new method of producing electricity is devised, it would seem reasonable to believe that engineers will continue to explore the possibilities of the regenerative cycle. The theoretical heat rates are now established with a high degree of precision, and from this paper one can determine quite easily the order of magnitude of improvement which still is possible. It appears from Fig. 5(*a*) and Table 2, that between good modern practice and the heat rate of an actual plant at the upper limit of this study (3200 psi at 1200 F), there is a margin of at least 1500 to 1700 Btu per kwhr (440 to 500 whr per kwhr).

Figure 5(*a*) also illustrates a point that has been made before, viz., that, as pressures and temperatures are increased, the rate of thermal economy improvement becomes smaller, thus making it more difficult to justify the improved conditions economically.

The authors have indicated, without elaboration, another use for these data in conjunction with the companion paper in establishing reasonable standards of plant operation by means of which it will be possible to estimate the degree of excellence with which a plant is operated. For many years it has been the practice in England to refer to some kind of standard for this purpose whereas in our country the emphasis has been more on designing the plant for economy and ease of operation and then expecting the operating staff to get the utmost in efficiency from the equipment that has been provided. One weakness of this arrangement is that it offers no incentive for careful operation of older plants in competition with newer ones. Perhaps Americans do not require a measuring stick for operating excellence, but for those who see merit in the idea the present paper offers data for determining a basis of comparison of regenerative-cycle plants.

The theoretical heat rates given in Table 1 are the result of a large amount of careful work for which the industry is grateful. The paper may develop into a tool of many uses.

A. A. BROOKS.[18] The writer believes that the requirement $dh(H - h)$ be constant, could be eliminated by using a sufficiently large number of steps with possibly less labor involved than recalculation to get equal steps.

[16] Professor of Mechanical Engineering, Columbia University, New York, N. Y. Mem. A.S.M.E.

[17] Engineering Division, The Detroit Edison Company, Detroit, Mich. Mem. A.S.M.E.

[18] Thermodynamic Engineer, Moore Steam Turbine Division, Worthington Pump and Machinery Corporation, Wellsville, N. Y.

No practical purpose is served for limiting the regeneration to saturated steam only. The use of superheated steam is simply a question of proportioning the heaters intelligently. It is doubtful if, in actual practice, it is feasible to get higher than the saturation temperature of the steam in the heater, and it would be interesting to see how figures on this basis compare with the author's figures. It is not clear whether the curves in Fig. 6, are given on this basis or on the basis of a perfect counterflow system for superheated steam.

That the cycle efficiency of better than 50 per cent for steam pressures has already been approached in actual practice is extremely interesting.

W. W. Dulmage.[19] In Table 2 of their paper Messrs. Selvey and Knowlton have applied design and performance factors for relating the operating results from three actual plants to the respective theoretical regenerative-cycle heat rates. Since further information of the same sort is needed for other plant cycles, the writer is pleased to furnish the following description of the cycle for River Rouge No. 1 power plant of the Ford Motor Co. with operating results for the year 1943.

In that power plant there are three steeple-compound condensing turbine-generators of 110,000-kw capacity each, and one 15,000-kw noncondensing turbine-generator. One of the large units operates on the reheating-regenerative cycle using throttle steam at 1200 psi 725 F and employing live-steam reheat to about 570 F at the crossover. The other two large units operate on the regenerative cycle without reheat, using throttle steam at 1200 psig 900 F. The noncondensing machine operates on throttle steam at 1200 psig 900 F and exhausts to large process evaporators at 250 psig. Since the paper deals only with the regenerative cycle the following remarks apply only to the two large units operating on that cycle, and are based on over-all plant data for the calendar year 1943 as adjusted to represent the performance of those two generating units. Several complications arise when attempting to allocate properly between the different cycles existing in the power plant such items, among others, as auxiliary power and soot-blowing steam. Therefore several of the factors of the authors' Table 2 have been grouped together in estimating the performance factors presented in Table 5 for the straight regenerative units. The cycle diagram for one of these units is given in Fig. 7 while the turbogenerator heat-rate curve obtained from tests[20] and corrected to standard conditions of throttle pressure and temperature and exhaust pressure is shown in Fig. 8.

[19] Power Department, Ford Motor Company, Dearborn Mich.

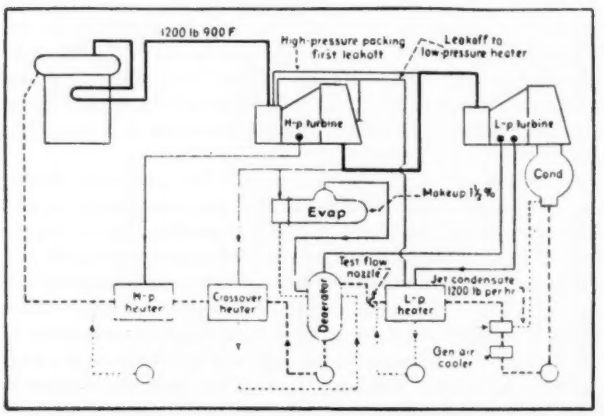


Fig. 7 Flow Diagram for Two 110,000 Kw Steeple-Compound Turbine-Generators Operating on 1200 Psig 900 F Regenerative Cycle in River Rouge No. 1 Power Plant of Ford Motor Co.

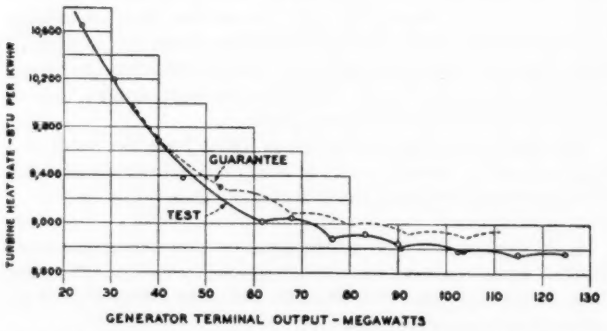


Fig. 8 Guarantee and Test Heat Rates for 110,000 Kw Steeple-Compound Turbine Generators Operating on 1200 Psig and 900 F Regenerative Cycle in River Rouge No. 1 Power Plant of Ford Motor Co.

Average values of the pertinent data for the year 1943 are as follows:

(1)	Over-all station heat rate, Btu per net kwhr	11,220
(2)	Over-all station coal rate, lb dry coal per kwhr	0.795
(3)	Heat value of coal, Btu per lb dry coal	14,107
(4)	Over-all boiler-room efficiency, per cent	87.1
(5)	Feedwater make-up, per cent	2.4
(6)	Auxiliary power, per cent of gross generation	4.5
(7)	Average load on regenerative units, kw each	52,600

TABLE 5 APPLICATION OF DESIGN AND PERFORMANCE FACTORS TO THEORETICAL REGENERATIVE-CYCLE HEAT RATES FOR RIVER ROUGE NO. 1 POWER PLANT OF FORD MOTOR CO.

		Factor	Btu per kwhr
(1)	Theoretical heat rate		6935
(2)	Engine-efficiency and exhaust-loss factor		
(3)	Cycle design factor		
(4)	Operating efficiency[a]	0.7497	
(5)	Mechanical and electrical efficiency		
(6)	Turbine heat rate, gross output (at average load)[a]		9250
(7)	Auxiliary-power usage factor		
(8)	Evaporated make-up factor		
(9)	Pipe-radiation-loss factor	0.9465	
(10)	Soot-blowing and miscellaneous-steam-usage factor		
(11)	Steam-generating efficiency	0.871	
(12)	Plant heat rate, net output		11,220
(13)	Plant-design and performance factor	0.6181	

[a] Average load was less than 50 per cent of rated capacity, which results in low value of item called Operating Efficiency in Table 2 of Selvey-Knowlton paper.

G. M. Dusinberre.[21] The authors ask for an explanation of the curvature of line A-B in Fig. 2(b). This line, by its deviation from the vertical, reflects the departure from reversibility in the feed-heating operation. This deviation is greatest at the top. Under the assumption of an infinite number of feed heaters, we are at this point using steam at 1200 F to heat water at 705 F, evidently with great thermal irreversibility. The situation is also apparent from the fourth line of Tables 3 and 4. Column 12 shows that we have extracted about 10 per cent of the throttle steam and column 2 shows that the through steam has done only 11 Btu of work per lb. This is not much different from heating the feed irreversibly in the boiler.

In their Appendix the authors state that a long form of computation would be necessary for investigation of the isothermal-compression regenerative cycle. This is true as regards pump and compressor work. But for net work or net heat rate, the calculations would be extremely simple. Such a cycle could ideally be made entirely reversible, internally, and the heat rejected per pound of throttle steam would be simply the tempera-

[20] See "Performance Test at Ford Motor Co.," by W. W. Dulmage and C. J. Walker, *Power*, vol. 85, July, 1941, p. 72.

[21] Assistant Professor of Mechanical Engineering, Virginia Polytechnic Institute, Blacksburg, Va. Now on duty at U. S. Naval Academy, Annapolis, Md. Mem. A.S.M.E.

ture at rejection times the change of entropy during heat supply. Thus, the "short-cut" formula, shown above Fig. 3 of the paper, would be precisely correct for this cycle.

The writer was impressed with the suggestion by A. A. Markson of an analysis based on a divided cycle and has prepared a brief outline of the form which the proposed tables might take. It is true that the work done by the saturated cycle can be obtained by multiplying its Carnot efficiency by the heat rejected by the superheat cycle, but there are certain advantages in having additional tables instead (Tables 6 and 7 of this discussion).

TABLE 6 SUPERHEAT-REGENERATIVE DATA

p	t	800	1000	1200
3200	q	378.7	562.5	697.5
	q'	316.7	500.5	635.5
	w	45.1	145.1	242.8
	y	0.570	0.531	0.524
	p_s	1343	385.8	141.0
(385.8)	q		1102.8	
	q'		318.5	
	w		337.1	
	y		0.786	
	p_s		13.0	

TABLE 7 SATURATED-REGENERATIVE DATA

p	tf	90	(79.03)	70	50
1400	w	273.0		283.9	294.9
	y	0.445		0.432	0.420
(1343)	w		282.0		
	y		0.446		
(385.8)	w		314.6		
	y		0.624		
(141.0)	w		293.0		
	y		0.720		
14	w	173.7		202.7	231.8
	y	0.881		0.861	0.842
(13.0)	w		185.2		
	y		0.875		

p—throttle (or reheat) pressure, psia
t—temperature at throttle (or after reheating), F
q—heat supplied to throttle steam, Btu/lb
q'—heat supplied to reheated steam, Btu/lb
w—work (net, turbine less feed pump) per lb steam supplied, Btu/lb
y—ratio of through steam to throttle steam
p_s—pressure at saturation, for isentropic expansion, psia
tf—condenser (or cooling water) temperature, F

The method of calculation was similar to the authors' short form except that no effort was made to keep the feed-heating increments equal as long as they were sufficiently small. The use of the tables may be illustrated by an example:

Throttle steam 3200 psia, 1200 F, lowest temperature 79.03 F (this temperature is chosen to agree with the authors' 1 in. Hg).

	Steam	Heat	Work
From superheat-regenerative Table 5	1.000	697.5	242.8
To saturated-regenerative at 141 psia	0.524		
Interpolating for 141 and 79.03			
Work, 293.0 × 0.524			153.5
Steam to condenser 0.720 × 0.524	0.377		
Totals		697.5	396.3

Heat rate 3413 × 697.5/396.3 = 6000 Btu per kwhr (5999 by authors)
Throttle steam/through steam 1/0.377 = 2.65 (2.6574 by authors)

So far, we have little that could not have been obtained more readily from the authors' tables. But what about reheat? Is it not possible and desirable to set an ideal standard for regenerative plants which is also applicable when reheat is employed?

The advantage of reheat lies in the reduction of moisture in the low-pressure stages of the turbine, rather than in any striking gain in ideal-cycle efficiency. Since this is the case, it would be logical to base a "standard" cycle on reheat at the pressure where the throttle isentropic reaches the saturation line. This would mean that reheat actually began with a moderate amount of superheat, which is not out of line with current practice.

If such a standard should be acceptable, the analysis of the ideal cycle can be made very readily with Tables 6 and 7, for example: Throttle steam 3200 psia, 1000 F, reheat to 1000 F, lowest temperature 79.03 F.

	Steam	Heat	Work
From superheat regenerative Table 5	1.000	562.5	145.1
To reheat regenerative at 385.8 psia	0.531		
Heat (use q') 318.5 × 0.531		169.1	
Work 337.1 × 0.531			179.0
Steam 0.786 × 0.531	0.417		
To saturated regenerative at 13.0 psia			
Work 185.2 × .417			77.2
Steam to condenser 0.875 × 0.417	0.365		
Totals		731.6	401.3

Heat rate 3413 × 731.6/401.2 = 6220 Btu per kwhr

This division of the cycle should lend itself better to the application of performance factors. The efficiency of a turbine, operating only in the superheat region, and of another operating only saturated, can be set forth in a more representative way than the efficiency of a turbine operating in both regions.

The saturated-regenerative Table 7, based on temperatures, can be used for condensation temperature or, as suggested by P. H. Hardie, for cooling-water temperature. This latter seems more logical in a study of purely ideal performance.

M. D. ENGLE.[22] A standard of measurement is a fundamental requirement of engineering progress. Many business enterprises having to do with the sale of a service have been really unsuccessful until a suitable device was developed to measure the service supplied. The electrical industry was greatly hindered in development until a suitable kilowatthour meter was developed. The hot-water district-heating business has never fully developed and one of the principal reasons for this lack of success is the nonexistence of a suitable device for measuring the service supplied. On the other hand, the district steam-heat business, having suitable measuring devices, is growing quite rapidly.

So it is in the business of designing and constructing steam-electric generating stations. While it is true that big advances have been made in design, we have long needed a suitable standard of measurement of the success of our design.

The net Btu per kwhr performance of a station is a useful factor but it does not really show how closely we have approached the ideal performance for the steam conditions and cycle adopted.

The data in this paper will be very useful to powerplant design engineers in calculating just how good a job they have done.

Furthermore, the careful analysis of the losses, as shown in Table 2, will more clearly focus the attention of the designers upon the particular items to be investigated for possible improvement.

We have been so much interested in the problem of keeping the turbine blades clean that probably very few have given much thought to the loss in station economy due to the blade deposits. Maybe such an analysis will show that we are justified in spending much more money in reducing the amount of deposit.

Likewise such an analysis will focus our attention upon the loss due to excessive auxiliary power usage, evaporated make-up losses due to avoidable steam leaks and condenser leakage, and the losses due to so-called "soot-blowing." (In this day and age that term should really be changed to "ash and slag" blowing.)

The operating engineers should also become more fully acquainted with such a detailed analysis of the possibilities of, and losses in, the stations which they are operating. They have of course studied station losses for years but, when they have the theoretical possibilities of their plant in mind, a more careful analysis of the losses will quite often pay handsome dividends.

[22] Assistant Superintendent of Engineering, Boston Edison Co., Boston, Mass. Mem. A.S.M.E.

The writer feels that both design and operating engineers will benefit greatly by the work done by the authors and is sure that they will co-operate by supplying the data which are needed to complete the study.

P. H. HARDIE.[23] The table of theoretical regenerative steam-cycle heat rates presented by the authors is a valuable contribution. The authors' suggested method of using this table as a basis for appraising plant performance should be adopted as an American standard, with possibly a slight modification which will be discussed later.

There are several points relating to the application of this table worth careful consideration. For example, the authors have proposed using the throttle steam conditions for the upper limit of the cycle instead of drum or superheater-outlet steam conditions. From a practical standpoint this would seem to be the best choice. However, for the lower boundary of the cycle, it would seem preferable to use the saturation pressure corresponding to the temperature of the condensing water, rather than the turbine exhaust pressure. This pressure is the theoretical minimum and will be more nearly constant for all units in a plant. Furthermore, it will not be affected by the differences in design, load, and cleanliness factor of the different condensers. These factors should properly appear in the plant-design-and-performance factor. If the authors agree to this change it would be helpful to have the data, presented in Fig. 5(*b*), replotted for condensing-water temperature.

No method has been proposed by the authors for computing the theoretical regeneration-steam-cycle heat rate of a plant having units operating at two or more pressures or temperatures. The theoretical heat rates of the different systems would have to be weight-averaged, but what is the proper basis of weighting? Boiler-steam output would not be satisfactory because of the differences in the enthalpy of the steam and/or the feedwater. Generator output would also be unsatisfactory because some of the steam may be throttled from the high-pressure system to the low-pressure system. Therefore fuel input would seem to be the only satisfactory basis for weight-averaging the theoretical regenerative-steam-cycle heat rates to determine the average for such plants.

The authors have shown good judgment in refraining from proposing the use of their table of the theoretical heat rates for appraising turbine performance. Barnard and Ellenwood's method of computing the ideal regenerative-cycle heat rates, based upon the actual number of heaters, is a more equitable standard for turbines. However when appraising the entire plant, the authors' tabular values for an infinite number of heaters should be used.

M. L. IRELAND, JR.[24] It would appear that the usefulness of the table of theoretical regenerative-steam-cycle heat rates presented in this paper can be increased by further comparison with the results obtained by "short-cut" formulas.

In the first place the comparison shown in Fig. 3 may give a somewhat exaggerated impression of the magnitude of error involved in the stated short-cut formula. When this error is expressed as a percentage correction and plotted against throttle temperature as shown in Fig. 9 of this discussion, it becomes apparent that up to about 2300 lb pressure, the correction is practically constant for a particular temperature, varying from about 0.2 per cent for 800 F to 1.2 per cent for 1200 F.

The necessity for a carefully prepared table such as is presented by the authors is particularly evident when considering steam temperatures above 1000 F and pressures over 2300 lb. However, the use of this table as a reference standard for actual power-plant cycles is subject to the basic disadvantage that actual cycles do not employ complete regeneration. A criterion based on actual or designed final feedwater temperature appears to be necessary. The short-cut formula, suitably corrected for additional feed-pump work done above the saturation pressure, corresponding to the final feed temperature, does supply such a criterion, but it is admittedly approximate. On the other hand, the computation of accurate results for individual cases by the authors' tabular integration method is quite laborious.

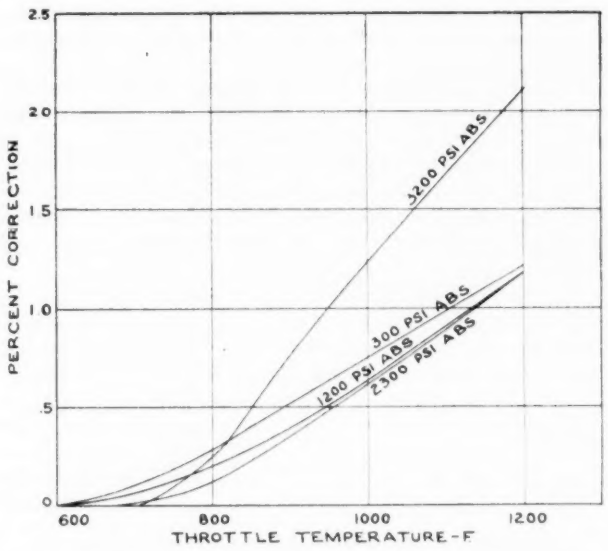


FIG. 9 CORRECTION TO APPROXIMATE REGENERATIVE-STEAM-CYCLE HEAT RATES OBTAINED BY "SHORT-CUT" FORMULA

It is understood that the authors intend to prepare a companion paper in which many such factors will be considered; however, in the meantime it would be helpful if the authors can suggest a means to make further corrections to the short-cut formula for computing heat rates of partial-regeneration cycles. It has occurred to this writer that, since the errors of the short-cut method are associated with regeneration by superheated steam, it might be satisfactory to use the correction curves of Fig. 9, at the pressure and temperature on the turbine-expansion line which correspond to the final feed temperature and saturation pressure.

A. A. MARKSON.[25] One who estimates the value of this paper by its literal applicability to design problems may be disappointed, but the student of such matters will find in it exactly what he needs. The cycle chosen by the authors is of high conceptual usefulness. It is defined incompletely in the paper despite the careful assumptions given. The additional statement that nowhere in such a cycle is there a degradation of energy which is not inherent in the cycle itself would complete the definition, as it would include frictional pressure drops, supersaturation, etc.

The authors have wisely chosen to represent this cycle in tabular form, giving efficiencies correlated with different throttle conditions and a constant condensing pressure. The writer believes that a conceptually more logical method of constructing such tables might be of interest. Inasmuch as the saturated region has Carnot efficiency, there is at once an alternate method of

[23] Engineer, Sanderson & Porter, New York, N. Y. Mem. A.S.M.E.

[24] Newport News Shipbuilding and Dry Dock Company, Newport News, Va. Mem. A.S.M.E.

[25] Hagan Corporation, Pittsburgh, Pa. Mem. A.S.M.E.

tabulation which eliminates the necessity of assuming a constant condenser pressure.

Starting with 1 lb of throttle steam as the basis, using throttle pressure and temperature as the main tabular entries, the efficiencies could be tabulated for the superheated expansion zone alone. The pressure at which the isentropic expansion crosses the saturation line is also tabulated. This completes the skeleton of the tables, but for convenience, the weight ratio passing to the saturated zone might be given. To use these tables to any saturated back pressure whatever, the user simply calculates the Carnot efficiency of his saturated cycle and makes a simple weighted average of this and the superheated cycle. This would eliminate the necessity for the exhaust-pressure corrections used by the authors, thus gaining considerable simplicity of concept.

The writer closes by suggesting that performance figures, such as shown in Fig. 5(*a*), be referred to as the "thermodynamic merit" of the cycle to avoid possibility of misunderstanding. Thus an actual cycle having a certain heat rate could be assigned an efficiency analogous to Rankine efficiency on the basis of the "thermodynamic merit" figure.

C. A. MEYER.[26] It appears to the writer that a simpler and more accurate definition for the theoretical regenerative-steam-cycle heat rate can be obtained by utilizing the well-known concept of available energy.

In any cycle in which heat (dQ) is added at variable temperature T (deg abs) and rejected at constant temperature T_e (deg abs), the maximum work obtainable (W_M) is given by

$$W_M = \int_{T_1}^{T_2} dQ \left(\frac{T - T_e}{T}\right) = Q_{1-2} - T_e \int_{T_1}^{T_2} \frac{dQ}{T} = Q_{1-2} - T_e(S_2 - S_1) \quad \ldots\ldots [1]$$

At constant pressure, the heat added is equal to the enthalpy rise

$$Q_{1-2} = h_2 - h_1$$

so that

$$W_M = (h_2 - T_e S_2) - (h_1 - T_e S_1) = A_2 - A_1 \quad \ldots\ldots [2]$$

where $A = h - T_e S$ is the total available energy measured above an arbitrary state point. The available energy at any state point is obtained as the difference between the value of A at the given state point and the value of A at the state point which we regard as having zero availability (atmospheric temperature and pressure). The relation Equation [2] is quite general and could have been written directly.

The maximum thermal efficiency of the regenerative cycle is then

$$\eta_M = \frac{(h_t - T_e S_t) - (h_f - T_e S_f)}{h_t - h_f} = 1 - \frac{T_e(S_t - S_f)}{h_t - h_f} \quad \ldots\ldots [3]$$

The theoretical heat rate is then

$$THR = \frac{3412.75(h_t - h_f)}{h_t - h_f - T_e(S_t - S_f)} \quad \ldots\ldots [4]$$

where h_t, S_t = throttle enthalpy and entropy, respectively
h_f, S_f = feedwater enthalpy and entropy, respectively
T_e = absolute temperature of cooling water

Relation, Equation [4], has been labeled "inaccurate" in the paper for reasons which are not clearly stated. However, Equation [4] gives the correct heat rate of the ideal cycle, defined by the four specifications given in the paper (perfect processes allowing for required pump work).

It is of interest to show that the theoretical heat rate of any cycle can be obtained in a similar manner. As an example, the efficiency of the Rankine cycle is easily written as

$$\eta_R = \frac{A_t - A_f}{h_t - h_f} = \frac{(h_t - T_e S_t) - (h_f - T_e S_f)}{h_t - h_f} \quad \ldots\ldots [5]$$

Since

$$T_e(S_2 - S_c) = h_2 - h_c \qquad S_2 = S_t$$
$$S_c = S_f \quad \text{and} \quad P = h_f - h_c$$

where P = pump work
h_c, S_c = enthalpy and entropy of condensate
h_2, S_2 = enthalpy and entropy at turbine exhaust

Equation [5] becomes the well-known expression for Rankine-cycle efficiency

$$\eta_R = \frac{h_t - h_2 - P}{h_t - h_c - P} \quad \ldots\ldots [6]$$

Returning to the regenerative cycle, a further point of interest is that factors correcting for the various inefficiencies in actual cycles can easily be defined. For instance by setting down the loss of available energy in an extraction turbine, a suitable correction factor for the inefficiency of the turbine can be obtained. The loss of available energy in a single extraction turbine is written as

$$L = G_t A_t - G_1 A_1 - G_e A_e - W$$

where L = loss of available energy in turbine
W = useful work output
$= G_t(h_t - h_1) + (G_t - G_1)(h_1 - h_e)$
G = flow
A = available energy $= h - T_e S$

Subscripts t, 1, e refer to throttle, bleed point, and exhaust, respectively.

The cycle efficiency (for losses in the turbine only) then becomes

$$\eta = \eta_M \times C_t = \left(\frac{A_t - A_f}{h_t - h_f}\right) \times \left(1 - \frac{L}{A_t - A_f}\right)$$

where $C_t = \left(1 - \dfrac{L}{A_t - A_f}\right)$ = turbine efficiency factor

Similar correction factors for terminal difference, mixing and pressure losses are easily obtainable from the losses in available energy due to these causes.

ERNEST L. ROBINSON.[27] Just 20 years ago the writer presented a chart showing the efficiencies of the theoretical extraction cycle in comparison with efficiencies obtainable with the Rankine cycle.[28] This was a small-scale diagram outlining in a general way the possibilities of cycle improvement. This diagram was extended to a temperature of 700 F and a pressure of 1000 psia, limits which were then thought to represent the fringes of possibility.

The calculations on which these efficiencies were obtained were based upon the Goodenough chart of 1917. Although we did not then know it, the Goodenough steam table at that time was an

[26] Research Engineer, Westinghouse Electric & Manufacturing Co., South Philadelphia Works. Mem. A.S.M.E.

[27] Turbine Engineering Division, General Electric Company, Schenectady, N. Y. Mem. A.S.M.E.

[28] "The Margins of Possible Improvement in the Central Station Steam Plant," by Ernest L. Robinson, Trans. A.S.M.E., vol. 45, 1923, p. 644.

excellent steam table. All circumstances considered, the efficiencies then given corresponded remarkably well with the heat rates given in this paper on the basis of present-day steam tables up to the values then used.

Ever since the steam tables have gone through the process of refinement and improvement to which they have been subjected during the past 20 years, the writer has felt that theoretical heat rates for the extraction cycle should be determined with the same degree of precision as the theoretical water rates for the Rankine cycle. This has never been done until the authors undertook the task a couple of years ago with the result which is now presented.

The authors have suggested certain further steps toward the analysis of station performance. The writer would like to mention one or two other investigations into the nature of steam which might well be undertaken.

The question of reheat factors has never been satisfactorily cleared up. Three important contributions on the subject appeared several years ago, one in England and two in this country. The excellent British article by Dr. D. M. Smith[29] was based upon an unjustified use of the moisture correction, and another paper by Dr. R. B. Smith[30] was based upon certain analytical assumptions. The writer would prefer to see reheat factors based strictly upon the steam table without any analytic assumptions. Such an attempt was made by Prof. C. G. Thatcher.[31] However, the writer's attempt to apply Professor Thatcher's results differed by as much as 1 per cent in turbine performance from Professor Thatcher's application of his own results. Without being completely in the dark as to the reasons for this uncertainty, it is evident that there is still a job to be done in the matter of reheat factors.

The evaluation of reheating effects in connection with the extraction cycle requires determination of the weight flow at various stages in the turbine and heat rates corresponding to actual stage efficiencies. The writer previously charted these quantities for expansion lines at 70 and 80 per cent efficiency.[32] Professor Thatcher's reheat factors were based on 85 per cent stage efficiency from which suitable correction to neighboring efficiencies may be made. A table of heat rates for a theoretical extraction cycle with 85 per cent stage efficiency would be a welcome contribution.

In addition to the heat rates to 1 in. Hg abs back pressure, it is advantageous for a number of reasons to know the weight flow at any point in the course of the expansion through the turbine. A knowledge of the weight flow is necessary for the proportioning of the areas of cross section of the many successive passages throughout the turbine. This is particularly true of the extraction cycle where the steam entering the throttle is likely to be in the order of 50 to 100 per cent more than what enters the condenser. This is the quantity $(1 + w)$ which appears throughout the formulas and tables in the paper. Mollier charts for the weight flow per pound of steam at 1 in. Hg abs back pressure were given in the writer's article[31] for expansion lines of 70 and 80 per cent efficiency. Under modern conditions, a chart for 85 per cent efficiency would be more useful.

A further advantage of the weight-flow data lies in the ability to determine over-all performance between any two levels of pressure without resorting to superheat, pressure, or vacuum corrections. The vacuum corrections given in the paper are good as long as the expansion ends in the wet region. However, if one wishes to know the performance of the high-pressure element of a cross-compound machine, it may be determined directly when the weight flows entering and leaving are known.

Data of this sort automatically include the evaluation of the reheating effect and indicate the energy actually available from the steam when expanding at a definite stage efficiency. Of course, in any case there must be suitable corrections for the deviation from an infinite number of turbine stages and points of extraction.

However, when weight-flow data are available, one may readily determine the heat rate and corresponding thermal efficiency for any particular initial steam conditions and back pressure. It is then approximately correct to assume a linear relation between the thermal efficiency and the stage efficiency. Thus, knowing the thermal efficiency for 85 and 100 per cent stage efficiencies, it may readily be determined for any stage efficiency between 80 and 90 per cent. Of course, the linear assumption could be avoided by preparing data at both 80 and 90 per cent as well as for 100 per cent. With such a line drawn for the steam conditions in question, it is as easy to determine the internal efficiency corresponding to a test result as it is to determine the expected performance corresponding to the internal efficiency of a design.

The writer believes this procedure to be one of the best methods, if not indeed the best, of taking complete account of the influence of the steam conditions on the turbine performance. (It does not deal with stage design.) Beyond this point the analysis of station performance might well follow the lines outlined by the authors.

J. Kenneth Salisbury.[33] In most studies of the regenerative cycle, the ultimate objective is to simplify the evaluation of power-plant turbine cycles, and to facilitate the comparison, on an extraction basis, of different steam conditions used with a given heater arrangement. At least two methods of approach are possible.

One is exemplified by the material presented by the present authors. They use as a basis the best possible heat rate which can be obtained in a conventional steam power plant, namely, the heat rate of a turbine having 100 per cent efficiency (and an isentropic expansion line) and heating its own feedwater in an infinite number of heaters to the saturation enthalpy corresponding to throttle pressure. Such a heat rate, when divided by the turbine-generator efficiency, yields the turbine-cycle heat rate, if a correction is made to a finite number of heaters operating at the desired final feedwater temperature, and "cycle corrections," etc., are neglected.

A second method of approach is that used by the writer in a paper presented before the A.S.M.E. in 1941.[34] In this method the actual nonextraction heat rate (including the actual turbine-generator efficiency) is used as a starting point. To this nonextraction heat rate is applied again factor $(1 - PG)$, which depends upon such parameters as the number of heaters used, the steam conditions, and the feedwater temperature. A small additional correction is required to obtain the actual heat rate because of departures of the actual cycle from the assumed cycle (a series of equally spaced contact heaters, each having no pressure drop in the extraction line, and no terminal difference).

---

[29] "Stage Efficiency, Cumulative Heat, and Reheat Factor of Steam Turbines," by D. M. Smith, Proceedings of The Institution of Mechanical Engineers, vol. 140, 1938, pp. 399–452.

[30] "The Calculation of Steam-Turbine Reheat Factors," by R. B. Smith, *Journal of Applied Mechanics*, Trans. A.S.M.E., vol. 60, 1938, pp. A-156–A-160.

[31] "Reheat Factors for Expansions of Superheated and Wet Steam," by C. G. Thatcher, *Journal of Applied Mechanics*, Trans. A.S.M.E., vol. 60, 1938, p. A-161.

[32] "Notes on the Comparison of Steam-Turbine Efficiencies," by Ernest L. Robinson, *General Electric Review*, vol. 29, 1926, pp. 503–510.

[33] Turbine Engineering Division, General Electric Company, Schenectady, N. Y. Mem. A.S.M.E.

[34] "The Steam-Turbine Regenerative Cycle—An Analytical Approach," by J. Kenneth Salisbury, Trans. A.S.M.E., vol. 64, 1942, pp. 231–245; see also, "A Short Cut to Turbine Cycle Heat Rates," by J. Kenneth Salisbury, *Power*, Oct., 1943, pp. 78–81, 144, 146, and Nov., 1943, pp. 78–80.

Neither of the two general methods can, in a simple straightforward manner, take care of all of the combinations and permutations which can be conceived by power-plant designers. It is necessary therefore that certain "cycle-correction" factors be applied for either method to take care of departures from the standard cycles. Such correction factors should meet the following requirements:

1 There should be a minimum number of corrections, for ease in handling.

2 The cycle corrections should be clearly defined and arranged so as to be easily applied to heat rates determined by test of operating units, thus greatly reducing the uncertainties and drudgery now involved in correction to standard conditions of such tests.

3 The corrections should, when possible, be independent of each other so as to permit isolation of the various losses and independent appraisal of various features of the cycle.

4 The corrections should, of course, be accurate, relative to the over-all heat rate, but since they are small, considerable tolerance may be allowed in the corrections themselves.

The writer's original conception of the problem was that, as a first step, a method should be devised which would properly consider the major variables, such as the following:

1 Number of heaters
2 Feedwater temperature
3 Operating steam conditions
4 Turbine efficiency.

This was accomplished in the original paper.[34] It was considered that the second step should be calculation of a set of correction factors, the function of which would be to increase the accuracy of the calculations made using the first set of data but which, in the meantime, could be estimated from experience. The entire analysis to be covered in the second step would be devoted to the accurate determination of the 1 to $1^1/_2$ per cent (total) correction to the heat rate found using the original data.

The present authors have embarked on a similar task by tabulating the heat rates for theoretical cycles at the optimum feedwater temperature (that is, saturation) for an infinite number of heaters. These heat rates are listed for intervals which are closer than required for accurate interpolation, but which are desirable for convenience in use with the present steam tables. The next step in the analysis, that is, corrections to these tabulated heat rates for cycles having a finite number of heaters at various final feedwater temperatures other than the optimum for an infinite number of heaters, will no doubt eventuate to be closely related to those given in the references cited.[34]

The necessary work has been completed, and will be published, on a method of correcting heat rates from the original somewhat idealized basis to the actual cycle.[35] All of these correction factors should be adaptable, with little change, to the present authors' data, with the exception of the boiler-feed-pump correction. An additional correction will, however, be required to correct the authors' state line (an isentropic line) to the actual case, that is, a state line having the applicable efficiency.

The corrections which have been analyzed by the writer are for the following:

1 Heater terminal difference.
2 Pressure drop in the extraction piping.
3 Flashing of one or more heaters to lower heaters with or without drip coolers, of any terminal difference.
4 Distribution of heaters.
5 Evaporators in cycle.
6 Heat-recovery apparatus in cycle.
7 Boiler-feed-pump loss.

(Suggestions are solicited as to other correction factors which might be required in heat-balance calculation.)

The present authors have used an isentropic state line which is never encountered in actual practice. It has, however, the merit of being easily and precisely defined, and of having the absolute support of classicism. The gain due to feedwater heating (the heat rate is not relevant, at the moment—only the gain) depends upon an average value of $(H - h)$, which was integrated essentially graphically by the present authors and analytically by the writer.[34] Since $(H - h)$ at a given extraction pressure or value of h depends only upon the location of the state line, the gain which is obtained by feedwater heating is a function both of the turbine efficiency and the assumed curvature, for given steam conditions. In obtaining actual heat rates from the authors' theoretical heat rates, an additional correction will therefore be required for these items. The correction may be from 0.5 to 1 per cent. This difference in state line assumption, plus the difference in the assumption relative to the boiler-feed-pump work, prevents valid cross checks between the authors' work and the writer's work. Making estimates of the effect of the foregoing items, it is, however, possible to arrive at reasonably close checks between the two sets of data.

A correction will have to be provided by the present authors for the use of a single boiler feed pump (or two boiler feed pumps) instead of the infinite number of pumps which have been used in their study. It is believed that the authors' data, as presented, properly charge the boiler-feed-pump loss for an infinite number of pumps having 100 per cent hydraulic efficiency, in that the power required to run the pumps is deducted from the main output, and the increase in enthalpy realized from the pumps is credited as heat. The data presented in the paper do not, without amplification, readily permit taking into account the effect of using a finite number of pumps, nor are the effects of extra pumping pressure and pump efficiency readily evaluated.

The writer evaluated the expression

$$\left(\frac{\text{P.W.}_{\infty}}{\text{P.W.}_{1}}\right)_{\text{1lb}} = \frac{\int_0^{P_1} V dP}{V_0(P_1 - P_0)}$$

(which neglects the small compressibility effect) to obtain an approximation of the power when using an infinite number of pumps

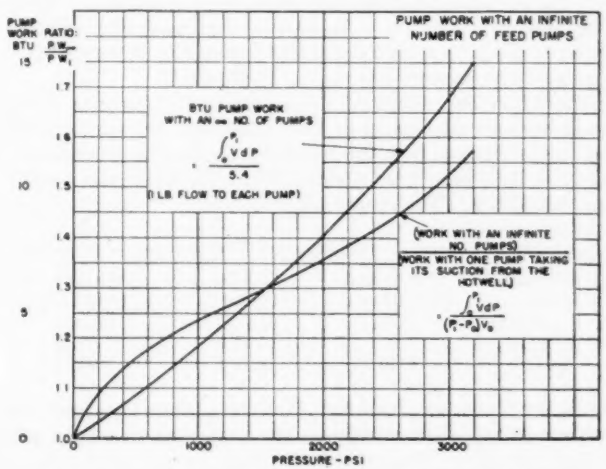


FIG. 10 PUMP WORK WITH AN INFINITE NUMBER OF PUMPS

[35] A few of the results of this work appear in vol. 2 of "Marine Engineering," Chapter 1, on "Heat Engineering and Thermodynamics," to be published by The Society of Naval Architects and Marine Engineers, New York, N. Y., 1944.

as compared with one hypothetical pump taking water from the hot well. The results, which are approximate only, are shown in Fig. 8 of this discussion, for equal flow to all pumps.

To obtain the true pump work included in the authors' heat rates with an infinite number of pumps, the expression used would have to include a term describing the flow to each infinitesimal pump

$$\left(\frac{\text{P.W.}_{\infty}}{\text{P.W.}_{1}}\right)_{(1+w)\text{ lb}} = \frac{\int_0^{P_1}(1+w)\ V dP}{(1+w)_t V_0(P_1 - P_0)}$$

where $(1 + w) = f(P$, etc.)
and $(1 + w)_t$ = throttle flow (= flow to pump when all drips are cascaded to hot well)

It may be found expedient in many cases to remove the loss due to boiler-feed-pump work so that, until corrections are available, the authors' theoretical heat rates will be of maximum usefulness. These data are apparently all available from the calculations made in obtaining the heat rates. Could the authors therefore undertake to present in their closure the boiler-feed-pump loss in some form such as the ratio just given, or in any other more suitable way?

A. H. SHAPIRO.[36] The exhaust-temperature correction for cycles supplied with wet steam can be derived directly and simply from the equations for the cycle efficiency, namely

$$\eta_0 = (T_1 - T_0)/T_1$$

and

$$\eta_T = (T_1 - T)/T_1$$

where η_0 and η_T are the thermal efficiencies for the throttle temperature T_1 and for exhaust temperatures T_0 and T, respectively. The ratio of heat rates at T_0 and T is given by the inverse ratio of efficiencies. Thus

$$F = HR_T/HR_0 = \eta_0/\eta_T$$

Elimination of η_T and T_1 from the system of three equations yields the expression

$$F = HR_T/HR_0 = \frac{\eta_0 T_0}{T_0 - T\,(1 - \eta_0)}$$

The authors point out that this correction loses validity when the throttle steam is superheated. Have calculations been carried out for cases involving large amounts of superheat to determine how large an error is incurred through using Fig. 5(*b*) and Table 1, rather than an independent calculation of the heat rate for an exhaust pressure other than 1 in. Hg abs?

The writer has compared the tabulated heat-rates of cycles using dry saturated steam at 3200, 1200, and 300 psia with the heat rates obtained from the expression for the Carnot efficiency, using for the temperature of absolute zero the two values —460 F and —459.69 F. The results are as follows:

Pressure, psia	Heat rates (Btu per kwhr) Selvey and Knowlton	Carnot (—460)	Carnot (—459.69)
3200	6351	6351.0	6349.3
1200	7181	7180.9	7178.7
300	8850	8850.4	8847.3

From the tabulation it appears that the authors have used the value —460 F when calculating the heat rates of cycles with saturated steam at the throttle. For the sake of thermodynamic consistency and of smoothness of the tables, the value —459.69 F would have been preferable, since this value is the one on which the "Steam Tables" of Keenan and Keyes is based and since most of the values in the heat-rate table are based in turn on the "Steam Tables."

The authors state that the intervals selected for the numerical integration of $\int dh/(H - h)$ must be so chosen that each of the intervals has the same value of $\Delta h/(H - h)$. From a mathematical standpoint there is no necessity for this restriction. The intervals Δh may be chosen at random, the sole requirement for application of the trapezoidal rule being that the quantity $1/(H - h)$ be linear with respect to h (to the degree of accuracy specified for the final results) throughout each interval Δh. There is an advantage in employing equal intervals of Δh, as either the trapezoidal rule or Simpson's rule may then conveniently be employed for calculating the total value of the integral between the condenser pressure and the throttle pressure.

In evaluating $\int dh/(H - h)$ the authors take the summation $\sum \frac{\Delta h}{(H - h)_{avg}}$. There should be employed instead the summation $\sum \left(\frac{1}{H - h}\right)_{avg} \Delta h$.

The difference between $\frac{1}{(H - h)_{avg}}$ and $\left(\frac{1}{H - h}\right)_{avg}$ is small when the two neighboring values of $(H - h)$ are nearly alike, but can appreciably affect the results when the two neighboring values of $(H - h)$ differ by more than a few per cent. In the example given by the authors, the error is of the order of two parts in 10,000 and will probably affect the heat rates by the same order of magnitude. The tabulated heat rates are therefore too small by about 1 or 2 Btu per kwhr.

There appears to be a fundamental inconsistency in the method of the authors for calculating the throttle flow. To begin with, the integral which is the starting point for the calculations, i.e.

$$\int_{h_e}^{h_t} dh/(H - h)$$

is not, as used by the authors, a true integral in the mathematical sense, since the summation of the infinitesimal values of dh is not equal to $h_i - h_e$. In other words, the integral is taken only over those portions of the $(h_i - h_e)$ interval which correspond to feedwater heating, the remaining portion of $(h_i - h_e)$ being accounted for by feed-pump work. The means employed by the authors for overcoming this difficulty seems (to the writer, at least) to involve the confusion of two fundamentally different methods of attack for calculating the throttle flow, namely:

Method 1. Calculations are made for a cycle with a finite number of heaters, the bleed rate to each heater being determined by a heat balance on the individual heater. In principle, the heat rate of the cycle with an infinite number of heaters may be calculated to any desired accuracy by selecting a large finite number of heaters.

Method 2. The differential equation for a single infinitesimal heater is developed and is then integrated to give the total throttle flow. For purposes of numerical integration, values of the integrand may be chosen at finitely separated intervals, but this in no way alters the distinction between the two methods, i.e., that in one case the heat rate for a finite number of heaters is calculated, while for the other case the heat rate for an infinite number of heaters is calculated.

The authors have used Method 1 for calculating the enthalpy change of the feedwater stream across each finite heater but have

[36] Assistant Professor, Department of Mechanical Engineering, Massachusetts Institute of Technology, Cambridge, Mass. Jun.A.S.M.E.

used an equation of Method 2 which applies to infinitesimal heaters for calculating the amount of steam bled to that heater. This combination of portions of two different procedures is inconsistent and leads to errors of unknown magnitude.

There follow the analyses for the two methods:

Method 1. Fig. 11 of this discussion shows a finite heater. A heat balance yields

$$\Delta w = \Delta(1 + w) = \frac{\Delta h}{H - h}(1 + w)$$

where h is the enthalpy of the feedwater stream entering the heater, Δh is the change in enthalpy of the feedwater stream across the heater, and $(H - h)$ pertains to that heater alone (in contrast to the procedure of the authors, in which $(H - h)$ is the average value for two neighboring heaters). Having tabulated

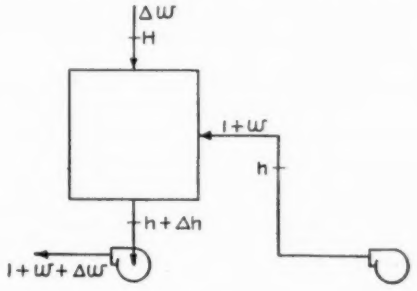


FIG. 11

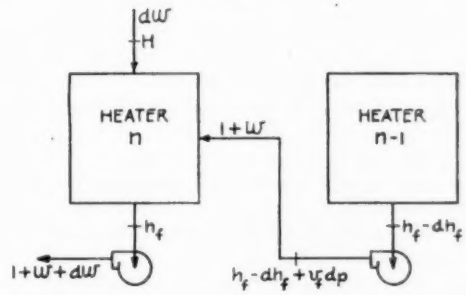


FIG. 12

the values of Δh and of $(H - h)$ for heaters at a number of different pressures, the bleed rate to each heater may be calculated in turn, starting from the low-pressure end. The throttle flow is then the sum of the bleeder flows and the condenser flow.

Method 2. Fig. 12 of this discussion shows two infinitesimal heaters. The symbol h_f refers to the enthalpy of saturated liquid leaving heater n. The enthalpy of saturated liquid leaving heater $n - 1$ is $h_f - dh_f$, and the enthalpy of the feedwater stream entering heater n is $h_f - dh_f + v_f dp$ (note [37]). Equating the enthalpy influx and outflux for heater n, as follows

$$(1 + w + dw)h_f = H\,dw + (h_f - dh_f + v_f dp)(1 + w) \quad \ldots\ldots [7]$$

there is obtained after rearrangement the expression

$$\frac{d(1 + w)}{1 + w} = \frac{dh_f}{H - h_f} - \frac{v_f}{H - h_f}dp \quad \ldots\ldots [8]$$

Integration of Equation [8] between condenser and throttle conditions yields for $(1 + w)$ at the throttle

$$\log_e (1 + w)_t = \int_{(h_f)_c}^{(h_f)_t} \frac{dh_f}{H - h_f} - \int_{p_c}^{p_t} \frac{v_f}{H - h_f}dp \quad \ldots\ldots [9]$$

The total feed-pump work is obtained from the integral

$$F = \int_{p_c}^{p_t} (1 + w)v_f dp \quad \ldots\ldots [10]$$

in which the value of $(1 + w)$ corresponding to any pressure p is found from an integral like that of Equation [9], except that the limits of Equation [9] are modified to correspond to condenser conditions and the conditions at the pressure p.

Analysis of an infinitesimal stage of the turbine yields for the turbine work the expression

$$dW = (1 + w + dw)(H + dH) - (1 + w)H \quad \ldots\ldots [11]$$

After rearrangement and combination of Equation [11] with Equation [8], the total turbine work may be written

$$W = \int_{\text{condenser}}^{\text{throttle}} (1 + w)\left[dH + \frac{H}{H - h_f}dh_f - \frac{v_f H}{H - h_f}dp\right] \quad \ldots [12]$$

The writer has used Equation [9] for calculating the throttle flow and the heat rate for the illustrative example given by the authors, i.e., throttle conditions of 3200 psia and 1200 F and condenser pressure of 1 in. Hg abs. The value of

$$\int_{(h_f)_c}^{(h_f)_t} \frac{(dh)_f}{H - h_f}$$

was determined numerically with Simpson's rule, using 16, 8, 4, and 2 intervals in $(h_t - h_c)$ to determine the necessary number of intervals. To avoid a separate series of steam-table calculations for the value of $\int_{p_c}^{p_t} \frac{v_f}{H - h_f}$ the expression $v_f/H - h_f$ was plotted against p for the same values of h_f which were previously used for the first integral of Equation [9]. From this plot there were read values of $v_f/H - h_f$ at equal intervals of pressure and the second integral of Equation [9] was evaluated with the aid of Simpson's rule. This semigraphical procedure was found to be amply precise for the second integral, because the value of the latter is very small as compared to the value of the first integral. The following table summarizes the results of the calculations:

$$\int_{p_c}^{p_t} \frac{v_f}{H - h_f}\,dp = 0.018089$$

Number of intervals	$\int_{(h_f)_c}^{(h_f)_t} \frac{dh_f}{H - h_f}$	$1 + w$	HR Btu per kwhr
16	0.995033	2.65632	6001.2
8	0.995032	2.65632	6001.2
4	0.995833	2.65844	5997.5
2	1.00524	2.68359	5955.3

The authors give for the heat rate 5999 Btu per kwhr. It appears from the tabulation that not more than 8 intervals are required in this case, as compared with 25 or 35 intervals used by the authors in conjunction with the trapezoidal rule.[38] For certain throttle conditions more than 8 intervals may be required, but the number of intervals will always be vastly less than that required with the trapezoidal rule.

The writer has pointed out what appear to him to be several defects in the construction of the table of heat rates. This

[37] From the thermodynamic expression $Tds = dh - vdp$ it follows that the change of enthalpy across an infinitesimal and reversible adiabatic pump is given exactly by the expression vdp, irrespective of volume changes.

[38] Simpson's rule requires that the relation between $1/H - h_f$ and h_f be of the third order or less throughout the chosen intervals of h_f. The trapezoidal rule requires that $1/H - h_f$ be linear with respect to h_f throughout the chosen intervals of h_f. Far fewer intervals may therefore be used with Simpson's rule than with the trapezoidal rule.

scarcely alters the worth of the table, since these defects generally cause errors only in the final digit of the tabulated heat rates. The introduction of these errors is unfortunate in the sense that the table of heat rates does not reflect the accuracy and precision of the thermal data on which the "Steam Tables" of Keenan and Keyes is based.

G. B. WARREN.[39] The work that led to this paper was started several years ago, following the quite successful application of a system of quickly determining turbine extracting performance which had been in use by the writer's company for some time.

This first system consisted of curves giving the heat consumption of turbines of 100 per cent efficiency based upon available energy and operating with two, three, four, or five extraction points, also with no pressure or temperature drop, and with the extracted steam mixed with the feedwater being heated. If to the data obtainable from such curves, internal turbine-efficiency figures similar to those given in the Knowlton and Warren paper[40] of 1941 are applied, corrections made for leaving loss and for the usually small departure of the actual from the ideal extraction cycle, a close approximation to the real turbine performance can be arrived at. If the feedwater temperature is known, and it can be chosen over quite a range without affecting greatly the foregoing results, the throttle and condenser flows can be easily obtained.

During the early study of this problem, it apparently appeared as though the original form of presenting these data should be modified, and it was put upon the basis of an infinite number of heaters heating the feedwater to the saturation temperature of the boiler, going back to a conception introduced in 1923, by Ernest L. Robinson.[41]

It is to be hoped that the present authors will have an opportunity to prepare the remaining portion of this work which will permit making full practical use of the data.

In the meantime, while the work from which this present paper was prepared was progressing rather slowly, J. K. Salisbury worked up his very excellent system of determining turbine-extraction performance,[34] based upon actual nonextraction heat rates. To some extent this followed an earlier method worked out by and used by the General Electric Turbine Division. This system also facilitated determination of over-all turbine-extraction performance from the nonextraction-turbine efficiencies obtainable from the Knowlton and Warren paper,[40] or from any other convenient source.

Power-plant engineers have at their command therefore published information from which complete and accurate studies of the relative heat consumption of any steam-turbine plant can be calculated. Knowledge of boiler performance and miscellaneous operating losses permits a close approximation of the over-all fuel consumption.

The authors are to be congratulated for carrying out a very long and laborious undertaking and can have the satisfaction of having made a lasting and fundamental contribution that should stand as long as the present steam tables maintain their acceptance and the many conditions of operation are not exceeded.

AUTHOR'S CLOSURE

The authors are gratified that so much worth-while discussion of their paper was forthcoming. The interest manifest in theoretical regenerative-steam-cycle heat rates has confirmed their opinion concerning the importance of this subject to steam-power engineers, and the need for basic data in a form convenient for applying to the solution of such problems. The discussers have brought to attention several points which can well be explained or amplified with a view to making the data more understandable and useful.

Professor Baumeister rightly states that the value of the paper rests in its utility to engineers engaged in designing and operating power plants and wishes to know whether it is proposed that the answers to several questions of detailed apparatus arrangements will be forthcoming. These answers are obviously not contained in the present paper, so that the question really is as to what is proposed for the future second part of the work. This second part has not been crystallized, but the general philosophy now existing regarding what should be done is about as follows:

The effects on performance of losses in any of the apparatus required in steam plants would be pointed out in some detail with the view to showing from past experience what should be reasonably attainable.

The fact that engine efficiencies and other factors change with steam conditions and with advances in the art of manufacturing turbines, as pointed out by Professor Baumeister, would seem to justify the development of the heat-rate tables on the basis of theoretical conditions as was done in the present paper. Thus the tabular values need not be changed (unless the steam tables are changed), and it is believed that correction factors can be worked out for different engine efficiencies so that the plant designer may use the engine efficiency which is applicable at the time of making his calculations.

It is not to be expected that such factors as can be evolved later will be sufficiently all inclusive to furnish an answer to every question; but in general it is hoped to give the plant designer enough information to permit him to assign an over-all efficiency to his plant, based upon actual or calculated heat consumption, and to show why this over-all efficiency is what it is assumed to be. When the major elements of a proposed cycle have been decided, it may then be necessary to make detailed calculations to evaluate the relative merits of minor refinements to the cycle such as changing the location in the cycle of an evaporator or of a heater-drain pump.

The data already presented also should be useful in making comparisons between different cycles, as Professor Baumeister suggests. These comparisons in practical cases require consideration of the effect on performance of many factors of an involved nature, although the net differences in the final answers may be small. A simple comparison of the theoretical heat rates will show the theoretical differences, which can be compared with the practical ones, whereby a better understanding of the reasons for discrepancies may be had.

Mr. Brooks raises a question as to the assumption made regarding the temperature to which feedwater is heated by superheated steam. This is stated in paragraph (2) of the paper under "Description." The curves in Fig. 6 are drawn from the figures in Table 1, simply to show the trend of decreasing heat rate with increasing temperature. With reference to the use of superheated steam in heaters, Mr. Brooks doubts that "it is feasible to get higher than the saturation temperature of the steam in the heater..." Actually several heater manufacturers are guaranteeing performance on the basis of heating the feedwater to a temperature several degrees above the saturated-steam temperature in the heater if the heater is supplied with superheated steam.

Commander Dusinberre, Mr. Markson, and Dr. Robinson apparently have a common idea, viz., that information concerning weight flows, as well as "parts" of complete cycles, should be made available. Commander Dusinberre has proceeded to make some sample figures and tabulations illustrating how this idea

[39] Turbine Engineering Division, General Electric Company, Schenectady, N. Y. Mem. A.S.M.E.

[40] "Relative 'Engine Efficiencies' Realizable From Large Modern Steam-Turbine-Generator Units," by G. B. Warren and P. H. Knowlton, Trans. A.S.M.E., vol. 63, 1941, pp. 125–135.

[41] "The Margins of Possible Improvement in the Central Station Plant," by Ernest L. Robinson, Trans. A.S.M.E., vol. 45, 1923, p. 644.

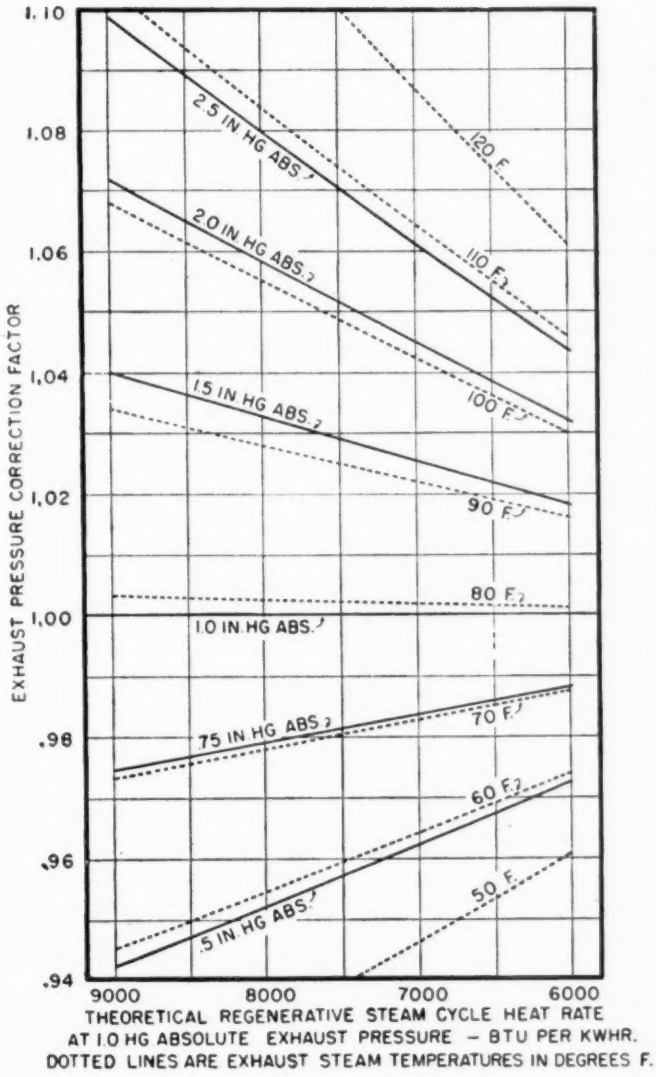


FIG. 5(*b*) REVISED CHART OF EXHAUST-PRESSURE CORRECTION FACTOR

(In the theoretical cycle, exhaust steam temperature is the same as condensing water supply temperature.)

might be carried out. The authors believe that such information, if completely worked out, would be useful. In fact, it may be the only good way of handling the reheat cycle but, at present, they are unable to do more than commend this suggestion to anyone having time to work on it.

In his statement concerning power-plant performance of River Rouge No. 1 Power Plant of the Ford Motor Company, Mr. Dulmage has made a welcome contribution to the store of information which will be needed in preparing the second paper. The authors appreciate this early co-operation. For further information about this plant, reference may be made to an article by W. W. Dulmage and C. J. Walker.[42]

Messrs. Engle and Benjamin both point out the possible value of the paper and its proposed sequel as a means of relating the actual performance of a plant to what can reasonably be expected of its cycle. Such uses are precisely along the lines of the authors' own ideas. There also may be considerable merit to the idea of rating the actual performance of a given plant upon the basis of what fairly can be expected of it, rather than upon the basis of comparison with a more modern or more complex plant.

The authors feel that Mr. Hardie has complimented them in suggesting that the heat-rate tables be adopted as an American Standard basis for appraising plant performance. His suggestion that the condensing-water temperature would be preferable to the turbine exhaust pressure as the lower boundary of the theoretical cycle is supported by the discussion of Commander Dusinberre. This suggestion appeals to the authors as well, since it serves to emphasize that in the theoretical cycle the exhaust steam would condense at the temperature of the cooling-water supply whereas in an actual cycle thermodynamic losses result from the necessity for a temperature rise in the cooling water, and a terminal temperature difference in the condenser. Accordingly, constant-temperature lines have been added to the chart in Fig. 5(*b*), which originally had exhaust pressure lines only. The revised Fig. 5(*b*) appears with this closure.

The authors had not considered the problem of appraising the performance of a mixed-pressure plant. It would seem that each section of such a plant could be appraised separately and a suitable basis of averaging arrived at. The suggested basis of fuel input may well be the most satisfactory for this purpose.

Mr. Hardie mentions the pressure loss from boiler drum to turbine throttle, which of course is not present in a theoretically perfect cycle. This is a practical loss, and presumably the actual plant should be charged with this loss, part of which occurs in the boiler and part in the piping.

Mr. Ireland has requested a basis for using a short-cut formula for computing heat rates of partial regeneration cycles on the assumption that, with the full regeneration heat-rate tables available, it would be possible to derive suitable correction factors for using a short-cut formula. In actual practice, the heater spacing is not ideal in all cases, only a small finite number of heaters are employed, and the same final feed temperature may be achieved using any number of feedwater heaters. For these reasons it does not appear that any simple set of corrections could be developed which would yield satisfactory results under all conditions when applied to the short-cut formula. If Mr. Ireland is thinking in terms of an actual turbine, the authors feel that the best way to accomplish what they believe he wants, the method developed by J. Kenneth Salisbury, referred to by other discussers, should be used, or the older methods of the large-turbine manufacturers.

On the other hand, if Mr. Ireland is thinking in terms of theoretical performance, with only partial regeneration, it is suggested that the results to be obtained from the short-cut formula with corrections could be derived rather easily by superimposing a Rankine cycle on a theoretical regenerative cycle having its initial pressure equal to that of the highest pressure bleed point. The bleed-point pressure would be the saturation pressure corresponding to the final feedwater temperature, and the exhaust pressure of the Rankine unit would have that same value. This suggestion is an application of the thoughts expressed by Commander Dusinberre and Mr. Markson. The heat rate of the regenerative portion of the cycle can be taken from the present paper while the heat rate of the Rankine portion of the cycle may be determined from published tables of theoretical steam rates.[43] The effect of partial regeneration would be covered in the correction factors of the proposed companion paper.

Mr. Meyer suggests that the calculations could be made by

[42] "Performance Test at Ford Motor Company," by W. W. Dulmage and C. J. Walker, *Power*, vol. 85, July, 1941, pp. 72–75.

[43] "Theoretical Steam Rate Tables," by J. H. Keenan and F. G. Keyes, published by THE AMERICAN SOCIETY OF MECHANICAL ENGINEERS, New York, N. Y., 1938.

formulas derived from the concept: "In any cycle in which heat (dQ) is added at variable temperature T (deg abs) and rejected at constant temperature T_s (deg abs) the maximum work obtainable (W_m) is given by" etc., from which he proceeds to derive the formula. This formula is the same as that given in the paper and labeled "inaccurate." The error of this formula is shown in Fig. 3 and comes about because the formula is only correct for a "reversible" cycle, whereas the cycle used by the authors contains an irreversible process whenever the throttle steam is superheated, this irreversible process being the transfer of heat from superheated steam to feedwater, which transfer involves a definite degradation of heat.

Professor Shapiro derives an expression for exhaust-pressure correction which is the equivalent of the one given in the paper. These expressions are exact, regardless of the initial condition of the steam, as long as the exhaust is in the wet region. Therefore there is no error in using Fig. 5(*b*) and Table 1. The authors believe Professor Shapiro must have misread the text since they did not intend to cast any doubt on the usefulness of the exhaust-pressure correction factors. Professor Shapiro's full discussion of the methods of calculation of the theoretical heat rates constitutes a valuable addition to the paper. The authors agree that his "Method 2" is an accurate means of performing the necessary integration, and that, even for the highest pressure cycles, a relatively small number of intervals is satisfactory. A similar method, although with not quite as precise a determination of the feed-pump work, was used in some of the calculations made in producing the heat-rate table. Unfortunately, a few computation errors were made, so that the true value of this method was obscured. Also, small errors in determining feed-pump work made the computations slightly inaccurate at the high pressures, which difficulty seems to have been overcome by Professor Shapiro. Regarding his statement as to the accuracy of the heat-rate table, we believe the figures to be correct within about $\pm$ 3 Btu per kwhr.

Dr. Robinson's remarks concerning the desirability of having weight-flow data available apparently reflect the same viewpoint as is expressed by Commander Dusinberre. The authors do not question the potential value of such information, if it could be prepared. Quite possibly it might be the most advantageous way of handling the reheat cycle for which Commander Dusinberre wants data. If such data were prepared it also would be desirable, as Dr. Robinson points out, to have figures based upon various practical turbine efficiencies.

Mr. Salisbury's remarks, comparing the present paper with his own excellent presentation, point out the differences as well as the similarities in the two approaches to this question of theoretical and practical steam-plant performance. The authors have hopes, with Mr. Salisbury's permission, of using some of his results, in preparing the proposed sequel to the present paper. It is thought that practically all of Mr. Salisbury's work is directly applicable except that, in general, his results must be cast into a somewhat different form. This is because he has dealt with "percentage gains," built up upon the nonextraction cycle, whereas the authors intended to deal with "percentage losses" from the theoretical regenerative cycle.

The authors do not agree with Mr. Salisbury that "it may be found expedient to remove the loss due to boiler-feed-pump work." In their opinion the feed-pump work is not a loss at all in the theoretical cycle, since the pump is a necessary part of the cycle. There are a number of practical ways in which the feed pump has been arranged in practical cycles, varying from a single pump to a separate pump for each of a finite number of feed heaters. It will eventually be necessary to work out the differences between the theoretical cycle infinite-number-of-steps pump and the practical one-or-more-step pump.

The authors appreciate the comments made by Mr. Warren, which present a concise picture of the way in which it is felt these theoretical heat rates will be of use. They also appreciate his constructive interest and consistent support accorded to this project.

Mechanical Features of the Glenville Impulse Turbine

By ARNOLD PFAU,[1] MILWAUKEE, WIS.

At the Glenville Plant of the Nantahala Power and Light Company near Franklin, N. C., is the only large impulse-wheel turbine unit east of the Rockies. Its performance has established a water-wheel efficiency record for the United States of practically 89 per cent. This paper is devoted to descriptive details of the unit, its operations, and performance.

THE Glenville Plant of the Nantahala Power and Light Company is located on the West Fork of the Tuckasegee River about 13 miles east of Franklin, N. C. It has the distinction of being the only large-capacity impulse turbine east of the Rocky Mountains. With a gross head of 1207 ft, a net head at maximum discharge of 1188 ft, and a rated capacity of 30,000 hp at 1150 ft, 27,000 kva, 21,600 kw, its capacity exceeds by far that of the few small impulse turbines in the East.

The Tuckasegee River at Glenville Dam has a drainage area of 39.4 sq miles and an average annual computed flow of 135 cfs. The dam with a height of 150 ft has a net storage volume of 68,000 acre-ft. Since the turbine uses about 275 cfs at full load, this unit will operate at approximately 50 per cent annual load factor, drawing out the available storage and generating power to suit the requirements of the downriver plants most advantageously.

General Operating Details

The Glenville unit is a horizontal-shaft single-jet double-overhung impulse wheel with shaft supported in two bearings and the generator rotor located between them. The turbine is rated 30,000 hp, 1150 ft net head, 257 rpm. One shaft end is extended for coupling to exciter, pilot exciter, and to the independent generator supplying current to the motors driving the flyballs of the governors.

Being of the double-overhung type, the two water wheels, one on each shaft end, constitute two independent hydraulic prime movers, each being provided with its own governor and gate valve, so that the water on one side can be shut off entirely without interfering with the operation of the other. When small outputs of less than 50 per cent are necessary or desirable, a better wheel efficiency can be maintained. Also, the individual control of each water wheel by its own governor assures a double safety, maintaining a control of one half of the output of the unit in case the governor of the other half should refuse to act properly.

This double control, two governors for one single generator, was successfully introduced by the company with which the author is connected and has since become a generally accepted design here and even abroad, not only for double-overhung impulse wheels but also for double-overhung Francis-turbine units, the first of this latter type having been furnished by the author's company in 1913, for the 18,000-hp unit at the Halsey Plant of the Pacific Gas & Electric Company of California.

The Glenville unit is designed for a static head of 1215 ft and rated two times 15,000 bhp under 1150 ft net head at 257 rpm. The generator is rated 27,000 kva maximum, 6600 v, 60 cycles, three phase. It is designed for the full runaway speed which the rotating parts may attain, with both jets wide open under 1150 ft net head and no load on the generator. Speed-and-pressure control of the unit is maintained by the individual governing mechanism of each water-wheel side.

To avoid dangerous pressure rises and surges in the pressure tunnel, which is several miles long, with no surge tank, the change of velocity of water under fluctuating load must be very gradual. To obtain quick response to load changes, the output of the unit must be changed quickly by a corresponding change of water quantity impinging upon the buckets. The most perfect method of quick control would be simply to control the impingement of the jets and to hold the flow-controlling needles stationary, i.e., water-wasting regulation. This is prohibitive when water is to be used economically. Here provision must be made to adjust the flow according to the load demand.

Since the Glenville plant does not permit of quick changes of flow in the tunnel and pressure pipe, it is realized that load increases can be taken care of only if so gradual that no serious pressure drops will be experienced. The two needles controlling the flow are therefore set to stop the flow at an average rate of 120 sec, slowing down near closed position to a rate of about 200 sec, and to accelerate to full flow in about 100 sec. Such rate of closing movement would involve a full runaway of the unit on full sudden load rejection such as is the case when the unit becomes detached from the power system. To hold the momentary speed rise within tolerable limits, the quantity of water directed upon the buckets must be changed more rapidly.

In the older art this was accomplished by moving the needle rapidly and by opening a relief outlet as synchronously as possible to discharge the amount shut off by the needle, and thereafter to close the relief outlet at a rate to prevent undesirable secondary pressure rises in the pipe line; in other words, a "switch-over" of flow out of the needle nozzle to relief outlet. This is ideal only if the two discharges are strictly inversed at all times so that the sum of the two discharges equals the former total discharge, i.e., that the velocity of water in the pipe line is not changed.

A practically perfect method, first introduced by the author's company in connection with the 60,000-hp impulse-wheel unit at the Big Creek 2-A Plant of the Southern California Edison Company, Los Angeles, Calif., is to provide means for diverting quickly the jet from the buckets and to let the flow-controlling needle follow the movement at a rate "independent" of the rate of deflection, but in strict accordance as dictated by the pipe-line characteristics.

The various processes are illustrated in Fig. 1 (*a*) for both relief outlet and jet deflection.

Relief Outlet. In Fig. 1 (*a*) at ordinate A-$A'T$ (governor time) = 0, the flow is 100 per cent (full load of unit). The load is suddenly dropped from A' to $A = 0$. The speed rises, but the flow-controlling needle does not start to move until time B is

---

[1] Consulting Engineer, Hydraulic Department, Allis-Chalmers Manufacturing Company.

Contributed by the Hydraulic Division and presented at the Annual Meeting, New York, N. Y., Nov. 29–Dec. 3, 1943, of The American Society of Mechanical Engineers.

Note: Statements and opinions advanced in papers are to be understood as individual expressions of their authors and not those of the Society.

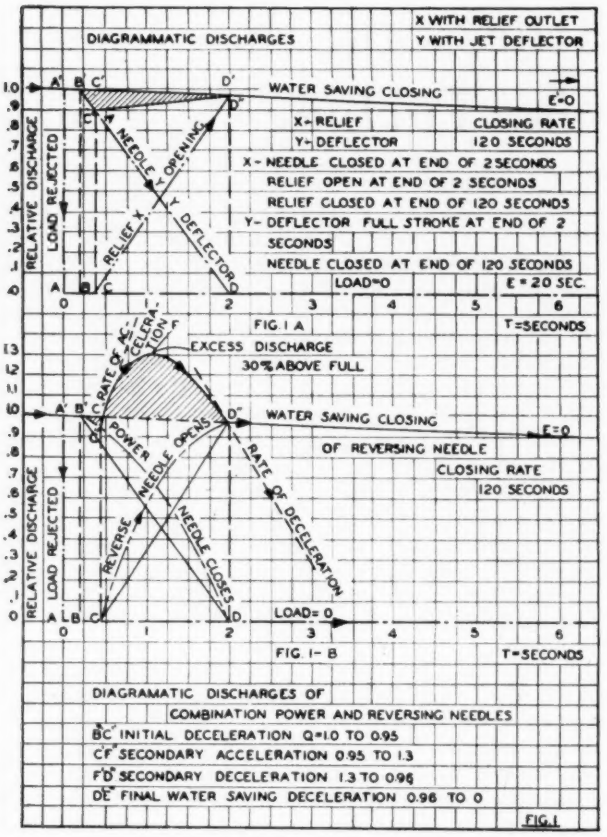


FIG. 1 DIAGRAMMATIC DISCHARGES OF COMBINATION POWER AND REVERSING NEEDLES

$B'C''$—Initial deceleration: $Q = 1.0$ to 0.95
$C''F$—Secondary acceleration: $Q = 0.95$ to 1.3
FD''—Secondary deceleration: $Q = 1.3$ to 0.96
$D''E'$—Final water-saving decelerations: $Q = 0.96$ to 0

reached. The flow through the needle is reduced along line B'-D and the flow upon the buckets is stopped in 2 sec from the beginning of load rejection. The movement of the needle acts upon the relief outlet which begins to open at time C, and its water-saving mechanism immediately starts its relative closing movement at a rate of 120 sec (from C' to E'). The delay BC, during which the relief outlet remains closed, causes a reduction of flow from B' to C'' at the full rate of closure of the needle, thereby producing a material initial pressure wave in the pipe line.

If the relief outlet has a capacity of 100 per cent of that of the needle, it opens the relief outlet wide at the time D, when the needle is closed. However, the relative water-saving movement reduces the flow to D'' instead of D'. If the discharge rates of the needle and relief outlet were linear, the resultant total discharge (being the sum of the ordinates of needle- and of relief-outlet discharges, respectively) would be as indicated by curve C''-D'', and the area $B'D'D''C''B'$ represents the change of velocity in the pipe line. It is obvious that any deviation from the straight lines B'-D and C-D'' causes even more serious changes of water velocity, as illustrated in Fig. 1 (*b*).

Jet Deflector. In Fig. 1 (*b*), the deflector is directly actuated by the governor. Therefore no additional initial delay BC is experienced. The output flow is reduced along line B'-D, and the needle controlling the flow in the pipe line is independently reduced to zero from B' to E'. The undesirable feature of change of resultant flow represented by former area $B'C''D''$ is reduced to $B'D''$. The diagram at once discloses that here the deflector movement from B' to D (taking the place of the former needle movement) can be made as quickly as is mechanically desirable.

Fig. 1 (*b*) represents the case of two reversing needles of approximately parabolic discharge characteristics, resulting in an initial deceleration $B'C''$ until the reversing needle begins to open, and changing suddenly into an acceleration $C''F$, diminishing to zero at F, where the total flow is a maximum, and changing into a deceleration from F to D'', reaching its maximum at D'', when the power needle is closed and the reversing needle wide open, and followed by the gradual deceleration $D''E'$, caused by the water-saving movement of the reversing needle to closed position at the end E' of 120 sec. Serious accidents to pipe lines and loss of life are on record caused by a faulty correlation in movements and discharge characteristics of such reversing needles.

Mechanical Features of Glenville Unit

Main Shaft. The main shaft is a hollow-bored steel forging with integrally forged flanges on each end for bolting the water-wheel runners to it. It is bossed up in the center so that the generator rotor can be brought into position over one of the flanges. It rests in two bearings of 22 in. diam, 18 ft apart. One end is arranged for flexible coupling to the direct-connected exciter.

Bearings. The total rotating weight (water wheels and generator rotor) of about 135 tons is carried in two ring-oiling pedestal-type bearings, each of 1450 sq in. bearing surface, in split, babbitt-lined shells with ball-and-socket seat, which permits of adjustment of the bearing surface in accordance with the deflection of the overhung portion of the shaft carrying the weight of wheel runner and the resultant impact force produced by the jet, which varies as the output of that side of unit varies. The two bearing shells are water-cooled, and lubrication is assured by five oiling rings which pick up the oil from the basin formed in the lower bearing housing and discharge it over the top of the shaft. Thus the normal operation is not in need of outside lubrication under pressure, but is self-contained. However, to facilitate starting the unit, when the contacting bearing surfaces may have become dry, provision is made to use oil under pressure from the oil-pressure system of the governors.

Temperature relays are provided which cause the governors to shut the unit down when the temperature becomes excessive. Excellent results have been obtained with this design of bearing, the largest being those at the Big Creek 2-A Plant with a shaft diameter of 32 in. operating at 250 and 300 rpm, delivering 50- and 60-cycle current at times, depending upon the network served.

Wheel Disks and Buckets. The forged-steel wheel disk is machined all over and is held to the forged-shaft flange by central-recess and ream-fit steel bolts with secured nuts. Twenty-one buckets of cast steel are held to the disk each by three taper ream-fit bolts with secured nuts on either end. From a point of view of mechanical strength, the design is liberal, involving only moderately high stresses of material even under maximum centrifugal force due to runaway speed, as also under conditions of rapid changes of impact force. It is not generally realized fully to what forces such a bucket is exposed, both as to amount and as to duration. At 257 rpm, a bucket passes through the jet 4.3 times per sec. When the full jet impinges, such as is the case here where the pitch is larger than the total length of intersection of the jet on the periphery of impingement, the impact force is 63,000 lb, beginning with zero value when the bucket lip enters the jet, reaching above maximum as long as the full jet impinges on the same bucket and reaching zero value again when the last particle of jet discharges from the bucket. This process takes

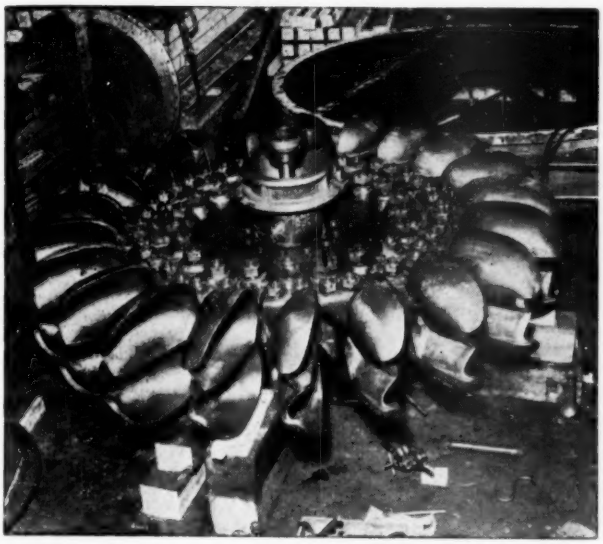


FIG. 2 SHOP-ASSEMBLED DISK AND BUCKETS FOR 10-IN-DIAM JETS

place over about 1/4 of the periphery of the wheel, therefore, in $\frac{1}{4 \times 4.3}$ or about $\frac{1}{17}$ sec.

This intense hammer blow (some practical engineers call it "a swift kick in the pants") must be resisted by the bolts holding the bucket to the disk, in addition to the steady centrifugal force of about 110,000 lb at normal speed, or about 370,000 lb at full runaway speed.

This explains the cause of serious accidents experienced early this century when buckets exploded, due to crystallization of bolts and breakage of bucket castings, and due to weakening on account of pitting because of faulty inlet and discharge angles of the bucket bowl.

Fig. 2 shows the shop-assembled bucket wheel with all bolt holes properly reamed and bolts and buckets fitted and assembled on the wheel disk. The weight of each rotating element is about 37,500 lb.

Nozzle Pipes. In the nozzle pipe, the energy of the flowing water (partly pressure and partly velocity), due to the total available net head of 1188 ft at the entrance to the nozzle pipe is transformed into kinetic energy which is contained in the jet after leaving the orifice. This process of transformation can be

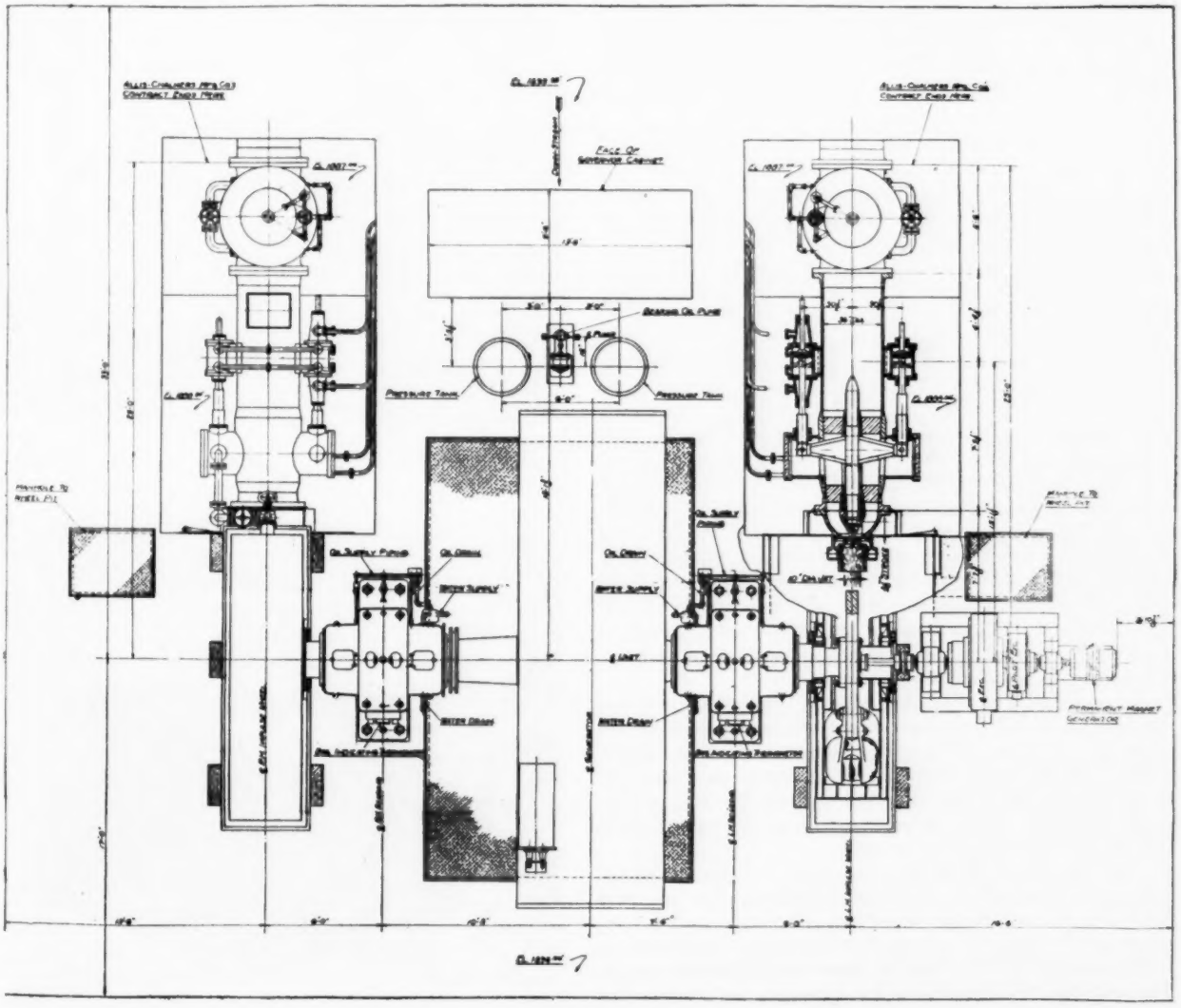


FIG. 3 PLAN OF HYDRAULIC IMPULSE-TURBINE UNIT AT GLENVILLE PLANT

accomplished more or less efficiently, depending upon the design and care of workmanship.

Let C_n be the velocity due to the net head H_n at the entrance to the nozzle pipe, and V the velocity of the jet. Thus the jet efficiency e is

$$e = 1 - \frac{M \times C_n^2}{2} - \frac{M \times V^2}{2} : \frac{M \times C_n^2}{2} \text{ or } \frac{(V)^2}{(C_n)}$$

If the jet velocity were equal to the available net velocity C_n, the efficiency of the jet would be 100 per cent. Naturally, the bucket, transforming the kinetic energy $\frac{M \times V^2}{2}$ in the jet into torque force, producing output, cannot do more than what it receives. This justifies the designer to endeavor to produce the best possible nozzle design. It at once cautions against using multiple-bend piping, such as is involved with a multiple-jet arrangement or crowded settings of the water wheel. This applies equally well to the Francis and propeller types.

The Glenville nozzles are of the patented design first used in 1927, in connection with the 40,000-hp water wheel at the San Francisquito No. 1 Plant of the Bureau of Power and Light, Los Angeles, Calif., and from which to date still issue the largest diameter of jets (14 in.) in the world.

Fig. 3 shows a plan view of the complete unit.

The nozzle pipe is made of welded steel with an inlet diameter of 36 in. for flanged connection to the gate valve. It is straight and slightly tapered, containing a four-arm spider forming the support of the needle stem carrying the steel needle tip. This needle tip is made of two removable parts to facilitate and economize repairs. The stem is provided with a crossarm, the two ends of which project into pockets on either side of the nozzle pipe where they are pivoted to plungers projecting through packing boxes to the outside where they are coupled to the piston rods of the servomotor jointly actuating the needle. The diameters of the plungers are so dimensioned that they partly offset the force tending to hold the needle tip against the orifice from which the jet issues. The downstream end of the nozzle pipe carries the cast-steel nozzle tip with renewable steel throat ring which, when the needle tip seats against it, closes the orifice tightly.

Fig. 4 shows the shop-assembled nozzles with needles, and mounted on them are:

The Jet Deflectors. These are disposed between the nozzle orifice and the rotating buckets, with a minimum space required to maintain compactness of the full jet impinging upon the buckets. The jet deflector surrounds the jet without interference when in neutral position to assure highest output efficiency. The portion surrounding the jet is lined with a renewable steel sleeve. The deflector is hinged and extended at the lower end for pivoted connections into the nozzle-pipe pit where it is coupled to its oil-pressure servomotor.

The orifice part of the nozzle pipe, consisting of the throat ring and needle tip, to a great extent affects the condition (or efficiency) of the jet, and since it is exposed to the high velocity of water issuing, it is essential that it be kept in good condition by frequent examination. For this purpose the supports for the hinges of the stream deflector can be readily moved out of the way for quick access to the orifice.

Upper and Lower Wheel Housing. Fig. 5 shows one of the housings shop-assembled. It is made of welded plate steel, suitably reinforced to minimize breathing. The lower part is completely grouted into the concrete foundation and is machined on top to form the base to which the upper wheel housing is bolted. The rear face is also machined for supporting and surrounding the nozzle pipe. A door is provided for access from the nozzle-

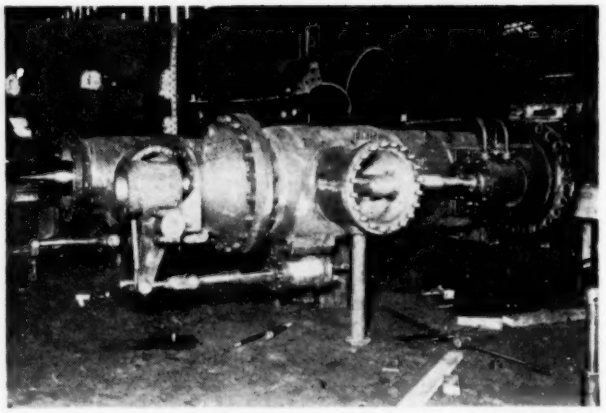


FIG. 4 NOZZLE WITH JET DEFLECTOR AND NEEDLE OPERATING CYLINDERS SET UP IN SHOP

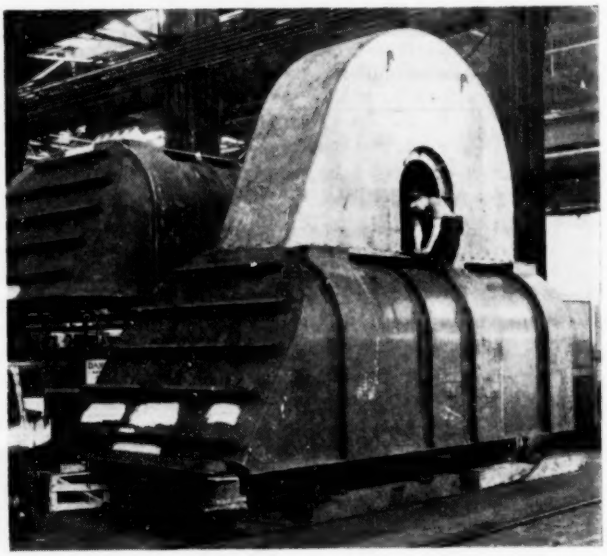


FIG. 5 UPPER AND LOWER WELDED-STEEL-PLATE IMPULSE-WHEEL HOUSINGS



FIG. 6 VIEW OF STILLING POOL

pipe pit to the front of the wheel pit. The downsteam face is inclined and heavily reinforced to be capable of receiving the full impact force of the jet when, due to runaway, the major portion of the jet passes forward without impinging upon the buckets. Proper baffles are provided in order to deflect the discharging water, rather than to throw it back against the buckets, or the orifice.

The upper housing is double-walled for stiffness and for the purpose of ventilation.

Where the main shaft projects through the housing, proper baffles are provided to prevent splash water from escaping along the shaft.

Wheel Pits. These are lined with steel on both sides, the bottom and the ceiling of the outlet.

Inspection shafts for access to the wheel pits are provided on each outer upstream end of the unit. They are covered by floor plates securely bolted to frames to avoid rattling caused by the heavy air-pressure fluctuations in the wheel pit when the jet becomes deflected on sudden load rejections.

Energy Translator. When the jet is fully deflected from the buckets by the sleeve in the jet deflector, it presses against the upper-cylinder portion of the sleeve and thus begins to spread, whereby it loses part of its impact force. This would still be so high as to cause destruction to the tailrace. Fig. 6 is a view of the stilling pool showing the water discharging when the jets are fully deflected. It was designed and built by the engineers of the Aluminum Company of America and is giving very satisfactory service. A combination of splitters is built into the end of the apron and these are assisted by the pool of water in the stilling pool itself. The splitters are wedge-shaped with the point of the wedge facing the unit, three to each water wheel, the center splitter being in line with the center line of the water wheel. This splits the deflected jet into seven parts. That part of the jet impinging against the wedgelike splitter is elevated, while the jet between the splitters and on either side of the end splitters goes out horizontally. This scheme has proved very satisfactory on full-load rejections, no water ever being spilled beyond the confining walls of the stilling pool when the full-load quantity of 270 cfs is discharged under 1188 ft net head with a velocity of about 264 fps.

Hydraulic Brake. The liberal flywheel effect of rotating parts of the two water-wheel runners and the generator rotor would keep the unit revolving for about 40 min after the water is shut off. In case of mechanical accident, this delay in coming to a stop may cause more damage. Provision is made to reduce this time materially by applying a water jet onto the buckets opposite to the direction of rotation. The brake jet is controllable by a hand-operated needle and a gate valve connected to the upstream side of the main gate valve, so that the brake can be applied even when the main gate valve has been closed.

Gate Valves. These are illustrated in Fig. 7, under actual water-pressure test in the shops with a pressure of 550 psi applied to the upstream side of valve plug. The valve, built of cast steel throughout, is of the single-seat parallel-face follower-ring type, as successfully used since 1913, for the eight 24-in. valves at Big Creek No. 1 and No. 2 Plants under heads up to 2350 ft. These are designed to be closed against the full flow of water under the maximum head. The filler ring is an extension, integral with and below the valve plug, which, when the valve is in the wide-open position, fits into the gap otherwise left in the valve housing. It thus protects the valve seat against scouring by sand, etc., passing through the valve during operation, and it serves as a guide for the plug to prevent chattering of the plug during closing or opening movement.

The valve plug is raised and lowered by a hydraulic piston and cylinder, with control valve admitting penstock pressure to the top and bottom, respectively, of the piston for closing and opening the valve.

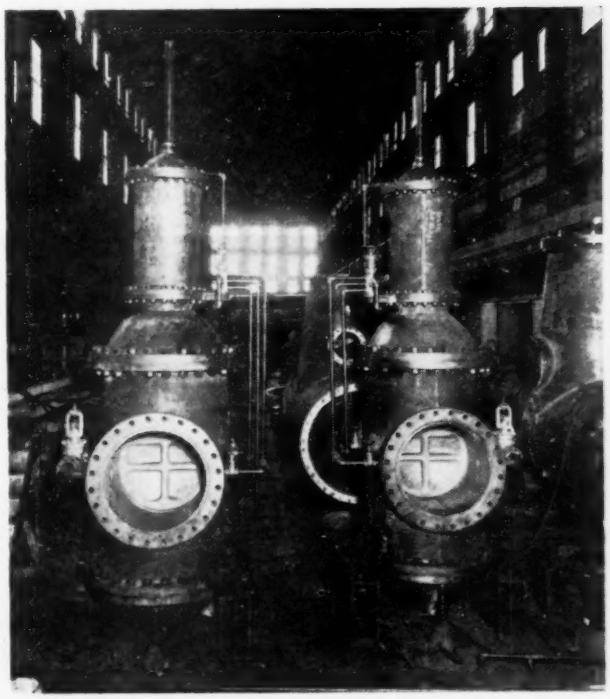


FIG. 7 TWO 36-IN. FOLLOWER-TYPE GATE VALVES FOR GLENVILLE UNIT UNDERGOING SHOP TESTS

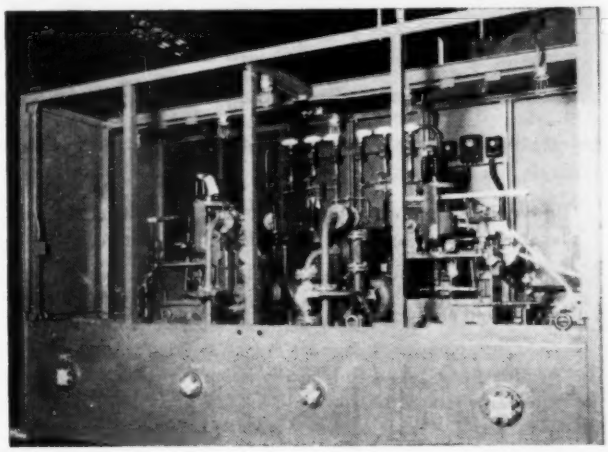


FIG. 8 REAR VIEW OF CABINET GOVERNOR FOR ONE DOUBLE-OVERHUNG IMPULSE WHEEL

Governors. As previously explained and diagrammatically illustrated in Fig. 1, speed and pressure regulation is accomplished by a combination of quick-acting water-wasting jet deflectors. Subsequent gradual movement of the flow-controlling needle is at a rate to assure protection of the pressure pipe line against undesirable pressure variations. Each water-wheel side has its own governor, with two servomotors attached to its nozzle pipe for movement of the needle, and one servomotor located below the nozzle pipe in the nozzle pit for the purpose of actuating the jet deflector.

The actuators of the governors are housed together in a cabinet near the upstream wall of the powerhouse, where the

two oil pump sets, pressure and receiver tanks are also located. Fig. 8 shows the rear of the cabinet opened up for a full view of the equipment and wiring circuits behind the front wall of the cabinet.

The principal elements of a modern governor are:

The speed-responsive part, or flyballs.

The control valve actuating the servomotor controlling the output producing flow of water.

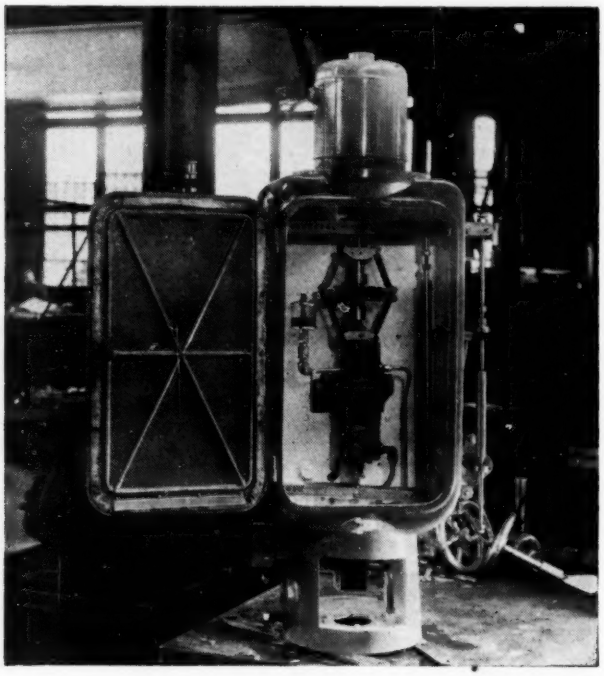


FIG. 9 SUPERSENSITIVE FLYBALLS FOR A RECONSTRUCTED GOVERNOR

The synchronizer for paralleling the unit, or shifting the load.

The speed droop device, for adjusting the difference between no-load and full-load speed.

The load-limiting device.

The solenoid shutdown.

The restoring mechanism which holds the control at rest at constant speed (or load).

The oil-pressure hand control.

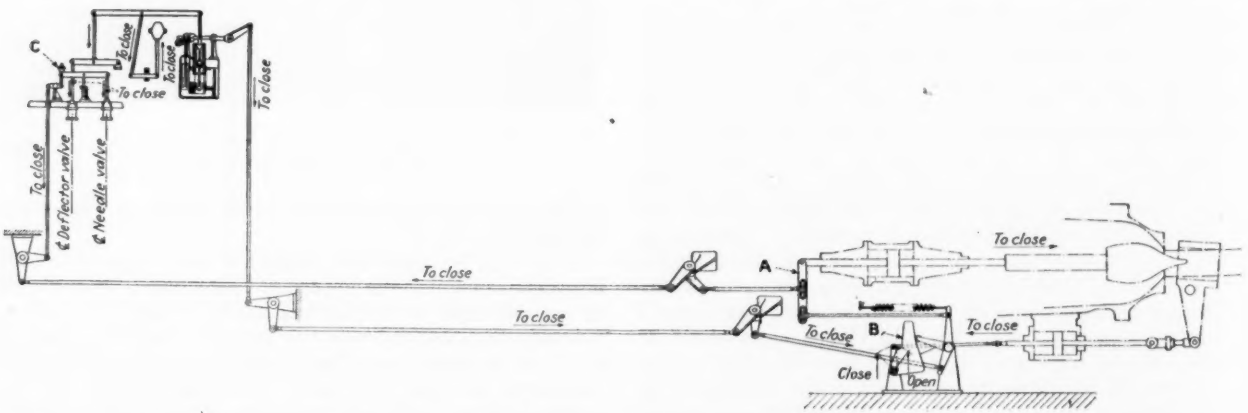
The oil-pressure supply system.

Flyballs. Fig. 9 shows the flyballs of a modernized governor of older design, mounted in a cabinet and directly coupled to the driving a-c motor operating in synchronism with the speed of the turbine. It is of the improved (patented) supersensitive, spring-balanced high-speed design in which the centrifugal forces are directly counteracted by adjustable springs, so that only the resultant governor force is transmitted to the flyball collar, no pivoted joints being employed. The flyball collar is flexibly coupled (however, without lost movement) to a stem which rotates with the flyballs and serves as a pilot for the servomotor actuating the levers leading to the control valve. Thus the pilot describes a high-speed rotary movement which, combined with the axial movement on speed changes, requires a minimum of energy for its operation, but produces a fixed force in the differential oil-pressure servomotor actuating the leverage leading to the control valve. The speed-responsive element is thus relieved of any mechanical duty, but acts merely as a speed-responsive device, which, by means of the servomotor, at once produces a liberal force available at the slightest speed change.

These flyballs respond safely to 0.01 per cent above and below speed, so that prompt control of the output is assured, resulting in sensitive speed control with practically entire absence of tendency to hunt. The servomotor is coupled to the center of a single-arm lever, one end being adjustable by a handwheel or by an electric motor for switchboard control, starting, paralleling, or stopping the unit, and for changing the output when paralleled.

The opposite lever end is pivoted to the main floating lever, one end of which actuates the control valve, the opposite end receiving the movement from the servomotor actuating the output control of the unit. An adjustable relay-compensating oil-dashpot device is inserted into the relay connection, which permits of small droop compensation when the movement of the servomotor is slow, and a temporary larger droop on quick movement with gradual return to the smaller droop, and which is adjustable from 6 per cent to $1^1/_2$, or even 0 per cent when the unit does not operate in parallel with other alternators.

An adjustable load-limit device, either hand- or remote-


C
To close
To close
To close

electric-operated, permits of holding the output within desired upper limits without preventing complete no-load action in case of total load rejection.

The solenoid shutdown device acts upon the load-limit device for the purpose of complete shutdown of the unit in case of failure of current to the flyball motor, or for any other protective features, such as excessive bearing temperature, overload, or overvoltage.

Where no independent mechanical hand control is combined with the main servomotor, a hand control by means of oil pressure is provided in order that the automatic parts of the governor can be examined or repaired without causing a shutdown of the unit.

The governors of the Nantahala unit are performing a combination of deflector and needle movement, involving two control valves and a combination relay mechanism. This is illustrated diagrammatically in Fig. 10.

The floating lever actuated by the flyball servomotor is pivoted not directly to a control valve but to the center of a single-arm lever with a fixed point on one end and connection on the opposite end to the control valve actuating the servomotor which moves the jet deflector, the movement of which is transmitted to a relay shaft carrying a lever B with a cam against which a roller is held by a tension spring. The roller is part of a lever keyed to a relay shaft carrying two levers, one with relay connection to the compensating oil dashpot actuating the end of the floating lever for the purpose of restoring neutral or dead-beat condition.

There is another lever keyed also to the relay shaft which transmits the movement of the roller to a floating lever, the outer end A of which receives the movement of the servomotor actuating the needle or, if the latter is stationary, serves as fulcrum and thus causes a second relay movement transmitted over a double-arm lever to the control valve actuating the needle. By proper cam movement the final dead beat or neutral position of the control is such that the jet deflector touches the jet so that water is not wasted, nor is there a dead or lost active movement of jet deflector, all of which assures prompt speed control.

Since the deflector can act quickly while the needle must move slowly only by reason of the rate-limit devices controlling the flow of oil directly in the needle servomotor, as required by the long pressure pipe line, the stroke at point C may cause an excessive stroke of needle-control-valve piston. To prevent this the fulcrum of this lever is made flexible; however, always tending to restore to normal position.

By means of a handwheel at C, the relative position can be changed between jet deflector and power needle.

Likewise, the shape of the cam surface of lever B can be so formed that at small outputs the jet deflector does not clear the jet until it has to assume a certain size in accordance with the output demand.

This particular feature has proved especially valuable, as will be set forth in the discussion of the special requirements of speed control of the local power system which the Glenville unit is to take care of at times.

Flyball Drive. Current to the motors driving the flyballs of both governors is supplied by an independent generator directly coupled to the exciter of the generator. It is of the permanent-magnet principle, 2-phase with common circuit for connection to the two flyball motors.

The oil-pressure system serves each governor independently, or can be interconnected. The 15-hp a-c-motor-driven oil pumps pick up the oil from the two-compartment receiver tank directly below, and deliver it to the respective pressure tank, a check valve preventing backflow when the pump does not deliver oil under pressure. Combined with the pump is an unloader valve which opens when an oil pressure of 300 psi is reached and closes at a lower limit of about 270 psi in the pressure tank. With the unloader is combined a relay switch which shuts the motor down when unloading and starts it when oil must again be delivered to the pressure tank.

The oil returning from the governor discharges over a strainer into the receiver tank. All individual elements of this pump system are arranged to be readily accessible.

Setting of Unit Due to Flood Conditions. Fig. 11 shows the complete hydroelectric unit. It will be noted that no windows are provided at elevations below the top of the generator stator.

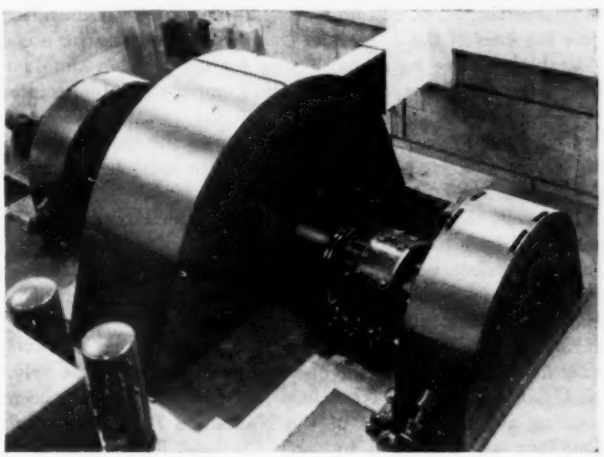


FIG. 11 INTERIOR OF STATION SHOWING TURBINE AND GENERATOR

The powerhouse is located in a gorge, and abnormal floods in the river might raise the water level so far above the floor that even the top of the generator would be submerged. This would drown the two water wheels, thereby materially reducing the output, if not rendering operation impossible. Since such floods are exceptional and of short duration only, it would be a waste of available head if the unit were placed safely above exceptional flood-water elevations. It was calculated that the kilowatthours permanently lost in normal times by this higher setting (and loss of head) would exceed the loss of kilowatthours output during the floods, with plant shut down completely. It was therefore economically feasible to locate the unit for the normal head condition, and merely shut it down during flood periods by providing tight-shutting gates at each wheel-pit outlet to keep the water from entering the wheel housings and putting them under pressure.

A system has been worked out which would permit setting the unit as high above lowest tail-water level as possible, putting the wheel housing under slight vacuum at the high head and under slight back pressure at extreme flood levels, however, without drowning the buckets. With this system the water level is held at safe distance by supplying compressed air, similar to what is now accomplished with Francis and propeller units, operated idly as synchronous condensers, so that they revolve in air instead of absorbing considerable power when revolving idly and submerged at normal speed. If the flood periods at Glenville were of longer duration it would have been economically feasible to provide for such an arrangement including auxiliary compressor equipment, which can be made automatic in case floods arrive unexpectedly.

Pressure and Speed Control. With a pressure conduit exceeding 16,000 ft in length, the critical time $\frac{2L}{a}$ at which a maximum

pressure rise of $\frac{aV}{g}$ will result is over 8 sec. Therefore, it necessitates a very gradual deceleration and acceleration of water on sudden load rejections and load increases in order to avoid pressure variations of a destructive value. Pressure control is assured by the rate of movement of the flow-controlling needles, which is fixed by admitting the oil into and out of the needle servomotors at a rate individual for each position of needle, entirely independent of the rate of governor action.

The system of the Nantahala Power and Light Company is connected through a rather long transmission line over mountainous country with the Aluminum Company's transmission line at Santeetlah, N. C. From Santeetlah the power is transmitted over the lines of the Aluminum Company of America for a considerable distance to Alcoa, Tenn., for use by the Aluminum Company. At Alcoa, the Aluminum Company's system is interconnected with the T.V.A. system.

Under these conditions, the regulation of the system will not be seriously affected when one of its large units becomes suddenly detached.

However, there are times when the Nantahala system is disconnected from the Aluminum Company's system at Santeetlah and is therefore isolated from both the Aluminum Company and T.V.A. systems. When this occurs, the system load of the Nantahala Power and Light Company amounts to a maximum of approximately 5000 kw. This remaining load has relatively wide fluctuations due to the operation of a paper mill at Sylva, N. C. Except for the Nantahala and Glenville plants, the remaining generator plants of the Nantahala Power and Light Company are too small to carry the load fluctuations satisfactorily.

The Glenville Plant was put into operation several months before the Nantahala Plant was completed.

The power company does not plan to use the Nantahala Plant for regulation of its local load due to the fact that it is a Francis-type turbine with a long tunnel and pipe line, operating under an exceptionally high head which requires slower governor-operating time, and which subjects the turbine parts to extreme cavitation and wear when operated at light loads.

It is therefore the duty of the Glenville unit to take care of the speed control when the load is restricted to the local system alone.

Under such conditions, prompter action is required than can be secured with the slow rate of movement of the needle. In other words, the water-wasting stream deflector must actively participate in the control of the momentary load changes of the isolated, small system.

When the unit operates in parallel with the Aluminum Company system, and in turn when that system is operating in parallel with T.V.A., the flywheel effect of all the rotating masses operating in synchronism is so large that even large, sudden load changes will cause only gradual changes in speed; in fact, so gradual that the slow-moving needle may be adequate to take care of it without causing the stream deflector to cut into the jet on sudden load rejections, i.e., if such load rejections do not increase the frequency more than 62 cycles.

At loads above 4000 kw per jet, the relative position of the deflector and needle is such that the deflector does not disturb the water stream issuing from the needle valve and therefore in no way influences the efficient operation of the unit.

At loads below 4000 kw per jet, the relation is such that the stream deflector remains partly in the jet, thereby deflecting some water from the buckets so as to be ready to back out of the jet promptly on load increases which the needle could not take care of by reasons of its slow rate of movement. Thus a materially better speed control is obtained for the small isolated system, although it inevitably involves a slight wastage of water at loads below 4000 kw.

Two requests of the power company had to be met:

1 That the frequency of the machine following full load rejection should be held to a minimum possible value, and that the unit should be promptly brought back to synchronous speed so as to be ready for prompt paralleling in a minimum length of time.

2 That penstock water-pressure swings, following full-load rejections and during light-load operation, should be held to a minimum.

To meet the first requirements, an overspeed switch was adjusted to close contacts at approximately 62 cycles. This over-

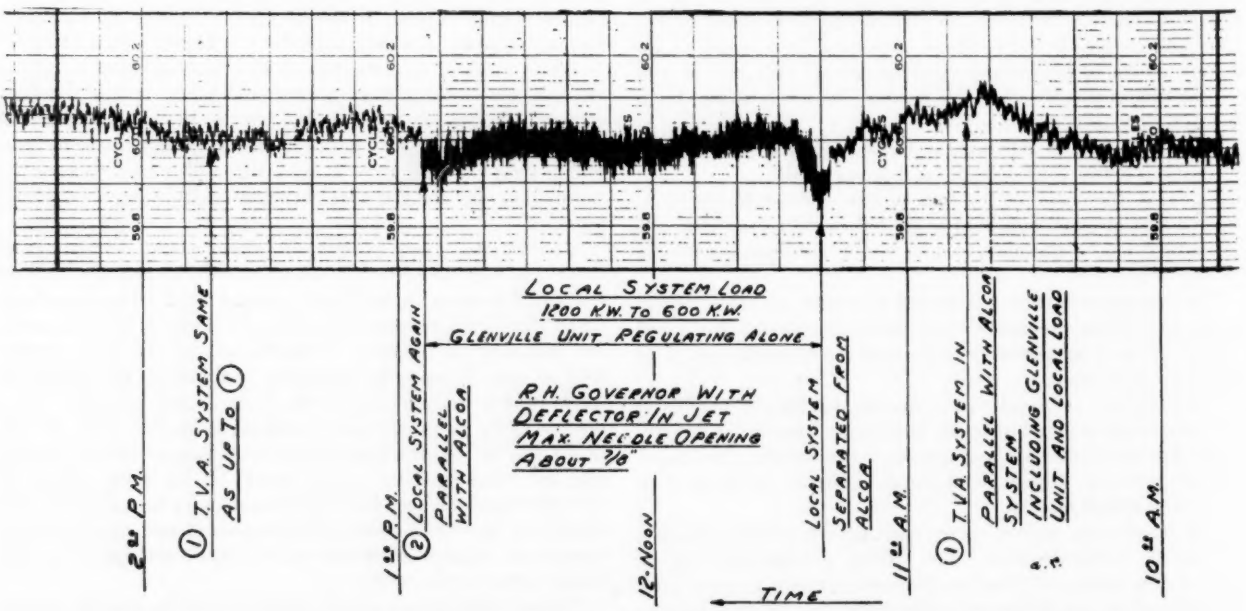


FIG. 12 RECORD OF CYCLES ON MARCH 31, 1942, UNDER DIFFERENT SYSTEM OPERATION OF GLENVILLE UNIT
(Voltage-limiting device is subsequently adjusted to release 15 sec earlier to allow voltage to return to normal in 40 sec after trip of breaker.)

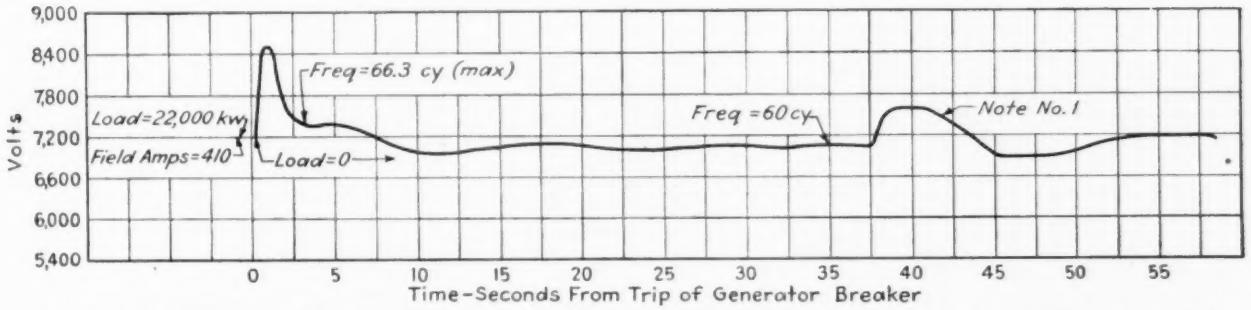


FIG. 13 CURVE SHOWING HOW VOLTAGE AT GENERATOR TERMINALS RETURNS TO NORMAL AFTER A LOAD REJECTION OF 22,000 KW

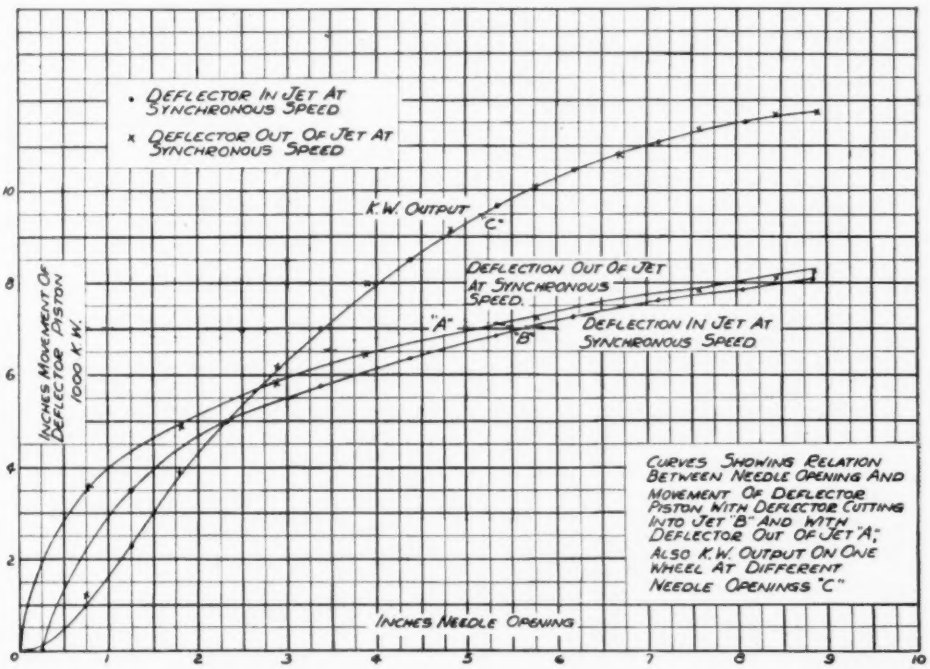


FIG. 14 CURVES SHOWING RELATION BETWEEN NEEDLE OPENING AND MOVEMENT OF DEFLECTOR PISTON WITH DEFLECTOR CUTTING INTO JET B, AND WITH DEFLECTOR OUT OF JET A; ALSO KW OUTPUT ON ONE WHEEL AT DIFFERENT NEEDLE OPENINGS, C

speed switch energizes a solenoid-operated valve to admit oil pressure to the deflector and also energizes the circuit to the synchronizing motor to operate it in the lowering direction. The synchronizing motor continues to operate until it returns the mechanism to the speed no-load position where the motor is stopped by means of a limit switch. The solenoid remains energized until the frequency returns to approximately 61.5 cycles. By means of these two devices, the latter of which was suggested by H. H. Gnuse, Jr., electrical engineer of the power company, the speed rise on rejection of 22,000 kw has been held to 66.3 cycles, as measured by a standard frequency meter, and the machine speed and voltage have returned to normal values within 35 sec, so that the unit was ready to be reparalleled with the system. These tests were made with a speed-droop setting of approximately 5 per cent.

During this load rejection, the penstock surges were very minor due primarily to the fact that, with the present adjustments, the needle never completely closes until the gate-limit adjustment has been operated to the zero position. The slight opening which remains in the needle valve very effectively prevents the customary penstock pressure surges which are obtained upon complete closure of such a valve.

Fig. 12 shows a record of the cycles on March 31, 1942. Up to point marked (1) it shows the cycles of the systems, Nantahala, Glenville, Alcoa, and T.V.A. interconnected, the Glenville unit operating with one water-wheel side only. At point (1) Glenville was detached from T.V.A. and Alcoa, to take care of the Nantahala system alone, with units at Franklin Plant and Bryson City operating on blocked governors to limit all frequency control to one Glenville governor. The load was around 600 kw with a total maximum of 1200 kw.

It will be noted that even one governor of the Glenville unit held the cycles within very satisfactory limits.

Fig. 13 is a record taken August 11, 1943, showing that voltage at generator terminals returns to normal after a sudden load rejection of 22,000 kw. The curve also indicates that the speed returned to normal 35 sec after the load change.

Fig. 14 shows the kilowatt output curve C and the inch movements of the servomotor piston actuating the deflector, curve A when the deflector does not cut into the jet under stationary needle positions, and B when it is set to cut into the jet. The points marked X on curve C apply to curve A, and those marked (·) apply to curve B. It will be noted that the outputs for the various needle openings do not vary appreciably whether the deflector cuts into the jet or not at normal speed. The adjustment, it will be noted, is so made that, at small jets (or needle

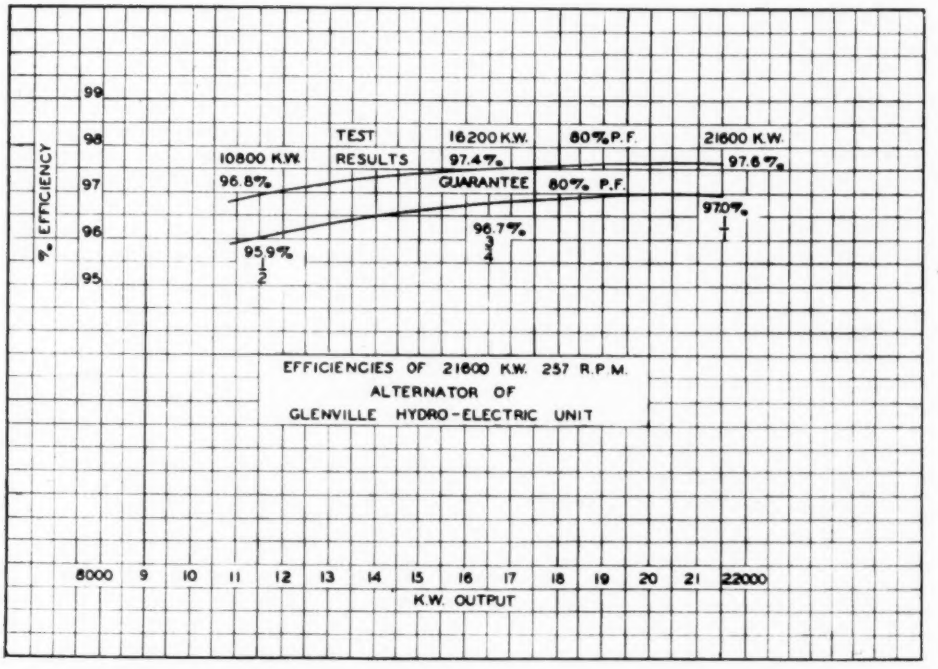


FIG. 15 EFFICIENCIES OF 21,500-KW 257-RPM ALTERNATOR OF GLENVILLE UNIT

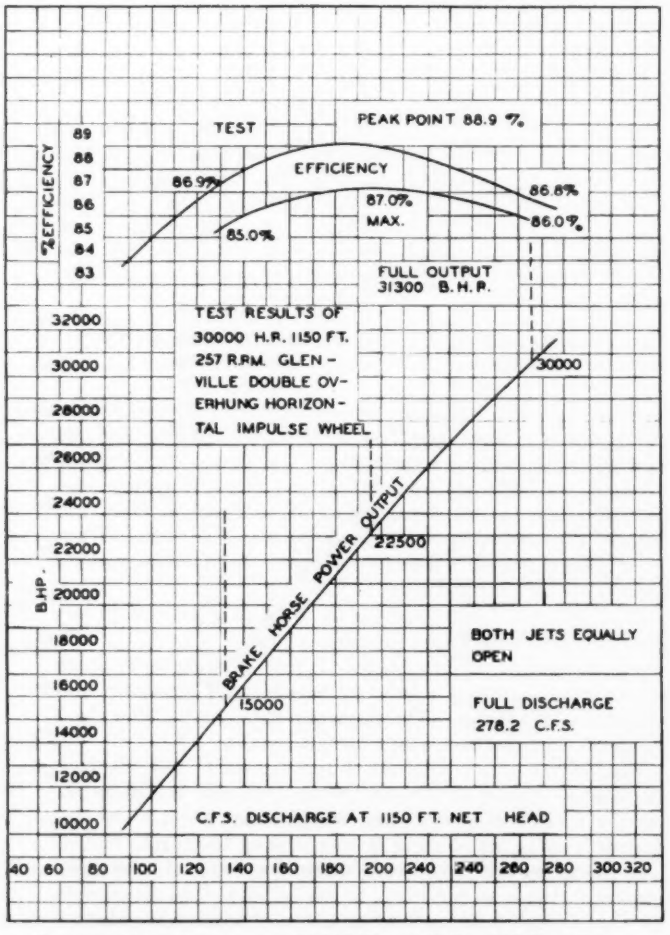


FIG. 16 TEST RESULTS OF 30,000-HP, 1150-FT, 257-RPM GLENVILLE DOUBLE OVERHUNG HORIZONTAL IMPULSE WHEEL

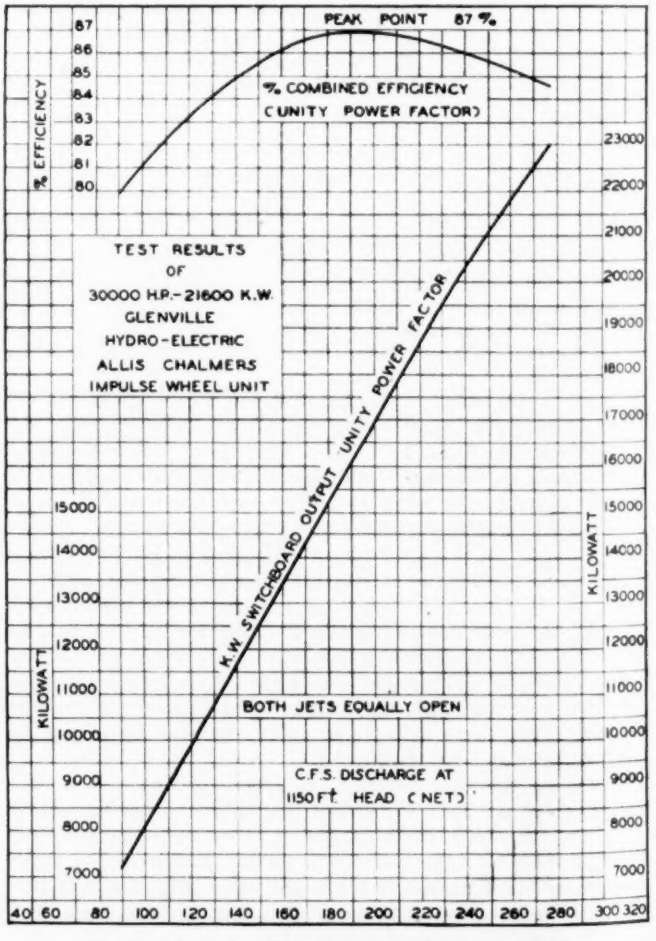


FIG. 17 OVER-ALL EFFICIENCIES OF GLENVILLE UNIT

strokes), the deflector cuts into the jet and is clear of the jet at larger needle strokes or outputs. This is desirable to insure equally close regulation on very small loads of the isolated Nantahala system.

Generator. The generator associated with this unit is rated 27,000 kva, 80 per cent power factor, 6600 v, three phase, 60 cycles, 257 rpm. The rotor is designed to provide the required 4,400,000 lb-ft² moment of inertia without the use of a separate flywheel. The poles are dovetailed into a laminated "floating" rim which is keyed to the fabricated spider. A damper winding is provided in the pole faces. The damper winding has no connections between poles but has the bars silver-soldered into the pole end plates. The stator core is made up of low-loss high-permeability silicon-steel laminations supported in a box-type welded plate steel yoke. The stator winding is of the double-layer lap-wound type, designed for minimum eddy-current loss.

A number of standard 10-ohm temperature-detector coils are embedded between coil sides. The generator is completely enclosed and is cooled by air circulated by axial-flow fans mounted on the generator rotor. Surface coolers are mounted below the generator to maintain the temperature of the in-going air to the generator at not more than 40 C. A main exciter and pilot exciter are direct-connected to the shaft. A rocking-contact-type regulator in the main exciter field controls the generator voltage.

The performance of this generator, as indicated by the tests made in August, 1942, and by the operating records is fully satisfactory. Conventional efficiency is more than 0.5 per cent above guaranteed values. Operating temperatures are well within those recommended by the standards.

Efficiency Tests

To determine the efficiencies of the entire hydroelectric unit, tests were made at the power plant, first to establish the generator efficiency to arrive at the actual brake-horsepower-output curve at the generator shaft.

The generator tests were made by purchasers' engineers and according to the A.I.E.E. Test Code.

Fig. 15 shows the guaranteed and the generator efficiencies actually obtained, indicating a substantial margin above the guarantees.

The water-wheel efficiency of the unit was determined by Dr. Norman R. Gibson's method, and in accordance with the rules of the A.S.M.E. Test Code in force.

Fig. 16 shows these guaranteed and the actually obtained efficiencies, indicating also a substantial margin above guarantees made.

Since the entire hydroelectric unit was designed and built "under one roof," so to speak, the individual test efficiencies of water wheel and of generator can be combined into one over-all efficiency from cfs discharge at normal contract net head to kilowatt output measured. These values are plotted in Fig. 17, as is also the corresponding over-all efficiencies as computed from the individual guarantees of water-wheel and generator efficiencies.

For a hydroelectric unit designed, built, and guaranteed by one single manufacturer, the "undivided responsibility" would permit of a simplification of the tests, in that a guarantee made from "water to switchboard" eliminates the necessity of establishing the individual efficiencies of the generator and turbine.

The Glenville unit is the only large impulse-wheel unit east of the Rockies, and its performance establishes a record in this country as regards water-wheel efficiency of practically 89 per cent.

Acknowledgments

The writer wishes to express his appreciation and thanks to Mr. J. E. S. Thorpe, president of the Nantahala Power and Light Company, and to his staff for the valuable assistance and co-operation rendered by contributing plans, photographs, and operating data.

Discussion

Robert Lowy.[2] Having had 25 years of experience in the construction of European Pelton wheels, the writer would like to point out certain differences between the trends of construction abroad and in this country, as follows:

1 The safety of the construction indicated in the paper is highly insured. The author himself mentions that the design, from a viewpoint of mechanical strength, is liberal. It may even be that the construction does not give a true picture of the current utilization of materials in the United States.

There was a great difference in Europe between constructions before and after the first world war; economy in the use of materials was far greater after the war.

This condition does not appear to have existed to anything like the same extent in the United States, owing to the fact that losses through the war were not as great, and there was no impoverishment. Perhaps this may change after the present war. However, we must not forget that, at the same time, impoverishment in Europe will be far greater than in America, and utilization of materials and labor in Europe will be forcibly magnified.

The construction of the Glenville plant as described is surely far safer than European installations. The principle of streamlining is also more highly developed than is the usual European practice.

2 A pertinent example is the construction of a turbine and generator for runaway speed. The price difference between a wheel which is built for a 1.8 runaway speed and for the runaway speed of only 1.2 is not very great; but, for the generator, the price difference is a multiple of the generator price. The runaway speed will in all likelihood never be reached. The European point of view is now that such constructions for complete runaway have in some way an exaggerated safety and indicate use of superfluous materials and labor. This amounts to a loss of national wealth. It would be the same as though a dam built for a 200-ft head were used for a 150-ft head. In Europe all large Pelton turbines have a special safety device which prevents racing of the turbine. This control is independent of the oil governor and also of the system of speed regulation. The safety device works hydraulically with the water pressure, sometimes with dead weight. Such constructions are indicated in a previous paper[3] by the writer.

A fundamental rule in using such safety devices is the instruction that these contrivances have to be tested either weekly or monthly. In this way operating personnel will become accustomed to having the unit running at higher speeds, limited by the safety device, and will not become alarmed in the event of racing.

Nevertheless, the generators for the Pelton plants in Europe are built up to date for the runaway speed, but owing to the safety device employed, the safety factor of the generator construction is tacitly lowered. Even with such construction, the safety of such units is far greater than that of steam turbines.

It seems there now exists an understanding among the producers in Europe to make the customer acquainted with the safety device to show that such a safety arrangement is more

[2] Baldwin Locomotive Works, Philadelphia, Pa. Mem. A.S.M.E.
[3] Yearbook of Waterpower, 1930–1931.

practical, more economical, and really provides a sufficient factor of safety. In a few years, maybe directly after the war, the construction of such turbine units to take care of runaway speed will be eliminated, and the arrangement of an efficient safety device will be all that is necessary, as in the case of steam turbines. As the price of the safety device is small in comparison with the construction for runaway speed, a real saving results. These remarks intend only to show the trend in Europe without recommending the use of them under existing economic conditions.

In studying the data given in the description of the Glenville Plant, the writer fails to find the closing time of the deflector servomotor. It would be interesting to know these relations because the speed rise by rejections of full power seems to be extremely high. The writer's experience indicates that to attain a smaller speed rise by full-power rejections is not so difficult. It is most difficult to obtain relatively small speed rise with small load rejection.

D. J. McCormack.[4] It is to be regretted that other American manufacturers have not accomplished any real development work on impulse wheels for many years past. European turbine builders have had engineers specializing on impulse turbines, and exhaustive studies and tests have been made continually to improve the results. Consequently, even 15 years ago, they were obtaining 89 to 91 per cent efficiency on field tests of impulse turbines. At that time American manufacturers thought they were achieving great results if they got 84.5 to 85.5 per cent efficiency. As a result, some of the large American installations were obsolete when they were installed. This turbine under discussion, showing 89 per cent efficiency on field test, is not in any way exceptional. If it showed 91 per cent efficiency or over, that would be notable. Seven years ago, the writer's company had field tests of 88 per cent on small units of only 2700 and 7000 hp.

Upon questioning, the author has stated that he would not take a chance with the American steel foundries, and cast the buckets solid with the disk or in a continuous ring. To date the writer's company has supplied 75 such runners up to 90 in. impulse diameter, which have stood up in service and are continuing to give fine results. Excellent castings are being produced which show up well under most rigid inspection. The construction is stronger, and a greater number of buckets can be used to obtain higher efficiencies. All buckets wear alike, so there is no advantage in replacing just one bucket. A whole new runner can be supplied for less than the cost of one set of buckets.

The author evidently does not favor the use of elbow-type nozzles. Of course, the answer to this is that higher efficiencies are being obtained with the elbow-type nozzle than with the straight-line nozzle originally developed by The Pelton Water Wheel Company, and the one under discussion which is only a slight modification of the Pelton design. However, the elbow-type nozzle must be designed properly.

E. B. Strowger.[5] The author has indicated that the pressure conduit of the Glenville unit is something over 16,000 ft long, and that no surge tank is installed. Further, the critical time of the pipe line is 8 sec. As a consequence, a long time of closure was chosen for deceleration of the flow. While the jet deflector acts to unload the wheel in about 2 sec, the needle stroke is timed to about 100 sec for full load.

The plant was tested by the Gibson method and, in view of the foregoing conditions, it may be of interest to describe briefly the application of this method and the results obtained. On

[4] Sales Manager, S. Morgan Smith Company, York, Pa. Mem. A.S.M.E.

[5] Hydraulic Engineer, The Niagara Falls Power Company, Niagara Falls, N. Y. Mem. A.S.M.E.

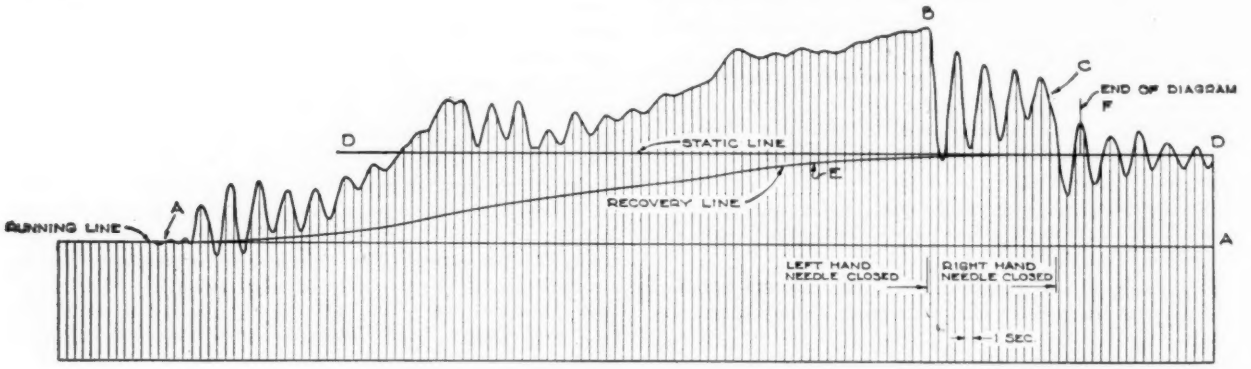


Fig. 18 Gibson Diagram 100 Per Cent Nozzle Opening
(Measured cubic feet per ser second, 280.1.)

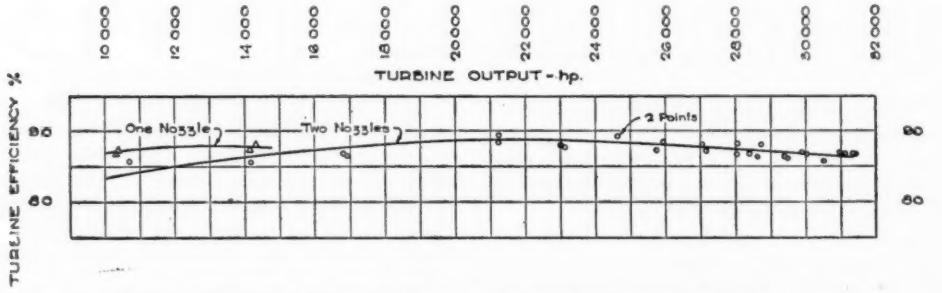


Fig. 19 Turbine-Efficiency Versus Turbine-Horsepower Curves

account of the long closing time, it was necessary to utilize a relatively long length of conduit in order to secure a pressure-time diagram of satisfactory size. The Gibson piezometers were therefore placed 378 ft apart. Using this length of pipe, the differential pressure-time diagram shown in Fig. 18 of this discussion, was obtained for the rejection of full load. The velocity in the pipe line was reduced from about 10 fps to zero during the gate closure.

The delineation of this diagram shows an area of approximately $13^1/_2$ sq in., which corresponds to a discharge of 280 cfs flowing in the pipe just before closure started. During each test run, the two nozzle openings were adjusted to the same value, and it was assumed that each wheel used 50 per cent of the total discharge. The timing of the two needles was not adjusted prior to the test to exactly the same value. For the diagram shown, the left-hand needle had a closing time of 88 sec, and the right-hand needle had a timing of 103 sec by stop-watch measurement. This can be checked from the diagram by counting the second marks from *A* to *B* for the left-hand needle and from *A* to *C* for the right-hand needle. *A*-*A* is the running line of the diagram, *D*-*D* the static line, and *A*-*E* the recovery line. The end of the diagram is at *F*.

Since the author showed the efficiency curve of the wheel plotted with cfs as abscissas, Fig. 19 is presented to show the variation of efficiency with turbine horsepower. The test points are shown on the curve which is very flat from 10,000 to 31,000 hp.

Author's Closure

Dr. Lowy's remarks that the safety factors of American waterwheel designs are materially higher than those of Europe are undisputed. It is a question as to whether the element of safety is to be invested in the unit itself, or into a safety device as an auxiliary. Today many power companies, well experienced by long years of operation of units, still prefer to witness a unit operating safely at its highest runaway speed without a safety device, because such a safety device does not guarantee absolute absence from failure even when its action is being witnessed during one test case.

Mr. McCormack's statement that field tests made seven years ago with units of his company's make showed efficiencies of 88 per cent should have been backed by a proof of authenticity equal to that of the Glenville test. It may be stated also that the author's company built impulse wheels with straight-flow needle-controlled nozzles as early as 1908, although not yet of the capacities of the world record as to physical size of the wheel at San Francisquito No. 1 plant of the Bureau of Power and Light, Los Angeles, Calif.

Mr. Strowger has answered Dr. Lowy's question by stating that the stream deflectors are moved in two seconds. This does not preclude the possibility of even a quicker rate if it should be desired.

Efficiency Analysis of Pelton Wheels

By ROBERT LOWY,[1] PHILADELPHIA, PA.

This paper is devoted to a discussion of the various flow losses in a Pelton bucket. Special attention is given to whether or not such losses are avoidable. Three phases of flow are investigated in detail, i.e., the entrance, the main flow, and the outlet. The author describes the application of a new method to study such movements. The investigation is carried out on a stationary bucket with a jet having the same entrance conditions as the jet on a rotating bucket. The influence of the lip on the entrance conditions is shown by example, and the conditions in the deflected part of the jet are indicated. The loss through the deflected jet is shown in kinetographic representation. A notable loss due to crossing of streamlines on a bucket is discussed. Finally, a list of all possible losses is tabulated.

THE efficiency of Pelton wheels heretofore built has been relatively high, and it is probable that the securing of such good efficiencies is the cause of the lack of much close study and analysis as applied to this type of unit. On the other hand, more study has been given to the reaction type of hydraulic turbines, both of the Francis and propeller type, due to the past necessity for improving the efficiencies of such units.

A stage has now been reached, however, where efficiencies of the reaction type often surpass those usually obtained from the impulse type; and it seems desirable to develop methods whereby the impulse-wheel efficiencies may be raised as the result of analyzing the various losses with a view to reducing them.

Thus it became obvious that the current simplified theory is not sufficient, and that a more exact and comprehensive examination of the flow would be necessary. The investigation of the flow of a jet on a revolving bucket is very complicated, and a complete theoretical examination is not feasible. It is possible to find certain hydraulic potential motions which have some resemblance to the flow mentioned; but these examples are relatively far from the true condition. Nevertheless, they are of great help in arriving at a better understanding and a clearer explanation of the actual phenomena.

Pelton-Wheel Nozzle and Bucket Details

The essential parts of a Pelton wheel involved in this analysis are the nozzle and the bucket. The nozzle consists of the orifice ring and the needle. Both parts form the control valve for the power-supply line. The bucket consists of two ellipsoidal half-shells connected with a common middle edge, the splitter. The outer edge of the bucket is provided with a lip which varies greatly in form for various designs. The lip results from the need to form a suitable entrance for the jet coming from the nozzle.

One of the principal differences in the general appearance of buckets lies in the depth. There are flat and relatively deep buckets. Nevertheless a practical investigation reveals that the relative depth has no determining influence on the efficiency, regardless of the specific speed.

The efficiency of a complete wheel, obviously, can be divided into efficiency of the nozzle and efficiency of the wheel itself, these parts being absolutely independent of each other.

The efficiency of a nozzle can be found by direct measurements; and it has been established that, in general, a loss of 2 to 3 per cent can be attributed to this part of the unit. A precise test of a special nozzle and needle at full opening gave the highest efficiency of 99.8 per cent. At 15.4 per cent opening the efficiency was 98.1 per cent. Material improvement of these values is not possible.

The efficiency of the wheel itself results from a great number of different losses. All these losses are relatively small, but in total they are considerable, so that the complete efficiency of a Pelton wheel reaches a maximum of 87 to 91 per cent.

Any increase in the efficiency can be obtained only by reducing, one by one, the separate losses. Therefore it is particularly essential to determine all the losses and to know how to deal with them.

This study will consider all losses in a bucket, and special attention will be given as to whether or not the loss is inevitable.

Losses in Pelton-Wheel Bucket

It has been found in many practical examples that low efficiency occurs mostly due to losses which are not known generally, and which are in some degree avoidable.

In considering the analysis of the losses, first we have those due to extraneous forces which are not dependent upon the flow. These are mechanical losses in friction in the bearings, and the air resistance of the rotating wheel. Both are inevitable and have to be minimized by proper adjustment.

Concerning the losses dependent upon the flow, we must distinguish principally three phases, as follows:

1 The entrance of the jet into the bucket, partially on the splitter, partially on the lip.
2 The flow in the bucket itself.
3 The discharge or the outflow from the bucket.

Each phase shows a loss which is necessary and which can be reduced only to a certain degree. A complete elimination of these losses is impossible. They are connected with the function of the flow itself and are in a certain sense necessary in the turbine system.

The principal loss is the discharge loss. It is necessary for the water to flow away from the bucket; and therefore some velocity head must be sacrificed to do this work. Then we have the loss due to friction on the surface of the bucket. Even the smoothest surface has some resistance, but with proper surface finish this loss can be reduced greatly. Finally we have the entrance loss, a singularly involved loss, which is dependent upon the specific speed.

These three losses are inevitable and cannot be avoided. Only arrangements with highly decreased losses are possible. The efficiency of a Pelton wheel is therefore determined by at least all these losses. It is necessary to take care of all the relevant circumstances to be able to reduce these losses, by proper adjustment, and to reach a high standard of performance.

In addition to the foregoing necessary losses, there may be other losses which appear not infrequently. Such losses are connected with the flow, but they are avoidable. Therefore an arrangement should be chosen so that such occurrences will be completely avoided, or the losses should at least be reduced as far as possible.

[1] Engineer, I. P. Morris Department, Baldwin-Southwark Division, Baldwin Locomotive Works. Mem. A.S.M.E.

Contributed by the Hydraulic Division and presented at the Annual Meeting, New York, N. Y., Nov. 29–Dec. 3, 1943, of The American Society of Mechanical Engineers.

Note: Statements and opinions advanced in papers are to be understood as individual expressions of their authors and not those of the Society.

Study of Flow in Bucket

To evaluate these losses, we have to investigate the flow in the bucket. It should be considered principally that the flow of the jet on the bucket changes because the nozzle through which the jet flows is fixed, whereas the bucket is moving. Of course, there is always an intermittent movement at the beginning of the impact of the jet. The impact of the jet on the bucket takes place both on the lip and on the splitter. Where the impact occurs on the lip, the jet is divided into two parts. One part remains flowing on the bucket and forms the impinging jet branch. The second part, the deviated jet branch, flows past the bucket and reaches the next bucket.

If the impact occurs on the splitter alone, two symmetrical jet branches result. These two branches of the jet on the bucket will then be turned back. The impact on the splitter takes place at different points, and, furthermore, every single water filament will have a different impact angle on encountering the splitter.

The construction of the impact angle, i.e., the entrance triangle, is well known and is represented in Fig. 1. In this figure, for one water filament a, the absolute velocity V, the peripheral velocity u, and the relative velocity v are indicated. Subsequently, the complete relative paths a', b', c', for three water filaments a, b, and c, are traced, which is a well-known construction. Furthermore six positions of a bucket are represented for the following cases:

1 First contact of a single water filament
2 First contact of the half jet
3 First contact of the complete jet
4 Last contact of the complete jet
5 Last contact of the half jet
6 Last contact of a single water filament.

It is necessary, of course, to choose the number of the buckets on a wheel so that the last drop encounters a bucket and no outflow between buckets is possible.

These procedures are generally known and used in practice. They contribute to a good efficiency of the bucket, but this alone does not give absolute assurance that a high efficiency will be reached.

Nevertheless, there have been cases in which buckets designed in conformity with these considerations, and with very smooth bucket curvatures, have given mediocre results. Investigations of the running wheel and the model, with and without stroboscopic instruments, have brought forth no explanations of such discrepancies. To study such cases and to find and eliminate disturbances, the author used an original method which gave excellent results.

Use of Fixed Bucket for Experiments

This method consists of a thorough investigation of the flow on a fixed bucket, but with a jet striking the bucket at the correct relative angle, under the same entrance conditions which exist on the running bucket.

The primary objection which can be made against this method is the fact that the flow on a stationary bucket is not identical with the flow on a rotating bucket. This is, in general, correct; however, the difference is not so far-reaching that this method cannot be applied. This can be proved easily by an examination of the flow.

We can distinguish three different kinds of flow motion:

1 The relative motion of the jet and the rotating bucket.
2 The absolute motion of the jet.
3 The flow of a jet on a fixed bucket with practically the same entrance conditions as for case 1. We designate this briefly as "absolute" motion but we repeat that this "absolute" motion has nothing in common with the motion in case 2.

This particular method involves an investigation of the motion in case 3 with the reservation that case 1 should be used.

We may now examine the difference between case 1, the relative motion, and case 3, the particular "absolute" motion. Regarding the course of the flow, the difference between the motions on the various parts of the bucket is not the same.

The greatest difference shows the part of a streamline which lies in a plane of rotation. This is the case which shows the relative paths in Fig. 1 (a', b', and c'). The absolute motion on the fixed bucket would be a straight line, the tangent to the relative path, therefore identical with the direction of the relative velocity v. A streamline on a bucket will run only to a small amount in a plane perpendicular to the axis of rotation. Therefore only a small difference between tangent and curved line can result.

No difference between "absolute" and relative motion will be found for a streamline which is formed by an enforced guidance in the bucket with a cylindrical surface, the cylinder being parallel to the axle of rotation. Here the relative path and the absolute path are always identical.

All other streamlines show differences which lie between these two extreme cases. If we desire to know the specific difference in the course of the flow on a bucket, we can trace a sketch which shows in which sense and to what extent such differences occur. Fig. 2 shows, on a bucket, different "absolute" and relative paths:

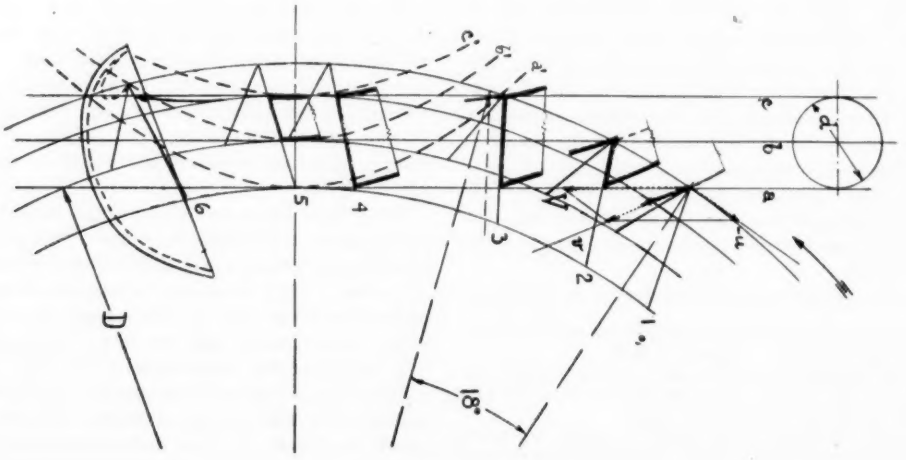


Fig. 1

The "absolute" paths are given in full lines 1, 5, the relative paths are given in dashed lines 1, 5. We conceive that the paths 1 and 5 in Fig. 2 are practically the same in both motions. The paths 2, 3, and 4 show deviation in a rotating system wherein path 3 shows the greatest deviation.

It is now essential to note that, even if relative and absolute courses of the flow are identical, the motions on the fixed bucket and the rotating bucket are not the same. This difference is, of course, due to the bucket rotation and is expressed by the value of the velocity.

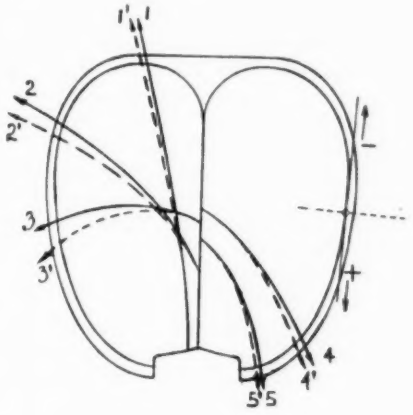


FIG. 2

In a stationary system, the velocity remains constant, if we do not take the losses into account. In a moving system with free flow, that is, with no essential pressure in the flowing liquid, the relative velocity is no longer constant but maintains the following relation according to the fundamental equation: For two points, 1 and 2, with the corresponding velocities, we have

$$\frac{u_2^2 - u_1^2}{2g} + \frac{v_1^2 - v_2^2}{2g} = 0 \quad \ldots\ldots [1]$$

where u_1 and u_2 are the peripheral velocities, and v_1 and v_2 are the relative velocities.

This is an equation which could be derived also from mechanical principles alone inasmuch as in the free flow there is no difference in pressure. The sense of this equation can more easily be understood by a simplified example. If we suppose that $u_2 = v_2$ (and this will be nearly the case with high efficiency), then also $u_1 = v_1$. Now it can be established in general that "the relative velocity in the rotating system changes in the same degree as the peripheral velocity."

We now see clearly that the motion on a bucket in a fixed system, as compared with a rotating system, has a different velocity, even if the path should be the same. If, for instance, the particle comes to a greater radius, the relative velocity increases and vice-versa. But, as we know, the difference in the peripheral velocity of a bucket is relatively small, due to the fact that the bucket for low and moderate specific speeds is small in comparison with the diameter of the wheel. Therefore, there can arise only a small degree of difference in the relative velocity.

Equation [1] provides an explanation of the mixing loss. We conceive that the relative velocity at one point of the water filament will be different from the relative velocity at another point of the water filament *c*. But both relative velocities are not connected by a relation similar to Equation [1]. This will be clear by the way in which the relative velocity was found, see Fig. 1. If the two water filaments, *a*, *c*, in the relative system, should represent only mechanically separate particles, and if the relative flow of these particles were in a manner free and independent, then the existence of different relative velocities would be possible.

But both filaments, *a*, *c*, are, in fact, not independent; they represent streamlines of a hydraulic continuity, i.e., confined flowing liquid, in which, between filaments, pressure transformations sometimes arise. The relation for this transformation can be given in a form similar to the Bernoulli equation for absolute motion. We have in an absolute system, the Bernoulli relation with

$$\frac{V^2}{2g} + \frac{p}{\rho} = \text{const} \quad \ldots\ldots [2]$$

In a relative system there exists the relation

$$\frac{v^2}{2g} + \frac{p}{\rho} = \text{const} + \frac{u^2}{2g} \quad \ldots\ldots [3]$$

It is important to know that such a connection exists between the velocities of a closed stream in a relative system. The constant can be regarded as similar to an energy capacity and remains, for a closed system, invariable. It is essential to understand that, in the present case, the single filaments do not have the same energy capacity, due to the fact that the relative velocity is not even at the same radius.

To explain this, we can make a comparison with a reaction turbine using water at different pressures. We conceive that in one runner this cannot be done without losses. If we try to use water at two different pressures in one runner, we receive a mixing of both pressures with a loss in energy. It is, in fact, necessary that an exchange in the energy capacity take place between the various water filaments on the bucket.

To show these relations in a practical example, consider Fig. 1, as the diagram for a wheel with the following data:

Head		1000 ft
Jet velocity	$V = \sqrt{(2gH)} =$	252 fps
Water quantity		24.2 cfs
Jet diameter	$d =$	4.2 in.
Wheel diameter	$D =$	59.6 in. = 4.97 ft
Power		2380 hp
Wheel speed	$n =$	450 rpm
Ratio	$D/d =$	14.2
Specific speed	$n_s =$	3.87

Now examine Fig. 1, position 3, "first contact of the complete jet," and we have the following velocities for the border filaments:

Peripheral velocities	113.5 fps	129.4 fps
Relative velocities	148.5 fps	133.0 fps
The corresponding heads are:		
For peripheral velocities	201 ft	261 ft
For relative velocities	345 ft	276 ft

The energy capacity measured in feet, as difference, is therefore 114 ft and 15 ft.

The jet on the surface of the bucket should present, in relative motion, a hydraulic continuity, with uniform energy capacity in every filament. But this is not the case. Therefore an energy exchange between the different filaments has to take place, owing to the fact that all filaments on the running wheel do not start with the same energy capacity.

The loss consists in the appearance of vortex motions between the various water filaments with an equalization of the different energy capacities, i.e., a mixing loss.

However, there is no need for a complete equalization of the energy to take place. If two filaments should be separated, then the closed system would be disturbed, and every filament could

remain separated with its own capacity, and no further mixing loss would occur.

This difference in energy capacity increases essentially with greater specific speed, that is, if the diameter of the jet is relatively larger in comparison with the diameter of the wheel. In this case, the influence of these appearances on the efficiency of the wheel is very unfavorable.

In case of an investigation of a stationary bucket, there is no mixing loss, the water impinging on the bucket with the same speed throughout. This fact consequently results in a difference between relative and "absolute" motion.

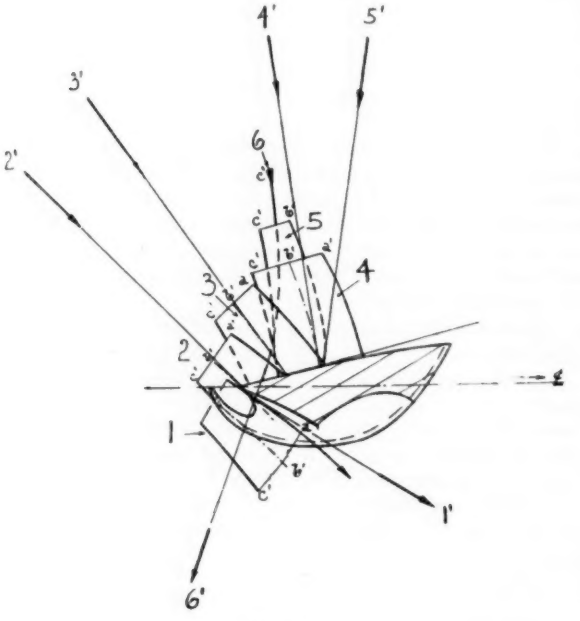


FIG. 3

Consideration and reflection show now that all these divergences and velocity differences are not so far-reaching that the general character of the flow would be changed. In fact, appearances in a stationary system are practically the same as in a rotating system.

By such means, it is possible to make an investigation of the flow on a stationary bucket, and this contributes deeply to the knowledge of the flow, as has been found by experience with this method. If desired, and as sometimes may be necessary for scientific investigations, it is also possible to rectify exactly the motion on a stationary bucket to obtain a precise reproduction of the flow in a rotating system. For practical purposes, however, an exact rectification is not necessary. Besides, we know that the flow of a jet on a surface takes place with a spreading effect, with an increase of the width. Then the outer water filaments of the surface are no longer parallel. The calculation could be made only for the filament which represents the center of gravity. But the side deviation of the border streamlines cannot be computed. The calculation is therefore from the beginning not very helpful.

We have defined the "absolute" motion as a flow on a bucket which shows the same entrance conditions as the flow in relative motion. In Fig. 3 the different positions of the impact of a jet on a stationary bucket are designated. This construction is developed from Fig. 1 which shows the same bucket in its six different positions. In the same way, in Fig. 3, we have six different positions for the jet on the stationary bucket.

It now becomes possible to form a simple arrangement to bring a nozzle into such position that the jet will have the same entrance conditions as in the relative motion. Such a testing arrangement was used for trial performance, and it was not difficult to make all necessary measurements.

The investigation of the flow on a stationary bucket seems to call for an arrangement where these various directions of the impinging jet will be secured; but it has been established that this sharp connection between jet and bucket is not necessary.

We know principally that the position of the impinging jet on the bucket is dependent upon the peripheral velocity, i.e., number of revolutions. With a change of the peripheral velocity, for instance, during speed regulations, or as a result of differences in pressure, a change of jet-impact conditions must take place. The flow should be regular without disturbances for a range of angles on the impinging jet; and therefore it is not advisable to make the investigation only for the computed main positions.

It is indeed practical to mark the main directions of the impinging jet on the bucket by painting. Nevertheless, the investigation will also embrace directions which are not far from these computed directions. In this way the investigation will be enlarged and will be made wider in scope than if merely fixed by the normal entrance conditions.

Cavitation and Bucket Efficiency

Now what can be proved by such an investigation on a "fixed" bucket? There are two principal factors which can be studied: The problem of cavitation and the problem of efficiency. Concerning the efficiency, we distinguish, as before, three phases of the flow, and consider first the discharge.

The best efficiency of a wheel will generally be reached if the value of the relative exit velocity is nearly identical with the value of peripheral velocity, or if the absolute exit velocity is perpendicular to the peripheral velocity. It is obvious that the absolute velocity has to be as small as possible, because the velocity head of the absolute exit velocity is a real inevitable loss, as previously mentioned.

To explain these relations, Fig. 4 shows all the relations at the discharge for a filament. We see in this figure that the absolute exit velocity consists of two components. The component perpendicular to the brim of the bucket is useful, inasmuch as this velocity carries the water away from the bucket. The second component which is directed parallel to the brim of the bucket and gives practically no help in discharging water is practically useless and should be eliminated completely, if possible.

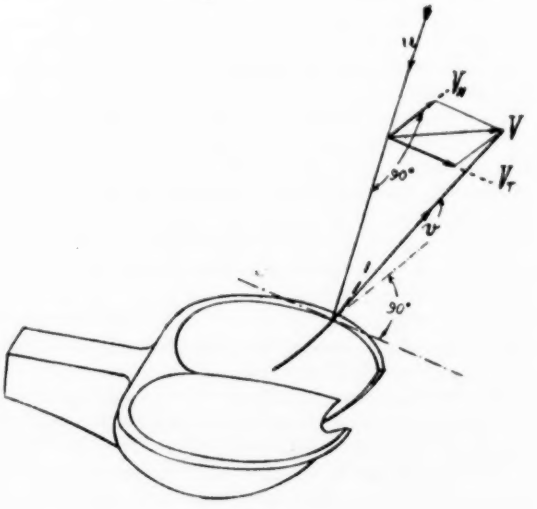


FIG. 4

We know that there is always a spreading of the jet on the bucket. Then the filaments on the border will always contain useless tangential components. Therefore a spreading with very inclined border lines should be avoided as far as possible. On the other hand, it should be borne in mind that the relative motion on the bucket is in a certain way different from the "absolute" motion on the fixed bucket. It is just this tangential component at the discharge which forms a principal difference between the two motions (Fig. 2).

Let us consider now the "absolute" flow on a fixed bucket, and imagine that we have found and tabulated the effective relations for each jet position. The tangential component of the exit velocity can be positive in some points, that is, directed outward, perhaps in some points negative (see Fig. 2). To arrive at a relative motion on the bucket, it is necessary to make the corrections with an additive positive tangential value; this means that points which show, in the absolute motion, an extreme negative tangential exit component will have an amelioration of the discharge on the rotating bucket. A flow on a fixed bucket, which shows a great positive tangential exit velocity, will suffer a deterioration in the case of the rotating bucket. In this case, a change of the bucket will be advisable, to reduce the tangential exit loss.

The examination of the discharge on the bucket is therefore reduced in finding the exact direction of the discharge velocity, especially with reference to the brim of the bucket. It is obvious that all positions of the jet under the corresponding impact angle should be investigated.

With these trials, it is necessary to determine that the jet coming from a bucket does not interfere with the preceding bucket.

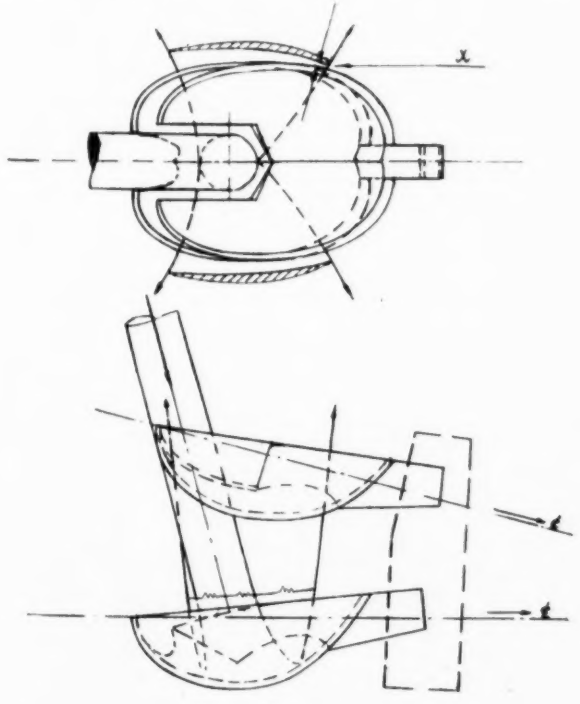


FIG. 5

There is a simple way to make all investigations in one by using a dummy bucket, Fig. 5. This dummy bucket has a far greater cutout than the normal bucket, so that the jet can be brought into the correct position with reference to the test bucket. In Fig. 5, the jet coming through the dummy bucket impinges on the test bucket, with nearly the same entrance conditions as on the rotating bucket. The discharge of the jet is, by this arrangement, clearly visible and easy to register.

In this way, it is possible to make exact measurements concerning the discharge of the jet. These measurements can be essentially simplified if two similar graduations are used on the test, and on the dummy bucket. It is also possible thereby to find the smallest clearance between jet and the preceding bucket, in this case the dummy bucket (see Fig. 5).

It is necessary to remark that a slight touching of the preceding bucket by the flow can be tolerated without sacrificing the efficiency, but such a condition can easily cause cavitation at high heads.

The inclination of the bucket relative to a radial line on the wheel should likewise be investigated. It is well known that there exists for the bucket a certain position with the highest efficiency. By changing this inclination slightly, there is almost no influence on the efficiency. On the stationary bucket, it will be found that by changing the inclination, a change in the discharge at the inner and outer part of the bucket brim will result. The discharge on the side of the brim remains practically unaltered.

Trials on a stationary bucket have proved, further, that the discharge from the bucket is not alone dependent upon the outlet form of the bucket, i.e., the brim itself, but also on the manner of the entrance relations. In this way, the splitter and the lips form a deciding factor for the discharge.

The investigation of the lip is now necessary in a twofold manner. We are interested in a correct form with reference to the discharge relations, that is, for the impinging branch of the jet. We are also interested in knowing what will happen to the deviated jet branch.

On Pelton buckets, there are now different forms of lips. The simplest form is that of an edge perpendicular to the splitter. Other forms have evolved by forming a bucket as a double ellipsoidal shell and by a cutout in the front of the bucket, the cutout being a surface of rotation with the center in the rotation axis. Another cutout is made with a cylindrical surface with its axis in the average path of the jet, and various other forms are also possible.

Thus quite diversified forms of lips may result, each form having certain advantages and disadvantages. The investigation of such lips gave such wide variety of results that it was practically impossible to classify them.

It was decided therefore to clarify the problem, and to study, first of all, the impact of the jet alone under simplified conditions. A series of tests was made to investigate the impact of a jet on specific plates under conditions similar to those arising in the bucket. This is practically equivalent to the arrangement of a lip with an edge perpendicular to the splitter.

EQUIPMENT AND TEST PROCEDURE

The testing equipment for this purpose is shown in Fig. 6. Testing plates are brought into a circular jet at different positions, Figs. 7 to 12, inclusive.

A description of the procedure is given, first, with an attempt to classify the measurements. The results in connection with the bucket will be discussed later. The results which were obtained with two test plates are shown as A and B, Fig. 7; Figs. 8 and 9 show the jet impinging on the plate A. Plate A was selected from a number of others as the most favorable arrangement. The thickness of plate A is very small, being only 6 per cent of the jet diameter. Experience has shown the importance of a clear distinction between the front part δ_f and rear part δ_r of the edge angle δ. The values of these angles are designated in Figs. 7 and 8.

The deformation of the deviated jet shows surprising forms. In Fig. 8 we see the form of the jet in two cross sections by using an

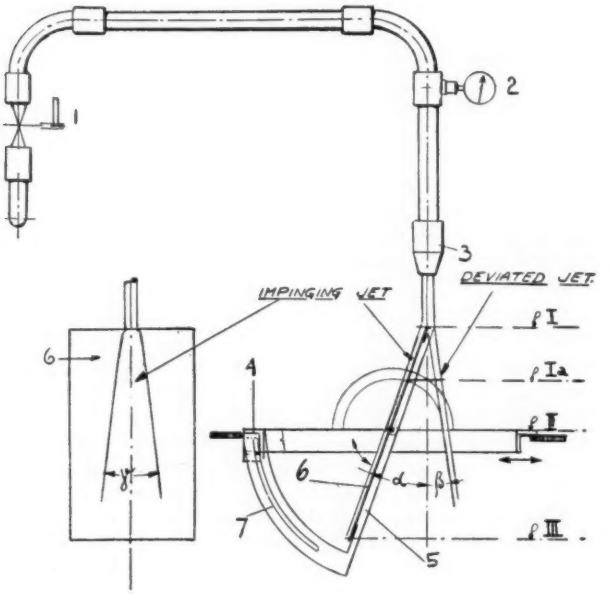


FIG. 6

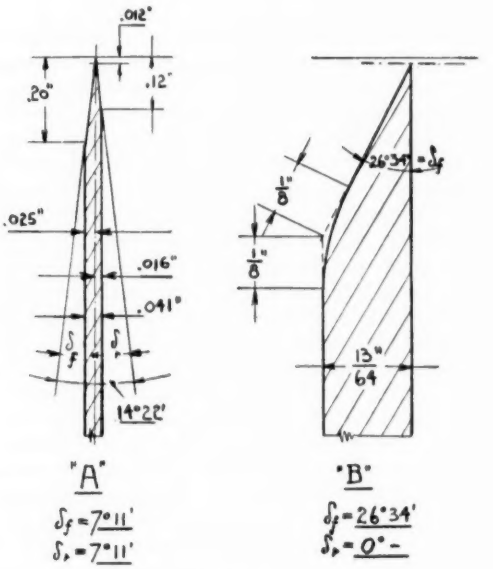


FIG. 7

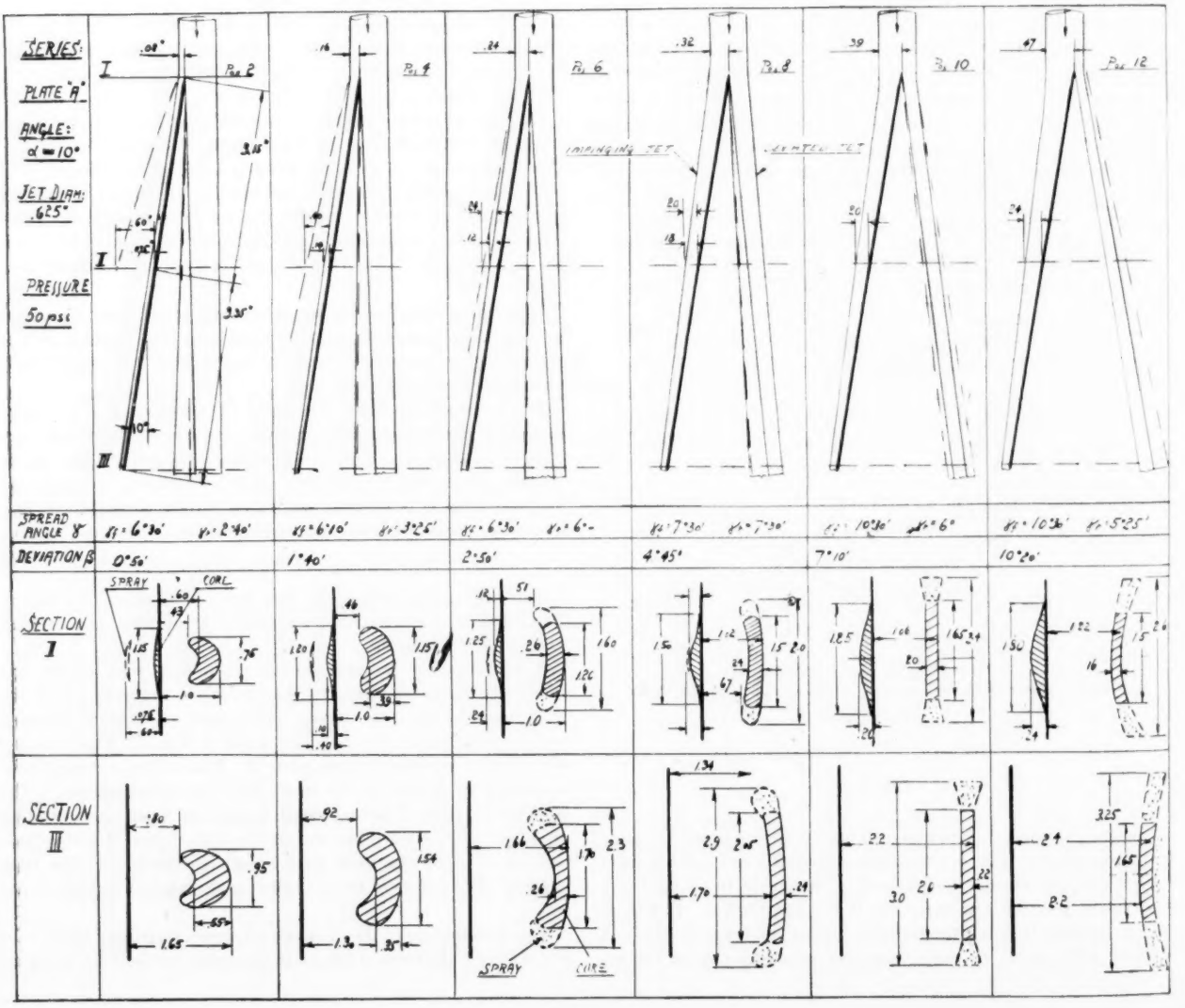


FIG. 8

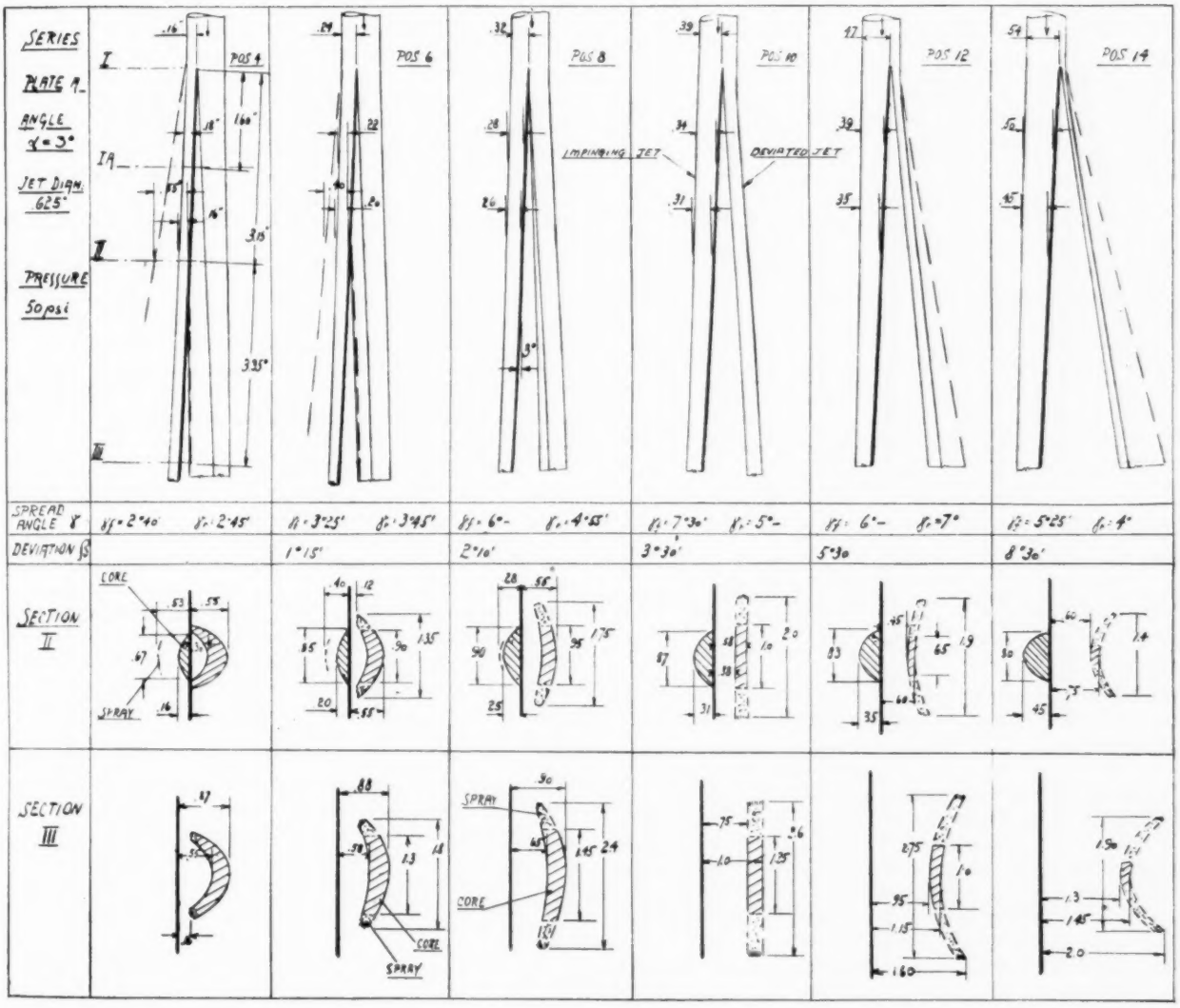


FIG. 9

impact angle of $\alpha = 10$ deg. The plate placed under this constant angle of 10 deg was shifted sidewise. The positions 2–12 in Fig. 8 correspond to the partition of the jet in its two branches, i.e., the impinging and the deviated jet. If the deviated jet is relatively large, (positions 2–6) from which it follows that the impinging jet branch is small, the cross section of the deviated jet is crescent-shaped, concave against the plate. With larger impinging jets, the crescent-shaped form changes to a flat rectangular cross section. With extremely small deviated jets, their cross sections will be curved in the direction opposite to the foregoing, i.e., convex against the plate. The deflection of the deviated jet will be greater with smaller jet. (Angle β is the angle of deviation.)

It should be mentioned that the cross section consists of two different parts; the core, which is practically filled with liquid, and the spray, which consists of numerous single separated water threads. The spray is developed extensively at a greater distance from the impact point, and, at certain positions of the deviated jet, the spray is at the point of impingement.

In addition to the deformation of the jet in the direction of deviation, there is also a spreading of the jet perpendicular to deviation. Both the impinging and the deviated jet spread on the plate, particularly with smaller thickness. (γ is the angle of

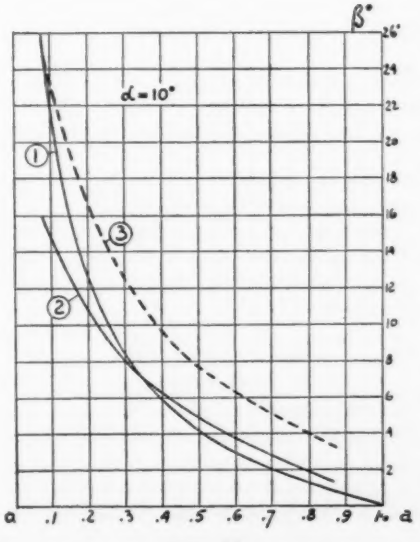


FIG. 10

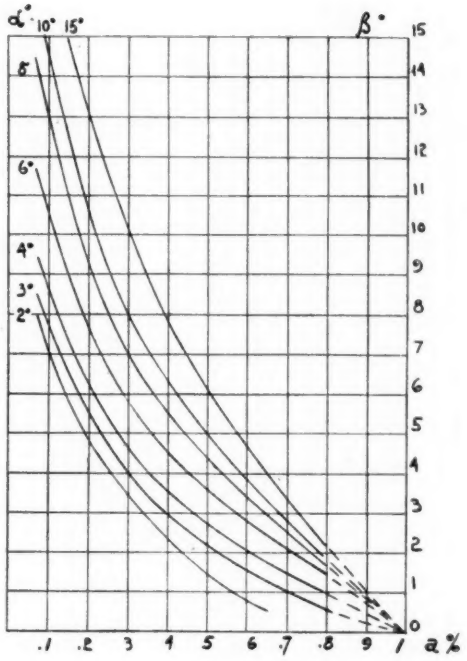


FIG. 11

spreading.) The angle of spreading of the impinging jet (γ_f), and the angle of spreading of the deviated jet (γ_r), should be clearly distinguished.

The plate was investigated at numerous impact angles. Fig. 9, for example, gives the appearances for an angle of 3 deg. The principal difference in these cases (angle 10 deg Fig. 8, and 3 deg Fig. 9) is that the curvatures of the cross sections are far more pronounced at 3 deg than at 10 deg. The cross section of a large jet deflection at 3 deg impact angle shows a cavity. The side ends of the deviated branch adhere to the plate; and under such conditions, cavitation is practically inevitable.

Figs. 8 and 9 indicate the angle of deviation β, i.e., the angle of the deviated jet, in relation to its initial direction. This angle can be calculated theoretically with relation to the reaction, and the following equation gives the value

$$a = \frac{1 - \cos \alpha}{1 - \cos (\alpha + \beta)} \quad \ldots\ldots\ldots\ldots\ldots [4]$$

In this equation α is the impact angle; β the angle of deviation, and a is the per cent area of jet deflection. (The complete jet has 100 per cent area and the impinging branch, the area $1 - a$ in per cent.)

Fig. 10 indicates the dependency of the deviation β as a function of jet deflection a for 10 deg impact angle. Line 1 gives the theoretical calculations according to Equation [4], and line 2 gives the measurements with plate A, according to Fig. 8. The values are not completely identical, but it is impracticable to discuss the differences here.

Results of Tests

In general, it has been established that the connection between deflected and impinging jets is uniform. Fig. 11 gives a complete diagram for plate A which shows all the deviations from 2 deg to 15 deg impact angles for all impinging jet areas.

As previously mentioned, plate A was selected from a variety of test plates. For example, in order to indicate the effects on another plate, Fig. 12 shows the conditions with jet impinging on plate B (Fig. 7). This was one of the first plates examined and has been developed from the lip forms used ordinarily.

In relation to the difference between plates (see enlarged sections in Fig. 7), the following comments are in order: While plate B is extremely thick in comparison with plate A, this alone does not constitute the essential difference. The edge angle on plate A is far smaller than on plate B. Moreover, the front edge angle δ_f on plate A is identical with the rear edge angle δ_r, whereas plate B has no rear edge angle at all.

By comparing the figures for plate B with those for plate A, it becomes evident that the results obtained with plate A are superior to those in the case of plate B. Both the impinging and deviated jets at plate B show disturbances which are not feasible under any conditions. To clarify these relations, the deviation for plate B under 10 deg impact angle is also noted in Fig. 8.

The principal differences in the impact conditions between plates A and B can best be defined as follows: Small impinging jets on plate B are not feasible, as the impinging jet will be deflected and sprayed.

With the same impact angle, the deviation for plate B is far greater than for plate A. The spreading of the jet is less favorable on plate B and is more developed.

A plate thinner than plate B, but with the same characteristic form, produces results analogous to plate B, with other limiting factors.

At this point, the influence of these investigations on the flow on a Pelton bucket should be discussed. We conceive from Figs. 8 to 12, inclusive, that the jet upon encountering a bucket has a tendency to deflect, this being forced to take another path, as presumed by the simple theory with the single water filament.

It is obvious that the relative paths a', b', c', in Fig. 1, are correct only in so far as they represent that portion of the jet which has not been deflected. The movement of that part of the jet which will be deflected is extremely complicated owing to certain cross sections being influenced by various deflections.

To make these relations as clear as possible, an attempt was made to develop a kinetographic representation. This has been accomplished in Fig. 13, by showing the wheel in a series of successive positions.

To simplify the representation, certain abstractions and suppositions were made as follows: The wheel should have 20 buckets (center angle 18 deg) similar to the case of Fig. 1 (buckets M, N, O). The lip of the bucket should have an edge, according to plate A, perpendicular to the splitter, so that the liquid will be caught up directly in the plane perpendicular to the plane of reproduction. The jet should be divided unequally (for practical reasons) into single segments. Their origin is as follows: The wheel will be presented in successive positions 10–20 (to 2 deg apart), affording uniform revolution.

The cross section 11 of the jet is determined by the end point of the bucket N in position 11 of the wheel. If bucket N arrives at position 12, the cross section 11 of the jet arrives simultaneously at the position indicated. In position 12, the end point of the bucket N determines the position of the cross section 12 in the jet, and so on.

This arrangement gives no uniform partition for the jet, but simplifies the representation. It is obvious that bucket O arrives at the location of bucket N in the successive ninth position. Positions 11 and 19 are identical.

The inclination of the lip was chosen of such a form that in the extreme position the relative velocity is exactly the direction of the lip entrance. It is assumed that if the lip enters into the jet, there will be a tendency toward deflection only for the critical cross section of the jet. The movement is now unsteady and it is therefore impossible to compute the exact influence on particles which are not in immediate proximity to the lip. A further sim-

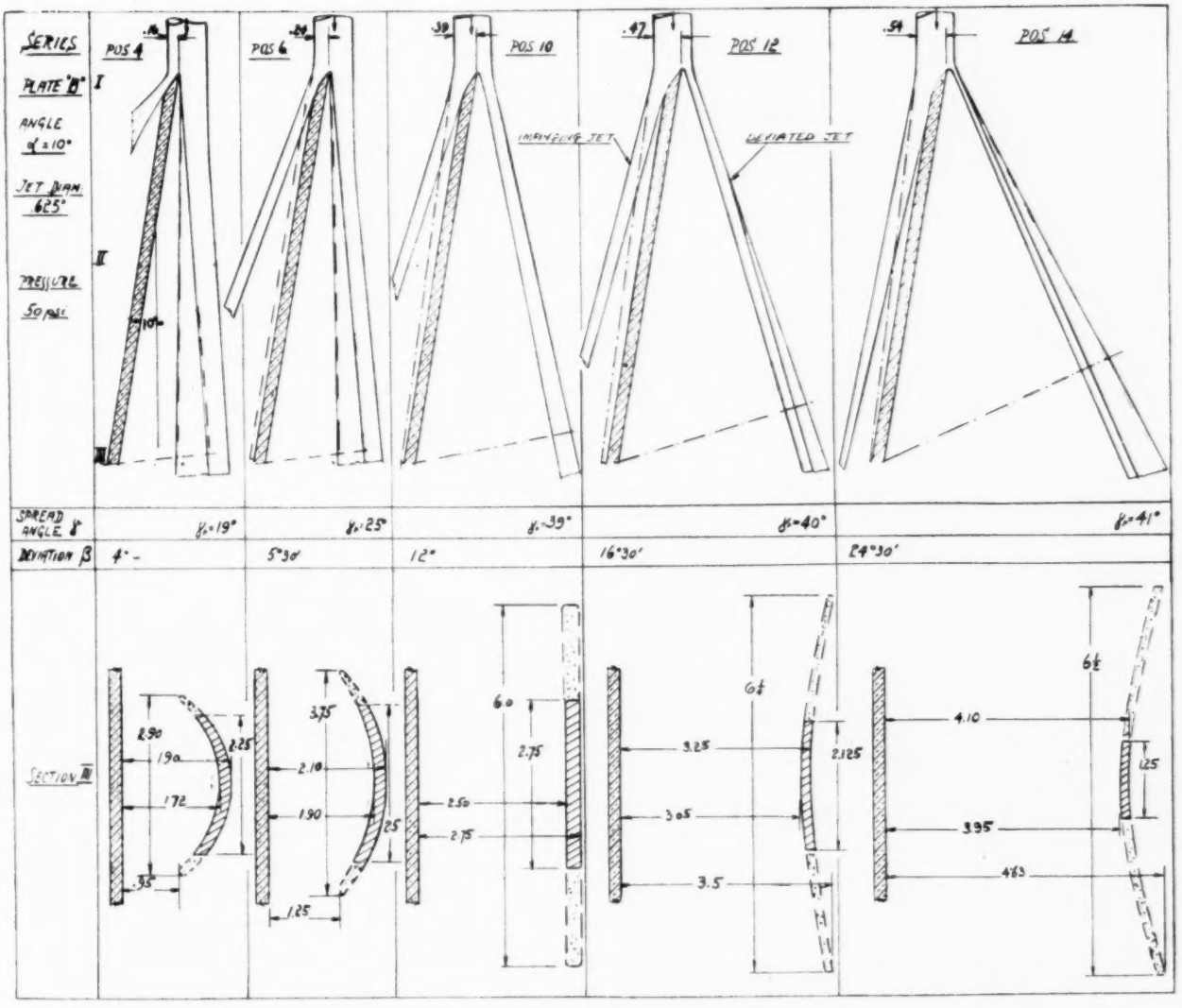


FIG. 12

plification can be made by disregarding the appearances of the width. We can therefore abstract the spreading and change of the cross section of the deviated jet. We assume further that the angle of deviation β in the relative system can be transferred unchanged in the absolute system. Therefore we co-ordinate to the influenced cross sections a deviation of the direction of the absolute speed according to the diagram, Fig. 11.

The affected cross sections of the jet are therefore not moving in the original direction; on the contrary, they will have individually different directions.

The kinetographic representation of the jet parts which form the admission for bucket M was made in this manner.

Fig. 13 represents a succession of positions of the three buckets M, N, O, and the relative position of the jet segments. Each second segment of the jet is hatched in the direction of motion. This figure represents clearly momentary positions, and it will be seen how a part of the jet between the cross sections 14–19 will be deflected so that it will not reach bucket M.

To find the loss, the volume of the part which does not reach the bucket is computed and divided by the volume of the jet per pitch length. The loss was found to be 5.8 per cent, which is excessive. An improvement can be effected in part by a greater number of buckets, and partly by increasing the wheel diameter.

These considerations have been abstracted from the form of the deflected jet. It has been established, Figs. 9 and 10, that there is a spread resulting in the form of the deviated jet being more or less rectangular, the longer side oblique to the splitter. It should be borne in mind that the deflected jet will be caught by the following bucket so that it will now be an impinging jet. The impact of such a rectangular jet on a bucket is certainly not favorable. The outer water filaments are likely to splash directly on the bottom of the bucket, guidance through the splitter thus being lost.

It is impossible to effect any material improvement of these particular conditions by changing the splitter. The lip, on the other hand, should be modified to avoid the appearance of such deviated and compressed jets. This is, in fact, the reason for the existence of special lip forms.

Relative to the impinging jet, it can be established that there is proper guidance only if the edge angle of the lip is very small. Sizable edge angles are inclined to produce a complete spray of the impinging jet. It has been demonstrated, furthermore, that the spread of the impinging jet is quite small if the impact angle is likewise small. It would be advantageous to arrange a bucket

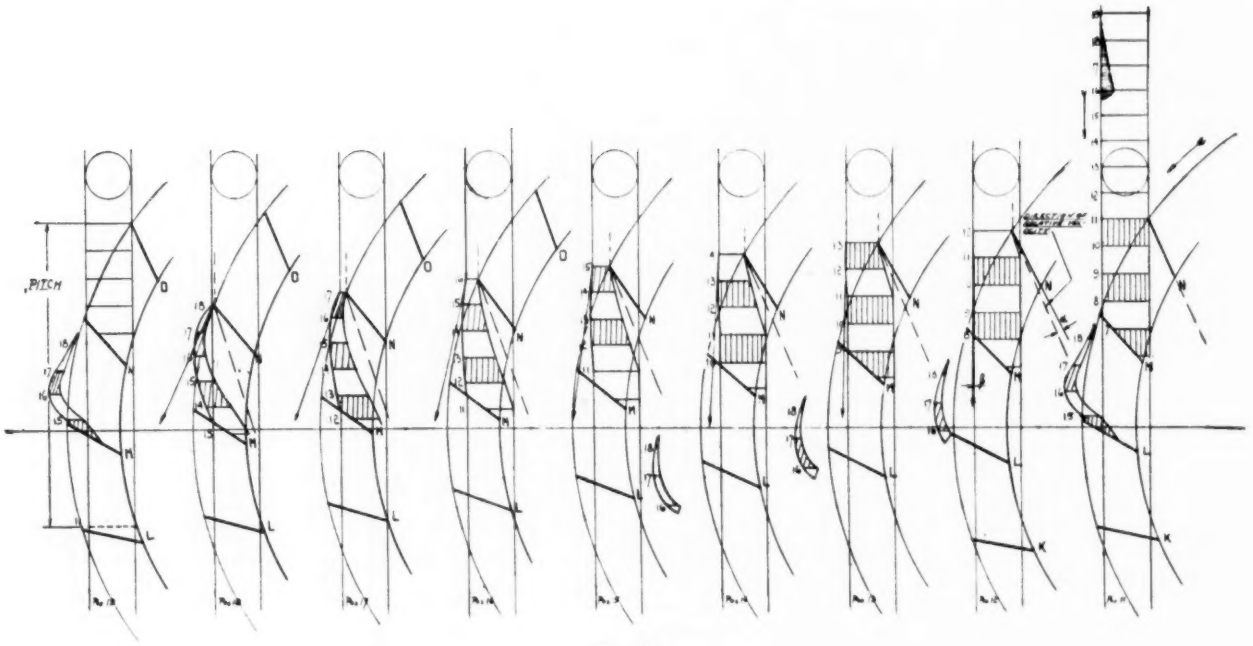


FIG. 13

so that small impact angles would be produced, but there are two reasons why this should not be done, as follows:

1 A very small impact angle at a given peripheral velocity results, at a greater peripheral velocity, in a jet impingement on the underside of the lip. This should be avoided because it decreases the efficiency.

2 Cavitation will inevitably be produced with smaller impact angles at higher heads.

On the other hand, a small edge angle on the lip is difficult to maintain, because such an edge will not stand up under high heads. Further, an uneven edge invariably causes cavitation; and it is therefore necessary to make the wall of the lip adequately thick.

It is obvious that the straight lip form does not give very favorable results (see Fig. 13). There are, however, various methods, forming other lips without the disadvantages just outlined.

As mentioned previously, the variety of the lips is so far-reaching that it is impossible to find a combination which can be regarded as best in every respect.

It develops that the method with the stationary bucket makes possible the study of all questions and problems connected with the form of the lip.

It has been said that the discharge on the Pelton bucket is influenced to a great extent by the entrance conditions, that is, by the form of the lip and of the splitter. We know now in what sense the lip is working, and that through the lip edge a spread of the impinging jet results.

The splitter also causes a spreading of the jet, and it can be stated generally that the spreading will be increased with greater splitter angle. Both edges, the splitter and the lip edge, have therefore a combined influence on the impinging jet. The form of the bucket should be a natural transition without sudden rupture in the curvature of the surface.

We assume that losses at the entrance are produced chiefly with the deflected jet, while losses at the entrance of the directly impinging jet are very rare, with suitable arrangement provided.

The losses of the deflected jet consist in not reaching the following bucket and in an impinging of a compressed jet on the adjacent bucket. By this means, the influence upon efficiency,

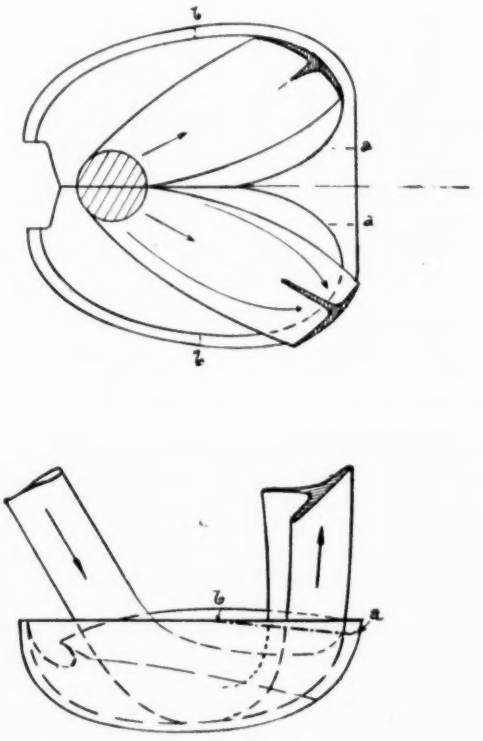


FIG. 14

both at the entrance and the discharge, can be established, resulting in considerable reduction of losses, if not completely eliminating them by proper arrangement. The final consideration is the possibility of avoidable losses during flow on the bucket itself.

It seems improbable that such losses could exist; however, with the method described, a hydraulic loss was found which caused further efficiency decrease. A runner which was built for a plant

according to a previous model did not show the efficiency expected. The bucket had smooth curvatures and had only slight differences in comparison with the model, which should have increased the efficiency.

Upon testing the bucket in the fixed position, this bucket showed a singular form of discharge. The cross section of the discharge was not flat or a more or less rectangular strip. On the contrary, it had a T-shaped form, Fig. 14.

It was established that this T-shaped cross section was produced by two streams, both originating on the splitter and working against each other. This was a steady appearance on the bucket, starting from a certain impact angle.

It was obvious that under such circumstances the discharging water came into strong interference with the preceding bucket. In this case it was possible to improve the efficiency largely by altering the discharge edge of the bucket alone. The bucket part on the rim between the points a and b (Fig. 14) was cut away as marked with dot-and-dash lines. However, a better correction would have involved a change in the curvature of the bucket.

Further investigations proved that such T-shaped discharge is not uncommon. In this case, the T-shaped form was a steady one, in another case it was found that such T-shaped form was produced by the continued succession of jet parts impinging under different angles.

These conditions can be studied easily in the case of the fixed bucket. It is doubtful whether it would have been possible to see them on a revolving wheel.

Upon becoming acquainted with the facts and knowing where to give our attention, it will be possible, with proper arrangements, to see these conditions on a revolving wheel with stroboscopic instruments.

Finally, there should be mentioned, among the avoidable losses, a disturbance which arises from the outflow, but which has its real cause in the enclosing housing. Sometimes the discharging water impinges against the walls of the housing or elsewhere and is deflected, after which it returns to the wheel, and in this way the power of the turbine is reduced.

In certain cases, the discharging water will be taken by the air rotating with the wheel, thus producing similar disturbances.

These losses cannot be traced back to the flow on the turbine; but they have their cause in the specific construction of the turbine itself, i.e., housing, air passages, baffle-plate arrangement, etc.

To avoid such conditions only one rule has to be observed. The outflow of the water from the bucket should be completely free of foreign matter which would interfere with the outflow; and it is advantageous to make arrangements whereby the outflow tendency can be increased.

Having established the relative outflow conditions on a bucket, it is possible to estimate the absolute flow and to decide whether interference is to be expected, and if such conditions exist, how to deal with them.

TABLE 1 ANALYSIS OF PELTON WHEEL LOSSES

1 Nozzle:
  Friction in nozzle and on needle
2 Wheel:
  (a) *Mechanical losses:*
    1 Friction in bearings
    2 Air resistance of turning wheel
  (b) *Hydraulic losses:*
    (a) Unavoidable losses
      1 Entrance; mixing loss
      2 On bucket; friction of flow on bucket
      3 Discharge; normal discharge loss
    (b) Avoidable losses:
      1 Entrance; deviation of jet on lip with outside pressing of jet parts. Spray-formation compression of jet parts with unfavorable impact on adjacent bucket
      2 On bucket; crossing of two streams; disturbances
      3 Discharge; tangential discharge; interference with preceding bucket; deflection of discharged jet on wheel housing and disturbances resulting therefrom.

With the method of the fixed bucket, the author has been enabled to study the flow on the bucket and to analyze the losses which determine the efficiency of the wheel. It is natural that this method alone is not sufficient to determine the efficiency which can be established only by testing the performance of the wheel. The losses on the bucket having been established, it is practical to summarize them for further investigation, as in Table 1.

Discussion

S. Logan Kerr.[2] This paper is of particular interest to the writer, as it fell to his lot to make a research investigation of some unhappy results of impulse-wheel performances when he was still in the hydraulic-turbine industry. Now after an absence of some 7 years, keeping meanwhile the position of "sitting on the lid of the Hydraulic Turbine Test Code Committee," the perspective attendant to a detached view of the "art" may be helpful as a contribution to the discussion of this paper.

Some 15 or 16 years ago, the writer had the privilege of visiting the plants of the principal manufacturers of turbines in Europe. They were most co-operative and put at his disposal much information which showed their superior performance, individually and collectively, with special attention to their improved performance in relation to the state of the art in America.

It was also his privilege to have entreé into the plants of the users of these superlative turbine units. Much "sales talk" was deflated thereby. But some things defined the debunking process; one in particular was the efficiency of impulse wheels.

Such "impossible" arrangements as a vertical shaft unit with a test efficiency of 90 per cent (with a penalty clause in the contract and a certified copy of the test results), and horizontal units of medium and large size that attained efficiencies of 88 to 91 per cent, seemed to be greatly at variance with reported "ceiling efficiencies" of 85 to 87 per cent in American practice, to say nothing of the horrible examples that slipped into the middle "seventies."

What was the answer to these major differences in performance?

There were many answers to that question given in writing, in polite conversation, and sometimes in conversation that was not so polite. Perhaps this view in retrospect will serve to bring the discussion of this controversial question down to a sound basis of an open-minded consideration of engineering and technical aspects and leave out completely the side issues of personal opinions and commercial issues, tradition, and other obscuring factors. Let us examine some fundamentals:

1 What is the efficiency of an impulse turbine? Is it not measured on the same basis as all other hydraulic prime movers as set forth in the A.S.M.E. Power Test Code for such equipment? Or should there be some other basis? The writer's committee[3] is vitally interested in knowing.

2 What elements determine the performance of an impulse turbine? Here we find an essential difference between the reaction turbine and the impulse turbine. In the reaction turbine, we have a single combined unit which permits various deviations in the individual elements that affect each other but can be compensated for in the design basis used.

In the impulse turbine, however, we find two units, the nozzle, and the bucket in series. The jet discharged by the nozzle must be solid and free from dispersion and distortion or else the most perfect bucket in the world cannot produce acceptable efficiencies. If the most perfect jet is impinged on a bucket not suited to it, the bucket cannot develop its best performance.

[2] United Engineers & Constructors, Inc., Philadelphia, Pa. Mem. A.S.M.E.

[3] Committee 18, Hydraulic Prime Movers, A.S.M.E.

We are then faced with two requirements: An efficient nozzle, delivering a solid compact jet to the bucket; and an efficient bucket capable of receiving it and converting this energy to the best possible degree.

4 The author gives a careful analysis and discussion of the elements of loss in the buckets upon receiving a good homogeneous jet of water from the nozzle. The writer recommends this paper; it merits careful study. It is the work of a distinguished engineer and scientist. Think well before taking issue, and then take issue only when full and accurate information to refute this exposition in part or in whole has been developed.

5 Make sure that the nozzle is free from rapid accelerations followed by retardations of flow; be sure that abnormally high velocities are eliminated from the approach passages of the nozzle; be sure that abrupt and unnecessary changes in direction are avoided in the nozzle and the approach to the nozzle; in brief, be sure that the most efficient bucket that can be designed has a good, solid, high-efficiency jet impinging upon it and can start its own work with a chance to contribute without impairment to the maximum over-all efficiency of the unit as a whole.

6 When these objectives have been attained, then test the scale model under conditions where there is sufficient turbulence to simulate accurately the behavior of the jet under full-scale velocity conditions of the design head, not the available test head for the model.

7 When these conditions have been thoroughly studied and complied with, then many of the mysterious discrepancies between the impulse-wheel laboratory work and the field performance will disappear, just as they did many years ago on the reaction turbine when the basic fundamentals of the relation between the model and full-sized-unit performance were reduced to an academic problem of slide-rule computation.

The impulse turbine has still to overcome the obstacles of insufficient relationship between experimental laboratory and full field performance, both as to the degree of efficiency attained at the maximum point and the ability to reproduce in the field the performance attained in the laboratory as to shape of curve and as to many other characteristics.

L. F. Moody.[4] It will be generally agreed that the Pelton wheel, while it has been developed into a thoroughly reliable and satisfactory prime mover, still has ample possibilities for further improvement. To hold that it has reached its ultimate state and that the room for betterment is too narrow for profitable investigation would represent a defeatist attitude not justified by analysis. Gains in efficiency of the order of some 5 per cent or more are easily conceivable. and when translated into values of generated power would justify intensive research.

As pointed out by the author, Pelton-wheel efficiencies have lagged considerably below those of reaction turbines; and it should be remembered in making this comparison that the installation efficiency of a Pelton wheel, which is the figure to be compared with the reaction-turbine performance, should include the head lost in the free fall from the buckets to the tail water, an element which is included in the reaction-turbine figures. Future development may show the practicability of regaining this loss, in spite of mechanical objections such as the closed outlet with shaft seals, ejector means for taking care of air accumulations, and float control of the water level.

The listing (Table 1 of the paper) of hydraulic factors involved in the Pelton-wheel action emphasizes the complexity of the flow in the bucket and the unattractiveness of attempting a completely theoretical analysis. In the hydraulic field, we have been long converted to the experimental method in attacking such problems. A mere comparison of over-all results with progressive changes in design is, however, a slow process, and a method of isolating parts of the problem and attacking them separately is greatly to be desired. The author's method of research should be of real value in giving us a deeper insight into the nature of the flow in the Pelton bucket.

Probably many have thought of using stationary buckets in experimental research on these wheels, or have actually made such experiments. The writer must admit, however, that before reading this paper he was inclined to think that conditions in the running wheel would be so different from those in the experiment that the results would be of doubtful value. The author shows convincingly that the differences are actually of a low order of magnitude; and that by the use of a dummy bucket, cut away to permit the jet to enter the preceding bucket at the correct relative direction, a close approximation to actual conditions can be secured. The author has thus introduced a new technique which should be of marked value in this field.

Without some method of this kind, it is difficult to know where to start in trying to improve bucket design; with the use of this method many unknown phenomena in the flow can be brought to light, the flow conditions can be determined at least qualitatively and directions of improvement shown.

The author has mentioned that not only can sources of loss of efficiency be detected, but that cavitation tendencies can also be discovered in some cases. One possible source of cavitation not included in the paper is the presence of a vortex core in the jet, which upon impinging on the bucket would produce all the essentials of cavitation.

The writer takes the opportunity to urge that more study be directed to Pelton-wheel cavitation and that statistical data be collected, as was done by the National Electric Light Association some years ago for reaction turbines, to show the general trend of the tendency toward pitting as a function of specific speed. With such data, we could plot curves of the Thoma cavitation factor sigma with respect to specific speed. For Pelton wheels having free discharge into the atmosphere, the static draft head term H_s disappears from the formula $\sigma = \frac{H_b - H_s}{H}$; giving simply $\sigma = H_b/H$, the ratio of the height of the barometric water column, at the elevation of the plant, to the effective head. With definite experience data plotted in this way we could more intelligently judge of the range of heads and speeds limiting the Pelton-wheel field.

Author's Closure

The author greatly appreciates the generous comments from such well-qualified sources as Mr. S. Logan Kerr and Prof. L. F. Moody.

Mr. Kerr states concisely the general principles which are absolutely necessary to obtain high efficiencies in Pelton wheels. Lower efficiencies in Pelton wheels can be attained very easily. One proof is that the old impulse wheel was built even a century ago in a primitive wooden form, sometimes with 75 per cent efficiency. This circumstance might be the reason for a certain superficial similarity between test and field arrangement. This neglect of nozzle arrangement and housing formation explains discrepancies between test and field performance.

The author agrees entirely with the remarks of Professor Moody, especially need of statistical survey concerning the cases of cavitation of Pelton wheels. It is obvious that cavitation is unavoidable in all kinds of turbines under certain conditions at a relatively high speed which is desired for economical reasons, and we urgently need to establish these limitations in order that cavitation may be avoided.

[4] Professor of Hydraulic Engineering, Princeton University, Princeton, N. J. Mem. A.S.M.E.

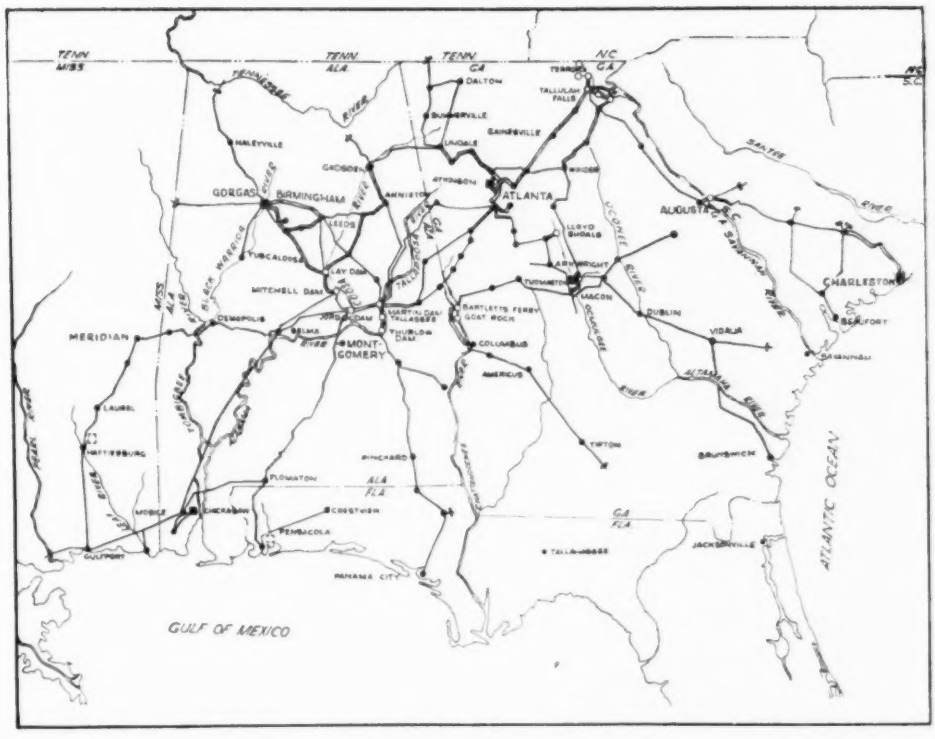


FIG. 1 EXTENT OF TERRITORY SERVED BY SOUTHEASTERN GROUP OF THE COMMONWEALTH & SOUTHERN CORPORATION

Range of Operation of Steam Plants in a Combined System of Steam and Hydro

BY A. T. HUTCHINS[1] AND HOWARD DURYEA[2]

The balance between hydro- and steam-plant power generation on the southeastern group of The Commonwealth & Southern Corporation during the postdepression period and later the period of peak war demands is explained in this paper for an understanding of the system's approach to the installation of steam plants. The discussion includes such data as area of the system, loads, plant capacities, and such pertinent factors as ratio of steam to hydro generation, the relation of steam to hydro capacity, etc. The unit principle is used in the steam-plant installations, i.e., one boiler supplies all steam requirements for one turbine unit. Details of the boilers, auxiliary equipment, operating experience, and results attained are comprehensively treated.

THE problem of fitting large and efficient steam units into utility loads during the depression years from 1930 through 1935 on the larger systems of the country has been much discussed. On the southeastern group system of The Commonwealth & Southern Corporation many of the steam plants were idle for long periods, and this was accentuated by the existence of hydro capacities that were relatively large in proportion to the total load. Seasonal changes in river flows necessitated wide variations in steam-plant loading to supplement hydro generation when flows were low and to utilize hydro generation and avoid wasting water during high flows. Postdepression and particularly the present high war loads are in sharp contrast to the foregoing conditions, as they require maximum continuous output from the more efficient steam plants and greatly increased generation from higher-cost plants.

EXTENT OF SOUTHEASTERN GROUP OF SYSTEM

The discussion of such operations is obviously more interesting if there is a general understanding of a system, its area, loads, and plant capacities, together with other pertinent factors, such as ratio of steam to hydro generation, the relation of steam to hydro capacity, etc. The small map, Fig. 1, has been prepared to show the extent of the territory served by the southeastern group of The Commonwealth & Southern Corporation. Because of lack of space it does not show all existing steam and hydroelectric plants, nor all of the transmission lines and substations.

[1] Production Consultant, The Commonwealth & Southern Corporation, Birmingham, Ala.

[2] Co-Ordinator of System Power Supply, The Commonwealth & Southern Corporation, Birmingham, Ala.

Contributed by the Power Division and presented at the Spring Meeting, Birmingham, Ala., April 3–5, 1944, of THE AMERICAN SOCIETY OF MECHANICAL ENGINEERS.

NOTE: Statements and opinions advanced in papers are to be understood as individual expressions of their authors and not those of the Society.

The data presented in this paper refer to the system shown in Fig. 1, corrections having been made for periods prior to 1940, when Tennessee Electric Power Company was included in this group. The present system includes South Carolina Power Company, Georgia Power Company, Alabama Power Company, Gulf Power Company, and Mississippi Power Company, listed in order from east to west. Again moving from east to west, the rivers supplying water to hydroplants are the Savannah, between Georgia and South Carolina; the Tallulah and Chattooga, whose confluence forms the Tugalo in northeast Georgia; the Oconee and Ocmulgee in north central Georgia; the Flint and Chattahoochee in southwest Georgia; and the Tallapoosa and Coosa in Alabama. Located as these rivers are in the southern foothills of the Appalachian range and above the fall line, they afford advantageous sites for hydro plant developments, starting with elevations of 1846 ft above sea level at the Burton site on the Tallulah River in northeast Georgia, with progressively lower elevations as one moves southwest.

Fig. 2 shows total load, expressed in million kilowatthours

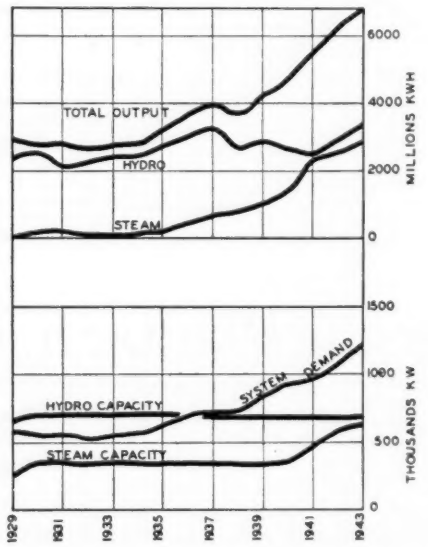


FIG. 2 TOTAL ANNUAL LOAD ON SYSTEM, RELATION OF HYDRO AND STEAM GENERATION, PEAK HOUR MAXIMUM DEMANDS, AND INSTALLED CAPACITY OF STEAM AND HYDRO POWER

annually, together with hydro and steam generation, and also peak hour maximum demands expressed in kilowatts, together with installed capacity of hydro and steam sources. Purchased energy is not shown because of lack of space and consequent confusion. The system has purchased large amounts of energy from outside sources, and the co-ordinated companies have purchased by-product generation from industrial concerns. For a few years one of them operated a plant to supply steam to an industrial customer, and thus secured a block of by-product energy. Purchases are based on requirements to supplement steam and hydro sources, availability, and relative cost.

In discussing the graphs, Fig. 2, depression loads are apparent from 1929 through 1934, followed by moderate increases in 1937. Loads near the close of 1937 and 1938 decreased, following which they again increased and assumed the present sharp upward slope characteristic of war production.

The lower section of Fig. 2 shows that there have been no increases in installed hydro capacity since 1930, and that steam capacity also remained practically constant from 1930 through 1940. This condition reflects the depression loads and the eventual loading of both hydro and steam plants until the war loads approached the existing capacity, about 1939, and resulted in the construction of additional steam facilities.

Fig. 1 shows the location of six hydro plants in extreme northeast Georgia; three on the Chattahoochee River above Columbus, Georgia, three on the Tallapoosa River, and three on the Coosa River in Alabama. In each of these groups the plants are in series so that water released from the upper plants is successively used by those below.

The total capacity of run-of-river plants is around 375,000 kw and that of the two principal storage groups is 350,000 kw, making the total installed hydro capacity some 725,000 kw. However, the annual generation is roughly two thirds from run-of-river plants and one third from storage plants. The total equivalent energy in storage is 450,000,000 kwhr, with some additional 15,000,000 kwhr in run-of-river ponds.

Referring to Fig. 2, curve "Steam," it will be noted that the output from steam plants was very low for the first 10 years shown. In fact, the composite plant factor for the steam capacity, as shown in the lower part of this figure, is approximately 10 per cent for this period. As previously mentioned, a load drop occurred in 1938, following which the sharp uptrend beginning in 1939, started a new era of steam-plant construction and operation in marked contrast to the previous periods. In 1939, the first unit of those shown in Table 1 was purchased and its initial operation, together with that of other added units, is given.

TABLE 1 STEAM PLANTS ADDED TO SYSTEM

Plant	Unit no.	Kilowatt rating	Throttle pressure, psi	Steam temperature, deg F	Revolutions, rpm	Generator cooling	Initial operation
Arkwright	1	40000	850	900	3600	Hydrogen	April, 1941
	2	40000	850	900	3600	Hydrogen	May, 1942
	3	40000	850	900	3600	Hydrogen	Nov., 1943
Chickasaw	1	40000	850	900	3600	Hydrogen	April, 1941
	2	40000	850	900	3600	Hydrogen	Mar., 1943
Atkinson	2	60000	425	750	1800	Air	Sept., 1941
Gorgas	5	60000	850	900	3600	Hydrogen	Dec., 1943

Although generating and transmission facilities, as well as distribution systems, are owned by the operating companies in the several states, planning studies for additions, design engineering, and subsequent direction of operations of power sources are coordinated by a service company mutually owned by the operating companies. The personnel of the service company for the southeastern group is located in Birmingham. By means of the co-ordination effected by the service company, the ultimate aim that power-producing facilities be most advantageously located, designed, maintained, and operated so as to produce the maximum amount of energy at lowest cost, and that each of the operating companies shall benefit therefrom is attained. In other words, all power-producing facilities are operated as a single group to provide capacity and energy for the total load. This method of operation takes advantage of all diversities of loads, stream flows, unit outages for inspection, maintenance, and emergencies that may occur between the individual operating companies' systems, as well as within the systems of each of them. Any action that materially reduces the area served and the facilities available to produce power would tend to lessen the economic value of the group.

SYSTEM RANKS HIGH IN PERFORMANCE

An indication that the size of this system tends toward economy in operation is its performance in comparison with other systems east of the Mississippi River. Of a load of 89 billion kwhr east of the Mississippi River in 1940, 44 per cent was generated by seven large generating and transmission systems that have been developed and operated under common ownership similar to the southern group of The Commonwealth & Southern Corporation. These seven systems generated an average of 4430 kwhr per kw

of dependable generating-plant capacity. This system stood third among these seven groups with a generation of 4413 kwhr per kw of dependable generating capacity.

The remaining load east of the Mississippi River was developed by a large number of smaller companies and systems. For the same year, these companies generated 3590 kwhr per kw of dependable generating-plant capacity. This is a rather striking comparison when it is realized that in this respect the seven systems under common ownership showed an increase in use factor of 23 per cent, as compared with the other systems.

Three factors undoubtedly contribute to these results:

(*a*) Diversity of peaks reserves the surplus capacity.

(*b*) Better planning, due to engineering staffs made practicable with size of operations.

(*c*) Greater use of interchange agreements where dispatching is handled by one co-ordinated organization.

The operation of all generating plants and the interchange of energy between companies within the group and with adjoining concerns is under the supervision of a central supervisory group of the service company, who work with the load-dispatching forces of the individual companies. Hourly load estimates for the entire group are maintained constantly and are projected into the future to provide hourly load schedules for hydro groups and steam units during critical daily and week-end periods. Arrangements are made to load and unload steam units so as to utilize, supplement, or conserve hydro flows; provide for outages for inspection, maintenance, and emergencies of steam and hydro units; insure sufficient free hydro-regulating capacity for tie-line control, spinning reserves, and minimum flows when and where required. Arrangements are made to receive energy from outside sources, to make deliveries to them, and to synchronize these transactions with hydro and steam operations on the system.

Unit Principle Used in Steam Plants

Since the short time peaks of load throughout the year are carried by the hydro plants, the units installed, as shown in Table 1, were all designed on the basis of carrying prescheduled loads. The extensive transmission system, interconnecting the load areas with their steam plants, makes conditions ideal for use of the unit principle of design, in which one boiler supplies all the steam requirements for one turbine. One exception among the units shown in Table 1 is unit No. 2 at Plant Atkinson, where there was some capacity available in existing boilers. Because of the importance of the load in the local area a cross connection was made between the steam lines of the two units at the Chickasaw Plant. It may be noted here that at the Gorgas Plant the steam conditions for No. 4 unit are 425 psi and 750 deg and No. 5 unit 850 psi and 900 deg, and no pressure-reducing and desuperheating equipment was installed.

The early plants in the 900-psi class were designed for 900 psi in the boiler drum and 850 psi at the turbine throttle. The design of superheaters to secure 900 F total steam temperature resulted in approximately 50 psi drop across the superheater at full load. When operated with a margin of 30 psi under popping pressure, and 20 psi drop through valves and piping, the pressure at the turbine approached 800 psi. In 1939, the requirement for safety valves designed to operate between 900 and 1500 psi was realized, and the purchase of the safety valves for the first boiler of the units, listed in Table 1, was delayed until such a valve was offered. Since that date boilers in this class have usually been built for 950 to 1000 psi at the boiler drum. This has resulted in securing the minimum of safety-valve operation.

All of these units in the 900-psi class are designed for four-stage extraction for feedwater heating, one heater being the direct-contact type arranged for very complete deaeration of the feedwater.

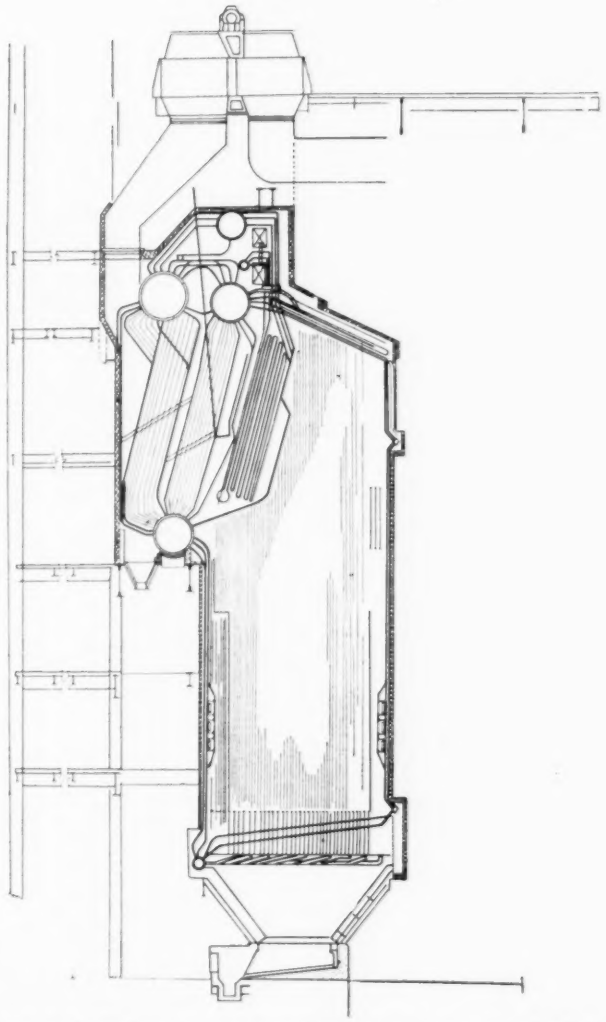


Fig. 3 Cross Section Through Steam Unit Rated at 400,000 Lb Per Hr, at 950-Psi Drum Pressure

Feedwater temperatures are approximately 375 F. Obviously, with the unit system, availability of the boiler for continuous operation over long periods is highly essential. Conventional types were selected and furnace design provided for reasonable heat liberation on the basis of four waterwalls and a dry ash pit.

Fig. 3 is a cross section of a unit rated at 400,000 lb per hr, 950 psi drum pressure, and 900 F. Three of these units were installed. The furnace of this unit has fin tubes on four sides and is tangentially fired with twelve burners, three at each corner. These three boilers and all others built with the units in Table 1 are each equipped with three pulverizers.

Fig. 4 is a cross section of one boiler built for the same capacity and steam conditions and differs primarily in the furnace bottom and the side-wall tubes. This arrangement of the furnace bottom is intended to be safe against damage to the hearth tubes from falling slag, which occurred in the other design, and also affords better protection for the dry-ash pit. The wall tubes are tangent tubes, 3 in. OD on $3^1/_8$-in. centers, which are connected to the headers with a forging which joins two tubes to a $3^1/_8$-in-OD nipple, which in turn is rolled into the header. Obviously, this results in a cooler furnace, which has proved to be less subject to slagging.

Fig. 5 is a cross section of a boiler built for the same steam con-

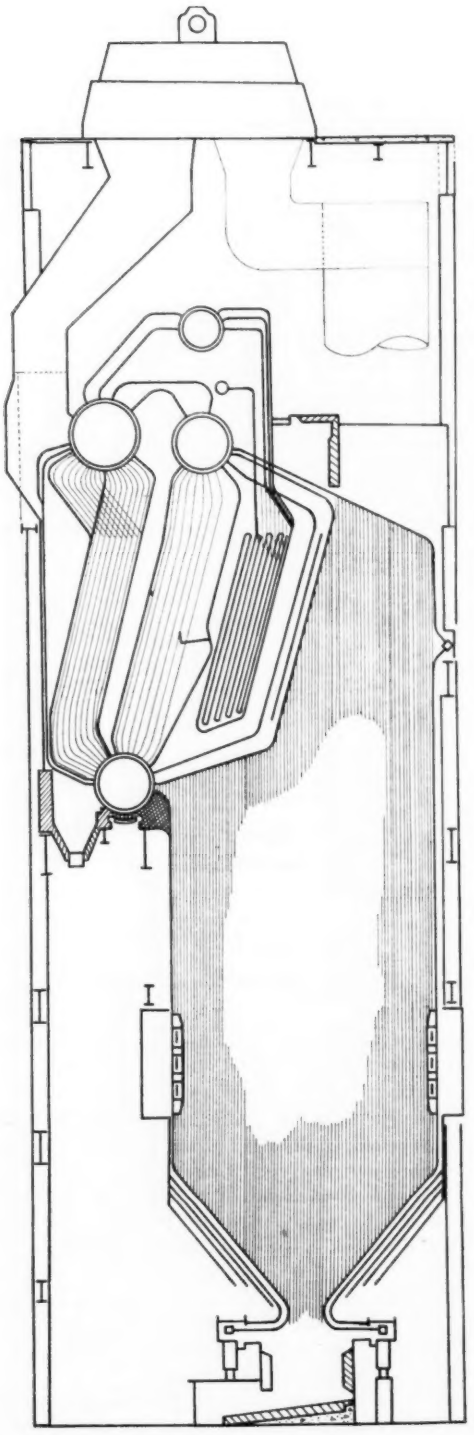


FIG. 4 CROSS SECTION THROUGH BOILER SHOWING VARIATIONS IN FURNACE BOTTOM AND SIDE-WALL TUBES

ditions but with a capacity of 600,000 lb per hr. The wall tubes and furnace bottom follow the pattern of Fig. 4; the design embodies an economizer and omits the dry drum. Similar to those just mentioned, this boiler is tangentially fired and all five units represented by Figs. 3, 4, and 5 are equipped with the regenerative-type air preheaters.

Fig. 6 is a cross section of another boiler of the 900-psi class and 400,000 lb per hr capacity. This unit is fired with six circular burners which are fitted with rings for burning gas, has a relatively large economizer and tubular air preheater. This unit has been in service only a short time, and it is too soon to report on several features of operation based on inspections, but tests show that carry-over from this boiler is a fraction of 1 ppm at rated load and with boiler water having from 340 to 835 ppm dissolved solids. This unit is installed with the primary-air fan ahead of the pulverizers, and comparative results will be studied with interest.

The reason for the selection of boilers with economizers designed to secure 2 to $2^1/_2$ per cent increased efficiency above that for the boilers, shown in Figs. 3 and 4, becomes evident when it is noted that these are the most recent units, will be assigned a more nearly base load, and the price increase was relatively small.

All of these units are arranged with by-pass dampers for control of superheat temperature, so that from 60 per cent to 100 per cent rating 860 F total steam temperature may be maintained. These dampers are manually controlled and for the type of load carried this has proved satisfactory.

Although one might not select the tangentially fired furnace for burning gas as fuel, a number of these have been fitted with gas

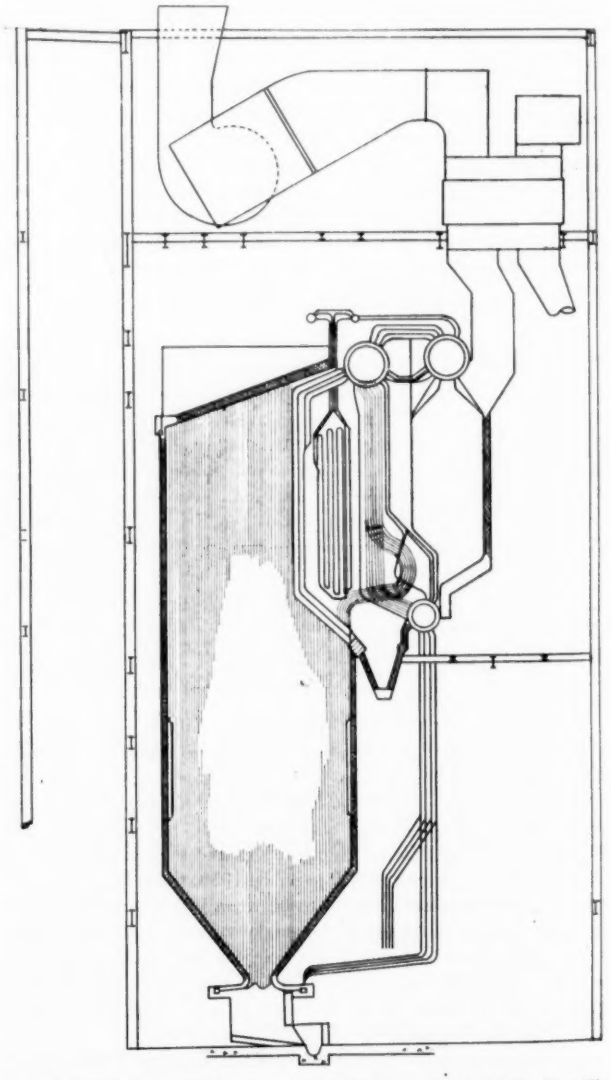


FIG. 5 CROSS SECTION THROUGH BOILER HAVING 600,000 LB PER HR CAPACITY

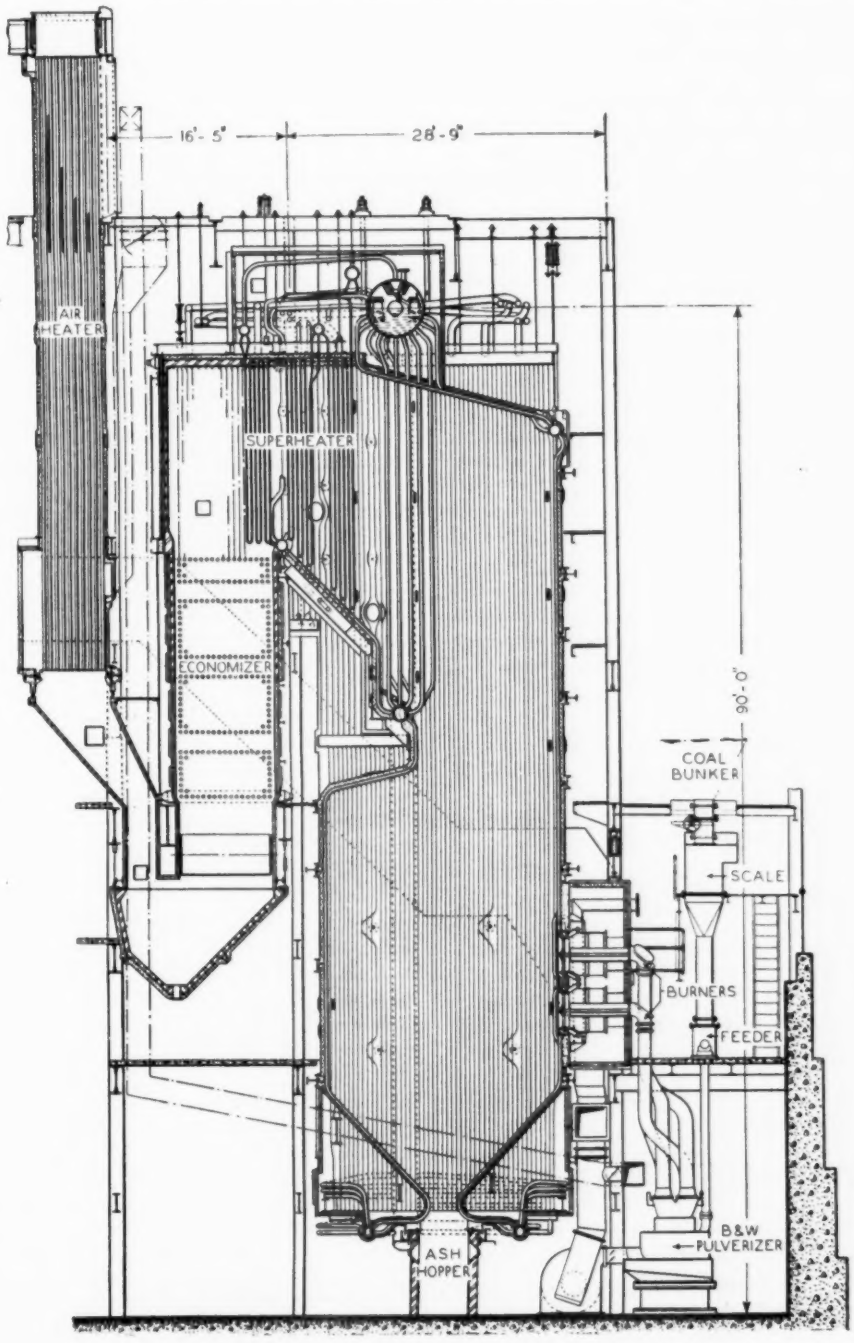


FIG. 6 CROSS SECTION THROUGH BOILER OF 900-PSI CLASS

burners and are performing fairly well. It is interesting to note that during summer months off-peak or "when available" supply of gas to plants Arkwright and Atkinson has approached 2 billion cu ft per month. The availability of burners and pulverizers installed with these units has been practically 100 per cent with no emergency outage. For the first 150,000 tons per mill, when pulverizing coal having a grindability of 45 to 50, there have been no replacements with the exception of exhauster-fan blades.

OPERATING EXPERIENCE WITH STEAM UNITS

In studying the performance of modern boilers, it is perfectly evident that the difficulty with handhole gaskets had caused considerable outage and particular effort was made in improving the design of previous units to reduce the extent of waterwall headers to an absolute minimum and thus eliminate handholes with their plates and gaskets. This was carried to the point of necessitating extremely long tubes, which were fabricated by welding, and required special arrangements for shipping. The cross sections of all these boilers clearly show this feature in the wall tubes. It is evident that a failure in one of these long tubes calls for repair by welding and this has been done successfully.

A study of the superheater of any of these boilers shows how

important it is that all portions of these tubes be free of faults and that no solids shall be deposited by the steam. In all cases tubes are made up with welded joints and at the outlet-header nipples are welded in and stresses relieved before shipping. None of these superheaters is drainable and great care must be taken to see that all condensed steam is evaporated before the tubes are subjected to gases at normal operating temperatures. One failure in the superheater of one of these boilers and of similar installations has been experienced, due to the presence of water in certain tubes, thus preventing the flow of steam and consequent overheating. In regard to the time element to secure safe starting, it may be noted that in general the elapsed time between the first indication of pressure rise in the boiler drum when starting from cold and the time for closing vent valves on the superheater outlet when steam is being supplied to the turbine is approximately $2^1/_2$ hours.

Other failures of superheater elements include erosion, due to leaking baffle, and one case of corrosion. The case of corrosion occurred near the upper end of the superheater element on the inlet side, and since there is no evidence of high temperature it must be assumed that the failure was due to oxygen attack which had been concentrated due to condensate flowing into the tube, or during the shutdown period when this element of the tube was nearly filled with water. This is mentioned because of the emphasis which it places on the necessity either for completely filling the superheater elements with water properly treated, or completely drying these elements when the unit is out of service. This latter is not easy of accomplishment.

Automatic combustion control providing only for the control of fuel and air to the pulverizers, secondary-air supply, and induced-draft-fan operation has been highly satisfactory.

With one exception the pumps for these units are all motor-driven with constant-speed motors, and the feedwater-control element consists of a single valve. Something over 2 years of service from one of these valves, which is provided with good hydraulic characteristics, has resulted in an almost perfect record, and the valve is now reported as being tight enough for shutoff purposes so that the boiler may be banked with a full pressure on the pump side of this valve. In contrast with requirements for boilers supplying steam at a rapidly fluctuating rate where three-element control is used, these valves operate from drum level only. By using a direct-contact heater for deaerating the feedwater and as a storage supply ahead of the boiler feed pump, one high-pressure closed heater has been eliminated. On the other hand, power for pumping increases somewhat, and we have found that pure water at 320 F attacks the steel in the pump more rapidly at points of high turbulence than at 235 F so frequently used. The cure for this has been coating such areas with a high-grade alloy metal or some recirculation of boiler salines.

Although the history of these units is not long enough to be conclusive in regard to carry-over, No. 1 unit at Chickasaw and No. 1 unit at Arkwright were each inspected after 2 years of operation and were found to be relatively free of blade deposits. In fact, this condition was such that continued operation throughout another year would have been satisfactory in this respect. The subject of carry-over embraces boiler performance, quality of feedwater, and finally quality of steam. To secure feedwater with low content of dissolved solids, make-up is secured from evaporators and special attention given to securing tight condensers.

Since the various manufacturers' recommendations were used in securing condenser tubes to the tube sheet, two methods were used. In one case, tubes are rolled at both ends, elongated by heating before rolling-in, and bowed slightly to take care of expansion. The other method calls for rolling at one end and packing at the other end of the tube, which was highly polished to avoid dragging the packing due to any movement caused by expansion. Both methods have proved highly satisfactory.

Starting with high-grade condensate secured from these condensers, water is supplied direct to the boilers without addition of chemicals but with thorough deaeration. Chemicals are supplied individually to each boiler through a chemical feed pump, and the initial operation of all boilers used the well-known phosphate treatment. Enough sodium sulphite was used to maintain from 10 to 15 ppm in the boiler water in order to take care of any residual oxygen or that picked up during shutdown periods. It may be noted here that the record of sulphite used in the case of 450 lb pressure and 850 lb pressure shows a considerable discrepancy, the easiest explanation being that in the higher pressure some of the sodium sulphite is broken up. About 15 or 20 ppm PO_4 in solution is maintained in the boiler water and pH of approximately 11. Under these conditions it was found that the first three boilers installed accumulated a considerable amount of fine black magnetic oxide in the boiler water. This oxide was present in quantities sufficient to cause considerable concern, and it should be noted here that the cure for it was considerably delayed due to the necessity of maintaining all boilers in operation. Some variation in boiler-water treatment was undertaken but without conclusive favorable results. Although no boiler failures have resulted from this type of corrosion, its prevention will be eagerly sought.

Turbogenerators and Fuel-Storage Methods

It will be noted from the data in Table 1, that six of the seven turbogenerator units installed in the last 4 years are equipped with hydrogen cooling for the generators. This has been highly satisfactory, hydrogen use has been less than specified by the manufacturer, and the control equipment has been trouble-free.

All of the 3600-rpm units in this group were built after the developments which provide for mounting the stator iron within a fairly rigid frame so that the 7200-cycle vibration, which has been objectionable in some earlier designs, was practically eliminated. The performance of the exciters on these units has been fairly satisfactory. The manufacturers supplied each turbine with pressure-relief diaphragms on the exhaust casing and automatic throttle closing in case of high back pressure, so that none of these units was equipped with atmospheric relief valves. This equipment has proved satisfactory on these and one 1929 unit.

At the time these plants were being designed, the use of tractors with bulldozers and carryalls for storing and reclaiming coal was gaining favor rapidly and after a test at Plant Atkinson, this equipment was put into use at the four plants: Atkinson, Arkwright, Chickasaw, and Gorgas. The advantages of using this equipment for storing and reclaiming coal are the wide range of operations permissible, low first cost, and the ability to store coal to any height of pile, as much as 30 to 40 ft. Over 200,000 tons have been stored in one pile with this equipment. Furthermore, the dense packing resulting reduces spontaneous combustion to a minimum; in fact, there have been no fires in such piles.

It is impossible to go into detail of all operating characteristics of these units, but it may be said that all changes in equipment worked out through co-operation with the manufacturer during the design of these plants have been quite satisfactory.

The longest forced outages have resulted from the damage to one superheater, previously noted, and the delay in putting two generators into regular service due to hot spots developing in the stator iron, which called for extensive rebuilding by the manufacturer. Erosion of induced-draft fans has caused repeated short outages, and plans are now under way for installing dust collectors ahead of these fans at one plant.

Shortage of manpower has prevented compilation of data to determine closely the performance of these units; such checks as have been made show they are surpassing design performance.

The Co-Ordinated Operation of Hydro and Steam Capacity in Electric Power Systems

By G. W. SPAULDING,[1] BALTIMORE, MD.

Two decades or more ago, numerous technical papers were written on the then popular subject of hydro *versus* steam power, but more recent discussions, presented both in society journals and in other engineering publications, have emphasized the advantages of the co-ordinated use of hydro *and* steam. These later papers have explored and charted that wide range of existing conditions where co-ordinated operation of hydro and steam will be more economical than use of either alone; and today the general principles involved in such co-ordinated operation are understood and applied in many regional power systems. In the first part of this paper, the historical development and the present status of co-ordinated operation in a specific regional power system are reviewed. This is followed by discussion of a possible approach to the use of pondage at run-of-river hydro plants as part of the system reserves, such use being predicated upon the probabilities of noncoincidence of maximum system loads, minimum river flows, and severe forced outage of steam capacity.

THE highly diversified industrial area in the Middle Atlantic States, including New Jersey, Delaware, Eastern Pennsylvania, Maryland, and the District of Columbia, is served by seventeen electric utility systems with power-generating resources of over 4,500,000 kw. The individual operating systems of the area, controlled by more than a dozen independent interests, have through the last decade been interconnected by high-voltage transmission lines to form an integrated regional system. Effective co-ordination of operation of the combined hydro and steam resources of this region has been established. The four companies operating in the southern portion of this area completely co-ordinated their hydro and steam operations over 10 years ago, while three of the larger companies in the northern portion began such operation at an even earlier date. Interconnection between the northern and southern parts of the area began about 1931, and over-all co-ordination has subsequently developed. Very recently, interconnections have been strengthened between the northern end of this regional power group and other regional systems in New York State and through them with power systems in New England.

Co-operative studies on a regional basis were initiated in the late 30's. These studies were gradually expanded to assure fullest utilization of the hydro and steam resources in the carrying of increased loads, in the scheduling of maintenance, and in meeting emergency outages of equipment. As a consequence, the production of power at the more economical steam-generating stations, in general without regard to location or company ownership, has resulted in operating economies and more effective utilization of available generating capacity. In addition to the co-ordinated scheduling and operation of capacity, there has been a continuing interchange of energy on an economy basis which has made possible, in the last 2 years, substantial conservation of much needed coal and fuel oil and in relief of fuel transportation.

[1] Vice-President, Pennsylvania Water & Power Company.

Contributed by the Power Division and presented at the Spring Meeting, Birmingham, Ala., April 3–5, 1944, of THE AMERICAN SOCIETY OF MECHANICAL ENGINEERS.

NOTE: Statements and opinions advanced in papers are to be understood as individual expressions of their authors and not those of the Society.

REGIONAL LOAD AND CAPACITY CONDITIONS

This regional power area is predominantly urban in character. The electrical-load requirements are typical of what might be expected in metropolitan areas in which are located large and diversified industries. The power resources of this area consist of approximately 85 per cent steam capacity and 15 per cent hydroelectric capacity. Of the effective hydro capacity of about 670,000 kw, nearly 90 per cent is installed in run-of-river plants along the lower reaches of the Susquehanna River, about 10 per cent is supplied from storage projects in the Delaware River drainage basin, while the balance is made up of numerous small hydro installations.

Since there is no upriver storage on the Susquehanna, the plants on this river are essentially run-of-river plants, the pondage at the plants being relatively small in comparison with installed capacities. The Susquehanna is subject to wide variations in natural flow. The flood stages of the river usually occur in the spring of the year, and the resultant reductions of head and capacity rarely adversely affect system capacity requirements, but the experienced low flows in the late summer, fall, and winter do have an important effect on the system capacity requirements. It is in the treatment of this capacity situation that this large interconnected group of utilities may be different from other power systems.

There has been co-ordinated hydro and steam operation in certain of the interconnected systems through varying forms of power contracts for over three decades. Because of this fact, most of their steam-capacity installations have been designed for sustained or base-load operations, that is, the turbines and more particularly the boilers have been designed and rated for operation for 12 or more hours a day, which operation is required with low river flow when the peak portion of the load is carried by the hydro plants. On other power systems in the area, experiencing generally the same daily and seasonal load shape, but with relatively less hydro capacity, the steam capacity has, through the years, been designed to carry a large portion of the daily peak loads, normally of short duration, and cannot be operated at maximum output for sustained periods. In co-ordinated operation, the normal limitation of this peak steam capacity must be recognized.

Under present-day conditions, with high-load-factor wartime loads, and absence of sharp evening peaks resulting from extension of daylight-saving time, and, until recently, curtailment of lighting in coastal areas, it has been necessary and desirable to use all steam capacity on a more or less sustained basis. This means that those plants designed for peak operation must now be operated for longer periods at reduced loading. The sharp peak loads, or what is left of them, are scheduled to be carried by hydro under critical capacity conditions.

ESSENTIAL FACTORS IN A CO-ORDINATED REGIONAL POWER SYSTEM

There are obviously several essentials to the complete and

full co-ordination of the combined generating facilities of a regional power system, in addition to the necessary physical facilities, particularly when the various operating systems in the power region are controlled by independent interests. These are as follows:

1 The first essential is the availability of power contracts or interconnection agreements between the several companies of the area which are sufficiently flexible to cover the wide range of required operation. Fortunately, there were such flexible interconnection agreements in this regional area, dating back at least 5 years. There must, of course, be an incentive for co-ordination, and this can best be provided within the framework of the power agreements.

2 Considerable operating experience is necessary before the fullest advantage from co-ordinated operation can be obtained. Our co-operative studies were expanded in both scope and detail in the light of experience gained during the several years preceding the present increased war loads, such experience establishing not only the basis for determining the amount of capacity gained from co-ordinated operation, but also the routine planning and scheduling of operation and of maintenance.

3 A procedure for day-to-day direction and control of co-ordinated operation is essential. Experience has indicated, when other essentials are provided for, that the maximum advantages can be obtained without a top regional power dispatcher, so long as there is a co-operative effort on the part of the several system dispatchers to work in the interest of over-all operating economy. This co-ordinated operation, which has been of such material aid in the war effort in this regional area, has been accomplished without encroachment upon the individual responsibilities of the many operating companies.

Joint Operating Problems Not Difficult to Handle

The operating problems of system frequency control, time variation, and tie-line controls have never been difficult, largely because of the capacity of the interconnecting transmission network. This consists primarily of two high-voltage 220-kv transmission systems, themselves interconnected by a grid of double-circuit 66, 110, and 132-kv lines. There are no automatic frequency controls or tie-line loading controls on the regional system. The responsibility for frequency control is assigned, from time to time, to one of the five larger systems.

Telemetering is used extensively in the several dispatching offices to give indications of tie lines, system loads, and station generations.

Problems of policy are considered by a "Steering Committee," consisting of the top operating executives of each operating company in the region, but experience has indicated that once the general principles are agreed upon, frequent meetings of this Steering Committee are not necessary. The detailed operating and accounting problems are handled through so-called "Operating Committees," on which each company or group of companies is represented by operating men.

One of the purposes of the continuing co-operative studies is the determination of the maximum firm hydro capacity available from the run-of-river hydro plants when operated as a co-ordinated part of the regional system capacity. Our problem was not one of determining whether hydro or steam capacity should be provided to serve the increasing system load, but rather how much more war load could be carried on the regional system by complete co-ordination of the three large run-of-river hydro plants and the available steam capacity. These hydro plants are owned by different utilities and, although geographically close together, are electrically connected with different parts of the regional system. While there were found to be minor limitations in the power that could be interchanged over the regional network, particularly between the northern and southern sections, these limitations did not impose any serious restrictions on the complete utilization of the available power resources. A detailed discussion of some of the general factors that enter into our studies of firm hydro capacity may be of interest in connection with further considerations of the economies of run-of-river hydroelectric developments.

Hydro Installation

There are four run-of-river hydroelectric plants within a 50-mile stretch in the lower reaches of the Susquehanna River adjacent to tidewater. Data on these plants are given in Table 1.

The operation of run-of-river hydro plants in a hydro-steam system has been frequently explained, and it is sufficient here to call attention only to the low ratio of hydro to steam capacity in this regional system. Under normal operating conditions, the Safe Harbor pond can be used for weekly regulations of low flows; but there are other conditions under which such operation is either not desirable or not possible. In general, the use of the Safe Harbor pondage differs for three possible conditions of operation, as follows:

1 When there is ample system capacity, i.e., an excess of reserve capability, the Safe Harbor pond elevation is scheduled to provide for most economical use of hydro energy on the combined system load. The use of pondage is so scheduled as to have the forebay at top elevation Monday morning.

2 When, because of low river flow or reduced steam reserve capability, the capacity situation appears critical, the Safe Harbor forebay is maintained as near top elevation as possible, at least during the first part of the week, in order that maximum pondage will be available in the event of forced loss of steam capacity, i.e., for emergency use.

3 When, because of low river flow, coincident with loss of steam capacity due to forced outages, there is a deficiency in steam-generating capacity on the system, i.e., an emergency exists, the Safe Harbor pondage may be drawn on to obtain the needed energy from the three lower plants. It should be recognized that the only alternative to such operation would be to curtail system load. As soon as steam reserves are again available, hydro generation is curtailed to restore the forebay to normal.

Load Shape and Maintenance Requirements

The 15-min integrated peak loads for each week in a wartime

TABLE 1 HYDRO PLANTS ON LOWER SUSQUEHANNA RIVER

Miles from tidewater	Plant	Year of initial operation	Number of units	Head, ft	Maximum plant discharge, cfs	Effective plant capacity, kw	Pondage, in terms of available energy,[a] kwhr
50	York Haven	1904	20	20	18000	20000	...
27	Safe Harbor	1931	7	55	65000	230000	10500000
19	Holtwood	1910	10	51	32000	104000	1200000
4	Conowingo	1928	7	89	44000	252000	5300000
				215		606000	17000000

[a] Energy that can be generated from useful pondage, including both generation at site and at downstream plants.

and a prewar year are shown in Fig. 1. The critical capacity conditions might be expected, from these data alone, to occur in December. In an all-steam system that conclusion would be obvious; but in a hydro steam system without storage, where hydro capacity varies from month to month depending upon river flow and reaches minimum values about September, the late summer loads may be the most critical. Maintenance requirements and condensing-water temperature effects on steam capacity also must be considered in this connection.

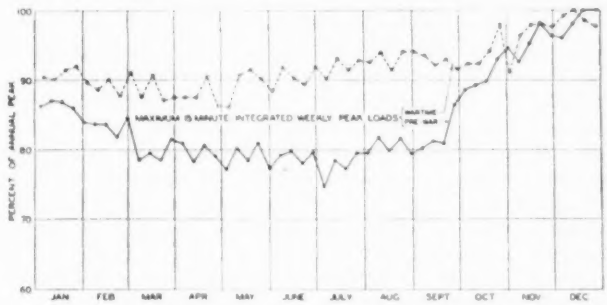


FIG. 1 ANNUAL LOAD SHAPES OF REGIONAL POWER SYSTEM

The valleys in the prewar annual load curves of the regional area and to a lesser extent in the wartime load curve, together with the seasonal variations in the amount of available hydro capacity, control to a large extent the scheduling of steam-unit maintenance; but because it is normally possible to schedule most maintenance at times other than the expected time of occurrence of system peak load, maintenance usually has little or no effect on system capacity requirements.

RIVER-FLOW EXPERIENCE

For many years, computations of firm hydro capacity have been based upon the most adverse river flows then of record, determining for such flows the hydro capacity that would be firm on maximum expected loads with pondage used over some specified period of time, determined by the assumed length of simultaneous forced outage of steam reserves. The improbability of the coincidence of all these conditions has led to a growing feeling that such assumptions are extremely "conservative."

The wartime need for using maximum-capacity resources gave added impetus to several earlier studies relating to the applicability to capacity computations of river flows somewhat greater than the minimum flows of record, but still coincident with the maximum system peak loads, and to the use of Safe Harbor pondage over a shorter period of time, which in turn is related to more recent experience on the probable length of simultaneous forced outages of steam units.

Prior to the increase in load resulting from war, the minimum weekly flows of record for each month were used in capacity computations; but currently the effective hydro capacity is computed for river flows that can be expected to be equaled or exceeded in about 93 per cent of the years (based upon flow records from 1891 to date). For the river flows thus selected for each low-flow month, the effective hydro capacity is determined for the maximum weekly load estimated for that month, with pondage used on a weekly cycle of drawdown and refill. This hydro capacity is then combined with steam capacity, adjusted for circulating-water temperatures, and for scheduled maintenance in arriving at the minimum total effective system capacity for that month, i.e., for load-carrying capacity and for system reserves. The excess of this computed capacity over the estimated system load is the capacity available for reserves and for new loads; the latter being of particular interest to the companies themselves and to the government agencies responsible for the location of war industries.

In the foregoing procedure, there are certain hydro resources which have not been fully evaluated. Additional hydro capacity is available for something less than 93 per cent of the time, resulting from river flows in excess of those used in capacity computations. Such capacity is valuable for the release of steam units for maintenance work in addition to that scheduled in advance, and much maintenance of this nature has recently been necessary. Additional hydro capacity is also available from the short-time use of pondage, when required by the simultaneous forced outage of a large number of steam units, even with stream flows lower than those used in capacity computations. The extent to which a system would be willing to rely on such capacity as firm would be influenced by the forced outage record of its own or similar steam-generating equipment, and upon the amount of other reserve capacity then available on the system.

Perhaps someone will eventually evaluate and properly combine all the pertinent factors by the application of a probability theory. As this theoretical solution now seems impracticable, an attempt has been made to approximate the possible use of pondage in the light of the forced-outage experience of steam-generating equipment, the ideal objective still being that a combined hydro and steam system should have substantially the same degree of reliability as an all-steam system.

FORCED-OUTAGE EXPERIENCE OF STEAM CAPACITY

Forced or emergency outages of steam turbines and boilers are of relatively infrequent occurrence; and only over a period

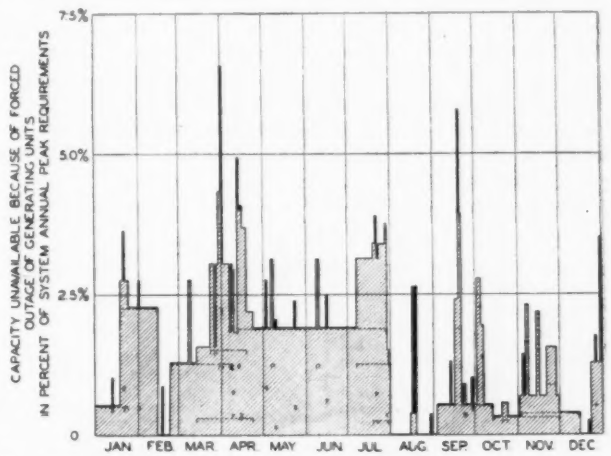


FIG. 2 ACTUAL FORCED OUTAGES OF GENERATING CAPACITY, 1943
(Exclusive of all scheduled outages or losses of capacity due to causes outside of the generating plants.)

of years could a system accumulate sufficient data to determine reasonably well the average forced-outage probabilities of its generating units. These probability factors may differ between systems in which there are different types of units or different operating requirements and maintenance practices. Although conclusions regarding either detailed differences or similarities in the probability factors must await collection of additional data, the general fact that simultaneous outages of a large number of generating units are infrequent and of short duration seems to be well established. This fact is fundamental in the determination of required system reserve capacity and the possible use that can be made of pondage.

The term "forced, or emergency outage" is sufficiently descriptive so that no precise definition is here required. We are interested only in the outages of facilities which have a bearing

upon the capacity resources of the power system, and we are not here concerned with scheduled outages for inspection, where such outages can be scheduled in advance.

It will be noted in Fig. 2 that a number of fairly long steam-unit outages were experienced on the regional system in 1943. Three of these prolonged outages existed concurrently on April 1, at the time of the largest total forced outage of capacity during the year. Yet, more than one half of this total simultaneous outage only lasted from 1 to 3 days. In spite of these several long outages, the average forced-outage time for this year was somewhat better than might have been expected from our own earlier experience; but such variations would be quite normal in year-to-year operation of any system.

Most of the individual and all of the more serious simultaneous outages, shown in Fig. 2, were of short duration. The absence in this one year of long severe simultaneous outages of capacity does not prove that such outages cannot exist, but the probabilities are decidedly against them. Data for earlier years generally confirm those shown for 1943, and give weight to the opinion that severe simultaneous forced outages of steam capacity are infrequent and of short duration. This point is important in connection with the use of pondage as firm capacity.

Use of Pondage for Short-Time Capacity

The pondage, which system operations have indicated as usable by the lower Susquehanna River plants, is equivalent to 17,000,000 kwhr. This is nearly $2^1/_2$ times the weekly hydro energy available from the lowest 7-day average river flow recorded in the month of December. Some portion of this pondage might be used (not to be confused with normal weekly use of pondage where the forebay is returned to top elevation on each Monday morning) as system reserve capacity on those infrequent occasions when severe multiple forced outages exist coincident with peak week loads and minimum flows. Such pondage operation is illustrated in Fig. 3, for the conditions assumed in capacity computations in contrast with conditions more likely to be met in actual operation.

The diagram at the left in Fig. 3 shows the assumed simultaneous outage of steam capacity equal to the ordinate Y. The energy made available by use of only 40 per cent of the available pondage, during the first 5 days of a period beginning Monday morning, would permit hydro capacity to replace an amount of steam capacity equal to the largest steam unit on the system (135 mw), or to the aggregate capacity of several smaller units. This capacity is indicated by the dimension X. (It is here assumed that there would be sufficient installed capacity at the hydro plants to permit such operation, which, however, is not presently the case.) By the following Monday morning, X capacity, out of the total forced out, is assumed to be returned to service. At that time about 60 per cent of the stored energy is still available as pondage, and this condition would be maintained until additional amounts of steam capacity are returned to service to permit gradual refilling of the ponds. The pondage will also be refilled in part as higher river flows are experienced or lighter system loads are encountered, both of which will have an appreciable influence, since it had been assumed from the beginning that such use of pondage coincided with maximum weekly loads and minimum river flow.

The diagram at the right in Fig. 3 assumes simultaneous outage of steam capacity such as was experienced by this system during the middle of April, 1943, the maximum of the simultaneous outage again being equal to Y capacity. In both diagrams the hatched areas indicate the capacity X and X_1 that could be obtained by drawing down the ponds of these three run-of-river hydro plants, while the cross-hatched portion represents capacity, which had been forced out at the beginning of the period but is returned to service, and the approximate time to bring the forebay back to top elevation. A comparison of the assumed and the more probable outage condition indicates that the assumption shown at the left is, indeed, conservative in the light of forced-outage experience; but it is an approach to the use of pondage for at least a portion of the system reserve.

It is necessary to emphasize that the amount of hydro capacity which may be available from drawdown cannot be considered as replacing the entire system reserve requirements. Obviously, it is impossible for pondage to be used as protection

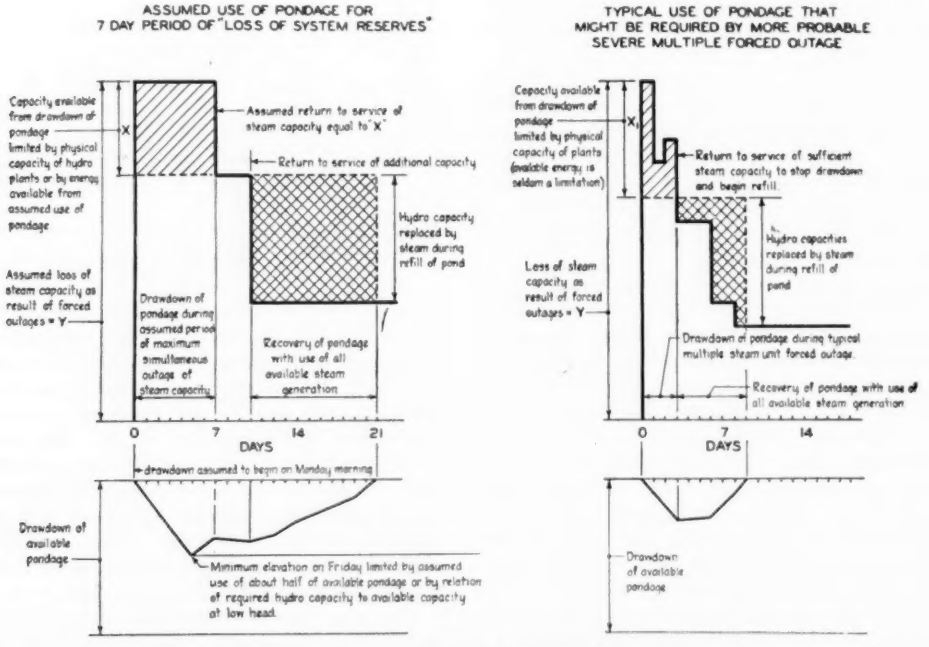


Fig. 3 Use of Pondage as Reserve Capacity

against all outages of steam capacity, for these are almost continuously existent; in low flow the available pondage would soon be exhausted as opportunities for refill would be inadequate. Neither could pondage provide protection against errors in load estimates which must be made several years in advance, nor could it provide capacity to cover scheduled maintenance where required during the peak load period of the year. However, under normal conditions, pondage might be considered for about one third of the total required system reserve.

Under present-day conditions, with necessity of meeting war loads with less system reserve than would be provided in normal times, together with the realization that any new loads added in the area might likely be of high load factor, it has been felt that the use of pondage should be limited in capacity estimates to that used on a weekly recovery cycle. It is appreciated that there is in storage, hydro energy available as emergency reserve.

Conclusion

The co-ordinated operation of all the interconnected utilities in this regional system, initiated by the utilities themselves for economic reasons even before the war clouds in Europe gathered, has proved of immense value in meeting electric-power demands of the national war effort. There has been considerable satisfaction in the realization that the saving of critical fuel and its transportation has been accomplished, and that the area has been able to absorb increased war loads because of such co-ordinated operation on a regional-system basis.

Evaluating Importance of the Physical and Chemical Properties of Fly Ash in Creating Commercial Outlets for the Material

By C. M. WEINHEIMER,[1] DETROIT, MICH.

The paper presents the reasons for emphasizing the physical properties rather than the chemical constituents in outlining an investigational program for fly-ash disposal and outlines the procedure followed in determining the potential consumers of this material. The results of a laboratory and field investigational program are presented and various methods and equipment for modifying the ash to meet special requirements are discussed. Commercial markets and other possible uses for fly ash are discussed together with the handling equipment and the storage facilities necessary in using bulk fly ash. Finally, certain conclusions are presented regarding the general problem of fly-ash disposal.

ANY company which operates pulverized-coal-burning equipment so located that collection of the fly ash is desirable and has available low-cost, adjacent land on which to dump it, is indeed fortunate. The company with which the author is associated is now in that enviable position; the long-time outlook, however, may not be so favorable. It is with this thought in mind that it has been considered advisable from time to time to sponsor work having as its purpose the development of revenue-producing outlets for fly ash. It is self-evident that any fly ash disposed of at a profit is not only a source of revenue in itself but at the same time eliminates disposal charges. It is conceivable that the profit derived from the sale of a portion of the fly ash might cover the cost of disposal of that portion for which there is no market.

In approaching the fly-ash-disposal problem, it can be considered that the value of the material lies in its physical and chemical properties, or in its chemical constituents.

The best hope for a satisfactory outlet seemed to be in capitalizing on the finely divided state in which all fly ash exists, and the major part of the investigational work was conducted with this property in mind. Nevertheless, it was felt that a certain amount of information on the chemical characteristics of fly ash would be necessary in order that we might talk intelligently with prospective customers, and, therefore, rather extensive chemical analyses were made of fly ash "as collected" and of a number of sieve fractions. In this connection it is well to make a distinction between chemical composition and chemical properties.

Laboratory Investigation

A laboratory program was undertaken, the object of which was to determine how fly ash compared physically and chemically with the materials that the ash might replace. Some of the physical and chemical properties and chemical constituents of fly ash are presented in Tables 1 and 2. Although most of this information is of a commonplace nature and is self-explanatory, a few of the properties, together with some not shown in the tables, warrant a brief discussion.

Physical Properties

Particle Size. In dealing with a material as fine as most fly ash, it is usually desirable to know more about the particle-size distribution than it is possible to learn from a sieve analysis. There are numerous ways of determining particle size in the subsieve-size range and a few of them as applied to fly ash will be discussed.

It was found that different technicians, using the hydrometer method, described by Biddle and Klein,[2] and the same suspension medium, could arrive at reproducible results within 5 per cent. However, when different suspension mediums were used, a wide divergence in results was obtained. The detailed results of this investigation are shown in Table 3.

Subsequent results obtained, using a Roller particle-size analyzer, indicate that the surface area ranges from 3500 to 4100 sq cm per g. Apparently, better dispersion is obtained when air is used for the suspension medium rather than water or kerosene.

In order to avoid the necessity for determining particle-size distribution by any one of the methods suitable for such determinations in the subsieve size ranges, in case such equipment was not available, an investigation was made of the possibility of making sieve analyses and obtaining the distribution of the finer particles by means of curves on logarithmic-probability paper. With the procedures used in this investigation, air elutriation and dry sieving, the results were not very encouraging.

Color. The color of fly ash is affected to a great extent by the carbon or coke particles. Even in those ashes that contain only a very small amount of carbon, the color is still some shade of gray. The results reported in Tables 1 and 2 show that the carbon content is much higher in the coarse than the fine-sieve fractions, yet the finest-sieve fraction with approximately one half the carbon content of the original material is reported as having the same color as the original material. In another case, where the carbon content was reduced to a little over 1 per cent, the color was distinctly gray. An explanation of this phenomenon is found in the fact that color is influenced to a greater extent by surface area than by weight. Thus in spite of the lower percentage by weight of carbon in the fine-sieve fractions, the surface area is probably much greater and the coloring effect more pronounced.

Fig. 1 shows two materials mixed in such a manner as to demonstrate this principle. These bottles contain mixtures of light and dark powders. The percentages by weight of the two powders is the same in each case, but the dark powder in the dark-appearing sample is of a much finer particle size than the dark powder in the light-appearing sample.

Particle Shape and Structure. There has always been con-

[1] Research Department, The Detroit Edison Company.

Contributed by the Fuels Division and presented at the Annual Meeting, New York, N. Y., Nov. 29–Dec. 3, 1943, of The American Society of Mechanical Engineers.

Note: Statements and opinions advanced in papers are to be understood as individual expressions of their authors and not those of the Society.

[2] "A Hydrometer Method for Determining the Fineness of Portland-Puzzolan Cements," by S. B. Biddle, Jr., and A. Klein, Proceedings of the A.S.T.M., vol. 36, Part 2, 1936, p. 310.

TABLE 1 CHEMICAL CONSTITUENTS OF PULVERIZED-COAL FLY ASH

Constituents	Ash as a whole, per cent	Per cent by weight of sample as collected, dried — Sieve fractions (Tyler Standard) — On 35	On 100	On 150	On 200	On 325	On 400	Through 400
Iron as Fe_2O_3	9.10	4.40	4.50	5.50	6.05	7.90	8.15	9.07
Carbon as C	10.64	76.30	60.50	31.60	24.75	16.36	13.49	5.20
Magnesium as MgO	0.83	0.19	0.22	0.24	0.81	0.83	0.86	1.09
Calcium as CaO	2.38	0.63	0.64	1.17	1.37	1.46	1.48	2.38
Aluminum as Al_2O_3	26.90	5.71	10.53	20.79	23.43	25.40	26.56	28.31
Sulphur as SO_3	1.28	0.60	0.70	1.00	0.92	0.86	0.58	1.20
Titanium as TiO_2	1.35	0.45	0.60	0.95	1.10	1.20	1.30	1.47
Carbonate as CO_3	0.01	0.03	0.01	0.01	0.02	0.01	0.01	0.004
Silicon as SiO_2	45.93	8.42	17.46	35.95	39.23	42.21	44.59	48.83
Phosphorus as P_2O_5	Trace	Trace	Trace	Trace	Trace	Trace	Trace	Trace
Undetermined	1.58	3.27	4.84	2.79	2.32	3.77	2.98	2.45

TABLE 2 PHYSICAL PROPERTIES

	Ash as a whole, per cent	Sieve fractions (Tyler Standard) — On 35	On 100	On 150	On 200	On 325	On 400	Through 400
Separated fractions retained on each sieve, per cent of sample sieved	....	0.1	3.3	3.0	4.6	8.6	7.0	73.2
Sieve fractions; expressed as cumulative per cent of sample sieved	....	0.1	3.4	6.4	11.0	19.6	26.6	....
Moisture, per cent by weight of dry sample	0.28	1.04	1.06	0.50	0.49	0.43	0.20	0.24
Solubility in water at 70 F, per cent by weight of dry sample	1.45[b]	3.44[a]	1.90[a]	1.37[a]	1.86[b]	2.33[b]	2.02[b]	1.51[b]
Solubility in water at 180 F, per cent by weight of dry sample	1.53[b]	3.19[a]	2.03[a]	1.55[a]	1.83[b]	2.35[b]	2.13[b]	1.55[b]
pH value of water in contact with ash 4 hr at 212 F	7.95[c]	2.75	3.25	5.90	4.00	3.50	3.95	8.00
Effect of dry ash on iron and lead	None	None	None	None	None	None	None	None
Effect of wet ash on iron, loss of weight in mg per sq cm exposed	1.94	2.56	6.48	2.62	1.53	2.63	0.82	0.73
Effect of wet ash on lead, loss of weight in mg per sq cm exposed	0.33	4.80	4.34	1.74	1.01	1.61	0.39	0.29
Settling rate in kerosene, per cent faster than asbestine	15	....	....	....	....	....	13	10
Linseed-oil absorption, ml of oil per 100 g of ash	....	....	....	....	....	....	92	46
Water preferential over asphalt oil, per cent in water phase	....	....	....	....	....	....	25	
Specific gravity, apparent	2.28	1.75	1.82	1.87	1.97	2.00	2.15	2.38
Unit weight, lb per cu ft	45.7	18.63	17.68	23.17	21.94	33.98	33.64	47.80
Color of fractions as sieved	Gray	Black	Black	Black and white	Black and white	Dark gray	Dark gray	Gray
Color of fractions burned free of carbon	Buff	Red-brown	Brown	Light brown	Dark buff	Buff	Buff	Light buff
Pyrometric cone equivalent:								
Initial deformation, deg F	2620	2430	2730	2730	2680	2680	2680	2620
Softening point, deg F	2690	2530	2820	2830	2750	2760	2750	2700
Initial fluidity, deg F	2800	2620	2840+	2840+	2810	2820	2810	2800

[a] Dissolved portion contained an appreciable amount of bituminous oil.
[b] Upon evaporation the solid matter consisted chiefly of gypsum.
[c] The pH value of pure water is 7.0 at 20 C.

TABLE 3 SPECIFIC SURFACES OF VARIOUS MATERIALS TESTED IN KEROSENE AND WATER MEDIUMS

Sample tested	Specific surface (sq cm per g) — in medium used in test — Kerosene (+ cp oleic acid)	Water — TDA[a]	Water — Saponin[a]
Portland cement (accepted value 2630)	2550	..	..
Sample B fly ash, as collected:			
Through 100-mesh Tyler sieve	1121	2332	2343
Through 325-mesh Tyler sieve	1097	2672	2705
Sample B fly ash, carbon-free:			
Through 100-mesh Tyler sieve	..	1398	..
Through 325-mesh Tyler sieve	2510	1777	1647
Weathered fly ash:			
Through 100-mesh Tyler sieve	1380	1789	..
Through 325-mesh Tyler sieve	1830	2326	..
Limestone dust:			
Through 100-mesh Tyler sieve	1196	1571	..

[a] Dispersing agents.

siderable verbal if not written discussion about the physical structure of fly-ash particles. From visual microscopic examinations of the ash itself and a study of photomicrographs, it is possible to make the following statements:

The carbon exists as irregular, porous, cokelike particles. The noncombustible particles generally have a spherical shape. A portion of the noncombustible particles, although apparently a small percentage, are thin-walled hollow glass spheres. Most of the dark-colored particles are cokelike material. The other dark-colored particles ordinarily spherical are believed to contain most of the iron compounds. Photomicrographs in Figs. 2 and 3 clearly show the physical condition of certain size fractions of fly ash and also how the condition is affected by burning out the carbon.

Thermal-Insulation Properties

The knowledge that some of the particles of fly ash are hollow glass balls invariably brings forth the idea that the loose ash

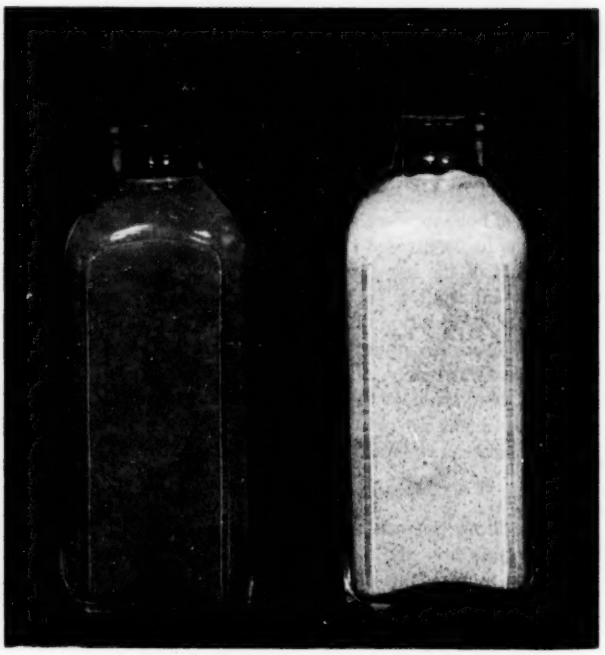


FIG. 1 INFLUENCE OF PARTICLE SIZE ON COLOR

Light Powder
90 per cent by weight of —150 + 200 mesh
10 per cent by weight of —400 mesh

Dark Powder
90 per cent by weight of —150 + 200 mesh
10 per cent by weight of —150 + 200 mesh

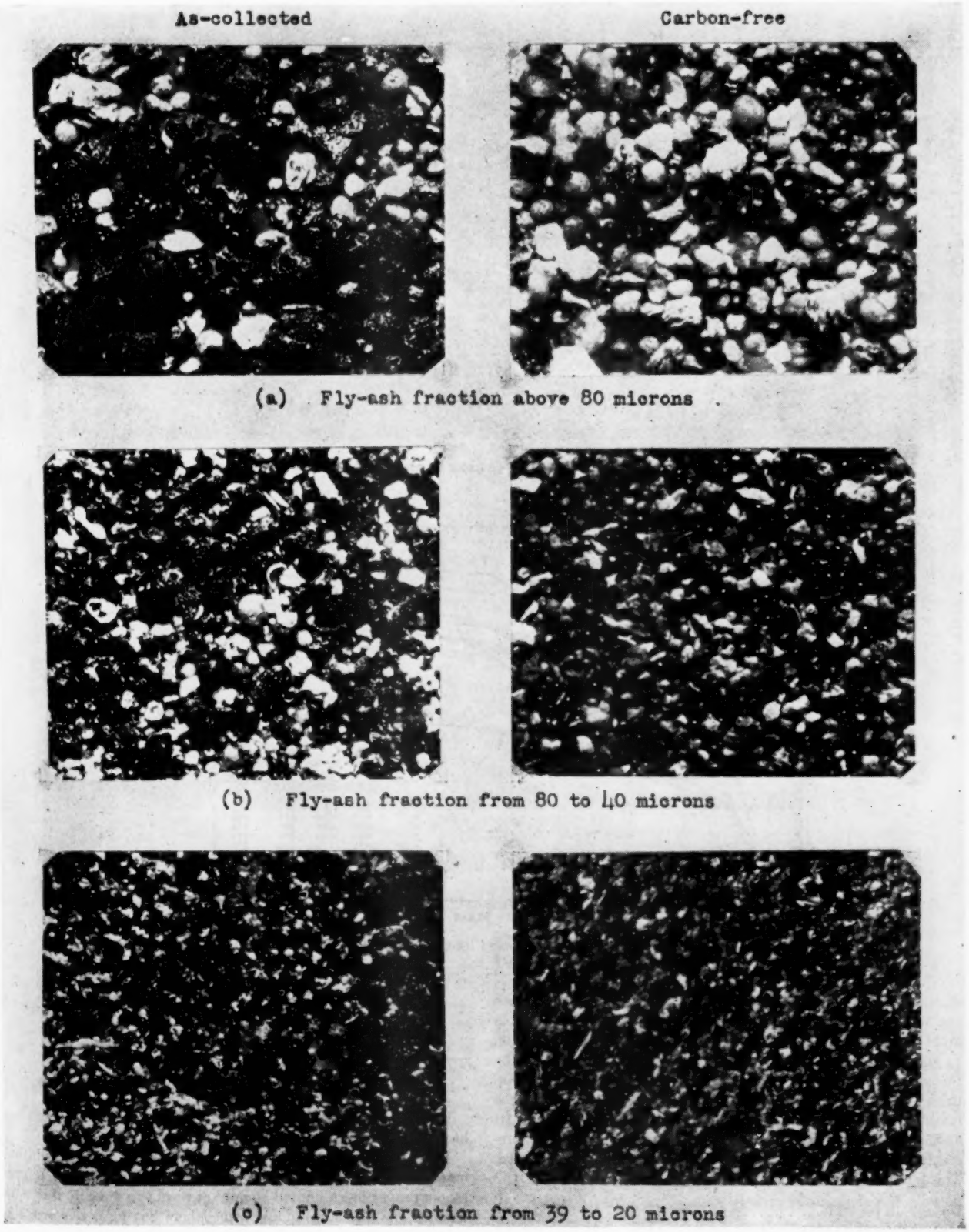


FIG. 2 PHYSICAL STRUCTURE OF FLY ASH IN THE "AS-COLLECTED" AND "CARBON-FREE" CONDITION; ×33

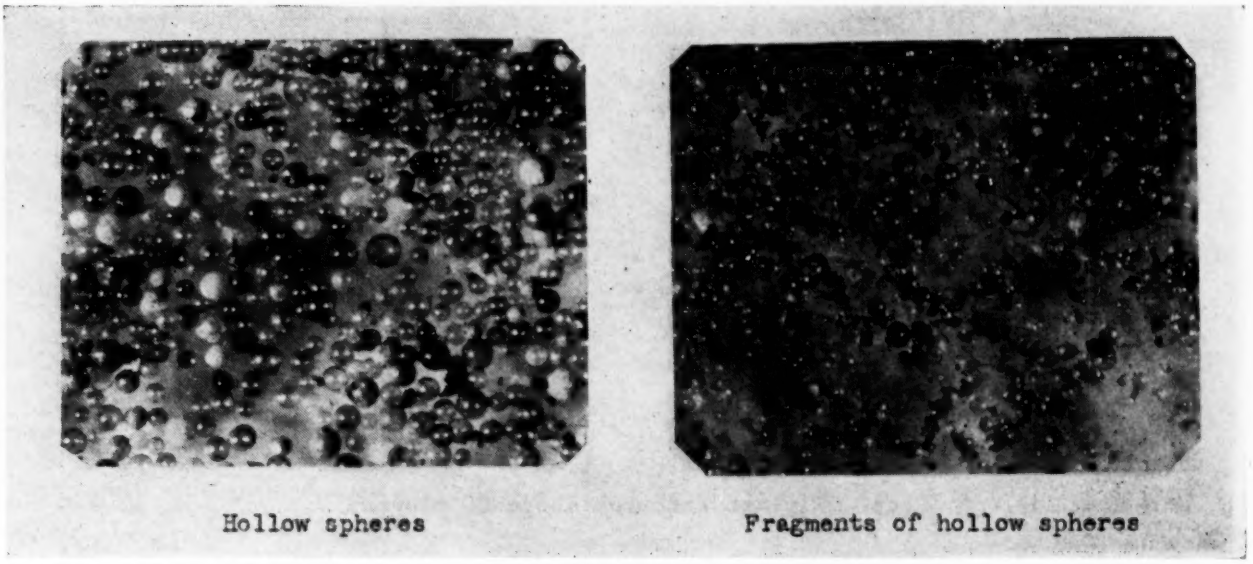


FIG. 3 EXAMPLE OF HOLLOW-SPHERE PARTICLES IN FLY ASH; ×33

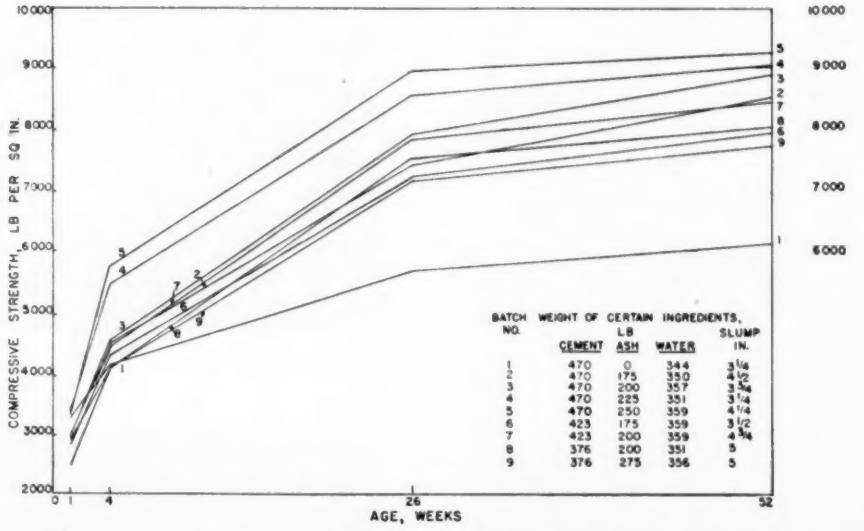


FIG. 4 EFFECT OF VARIOUS CEMENT AND ASH CONTENTS ON COMPRESSIVE STRENGTH OF SLAG-SAND-ASH CONCRETE

should make a good thermal insulator. These hollow spheres are very friable, however; hence it is quite probable that a great many of them are broken in the course of normal handling. In spite of this apparent weakness, it was decided to obtain the thermal conductivity value k, Btu per sq ft per hr per in. thickness per deg F, for bulk fly ash. The values obtained in the investigation ranged from 0.74 at 75 F mean temperature to 1.04 at 356 F mean temperature. Apparently the k value is appreciably affected by the degree to which the ash is consolidated. This is clearly illustrated by the following data:

Density, lb per cu ft	46.7	47.5	50.1	50.0
Mean temperature, deg F	74.9	75.0	74.6	76.0
k value	0.740	0.768	0.863	0.868

A test made on an 8-in. wall of Cottrell block 5 ft square revealed the following information:

Type of insulation	U[a]
None	0.383
Rock wool	0.159
Bulk fly ash	0.179

[a] Over-all conductivity coefficient corrected to a 15-mph wind velocity.

In a number of houses constructed of Cottrell block, fly ash has been used as insulation with apparent satisfaction.

Inasmuch as widespread use of fly ash as a loose insulation material would not be made without information on its hygroscopic properties, a limited amount of work was done in this connection. With a surrounding atmosphere having a relative humidity of approximately 36 per cent, it was found that the ash absorbed 0.15 per cent of its weight in 20 min. The rate of absorption decreased rapidly after the initial period and at 160 hr had reached an equilibrium state at 0.48 per cent.

TABLE 4 RESULTS OF AN INDUSTRIAL SURVEY OF FLY-ASH DISPOSAL

Industry	Material previously used	Can ash be used—Technically	Can ash be used—Commercially	Remarks
Acoustic				
dum dum	Slag dust	Questionable	Yes	Too light in weight
Agriculture				
fertilizer	Spent sand	No	No	Too fine; spent foundry sand delivered for $0.40 per ton
Soil-amendment agent	Unknown	Yes	Yes	Probably would not produce any revenue
Alumina	Bauxite	Yes	No	Uneconomic under present conditions
Building block:				
Cement block	Cement	Yes	No	Detroit market demands light-colored block
Cinder block		Yes	Yes	Improved quality of block
Cottrell block		Yes		
Glazed block		Yes	Yes	Glazed, colored tile for decorative work
Building brick:				
Fired	Clay	No	No	Unsatisfactory product
Sand lime	Sand	No	No	Unsatisfactory product, dark color
Ceramic industry:				
Drain tile	Clay	Yes	No	No improvement in quality of product and cost of manufacture increased
Hollow tile	Clay	Yes	No	
Flower pots	Clay	Yes	No	
Concrete:				
Transit mixed	Cement	Yes	Yes	Improves quality, reduces cost
Cinder ash		Yes	Yes	Lightweight concrete
Floor tile:				
Asphalt tile	Clay	Yes	No	Shipping distance too far. Color limitation
Foundry:				
Core sand	Sand	No	No	Too fine; makes a dense core
Parting sand	Limestone dust	Yes	Yes	Aluminum and magnesium foundries
Facing sand	Sand	No	Yes	Softening point too low for steel
Hot tops	Calcined clay	Unknown	No	Believed to be unsatisfactory
Gaskets	Clay	Unknown	Yes	Believed to be unsatisfactory
Paint	Extender	Questionable	Yes	Lacks covering power; difficult to disperse
Paper	Clay	No	Yes	Color, no matting properties
Plastics	Diatomaceous earth	Questionable	Yes	Poor quality of product
Polishing:				
Buffing compound	Pumice	No	Yes	Does not produce desired finish
Tooth paste	Whiting	No	Yes	Too hard
Portland cement:				
Raw material	Clay	Questionable	Yes	High alumina content is objectionable
Purification:				
Water filter	Sand	Questionable	...	Market small; properly graded material required
Oil	Fuller's earth	No	Yes	Does not produce clarification
Filter aid	Diatomaceous earth	No	...	Does not function as such; wrong type of particle
Zeolite	Zeolites	Yes	No	Small fraction satisfactory; low capacity
Putty:				
Furnace cement	Whiting	...	...	No information was obtainable
Sash putty	Whiting	Questionable	...	Dark color objectionable
Caulking compound	Asbestine	Questionable	...	Dark color objectionable
Road:				
Asphalt	Limestone	Yes	Yes	Lower cost
Concrete	Cement	Yes	Yes	Lower cost; improved product
Oil aggregate	Limestone	Yes	Yes	Lower cost
Roofing	Filler	Unknown	No	No market
Roofing	Slate granules	No	Yes	Too fine
Rubber	Clay	Questionable	Yes	Seems to have possibilities
Soap mechanic's	Pumice	Unknown	Yes	Small market; dark-colored soap
Thermal insulation:				
Insulating cement	Calcined clay	Yes	Yes	Improved product
Loose fill	Mineral wool or vermiculite	Yes	No	Can be used only in the cells of masonry building blocks

Since the thermal insulating value k is very sensitive with respect to the unit weight, the maximum compressibility of the bulk fly ash is important. Again, there are a number of variables, such as original condition of the ash and dimensions of the test specimen, that must be considered in interpreting the results.

Using a cylinder 13.54 in. diam (1 sq ft) and 1 ft high, it was found that with rodded ash the over-all height could be reduced 1.10 in. under a total load of 300 lb. With aerated ash, this reduction increased to 2.15 in. These results indicate that even under a loading of 300 psf, the unit weight would not be more than 48.5 lb per cu ft. If no vibration were present, this might be so, but unit weights of 54.7 lb per cu ft have been produced by vibration alone without any external pressure. On the basis of these data, it appears probable that loose ash in a wall or similar container would acquire a unit weight of at least 50 lb per cu ft.

Chemical Properties

As previously stated, most of the investigational work dealt with the physical properties of fly ash. All of these have been reported and the unusual properties discussed. Earlier in the paper a rather elaborate chemical analysis of fly ash was presented. Fly ash has a few chemical properties, independent of the chemical composition, that warrant discussion.

Certain types of materials are known as "pozzolanas." A "pozzolana" can be defined as a siliceous material that, although not cementitious in itself, contains constituents that at ordinary temperatures will combine with lime in the presence of water to form compounds that have a low solubility and possess cementing properties. Since volcanic tuffs, burnt clays and shales, and pumicite are pozzolanas, it is logical that fly ash should have pozzolanic properties inasmuch as all these materials have a similar chemical composition and have been subjected to a

calcination temperature. Evidence that fly ash is a pozzolana is shown in an indirect manner later on in the paper where concretes containing fly ash are discussed. If increase in compressive strength of concrete is a measure of pozzolanic activity, then the results, shown in Fig. 4, clearly demonstrate that this fly ash is a pozzolana or has pozzolanic properties.

Sales Program

Following the accumulation of these rather complete data on the properties of fly ash, a canvass was made of the potential users located within the area of economic shipment. If possible, a personal call was made to discuss the matter with both the purchasing and technical departments. If information was requested on specific properties of fly ash that had not already been obtained, an attempt was made to furnish it to the prospective customer either by work in our own research laboratory or by sponsoring investigational work in an outside organization. If there was any possibility of substituting ash for a material being used by the customer, a sample of ash was provided. Often these interviews resulted in requests to supply ash in a modified form. Wherever possible this was done. The methods employed to provide the processed ash will be described in detail later. A subsequent attempt was made to learn the results of the experiments using the ash. Sometimes, however, it was impossible to get any worth-while information. The results of this sales program are given in Table 4. The conclusions to be drawn are as follows:

1 There are only a few industries that can use the quantity of ash produced by a large steam power plant.

2 The only reason for attempting to develop the small-consumer market is for greater diversification of sales and to improve the yearly load factor inasmuch as the requirements of the large consumer are apt to be very seasonal.

3 In general, the ceramic industry is not an outlet for ash because ash does not improve the product and clay can be delivered in the plant at a cost below that at which it would be possible to supply ash, except under unusual circumstances.

Modifying Processes

Sometimes it appeared that a prospective customer might be able to use ash if it were modified in some way. The usual requirement was that certain coarse fractions or certain chemical ingredients be eliminated. These cases led to investigations of commercial ways for modifying the ash by some process.

Air Classification. It was found that, by passing ash through an air classifier, a filler material could be obtained which would meet the physical requirements of the rubber and plastics industries. The results of air classification are shown in Table 5.

In doing this work no adjustments were made to the air classifier other than those possible on standard equipment. It is believed that possibly a larger recovery of fines in one processing could be obtained with a small amount of experimentation in adjustments. It should be noted that (1) the fines of Run A meet the physical requirements for rubber and plastic fillers, (2) the tailings of Run A meet the physical requirements for asphalt filler, (3) the fines of Run B meet the requirements for asphalt filler, and (4) inasmuch as the tailings from Run B contain approximately 20 per cent carbon, they might be returned to the furnace as fuel. Since these tailings represent less than 15 per cent of the ash produced, it is doubtful that the dust-collecting equipment would be overloaded by the additional burden.

Carbon Removal. Freedom from carbon is a requirement in many instances, chiefly because of the color effect mentioned previously.

Several ways of removing carbon or reducing the carbon content were investigated but none was found to be satisfactory from both the technical and the economic viewpoints. While none of the modern flotation methods was investigated, some elementary work on this type of processing was done in the laboratory, based on information from Germany, in which it was claimed that the carbon content, which was high in the case discussed, could be reduced by a flotation method using an oil-water emulsion. Our limited work indicated that (1) with carbon contents of approximately 10 per cent no carbon reduction was obtainable, (2) the loss of the flotation medium was excessive, (3) the final product would not have been satisfactory for the intended use even had the carbon content been satisfactory.

The production of carbon-free ash by the continuous-ignition process proved to be technically possible but not commercially

TABLE 5 SOME PROPERTIES OF AIR-CLASSIFIED FLY ASH

Sample		As collected	Run A		Run B[a]	
Sieve fraction		Sieve Analysis (Tyler Sieves)				
		Per cent by weight				
			Fines	Tailings	Fines	Tailings
	Retained on 16 mesh	0.0	0.0	0.0	0.0	0.0
Passing 16 mesh	35	0.1	0.0	0.8	0.0	1.2
35	100	3.3	0.0	6.2	0.8	18.9
100	150	3.0	0.1	5.3	1.8	14.5
150	200	4.6	0.3	7.0	3.9	16.5
200	325	8.6	1.3	11.3	9.1	17.8
325	400	7.0	2.8	9.0	9.0	8.9
400		73.2	94.8	59.6	74.6	21.2
	Unaccounted for	0.2	0.7	0.8	0.8	1.0
	Total	100.0	100.0	100.0	100.0	100.0
	Per cent recovered in each fraction		45.6	54.4	76.7	23.3
		Chemical Properties				
	Carbon content, per cent	10.64	7.68	13.75	11.67	19.28
	pH value	7.95	7.80			

[a] Run B is a reclassification of the tailings of run A.

TABLE 6 RESULTS OF CARBON REMOVAL BY SOLUTION METHOD[a]

Sample no.	Quantity of fly ash digested	Quantity of digestive agent used,[b] ml	Carbon in sample, per cent by weight	Ash dissolved, per cent by weight of sample	Carbon removed, per cent by weight of sample	Carbon remaining, per cent by weight of sample	Carbon removed, per cent by weight of total carbon
1	5	50	21.82	12.45	6.60	15.22	30.24
2	5	100	21.82	19.69	13.61	8.20	62.40
3	5	200	21.82	26.67	20.37	1.43	93.40
4	5	300	21.82	27.96	21.36	0.46	97.89
5	5	400	21.82	33.84	21.44	0.38	98.30

[a] Time of digestion varied from 15 min for the smallest quantity of solution to 30 min for the largest quantity.
[b] Chromic acid.

practical. Using an externally fired, rotating, inclined kiln, it was possible to reduce the carbon content from approximately 6 per cent to less than 0.5 per cent. The kiln was operated at approximately 1500 F, and the output was 25 lb of ash per hr. It was found that the introduction of a small quantity of air at low velocity greatly aided the carbon reduction. However, the high fuel cost and limited output possible from this type of equipment prohibit its becoming commercially useful. Approximately 1500 lb of ash were processed in this equipment.

Another attempt was made in the laboratory to remove the carbon by mixing air and ash, both of which had been preheated, in an externally heated chamber. For operating temperatures up to 1800 F, it appears impossible to reduce the carbon content below 2 per cent with this arrangement of equipment.

Further efforts were made to remove the carbon by solution methods. While a number of acids could be used as the reagent to perform this function, our work was limited to the use of cleaning solution (chromic acid). The results are given in Table 6. These results show that, in addition to carbon, other ingredients, probably iron, are removed by this treatment. The fact that the residue retains its white color even after heating to 1800 F in an oxidizing atmosphere, further substantiates the conjecture that the iron compounds are removed. Because of the high cost of processing and the substantial loss of material by this digestive process, it is believed to be uneconomical to treat fly ash with acids for carbon removal.

A final attempt to remove the carbon was made using a contact potential separator at the U. S. Bureau of Mines. Starting with a material containing 7.32 per cent of carbon, two passes through the separator produced a material containing only 1.3 per cent of carbon. The yield of low-carbon material was approximately 55 per cent of the ash charged. Combining certain fractions of high-carbon material and reprocessing them would undoubtedly increase the yield of low-carbon ash without substantially increasing the carbon content. This method appears to offer the possibility of producing a low-carbon and extremely fine material in one processing. In spite of the low carbon content, the material still possessed a light-gray color which is in distinct contrast to the buff-colored material of similar carbon content produced by burning the carbon. This process seems to have definite commercial possibilities for producing a low-carbon fly ash.

Iron-Compound Removal. The general chemical composition of the ash indicated that it could be used as a raw material in the manufacture of glass if the iron compounds were removed. With this in mind, various processes aiming to reduce the iron content were investigated, but none was found which accomplished the purpose.

As previously mentioned, under the process for reducing the carbon content by treating the ash with chromic acid, the iron as well as the carbon was removed. The cost of treatment in this process made such processing economically unsound even if the process yielded a satisfactory material. A subsequent laboratory investigation disclosed that solution methods using hydrochloric, sulphuric, and chromic acids failed in all cases to reduce the iron content below 6 per cent. The original material contained 9.10 per cent iron in the form of an oxide.

Failing to produce a material of low iron content by the solution method, commercial magnetic-processing equipment was investigated. In no case was it possible to produce a material with an iron content of less than 5 per cent.

On the basis of the equipment and processes now available it appears impossible to process fly ash to produce a material containing less than 1 per cent iron which is the maximum permissible for use in the glass industry.

Commercial Markets

As a result of this extensive amount of laboratory and field investigational work, what can be stated regarding the prospects of developing commercial markets that will yield some revenue and use sufficient tonnage to take a substantial portion of the fly-ash production?

Concrete. That certain fly ashes improve the quality of concrete is no longer a debatable question, and the real problem in the use of them in this field is one of economics and sales resistance. In order to obtain data on the value of fly ash in concrete made with the cements and aggregates available in the Detroit area, considerable laboratory and field investigational work has been conducted. This work, part of which was previously discussed, confirmed the findings obtained by other investigators that fly ash has pozzolanic properties.

The chief benefits to be derived from using fly ash in concrete containing pebbles, crushed slag, or stone as the coarse aggregate are (1) greater long-time strength, (2) improved workability, (3) greater resistance to attack by ground waters, (4) lower permeability, (5) lower cost, (6) less bleeding.

Pebble-sand and slag-sand concretes containing fly ash and cinder-ash concrete have been used satisfactorily on a number of projects of the author's company.

The type of concrete and manner of use are as follows:

Type of Concrete	Use
Pebble-sand-ash	Roadways, building structures, machine foundations, cable ducts
Slag-sand-ash	Roadway
Cinder-ash	Lightweight concrete

The fact that the use of fly ash in pebble-sand concrete makes possible a decrease in cement content without sacrificing strength is clearly shown in Fig. 5. As would be expected, because of the

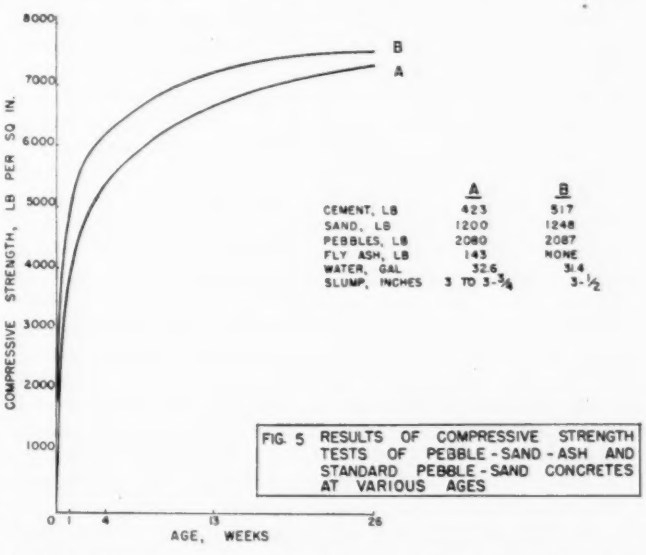


Fig. 5 Results of Compressive Strength Tests of Pebble-Sand-Ash and Standard Pebble-Sand Concretes at Various Ages

lower cement content, the pebble-sand-ash concrete had a lower early strength. However, after 6 months aging, both types of concrete reached approximately the same compressive strength value of 7400 psi, which is excellent concrete. Although in this case it took approximately 6 months for the two concretes to arrive at the same compressive-strength value, other tests have

shown that this point may be reached in a minimum of 28 days and a maximum of 1 year.

In an article[3] by F. R. McMillan and T. C Powers, a method is given for determining the relative values of admixtures and Portland cement in producing workability in concrete. Fly ash was one of the materials tested and in this case was approximately 11 per cent more effective than Portland cement in improving workability. No information was given as to the properties of the fly ash, but it is believed that its efficacy would be considerably influenced by the surface area, specific gravity, and possibly the carbon content. That the addition of finely divided materials is an accepted method for improving workability is evidenced by a statement taken verbatim from the article mentioned: "For example, if it is desired to bring about an improvement in workability, that may be done by enriching the mix, by correction of aggregate graduation, or by the use of almost any one of a host of available finely powdered materials."

Obviously, any material which not only is more efficient than Portland cement in producing workability but also contributes other valuable properties to the concrete should be given serious consideration, especially since the material is available at a fraction of the cost of Portland cement.

The presence of jagged and irregular particles in crushed-stone and to a greater extent in crushed-slag coarse aggregate leads to harshness and poor workability in concretes. The advantages, both as to workability and compressive strength, of using fly ash in slag concrete are shown in Fig. 4.

Recent permeability tests, conducted in the course of this investigational work on fly ash in concrete, were inconclusive in that it was not possible at pressures up to 90 psi to permeate sufficient water for accurate measurement. C. F. Ramseyer, formerly of the Chicago District Electric Generating Corporation, was more successful in his experimental work. In an article[4] reporting his results, curves are presented which show the relative permeabilities of different concrete mixes. The total water-loss permeation through a 28-day-old test specimen made from 6-bag per cu yd concrete was 340 cc at the end of a 7-day test period. The loss during the same period of time on a similar specimen, made from concrete containing 5 bags of Portland cement and 1 bag of fly ash per cu yd was 50 cc, a ratio of nearly 7 to 1. Low permeability is especially desirable in concretes exposed to frost action and ground waters.

From time to time there has been considerable discussion, both written and verbal, concerning the resistance of concretes containing fly ash to the deteriorating effects of alternate freezing and thawing. Some of the investigational work has been carried out on small specimens and it was necessary to screen out of the test-concrete mix part of the coarse aggregate. In order to approach field conditions as closely as possible, freezing-and-thawing tests were run on test specimens consisting of 8-in. concrete cubes from which no aggregate had been screened. The appearance of two tested cubes of pebble-sand-ash concrete is shown in Fig. 6. The results of this test and others indicate no reason to believe that concretes containing fly ash are particularly sensitive to freezing and thawing.

In certain locations, such as caissons or footings, substructures, and underground-cable duct, the resistance of concrete to the ground waters is very important. A great deal of investigational work has been carried on especially in Europe on the effect of

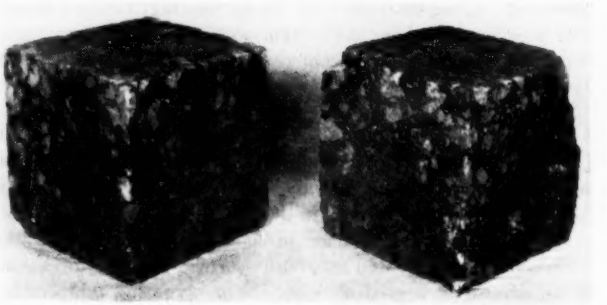


FIG. 6 8-INCH CONCRETE CUBES AFTER SUBJECTION TO 225 CYCLES OF FREEZING AND THAWING
(4½ bags cement, 150 lb fly ash, 36 gal water per cu yd concrete.)

ground waters on concrete. In a book[5] by F. M. Lea and C. H. Desch, a summary is given of the work of a number of investigators who have conducted experimental work on the effect pozzolanas have in increasing the resistance of concrete to the action of ground waters. In general, the results are favorable. In order to determine the effect of sulphur water on the concrete caissons of a powerhouse, an experiment was started by the company with which the author is associated, approximately 15 years ago in which various concretes were exposed to the particular sulphur water in question. An analysis of this water indicates that, in addition to hydrogen sulphide, it contains sulphates commonly found in ground and sea water and is practically neutral, that is, neither acidic nor basic. Some of the concrete cylinders exposed to this sulphur water contain fly ash. The last progress report[6] on this test contains the following conclusions:

1 The concrete should have a high cement content.

2 The concrete should have a minimum slump consistent with good placeability for a dense concrete.

3 The addition of fly ash up to 35 per cent by weight of the cement content is desirable.

This discussion regarding concrete has dealt with improving the quality of the product. In approaching a prospective user of fly ash, a sales argument that shows him how he can reduce his costs has much more appeal than one concerning improvement of his product. This is natural in that he is now selling his product and, therefore, believes it must be good enough for the job. The chance of making any substantial saving in the cost of concrete other than by a reduction in cement content is remote. Cement is a comparatively cheap material. Therefore, it is essential that there be a sufficient differential between the cost of cement and of fly ash to make it worth while to handle an extra material. Part of the delivered cost of fly ash is in the handling; this matter is discussed later on.

All the foregoing discussion has dealt with a standard concrete modified by the addition of fly ash. A new lightweight concrete is now available that uses fly ash in large quantities. It is known as cinder-ash concrete[7] and can be used wherever lightweight concrete is acceptable. All the floors and the roof in a six-story office building of a volume of 2,000,000 cu ft are constructed of this material. Before proceeding with the use of cinder-ash concrete in this structure, an extensive investigation was made of properties of the concrete. The results of this investigation are given in Table 7.

[3] "A Method of Evaluating Admixtures," by F. R. McMillan and T. C. Powers, *Journal of the American Concrete Institute*, vol. 5, March–April, 1934, pp. 325–344.

[4] "Solving the Fly-Ash Problem," by C. F. Ramseyer, *Electric Light & Power*, vol. 17, February, 1939, pp. 44–47, 66.

[5] "The Chemistry of Cement and Concrete," by F. M. Lea and C. H. Desch, E. Arnold & Company, London, 1935.

[6] "Concrete Exposed to Sulphur Water," by J. S. Nelles (Progress Report on Tests), Proceedings of the American Concrete Institute, vol. 37, 1941 pp. 441–452.

[7] U. S. Patent 2,250,107.

TABLE 7 RESULTS OF INVESTIGATION ON LIGHTWEIGHT CONCRETE

Physical Properties of a 5½-Bag Cinder-Ash Concrete

Weight, lb per cu ft	100
Modulus of elasticity (3000 psi compressive strength):	
At 20 per cent of compressive strength	$1.6–2.0 \times 10^6$
At 50 per cent of compressive strength	$1.5–1.7 \times 10^6$
Compressive strength, psi:	
At 7 days	1600
At 28 days	3000
Slump, in.	6–7

Typical 1-Cu-Yd Batch Design Data

Ingredient	Weight, lb
Cement (5½ bags)	517
Ash (dry)	500
Cinders (24 cu ft)	1450
Total water (63 gal)	525

Sieve Analysis of Cinder Aggregate

Sieve fraction, retained on	Cumulative per cent by weight
1½ in.	1.70
¾ in.	17.40
⅜ in.	41.70
No. 4	60.00
No. 8	72.50
No. 14	80.80
No. 28	87.00
No. 48	91.50
No. 100	100.00

The extensive use of this type of concrete would create a large market for fly ash because of the high ash content. The ash supplied for the cinder-ash concrete used in the building mentioned had about 25 per cent moisture by weight of dry ash. This in itself may seem a bit unusual and contrary to accepted practice. Early in this paper, it was stated that fly ash was a pozzolana and, according to the definition, a pozzolana was not cementitious in itself. Therefore there seems to be no reason that moist ash could not be used in all types of concrete. An investigation of this deduction disclosed that as good concrete can be produced with moist fly ash as with dry. However, it should be pointed out that the problems encountered in handling moist fly ash are quite formidable and any shipping advantages obtained from using the moist ash may be offset by local handling difficulties.

Bitumastic Road Fillers. Trinidad asphalt was at one time about the only bitumastic material available for road construction. Now, however, by-product materials from the oil refineries and the coke ovens provide a large amount of binder material. Trinidad asphalt is in fact a mixture of asphalt and mineral filler. From the chemical composition and the appearance of the particles, this filler evidently is pumice which is of volcanic origin. In the course of our investigational work in connection with the use of fly ash as a mineral filler in asphalt topping, an incomplete chemical analysis was made of the mineral filler in Trinidad asphalt. A comparison of certain chemical ingredients of fly-ash and Trinidad-asphalt-mineral filler is given in Table 8.

TABLE 8 PRINCIPAL INGREDIENTS OF ASPHALT FILLERS

Material	Composition, per cent by weight—SiO_2	Al_2O_3	Fe_2O_3	Total
Fly ash, as collected	45.9	26.9	9.1	81.9
Fly ash, burned free of carbon	51.4	30.1	10.2	91.7
Trinidad-asphalt filler	67.6	18.9	6.4	92.9

The use of fly ash as a mineral filler in bitumastic road construction is now definitely established in the Detroit area. This use was arrived at, however, only after an extensive period of experimentation and by overcoming a considerable amount of sales resistance. The fly ash is being used as a mineral filler in both asphalt and oil-aggregate or black-top types of roads.

The original installation of asphalt topping or wearing surface was installed on a heavily traveled thoroughfare in 1931, and it is still in use. Since 1939, approximately 1,325,000 sq yd of fly-ash-asphalt topping has been installed. Design data typical of this material are as follows:

Ingredient	Per cent by weight
Sand	76.7
Fly ash	13.0
Asphalt	10.3
Total	100.0

This mixture, when tested in a Hubbard-Field stability tester, gives a stability value of 1925 lb.

Oil-aggregate or black-top roads differ from asphalt topping in that the binding agent in the former is a slow-curing asphaltic oil, while in the latter it is asphalt. There is also a considerable difference in particle size and gradation of the aggregate, the oil aggregate having much larger particles and less mineral filler. Oil absorption by the filler is an important item in the cost and should be determined. The amount of absorption would undoubtedly be different for various ashes, depending probably upon the surface area and carbon content.

Rubber. In both of the large outlets for fly ash previously discussed, the delivery demands fluctuate widely and seasonally, there being practically no demand in the winter months. An attempt to improve this yearly load factor led to a rather extensive investigation of the possibility of substituting fly ash in some form for the clays and whiting now used as inert fillers in certain rubber products. It was realized that the "as-collected" fly ash would not meet the fineness requirements for rubber filler, but the air-classification process previously described did permit the recovery of approximately 50 per cent of the ash in a satisfactory particle size for use as a rubber filler. The estimated cost of classification was sufficiently low to make the process a commercial possibility. As previously mentioned, a considerable amount of ash was air-classified and a portion of this was burned free of carbon. Quantities of these materials were supplied for test purposes to a rubber company whose products were mechanical goods, such as floor mats, pedal covers, running-board mats, etc. The resulting rubber product was reported as having a tensile strength 10 per cent lower than that of the present material and of a darker color.

For the type of product being made, the limited color range did not seem particularly important to the author but it was just another hurdle to be overcome in breaking down the sales resistance. Considering the fact that, on the first trial, rubber was produced whose only limitations were color and a reduction of 10 per cent in the tensile strength, it does not seem that the door is completely closed yet in this field. Any company that is interested in the fly-ash-disposal problem should investigate the possibility of substituting processed fly ash for the present inert filler in low-cost mechanical rubber goods, because it affords a profitable outlet with a good yearly load factor and may also provide the rubber company with a satisfactory filler at a price advantage.

Handling Facilities

Because fly ash is usually sold in competition with low-cost materials, the desirable way of handling the ash is in bulk shipments. In some instances the ash must be handled in bulk because of the handling equipment available, while in others bulk use is necessary from an economic standpoint.

Fly ash has a very unfavorable reputation with respect to handling properties. In part, this reputation is deserved owing to the combination of small particle size and low specific gravity. When air becomes entrained, a light, fluffy, bulky product results, which flows very readily and leaks through very small openings. On the other hand when no air is entrained or when the material is allowed to settle for a long period of time, the ash is likely to pack hard in the bin and bridge over.

A large part of this poor reputation may be attributable to the attempts that have been made to handle fly ash with equipment

that was never intended to handle such fine material. Nevertheless, it is often the case that the equipment is already installed and, if fly ash is to be used, it must be handled with available machinery.

In using fly ash as a mineral filler in asphalt topping it was necessary to devise some means for handling the ash, as otherwise it would not be used even though the topping was technically satisfactory. A portable Fuller-Kinyon pump had been used for unloading bulk limestone dust from boxcars. This equipment, as built, could not be used to handle bulk fly ash. The problem was solved by delivering the ash in bulk-cement trucks, providing an adapter, and modifying the pump. This combination is shown in Fig. 7. However, it was found that trucks, which

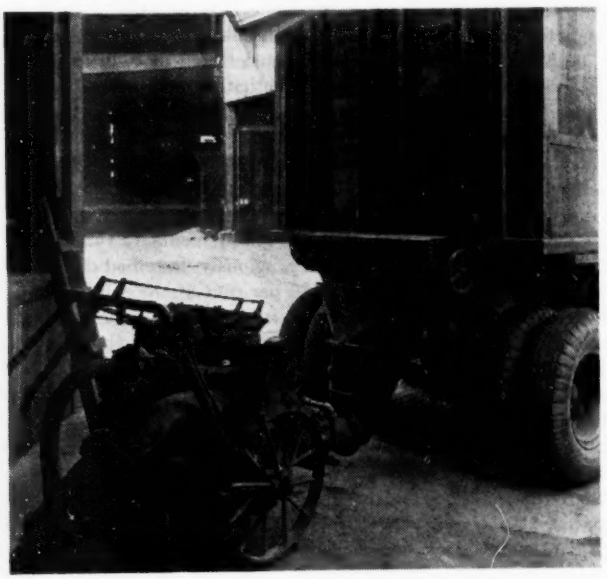


FIG. 7 UNLOADING DEVICE FOR BULK FLY ASH

were satisfactory for bulk cement, were not satisfactory for fly ash. The stop-gate construction at the rear had to be improved and holes in the body, that were not troublesome when the trucks were used for cement, had to be sealed.

At another asphalt plant, the ash is delivered in bulk cement cars and unloaded by means of a stationary Fuller-Kinyon pump located in a pit beneath the tracks. It is also possible to deliver ash by truck to this same plant, as shown in Fig. 8. If a portable Fuller-Kinyon pump is available, it can be converted to handle ash from the bulk-cement cars.

At the power plants, both the trucks and the cars are loaded from overhead bins through a rubber hose that is dropped into open hatches in the top of the conveyance. Between the bin and the hose line there should be installed a star-feeder to facilitate control of the rate of flow through the hose. A small vacuum breaker at the top of the hose line produces a much more uniform flow of ash than is obtainable if the hose line is sealed tightly. Because of the low specific gravity of fly ash and its tendency to aerate readily, the capacity by weight of bulk-cement conveyances is reduced when carrying the ash. This tends to increase the hauling charges. Laboratory investigations showed that by vibrating the receptacle with a commercial electric vibrator the unit weight of ash could be increased from 39.9 to 54.7 lb per cu ft, or 37.1 per cent, which would approach the bulk weight of uncompacted cement.

At a transit-mixed concrete plant and at an oil-aggregate batching plant, the ash is being handled successfully in bucket conveyers. The rate of discharge is somewhat slower than when handling cement or limestone dust. Precautions must be taken to keep the ash from bridging over in the feeding hopper to the conveyer, and better results are obtained if the speed of the bucket conveyer is kept below that recommended for use when handling cement.

At this point it is well to consider storage facilities. Previously it has been mentioned that the ash demand is seasonal for concrete and roads. Since both of these uses are dependent to some extent upon the weather conditions, there is a considerable fluctuation in day-to-day requirements. Also, if a contractor for a large project were considering the use of fly ash, it would be necessary to assure him that the ash could be delivered at the rate necessary to meet his requirements. These daily requirements might be considerably above the average daily ash output of the power plants. This means that adequate storage facilities must be provided, either by the producer or the consumer of the ash.

Of course, fly ash can always be furnished in paper bags similar to those used for Portland cement, but of a greater volume if it is desired to have the same weight of fly ash as cement. As a general rule bagged ash is supplied only to the small consumer. If a fly-ash producer should be so fortunate as to develop a large

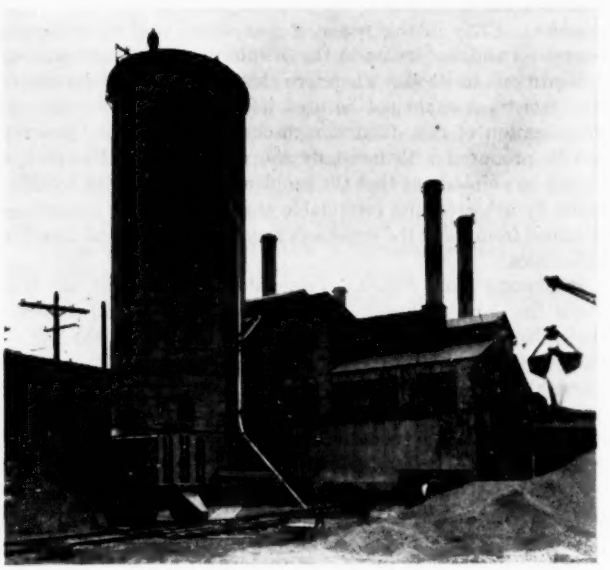


FIG. 8 CONVEYING, UNLOADING, AND STORAGE FACILITIES FOR BULK FLY ASH AT AN ASPHALT PLANT
(Unloading bulk fly ash from a truck with the same unloading unit as used with a bulk cement car.)

number of small customers, it might be well to consider a delivery unit that would be self-contained, that is, the customer would provide the bin, piping, and possibly compressed air, and the remaining equipment necessary to discharge the ash into the bin would be a part of the truck or semitrailer. Such an arrangement would eliminate the expensive bagging operation, cut the cost to the consumer, and decrease the handling cost.

In interviewing a prospective customer, it is essential that one be able to discuss intelligently means of handling the fly ash. This is important because in a great many cases the bad reputation of ash is already known to the customer, and, unless proper facilities are provided for handling the material, the results will be unsatisfactory.

Other Possible Uses

Being of such fine particle size, fly ash has not been considered a satisfactory ground-fill material. Nevertheless, the experience of the author's company with several fills along the water front indicates that, if properly handled, filled-in land of this sort can be made capable of sustaining coal piles 35 ft high. In one case, the fill, which in places contained 15 ft of fly ash, part of which was submerged in water, has sunk about 1 ft after several years of storage of coal.

An attempt was made to produce a satisfactory fill material by combining fly ash with an impure limestone that is available in large quantities as a by-product from the soda-ash and acetylene-gas industries. The production of a suitable fill material was unsuccessful because of the difficulties encountered in mixing the two ingredients mechanically. However, a material was produced that was quite comparable, in resistance to disintegration and compressive strength, to well-designed soil-cement stabilization mixtures.

In Table 4, dealing with possible uses of fly ash, reference is made to the use of fly ash as a filler in agricultural fertilizer, and the reason for its being unsuccessful. Fly ash, however, does produce certain beneficial effects in heavy clay soils. That is, it is a soil-amendment agent. Such an agent may not have any fertilizing value but does benefit the soil by improving its mechanical properties. When thoroughly mixed with heavy clays, fly ash, being a highly vitrified material, tends to decrease the tendency to bake hard, crack, and ball up, and to increase the capacity to hold moisture. Heavy clays may require an addition of 50 per cent by weight of fly ash in order accomplish to the desired results. It is realized that this market offers very little opportunity for revenue, but it might eliminate haulage charges for dumping. Since the fall and winter months are the ideal time to place the ash on farmland, such an outlet would fit in nicely with the bitumastic road and concrete requirements.

Conclusions

As a result of this extended investigation, conducted both in the laboratory and in the field, it appears possible to arrive at certain general conclusions regarding the fly-ash market.

1 There are only a few industries that can use the quantity of ash produced by a large steam power plant.

2 The ceramic industry, which is a large consumer of clays, is not likely to become a user of fly ash because of the cheapness with which clays are delivered to the ceramic plants and because the ash does not generally have the proper properties to improve the quality of the product.

3 Certain types of fly ash are satisfactory as mineral fillers in bitumastic road construction.

4 Certain types of fly ash improve the quality of standard concrete, make possible a new lightweight concrete, and also open the way to a possible reduction in the cost of concrete.

5 The seasonal load factor of the mineral-filler and concrete markets makes it desirable to develop a year-round outlet of large tonnage such as in the fields of rubber or plastic fillers.

6 Regardless of the merits of fly ash as a material, it cannot be sold commercially unless the customer's handling problem is satisfactorily solved.

7 There will be no fly-ash-disposal problem if the sales resistance of the concrete industry and the bitumastic road industry can be overcome.

Radio-Frequency Technology in Wood Application

By G. F. RUSSELL[1] AND J. W. MANN,[2] TACOMA, WASH.

As a basis for understanding the principles involved in applying radio-frequency heating to the resin-bonding of wood, the author explains certain fundamentals of radio theory which are involved. A particular quality of the radio-frequency field is its selectivity which results from the tendency of the field to follow the most conductive path between electrode extremities. Originally operations of bonding materials by this means placed alternate layers of wood and glue in the field so that the glue lines were established parallel with the electrodes causing the field to be perpendicular to the glue line. More recently it has been established that the normal resin-glue line is more conductive than the wood with which it is associated, and the technique of "parallel bonding" in which the field is parallel with the glue line has been developed. Details of the process, application of radio-frequency heating to specific cases, most efficient electrode arrangements, and results attained are treated comprehensively.

Technical Background

CERTAIN fundamentals of radio theory are essential to a proper understanding of radio-frequency heating effects. An electromagnetic field of force evidences itself through rapid alternations of charge on electrodes which constitute elements of the output circuit of a radio-frequency generator. When one electrode is charged highly negative, the opposite electrode is relatively highly positive. The next half-cycle results in a reversal of this relationship with the negatively charged electrode becoming the positive, and the positive becoming the negative. The electrodes with their connecting inductance constitute a simple oscillatory circuit. The space between the electrodes constitutes the part of the circuit wherein the dielectric is placed for heating.

When air is the dielectric between the electrodes, no loss takes place in the area. When other dielectrics are placed between the electrodes, however, a loss will result. When an energy-absorbing dielectric is introduced into a radio field of force, a phase shift takes place according to the standard laws

$$E\,I\cos\theta$$

which measures the total of real power. If wood of a certain density is introduced, a certain resistance will result. If wood of another density is introduced another phase shift will result. The energy absorption of the dielectric employed in the field has a major bearing upon the resultant phase shift.

Between the electrodes acting as boundaries of the capacitance portion of the circuit, there exists a half-standing wave of electromagnetic energy. This half-standing wave is a balance and a supplement to the half-standing wave resident in the inductance portion of the same circuit. When no resistance exists between the electrodes, there is a 90-deg out-of-phase relationship between voltage and current in the capacitive area established by the electrode boundaries, while the out-of-phase relationship in the inductance portion is in proportion to its ohmic resistance.

Radio-frequency waves are analogous to sound and similar to light waves. Each has the peculiar quality either of standing or traveling. The fundamental difference involved here is between the standing and the traveling wave. It is this difference which led to the discovery of and proof that there exists a half-standing wave in the capacitance portion of an oscillating circuit, and a half-standing wave in the inductance portion.

In electrical engineering language where there is no energy absorption in a circuit operating on 60 cycles, a 90-deg out-of-phase relationship exists between current and voltage. When resistance is introduced into this 60-cycle circuit, a phase shift results, and power loss may be calculated effectively by the vector method which shows total average power expended. This vector engineering is satisfactory when a traveling wave is considered to be active in the circuit study. It fails to show the placement of power loss when a circuit involving a standing wave is considered, because it only shows a total of the whole effect. The fundamental difference between a traveling wave as studied by vector diagrams and the standing wave which must be studied by chart diagrams is that the traveling wave averages its effect over a long distance, while the standing wave does not average its effect but in another manner maintains fixed and identifiable positions of energy conversion. The difference between the traveling-wave concept and that of the standing wave is observed to be the difference between averages of the whole effect and instantaneous values as fixed positions of power loss.

To return now to the half-standing wave between the electrodes of an oscillating circuit, it can be noted that the values are not averages, as would be the case of a vector analysis, but result in fixed but varying effects throughout the area wherein resistance is effective on the field of force. When a problem of heat placement is considered, the vector method of analysis might lead to the belief that heat distribution, as a result of natural forces, would be uniform. In this new approach, namely, the analysis of heat distribution by standing-wave instantaneous values, placement of the heat effect in its nonuniform distribution is almost exactly determinable.

Most investigators dealing with this problem of dielectric heating have discovered that greater heat exists in the center of a package of dielectric than on the outer edges of such a package. On the basis of analyzing the effect through vectors and averages, it naturally might be assumed that the less heating effect on the outer edges of the package is caused by radiation through the electrodes and through the outer atmosphere where there is a gradient of heat between the block and outside area. When the analysis of heat distribution is made by standing-wave method, the fallacy of even heat distribution in the radio-frequency field of force becomes apparent. Several simple steps show nonuniformity of heating effect in the radio-frequency field, the

[1] President, Northwest Syndicate, Inc., Tacoma, Washington.
[2] President, Mann Capacitherm Company, Vice-President, Northwest Syndicate, Inc.

Contributed by the Wood Industries Division and presented at the Annual Meeting, New York, N. Y., Nov. 29–Dec. 3, 1943, of THE AMERICAN SOCIETY OF MECHANICAL ENGINEERS.

NOTE: Statements and opinions advanced in papers are to be understood as individual expressions of their authors and not those of the Society.

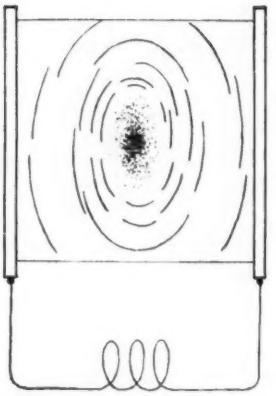


FIG. 1

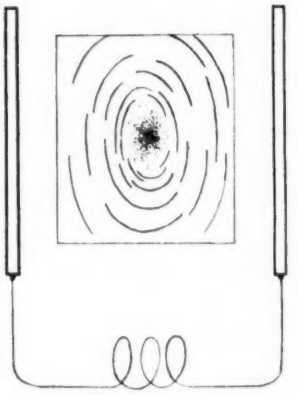


FIG. 2

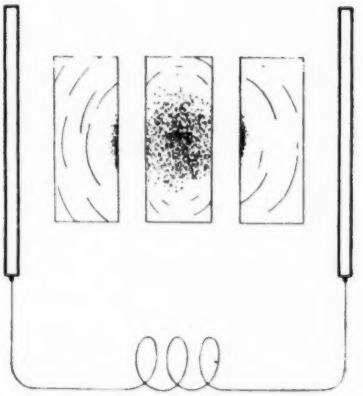


FIG. 3

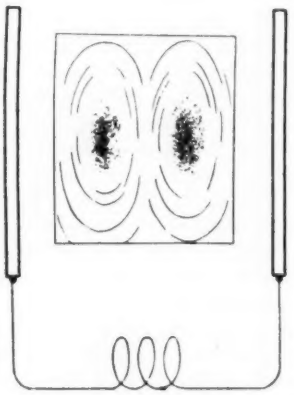


FIG. 4

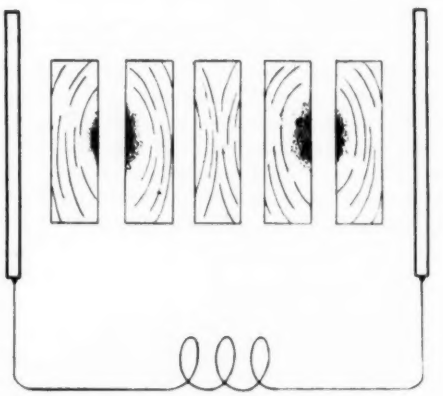


FIG. 5

first being to burn a single block in the center with electrodes contacting the outer face of the block as in Fig. 1. A second step is to separate the electrodes from the side of the block and burn it in a similar manner, as in Fig. 2. If radiation from the outer edges were the proper answer to the uneven burned effect of the dielectric, this could readily be proved by placing three blocks of dielectric in the field of force and having each separated from the other by an equal air space. This effect results in the center of the three pieces of dielectric being charred to an extreme, and the inside faces of the outer two grading down, leaving the outside faces of the outer two blocks unaffected by charring, as in Fig. 3. If the radio-frequency field of force were uniform, the three blocks would each be burned, respectively, at their centers.

It might be argued, at this point, that radiation still has its effect even on the three separated blocks and this, in part should not be denied, and so our studies should be carried a step further and show the effect of smaller phase shifts than occur in the examples of Figs. 1, 2, and 3. Producing this result shows a double burned area, with one burned spot on the left of the center and one on the right of the center, with the center and the two outsides remaining unaffected by charring, as in Fig. 4. The burned areas are the direct results of a shift in phase of less than that which causes the center burn in the other blocks. The conclusion of the series of experiments brings into the field five separated blocks with burned areas in the blocks next to the center one and also next to the outside ones, as in Fig. 5, reproducing the pattern shown in the single block, Fig. 4. All of the burns shown in the five illustrations are the result of double burned areas; but in the first three the two spots are merged into what appears as a single spot, the phase shift being greater and in phase relationship between the electrical components being closer than in the last two.

When a phase angle approaches 90 deg, but some energy absorption is effective, the two burned areas will be found at one quarter and three quarters of its thickness. When the phase angle approaches 0 deg and maximum energy absorption is effective, the two burned areas merge to form a single peaked area at the center of the thickness. In this latter case, heat distribution approaches the square of the instantaneous values of a half-standing wave of current. Returning therefore to the original formula for power, it can be said that $E\ I \cos \theta$, which shows total power does not show the distribution of a radio-frequency field of force, and that the relationship of power distribution to dielectric materials varies in uniformity with the adsorptive qualities of the load, and the effectiveness of the dielectric to produce a resistive effect.

The foregoing discussion is offered as in opposition to the uniformity theory, not to conclude that all that has gone before is wrong, but to see another side of the matter which results from a study of the physics of wave structure and electron motion, with the admonition to think twice before too much is assumed, based upon the vector engineering of 60-cycle alternating current.

The fact that the heating effect of the radio field can be predetermined; that its heat effect can be controlled; that its effect through the thickness of the material, while not uniform, is instantaneous and simultaneous makes it a new and useful tool for industry in many wood, plastic, and other applications. However, the primary concern in this discussion is with adaptations

to wood treatment and glue-setting technique in wood which stem from some of its unique, nonuniform, and selective qualities.

Gluing Technique

A particular quality of the radio-frequency field is its selectivity. This results from the tendency of the field to follow the most conductive path between electrode extremities.

Original operations of bonding materials with radio frequency placed alternate layers of wood and glue in the field so that the glue lines were established parallel with the electrodes. This means simply that the established lines of force between the electrodes would be perpendicular to the respective glue lines. There being no one path between the electrodes, under this situation, which would be any more conductive than any one other path, it was perfectly natural to bring the entire package of wood and glue up to the critical setting temperature of the glue for purposes of bonding the mass. It has been incorrectly assumed that it made little difference whether the glue lines were perpendicular to or parallel to the lines of force.

Parallel Bonding. Now it has been determined, however, that the normal resin-glue line is much more conductive than the wood with which it is associated, so we can adapt this knowledge of conductivity and selectivity to gluing technique and place the glue lines in the field so that they substantially parallel the main lines of force rather than exist perpendicular to them. This technique of gluing is called "parallel bonding" and differs materially from the older technique of "perpendicular bonding" in that it allows the concentration of the entire effect of the field on the glue joint, avoiding the necessity of wasting much heat in bringing the wood up to the same critical temperature as is required to set the resin glue. In some cases it had been found that in thick laminations only a small portion of the heat from the radio field is required to set a given package by the parallel-bonding method as was required to set an equal passage by the perpendicular process.

It should be pointed out however that, as the critical setting temperature of the resin is increased to a point approaching 212 F, the effect of parallel bonding diminishes, and that if the critical setting temperature of the resin is substantially above the boiling point as is the case of high-temperature phenol resins, little if any advantage remains through the use of parallel-bonding methods, as compared with perpendicular methods. This is due in part to the fact that much energy will be expended from the hot glue lines by conduction to the wood itself before the temperature reaches 212 F, and also in part to the fact that the moisture in the wood will be acted upon equally with or to the exclusion of the conductivity of the glue lines above 212 F. The selective effect of the radio field therefore has led to interesting and advantageous methods of gluing wood and the treatment of other materials.

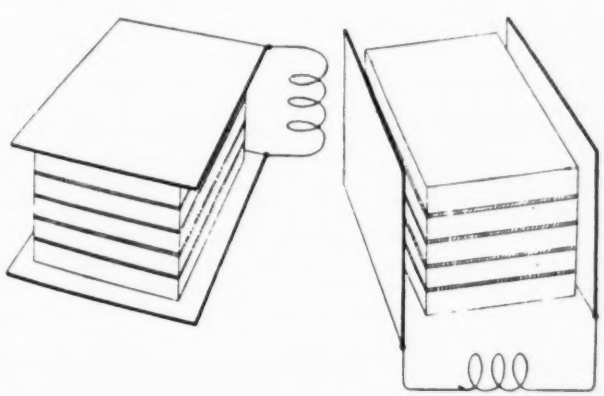


Fig. 6

Resins. This selectivity may best be utilized by parallel bonding techniques, using ureas, melamines, and the very new types of phenol resins, which are in time, cold-setting, or at least set below the boiling point. Heat will accelerate practically any resin adhesive, so if a cold-setting resin is used heat will accelerate its chemical reaction and complete polymerization in rapid order. Rather than spend time describing glues, our primary interest is in applications of varying techniques and electrode arrangements. It is one job to create a radio-frequency oscillator, but it is still another to apply it properly to a gluing operation. Fig. 6 illustrates the two general types of electrode arrangement used in most operations; the sandwich or perpendicular method and the parallel bonding method. The differences between these types has been described but some general principles can be illustrated from them.

Applying the Radio-Frequency Oscillator

In both methods, pressure is applied to the top and bottom of the package, the electrodes in the perpendicular method being between the package and the pressure sources. Surplus glue may squeeze out, fall downward toward the bottom plate electrode, and if the spread is not very carefully controlled to prevent this squeeze-out, the glue excess will start a high-frequency arc and carbonize a path between the electrodes which not only is dangerous as it reflects back into the oscillator or amplifier, but it may easily ruin the entire batch of material. In parallel bonding, since the electrodes do not have to contact the work, squeeze-out as a danger is entirely avoided.

In determining which method to use for a specific job, frequency of the package, which is dependent upon its size, shape, moisture content, and glue is sometimes a determining factor. With a fixed-frequency oscillator, of course, less flexibility in package dimension and electrode placement is permissible than with a variable-frequency oscillator. The latter types are variable, even so, only over the range of their variable capacitances. The lamination of ten plies of veneer $^1/_8$ in. thick with $^1/_8$-in. cauls above and below in a size 7 in. × 14 in., for example, can be treated at different frequencies, but its fundamental, using the sandwich method with plattens above and below, is in the neighborhood of 25 meters or 12 megacycles. With parallel-bonding electrodes on either side of the same-size package, its frequency fundamental is 10 meters or 30 megacycles. In a scarfed joint the same size and thickness, the fundamental frequency is slightly higher, due to a lesser content of resin glue. Frequency of oscillation, or wave length, undoubtedly has its effect upon speed of setting and effective heat penetration and conversion, but the study by Von Hipple and Deitz was inconclusive in this regard. It has been said that the higher frequencies are more effective in heat generation than are the lower ones, which in general may be accepted as founded on some logic, but it is believed that power input and conversion efficiency of the oscillator have a greater effect upon heating than does the variation of frequency within limits, for example, between 10 and 50 megacycles. At the lower frequencies, which is to say, under 6 megacycles, some noticeable reduction in heat-conversion efficiencies should become apparent.

Almost any wood-bonding load can be matched, one way or another within the range of between 10 and 50 megacycles. Simpler apparatus at these wave lengths is just another reason to go higher and higher in oscillating frequency. But limitations of power, because of the capacitances of the vacuum tubes, prevent large packages being operated upon at very high frequencies. Some day these limitations will be breached, and progress in that direction is currently very rapid.

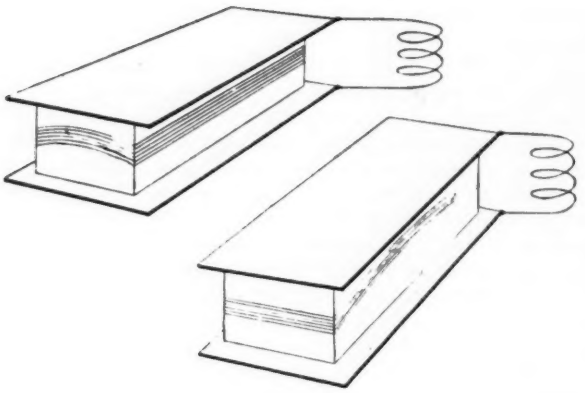


FIG. 7

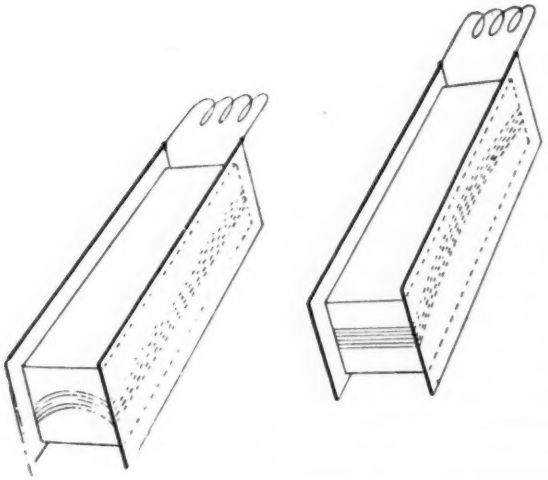


FIG. 8

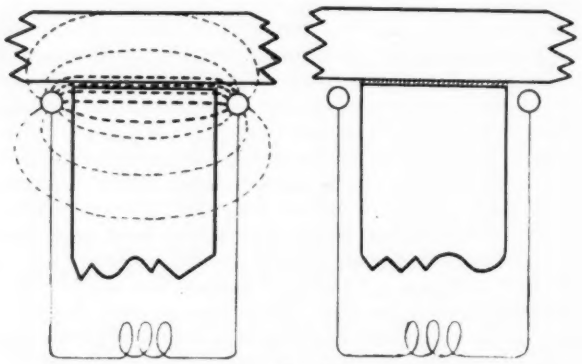


FIG. 9

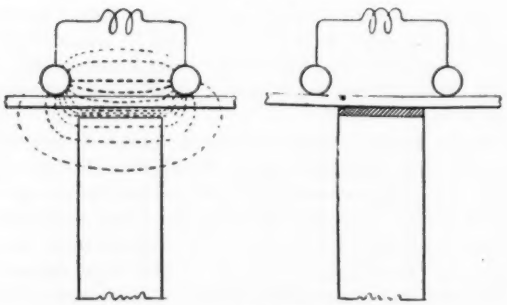


FIG. 10

Fig. 7 shows a perpendicular bonding setup which employs the advantages of and also approaches the effectiveness of parallel bonding. Here curved shapes may be bonded between male and female forms. Fig. 8 shows these two same curved shapes set up on a pure parallel-bonding method. The time of bonding using the same input power will be about one fifth as long with the parallel bonding means as with the perpendicular means, with a glue which sets below 212 F.

Fig. 9 shows an accessible butt joint with electrode arrangement and field distribution. This is a simple means of bonding joints quickly. Fig. 10 shows a similar application, but in the case of a thin skin abutting an inaccessible rib or other member. The field distribution shows how the energy seeks the conductive

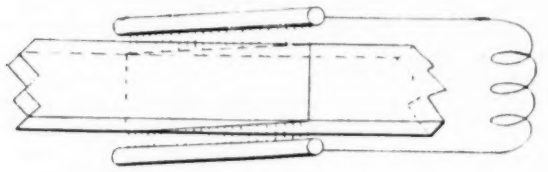


FIG. 11

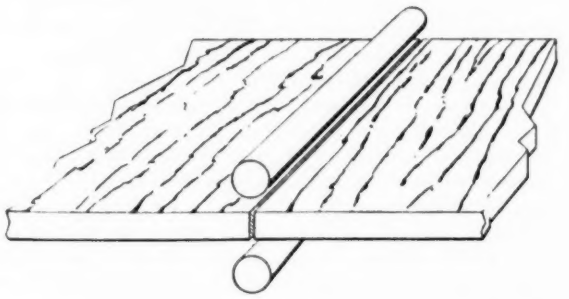


FIG. 12

glue line through the skin surface and accelerates its setting even through relatively thick sections. This application is one means of spot-welding wood or sewing thermoplastics. No matter what the accessibility of the joint, so long as no metal parts parallel the field of force and detract from the conductivity of the glue line, some method can usually be worked out to accomplish the job, and some system of electrode arrangement devised to supply properly radio-frequency energy to the joint.

MOST EFFICIENT ELECTRODE ARRANGEMENTS

A straight scarf, such as is employed in aircraft work shown in Fig. 11, when pressed from top and bottom, presents no problem when the scarf is under 6, 8, or even 12 in. in width. Rods or tubes placed along either side of the scarf, their centers aligned with the glue line and supported by standoff insulators, suffice for electrodes, either center or end fed. The field lines of force literally spit through the glue line in this setup but care should be taken either to space the electrodes away from direct contact with the glue lines, or to place a thin wood or other dielectric caul between them. An air gap when not too wide, say, $^1/_2$ or $^3/_4$ in. on either side of the scarf, will cause no material slowing of the reaction of the glue, as compared to using a thin caul and no air gap. A bar or tube rather than the conventional flat plate, as shown in Fig. 6, may be employed in order to concentrate emission from the surface closest to the glue line. Stray and therefore wasted field lines of force are minimized with rods, but are greatly increased when an electrode area of great width is presented to a single glue-line application.

The principle of presenting the minimum of electrode-surface

area to the glue line is well illustrated in Fig. 12, which shows a tube-electrode application to edge-glued lumber or veneer, employing the parallel bonding method. This means is employed on a continuous machine being developed to take the place of the tape splicer and also the hot-plate tapeless splicer

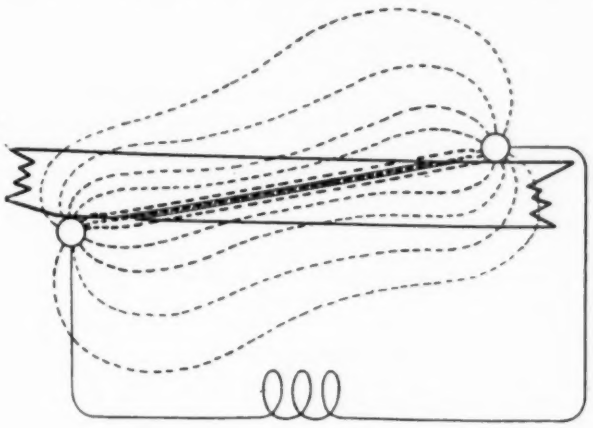


FIG. 13

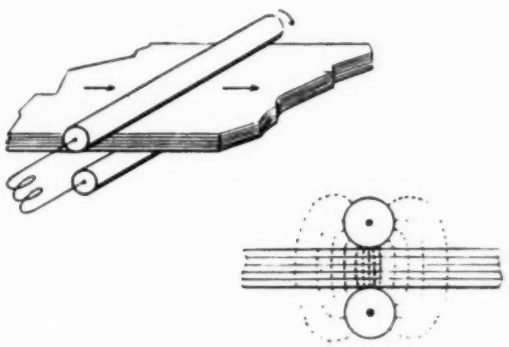


FIG. 14

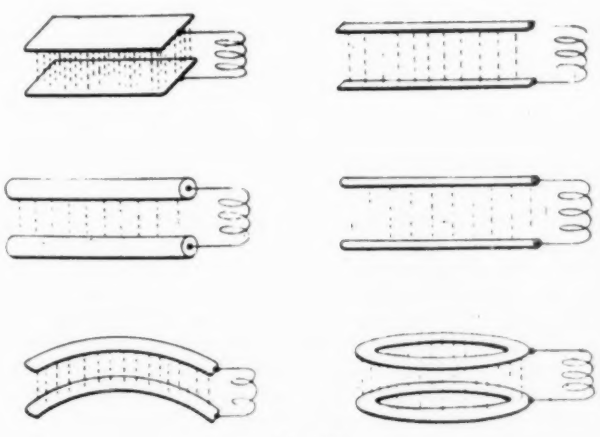


FIG. 15

used for core work in plywood, veneer, and furniture manufacture. It is anticipated that we will shortly see in operation such a machine running at a speed of between 50 and 100 fpm.

Fig. 13 illustrates parallel bonding applied to a scarf joint which is very wide, for example, in the 4- or 8-ft side of a sheet of plywood. These joints, 10 or 12 in. through and 4 ft long, are such as those used on the bottom of PT boats. It would be impractical to apply an electrode arrangement such as shown in Fig. 11, because its frequency would be much too high to come within the range of any currently used radio-frequency machines. It might even reach 300 or 400 megacycles or even into the microwave strata. Long tubes can be used running the entire length of the scarf and still take advantage of the parallel bonding method. These electrodes, supported by standoff or other insulators, run the entire length of the scarfed joint. Using tubes 3 in. diam and 50 in. long, as shown in Fig. 13, a frequency of 15 megacycles, and a wave length of 20 meters, creates a nice operating load. When these electrodes are extended to longer lengths and the width of the scarf widened also, the frequency is maintained at 15 megacycles.

For certain operations such as bonding plywood on a continuous basis roller electrodes are employed successfully. With one roller above and another below the package, the established field lines operate perpendicular to the glue lines. Such an operation, as shown in Fig. 14, not only applies to plywood bonding, but to the drying of wood, the treating of cellulose-plastic compounds, the dehydration of food products, and many other uses.

By reference to the several illustrations, possible electrode arrangements are shown for several different uses. These are but a few, and to show others would be to repeat largely the lessons evolved from the various types of placement. The shape of electrodes may vary even more widely than their relative placement. Fig. 15 has six separate shapes, plates, strips, rollers, bars, curves and circles, all of which with equal efficiency may be adapted to their special uses.

It might be asked how the two-spot heating effect, or even that of the single spot affects gluing procedures. On loads of relatively light power absorption or power factor, as some call it, the two-area heating will be encountered in parallel bonding. In perpendicular bonding, no such light load is apt to be encountered. The two hottest areas, in a light resistive load, will spread their temperature rise rapidly to adjacent glue-line areas, and in a flash which is so fast as almost to prevent stop-watch timing, distribute enough heat to polymerize the resin in the entire glue line.

One very interesting case occurred in bonding a small scarf joint $1^1/_2$ in. wide and 4 in. long in $^1/_4$-in. spruce aircraft stock, using tubular electrodes, and the method shown in Fig. 11. A 2-sec exposure to the field of a generator having an output rating of 2200 Btu per hr cured the two outer edges and into the scarf some distance, but when broken immediately after release from the press an uncured center showed up about $^1/_2$ in. through the glue line. This indicates quite clearly the two-spot heating effect. When exposed 5 sec, the entire scarf-joint glue line was cured throughout. Normally one might not encounter usual evidences of the two-spot heating effect, but it is there nevertheless and should be considered in gluing light resistive loads.

An Introduction to Aircraft Hydraulic Systems

By HOWARD FIELD, JR.,[1] INGLEWOOD, CALIF.

This paper traces the evolution of hydraulic systems for airplanes, from the hand-actuated piston pump and "motor" piston, through the stage of motor-driven gear pumps, down to the present-day systems which derive their power directly from the airplane engine. Three general methods of pump control have been developed which permit rotation of the pump but prevent build-up in the hydraulic system, since the pump operates continuously. These methods include "the constant-pressure," the "manual by-pass," and the "automatic by-pass," all of which are in wide use. Special applications of hydraulic control are described in the "power-amplifier" or "load-feel" system, the "follow-up" system, "follow-up plus load-feel" system, and the "full-automatic" system.

THERE are many means of transmitting power from its source to the place where it is to be used, among which are electrical, steam, mechanical, hydraulic, etc. Each has advantages and disadvantages which become of greater or lesser importance depending upon the particular problem at hand.

Having no regard for relative importance, and in fact, the relative importance is not constant, the advantages of hydraulic systems in aircraft are as follows:

1 Light weight per horsepower required.

2 Low inertia of moving parts, making quick starts and stops possible without undue stresses being set up.

3 Controllability to any degree of accuracy and sensitivity required.

4 Great flexibility of installation not only because tubes can be run anywhere but also because the same system can develop great forces or light rapid motions.

5 Ability to withstand large amounts of abuse without complete breakdown.

6 Reliability greater than many other competing forms of power transmission.

Since the hydraulic system is a method of transmitting power, it is obvious that there must be a means of applying the power at one end of the chain, in other words, a pump. This pump may be either hand- or power-operated, the simplest form being a cylinder containing a piston which may be manually moved. Next, a line or tube to convey the power to the output end of the chain, and a motor to reconvert the hydraulic power to mechanical motion and force are required. This "motor" may likewise be a simple cylinder and piston. If this "motor" piston be arranged to be returned by a spring, and a reservoir to take care of leakage or volume changes be added, the result is the well-known automobile hydraulic brake. Many small airplanes use this identical system for brake actuation, as shown in Fig. 1. It will be noted that none of the diagrams in this paper makes any pretense of showing the actual physical embodiment of the circuits or devices. They are intended to be only the simplest possible representation of principles. In many cases, undesirable devices have been represented rather than more desirable but more complicated ones, which would be more confusing. In general, no packings have been shown, although they are obviously necessary in the actual devices.

By substituting an ordinary double-acting pump for the simple master cylinder, a double-acting cylinder for the brake cylinder, and adding another line and directional-control valve, the resulting system (diagrammatically shown in Fig. 2) is complete. This was the first system used in aircraft for actuating mechanisms other than brakes. There are many control-valve designs, but all accomplish the same end. These valves are usually known as "selector valves," or "4-way valves."

The next step was to add another unit to be operated from the same pump and reservoir. This can be done by having the second unit in series or in parallel with the first. Since the series arrangement requires the use of tail rods or different sizes of cylinders to provide identical motions it is not used for the following reasons:

1 Tail rods require extra packings.

2 Different sizes complicate manufacture, and they might be improperly installed.

3 There is no way to bleed the trapped portion of the circuit between the two cylinders.

4 Thermal changes in volume or slight leakages would throw the cylinders out of synchronism.

5 The pressure is divided between the two cylinders; hence it is necessary to make them large and consequently heavy.

There are ways to overcome faults 3 and 4, but series cylinders

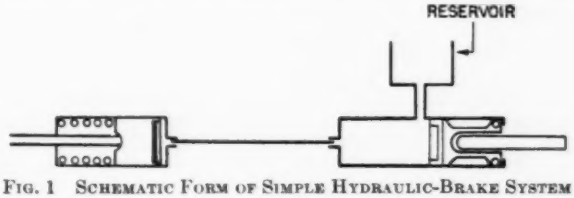


FIG. 1 SCHEMATIC FORM OF SIMPLE HYDRAULIC-BRAKE SYSTEM

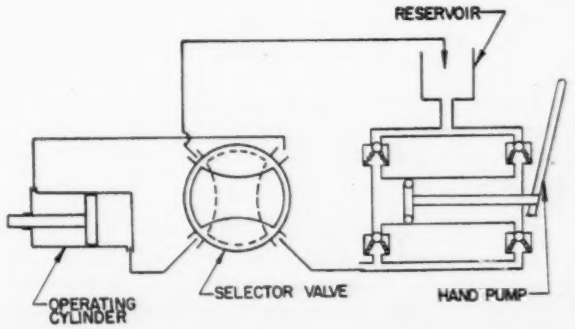


FIG. 2 DIAGRAM OF SYSTEM IN WHICH DOUBLE-ACTING PUMP AND CYLINDER WITH "SELECTOR VALVE" ARE SUBSTITUTED FOR SIMPLE FORM OF FIG. 1

[1] Consulting Engineer. Formerly Hydraulics Engineer, North American Aviation, Inc.

Contributed by the Aviation and Hydraulic Divisions and presented at the Semi-Annual Meeting, Los Angeles, Calif., June 14–17, 1943, of THE AMERICAN SOCIETY OF MECHANICAL ENGINEERS.

NOTE: Statements and opinions advanced in papers are to be understood as individual expressions of their authors and not those of the Society.

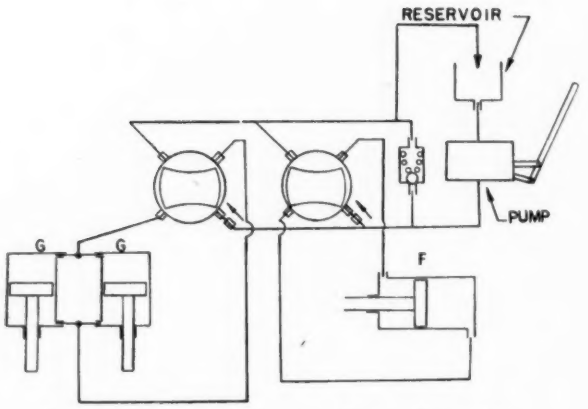


FIG. 3 SYSTEM WITH PRESSURE-RELIEF VALVE ADDED

are never used unless there are overwhelming reasons for so doing. All five of these difficulties are avoided by connecting the cylinders in parallel, although this introduces a new problem. The cylinder which, for any reason, moves easiest moves first. It is seldom that this causes actual difficulties and, where it does, corrective steps can be taken. For example, it may add aesthetic value to have both wheels of an airplane retract in unison, but it is not usually essential that they do so.

The addition of a relief valve to prevent excessive pressures from being built up in the pressure lines results in a circuit like Fig. 3, and consideration must be given to what would happen if the pilot should open both selector valves at the same time. In any system, there is a tendency for all potentials to seek a common level, and a hydraulic system is no exception. Assume that an airplane is coming in for a landing and the pilot pumps his flaps down; this may require 600 psi in the flap-actuating cylinder (cylinder *F* in Fig. 3). The pilot moves his landing-gear selector valve to "gear down." The gear falls part way by gravity, which requires no pressure, so the fluid runs out of the flap cylinder and into the landing-gear cylinders (cylinders *G* in Fig. 3). Since there is nothing holding the flap down, it moves to a trailing position, which reduces the lift and may result in a crash. Of course, if he had lowered his gear first, this would not have happened, but the simple addition of check valves at the fluid-pressure ports of the selector valves will prevent unwanted interflow between selector valves, although this introduces another difficulty.

Hydraulic fluid expands about $4^1/_2$ per cent per 100 deg F (much more than the metallic parts expand), and the check valves block off any chance of relieving excess pressures due to thermal expansion in the cylinders and lines through the relief valve. This can be overcome either by making the check valves "leaky" so they will permit the very slowly expanding fluid to pass, or by putting additional relief valves at each selector-valve pressure port. Circumstances dictate which method shall be used. The first would let the flaps creep up slowly (disadvantageous but not usually critical), while the second entails manufacture of more relief valves. Strangely enough, even though very simple, good relief valves are among the most difficult hydraulic parts to make.

General Power System

As airplanes grew in size, it became evident that some sort of power would have to be applied to hydraulic systems, since a pilot cannot be expected to produce more than about $^1/_5$ hp, and that only for a limited period of time. It was also true that as airplanes grew larger, the pilot had more to do and no longer had time to spend in purely manual labor. When airplane systems required 1 or 2 hp, it seemed a logical development to apply an electric motor to drive the hydraulic pump, which was generally of a positive-displacement type, such as a gear pump. This entailed the addition of a relief valve to provide a path for unused fluid to return to the reservoir.

Further experience showed that the pilot neglected entirely to turn off the motor when the operation was completed, and the system continued to run, heating up the oil. It then became necessary to connect a pressure-operated device to the switch so that, when a predetermined pressure was reached, the switch would operate automatically. Of course, the relief valve was set higher than the amount of pressure which was expected to be used. Fig. 4 shows the resulting power circuit. This automatic pressure "kick-out" device relieved the pilot but it had faults of its own. For example, the pressure had to be set very much higher than required for an operation or the switch would kick out when accelerations acted on the landing gear. Thus the system had to be designed for much higher pressures which shortened the pump life and made everything heavier.

No good solution was ever found for this condition because other factors increased the power requirements so fast that it became impracticable to draw the power from the airplane electrical

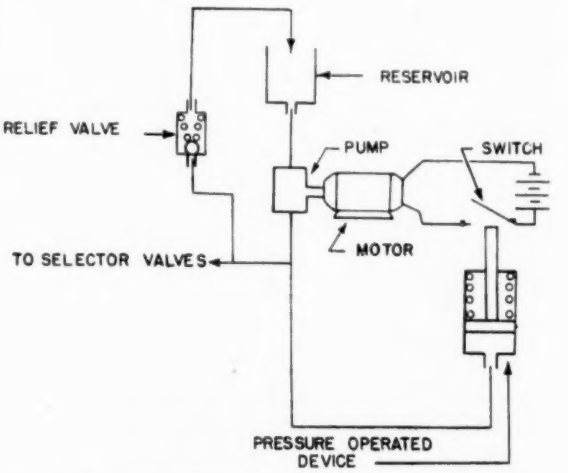


FIG. 4 HYDRAULIC CIRCUIT WITH ELECTRIC POWER ADDED

system. The obvious answer was to connect the pump to the engine, and thus to use the engine power directly, instead of indirectly through the storage battery and motor. With the pump driven by the engine, there was no such thing as turning it on when required unless some sort of clutch device were interposed between the engine and the pump. The idea of using the clutch was abandoned, as investigation showed that this would be cumbersome and heavy and would probably lead to service difficulties. Thus it was necessary for the pump to operate continuously whenever the engines were running, which meant that fluid was always being pumped.

By-Pass Methods of Relieving Hydraulic Systems

One method of relieving the hydraulic system and the pump when it was not required was to by-pass the fluid which was being pumped all the time the engine was in operation. This general scheme is the one used in almost every hydraulic system at the present time. This method of by-passing the pump may be subdivided into three general classes:

1 The class, known as the "constant-pressure" system, may in turn be subdivided into two classes:

(*a*) This class utilizes a relief valve to limit the pressure. In

this system, the fluid when otherwise not being used, constantly runs through this relief valve, which is undesirable, since the power put into the fluid by the engine-driven pump is wasted or turned into heat. Although this type of "constant-pressure" system is sometimes applied, it is limited to approximately $^1/_3$ hp because of the large heat-rejection problem.

(*b*) A variation of the "constant-pressure" system which is used to some extent, particularly in Europe, is one in which a variable-delivery pump is connected to the engine. This pump is so constructed that, as the pressure which it produces is increased, the amount of oil or fluid which it pumps is decreased. Thus when the pressure rises to some predetermined point, which is somewhat above that required for operation, the volume of fluid delivered falls to zero and no further pressure increase occurs. The pressure in the system remains at "cut-out" values, but since there is no volume being moved, the power absorption and consequent heat rejection is zero, except for the power required to overcome pump friction.

2 A method of relieving the hydraulic system, known as the "manual by-pass" system, is usually semiautomatic in that the pilot turns on the pressure, but it is relieved automatically. This method may again be subdivided as follows:

(*a*) An application, which uses a special by-pass valve for operation at some predetermined pressure, is utilized in the power system shown schematically in Fig. 5. The by-pass valve is constructed so that the pilot pushes the plunger "in" (to the left in Fig. 5), where it is latched. There it remains until the pressure in the release mechanism (shown as a cylinder and piston, restrained by a strong spring, in Fig. 5) builds up to a point where the latch is released, and the plunger is returned to an "open" position by the light spring behind it. The by-pass valve performs much the same function as the switch in an electrically operated system, in that the pilot closes it and it opens automatically. Unfortunately, it is subject to the same disadvantages as the electrically driven pump system because the pressure must be set at a higher point than is desirable, in order that the valve may not be operated by a surge in the hydraulic lines and thus stop operations which are not complete.

(*b*) Another scheme uses a special by-pass valve which opens a certain length of time after it is closed. This by-pass valve is shown in Fig. 6. This would connect to the general hydraulic system in the same manner as the by-pass valve in Fig. 5. In Fig. 6, a plunger is adapted to close the pressure line when it is pushed into its seat by the pilot. Then the pressure from the line exerts a force to push the piston to the right and withdraw the plunger, but an equal and opposite force is exerted by the fluid which runs through the check valve and acts against the right-hand side of the piston. Thus the hydraulic forces are in balance but the spring shown tends to move the piston to the right. In order to accomplish this, it is necessary that the fluid to the right of the piston escape to the return line. This is controlled by a properly chosen restrictor valve in the line connecting both ends of the valve. A number of trainer type airplanes use this scheme of operation.

(*c*) Yet another application of the "manual by-pass" system makes use of a special type of selector valve known as an "open-center" type. When in the neutral position, the fluid from the engine pump circulates through the valve and back to the reservoir. When any of the valves is displaced to operate some unit, this by-pass is shut off and the fluid is then directed to the proper operational device. The early versions of this open-center type depended upon the pilot returning the valve to neutral position when the desired operation was completed, and again the pilot forgot to do so, which left the oil at full pressure and being relieved through a pressure-relief valve. To avoid this difficulty, pressure-operated devices were arranged to return the valve to

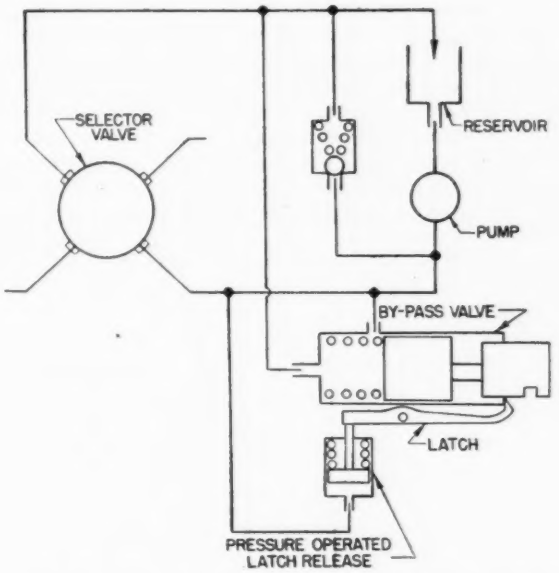


Fig. 5 Manual By-Pass System of Pump Relief With By-Pass Valve Operating at Predetermined Pressure

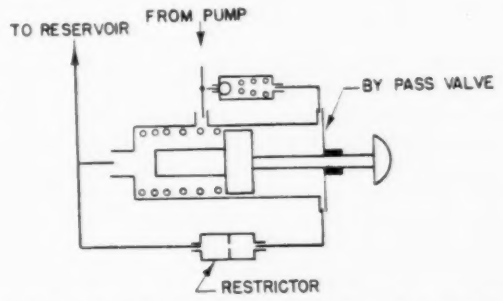


Fig. 6 By-Pass Valve Operating on Time-Lag Principle

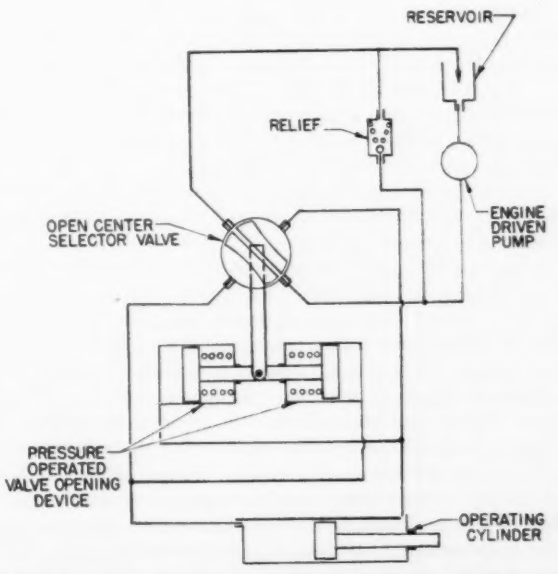


Fig. 7 Manual By-Pass System of Pump Relief Employing "Open-Center" Type of Selector Valve

neutral automatically when the end of an operation was reached. Schematically, this system is shown in Fig. 7. Here again, the pressure must be set higher than is desirable in order to keep the valve from being moved to neutral by pressure surges in the system. Although somewhat undesirable, this system is in use in some airplanes at the present time.

3 Another general method of relieving the pump is known as the "automatic by-pass" or "unloader" system. This method is now used on practically all airplanes built in the United States. The heart of the system is an "unloader" valve which is shown diagrammatically in Fig. 8. This valve is placed in a circuit with

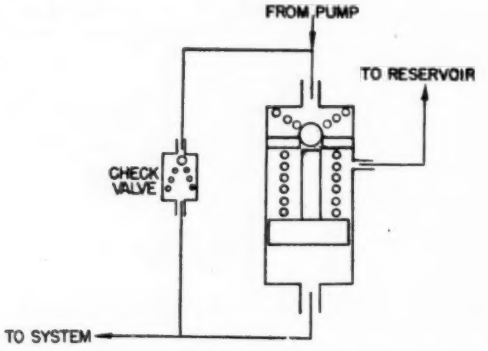


FIG. 8 DIAGRAMMATIC REPRESENTATION OF PUMP RELIEF BY MEANS OF "AUTOMATIC BY-PASS" OR "UNLOADER" SYSTEM

the fluid from the pump entering the valve as shown, and also flowing through the check valve and to the general hydraulic system. A small ball, seated in the partition across the valve body, forces the fluid to flow through the check valve and to the general system, since the ball prevents the oil from going through the valve seat and out through the side port and back to the reservoir. The pressure in the system is carried to the bottom of the piston which is shown as having an extension reaching the ball valve. The pressure acting below the piston tends to lift the ball from its seat. This is resisted by two forces, (1) the heavy spring whi h tends to push the piston downward and (2) the pressure acting on top of the ball tending to hold it to its seat. As the pressure increases, a point is reached where the pressure below the piston overcomes the spring and lifts the ball from its seat, thus losing the pressure which tended to hold it down, consequently the piston moves up rapidly opening the valve wide. Now, the fluid from the pump has free passage to the reservoir and, consequently the pressure drops. Obviously, the check valve, shown at the left, is required; if it were not for the check valve, the pressure would also drop in the rest of the system which would permit the piston again to return to its original position and thus close the ball valve, resulting in a system that was constantly opening and closing.

In this system an additional supply of fluid must be provided to react against the bottom of the piston in order.to keep it moving in an upward direction. Without this extra fluid supplied below the piston, the piston would move up only to a point at which the ball would rise off its seat a sufficient amount for the pressure loss through it to reduce the pressure below the piston to a degree that would cause the valve to stay in that position. To overcome this, an elastic device, which is known as an accumulator, is used in the line to the system. Originally, accumulators were simply cylinder-piston combinations which were loaded by means of heavy springs, but, since operating pressures increased to the neighborhood of 1000 psi, this type of accumulator became impracticable because of the excessive spring weight. Later, accumulators were designed which used compressed air in place of the spring. This proved much lighter than the old spring-loaded type and has been in continuous use since then.

The air-loaded accumulator consists of a chamber, usually spherical in shape, which is divided at its diameter by a diaphragm of flexible material. The chamber on one side of the diaphragm is pumped up to some initial-charge pressure, such as 400 psi, through an air valve, the diaphragm serving to separate the air from the oil which is admitted to the other side of the accumulator. Obviously, as the pressure in the fluid is increased, the air is reduced in volume so that it functions in the same manner as did the spring in the earlier design; but the air is practically weightless.

There have been numerous difficulties with this type of accumulator, most of which have been due to the requirements of the diaphragm material. It not only must be immune to attack by the fluid but also must have flexibility at very low temperatures. Improved synthetic-rubber materials have been developed which now make this type of accumulator entirely practicable.

A third type of accumulator, coming into wider use, is something of a combination of the two former types in that it consists of a cylinder having a piston to separate the oil and the air, but utilizes air above the piston instead of a spring. Early attempts to construct this type of accumulator were generally unsuccessful because of the difficulty of making packings which seal properly when the pressure on both sides are equal. Some of the newer type packings solve this problem satisfactorily.

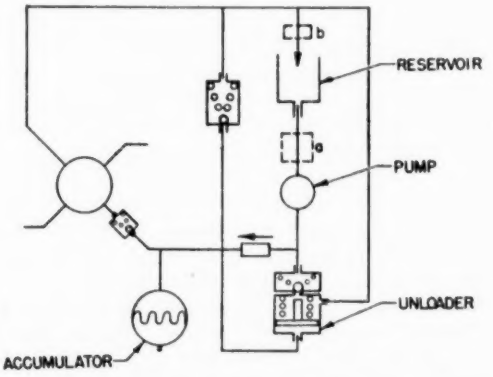


FIG. 9 DIAGRAM SHOWING UNLOADER VALVE AND ACCUMULATOR CONNECTED INTO POWER CIRCUIT

The unloader valve and the accumulator are connected into the power circuit as shown in Fig. 9. Here the pump draws the supply of oil from the reservoir and then discharges it to the upper portion of the unloader valve and also to the general system. The accumulator is shown connected to the general system at the left. It is obvious that if the selector valve, or valves, be closed, the oil delivered by the pump will first be used to charge the accumulator; and when that is accomplished, the pressure will rise to a point at which the unloader will open, thus permitting the pump to circulate the oil freely through the unloader valve and back to the reservoir. When a selector valve is opened, the pressure tends to fall, and the oil is drawn from the accumulator which starts the operation desired. As the pressure reaches the level at which the unloader valve again closes, the pump will discharge to the system and to the accumulator instead of back to the reservoir. Of course, when the pressure is again increased, the pump is again unloaded.

In Fig. 9 the dotted rectangles are shown as possible locations of filters. While location (*a*) is more desirable, since fluid is filtered before it goes to the pump, this location is seldom used because of the increased losses in the intake pressure at the

pump. If the filter be installed in location (*b*), this difficulty is avoided.

Special Power System

Among the advantages of the hydraulic system, as applied to aircraft, has been "greater flexibility of installation." Examination of one or two simple devices might illustrate this point. Suppose that the general hydraulic system was designed to operate at a pressure of 1000 psi, and then an additional device such as, for example, an automatic pilot which operates at a pressure of approximately 200 psi were added. By connecting a pressure supply for this device properly, it can be operated from the general system without endangering the system at all. Fig. 10 shows a method of connecting the reduced-pressure system into the general hydraulic system. Here, the unloader valve and check valve to the full-pressure system are exactly as shown previously. The check valves between the engine-driven pumps and the general system prevent by-passing of fluid through either pump in case of shaft failure. Between one pump and its check valve, what is known as a selective relief valve is inserted, and immediately above that a tap-off of fluid to the reduced-pressure system. Of course, a shutoff valve to prevent flow in this reduced-pressure system when it is not being used and an ordinary relief valve, connected to this reduced-pressure system to eliminate overpressures, are necessary.

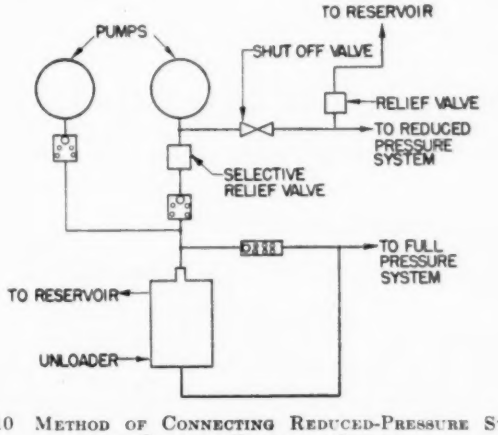


Fig. 10 Method of Connecting Reduced-Pressure System Into General Hydraulic System

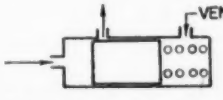


Fig. 11 Selective Relief Valve Diagram

The selective relief valve is somewhat similar to the ordinary relief valve and is shown diagrammatically in Fig. 11. Here, the fluid enters the valve from the left where it acts upon a piston. When the entering pressure is low, this piston covers up the outlet port and, consequently, there is no flow through the valve. However, as the pressure increases, the piston moves to the right a sufficient distance to make the loss through the valve equal to whatever pressure the spring was set to produce, as shown in the right-hand end of the valve.

The real difference between the ordinary relief valve and the selective relief valve is that the piston in the selective relief valve is packed and the rear of the piston is open to the atmosphere. Then the valve is unaffected by back pressures in the outgoing line, because these back pressures cannot act against the back of the piston. Hence it tends to hold the entering pressure to a definite figure or a definite amount above atmospheric rather than above return-line pressure; any higher pressure merely holds it wide open.

As this valve is installed in a system corresponding to Fig. 10, the oil from the right-hand pump enters the end port of the selective relief valve and discharges through the side port, through the check valve, the unloader, and the general hydraulic system. If the shutoff valve be opened to use the reduced-pressure system, this selective relief functions to maintain the predetermined pressure in the lines going to the reduced-pressure system, but it does not prevent the pump being used in the general or full-pressure system whenever the reduced-pressure system is turned off. It is, of course, true that all the time that the pump operates, it is operating against the pressure established by the selective relief valve. However, this is usually of so low a value that the pump can operate against it indefinitely. This results in a flexible arrangement in which both pumps can be used to operate the general system. Whenever the reduced-pressure system is being used, one pump is always available to the full-pressure system, and the other pump operates the reduced-pressure system.

This selective-relief-valve installation is shown merely as an example of what may be done with the hydraulic system in an airplane. It would be difficult even to begin to enumerate all the special conditions which are being provided for hydraulically in various airplanes at the present time. All sorts of sequence-operating devices are being hydraulically controlled, and many complicated actions have been made possible by proper valving. In many cases, it has been impossible to accomplish the desired result by any means other than hydraulic.

Special Control Systems

Some of the rather special systems which are used primarily because of the great degree of controllability or sensitivity are of interest. Among these are units in which the pilot must not only be able to direct the fluid or the power to the desired operational unit, but he must also be able to feel the load of the operational unit and to know its position at all times. Actually, four definite types of systems are used because of this great degree of controllability:

1 In the "power-amplifier" or "load-feel" system, the pilot supplies part of the energy for the operation, and the hydraulic system supplies the remainder. This system can be arranged so that the pilot supplies most of the power or, on the other hand, he may not supply more than 0.1 per cent of the power, but the part that he does supply is always in definite relation to the total amount required.

2 A second type of control is known as a "follow-up" system, which may be subdivided into mechanical and hydraulic types of positional transmission, both of which will be shown later. These are devices in which the pilot selects the position to which he wants some operational unit to move and, upon completion of this movement, the system automatically stops. Such a system is frequently used to operate landing flaps. In this case, the pilot merely moves his flap-control handle to whatever position he desires, say, for example, 30-deg flaps. The flaps move to that position and stop of their own accord. It is the fact that it is not necessary for the pilot to know what load is required to move the flap to the selected position, which differentiates the "follow-up" system from the "power-amplifier" system.

3 A type of control system which combines the two previous ones is usually known as a "follow-up plus load-feel" system. This is the type of system used for surface-control boosters. In these, the pilot must know not only in what position his control surfaces are, but he must also supply some of the power required to move the controls to this position. While it would be possible to handle control surfaces by means of a power follow-up system,

moving the controls very lightly from one position to another, he would have no conception of how hard it is to get them there. Unless the pilot has some idea of the amount of energy required, he is apt to force the ship into a more violent maneuver than it was designed to withstand, so the use of the "follow-up plus load-feel" system is indicated.

4 The fourth control type might be classified as the "full-automatic" system. Many different services are performed by the hydraulic system without any attention whatever from the pilot. A good example of these is the automatic temperature control for engines.

Application of the "Load-Feel" System

One of the most common examples of the "load-feel" system is the power brake valve. This form of valve control is shown diagrammatically in Fig. 12. The pilot does not want to know the

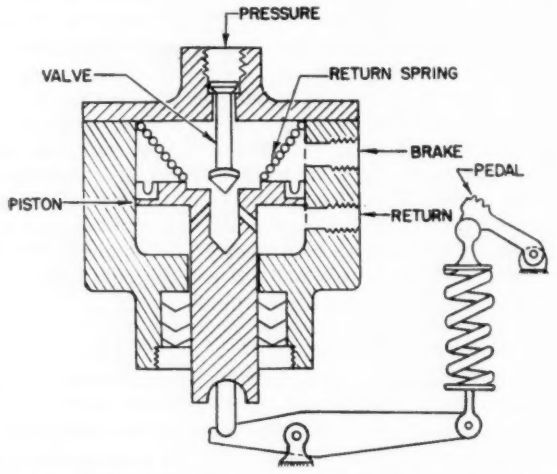


Fig. 12 Application of "Load Feel" System to Power Brake Valve

exact positions of the brake shoes or disks, the only thing which interests him is the pressure that is being applied to them. On smaller airplanes, the pilot was able to supply sufficient energy to operate the brakes without assistance from the main power supply. However, for airplanes having gross weights of about 10,000 lb or more, few pilots are physically capable of applying the brakes without assistance.

In the brake valve, shown in Fig. 12, the inlet for the pressure from the hydraulic system is at the top. Since the valve is shown in the closed, or brake-off position, this pressure is prevented from going to the brake by the cone-shaped valve closing the port. On the other hand, the brake line is open to the return port. This insures that the brakes will not be applied until the valve is moved. When the pilot applies the brake, he pushes down on the pedal as shown. This motion is carried through the brake-valve lever at the bottom of the figure and results in the upward movement of the piston in the valve. The first effect of this movement is to close off the return port by seating of the lower cone of the return valve, thus preventing any pressure admitted to the brake line from escaping through the return line. A very slight further movement of the piston in an upward direction will then open the pressure valve admitting pressure to the brake. As this pressure builds up, it will act downward against the piston in exact proportion to the pressure in the brake. This downward force on the piston is transmitted through the brake-valve lever and up to the pedal so the pilot feels the reaction on his foot. Obviously, if he pushes only lightly on the pedal, the pressure builds up in the brake valve to such an intensity that the piston reacts strongly enough to move his foot back a few thousandths of an inch, no more pressure passes into the brakes, and the result is a very light application of the brakes. As the pilot pushes harder on the pedal, the pressure in the brake valve builds up higher and greater brake action is achieved.

Notice that the actual movement of the brake pedal is very small, as a matter of fact, only a few thousandths of an inch. The valve acts perfectly. It does what is required but it feels unnatural to the pilot, since he has been accustomed to mechanically operated brake pedals in smaller airplanes, or to automobile brakes in which the pedals have a substantial movement. It does not feel natural to push on a pedal which is apparently as unyielding as a brick wall. To make this feel more natural to the pilot, a spring is introduced between the pedal and the piston. In Fig. 12, this is shown as though it were directly in connection with the pedal itself. This spring does not have any actual function in so far as the brake valve is concerned. It is merely introduced to make it feel more natural to the pilot. Here is an example of a power amplifier in which the pilot's first effort is amplified by the hydraulic system and then applied to the brake. There is apparently no particular limitation as to the amount of power which may be controlled by the brake valve, and it is to be expected that, as airplanes continue to get larger, the pilot will actually supply only about 1 or 2 per cent of the power required to apply the brakes.

Preselective Flap Control, Example of "Follow-Up" System

The mechanical version of the second class of control system, called the "follow-up" system, is illustrated in Fig. 13. This is a system which might be used as a preselective flap control. When

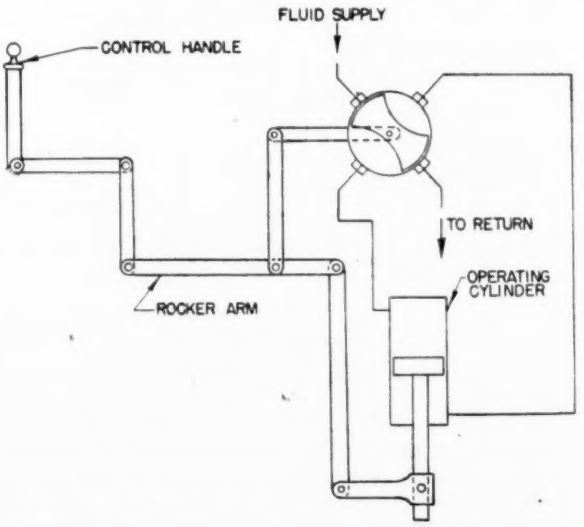


Fig. 13 Mechanical Follow-Up Type of Control System

the pilot moves his control handle to some position, the valve is opened and the resulting motion of the operational unit is transmitted mechanically to the valve through a rocker arm so that, when the desired position is reached, the valve has been brought back to neutral and the operation ceases. This mechanical position-transmitting type of "follow-up" system is seldom used, except where the power required for the operation is fairly large or where structural considerations make its application easy.

If the power requirement is low and installation difficulties prevent direct mechanical connections between the control handle

and the unit to be operated, a "follow-up" system having hydraulic positional transmitting connections may be used, Fig. 14. In this system, the operating unit, which is known as a "slave unit," is connected by lines to a follow-up cylinder and a valve whose body is fastened to the follow-up cylinder and moves with it. In the figure, the piston rod is shown as being anchored, and the valve lever is connected to a handle for pilot operation. If the handle be moved in the direction shown by the arrow, pressure will be admitted to the right-hand end of the follow-up cylinder. This pressure will push the cylinder itself toward the right, reducing the space in the left-hand end of the cylinder, thus forcing the fluid to flow through the pipe to the right-hand end of the slave unit. Since the slave unit is fixed, the piston will move to the left, and the oil returning from the left-hand end of the slave unit passes through the valve and is returned. It is evident that, as the follow-up cylinder moves to the right, it will move the valve body to the right, and, since the pilot's control handle is in a fixed position at that time, the valve will automatically

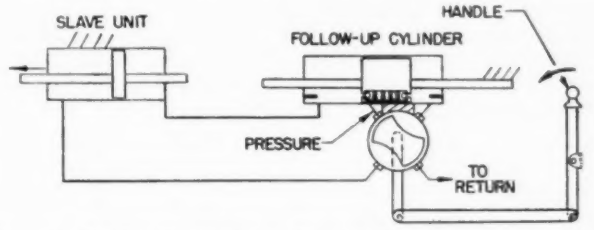


Fig. 14 Follow-Up Control System With Hydraulic Positional Transmitting Connection

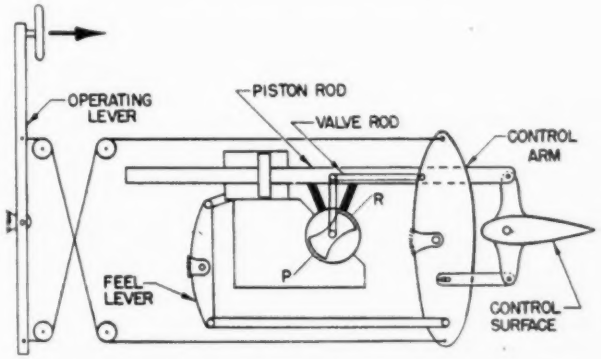


Fig. 15 "Follow-Up Plus Load-Feel" Type of Control Unit

close off when the position of the slave unit corresponds to that of the handle.

This type of circuit is, in effect, two cylinders in series and, in order to compensate for thermal expansion of the fluid or leakage, check valves are placed within the piston of the follow-up cylinder, and lifters are arranged at the ends of the cylinders so that whenever an extreme position either right or left is reached, one or the other of the check valves will be raised from its seat, permitting fluid to equalize between the follow-up cylinder and the slave unit and thus resynchronize.

"Follow-Up Plus Load-Feel" System of Control

The type of control known as the "follow-up plus load-feel" is used where the pilot must not only know the position of the controlled unit but also have some realization of the loads required to move it to that position. Fig. 15 shows such a system connected up as a surface-booster mechanism. The operating lever in the left-hand side is connected by cables to a control arm. The piston rod of the operating cylinder is connected to a horn attached to the control surface and, at the same distance from the center, a valve rod which operates the valve is connected about as shown. The valve body is fastened to the piston rod and moves with it. If the operating lever be moved in the direction of the arrow, that is, to the right, the control arm is pushed in the opposite direction. This moves the valve rod and opens the valve in a direction which will permit pressure to enter the right-hand end of the cylinder. This pressure entering will move the piston rod to the left thus moving the control surface in the desired direction. If the piston rod moves to the left, it carries the valve body with it and, since the valve rod is fixed in position, the valve will close when the piston has moved a sufficient distance to bring it into synchronism with the control arm. There is no need of having any connection between the control arm and the control surface, but a connection having lost motion is used because in the event of failure in the hydraulic system, the pilot would wish to have control of the airplane by manual means even though he might have to push very hard for the controls to accomplish the desired results.

Referring again to the operating cylinder, notice that it is not fixed to the structure but is connected through a lever and rod back to the control arm. The cylinder could have been fixed but, if it had been, an irreversible system would have resulted and the pilot would not have any "feel" of the loads required. By connecting the cylinder back through this lever and rod, the position of the pivot about which this lever moves can be so varied that the force transmitted to the control arm is in any desirable proportion to the effort which is exerted by the cylinder. If the pivot be put nearer the cylinder, the pilot will feel only a small portion of the effort.

It is, of course, obvious that the type of valve, shown in this diagram (Fig. 15) and also in the previous one, is not at all suitable for this use, since it is not sensitive in action and must be rotated through large angles. However, it was used merely for illustration since the principle is the same, and the rotary valve is much easier to understand in a diagram than the somewhat complicated but more sensitive valve which is actually used in practice.

Fully Automatic Type of Hydraulic Control

The final type of system is the fully automatic one in which the pilot has nothing to do with the operation. Such controls are used frequently as temperature controls, manifold-boost controls, or propeller controls. A fully automatic temperature control is illustrated in Fig. 16, which shows an operating cylinder, the piston rod of which is connected to a bell crank so that as the piston moves to the left, the scoop is opened wider. At the right-hand side is shown a rotary valve with its operating lever connected to a sylphon bellows which expands when heated. This bellows would be placed in the coolant circuit and, as the engine increases in temperature, the coolant temperature would increase and the sylphon bellows would expand. This would rotate the valve in a clockwise direction, admitting pressure to the right-hand end of the operating cylinder, thus moving the piston to the left and

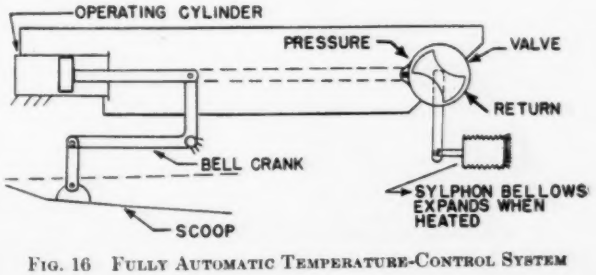


Fig. 16 Fully Automatic Temperature-Control System

opening the cooling scoop further. It is probable that the scoop would operate a great deal faster than the temperatures of the engine, and, consequently, the bellows would change so the scoop would be opened completely before the bellows had a chance to contract and close the valve. The scoop, being too far open, would overcool the engine and the sylphon bellows would contract, thus opening the valve in the opposite direction and closing the scoop. This would go on indefinitely, resulting in the scoop alternately opening and closing fully all the time.

Of course, restrictors might be placed in the lines so that the scoop could only move slowly. It is not advisable to control the hunting tendency in this manner since it limits the rapidity with which the scoop can be moved, and many times it is necessary to open a scoop quickly.

Another way of controlling this hunting would be to connect the valve body with the piston rod by a connection which is shown in dotted lines. Then, if the bellows heats up, the valve opens admitting pressure to the right-hand end of the cylinder and the piston moves to the left thus opening the scoop, but at the same time the valve body moves to the left which tends to close the valve. Now, if the engine should get warmer, the bellows would expand further, again opening the valve, and the scoop would open still further. Hence it is evident that the temperature of the sylphon bellows will have to be somewhat higher when the scoop is fully open than it would be when the scoop is nearly closed. In other words, a definite fixed temperature cannot be held regardless of the opening of the scoop. The relation between this range of temperature and the valve operation gives the system what is known as "drooping" characteristics.

Nearly all fully automatic controls require that there be some droop in the characteristics, in order to avoid hunting. The amount of droop depends upon the particular application and circumstances. It is expected that many more fully automatic controls will be used in airplanes in the future as designers become familiar with the simplicity of these automatic devices and learn that the most important feature about them is to select properly the amount of droop in their characteristics.

The discussion of various types and details of aircraft hydraulic systems might be continued indefinitely, although the basic ideas have been shown.

The detail design of hydraulic units and systems is based upon just three factors: (1) an understanding of the principles which have been illustrated, (2) a knowledge of fluid mechanics, and (3) experience. Most of the difficulties in connection with present-day hydraulic systems are due to the inexperience of the designers of the particular system or, in some cases, lack of test information, both of which are inherent in such a new and rapidly growing field of endeavor.

Controversy Over the Choice of a Medium for Aircraft Power Transmission

By RICHARD L. HAYMAN,[1] BURBANK, CALIF.

The growth in size and the increase in speed of modern aircraft has created the need for powered operation of many controls, accessories, etc., to supplement the work performed by the crew. The services performed by engine power and remotely transmitted to various parts of the airplane are too numerous to mention here but are tabulated in part in the paper. The choice of a medium for the transmission of this engine power to remote points has provoked one of the most intense controversies of aircraft engineering. In spite of the bitterness of the controversy that has at times prevailed, it has probably proved to be a dominant factor in the improvement of the two major surviving media, namely, hydraulics and electricity. This paper sets forth the cause of the controversy and presents a fair evaluation of each system of power transmission.

Introduction and General Explanation

MOST powered operations on aircraft can and have been performed by either the hydraulic or the electrical method, although perhaps not as conveniently one way as another. The choice actually resolves itself down to an evaluation of the comparative advantages and disadvantages of these two media for the particular job at hand. Certain companies subscribe almost completely to all-hydraulic operations; others cling to all-electric operations, while the majority hover between the two. This would verify the fact that opinions differ widely as to the proper evaluation of the services. To understand this radical difference in opinion of sound engineering minds one must study the complexity of the problem. This paper will attempt to present some aspects of the controversy in its present stage of development.

The problem is rightfully divided into two parts: (1) the transmission of power from one point to another, and (2) the conversion of this power into useful work. While no attempt will be made to treat these parts separately, the division should nevertheless be borne in mind.

Three Basic Forms of Power Transmission

The three basic forms of power transmission (other than purely mechanical) in common use in modern aircraft are hydraulic, electric, and pneumatic (including vacuum). Of these three basic services, electricity alone is an absolute necessity. Lighting and communications are two chores that make the use of electrical power mandatory. Since it is desirable to keep the number of different types of power media to a minimum, this fact is a strong argument for the use of all-electric power.

The use of vacuum and compressed air is relatively minor at this time in this country and will be neglected in this paper. Certain instruments have utilized vacuum for their operation for some time. The vacuum pumps necessary for this work have served double duty by providing the low-pressure air used by the inflatable wing-deicer boot. The use of electrically operated gyros and heat deicers may make obsolete these services. The use of hydraulics is universal, however, in spite of the fact that most of the services performed by it could be done electrically. To understand this we must enumerate the requirements of a power medium.

A brief explanation of the three basic services follows:

Aircraft hydraulics utilizes a low-viscosity mineral oil, and operates (in this country) at pressures ranging up to 3000 psi. Aircraft electricity consists of 12 and 24-v d-c systems, 110-v a-c systems, and an experimental 208-v, 3-phase, 400-cycle a-c system. Pneumatic power ranges from vacuum air systems to high-pressure air systems.

Choosing a Medium for Power Transmission

The Requirements. If the requirements for a power-transmission medium were to be listed in the order of their importance, they might read as follows:

1 Reliability (including lack of vulnerability).
2 Functional suitability.
3 Low weight (including efficiency).
4 Simplicity (from both development and maintenance standpoint).
5 Low cost (in terms of time and material now; in terms of money after the war).
6 Compactness.

There are probably others that could be added under separate headings, but we will try to include all requirements under one of those listed. The order of importance of the requirements may vary with the size, type, and function of the airplane and is therefore subject to change. All of the requirements listed necessarily overlap to a certain extent, so that it is impossible to discuss one without referring to others. Thus reliability and simplicity will go hand in hand. Simplicity and functional suitability will combine, and simplicity and cost will be contested as being synonymous. Low weight and compactness will fall into a similar category.

Reliability. The relative reliability of electrical and hydraulic systems has been strenuously contested verbally, but very little

TABLE 1 UNITS FREQUENTLY OPERATED BY CYLINDERS OR MOTORS IN LIEU OF MANUAL OPERATION[a]

Power Plant	Flight Controls
Starter	Surface-control power boost
Cowl flaps	Dive flaps or brakes
Oil-cooler flaps	Tabs
Prestone radiator flaps	Wing flaps
Carburetor hot-air valve	Automatic pilot
Carburetor air-filter control	Slots
Two-speed supercharger contr	**General**
Propeller-feathering pump	Landing gear and landing-gear door
Propeller deicing pump	Floats
Fuel booster or assist pump	Folding wings
Armament	Brakes
Gun chargers	Steering
Ammunition boosters	Fans (heating and ventilating)
Elevation boosters	Cabin supercharger
Gun turrets	Winches (for loading, etc.)
Bomb doors	Dump valves and chutes
	Landing lights
	Deicer pumps and controls

[a] The list is not necessarily complete.

[1] Hydraulics Engineer, Lockheed Aircraft Corporation.

Contributed by the Hydraulic and Aviation Divisions and presented at the Semi-Annual Meeting, Los Angeles, Calif., June 14–17, 1943, of The American Society of Mechanical Engineers.

Note: Statements and opinions advanced in papers are to be understood as individual expressions of their authors and not those of the Society.

conclusive proof has been brought forward to substantiate a claim for either medium. Actually it is extremely difficult to make a good comparison and arrive at any definite conclusion. In every case unreliability of one or the other is a function of poor design, installation, or maintenance. Since, however, we will always be limited by human ability to perform these functions, we can do no more than take actual cases as a parameter to compare the two services.

In an endeavor to make an evaluation of any usefulness, it was felt that actual service records should be explored. Service reports on types and makes from many different companies, covering a period of several years, were studied toward this end. In every case of failure of electrical or hydraulic equipment or systems, the seriousness of the failure naturally depended on the nature and the importance of the units being powered. Both systems have necessarily gone through a period of strenuous development. Aircraft hydraulics is newer than aircraft electricity and, although lacking the standardization that electrical-parts manufacturers have achieved, concedes no ground to electrical systems in reliability.

We find in practically every case that trouble was due to lack of experience, either on the part of the equipment manufacturer, the aircraft manufacturer, or the ultimate operator of the aircraft. Since the use of these auxiliary powers to such a great extent in aircraft is really quite new, lack of experience is natural. Both systems went through similar epidemics of trouble. In the hydraulics field at certain times, there were numerous failures of regulators, accumulators, ball-check valves, and packing. Sheared pump shafts provided another flurry of trouble and less predominant were hose failures and control-valve failures. In the electrical field, the same period was marked by frequent generator, voltage-regulator, inverter, limit-switch, and starter failures, and burned-out or broken wires or plugs. Less frequent were motor failures, fused battery solenoids, and burned-out relays. Cold-weather operation caused trouble to both systems, although perhaps more to hydraulics, while high-altitude trouble was more serious to the electrical systems. No one of the troubles developed in either system has been insurmountable. All have been susceptible of solution, the net result being a marked improvement in the equipment of all manufacturers.

For purposes of comparison, three different airplanes, representing three different manufacturers, were singled out. Service troubles were totaled for both electrical and hydraulic systems for these airplanes over a given period of time. It will be evident that these reports occurred during epidemics of trouble. They do not, however, represent all of the failures that occurred, as a large percentage are never formally reported. The reports cover a considerable number of airplanes and represent a long period of time.

The figures, as noted, list the number of unsatisfactory reports received on airplane No. 1 for a given period, but do not necessarily mean the total number of failures, as several unsatisfactory reports include more than one failure. In this airplane, the electrical-system source was capable of a maximum of approximately 3.25 hp delivery, while the hydraulics source delivered a peak of approximately 5.5 hp at any one time.

Hydraulic Failures

1 Packing failures: 27 unsatisfactory reports, comprising 28 or more[2] occurrences; of these, three reported belly landings due to the failure.

2 Hose failures: 4 unsatisfactory reports; one reported belly landing due to the failure.

3 Broken lines or fittings: 4 unsatisfactory reports; three due to interference.

4 Pump failures: 4 unsatisfactory reports; comprising four or more[2] occurrences.

5 Cylinder failures: 11 unsatisfactory reports of which 9 were structural failures.

Electrical Failures

1 Burned or fused wires or groups of wires or plugs: 24 unsatisfactory reports, comprising 32 or more[2] occurrences; of these, 9 reported complete electrical-system failure, of which 6 reported forced landings due to runaway propellers.

2 Voltage regulators: 3 unsatisfactory reports; one reported 30 per cent of all voltage regulators tested were out of adjustment.

3 Inverter failures: 4 unsatisfactory reports, comprising 21 or more[2] occurrences; 18 were reported due to high altitude.

4 Generator failure: 8 unsatisfactory reports, comprising 22 failures; average life reported to be 15 hr.

5 Starter failure: 4 unsatisfactory reports.

6 Relay failure: 5 unsatisfactory reports comprising 7 occurrences.

7 Fused battery solenoids: 4 unsatisfactory reports, comprising 4 or more[2] occurrences.

There were other miscellaneous trouble reports in both systems, but since they were not repetitive, no inclusion was made in the foregoing list.

Both electric and hydraulic motors were in use on this airplane, and only one unsatisfactory report on an electric motor was received.

Another airplane of a different type, made by a different manufacturer, indicated a total of 108 unsatisfactory reports for hydraulics, and 110 unsatisfactory reports for electrical equipment for the same period of time. Only basic electrical-system failures were included here; no heating, lighting, communications, or instrument failures were listed. Airplane No. 3 of a different type by a different manufacturer shows 63 reports of trouble with hydraulic pumps against 38 reports of trouble with generators, voltage regulators, and relays. Total maximum horsepower available from the hydraulic pumps was approximately 45, as compared to approximately 13 delivered by the electrical generators.

If these troubles were summarized, they would probably prove to be nearly equal. If, however, a comparison is made on the basis of number of troubles experienced per horsepower transmitted, the favor rests rather heavily with hydraulics. It may be disputable as to whether or not the power comparison is a fair yardstick, but for want of a better one it will have to suffice.

In passing, a plea should be made for more immediate action on service complaints. They are all eventually acted upon, but the length of time that often elapses before any action is taken is appalling. This has undoubtedly done more toward prejudicing certain persons against one or the other system than any other avoidable cause.

Vulnerability. The subject of relative vulnerability of hydraulic systems and electrical systems is a delicate one indeed. In order to be clear on all fronts, we will define vulnerability as lack of ability to survive gunfire.

The first, and natural, and perhaps correct assumption is that electrical systems are less vulnerable. Foremost and insurmountable is the fact that there is no fluid to be lost in electrical systems, and any number of minor lines may be severed without damage to the rest of the system. Although fusing of wires or plugs from short-circuits is not infrequent, it is seldom that a serious fire results from this cause. In a hydraulic system, however, we are carrying an inflammable fluid around in pipes to

[2] One or more unsatisfactory reports noted "many failures," but did not specify how many.

most parts of the airplane. Thus, while the hydraulic system itself may be incapable of starting a fire through its own operation, the fluid it utilizes may be ignited from the incendiary projectile that breaks the line or unit containing the fluid. The same projectile that would break a hydraulic line, but fail to ignite the fluid, might conceivably break electrical connections in the immediate vicinity, creating a short that would ignite the fluid. While this may or may not be a far-fetched conclusion, the blame for the fire would rest with the hydraulic fluid, since the electrical wires were there of necessity.

In contrast to these arguments it can and has been theoretically shown that hydraulic systems can be made less vulnerable than comparable electromechanical systems by virtue of the smaller exposed vulnerable area. Where gravity cannot be utilized emergency measures can usually be applied more readily to a cylinder than to an electric motor-gearbox combination. Relative to emergency means of operation, the advantage enjoyed by a gravity extendable hydraulic landing gear over the electromechanical gear disappears with the use of the ball-bearing screw jack. A functional advantage may still rest with the cylinder for the gravity extension by use of the dashpot. The same thing may be accomplished on the electric drive by means of a centrifugal-governor-operated brake, but not so simply as the dashpot on the cylinder.

Enough more could be said on this subject of vulnerability to make a separate paper. It is certain, however, that those best qualified to present the facts are too busy fighting to keep the airplanes in the air to take time out to write about it. Unfortunately, the information that does filter back is often as conflicting as the arguments which arise over the basic subject under discussion.

Functional Suitability. By functional suitability, we mean a solution to a mechanical problem that gives us the exact operation we are seeking in the simplest, most direct manner possible. It is here that hydraulics enjoys one of its greatest advantages. As stated earlier, the problem of translating transmitted power into useful work is practically a separate and distinct problem from the transmission of power itself. It is in this translation of power into useful work that the hydraulic cylinder plays a principal role.

As has been said so many times before, the straight-line motion of the cylinder has no satisfactory electrical counterpart. There is more, however, to the advantage of the cylinder than just straight-line motion. The starting, stopping, and rate of travel of the cylinder are very simply controlled. The cylinder is its own basic travel-limit device for both extremes of its stroke. By means of the dashpot, the rate of travel of the cylinder during part of the stroke may be effectively governed. No special means have to be provided to start and stop the cylinder anywhere in its travel, as we are dealing with lightweight parts, traveling at low speed, immersed in oil. The electric motor-screw jack combination does not offer a favorable comparison with this operation. Limit switches must be provided to govern the length of stroke, and magnetic clutches or brakes must be employed to start and stop the unit with any reasonable accuracy. For use in areas subject to extreme vibration, the cylinder is ideal and natural. As a vibration damper, the oil column serves a very useful purpose. Use of a screw jack, gearing, and flexible shafting in a function in which vibration defies stress analysis does not seem logical. Electromechanical units have been developed through years of experience, however, that will withstand this vibration. Similarly, electrical brakes and purely electrical power turrets have been developed that have been operated successfully. These electrical uses, however, are functionally about as natural as the use of phosphorescent hydraulic oil for lighting.

The transmission of power from one point to another cannot be done so simply or economically with hydraulics as with electricity. In this regard, the electrohydraulic gun turret offers a common-sense solution to a difficult mechanical problem. It enjoys the simplicity and lack of vulnerability of the electrical transmission system, but utilizes the compactness and natural sensitivity of control and response of the hydraulic system. It might be said that this is an ideal example of intelligent use of both media. This should not necessarily be inferred as being a recommendation for the use of an electric-motor-driven pump for each and every piston in the airplane; rather, it is a plea for open-minded intelligent use of both media, employing them to their best advantage wherever possible.

It was stated earlier that the cylinder had no electrical counterpart; this is not strictly true. The solenoid is essentially similar to the cylinder in its action. For aircraft use it is limited by size and weight to light duty. This can be put to excellent use in the hydraulic system itself. The directional-control valves for landing gear, flaps, power-plant-cooling flaps, etc. present a problem in remote control all their own. The problem can be solved by two basic methods: (1) either the control valves can be located in the cockpit and directly controlled, or (2) they can be located at the unit to be remotely controlled. To locate them at the unit to be controlled obviously provides the cleanest hydraulic system from the standpoint of plumbing complications. It is in this remote control that the solenoid finds an ideal use. The solenoid-operated valve presents another common-sense solution to a problem involving the use of both media.

It has been said that to combine both systems is to double the vulnerability and be subject to the malfunctioning of both. The following statements would prove this untrue:

1 Conceding that present electrical systems are less vulnerable to gunfire than present hydraulic systems and that the installation of double wiring is feasible for such valves, we are not doubling our vulnerability.

2 A magnificent reduction in piping and cables can be made by the use of solenoid-operated valves. Reducing the quantity of piping involved reduces the vulnerability in direct proportion. This can only too readily be demonstrated on many airplanes where the multiplicity of piping strains the imagination as to how a projectile could possibly miss all of it.

3 Whether the valve be directly controlled in the cockpit, remotely controlled by cable, or remotely controlled by electricity, a suitable emergency means of operation must be provided if the operation involved is of major magnitude. The use of solenoid valves for these operations does not change this.

4 The design of solenoid-operated valves has progressed to the point where they can no longer be regarded as being in the experimental development stage. It is only extensive use that will provide the opportunity to prove them to the point where their use is as natural as direct control.

Returning to the subject of functional suitability, we find that the smoothness of operation that can be obtained with calibrated valves, as used on power turrets, on surface-control power boost, or similarly as the metering pin on oleo struts cannot be so simply duplicated electrically. Similarly, the ability of hydraulics to transmit true "feel" through its transmission lines is an advantage readily utilized by the hydraulic brake. It might also be worth mentioning that the ability of a hydraulic cylinder or motor to absorb an overload indefinitely without damage cannot be so naturally accomplished electrically.

Electricity, on the other hand, presents many functional advantages which cannot be equaled hydraulically. For very low power requirements, hydraulic power transmission is not economical, and we naturally turn to electricity. Units utilizing high-speed rotary motion, such as centrifugal pumps, are ob-

viously better done electrically, and the synchronous electric motor will find many unparalleled uses. The ability to store energy for ground operation is readily accomplished by the battery for the direct-current electrical system. Size and weight limitations of the battery, however, make the compressed-air bottle or hydraulic accumulator more satisfactory for storing large amounts of energy for emergency operations requiring heavy work, so that no advantage can be conceded to the battery. The alternating-current electrical system, unless augmented by direct-current service, is no better than a hydraulic system for ground operation and lacks the ability of the compressed-air bottle for emergency duty.

Other advantageous properties that must be conceded to electrical-power transmissions are its cleanliness and its relative independence of normal operating temperatures. Gearbox and motor lubricants, mechanical clearances, etc., are affected by temperature, but they do not present the design problem that an expanding and contracting fluid offers.

Summarizing, it may be safe to assume that, for most purposes, hydraulics is more suitable as a solution to mechanical problems involving relatively large forces or power, while electricity is more suited to light-duty work.

Low Weight. It is believed that no voice will be raised too strongly in objection to the statement that, power for power, present-day direct-current electrical systems are heavier than equivalent hydraulic systems of the 1000 to 1500-psi range. This fact has been one of the main talking points other than functional suitability for the use of hydraulics to supplement electricity.

Power for power, hydraulic pumps are lighter by far than electrical generators, be they direct-current generators or alternating-current alternators. Likewise, the hydraulic motor is lighter for an equivalent power rating than even the presently proposed high-speed alternating-current electric motors, and by far lighter than direct-current motors. For example, a piston motor has been successfully run continuously at 4000 rpm at 1500 psi, delivering approximately 8.6 hp. This motor weighs 4.3 lb, thus giving a ratio of 0.5 pound per hp. For intermittent duty, the motor has been run at higher speeds and higher pressures. An intermittent-duty 8-hp d-c motor running at about 5500 rpm is quoted at approximately 17 lb, while a 12,000-rpm intermittent-duty 8-hp a-c motor weighs approximately 14 lb. For continuous duty at this power, no actual figures could be obtained, but an approximation of 30 to 40 lb seems to be in order. The analogy breaks down, however, for small power requirements, and the electric motor becomes lighter than the hydraulic motor. In transmission, electric wires are lighter than equivalent hydraulic lines and oil, for small power on 24-v direct current, and for all power on the higher-voltage alternating-current systems.

The weight and size of the cylinder are dependent upon the total work performed, and the efficiency of the stroke, not upon the rate of operation. Thus for a given operating pressure, it is the peak load on the stroke-load curve which determines the cylinder diameter. It is desirable, of course, to keep this peak load as small as possible. On a landing-gear cylinder, where the cylinder size and time of retraction may well dictate the size of hydraulic pump and lines required, this becomes of extreme importance. Thus in Fig. 1 we have a typical landing-gear-cylinder load curve.

Assuming that this cylinder is used in a system with a peak design pressure of 1500 psi, the cylinder diameter required would be 6 $^{7}/_{8}$ in. (neglecting rod area). The cylinder volume would then be 2.57 gal on the retraction side. If it is desired to retract this gear in 10 sec, approximately 15.4 gpm must be fed to each gear cylinder. Assuming for simplicity that the nose gear would have the same load curve as the two main gears, the total flow required from the power pumps would then be 3 × 15.4 or 46.2 gpm. By attaching the cylinder to the drag-link fulcrum horn by means of differential linkage, the peak load was reduced to 36,000 lb as shown in Fig. 2. The cylinder diameter required for this condition was then 5 $^{5}/_{8}$ in.; the volume was reduced to 1.72 gal. The rate of flow to each cylinder now became 10.3 gpm, and the total flow required from the power pumps was 30.9 gpm. The added weight of linkages was more than compensated for by the reduction in cylinder weight alone, while the weight saved in line-size reduction, oil, power pumps, and the attachment structure for the cylinder was pure gain.

Utilizing the higher pressures (1500 to 3000 psi) and taking as full advantage as possible of design features as just illustrated,

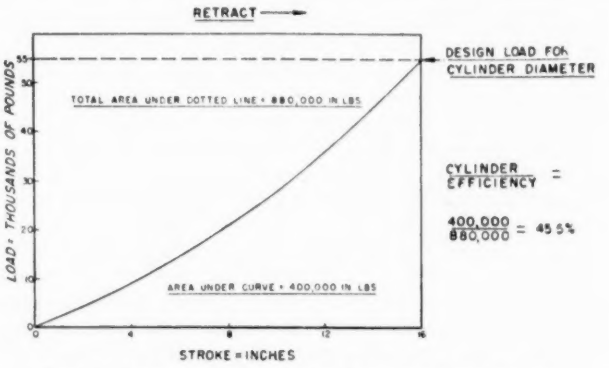


FIG. 1 TYPICAL LANDING-GEAR-CYLINDER LOAD CURVE

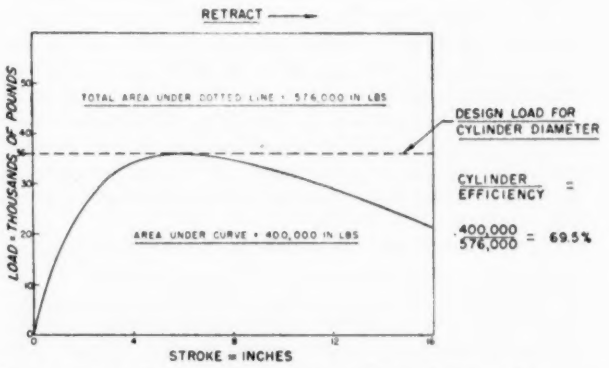


FIG. 2 CURVE SHOWING REDUCTION OF PEAK LOAD IN LANDING-GEAR CYLINDER

the weight superiority of hydraulic systems over 24-v d-c systems can be maintained in most cases over a-c systems. This is true, however, only as long as we are dealing with relatively high power requirements. As allowable gear- and flap-retraction times are increased and the power requirement drops, a turning point is reached where the electrical system enjoys a weight advantage over the hydraulic system. Where this point lies must be determined for each different airplane, unless a cursory inspection of conditions makes it self-evident.

In this regard, the a-c alternator has a property that must not be overlooked, i.e., the ability to absorb approximately 50 per cent overload for 5 min without damage. Thus it is conceivable that, on a large cargo and/or passenger airplane, the alternator size, as dictated by lighting, heating, communications, equipment, air conditioning, and other ordinary duty, will be sufficient to handle landing gear and flap loads without any increase in size, merely by being overloaded for a short period of time. If there is no duty which requires hydraulic service, the

total weight of the complete hydraulic-power system must be added to the comparable weight analysis of cylinders versus motors and gearboxes, etc. This free power may well place the weight advantage in electrical operation many times. The comparative weight between high-pressure hydraulic systems and a-c electrical systems then resolves itself down to particular cases.

Simplicity. It would seem logical that hydraulics, since it is really the mechanics of fluids, would be far simpler than electricity. Practically, it may be said that this is reasonably true. The hydraulic cylinder by no means presents the design problem that the gearbox does. With the use of "O" ring packing and the establishment of standard clearances, cylinder design has become extremely simple. Similarly, the development and testing of the cylinder is much simpler than that of a high-reduction gearbox. Providing both cylinder and gearbox satisfactorily pass a life test, there should be no service required other than a periodic drain and flush for the gearbox lubricant and a periodic check of the cylinder packing.

As a balancing factor against the mechanical development time required by the gearbox is the standardization of electrical parts. In practically every case 100 per cent of the purely electrical equipment is purchased from electrical-equipment manufacturers, and the development cost of such equipment is amortized over many different companies. The aircraft electrical engineer's job, then, is one of installation, rather than of design and development.

Aircraft hydraulics, however, is relatively new. We have not settled as yet the majority of problems that will have to be resolved before we can begin to use standard items "out of stock." It may be a long time before we are ready to agree on a type of system, an operating pressure, and even upon such basic parts as a suitable leakproof coupling. Consequently, the aircraft hydraulic engineer's problem is one of design and development as well as installation. It is realized, of course, that electrical systems will undergo a period of development with the advent of a-c systems, but such development work will be a function of the electrical-equipment manufacturers rather than the ultimate users, even though they be the guinea pigs for its testing.

In the field of hydraulics, there is no parallel gigantic research organization to which we can present our problems and know they will be worked out from beginning to end. There is no one organization set up to engineer, develop, and manufacture a complete hydraulic system from reservoir, to pump, to valve, to cylinder. Each aircraft company is dependent upon its own engineers plus those of a multitude of vendors. Undoubtedly, there is room in the hydraulics field for such a complete organization. Perhaps we shall someday see one.

Simplicity of maintenance, like reliability, is very close to being a stand off between the two systems. A mechanic with only a smattering of electrical knowledge will favor the hydraulic system because it is basically easier to visualize what goes on in a pump or cylinder or valve, than in a generator, electric motor, or relay. Similarly, the trouble is ordinarily easier to trace in a hydraulic system, although on occasions this can be a drawback.

In military theaters, the necessity of stocking hydraulic oil is undoubtedly a nuisance. If, however, this hydraulic oil is the only satisfactory low-temperature lubricant for gearboxes, etc., its use might be justified. It would seem easier, also, to replace a shot-up wire or bundle of wires than a similar group of prefabricated tubing. If we consider, though, that the tubes and hydraulic cylinders are replacing gearboxes, torque tubes, flexible shafts, and cables, we are not so prone to concede the advantage. As it is necessary to have trained mechanics and trained electricians wherever the aircraft goes, any claim to advantage in one or the other system would seem purely academic.

Low Cost. Low cost is closely allied with simplicity, and the same remarks apply to it as to simplicity. The cylinder is basically cheaper than the motor-gearbox combination, but the standardization of electrical parts is much superior to hydraulics standardization, thus resulting in somewhat of a balance. If the electrical engineer is forced to use special generators, special voltage regulators, special motors, etc., his cost would probably be greater than a similar hydraulic arrangement.

It is too often believed that cost should not be considered in time of war. Cost, we must remember, however, is a measure of time and material, and time and material is a measure of quantity of production. Thus to achieve the correct balance, we must weigh cost carefully with function to make sure that the time and material expended justify the purpose. Too often recently we have seen numerical superiority prove more important than quality. To strike a happy medium, then, is the purpose of every conscientious engineer and manufacturer.

Compactness. A strong case can be made for the hydraulic cylinder when space is at a premium. In a small fast pursuit plane, where every nook and cranny contains some piece of equipment, the ability of a cylinder to change its "gear ratio" by changing its diameter and stroke, and yet do the same amount of work, is extremely useful. It is usually in such planes that rapid rates of gear retraction are demanded, thus making the job a natural for hydraulics. Small motor - gear screw combinations can be made, but they cannot compete with the cylinder on a power basis simply because the cylinder is independent of rate of operation while the motor is not. Plumbing, however, outdistances wiring by a great deal in space consumed. Thus from a compactness point of view, the choice depends upon where the compactness is wanted if it is going to be a contributing factor to the decision.

Aside from the solenoid, electrical power is limited to high-speed rotary motion. To convert this into low-speed rotary motion or linear motion requires gearing of some sort or other. Such gearing, however, as developed by electrical-equipment manufacturers is not necessarily extremely heavy or inefficient. The use of precision-built planetary gearing in steps provides very high reductions with amazing efficiency for relatively low weight. A new design of ball-bearing screw jack has opened up new fields for electric motors by its very high efficiency. Thus with spur gearing and the ball-bearing screw jack, one may conceivably go through a very high gear reduction, translate into linear motion, and emerge with a relatively high mechanical efficiency. Such gearboxes may also contain torque limiters, magnetic brakes, speed limiters of the centrifugal type, and all the necessary bearings and still be compact and relatively light in weight.

Evaluation of the Two Media

As previously stated, the evaluation of the comparison between the two media is probably the most opinionated part of the whole controversy. To those who say that everything must be sacrificed to vulnerability during the present emergency, the obvious answer seems to rest with all-electrical service. The weight, simplicity, and functional advantage usually resting with hydraulics, however, would seem to justify its use, even though necessary to employ some armor and self-sealing tanks. That this view is held by certain German designers is evident from some of their more recent designs.

Any tendency to adopt all-electrical service could be construed as being partially a fault of the hydraulics engineers in that we have not worked together perhaps as closely as we might have. That this was originally due to competition is undoubtedly true. Nevertheless, our aircraft electrical men were compelled to work together by being so dependent upon outside

sources, and in so doing have gained very definite advantages.

Through simplification of existing systems and careful design of future systems, hydraulics can be made, it is believed, no more vulnerable than a comparable electrical system. For civil aircraft where vulnerability to gunfire is of no concern, hydraulics should again be the favorite it has been in the past. Surface-control power boost will play no small part in more firmly establishing hydraulics as a power-transmission medium. With the advent of larger and faster aircraft, the power requirements will grow accordingly and with this we shall probably see general use of a-c electrical systems and 1500- to 3000-psi hydraulic systems.

In the field of naval vessels, the same trend to all-electric operation and control was made. The pendulum is now swinging back again, and the newest electrohydraulically controlled ships have proved themselves so well in actual combat that a definite movement to extensive electrohydraulic control is foreseen.

A decision to restrict all new military aircraft to all-electric control on the basis of past performance would therefore seem unwarranted and short sighted at this time. There are very definite advantages to be gained through the use of hydraulics in military aircraft as well as in civil aircraft. It is recommended, then, that the best uses of both systems continue to be utilized, even though it may mean mergers of the services in some cases to achieve ideal conditions.

BIBLIOGRAPHY

1 "The Problem of Ancillary Power Service on Aircraft," by R. H. Chaplin and F. Nixon, *Journal of the Royal Aeronautical Society*, vol. 43, 1939, pp. 942–991.

2 "Relative Vulnerability to Gunfire of Hydraulic Systems Versus Mechanical and Electrical Systems," U. S. Army Air Forces, AC ESMR EXP-M-41/AD745, Wright Field, Dayton, Ohio, July 29, 1940.

Discussion

H. F. Rempt.[3] The author's presentation is so fair that it is quite difficult for the writer to pick out exactly where the aircraft electrical system is really stepped on. However, since the problem is a controversial one, the following comments are given on parts of the paper, in the order that they were presented:

The two main parts of the problem were expressed as "transmission of power" and "conversion of power." It is believed that a third part should be included, namely, "remote control of power." In the present airplanes, it is hard to find one application of power that is not remotely controlled.

[3] Electrical Engineer, Lockheed Aircraft Corp., Burbank, Calif.

The author states, "of the three basic services, electricity alone is an absolute necessity." If this fact is conceded, then it is necessary for every hydraulic application not only to compare favorably with the same electrical application, but also to justify its share of the installation of the entire hydraulic system.

Under "failures," the number of unsatisfactory reports for hydraulic and electrical operation was approximately the same. However, the statement was made, "the favor rests rather heavily with hydraulics if the comparison is made on the basis of number of troubles experienced per horsepower transmitted." Rather than use horsepower as a comparison, it is believed the number of systems or units should be used.

The assumption that electrical systems are less vulnerable than hydraulic systems is true, particularly if the comparison is made by similar systems.

The writer differs with the statement under "Suitability," that electrical power turrets are not functionally natural. Since the guns elevate in an arc and the turrets revolve, it is believed an electric turret is a natural application for rotating power.

The mention of some type of operation "providing the cleanest hydraulic system" does not agree with the writer's experience when standing in wheel wells. The writer does not believe there can be a clean hydraulic system.

The comparison of compressed-air bottles and accumulators to the battery is in error, since the battery is in the airplane anyway and the bottles and accumulators then become added weight.

The writer cannot subscribe to the statement, "the aircraft electrical engineer's job is one of installation rather than design and development." Most of the new developments in aircraft electricity come about by a design and development program undertaken by an electrical manufacturer in conjunction with preliminary design information from the aircraft electrical engineer. The main difference between electrical and hydraulic equipment is that the electrical equipment is not usually made in an aircraft plant because of the special machinery and technique that is required.

For simplicity, the engineer's ideal of a "little black box that snaps in place" is practically answered by present-day electrical equipment. The airplane will be simple to service if the parts are simple to install. By means of bench-testing of complete electrical systems, the installation problem is also simplified. There is no comparable method of bench-testing complete hydraulic systems.

The writer considers the use of electrohydraulic control a step in the right direction. It will be only a matter of 5 or 6 years before the complexity of control requirements will make the all-electric airplane a reality.

The Evolution of the Hydraulic Pump as Applied to Aircraft

By DALE HERMAN,[1] BEVERLY HILLS, CALIF.

Having passed through a period of manual control of auxiliary power functions on earlier aircraft, and later the hand-pump and low-pressure vane- and gear-pump stages, continued demands for higher pressure eventually led to the present-day types of piston pumps which supply necessary power to hydraulic systems of control. The author outlines the basic requirements for well-designed oil-hydraulic equipment including pumps, and then in detail describes the gear pump and the axial-piston pump in both the constant- and variable-delivery designs. Considerations in selecting pumping equipment and the design of the hydraulic circuit are stated.

EXCEPT for earlier simple types of aircraft and small craft of current design, power to perform many auxiliary operations formerly handled by direct manual control has long been a necessity. Power was first introduced in the form of hand pumps, actuated by the pilot, to operate retractable landing gear and brakes.

Being capable of high pressures at reduced volumes, these pumps are still widely used for emergency service. With the advent of larger and faster aircraft, power-operated pumps became necessary, and the earlier hydraulic systems were equipped with low-pressure vane and gear pumps. Continued progress made it expedient to provide more power for the hydraulic system, necessitating higher pressures, and consequent improved designs of gear pumps, and later the introduction of piston pumps to cope with the loads. Today the engine- or electric-motor-driven pump is the heart of the aircraft hydraulic system, and the trend is definitely toward higher pressures on military, transport, and cargo planes.

Basic Pump Requirements

Well-designed oil-hydraulic equipment, including pumps, as used for aircraft, should be neither heavy nor bulky and should transmit power efficiently. Consequently, pump bearing loads lean toward the permissible maximum in order to reduce bulk, and operating clearances are held to a minimum to reduce leakage losses, commonly termed "slip" in pumps, and higher speeds are used to reduce weight per horsepower.

The weight feature of the pump and of other hydraulic equipment is carefully evaluated by every aircraft engineer when undertaking a new design. The efficiencies of the accessory items, such as the hydraulic pumps, which are being added to the engine loads, are not always given as close attention. The hydraulic horsepower generated by a pump is expressed by the following commonly accepted formula:

$$\text{Hydraulic horsepower} = \text{displacement (gpm)} \times \text{pressure (psi)} \times 0.00058$$

The engineer should study the characteristics of the pump selected, from the standpoint of power input under system operating conditions, as well as from the hydraulic output, as represented by this formula, to determine efficiency, and to evaluate the useful work transmitted.

The component parts of hydraulic pumps, designed for high-pressure service, must be manufactured with precision, and ample provision must be made to lubricate properly all working parts, which are in turn suitably housed to protect them from dust, moisture, etc. present in the atmosphere. However, the efficiency and life of the pump, like that of any other piece of precision machinery, incorporating bearings and close running fits, will depend largely upon the care with which it is installed and the attention it receives while in service.

Oil under pressure tends to leak through small running clearances, however minute. All such leakage represents a loss in the applied energy without accomplishing useful work. Such loss in energy is transformed into heat, raising the oil temperature, and if considerable leakage is present, auxiliary cooling may become necessary. Consequently, clearances between moving parts, subject to pressure, must be held to a minimum to insure high operating efficiency. These must be more closely controlled in high-pressure pumps.

If foreign matter of an abrasive nature is allowed within the hydraulic system due to inadvertent carelessness while installing or maintaining the equipment, it will impair the life of all operating parts in the pump, valves, and motors comprising the system. It is noted, therefore, with considerable satisfaction, that the aircraft manufacturers who are pioneering higher operating pressures in hydraulic systems have not overlooked the matter of improved oil filters. This subject is covered in detail in a paper by W. W. Thayer.[2]

In his connection with a manufacturer of vane, gear, and piston pumps for industrial and marine service, the author has acquired considerable experience with the gear and piston designs, which are employed exclusively on aircraft systems, and thus is qualified to discuss the merits of each design, and the class of service for which each is best adapted.

Gear Pump

A large percentage of aircraft systems to date has employed the gear-type hydraulic pump, as pressures below 1000 psi have predominated. The gear pump which is relatively simple in construction, consisting of two accurately machined and fitted gears in mesh, occupied a prominent place in the field until pressure and volume characteristics reached a point at which the requirements exceeded the efficiency limitations of this construction. Gears and the bores in which they operate can admittedly be machined to the same degree of accuracy as pistons. However, due to the larger critical dimensions of the gears, as compared with pistons, to obtain required displacements, these parts have greater linear expansion with temperature change, and must therefore be fitted initially to insure adequate running clearances at the two temperature extremes to which they are subjected in service. Fits on both the width of the gears and the diameter have a bearing on the internal slip or leakage of

[1] West Coast Engineer for Vickers, Inc., Detroit, Mich.

Contributed by the Aviation and Hydraulic Divisions and presented at the Semi-Annual Meeting, Los Angeles, Calif., June 14–17, 1943, of The American Society of Mechanical Engineers.

Note: Statements and opinions advanced in papers are to be understood as individual expressions of their authors and not those of the Society.

[2] "The Modern Hydraulic Reservoir," by W. W. Thayer, appearing on p. 589, of this issue of the Transactions.

the pump and therefore on its volumetric and over-all efficiencies.

In developing a line of hydraulic equipment for machinery manufacturers, and subsequently for aircraft, first consideration was given to the design of a suitable pump with constant-displacement characteristics. The gear pump, which was most commonly used, was first considered but discarded because this pump is hydraulically unbalanced over the projected area of each gear, as illustrated in Fig. 1. While running, the extent of this unbalance undoubtedly will exceed that shown on the diagram,

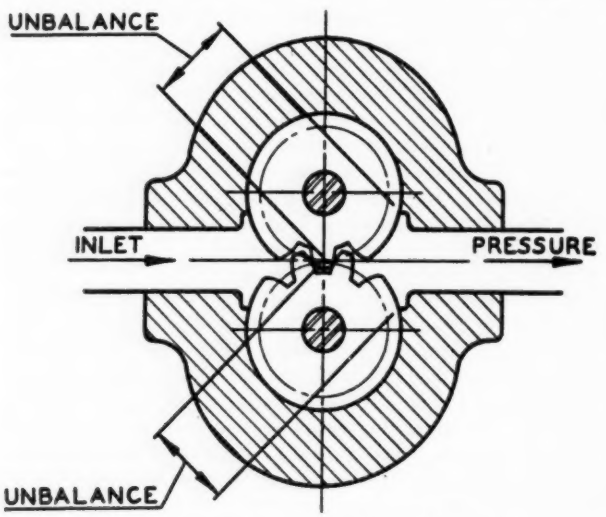


FIG. 1 UNBALANCED GEAR-PUMP DESIGN

because the pressure will tend to distribute itself around the periphery of each gear, being maximum at the discharge port and decreasing toward the suction port. Since the bearing diameters must necessarily be smaller than the periphery of the gears, it is necessary to increase the length of the bearings in proportion to the width of the face of the gears, in a conventional design, to keep the projected areas and the resulting bearing loads within safe operating limits. This also tends to limit the maximum pressure and displacement characteristics of such a pump.

It therefore became apparent that the necessary running clearances between the outside diameters of the gears and the pump body, as well as that of the bearings to their bores, had to be accurately maintained or the radial loading, combined with the differential expansion of the respective parts due to temperature changes, would cause the periphery of the gears to come into metal-to-metal contact with the housing. This would cause scoring and loss of efficiency. Bearing wear, resulting from this unbalanced hydraulic loading, which is accelerated by the presence of foreign materials in the oil, will therefore result in rapid deterioration of the pump.

The design was then modified to balance the gears hydraulically by arranging porting that would apply pressure on the periphery of each gear diametrically opposite to the discharge port and of like area. Gear motors, balanced in this manner, have been used on aircraft, as well as on marine and industrial applications, but their efficiency due to slip does not compare with the piston motor; and the same condition holds true when they are used as pumps.

On most gear pumps the running clearance over the side faces of the gears is fixed to conform with thermal-expansion and lubrication requirements. One manufacturer has introduced an innovation in the normal recognized construction of gear pumps, to control the running clearances over the width of the gear. In certain capacities, this design has been recommended and approved for 1500-psi service.

Gear pumps are made commercially having constant-delivery characteristics, the delivery per revolution being fixed except for slip which increases with pressure. Hence it is necessary to use such pumps with an accumulator system where variable volumes are required for operating different devices, for best efficiency.

As an alternative, on extremely low-pressure systems, where pumps of small displacement are used, such as on gyropilot systems, the delivery of the pump beyond system requirements is by-passed through a relief valve at a constant pressure, thus converting the unused energy into heat. To avoid the necessity for such a second low-pressure pumping system, the use of a pressure-reducing valve is recommended. This takes oil from the high-pressure system on the plane and reduces it to the low pressure required for the automatic pilot or similar auxiliary controls.

AXIAL-PISTON PUMP

The axial-piston pump is essentially a multipiston engine, the stroke of the pistons being determined by the angle of the rotating group, including cylinder block, pistons etc., to the drive shaft. These units were first developed in larger sizes for industrial-machinery applications, and a wealth of experience was available as a result, when the design of lightweight aircraft models was undertaken. Pumps of this same design have been in use in marine, ordnance, and machinery service for power transmission for 8 years. Sizes are available from the smallest constant-delivery aircraft unit that weighs $3^1/_4$ lb and develops 4 hp at 4200 rpm and 1000 psi, to marine gears requiring variable-displacement pumps, operating at 850 rpm and developing up to 300 hp.

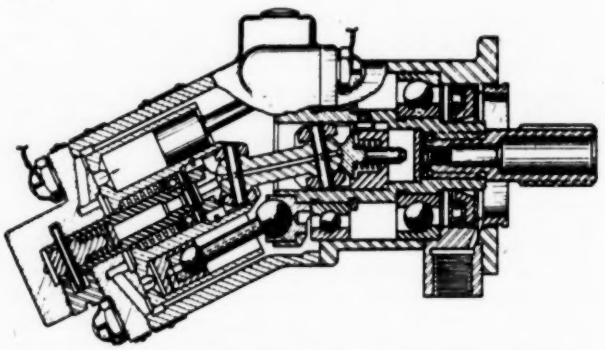


FIG. 2 CONSTANT-DELIVERY TYPE OF AXIAL-PISTON PUMP

The design is well adapted to aircraft service because the bearings can be small in diameter, permitting high-speed operation; and rotating parts are compactly spaced in a manner to minimize weight. The units operate equally well as motors or as pumps, and at the same time offer the advantages of interchangeability of the rotating group of parts as a service consideration. Of equal importance, they may be constructed for variable-delivery output.

These pumps are now available in aircraft types with constant- or variable-delivery characteristics. Basically they have seven or nine pistons that are joined to the drive shaft by connecting rods, the latter having ball-and-socket bearings on both ends. No piston rings are used, but the pistons are fitted to the bores of a bronze cylinder block to a clearance of a few ten-thousandths of an inch, depending upon their diameter. The cylinder block is in turn mounted on a stub shaft and is driven by a universal shaft, having a universal joint at either end to insure that the

speed of the cylinder block corresponds to that of the drive shaft. This universal drive merely acts as a timing member, and overcomes bearing friction within the cylinder block. It does not transmit power, as all working loads are transmitted from the drive shaft directly through the rods to the pistons.

In the constant-delivery type of pump shown in Fig. 2, the angular position of the cylinder block is fixed as determined by the housing. These angles vary from 10 to 25 deg, depending upon the delivery required, as this angle determines the stroke of the pistons and thereby the displacement.

The drive shaft is, of course, mounted on ball bearings, with the angular-contact type taking the thrust produced by the pressure on the pistons, and the radial bearing carrying the radial load imposed by the angular position of the pistons. On pumps designed for pressures over 1000 psi, two radial and one angular-contact thrust bearings are incorporated.

The valve porting in the cylinder block and valve plates of these pumps is clearly illustrated in Fig. 3 and is designed to balance hydraulically most of the hydraulic thrust equivalent to the effective piston area subjected to pressure. Therefore, the Kingsbury type bearing, on the periphery of the hardened and lapped steel valve plate, carries relatively low loads.

These constant-delivery pumps are available in various capacities up to a displacement of 0.507 cu in. per revolution, and for three pressure ranges, as follows:

1000 psi continuous duty	1250 psi intermittent duty
1500 psi continuous duty	2000 psi intermittent duty
2000 psi continuous duty	3000 psi intermittent duty

Although the principal working parts of these pumps are interchangeable, the shafts, bearings, housings, and valve plates must necessarily be proportioned for the pressure service. In other words, it was not necessary when designing for higher pressures to decrease clearances or to add any parts or stages to the lower-pressure design. The addition of stages would naturally reduce the over-all efficiency by the introduction of additional parts, creating friction and other internal-leakage points.

The largest constant-delivery piston pump available, rated for 1500-psi service, which delivers 6.4 gpm at 3000 rpm cruising and at rated pressure, weighs 5 lb. The weight per gpm at rated pressure is 0.8 lb. This is a more favorable weight-performance ratio than for any other aircraft pump design of comparable capacity known to the author. The input is 6 hp under these conditions.

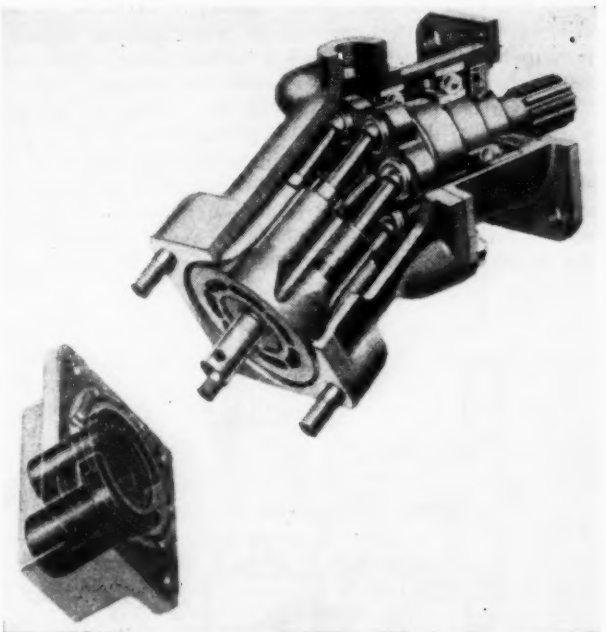


FIG. 3 VALVE PORTING IN CYLINDER BLOCK AND VALVE PLATES OF CONSTANT-DELIVERY AXIAL-PISTON PUMP

Another design of this pump, rated for 2000 psi, is being used by one manufacturer intermittently on an accumulator circuit operating at 3000 psi. At the latter pressure the delivery is 6.3 gpm at 3000 rpm cruising, and the pump weighs 6 lb. The weight per gpm under these operating conditions is 0.95 lb.

The reduced running clearances on the piston-type pump, as

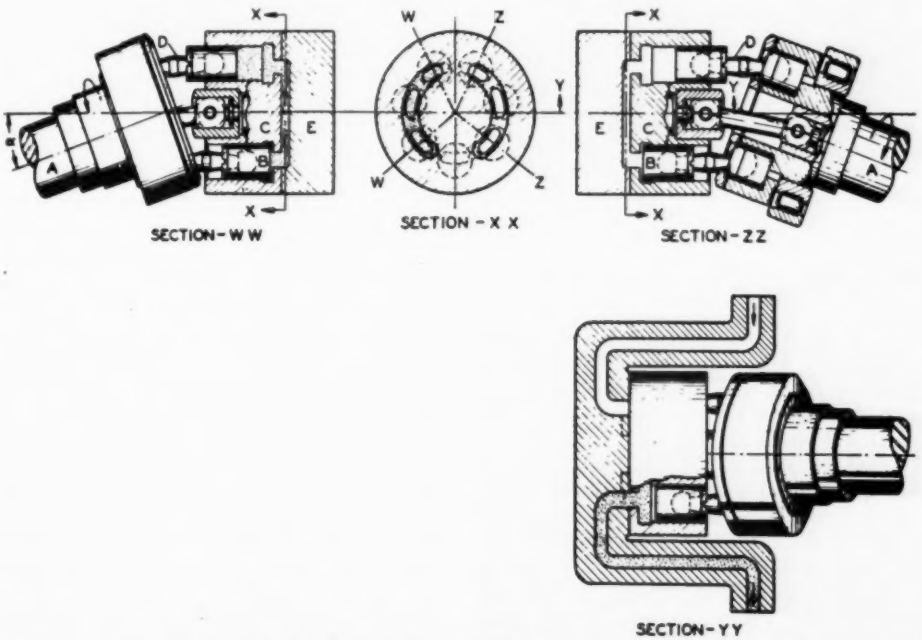


FIG. 4 OPERATION OF VARIABLE-DELIVERY TYPE OF AXIAL-PISTON PUMP

compared with the gear pump, materially improves its self-priming characteristics, particularly when starting against a pressure head, and when there is air in the system. This condition might be encountered in an accumulator circuit.

The variable-delivery version of the axial-piston pump is essentially like the fixed-stroke type, except that the angular position of the cylinder block can be changed relative to the shaft, while in operation. The degree of angle determines the amount that the pistons may reciprocate in their bores, creating suction during one half of the revolution and discharging during the other half, thus varying the delivery. By moving the

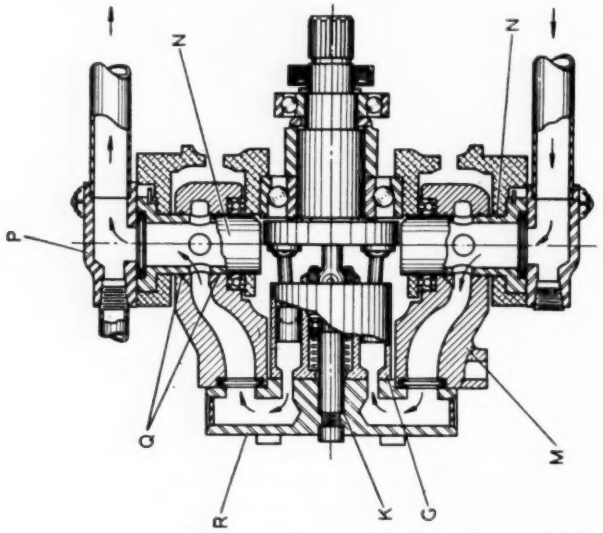


FIG. 5 CONSTRUCTION FOR SWINGING CYLINDER BLOCK TO OBTAIN VARYING VOLUME

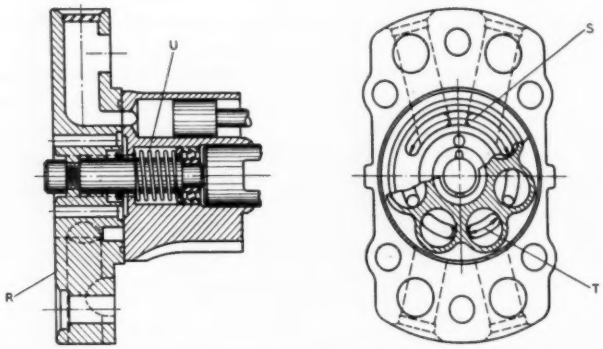


FIG. 6 DETAILS OF PORTING IN CYLINDER BLOCK AND VALVE PLATES OF VARIABLE-DELIVERY AXIAL-PISTON PUMP

cylinder block across the center, the direction of flow through the pump may be reversed. This latter feature is used to advantage on certain rotary drives such as are employed on gun turrets, where both directions of rotation are required. The operation of this pump is illustrated in Fig. 4.

The construction used for swinging the cylinder block to obtain varying volume is shown in Fig. 5. A yoke containing the stub shaft on which the cylinder block is mounted is supported on two stationary pintles, and ball bearings are inserted in the arms of the yoke to reduce friction to a minimum. The porting of the oil to and from the cylinder block through the yoke and pintles is indicated by arrows. Flanges mounted on the pump housing, which is not shown on this schematic drawing, sealed by neoprene Vickerseals, retain the pintles and contain the connections. Circular seals are inserted into the yoke arms, and pressure is applied to their outside diameters to insure a minimum of leakage between the swinging yoke and the pintle.

Fig. 6 shows further details of the porting in the cylinder block and valve plate.

Several methods of controlling the flow from these variable-delivery pumps are used in production. The first consists of a mechanical linkage, by which the operator can vary the delivery of the pump by moving a lever or cam. A hydraulic servo or power booster is sometimes introduced between the linkage and the pump yoke, to minimize the manual effort. The latter control is also used in conjunction with syncromotors for remote electrical control and is employed on armament equipment.

The method commonly employed on engine-driven pumps is the self-actuated pressure compensator. This in its simplest form is a spring-loaded piston connected to the yoke, which normally holds it in the maximum displacement position, whereby, with pressure connected from the discharge of the pump acting on the piston, it overcomes the spring load and strokes the pump to the neutral position. Such a control causes the delivery to vary approximately inversely with the pressure. The conventional control of this type requires a heavy spring for high pressure and smooth operation and becomes quite bulky. Besides, on most installations the change from full pump volume to zero stroke must be accomplished with a minimum pressure differential, say, from 1500 to 1700 psi. This makes a practically constant pressure available to the system regardless of pump delivery. To accomplish this a compact pilot pressure-controlled device, providing convenient pressure adjustment has been designed, which insures accurate smooth regulation within the desired range. The differential rate generally employed is from 100 to 200 psi. This control is designed so that two or more pumps can be operated in parallel on the system, and each will supply its portion of the variable demand. With this type of control, and all valves in the system closed, resulting in no demand, the pump will maintain a constant preadjusted pressure, pumping only sufficient volume to compensate for slip within the pump itself, and in valves which are exposed to pressure.

Pumps of this general type for 1500-psi 15-hp service were first furnished to an aircraft manufacturer in 1939, and are now available for applications requiring maximum pressures from 800 to 2000 psi. Pumps furnished for 1700 psi have a maximum displacement of 1.518 cu in. per revolution, providing 25 gpm at 3750 rpm, during take-off, and 19 gpm at 3000 rpm, when cruising. The maximum input approximates 28 hp, and this unit weighs 25 lb.

SELECTION OF PUMPING EQUIPMENT

When selecting a hydraulic pump for a new design, the engineer must first consider the total hydraulic horsepower to be transmitted in terms of the formula previously mentioned. The two factors entering into this equation are the maximum pressure for which the system is to be designed, and the maximum displacement required for the limiting operation, which on many installations is that required to operate the landing gear. The pressure selected is generally determined by the size of the ship, taking into consideration weight and availability of the pump and all other accessories used in the system, such as unloading valves, relief valves, accumulators, hydraulic fittings, tubing, etc. The average pressure in use today would fall somewhere between 1000 and 1500 psi in production aircraft, but the tendency on new designs is to consider higher pressures. One manufacturer has designed a satisfactory system, functioning to a maximum pressure of 3000 psi. The power-driven pump must operate intermittently at this pressure, as a conventional unloading-valve and accumulator system is employed, requiring

that the pump obtain this maximum pressure only while charging the accumulator.

Rather than attempt to take sides in a controversial matter, the author prefers to point out the features which favor the use of higher-pressure systems and those substantiating a more conservative viewpoint, which would approach the matter of higher pressures more gradually. The arguments advanced for higher pressures are that they will permit the use of smaller sizes of tubing and fittings, as well as valves, cylinders, pumps, and hydraulic motors, resulting in considerable weight saving. Such savings will obviously add to pay-load capacity and also allow steel fittings at many points, thereby increasing ruggedness and decreasing bulk.

On the other hand, experience with systems of this type is at present somewhat limited and the necessary auxiliary equipment required for a complete system is not available to the same extent as for lower pressures. Closer manufacturing limits will be necessary in order to obtain the fits required in certain of these accessories, thereby in some cases increasing manufacturing costs. Control valves of the type that meter or throttle the oil flow for control purposes will present more of a problem because of the smaller sizes of the orifices necessary to obtain nicety of operation; and lint and other foreign substances in the system will become more critical in valves of this type. More consideration will have to be given to distortion of valves and other portions of the system resulting from pressure changes. The combination of vibration and high pressures will present difficulties in maintaining seals at fittings and flange joints of the respective units incorporated in the system.

The foregoing represents an unbiased viewpoint since the author's company manufactures certain equipment for systems falling within this range of pressure. It would, however, seem that any transition should be along conservative lines.

In the case of hydraulic circuits on machine tools on which we have had broad experience, the maximum pressure used approximates 1000 psi, as on this class of equipment nicety of control on fine feeds and reversal together with long life are the paramount considerations.

Another design problem which must be considered is whether or not a constant-volume pump, which is generally used in conjunction with an accumulator system, or a variable-volume pump should be used. In making this choice, the engineer should take into consideration the equipment which is hydraulically actuated by the circuit.

The majority of military and transport ships now in production employ the constant-delivery pump, with an accumulator suitable for supplying intermittent high demands and also providing a source of pressure for the brakes when the plane is on the ground and the engines are not running. Our observations are that such a system is most desirable on installations requiring intermittent hydraulic demands in flight. Most of the unloading-valve systems at this time function only during take-off and landing, and the remainder of the time the accumulator remains charged and the unloading valve cut out. During this time the pump will circulate freely to the reservoir during flight, unless there is an occasional demand, or some leakage from the accumulator portion of the system, in which case it may require intermittent recharging from the pump. The equipment operated from a system of this type generally includes: landing gear, flaps, oil coolers, wing floats, cowl flaps, power brakes, bomb doors, and wing-folding operations.

The use of a variable-volume pump would on such installations only eliminate the unloading valve and possibly the accumulator from the main system. Therefore, it would not offer any great weight saving or other economy.

The constant-delivery pump on such a system is subject only to intermittent service at system pressure, which is a desirable feature, as it tends toward long pump life.

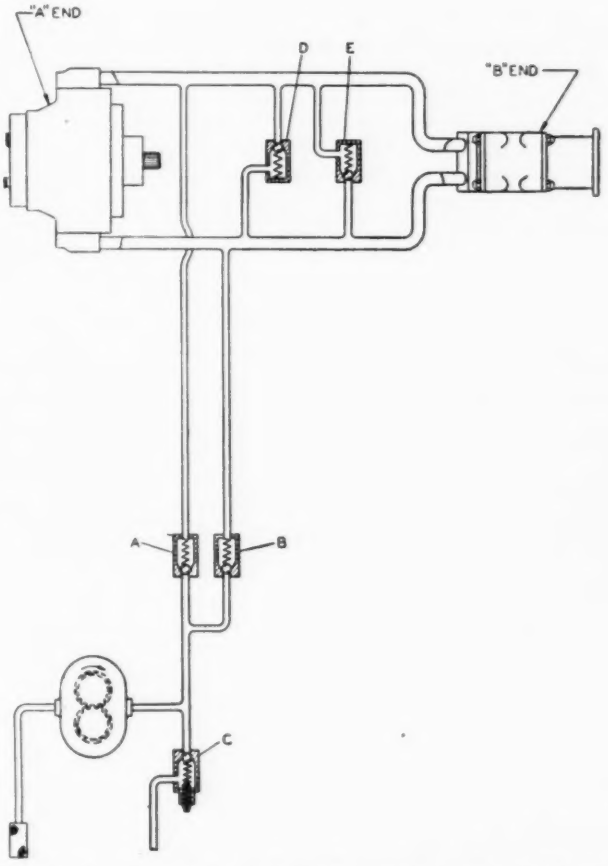


FIG. 7 VARIABLE PUMP AND FIXED-DISPLACEMENT PISTON MOTOR COMBINED IN LOCKED CIRCUIT FOR CONTROL OF ARMAMENT EQUIPMENT

The repeated stressing and relieving from pressure in the lines between the pump and unloading valve introduces some line shock and fatigue in this portion of the circuit. This becomes more pronounced at higher pressures. A properly designed unloading valve, however, minimizes this objectionable feature.

The variable-volume pump is gaining more acceptance on the larger-plane designs, where larger volumes of oil are required, and there is a continuous varying demand for hydraulic power during flight. Another feature of the variable-volume pump is that it will supply a system requiring a constant maximum volume in flight, irrespective of engine speed. The pump will operate at relatively short stroke during take-off, but at maximum stroke while the engine is idling, so that its delivery will remain constant throughout the normal operating speed range of the engine. Some of the controls which favor the use of the variable pump are (1) power boosters for control surfaces; (2) cabin supercharger drives, using hydraulic motors; (3) fan drives, employing hydraulic motors; (4) turret drives; (5) constant-speed accessory drives.

It is obvious on hydraulic circuits with the operations listed, that the steady usage would cause the unloading valve on a constant-delivery system to operate frequently in flight, and the pressure surges might introduce complications within the power-booster system, for example. The maintenance of steady pressure with a variable pump that would adjust itself to demands is conceivably better for such an installation.

The sensitivity of control, combined with reversible flow without a dead spot, made possible with the variable pump and fixed-displacement piston motor offers decided advantages for the operation of armament equipment. An infinite range of speed control, relatively unaffected by varying loads, due to the position of the guns in the slip stream, from the slow rates necessary for tracking the target to high slewing speeds, is possible with such a system. A typical locked circuit of this type is shown in Fig. 7. Control of this type is used on turrets in "Flying Fortresses," on various antiaircraft mounts, tank turrets, and in the largest gun turrets on ships. The low moment of inertia characteristics of the hydraulic motor and its corresponding high torque for a minimum of weight combine to make this type drive ideal for this service.

As a summary, it would be apparent that each design or type of construction has merit in one or more applications, and full consideration must be given to the circuit before selection is made.

The Modern Hydraulic Reservoir: How It Provides Micron-Range Filtration and Pump Supercharging

By W. W. THAYER,[1] LOS ANGELES, CALIF.

At the present time, the term "high pressure," with reference to aircraft hydraulic systems, means 3000 psi. Successful design of such systems, now in quantity production by the author's company, depends upon careful consideration of details, rather than upon the adoption of any features that might be classed as unorthodox. For instance, detailed attention has been given to an improvement in service life of certain hydraulic units whose operation depends upon close-fitted sliding parts. This consideration, resolving into a study of methods for combating abrasion and cavitation, has led to the development of a filter for the removal of particles as small as 10 microns, and a simple arrangement for reducing pump cavitation by building up a supercharging pressure in the hydraulic-system reservoir.

WHEN contemplating the design of large airplanes, almost without exception, the aircraft designer is thinking in terms of high pressures for the hydraulic system that will operate landing gears, bomb doors, wing flaps, and other services. It has become traditional in the aircraft industry to refrain from defining the word "large," as applied to airplanes. However, "high" as applied to hydraulic pressures, means, at least for the moment, 3000 psi. This is twice as high as the next highest pressure in common use.

The author's company has been the first to go into quantity production of airplanes with 3000-psi hydraulic systems. Obviously, the higher pressures yield major savings in weight and space. Experience has been that design practices for the higher pressures are consistent with the same fundamental principles that have been well established at low pressure. It has not been necessary to resort to any engineering trickery to make high-pressure systems work, but painstaking attention to design detail has been essential.

Improving Service Life of Hydraulic Units

As an example of design detail, this paper will describe the work that has been done toward improving the service life of hydraulic units, which, because of some specialized function, depend for leakage control upon close-fitting sliding contact between metallic parts, rather than the well-known V-ring or O-ring packings. Common examples of such units are pressure regulators, surface control booster valves, wing-flap synchronizers, constant-flow valves, and piston pumps.

Such hydraulic units are subject to wear because abrasive particles find their way into the hydraulic fluid, despite all practical precautions. Contamination may result from the natural wear of metal parts, from the flaking-off of protective plate, from dust sucked in as the reservoir breathes, from machining chips or free abrasives remaining in parts after washing, from particles broken loose by screwing in fittings, flaring lines, and tightening connections, from attaching the system to portable test stands that may have accumulated dirt, from dirt that enters past piston-rod packings or when filling the reservoir with oil, from blowing out tubing with an air hose, etc.

In addition to the effects of abrasive wear, deterioration of pumps may be accelerated by prolonged operation under conditions of cavitation. Sizable pits frequently occur where least desired, even in steel parts that have been hardened and ground. Furthermore, torque pulsations in a pump, running under cavitating conditions, may lead to the serious consequence of drive-shaft fatigue failure.

A typical aircraft hydraulic-pump installation is illustrated in Fig. 1. (A fixed-displacement pump is shown, rather than a variable-displacement type, due to the rather limited application of the latter in aircraft up to the present time.) The pump runs whenever the engines are running. As long as there is sufficient pressure in the "accumulator" to hold the "pressure regulator" in the by-pass position, the discharge from the pump is returned directly to the reservoir, at essentially zero pressure. Whenever the accumulator pressure falls, as it does whenever a hydraulic-operating cylinder begins to move, the pressure regulator acts to divert the pump discharge into the power system.

In the unloaded condition, the torque pulsations in a cavitating pump are probably less severe than if it were loaded, but the forces tending to cause pitting are undiminished.

Various changes were necessary to free the ordinary hydraulic system from the effects of abrasion and cavitation. It was the development of these protective measures which brought the commonplace hydraulic reservoir out of obscurity and into the center of interest.

There are few units in the hydraulic system which give the service mechanic, the design engineer, or the test pilot the same feeling of self-confidence as that engendered by the hydraulic-system reservoir. Everyone, with the possible exception of the weight engineer, casts a friendly eye on its bland, rotund exterior. They know that it is nothing but a hollow sheet-metal shell, conceived according to easily applied formulas set forth in Army-Navy specifications; so much foam space, so much basic volume, so much hand-pump reserve, etc. The reservoir has consistently been the one item in the hydraulic system which could be identified, and thoroughly understood, without the aid of a schematic diagram.

During the last year, even reservoirs have "gone modern;" incorporating a built-in filter working in the micron range, and air injectors for automatic self-pressurizing. The modern reservoir has acquired, as service mechanics found if they unscrewed the filler cap without heeding placarded instructions, a literal, as well as a figurative, "air of mystery."

By the time the first of these super reservoirs was actually installed in an airplane, the filter, originally designed solely for dirt removal, had become so important that the pumps could

[1] Mechanical Test Engineer, Douglas Aircraft Co., Inc.

Contributed by the Aviation and Hydraulic Divisions and presented at the Semi-Annual Meeting, Los Angeles, Calif., June 14–17, 1943, of The American Society of Mechanical Engineers.

Note: Statements and opinions advanced in papers are to be understood as individual expressions of their authors and not those of the Society.

scarcely operate without it, and the automatic self-pressurizing device was serving an auxiliary function that alone would have justified its inclusion in the hydraulic system.

Analysis of Filter-Performance Requirements

About 3 years ago, a search was begun to find a filter suitable to protect hydraulic units for 3000-psi systems. In most cases, these units already employed the hardest practical materials, to minimize the effect of abrasive particles. After more than a dozen filter vendors had been contacted, it was obvious that no one had made a thorough analysis of the requirements of such a filter. The problem resolved itself into the following four highly controversial questions:

1 Where should the filter be located in the circuit?
2 What size are the finest particles it must remove?
3 What flow resistance or how large a filter could be tolerated?
4 How long a life could be reasonably demanded, or what service or maintenance responsibilities must be accepted?

There were several possible answers to the question as to where the filter should be installed, as follows:

1 A single filter, through which all the oil must pass before reaching the pumps, would provide the best protection for the entire hydraulic system, provided that it removed small enough particles. The original prospects of obtaining a suitable filter for this location seemed remote indeed, since the location combined the maximum flow rate found anywhere in the system with the minimum amount of pressure available to force oil through the filter. Actual flow rates reached as high as 30 gpm, in the particular airplane for which a filter was immediately required, while even the most optimistic estimates allowed no more than 2 psi to force this amount of oil through the filter, at 70 F, if the hydraulic pump had to provide the necessary suction. Actually, as will be shown later, when the need for pump supercharging is discussed, even this amount of pressure was not available. Since the maximum flow resistance of the filter was to be no more than 2 psi, and since flow resistance increases as the filters accumulate dirt, the resistance of a new clean filter was limited to something on the order of 1 psi. Furthermore, in order to conserve space and reduce weight to a minimum by the elimination of a separate housing, the size of such a filter was arbitrarily limited by the largest object that could be conveniently taken in and out of the hydraulic reservoir under consideration, this being a cylinder about 6 in. diam and 9 in. long.

2 The finest practical filter, with an acceptable flow resistance, could be located ahead of the pumps, and as fine a filter as necessary could be located ahead of each one of the critical units, where flows were relatively low. This arrangement sacrifices a certain amount of protection for the pumps, where it is vitally needed, requires more maintenance, and is contrary to the present emphasis on standardization, because of the wide range of flows and operating pressures which must be accommodated.

3 Another alternative consists of installing a by-pass-type filter at any convenient point in the system, such as the regulator return line. This system obviously offers less protection against abrasive particles than either of the other two systems.

Evaluation of Critical Particle Size

Before making a choice of one of these three installations, it was necessary to determine the smallest dirt particle that it would be advisable to remove. A large number of simple slide valves (as shown in Fig. 2), with 0.0003 to 0.0005 in. initial diametral clearance were built and wear-tested. The wear tests consisted essentially of cycling the valves, while oil containing a known percentage of a known size abrasive passed through them.

A simple hydraulic system was proposed for the cycling test. The slide valve was located between two reservoirs, and oil forced back and forth between them by applying air pressure alternately to one reservoir and then to the other. The need for a filter in an airplane hydraulic system, with hundreds of feet of tubing and dozens of valves and cylinders, was strikingly demonstrated by the troubles experienced when this simple arrangement was used in an initial run to establish a reference datum for operation under supposedly ideal conditions, with clean parts and new oil. It was found to be impossible to operate the valves even a few thousand cycles without scratching.

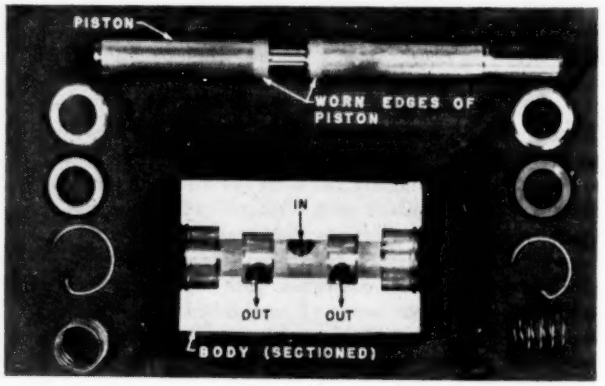


Fig. 2 Construction of Typical Valve Used to Evaluate Critical Particle Size

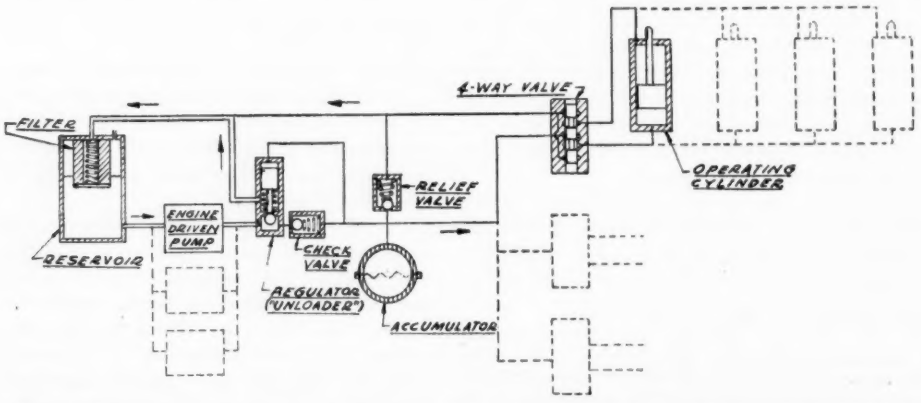


Fig. 1 Schematic Diagram Showing the Basic Parts of an Aircraft Hydraulic System

Finally, after a number of unsuccessful attempts to clean the system thoroughly, a slide valve was operated with only standpipes full of oil at each port. When this valve did not scratch, it was evident that scratching was not inherent in the valve itself, as it was almost beginning to seem, but must be due to dirt.

In slightly revised form, this simplified system was used to test the relative rates of wear of seven grades of abrasives, having nominal sizes ranging from 3 to 58 microns. A micron (μ) is 0.000001 meter, and 1 μ-in. is 0.000001 in., so that 1 μ is 39 μ-in. It is an interesting side light that the very character of the word "micron" may have been responsible, in no small measure, for the success of the entire development program. The filter manufacturers were quick to realize that something about the word attracted popular attention; its applicability to future advertising may well have mitigated the usual difficulty in obtaining research funds necessary for this type of work. Now, after three years, the word is widely used throughout the aircraft hydraulic industry, symbolizing a distinct change in the concept of satisfactory filter performance.

All the abrasives used in the test program caused some change in the valves, but there was a tremendous difference depending upon the particle size. From a study of the leakage measurements, wear measurements, and appearance of the pistons, some of which are shown in Fig. 3, it was decided that all 10-μ-size particles should be removed, and as many as possible of the 5-μ size. Indications were that particles as small as 1 μ would not be very serious.

In order to obtain some idea of the amount of dirt that a suitable filter must be capable of absorbing, the dirt content of several samples of hydraulic fluid that had been in service for 1000 hr was measured. From this it was estimated that the filter should be capable of absorbing 2 or 3 cu in. of dirt before requiring service or replacement, on the basis of service periods not more often than every 2000 hr flying time.

Thus the requirements for the type of installation in which all the oil is filtered each time it flows through the reservoir may be summarized by the following:

1 Remove all particles larger than 10 μ.

2 Pass 30 gpm at 70 F, with 2 psi pressure drop, after collecting 3 cu in. of dirt.

3 Occupy a space no larger than 6 in. diam × 9 in. length.

These requirements are so difficult to meet that for a long time it was necessary to maintain active interest in the other types of filter installations that have been mentioned, so remote did it seem that any satisfactory filter of the type 1 would be found. The first thing that was brought out by detail tests on various filter media, particularly felt and paper, was that a tremendous surface area would be required for such a filter, and that the thicker the filter medium, the greater would be the required area. This narrowed the field to the use of paper, or some other very thin filter medium, for in no other way could so much area be built into such a small space.

The problem of the filter manufacturer then became one of arranging the paper in the best possible manner. If too much paper is used, the internal passageways will become too small and tortuous, and may perhaps clog up, shutting off large areas of the filter. If too little paper is used, the flow rate per unit area will be high, and so will be the pressure drop. As the result of considerable development work, several successful designs are now available.

Approval of the retentivity of the filter papers used in these designs was granted after tests using the same graded abrasives that had been used for the wear tests.

Measurement of Filter Flow Resistance

The measurement of flow resistance through such a filter proved to be a more interesting matter than had been anticipated, for it was here that the filtering and pumping problems became interwoven. In the first place, the flow rate into the particular reservoir for which this filter was originally designed is quite high, amounting nearly to 5 changes per min. The reason for the high flow is that airplane operators feel it is well worth while to be able to retract the landing gear in a matter of seconds, and, in this case, 45 hp is available for the purpose. At 3000 psi, this requires a flow of about 25 gpm. (When this figure is compared to the 75 gpm that it would take to do the same work at 1000 psi, the reason for widespread interest in high-pressure hydraulic systems is obvious.)

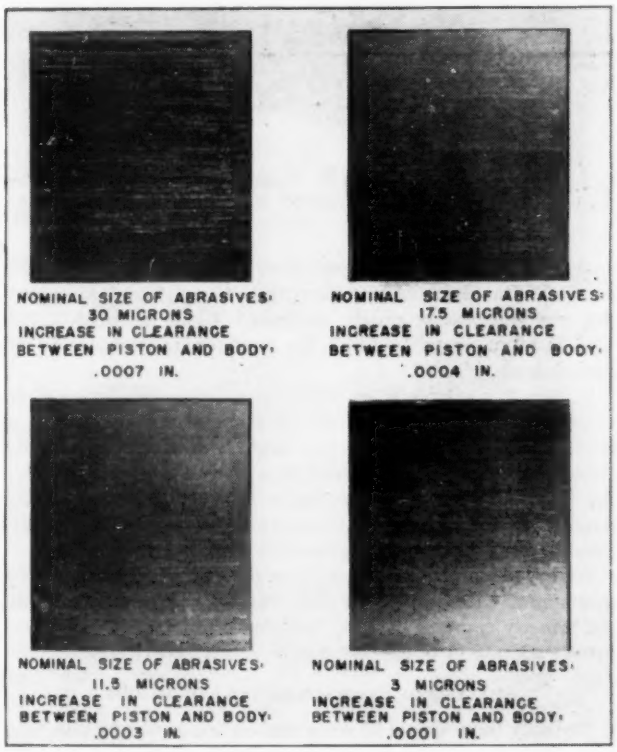
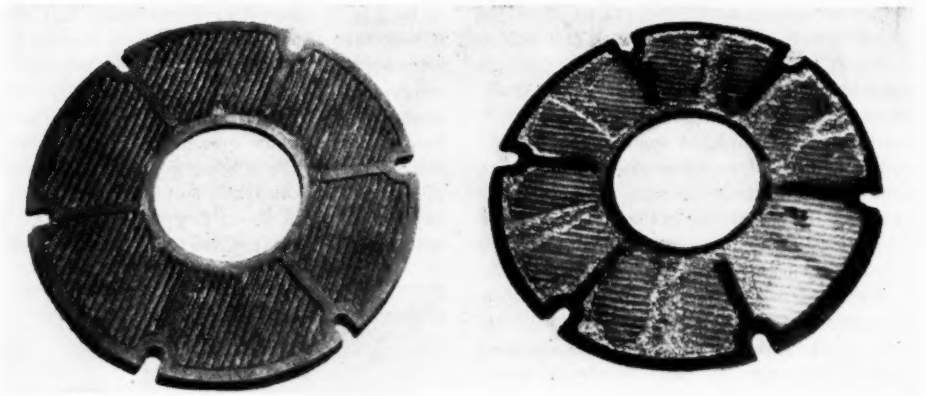


Fig. 3 Partial Summary of Wear-Test Results

It had been the original intention to discharge the return oil into the reservoir tangentially, and suck it out to the engine-driven pumps through the filter. When an attempt was made to measure the flow resistance of the filter using this arrangement, it was not only impossible to obtain accurate readings, but the energy in the return oil was sufficient to set the entire content of the reservoir in rapid rotation, promoting so much air entrainment and foaming that it was virtually impossible for the pumps to operate. A number of modifications were tried without success. Finally, the filter was utilized as a diffuser, through which the oil was discharged into the reservoir. In this case, instead of entering tangentially at 30 fps the oil entered radially with a velocity of less than $^1/_2$ fps. This arrangement effectively eliminated all troubles due to foaming.

In addition, this revised installation yielded a particularly accurate means for measuring flow resistance of the filter. A hole was simply tapped into the unfiltered oil region, inside the filter, and a standpipe extended up from it. Oil was circulated through the filter at the required rate, and the pressure drop was determined by measuring the height of the oil in the standpipe, above the oil level in the reservoir. By injecting measured



(*a*) (*b*)

FIG. 4 SAMPLE FILTER DISKS; FILTER ASSEMBLY CONSISTS OF MANY SUCH DISKS
(*a*, Shows amount of dirt collected during 1000 hr of service in an airplane. *b*, Shows amount of dirt collected during test without causing objectionable flow resistance.)

amounts of dirt into the oil just ahead of the filter, the dirt capacity of the elements was investigated, and found to exceed the requirements originally estimated. This completed the final tests necessary to fulfill the predetermined standards of performance.

In Fig. 4, a sample filter disk from a laboratory-tested filter is compared to a disk, obtained at a much later date, from a filter assembly with 1000 hr of aircraft service. The ample dirt-storage capacity of the design is obvious. Unfortunately, the illustration does not emphasize the fact that, despite its relatively clean appearance, the service-tested disk has actually caught a large number of dangerous dirt particles.

While the completion of these filter tests provided considerable reassurance with respect to slide valves, where abrasion was the primary cause of concern, additional problems were anticipated with respect to the piston pumps, due to cavitation.

ANALYSIS OF PUMP OPERATING CONDITIONS

Probably there should be some explanation as to why pumping problems still exist, after airplane hydraulic systems have been built for so many years. For example, operators are demanding satisfactory operation at higher altitudes, and more hydraulic operations are being required at altitude conditions. Whereas, the commonest employment of the hydraulic system has hitherto been landing gear and wing-flap operation near airport levels, now surface-control boosters, turrets, bomb doors, etc., find frequent use at service ceiling. Even if the hydraulic pumps are running unloaded, injurious cavitation may occur at high altitude, at low temperature, or at high pump speed. Furthermore, the trend to larger airplanes moves the pumps farther and farther away from the hydraulic reservoir, perhaps 30 to 50 ft. It is frequently impossible to locate the reservoir higher than the pumps, and the line connecting the reservoir and pump must be kept as small as possible to reduce weight and facilitate installation.

Operation of pumps under conditions of cavitation can be dangerous in at least four different ways. If carried to the extreme, the hydraulic system will be rendered useless because of lack of oil supply. Before this condition is reached, pump efficiency may fall so low that overheating and seizure may result. As an even earlier effect, the extreme vibration attendant upon partial cavitation may cause fatigue failure of the pump shaft. Still another effect is the formation of small pits frequently in parts which must remain smooth for sealing purposes.

Sufficient study has been made of the pressure losses between reservoir and pump to conclude that some form of supercharging is justified from the weight standpoint, and is the only answer for high-altitude operation.

The minimum allowable absolute pressure in the hydraulic-system reservoir is essentially the sum of the following major pressure losses:

1 Line loss, plus the difference in head between pumps and reservoir.
2 Valve-port loss, getting the oil into the pump cylinder.
3 "Unavailable pressure," due to vaporization of oil and to dissolved or entrained air.

If atmospheric pressure at the altitude of flight does not exceed the sum of these losses, cavitation will exist unless supercharging is provided.

It is not necessary to determine the magnitude of these losses with scientific accuracy in order to determine which factors are most important from the standpoint of making a general improvement in pump operating conditions.

SURVEY OF PRESSURE LOSSES ON INLET SIDE OF A PUMP

Line loss may be readily calculated from well-known and reliable formulas, which are further simplified because the calculations of interest usually fall in the laminar-flow range. Such calculations show that the use of larger lines to reduce pressure loss is extremely limited and costly. The use of the next size larger lines in one particular airplane would involve a 23-lb increase in weight, and save only slightly more than 1 psi line loss at 70 F, or, if viewed from the temperature standpoint, would permit operation with oil about 20 deg F lower in temperature. Temperature has such a tremendous effect on line loss that it is impossible to take care of very cold oil by increasing line sizes. Fortunately, the flows are usually low when the oil is cold, because under these conditions the main engines, which drive the pumps, are likewise cold and must be run slowly. As the engines warm up, the oil may be expected to warm up also, due to the friction of circulating it through the lines. Of course it is always possible to provide additional resistance in the circuit, if necessary to accelerate warm-up, at the expense of adding a thermally controlled relief valve.

Losses through the various expansions and contractions at the inlet to a pump cylinder may be approximated using formulas and coefficients available in any hydraulics textbook. It requires a bit of optimism to trust such calculations to any great

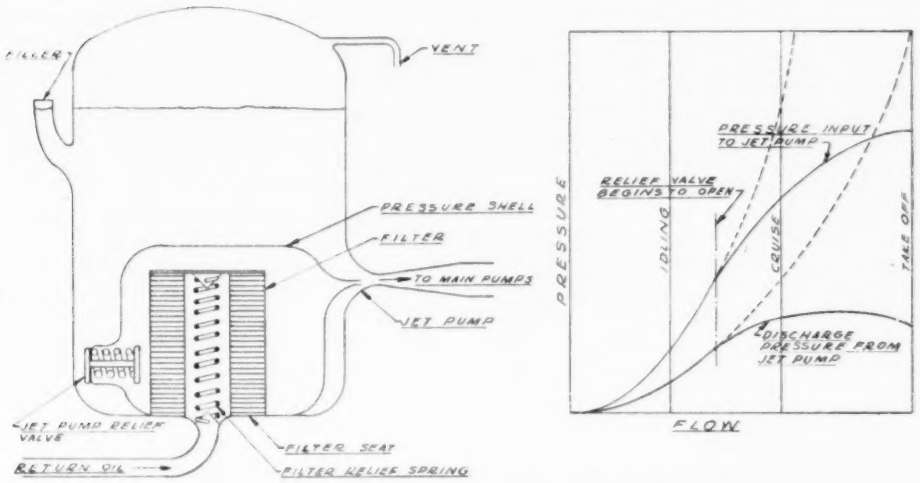


FIG. 5 JET-PUMP METHOD OF PUMP SUPERCHARGING; RESERVOIR UNPRESSURIZED

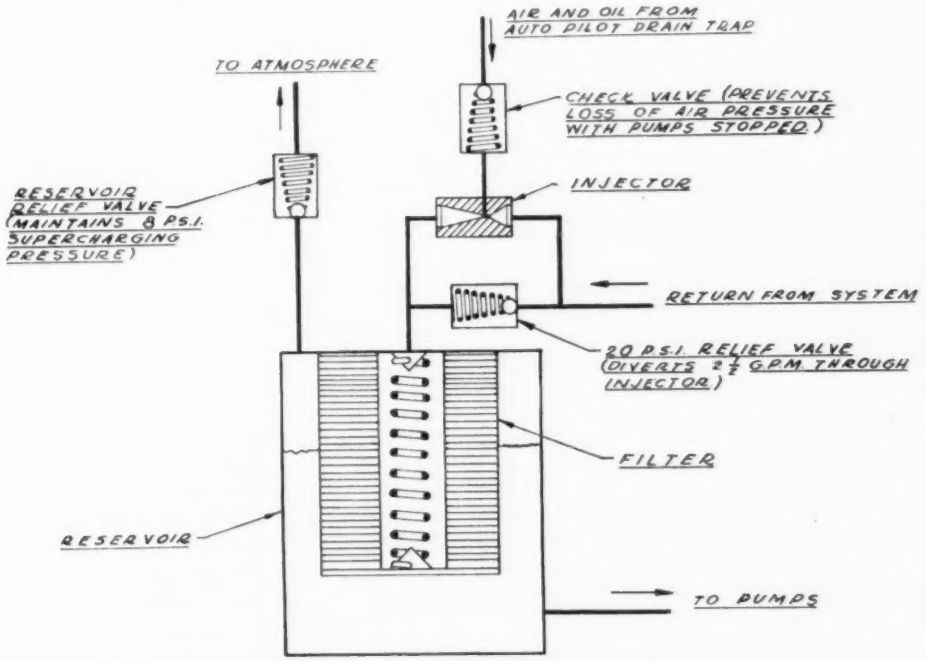


FIG. 6 AIR-INJECTION METHOD OF PUMP SUPERCHARGING; PRESSURIZED RESERVOIR

extent, because the resemblance between the passageways in the pump and those in the textbooks is rather remote. Furthermore, there is a surprising lack of agreement among texts as to the coefficient for sudden contractions under ideal conditions. The calculated losses for one particular pump amounted to 2.7 psi, which, when added to the other calculated operating losses, yielded a total that was quite closely confirmed by test. This restored a measure of confidence in these methods, which, if correct, bring out the point that even if the port losses could be cut in half the increase in safe operating altitude would be small.

The loss due to oil vaporization is in a similar category. It is probably impractical to effect any improvement, but, before making such a decision, it is necessary to have some idea as to what the magnitude of the loss might be. The fact that some oil actually turns into vapor in a pump chamber is substantiated by an observed decrease in volumetric efficiency, above a critical speed, for a positive-displacement pump, operating at constant discharge pressure. Since the pump chambers are not running full of oil, the remaining space must be occupied by vapor. This would seem to indicate that an extremely low absolute pressure is reached in the pump, since one vendor of hydraulic fluid quotes a vapor pressure as low as 5 mm of mercury at 175 F. However, this vapor-pressure figure may be very misleading, because oil, being a mixture of hydrocarbons, has no fixed boiling point.

Vapor pressure is frequently measured by allowing the liquid to vaporize until it fills a space several times as large as the liquid volume. In pumps, the vapor volume becomes important while yet a small fraction of the liquid volume. For this reason, the vapor pressure of interest to aircraft hydraulic engineers is not the vapor pressure that is likely to be quoted in good faith by a chemistry laboratory.

When this point was investigated further, measurements of the gas volumes developed from hydraulic fluid, maintained at

150 F, and a vacuum of 25 in. of mercury, until gassing stopped, yielded a value nearly equal to one half the liquid volume. In a hydraulic pump, the liquid has only an instant to flash into vapor, so that there is an additional factor, time, of unknown importance. Furthermore, no line has yet been drawn to define the critical ratio of gas to liquid volume. The one item which has been established is that the pressure rendered unavailable to the pumps, due to oil vaporization, is of the order of 5 in. of mercury, rather than 5 mm.

If this figure of 5 in. of mercury is accepted as the minimum absolute pressure normally attainable in the cylinder of a pump handling hydraulic fluid, then the importance of entrained or dissolved air becomes greatly minimized. For instance, the fluid would have to contain 14 per cent air, by volume, at sea-level pressure, in order to amount to half air and half liquid at 5 in. of mercury abs. However, if the pressure could fall to 5 mm of mercury abs, it would take less than 1 per cent of air at sea-level pressure to reach this same ratio.

When all of the foregoing losses are considered, it is apparent that the volumetric efficiency of the pumps on an airplane would begin to decline, well below the service ceiling demanded by current airplanes, even if the pumps were mounted in the hydraulic-system reservoir.

No one is prepared to say how low a volumetric efficiency is safe for continuous operation, but there is obviously no reason to take chances, if a supercharging pressure can be readily obtained.

Methods of Pump Supercharging

Various systems for boosting the inlet pressure at the engine-driven pump have been suggested, but most of the obvious ones can be discarded because they involve moving parts, or make the reliability of the hydraulic system depend upon the reliability of some other apparatus that is relatively complicated. The author's company has developed a satisfactory arrangement using a jet pump, Fig. 5, but this was not selected, because another method is available which pressurizes the reservoir with equipment that is already required to perform another service.

The system finally adopted, Fig. 6, employs a simple Venturi, which, acting as an air injector, builds up a pressure of about 8 psi in the sealed hydraulic-system reservoir. In addition, it serves to inject into the reservoir the hydraulic leakage from several unpacked lap-fitted slide valves that are component parts of the autopilot system. The latter function requires the Venturi to provide a subatmospheric pressure at the autopilot drain connection, at all times when the engines are running; that is, the Venturi must never stall, either because the reservoir pressure becomes too high for it to pump against, or because the fluid flow through it is reduced.

In order to insure that stalling can never take place, it is necessary to provide the Venturi with a flow that is never less than a predetermined minimum, and set the reservoir relief valve, which governs the pressure against which the Venturi is pumping, at some pressure less than that which the Venturi is capable of producing, when supplied with minimum oil flow. The flow provision is a simple matter. Whenever the engines are running, oil is circulated through the reservoir. It is only necessary to add a spring-loaded valve in the reservoir return line, and locate the Venturi in parallel with it. Since too much air added to the oil tends to defeat the basic purpose of the system, which is, of course, to force solid oil into the pumps, it is wise to design this spring-loaded valve so that its resistance is essentially independent of flow, and thus introduce no more air into the oil than is absolutely necessary.

The rate of introducing air was chosen so that the supercharging system would maintain sea-level pressure in the reservoir, if the airplane took off with an initially unpressurized reservoir and climbed directly to its service ceiling. Ordinarily, the reservoir will never be unpressurized, because a check valve in the air-inlet line prevents the escape of pressure back through the Venturi when the engines are stopped.

Every pound per square inch of pressure in the reservoir is purchased at the expense of about 3 times that much "back pressure" on the oil returning to the reservoir; that is, the nominal setting of the spring-loaded valve which controls flow rate through the venturi is roughly 3 times the minimum amount of supercharging pressure that is provided. This additional pressure is expended in overcoming the resistance of the check valve in the air-inlet line, in overcoming pipe friction, venturi inefficiency, and pressure loss through the filter, and in providing a margin for tolerance on the pressure settings of the reservoir relief valve and the valve controlling venturi flow rate.

Each major unit in the hydraulic system has had its share of notoriety in past years; the power brake valves, pressure regulators, accumulators, surface-control boosters, brake de-boosters, emergency air valves, 3000-psi pumps. It is truly a fitting reward for loyal service that the lowly and obscure hydraulic reservoir, now with built-in pump supercharging and micron-range filtration, at least achieves in some measure, the attention that has been accorded its associated units.

Aircraft-Engine Temperature Control

By WILLIAM A. RAY,[1] GLENDALE, CALIF.

Exposed to variations of as much as 200 deg F in ambient temperatures over short periods of time, the aircraft-engine temperature-control problem is a vital consideration of design and operation both of military and commercial aircraft. Weight, compression ratios, combustion rates, factors of safety, efficiency, ambient temperatures, and general operating conditions are all factors contributing to the necessity of controlling engine temperatures. The author undertakes an objective analysis of the problem and describes a system of hydraulic control which has been developed and which has proved satisfactory in service.

A PROPER appraisal of aircraft-engine temperature control should be based upon an objective view of the engine itself, its work load, and its surroundings, as compared with typical internal-combustion engines with which most engineers are familiar, either in stationary or automotive work.

The most obvious difference between internal-combustion engines and aircraft engines is that of weight; the former seldom being lighter than 5 or 6 lb per hp, whereas aircraft engines will average just over 1 lb per hp. Combustion rates and compression ratios are high on aircraft engines, whereas the factor of safety on mechanical stresses is generally low by comparison. On the heavier internal-combustion engines, high factors of safety on mechanical stresses are used to overcome those normal defects which occur in all mechanical structures but which cannot be economically sought out, at least up to the present time, on automotive or stationary engines. Aircraft engines necessarily light and safe from an economic standpoint justify extreme care in manufacture. There are no marginal factors of safety to cover these typical manufacturing defects. All aircraft engines must be normal or better.

On the operating side, aircraft engines also have their distinct differences. Over-all operating efficiency must be a maximum. Inefficiency cannot be tolerated since extra fuel would be required, thus seriously reducing pay load and cruising range, particularly on ocean flying where landing fields may not exist for 2000 or 3000 miles.

With the average internal-combustion engine employing customary cooling methods, it is usually impossible to operate at too hot or too cold a temperature from a safety standpoint. However, this can easily occur on an airplane, since any substantially fixed cooling arrangement, which may be used on most other engines, can never meet all conditions that occur on an airplane, with the result that an engine may get too hot, resulting in fire; or too cold, resulting in misfiring. The latter often occurs, particularly on military airplanes, when the need for maximum power exists, as, for example, when pulling out of a glide dive.

The aircraft engine is also subjected to wider ambient temperatures on the cooling medium than almost any other type of engine, it being quite possible to have changes in the temperature of the air medium through which the plane is flying approaching 200 deg. The effectiveness of this cooling medium is further complicated by the variation in speed of the airplane, most variations of necessity having no relation to the cooling needs of the engine.

Furthermore, from an operating standpoint, for the sizes of the engine involved or horsepower output, all airplane engines are warmed up faster than any other type, particularly on military planes which are subjected to widely variable and sudden load changes.

These questions of weight, compression ratios, combustion rates, factors of safety, efficiency, ambient temperatures, and general operating conditions have all contributed toward the necessity for control of engine temperatures. All these factors likewise accentuate the time function, requiring both responsive and watchful temperature control.

Analyzing the Engine-Cooling Problem

An objective analysis should include a scrutiny of the cooling job itself. There are normally three ways that heat may be dissipated from aircraft engines, two of which are always used depending upon the type of engine, that is, whether it is air-cooled or liquid-cooled. Both types dissipate a great deal of heat to the lubricating oil, in contrast with stationary-engine practice where little or no effort is made to dissipate heat through this medium. However, the design of aircraft engines for higher work rates makes it imperative to dissipate substantial amounts of heat through the lubricating oil. Thus the lubricating oil, distinctly a cooling agent and subjected to extremes of temperature may catch fire at one extreme, yet freeze to a solid at the other. This heat in the oil is usually dissipated through a radiator, the effectiveness of which is dependent upon the atmospheric conditions through which the airplane is flying. The air-cooled engine dissipates additional heat from cylinder walls or finned heads. Here again extreme temperatures may at one end result in loss of strength of the engine parts, and at the other end misfiring, because cylinder and head temperatures affect ignition. The liquid-cooled engine, originally using water as a coolant, now uses a chemical (ethylene glycol, commonly known as prestone) as a coolant, because of the more desirable properties of this chemical as compared with water. On a liquid-cooled engine this coolant collects that heat occurring at the cylinder walls and cylinder in the same manner as in the air-cooled engine. The coolant heat is then dissipated by a radiator in the air stream. Here again extremes of temperatures will result in engine failure or misfiring.

Hence it is important to control the air flow over these cooling elements, whether in the form of the lubricating-oil radiator, the prestone radiator, or the air-cooled engine cooling fins. This control is usually obtained by suitable flaps that permit or restrict the air flow. These flaps are desirably located around the engine, a point more often than not remote from the pilot's control, making it necessary to obtain some kind of a remote operation of the flap. Mechanical operation is not always satisfactory because of the work loads involved, and the difficulty of working the operating gear through the airplane structure. The result is that on most airplanes, a more flexible, outside, work-doing medium is used to power the flaps and secure remote control. Until quite recently, this remote control has been mainly manual. The pilot or flight engineer periodically checked engine temperatures and corrected the flap position as required.

[1] Chief Engineer, General Controls Company.

Contributed by the Aviation and Hydraulic Divisions and presented at the Semi-Annual Meeting, Los Angeles, Calif., June 14–17, 1943, of The American Society of Mechanical Engineers.

Note: Statements and opinions advanced in papers are to be understood as individual expressions of their authors and not those of the Society.

Thus on the typical airplane, there has existed a means for operating the temperature flaps, so in order to secure automatic control, it has only been necessary to provide some automatic piloting method to control the operating medium. The sensitive thermal element of the automatic control is usually more accurate, minimizes the human element, and stays on the job at all times.

The ease with which automatic temperature control can be adapted to the usual flap-operating gear, also makes it possible, in most cases, readily to switch back to manual control for such occasions when only human perception can decide the best condition, such as for take-off, landing, or fast warm-up. However, if the ship has automatic controls sensing such functions, they can be made automatic as well. Thus if desired to minimize head resistance, as when taking off heavily loaded ships, flaps can be retracted more than usual; or when landing, when head resistance may be desirable, flaps can be opened more than usual.

Hydraulic Controls Developed

Development work, as done by the author's group, has hinged around hydraulic operation, as it was felt that this actuating medium was more reliable and more easily repaired, because of its mechanical simplicity and the ease with which faults in the system may be detected. Electric operation, lubricating oil under pressure, air under pressure or vacuum, and even direct thermal operation are possible alternatives. Direct operation, consisting of a thermal unit powerful enough to position flaps, is not practical for larger engine installations.

However, hydraulic operation as mentioned, is believed to be admirably adaptable to most temperature applications and readily lends itself to constant operation without destruction either to control valves or operating cylinders, has very few moving parts, and the weight is well in line. Hydraulic operation has further advantages in that in most cases of system failure, the flaps will fair or trail. Although maximum engine power is not always obtainable with faired flaps, and retirement from combat may be necessary, sufficient engine power is available for safe operation of the airplane. In fact, on most aircraft, the design is such that the flaps will fair or trail at cruising speed.

The selection of hydraulic oil as the working medium resulted in the initial development of a temperature control that is adaptable either to lubricating oil or engine coolant. This particular control is operated by a sensing element or thermal element of the liquid-expansion type. This element was selected because of its great work-doing possibilities, compared to other types of sensing elements, such as bimetal expanding or bending members, thermocouples, vapor-tension or gas expansion. A liquid element is particularly suited to aircraft work in that it is not responsive to altitude conditions; hence it holds its temperature calibration regardless of atmospheric pressure, provides a hard working force, and in general, does not require compensating means or glands. Development work has also overcome the slowness of response of this type of unit to a point at which it is comparable, for example, with bimetal immersed directly in the fluid.

This liquid-charged element operates a four-way selector valve which, in a sense, is an amplifier, since a small work load of the order of 0.01 to 0.02 in-lb will cause or prohibit the operation of 1 hp of net work at the flap, the smaller work being provided by the thermal element. The four-way selector-valve operation controls the flow of hydraulic oil usually at 1500 psi pressure to the hydraulic cylinder or strut, which in turn operates the air-controlling flap. This arrangement is additionally effective in that hydraulic oil or pressure is readily convertible to force in its most usable form in so far as flap operation is concerned, hence the efficiency of this working medium is very high.

The most desirable type of control is one that will modulate the flap, that is, not open or close only, but assume some position best suited to obtain the correct temperature control. Operating efficiency of the engine installation virtually requires modulating control, not only to maintain actual engine efficiency by holding correct temperatures, but maximum aerodynamic efficiency by lessening unnecessary flap opening. However, modulating controls have an inherent weakness, that is, a tendency toward instability, to "hunt," or to oscillate about the desired position. This is overcome in nearly all modulating mechanisms by what is known as the reset or follow-up mechanism. This mechanism readjusts the calibration point of the temperature control for the particular flap position. Thus when the engine is cold, and the flaps are closed, the temperature control will respond at a temperature 20 deg, 30 deg, or 40 deg F, as the case may be, lower than it would if the flaps were open.

Modulated Temperature Control

A typical modulating control does not have a fixed temperature-responsive point in the sense that we understand the typical thermostat to have. For example, a typical on-and-off thermostat would turn on at a certain temperature, say 210 F, and turn off at 220 F. The 10 deg F difference is known as differential, and the operated unit would open or close, only in response to such a control unit. The modulating control may start at 210 F and initiate opening of the flap, the resultant operation of which would shift the range of the control, resulting in a small movement suited to the cooling needs. The flap would not open fully, but would open, for example, at 20 per cent, and additionally, the control point or response point of the control would be shifted from 210 to 216 F. Another rise in temperature would cause a further opening of the flaps, an increment suited to the rise of temperature. The flaps would be fully open, for example, at 240 F, and the new response point of the control, because of the reset mechanism, would be at 240 F. The temperature dropping some amount below 240 F would result in a closing of the flap again an incremental amount as needed. Thus with a reset mechanism, an actual closing condition is obtained which may be higher in temperature response than another point at which the flaps would open. The reset mechanism is solely responsible for this condition, and ideally prevents "hunting," or oscillating about the control point, or unnecessary flap operation.

The range, in this case, from 210 to 240 F is known as the reset range, and is here 30 deg F. As compared to the on-and-off control, first mentioned, it appears to be wide, and would result in a wide controlling temperature. However, the on-and-off control is subject to swing in control. For example, a control which shuts off at 220 F, as just outlined, does not result in holding the control medium at 220 F. A swing occurs which will carry it greatly beyond this point, depending upon the characteristics of the medium and system on which the control is being used. A properly designed reset range, and it should always be wide enough to be so designed, will result in holding the control temperature entirely within that range, particularly if the control is rapidly responsive. Hence although the reset range of the modulating control is wider than the differential of typical on-and-off control, the actual control temperature is more often closer or narrower than that obtained with an on-and-off type. Therefore, a reset mechanism was included in the control, not only to prevent "hunting" but for closeness of control.

Pilot supervisory control can be exercised taking the flap control completely away from the automatic control. This can be done mechanically, electrically, or hydraulically as the work

involved is slight, and hence reasonable, regardless of the medium used. The medium to be used depends upon the remoteness of the location as well as upon the reliability of the types available. The use of certain mediums is precluded because of inaccessibility. The particular control in question may be overridden either mechanically, electrically, or hydraulically. Each will work equally well. The mechanical method of overriding has the obvious advantage of providing a direct operation in the event of either electric- or hydraulic-system failure, particularly in view of the fact that the hydraulic temperature control will fair the flaps upon proper operation of the selector valve. However, electrical or hydraulic operation is used where it may be physically impossible to reach the control mechanically. The overriding control thus provides four positions, i.e., automatic, open flap, closed flap, locked flap. Predetermined flap positions are possible or manual modulation may be used, according to needs.

An engine temperature control using a hydraulic work medium is successfully operable from either lubricating-oil or engine-coolant temperatures. In addition, operation is fast enough to cover all flight conditions, even those existing in pursuit ships. In fact, actual test curves on one of the fast pursuits shows that the control is never lost—never has to overshoot to catch up with its position. Also, overriding or pilot supervision is just as effective as if the temperature control never existed. The weight is low. Field experience and operating life have been satisfactory.

The development and subsequent operation of this contro have demonstrated the excellent possibilities of hydraulic operation of engine temperature control. Further advancement gives indication that air-cooled-engine cowl-flap control may be solved hydraulically. Advances in the art, accelerated by the substantial production now existing, will most certainly result in even greater reliability, lower weight, lower cost and accuracy for any aircraft temperature-control problem.

High- and Low-Pressure Airplane Hydraulics in Europe

By JEAN MERCIER,[1] NEW YORK, N. Y.

Development of hydraulic control systems for aircraft began to make progress in Europe about 1936, the trend being toward pressures of 5000 psi and higher. Details of the equipment comprising the hydraulic systems, applications made, and lines of development when the war interrupted the program are treated in this paper.

IT may be recalled that during the heroic phase of the airplane in the first world war, the kinetic energy of any abnormal landing shock was absorbed, as is said in French, by "breaking wood." The wood referred to was, of course, the wooden undercarriage, even when it ceased to be made of wood as originally.

So many of the Allied planes were thus immobilized that the author's father, Henri Mercier, who at the time was Director of the Mechanical Section of Inventions of the War Department in France, suggested what he and his colleagues termed "a pneumatic shock absorber with a very long stroke!" Compared with the shock absorber of today, the very long stroke, which was 30 in., will surely bring a smile. To avoid any drag which might disturb the flight, a telescopic retracting system was developed.

The Armistice of 1918 interrupted this research before any test flights were made. Incidentally, the fluid retraction of the landing gear was not hydraulic but pneumatic; a small Letombe compressor actuated by a propeller was the prime mover.

Twelve years passed before another French engineer, the late Georges Messier, took up the problem. His was a hybrid development. By combining Col. Deport's oleo-pneumatic gun recoil with samples of the American Lockheed automobile hydraulic-actuating cylinders, he built probably the first modern hydraulically retractable landing gear. The Olaer Company, which the author directed, was working on similar problems for automobiles at that time and decided to enter the airplane field. To have the best chance against competition by electric controls using high voltage, it seemed necessary that an equivalent high "voltage" hydraulic system, foolproof and unaffected by wear, tear, cold, and age, be first scientifically developed.

Advantages of High Pressures

The following illustrations may help to clarify the analogy between high voltage and high pressure in hydraulics:

A few volts permit the handling of a good-sized telephone bell; a few pounds' pressure are just good enough to actuate a windshield wiper; 1000 lb will hold its own against a 20-v motor. The future will certainly bring into competition systems of several hundred volts, such as are already being applied in ships with installations of several thousand pounds per square inch. In other words, high pressure is comparable to high voltage, thus affording an efficient way of producing and transporting energy without the corresponding trouble of handling great volumes of oil or conducting many amperes of electricity.

The enormous advantages of high voltage are thus balanced, and hydraulics will be free to develop its potentialities of easy maintenance, light weight, and flexibility. The value of these qualities is particularly potent in the high-pressure hydraulic accumulator which is able, in a fraction of a second, to start off the heaviest engines.

Having adopted this point of view and before determining the optimum operative pressure, it was essential to learn the reaction of European aeronautical engineers and test pilots compelled to fly with apparatus under such apparently eruptive pressures. It is hard to believe the great difficulties encountered by the author in promoting the idea that the damage caused by the explosion of an accumulator is related to the amount of energy thus liberated, e.g., the energy stored in a 50-cu-in. accumulator at 5000 psi is not much greater than 1 gal at 1000 psi.

The best illustration of the present status of the art in the United States is Harold Adams' very interesting work,[2] in which the optimum operating pressure is calculated, and which proves that above 3000 psi there is practically no saving of weight, either in tubing or in actuating cylinder walls, if the same load factor is maintained for both high- and low-pressure hydraulic systems.

While the author is in full agreement with Mr. Adams' calculations concerning the parts involved, he has found that above 3000 psi there is still a marked saving in cylinder heads and tube fittings, as well as in the actual weight of oil involved. In addition to this, higher pressures should be of great interest for the following reasons: The smaller the apparatus, the less will be the modifications necessary in the structural design of the plane, thus saving an incredible amount of weight, space, and last but not least, headaches. One is led to the conclusion that too low a pressure, even 3000 psi, limits the free development of optimum structural design.

Furthermore, a constant pressure drop in the line of a few hundred pounds is necessary to transmit the energy from the pump to the actuating cylinder. Those hundred pounds become a relatively smaller percentage in a 9000-psi system than in one of 3000 psi. The corresponding tubing, being necessarily thicker, resists external stress and vibrations so well that the factor of safety can be reduced to the one adopted for cylinders, thus giving nearly 50 per cent weight saving. Once again, there is a point of comparison with the high voltage in electrical-power transmission.

TABLE 1 WEIGHT SAVING COMPARISON BETWEEN 5000-PSI AND 1000-PSI HYDRAULIC SYSTEMS

	Weight saved, lb	Per cent saved
Tubings, fittings, and supports	5	50
Oil	30	75
Pump	0	0
Selector valve	1	50
Landing-gear cylinders	5	60
Dive-flaps cylinder booster of pressure	11	70

As an illustration of weights saving, Table 1 summarizes the case of an airplane weighing 7000 to 8000 lb, with a hydraulic

[1] Consulting Engineer, Simmonds Aerocessories, Inc.; President, Ol-Aer Patent Company.

Contributed by the Aviation and Hydraulic Divisions and presented at the Semi-Annual Meeting, Los Angeles, Calif., June 14–17, 1943, of The American Society of Mechanical Engineers.

Note: Statements and opinions advanced in papers are to be understood as individual expressions of their authors and not those of the Society.

[2] "Design and Shape Problems in High-Pressure Hydraulic Systems," by Harold Adams, *S.A.E. Journal*, September, 1940.

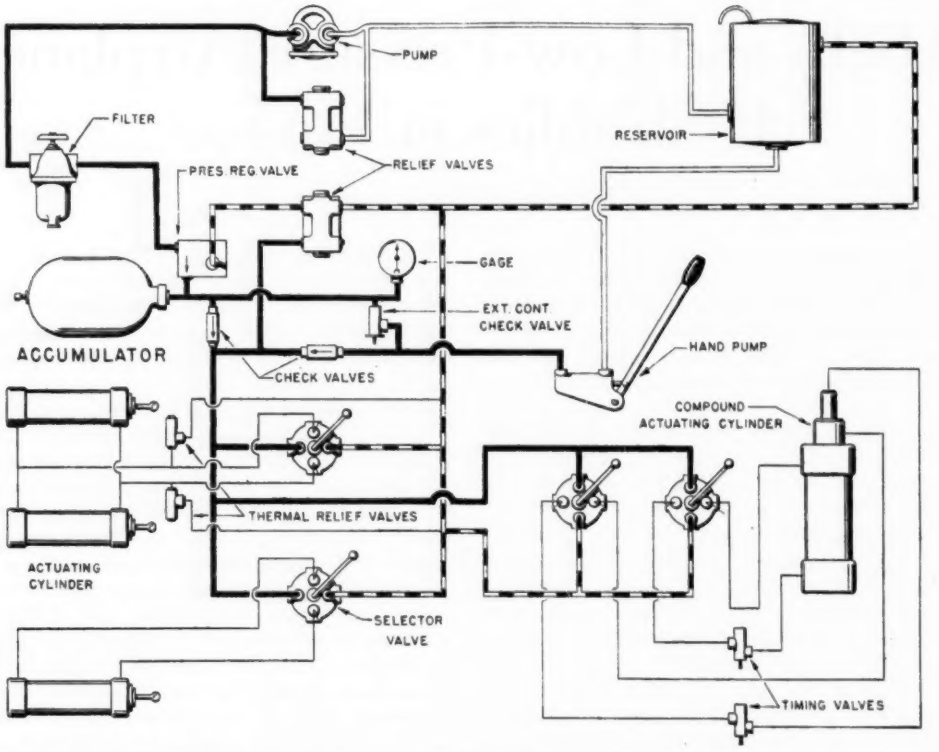


FIG. 1 SCHEMATIC DRAWING OF TYPICAL OLAER MERCIER HYDRAULIC SYSTEM SHOWING INSTALLATION OF ACCUMULATOR AS IN REGULAR USE IN FRANCE IN 1936, AND AS IN USE ON AMERICAN AIRCRAFT IN 1943
(When a variable-delivery pump, Dowty, England; Olaer Mercier, France, is used, the pressure-regulator valve is suppressed.)

system utilizing 5000 psi, compared to one at 1000 psi (Fig. 1). In this instance, the total weight saving appears to be over 60 per cent.

In Europe, prior to 1935, to the best of the author's knowledge no planes had flown with a hydraulic system operated at a pressure appreciably over 1000 psi.

It was difficult to get the French Bureau of Aeronautics to have little more than faint sympathy for such evident madness as the proposal of the Olaer Company. However, after 2 months of completely successful trials at 8000 psi, it was agreed, much to the relief of the bureau, to drop the pressure to 4000 psi. In 1935, the Morane Saulnier fighter 405–406, equipped with Olaer-Mercier hydraulic system at 4000 psi, took off from the Villacoublay Airport, piloted by an amazingly confident man, Michel Detroyat.

HIGH-PRESSURE SYSTEMS ADOPTED FOR MILITARY AIRCRAFT IN 1936

Interesting items at that time were the automatic thermostatic actuation of the selector valve, controlling the position of the radiator-actuating cylinder and the follow-up flap control, permitting their immobilization at any degree of their travel. There were, also, separate piston-type accumulators with metallic glands, permitting independent emergency movements of flaps and undercarriages.

In 1936, the Fokker Gl light bomber adopted the same system at an operative pressure of 4500 psi. Both types of planes have since been manufactured in regular line production. The basic scheme of the hydraulic system of both of these planes is the same. In the Fokker, the following functions were controlled by the Olaer-Mercier system: Retractable landing gear with mechanical lock hydraulically operated by special cylinder, landing flaps with a safety valve allowing for automatic adjustment at high speed, dive flaps, bomb doors, cockpit opening, and cooling flaps.

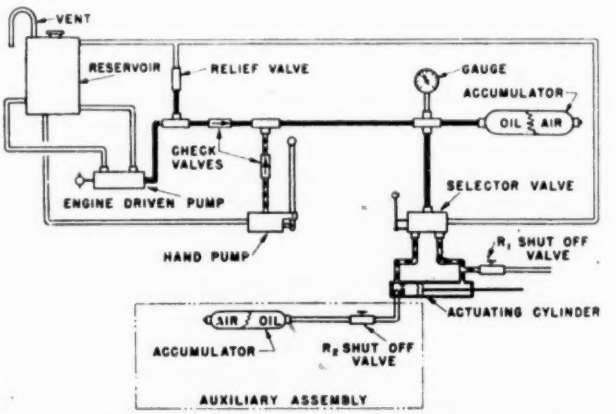


FIG. 2 SCHEMATIC DIAGRAM SHOWING ELEMENTS OF TYPICAL OLAER MERCIER INSTALLATION WITH SELF-REGULATING PUMP
(Note independent circuit and emergency outlet. In case of pressure failure in line 1, pilot opens valve R_2 and, if necessary, R_1 to lower landing gear. In use in Holland, Switzerland, Italy, France, 1936.)

Special mention must be made of the emergency hydraulic pressure conducted to the hydraulic-flap and landing cylinders, utilizing an automatic transfer valve on the cylinder head, isolating the normal hydraulic circuit in case of its failure (see Fig. 2). The energy for this was provided by an air bottle or an accumulator preloaded at 5000 psi, thus doing away with the hand pump. Bristol, in England, and others use a similar transfer valve to connect a gas-charge-producing cartridge device. At the same time, Caproni in Italy acquired the Olaer license in order to equip its series of light bombers 310. The chief char-

acteristic of this modified installation was a complete dual hydraulic system up to the jack, with two independent pumps, one on each engine, the pilot thus having the choice of shifting from one to the other, provision having been made for automatic transfer valves. Since then, the high-pressure hydraulic system has been adopted in Switzerland, and in Czechoslovakia by Skoda for its Avia 35. In 1938, the French fighter Dewoittine 520 also adopted Olaer. The different components of this system were on view, in operative condition, at the hydraulics meeting in Los Angeles, November, 1941, under the chairmanship of Commander Harry Marx of the Bureau of Aeronautics, and of Mr. Bashark of Wright Field.

The parts shown consisted of a complete retractable landing gear, composed of a magnesium wheel, specially coated with metallic salts, resisting 1000 hr of exposure to salt spray (which coating process is now in use in Germany and was recently found satisfactory by Northrop laboratories), and of brakes of the inflated-bag type having an extremely large brake drum located inside of the wheel contour, thus enabling the dispersion of the heat generated when landing at very high speed, i.e., 100 mph. This last-mentioned characteristic was found necessary, if not always for actual landing, at least for taxiing rapidly along the ground to shelter in war operations.

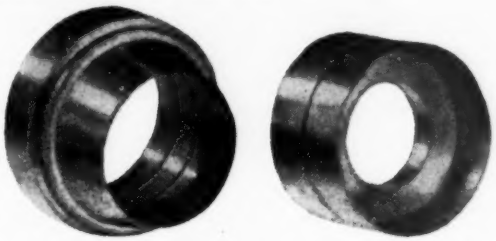


FIG. 3 OLAER MERCIER METALLIC GLAND FOR PRESSURE UP TO 30,000 PSI AND TEMPERATURE RANGE FROM —100 F TO +400 F
(In use in France, Holland, and Switzerland since 1936.)

Shock struts were provided with the Olaer metallic glands (Fig. 3), adequate to resist excessively low temperatures such as found in Russia and Alaska. A complete retracting system, with the nut-cracker link actuated by a cylinder having no fixed point on the airplane structure, was simultaneously developed by Bristol in England, and by Olaer in France. Here the mechanical lock is included in the hydraulic cylinder (Fig. 4), and operated by a subsidiary piston actuated by the pressure existing in the cylinder itself, thus suppressing external connections. This feature has since been adopted by the Messerschmitt fighter.

As to the simultaneous problems of fittings and flexible hose, they were very easily solved by the Ermeto fittings (Weatherhead) as long as the wall thickness of the tube is over 0.04 in., and the ordinary Alemite flexible hose, provided the inside diameters remained under $^3/_{16}$ in. For operations at very low temperatures, a carefully designed horn-shaped metallic tubing gives a foolproof solution, so long as the displacement of the units to be connected is not too great.

OTHER NOTABLE DEVELOPMENTS IN EUROPE

It may be worth while to mention some other characteristic devices developed in Europe. To replace the mechanical push-pull control, the Exactor system, initiated in England and since licensed in the United States, has taken a leading place. Messier developed a similar system, characterized by keeping the oil under pressure in both circuits, forward and backward; the total of the pressure in both lines is kept constant due to a single spring acting on two independent compensating pistons.

Except for the Letombe Viet air compressor, which is after all

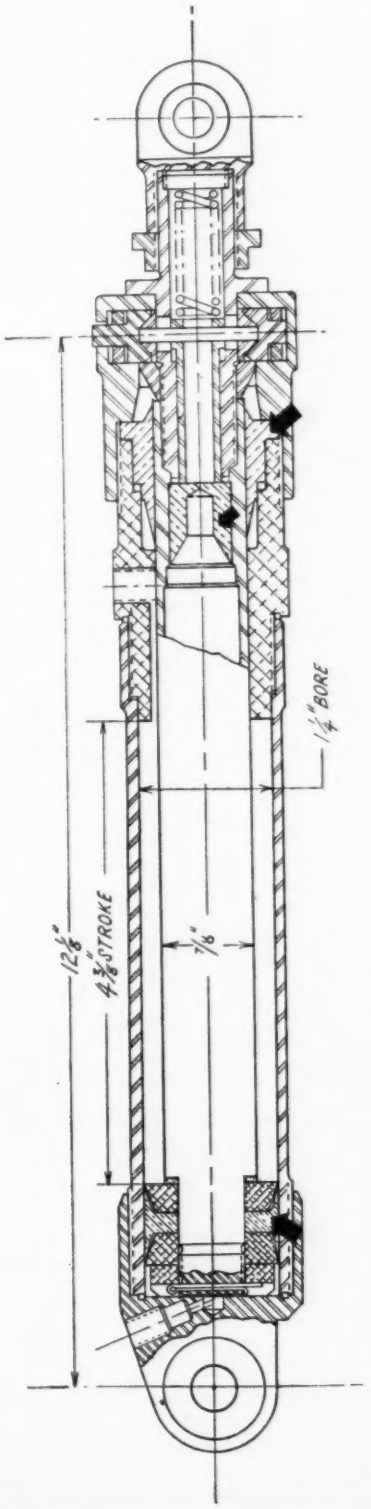


FIG. 4 TYPICAL LANDING-GEAR-ACTUATING CYLINDER FOR CURRENT TYPE PURSUIT AIRPLANES, WEIGHING ABOUT 6000 LB
(The Olaer Mercier metallic gland, indicated by arrows, replaces the old-fashioned packing subject to aging, leakage, and rapid deterioration unless periodically renewed. The gland acts as a bearing, occupies less space, and weighs no more than the cap required to fix the old packing and the retainers. It flexes sufficiently to adapt to the cylindrical form of the piston itself, demands but slight refinement of tolerance.)

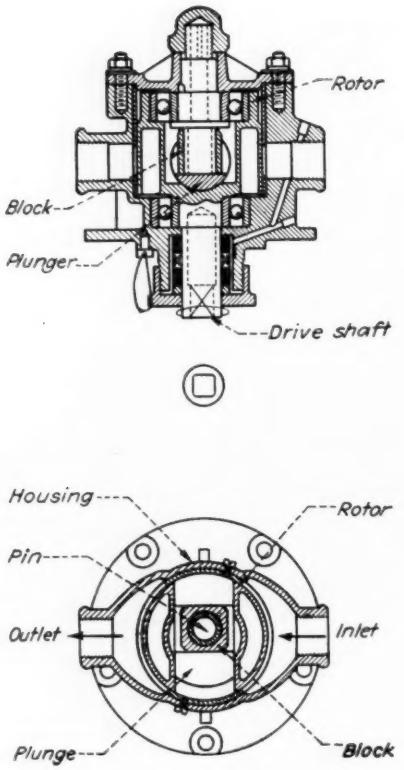


FIG. 5 ROTO PLUNGE RECIPROCATING PUMP, ENGLAND

not a pump, the first application of reciprocating pumps was made in England under the name of the "Roto-Plunge" pump, manufactured by T. H. and J. Daniels Company (Fig. 5). Later on Vickers Aviation Company, Ltd., in England (which has no connection with the Vickers Company of Detroit) produced a two-cylinder pump for use in aircraft (Fig. 6).

In 1935, Bristol developed a three-stage gear pump with a normal delivery of $2^3/_4$ gpm at 1500 psi, at a speed of 2400 rpm. Between 1930 and 1933, de Boysson in France developed a very fine radial-piston pump for turret control. This pump, adopted by Messier, is shown in Fig. 7. Some 5 years ago, an automatic clutch device, controlled by hydraulic pressure,

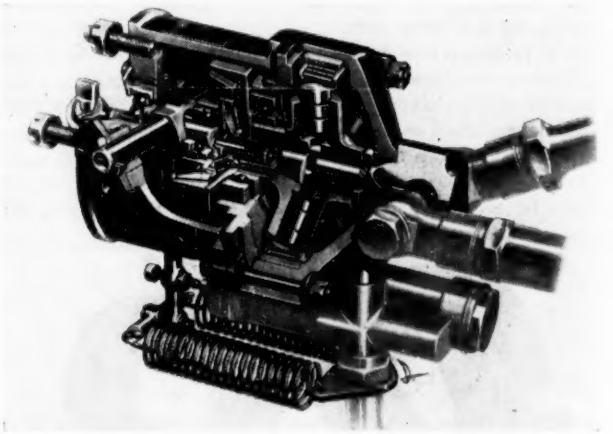


FIG. 7 DE BOYSSON PUMP, IN USE IN FRANCE ON MESSIER HYDRAULIC CONTROLS

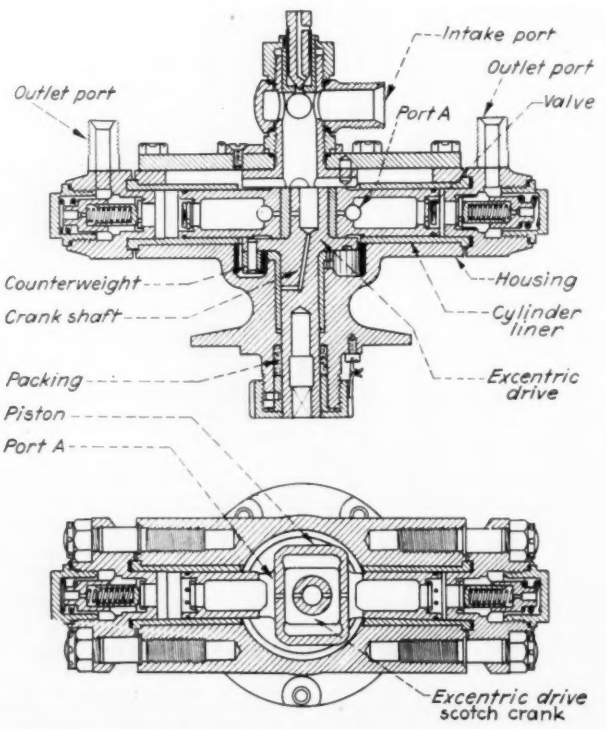


FIG. 6 VICKERS, LTD., HORIZONTALLY OPPOSED TWO-CYLINDER RECIPROCATING PUMP

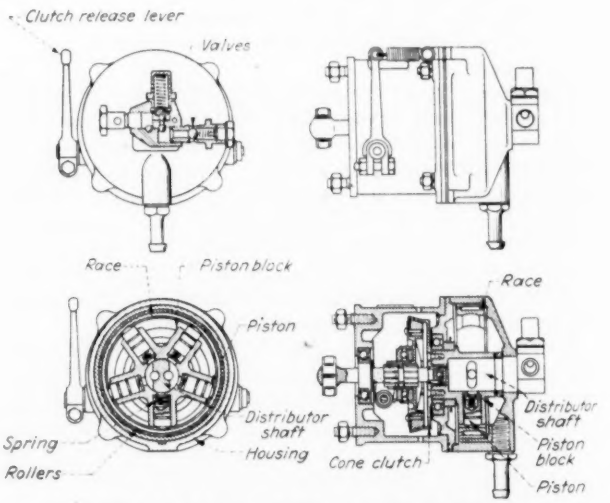


FIG. 8 DE BOYSSON MESSIER PUMP, FRANCE

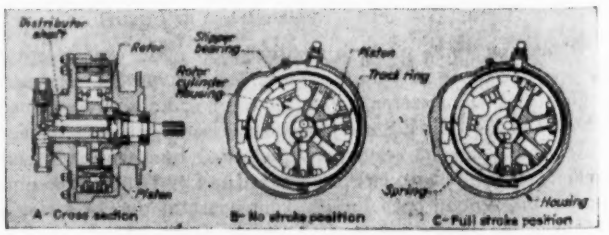


FIG. 9 CROSS SECTION DOWTY, ENGLAND, LIVE-LINE PUMP

was evolved jointly by de Boysson and Messier (Fig. 8). On the same general principle, Dowty adopted a pump which a few years ago was transformed into a self-regulating pump by the addition of a spring limiting the torque (Fig. 9). This is known today as the "Live-Line" system in which the only, but very interesting, improvement over the Olaer self-regulating system consists in the elimination of the accumulator, a bigger pump taking care of the instantaneous flow requirements. This carries the risk that, in case of pump or engine failure, no energy is available.

The Olaer pump (Fig. 10), developed in the period 1935–1938, and since adopted in several European countries, is somewhat similar to the well-known Vickers wobble-plate type, described fully in a paper by Dale Herman.[3] Its characteristics are (1)

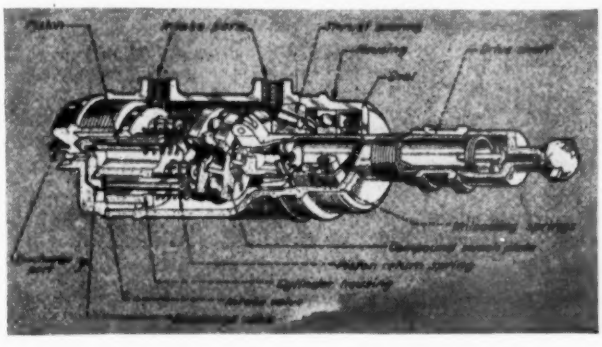


FIG. 10 OLAER MERCIER PUMP, 5000 PSI, WEIGHT, 2.2 LB
(In use in France, Holland, Italy, and Switzerland.)

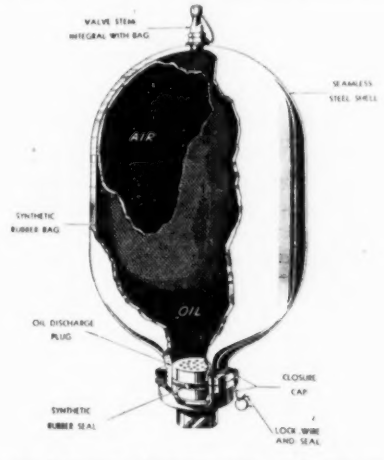


FIG. 11 OLAER MERCIER ACCUMULATOR AS BUILT IN THE UNITED STATES

supercharging, thus avoiding cavitation at high speed; (2) self-regulation by a spring concentric to the axis; and (3) lightness of weight, 2.2 lb for a 1/4-gpm, 5000-psi pump. The basic design for all these pumps, as also for many of the ultramodern hydraulic devices, can be found in the hydraulic controls used on battleships for the last 40 years. Hele-Shaw (England) and Waterbury (England) have contributed largely to their development. Happily for us aviation hydraulics engineers, the prohibitive weight of these known devices makes their use in aviation impossible. The hydraulic cylinders, utilizing rubber or leather glands, are more or less similar to the American practice.

Fig. 11 shows the Olaer-Mercier bag-type accumulator, and Fig. 4 the Olaer jack, also developed in 1936, the latter having an internal self-locking device and metallic glands as shown in Figs. 3 and 4.

The similarity holds good for European and American globe, check, regulating, pressure-reducing, safety, and selector valves.

In Europe, faith in hydraulics led to the development of hydraulic valve locks to prevent eccentric movements. Bristol and Olaer use a valve operated by a connecting rod which, by shutting off the line when the weight of the airplane telescopes the oleo strut, makes it impossible for the undercarriage to retract on the ground. A variant feature of this device prevents the outflow of oil from the jack when external force tends to displace the piston. Bristol applies his double hydraulic lock on bomb doors. This lock consists of spring-loaded poppet valves independent of the jack. The Olaer system is based on a sliding head of the jack itself, which closes the hydraulic circuit when the head tends to telescope into the cylinder due to external forces. When the internal pressure is again applied it pushes out the head thus reopening the oil circuit.

WAR INTERRUPTS WORK ON EXTENSIVE HYDRAULICS APPLICATIONS

There were three more interesting developments in process at the outbreak of the war in Europe. One, in collaboration with the French Navy, for watertight compartments, was later proposed for very large airplanes. If the weight increase, necessitated by the increasing distance between the hydraulic units and the increased energy to be transmitted on the "bigger and better" planes now on their way, were not provided for, the planes would soon carry more tubing than freight. A patented solution to this was found in providing, close to each hydraulic cylinder, two accumulators, one of high pressure to store the local energy, and the other of low pressure to absorb locally the outlet flow required during rapid actuation, as well as a local selector valve, controlled electrically at distance by the pilot or, in case of emergency, by hand. An enclosed hydraulic circuit, independent of the atmospheric pressure and particularly noteworthy for stratospheric flying, is thus obtained automatically by the elimination of the oil reservoir rendered unnecessary by the presence of the low-pressure accumulators. The combination of an electrical remote-control system, with hydraulic-actuating cylinders, may be compared with the nervous system of the human body in controlling the flow of blood to the muscles for actuation. This organic union might well encourage the electrical engineer to accept hydraulics "for better or for worse," or at any rate until rotary high-speed servomotors take its place.

Another development of note was a hydraulic steering device for the front wheel of the Fokker D23, a tricycle landing gear similar to the follow-up rudder control of ships, which sooner or later will be applied to airplanes.

A still further interesting point was the hydraulic control of two or more landing flaps, operating simultaneously without any mechanical connection. Instead of controlling the amount of fluid to be admitted to or exhausted from each of the operative jacks, the problem was reversed. If a disequilibrium should occur, the pilot would correct it in the normal way by means of the stick, thus automatically bringing into action a special distributing valve, which in turn corrects the amount of fluid needed for an exact symmetrical displacement of the flaps.

Of course, some additional features are required to permit the correction being made while lowering or raising the flaps. A leak in any part of the line would be taken care of automatically, because the control is not affected by the distribution of the oil, nor by the movement of the flaps themselves when not absolutely symmetrical, but by the stability of the plane itself.

[3] "The Evolution of the Hydraulic Pump as Applied to Aircraft," by Dale Herman, appearing on pages 583–588 of this issue of the Transactions.

A two-position actuating cylinder was used to permit different landing and taking-off flap positions.

ACKNOWLEDGMENT

The author wishes to express his appreciation for the courtesy and help of Commander Harry Marx, U.S.N.R., who is in charge of hydraulics at the Bureau of Aeronautics of the Navy; of Mr. Edward Greer of Greer Hydraulics Co.; and of Simmonds Aerocessories, Inc., for the use of the illustrations in this paper.

Maintenance of Aircraft Hydraulic Systems in the Field

By R. E. MIDDLETON,[1] BURBANK, CALIF.

This paper deals with certain aspects of the aircraft-accessories maintenance problem, under wartime conditions, and sets forth some suggestions as to how manufacturers of aircraft hydraulic equipment might assist in its solution. The comparative merits of hydraulic systems and electrical-mechanical systems for operating airplane accessories are discussed from the standpoint of maintenance and repair.

IN contrast to peacetime when Army aircraft could be serviced under the best possible shop conditions by a thoroughly trained and experienced staff, highly complex and delicate aircraft accessories are today overhauled, repaired, and adjusted oftentimes in the open, exposed to extremes of weather and with only the most limited tools and equipment. It is true that all large well-equipped air bases have proper maintenance facilities but under combat conditions, so long as an airplane will fly, it is usually operated from outposts far removed from such shops.

Through the courtesy of the Army Air Forces, the author has had an opportunity to become quite thoroughly acquainted with the conditions under which airplanes being used in the Alaskan theater of operations are being serviced and kept in proper flying condition. This study involved observation of the maintenance and service operations at various bases, including actual combat squadrons.

Improvement Necessary in Servicing Hydraulic Equipment

This study of conditions in the field demonstrated the eagerness of the Army Air Forces' personnel to avail themselves of all constructive advice and help forthcoming from civilian technicians and representatives of equipment manufacturers. In the case of hydraulic equipment, which is doing a fine job in the field, the results are being accomplished with wholly inadequate field service provided by manufacturers of this type of equipment, and in spite of certain quite serious handicaps. In general, manufacturers have not furnished the caliber of field service essential to the most advantageous operation of the equipment and the least interference with operation of the airplane, at all times. Of course, one important reason for this is the tremendous expansion in the Army Air Forces without corresponding increase in available personnel, with a thorough knowledge of hydraulics.

It is believed that the greatest field for improvement in the operation of hydraulic systems under service conditions lies in the expansion by hydraulic-equipment manufacturers of the facilities for educating service personnel; and in furnishing the proper tools, equipment, and service manuals pertinent to the maintenance, adjustment, and repair of these accessories.

Of course, it would not be accurate to assume that similar service difficulties are not encountered in electrical-mechanical systems for operating accessories. During the tour in Alaska it was possible to observe many instances where electrical equipment of various kinds was being removed, repaired, or replaced. Actually, the percentage of such replacements appeared to be higher than the percentage of replacements of hydraulic equipment. In connection with such comparisons, it should be borne in mind that the total quantity of hydraulically operated accessories now in use on standard military airplanes exceeds considerably the total of electrically operated accessories. Therefore, even though the percentage of replacements of hydraulic equipment is low, the actual number of such replacements may still be greater than the actual number of replacements of electrically operated equipment.

More Rugged and Serviceable Designs Will Help

The following suggestions are made to manufacturers of hydraulic equipment in the interest of remedying at least partially some of the failures of hydraulic equipment to give the best possible service. By improving field conditions, one of the greatest obstacles to present and future progress in the use of hydraulics in aircraft will be removed.

It is the author's belief that hydraulic-accessories manufacturers have not in the past assumed their full responsibility for the successful and trouble-free operation of their equipment in the field. In many cases, the design of such equipment does not provide the reliable and rugged construction which is necessary for it to stand up under varying and adverse atmospheric, weather, and ground conditions which prevail in many theaters throughout the world where American-built aircraft are called upon to operate. In partial justification, it is true that sufficient time has not been available for developing and testing design features of the equipment which may later cause trouble. Obviously in many cases the airplane itself has had to be the proving ground for the equipment. Consideration must also be given to the extreme urgency under which manufacturers have been operating. They have been called upon to produce equipment within the most stringent delivery schedules. Nevertheless, it is believed to be entirely feasible for the accessories manufacturer to work out a comprehensive program which will allow sufficient time to find and correct the majority of the weak points of his equipment through careful test and improvement.

The facts demonstrate that in the few cases where such procedure has been followed, even to the point of apparent overcaution in proving equipment before it is installed in airplanes, the greatest serviceability in the field has been achieved.

Another important design consideration relates to the tools and methods required for maintenance and service. Many instances are on record of units which required special wrenches, holding fixtures, and adjusting tools, for their proper adjustment and repair. These may be quite acceptable where the units can be serviced in well-equipped base repair depots, which can maintain supplies of such tools, fixtures, and gages. Under war conditions, in practically no case is sufficient equipment available at the points where airplanes are actually being operated in service, and where it is necessary for mechanics to keep them flying.

Whether it is hydraulic, electrical, or mechanical, the ac-

[1] Chief Engineer, Hydraulics Division, Aircraft Accessories Corp. Mem. A.S.M.E.

Contributed by the Aviation and Hydraulic Divisions and presented at the Semi-Annual Meeting, Los Angeles, Calif., June 14–17, 1943, of The American Society of Mechanical Engineers.

Note: Statements and opinions advanced in papers are to be understood as individual expressions of their authors and not those of the Society.

cessory equipment which literally can be taken apart and put together again on the upturned bottom of a packing case, with the ordinary mechanic's tool kit, will in general be successful. Certainly it will have to be rugged equipment. Experience would appear to prove that hydraulic equipment is much more susceptible to design which is capable of this type of servicing than are electrical-mechanical devices, which are more delicate, more needful of special tools, and more difficult to repair in the field.

Another major point in a program of service improvement is the assumption on the part of the accessories manufacturer of a greater share of the responsibility for actual servicing of the equipment in the field. The first step is for each manufacturer, within his ability to do so, to assure that full information and instructions are made available to all squadrons flying airplanes in which his equipment is installed, and also to make a greater effort to furnish the necessary tools and spares at points where they are needed. It is believed that this can best be accomplished through the efforts of qualified service representatives of the accessories manufacturers who, under the auspices of the Air Service Command, can work with the Army and Navy personnel. They can serve as advisers, guides, helpers, and liaison between the service organizations, which must use and maintain the equipment, and the factories which, because they are so far removed from the battle fronts, usually tend to lose sight of their great responsibility and the tremendous job that must be done in keeping the equipment working and the airplanes flying.

As has been amply demonstrated by the aircraft manufacturers, a sufficient number of qualified service representatives can be invaluable in aiding the personnel of the armed services to become thoroughly familiar with the highly specialized, intricate and, at best, rather delicate accessory equipment. They can go far toward attaining the degree of co-operation between the accessories manufacturers and the actual users of the equipment, which will not only insure long life but also reliable operation.

Centrifugal Casting of Steel

By S. D. MOXLEY,[1] BIRMINGHAM, ALA.

This relatively new method of casting is being applied to great advantage in the economic production of high-quality engineering parts. The three methods generally used are true centrifugal casting, semicentrifugal casting, and centrifuging. The author gives a comprehensive description of each method, the work for which it is best adapted, the machines used, details of molds, and physical properties of the resulting products.

THE casting of metals centrifugally is basically "pressure casting." In static molding, feeding is done by atmospheric pressure and gravity, and the pressure under which the metal is cast is dependent upon the height of the gates and risers. In centrifugal casting, the metal is forced against the mold wall and into the cavities under much higher pressures resulting from centrifugal force imparted by the revolving mold.

Generally, the methods of centrifugal casting are (1) true centrifugal casting, (2) semicentrifugal casting, (3) centrifuging.

The "true centrifugal" method consists of spinning the casting about its own axis and using centrifugal force to hold the metal on the wall of the mold, thus forming the inside without the use of a center core. When a mold is spun about a horizontal axis, the interior cavity formed by the molten metal is a true cylinder, regardless of the shape of the outside of the casting. Its inside diameter is determined by the volume of metal poured.

Fig. 1 shows a cylindrical flask lined with sand and provided with suitable end fixtures. If the mold is spun at sufficient speed and metal is poured into it, a cylindrical tube, as indicated, is cast.

If more than one inside diameter is required in a casting, the larger inside diameters may be formed by cores extended from the ends of the mold, leaving the smaller diameter to be formed by centrifugal force. Fig. 2 shows a conventional mold for making cast-iron pressure pipe. Note that the inside diameter of the socket is larger than the inside diameter of the pipe and is made with a core.

This method has been used in the mass production of cast-iron pipe for more than 20 years. During that period both sand-lined mold and metal-mold processes have been in successful commercial use, and their economic soundness has long since been proved. Higher physical properties have been obtained, and this has resulted in a reduction in the required thickness and weight of the pipe for a given service. Alloy-steel gun barrels are centrifugally cast in horizontal metal molds by a process developed over a long period of years at Watertown Arsenal.

True horizontal centrifugal casting is well adapted to the manufacture of short and long tubes in various sizes where the inside cavities are cylindrical. Steel tubes, ranging from several inches in diameter up to 50 in. diam, can now be made by the author's company in lengths of 16 ft. Typical products of this method are pipe, various kinds of tubing, radial-engine cylinder barrels, hollow ship shafts, weld-neck castings, bearings, sleeves, etc.

Vertical True Centrifugal Casting

True centrifugal casting is also done by spinning the mold about a vertical or an inclined axis. When this is done the resulting interior cavity is a paraboloid. The shape of this paraboloid is dependent upon (1) the speed of rotation of the mold, (2) the diameter of the closing fixture at the top of the mold, and (3) the angle of inclination of the axis of rotation. Assuming a fixed diameter at the top of the inside cavity, and a fixed angle of inclination, the depth of the paraboloid is increased by an in-

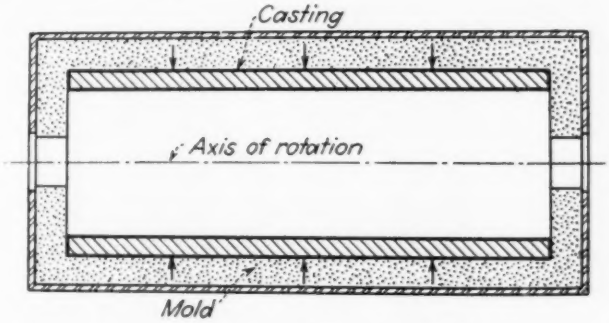


Fig. 1 Cylindrical Flask Lined With Sand

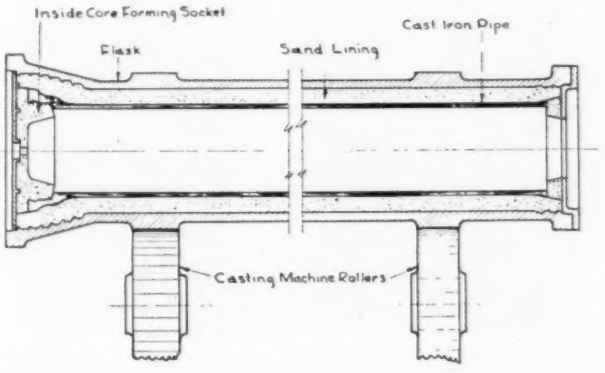


Fig. 2 True Centrifugal Mold for Making Cast-Iron Pipe

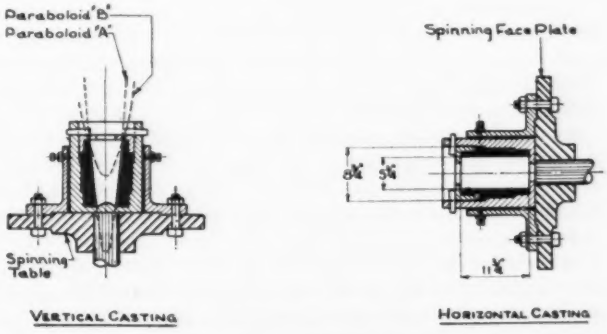


Fig. 3 True Centrifugal Method of Casting Radial-Engine Cylinder Barrels

[1] Chief Engineer, American Cast Iron Pipe Company. Mem. A.S.M.E.

Contributed by the Metals Engineering Division and presented at the Spring Meeting, Birmingham, Ala., April 3–5, 1944, of The American Society of Mechanical Engineers.

Note: Statements and opinions advanced in papers are to be understood as individual expressions of their authors and not those of the Society.

crease of speed. Likewise, the paraboloid will be shortened with slower speed.

Fig. 3 shows radial-engine cylinder barrels being cast by the horizontal and the vertical methods. At the right the mold is spun about a horizontal axis, and the inside cavity is cylindrical. At the left the mold is spun vertically and the inside cavity is parabolic in shape. At a certain speed of rotation the inside cavity will take the shape of paraboloid *A* as shown, while at some lower speed the inside cavity will be formed on the line of paraboloid *B*. In either case, the top diameter of the inside cavity will be larger than the bottom diameter. These castings ($8^3/_4$ in. OD × $11^3/_4$ in. long) are now being made horizontally at speeds of 975 rpm and lower, and vertically at speeds approaching 1200 rpm. The mathematics for calculating the shape of the inside paraboloid is relatively simple and is in the record.[2] Fig. 4 shows a comparison of an actual paraboloid as cast with the shape of cavity as calculated.

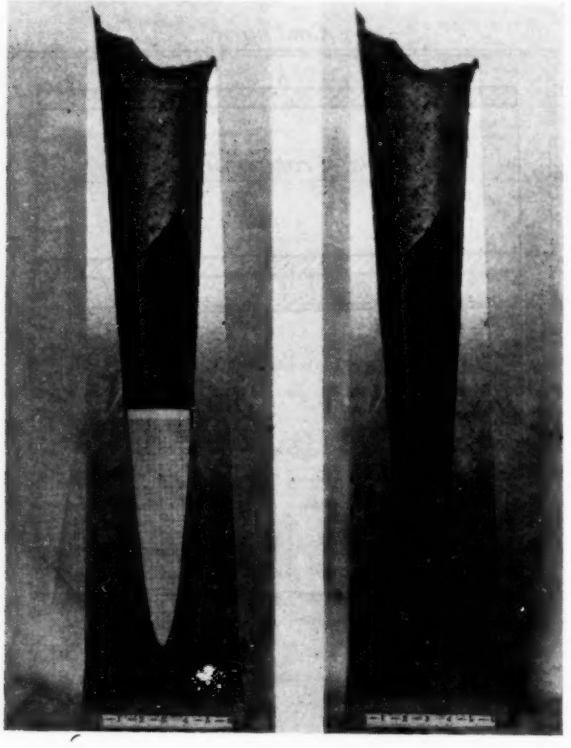


FIG. 4 COMPARISON OF ACTUAL PARABOLOID AS CAST WITH CALCULATED SHAPE OF CAVITY

Advantages. The horizontal and vertical methods of producing castings have many advantages. In static castings a large proportion of the critical defects are subsurface imperfections, detectable only by expensive and time-consuming methods. When spun, the impurities such as dirt, sand, and slag, having lower specific gravity, are forced to the inside surface of the casting by centrifugal force. Any gas or air pockets are likewise eliminated. The elimination of these foreign inclusions results in a sounder casting, and the product is more uniform. A centrifugal casting is more dense than a static casting. It is doubtful that the method of casting steel would change the specific gravity of the metal, but being free of these foreign inclusions or voids would naturally make a casting more dense, or rather, heavier per unit volume.

[2] R. F. Wood, U. S. Patent No. 1,533,780.

Directional solidification is very important in any method of molding. In true centrifugal casting, this occurs naturally, since the metal is cooled from the outside toward the center. Inspection of the castings is greatly simplified, since such defects as are found are in nearly all cases on the inside or outside surface of the castings, thus making them more readily detectable.

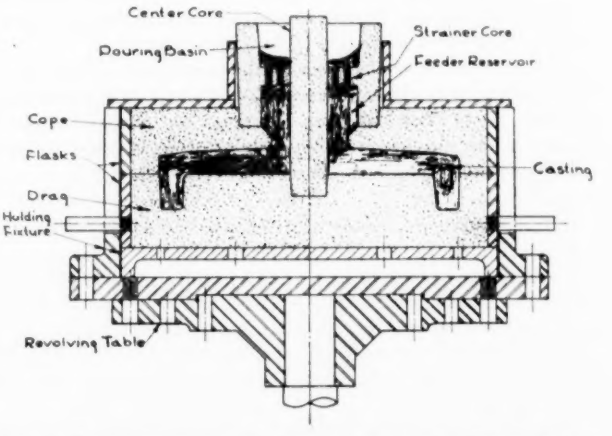


FIG. 5 SEMICENTRIFUGAL CASTING OF FLYWHEEL WITH CENTER CAVITY

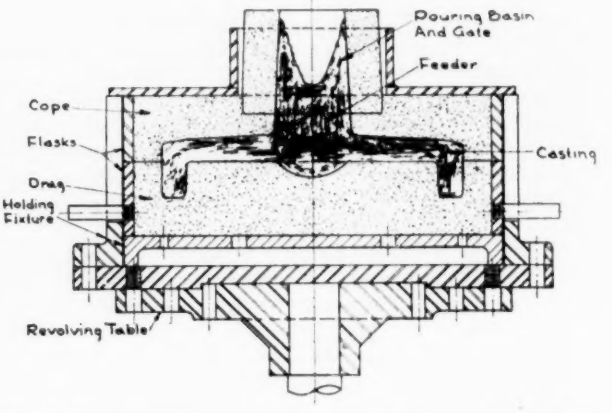


FIG. 6 SEMICENTRIFUGAL CASTING OF FLYWHEEL WITH SOLID CENTER

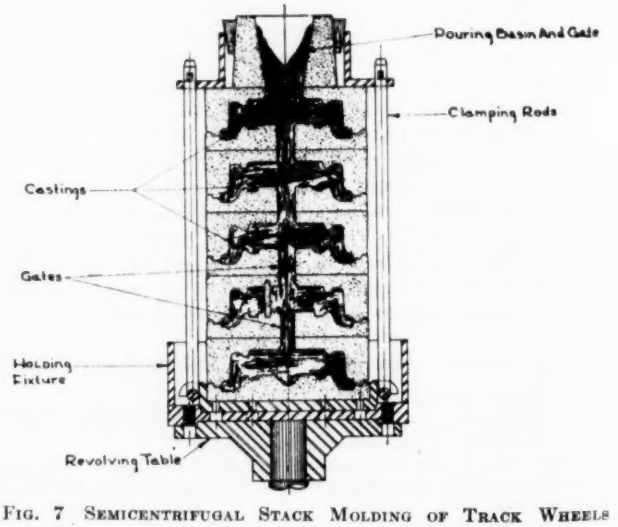


FIG. 7 SEMICENTRIFUGAL STACK MOLDING OF TRACK WHEELS

The elimination of inside cores greatly reduces the costs in the foundry as well as in the cleaning shed.

The elimination of gates and risers greatly increases the yield and in some cases 100 per cent yield is obtained. Cases in which 100 per cent yield is obtained include cast-steel hollow ship shafts, various tubing, cast-iron pipe, etc., where inside machining is not required. In castings such as radial-engine cylinder barrels where the inside machined surface is highly important, the wall is poured thicker than required. This extra thickness on the inside serves very much as an inside gate or feeder and is later removed by machining. Thus in such cases the actual yield is lower. The centrifugal method is highly adaptable for mass production of identical castings.

Semicentrifugal Method

Semicentrifugal casting consists of spinning a casting about its own axis—usually about the vertical axis. If the casting has a center cavity, this cavity is often formed with a center core, and the casting is fed by a center gate passing down around this core. Fig. 5, demonstrating this method, shows a cross section through a sand mold mounted on the revolving table of a vertical casting machine. This is a flywheel casting and is typical of the semicentrifugal method.



Fig. 8 Semicentrifugal Casting; Stack Molding of Tractor Wheels
(Mold made up ready for placing on casting machine.)

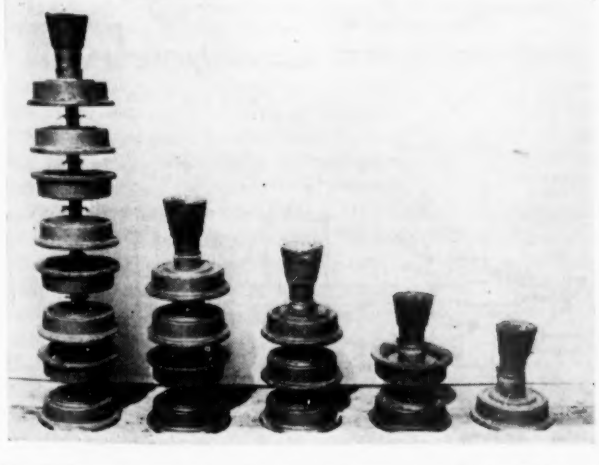


Fig. 9 Semicentrifugal Casting, Illustrating Stack Molding of Tractor Wheels

In many cases, the center is cast solid and the center cavity, if any, is machined out, or removed by an oxyacetylene torch. This is shown in Fig. 6 where the same flywheel is cast with a solid center.

Metal molds and a combination of metal and sand molds are also used. Stack molding, where a number of castings are made in one pour, is well adapted to this method. This is illustrated in Fig. 7. Fig. 8 shows a built-up stack mold ready to place on the casting machine. Fig. 9 serves to illustrate the possibilities of stack molding. On the right is a wheel casting made one in a mold, while at the extreme left it will be noted that eight castings are made on the stick. The only limitation on the number of layers used in stack molding is the convenience and economics of the handling operations. Usually a greater number of castings made on a single stick increases the foundry yield, and this factor must be considered against the problems of handling, pouring, shakeout, and other foundry problems.

Very often it is found advisable to change somewhat the design of the casting to favor gating, feeding, and directional solidification in order to obtain more uniformly sound castings. Ordinarily, this can be done without altering the usefulness of the casting, if the engineer and foundryman will cooperate.

In good practice, the gating, feeding, and provision for directional solidification are different in centrifugal molding. The gates and feeders must be designed to suit this type of molding. The foundry technique also must be changed to suit the method. Most successful foundries have found it necessary to engineer carefully each job that is to be spun, and many jobs are found better suited for static molding.

The speed of rotation in semicentrifugal casting is lower than that used in true centrifugal casting, and hence the centrifugal pressure is less. However, this rotation keeps the liquid metal in motion. This action aids in flowing the metal into all of the cavities of the mold, and in more completely feeding the casting. It further insures against blows and voids caused by contraction during solidification. This produces sounder and more uniform castings.

This method is particularly adaptable for casting wheels, gear blanks, and other circular shapes.

Centrifuging

In the "centrifuging method" the molds forming the useful castings are positioned near the periphery of the revolving table. The metal is poured into a gate located on the axis of rotation and is fed into the molds by radial sprues. Centrifugal force is used merely to provide liquid pressure. Usually, two or more castings are made in each mold.

One of the earliest applications of this method is the old-time inlay-casting machine used in dentistry, as shown in Fig. 10. A plaster-of-Paris mold was attached to one end of an arm. The other end of the arm was pivoted to and supported by a pedestal; the arm being free to revolve around the pivot. Molten gold was poured into the mold and the mold was rapidly spun around the pivot by hand. The centrifugal force of spinning forced the molten gold into the intricate cavities of the mold resulting in a very sound casting accurately shaped.

A typical example of centrifuging is shown in Fig. 11, where five bogie-wheel hub castings are made in one mold. The center gate with the five radial sprues to feed the castings is shown.

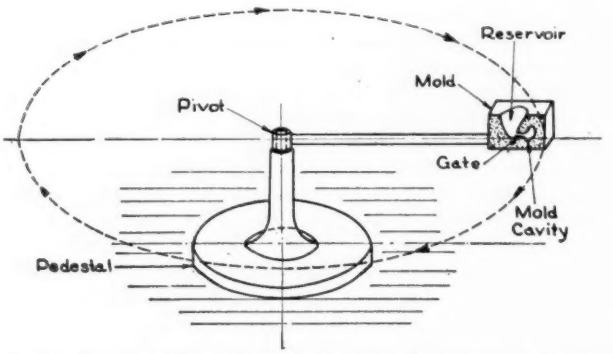


FIG. 10 DENTISTS' INLAY-CASTING MACHINE, ILLUSTRATING CENTRIFUGE CASTING

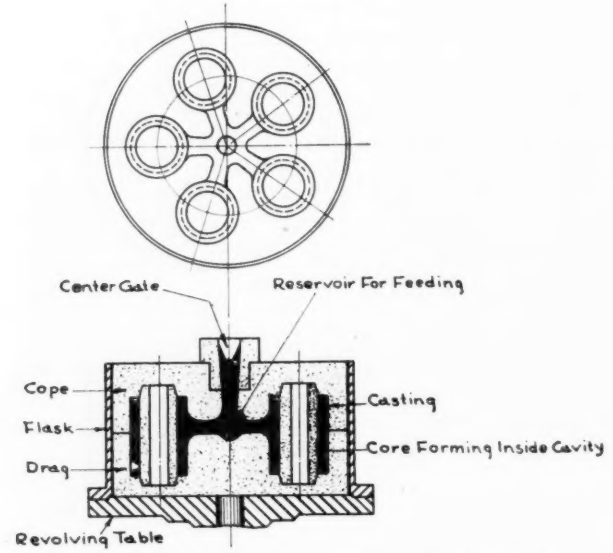


FIG. 11 CENTRIFUGE CASTING OF BOGIE-WHEEL HUBS

In this case a core is used to form the inside cavity of each casting. This method is also well adapted to stack molding, and many odd-shaped castings are made by this process. This is illustrated in Fig. 12 which shows bracket castings made by this method in one layer, and the same castings made by stack molding in eight layers.

The advantages of centrifuged casting are substantially the same as obtained in semicentrifugal casting. Yields above 85 per cent have been reported on jobs where formerly in static casting they were less than 50 per cent. On single-mold casting by the semicentrifugal method, yields have been increased from approximately 30 per cent to more than 70 per cent. The casting machines can be of simple construction, and therefore not too expensive, either in first cost or in maintenance. Floor-type units may be used which can be moved from one location in the foundry to another at little cost or inconvenience.

MACHINE CONSTRUCTION

Many different designs of centrifugal-casting machines are used. Those used in "true centrifugal" castings are of two types, i.e. (1) indirect-driven, and (2) direct-driven. In indirect-driven machines, the mold usually rests on four rollers. Two or more of these rollers are connected to an electric motor or other driving unit. Sometimes top rollers are used. A suitable pouring basin with spout, or orifice, is provided on the pouring end of the machine. This orifice, or trough, projects slightly inside the pouring end of the revolving mold. The principle of design is the same with relatively long casting machines as with short ones. Fig. 13 illustrates the usual design of this type of machine.

In making short-length castings, the mold is sometimes bolted to a face plate which is mounted on a shaft, and thus the mold is directly driven. This type design is shown in Fig. 14. There are many variations, but these two general types serve the purpose here. With both types of machines sand and metal molds are used.

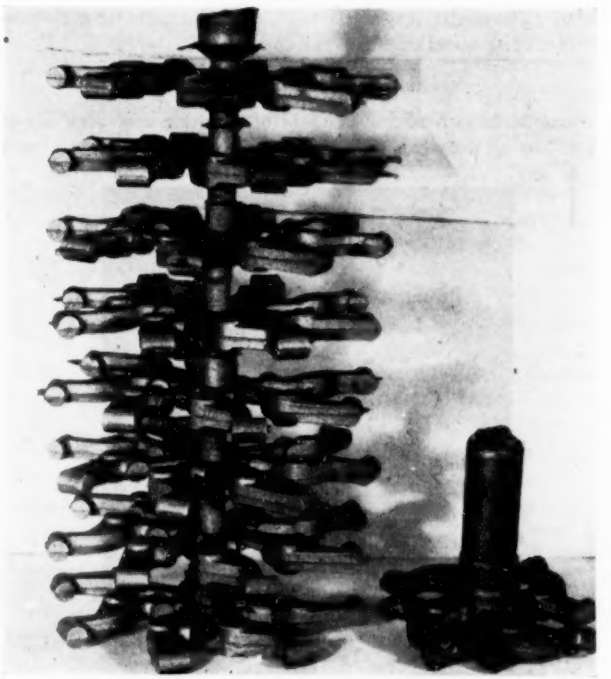


FIG. 12 BRACKET CASTINGS MADE BY CENTRIFUGING IN ONE LAYER (RIGHT); AND BY STACK MOLDING IN EIGHT LAYERS

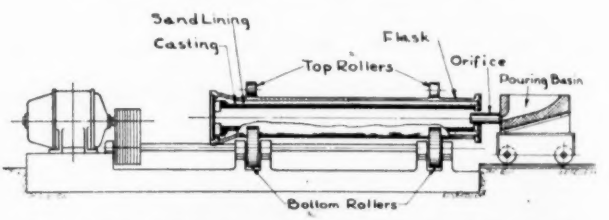


FIG. 13 TRUE CENTRIFUGAL MACHINE FOR LONG CASTINGS

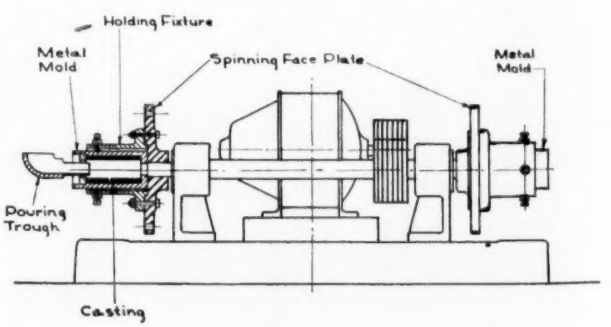


FIG. 14 TRUE CENTRIFUGAL CASTING MACHINE WITH MOLD DIRECT-DRIVEN

The machine used in the semicentrifugal method is identical with the one used in the centrifuge method. It consists usually of a vertical spindle on which a table is mounted, the flask being centered and securely clamped to the table, as shown in Fig. 15. Sometimes floor-mounted units with bevel-geared drives are used. This type of machine is illustrated in Fig. 16.

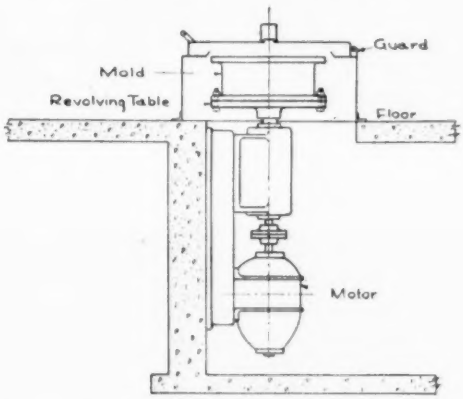


FIG. 15 PIG-TYPE CENTRIFUGAL CASTING MACHINE

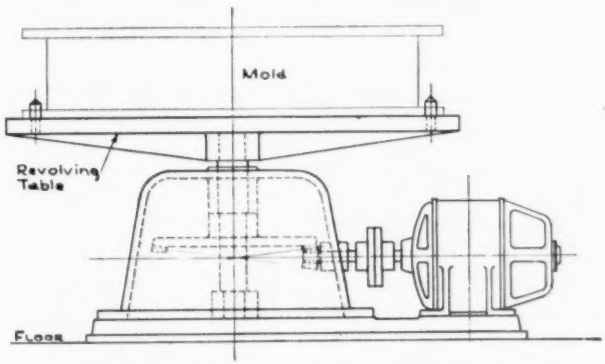


FIG. 16 FLOOR-TYPE CENTRIFUGAL CASTING MACHINE

Drives. Many types of motors have been used to drive centrifugal casting machines. Usually a speed range of 3 or 4 to 1 will meet all the requirements, and any driving unit with this range will be adequate.

TYPES OF MOLDS USED

Both metal and sand molds are being used extensively in producing castings by this method. Carbon or graphite molds have also been used for casting nonferrous metals. Each kind of mold has its place in centrifugal casting, and the type of casting to be produced usually determines the kind of mold best suited.

Permanent molds are best adapted (1) where large quantities of identical castings are to be made, (2) where the outside contour of the casting is such that it can be readily withdrawn from the mold after casting, and (3) where a fast cooling rate from the outside inward with attendant fine grain is desirable. They are also better suited for castings which have relatively uniform wall thicknesses, or without abrupt changes in wall thickness.

Permanent molds are usually made of cast iron or steel. When cast-iron molds are used, it has been found desirable to have a cross-sectional area of the mold 4 to 5 times that of the casting produced. The life of a permanent mold is dependent upon many factors and foundry techniques which have not yet been fully explored. Usually metal molds are kept at temperatures between 400 F and 800 F, during the casting operation. It is the usual practice to coat the mold with some form of facing between casts to protect it.

Sand molds are generally preferred (1) in the casting of long tubes where the metal must flow relatively long distances over the mold surface, (2) where the shape of the casting is such that the mold must be broken down to remove it, (3) where it is essential to be able to vary the dimensions and shapes of similar castings, (4) where relatively few identical castings are to be made, and (5) where a relatively uniform cooling rate through a thick section is desirable. Sand molds more commonly used are dry-sand, skin-dried, and oil-sand, and they are usually faced to prevent cutting. The cooling time of castings made in sand molds is much longer than in metal molds, thus the casting is free of chilled surfaces and is likely to have fewer casting strains. The sand used for centrifugal molding must be much stronger than in static molding to resist the added pressure and vibration caused by spinning. Usually it is found advisable to have a sand with higher permeability than that used in static molding.

Quite often a combination of metal molds and sand molds is used. Where it is desired to core holes of various shapes in castings, cores are used with the metal molds for this purpose. Often it is desirable to relieve the chill in certain portions of the casting, and this is done by using dry-sand cores. In some cases, there is a serious cutting action on the mold where the metal enters during the casting operation. A dry-sand splash core inserted in the metal mold to prevent this cutting action will materially lengthen the life of the metal mold.

MANY SPEEDS USED IN CENTRIFUGAL CASTING

In the manufacture of centrifugal castings a wide variety of mold speeds is used. The terms usually referred to are "peripheral velocity," and number of "times gravity" centrifugal force, or pressure, against the mold wall. The casting speed is linked with a number of other factors, such as pouring time, size and shape of casting, wall thickness, method of centrifugal casting being used, and others.

A general rule in the manufacture of relatively thin-wall tubes by the horizontal true centrifugal method in sand-lined molds is a speed of rotation which will produce a centrifugal force of 75 times gravity. Although this rule is generally accepted, it might be said that a favorable speed would be the lowest which would prevent "raining" during the pouring operation and yet provide enough force to squeeze out the foreign inclusions in the metal.

In practice the rotational speed of metal molds usually will be found lower than with sand molds, approximately 60 times gravity. This is because the chilling effect of the mold causes the molten metal to "pick up" more readily than in the refractory sand mold.

In the manufacture of cast-iron pipe in sand molds, the general rule is 75 times gravity. The general rule in the manufacture of cast-iron pipe in water-cooled steel molds is from 900 to 1250 fpm peripheral velocity, depending upon the size and thickness of the pipe to be cast.

An examination of the rotational speeds used by the various successful steel foundries leads to the conclusion that speed is not critical. Certainly it can be said that the ideal rotational speed cannot be determined at present, in the light of the many variables involved in true centrifugal casting of metals.

Likewise, there is a wide variation of rotational speeds used in semicentrifugal casting and in centrifuging. By both of these methods castings are being successfully made with peripheral speeds on the outermost part of the casting of from 100 to 1000 fpm. Here again, factors such as gating, pouring time, size and shape of casting, and type of mold used are to be considered. In

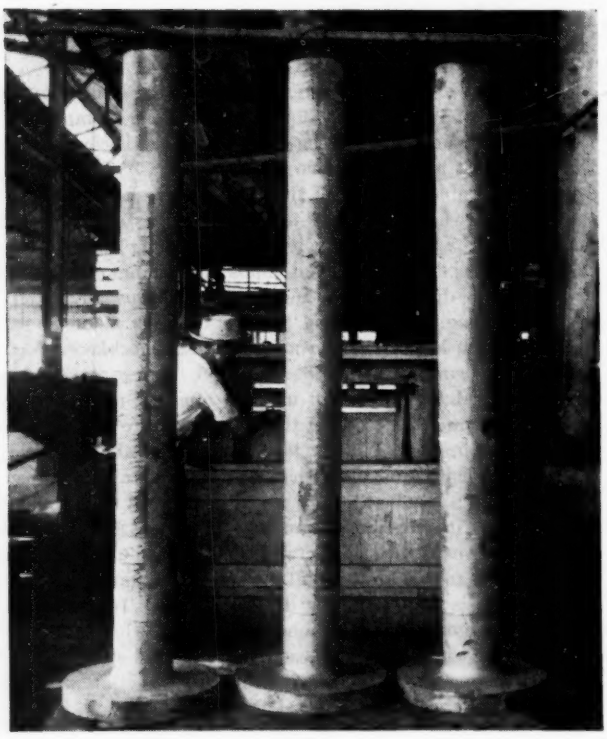


FIG. 17 RUDDER STOCK, FABRICATED FROM CENTRIFUGALLY CAST TUBING, WELDED TO STATICALLY CAST FLANGE SECTION

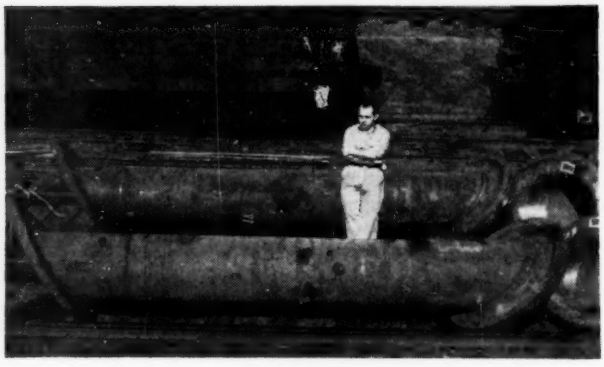


FIG. 18 HAWSE PIPE FOR SHIPS
(Main section centrifugally cast as a tube. Welded-on deck and shell bolsters were statically cast.)



FIG. 19 SHAFTING FOR SHIPS
(Centrifugally cast in 16-ft lengths.)

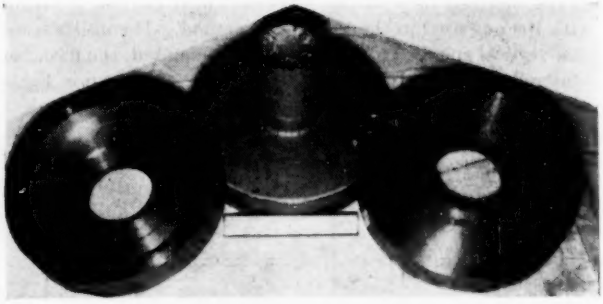


FIG. 20 ENGINE FLYWHEELS
(Centrifugally cast in vertical-axis machines in sand molds.)

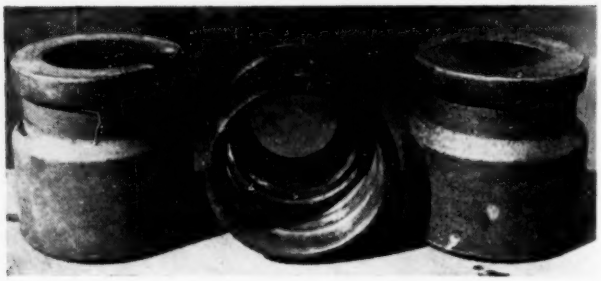


FIG. 21 IDLER WHEEL HUBS
(Centrifugally cast in horizontal-axis machines, using sand-lined molds and cores.)



FIG. 22 CYLINDER BARRELS FOR RADIAL ENGINES
(*Left:* As cast. *Center:* Rough-bored and turned. *Right:* As finished by the engine builder.)

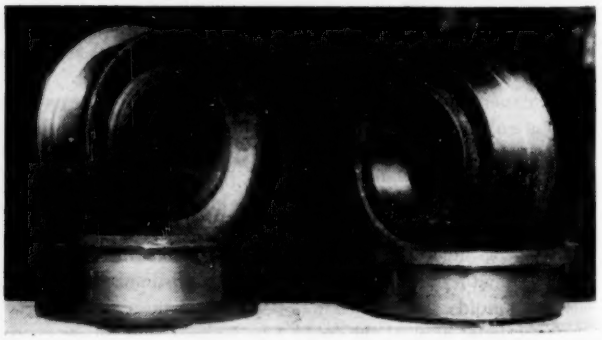


FIG. 23 TRACK-WHEEL RIMS FOR CRAWLER-TYPE TRACTORS
(Single-flange and double-flange track roller rims, cast centrifugally in vertical-axis machines. High-carbon steel for special quench heat-treatment to provide shrink fit on hubs.)

some cases the mold is filled with molten metal before revolving. In other cases the mold is poured at slow speed and then brought up to full casting speed.

Typical examples of centrifugal castings made by the author's company are shown in Figs. 17 to 23.

Physical Properties

The present emergency has given sharp impetus to the development and the production of centrifugal steel castings, not only as an improvement over static casting methods, but to produce parts formerly thought possible only by forging. Most of the physical properties of these castings have been found to compare favorably with those of forgings and, in many cases, to be better, depending upon how the casting is used.

The physical properties of centrifugal castings are practically the same as sound static castings. However, the ability to consistently produce sound homogeneous castings has made it possible to cast engineering parts that were not thought possible a few years ago. Once the foundry routine is adjusted, greater uniformity of product is usually obtained.

Compared with forgings it may be said that some centrifugal castings can be produced nearer to finished dimensions with consequent saving in machining cost. To illustrate, Fig. 24 shows

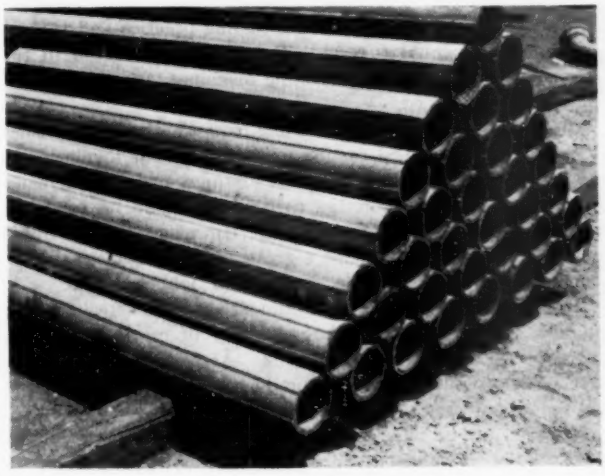


Fig. 24 Fluted-Tubes Stators

fluted tubes cast in 16 ft 0 in. lengths, later fabricated into small electric-motor stators. The as-cast tube is $4^{3}/_{4}$ OD and $4^{1}/_{16}$ ID. The OD tolerance of the casting is $\pm^{1}/_{64}$ in.; ID is $\pm .08$.

In forgings the physical strength and ductility values are higher in the direction of rolling than those taken across the direction of rolling. In a sound steel casting these values are equal in all directions, and in many cases advantage can be taken of this characteristic. Cone[3] has reported bursting tests of forged vs. centrifugally cast airplane cylinder barrels. The forgings split longitudinally at lower pressures than the bursting pressures of cast barrels. The cast barrels also showed greater "bulge" deformation. McCarroll[4] has also reported centrifugally cast gears to have better over-all properties than forged gears.

It should be pointed out that the chief advantage of this process is its ability to produce *high-quality* castings rather than low-cost castings. Adequate equipment and competent personnel for making chemical and physical tests on the product are essential. Rigid routine control on metallurgy, melting, sand conditioning, and the other factors of the process must be maintained to insure high-quality castings.

[3] "Centrifugally Cast Cylinder Barrels for Airplane Engines," by E. F. Cone, *Metals and Alloys*, vol. 16, no. 6, December, 1942, pp. 1062–1066.

[4] "Progress in Automotive Steel Castings," by R. H. McCarroll, *The Foundry*, vol. 66, no. 10, October, 1938, pp. 30, 31, 72, 74, and 77.

Conclusions

No one experienced in the art would venture to say that these methods of molding will revolutionize the steel-foundry industry or replace the great bulk of work done by forging. The size and shape of the casting place definite limitations on the process. However, the centrifugal method of casting is ideally suited for producing a vast variety of work. It is a relatively new method that is rapidly finding its place in the economic production of high-quality engineering parts.

Discussion

J. B. Caine.[5] This paper describes a noteworthy contribution to this increasingly important method of forming metals. To the writer, at least, the economic importance of this new process should not be overlooked. It is incontestable from the theoretical standpoint that the most efficient method of forming a shape slightly more complicated than a round or flat is by casting. The reason that steel castings have not been able to compete in price with other methods of forming relatively simple shapes in quantity has been the necessity of making an individual mold for each casting and that steel shrinks during solidification. This solidification shrinkage necessitates the use of such large risers to supply liquid steel to the solidifying casting that the steel foundry must pour twice as much metal in the average mold as that required for the casting.

If the design of the part permits the use of permanent molds and the true centrifugal process, an individual mold for each casting is not required, and, as the author states, yields approach 100 per cent. Casting is then the most efficient method known of forming these parts. If the part is more complicated, the semicentrifugal and centrifuging processes, although requiring an individual mold for each casting or group of castings, increase the all-important yield and therefore improve the competitive position of castings.

There is at least one other advantage that the author has not stressed, namely, the use of centrifugal force to impel molten metal into thinner sections than can be cast statically. With increasing emphasis on strength-weight ratios, it will be necessary to cast thinner and thinner sections to take full advantage of high-strength cast steels. A corollary of this is, of course, the use of centrifugal force to cast fine detail and within tolerances measured in thousandths of an inch.

Nathan Janco.[6] This paper is an excellent summation of the centrifugal process of casting steel, and its progress up to the present time. The various methods of centrifugal casting are clearly outlined, as well as some of the details of the actual production methods. The paper certainly should be of considerable interest to practical foundrymen, as well as to mechanical engineers concerned with the design of steel parts.

In the production of semicentrifugal castings, or castings produced by the centrifuging method, it is essential that conditions for directional solidification be set up, in order to obtain perfect castings. In a great many cases this can be accomplished only by pouring the metal into the mold while the mold is revolving. However, if the metal is poured into the mold at the usual speeds

[5] Metallurgist, Sawbrook Steel Castings Company, Lockland, Ohio.

[6] Chief Engineer, The Centrifugal Casting Machine Company, Tulsa, Okla. Mem. A.S.M.E.

used for spinning, the erosive action of the metal upon the sand-mold surface will be excessive and dirty castings will result. This is extremely important as it is to no avail if metallurgically perfect castings are produced and then have to be scrapped because they are dirty. During the past few years, this difficulty has been overcome by pouring the metal into the mold while the mold is rotating at speeds between 10 and 25 rpm. After the mold is full, or partially full, it is accelerated to the proper spinning speed. This has been found to be very successful in the elimination of dirty castings. A greater speed range than 3 or 4 to 1 is necessary in a centrifugal casting machine in order to accomplish the desired result.

The writer's experience concerning rotative speeds agrees with that of the author. A general average of the speeds used for the various types of centrifugal casting work, and which covers a very large percentage of all types of castings is as follows:

True Centrifugal Castings:

1 Sand-lined molds; speed, 60 to 75 times gravity.

2 Metal molds; speed, 40 to 60 times gravity.

3 Sand or metal molds, vertically spun; (generally castings whose length does not exceed 2 times the casting inside diameter); speed, 75 to 125 times gravity.

Semicentrifugal or Centrifuging Methods: Speed 600 to 1000 fpm; average, 800 fpm.

Centrifugal castings produced by the precision casting method, or "lost-wax" process, are castings which generally have very thin metal sections and usually are spun at rotative speeds below 600 fpm. In this case no advantage is being taken of the pressure of metal resulting from centrifugal force. The centrifugal casting machines are used only to provide a method of keeping the metal in motion, and thus permit the metal to run into thin sections and to obtain sharp definition.

The density and other physical properties of a perfect centrifugal casting do not differ from those obtained from a statically cast test bar which is a perfect casting. The principal advantage of centrifugal casting is that it is practical to produce castings in quantity which have physical properties approaching the best obtained in a test bar and yet achieve a high metal yield. To obtain such results by static casting methods is likely to be difficult and expensive.

E. C. Jeter.[7] There is a definite opportunity for the expansion of the already wide field of centrifugal castings. Sometimes, however, certain groups are prone to become overenthusiastic and to apply this method to a wide variety of parts, many of which would better have remained as forgings or as static castings.

Some of these are of such a design that centrifugal casting methods could not guarantee freedom from defects, and thus centrifugal castings would not be good enough from a quality standpoint. Physical-property requirements might be above those which can be met by centrifugal castings, although there probably would not be many such cases.

Other parts might be of such design that static castings would be of high enough quality and more economical. The simplicity of design might indicate that a forging would be more economical than either a centrifugal or a static casting. Unless castings are of such design as to be centrifugal "naturals," such as flanged cylinder barrels and symmetrical castings of that type, a static casting might be good enough or be more economical, unless for some reasons of design a very great saving in gates and risers is obtained.

In the final analysis the centrifugal method of casting should be applied intelligently to the parts for which it is best suited. Promiscuously making a wide variety of castings, many of which are not adapted to centrifugal casting methods, will do more harm to this field than any other one thing.

Anton Johnson.[8] The author has described comprehensively the various methods of centrifugal casting practice and the applications best suited to each. Details are also given in the paper of types of centrifugal casting machines, and the jobs for which each is adapted.

Confirming the author's concluding remarks, the writer wishes to state that centrifugal casting methods will not revolutionize the steel-foundry practice of static castings, owing principally to the fact that large-tonnage castings can now be produced statically, with resultant high yields. However, the centrifugal casting method can be applied a great deal more widely than is commonly believed possible, even in a jobbing shop. The writer's company operates a medium-sized electric steel jobbing foundry, which produces a large variety of castings with an average weight of 20 lb per casting. As high as 25 per cent of the monthly output has been produced by the semicentrifugal and the centrifuging methods?

Will the author please advise what is the dry permeability of the sand in centrifugal practice, and why a higher permeability is used than in static practice? Also, what method is used in pouring stack molds, i.e., are they stationary when poured, and then spun? If spun, what has been the author's experience, if any, with misruns or cutting of molds?

[7] Ford Motor Company, Dearborn, Mich.

[8] Works Manager, Oklahoma Steel Castings Company, Tulsa, Okla.

Some Characteristics of Rotary Pumps in Aviation Service

By R. J. S. PIGOTT,[1] PITTSBURGH, PA.

Only within recent years have rotary pumps been accorded a semblance of the technical consideration which has been expended upon the piston or plunger reciprocating type, and the centrifugal and turbine types, between which two groups occurs its sphere of greatest usefulness. The rotary can handle all pumpable viscosities at any pressure up to 1000 psi. It has other qualities such as the ability to handle liquids with considerable gas or vapor present. The present paper is devoted to a discussion of characteristics of gear- and vane-type rotary pumps which make them widely adaptable to lubrication-oil, fuel-oil supply, and other aircraft uses in which they predominate.

THE group of positive-displacement pumps generally known as rotary pumps lies between the piston or plunger reciprocating pumps, which are also positive displacement, and the centrifugal and turbine pumps, which are not. Rotary pumps have never received the amount of technical attention accorded the two other large groups, chiefly because, like the bat, they occupied a position between the "birds and the beasts." However, this stepchild of the pump family has come in for much more attention during the last 10 years than formerly, since it has been finally discovered that, given the same degree of design skill, the rotary pump is quite as good as, and in many cases better, than the other two general types, when applied in its proper sphere. The following generalizations can be made which apply to the whole field of applications:

Centrifugal pumps are best on low-viscosity liquids, such as water or light oil, and relatively large quantities at low or moderate pressure. The efficiency falls off badly at 2500 sec S.U. viscosity, and centrifugals are of no use whatever above 5000 sec S.U. The efficiency also falls off rapidly with reduction of size below 100 gpm, unless particularly fine design and smooth finish of impellers and passages are employed. The reciprocating pump is good on either high- or low-viscosity liquids, for all pressures, especially for high pressure, and for any size above 1 gpm. The centrifugal is always cheapest and smallest, in the field where it is best fitted. The reciprocating pump is always largest and most expensive, but has the high-pressure field (1000 psi up, at moderate to large size, all viscosities) almost to itself. There lies in between a field which the rotary may often fill better than either; it can handle all pumpable viscosities in any size, at any pressure up to 1000 psi. Two particular designs are satisfactory up to 3000 psi in small sizes, the radial-plunger and the axial-plunger designs. Durability is, in general, less than that of reciprocating pumps.

The rotary can also handle liquids with considerable gas or vapor present; the reciprocating pump is apt to develop difficulties under these circumstances, and the centrifugal gives up completely.

The rotary has now taken a prominent position in machine-tool operations, including presses for all sorts of oil-pumping duty, and may handle a variety of queer liquids like glue and tomato sauce, that are not very manageable with the two older and more considered types.

But in airplane service, practically all the pumps used are rotaries, mostly gear and vane types for lubrication and fuel supply, with some axial plunger types for hydraulic operations. We therefore become immediately interested in a study of inlet-side losses, as well as in general performance with and without air or vapor present in quantity. There have been serious failures of such pumps at high altitudes, particularly when air or vapor is present.

It is high time some of the hydraulics of such pumps were given the attention needed to provide good designs and installations for the purpose, i.e., successful high-altitude operation.

So little seems to be clearly perceived about capacity and efficiency that it even appears necessary to restate some principles which should be obvious.

The principal types of rotary pumps are as follows:

1 Gear: (*a*) Spur or helical external gear (any lube pump, aeronautic). (*b*) Straight or helical internal gear (Feuerheerd, Hill, Pigott).

2 Vane (Pesco, Chandler Evans, Vickers).

3 Oscillating piston (Kinney).

4 Screw: (*a*) Two screw (Quimby). (*b*) Three screw (Imo)

5 Plunger: (*a*) Radial plunger (American Engineering, Oil Gear, Northern). (*b*) Axial plunger (Waterbury, Vickers).

6 Lobular (Roots, Northern).

The following discussion applies to all types, but since we are for the moment most interested in the aviation applications, the examples and test data will be largely from gear and vane types.

Displacement of Gear Pumps

Many formulas for the displacement of spur and helical external-gear pumps have been used and published. All of those with which the author is familiar are based upon incorrect theory of what constitutes clearance volume, and some in rather general use are as much as 15 to 20 per cent in error.

The proof of this statement is that for years pump manufacturers have published test curves showing, for example, volumetric efficiency of 85 per cent at zero pressure difference. How can there be any leakage, or "slip," if there is no pressure difference? A pump always delivers substantially its full displacement at zero pressure difference, unless it is so badly designed as to be cavitating, or there is gas or vapor present.

Referring to Fig. 1, in a spur-gear pump, the full tooth-space volume of both gears is delivered around the outer side of the gears from suction to discharge side. The volume that is returned to suction from the discharge side is that which is sealed off from both sides, at the instant when two pairs of teeth first contact (seal point, see Fig. 1*a*). It is quite apparent that this volume has no relation to the volume under one tooth when fully meshed with the mating teeth on the center line between gears;

[1] Chief Engineer, Gulf Research & Development Company. Fellow, A.S.M.E.

Contributed by the Hydraulic Division and presented at the Semi-Annual Meeting, Pittsburgh, Pa., June 19–22, 1944, of The American Society of Mechanical Engineers.

Note: Statements and opinions advanced in papers are to be understood as individual expressions of their authors and not those of the Society.

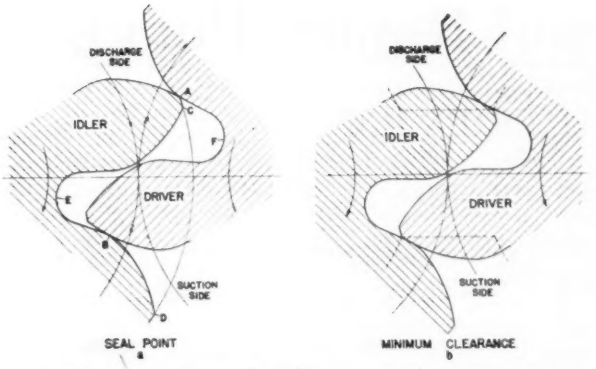


FIG. 1 SPUR-GEAR PUMP, SEAL-POINT, AND MINIMUM-CLEARANCE DIAGRAMS

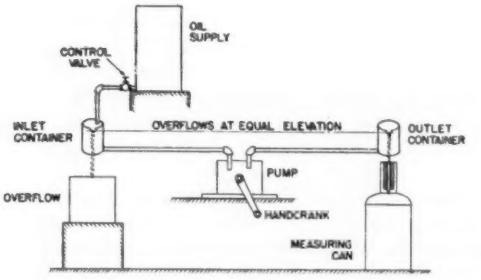


FIG. 2 HAND-CRANK DISPLACEMENT TEST

the latter is the usual clearance volume used for most displacement formulas.

Referring to Fig. 1*b*, the two pairs of teeth are now symmetrically placed on either side of the center line; this is the position of minimum volume and is 1 to $1^1/_2$ per cent less than that at the seal point, depending upon the number of teeth and the angle of attack. This seal-point area, and that of the tooth space, can be accurately planimetered, say on 10-times-scale drawing. The proof that this operation gives displacement and clearance volume correctly is as follows:

Fig. 2 shows a pump set up for the "hand-crank test." The two reservoirs are arranged with weirs for holding the static head the same on suction and discharge; the intake side is slightly oversupplied from another tank, so that there is always a slight overflow at the weir. The pump is then slowly hand-cranked, say 100 revolutions, and the overflow from the discharge-tank weir is measured in a suitable container, i.e., a glass graduate, or a standard test can. Since there is no difference in static head, and no measurable flow loss in the pump, at very slow rotation, there can be no slip.

The results of many hand-crank tests check planimeter values within 0.1 to 0.2 per cent, much better than usual pump-test deviations. It is important to have the displacement value as nearly exact as possible, since all systematic analyses of slip and mechanical losses depend upon it, and the effect of air or other compressibles can be calculated correctly only when the displacement and clearance volume are accurately known.

A convenient proof of no slip is to perform the hand-crank test on two liquids of widely different viscosity, for example, kerosene and an S.A.E. 30 lube oil. Since the slip is inversely proportional to viscosity and directly as pressure, the two values for displacement will always differ, if there is any pressure difference in the pump due to internal losses dependent upon speed of rotation. This can be shown by cranking too fast. When the two values agree, there is no slip and no pressure difference; the value is then exactly the displacement.

SLIP AND MECHANICAL LOSSES

The losses in any rotary pump can be divided into two classes, which can easily be segregated in an ordinary performance test. We can, from the test and the displacement, obtain delivery in gallons per minute, displacement gallons per minute, water horsepower, displacement horsepower, and brake horsepower.

If we divide total losses into slip and mechanical losses, we can get two general values of considerable usefulness. These two values aid in detecting what details of a pump should be changed to obtain improved results.

Slip, obtained from (displacement gallons per minute—delivery gallons per minute) can be correlated with pressure difference across the pump, viscosity, and speed. Mechanical losses comprise bearing and shaft-packing friction, viscous shear in running fits at teeth or vanes, and sides of rotor, and for convenience, the hydraulic inlet and outlet losses, such as port skin friction, losses due to turns in ports, or diffusion streams, and centrifugal

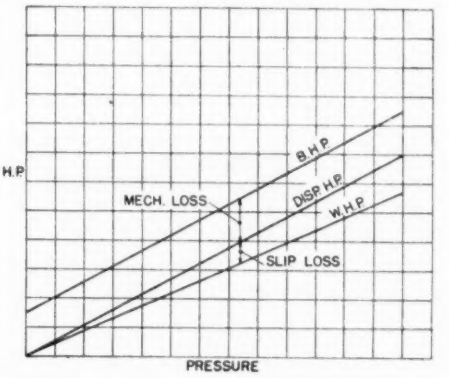


FIG. 3 CONSTANT SPEED AND VISCOSITY, VARYING PRESSURE

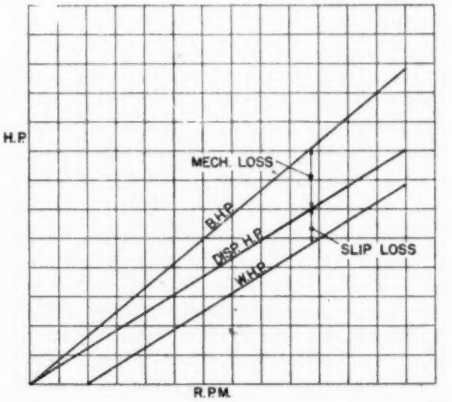


FIG. 4 CONSTANT PRESSURE AND VISCOSITY, VARYING SPEED

effects. Every positive-displacement pump pumps the full displacement volume, but some leaks back to suction, after the work has been done on it. Slip horsepower loss is therefore merely the difference between displacement horsepower and water horsepower as delivered. Friction horsepower, or mechanical loss, is the difference between brake-horsepower input and displacement horsepower. Fig. 3 shows the analysis for a pump running at constant speed and viscosity of liquid, varying pressure. Fig. 4 shows the same for varying speed, pressure difference, and viscosity constant.

After some struggles, we succeeded in calculating the slip and friction of rotary pumps closely enough to predict what the per-

formance should be on test, within a few per cent. It is a somewhat tedious job, but mathematically simple. Some general forms indicate the nature of the losses.

Since all rotary pumps are capillary-sealed, i.e., close fits, the flow for most liquids above water in viscosity and at pressures less than 500 psi will be in the viscous region and follow the general formula

$$\Delta p = \frac{0.00173\ \mu l v}{b^2}$$

where

Δp = pressure drop, psi
μ = viscosity, Reyns (= centipoises × 0.000672)
l = length of capillary path, ft
v = velocity, fps
b = clearance, ft

If the value of $\frac{2b\rho v}{\mu}$ is greater than 1200, the flow is turbulent and follows the law

$$\Delta p = \frac{0.000054\ f l \rho v^2}{b}$$

where f is the friction factor and ρ is the density in lb per cu ft.

If the clearances are not in excess of 0.010 in., and ordinary ground finishes are used, the passage may be considered rough, f becomes constant at 0.054, and viscosity has no effect. For finer finish and larger clearances, roughness is low enough to make f vary with Reynolds number, and the author's curves[2] for this purpose may be used. The maximum effect of viscosity with perfectly smooth passages would be 0.25 power of μ.

The teeth of gears not in pressure contact, such as may be found in the internal-gear pumps at the out-of-mesh position, and the rounded tips of vanes have substantially a line seal, consequently, they may be treated as rounded-approach orifices; they will be in the turbulent region at considerably higher viscosity or lower pressure than the relatively long path seals. Sides of gears, vanes or rotors, and square tops of external-gear-pump teeth will nearly always be in viscous flow.

In pumps operating at fairly high rotative speed, low or moderate pressure and very viscous liquids, there is a noticeable temperature effect, owing to the high rate of viscous shear in the capillary-seal areas, and to heat added by the energy loss from slip.

This effect may be great enough to reverse the expected and usual reduction of slip, with increase of viscosity, by heating the liquid in the clearance spaces and thus reducing the viscosity therein. For example, a pump running at 1150 rpm, peripheral speed of gear 34 fps, 100 psi pressure, the slip reaches a minimum at about 1500 sec Saybolt viscosity, and thereafter increases with viscosity of the pumped liquid.

From the foregoing, external-gear-pump slip will be largely in the viscous region for aviation lubrication pumps and slip will therefore vary chiefly as p/μ. In any case, the majority of the pumps in aviation service operate at pressure ranges from 10 to 100 psi and on viscosities of not less than 30 cp (hot), so that the slip is not very large anyway, usually 3 to 6 per cent.

The mechanical losses are more troublesome to calculate, and since there is not much interest in the matter for airplane pumps except perhaps the hydraulic pumps, it will not be detailed here.

[2] "The Flow of Fluids in Closed Conduits," by R. J. S. Pigott, *Mechanical Engineering*, vol. 55, 1933, pp. 497–501, 515; also Kent's "Mechanical Engineer's Handbook," John Wiley & Sons, Inc., New York, N. Y., 1936.

Inlet-Side Losses

The inlet-side losses become extremely important for both oil and fuel pumps in high-altitude flying, and hitherto this interesting and valuable field of investigation has been almost completely neglected. A vacuum gage at the inlet connection of a pump gives slight indication of the minimum absolute pressure within the running parts of the pump.

Referring to Fig. 5, it is seen that one of the forces opposing

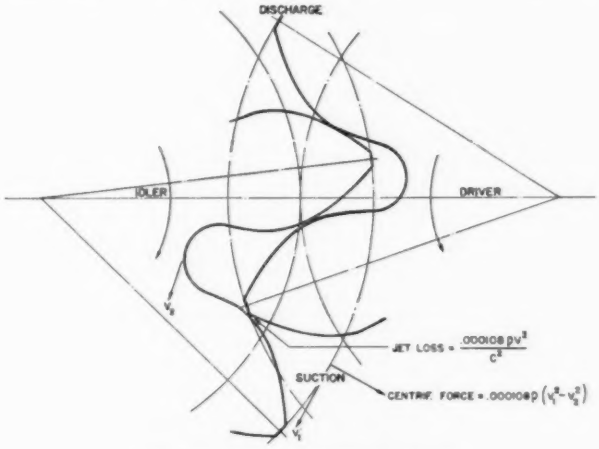


Fig. 5 Spur-Gear-Tooth Loss

flow is the centrifugal force of the ring of oil in the teeth; the second loss is the jet head required to flow the oil between the tip of one tooth and the side of the mating tooth, so as to supply the increasing volume of the space enclosed by these teeth. A third loss is the suction chamber, or port loss, and consists of the skin friction, and the diffusion of the stream from a round pipe to a much larger square section in a very short distance.

While the author has calculated these losses with quite reasonable success, fortunately it is unnecessary to depend upon any estimates, as the inlet-side loss is very easily measured.

The theoretical analysis shows, however, that the suction-side loss does vary at different positions of the gear teeth or vanes, and the measured loss by test is an intermediate value between the maximum and minimum calculated loss.

Two test methods will yield the total inlet-side losses directly. It is necessary that the liquid used have a very low vapor pressure, and be substantially free of dissolved gases. Ordinary lubricating oil, S.A.E. 10 to 50, has a very low vapor pressure, but may contain dissolved air up to 8 or 9 per cent by volume, at 1 atm and 68 F. A convenient stripping method is to restrict the inlet of the pump by means of a valve, and operate the weigh system with the pump cavitating 50 or more per cent of its normal capacity, circulating the whole body of oil in the system 5 to 10 times. Then make the cavitation tests immediately, before any appreciable air is reabsorbed. This method does quite well for most tests, but since air is slowly reabsorbed, and moreover does not strip completely, the method is not rigorous but represents rather closely the best that may be obtained in flight. A better method for air-free determinations is to use a vacuum tank weigher and operate the whole system under vacuum, sealing at possible leak points such as pump-shaft packing and valve stems with suitable oil supply. By this method, all air is positively stripped out. One method of test is to run the pump at constant differential pressure, increasing speed until the pump begins to cavitate. Fig. 6 shows such a test. Up to the cavitation point, since slip varies with $\Delta p/\mu$, and both Δp and μ are constant, the slip is constant, and the delivery line parallels the displacement.

At the point where the delivery line first departs from parallelism to the displacement line, the remaining pressure difference between the absolute pressure, measured at the inlet flange, and the barometer, is equal to the required pressure to deliver full flow to the pump.

By restricting the inlet with a valve, the pumps can be made to

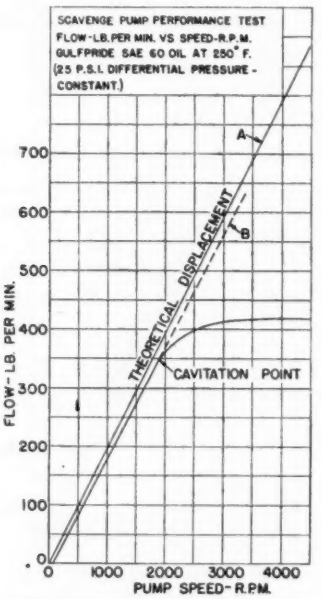


FIG. 6 SCAVENGE-PUMP PERFORMANCE TEST

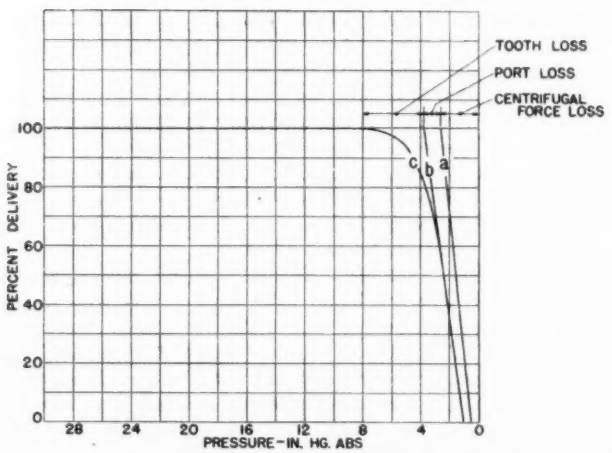


FIG. 7 CAVITATION TEST, CONSTANT SPEED

cavitate at a lower speed, and a plot made of pump loss versus speed.

The other method is to operate at one or more fixed speeds, constant pressure differential, and restrict the inlet until the pump cavitates, and this can be continued down to the point of pump instability. This method yields the same results and also gives performance curves exactly as the pump behaves in high-altitude flying. Moreover, it is a more convenient plot for performance testing with entrained air present, as also occurs in flight. This method of test is shown in Fig. 7. The centrifugal force is shown at a. Its value decreases from the full amount, $\Delta p = 0.000108\rho(v_1^2 - v_2^2)$ with "solid" oil, to 20 to 30 per cent of this amount at zero delivery. The reason is plain—as the pump goes into cavitation the amount of oil does not fill the tooth space. The remainder is oil vapor (no air is present). The effective density is therefore reduced and with it the centrifugal force. Centrifugal force does not decrease to zero at zero delivery, because if the differential pressure across the pump is maintained, the slip remains the same and returns to suction, and the clearance volume is also returned to suction, so that the pump at zero delivery must actually still be pumping slip and clearance volume in order to maintain pressure.

For example, in Fig. 7, the full centrifugal force is 2.77 in. Hg with the tooth spaces full of oil. The slip is 5.69 per cent of displacement, clearance volume 25.8 per cent of displacement, a total of 31.49 per cent. This value must be reduced to tooth volume as follows, remembering tooth space is displacement plus clearance: $\frac{31.49}{1.258} = 25.0$ per cent.

That is, the tooth space is 25 per cent oil, 75 per cent air or oil vapor. Neglecting vapor weight, the effective density is then 25 per cent of that full of oil, and the zero delivery centrifugal force will therefore be $2.77 \times 0.25 = 0.69$ in.

The calculated port loss added to the centrifugal force (line a) gives line b which coincides with the test line c from zero delivery up to about two thirds of full delivery, when the test line c shows a further loss, i.e., the tooth loss (see also Fig. 5). This curve shows an effect that is logically to be expected. Calculation of this loss from the simultaneous values of increasing volume and the area of the opening between the teeth, including side pockets (if any) shows that the initial tooth loss is high at the seal point, decreases rapidly as the teeth come out of mesh, and vanishes when the teeth are fully out of mesh; about 45 deg with seven teeth, for example. When inlet absolute pressure exceeds the full tooth loss, this region of high loss has a pronounced effect, but as the inlet pressure is reduced, cavitation starts in the full-mesh region in each pair of teeth and extends farther and farther as the inlet pressure is reduced an additional amount. The result is

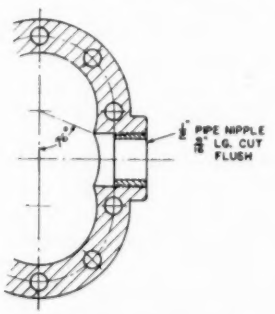


FIG. 8 SPUR-GEAR PUMP, CONDITION NO. 1

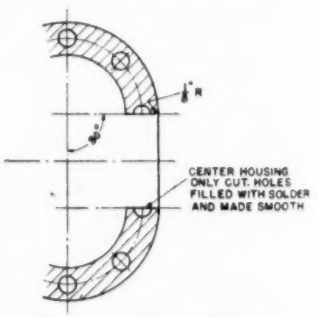


FIG. 9 SPUR-GEAR PUMP, CONDITION NO. 1-A

that the high-loss region is less and less well filled, consequently, the average tooth resistance drops off and finally vanishes altogether. At this time most of filling is done in the open region after the teeth are out of mesh, where there can be no tooth resistance.

These calculations are made mainly to disclose the nature and variation of the three losses; quantitative results are easily obtained by test. But such calculations show the path for improvement.

For example, one immediate indication is that the arc of gear exposed to entry of fluid on the suction side has importance. Many gear pumps are built, as shown in Fig. 8, with very little arc exposed to suction side. When opened up to 90-deg exposure, the reduction of break-point was from 7 in. to 5 in. Hg. The optimum arc exposed is 90 deg to not over 135 deg, from the center line of the gears, shown in Fig. 9.

Effect of Clearance Volume and Air

Clearance volume in a rotary pump corresponds, in a piston pump, to the space between piston and cylinder head at the end of the stroke, together with the volume of the ports from the cylinder to the valves. There is, however, a difference in operation; in the piston or plunger pump, the clearance volume is never delivered to the discharge chamber, whereas in a gear pump, the whole tooth space (which includes the clearance volume) delivers to the discharge chamber, and the clearance volume then takes a fraction of this volume back again to the suction.

If a liquid, no gas present, is handled, the clearance has no effect on the delivery; it is simply displacement minus slip. But if air or other compressible gas is present, the clearance has a pronounced effect upon performance, much the same as in a compressor.

The tooth space supplies all the oil that will reach the discharge chamber, but a volume of oil leaks back as slip, mixed of course with the compressed air, and a volume of oil and air is also returned to the suction in the clearance volume. All quantities as fractions of tooth space:

Q_t = tooth-space volume per unit of time delivered to discharge side (= 1.000)
Q_c = clearance volume oil returned to suction
Q = delivery of pump
a_t = air/mixture at tooth inlet side pressure p_t
a_2 = air/mixture at discharge pressure p_2
a_1 = air/mixture at inlet pressure p_1
p_1 = inlet pressure, in. Hg abs
p_t = tooth pressure inlet side, in. Hg abs
p_2 = discharge pressure, in. Hg abs
s_t = slip, a function of $\dfrac{\text{pressure difference}}{\text{viscosity}}$ $\left(= \dfrac{s_d}{(1 + c_d)}\right)$
c_t = clearance volume $\left(= \dfrac{c_d}{1 + c_d}\right)$
s_d = slip, c_d = clearance } in the usual term, fraction of displacement

The air delivered to the discharge side is compressed to a reduced volume.

$$a_2 = \frac{\left(\dfrac{a_t p_t}{p_2}\right)}{(1 - a_t) + \left(\dfrac{a_t + p_t}{p_2}\right)}$$

It is evident, then, that the clearance volume fills with a mixture of very much higher oil concentration than that which entered the teeth. The value for oil returned in the clearance is

$$Q_c = c_t - \frac{c_t\left(\dfrac{a_t p_t}{p_2}\right)}{(1 - a_t) + \left(\dfrac{a_t p_t}{p_2}\right)}$$

The delivery, in fraction of tooth space, is

$$Q = Q_t - s_t - Q_c - a_t$$

$$= (1.000 - c_t - s_t) - a_t + \frac{c_t\left(\dfrac{a_t p_t}{p_2}\right)}{(1 - a_t) + \dfrac{a_t p_t}{p_2}}$$

The first parenthesis is the normal full liquid delivery of the pump, no air present. The second portion is the effect of air.

To avoid confusion, it should be made clear that slip is still a function of p/μ, and it is not affected by the air present, provided the flow is viscous. In turbulent flow, the pressure drop for a given liquid flow goes up in proportion to the volume of air present, but rationalizing from the usual formulas and tests shows that it has no effect in viscous flow. We are concerned almost exclusively with viscous flow in the capillary seals of aviation pumps, on account of the small hydraulic depth and relatively high viscosity. Under these circumstances, the slip can be taken as constant, regardless of air present in the mixture, provided pressure difference and viscosity are constant.

Calculating for a series of values of a_t from 0.05 to 0.40, we get delivery, Q. Having deliveries, we can now take the pump inlet loss from a curve such as Fig. 7 for the particular pump involved, which added to p_t will yield p_1.

Having found p_1, we can convert the selected values of a_t to a_1 the air percentage at the inlet (where it will ordinarily be possible to measure it by test). Then by plotting p_1 versus a_1 and Q versus a_1, we can take simultaneous values of Q and p_1 for selected values of a_1, such as 5, 10, 15 per cent and cross plot in the form we want as shown in Fig. 10. This form of plot is the most convenient for test results likewise. In this figure, the vacuum test of the actual pump for cavitation air-free is for a pressure pump operating at 2700 rpm, 90 psig discharge pressure, aviation 120 oil at 185 F. For any other speed or discharge pressure, the figures of course change, since slip or displacement change; a change of oil temperature or viscosity alters the plots very little, since the slip is small in any case.

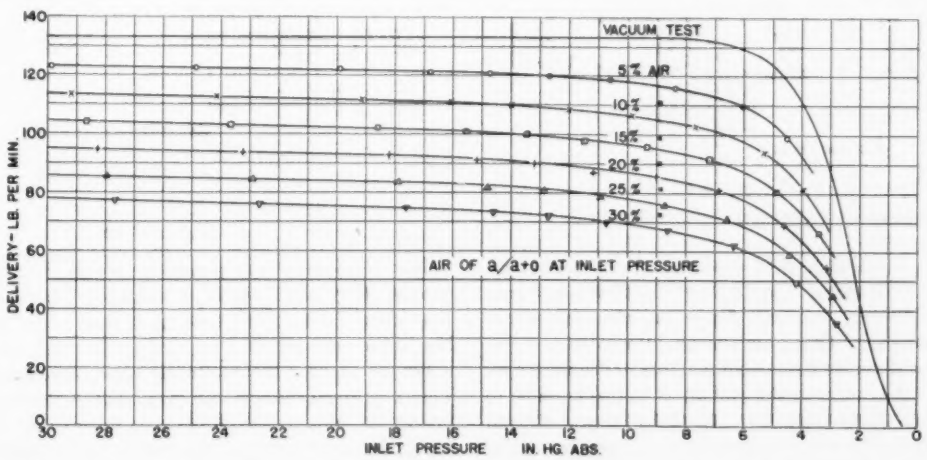


Fig. 10 Calculated Performance, Standard Spur-Gear Pressure Pump, 90 Psi Discharge Pressure

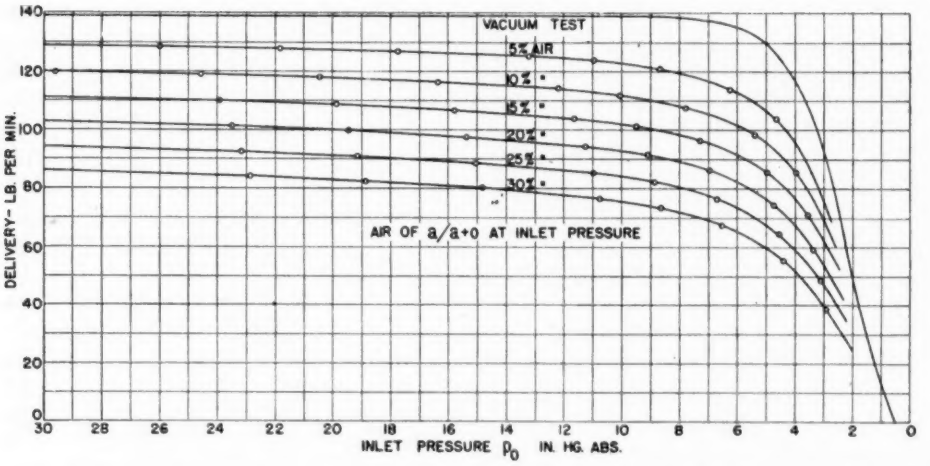


FIG. 11 CALCULATED PERFORMANCE, STANDARD SPUR-GEAR PRESSURE PUMP, 20 PSI DISCHARGE PRESSURE

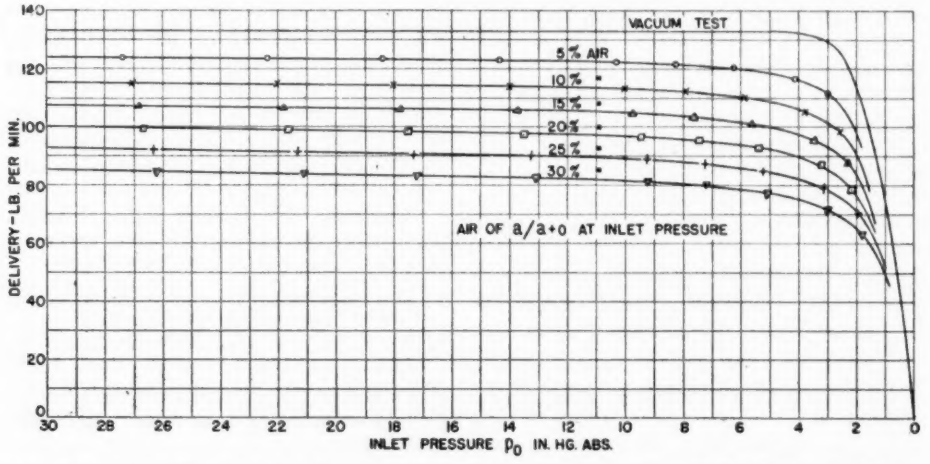


FIG. 12 CALCULATED PERFORMANCE, INTERNAL-PORTED EXPERIMENTAL PUMP, 90 PSI DISCHARGE PRESSURE

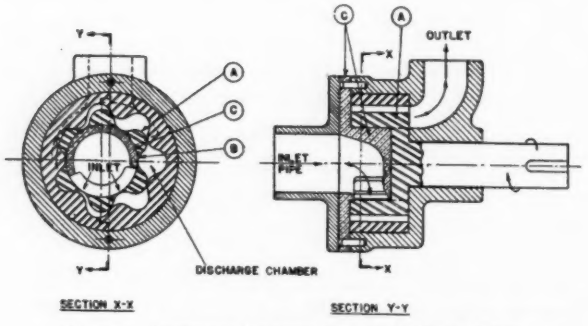


FIG. 13 INTERNAL-PORTED INTERNAL-GEAR PUMP

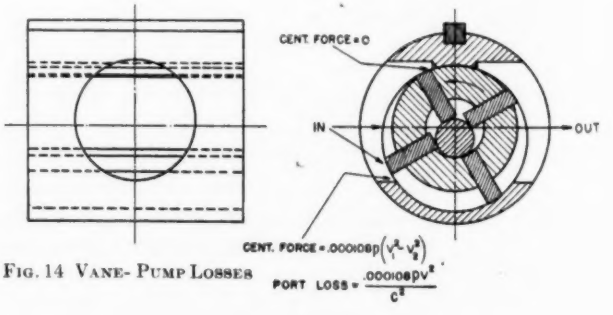


FIG. 14 VANE-PUMP LOSSES

Fig. 11 shows a recalculation of the same pump for 20 psi discharge pressure, scavenging. Fig. 12 shows the 90-lb conditions for a pump, same delivery, but only 5 per cent clearance and a much lower intake loss. This pump is an internal-gear type, shown in Fig. 13, and avoids the centrifugal loss in the intake by taking in the oil at the center of the pinion; it is also possible to get very low values of clearance with the internal-gear design, since the tooth practically fills the tooth space; in a spur gear, clearance cannot be reduced below about 12 per cent.

VANE PUMPS

The situation in vane pumps is very nearly parallel to the gear pumps; they both take in oil at the periphery, so are subject to centrifugal force; both have port loss. But there is no tooth loss in the vane pump.

Fig. 14 shows a diagrammatic view as commonly constructed. The centrifugal force at the beginning of the suction "stroke" is practically zero, as the oil between rotor drum and sleeve has no depth, but at the end of the stroke as the blade is just meeting the lower abutment, the depth is nearly twice the eccentricity so

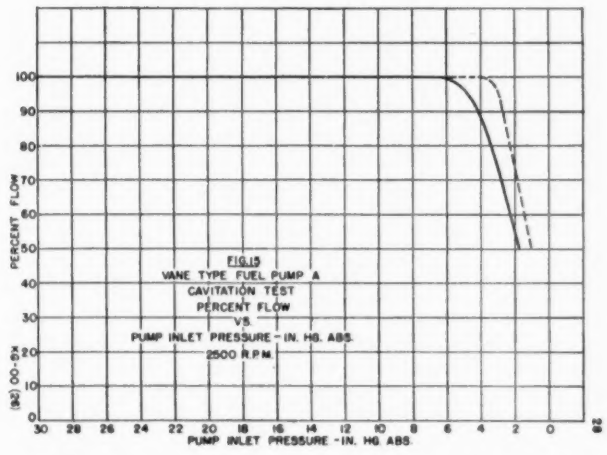


FIG. 15 VANE-TYPE FUEL PUMP A, CAVITATION TEST

that the centrifugal force is nearly double that of a gear pump of corresponding diameter. The port, which is in the sleeve, is usually a round hole and therefore the area for filling, under the edge of the descending blade and the lower edge of the port, is decreasing much faster than the required rate of filling of the space between rotor blades and sleeve. Consequently, the port loss becomes quite substantial.

The cavitation test on such a pump is shown in Fig. 15 and is worse than that of a gear pump of the same diameter and speed. There is, moreover, little need for so much loss. A simple change in the port for better terminal velocities lowered the losses 30 per cent. This pump is typical of several made by different manufacturers, and it is obvious that the designers have not yet paid enough attention to the hydraulics of the operation.

SOME GENERAL DATA

The following is a summary of the pump situation at the present time:

Taking a pump of $1^1/_2$ in. gear or sleeve diameter, or a centrifugal of the same eye diameter, and running at 2700 rpm on aviation oil, the losses are about as follows, at the point of cavitation:

1 External gear pump, 7 in. Hg best, many designs now in actual flight up to 11 in. Hg.

2 Vane pump, 5 in. Hg best, most designs now in use 6.5 to 7 in.

3 Internal-gear pump, Fig. 13, 3.0 in. Hg.

4 Centrifugal boosters, as in use 3.5 to 5 in. Hg.

It is perfectly obvious that if we are to fly these pumps satisfactorily at 50,000 ft, which is the present aim, the total losses in suction piping from tank and to the interior of the pump must be less than 3.43 in., the barometric pressure at that altitude.

Since the piping may have losses from 1 in. Hg at full flow to as high as 7 or 8 in. in some bad cases, not much is left to fill the pump. Clearly the pumps must be designed for a total loss on the suction side of the pump which, including any pipe losses from the tank, does not exceed the barometric pressure at the maximum altitude desired.

We have several ways of attaining this end:

1 Design the pumps for low inlet loss.

2 Design the piping for lower loss than is now common, eliminating all sharp ells, restrictions, and quick disconnects, possible.

3 Put the pump drowned at the sump or tank, and avoid all inlet piping.

4 For those cases where a considerable change of piping and pump is not a feasible fix for designs now flying, use low-loss boosters at the sump or tank.

It is of course true that we can always take some advantage of the reduction of inlet loss when the pump operates below its cavitation point, which is usually the condition where failure will occur (see Figs. 10 and 12, for example), and that is where the pumps usually are operating in flight, since some entrained air is always present in the oil and probably always will be. The path for successful selection of a pump is therefore rather clearly indicated. Let us use the pressure pump as an example; to fly at 50,000 ft means 3.43 in. barometer. For a normal short line from tank to pump, we can assume the line can be designed for, say, 1.0 in. loss at 110 per cent of normal new engine flow. That will leave 2.43 in. for the pump loss. About 10 per cent air at tank at present should be allowed for a poor tank at low level of oil, and the pump can then be selected that will deliver the required 110 per cent of new engine flow, with 10 per cent air at the tank, and at 2.43-in. pump loss, from curves such as Fig. 7.

Even without any tests, these losses may now be quite accurately and safely calculated so that the design can be assured of success before building the job.

The foregoing discussion on pumps has only touched on major points; it is hoped that this sort of study will be carried further by those directly interested in building engines, pumps, and planes.

Discussion

R. A. JEHEBER.[3] Referring to the section entitled, "Slip and Mechanical Losses," there are some statements which the writer feels are somewhat oversimplified and do not reveal what is actually happening in many cases. These are: "Every positive-displacement pump pumps the full displacement volume, . . . Slip-horsepower loss is therefore merely the difference between displacement horsepower and water horsepower as delivered. Friction horsepower, or mechanical loss, is the difference between brake-horsepower input and displacement horsepower." Figs. 3 and 4 of the paper are based on these statements.

The writer bases his opinion on past experience with reciprocating pumps; it should apply to rotary pumps as well, as they are the same type, that is, positive displacement. Several years ago when the majority of liquids pumped (mostly water) were practically incompressible, the author's statements would have corresponded closely to the truth. Developments in oil-refinery practice, however, soon showed that the word "slip" contained more than one type of loss.

If we start from the common accepted definition of "slip" as used by the author (displacement in gallons per minute minus delivery in gallons per minute), we can divide this slip into two main types as follows:

1 *Full Power-Loss Slip.* In other words liquid which leaks back to the suction after full discharge pressure has been built up in it. Examples of such slip are leakage past valves or pistons (in reciprocating pumps), or clearances (in rotary pumps) from full discharge pressure to suction pressure.

2 *No (or Low) Power-Loss Slip.* In this category we have such types as the following:

(a) Liquid which falls back to the suction before pressure builds up (for example, the liquid which falls back through the suction valves of a reciprocating pump while they close, before the build-up of pressure. Another example, rather extreme to illustrate the point, would be a four-plunger pump with one suc

[3] Director of Research, Mack Manufacturing Corporation, Plainfield, N. J. Mem. A.S.M.E.

tion valve stuck open so that one plunger, although it travels back and forth, does not do any effective work; assuming ideal operation for the other three plungers this positive-displacement pump would pump only three quarters of the full displacement volume).

(*b*) Liquid which cannot be drawn in because it has been displaced by air or vapor (an extreme example of this would be to connect air instead of the liquid to the suction valve[s] of one plunger. In a four-plunger pump, this would again mean that this positive-displacement pump would pump no more than three quarters of the full displacement volume).

(*c*) Liquid which cannot be drawn in because of expansion of the liquid trapped in the clearance space. To illustrate, let us imagine a pump handling compressible liquids which expand in the clearance space so that its plungers travel one quarter of their suction stroke before the suction valves can open; here again this positive-displacement pump would pump no more than three quarters of the displacement volume.

There are of course some volumetric losses which fall partly in the first and partly in the second category, such as, for example, liquid which leaks back while the pressure is only partly built up. In a 1000-lb differential-pressure pump, for instance, the amount which leaks back from 250 lb differential pressure might be one-quarter loss of the first type and three quarters loss of the second type.

This second type of slip is far from negligible for such liquids as hot oil or propane close to the boiling point where they are quite compressible and may also pull vapor.

As a matter of fact this was brought forcefully to the writer's attention in some tests with large reciprocating-plunger pumps where the effect of this second type of slip was so great that the brake horsepower required to drive the pump was less than the displacement horsepower based upon geometrical displacement (geometrical displacement of the pump in gallons per minute times differential pressure of pump in pounds per square inch divided by 1715). In plunger pumps there is not much argument as to what constitutes the geometrical displacement.

It might be said that this is a special case of a pump which functions partly as a compressor. This may be true, but there are enough modern applications in oil-refinery work and high-altitude flying to warrant its recognition.

The author is fully aware of this second type of slip, or should we say, volumetric loss; he recognizes some of it in other parts of his paper as "effect of air or other compressibles" also "effect of clearance volume and air;" only he does not call it "slip." This would suggest that the disagreement could perhaps be one of definitions and words rather than one of principle. Possibly the author has in mind making a correction to a "reduced displacement" which would be equal to the geometric displacement minus a certain value representing this second type of slip. If this is the case, it would be interesting to know how the various factors are evaluated in such a correction.

It is agreed with the author that theories used in the pump industry should undergo a general overhaul so that they can be adapted to problems encountered in present-day practice.

W. L. Weeks.[4] During the past 2 years or so the Wright Aeronautical Corporation has worked very closely with the author's organization on problems of air entrainment and of refinement of oil-pump design.

Since the investigation of inlet ports and tooth-loss effects, made by progressively cutting away the inlet side of a submerged pump, was one of the jobs they did for us, it is natural that we are in general agreement with this paper.

[4] Project Engineer, Wright Aeronautical Corporation, Paterson, N. J.

In the successful effort in making his paper a digest, some points are necessarily condensed. With some slight urging, the author might expand a few points. For instance, a more detailed concept of the centrifugal-loss line *a* in Fig. 7 might be of interest. The author might explain that, while for purpose of general discussion, this line may be considered straight, it actually is a slightly curved one as calculated for conditions beyond the start of cavitation. To us it is an interesting even if not a highly important point.

Another item which is interesting in some phases beyond the present exposition is the one the author calls "jet loss."

When we started the research with Gulf, we already knew inlet ports could be bad if too narrow. As a matter of fact, we had widened them in some pumps where the location of studs would permit. But the pump's volumetric efficiency at altitude still left much to be desired. At that time we had no evidence that the spur-gear pump was not as good a type as any, for the job; and we had investigated others.

The question of volumetric efficiency being tied in with pump gear-tip speed gave us an incentive to check empirical figures we had heard on tip-speed practice. All told, we felt that every factor in the action of a spur-gear pump should have its possibilities exhausted by research.

We soon found that our program dovetailed very well with some analytical studies the author had made. The now completed research leaves the spur-gear-pump ceiling quite predictable and the limitations of this type pump well established before we adopt other types.

A very clear picture of various loss factors is given in this paper, but one which concerned us a year ago is slighted. It deserves consideration.

The author has pointed out that loss by centrifugal force can be evaluated. He shows that loss in the unmeshing process of the gears, labeled "jet loss," is not only a difficult one to evaluate, but that it can easily be avoided by making the inlet port reasonably wide.

In the research with the mutilated and submerged oil pump, one factor we tried to clarify was that called shock loss, namely, the loss caused by the struggle of the liquid to get in behind a gear tooth as it speeds across, and even partly against, the path of liquid flow through the inlet port.

Referring to Fig. 7 of the paper, and the "test line *c*," it may be said that even in the flow plot of a pump with a very wide inlet port, this line *c* is still a fairly easy curve, showing a loss imposed aside from the computable port and centrifugal ones. And yet, with such a wide inlet port, the author says (and we certainly subscribe) the "jet loss" is practically negligible. A reasonable deduction might be, then, that test line *c* represents the loss due to shock of sudden change of direction of liquid entering the rotors, even during exposure of wide-open tooth spaces. In fact this interpretation is indicated in the report of the tests thus: ". . . . the shock losses are practically independent of the gear exposure." Also, in the discussion section of the report, where housing-inlet, centrifugal, and acceleration losses (the latter, the author has spoken of, in his present paper as jet loss) are treated, the last item is shock loss. But, although given last place in discussed losses, this loss is evaluated in the over-all, as follows: "The major portion of the loss indicated by the tests, after deducting the calculated centrifugal and inlet friction losses, is that due to shock brought about by sudden changes in the velocity and direction of oil flow." We certainly agree with the report statement.

It is believed the author will agree that the flow curves from the internal-ported gear-type pump, shown in section in Fig. 13, show more delay in cavitation than can be explained by centrifugal aid to rotor filling, and designedly low inlet-port loss, when

compared with the flow curve from a wide-ported spur-gear pump. This could be explained by the fact that, although in both types of pump the teeth move practically crosswise of oil flow, the cross-sectional shape of the pinion (or inner rotor) teeth and the profile of the teeth of the outer rotor in the I. P. pump are much cleaner in point of flow lines, than are spur-gear teeth to radial entry of liquid.

Does the author feel that this comparison further supports the status given to shock loss, or what we like to call tooth turbulent-entry loss, in spur-gear pumps, as stated in the test report?

In no sense is the foregoing questioned correlation pertinent to the status of the internal-ported pump in the aviation industry. If its outstanding volumetric efficiency at extremely low inlet absolute pressures is 99 per cent due to centrifugal aid to rotor filling, we do not care in the least. This new and cleverly developed type of pump has become available almost exactly when we are convinced that the inherent limitations of the spur-gear type shows it to be unsatisfactory for service at altitudes of 40,000 ft and upward. Although the author has not pushed this new development particularly, the writer takes the opportunity to say that we cannot afford to neglect its potentialities.

Author's Closure

Referring to the discussion by W. L. Weeks, possibly he has confused the losses in the inlet port with those which may occur in the inlet chamber between the pipe port and the gears. The normal losses in the port and the inlet chamber are, in all cases, relatively small for any reasonably well-designed pump, but the amount of the pinion arc that is exposed to the suction chamber is quite important. This situation has been discussed in the paper and is also covered by Mr. Weeks.

With regard to his point that the jet loss, by which the author means the flow between the tip of one tooth and the flank of the next, can be eliminated by making the inlet port reasonably wide, while this is not subject to exact determination, in general, the statements made in the paper and those by Mr. Weeks are in agreement. The jet loss still exists in reduced amount when the pump is in cavitation, but by exposing more arc of the teeth in the unmeshed region, a greater time is allowed for filling the incompletely filled teeth, and therefore the loss occurring in the meshed region may not be appreciable or even detectable. It is somewhat difficult to get exact terminology to describe these situations, but in Fig. 7 of the paper, the port loss as indicated in this figure includes any loss due to the pipe opening into the pump, the skin friction in the inlet chamber, and any velocity-head-type loss due to changes of direction of the stream from the usually circular inlet pipe to the usually rectangular configuration where the oil enters the gears. It will be seen from the diagram that the port or intake-chamber loss forms a relatively small percentage of the total when the pump is either not cavitating or is in low order of cavitation, but assumes a somewhat larger percentage of the total after the tooth loss has substantially vanished in the high order of cavitation. It is possible that Mr. Weeks has misunderstood the application of the term "jet loss." The author was thinking almost exclusively of the high-speed jet occurring between the tip of one tooth and the flank of the next, which is actually the bulk of the tooth loss. The other velocities elsewhere, particularly in the port and intake chamber, are relatively rather low.

With regard to Fig. 13 of the paper, part of the gain shown by this design of pump is of course elimination of centrifugal force. Another fraction of the gain is due to proper shaping of the gear-tooth ports for good pickup, just as in a centrifugal pump; and another fraction of the gain is due to the great reduction in clearance. His point is correct, that the proper shaping of the intake edge of the gear teeth, so as to introduce the liquid radially from the intake cup without shock, is quite important. The difference between a plain radial port and the ports as now shaped amounts to as much as $1^1/_2$ to 2 in. Hg. It is the author's feeling that the improvement in this pump is not traceable to any one cause but to several of the structural changes that have been accomplished. These are about as follows:

1 Elimination of centrifugal resistance.

2 Good turn conditions and faired shapes in the inlet cup.

3 Proper proportioning of the port area in the gear, together with proper angle of the inlet edge to reduce, as far as possible, any shock loss or change in direction of the fluid as it enters the teeth.

4 The reduction of clearance from approximately 20 per cent to around 5 per cent.

In response to Mr. Week's kind remark about the potentialities of this design, the author has rather avoided pushing this design too much, since this is a technical paper, and presumably quite unbiased. However, it is within the bounds of propriety to say that, at the present time, this pump has the lowest inlet loss of any we have investigated, including some centrifugal boosters.

In reply to Professor Schweitzer's oral comments the author is in agreement that, in some sense at least, displacement is a conventional term. However, the reason why we have adopted displacement in the form given in the paper is: (1) It is in exactly the same status as the displacement of a reciprocating pump and in all of the commercial rotary pumps, and therefore has very widespread use. (2) The distinction between slip and mechanical loss can only be made correctly upon the basis of this form of displacement. They do not correlate properly with the geometric displacement described by Professor Schweitzer which in effect corresponds in the present paper to the tooth space. Mr. Hambling of the Thornton Laboratories in England also applied Professor Schweitzer's method of using the geometric displacement, with the result that all analyses based upon volumetric efficiency give very deceptive values.

With regard to the assumption that slip may occur elsewhere than from the discharge side to the inlet, two points should be made as follows:

In the analysis as made in the paper and in 90 per cent of the pumps, there is no external shaft leakage because for a commercial pump the shaft is packed. The only case where shaft leakage is permitted is in aviation pumps where leakage along the shaft either passes back to a sump or travels through to another pump in the same case. It is believed Professor Schweitzer's assumption that some of the leakage may have come from oil carried into the tooth space on its way from suction to discharge, and leak out before it reaches the discharge, is an incomplete rationalization. It must be realized that, while some of this leakage is taking place all along this path, what material does leak out is from an intermediate-pressure region and the tooth must be refilled from some other source or the leakage would not take place. Now it is obvious that between the point where this particular quantity of oil has leaked back before completing the path from suction to discharge chambers, there is also pressure difference between this pressure and the discharge, and leakage comes down from discharge to this point to replace that which has leaked out at the lower pressure point. The net result is, therefore, that the entire displacement work is done on the total difference of pressure, and all leakage is truly represented by calculation on the total pressure difference between inlet and discharge. It is therefore clear that the work done on the liquid in the pump is always that of pumping the entire displacement against the difference of pressure between inlet and discharge and is not in any way affected by what place, in the pump, any particle of oil came from to join the leakage. This situation is not an approximation, it is entirely rigorous.

Effect of Combined High Temperature and High Humidity on the Corrosion of Samples of Various Metals

By W. L. MAUCHER[1] AND B. W. JONES,[2] SCHENECTADY, N. Y.

The atmosphere around and in oil refineries is corrosive; and when these refineries are located in hot humid locations, this atmosphere attacks various metals actively. Four groups of eighteen selected metal specimens were subjected to this corrosive atmosphere in a refinery along the Gulf Coast. Two groups were located indoors and two groups outdoors for about one year. This paper is a report of how these specimens withstood this hot, humid, corrosive atmosphere.

VARIOUS metals when subjected to the combination of high temperatures, high saline humidity, and to the gases which are found around and in the various oil refineries along the Texas Gulf Coast exhibit a very high rate of corrosion. This condition has been the cause of much destruction to enclosing cases, structural members, and to electrical parts which are magnetic. This gas also rapidly attacks current-carrying parts such as copper, cadmium, silver, and other materials, so that the maintenance personnel in these plants would welcome any suggestions that would reduce this type of corrosion.

The present paper is a report of some work done to ascertain the degree of corrosion which this condition would have on eighteen selected materials or platings. Four groups of these eighteen selections per group were placed in four selected locations of an oil refinery which was adjudged to be the most severe plant in that area as regards corroding. Each specimen was hung on a porcelain-enameled hook so that the specimen did not touch any other member. No. 1 location was inside a power plant; No. 2 location was outside this same power plant, where the samples were subjected to the rain and sun; No. 3 location was inside a chilling pump house; and No. 4 location was outside this same chilling pump house.

A competent person inspected these seventy-two specimens at the expiration of 7, 14, 35, 72, 129, and 225 days at the test sites, and Tables 1 to 4, inclusive, are his report. These specimens were returned to the laboratory after 1 year exposure and W. L. Maucher who originally prepared them also inspected them on their return. Tables 5 and 6 are from his report. Therefore, these two reports give a comprehensive description of what occurred during this period of 1 year in a saline atmosphere containing a substantial concentration of sulphur acids, such as hydrogen sulphide and sulphurous and sulphuric acids, and we should be able to draw a few useful conclusions from the results. The list of metals as shown in the next column might be generalized as follows: (*a*) Five simple elements; (*b*) electroplated coatings on copper; (*c*) chromium alloys; (*d*) copper alloys; and (*e*) nickel alloys.

LIST OF 18 DISTINCTIVE SPECIMENS OF METALS

Specimen number	Material
1	Rolled copper
2	Rolled copper with 0.001 in. silver electroplate per side
3	Rolled copper with 0.001 in. lead electroplate per side
4	Rolled copper with 0.001 in. tin electroplate per side
5	Rolled copper with 0.001 in. cadmium electroplate per side
6	Rolled nickel
7	Type 410 12 per cent chrome steel passivated
8	Nichrome V
9	Lead
10	Type 302 18-8 stainless steel passivated
11	2S aluminum
12	2S aluminum anodized for 20 min
13	Cold-rolled steel
14	Fine silver
15	Monel
16	Everdur
17	Red brass (85 Cu, 15 Zn)
18	25 per cent chrome steel passivated

1 Of the four electroplated coatings on copper, the tin appeared to stand up best. The cadmium was completely gone and the silver showed heavy attack, as evidenced by the scaly black deposit which was probably silver sulphide. The lead plating did not look so bad on the surface but on closer inspection, deep pits of the copper base metal were noted.

2 Rating the chromium alloys in their order of merit, 18-8 stainless steel and Nichrome V average up about the same and rate about the best in this test. The 25 per cent chrome steel was somewhat worse, and 12 per cent chrome steel was decidedly inferior to the other three.

3 While aluminum, untreated, showed a uniform corrosion coating and the anodized aluminum had scattered pits, it is felt that this metal showed up nearly as well as did the 18-8 stainless steel. Considering price, it is the consensus of opinion that aluminum, anodized or otherwise properly treated for paint, and then given two or more coats of suitable aluminum paint, would provide one of the most corrosion-resistant combinations.

4 The test on copper and copper alloys showed conclusively that the high-copper metals have a low resistance to corrosion in this kind of atmosphere and should not be used unless protected by some protective coating.

5 A comparison of monel and nickel indicate that nickel was not attacked as much as was monel.

6 The extremely bad corrosion of the unprotected cold-rolled steel indicates the severity of the corrosive atmosphere at this location and emphasizes the necessity for maintenance painting on any steel parts.

7 Lead showed up outstandingly well but because of its low physical properties would not lend itself to many applications.

8 The interesting observation on silver was that, although it was heavily attacked, there was no sign of pitting or noticeable etching. The metal underneath the corrosion film was very smooth. On large knife switches, the silver surfaces continued to carry their currents satisfactorily.

[1] Works Laboratory, General Electric Co.

[2] Industrial Control Engineering Division, General Electric Co.

Contributed by the Aviation Division and presented at the Semi-Annual Meeting, Pittsburgh, Pa., June 19–22, 1944, of THE AMERICAN SOCIETY OF MECHANICAL ENGINEERS.

NOTE: Statements and opinions advanced in papers are to be understood as individual expressions of authors and not of the Society.

TABLE 1 RESULTS OF EXPOSURE OF SPECIMENS TO CORROSION GASES
(Field Inspections)

	SPECIMEN NUMBER	2-20-40 7 DAYS EXPOSURE	2-27-40 14 DAYS EXPOSURE	3-19-40 35 DAYS EXPOSURE
INSIDE POWER PLANT	1	Colored Red & Green. Spotted.	Gray Film Some Copper Showing.	Dark Gray
	2	Dark Brown Coating. Spotted.	Coated Greenish Blue.	Dark Brown all over.
	3	Slightly tarnished. Clear	Tarnished to Bluish Gray.	Slate Gray. Spotted.
	4	Very Slightly Tarnished. Clear	Light Gray Coating.	Dull Gray. Clear
	5	Bright. Several Dark Spots.	Bright. Silvery Color. Few Spots	Semi-Bright. Rainbow Colors.
	6	Very Slightly Dulled. Clear.	Slightly Dulled. Clear	Dull Gray. Clear.
	7	Very Slightly Dulled. Clear.	Slightly Dulled. Clear.	Dull. Clear.
	8	Bright - Like New.	Bright - Clear.	Slightly Dulled. Clear.
	9	Darkened. Clear	Darkened. Clear.	Dull. Clear.
	10	Bright and Clear.	Bright - Clear.	Semi Bright - Clear.
	11	Bright and Clear.	Bright - Clear.	Bright - Clear.
	12	Bright and Clear.	Bright - Clear.	Bright - Clear.
	13	Darkened - Clear.	Light Coat of Rust. All over.	Rust all over.
	14	Very Tarnished. Spotted.	Very Tarnished.	Very Tarnished.
	15	Tarnished. Clear.	Dull Gray. Clear.	Dull - Rust Color.
	16	Rainbow Colored.	Tarnished - Spotted.	Very Dark with few Bright Colors.
	17	Colored Green & Red.	Tarnished - Spotted.	Very Dark - Spotted.
	18	Bright and Clear	Bright and Clear.	Semi Bright and Clear.
OUTSIDE POWER PLANT	1	Rainbow Colored - Dark Spots.	Tarnished - Very Spotted.	Dull Gray. Black Spots (rough).
	2	Blue Cast with Red Spots.	Tarnished. Brown Spots.	Dull Gray - Black Spots (Rough).
	3	Gray - Spotted.	Dull Gray. Spotted.	Dull Gray - Black Spots (Rough).
	4	Slate Colored.	Dull Slate Color	Dull Gray - Black Spots (Rough).
	5	Bright-Some Green Spots.	Yellow Powdery Coating.	Yellowish Green -Rough
	6	Darkened - Clear.	Dull, Many Dark Spots.	Black, Spotted, Rough
	7	Large Rust Spots.	Rusted all over.	Rust all over.
	8	Slightly Dull - Clear	Dulled - Mottled.	Dull Gray - Spotted.
	9	Darkened - Some Spots	Dull - Spotted.	Dull - Spotted.
	10	Bright and Clear	Rust Spots Showing, Dull.	Dull - Brown Spots.
	11	Bright and Clear	Dull, Gray Powder Coating.	Dull - Rough
	12	Bright and Clear	Bright - Clear.	Semi Bright, Rough Black Spots.
	13	Rusted all over.	Rust all over.	Very Rusty all over.
	14	Tarnished near Black	Tarnished Dull Gray	Tarnished near Black
	15	Slight Tarnish, Clear.	Tarnished Dull Gray	Dull Gray - Rough
	16	Tarnished - Spotted.	Dull - Spotted	Dull Gray - Rough
	17	Tarnished - Spotted.	Dull - Spotted	Dull Gray - Rough
	18	Bright and Clear	Bright - Clear	Some Bright Areas - Brown Spots, Rough.

TABLE 2 RESULTS OF EXPOSURE OF SPECIMENS TO CORROSION GASES
(Field Inspections)

	SPECIMEN NUMBER	4-26-40 72 DAYS EXPOSURE	6-26-40 129 DAYS EXPOSURE	10-1-40 225 DAYS EXPOSURE
INSIDE POWER PLANT	1	Black Sooty Film - Easily Rubbed Off.	Rough - Black	Rough - Black
	2	Black, Spotted, Smooth.	Slightly Rough, Dull Black.	Slightly Rough - Plating O.K.
	3	Slate Gray, Smooth, Some Spots.	Dull Gray - Smooth.	Smooth - Dull. Plating O.K.
	4	Light Gray, Smooth Clear.	Dull Gray - Smooth.	Smooth - Dull. Plating O.K.
	5	Yellowish & Iridescent- Smooth.	Yellowish - Smooth.	Smooth - Yellowish Plating Oxidizing.
	6	Dull Gray, Clear, Smooth.	Dull Gray, Smooth, Clear.	Considerably Etched.
	7	Dull Gray, Clear, Slightly Rough.	Dull Gray, Slightly Rough, Clear.	Slight Rust Showing.
	8	Semi Bright-Slightly Rough.	Semi Bright, Smooth Clear.	Etched.
	9	Dark Gray, Smooth, Clear.	Lead Color, Smooth Clear.	Lead Gray Color. Smooth.
	10	Semi-Bright, Smooth Clear.	Semi-Bright, Smooth Clear.	Good Condition
	11	Bright Smooth Clear	Bright Smooth Clear	Slightly etched.
	12	Bright Smooth Clear	Bright Smooth Clear	Very Good.
	13	Rusted all over, Very Rough.	Very Rusty & Rough	Very Rusty & Rough
	14	Dark Smooth Spotted	Very Dark, Smooth, Spotted.	Very Tarnished - Smooth.
	15	Black Smooth Clear	Black, Slightly Rough	Slightly Etched.
	16	Black Smooth, Some Spots.	Black, Slightly Rough	Coated with Copper Sulphide.
	17	Black Smooth Flaking	Bluish Black, Slightly Rough	Coated with Copper Sulphide.
	18	Bright Clear Smooth	Bright - Smooth.	Very Good Condition.
OUTSIDE POWER PLANT	1	Dark, Iridescent, Spotted, Rough	Blue-Black, Very Rough	Severely Corroded, Rough, Black
	2	Dark Gray, Spotted Rough.	Dull Gray, Very Rough.	Severely Corroded, Dull Gray.
	3	Light Gray, Rough, Black Spots.	Blue-Black, Slightly Rough.	Plating OK except when Samples Rubbed.
	4	Light Gray-Rough, Black Spots.	Dull Gray, Slightly Rough.	Plating OK except when Samples Rubbed.
	5	Yellow-Rough Flaking	Yellowish, Very Rough	Plating Wearing Off by Flaking.
	6	Black, Rough, Spotted.	Tarnished Bronze Slightly Rough.	Thick Coating, Etched
	7	Rusted all over. Rough	Rusted all over Rough.	Very Rusted & Pitted
	8	Dull Gray, Slightly Rough, Spotted.	Dull Gray - Rough.	Thin Coating, Badly Etched.
	9	Dull, Slightly Rough.	Lead Color, Slightly Rough.	Etched.
	10	90% Area Rusted	95% Area Rusted, Rough.	Covered with Rust Spots

TABLE 2 (*Continued*)

	SPECIMEN NUMBER	4-26-40 72 DAYS EXPOSURE	6-26-40 129 DAYS EXPOSURE	10-1-40 225 DAYS EXPOSURE
OUTSIDE POWER PLANT	11	Dull, Very Rough.	Dull, Very Rough.	Dull, Rough Coating.
	12	Semi-Bright, Rough Black Spots.	Dull & Semi-Bright Spots. Rough.	Semi-Bright to Dull Rough.
	13	Very Rusty all over, Rough.	Rusted all over, very rough.	Very rusty.
	14	Tarnished to near black. Spotted Flaking.	Blue-Black. Smooth	Tarnished to Blue-Black.
	15	Dark Gray - Rough.	Blue-Black. Very Rough.	Severely etched.
	16	Flaked to Bright Surface. 75% Balance Rough.	Blue-Black. Very Rough.	Severely etched.
	17	Flaked to Bright Surface. 75% Balance Rough	Blue-Black. Very Rough.	Thick Coating
	18	90% Area Rusted. Rough.	95% Area Rusted. Very Rough.	Covered with Rust Spots.

TABLE 3 RESULTS OF EXPOSURE OF SPECIMENS TO CORROSION GASES

(Field Inspections)

	SPECIMEN NUMBER	2-20-40 7 DAYS EXPOSURE	2-27-40 14 DAYS EXPOSURE	3-19-40 35 DAYS EXPOSURE
INSIDE CHILLING PLANT	1	Very Spotted & Tarnished.	Red, Green & Copper Colors	Brown, Red & Gray Casts.
	2	Colored to varying shades of brown.	Mottled - Brown.	Varying shades of brown.
	3	Dark Gray, Clear.	Dark Gray, Clear.	Dark Gray, Clear.
	4	Light Slate Color, Clear.	Slate Colored, Clear.	Slate Colored, Clear.
	5	Bright - Clear.	Bright - Clear.	Bright - Clear.
	6	Bright - Clear.	Bright - Clear.	Bright, Few Brown Stains
	7	Dull - Clear.	Dull - Clear.	Dull Gray - Clear.
	8	Bright, Like New.	Bright - Clear.	Bright - Clear.
	9	Dull, Some Spots.	Dull, Spotted.	Dull, Clear.
	10	Dull, Clear	Dull, Clear.	Semi-Bright, Clear.
	11	Bright, Clear.	Bright, Clear.	Bright, Clear.
	12	Bright, Clear.	Bright, Clear.	Semi-Bright, Clear.
	13	Bright, Clear.	Bright, Pimply Spots	Bright, Pimply Spots
	14	Very Tarnished	Tarnished Black & Red Casts.	Tarnished Black & Red Casts
	15	Bright - Clear.	Bright - Clear.	Semi-Bright, Clear.
	16	Stained with Dark Brown Spots.	Bronze Color - Large Brown Spots	Brown-Red & Gray Mottled
	17	Stained with Dark Brown Spots.	Bronze Color - Mottled	Bronze Color, Red & Brown Mottled.
	18	This sample was Lost		

TABLE 3 (*Continued*)

OUTSIDE CHILLING PLANT

SPECIMEN NUMBER	2-20-40 7 DAYS EXPOSURE	2-27-40 14 DAYS EXPOSURE	3-19-40 35 DAYS EXPOSURE
1	Very Tarnished and Spotted	Tarnished Black & Green	Black & Red Casts - Rubs Off
2	Very Tarnished and Spotted	Tarnished, very dark, Spotted	Very dark, Spotted
3	Tarnished to Dull Gray	Tarnished, Spotted	Gray, Spotted
4	Tarnished Dull Gray	Tarnished, Dull Gray	Dull Gray, Spotted
5	Tarnished to Green & Gray Colors	Gray, Mottled	Dull Gray, Rough, Powdery.
6	Tarnished Dull Gray	Very Dull, Clear	Dull Gray, Yellowish, Rough
7	Large Rust Spots	Rust all over	Rust all over
8	Bright Like New	Dull Gray, Clear	Dull, Green Spots, Raised.
9	Dull, Some Spots	Dull, Spotted	Dull
10	Bright, Some Spots	Dull & Bright Areas	Dull and Bright Areas
11	Bright & Clear one side. Spotted on South Side	Gray Powder Coat - Dull	White, Rough, Coating
12	Bright & Clear	Some Gray Powder - Bright	Semi-Bright, Rough with white spots
13	Rusted all over	Rusted all over	Heavy rust coating
14	Very Tarnished	Tarnished, Black & Red Casts	Tarnished Black
15	Tarnished & Spotted	Dark - Spotted	Black, Some Green Spots
16	Very Tarnished and Spotted	Tarnished, Green Spots	Black, Some Green Spots
17	Very Tarnished and Spotted	Tarnished to Black	Black, Some Geeen Spots
18	Bright and Clear	North Side Bright, Mottled, South Side Brown Spots	North Side Bright, South Side Brown Spots

TABLE 4 RESULTS OF EXPOSURE OF SPECIMENS TO CORROSION GASES
(Field Inspections)

	SPECIMEN NUMBER	4-26-40 72 DAYS EXPOSURE	6-26-40 129 DAYS EXPOSURE	10-1-40 225 DAYS EXPOSURE
Inside Chilling Plant	1	Brown, Red & Gray Casts, Smooth	Bronze & Black Spots Smooth	Tarnished to Bronze and Black Spots
	2	Varying Light & Dark Shades of Brown, Smooth	Light & Dark Brown Smooth	Tarnished Plating O.K.
	3	Bluish Gray, Smooth	Lead Gray, Smooth	Gray, Plating O.K.
	4	Light Gray, Smooth	Light Gray, Smooth	Gray, Plating O.K.
	5	Bright, Smooth, Clear	Yellow (Pale), Smooth	Lemon Yellow, Plating O.K.
	6	Bright, Smooth, Some Brown Stains	Bright, Smooth, Few Spots	Dulled, O.K.
	7	Dull Gray, Smooth, Clear	Dull Gray, Smooth, Few Spots	Dulled, O.K.
	8	Bright, Smooth, Clear	Bright, Smooth	Dulled, O.K.
	9	Dull, Smooth, Clear	Lead Color, Smooth	O.K.
	10	Semi-Bright, Smooth Clear	Dull, Smooth	O.K. (Dulled)
Inside Chilling Plant	11	Bright, Smooth, Clear	Bright, Smooth	Bright, O.K.
	12	Semi-Bright, Smooth, Clear	Bright, Smooth	Bright, O.K.
	13	Bright, Pumply Spots	Bright, Smooth	Very Rusty
	14	Tarnished to Black and Red, Smooth	Nearly Black, Smooth	Tarnished Blue-Black
	15	Semi-Bright, Smooth Clear	Semi Bright, Smooth	Dull, Spotted
	16	Gray, Red & Brown Mottled, Smooth	Black & Bronze, Smooth	Tarnished - Varigated Colors
	17	Red & Brown, Smooth	Spotted Red & Bronze Smooth	Tarnished, Black and Bronze
	18	This sample was lost		

TABLE 4 (*Continued*)

Outside Chilling Plant

SPECIMEN NUMBER	4-26-40 72 DAYS EXPOSURE	6-26-40 129 DAYS EXPOSURE	10-1-40 225 DAYS EXPOSURE
1	Gray - Smooth	Black to Bronze, Smooth	South Side Badly Attacked, North Side not so bad.
2	Very dark, rough	Dark Brown, Spotted, Rough	Plating Good, Few Rough Spots
3	Gray, Rough, Spotted	Lead Gray, Smooth	Plating Good, Few Rough Spots
4	Light Gray, Rough Spotted	Gray, Very Rough, Spotted	Much of Plating Gone, Pitted.
5	Dull Gray, Rough, Powder Surface	Yellowish, Slightly Rough	Plating all gone.
6	Green & Yellow, Rough	Spotted, Smooth	Tarnished, Slightly Rough
7	Rusted all over, Rough	Rusted all over Very Rough	Rusted all over
8	Green Cast - Rough	Dull, Slightly Rough	Etched & Slightly Rough
9	Dull, Smooth, Spotted	Lead Color, Smooth	Turned to Light Gray
10	75% Area Rusted - Rough	80% Area Rusted - Rough	Covered with Rust Spots
11	Dull - Very Corroded	Very Much Corroded, Rough	Very Corroded
12	Dull, Rough	Very Much Corroded, Rough	Very Corroded (Not as bad as #11)
13	Rusted all over, Rough	Rusted all over, Scaling off	Plate 50% Gone
14	Tarnished Black, Spotted, Smooth	Tarnished & Black, Smooth	Tarnished, Smooth
15	Black, Smooth	Very Rough	Tarnished & Rough
16	Black & Brown, Rough	Very Rough	Very Rough Coating
17	Black & Brown, Rough	Very Rough	Very Rough Coating
18	North Side Dull, South Side 15% Area Rusted	North Side Dulled, South Side Rusted	South Side Rusted, North Side Some Rust

TABLE 5 LABORATORY INSPECTION RESULTS OF ONE YEAR OF EXPOSURE TO CORROSIVE GASES

SPECIMEN NUMBER	LOCATION A OUTSIDE #3 POWER PLANT	LOCATION B INSIDE #3 POWER PLANT
1	Heavy black corrosion incrustation. Metal etched and pitted.	Heavy incrustation of dark corrosion products. Metal etched.
2	Medium black corrosion. No pitting. Some silver plate still present.	Thin, uniform dark corrosion coating. No etching or pitting.
3	Uniform black corrosion. Some pitting.	Same as No. 2
4	Uniform black corrosion. No noticeable pitting.	Thin, uniform gray corrosion coating. No etching or pitting.
5	Cadmium plate all gone. Similar in appearance to #1.	Uniform yellow corrosion coating. No pitting or etching.
6	Uniform green and black corrosion. No pitting.	Uniform light green corrosion coating. No pitting or etching.
7	General rusting over all. Shallow pits.	Numerous scattered rust spots. Metal etched.
8	Thin green-gray corrosion over all.	Same as No. 6
9	Missing	Thin dark corrosion film. No pitting.
10	Scattered rust spots over all. Shallow pits.	No appreciable corrosion. Metal slightly dulled.
11	Moderate gray uncrustation. Uniformly etched.	Numerous pits scattered over surface.
12	Light corrosion with scattered shallow pits.	Practically perfect. One pit noted.
13	Badly corroded. Metal thinned by extreme rusting	Over all rust
14	Uniform black corrosion scale. No noticeable pitting	Thin uniform smooth black scale. No pitting
15	Heavy black incrustation. Metal etched but not pitted (not as good as nickel.)	Moderately heavy black incrustation. Metal etched.
16	Same as No. 1.	Same as No. 1.
17	Same as No. 1.	Slightly better than No. 1 or No. 16 but of the same order.
18	Scattered rust over all. Shallow pits.	No attack. In excellent condition.

TABLE 6 LABORATORY INSPECTION RESULTS OF ONE YEAR OF EXPOSURE TO CORROSIVE GASES

SPECIMEN NUMBER	LOCATION C OUTSIDE CHILLING PUMP HOUSE	LOCATION D INSIDE CHILLING PUMP HOUSE
1	Heavy incrustation of dark corrosion products. Metal etched.	Black film overall. Somewhat etched.
2	Medium incrustation. No pitting. Some silver plate still present.	Uniform black coating. No etching or pitting.
3	Medium incrustation. Deep pits in basis metal.	Tarnished but otherwise O.K.
4	Fairly heavy incrustation. Shallow pits of basis metal.	No appreciable change. In excellent condition.
5	Medium incrustation. No cadmium plate left. No appreciable pitting.	Uniform yellow color. Otherwise O.K.
6	Moderate uniform corrosion products. No pitting.	Slightly tarnished. Otherwise in perfect condition.
7	Heavy rust overall. Metal etched with shallow pits.	Same as No. 4.
8	Thin gray surface film. No pitting or etching.	Same as No. 4.
9	Moderate uniform gray film over all. No pitting.	Tarnished and a few shallow pits.
10	Numerous scattered small rust spots which show shallow pits underneath.	Same as No. 4.
11	Moderate gray incrustation. Metal etched.	Same as No. 4.
12	Scattered corrosion pits.	Same as No. 4.
13	Very heavy rust.	Rust over all.
14	Thin uniform smooth corrosion scale (.0004" thick). No pitting.	Uniform black tarnish coating. No pitting or etching.
15	Moderately heavy corrosion products over all. Metal surface etched.	Tarnished but not appreciably etched or pitted.
16	Same as Copper (#1).	Same as #1.
17	Same as Copper (#1).	Similar to #1 & #16 but slightly better.
18	Missing	General rusting and pitting.

R. B. MEARS.[3] We were very much interested in the paper by Mr. Maucher and Mr. Jones. Naturally, we were gratified by the good resistance to attack exhibited by the bare and anodically coated aluminum samples. These results are supported by a considerable amount of other data obtained both by our own laboratories and elsewhere. These other tests unite in revealing that many aluminum-base materials are highly resistant to outdoor exposure conditions, even in damp or seacoast locations. It is also well known that sulphur compounds do not attack any of the commercial aluminum-base alloys. Thus the high resistance of the aluminum-base alloys to atmospheric conditions coupled with their specific resistance to sulphur compounds indicates that oil-refinery people could well afford to give serious consideration to the use of aluminum alloys.

Data from extensive atmospheric exposure tests conducted by A.S.T.M. Committee B-3, Subcommittee VI, for periods up to ten years are now available. These tests were conducted at seven different outdoor exposure sites, including exposures at Altoona, Pa.; New York N. Y.; State College, Pa.; Phoenix, Arizona; Sandy Hook, N. J.; Key West, Fla.; and La Jolla, Calif.

Aluminum alloys 2S, 3S, and Alclad 17S-T proved highly resistant at all locations. Rather similar tests conducted by the Aluminum Research Laboratories indicate that some of the newer sheet alloys such as 52S, 53S, Alcald 3S, and Alclad 24S-T are also highly resistant in outdoor exposures.

Aluminum alloys have been used to some extent in roofs for oil tanks handling sour crudes. About 60 unpainted aluminum-alloy (3S) roofs have been used. In all cases it is understood that these roofs resisted both the outdoor atmospheric exposures and the moist air containing H_2S in the tank interiors very satisfactorily.

Because of the high resistance of aluminum alloys to sulphur compounds and to ammonia (or ammonium hydroxide), aluminum-alloy tubes can often be used advantageously in heat exchangers and condensers in refineries. For such applications, the use of Alclad 3S alloy tubing or of cathodic protection by zinc attachments is advantageous in minimizing the effects of corrosive cooling waters.

Aluminum wires are used for telephone lines in atmospheres containing hydrogen sulphide, because of their high resistance to attack by sulphur compounds.

Aluminum alloy (17S-T) nails are extensively employed for use in wooden structures in oil fields, again because of their resistance to sulphur compounds.

Large processing equipment for gas purification can often be made of aluminum alloys advantageously. Here the high resistance to both CO_2 and H_2S is valuable.

AUTHORS' CLOSURE

We appreciate Dr. Mears's discussion concerning the behavior of aluminum and its alloys under test and service conditions related to those which prevailed in this investigation. It is gratifying to note that the data obtained by the authors are in substantial agreement with Dr. Mears's extensive observations and experience.

[3] Chief, Chemical Metallurgy Division, Aluminum Research Laboratories, Aluminum Company of America, New Kensington, Pa.

An Investigation of Radial Rake Angles in Face Milling

By J. B. ARMITAGE[1] and A. O. SCHMIDT,[2] MILWAUKEE, WIS.

The object of this investigation was to determine the effect of negative and positive radial rake angles in milling cutters upon the power required for the cutting action, the tool life of the cutter, the surface finish, and temperature of the workpiece. Tests were conducted with 2-in. face mills which had two brazed carbide tips. All cutters had the same dimensions except for the radial rake angles which included 30 deg, 15 deg, 6 deg positive; 0 deg, 6 deg, 12 deg, 20 deg, and 30 deg negative. The axial rake angle was 0 deg on all of the cutters. Cutting speeds were varied in seven steps between 106 and 785 fpm; different feeds were used with each speed and the depth of cut was constant at 0.125 in. Test bars were made of normalized S.A.E. 1055 hot-rolled stock. This steel was used throughout the investigation except for the tool-life tests in which S.A.E. 1020 was also used. Equipment and procedure used in the tests are discussed and the results illustrated by several graphs. Clearly defined conclusions are drawn from the investigation.

Discussion of Previous Investigations

NUMEROUS articles recommending negative radial rake milling have appeared in technical publications and bulletins, most of them reporting on over-all performance. The following is stated in one such reference (1):[3] "While the cutting force with a 10-degree NEGATIVE rake is higher than that of a 10-degree positive rake cutter at low speeds, there is always a point at which they are equal, and if a sufficiently high speed is used, the force on the NEGATIVE rake cutter is less than on the positive rake cutter."

At the 1943 Annual Meeting of the Society, a paper was given by Hans Ernst (2), in which were shown several graphs of test data and diagrams with a single-point-tool dynamometer. The results indicated an increase of tool force at high speeds for a 10-deg positive radial rake angle and a decrease of tool force at high speeds for a 10-deg negative radial rake angle. It was stated: "Careful investigations over a wide range of speeds and with various work materials have shown that the power required with negative rake angles decreases steadily with increase in speed. In fact, it has been found in several cases that beyond a certain speed, the specific power consumption with negative rake angles is actually less than with positive rake angles."

At the same meeting, in a companion paper (3), Wallace E. Brainard showed that the tool forces do not vary with the cutting speed from 200 to 1500 fpm. In his investigation, he used an electrical strain gage to determine the tool forces.

For negative radial rake angles, 50 per cent increase in horsepower over present machines and cutting speeds from 375 to 1000 fpm are recommended by R. G. Owen (4). It is also stated that a feed of 0.0005 in. per tooth will dull a cutter after 3 to 5 min cutting time.

C. H. Bodner (5) suggests a heavy cutter body and finds negative blade angles of 10 deg for axial and radial rake the best, in spite of the fact that they require more power to drive the machine tool than positive angles. Climb-milling on machines without backlash and a feed of 0.006 in. per tooth are also recommended.

In a paper by Fred W. Lucht (6), which was presented at the 1943 Annual Meeting of the Society, the following information was given:

"As a rule, positive rake angles result in less power consumption and permit deeper cuts and heavier feeds than do negative rake angles, but the latter should be employed only when necessary to strengthen the cutting edge. Carbide blades 30 to 50 per cent thicker than those used for cast iron permit optimum results when milling steel. A minimum feed of 0.005 in. per tooth is also recommended for steel."

Procedure and Equipment for High-Speed Milling Tests

For this milling investigation a special setup had to be developed to measure the power at the cutting edge accurately at both low and high speeds. All tests were carried out on a Milwaukee 2-K vertical milling machine which had a wide range of feeds and speeds and permitted a maximum cutting speed of 785 fpm with a 2-in. face mill. For checking purposes, an Esterline-Angus recording wattmeter was connected with the milling-machine-drive motor. The surface temperature of the test specimen was measured immediately before and after cutting with an "Alnor" low-range thermocouple. Surface finish on the test bars was checked with a profilometer.

During this investigation, the power required by the tool was measured with a calorimeter from which the heat in the chips was determined. This method proved to be simple and reliable.[4] The measuring of tool forces has been generally effected by the use of mechanical, optical, and electrical means, while the temperature of the cutting edge during the cutting operation has been measured by thermoelectrical devices. In the reported test, distilled water is employed as a means of measuring the quantity of heat generated by a combination of friction and deformation during the cutting operation. Because of the effect which water may have in a milling operation, it was decided to cut the test bars dry and measure only the heat of the chips in the calorimeter. When work is transformed into heat or heat into work, a quantity of work is the mechanical equivalent of a quantity of heat.

Discussion and Interpretation of Results

The main advantage of the calorimetric method used in these tests is that it permits in a simple way the measurement of power at the cutting tool at any cutting speed. Prof. G. Schlesinger

[1] Vice-President in Charge of Engineering, Kearney & Trecker Corporation. Mem. A.S.M.E.

[2] Research Engineer in Charge of Metal Cutting Research, Kearney & Trecker Corporation. Mem. A.S.M.E.

[3] Numbers in parentheses refer to the Bibliography at the end of the paper.

Contributed by the Production Engineering Division and presented at the Semi-Annual Meeting, Pittsburgh, Pa., June 19–22, 1944, of The American Society of Mechanical Engineers.

Note: Statements and opinions advanced in papers are to be understood as individual expressions of their authors and not those of the Society.

[4] For more detailed information see the paper, "Determining Tool Forces in High-Speed Milling by Thermoanalysis," by A. O. Schmidt, presented as a companion paper, at the Semi-Annual Meeting of the Society.

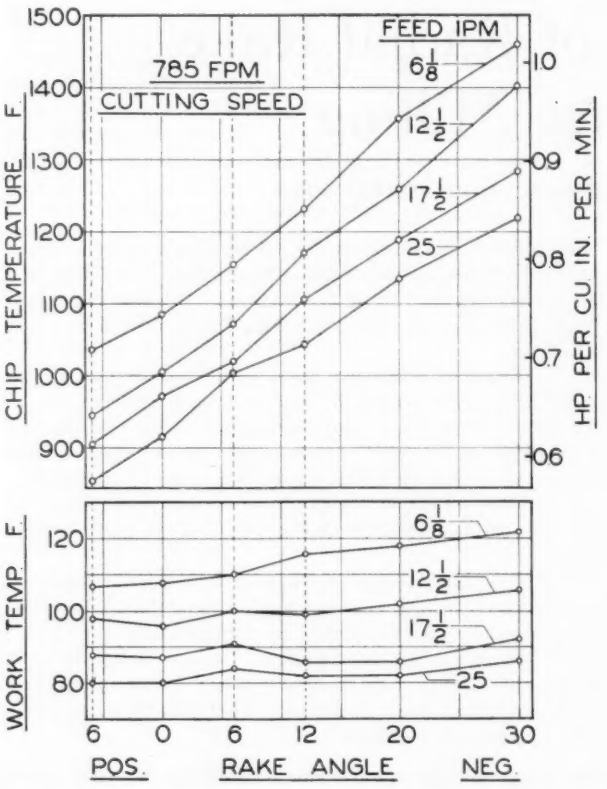


FIG. 1 GRAPHS SHOWING TEMPERATURE OF CHIPS, HORSEPOWER PER CU IN. PER MIN, AND SURFACE TEMPERATURE OF WORKPIECE

(Top: Temperature of chips and horsepower per cubic inch per minute in relation to radial rake angles at 785 fpm cutting speed and various feeds. Material cut is S.A.E. 1055, 1 in. diam, hot-rolled, and normalized. Depth of cut is 0.125 in. Bottom: Surface temperature of workpiece measured with thermocouple immediately after taking cuts plotted in upper graph. Room temperature is constant at 70 F.)

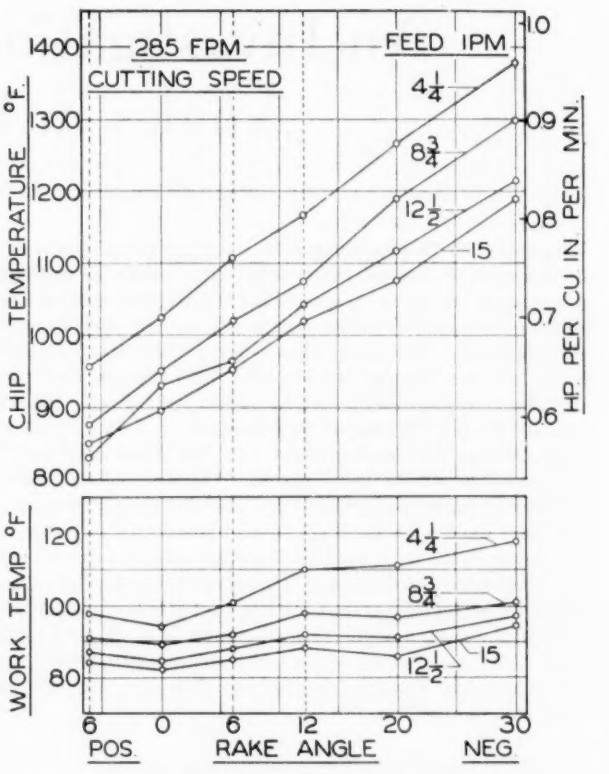


FIG. 2 GRAPHS SHOWING TEMPERATURE OF CHIPS, HORSEPOWER PER CU IN. PER MIN, AND SURFACE TEMPERATURE OF WORKPIECE

(Top: Temperature of chips and horsepower per cubic inch per minute in relation to radial rake angles at 285 fpm cutting speed and various feeds. Material cut is S.A.E. 1055, 1 in. diam, hot-rolled, and normalized. Depth of cut is 0.125 in. Bottom: Surface temperatures of workpiece measured with thermocouple immediately after taking cuts plotted in upper graph. Room temperature is constant at 70 F.)

(7) has stated that in customary shop tests in metal cutting, variations in the results up to 20 per cent may occur. There are inevitable differences in the elements of the test which are due to the following:

1 The efficiency of the motor which may vary from 5 to 8 per cent because of irregular heating due to load variations during the testing period.

2 The efficiency of the gears which may vary from 3 to 8 per cent because of difficulties in keeping the lubrication factors constant and to the heating caused by a change of load.

3 The variations of 5 to 10 per cent in the test material.

4 Variations in the heat-treatment of the tool, which may vary between 5 and 20 per cent in high-speed tools. (The authors have found that the same percentages will apply to brazed tungsten-carbide tips.)

Data plotted in the accompanying graphs constitute the average of at least three individual tests and are based upon the measurements taken with the calorimeter. This excludes errors due to motor and gear variations. Test bars were taken from the same piece of material and were normalized. A close check was maintained in order to eliminate those bars which would repeatedly give results more than 5 per cent above or below the average temperature value measured in the calorimeter for identical tests.

Care was taken to use carbide tips from the same batch and to have them carefully brazed and ground. Another source of error is the wear to which the carbide tip is exposed as soon as it begins to cut metal. During the power tests, tips were inspected after each cut on a test bar. Cutters were eliminated if they showed any sign of wear under the illuminated magnifying glass, and in most cases were used on three test bars removing 0.3 cu in. of metal and not on more than six test bars. During these tests, the cutters were considered to be sharp. A very close check on the cutting edge was also possible because a rise in the calorimeter readings and the surface-temperature readings would always indicate a hard spot in the test bar or wear and chipping of the cutting edge. In some cases this could also be noticed by a rise in the wattmeter reading and could be seen with the magnifying glass as wear on the cutting edge.

Changes in the power required by the two-lip milling cutter in relation to the rake angle were investigated first. The initial series of tests was conducted at a cutting speed of 427 fpm and varying feeds with the 6-deg positive radial rake and 0 deg, 6 deg, 12 deg, 20 deg, and 30-deg negative radial rake angles. A second series of more than 1000 tests was run under identical conditions except that the cutting speed was increased to 523 fpm.

In order to study the effect of the negative radial rake angles at lower speeds, tests were conducted at 285, 192, and 106 fpm cutting speeds. At these speeds the surface of the specimen would show conspicuous chatter marks for all negative radial rake angles larger than 6 deg. Considerable vibration was induced in the machine. At 106 fpm the surface of the specimen was also badly torn and cracked by the negative radial rake cutters.

Several series of tests were conducted at 638 and 785 fpm, and the results were found to agree substantially with those at the lower speeds. From the computed average temperature of the chips, it can be seen that the melting temperature of S.A.E. 1055 was not approached in any test. Observation indicates that

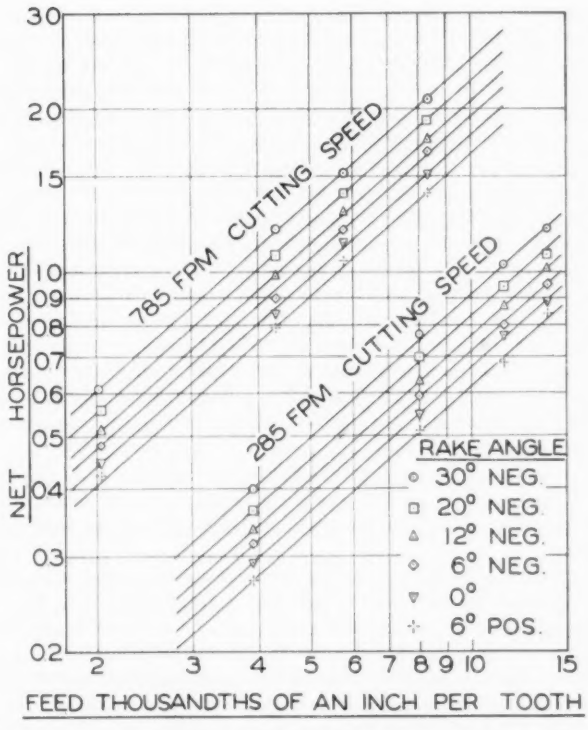


FIG. 3 COMPARISON OF NET HORSEPOWER REQUIREMENTS OF DIFFERENT RADIAL RAKE CUTTERS OPERATING AT CONSTANT CUTTING SPEEDS, 0.125 IN. DEPTH OF CUT, AND VARIOUS FEEDS AS COMPUTED FROM HEAT IN THE CHIPS

(Material, S.A.E. 1055; normalized; Bhn 205.)

the average temperature is the actual temperature of the chips only at fine feeds, while a heavier chip has a different temperature on each side, the higher one on the side away from the tool. This is indicated by the difference in color in individual chips.

When cutting tests are made at heavy feeds and at high speeds, chips and minute particles from the workpiece come off simultaneously. These small particles usually become so overheated, because of their smaller heat-carrying capacity, that they fly off as sparks, while the heavier chips are blue on the side away from the tool and still have the silvery steel color on the side which has just been separated from the workpiece.

From the temperature rise of the calorimeter the average temperature rise of chips, the horsepower per cubic inch per minute, and the net horsepower could be determined.

Values for average chip temperature and horsepower per cubic inch per minute thus arrived at are plotted in Figs. 1 and 2. It can be seen that the chip temperatures increase as the radial rake angle becomes more negative. Because these negative radial rake angles required more net horsepower, it follows that there was more heat generated during the cutting operation. The plotted temperatures further substantiate this statement. Chip temperatures were computed from the calorimeter readings for a constant specific heat. Actually, the specific heat of steel must be assumed to increase at high temperatures and the true chip-temperature values are lower than those plotted.

From the surface temperatures of the workpiece which were measured with the "Alnor" low-range thermocouple immediately before and after the cutting of the test bar, it can be seen that workpiece temperatures depend less upon the radial rake angle than upon the feed (see lower part of Figs. 1 and 2). The temperature of the workpiece and chips varies inversely as the feed. This general tendency was also found to be true in the tool-life tests when the same test bar was used continuously until the cutter had failed.

The net horsepower values, as computed from the calorimeter temperature rise, in relation to the feed per tooth as used in the tests are plotted with a logarithmic scale in Fig. 3, for a cutting speed of 785 and 285 fpm. This relationship between the values for different radial rake angles at other cutting speeds was found to remain substantially the same.

For a given radial rake angle, the increase in net horsepower with an increase in feed has a relationship which is always definite and can be determined from the logarithmic graphs as

$$\text{hp} = CnNf^a$$

in which

C = constant depending upon the radial rake angle
n = number of cutter revolutions per minute
N = number of teeth in cutter
f = feed in inches per tooth
a = exponent determined as 0.85 from values plotted on log-log paper

Net horsepower values computed by the foregoing formula were found to agree within close limits with actual test results. This was a further check that the tool forces were not reduced by negative radial rake angles or high cutting speed, but remained constant for a given chip cross section and changed with the radial rake angle, as shown in Figs. 12 and 13.

During these tests conducted at 427, 523, 638, and 785 fpm cutting speeds, various feeds, and a constant depth of cut, the following observations were made:

1 In taking the first six cuts with sharp cutters on a test bar the power requirement of the cutter with positive radial rake is less than that for cutters with negative radial rake angles.

2 After the negative and positive radial rake cutters have cut an equal amount of metal and all show wear on the cutting edge, the negative radial rake cutters will require less power.

3 In comparison with positive radial rake cutters, the cutter with negative radial rake angles will stand up longer and show less wear.

4 A cutter with negative radial rake angles is more effective at higher cutting speeds because of its inherent additional strength at the cutting lip.

5 Cutters with 20- and 30-deg negative radial rake angles left more pronounced chatter marks on the workpiece and frequently induced machine vibration.

6 Observations for tests run at 427, 523, 638, and 785 fpm agree substantially for tests run at 285 and 192 fpm cutting speed. However, surfaces showed conspicuous chatter marks for all negative radial rake angles above 6 deg even at low feeds.

7 At 106 fpm the surface of the specimen was badly torn and cracked by all negative radial rake cutters. In every specimen, the edge at which the cut was completed was ragged and chipped below the surface plane, indicating that the edge of the test bar had been broken rather than milled off. Induced vibration of the machine was very noticeable during these low-speed tests with the various negative radial rake cutters.

8 The surface temperature of the workpiece decreases with increasing feed rate and is proportional to the temperature of the chips.

The horsepower per cubic inch of metal removed per minute by the cutters with different radial rake angles at a cutting speed of 785 fpm is plotted in Fig. 1. The highest values were obtained with the 30-deg negative radial rake cutter and the lowest with the 6-deg positive radial rake cutter. In spite of the fact that data points are somewhat scattered due to the inevitable test variations, it can be seen that there is a tendency of the horse-

power per cubic inch per minute to decrease with increasing feed. This really means that the work required to remove a cubic inch of metal is less with a coarse feed than with a fine feed. One good reason for the better power economy at coarser feeds is the fact that a coarse feed F, which is twice the fine feed f, is separating a smaller suface in relation to the volume removed. As can be seen in the simplified diagram, Fig. 4, the fine feed will separate a surface area of $2(f + d) \times l$ which is $(d \times l)$ larger than the surface area of separation for the coarse feed which is $(2f + d) \times l$. But in each case the same volume of metal will be removed and a coarse feed will result in more economical power consumption.

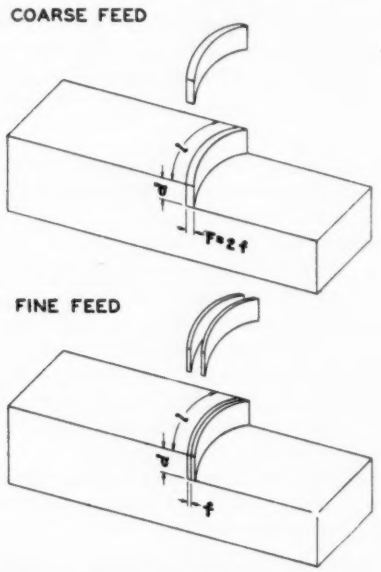


FIG. 4 RELATIONSHIP BETWEEN ONE COARSE CHIP AND TWO FINE CHIPS IN REMOVING SAME AMOUNT OF METAL

The advantage in power economy gained with heavier feed is illustrated in Fig. 5, in which the feed in inches per tooth is plotted on the abscissa, 1 f being the feed which is so fine that there is only minimum deformation in the workpiece and chip. For this reason the cutting force is assumed to be directly proportional to the area of the surfaces of separation and to the volume of metal removed. On the right-hand ordinate are given values for the cutting force per chip and also area of the surfaces which are separated when cutting a particular chip. Volume of the chip is indicated on the left-hand ordinate. If it were possible to separate the metal chips from the workpiece in one plane only, e.g., without disturbing the adjacent layers in the metal, the increase in the cutting forces with increase in feed per tooth would be very small and would coincide with the increase in the area of the surfaces of separation. The volume of metal removed will increase more rapidly as can be seen from the upper line.

However, besides separation of the metal planes, compression, bending, friction, and other phenomena in a metal-cutting operation which can be observed as deformation also occur. Since this deformation in the chip and in adjacent layers of the workpiece is proportional to the feed, the tool forces become greater with an increase in feed.

When the volume of metal being cut is removed in fine chips of 1 f thickness, the force line would coincide with the volume line because of the large proportional increase in the areas of separation.

The ordinate b-c between the first and second curve can be considered as representing the increase in the cutting force due to deformation of the heavier chips. If the force of separation were the only force necessary to cut metal, then the cutting force would be directly proportional to the surface areas of separation, and the increase in cutting force would equal a-b. It is evident that one thick chip is more economical than several fine chips in removing an equal volume of metal from the difference in the ordinate of the same chip for the force and volume curve. The volume curve would indicate the sum of the forces necessary to remove 10 fine chips of 1 f thickness, while the force curve represents the actual force necessary to remove one thick chip of 10 f thickness. The difference, c-d, in the height of the ordinate equals the decrease in force in the latter case.

For this particular feed of 10 f, the increase in volume of the metal removed is 1000 per cent in comparison to a feed of 1 f, while the increase of the cutting force is only 720 per cent. If there were no deformation in the chip and workpiece, the cutting force would have increased only slightly less than 10 per cent be-

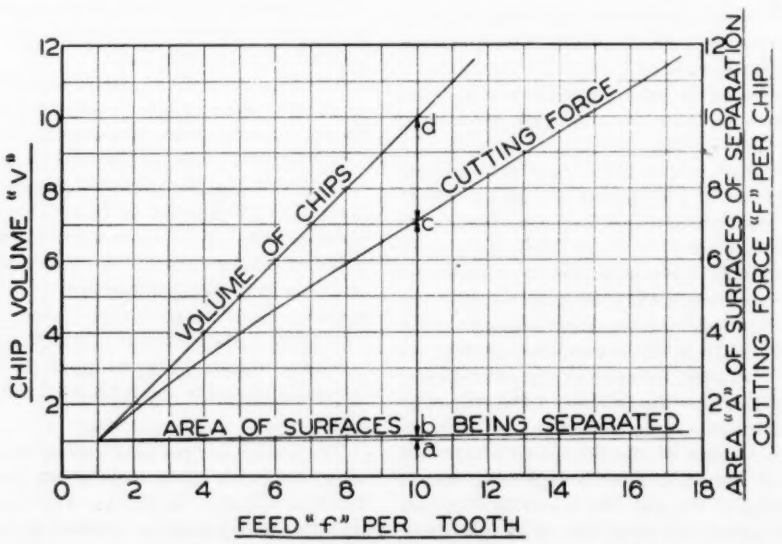


FIG. 5 RELATIONSHIP OF VOLUME OF CHIPS REMOVED, AREA OF SURFACES OF SEPARATION, AND CUTTING FORCE TO FEED PER TOOTH OF CUTTER

cause it would have equalled the small increase in the area of surfaces being separated. Therefore, this one chip of 10 f required almost 7 times as much force due to deformation as was required for its separation.

But no matter how fine a chip is cut, there is always more work done in deforming the metal than in separating it. As just pointed out, separation of metal is only a small part of metal-cutting. This can be seen from the appearance of heavier steel chips, which will often retain the steel color in the cutting plane and be heavily oxidized on the side away from it, indicating that more heat was generated through deformation than cutting of the chip.

From the heat values of the calorimeter, the average temperatures of the various chips were computed. Increasing the chip thickness will lower the average temperature because, with increasing feed, the volume of the chips increases more rapidly than the cutting forces. Therefore, the average temperature of the chips will vary inversely as the chip thickness.

The graph in Fig. 5 has been plotted with values of depth of cut and feed corresponding to the ones used in the tests, as have the force values. If another ratio of depth of cut to feed were to be used, the line for the areas of separation would be steeper for a smaller ratio and have still less slope if the ratio between depth of cut and feed were larger.

Comparative Tool-Life Tests

During the tests for power consumption, it was found that the positive radial rake cutters would frequently fail after the first cut on the test bar. For this reason numerous comparative tool-life tests were made following the procedure subsequently described. Since the cutters with 20- and 30-deg negative radial rake angle induced too much vibration, very few tool-life tests were run with them. Cutters with 15- and 30-deg positive radial rake were excluded from the tool-life tests because they failed too easily.

Three readings on test bars of S.A.E. 1055 (the same as used in the tests for power consumption) were taken first. Then 16 cuts which removed 28 cu in. of metal were made on S.A.E. 1020. Following this, three test bars were again cut for comparison. Depth of cut was 0.125 in. for all tests; the feed was constant at 15 ipm with a cutting speed of 523 fpm.

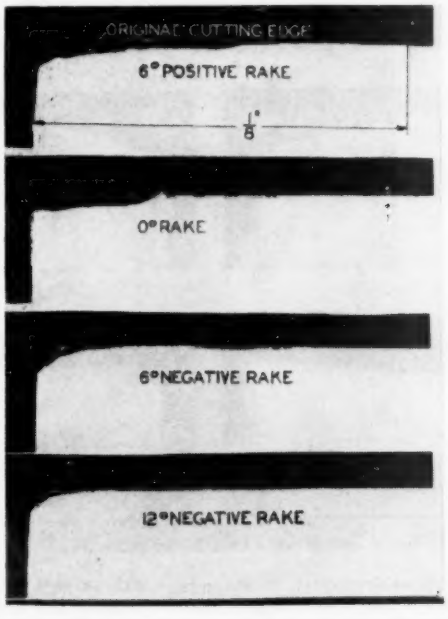


Fig. 6 Silhouettes of Cutting Edges of Various Cutters in Plane Parallel to Axis of Rotation Taken on a Jones and Lamson Optical Comparator

(Each cutter has removed 28 cu in. of S.A.E. 1020 cold-rolled steel and 0.59 cu in. of S.A.E. 1055 at a cutting speed of 523 fpm, a feed of 0.0075 in. per tooth, and 0.125 in. depth of cut.)

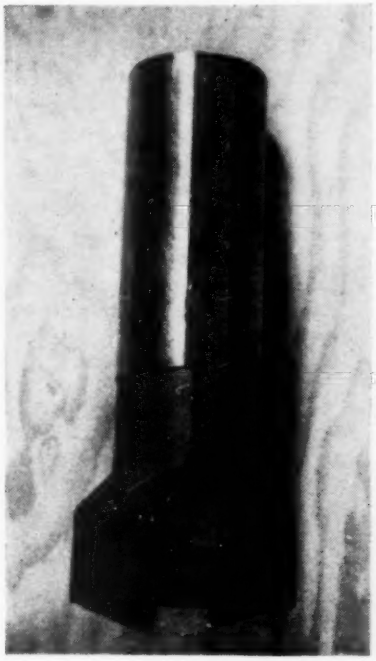


Fig. 7 Two-Bladed Face-Milling Cutter Which Was Used in Tests and Was Provided With Blades of Various Radial Rake Angles

The following observations and measurements are typical and representative of the results in the comparative tool-life tests:

1 After the same amount of metal had been cut with each cutter the increase in power consumption was as follows:

6-deg positive radial rake cutter	34 per cent increase in power
0-deg radial rake cutter	24 per cent increase in power
6-deg negative radial rake cutter	16 per cent increase in power
12-deg negative radial rake cutter	12 per cent increase in power

2 The wear on the cutting edge of the 6-deg positive, 0-deg and 6-deg negative radial rake cutters was due to minute chipping of the carbide tips. On the cutting edge of the 12-deg negative radial rake cutter only fine abrasion was visible, see Fig. 6.

3 Average profilometer readings in microinches on the surface of the test bars at the beginning and end of test were as follows:

Cutter	Reading at beginning	Reading at end
6-deg positive radial rake	140	53
0-deg radial rake	23	26
6-deg negative radial rake	45	80
12-deg negative radial rake	22	80

4 The average surface temperature rise of the specimen would increase between 200 and 400 per cent for the last cuts taken with the partly failed and worn cutter.

Comparative Tool-Life Tests of Cutters Provided With Double Radial Rake Angle Tips

It was established without doubt by numerous tests at cutting speeds ranging from 100 to 800 fpm that the tool forces are higher

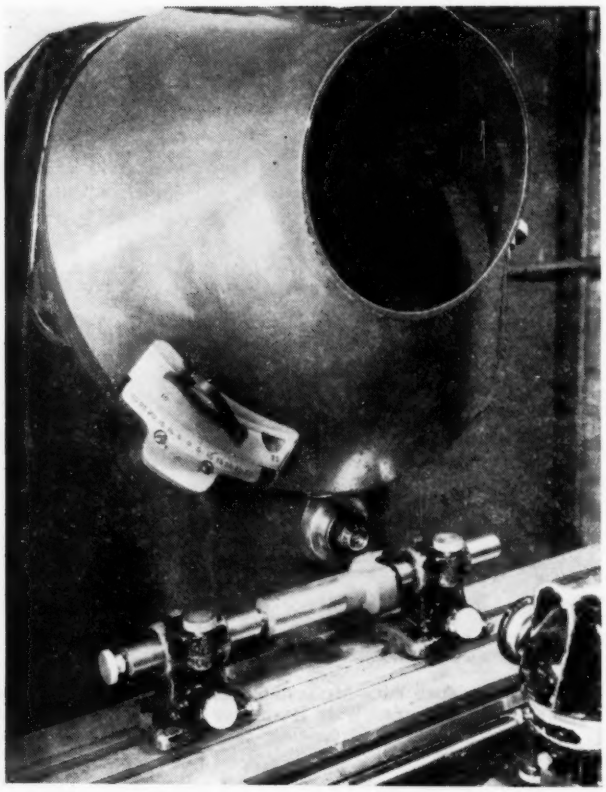


FIG. 8 JONES AND LAMSON OPTICAL COMPARATOR USED FOR INVESTIGATION AND RECORDING OF TIP FAILURE

for cutters with negative radial rake angles than for positive radial rake angles. However, the cutters with negative radial rake angles will stand up much better and their power requirements will increase more slowly than those with positive radial rake angles. This increase in power consumption during the cutting operation is due to the wear to which any cutter is exposed while in operation. Only because of the more rapid wear may it actually happen that a positive radial rake cutter will entail higher cutting forces than one with negative radial rake angles.

From Fig. 5, it is evident that the cutting forces are invariably several times greater due to deformation of the metal than to separation in the cutting plane. This deformation is always present no matter which angles are provided on the cutter and will be more evident with negative radial rake angles than with positive radial rake angles. A very sharp tool would induce little deformation in the chip or workpiece but tool life would be very low if one would go to the extreme and use a metal-cutting tool similar to a razor blade.

There are therefore two major requirements for a cutter which will give satisfactory cutting action and tool life:

1 A cutting edge which will stand up and not wear or chip readily.

2 A tool shape which will reduce the deformation in the chips and workpiece.

As the cutting speed and hardness of the workpiece material increase, these two requirements assume greater importance. The first requisite can be satisfied with negative radial rake angles and carbides on the cutting tips; the second is achieved by simultaneously providing a positive radial rake angle for improving chip flow.

In accordance with the foregoing conclusions, it was found that cutters which had positive secondary radial rake angles with negative primary radial rake angles imposed at the cutting edge gave better tool life and required less power than cutters with negative radial rake angles. In the text the term "primary" radial rake refers to the radial rake angle at the cutting edge. "Secondary" radial rake refers to the radial rake angle behind the primary radial rake angle (see Fig. 9, *A* and *C*.)

Similar designs for rake angles on single-point tools have been used by DeLeeuw, E. G. Herbert, and Klopstock and are discussed in their application to high-speed tools by O. W. Boston (8). The use of negative and positive rake angles on carbide lathe tools for the machining of steel has recently been reported by Einar Almdale (9).

For the experimental investigation of the double radial rake angles, the first two cutters tested had been given a negative primary radial rake angle of 12-deg, 0.005 in. wide at the cutting edge of a 15-deg positive secondary radial rake tooth. This cutter was tested at 523 fpm cutting speed and compared with cutters of 6-deg positive radial rake angle and 12-deg negative radial

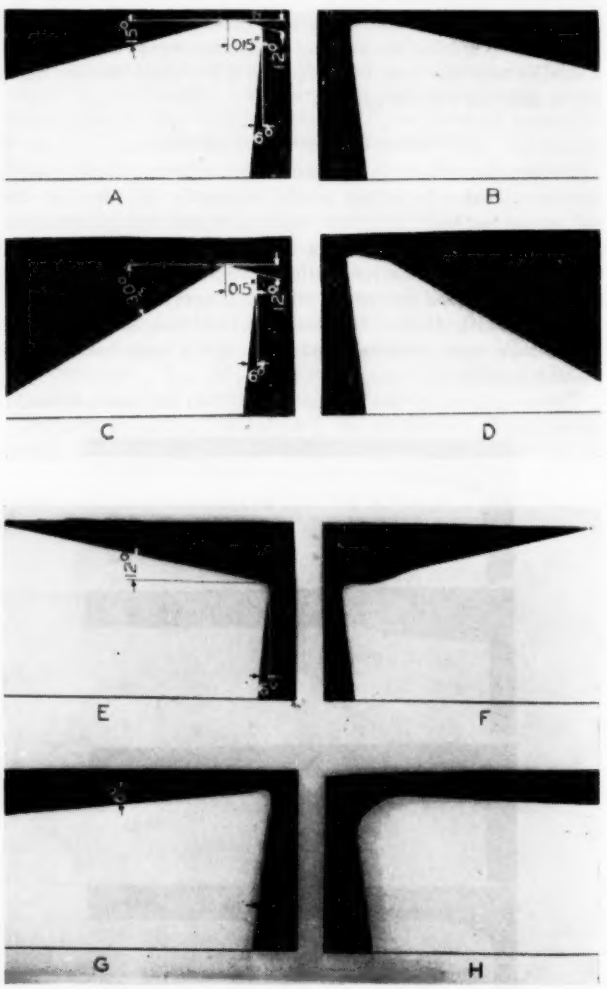


FIG. 9 CROSS-SECTIONAL SILHOUETTES OF CARBIDE CUTTING TIPS IN A PLANE NORMAL TO AXIS OF ROTATION BEFORE AND AFTER THEY HAD REMOVED EQUAL AMOUNTS OF METAL

(Double radial rake cutter blades are shown in *A*, *B*, *C*, and *D*. The 12-deg negative radial rake angle is the primary radial rake angle and the 15- or 30-deg positive radial rake angle behind it is the secondary radial rake angle. Negative and positive radial rake angles are shown in *E*, *F*, *G*, and *H*. Illustrations at left show the angles of a sharp cutter blade, while those at right show type of wear which was most frequently encountered in tips provided with the respective radial rake angles.)

rake angle. The feed per tooth in this test was 0.0075 in. and it was observed that the cutter with the double radial rake angles used less power than the cutter of 6-deg positive radial rake angle. It was also standing up better, but not as well as the cutter with 12-deg negative radial rake angle. After the cutter had removed a comparatively small amount of metal, a crater started to form behind the cutting edge and eventually caused the edge to fracture.

The next comparative test was made with the same cutters except that the negative primary radial rake angle of 12 deg on the double radial rake cutter was increased in width to 0.007 in. The result was practically the same as in the first series of tests.

A third series of tests was conducted with identical cutters. The ones with double radial rake were given a negative primary radial rake of 12 deg, 0.020 in. wide, and the feed per tooth was 0.0105 in. In these tests, the double radial rake cutter required approximately the same power as the 6-deg positive radial rake cutter at the beginning of the test. Later, after it had machined the same amount of metal as the others, its power requirements were less than either of the other cutters. At this point the 6-deg positive radial rake cutter had failed completely and the 12-deg negative radial rake cutter had worn more than the double radial rake cutter. A comparison of the actual power consumption shows that after the double radial rake cutter had machined 16.8 cu in. of metal its power requirement was equal to that of the 12-deg negative radial rake cutter at the beginning of the test. Workpiece temperature was also lower than for the other cutters.

After these tests a large number of cutters with 30-deg positive secondary radial rake angles provided with a negative primary radial rake angle were tested. The positive secondary radial rake angle of 30-deg behind the negative primary radial rake angle of 12-deg brought about an additional decrease in tool force, power consumption, and tool wear, Figs. 9, 12, and 13.

The most obvious indication of improved cutting action was the shape and color of the chips. Those made by a double radial rake angle cutter showed little deformation, Fig. 14. They were almost flat (cutting S.A.E. 1020) and the color ranged from straw for the 15-deg positive secondary radial rake cutter with 12-deg negative primary radial rake to white for the 30-deg positive secondary radial rake cutter with 12-deg negative primary radial rake, Fig. 16.

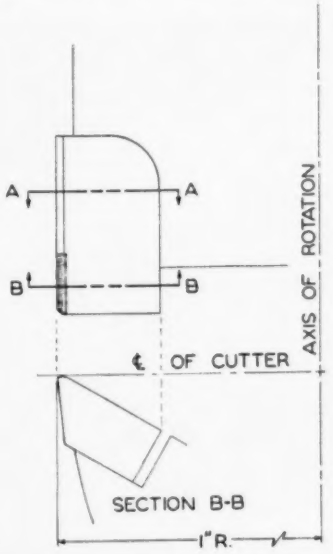


FIG. 10 DIAGRAM INDICATING LOCATION OF CROSS SECTIONS SHOWN IN FIG. 9

(Section *A-A* is new blade as shown on the left side in Fig. 9, while section *B-B* is worn portion shown on right side.)

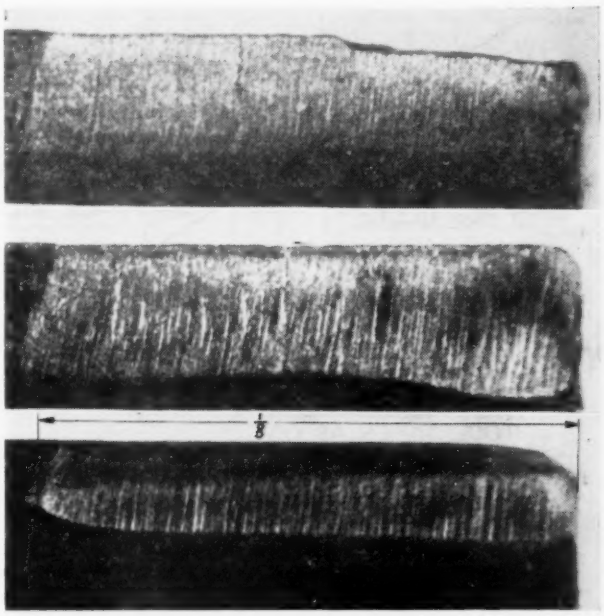


FIG. 11 TYPES OF WEAR AND FAILURE ON DIFFERENT CUTTING TIPS MADE OF TUNGSTEN CARBIDE

(Top: Positive and 0-deg radial rake angles. Center: Negative radial rake angles. Bottom: Double radial rake angles. All these tips had been working equal amounts of metal.)

SURFACE FINISH AND TEMPERATURE OF WORKPIECE

In order to obtain a measure of the surface finish of the workpiece produced by milling cutters with various radial rake angles, profilometer readings were taken of the finish of each S.A.E. 1055 test bar or every third one in the tests which were repeated more than three times. In either case the first test bar cut with a new cutter and the last one of the test or series of tests were always checked for surface finish with the profilometer.

After comparing several thousand readings of surface finish produced at different speeds and feeds, the following statements can be made:

The best surface finish of 8 to 50 microinches is attained at cutting speeds from 500 to 800 fpm and a small feed of 0.0005 to 0.001 in. per tooth. At these feeds no difference could be established between the surfaces produced by the different cutters with various radial rake angles. However, when the feed was increased from 0.003 to 0.012 in. per tooth, the negative radial rake cutters gave a better finish than the cutters with positive radial rake. The best finish at these speeds was produced by the 12-deg negative radial rake cutter and had profilometer readings from 20 to 70 μ in. while the 6-deg positive radial rake cutter produced a finish from 30 to 145 μ in.

For a series of tests made at 427 fpm, the cutter with the 12-deg negative radial rake angles produced the best surface finish.

At speeds of 285, 192, and 106 fpm, with feeds from 0.0036 to 0.0130 in. per tooth, the surface finish was a little better with the 6-deg positive radial rake cutter than with the negative radial rake cutters. All the surface finishes were very poor, ranging from 90 to 245 μ in. for the 6-deg positive radial rake cutter to 170 to 290 μ in. for the 12-deg negative radial rake cutter.

It was found that the 6-deg positive radial rake cutter would produce a better surface at the higher cutting speeds after the cutting edges had become slightly worn.

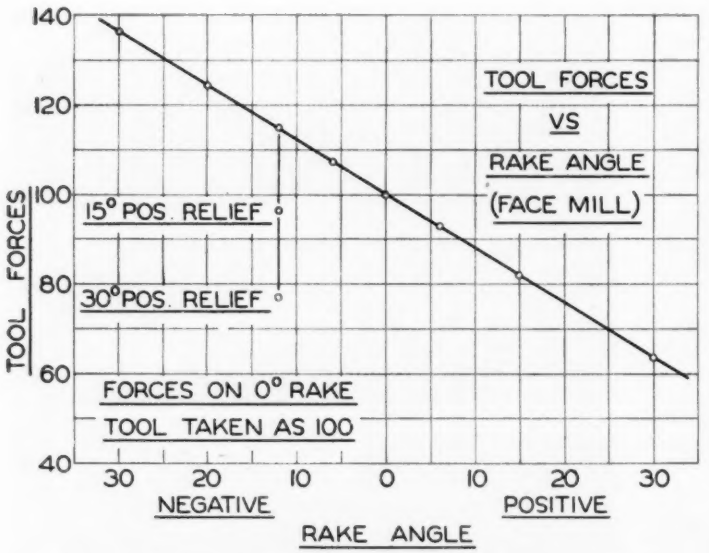


FIG. 12 EFFECT OF VARIOUS RADIAL RAKE ANGLES ON TOOL FORCES ACTING ON A FACE-MILLING CUTTER

(Points indicated as 15- and 30-deg positive relief represent cutters which had a negative primary radial rake angle of 12 deg, and a positive secondary rake angle of 15 or 30 deg.)

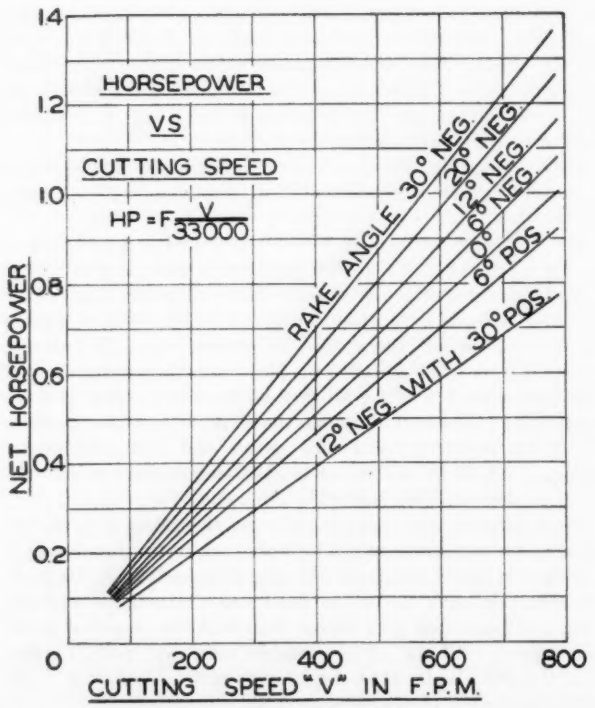


FIG. 13 VARIATION OF NET POWER REQUIREMENTS WITH CUTTING SPEED FOR VARIOUS RADIAL RAKE ANGLES

(Line designated 12-deg neg. with 30-deg pos. represents the cutter with 12-deg negative primary radial rake angle and a 30-deg positive secondary radial rake angle.)



FIG. 14 PHOTOMICROGRAPHS OF S.A.E. 1020 COLD-ROLLED STEEL USED IN TOOL-LIFE TESTS; ×100

(Top: Microstructure of parent metal. Center: Microstructure of badly deformed chips as produced by a 12-deg negative radial rake angle. Bottom: Microstructure of chip produced by 12-deg negative primary radial rake angle and 30-deg positive secondary radial rake angle. Very little deformation is visible.)

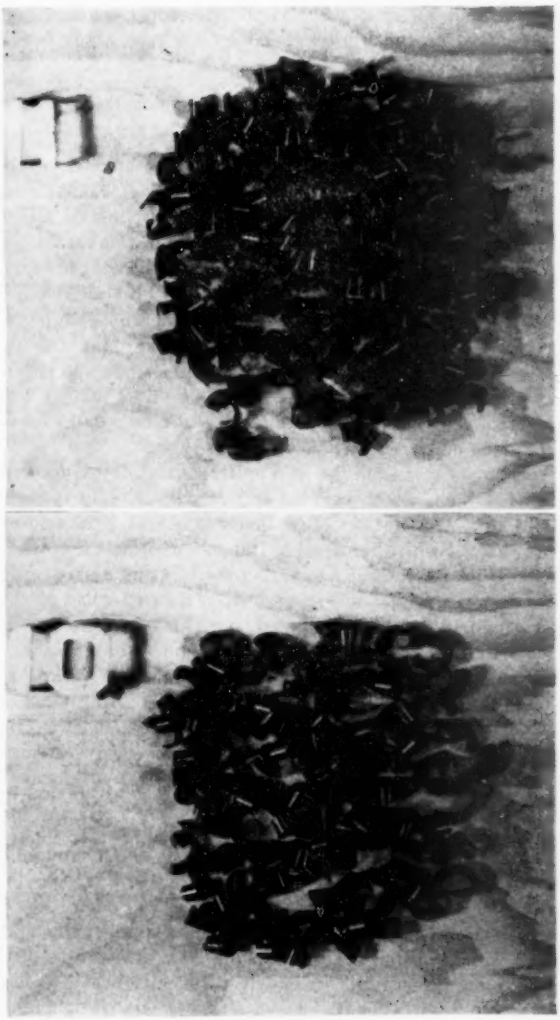


FIG. 15 CHIPS FROM S.A.E. 1020 PRODUCED AT 523 FPM CUTTING SPEED WITH FEED OF 0.0105 IN. PER TOOTH
(Top: By cutter with 12-deg negative radial rake angle. Bottom: By cutter with 6-deg positive radial rake angle.)

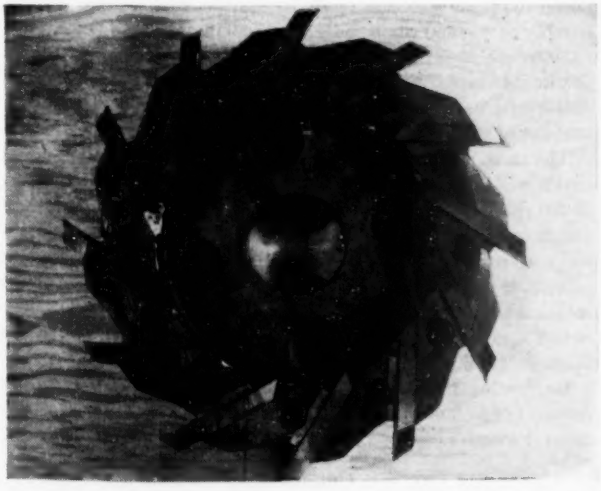


FIG. 17 CUTTER WITH 12 BLADES PROVIDED WITH 30-DEG POSITIVE SECONDARY RADIAL RAKE AND NEGATIVE PRIMARY RADIAL RAKE OF 6 DEG

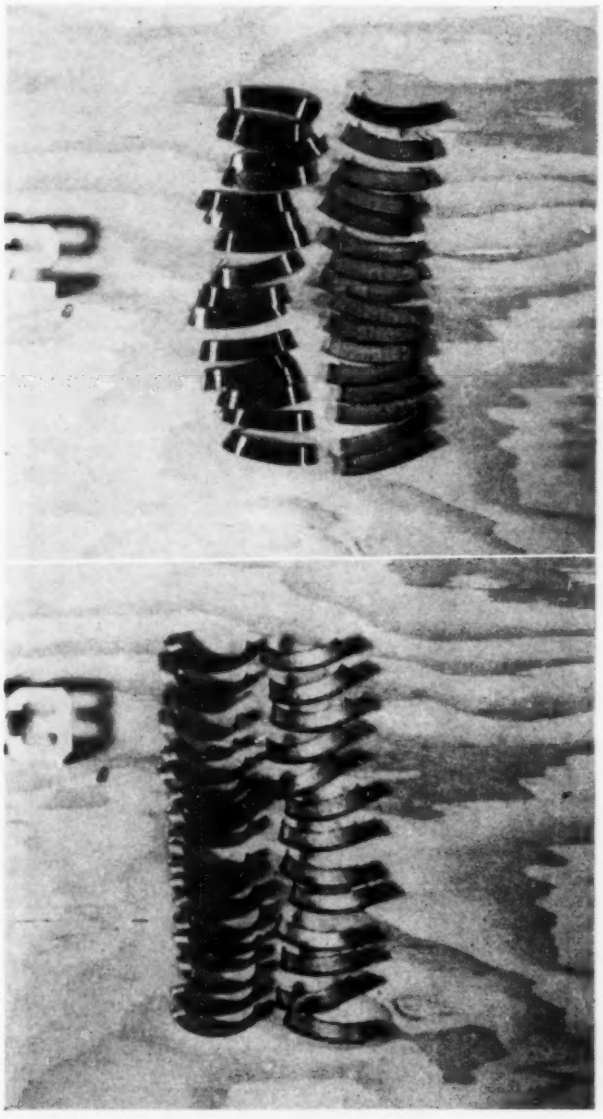


FIG. 16 CHIPS FROM S.A.E. 1020 PRODUCED AT 523 FPM CUTTING SPEED WITH FEED OF 0.0105 IN. PER TOOTH
(Top: By cutter with 12-deg negative primary radial rake angle and 15-deg positive secondary radial rake angle. Bottom: By cutter with 12-deg negative primary radial rake angle and 30-deg positive secondary radial rake angle.)

The surface temperatures of the test bars were measured immediately before and after the cut. It can generally be stated that temperature of the workpiece is influenced by the radial rake angles of the cutter but is more dependent upon the cutting speed and feed. Surface temperature of the workpiece will vary directly as the cutting speed and inversely as the feed, see lower part of Figs. 1 and 2. The cutter which cuts with a smaller force, e.g., the 6-deg positive radial rake angle, will also entail a lower surface temperature as long as its cutting edge is sharp. As soon as its cutting edge is slightly worn, the surface temperature of the workpiece will increase beyond the temperatures generated by cutters with negative radial rake angles which have removed an equal amount of material. A cutter with negative radial rake angles, because of better wearing qualities, will generally give a somewhat lower surface temperature in workpieces than a positive radial rake cutter.

The foregoing statements apply only in those cases in which



FIG. 18 DIFFERENT TYPES OF CHIPS, AS PRODUCED WITH CUTTER IN FIG. 16, WHEN CUTTING A 4-IN. TEST BAR OF S.A.E. 1020

(Top: Washerlike chips cut at a feed of 30 ipm. Center: Chips cut at 30 ipm by same cutter after a corner angle of 20 deg had been added. Bottom: Chips from same cutter, 20-deg corner angle, operating at 60 ipm feed.)

the chips will not be deposited upon the workpiece and will not transfer heat to the workpiece after their separation from the stock.

PRACTICAL APPLICATION OF DOUBLE RADIAL RAKE ANGLE

Performance of the double radial rake angle cutters with the experimental setup indicated a definite superiority over cutters with a single positive or negative radial rake angle. To check the action of double radial rake angles in a production setup, an 8-in-diam cutter, Fig. 17, was designed for the machining of mild steel. This cutter was made for comparison with existing cutters with negative radial rake angles and therefore was provided with 12 teeth. Blades made of solid carbide were ground and lapped so they could be held by wedges in ground slots in the cutter body. No axial rake angle or corner angle was provided. The positive secondary radial rake angle of the blades was 30 deg, and a negative primary radial rake of 6 deg, 0.015 in. wide, was ground on the cutting edge.

This cutter was operated at a cutting speed of 465 fpm and a feed of 30 ipm, which resulted in a maximum chip thickess of 0.0113 in. A $4 \times 4 \times 12$-in. block of S.A.E. 1020 cold-rolled steel with a Brinell hardness of 160 was used as the workpiece. Flat circular chips similar to spring washers and almost white in color were cut, see top of Fig. 18. After the cutter had machined approximately 300 cu in. of metal, signs of wear were detectable chiefly from the tendency of chips to assume a bronze tint. Interference of chips between the cutting blade and workpiece led to chipping of the cutting edge.

To increase cutter strength, a corner angle of 20 deg was ground on the blades. Chip clearance was improved by setting the blades out farther. The cutting edge was given a negative primary radial rake of 6 deg, but the width was increased to 0.025 in. This cutter was operated at various cutting speeds with feeds ranging from 35 to 60 ipm. Consequently, the maximum chip thickness was varied between 0.019 and 0.023 in. per tooth. Depth of cut was held constant at 0.125 in.

Chips cut with the second cutter were flat, semicircular, and almost white in color, see center of Fig. 18. After signs of wear began to appear on the cutting edge, the chips began to show a bronze coloring. One tip of the cutter was slightly damaged after operating for two hours by a chip which was carried around and caught between the blade and workpiece.

As can be seen from the chips in the lower part of Fig. 18, the chief disadvantage in this cutter design was inadequate chip clearance which allowed the chips to hit the cutter body and curl sharply at one end when the feed was 60 ipm.

However, these tests were sufficiently conclusive to prove that the double radial rake angle cutters require less power than the cutter with negative radial rake only and still provide a maximum amount of strength in the cutting edge.

The main advantage of the double radial rake on a face milling cutter will be that one cutter of basic design, e.g., 30-deg positive radial rake, can be used for mild-steel and nonferrous metals by grinding a primary negative radial rake on the cutting edge in the case of steels or a positive primary radial rake in the case of nonferrous metals. A cutter with a 15-deg positive secondary radial rake and a negative primary radial rake will be a stronger cutter and could be used in machining steels with a hardness in excess of 200 Bhn.

Regrinding of the double radial rake cutter will not require the removal of as much of the carbide tip as either a positive or negative rake cutter.

CONCLUSIONS

Negative radial rake angles were found to produce stronger

cutting tips, the cutting edges of which are generally not as liable to fail from impact and shock when entering a workpiece of hard material as are the cutting edges formed by positive radial rake angles.

Power required at the cutting edge is higher for the negative radial rake cutter than for cutters with positive radial rake angles. This holds true for conventional cutting speeds as well as higher cutting speeds up to 785 fpm.

Cutters with negative radial rake angles will stand up longer at the higher speeds than positive radial rake cutters under identical conditions.

Wear and failure at high speeds on the cutting edge of a positive radial rake angle cutter will soon increase its power consumption above that of a cutter with negative radial rake angles.

Best surface finish in high-speed milling is produced with a negative radial rake cutter at cutting speeds between 500 and 800 fpm. A feed of 0.001 in. per tooth or less will give the smoothest surface but will also result in more rapid abrasion at the cutting edge than with coarser feeds.

At 192 and 106 fpm cutting speed, the surface of the test specimens was badly torn and cracked by the negative radial rake cutters. This did not happen at higher cutting speeds.

Average temperature of the chips produced by ordinary feed does not approach the melting temperature of steel even at high speeds.

Heat in the workpiece and chips is due more to deformation of the metal than to separation in the cutting planes.

When removing a chip there is always more work done in deforming the metal than in separating it. The various elements like compression, bending, work-hardening, shearing, and friction enter into what is commonly called "metal-cutting."

A cutter with negative radial rake angles will generally give a somewhat lower surface temperature in the workpiece because it does not wear as rapidly as the positive radial rake cutter. However, as long as the positive radial rake cutter has a sharp cutting edge it will maintain lower temperatures in the workpiece.

A cutter with a 15- or 30-deg positive secondary radial rake angle and provided at the cutting edge with a negative primary radial rake angle 1 to 2 times the width of feed per tooth was found to be a more effective cutter, since it combined the increased strength of the cutting edge afforded by negative radial rake angles and the lower power requirement of the cutter with positive radial rake angles.

When running tool-life tests, it was found that the tool life of the carbide tips may vary as much as 50 per cent for the same cutters under identical conditions. This was due to variations of the quality between batches of carbide inserts of the same brand. Since tungsten from different sources is used by the carbide makers, this may be one of the most likely causes for the variation in cutter performance.

From the net horsepower at the cutter, as determined by the calorimeter, the tool forces were computed for the different rake angles by the formula

$$\text{hp} = \frac{F \times V}{33{,}000}$$

$$F = \frac{\text{hp} \times 33{,}000}{V}$$

This force F is the resultant force of several component forces, and it can be seen in Fig. 12 that it increases with the negative radial rake angle and decreases with the positive radial rake angle. It also shows how much the tool forces on a cutter with 12-deg negative primary radial rake are reduced by the application of a positive secondary radial rake angle of 15 or 30 deg.

The graph in Fig. 13 illustrates that the horsepower is a straight-line relationship to the cutting speed when depth of cut and feed are constant. The force F has a particular value for each radial rake angle and chip cross section. This value does not vary with cutting speed.

Acknowledgment

Mr. J. R. Roubik of the Department of Engineering Development, Kearney & Trecker Corporation, assisted in carrying out and evaluating the reported tests. Grateful acknowledgment is also made to J. P. Bunce for his help in checking the manuscript.

BIBLIOGRAPHY

1 "Hyper Milling," Engineering Bulletin No. FE-106, Firth-Sterling Steel Company, p. 10.

2 "High-Speed Milling With Negative Rake Angles," by Hans Ernst, *Mechanical Engineering*, vol. 66, 1944, pp. 295–299.

3 "Determining Tool Efficiency in High-Speed Milling," by W. E. Brainard, *Mechanical Engineering*, vol. 66, 1944, pp. 301–302.

4 "Vega's Experience With Carbide Milling Cutters," by R. G. Owen, *Machinery*, vol. 49, July, 1943, pp. 152–159.

5 "Hi-Cycle and Hyper Milling on Aircraft Parts," by C. H. Bodner, *American Machinist*, vol. 87, June 10, 1943, pp. 103–106.

6 "Carbide-Tipped Cutters Speed Steel Milling," by F. W. Lucht, *American Machinist*, vol. 87, Dec. 23, 1943, pp. 105–114.

7 "Die Kraefte in der Werkzeugmaschine," by G. Schlesinger, *Zeitschrift des Vereines deutscher Ingenieure*, vol. 74, 1930, pp. 1067–1068.

8 "Engineering Shop Practice," by O. W. Boston, John Wiley & Sons, Inc., New York, N. Y., vol. 1, 1933, pp. 117–119.

9 "Chip Control When Machining Steel With Carbides," by Einar Almdale, *Tool and Die Journal*, vol. 9, Dec., 1943, pp. 105–109.

Effect of Grain Size and Subzero Treatment on Productivity of Four High-Speed Steels

By S. M. DEPOY,[1] DAYTON, OHIO

In the investigation reported, the effect of grain size and subzero treatment on the productivity of four high-speed steels was studied by means of a series of turning tests on one alloy steel at a preselected uniform hardness. The material being cut, the shape of the tool bit, and the speed, feed, and depth of cut on the turning operation were held constant. Standard and subzero treatments were used at different hardening temperatures to develop different grain sizes and different hardening products. The results obtained show that the grain size, carbide solution, and type of martensite formed in the tool have a very marked effect on its cutting ability. It appears that subzero treatment is much more effective, when large grain sizes are developed.

THE purpose of the research was as follows:

1 To determine the difference in cutting ability between four types of high-speed steel.

2 To determine the difference in cutting ability which may exist between standard-treated cutting tools and those that are subzero-treated between subsequent tempers.

3 To determine the effect of ultimate grain size on the cutting ability of cutting tools.

The equipment and materials used in the research were as follows:

1 Model C Monarch toolroom lathe, 14 in.

2 Battery of Ajax electric salt-bath furnaces.

3 Subzero unit; simple container filled with dry ice and methanol.

The materials utilized consisted of one alloy machinery steel, N.E. 8620, and four types of high-speed tool steel. The source, heat number and chemistry of these materials are given in Table 1.

TABLE 1 SOURCE, HEAT NUMBER, AND CHEMISTRY OF STEELS USED IN TESTS

Spec. no.[a]	Trade name	Source	Heat no.	Chemical composition, per cent C	Mn	Si	P	S	Cr	W	Mo	Va	Co	Ni
NE-8620	NE-8620	Timken Steel & Tube Div.	...	0.20	1.03	0.29	0.014	0.016	0.49	...	0.17	...	...	..
M-2	Electrite Double Six	Latrobe Electric Steel Co.	20392	0.85	0.29	0.21	0.028	0.012	4.12	5.78	4.57	1.59	...	..
M-36	Electrite CO-6	Latrobe Electric Steel Co.	44038	0.86	0.31	0.33	0.022	0.014	4.07	5.39	4.41	1.65	8.63	..
T-1	Electrite no. 1	Latrobe Electric Steel Co.	21003	0.73	0.34	0.32	0.029	0.009	4.07	17.76	...	1.07	...	..
T-5	Electrite Super Cobalt	Latrobe Electric Steel Co.	44041	0.85	0.29	0.25	0.027	0.012	4.30	18.03	0.78	1.94	8.56	..

[a] Specification for high-speed steels in this column were recently adopted by three large automotive manufacturers.

Procedure Followed in Tests

All high-speed steel bits (3/8 in. square × 3 in. long) were hardened in the Ajax salt-bath furnaces using Houghton liquid heat N.D. salt and Houghton liquid heat 2400 C salt in the preheat and high-heat furnaces, respectively. Park No. 100 salt was used in the quenching bath. The following are the treatments used:

Treatment No. 1. Preheat at 1650 F for 30 min; high heat at 2175 F for 2 1/2 min; quench at 1100 F for 3 min; cool in air to 100–150 F; wash thoroughly (hot water not less than 150 F); double temper at 1050 F, 2 hr + 2 hr.

Note: Care was taken that the bits cooled to room temperature between the temper cycles on all treatments.

Treatment No. 2. Preheat at 1650 F for 30 min; high heat at 2225 F for 2 1/2 min; quench at 1100 F for 3 min; cool in air to 100–150 F; wash thoroughly; double temper at 1050 F, 2 hr + 2 hr.

Treatment No. 3. Preheat at 1650 F for 30 min; high heat at 2275 F for 2 1/2 min; quench at 1100 F for 3 min; cool in air to 100–150 F; wash thoroughly; double temper at 1050 F, 2 hr + 2 hr.

Treatment No. 4. Preheat at 1650 F for 30 min; high heat at 2300 F for 2 1/2 min; quench at 1100 F for 3 min; cool in air to 100–150 F; wash thoroughly; double temper at 1050 F, 2 hr + 2 hr.

Treatment No. 5. Preheat at 1650 F for 30 min; high heat at 2325 F for 2 1/2 min; quench at 1100 F for 3 min; cool in air to 100–150 F; wash thoroughly; double temper at 1050 F, 2 hr + 2 hr.

Treatment No. 6. Preheat at 1650 F for 30 min; high heat at 2350 F for 2 1/2 min; quench at 1100 F for 3 min; cool in air to 100–150 F; wash thoroughly; double temper at 1050 F, 2 hr + 2 hr.

Treatment No. 7. Preheat at 1650 F for 30 min; high heat at 2410 F for 2 1/2 min; quench at 1100 F for 3 min; cool in air to 100–150 F; wash thoroughly; double temper at 1050 F, 2 hr + 2 hr.

A duplicate of each standard bit was made, and these duplicates were treated at 105 F below zero (—105 F). The bits were subjected to the subzero treatment between the two tempers. The refrigeration cycle was 3 hr. An Izod impact specimen was treated with each bit, and the relative impact values determined. Microsections were made on each bit, and the grain count was

TABLE 2 HARDNESS, IMPACT VALUE, AND GRAIN COUNT OF BITS TREATED AT —105 F

Material	Treatment	Hardness, Rockwell Standard	Hardness, Rockwell Subzero	Impact, ft-lb Standard	Impact, ft-lb Subzero	Grain count (intercept) Standard	Grain count (intercept) Subzero
M-2	1	63.5	65.0	33	29	9 1/2	10
M-2	2	63.5	66.5	42	15	10 1/2	6 1/2
M-2	3	64.0	67.0	7	6	8	7
M-36	1	64.0	66.5	18	12	8 1/2	8
M-36	2	64.0	67.0	21	7	8	6 1/2
M-36	4	64.5	67.5	4	4	4	4 1/2
T-1	3	63.0	65.0	31	32	11	11 1/2
T-1	5	63.5	65.5	20	51[a]	10	12
T-1	7	63.5	66.5	8	8	5	6
T-5	4	64.0	66.5	15	13	10 1/2	7 1/2
T-5	6	64.5	68.0	4	4	6	6
T-5	7	65.5	67.0	4	4	5 1/2	5

[a] Questionable; no explanation for high value.

[1] Metallurgist, Delco Products Division, General Motors Corporation.

Contributed by the Research Committee on Metal Cutting Data and Bibliography and presented at the Semi-Annual Meeting, Pittsburgh, Pa., June 19–22, 1944, of The American Society of Mechanical Engineers.

Note: Statements and opinions advanced in papers are to be understood as individual expressions of their authors and not those of the Society.

determined by the intercept method. Table 2 records the hardness, impact value, and grain count on each bit.

Following the heat-treatment all bits were ground to conform to the following specifications:[2] Back rake, 8 deg; side rake, 14 deg; front relief angle, 6 deg; side relief angle, 6 deg; end cutting angle, 6 deg; side cutting angle, 15 deg; nose radius, $^3/_{64}$ in. Care was taken that all bits were ground exactly alike.

When the bits were completely finished a 5-in-diam bar of N.E. 8620 of 240 Bhn, was set up in a 14-in. Model C Monarch toolroom lathe, and a preliminary cut made on it to remove the hot-rolled surface, reducing it to 4.950 in. diam. The bar was 23 in. long, having an available machining surface of 20 in. By varying the revolutions per minute (rpm) with respect to the diameter, a surface speed of 200–219 fpm was maintained, according to the following formula:

Surface speed = 0.262 × diam of bar × rpm of chuck

The cutting point of the tool was set on the center of the bar, and the shank of the tool was at 90 deg to the center axis of the bar. The depth of cut was held uniform at 0.050 in., and the feed at 0.0075 in. per revolution. The operation time of each bit was timed with a stop watch. The point of failure of each bit was obvious and abrupt. After failure, each bit was reground and made ready for a repeat test. All 24 bits were tested five times. It should be noted that small pieces of the tool bit were left in the bar at the point of failure. It was necessary to remove these and the "glazed" surface before starting another test bit.

Results of Tests

After tabulating the operating time on each bit, the average time was calculated for the five test runs. In order to present the comparison of the results on the various materials and heat-treatments, an arbitrary figure, which will be referred to as the "productivity" of the tool, was developed. This figure was arrived at by calculating the volume of metal removed, according to the following formula:

Volume of metal removed (cu in.)
= depth of cut × 12 × speed (fpm) × feed × operating time

With the feed depth of cut constant, the formula reduces to

Volume of metal removed = 0.0045 × speed × operating time

or

$$V = 0.0045\,ST = \text{productivity} = P$$

Thus

$$P = 0.0045\,ST$$

From this formula the productivity was calculated for each test run, and the average productivity determined for each bit.

TABLE 3 AVERAGE OPERATING TIME AND PRODUCTIVITY OF TOOLS TESTED

Material	Treatment	Average operating time, min: Standard	Average operating time, min: Subzero	P: Standard	P: Subzero	Increase in P, subzero over standard, per cent
M-2	1	15.85	17.60	15.00	16.88	12.5
M-2	2	20.36	29.20	19.80	27.38	38.3
M-2	3	29.29	45.32	27.20	42.60	56.5
M-36	1	3.22	3.50	2.98	3.22	8.0
M-36	2	20.86	28.95	19.10	27.40	43.5
M-36	4	32.18	47.38	30.85	46.00	49.0
T-1	3	4.26	4.69	4.00	4.35	8.5
T-1	5	15.18	20.10	14.30	18.55	29.8
T-1	7	20.52	29.02	18.83	26.58	41.0
T-5	4	2.41	3.18	2.28	3.05	33.7
T-5	6	13.65	18.61	13.30	17.43	31.2
T-5	7	34.21	49.15	31.80	46.30	45.5

Table 3 lists the average operating time and the average productivity for each tool tested.

[2] "The Effect of Hardness on the Machinability of Six Alloy Steels," by O. W. Boston and L. V. Colwell, Trans. American Society for Metals, 1943, vol. 31, pp. 955–979.

Interpretation of Results

From examination of Table 3, it is immediately apparent that the low refrigeration treatment is immensely effective. Further, it may be noted that refrigeration is much more effective on the steel when it is austenitized at comparatively high temperatures.[3] It may also be noted that the higher austenitizing temperatures produce a superior cutting tool even when the tool is not subjected to refrigeration. However, this does not mean that high-speed tool steels may be heated at or over the top of the austenitizing range promiscuously. It must be remembered that these treatments were controlled very closely both regarding time of soak and temperature range. A small increment of prolonged soaking time or higher temperature would cause incipient fusion, thus producing a "burned structure." This structure would be extremely brittle and would be practically useless in operation.



Fig. 1 M-36 Steel, No. 4 Standard Heat-Treatment (Aqua regia etch; ×1000.)

The superiority of the bits that are austenitized at the top of the range is probably due to the more complete solution of the carbides contained in the steel. Microsections of these treatments show very little free carbide areas. In contrast to this, the bits that were austenitized at temperatures on the low side of the range or below, revealed very high percentages of free carbides. The carbides are much more effective as abrasive resistors when they are in solution. Consequently, it should be the object of the hardener to get as much solution as possible. There are patented and so-called "secret processes" which utilize this fact as a basis for their treatment. However, they use very high temperatures (2500–2700 F) in the austenitizing cycle and depend solely upon the operator to remove them before damage is done to the tool. It is believed that the same results may be obtained by close temperature control at the top of the austenitizing range.

Photomicrographs reveal a very definite structure is caused by subzero treatment. This structure is decidedly different from that obtained by standard treatments. Further, this in-

[3] "The Transformation of Retained Austenite in High Speed Steel at Subatmospheric Temperatures," by P. Gordon and M. Cohen, Trans. American Society for Metals, 1942, vol. 30, pp. 569–591.

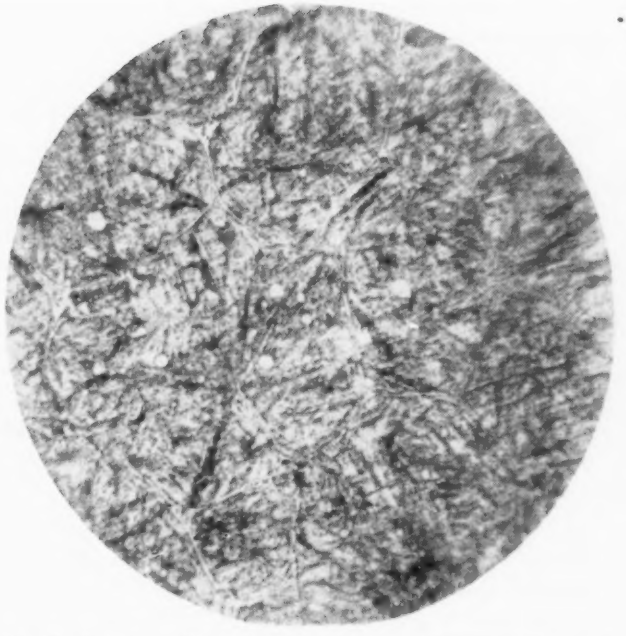


FIG. 2 STEEL OF FIG. 1 SUBZERO-TREATED BETWEEN TEMPERS
(Aqua regia etch; ×1000.)

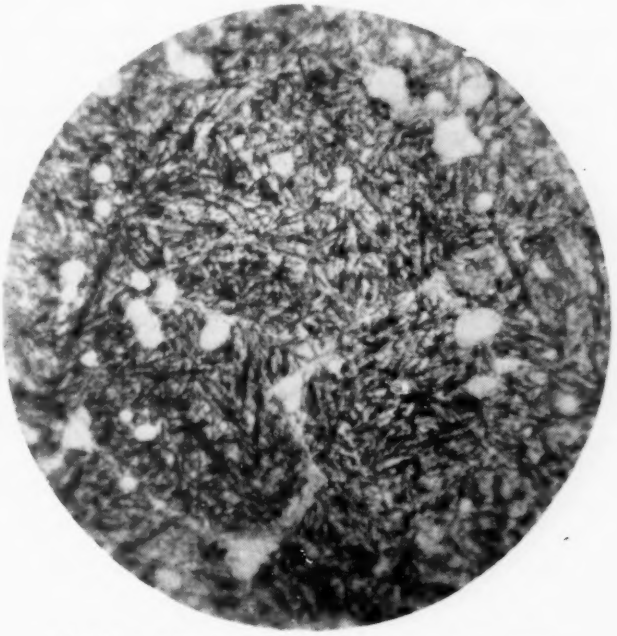


FIG. 3 M-2 STEEL, NO. 3 STANDARD HEAT-TREATMENT
(Aqua regia etch; ×1000.)

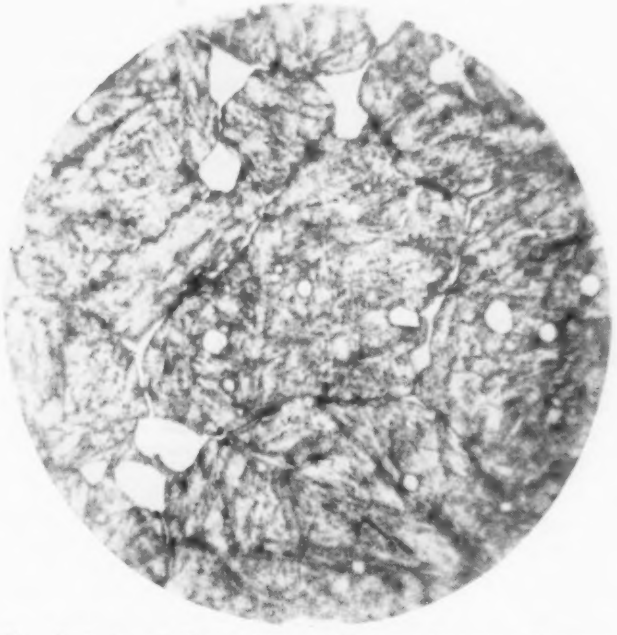


FIG. 4 STEEL OF FIG. 3, SUBZERO-TREATED BETWEEN TEMPERS
(Aqua regia etch; ×1000.)

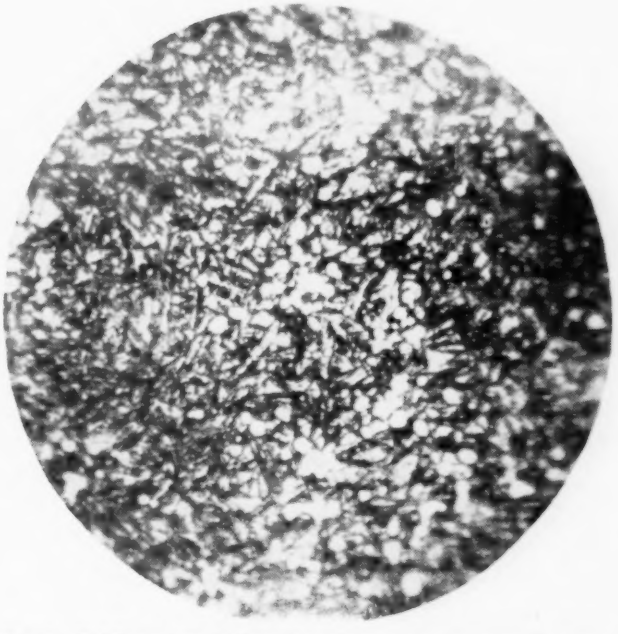


FIG. 5 M-2 STEEL, NO. 2 HEAT-TREATMENT, AND SUBZERO-TREATED AT —85 F BETWEEN TEMPERS
(Aqua regia etch; ×1250.)

vestigator has not been able to produce the de-ired structure or productivity on tools that are treated at —90 F or higher.

Fig. 1 is a photomicrograph of M-36 steel treated with No. 4 treatment, but not subzero-treated. The familiar acicular formation of the marten ite is apparent. Fig. 2 reveals the structure obtained in the same steel with the same treatment only that it has been subzero-treated between the tempers. It may be seen that the martensite is no longer heavy acicular, but rather fine, giving a peppery structure. The same phenomenon is present in Figs. 3 and 4. The microsections were taken of M-2 steel using No. 3 heat-treatment. Fig. 3 is standard-treated, and Fig. 4 is subzero-treated. The apparent absence of the familiar carbides in Figs. 1 and 2 is the result of the extreme austenitizing temperature. This temperature has caused almost all of the carbides to go into solution.

The formation of the fine martensitic structure on the refrigerated material is believed by the author to be caused by the intense internal strains and pressures caused by the extreme low temperature. It is suggested that these pressures also caused the transformation of austenite to martensite to go to completion. Fig. 5 is a microsection of M-2 steel which was treated ac-

cording to No. 2 treatment, and refrigerated at —85 F, between the tempers. The heavy acicular martensitic structure is still present and blocky austenite may be seen. It may also be noted that the results obtained on cutting tests were very much the same as on an unrefrigerated tool. Consequently, it is believed that the pressures set up at —85 F are not sufficient to affect the structure of a material that has high alloy content, and the sluggish transformation properties that are present in high-speed steels.

Conclusions

The following general conclusions have been arrived at by a study of the results of this research:

1 High austenitizing temperatures should be used to produce the best structure for metal removal. However, the control of these temperatures and the austenitizing time must be accurate.

2 Refrigeration treatment of high-speed steel at —100 F or lower between the tempers will produce a superior tool.

3 Low austenitizing temperatures leave too many undissolved carbides, thus producing an inferior tool. Therefore, they should be avoided.

4 For cutting operations on hard alloy material, where intense heat is generated at the cutting edge, cobalt-bearing high-speed steel will generally prove superior.

Acknowledgment

Acknowledgment is given to Mr. Ray P. Kells of the Latrobe Electric Steel Company for furnishing the high-speed steel used in this research and the many suggestions that he made to the investigator.

BIBLIOGRAPHY

1 "The Transformation of Retained Austenite in High Speed Steel at Subatmospheric Temperatures," by P. Gordon and M. Cohen, Trans., American Society for Metals, vol. 30, 1942, pp. 569–591.

2 "The Effect of Hardness on the Machinability of Six Alloy Steels," by O. W. Boston and L. V. Colwell, Trans., American Society for Metals, vol. 31, 1943, pp. 955–979.

Machinability of Plain-Carbon, Alloy, and Austenitic (Nonmagnetic) Steels, and Its Relation to Yield-Stress Ratios When Tensile Strengths Are Similar

By E. J. JANITZKY,[1] CHICAGO, ILL.

It is possible by the use of yield-stress ratios of plain-carbon, alloy, and austenitic (nonmagnetic) steels of the same tensile strength to obtain an index of machinability for rough-turning. The relation between Taylor speed and yield-stress ratios of the same tensile strength is expressed mathematically in the paper. A graphical presentation is also given. The yield-stress ratios of steels of the same tensile strength allow co-ordination of machinability of the types of steel listed by the same method, a distinct advantage over the use of any one of the four components of the tensile test alone, or a combination of stress and strain.

THE quest for an index of machinability began with Taylor's[2] establishment of the conception that the measure of machinability may be expressed by the cutting speed at which a standard tool will last for periods of 20 min, 1 hr, or more.

Taylor also found that the change of life of a high-speed steel tool, resulting from a change in the cutting speed, could be represented approximately by an empirical equation

$$VT^n = C \quad \ldots\ldots\ldots\ldots\ldots\ldots [1]$$

in which

V = cutting speed, fpm
T = tool life, min
n = an exponent
C = constant which is dependent for its numerical value upon exact cutting conditions (other than speed). It will vary with the form and size of tools, the material cut, the steel and treatment of the steel from which the tools are prepared, the feed and depth of cut

Curves from which V is deduced are generally called TV curves.

Taylor also developed an empirical relation for carbon steels between cutting speed and the tensile properties of the steel tested by using the tensile strength and elongation. The equation gives some indication regarding machinability but, with the advent of alloy steels, it lost its usefulness. Taylor, however, was not satisfied with the evaluations by this equation.

The present tendency to judge machinability by tensile strength, yield stress, Brinell hardness number or reduction of area, separately, is not satisfactory. Two steels with equal tensile strength or equal yield stress may have different machining properties depending upon the ratio of yield stress to the tensile strength. Likewise two equal Brinell hardness numbers do not necessarily signify equal machinability.

Relationship of Stress and Strain

Before going into the discussion of machinability of steel and its relation to yield-stress ratios when the tensile strengths are similar, it is advisable to consider the relation of stress and strain as they manifest themselves in the tensile test.

A statistical analysis of the relation of the yield-stress ratio to the deformation ratio may be helpful in arriving at a better understanding of the subject.

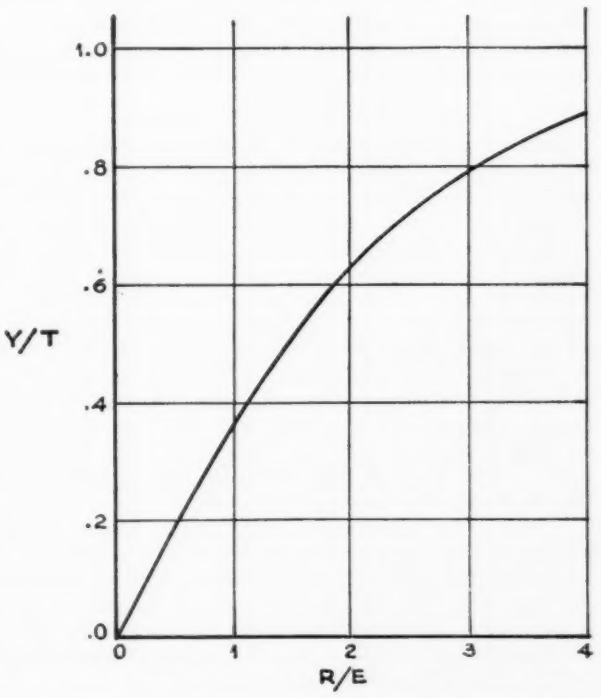


Fig. 1 Illustrating Relation of Deformation Ratio to Yield-Stress Ratio

Yield-stress ratio is defined as the ratio of yield stress to tensile strength, and deformation ratio, the ratio of reduction of area to elongation.

By plotting yield-stress ratios (Y:T) against deformation ratios (R:E), one obtains a curve as shown in Fig. 1.

The curve may be expressed by the equation

[1] Consulting Metallurgical Engineer, Carnegie-Illinois Steel Corporation, South Works.

[2] "On the Art of Cutting Metals," by F. W. Taylor, Trans. A.S.M.E., vol. 28, 1906, pp. 31–279.

Contributed by the Research Committee on Metal Cutting Data and Bibliography and presented at the Semi-Annual Meeting, Pittsburgh, Pa., June 19–22, 1944, of The American Society of Mechanical Engineers.

Note: Statements and opinions advanced in papers are to be understood as individual expressions of their authors and not those of the Society.

$$\frac{Y}{T} = 1 - e^{-0.446}\left(\frac{R}{E}\right)^{1.133} \quad \ldots\ldots\ldots\ldots [2]$$

where

T = tensile strength, psi $\times 10^{-3}$
Y = yield stress, psi $\times 10^{-3}$
R = reduction of area, per cent
E = elongation, per cent, in a gage length 4 times diameter
e = base of natural logarithm

The equation was developed by using yield stress at a set of 0.2 per cent gage length and a pulling speed of 0.11 ipm.

From Equation [2], we perceive that, for a given deformation ratio, there is a corresponding yield-stress ratio. We also perceive that at constant tensile strength with increasing deformation ratio, the yield-stress ratio increases and, consequently the yield stress and vice versa.

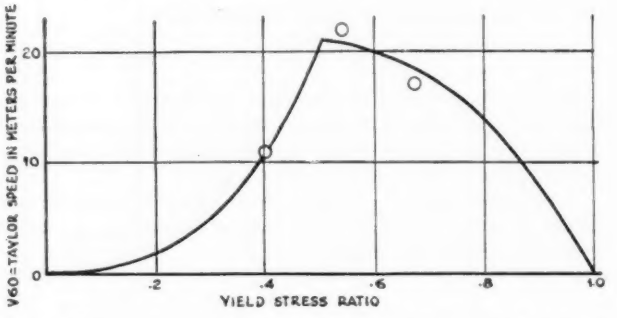


FIG. 2 REPRESENTING AN ISOROTIC CYCLE FOR A TENSILE STRENGTH OF 64.5 KG PER SQ MM OR 91.5 PSI $\times 10^{-3}$ AND DIFFERENT YIELD-STRESS RATIO

From the foregoing observations, it is also evident that co-ordination of machinability with any of the four properties reported in making the tensile test is impossible and leads to erroneous conclusions. The use of indentation hardness for co-ordination of machinability properties may also result in misleading conclusions. An austenitic steel (nonmagnetic) may possess the same Brinell hardness numeral as a quenched and tempered or annealed plain-carbon or alloyed steel and have different tensile properties and, therefore, different machinability properties.

As already mentioned, steels of the same tensile strength may possess different yield-stress ratios and, consequently, different machinability properties. Thus a plot of different yield-stress ratios, but of the same tensile strength, against Taylor speed appears to be the clue to the present enigma.

However, some steels of the same tensile strength but different yield-stress ratio may possess the same Taylor speed. This coincidence manifests itself in nonmagnetic steels of austenitic structure or very low-carbon steels of ferritic structure; that is, in steels of a yield-stress ratio lower than 0.5. Thus the coincidence suggests a family of reversing cycles of the same tensile strength but different yield-stress ratios.

When Taylor speeds are plotted on the ordinate and yield-stress ratios of the same tensile strength on the abscissa, a reversing cycle is obtained.

The cycle, as illustrated in Fig. 2, starts at a yield-stress ratio of 0 and ascends up to a yield-stress ratio of 0.5. From this point the cycle descends to the X axis and terminates at a yield-stress ratio of 1.0.

In Fig. 2, the cycle represents steels of a tensile strength of 64.5 kg per sq mm or 91.5 psi $\times 10^{-3}$, including a nonmagnetic stainless steel of the S-18-8 grade with a yield-stress ratio of 0.4 (own datum).

TABLE 1 COMPILATION OF DATA ON MATERIAL UNDER TAYLOR TEST (LANGENBACH)

1	2	3		4	5	6	7
No.	S.A.E. grade	Heat-treatment, deg C		Tensile strength, kg per sq mm	Yield stress, kg per sq mm	Taylor speed V_{60}, m per min Observed	Calculated
1	1020	N 920 C 1688 F		37.5	22.0	39.5	39.2
2	1025	N 880 C 1616 F	T 700 C 1292 F	46.3	26.3	31.5	30.7
3	1035	O 850 C 1562 F	T 720 C 1328 F	55.0	28.0	26.5	25.5
4	1045	O 850 C 1562 F	T 720 C 1328 F	64.7	34.0	21.5	20.9
5	1070	A 720 C 1328 F		75.4	39.5	19.0	17.4
6	1075	O 850 C 1562 F	T 650 C 1202 F	83.5	43.2	18.0	15.5
7	1080	O 850 C 1562 F	T 650 C 1202 F	90.0	45.7	16.5	14.1
8	X-1020	W 820 C 1508 F	T 650 C 1202 F	51.5	30.5	24.0	26.7
9	X-1030	W 820 C 1508 F	T 650 C 1202 F	63.1	38.8	20.0	20.5
10	T-1340	O 850 C 1562 F	T 680 C 1256 F	74.2	50.5	15.0	15.5
11	2320	O 850 C 1562 F	T 670 C 1238 F	58.6	39.2	19.0	20.9
12	2520	O 850 C 1562 F	T 670 C 1238 F	61.8	41.7	17.5	19.4
13	2330	O 830 C 1526 F	T 500 C 932 F	65.6	45.0	17.0	17.7
14	5130	O 840 C 1544 F	T 550 C 1022 F	81.5	53.0	14.0	14.5
15	5140	O 840 C 1544 F	T 550 C 1022 F	87.5	65.6	12.5	11.6
16	5160	O 840 C 1544 F	T 550 C 1022 F	96.6	70.3	11.5	10.7
17	3230	O 850 C 1562 F	T 670 C 1238 F	58.5	42.0	18.5	19.2
18	3330	O 820 C 1508 F	T 680 C 1256 F	76.3	56.5	14.0	13.3
19	3340	O 820 C 1508 F	T 620 C 1148 F	93.4	72.5	10.0	9.4
20	5 per cent Ni 1.5 per cent Cr	O 820 C 1508 F	T 550 C 1022 F	118.5	94.0	7.5	6.7

NOTE: N = normalized, A = annealed, O = oil-quenched, W = water-quenched, T = tempered.

The cycle may be identified as reversing parabolic cycle with the ascending branch of the paraboła (a cubic parabola) having its vertex at 0 yield-stress ratio and the descending branch (an ordinary parabola) having its verfex at the maximum V_{60}, corresponding to a yield-stress ratio of 0.5.

Thus we may express the ascending part of the cycle

$$V_{60} = c_1\left(\frac{Y}{T}\right)^3 \quad \ldots\ldots\ldots\ldots [3]$$

and the descending part of the cycle

$$V_{60} = c_2\left[0.25 - \left(\frac{Y}{T} - 0.5\right)^2\right] \quad \ldots\ldots\ldots [3a]$$

where

$\frac{Y}{T}$ = yield-stress ratio (Y = yield stress, T = tensile strength)
V_{60} = Taylor speed in meters or feet per minute
c_1 and c_2 = factors

Calculating the factor c_2 from data of Langenbach,[3] given in

[3] "Die Zerspannbarkeit-Kennziffer V_{60} in ihrer Beziehung zur Zugfestigkeit und Streckgrenze beim Schrupp-Dreh Vorgang von legierten und unlegierten Staehlen," by F. Langenbach, Technische Hochschule, Aachen, 1932.

Table 1, and plotting it against the corresponding tensile strength, we obtain a hyperbolic relation that is

$$c_2 = \frac{12{,}500}{T^{1.2}}$$

By interpolating the data from the stainless steel

$$c_1 = \frac{25{,}000}{T^{1.2}}$$

Thus Equation [3] will read

$$V_{60} = \frac{25{,}000}{T^{1.2}} \left(\frac{Y}{T}\right)^3$$

and Equation [3*a*]

$$V_{60} = \frac{12{,}500}{T^{1.2}} \left[0.25 - \left(\frac{Y}{T} - 0.5\right)^2\right]$$

In order to transfer the equation into feet per minute when T is expressed in psi $\times 10^{-3}$, $c_1 = 116{,}642$ and $c_2 = 58{,}464$. The factors c_1 and c_2 in this special case are for the dimension of the tool, for its heat-treatment and chemical composition, the depth of cut, and feed.

Credence to these equations is given in Table 1. Data of observed values are in column 6 and the approximated values are in column 7. A family of cycles in steps of 10 kg per sq mm or 14.2 psi $\times 10^{-3}$ is also given in Fig. 3, for comparing relative machinability.

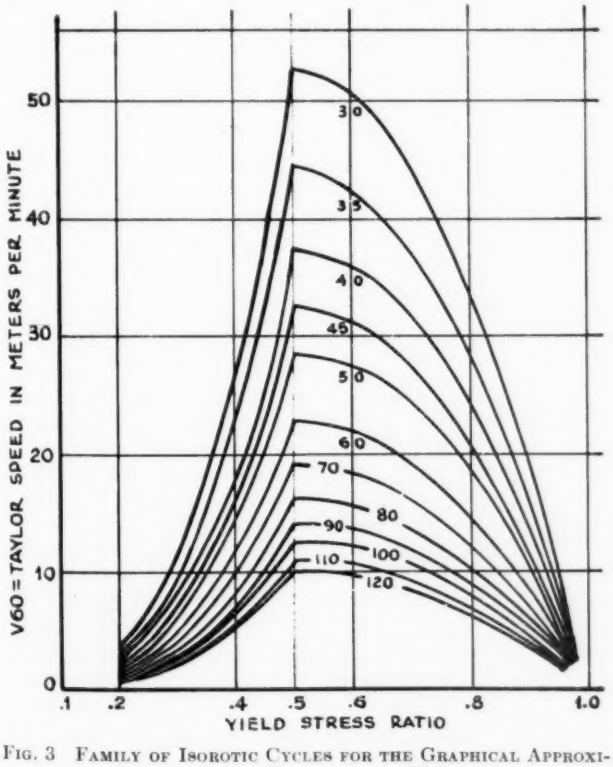


FIG. 3 FAMILY OF ISOROTIC CYCLES FOR THE GRAPHICAL APPROXIMATION OF TAYLOR SPEED (V_{60})
(Numerals at each cycle are kg per sq mm.)

It will be noted by comparison of calculated and actual Taylor speed, that variation in chemical composition does not influence machinability, provided that the steels can be heat-treated to have the same tensile properties. In other words, if two steels are heat-treated to have the same tensile properties (tensile strength, yield stress, elongation, and reduction of area), assuming such heat-treatment is possible, they will be equal in regard to machinability. Leaded, sulphurized, or phosphorized steels, or steels containing other elements as selenium, etc., are exceptions and must be co-ordinated as such. Another method of co-ordination may be applied by including tool angles, that is, the most efficient tool angle for yield-stress ratios of the same tensile strength.

Co-ordination of cold-worked steels of the same tensile strength but different yield-stress ratios may also be accomplished. It is known that cold-drawn or cold-rolled bars machine easier than bars in their natural conditions. It is also known that by cold deformation the yield-stress ratio and also the tensile strength are raised above those in their prior condition. Thus, the machinability of cold-work-processed steels may be also co-ordinated.

When using the same tool and the same feed and depth of cut for steels cold-work-processed to the same tensile strength but different yield-stress ratios, machinability will increase with increasing yield-stress ratio. However, the higher the yield-stress ratio of the steel before cold-processing, the less increase in machinability is to be expected, and cold-work-processing becomes impracticable or technically impossible.

In order not to confuse the conception of machinability, one has to consider that it is a different matter when speed of machining is the primary object and surface finish secondary. In the first case it is desirable to have a lower yield-stress ratio than in the second case, when the material is of the same tensile strength.

Cutting-speed variations also influence the surface finish, that is, the higher the permissible speed the better the surface appearance.

DETAILS OF MACHINABILITY TEST

Following are the details of the machinability test on which the development is based. The data were taken from F. Langen-

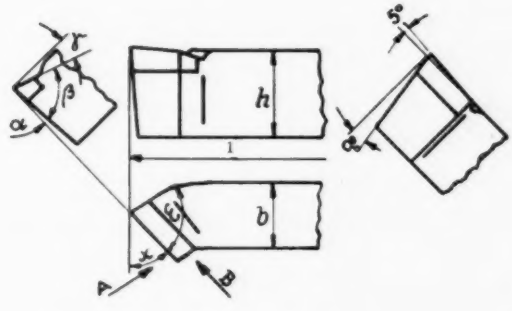


FIG. 4 DIMENSIONS OF TOOL
(Arrows *A* and *B* direction of view. $h = 1.574$ in.; $b = 1.18$ in.; $1 = 13.$ in.; $\alpha = 6$ deg; $\beta = 65$ deg; $\gamma = 19$ deg; $\varepsilon = 45$ deg; $\epsilon = 80$ deg.)

bach's machinability test and selected not only because of the wide range of analyses represented, but also because of precautions used in making the tests, and the fact that only a limited zone was used for making both the machinability tests and the tests for physical properties. As the material under test (bars from 6 to 8 in. diam, and from 60 to 120 in. long) was in the heat-treated condition, it is very important how deep the ma-

chining was performed in regard to the diameter or the location of the tests taken for tensile strength. Fortunately, the machining depth was limited to 2 inches maximum in order to avoid discrepancies on account of hardness gradients, and the tensile-test specimens were taken longitudinally, close to the surface at the ends of the rounds (gage length, 5 times the diameter); yield stress at 0.2 per cent of gage length.

The machining was of the roughing type and dry. The tools were of 18-4-1 composition and the dimensions are given in Fig. 4. The recorded data on machinability represent a depth of cut of 0.236 in. and a feed of 0.039 in. per revolution. The Taylor speed, V_{60}, was obtained by Taylor's method from the TV curves. Each of the TV curves was duplicated and the data so obtained were averaged. If the duplicate tests were not in agreement a triplicate test was run.

The motive of Langenbach's work was to investigate the influence of yield stress on the machinability of steels, as he was aware of the fact that machinability of steels of the same tensile strength decreased with increasing yield stress, however, a co-ordination was not attempted. The present paper deals with the co-ordination. It is perhaps not out of place to mention that the second object of these tests was to establish whether there was a difference between tipped tools when compared with standard tools. Therefore, the machinability of each steel was determined with tipped tools and with standard tools and was found to be independent of the type of tool used.

The Influence of Through-Metal on the Heat Loss From Insulated Walls

By VICTOR PASCHKIS[1] and M. P. HEISLER,[2] NEW YORK, N. Y.

The heat flow through insulation containing "through-metal," or "thermal short-circuits" has been investigated. The heat flow through such a structure (occurring, for example, in the insulation of ship hulls) can be considerably larger than would be found from adding to the heat flow through the insulation that contributed by the "through-metal," as if the two were independent. Thus the apparent effectiveness of an insulation can be very much smaller than would be calculated from the thermal conductivity alone. From the many different forms of thermal short-circuits, one specific type has been selected for investigation, i.e., that of metal strips or fins extending through insulation which is covered on its surfaces by sheet metal. General curves are developed and their application explained, from which an "increase factor" for any condition (conductivity and thickness of the insulation, conductivity and thickness of the strips, outside film conductance) can be read. The "increase factor" is defined as the ratio of the heat flow through an actual structure, compared with the flow that would occur if the insulation and heat flow through metal strips were independent of each other. The method of developing these general curves and the basis of the experimental technique used are explained in two Appendixes.

Statement of Problem

FREQUENTLY, in the practical application of thermal insulation "through-metal" has to be used. The term "through-metal" is here used for any metal extending from the hot surface to the cold one. Because metal has a very much higher conductivity than any insulating material, such through-metal acts like a thermal short-circuit, and therefore greatly influences the flow of heat through a structure. The present paper deals with some problems in connection with the heat losses caused by "through-metal."

Out of the great variety of possible shapes and sizes of such through-metal, one arrangement has been selected as the object of the investigations; the case of a strip of metal connecting the hot surface with the cold surface. Fig. 1 is an isometric sketch of this arrangement. It shows an insulation (of thickness L) covered by sheet metal a and b (thickness W_M). The insulation is assumed to extend infinitely in the x- and y-directions, but in the x-direction it is interrupted by infinitely long strips c (thickness $2\,W_M$) which are spaced at regular intervals W_I. (In case of block insulation W_I represents the width of an individual block.) Arrangements as shown in Fig. 1 are frequently used. Typical examples are the insulated hulls of ships, walls of stratochambers, and industrial ovens with metallic walls. Similar problems occur in almost all insulating practice. By way of example, the following cases may be mentioned: Metal-enclosed bricks such as are used in electric furnaces and in open-hearth furnaces; pipe flanges extending through the pipe insulation; anchor bolts and pipes used in boiler insulation; and mortar joints in brick walls.

It is obvious that such through-metal influences the heat loss of the structure, and also that, at any appreciable distance from the surface, the metal will influence the temperatures in the adjacent insulation.

In determining the heat loss from a structure incorporating through-metal, the oldest and empirical way is to estimate the increase of heat loss due to the metal and account for this increase by an additive, or by a multiplication correction factor, found from experience with similar arrangements.

A distinct step forward is the separate calculation of the heat flowing through the insulation and through the metal, and adding both heat flows. This method is based upon the assumption that the metal does not influence the temperatures in the surrounding insulation. This assumption, however, is in many cases not tenable, as will be evident from this paper. The correct approach must take the lateral flow into consideration.

A general solution for this problem, covering any thickness L of the structure, any spacing W_I of the strips, any thickness W_M of the metal, as well as any conductivity of insulation k_I and metal k_M, is the main object of this report. Only three assumptions have been made which limit the generality:

1 The film conductance on the hot surface is considered to be infinite (this means that the hot surface has the same temperature as the adjacent air (ambient).

2 The thickness of the metallic strips is twice that of the sheet metal covering the surfaces.

3 The thermal properties (conductivities and cold-side film conductance) do not change with temperature.

Lateral Heat Flow

Assume a wall of thickness L (Fig. 2). The hot side is maintained constantly at a temperature t_h, the cold side at a temperature t_{cs}. Now if the wall is homogeneous, then independent of the thermal conductivity of the material of the wall, the temperature at any given distance l from the hot surface always has the same value as given by

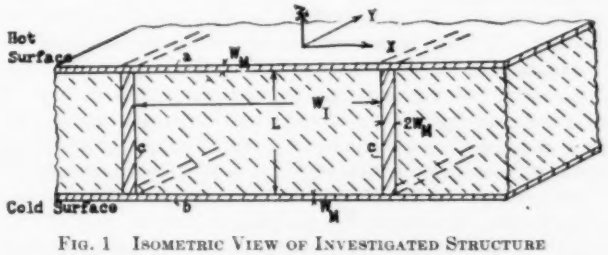


Fig. 1 Isometric View of Investigated Structure

$$t = t_{cs} + \frac{L - l}{L}(t_h - t_{cs}) \qquad [1]$$

If (Fig. 3) two materials with thermal conductivities k_1 and k_2

[1] Research Associate in Mechanical Engineering, Columbia University; Charge of Heat and Mass Flow Analyzer Laboratory.

[2] Assistant in the Heat and Mass Flow Analyzer Laboratory, Department of Mechanical Engineering, Columbia University.

Contributed by the Heat Transfer Division and presented at the Spring Meeting, Birmingham, Ala., April 3–5, 1944, of The American Society of Mechanical Engineers.

Note: Statements and opinions advanced in papers are to be understood as individual expressions of their authors and not those of the Society.

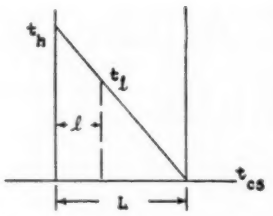


FIG. 2 TEMPERATURE DROP THROUGH HOMOGENEOUS WALL

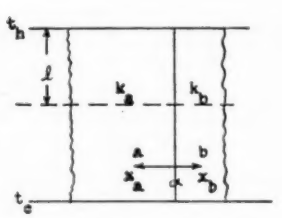


FIG. 3 INTERFACE BETWEEN TWO MATERIALS

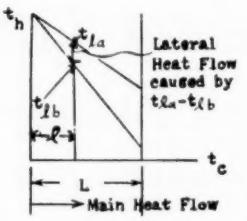


FIG. 4 TEMPERATURE DROP CAUSING LATERAL FLOW

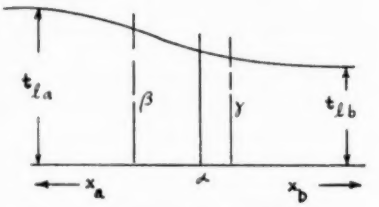


FIG. 5 TEMPERATURE DISTRIBUTION NEAR INTERFACE

are subjected in parallel to the same temperature difference, then their temperatures at a distance l from the hot surface are the same. Between points of equal temperature, no heat transfer can of course occur.

Matters are different however if the cold surface, instead of being held at a constant value, is (Fig. 4) facing an ambient of constant temperature t_c. Now the temperature at point l is not only a function of the quantities appearing in Equation [1] but also of the conductivity k of the material and the film conductance h at the cold surface. The temperature at l can now be found from

$$t_l = t_c + (t_h - t_c)\left(1 - \frac{l}{1 + \frac{k}{h}}\right) \quad \ldots\ldots\ldots [2]$$

Considering again the arrangement in Fig. 3, it is obvious that, since the two materials have different thermal conductivities, there will result different temperatures at each and any level l. Fig. 4 contains two such temperature lines for materials of different conductivities. At distance l from the hot surface, material a will have temperature t_{la} and material b temperature t_{lb}. Of course heat will flow from the point of higher temperature to that of lower temperature. This flow of heat is perpendicular to the main flow, which goes from the hot to the cold surface. It is called hereafter the "lateral" heat flow. The lateral heat flow is proportional to the difference of temperatures $(t_{la} - t_{lb})$. This difference in turn depends upon the relative magnitude of the values k_a/h and k_b/h, as becomes obvious from Equation [2]. If h approaches infinity ($h = \infty$ is the mathematical expression for the surface having the same temperature as the ambient), Equation [2] becomes identical with Equation [1]. No lateral heat flow occurs. If h approaches zero (which is the mathematical expression for a wall covered on the cold side by an absolute insulator), t_l becomes t_h and the entire wall is at uniform temperature equal to the hot-surface temperature.

The lateral heat flow does not leave the temperature field unchanged. If there is no contact resistance between the two materials (Fig. 3), the interface will show a temperature drop line, which lies between that for material a and material b. Adjacent strata will have almost the same temperatures, and only at some distance from α will the influence of the other material be no longer noticeable. Fig. 5 shows schematically the temperatures at level l. The distances x are plotted as abscissas on both sides of position α; temperatures are plotted as ordinates. If in either material the temperatures are taken close to α, say at β and γ, then different temperatures are obtained from those which would be expected if no lateral heat flow occurred; namely, different from t_a and t_b.

Referring to Fig. 1, let $W_I = 2.5$ in., $L = 9$ in., and the thickness $2\,W_M$ of the metal strips c be $^1/_8$ in. Let the conductivity of the insulation be 0.25 Btu/ft, hr, F, the conductivity of the metal strips and sheets be 25 Btu/ft, hr, F, and the film conductance h be 2 Btu/sq ft, hr, F.

In Fig. 6 the thickness L is plotted as abscissa, and temperature as ordinate. The two dotted lines show the temperatures that would exist if no lateral flow occurred. Because of the lateral flow, however, the temperatures approach each other. Near the metal, the line s prevails and in the center of the brick, the line c.

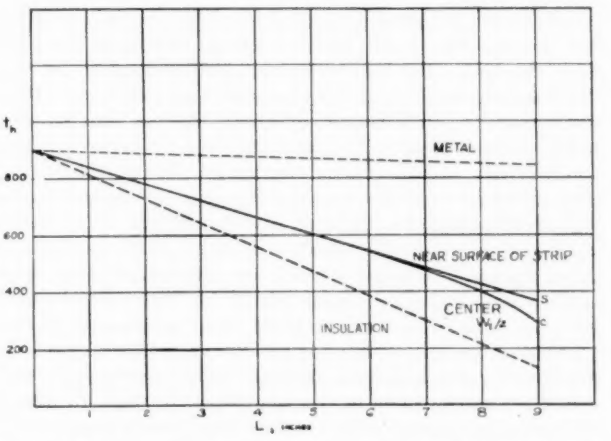


FIG. 6 TEMPERATURE DISTRIBUTION WITH "THROUGH-METAL"

LIST OF VARIABLES

In order to obtain a general solution, a survey of the variables which influence the heat flow was made. The heat flow Q for a structure, as shown in Fig. 1, is governed by the following:

1 The temperature difference between the hot surface and the cold ambient.
2 The net spacing W_I of the strips.
3 The thickness L of the insulation.
4 The thickness W_M of the strips.
5 The conductivities k_I of the insulation and k_M of the strip.
6 The surface-film conductance h.

Instead of plotting a great number of values of Q for many different combinations of the properties involved, it appeared simpler to compare the actual heat loss with a standard value. Although different possibilities for this value are available, it was decided to compare Q with the value that would be obtained if no lateral heat flow occurred. The ratio thus observed

$$\frac{\text{Actual heat loss with lateral heat flow}}{\text{Heat loss with no lateral heat flow}}$$

is called the "increase factor," and is abbreviated hereafter by I.

In order to determine the heat loss for any actual structure, such as Fig. 1, proceed as follows:

1 Determine the heat loss Q_s, i.e., the heat loss assuming no lateral heat flow.
2 Determine the value of I (see "Presentation of Results").
3 Multiply Q_s by I; this gives the actual heat loss Q with lateral heat flow.

4 Q_s can be found from Equation [3], which represents the basic law of steady-state heat flow

$$Q_s = (t_h - t_c)\left(\frac{W_I}{\frac{L}{k_I} + \frac{1}{h}} + \frac{W_M}{\frac{L}{k_M} + \frac{1}{h}}\right) \quad \ldots\ldots\ldots [3]$$

In this equation, as in the entire paper, it is assumed that the strips repeat at equal distances, so that it is sufficient to consider one space W_I and one strip c.

Method of Experiments

All experiments described in this paper were carried out by the "electric analogy method" on the "heat and mass flow analyzer" at Columbia University. This method is based on the identity of laws governing the flow of electricity and of heat in a body. Appendix 1 contains a more detailed discussion and description of the method. Here it may suffice to say that in the analogy:

Electric conductivity represents thermal conductivity.
Voltage represents temperature difference.
Current represents heat flow.

The application of the method consists of building an electrical circuit which is analogous to the structure, measuring the current through the structure for applied voltage (which corresponds to the temperature difference across the structure), and translating the measured current into heat units.

Influence of Individual Variables

It is of interest to study the influence of the different variables just mentioned on the increase factor I.

The temperature difference $t_h - t_c$ has no influence on I. Q_s as well as Q is proportional to the temperature difference, and therefore, I, which by definition is $I = \frac{Q}{Q_s}$, is independent of temperature.

If W_I becomes very small and approaches zero, the influence of the insulating material as compared with the metal strips vanishes. Consequently, for $W_I = 0$, I becomes unity. On the other hand, if W_I becomes very large, the influence of the strips vanishes, and the structure behaves as if it consisted only of insulating material. For $W_I = \infty$, therefore, I again approaches unity. Between $W_I = 0$ and $W_I = \infty$, however, I must have values larger than 1. At some value a maximum will occur.

If L is very small, the thermal resistance of the insulation as well as of the strip becomes very small; the major part of the resistance then lies in the surface film. There will be almost no temperature differences within the structure; therefore very little lateral heat flow occurs, and, as a limit, I becomes unity (for $L = 0$). If, on the other hand, L becomes extremely large, the resistance in the film becomes insignificant; and all points at the same distance l from the hot surface have the same temperature, independent of the material involved. Again no lateral heat flow can develop, and I becomes unity when L equals infinity. The character of the curve is the same as that shown in Fig. 7, for W_I.

It is obvious that a change of W_M will result in a similar curve. If W_M approaches zero, almost all heat flow is limited to the insulation. If on the other hand W_M becomes exceedingly large the influence of the heat flow through the insulation can be entirely neglected, making I equal to unity.

If either of the two conductivities (k_I or k_M) becomes zero or infinite, the importance of the part of the structure having the other conductivity becomes either alone dominant or entirely insignificant, e.g., let $k_I = 0$. Then only the heat flow through

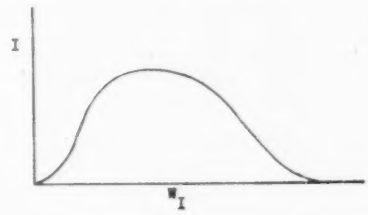


Fig. 7 Characteristic Shape of I—W_I Function

c, the metal strips, with the width W_M remains. If $k_I = \infty$, the heat flow through c becomes entirely insignificant. (If k_M changes, the situation is correspondingly reversed.) Consequently, either of the two conductivities will yield a curve for I of the same character as that shown in Fig. 7 for W_I.

It has been mentioned that for $h = 0$ and for $h = \infty$, the value of I becomes unity, while for other values of h, I is larger than unity.

Summarizing, it can be stated that the curve for I plotted against any single variable (the other variables held constant) yields curves of the same general character: For the two limiting cases, the variable being zero or infinity, I is unity; for all values of the variable in between, I is larger than unity.

Presentation of Results

The presentation of I as a function of six different variables would call for a vast number of charts, which would take long to plot, and then would still be unwieldy to use. Fortunately, however, the six variables can be grouped in four parameters, which will be mentioned. Thus plotting is greatly simplified. The deduction of these parameters, and the proof of their validity, is given in Appendix 2.

The four parameters are as follows

$$f_1 = \frac{W_M}{W_I}, \quad f_2 = \frac{W_I}{L}, \quad f_3 = \frac{k_I \cdot L}{k_M \cdot W_M}, \quad f_4 = \frac{k_I}{h \cdot W_I} \quad \ldots [4]$$

The values of the parameters to be used in the charts were so selected that at least the following limits for the individual variables are covered by the graphs:

W_I = $^1/_{12}$ to $1^1/_4$ ft
W_M = $^1/_{192}$ to $^1/_{24}$ ft (= $^1/_{16}$ to $^1/_2$ in.)
L = $^1/_6$ to $1^1/_2$ ft
k_I = 0.025 to 1.5 Btu/ft, hr, F
k_M = 2.5 to 200 Btu/ft, hr, F
h = 1 to 8 Btu/sq ft, hr, F

For practical purposes, a greater range is covered, since any two of the variables will seldom approach their limit at the same time. Because of the relationship in Equation [4] any one of the values can become larger, if at the same time the other values change accordingly. The values are so selected that f_1 to f_4 can be obtained even if the individual magnitudes are as unfavorable as possible. For example f_1 has been investigated within the limits 0.004 to 0.5 $\left(\text{i.e., } \frac{1}{192 \times 1.25} \text{ to } \frac{12}{24}\right)$.

The results are presented in Table 1 and in charts. In all charts, values of I are plotted as ordinates and values of f_4 as abscissas. Each chart contains several curves, each curve holding for a different but constant value of f_3.

In order to enable proper interpolation, charts are presented for four different values of f_1 and four different values of f_2. Inasmuch as f_1 and f_2 can vary independently, sixteen different combinations are necessary.

The four values of f_1 are 0.004, 0.020, 0.100, 0.500.

The four values of f_2 are 0.25, 0.5, 0.5, 1.5, 7.5.

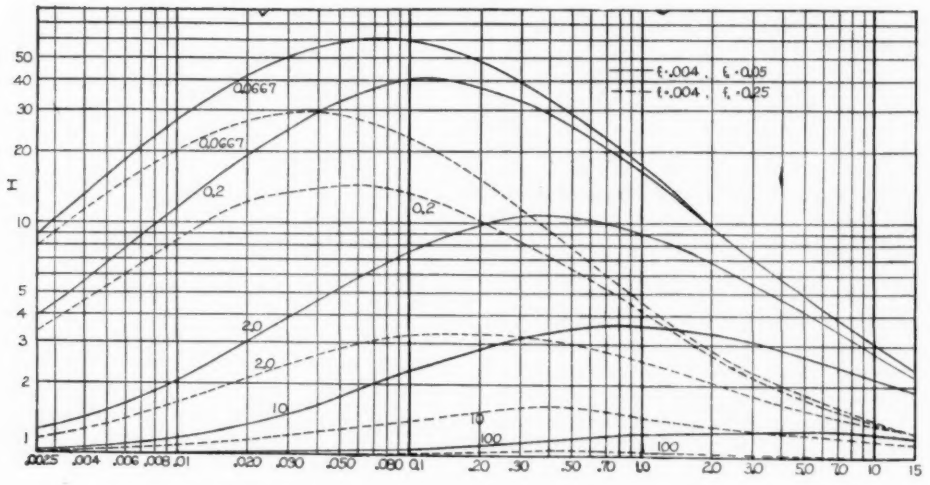


FIG. 8 INCREASE FACTOR I PLOTTED AGAINST f_4 FOR VARIOUS VALUES OF f_3

As explained, each value of f_1 can combine with any of the four values of f_2.

A first survey of the results may be obtained from Table 1, which contains the maximum values of I for different combinations of the values for f_1, f_2, f_3.

The results are shown in Figs. 8 to 14, inclusive. Table 2 shows the combinations of the different parameters to be found in the various figures.

TABLE 1 MAXIMUM VALUES OF "INCREASE FACTOR" I

f_1	f_2	0.05	0.25	1.5	7.5
0.004	f_3 = 0.0667	60.0	29.3	8.90	2.30
	0.2	41.0	14.2	3.40	1.56
	2.0	10.8	3.32	1.36	1.09
	10	3.62	1.64	1.05	1
	100	1.30	1.06	1	1
	500	1.0	1	1	1
	f_3 = 0.0667	15.4	12.1	3.2	2.03
	0.2	14.0	6.9	2.3	1.35
0.020	2.0	6.1	2.5	1.29	1
	10	2.69	1.4	1	1
	100	1.17	1	1	1
	500	1	1	1	1
	f_3 = 0.0667	5.14	4.17	2.26	1.25
	0.2	4.50	3.20	1.64	1.09
0.100	2.0	2.80	1.61	1.05	1
	10	1.67	1	1	1
	100	1	1	1	1
	500	1	1	1	1
	f_3 = 0.0667	1.21	1.168	1.27	1.02
	0.2	1.175	1.122	1.09	1
0.500	2.0	1.097	1.037	1	1
	10	1.028	1	1	1
	100	1	1	1	1
	500	1	1	1	1

TABLE 2 COMBINATIONS OF DIFFERENT PARAMETERS ILLUSTRATED IN FIGS. 8 TO 14

f_1	f_2 = 0.05	0.25	1.5	7.5
0.004	Fig. 8	Fig. 8	Fig. 9	Fig. 9
0.020	Fig. 10	Fig. 10	Fig. 11	Fig. 11
0.100	Fig. 12	Fig. 12	Fig. 13	Fig. 13
0.500	Fig. 14	Fig. 14	Fig. 13	

Wherever Table 1 shows amaximum (for I) of 1.0, no curve appears in the graphs, because I has the value 1 over the entire range of f_4.

DISCUSSION OF EXPERIMENTAL RESULTS AND APPLICATION OF CHARTS

Discussion. High values of I occur with low values of f_1 and f_3. The meaning of f_1 and f_2 is so simple (from Equation [4]) that no comment appears to be necessary. The parameter f_3, however, is a complex expression

$$f_1 \cdot f_2 \cdot f_3 = \frac{k_I}{k_M}$$

A low f_3, with other f's unchanged means therefore a very high-grade insulating material with steel, or a medium insulating material with copper for the strips, etc. At high values of f_3, I becomes appreciable only under extreme conditions for the other f values (f_1 low, f_2 medium).

The parameter f_4 definitely shows a critical range in the neighborhood of 0.5. It determines the spacing of the strips and indicates that the spacing exerts its influence not directly but in combination with the thickness of the insulation. If I becomes smaller with decreasing f_2 (i.e., if the spacing of the strips becomes smaller), the heat losses do not necessarily decrease also. The heat losses are the product of the value $Q_s \cdot I$. This is important to keep in mind, because a drop in I might lead to the erroneous assumption that the heat loss drops.

Application of Curves. The curves shown in Figs. 8 to 14, inclusive, enable the determination of the actual heat loss for any condition covered by the general program outlined under "Statement of Problem." The use of the dimensionless parameters f_1 to f_4 makes the trends less easily recognized. Their use, however, is the only means of presenting the results in a practicable way. The use of the curves is best demonstrated in three examples which will cover two different insulating materials. The examples will also show how to use the curves to detect the influence of change in design.

Example 1: An insulation, L = 8 in. (0.667 ft) thick, is reinforced by steel strips $2W_M$ = 1/8 in. (0.0104 ft) thick. The insulation is covered on both sides by steel sheets of the thickness W_M = 1/16 in. (0.0052 ft). The temperature of the hot side of the structure is 570 F; the ambient facing the cold side is 70 F. The film conductance on the cold side is 2 Btu/sq ft, hr, F. The thermal conductivity of the insulating material is 0.08 Btu/ft, hr, F; that of the steel is 26 Btu/ft, hr, F.

(*A*) What is the heat loss if the strips are spaced W_I = 8 in. (0.667 ft) apart?

(*B*) How is the heat loss changed if the spacing changes to W_I = 4 in., 6 in., 12 in., 16 in.?

In order to answer these two questions, the values of the f's must be determined. The parameter f_3 is not influenced by W_I, and therefore has a constant value, f_3 = 0.394. The values of f_1, f_2, f_4 change with W_I, as shown in Table 3.

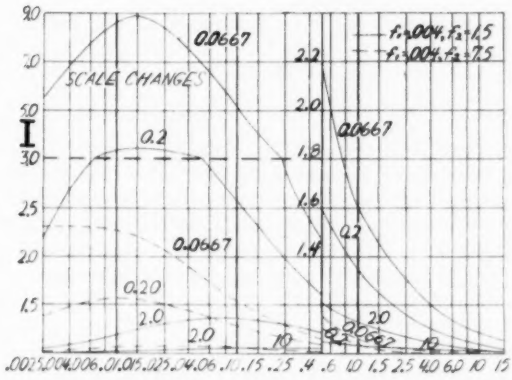


FIG. 9 INCREASE FACTOR I PLOTTED AGAINST f_4 FOR VARIOUS VALUES OF f_3

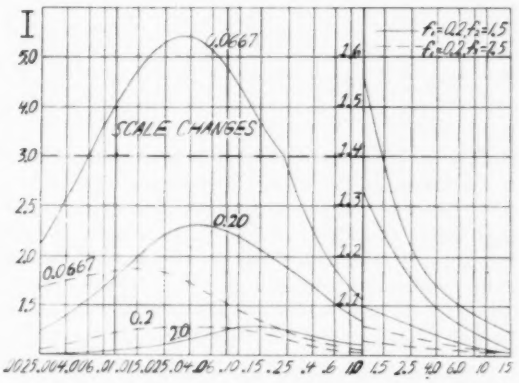


FIG. 11 INCREASE FACTOR I PLOTTED AGAINST f_4 FOR VARIOUS VALUES OF f_3

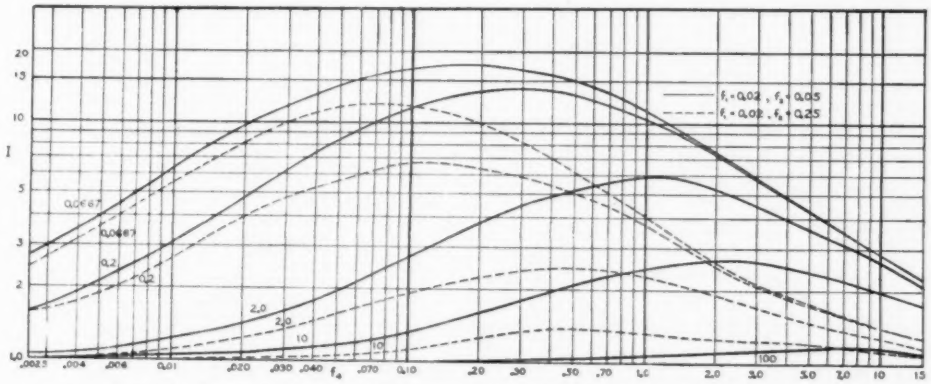


FIG. 10 INCREASE FACTOR I PLOTTED AGAINST f_4 FOR VARIOUS VALUES OF f_3

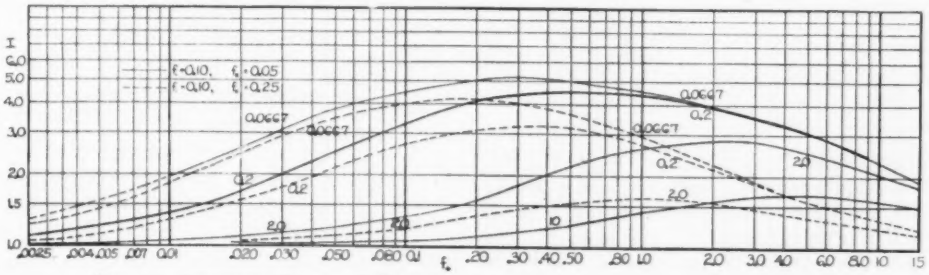


FIG. 12 INCREASE FACTOR I PLOTTED AGAINST f_4 FOR VARIOUS VALUES OF f_3

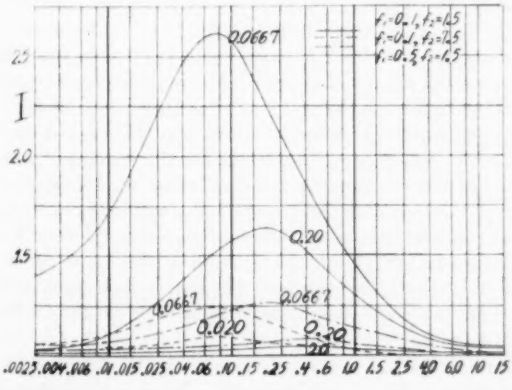


FIG. 13 INCREASE FACTOR I PLOTTED AGAINST f_4 FOR VARIOUS VALUES OF f_3

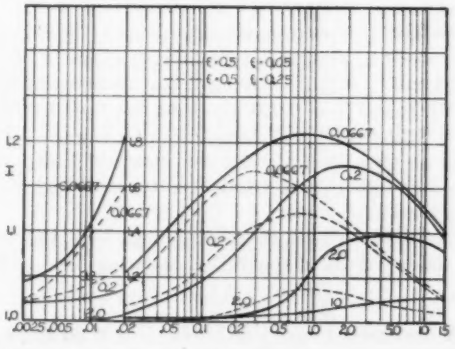


FIG. 14 INCREASE FACTOR I PLOTTED AGAINST f_4 FOR VARIOUS VALUES OF f_3

TABLE 3 VALUES OF PARAMETERS f_1, f_2, AND f_4

W_1	f_1	f_2	f_4
4	0.0156	0.5	0.12
6	0.0104	0.75	0.08
8	0.0078	1.0	0.06
12	0.0052	1.5	0.04
16	0.0039	2	0.03

The values for f_4 can be read directly on the abscissa of the charts; the values of the other f's, however, cannot be read directly. Therefore, the I values for these f's have to be found by interpolation. This interpolation is shown here for $W_I = 8$ in. The values of I for $f_3 = 0.394$ are not directly available in the charts. In order to interpolate, cross-curves have to be drawn (see Fig. 15). Values of f_3 are plotted as abscissas, and I as ordinates. Three curves (full lines) are drawn, each for a

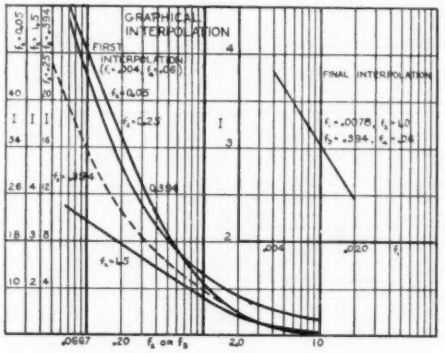


FIG. 15 GRAPHICAL INTERPOLATION

different value of f_2. (Each of the three curves has a different ordinate scale; for curve f_2 use the scale marked $f_2 = 0.05$, etc.) All curves are for $f_1 = 0.004$.

The values of I for $f_3 = 0.394$ (abscissa) are now read as follows:

	I for $f_3 = 0.394$
Curve $f_2 = 0.05$	22.7
Curve $f_2 = 0.25$	8.6
Curve $f_2 = 1.5$	2.45

The value of f_2 in the example ($W_I = 8$ in.) is $f_2 = 1$. For this value interpolation is again necessary. Because $f_2 = 0.25$ and $f_2 = 1.5$ are too far apart for accurate interpolation, a curve with all three values is drawn (dashed curve); f_2 is plotted on the abscissa, I on the ordinate. At $f_2 = 1$, the value of $I = 3.8$ is read on the ordinate. This is the increase factor I for $f_1 = 0.004$ $f_2 = 1.0$, $f_3 = 0.394$, and $f_4 = 0.06$.

A similar chart (not included in this paper) may now be drawn for $f_1 = 0.02$. From this chart, the value of I for $f_1 = 0.02$, $f_2 = 1$, $f_3 = 0.394$, $f_4 = 0.06$ is found to be 2.45.

Now the final interpolation is made (see insert in Fig. 15); f_1 is plotted as abscissa, while the ordinates give values of I for $f_2 = 1$, $f_3 = 0.394$ and $f_4 = 0.06$. By interpolating between the values for $f_1 = 0.004$ and $f_1 = 0.020$, the value for $f_1 = 0.0078$ can be read; $I = 3.22$.

This means that due to lateral heat flow, the heat loss for the structure described in case (A) is 3.22 times as high as if there were no lateral flow.

In order to determine the actual heat loss, the heat flow through the metal and through the insulation have to be calculated

$$\text{Metal heat flow } \frac{(570 - 70)^1/_8 \times {}^1/_{12}}{\frac{8}{12 \times 26} + \frac{1}{2}} = 9.90 \text{ Btu per hr}$$

$$\text{Insulation } \frac{(570 - 70) \times 8 \times {}^1/_{12}}{\frac{8}{12 \times 0.08} + {}^1/_2} = 37.6 \text{ Btu per hr}$$

Total $9.9 + 37.6 = 47.5$ Btu per hr

The actual heat loss is $47.5 \times 3.08 = 146$ Btu per hr

The influence of the spacing (case B) has been studied by similar interpolations. In order to compare the results, it seemed advisable to reduce all of them to a width of 1 ft; inasmuch as the length (of the infinite structure) under consideration is also 1 ft, the results then apply to 1 sq ft. The reduction is carried out by dividing the heat loss by $(W_I + 2W_M)$, where W_I and W_M are expressed in feet.

The results are shown in Fig. 16, in which spacing W_I is plotted as abscissa. Two ordinate scales are used; one for heat flow in Btu/sq ft, hr, the other (dimensionless) for I. Three curves are shown: the full line is for I; the dotted line is for the heat loss without lateral flow (sum of flow through metal and through insulation); the broken line is the actual heat loss with lateral heat flow.

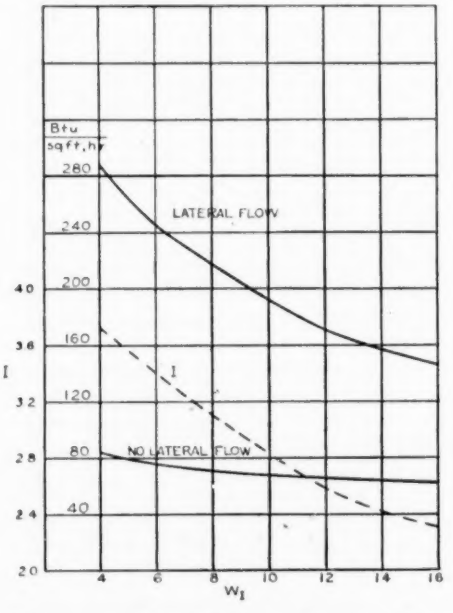


FIG. 16 VARIATION OF HEAT LOSS AND INCREASE FACTOR WITH SPACING OF STRIPS; $h = 2$

Example 2: What is the influence of the cold-side film conductance for the wall described in Example 1? How do the heat losses change if $h_0 = 1.5$, 2.5, or 3.5 instead of 2 as in Example 1?

Changing the film conductance influences only f_4; nevertheless all the interpolations have to be repeated. The results are given in Fig. 17, which shows the actual heat loss and the increase factor, both plotted as ordinates against the spacing W_I of the strips. Each curve is for a different value of h indicated on the curve. Changing the film conductance within the range of the example has relatively small influence on either the heat loss or the increase factor; more than doubling the value of h (3.5 instead of 1.5) increases the heat loss only something like 20 to 35 per cent. Of course conditions may be different for a different value of k_I or L.

Example 3: What is the influence of the thickness of insulation on increase factor and heat loss? What is the influence of the thermal conductivity of the insulation?

The results for this example are shown in Fig. 18. The ex-

ample has been carried through for a spacing of the strips, $W_I = 8$ in.; thickness of the metal, $W_M = {}^1/_{32}$ in.; conductivity of the metal, 26 Btu/ft, hr, F; film conductance, $h = 2$ Btu/sq ft, hr, F.

Thickness L of the insulation is plotted as abscissa. The ordinates have two scales, i.e., one for the heat losses per square foot (Btu/sq ft, hr), one dimensionless for I. The broken lines show the heat loss without lateral heat flow, the full lines the heat loss with lateral heat flow, and the dashed lines the increase factor. There are two curves of each type, i.e., one for a conductivity of the insulation $k_I = 0.08$, the other for $k_I = 0.05$. The values of the conductivities are noted on the curves. The increase factor for $k_I = 0.05$ goes through a maximum, while the corresponding curve of total heat loss does not show a maximum.

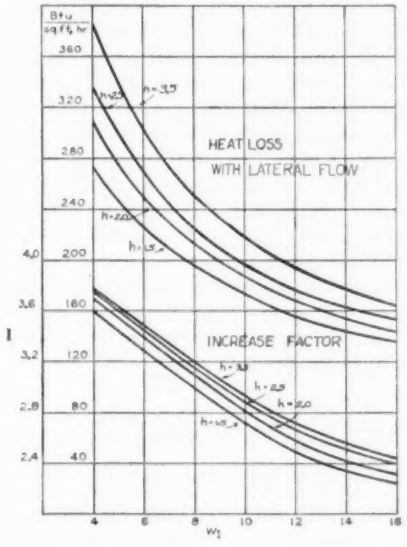


FIG. 17 VARIATION OF HEAT LOSS AND INCREASE FACTOR WITH SPACING OF STRIPS W_I FOR VARIOUS VALUES OF BOUNDARY CONDUCTANCE h

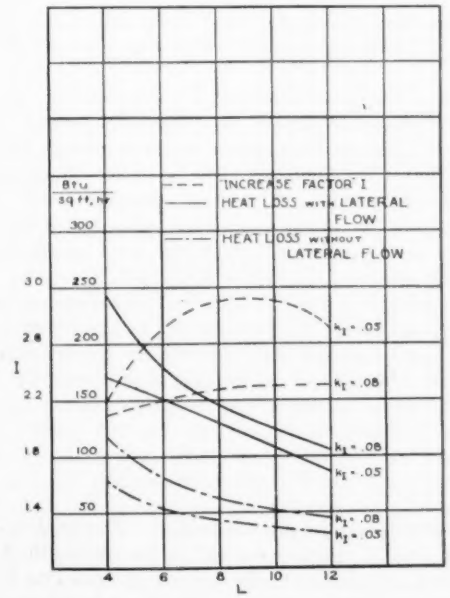


FIG. 18 VARIATION OF HEAT LOSS AND INCREASE FACTOR WITH THICKNESS L, OF INSULATION FOR DIFFERENT THERMAL CONDUCTIVITIES k_I OF THE INSULATION

Conclusions and Verifications. The extremely high values of the increase factor look alarming. Some preliminary tests indicate that the larger part of the additional heat loss can be attributed to the influence of the steel enclosure on both surfaces of the insulators. This should be further investigated, and (in further tests) if it should prove to be true, important design factors may result, e.g., insulation inserted between the strips and the covering sheets would do much to decrease the loss. From these considerations it also follows that a contact resistance between insulation and through-metal, or insulation and covering sheets, would not affect the results materially. Further investigations to verify this point would be desirable.

By way of a general confirmation as to the order of magnitude of the increase factor, reference is made to an article by J. G. Bergdoll (1),[3] in which the author states that in insulating a strato chamber it has been found that, due to thermal short circuits, the actual heat loss was 4 times as high as expected for the conductivity and thickness of the insulation.

SUMMARY

1 The heat flow through a structure composed of an insulation covered by sheet metal and interspersed with metal strips (through-metal) is discussed.

2 The cause of "lateral heat flow" occurring at any plane or level parallel to the surface of the structure, is explained and related to the cold-side film conductance.

3 An "increase factor" is defined as the ratio of the actual heat loss, including lateral heat flow, to the heat flow that would occur if no lateral heat flow existed.

4 The factors influencing the increase factor are discussed.

5 General curves giving the increase factor for various conditions are presented.

6 The use of these general curves is explained by means of examples. The examples show in a readily understandable way the influence of the thermal conductivity of the insulation, its thickness, the spacing of the metal strips, and the film conductance in specific cases.

7 In two Appendixes which follow the experimental technique and the mathematical deductions for the paper are presented.

Appendix I

ELECTRIC ANALOGY METHOD

Ohm's law for the flow of electricity through a conductor is expressed by

$$e = ir \qquad [5]$$

where

e designates voltage
i designates current
r designates resistance

Similarly, Fourier's law for steady-state heat flow through a body can be written

$$t = Q \cdot R \qquad [6]$$

where

t designates temperature difference
Q designates rate of heat flow
R designates thermal resistance

Both the electrical resistance and the thermal resistance are

[3] Numbers in parentheses refer to the Bibliography at the end of the paper.

proportional to the length L of the path traveled by the medium (current or heat) and inversely proportional to the area S of flow; both are proportional to the resistivity (ρe and ρt) of the material involved (in case of heat flow, it is more common to use the reciprocal value of the resistivity, namely, the thermal conductivity, $k = \frac{1}{\rho t}$). Therefore, r and R can be expressed by

$$r = \rho e \cdot \frac{L}{A} \quad \ldots\ldots\ldots\ldots\ldots\ldots [7a]$$

$$R = \frac{1}{k} \cdot \frac{L}{A} \quad \ldots\ldots\ldots\ldots\ldots\ldots [7b]$$

From the mathematical identity of Equations [5] and [6] and that of Equations [7a] and [7b], it follows that thermal phenomena can be studied by carrying out certain electrical measurements. (Incidentally, the method is widely inclusive and can be used to analyze the transient state as well as the steady state.)

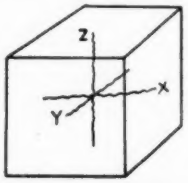


FIG. 19 VIEW OF LUMP WITH RESISTORS REPRESENTING THREE-DIMENSIONAL FLOW

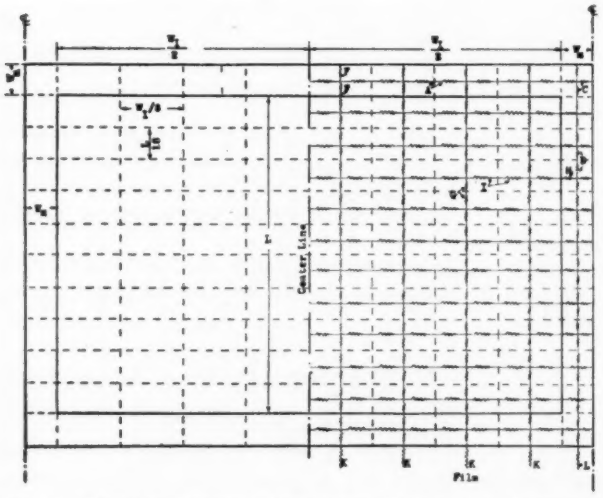


FIG. 20 DIAGRAM SHOWING SECTIONING LAYOUT AND RESISTORS

The equipment at Columbia University, known as the "heat and mass flow analyzer," has been especially devised to handle complex problems of the transient state. The method and the laboratory have been described elsewhere (2). As is evident from this paper, it can be usefully employed for analyzing complicated steady-state problems.

One method of studying steady-heat flow by electric analogy consists in setting up a body which is geometrically identical to the body subjected to heat flow and filling this body with a semiconductor. Electrical measurements then disclose the heat flow, even in odd shapes. Langmuir (3) probably was the first to use this method.

For the present experiments, the analyzer, primarily designed for transient flow, has been used. In this method the body which is to be analyzed is thought of as cut into a number of sections or lumps. The resistance in each of the three directions is considered concentrated in the three axes, as indicated by the isometric sketch, Fig. 19.

The structure being of infinite length in the Y direction, there can be no heat flow in the Y direction, and the problem reduces to one involving only two dimensions.

Thus a network is built up having "horizontal" resistors for flow in the direction X, and "vertical" resistors for flow in the direction Z. Fig. 20 shows the wiring diagram. Because of symmetry, it is sufficient to build up a circuit representing $W_I/2$ and W_M. L has been divided into 10 sections, and $W_I/2$ into four sections. Fig. 20 shows the geometrical meaning of the sections. It is a cross section, showing the same view as the isometric sketch, Fig. 1, with the limits of the sections noted. The film conductance on the cold surface is represented by additional resistors. The letters at each resistor refer to Appendix 2, where the deduction of the dimensionless units is discussed.

A word of comparison with the other electrical method (with geometrical similarity) may not be amiss. The "lumping" method used here is probably more complicated than the "similarity" method. With only 115 sections available, the "lumping" is rather crude. (Previous experiments (4) have shown, however, that this does not affect the accuracy to any appreciable extent.) One great advantage, on the other hand, may be claimed for the "lumping" method; it is easily possible to study separately the influence of the thermal conductivities of the various materials involved.

Appendix 2

DERIVATION OF DIMENSIONLESS UNITS

If two different thermal arrangements lead to the same circuit, they have the same value I. If, once a network is established, all resistors are changed in the same ratio, e.g., all resistors are doubled or halved, the outcome of the experiments is not changed; merely the "scale factor" between Ohm's law and Joule's law is different.

The first step then in deriving the dimensionless units consists in writing the equations for all resistors, Equations [9] to [17]. Resistors having the same letter always have the same value and are changed in value only after the individual test is over.

The next step consists in forming resistor ratios. Here all resistors were compared with R_I as "standard." Any of the other resistors (R_A, R_B, etc.) would have done just as well; all resistors, however, must be compared with the same "standard" (R_I), Equations [18] to [25]. If in these equations certain variables always appear in the same grouping, then this group may be taken as one parameter. Thus the four parameters were empirically evolved. In writing Equations [9] to [18], a value z has been used; z is the "scale factor" transforming heat units into electrical units. The scale factor z in (megohms $\times$ Btu/hr, F) ties in each individual resistor with the thermal resistance it represents. For example, in the case of resistance R_G; the thermal resistance R_{Gt} for this section is expressed by

$$R_{Gt} = \frac{8}{10} \frac{L}{k_I \cdot W_I \cdot 1} \quad \ldots\ldots\ldots\ldots\ldots\ldots [8]$$

This equation is easy enough to find. The total thickness L is divided into 10 sections; one section has for length of the heat path only $L/10$; similarly, the width is divided into 8 sections. Hence, the area is proportional to $W_I/8$. A length in the direction Y of 1 ft is considered. If L and W_I are expressed in feet, k_B in Btu/ft, hr, F, then R_{Gt} is expressed in F, hr/Btu. In

order to obtain the resistance R_G in megohms, R_{Gt} has to be multiplied by z

$$R_G = \frac{8 \cdot z \cdot L}{10 \cdot k_I \cdot W_I} \quad [9]$$

Similarly the other Equations [10] to [17], for the resistors have been found.

$$R_I = \frac{10 \cdot z \cdot W_I}{8 \cdot k_I \cdot L} \quad [10]$$

$$R_A = \frac{1 \cdot z \cdot W_I}{8 \cdot k_M \cdot W_M} \quad [11]$$

$$R_D = \frac{1 \cdot z \cdot L}{10 \cdot k_M \cdot W_M} \quad [12]$$

$$R_L = \frac{z}{h \cdot W_M} \quad [13]$$

$$R_K = \frac{8 \cdot z}{h \cdot W_I} \quad [14]$$

$$R_C = \frac{z \cdot W_M \cdot 1}{k_M \cdot 2 \cdot W_M} = \frac{z}{2k_M} \quad [15]$$

$$R_H = \frac{z \cdot W_M \cdot 10}{k_M \cdot 2 \cdot L} \quad [16]$$

$$R_F = \frac{z \cdot W_M \cdot 8}{k_M \cdot 2 \cdot W_I} \quad [17]$$

Now by comparing each of these resistors with R_I it can readily be found that the variables always appear in given ratios, and only in these ratios. They therefore are selected as parameters. They were given in Equations [4], which, for convenience, are repeated here

$$f_1 = \frac{W_M}{W_I};\ f_2 = \frac{W_I}{L};\ f_3 = \frac{k_I \cdot L}{k_M \cdot W_M};\ f_4 = \frac{k_I}{h \cdot W_I} \quad [4]$$

With these parameters, equations for various resistors read

$$R_G = 0.64 \cdot \frac{R_I}{f_2^2} \quad [18]$$

$$R_A = 0.1 \cdot f_3 \cdot R_I \quad [19]$$

$$R_D = 0.08 \frac{f_3}{f_2} \cdot R_I \quad [20]$$

$$R_L = 0.8 \frac{f_4}{f_1 \cdot f_2} \cdot R_I \quad [21]$$

$$R_C = 0.4 \cdot f_1 \cdot f_3 \cdot R_I \quad [22]$$

$$R_H = 4 \cdot f_1^2 \cdot f_2 \cdot f_3 \cdot R_I \quad [23]$$

$$R_F = 3.2 \cdot f_1^2 \cdot f_3 \cdot R_I \quad [24]$$

$$R_k = \frac{6.4 f_4}{f_2} \cdot R_I \quad [25]$$

The four parameters used are by no means the only ones possible. There are certainly other combinations available. The validity of the parameters chosen was checked twice; once by "dimensional analysis" (5), which shows possible selections of parameters. A second practical test was made by setting up one set of conditions. Then one value, say W_I, was changed. Following Equations [4] this means a change of W_M and L if f_1 to f_4 are to remain unchanged, which in turn calls for other changes. By systematically changing the conditions and corresponding circuits, one must return to the original circuit if the parameters are to be correct. The method of finding the parameters, as just described, is generally applicable in working with the heat and mass flow analyzer, and is in many cases very promising. For specific cases, it yields answers avoiding lengthy and extended mathematical analysis. In other cases of course it would be easier to determine the (dimensionless) parameters mathematically and arrange the experiments accordingly.

BIBLIOGRAPHY

1 "Recent Developments in Strato Chambers," by J. G. Bergdoll, *Refrigerating Engineering*, (Journal A.S.R.E.), vol. 45, 1943, pp. 25–33.

2 "A Method for Determining Unsteady State Heat Transfer by Means of an Electrical Analogy," by V. Paschkis and H. D. Baker, Trans. A.S.M.E., vol. 64, 1942, pp. 105–112.

"Electrical Machine Solves Heat Transfer Problems," by P. Swain, *Power*, vol. 85, 1941, pp. 76–78, 170, 172, 174.

"Electrical Analogy Method for the Investigation of Transient Heat Flow Problems," by V. Paschkis, *Industrial Heating*, vol. 9, 1942, pp. 1162, 1164, 1166, 1168, and 1170.

3 "Flow of Heat Through Furnace Walls," by I. Langmuir, E. Q. Adams, and G. S. Meikle, Trans. American Electrochemical Society, vol. 24, 1913, pp. 53–84.

"The Effect of Shape on the Heat Loss Through Insulation," by J. H. Awbery and F. H. Schofield, 5th International Congress of Refrigeration, Rome, 1928.

4 "Application of an Electrical Model to the Study of Two-Dimensional Heat Flow," by M. Avrami and V. Paschkis, Trans. American Institute of Chemical Engineers, vol. 38, 1942, pp. 631–652.

5 "Mathematics of Modern Engineering," by R. E. Doherty and E. G. Keller, John Wiley & Sons, Inc., New York, N. Y., 1936, p. 130

Discussion

C. E. Ernst.[4] The influence of through-metal in limiting the effectiveness of insulation has long been realized, but this paper presents what is apparently the first concrete information on the extent of this influence. A true appreciation of the importance of such information can be gained from a consideration of the economics involved.

Thermal insulation for any specific condition should be applied in a thickness consistent with its cost and efficiency and the cost of heat-energy loss. In other words, the economic thickness is that thickness at which the sum of the cost of insulation per year and the cost of heat-energy loss is a minimum.

Through-metal, however, has the effect of reducing the efficiency of insulation, and the greater the amount of through-metal the less the thickness of insulation that can be justified. In other words, if the amount of through-metal is sufficient to nullify the effect of the insulation, the elimination of the insulation can be economically justified.

While, for the present, construction methods apparently do not allow complete elimination of thermal short-circuiting paths through insulation, common sense tells us that it is certainly of economic advantage to reduce them to a minimum.

Herein lies the importance of the present work which is a good start in the right direction. Further work along these lines should lead to better design and construction methods for the incorporation of thermal insulation into all kinds of heated and refrigerated equipment with the efficiency of the insulation in place approaching that of the material alone, while maintaining the required mechanical strength of the structure.

G. M. Dusinberre.[5] The practical use of the authors' curves is considerably restricted by the lack of generality in the basic assumptions. For example, one of the metal walls will generally be designed for structural strength and will be rela-

[4] Johns-Manville Corporation, New York, N. Y.

[5] Department of Mechanical Engineering, Virginia Polytechnic Institute, Blacksburg, Va. Now on duty at U. S. Naval Academy, Annapolis, Md. Mem. A.S.M.E.

tively thick, while the other wall will merely serve as a retainer for the insulation and will be relatively thin. The through-metal will often, as in ship construction, serve a structural purpose in stiffening the strength bulkhead, and the web thickness will be related to the thickness of this bulkhead.

Another serious lack of generality lies in the assumption that the surface resistance can be neglected on one side. There are a great many practical cases where this cannot be done.

Fortunately, the engineer who has to grind out an answer for this type of problem has at his disposal the greater flexibility, generality, speed, and lucidity of the numerical method outlined by Emmons.[6]

The writer worked the authors' Example 1A by this method, using the same assumptions except that the temperature gradient in the thin direction of the metal was neglected.[7] The time required was 2 hr for a 4-in. and a 2-in. network spacing. Additional solutions on the 2-in. spacing would take about $^1/_2$ hr each. This is probably more rapid than the authors' method, considering the intricate interpolation procedure which they describe.

In the numerical method, we work directly in temperatures, and trends are readily recognized. The authors note that the opposite is true when working with parameters. In the numerical method we acquire, incidentally, some other information of value, such as the maximum cold-surface temperature. This is a matter which insulation engineers are sometimes called upon to guarantee.

The temperature-distribution pattern was found to be as indicated in Fig. 21. This pattern is reversed on either side, by symmetry.

The heat flow can be calculated from the various layers. For example, from the cold surface to ambient, we have a mean temperature difference of 123 F. The width of a unit panel is $^2/_3$ ft and the surface coefficient is 2. Then $123 \times {}^2/_3 \times 2 = 164$ Btu per hr. Checking with the second layer in Fig. 21, we have

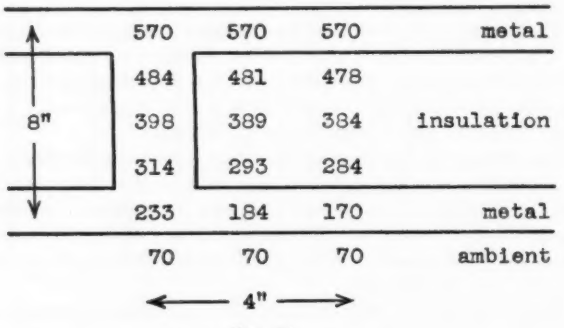


FIG. 21

a temperature difference of 84 F in the metal, and a mean temperature difference of 94 F in the insulation. Then $84 \times 26 \times 6 \times {}^1/_{96} = 137$ Btu per hr for the steel, and $94 \times 0.08 \times 6 \times {}^2/_3 = 30$ Btu per hr for the insulation, a total of 167 Btu per hr. The hot-side layer figures 169 Btu per hr, which is close enough to give the answer as 167 ± 3 Btu per hr.

This does not agree with the authors' figure of 146 Btu per hr. If the authors would publish a temperature-distribution diagram for this example, it might indicate where the discrepancy lies.

H. G. ELROD, JR.[8] For the conditions outlined by the authors, the heat flow per section may be obtained from the following formula

$$Q = \frac{t_h - t_c}{\frac{L}{k_I} + \frac{1}{h}} \left[W_I + \frac{k_M}{k_I}(2W_M) - \left\{ \frac{(2W_M)}{L\,W'_M} \left(1 - \frac{k_I}{k_M}\right) \frac{\tanh \alpha \frac{W_I}{2} + \frac{k_M}{k_I}(W_M)}{\alpha \tanh \alpha \frac{W_I}{2} + \beta W_M} \right\} \right]$$

where

$$\alpha^2 = \frac{\frac{k_I}{L} + h}{k_M W_M'}$$

and

$$\beta = \frac{\frac{k_M}{L} + h}{k_M W_M'}$$

W_M' the thickness of the metal walls need not be one half of the thickness of the through-metal strips.

The foregoing formula was derived by neglecting the temperature drop in the thin direction of the metal, and the lateral heat flow in the insulation. The first assumption is obviously allowable; the second assumption, because it arbitrarily restricts the heat flow, should cause the formula to yield values of heat flow smaller than actually found. Nevertheless, the formula values consistently exceed those shown by the authors in Fig. 17. On the other hand, the formula agrees well with the numerical method. The following is a comparison between formula and numerical method for the authors' example (1*a*):

	Formula	Numerical method	Authors' value
Over-all heat flow, Btu per hr	165	167 ± 3	146
Cold-surface temperatures,[a] deg F	168	170	
	184	184	
	238	233	

[a] Obtained using a temperature-distribution formula based upon precisely the same assumptions as used for the formula given in this discussion.

The writer's formula can be applied to the case where the metal-wall thicknesses and film coefficients are the same on both sides of the insulation. For this case, L should stand for one-half of the thickness of the insulation, and $t_h - t_c$ should be replaced by one half the total temperature difference.

The solution for cylindrical through-metal (bolts and pipes) has already been illustrated.[9]

AUTHORS' CLOSURE

Mr. Ernst stresses the fact that through-metal greatly increases the heat losses of insulated structures, and that the value of insulation is therefore decreased. Examination of this problem shows that the economic thickness of insulation is greater for structures with thermal short circuits than for those without. Quite apart from any numerical examination, pure reasoning can prove that this must be so. With increasing thickness, the influence of the thermal short circuit decreases; therefore, greater thickness results in a smaller increase factor. However,

[6] "The Numerical Solution of Heat-Conduction Problems," by H. W. Emmons, Trans. A.S.M.E., vol. 65, 1943, p. 607–615.

[7] This gradient works out to be on the order of 0.01 deg F in the present example. It seems surprising that the authors used two resistances in series to subdivide such a relatively small quantity.

[8] Department of Marine Engineering, U. S. Naval Academy, Annapolis, Md. Jun. A.S.M.E.

[9] "Applied Mathematics in Chemical Engineering," by T. K. Sherwood and C. E. Reed, McGraw-Hill Book Company, Inc., New York, N. Y., 1939, p. 207.

no increase in thickness within practical limits can offset the increased losses due to through-metal. Therefore, every care should be taken in design of equipment to avoid through-metal as far as possible. After the limit has been reached, the economic thickness of the insulation should be determined, and this can best be done by using curves such as are contained in this paper.

With regard to the example checked by Messrs. Dusinberre and Elrod, it should be noted that in the paper an increase factor of 3.08 was inadvertently introduced in place of the actual value 3.22 found from the graphical interpolations. If 3.22 is used, as should have been done, the heat loss becomes $3.22 \times 4.75 = 153$ Btu per hr. This is about 7 per cent less than the loss calculated by the discussers, and the difference must be attributed to the many steps in the interpolation. This was verified by setting up the network for this specific case and measuring the heat loss, which was found to be approximately 165 Btu per hr.

In specific reply to Mr. Dusinberre's comments it can be agreed that the present curves do not cover all cases which he mentions as important. If only one case at a time has to be solved, the use of the numerical method may be helpful, if no network or analyzer is quickly available. If, however, a larger number of such cases have to be solved, the development of curves would be desirable, because the practicing engineer will rarely find the time for the calculations entailed by the numerical method.

Mr. Dusinberre's statement that in the numerical method trends are more readily recognized than when working with parameters is misleading. The statement that trends are not readily seen when working with parameters refers to the trends due to the individual variables, as conductivity, spacing, etc. Such trends cannot be found by solving only one problem, either by the numerical method or on the analyzer. They can be detected only by solving a number of problems sufficient to cover the range it is desired to investigate. The best presentation of a large number of tests is by dimensionless parameter as used in this paper.

The maximum cold-surface temperatures can be found on the analyzer without additional work. They could be presented in graphs similar to those shown in the paper.

Network spacings of 2 in. and 4 in., as used by Mr. Dusinberre, are sufficient in the present example. In many instances, they will not yield accurate results, in which case the work involved by the numerical method increases considerably.

In his footnote,[7] Mr. Dusinberre overlooks the fact that the network, as shown in Fig. 20, refers not only to the example discussed by him but also to broader cases in which the subdivision as shown is necessary because the temperature gradient in the thin direction of the metal cannot be neglected.

Mr. Elrod's formula is interesting, and it would be desirable that he publish proof. The assumptions made are rather broad for certain conditions, and the value of the equation would be enhanced if Mr. Elrod would determine the limits (perhaps expressed in f_1, f_2, f_3, and f_4) within which his formula can be safely used.

Formulas for Calculating the Temperature Distribution in Electrical Coils of General Rectangular Cross Section

By T. J. HIGGINS,[1] CHICAGO, ILL.

In a recent paper (1)[2] Prof. Max Jakob outlined a procedure for calculating the temperature at any point T, the maximum temperature T_m, and the average temperature T_a in an electrical coil maintained at uniform surface temperature. Mr. Jakob derived explicit formulas for certain simple coils, i.e., the circular cylindrical coil, the infinite-plate coil, the spherical coil. The present paper is devoted to effecting formulas for T, T_m, and T_a for the very important case of the toroidal coil of general rectangular cross section. Following Jakob, the procedure is to pose determination of T as a boundary-value problem in the mathematical theory of heat; effect the formal solution for T; and obtain the corresponding formulas for T_m and T_a by use of their known relationship with T. Illustrative of application of the general formulas derived in the present paper, the maximum and average temperatures in a coil of given dimensions are calculated and are found to be in excellent agreement with the known measured values.

1 General Remarks

A current-carrying toroidal coil of rectangular cross section, composed of many turns of insulated wire of circular or of rectangular cross section, is an important component of many electrical devices. Commonly, the coil is either exposed to the atmosphere, e.g., the field coils of a dynamo, or is submerged in a liquid, e.g., the coils of a transformer. Usually, conditions are such that the temperature distribution in the coil is substantially independent of the angular co-ordinate of a system of cylindrical co-ordinates, the axis of which is the axis of the coil. If so, the temperature distribution is two-dimensional, i.e., it is the same over any cross section of the coil. Only this case will be considered.

In use, the heat generated in the coil results in a general temperature rise throughout the coil. In consequence, a point of maximum temperature is to be found in the cross section of the coil. By virtue of the assumed angular symmetry, this maximum temperature is the maximum temperature in the coil. Because the permissible maximum coil current is that which produces a specified maximum temperature in the coil, and because the "hot" or "operating" resistance of the coil depends upon, and can be calculated from, the average (mean) temperature of the coil, formulas for predetermining the temperature distribution, maximum temperature, and average temperature are of considerable interest to the designer of toroidal coils. Unfortunately, but few such formulas are available to him in the literature.

Undoubtedly, this paucity of formulas stems from the analytical difficulties posed by the various factors which affect the temperature distribution in the coil. In the main, the temperature at an arbitrary point in the coil is determined by (*a*) the geometry of the coil, (*b*) the surface conditions, (*c*) the current density in the metal, (*d*) the temperature variations of the thermal conductivities of the insulation and of the metal, and (*e*) the temperature variation of the electrical resistivity of the metal. If each of these quantities is specified analytically, determination of the temperature distribution can be set as a problem in the mathematical theory of heat. Theoretically, a rigorous solution of this problem is possible. Practically, such a solution is mathematically intractable.

Thus for specification of even the simplest conditions for items (*b*) to (*e*), i.e., uniform surface temperature and uniform current density, thermal conductivities and electrical resistivity independent of the temperature, the writer is unacquainted with any analysis, rigorous or approximate, wherein the actual toroidal geometry of the coil is taken into account. The mathematical analysis prerequisite to such a solution is so severe that, perforce, those who have worked on the problem have limited themselves to analyzing coils of simple geometry in which the temperature distribution approximates (so it is thought) that in certain special shapes of toroidal coils.

For example, a rectangular cylinder (i.e., an infinite cylinder of rectangular cross section) can be considered as a torus of the same cross section and of infinite inner radius. If, then, a toroidal coil of rectangular cross section is such that the inner radius is large compared with either dimension of its cross section, the temperature distribution in it tends to that in a rectangular cylindrical coil of the same cross section.

If, further, the length of the radial side (width) of the rectangular cross section of the toroidal coil is small, compared with that of the axial side (height), the temperature distribution in both the toroidal and the cylindrical coils tends to that in the geometrically simpler plate coil (i.e., a cylindrical coil with cross section an infinite strip of definite width). Accordingly, if the toroidal coil tends to either of these two limiting shapes, it can be conjectured that an approximate formula for the temperature distribution in the toroidal coil is afforded by the formula for the corresponding rectangular cylindrical or plate coil.

However, for these simpler coils, as for the more complex toroidal coil, the author is unacquainted with any rigorous solution for the temperature distribution. Neither is it to be expected that any exists. For even if temperature variations in the thermal conductivities and electrical resistivity be neglected, in a rigorous solution (as a problem in the mathematical theory of heat), account must yet be taken (*a*) of the discrete distribution of current density over the cross section, zero in the insulation, practically uniform in the metal, and (*b*) of the boundary conditions at the interfaces between the insulation and the metal, continuity of the temperature and of the normal component of heat-flux density. While it is not difficult to take the first factor into account, the second renders a rigorous solution mathematically intractable.

---

[1] Associate Professor of Electrical Engineering, Illinois Institute of Technology.

[2] Numbers in parentheses refer to the Bibliography at the end of the paper.

Contributed by the Heat Transfer Division and presented at the Annual Meeting, New York, N. Y., Nov. 29–Dec. 3, 1943, of The American Society of Mechanical Engineers.

Note: Statements and opinions advanced in papers are to be understood as individual expressions of their authors and not those of the Society.

Aware, explicitly or intuitively, of this intractableness, yet desirous of obtaining some approximation to the rigorous formulas for temperature distribution in these simpler coils, those who have worked at this problem have resorted, perforce, to various artifices. These latter comprise two categories, as follows:

1 Physical considerations serve as bases for the deduction of empirical formulas for the maximum and the average temperatures.

2 Formulas for the temperature distribution, maximum temperature, and average temperature in a homogeneous infinite plate or a homogeneous rectangular cylinder, subject to certain conditions of surface temperature and internally generated heat, are affected rigorously by application of the mathematical theory of heat. It is then implied that these formulas can be utilized either directly, in conjunction with certain measurements, or in combination with empirically calculated physical "constants," to calculate the corresponding temperatures in plate or in rectangular cylindrical coils.

In one or the other of these fashions formulas have been effected by Binder (2), Humburg (3), Jakob (1, 4), Ott (5), Punga (6), Rogowski (7), and Vidmar (8). The most recent, most inclusive, and most applicable work is that of Jakob (1). His analysis encompasses an important factor neglected by the others, i.e., the temperature variation of the resistivity of the conducting metal.[3] This factor has a decided effect upon the temperature distribution in the coil.

We epitomize Jakob's analysis:[4] If a toroidal coil is of such inner radius that it can be approximated by a cylindrical coil of the same cross section, and if the toroidal coil is composed of many turns of light wire, then:

1 We identify the temperature distribution T, the maximum temperature T_m, and the average temperature T_a for the coil with the corresponding quantities in a homogeneous cylinder of the following characteristics:

(*a*) Of the same cross section as the coil.

(*b*) Of "equivalent" thermal conductivity k (calculated as outlined in Section 4).

(*c*) Maintained at the same surface conditions as the coil.

(*d*) And wherein q, the heat generated per unit volume per unit time, is $q_0[1 + \alpha_0 T]$; T_s is the surface temperature; α_0 the temperature coefficient of resistivity of the conducting metal at 0 deg C; and $q_0 = I^2R_0/V$, I being the coil current, V the volume of the coil, and R_0 the coil resistance when the entire coil is at temperature 0 deg C.

2 And proceed to determine T, T_m, and T_a for the homogeneous cylinder as a problem in the mathematical theory of heat.

For the boundary condition of uniform surface temperature, Jakob obtains formulas for T, T_m, and T_a for the one-dimensional problems of the circular cylinder, and the infinite plate of definite thickness (and also the sphere). These formulas obtained, Jakob suggests that the formulas for T, T_m, and T_a for the circular cylinder can be used to approximate the corresponding quantities in the toroidal coil of square cross section, and that those for the infinite plate can be used similarly for toroidal coils of quite elongated rectangular cross section. In support of this suggestion and illustrative of his analysis in general, the formulas for T_m and T_a for the circular cylinder are used to calculate T_m and T_a in the toroidal coil of square cross section utilized in the experiments of Rogowski and Vieweg (11). The values thus calculated are found to be in substantial agreement with the known measured values.

Now most rectangular toroidal coils are neither of square nor of quite elongated rectangular cross section. In consequence, it is most desirable to have formulas for T, T_m, and T_a that are applicable for the general rectangular cross section. Such formulas are derived in Sections 2 to 4. Illustrative of their use and substantiative of their correctness, the formulas for T_m and T_a are then utilized to calculate these temperatures in the same coil as that used by Jakob in his numerical example. Seemingly, no other experimental data are available. Excellent agreement is obtained between the calculated and the measured values.

2 Solution of the Associated Heat Problem

The axis of a homogeneous infinite rectangular cylinder of thermal conductivity k watts cm^{-1} deg C^{-1} is coincident with the z axis of a Cartesian system of co-ordinates, the sides of the right cross section are parallel to the x and y axes (Fig. 1). The surface of the cylinder is maintained at uniform temperature T_s deg C. Heat per unit volume per unit time is developed in the cylinder at the rate of $q_0(1 + \alpha_0 T)$ watts cm^{-3}, q_0 and α_0 being constant and T a function of x and y alone. Required: The expressions for the temperature $T(x, y)$ at any point in the cylinder, the maximum temperature T_m, and the average temperature T_a.

From the mathematical theory of heat, the expression for T is that solution of the partial-differential equation

$$\partial^2 T/\partial x^2 + \partial^2 T/\partial y^2 = -q_0(1 + \alpha_0 T)/k \quad [1]$$

which satisfies the given boundary condition

$$T = T_s \quad [2]$$

at $$x = \pm a, \quad y = \pm b$$

and the condition stemming from the symmetry of the problem

$$T(x, y) = T(\pm x, \pm y) \quad [3]$$

By virtue of Equation [3], the temperature T is an even function of x and of y. Accordingly, T can be expressed by the double Fourier cosine series

$$T = A_0 + \sum_{i=1}^{\infty} \sum_{j=1}^{\infty} A_{ij} \cos M_i x \cos N_j y \quad [4]$$

in which A_0, A_{ij}, M_i, and N_j are constants to be determined from Equations [1] and [2]. Substituting Equation [4] in Equation [2], we find Equation [4] satisfies Equation [2] providing

$$M_i = \pi(2i - 1)/2a \qquad i = 1, 2, 3 \quad [5]$$

$$N_j = \pi(2j - 1)/2b \qquad j = 1, 2, 3 \quad [6]$$

and

$$A_0 = T_s \quad [7]$$

We determine A_{ij} from Equation [1] in the usual fashion. Substituting Equation [4] in [1]

[3] Jakob (1) remarks, and it is also so mentioned in the discussions of Davis and Tramontini appended to his paper, that his analysis encompasses the effects of the temperature variation of the thermal conductivity. In the opinion of the author, this is not so. For if the thermal conductivity k were a function of the temperature θ, then the correct form of Equation [5] of Jakob's paper would be $\partial(k\ \partial\theta/\partial x)/\partial x = -q'''$, whence assumption of some analytical expression of k as a function of θ gives rise to a more or less complicated differential equation. The correct interpretation of the constants in Equations [5] and [6] of Jakob's paper is that k is constant and q''' is a linear function of temperature $q_s(1 + \epsilon_s\theta)$, q_s a constant, and ϵ_s a temperature coefficient of resistivity at s deg C. Hence Equation [6] becomes $q'''/k = m(1 + \epsilon\theta) = (q_s/k)(1 + \epsilon_s\theta)$. Note that in his numerical example Jakob himself identifies ϵ with the temperature coefficient of electrical resistivity. For further discussion of the temperature variation of thermal conductivity see Section 4 of the present paper.

[4] This is the writer's interpretation as deduced from study of the numerical example in Jakob's paper. For a qualitative discussion of the correctness of this procedure see Section 4 of the present paper.

$$\sum_{i=1}^{\infty}\sum_{j=1}^{\infty} A_{ij}(M_i^2 + N_j^2 - C^2)\cos M_i x \cos N_j y = C' \quad [8]$$

in which

$$C^2 = q_0\alpha_0/k;\ C' = q_0(1 + \alpha_0 T_s)/k;\ C'/C^2 = T_s + \alpha_0^{-1} \quad [9]$$

multiplying each member of Equation [8] by $\cos M_p x \cos N_q y$, p, and q arbitrary positive integers; integrating over a quadrant of the cross section shown in Fig. 1

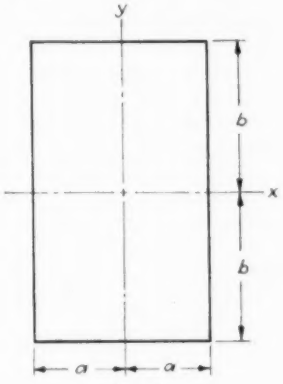


FIG. 1

$$\sum_{i=1}^{\infty}\sum_{j=1}^{\infty} A_{ij}(M_i^2 + N_j^2 - C^2)\int_0^a\int_0^b \cos M_i x \cos M_p x \cos N_j y \cos N_q y\, dy\, dx = 4C'\int_0^a\int_0^b \cos M_p x \cos N_q y\, dy\, dx \quad [10]$$

evaluating the double integrals (all integrals on the left-hand side vanish except those for which $p = i$, $q = j$); simplifying by use of Equations [5] and [6]; and solving for A_{ij} yields

$$A_{ij} = (4C'/ab)(-1)^{i+j}/M_i N_j(M_i^2 + N_j^2 - C^2) \quad [11]$$

Substituting Equations [7] and [11] in Equation [4], we have

$$T = T_s + (4C'/ab)\sum_{i=1}^{\infty}\sum_{j=1}^{\infty}(-1)^{i+j}\cos M_i x \cos N_j y/M_i N_j(M_i^2 + N_j^2 - C^2) \quad [12]$$

We can transform Equation [12] into forms more convenient for numerical computation by use of the identities[5]

$$(2/b)\sum_{j=1}^{\infty}(-1)^{j-1}\cos N_j y/N_j(N_j^2 + K_i^2) = (1/K_i^2)(1 - \cosh K_i y \operatorname{sech} K_i b) \quad [13]$$

in which $K_i^2 = M_i^2 - C^2$ and K_i is the positive root; and

$$(2/a)\sum_{i=1}^{\infty}(-1)^{i-1}\cos M_i x/M_i K_i^2 = \begin{cases} (1/C^2)(1 - \cosh Cx \operatorname{sech} Ca),\ C^2 < 0 \\ (-1/C^2)(1 - \cos Cx \sec Ca),\ C^2 > 0 \end{cases} \quad [14]$$

[5] "Sur une méthode de sommation de certaines series de Fourier," by E. Roth and G. Kouskoff, *Revue Gènèrale de l'Electricité*, vol. 23, 1928, pp. 1061–1073.

Substituting Equation [13] in Equation [12] yields

$$T = T_s + (2C'/a)\sum_{i=1}^{\infty}(-1)^{i-1}\cos M_i x(1 - \cosh K_i y \operatorname{sech} K_i b)/K_i^2 M_i \quad [15]$$

Simplifying Equation [15] by use of the second form of Equation [14], we have

$$T = T_s - (C'/C^2)(1 - \cos Cx \sec Ca) - (2C'/a)\sum_{i=1}^{\infty}(-1)^{i-1}\cos M_i x \cosh K_i y/K_i^2 M_i \cosh K_i b \quad [16]$$

in which $C^2 > 0$.

By virtue of the symmetry of Equation [12], an alternative form of Equation [16] can be obtained by interchanging a and b, x and y, M_i and N_j, K_i and $K_j (= N_j^2 - C^2)$. As this is easily done, we shall not write down this alternative form.

The maximum temperature T_m occurs at the center of the cross section. Substituting $x = 0$, $y = 0$ in Equation [16], we have

$$T_m = T_s - (C'/C^2)(1 - \sec Ca) - (2C'/a)\sum_{i=1}^{\infty}(-1)^{i-1}/K_i^3 M_i \cosh K_i b \quad [17]$$

The average temperature T_a over the cross section is given by

$$T_a = (1/4ab)\int_{-a}^{a}\int_{-b}^{b} T\,dy\,dx \quad [18]$$

Substituting Equation [16] in Equation [18], and integrating, yields

$$T_a = T_s - (C'/C^2)(1 - \tan Ca/Ca) - (2C'/a^2 b)\sum_{i=1}^{\infty}(-1)^{i-1}\sin M_i a \tanh K_i b/K_i^2 M_i^2 \quad [19]$$

3 Special Cases of the General Heat Problem

Certain special cases of the general problem are of particular interest.

Rectangular Cylinder and Uniform Heat Density. If $\alpha_0 = 0$, whence $C^2 = 0$, q is uniform throughout the cylinder. Taking the limit as $C^2 \to 0$ of the right-hand members of Equations [16], [17], and [19] (the details are contained in the Appendix), yields

$$T = T_s + C'(a^2 - x^2)/2 - (2C'/a)\sum_{i=1}^{\infty}(-1)^{i-1}\cos M_i x \cosh M_i y/M_i^3 \cosh M_i b \quad [20]$$

$$T_m = T_s + C'a^2/2 - (2C'/a)\sum_{i=1}^{\infty}(-1)^{i-1}/M_i^3 \cosh M_i b \quad [21]$$

$$T_a = T_s + C'a^2/3 - (2C'/a^2 b)\sum_{i=1}^{\infty}(-1)^{i-1}\sin M_i a \tanh M_i b/M_i^4 \quad [22]$$

This case was studied by Humburg (3), and later by Jakob (4). The latter's formulas for T, T_m, and T_a are less compact than the author's; they are expressed in terms of double-infinite

series whereas the present ones are expressed in terms of single-infinite series. The two forms are equivalent, however, in that Equations [20], [21], and [22] can be transformed into the corresponding Equations [17], [19], and [21] of Jakob's paper (1).

Infinite Plate and Nonuniform Heat Density. As $b \to \infty$, the rectangular cross section tends to an infinite strip of thickness $2a$, whence the rectangular cylinder tends to an infinite plate of thickness $2a$. Substituting $b = \infty$ in the right-hand members of Equations [16], [17], and [19], yields

$$T = T_s - (C'/C^2)(1 - \cos Cx \sec Ca) \quad [23]$$

$$T_m = T_s - (C'/C^2)(1 - \sec Ca) \quad [24]$$

$$T_a = T_s - (C'/C^2)(1 - \tan Ca/Ca) \quad [25]$$

Jakob (1) has recently considered this case in detail. Corroborative of the present analysis, Equations [23], [24], and [25] are identical (aside from notation) with the corresponding Equations [14], [15], and [16] of Jakob's paper (1).

Infinite Plate and Uniform Heat Density. Substituting $b = \infty$ in Equations [20], [21], and [22], yields

$$T = T_s + C'(a^2 - x^2)/2 \quad [26]$$

$$T_m = T_s + C'a^2/2 \quad [27]$$

$$T_a = T_s + C'a^2/3 \quad [28]$$

This case was studied first by Rogowski (7). The present equations for T, T_m, and T_a are identical with his.

4 Application of the Heat Problem to Electrical Coils

The formulas of Sections 2 and 3 can be utilized to calculate temperatures in electrical coils, provided we interpret q_0, α_0, and k as deduced in this section.

Inasmuch as the wire comprising an electrical coil is insulated, the same current I flows through any cross section of the wire. If R_0 is the resistance of the coil when its temperature is uniform at 0 deg C, the Joulean power developed in the coil at this temperature is I^2R_0; whence the average power per unit volume is I^2R_0/V. Now if the coil were composed of wire of zero thickness of insulation, I^2R_0/V would be identical with $q_0 (= i^2\rho_0)$ (i being the current density, and ρ_0 the resistivity at 0 deg C of the metal), the power per unit volume developed at any point in the coil. If the coil were composed of thinly insulated wire, the average of q_0 over the sectioned metal and insulation of a cross section of the wire would closely approximate I^2R_0/V. Accordingly, if we restrict ourselves to coils composed of thinly insulated wire (and commonly the wire is thus insulated), it is rational to identify q_0 in the equations of Sections 2 and 3 with I^2R_0/V.

In use, both the temperature T and the power density q vary from point to point in the coil. If, in addition, we assume that the coil is composed of wire of cross section small in comparison with that of the coil,[6] which is the case if (as is usual) the coil is composed of many turns of light wire, the current density i over any cross section of the (metal of the) wire is substantially uniform; whence variation in $q (= i^2\rho)$ from point to point in the coil must be attributed to variation in the resistivity of the metal from point to point. As a function of temperature $\rho = \rho_0(1 + \alpha_0 T)$; from which we derive $q = q_0(1 + \alpha_0 T)$. Accordingly, we identify α_0 in the equations of Sections 2 and 3 with the temperature coefficient of resistivity at 0 deg C of the metal of the coil.

The thermal conductivities k_m and k_i of the metal and of the insulation of a coil are quite different. Commonly, k_m is several thousand times greater than k_i. Accordingly, k in the formulas of Sections 2 and 3 is to be identified with the "equivalent thermal conductivity" of the coil.[7] The equivalent thermal conductivity of an array of parallel circular cylindrical metallic conductors embedded in a homogeneous insulation can be determined from curves due to Richter (9). These curves are reproduced in a text on electrical design by Moore (10).

If, as is frequently the case, the wire is of square or of not too elongated rectangular cross section, Richter's curves can yet be used through the device of replacing the rectangular cross section by an "equivalent" circular cross section of the same area. Alternatively, the areas of sectioned metal and insulation, comprising the cross section of a coil, can be taken as comprising a network of thermal conductances; these conductances are combined into a single equivalent thermal conductance in the same fashion as a series-parallel network of electrical conductances is reduced to a single equivalent conductance; and the equivalent conductivity k determined therefrom. This method of calculating k is made use of in Jakob's paper (1).

In general, despite the large ratio of k_m/k_i, k is only several times larger than k_i. Accordingly, if we were to attempt to take the variation of the thermal conductivities of k_i and k_m into account, it would be rational to do so by identifying the variation in k with that in k_i. Few quantitative data are available, however, on the temperature variations of the thermal conductivities of insulating materials. Nor, for that matter, are the k_i values known accurately at any particular temperature. In consequence although it is possible to effect a solution for the heat problem of Section 2, in which k as well as q is taken as a linear function of the temperature (in fact, the writer has done so), such a refinement as applied to calculation of the temperature in electrical coils would be meaningless.

In the light of the discussion to this point, we may expect that if a coil comprises many turns of thinly insulated wire of comparatively small cross section, and if the constants q_0, α_0, and k are interpreted as outlined in this section, the formulas of Sections 2 and 3 will yield fairly accurate values of temperature. Comparatively few experimental data are available for affording, through comparison of known test values with calculated values, either confirmation or disproval of this statement. Seemingly, the only available published data suitable to this purpose are those of Rogowski and Vieweg (11). Certain of their data were used by Jakob (1) to illustrate use of the formulas and procedure advanced in his paper. The author utilizes these same data in the numerical example of Section 5.

5 Numerical Example

We consider the following problem: To calculate the maximum temperature attained in the rectangular toroidal coil during Run 2 of the experiments of Rogowski and Vieweg (11). This particular run is selected in the thought that the surface condition apposite to the formulas derived in this paper, i.e., uniform surface tem-

[6] If the cross section of the wire is large, the current density will be nonuniform over the cross section. For, since the resistivity of different filaments of the wire will vary with the temperature variation over the cross section, and since all filaments are connected in parallel, whence the voltage gradient ϵ along each filament must be the same, the current density $i = \epsilon/\rho$ will necessarily vary over the cross section. Thus in the case of a single heavy circular cylindrical conductor, the current density is a minimum at the center of the cross section, at which point the temperature is greatest.

[7] Our reason for doing so is as follows: In various problems having to do with the flow of heat in materials which are not homogeneous from point to point but which are homogeneous in a "fine-grained" sense (a nonhomogeneous pattern of small area is regularly ranked to form a comparatively large area, thus the cross section of the coil is composed of a regular array of identical nonhomogeneous cross sections of the wire), experience is to the effect that utilization of such an equivalent thermal conductivity permits satisfactory analytical formulation of an otherwise intractable problem. Thus, heat-flow problems in cellular materials are handled in precisely this fashion.

perature, is more closely approximated in Run 2 than in the other runs. In Run 2 the coil is cooled on all sides by an air blast.

Given Data: Toroidal coil with square cross section; inner radius 4 cm; winding composed of 1416 turns of 0.1-cm-diam copper wire insulated with lacquer-soaked silk; these turns are arranged in coaxial layers, each layer composed of 40 turns; surface temperature 76.1 C; maximum temperature 122.4 C; mean temperature calculated from the "hot" or operating resistance 96.7 C; cold resistance ≈ 11 ohms; coil current 3 amp.

Derived Data: Using the given data, we find the volume V of the coil to be 754 cu cm. The percentage conductivity of the copper wire is not stated. Taking it to be 100 per cent, we find (as can be found in any electrical handbook) that $\alpha_0 \approx 0.00423$ deg C^{-1} and $\alpha_{20} = 0.00393$ deg C^{-1}. The temperature at which the "cold" resistance ≈ 11 ohms was measured is not stated. We assume 20 deg C (68 F). Then $R_0 = 11[1 - 0.00393 \times 20]$ 10.13 ohms; whence $q_0 = I^2R_0/V = 0.1207$ cm^{-3}. Jakob (1) has calculated the equivalent conductivity of the coil to be $k = 0.00531$ watt cm^{-1} deg C^{-1}.

Using these derived values of α_0, q_0, and k, we find by direct computation

$$C^2 = 0.0963;\ C' = 29.9;\ C'/C^2 = 310.6;\ Ca = 0.683$$
$$M_1 = 0.714;\ M_1^2 = 0.5098;\ K_1^2 = 0.4135;\ K_1 = 0.643;\ K_1b = 1.415$$
$$M_2 = 2.142;\ M_2^2 = 4.588;\ K_2^2 = 4.492;\ K_2 = 2.119;\ K_2b = 4.651$$

These values were calculated on a 20-in. slide rule. Substituting appropriately in Equations [17] and [19], we have

$$T_m = 76.1 + 89.8 - (42.2 - 0.11) = 123.8 \text{ deg C}$$

$$T_a = 76.1 + 58.8 - (136.7 - 0.13) = 98.3 \text{ deg C}$$

The terms within the parentheses are those contributed by the infinite series in Equations [17] and [19]. We note that these series converge so rapidly that generally it is necessary to compute only the first term; the second term is certainly much smaller than the error inherent in the general procedure.

Comparing these calculated values with the corresponding measured values,[8] $T_m = 122.4$ deg C and $T_a = 96.7$ deg C, we find differences of 1.4 deg C and 1.6 deg C. These differences are 1.15 per cent and 1.65 per cent, respectively, of T_m and T_a.

Considering the various assumptions made in Section 4, and the uncertainties in the given data, this substantial agreement between calculated and measured values is most gratifying. For, although success in this one numerical example hardly constitutes a general validification of the formulas given in this paper and although it is most desirable to obtain additional and more precise experimental data for use in effecting similar comparisons, it is substantiative of the author's opinion that the formulas of this paper will yield satisfactory numerical values of the temperature in rectangular toroidal coils, providing the coil geometry and surface conditions are such that application of these formulas is justifiable.

ACKNOWLEDGMENT

The author is indebted to Prof. M. Jakob for calling attention to the subject of this paper, and for personal discussion of certain points of his previous paper (1).

BIBLIOGRAPHY

1 "Influence of Nonuniform Development of Heat Upon the Temperature Distribution in Electrical Coils and Similar Heat Sources of Simple Form," by M. Jakob, Trans. A.S.M.E., vol. 65, 1943, pp. 593–605.

2 "Über die Berechnung der Temperaturen im Innern von Magnetspulen," by L. Binder, *Archiv für Elektrotechnik*, vol. 2, 1913, pp. 131–148.

3 "Die Temperaturverteilung im Innern von Magnetspulen mit rechteckigem Querschnitt," by K. Humburg, *Electrotechnik und Maschinenbau*, vol. 27, 1909, pp. 677–681 and 696–703.

4 "Die Temperaturverteilung in einer elektrischen Wicklung von recteckigem Querschnitt," by M. Jakob, *Archiv für Electrotechnik*, vol. 8, 1919–1920, pp. 117–126.

5 "Untersuchungen zur Frage der Erwärmung elektrischer Maschinen," by L. Ott, *Mitteilungen über Forschungsarbeiten auf dem Gebiets des Ingenieurwesens*, Heft 35 and 36, 1906, pp. 53–107.

6 "Die Maximale Temperatur von Feldspulen," by F. Punga, *Archiv für Elektrotechnik*, vol. 21, 1928–1929, pp. 97–105.

7 "Erganzung der Erwarmungsvorschriften: Zum Vorschlag des Herrn Vidmar," by W. Rogowski, *Archiv für Elektrotechnik*, vol. 7, 1918–1919, pp. 41–47.

8 "Ein Vorschlag zür Ergänzung der Erwärmungsvorschriften," by M. Vidmar, *Elektrotechnik und Maschinenbau*, vol. 36, 1918, pp. 49–52, and 64–66.

9 "Elektrische Maschinen," by R. Richter, Julius Springer, Berlin, 1924.

10 "Fundamentals of Electrical Design," by A. D. Moore, McGraw-Hill Book Company, Inc., New York, N. Y., 1927, pp. 95–96.

11 "Höchsttemperatur stromdurchflossener Spulen," by W. Rogowski and V. Vieweg, *Archiv für Elektrotechnik*, vol. 8, 1919–1920, pp. 329–332.

Appendix

To obtain the limit as $C^2 \to 0$ of the right-hand member of Equation [16], we note that

$$\lim_{C^2 \to 0} K_i = M_i$$

and that

$$\lim_{C^2 \to 0} (C'/C^2)(1 - \cos Cx \sec Ca)$$
$$= \lim_{C^2 \to 0} (C'/C^2)[1 - (1 - C^2x^2/2! + C^4x^4/4! - \ldots)(1 - C^2a^2/2! + C^4a^4/4! - \ldots)^{-1}]$$
$$= \lim_{C^2 \to 0} (C'/C^2)[1 - 1 + C^2(x^2 + a^2)/2! - C^4(a^4/4! + x^4/4! + a^2x^2/2 \cdot 2!) + \ldots]$$
$$= C'(x^2 + a^2)/2!$$

Taking the limit as $C^2 \to 0$ of the right-hand member of Equation [16] and making use of the foregoing evaluations yields Equation [20].

In similar fashion, Equation [22] follows from Equation [19] by making use of the identity

$$\lim_{C^2 \to 0} (C'/C^2)(1 - \tan Ca/Ca)$$
$$= \lim_{C^2 \to 0} (C'/C^2)[1 - (Ca + C^3a^3/3 + 2C^5a^5/15 + \ldots)/Ca]$$
$$= C'a^2/3$$

Discussion

VICTOR PASCHKIS.[9] Electrical coils are usually operated at constant voltage. Thus, if for reasons of poor design the temperature and therewith the electrical resistance would increase considerably, the current would drop.

It would be of considerable interest if the author's investigation could be extended to include the case of constant voltage, and a current initially not known but dependent upon the resulting temperatures.

In discussing the paper orally, Prof. L. M. Boelter mentioned some desirable refinements which may make the problem mathematically unsolvable. If this should be the case, investigation on

[8] Jakob (1) states that the measured value was 100 deg C (= 76.1 + 23.9), but Rogowski and Vieweg definitely state 96.7 deg C for T_a.

[9] Research Associate, Department of Mechanical Engineering, Research Laboratories, Columbia University, New York, N. Y.

the "heat and mass-flow analyzer" might offer a solution. The desirability was mentioned of determining the apparent thermal conductivity of laminated materials, such as cores of transformers, etc. Such determination would also be highly desirable in connection with heat flow in strip coils and staples of metal sheets. For this purpose a temperature range up to 1600 F or 1800 F should be investigated.

Knowledge of the thermal conductivity under these conditions would make possible a rational analysis of uniformity in heat-treating practice.

Friction Factors for Pipe Flow

By LEWIS F. MOODY,[1] PRINCETON, N. J.

The object of this paper is to furnish the engineer with a simple means of estimating the friction factors to be used in computing the loss of head in clean new pipes and in closed conduits running full with steady flow. The modern developments in the application of theoretical hydrodynamics to the fluid-friction problem are impressive and scattered through an extensive literature. This paper is not intended as a critical survey of this wide field. For a concise review, Professor Bakhmeteff's (1)[2] small book on the mechanics of fluid flow is an excellent reference. Prandtl and Tietjens (2) and Rouse (3) have also made notable contributions to the subject. The author does not claim to offer anything particularly new or original, his aim merely being to embody the now accepted conclusions in convenient form for engineering use.

IN the present pipe-flow study, the friction factor, denoted by f in the accompanying charts, is the coefficient in the Darcy formula

$$h_f = f \frac{L}{D} \frac{V^2}{2g}$$

in which h_f is the loss of head in friction, in feet of fluid column of the fluid flowing; L and D the length and internal diameter of the pipe in feet; V the mean velocity of flow in feet per second; and g the acceleration of gravity in feet per second per second (mean value taken as 32.16). The factor f is a dimensionless quantity, and at ordinary velocities is a function of two, and only two, other dimensionless quantities, the relative roughness of the surface, $\frac{\epsilon}{D}$ (ϵ being a linear quantity in feet representative of the absolute roughness), and the Reynolds number $\mathbf{R} = \frac{VD}{\nu}$ (ν being the coefficient of kinematic viscosity of the fluid in square feet per second). Fig. 1 gives numerical values of f as a function of $\frac{\epsilon}{D}$ and $\mathbf{R}$.

Ten years ago R. J. S. Pigott (4) published a chart for the same friction factor, using the same co-ordinates as in Fig. 1 of this paper. His chart has proved to be most useful and practical and has been reproduced in a number of texts (5). The Pigott chart was based upon an analysis of some 10,000 experiments from various sources (6), but did not have the benefit, in plotting or fairing the curves, of later developments in functional forms of the curves.

In the same year Nikuradse (7) published his experiments on artificially roughened pipes. Based upon the tests of Nikuradse and others, von Kármán (8) and Prandtl (9) developed their theoretical analyses of pipe flow and gave us suitable formulas with numerical constants for the case of perfectly smooth pipes or those in which the irregularities are small compared to the thickness of the laminar boundary layer, and for the case of rough pipes where the roughnesses protrude sufficiently to break up the laminar layer, and the flow becomes completely turbulent.

The analysis did not, however, cover the entire field but left a gap, namely, the transition zone between smooth and rough pipes, the region of incomplete turbulence. Attempts to fill this gap by the use of Nikuradse's results for artificial roughness produced by closely packed sand grains, were not adequate, since the results were clearly at variance from actual experience for ordinary surfaces encountered in practice. Nikuradse's curves showed a sharp drop followed by a peculiar reverse curve,[3] not observed with commercial surfaces, and nowhere suggested by the Pigott chart based on many tests.

Recently Colebrook (11), in collaboration with C. M. White, developed a function which gives a practical form of transition curve to bridge the gap. This function agrees with the two extremes of roughness and gives values in very satisfactory agreement with actual measurements on most forms of commercial piping and usual pipe surfaces. Rouse (12) has shown that it is a reasonable and practically adequate solution and has plotted a chart based upon it. In order to simplify the plotting, Rouse adopted co-ordinates inconvenient for ordinary engineering use, since f is implicit in both co-ordinates, and $\mathbf{R}$ values are represented by curved co-ordinates, so that interpolation is troublesome.

The author has drawn up a new chart, Fig. 1, in the more conventional form used by Pigott, taking advantage of the functional relationships established in recent years. Curves of f versus $\mathbf{R}$ are plotted to logarithmic scales for various constant values of relative roughness $\frac{\epsilon}{D}$; and to permit easy selection of $\frac{\epsilon}{D}$, an accompanying chart, Fig. 2, is given from which $\frac{\epsilon}{D}$ can be read for any size of pipe of a given type of surface.

In order to find the friction loss in a pipe, the procedure is as follows: Find the appropriate $\frac{\epsilon}{D}$ from Fig. 2, then follow the corresponding line, thus identified, in Fig. 1, to the value of the Reynolds number $\mathbf{R}$ corresponding to the velocity of flow. The factor f is thus found, for use in the Darcy formula

$$h_f = f \frac{L}{D} \frac{V^2}{2g}$$

In Fig. 2, the scales at the top and bottom give values of the diameter in both feet and inches. Fig. 1 involves only dimensionless quantities and is applicable in any system of units.

To facilitate the calculation of $\mathbf{R}$, auxiliary scales are shown at the top of Fig. 1, giving values of the product (VD') for two fluids, i.e., water and atmospheric air, at 60 F. (D' is the inside diameter in inches.) As a further auxiliary, Fig. 3 is given, from which $\mathbf{R}$ can be quickly found for water at ordinary temperatures, for any size of pipe and mean velocity V. Dashed lines on this chart have been added giving values of the discharge or quantity of fluid flowing, $Q = AV$, expressed in both cubic feet per second and in U. S. gallons per minute.

---

[1] Professor, Hydraulic Engineering, Princeton University. Mem. A.S.M.E.

[2] Numbers in parentheses refer to the Bibliography at the end of the paper.

Contributed by the Hydraulic Division and presented at the Semi-Annual Meeting, Pittsburgh, Pa., June 19–22, 1944, of THE AMERICAN SOCIETY OF MECHANICAL ENGINEERS.

NOTE: Statements and opinions advanced in papers are to be understood as individual expressions of their authors and not those of the Society.

[3] Rouse, reference (3), p. 250; and Powell, reference (10), p. 174.

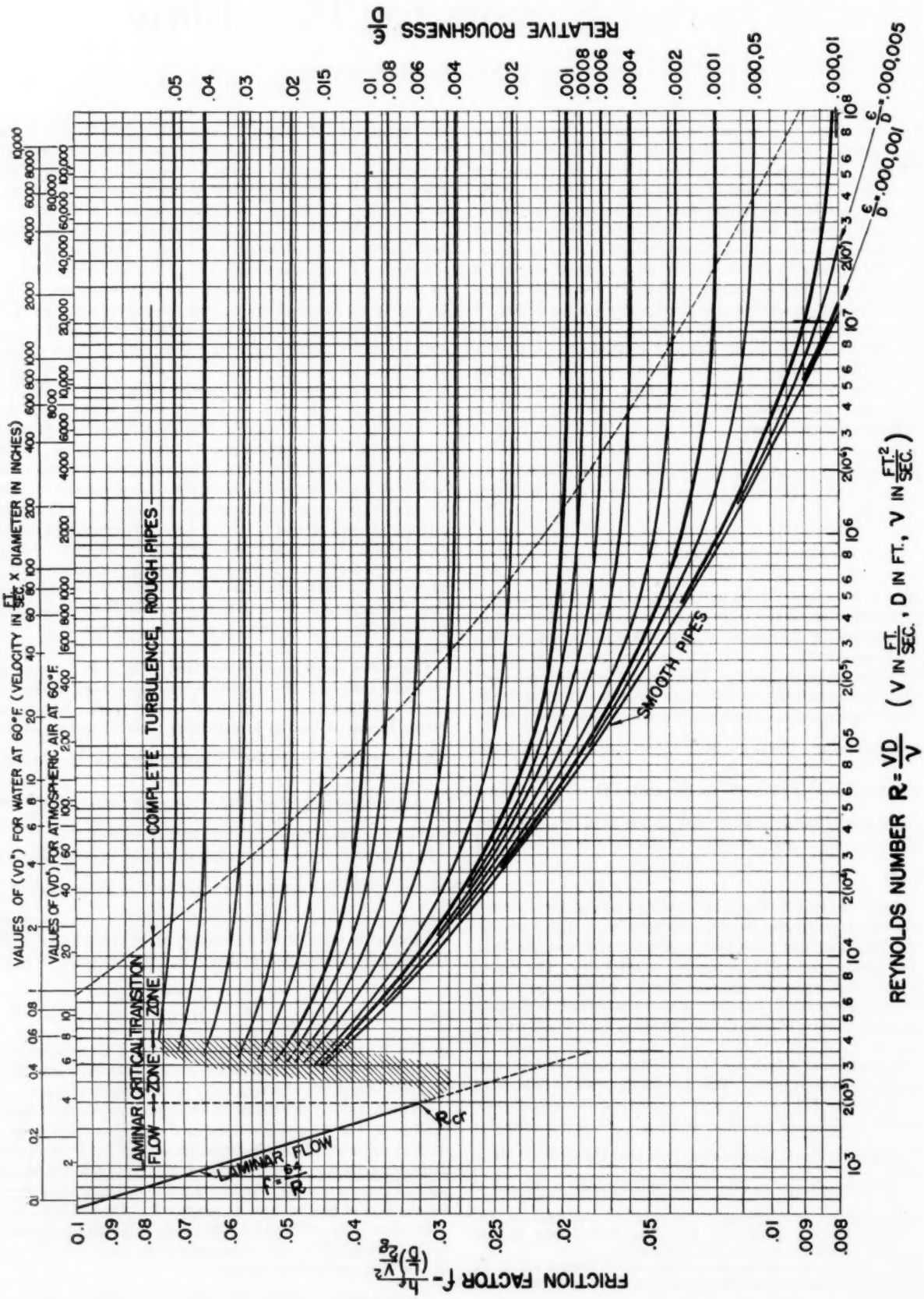

RELATIVE ROUGHNESS ε/D
.05
.04
.03
.02
.015
.01
.008
.006
.004
.002
.001
.0008
.0006
.0004
.0002
.0001
.000,05
.000,01
ε/D=.000,001
ε/D=.000,005
VALUES OF (VD') FOR WATER AT 60°F. (VELOCITY IN FT./SEC. X DIAMETER IN INCHES)
VALUES OF (VD') FOR ATMOSPHERIC AIR AT 60°F.
LAMINAR FLOW
CRITICAL TRANSITION ZONE
COMPLETE TURBULENCE, ROUGH PIPES
SMOOTH PIPES
LAMINAR FLOW f=64/R
Rcr
FRICTION FACTOR f=(h_f/(L/D))(2g/V²)
REYNOLDS NUMBER R=VD/ν (V IN FT./SEC., D IN FT., ν IN FT.²/SEC.)

Fig. 1

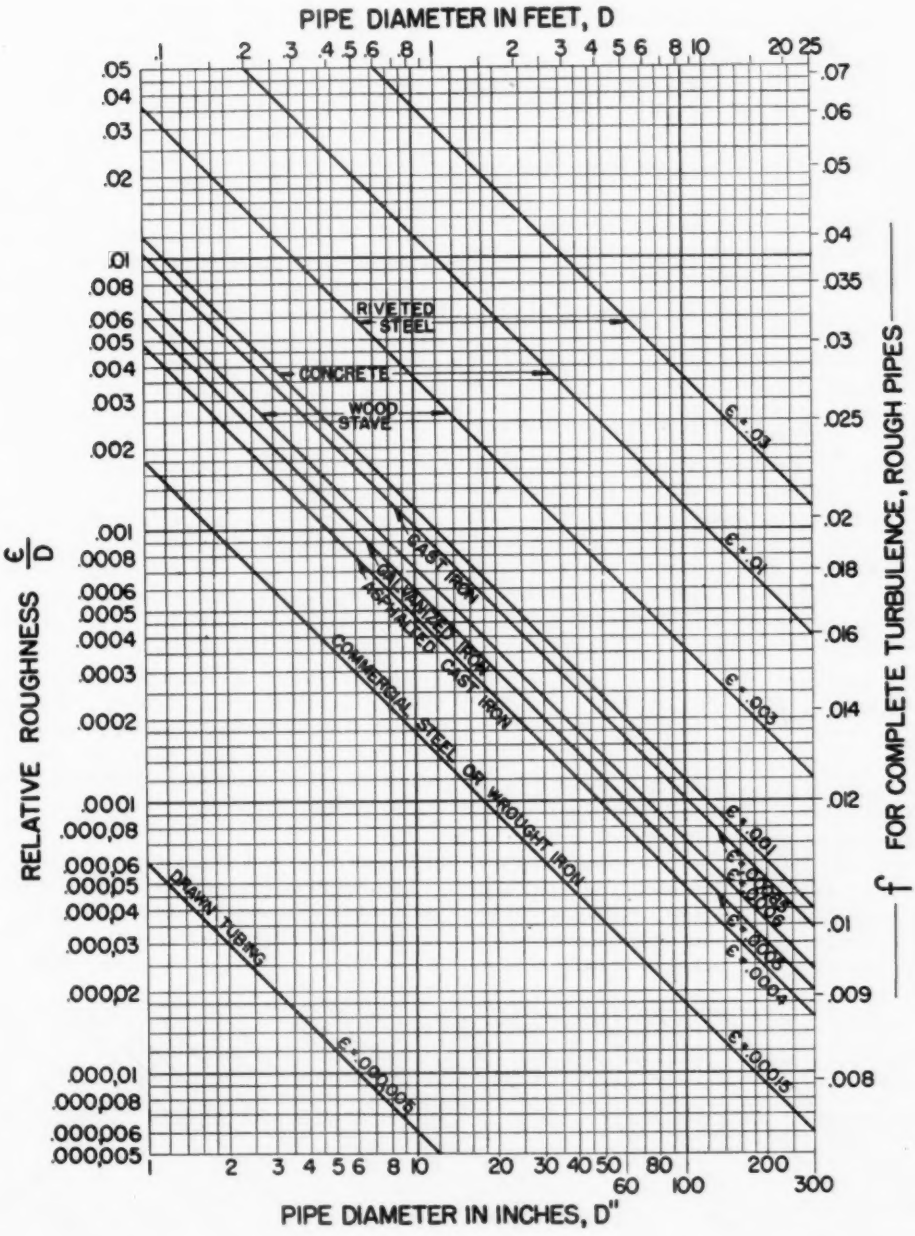


FIG. 2

For other fluids, the kinematic viscosity ν may be found from Fig. 4, which with Prof. R. L. Daugherty's kind permission has been reproduced.[4] To enable **R** to be quickly found for various fluids, Fig. 4 includes an auxiliary diagram constructed by Dr. G. F. Wislicenus, which gives **R** for various values of the product VD'' shown by the diagonal lines. For any value of ν in the left-hand diagram, by following a horizontal line to the appropriate diagonal at the right, the corresponding **R** may be read at the top of the auxiliary graph.

Over a large part of Fig. 1, an approximate figure for **R** is sufficient, since f varies only slowly with changes in **R**; and in the rough-pipe zone f is independent of **R**. From the last consideration, it becomes possible to show, in the right-hand margin of Fig. 2, values of f for rough pipes and complete turbulence. If it is seen that the conditions of any problem clearly fall in the zone of complete turbulence above and to the right of the dashed line in Fig. 1, then Fig. 2 will give the value of f directly without further reference to the other charts.

[4] Reference (13) and reference (5).

ILLUSTRATION OF USE OF CHARTS

Example 1: To estimate the loss of head in 200 ft of 6-in. asphalted cast-iron pipe carrying water with a mean velocity of 6 fps: In Fig. 2, for 6 in. diam (bottom scale), the diagonal for "asphalted cast iron" gives $\frac{\epsilon}{D} = 0.0008$ (left-hand margin). In Fig. 3, for 6 in. diam (left-hand margin), the diagonal for $V = 6$ fps gives $\mathbf{R} = 2.5\ (10^5)$ (bottom scale) (or, instead of using Fig. 3, compute $VD'' = 6 \times 6 = 36$). In Fig. 1, locate from the right-

hand margin the curve for $\frac{\epsilon}{D} = 0.0008$ and follow this curve to a point above $\mathbf{R} = 2.5\ (10^5)$ on the bottom scale (or below $VD'' = 36$ on the top scale). This point gives $f = 0.02$ (left-hand margin); then

$$h_f = f\frac{L}{D}\frac{V^2}{2g} = 0.02\,\frac{(200)}{(0.5)}\,\frac{(6)^2}{64.3} = 4.5 \text{ ft friction loss}$$

Example 2: To estimate the loss of head per 100 ft in a 15-in. new cast-iron pipe, carrying water with a mean velocity of 20 fps: In Fig. 2, for 15 in. diam (bottom scale), the diagonal for "cast iron" gives $\frac{\epsilon}{D} = 0.0007$ (left-hand margin). In Fig. 3, for 15 in. diam (left-hand margin), the diagonal for $V = 20$ fps gives $\mathbf{R} = 2\ (10^6)$ (or, instead of using Fig. 3, compute $VD'' = 20 \times 15 = 300$). In Fig. 1, the curve for $\frac{\epsilon}{D} = 0.0007$ (interpolating between 0.0006 and 0.0008, right-hand margin), at a point above $\mathbf{R} = 2\ (10^6)$ (bottom scale) (or below $VD'' = 300$, top scale) gives $f = 0.018$ (left-hand margin). In this case the point on Fig. 1 falls just on the boundary of the region of "complete turbulence, rough pipes." Here $\mathbf{R}$ or VD'' need only be approximated sufficiently to see that the point falls in the complete turbulence region, and f can then be found directly from the right-hand margin in Fig. 2 without further reference to Fig. 1; then

$$h_f = f\frac{L}{D}\frac{V^2}{2g} = 0.018\,\frac{(100)}{(1.25)}\,\frac{(20)^2}{64.3}$$

$$= 8.95 \text{ or, say, 9 ft friction loss}$$

It must be recognized that any high degree of accuracy in determining f is not to be expected. With smooth tubing, it is true, good degrees of accuracy are obtainable; a probable variation in f within about ±5 per cent (14), and for commercial steel and wrought-iron piping, a variation within about ±10 per cent. But, in the transition and rough-pipe regions, we lack the primary and obvious essential, a technique for measuring the roughness of a pipe mechanically. Until such a technique is developed, we have to get along with descriptive terms to specify the roughness; and naturally this leaves much latitude. The lines in Fig. 2 might be more graphically represented by broad bands rather than single lines, but this is not practical due to overlapping.

Even with this handicap, however, fairly reasonable estimates of friction loss can be made, and, fortunately, engineering problems rarely require more than this. It will be noted from the charts that a wide variation in estimating the roughness affects f to a much smaller degree. In the rough-pipe region, for the reasons just explained, the values of f cannot be relied upon within a range of the order of at least 10 per cent.

The charts apply only to new and clean piping, since the rapidity of deterioration with age, dependent upon the quality of the water or fluid and that of the pipe material, can only be guessed in most cases; and in addition to the variation in roughness there may be, in old piping, an appreciable reduction in effective diameter, making an estimate of performance speculative.

Although we have no accepted method of direct measurement of the roughness, in any case where we have a sample of pipe of the same surface texture available for test in the laboratory or in the field, then from a test of such a pipe in any size we can, by aid of the charts, find the absolute roughness corresponding to its performance. Thus we have a means for measuring the roughness hydraulically. The scale of the absolute roughness ϵ used in plotting the charts is arbitrary, based upon the sand-grain diameters of Nikuradse's experiments.

The field covered by Fig. 1 divides itself into four areas representing distinct flow characteristics. The first is the region of laminar flow, up to the critical Reynolds number of 2000. Here the flow is fully stabilized under the control of viscous forces which damp out turbulence, permitting a completely rational solution. The values of f are here given by a single curve, $f = \frac{64}{\mathbf{R}'}$, independent of roughness, representing the Hagen-Poiseuille law.

Between Reynolds numbers of 2000 and 3000 or 4000, the conditions depend upon the initial turbulence due to such extraneous factors as sudden changes in section, obstructions, or a sharp-edged entrance corner prior to the reach of pipe considered;

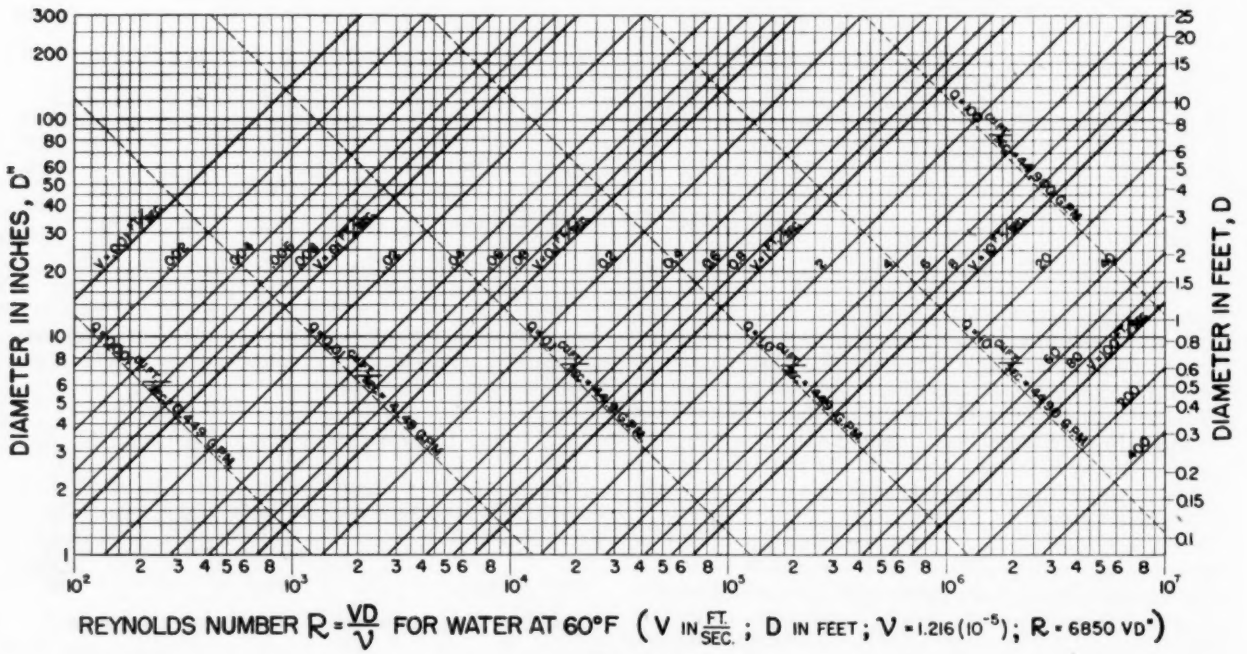


FIG. 3

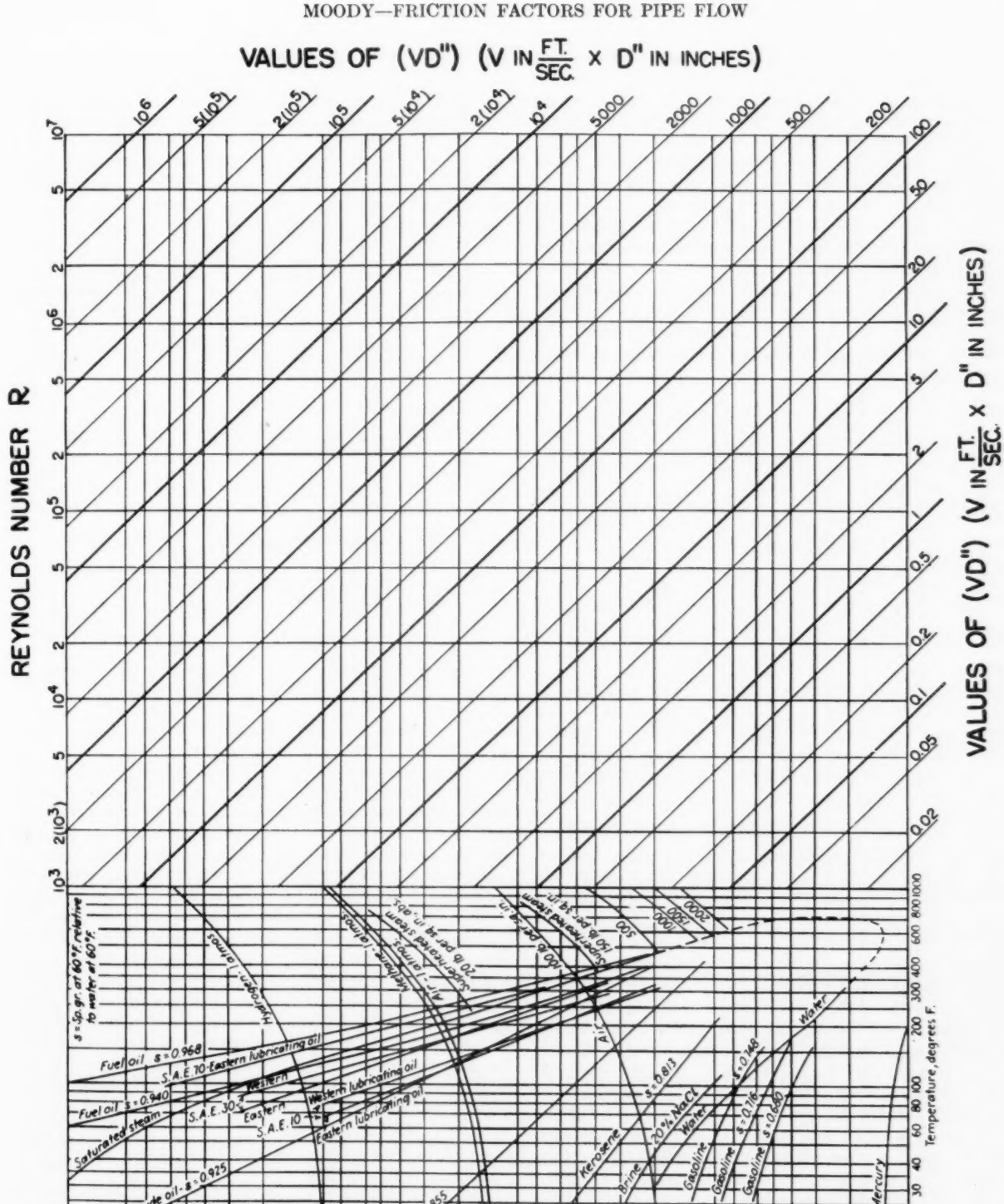

VALUES OF (VD") (V IN FT./SEC. x D" IN INCHES)
REYNOLDS NUMBER R
VALUES OF (VD") (V IN FT./SEC. x D" IN INCHES)
Kinematic viscosity, sq. ft per sec.
Temperature, degrees F.
s = Sp. gr. at 60°F. relative to water at 60°F.
Hydrogen
Air
Fuel oil s = 0.968
S.A.E. 10-Eastern lubricating oil
Fuel oil s = 0.940
S.A.E. 30-Eastern
S.A.E. 10-Eastern
Western lubricating oil
Eastern lubricating oil
Saturated steam
Crude oil s = 0.925
Crude oil s = 0.855
Kerosene
Brine
20% NaCl
Water
Gasoline s = 0.748
Gasoline s = 0.716
Gasoline s = 0.680
Mercury
Water

FIG. 4

and the conditions are probably also affected by pressure waves initiating instability. This region has been called a critical zone, and the indefiniteness of behavior in this region has been indicated by a hatched area without definite f lines. The minimum limit for f values is the dotted continuation of the laminar-flow line, corresponding to very smooth and steady initial flow. When there is distinct turbulence in the entering fluid, the flow in the critical zone is likely to be pulsating (2) rather than steady. The effects of strong initial turbulence may even extend into the laminar-flow zone, raising the f values somewhat, as far as to a Reynolds number of about 1200.

Above a Reynolds number of 3000 or 4000, conditions again become reasonably determinate. Here we find two regions, namely, the transition zone and the rough-pipe zone. The transition zone extends upward from the line for perfectly smooth pipes, for which the equation is

$$1/\sqrt{f} = 2\log_{10}\frac{\mathbf{R}\sqrt{f}}{2.51};\ \text{or}\ 1/\sqrt{f} = 2\log \mathbf{R}\sqrt{f} - 0.8$$

(Kármán, Prandtl, Nikuradse) to the dashed line indicating its upper limit, plotted from the relation

$$\frac{1}{\sqrt{f}} = \frac{\mathbf{R}}{200}\frac{\epsilon}{D}$$

(following the corresponding line in Rouse's chart, reference 12). In the transition zone the curves follow the Colebrook function

$$1/\sqrt{f} = -2\log\left(\frac{\epsilon/D}{3.7} + \frac{2.51}{\mathbf{R}\sqrt{f}}\right)$$

These curves are asymptotic at one end to the smooth pipe line and at the other to the horizontal lines of the rough-pipe zone. Actually, the curves converge rapidly to these limits, merging with the smooth pipe line at the left, and at the right, beyond the dashed line, becoming indistinguishable from the constant f lines for rough pipe.

The Colebrook Function

The basis of the Colebrook function may be briefly outlined. Von Kármán had shown that, for completely turbulent flow in rough pipes, the expression $1/\sqrt{f} - 2\log(D/2\epsilon)$ is equal to a constant (1.74), or, as expressed by Colebrook, $2\log\frac{3.7D}{\epsilon} - 1/\sqrt{f}$ is equal to zero. In the transition region of incomplete turbulence von Kármán's expression is not equal to a constant but to some function of the ratio of the size of the roughnesses to the thickness of the laminar boundary layer. Accordingly, Nikuradse had represented his experimental results on artificially roughened pipes by plotting $1/\sqrt{f} - 2\log(D/2\epsilon)$ versus ϵ/δ, in which δ is the laminar layer thickness. By this method of plotting, the results for all types of flow and degrees of roughness were shown to fall on a single curve. Using logarithmic scales, the smooth-pipe curve becomes an inclined straight line, and the rough-pipe curves merge in a single horizontal line.

Colebrook (11), using equivalent co-ordinates,[5] plotted in his Fig. 1, here reproduced as Fig. 5, the results of many groups of tests on various types of commercial pipe surfaces. He found that each class of commercial pipe gave a curve of the same form, and while these curves are quite different from Nikuradse's sand-grain results, they agree closely with each other and with a curve representing his transition function.

[5] ϵ/δ may be expressed in alternative forms as proportional to $\frac{\mathbf{R}\sqrt{f}}{r/k}$ in which $r = D/2$, $k = \epsilon$; or to $\rho\frac{V_*k}{\mu}$ in which $V_* = \sqrt{\frac{\tau_0}{\rho}}$. τ_0 being the shearing stress at the pipe wall, ρ the mass density of the fluid and μ its absolute or dynamic viscosity.

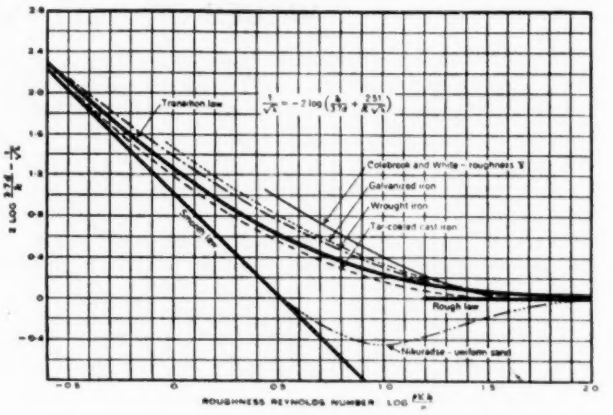


FIG. 5

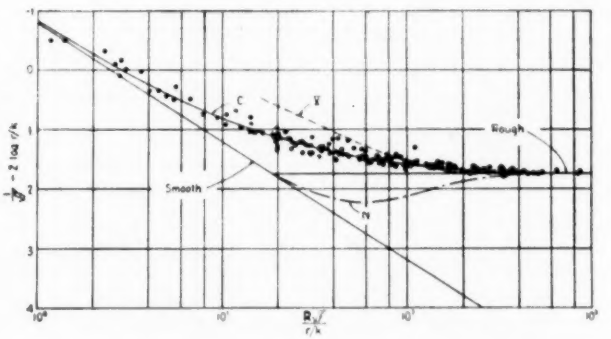


FIG. 6

Rouse (12), also using equivalent co-ordinates, has plotted in his Fig. 6, here reproduced as Fig. 6, a large number of points each of which represents a series of tests on a given size of commercial pipe, together with the Colebrook curve. As he points out, the deviation of the points from the Colebrook curve "is evidently not much greater than the experimental scatter of the individual measurements in any one series."

When the thickness of the laminar layer, which decreases with increasing Reynolds number, becomes so small, compared to the surface irregularities, that the laminar flow is broken up into turbulence, the flow conditions pass over into the zone of "rough pipes," with complete turbulence established practically throughout the flow. Viscous forces then become negligible compared to inertia forces, and f ceases to be a function of the Reynolds number and depends only upon the relative roughness, giving horizontal lines of constant f in the chart. These lines agree with the von Kármán rough-pipe formula

$$1/\sqrt{f} = 2\log\left(\frac{3.7}{\epsilon/D}\right),\quad \text{or}\quad 1/\sqrt{f} = 1.74 - 2\log\left(\frac{2\epsilon}{D}\right)$$

Since f depends upon the relative roughness, the ratio of the absolute roughness to the pipe diameter, even a fairly rough surface in a very large pipe gives a small relative roughness. Thus Colebrook plots the results obtained on the penstocks of the Ontario Power Company, where metal forms and specially laid concrete produced a very smooth example of concrete surface. This in combination with the large diameter gave a relative roughness comparable to drawn brass tubing, with f values falling practically on the "smooth pipe" line of Fig. 1. Such specially fabricated welded-steel pipe lines as those of the Colorado aqueduct system would probably give values along the same curve.

On the other hand, at very high velocities in drawn tubing of

small diameter, even the small absolute roughness is sufficient to break up the laminar boundary layer, and the tubing becomes in effect a "rough pipe." Very few experiments have carried the velocities and Reynolds numbers high enough to permit a close estimate of ϵ for drawn brass, copper, or similar tubing; but by applying the Colebrook function to the available data (14, 15), for the smoothest surfaces reported upon, ϵ was estimated as of the order of 0.000005; and a line corresponding to this value has been drawn in Fig. 2, serving as a minimum limit for surfaces likely to be encountered in practice.

Pipe Friction Factors Applied to Open-Channel Flow

Pipe friction factors have sometimes been applied to open-channel flow, and more commonly the friction losses in large pipes and other closed conduits have been computed from open-channel formulas. The Chezy formula for open channels is $V = C\sqrt{mS}$ in which V is the mean velocity; m the hydraulic mean depth or "hydraulic radius," the sectional area divided by the wetted perimeter; S the slope, the loss of head divided by length of channel, and C a coefficient. The Chezy formula is equivalent to the Darcy formula for pipes, the Chezy coefficient C being convertible into f by the relation $f = \frac{8g}{C^2}$. It should be considered, however, that the Chezy coefficients have been derived principally from observations on relatively wide and shallow channels of large area and rough bottoms, far from circular in shape, and that they involve a free water surface not present in closed conduits, so that, even when the flow is uniform, the problem is highly complex. Consequently, such formulas as Manning's are recommended for open channels in preference to the use of values of C derived from the pipe friction factors.

Open channels dealt with in engineering practice are usually rough-surfaced and of large cross section, corresponding to large Reynolds numbers and falling in the zone of complete turbulence, so that the friction factors are practically independent of Reynolds number. The presence of a free surface, however, with surface waves or disturbances, introduces a consideration not involved in closed-conduit flow. It is therefore the author's view that while, for open channels, we can drop the Reynolds number as an index of performance, we should replace it by a new criterion, the Froude number relating the velocity head and depth, which can be expressed as $\frac{V^2}{2gm}$ or $\frac{V}{\sqrt{gm}}$; or more strictly $\frac{V}{\sqrt{g\mathfrak{d}}}$, in which $\mathfrak{d}$ denotes the average depth or sectional area divided by the surface breadth; the latter form representing the ratio of mean velocity to the gravitational critical velocity or velocity of propagation of surface waves.

This proposed criterion defines whether the flow falls in the "tranquil," "shooting," or critical state. The neglect of this factor may at least partially account for inconsistencies between various open-channel formulas, and between open-channel and pipe-friction formulas, and casts particular doubt on accepted formulas for open-channel friction in the critical or shooting-flow regions. These considerations suggest the plotting of open-channel friction factors as a function of the relative roughness and the Froude number, in similar manner to the plotting of f as a function of the relative roughness and the Reynolds number for closed conduits.

For the foregoing reasons, Fig. 1 is not recommended with much confidence for general application to open channels, for which a formula such as Manning's better represents the available information. The charts can however be applied, at least as an approximation, to noncircular closed conduits of not too eccentric a form or not too different from a circular section, by using an equivalent diameter

$$D = 4m = 4\left(\frac{\text{Sectional area}}{\text{Length of perimeter}}\right)$$

Since civil engineers usually classify surface roughness by the Kutter and Manning roughness factor n, it would be helpful in selecting a value of ϵ for such variable surfaces as concrete, if we could correlate ϵ and n. P. Panagos[6] has applied the Colebrook function to the test data collected by Scobey (16) and finds the following values of ϵ corresponding to the Kutter n ratings given by Scobey, which may be at least tentatively utilized:

Kutter n.....	0.0105	0.011	0.012	0.013	0.014	0.015	0.016
Absolute roughness ϵ.....	0.00015	0.0005	0.002	0.005	0.011	0.02	0.03

Accordingly, on the basis of Scobey's data the lines given in Fig. 2 for concrete may be somewhat more definitely described as follows:

ϵ	n	
0.001	0.0115	Highest practical grade of concrete. Surface and joints smooth
0.003	0.0125	
0.01	0.014	Concrete surface with slight form marks, fairly smooth joints or roughly troweled
0.03	0.016	Prominent form marks or deposits of stones on bottom

Although the curves in Fig. 1 are plotted from definite functional forms which can be accepted with some confidence within the degree of accuracy required in engineering use, further information will be welcomed which would improve the location and definition of the lines in Fig. 2, or which would add new lines for other materials. Any tests of friction head in pipe of any material can be applied to Fig. 1, and corresponding points can be readily located in Fig. 2. A 45-deg line through a point so located can then be added to Fig. 2, to represent a particular kind of pipe surface.

Acknowledgment

For helpful suggestions and assistance, the author is particularly indebted to Prof. B. A. Bakhmeteff, Mr. Ralph Watson, Dr. G. F. Wislicenus, Dr. A. T. Ippen; and to Mr. P. Panagos for collecting data and numerical checking.

BIBLIOGRAPHY

1 "The Mechanics of Turbulent Flow," by B. A. Bakhmeteff, Princeton University Press, 1936.

2 "Applied Hydro- and Aeromechanics," by L. Prandtl and O. G. Tietjens, Engineering Societies Monographs, McGraw-Hill Book Company, Inc., New York, N. Y., 1934.

3 "Fluid Mechanics for Hydraulic Engineers," by H. Rouse, Engineering Societies Monographs, McGraw-Hill Book Company, Inc., New York, N. Y., 1938.

4 "The Flow of Fluids in Closed Conduits," by R. J. S. Pigott, *Mechanical Engineering*, vol. 55, 1933, pp. 497–501, 515.

5 "Hydraulics," by R. L. Daugherty, McGraw-Hill Book Company, Inc., New York, N. Y., 1937.

6 "A Study of the Data on the Flow of Fluid in Pipes," by E. Kemler, Trans. A.S.M.E., vol. 55, 1933, paper Hyd-55-2, pp. 7–32.

7 "Strömungsgesetze in Rauhen Rohren," by J. Nikuradse, *V.D.I. Forschungsheft* 361, Berlin, 1933, pp. 1–22.

8 "Mechanische Ähnlichkeit und Turbulenz," by Th. von Kármán, *Nachrichten von der Gesellschaft der Wissenschaften zu Göttingen*, 1930, Fachgruppe 1, Mathematik, no. 5, pp. 58–76. ("Mechanical Similitude and Turbulence," Tech. Mem. N.A.C.A., no. 611, 1931.)

9 "Neuere Ergebnisse der Turbulenzforschung," by L. Prandtl, *Zeitschrift des Vereines deutscher Ingenieure*, vol. 77, 1933, pp. 105–114.

10 "Mechanics of Liquids," by R. W. Powell, The Macmillan Company, New York, N. Y., 1940.

11 "Turbulent Flow in Pipes, With Particular Reference to the Transition Region Between the Smooth and Rough Pipe Laws," by C. F. Colebrook, *Journal of the Institution of Civil Engineers* (London, England), vol. 11, 1938–1939, pp. 133–156.

12 "Evaluation of Boundary Roughness," by H. Rouse, Proceed-

[6] Assistant in Mechanical Engineering, Princeton University, Princeton, N. J.

ings Second Hydraulic Conference, University of Iowa Bulletin 27, 1943.

13 "Some Physical Properties of Water and Other Fluids," by R. L. Daugherty, Trans. A.S.M.E., vol. 57, 1935, pp. 193–196.

14 "The Friction Factors for Clean Round Pipes," by T. B. Drew, E. C. Koo, and W. H. McAdams, Trans. American Institute of Chemical Engineers, vol. 28, 1932, pp. 56–72.

15 "Experiments Upon the Flow of Water in Pipes and Pipe Fittings," by J. R. Freeman, published by THE AMERICAN SOCIETY OF MECHANICAL ENGINEERS, 1941.

16 "The Flow of Water in Concrete Pipe," by F. C. Scobey, Bulletin 852, U. S. Department of Agriculture, October, 1920.

Discussion

R. L. DAUGHERTY.[7] The writer has nothing but commendation for this excellent paper. The author has presented the latest theory combined with the available experimental data in a manner which makes it more convenient for use than has been the case heretofore. His evaluation of relative roughness for different types and sizes of pipes is a step forward.

While this paper deals primarily with pipe friction it is interesting to note the suggestions made concerning the treatment of the flow in open channels. The latter has not been given the attention from the standpoint of rational analysis that has been devoted in the past to pipes. It is to be hoped that developments in this field may be made along the lines suggested by the author.

The author calls attention to the well-known fact that in the transition zone the Nikuradse curves for his artificial sand-grain roughness are quite different from those obtained with commercial pipes. The writer would like to know if the author has any explanation to offer for this marked difference.

C. W. HUBBARD.[8] This paper is of interest to engineers who must estimate fluid-friction loss closely for certain types of problems. Ordinarily the Manning type of formula is preferred, since the roughness value may be determined from the type of surface of the wall as contrasted to the Darcy formula where the roughness coefficient varies with the size of pipe and is difficult to estimate. The author's Fig. 2 allows a quantitative wall roughness estimated from the type of wall to be used.

During some recent tests made to select a protective paint for steel which would also have a low friction loss, it was found that several coatings, particularly those consisting of certain bitumastic constituents which required them to be applied thickly to the wall, gave low flow-resistance values. The tests, made in 3-in. pipes, which were split longitudinally to allow proper application of the coating, showed roughness values of the order of those obtained with drawn-brass tubing. However, the appearance of the coating was not as smooth as drawn tubing. The writer had previously experienced this effect with similar coatings. There seems to be little published material on the friction loss produced by various protective paints and coatings on pipe walls, particularly on small pipes when the flow is likely to occur in the transition range where the friction loss is dependent upon Reynolds number. Apparently the roughness of such surfaces is of the wavy type which cannot be evaluated on the same basis as the same magnitude of roughness which is of the granular type.

A. T. IPPEN.[9] The author has ably satisfied the object of his paper stated in the beginning with an extremely timely and practical summary of the latest information available on pipe friction. Academic research in this field over the last 30 years conducted on a fundamental basis has finally yielded a satisfactory explanation of the nature of the laws of pipe friction and has cleared up the concepts of energy dissipation in conduits and channels.

The evidence for the adoption of the methods for determining the pipe friction factor as presented by Colebrook is rather astonishing. Some experiences in this connection may be contributed here. The writer has computed two comprehensive sets of data on pipe friction, one by John R. Freeman and another by L. H. Kessler. The former completed his experiments during the years 1889 to 1893 and his data were published by this Society in a special volume (15)[10] in 1941. The second set of data was obtained from pipe-friction experiments at the Wisconsin Experimental Station, the results of which were published in 1935. Both experimenters performed tests on $^1/_4$ in- to 8 in-diam wrought-iron pipes in new condition covering the maximum range in Reynolds numbers possible under their experimental conditions. After plotting these results every one of their runs shows essentially the f versus $\mathbf{R}$ curve indicated by Colebrook and ϵ values calculated for all the various sizes come out very close to the average value stated for wrought-iron pipe in the present paper. It must be remembered that Kessler's data were obtained 40 years after those of Freeman and that it can hardly be assumed that manufacturing processes remained identical during that period.

Another fact of importance to the practical engineer from this analysis of Freeman's and Kessler's data is worth mentioning. Rouse and Moody in their f versus $\mathbf{R}$ curves terminate the transition range from smooth- to rough-pipe flow along a line corresponding to a ratio of absolute roughness ϵ to the laminar boundary-layer thickness δ of 6.08. Kessler's and Freeman's data do not give a single value that high in all their runs; their highest values obtained were about $\frac{\epsilon}{\delta} = 2.5$. Under practical conditions of use therefore the flow of water in pipes occurs well in the transition range from smooth- to rough-pipe flow.

This fact easily explains why a final solution of the pipe-friction problem was possible only after the concepts of "smooth-pipe" and "rough-pipe" flow had been established separately. While Nikuradse's results on uniformly sand-coated pipe were helpful in this respect, they also resulted in more complicated transition curves than are obtained from tests with the statistical roughness patterns encountered on most commercial pipe surfaces. The Colebrook universal function seems to fit the better in this transition range; the more the roughness irregularities are statistically distributed as far as size and shape are concerned and vice versa, the more regular the size and pattern of the irregularities the closer Nikuradse's transition curves are approached, where finally the critical velocity for all roughness bodies is the same in the ideal case of completely uniform size.

The familiar functions for the pipe friction factor f may be written in the following form

$$\frac{1}{\sqrt{f}} = 1.74 - 2 \log \frac{18.6}{\mathbf{R}\sqrt{f}} \quad \ldots\ldots [1]$$

for smooth-pipe flow

$$\frac{1}{\sqrt{f}} = 1.74 - 2 \log \frac{\epsilon}{r} \quad \ldots\ldots [2]$$

for rough-pipe flow

$$\frac{18.6}{\mathbf{R}\sqrt{f}} = 0.282 \frac{\delta}{r} \quad \ldots\ldots [3]$$

for laminar boundary-layer thickness.

[7] Professor of Mechanical Engineering, California Institute of Technology, Pasadena, Calif.

[8] Lieutenant Commander, U.S.N.R. Mem. A.S.M.E.

[9] Assistant Professor, Hydraulic Laboratory, Lehigh University, Bethlehem, Pa.

[10] Numbers in parentheses throughout the discussion refer to the Bibliography at the end of the author's paper.

According to Colebrook, Equations, [1] and [2] are combined into the following universal function

$$\frac{1}{\sqrt{f}} = 1.74 - 2 \log \left(\frac{18.6}{\mathbf{R}\sqrt{f}} + \frac{\epsilon}{r} \right) \quad [4]$$

This function reverts to either Equation [1] or Equation [2], if either the influence of the relative roughness disappears or when the viscous influence becomes insignificant. By use of Equation [3], the Colebrook function may be written in the alternative form

$$\frac{1}{\sqrt{f}} = 1.74 - 2 \log \frac{\epsilon}{r} \left(1 + 0.282 \frac{\delta}{\epsilon} \right) \quad [5]$$

This equation clearly brings out the dependence of the pipe friction phenomena upon the thickness of the laminar boundary layer, i.e., on the viscosity of the fluid. It will be found in practical calculations that this influence is very seldom absent. The proposed ultimate value of $\frac{\mathbf{R}\sqrt{f}}{r/\epsilon} = 400$ is equivalent to a value of $\frac{\epsilon}{\delta}$ of 6.08.

It is evident that aging of pipes under varying conditions of use will result in new values of absolute roughness which at present are not easily predicted. From experiments on galvanized steel pipe of 4 in. diam at the Hydraulic Laboratory of Lehigh University, an initial average value of $\epsilon = 0.00045$ ft was obtained. This value of ϵ was doubled within 3 years as a result of the change in surface conditions with aging under moderate conditions of use. It must be remembered here that this change in ϵ represents only about a 20 per cent increase in the Darcy-Weisbach factor f, since the ϵ value is a much more sensitive indicator of pipe roughness than the factor f.

In conclusion, it may be hoped that this paper will bring the general adoption of this relatively easy and reliable method of determining pipe friction and thereby establish a standard procedure in practice which is based upon sound analytical and experimental evidence.

W. S. Pardoe.[11] In the following tests on pipes of various diameters and materials, the exponent n in the exponential formula

$$V = Kd^m S^n$$

varied from 0.535 to 0.546, thus checking Williams' and Hazen's formula

$$V = 1.318\, C_w r^{0.63} S^{0.54}$$

very closely. The maximum value of **R** was about 1,250,000 for 8-in. Neoprene dock-loading hose (very smooth) which is much below the "complete turbulence zone." The tests included:

6-in. Italite cement-asbestos pipe (predecessor of Transite)
4-in. Ruberoid cement-asbestos extruded pipe
4-in. fiber conduit
6-in. and 8-in. Neoprene dock-loading hose for E. I. du Pont de Nemours
2-in. to 12-in. steel pipe
8-in. rubber dock-loading hose with 1-in. × 1/8-in. helical metal band on inside

In no case except the last did the exponent n show even a tendency of decreasing, let alone approaching a value of 0.5 or complete turbulence. This must be due to the smoothness of the materials and the low value of Reynolds number. In the last case, the values of f did show a tendency to become constant, the value of ϵ/D being quite large.

The writer has not conducted a sufficient number of tests on pipes and is far from a pundit on this subject. At some time in the future, he will attempt to work into the "complete turbulence zone," if such there is, even if he must use a bit of 4-in. turberculated cast-iron pipe.

Mr. Pigott in his discussion has mentioned my insistence on the fact that the coefficients of Venturi meters become constant. This coefficient may be approximated by the formula

$$C = \sqrt{\frac{1 - \beta^4}{1 - \beta^4 + K}}$$

in which β is the diameter ratio d_2/d_1 and K is the coefficient of loss in

$$h_f = K \frac{V_2^2}{2g}$$

The value of K on the flat part of tests of 85 cast-iron Venturi meters approximates

$$K = \frac{0.0435}{(d_2'')^{0.25}}$$

As the absolute roughness is constant, the proportional roughness varies inversely as the diameter or the coefficient increases with the diameter. The tests ran to quite high values of Reynolds number in terms of $\frac{V_2 d_2 \rho}{\mu}$, thus indicating there is such a thing as complete turbulence. Solving the foregoing expression

$$K = \frac{1 - \beta^4}{c^2} - (1 - \beta^4)$$

Hence a constant value of c gives a constant K, or h_f varies as V^2.

This is of course arguing from the writer's experience with Venturi meters to make up for his lack of adequate experimental knowledge of the subject under discussion.

Professor Moody says f is a function of "two and only two" dimensionless quantities ϵ/D and $\frac{VD\rho}{\mu}$. The writer has found in his work on Venturi meters a variation of over 1/2 per cent, due to the effect of the ambient temperature.[12]

As a variation of 1/2 per cent in c requires a variation of 25 per cent in k it seems to the writer the effect of a difference of temperature of 20 deg F on f at low value of **R** might be considerable. This effect is brought about by a change in the boundary shear; thus

$$\tau_0 = \frac{f\rho V^2}{8} = \mu \frac{dv}{dy}$$

If Q is kept constant dv/dy will also be constant, and μ corresponds to the temperature of the inside wall of the pipe, which will lie between the ambient temperature and that of the water. It will decrease as the velocity increases as a result of the heat being conducted away more rapidly. This the writer will check in future experiments; it may throw some light on the upper limit of the critical or unstable zone. The effect is a function of Reynolds and Prandtl's or Nusselt's numbers, and the writer is not certain "what the price of cheese in Denmark does to effect f."

[11] Department of Civil Engineering, University of Pennsylvania, Philadelphia, Pa.

[12] "Effect of High Temperatures and Pressures on Cast-Steel Venturi Tubes," by W. S. Pardoe, Trans. A.S.M.E., vol. 61, 1939, p. 247.

Professor Moody is to be congratulated on producing a very usable plot of friction factors which in due time may replace the Pigott and Kemler curves which have to date been extensively quoted and used by engineers. Thus do we progress.

R. J. S. PIGOTT.[13] This study of friction factor in pipes is particularly interesting to the writer, as it is a valuable further rationalization of a situation which has been unsatisfactorily empirical.

At the time the writer's own correlation (4) was presented (1933) there was almost complete lack of uniformity between various formulations in general use, wandering all the way from Kutter, Hazen, and Williams tables, to Aisenstein's averaged values.

There was great need to prepare a formulation that would work satisfactorily for all kinds of conduit, from brass tubing to brick ducts, and for all fluids.

Dr. Kemler, then on the writer's staff, did the laborious part of the job, in correlating the results of all the experiments published up to that time, culling all those with incomplete data (6). The writer summarized this work, in form for direct application generally, introducing the roughness effect by rather strong-arm empirics, but at any rate the resulting chart worked well and has been growing in use.

The great value of the author's study is that it puts the roughness effect, at last, on a much better justified basis. For example, Buckingham (Fig. 1, reference 5) drew the lines for different sizes of steel pipe curved as they approached the viscous region, the same as the author now shows them; Stodola (Fig. 1, ref. 5) shows them straight and intercepting.

The later material used by the author shows that they are curved. Another important point settled by the author is that the lines for all roughnesses finally reach a constant value. The point at which this condition obtains is plainly shown to be a function of relative roughness, and so solves a difficulty Dr. Kemler and the writer had, in correlating some of the test material. Some of the experimental results showed rather flat coefficients that were unexpected in regions of moderate roughness. But this constant value of f is confirmed by Professor Pardoe's findings on Venturi discharge coefficients. He has been pointing out for years that the coefficient reaches a constant value at some Reynolds number that increases with size. Since most Venturis above rather small sizes are made with cast approach cones and the losses are substantially represented by pipe friction, this situation corresponds to flat final value of f at complete turbulence, and a decrease of the value of f with decrease of roughness.

Some engineers may be interested in the flow of queer materials like greases, muds, cement slurries, etc., that have thixotropic properties (quoted from the rheologists), that is, they have plasticity mixed in with viscosity. All these materials have apparent viscosities which decrease with increase of shear rate, but, when they finally reach turbulent flow, behave like true liquids of rather low viscosity. Such activities as oil-well drilling, cement-gun and grouting operations, automotive greasing equipment, and ball bearings involve such materials. In food industries, one gets tomato ketchup and pea soup; glue and soap solutions, paint and varnish operations, and various queer materials in the rayon and plastics industries. For those interested, a paper[14] by the writer presents more or less a rational solution that has been quite satisfactorily supported by tests.

In Fig. 1, the author has drawn his dotted line of complete turbulence somewhat in advance of the Reynolds number values at which the friction factor becomes a constant quantity. The writer finds that the expression

$$\frac{3500}{\frac{\epsilon}{D}} = \mathbf{R}_t$$

represents, as closely as can be determined from the small-scale diagram, the point at which the friction factor becomes absolutely constant. It is curious and probably only accidental that the value 3500 corresponds about to the upper limit of the critical zone.

HUNTER ROUSE.[15] Important results of laboratory research frequently do not reach the hands of practicing engineers until many years after the original papers have been published. A salient case in point is the discovery by Blasius in 1913 of the dependence of the Darcy-Weisbach resistance coefficient f upon the Reynolds number $\mathbf{R}$, which did not come into general engineering use until perhaps a decade ago. It often happens, however, that once engineers have accepted a new idea they are loath to modify it in any way. The paper under discussion is a very commendable endeavor to make recent experimental findings immediately useful to the engineer, but the writer feels that it still caters to a regrettable degree to the engineer's innate conservatism.

If the writer's belief is correct, this paper is intended to fulfill the same purpose as that which prompted the writer to present a somewhat similar paper (12) and resistance chart at the Second Hydraulics Conference in 1942. The author claims that in this chart, which is reproduced herewith in slightly modified form,[16] the writer adopted co-ordinates inconvenient for ordinary engineering use. Such criticism resulted from the writer's deliberate advancement beyond the now familiar Blasius f-versus-$\mathbf{R}$ notation in the belief that both greater convenience and greater significance would be attained thereby. Since these two papers of identical purpose thus differ in their basic method of approach, a criticism of the one point of view must necessarily involve a defense of the other.

Although Blasius' original dimensional analysis of the variables involved led to his adoption of the form VD/ν as the most significant grouping of terms upon which f should depend, it must be realized that the following three different combinations of the same variables are all equally valid for the basic case of a smooth pipe:[17]

$$f = \frac{2gh_fD}{LV^2} = \varphi_1\left(\frac{VD}{\nu}\right) = \varphi_1(\mathbf{R})$$

$$f = \frac{2gh_fD}{LV^2} = \varphi_2\left(\frac{2gh_fD^3}{L\nu^2}\right) = \varphi_2'(\mathbf{R}\sqrt{f})$$

$$f = \frac{2gh_fD}{LV^2} = \varphi_3\left(\frac{2gh_fQ^3}{L\nu^5}\right) = \varphi_3'(\mathbf{R}f^{1/3})$$

The combination now most familiar to the engineer, of course, is the first, although it has long since been proved that it will yield a linear plot on logarithmic paper for only the laminar zone. The second, on the other hand, is the basis of the Kármán-Prandtl analysis of the turbulent zone, the general functional relationship simply being written in the specific form

[13] Chief Engineer, Gulf Research and Development Company, Pittsburgh 30, Pa. Fellow A.S.M.E.

[14] "Mud Flow in Drilling," by R. J. S. Pigott, Drilling and Production Practic A.P.I., 1941, pp. 91–103.

[15] Director, Iowa Institute of Hydraulic Research, University of Iowa, Iowa City, Iowa.

[16] "Elementary Mechanics of Fluids," by Hunter Rouse; John Wiley & Sons, Inc., New York, N. Y. (in Press).

[17] "Solving Pipe Flow Problem With Dimensionless Numbers," by A. A. Kalinski, *Engineering News-Record*, vol. 123, 1939, p. 23.

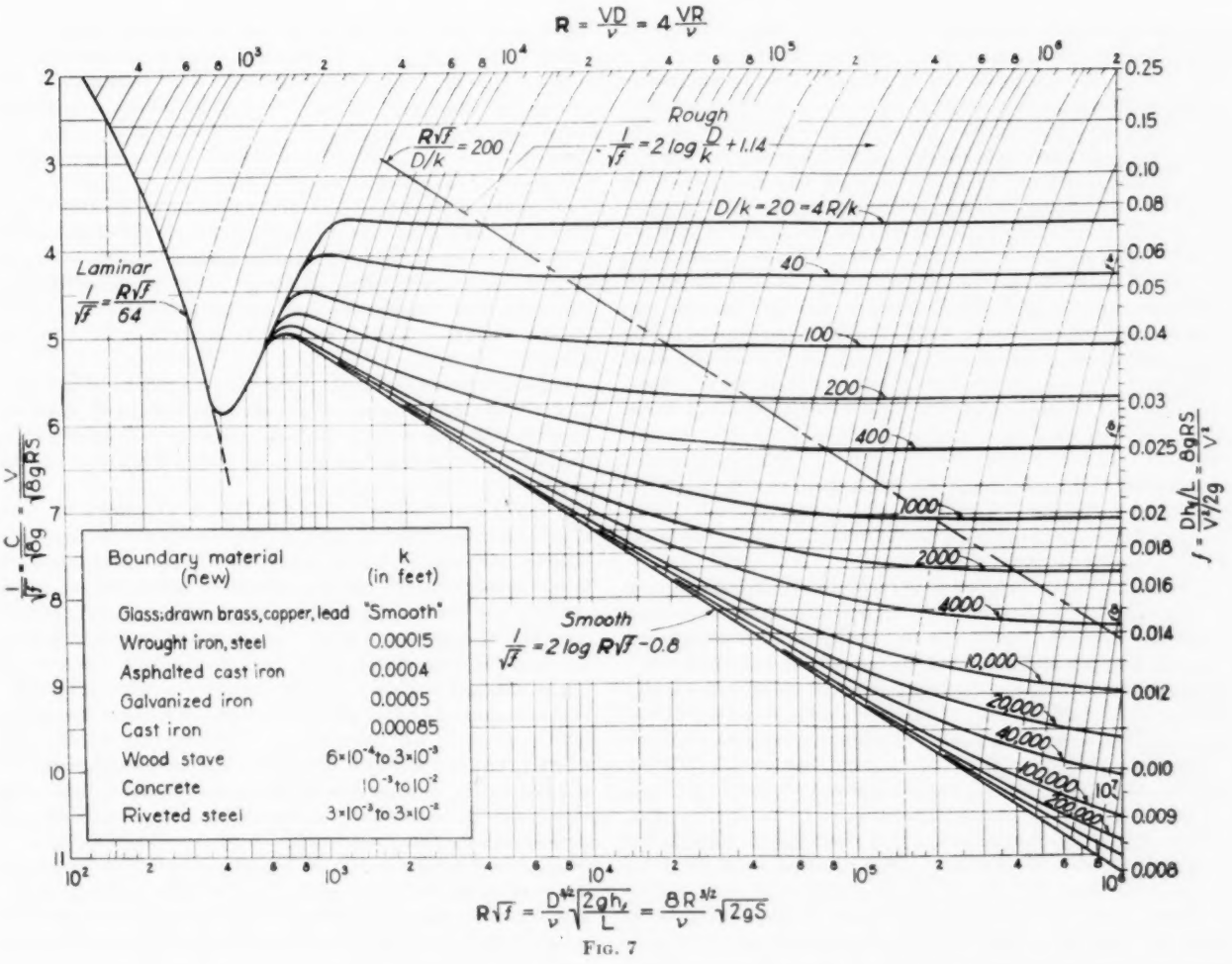


FIG. 7

$$1/\sqrt{f} = A + B \log (\mathbf{R}\sqrt{f})$$

Despite the author's indication to the contrary, f is not inextricably embodied in the second term of this relationship, as may be seen from the identity $\mathbf{R}\sqrt{f} = \sqrt{(2gh_fD^3/L\nu^2)}$. If the Kármán-Prandtl parameters are chosen as the basis of a semilogarithmic chart, as in the accompanying figure, not only will the smooth-pipe relationship plot as a straight line, but all transition curves from the smooth to the rough relationship will be geometrically similar. It would appear to the writer that this combines ease in interpolation (and hence convenience) with greater significance than the Blasius plot will permit. This, therefore, is one of the writer's two reasons for continuing to recommend the newer type of chart in preference to that of the author.

The writer's second reason will be evident after further inspection of the foregoing functional relationships. The first relationship will be directly useful in graph form only if the velocity or rate of flow is known; otherwise the desired coefficient may be evaluated from the graph only through the inconvenient process of trial and error. If the velocity or rate of flow is not known, on the other hand, a graph of the second functional relationship will make the desired coefficient immediately available. In order to provide a single chart which would satisfy both sets of requirements, the writer supplied ordinate scales of both f and $1\sqrt{f}$ (the latter being proportional to the Chezy C) and abscissa scales of both $\mathbf{R} = VD/\nu$ and $\mathbf{R}\sqrt{f} = \sqrt{2g\,h_f/L}\;D^{3/2}/\nu$. Since the parameters $1/\sqrt{f}$ and log $(\mathbf{R}\sqrt{f})$ were selected by the writer for the primary ordinate and abscissa scales, the alternative abscissa parameter log $\mathbf{R}$ is necessarily represented by curved lines over a portion of the writer's chart. Had log f and log $\mathbf{R}$ been chosen as the primary parameters, log $(\mathbf{R}\sqrt{f})$ would still have required sloping lines in the grid; such choice therefore involves no particular advantage over the writer's but rather defeats the writer's purpose owing to the accompanying distortion of the entire system of transition curves. The author's graph, of course, contains no secondary grid system simply because it permits direct solution for only one of the several variables.

Brief mention might be made of the third possible combination of variables, which is evidently applicable to problems in which the diameter is the unknown quantity. So long as the pipe is smooth, such a plot will be of use, but the adoption of a similar function for the case of rough surfaces will still require a trial-and-error solution, unless the graph is made hopelessly complex, owing to the fact that for a given boundary material the pipe diameter must be known before the relative roughness may be evaluated. Solution by trial might therefore proceed just as well from either of the other two functional relationships contained in the writer's diagram.

The writer commends the author's presentation in graph form of the values of absolute roughness given in the writer's paper, but notes with interest that this plot is consistent with the writer's rather than the author's choice of basic parameters. Such a graph would therefore have its greatest value when prepared as

a marginal extension of the writer's resistance chart, for then no relative-roughness computations would have to be made.

So far as the author's discussion of open-channel resistance is concerned, the writer takes exception to two points of fundamental importance: First, the author states that such relationships as the Manning formula should be used in open-channel computations in preference to values derived from pipe tests, implying that the familiar empirical open-channel formulas are inherently more valid. It is known, however, that the Manning formula (not to mention those of Bazin and Kutter) is not in accordance with the logarithmic law of relative roughness upon which the author's paper is based. So far as the writer can ascertain, the only reason pipe tests could not generally be used in evaluating open-channel resistance lies in the fact that few open-channel boundary surfaces are suitable to testing in pipe form. Aside from the moot question of the effect of cross-sectional shape (which the empirical open-channel formulas in no way answer), it would appear to the writer that a general resistance graph for uniform open channels should differ little from that for pipes, except in that the familiar parameters C and S might conveniently be included in the co-ordinate scales; this has been done in the present form of the writer's chart.

The writer's second objection to the author's closing section is in regard to his implication that the Froude number should replace the Reynolds number as the fundamental resistance parameter for open-channel flow. So far as boundary resistance is concerned, the writer can see no possibility of the Froude number playing a comparable role. It is true that viscous shear is of little significance in comparison with boundary roughness in most open-channel problems, but it is also true that the effect of surface waves upon the internal resistance to flow has not yet been ascertained. The open-channel problem is, in fact, quite analogous to that of ship resistance, in which the matter of surface drag is considered wholly independent of the Froude number. If, to be sure, the phenomena of slug flow, atmospheric drag, and air entrainment prove to govern the resistance in the comparatively infrequent case of supercritical flow in open channels, then the Froude number may well become an appropriate resistance criterion, as it already is for cases of channel transition. But to imply that it should replace the Reynolds number as a resistance parameter whenever a free surface exists seems rather untimely to the writer, in that it could lead to serious misinterpretation of those few principles of boundary resistance which have been definitely established.

P. H. Schweitzer.[18] Lest the author's charts, presented in delightfully handy forms, be used indiscriminately, it is perhaps in order to add one note of caution. Most of the statements, formulas, and charts are valid only for "long" pipes. For short pipes, the rules controlling turbulence are different, and Reynolds number is not the sole or deciding criterion for the state of flow.

If the velocity of flow in a long tube is decreased below the "critical" value, a change from turbulent to laminar flow takes place rather abruptly. The author sets the indeterminate region between 2000 and 4000 Reynolds number. Even that represents a rather narrow strip in the total range covered by the flow of such liquids as water or light oil. Outside of this indeterminate region, the flow is either completely laminar or decidedly turbulent, ignoring the rather thin laminar-boundary layer.

While this is true of relatively long tubes, for short tubes or nozzles it is not. In a short tube, as was shown by the writer,[19] the normal state may be described as "semiturbulent flow," which may be visualized as a turbulent core in the center and a laminar envelope near the periphery. The thickness of the laminar envelope may vary between wide limits. The change from turbulent to laminar flow or the reverse takes place in a short tube so gradually that the intermediate stage usually covers the whole practical region.

Of course, in both long and short tubes, turbulent flow is promoted by high flow velocity, large tube size, curvature of the tube, divergence of the tube, rapid changes in direction and cross-sectional area of the tube. Laminar flow is promoted by high liquid viscosity, laminar approach, rounded entrance to the tube, slight convergence of the tube, absence of curvature and disturbances.

Irrespective of the length of the tube an originally turbulent flow will remain turbulent, if its Reynolds number $\mathbf{R} = vd/\nu$ is greater than the critical Reynolds number. Conversely, an originally laminar flow will remain laminar if $\mathbf{R}$ is lower than the number.

If the flow at the entrance is turbulent but its Reynolds number in the tube is lower than the critical, the flow will turn purely laminar if the tube is straight, reasonably smooth, and sufficiently long. If the flow at the entry of the tube is laminar but its Reynolds number is above the critical, it is hard to predict the character of the ensuing flow. If the entry is smooth and rounded and the tube free from disturbances and irregularities, the flow will remain laminar even at Reynolds numbers[20] as high as 15,000.

In a complete absence of all disturbances, a laminar flow probably never turns turbulent, no matter how high its Reynolds number, but the slightest disturbance will ultimately cause turbulence if the Reynolds number is above the critical. The higher the Reynolds number the greater the disturbance, the shorter the tube travel necessary for turbulence to set in.

In a short tube the critical Reynolds number is not the one above which the flow generally or in a particular case is turbulent. The flow is frequently laminar at Reynolds numbers above the critical and it may be turbulent or semiturbulent at Reynolds number below the critical.

The critical Reynolds number is the one below which, in a straight long cylindrical tube, disturbances in the flow will damp out. Above the critical Reynolds number disturbances (approach, entry, etc.) never damp out, no matter how long the tube is. The critical Reynolds number so defined was found by Schiller[21] to be approximately 2320.

In short tubes, or nozzles, the length is not nearly enough for the flow to assume a stable condition. Under the circumstances, a Reynolds number higher than critical will have a tendency toward turbulence and vice versa, but it may take a tube travel of 60 times diameter before a stable velocity distribution is developed. The actual flow in the nozzle will be influenced considerably by the state of flow before the orifice and the disturbances in the approach and within the nozzle. The combination of these factors in addition to the Reynolds number will determine the state of turbulence at the exit of the short tube. For a given short tube or nozzle, the influence of the nozzle factors can be considered the same; therefore the Reynolds number alone will determine the character of the flow.

With decreasing Reynolds number, the thickness of the laminar layer increases and the turbulent inner portion decreases until it finally disappears. It is peculiar to nozzles or short tubes that the change from turbulent to laminar flow (or vice versa)

[18] Professor of Engineering Research, The Pennsylvania State College, School of Engineering, State College, Pa. Mem. A.S.M.E.

[19] "Mechanism of Disintegration of Liquid Jets," by P. H. Schweitzer, *Journal of Applied Physics*, vol. 8, 1937, pp. 513–521.

[20] With a convergent tube of 10-deg cone angle Gibson (Proceedings of the Royal Society of London, vol. A83, 1910, p. 376), observed laminar flow at $\mathbf{R} = 97{,}000$.

[21] "Untersuchungen über laminare und turbulente Strömung," by L. Schiller, *V.D.I. Forschungsarbeiten*, vol. 248, 1922.

takes place gradually rather than abruptly. The semiturbulent state extends over a wide range of Reynolds numbers, differing only in the relative thickness of the turbulent core and laminar envelope.

Author's Closure

The paper was intended for application to normal conditions of engineering practice and specifies a number of qualifications limiting the scope of the charts, such as their restriction to round (straight) new and clean pipes, running full, and with steady flow. Under such conditions it was stated, as noted by Professor Pardoe, that the friction factor f "is a dimensionless quantity, and at ordinary velocities is a function of two, and only two, other dimensionless quantities,—the relative roughness of the surface and the Reynolds number."

Under abnormal conditions f could of course be affected by other dimensionless criteria. In closed conduits at very high velocities or with rapidly varying pressures it depends on the Mach or Cauchy number introducing the acoustic velocity. In open channels, as pointed out, free surface phenomena, gravity waves, make it logically dependent on Froude's number. At very low velocities in shallow open troughs it would conceivably be controlled also by the Weber number for surface tension and capillary waves. Capillary forces while important to insects, as to a fly on flypaper, are negligible to us in problems of engineering magnitude. Under usual conditions of pipe flow only the two dimensionless ratios mentioned need be considered, and it is possible to present the relations between the factors in a chart such as Fig. 1.

The discussions have brought out a number of other departures from normal conditions and further limitations to the scope of the charts. Professor Pardoe reminds us that a considerable temperature difference between the fluid and pipe wall may have a measurable effect on the shear stresses, due to ambient currents which would increase the momentum transfer in similar manner to turbulent mixing. This effect would probably be of importance only at the lower Reynolds numbers and with material temperature differences.

Mr. Pigott reminds us that the scope is limited to simple fluids and does not cover "queer materials like greases, muds, cement slurries" and mixtures with suspended solids. Professor (now Commander) Hubbard and Professor Pardoe mention some unusual forms of pipe surfaces. The author thinks that most of these, including paint coatings, will follow the lines of the charts closely enough for practical purposes if the proper roughness figures are determined; but the rubber dock-loading hose with helical internal band will probably follow a curve similar to curve V in Fig. 6, which Colebrook and White obtained for spiral-riveted pipe.

Dr. Ippen mentions the rate of increase of roughness from corrosion and gives some useful test information. Colebrook found that corrosion usually increases the value of ϵ at substantially a uniform rate with respect to time. Professor Schweitzer calls attention to the point that the pipe must be long, with an established regime of flow, and that the charts do not apply to the entrance or "smoothing section" which require separate allowances. Fortunately we are seldom concerned with close estimates of friction loss in short tubes, where friction is a minor element in the total loss of head.

Dr. Ippen's discussion admirably summarizes the basic structure of the charts and gives supporting evidence. His own studies of the problem had, the author believes, led him independently to conclusions similar to Colebrook's.

The Colebrook function has given us a practically satisfactory formulation bridging the previous gap in our theoretic structure, a region in which the majority of engineering problems fall. It has the further useful property of covering in a single formula the whole field of pipe flow above the laminar and critical zones; and throughout the field agrees with observations as closely as can be reasonably demanded within the range of accuracy available in the measurements, particularly in the evaluation of the boundary roughness.

Referring to a question raised by Professor Daugherty, the inconsistency between Nikuradse's tests in the transition zone and those from commercial pipe is usually attributed either to the close spacing of the artificially applied sand grains, such that one particle may lie in the wake behind another, or to the uniformity of Nikuradse's particles in contrast to the usual commercial surface, which is probably a mixture of large and small roughnesses distributed at random. The latter explanation seems particularly plausible, since a few large protuberances mixed with smaller ones could project far enough into the laminar boundary layer to break it up, while a uniform layer of projections of average size would all remain well within the same thickness of layer. Thus Nikuradse's curve clings closely to the smooth pipe line much farther than the curve for commercial surfaces. At any rate the artificial character of Nikuradse's surfaces weighs against the use of his values in the region where the discrepancies appear.

Mr. Pigott reviews the progress in charting friction factors and gives evidence supporting the laws adopted. At the end of his discussion he brings up an interesting question, the form and location of the dashed line in Fig. 1 marking the boundary of the rough pipe zone for complete turbulence, beyond which the friction factors become practically horizontal. With his gift for detecting relationships he arrives at a modified equation for this curve.

Referring to Figs. 5 and 6 it will be noted that Nikuradse's experiments on artificial roughness gave a curve which dropped below the "rough pipe" line and then approached it from below, while ordinary commercial pipes give points which approach the rough pipe line from above, and that both sets of points seem to merge with the rough pipe line at about $\frac{\mathbf{R}\sqrt{f}}{D/2\epsilon} = 400$, which Rouse accordingly adopted as the equation of the boundary of the rough pipe zone, the dashed line shown in Fig. 1. If, however, we adopt the Colebrook function for the transition region to the left of this boundary curve, strictly speaking the Colebrook curves never completely merge with the constant f lines but are asymptotic to them; so that on the basis of the Colebrook function there is no definite boundary to the rough pipe region.

Practically however the Colebrook function converges so rapidly to the horizontal f lines that beyond Rouse's dashed curve the differences are insignificant. Considering the practical difficulties of measurement and consequent scatter of the test points, and the fact that the Colebrook function is partly empirical and merely a satisfactory approximation, it seems hardly justifiable to draw fine distinctions from an extrapolation of this function. If the function could be accepted as completely rational it would be more logical to locate the boundary curve so that it would correspond to some fixed percentage of excess in f over the f for complete turbulence.

Prompted by Mr. Pigott's suggestion, the author has analyzed the Colebrook equation from this point of view. Calling f the value of the friction factor according to Colebrook, and f_k the value for complete turbulence according to von Kármán, the Colebrook equation can be expressed

$$1/\sqrt{f_k} - 1/\sqrt{f} = 2\log\left(1 + \frac{3.7 \times 2.51}{\epsilon/D\,\mathbf{R}\sqrt{f}}\right)$$

Calling $\frac{3.7 \times 2.51}{\epsilon/D\ \mathbf{R}\sqrt{f}} = x$, a small quantity compared to 1 (of the order of 0.05 or less in the region of the boundary curve) then $\log (1 + x)$ can be expanded in a series giving

$0.4343\left(x - \frac{x^2}{2} + \frac{x^3}{3} - \ldots\right)$; and neglecting x^2 and higher powers

$1/\sqrt{f_k} - 1/\sqrt{f} = 0.8686x.$

If now we denote by s the *proportional* change in f, that is $s = \frac{f - f_k}{f_k} = \frac{f}{f_k} - 1$, s being small compared to 1, then

$$1/\sqrt{f_k} - 1/\sqrt{f} = 1/\sqrt{f}\left(\sqrt{f/f_k} - 1\right)$$
$$= 1/\sqrt{f}\left(\sqrt{1+s} - 1\right)$$

which, expanding by the binomial formula, is very nearly

$$1/\sqrt{f}\ (1 + s/2 - 1) = s/2\sqrt{f}$$

Hence

$$s/2\sqrt{f} = 0.8686x = \frac{0.8686 \times 3.7 \times 2.51}{\epsilon/D\ \mathbf{R}\sqrt{f}};\ \text{and}\ s = \frac{16.1}{\epsilon/D\mathbf{R}}$$

is the proportional change in f caused by the Colebrook function.

In plotting Fig. 1, the author, instead of continuing indefinitely with the insignificant effect of the small term, and favoring the view that f should become substantially constant in the rough pipe zone, adopted the compromise of ignoring the variation when it fell below about one half of one per cent; and beyond this point the f lines were drawn horizontally at the Kármán value. That is, the chart applied the Colebrook formula only to the transition zone.

Putting $s = .005 = \frac{16}{\epsilon/D\mathbf{R}}$, we have $\mathbf{R} = \frac{3200}{\epsilon/D}$, practically confirming Mr. Pigott's deduction. If we adopt a one per cent variation of f as a reasonable allowance, the boundary curve could be plotted from $\mathbf{R} = \frac{1600}{\epsilon/D}$. It might be more logical, to be consistent with the Colebrook function, to use this formula for the boundary curve instead of Rouse's form. The two curves differ but little, and the choice seems more a matter of academic preference than practical importance; the scatter of test observations obscures a final answer.

As noted in numerous references in the paper the author has been indebted to Professor Rouse for his contributions to the subject, particularly his valuable paper at the Iowa Hydraulic Conference. Professor Rouse's inclusion in his discussion of his chart, Fig. 7, from the latter paper, is a useful addition to the material here collected. The co-ordinates selected for this chart bring out the functional relationships in a simple manner; and those who prefer to adopt this form of chart now have it at hand.

The author still considers it less convenient for usual engineering problems than his Fig. 1. While the horizontal scale of Fig. 7 can be expressed in terms of the frictional loss of head in place of f, this is of no help where the velocity is given and the friction loss is to be found, nor is it of much help in usual engineering problems where the total head is given and the velocity is to be found. The total head almost always includes not only the friction loss in a pipe system, but also the exit loss, and the losses at entrance and in fittings, bends, and changes in section; and we can seldom assign in advance the value of the friction head or slope of the hydraulic gradient; so that successive approximations or trial-and-error solutions are still required. While Rouse's chart is easier to construct, for the reasons explained the author adopted the form of Fig. 1 as easier to use.

Regarding the author's suggestions as to open channels, the questions raised by Professor Rouse are probably due mainly to the omission of fuller explanation in the paper. It was not the intention to imply that at low velocities in relatively smooth open channels the friction loss would be independent of Reynolds number, and it may well be found that in this region the logarithmic laws may continue to apply, at least in modified form, and that, as Professor Rouse states, "a general resistance graph for uniform open channels should differ little from that for pipes."

The author was speaking of another region, "open channels dealt with in engineering practice...usually rough-surfaced and of large cross section, corresponding to large Reynolds numbers and falling in the zone of complete turbulence." With fairly high velocities, corresponding to large Reynolds numbers, in the presence of a free surface, dimensional considerations require us to include the Froude number as a criterion; and in the region of complete turbulence we can fortunately afford to omit the Reynolds number as a controlling factor so that we do not have too many variables to handle. The author did not intend to imply that the Froude number "should replace the Reynolds number as a resistance factor *whenever a free surface exists*" but only in the region described, which however is within the range of ordinary practice.

Professor Rouse recognizes that free-surface phenomena comprise a factor in the problem; his objection to including the Froude number is merely that "the effect of surface waves upon the internal resistance to flow has not yet been ascertained—" which calls on us to investigate the effect rather than to ignore it. Certainly wave-making resistance is a very real factor both in ship resistance, and in open channel flow in the region of the gravitational critical velocity. Even in tranquil flow it still may have a measurable effect; the location of the maximum velocity point below rather than at the surface suggests an influence of this factor.

The author is confident that Professor Rouse will agree with his belief that further research on open channel friction is much needed; and he commends such a project particularly to the civil engineers. Neither the f versus $\mathbf{R}$ charts nor such formulas as Manning's, Kutter's or Bazin's are believed to take into account all of the major controlling factors, and a statistical analysis of available data along the lines suggested, supplemented by further experiments, may yield working charts or formulas of great value to engineers.

It is regretted that Professor (now Major) Colebrook, who has been serving in the British Army since 1939, was unable to submit a discussion. The author wishes to thank all of the discussers for their useful contributions, and also to thank Mr. Richard B. Willi for his able presentation of the paper at the Pittsburgh meeting on behalf of the author.

Factors Affecting the Thickness of Coal-Ash Slag on Furnace-Wall Tubes[1]

By W. T. REID[2] and P. COHEN,[3] PITTSBURGH, PA.

Modern central-station power plants generating steam in slag-tap pulverized-coal-fired furnaces often report difficulties in operation as the result of excessive accumulations of slag on the heat-absorbing surfaces of the furnace. Such deposits of slag interfere with the expected transfer of heat from the furnace to the tube metal, and not only may cause trouble in maintaining superheat temperatures at proper levels, but also may be responsible for troubles experienced with circulation. Few means have been available in the past to evaluate the tendency of slags to form objectionable deposits. This paper describes methods of predicting the relative thickness of slag deposits on heat-absorbing surfaces and is based upon the application of data obtained in the laboratory on the flow properties of coal-ash slags at high temperatures. Although based on idealized furnace conditions, it should serve as a guide in comparing the behavior of different coal ashes in the same furnace under similar operating conditions, or in predicting the effect of change in these conditions on the action of a given coal ash. Also, it should serve as a guide for field tests of the effect of slag on furnace performance.

As a result of increased interest in the effect of slag on the performance of modern central-station boiler furnaces burning pulverized coal, recent studies in this laboratory have been directed largely toward determining the fundamental properties of coal-ash slags at high temperatures. Such data are useful in studying the accumulation of slag on heat-absorbing surfaces, such as furnace-wall tubes. One of the problems facing both designers and operators of these furnaces is the effect of deposits of slag in decreasing the normal transfer of heat from the furnace cavity to the tube metal, resulting in unpredictable and variable fluctuations in the temperature of the furnace gases. This usually causes difficulty in maintaining a desired superheat temperature, while troubles experienced with circulation often have been attributed to unexpected variations in the rate of heat transfer to certain sections of waterwalls caused by unforeseen slag accumulations.

Design rates of heat transfer based upon previous experience with a certain coal may not be attainable when other coals are burned because of differences in the composition of the ash, which may result in thicker slag deposits and, consequently, greater insulating effects. A proper knowledge of slag characteristics and of the behavior of slag in the furnace should permit the design of furnaces having predictable heat-absorbing characteristics when fired with coal having ash of known composition and would make it possible to select coals upon the basis of slag performance rather than upon the now generally used guide of the cone-softening temperature.

Only recently has that fundamental information been obtained which makes possible a critical analysis of the action of slag on heat-absorbing surfaces. The development in 1940 by the Bureau of Mines of a high-temperature viscometer[4] for measuring the flow properties of coal-ash slag at temperatures where the slag behaved as a true liquid and, in 1943, of a modification,[5] permitting study of the region where the slag behaved as a plastic rather than a viscous material, furnished methods of obtaining the required data. A preliminary discussion of a means of calculating the thickness of slag deposits on heat-absorbing surfaces based on the flow properties of the slag was given in the second report,[5] but its importance seemed to warrant additional explanation. Consequently, the study was carried further

The present paper reviews the information included in a forthcoming Technical Paper of the Bureau of Mines,[6] in which the subject is treated in considerable detail and in which the mathematical derivations of the complex relationships are given. The present paper describes the principal elements included in that publication to show the factors which are of importance in fixing the thickness of slag deposits on heat-absorbing surfaces but does not include specific details as to the means of arriving at the relationships obtained. It is expected that much of the information included will be used in a field study of the action of coal ash in boiler furnaces now being conducted in co-operation with the Special Research Committee on Furnace Performance Factors; thus the present paper may be considered as a preliminary report to that committee. Others interested in the effect of slag on heat transfer in boiler furnaces may find the method advantageous over purely speculative schemes based upon empirical considerations.

The factors involved in this study can be divided into two classes, one fixed by the properties of the slag and the other dependent on furnace conditions; one example of this is the rate of supply of slag to the wall from the flame. Factors depending on the flow properties of the slag will be discussed first.

Properties of Slag Affecting Its Behavior on Furnace Walls

This report refers only to the deposition of slag on the walls of that part of the furnace where the slag surface is molten and a continuous surface flow of slag occurs. On other sections of the furnace, such as on generating tubes, where adherent but nonflowing deposits are formed, or where the deposits break off after reaching considerable thickness, the conditions are less susceptible to analysis and will not be considered here. Because of the

---

[1] Published by permission of the Director, Bureau of Mines, United States Department of the Interior.

[2] Supervising engineer, Fuel Section, Central Experiment Station, Bureau of Mines. Mem. A.S.M.E.

[3] Fuel engineer, Fuel Section, Central Experiment Station, Bureau of Mines.

Contributed by the Fuels Division and presented at the Semi-Annual Meeting, Pittsburgh, Pa., June 19–22, 1944, of The American Society of Mechanical Engineers.

Note: Statements and opinions advanced in papers are to be understood as individual expressions of their authors and not those of the Society.

[4] "Viscosity of Coal-Ash Slags," by P. Nicholls and W. T. Reid, Trans. A.S.M.E., vol. 62, 1940, pp. 141–153.

[5] "The Flow Characteristics of Coal-Ash Slags in the Solidification Range," by W. T. Reid and P. Cohen. Published in pamphlet, "Furnace Performance Factors," The American Society of Mcehanical Engineers, May, 1944.

[6] "The Flow of Coal-Ash Slag on Furnace Walls," by P. Cohen and W. T. Reid, Tech. Paper 663, Bureau of Mines, in press.

high rate of heat transfer in the slagging zone, an analysis confined to that part of the furnace is most important.

Physical Structure of Slag Deposits. Examination of a section of slag, taken from the wall of a slag-tap furnace in the slagging zone, often gives a visual indication of the flow process. Fig. 1 shows a representation of a typical deposit. Immediately adjacent to the surface of the tube is a thin, semiporous, irregular layer of partly melted ash, through which the slag adheres to the tube. Next, is a dense, crystalline layer of slag, which usually makes up the largest part of the deposit. Finally, there is a layer of glassy slag which extends to the surface, the boundary between it and the crystalline layer usually being sharply defined. The arrangement of these layers results from the temperature gradient through the slag which existed during operation of the furnace, and does not result from events subsequent

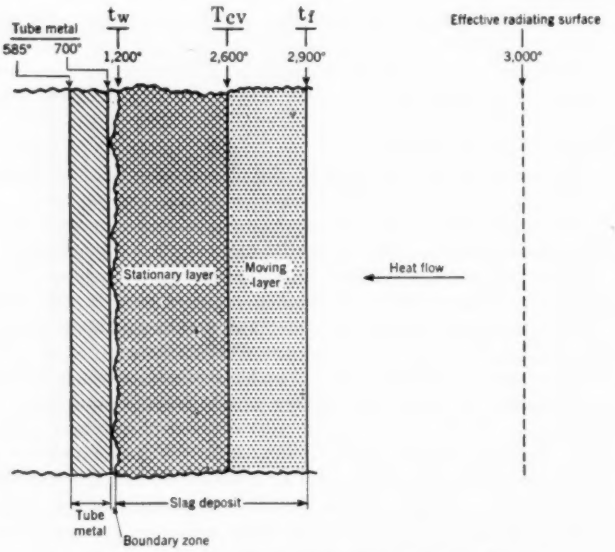


FIG. 1 TEMPERATURE DISTRIBUTION IN SLAG DEPOSIT

to taking the furnace off the line, in which case the glassy layer would have been next to the tube surface, having there been cooled most rapidly. It is evident, then, that when a furnace is operating, the part of the slag deposit nearest the tube is maintained at a sufficiently low temperature for the slag to crystallize, whereas on the furnace side the slag is molten.

Flow Properties of Coal-Ash Slags. Laboratory studies have shown that coal-ash slags are not true liquids over a wide range of temperatures. Most slags on being cooled slowly from high temperatures where they exist as true liquids, at some point, depending upon the composition of the slag and the state of oxidation of its iron content, and somewhat on the thermal history of the melt, begin to separate solid material from the otherwise liquid slag. This solid matter, usually present as very small crystals, causes the slag to become plastic rather than viscous. The essential characteristics of this plastic state are that a definite shear stress (the internal yield stress) is necessary to produce flow and that the rate of flow is proportional to the excess of the applied shear stress over this minimum value. The temperature at which this transition occurs is called the "temperature of critical viscosity," T_{cv}; values of this constant have been determined for a wide range of composition of coal-ash slags, including variation in the state of oxidation of the iron in the slag that is significant. Because both the internal yield stress and the plastic viscosity increase rapidly with decrease in temperature below T_{cv} and, furthermore, at low applied shear stress the effect of even slight internal yield stress is such as to make the apparent viscosity very high, the important assumption is made that the flow of slag at temperatures below T_{cv} is insignificant as compared with flow at higher temperatures. In other words, for all practical purposes where the applied stress is low (as by the action of gravity), the point at which the temperature of critical viscosity occurs in a slag deposit represents an abrupt change in physical properties; slag at a lower temperature behaves as a solid, while hotter slag flows like any liquid; the slightest application of force producing a corresponding flow. Thus it is reasonable to believe that the demarcation between the crystalline stationary layer and the glassy flowing layer of slag on furnace walls occurs at the temperature of critical viscosity.

In the flowing liquid layer of slag, the low-temperature boundary will be at the temperature of critical viscosity, while the high-temperature boundary will be at the furnace temperature; thus usually there will be a temperature difference of several hundred degrees between the two sides of the layer. The viscosity of the liquid slag and its variation with temperature will determine the thickness of the liquid layer required to carry off the slag being supplied. Data obtained from a great many determinations of the viscosity of coal-ash slags in the liquid region, that is, at temperatures higher than T_{cv}, show that the variation of viscosity with temperature can be expressed in the form $\eta^{-z} = At - B$ where η is the viscosity in poises; Z and A are constants for the entire field of composition normally found and are equal numerically to 0.1614 and 0.000452, respectively; t is the temperature in degrees F; and B depends on the composition of the slag. Knowing the viscosity of any slag at a particular temperature, B can be computed from the known values of Z and A.

The flow properties important in fixing the thickness of a slag deposit on a heat-absorbing surface are, therefore, (1) the temperature of critical viscosity, because it fixes the lower temperature of the flowing layer and determines the fraction of the total deposit that effectively will be solid and thus can be considered to be fixed in position; (2) the relationship between temperature and viscosity of the liquid layer, which will control the rate at which the slag can flow to cause a decrease in the over-all thickness. Obviously, as the temperature of critical viscosity increases, the fraction of the total deposit of slag which is stagnant will also increase, and the thickness of the layer will be greater. Likewise, as the viscosity of the liquid layer of slag increases at any fixed temperature, the rate of flow of the slag will be decreased, and the slag thickness will be greater. Thus if these properties of the slag are known from measurements made in the viscometer and correlated with composition, it is possible to predict actions of the slag in the furnace.

EFFECT OF FURNACE CONDITIONS

Factors other than the fundamental flow properties of coal-ash slags are important in fixing the thickness of slag on heat-absorbing surfaces. These include (1) temperatures in the furnace and of the slag deposit; (2) the quantity of slag being supplied to the surface from the furnace gases per unit of time; (3) the height in the furnace at which flow begins; (4) the height at which the thickness of slag is to be considered; (5) the angle of inclination of the flowing slag (essentially that of the furnace wall); and (6) the rate of heat transfer through the layer of slag. Additional factors dependent upon slag properties other than flow include (1) the thermal conductivity of the slag, and (2) the density of the slag.

The importance of temperature is obvious, because the flow properties of any given slag depend principally on that factor. Further, assuming that the temperature gradient through the slag deposit is linear, the thickness of the flowing layer of slag

will depend on the temperature of its boundaries, this layer then being a definite fraction of the total thickness of the deposit. For instance, if the furnace side of the slag deposit is at a temperature of 2900 F, the tube side is at 1200 F, and the temperature of critical viscosity is 2600 F, the flowing layer is $\frac{2900 - 2600}{2900 - 1200} = 0.18$ of the total thickness of the deposit, and the stationary layer is 0.82 of the total thickness. In this case the total thickness of the deposit will be 5.6 times that of the flowing layer.

If the furnace is operating under steady conditions, so that equilibrium occurs and no change takes place in any factor, the volume of slag flowing past a given position in the furnace must equal the total volume of slag deposited on the furnace wall in the slagging zone above that position. Therefore, the quantity of slag being deposited from the flame is important. It is also evident that the height of the slagging zone in the furnace, and the position of the area being considered, will affect the quantity of slag flowing past any given point. Because the quantity of slag reaching the wall is difficult to determine, comparisons in this report are based upon an arbitrary quantity of slag flow, and two different slags are compared by considering the ratio of the thicknesses that would be obtained for the same flow of slag in each case. By taking this ratio for all slags relative to a "standard" slag and fixed furnace conditions, a set of relative thicknesses is obtained.

The angle of the flowing layer of slag will affect its thickness in a simple manner. Although wall tubes are usually vertical, this factor has been included to permit consideration of special cases.

The point of major interest is of course the rate of heat transfer from the furnace through the slag to the tubes. For a given temperature drop through the deposit, the rate of heat transfer is proportional to the reciprocal of the total thickness of slag, the proportionality factor being the thermal conductivity. Lacking any information at present on the thermal conductivity of coal-ash slags, this factor can be assumed to be independent both of composition and temperature, and the relative rates of heat transfer of the deposits can be obtained from their relative thickness. Lack of information on absolute values of rate of slag deposition, thickness of the deposit, or the rate of heat transfer need not detract from the usefulness of this study; when the data are available, the absolute values can be computed by these same methods.

Equation for Computing Thickness of Slag Deposits

The assumptions made in deriving the equation for the thickness of slag on heat-absorbing surfaces are (1) the flow of slag at temperatures below that of the critical viscosity is insignificant; (2) the thermal gradient through the slag deposit is constant; (3) the slag density is independent of composition and temperature; and (4) the slag exists on a plane surface and heat transfer occurs normal to that surface.

The equation, the derivation of which is given in another publication,[6] is long and involved, including, as it does, approximately 10 parameters. Those interested in the mathematical method may wish to follow the derivation step by step; others interested solely in the action of slag in furnaces can better understand its usefulness by referring to the figures given later. The equation is

$$D = \frac{0.00115\ \Delta t \left(\int_h^{h_m} V_s\, dh \right)^{1/3}}{(\rho\ \sin\alpha)^{1/3}\ [\ ]^{1/3}}$$

where

$$[\ ] = \left[\left(\frac{\omega + A'\Delta t}{7.20} \right) \left\{ \frac{(\omega + A'\Delta t)^{8.20} - (\omega + A'\beta\Delta t)^{8.20}}{8.20} - (\omega + A'\beta\Delta t)^{7.20}(1 - \beta)(A'\Delta t) \right\} \right.$$

$$\left. -0.122 \left\{ \frac{(\omega + A'\Delta t)^{9.20} - (\omega + A'\beta\Delta t)^{9.20}}{9.20} - (\omega + A'\beta\Delta t)^{8.20} (1 - \beta)(A'\Delta t) \right\} \right]$$

The nomenclature used is as follows:

- t_f = temperature, deg F, of furnace side of slag deposit
- t_w = temperature, deg F, of wall side of slag deposit
- T_{cv} = temperature of critical viscosity, deg F, below which no flow is assumed to occur
- $\Delta t = t_f - t_w$, temperature drop across slag deposit, deg F
- D = total thickness of slag deposit, in.
- ρ = density of slag, assumed constant, lb mass per cu ft
- h_m = height in furnace at which flow begins, above datum line, ft
- h = height above datum line in furnace, ft
- V_s = volume of slag supplied to wall at height h, ft³ per ft² per sec
- V = volume of slag flow at height h, ft³ per ft² per sec
- α = angle of inclination of wall from horizontal, deg
- $\beta = \frac{T_{cv} - tw}{\Delta t}$ = fraction of deposit which does not flow
- $A' = 1.546A = 0.000699$
- $B' = 1.546B$
- $\omega = A't_w - B'$
- t_g = temperature of gas, deg F
- T_g = temperature of gas, deg R
- t_a = adiabatic combustion temperature, deg F
- T_f = temperature of furnace side of slag deposit, deg R

Application of Equation

Effect of Change in Viscosity and Temperature of Critical Viscosity. The effect on the thickness of slag deposits caused by change in the flow properties of the slag is shown in Fig. 2; the data were calculated by the equation just described. This and

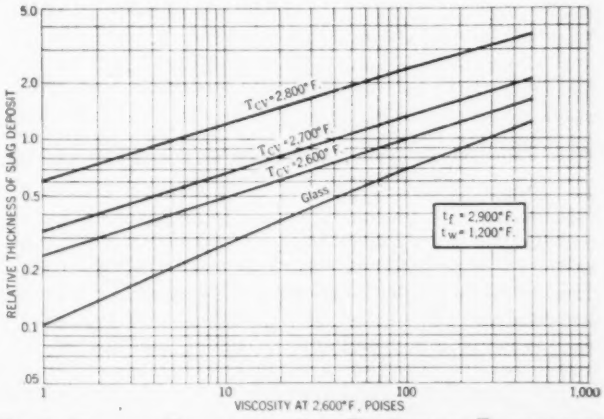


Fig. 2 Relative Thickness of Slag Deposits for Temperature of Furnace Side of Slag Deposit of 2800 F

the succeeding plots express the thickness of slag in terms of the relative thickness compared with a "standard" slag having a viscosity of 100 poises at 2600 F, and a temperature of critical viscosity of 2600 F. They show that the effect of change in viscosity is only slightly greater than change in the temperature of critical viscosity, T_{cv}. For instance, with a slag for which T_{cv} is 2600 F, decreasing the viscosity from 100 to 10 poises, as measured at 2600 F, decreases the slag thickness to 48 per cent of the

original thickness and, if the viscosity were reduced to 1 poise, to 23 per cent. However, if T_{cv} is changed from 2600 F to its minimum value, which would be the case for a slag which acted as a glass, the thickness would be 55 per cent of the original if the viscosity were maintained at 100 poises and 31 per cent if the comparison were made at a viscosity of 1 poise for both slags. It should be noted that as T_{cv} approaches the temperature of the furnace side of the slag deposit, there is a sharp increase in relative thickness at all viscosities, whereas when T_{cv} decreases to approximately 2000 F, the properties approach that of a glass.

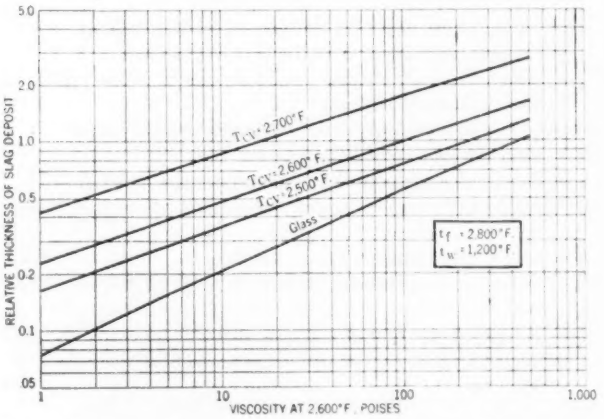


FIG. 3 RELATIVE THICKNESS OF SLAG DEPOSITS FOR TEMPERATURE OF FURNACE SIDE OF SLAG DEPOSIT OF 2900 F

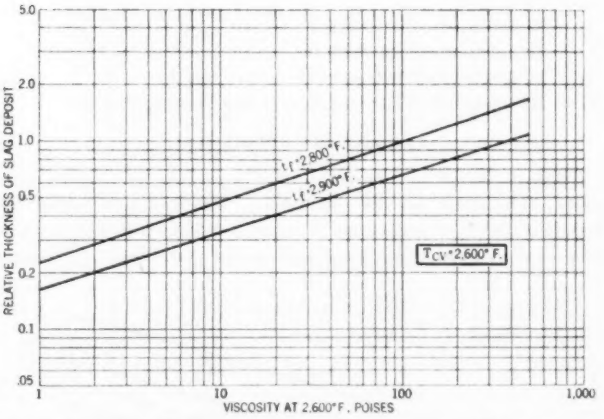


FIG. 4 RELATIVE THICKNESS OF SLAG DEPOSITS FOR TEMPERATURE OF CRITICAL VISCOSITY OF 2600 F

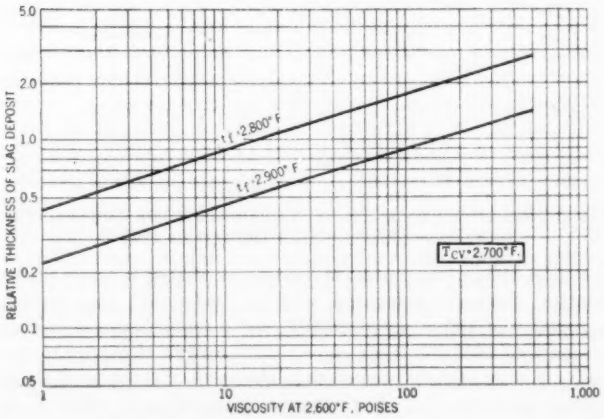


FIG. 5 RELATIVE THICKNESS OF SLAG DEPOSITS FOR TEMPERATURE OF CRITICAL VISCOSITY OF 2700 F

Effect of Change in Furnace Conditions. Changing the rate of heat release in a furnace will affect the temperature of the furnace side of the slag deposit, t_f. Fig. 3 shows the result of increasing t_f to 2900 F, the principal change being a slight decrease in the spacing of the curves. Viscosity and temperature of critical viscosity are again approximately of equal significance in affecting the thickness of the slag deposit.

A different method of expressing the same data is shown in Fig. 4, where the effect of change in furnace temperature on thickness is shown for slags of varying viscosity but with a fixed temperature of critical viscosity of 2600 F. It is apparent that increasing t_f from 2800 to 2900 F decreased the thickness at 100 poises to 66 per cent of the original thickness, and that the percentage decrease of thickness is approximately the same for a given change in t_f independent of the viscosity of the slag. In Fig. 5, where the same type of plot is used, except that T_{cv} is increased to 2700 F, similar effects are observed, except that increasing t_f from 2800 to 2900 F decreased the relative thickness at 100 poises from 1.8 to 0.9, or to 50 per cent of the original thickness. Again, because the isotherms are parallel lines, this percentage change will be constant over the range of viscosities studied.

As noted previously, both the viscosity and the temperature of critical viscosity of coal-ash slags have been determined experimentally for a wide range of compositions. These data have been correlated so that knowledge of the chemical analysis of the slag permits prediction of these properties. Such correlations have been used in Fig. 6, in expressing the relative thickness of slag deposits as a function of composition. Thus knowing the composition of two slags being deposited on the wall tubes of a furnace under identical conditions, a prediction can be made of the relative thickness of the two deposits.

Fig. 6 shows that increase in the equivalent Fe_2O_3 content of the slag results in decreased thickness and that decreasing the ferric percentage, that is, increasing the state of reduction of the iron oxides, decreases the thickness of the deposit. The action of CaO is also to decrease the thickness of the slag as its content increases, the effect being greatest with slags containing less than 20 per cent equivalent Fe_2O_3. For instance, with a slag containing 15 per cent equivalent Fe_2O_3, at a ferric percentage of 20, the thickness with 10 per cent CaO is 44 per cent of that for a slag having 5 per cent CaO, while at 30 per cent equivalent Fe_2O_3 the thickness would be 73 per cent that for a slag containing 5 per cent CaO. Although these relationships may appear complex, by reference to this figure they can be made relatively simple. It is important to note that the use of this figure is limited to slags having a silica : alumina ratio of 2; experimental work now in progress will extend it later to cover a wider range of compositions, including most commonly occurring slags.

Relative Rates of Heat Transfer Through Slag Deposits. The relative rate of transfer of heat through two slags is shown in Fig. 7, as a function of the temperature of the furnace side of the slag deposit; the slags had viscosities of 5 and 100 poises, respectively, and a temperature of critical viscosity of 2600 F. It is obvious that normal change in the viscosity of the slag is more important than change in furnace temperature in affecting the rate of heat transfer. Also, as the furnace temperature approaches the temperature of critical viscosity, the rate of heat transfer will approach zero. This is true of course because under these conditions the thickness of slag increases markedly; because such slag deposits probably would not be physically strong enough to build up indefinitely, this region of the curve has theoretical significance only.

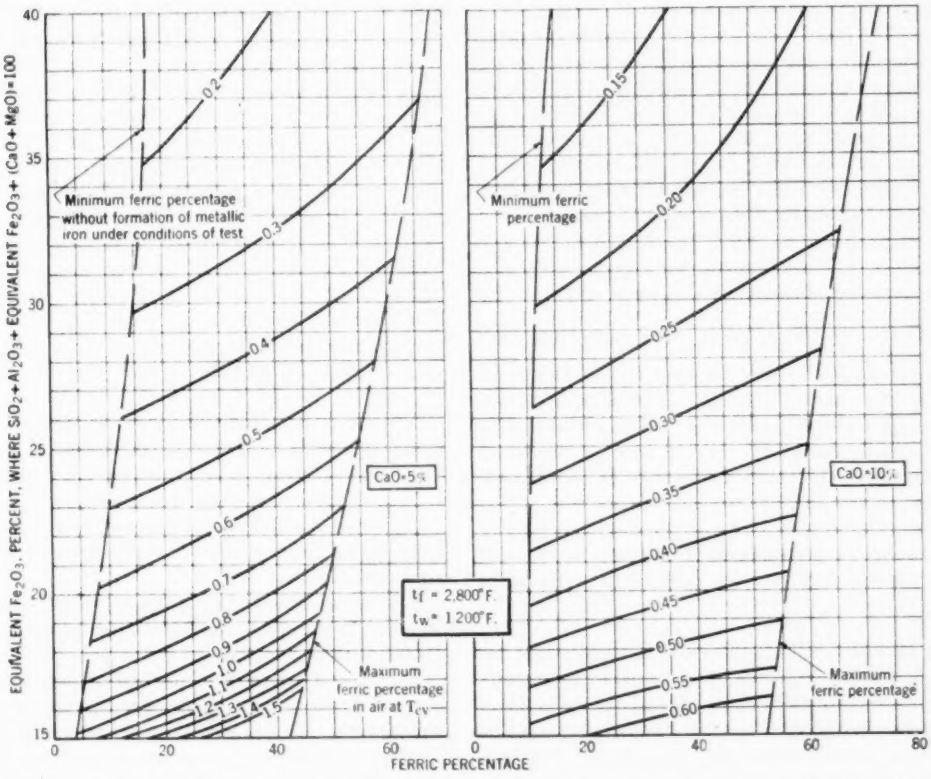


FIG. 6 RELATIVE THICKNESS OF SLAG DEPOSITS AS FUNCTION OF COMPOSITION AND FERRIC PERCENTAGE FOR A SILICA: ALUMINA RATIO OF 2

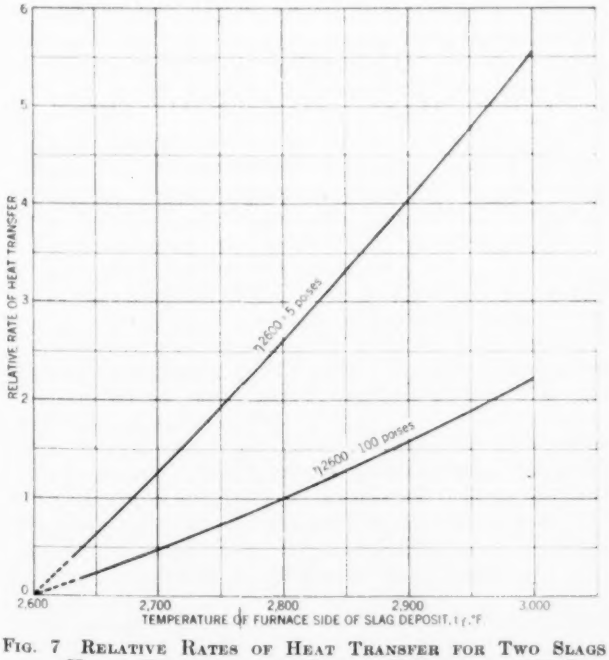


FIG. 7 RELATIVE RATES OF HEAT TRANSFER FOR TWO SLAGS HAVING TEMPERATURE OF CRITICAL VISCOSITY OF 2600 F

EFFECT OF SLAG ON RATE OF HEAT TRANSFER UNDER FURNACE CONDITIONS

The principal interest in the thickness of slag on furnace-wall tubes, of course, is based upon its effect on the rate of transfer of heat. This has already been described briefly, but for a model furnace where conditions are assumed constant over the entire area under study; actually, in an operating furnace they would vary from point to point in an unknown manner. The problem of taking these variations into account would be enormous, even if the distribution of thermal energy were known or if the rate of supply of slag to the walls could be accurately determined. Also, if the conditions in the furnace were uniform throughout, comparison between different slags would be complicated by the fact that any change would result in a different rate of heat transfer, and the temperatures in the furnace would be different unless there had been some accidentally correct change in the rate of firing. However, a means of making the necessary corrections is available and will be described briefly.

A method of determining the heat absorbed by furnace walls has been described by Wohlenberg and others[7] who measured the temperature of furnace-exit gases with high-velocity thermocouples. Mullikin,[8] using the Stefan-Boltzmann law, determined the fraction of the total heat supplied which was absorbed in the furnace and estimated the effects of the slag accumulation. More recently Bailey[9] studied the effect of slag on the heat absorption in steam-generating units, using the cone-fusion temperature as a measure of the flow properties of the slag. He obtained a relationship, called the "gas-ash temperature graph," between the properties of the slag and the temperature measured in several typical furnaces.

[7] "An Experimental Investigation of Heat Absorption in Boiler Furnaces," by W. J. Wohlenberg, H. F. Mullikin, W. H. Armacost, and C. W. Gordon, Trans. A.S.M.E., vol. 57, 1935, paper RP-57-4, pp. 541–553.

[8] "Evaluation of Effective Radiant Heating Surface and Application of the Stefan-Boltzmann Law to Heat Absorption in Boiler Furnaces," by H. F. Mullikin, Trans. A.S.M.E., vol. 57, 1935, paper RP-57-2, pp. 517-529.

[9] "Modern Boiler Furnaces," by E. G. Bailey, Trans. A.S.M.E., vol. 61, 1939, pp. 561–576.

The method used in the present investigation is described in detail in Appendix II of reference 6. Briefly, it may be described as follows: If all the heat transfer in the slagging zone is assumed to occur by radiation, then the sensible-heat loss of the furnace gases between the adiabatic temperature t_a, and the furnace gas temperature t_g, must equal the heat transfer by radiation from the furnace gases at temperature t_g to the furnace wall at temperature t_f. Further, this must equal the heat conducted through the slag layer from the furnace side at temperature t_f to the tube side at temperature t_w. If the sensible-heat loss is proportional to $t_a - t_g$, the heat transfer by radiation to $T_g^4 - T_f^4$, the capitals denoting absolute temperatures, and the heat transfer by conduction to $\frac{t_f - t_w}{D}$, then these three quantities are mutually proportional, and a change in any one factor will result in changes in the others, which can be calculated. Thus in a given furnace, if a change is made in the coal fired so that the thickness of slag deposited on the wall tubes is decreased, other things being equal, the heat transfer through the slag will be increased, and, as a result, the furnace temperature will be lowered. Knowing the expected change in slag thickness resulting from a change in composition of the ash in the coal, therefore, allows prediction of the effect on furnace performance.

Summary

The increasing importance of slag deposits to the designer and operator of slag-tap pulverized-coal boiler furnaces has created a demand for more quantitative knowledge of the behavior of slag under furnace conditions. Recent developments in the study of these slags have furnished data from which the thickness of slag deposits can be calculated for idealized conditions.

An equation is given relating the thickness of the slag deposit to the flow properties of the slag, the temperature of the hot and cold sides of the deposit, and the volume of slag flow. The relative thickness of slag deposits for typical conditions can be calculated from this equation, thus providing a method of comparing the behavior of different coal ashes on furnace walls.

It is shown that for fixed furnace conditions, increase in the temperature of critical viscosity, that is, the temperature at which the slowly cooled slag changes from the liquid to the plastic state, and increase in the viscosity of the slag cause approximately equal increases in the thickness of the slag deposit. As the temperature of critical viscosity approaches the temperature of the furnace side of the slag deposit, there is a large increase in the thickness for all viscosities. It is shown that, for a fixed temperature of critical viscosity, there is an equal percentage decrease in the thickness of the deposit for all viscosities as the temperature of the furnace side of the slag deposit is increased.

The relationship between slag composition and relative thickness of deposit is shown for part of the field of composition of coal-ash slags. Increase in equivalent Fe_2O_3 content and decrease in ferric percentage decrease the thickness of the deposit; CaO also decreases the deposit thickness as its content increases, the effect being greatest with slags containing less than 20 per cent equivalent Fe_2O_3.

Change in viscosity of slag due to change in composition of ash is shown to be more important than normal change in furnace temperature in affecting the rate of heat transfer.

Reference is made to a method of determining the effect on furnace temperatures of changes in the rate of heat transfer through the slag deposit, thus permitting the correlation of all the factors involved. Although the method applies strictly only to a model furnace, its application to operating furnaces should assist in studying the part taken by slag in affecting furnace performance.

Draft-Gear Action in Train Service

By O. R. WIKANDER,[1] PITTSBURGH, PA.

In order to investigate the most desirable characteristics of a draft gear by mathematical analysis, a study has been made of the mechanics of an elastic bar, which is subjected to external forces that correspond to those acting in trains under various service conditions. The results of this study, including the derivation of the various equations governing the behavior of an elastic bar, solid or with free slack, are given in another paper by the author.[2] The present paper contains substantially the same equations but transcribed so as to apply to railway trains. Numerical examples are given showing the applications of these equations to assumed test trains.

Definition of Terms

THE "capacity" of a draft gear is the amount of energy required to close it solid in drop test under a 27,000-lb tup, ft-lb.

The "recoil energy" of a draft gear is the amount of work, expressed in ft-lb or as a fraction or percentage of the draft-gear capacity, which the gear performs when it recoils the full distance of its service travel.

The "free slack" per coupling is the maximum relative movement between two adjacent cars, which can be made without compressing the draft gears.

The "controlled slack" per coupling is the amount of movement between adjacent cars, which is resisted by draft-gear action.

The "residual slack" per coupling is the amount of controlled slack which is released between two adjacent cars when, during a train operation, a previously compressed train is stretched, or a previously stretched train is compressed. (The effect is substantially that of increasing the free slack by the amount of the residual slack.)

The "propagation speed" is the speed at which a force or vehicle speed is transmitted through a train without free slack.

The "rate of progressive force application" is the speed at which a serial force application progresses through a long train.

The "propagation ratio" is the ratio of the propagation speed to the rate of progressive force application.

The "passing point," existing under certain conditions in elastic bars or long trains with free and residual slack, is the point at which the slack take-up passes the force application, and is defined by the number of the car at which it occurs, counted from the end of the bar or the train, at which the progressive external forces were originally applied.

The "critical train slack" is the amount of free plus residual slack per coupling which, in case of emergency-brake application, will place the passing point at the rear end of a train. A decrease below this amount of slack will move the passing point toward the front end of the train, and an increase will move it to an imaginary point beyond the rear end of the train.

Equations Governing Train Dynamics

The following nomenclature will be used:

C = capacity of one draft gear, ft-lb
e = base of natural logarithms
F = retarding force per car, lb
L_1 = length per car between buffing surfaces, ft
M = mass per car, slugs
M_1 = mass of locomotives and tender, slugs
n = number of cars or number of car in train
n_1 = number of car at passing point
n_2 = number of car of maximum coupler pressure in train without free slack
P = drawbar pull of a locomotive, lb
P_1 = tractive effort of a locomotive, lb
p = propagation ratio
q = full travel per draft gear, ft
s_1 = free plus residual slack per coupling, ft
s_2 = critical free plus residual slack per coupling, ft
t_1 = time interval between emergency brake or other force applications on adjacent cars, sec

Starting a Train

It will be assumed for the present that the train is started down a hill of such a grade that the frictional and gravitational forces balance. The entire power of the locomotives is thus applied to acceleration of the masses. Different equations apply, depending upon whether the train is started stretched or with free slack, and also whether the drawbar pull or the tractive effort of the locomotive is assumed to be constant during the starting period.

In any stretched train the drawbar pull P will be transmitted through the train at a constant propagation speed V which may be expressed as

$$V = (L_1/q)\sqrt{(C/M)} \quad [1]$$

Case 1. A locomotive of constant drawbar pull starts a train without free slack:

In this case the pickup speed v of the individual cars is also constant and may be expressed as

$$v = Pq/\sqrt{(CM)} \text{ or } P = (v/q)\sqrt{(MC)} \quad [2]$$

The time t required to set the train of n cars in motion, or the duration of the starting period, is

$$t = nq\sqrt{(M/C)} \quad [3]$$

The distance D traveled by the locomotive during the time t may be expressed as

$$D = nPq^2/C \quad [4]$$

After the time t, the train as a whole would, in this as well as in the following three cases, accelerate at the rate of $P/(M_1 + nM)$ if no external forces were impeding its motion.

Case 2. A locomotive of constant tractive effort starts a train without free slack:

During the starting time t, between the application of the tractive effort P_1 and until the last car begins to move, the speed of the locomotive increases according to the equation

$$v = [P_1q/\sqrt{(MC)}][1 - e^{-t\sqrt{(MC)}/(qM_1)}] \quad [5]$$

---

[1] Mechanical Engineer, Ring Spring Department, Edgewater Steel Company. Mem. A.S.M.E.

[2] "Dynamics of an Elastic Bar," by O. R. Wikander. To be presented at the Annual Meeting, Nov. 27–Dec. 1, 1944, of the A.S.M.E.

Contributed by the Railroad Division and presented at the Semi-Annual Meeting, Pittsburgh, Pa., June 19–22, 1944, of The American Society of Mechanical Engineers.

Note: Statements and opinions advanced in papers are to be understood as individual expressions of their authors and not those of the Society.

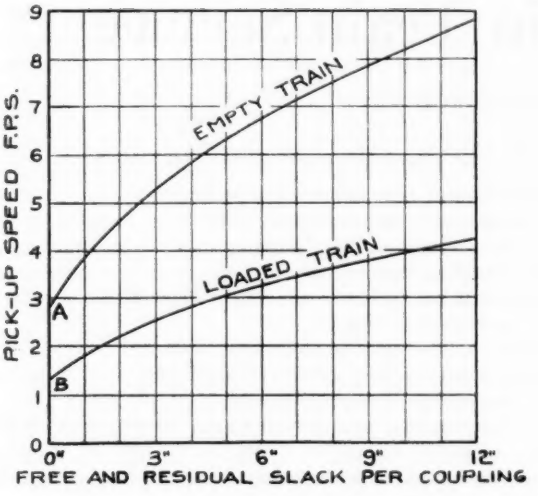


FIG. 1 PICK-UP SPEEDS OF EMPTY AND LOADED TRAINS AT CONSTANT DRAWBAR PULL

The duration t of this starting period is given in Equation [3].

Substituting this value in Equation [5], the latter takes the form

$$v = [P_1q/\sqrt{(MC)}][1 - e^{-nM/M_1}] \quad [5a]$$

This equation expresses the speed of the locomotive at the time when car n begins to move.

The drawbar pull at that time is

$$P = P_1(1 - e^{-nM/M_1}) \quad [6]$$

Case 3. A locomotive of constant drawbar pull starts a train with free slack:

The pick-up speed of the individual cars is constant and can be expressed as

$$v = [P_1q/\{2\sqrt{(CM)}\}][1 + \sqrt{\{1 + 4s_1C/(P_1q^2)\}}] \quad [7]$$

The duration of the starting period or the time t at which car n is set in motion is

$$t = [nq\sqrt{M}/(2\sqrt{c})][1 + \sqrt{\{1 + 4s_1C/(P_1q^2)\}}] \quad [8]$$

The distance D traveled by the locomotive during the starting time t or until the last car is picked up may be expressed as

$$D = n[s_1 + (P_1q^2/\{2c\})(1 + \sqrt{\{1 + 4s_1C/\{P_1q^2\}\}})] \quad [9]$$

Case 4. A locomotive of constant tractive effort starts a train with free slack:

The pickup speeds v of the individual cars increase with the number of the car n counted from the locomotive. The relationship between v and n under the assumption that all bunched cars have a uniform speed is expressed by the equation

$$n = (M_1/M)\{[\sqrt{(s_1C)}/\sqrt{(s_1C + P_1q^2<x - x^2>)}]$$
$$[(a^2 + 2ax + 2x - 1)/(a^2 - 2ax + 2x - 1)]^{1/(2a)} - 1\} \quad [10]$$

where $x = v\sqrt{(CM)}/(P_1q)$ is a parameter and $a = \sqrt{(1 + 4s_1C/[P_1q^2])}$ is a constant.

This equation permits the computation of n for assumed values of v and makes it possible to plot the vn curve.

The duration of the starting period t for a train with n cars may be expressed as

$$t = (v/P_1)(M_1 + Mn) \quad [10a]$$

where v has the value on the vn curve corresponding to the number of the car n. For large values of n the value of v from Equation [7] gives a good approximation. Substituting this latter value in Equation [10a] gives

$$t = [(M_1 + Mn)/\{2\sqrt{(CM)}\}][1 + \sqrt{\{1 + 4s_1C/(P_1q^2)\}}] \quad [11]$$

The distance traveled by the locomotive during the starting period may be expressed as

$$D = s_1n + Aq\sqrt{(M/C)} \quad [12]$$

where A represents the area under the vn curve from the origin to the car number n.

BRAKING A TRAIN

The following equations, governing the braking of a train, apply also, if the proper constants are used, to its behavior during a change in the grade of the track:

A train constant, which is very important since it affects practically every characteristic of a train, is its "propagation ratio" p.

The value of p is computed from the equation

$$p = (t_1/q)\sqrt{(C/M)} \quad [13]$$

Braking a Train Without Free Slack. If the train is bunched when the brakes are applied from the front or stretched when they are applied from the rear, its behavior will correspond to that of a solid elastic bar to which uniformly distributed external forces are serially applied.

It will be different, depending upon whether the propagation ratio is higher than, equal to, or lower than unity and these three cases will therefore be treated separately.

Case 1. Propagation ratio is higher than unity: The relative impact speed between adjacent cars in such a train is zero, since the compression speed between adjacent cars gradually increases from zero.

The time required for the brake application to reach the first car in the train will be designated as t_1, which is also the time interval between the brake application on adjacent cars; hence, the brakes will be applied to car n at the time nt_1. Maximum gear compression and coupler pressure is reached at the time

$$t = 2nt_1/(p + 1) \quad [14]$$

This maximum coupler pressure may be expressed as

$$P_m = 2Fnp/(p + 1)^2 \quad [15]$$

It is located at car number n_2, counted from the locomotive; it is

$$n_2 = 2n/(p + 1) \quad [16]$$

The contraction of the train during the time t is

$$D = (Fq^2n^2/c)(p/[p + 1]^2) \quad [17]$$

Case 2. Propagation ratio is equal to unity:

The maximum coupler pressure amounts to

$$P_m = Fn/2 \quad [18]$$

It occurs at the car number $n_2 = n$, counted from the front end of the train.

The relative car impact speed, due to the instantaneous rise of pressure is

$$v = Fqn/[2\sqrt{(CM)}] \quad [19]$$

The time t required for the coupler pressure and for the force application to reach the end of a train of n cars is

$$t = nt_1 \quad [20]$$

The contraction of the train during the time t is

$$D = Fq^2n^2/(4C) \quad [21]$$

Case 3. Propagation ratio is lower than unity:
The maximum coupler pressure in such a train amounts to

$$P_m = Fnp/2 \quad [22]$$

and occurs at car number n_2 from the front end, expressed as

$$n_2 = n(p + 1)/2 \quad [23]$$

The relative impact speed between adjacent cars is zero. The time t required for the maximum coupler pressure to form may be expressed as

$$t = nt_1(p + 1)/(2p) \quad [24]$$

The contraction of the train at the time t may be expressed as

$$D = Fq^2n^2p/(4C) \quad [24a]$$

Braking a Train With Free Slack. If a train is stretched when the brakes are applied from the front, or bunched when they are applied from the rear, a certain amount of free slack will be taken up during the braking period.

In such a train the conditions will be different, depending upon whether the car under consideration is located:

1 Before the passing point or in a train which has no passing point.
2 At the passing point.
3 Beyond the passing point.

These three cases will be considered separately.

Case 1: Conditions in a train without a passing point or before that point is reached:
The relative car impact speed v at which the car $(n + 1)$ collides with a string of n bunched cars is

$$v = Fnt_1/(2M) \quad [25]$$

The time t' at which the car number $(n + 1)$ collides with the string of n bunched cars is

$$t' = s_1M/(Ft_1) + nt_1(2p + 1)/(3p) \quad [26]$$

According to this equation the time t', plotted against the car number n, is a straight line, beginning at the point $n = 0$, $t' = s_1M/Ft_1$ and rises from the n axis at a slope of $t_1(2p + 1)/(3p)$. For $p = 1$, nt_1 and t' are represented by parallel lines, while for $p < 1$ these lines are divergent and in neither case has the train a passing point.

For $p > 1$ and only in that case, the lines are convergent, and the train has a passing point.

The contraction of the train at the time t' is

$$D = s_1^2M/(2Ft_1^2) + s_1n(2p + 1)/(3p) + [Fn^2t_1^2/(2M)]\left(\frac{1}{9} + \frac{5}{18p} + \frac{1}{9p^2}\right) \quad [27]$$

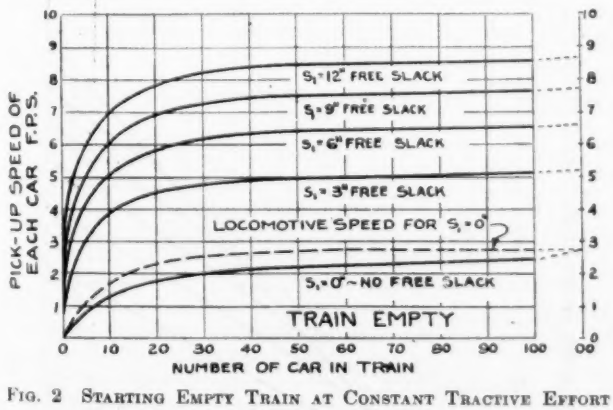


FIG. 2 STARTING EMPTY TRAIN AT CONSTANT TRACTIVE EFFORT

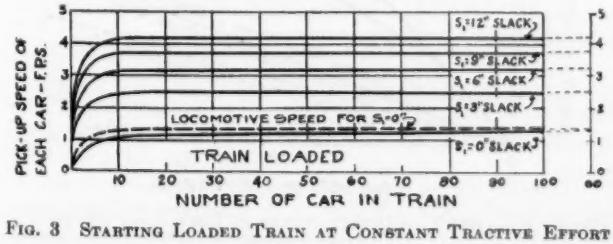


FIG. 3 STARTING LOADED TRAIN AT CONSTANT TRACTIVE EFFORT

Case 2. Conditions in a train at the passing point:
The location of the passing point at car number n_1 is expressed as

$$n_1 = [Ms_1/(Ft_1^2)][3p/(p - 1)] \quad [28]$$

The relative car impact speed v_1 of the number n_1 car is

$$v_1 = (s_1/t_1)[3p/[2(p - 1)]] \quad [29]$$

The time t_2 at which the passing point is reached is

$$t_2 = [s_1M/(Ft_1)][3p/(p - 1)] \quad [30]$$

The contraction of the train at the time t_2 is

$$D_1 = [s_1^2M(Ft_1^2)][3p(4p - 1)/[4(p - 1)^2]] \quad [31]$$

Case 3. Conditions in a train beyond the passing point:
In braked trains with a propagation ratio greater than unity and small or moderate amounts of free slack, and in trains with any reasonable amount of slack, subjected to a change in grade of the track, the car impact point will pass beyond the point of force application and from then on the relative car impact speed v will increase in a much slower tempo.

The relationship between the loss in speed of a group of n bunched cars, assumed to travel at a uniform speed, or their relative collision speed with the car number $(n + 1)$, as yet unretarded, is expressed by the equation

$$dv/dn = \sqrt{[2F/(Mt_1)]}[s_1/\sqrt{(vn)} + (t_1/p)\sqrt{(v/n)}] - v/n \quad [32]$$

The solution of this equation is as yet unknown, and it is therefore necessary to use approximative integration, using the Simpson rule or some equivalent method to construct the nv curve for cars beyond the passing point.

From the origin and up to the passing point n_1v_1 the nv curve is computed from Equation [25] and is thus a straight line. At that point it bends sharply to the slope dv/dn expressed by the equation

$$dv/dn = [Ft_1/M][(p + 2)/(6p)] \quad [33]$$

It can be seen from this equation that all the v-n curves have the same slope at the passing point, regardless of the location of the latter which is governed by the amount of train slack.

The time t' required to bunch a group of n cars may be expressed as

$$t' = nt_1 + s_1A_1/L_1 \quad [34]$$

where A_1 is the area in the $\frac{1}{v}$ n diagram, located between the $\frac{1}{v}$ curve and the n axis, and between the verticals at n_1 and n.

The amount of contraction of the train after the bunching of n cars is

$$D = 3Ms_1/t^2 + s_1n + A(t_1/p) \quad [35]$$

where A is the area in the n-v diagram, located between the v-curve and the n axis and between the verticals n_1 and n.

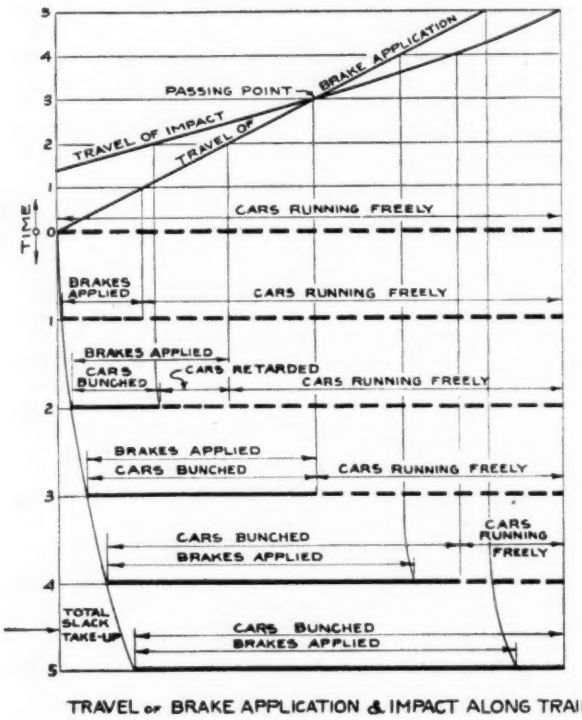


FIG. 4 TRAVEL OF BRAKE APPLICATION AND IMPACT ALONG TRAIN

BRAKE ACTION IN A LONG TRAIN

Fig. 4 illustrates, in diagram form, the conditions under which the brake application and the resulting car impacts proceed in a train with free slack.

The freely running train is represented at the time zero by a horizontal broken line, in which each dash represents a car or a group of cars. Before the application of the brakes, the cars are assumed to be moving uniformly toward the left. The brakes are applied aerially from the front of the train.

The forward motion of the train as a whole is not shown.

The conditions of the train after the periods of time, represented by the horizontals 1 to 5 above the zero line, are shown on the horizontal train diagrams below the zero time line, designated by the same numbers.

Fig. 4 represents a case where the propagation ratio of the train is $p > 1$ and the two inclined diagram lines intersect at the "passing point."

If $p = 1$ these lines are parallel, if $p < 1$ they are divergent, and in neither case has the train a passing point.

CRITICAL TRAIN SLACK

Beyond the passing point, the impact speed v increases at a slower rate and the critical slack, defined as the amount of free plus residual slack per coupling, which will place the passing point at the end of the train therefore produces the highest possible car impact speed.

In a train of n cars, the critical slack s_2 may be computed from Equation [28] by substituting $s_2 = s_1$ and $n = n_1$

$$s_2 = [Ft^2n/(3M)]/[(p-1)/p] \quad \ldots\ldots\ldots\ldots [36]$$

In cases where p is equal to or smaller than unity, s_2 is infinite, and the car impact speed is entirely independent of the amount of free or residual slack in the train.

APPLICATION OF EQUATIONS

The use of the equations will be illustrated by a few examples, in which they will be applied to assumed test trains made up of identical cars. The following values are given:

C = capacity of one draft gear, 26,300 ft-lb
g = total travel of each gear = 0.219 ft (= $2^5/_8$ in.)
F = external force acting on each car during emergency-brake application
= 7500 lb, when type K brake is used
= 3750 lb, when type AB brake is used as an initial application, which has the main purpose of bunching a stretched train before the full retarding force of 7500 pounds is applied
M = mass per car
= 1550 for empty car weighing 50,000 lb
= 6500 for loaded car weighing 210,000 lb
M_1 = mass of locomotives and tender
= 17,100 for a combined weight of 550,000 lb
P_1 = tractive effort of locomotive, = 80,000 lb
P = drawbar pull of locomotive, lb
t_1 = time between emergency-brake application on adjacent cars, sec
= 0.092 sec for type K brake
= 0.0612 sec for type AB brake

Example 1. A locomotive of constant drawbar pull starts a stretched train:

In this case the pickup speed v of the individual cars is constant during the whole starting period and can be computed from Equation [2].

For the empty test train, it is represented in Fig. 1, by the vertical OA. For the loaded one it is represented by the vertical OB in the same figure.

Example 2. A locomotive of constant tractive effort starts a stretched train:

In this case the speed v of the locomotive at the time of starting of each individual car is different, depending upon the car number

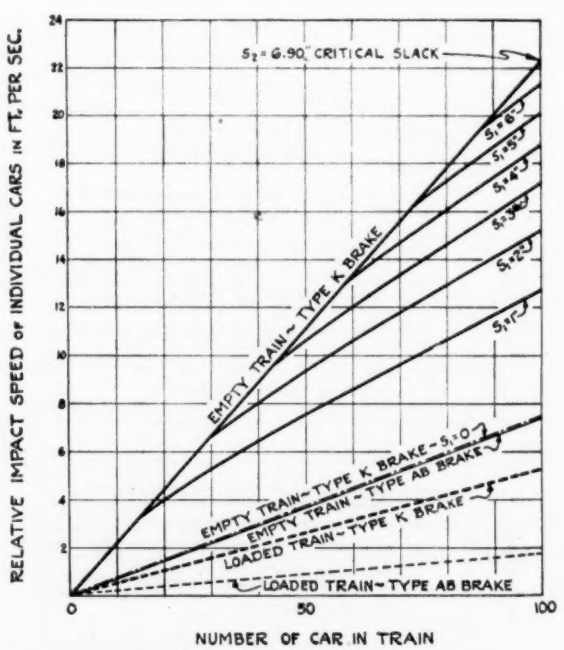


FIG. 5 RELATIVE CAR IMPACT SPEEDS IN EMERGENCY BRAKING OF LONG TRAINS

n counted from the locomotive, and may be computed from Equation [5a].

For the empty train, this speed is represented in Fig. 2 by the dotted curve marked "locomotive speed" for $s_1 = 0$. For the loaded train it is represented by the corresponding dotted curve in Fig. 3.

Example 3. A locomotive of constant drawbar pull starts a train with free slack:

For a given train slack, the pick-up speed of the individual car is constant during the entire starting period and can be computed from Equation [7].

The computed car impact speeds for the empty and loaded test trains are plotted in Fig. 1, against the amount of free plus residual slack per coupling. It will be seen from the curves that the constant pickup speed v of the individual cars in empty as well as in loaded trains increases sharply with the amount of free and residual slack between the individual cars.

Fig. 1 shows that the pickup speed of the loaded train is only about one half that of the empty one, but the mass of the individual car is about 4 times larger, and thus the impact energies of the individual cars are the same regardless of whether the cars are loaded or empty.

Example 4. A locomotive of constant tractive effort starts a train with free slack:

Referring to Fig. 2, the pickup speeds of the individual cars, from 1 to 100 in the empty train have been computed from Equation [10], and for various values of the free plus residual slack s_1 from 0 to 12 in. per coupling under the assumption that the tractive effort P_1 of the locomotive is constant.

It is seen that these curves, rising from zero at the first car, rapidly approach horizontal asymptotes, which latter represent the pickup speeds of all the cars in the train under the assumption of a constant drawbar pull P_1 equal to the tractive effort of the locomotive.

It will be seen that beyond car 50, the computed pickup speed would be practically the same regardless of whether the train were started with a constant drawbar pull or an equal constant tractive effort.

Example 5. Computation of the propagation ratios during emergency braking of the assumed test trains:

By substituting the proper constants in Equation [13], the values of p, listed in Table 1, are obtained.

TABLE 1 PROPAGATION RATIOS p FOR VARIOUS TEST TRAINS

	Type K brake	Type AB brake
Empty train, p =	1.73	1.155
Loaded train, p =	0.845	0.563

Example 6. Relative car impact speeds:

How to compute the relative car impact speeds of all the cars in a 100-car train in case of emergency braking from the front.

(*a*) *Empty Train, Type K Brakes.* In all the empty trains, the relative car impact speeds before the passing point are independent of the draft-gear characteristics and are located on the straight line through the origin defined by Equation [25].

The location of the passing point on this line at car n_1 and the corresponding relative car impact speed v_1 are determined by Equations [28] and [29], respectively.

The relative impact speeds of the cars beyond the passing point are governed by the differential Equation [32].

Fig. 5 shows in heavy full lines the nv curves of the empty train with type K brakes for various values of the free plus residual slack s_1 up to its critical value, $s_2 = 6.90$ in., the latter to be computed from Equation [36].

The curves beyond the passing point were constructed by approximative integration from Equation [32], using a method similar to the Simpson rule.

(*b*) *Loaded Trains, Type K Brakes.* For these trains the propagation ratio is less than unity, as shown in Table 1. The relative car impact speeds v are therefore independent of the amount of free plus residual slack per coupling s_1 and may be computed from Equation [25]. They are shown in heavy dotted lines in Fig. 5.

Example 7. Computation of the propagation ratios for a train passing through a change in the grade of slack:

Let us assume that the test trains coast at a speed of 40 mph and are subjected to a change in grade of 4 per cent.

The gravitational forces will produce a change in force per car equal to 4 per cent of its weight, and therefore

$$F = 0.04 \times 50{,}000 = 2000 \text{ lb for empty cars and}$$
$$= 0.04 \times 210{,}000 = 8400 \text{ lb for loaded cars}$$

The time t_1 between force applications on adjacent cars at a train speed of 40 mph (= 58.6 fps) and for a car length of 50 ft is

$$t_1 = 50/58.6 = 0.852 \text{ sec}$$

Substituting these constants in Equation [13], the propagation ratios are found to be recorded as follows:

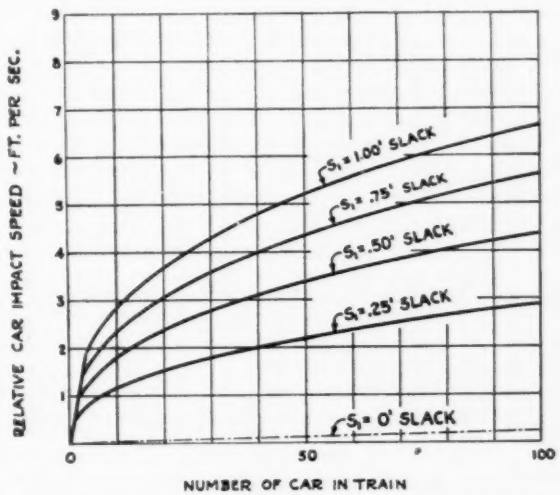


FIG. 6 RELATIVE CAR IMPACT SPEEDS IN EMPTY TRAINS RUNNING THROUGH DIP IN TRACK AT 40 MPH, 4 PER CENT CHANGE IN TRACK GRADE

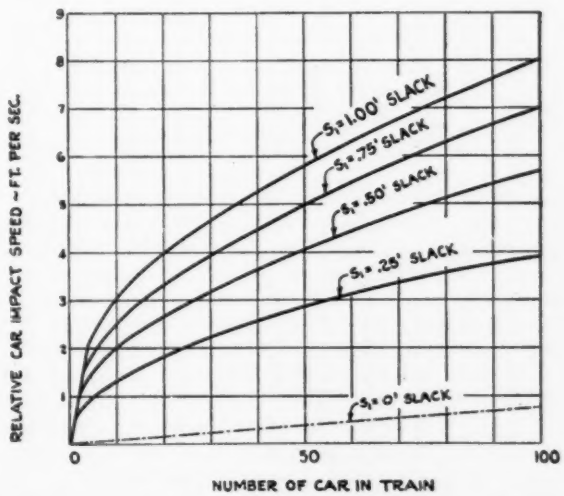


FIG. 7 RELATIVE CAR IMPACT SPEEDS IN LOADED TRAINS RUNNING THROUGH DIP IN TRACK AT 40 MPH, 4 PER CENT CHANGE IN TRACK GRADE

TABLE 2

In empty trains, $p = 16.1$
In loaded trains, $p = 7.83$

Example 8. Relative car impact speeds:

This covers the computation of the relative car impact speeds of all cars in the test trains when passing through a 4 per cent dip at a train speed of 40 mph for different values of the free plus residual slack per coupling. For all the cars before the passing point, these speeds are located on the straight line through the origin, defined by Equation [25]. The locations of the passing points on this line are computed from Equations [28] and [29] and are plotted in Fig. 6.

The nv curves for empty and loaded trains beyond the passing point were computed by approximate integration from Equation [33] and plotted in Fig. 6 for empty trains, and in Fig. 7 for loaded trains.

Energy Intake and Gear Reaction

The foregoing equations and examples refer mostly to gear reactions in trains without free or residual slack, and to relative car impact speeds in trains with free and residual slack. A few remarks regarding the relationship of car impact speeds to energy intake and gear reaction are therefore indicated.

If two cars, each of the mass M, collide at the relative impact speed v, their draft gears will be compressed until the car speeds are equalized. At that time one of the cars will have gained and the other one will have lost a speed, equal to $v/2$ and, disregarding the elasticity of the car bodies, the energy taken up by each of the two coacting gears is, therefore

$$(1/2)M(v/2)^2 = Mv^2/8$$

Likewise, if a single car strikes a group of cars and if the draft gears of the struck cars were fully expanded before the impact occurred, the same relative impact speed v will cause the same energy intake per gear as just given.

If, however, a car strikes a group of bunched cars with fully compressed draft gears, the relative kinetic energy of the moving car, amounting to $Mv^2/2$, will be taken up by the two impacting gears, each taking up the energy $Mv^2/4$.

In the latter case and if the draft gears have a capacity of C ft-lb and a total travel of q ft, the gear reaction P produced by the energy intake of $Mv^2/4$ would be the one given in Equation [2].

Instead of computing the gear reaction from this equation and since most draft gears do not have a straight compression line, it is recommended to use a curve, obtained by laboratory test, where the gear reaction, as established by drop test, is plotted against the energy intake of the gear.

Draft-Gear Recoil

The foregoing equations as well as the curves plotted from the computations in the various examples show, and practical experience confirms, that free and residual slack increases the relative car impact speeds, and causes undesirably high gear reactions in a train, during starting, braking, and passing over changes in the grade of the track.

The free slack is mainly composed of clearances in couplers and draft-gear attachments, and is therefore largely beyond the control of the draft-gear designer.

The residual slack, which is equally undesirable, is caused by sticking draft gears and by gears of insufficient recoil energy to expand a partly or fully compressed train or to contract a partly or fully stretched one.

It is therefore desirable to design draft gears with ample recoil energy so as to prevent sticking and reduce the residual slack.

It is also desirable to design them with high initial recoil force in order to reduce the residual slack, even after comparatively light train compressions.

Acknowledgment

The author is indebted to the Edgewater Steel Company for sponsoring this investigation; to Mr. L. H. Fry for deriving some of the more important equations by a different method, thus checking the validity of the elastic-bar method; and to Dr W. M. Dudley for helpful suggestions.

Temperature Distribution Within Boiler Tubing Under Oblique Radiation

By W. S. KIMBALL,[1] ANNAPOLIS, MD.

The surface and interior temperature distribution in a section of boiler tubing under normal symmetric radiation from the furnace has been investigated by G. M. Dusinberre and others, and reported on in a discussion of data furnished by W. F. Davidson.[2] In the same issue such problems in heat conduction are also treated by Paschkis[3] using the method of electrical analogy, and by Emmons[4] using the numerical method of obtaining approximate solutions; and in the reported discussion of the latter Dusinberre points out that the numerical method, carried out to the needed accuracy, checks the analytical solution and results are obtained with greater ease. The analytical method of Fourier, previously confined to the symmetric case of normal radiation, is here extended to the unsymmetric case where radiation from the fire is received obliquely and with consequent shadowing effect from adjoining tubes. An advantage of this investigation is that it supplies a general mathematical expression for temperature distribution under parallel radiation received at any angle with the boiler wall normal, thus affording a check on results that sometimes may be obtained easier by other methods. A further advantage is that this general mathematical expression makes it fairly easy to compare temperature gradients and hence rates of the heat transfer as done herein for various obliquity angles of received radiation.

IN the present study of temperature distribution in boiler tubing, it is assumed that interface resistance and external convection and conduction are negligible. These assumptions are in line with the conclusions of the authors mentioned, when conduction is ruled out by having insulated refractory backing at practically tube-surface temperature. Thus no heat transfer across the outer tube surface occurs except by radiation.

It is further assumed, as formerly, that a tube receives radiation uniformly per unit projected area as from a distant source. For symmetric radiation previously treated this leads to the temperature-slope condition at the outer tube surface

$$\frac{\partial T}{\partial r} = \frac{Q}{K} \cos \theta$$

where θ is the angle between the received radiation and the tube surface normal. For oblique radiation now treated, the foregoing condition is replaced by condition, Equation [3] with $\theta - \beta$ in place of θ, since β measures the obliquity of the radiation.

The general temperature expression here derived includes the special symmetric case where the obliquity angle is zero and the received radiation comes in normal to the boiler wall with formula given by Equation [13] of the Davidson paper[2] and graphed in his Fig. 48. In all cases herein parallel radiation is assumed,[5] making a given obliquity angle β with the boiler wall normal, and the wall is made up of cylindrical tubes in contact.

This new general temperature expression is here studied for a series of obliquity angles for the received radiation. With all of these, the surface exposed to radiation is reduced by shadowing of adjoining tubes below the 180 deg exposure, or semicircumference opposite the fire for normal radiation.

Special attention and graphs are given for four typical cases, (*a*) where 120 deg of tube surface is exposed to radiation of exactly three quarters of the amount of normal heat radiation, (*b*) where 90 deg of tube surface is exposed, receiving exactly one half the amount of normal radiation per tube, (*c*) where 60 deg of tube surface is exposed, receiving exactly one quarter of the normal radiation per tube, and (*d*) where 30 deg of tube surface is exposed, receiving one fifteenth of the normal radiation.

For the 120-deg exposure or two thirds the normal, the radiation comes in at an obliquity angle of 41°25′ with the boiler wall normal. For 90 deg or one half the normal exposure to radiation, the radiant heat comes in at a 60 deg angle of obliquity with the boiler wall normal, and for a 60-deg tube exposure or one third the normal, the radiation comes in at a 75°30′ angle with the boiler wall normal. When only 30 deg or one sixth of the tube surface is exposed, the radiation comes at an angle of 86 deg with the boiler wall normal, being only 4 deg short of the grazing angle of tangency with the wall, with the amount of received radiation one fifteenth that of the normal radiation per tube.

The temperature graphs show that the hot point of highest temperature is not where the oblique radiation comes in normal to the tube surface, but is shifted back toward the symmetric point opposite the fire cavity where the tube surface parallels the boiler wall, and where the hot point would be in case of radiation normal to the boiler wall. This hot-point shift occurs in the direction of the geometrical center of the received radiation, as is to be expected.

A most interesting result is the way the temperature gradient or difference between outer and inner tube-surface temperatures falls off with increased angle of obliquity, assuming the same density of radiation. Where the received radiation is three quarters the normal radiation, and comes at a 41-deg angle with 120 deg of tube surface exposed to it, there is only a 2 per cent drop in temperature gradient, the distribution being merely shifted around the tube in the direction of the received radiation.

When one half the normal radiation is received over 90 deg of exposed surface, coming in at 60 deg to boiler wall normal, there is a 14 per cent loss in the temperature gradient, and when only one quarter of normal radiation is received over one third as much tube surface exposed (60 deg), then the loss in temperature drop is 50 per cent, as compared with that for normal radiation.

[1] Lieutenant Commander, Department of Marine Engineering, U. S. Naval Academy.

[2] "Studies of Heat Transmission Through Boiler Tubing at Pressures From 500 to 3300 Pounds," by W. F. Davidson, P. H. Hardie, C. G. R. Humphreys, A. A. Markson, A. R. Mumford, and T. Ravese, Trans. A.S.M.E., vol. 65, 1943, pp. 553–579, and discussion, pp. 579–591.

[3] Ibid., p. 587, discussion by V. Paschkis.

[4] "The Numerical Solution of Heat-Conduction Problems," by H. W. Emmons, Trans. A.S.M.E., vol. 65, 1943, pp. 607–612.

Contributed by the Heat Transfer Division and presented at the Spring Meeting, Birmingham, Ala., April 3–5, 1944, of THE AMERICAN SOCIETY OF MECHANICAL ENGINEERS.

NOTE: Statements and opinions advanced in papers are to be understood as individual expressions of their authors and not those of the Society.

[5] See reference 2, Appendix, p. 581, Max Jakob.

And when about one fifteenth the normal radiation is received at only 4 deg short of grazing angle with 30 deg of exposed surface (one sixth of the normal), then the temperature drop is about 15 per cent of normal radiation, representing an 85 per cent reduction in gradient.

These results indicate that the ease or efficiency with which heat is disposed of decreases with increased obliquity angle, since the shortage of heat supplied from the fire falls off with increasing obliquity angle much faster than the corresponding temperature gradients.

A further point to be noted is that the sum of these temperature expressions as solutions of Laplace's equation is still such a solution and would represent a physical situation corresponding to a superposition of the conditions they separately represent, likewise, if different values of Q, the normal heat flux per unit area, were used for the various cases. Thus any condition equivalent to and separable into two or more cases of parallel radiation acting in unison could be represented by a temperature expression given by the sum of such series as here shown.

Nomenclature

The following nomenclature will be used in succeeding sections of the paper:

T = temperature
T_0 = temperature at inner tube radius $r_0 (= 0$, for convenience)
r = radial distance from tube center
θ = angle measured from an axis normal to boiler wall and extending into fire
r_0 = inside radius of boiler tube
r_1 = outside radius of boiler tube
Q = maximum heat flux at r_1, i.e. the density of radiant heat
K = thermal conductivity of metal
β = angle between boiler wall normal and direction of oblique radiation
γ = shadow angle, measuring from boiler wall, the extent of tube surface that receives no radiation owing to shadow from the adjoining tube (see Fig. 1).
$\pi - \beta - \gamma = \pi - 2\alpha$ = angular range of received radiation on a tube
$\alpha = \dfrac{\beta + \gamma}{2}$ = auxiliary angle, measuring one half reduction in angular range from π, corresponding to normal radiation
$\phi = \theta - \dfrac{\beta - \gamma}{2} = \theta - (\beta - \alpha)$ = position angle measured from the mid-point, $\beta - \gamma/2$ of angular range exposed to oblique radiation (see Fig. 1)
$\rho = \dfrac{r}{r_0}$ = dimensionless ratio for radial distance r
$\rho_1 = \dfrac{r_1}{r_0}$ = dimensionless ratio at outer tube radius r_1 (= 1.5 throughout this paper)
A_m, B_m, A'_m, B'_m are Fourier constant coefficients evaluated later

Assumptions and Boundary Conditions

Three basic assumptions are made as follows

$$T_0 = \text{constant } (= 0) \qquad [1]$$

at inner boundary where $r = r_0$ which implies negligible interface resistance at the inside of the tube in contact with the steam.

$$\left(\frac{\partial T}{\partial r}\right)_{r=r_1} = 0 \qquad [2]$$

for $$\left(\frac{\pi}{2} - \gamma\right) < \theta < \left(\frac{3\pi}{2} + \beta\right)$$

Condition Equation [2] says there is no heat transfer across the entire outer boundary where $r = r_1$ except where radiation is received between angles β and γ shown in Fig. 1. The back part is assumed to be insulated and the part of the circumference toward the fire that receives no radiation is assumed to be in equilibrium with the surroundings.

The third basic assumption gives the condition for absorption of radiant energy, as follows

$$\left(\frac{\partial T}{\partial r}\right)_{r=r_1} = \frac{Q}{K}\cos(\theta - \beta) \qquad [3]$$

for $$-\left(\frac{\pi}{2} - \beta\right) < \theta < \left(\frac{\pi}{2} - \gamma\right)$$

This condition refers to parallel radiation of uniform density received on the tube surface at angle $\theta - \beta$ with the tube surface

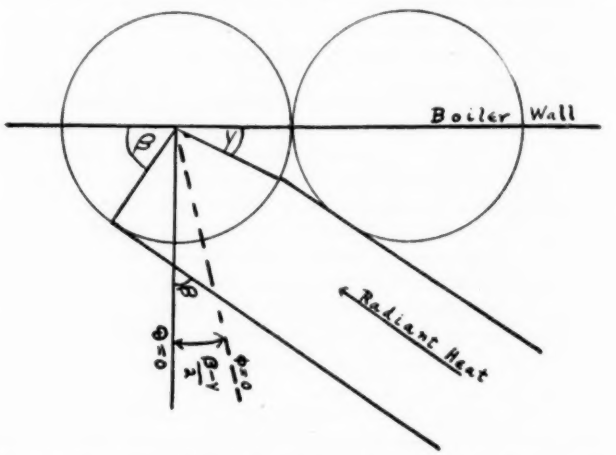


Fig. 1 Obliquity Angle β, Shadow Angle γ, and Mid-Point $\theta = \dfrac{\beta - \gamma}{2}$ of Surface Exposed to Oblique Radiation

normal. Unit cross section of radiation will be spread over an area equal to sec $(\theta - \beta)$ so that the fraction of Q, the radiation density that is conducted away through unit surface area, will be reduced by this same proportion according to Equation [3].

When conditions, Equations [2] and [3], are referred to the angle ϕ and constant angle α which are symmetric about the dotted center line $\phi = 0$ of exposed tube surface, shown in Fig. 1, Equations [2] and [3] take a symmetric form adapted to computation of the Fourier coefficients.

$$\left(\frac{\partial T}{\partial r}\right)_{r=r_1} = 0 \qquad [4]$$

for $$\left(\frac{\pi}{2} - \alpha\right) < \phi < \left(\frac{3\pi}{2} + \alpha\right)$$

$$\left(\frac{\partial T}{\partial r}\right)_{r=r_1} = \frac{Q}{K}\cos(\phi - \alpha) = \frac{Q}{K}(\cos\alpha\cos\phi + \sin\alpha\sin\phi) \qquad [5]$$

for $$-\left(\frac{\pi}{2} - \alpha\right) < \phi < \left(\frac{\pi}{2} - \alpha\right)$$

Relation Between Obliquity Angle β, and Shadow Angle γ

The relation between the obliquity of radiation β and the shadow angle γ is most easily obtained by applying the law of sines to the triangle made by extending the straight-line tangent to the right-hand circle in Fig. 1, until it hits the line of centers of the two circles. We then have

$$\cos(\beta + \gamma) = 2\cos\beta - 1 = \cos 2\alpha \quad \ldots\ldots\ldots\ldots\ldots [6]$$

where on the right the symmetric auxiliary angle α is introduced, defined according to the nomenclature. This relation is essential to obtaining the graphs which follow. Note $\cos^2\alpha = \cos\beta$.

Temperature Within a Boiler Tube Under Oblique and Normal Radiation

Expressions for the temperature within a boiler tube under radiation are obtained by solving Laplace's equation and computing the Fourier coefficients in the usual way. When the exposed surface includes the angular range $\pi - 2\alpha = \pi - \beta - \gamma$, according to the nomenclature, we have in terms of α and the ratios $\rho = \frac{r}{r_0}$ and $\rho_1 = \frac{r_1}{r_0}$ of the radii

$$\left.\begin{aligned} T = \frac{Qr_1}{\pi K}\Bigg[& \cos^2\alpha \log\rho + \frac{\rho_1}{2\rho}\left(\frac{\rho^2-1}{\rho_1^2+1}\right)\Big\{(\pi - 2\alpha \\ & - \sin 2\alpha)\sin\alpha\sin\phi + (\pi - 2\alpha + \sin 2\alpha)\cos\alpha\cos\phi\Big\} \\ & + \frac{\rho_1^2}{6\rho^2}\left(\frac{\rho^4-1}{\rho_1^4+1}\right)\Big\{(3\cos\alpha + \cos 3\alpha)\sin\alpha\sin 2\phi \\ & + (3\cos\alpha - \cos 3\alpha)\cos\alpha\cos 2\phi\Big\} \\ & + \frac{\rho_1^3}{12\rho^3}\left(\frac{\rho^6-1}{\rho_1^6+1}\right)\Big\{(2\sin 2\alpha + \sin 4\alpha)\sin\alpha\sin 3\phi \\ & + (2\sin 2\alpha - \sin 4\alpha)\cos\alpha\cos 3\phi\Big\} \\ & - \frac{\rho_1^4}{60\rho^4}\left(\frac{\rho^8-1}{\rho_1^8+1}\right)\Big\{(5\cos 3\alpha + 3\cos 5\alpha)\sin\alpha\sin 4\phi \\ & + (5\cos 3\alpha - 3\cos 5\alpha)\cos\alpha\cos 4\phi\Big\} + \ldots\ldots\ldots \end{aligned}\right\} \ldots [7]$$

The most important special case of Equation [7] occurs when the radiation is normal to the boiler wall and the angular range of exposed tube surface is 180°, with obliquity angle $\beta = 0$. We see from Equation [6] and Fig. 1, that in this case angles α and γ are also zero, hence $\sin\alpha = 0$ and $\cos\alpha = 1$, and likewise with the sines and cosines of all multiples of α. Hence Equation [7] reduces to

$$T = \frac{Qr_1}{\pi K}\left[\log\rho + \frac{\pi\rho_1}{2\rho}\left(\frac{\rho^2-1}{\rho_1^2+1}\right)\cos\theta + \frac{\rho_1^2}{3\rho^2}\left(\frac{\rho^4-1}{\rho_1^4+1}\right)\cos 2\theta - \frac{\rho_1^4}{30\rho^4}\left(\frac{\rho^8-1}{\rho_1^8+1}\right)\cos 4\theta + \frac{\rho_1^6}{105\rho^6}\left(\frac{\rho^{12}-1}{\rho_1^{12}+1}\right)\cos 6\theta + \ldots\right] [8]$$

This is the same temperature expression as given by Equation [13] in the appendix of the Davidson paper[2] and graphed there in Fig. 48. Equation [8] herewith is expressed in terms of the dimensionless variable $\rho = \frac{r}{r_0}$ and constant $\rho_1 = \frac{r_1}{r_0}$ instead of the r's, thus checking the previous result.

Temperature Distribution Under Radiation of 41°25′ Obliquity and 120° of Exposed Tube Surface With Three Quarters of the Heat Supply of Normal Radiation and 2 Per Cent Loss of Temperature Gradient

The angular range (see nomenclature) determines α

$$\pi - 2\alpha = \frac{2}{3}\pi, \text{ therefore } \alpha = \frac{\pi}{6} = 30 \text{ deg}$$

Hence from Equation [6]

$$\cos\beta = \frac{3}{4}; \quad \beta = 41°\,25'$$

$$\gamma = 18°35'$$

and the mid-point of the angular range of exposed radiation (nomenclature) is

$$\theta_0 = \beta - \alpha = 11°25'$$

where $\phi = 0$.

Since Q, the radiation density, is the same as for normal radiation, and since the entire beam of received radiation is for 120 deg of exposed surface, just $^3/_4$ the breadth of the normal radiation beam, we see that the total heat supplied is exactly $^3/_4$ of that supplied under normal radiation.

Using $\alpha = \frac{\pi}{6}$ in Equation [7] gives the formula for this distribution

$$\left.\begin{aligned} (a)\quad T = \frac{Qr_1}{\pi K}\Bigg[& \frac{3}{4}\log\rho + \frac{\rho_1}{4\rho}\left(\frac{\rho^2-1}{\rho_1^2+1}\right)\Big\{\Big(\frac{2}{3}\pi \\ & - \frac{\sqrt{3}}{2}\Big)\sin\phi + \Big(\frac{2}{3}\pi + \frac{\sqrt{3}}{2}\Big)\sqrt{3}\cos\phi\Big\} \\ & + \frac{\rho_1^2}{8\rho^2}\left(\frac{\rho^4-1}{\rho_1^4+1}\right)\Big(\sqrt{3}\sin 2\phi + 3\cos 2\phi\Big) \\ & + \frac{\rho_1^3}{16\rho^3}\left(\frac{\rho^6-1}{\rho_1^6+1}\right)\Big(\sqrt{3}\sin 3\phi + \cos 3\phi\Big) \\ & + \frac{\rho_1^4}{80\rho^4}\left(\frac{\rho^8-1}{\rho_1^8+1}\right)\Big(\sqrt{3}\sin 4\phi - 3\cos 4\phi\Big) + \ldots\ldots \end{aligned}\right\} \ldots [9]$$

Temperature Distribution Under Radiation of 60 Deg Obliquity and 90 Deg of Exposed Tube Surface With One Half the Heat Supply of Normal Radiation and 14 Per Cent Loss of Temperature Gradient

Angle α is determined by the exposed angular range

$$\pi - 2\alpha = \frac{\pi}{2}; \quad \alpha = \frac{\pi}{4} = 45°$$

Hence from Equation [6]

$$\cos\beta = \frac{1}{2}; \quad \beta = 60°$$

$$\gamma = 30°$$

and the mid-point of angular range exposed to radiation is

$$\theta_0 = \beta - \alpha = 15°$$

where $\phi = 0$.

With the same radiation density Q as before and one half the breadth of the beam, we have exactly one half the heat supply. We note that the hot point is now at only 86 per cent of the 100 deg taken as a comparison standard, being the temperature drop for the hot point under normal radiation. The hot point here

is no longer under the radiation that hits the tube normally at $\theta = 60$ deg because this is the outer edge of the radiation beam, but is shifted some 25 deg or 30 deg toward the center of the radiation beam.

The formula for this distribution is given by Equation [7] using $\alpha = \frac{\pi}{4}$

$$(b)\quad T = \frac{Qr_1}{\pi K}\left[\frac{1}{2}\log\rho + \frac{\rho_1\sqrt{2}}{4\rho}\left(\frac{\rho^2-1}{\rho_1^2+1}\right)\left\{\left(\frac{\pi}{2}-1\right)\sin\phi + \left(\frac{\pi}{2}+1\right)\cos\phi\right\}\right.$$
$$+ \frac{\rho_1^2}{6\rho^2}\left(\frac{\rho^4-1}{\rho_1^4+1}\right)(\sin 2\phi + 2\cos 2\phi)$$
$$+ \frac{\sqrt{2}\rho_1^3}{12\rho^3}\left(\frac{\rho^6-1}{\rho_1^6+1}\right)(\sin 3\phi + \cos 3\phi)$$
$$\left. + \frac{\rho_1^4}{60\rho^4}\left(\frac{\rho^8-1}{\rho_1^8+1}\right)(4\sin 4\phi + \cos 4\phi) + \ldots\right] \quad \ldots [10]$$

TEMPERATURE DISTRIBUTION UNDER RADIATION OF 75°30′ OBLIQUITY AND 60° OF EXPOSED TUBE SURFACE WITH ONE QUARTER OF THE HEAT SUPPLY OF NORMAL RADIATION AND 50 PER CENT LOSS OF TEMPERATURE GRADIENT

Angle α is determined by the exposed angular range

$$\pi - 2\alpha = \frac{\pi}{3} = 60° = \alpha$$

Hence from Equation [6]

$$\cos\beta = 1/4;\ \beta = 75°30'$$
$$\gamma = 44°30'$$

and the mid-point of the angular range exposed to radiation is

$$\theta_0 = \beta - \alpha = 15°30' \text{ where } \phi = 0$$

The temperature distribution of Fig. 4 is given by using $\alpha = \frac{\pi}{3}$ in Equation [7]

$$T = \frac{Qr_1}{\pi K}\left[\frac{1}{4}\log\rho + \frac{\rho_1}{4\rho}\left(\frac{\rho^2-1}{\rho_1^2+1}\right)\left\{\left(\frac{\pi}{\sqrt{3}}-\frac{3}{2}\right)\sin\phi\right.\right.$$
$$\left.+\left(\frac{\pi}{3}+\frac{\sqrt{3}}{2}\right)\cos\phi\right\} + \frac{\rho_1^2}{24\rho^2}\left(\frac{\rho^4-1}{\rho_1^4+1}\right)(\sqrt{3}\sin 2\phi$$
$$+ 5\cos 2\phi) + \frac{\rho_1^3}{16\rho^3}\left(\frac{\rho^6-1}{\rho_1^6+1}\right)(\sin 3\phi + \sqrt{3}\cos 3\phi)$$
$$\left. + \frac{\rho_1^4}{240\rho^4}\left(\frac{\rho^8-1}{\rho_1^8+1}\right)(7\sqrt{3}\sin 4\phi + 13\cos 4\phi) + \ldots\right] \quad \ldots [11]$$

TEMPERATURE DISTRIBUTION UNDER RADIATION OF 86°10′ OBLIQUITY, RECEIVED OVER 30° OF EXPOSED TUBE SURFACE ABSORBING ONLY ONE FIFTEENTH OF THE NORMAL RADIATION, AND WITH TEMPERATURE GRADIENT 15 PER CENT OF THE GRADIENT UNDER NORMAL RADIATION

The angular range determines angle α

$$\pi - 2\alpha = \frac{\pi}{6};\ \alpha = \frac{5}{12}\pi = 75°$$

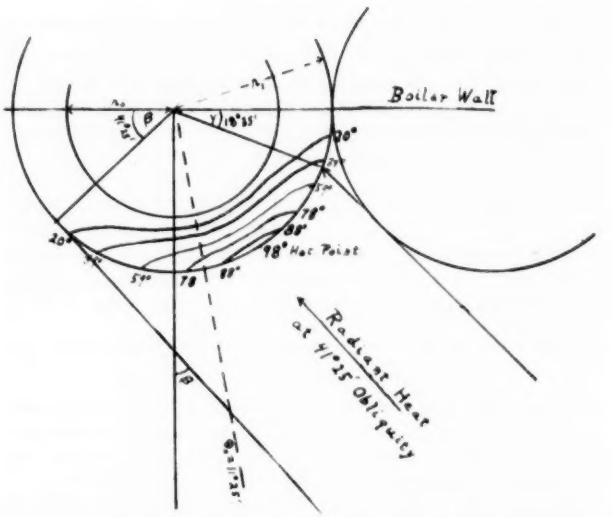


FIG. 2 RADIATION AT 41°25′ OBLIQUITY, OF THREE QUARTERS THE AMOUNT, AND RECEIVED BY TWO THIRDS THE SURFACE EXPOSED TO NORMAL RADIATION

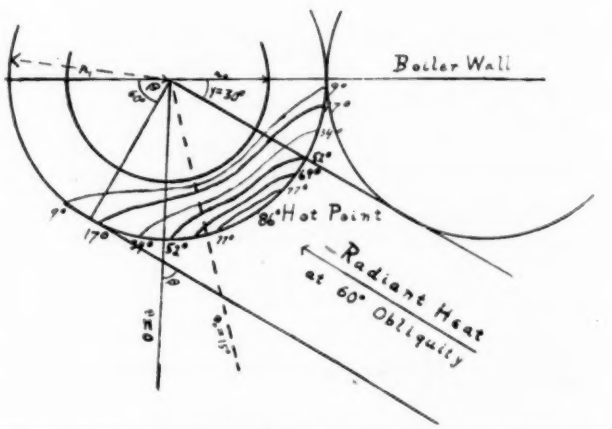


FIG. 3 RADIATION AT 60 DEG OBLIQUITY, OF ONE HALF THE AMOUNT, AND RECEIVED BY ONE HALF THE SURFACE EXPOSED TO NORMAL RADIATION

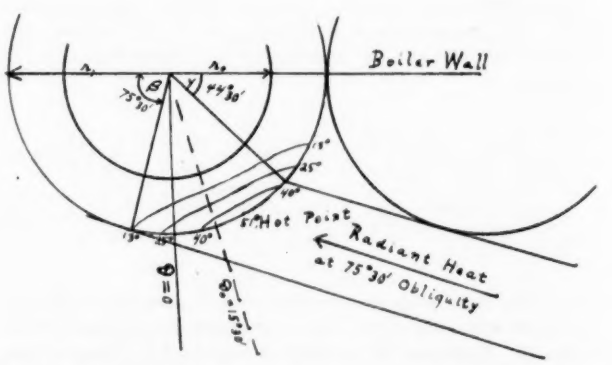


FIG. 4 RADIATION AT 75°30′ OBLIQUITY, OF ONE QUARTER THE AMOUNT, AND RECEIVED BY ONE THIRD THE SURFACE EXPOSED TO NORMAL RADIATION

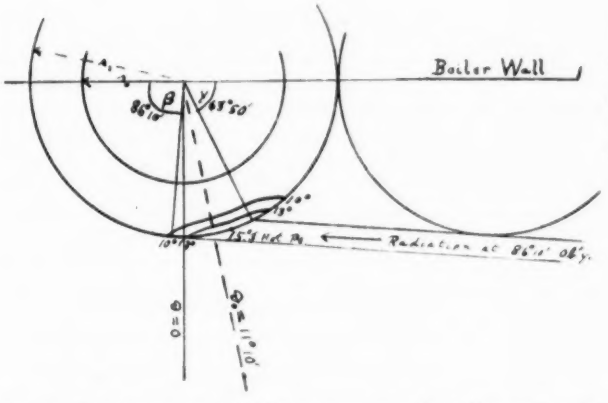


FIG. 5 RADIATION AT 86°10′ OBLIQUITY, OF ONE FIFTEENTH THE AMOUNT, AND RECEIVED BY ONE SIXTH THE SURFACE EXPOSED TO NORMAL RADIATION

Hence from Equation [6]

$$\cos \beta = 0.067; \ \beta = 86°10'$$
$$\gamma = 63°50'$$

and the center line of the exposed surface is at

$$\theta_0 = \frac{\beta - \gamma}{2} = 11°10'$$

where $\phi = 0$.

The temperature expression for the foregoing distribution comes from introducing $\alpha = 75$ deg in Equation [7]

$$T = \frac{Qr_1}{\pi K}\left[0.067 \log \rho + \frac{1}{4}\frac{\rho_1}{\rho}\left(\frac{\rho^2 - 1}{\rho_1^2 + 1}\right)\right.$$
$$\left\{\left(\frac{\pi}{3} - 1\right)0.9659 \sin \phi + \left(\frac{\pi}{3} + 1\right)0.2588 \cos \phi\right\}$$
$$+ \frac{\rho_1^2}{6\rho^2}\left(\frac{\rho^4 - 1}{\rho_1^4 + 1}\right)(0.0657 \sin 2\phi + 0.3294 \cos 4\phi) \quad \left.\right\} \ldots [12]$$
$$+ \frac{\rho_1^3}{12\rho^3}\left(\frac{\rho^6 - 1}{\rho_1^6 + 1}\right)(0.129 \sin 3\phi + 0.4829 \cos 3\phi)$$
$$\left. + \frac{\rho_1^4}{60\rho^4}\left(\frac{\rho^8 - 1}{\rho_1^8 + 1}\right)(0.616 \sin 4\phi + 1.65 \cos 4\phi) + \ldots\right]$$

HEAT TRANSFER PER DEGREE OF TEMPERATURE DROP AS A FUNCTION OF OBLIQUITY ANGLE

The radiant heat transfer per unit tube length is evidently $H_0 = 2r_1Q$ for the normal radiation case where $2r_1$ is the breadth of the beam and Q is its density or heat flux per unit cross section. In case heat comes obliquely, the total amount received per tube is seen to be $H = H_0 \cos \beta$ since the breadth of the beam received by a tube is now $2r_1 \cos \beta$. Note that when only one fourth the normal radiation is received (Fig. 4) over one third the normal receiving area, the temperature drop is only one half that for normal radiation, showing that the heat disposed of per degree of temperature drop between outer and inner tube is one half as great for 75 deg obliquity of radiation as for normal radiation, due possibly to less cramped (from adjoining beams) means of heat disposal. This result, for various obliquity angles, may be graphed most conveniently by plotting H/T against cos β. Thus, in Fig. 6 the ordinate is heat transfer per tube per temperature drop between outer and inner tube since $\Delta T = T - T_0 = T$ taking $T_0 = 0$ according to the nomenclature.

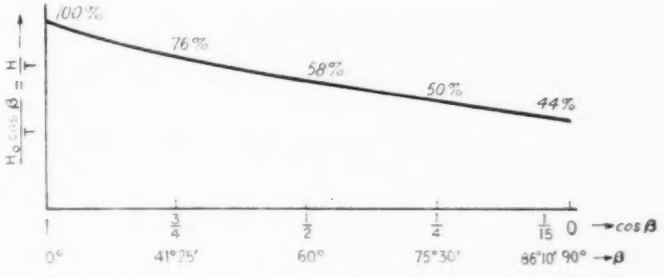


FIG. 6 DECREASE IN HEAT TRANSFER PER DEGREE OF TEMPERATURE GRADIENT AS OBLIQUITY OF RADIATION INCREASES

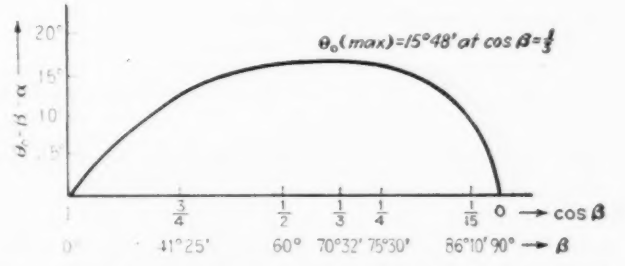


FIG. 7 SHIFT θ_0 OF CENTER OF RECEIVED RADIATION AS A FUNCTION OF OBLIQUITY AND OF COS β

These are shown in percentages of heat transfer per degree, relative to the ratio for normal radiation taken as 100 per cent. They are not efficiencies in the true sense of the term, since there are no heat losses under any of the situations here treated (true efficiencies are all 100 per cent) but are perhaps due to greater spreading of heat through areas not exposed under oblique radiation.

SUMMARY OF RESULTS

The distribution of temperature inside boiler tubes in contact under parallel oblique radiation of any obliquity angle β is given by Equation [7], assuming no heat transfer at back or anywhere across outer tube surface, except where it is under radiation from the fire.

The hot point on the boiler tube is near the center of the received radiation beam but shifted toward the surface point where the radiation strikes or would strike (except for shadowing) the surface normally for that obliquity angle.

The temperature drop between outer and inner tube surface is greater for a given quantity of received oblique radiation than for normal radiation, up to angles of extreme obliquity approaching 90 deg. This may be due to greater concentration of heat under oblique radiation, corresponding to greater ease in disposing of it under normal radiation. Fig. 6 shows how the heat transfer per degree of temperature drop decreases under oblique radiation continuously.

The center of the tube-surface area exposed to radiation given by $\theta = \beta - \alpha$ does not shift from its normal position $\theta = 0$ opposite the fire in the same way as the obliquity angle does, due to shadowing effect of adjoining tubes. Its maximum (see Appendix 2) occurs at radiation obliquity of $\beta = 70°32'$, where the central angle θ_0 of surface exposed to radiation is 15°48′ representing maximum eccentricity of received radiation. When the eccentricity angle θ_0 is plotted against the cosine of obliquity angle β for received radiation, we have a graph of Equation [6] which is shown in Fig. 7.

Appendix 1

Derivation of Temperature Distribution Under Oblique Radiation

Taking account of the first assumption or boundary condition, Equation [1], we have for the solutions of Laplace's equation

$$T = (r^m - r_0^{2m} r^{-m})(A_m \sin m\theta + B_m \cos m\theta);\ m \neq 0 \quad \ldots\ldots [13]$$

$$T = c \log \frac{r}{r_0};\ m = 0$$

which includes terms in sin $m\theta$ as well as in cos $m\theta$ because of the unsymmetric type of distribution. We now introduce variable angle ϕ, measured from the center of the area exposed to radiation, and related to θ according to the nomenclature. Then, using new Fourier coefficients A' and B' in Equation [13], we have for our temperature expression

$$T = c \log \frac{r}{r_0} + \sum_{m=1}^{\infty} (r^m - r_0^{2m} r^{-m})(A'_m \sin m\phi + B'_m \cos m\phi) \quad [14]$$

where, according to the nomenclature, the constants are related by

$$\begin{aligned} A_m &= A'_m \cos m(\alpha - \beta) - B'_m \sin m(\alpha - \beta) \\ B_m &= A'_m \sin m(\alpha - \beta) + B'_m \cos m(\alpha - \beta) \end{aligned} \quad \ldots\ldots [15]$$

The Fourier coefficients of Equation [14] are computed in the usual way taking account of Equations [4] and [5]

$\frac{\partial T}{\partial r}$ at $r = r_1$ is, for the mth term of the series Equation [14]:

(for $m \neq 0$)

$$\left(\frac{\partial T}{\partial r}\right)_{r=r_1} = \frac{m}{r_1}\left(\frac{r_0^{2m} + r_1^{2m}}{r_1^m}\right)(A'_m \sin m\phi + B'_m \cos m\phi)$$

$$= \frac{Q}{K}(\sin\alpha \sin\phi + \cos\alpha \cos\phi)$$

The odd series coefficients are obtained by multiplying the foregoing odd functions by sin $m\phi$ and integrating, and the even terms by multiplying the even functions by cos $m\phi$ and integrating (between limits 0 to π on left and from 0 to $\frac{\pi}{2} - \alpha$ on the right). Thus

$$\frac{m}{r_1}\frac{(r_0^{2m} + r_1^{2m})}{r_1^m} A'_m \frac{\pi}{2} = \frac{Q}{K}\sin\alpha \int_0^{\frac{\pi}{2}-\alpha} \sin\phi \sin m\phi d\phi$$

$$= \frac{Q}{2K}\sin\alpha \int_0^{\frac{\pi}{2}-\alpha} [\cos(m-1)\phi - \cos(m+1)\phi]\, d\phi$$

$$\frac{m}{r_1}\left(\frac{r_0^{2m} + r_1^{2m}}{r_1^m}\right) B'_m \frac{\pi}{2} = \frac{Q}{K}\cos\alpha \int_0^{\frac{\pi}{2}-\alpha} \cos\phi \cos m\phi d\phi$$

$$= \frac{Q}{2K}\cos\alpha \int_0^{\frac{\pi}{2}-\alpha} [\cos(m-1)\phi + \cos(m+1)\phi]\, d\phi$$

where the integral on the right vanishes according to Equation [4] beyond the indicated upper limit of integration. When the values of A'_m and B'_m so determined are substituted in Equation [14] we have

$$T = \frac{Qr_1}{\pi K}\left[\cos^2\alpha \log\frac{r}{r_0} + \frac{r_1}{2}\frac{(r - r_0^2 r^{-1})}{(r_1^2 + r_0^2)}\left\{(\pi - 2\alpha - \sin 2\alpha)\sin\alpha\sin\phi + (\pi - 2\alpha + \sin 2\alpha)\cos\alpha\cos\phi\right\}\right.$$
$$+ \frac{r_1^2}{6}\left(\frac{r^2 - r_0^4 r^{-2}}{r_0^4 + r_1^4}\right)\left\{(3\cos\alpha + \cos 3\alpha)\sin\alpha\sin 2\phi + (3\cos\alpha - \cos 3\alpha)\cos\alpha\cos 2\phi\right\}$$
$$+ \frac{r_1^3}{12}\left(\frac{r^3 - r_0^6 r^{-3}}{r_0^6 + r_1^6}\right)\left\{(2\sin 2\alpha + \sin 4\alpha)\sin\alpha\sin 3\phi + (2\sin 2\alpha - \sin 4\alpha)\cos\alpha\cos 3\phi\right\}$$
$$\left. - \frac{r_1^4}{60}\left(\frac{r^4 - r_0^8 r^{-4}}{r_0^8 + r_1^8}\right)\left\{(5\cos 3\alpha + 3\cos 5\alpha)\sin\alpha\sin 4\phi + (5\cos 3\alpha - 3\cos 5\alpha)\cos\alpha\cos 4\phi\right\} + \ldots\ldots\right] \quad \ldots [16]$$

When the dimensionless variable and constant $\rho = \frac{r}{r_0}$ and $\rho_1 = \frac{r_1}{r_0}$ are used in Equation [16], we obtain series Equation [7].

Appendix 2

Center of Area Exposed to Radiation as a Function of Obliquity Angle

If we solve Equation [6] for α, we have

$$\alpha = {}^1/_2 \text{ arc cos } (2\cos\beta - 1) \quad \ldots\ldots [17]$$

and hence for the center of the area exposed to radiation according to Fig. 1 and the nomenclature

$$\theta_0 = \beta - \alpha = \beta - {}^1/_2 \text{ arc cos } (2\cos\beta - 1) \quad \ldots\ldots [18]$$

The derivative of this is readily seen to be

$$\frac{d\theta_0}{d\beta} = 1 - \frac{\sin\beta}{2\sqrt{\cos\beta - \cos^2\beta}} \quad \ldots\ldots [19]$$

Setting this equal to zero gives

$$\left.\begin{aligned} \cos\beta &= {}^1/_4 \\ \beta &= 70°32' \end{aligned}\right\} \quad \ldots\ldots [20]$$

for the obliquity angle of maximum θ_0 being the center of the area exposed to radiation. The position of this maximum shift of the center is obtained by substituting Equation [20] in Equation [18].

$$\theta_{0(\max)} = \beta - {}^1/_2 \text{ arc cos } (-{}^1/_4) = \beta - {}^1/_2\,(109°28')$$
$$\theta_{0(\max)} = 70°32' - 54°44' = 15°48' \quad \ldots\ldots [21]$$

This is the most eccentric position of the surface exposed to oblique radiation. Note that it is less than 1 deg out from the center of the radiation beam of 60 deg obliquity ($\theta_0 = 15°$) and of 75°30′ obliquity ($\theta_0 = 15°30'$) of Figs. 3 and 4, and greater than 70°32′ angles of obliquity reduce the eccentricity of the exposed surface. Thus Fig. 5 shows that for an 86°10′ obliquity angle the center of the area exposed to radiation is given by $\theta_0 = 11°10'$, being less eccentric than the distribution of Fig. 2, for 41 deg obliquity of radiation when the eccentric angle $\theta_0 = 11°25'$ gives the shift of the center from its position $\theta_0 = 0$ opposite the fire in case of normal radiation.

Discussion

G. M. Dusinberre.[6] The section, "Heat Transfer per Degree of Temperature Drop as a Function of Obliquity Angle β," opens an interesting line of study, for it shows that the maximum temperature gradient in the metal falls off surprisingly slowly as the heat transfer decreases (owing to location of the tube), under the author's assumptions. As the heat transfer and internal turbulence decrease, the temperature gradient between metal and boiling liquid will no longer be negligible. But according to the studies of Jakob[7] this gradient may well be constant about the inner circumference. If so, the author's temperature distributions would remain qualitatively correct. Now, if the interior surface gradient should become greater than the decrease of gradient in the metal, then a tube at the end of the wall, although receiving less heat, might attain a higher surface temperature than a tube opposite the flame. This high temperature would, moreover, be quite localized.

The practicing engineer who has not the author's thorough command of differential equations will find that solutions of this type of problem are readily obtained by the numerical method outlined by Emmons.[4] The precision of the method depends only upon the time spent, and this is equally true of the analytical solution, for one computes only as many terms of the series as is judged to be necessary for the purpose at hand. For a degree of precision consistent with that of most engineering data, the numerical method offers a tremendous saving of time.

The writer's experience shows that a particular case, such as is represented by one of the author's diagrams, can be solved from the beginning in the time required for the final computations alone in the analytical solution. Thus one saves the time required for solving the differential equation and for calculating the numerical constants in the series. The numerical method is also more flexible. As Emmons has pointed out, there is only slightly more difficulty in the treatment of a fin or stud tube, whereas these would greatly complicate an analytical solution. The same may be said for the effect of a slag layer such as occurs in pulverized-coal firing.

[6] Assistant Professor of Mechanical Engineering, Virginia Polytechnic Institute, Blacksburg, Va. Now on duty at U. S. Naval Academy, Annapolis, Md. Mem. A.S.M.E.

[7] Reference 5 of paper, p. 585, discussion by Max Jakob.

Author's Closure

The main advantage of the present treatment over the numerical method discussed by Mr. Dusinberre seems to lie in its dual nature in that it supplies first the mathematical formula and secondly the graph for any oblique distribution within the scope of the subject matter, such as the four special series herein and their temperature distribution graphs. Its application involves, of course, the selection of a given obliquity angle β and its incorporation into Equation [7] and corresponding graph as preliminary to any special detailed study of the situation it represents; but now that [7] is supplied, the time involved may be of the same order of magnitude as for obtaining from the beginning a graph by the numerical method. And the present method is then roughly of twice the productivity in that it supplies the mathematical series as well as the graph.

One does not need to enlarge upon the power and completeness of any mathematical solution that is true to the facts of any problem. It usually involves hidden truths to be unraveled by further study of the formulas, as well as often unexpected though mathematically obvious relations such as that herein shown and discussed concerning the temperature drop as a function of the obliquity angle.

The greater flexibility of the numerical method is readily conceded, but flexibility of method is usually accompanied by corresponding handicaps. A more flexible analytical method is usually the more difficult one, witness Weierstrass elliptic functions as compared with the more frequently used Legendre functions. In the present instance the flexibility of the numerical method is obtained at the expense of any mathematical representation at all, and so in this regard it has only half the thoroughgoing completeness of the twofold treatment herein.

Ratio and Multiple-Fuel Controls in the Steel Industry

By HERBERT ZIEBOLZ,[1] CHICAGO, ILL.

The need for accurate control of the furnace atmosphere in the steel industry has brought about the development of a variety of designs and basic circuits to solve this problem. The methods used and the apparatus which were developed are briefly discussed, i.e., (1) the basic ratio control, (2) the control mixing stations, and (3) the controls available for burning several fuels simultaneously with only one common supply for combustion air.

Reason for Use of Ratio Controls in Steel Industry

THE development of automatic controls and instruments in the steel industry followed a course somewhat different from that in other industries. Relatively great forces had to be handled. Many of the plants were old and out-dated, and the original designers had rarely considered the requirements of controls and instruments. Consequently, most of the installations had to be designed to meet individual requirements.

The last ten years have fortunately brought about a better understanding of the mutual problems, and the importance of this co-operation can hardly be overemphasized.

Generally speaking, there are three major problems, typical of the steel industry:

1 Chemically changing the material handled.
2 Changing its physical shape.
3 Raising its temperature prior to (1) and (2).

The diagram, Fig. 1, showing the variables entering into problem 3, i.e., the heating of carbon steel, gives a general view of the subject covered by this paper. The vertical *Z* axis shows the products of combustion of the most expensive fuel in the entire steel plant, i.e., scale. The *X* axis gives the percentages of excess and deficiency of combustion air, the *Y* axis gives various steel temperatures. It will also be noticed that the heating time, during which the steel is exposed to these temperatures and atmospheres, is indicated. This diagram gives in concise form the story of heating steel, and it will be observed that if it is required to bring a piece of steel to a given temperature with a minimum and controlled type of scale formation, two variables must be taken into account, as follows:

(*a*) Rate of temperature increase.
(*b*) Atmosphere control.

The purpose of this paper is to discuss the latter problem and, in particular, the mechanisms developed for combustion or atmosphere control. This includes the premixing of fuels to be used in the burners.

An attempt will be made to show the reasoning behind various solutions from the viewpoint of the oft forgotten designer, as a more general knowledge of his problems may well be of value in the future development of the art.

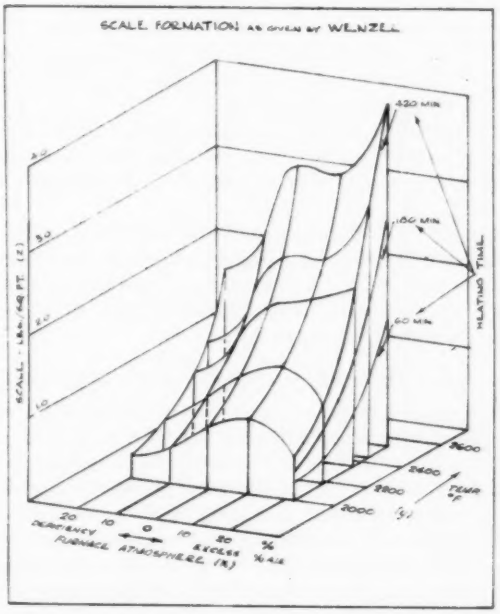


Fig. 1 Scale Formation of Carbon Steel as Function of Atmosphere, Temperature, and Heating Time for Carbon Content of 0.35 to 0.61 Per Cent

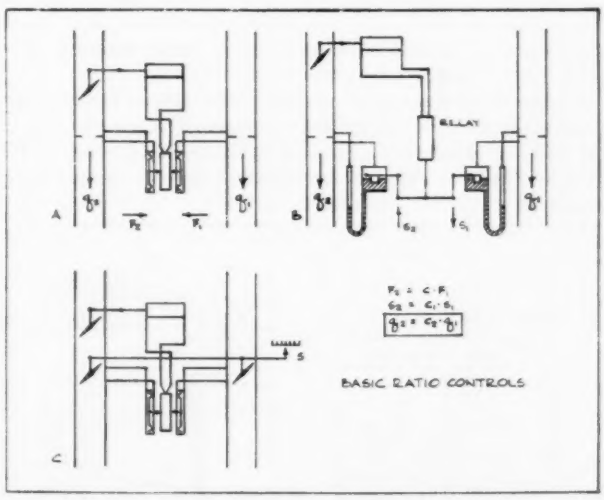


Fig. 2 Basic Ratio Controls

(*A*, Balancing of forces produced by pressures across fixed orifice plates. *B*, Balancing of movements created by pressures across fixed orifice plates *C*, Balancing of forces produced by pressures across orifice plates.)

Basic Ratio-Control Principles

In order to control the proportion between fuel and air, and thus atmospheres, we must first measure the rates of flow. Two alternate methods are generally available:

1 The use of a fixed orifice with varying differential.
2 The use of a variable orifice with a fixed differential.

---

[1] Vice-President, Askania Regulator Company. Jun. A.S.M.E.

Contributed by the Industrial Instruments and Regulators Division and presented at the Spring Meeting, Birmingham, Ala., April 3–5, 1944, of The American Society of Mechanical Engineers.

Note: Statements and opinions advanced in papers are to be understood as individual expressions of their authors and not those of the Society.

It should also be borne in mind that most ratio- or mixing-control jobs demand a constant or varying ratio on a weight basis rather than on a volumetric basis. Thus the factor of density enters into the picture, and we can expect that in the future more consideration will be given to its measurement. Keeping this in mind, we can now consider basic solutions of ratio-control problems.

Fig. 2(*A*) shows the typical method of balancing two differentials against each other. As long as the two forces F_2 and F_1 are proportional the corresponding pressure drops and thus the rate of flows q_2 and q_1 are proportional. We shall use this diagram as a symbol rather than as representative of a particular design in the following schematic sketches.

As an alternative, we can match the strokes S_1 and S_2, Fig. 2(*B*), instead of forces, if we make provision that these movements are proportional to the differential pressures. The diagram is self-explanatory.

In Fig. 2(*C*) we find the same ratio control as in Fig. 2(*A*), with the modification that variable orifices are used to increase the range of operation. In this particular instance, butterflies of identical characteristics (with geometric proportionality and with the same Reynolds numbers) are used.

Central Gas-Mixing Stations for Interchangeable Fuels

Fortunately for the steel industry, it frequently has a number of sources of fuel gas at its disposal. To use these fuels without the need for repeated burner- and combustion-control adjustments, it is necessary to provide central or individual gas-mixing stations, in order to provide an interchangeable fuel at all times.

Owing to the wide variations in fuel demand in central mixing stations, it is obvious that only variable orifices can be used in such stations. Fig. 3(*A*) shows a "wide-range mixing station in which the variable orifices are operated by means of a differential controller which keeps constant the pressure drop across one of the variable orifices, q_1. The ratio-controller's job is to proportion the pressure drop produced by the other rate of fluid flow q_2, to that produced by q_1 across the primary variable orifice. Both orifices move simultaneously and are so connected as to give (directly) proportional free areas.

A supervising control, responding to the Btu of the mixture, density, or any other representative variable, is used to correct the ratio by adjusting s. Such additional controls serve at the same time as a correction for discrepancies between the flow characteristics of the variable orifices.

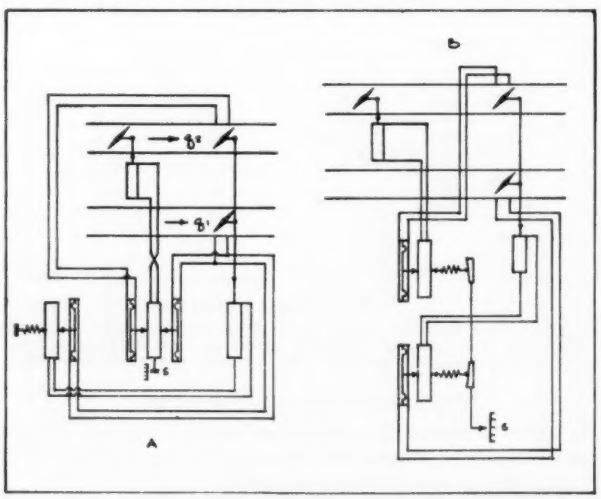


Fig. 3 Wide-Range Ratio Control
(*A*, With one differential and one ratio control. *B*, With two differential controls.)

From the foregoing, it seems logical to develop an alternative scheme, Fig. 3(*B*). If the differential across one of the orifices is kept constant, it is unnecessary to measure it a second time. A spring can thus be substituted for the right-hand diaphragm of Fig. 3(*A*), or to make the control more flexible, a cam can be used which simultaneously changes the differential-pressure settings of the primary- and secondary-flow-rate controllers. An adjustment of the cam s will change the ratio between the two flow rates, and thus obtain any desired relationship between s and the ratio between the two fluids.

Fig. 4 shows how the change of ratio setting is accomplished.

Typical Means for Varying Ratio Setting

The ratio adjuster as shown in Fig. 4(*a*) and in two typical controller designs has a particular characteristic, i.e., the relationship between its stroke and the ratio established for the opposing forces F_1 and F_2.

This ratio is given in Fig. 4(*b*) and represents a hyperbolic function. Fortunately, the hyperbola coincides to an unexpectedly high degree of accuracy with a logarithmic curve within the range of values of R between 2 and 0.5 in., which is typical for ratio adjustments. This makes an adjustment of the ratio slider possible without a recalibration of scales, as any correction factor can be introduced into the mechanism by means of a shift of the ratio scale. The reason for this is the fact that the log of the product of two variables is the sum of the logs of the two variables. It also allows the mechanical addition of movements representing correction factors, such as barometric pressure, temperature, Btu content, humidity, density, and other variables.

This ratio variation, produced by increasing one of the differentials of a ratio control relative to the magnitude of the other is shown in Fig. 4(*d*), where one orifice is fixed, the other variable, and in Fig. 4(*e*), where the free areas of both orifices change in opposite direction.

Another scheme which may at first glance appear rather elaborate is shown in Fig. 4(*f*). A ratio control establishes a pilot flow of low-pressure air which is directly proportional to the main flow. A double orifice of the type shown in Fig. 4(*e*) is used to split this pilot flow into two proportional branches. The flow through one of these branches is used to produce a signal which controls the rate of flow q_2, by means of a second ratio control. Thus depending upon the position of the double orifice in the pilot line, various ratios of q_1/q_2 can be obtained.

Compensation for Air Infiltration or Constant Amount of Primary-Air Supply

So far, we have only considered the control of one rate of flow proportionally to a second one and have solved our multiple-fuel problem by proportioning the individual fuels to each other, so as to produce a new composite fuel which can then be proportioned to air.

The simplest solution of a multiple-fuel problem is to provide a separate air supply for each fuel. Although this design is quite frequently used, it requires surplus capacity of fans and ducts, as, if 100 per cent of any fuel should be used at any time, the total air must be delivered from its particular source.

In this connection it may be well to recommend thinking of air as a fuel of about 100 Btu per standard cu ft which can be burned with various fluids.

Given two fluids with flows q_a and q_b, which are measured by their respective pressure drops h_a and h_b, with the flow constant c_a and c_b, the problem of controlling a third rate of flow q_c with h_c and c_c proportional to their sum takes the following form

$$(q_a + q_b) = q_c$$
$$(c_a \sqrt{h_a} + c_b \sqrt{h_b}) = c_c \sqrt{h_c}$$

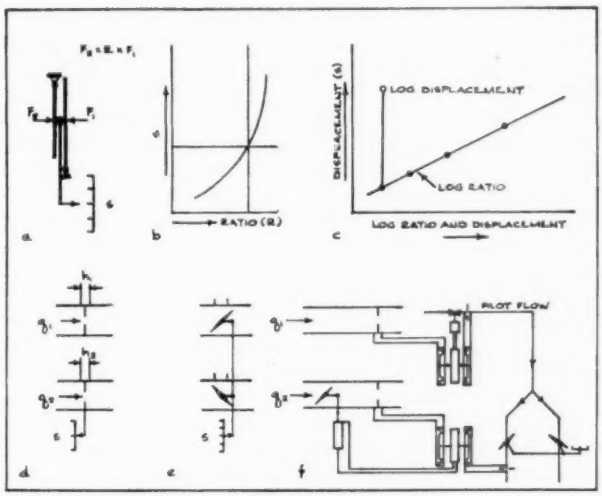


FIG. 4 RATIO-VARYING DEVICES

(*a*, Ratio slider; *b* and *c*, relationship between stroke and ratio; *d* and *e*, ratio change by means of variable orifice; *f*, ratio change by means of controlling pilot flows.)

$$(c_a^2 \cdot h_a + c_b^2 \cdot h_b) + 2 \cdot c_a \cdot c_b \cdot \sqrt{h_a \cdot h_b} = c_c^2 \cdot h_c$$

This equation shows that h_c cannot be made proportional to $c_a^2 \cdot h_a + c_b^2 \cdot h_b$, as is time and again suggested even by engineers who should know better.

One typical example is the case where the fuel has to be proportional to the sum of two air flows. These two air supplies may be as follows:

(*a*) Combustion air + air infiltration; or
(*b*) Combustion air + primary air.

It is in such cases often erroneously suggested to provide an additional spring loading on one of the diaphragms to compensate for or to represent the rate of air infiltration or primary-air flow which is assumed to be constant.

In Fig. 5, the result of this method is shown giving the possible compensation for constant "air infiltration" of 5 per cent and 15 per cent maximum flow q_2.

The diagram, Fig. 6, proves that it is possible to improve greatly the effect of this compensation by using 3 times the equivalent force of the amount of infiltration as the spring tension to be added. This gives satisfactory results down to as low as 30 per cent of the maximum rate of flow.

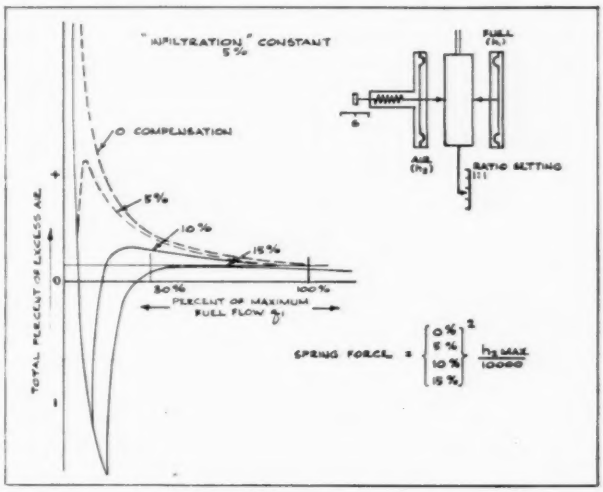


FIG. 6 EFFECT OF VARIABLES OR CONSTANT FORCES ADDED TO RATIO REGULATORS FOR COMPENSATION OF INFILTRATION

However, since at 10 per cent flow, the force of the diaphragm is equal to $^1/_{100}$ of the maximum force obtained from full flow, it becomes apparent how critical is this adjustment and that it should be used only in emergencies, and by men who know exactly its effect. A variation of infiltration with time, and an attempt to compensate for it by the foregoing method seems therefore not to be too desirable as a plant-maintenance job.

It seems promising to try a solution in which a model of the actual flow distribution is established and the same flow pattern is repeated on a smaller scale. Fig. 7 shows this method. A pilot flow is established, which is directly proportional to the total air requirements of the fuel q_1. Downstream from the pilot-flow valve, an orifice produces a signal differential which is used to act upon the main air-flow regulator. The orifice for the first ratio control, which establishes the pilot flow, is upstream from the pilot-flow valve. By bleeding various amounts of air between this valve and the upstream orifice, an amount of air can be deducted from the downstream pilot flow which is directly proportional to the air infiltration.

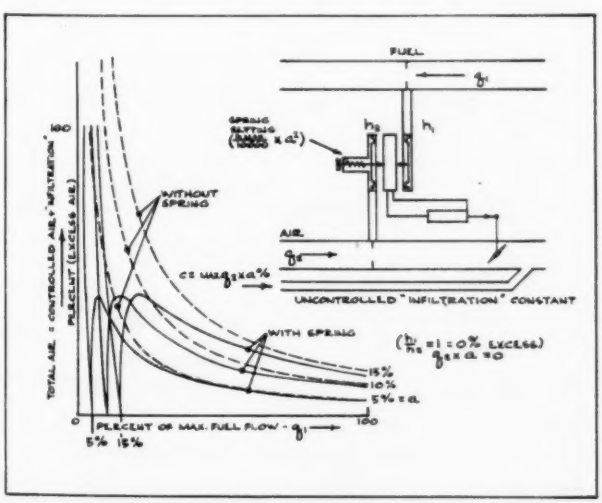


FIG. 5 CORRECTION FOR INFILTRATION BY ADDING CONSTANT FORCES ON RATIO REGULATORS

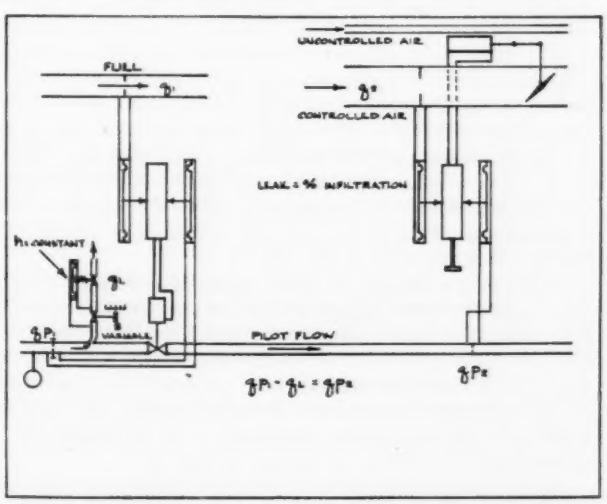


FIG. 7 CORRECTION FOR UNCONTROLLED AIR FLOW BY MEANS OF PILOT FLOWS

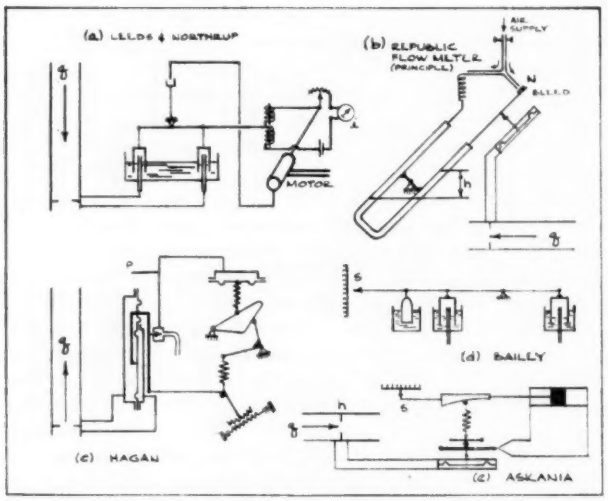


FIG. 8 VARIOUS METHODS TO EXTRACT SQUARE ROOTS AND FOR GETTING SECOND-POWER FUNCTIONS

A differential regulator is shown making the adjustment of the bleed-off valve a direct function of the bleed-off flow.

The basic reason for the success of this arrangement is the fact that the square functions, i.e., the differential pressures, are converted into linear functions of flow rates. These functions can then be added or subtracted without introducing an error.

METHODS AND DEVICES FOR "MODULATING" SIGNALS

It has been shown that the basic problem in multiple-fuel control is the conversion of square functions into linear functions, and the provision of means for adding and subtracting values representing individual flow rates or air requirements.

It seems desirable therefore to study some of the methods developed by various designers to solve this problem before we discuss the complete controls available for multiple-fuel-control problems.

In Fig. 8(*a*), one solution is found in the use of a Kelvin balance (Leeds & Northrup Company) which produces a "pilot" flow of electrical current which is directly proportional to the fuel flow or its air requirements.

As the force developed by the two coils in series is proportional to the square of the current flowing through them, and the force exerted on the pressure bells is proportional to q^2, we obtain a current which is directly porportional to the flow rate q. The current is controlled by a rheostat and a motor which reverses its direction of rotation, depending upon the direction of the unbalanced movement of the instrument. While previously an energy rate of flow was obtained in the form of a fluid pilot flow, the device mentioned produces a directly proportional electric-energy flow rate represented by the current i. This current, as we shall see later, lends itself just as well as the fluid pilot flow to summarizing and subtracting problems.

In Fig. 8(*b*), a mechanical device is shown in which the differential pressure across an orifice (a second power function of the flow rate) is translated into a pressure which is a linear function of the flow. The differential across the orifice tilts a U-tube and thereby simultaneously increases the pressure in a relay nozzle N. The pressure thus produced is transmitted to one leg of the U-tube and thereby causes the liquid level to change by an amount h.

As the counteracting or feedback moment is proportional to h times the distance of the displacement center of gravity ($c_1 \cdot h$) the moment becomes equal to ($c_1 \times h^2$), or, when in the balanced condition, h becomes directly proportional to q. The device thus takes the square root out of the flow signal. Reversing the design, it is possible to produce an h_2 which is porportional to the square of h_1 (Republic Flow Meters Company's "modulator").

Another company (Hagan Corporation) introduces the additional parameter s, a stroke. The differential pressure acts upon a diaphragm, Fig. 8(*c*), thus creating a force directly proportional to the square of the flow rate q. This force is transmitted to the outside through a stuffing box (diaphragm type) and controls a relay valve which produces a pressure on top of a spring-opposed diaphragm. For every pressure on the diaphragm, a stroke is obtained which is modified by a cam, and reconverted into a force which finally opposes the primary-flow-rate signal. Thus a feedback establishes a balance between forces and produces a pressure p which, by use of a proper cam, can be made directly proportional to q.

A ratio adjuster working on the force-vector principle allows a change of the proportionality factor. The translation is thus accomplished in steps following the sequence:

From flow energy to differential pressure to force(I) to stroke; to a modified stroke to a force(II), with a feedback circuit between force(I) and force(II).

We will find such translators in series in most of our multiple-fuel-control solutions. Again the device can be reversed, with slight changes, to produce a differential h^2 for any given p or h.

In Fig. 8(*d*), the same problem is solved (by Bailey Meters Company) with the use of displacement bodies and floating inverted bells.

The translation follows the lines:

Energy flow—differential pressure—force(I)—stroke—force(II) (counteracting buoyancy). Feedback is established between force(I) and force(II) with the result that the stroke s becomes directly proportional to q, the flow rate.

Fig. 8(*e*) shows another method (Askania Regulator Company) in which the translation is obtained by means of a force feedback, represented by a spring counteracting the diaphragm force. By the use of an adjustable cam, which can be easily adjusted in the field, any relationship between h and s can be produced. This is particularly advantageous if the flow signals, as frequently happens, do not follow second power or any other predictable or simple laws.

We recall that the reason for the existence of all these translating devices is that the square of the sum is not equal to the sum

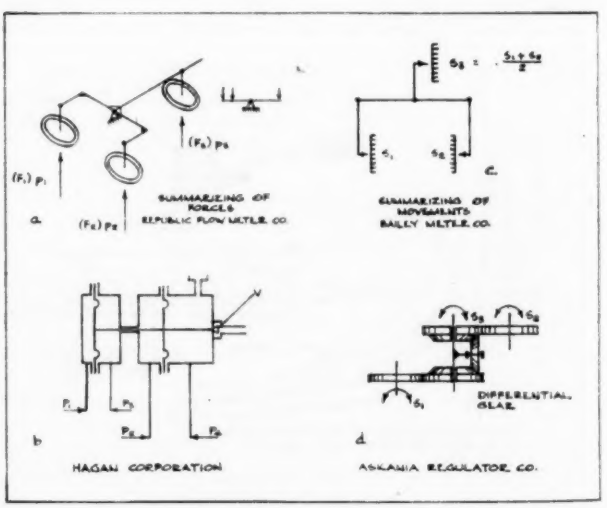


FIG. 9 VARIOUS SUMMARIZING DEVICES FOR FORCES *a* AND *b* AND MOVEMENTS *c* AND *d*

of the squares, and that directly proportional variables must be obtained for summarization.

Means for Summarization of Signals Representing Flow Rates

Before describing the individual basic solutions of the multiple-fuel problem as they are now available to the steel industry, we shall discuss briefly some typical summarizing devices for pressures and strokes as they are found in many various controllers. As it is impossible to summarize pressures directly, a detour becomes necessary.

Fig. 9(*a*) uses for that purpose a forked lever with pressures p_1 and p_2 applied to individual diaphragms. A pilot (not shown) produces a pressure p_3, which is used as a feedback into a third diaphragm, producing a balancing force F_3. Then F_3 becomes the sum of $(F_1 \cdot c_1 + F_2 \cdot c_2)$ with c_1 and c_2 as constants (Republic Flow Meters Company). Basically, the same idea is used in design Fig. 9(*b*), in which two or three pressures are added or subtracted by means of diaphragms in series. Pressure p_4 is the resulting pressure counteracting $(c_1 \cdot p_1 + c_2 \cdot p_2 - c_3 \cdot p_3)$ and controlled by a bleed-off valve v (Hagan Corporation).

In the class of the stroke summarizers, we find the whiffletree, Fig. 9(*c*) (Bailey Meter Company), and the differential gearbox Fig. 9(*d*) (Askania Regulator Company). Both of these devices are too well known to need any further explanation.

Methods and Devices for Combustion Controls Using Several Fuels but Only One Air Supply

Thus prepared, we can finally analyze the various designs of actual controllers used in multiple-fuel controls.

We have seen that producing a proportional pilot-flow model offers a particularly flexible solution. In Fig. 10 (Leeds & Northrup Company), we note that the summarization is accomplished by the addition of two (or more) currents which are directly proportional to the individual air requirements.

New in this picture is the use of a positive-displacement meter for measuring the fuel-oil rate of flow by means of a generated voltage directly proportional to the speed of the meter. The generated voltage is balanced by a potentiometer controller against the voltage due to the current (i_2 current) flow in the pilot circuit. The potentiometer adjusts the rheostat to maintain this voltage. This current is added to that produced by the Kelvin bridge. The square-root symbol indicates the linearity of the controlled strokes. No special summarizing devices are necessary,

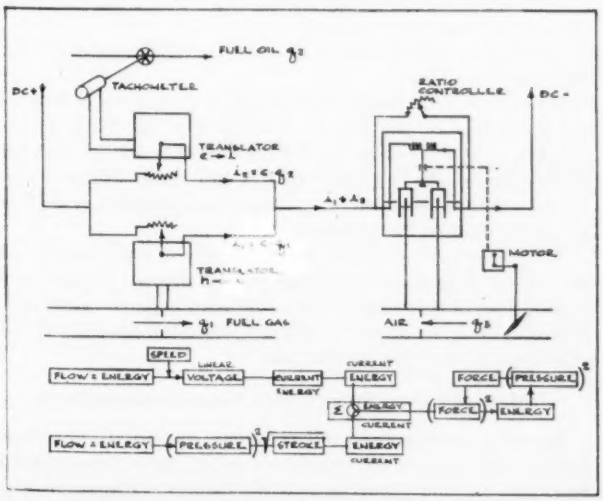


Fig. 10 Multiple-Fuel Control; Leeds & Northrup Company

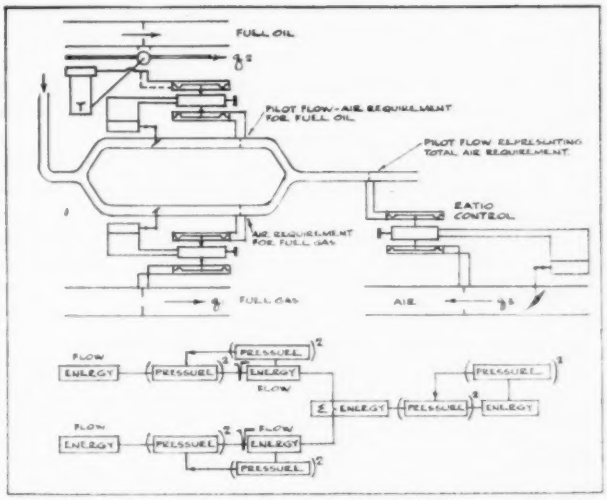


Fig. 11 Multiple-Fuel Control; Askania Regulator Company

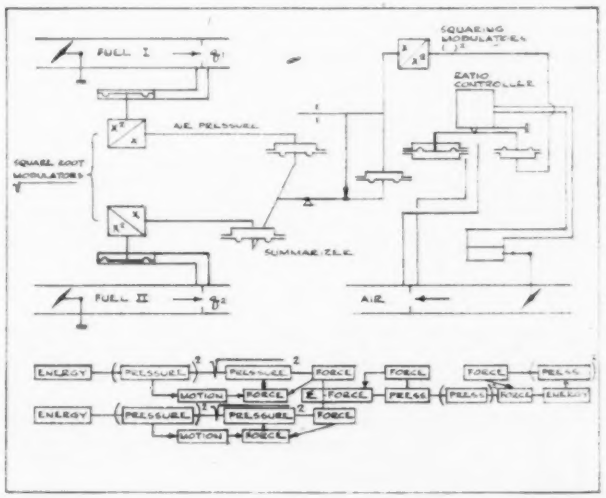


Fig. 12 Multiple-Fuel Control; Republic Flow Meters Company

as the currents flow together in accordance with Kirchhoff's law. The sum total produces a force proportional to i^2 and controls the flow of air needed for combustion.

The ratio controller is basically the Kelvin balance in reverse. The air-flow energy produces a second-power pressure, which, translated into a force, is fed back against the current force.

A ratio adjuster in the form of a rheostat permits the adjustment of the ratio from excess to deficiency.

An attempt is made in Fig. 10 and the following diagrams to present the individual steps of translations in a block diagram.

For want of a definite standard way of using symbols for such translators these diagrams are tentative only and should be modified as soon as a general agreement on these symbols has been or can be reached. For the purpose of the present paper, however, these diagrams may be sufficiently clear to demonstrate the approach to the circuit analysis, although it would be desirable to develop a more universally acceptable way of presentation.

Fig. 11 is basically the same circuit with the exception that fluid pilot flows are used instead of the electrical currents (Askania Regulator Company).

Of interest is the possibility of using alternative fuels by the application of the device which translates the speed of the posi-

tive-displacement oil meter into square-function air pressures. By matching the fluid pressure produced by this device to that obtained from an orifice in the alternate fuel line in such a manner that it represents the same air requirement, the pneumatic tachometer T can be switched off, and its signal can be replaced by the gas differential without any changes in the circuit.

For convenience, the orifices in the pilot lines are adjustable, thus greatly facilitating adjustments for varying operating conditions.

As the two pilot flows can be easily combined and the totalized flow produces a square function across the totalizer orifice in the common conduit, no additional translating devices are needed. Feedback is established by balancing pressure differentials, or to be more precise, forces.

In Fig. 12, the summarization is accomplished by adding pressures or forces which are directly proportional to the flow rates (Republic Flow Meters Company). To do this, "modulators" converting square functions into linear functions (symbol x^2/x) are used, and summarizers as shown in Fig. 9(a). The sum is "modulated" into a square function (symbol x/x^2) and applied to a ratio regulator which controls the total combustion air. The air differential is fed back into the ratio control to re-establish balance.

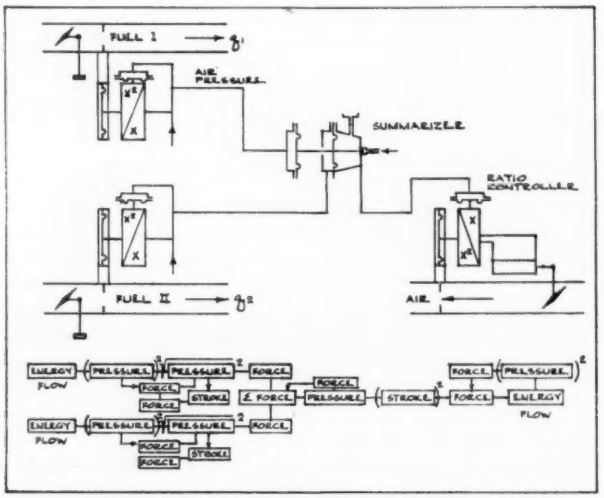


FIG. 13 MULTIPLE-FUEL CONTROL; HAGAN CORPORATION

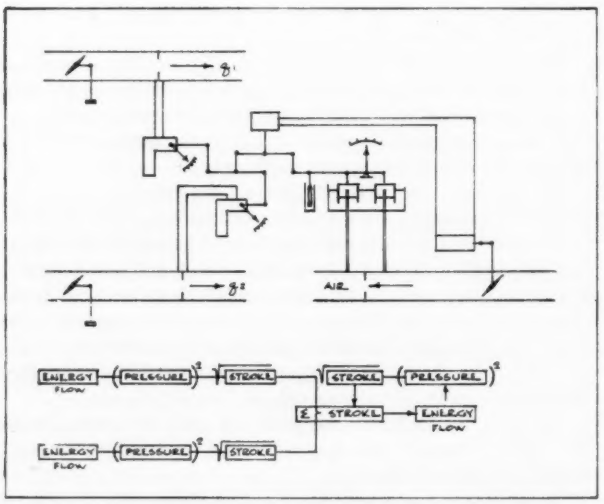


FIG. 14 MULTIPLE-FUEL CONTROL; BAILEY METER COMPANY

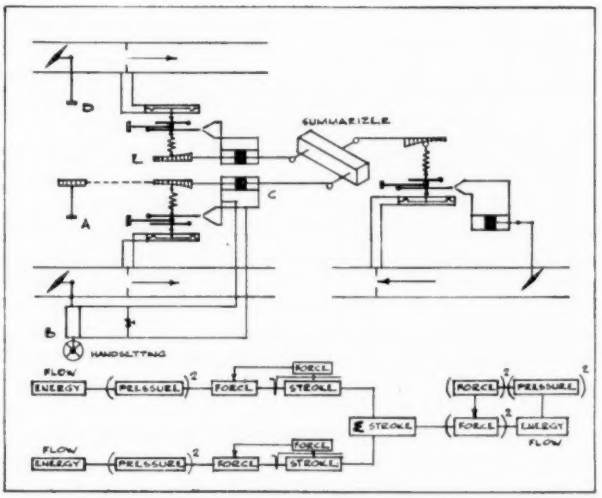


FIG. 15 MULTIPLE-FUEL CONTROL; ASKANIA REGULATOR COMPANY

Basically, the same line of thinking is found in the solution of Fig. 13 (Hagan Corporation), although, as previously shown, the details of the modulator design are different. For the purpose of clarity the same box symbols for the modulators are shown as in Fig. 12.

In Fig. 14, the summarization is accomplished by means of the whiffletree shown in Fig. 9. Individual flowmeters add their pointer movements (without additional power amplifiers) and produce linear movements by suitable float arrangements (stroke modulators) or displacement bodies (force modulators) (Bailey Meter Company). The diagram is self-explanatory. Feedback is accomplished by comparing movements of "strokes."

The last example, Fig. 15, shows a stroke feedback with power amplification (Askania Regulator Company). The modulator, previously discussed in connection with Fig. 8(e), will be recognized.

The diagram shows an alternative adjustment of A or B. If the cam is set by hand, adjustment A, the butterfly valve is controlled, and thus the fuel flow becomes constant, regardless of any variations in the fuel-supply line. If B is set by hand, the flow regulator acts as a "flowmeter." Adjustable cams permit not only correction for second-power flow signals, but permit also:

(a) Correct compensation for any air infiltration (either constant or varying with the load).

(b) The varying of setting of excess and deficiencies of air for different heat inputs.

How this same principle can be applied to wide-range flow-mixing or combustion problems is shown in Fig. 16. With the same number of controls as in Fig. 15, and variable orifices, any turndown range can be handled. In this case again strokes are used as the common parameters, strokes are summarized, and strokes are used in the feedback system.

With these tools available, we are finally in a position to solve practically all problems of multiple-fuel controls. As most of the applications have been previously discussed in papers given by the individual manufacturers, a detailed discussion would only be a repetition of available information.

MAKE-UP FUEL STARTED AT A PREDETERMINED RATE

Recently another problem has become more and more important, i.e., the need for starting the secondary fuel at some minimum flow rate, as there is usually a certain minimum rate below which a burner cannot operate satisfactorily. If a deficiency of pri-

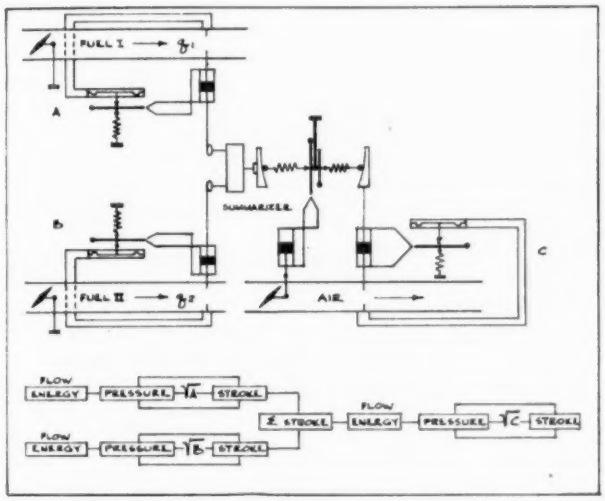


FIG. 16 WIDE-RANGE MULTIPLE-FUEL CONTROL; ASKANIA REGULATOR COMPANY

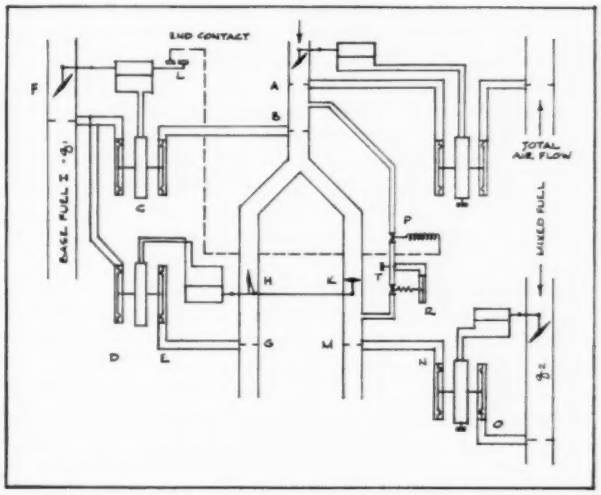


FIG. 17 MULTIPLE-FUEL CONTROL WITH MINIMUM SETTING OF SECONDARY FUEL

mary fuel therefore demands a start of secondary fuel, means have to be found to start the secondary-fuel flow at once at this minimum rate, and simultaneously to reduce the primary-fuel flow by an equivalent amount of Btu supply.

Fig. 17 shows one possible solution which uses pilot flows to represent air flow or Btu rates per time unit (Askania Regulator Company). The total air flow, or the rate of total Btu supply, is replaced by a pilot flow which branches into two lines representing the Btu rates of the individual fuels.

An orifice in the main pilot line B produces a signal representing a certain amount of Btu of fuel I (q_1). As long as ratio regulator C can satisfy this demand, and controls butterfly F, the differential acting on D is equal or slightly greater than that produced by G. Under these conditions, butterfly H is open and butterfly K closed.

Both butterflies are operating in opposite directions H, opening when K closes and vice versa.

If there is a deficiency of the primary fuel, butterfly F opens wide in an attempt to satisfy the demand, and thus closes contacts L, which energize a solenoid valve P, and thereby a passage for bleeding a definite amount of pilot flow from a point between A and B to a point ahead of M, which determines the rate of fuel demand for the secondary fuel.

This fuel rate is controlled by means of the ratio regulator N–O. A differential control valve in R the by-pass, and an adjustable restriction T, assure a definite rate of flow which represents the minimum flow rate for the secondary-fuel burner.

It will be noted that the diversion of flow from the left branch to the right decreases the loading on ratio control C. Butterfly F therefore reduces the flow rate (q_1) by at least the amount of the by-passed pilot flow, and ratio control D–E cuts down the pilot flow through H and increases the flow through K so that the difference is always diverted to orifice M. The design is intentionally so arranged that the secondary-fuel burners remain in operation until an operator manually disconnects them from the line. All that is necessary for this purpose is to de-energize solenoid P, which incidently can also be done automatically.

It appears that all of the foregoing solutions offer a great help to the operator and simplify his job of operating a furnace.

The question which is still open, and which this paper did not attempt to cover, is: What is the best setting of these calculating and controlling devices assuming optimum operating conditions?

We must not forget that the equipment, even if its performance is beyond reproach, is just as capable of maintaining the wrong operating conditions as it is of maintaining the correct ones.

ACKNOWLEDGMENT

The author is indebted for assistance in the preparation of the paper to Messrs. M. J. Boho, Hagan Corporation; C. J. Geiser, Republic Flow Meters Co.; J. C. Peters, Leeds & Northrup Company, H. E. Weaver, Bailey Meter Company, and P. W. Keppler, Foxboro Co.

BIBLIOGRAPHY

1 "Open Hearth Furnace Control," by M. J. Bradley, *Iron and Steel Engineer*, vol. 18, June, 1941, pp. 35–45, 50.

2 "Modulator Controls for Multi-Fuel-Fired Furnaces," by C. J. Geiser, *Iron and Steel Engineer*, vol. 20, August, 1943, pp. 35–39.

3 "Fuel Air Control for Open-Hearth Furnaces," by T. A. Peebles, *Blast Furnace and Steel Plant*, vol. 26, 1938, pp. 404–405.

4 "Recent Advances in the Control of Multi-Fired Furnaces," by J. C. Vaaler, *Iron and Steel Engineer*, vol. 19, September, 1942, pp. 134–140.

5 "Versuche über den Abbrand in Walzwerksöfen—IV," by Fritz Wenzel, *Stahl und Eisen*, vol. 58, 1938, pp. 481–491.

6 "Characteristics of Hydraulic and Pneumatic Relays as Energy-Converting Devices," by H. Ziebolz, *Instruments*, vol. 15, 1942, pp. 340–345.

"Basic Solutions for Flow Measurement," by H. Ziebolz, *Review of Scientific Instruments*, vol. 15, April, 1944, pp. 80–87.

"Relay Devices and Their Application to the Solution of Mathematical Equations," by H. Ziebolz, Askania Regulator Company, Chicago, Ill., vols. 1 and 2, 1944.

Discussion

C. J. GEISER.[2] The author has contributed a commendable paper, presenting the general problems of ratio and multiple-fuel controls in the steel industry and a brief description of the various designs of systems used to solve these problems.

The problem of uncontrolled air infiltration has always presented difficulties on actual applications. Limitations of burners at low rates of firing and limitations as to the minimum amount of combustion air (cold or preheated) required at the burner at low rates of firing for proper combustion will necessarily limit the extent to which full compensation can be provided. Each individual furnace usually presents an individual problem in this respect requiring extensive test work to determine optimum settings

[2] Republic Flow Meters Company, Chicago, Ill.

for various firing rates and for various phases of the furnace cycle.

The method of compensation described by the author, and illustrated in Figs. 5 and 6, is useful for obtaining a close approximation of theoretically correct total combustion air for the limited firing range specified. Whether or not a furnace will give its best performance with theoretically correct total combustion air (full air-infiltration compensation) at the lower rates of firing, say between 50 and 30 per cent of maximum, can be determined only by actual tests. Due to other considerations, partial compensation (illustrated by the 10 per cent curve of Fig. 6) may possibly give superior over-all results.

It is obvious that higher percentages of air infiltration adversely affect the range of operation of fuel-air ratio control and the attempts to compensate for the infiltration. For example, as an extreme condition, if the air infiltration is equal to 50 per cent of the controlled maximum air flow, the ratio regulator could not possibly control the first $33^1/_3$ per cent of total air flow. Also, using the method of compensation illustrated in Fig. 6, the fuel-flow range would be reduced to a range of approximately 60 per cent to 100 per cent.

The means of compensation shown in Fig. 7 of the paper provides a method for obtaining the correct characteristic for a constant quantity of air infiltration for a particular setting of variable S. It may not be immediately apparent that another means of obtaining exactly the same characteristic is available on the design shown in Fig. 12. Having established an air pressure which is directly proportional and linear with respect to fuel-flow (or total fuel flow on the multiple-fuel control), spring or weight loading of an air-pressure relay (or the summarizer) will exactly compensate for a constant quantity of air infiltration.

Generally, the application of ratio and multiple-fuel controls, particularly on fuel-fired furnace in the steel industry, might be divided into two very broad divisions:

1 The applications on newly designed and built furnaces.
2 The applications on outmoded, existing furnaces.

New furnaces which are carefully designed to minimize air infiltration and to accommodate a wide range of firing, will unquestionably prove the most easily adaptable to the application of these controls. However, the possibilities of applications to the older, existing equipment cannot be overlooked, merely because these applications may introduce difficult problems of maintaining the required combustion analysis due to excessive air infiltration or other limitations. While the older equipment may introduce greater problems for successful application, careful attention by the plant combustion personnel in applying the control, to obtain optimum control settings, will show a great improvement in over-all furnace performance compared to uncontrolled operation.

The vast majority of ratio and similar controls, applied to the steel industry, are entirely dependent upon the judgment of combustion engineers (or other authorized operators) to determine and set the values of pressure, flow, ratio, etc., which the control will maintain throughout the various cycles of the process. As pointed out by the author (and possibly this point cannot be overemphasized), "the control is just as capable of maintaining the wrong operating conditions as it is of maintaining the correct ones." The personnel factor, therefore, enters into the over-all application problem to a large degree and should be given very serious consideration when determining the features which are to be incorporated into any particular design of these controls for a particular application. Considering the physical condition and other limitations of older, existing mill equipment, as well as the deep-rooted precedents which have been established during a long period of use by the operators, the greatest care and attention are required for the successful application on old furnaces.

Summarizing the features of combustion-control equipment which is today available to progressive combustion engineers:

1 Standard fuel-air ratio controls may be compensated for air infiltration, within limits.

2 An almost unlimited number of control-characteristic combinations are available to permit addition and subtraction, multiplication and division of control factors, with designs that can be readily tailor-made to fit the exact requirements of a single application.

3 The extent of control refinements possible is limited in most cases only by the ability of the plant personnel to use the control equipment successfully.

Stress Coefficients for Rotating Disks of Conical Profile

By K. E. BISSHOPP,[1] BELOIT, WIS.

The solution of this problem involves calculations with infinite series which satisfy a hypergeometric differential equation of exponent difference 2. Numerical evaluation of the coefficients is facilitated by employing the linear relations between the hypergeometric functions of arguments x and $1 - x$. These linear relations are derived by an elementary method, which it is believed, has not been described heretofore in engineering literature. The formulas obtained by this method were used to compile tables of the hypergeometric function and the related stress coefficients for various values of Poisson's ratio. The application of these stress coefficients to an illustrative example which had been calculated with a system of uniform disks clearly shows the advantages obtainable with a system of conical profiles.

Nomenclature

THE following nomenclature is used in the paper:

a, b, c α, β, γ	=	elements of hypergeometric equation
A, B	=	arbitrary constants
C_1, C_2, C_3	=	constants which express linear relations between the hypergeometric functions of x and $1 - x$
h	=	one-half thickness of disk at any radius
m, n	=	integers
p, p', p''	=	radial stresses
q, q', q''	=	tangential stresses
r	=	radius
t	=	$1 - x$
u_n	=	coefficient of x^n
x	=	r/R
P	=	$(1 - x)p$
Q	=	$P + xdP/dx$
R_m	=	remainder term
$S_1(x), S_4(x)$	=	infinite series involving x
$S_2(t), S_3(t)$	=	infinite series involving t
Φ_n		defined by Equation [24] or [38]
$\psi(x)$		defined by Equation [25]
$\Psi(x)$		defined by Equation [27]
$\Gamma(x)$	=	Gamma function
γ	=	0.577,215,665 . . . (Euler's constant)
σ	=	Poisson's ratio
ρ	=	mass density
ω	=	angular velocity, radians per sec.

[1] Design Calculator, Fairbanks, Morse & Company.

Presented at the Annual Meeting, New York, N. Y., Nov. 29–Dec. 3, 1943, of The American Society of Mechanical Engineers.

Discussion of this paper should be addressed to the Secretary, A.S.M.E., 29 West 39th Street, New York, N. Y., and will be accepted until April 10, 1944, for publication at a later date. Discussion received after the closing date will be returned.

Note: Statements and opinions advanced in papers are to be understood as individual expressions of their authors, and not those of the Society.

Purpose of Study

Stress coefficients for rotating disks of conical profile were obtained from power-series solutions of a hypergeometric differential equation (1)[2] of integral exponent difference by Martin (2) and Honegger (3), who recognized the objections to this method of calculation. Numerical evaluation of the coefficients corresponding to the values of the argument near which these series converge slowly or diverge becomes laborious, and in some cases asymptotic approximations may be necessary. Furthermore, the inadequacy of power series alone for calculating uniformly accurate coefficients is shown by the limitations of the published tables. This paper describes a more convenient form of the solution which avoids these difficulties of computation and at the same time substantiates the results of previous investigators.

The easiest solutions to construct are the two series in ascending powers of x and $1 - x$, respectively, given by Martin (2) and Honegger (3). There are also two other expansions in terms of x and $1 - x$ which the integral exponent difference of the differential equation shows involve logarithms. A more convenient method of calculation can be obtained by using linear combinations of all four solutions. The appropriate factors are determined by the asymptotic behavior of the hypergeometric function and/or its derivatives in the neighborhood of the poles. This procedure gives the principal part of the logarithmic solution in finite form near $x = 0$ instead of a slowly convergent series in powers of $1 - x$. The method retains its advantages when applied to the evaluation of the power series solution near $x = 1$ even though this series does converge absolutely at that point.

The difficulties of the power-series method cannot be removed by transformation since the singularities of the stress functions remain unchanged. This can be seen in reference (3), where the solution is obtained from a differential equation of exponent difference 2, involving the radial strain. Except for small differences, Honegger's results can be verified from the tables at the end of this paper by introducing factors of proportionality which are finally absorbed in the arbitrary constants of the general solution. The point of view assumed here in deriving the basic differential equation parallels Martin's analysis which gives the stress coefficients directly without transformation.

Derivation of Differential Equation (4)

In Fig. 1, let p and q denote mean radial and hoop stresses at r, and let the variable thickness be $2h$ so that for a conical profile $2h = 2H(1 - r/R)$ where H is a constant. If ρ is the mass density of the material and ω the angular velocity of rotation in radians per second, there is obtained by equating forces acting on an infinitesimal element of volume

$$4hqdr \sin {}^1/_2(d\theta) - 2d(hrp)d\theta = 2\rho h\omega^2 r^2 dr d\theta \ldots\ldots [1]$$

$$(1 - r/R)q - (1 - 2r/R)p - r(1 - r/R)dp/dr = \rho\,(1 - r/R)\,r^2\omega^2 \ldots\ldots [2]$$

[2] Numbers in parentheses refer to the Bibliography at the end of the paper.

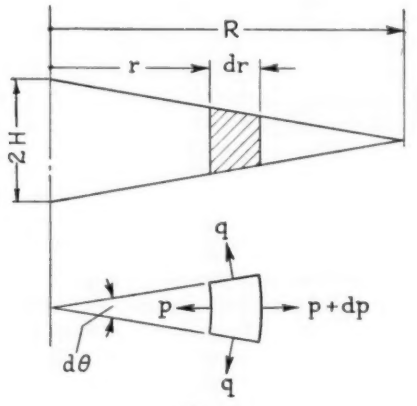


FIG. 1

The condition for compatibility between stress and strain requires

$$p - \sigma q = d/dr(rq - \sigma rp) \quad \ldots\ldots [3]$$

where σ is Poisson's ratio.
Differentiating Equation [2] and setting $r = Rx$ gives

$$x\frac{d^2p}{dx^2} - \frac{3x-2}{1-x}\cdot\frac{dp}{dx} - \frac{dq}{dx} - \frac{p}{(1-x)^2} = -2\rho R^2\omega^2 x \quad \ldots [4]$$

The result of eliminating q and dq/dx from Equations [2], [3], and [4], after making the substitution $P = (1-x)p$ is

$$x(1-x)\frac{d^2P}{dx^2} + (3-2x)\frac{dP}{dx} + (1-\sigma)P = -(3+\sigma)\rho R^2\omega^2 x(1-x) \quad \ldots [5]$$

the left-hand side of which is recognized to be of hypergeometric type, such as (reference 5)

$$x(1-x)\frac{d^2P}{dx^2} + [c-(a+b+1)x]\frac{dP}{dx} - abP = 0 \quad \ldots [6]$$

where $c = 3$, $a + b = 1$, and $ab = \sigma - 1$.
The substitution of $1 - x = t$ in Equation [6] gives

$$t(1-t)\frac{d^2P}{dt^2} + [a+b+1-c-(a+b+1)t]\frac{dP}{dt} - abP = 0 \quad \ldots\ldots [7]$$

the convenience of which will appear later. Since c is independent of σ, the numerical value of c will be used in the remaining equations, except when it is desired to emphasize general characteristics of the hypergeometric function. Numerical calculations were made for fundamental solutions of Equation [6] and the stress coefficients with $\sigma = 0.24, 0.27, 0.30, 0.33$, and 0.36,[3] corresponding to positive values of x between zero and unity.

SOLUTIONS OF THE DIFFERENTIAL EQUATIONS

The general solution of Equation [5] is

$$P(x) = AP_1(x) + BP_2(x) + P_3(x) \quad \ldots\ldots [8]$$

where $P_1(x)$ and $P_2(x)$ are the complementary functions, and $P_3(x)$ is the particular integral. It can be verified by direct substitution or otherwise, that

$$P_3(x) = \rho\frac{R^2\omega^2(3+\sigma)}{11+\sigma}\left[x^3 - \frac{7+2\sigma}{5+\sigma}x^2 - \frac{1-\sigma}{5+\sigma}x + \frac{3}{5+\sigma}\right] \quad \ldots\ldots [9]$$

Referring to Equation [6] the stated relations between the elements a, b, 3, show that the roots of the indicial equation (reference 6) are 0 and -2. The integral which belongs to the exponent 0 is, in the notation of the hypergeometric function

$$F(a, b, 3, x) = S_1(x) = 1 + \frac{a.b}{1\cdot 3}x + \frac{a(a+1)b(b+1)}{1\cdot 2\cdot 3\cdot 4}x^2 + \ldots \quad \ldots\ldots [10]$$

$$\text{Coefficient of } x^n = u_n = \frac{2(a+n-1)\ldots a(b+n-1)\ldots b}{n!(n+2)!} = \frac{2(n+1)}{n+2}\cdot\frac{\Gamma(n+a)\Gamma(n+b)}{\Gamma(a)\Gamma(b)[\Gamma(n+2)]^2} \quad \ldots\ldots [11]$$

The application of Stirling's expansion (7) to the general case yields

$$\lim_{n\to\infty} n^{c-a-b+1}u_n = \Gamma(c)/\Gamma(a)\Gamma(b)$$

The relation between the elements now gives

$$\lim_{n\to\infty} n^2 u_n = 2/\Gamma(a)\Gamma(b) = (2/\pi)\sin a\pi \quad \ldots\ldots [12]$$

since $a + b = 1$ and $\Gamma(a)\Gamma(b) = \pi \csc a\pi$. Comparison of series, Equation [10], with $\sum_{n=1}^{\infty} n^{-2}$ gives the remainder (8) after m terms to be

$$R_m < \frac{(m+2)x^m \sin a\pi}{\pi m^2} \quad \ldots\ldots [13]$$

which may be used to estimate the number of terms required to calculate $S_1(x)$ to any degree of accuracy for suitable values of x. Inspection of the remainder, term [13], shows that there is a value of $m > N_0$ for $|x| \leq 1$ which makes the sum of almost all of the terms in the series arbitrarily small. This proves that the series, Equation [10], is absolutely and uniformly convergent whenever $|x| \leq 1$.

The derived function may be obtained directly from $S_1(x)$ and satisfies the relation

$$d/dx\, S_1(x) = S_1'(x) = \frac{ab}{3}F(a+1, b+1, 4, x) \quad \ldots\ldots [14]$$

In exactly the same manner as before it is found that the remainder after m terms of the derived series is

$$R_m < \frac{2(m+1)x^m \sin a\pi}{\pi m^2}$$

so that this series also is absolutely and uniformly convergent in the interval $|x| \leq 1$.

The next solution in order of difficulty satisfies Equation [7]. In reality this solution is a function of x, but the algebra is simplified somewhat by using t for the independent variable where $1 - x = t$. The roots of the indicial equation are 0 and 2 and the corresponding integral of index 2 is

$$t^2F(a+2, b+2, 3, t) = S_2(t) = \frac{2t^2}{ab+2}\left[\frac{ab+2}{2} + \frac{(a+1)(b+1)}{1!3!}t + \frac{(a+1)(a+2)(b+1)(b+2)}{2!4!}t^2 + \ldots\right] \quad \ldots\ldots [15]$$

[3] Tables for $\sigma = 0.30$ and 0.36 are included in this paper. Copies of the remaining tables may be had on application to Fairbanks, Morse & Company, Beloit, Wis.

$$u_n = \frac{(n+a+1)\ldots(a+1)(n+b+1)\ldots(b+1)}{n!(n+2)!}$$

$$= \frac{n+1}{n+2} \cdot \frac{\Gamma(a+n+2)\Gamma(b+n+2)}{\Gamma(a+1)\Gamma(b+1)[\Gamma(n+2)]^2}$$

$$\lim_{n\to\infty} \frac{u_n}{n} = \frac{\sin a\pi}{\pi ab} \ldots\ldots\ldots [16]$$

The limiting form of the nth term of a hypergeometric series obeys a simple law (9) so that its asymptotic behavior for $\alpha + \beta - \gamma$ an integer exceeding zero is

$$F(x) \underset{x\to 1}{\sim} \frac{\Gamma(\gamma)\Gamma(\alpha+\beta-\gamma)}{\Gamma(\alpha)\Gamma(\beta)} (1-x)^{\gamma-\alpha-\beta} \ldots\ldots [17a]$$

when $\alpha + \beta = \gamma$

$$F(x) \underset{x\to 1}{\sim} \frac{\Gamma(\alpha+\beta)}{\Gamma(\alpha)\Gamma(\beta)} \log_e \frac{1}{1-x} \ldots\ldots\ldots\ldots [17b]$$

The application of this theorem to series, Equation [15], shows that

$$S_2(t) \underset{t\to 1}{\sim} \frac{\Gamma(3)\Gamma(2)(1-t)^{-2}}{a(a+1)b(b+1)\Gamma(a)\Gamma(b)} = \frac{2\sin a\pi}{\pi ab(ab+2)(1-t)^2}$$

which is also the form of the remainder term when t approaches unity. A better approximation to the sum gives

$$S_2(t) = \frac{2t^2}{ab+2}\left[\sum_{n=0}^{m-1} u_n t^n + R_m\right] \ldots\ldots\ldots [18]$$

where

$$R_m < \frac{\sin a\pi}{\pi ab(1-t)}\left[m + \frac{t}{1-t}\right] t^m \ldots\ldots\ldots [19]$$

Similarly

$$S_2'(t) = \frac{2t}{ab+2}\left[\sum_{n=0}^{m-1} (n+2)u_n t^n + R_m\right] \ldots\ldots [20]$$

where

$$R_m < \frac{\sin a\pi}{\pi ab(1-t)}\left\{m(m+2) + \frac{(2m+3)t}{1-t} + \frac{2t^2}{(1-t)^2}\right\} t^m \quad [21]$$

The form of the remainders in Equations [19] and [21] is useful for obtaining greater numerical accuracy from a given number of terms in the series. The accuracy of R_m is equal to the number of significant figures common to $|u_{m-1} - u_m|$ and $\lim_{n\to\infty} \frac{u_n}{n}$.

The remainder, term [13], shows that series, Equation [10], converges so slowly near $x = 1$ that 100 terms would be required to approach an accuracy of 5 significant figures in the sum, while series, Equation [15], diverges when $t = 1$. As would be expected, these difficulties are increased when calculating the derivatives with infinite series for values of x or t near unity.

Numerical results, accurate to 8 significant figures for all positive values of $x \leq 1$ (exclusive of values where the functions are known to be infinite) can be obtained from series, Equations [10], [14], [15], and [20], together with the logarithmic solutions without exceeding 30 terms in any of the expansions involved. The logarithmic solutions introduce two more series which also converge rapidly when x and t are near zero. As a consequence of the relation $1 - x = t$ the latter two series may be used to construct a convenient form of the function for calculation with those values of x and t which previously were troublesome. For the purposes of numerical calculations it was found sufficient to restrict x and t to positive values between 0 and $^1/_2$ in all four series and their derivatives. The first step in the development of this procedure is the derivation of the logarithmic solutions of Equations [6] and [7].

Logarithmic Solutions

The second solution of Equation [7] involves logarithms (10) whenever the difference of the roots is an integer unless a or b is zero or a negative integer not less than $a + b + 1 - c$. According to the general theory, this solution is

$$\bar{S}_2(t) = -\frac{a(a+1)b(b+1)}{2} S_2(t) \log_e t + S_3(t) \ldots [22]$$

where

$$S_3(t) = 1 - abt - \sum_{n=2}^{\infty} \frac{(n-1+a)\ldots a(n-1+b)\ldots b}{n!(n-2)!} t^n \Phi_n$$

$$\ldots\ldots [23]$$

and

$$\Phi_n = \frac{1}{a} + \ldots + \frac{1}{a+n-1} + \frac{1}{b} + \ldots + \frac{1}{b+n-1}$$

$$-1 - \frac{1}{2} - \ldots - \frac{1}{n-2} - 1 - \frac{1}{2} - \ldots - \frac{1}{n} \ldots [24]$$

or

$$\Phi_n = \psi(n-1+a) + \psi(n-1+b) - \psi(n-2) - \psi(n) \ldots [25]$$

The expression for the limiting form of the nth term of $S_3(t)$ requires the evaluation of $\lim_{n\to\infty} \Phi_n$ which can be done with the aid of the logarithmic derivative of the gamma function. The necessary relations are (11, 12), for positive argument,[4] x

$$\Psi(x) = \frac{\Gamma'(x+1)}{\Gamma(x+1)} = -\gamma + \lim_{n\to\infty} \sum_{m=1}^{n} \left(\frac{1}{m} - \frac{1}{m+x}\right) \ldots [26]$$

where $\gamma = 0.577{,}215{,}665 \ldots$ (Euler's constant).
Numerical values of $\Psi(x)$ are obtained readily from the formulas

$$\Psi(x) = \log_e x + \frac{1}{2x} - \frac{1}{12x^2} + \frac{1}{120x^4} - \frac{B_3}{6x^6} + \frac{B_4}{8x^8} - \ldots [27]$$

where the B's are Bernoulli's numbers. When n is an integer

$$\Psi(x+n) = \Psi(x) + \left[\frac{1}{x+1} + \ldots + \frac{1}{x+n}\right] \ldots [28]$$

and generally

$$\Psi(-x) = \Psi(x-1) + \pi \cot \pi x \ldots\ldots\ldots [29]$$

Equation [28] may be used when increasing the argument to a convenient value for calculation with Equation [27]. Equation [29] is used in conjunction with the relation $a + b = 1$.

The form of $\lim_{n\to\infty} \Phi_n$ suitable for numerical evaluation now becomes

$$\lim_{n\to\infty} \Phi_n = 2\left[\frac{1}{a} - \gamma - \Psi(a)\right] - \pi \cot a\pi \ldots\ldots [30]$$

[4] Not to be confused with r/R.

Also

$$\lim_{n\to\infty}\frac{u_n}{n}=\lim_{n\to\infty}\frac{(n-1+a)\dots a(n-1+b)\dots b}{n!(n-2)!n}=\frac{\sin a\pi}{\pi}\qquad\dots\dots[31]$$

After some reduction, the approximate value of $S_3(t)$ is

$$S_3(t)=1-abt-\left[\sum_{n=2}^{m-1}u_nt^n\Phi_n+R_m\right]\qquad\dots\dots[32]$$

$$R_m<\lim_{n\to\infty}\frac{u_n\Phi_n}{n}\left(m+\frac{t}{1-t}\right)\frac{t^m}{1-t}\qquad\dots\dots[33]$$

and

$$S_3'(t)=-ab-\left[\sum_{n=2}^{m}nu_nt^{n-1}\Phi_n+R_m\right]\qquad\dots\dots[34]$$

$$R_m<\lim_{n\to\infty}\frac{u_n\Phi_n}{n}\left\{m(m+2)+\frac{(2m+3)t}{1-t}+\frac{2t^2}{(1-t)^2}\right\}\frac{t^m}{1-t}\qquad\dots\dots[35]$$

The $\lim_{n\to\infty}\frac{u_n\Phi_n}{n}$ is the product of the limits given by Equations [30] and [31]. The accuracy of R_m is the same as in Equations [19] and [21].

Returning to Equation [6], with suitable restrictions on the elements (10), the general theory yields a second solution in the form

$$\bar{S}_1(x)=-\frac{ab(ab+2)}{2}S_1(x)\log_e x+\frac{1}{x^2}-\frac{ab+2}{x}-S_4(x)\qquad[36]$$

$$S_4(x)=\sum_{n=2}^{\infty}\frac{(n+a-3)\dots(a-2)(n+b-3)\dots(b-2)}{n!(n-2)!}\times x^{n-2}\Phi_n\qquad\dots\dots[37]$$

$$\Phi_n=\psi(n-3+a)+\psi(n-3+b)-\psi(n-2)-\psi(n)\qquad[38]$$

$$\lim_{n\to\infty}\Phi_n=\frac{1}{a-2}+\frac{1}{a-1}+\frac{1}{a}-\frac{1}{a+1}-2\gamma-2\Psi(a)-\pi\cot a\pi\qquad\dots\dots[39]$$

$$\lim_{n\to\infty}n^3u_n=\frac{ab(ab+2)\sin a\pi}{\pi}\qquad\dots\dots[40]$$

The remainder after m terms is

$$R_m<\frac{(m+2)x^m}{2m^3}\lim_{n\to\infty}n^3u_n\Phi_n\qquad\dots\dots[41]$$

where $\lim_{n\to\infty}n^3u_n\Phi_n$ is equal to the product of the limits, Equations [39] and [40]. Similarly the remainder for the derived series $S'_4(x)$ is

$$R_m<\frac{(m+1)x^m}{m^3}\lim_{n\to\infty}n^2u_n\Phi_n\qquad\dots\dots[42]$$

Equations [41] and [42] show that both $S_4(x)$ and $S_4'(x)$ are absolutely and uniformly convergent whenever $|x|\leq 1$.

Linear Dependence of the Solutions

The four solutions, Equations [10], [15], [22], and [36] are linearly dependent since they satisfy two second-order differential equations which are connected by a linear transformation that does not alter the common interval of convergence. This property enables the functions of arguments t and x to be correlated by a proper choice of the constants of integration. The elementary method (13) used to obtain these constants depends upon the asymptotic form of the hypergeometric function in the neighborhood of its poles.

Since $1-x=t$, the general solution involving $S_2(t)$ and $\bar{S}_2(t)$ is identically equal to $S_1(x)$ in the interval between zero and unity; that is

$$P(t)=C_2S_2(t)+C_1\bar{S}_2(t)=S_1(x)\qquad\dots\dots[43]$$

where C_1 and C_2 are determined by the following conditions (reference 14):

$$\lim_{t\to0}P(t)=\lim_{x\to1}S_1(x)=\frac{2\sin a\pi}{\pi ab(ab+2)}\qquad\dots\dots[44]$$

$$\lim_{t\to1}P(t)=\lim_{x\to0}S_1(x)=1\qquad\dots\dots[45]$$

Equations [22], [43], and [44] show that

$$C_1=(2\sin a\pi)/\pi ab(ab+2)$$

The remainder formulas [19] and [33] show that $S_2(t)$ and $\bar{S}_2(t)$ have the same order of singularity at $t=1$. The constant C_2 may be chosen so that $\lim_{t\to1}P(t)$ remains finite and satisfies Equation [45]. After some reduction it is found that

$$C_2=\frac{2\sin a\pi}{\pi}\left[\frac{1}{a}-\gamma-\Psi(a)\right]-\cos a\pi\qquad\dots\dots[46]$$

Equations [8] and [43], together with the relation $1-x=t$ give

$$AP_1(x)=AS_1(x)\qquad\dots\dots[47a]$$

$$=A\left\{C_2S_2(1-x)+C_1\bar{S}_2(1-x)\right\}\qquad\dots\dots[47b]$$

Equation [47a] converges very rapidly near $x=0$, while Equation [47b] does the same near $x=1$, which is precisely the most desirable characteristic for making numerical calculations.

The second solution is treated in a similar manner. Let the general solution with argument x be

$$P(x)=C_3S_1(x)+C_4\bar{S}_1(x)\qquad\dots\dots[48]$$

subject to the conditions

$$\lim_{x\to0}P(x)=\lim_{t\to1}S_2(t)\sim\frac{C_4}{(1-t)^2};\quad\lim_{x\to1}P(x)=\lim_{t\to0}S_2(t)=0\qquad\dots\dots[49]$$

Equation [17a] shows that C_4 remains unchanged. Furthermore Equations [14] and [17b] show that $S_1''(x)$ and $\bar{S}_1''(x)$ have a logarithmic singularity at $x=1$ and $\lim_{t\to0}S_2''(t)$ is finite, which gives

$$C_3=\frac{\sin a\pi}{\pi}\lim_{n\to\infty}\Phi_n\qquad\dots\dots[50]$$

where $\lim_{n\to\infty}\Phi_n$ is evaluated by Equation [39]. Equations [8] and [48], together with the relation $1-x=t$ show that

$$BP_2(x)=BS_2(1-x)\qquad\dots\dots[51a]$$

$$=B\left\{C_3S_1(x)+C_4\bar{S}_1(x)\right\}\qquad\dots\dots[51b]$$

which readily is seen to be a convenient form for numerical work. The derivatives with respect to x now can be calculated directly from Equations [47a], [47b], [51a], and [51b].

Stress Calculations

From Equation [2] with $r=Rx$ the relations between P and Q are found to be

$$\left.\begin{aligned} Q_1 &= P_1 + x dP_1/dx \\ Q_2 &= P_2 + x dP_2/dx \\ Q_3 &= P_3 + x dP_3/dx + \rho R^2\omega^2 x^2(1-x) \end{aligned}\right\} \ldots\ldots [52]$$

where $P = (1-x)p$ and $Q = (1-x)q$. Equations [52] give the "stress coefficients"

$$\left.\begin{aligned} p_1 &= P_1/C_1(1-x) \qquad q_1 = Q_1/C_1(1-x) \\ p_2 &= -P_2/(1-x) \qquad q_2 = -Q_2/(1-x) \\ p_3 &= \frac{3+\sigma}{11+\sigma}\left[-x^2 + \frac{2+\sigma}{5+\sigma}x + \frac{3}{5+\sigma}\right] \\ q_3 &= \frac{3+\sigma}{11+\sigma}\left[-\frac{1+3\sigma}{3+\sigma}x^2 + \frac{1+2\sigma}{5+\sigma}x + \frac{3}{5+\sigma}\right] \end{aligned}\right\} \ldots [53]$$

which express the stresses p and q in the following form

$$p = Ap_1 + Bp_2 + \rho R^2\omega^2 p_3 \ldots\ldots [54]$$

$$q = Aq_1 + Bq_2 + \rho R^2\omega^2 q_3 \ldots\ldots [55]$$

Numerical values of the fundamental solutions of the hypergeometric Equation [6] were tabulated for the values of Poisson's ratio (σ) designated in the titles of the tables. The corresponding tables of stress coefficients were calculated from Equations [53] and tabulated at intervals of $r/R = 0.01$ between zero and unity. The tables are accurate to within 5 parts in 2,000,000. Slide-rule accuracy is obtainable from linear interpolation of the tabulated values. If greater accuracy is required for intermediate values, interpolation methods may be used. References (15), (16), and (17) may be consulted with advantage in this connection.

Illustrative Example

An aluminum supercharger rotor, the details of which are shown in Fig. 2, was calculated by replacing the actual disk profile with (I) a system of disks of uniform thickness, and (II) a system of conical profiles. In both cases Poisson's ratio was taken as 0.36 with $\rho = 2.5904 \times 10^{-4}$ for $r < 5^3/_8$ in. and $\rho = 3.6180 \times 10^{-4}$ when $r > 5^3/_8$ in. to compensate for the mass of the vanes.[5]

The tabular solutions about to be described were made for $\omega = 1000$, in order to simplify the calculations. The stresses for any other value of ω are obtained by multiplying the results for $\omega = 1000$ by $\omega^2 \times 10^{-6}$.

Case I. Method of Uniform Disks:

These calculations depend upon the following general formulas for mean radial and tangential stresses in a uniform rotating disk (18)

$$\left.\begin{aligned} p &= A - B/r^2 - {}^1/_8(3+\sigma)\rho\omega^2 r^2 \\ q &= A + B/r^2 - {}^1/_8(1+3\sigma)\rho\omega^2 r^2 \end{aligned}\right\} \ldots\ldots [56]$$

Let r_n be the radius to the nth boundary between approximating disks of different thicknesses, then if p'_n, q'_n and p''_n, q''_n are the corresponding radial and tangential stresses on the material outside and inside of this boundary, respectively, Equations [56] give

$$\left.\begin{aligned} p''_{n+1} + q''_{n+1} &= p'_n + q'_n - {}^1/_2(1+\sigma)\rho\omega^2(r^2_{n+1} - r_n^2) \\ p''_{n+1} - q''_{n+1} &= (p'_n - q'_n)r_n^2/r^2_{n+1} \\ &\quad - {}^1/_4(1-\sigma)\rho\omega^2(r^2_{n+1} - r_n^2)(1 + r^2_n/r^2_{n+1}) \end{aligned}\right\} \ldots [57]$$

Denoting by h_n one half the thickness of the disk whose inner and outer radii are r_n and r_{n+1}, respectively, the following relations are satisfied by the stresses on either side of the $(n+1)$th boundary:

$$\left.\begin{aligned} h_{n+1}p'_{n+1} &= h_n p''_{n+1} \\ q'_{n+1} &= \sigma(h_n/h_{n+1} - 1)\,p''_{n+1} + q''_{n+1} \end{aligned}\right\} \ldots\ldots [58]$$

Equations [57] and [58] can be arranged conveniently for tabular solution in a manner analogous to Donath's sum-and-difference method (18).

Table 1 contains the calculation factors which depend only upon the configuration of the disk, the angular velocity, and the material. The solution for the stresses is obtained by using these factors to calculate Table 1(a) with assumed values of q'_1 for any particular value of p'_1 determined by the hub fit. Calculations with Table 1(a) are repeated until a value of q'_1 has been found which makes the final value of p'' equal to the known radial stress at the periphery of the disk. A refinement of this method (18) makes it possible to obtain the final stresses from three calculations with Table 1(a).

Let it be assumed that the choice of $(q'_1)_1$ does not give the known peripheral stress p_{14}. A suitable static stress distribution which will reduce $(p''_{14})_1$ to its proper value by superposition is obtained as follows:

Table 1(a) is worked out for an arbitrary value of q'_1 say $(q'_1)_2$ with $\omega = 0$, which requires the omission from the calculation of the factors in columns 9 and 10 of Table 1. The final stress distribution which produces the required radial stress at the periphery of the disk is

$$q'_n = (q'_n)_1 + (q'_n)_2\left[\frac{p_{14} - (p''_{14})_1}{(p''_{14})_2}\right] \ldots\ldots [59]$$

together with an analogous equation for p'_n. This stress system

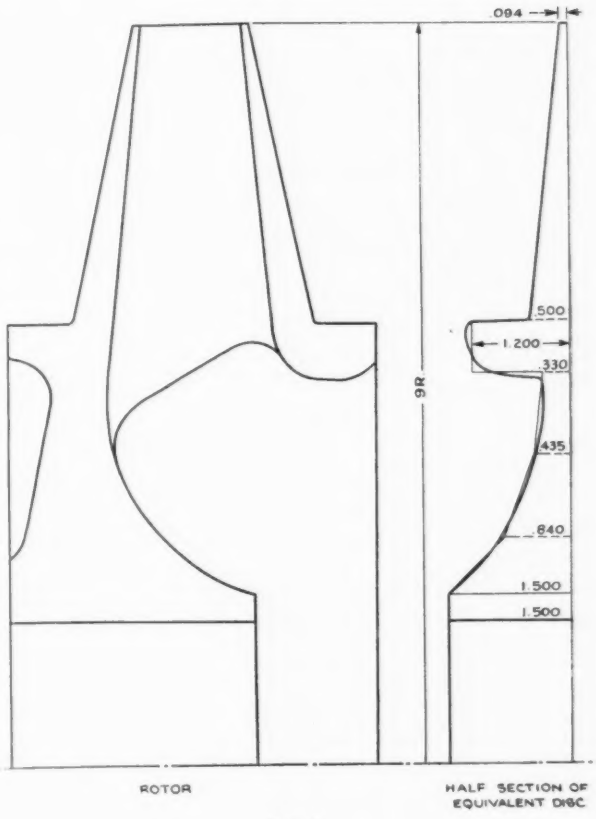


Fig. 2

[5] It is not the purpose of this example to justify the method of determining the equivalent disk.

TABLE 1

n	1 r_n	2 h_n	3 $\frac{h_n}{h_{n+1}}$	4 $\sigma\left(\frac{h_n}{h_{n+1}}-1\right)$	5 r_n^2	6 $r_{n+1}^2-r_n^2$	7 $\left(\frac{r_n}{r_{n+1}}\right)^2$	8 $\frac{(r_{n+1}^2-r_n^2)}{(1+\sigma+\sigma r_n^2/r_{n+1}^2)}$	9 $\frac{\rho k}{8}(1+\sigma)$ × COL(6) × 10^6	10 $\frac{\rho k}{8}(1-\sigma)$ × COL(8) × 10^6
1	1.7500	1.5000			3.0625					
2	2.0000	1.2806	1.1713	.0617	4.0000	.9375	.7656	1.6852	165.	69
3	2.5000	.8771	1.4600	.1656	6.2500	2.2500	.6400	3.6900	396.	153.
4	3.0000	.6262	1.4007	.1443	9.0000	2.7500	.6944	4.6996	484.	193
5	3.5000	.4432	1.4129	.1486	12.2500	3.2500	.7347	5.6378	572.	234
6	4.2500	.3550	1.2485	.0895	18.0625	5.8125	.6782	9.7545	1024.	404
7	4.6875	.8800	.4034	-.2148	21.9727	3.9102	.8220	7.1244	689.	292
8	4.9375	1.2229	.7196	-.1009	24.3789	2.4062	.9013	4.5749	424.	190.
9	5.3750	.4661	2.6237	.5845	28.8906	4.5117	.8458	8.3187	795.	345
10	6.0000	.3856	1.2088	.0752	36.0000	7.1094	.8025	12.8147	1749.	742
11	6.7500	.3025	1.2747	.0989	45.5625	9.5625	.7901	17.1178	2358.	991
12	7.5000	.2194	1.3788	.1364	56.2500	10.6875	.8100	19.3444	2629.	1120.
13	8.2500	.1349	1.6264	.2255	68.0625	11.8125	.8264	21.5744	2906.	1249
14	9.0000				81.0000	12.9375	.8408	23.8089	3183.	1378

TABLE 1(a)

n	11 t'_n / COL(3)×COL(9)+COL(10)	12 q'_n / COL(4)×COL(9)+COL(11)	13 $t'_n+q'_n$	14 $t'_n-q'_n$	15 $t'_n+q'_n$ / COL(13)−COL(10)	16 $t'_n-q'_n$ / COL(14)×COL(7) − COL(12)	17 t'_n / 2	18 q'_n / 2	19 COL(4) × COL(17)
1	0	10249.	10,249.	-10,249.					
2	1270.	9067.	10,337.	-7797.	10,084.	-7916.	1084.	9000.	67.
3	3503.	7939.	11,442.	-4436.	9941.	-5143.	2399.	7542.	397.
4	5381.	7610.	13,051.	-2289.	10,958.	-3273.	3842.	7116.	554.
5	7463.	7983.	15,446.	- 520.	12,479.	-1916.	5282.	7198.	785.
6	8530.	8201.	16,731.	- 329.	14,422.	- 757.	6832.	7590.	611.
7	3231.	6311.	9,542.	-3080.	16,042.	- 22.	8010.	8032.	-1721.
8	2219.	5732.	7,945.	-3519.	9118.	-2966.	3076.	6042.	-310.
9	5032.	6353.	11,385.	- 1321.	7150.	-3314.	1918.	5232.	1121.
10	4755.	6014.	10,749.	-1279.	9636.	-1802.	3917.	5719.	295.
11	4075.	5515.	9,590.	-1440.	8996.	-2002.	3197.	5199.	316.
12	3224.	4943.	8,167.	-1719.	6961.	-2286.	2938.	4624.	319.
13	2108.	4258.	6,366.	-2150.	5261.	-2670.	1296.	3966.	242
14					3183.	-3185.	1.	3184.	

satisfies the boundary conditions when substituted in Table 1(a) with the original value of ω.

The column numbers from Table 1 have been continued through Table 1(a) to avoid confusion. Table 1(a) appears here in its final form where the last value of $p''_{14} = 1$ which is sufficiently near zero for the number of significant figures carried in the calculation.

Case II. Method of Equivalent Conical Profiles:

This method is based on the replacement of the actual disk by portions of cones, as shown in Fig. 2. Let r_{n+1} be the radius to the intersection of the conical surfaces, whose base radii are R_n and R_{n+1} (Fig. 3), respectively. Using the notation of Case I for boundary stresses, Equations [54] and [55] become

$$\left.\begin{aligned} p'_n &= A_n p'_{1n} + B_n p'_{2n} + \rho R_n^2\omega^2 p'_{3n} \\ q'_n &= A_n q'_{1n} + B_n q'_{2n} + \rho R_n^2\omega^2 q'_{3n} \end{aligned}\right\} \quad \ldots\ldots [60]$$

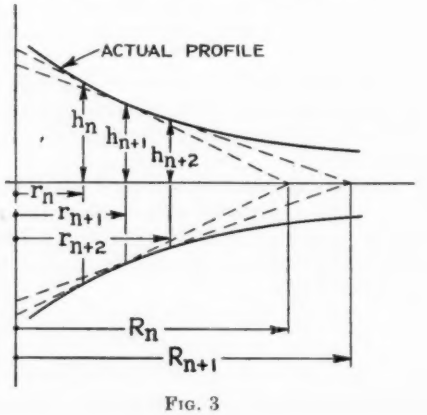


FIG. 3

$$\left.\begin{aligned} p''_{n+1} &= A_n p''_{1n} + B_n p''_{2n} + \rho R_n^2\omega^2 p''_{3n} \\ q''_{n+1} &= A_n q''_{1n} + B_n q''_{2n} + \rho R_n^2\omega^2 q''_{3n} \end{aligned}\right\} \quad \ldots [61]$$

If some of the approximating sections are cylinders, Equations [56] can be expressed in the foregoing form by making the following changes, which were applied to lines 1 and 5 of Table 2.

$$\left.\begin{aligned} p'_{1n} &= q'_{1n} = 1 & p''_{1n} &= q''_{1n} = 1 \\ -p'_{2n} &= q'_{2n} = 1/r^2_n & -p''_{2n} &= q''_{2n} = 1/r^2_{n+1} \\ p'_{3n} &= -1/8(3+\sigma) & p''_{3n} &= p'_{3n}\cdot r^2_{n+1}/r^2_n \\ q'_{3n} &= -1/8(1+3\sigma) & q''_{3n} &= q'_{3n}\cdot r^2_{n+1}/r^2_n \\ R_n &= r_n & R_n &= r_n \end{aligned}\right\} \quad \ldots [62]$$

The twelve quantities $p'_{1n}, \ldots q'_{3n}, p''_{1n}, \ldots q''_{3n}$ appearing in Equations [60] and [61] are obtained from the tables of stress coefficients. The argument for the singly primed quantities is r_n/R_n, while that for the doubly primed ones is r_{n+1}/R_n. The calculation consists of finding A_n and B_n from Equations [60] which values in turn are used to calculate p''_{n+1} and q''_{n+1} with Equations [61]. Following this calculation, p'_{n+1} and q'_{n+1} are found by Equations [58] where h_n and h_{n+1} now are replaced by the half thicknesses of the disk at $r_{n+1} - 0$ and $r_{n+1} + 0$, respectively. This process then is repeated with the indices increased by unity each time until the periphery is reached where the radial stress is known.

The solution can be arranged conveniently in tabular form, as shown in Table 2, where columns 1 to 23, inclusive, contain all necessary calculation constants which do not depend upon the stresses. Columns 7 to 18, inclusive, except lines 1 and 5, were obtained by linear interpolation from the tables of stress coefficients for $\sigma = 0.36$. Beginning with the assumed value of $(q'_1)_1 = 12{,}000$ and $(p'_1)_1 = 0$, the first approximation to the stresses was obtained with Table 2(a). The static stress dis-

TABLE 2

n	1 r_n	2 R_n	3 $\frac{R_n^2}{\rho k}$ OR $\frac{R_n^2}{p''_{3n}}$	4 r_n/R_n	5 r_{n+1}/R_n	6 $\frac{\rho R_n^2}{\rho k}\times 10^6$	7 COEFFICIENTS FOR VALUES OF r_n/R_n: t'_{1n}	8 t'_{2n}	9 t'_{3n}	10 q'_{1n}	11 q'_{2n}	12 q'_{3n}
1	1.7500	∞	3.0625	0	0	793.91	1.0000	-.9265	-.4200	1.0000	.9265	-.2600
2	2.0625	3.625	13.1406	.5690	.7586	3403.9	2.783	-1.1983	1.4388	2.279	4.169	1.6027
3	2.7500	4.824	23.271	.9701	.7774	6028.1	2.788	-1.1908	1.4366	2.283	4.157	1.6015
4	3.7500	7.893	62.299	.4751	.6018	16138.	2.352	-2.037	1.6065	2.024	5.427	1.6930
5	4.7500	∞	22.562	0	0	5844.5	1.0000	-.04432	-.4200	1.0000	.04432	-.2600
6	5.3750	9.839	96.806	.5463	.9147	35025.	2.663	-1.3599	1.4841	2.209	4.420	1.6275
7	9.0000											

TABLE 2 (*Continued*)

n	13 COEFFICIENTS FOR VALUES OF r_{n+1}/R_n: t''_{1n}	14 t''_{2n}	15 t''_{3n}	16 q''_{1n}	17 q''_{2n}	18 q''_{3n}	19 $t'_{1n}q'_{1n}$ / $t'_{2n}t''_{1n}+t''_{2n}q'_{1n}$	20 $t'_{2n}t''_{2n}$ / $t'_{3n}t''_{3n}+t''_{3n}q'_{3n}$	21 $t'_{3n}q'_{2n}$ / $q'_{1n}t''_{3n}+t''_{1n}q'_{3n}$	22 COL(19) × COL(6)	23 COL(20) × COL(6)
1	1.0000	-.2351	-.8634	1.0000	.2351	-.3611	.1600	-.3220	.6530	126.93	-176.11
2	4.650	-.3970	.09412	3.274	2.818	.13218	.11813	.7919	14.933	402.1	2696.
3	5.006	-.3502	.08803	3.449	2.730	.12067	.11868	.7879	14.312	715.4	4750.
4	2.981	-.9989	.15479	2.592	3.853	.15695	.07304	1.2167	16.887	1178.7	19695
5	1.0000	-.09461	-.5978	1.0000	.09461	-.3928	.1600	-.05014	.06864	995.1	-176.15
6	12.291	-.1001	.03719	6.709	2.226	.09916	.10557	.8773	14.774	3648	30.727

$(q'_1)_1 = 12{,}000$ TABLE 2(a)[a] $\omega = 1000$

n	24 t'_{1n}	25 q'_{1n}	26 $t'_{1n}q'_{2n}$	27 $t'_{2n}q'_{1n}$	28 $q'_{1n}t'_{3n}$	29 $q'_{1n}t'_{2n}$	30 $\frac{A_n}{(23)-(24)-(25)}$ / (25)	31 $\frac{B_n}{(26)-(27)-(28)}$ / (27)	32 $t'_{1n+1}=(18)\times(30)+(14)\times(29)+(15)\times(6)$	33 $q'_{1n+1}=(16)\times(30)+(17)\times(29)+(18)\times(6)$
1	0	12000	0	0	12000	-.3918	6270	18182	1593	10258
2	1593	10258	3494	6391	28548	-12.292	1115.4	17199	4824	8948
3	4824	8948	11013	20053	24956	-10.655	18197	924.2	9286	9554
4	9286	9554	18795	50395	22471	-19.461	2973	147.88	10922	10204
5	3004	7353	3004	138.13	7353	-.325.9	7166	36814	2690	6853
6	6456	7909	14261	28596	21062	-10.755	5197	210.0	8407	7830
7	8407	7830								

[a] Numbers in parentheses in Tables 2(a), (b), and (c) denote operations on values in corresponding columns.

$(q'_1)_2 = 1000$ TABLE 2(*b*) $\omega = 0$

	24	25	26	27	28	29	30	31	32	33
n	p'_n	q'_n	$p'_n q'_{1n}$	$p'_n p'_{1n}$	$q'_n p'_{1n}$	$q'_n q'_{1n}$	$A_{n+1} = \frac{(27)-(24)}{(21)}$	$B_{n+1} = \frac{(28)-(26)}{(21)}$	$p'_{n+1} = (13)\times(30) + (14)\times(31)$	$q'_{n+1} = (16)\times(30) + (17)\times(31)$
1	0	1000	0	0	1000	-3265	500.0	1531.4	140	860
2	140	860	319.1	583.7	2393	-10305	112.62	144.69	466.2	776.5
3	466.2	776.5	1064.3	1938.0	2186	-924.7	200.0	76.98	974.2	900.0
4	974.2	900.0	1971.8	52870	2117	-1833.3	421.6	8.599	1248.2	1041.6
5	343.3	715.8	343.3	18 215	715.8	-31.72	529.5	4202.	984.1	674.9
6	921.8	868.5	2036	4074	2515	-1181.1	358.7	18.78	4970	2428
7	4370	2428								

$q'_1 = 10{,}076$ TABLE 2(*c*) $\omega = 1000$

	24	25	26	27	28	29	30	31	32	33
n	p'_n	q'_n	$p'_n q'_{1n}$	$p'_n p'_{1n}$	$q'_n p'_{1n}$	$q'_n q'_{1n}$	$A_{n+1} = \frac{(27)-(24)-(28)}{(21)}$	$B_{n+1} = \frac{(28)-(26)-(22)}{(21)}$	$p'_{n+1} = (13)\times(30) - (14)\times(31) - (15)\times(32)$	$q'_{n+1} = (16)\times(30) + (17)\times(31) + (18)\times(32)$
1	0	10,076	0	0	10076	-3290	5308	15236	1263	8804
2	1263	8604	2878	5265	23945	-10310	898.6	1441.8	3926	7455
3	3926	7455	8963	16320	20792	-8877	1428.7	776.5	7411	7823
4	7411	7823	15000	40219	18400	-15995	2163	131.54	8524	8204
5	2344	5979	2344	103.89	5979	-2650	6149	90.459	1952	5258
6	4685	6242	10349	20708	16622	-8488	-103.63	174.29	-11	3166
7	- 11	3166								

ACKNOWLEDGMENT

The tables were constructed with the aid of the staff of the Calculation Department of Fairbanks, Morse & Company, Beloit, Wis., to whom acknowledgment hereby is made.

BIBLIOGRAPHY

1 "A Course of Modern Analysis," by E. T. Whittaker and G. N. Watson, fourth edition, Cambridge University Press, London, England, 1927, chapt. 14. This reference contains a bibliography and numerous examples.

2 "Stress Distribution in Rotating Disks of Conical Profile," by H. M. Martin, *Engineering*, vol. 115, 1923, pp. 1–3, 115–116, 407 and 630.

3 "Festigkeitsberechnung rotierender Scheiben," by I. Malkin, J. Springer, Berlin, Germany, 1935, pp. 61–62.

4 "Applied Elasticity," by J. Prescott, Longmans Green & Company, London, England, 1924, p. 343.

5 Reference (1), p 283.

6 Reference (1), p. 198.

7 Reference (1), p. 253.

8 Reference (1), p. 71.

9 "Theory of Functions," by E. C. Titchmarsh, Oxford University Press, New York, N. Y., 1932, p. 224.

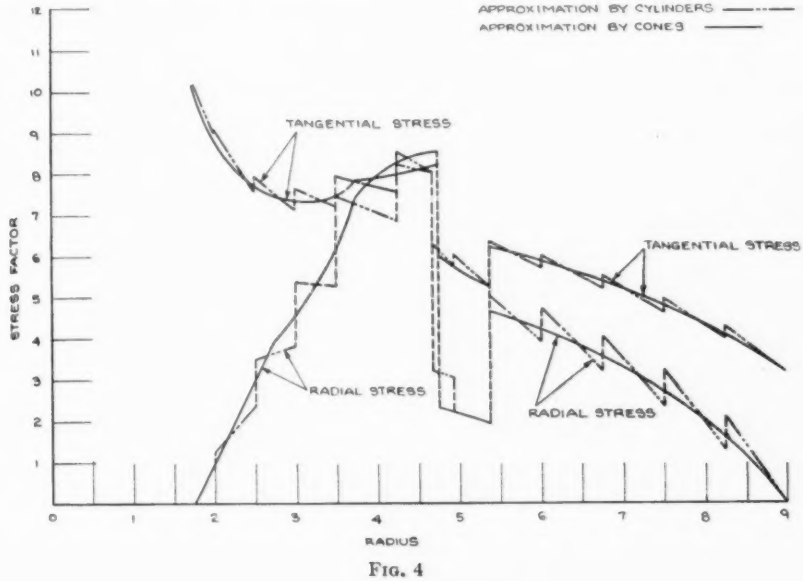


FIG. 4

tribution for $(q'_1)_2 = 1000$ and $(p'_1)_2 = 0$ with $\omega = 0$ was calculated with Table 2(*b*). The resultant stress distribution could have been obtained by interpolating columns 24, 25, 32, and 33 of Tables 2(*a*) and 2(*b*) with Equation [59]; however, a recalculation with Table 2(*c*), using $p_1' = 0$ and $q'_1 = 12{,}000 + (0 - 8407) \times 1000/4370 = 10{,}076$ and $\omega = 1000$ gives this information and at the same time provides a final check on all of the numerical work.

These calculations show that the advantages obtainable by approximating an arbitrary disk profile with portions of cones are as follows:

1 There are no discontinuities in the final stress-distribution curve except those caused by an abrupt change in the actual profile.

2 Considerably fewer steps are required than with the uniform-disk method.

10 "Theory of Differential Equations," by A. R. Forsyth, Cambridge University Press, London, England, vol. 4, 1902, part 3, p. 147.

11 Reference (1), p. 247.

12 "Tables of Functions," by E. Jahnke and F. Emde, Teubner, Leipzig, Germany, 1938, p. 19.

13 "The Interrelations of the Fundamental Solutions of the Hypergeometric Equation; Logarithmic Case," by L. E. Mehlenbacher, *American Journal of Mathematics*, vol. 60, 1938, p. 120. A complex variable method is discussed in this paper.

14 Reference (1), p. 282.

15 "Mathematical Tables," by H. B. Dwight, McGraw-Hill Book Company, Inc., New York, N. Y., 1941, p. 186.

16 "Numerical Mathematical Analysis," by J. B. Scarborough, Johns-Hopkins Press, Baltimore, Md., 1930.

17 "Calculus of Observations," by E. T. Whittaker and G. Robinson, Blackie & Son, Ltd., Glasgow, Scotland, second edition, 1937.

18 "Strength of Materials," by S. Timoshenko, D. Van Nostrand Co., Inc., New York, N. Y., 1930, p. 545.

FUNDAMENTAL SOLUTIONS OF HYPERGEOMETRIC EQUATION, $\sigma = 0.30$

ξ	F_1	$-F_1'$	F_2	$-F_2'$	ξ	F_1	$-F_1'$	F_2	$-F_2'$
.00	1.000000	.233333	∞	∞	.50	.871627	.286191	.871627	6.68682
.01	.997663	.234096	6881.56	1385642.	.51	.868757	.287716	.807239	6.19769
.02	.995318	.234866	1696.842	172059.7	.52	.865872	.289269	.745739	5.74857
.03	.992966	.235645	743.515	50638.7	.53	.862972	.290852	.692147	5.33599
.04	.990605	.236433	412.166	21217.8	.54	.860055	.292467	.640719	4.95532
.05	.988237	.237229	259.865	10788.58	.55	.857122	.294114	.592942	4.60470
.06	.985861	.238034	177.7145	6199.66	.56	.854173	.295794	.548535	4.28102
.07	.983476	.238848	128.5319	3876.41	.57	.851206	.297509	.507240	3.98183
.08	.981084	.239671	96.8402	2578.15	.58	.848222	.299261	.468824	3.70496
.09	.978683	.240503	75.2709	1797.453	.59	.845221	.301050	.433073	3.44846
.10	.976273	.241346	59.9568	1300.595	.60	.842201	.302878	.399793	3.21056
.11	.973856	.242198	48.7112	969.773	.61	.839163	.304747	.368805	2.98970
.12	.971429	.243060	40.2232	741.238	.62	.836106	.306659	.339947	2.78443
.13	.968994	.243932	33.6688	578.458	.63	.833030	.308615	.313069	2.59348
.14	.966551	.244814	28.5090	459.475	.64	.829934	.310617	.288033	2.41568
.15	.964098	.245708	24.3796	370.562	.65	.826817	.312669	.264715	2.24997
.16	.961637	.246612	21.0274	302.834	.66	.823680	.314771	.242997	2.09540
.17	.959166	.247527	18.27221	250.373	.67	.820522	.316926	.222773	1.951105
.18	.956686	.248454	15.98270	209.135	.68	.817341	.319138	.203943	1.816284
.19	.954197	.249392	14.06162	176.2906	.69	.814139	.321408	.186411 77	1.690219
.20	.951698	.250342	12.43569	149.8239	.70	.810913	.323741	.1701118	1.572254
.21	.949190	.251304	11.04881	128.2709	.71	.807664	.326138	.154 9477	1.461787
.22	.946672	.252279	9.85752	110.5515	.72	.804390	.328605	.140 8529	1.358270
.23	.944144	.253267	8.82772	95.8574	.73	.801091	.331145	.1277607	1.261200
.24	.941607	.254267	7.93235	83.5756	.74	.797767	.333762	.1156090	1.170116
.25	.939059	.255281	7.14974	73.2358	.75	.794416	.336460	.104 3399	1.084594
.26	.936501	.256309	6.46238	64.4729	.76	.791037	.339246	.0938998	1.004247
.27	.933933	.257351	5.85599	57.0008	.77	.787631	.342125	.0842389	.928717
.28	.931354	.258406	5.31882	50.5933	.78	.784195	.345102	.0753105	.857676
.29	.928764	.259477	4.84118	45.0697	.79	.780728	.348186	.0670714	.790819
.30	.926164	.260563	4.41497	40.2648	.80	.777230	.351384	.0594811	.727868
.31	.923553	.261664	4.03342	36.1208	.81	.773700	.354705	.0525019	.668564
.32	.920931	.262782	3.69081	32.4818	.82	.770136	.358158	.046 0585	.612669
.33	.918297	.263915	3.38230	29.2888	.83	.766536	.361755	.040 2379	.559962
.34	.915653	.265065	3.10376	26.4767	.84	.762900	.365508	.035 8893	.510239
.35	.912996	.266233	2.85168	23.9913	.85	.759226	.369433	.0300238	.463310
.36	.910328	.267418	2.62300	21.7874	.86	.755511	.373545	.025 6144	.419000
.37	.907648	.268622	2.41512	19.82699	.87	.751754	.377865	.0216356	.377146
.38	.904955	.269844	2.22576	18.0736.2	.88	.747953	.382416	.018 06377	.337597
.39	.902251	.271085	2.05254	16.51333	.89	.744105	.387226	.014 87617	.300212
.40	.899534	.272346	1.89 4953	15.10980	.90	.740207	.392328	.01205276	.264859
.41	.896804	.273628	1.750276	13.84766	.91	.736257	.397764	.00957291	.231418
.42	.894061	.274931	1.617595	12.70997	.92	.732251	.403585	.007 71840	.199 7747
.43	.891305	.276255	1.495711	11.68213	.93	.728184	.409859	.00557178	.169 8227
.44	.888536	.277601	1.383619	10.75153	.94	.724052	.416673	.001 01663	.141 6646
.45	.885753	.278971	1.280332	9.90725	.95	.719848	.424169	.00273750	.115 6059
.46	.882956	.280364	1.185218	9.13977	.96	.715566	.432462	.00171980	.0891625
.47	.880146	.281782	1.097368	8.44081	.97	.711196	.441888	.0009 6980	.0650531
.48	.877321	.283225	1.016197	7.80312	.98	.706723	.452908	.000 41454	.042 9825
.49	.874481	.284695	.941123	7.22032	.99	.702129	.466581	.00013179	.0205401
.50	.871627	.286191	.871627	6.68682	1.00	.697370	.488159	0	0

STRESS COEFFICIENTS FOR ROTATING DISKS OF CONICAL PROFILE, $\sigma = 0.30$

$\frac{r}{R}$	p_1	$-p_2$	p_3	$\frac{r}{R}$	p_1	$-p_2$	p_3
.00	1.433959	∞	.1653031	.50	2.09975	1.743253	.1556604
.01	1.441058	6951.07	.1665412	.51	2.542237	1.647427	.1539781
.02	1.456373	1731.472	.1677209	.52	2.58672	1.557374	.1523375
.03	1.467909	766.511	.1688422	.53	2.63291	1.472654	.1504385
.04	1.479674	429.340	.1699051	.54	2.68105	1.392866	.1485810
.05	1.491675	273.542	.1709096	.55	2.73128	1.317649	.1466651
.06	1.503919	189.0980	.1718557	.56	2.78375	1.246670	.1446909
.07	1.516414	138.2064	.1727434	.57	2.83859	1.179628	.1426582
.08	1.529167	105.2611	.1735726	.58	2.89599	1.116248	.1405671
.09	1.542188	82.7153	.1743435	.59	2.95613	1.056276	.1384176
.10	1.555485	66.6187	.1750559	.60	3.01921	.999182	.1362097
.11	1.569067	54.7317	.1757100	.61	3.085 45	.945654	.1339434
.12	1.582943	45.7082	.1763056	.62	3.15511	.894597	.1316187
.13	1.597125	38.6998	.1768429	.63	3.228 46	.846132	.1292356
.14	1.611621	33.1500	.1773217	.64	3.30581	.800093	.1267941
.15	1.626444	28.6619	.1777421	.65	3.387 49	.756528	.1242941
.16	1.641604	25.0327	.1781041	.66	3.47389	.715697	.1217358
.17	1.657114	22.0147	.1784077	.67	3.565 44	.675068	.1191190
.18	1.672986	19.49109	.1786529	.68	3.66261	.637322	.1164439
.19	1.689234	17.36003	.1788397	.69	3.76594	.601347	.1137103
.20	1.705870	15.54461	.1789681	.70	3.87605	.567039	.1109181
.21	1.722911	13.98583	.1790381	.71	3.99364	.534302	.1080680
.22	1.740370	12.63785	.1790497	.72	4.11951	.503046	.1051592
.23	1.758265	11.46157	.1790028	.73	4.25456	.473188	.1021920
.24	1.776612	10.43730	.1788976	.74	4.39987	.444650	.0991664
.25	1.795429	9.53299	.1787339	.75	4.55664	.417360	.0960824
.26	1.814735	8.73295	.1785119	.76	4.72631	.391249	.0929400
.27	1.834550	8.02190	.1782314	.77	4.91057	.366256	.0897392
.28	1.854894	7.38726	.1778925	.78	5.11138	.342321	.0864800
.29	1.875789	6.81856	.1774953	.79	5.33111	.319386	.0831623
.30	1.897260	6.30710	.1770396	.80	5.57258	.297406	.0797863
.31	1.919330	5.84553	.1765255	.81	5.83923	.276326	.0763518
.32	1.942026	5.42766	.1759530	.82	6.13521	.256103	.0728590
.33	1.965375	5.04821	.1753221	.83	6.46578	.236694	.0693077
.34	1.989407	4.70267	.1746328	.84	6.83730	.218058	.0656980
.35	2.014155	4.38719	.1738850	.85	7.25799	.200159	.0620300
.36	2.039665	4.09844	.1730789	.86	7.73837	.1829599	.0583035
.37	2.066592	3.83352	.1722144	.87	8.29219	.1661279	.0545186
.38	2.09301	3.58993	.1712914	.88	8.93778	.1505314	.0506753
.39	2.12097	3.36548	.1703101	.89	9.70015	.1352406	.0467736
.40	2.14902	3.15825	.1692703	.90	10.61127	.1205276	.0428135
.41	2.17963	2.96657	.1681722	.91	11.73070	.1063657	.0387950
.42	2.21043	2.78894	.1670156	.92	13.12522	.0927300	.0347180
.43	2.24227	2.62405	.1658006	.93	14.91694	.0795969	.0305827
.44	2.27522	2.47075	.1645272	.94	17.30435	.0669438	.0263890
.45	2.30933	2.32799	.1631954	.95	20.64147	.0547500	.0221368
.46	2.34467	2.19485	.1618052	.96	25.6523	.0429950	.01782629
.47	2.38131	2.07051	.1603566	.97	33.9942	.0316601	.0134732
.48	2.41931	1.95 4285	.1588496	.98	50.6706	.0207272	.00902995
.49	2.45876	1.84 5340	.1572842	.99	100.6824	.01017919	.00454118
.50	2.09975	1.743253	.1556604	1.00	∞	0	0

$\frac{r}{R}$	q_1	q_2	q_3	$\frac{r}{R}$	q_1	q_2	q_3
.00	1.433959	∞	.1653031	.50	2.09937	4.94357	.1673485
.01	1.441668	7045.31	.1661679	.51	2.11296	4.80323	.1665319
.02	1.459500	1779.952	.1669990	.52	2.13735	4.67024	.1656816
.03	1.457459	799.636	.1677966	.53	2.16259	4.54407	.1647978
.04	1.465548	454.739	.1685605	.54	2.18873	4.42425	.1638802
.05	1.473771	294.278	.1692908	.55	2.21582	4.31032	.1629291
.06	1.482132	206.665	.1699874	.56	2.24391	4.20190	.1619444
.07	1.490634	153.5664	.1706505	.57	2.27308	4.09861	.1609260
.08	1.499282	118.9261	.1712799	.58	2.30339	4.00013	.1598740
.09	1.508080	95.0548	.1718757	.59	2.33491	3.90611	.1587883
.10	1.517031	77.8919	.1721378	.60	2.36773	3.81636	.1576691
.11	1.526142	65.1279	.1729663	.61	2.40195	3.73054	.1565162
.12	1.535415	55.3697	.1734612	.62	2.43765	3.64842	.1553296
.13	1.544857	47.7364	.1739225	.63	2.47495	3.56979	.1541095
.14	1.554473	41.6484	.1743501	.64	2.51396	3.49444	.1528557
.15	1.564267	36.7114	.1747441	.65	2.55483	3.42219	.1515683
.16	1.574246	32.6500	.1751045	.66	2.59771	3.35285	.1502473
.17	1.584415	29.2666	.1754312	.67	2.64275	3.28627	.1488926
.18	1.594780	26.4.166	.1757243	.68	2.69014	3.22228	.1475043
.19	1.605348	23.9921	.1759839	.69	2.74010	3.16075	.1460824
.20	1.616125	21.9114	.1762097	.70	2.79285	3.10155	.1446268
.21	1.627119	20.1115	.1764020	.71	2.84866	3.04456	.1431376
.22	1.638336	18.54334	.1765606	.72	2.90783	2.98965	.1416148
.23	1.649785	17.16616	.1766855	.73	2.97071	2.93672	.1400584
.24	1.661473	15.95500	.1767769	.74	3.03769	2.88568	.1384683
.25	1.673408	14.87894	.1768346	.75	3.10923	2.83642	.1368446
.26	1.685601	13.91969	.1768587	.76	3.18584	2.78887	.1351873
.27	1.698059	13.06060	.1768492	.77	3.26815	2.74293	.1334964
.28	1.710793	12.28792	.1768060	.78	3.35686	2.69853	.1317718
.29	1.723813	11.59018	.1767292	.79	3.45284	2.65560	.1300136
.30	1.737130	10.95779	.1766188	.80	3.55710	2.61407	.1282217
.31	1.750754	10.38265	.1764748	.81	3.67085	2.57387	.1263963
.32	1.764699	9.85787	.1762971	.82	3.79558	2.53494	.1245372
.33	1.778977	9.37761	.1760858	.83	3.93310	2.49721	.1226445
.34	1.793601	8.93682	.1758408	.84	4.08565	2.46070	.1207181
.35	1.808585	8.53119	.1755623	.85	4.25607	2.42526	.1187582
.36	1.823945	8.15697	.1752501	.86	4.44796	2.39090	.1167645
.37	1.839696	7.81090	.1749043	.87	4.66601	2.35755	.1147373
.38	1.855855	7.49015	.1745248	.88	4.91641	2.32518	.1126764
.39	1.872439	7.19222	.1741118	.89	5.20754	2.29375	.1105820
.40	1.889468	6.91194	.1736651	.90	5.55103	2.26321	.1084538
.41	1.906962	6.65638	.1731847	.91	5.96355	2.23353	.1062921
.42	1.924942	6.41883	.1726708	.92	6.46989	2.20468	.1040967
.43	1.943431	6.18878	.1721232	.93	7.10866	2.17662	.1018677
.44	1.962453	5.97688	.1715420	.94	7.94365	2.14933	.0996051
.45	1.982034	5.77794	.1709271	.95	9.08861	2.12276	.0973088
.46	2.00220	5.59089	.1702786	.96	10.76913	2.09690	.0949789
.47	2.02299	5.41174	.1695966	.97	13.50620	2.07172	.0926154
.48	2.04442	5.24665	.1688808	.98	18.84745	2.04719	.0902183
.49	2.06653	5.09183	.1681315	.99	34.44457	2.02329	.0877875
.50	2.08937	4.94357	.1673485	1.00	∞	2.00000	.0853231

FUNDAMENTAL SOLUTIONS OF HYPERGEOMETRIC EQUATION
$\sigma = 0.36$

x	P_1	$-P'_1$	P_2	$-P'_2$	x	P_1	$-P'_1$	P_2	$-P'_2$
.00	1.000000	.213333	∞	∞	.50	.882108	.264085	.882108	6.79278
.01	.997863	.211063	7099.49	1429933.	.51	.879660	.265551	.816711	6.29386
.02	.995719	.211800	1749.583	177505.7	.52	.876747	.267051	.756095	5.83587
.03	.993567	.215545	766.201	52225.6	.53	.871119	.266578	.699871	5.41186
.04	.991408	.216298	424.513	21876.1	.54	.871426	.270135	.647686	5.02730
.05	.989241	.217060	267.508	11119.84	.55	.868716	.271722	.599223	4.67008
.06	.987067	.217831	182.8471	6388.05	.56	.865991	.273343	.554193	4.34039
.07	.984884	.218610	132.1773	3992.96	.57	.863249	.274998	.512332	4.03575
.08	.982694	.219398	99.5374	2654.84	.58	.860491	.276688	.473402	3.75392
.09	.980496	.220195	77.3298	1850.342	.59	.857716	.278415	.437184	3.49290
.10	.978290	.221002	61.5674	1338.443	.60	.854923	.280179	.403481	3.25089
.11	.976076	.221818	49.9963	997.679	.61	.852112	.281984	.372109	3.02627
.12	.973854	.222643	41.2654	762.328	.62	.849283	.283830	.342902	2.81759
.13	.971623	.223479	34.5255	594.727	.63	.846435	.285720	.315708	2.62352
.14	.969384	.224325	29.2214	472.248	.64	.843568	.287655	.290387	2.44288
.15	.967137	.225181	24.9778	380.742	.65	.840682	.289637	.266809	2.27458
.16	.964881	.226047	21.5341	311.091	.66	.837775	.291669	.244857	2.11764
.17	.962616	.226924	18.7047	257.087	.67	.834848	.293753	.224422	1.97118
.18	.960342	.227813	16.3540	211.674	.68	.831900	.295892	.205402	1.83438
.19	.958060	.228712	14.3828	180.9015	.69	.828930	.298088	.187704	1.70652
.20	.955768	.229623	12.7118	153.6931	.70	.825938	.300345	.171236	1.58691
.21	.953467	.230546	11.2917	131.5410	.71	.822923	.302665	.155904	1.47494
.22	.951157	.231481	10.0702	113.3332	.72	.819885	.305053	.141710	1.37006
.23	.948837	.232428	9.01169	98.2376	.73	.816822	.307512	.128572	1.27176
.24	.946508	.233388	8.0972	85.6231	.74	.813734	.310047	.116265	1.17930
.25	.944170	.234361	7.29559	75.0056	.75	.810621	.312661	.104907	1.09276
.26	.941821	.235347	6.59173	66.0095	.76	.807481	.315361	.094388	1.01168
.27	.939463	.236347	5.97098	58.3104	.77	.804313	.318151	.084656	.935305
.28	.937094	.237361	5.42128	51.7654	.78	.801117	.321039	.075663	.863188
.29	.934715	.238389	4.93265	46.0988	.79	.797892	.324030	.067373	.795929
.30	.932326	.239432	4.49677	41.1912	.80	.794636	.327133	.059735	.732852
.31	.929927	.240489	4.10670	36.9215	.81	.791349	.330356	.052714	.674164
.32	.927516	.241563	3.75655	33.1910	.82	.788029	.333709	.046274	.619051
.33	.925095	.242652	3.44135	29.9185	.83	.784674	.337202	.040382	.567878
.34	.922663	.243757	3.15688	27.0371	.84	.781284	.340849	.035007	.520736
.35	.920220	.244879	2.89969	24.4911	.85	.777857	.344663	.030118	.476834
.36	.917766	.246018	2.66609	22.2340	.86	.774390	.348661	.025695	.436791
.37	.915300	.247175	2.45398	20.2268	.87	.770883	.352863	.021694	.378641
.38	.912822	.248350	2.26083	18.4356	.88	.767332	.357291	.018106	.338831
.39	.910333	.249544	2.08462	16.83533	.89	.763736	.361974	.014910	.301216
.40	.907831	.250757	1.923576	15.39940	.90	.760092	.366943	.012077	.265664
.41	.905318	.251990	1.776150	14.10845	.91	.756396	.372239	.009590	.232050
.42	.902791	.253243	1.640982	12.94511	.92	.752646	.377914	.007430	.200259
.43	.900253	.254517	1.516672	11.89436	.93	.748836	.384034	.005579	.1701826
.44	.897701	.255813	1.402762	10.94329	.94	.744963	.390684	.004021	.1417206
.45	.895136	.257131	1.297712	10.08066	.95	.741021	.397985	.002714	.1147789
.46	.892558	.258473	1.200887	9.29671	.96	.737001	.406110	.001721	.0892700
.47	.889967	.259838	1.111544	8.58295	.97	.732895	.415329	.000950	.0651119
.48	.887361	.261228	1.029019	7.93195	.98	.728689	.426119	.000411	.0422279
.49	.884742	.262643	.952718	7.33712	.99	.724364	.439521	.000101	.0205463
.50	.882108	.264085	.882108	6.79278	1.00	.719877	.460722	0	0

STRESS COEFFICIENTS FOR ROTATING DISKS OF CONICAL PROFILE, $\sigma = 0.36$

r/t	P_1	$-P_2$	P_3	r/t	P_1	$-P_2$	P_3
.00	1.389125	∞	.1655455	.50	2.45072	1.761217	.1567164
.01	1.400158	7171.20	.1668182	.51	2.49323	1.666758	.1550314
.02	1.411106	1785.288	.1680318	.52	2.53746	1.575198	.1532372
.03	1.422875	789.898	.1691862	.53	2.58353	1.489087	.1511838
.04	1.434573	442.201	.1702814	.54	2.63156	1.408014	.1496214
.05	1.446505	281.588	.1713175	.55	2.68168	1.331608	.1476997
.06	1.458680	194.5182	.1722945	.56	2.73402	1.259529	.1457189
.07	1.471105	142.1261	.1732122	.57	2.78875	1.191470	.1436789
.08	1.483789	108.1928	.1740709	.58	2.84602	1.127147	.1415798
.09	1.496739	84.9778	.1748704	.59	2.90604	1.066303	.1394215
.10	1.509964	68.4083	.1756107	.60	2.96899	1.008701	.1372041
.11	1.523475	56.1756	.1762918	.61	3.03510	.954125	.1349275
.12	1.537279	46.8925	.1769139	.62	3.10463	.902374	.1325918
.13	1.551387	39.6645	.1774767	.63	3.17785	.853265	.1301969
.14	1.566810	33.9783	.1779804	.64	3.25506	.806630	.1277429
.15	1.580558	29.3957	.1784250	.65	3.33661	.762312	.1252297
.16	1.595643	25.6359	.1788103	.66	3.42287	.720169	.1226573
.17	1.611077	22.5356	.1791366	.67	3.51427	.680066	.1200258
.18	1.626873	19.9693	.1794037	.68	3.61129	.641880	.1173351
.19	1.643043	17.75603	.1796116	.69	3.71448	.605497	.1145853
.20	1.659602	15.89272	.1797604	.70	3.82444	.570812	.1117763
.21	1.676564	14.29330	.1798500	.71	3.94187	.537726	.1089082
.22	1.693944	12.91057	.1798804	.72	4.06758	.506147	.1059809
.23	1.711759	11.70739	.1798517	.73	4.20247	.475990	.1029945
.24	1.730025	10.654.26	.1797639	.74	4.34761	.447176	.0999489
.25	1.748760	9.72745	.1796169	.75	4.50421	.419631	.0968441
.26	1.767985	8.90774	.1794107	.76	4.67372	.393286	.0936802
.27	1.787714	8.17942	.1791454	.77	4.85779	.368077	.0904572
.28	1.807974	7.52955	.1788209	.78	5.05842	.343942	.0871749
.29	1.828784	6.94.759	.1784373	.79	5.27796	.320827	.0838336
.30	1.850169	6.42396	.1779945	.80	5.51925	.298678	.0804330
.31	1.872152	5.95174	.1774926	.81	5.78570	.277445	.0769734
.32	1.894760	5.52834	.1769315	.82	6.08150	.257082	.0734545
.33	1.918020	5.13639	.1763113	.83	6.41163	.237545	.0698765
.34	1.941962	4.78315	.1756319	.84	6.78313	.218794	.0662394
.35	1.966617	4.46076	.1748933	.85	7.20360	.200790	.0625431
.36	1.992013	4.16577	.1740956	.86	7.68375	.183492	.0587876
.37	2.01820	3.89521	.1732387	.87	8.23733	.1668794	.0549730
.38	2.04520	3.64650	.1723227	.88	8.88267	.1509071	.0510993
.39	2.07306	3.41741	.1713476	.89	9.64477	.1355490	.0471663
.40	2.10182	3.20596	.1703132	.90	10.55363	.1207766	.0431743
.41	2.13152	3.01012	.1692197	.91	11.67477	.1066428	.0391230
.42	2.16222	2.82928	.1680671	.92	13.06399	.0928822	.0350127
.43	2.19397	2.66118	.1668553	.93	14.86040	.0797109	.0308431
.44	2.22682	2.50493	.1655841	.94	17.21746	.0670258	.0266144
.45	2.26083	2.35948	.1642542	.95	20.5871	.0548056	.0223266
.46	2.29607	2.22386	.1628650	.96	25.5917	.0430298	.0179796
.47	2.33260	2.09725	.1614166	.97	33.9361	.0316793	.0135734
.48	2.37049	1.978885	.1599090	.98	50.6120	.0207355	.0091081
.49	2.40984	1.868075	.1583423	.99	100.6233	.0101412	.0045836
.50	2.45072	1.761217	.1567164	1.00	∞	0	0

r/t	q_1	q_2	q_3	r/t	q_1	q_2	q_3
.00	1.389125	∞	.1655455	.50	2.08387	5.02857	.1672272
.01	1.397155	7272.56	.1664763	.51	2.10928	4.88399	.1663271
.02	1.405317	1537.277	.1673705	.52	2.13558	4.74699	.1653903
.03	1.413615	825.328	.1682281	.53	2.16282	4.61703	.1644169
.04	1.422053	469.304	.1690491	.54	2.19105	4.49360	.1634068
.05	1.430635	303.667	.1698334	.55	2.22034	4.37627	.1623602
.06	1.439366	213.230	.1705811	.56	2.25076	4.26461	.1612769
.07	1.448248	158.4193	.1712922	.57	2.28237	4.15825	.1601570
.08	1.457287	122.6630	.1719667	.58	2.31525	4.05684	.1590005
.09	1.466487	98.0289	.1726046	.59	2.34949	3.96007	.1578074
.10	1.475853	80.3076	.1732058	.60	2.38518	3.86763	.1565777
.11	1.485391	67.1330	.1737704	.61	2.42243	3.77928	.1553113
.12	1.495104	57.0613	.1742984	.62	2.46134	3.69475	.1540083
.13	1.504999	49.1829	.1747898	.63	2.50205	3.61381	.1526687
.14	1.515082	42.8993	.1752446	.64	2.54468	3.53626	.1512925
.15	1.525357	37.8040	.1756627	.65	2.58940	3.46190	.1498796
.16	1.535832	33.6125	.1760442	.66	2.63637	3.39055	.1484302
.17	1.546513	30.1208	.1763891	.67	2.68578	3.32203	.1469441
.18	1.557406	27.1796	.1766974	.68	2.73785	3.25619	.1454214
.19	1.568519	24.6777	.1769691	.69	2.79281	3.19289	.1438621
.20	1.579858	22.5306	.1772041	.70	2.85093	3.13199	.1422661
.21	1.591432	20.6733	.1774025	.71	2.91252	3.07336	.1406336
.22	1.603249	19.0522	.1775642	.72	2.97792	3.01688	.1389644
.23	1.615316	17.6630	.1776895	.73	3.04752	2.96244	.1372586
.24	1.627644	16.4862	.1777781	.74	3.12179	2.90995	.1355162
.25	1.640241	15.4243	.1778300	.75	3.20124	2.85930	.1337371
.26	1.653117	14.4479	.1778454	.76	3.28648	2.81040	.1319215
.27	1.666282	13.5663	.1778241	.77	3.37821	2.76316	.1300692
.28	1.679748	12.7615	.1777662	.78	3.47738	2.71752	.1281803
.29	1.693525	11.8871	.1776716	.79	3.58466	2.67338	.1262548
.30	1.707626	11.2291	.1775405	.80	3.70153	2.63069	.1242926
.31	1.722062	10.6319	.1773727	.81	3.82931	2.58938	.1222939
.32	1.736849	10.0894	.1771683	.82	3.96972	2.54937	.1202585
.33	1.751999	9.59963	.1769273	.83	4.12486	2.51062	.1181865
.34	1.767527	9.11606	.1766496	.84	4.29736	2.47307	.1160779
.35	1.783450	8.72476	.1763354	.85	4.49052	2.43667	.1139326
.36	1.799784	8.34087	.1759845	.86	4.70856	2.40136	.1117508
.37	1.816546	7.98404	.1756970	.87	4.95696	2.36710	.1095323
.38	1.833756	7.65332	.1751729	.88	5.24297	2.33385	.1072772
.39	1.851432	7.34616	.1747122	.89	5.57645	2.30156	.1049855
.40	1.869597	7.06050	.1742148	.90	5.97107	2.27020	.1026571
.41	1.888273	6.79376	.1736809	.91	6.44445	2.23972	.1002922
.42	1.907483	6.54176	.1731103	.92	7.03183	2.21010	.0978906
.43	1.927254	6.31176	.1725031	.93	7.77285	2.18129	.0954524
.44	1.947611	6.09337	.1718592	.94	8.74501	2.15326	.0929776
.45	1.968586	5.88833	.1711788	.95	10.08321	2.12599	.0904662
.46	1.990207	5.69556	.1704617	.96	12.05557	2.09945	.0879181
.47	2.01251	5.51405	.1697080	.97	15.03147	2.07360	.0853334
.48	2.03553	5.34290	.1689177	.98	21.6073	2.04843	.0827121
.49	2.05930	5.18152	.1680904	.99	40.1758	2.02390	.0800542
.50	2.08387	5.02857	.1672272	1.00	∞	2.00000	.0773597

Studies in Three-Dimensional Photoelasticity

Stresses in Bent Circular Shafts With Transverse Holes—Correlation With Results From Fatigue and Strain Measurements

By M. M. FROCHT,[1] PITTSBURGH, PA.

Bent circular shafts with holes in the plane of bending are of frequent occurrence in modern machines. They often form a part of the lubricating system as, for example, in the crankshafts of aircraft engines. Considerable work has been done to determine the maximum stresses and the factors of stress concentration in such shafts. The author presents a simple method of calculating such stresses for transverse holes in pure bending. Experimental photoelastic evidence that led to this method is given. A comparison of the stress-concentration factors obtained by it is made with the published results from fatigue tests and strain measurements from large steel shafts, which were performed a number of years ago at the Westinghouse Research Laboratories.

Introduction

IN this paper are reported the results of a photoelastic investigation of the stress concentrations produced around open transverse holes in circular shafts which are subjected to pure bending, the axis of the hole and the bending couples being in one plane with the axis of the shaft. This problem is not only of scientific interest but is also of practical importance. Open holes in shafts often form a part of the lubricating system of a machine. The oil holes in crankshafts are one example. Considerable research work in that direction has already been done by means of strain gages and fatigue tests.[2] The development of three-dimensional photoelasticity makes it possible to study this problem by the optical method. Some work on this problem has been done by Hetényi.[3]

Method and Models. The method employed was that of freezing or fixing the stresses into a Bakelite model and subsequently cutting it into slices for individual observation in the polariscope.[4] The model shafts were all of Bakelite BT-61-893, approximately 1 in. diam and 7 in. long. They were heated for 2 to 3 hr, and slowly cooled under load to room temperature, the time of cooling being about 12 to 14 hr. A typical frozen stress pattern of a shaft as a whole is shown in Fig. 1. All sections were made perpendicular to the axis of the hole, so that each section represented a plate with a central transverse circular hole. The general dimensions of the models and the manner of slicing will be shown later.

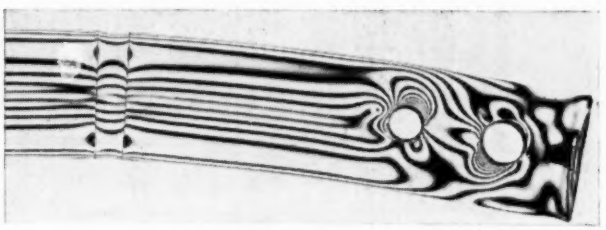


FIG. 1 FROZEN STRESS PATTERN OF A CIRCULAR SHAFT WITH TRANSVERSE HOLE IN PURE BENDING
(D = 0.980 in.; r = 0.110 in.; r/d = 0.145, initial dimensions; M = 2.57 lb-in.)

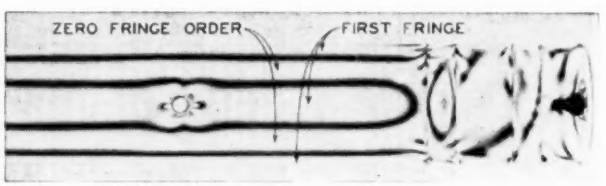


FIG. 2 FROZEN STRESS PATTERN OF A CIRCULAR SHAFT WITH TRANSVERSE HOLE IN PURE BENDING VIEWED WITH LIGHT PARALLEL TO AXIS OF HOLE
(Plane of bending was also parallel to axis of hole. D = 1.058 in.; r = 0.065 in.; r/d = 0.070; M = 3.33 lb-in.)

Boundary Difficulties. The greatest difficulty in studying stress concentrations photoelastically is the difficulty of making the boundaries and the boundary stresses visible, especially at the sources of stress concentration. Unfortunately, these difficulties, which have been successfully disposed of in two-dimensional problems, recur again in three-dimensional work.[5]

The causes of the present boundary disturbances are (1) time stresses, resulting from the relatively long period of time needed for heating, cooling, and machining, and (2) the inevitable deformations and distortions which are present in three-dimensional problems. The presence of time stresses is clearly shown in the stress pattern, Fig. 2. The region in pure bending would all be of zero fringe order were it not for the initial stresses. In view of the care which was taken in the machining of the model the observed effects are in the main due to time stresses.

The use of thin plates or sections effectively removes the shadows or space effects. We have used slices as thin as $^1/_{16}$ in. with fairly good results. When very thin plates are employed, it may

---

[1] Associate Professor of Mechanics in Charge of Photoelastic Laboratory, Carnegie Institute of Technology. Mem. A.S.M.E.

[2] "Two and Three Dimensional Cases of Stress Concentration and Comparison With Fatigue Tests," by R. E. Peterson and A. M. Wahl, JOURNAL OF APPLIED MECHANICS, Trans. A.S.M.E., 1936, p. A-15.

[3] "Photoelastic Stress Analyses Made in Three Dimensions," by M. Hetényi, *Machine Design*, vol. 10, Dec., 1938, pp. 40-41.

[4] For a discussion of the theory of the frozen stress pattern see "Photoelasticity," by M. M. Frocht, John Wiley & Sons, Inc., New York, N. Y., vol. 1, 1941, sections 10.7 through 10.11; or "The Fundamentals of Three-Dimensional Photoelasticity," by M. Hetényi, JOURNAL OF APPLIED MECHANICS, Trans. A.S.M.E., vol. 60, 1938, p. A-149; also ref. 3.

Presented at the National Meeting of the Applied Mechanics Division, Pittsburgh, Pa. June 25-26, 1943, of THE AMERICAN SOCIETY OF MECHANICAL ENGINEERS.

Discussion of this paper should be addressed to the Secretary, A.S.M.E., 29 West 39th Street, New York, N. Y., and will be accepted until April 10, 1944. Discussion received after the closing date will be returned.

NOTE: Statements and opinions advanced in papers are to be understood as individual expressions of authors, not of the Society.

[5] For an explanation of the causes of boundary vagueness and the proper technique of making it clearly visible, see ref. 4, vol. 1, sections 11.4 through 11.8; also "Studies in Photoelastic Stress Concentrations," by E. E. Weibel, Trans. A.S.M.E., vol. 56, 1934, pp. 637-658; and "Stress Concentrations Produced by Holes and Notches," by A. M. Wahl and R. Beeuwkes, Trans. A.S.M.E., vol. 56, 1934, pp. 617-625.

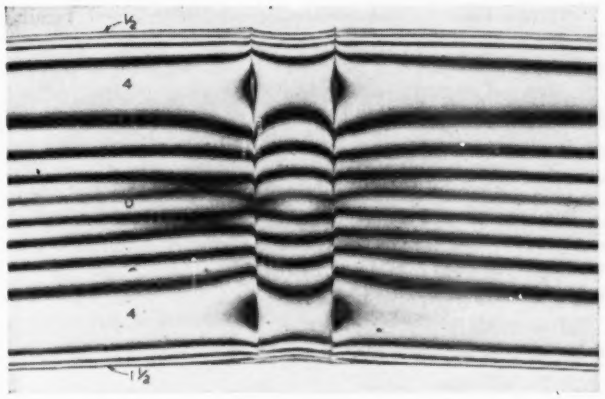


FIG. 3 ENLARGED VIEW OF SECTION AT HOLE OF FROZEN STRESS PATTERN OF CIRCULAR SHAFT WITH TRANSVERSE HOLE IN PURE BENDING

(D = 0.980 in.; r = 0.110 in.; r/d = 0.145, initial dimensions; M = 2.57 lb-in.)

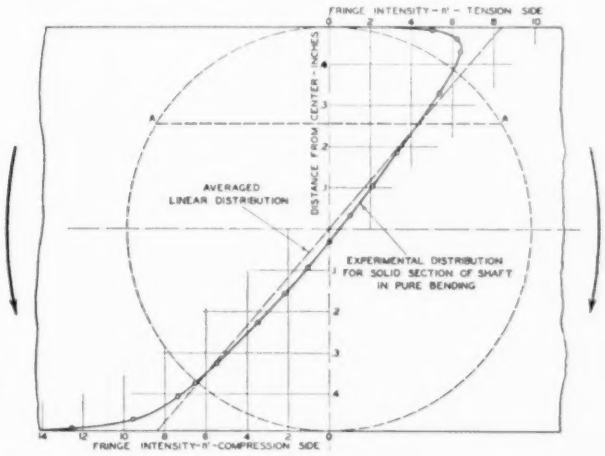


FIG. 4 CURVE SHOWING EFFECT OF TIME STRESSES ON FRINGE INTENSITY, I.E., STRESS IN FRINGES, IN A CIRCULAR SHAFT WITH TRANSVERSE HOLE IN PURE BENDING AT A SECTION AWAY FROM INFLUENCE OF HOLE

(Plotted from stress pattern shown in Fig. 3.)

become necessary to resort to the doubling polariscope, or the Babinet compensator.

Method of Loading. Some difficulty was encountered in producing pure bending. The best alignment was obtained when the metal clevices were replaced by loops of twine or strong string. These were formed into closed bands, put through the holes in the bars of the loading frame, and the ends slipped over the pins passing through the bar. In order to eliminate axial stresses the strings should be fairly long. It should perhaps be added that even greater difficulties are encountered in producing uniform tension or compression.

Fringe Order. In the case of pure bending, the fringe order can be readily determined at every point of the shaft. This is due to the presence of a neutral surface along the middle region of the shaft, which can be used as a reliable origin from which the fringe order at any other point can be determined. The fringe orders are shown in Fig. 3. It should be noted that although the extreme fibers are also of zero fringe order they are not reliable origins. The distances from these edges to the first fringe may be too small for this fringe to be clearly visible in the stress pattern. Inspection of Fig. 3 shows that on the compression side the lowest discernible fringe is of order 1½, although on the tension side it is ½. These difficulties increase under higher loads and are especially troublesome in shafts in pure tension where the zero fringe order is confined to the edges.

The differences in the spacings of the fringes on opposite sides of the shaft is due to the time stresses, which form in Bakelite models after several hours.

Fringe Value. It will be shown later that in the problem under consideration the factor of stress concentration is independent of the fringe value, or more precisely this factor can be determined without the fringe value. Should the fringe value be desired it can be calculated from the established fringe order; care must be taken, however, to eliminate the effect of the time stresses. In the case of pure bending the mean values from the fringe orders on the tension and compression sides cancel effectively the time stresses and yield a good approximation to the true fringe value. In the case of a shaft in tension the determination of the true fringe value is considerably more involved.

The full curve of Fig. 4 shows the effect of the time stresses on the fringe intensities n', which are defined as the number of fringes per unit of thickness measured along a line parallel to the direction of the light, i.e., parallel to the neutral axis in a transverse section of the shaft, such as line A-A. Owing to the fact that the time stresses are compressive on the surface of the shaft, the boundary stresses are considerably reduced on the tension side and increased on the compression side. The mean values of the fringe intensities on opposite sides of the neutral surface fall very close to the straight dashed line in Fig. 4.

Experiments show that in order to bring a shaft 1 in. diam to a uniform temperature at which the primary bonds alone function it is necessary to heat the model considerably above 230 F, which temperature was found sufficient for a bar ¼ in. thick for two-dimensional purposes. We found a temperature of about 260 to 265 F, and a heating time of about 2 hr, to give satisfactory results.

STRESS DISTRIBUTIONS AND FACTORS OF STRESS CONCENTRATIONS IN SHAFTS WITH TRANSVERSE HOLES IN PURE BENDING

Case 1: (r/d = 0.145)

D = diameter of shaft before loading = 0.980 in.

$2r$ = diameter of hole = 0.220 in.

d = $(D - 2r)$ = 0.760 in.

r/d = 0.145 (initial dimensions)

I_1 = moment of inertia of solid transverse section = 0.0453 in.⁴ (initial dimensions)

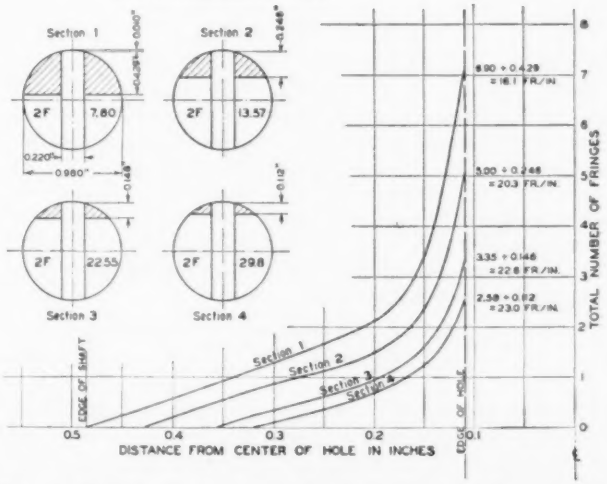


FIG. 5 CURVES OF $(p - q)$ AT SECTION OF HOLE FOR FOUR SUCCESSIVE PLATES TAKEN FROM TENSION SIDE OF CIRCULAR SHAFT WITH TRANSVERSE HOLE IN BENDING; r/d = 0.145

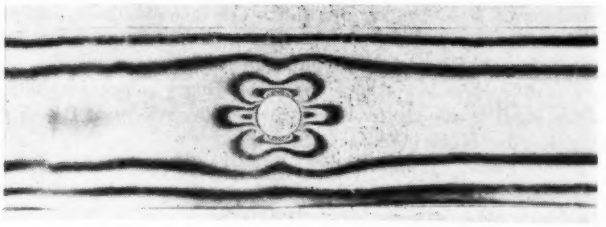


FIG. 6 FROZEN STRESS PATTERN OF TENSION HALF OF CIRCULAR SHAFT WITH TRANSVERSE HOLE IN PURE BENDING
$D' = 0.971$ in.; $r = 0.110$ in.; $r/d = 0.145$; $t = 0.430$; n_{max} [extrapolated] = 6.90 fringes.)

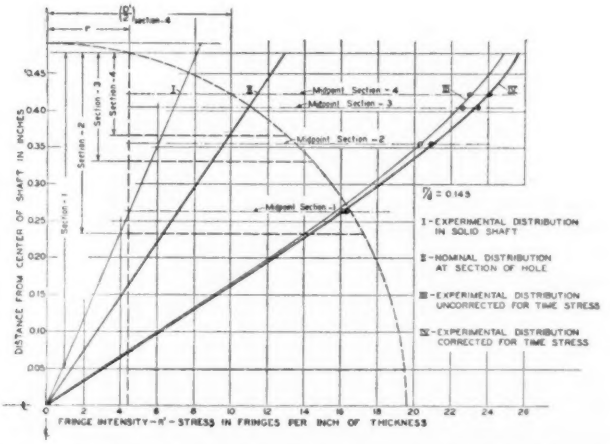


FIG. 7 CURVES SHOWING EXPERIMENTAL STRESS DISTRIBUTION AT SECTION THROUGH HOLE FOR TENSION SIDE AS DETERMINED FROM THE FOUR INDICATED PLATES; $r/d = 0.145$

I_2 = moment of inertia of transverse section through hole = 0.0286 in.^{4}, approx. (initial dimensions)
P = load = 3.50 lb
a = moment arm = 0.735 in. (final dimensions)
M = bending moment = 2.57 lb-in.
N_1' = maximum stress intensity in fringes at solid transverse section in pure bending = 8.3
N_2' = maximum stress intensity in fringes at transverse section through hole determined photoelastically = 25.5
$(N_2')_{\text{nominal}}$ = nominal maximum at hole = 12.8

Fig. 5 shows the dimensions of the four successive plates cut from the tension half of the shaft and the resulting curves of $(p - q)$. A typical stress pattern obtained from these plates is shown in Fig. 6. Fig. 7 shows the nominal and photoelastic stress distributions for a transverse section through the hole. Curve I gives the nominal stresses for a transverse section through a solid portion of the shaft in pure bending. This is the mean curve found in Fig. 4. Curve II of Fig. 7 is the nominal stress distribution through the hole. It is obtained from curve I by means of the simple relation

$$(n_2')_{\text{nominal}} = n_1' \frac{I_1}{I_2} \quad \ldots\ldots\ldots\ldots\ldots\ldots [1]$$

in which n_2' and n_1' are, respectively, the nominal stresses in the same fiber in a solid section in pure bending and at a section through the hole. From Equation [1] it follows that

$$\left(N_2'\right)_{\text{nominal}} = N_1' \frac{I_1}{I_2} \quad \ldots\ldots\ldots\ldots\ldots\ldots [2]$$

Curve III shows the photoelastically determined bending stresses at the hole. On plotting this curve the average fringe intensity obtained for a plate was placed at the mid-point of the plate. The curve obtained in this manner is straight for a considerable distance from the center of the shaft and does not differ radically from a straight line thereafter. The assumption that the mean stress intensity corresponds to the mid-point of the plate is therefore justified for all practical purposes. Curve IV gives the same data as curve III corrected for time stresses. The manner in which the correction is generally obtained in pure bending is shown in Figs. 4 and 11.

Case 2: $(r/d = 0.07)$
D = 1.058 in.
$2r$ = 0.13 in.
d = 0.928 in.
r/d = 0.07
I_1 = 0.0615 in.^{4}
I_2 = 0.049

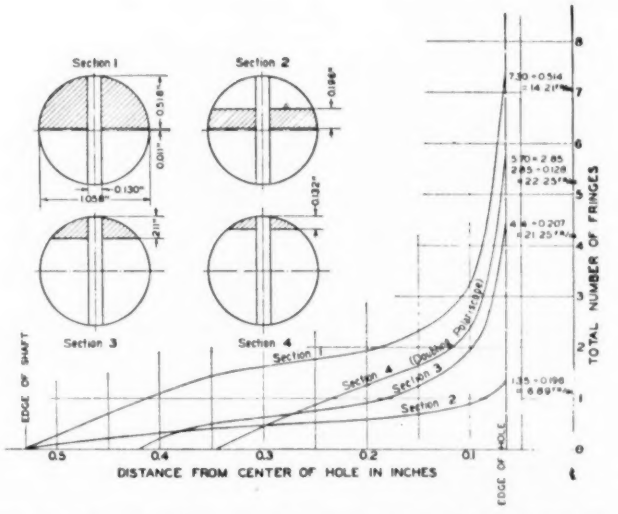


FIG. 8 CURVES OF $(p - q)$ AT SECTION THROUGH HOLE FOR FOUR PLATES TAKEN FROM TENSION SIDE OF CIRCULAR SHAFT WITH TRANSVERSE HOLE IN PURE BENDING; $r/d = 0.070$

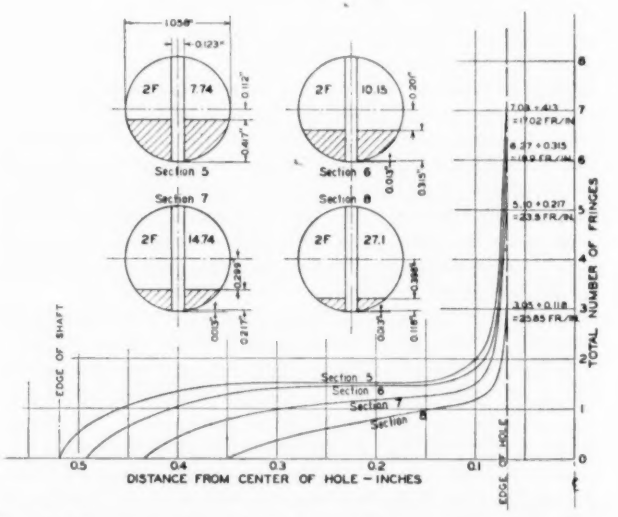


FIG. 9 CURVES OF $(p - q)$ AT SECTION THROUGH HOLE FOR FOUR SUCCESSIVE PLATES CUT FROM COMPRESSIVE SIDE OF CIRCULAR SHAFT WITH TRANSVERSE HOLE IN PURE BENDING; $r/d = 0.070$

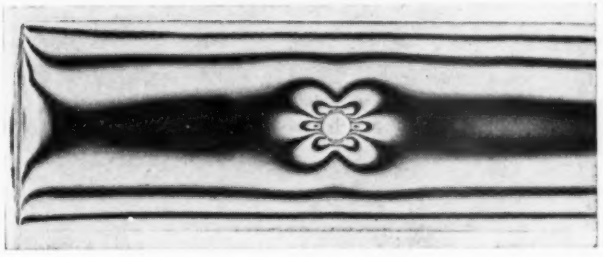


FIG. 10 FROZEN STRESS PATTERN OF TENSION HALF OF CIRCULAR SHAFT WITH TRANSVERSE HOLE IN PURE BENDING
(D' = 1.058 in.; r = 0.065 in.; r/d = 0.070; t = 0.518 in.; n_{max}, [extrapolated] = 7.30 fringes.)

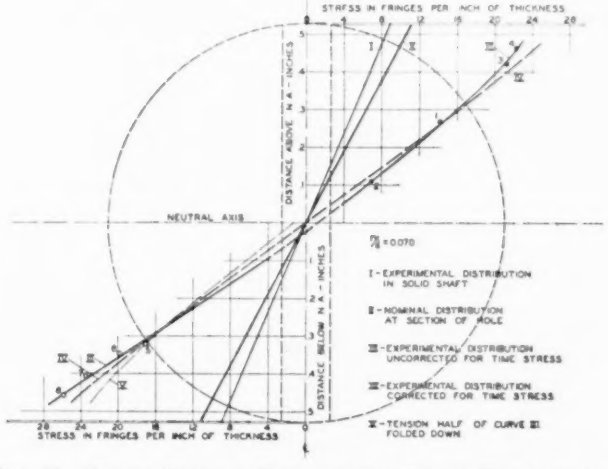


FIG. 11 CURVES SHOWING EXPERIMENTAL STRESS DISTRIBUTION AT SECTION OF HOLE IN CIRCULAR SHAFT WITH TRANSVERSE HOLE IN PURE BENDING; r/d = 0.070

P = 4.44 lb
a = 0.75 in.
M = Pa = 3.33 lb-in.
N_1' = 8.95 fringes per in.
N_2' = 26 fringes per in. at extreme fibers
$(N_2')_{nominal}$ = 11.2 fringes per in.

Figs. 8 and 9 show the plates cut from the tension and compression half, respectively, and the resulting curves of $(p - q)$. A typical stress pattern on which these curves are based is shown in Fig. 10. The resulting stress distribution is shown in Fig. 11.

Photoelastic Factors of Stress Concentration. By definition the factor of stress concentration k_3 is given by

$$k_3 = \frac{\sigma_{max}}{\sigma_{nominal}} \quad \ldots\ldots [3]$$

$$= \frac{N_2' \times 2f}{\frac{Mr}{I_2}} \quad \ldots\ldots [4]$$

in which $2f$ is the fringe value in tension or compression per inch of thickness. Remembering that

$$2f = \frac{Mr}{I_1 N_1'} \quad \ldots\ldots [5]$$

we obtain after substitution

$$k_3 = \frac{N_2' I_2}{N_1' I_1} \quad \ldots\ldots [6]$$

Using Equation [2], this becomes

$$k_3 = \frac{N_2'}{(N_2')_{nominal}} \quad \ldots\ldots [7]$$

Equation [6] shows that the factor of stress concentration k_3 can be calculated without the fringe value or bending moment, thereby eliminating one or two possible sources of error. The only experimental data needed to evaluate this factor are the maximum nominal fringe intensity N_1' in the solid portion of the shaft which is in pure bending and the maximum photoelastic fringe intensity N_2' at the hole. The ratio I_1/I_2 is taken from the initial dimension of the shaft and this may introduce a small error.

For purpose of calculation Equation [7] is the most convenient since both N_2' and $(N_2')_{nominal}$ are given directly by the curves of Figs. 7 and 11. Using these curves, we find that

$$(k_3)_{r/d = 0.145} = \frac{25.5}{12.8} = 1.98 \text{ approx.}$$

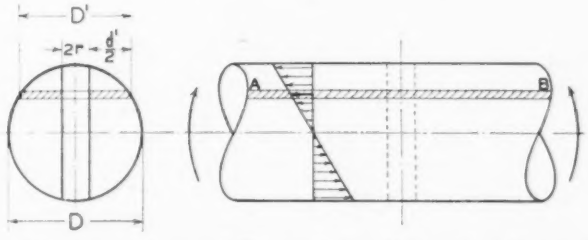


FIG. 12 SKETCH SHOWING NOTATION AND MEANING OF LAMINAR ACTION FOR CIRCULAR SHAFTS IN BENDING

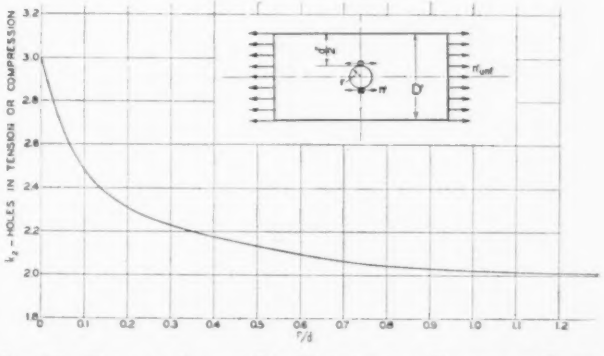


FIG. 13 CURVE OF k_2, THE TWO-DIMENSIONAL FACTORS OF STRESS CONCENTRATION, FOR HOLES IN TENSION OR COMPRESSION AS APPLIED TO A SINGLE PLATE OR LAMINA IN A CIRCULAR SHAFT WITH TRANSVERSE HOLE IN BENDING
(This curve can be found in author's paper "Photoelastic Studies in Stress Concentrations," *Mechanical Engineering*, vol. 58, 1936, pp. 485–489, or in "Strength of Materials," by N. C. Riggs and M. M. Frocht, Ronald Press Company, New York, N. Y., 1938.)

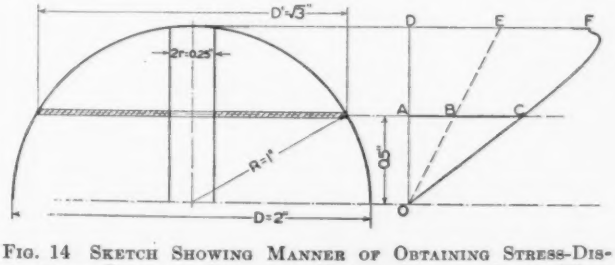


FIG. 14 SKETCH SHOWING MANNER OF OBTAINING STRESS-DISTRIBUTION CURVES AT SECTION OF HOLE IN CIRCULAR SHAFTS WITH TRANSVERSE HOLE IN BENDING BY APPLYING THE THEORY OF LAMINAR ACTION

and

$$(k_3)_{r/d\,=\,0.07} = \frac{26}{11.2} = 2.32, \text{ approx.}$$

A third case in which $r/d = 0.058$ was investigated and it gave a value of $k_3 = 2.16$.

In calculating these factors the experimental curves were extrapolated to the extreme fibers on the assumption that the maximum stresses occur there. It will be shown later that a strong probability exists that this assumption is not always true, and specifically that the maximum bending stress may actually be developed at a point some small distance away from the extreme fibers. The effect of this will be to reduce the factor k_3, for small values of r/d.

Theory of Laminar Action

The experimental results, shown in Figs. 7 and 11, can be explained by assuming:

1 That in transverse sections far from the hole the longitudinal stresses follow the linear distribution given by the elementary flexure formula

$$\sigma = \frac{My}{I} \quad \ldots\ldots\ldots\ldots\ldots\ldots\ldots\ldots [8]$$

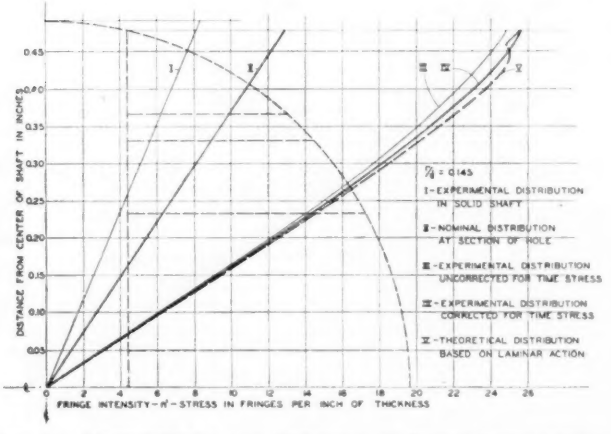


Fig. 15 Experimental and Theoretical Stress Distribution at Section of Hole in Circular Shaft in Pure Bending (Case 1: $r/d = 0.145$.)

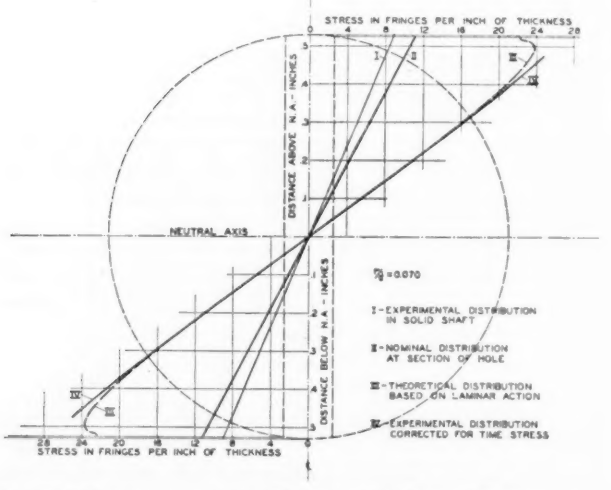
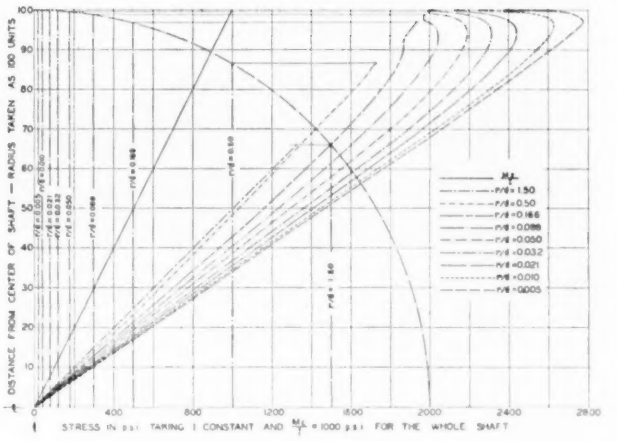
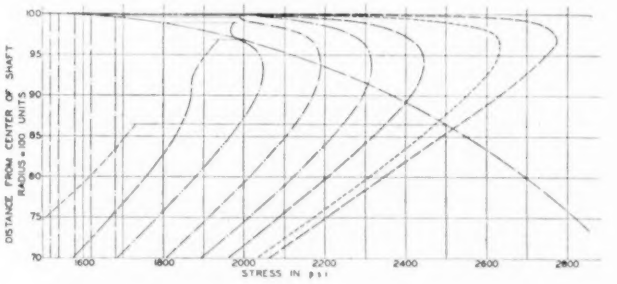


Fig. 16 Experimental and Theoretical Stress Distribution at Section of Hole in Circular Shaft in Pure Bending (Case 2: $r/d = 0.070$.)



(a)



(b)

Fig. 17 Curves Showing Distribution of Bending Stresses (a Curves giving theoretical stress distribution on assumption of laminar action at section of hole. Nine different values of r/d for circular shafts with transverse hole in bending are shown. b Enlargement of top portion of curves in a.)

2 That each thin plate, or lamina, parallel to the neutral surface behaves like a two-dimensional bar in pure tension or compression, Fig. 12.

One consequence of this assumption is that the factor of stress concentration around the hole in each plate is exactly the same as the two-dimensional factor k_2 for the same ratio r/d, Fig. 13.

As an illustration, consider a shaft 2 in diam with a $^1/_4$-in. hole, Fig. 14. At a point $^1/_2$ in. above the neutral axis, the length of the chord $D' = \sqrt{3}$, and $d' = D' - 2r = 1.482$ in. The corresponding r/d' is given by

$$\frac{r}{d'} = \frac{0.125}{1.482} = 0.0843 \text{ in.}$$

From the curve in Fig. 13, we find that the stress-concentration factor k_2 for this plate is 2.53, approximately. The maximum bending stress σ in this strip is then

$$\sigma = 2.53 \times \frac{My}{I}$$

The values of σ would then follow some such curve as OCF, Fig. 14, in which

$$\frac{AC}{AB} = (k_2)_{r/d' = 0.843} = 2.53$$

and

$$\frac{DF}{DE} = (k_2)_{r/d' = \infty} = 2$$

The stress distributions which follow from the foregoing assumptions, and the corresponding photoelastic values for $r/d = 0.145$ and $r/d = 0.070$, are shown in Figs. 15 and 16, respectively. The dashed curves represent the distribution from the assumption of laminar action. The other curves are the same as in Figs. 7 and 11.

The distribution of the bending stresses on the assumption of laminar action for nine different ratios of r/d are shown in Fig. 17 (a), and an enlarged view of the same curves in the proximity of the extreme fibers is shown in Fig. 17(b). Inspection of these curves shows that, for values of r/d less than 0.14, the maximum bending stresses may occur below the extreme fibers. It should, perhaps, be added that the assumption of laminar action satisfies the laws of equilibrium, since the resultant force in each separate lamina remains equal to that given by the flexure formula.

Factors of Stress Concentration on the Assumption of Laminar Action. Assuming laminar action the three-dimensional factors of stress concentrations k_3 would be given by

$$k_3 = \frac{k_2 \dfrac{My_m}{I_2}}{\dfrac{Mr}{I_2}}$$

or

$$k_3 = k_2 \frac{y_m}{r} \qquad [9]$$

in which y_m denotes the distance from the neutral axis to the point of maximum bending stress, in what we may briefly call the theoretical curves, and, for small holes, r equals the radius of the shaft approximately. Inspection of Fig. 17(b) shows that $(r - y_m)$ is very small. Thus for $r/d = 0.005$, $y_m = 0.995\,r$, and for $r/d = 0.9$, $y_m = 0.93\,r$ approx.

Since $\dfrac{y_m}{r}$ is never greater than unity it follows that k_3 is never greater than the maximum value of k_2. From two-dimensional studies we know that the maximum value of k_2 is 3. Hence assuming laminar action, k_3 cannot possibly exceed that value. For r/d greater than 0.14, the maximum bending stress occurs in the extreme fibers and $k_3 = 2$; and for r/d less than 0.14, k_3 is greater than 2.

Comparison With Results From Fatigue Tests and Strain Measurements. Factors of stress concentration k_3, based on the assumption of independent laminar action, i.e., on the curves of Fig. 17, are given by curve I of Fig. 18.

Superimposed over this curve are the three points from the photoelastic tests reported in this paper and seven additional points from fatigue tests and strain measurements determined by Peterson and Wahl.[2] Inspection of this curve shows that all but two, the points from fatigue tests from small shafts (0.5 in. diam), fall well on the curve.

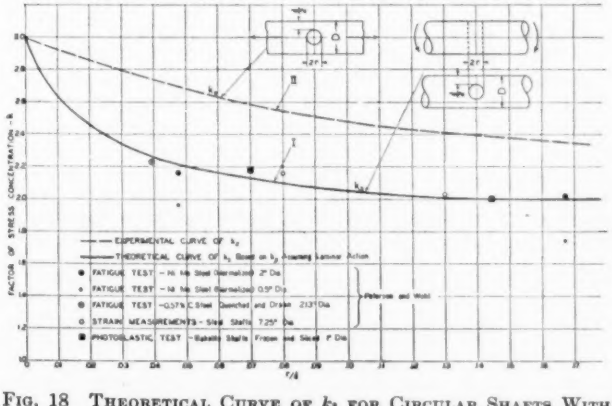


FIG. 18 THEORETICAL CURVE OF k_3 FOR CIRCULAR SHAFTS WITH TRANSVERSE HOLE, BASED ON THE THEORY OF LAMINAR ACTION WITH POINTS FROM A NUMBER OF TESTS MADE AT VARIOUS TIMES USING VARIOUS KINDS OF MATERIAL

(The three photoelastic tests are marked with solid squares.)

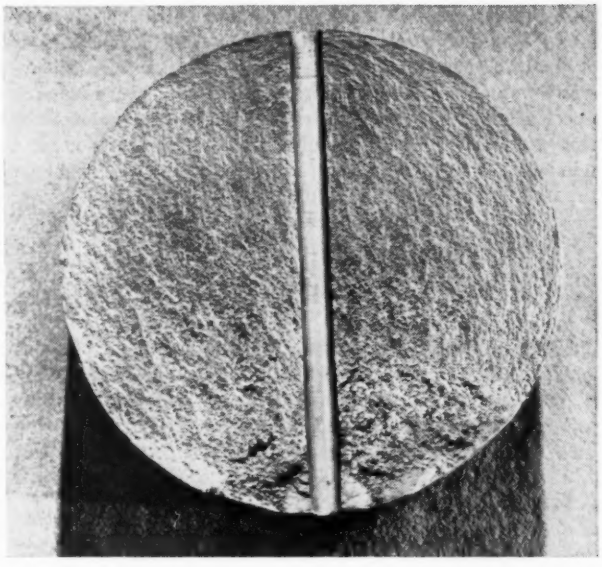


FIG. 19 PHOTOGRAPH OF FRACTURE OF A STEEL SHAFT SHOWING EVIDENCE THAT MAXIMUM STRESS OCCURS BELOW SURFACE OF SHAFT; NOTE CRACK NEAR TOP OF HOLE

($D = 3$ in.; $r = 0.187$ in.; $r/d = 0.0334$. Photograph by courtesy of R. E. Peterson, Westinghouse Electric & Manufacturing Co.)

Moreover there is some direct experimental evidence tending to show that in shafts with small holes the maximum stress is not developed in the extreme fibers but at points some distance below. Examination of fractures from fatigue tests seems to substantiate this conclusion. Fig. 19 shows one such fracture. Inspection of this illustration shows a crack on both sides of the hole well below the extreme fibers. Further, the position of this crack agrees substantially with that given by the theoretical curve for the same ratio r/d.

Returning now to the photoelastic results for curve II, in which $r/d = 0.07$, and assuming that the maximum bending stresses do not occur at the extreme fibers but at the points indicated by the theoretical curves, the factor k_3 from the photoelastic data would become

$$k_3 = \frac{24.4}{11.2} = 2.18$$

instead of the previously calculated 2.32. This value is in closer agreement with the results from fatigue tests and strain measurements, as well as with the curve based on laminar action.

Sources of Errors. Bakelite, which is a well-nigh perfect material, for two-dimensional models at room temperature, has several inherent weaknesses when used for three-dimensional problems. At high temperature it produces large deformations even under moderate stresses, it gives rise to annoying time stresses, and at present it is available only in blocks approximately 12 in. × 7 in. × 1 in. in size.

The main source of error in the work described in this paper arises from the first-mentioned weakness. In order to avoid large deformations and the resulting changes in the shape of the hole and in the value of r/d the bending moment was deliberately kept low. To compensate for the small stresses in the shaft, relatively thick plates or sections were employed. This in turn

obscured the true boundary and made it necessary to resort to extrapolation in the determination of the maximum fringe order at the hole. The main errors spring from the extrapolation. It will be observed, however, Figs. 5 and 9, that near the extreme fibers where the stresses are critical our plates were relatively thin and we employed a doubling polariscope to increase the number of fringes. The use of this plate will in general eliminate the need for extrapolation and should lead to a greater accuracy. But here the time stresses become a disturbing factor. In the problem under consideration the time stresses tend to cancel out and the errors due to this cause are probably small. The same conclusion holds for the error arising from the changes in the values of r/d.

Since the fringe value and the bending moment do not enter into Equation [7], the expression used to calculate the value of k_3, it means that the effect of friction on the load, and the accuracy of measuring the bending moment, do not affect our results, although precautions were taken to free the pivot in the straining machine of frictional forces and to measure the bending moment accurately.

Conclusions

The photoelastic results suggested the hypothesis of independent laminar action, which, although not conclusively proved here, is strongly supported by the available data from fatigue tests and strain measurements. This hypothesis leads to a simple method of calculation of maximum bending stresses and theoretical factors of stress concentrations. The first important conclusion is that the theoretical stress-concentration curve obtained on the assumptions of laminar action is in good agreement with the results from fatigue tests, strain measurements, and the photoelastic tests. We thus have a simple and effective correlation between stress and failure. Large (2 in.) normalized Ni-Mo shafts with transverse holes in pure bending in fatigue seem to break at a stress equal to the endurance limit divided by the theoretical factor of stress concentration. The behavior of such shafts is then similar to that of a brittle material except that the endurance limit replaces the ultimate tensile strength.

We further conclude that, except for the limiting values, the three-dimensional factors k_3 are considerably smaller than the two-dimensional factors k_2 for the same ratio of r/d.

Inspection of Fig. 18 shows that k_3 like k_2 approaches 2 as the lower limit, only k_3 reaches this limit more rapidly than k_2. Thus at $r/d = 0.14$, k_2 is already equal to 2, whereas k_3 approaches this value only when r/d becomes infinite.

The upper branch of the curve of k_3 for values of r/d less than 0.04 is at the moment without experimental corroboration, and further work is needed on shafts with very minute holes. In view of the limitation in the dimensions of good photoelastic material for three-dimensional studies it seems probable that more pertinent information can at the present time be expected from fatigue tests especially designed for this purpose. This would also throw further light on the hypothesis of laminar action. However, further photoelastic work using built-up beams is contemplated.

The scope of three-dimensional photoelasticity is circumscribed only by the quality and size of the material available for models, and the over-all accuracy of three-dimensional photoelastic analyses is at present somewhat lower than that of two-dimensional investigation. Nevertheless, the optical method is yielding valuable stress data for space problems even under the present limitations. With the development of an improved material on which some laboratories are now working, a material which would permit the molding or casting of complicated shapes, which would be optically sensitive and free from time stresses, the power of the photoelastician will sharply mount.

Acknowledgment

The author expresses his acknowledgment to the administration of the Carnegie Institute of Technology for support of this work. Mr. John Robert McDowell, mechanician in the Photoelastic Laboratory, assisted in the calculations, photography, and drawings. Mr. M. M. Leven, now a Lieutenant in the United States Navy, assisted in obtaining the original photoelastic data for cases 1 and 2. The author also wishes to thank Mr. R. E. Peterson from the Westinghouse Research Laboratories for making available to him the photograph of the fracture showing the crack below the extreme fibers.

The Stresses in Cemented Joints

By M. GOLAND,[1] BUFFALO, N. Y., and E. REISSNER,[2] CAMBRIDGE, MASS.

The determination of the stresses in cemented lap joints has become of practical importance because of the development of new methods which permit a strong bond to be established between wood, plastic, or metal sheets, or combinations of them by the use of cement adhesives. In this paper, the problem is divided into two parts, (*a*) determination of the loads at the edges of the joint; (*b*) determination of the stresses in the joint due to the applied loads. Solutions are obtained for two limiting cases, i.e., where the cement layer is so thin that its effect on the flexibility of the joint may be neglected; and where the joint flexibility is mainly due to that of the cement layer. In both cases expressions are obtained for the shearing stresses in the cement, and for the normal stresses in the cement in a direction perpendicular to the plane of the joint.

THE present paper deals with the determination of the stresses in cemented lap joints. The problem has become of practical importance as a result of the development of new methods which permit the joining of wooden or metal sheets, or a combination of the two, by means of cement adhesives in such a manner that a very strong bond is established.

The problem is subdivided into two parts. The first part is concerned with the determination of the loads at the edges of the joint. It is recognized that this is a problem in which the deformation of the jointed sheets must be taken into account, using the finite-deflection theory of cylindrically bent plates. The second part is concerned with the determination of the stresses in the joint due to the applied loads. This problem is formulated as one in plane strain. Explicit solutions are obtained for two limiting cases, (*a*) the case where the cement layer is so thin that its effect on the flexibility of the joint may be neglected; (*b*) the case in which the joint flexibility is mainly due to that of the cement layer. Case (*b*) is significant for the analysis of cemented metal sheets. Case (*a*) is of practical interest in the study of cemented wooden and plastic sheets. In both cases, expressions are obtained for the shearing stresses in the cement and for the normal stresses in the cement in a direction perpendicular to the plane of the joint. For these latter stresses, the name "tearing stresses" is suggested, as they are thought to explain the tearing failures observed to take place at the edges of lap joints.

Related problems on the strength of welded or riveted joints have been considered by several previous writers (1, 2, 3, 4, 5, 6)[3] The main interest in these previous publications was the distribution of the shearing stresses, and neither the effect of the deflection of the jointed members due to plate bending nor the effect of the tearing-stress component was taken into consideration. It is shown here that consideration of these effects is essential for the analysis of cemented lap joints and the mathematical formulation of the problem in this manner leads to a system of equations which, to the authors' knowledge, has not been established previously.

Formulation of the Problem

Given are two rectangular sheets of equal thickness t, of unit width and of length $(l + 2c)$. The two sheets are lap-jointed over the length $2c$. The bond between the two sheets is established by means of a cement layer whose thickness η is small compared with those of the sheets. The unjointed ends of the sheets may be assumed to be simply supported and acted upon by tensile forces of magnitude T per unit of sheet width, Fig. 1.

The main problem is the determination of the shearing and normal stresses in the cement. Due to the fact that the sheet width is large compared with the sheet thickness, this may be considered as a problem in plane strain. The problem is subdivided into two parts. Part one concerns the determination of the loads applied to the rectangular joint section of length $2c$ and thickness $(2t + \eta)$. Assuming that it is satisfactory to approximate the applied loads by a linear normal stress and a parabolic shear distribution, this problem may be considered as one of beam theory, or rather, of cylindrically bent-plate theory. The two overlapping sheets are considered as one homogeneous plate with a discontinuous thickness variation and a neutral plane discontinuous at the ends of the joint section. Moreover, it is found necessary to take into account the effect which the deflection of the joint section has on the moment distribution, Fig. 2. The solution of this problem is given in Part 1 of the present paper.

Having the distribution of loads along the edges of the joint, it remains to solve a problem in plane strain in order to determine the stresses in the cement. The complete solution of this boundary problem is of considerable difficulty. Its proper execution requires that the deformation of the sheets due to the three stress components σ_x, σ_y and τ_{xy} be taken into account, as well as the deformation of the cement layer due to the corresponding three stress components.

However, the relative thinness of the cement layer and the smallness of its elastic moduli, as compared with the elastic moduli of the sheet material, allow several simplifications to be made, i.e., neglect of the normal stress in the cement parallel to the layer and the assumption that the remaining stresses in the cement do not vary across the thickness of the layer.

On the basis of these assumptions, the strain energy of the joint, expressed in terms of the stresses, is given by

$$W = \int_{-c}^{c} \int_{0}^{t} \left\{ \frac{1-\nu^2}{E} \left[\sigma_x^2 + \sigma_y^2 - \frac{2\nu}{1-\nu} \sigma_x \sigma_y \right] + \frac{1}{G} \tau_{xy}^2 \right\} dx dy + \frac{1}{2} \eta \int_{-c}^{c} \left\{ \frac{1}{E_c} \sigma_c^2 + \frac{1}{G_c} \tau_c^2 \right\} dx \quad \ldots\ldots [1]$$

Here E, G, and ν represent the Young's modulus, the shear modulus, and the Poisson's ratio, respectively, of the sheet material and E_c and G_c refer to the Young's and shear moduli, respectively, of the cement material. The sheet normal stress σ_x is parallel to the plane of the joint and the normal stress σ_y is per-

---

[1] Research Engineer, Research Laboratory, Curtiss-Wright Corporation, Airplane Division.

[2] Consultant, Research Laboratory, Curtiss-Wright Corporation, Airplane Division, Assistant Professor of Mathematics, Massachusetts Institute of Technology.

[3] Numbers in parentheses refer to the Bibliography at the end of the paper.

Presented at the Annual Meeting, New York, N. Y., Nov. 29–Dec. 3, 1943, of The American Society of Mechanical Engineers.

Discussion of this paper should be addressed to the Secretary, A.S.M.E., 29 West 39th Street, New York, N. Y., and will be accepted until April 10, 1944, for publication at a later date. Discussion received after the closing date will be returned.

Note: Statements and opinions advanced in papers are to be understood as individual expressions of their authors and not those of the Society.

pendicular to this plane. The sheet shear stress τ_{xy} acts on planes parallel to the directions of σ_x and σ_y. The cement stresses σ_o and τ_o represent, respectively, the normal "tearing stress" in the cement and the shear stress acting on planes parallel to that of the cement layer.

The correct stress distribution is distinguished from all stress distributions satisfying the equilibrium equations and the boundary conditions of the joint problem by the fact that it minimizes the strain energy W.

On the basis of this energy consideration, an estimate can be made of the range of validity of the two approximate treatments which are given in what follows.

The first approximate treatment neglects the flexibility of the cement layer; i.e., the work of the stresses σ_o and τ_o in the cement compared with the work of the stresses σ_y and τ_{xy} in the sheet. Since, approximately

$$\int_0^t \frac{\sigma_y^2}{E}\, dy \approx \frac{t}{2E}\,\sigma_o^2 \qquad [2]$$

with a corresponding estimate for τ_{xy}, it follows that the flexibility of the cement layer may be neglected when the following order of magnitude relation is satisfied:

$$\frac{\eta}{E_c} \ll \frac{t}{E}, \quad \frac{\eta}{G_c} \ll \frac{t}{G} \qquad [3]$$

and acceptable results should be obtained when

$$\frac{\eta}{E_c} \lesssim \frac{1}{10}\cdot\frac{t}{E}, \quad \frac{\eta}{G_c} \lesssim \frac{1}{10}\cdot\frac{t}{G} \qquad [4]$$

This inequality means, for example, when the elastic moduli of the cement are 1/100, (1/1000) of the elastic moduli of the sheet material, the thickness of the cement layer must be not more than 1/1000, (1/10,000) of the sheet thickness, in order that this part of the theory give quantitative information.

The second approximate treatment neglects, in effect, the work of the stresses σ_y and τ_{xy} in the sheet as compared with the work of the stresses σ_o and τ_o in the cement. As before, Equation [2] may be assumed to hold, and consequently the order of magnitude relations describing the range of validity of this approximate theory become

$$\frac{t}{E} \ll \frac{\eta}{E_c}, \quad \frac{t}{G} \ll \frac{\eta}{G_c} \qquad [5]$$

which conditions may be replaced by

$$\frac{t}{E} \lesssim \frac{1}{10}\cdot\frac{\eta}{E_c}, \quad \frac{t}{G} \lesssim \frac{1}{10}\cdot\frac{\eta}{G_c} \qquad [6]$$

Thus if the elastic moduli of the cement are 1/100, (1/1000) of the elastic moduli of the sheet material, the thickness of the cement layer must be not less than 1/10, (1/100) of the thickness of the sheet, in order that this part of the theory be applicable.

It is recognized from these order-of-magnitude considerations that the second approximate treatment is well adapted to the analysis of metal joints of the dimensions occurring in airplane structures, while the first treatment is of value in the study of the cementing of relatively thick wood and plastic sheets.

Results and Discussion of Results

The results of major interest are those pertaining to the values of the stresses in the cement layer of a loaded joint. Prior to investigating the cement stresses, however, it is necessary to evaluate the forces and moments transmitted by the unjointed-sheet portions to the lapped-joint portion.

The loads transmitted by the sheets to the edges of the joint consist of a tension T, a moment M_o and a transverse shearing force V_o, each per unit of joint width, Fig. 1. The moment M_o is directed so as to introduce tensile stresses in the sheet fibers nearest to the cement layer. It is found, in section 1, that the magnitudes of the moment M_o and the shearing force V_o are dependent upon the value of the tensile stress p in the unjointed sheet, the joint dimensions, and the physical properties of the sheet material. The precise nature of this dependence is indicated by Table 1 and Fig. 3 of this paper. Fig. 3 is a plot of the nondimensional factor $k = \dfrac{2M_o}{pt^2}$ versus the parameter $\dfrac{c}{t}\sqrt{\dfrac{p}{E}}$, where the factor k is the ratio of the magnitude of the edge moment M_o and the value of this moment in a nondeformable system, and p represents the mean stress T/t in the sheets away from the joint. Values of $\dfrac{V_o c}{pt^2}$ for various $\dfrac{c}{t}\sqrt{\dfrac{p}{E}}$ are given in Table 1.

In representative joints composed of cemented aluminum-alloy sheets, the value of k is reduced to as little as 35 per cent of its initial value, as the sheet stress p is raised from zero to 40,000 psi. The edge-shearing force in these sheets is never in excess of $0.02T$.

For joints with relatively inflexible cement layers, i.e., for joints where $\dfrac{\eta}{E_c} \lesssim \dfrac{1}{10}\cdot\dfrac{t}{E}$ and $\dfrac{\eta}{G_c} \lesssim \dfrac{1}{10}\cdot\dfrac{t}{G}$, very high concentrations of stresses are found at the joint edges. Fig. 7 shows the maximum values of these stresses, plotted as a function of the moment factor k. The normal stress σ_o in the cement, acting in a direction perpendicular to the plane of the joint, has the surprisingly large value 4.3 p for $k = 1.0$. As the value of k is reduced, due to an increase in the applied sheet stress p, the σ_o concentration also decreases, reaching the value 2.1 when $k = 0.4$. The higher sheet stresses are thus accompanied by lower σ_o concentrations. It is to be noted, however, that the numerical magnitude of σ_o increases steadily with the sheet stress p.

The magnitude of the maximum shear stress τ_o in the cement plane is likewise large. At the start of loading ($k = 1.0$), the peak shear stress value is 0.79 p; the shear-concentration factor decreases to 0.45 for $k = 0.4$. The numerical magnitude of the maximum shear stress is again found to increase steadily with the sheet stress p.

It is of extreme interest to note the existence of such large cement stresses, particularly with regard to the σ_o stresses. It is observed, during actual joint tests, that the start of failure is characterized by a splitting apart of the two sheets at the joint edges. This action is explained by the presence of the high σ_o stresses. For easy reference, a descriptive title for the σ_o stresses is desirable; the name "tearing stresses" is suggested as being appropriate for this purpose.

The third stress, shown in Fig. 7, is the longitudinal tensile stress σ_f in the most highly loaded sheet fiber adjacent to the cement layer. As do those of σ_o and τ_o, the concentration factor for σ_f markedly decreases as the joint load increases, i.e., as the value of k decreases.

Fig. 6 shows the stress distribution along the shear plane of the joint in the vicinity of the edges, calculated for a value $k = 1.0$. The σ_o stress is highest at the joint edge and rapidly damps out to a small value (0.1 p) within a distance along the shear plane of about two sheet thicknesses; the reversal of the σ_o stress from a tensile to a compressive stress within this distance is of interest. The τ_o stress has the value zero at the joint edges; it rapidly rises to a peak value and once more decays to almost zero within a distance of two sheet thicknesses. Finally, the sheet fiber stress σ_f rapidly decreases to its nominal value 0.5 p within this same distance along the shear plane. In joints with relatively inflexible cement layers, therefore, the tearing and shear stresses in the

cement are concentrated in small regions near the ends of the joint. The middle-joint portions are under practically pure tension of amount 0.5 p in the sheets.

For joints with relatively flexible cement layers, i.e., for joints where $\frac{t}{E} \leq \frac{1}{10} \cdot \frac{\eta}{E_c}$ and $\frac{t}{G} \leq \frac{1}{10} \cdot \frac{\eta}{G_c}$, results of entirely different nature are obtained. To begin with, whereas the stress distribution in the cement for the inflexible-layer case is independent of both the joint dimensions and the physical properties of the cement material, the cement stresses in flexible layers are dependent upon both of these factors. Furthermore, the cement stresses are no longer restricted to small end zones in flexible layers, but are of appreciable magnitude over the whole of the shear plane.

Fig. 9 shows typical σ_o and τ_o distributions in joints with flexible cement layers, calculated for several k values. The joints are composed of representative materials and dimensions (say, aluminum-alloy sheets cemented with a typical resin adhesive and with a joint overlap to joint thickness ratio of 5), as specified by the values of the parameters given on the sketch. It is evident that the increased flexibility of the cement layer causes the shear stress τ_o in the cement to be more uniformly distributed over the joint shear plane. Nevertheless, the distribution still indicates a sizable concentration of shear in the end regions of the joint. The σ_o stresses again reverse their sign near the joint edges, but are not damped away as quickly as they were in inflexible cement layers. The peak τ_o and σ_o values still occur at the joint edges.

It is at once clear that the magnitudes of the peak cement stresses are very much lower in joints with flexible-cement layers than in joints with relatively inflexible layers. Their orders of magnitudes for representative joints are indicated in Fig. 9. For $\frac{c}{t} = 5$, the maximum σ_o value is about 0.12 p and that of τ_o is approximately the same magnitude. It is to be noted that even more pronounced reductions in the σ_o values than in the τ_o values are brought about by increased cement-layer flexibilities.

Figs. 10 and 11 are plots of the maximum values of the tearing stress σ_o and the shear stress τ_o in the cement. The plots are arranged to include the effects of variations in the semi-lap length to sheet thickness ratio $\frac{c}{t}$, as well as the effects of variations in the sheet and cement materials. The definitions of β and γ, which appear on the figures are

$$\beta = \sqrt{8 \frac{G_c}{E} \cdot \frac{t}{\eta}}, \quad \gamma = \sqrt[4]{6 \frac{E_c}{E} \cdot \frac{t}{\eta}}$$

The flexible-cement-layer analysis is applicable to joints composed of thin metal sheets cemented together. The adhesive materials used in such joints are particularly weak in tension. Hence the σ_o stresses, although smaller than those encountered in inflexible-layer joints, are still of sufficient magnitude to cause a splitting failure at the joint edges.

It may be noted that several interesting extensions of the work presented in this paper are possible. For example, the joint edge loads could be determined for sheets which are not initially flat, but which are instead crimped near the overlap region. By proper crimping, it is possible to greatly reduce the values of the edge bending moments and thereby the values of the tearing stress concentration. The effects of lateral loads, normal to the plane of the sheets, could also be studied. Furthermore, the methods of this paper can be extended so as to cover such cases as the joining of two sheets of unequal thickness and the problem of one sheet, to which are cemented two side sheets (the double shear joint).

DERIVATION OF RESULTS

1 Determination of the Joint Edge Loads

It is proposed to determine the loads acting upon the edges of the joint by considering the joint and the neighboring sheet to act as a cylindrically bent plate of variable cross section and

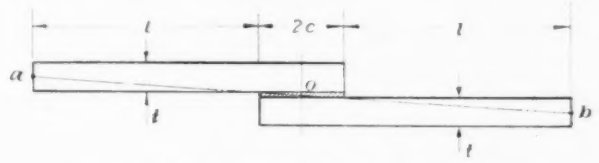


Fig. 1 Profile View of Cemented-Joint System

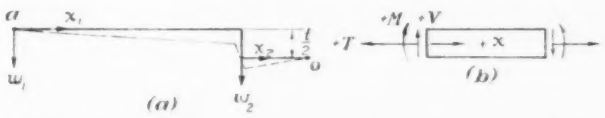


Fig. 2 Load Applied to Cemented-Joint System in Fig. 1 (a, Neutral plane of joint before and after application of load. b, Positive conventions for M, V, and T, as used in Section 1.)

variable neutral plane. The required results indicate that account must be taken of the effects of the transverse deflections of the sheet and joint on the values of the edge loads.

A graphical representation of a section of an unloaded joint is shown in Fig. 1. The joint (overlap) length is notated $2c$, the two joined sheets are considered to be of equal thickness t and are presumed to extend a distance l to either side of the joint. The joint width, in a direction normal to the plane of the section shown, is assumed to be large compared with the sheet thickness. If the system is now loaded by tensile forces T per unit of sheet width at the supports a and b, the line of action of the forces will be aob. The order of magnitudes of the joint edge loads can at once be recognized. For reasonably small deformations of the system, the tensile force in the sheet per unit of width remains very nearly equal to T, and the sheet moment at the joint edges is of the order $\frac{1}{2}Tt$. Since the order of magnitude of the transverse deflections observed during actual joint tests is t, the need for including the effects of the sheet and joint deflections in determining the edge loads is apparent.

The solid line of Fig. 2 represents the elastic axis of a longitudinal cross section of the lap joint. Since the form of the axis will always remain antisymmetrical about the mid-point o of the joint, only the left-hand sheet and the left portion of the joint are shown in Fig. 2. In the cemented region, the axis is along the mid-plane of the joint and hence, presuming always a cement layer of small thickness compared with that of the sheet, the elastic axis has a discontinuity of amount $t/2$ at the joint edges. (The discontinuity is drawn to a magnified scale on the figure for purposes of clarity.) Under load, the elastic axis deflects to some form such as that of the dotted line in Fig. 2. In order to study the system deformations, it is convenient to introduce two coordinate systems (x_1, w_1) and (x_2, w_2). The first system is used to analyze the behavior of the left-hand sheet under load; the x_1 co-ordinate has its origin at the support a, extends along the gravity axis of the sheet and is positive to the right. The w_1 coordinate represents transverse deflections of the sheet from the unloaded condition and is positive downward. A similar definition is taken for (x_2, w_2) with reference to the joint, as shown in Fig. 2.

Setting M_1 equal to the bending moment in the sheet at station x_1 and M_2 equal to the moment in the joint at station x_2, each per unit of width, then

$$\left.\begin{aligned} M_1 &= T[\alpha_n x_1 - w_1] \text{ for } 0 \le x_1 \le l \\ M_2 &= T\left[\alpha_n(l + x_2) - w_2 - \frac{t}{2}\right] \text{ for } 0 \le x_2 \le c \end{aligned}\right\} \quad \ldots\ldots [7]$$

Here α_n represents the angle between the x_1 (or x_2) co-ordinate and the line of action *aob* of the applied forces and is very nearly equal to

$$\alpha_n = \frac{1}{2}\,\frac{t}{(l + c)}$$

The positive conventions chosen for the moments M_1 and M_2 and for the transverse shearing forces per unit of width V_1 in the sheet and V_2 in the joint, to be introduced in the later work, are shown in Fig. 2.

According to the theory for the small bending of thin, cylindrically bent plates, the differential equations for the transverse deflections of the sheet and joint become

$$\left.\begin{aligned} \frac{d^2w_1}{dx_1^2} &= -\frac{M_1}{D_1} = -\frac{T}{D_1}\,[\alpha_n x_1 - w_1],\ 0 \le x_1 \le l \\ \frac{d^2w_2}{dx_2^2} &= -\frac{M_2}{D_2} = -\frac{T}{D_2}\left[\alpha_n(l + x_2) - w_2 - \frac{t}{2}\right],\ 0 \le x_2 \le c \end{aligned}\right\} \quad \ldots\ldots [8]$$

where D_1 and D_2 are the flexural rigidities of the sheet and joint respectively.

The two preceding Equations [8] have solutions of the form

$$\left.\begin{aligned} w_1 &= A_1 \cosh u_1x_1 + B_1 \sinh u_1x_1 + \alpha_n x_1,\ 0 \le x_1 \le l \\ w_2 &= A_2 \cosh u_2x_2 + B_2 \sinh u_2x_2 + \alpha_n\left(l + x_2 - \frac{t}{2}\right),\ 0 \le x_2 \le c \end{aligned}\right\} \quad \ldots\ldots [9]$$

where

$$u_1 = \sqrt{\frac{T}{D_1}} \quad \text{and} \quad u_2 = \sqrt{\frac{T}{D_2}}$$

The four constants of Equations [9] are readily evaluated from the four conditions

$$\left.\begin{aligned} &\text{at } x_1 = 0 && w_1 = 0 \\ &\text{at } x_1 = l,\ x_2 = 0 && w_1 = w_2 \\ &\text{at } x_1 = l,\ x_2 = 0 && \frac{dw_1}{dx_1} = \frac{dw_2}{dx_2} \\ &\text{at } x_2 = c && w_2 = 0 \end{aligned}\right\} \quad \ldots\ldots [10]$$

The moment and shearing force at the transition section then become

$$\left.\begin{aligned} M_o &= (M_1)_{x_1=l} = -D_1\left(\frac{d^2w_1}{dx_1^2}\right)_{x_1=l} \\ &= \frac{Tt}{2}\left\{\frac{\cosh u_2c \sinh u_1l}{\sinh u_1l \cosh u_2c + \dfrac{u_1}{u_2}\cosh u_1l \sinh u_2c}\right\} \end{aligned}\right\} \quad \ldots\ldots [11]$$

and

$$\left.\begin{aligned} V_o &= (V_1)_{x_1=l} = \left(\frac{dM_1}{dx_1}\right)_{x_1=l} \\ &= u_1\frac{Tt}{2}\left\{\frac{\cosh u_2c \cosh u_1l}{\sinh u_1l \cosh u_2c + \dfrac{u_1}{u_2}\cosh u_1l \sinh u_2c}\right\} \end{aligned}\right\} \quad \ldots\ldots [12]$$

Letting p represent the applied tensile stress in the plate (so that $T = pt$) and E and ν the Young's modulus and the Poisson's ratio, respectively, of the sheet material, then since the joint is very nearly twice the thickness of the sheet

$$D_1 = \frac{D_2}{8} = \frac{Et^3}{12(1 - \nu^2)}$$

and

$$\left.\begin{aligned} u_1l &= 2\sqrt{3(1 - \nu^2)}\,\frac{l}{t}\sqrt{\frac{p}{E}} \\ u_2c &= \sqrt{\frac{3(1 - \nu^2)}{2}}\cdot\frac{c}{t}\sqrt{\frac{p}{E}} \end{aligned}\right\} \quad \ldots\ldots [13]$$

In all practical cases, the value of u_1l is sufficiently large to permit taking

$$\sinh u_1l \approx \cosh u_1l \approx \frac{1}{2}\,e^{u_1l} \quad \ldots\ldots [14]$$

Equations [11] and [12] then reduce to the simplified forms

$$M_o = k\,\frac{Tt}{2},\ V_o = kT\sqrt{3(1 - \nu^2)}\,\frac{p}{E} \quad \ldots\ldots [15]$$

where the value of the factor k is dependent upon the sheet stress p, the joint dimensions and the physical properties of the sheet material in the following manner:

$$k = \frac{\cosh u_2c}{\cosh u_2c + 2\sqrt{2}\sinh u_2c} \quad \ldots\ldots [16]$$

Values of $k = \dfrac{2M_o}{Tt}$ and of $\dfrac{V_oc}{Tt}$ for various values of $\dfrac{c}{t}\sqrt{\dfrac{p}{E}}$ are given in Table 1; Fig. 3 is a graphical plot of the factor k versus $\dfrac{c}{t}\sqrt{\dfrac{p}{E}}$. For average values of overlap and for plate stresses as high as 40,000 psi in joints composed of cemented aluminum-alloy sheets, a practical lower limit of about 0.35 is established for k. Hence it is evident that the joint-edge moments are considerably reduced under load from the initial value $^1/_2\,Tt$, the amount of

TABLE 1 VALUES OF $k = \dfrac{2M_o}{Tt}$ AND $k' = \dfrac{V_oc}{Tt}$ FOR VARIOUS $\dfrac{c}{t}\sqrt{\dfrac{p}{E}}$

$\frac{c}{t}\sqrt{\frac{p}{E}}$	$k = \frac{2M_o}{Tt}$	$k' = \frac{V_oc}{Tt}$
0	1.00	0
0.1	0.75	0.039
0.2	0.61	0.064
0.3	0.51	0.080
0.4	0.45	0.094
0.5	0.40	0.104
0.6	0.37	0.116
0.65	0.36	0.122

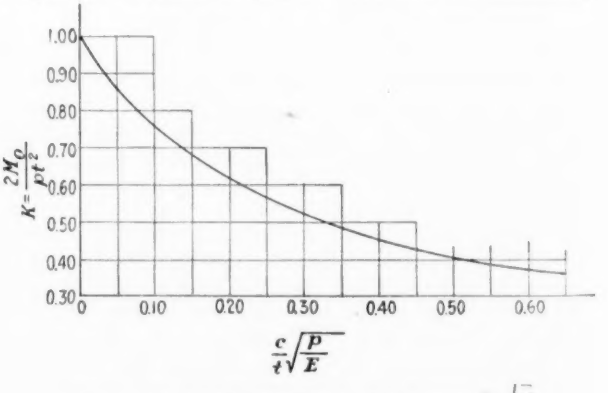


FIG. 3 PLOT OF MOMENT FACTOR k VERSUS $\dfrac{c}{t}\sqrt{\dfrac{p}{E}}$

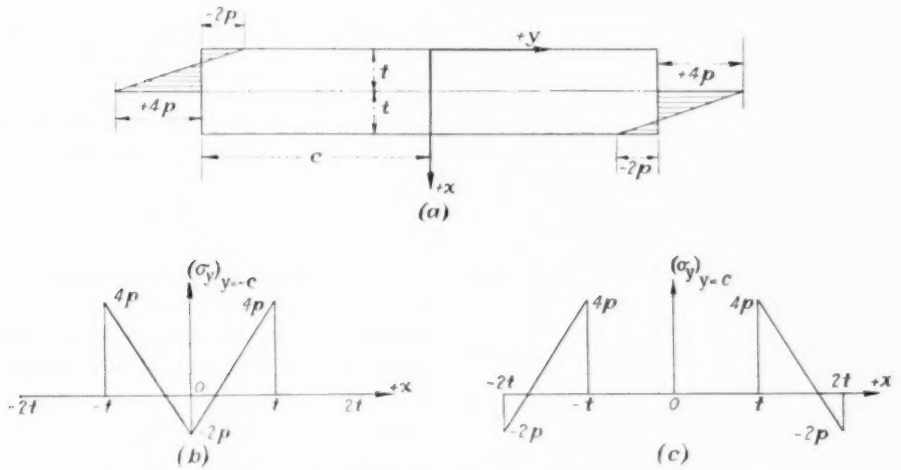


FIG. 4 DIAGRAM OF JOINT WITH RELATIVELY INFLEXIBLE CEMENT LAYER
(*a*, Profile of joint, showing edge stress distribution; *b*, periodic function for stress on joint edge $y = -c$; *c*, periodic function for stress on joint edge $y = c$. For $k = 1.0$.)

reduction being as much as 65 per cent in practical cases. It is also clear, from the values of Table 1, that only small transverse shearing forces are introduced at the joint edges of loaded systems with reasonable overlap. The shearing forces are never in excess of 0.02 T in actual joints.

2 STRESS DISTRIBUTION IN JOINT FOR RELATIVELY INFLEXIBLE CEMENT LAYERS

If the thickness of the cement layer in a joint is exceedingly small compared with that of the sheet, the presence of the cement can be ignored in the calculation of the stress distribution in the joint. For, in the case of very thin layers, the variations in stress and the magnitudes of the deformations in the cement are insignificantly small and, consequently, do not appreciably affect the stress distribution in the two adjoining sheet portions. For purposes of analysis, therefore, the joint can be assumed to consist of a homogeneous slab of thickness $2\ t$, length $2\ c$, large width and with the same physical properties throughout as those of the sheet material. It is to be noted that this treatment is valid even for cement layers of appreciable thickness, providing the cement material is relatively stiff, i.e., providing its physical properties are at least of the same order of magnitude as those of the sheet material.

The loads transmitted by the sheet to the edges of the joint have been determined in Section 1 of the paper. They are found to consist of a tension T, a moment $M_o = k\dfrac{Tt}{2}$ (each per unit of joint width), and a small transverse shearing force. In this first analysis, the transverse shearing forces are neglected, the tension T is assumed to be uniformly distributed over the sheet cross section and the moment M_o is considered to arise from the usual elementary linear stress distribution. It is evident, from past experience with similar problems, that the first two assumptions do not introduce appreciable error; the last assumption implies that sheet cross sections remain plane near the edges of the joint and has, for verification, the results of a series of photoelastic tests. The tests, reported by Tylecote (7), were made on homogeneous, short joints. The departure from a linear normal stress distribution at the joint edges should presumably be a maximum in short joints; the test results indicate, nevertheless, a remarkable degree of linearity.

The normal stresses on the joint edges over the regions where the sheet attaches to the joint are then given by expressions of the type

$$p + \frac{12M_o}{t^3}z$$

where z refers to the distance from the elastic axis of the sheet to a sheet fiber stressed in tension by the bending moment M_o. The normal stress distribution at the two edges is shown schematically in Fig. 4(*a*).

Let a co-ordinate x be defined in the direction of the joint thickness, with its origin at the upper surface of the joint, Fig. 4(*a*). The co-ordinate y is taken with its origin at the mid-point of the joint length and is measured positively to the right. The normal stress distribution of Fig. 4(*a*) then becomes

$$\left.\begin{array}{lll} \text{at} \quad y = -c, (\sigma_y)_{y=-c} & \begin{cases} = p + pk\left(6\dfrac{x}{t} - 3\right), & 0 \leqslant x < t \\ = 0, & t < x \leqslant 2t \end{cases} \\ \text{at} \quad y = c, (\sigma_y)_{y=c} & \begin{cases} = 0, & 0 \leqslant x < t \\ = p + pk\left(9 - 6\dfrac{x}{t}\right), & t < x \leqslant 2t \end{cases} \end{array}\right\} \quad \ldots\ldots\ldots\ldots [17]$$

The evaluation of the stress distribution in the joint is thus transformed to the solution of the plane-strain problem involving the boundary stresses of expressions [17], acting on the edges of a wide, rectangular slab of length $2\ c$ and thickness $2\ t$. The boundary stresses, expressions [17], will first be written as Fourier series, and a stress distribution, satisfying the conditions at the edges $y = -c$ and $y = c$, will be determined with their aid. This solution will, however, introduce undesirable normal and shear stresses on the joint surfaces $x = 0$ and $x = 2t$. An approximate method is used to remove these stresses, employing the known results for a series of concentrated forces distributed over the plane boundary of a semi-infinite elastic solid.

The edge stress conditions, expressions [17], are made into periodic functions as shown in Figs. 4(*b*) and (*c*). Writing

$$\left.\begin{array}{l} (\sigma_y)_{y=-c} = a_o + \displaystyle\sum_{n=1}^{\infty} a_n \cos\frac{n\pi}{2t}x \\ (\sigma_y)_{y=c} = b_o + \displaystyle\sum_{n=1}^{\infty} b_n \cos\frac{n\pi}{2t}x \end{array}\right\} \quad \ldots\ldots [18]$$

the Fourier constants become

$$\left.\begin{aligned} a_o &= b_o = \frac{1}{2}\,p \\ a_n &= \frac{2p}{n\pi}\left\{\frac{12k}{n\pi}\left(\cos\frac{n\pi}{2}-1\right)+(3k+1)\sin\frac{n\pi}{2}\right\} \\ b_n &= \frac{2p}{n\pi}\left\{\frac{12k}{n\pi}\left(\cos\frac{n\pi}{2}-\cos n\pi\right)-(3k+1)\sin\frac{n\pi}{2}\right\} \end{aligned}\right\} \quad \ldots [19]$$

According to the theory for plane strain, there exists a stress function φ_1 such that

$$\sigma_x = \frac{\partial^2\varphi_1}{\partial y^2}, \quad \sigma_y = \frac{\partial^2\varphi_1}{\partial x^2}, \quad \tau_{xy} = -\frac{\partial^2\varphi_1}{\partial x\partial y} \quad \ldots [20]$$

where σ_x, σ_y, τ_{xy} are stress notations as defined in reference 8. It is appropriate to take

$$\varphi_1 = \frac{px^2}{4} + \sum_{n=1}^{\infty} Y_n \cos\frac{n\pi}{2t}\,x \quad \ldots [21]$$

where Y_n is a function of n and the variable y only. The requirement that $\nabla^4\varphi_1 = 0$ fixes the form of Y_n as

$$Y_n = C_1\cosh\alpha y + C_2\sinh\alpha y + C_3 y\cosh\alpha y + C_4 y\sinh\alpha y \ldots [22]$$

where $\alpha = \dfrac{n\pi}{2t}$. Then, denoting the derivatives of Y_n with respect to the variable y by primes, the three stresses become

$$\left.\begin{aligned} \sigma_x &= \sum_{n=1}^{\infty} Y_n''\cos\alpha x \\ \sigma_y &= \frac{p}{2} - \sum_{n=1}^{\infty}\alpha^2 Y_n\cos\alpha x \\ \tau_{xy} &= \sum_{n=1}^{\infty}\alpha Y_n'\sin\alpha x \end{aligned}\right\} \quad \ldots [23]$$

The four constants appearing in the function Y_n are determined from the boundary conditions, previously decided upon

$$\left.\begin{aligned} &\text{at } y = -c, && \tau_{xy} = 0 \\ & && \sigma_y = (\sigma_y)_{y=-c} \\ &\text{at } y = c, && \tau_{xy} = 0 \\ & && \sigma_y = (\sigma_y)_{y=c} \end{aligned}\right\} \quad \ldots [24]$$

and the three stresses σ_x, σ_y, and τ_{xy} then assume the forms

$$\left.\begin{aligned} \sigma_x &= \sum_{n=1}^{\infty}[A_n y_1 + B_n y_2]\cos\alpha x \\ \sigma_y &= \frac{p}{2} + \sum_{n=1}^{\infty}[A_n y_3 + B_n y_4]\cos\alpha x \\ \tau_{xy} &= \sum_{n=1}^{\infty}[A_n y_5 + B_n y_6]\sin\alpha x \end{aligned}\right\} \quad \ldots [25]$$

where $A_n = b_n + a_n$, $B_n = b_n - a_n$ and $y_1, y_2, \ldots, y_6$ are six functions of y only. A typical form is

$$y_1 = \frac{\cosh\alpha y\,(\sinh\alpha c - \alpha c\cosh\alpha c) + \alpha y\sinh\alpha c\sinh\alpha y}{\sinh 2\alpha c + 2\alpha c} \quad \ldots [26]$$

The fact that the length of the joint is always large compared with its thickness leads to a considerable simplification of expressions [25]. For then c is large compared with t and

$$\left.\begin{aligned} \sinh\alpha c &\approx \cosh\alpha c \approx \frac{1}{2}\,e^{\alpha c} \\ \sinh 2\alpha c &\pm 2\alpha c \approx \sinh 2\alpha c \approx \frac{1}{2}\,e^{2\alpha c} \end{aligned}\right\} \quad \ldots [27]$$

Furthermore, confining attention to the joint regions near the edges, where the stress distribution is of most interest, then with small error

$$\sinh\alpha y \approx \cosh\alpha y \approx \frac{1}{2}\,e^{\alpha y}$$

With these approximations, the complexity of the forms describing $y_1, y_2, \ldots, y_6$ is reduced and the stresses can be written as

$$\left.\begin{aligned} \sigma_x &= \sum_{n=1}^{\infty}(A_n + B_n)\left\{\frac{1}{2}\,e^{\alpha(y-c)}\,[\alpha(y-c)+1]\right\}\cos\alpha x \\ \sigma_y &= \frac{p}{2} + \sum_{n=1}^{\infty}(A_n + B_n)\left\{\frac{1}{2}\,e^{\alpha(y-c)}[\alpha(c-y)+1]\right\}\cos\alpha x \\ \tau_{xy} &= \sum_{n=1}^{\infty}(A_n + B_n)\left\{\frac{1}{2}\,e^{\alpha(y-c)}[\alpha(y-c)]\right\}\sin\alpha x \end{aligned}\right\} \quad \ldots [28]$$

where

$$A_n + B_n = 2b_n = \frac{4p}{n\pi}\left\{\frac{12k}{n\pi}\left(\cos\frac{n\pi}{2} - \cos n\pi\right) - (3k+1)\sin\frac{n\pi}{2}\right\} \quad \ldots [29]$$

During the calculation of the values of the stresses, Equations [28] in the vicinity of the joint edges, the series converge fairly rapidly.

It has already been mentioned that the stress function φ_1 does not maintain the necessary stress-free conditions on the joint surfaces $x = 0$ and $x = 2t$. In fact, it is found that large normal and shearing stresses remain on both of these faces. In order to remove these objectionable stresses, an approximate method described in reference (8) is used. It employs the results, first obtained by Boussinesq, for the plane-strain problem of an inclined force applied to the plane edge of a semi-infinite elastic slab.

The left joint edge is shown in Fig. 5 with the joint material arbitrarily extended infinitely to either side of the joint in the x direction. The plane boundary at $y = -c$ is maintained. A series of concentrated forces may now be applied to the plane boundary outside of the region from $x = 0$ to $x = 2t$ without introducing any surface stresses over the joint edge. Either forces parallel or perpendicular to the plane boundary can be applied at will. Let m such separate forces be applied and consider the resulting stresses at points along the two planes $x = 0$ and $x = 2t$. It is obvious that if any combination of m normal and shear stresses σ_x and τ_{xy}, acting at arbitrarily specified points along these planes, are chosen for reference, then the magnitudes of the m applied forces can be so adjusted as to fix these stresses

at any desired values. It is the purpose here to set these m values of σ_x and τ_{xy} of equal magnitude and opposite sign to those remaining on the joint surfaces due to the stress function φ_1, and by choosing m sufficiently large, to obtain reasonable correspondence between the surface stresses due to the two stress systems over the entire semi-length c of the joint. By superposition of the two systems, the surfaces $x = 0$ and $x = 2t$ are then left free of stress. It is allowable then to ignore the portions of the slab outside of the two surfaces and to study only the joint itself. If φ_2 refers to the stress function describing the application of the m forces, the stress distribution in the joint is obtained from the total stress function

$$\varphi = \varphi_1 + \varphi_2 \quad \ldots\ldots\ldots\ldots\ldots\ldots\ldots\ldots [30]$$

The form of the stress function φ_2 is obtained from well-known results (8) and will not be given here in detail for reasons of brevity.

By trial and error, it is found that six concentrated forces, ap-

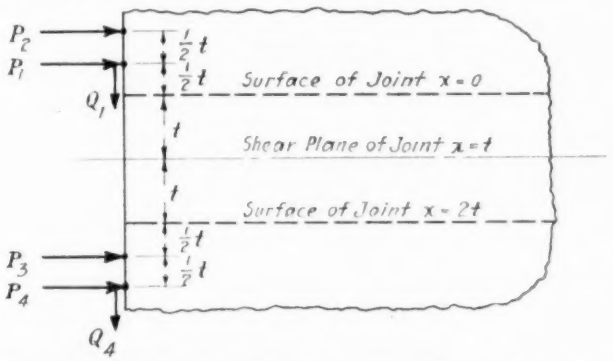


FIG. 5 FORCE PATTERN USED TO CLEAR THE SURFACES $x = 0$ AND $x = 2t$ OF STRESS

plied as shown in Fig. 5, are sufficient to remove almost completely the surface shearing stresses introduced by φ_1. Their positions are dimensioned in Fig. 5, and their magnitudes are, each per unit of joint width

$$\left.\begin{aligned} P_1 &= (-0.07 + 0.77k)\pi tp \\ P_2 &= -0.30k\,\pi tp \\ P_3 &= (0.14 - 0.30k)\pi tp \\ P_4 &= 0.16\,\pi tp \\ Q_1 &= (0.13 - 0.75k)\pi tp \\ Q_4 &= (0.25 - 0.25k)\pi tp \end{aligned}\right\} \quad \ldots\ldots\ldots\ldots [31]$$

The values of the shearing stresses yet remaining on the surfaces $x = 0$, $x = 2t$ of the joint in the neighborhood of the joint edge are given in Table 2 and are seen to be quite small for all values of k. The remaining normal stresses σ_x are also given and are of considerably larger magnitude. Since the joint is relatively thin compared with its length, it is allowable to consider the mean of the two remaining surface-pressure distributions to be transmitted directly through the sheet without change of form. Hence, this component can be subtracted from the total stress distribution and the net remaining surface pressures are given by the differences between the original and the removable mean stresses,

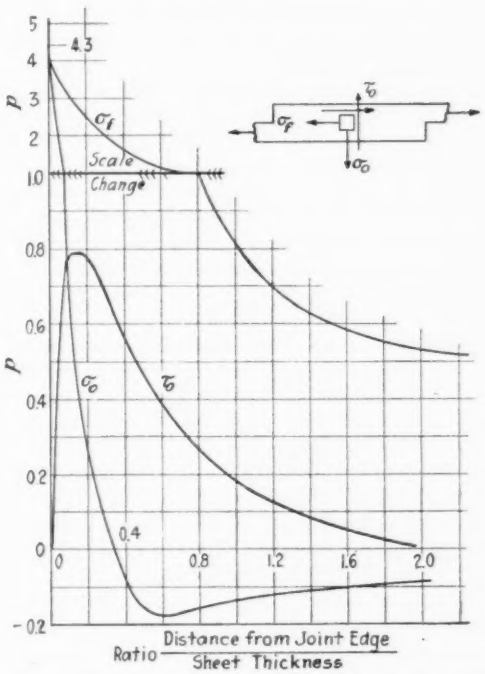


FIG. 6 STRESS DISTRIBUTION ALONG SHEAR PLANE IN JOINTS WITH RELATIVELY INFLEXIBLE CEMENT; FOR $k = 1$

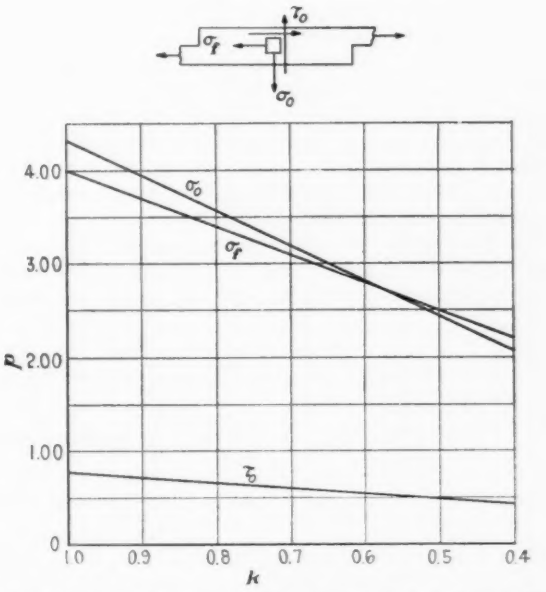


FIG. 7 MAXIMUM STRESSES IN SHEAR PLANE FOR JOINTS WITH RELATIVELY INFLEXIBLE CEMENT LAYERS, PLOTTED VERSUS MOMENT FACTOR k

TABLE 2 STRESSES REMAINING ON JOINT SURFACES, $x = 0$ AND $x = 2t$

Distance from joint edge $c - y$	Shear stress τ_{xy} on $x = 0$ $+ p$	Shear stress τ_{xy} on $x = 2t$ $+ p$	Normal stress σ_x on $x = 0$ $+ p$	Normal stress σ_x on $x = 2t$ $+ p$	Mean normal stress σ_x on $x = 0$, $x = 2t$ $+ p$	Final normal stress σ_x on $x = 0$ $+ p$	Final normal stress σ_x on $x = 2t$ $+ p$
0	0	0	$-0.100 + 0.100k$	$0.166 - 0.166k$	$0.033 - 0.033k$	$-0.133 + 0.133k$	$0.133 - 0.133k$
$0.5t$	$0.015 - 0.047k$	$-0.075 + 0.093k$	$-0.090 + 0.544k$	$0.150 + 0.256k$	$0.030 + 0.400k$	$-0.120 + 0.144k$	$0.120 - 0.144k$
$1.0t$	$0.021 + 0.058k$	$-0.017 - 0.079k$	$0.011 + 0.309k$	$0.008 + 0.158k$	$0.010 + 0.234k$	$0.001 + 0.075k$	$-0.002 - 0.076k$
$1.5t$	$0.026 + 0.070k$	$-0.005 - 0.054k$	$0.029 + 0.156k$	$-0.040 + 0.075k$	$-0.005 + 0.116k$	$0.034 + 0.040k$	$-0.035 - 0.041k$
$2.0t$	$0.025 + 0.048k$	$+0.006 - 0.037k$	$0.023 + 0.067k$	$-0.042 + 0.042k$	$-0.010 + 0.055k$	$0.033 + 0.012k$	$-0.032 - 0.013k$

as indicated by the last column of Table 2. No attempt will be made to remove the small normal and shearing stresses which persist on the joint surfaces.

It is pertinent to study the probable errors resulting from the small stresses remaining on the surfaces $x = 0$ and $x = 2t$. These are best investigated by noting the effect of changing the magnitudes of the applied concentrated forces on the stress distribution in the joint. It is found that large changes in the values of these forces result in relatively small changes in the stress distribution across the shear plane $x = t$ of the joint. Since this is the region of greatest practical significance, it is concluded that the approximate method used to remove the undesirable surface stresses is of sufficient accuracy.

Fig. 6 is a plot of the stress distribution along the mid-plane $x = t$ of the joint for the case $k = 1$. This plane corresponds with that of the cement layer and hence the stresses τ_{xy} and σ_x shown are those to which the cement material is subjected in a loaded joint. The stresses are highest near the joint edges and only this region is shown in Fig. 6. The stresses in the other regions of the joint are of lesser interest, since joint failure is usually precipitated by fracture of the relatively weak cement material.

It is recognized that the peak values of σ_x and τ_{xy} at the shear plane will change with the factor k. Fig. 7 shows this variation by plotting the maximum values of the cement stresses $\sigma_x = \sigma_o$ and $\tau_{xy} = \tau_o$ as a function of k. The change in the longitudinal stress σ_f in the sheet fibers adjoining the cement, brought about by a change in the value of k, is also indicated on this plot. The significance of Figs. 6 and 7 in explaining joint behavior has already been discussed.

3 Stress Distribution in Joint for Relatively Flexible Cement Layers

In this section, joints are considered for which the following assumption is permissible: The transverse normal strain and shear strain in the jointed sheets are negligibly small compared with the corresponding strains in the cement layer. Assuming, then, that the deformation of the sheets is due solely to the longitudinal normal stress σ_x, it is apparent that the sheets may be treated as cylindrically bent plates, whereas the role played by the cement layer is analogous to that of a system of infinitesimal coil springs positioned between the two plates.

Fig. 8 represents the cemented joint with the loads, as determined in Section 1, applied to it. The co-ordinate x is defined in the direction of the joint length, with its origin at the mid-point of the joint and its positive direction to the right. The bending moments, vertical shear, and axial tension in the sheets are denoted by M, V, and T, respectively, and the subscripts u and l designate quantities pertaining to the upper or lower sheet, respectively. The transverse normal (tearing) stress and the shear stress in the cement are notated σ_o and τ_o, respectively Figs. 8(b) and (c) show elements of the upper and lower sheet, with the sign conventions chosen for moments and forces indicated.

The conditions of moment equilibrium for the elements of the sheet are

$$\left.\begin{aligned} \frac{dM_u}{dx} - V_u + \tau_o \frac{t}{2} &= 0 \\ \frac{dM_l}{dx} - V_l + \tau_o \frac{t}{2} &= 0 \end{aligned}\right\} \quad \ldots\ldots\ldots\ldots [32]$$

The conditions of horizontal force equilibrium are

$$\left.\begin{aligned} \frac{dT_u}{dx} - \tau_o &= 0 \\ \frac{dT_l}{dx} + \tau_o &= 0 \end{aligned}\right\} \quad \ldots\ldots\ldots\ldots\ldots [33]$$

The conditions of vertical force equilibrium are

$$\left.\begin{aligned} \frac{dV_u}{dx} - \sigma_o &= 0 \\ \frac{dV_l}{dx} + \sigma_o &= 0 \end{aligned}\right\} \quad \ldots\ldots\ldots\ldots\ldots [34]$$

Denoting by v_u and v_l the transverse deflections of the upper and lower sheets, respectively, both measured positively upward, then from thin plate theory

$$\left.\begin{aligned} \frac{d^2v_u}{dx^2} &= -\frac{M_u}{D} \\ \frac{d^2v_l}{dx^2} &= -\frac{M_l}{D} \end{aligned}\right\} \quad \ldots\ldots\ldots\ldots\ldots [35]$$

where $D = \dfrac{Et^3}{12(1-\nu^2)}$ refers to the flexural rigidity of the sheets.

Let u_u and u_l represent the longitudinal displacements of the

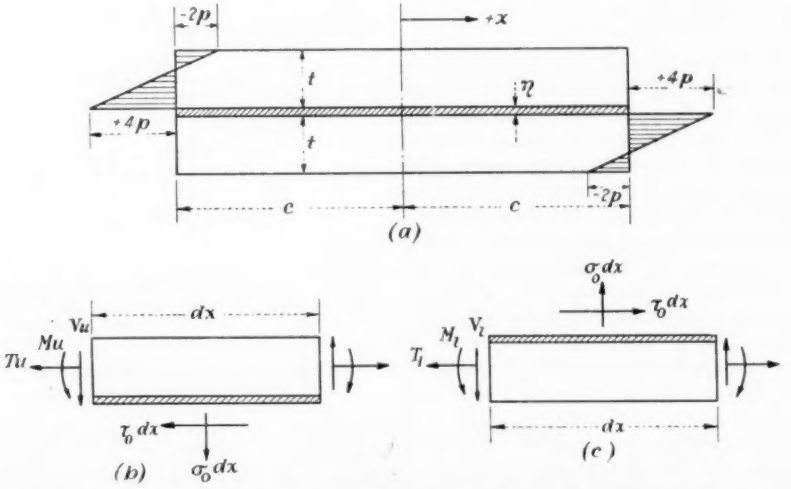


Fig. 8 Diagram of Joint With Relatively Flexible Cement Layer

(a, Profile of joint, showing longitudinal stress distribution on edges; b, element of upper sheet; c, element of lower sheet. For $k = 1.0$.)

sheet at the sheet boundaries adjacent to the cement. Then, the stress-strain relations give

$$\left.\begin{aligned} \frac{du_u}{dx} &= \frac{1}{E}\left(\frac{T_u}{t} - 6\frac{M_u}{t^2}\right) \\ \frac{du_l}{dx} &= \frac{1}{E}\left(\frac{T_l}{t} + 6\frac{M_l}{t^2}\right) \end{aligned}\right\} \quad \ldots\ldots\ldots\ldots [36]$$

where the terms on the right side of Equations [36] are the known combinations of bending and direct stress in the outermost fibers of a loaded beam.

The required system of equations is completed by the relations between the stresses and strains in the cement. For an elastic cement they are

$$\left.\begin{aligned} \frac{\tau_o}{G_c} &= \frac{u_u - u_l}{\eta} \\ \frac{\sigma_o}{E_c} &= \frac{v_u - v_l}{\eta} \end{aligned}\right\} \quad \ldots\ldots\ldots\ldots [37]$$

It might be remarked that the linear stress-strain relations of Equations [37] could be replaced by nonlinear expressions without making the solution of the problem of prohibitive difficulty.

The edge conditions for the two sheets are

$$\left.\begin{aligned} &\text{at} \quad x = c, \begin{cases} M_u = T_u = V_u = 0 \\ M_l = M_o,\ V_l = V_o,\ T_l = T \end{cases} \\ &\text{at} \quad x = -c, \begin{cases} M_l = T_l = V_l = 0 \\ M_u = -M_o,\ V_u = V_o,\ T_u = T \end{cases} \end{aligned}\right\} \ldots [38]$$

The system of Equations [32] to [38], inclusive, is now to be reduced to two differential equations for σ_o and τ_o and to boundary conditions in terms of these two quantities. Combining Equations [36] and the first of Equations [37], there follows

$$\frac{\eta}{G_c}\cdot\frac{d\tau_o}{dx} = \frac{1}{E}\left(\frac{T_u - T_l}{t} - 6\frac{M_u + M_l}{t^2}\right) \ldots\ldots [39]$$

Differentiating once and observing Equations [32] and [33]

$$\frac{\eta}{G_c}\cdot\frac{d^2\tau_o}{dx^2} = \frac{1}{E}\left(2\frac{\tau_o}{t} + 6\frac{\tau_o}{t} - 6\frac{V_u + V_l}{t^2}\right) \ldots\ldots [40]$$

Differentiating once more and noting Equations [34], an equation in τ_o only results,

$$\frac{d^3\tau_o}{dx^3} - \frac{8G_c}{Et\eta}\cdot\frac{d\tau_o}{dx} = 0 \ldots\ldots\ldots\ldots [41]$$

An equation for σ_o is found by first differentiating the second of Equations [37] twice and introducing Equations [35]. Then

$$\frac{1}{E_c}\cdot\frac{d^2\sigma_o}{dx^2} = \frac{1}{\eta}\cdot\frac{M_l - M_u}{D} \ldots\ldots\ldots\ldots [42]$$

From Equations [32], it follows that

$$\frac{1}{E_c}\cdot\frac{d^3\sigma_o}{dx^3} = \frac{1}{\eta D}\cdot(V_l - V_u) \ldots\ldots\ldots\ldots [43]$$

and from Equations [34], finally

$$\frac{1}{E_c}\cdot\frac{d^4\sigma_o}{dx^4} = -\frac{2}{\eta D}\sigma_o \ldots\ldots\ldots\ldots [44]$$

or

$$\frac{d^4\sigma_o}{dx^4} + \frac{24(1-\nu^2)E_c}{\eta t^3 E}\sigma_o = 0 \ldots\ldots\ldots\ldots [45]$$

The boundary conditions for τ_o and σ_o are obtained by combining Equations [38], [39], [42], and [43]. The conditions for τ_o are

$$\text{at} \quad x = \pm c, \quad \frac{d\tau_o}{dx} = \mp\frac{G_c}{Et\eta}\left(T + 6\frac{M_o}{t}\right) \ldots\ldots [46]$$

to which is added the equilibrium condition

$$\int_{-c}^{c}\tau_o dx + T = 0 \ldots\ldots\ldots\ldots [47]$$

The conditions for σ_o are

$$\text{at} \quad x = \pm c \left\{\begin{aligned} \frac{d^2\sigma_o}{dx^2} &= \frac{E_c}{\eta D}M_o \\ \frac{d^3\sigma_o}{dx^3} &= \pm\frac{E_c}{\eta D}V_o \end{aligned}\right\} \ldots\ldots [48]$$

It may be noted that Equations [45] and [48] for σ_o are analogous to the equations for the deflection of a beam on elastic foundation, acted upon by edge forces and moments.

On the basis of the differential Equation [41] and the boundary conditions, Equations [46] and [47], the distribution of shear stress in the cement is obtained in the form

$$\frac{\tau_o}{p}\frac{c}{t} = -\frac{1}{8}\left\{\frac{\beta c}{t}(1+3k)\frac{\cosh\frac{\beta c}{t}\cdot\frac{x}{c}}{\sinh\frac{\beta c}{t}} + 3(1-k)\right\} \ldots [49]$$

where

$$\beta^2 = 8\frac{G_c}{E}\cdot\frac{t}{\eta}$$

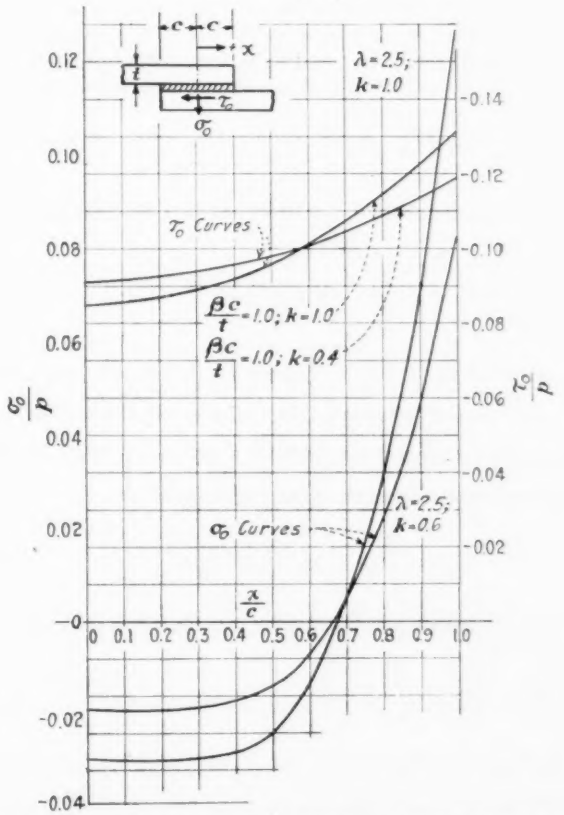


FIG. 9 STRESS DISTRIBUTION IN CEMENT IN JOINTS WITH RELATIVELY FLEXIBLE CEMENT LAYERS

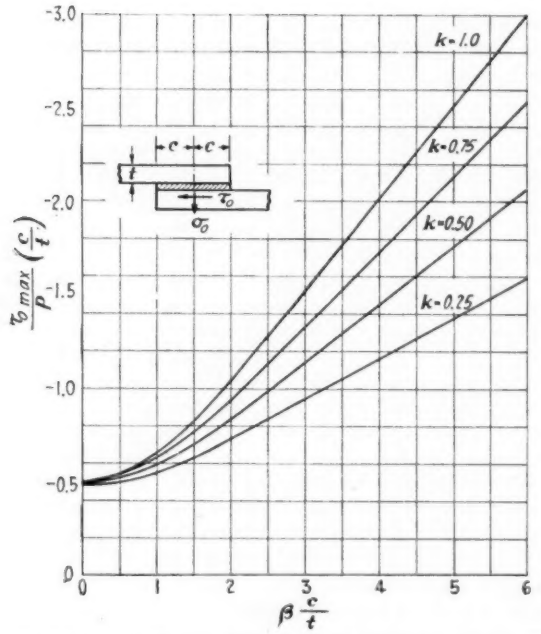


FIG. 10 MAXIMUM SHEAR STRESS IN CEMENT IN JOINTS WITH RELATIVELY FLEXIBLE CEMENT LAYERS

This expression may be compared with the average shear

$$(\tau_o)_{avg} = -\frac{pt}{2c} \quad \ldots\ldots\ldots\ldots\ldots\ldots [50]$$

Fig. 9 shows a typical distribution of τ_o in a joint of representative dimensions and materials and for values of the factor k of 1 and 0.60. It should be noted that, as expected, Equation [49] indicates a substantially uniform shear distribution in short joints. For longer joints, say for $\frac{\beta c}{t} > 0.5$, this is no longer the case.

The maximum value of τ_o is found at the edge of the joint and is

$$\frac{(\tau_o)_{max}}{p}\cdot\frac{c}{t} = -\frac{1}{8}\left[\frac{\beta c}{t}(1+3k)\coth\frac{\beta c}{t} + 3\ (1-k)\right]. \quad [51]$$

Fig. 10 is a plot of $\frac{(\tau_o)_{max}}{p}\cdot\frac{c}{t}$ versus $\frac{\beta c}{t}$ for various values of k. An inspection of Equation [51] indicates that increasing the length of joint beyond the limit $\frac{\beta c}{t} \approx 25$ has no effect on the magnitude of the maximum shear, which remains

$$(\tau_o)_{max} = -\frac{p}{8}\ (1+3k)\sqrt{8\frac{G_c}{E}\cdot\frac{t}{\eta}} \quad \ldots\ldots\ldots [52]$$

The σ_o distribution is found to be, on the basis of Equations [45] and [48]

$$\frac{\sigma_o}{p}\left(\frac{c}{t}\right)^2 = \frac{1}{\Delta}\left[(R_2\lambda^2\frac{k}{2} + \lambda k'\cosh\lambda\cos\lambda)\cosh\lambda\frac{x}{c}\cos\lambda\frac{x}{c} + (R_1\lambda^2\frac{k}{2} + \lambda k'\sinh\lambda\sin\lambda)\sinh\lambda\frac{x}{c}\sin\lambda\frac{x}{c}\right] \quad \ldots\ldots\ldots [53]$$

where $\gamma^4 = 6\frac{E_c}{E}\cdot\frac{t}{\eta}$, $\lambda = \gamma\frac{c}{t}$

$$R_1 = \cosh\lambda\sin\lambda + \sinh\lambda\cos\lambda$$
$$R_2 = \sinh\lambda\cos\lambda - \cosh\lambda\sin\lambda$$
$$\Delta = \frac{1}{2}(\sinh 2\lambda + \sin 2\lambda)$$

and, from Section 1

$$\frac{2M_o}{pt^2} = k, \quad \frac{V_o c}{pt^2} = k'$$

The maximum value of σ_o acts at the joint edges and is given by

$$\frac{(\sigma_o)_{max}}{p}\left(\frac{c}{t}\right)^2 = \lambda^2\frac{k}{2}\cdot\frac{\sinh 2\lambda - \sin 2\lambda}{\sinh 2\lambda + \sin 2\lambda} + \lambda k'\frac{\cosh 2\lambda + \cos 2\lambda}{\sinh 2\lambda + \sin 2\lambda} \quad \ldots\ldots\ldots [54]$$

For long joints, defined by λ greater than, say, 5/2 this becomes

$$\frac{(\sigma_o)_{max}}{p} = \frac{k}{2}\sqrt{6\frac{E_c}{E}\cdot\frac{t}{\eta}} + k'\frac{t}{c}\sqrt[4]{6\frac{E_c}{E}\cdot\frac{t}{\eta}} \quad \ldots\ldots\ldots [55]$$

It is noteworthy that, for long joints, the transverse normal stress and shear stress in the cement layer depend in essentially the same way on the elastic-moduli ratio and the thickness ratio of the sheet and cement. While, however, the shear stress τ_o is due in equal measure to the direct sheet stress and the sheet bending stress, the normal stress σ_o is almost entirely due to the existence of the sheet bending stress.

Fig. 11 is a plot of $\frac{(\sigma_o)_{max}}{p}\left(\frac{c}{t}\right)^2$ versus λ for various values of the factor k. A typical σ_o distribution in a representative joint is shown in Fig. 9. The end concentration of σ_o is of interest, showing the existence of tearing stresses of appreciable magnitude (see section on "Results and Discussion of Results"). It is of interest also to note that increasing overlap ratios c/t result in decreasing values of the maximum tearing stress $(\sigma_o)_{max}$ at the joint edges.

ACKNOWLEDGMENT

The authors are indebted to Mr. E. S. Jenkins, Chief of Ma-

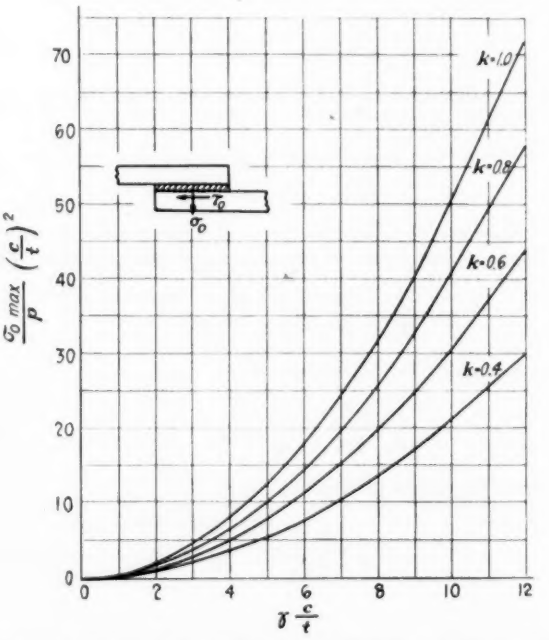


FIG. 11 MAXIMUM TEARING STRESS IN CEMENT IN JOINTS WITH RELATIVELY FLEXIBLE CEMENT LAYERS

terials and Structures Research, Research Laboratory, Curtiss-Wright Corporation, Airplane Division, for the suggestion to undertake this investigation and for permission to publish its results. During the course of the work, helpful advice was received from Mr. Jenkins and from Mr. A. F. Donovan, Head of Structures Group, Research Laboratory, Curtiss-Wright Corporation.

BIBLIOGRAPHY

1 "The Stress Distribution in Welds," by W. Hovgaard, Proceedings National Academy of Sciences, vol. 16, 1930, pp. 667–673; also "The Stress Distribution in Welded Overlapped Joints," by W Hovgaard, Proceedings National Academy of Sciences, vol. 16, 1930, pp. 673–678.

2 "The Distribution of Stresses in Welded and Riveted Connections," by W. Hovgaard, Proceedings National Academy of Sciences, vol. 17, 1931, pp. 351–359.

3 "An Investigation of the Stresses in Longitudinal Welds," by W. Hovgaard, Proceedings National Academy of Sciences, vol. 20, 1934, pp. 17–23.

4 "The Stress Distribution in Longitudinal Welds and Adjoining Structures," by W. Hovgaard, *Journal of Mathematics and Physics*, vol. 13, 1934, pp. 195–248.

5 "Distribution of Shear in Welded Connections," by H. W. Troelsch, Trans. A.S.C.E., vol. 99, 1934, pp. 409–436.

6 "Stress Distribution in Side-Welded Joints," by W. H. Weiskopf and M. Male, *Journal of the American Welding Society*, vol. 9, Sept., 1930, pp. 23–48, and Dec., 1930, pp. 68–82.

7 "Spot Welding," by R. F. Tylecote, *Welding Journal*, Welding Research Supplement, vol. 20, Aug., 1941, pp. 359–368.

8 "Theory of Elasticity," by S. Timoshenko, McGraw-Hill Book Co., Inc., New York, N. Y., 1934, pp. 82–93.

Relations Between the Notched Beam Impact Test and the Static Tension Test

By C. W. MacGREGOR[1] and J. C. FISHER,[2] CAMBRIDGE, MASS.

Results of static tension tests of both notched and uniform bars are compared with notched beam impact tests through the use of true stress-strain values. For the materials tested and under the temperature conditions imposed, it was found that the effect of drawing and testing temperatures on the energy absorbed per unit of volume was essentially the same for both static notched tension and notched beam impact tests.

THE notched-beam impact test has been of considerable value in determining the effect of various metallurgical and mechanical conditions on the suitability of materials for different applications. Experience has demonstrated that the effect of some of these conditions cannot be detected by the ordinary form of tension test. The present state of the notched beam impact test has been thoroughly covered in various papers presented at the "Symposium on Impact Testing" during the 1938 meeting of the American Society for Testing Materials. A very extensive literature has developed on the subject and although space limitations will not permit detailed reference and discussion of many of the individual contributions to the field, mention will be made of some of those more closely related to the immediate problem under discussion. McAdam (1)[3] and Clyne (1) have given a very complete discussion of the effects of such variables as heat-treatment, testing temperature, the geometry of the test bar, velocity, etc., on the energy values obtained in the notched bar impact test as reported by many of the early investigators in the field such as Greaves and Jones, Maurer and Mailander, Moser, Stribeck and others.

The ratio of the technical cohesive strength to the shear strength and its effect on impact values has been discussed by Hoyt (2) and McAdam and Clyne (1). The technical cohesive strength has been the subject of considerable study by Kuntze (3), Gensamer (4), McAdam (5, 6) and Mebs (6) and others.

One of the shortcomings of the notched beam impact test has always been that it provides only energy values and hence gives no stress-strain information which might be used directly in design. Realizing this, a number of studies (7–12) have been made in recent years of the stress-strain relations in rapid tension or tension impact tests. Most of these have shown for the ductile metals, excluding low-melting metals such as lead and tin, that at normal temperatures rather large speed ratios are necessary before important speed effects are observed.

Various investigators have reported that the ordinary form of static tension test in many cases does not detect certain properties which are disclosed by the notched beam impact test. For example, Riegel and Vaughn (13) have demonstrated that two mill heats of the same typical chemical composition and almost identical ordinary tension properties may possess very different notched beam impact values.

Experiments by Greaves and Jones (14) support the view that the difference in results obtained from the notched beam impact test and the slow-speed tension test are due mainly to the notch effect rather than to the difference in the speed of the testing machines. Impact tests made on ingot iron with and without notches showed that while the temperatures of hot brittleness for the unnotched bars in impact agreed well with those determined from static tension tests, the notched impact specimens gave temperatures of hot brittleness which were much in excess of those determined statically.

More recently, tests conducted by Jones (15) disclosed the fact that the total impact energies for notched tension and notched beam impact specimens were affected in a similar manner by changing the testing temperature. On the other hand, his experiments with unnotched tension impact specimens exhibited no correlation with the notched beam impact results.

The inability of the ordinary tensile properties to reveal the practical performance characteristics of certain heat-treated low-alloy steels has been brought out in a series of experiments by Sachs and Lubahn (16). They found that notched static tension tests were more valuable in this respect. In addition, a comparison was made between the total energies for notched beam impact specimens and the product of the ordinary tensile strength and the ordinary reduction of area at fracture obtained from static notched tension tests. The results disclosed that both quantities were similarly affected by the testing temperature. This provides additional evidence that the effects usually observed in standard notched-beam impact tests are due mainly to the presence of the notch and not so much to the speed of the testing machine.

The notched beam impact test has always been difficult to correlate with other forms of tests. It has been the authors' feeling, however, that if any correlation existed between the notched-beam impact test and the static-tension test, it might best be approached through the use of true stress-strain values (17, 18). Accordingly an experimental program was undertaken with the object of ascertaining if the static-tension test in its more rational form could be used to show essentially the same effects of certain mechanical and metallurgical conditions on energy values as were portrayed by the notched-beam impact test. If this were possible, the tension test would have the added advantage of supplying stress-strain values not determined in the other form of test.

The first part of the following discussion is devoted to a description of the general testing procedure together with some preliminary results obtained using uniform tension specimens. A comparison then is made of the effects of heat-treatment and testing temperature on the variation of the *energy per unit of deformed volume* from notched-beam tests (as originally suggested by Moser (19)), and from static tension tests of the true stress-strain type on notched specimens.

---

[1] Professor of Applied Mechanics, Department of Mechanical Engineering, Massachusetts Institute of Technology. Mem. A.S.M.E.

[2] Assistant, Department of Mechanical Engineering, Massachusetts Institute of Technology.

[3] Numbers in parentheses refer to Bibliography at end of the paper.

For presentation at the Annual Meeting, New York, N. Y., Nov. 29–Dec. 3, 1943, of THE AMERICAN SOCIETY OF MECHANICAL ENGINEERS.

Discussion of this paper should be addressed to the Secretary, A.S.M.E., 29 West 39th Street, New York, N. Y., and will be accepted until April 10, 1944, for publication at a later date. Discussion received after the closing date will be returned.

NOTE: Statements and opinions advanced in papers are to be understood as individual expressions of their authors and not of the Society.

TABLE 1 MATERIALS AND HEAT-TREATMENTS

Material	Heat-treatment
S.A.E. 1020	Annealed for one hour at 1650 F and furnace cooled.
S.A.E. 1112	Annealed for one hour at 1650 F and furnace cooled.
S.A.E. 1045	Heated to 1550 F, quenched in water, and drawn at various temperatures. Tensile specimens held at drawing temperature for 45 min. Impact specimens held at drawing temperature for 20 min.
S.A.E. 3140	Annealed for one hour at 1550 F and furnace cooled.

NOTE: At least two impact and tension specimens were tested for each temperature condition.

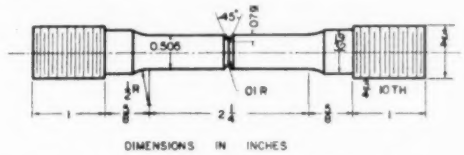


FIG. 1 NOTCHED TENSION SPECIMEN

TESTING PROCEDURE

The materials investigated together with their heat-treatments are listed in Table 1. They were received in the form of $^3/_4$-in. round bars and with the exception of the S.A.E. 1112 steel were in the hot-rolled condition. The S.A.E. 1112 was received as cold drawn.

Standard 0.505-in. diam uniform tension specimens were prepared from some materials, while notched-tension specimens were prepared from all materials. The dimensions of the notched-tension test pieces are given in Fig. 1. The 45-deg notch was produced by using as a lathe tool a tooth of the same milling cutter with which the notch in the notched beam specimens was formed. The S.A.E. 1045 specimens were notched after heat-treating.

Standard notched-beam impact specimens (Charpy impact specimens) were machined following the A.S.T.M. specifications. These specimens contained a single 45-deg notch 0.079 in. deep with a 0.01-in. radius at the base. Hence the notches in both tension and impact specimens were essentially the same.

The tension tests were performed on a 60,000-lb capacity Baldwin Southwark hydraulic testing machine having in addition both 2400- and 12,000-lb ranges. The procedure was to take simultaneous readings of load and minimum diameter throughout the tests. A special dial gage and clamp (17,18) was used to measure the diameter of the uniform specimens. For the notched bars, the minimum diameters were read with a measuring microscope. A special tank consisting of a metal tube 3 in. in diameter and 8 in. high surrounded the test pieces during the constant-temperature tests. The tank was fitted with two plastic windows which permitted observation of the specimen during the test, and measurement of the minimum diameter with the measuring microscope. For the higher temperatures the tank was filled with mineral oil which was electrically heated and circulated. The low temperatures were obtained by using alcohol with the addition of dry ice. The temperatures were held to plus or minus three degrees centigrade during each test. From the data so obtained the average true stress[4] $s = P/A$ was plotted versus the true strain $\epsilon = q' = \log_e A_0/A$ where P, A, A_0, ϵ, and q' are the instantaneous load, the instantaneous true area, the original area, the true strain and the true reduction of area respectively (17). A list of the symbols employed is given in Table 2. The values of energy absorbed per unit of volume up to fracture (E_s) were determined by computing

$$E_s = \int_0^{\epsilon_b} s \cdot d\epsilon$$

or the area under the true stress-strain curve where ϵ_b is the true fracture strain.[5]

TABLE 2 NOMENCLATURE

P = Axial load on tension test bar (Lb)
A_0 = Original area of cross section (In.)^2
A = Actual instantaneous area of cross section (In.)^2
L_0 = Original gage length (In.)
L = Actual gage length (In.)
A_u = Actual area of cross section at maximum load (In.)^2
A_b = Actual fracture area of cross section (In.)^2
ϵ = True strain = $\log_e A_0/A = \log_e L/L_0$
q' = True reduction of area = $\log_e \frac{A_0}{A} = \log_e L/L_0$
E_s = Energy per unit of volume = $\int_0^{\epsilon_b} s \cdot d\epsilon$ (Lb/In.^{2})
ϵ_b = True fracture strain = $\log_e A_0/A_b$
ϵ_u = True uniform strain = $\log_e A_0/A_u$
ϵ_n = True local necking strain = $\log_e A_u/A_b$
$\frac{\partial s}{\partial \epsilon}$ = Minimum modulus of strain hardening (Lb/In.^{2})

[4] For the notched specimens, the stress computed by dividing the load by the actual area represents an average of the true axial stresses. In order to save constant repetition, however, the word "average" will be omitted many places in the text.

[5] The value of the energy absorbed per unit of volume can be determined as follows: The total energy absorbed is equal to the work done on the specimen by the external forces. Let us first consider a uniform specimen. Then

$$\text{Total energy} = \int_{L_0}^{L} P \cdot dL = \int_{L_0}^{L} s \cdot A \cdot dL \quad \ldots\ldots [1]$$

where L and L_0 are the final and initial gage lengths and A and A_0 the final and initial areas of cross section. Since the volume remains constant

$$A \cdot L = A_0 \cdot L_0 \quad \ldots\ldots [2]$$

and hence

$$dL = -A_0 L_0 \frac{dA}{A^2} \quad \ldots\ldots [3]$$

Substituting Equation [3] in [1] gives

$$\text{Total energy} = A_0 L_0 \int_{A_0}^{A} s \left(-\frac{dA}{A}\right) = V_0 \int_{A_0}^{A} s \left(-\frac{dA}{A}\right) \quad [4]$$

where V_0 is the initial volume of material. But

$$V = A \cdot L = V_0 = \text{constant} \quad \ldots\ldots [5]$$

$$\text{Hence } dV = A dL + L da = 0 \quad \ldots\ldots [6]$$

$$\text{and } \frac{dL}{L} = -\frac{dA}{A} = d\epsilon \quad \ldots\ldots [7]$$

(From Equation [7] note that

$$\epsilon = \int_{L_0}^{L} \frac{dL}{L} = -\int_{A_0}^{A} \frac{dA}{A} = q' = \log_e \frac{L}{L_0} = \log_e \frac{A_0}{A}$$

which [17] are our definitions of true strain ϵ and true reduction of area q'.)

Substituting Equation [7] in [4] one obtains

$$\text{Total energy} = V \int_0^{\epsilon} s \cdot d\epsilon \quad \ldots\ldots [8]$$

The energy per unit of volume, or specific energy E_s corresponding to any strain value ϵ becomes

$$E_s = \int_0^{\epsilon} s \cdot d\epsilon \quad \ldots\ldots [9]$$

or the area under the true stress-strain curve.

When a uniform specimen begins to neck down (or for an initially notched test bar), the total energy calculated above refers only to an

The notched-beam impact specimens were tested in a standard Charpy impact machine having a striking velocity of 17.4 fps. For variation of testing temperature the specimens were immersed in oil at medium and higher temperatures, or in alcohol and dry ice at low temperatures, and were left in the bath until equilibrium was reached. They were then removed and tested as quickly as possible. The average time between removal from the bath and fracture was about four seconds.

In order to compare in a rational manner the static tension test results, where the energy per unit of volume was determined, with the results of the Charpy impact test, the energy absorbed per unit of deformed volume for the Charpy test was determined as originally suggested by Moser (19). After the notched beam impact specimens were machined, they were polished on one side and a fine network of lines 0.04 in. apart was marked on the surface with a diamond scriber. The network was measured before the test with a measuring microscope. After fracture the network was again carefully measured. The material which had a permanent strain of ± one per cent or greater was taken as the deformed volume. The limit of one per cent was chosen because

element in the most severely deformed region, and not to the over-all work done on the entire bar. In these cases such an element is subjected to both axial and radial stresses. Equation [9] represents then only that portion of the energy absorbed per unit of most severely deformed volume contributed by the axial stresses. Since the contribution by the radial stresses is neglected in Equation [9], the Equation must be taken as an approximation. While the effect of the radial stresses is probably not large for the uniform specimens, it is not negligible for severely notched bars. The value or distribution of the radial stresses in the plastic range for notched bars is not known at the present time. However, since the relative magnitude of the radial stress is determined mainly by the notch itself, it was felt that for a given notch and material the effect of various tempering and testing temperatures on the energy absorbed per unit volume might be adequately reflected by the value given in Equation [9]. The experiments described in this paper lend support to this view.

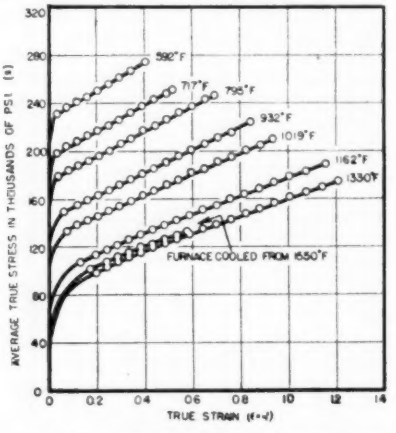


FIG. 2 AVERAGE TRUE STRESS-STRAIN CURVES OBTAINED WITH UNIFORM SPECIMENS OF S.A.E. 1045 STEEL QUENCHED FROM 1550 F IN WATER AND DRAWN TO THE TEMPERATURES INDICATED
(Circles indicate points from maximum load to fracture.)

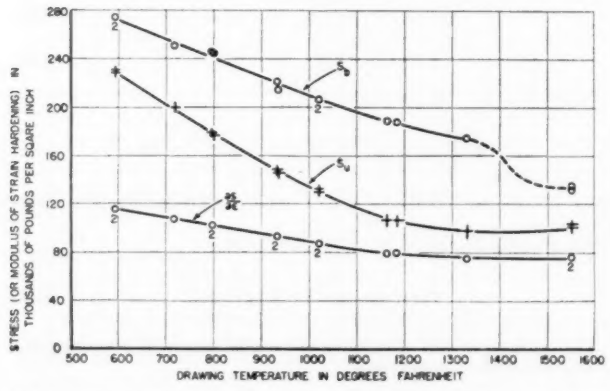


FIG. 3 TRUE STRESS AT FRACTURE (S_b), TRUE STRESS AT MAXIMUM LOAD (S_u), AND MINIMUM MODULUS OF STRAIN HARDENING $\frac{\partial s}{\partial \epsilon}$ AS FUNCTIONS OF DRAWING TEMPERATURE, FOR QUENCHED AND DRAWN S.A.E. 1045 STEEL. DATA OBTAINED FROM UNIFORM SPECIMENS

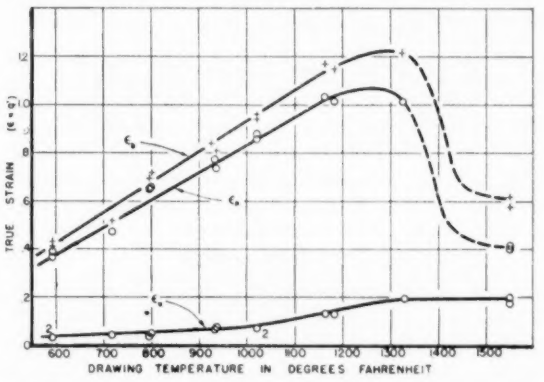


FIG. 4 TRUE UNIFORM STRAIN (ϵ_u), TRUE LOCAL NECKING STRAIN (ϵ_n), AND TRUE FRACTURE STRAIN (ϵ_b) AS FUNCTIONS OF DRAWING TEMPERATURE, FOR QUENCHED AND DRAWN S.A.E. 1045 STEEL. DATA OBTAINED FROM UNIFORM SPECIMENS

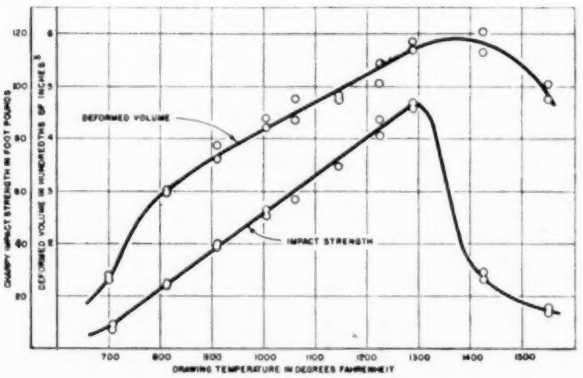


FIG. 5 TOTAL IMPACT STRENGTH AND TOTAL DEFORMED VOLUME FOR CHARPY IMPACT TESTS ON QUENCHED AND DRAWN S.A.E. 1045 STEEL, AS FUNCTIONS OF DRAWING TEMPERATURE

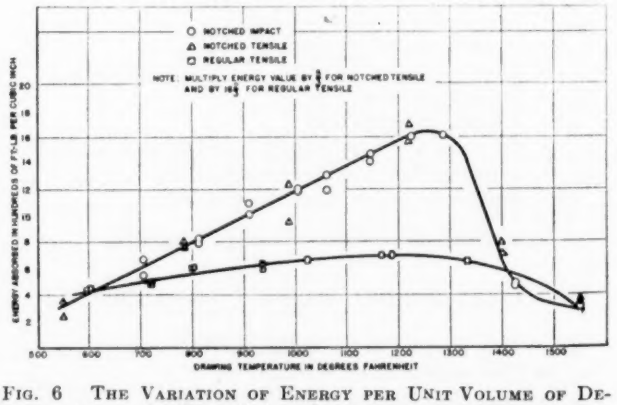


FIG. 6 THE VARIATION OF ENERGY PER UNIT VOLUME OF DEFORMED METAL (S.A.E. 1045 STEEL) AS DETERMINED FROM NOTCHED BEAM IMPACT, UNIFORM TENSION, AND NOTCHED TENSION TESTS PLOTTED VERSUS DRAWING TEMPERATURE

it was about the smallest value which could be reliably measured. The energy per unit of deformed volume then was obtained by dividing the total energy as read on the Charpy machine by the deformed volume determined in the manner described above.

Preliminary Results With Uniform Static Tension and Notched Beam Impact Specimens

Static true stress-strain tension tests were first made on uniform diameter specimens of S.A.E. 1045 steel which had been quenched from 1550 F and drawn at various temperatures. At least two specimens for each heat-treated condition were tested and Fig. 2 shows a typical set of curves obtained.[6] It will be noted that straight lines maintain from the maximum load to fracture. Figs. 3 and 4 show the variation of the true stress at maximum load (s_u), the true stress at fracture (s_b), the minimum modulus of strain hardening $\left(\frac{\partial s}{\partial \epsilon}\right)$, the true uniform strain (ϵ_u), the true local necking strain (ϵ_n), and the true fracture strain (ϵ_b) with the drawing temperature. Whenever the figure "2" appears on these curves, it indicates that two observed values are coincident. It is seen from Fig. 3 that the stress and modulus of strain hardening values decrease as the drawing temperature increases. As indicated in Fig. 4 the true fracture strain (ϵ_b) and the true local necking strain (ϵ_n) are affected in a very similar manner by the drawing temperature, while the true uniform strain (ϵ_u) behaves quite differently from these.

A series of notched beam impact tests were conducted on the S.A.E. 1045 steel in the manner previously described and for essentially the same heat-treated conditions used in the static tension tests. Fig. 5 includes the variation of the total impact energy and deformed volume as depending on the drawing temperature for this material. The notched-beam impact energies per unit of deformed volume are plotted versus the drawing temperature in Fig. 6. The areas under the curves of Fig. 2 for the uniform tension tests, i.e., the energy per unit of volume, were also plotted in Fig. 6 for comparison. These latter values form the lower curve in the figure. It can be seen that the uniform tension specimen values, while showing some variation with temperature, are not nearly as sensitive to this variable as the notched beam impact values, and do not reproduce the same type of variation.

Comparison of Energy Values Using Notched Specimens for Both Static Tension and Beam Impact Tests

Since the uniform tension tests did not correlate very well with the notched beam impact results, notched static-tension tests were performed as described above on specimens of the type shown in Fig. 1. Average true stress-strain curves were constructed and the areas under them determined. The energies per unit of volume obtained in this way are shown plotted versus the drawing temperature in Fig. 6, for the S.A.E. 1045 steel. It can be seen from this figure that the notched static tension tests correlate very closely with the notched beam impact tests. Since the energy per unit of deformed volume values for the notched beam impact tests represent an average over the deformed portion of the test piece, and the corresponding values for the notched tension specimens are measured at the most severely deformed portion only, it is natural that these curves should differ by a factor. It was found that the notched tensile specific energies agreed quantitatively with the notched beam specific energies when multiplied by the constant factor $^5/_8$. This result would

[6] After this paper was submitted to the A.S.M.E. it came to the authors' attention that similar true stress-strain curves for this material are contained in a paper presented at the National Metals Congress in Chicago on Oct. 19, 1943, by Lieutenant J. H. Hollomon of the Watertown Arsenal.

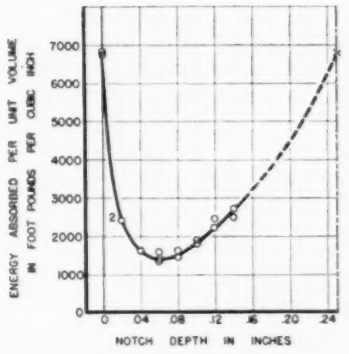


Fig. 7 Variation of Energy Absorbed per Unit of Volume With Notch Depth for Tension Tests on Annealed S.A.E. 1020 Steel

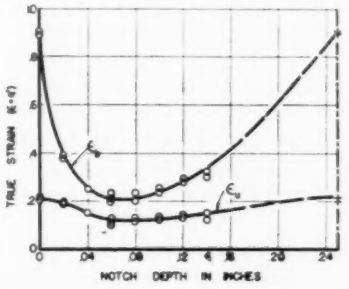


Fig. 8 True Fracture Strain (ϵ_b) and True Uniform Strain (ϵ_u) as a Function of Notch Depth for Tension Tests on Annealed S.A.E. 1020 Steel

seem to indicate that the notched static tension test performed in this way can yield the same information regarding the effect of heat treatment on specific energy values as the notched beam impact test, while at the same time providing additional strength and ductility data. It also indicates that the main effect is due to the notch rather than to the speed of the testing machine. This is in agreement with the results of other investigators. While quantitatively the energies per unit of volume for a given material differ by a constant factor in the two types of tests, this is not important since as pointed out by McAdam (1) and Clyne (1) it is not the actual numerical value of energy obtained from the notched beam impact test but its variation with different conditions that is the important feature of the test.

In order to investigate further the correlation of the static notched tension and the notched beam impact tests, additional experiments were carried out on other materials and under different conditions.

First, the variation of the energy per unit of volume with the depth of the notch in the tension test piece was determined for annealed S.A.E. 1020 steel as indicated in Fig. 7. Since the notch depth used in these experiments was 0.079 in., it can be seen that with a 45 deg angle and a radius of 0.01 in. at the base of the notch, this depth provided a minimum of energy per unit of volume. This is the same depth and shape of notch used in the notched beam impact specimen. Fig. 8 shows that the true uniform strain (ϵ_u) and true fracture strain (ϵ_b) are also a minimum near this depth of notch. It can be seen from this figure that the true uniform and fracture strains are affected somewhat differently by the notching procedure.

Since it is known that the testing temperature has an important effect on impact values, notched static tension and notched beam impact tests were conducted on S.A.E. 1020, 3140, and 1112 steels at various temperatures in order to compare further the results of these two forms of test.

The general effect of the testing temperature on the deformed volume and on the total energy absorbed in notched beam impact can be seen in Figs. 9, 10, and 11 for the three materials mentioned. From these curves it appears that the testing temperature affects the deformed volume in a manner similar to its influence on the total energy. An interesting result is shown in Fig. 11. The total absorbed energy curve has a discontinuity at 110 F. A similar discontinuity appears at this temperature in the deformed volume curve. The curve of energy per unit of deformed volume, however, is continuous throughout. Examina-

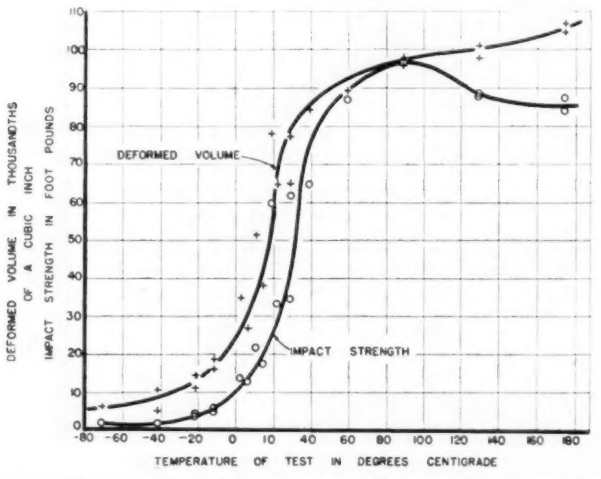


FIG. 9 TOTAL NOTCHED BEAM IMPACT ENERGY AND DEFORMED VOLUME FOR ANNEALED S.A.E. 1020 STEEL AS AFFECTED BY TESTING TEMPERATURE

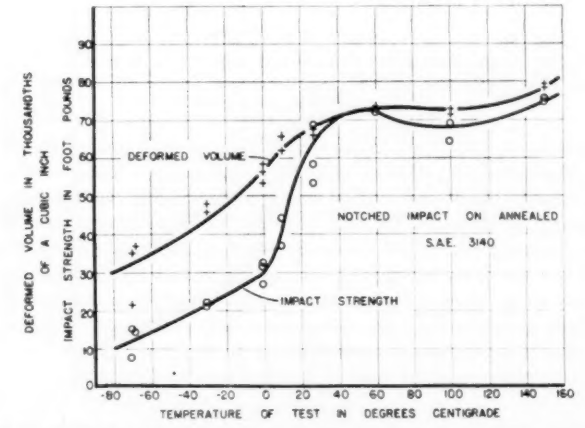


FIG. 10 TOTAL NOTCHED BEAM IMPACT ENERGY AND DEFORMED VOLUME FOR ANNEALED S.A.E. 3140 STEEL AS AFFECTED BY TESTING TEMPERATURE

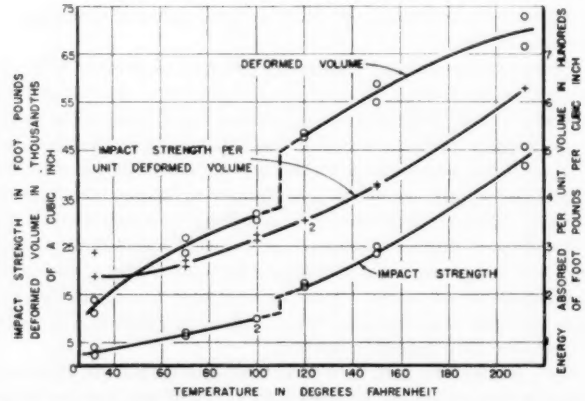


FIG. 11 TOTAL NOTCHED BEAM IMPACT ENERGY, DEFORMED VOLUME, AND ENERGY PER UNIT VOLUME OF DEFORMED METAL FOR ANNEALED S.A.E. 1112 STEEL AS AFFECTED BY TESTING TEMPERATURE

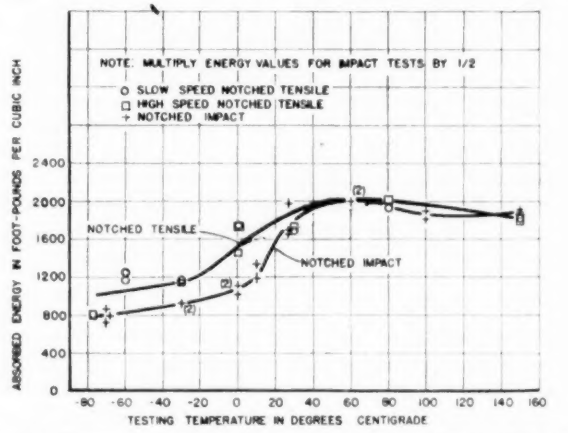


FIG. 12 ENERGY PER UNIT OF DEFORMED VOLUME FOR S.A.E. 3140 STEEL AS A FUNCTION OF TESTING TEMPERATURE AS DETERMINED BY NOTCHED TENSION AND NOTCHED BEAM IMPACT TESTS

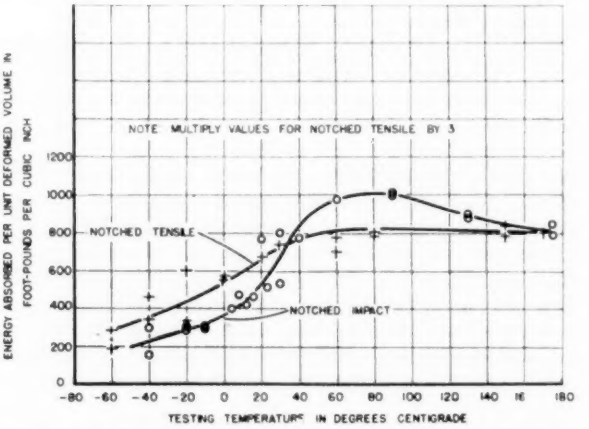


FIG. 13 RELATION OF THE ENERGY PER UNIT OF DEFORMED VOLUME TO THE TESTING TEMPERATURE FOR ANNEALED S.A.E. 1020 STEEL AS DETERMINED BY RAPID NOTCHED TENSION TESTS AND CHARPY IMPACT TESTS

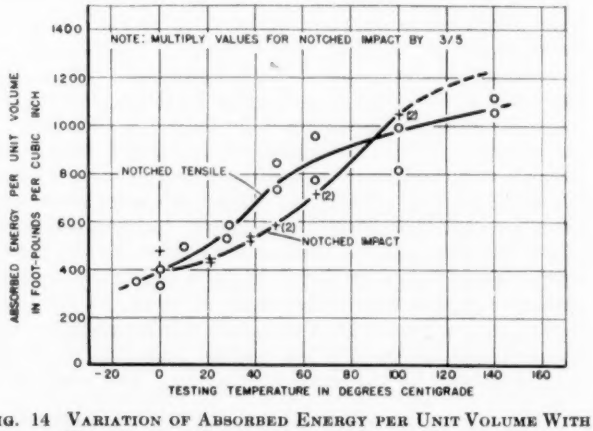


FIG. 14 VARIATION OF ABSORBED ENERGY PER UNIT VOLUME WITH TESTING TEMPERATURE DETERMINED BY RAPID NOTCHED TENSION TESTS AND NOTCHED BEAM IMPACT TESTS ON ANNEALED S.A.E. 1112 STEEL

tion of the test pieces showed that the specimen deforms only in a region near the notch below 110 F while above this temperature general plastic bending of the test piece results. The discontinuity then is not due to any change in the properties of the material at the notch but merely due to bending in a region removed from it. This provides added evidence that the energy per unit of volume is of more fundamental significance than total energy.

While the speed of testing was not found to be critical for the S.A.E. 1045 steel discussed earlier, or for the S.A.E. 3140 steel, the average testing time being 35 min for these materials, the onset of strain aging occurring during the tension tests at the higher temperatures for the low carbon steels necessitated for the S.A.E. 1020 and 1112 increased testing velocities if the results were to be compared with the notched beam impact tests. In fact the notched beam impact tests were completed before strain aging could be effective. Preliminary notched tension tests lasting 35 min on the two low-carbon steels showed that no correlation would be possible at the higher temperatures due to this aging effect. Consequently, the speeds of these tension tests were increased to 4 in. per min, providing a testing period of only a few seconds.

A comparison of the energies per unit of volume for the notched tension and the notched beam impact tests for these three steels, as affected by the testing temperature, can be made by referring to Figs. 12, 13, and 14. In Fig. 12 values from both slow and rapid tension tests are included. It can be seen that the testing velocity is not particularly important for the S.A.E. 3140. Further, the notched impact and the notched tensile specific energies show similar trends with the testing temperature. An examination of Figs. 13 and 14 for the S.A.E. 1020 and 1112 steels leads to a similar conclusion.

Although more experiments should be made with other materials and under other conditions of heat treatment, testing temperature, etc., in order to determine possible exceptions, these results seem to indicate that static notched tension tests of the true stress-strain type can be used to obtain essentially the same specific energy information as yielded by the notched beam impact test, while at the same time supplying useful stress-strain data not obtainable with the notched beam test.

Conclusion

The following conclusions may be drawn from these experiments:

1 For the same materials and conditions maintaining as in the present investigation, a reasonably good correlation exists between the notched beam impact test and the static notched tension test when true stress-strain values are employed. Both forms of test display essentially the same effects of drawing and testing temperatures on the specific energy for fracture.

2 While the main characteristics of the notched beam impact test in these experiments appear to be due to the notch rather than to the testing machine speed, the duration of the test is important where such effects as strain aging are pronounced. For a material subject to such changes in properties during the test, the duration of the tension test must approach that of the impact test in order for the correlation mentioned in (1) to hold. It is also apparent that when tests are conducted at temperatures considerably in excess of those employed in these experiments, or when low melting alloys are investigated at normal temperatures, the testing speed is of considerable importance.

3 Although the notched beam impact test appears to correlate with the notched static tension test better than with the uniform static tension test, this does not detract from the great value and significance of the tension test on uniform specimens. The latter are especially important where correlations are desired between tension values and results from other forms of tests such as torsion tests, combined stress tests of many kinds, metal forming operations such as drawing, rolling, etc. It is evident that no one form of tension test is the best for all purposes. The notched tension test seems to be particularly useful in those applications where the notched beam impact test has proved of value.

4 Attention should also be invited to the fact that while the notched static tension test takes longer to perform than the standard notched beam impact test where total energies only are determined, it has the added advantage of supplying stress-strain data not obtainable in the impact test. It appears that the energy per unit of deformed volume (specific energy) from the notched beam impact test is of more fundamental significance than total energy. If the former is determined in the impact test the time consumed is usually in excess of that required for the notched static tension test.

Acknowledgment

The experimental work described in this paper was performed in the laboratories of the Department of Mechanical Engineering at the Massachusetts Institute of Technology, and the authors wish to acknowledge the interest and support given the project by Dr. Compton and by Dr. Hunsaker. The careful machining of the test specimens was carried out by Mr. Herbert Johnson, and assistance in the experiments was given by Messrs. J. C. Crowley and H. J. Maier.

BIBLIOGRAPHY

1 "The Theory of Impact Testing etc.," by D. J. McAdam, Jr., and R. W. Clyne, Symposium on Impact Testing, American Society for Testing Materials, 1938, pp. 112–132.

2 "Notched Bar Testing and Impact Testing," by S. L. Hoyt, Symposium on Impact Testing, American Society for Testing Materials, 1938, pp. 162–177.

3 "Kohäsionsfestigkeit," by W. Kuntze, Mitteilungen aus der deutscher Materialprüfungsanstalten, Sonderheft 20, Julius Springer, Berlin, Germany, 1932.

4 "Static Crack Strength of Metals, Its Determination and Significance," by M. Gensamer, *Metal Progress*, vol. 38, 1940, pp. 58–64.

5 "The Technical Cohesive Strength of Metals," by D. J. McAdam, Jr., Journal of Applied Mechanics, Trans. A.S.M.E., vol. 63, 1941, pp. A155–165. "The Technical Cohesive Strength and Yield Strength of Metals," A.I.M.E. Technical Publication No. 1414, *Metals Technology*, January, 1942.

6 "An Investigation of the Technical Cohesive Strength of Metals," by D. J. McAdam, Jr., and R. W. Mebs, *Metals Technology*, August, 1943, pp. 1–63.

7 "High Velocity Tension-Impact Tests," by H. C. Mann, Proceedings, American Society for Testing Materials, vol. 36, part 2, 1936, pp. 85–97.

8 "Stress-Strain Relations Under Tension Impact Loading," by D. S. Clark and G. Dätwyler, Proceedings, American Society for Testing Materials, vol. 38, part 2, 1938, pp. 98–106.

9 "High-Speed Tension Tests at Elevated Temperatures," by A. Nadai and M. Manjoine, Proceedings, American Society for Testing Materials, vol. 40, 1940, pp. 822–837. Also Parts 2 and 3, Journal of Applied Mechanics, Trans. A.S.M.E., vol. 63, 1941, pp. A77–A91.

10 "Some Factors Affecting the Plastic Deformation of Sheet and Strip Steel and Their Relation to the Deep Drawing Properties," by J. Winlock and R. W. E. Leiter, Transactions, American Society for Metals, vol. 25, 1937, pp. 163–184.

11 "Experimentelle Untersuchungen über die Abhängigkeit der Zugspannungen von der Verformungsgeswindigkeit," by H. Deutler, Phys. Ztsch., vol. 33, 1932, pp. 247–259.

12 "Rapid Tension Tests Using the Two-Load Method," by A. V. DeForest, C. W. MacGregor, and A. R. Anderson, Technical Publication No. 1393, A.I.M.E., *Metals Technology*, December, 1941, pp. 1–9.

13 "Practical Application of the Notched-Bar Impact Test," by G. C. Riegel and F. F. Vaughn, Symposium on Impact Testing, American Society for Testing Materials, 1938, pp. 60–66.

14 "The Effect of Temperature on the Behavior of Iron and Steel in the Notched Bar Impact Test," by R. H. Greaves and J. A. Jones, *Journal Iron and Steel Institute*, no. 2, vol. 112, 1925, p. 152.

15 "On the Transition From a Ductile to a Brittle Type of Fracture in Several Low-Alloy Steels," by P. G. Jones, presented at the A.S.T.M. meeting in Pittsburgh July, 1943.

16 "Notched Bar Tensile Tests on Heat-Treated Low Alloy Steels," by G. Sachs and J. D. Lubahn, Transactions, American Society for Metals, vol. 31, no. 1, March, 1943, pp. 125–157.

17 "Relations Between Stress and Reduction in Area for Tensile Tests of Metals, by C. W MacGregor, Transactions A.I.M.E., vol. 124, 1937, p. 208. "Differential Area Relations in the Plastic State for Uniaxial Stress," S. Timoshenko Anniversary Volume, 1938, The MacMillan Co., New York, N. Y. "The Tension Test," Proceedings, American Society Testing Materials, vol. 40, 1940, pp. 508-534. "A Two-Load Method of Determining the Average True Stress-Strain Curve in Tension," *Journal Applied Mechanics*, vol. 6, no. 4, December, 1939.

18 "True Stress-Strain Relations at High Temperatures by the Two-Load Method," by C. W. MacGregor and L. E. Welch, Technical Publication No. 1507, A.I.M.E. *Metals Technology*, September, 1942.

19 "Zur Gesetzmässigkeit der Kerbschlagprobe," by M. Moser, Kruppsche Monatshefte, vol. 2, 1921, p. 225. "Die Ergebnisse des Kerbschlagversuches," Kruppsche Monatshefte, vol. 5, 1924, p. 48.

The Effects of Web Deformation on the Torsion of I-Beams

By J. N. GOODIER[1] and M. V. BARTON[2]

An analysis of the I-beam in nonuniform torsion, as for instance, when a built-in end or section of symmetry is prevented from warping, is made which includes not only the bending of the flanges in their own planes (as considered previously by Timoshenko) but also a deformation of the web cross section. This extends the theory to thinner webs and permits the satisfaction of more general end conditions. Numerical examples worked out for three sections, differing in web thickness only, show that the stress and deformation are significantly modified by the web flexibility when the web is sufficiently thin, and that there are then bending stresses in the web which may be larger than the bending stresses in the flanges. Only the unbuckled state of the web is considered.

WHEN I-beams are subject to a nonuniform torsional deformation, in which the angle of twist β at a section with axial co-ordinate z is not simply proportional to z (or linear in z), the center lines of the flanges become curves,[3] Fig. 1, and

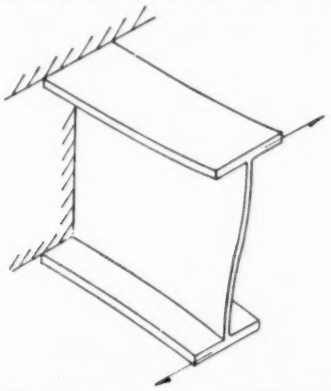


FIG. 1 FLANGE BENDING SHOWING SHEAR FORCES

each flange is in the condition of a beam with bending moments and shearing forces. The two shearing forces in the two flanges form an axial couple which combines with the ordinary Saint Venant couple of the torsional shearing stress to balance the axial couple, at the section, due to applied twisting moments. A theory of this behavior has been worked out by Timoshenko,[4] who applied it to the analysis of the twisted I-beam, and other sections, when warping of the cross section is prevented at one or both ends. Timoshenko's differential equation[5] may be written

$$\frac{1}{2}EI_f h^2 \beta''' - GC\beta' = -T$$

where EI_f is the flexural rigidity of one flange as a beam bent in its own plane, h is the distance between flanges, GC is the Saint Venant torsional rigidity of the whole section, and T is the twisting moment which must be balanced by the stresses on the section z. Primes denote differentiation with respect to z. The deflection of a flange as a beam is $\beta h/2$, Fig. 3*a*.

The solution for a beam built-in (warping prevented) at $z = 0$ and twisted by a moment T at the other end $z = l$ is such that

$$\beta' = \frac{T}{GC}\left\{1 - \frac{\cosh r(l-z)}{\cosh rl}\right\}$$

where $1/r^2 = EI_f h^2/2GC$. Thus (unless l is infinite) β''' is not zero at the end $z = l$, and the flange bending torque $EI_f(h^2/2)\beta'''$ is not zero. The moment T at $z = l$ must therefore, for the analysis, to be valid at both ends, be applied as a mixture of Saint Venant torque $GC\beta'$ and flange bending torque, in proportions which we are not free to assign. In fact, since the equation is of the third order, only three end conditions can be satisfied.

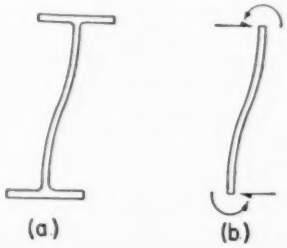


FIG. 2 WEB DEFORMATION

From the fact that the analysis treats the whole beam as twisted, and the flanges as beams bent in their planes, we should expect to be able to satisfy two conditions at each end of the flange, as for a beam, and one condition on the torsion of the beam as a whole for each end. At least we may expect to be able to assign the contributions to the total torque at each end of the Saint Venant torque and the torque of the flange shearing forces. The analysis of Timoshenko is not sufficiently general to permit this. The inference is therefore that it disregards some aspect of the problem which is significant in the bending of the flanges as beams and the torsion of the beam as a whole. It is shown in this paper that the desired generality may be obtained by considering a deformation of the web. At the same time it is shown that certain bending stresses exist in the web which become important when the web is thin. The analysis may also elucidate some problems in the deformation of "beams" formed of two flanges connected by a lattice "web," the latter being thought of as replaced by a thin continuous web. The

[1] Professor of Engineering Mechanics, Cornell University, Ithaca N. Y. Mem. A.S.M.E.

[2] Professor of Aeronautical Engineering, University of Texas, Austin, Texas. Mem. A.S.M.E.

[3] The helical forms corresponding to uniform torsion are identified with straight lines for a limited length.

[4] (*a*) "Strength of Materials," by S. Timoshenko, second edition, D. Van Nostrand Company, Inc., New York, N. Y., vol. 2, 1941, p. 282. (*b*) "Theory of Elasticity," by S. Timoshenko, McGraw-Hill Book Company, Inc., New York, N. Y., 1934, p. 256.

Presented at the Annual Meeting, New York, N. Y., Nov. 29–Dec. 3, 1943, of THE AMERICAN SOCIETY OF MECHANICAL ENGINEERS.

Discussion of this paper should be addressed to the Secretary, A.S.M.E., 29 West 39th Street, New York, N. Y., and will be accepted until April 10, 1944, for publication at a later date. Discussion received after the closing date will be returned.

NOTE: Statements and opinions advanced in papers are to be understood as individual expressions of their authors and not those of the Society.

[5] Reference 4(*b*), p. 257.

lateral buckling of such beams is known to involve the type of deformation indicated in Fig. 2, rather than the simple rotation of cross sections assumed in the present theory of lateral buckling, and an analysis of lateral buckling taking this into account can be developed from the results which will be given.

The existence of web deformation, as indicated in Fig. 2, is to be expected from the consideration that the deflection of a flange in its own plane as a beam will in general have a nonzero fourth derivative, corresponding to some distributed load on the flange. This load (at least in part, when there is external distributed load on each flange) must be applied by the web. Correspondingly there are reactive lateral forces and accompanying moments on the web, as indicated in Fig. 2(*b*), and these cause the web cross section to become curved.

Again, if we consider the influence of web thickness on the behavior of an I-beam, it soon becomes apparent from examples that such deformation can be important. Consider a long I-beam built-in at one end, and twisted by two equal and opposite flange shears at the other end, Fig. 1. This couple is transformed more or less gradually as we proceed along the beam into the Saint Venant shearing stresses of torsion, the flange shears disappearing. This much follows from Saint Venant's principle. But the limiting case of the very thin web would be a web of negligible influence on the flanges. Then they are independent cantilevers, and the same shear force persists all along. The flanges are not twisted. When the web is very thin, therefore, it must have the deformation shown in Fig. 2, and its thickness must govern closely the manner in which the total torque at a section is shared between the Saint Venant torsional couple and the couple formed by the flange shear forces

Saint Venant's principle would indicate that simple (Saint Venant) torsion would be established in a distance from the end comparable with the "dimensions of the end." We find in this case, however, that the governing dimension is not the over-all size of the end, that is, the cross section, but something involving the thickness of the web in relation to the other cross-sectional measurements.

The Differential Equations

Fig. 3(*a*) indicates the rotation β of the section without deformation, which is assumed in Timoshenko's theory. Fig. 3(*b*) indicates how the web bending is specified by the angle α. Thus each flange is a beam bent in its own plane to a deflection $\beta h/2$, and twisted through an angle $\beta - \alpha$ at a section z. A distribution of lateral load q per unit length acts on it, as indicated in Fig. 4, and also a distribution of twisting couple m per unit length, both exerted by the web. The equations of bending and twisting may thus be written

$$\frac{1}{2} hEI_f\beta^{iv} = q \qquad [1]$$

$$GC_f(\beta' - \alpha') = -m \qquad [2]$$

where GC_f is the torsional rigidity of one flange alone, G being the shear modulus.

The web is a rectangular strip twisted to the angle β, but also deformed, as shown in Fig. 4, by the forces q and the couples m. These constitute a distribution of twisting moment $2m + qh$ per unit length, and the torsional equation is

$$GC_w\beta' = 2m + qh \qquad [3]$$

where GC_w is the torsional rigidity of the web alone. The angle α can be calculated in terms of the forces acting on a slice of the web between the sections z and $z + dz$. This strip may be regarded as bent (Fig. 5) by the end forces and couples qdz and mdz, and by the distributed bending couple formed by the difference in the Saint Venant shearing stresses on the two sections. The difference of torsional couple is $GC_w\beta'dz$ and this is distributed along the length h of the strip in Fig. 5, thus giving a distribution of couple $(GC_w/h)\beta'dz$ per unit length, which is a bending couple with reference to the bending indicated in Fig. 5. From the solution of this beam problem we find

$$m = \frac{6D_w}{h}\alpha \qquad [4]$$

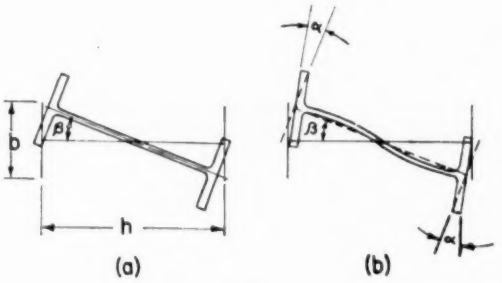


Fig. 3

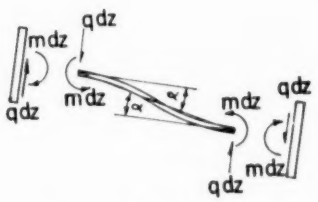


Fig. 4

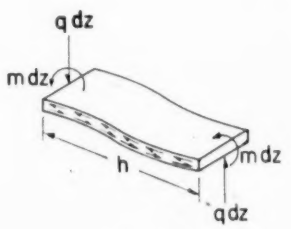


Fig. 5

where $D_w = Et_w^3/12(1 - \nu^2)$, t_w being the web thickness, and the factor $(1 - \nu^2)$ with ν as Poisson's ratio occurring in virtue of the prevention of anticlastic curvature in the strip by its attachment to the rest of the web.

Equations [1], [2], [3], and [4] are four equations for β, α, m, and q. On elimination of m and q we find the two equations

$$GC_f(\beta' - \alpha') + 6\frac{D_w}{h}\alpha = 0 \qquad [5]$$

$$\frac{1}{2}EI_fh^2\beta^{iv} - GC_w\beta' + 12\frac{D_w}{h}\alpha = 0 \qquad [6]$$

for α and β.

If T is the twisting moment produced by all forces beyond the section z, in the clockwise sense looking along the z axis, Fig. 6, this moment is balanced by the stress on the section, and

$$T = GC_w\beta' + 2GC_f(\beta' - \alpha') - \frac{1}{2}EI_fh^2\beta'''$$

or

$$T = GC\beta' - 2GC_f\alpha' - \frac{1}{2}EI_f h^2\beta''' \quad \ldots\ldots [7]$$

where GC is the torsional rigidity of the whole section. This follows at once from the fact that the web is twisted to the angle

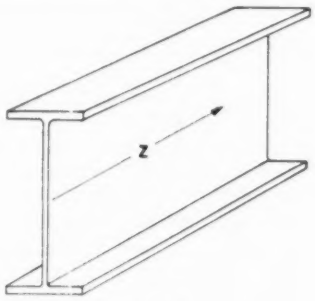


FIG. 6

β, each flange to the angle $\beta - \alpha$, and that there is a shearing force $\frac{1}{2}EI_f h\beta'''$ in each flange. Equation [7] may thus, when it is convenient, replace one of the Equations [1], [2], [3], or [4].

Using the dimensionless coefficients

$$\left.\begin{aligned} k_1 &= \frac{EI_f}{2GC} \\ k_2 &= \frac{C_w}{C} \\ k_3 &= \frac{C_f}{C} \\ k_4 &= \frac{6D_w h}{GC} \end{aligned}\right\} \quad \ldots\ldots [8]$$

Equations [5] and [6] may be written

$$k_3 h^2(\beta'' - \alpha'') + k_4\alpha = 0 \quad \ldots\ldots [9]$$

$$k_1 h^4\beta^{iv} - k_3 h^2\beta'' + 2k_4\alpha = 0 \quad \ldots\ldots [10]$$

SOLUTION OF THE DIFFERENTIAL EQUATIONS

The equations, being linear with constant coefficients, have solutions of the form $\beta = C_1 e^{\lambda z}$, $\alpha = C_2 e^{\lambda z}$, in addition to the obvious solution

$$\beta = A_1 + A_2 z, \quad \alpha = 0 \quad \ldots\ldots [11]$$

which corresponds to ordinary (Saint Venant) twisting. On substitution of the exponential forms we have

$$\left.\begin{aligned} (k_3\lambda^2 h^2 - k_4)C_1 - k_3\lambda^2 h^2 C_2 &= 0 \\ 2k_4 C_2 + (k_1\lambda^4 h^4 - k_3\lambda^2 h^2)C_1 &= 0 \end{aligned}\right\} \quad \ldots\ldots [12]$$

which can only be satisfied with C_1, C_2 different from zero if

$$\lambda^2 h^2(k_3\lambda^2 h^2 - k_4)(k_1\lambda^2 h^2 - k_3) + 2k_3 k_4\lambda^2 h^2 = 0 \quad \ldots\ldots [13]$$

The root $\lambda^2 h^2 = 0$ corresponds to the simple torsional solution previously mentioned. When the factor $\lambda^2 h^2$ is removed, Equation [13] becomes a quadratic in $\lambda^2 h^2$ with roots given by

$$\frac{2}{K_1}(\lambda h)^2 = 1 \pm \sqrt{1 - K_2} \quad \ldots\ldots [14]$$

where

$$K_1 = \frac{k_3}{k_1} + \frac{k_4}{k_3} = \frac{2GC_w}{EI_f} + \frac{6D_w h}{GC_f} \quad \ldots\ldots [15]$$

$$K_2 = \frac{4\frac{k_4}{k_1}\left(2 + \frac{k_3}{k_3}\right)}{\left(\frac{k_3}{k_1} + \frac{k_4}{k_3}\right)^2} = 48\frac{D_w h}{EI_f}\left(2 + \frac{C_w}{C_f}\right)\Big/\left(\frac{2GC_w}{EI_f} + \frac{6D_w h}{GC}\right)^2 \quad \ldots [16]$$

Thus the dimensionless group $(\lambda h)^2/K_1$ is a function of the group K_2 only. In any given case K_1 and K_2 can be calculated from the data and the two values of $(\lambda h)^2$ found. These are real or complex according as K_2 is less than or greater than 1. It appears from the calculations already made that they are complex if the web is sufficiently thin, being real for thick webs. The two cases are now discussed separately.

Real Roots. There are two real values of λ^2. Let these be denoted by λ_1^2, λ_2^2 where λ_1, λ_2 are positive. Then we have the four possible values of λ, $\pm\lambda_1$, $\pm\lambda_2$. The complete solution for β is

$$\beta = A_1 + A_2 z + A_3 e^{\lambda_1 z} + A_4 e^{-\lambda_1 z} + A_5 e^{\lambda_2 z} + A_6 e^{-\lambda_2 z} \quad \ldots [17]$$

where A_1, A_2, etc., are arbitrary constants. The corresponding constants in α are related to these as C_1 and C_2 are related by either of the Equations [12], and we have as the complete solution for α

$$\alpha = [k_5(\lambda_1 h)^2 - k_6(\lambda_1 h)^4][A_3 e^{\lambda_1 z} + A_4 e^{-\lambda_1 z}] + [k_5(\lambda_2 h)^2 - k_6(\lambda_1 h)^4][A_5 e^{\lambda_2 z} + A_6 e^{-\lambda_2 z}] \quad \ldots\ldots [18]$$

where $k_5 = k_2/2k_4$, $k_6 = k_1/2k_4$.

Complex Roots. When the two possible values of λ^2 are complex, they will yield four possible complex values δf λ in the form $\pm(\xi \pm i\eta)$. The solution for β becomes

$$\beta = B_1 + B_2 z + e^{\xi z}(B_3 \cos \eta z + B_4 \sin \eta z) + e^{-\xi z}(B_5 \cos \eta z + B_6 \sin \eta z)$$

where B_1, B_2, etc., are real constants. The solution for α in terms of these same constants then follows from Equation [10].

In the four values of λ, $\pm(\xi \pm i\eta)$, it is evident that whether ξ, η be positive or negative two of the values will have positive real parts, the other two negative. It is then permissible to take ξ (and η) as positive. Then with $\lambda_1 = \xi + i\eta$, $\lambda_2 = \xi - i\eta$ the four values are $\pm\lambda_1$, $\pm\lambda_2$, the values λ_1, λ_2 having positive, and $-\lambda_1$, $-\lambda_2$ negative, real parts. With this notation, the solution of Equations [17] and [18] covers both real and complex roots. In the latter case A_3, A_4, A_5, A_6 are complex. Then the real parts of β and α and the imaginary parts must satisfy Equations [9] and [10] separately, since these are linear equations with real coefficients. The imaginary parts may thus be discarded, but this may be done before or after β and α have, with the appropriate derivatives, been made to assume the required (real) end values of the particular problem.

End Conditions. If at a "fixed" end, the beam is rigidly attached by the flanges only (Fig. 7), the end of the web being free, each flange, as a beam in its plane, is built in with zero deflection. We have, therefore, $\beta = 0$ and $\beta' = 0$. Also, since there is no twisting rotation of the flange end, $\beta - \alpha = 0$. The web end is free from torsional shearing stress, requiring again $\beta' = 0$. The conditions are thus $\alpha = \beta = \beta' = 0$.

If the web is rigidly held, as well as the flanges, the condition

on the web is $\alpha = 0$ and the conditions are still the same. Fixing the web thus has no effect so long as the flanges are fixed.

If, however, the web is fixed but the flanges are free (Fig. 8), we have for the web

$$\alpha = 0, \quad \beta = 0$$

for the flange

$$\beta = 0, \quad \beta' - \alpha' = 0, \quad \beta'' = 0, \quad \beta''' = 0 \ldots\ldots [19]$$

the flange conditions corresponding, respectively, to zero deflection, zero torsional shearing stress, zero longitudinal (flange bending) stress, and zero transverse shear force. However, all these conditions cannot be satisfied by the present theory except of course in the trivial case of the completely unloaded condition. This is shown, and some explanation offered, in the next section.

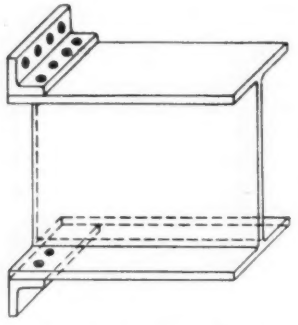


FIG. 7 FLANGES FIXED

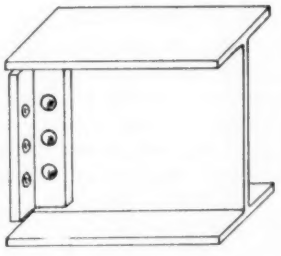


FIG. 8 WEB FIXED

THE LONG BEAM

Flanges Fixed at $z = 0$. If the beam is sufficiently long, the state of stress found at the fixed end will merge into that of ordinary torsion. Thus we may take besides the conditions

$$\alpha = \beta = \beta' = 0 \text{ at } z = 0$$

the condition that β approaches a linear function of z as z increases. We must then discard the positive exponentials in Equations [17] and [18], and take

$$\beta = A_1 + A_2 z + A_4 e^{-\lambda_1 z} + A_6 e^{-\lambda_2 z} \ldots\ldots [20]$$

$$\alpha = [k_5(\lambda_1 h)^2 - k_6(\lambda_1 h)^4] A_4 e^{-\lambda_1 z} + [k_5(\lambda_2 h)^2 - k_6(\lambda_2 h)^4] A_6 e^{-\lambda_2 z} \ldots\ldots [21]$$

This covers complex λ's as well as real, since in the former case λ_1 and λ_2 have been defined as having positive real parts; as

$$z \to \infty, \ \beta \to A_1 + A_2 z \text{ and } \beta' \to A_2$$

Thus the axial couple transmitted by the beam is $GCA_2 = T$. The conditions at $z = 0$ require

$$A_1 + A_4 + A_6 = 0, \qquad A_2 - \lambda_1 A_4 - \lambda_2 A_6 = 0$$

$$[k_5(\lambda_1 h)^2 - k_6(\lambda_1 h)^4] A_4 + [k_5(\lambda_2 h)^2 - k_6(\lambda_2 h)^4] A_6 = 0$$

whence

$$A_4 = \frac{A_2}{\lambda_2} \cdot \left[\frac{\lambda_1}{\lambda_2} - \frac{k_5(\lambda_1 h)^2 - k_6(\lambda_1 h)^4}{k_5(\lambda_2 h)^2 - k_6(\lambda_2 h)^4} \right]^{-1},$$

$$A_6 = \frac{A_2}{\lambda_1} \left[\frac{\lambda_2}{\lambda_1} - \frac{k_5(\lambda_2 h)^2 - k_6(\lambda_2 h)^4}{k_5(\lambda_1 h)^2 - k_6(\lambda_1 h)^4} \right]^{-1}$$

in which A_2 can be replaced by T/GC.

The quantity A_1, given by $-(A_4 + A_6)$ represents the effect on the angle of twist $(A_1 + A_2 z)$ of a long length, of the flange bending and web deformation near $z = 0$, since without this local condition there would be simple torsion $\beta = A_2 z$ with $GCA_2 = T$.

The results of such calculations for an I-beam with three different web thicknesses are given in the next section.

Web Fixed, Flanges Free. The end conditions (at $z = 0$) are given by Equation [19], and must be satisfied by Equations [20] and [21]. If we take only the conditions on the flange, the second line of Equation [19], we find at once from

$$\beta = \beta'' = \beta''' = 0 \quad \text{that} \quad A_1 = A_4 = A_6 = 0$$

and thus that $\alpha = 0$ all along the beam. Then the remaining flange condition $\beta' - \alpha' = 0$ reduces to $\beta' = 0$ and gives $A_2 = 0$. All the A's are now zero, and the beam is in the unloaded condition. The conclusion is that fixture of the web only involves a state of deformation which cannot be represented at all by the web twisting and bending, and flange twisting and bending, of the present theory. Some yet more highly localized and complex stress distribution is to be expected near the end, depending upon the details of the fixture.

THE FINITE BEAM

Flanges Rigidly Attached at Both Ends to Plates Which Remain Normal to Axis. The beam is twisted by moments applied to the plates to which the flange ends are fixed, Fig. 9. These plates rotate (by equal amounts β_1 in opposite directions) in their own planes. If we take the origin at the middle, β will be an odd function of z, and we may take

$$\beta = A_2 z + B_3 \sinh \lambda_1 z + B_5 \sinh \lambda_2 z$$

$$\alpha = [k_5(\lambda_1 h)^2 - k_6(\lambda_1 h)^4] B_3 \sinh \lambda_1 z + [k_5(\lambda_2 h)^2 - k_6(\lambda_2 h)^4] B_5 \sinh \lambda_2 z$$

with $\alpha = \beta' = 0, \quad \beta = \beta_1, \quad \text{at } z = l$

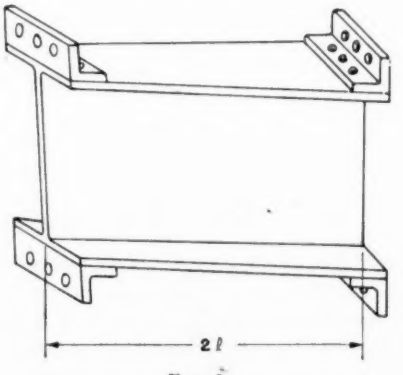


FIG. 9

These conditions yield three equations whence A_2, B_3, B_5 can be found in terms of β_1. The relation between β_1 and the applied twisting moment T can then be found from Equation [7].

NUMERICAL EVALUATIONS

Figs. 11 to 18 show the results of calculations for the section shown in Fig. 10, with three values of the web thickness, 0.35 in., 0.175 in., and 0.0875 in., respectively. Figs. 11, 12, 13 are for a beam of infinite length, built-in at the left end and twisted by a torque T at the other end, as discussed under the heading "The Long Beam: Flanges fixed at $z = 0$." Each figure is for a particular web thickness and shows the rotation of the cross section β, the bending moment (per unit axial length) m in the web, and the flange bending moment M. It will be observed that β and M show only small departures from the values found

from Timoshenko's analysis, the departures being most pronounced for the thinnest web.

There are radical differences however in m. The theory of this paper differs from the Timoshenko theory in the introduction of the angle α and reduces to it when α is taken as zero. Then Equation [2] gives $m = -GC_f\beta''$ for the calculation of m, according to the Timoshenko theory. This has its greatest value at the fixed end. On the other hand, the theory of the present paper gives m according to Equation [4], and since α vanishes at the fixed end, m does also.

The stress corresponding to m is called "web bending stress." It attains significant magnitudes, being greater for the thinner webs. Its ratio to the flange bending stress (using greatest values) is 0.19 for $t = 0.35$ in., but 1.02 for $t = 0.0875$ in. The ratio of flange bending stress to (Saint Venant) torsional shear stress is 1.85 for $t = 0.35$ in., and 1.35 for $t = 0.0875$ in.

It must be remarked, however, that Equation [4] is accurate only when m varies little in an axial length equal to the depth

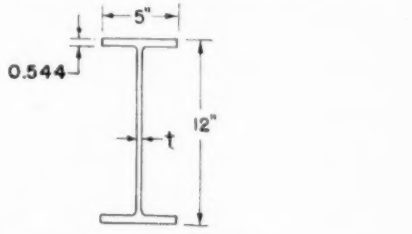


FIG. 10 DIMENSIONS OF CROSS SECTION
(t varies from 0.35 in. to 0.0875 in.)

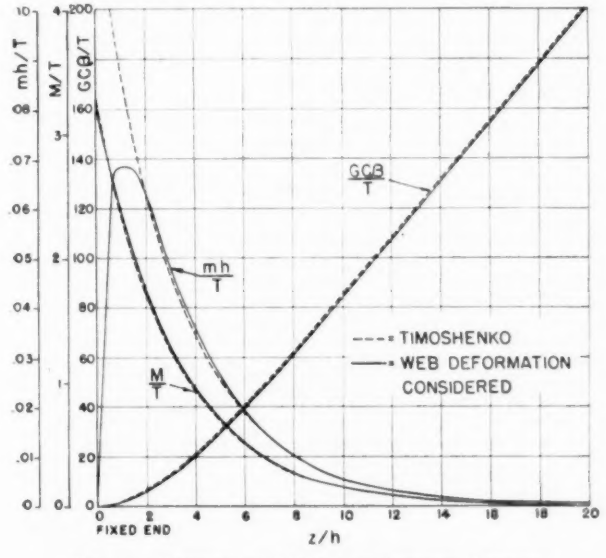


FIG. 11 TORSION OF I-BEAM OF INFINITE LENGTH
(Web thickness = 0.35 in.)

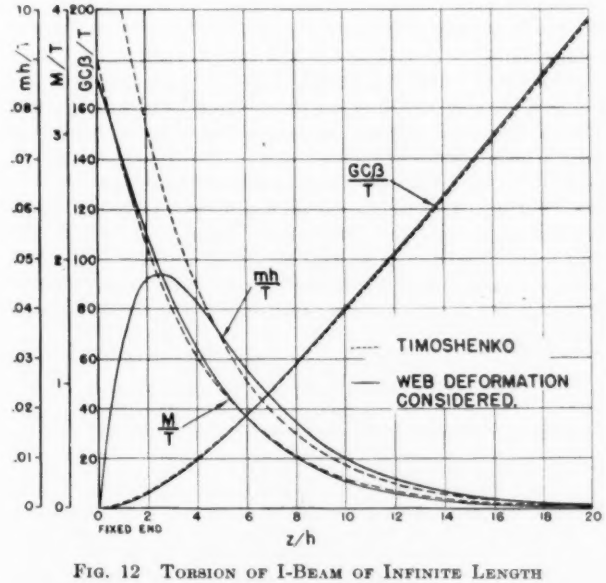


FIG. 12 TORSION OF I-BEAM OF INFINITE LENGTH
(Web thickness = 0.175 in.)

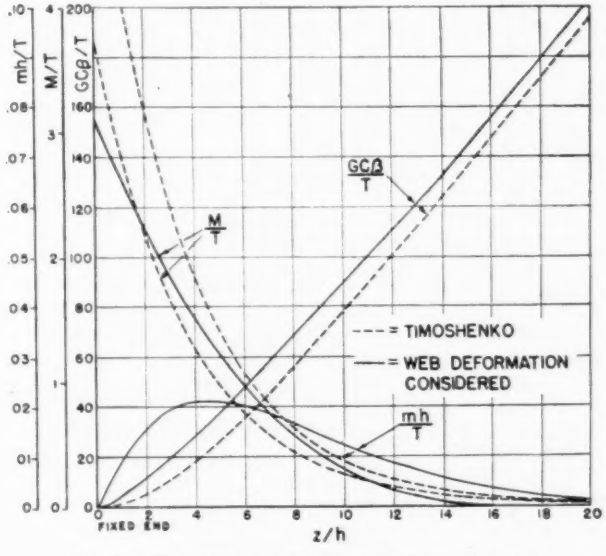


FIG. 13 TORSION OF I-BEAM OF INFINITE LENGTH
(Web thickness = 0.0875 in.)

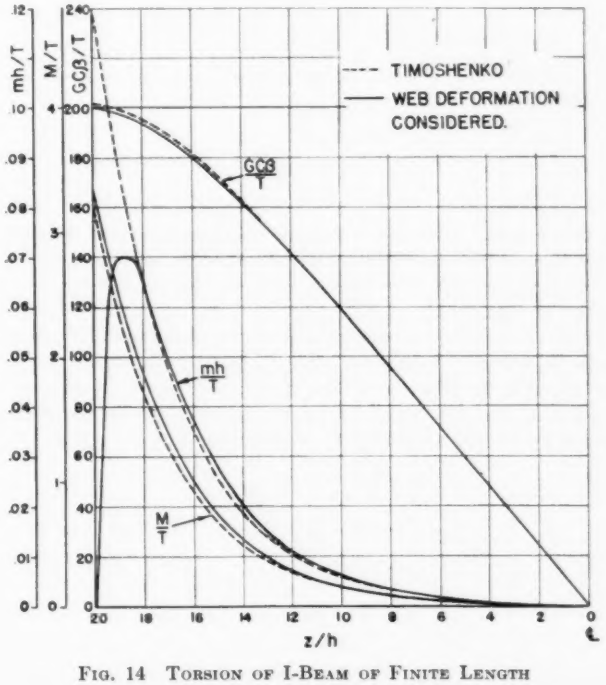


FIG. 14 TORSION OF I-BEAM OF FINITE LENGTH
(Length = 40 h; web thickness = 0.35 in.)

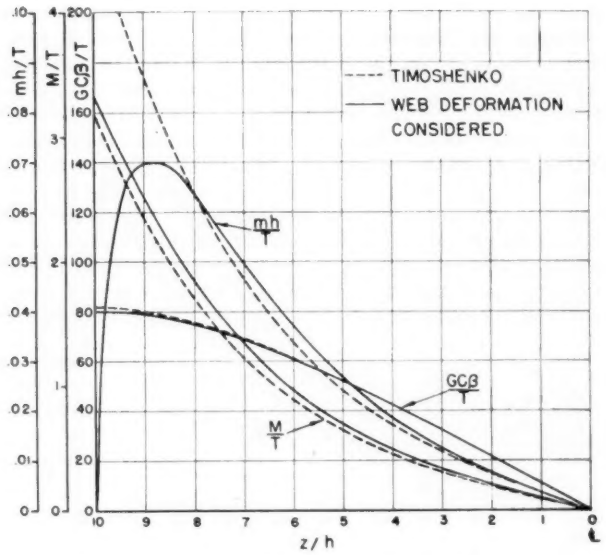


FIG. 15 TORSION OF I-BEAM OF FINITE LENGTH
(Length = 20 h; web thickness = 0.35 in.)

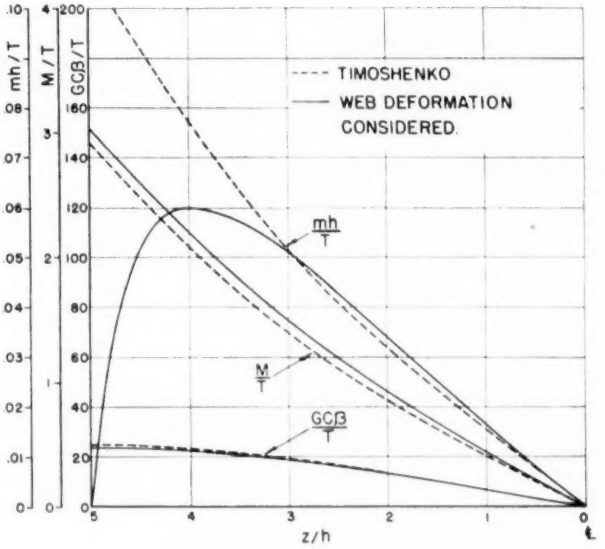


FIG. 16 TORSION OF I-BEAM OF FINITE LENGTH
(Length = 10 h; web thickness = 0.35 in.)

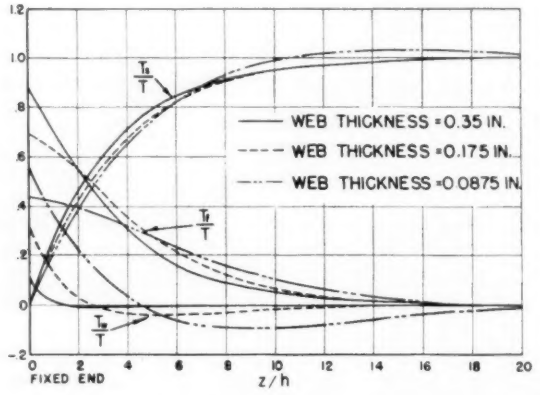


FIG. 17 TORQUE DIVISION FOR I-BEAM OF INFINITE LENGTH

T_s = Saint Venant shear torque
T_f = Flange shear torque
T_w = Torque modification due to web deformation

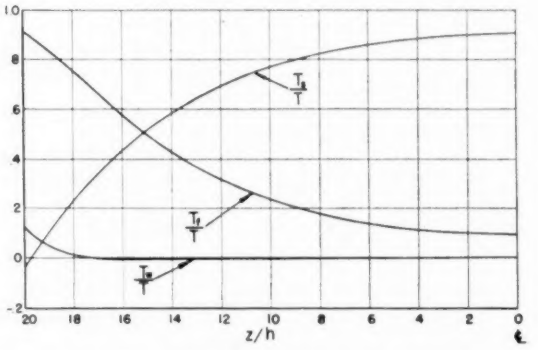


FIG. 18 TORQUE DIVISION FOR I-BEAM OF FINITE LENGTH
(Length = 20 h; web thickness = 0.35 in.)

h of the web. The variation found near the fixed end is rapid, and the results may therefore be subject to some correction on this account. The correction could be determined by more elaborate analysis.

Fig. 17 exhibits the relative magnitudes of the terms of Equation [7] for the total torque. The second term of course would be absent in the Timoshenko theory (and the value of β different). In Fig. 17, the first term of the right side of Equation [7] is denoted by T_s, the second by T_w, and the third by T_f. It will be observed that the second term, arising directly from the bending of the web, becomes important near the fixed end when the web is thin.

Another set of results is shown in Figs. 14, 15, 16, and 18 for the beam of finite length in the condition discussed under the heading "The Finite Beam: Flanges Rigidly Attached at Both Ends to Plates Which Remain Normal to Axis." In Figs. 14, 15, and 16, however, the web thickness is the same (0.35 in.) in each case. It is the length of the beam which is different. Again, there is little departure from the Timoshenko values in β and M, but pronounced departure in m near the end. In these three diagrams, the right end of the horizontal axis is the mid-section of the beam, the deformation being antisymmetrical about the plane of this section.

Pi-Tee Transformations in the Analysis of Mechanical Transmission Lines

By G. HORVAY[1] and S. PINES,[2] WASHINGTON, D. C.

A method is given which simplifies the analysis of mechanical transmission systems without making use of "electrical analogies." The method is applied to the problem of the viscous vibration damper.

1—Introduction

THE solution of the vibration problem of a shaft system is often facilitated by the replacement of certain portions of the system by simpler dynamical equivalents. For instance, the two shafts K_1, K_2, Fig. 1(*a*), connecting the masses M_1 and M_2 of a given system, can be replaced by a shaft of stiffness

$$K = K_1 + K_2 \quad [1]$$

Fig. 1(*b*), in all vibration calculations.* We shall refer to this replacement as "substitution I." Likewise, the two shafts K_α, K_β of the partial system shown in Fig. 2(*a*) can be replaced by the single equivalent shaft

$$K = \frac{1}{1/K_\alpha + 1/K_\beta} \quad [2]$$

as shown in Fig. 2(*b*). We shall call this "substitution II."

Other substitutions permit the simplification of geared systems. These substitutions are well known[3, 4, 5] and will not concern us. In this paper our main interest is centered on what we shall call "substitution III," the replacement of the partial system $[K_1, M_3, K_2]$ of Fig. 3(*a*) by the dynamically equivalent partial system $[M_1', K_3', M_2']$ of Fig. 3(*b*).

A given system, of which $[K_1, M_3, K_2]$ forms a part, transmits to shaft K_1 at point 1 a harmonic force $f_1(t) = F_1 e^{j\omega t}$ and a harmonic displacement

$$x_1(t) = X_1 e^{j\omega t} \quad [3a]$$

The partial system $[K_1, M_3, K_2]$ modifies the force and the motion, with the result that the force and the displacement delivered to the remainder of the system at point 2 assume the new values $f_2(t) = F_2 e^{j\omega t}$ and



Fig. 1 The System in Diagram (*b*) Is Equivalent to the System in Diagram (*a*) by Virtue of Equation [1]



Fig. 2 The System in Diagram (*b*) Is Equivalent to the System in Diagram (*a*) by Virtue of Equation [2]



Fig. 3 The System in Diagram (*b*) Is Equivalent to the System in Diagram [*a*] by Virtue of Equations [4]

$$x_2(t) = X_2 e^{j\omega t} \quad [3b]$$

If $[M_1', K_3', M_2']$ is the dynamical equivalent of $[K_1, M_3, K_2]$, then the application of the foregoing x_1 and f_1 at point 1′ results in the same x_2 and f_2 at point 2′ as resulted at point 2. Thus our problem is to determine the quantities M_1', K_3', M_2' which yield the correct x_2 and f_2.

The solution of the problem at any frequency ω is

$$M_1' = \frac{K_1 M_3}{K_1 + K_2 - M_3\omega^2}, \quad M_2' = \frac{K_2 M_3}{K_1 + K_2 - M_3\omega^2}$$

$$K_3' = \frac{K_1 K_2}{K_1 + K_2 - M_3\omega^2} \quad [4a]$$

We denote these equations more simply by

$$K_1' = K_1K_3/K, \quad K_2' = K_2K_3/K, \quad K_3' = K_1K_2/K \quad [5a]$$

where

$$K_1' = -M_1'\omega^2, \quad K_2' = -M_2'\omega^2, \quad K_3 = -M_3\omega^2,$$

$$K = K_1 + K_2 + K_3 \quad [5']$$

The inverse transformation, which leads from Fig. 3(*b*) to Fig. 3(*a*), is given by the formulas

$$\left.\begin{aligned} K_1 &= (1 + M_1'/M_2')K_3' - M_1'\omega^2 \\ K_2 &= (1 + M_2'/M_1')K_3' - M_2'\omega^2 \\ M_3 &= M_1' + M_2' - M_1'M_2'\omega^2/K_3' \end{aligned}\right\} \quad [4b]$$

In an abbreviated form these can be written as

$$K_1 = K'^2/K_2', \quad K_2 = K'^2/K_1', \quad K_3 = K'^2/K_3' \quad [5b]$$

where

$$K'^2 = K_1'K_2' + K_2'K_3' + K_3'K_1' \quad [5'']$$

The transformation [5*a*] is known in Electrical Engineering literature as a $\Pi - T$ (or $\Delta - Y$) transformation, the inverse

---

[1] Associate Mathematician, the David Taylor Model Basin; instructor of Engineering Mathematics, University of Cincinnati, Cincinnati, Ohio (on leave).

[2] Research Test Engineer, Chance-Vought Aircraft Corp., Stratford, Conn. Formerly Junior Mathematician, the David Taylor Model Basin.

[3] "Vibration Problems in Engineering," by S. Timoshenko, D. Van Nostrand Co., Inc., New York, N. Y., 1937, p. 256.

[4] "Mechanical Vibrations," by J. P. Den Hartog, McGraw-Hill Book Co., Inc., New York, N. Y., 1940, p. 160.

[5] "Electrical Circuit Analysis of Torsional Oscillations," by L. A. Pipes, *Journal of Applied Physics*, vol. 14, 1943, p. 352.

* The authors consider only longitudinal (or torsional) harmonic vibrations.

Presented at the Annual Meeting, New York, N. Y., Nov. 29–Dec. 3, 1943, of The American Society of Mechanical Engineers.

Discussion of this paper should be addressed to the Secretary, A.S.M.E., 29 West 39th Street, New York, N. Y., and will be accepted until April 10, 1944, for publication at a later date. Discussion received after the closing date will be returned.

Note: Statements and opinions advanced in papers are to be understood as individual expressions of authors and not of the Society.

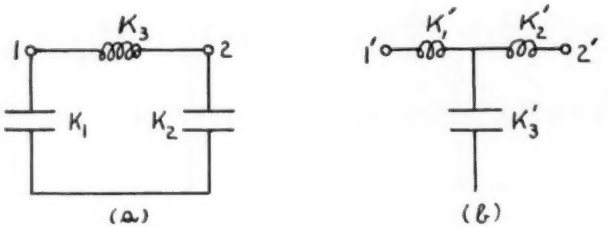


FIG. 4 PI AND TEE CIRCUITS

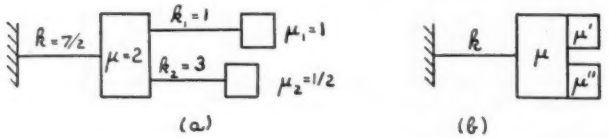


FIG. 5 REDUCTION OF A BRANCHED SYSTEM TO A SIMPLE SYSTEM

transformation [5b] is known as a $T - \Pi$ (or $Y - \Delta$) transformation. The Π and T circuits are illustrated in Figs. 4(*a*, *b*); the impedances are denoted by K_1, K_2, K_3, and by K_1', K_2', K_3', respectively. The equivalence of Figs. 3(*a*) and 4(*a*), and of Figs. 3(*b*) and 4(*b*) will become apparent in section 2. (Equations [7] and [8] apply both to the mechanical systems, Fig. 3, and to the electrical systems, Fig. 4. We shall not make use of this correspondence, as our aim is to analyze mechanical transmission systems without an appeal to "electrical analogies.")

As a simple illustration, we consider the problem of determining the natural frequencies of the branched system, Fig. 5(*a*). We replace the upper shaft k_1 and mass μ_1 by an equivalent mass μ' as follows: For the quantities $[K_1, M_2, K_2]$ of Fig. 3(*a*), we take $[k_1, \mu_1, 0]$ in Fig. 5(*a*). Equations [5*a*] then give $K_2' = K_3' = 0$, and

$$-\mu'\omega^2 = K_1' = \frac{K_1K_3}{K_1 + K_2 + K_3} = -\frac{k_1\mu_1\omega^2}{k_1 - \mu_1\omega^2}$$

from which

$$\mu' = \frac{k_1\mu_1}{k_1 - \mu_1\omega^2} \qquad [6]$$

In terms of the given numerical values $\mu' = 1/(1 - \omega^2)$.

Similarly, the lower shaft k_2 and mass μ_2 can be replaced by an equivalent mass μ''

$$\mu'' = \frac{k_2\mu_2}{k_2 - \mu_2\omega^2} = \frac{3/2}{3 - \omega^2/2}$$

Thus for the dynamically equivalent system, Fig. 5(*b*)

$$\omega^2 = \frac{k}{\mu + \mu' + \mu''} = \frac{3.5}{2 + 1/(1 - \omega^2) + 1.5/(3 - 0.5\,\omega^2)}$$

Clearing fractions and collecting terms, we get

$$\omega^6 - \frac{43}{4}\,\omega^4 + \frac{91}{4}\,\omega^2 - \frac{21}{2} = (\omega^2 - 2)\left(\omega^4 - \frac{35}{4}\,\omega^2 + \frac{21}{4}\right) = 0$$

from which $\omega = \sqrt{0.648},\ \sqrt{2},\ \sqrt{8.102}$ are obtained as the natural frequencies of the system.

Substitution III is one of the most powerful tools of electrical-circuit analysis. It also plays a fundamental role in shaft-vibration problems. An independent derivation of Equations [5*a*, *b*], using mechanical engineering terminology, seems therefore justified and is given in section 2. The method is applied to the problem of the viscous vibration damper in section 3. Two successive $\Pi - T$ transformations bring the system to a form which then can be treated by Holzer's method. For purposes of comparison Appendix 1 includes an outline of the solution of the same problem by means of the "electrical-analogy" method. This method appears artificial and lengthy compared to the direct approach.

2—THE $\Pi - T$ TRANSFORMATION

We begin with the inverse transformation. The equations of motion of the $[M_1', K_3', M_2']$ system, Fig. 3(*b*), are

$$M_1'\ddot{x}_1' + K_3'(x_1' - x_2') = \mathfrak{F}_1'e^{j\omega t}$$

$$K_3'(x_2' - x_1') + M_2'\ddot{x}_2' = \mathfrak{F}_2'e^{j\omega t} = -F_2'e^{j\omega t}$$

The force applied at point 1′ is denoted by $\mathfrak{F}_1'$. The force delivered at point 2′ is denoted by F_2'; the balancing force, $-F_2'$, is denoted by $\mathfrak{F}_2'$. In the notation of Equations [3*a*, *b*] and [5′], the foregoing equations can be written in the form

$$\left.\begin{aligned}(K_1' + K_3')X_1' - K_3'X_2' &= \mathfrak{F}_1' \\ -K_3'X_1' + (K_2' + K_3')X_2' &= \mathfrak{F}_2'\end{aligned}\right\} \qquad [7]$$

Let the quantities X_1' and $\mathfrak{F}_1'$ at terminal 1′ be given. Then the quantities X_2' and $\mathfrak{F}_2'$ at terminal 2′ are uniquely fixed in terms of X_1', $\mathfrak{F}_1'$ and the parameters K_1', K_2', K_3'.

The equations of motion of the system of Fig. 3(*a*) are

$$\begin{aligned}K_1(x_1 - x_3) &= \mathfrak{F}_1e^{j\omega t} \\ K_1(x_3 - x_1) + M_3\ddot{x}_3 + K_2(x_3 - x_2) &= 0 \\ K_2(x_2 - x_3) &= \mathfrak{F}_2e^{j\omega t}\end{aligned}$$

The motion of the mass M_3 is represented by $x_3(t) = X_3e^{j\omega t}$. We can rewrite these equations in the form

$$\left.\begin{aligned}K_1X_1 - K_1X_3 &= \mathfrak{F}_1 \\ -K_1X_1 + (K_3 + K_1 + K_2)X_3 - K_2X_2 &= 0 \\ -K_2X_3 + K_2X_2 &= \mathfrak{F}_2\end{aligned}\right\} \qquad [8]$$

By assumption $X_1 = X_1'$, $\mathfrak{F}_1 = \mathfrak{F}_1'$. The problem is to find the values K_1, K_2, K_3 which will result in $X_2 = X_2'$, $\mathfrak{F}_2 = \mathfrak{F}_2'$. Instead of fixing $X_1 = X_1'$, $\mathfrak{F}_1 = \mathfrak{F}_1'$, and solving the equations $X_2 = X_2'$, $\mathfrak{F}_2 = \mathfrak{F}_2'$ for K_1, K_2, K_3, we can prescribe more conveniently $\mathfrak{F}_1 = \mathfrak{F}_1'$, $\mathfrak{F}_2 = \mathfrak{F}_2'$, and solve for K_1, K_2, K_3 from $X_1 = X_1'$, $X_2 = X_2'$.

From Equations [7] we obtain

$$\left.\begin{aligned}X_1' &= \frac{K_2' + K_3'}{K'^2}\,\mathfrak{F}_1' + \frac{K_3'}{K'^2}\,\mathfrak{F}_2' \\ X_2' &= \frac{K_3'}{K'^2}\,\mathfrak{F}_1' + \frac{K_1' + K_3'}{K'^2}\,\mathfrak{F}_2'\end{aligned}\right\} \qquad [9]$$

From Equations [8], we obtain

$$\left.\begin{aligned}X_1 &= \left(\frac{1}{K_1} + \frac{1}{K_3}\right)\mathfrak{F}_1 + \frac{1}{K_3}\,\mathfrak{F}_2 \\ X_2 &= \frac{1}{K_3}\,\mathfrak{F}_1 + \left(\frac{1}{K_2} + \frac{1}{K_3}\right)\mathfrak{F}_2\end{aligned}\right\} \qquad [10]$$

The corresponding coefficients in Equations [9] and [10] must be equal. This leads to the relations, *independent* of $\mathfrak{F}_1$ and $\mathfrak{F}_2$

$$\frac{1}{K_3} = \frac{K_3'}{K'^2}, \qquad \frac{1}{K_1} + \frac{1}{K_3} = \frac{K_2' + K_3'}{K'^2}, \qquad \frac{1}{K_2} + \frac{1}{K_3} = \frac{K_1' + K_3'}{K'^2}$$

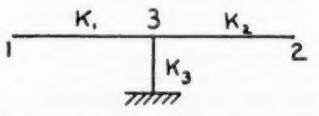


FIG. 6 REPLACEMENT OF MASS M_3 OF FIG. (3*a*) BY A SHEARED SHAFT K_3

These are Equations [5b] in a rearranged form. Equations [5a] are then obtained by solving Equations [5b] for K_1', K_2', K_3'. This completes the proof.

In Fig. 3(a), the motion x_3 of mass M_3 resulted from a force $K_3x_3 = -M_3\omega^2x_3$. In Fig. 6, the motion of the end point 3 of the (sheared) shaft K_3 is due to a force K_3x_3. Equations [5] apply also in this case. In general K_3x_3 stands for the force on any element which performs the absolute motion x_3, and the "stiffness" K_3 is merely an abbreviation for force per unit displacement. Similarly, $K_1(x_3 - x_1)$, in Fig. 3(a), represents the force on any circuit element which performs the relative motion $x_3 - x_1$. Thus, the "stiffness" terms K_i, K_i' of substitution III represent general mechanical impedances.

3—The Viscous Vibration Absorber[6,7]

The spring k_1 and the mass μ_1 constitute the main system. The absorber mass μ_2 is connected to μ_1 by the spring k_2, and by the damping device which consists of the two shafts k_α and k_β, of the two masses μ_α and μ_β, and of the damping fluid of damping constant ρ, see Fig. 7.

The springs k_1, k_2, k_α, k_β have distributed masses m_1, m_2, m_α, m_β. The mass μ_α is the effective plunger mass.[8] It is the sum of μ_α', the actual mass of the plunger, and of μ_α'', the mass of the fluid entrained by the plunger

$$\mu_\alpha = \mu_\alpha' + \mu_\alpha''$$

The mass μ_β is the effective dashpot mass. It is the sum of μ_β', the actual mass of the dashpot, and of μ_β'', the mass of the fluid which moves with the dashpot

$$\mu_\beta = \mu_\beta' + \mu_\beta''$$

The problem is to find the amplitude of motion of mass μ_1 under the action of an applied force $\mathfrak{F}e^{j\omega t}$. The (absolute) displacement of the masses μ_1, μ_2, μ_α, μ_β are denoted by x_1, x_2, x_α, x_β. As usual, $x_i(t) = X_ie^{j\omega t}$.

The problem is solved in two steps. First, the system, shown in Fig. 7, is reduced to that in Fig. 8, where $\mathfrak{K}_1$, $\mathfrak{K}_2$, $\mathfrak{M}_1$, $\mathfrak{M}_2$ denote certain effective spring constants and masses. Second, Holzer's method is applied to the system of Fig. 8, and the response $X_1e^{j\omega t}$ of mass μ_1 to the applied force is calculated.

We shall solve the problem in three successive approximations: (1) We shall assume that the shaft masses $m_1 = m_2 = m_\alpha = m_\beta = 0$, and that $\mu_\alpha = \mu_\beta = 0$, and $k_\alpha = k_\beta = \infty$. This is the usual procedure and is discussed by Den Hartog.[7] (2) We shall assume the correct values k_α, k_β for the damper springs, but leave the shaft masses $= 0$, and $\mu_\alpha = \mu_\beta = 0$, as in the preceding case. (3) We shall take all masses into account in an "appropriate approximation."

For numerical values we select $k_1 = 20$, $k_2 = 1$, $k_\alpha = 2$, $k_\beta = \infty$, $m_1 = 1.20$, $m_2 = 0.12$, $m_\alpha = m_\beta = 0.06$, $\mu_\alpha = \mu_\beta = 0.12$, $\rho = 0.2$, and finally, $\mathfrak{F} = 1$, $\omega = 0.9$.

First Approximation:

$$m_1 = m_2 = m_\alpha = m_\beta = \mu_\alpha = \mu_\beta = 0;\ k_\alpha = k_\beta = \infty$$

Since $k_\alpha = k_\beta = \infty$, the motions x_α and x_β are the same as x_1 and x_2. The damper is acted upon by the force

$$\rho(\dot{x}_\beta - \dot{x}_\alpha) = \rho(\dot{x}_2 - \dot{x}_1) = j\rho\omega(x_2 - x_1)$$

We denote this by $k_\gamma(x_2 - x_1)$. Using substitution I for the combination of springs k_γ and k_2, we obtain the system shown in Fig. 8, where

$$\begin{aligned}\overline{cb} &= \mathfrak{K}_2 = k_2 + k_\gamma = 1 + 0.18j\\ \overline{0a} &= \mathfrak{K}_1 = k_1 = 20\\ \overline{a1} &= \mathfrak{M}_1 = \mu_1 = 20\\ \overline{b2} &= \mathfrak{M}_2 = \mu_2 = 1\end{aligned}$$

The applied force is $\mathfrak{F}$ represented by $\overline{1c}$.

Holzer's method can be applied at once to the system of Fig. 8, as follows: We *assume* that $\mathfrak{M}_1$ vibrates with an amplitude $X_{au} = X_{1u} = 1$. (The subscript u stands for "unadjusted." See the schematic displacement-force diagram, Fig. 9; $P_{au} = [X_{au}, F_{au}]$.) The tension in the spring $\mathfrak{K}_1$ is $F_{au} = \mathfrak{K}_1X_{au} = \mathfrak{K}_1$. The mass $\mathfrak{M}_1$ takes up a force $\mathfrak{M}_1\ddot{x}_1 = -\mathfrak{M}_1\omega^2x_1$ and reduces the acting force from F_{au} at a to $F_{1u} = \mathfrak{K}_1 - \mathfrak{M}_1\omega^2$ at 1. This determines the dashed line $P_{0u}P_{au}P_{1u}$ of the diagram.

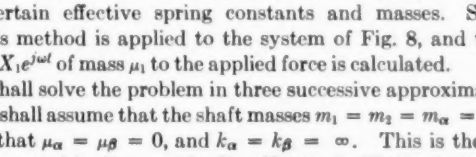


Fig. 7 Viscous Vibration Absorber

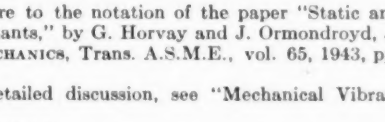


Fig. 8 The System in Fig. 8 Is Equivalent to the System in Fig. 7, by Virtue of Equations [14] and [15]

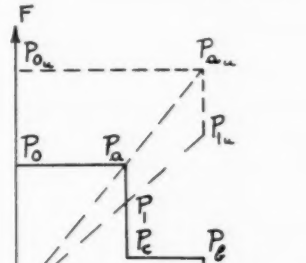


Fig. 9 Illustration of Holzer's Method

Next, we *assume* that $\mathfrak{M}_2$ vibrates with an amplitude $X_2 = X_b = 1$. Since the end 2 of the system is free, no force is acting on it. Thus, the amplitude of the force at point b is

$$F_b = \mathfrak{M}_2\omega^2X_b = \mathfrak{M}_2\omega^2$$

Under the action of this force the spring $\mathfrak{K}_2$ is extended by an amount

$$X_b - X_c = F_b/\mathfrak{K}_2 = \mathfrak{M}_2\omega^2/\mathfrak{K}_2$$

from which

$$X_c = X_b - \mathfrak{M}_2\omega^2/\mathfrak{K}_2 = 1 - \mathfrak{M}_2\omega^2/\mathfrak{K}_2$$

This fixes the full line $P_2P_bP_c$. (In Fig. 9 the complex quantity $X_b - X_c$ is represented by the real line P_cP_b.) But the points P_c and P_1 of Fig. 9 must have the same abscissa; the line P_cP_1 represents the applied force $\mathfrak{F} = F_1 - F_c$ and therefore must be vertical. We make it vertical by reducing the $P_{0u}P_{au}P_{1u}$ portion of the displacement-force diagram in the ratio

[6] We adhere to the notation of the paper "Static and Dynamic Spring Constants," by G. Horvay and J. Ormondroyd, Journal of Applied Mechanics, Trans. A.S.M.E., vol. 65, 1943, pp. A-213 to A-219.

[7] For a detailed discussion, see "Mechanical Vibrations,"[4] pp. 115–129.

[8] See Appendix 2.

$$\frac{X_c}{X_{1s}} = \frac{1 - \mathfrak{M}_2\omega^2/\mathfrak{C}_2}{1}$$

This leads to the adjusted points P_0, P_a, P_1. We now have

$$X_1 = X_c = 1 - \mathfrak{M}_2\omega^2/\mathfrak{C}_2 \quad [11a]$$

and

$$\mathfrak{F} = F_1 - F_c = (\mathfrak{C}_1 - \mathfrak{M}_1\omega^2)X_1 - \mathfrak{M}_2\omega^2 \quad [11b]$$

Since the force $\mathfrak{F}e^{j\omega t}$ causes a displacement of amplitude X_1, the force $1 \times e^{j\omega t}$ causes a displacement of amplitude

$$\overline{X} = X_1/\mathfrak{F} \quad [12]$$

This is the quantity we wish to evaluate.[9]

In our case

$$X_1 = 1 - \frac{1 \times 0.9^2}{1 + 0.18j} = 1 - \frac{0.81(1 - 0.18j)}{1.0324} = 0.2154 + 0.1413j = 0.2576 \angle 33.2 \text{ deg}$$

$$\mathfrak{F} = (20 - 20 \times 0.9^2)(0.2154 + 0.1413j) - 1 \times 0.9^2 = 0.0086 + 0.537j = 0.537 \angle 89.1 \text{ deg}$$

Thus $\overline{X} = X_1/\mathfrak{F} = 0.480 \angle -55.9$ deg. This compares with the static displacement $X_{stat} = 1/k_1 = 0.05$, giving $|\overline{X}/X_{stat}| = 9.60$. The reader will readily identify our example with the system $c/c_c = 0.10$ of Den Hartog, Fig. 79.[7] Mass μ_1 has maximum amplitude at the resonant frequency $\omega = 0.900$.

Second Approximation:

$$m_1 = m_2 = m_\alpha = m_\beta = \mu_\alpha = \mu_\beta = 0;\ k_\alpha = 2,\ k_\beta = \infty$$

Substitution II permits the replacement of shafts k_α, k_γ, k_β by an equivalent shaft

$$k_2' = (k_\alpha^{-1} + k_\gamma^{-1} + k_\beta^{-1})^{-1} = \left(\frac{1}{2} + \frac{1}{0.18j} + 0\right)^{-1} = \frac{0.18j}{1 + 0.09j} = 0.0161 + 0.1786j$$

which in combination with k_2 gives

$$\mathfrak{C}_2 = k_2 + k_2' = 1.0161 + 0.1786j$$

The constants $\mathfrak{C}_1$, $\mathfrak{M}_1$, $\mathfrak{M}_2$ are as in the preceding approximation. We find

$$X_1 = 1 - \frac{0.81}{1.0161 + 0.1786\,j} = 0.2267 + 0.1359\,j = 0.2643 \angle 30.9 \text{ deg}$$

$$\mathfrak{F} = 3.8(0.2267 + 0.1359\,j) - 0.81 = 0.0514 + 0.516\,j = 0.519 \angle 84.3 \text{ deg}$$

and

$$\overline{X} = X_1/\mathfrak{F} = 0.509 \angle -53.4 \text{ deg}$$

In this case, $|\overline{X}/X_{stat}| = 10.19$. The result is close to the previous value, 9.60.

[9] Equation [12] can be obtained more readily by applying a $\Pi - T$ transformation to the $[\mathfrak{C}_2, \mathfrak{M}_2, 0]$ end of the system of Fig. 8. This leads to a one-degree-of-freedom system, consisting of a shaft $\mathfrak{C}_1$, and of an end mass $\mathfrak{M}_1' = \mathfrak{M}_1 + \mathfrak{C}_2\mathfrak{M}_2/(\mathfrak{C}_2 - \mathfrak{M}_2\omega^2)$, cf. Fig. 5. The amplitude of motion of mass $\mathfrak{M}_1'$ (and also of mass $\mathfrak{M}_1$) under the action of a force $1.e^{j\omega t}$ is then given by $\overline{X}_1 = 1/(\mathfrak{C}_1 - \mathfrak{M}_1'\omega^2)$. This is Equation [12]. The vibration problem of any arrangement, involving a sequence of masses and elasticities, can thus be solved by successive $\Pi - T$ transformations, but ordinarily such a process is more laborious than Holzer's method.

Appropriate Approximation. The appropriate approximation consists in replacing a shaft k with distributed inertia m by a weightless shaft of stiffness $K = k + m\omega^2/6$ which carries masses $m/2$ at each end.[6, 10] This leads to the dynamic spring constants

$$K_1 = 20 + 0.2\,\omega^2 = 20.162,\quad K_2 = 1 + 0.02\,\omega^2 = 1.0162,$$

$$K_\alpha = 2 + 0.01\,\omega^2 = 2.0081,\quad K_\beta = \infty$$

The masses μ_1, μ_2, μ_α, μ_β are now replaced by the dynamic masses

$$M_1 = \mu_1 + \frac{1}{2}m_1 + \frac{1}{2}m_2 + \frac{1}{2}m_\alpha = 20 + 0.6 + 0.06 + 0.03 = 20.69,\quad M_2 = \mu_2 + \frac{1}{2}m_2 + \frac{1}{2}m_\beta = 1.09,$$

$$M_\alpha = \mu_\alpha + \frac{1}{2}m_\alpha = 0.15,\quad M_\beta = \mu_\beta + \frac{1}{2}m_\beta = 0.15$$

The mass

$$M_\gamma = -j\rho/\omega = -0.2\,j/0.9 = -0.2222\,j$$

is the effective "damper" mass of the fluid.[8]

We apply a $\Pi - T$ transformation to the partial system of damping fluid $K_\gamma = -M_\gamma\omega^2$, dashpot M_β, and dashpot shaft K_β, which now play the role of $[K_1, M_3, K_2]$ of Fig. 3(*a*). Then we obtain an $[M_1', K_2', M_2']$ system which we denote by the letters M', K', μ'. By Equations [5*a*]

$$-M'\omega^2 = \frac{M_\beta M_\gamma\omega^4}{K_\beta - (M_\beta + M_\gamma)\omega^2},\quad K' = \frac{-K_\beta M_\gamma\omega^2}{K_\beta - (M_\beta + M_\gamma)\omega^2},$$

$$-\mu'\omega^2 = \frac{-K_\beta M_\beta\omega^2}{K_\beta - (M_\beta + M_\gamma)\omega^2} \quad [13]$$

A second $\Pi - T$ transformation, applied to $[K_\alpha, M_\alpha + M', K']$, leads to auxiliary quantities μ_1', K_2', μ'', where

$$-\mu_1'\omega^2 = -\frac{K_\alpha(M_\alpha + M')\omega^2}{K_\alpha + K' - (M_\alpha + M')\omega^2},$$

$$K_2 = \frac{K_\alpha K'}{K_\alpha + K' - (M_\alpha + M')\omega^2},$$

$$-\mu''\omega^2 = -\frac{K'(M_\alpha + M')\omega^2}{K_\alpha + K' - (M_\alpha + M')\omega^2}$$

In view of Equations [13] we can write

$$\mu_1' = K_\alpha(K_\beta M_\alpha - M^2\omega^2)/D \quad [14a]$$

$$K_2' = -K_\alpha K_\beta M_\gamma\omega^2/D \quad [14b]$$

$$\mu'' + \mu' = \mu_2' = K_\beta(K_\alpha M_\beta - M^2\omega^2)/D \quad [14c]$$

where M^2 and D are the abbreviations.

$$M^2 = M_\alpha M_\beta + M_\beta M_\gamma + M_\gamma M_\alpha$$

$$D = K_\alpha K_\beta - K_\alpha(M_\beta + M_\gamma)\omega^2 - K_\beta(M_\alpha + M_\gamma)\omega^2 + M^2\omega^4 \quad [14']$$

The system of Fig. 7 is now reduced to the system of Fig. 10, and the final reduction to Fig. 8 consists in taking

$$\mathfrak{C}_1 = K_1,\ \mathfrak{M}_1 = M_1 + \mu_1',\ \mathfrak{M}_2 = M_2 + \mu_2',\ \mathfrak{C}_2 = K_2 + K_2' \quad [15]$$

The numerical substitutions give

$$M^2 = 0.15^2 - 2 \times 0.15 \times 0.2222\,j = 0.0225 - 0.06667\,j$$

$$D = [K_\alpha - (M_\alpha + M_\gamma)\omega^2]K_\beta = (1.8866 + 0.18\,j)K_\beta$$

[10] "The Appropriate Lumped Constants of Vibrating Shaft Systems," by G. Horvay and J. Ormondroyd, JOURNAL OF APPLIED MECHANICS, Trans. A.S.M.E., vol. 65, 1943, pp. A-220 to A-224.

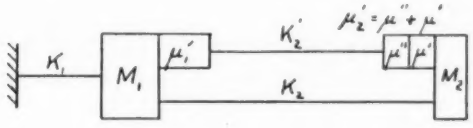


FIG. 10 INTERMEDIATE STEP IN REDUCTION OF SYSTEM OF FIG. 7 TO SYSTEM OF FIG. 8

$$\mathfrak{M}_1 = M_1 + K_\alpha K_\beta M_\alpha/D = 20.69 + \frac{2.0081 \times 0.15\,K_\beta}{(1.8866 + 0.18\,j)K_\beta} =$$

$$20.69 + \frac{0.30121\,(1.8866 - 0.18\,j)}{3.5917} = 20.848 - 0.01510\,j$$

$$\mathfrak{M}_2 = 1.09 + \frac{0.3012 - 0.01822 + 0.054\,j}{1.8866 + 0.18\,j} = 1.2414 + 0.01418\,j$$

$$\mathfrak{K}_2 = 1.0162 + \frac{2.0081 \times 0.18\,j}{1.8866 + 0.18\,j} = 1.0343 + 0.1899\,j, \mathfrak{K}_1 = 20.162$$

The constants of Fig. 8 are now determined, and Equations [11*a*,*b*] apply. We find

$$X_1 = 1 - \mathfrak{M}_2\omega^2/\mathfrak{K}_2 = 0.0576 + 0.1619\,j = 0.1718 \angle 70.4 \text{ deg}$$

$$\mathfrak{F} = (\mathfrak{K}_1 - \mathfrak{M}_1\omega^2)X_1 - \mathfrak{M}_2\omega^2 = -0.819 + 0.519\,j = 0.970 \angle 147.6 \text{ deg}$$

By Equation [12]

$$\overline{X} = X_1/\mathfrak{F} = 0.1771 \angle -77.2 \text{ deg}$$

Finally

$$|X/X_{\text{stat}}| = 3.54$$

This result differs considerably from the two previous approximations and shows the importance of accounting appropriately for all distributed and concentrated masses.

ACKNOWLEDGMENT

The authors are indebted to Commander J. P. Den Hartog, for suggesting the problem. They are also indebted to the referee, Prof. F. M. Lewis, for several improvements, particularly for the shortcut in footnote 9, and for an improved interpretation of the expression for fluid energy, Appendix 2.

Appendix 1

THE "ELECTRICAL-ANALOGY" METHOD

We assign a length $l_1 = L_1$ to shaft k_1 of Fig. 7; a length $l_2 = L_2 - L_1$ to shaft k_2; a length $l_\alpha = L_\alpha - L_1$ to shaft k_α; a length $l_\beta = L_2 - L_\beta$ to shaft k_β. We use $x_l(\xi, t) = X_l(\xi)e^{j\omega t}$ to denote the instantaneous displacement along the lower shaft k_2; we use $x_u(\xi, t) = X_u(\xi)e^{j\omega t}$ to denote the displacement along the upper shafts k_α, k_β. The abscissa ξ is the running co-ordinate. Then the kinetic energy of the system is given by [8,10]

$$T = \frac{1}{2}\mu_1\dot{x}_1^2 + \frac{1}{2}\mu_2\dot{x}_2^2 + \frac{1}{2}\mu_\alpha\dot{x}_\alpha^2 + \frac{1}{2}\mu_\beta\dot{x}_\beta^2 - \frac{1}{2}\frac{j\rho}{\omega}(\dot{x}_\beta - \dot{x}_\alpha)^2 + \frac{1}{2}\frac{m_1}{l_1}\int_0^{L_1}\dot{x}^2d\xi + \frac{1}{2}\frac{m_2}{l_2}\int_{L_1}^{L_2}\dot{x}_l^2d\xi + \frac{1}{2}\frac{m_\alpha}{l_\alpha}\int_{L_1}^{L_\alpha}\dot{x}_u^2d\xi + \frac{1}{2}\frac{m_\beta}{l_\beta}\int_{L_\beta}^{L_2}\dot{x}_u^2d\xi \quad [16a]$$

and the potential energy is given by

$$V = \frac{1}{2}k_1l_1\int_0^{L_1}x'^2d\xi + \frac{1}{2}k_2l_2\int_{L_1}^{L_2}x_l'^2d\xi + \frac{1}{2}k_\alpha l_\alpha\int_{L_1}^{L_\alpha}x_u'^2d\xi + \frac{1}{2}k_\beta l_\beta\int_{L_\beta}^{L_2}x_u'^2d\xi \quad [16b]$$

Assuming a linear variation for $X(\xi)$, the energy expressions become[10]

$$T = \frac{1}{2}\mu_1\dot{x}_1^2 + \frac{1}{2}\mu_2\dot{x}_2^2 + \frac{1}{2}\mu_\alpha\dot{x}_\alpha^2 + \frac{1}{2}\mu_\beta\dot{x}_\beta^2 - \frac{1}{2}\frac{j\rho}{\omega}\cdot(\dot{x}_\beta - \dot{x}_\alpha)^2 + \frac{1}{6}m_1\dot{x}_1^2 + \frac{1}{6}m_2(\dot{x}_1^2 + \dot{x}_1\dot{x}_2 + \dot{x}_2^2) + \frac{1}{6}m_\alpha(\dot{x}_1^2 + \dot{x}_1\dot{x}_\alpha + \dot{x}_\alpha^2) + \frac{1}{6}m_\beta(\dot{x}_2^2 + \dot{x}_2\dot{x}_\beta + \dot{x}_\beta^2) \quad [17a]$$

$$V = \frac{1}{2}k_1x_1^2 + \frac{1}{2}k_2(x_2 - x_1)^2 + \frac{1}{2}k_\alpha(x_\alpha - x_1)^2 + \frac{1}{2}k_\beta(x_2 - x_\beta)^2 \quad [17b]$$

We form the Lagrangian equations of motion

$$\frac{d}{dt}\frac{\partial T}{\partial \dot{x}_i} + \frac{\partial V}{\partial x_i} = \mathfrak{F}_ie^{j\omega t} \quad [18]$$

associated with the approximate energy expressions [17], and obtain

$$\left.\begin{aligned} x_1&: M_1\ddot{x}_1 + K_1x_1 + K_2(x_1 - x_2) + K_\alpha(x_1 - x_\alpha) = \mathfrak{F}e^{j\omega t}\\ x_2&: M_2\ddot{x}_2 + K_2(x_2 - x_1) + K_\beta(x_2 - x_\beta) = 0\\ x_\alpha&: M_\alpha\ddot{x}_\alpha + M_\gamma(\ddot{x}_\alpha - \ddot{x}_\beta) + K_\alpha(x_\alpha - x_1) = 0\\ x_\beta&: M_\beta\ddot{x}_\beta + M_\gamma(\ddot{x}_\beta - \ddot{x}_\alpha) + K_\beta(x_\beta - x_2) = 0 \end{aligned}\right\} \quad [19]$$

We used the abbreviations

$$M_1 = \mu_1 + \frac{1}{2}(m_1 + m_2 + m_\alpha), \qquad M_2 = \mu_2 + \frac{1}{2}(m_2 + m_\beta),$$

$$M_\alpha = \mu_\alpha + \frac{1}{2}m_\alpha, \qquad M_\beta = \mu_\beta + \frac{1}{2}m_\beta, \qquad M_\gamma = -j\rho/\omega,$$

$$K_1 = k_1 + \frac{1}{6}m_1\omega^2, \qquad K_2 = k_2 + \frac{1}{6}m_2\omega^2,$$

$$K_\alpha = k_\alpha + \frac{1}{6}m_\alpha\omega^2, \qquad K_\beta = k_\beta + \frac{1}{6}m_\beta\omega^2$$

Equations [19] are recognized as the equations of charge displacement in the loops (1), (2), (α), (β), of Fig. 11, where K_i denotes reciprocal capacities, M_i denotes inductances.

Two successive $\Pi - T$ transformations, applied to the α, β loops, reduce Fig. 11 to Fig. 12, which corresponds to Fig. 10 of the mechanical system. Finally, the combinations $\mathfrak{K}_2 = K_2 + K_2'$, $\mathfrak{M}_1 = M_1 + \mu_1'$, $\mathfrak{M}_2 = M_2 + \mu_2'$ reduce Fig. 12 to an electrical system equivalent to Fig. 8. Whereas in the "electrical-analogy" method the calculations are carried out in connection with the electrical system, and the results are retranslated into mechanical engineering terminology, the direct method of section 3 eliminates all intermediate steps.

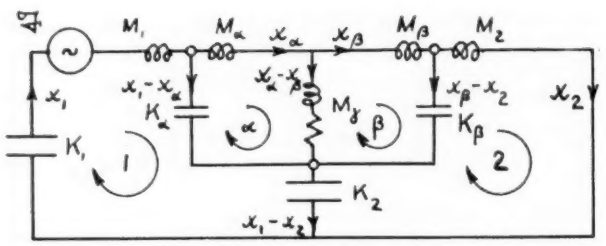


FIG. 11 ELECTRICAL ANALOGUE OF SYSTEM IN FIG. 7

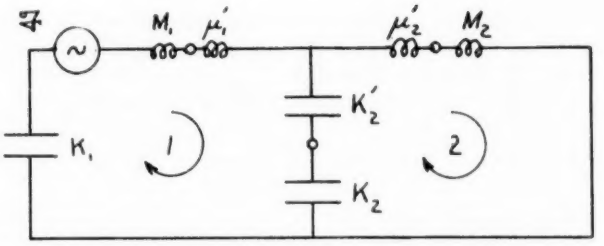


FIG. 12 ELECTRICAL ANALOGUE OF SYSTEM IN FIG. 10

Appendix 2

THE ENERGY EXPRESSION OF THE FLUID

Since some fluid particles move with the velocity $\dot{x}_\alpha$ of the plunger, others with the velocity $\dot{x}_\beta$ of the dashpot, the kinetic energy of the fluid is to a good approximation a quadratic form in $\dot{x}_\alpha$ and $\dot{x}_\beta$

$$T_{fl} = \alpha\dot{x}_\alpha^2 + \beta\dot{x}_\beta^2 + \gamma\dot{x}_\alpha\dot{x}_\beta$$

A more convenient way of writing this is[11]

$$T_{fl} = \mu_\alpha''\dot{x}_\alpha^2/2 + \mu_\beta''\dot{x}_\beta^2/2 + M_\gamma(\dot{x}_\beta - \dot{x}_\alpha)^2/2$$

Here μ_α'' denotes the mass of the fluid which moves with the plunger. We incorporate it into μ_α, the effective plunger mass. The mass μ_β'' moves with the dashpot. We incorporate it into μ_β, the effective dashpot mass. The mass $M_\gamma = \mu_\gamma - j\rho/\omega$ is the effective "damper" mass of the fluid. Whereas the μ_α'' and μ_β'' energy terms change periodically into potential energy, the M_γ term, which depends upon the relative motion of plunger and dashpot, converts almost immediately into heat. Thus the nondissipative term $\mu_\gamma(\dot{x}_\beta - \dot{x}_\alpha)^2/2$ can be considered as negligibly small, and $\mu_\gamma = 0$ can be used. This we did throughout the text.

[11] The corresponding expressions for shaft k_2 (see Equation [17a]) are

$$T_{\text{shaft}_2} = \frac{1}{6}\, m_2(\dot{x}_1^2 + \dot{x}_2^2 + \dot{x}_1\dot{x}_2)$$

$$= \frac{1}{2}\left[\frac{1}{2}\, m_2\dot{x}_1^2 + \frac{1}{2}\, m_2\dot{x}_2^2 - \frac{1}{6}\; m_2\,(\dot{x}_2 - \dot{x}_1)^2\right]$$

The term $\frac{1}{6}\, m_2\omega^2\,(x_2 - x_1)^2$ manifests itself in an increase in the stiffness of the shaft.

Design Data

It is important that the data contained in technical papers be made readily available to designing engineers. In order to satisfy these needs of industry, this section of the Journal includes a concise presentation of data and information drawn chiefly from papers previously published by the Applied Mechanics Division of The American Society of Mechanical Engineers.

The data have been prepared by a subcommittee of the Applied Mechanics Division—S. Timoshenko, R. E. Peterson, J. Ormondroyd, J. N. Goodier, and J. M. Lessells.

Balancing of Rotating Apparatus—II*

By R. P. KROON,[7] PHILADELPHIA, PA.

Shop Balance Methods

IT is customary to balance rotors at relatively low speed in balancing machines in the shop. These detect the unbalances by the vibration produced in the balancing machine. Fig. 16 shows the principles of such a machine. The bearings are supported on thin strips g, flexible in the lateral direction. The vibration can be measured at A and B by dial indicators or by other instruments.

Balancing in its most primitive form, popular in shops where it is not a mass-production operation, consists in principle of the following:

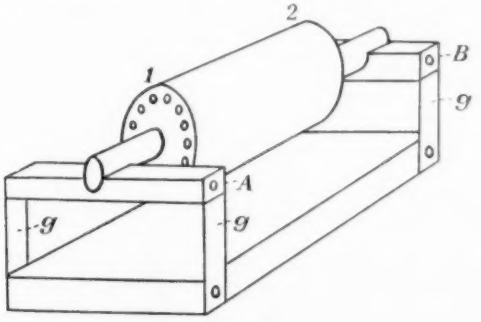


Fig. 16

One bearing, say B, is locked so that it cannot move laterally and the rotor is brought up through the critical speed (of the rotor on the flexible bearing A). The rotor can be speeded up by an air jet or by a motor-driven belt passing over the rotor. While coasting down through the critical speed, the horizontal motion at A is measured. Corrections are now made (usually by cut-and-try methods) in plane 1 until this amplitude is reduced to zero. This can be facilitated by holding a pencil against the rotor, scribing the high spot.

Now the other bearing is locked and the motion at B is reduced to zero by placing corrective weight in plane 2.

Some machines are built with a frame which allows the locking of a fulcrum exactly in the balance plane (say, 2). Then the corrective weight put in plane 1 is indeed final. Where this is not the case one can scuttle back and forth, locking first one bearing, then the other, then going back to the first, etc., until a satisfactory balance is obtained; which can be checked by running with both bearings unlocked, or the correct weight can be immediately determined by means of the following consideration:

Let the original unbalance be such that it can be represented by a weight W_I in plane 1 and another weight W_{II} in plane 2, Fig. 17 (*a*). Now when bearing B is locked, the correction weight w_1, in plane 1, which reduces the motion at A to zero can

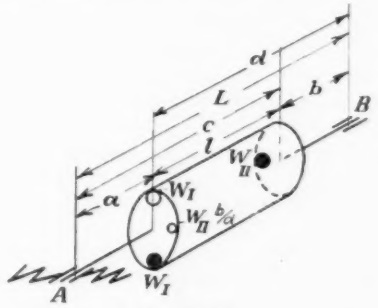


Fig. 17 (*a*)
(Bearing B locked; motion at A reduced to zero.)

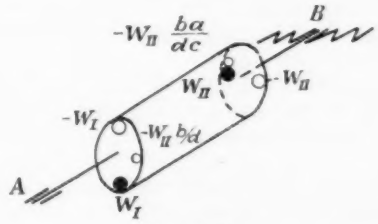


Fig. 17 (*b*)
(Bearing A locked; motion at B reduced to zero.)

be thought of as consisting of two parts. One component ($-W_I$) corrects the unbalance W_I in plane 1. The second part ($-W_{II}\,b/d$) is necessary to offset the moment about B caused by W_{II}. Now when bearing A is locked (with w_1 left in place) and bearing B is left free to float, the weight w_2, in plane 2, which cuts down all vibration of B, must compensate not only for W_{II}, but also for the moment from the portion $-W_{II}\,b/d$ of weight w_1, Fig.

* Part I of this paper was published in the Journal of Applied Mechanics, Trans. A.S.M.E., vol. 65, December, 1943, p. A-225.

[7] Manager, Development Division, South Philadelphia Works, Westinghouse Electric & Manufacturing Co. Mem. A.S.M.E.

Discussion of this paper should be addressed to the Secretary, A.S.M.E., 29 West 39th Street, New York, N. Y., and will be accepted until April 10, 1944. Discussion received after the closing date will be returned.

17 (*b*). Therefore, weight w_2 can again be resolved into two components, one weight $-W_{II}$ and another, $W_{II}\frac{ba}{dc}$ diametrically opposite.

Since
$$w_2 = -W_{II} + W_{II}\frac{ba}{dc}$$

$$W_{II} = \frac{-w_2}{1 - \frac{ab}{cd}} = -w_2\frac{cd}{lL}$$

Therefore, after the location and amount of w_2 in plane 2 has been found with bearing A locked, the amount is increased in the ratio cd/lL. Then, in plane 1, one adds a weight $-W_{II}\frac{b}{d} = w_2\frac{bc}{lL}$ exactly on the opposite side of the rotor. These weights and w_1 which was left in the rotor, will provide complete balance.

More Elaborate Shop Balancing; Field Balancing

The more efficient shop-balancing methods (in which both bearings are left unlocked) and the procedures used in field balancing are not fundamentally different. Shop balancing is simpler in so far as the vibratory system can be so designed that the angle of lag is known ($\varphi = 90$ deg for operation at resonance of the rotor on its flexible supports, $\varphi = 180$ deg for operating far above resonance, now preferred, because of greater independence of variations in speed and damping). There exist a great many methods relying either on using amplitudes alone, or phase angles and amplitudes on one side at a time, etc., but the most efficient methods use as much information as can be gathered during a run; i.e., both amplitude and phase measured in as many places as is necessary. This presupposes that instruments are available to measure both amplitude and phase accurately.

The term "angle of lag" (sometimes called "phase angle") has so far been used to designate the angle φ between the direction of the eccentricity and the direction of the center of gravity S, Fig. 5. While balancing, the position of S is unknown. The phase angle ϕ is measured between the high spot T and an arbitrary reference point R on the shaft, Fig. 18.

The high spot T may be the physical point on the shaft touched by a marking pencil. But generally, and this applies to shaft as well as to bearing vibration, the high spot T can be defined as the point on the rotor which passes some arbitrary reference mark C when the vibratory motion reaches its maximum positive value. The phase angle ϕ is the angle between the high spot T and a given reference point R on the rotor.

It is customary always to show the diagram, Fig. 18, with the reference point R (say, No. 1 balance hole) on top and to draw the arrow OA to represent the amplitude to a certain scale, Fig. 19.

The vibration of a two-bearing unit, Fig. 20, which we shall suppose vibrates in one direction only (say, vertically) can thus be represented by two of these vector diagrams, one for bearing A and one for B. Notice that the direction of rotation is the same in both diagrams. Here A_0 and B_0 are the amplitudes measured at A and B, and ϕ_A and ϕ_B are phase angles between the vibration and a common reference point R.

Weights should be applied in the balance planes 1 and 2 in such a fashion as to eliminate the vibration of both bearings. A trial weight w_1 is now put in plane 1. This affects the vibration. For example, the vibration at bearing A has now changed from A_0 to A_{01}, Fig. 21; there is a different amplitude and a different

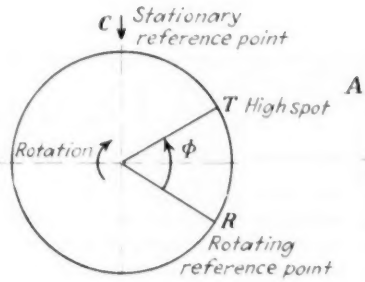


Fig. 18

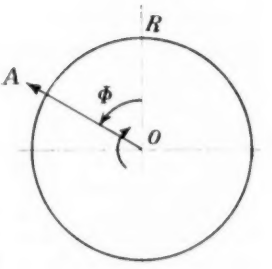


Fig. 19

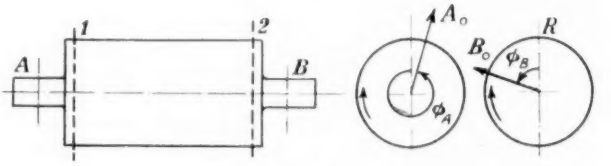


Fig. 20

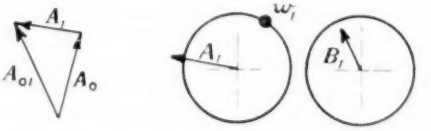


Fig. 21

Fig. 22

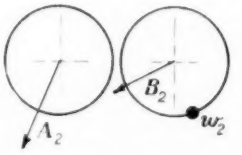


Fig. 23

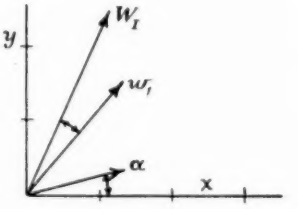


Fig. 24

high spot. The difference in vibration is expressed vectorially by A_1.

Thus Fig. 22 may represent the changes in vibration (the increment) caused by the trial weight w_1. A trial weight w_2 in the other balance plane 2 again produces changes in vibration, shown in Fig. 23. The original vibration measurements and the two trial runs yield all the necessary information to find the amount and location of the final balance weights.

A speedy solution (6, 7)[8] hinges around a convenient method to describe the vibration from any balance weight. The theory of complex numbers has provided an operation which does just this thing; namely, if the vector w_1 (Fig. 24) represents the weight w_1, both in magnitude and direction (location), multiplication with another vector α gives, by definition, another vector having a magnitude equal to the product of the magnitudes of w_1 and α and enclosing an angle with the x axis equal to the sum of the angles between the x axis and w_1 and α, respectively. Therefore, varying α both in magnitude and direction, any unbalance weight $W_1 = \alpha w_1$ in plane 1 can be described.

In all analytical balance methods, a linear system is assumed. The vibration due to a weight in a certain plane is taken to be proportional to the amount of weight. The phase angle between weight and vibration is assumed to stay constant.

[8] Numbers in parentheses refer to the Bibliography, at the end of this section of the design data.



FIG. 25

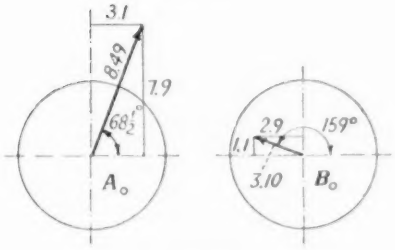


FIG. 26

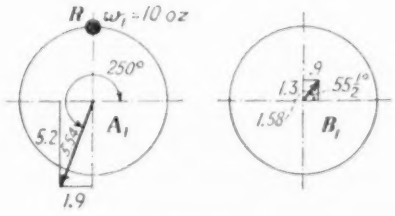


FIG. 27

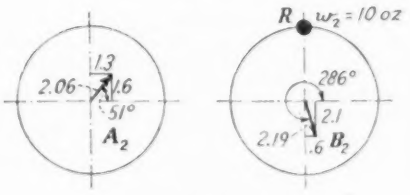


FIG. 28

Then the vibratory effect of W_I in plane 1 can be obtained by multiplying the vectors A_1 and B_1 (due to the trial weight w_1) with the vector α (Fig. 25).

Similarly, the vibration produced by weight $W_{II} = \beta w_2$ will be βA_2 in plane A and βB_2 in plane B.

Let W_I and W_{II} now be defined as those weights which together, on an initially balanced rotor, would produce the vibrations A_0 and B_0; then

$$\left.\begin{aligned} \alpha A_1 + \beta A_2 &= A_0 \\ \alpha B_1 + \beta B_2 &= B_0 \end{aligned}\right\} \quad \ldots\ldots\ldots\ldots\ldots [11]$$

Note that all symbols in the equations represent complex numbers. The solutions

$$\left.\begin{aligned} \alpha = \frac{W_I}{w_1} &= \frac{A_0B_2 - A_2B_0}{A_1B_2 - A_2B_1} \\ \beta = \frac{W_{II}}{w_2} &= \frac{A_1B_0 - A_0B_1}{A_1B_2 - A_2B_1} \end{aligned}\right\} \quad \ldots\ldots\ldots\ldots [12]$$

determine the weights W_I and W_{II} in terms of the trial weights w_1 and w_2. The corrections to be made are $-W_I$ in plane 1 and $-W_{II}$ in plane 2.

Equations [12] can be solved either graphically or analytically by means of the complex number notation $a + bj$ for any of the vectors.

To illustrate the vector algebra method, a simple example is treated here. The initial conditions are shown in Fig. 26. They might be written as follows:

$$A_0 = 3.1 + 7.9\,j$$

$$B_0 = -2.9 + 1.1\,j$$

A trial weight of 10 oz is inserted at balance hole 1, point R, in balance plane 1. Its effect (the vectorial change in vibration it produces) is shown in Fig. 27.

The same unbalance weight, removed and inserted at R in balance plane 2, produces the changes given in Fig. 28.

Applying Equation [12]

$$\alpha = \frac{W_I}{w_1}$$

$$= \frac{(3.1 + 7.9j)\,(0.6 - 2.1\,j) - (1.3 + 1.6\,j)\,(-2.9 + 1.1\,j)}{(-1.9 - 5.2\,j)\,(0.6 - 2.1\,j) - (1.3 + 1.6\,j)\,(0.9 + 1.3\,j)}$$

$$= \frac{23.96 + 1.44\,j}{-11.15 - 2.26\,j}$$

$$\beta = \frac{(-1.9 - 5.2\,j)\,(-2.9 + 1.1\,j) - (3.1 + 7.9\,j)\,(0.9 + 1.3\,j)}{(-1.9 - 5.2\,j)\,(0.6 - 2.1\,j) - (1.3 + 1.6\,j)\,(0.9 + 1.3\,j)}$$

$$= \frac{18.71 + 1.85\,j}{-11.15 - 2.26\,j}$$

Carrying out the division

$$\alpha = -2.09 + 0.295\,j, \qquad \beta = -1.64 + 0.167\,j$$

The 10-oz trial weight at point R can be described by

$$w_1 = w_2 = 10\,j$$

Then

$$W_I = \alpha\, w_1 = -2.95 - 20.9\,j$$

$$W_{II} = \beta\, w_2 = -1.67 - 16.4\,j$$

and the corrective weights are $-W_I = 2.95 + 20.9\,j$ in plane 1, and $-W_{II} = 1.67 + 16.4\,j$ in plane 2.

The amount of $-W_I$ is $\sqrt{2.95^2 + 20.9^2} = 21.1$ oz. This corrective weight should be put at an angle arc $tg \frac{20.9}{2.95} = 82$ deg from the positive horizontal axis, that is, 8 deg clockwise from R. The size of weight $-W_{II}$ is $\sqrt{1.67^2 + 16.4^2} = 16.5$ oz, and it should be located at an angle of arc $tg \frac{16.4}{1.67} = 84$ deg from the real positive axis, or 6 deg to the right of R.

Another way of finding the corrective weight for the same example is shown in Fig. 29. Here are plotted the vector products A_0B_2, A_2B_0, A_1B_0, A_0B_1, A_1B_2, A_2B_1. With A_0 being 8.49 units long and enclosing an angle of $68\frac{1}{2}$ deg with the positive horizontal axis; B_1 being a vector 1.58 units making an angle $55\frac{1}{2}$ deg with the horizontal axis; A_0B_1 is a vector $8.49 \times 1.58 = 13.40$ units long at an angle $68\frac{1}{2}$ deg + $55\frac{1}{2}$ deg = 124 deg with the horizontal.

The vector subtractions $A_1B_0 - A_0B_1$, etc., are done graphically.

The values α, β in Equations [12] are determined arithmetically. When $A_1B_0 - A_0B_1$ is found to be 18.8 units long at an angle of $5\frac{1}{2}$ deg and $A_1B_2 - A_2B_1$ comes out 11.4 units long, with an angle of $191\frac{1}{2}$ deg, β is $\frac{18.8}{11.4} = 1.65$ and includes an angle $365\frac{1}{2} - 191\frac{1}{2} = 174$ deg with the positive x axis. Thus $-W_{II}$ is

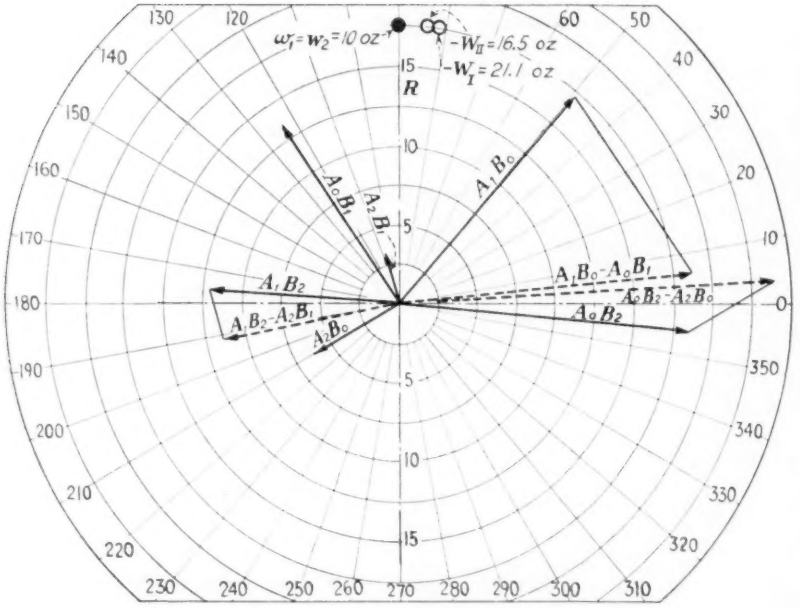


FIG. 29

$1.65 \times 10 = 16.5$ oz, it should be put at an angle (174 deg + 90 deg) —180 deg = 84 deg away from the positive axis (6 deg from R).

Trial-and-Error Solution. The analytical method just described can be applied to units with more than two bearings. However, in such cases it is usually more convenient to find the corrective weights by trial and error rather than by solving complicated determinants. This is done by manipulating the vectors from the trial weights, changing both amount and location of the weights and noticing their combined effect on the initial vibration.

General Discussion of Field Balancing

Because of the complexity of the vibratory systems on large machines, several points require special consideration.

Nonlinearity. Many machines are found to be nonlinear, that is, the vectorial changes produced by a certain amount of weight, vary. On rough-running units, correction weights made up according to Equations [12] may not altogether eliminate the vibration. One can then make a second approximation, using the old effects (A_1, B_1, A_2, B_2) on the new "initial condition." In cases of bad nonlinearity, it may be necessary to find new effects after reasonably smooth running has been obtained.

Operating Conditions. Machines operating under widely varying conditions may show a variation in vibration. To insure that this variation does not result in false readings for the effects of the trial weights, runs must be made under the same operating conditions and after making sure that steady conditions prevail.

New Balance Planes. In balancing flexible shafts such as long generator rotors (8), the balance planes can be so situated that no satisfactory balance can be obtained. For example, a balance weight in the center of the shaft (the node) of Fig. 12, would have to be infinite to counteract an unbalance in any other place.

A different but equally unsatisfactory condition exists when the denominator $A_1B_2 - A_2B_1$ equals zero. This again would require infinite weights according to Equation [12]. In this condition $\frac{A_1}{B_1} = \frac{A_2}{B_2}$; in other words, no matter whether we put the corrective weight in plane 1 or in plane 2, the change in vibration at bearing A always bears a certain relation to that at B, and it is impossible to neutralize any arbitrary initial vibration at A and B. In such cases the selection of a new balance plane is indicated.

On machines such as turbogenerators, it is customary to take vibration measurements in three directions (vertical, lateral, and axial) on all bearings and at whatever other locations (shaft, bedplate, columns, floors, etc.) as are of interest. It can happen that the corrective weight decreases all these vibrations simultaneously. But it also can happen on complicated dynamic systems where moments as well as forces on the bearings may be important that one can eliminate, say, the vertical vibration only by making the horizontal vibration worse. In the latter cases there are two choices; (*a*) to achieve a compromise, (*b*) to select additional balance planes.

Local Resonance. Occasionally local resonances can exist (of floor plates, columns, etc.). To eliminate vibration at such points may require such smooth running as would be impossible or impractical to maintain. When this is the case, one should detune the part in question by changing its mass or its rigidity (3).

Vibration Spells. Where variable vibration of running frequency occurs, the balancing operation can be expected only to eliminate a certain average "steady component." Where the variation is pronounced, the only remedy lies in abolishing the cause of the variation (9, 10). For permissible amplitudes refer to a paper by Rathbone (12).

BIBLIOGRAPHY

1 "Theory of Sound," by Lord Rayleigh, Macmillan & Company, London, England. See 1894 edition, reprinted 1926.

2 "Steam and Gas Turbines," by A. Stodola and L. C. Loewenstein, McGraw-Hill Book Company, Inc., New York, N. Y., vol. 1, 1927, pp. 416–430.

3 "Turbine Vibration and Balancing," by Thomas C. Rathbone, Trans. A.S.M.E., vol. 51, part 1, 1929, paper APM-51-23.

4 "Vibration Problems in Engineering," by S. Timoshenko, D. Van Nostrand Company, Inc., New York, N. Y., Third printing, 1935, pp. 38–52.

5 "Mechanical Vibrations," by J. P. Den Hartog, McGraw-Hill Book Company, Inc., New York, N. Y., first edition, 1934, p. 237.

6 "Dynamic Balancing of Rotating Machinery in the Field," by E. L. Thearle, Trans. A.S.M.E., vol. 56, 1934, paper APM-56-19.

7 "Balancing Rotors by Means of Electrical Networks," by J. G. Baker and F. C. Rushing, *Journal of The Franklin Institute*, vol. 222, no. 2, 1936, pp. 183–190.

8 "Balancing Rotating Machines in the Field," by F. C. Rushing and B. A. Rose, *Electric Journal*, vol. 34, 1937, pp. 441–444.

9 "Methods of Rotor Unbalance Determination," by J. G. Baker, JOURNAL OF APPLIED MECHANICS, Trans. A.S.M.E., vol. 61, 1939, p. A-145.

10 "Spiral Vibration of Rotating Machinery," by R. P. Kroon and W. A. Williams, Proceedings of the Fifth International Congress for Applied Mechanics, John Wiley & Sons, Inc., New York, N. Y., 1938.

11 "Erratic Vibration," by R. P. Kroon, *Power*, vol. 84, April, 1940, p. 66.

12 "Vibration Tolerances," by Thomas C. Rathbone, *Power Plant Engineering*, vol. 42, 1939, p. 721.

Circular Beams Loaded Normal to the Plane of Curvature—2

By MERVIN B. HOGAN,[1] SALT LAKE CITY, UTAH

Expressions are presented in this paper for the deflection, angle of slope, and angle of twist of the free end of a circular cantilever beam with a bending moment applied at the free end. Like expressions are also given for the same beam with a twisting moment acting at the free end. The values of the reaction and the angles of slope and twist at the simple support are given for a circular beam built in at one end, simply supported at the other, and loaded as in each of the foregoing cases. Also, equations are included for the three internal reactions, i.e., bending moment, twisting moment, and shear existing at the plane of symmetry of a cantilever arc beam, built in at both ends, with an arbitrarily placed concentrated load acting perpendicular to the plane of the beam, and at its center line. Corresponding expressions for the same element with a uniformly distributed load covering the half of the beam to one side of the axis of symmetry, and an expression for the bending moment at the plane of symmetry of the same beam when its entire length is uniformly loaded, are also stated.

Introduction

THIS paper is supplementary to a previous one by the author.[2] The curves here presented are for the same three cross sections, with steel as the chosen material, as those used in that paper. The nomenclature is the same except for the two additional items j and k. These two ratios are clearly

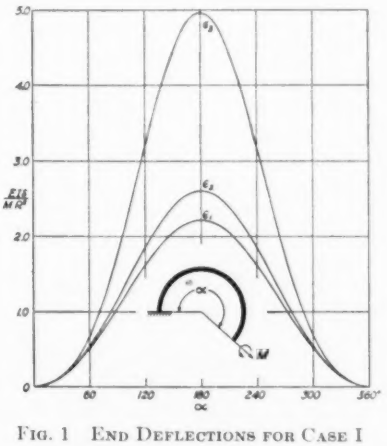


FIG. 1 END DEFLECTIONS FOR CASE I

defined in Fig. 5. The same method of derivation was employed as in the former case, and the same remarks concerning the use of the principle of superposition are applicable here.

All the expressions for the different beams and loadings are given in Table 1.

[1] Professor of Mechanical Engineering, University of Utah. Mem. A.S.M.E.

[2] "Circular Beams Loaded Normal to the Plane of Curvature," by Mervin B. Hogan, JOURNAL OF APPLIED MECHANICS, Trans. A.S.M.E., vol. 60, 1938, p. A-81.

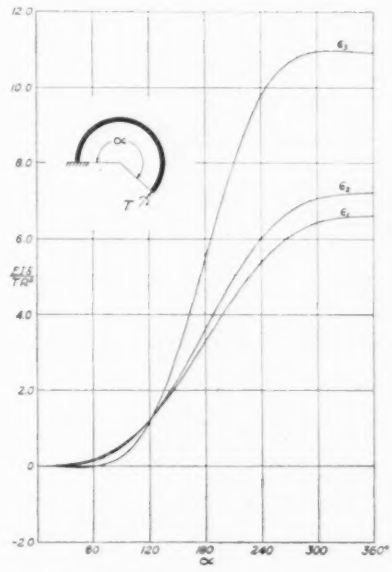


FIG. 2 END DEFLECTIONS FOR CASE II

TABLE 1 EXPRESSIONS FOR THE VARIOUS BEAMS AND LOADINGS

Case I	$\delta_1 = \frac{MR^2}{EI}\left[\frac{(1-\epsilon)}{2}(1+\cos\alpha)+\epsilon\right](1-\cos\alpha)$ $\theta_1 = \frac{MR}{EI}\left[\frac{(1+\epsilon)}{2}(\alpha+\sin\alpha\cos\alpha)-\epsilon\sin\alpha\cos\alpha\right]$ $\beta_1 = \frac{MR}{EI}\left[\frac{(1-\epsilon)}{2}\sin^2\alpha\right]$
Case II	$\delta_2 = \frac{TR^2}{EI}\left[\frac{(1+\epsilon)}{2}(\alpha-\sin\alpha\cos\alpha)-\epsilon\sin\alpha(1-\cos\alpha)\right]$ $\theta_2 = \frac{TR}{EI}\left[\frac{(1-\epsilon)}{2}\sin^2\alpha\right]$ $\beta_2 = \frac{TR}{EI}\left[\frac{(1+\epsilon)}{2}(\alpha-\sin\alpha\cos\alpha)+\epsilon\sin\alpha\cos\alpha\right]$
Case III	$F_3 = \frac{EI}{R^3D_1}\frac{k}{j}$; $\delta_3 = \delta_1 - \frac{F_3R^3}{EI}N_1$; $\beta_3 = \beta_1 - \frac{F_3R^2}{EI}N_1$ — WHERE: $D_1 = \frac{(1+3\epsilon)}{2}(\alpha-\sin\alpha\cos\alpha)-2\epsilon\sin\alpha(1-\cos\alpha)$
Case IV	$F_4 = \frac{EI}{R^3D_1}\frac{k}{j}$; $\theta_4 = \theta_2 - \frac{F_4R^2}{EI}N_1$; $\beta_4 = \beta_2 - \frac{F_4R^2}{EI}N_1$ — $N_1 = \left[(1+\epsilon+(1-\epsilon)\cos\alpha)\frac{(1-\cos\alpha)}{2}\right]$; $N_2 = \left(\frac{1+\epsilon}{2}\right)(\alpha-\sin\alpha\cos\alpha)-\epsilon\sin\alpha(1-\cos\alpha)$
Case Va	$M_5 = \frac{PR}{2}\left[\frac{(1+\epsilon)\{\sin\alpha\sin(\alpha-\Sigma)-(\alpha-\Sigma)\sin\Sigma\}-2\epsilon\{\sin\alpha\sin(\alpha-\Sigma)+\cos\alpha-\cos\Sigma\}+2K\{\frac{k}{2}\cos\alpha+(1-\epsilon)\cos\alpha\sin(\alpha-\Sigma)+\epsilon(\sin\alpha-\sin\Sigma)\}}{(1+\epsilon)(\alpha+\sin\alpha\cos\alpha)-2\epsilon\sin\alpha\cos\alpha+2K\{(1-\epsilon)\sin^2\alpha+\epsilon\}}\right]$ $T_5 = \frac{PR}{2}\left[\frac{AF-BE}{AC-BD}\right]$; $V_5 = \frac{P}{2}\left[\frac{CE-DF}{AC-BD}\right]$ — WHERE: $A = K^2\left\{\frac{3\sin\alpha}{2}+\frac{k^2}{8}\right\}+\epsilon\{\alpha\cos\alpha+K(1-\cos\alpha)\}$; $B = \frac{(1+\epsilon)}{2}(\alpha-\sin\alpha\cos\alpha)-\epsilon\sin\alpha(1-\cos\alpha)+K\{(1-\epsilon)\sin^2\alpha+\epsilon(1-\cos\alpha)\}+\frac{k^2}{2}\sin\alpha$; $C = \frac{(1+\epsilon)}{2}(\alpha-\sin\alpha\cos\alpha)+\epsilon\sin\alpha\cos\alpha+K\{(1-\epsilon)\sin^2\alpha+\epsilon\}$; $D = \frac{k^2}{2}\sin\alpha-\epsilon(\sin\alpha+K\cos\alpha)$; $E = K^2\left\{\frac{3\sin(\alpha-\Sigma)}{2}+\frac{k^2}{8}\right\}+\epsilon\{\alpha-\Sigma-\sin\alpha(\alpha-\Sigma)+K\{1-\cos\alpha(\alpha-\Sigma)\}\}$; $F = \frac{(1+\epsilon)}{2}\{\alpha-\Sigma\}\cos\Sigma-\sin\alpha\cos\{\alpha-\Sigma+\sin\Sigma\}-\epsilon\sin\alpha\{1-\cos(\alpha-\Sigma)\}+K\{(1-\epsilon)\sin\alpha\sin(\alpha-\Sigma)+\epsilon\{\sin\Sigma-\cos\alpha\}+\frac{k^2}{2}\sin\alpha$
Case Vb	$M_6 = \frac{PR}{2\Sigma_6}K^2(1-j)^2\cos\alpha$; $T_6 = \frac{PR}{4}K^2(1-j)^2\left[\frac{A\sin\alpha-B\frac{k^2}{8}(2+j)}{AC-BD}\right]$; $V_6 = \frac{P}{4}K^2(1-j)^2\left[\frac{C\frac{k^2}{8}(2+j)-D\sin\alpha}{AC-BD}\right]$ — WHERE: $\Sigma_6 = (1+\epsilon)(\alpha+\sin\alpha\cos\alpha)-2\epsilon\sin\alpha\cos\alpha+2K\{(1-\epsilon)\cos^2\alpha+\epsilon\}$; SYMBOLS SAME AS ABOVE
Case VI	$M_7 = \frac{WR}{2(\alpha+K)\Sigma_7}\left[(2-\cos\alpha)\sin\alpha-\alpha+\epsilon\left\{\sin\alpha-\alpha\cos\alpha-(1+\cos\alpha)(\alpha-\sin\alpha)\right\}+2K\left\{\sin\alpha\left(\frac{k^2}{8}+\frac{3}{2}\alpha+\frac{1}{2}\alpha\cos\alpha\right)+\epsilon\sin\alpha(\alpha-\sin\alpha)\right\}\right]$
Case VII	$M_8 = \frac{WR}{2(\alpha+K)\Sigma_8}\left[(2-\cos\alpha)\sin\alpha-\alpha+\epsilon\left\{\sin\alpha-\alpha\cos\alpha-(1+\cos\alpha)(\alpha-\sin\alpha)\right\}+2K\left\{\sin\alpha\left(\frac{k^2}{8}+\frac{3}{2}\alpha+\frac{1}{2}\alpha\cos\alpha\right)+\epsilon\sin\alpha(\alpha-\sin\alpha)\right\}\right]$ $T_8 = \frac{WR}{2(\alpha+K)}\left[\frac{A\left\{F+\frac{K^2\sin\alpha}{8}\right\}-B\left\{E+\frac{k^2}{8}\right\}}{AC-BD}\right]$; $V_8 = \frac{W}{2(\alpha+K)}\left[\frac{C\left\{E+\frac{k^2}{8}\right\}-D\left\{F+\frac{K^2\sin\alpha}{8}\right\}}{AC-BD}\right]$ — NOTATION SAME AS ABOVE

Statically Determinate Cases

The circular cantilever beam of arc α with a bending moment M acting at the free end is shown in Fig. 1. The curves are presented for three different cross sections showing the variation in the end deflection as α increases from 0 to 360 deg. The expressions for δ, β, and θ are given in Table 1 for this beam under the heading of Case I.

The same beam with a twisting moment T acting at the free

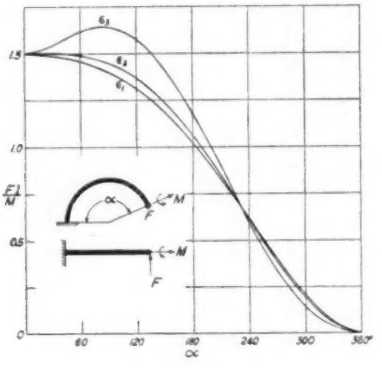


Fig. 3

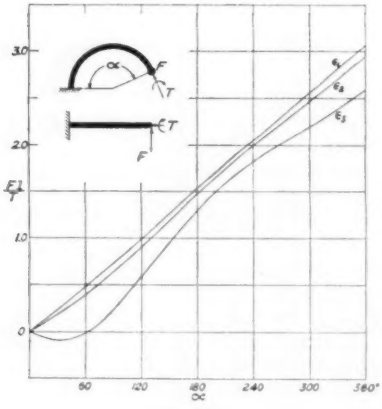


Fig. 4

end is denoted Case II and is shown in Fig. 2. There also is visualized the variation in the end deflection for the three cross sections, as α varies from 0 to 360 deg. Case II of Table 1 gives the expressions for δ, β, and θ for this loading.

Statically Indeterminate Cases

Cases I and II become statically indeterminate when a simple support is placed at the free end. Case I then becomes that denoted as Case III, and Case II that entitled Case IV.

The ratio of the product of the reaction F and the length l of the curved beam to the moment M is graphically shown in Fig. 3, for the angle of arc α from 0 to 360 deg. In Fig. 4, the ratio of the product Fl to the twisting moment T is likewise presented as a function of the arc angle α through the same range. In both figures, the curves are drawn for the three indicated cross sections.

The cantilever arc beam is shown in Fig. 5. It consists of a circular arc of angle 2α with two equal tangential legs of length l. Due to the discontinuity of the structure, two sets of expressions are necessary for the reactions M_0, T_0, and V_0 at the plane of symmetry of the beam. One group of expressions is valid for the load P at any position on the arc, denoted by the angle γ, as shown in Fig. 5(a). The second set of equations holds for the load P at any position on the leg, as indicated by the distance a in Fig. 5(b). For the loading presented in Fig. 5(a) the designation Case Va is used, while for the loading of Fig. 5(b) the notation is Case Vb.

The positive sense of the three reactions, i.e., bending moment M_0, twisting moment T_0, and shear V_0 at the plane of symmetry of the beam is indicated in Fig. 5. As shown, P is a concentrated load acting downward and perpendicular to the plane of the beam on the left-hand side of the axis of symmetry of the beam. The shear reaction V_0 acts in the same direction as P on the right-hand half and in the opposite direction (upward) on the left-hand half.

The variation in the ratio of M_0 to PR is shown in Fig. 6 for

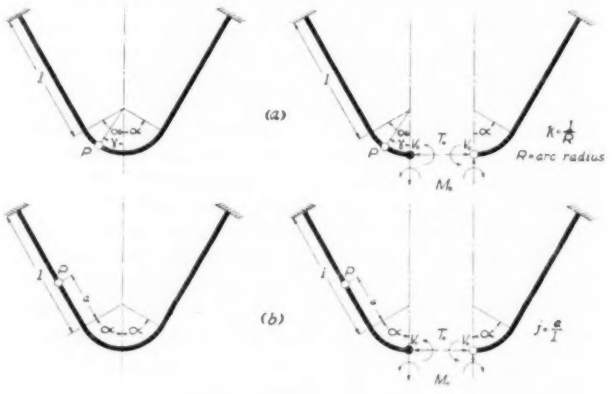


Fig. 5

various positions of the load P on the arc α, as denoted by the ratio γ/α. Curves are there plotted for values of $k = 0.5$, 1.0, and 2.0, and of α from 0 to 90 deg for the three cross sections. Like results are given in Fig. 7 for any position of P on the leg l of the beam. This position is indicated by the ratio j.

The ratio of T_0 to PR as a function of α is shown in Fig. 8 for the three cross sections and values of $k = 0.5$, 1.0, and 2.0. Curves are plotted for various positions along both the arc and the leg of the beam. Fig. 10 presents the ratio of T_0 to PR as a function of the position of the load, i.e., γ/α and j, for the steel circular cross section, $\epsilon = 1.3$, and values of $k = 0.5$, 1.0, and 2.0. These curves clearly show the variation in T_0 from zero with the load P at the axis of symmetry of the beam, to a maximum and then to zero again at the built-in support.

In Fig. 9 is plotted the variation in the ratio of V_0 to P as a function of α for values of α from 0 to 90 deg. The results for the three cross sections, and $k = 0.5$, 1.0, and 2.0, are given for various values of γ/α and j.

The substitution of a differential load $wRd\gamma$ for P in the expressions of Case Va, followed by an integration between the limits of 0 and α, gives results for M_0, T_0, and V_0 due to a uniformly distributed load of intensity w over the left-hand arc α. A similar substitution of a differential load wdx for P in the expressions for Case Vb, followed by an integration between the limits of 0 and l, gives corresponding results due to a uniformly distributed load of intensity w over the left-hand leg l. The sum of these two results for the bending moment gives an expression for the bending moment M_0 at the plane of symmetry of the beam due to a uniformly distributed load of intensity w over the left-hand side of the beam. Similarly, the expressions for the twisting moment T_0 and the shear V_0 at the same point are obtained. These results are tabulated in Table 1 as Case VII.

The use of the results of Case VII and the principle of super-

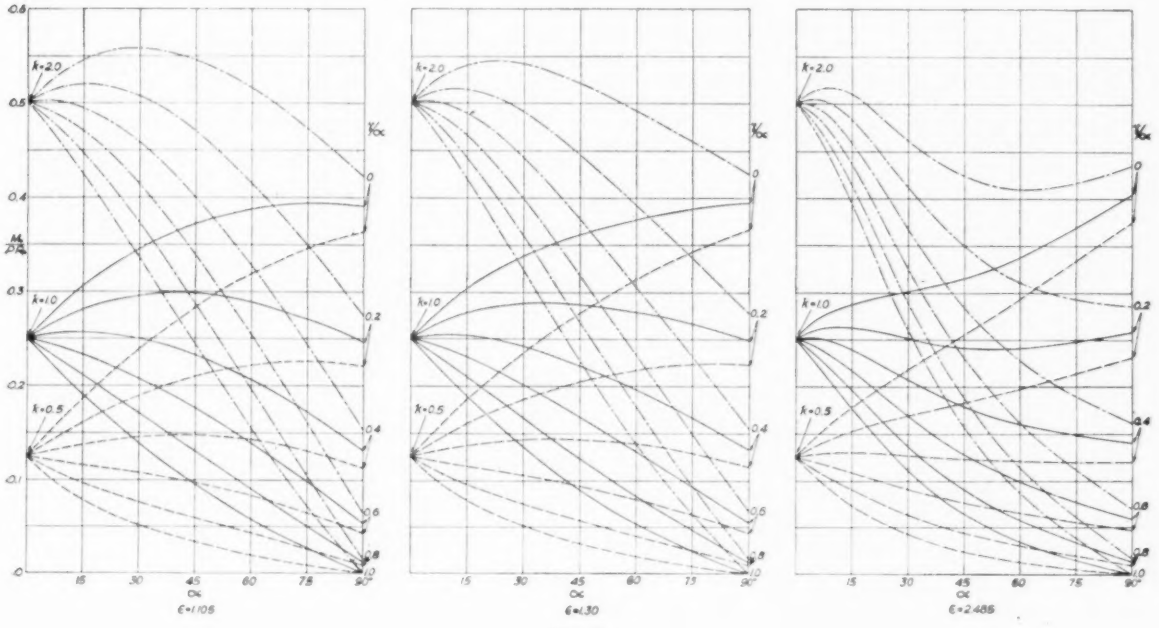

k=2.0
k=1.0
k=0.5
M/PR
Y/c
α
ε=1.105
ε=1.30
ε=2.485

FIG. 6

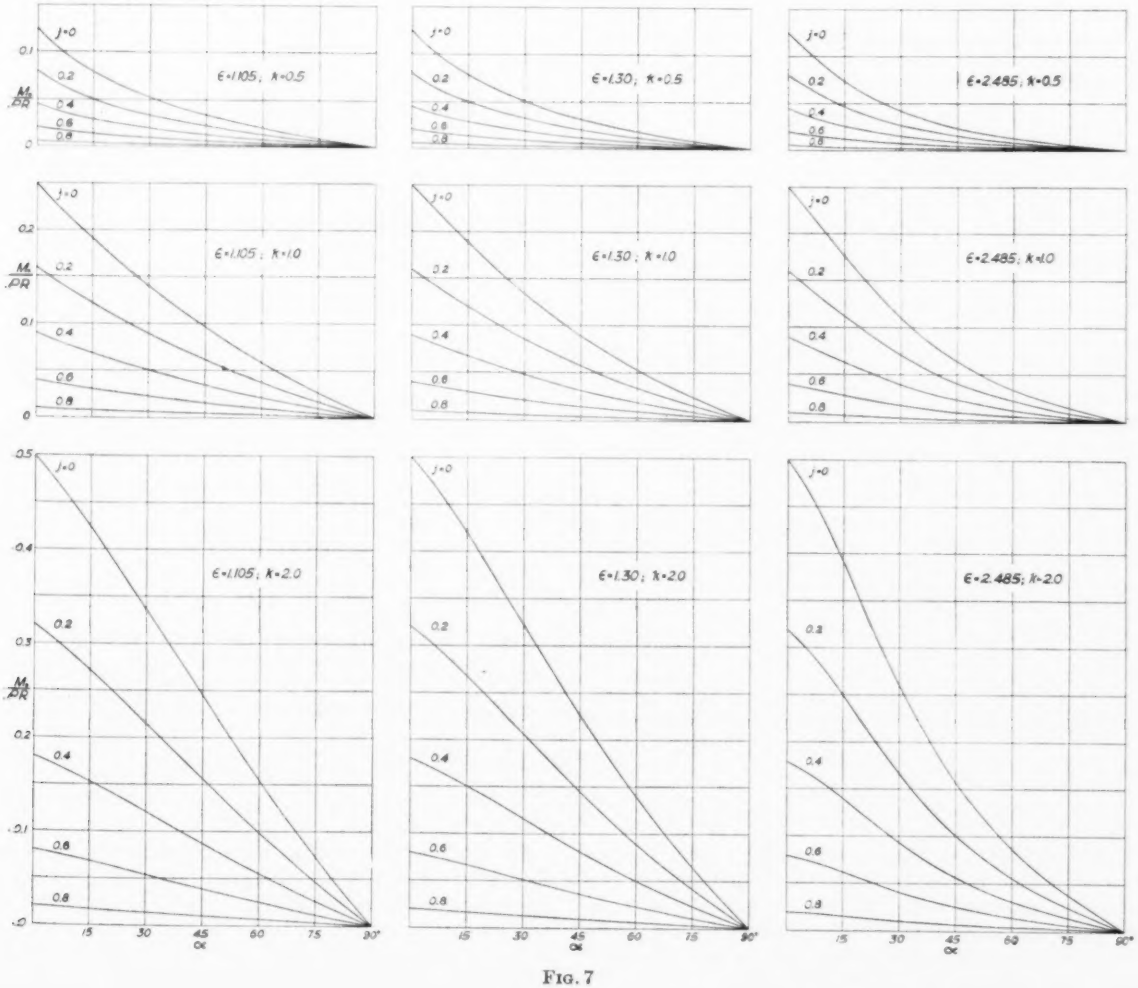

ε=1.105; k=0.5
ε=1.30; k=0.5
ε=2.485; k=0.5
ε=1.105; k=1.0
ε=1.30; k=1.0
ε=2.485; k=1.0
ε=1.105; k=2.0
ε=1.30; k=2.0
ε=2.485; k=2.0
j=0
M/PR
α

FIG. 7

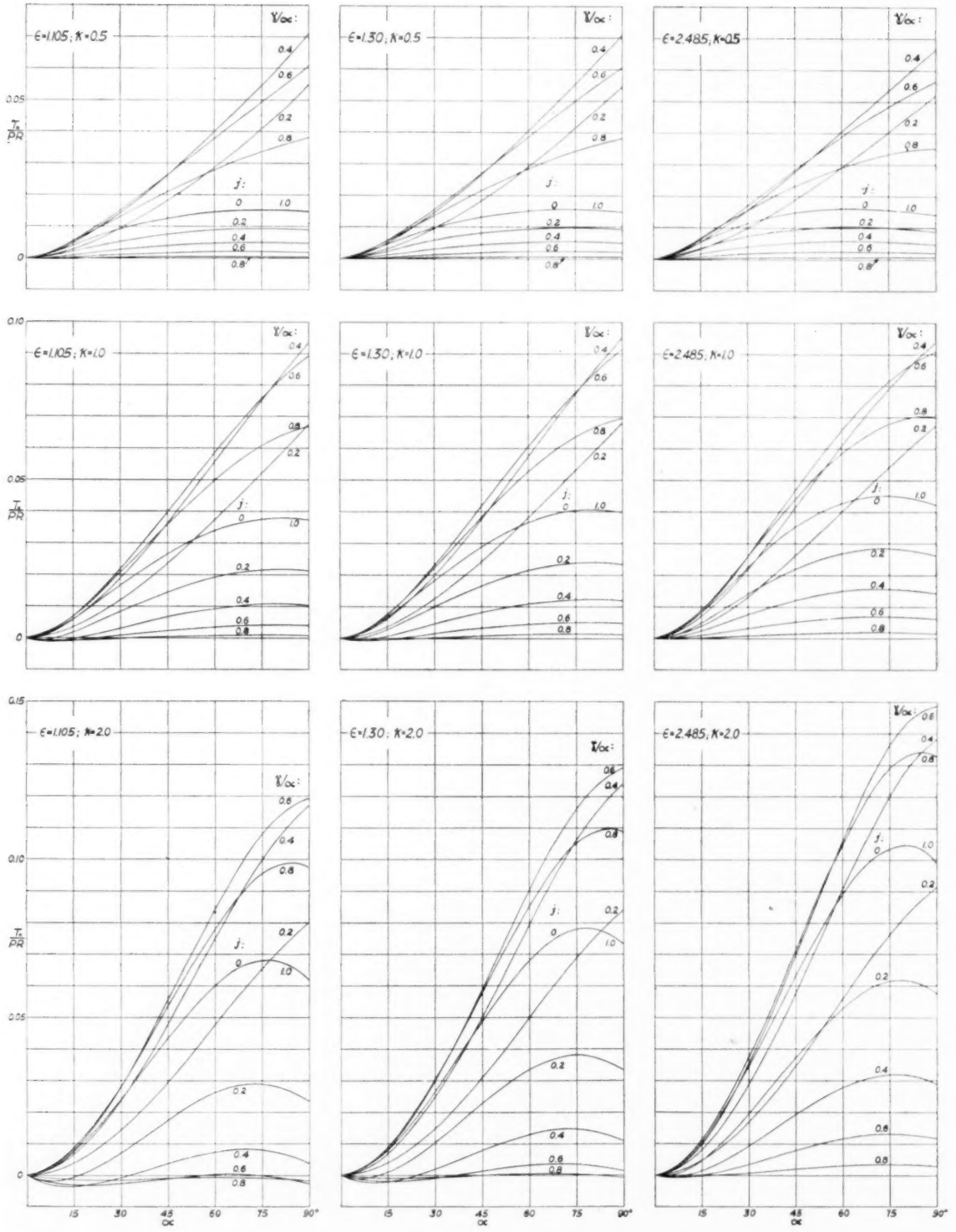


FIG. 8

position immediately give the corresponding results for the cantilever arc beam in Fig. 11, subjected to a uniformly distributed load of intensity w over its entire length. Then $T_0 = 0$, $V_0 = 0$, and M_0 is given under the heading of Case VI in Table 1. It should be observed that the total transverse load W in Case VI is just twice the value of W in Case VII.

The ratio of M_0 to WR for the uniformly loaded cantilever arc beam is presented in Fig. 11, for values of $k = 0$, 0.5, 1.0, and 2.0, and arc angle α from 0 to 90 deg. Curves are presented in each case for the three cross sections. The same curves for the case of $k = 0$, the built-in circular beam of arc angle 2α, are plotted in Fig. 12 for values of α from 0 to 180 deg.

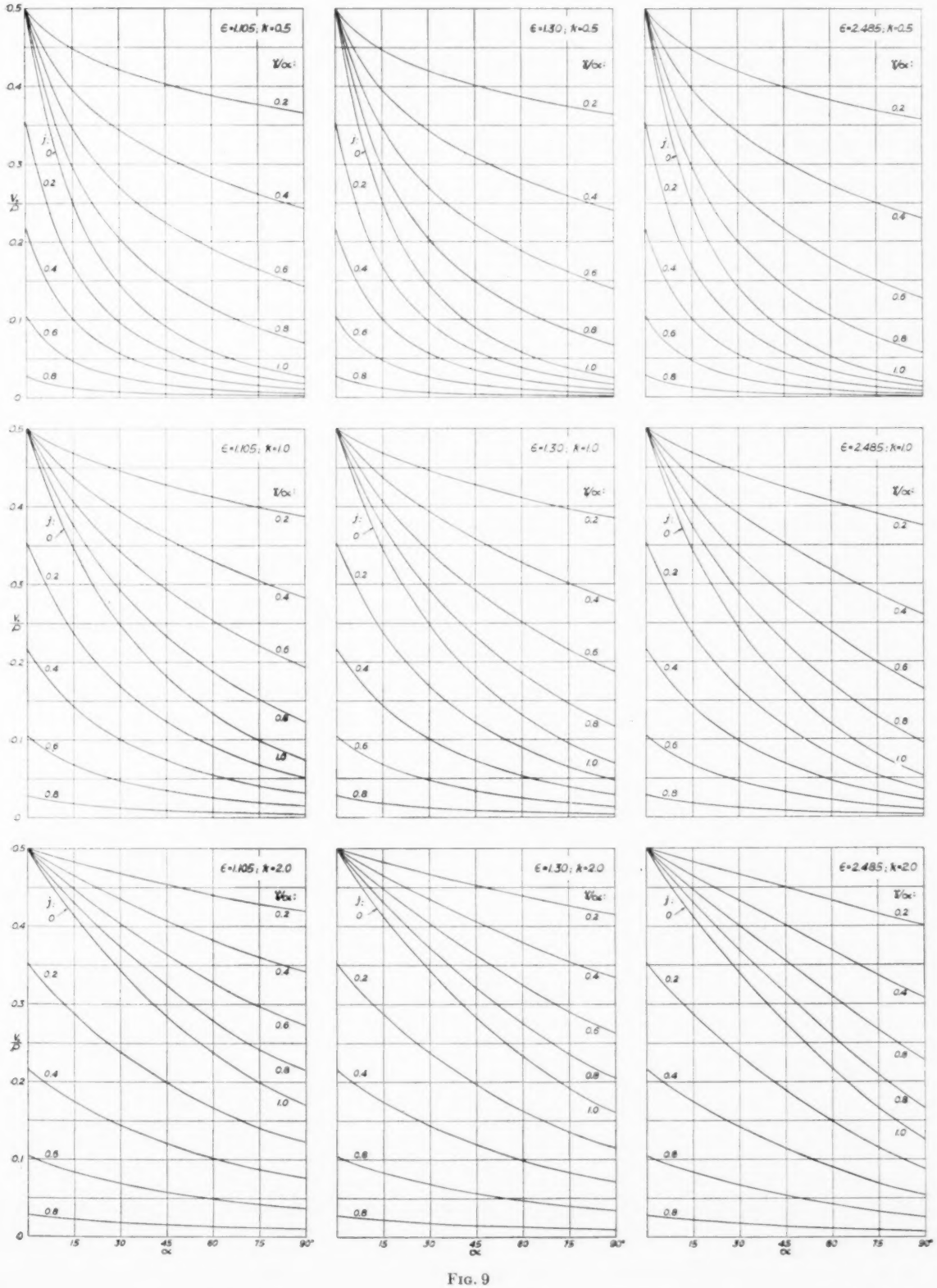


FIG. 9

LIMITING VALUES

For the statically determinate Cases I and II there are two possibilities as α approaches zero. The first is that the radius R remains constant as α approaches zero. Then the result is simply that of the curved beam of zero length. If, however, as α approaches zero, the length of the beam remains finite, the radius R approaches infinity, and the product αR approaches the length l of a straight beam. This leads to the results for straight

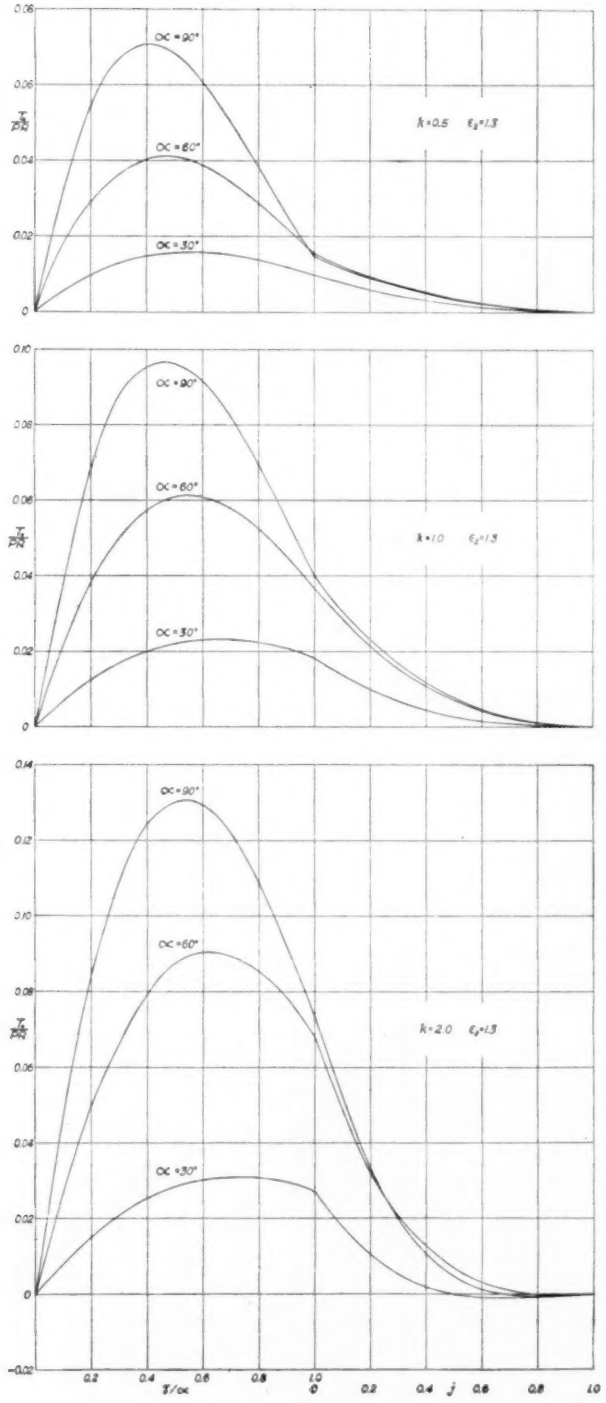


FIG. 10

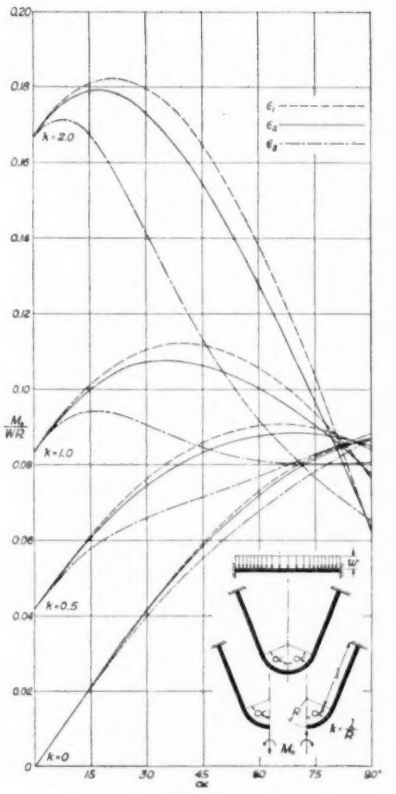


FIG. 11

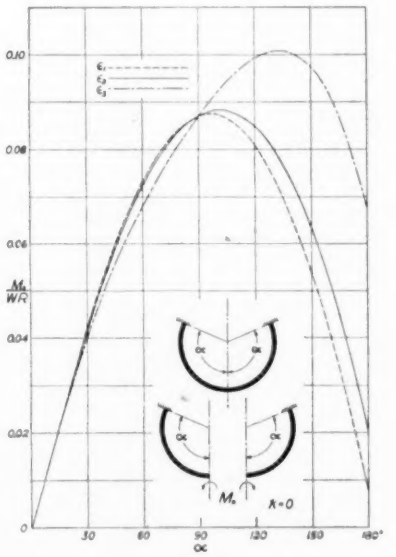


FIG. 12

beams with the same loadings. For Cases III and IV the values of the reactions F approach those of straight beams with corresponding loads as α approaches zero.

As α approaches zero Case V*a* degenerates into a straight beam of length $2l$ with the load P at mid-span while Case V*b* becomes that of a straight beam of length $2l$ with the load P at the distance a to the left of mid-span. Similarly, Case VII degenerates into a straight beam of length $2l$ with a uniformly distributed load over the left half and Case VI into the same beam with the distributed load extending over the entire length $2l$.

Discussion

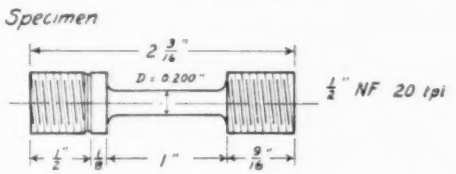
Measurement of Dynamic Strain[1]

LEVAN GRIFFIS.[2] The writer participated in developing bonded "metalectric" strain gages for recording complete stress-strain curves during tensile impact tests.[3] Specimens of 1 in. gage and 1/8 in. diam were tested at velocities of 10 to 250 fps.[4]

The authors' Fig. 11, referring to elastic longitudinal impact stresses, recorded and compared to theoretical values is of particular interest. Electric strain gages are also used to record plastic stresses, e.g., tensile impact stress-strain curves. This requires a wire resistor bonded to a dynamometer bar holding the specimen (Fig. 1 of this discussion). This bar is alloy steel, longitudinally wound with resistance wire, of sufficient section to insure that all stresses applied to it are in the elastic range, although the specimen is tested to failure. An early criticism of such gages was that, calibrated statically, they are used dynamically, with no proof that dynamic and static behavior should coincide. On the basis of elementary wave mechanics, one can predict the dynamic response of such a gage to any force-time function and show that it is reliable. A simplified form of such analysis was made by G. Datwyler and L. Griffis in June, 1938, as part of the research program.[3]

The analysis is generalized from a paper by L. H. Donnell,[5] a section of which deals with waves in materials which do not obey Hooke's law. The speed of an elastic stress wave front in a material is $c_0 = \sqrt{\frac{E_0}{\rho}}$ in which E_0 is the elastic modulus, ρ is density. For a material with curves stress-strain (σ-δ) diagram (Fig. 2 of this discussion), the speed of an inelastic stress increment ($\Delta\sigma$) at σ_1 is $c_1 = \sqrt{\frac{E_1}{\rho}}$ where the E_1 is the slope of the (σ-δ) curve at σ_1. A wave of intensity σ_1 will travel with a changing curved wave front whose shape depends upon $d\sigma/d\delta$, since each increment travels with slower speed than a lower increment. As a wave-front increment $\Delta\sigma$ passes a section Δx of a bar, that section will acquire a change in velocity due to the impulse applied; force-time $= A \cdot \Delta\sigma \cdot \frac{\Delta x}{c} = \rho \cdot A \cdot \Delta x \Delta V$. Therefore a velocity of impact V at a section will produce a succession of stress increments from zero to σ_a, depending upon ρ and the (σ-δ) curve. Velocity V determines σ_a, since from the preceding equation $V = \frac{1}{\rho} F(\sigma)$, where $F(\sigma)$ is a function only of the stress-strain curve and may be plotted graphically: $\sum_{\sigma_a}^{n} \left(\frac{\Delta\sigma}{c}\right)$.

When a wave front strikes a section of increased or decreased area, or when opposing wave fronts meet, the transmitted (σ_t) and reflected (σ_r) stresses (waves) are determined by the facts that, on each side of that section, (1) final particle velocities must be equal and, (2) total forces must be equal. A fixed end is equivalent to infinite increase in section; a free end to a decrease in section to zero. Equating impulse to momentum change for particles on each side of the discontinuity determines



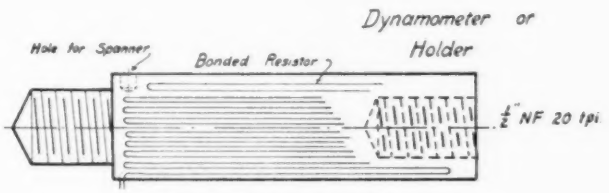


FIG. 1 SPECIMEN AND HOLDER

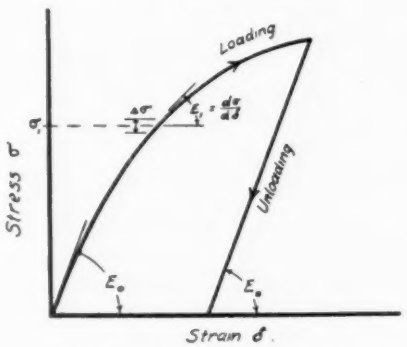


FIG. 2 STRESS-STRAIN CURVE

the magnitude of σ_r and σ_t. A discontinuity in material of a bar may be reduced to an equivalent change in sectional area. At increases in section, $\sigma_r > \sigma_a$ and $\sigma_t < \sigma_a$; at decreases in section, $\sigma_r < \sigma_a$ and $\sigma_t > \sigma_a$.

The shapes of the transmitted and reflected wave fronts are obtained by dividing the original waves into steps, each with its own speed $c_n = \sqrt{\frac{E_n}{\rho}}$. The time-position picture of these increments, and of all reflected and transmitted increments, can be constructed if these characteristic speeds are known. By carrying out a simultaneous computation of transmitted and reflected stress magnitudes for all increments, during meetings of waves or at discontinuities in section, the speeds are found from the (σ-δ) curve, using $c = \sqrt{\frac{E}{\rho}}$. The time-position of any stress is indicated by a ray whose slope with the time axis equals the speed. This determines the complete time-space-stress function for the bar up to necking, for any case of longitudinal impact. From the stress, the strain distribution may be found. If a

[1] By C. O. Dohrenwend and W. R. Mehaffey, published in the June, 1943, issue of the JOURNAL OF APPLIED MECHANICS, Trans. A.S.M.E., p. A-85.

[2] Assistant Professor of Mechanics, Illinois Institute of Technology, Chicago, Ill.

[3] Impact Research Laboratory, California Insitute of Technology, 1938–1941.

[4] "Effect of the Rate of Deformation on the Behavior of Materials in Tension," by L. Griffis, Doctor's Dissertation, California Institute of Technology, 1941.

[5] "Longitudinal Wave Transmission and Impact," by L. H. Donnell, Trans. A.S.M.E., vol. 52, 1930, paper APM-52-14.

material unloads along an elastic line from any stress, Fig. 2 of this discussion, an elastic unloading wave may be added to the picture under certain conditions, permitting analysis of stress conditions in the dynamometer after the specimen fails.

To illustrate, assume a specimen and holder as in Fig. 3, herewith. An instantaneous impact velocity V applied at A at time t_0 will set up a continuous tensile-stress wave front of intensity σ_a traveling toward B. This will strike B, beginning at time t_1, then be partially transmitted to the holder as an elastic tensile wave front σ_t, and also be reflected as a tensile wave front σ_r superimposed upon σ_a. The elastic wave σ_t proceeds to the rigid end C where, beginning at time t_2, it reflects as an elastic wave of intensity $2\,\sigma_t$. Simultaneously σ_r returns toward A where it reflects at t_3

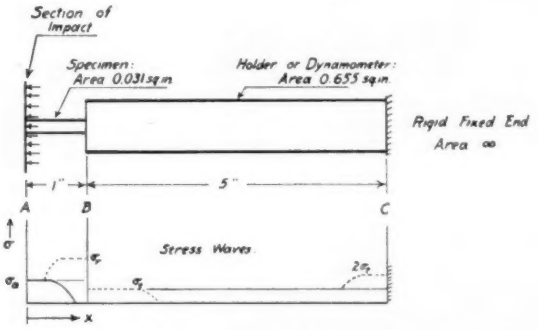


FIG. 3 WAVE PROPAGATION IN SPECIMEN AND HOLDER

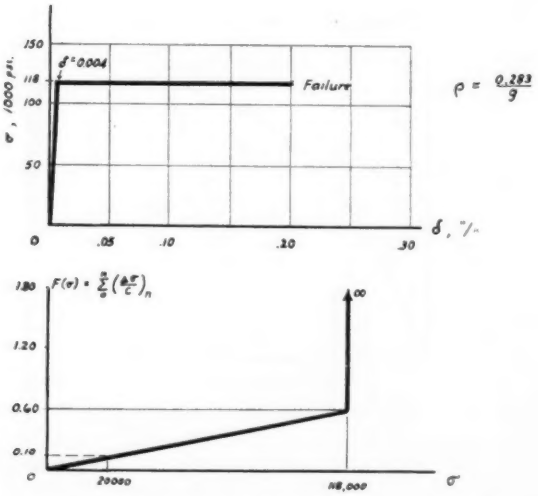


FIG. 4 ASSUMED STRESS-STRAIN CURVE FOR STEEL, AND COMPUTED CURVE OF $F(\sigma)$

as another tensile wave front σ_a', as if A were a rigid end. The wave $2\,\sigma_t$ will reach B at t_4 where, at this decrease in section, it is partially reflected as a wave front of less intensity than $2\,\sigma_t$, and partially transmitted to the specimen as a tensile wave of increased intensity. (Imagine a large mass striking a small mass inelastically.) This might cause necking in the specimen near C, simultaneously with necking near A, if stress intensities were of proper amounts. Or, such transmissions and reflections at A, B, and C may continue if the specimen stress has not built up to the ultimate, until at some point (which might be predicted) necking and failure result. The response of the strain gage at any instant depends upon the intensity and distribution of the elastic waves in the holder.

As an example, assume specimen and holder to be steel, the specimen having simple (σ-δ) and $F(\sigma)$ curves as in the writer's Fig. 4. For an impact velocity of 11.3 fps, one finds that $F(\sigma_a) = 0.10$ lb-sec per cu in., $\sigma_a = 20{,}000$ psi, and $c_0 = 196{,}000$ in per sec. In this simple case, all waves in the specimen have velocities c_0 up to the instant of yield, then have zero velocity; $6\cdot\sigma_a$ is required to produce yield. In this case it is simpler to use forces f instead of stresses σ, since a force wave intensity distributed along the entire holder, and equal to the specimen force at the same instant, corresponds to 100 per cent response. At section B (time t_1), $f_t = 1.91\cdot f_a$ and $f_r = 0.91\cdot f_a$. Also, the required $6\cdot f_a$ will develop in the specimen before $2\cdot f_t$ returns to B, after which B becomes in effect a free end.

Fig. 5 of this discussion shows the stress-time-space picture, with each ray indicating a force intensity moving at speed c_0. Polygons in the diagram indicate at any time the distribution of constant force in the specimen or holder, of intensity as noted in small print.

Fig. 6 (dotted) shows the curve of holder response, based upon 100 per cent response equal to yield force in the specimen. No damping of stress intensity is assumed in specimen or holder.

Assuming for metals that the damping of waves or vibrations is proportional to intensity, and to distance which the wave has traveled, Fig. 6 shows (dashed) the curve of holder response calculated as before, but assuming that in one holder length, a wave intensity f damps to intensity $^3/_4 f$ (25 per cent damping). Similar results are shown (solid curve) in Fig. 6 for 50 per cent damping in one holder length. In each case, perfect holder response would be indicated by the heavy line rising directly to 118,000 psi and then becoming horizontal. The mean line through the gage response vibrations is then the correct and reliable response. The gage does not respond at all until time t_1 ($0.5\cdot10^{-5}$ sec after impact). Clearly, a dynamometer should have a high natural frequency compared to the phenomenon being recorded. For

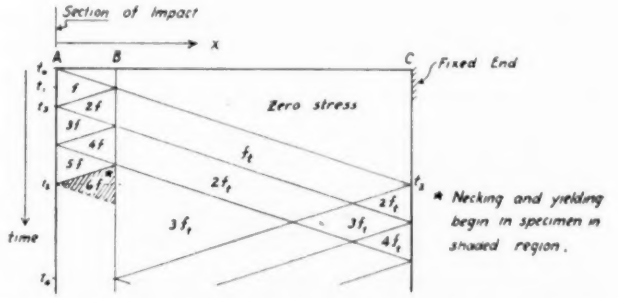


FIG. 5 BEGINNING OF FORCE-SPACE-TIME DIAGRAM FOR SPECIMEN AND HOLDER

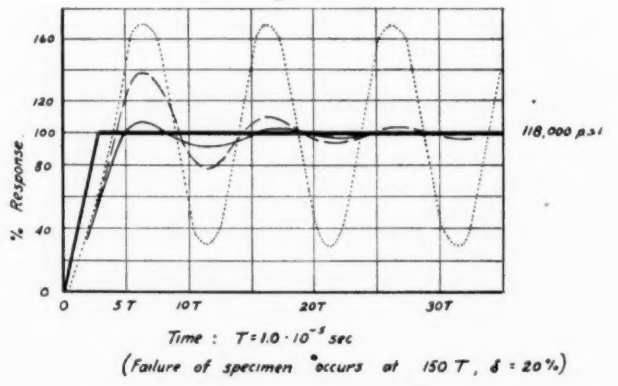


FIG. 6 DYNAMOMETER RESPONSE, IN PER CENT OF YIELD STRESSES

higher velocity impact tests, a shorter dynamometer would be desirable.

Fig. 7 herewith shows a force-time elongation diagram for an aluminum specimen tested at 20 fps. The force calibration (2590 lb) is made by introducing a known resistance into the oscillograph circuit, corresponding to a definite force required to produce an equal resistance change in the strain gage. A modulated timing wave (5000 kc) is shown, the time for tensile fracture being 0.0028 sec. Modulations on the force-time

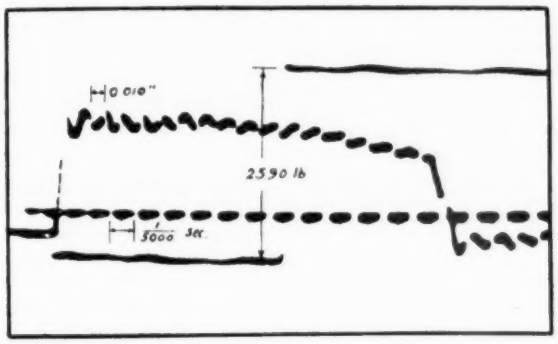


FIG. 7

curve are produced by recording the forward motion of the section of impact using a scratch gage. This device alternately makes and breaks a contact at each 0.01 in. of forward motion.

J. H. MEIER.[6] The Bucyrus-Erie Company's Research Department has developed a somewhat similar unit for field measurement of strains on large excavators.[7] The amplitude modulation scheme was chosen as it is well capable of covering the range of mechanical frequencies encountered on heavy machines. Carrier frequencies up to 3000 cycles per sec have been used successfully; thus mechanical vibrations up to 500 cycles per sec can be recorded without appreciable loss in accuracy of peak values.

The bridge circuit employed is shown in Fig. 8 of this discussion. Like the authors' arrangement it is symmetrical. Phase balancing is identical; however, resistance balancing is considerably simpler. It is achieved by means of a large fixed resistor across one arm of the bridge and a variable resistor across the adjoining arm, the common point being ground. A decade box is used as variable resistor; contact resistance is not critical because of the high shunt resistance. With this arrangement the balance point is found easily and rapidly, thus the disadvantage of hunting for the correct setting as described by the authors is overcome. Also, sensitivity adjustment and calibration are greatly simplified. From the gage factor and the balance setting the resistance offset causing the same signal as a convenient strain, for instance 0.001, can be computed easily. The decade box is offset by this amount, and after proper adjustment of amplifier gain, the oscillograph deflection is photographed and serves as calibration for the record. Proper functioning of the setup can be checked readily by offsetting the decade box 500 or 1000 ohms.

All four arms of the bridge are arranged near the active strain gage. This requires four leads between gages and recording equipment, while the authors' arrangement requires only three. The inconvenience is small, however, since three leads in a shield can be handled easily. Two leads feed the bridge, while one lead and the shield carry the signal. The great advantage of this scheme is that relatively large changes in lead resistance affect the signal but slightly. This is particularly important when using trailing cables from moving objects, since these cables are apt to be stressed and act as undesirable strain gages of their own. Furthermore, the effect of lead resistance on calibration is much smaller than in the authors' scheme. Also, the undesirable influence of the distributed capacity of the leads is substantially reduced.

Electrical-resistance gages have linear response within the range of strains covered by the authors' investigation.[8] The authors' nonlinear calibration curve is therefore a characteristic of the circuits described. Linearity of response is desirable in several respects, as follows:

1 It greatly facilitates the checking of equipment and performance, and it is of importance in detecting pickup and other disturbances affecting the accuracy of the results.

2 It renders calibration easy and reliable.

3 It permits making full use of the available oscillograph screen width; thus greatest possible accuracy can be expected.

With equipment of sufficient sensitivity available to measure very small strains, an initial offset corresponding to a multiple of the strains to be observed is a certain disadvantage. When the sign of strain is known (as for instance when rope pulls are measured by means of calibrated links), the drawback of the initial offset to eliminate the nonlinear portion is particularly apparent.

The cathode-ray oscillograph will be of great help in determining the cause of nonlinearity. Although the authors claim that the plot represents the unbalanced voltage, it appears from their diagram, Fig. 4, that at least part of the nonlinearity may

[6] Research Engineer, Bucyrus-Erie Company, South Milwaukee, Wis.

[7] Recording Unit for Strain and Timing Functions, *Electronics*, April, 1943.

[8] "The Development of an Electrical Strain Gage," by J. H. Meier, Doctor's Thesis, Department of Civil and Sanitary Engineering, Massachusetts Institute of Technology, 1939.

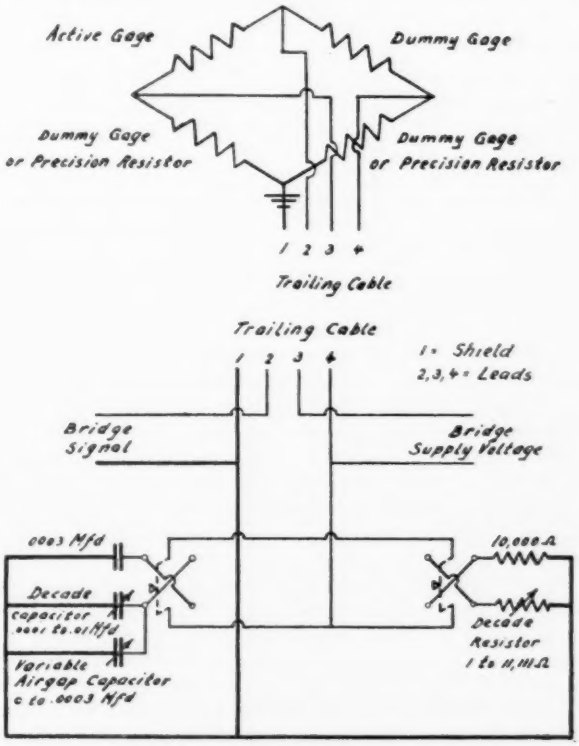


FIG. 8 BRIDGE ARRANGEMENT AND CONTROL

be the characteristic of the rectifier-meter system. It could be greatly improved by using higher amplification, an electronic-tube rectifier, and a high series resistance in the meter circuit. The nonlinearity observed in the rectifier-meter system of the writer's company is less than 2 per cent of that shown by the authors. The meter is used primarily for observation while photographic records are being taken.

If the bridge is working properly, the response of the cathode-ray oscillograph is perfectly linear and the deflection for zero strain is zero. It is important that this be verified for each setup, in order to secure proper phase balancing. If phase balance is not obtained the bridge signal is not proportional to the strain and considerable errors may result. As phase balance is different for each installation, it cannot be accounted for by calibration.

Readings and records should not be taken before zero deflection on the oscillograph screen can be obtained. Phase balancing should then not be disturbed for the entire test period. Failure of the signal to become zero reveals a potential source of error. It is usually due to pickup or to harmonics in the carrier wave which cannot be balanced simultaneously.

H. C. Roberts.[9] Although for several years there has been available excellent commercial equipment for recording mechanical strains and movements, there is still a shortage of usable published material dealing with methods and instruments. For this reason, such papers as do appear are likely to be studied with great interest by test engineers. This writer feels that with regard to the authors' present paper several omissions of some importance should be pointed out.

The authors have in no manner indicated the differences in the nature of the technical problem which appear when a measuring circuit is transferred from a single-channel setup under well-controlled conditions to a multichannel apparatus which will simultaneously record dynamic phenomena from a number of gages under conditions of field or factory operation. For industrial measurements, in general a ten-channel apparatus is much more than 10 times as useful as a single-channel apparatus. The experimental difficulties are likewise greater, but by proper selection of equipment the operating difficulties connected with a ten-channel apparatus may be made little greater than with a two-channel apparatus.

For multichannel recording, the electromagnetic oscillograph, recording a number of traces on the same strip of photographic film, together with a time indication, and with sequence or operation indications, is unexcelled within its frequency range. Such an oscillograph can be made to record satisfactorily as high as 10,000 cycles per sec, and at film speed as high as 50 ips for continuous drive; much higher speeds are available in the drum-type drive. These data refer to standard-model commercially available instruments. With such an oscillograph, all data as recorded are correlated against time, and thus a correlation also exists between all the traces. The magnetic oscillograph is a robust self-contained instrument, extremely efficient and flexible in operation. Its only serious handicap is a loss of response at extremely low operating temperatures; many commercial instruments have thermostatic control of temperature, thus eliminating this defect.

The writer feels also that the carbon-type resistance strip strain gage is being unjustifiably neglected. Admittedly it has its faults; at the same time it has some very appreciable advantages. There are now available some half-dozen commercial gages of this type, with a wide range of characteristics. A degree of stability is easily attainable which is satisfactory for practically all dynamic measurements; for tests involving weeks or months of elapsed time no gage now available can be used without rather elaborate precautions. For work which requires the use of many gages simultaneously, the ability to remove and re-use the same gage is worth while; this is not because of the cost of the gages, but because a gage can be calibrated experimentally and re-used many times. The principal disadvantage of the carbon-type gage is its relatively high cross-sensitivity; however, the wire-type resistance strip gage is not free from this fault.

The higher sensitivity of the carbon-type resistance strip gage permits the design of direct-coupled amplifiers having a high degree of stability. Such amplifiers are at this time giving satisfactory service; they have been in use for several years.

No mention is made of that most useful device, the carrier-type amplifier. With such an amplifier, the response may be maintained from static conditions (zero frequency) up to the highest frequencies normally encountered, and far above those which can be recorded with the magnetic galvanometer. Amplifiers of this type have been used to record phenomena well up into the tens of thousands of cycles per second. At the same time the gage circuit is excited with direct current and is thus freed from many operating difficulties which appear with alternating-current bridge circuits. The accuracy and stability of such an amplifier are comparable to that of an alternating-current amplifier. Such apparatus is sometimes deranged by extreme conditions of humidity, unless constructed with suitable precautions; the same is true of the cathode-ray oscillograph and of any other instrument utilizing high voltages or high-impedance circuits.

By means of either the direct-coupled amplifier or the carrier-type amplifier, operating into the magnetic oscillograph, it is possible to record phenomena at frequencies ranging from static conditions up to several thousand cycles per second. At the same time the records appear as single-line traces, which are easier to read and somewhat more accurate than the amplitude-modulated trace; this is especially true when several traces are recorded upon the same film.

It is of course true that the magnetic strain gage is limited in its applications; for example, its frequency response is necessarily limited by the frequency of the exciting current, and by other factors. Excitation frequencies as high as 50,000 cycles per sec have been used; there is, however, considerable doubt if even with this frequency of excitation the recording ability extended as high as the 9000 to 10,000 cycles per sec that such a frequency of excitation would indicate. At frequencies higher than perhaps 2500 cycles per sec, a magnetic gage is likely, because of its mechanical inertia, to act as an accelerometer.

Within its range of frequencies, and upon specimens to which it can be satisfactorily attached, the modern magnetic strain gage is the most reliable, the most stable, and the least difficult of operation of all the electrical strain gages. The push-pull type of gage, attached by clamping with its knife-edge feet, is least disturbed by time and temperature changes of all such equipment. The magnetic gage is normally a low-impedance device and is not disturbed by random fields or by changes in length of connecting cable; this because, although its total impedance is low, still the largest component of that impedance is inductance, and the effect of ohmic resistance, and of changes in ohmic resistance, can be made small. The magnetic gage does not normally require an amplifier and can be made to provide sufficient output to operate a recording galvanometer. It is of course necessary to provide an excitation current, which must be well regulated, so that changes in the amount of power absorbed by the gage, and changes in the voltage of the power-line supply, will not produce changes in the voltage applied to the gage. This equipment is also well developed and is commercially available.

With some types of magnetic gages, the effective level of measurement is above the surface of the specimen, and bending stresses will therefore introduce inaccuracy; with other types this is not the case. Few of the commercial magnetic strain gages now available are so constructed that the specimen is made part of the magnetic circuit; they may therefore be used on specimens of nonmetallic materials and may be attached by clamps, by screws, or by any other convenient method. In the

[9] Special Research Associate, Engineering Experiment Station, University of Illinois, Urbana, Ill.

'Progress Reports of the Stresses in Track Investigation" of the Association of American Railroads, several very informative discussions of such gages have appeared; the work of this organization with this equipment extends back to about 1930.

The magnetic strain gage has one advantage shared only by the capacity type among the electrical gages, that is, its ability to operate at different gage sensitivities and over wide ranges of strain. There are types of magnetic gages available for measuring movements of several inches, or even several feet, if necessary. All of these gages employ the same auxiliary equipment, thus increasing the flexibility of the entire group. Accelerometers are also available, operating from conditions of constant acceleration up to frequencies of change of acceleration as high as several hundred sinusoidal cycles per second.

The capacity type of strain gage is not especially well suited for use except under very closely controlled conditions, if it is to be calibrated quantitatively. Yet, since the early announcement of the Whiddington ultramicrometer in 1919, many capacity gages have been used. They are capable of an extremely high sensitivity, but their disadvantage is that it is very difficult to so construct them that there will be no change of capacity excepting that due to the strain. They are especially susceptible to humidity changes. Transducer circuits having an exceptionally high electrical stability have been developed, but this electrical stability does not compensate for errors coming from without the instrument. In the laboratory, or in applications in which the shape and variation in magnitude of a wave form are more important than its absolute magnitude, the capacity gage is often quite suitable.

Both the capacity gage and the magnetic gage are superior to the resistance types in that they impose no restraint upon the specimen other than that due to the weight of the gage itself. Most types of resistance gage impose quite a considerable restraint upon the specimen; this restraint appears as a shear in the adhesive by which the gage is attached, and there is thus usually a reasonable doubt in the mind of the worker as to whether or not there is creepage in the adhesive. With most of the available adhesives, this doubt is well founded. It is also true that with the magnetic and the capacity gages, there is no cross sensitivity.

The writer does not wish to criticize any type of gage unduly, but experience has convinced him that few electrical strain gages are at the present time in such form that their application and operation can be considered an exact science. For this reason, the type of gage selected should be affected by the character of the personnel which is to operate the equipment as well as by the type of measurement to be made.

A. V. de Forest[10] and A. C. Ruge.[11] This paper is timely in adding pertinent information on the many uses of the wire resistance strain gage. As the authors point out, the associated equipment for measuring the gage response is the all-important part of successful operation.

A few additional types of equipment which may be useful in certain instances might well be added to the list described by the authors of the paper. We have found many instances where the rate of application of load is reasonably slow, as in stresses in moving vehicles and landing stresses in airplanes, and where a pen-and-ink recorder, operating on a modulated 60- or 120-cycle alternating bridge, is more convenient and lighter in weight than an oscillograph. The Brush crystal recorder has been used very successfully in this field.

For high-speed work, particularly in preliminary investigations of transients, we have had good success in photographing a 5-in. cathode-ray tube with a still camera using a recurrent sweep. This process normally gives some distortion of the time scale but the system is so simple that where a transient may conveniently be repeated the records have proved to be valuable.

For high-speed work, where accurate timing is necessary, we have found the Dumont 208 cathode-ray oscillograph to have excellent frequency response and sufficient sensitivity to operate on large stresses without any additional amplification. Two, three, or four oscillographs may be photographed simultaneously with a drum camera. In using this equipment, it is frequently desirable to introduce a pulser circuit so that the oscillograph spot only remains on the screen for 1 revolution of the drum.

In all cases involving amplification and oscillograph measurements, we have found it desirable to calibrate the deflection directly in terms of a change in resistance. This is most easily accomplished by shunting the measuring gage through a resistance which changes the total to an amount corresponding to the approximate range of stress for which the oscillograph is set up. The calibration and the record are both photographed on the same film. There is then no question of interpreting the record later on. This method of procedure is applicable because the sensitivity of the original gage is highly dependable. The calibrating equipment mentioned by the authors is well suited for determining this strain sensitivity in the case of unknown gages.

Where the frequency response of amplifiers and oscillographs is in question, we have found it convenient to measure the response of this portion of the measuring device by the normal means of a variable-frequency oscillator rather than by means of the tuning fork described in the paper. The tuning-fork method is, of course, an extremely simple method of generating a fixed frequency. Where this is sufficient, it becomes a most practical solution to the problem. Additional points regarding the use of the strain gages are covered in a paper by one of the writers.[12]

C. W. Gadd.[13] The writer considers this paper a very worthwhile contribution to the literature available to the mechanical engineer interested in strain measurements, particularly because it sets down in concrete and immediately applicable form the essential information required to apply the wire-gage technique to dynamic studies. Since wire gages were made available there has been considerable duplication of effort in the development of equipment for dynamic-strain measurement with the gages, and much should be gained from this paper, particularly by organizations who either are not equipped or do not have the time to develop their own instrumentation.

In regard to static versus dynamic strain measurements, the writer believes that either or both are necessary, depending upon the problem at hand. It is often best to determine, first, with dynamic gages, the service loads and distortions of the part in question and then to analyze by means of a laboratory test, using one of the static-strain-measuring methods, for the effects of design changes. This procedure will often be advantageous from the standpoint of economy of time, control over the variables affecting the test results, and ease of measurements in fillets and other points difficult of access with dynamic gages.

As for the electrical circuits themselves, the writer believes that the usefulness of the potentiometer type could be empha-

[10] Professor, Massachusetts Institute of Technology, Cambridge, Mass.

[11] Associate Professor, Massachusetts Institute of Technology, Cambridge, Mass.

[12] "Characteristics and Aircraft Applications of Wire Resistance Strain Gages," by A. V. de Forest, *Instruments*, vol. 15, April, 1942, p. 112.

[13] Research Engineer in Mechanical Engineering, No. 6, Research Laboratories Division, General Motors Corporation, Detroit, Mich.

sized somewhat. In many practical problems, where variables of the order of 5 per cent or more will exist, the practical low limit of the alternating-current amplifier frequency response should be considered as only a few cycles per second. In regard to the degree of amplification required, general-purpose equipment should include amplifiers such as those described in the paper, particularly if low-resistance gages are to be employed; however, the use of gages of several hundred ohms with no amplifier other than that with which the oscilloscope is equipped might be kept in mind as the simplest practical method of making dynamic measurements.

Authors' Closure

The application of the wire gage, as explained by Le Van Griffis, is extremely interesting, especially since the gage was used to record plastic strains. It might be well to point out that for large strains, such as are obtained in the plastic regions, the creep of the binding material may become a major factor and care must be exercised in making such applications. The authors have found the information concerning the shapes of wave fronts, as explained by this discussion, very interesting. The work on longitudinal impact as mentioned in the original paper, however, was presented only to show the characteristic of the amplifier used.

Mr. Meier's comments relating to the curvature of the calibration curve of the auxiliary meter for static work with the amplitude modulation unit are of interest. In any case both the vacuum-tube and copper-oxide rectifiers have an appreciable internal impedance and if curvature of the calibration curve is to be eliminated, extremely high series resistances must be used in the rectifier circuit. This high resistance will limit the current to a very small value and therefore a sensitive spotlight galvanometer must be used. If the designer is willing to accept a small amount of curvature in the calibration curve a rugged 1-ma meter can be used and this is more suitable for field use than a delicate galvanometer.

It should also be pointed out that the effect of curvature at the origin is negligible if the operating point is selected at mid-scale by unbalancing the bridge as suggested in the paper.

The amplifier and oscilloscope used with the amplitude-modulation unit are linear so there is no curvature of the oscilloscope calibration curve.

In the three-wire system, as described in the paper, one wire of the cable is a part of the standard arm of the bridge and a second wire is part of the variable arm of the bridge; normally both wires are subject to the same temperature and strain conditions. Therefore both temperature and strain effects on the cables will tend to cancel leaving only changes due to strain in the measuring gage. If the cables are allowed to hang, the swaying due to wind will be a bending condition, and therefore the wires will be subject to different strain conditions. An error due to strain may result.

The four-wire system has a complete bridge circuit located at the measuring point. Therefore the effect of strain and temperature on the resistance of the cables is eliminated, but since the four-wire cable includes both leads to the amplifier input and oscillator leads for power to the bridge, some trouble may be encountered with direct pickup of oscillator output by the amplifier. This will limit the degree of amplification so that only large strains can be measured.

The four-wire arrangement is very useful in applications in which slip rings must be used to take off a signal from a rotating member. The effect of contact resistance of clean slip rings is negligible with this system.

In applications in which many measuring points are used the three-wire system is more convenient as simpler switching systems and fewer gages are required.

Mr. Roberts' remarks concerning the usefulness of a multichannel set as compared to a single channel is well taken. However, difficulties of multichannel units are not serious and the danger of cross talk and oscillation is well known to amplifier designers. The string type of oscilloscope can give good results in laboratory practice; however, in the field it proves a bulky piece of equipment quite sensitive to mechanical shock. There are, however, many applications where pen-and-ink or chemical recorders can be used to good advantage.

The fault of cross sensitivity of the wire gage as pointed out by Mr. Roberts is present, but its magnitude is less than the accuracy of the auxiliary equipment used with the gage and is therefore of little consequence. Mr. Roberts is not too clear in his remarks concerning the carrier type of amplifier, which appears to be, from his description, quite similar to the type labeled amplitude modulation by the authors. For direct-current amplifiers the gain required for good results is so high as to require very high amplification leading to instability.

The suggestion of Mr. Roberts that it would be simple to detect the amplitude-modulated wave and obtain the envelope by filtering off the carrier-frequency wires was tried originally and gave good results, but since the choice of time constants is critical in order to respond to peak values, we feel it is safer to record the amplitude-modulated carrier. One advantage is that the carrier provides a good time axis.

In the authors' opinion the magnetic type of gage is quite useful when large displacements are to be measured. For dynamic-strain measurements, or normal-strain measurements, the application is too complicated to make it a good device for strain analysis, especially since magnetic shielding is essential; also the application requires holes, or attachments of some variety, and the action of these disturbances is indeterminate.

There is no doubt that this type of gage is excellent for certain purposes; high-speed dynamic strain is not one of them. Mr. Roberts is of the opinion that the application of the electrical strain gage cannot be considered an exact science. The authors would like to point out that even though this be the case, one must learn to creep before he walks and walk before he runs. The electrical gage, especially the wire type, has allowed measurements by the mechanical engineer never before possible. In dynamic measurement, the type of personnel cannot at present control the type of gage required. The personnel must of necessity be more elastic than the laws of nature they are trying to interpret.

The authors agree with Messrs. deForest and Ruge in their statement that the sensitivity of the original gages is highly dependable and the electrical method of calibration good for such gages.

The remarks of Mr. Gadd, stating that the dynamic gage can be of use to determine service loads or distortions and to make the analysis in the laboratory by use of static-strain-measuring methods, is well taken.

In summary, the authors wish to express their appreciation to the discussers for the time they have given and feel that each has added much to help in the understanding of the limitation of the measurements of dynamic strain. It may also be well to point out that the applications of electrical measurements in mechanics are undergoing rapid development and all the instrumentation is in a state of continual change.

There is one error in the original paper: In Fig. 2 the condenser C_2 was marked 0.01 mfd and it should be marked 10 mfd.

Book Reviews

Vector and Tensor Analysis

VECTOR AND TENSOR ANALYSIS. By Homer Craig, professor of applied mathematics and astronomy, University of Texas. McGraw-Hill Book Company, Inc., New York, N. Y., 1943. Cloth, 6 × 9 in., xiv and 434 pp., $3.50.

REVIEWED BY ALBERT E. HEINS[1]

VECTOR and Tensor Analysis" by Homer Craig was written with a threefold purpose in mind. Briefly the aims are the following: (*a*) To supply the necessary material to bridge the gap between the elementary calculus and the study of vector and tensor analysis; (*b*) to give a treatment of vector and tensor analysis; and finally, (*c*) to emphasize the concept of the invariant. The book is accordingly divided into four parts. Part *A* deals with the additional mathematical background mentioned in (*a*). In this section we find a discussion of such topics as the real number system, infinite sequences, the calculus of functions of two variables, parameterization of arcs and co-ordinate transformations including some remarks on Jacobians. This background is certainly adequate to orient the reader into what is to follow.

Parts *B* and *C* are concerned with a treatment of vector and tensor analysis. In these sections there is a discussion of the algebra and calculus of vectors and tensors. Some applications of vector analysis to the differential geometry of curves and surfaces are given. The section on the calculus of vectors also includes line, surface, and volume integrals, and the theorems of Gauss, Stokes, and Green which play such a prominent role in certain developments in the dynamics of continuous media. The last part of the book gives a discussion of the applications of Parts *B* and *C* to classical dynamics, special and general relativity.

A study of this book will reward the student of mathematics, engineering, or physics with a good working knowledge of vector and tensor analysis. The indicated applications to geometry and dynamics serve to illustrate the use of vector and tensor analysis in pure and applied mathematics. A useful bibliography is appended to each part.

Proceedings of the Society for Experimental Stress Analysis

PROCEEDINGS OF THE SOCIETY FOR EXPERIMENTAL STRESS ANALYSIS. Volume 1, No. 1. Papers presented at the Seventeenth Eastern Photoelasticity Conference and Experimental Stress Symposium. Held Under the Auspices of the Chrysler Institute of Engineering, Detroit, Michigan, May 13, 14, and 15, 1943. Published by Addison-Wesley Press, Inc., Cambridge, Mass. Cloth, 8½ × 11 in., xvi and 156 pp., figs., tables, $3.

REVIEWED BY A. M. WAHL[2]

THIS volume, edited by Dr. C. Lipson and Prof. W. M. Murray, consists of a collection of papers presented at the seventeenth Eastern Photoelasticity Conference and Experimental Stress Symposium held at Detroit during May, 1943. It also represents the first volume of the proceedings of the newly formed Society for Experimental Stress Analysis.

Although the S.E.S.A. is an outgrowth of the Photoelastic Conference which, at first, was devoted largely to papers on photoelastic-stress analysis, the wartime trend in emphasis toward strain measurements on actual structures or machine parts is exemplified in this volume by the predominant number of papers discussing uses and applications of electric gages or brittle coating methods. Thus out of the seventeen papers in this volume, about one half are concerned with the description, use, or application of electric strain gages and associated instrumentation. This reflects the increasing importance of electrical strain measurements, particularly in aircraft and automotive design problems.

Those engineers who are interested in the technique of using the resistance-wire type of gage together with the associated instrumentation will find much data of interest in the papers by Gibbons, Hathaway, Grover, and Dohrenwend. The paper by Gibbons discusses many technical problems arising in the use of the resistance-wire gage while that by Hathaway treats not only resistance-type gages but also electromagnetic types together with associated control, power supply, and recording equipment. The use and application of resistance-type gages to the measurement of dynamic strains, particularly in fatigue testing, is described in the paper by Grover. A paper of considerable interest to spring designers is that by Dohrenwend,who investigated the stress distribution and eccentricity of loading in volute springs.

A considerable number of papers in this volume treat applications of strain measurements to aircraft and automotive design problems. There is an interesting paper by Tucker which discusses the use of resistance gages in aircraft-engine parts where elevated temperatures (up to around 500 F) are involved. Results of strain measurements thus obtained on aircraft cylinder-barrel flanges and cylinder studs are given. The increase in dynamic stress due to insufficient tightening of the cylinder studs is shown by the test results. This paper also emphasizes the obvious truth that it is not enough to merely measure stresses; they must also be evaluated by the designer in terms of fatigue life or margin of safety. This latter phase of the problem is often the more difficult one. Other papers involving strain measurements include that by Lipson on stresses in connecting-rod bearings and by Ellis which treats of an analysis of an aircraft-engine-cylinder failure using the brittle-lacquer method. This latter paper should be of considerable interest to engineers interested in the technique involved in such measurements and the application of brittle coating methods to dynamic- and static-strain measurements. A paper by Gadd discusses the results of strain measurement with a short-gage-length extensometer on an engine crankshaft together with other stress-analysis problems in engine design.

An interesting discussion of the determination of aircraft-engine-piston operating temperatures by means of hardness changes during operation is given by R. G. Anderson. This paper also records the results of brittle-lacquer measurements on actual pistons. These data are correlated with fatigue-test results on pistons, using a hydraulic type of machine in which operating temperature gradients are simulated.

An investigation of the stress distribution around an elliptical hole in a plate under biaxial stress using photoelastic and brittle-lacquer methods is reported by Durelli and Murray. The usefulness of the brittle-lacquer method in order to determine the

[1] Assistant Professor of Mathematics, Purdue University, Lafayette, Ind. (Pro tem on leave of absence.)

[2] Research Engineer, Westinghouse Electric & Manufacturing Co., East Pittsburgh, Pa. Mem. A.S.M.E.

principal stress directions is brought out very well in this paper.

A paper of direct practical interest to machine designers is that by Hetényi which treats of the stress distribution in threaded connections using both plane and three-dimensional photoelastic methods. It is shown that approximately 40 per cent reduction in peak stress for elastic conditions may be obtained by using a nut with a tapered thread or a tapered lip. The results of comparative photoelastic tests on U. S. Standard, Whitworth, and Aero-Thread forms are also presented.

A mechanical device for evaluating strain rosette readings in terms of principal stresses and stress directions forms the subject of a paper by Murray. Such a device should be quite useful where a large amount of test data must be worked up. In discussions of this paper, three graphical solutions of this problem are presented by Meier, Hansen, and Baumberger. The latter presents a particularly simple solution for the 45-deg rosette gage with three components.

Two papers involving fatigue studies are included. The first by Horger, Neifert, and Regen describes residual stress measurements on $2^3/_{16}$-in. round bars of heat-treated S.A.E. 1045 steel, electric strain gages being used. Of interest is the nonsymmetrical stress distribution found. The results of fatigue tests on 2-in. alloy-steel bars with very small transverse holes are also given to show the improvement produced by surface rolling. The second paper by Peterson shows how the results of photoelastic tests or strain measurements may be correlated with strength-reduction factors obtained by means of fatigue tests on specimens with notches or grooves. This paper represents further progress on the general problem of evaluating the results of strain measurements of photoelastic tests in terms of danger of failure, particularly where fatigue is involved.

In general, it may be said that this first volume of the newly formed S.E.S.A. contains a great deal of information of interest not only to engineers directly concerned with the experimental determination of stress in machines or structures but also to design engineers and stress analysts in general.

Dynamical Analogies

DYNAMICAL ANALOGIES. By Harry F. Olson, acoustical research director, RCA Laboratories, Princeton, N. J. D. Van Nostrand Company, Inc., New York, N. Y., 1943. Cloth, $5^1/_2 \times 8^1/_2$ in., xi and 196 pp., $2.75.

REVIEWED BY J. P. DEN HARTOG[3]

THIS is a small and extremely useful book by a well-known engineer in the acoustic field. In a previous book by the same author, "Elements of Acoustical Engineering," D. Van Nostrand, 1940, which incidentally is also highly recommended, there appears a chapter on "Electrical, Mechanical, and Acoustical Analogies," which forms the basis of the work now under review.

It gives in a concise and clear form, without derivations, but with adequate definitions, the principal formulas and pictures showing four equivalent systems: linear mechanical, rotational mechanical, electrical, and acoustical. The author confines the analogy to the usual one where mechanical velocity corresponds to electric current. Other proposals, the best known of which is due to Firestone, are mentioned in a footnote, but since they are not widely used they are not discussed further in the book. The "acoustical" system differs from the "linear mechanical" mainly by the substitution of pressure in lb per sq in. for force in lb. The book is nicely illustrated by groups of five figures showing sketches of the four different systems and a small diagram with their common characteristics.

The detailed contents of the various chapters follow:

Chapter 1 gives definitions, clear and concise, of all the quantities discussed, some hundred of them.

Chapter 2, entitled "Elements," gives pictures and tables showing the correspondence between "mass" and "inductance," etc., as well as between the various kinds of impedance with their dimensions.

Chapter 3 deals with single-degree-of-freedom systems, and chapter 4 with systems of two and three degrees of freedom, giving pictures and listing the principal differential equations and formulas for the natural frequencies, impedances, and other characteristics.

Chapter 5 is entitled "Corrective Networks" and could also appropriately be called "Compounding of Elements." It shows various series and parallel connections of elements, usually not involving more than three such elements. Again, comparative figures with little diagrams showing transmissibility vs. frequency are the main contribution.

Chapter 6, "Wave Filters," extends the subject of the previous chapter to more than three elements and presents the matter in the same form with a good collection of formulas showing cutoff frequencies.

Chapter 7, "Transients," gives a statement of Heaviside's unit function and the response of the four kinds of systems to it and also a short exposition of how the response of such a system to an arbitrary exciting force can be found by integration of the response to the unit function.

Chapter 8 deals with "Driving Systems" or "Transducers," being devices for converting electric currents into mechanical vibrations, mainly for loudspeakers and phonograph recorders It discusses the electrodynamic, electromagnetic, electrostatic, magnetostrictive and piezoelectric systems and gives the electric circuit diagrams and the pertinent formulas both for the electrical and the mechanical parts of the system.

In chapter 9 "Generating Systems" are treated, which are devices operating on the same principle but opposite to those of the previous chapter in that they convert mechanical vibrations into electric currents, with applications mainly to microphones and phonographs.

Chapters 10 and 11 state some theorems and give a few applications to mechanical engineering, such as vibration and shock-mounting of engines and instruments, mufflers, and automobile suspensions.

All in all, a very readable book which will be useful to engineers dealing with vibration—mechanical, as well as electrical or acoustical.

[3] Comd., U.S.N.R., Bushipa, Washington, D. C. Mem. A.S.M.E.

Measurement of Dynamic Stress and Strain in Tensile Test Specimens

By R. O. FEHR,[1] E. R. PARKER,[2] AND D. J. DEMICHEAL[1]

In the investigation detailed in this paper, the tensile strength, the yield strength, and the breakage energy of test specimens (cold-rolled steel and dural) were measured while the specimens were being broken by a force applied at a high rate of speed in a commercial high-velocity impact-testing machine. The dynamic tensile strength, the dynamic yield strength and the dynamic breakage energy were found to be higher than the static values up to the maximum impact velocities of these tests (100 fps). The paper contains: (1) A presentation of some results of these tests. (2) A description of the technique used. (3) A description of the analysis used.

Introduction

FOR rational design, the dynamic characteristics, such as strength and breakage energy, of materials used in apparatus subjected to impact need to be known. However, at the present time, designs of apparatus are mostly based upon the static characteristics of the different materials even when the apparatus is subjected to impacts. When the dynamic breakage strength is lower than the static breakage strength, the apparatus may not withstand the impact, and when the dynamic breakage strength is above the static value, the weight of the apparatus may be unnecessarily high. Design of apparatus subjected to dynamic loads can, therefore, be improved when the design is based upon the dynamic characteristics of materials.

The determination of the relative dynamic characteristics of different materials is of special importance when materials which are now scarce have to be replaced by substitute materials.

In the tests reported in this paper, measurements of stress and strain have been made on test samples of cold-rolled steel (S.A.E-X-1112), and of dural (17-ST), while specimens made from these materials were being broken by a force applied at a high rate of speed in a commerical high-velocity impact-testing machine,[3] shown in Fig. 1.

The object of this paper is to present some results of these tests, to explain the technique and the analysis used, and to demonstrate the adequacy of this technique and analysis.

Summary of Test Results

The dynamic tensile strength, the dynamic yield strength, the dynamic breakage energy, and the dynamic elongation of the tested materials were found to be higher than the corresponding values obtained in the static tensile test.

The values for these four material characteristics increased with increasing striking velocity. The increase of the strength value above the static-strength value was in most cases less than 50 per cent up to a striking velocity of 100 fps, which was the highest test velocity.

The dynamic tensile strength and the dynamic yield strength versus the striking velocity are shown in Fig. 2 (*a*) for cold-rolled steel and in Fig. 2 (*b*) for dural; the dynamic breakage energy versus the striking velocity is shown in Fig. 3; and the dynamic elongation versus the striking velocity is shown in Fig. 4.

Limitations of High-Velocity Impact-Testing Machine

Only the dynamic breakage energy and the dynamic elongation, not the dynamic strength values, are obtainable from the conventional high-velocity impact-testing machine in the absence of special strain-gage equipment. It is, therefore, important to consider to what extent the dynamic strength values are indicated by the values for dynamic breakage energy and dynamic elongation.

The test results here presented indicate that, for the materials tested, the strength values vary only qualitatively, not in quantitative proportion, with the energy and elongation values. No definite relationship between the strength values and the energy or elongation values is evident.

The conventional high-velocity impact-testing machine will, therefore, require addition of strength-measurement equipment, such as the strain gages here discussed, when quantitative results on dynamic-strength characteristics are desired.

Recommendations for Use of Strain Gages

Results of the present investigation seem to warrant the follow-

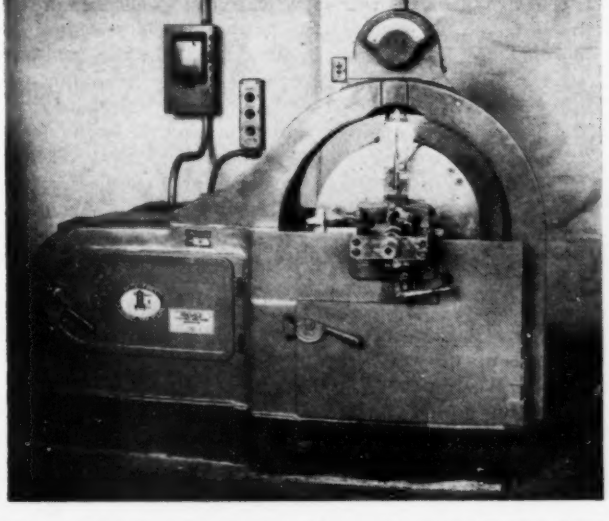


Fig. 1 High-Velocity Impact-Testing Machine, Outside View

[1] General Engineering Laboratory, General Electric Company, Schenectady, N. Y.

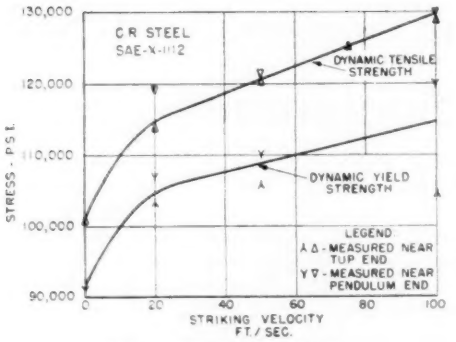
[2] Research Laboratory, General Electric Company, Schenectady, N. Y.

[3] "High Velocity Tension Impact Tests," part 2, by H. C. Mann, Proceedings A.S.T.M., vol. 36, 1936, pp. 85–109.

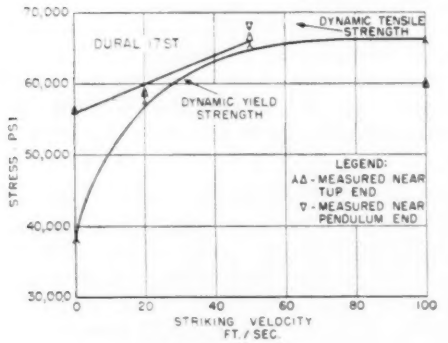
Contributed by the Applied Mechanics Division of The American Society of Mechanical Engineers and presented at a joint meeting with the Society for Experimental Stress Analysis, in conjunction with the Annual Meeting, New York, N. Y., Nov. 29–Dec. 3, 1943, of The American Society of Mechanical Engineers.

Discussion of this paper should be addressed to the Secretary, A.S.M.E., 29 West 39th Street, New York, N. Y., and will be accepted until July 10, 1944, for publication at a later date. Discussion received after the closing date will be returned.

Note: Statements and opinions advanced in papers are to be understood as individual expressions of their authors and not those of the Society.



(*a*) For steel; S.A.E-X-1112



(*b*) For Dural; 17-ST

FIG. 2 DYNAMIC YIELD STRENGTH AND DYNAMIC TENSILE STRENGTH VERSUS STRIKING VELOCITY

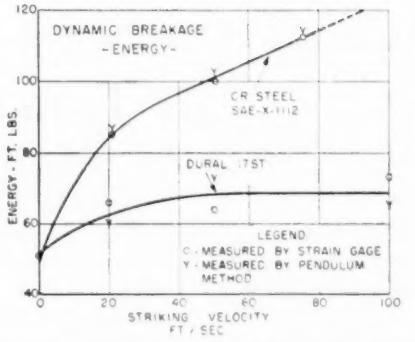


FIG. 3 DYNAMIC BREAKAGE ENERGY VERSUS STRIKING VELOCITY

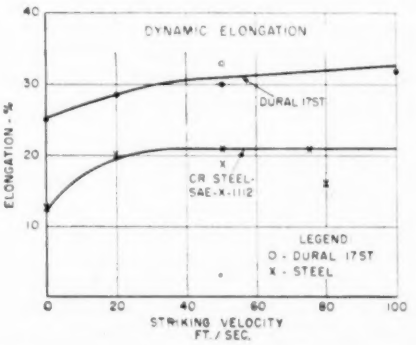


FIG. 4 DYNAMIC ELONGATION VERSUS STRIKING VELOCITY

ing recommendations in future applications of strain gages to measurements of dynamic strength in the high-velocity impact-testing machine:

1 The strain gage should be attached to the pendulum end, not the tup end, of the specimen.

2 The strain gage should be attached as close to the small cross section of the test specimen as practicable.

3 The length of the strain gage should be as short as practicable.

DESCRIPTION OF EQUIPMENT

The measurements were made while test specimens were being fractured in a high-velocity impact-testing machine. This machine consisted essentially of a flywheel, from which two striking horns could be thrust, and a heavy pendulum which supported the specimen. These are shown schematically in Fig. 5. The striking horns were thrust out after the circumferential speed of the wheel had attained the desired velocity. The specimen was fractured when the striking horns engaged a tup attached to the front end of the specimen. The holding force was the very high inertia force of the pendulum. The breakage energy could be calculated from the swing of the pendulum after the impact.

The shape of the test specimens, which were used for the dynamic tensile tests, was similar to a specimen shape which is in common use for static tensile tests. The specimens used are shown in Fig. 6.

The stress in the tensile test specimen was measured with a resistance-type electric strain gage,[4] in most cases attached to a large-diameter section adjacent to the test section of the speci-

[4] "Some Complexities of Impact Strength," by A. V. deForest, American Institute of Mining and Metallurgical Engineers, Technical Publication No. 1341.

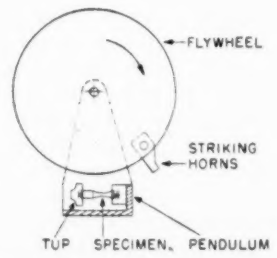


FIG. 5 HIGH-VELOCITY IMPACT-TESTING MACHINE, SCHEMATIC DIAGRAM

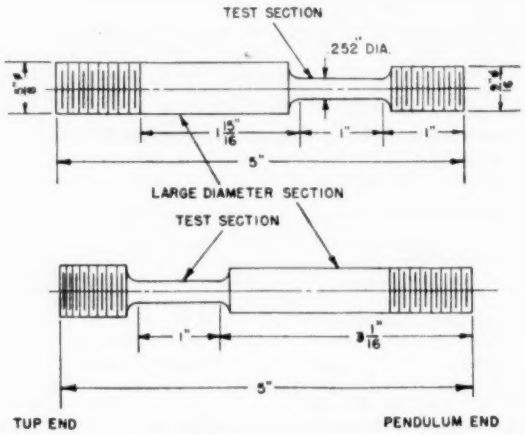


FIG. 6 SPECIMENS FOR HIGH-VELOCITY IMPACT-TESTING MACHINE (*a*, For strain measurements at the tup end of the specimen. *b*, For strain measurements at the pendulum end of the specimen.)

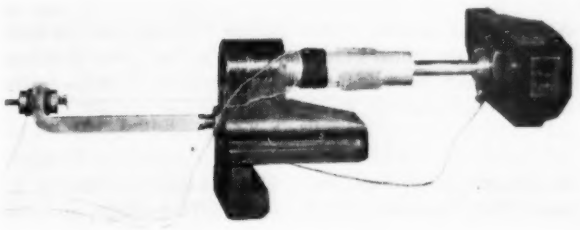


FIG. 7 SPECIMEN ASSEMBLY FOR STRAIN MEASUREMENTS AT PENDULUM END OF SPECIMEN

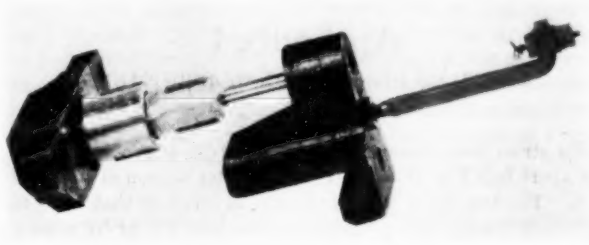


FIG. 8 SPECIMEN ASSEMBLY FOR STRAIN MEASUREMENTS AT TUP END OF SPECIMEN

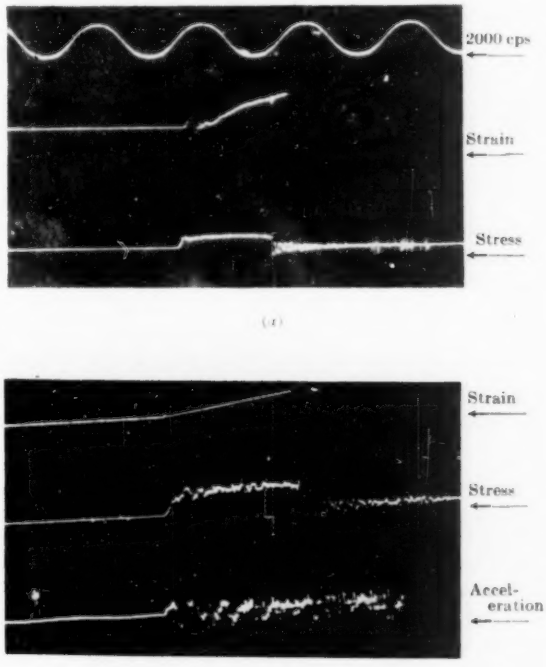


FIG. 9 TYPICAL OSCILLOGRAMS

(*a*, Strain measurements at pendulum end of specimen. *b*, Strain measurements at tup end of specimen.)

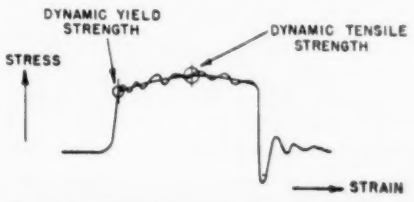


FIG. 10 TYPICAL STRESS-STRAIN DIAGRAM

men (Fig. 7), or in some cases attached to a cylindrical specimen holder.

The elongation of the specimen was measured with a thin nichrome wire stretched between the two ends of the specimen, Fig. 7. The elongation of this wire equaled the elongation of the specimen, and the resistance change in this wire due to this elongation was recorded.

The acceleration of the tup was measured by recording the stress produced solely by the acceleration force in a hollow cylinder attached to the tup, Fig. 8. This stress was measured with a resistance-type electric strain gage.

The resistance change in these gages was recorded on photographic film by means of a cathode-ray oscillograph and a high-speed camera. A record was obtained which showed the stress, strain, and, in some cases, the acceleration as a function of time. Two typical records are shown in Figs. 9 (*a*) and 9 (*b*).

This equipment is described in greater detail in Appendix 1.

EVALUATION OF TEST RESULTS

The object of the tests was to determine the values of the dynamic tensile strength, of the dynamic yield strength, and of the breakage energy of test specimens as a function of the striking velocity. The following procedure was used:

Stress versus time curves were obtained from measurements with strain gages which measured the stress in the large diameter section adjacent to the smaller diameter test section in which the break occurred. The stress in the test section was usually obtained by a simple multiplication of the stress in the larger diameter section, provided the measurements were made near the pendulum end. When the measurements were made near the tup end, the stress due to the inertia forces was first deducted from the recorded stress values before applying the multiplication factor. These curves were replotted as stress versus strain curves using the strain versus time records, which were obtained from oscillographic records, such as shown in Fig. 9. This analysis is discussed at greater length in Appendix 2.

The dynamic tensile strength is the stress in the test section corresponding to the highest point of the average line in the stress-strain curve in Fig. 10. The dynamic yield strength is that value of stress at which the rate of change of elongation for a constant increment of stress begins to increase.

Values for the dynamic tensile strength were also obtained from measurements with strain gages cemented, not to the specimen itself, but to a strain-sensitive specimen holder which was attached to the pendulum end. This arrangement was used when a large number of specimens was to be tested, since it made it unnecessary to attach strain gages to the individual specimens. The stress versus time records obtained by this arrangement showed large peaks, in contrast to the rather smooth stress versus time record obtained by a gage attached to the large-diameter section of the specimen, and placed in an identical location.

The energy values were obtained by integration of the stress-strain curves. The values obtained checked closely those energy values which had been obtained by the measurement of the pendulum swing[5] (see graph in Fig. 3).

ADEQUACY OF TEST TECHNIQUE

To establish the adequacy of the technique, it has to be demonstrated that measurements with a strain gage in the chosen location yield the proper results.

Stress measurements were made on the specimen at two locations, i.e., one between the point of rupture and the fixed specimen holder, and the other between the point of rupture and the point

[5] "The Effect of Strain Rate Upon the Tensile Impact Strength of Some Metals," by E. R. Parker and C. Ferguson, Trans. American Society for Metals, vol. 30, 1942, pp. 68–85.

of impact. Analysis in Appendix 2 indicates that for the specimen shape used the stress measurements at the first of these locations should give directly an approximate value for the stresses in the test section. The analysis shows, moreover, that the stresses in the test section could be determined approximately also from records taken at the other location, provided inertia effects were taken into consideration. The values obtained both ways were found to be in good agreement; this fact provides a confirmation of the analysis as well as of the validity of the strength values obtained.

Inadequacy of Reference Velocity

The true impact velocity at the critical region of fracture was decidedly not equal to the striking velocity (velocity of the striking horns) at the characteristic moment of the beginning of plastic flow. The value of this important true impact velocity could not be obtained offhand from the records, or from readings of the instruments on the machine. The answer to the question

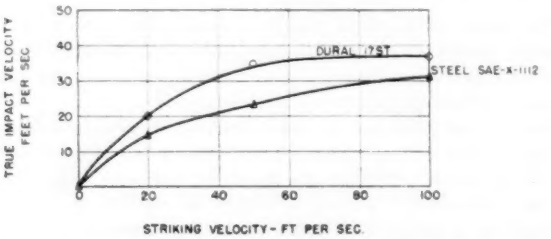


Fig. 11 True Impact Velocity, at Which Yield Strength Is Reached, Versus Striking Velocity

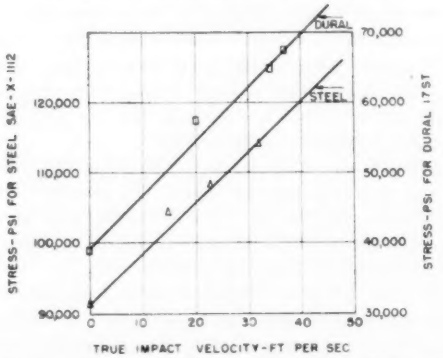


Fig. 12 Dynamic Yield Strength Versus True Impact Velocity

as to what the true value of this impact velocity is, was obtained from the analysis by stress waves discussed in Appendix 2. It was found from this analysis that the true impact velocity was generally far below the striking velocity at the critical instant at which the yield strength was reached (see Fig. 11). The true impact velocity was found to give a simpler correlation of yield strength than the striking velocity gave.

When the yield strength was plotted as a function of the true impact velocity, it was found to approximate a straight line while the conventional plot of the same value versus the striking velocity gave a curve which apparently approached a finite value, as illustrated by comparison of Fig. 12 with Fig. 2 (*a*) and (*b*).

The striking velocity was, nevertheless, chosen as the velocity of reference in correlating the effect of velocity on the strength and energy results. This choice seemed advisable for practical reasons. The striking velocity could be obtained directly from the speedometer on the testing machine, whereas the true impact velocity could be obtained only by cumbersome calculations impractical for general use. Moreover, the plot of the strength and energy values as a function of the true impact velocity would not be of much greater practical significance than the plot of these values as a function of the striking velocity, since in most practical cases the impact is transmitted to the place of failure through some sort of structure as is also the case for specimens tested in the high-velocity machine.

Acknowledgment

The authors are indebted for helpful comments to Prof. A. V. deForest of the Massachusetts Institute of Technology, and also for suggestions and advice to a number of individuals in the General Electric Company organization. They particularly wish to acknowledge the help of Mr. R. H. Norris and the suggestions of Mr. D. C. Prince, Jr.

Appendix 1

Detailed Description of Equipment

Strain Gages

For stress measurements, two wire gages[4] were cemented 180 deg apart (see Fig. 7) to the large-diameter section of the specimen. The two gages were connected in series so that the total resistance change was produced by compression or by tension, and so that no resistance change was produced by bending.

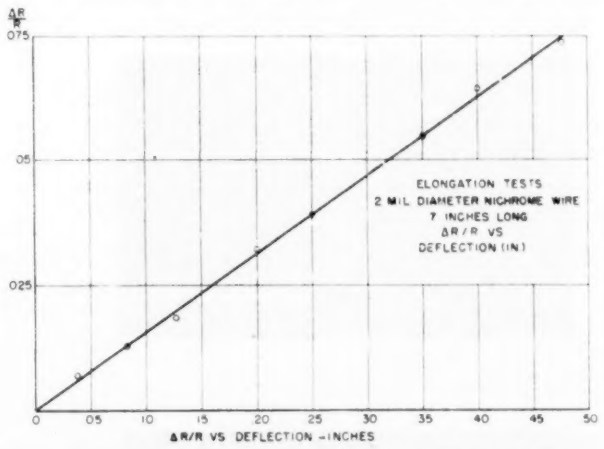


Fig. 13 Single-Wire Strain-Gage Resistance Change Versus Elongation

For acceleration measurements, the same type of wire gages was applied. A pair of these gages was cemented to a hollow cylinder which was used as acceleration-sensitive element (see Fig. 8). The gages were connected in series so that no resistance change was caused by bending. It was assumed that the strain in the cylinder was caused by the force necessary to accelerate the mass of that section which was located between the center of the strain gage, and the free end.

For strain measurements, a 2-mil-diam nichrome wire, 7 in. long, was stretched between two anchor points, one of them on the tup, and the other one on an arm attached to the pendulum, Fig. 7. This anchor point for the wire was isolated from the arm, and provisions were made for putting the wire under tension after it had been soldered.

This arrangement made the stress in the wire near the soldered joint very small even when the impact occurred. This provision was necessary as experience has shown that thin wires break near soldered junctions when relatively small stresses occur.

The gage factor[6] was determined by elongating the wire stati-

[6] "The Development of Electrical Strain Gages," by A. V. deForest and H. Lederman, National Advisory Committee for Aeronautics, Technical Notes No. 744.

cally, and by simultaneous measurement of the relative resistance and of the relative elongation. To make these measurements, the wire was cemented to a rubber strip, suspended vertically. The lower end of the rubber strip carried a platform on which weights could be placed. The elongation was measured by a scale observed with a magnifying glass. The resistance change was measured by a standard bridge. The relative resistance change is plotted as a function of relative elongation in Fig. 13, and it should be noted that this function is a straight line which extends well into the plastic range of the wire. This is not necessarily true, however, when the stress is reduced after the yield strength has been exceeded.

Attention was given to the attachment of the leads to the gages near the tup to prevent breakage due to the high acceleration, and due to the approximate 2-ft travel of the tup end after the fracture of the specimen. The terminals of the gages were soldered to cotton-covered insulated copper wire of 10 mils diam. The terminals and the wire were tied to the specimen and to the tup by friction tape and by transparent Scotch tape, as can be seen in Fig. 7.

Electrical Circuit

The electrical circuits associated with the strain gages for the measurement of stress, strain, and acceleration were identical. A schematic diagram of this circuit is shown in Fig. 14.

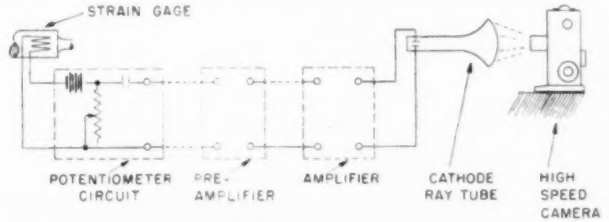


Fig. 14 Electrical Equipment and Recording Equipment Associated With Strain Gages

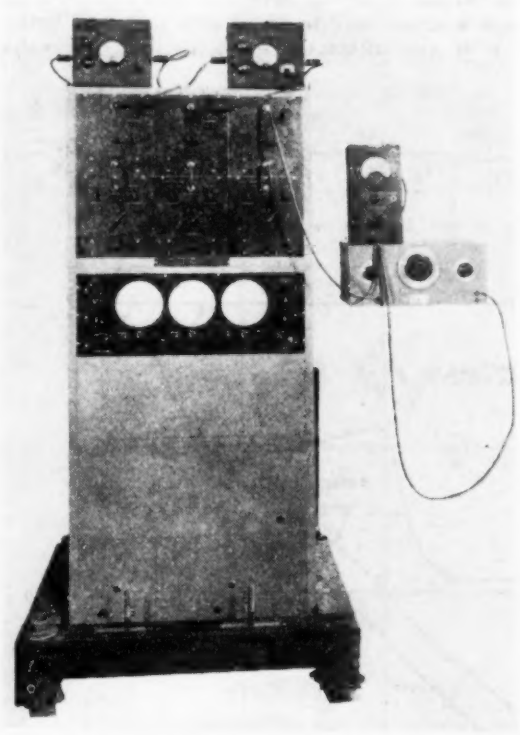


Fig. 15 Cathode-Ray Oscillograph for Simultaneous Recording of Three Signals

The changing resistance of the gage wire due to the elongation or compression of the specimen was converted to an alternating voltage in the potentiometer circuit. The output of the potentiometer circuit was supplied to the low-level amplifiers of a commercial three-tube cathode-ray oscillograph, which is shown in Fig. 15. In this illustration, the cabinets containing the potentiometer circuits are placed on top of the oscillograph. The oscillator and the vacuum-tube voltmeter seen at the right are used to calibrate the circuit, and to put a 2000-cps timing wave on the record. The gain of the electrical circuit was constant within 5 per cent for sinusoidal input voltages from 10 to 100,000 cps. An input voltage having a square wave shape did not excite any oscillations which would be noticeable on the records. The available gain of the amplifiers was 1,000,000. A gain of approximately 100,000, however, was sufficient for most tests.

Appendix 2

Effect of Location of Strain Gage

Forces in Test Section and in Large-Diameter Sections

The force distribution in the specimen was analyzed. The stress in the test section in which fracture took place was determined from measurements of the strain in one or both of the adjacent sections of larger diameter, since strain measurements by wire-type strain gages could not, of course, be made in the test section itself. The relations between the forces in the test section and the forces in each of the large-diameter sections were found by analysis and confirmed by the consistency of results, as mentioned elsewhere.

The following equation was used to calculate the stresses in the test section from the strain measurements in either one of the large-diameter sections

$$\sigma_{TS} = \left(\epsilon_{LS} E_{LS} \pm \frac{ma}{A_{LS}}\right) \frac{A_{LS}}{A_{TS}} \quad \ldots\ldots\ldots\ldots [1]$$

where σ = stress
ϵ = strain
E = modulus of elasticity
A = area
m = mass between center line of strain gage in large-diameter section and line of rupture
a = acceleration of mass m
Subscript (LS) indicates the large-diameter section, and subscript (TS) indicates the test section.

The plus sign was used in Equation [1], when the strain measurements were made near the tup end and the minus sign was used when strain measurements were made near the pendulum end, although for this latter case the term for the stress due to the inertia effect $\frac{ma}{A_{LS}}$ was in general very small (less than 5 per cent of the total stress). The stress was obtained with sufficient accuracy for most practical purposes for measurement made near the pendulum end from the simplified equation

$$\sigma_{TS} = \epsilon_{LS} E_{LS} \frac{A_{LS}}{A_{TS}} \quad \ldots\ldots\ldots\ldots\ldots\ldots [2]$$

Equations [1] and [2] were derived from the analysis of the equivalent "mass-and-spring" system. The same Equation [2] was obtained by an additional analysis by "stress waves." This latter analysis is independent of the previously mentioned analysis. Both methods of analysis will be discussed in detail.

The strain value ϵ_{LS} and the acceleration values a, were ob-

tained as a function of time from oscillograms, such as shown in Fig. 9 (*b*).

Analysis as "Mass-and-Spring" System

In this analysis the specimen was considered as a system split up into one mass and two springs. (The justification and limitations are discussed later.) The "mass-and-spring" system for that case in which the strain gage was attached near the tup end is shown in Fig. 16. The spring k_1 represents that portion of the large-diameter section covered by the strain gage, and the spring k_2 represents that portion of the small-diameter section in which yielding occurred. The mass represents the mass of the specimen between the center of the strain gage and the point of rupture. The strain gage attached to the large-diameter section measured the force F_1 through the spring k_1, while the force F_2 through the spring k_2 ruptured the specimen. The relation between those two forces is then

$$F_1 = ma + F_2$$

where a = acceleration of the mass.

Equation [1] is obtained from this equation by substitution of corresponding stresses in place of the forces.

The stress in the large-diameter section was, therefore, mainly produced by a force which was equal to the tensile force on the specimen at the point of rupture, the value of which was desired to be known, plus the force required to accelerate that section of the specimen which was between the gage and the point of rupture.

When the strain gage was attached near the pendulum end, the "mass-and-spring" system in Fig. 16 was applicable except that the tup and the pendulum are now interchanged in the sketch in Fig. 16, and that the force F cuts in the opposite direction.

The foregoing analysis can be justified as providing a reasonable approximation for the period of plastic deformation which is the greater part of the time interval of the total rupture period, and which lasts from 250 to 1000 μ sec, depending upon the striking velocity. This "mass-and-spring" system analysis, however, should preferably not be used for the short time interval of elastic deformation, lasting only 30 to 60 μ sec, since it does not furnish information on the details of the force fluctuations during certain small time intervals. This interval is the time it takes a stress wave to travel once back and forth. This time is 40 μ sec within the specimens used. To analyze the

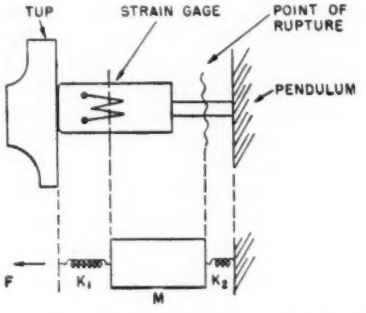


Fig. 16 Equivalent "Mass-and-Spring" System of Specimen

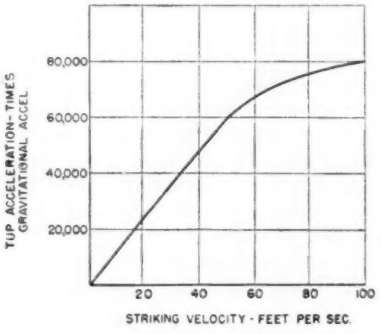


Fig. 17 High-Velocity Impact-Testing Machine; Tup Acceleration Versus Striking Velocity

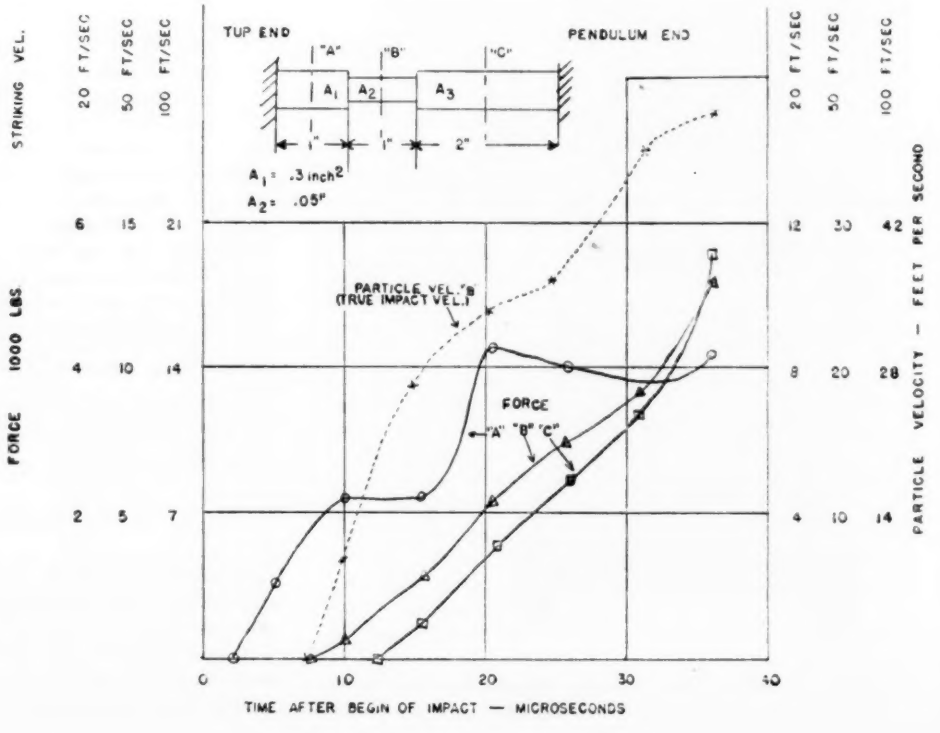


Fig. 18 Constructed Forces and Particle-Velocity Curves (*a*, Specimen for stress wave analysis. *b*, Force versus time curves. *c*, Particle velocity versus time curves.)

stresses during this time interval, the analysis by stress waves was used.

Analysis by Stress Waves

For the analysis by means of stress waves, certain assumptions seemed necessary. The acceleration of the tup end of the specimen was assumed to be constant from the instant of the impact to that instant at which the front end of the specimen attained the velocity of the striking horns, and for the succeeding time intervals the acceleration was assumed to be zero. The value of this initial constant acceleration was chosen as the maximum acceleration measured, Fig. 17. It was further assumed that both the pendulum end of the specimen and also the tup end were attached to masses which were very large compared with the mass of the specimen. The specimen for which this analysis was made is shown in Fig. 18(*a*).

The process of this analysis has been described by Donnell.[7]

[7] "Longitudinal Wave Transmission and Impact," part 1, by L. H. Donnell, Trans. A.S.M.E., vol. 52, 1930, p. 153.

The magnitude of force in each section of the specimen during the time intervals after the impact was obtained from the analysis, and these forces were plotted as a function of time in Fig. 18(*b*). A similar analysis and curves of somewhat similar shape were obtained for the magnitudes of the particle velocity to obtain the actual impact velocities when the yield strength was reached, Fig. 18(*c*).

The analysis was carried out only for the range of elastic deformation, i.e., up to that instant at which the yield strength was reached; and, hence, the curves in Fig. 18(*b*) cover stresses only below the yield strength. The values for the yield strength were taken from the yield strength versus striking velocity curves, Fig. 2(*a*) and (*b*).

The forces within the test section are in fair agreement with the forces in the larger diameter section near the pendulum end at the instant at which the yield strength is reached. This is important as the yield strength in the test section was determined from measurements in the large-diameter section. This fair agreement leads to the same Equation [2] which resulted from the previous analysis.

Heat Effects in Lubricating Films

By A. C. HAGG,[1] EAST PITTSBURGH, PA.

Heat effects in lubricating films are analyzed on the basis of simple shear of the lubricant, Reynolds logarithmic formula relating lubricant viscosity and temperature, and an equation relating the heat generation and heat flow in the film. The film-temperature dependence on velocity is determined, and the result is used to obtain the shearing stress and shearing rates. The formulas thus derived are useful in analyzing the performance of oil-film bearings. Experiments have been carried out with measurement of shaft- and bearing-surface temperatures, as well as friction; the tests support the analytical results. An approximate means for judging the importance of film heating in a given case in terms of velocity and lubricant viscosity is suggested.

Nomenclature

THE following nomenclature is used in the paper:

Symbol			Dimensions
θ	=	temperature at any point in film	θ
θ_1	=	temperature at surface of bearing	θ
θ_2	=	temperature at surface of journal	θ
θ_0	=	maximum temperature in film	θ
h	=	film thickness	L
y	=	distance from bearing surface to point in film	L
U	=	velocity of journal	LT^{-1}
u	=	velocity of lubricant at y	LT^{-1}
u_0	=	velocity of lubricant where $\theta = \theta_0$	LT^{-1}
μ	=	viscosity of lubricant	$ML^{-1}T^{-1}$
μ_1	=	viscosity of lubricant where $\theta = \theta_1$	$ML^{-1}T^{-1}$
μ_2	=	viscosity of lubricant where $\theta = \theta_2$	$ML^{-1}T^{-1}$
μ_0	=	viscosity of lubricant where $\theta = \theta_0$	$ML^{-1}T^{-1}$
α	=	coefficient in expression for viscosity	$ML^{-1}T^{-1}$
β	=	coefficient of exponent in expression for viscosity	θ^{-1}
S	=	shearing stress in lubricant	$ML^{-1}T^{-2}$
H	=	heat flow normal to surfaces at y	MT^{-3}
K	=	thermal conductivity of lubricant	$MLT^{-3}\theta^{-1}$

Introduction

The first considerations of heat effects in lubricating films were approximations based upon the assumption that the viscosity of the lubricant was not appreciably affected by the temperature differences within the film; the formal results were confined to defining the temperature distribution across the film.[2] Later, Kingsbury devised a graphical method for solving the temperature-distribution problem when the temperature variation is considerable;[3] the method also yields the shearing stress and other film characteristics.

The purpose of the present consideration of heat effects in lubricating films was to obtain usable formulas defining film conditions, taking account of the variable viscosity across the film thickness, and to check experimentally the results for comparatively high journal velocities, and high shear rates.

1 Analysis

The analysis is based on (1) simple shear of the lubricant as defined by Newton's law of viscosity; (2) Reynolds' logarithmic formula relating lubricant viscosity and temperature; and (3) Fourier's equation written for the heat generation and heat flow in the film. Further, it is assumed that the lubricant flow is laminar in character and bounded by parallel planes, and that the conduction of heat through the lubricant is not affected by its motion; normal temperature gradients are assumed to occur in the region of the boundary layers of the film and surfaces. The change in heat conductivity with temperature of ordinary lubricants is small and will be considered negligible

We can write the following three equations

$$S = \mu \frac{du}{dy} \quad [1]$$

$$\mu = \alpha e^{-\beta\theta} \quad [2]$$

$$H = S(u - u_0) = -K \frac{d\theta}{dy} \quad [3]$$

Film Temperatures

Substituting Equations [1] and [2] in Equation [3]

$$(u_0 - u)du = \frac{K}{\alpha} e^{\beta\theta} d\theta \quad [4]$$

Integrating

$$u_0 u - \frac{1}{2}u^2 = \frac{K}{\alpha\beta} e^{\beta\theta} + C \quad [5]$$

Evaluating the constant of integration, at $u = 0$, $\theta = \theta_1$

$$C = -\frac{K}{\alpha\beta} e^{\beta\theta_1}$$

Substituting the value of C in Equation [5] and solving for θ

$$\theta = \frac{1}{\beta} \ln \left(e^{\beta\theta_1} + \frac{\alpha\beta u_0}{K} u - \frac{\alpha\beta}{2K} u^2 \right) \quad [6]$$

where the value of u_0 can be obtained from Equation [4] by integrating between the limits $(U, 0)$ and (θ_2, θ_1)

$$\int_0^U (u_0 - u)du = \int_{\theta_1}^{\theta_2} \frac{K}{\alpha} e^{\beta\theta} d\theta$$

and

$$u_0 = \frac{U}{2} + \frac{K}{\alpha\beta U} \left(e^{\beta\theta_2} - e^{\beta\theta_1} \right) \quad [7]$$

---

[1] Westinghouse Research Laboratories.

[2] See for example "Theory of Lubrication," by Mayo D. Hersey, John Wiley and Sons, Inc., New York, N. Y., 1938, p. 115.

Contributed by the Applied Mechanics Division and the Special Research Committee on Lubrication and presented at the Annual Meeting, New York, N. Y., Nov. 29–Dec. 3, 1943, of The American Society of Mechanical Engineers.

Discussion of this paper should be addressed to the Secretary, A.S.M.E., 29 West 39th Street, New York, N. Y., and will be accepted until July 10, 1944, for publication at a later date. Discussion received after the closing date will be returned.

Note: Statements and opinions advanced in papers are to be understood as individual expressions of authors and not of the Society.

[3] "Heat Effects in Lubricating Films," by Albert Kingsbury, *Mechanical Engineering*, vol. 55, 1933, pp. 685–688; discussion, vol. 56, 1934, pp. 120, 121.

Equation [7] can also be written

$$u_0 = \frac{U}{2} + \frac{K}{\beta U}\left(\frac{1}{\mu_2} - \frac{1}{\mu_1}\right) \quad \ldots\ldots [7a]$$

At the point of maximum temperature, $u = u_0$ and thus

$$\theta_0 = \frac{1}{\beta}\ln\left(e^{\beta\theta_1} + \frac{\alpha\beta}{2K}u_0^2\right) \quad \ldots\ldots [8]$$

In many practical cases, the heat conduction axially along a journal is negligible after equilibrium conditions have been reached; thus the journal can be considered as neither receiving nor giving up heat, and $u_0 = U$ and $\theta_0 = \theta_2$. Dividing Equation [8] by $e^{\beta\theta_1}$ the temperature drop across the film is

$$(\theta_2 - \theta_1) = \frac{1}{\beta}\ln\left(1 + \frac{\beta\mu_1}{2K}U^2\right) \quad \ldots\ldots [9]$$

For small values of $\frac{\beta\mu_1}{2K}U^2$ compared to unity, the right side of Equation [9] closely approaches $\frac{\mu_1}{2K}U^2$, and we can write to a close approximation

$$(\theta_2 - \theta_1) = \frac{\mu}{2K}U^2 \quad \ldots\ldots [10]$$

or

$$(\theta_0 - \theta_1) = \frac{\mu}{2K}u_0^2 \quad \ldots\ldots [10a]$$

Equation [10] corresponds to the simplified result obtained on the assumption that the viscosity of the lubricant is not appreciably affected by temperature differences within the film.[3]

Shearing Stress

The value of the shear stress can be obtained from Equations [1] and [2] combined with a previous result Equation [6], relating θ as $f(u)$, thus

$$Sdy = \alpha e^{-\beta[f(u)]}\,du \quad \ldots\ldots [11]$$

where

$$f(u) = \frac{1}{\beta}\ln\left(e^{\beta\theta_1} + \frac{\alpha\beta u_0}{K}u - \frac{\alpha\beta}{2K}u^2\right)$$

taking the logarithm of Equation [11]

$$\ln Sdy = \ln\alpha - \beta[f(u)] + \ln du$$

or

$$Sdy = \frac{\alpha\,du}{\left(e^{\beta\theta_1} + \frac{\alpha\beta u_0}{K}u - \frac{\alpha\beta}{2K}u^2\right)} \quad \ldots\ldots [12]$$

using the following relations

$$\left.\begin{aligned} a &= e^{\beta\theta_1} \\ b &= \frac{\alpha\beta u_0}{K} \\ m &= -\frac{\alpha\beta}{2K} \\ q &= b^2 - 4am \end{aligned}\right\} \quad \ldots\ldots [13]$$

the solution of Equation [12] is

$$Sy = \frac{-2\alpha}{\sqrt{q}}\tanh^{-1}\frac{2mu + b}{\sqrt{q}} + C \quad \ldots\ldots [14]$$

at $y = 0$, $u = 0$, and the constant of integration is

$$C = \frac{2\alpha}{\sqrt{q}}\tanh^{-1}\frac{b}{\sqrt{q}}$$

and

$$S = \frac{2\alpha}{y\sqrt{q}}\left[\tanh^{-1}\frac{b}{\sqrt{q}} - \tanh^{-1}\frac{2mu + b}{\sqrt{q}}\right] \quad \ldots [15]$$

Remembering that at $y = h$, $u = U$, Equation [15] becomes

$$S = \frac{2\alpha}{h\sqrt{q}}\left[\tanh^{-1}\frac{b}{\sqrt{q}} - \tanh^{-1}\frac{2mU + b}{\sqrt{q}}\right] \quad \ldots [16]$$

which is the general result desired.

Equation [16] can be converted to the normal nomenclature by making use again of the relations [13] and Equation [8], thus the shearing stress becomes

$$S = \frac{1}{h\sqrt{\frac{\beta}{2K\mu_0}}}\left[\tanh^{-1}\sqrt{\frac{\beta\mu_0}{2K}}u_0 + \tanh^{-1}\sqrt{\frac{\beta\mu_0}{2K}}(U - u_0)\right] \quad \ldots\ldots [17]$$

An important special case occurs when the maximum temperature is at the moving surface, i.e., $u_0 = U$, and $\mu_0 = \mu_2$, and thus Equation [17] reduces to

$$S = \frac{1}{h\sqrt{\frac{\beta}{2K\mu_2}}}\tanh^{-1}\sqrt{\frac{\beta\mu_2}{2K}}U \quad \ldots\ldots [18]$$

Another special case is when the boundary surfaces are at the same temperature, i.e., $u_0 = \frac{U}{2}$, and the shearing stress becomes

$$S = \frac{2}{h\sqrt{\frac{\beta}{2K\mu_0}}}\tanh^{-1}\frac{1}{2}\sqrt{\frac{\beta\mu_0}{2K}}U \quad \ldots\ldots [19]$$

Equations [17], [18], and [19] reveal that for a given minimum viscosity in the lubricant film, the shearing stress increases at an increasing rate with increase in velocity U. The velocity is finally limited by the infinite rate at which the shearing stress increases, i.e., when the arguments reach unity. Doubtless the assumptions upon which the development is based break down before the limiting condition is reached, and probably the maximum velocity thus defined is somewhat low. With the help of Equations [2] and [8], we can substitute for μ_2 in Equation [18] its value

$$\mu_2 = \frac{\mu_1}{1 + \frac{\beta\mu_1}{2K}U^2} \quad \ldots\ldots [20]$$

and we can see that, with a given maximum viscosity, the shearing stress increases at a decreasing rate with increase in U. A maximum shear stress is finally reached, and with further increase in U the shear stress diminishes slowly. A curve showing this effect, calculated on the basis of a typical mineral oil, is given in Fig. 1. It is expected that the theory would be valid, at least to velocities corresponding to the maximum shear stress.

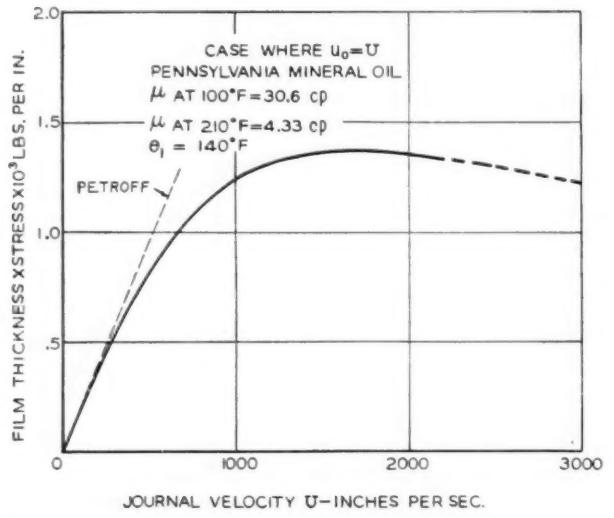


FIG. 1 SHEARING STRESS FOR CONSTANT BEARING TEMPERATURE

It can be noted that for small values of U, Equations [17], [18], and [19] reduce to a good approximation

$$S = \mu \frac{U}{h} \quad \ldots\ldots\ldots\ldots\ldots\ldots [21]$$

which is the basis for Petroff's equation.

RATE OF SHEAR

The rate of shear in the film can be obtained for all values of μ, and, consequently, for all values of u by rewriting Equation [11]

$$\frac{du}{dy} = \frac{S}{\alpha e^{-\beta[f(u)]}} \quad \ldots\ldots\ldots\ldots\ldots\ldots [11a]$$

Similarly for any value of θ, u, μ, or $\frac{du}{dy}$ the corresponding value of y/h can be obtained from Equations [15] and [16].

2 EXPERIMENTS

Equations [9] and [18] of the analysis were chosen as a basis for designing the experiments and apparatus because it appeared that the condition of negligible heat flow to or from a journal could be closely approached, and in a steady state. Under this condition, film heating is disclosed most prominently in the effect upon friction; moreover, the maximum and minimum temperatures in the film occur at the journal and bearing surfaces, respectively, and measurement of journal and bearing temperatures leads to a direct check on the derived results. The independence of the temperature drop on the film thickness enhances the attractiveness of the latter test. The velocity distribution, and the temperature distribution in the film under the test conditions are shown in Fig. 2.

APPARATUS AND TEST PROCEDURES

The apparatus, as designed and used for the tests is shown in section in Fig. 3. A ground and polished plug shaft $1^1/_2$ in. diam of hardened tool steel was arranged to rotate in a steel ring. The bearing surface was a tin-base babbitt metal about $^1/_{32}$ in. thick, considerable care being taken to obtain a uniformly good bond between the babbitt metal and the steel to avoid the possibility of any abnormal temperature gradients at or near the

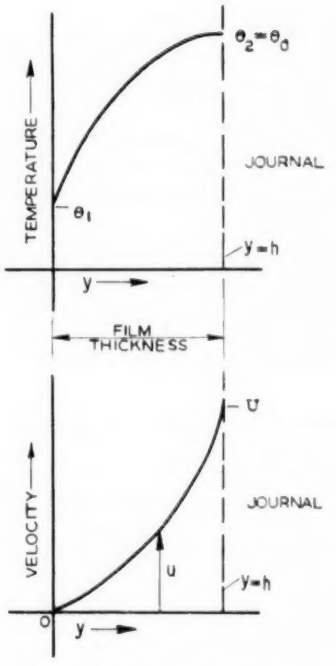


FIG. 2 FILM TEMPERATURE AND VELOCITY DISTRIBUTION UNDER TEST CONDITIONS

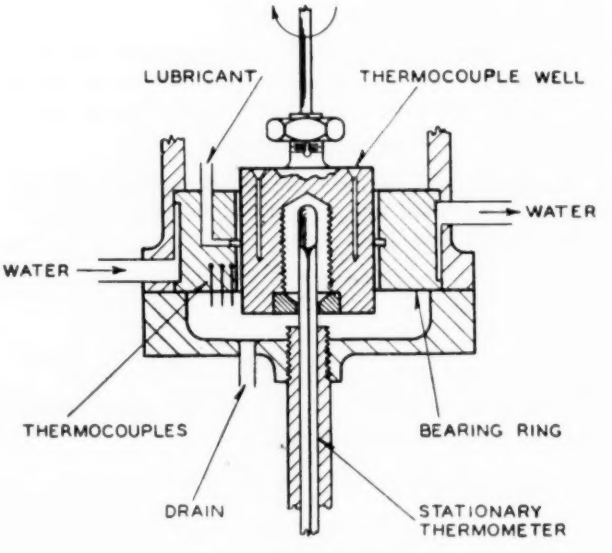


FIG. 3 TEST MACHINE

bonding area. The outer surface of the ring was arranged for water cooling, which arrangement afforded a simple thermal means for measuring the bearing friction.

The loss of heat from the plug shaft through normal modes of heat transfer was calculated to be negligibly small under contemplated conditions, compared to the heat generated within the film. Thus it was concluded that the shaft temperature would be very nearly uniform throughout. To determine this temperature, the bulb of a mercurial thermometer was arranged to project into an axial hole in the shaft; the radial clearance between the stationary thermometer and the hole entrance being made as small as practicable, or about 0.005 in. Under test

conditions, the oil pan and thermometer support, and the enclosed volume were at a temperature not far removed from the shaft temperature, so that any small interchange of air and oil vapor between the oil-pan volume and the shaft cavity, or heat conduction along the thermometer barrel, was believed to have negligible effect on the thermometer reading.

The temperature of the bearing surface was determined by the extrapolation of temperature data obtained by means of thermocouples at several radii. The extrapolation was simplified by recalling the formula for the outward radial heat conduction in a ring or plate; viz.

$$\theta = -\frac{H}{2\pi K} \ln r + C$$

Thus, the temperature data can be plotted on semi-logarithmic co-ordinates, and the extrapolation made conveniently by a straight line. A typical extrapolation is shown in Fig. 4.

The emf's of the copper-constantan thermocouples were indicated on a Leeds and Northrup 8657-C potentiometer, and calibrated against the shaft thermometer. It is believed that, relatively, the temperatures could be determined within $^1/_2$ deg F.

The lubricating system was a recirculating type with the supply reservoir kept under reduced pressure of 1 mm of mercury abs to eliminate absorbed air in the lubricant. The lubricant was pumped from the reservoir and supplied to the test bearing at a gage pressure of 10 to 15 psi. Two low-viscosity mineral oils were used in the tests; their viscosity characteristics being calculated from Saybolt readings made before and after each test. The accepted values were believed to be accurate to within ±3 per cent.

Speed measurements were made with a General Radio "Strobotac," the calibration against line frequency being carefully checked before and after each reading. The accuracy of the speed measurements is considered to be within ±0.5 per cent.

Test runs were carried out under steady-state conditions as indicated by constant temperature readings. Measurements of speed, temperatures, and friction were made in order; the measurements being repeated until three successive sets of data were in good agreement. The average values of these data were accepted as a test result. The friction values included minor corrections as determined from the bearing end leakage, and temperature gradients in the machine frame.

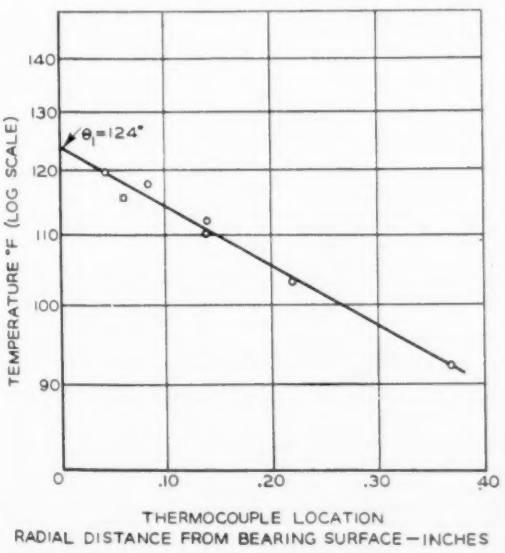


FIG. 4 TYPICAL EXTRAPOLATION FOR BEARING TEMPERATURE

TEST RESULTS AND COMPARISON WITH THEORY

The principal test results are given in Table 1; the dimensional units employed are the inch, the pound, the second, and deg F. The given values of the film thickness were determined from the average of a number of careful measurements of bearing and shaft diameters, and corrected for thermal-expansion effects. The basic measurements were made with telescopic and micrometer gages.

TABLE 1 TEST DATA

Run no.	Journal speed U, ips	Film temperature at journal θ_2, deg F	Film temperature at bearing θ_1, deg F	Film temperature drop ($\theta_2 - \theta_1$) deg F	Shearing stress S, psi	Film thickness h, in. × 10^3	Oil thermal conductivity[b] K, lb/sec per deg F	Oil[a]
1	786	136.5	125	11.5	0.787	0.60	0.017	A
2	790	136	124	12.0	0.805	0.60	0.017	A
3	1180	179	159	20.0	0.744	0.55	0.0165	A
4	1290	179	156	23.0	0.882	0.55	0.0165	A
5	935	144.5	121	23.5	0.815	1.20	0.017	B
6	1035	155.5	131	24.5	0.780	1.20	0.017	B
7	1185	160.5	127.5	33.0	0.750	1.15	0.0165	B
8	780	143	125	18.0	0.660	1.20	0.017	B

[a] For oil A: μ at 130 F = 4.44 cp; μ at 170 F = 2.76 cp. $\alpha = 3.06 \times 10^{-6}$ lb-sec/in.^{2}; $\beta = 1.20 \times 10^{-2}$ reciprocal deg F.
For oil B: μ at 130 F = 7 cp, μ at 170 F = 4.04 cp. $\alpha = 5.94 \times 10^{-6}$ lb-sec/in.^{2}; $\beta = 1.36 \times 10^{-2}$ reciprocal deg F.
[b] From J. F. D. Smith, Ind. and Eng. Chem., vol. 22, 1930.

It can be noted from the table that the temperature difference across the film was considerable in each case, and, consequently, the conclusions can hardly be influenced by small errors in the temperature measurements.

The comparison of theory and experiment can be made conveniently by plotting the results in dimensionless form. Multiplying Equation [9] by β, we have

$$\beta(\theta_2 - \theta_1) = \ln\left(1 + \frac{\beta\mu_1}{2K} U^2\right) \quad \ldots\ldots\ldots\ldots [9a]$$

and the dimensionless parameters are $\beta(\theta_2 - \theta_1)$ and $\frac{\beta\mu_1}{2K} U^2$.

Similarly Equation [18] can be rewritten as

$$h\sqrt{\frac{\beta}{2K_{\mu_2}}}\, S = \tanh^{-1}\sqrt{\frac{\beta\mu_2}{2K}}\, U \quad \ldots\ldots\ldots\ldots [18a]$$

and the dimensionless parameters are $h\sqrt{\frac{\beta}{2K_{\mu_2}}}\, S$ and $\sqrt{\frac{\beta\mu_2}{2K}}\, U$.

The resulting curves are shown in Figs. 5 and 6.

Referring to Fig. 5, the measured temperature drops across the film are in relatively close agreement with theory. These results are considered the more significant because of their independence on film thickness. The trend of the test points on oil B suggest some error in the accepted μ, or K or in both.

The measured shearing stresses in the film, shown in Fig. 6, are also in good agreement with theory, although the scatter of the test points is more pronounced than in the case of the film-temperature drops. Inaccuracies, which are difficult to avoid in the many measurements required in this test, probably account for the discrepancies.

The foregoing considerations of theory and experiment suggest an importance of heat effects in lubricating films; it appears that the degree of importance should be qualified by some convenient criterion involving the principal operating variables of velocity and lubricant viscosity.

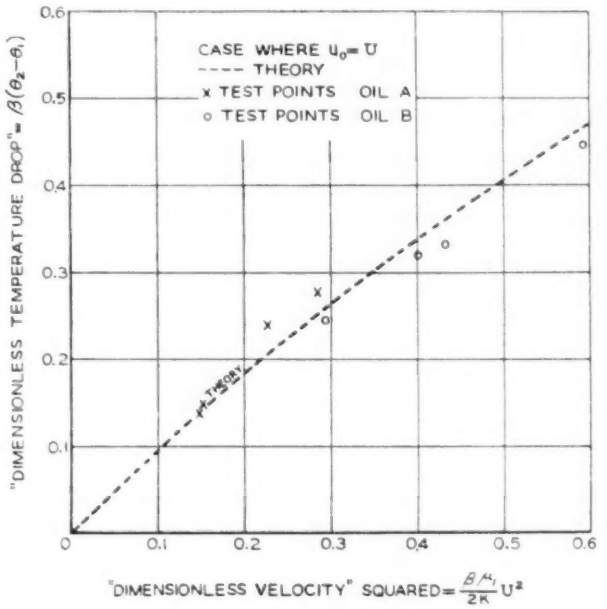


FIG. 5 TEMPERATURE DROP ACROSS OIL FILM

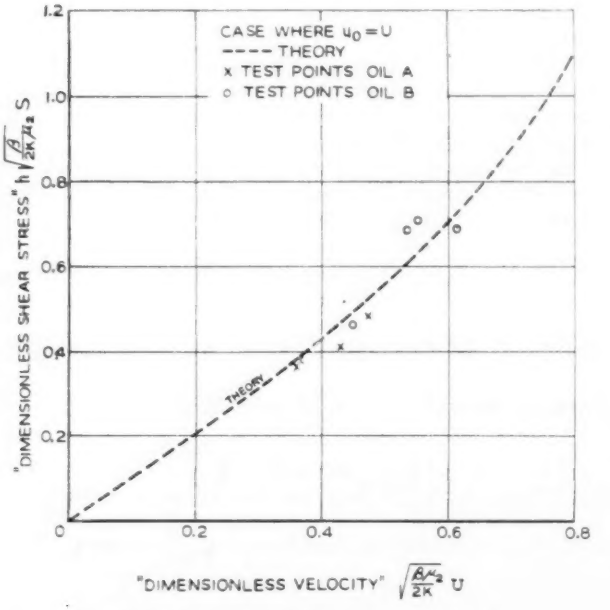


FIG. 6 SHEARING STRESS IN OIL FILM

The effect of operating variables on shearing stress are defined for limiting conditions of bearing and shaft temperatures by Equations [18] and [19]. The appropriate comparison with the shear stress, as defined by Equation [21] and evaluated using the maximum film viscosity, is an indication of the effect of film heating. Letting S_1 and S_2 refer to the shearing stress, as defined by Equations [18] and [21], respectively, we might write the percentage decrease in shear stress due to film heating

$$\text{Per cent decrease} = \frac{S_2 - S_1}{S_2} \quad \ldots\ldots\ldots\ldots [22]$$

Using an average value of $K = 0.0165$ and of $\beta = 0.015$, with the help of Equation [20], we can determine the approximate values of lubricant viscosity and velocity for a given percentage effect on shear stress. The results have been determined for 2, 5, and 10 per cent decrease in shearing stress; for the cases where film heating is manifest most prominently, Equation [18]; and where heat effects are least pronounced, Equation [19]. These results, as shown in Fig. 7, afford an approximate means for judging the importance of film heat effects. It should be remembered that, when the heat carried away by end leakage of the lubricant is appreciable compared to the total heat generated, the film heat effects are diminished.

SUMMARY

Formulas have been derived for the temperature distribution in lubricating films, and the shearing stress has been evaluated taking account of the variable viscosity across the film thickness. The results are useful in analyzing the performance of oil-film bearings. The formulas for shearing stress are useful in determining the friction in high-speed, lightly loaded guide or journal bearings.

Experimental results are in good agreement with theory for velocities up to 1290 ips, and shearing rates in excess of 2×10^6 reciprocal seconds. The viscosity characteristics of the oils tested were apparently not influenced by shear rate within the limits of the experiments.

The approximate effect of film heating in a given case can be judged from Fig. 7.

ACKNOWLEDGMENT

The author wishes to express his thanks to Mr. R. E. Peterson and to Mr. M. D. Hersey for their interest and suggestions, and also to Mr. Carl Green for carefully carrying out the test program.

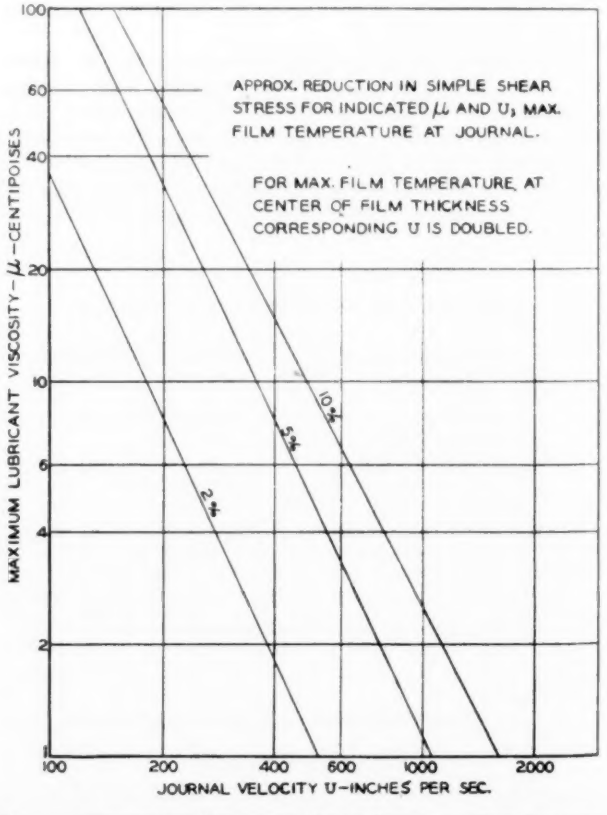


FIG. 7 APPROXIMATE EFFECT ON SHEAR STRESS BY FILM HEATING

Shrink-Fit Stresses and Deformations

By A. W. RANKIN,[1] SCHENECTADY, N. Y.

In this paper are derived the expressions for the stresses in a solid cylinder of infinite length caused by the action of an applied radial stress distributed uniformly over a single circumferential ring of finite length on the surface of the cylinder. An example of stresses of this type would be a long solid shaft with a uniform pressure applied on the surface for a short axial length. The practical worth of the results presented in this paper lie in their approximate applications to shrink fits. Test measurements of shaft deformations due to shrink pressures are included to illustrate the application of the theoretical results.

Nomenclature

The following nomenclature is used in the paper:

a = one half of axial length over which radial stress p is applied

a_0, a_1 = constants in solution for ϕ

E = modulus of elasticity

i = $\sqrt{-1}$

i_n = partial Bessel defined by $I_n(u) = \dfrac{e^u}{\sqrt{2\pi u}}\, i_n(u)$

I_n = modified Bessel of nth order and first kind, defined by $J_n(i\lambda r) = i^n I_n(\lambda r)$

J_n = Bessel of nth order and first kind

k = constant giving "effective" length of a long shaft subjected to a radial stress applied over a short axial length

m = constant which takes the values of m_1 and m_2 only

m_1 = $\dfrac{a + z}{r_0}$

m_2 = $\dfrac{a - z}{r_0}$

p = applied radial stress

r = radial distance

r_0 = shaft radius; also used to denote inside radius of ring to be shrunk on shaft

r_1 = outside radius of ring to be shrunk on shaft

u = radial deformation

u_0 = total shrink allowance

u_r = deformation of shrink ring

u_s = deformation of shaft surface

z = axial distance

$\gamma_{1.0}$ = $(1 - 2\nu - \rho) i_0(\lambda r_0) + \left(\lambda r_0 + \dfrac{\rho}{\lambda r_0}\right) i_1(\lambda r_0)$

$\gamma'_{1.0}$ = $(1 - 2\nu - \rho) I_0(\lambda r_0) + \left(\lambda r_0 + \dfrac{\rho}{\lambda r_0}\right) I_1(\lambda r_0)$

δ = *average* deformation of shaft surface within the planes of $z = \pm a$

λ = variable of integration used in Fourier integral. (Note that the variable λ would disappear if the indicated integrations could be completed; λ has in itself no direct physical significance)

ν = Poisson's ratio ($\nu = 0.30$ has been used for all the numerical work of this paper)

ρ = $2(1 - \nu) + \lambda r_0 \dfrac{i_0(\lambda r_0)}{i_1(\lambda r_0)}$

σ_r = radial stress

$\bar{\sigma}_r$ = radial-stress component

σ_θ = tangential stress

$\bar{\sigma}_\theta$ = tangential-stress component

σ_z = axial stress

$\bar{\sigma}_z$ = axial-stress component

τ_{rz} = shear stress

$\bar{\tau}_{rz}$ = shear-stress component

ϕ = stress function

General Considerations

In a considerable number of shrink-fit problems, a ring of short axial length is shrunk on a shaft whose length is so much greater than the length of the shrink ring that for practical purposes it may be considered infinite. It then becomes of great practical importance to determine the relation in the shaft between the radial stress on the outer surface and the radial deformation of this surface in order to calculate the resulting shrink-fit pressure between the ring and the shaft.

In an actual shrink-fit problem, a determination of the actual stresses would be extremely complex since it would be necessary to consider the stress distribution in the short ring as well as in the long shaft. It is well known, however, that the actual radial stress between the short ring and the long shaft is essentially constant in magnitude along the axial length of the shrink ring except close to the ends at which point the radial stress reaches a high value. Since the increase in the radial stress occurs only close to the ends, it follows that a good approximation to the average deformation of the shaft surface could be obtained by ignoring the radial-stress variations and considering only a long shaft with a uniform radial stress applied to the surface over a ring of short axial length. Such an approximation will not give the true stress distribution present in an actual shrink fit, but the average shrink pressure so calculated should be much closer to the true average than is now ordinarily calculated.

It is the purpose of this paper to present an analysis based on the uniform-stress conditions outlined previously, and to show how the results of this analysis may be used in shrink-fit problems; the physical conditions of the subject analysis are illustrated in Fig. 1.

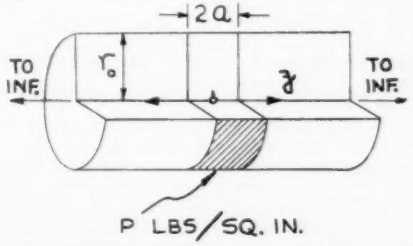


Fig. 1 Illustration of Physical Conditions of Subject Problem

---

[1] Central Station Engineering Division, formerly of Turbine Generator Engineering Division, General Electric Company.

Presented at the Annual Meeting, New York, N. Y., Nov. 29–Dec. 3, 1943, of The American Society of Mechanical Engineers.

Discussion of this paper should be addressed to the Secretary, A.S.M.E., 29 West 39th Street, New York, N. Y., and will be accepted until July 10, 1944, for public2tion at a later date. Discussion received after the closing date will be returned.

Note:. Statements and opinions advanced in papers are to be understood as individual expressions of their authors, and not those of the Society.

Curves will be given showing the radial, tangential, axial, and shear stresses throughout a long solid cylinder in which the applied radial stress is distributed on the shaft surface over a single circumferential band whose length is 15 per cent of the shaft diameter; charts are also given from which similar curves may be plotted for cases in which the length of the band over which the radial stress is applied varies from zero up to the diameter of the cylinder. Curves are plotted showing the radial deformation of the shaft surface for various ratios of band length to shaft diameter; also, a simple curve is given from which may be calculated the *average* radial deformation of the shaft surface under the band over which the applied radial stress is distributed. Also included are test data to illustrate the validity of the theoretical results.

It should be noted at this point that the method employed in the present analysis is given in some detail by Timoshenko (1),[2] although without any numerical results; an approximation to the present problem is also treated by Föppl (2), although again without giving any numerical results. The work of Timoshenko (1) actually considers an applied radial-stress system which would represent an infinite series of rings shrunk on a shaft, and is not directly applicable to the present problem which considers only one shrink ring. Timoshenko's solution considers an applied stress system which can be represented by a Fourier series rather than the stress system of the present problem which requires a Fourier integral representation.

The work of Föppl (2) assumes the applied force to be concentrated on the surface on a ring of infinitesimal length (thereby resulting in infinite stresses under the applied force). It would be necessary to apply still another integration in Föppl's analysis in order to consider the present case of radial stresses applied over a ring of finite length.

Methods of Analysis Based on Uniform-Stress Conditions

A series solution of the uniform-stress problem of this paper was published by M. V. Barton (3),[3] using a Fourier series of the general type given by Timoshenko (1), but with the fundamental period of the series sufficiently large so that the effects of neighboring pressure rings were small. The larger the fundamental period of the series the closer will the stress distribution approach that of a single ring, but the slower will be the convergence. Especially is this true around the points of discontinuity of the Fourier series as these are the points to exhibit the slowest convergence. The solution presented in the present paper, however, considers the stress distribution of a single ring directly and presents the results in Fourier integrals; the integrals are then evaluated to any desired degree of accuracy by using numerical integration in conjunction with the Si (x) and Ci (x) functions (4).

Comparison of the Fourier integral results with the series results of Barton (3) show close correspondence in all except minor details. In particular, the stress curves of the integral solution give slightly higher stresses near the ends of the applied stress p (z close to $\pm a$) for values of r approaching r_0, but these differences are never large enough to be of importance.

Assumptions

The major assumptions used in the present analysis are those in general use in most stress calculations; namely, it is assumed that the material is homogeneous and continuously distributed, is isotropic, perfectly elastic, and that the stresses do not exceed the elastic range. In addition to these general assumptions, the following are used to simplify the present specific problem:

1 It is assumed that there is no restraint to movement in the axial, or z, direction.

2 It is assumed that no bore hole is present in the shaft.

3 All the calculations have been based upon a value of Poisson's ratio $\nu = 0.30$.

Results

The radial deformation of the surface of a cylinder subjected to a radial stress p, distributed over the entire peripheral surface, may be put in the following form if it is assumed that σ_z and τ_{rz} (axial and shear stresses, respectively) are negligible

$$u = \frac{(1 - \nu) r_0 p}{E} \qquad [1a]$$

Similarly, the average deformation of the surface of the shaft of the present problem $\left(\text{average between the cross sections } \frac{z}{r_0} = \pm \frac{a}{r_0}\right)$ may be put in the following form

$$\delta = \frac{(1 - \nu) r_0 p}{kE} \qquad [1b]$$

The value of the constant k has been calculated for various values of the ratio $\frac{a}{r_0}$, and these are plotted in Fig. 2. The practical use of Equation [1b] is shown in the numerical example in the section, "Stress and Strain Curves, and Discussion."

Curves showing the distribution of the radial, tangential, axial, and shear stresses for the ratio $\frac{a}{r_0} = 0.150$ are given in Figs. 3 to 6, inclusive. In Fig. 7 has been plotted the direction of one of the principal stresses for the same value of the ratio $\frac{a}{r_0}$, and several stress trajectories are shown in this figure; the second principal stress is at right angles to the principal stress shown in Fig. 7, while the third principal stress is the σ_θ stress and is in the circumferential direction.

In Fig. 8 has been plotted the radial deformation of the shaft surface for the ratio of $\frac{a}{r_0} = 0.150$. Note that all these curves have been plotted against the ratio $\frac{z}{r_0}$, or axial distance expressed as a decimal of the shaft radius.

Fig. 9 gives the radial deformation of the shaft surface for several values of $\frac{a}{r_0}$, but on this curve the abscissa is $z/2a$, or axial distance expressed as a decimal of the axial length of the applied load. The latter abscissa was chosen for Fig. 9 so that the limit which the deformation approaches as $\frac{a}{r_0}$ approaches infinity may be clearly shown.

The radial, tangential, axial, and shear stresses in the solid cylinder of the subject problem are given explicitly by the infinite integrals Equations [18a] to [18d], inclusive, of the Appendix. Since, however, these expressions cannot be integrated, it is necessary to resort to numerical integration, and for that reason the curves given in Figs. 10 to 13, inclusive, have been prepared. The expressions evaluated by these curves are termed "stress

[2] Numbers in parentheses refer to the Bibliography at the end of the paper.

[3] The solution of reference (3) was unfortunately overlooked until the major portion of the present paper had been completed. Because of the importance of the approximate application to the universal problem of shrink fits, which was not discussed in detail in reference (3), it was felt that the integral and series methods presented very desirable complementary solutions.

components" since these curves are used to determine the actual stresses. The latter are obtained from the stress components by the following relations

$$\left.\begin{aligned}\sigma_r\left(\frac{r}{r_0},\frac{a}{r_0},\frac{z}{r_0}\right) &= \bar{\sigma}_r\left(\frac{r}{r_0},m_1\right)+\bar{\sigma}_r\left(\frac{r}{r_0},m_2\right)\\ \text{with } \bar{\sigma}_r\left(\frac{r}{r_0},-m\right) &= -\bar{\sigma}_r\left(\frac{r}{r_0},+m\right)\end{aligned}\right\}\quad\ldots[2a]$$

$$\left.\begin{aligned}\sigma_\theta\left(\frac{r}{r_0},\frac{a}{r_0},\frac{z}{r_0}\right) &= \bar{\sigma}_\theta\left(\frac{r}{r_0},m_1\right)+\bar{\sigma}_\theta\left(\frac{r}{r_0},m_2\right)\\ \text{with } \bar{\sigma}_\theta\left(\frac{r}{r_0},-m\right) &= -\bar{\sigma}_\theta\left(\frac{r}{r_0},+m\right)\end{aligned}\right\}\quad\ldots[2b]$$

$$\left.\begin{aligned}\sigma_z\left(\frac{r}{r_0},\frac{a}{r_0},\frac{z}{r_0}\right) &= \bar{\sigma}_z\left(\frac{r}{r_0},m_1\right)+\bar{\sigma}_z\left(\frac{r}{r_0},m_2\right)\\ \text{with } \bar{\sigma}_z\left(\frac{r}{r_0},-m\right) &= -\bar{\sigma}_z\left(\frac{r}{r_0},+m\right)\end{aligned}\right\}\quad\ldots[2c]$$

$$\left.\begin{aligned}\tau_{rz}\left(\frac{r}{r_0},\frac{a}{r_0},\frac{z}{r_0}\right) &= -\bar{\tau}_{rz}\left(\frac{r}{r_0},m_1\right)+\bar{\tau}_{rz}\left(\frac{r}{r_0},m_2\right)\\ \text{with } \bar{\tau}_{rz}\left(\frac{r}{r_0},-m\right) &= +\bar{\tau}_{rz}\left(\frac{r}{r_0},+m\right)\end{aligned}\right\}\quad\ldots[2d]$$

Stress and Strain Curves, and Discussion

In Fig. 2 is plotted a curve giving, for various values of $\frac{a}{r_0}$, the *average* radial deformation of the shaft surface under the band over which the radial stress is applied. By average deformation is meant the average radial deformation of the shaft surface between the planes $z = \pm a$. This is the curve whose use is recommended for calculating shrink fits and shrink-fit pressures between a ring of short axial length and a solid shaft whose length is much longer than that of the ring.

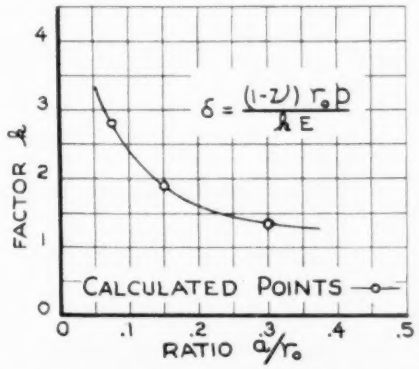


Fig. 2 Factor k for Computing Average Deformation on Radius of Shaft Surface Under Applied Radial Stress

As an illustration of the use of Fig. 2, assume that a ring of inner radius r_0 and outer radius r_1, and of short axial length, is shrunk on a solid shaft of much greater length, with a shrink of u_0 inches on the radius. If p is the average radial pressure between the ring and the shaft, the radial movement of the inside of the short ring will be

$$u_r = \frac{r_0 p}{E}\left[\frac{(1+\nu)+(1-\nu)\left(\frac{r_0}{r_1}\right)^2}{1-\left(\frac{r_0}{r_1}\right)^2}\right]\quad\ldots\ldots[3]$$

From Fig. 2, the average deformation of the surface of the solid shaft will be

$$u_s = \frac{(1-\nu)r_0 p}{kE}\quad\ldots\ldots[4]$$

with the value of k selected from Fig. 2 for the given ratio of $\frac{a}{r_0}$.

The total deformation must equal the specified shrink, or

$$u_0 = u_r + u_s\quad\ldots\ldots[5]$$

Solving for the radial pressure in terms of u_0

$$p = \frac{\frac{u_0}{r_0}E}{\left[\frac{(1+\nu)+(1-\nu)\left(\frac{r_0}{r_1}\right)^2}{1-\left(\frac{r_0}{r_1}\right)^2}+\frac{(1-\nu)}{k}\right]}\quad\ldots\ldots[6]$$

As a numerical example, assume the following

$r_0 = 10$ in. $\quad r_1 = 18$ in. $\quad a = 1.5$ in. $\quad \frac{u_0}{r_0} = 1.0 \times 10^{-3}$

$\nu = 0.30 \quad E = 30 \times 10^6 \quad k = 1.9$ (Fig. 2)

Substituting in Equation [6] gives

$$p = 11{,}700 \text{ psi}$$

If the effect of that portion of the shaft beyond the ring is neglected, then $k = 1$ in Equation [6], and the radial pressure between the ring and the shaft would be

$$p = 10{,}300 \text{ psi}$$

Consideration of the entire shaft has therefore increased the shrink pressure over 10 per cent.

Proceeding to Fig. 3, the radial stress σ_r is there plotted for the ratio $\frac{a}{r_0} = 0.150$. It is interesting to note here that for this ratio of $\frac{a}{r_0}$, the radial pressure at the center of the shaft is only 30 per cent of the applied radial stress instead of being equal to the

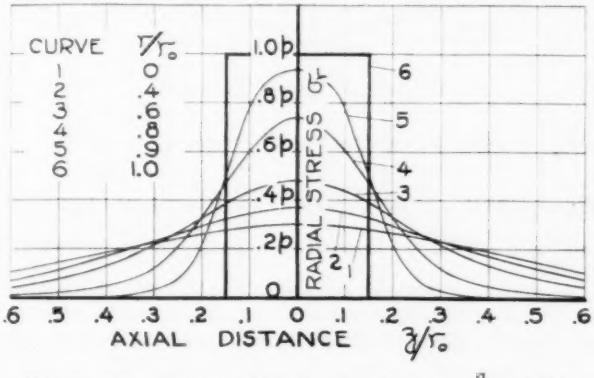


Fig. 3 Distribution of Radial Stress σ_r, for $\frac{a}{r_0} = 0.150$

applied radial stress as is implied when one neglects that portion of the length of the shaft beyond the ring over which the applied radial stress is distributed.

The distribution of tangential stress σ_θ has been plotted in Fig. 4 for the same ratio of $\frac{a}{r_0}$ (= 0.150). Note that at the center of

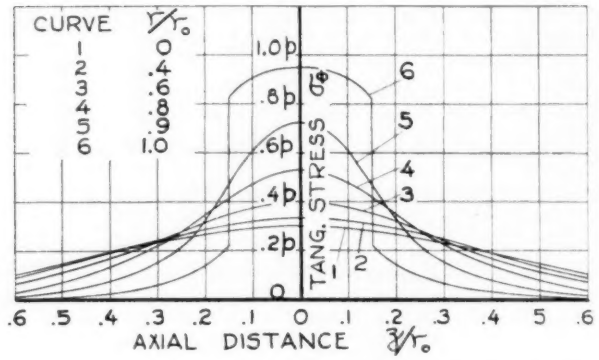


FIG. 4 DISTRIBUTION OF TANGENTIAL STRESS σ_θ, FOR $\frac{a}{r_0} = 0.150$

the shaft σ_θ is reduced to only 30 per cent of the applied radial stress; note also that on the surface of the shaft σ_θ is discontinuous at the lines of discontinuity of the applied radial stress.

The distribution of axial stress σ_z has been plotted in Fig. 5 $\left(\text{for } \frac{a}{r_0} = 0.150\right)$, and the rapidity with which σ_z changes magnitude may be seen by noting that σ_z has decreased from its maximum value (at $r = r_0$) to zero and has changed sign all within the outer 15 per cent of the shaft radius. The axial stress is actually discontinuous on the surface $r = r_0$ at the lines of discontinuity of the applied radial stress, changing from the maximum positive value to the maximum negative value at this point.

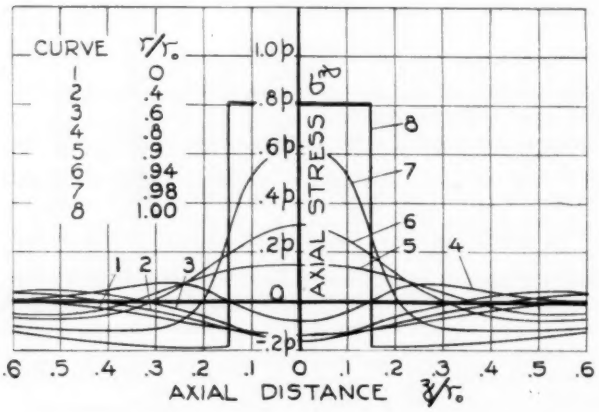


FIG. 5 DISTRIBUTION OF AXIAL STRESS σ_z, FOR $\frac{a}{r_0} = 0.150$

The distribution of shear stress τ_{rz} has been plotted in Fig. 6 for the ratio $\frac{a}{r_0} = 0.150$. It may be observed from this figure that the shear stress is zero for the center of the shaft, and is also zero at the shaft surface $r = r_0$ with the exception of the lines of discontinuity of the applied radial stress; at the latter lines, for $r = r_0$, the shear stress reaches its maximum value of $\pm \frac{p}{\pi}$. For intermediate values of r, the shear stress varies from zero, at the cross section representing the center line of the applied radial stress, to a maximum value which approaches $\frac{p}{\pi}$ as r approaches r_0, and then decreases to zero for cross sections remote from the applied radial stress. It is extremely interesting to note that this type of shear pattern, which gives a maximum shear at the surface of the shaft with zero shear at the shaft center line, is remarkably close to the shear patterns given by Timoshenko,[4] which actually apply to short beams under concentrated loads. The parabolic distribution which elementary theory gives for the shear in beams actually applies only to cross sections remote from the applied loads; near the applied loads, the shear in a beam is actually zero at the beam axial center line, and has a maximum value which approaches the outer surface of the beam as the point of application of the applied load is approached.

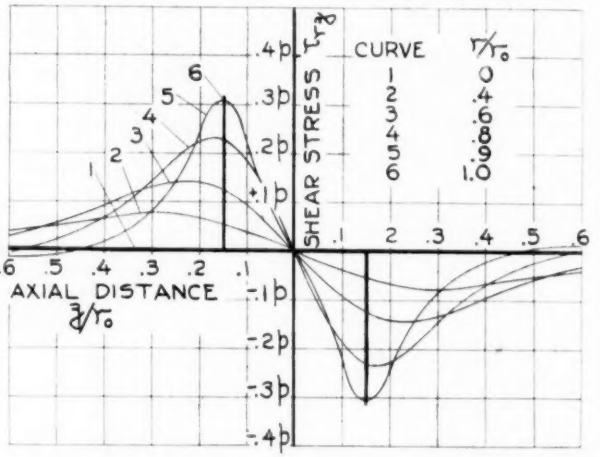


FIG. 6 DISTRIBUTION OF SHEAR STRESS τ_{rz}, FOR $\frac{a}{r_0} = 0.150$

Plotted in Fig. 7 are the stress trajectories formed by one of the principal stresses. These trajectories serve to illustrate clearly how the stress flows axially along the shaft so that the length of the latter external to the applied radial stress also tends to carry some of the load.

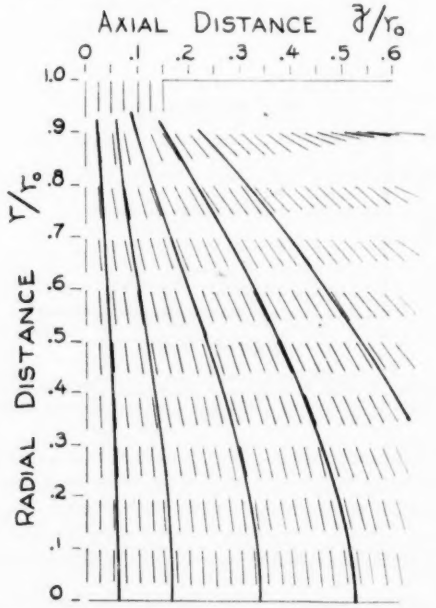


FIG. 7 DIRECTIONS OF ONE PRINCIPAL STRESS, AND STRESS TRAJECTORIES, FOR $\frac{a}{r_0} = 0.150$

[4] Bibliography, ref. (1), p. 49.

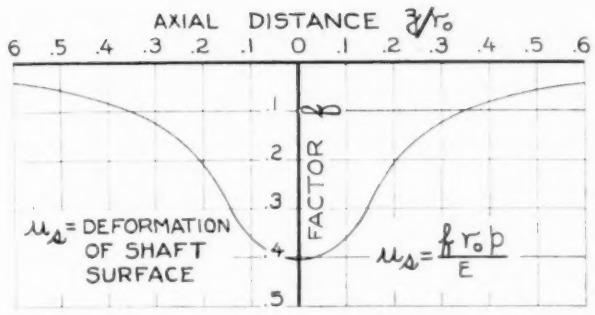


FIG. 8 DEFORMATION OF SHAFT SURFACE, FOR $\frac{a}{r_0} = 0.150$, PLOTTED AGAINST z/r_0

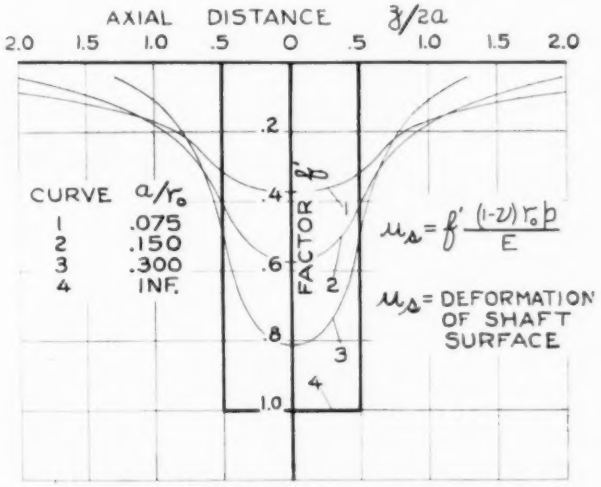


FIG. 9 DEFORMATION OF SHAFT SURFACE, FOR VARIOUS VALUES OF $\frac{a}{r_0}$, PLOTTED AGAINST $z/2a$

The radial deformation for the case of axial symmetry is given by

$$u = \frac{r}{E}\left[\sigma_\theta - \nu(\sigma_z + \sigma_r)\right] \quad \ldots\ldots\ldots\ldots\ldots [7]$$

and the deformation of the shaft surface has been plotted in Fig. 8 from this equation. Fig. 8 gives the shaft surface deformation, for the ratio $a/r_0 = 0.150$, plotted against z/r_0. In Fig. 9, the deformation of the shaft surface has been plotted for several values of a/r_0, but in this figure the plotting is against the axial distance $z/2a$.

In Figs. 10 to 13, inclusive, have been plotted the stress components whose use has been described in the section headed "Results" and whose derivation is given in the appendix. To illustrate numerically the use of these stress components, assume that σ_r is desired for the following point:

$$\frac{r}{r_0} = 0.80 \qquad \frac{a}{r_0} = 0.150 \qquad \frac{z}{r_0} = 0.20$$

then

$$m_1 = 0.15 + 0.20 = +0.35 \qquad \bar{\sigma}_r\left(\begin{matrix} m_1 = +0.35 \\ \frac{r}{r_0} = 0.80 \end{matrix}\right) = +0.48p$$

$$m_2 = 0.15 - 0.20 = -0.05 \qquad \bar{\sigma}_r\left(\begin{matrix} m_2 = -0.05 \\ \frac{r}{r_0} = 0.80 \end{matrix}\right) = -0.15p$$

$$\therefore \bar{\sigma}_r\left(\frac{r}{r_0} = 0.80;\ \frac{a}{r_0} = 0.150;\ \frac{z}{r_0} = 0.20\right) = +0.48p - 0.15p = +0.33p$$

In a similar fashion, σ_r, σ_θ, or σ_z may be plotted for any point within the cylinder. The shear-stress component $\bar{\tau}_{rz}$ is plotted in Fig. 13, and this component differs from $\bar{\sigma}_r$, $\bar{\sigma}_\theta$, and $\bar{\sigma}_z$ in that the integral contains a cosine term, and the sign of $\bar{\tau}_{rz}$ differs from the sign of τ_{rz}: since the integral contains a cosine term, the sign of $\bar{\tau}_{rz}$ is independent of the sign of m_1 or m_2. Assume τ_{rz} is desired for the following point:

$$\frac{r}{r_0} = 0.80 \qquad \frac{a}{r_0} = 0.150 \qquad \frac{z}{r_0} = 0.20$$

then

$$m_1 = 0.15 + 0.20 = +0.35 \qquad \bar{\tau}_{rz}\left(\begin{matrix} m_1 = +0.35 \\ \frac{r}{r_0} = 0.80 \end{matrix}\right) = +0.02p$$

$$m_2 = 0.15 - 0.20 = -0.05 \qquad \bar{\tau}_{rz}\left(\begin{matrix} m_2 = -0.05 \\ \frac{r}{r_0} = 0.80 \end{matrix}\right) = -0.21p$$

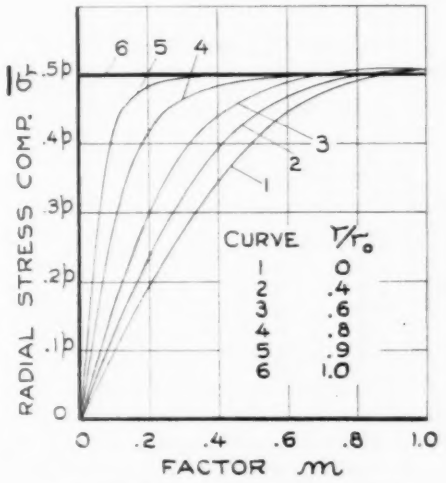


FIG. 10 RADIAL-STRESS COMPONENT $\bar{\sigma}_r$

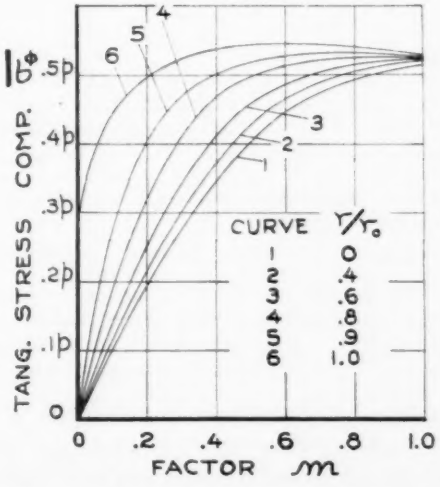


FIG. 11 TANGENTIAL-STRESS COMPONENT $\bar{\sigma}_\theta$

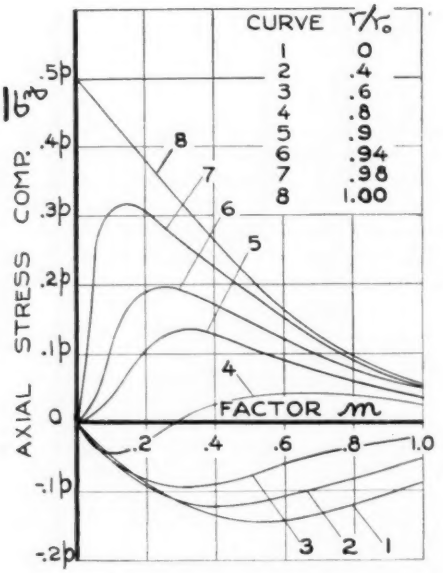


FIG. 12 AXIAL-STRESS COMPONENT $\bar{\sigma}_z$

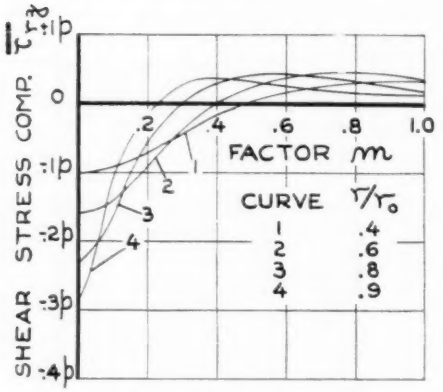


FIG. 13 SHEAR-STRESS COMPONENT $\bar{\tau}_{rz}$

(For $r = 0$, $\bar{\tau}_{rz}$ is zero for all values of m; for $r = r_0$ τ_{rz} is zero for all values of m except $m = 0$ at which point $\bar{\tau}_{rz} = -0.318p$.)

$$\therefore \tau_{rz}\left(\frac{r}{r_0} = 0.80;\ \frac{a}{r_0} = 0.15;\ \frac{z}{r_0} = 0.20\right) = -0.02p - 0.21p$$

$$= -0.23p$$

From the $\bar{\sigma}_r$ and $\bar{\sigma}_\theta$ curves, it is interesting to note than σ_r and σ_θ may both reach values exceeding the applied radial stress p. In Fig. 11, note that it is possible for the tangential stress to reach a value about 9 per cent greater than the applied radial stress p. This maximum is reached for a value of $\frac{a}{r_0} = 0.60$ and occurs at the surface $r = r_0$. For greater values of $\frac{a}{r_0}$, σ_θ decreases to its limiting value of unity, which value is approached for all points within the shaft. This limiting value is the value to be expected from the analysis of a long solid shaft subjected to an applied radial stress over its entire surface. It might also be noted that for large ratios of $\frac{a}{r_0}$ or for points on the shaft remote from the applied stress, the tangential stress can change sign and become negative; this may be seen by noting that the $\bar{\sigma}_r$ curves have a maximum value at the point $m = 0.6$. This reversal of tangential stress is similar to the reversals of stress which may be noted when subjecting a beam on an elastic foundation to a concentrated load.

From the $\bar{\sigma}_r$ curves (Fig. 10), it may be seen that it is possible for σ_r to exceed the applied radial stress p; the excess, however, is small and occurs at some point below the shaft surface.

It will be noted that all the stress-component curves are plotted only to the value $m = 1.0$. Beyond this value of m, however, the stress components are sufficiently close to their limiting values so that the latter may be used. These curves are consequently approximately valid for all values of the ratio $\frac{a}{r_0}$, but if the stresses are desired only on the shaft cross section at the center of the applied radial stress, the stress-component curves indicate that the analysis of a long solid cylinder with an applied radial stress over the entire surface may be used if $\frac{a}{r_0}$ becomes greater than unity.

TEST RESULTS

In order to check the validity of the results presented by this analysis, several tests were conducted in which the deformation of the surface of a shaft subjected to a shrink pressure was accurately measured. No attempt was made to measure the shaft-surface deformations under the shrink rings; only the shaft-surface deformations external but closely adjacent to the shrink rings were measured. As shown in Figs. 14 and 16, the theoretical results were closely duplicated.

For the first test, a solid steel shaft 4 in. diam and 8 in. long was obtained, and the surface accurately mapped by an electric gage[5] of the type described by Hathaway and Lee (5), and Kuehni (6). A steel ring of $^5/_8$ in. axial length and with a shrink of 9.5 mils on the diameter was then shrunk on the shaft, and, after cooling, the shaft surface was again accurately mapped. The shaft was sufficiently long that points could be obtained at a distance so remote from the shrink ring that no effects of the shrink

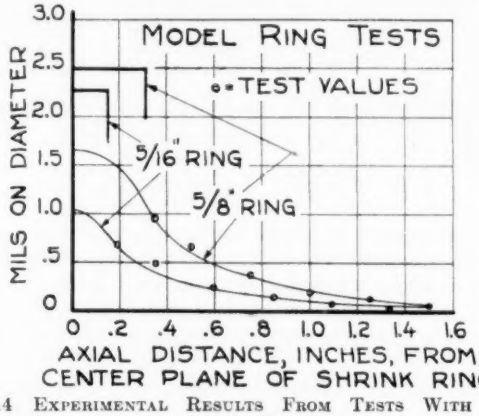


FIG. 14 EXPERIMENTAL RESULTS FROM TESTS WITH MODEL SHRINK RINGS

pressure could be observed, and these points could be used as reference levels to correlate the surface mappings with and without the shrink rings. As a consequence, the shaft-surface deformation due to the shrink ring could be obtained very accurately.

The test results obtained with the $^5/_8$-in. shrink ring are shown in Fig. 14; also shown in this figure are the test results obtained when a ring of $^5/_{16}$ in. axial length was substituted for the $^5/_8$-in. ring. The shrink on the $^5/_{16}$-in. ring was only 8.6 mils in place of the 9.5 mils of the $^5/_8$-in. ring. The two lower curves in Fig. 14

[5] The elements of this electric gage were developed by the company by whom the writer is employed and are used in the well-known precision Electrolimit gages of the Pratt and Whitney Division of the Niles-Bement-Pond Company.

were plotted from the analysis presented in this paper, and the correlation between the test and calculated results is surprisingly good. The two rectangular curves, shown in the upper half of Fig. 14, are the shaft-surface deformations calculated by the two-dimensional theory usually employed which ignores the effect of the shaft external to the axial length of the ring. It should be noted that the subject analysis and the test results indicate that the tangential stress in the $^5/_{16}$ in. ring is 20 per cent greater than the usual two-dimensional analysis would show; for the $^5/_8$ in. ring, the tangential stress is 13 per cent greater than the two-dimensional analysis would show. These are average values and do not consider the stress concentrations at the inner edges of the rings.

Fig. 15 is the testing equipment used for the foregoing tests, showing the shaft with the $^5/_{16}$-in. ring in place and resting on a

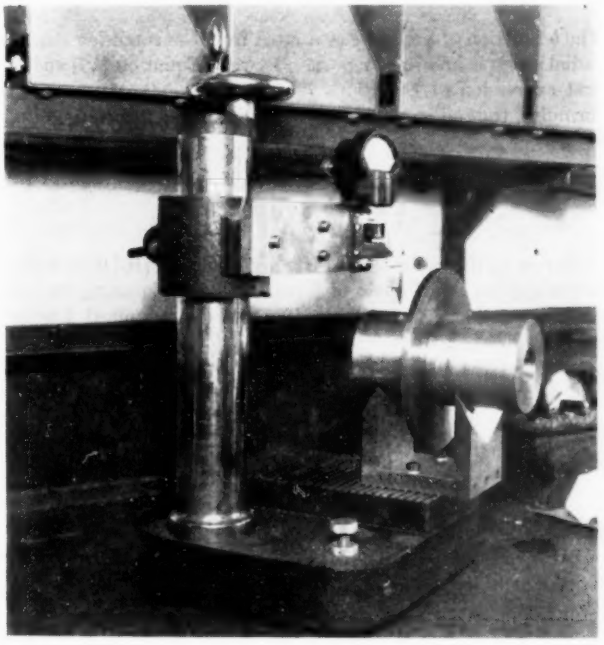


FIG. 15 ELECTRIC GAGE STAND FOR MEASURING SHAFT-SURFACE DEFORMATIONS; MODEL SHAFT WITH $^5/_{16}$-IN. SHRINK RING IN PLACE

Vee-block anvil used as a base. The measuring head of the gage can be seen above the far portion of the shaft, and the indicating meter which gives the surface deformation in tenths of a mil can be seen directly above the measuring head. The major portion of the credit for the gratifying results obtained in the tests must be given to the electric gage. It showed no tendency to drift or exhibit hysteresis and consistently duplicated its readings in a most satisfactory manner.

The results of a third test are shown in Fig. 16. In this test, a turbine shaft of 21 in. diam was used, and a small portion of the shaft between the turbine wheels and an impeller sleeve was closely measured before and after shrinking on the wheels and the sleeve. In Fig. 16, negative values of inches to the left of the zero give distances measured under the turbine wheels; the edge of the impeller sleeve is shown about 4.5 in. to the right of the edge of the last wheel. The dashed horizontal line at 8.2 mils gives the calculated surface deformation under the turbine wheels at a considerable distance to the left of the zero line; the full curve shown is a plot of the surface deformation as calculated by the methods suggested in this paper. The stiffness of the turbine wheels was calculated by the methods shown by S. H. Weaver (7). The test values as obtained are indicated by the small circles, and these values with a 5-F temperature correction are shown by the small crosses. It was necessary to include the latter correction as the shaft felt slightly warm, and factory production schedules prohibited holding the shaft until room temperature had been obtained. Considering that the data shown in Fig. 16 were obtained from factory measurements with a micrometer, and are probably correct only to $^1/_2$ mil, the correspondence between the test values and the calculated curve is satisfying.

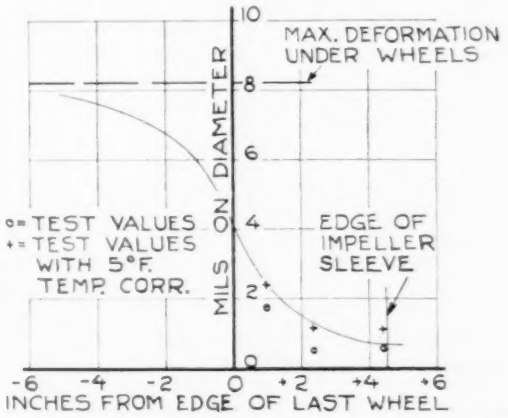


FIG. 16 EXPERIMENTAL RESULTS ON 21-IN-DIAM TURBINE SHAFT

Appendix

STRESS DISTRIBUTION ANALYSIS

It is the purpose of the following analysis to calculate the stress distribution throughout a solid circular cylinder of infinite length due to the action of a radial stress of p units magnitude applied to the surface over a single circumferential band of finite length; the application of this radial stress is shown in Fig. 1.

In order to calculate the stress within the cylinder, it will be necessary to express the applied radial stress p as a Fourier integral; one method of doing this is outlined in reference (8). Applying this method gives the following expression for the applied radial stress of Fig. 1

$$\sigma_r = \frac{2p}{\pi}\int_0^\infty \frac{\sin \lambda a}{\lambda} \cos \lambda z d\lambda \quad \ldots\ldots\ldots [8a]$$

That Equation [8a] actually represents the applied-stress distribution of Fig. 1 may be proved by means of the following definite integral[6]

$$\left.\begin{aligned} \int_0^\infty \frac{\sin mx}{x} dx &= +\frac{\pi}{2} \text{ for } m > 0 \\ &= 0 \text{ for } m = 0 \\ &= -\frac{\pi}{2} \text{ for } m < 0 \end{aligned}\right\} \quad \ldots\ldots\ldots [8b]$$

Rewriting Equation [8a] as the sum of two integrals, there results

$$\sigma_r = \frac{p}{\pi}\int_0^\infty \frac{\sin \lambda (a+z)}{\lambda} d\lambda + \frac{p}{\pi}\int_0^\infty \frac{\sin \lambda (a-z)}{\lambda} d\lambda \quad [8c]$$

Now if $z < a$, m is positive for both integrals of Equation [8c], and the latter reduces to p; if $z = a$, m is positive for the first integral of Equation [8c] and zero for the second, and Equation [8c] reduces to $^1/_2 p$; if $z > a$, m is positive for one integral of

[6] Reference (9), Equation 858.5.

Equation [8c] and negative for the second, and the algebraic sum reduces to zero as needed.

With the applied radial stress given mathematically by Equation [8a], it is now necessary to obtain a solution of the equations of elasticity such that the radial stress reduces to Equation [8a] on the surface. It has been shown[7] that for axially symmetrical stress distribution in a solid of revolution, the equations of equilibrium and the equations of compatibility are all satisfied by a stress function ϕ given by

$$\nabla^4\phi = \nabla^2\nabla^2\phi = 0 \quad [9a]$$

if the stresses are taken as

$$\left.\begin{aligned} \sigma_r &= \frac{\partial}{\partial z}\left(\nu\nabla^2\phi - \frac{\partial^2\phi}{\partial r^2}\right) \\ \sigma_z &= \frac{\partial}{\partial z}\left[(2-\nu)\nabla^2\phi - \frac{\partial^2\phi}{\partial z^2}\right] \\ \sigma_\theta &= \frac{\partial}{\partial z}\left(\nu\nabla^2\phi - \frac{1}{r}\cdot\frac{\partial\phi}{\partial r}\right) \\ \tau_{rz} &= \frac{\partial}{\partial r}\left[(1-\nu)\nabla^2\phi - \frac{\partial^2\phi}{\partial z^2}\right] \end{aligned}\right\} \quad [9b]$$

with

$$\nabla^2 = \frac{\partial^2}{\partial r^2} + \frac{1}{r}\frac{\partial}{\partial r} + \frac{\partial^2}{\partial z^2} \quad [9c]$$

Assume a solution in the form

$$\phi = \int_0^\infty Rb \sin \lambda z d\lambda \quad [10]$$

in which R is a function of r alone, and b is a function of λ alone. Note that λ is merely a new variable which is used only in the integral, Equation [10], and which disappears when the integration is performed; λ has, in itself, no direct physical significance.

Substituting Equation [10] into Equation [9a], the equation for R is obtained as

$$\left(\frac{d^2}{dr^2} + \frac{1}{r}\cdot\frac{d}{dr} - \lambda^2\right)\left(\frac{d^2}{dr^2} + \frac{1}{r}\cdot\frac{d}{dr} - \lambda^2\right)R = 0 \quad [11]$$

The solution of Equation [11] is

$$R = a_0 J_0(i\lambda r) + a_1 i\lambda r\, J_1(i\lambda r) \quad [12]$$

in which J_0 and J_1 are Bessel functions of the zero and first orders, respectively, as defined in reference (9).[8] The symbol i in Equation [12] is $\sqrt{-1}$. It should be noted that the complete solution of Equation [11] contains two Bessel functions of the second kind (K_0 and K_1, as defined in reference (9),[9] as well as the two Bessels of the first kind as given by Equation [12], thereby resulting in the necessary four undetermined constants. The two Bessels of the second kind approach infinity as r approaches zero, however, and since the present problem treats only a solid cylinder with no internal bore hole, it is necessary that the coefficients of the Bessels of the second kind be zero. Equation [12], therefore, is the complete solution of R needed for the present problem.

Defining ρ as the ratio of a_0 to a_1, and removing the $\sqrt{-1}$ from Equation [12] by substituting the modified Bessels defined in the nomenclature, ϕ may be written as

$$\phi = \int_0^\infty [\rho I_0(\lambda r) - \lambda r I_1(\lambda r)]a_1 b \sin \lambda z d\lambda \quad [13]$$

[7] Reference (1), Chapt. 11.
[8] Reference (9), Equations 807.1 and 807.2.
[9] Ibid., Equations 815.1 and 815.2.

Note that a_1 is now grouped with the b function of λ, and the two will be evaluated simultaneously; ρ may be evaluated easily from the condition that there is no shear on the surface $r = r_0$.

Between Equation [13] and the last of Equations [9b], the following expression may be obtained for the shear stress

$$\tau_{rz} = \int_0^\infty \left[\begin{array}{l} \rho\lambda I'_0(\lambda r) - \lambda^2 r I_1'(\lambda r) - \\ \lambda I_1(\lambda r) - 2\lambda(1-\nu)I'_0(\lambda r) \end{array}\right] \lambda^2 a_1 b \sin \lambda z d\lambda \quad [14]$$

in which the prime values indicate differentiation with respect to λr. At $r = r_0$, there is to be no shear; this condition can be satisfied by equating the bracketed term to zero for $r = r_0$. Then, using the Bessel recurrence formulas, given by reference (9), the following expression may be obtained for ρ

$$\rho = 2(1-\nu) + \lambda r_0 \frac{I_0(\lambda r_0)}{I_1(\lambda r_0)} \quad [15]$$

The b function of λ may be evaluated from the condition that the radial stress is known at $r = r_0$. Between Equation [13] and the first expression of Equations [9b], and using Bessel recurrence formulas, the radial stress may be expressed as follows

$$\sigma_r = \int_0^\infty \left[\begin{array}{l} (1-2\nu-\rho)I_0(\lambda r) + \\ \left(\lambda r + \dfrac{\rho}{\lambda r}\right) I_1(\lambda r) \end{array}\right] \lambda^3 a_1 b \cos \lambda z d\lambda \quad [16]$$

At $r = r_0$, the radial stress given by Equation [16] must reduce to the applied radial stress of Equation [8a]. Equating [8a] and [16], the following is obtained for the undetermined function $a_1 b$

$$a_1 b = \frac{\dfrac{2p}{\pi\lambda^4}\sin \lambda a}{\left[\begin{array}{l} (1-2\nu-\rho)\, I_0(\lambda r_0) + \\ \left(\lambda r_0 + \dfrac{\rho}{\lambda r_0}\right) I_1(\lambda r_0) \end{array}\right]} \quad [17]$$

Between Equations [9], [13], [15], and [17], the stresses may be written as follows

$$\sigma_r = \int_0^\infty \frac{\left[\begin{array}{l} (1-2\nu-\rho)I_0(\lambda r) + \\ \left(\lambda r + \dfrac{\rho}{\lambda r}\right) I_1(\lambda r) \end{array}\right]}{\gamma'_{1\cdot 0}} \cdot \frac{2p}{\pi} \cdot \frac{\sin \lambda a \cos \lambda z d\lambda}{\lambda} \quad [18a]$$

$$\sigma_\theta = \int_0^\infty \frac{\left[\begin{array}{l} (1-2\nu)I_0(\lambda r) - \\ \dfrac{\rho}{\lambda r} I_1(\lambda r) \end{array}\right]}{\gamma'_{1\cdot 0}} \cdot \frac{2p}{\pi} \cdot \frac{\sin \lambda a \cos \lambda z d\lambda}{\lambda} \quad [18b]$$

$$\sigma_z = \int_0^\infty \frac{\left[\begin{array}{l} (\rho + 2\nu - 4)I_0(\lambda r) \\ - \lambda r I_1(\lambda r) \end{array}\right]}{\gamma'_{1\cdot 0}} \cdot \frac{2p}{\pi} \cdot \frac{\sin \lambda a \cos \lambda z d\lambda}{\lambda} \quad [18c]$$

$$\tau_{rz} = \int_0^\infty \frac{\left[\begin{array}{l} (\rho + 2\nu - 2)I_1(\lambda r) \\ - \lambda r I_0(\lambda r) \end{array}\right]}{\gamma'_{1\cdot 0}} \cdot \frac{2p}{\pi} \cdot \frac{\sin \lambda a \sin \lambda z d\lambda}{\lambda} \quad [18d]$$

Since the foregoing expressions cannot be integrated, it is necessary to resort to numerical integration, and for this method it is more convenient to rewrite them as follows:

Let the Bessel functions be replaced by the following asymptotic expressions[10]

$$I_0(\lambda r) = \frac{e^{\lambda r}}{\sqrt{2\pi\lambda r}} i_0(\lambda r) \qquad I_1(\lambda r) = \frac{e^{\lambda r}}{\sqrt{2\pi\lambda r}} i_1(\lambda r) \quad . . [19]$$

with

$$i_0(\lambda r) = 1 + \frac{0.12500}{(\lambda r)} + \frac{0.07031}{(\lambda r)^2} + \frac{0.07324}{(\lambda r)^3} + \frac{0.11215}{(\lambda r)^4} + \longrightarrow \ldots\ldots [20a]$$

$$i_1(\lambda r) = 1 - \frac{0.37500}{(\lambda r)} - \frac{0.11719}{(\lambda r)^2} - \frac{0.10254}{(\lambda r)^3} - \frac{0.14420}{(\lambda r)^4} - \longrightarrow \ldots\ldots [20b]$$

σ_r as given by Equation [18a] may now be written as follows

$$\sigma_r = \frac{p}{\pi} \int_0^\infty \frac{\left[(1 - 2\nu - \rho) i_0 \left(\lambda r_0 \frac{r}{r_0} \right) + \left(\lambda r_0 \frac{r}{r_0} + \frac{\rho}{\lambda r_0 \frac{r}{r_0}} \right) i_1 \left(\lambda r_0 \frac{r}{r_0} \right) \right]}{\sqrt{\frac{r}{r_0}} \gamma_{1.0}\, e^{\lambda r_0 \left(1 - \frac{r}{r_0}\right)}} \times \frac{\left[\sin \lambda r_0 \frac{a+z}{r_0} + \sin \lambda r_0 \frac{a-z}{r_0} \right]}{\lambda r_0} d(\lambda r_0) \ldots\ldots [21]$$

Let the stress component $\bar{\sigma}_r$ be defined as follows

$$\bar{\sigma}_r = \frac{p}{\pi} \int_0^\infty \frac{\left[(1 - 2\nu - \rho) i_0 \left(\lambda r_0 \frac{r}{r_0} \right) + \left(\lambda r_0 \frac{r}{r_0} + \frac{\rho}{\lambda r_0 \frac{r}{r_0}} \right) i_1 \left(\lambda r_0 \frac{r}{r_0} \right) \right]}{\sqrt{\frac{r}{r_0}} \gamma_{1.0}\, e^{\lambda r_0 \left(1 - \frac{r}{r_0}\right)}} \times \frac{\sin m\lambda r_0}{\lambda r_0} d(\lambda r_0) \ldots\ldots [22]$$

[10] The values of λr for which these asymptotic expressions yield slow convergence are also sufficiently small so that the limiting values of the integrals may be used directly.

From the two expressions, Equations [21] and [22], σ_r may be evaluated for any point by taking the sum of the two values of $\bar{\sigma}_r$ determined for the two values of m

$$m_1 = \frac{a+z}{r_0} \qquad m_2 = \frac{a-z}{r_0} \ldots\ldots [23]$$

By applying the same reasoning to σ_θ, σ_z, and τ_{rz}, the stress-component relations given by Equation [2] may be derived. Figs. 10 to 13, inclusive, give curves of the stress components versus m, and the actual stresses are obtained from these curves as shown by the numerical examples in the section headed "Stress and Strain Curves, and Discussion." As a matter of note, these curves were obtained by numerical integration using the Si (x) and Ci (x) functions of reference (4).

Acknowledgment

The author expresses his appreciation to the following members of the General Electric Company, Schenectady, New York: to H. D. Taylor of the Turbine Generator Engineering Division for suggesting this problem and for indicating the practical importance of the solution, and for his many valued suggestions; to H. P. Kuehni and A. R. Hand of the General Engineering Laboratory for their assistance and instruction in the use of the electric gage; to R. Patterson of the Turbine Generator Engineering Division for his discussions of the mathematical work and his assistance with the experimental measurements; and to M. A. Savage of the Turbine Generator Engineering Division for suggesting the publication of these results.

BIBLIOGRAPHY

1 "Theory of Elasticity," by S. Timoshenko, McGraw-Hill Book Company, Inc., New York, N. Y., 1934, pp. 352–354.

2 "Drang und Zwang," by A. Föppl and L. Föppl, R. Oldenbourg, Munich, Germany, 1928, pp. 168–190.

3 "The Circular Cylinder With a Band of Uniform Pressure on a Finite Length of the Surface," by M. V. Barton, JOURNAL OF APPLIED MECHANICS, Trans. A.S.M.E., vol. 63, 1941, p. A-97.

4 "Tables of Functions," by E. Hahnke and F. Ende, B. G. Teubner, Berlin, Germany, 1938.

5 "The Electric Gage," by C. M. Hathaway and E. S. Lee, *Mechanical Engineering*, vol. 59, 1937, p. 653.

6 "Electric Gages," by H. P. Kuehni, *General Electric Review*, vol. 45, 1942, p. 533.

7 "Disk-Wheel Stress Determinations," by S. H. Weaver, Trans. A.S.M.E., vol. 39, 1917, p. 173.

8 "Mathematical Methods in Engineering," by Th. von Kármán and M. W. Biot, McGraw-Hill Book Company, Inc., New York, N. Y., 1940, pp. 343–347.

9 "Tables of Integrals and Other Mathematical Data," by H. B. Dwight, MacMillan Company, New York, N. Y., 1934.

Measurement of the Damping of Engineering Materials During Flexural Vibration at Elevated Temperatures

By CARL SCHABTACH[1] and R. O. FEHR,[2] SCHENECTADY, N. Y.

The method and equipment developed and used by the authors for measuring the damping of materials are described. A tuning-fork specimen is set into vibration by jerking a spreader from the gap between the ends of the tines. The damping is expressed in terms of the logarithmic decrement of the decaying vibration, which is measured and recorded by means of a magnetic oscillograph, amplifiers, and a resistance-type electric strain gage cemented to the specimen. The results include (1) the damping of a number of materials during flexural vibration at approximately 1000 cycles per sec, at maximum bending stresses up to 40,000 psi, and at temperatures up to 1400 F; (2) the variation in modulus of elasticity with temperature, as determined from the specimen vibration frequencies.

Introduction

THE damping of a material is a measure of its ability to dissipate energy when subjected to fluctuating stresses. (The terms "internal friction," "mechanical hysteresis," "damping capacity," and "specific damping capacity" are used also to describe this property.) Fluctuating stresses in machine or structural elements may reach destructive size under resonance conditions, i.e., when the frequency of force pulsations applied to a system coincides with the natural frequency of the system. Under such conditions, these fluctuating stresses are limited only by damping.

In many structures, high damping is assured, regardless of the properties of the materials, by friction in mechanical connections, fluid friction, mechanical impacts, or component damping devices such as dashpots. Where these are effective in only minor degree, we must look to damping in the materials themselves for protection against excessive vibratory stresses at resonance. To this end, we must know the damping, along with other properties of materials, under conditions as nearly as possible the same as those to which they will be subjected in service.

While the results of many investigations of the damping of engineering materials have been reported,[3] the data so accumulated are meager, and our understanding of the phenomenon is, insufficient to permit application of available data to conditions materially different from those under which they were obtained.

It is the purpose of this paper to describe equipment suitable for measuring the damping of materials at temperatures up to 1400 F, over a wide range of stresses caused by bending at frequencies from 100 to 3000 cycles per sec. These cover the range of conditions under which the buckets and wheels of some steam and gas turbines operate, and for which data are needed concerning the materials used in their construction. Representative results are included, but more comprehensive data will be published later.

General Description of Equipment

There are, broadly, two ways to determine damping; one involves measuring the power required to sustain a specimen in vibration, the other measuring the rate at which a free vibration decays. The free-vibration-decay method, using a tuning-fork specimen, was adopted.

A tuning fork, Fig. 1, having a frequency of about 1000 cycles

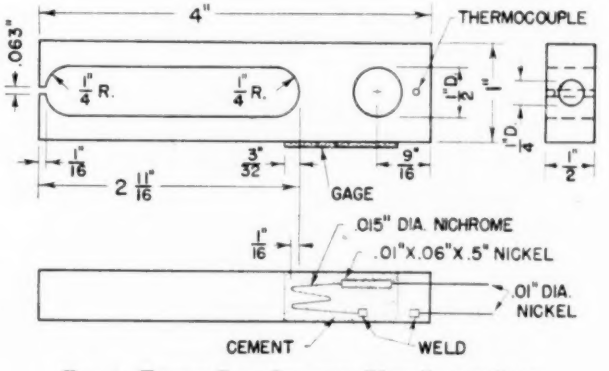


Fig. 1 Tuning-Fork Specimen With Strain Gage

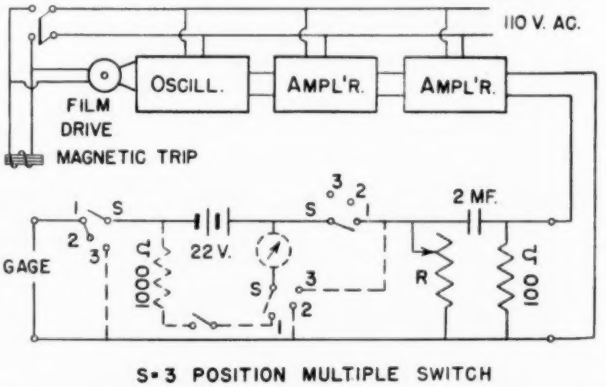


Fig. 2 Connection Diagram for Strain Gage, Potentiometer, Amplifiers, and Oscillograph, With Details of Potentiometer Circuit

[1] Turbine Engineering Division, Rotor and Diaphragm Section General Electric Company. Mem. A.S.M.E.

[2] General Engineering Laboratory, General Electric Company.

[3] "Vibration Problems—Friction and Damping in Vibrations," by A. L. Kimball, Journal of Applied Mechanics, Trans. A.S.M.E., vol. 63, 1941, part 4, pp. A-37 to A-41; part 5, pp. A-135 to A-140. These contain an exhaustive summary of damping data, and part 5 contains an extensive Bibliography on damping.

Presented at the Annual Meeting, New York, N. Y., Nov. 29–Dec. 3, 1943, of The American Society of Mechanical Engineers.

Discussion of this paper should be addressed to the Secretary, A.S.M.E., 29 West 39th Street, New York, N. Y., and will be accepted until July 10, for publication at a later date. Discussion received after the closing date will be returned.

Note: Statements and opinions advanced in papers are to be understood as individual expressions of their authors and not those of the Society.

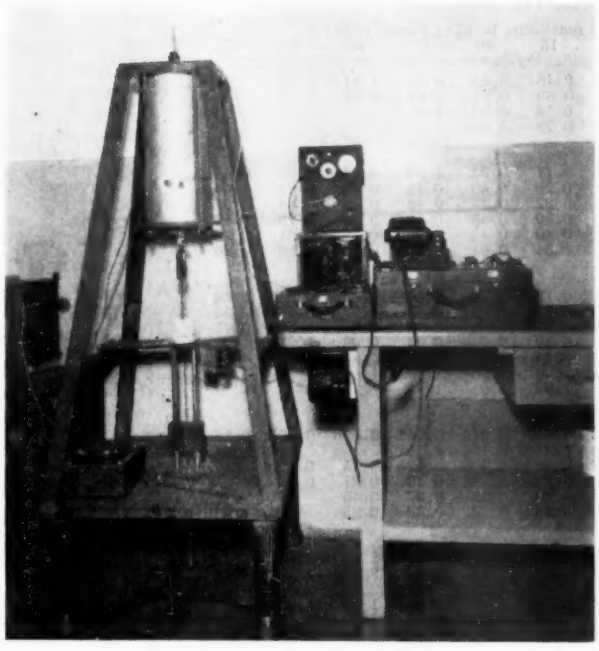


FIG. 3 VIEW OF TEST EQUIPMENT

per sec, is set into vibration by jerking a spreader from the gap between the feet on the ends of the tines. The subsequent vibration is measured with a resistance-type electric strain gage attached to the fork and is recorded on photographic film by means of a magnetic oscillograph.

Fig. 2 shows the details of the potentiometer circuit and a connection diagram for the amplifiers used in conjunction with the strain gage and oscillograph.

The equipment used for supporting and heating the specimen, and setting it into vibration is shown in Fig. 3, together with the amplifiers and oscillograph.

Details of the test equipment and the method of conducting tests are explained and discussed fully in Appendix 1.

Fig. 4 illustrates a specimen suitable for use in determining the influence of vibration frequency on damping. By cutting off the tines successively at each of the projections, the frequency is increased progressively from about 150 to 3000 cycles per sec. All of the results reported in this paper were obtained with specimens of the proportions shown in Fig. 1.

DISCUSSION OF TEST CONDITIONS AND METHOD OF COMPUTING RESULTS

At the instant the vibration starts, it comprises all modes in the same degree and phase relation that they were represented in the static deflection caused by the spreader. The vibration amplitude in the fundamental mode is by far the largest. In the second mode, whose frequency is about 6.3 times the fundamental, and which has a node about 17 per cent of the length from the free end of the tine, the amplitude is only 2 or 3 per cent of the fundamental.

Only the fundamental component of the vibration is recorded by the oscillograph, if the specimen frequency exceeds about 500 cycles per sec. The characteristics of the measuring equipment are such that the small-amplitude higher-frequency components are practically eliminated. If the frequency is below 500 cycles per sec, the second-mode vibration is recorded, but can readily be separated from the record of the fundamental.

The damping is expressed in terms of the logarithmic decrement of the fundamental mode. It is assumed that the vibration in each mode dies out independently of the others. This seems justified by the poor coupling between the different modes of vibration of the tines and by the smallness of the higher mode components. It was checked experimentally by using a fork having the feet located some distance back from the free ends of the tines, so that the static-deflection shape approximated the vibration shape more nearly and the second-mode component was much reduced. The decrement of the fundamental mode did not differ appreciably from that obtained from the same fork when the feet were located at the ends of the tines.

The rates of energy dissipation and vibration-amplitude decay are simply related to the logarithmic decrement. Provided the latter is small (less than 10 per cent), then with very little error, the percentage reduction in amplitude per cycle is equal to the percentage logarithmic decrement; the percentage loss of energy per amplitude cycle, called "specific damping capacity," is equal to twice the percentage logarithmic decrement.

The initial-vibration amplitude in the fundamental mode is determined by and from the static deflection before release. It is assumed that components of the vibration in modes higher than the second are negligible. The amplitudes of the fundamental and second mode are determined to satisfy the initial static deflection at the free ends and at the middle of the tines of the tuning fork. This fixes the fundamental amplitude of the end of the tine at 97.4 per cent of the static deflection, and of the second mode 2.6 per cent (see Appendix 2).

The bending moment at the fixed end of each tine is the sum of the inertia moments of the tine and foot due to vibration in the fundamental mode. It is assumed that the tine is fixed at a section through the bottom of the slot between tines.

All stresses are expressed in terms of the nominal maximum bending stress, obtained by dividing the bending moment at the fixed ends of the tines, as determined previously, by the section modulus of the tine. If the proportions of the specimen are reasonably close to those specified in Fig. 1, the nominal maximum bending stress at the instant the vibration starts

$$S = 0.192 \frac{f_1^2 \gamma l^2}{h} Y,$$

in terms of the nomenclature given in Appendix 2. As the vibration decays, the stress decreases in proportion to the recorded amplitude.

It should be noted that the nominal maximum bending stress neglects the effect of the fillet at the fixed ends of the tines. This is in accordance with common engineering practice, wherein the

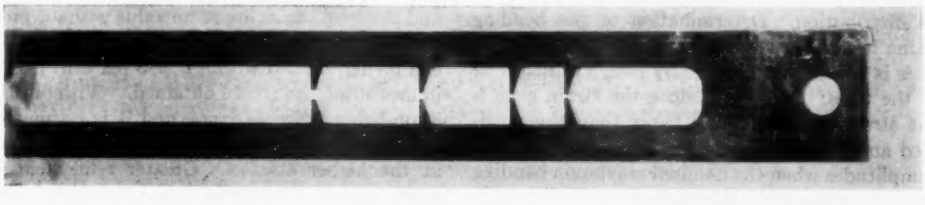


FIG. 4 TUNING-FORK SPECIMEN FOR DETERMINING EFFECT OF FREQUENCY ON DAMPING

TABLE 1 DAMPING AND RELATIVE MODULUS

Material	Temp, F	Relative modulus	Nominal maximum bending stress, 1000 psi: 5	10	15	20	25	30	35	40
			Damping; log decrement, per cent							
SAE 1020	75	1.00	0.11	0.28	0.40	0.48	0.52	0.54	0.55	
	300	0.92	0.30	0.49	0.60	0.67	0.69	0.72	0.74	
	500	0.88	0.20	0.45	0.76	0.96	1.0			
	700	0.86	0.50	0.73	0.78	0.80				
SAE 4140	75	1.00		0.11	0.17	0.23	0.29	0.34	0.38	0.41
	300	0.98		0.17	0.28	0.40	0.51	0.58	0.61	0.64
	500	0.96		0.19	0.27	0.35	0.42	0.49	0.54	0.59
	700	0.93		0.20	0.30	0.40	0.50	0.60	0.70	0.80
	900	0.90		0.32	0.40	0.44	0.50	0.59	0.61	0.62
	1200	0.85		0.41	0.54	0.61	0.63	0.63	0.65	0.76
3.5% Ni Steel	75	1.00	0.065	0.10	0.17	0.25	0.36	0.45	0.51	0.54
	300	0.94	0.050	0.13	0.24	0.36	0.47	0.52	0.54	0.55
	500	0.90	0.050	0.13	0.30	0.50	0.59	0.64	0.69	0.77
	700	0.86	0.142	0.37	0.59	0.74	0.87	0.99	1.08	
	900	0.83	0.095	0.26	0.46	0.62	0.74	0.83	0.90	
	1050	0.81	0.20	0.58	1.00	1.16	1.19	1.11		
	1200	0.80	0.63	0.96	1.04	1.05	1.05			
Cr-Mo-Va Steel	75	1.00	0.042	0.042	0.043	0.046	0.056	0.070	0.105	0.15
	300	0.96	0.040	0.054	0.076	0.105	0.141			
	500	0.93	0.075	0.082	0.092	0.106	0.125	0.15	0.19	
	700	0.91	0.102	0.110	0.123	0.144	0.18	0.21	0.23	
	900	0.90	0.080	0.135	0.20	0.28	0.37	0.40		
	1050	0.89	0.090	0.136	0.18	0.23	0.30	0.35		
13% Cr Iron	75	1.00	0.20	0.56	1.28	1.87	2.09	2.10	2.18	2.36
	300	0.98	0.28	0.85	1.60	1.98	2.05	2.06	2.10	2.16
	500	0.96	0.33	1.15	1.92	2.16	2.21	2.24	2.26	
	700	0.94	0.57	1.35	1.76	1.85	1.84	1.86	1.90	
	900	0.92	0.62	1.10	1.39	1.39	1.33	1.30	1.29	
	1050	0.89	1.02	1.23	1.31	1.34	1.37	1.39		
Inconel	75	1.00	0.035	0.031	0.031	0.032	0.035	0.037	0.038	0.040
	300	0.97	0.045	0.040	0.038	0.040	0.042	0.044	0.043	0.041
	500	0.95	0.055	0.050	0.049	0.051	0.052	0.052	0.052	0.051
	700	0.92	0.050	0.055	0.057	0.055	0.057	0.062	0.065	0.067
	900	0.89	0.085	0.084	0.077	0.070	0.068	0.069	0.066	
	1050	0.86	0.120	0.115	0.121	0.120	0.112	0.103	0.098	
	1200	0.83	0.067	0.056	0.050	0.053	0.061	0.067	0.070	
N-153	75	1.00		0.080	0.087	0.104	0.14	0.21	0.36	
	500	0.95		0.081	0.083	0.088	0.10	0.122		
	700	0.91		0.051	0.058	0.069	0.083	0.102		
	900	0.86		0.060	0.080	0.080	0.091	0.115		
	1050	0.84		0.053	0.065	0.068	0.073	0.088		
	1200	0.83		0.065	0.087	0.085	0.098	0.102		
	1300	0.82	0.054	0.088	0.096	0.106	0.110	0.102		
S-495	75	1.00	0.043	0.085	0.13	0.18	0.22	0.27	0.32	0.38
	300	0.96	0.065	0.10	0.15	0.22	0.31	0.37	0.39	0.41
	500	0.92		0.11	0.21	0.31	0.40	0.47	0.54	0.59
	700	0.89	0.038	0.11	0.18	0.23	0.28	0.33	0.37	
	900	0.85	0.055	0.058	0.060	0.073	0.09	0.10	0.12	
	1050	0.82		0.055	0.070	0.081	0.09	0.09	0.10	
	1200	0.78		0.080	0.085	0.095	0.10	0.10		
	1300	0.76		0.085	0.095	0.105	0.11	0.11		
	1400	0.74		0.12	0.14	0.15	0.15	0.14		
Vitallium	75	1.00	0.017	0.018	0.019	0.022	0.025	0.031	0.038	0.041
	300	0.96	0.020	0.022	0.025	0.028	0.033	0.038	0.044	
	500	0.92	0.023	0.027	0.031	0.036	0.041	0.048	0.053	
	700	0.88	0.050	0.048	0.053	0.061	0.073	0.087	0.103	
	900	0.84	0.141	0.120	0.107	0.113	0.15	0.19	0.24	
	1100	0.79	0.155	0.151	0.15	0.16	0.19	0.24		
	1200	0.77	0.136	0.123	0.13	0.16	0.22	0.30		

effect of fillets at changes of section is included in a stress-concentration factor applied to the nominal stress.

It should be noted also that the nominal-maximum-stress calculation assumes that the surface stresses are below the elastic limit of the material. For surface stresses above the elastic limit, the bending moment must be divided by something greater than the section modulus of the tine, using one of the approximate methods of analysis which are available for determining the actual stress distribution. Determination of the bending moment is the same in either case, however, since the moment of the inertia forces is not greatly affected by local yielding near the fixed ends of the tines. Moreover, since the strain gage is located where the stress is considerably lower than the maximum, the recorded amplitudes will continue to be proportional to the vibration amplitudes when the nominal maximum bending stress is considerably in excess of the elastic limit.

The variation in the elastic modulus of materials with temperature is a useful by-product of the damping measurements. The square root of the ratio of the frequencies of a tuning-fork specimen at any two temperatures is equal to the ratio of the moduli of elasticity at those temperatures. The frequencies are measured at small vibration amplitudes, with nominal maximum bending stresses of the order of 5000 to 10,000 psi. The frequencies themselves have not been reported, since the proportions of many of the specimens tested so far differ slightly, and the frequencies are of no value without proper correction.

With regard to accuracy, it is estimated that damping values can be determined within 2 or 3 per cent if extreme care is used in measuring the record obtained. With ordinary care, the error is probably twice as large, and it is estimated that the results given here may be in error by as much as 5 per cent, particularly at the higher stresses. Greater refinement is not considered worth while. The stress values should be correct within 2 or 3 per cent, and the modulus ratios within 1 per cent.

TABLE 2 PHYSICAL PROPERTIES AT ROOM TEMPERATURE

Material	Tensile strength, psi	Proportional limit, psi	Elongation, per cent in 2 in.	Reduction in area, per cent
S.A.E. 1020	64900	40400	35	63.9
S.A.E. 4140	107000	71900	24	55.
3.5 Per cent Ni steel	123700	104900	21.5	62.4
CR-Mo-Va steel	133400	126900	21.5	55.4
13 Per cent Cr iron	104300	75000	21.7	69.5
N-153	176000	146000[a]	15[b]	30
S-495	135000	82000[a]	13[b]	15
Vitallium	116000	.....	12[c]	26

[a] Yield strength (0.0002)
[b] Per cent in 1 in.
[c] Per cent in 1/2 in.

TABLE 3 CHEMICAL COMPOSITION AND HEAT-TREATMENT

Material	Composition	Heat-treatment
S.A.E. 1020	0.18/0.23 C, 0.4/0.6 Mn, 0.04 P max, 0.05 S max	Hot-rolled
S.A.E. 4140	0.42 C, 0.78 Mn, 0.23 Si, 0.89 Cr, 0.18 Mo	950 C—6 hr—AC 600 C—4 hr—AC
3.5% Ni Stl	0.38/0.43 C, 0.7/0.9 Mn, 0.15/0.30 Si, 0.04 P max, 0.04 S max, 3.25/3.75 Ni	850 C—OQ 625 C—AC
Cr-Mo-Va Stl	0.5 C max, 0.4/0.7 Mn, 0.20/0.35 Si, 0.04 P max, 0.045 S max, 0.8/1.1 Cr, 0.45/0.65 Mo, 0.25/0.35 Va	900 C—8 hr—OQ 675 C—4 hr—AC
13% Cr Iron	0.06/0.13 C, 0.25/0.80 Mn, 0.5 Si max, 0.03 S max, 0.03 P max, 0.5 Ni max, 11.5/13 Cr	950 C—OQ 600 C—AC
Inconel	0.04 C, 0.73 Mn, 0.52 Si, 0.01 S, 73.98 Ni, 15.02 Cr, 2.42 Ti, 0.49 Al, 6.7 Fe	1975 F—2 hr—WQ 1300 F—16 hr—AC
N-153	0.35/0.45 C, 1.25/1.75 Mn, 0.60 Si, 15/16 Ni, 15/16 Cr, 1.25/1.75 W, 3.75/-4.25 Mo, 11/13 Co, 0.80/1.20 Cb	2175 F—1/4 hr—WQ 1400 F—cold-worked, 25% R.A. 1500 F—2 hr—AC
S-495	0.43 C, 0.64 Mn, 0.93 Si, 0.016 S, 0.016 P, 19.74 Ni, 14.18 Cr, 4.00 W, 3.55 Mo, 3.68 Cb	2175 F—1/4 hr—WQ 1400 F—cold-worked, 10% R.A. 1500 F—2 hr—AC
Vitallium	0.2 C, 0.5 Mn, 0.5 Si, 29 Cr, 5 Mo, balance Co	Cast, 1500 F—FC

Errors in the measured values of damping caused by energy losses outside the specimen, were investigated in detail and found to be negligible (see Appendix 1).

Results

Table 1 contains the damping in per cent logarithmic decrement, measured on a number of materials as a function of temperature and nominal maximum bending stress, using the specimen shown in Fig. 1. It includes also the ratios of the moduli of elasticity at elevated temperatures to the moduli at room temperature, in the column headed "Relative Modulus."

Table 2 contains the physical properties, and Table 3, the chemical composition and heat-treatment of the materials included in Table 1.

Conclusion

The materials tested differ widely in damping and in their variation in damping with temperature. Explanation of these differences, or correlation of them with other of the material properties, is beyond the purpose of this paper and probably beyond the potentialities of the data as well.

Comparison of the results with damping values measured under different types of stress and at different frequencies should recognize the effect of these factors. In a torsion-test specimen, the entire surface of the specimen is subjected to the maximum stress, whereas the maximum stress in a tuning-fork specimen is highly localized. Since damping usually increases with stress, it follows that the damping measured in torsion will be higher than that in bending, if the maximum significant stress is the same in both cases. Just what this significant stress is, i.e., whether the resultant tension or shear stress, or some more complex function of the stresses, we do not know. We do know, however, that the logarithmic decrement of a vibrating cantilever at a given maximum bending stress will differ from, and probably will be less than, that of a vibrating torsional pendulum under an equal maximum shear stress. It is generally recognized, too, that damping depends upon the frequency of stress fluctuation, although the effect of frequency is usually considered to be smaller than that of stress or temperature.

For these reasons, damping data should be obtained under conditions closely similar to those for which they are to be used. Data obtained from tuning-fork specimens are directly applicable to parts subjected to vibratory bending, whereas those obtained from the commonly used low-frequency torsional machine are particularly applicable to parts such as shafting which may vibrate in torsion. Either test, perhaps, is suitable for classifying materials as to damping under any condition of stress, but this has still to be established by carefully conducted comparative tests.

Appendix 1

Details of Test Equipment and Procedure

Mechanical Equipment

The solid portion of the fork is screwed to the lower end of a 3/8-in-diam stainless-steel rod, whose upper end is gripped in a collet fastened to a rigid framework. The spreader is screwed to the upper end of a trip rod which is positioned by guide bushings in two horizontal plates of the framework so that its axis coincides with the axis of the rod supporting the fork. The trip rod passes through a hole in the center of a 5-lb weight, which is guided parallel with the trip rod. By striking a shoulder on the bottom of the trip rod, the weight jerks the spreader from between the tines of the fork, and the specimen vibrates with an amplitude which is equal approximately to the deflection caused by the spreader.

The weight is held at the upper limit of its travel by a solenoid-operated latch connected electrically, through an adjustable time-delay relay, in parallel with the film-driving motor on the oscillograph. The fork vibration may thus be started automatically so that it is recorded at the beginning of the film.

The fork and its supporting rod are enclosed by a furnace 3 in. diam × 16 in. long inside, with a removable cover at the bottom. The spreader and trip rod are inserted through a small hole in the cover. Fig. 3 shows the cover removed and the fork lowered outside the furnace. During test, the bottom of the fork is opposite a sight hole in the side of the furnace, so that insertion of the spreader between the tines of the specimen, employing an offset spreading tool, can be viewed.

The furnace is heated electrically with alternating current through a nichrome winding around the quartz tube forming the inner wall. The temperature variation in the section occupied by the test specimen does not exceed 2 per cent of the test temperature, in degrees F, and most of this occurs in the section near the free ends of the tines which contributes very little to the damping.

The temperature is measured with a chromel-alumel thermocouple inserted in a 1/16-in-diam hole in the specimen, Fig. 1. Leads are brought out through the top of the furnace.

Since the furnace winding is inductive, and the damping capacity of magnetic materials is influenced by magnetic fields, the current must be shut off and the specimen demagnetized before taking the vibration decrement. This is accomplished by reducing slowly the current through the furnace winding to zero, using a potentiometer arrangement of resistance boxes.

Lead wires to the strain gage are connected to the 0.010-in-diam nickel leads on the fork at a terminal block clamped to the support rod just above the fork. Simple pressure-contact con-

nections are satisfactory, but the screw threads must be lubricated with a high-temperature bolting compound. One of the terminals is grounded, the other is carried by an asbestos insulating strip.

Specimen and Strain Gage

The gap between the little feet on the free ends of the tines of the tuning-fork specimen, Fig. 1, is made only large enough so that it will not close when the fork is vibrating. This is important for, with a large gap, slight misalignment of the spreader as it is jerked out will cause it to break contact with one tine before the other, with the result that some of the energy stored in the fork is imparted to the spreader and trip rod, and the two tines tend to begin vibrating with unequal amplitudes. It is important, too, that the corners on the edges of the feet and the spreader be square and sharp, so that they "break clean" and the initial vibration amplitude equals the static deflection. A slight taper on these surfaces is particularly to be avoided, since the tines will follow the contour as the spreader is withdrawn; they will not, however, follow the contour of a very small chamfer because of the high velocity at which the spreader moves (about 100 ips), compared to the transverse velocity at which the tines approach it.

The $^1/_2$-in-diam hole in the solid portion of the fork accommodates a nut on the end of the support rod and can be omitted if the material is such as to permit threading the $^1/_4$-in-diam hole at right angles to it.

No extraordinary precautions need be taken to make the frequencies of the two tines the same. Slight differences between the tines seem to have no appreciable effect on the damping, although it seems likely that if they are badly unbalanced, the energy dissipation to the support rod will be increased.

The resistance-type electric strain gage operates on the change in resistance of a wire with strain. The authors have developed a technique of using such gages suitable for measuring dynamic strains at high temperatures.[4] They consist of 0.0015-in-diam nichrome gage wire cemented to the specimen with Sauereisen No. 31 cement[5] and are built up on the specimen as follows:

The surface of the metal is roughened by cutting many shallow nicks with a sharp cold chisel. Grease and dirt are removed by washing with alcohol, and a thin coat of cement is applied. On this, the gage wire is arranged in a "W" and held in place with three loops of hair stuck to the fork. One end of the gage wire is grounded to the fork by folding a small piece of nickel ribbon around it and spot-welding. To the other end is welded a second piece of nickel ribbon $^1/_2$ in. long, insulated from the fork by cement. The ground connection, and one-half the nickel-ribbon strip are covered with a second coat of cement, which is allowed to dry and then baked at 500 F. Finally, 0.010-in-diam nickel wires are welded to the strip and fork, respectively.

Location of the gage on the fork, as shown in Fig. 1, is suitable for damping measurements; if it is moved toward the free ends of the tines, the energy absorbed by the gage increases; if it is moved in the opposite direction its sensitivity is reduced.

Such gages stand up satisfactorily at 1100 F. They usually last for 1 to 2 hr at 1300 F and sometimes long enough for a damping test at 1400 F.

[4] Gages suitable for use at temperatures up to 500 F are sold by the Baldwin Southwark Division of the Baldwin Locomotive Works under the name of SR-4 bonded resistance-wire strain gages. These are applied to the specimen by polymerization of a cementing medium in place in the presence of heat and pressure. Patent licenses for developments using wire gages of the bonded type are available from the Baldwin Locomotive Works.

[5] Obtained from Sauereisen Cements Company, Pittsburgh, Pa.

Measuring Circuit

The fluctuating resistance of the gage wire, accompanying vibration of the specimen, is converted to an alternating voltage at the output of the potentiometer circuit. The essential elements of the latter are shown in full lines in Fig. 2. The dashed lines define an auxiliary circuit used for adjusting the resistance R to equal the gage resistance and checking the battery voltage.

The output of the potentiometer circuit is supplied through two amplifiers to the oscillograph. These are standard equipment and are shown at the right in Fig. 3. One of the two oscillograph galvanometers is used for a 60-cycle timing wave. Records are made on Kodak No. 120 verichrome film, using a standard continuous-drive film holder.

Characteristics of Measuring Circuit

Gages constructed and located as described have about 50 ohms resistance and a nominal sensitivity factor of about 0.6, that is, the fractional change in resistance is about 0.6 of the strain which would be produced by a uniform stress equal to the nominal maximum bending stress. Hence a nominal maximum bending stress of 30,000 psi, in a specimen of material having a 30,000,000-psi modulus of elasticity, produces a change in resistance of $0.6 \times 0.0001 \times 50$ or 0.003 ohm in the gage wire.

At 1000 cycles per sec frequency, the corresponding alternating voltage across the output resistor of the potentiometer circuit is about 2 mv (rms). This is amplified to produce full-scale deflection (50 mm) of the oscillograph galvanometer, whose sensitivity is 1.6 mv (rms) per mm and whose resistance is 0.9 ohm.

The transient response of the measuring circuit to the impulse occurring when the vibration starts is such that an approximately true record is obtained after about 1/1000 sec or 1 cycle, from the start of the vibration. The impulse results from the abrupt change in the average gage resistance at the instant of release. The first $^1/_2$ cycle recorded is about 25 per cent too high, but this is not objectionable unless the damping is extremely high, i.e., 5 per cent logarithmic decrement or above.

Accuracy of Results

The equipment was investigated in detail for sources of error in the measured values of damping. Errors may arise from energy losses outside the specimen, nonlinearity between the actual specimen vibration amplitude and the recorded vibration amplitude, and inaccuracy in calculating the logarithmic decrement from the vibration record. The latter constitutes the only appreciable source of error, in so far as could be determined.

Energy losses outside the specimen may occur in the support rod and frame, in the strain gage, or from fluid friction in the air. A specimen of very low damping material (vitallium) suspended from a loop of fine cotton thread showed the same damping as it did when screwed to the support rod. While this does not eliminate all question of losses to the support, it seems to indicate that they are extremely small. The damping of the specimen in this case was of the order of 0.02 to 0.04 per cent logarithmic decrement, and a difference of 5 per cent of this between the decrements obtained with the two methods of support would have been discernible.

The same specimen was used to check possible energy loss in the gage by the simple expedient of testing first with two gages (one on each tine) then with one. No difference in the results could be seen.

A rough computation indicates that fluid-friction losses to the air can hardly account for more than 0.002 per cent logarithmic decrement.

Linearity between actual vibration amplitude and the recorded amplitude depends upon the characteristics of the strain gage and measuring circuit. The latter was checked electrically by observing that the oscillograph deflection was proportional to a 1000-cycle voltage applied across the gage. The gage characteristics were investigated by using a special fork, similar to the test specimen but having tines 12 in. long. The change in resistance of the gage was measured as a function of the deflection at the free ends of the tines. The relation was found to be linear at any temperature up to 1200 F, for deflections corresponding to bending stresses at the fixed ends of the tines up to 35,000 psi. It is believed the linearity will hold at higher temperatures and stresses under elastic conditions at the gage.

It has been found that log decrements calculated from the same vibration record by different persons using average care may differ by 6 or 8 per cent; with extreme care agreement within 2 or 3 per cent can be obtained.

Test Procedure

While the manner of conducting a test will be fairly apparent from the description of the test equipment, certain details of the actual procedure require further comment.

Before testing, the width of each specimen is measured at the free ends of the tines with a micrometer, and the width of the gap between the feet is measured with a taper gage.

From the properties of the material, the maximum stress at which measurements are to be made is chosen. Two spreaders are selected, one large enough to produce this maximum stress, the other to produce a stress about 40 per cent as great. The deflection produced by each is checked by inserting it in the gap and measuring the width of the fork at the ends of the tines.

The fork is connected for test and tripped 2 or 3 times until the amplifiers are adjusted for full-scale deflection on the oscillograph, and a rough estimate of the damping is made so that the film-travel speed can be chosen to obtain a decrement curve suitable for analysis.

Oscillograms are taken using first the larger, then the smaller, of the two spreaders at each test temperature, starting at room temperature and increasing. After testing at each temperature, the gap is checked with the taper gage. If yielding has occurred, the test may be stopped, or continued at lower stresses. After the test is completed and the fork has cooled, the width is checked again to determine any final permanent set, and to check the taper-gage readings taken while the fork was hot.

The specimen is held at each test temperature for about 10 min before testing. Since the bottom of the furnace is removed momentarily while the spreader is inserted, the temperature of the specimen drops slightly before the vibration is started. To compensate for this, the spreader is inserted when the specimen is a few degrees above the test temperature.

With very low-damping materials, the film-travel speed must be so low that individual cycles cannot be discerned in the record. In such cases, an additional record for frequency measurement is taken at selected temperatures, using a higher film-travel speed.

The vibration-decay records taken with the two spreaders of different size afford several useful checks on the results. Since, in general, the recorded amplitudes at the start of the vibration are proportional to the initial static deflections produced by the respective spreaders, the amplitude linearity of the vibration-measuring system is substantiated. Moreover, if it is found in certain cases that this proportionality is imperfect, those cases can be examined for the cause. Finally, the two records provide a check on the calculation of the log decrement in the medium-stress range which is usually covered by both.

Appendix 2

Mathematical Analysis and Calculations

Nomenclature

The following nomenclature is used in Appendix 2:

α = constant
b = width of tine, in.
c = distance from neutral axis to extreme fiber in bending, in.
δ = log decrement of vibration
E = modulus of elasticity, psi
f_1, f_2, f_i = vibration frequency in fundamental, second and ith modes, respectively, cycles per sec
g = acceleration of gravity, ipsps
h = thickness of tine, in.
γ = density of material, pci
I = moment of inertia of cross section of tine about neutral axis in bending, in.[4]
l = length of tine from bottom of slot, in.
$M = M_T + M_F$
M_T, M_F = bending moment at fixed ends of tine due to inertia forces of tine and foot, respectively, lb-in.
$m_1, m_2, m_i = \left(\frac{\gamma f^2 bh}{gEI}\right)^{1/4}$ for $f = f_1, f_2, f_i$, respectively
N = number of vibration cycles, measured from start of vibration
S = nominal maximum bending stress at fixed ends of tines, psi
t = time from start of vibration, sec
V = volume of foot on end of tine, in.
x = distance along tine from bottom of slot, in.
x_F = distance from bottom of slot to center of gravity of foot, in.
Y = vibration amplitude of end of tine at time t, in.
Y_1, Y_2, Y_i = initial vibration amplitude of end of tine in fundamental, second and ith modes, respectively, in.
Y_s = static deflection of end of tine due to spreader, in.
y_1, y_2, y_i = initial vibration amplitude at any point on tine in fundamental, second and ith modes, respectively, in.
y_s = initial static deflection at any point on tine due to spreader, in.
y_F = initial vibration amplitude in fundamental mode, of center of gravity of foot, in.

Initial Vibration Amplitude

Before release, with the spreader between the feet, the deflection of the tines corresponds to that of a fixed-free beam with a terminal load, and at any point[6]

$$y_s = Y_s\left[\frac{3}{2}\left(\frac{x}{l}\right)^2 - \frac{1}{2}\left(\frac{x}{l}\right)^3\right] \quad \text{[1]}$$

At the instant following release, assuming the amplitudes of modes of vibration higher than the second are negligible, the amplitudes of the fundamental- and second-mode components of the vibration must satisfy the relation

$$y_s = y_1 + y_2 \text{ at } \frac{x}{l} = 1, 0.5 \quad \text{[2]}$$

The deflection at any point of a fixed-free beam vibrating at its natural frequency in the ith mode[7]

[6] This is given in most strength-of-materials textbooks.

[7] See "Applied Elasticity," by J. Prescott, Longmans, Green & Company, New York, N. Y., 1924, for derivation of Equations [3], [4], and [5].

$$y_i = \frac{Y_i}{k_i}\left[\frac{\cosh m_i x - \cos m_i x}{\cosh m_i l + \cos m_i l} - \frac{\sinh m_i x - \sin m_i x}{\sinh m_i l + \sin m_i l}\right] \quad [3]$$

where

$$k_i = \left[\frac{\cosh m_i l - \cos m_i l}{\cosh m_i l + \cos m_i l} - \frac{\sinh m_i l - \sin m_i l}{\sinh m_i l + \sin m_i l}\right] \quad [4]$$

For the fundamental and second modes, $i = 1$ and $i = 2$, respectively

$$\left.\begin{aligned} m_1 &= \frac{1.875}{l} \\ m_2 &= \frac{4.6944}{l} \end{aligned}\right\} \quad [5]$$

By substituting Equations [1], [3], [4], and [5] in [2]

$$Y_1 = 0.9744\ Y_s \quad [6]$$

$$Y_2 = 0.0256\ Y_s \quad [7]$$

or the amplitude in the fundamental mode is 97.44 per cent of the static deflection before release, and in the second mode 2.56 per cent.

Nominal Maximum Bending Stress

The nominal maximum bending stress at a section through the tine at the base of the slot

$$S = M\frac{c}{I} \quad [8]$$

The bending moment on this section is equal to the sum of the moments of the inertia forces of the tine and foot, due to vibration in the fundamental mode, or

$$M = M_T + M_F \quad [9]$$

Due to the tine

$$M_T = \int_0^l \frac{\gamma(2\pi f_1)^2}{g}\, y_1\, x dx \quad [10]$$

whence, using y_1 from Equations [3], [4], and [5], and performing the integration

$$M_T = 0.283\,\frac{4\pi f_1^2 \gamma b h}{g}\, Y_1\, l^2 \quad [11]$$

Due to the feet, similarly

$$M_F = \frac{4\pi^2 f_1^2 \gamma V}{g}\, y_F x_F \quad [12]$$

From the proportions of the specimen, Fig. 1

$$x_F = 0.972l \quad [13]$$

and from Equations [3], [4], [5], and [6], using $i = 1$

$$y_F = 0.961\ Y_1 = 0.936\ Y_s \quad [14]$$

The section modulus of the tuning-fork tine

$$\frac{I}{c} = \frac{bh^2}{6} \quad [15]$$

By substituting Equations [13] and [14] in [12], and the result, together with Equations [11] and [15] in [9], and [8]

$$S = 0.9744\,\frac{24\pi^2}{g}\left[0.283 + \frac{0.936V}{bhl}\right]\frac{f_1^2\gamma l^2}{h}\, Y_s \quad [16]$$

Since the second term in brackets is small, its contribution to the total will not be changed appreciably by small variations in h, l, and b. Hence it may be evaluated once and for all by using the nominal dimensions of the specimen, viz., from Fig. 1

h = 0.25 in.
b = 0.5 in.
l = 2.688 in.
V = 0.0136 cu in.
g = 386 ipsps

and Equation [16] may then be reduced to

$$S = 0.192\,\frac{f_1^2\gamma l^2}{h}\, Y_s \quad [17]$$

It will be noted that no allowance has been made for the effect of the feet on the shape of the vibration-deflection curve. The resulting error in S may be estimated by comparing the actual case with the extreme case where the mass of the tine is negligible compared to the mass of the feet. Then the deflection shape during vibration would be defined by Equation [1] instead of Equation [3], and M_T would be 3 per cent less than the value given by Equation [11]. Actually, since M_F is only about 12 per cent of M, as may be seen from Equation [16], the value of S given by Equation [17] is only about $^1/_3$ of 1 per cent too high.

Logarithmic Decrement

If a sinusoidal vibration decays at a rate proportional at any moment to its amplitude, its amplitude

$$Y = Y_1 \epsilon^{-\alpha t} \quad [18]$$

By definition, the log decrement

$$\delta = \ln \frac{Y_1}{Y_1 \epsilon^{-\alpha/f_1}} = \frac{\alpha}{f_1} \quad [19]$$

Hence, since

$$N = f_1 t \quad [20]$$

Equation [18] may be written

$$Y = Y_1 \epsilon^{-N\delta} \quad [21]$$

and by differentiation

$$\frac{dY}{dN} = -\delta Y_1 \epsilon^{-N\delta} = -\delta Y$$

whence

$$\delta = -\frac{1}{Y}\cdot\frac{dY}{dN} \quad [22]$$

By employing Equation [22], δ may readily be evaluated by drawing tangents to a curve of Y versus N.

Nozzles for Supersonic Flow Without Shock Fronts

By ASCHER H. SHAPIRO,[1] CAMBRIDGE, MASS.

Flow patterns for compressible fluids at supersonic velocities are discussed, and it is shown that shock fronts form when neighboring Mach lines (envelopes of wave fronts originating from point disturbances) intersect. A criterion for divergence of Mach lines is developed for cases in which the passage is symmetrical in two or three dimensions and has a straight axis. This criterion is used as the basis for designing supersonic nozzles and diffusers. The analysis indicates that only a nozzle of infinite length can discharge a parallel stream into a tube of constant cross section without the formation of shock fronts. Methods are presented for designing nozzles of finite length, with the intensity of shock fronts reduced to as small a value as possible, and it is shown that nozzles of reasonable length may be designed so that shock fronts are insignificant. Experimental observations indicate that the proposed method of nozzle design is a practical one. With regard to supersonic diffusers having a straight axis, it is shown that shock fronts cannot be avoided, even though the diffuser is of infinite length. However, the methods of this paper may be used as an aid in determining the best diffuser design.

Nomenclature

The following nomenclature is used in the paper:

A = cross-sectional area of passage
A_t = value of A at section where stream velocity equals local sound velocity (throat area)
k = ratio of specific heat at constant pressure to specific heat at constant volume
M = Mach number (ratio of local stream velocity to local velocity of sound)
S = projection on a line perpendicular to axis of passage, of distance required for neighboring Mach lines to intersect, Fig. 4
x = distance along nozzle axis
y = distance of wall from nozzle axis
y_t = value of y at section where stream velocify equals local sound velocity
α = Mach angle = arc sin $1/M$
β = angle of passage wall with respect to axis of passage
μ = $d(dy/dx)/d\alpha$. Defined by Equation [2]
$d\phi$ = angle between Mach lines which originate at two points on the wall an infinitesimal distance apart

Subscripts

t = throat of nozzle
1 = beginning of curved contour of nozzle
2 = end of nozzle

Introduction

Nature of Problem. A characteristic which distinguishes compressible flow at supersonic velocities from flow at subsonic velocities is the possibility that discontinuities in the supersonic flow pattern may occur, accompanied by abrupt rises in pressure along a "shock front." Since the discontinuities are irreversible in the thermodynamic sense, they reduce the efficiency of any flow passage in which they occur. Furthermore, separation of the stream from the walls may take place in consequence of the large negative pressure gradients in the boundary layer at the point where the shock occurs. It is therefore important to design ducts so that shock waves are avoided, or reduced to small proportions.

Object. It is the purpose of this paper to present a method for the design of supersonic passageways which are symmetrical in two or three dimensions and which have a straight axis. Practical applications include the design of nozzles for wind tunnels and for steam and gas turbines, and the design of supersonic diffusers.

Previous Work. Meyer (1)[2] analyzed the two-dimensional parallel flow of a gas at supersonic velocities when the stream turns a sharp bend so that the flow is subsequently parallel but in a new direction. Accelerating flow around a bend (from a region of high pressure to one of low pressure) was analyzed on the basis of irrotational flow, with the special assumption that the region of changing pressure and velocity would be wedge-shaped, with its apex at the corner, and that all stream velocities would be constant along any radius within the wedge-shaped region. It was shown that the decelerating flow around a sharp bend is discontinuous, the rise in pressure and decrease in stream velocity occurring along an oblique shock front which is represented by a straight line originating at the sharp corner. Meyer further presented Schlieren photographs of a parallel stream issuing from a nozzle and passing into regions of high and low pressure, illustrating the wedge-shaped expansion for accelerating flow and the oblique shock front for decelerating flow.

Prandtl and Busemann (2) used Meyer's analysis of parallel flow around a sharp corner as the basis for an approximate method of designing the diverging portion of a two-dimensional nozzle to produce a parallel, supersonic stream at its exit. They proposed a step method in which small parts of the flow pattern for flow around a corner are transferred to the flow within the nozzle walls, yielding a nozzle contour which is wedge-shaped near the throat and tangent to a parallel section at the nozzle exit. This procedure involves the application of a flow pattern pertaining to a specific set of boundary conditions to a problem having a different set of boundary conditions. The method is therefore approximate and involves errors of uncertain magnitude.

Busemann (3) gave Schlieren photographs of the flow within the diverging portions of two-dimensional Laval nozzles having walls which become parallel at exit. The photographs showed

[1] Instructor in Mechanical Engineering, Massachusetts Institute of Technology. Jun. A.S.M.E.

Presented at the Annual Meeting, New York, N. Y., Nov. 29–Dec. 3, 1943, of The American Society of Mechanical Engineers.

Discussion of this paper should be addressed to the Secretary, A.S.M.E., 29 West 39th Street, New York, N. Y., and will be accepted until July 10, 1944, for publication at a later date. Discussion received after the closing date will be returned.

Note: Statements and opinions advanced in papers are to be understood as individual expressions of their authors and not those of the Society.

[2] Numbers in parentheses refer to the Bibliography at the end of the paper.

that the curvature of the walls was the chief factor in the formation of oblique shock fronts. Specifically, when the curvature at any point along the nozzle contour was too great, an oblique shock front was formed within the nozzle. A parallel stream without visible shock fronts was produced at the nozzle exit only when the curvature of the walls was very small.

Formation of Shock Fronts

Propagation of Disturbances. A small disturbance in a stream of fluid is propagated in all directions with respect to the fluid at the speed of sound (4). When the stream itself is moving at subsonic velocities, the disturbance can be propagated upstream; therefore, the flow pattern upstream of an obstacle is affected by the presence of the obstacle. If the stream is moving at supersonic velocity, a small disturbance cannot be propagated upstream, since the velocity of the stream exceeds the velocity with which a disturbance can be propagated relative to the stream. Therefore, the flow pattern of a stream approaching an obstacle at supersonic velocity is altered only in a region downstream of the obstacle. For example, Fig. 1 shows a parallel stream approaching a thin sharp-pointed object. The disturbance caused by the sharp point is propagated into the stream along the wave front shown by the dotted lines, the latter being known as Mach lines. The angle α is called the Mach angle, and its magnitude is determined by the ratio of the stream velocity to the local velocity of sound in the fluid, thus (5)

$$\sin \alpha = 1/M$$

where M represents the Mach number and is defined as the ratio of the local velocity of the stream to the local velocity of sound. The disturbance caused by the point affects the stream only in the cone of angle 2α.

Accelerating Flow. At supersonic velocities, acceleration of a stream is accompanied by a divergence of the streamlines. Fig. 2 (6) shows a parallel two-dimensional flow approaching a curved foil which, for analysis, is divided into an infinite number of short chords, each infinitesimal in length. Above the foil the streamlines tend to diverge, so that the velocity of the stream increases while the pressure drops in the direction of flow. However, no

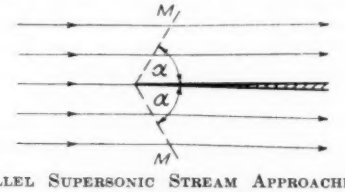


Fig. 1 Parallel Supersonic Stream Approaching a Sharp-Pointed Obstacle

The dotted line M represents the envelope of pressure waves which are propagated into the stream from the point disturbance.)

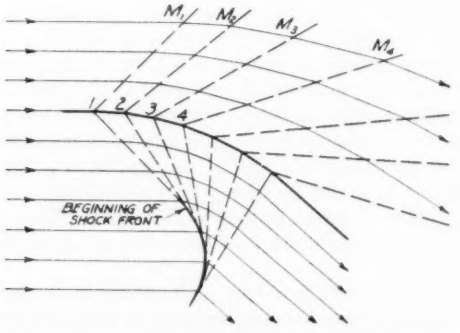


Fig. 2 Parallel Supersonic Stream Approaching a Curved Foil

(Mach lines originating on the top surface diverge. Mach lines originating on the bottom surface converge and form a shock front.)

change occurs until the stream reaches the Mach line M_1, at which point the stream bends downward in response to the disturbance caused by the corner 1. The influence of the corner 2 is not felt until the stream approaches the Mach line M_2, which is propagated into the fluid at a Mach angle corresponding to the local stream velocity and the local velocity of sound. If the flow takes place without friction and without heat transfer (that is, isentropically), an increase in velocity will result in a decrease in temperature and a consequent decrease in the local sound velocity. It follows that along the upper side of the foil, the Mach number increases and the Mach angle decreases. Neighboring Mach lines must therefore diverge, both from the standpoint of the change in stream direction and from the standpoint of the change in Mach angle.

Decelerating Flow. The flow under the foil of Fig. 2 is accompanied by a rise in pressure and a decrease in velocity, since the streamlines are caused to converge by the presence of the foil. The changes in pressure and in velocity are propagated along Mach lines which originate at each corner and which cross the streamlines at the local Mach angle. Since a decrease in velocity causes a rise in temperature and, in turn, an increase in the local velocity of sound, the local Mach angle increases in the direction of flow. This, together with the change in direction of the stream, causes neighboring Mach lines to converge. The chords into which the foil is divided are infinitesimal in length, and each makes an infinitesimal angle with its neighbor. Therefore, the change in pressure and change in velocity across each Mach line are infinitesimal, and, were it not for the convergence of Mach lines, the pressure and velocity fields would be everywhere continuous. However, along the envelope of converging Mach lines, shown by the heavy line in Fig. 2, the infinitesimal changes in pressure and velocity of many Mach lines accumulate, so that this line becomes a discontinuous shock front across which both pressure and velocity change by a finite amount in an infinitesimal distance, corresponding to infinite pressure gradients and accelerations. In the illustration shown, the shock front is detached from the body. When the body itself has sharp bends in it (or the limiting case of a smooth bend with zero radius of curvature), as in Fig. 3, the shock front starts at the sharp bend.

As further instances of shock fronts caused by convergence of neighboring Mach lines, Fig. 3 shows two examples. In Fig. 3(*a*) a parallel stream at supersonic velocity enters a conical diffuser which is joined to the straight passage by a sharp angle. An oblique shock front starts at the corner. In Fig. 3(*b*), a stream leaving the conical section of a converging-diverging nozzle enters a straight passage of constant cross section, with a finite angle at the joint. Although there is no change in cross-sectional area across the joint, a shock front is formed because the change in the direction of the stream results in a convergence of the Mach lines immediately before and after the sharp corner.

Criterion for Avoidance of Shock Fronts. It may be concluded from the foregoing discussion that, if shock fronts are to be absent, the boundaries of a stream must be curved in such a manner that neighboring Mach lines do not intersect. In the following analysis this criterion is given mathematical form for the case of flow within a passageway having a straight axis, and it is

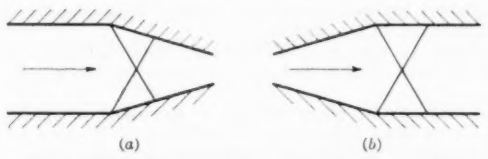


Fig. 3 Shock Fronts Caused by Convergence of Neighboring Mach Lines

(*a*, Parallel supersonic stream entering a diffuser. *b*, Stream leaving the conical portion of a supersonic nozzle and passing into a straight tube.)

shown how this mathematical statement may be used as a basis of nozzle design.

The Design of Shockless Passages

Assumptions. The following assumptions are made:

1 The axis of the passage is a straight line.

2 The passage may be two-dimensional, with a rectangular cross section; or three-dimensional, with a circular cross section.

3 The angle between the passage wall and the axis is small enough so that the tangent of the angle may be taken equal to the angle itself.

4 The velocity of the stream is uniform over any cross section perpendicular to the axis of the passage. This will be satisfied when the angle between the passage walls is small and when frictional effects are absent.

5 The direction of the stream at the solid boundary is identical with the tangent to the solid boundary.

6 Velocities are supersonic.

Criterion for Shockless Flow. Consider a short section of passage of length dx, as shown in Fig. 4. The distance y represents

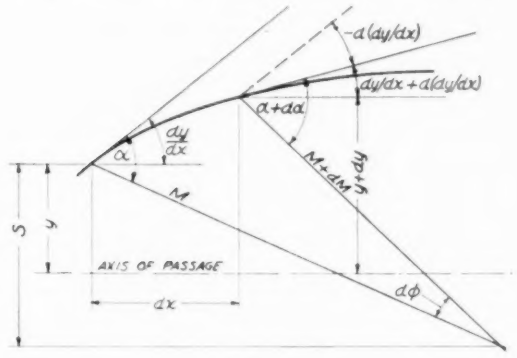


Fig. 4

one half the width of a rectangular passage for two-dimensional flow, and the radius of a circular passage for three-dimensional flow. A geometric analysis shows that the angle between two neighboring Mach lines, originating at points on the boundary an infinitesimal distance apart, is given by[3]

$$d\phi = d\alpha - d(dy/dx) \quad [1]$$

If μ is defined arbitrarily by the relation

$$d(dy/dx) = \mu d\alpha \quad [2]$$

it follows from Equation [1] that

$$d\phi = (1 - \mu)\, d\alpha \quad [3]$$

In a symmetrical passage, the slope of the streamlines and the rate of change of slope with respect to distance along the axis will increase as the distance from the passage axis increases. On the other hand, the Mach angle α is uniform over a cross section perpendicular to the axis. It follows that the angle between neighboring Mach lines is greatest at the wall, so that the criterion for the generation of shock fronts may, for the simple case of flow within a symmetrical passage having a straight axis, be expressed in terms of conditions at the wall.

Shock fronts will be absent when the angle $d\phi$ is negative (or in the limit, zero) at all points along the passage, since positive values of $d\phi$ correspond to convergence of neighboring Mach lines. Therefore, the criterion for the absence of shock fronts is

$$(1 - \mu)\, d\alpha \leq 0 \quad [4]$$

When the stream accelerates in the direction of flow, the Mach number increases and the Mach angle decreases; it follows from Equation [4] that for shockless flow in a diverging passage

$$\mu \leq 1 \quad [5a]$$

In similar fashion it may be shown that for shockless flow in a converging passage

$$\mu \geq 1 \quad [5b]$$

Likewise, shock fronts will occur in a diverging passage when $\mu > 1$; and in a converging passage when $\mu < 1$.

Since the value of μ is arbitrary, it may be constant over the length of the passage, or it may be an arbitrary function of α.

Application to Design of Nozzles. The foregoing criteria will be applied to the design of a nozzle passage of the type shown in Fig. 5. The contour t–1 is wedge-shaped or cone-shaped, with walls at an angle β_1 to the axis of the nozzle. The contour 1–2 is tangent to the contour t–1 at section 1 and to a passage of constant cross section at section 2 and is curved to avoid shock fronts.

Equation [2] shows that the value of μ is zero for the contour t–1, so that shock fronts cannot form in this section of the nozzle.

The contour between sections 1 and 2 will be based upon the criterion for shockless flow, employing a constant value of μ. Equation [2] may be integrated, thus

$$d(dy/dx) = \mu d\alpha \quad [2]$$

$$dy/dx = \mu\alpha + c_1 \quad [6]$$

where the constant of integration c_1 is evaluated with the aid of either of the following boundary conditions

when $dy/dx = 0$, then $\alpha = \alpha_2$ [7a]

when $dy/dx = \tan \beta_1$, then $\alpha = \alpha_1$ [7b]

Combination of Equations [7a] and [7b] yields an important relation between the boundary variables, as follows

$$c_1 = -\mu\alpha_2 = \tan \beta_1 - \mu\alpha_1$$

or

$$\tan \beta_1 = \mu(\alpha_1 - \alpha_2) \quad [7c]$$

Substitution of Equation [7a] into Equation [6] yields the equation

$$dy/dx = \mu\,(\alpha - \alpha_2) \quad [8]$$

After rearrangement and integration, Equation [8] becomes

$$\frac{x - x_1}{y_t} = \frac{1}{\mu} \int_{(y/y_t)1}^{(y/y_t)} \frac{d\,(y/y_t)}{\alpha - \alpha_2} \quad [9]$$

The value of y/y_t is related to the area ratio A/A_t, which in turn is related to the Mach angle α. Integration of Equation [9] yields the curved contour between sections 1 and 2 of Fig. 5.

For a two-dimensional nozzle

$$y/y_t = A/A_t \quad [10a]$$

and for a three-dimensional nozzle

$$y/y_t = \sqrt{A/A_t} \quad [10b]$$

The relation between the area ratio A/A_t and the Mach angle α depends upon the properties of the gas and on the wall friction at the solid boundaries. For frictionless adiabatic flow of a perfect gas, this algebraic relationship is given by

[3] This equation gives the angle between neighboring Mach lines at the wall; the angle between the same pair of Mach lines may be different in the core of the stream.

$$\frac{A}{A_t} = \frac{\sqrt{\left(\frac{k-1}{k+1}\right)\left(\frac{2}{k+1}\right)^{\frac{2}{k-1}}}}{\sqrt{\frac{Z-1}{Z^{(k+1)/(k-1)}}}}$$

where

$$Z = 1 + \left(\frac{k-1}{2}\right)\left(\frac{1}{\sin \alpha}\right)^2$$

This expression is sufficiently complex so that the right-hand side of Equation [9] does not appear to be algebraically integrable by ordinary methods. The integration may be carried out either graphically or numerically. For the latter purpose, a table relating $\sqrt{A/A_t}$ and α, and having equal intervals in $\sqrt{A/A_t}$, permits the numerical integration to be carried out simply and rapidly with the aid of the trapezoidal rule or Simpson's rule. Table 1 gives this relationship for the isentropic flow of a perfect

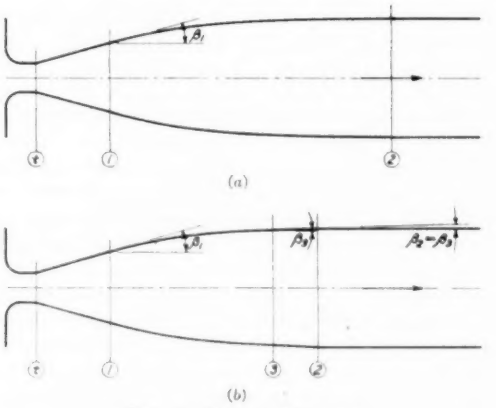


FIG. 5 · NOZZLE DESIGNS

(*a*, Nozzle design in which a curved contour connects a straight tube to a wedge-shaped or cone-shaped section. *b*, Nozzle design in which a curved contour connects two wedge-shaped or cone-shaped sections.)

TABLE 1 SQUARE-ROOT OF AREA-RATIO AS A FUNCTION OF MACH ANGLE FOR ISENTROPIC FLOW OF A PERFECT GAS WITH $k = 1.4$

A = Cross-section area A_t = minimum cross-section area of passage α = Mach angle, radians

$\sqrt{A/A_t}$	α	$\sqrt{A/A_t}$	α	$\sqrt{A/A_t}$	α	$\sqrt{A/A_t}$	α	$\sqrt{A/A_t}$	α	$\sqrt{A/A_t}$	α	$\sqrt{A/A_t}$	α
1.00	1.5708	1.30	0.5231	1.60	0.4172	1.90	0.3609	2.20	0.3241	2.50	0.2975	2.80	0.2771
1.01	1.0396	1.31	0.5179	1.61	0.4148	1.91	0.3594	2.21	0.3230	2.51	0.2967	2.81	0.2765
1.02	0.9474	1.32	0.5129	1.62	0.4125	1.92	0.3580	2.22	0.3220	2.52	0.2960	2.82	0.2759
1.03	0.8899	1.33	0.5080	1.63	0.4102	1.93	0.3566	2.23	0.3210	2.53	0.2952	2.83	0.2753
1.04	0.8477	1.34	0.5033	1.64	0.4079	1.94	0.3552	2.24	0.3200	2.54	0.2944	2.84	0.2747
1.05	0.8132	1.35	0.4987	1.65	0.4057	1.95	0.3538	2.25	0.3190	2.55	0.2937	2.85	0.2742
1.06	0.7845	1.36	0.4943	1.66	0.4035	1.96	0.3524	2.26	0.3181	2.56	0.2930	2.86	0.2736
1.07	0.7601	1.37	0.4900	1.67	0.4014	1.97	0.3510	2.27	0.3171	2.57	0.2923	2.87	0.2730
1.08	0.7386	1.38	0.4858	1.68	0.3993	1.98	0.3497	2.28	0.3162	2.58	0.2916	2.88	0.2724
1.09	0.7194	1.39	0.4818	1.69	0.3972	1.99	0.3484	2.29	0.3153	2.59	0.2909	2.89	0.2719
1.10	0.7024	1.40	0.4780	1.70	0.3951	2.00	0.3471	2.30	0.3143	2.60	0.2902	2.90	0.2713
1.11	0.6868	1.41	0.4742	1.71	0.3931	2.01	0.3458	2.31	0.3134	2.61	0.2895	2.91	0.2707
1.12	0.6726	1.42	0.4705	1.72	0.3912	2.02	0.3446	2.32	0.3125	2.62	0.2888	2.92	0.2702
1.13	0.6595	1.43	0.4668	1.73	0.3893	2.03	0.3433	2.33	0.3116	2.63	0.2881	2.93	0.2696
1.14	0.6473	1.44	0.4632	1.74	0.3874	2.04	0.3421	2.34	0.3107	2.64	0.2874	2.94	0.2691
1.15	0.6360	1.45	0.4597	1.75	0.3855	2.05	0.3408	2.35	0.3098	2.65	0.2867	2.95	0.2685
1.16	0.6254	1.46	0.4564	1.76	0.3837	2.06	0.3396	2.36	0.3089	2.66	0.2860	2.96	0.2680
1.17	0.6154	1.47	0.4532	1.77	0.3819	2.07	0.3384	2.37	0.3080	2.67	0.2853	2.97	0.2674
1.18	0.6059	1.48	0.4500	1.78	0.3801	2.08	0.3373	2.38	0.3072	2.68	0.2846	2.98	0.2669
1.19	0.5970	1.49	0.4469	1.79	0.3784	2.09	0.3361	2.39	0.3063	2.69	0.2840	2.99	0.2664
1.20	0.5886	1.50	0.4439	1.80	0.3767	2.10	0.3350	2.40	0.3055	2.70	0.2834	3.00	0.2658
1.21	0.5807	1.51	0.4410	1.81	0.3750	2.11	0.3338	2.41	0.3047	2.71	0.2827	3.01	0.2653
1.22	0.5731	1.52	0.4381	1.82	0.3734	2.12	0.3327	2.42	0.3038	2.72	0.2820	3.02	0.2648
1.23	0.5659	1.53	0.4353	1.83	0.3717	2.13	0.3316	2.43	0.3030	2.73	0.2814	3.03	0.2643
1.24	0.5590	1.54	0.4325	1.84	0.3701	2.14	0.3304	2.44	0.3022	2.74	0.2808	3.04	0.2638
1.25	0.5524	1.55	0.4298	1.85	0.3685	2.15	0.3294	2.45	0.3014	2.75	0.2802	3.05	0.2633
1.26	0.5461	1.56	0.4272	1.86	0.3670	2.16	0.3283	2.46	0.3006	2.76	0.2795	3.06	0.2628
1.27	0.5400	1.57	0.4246	1.87	0.3654	2.17	0.3272	2.47	0.2998	2.77	0.2789	3.07	0.2623
1.28	0.5341	1.58	0.4221	1.88	0.3639	2.18	0.3262	2.48	0.2990	2.78	0.2783	3.08	0.2618
1.29	0.5285	1.59	0.4196	1.89	0.3624	2.19	0.3251	2.49	0.2982	2.79	0.2777	3.09	0.2613

TABLE 1 (*Continued*)

$\sqrt{A/A_t}$	α	$\sqrt{A/A_t}$	α	$\sqrt{A/A_t}$	α	$\sqrt{A/A_t}$	α	$\sqrt{A/A_t}$	α	$\sqrt{A/A_t}$	α
3.10	0.2608	3.40	0.2473	3.70	0.2359	4.00	0.2262	4.30	0.21766	4.60	0.21014
3.11	0.2604	3.41	0.2469	3.71	0.2355	4.01	0.2259	4.31	0.21738	4.61	0.20990
3.12	0.2599	3.42	0.2465	3.72	0.2351	4.02	0.22558	4.32	0.21712	4.62	0.20966
3.13	0.2594	3.43	0.2461	3.73	0.2348	4.03	0.22526	4.33	0.21686	4.63	0.20944
3.14	0.2589	3.44	0.2457	3.74	0.2345	4.04	0.22496	4.34	0.21660	4.64	0.20920
3.15	0.2584	3.45	0.2453	3.75	0.2341	4.05	0.22466	4.35	0.21634	4.65	0.20898
3.16	0.2580	3.46	0.2449	3.76	0.2338	4.06	0.22438	4.36	0.21608	4.66	0.20874
3.17	0.2575	3.47	0.2445	3.77	0.2334	4.07	0.22408	4.37	0.21582	4.67	0.20852
3.18	0.2570	3.48	0.2441	3.78	0.2331	4.08	0.22378	4.38	0.21556	4.68	0.20828
3.19	0.2566	3.49	0.2437	3.79	0.2328	4.09	0.22350	4.39	0.21530	4.69	0.20806
3.20	0.2561	3.50	0.2433	3.80	0.2325	4.10	0.22320	4.40	0.21506	4.70	0.20784
3.21	0.2556	3.51	0.2429	3.81	0.2321	4.11	0.22292	4.41	0.21480	4.71	0.20762
3.22	0.2552	3.52	0.2426	3.82	0.2318	4.12	0.22264	4.42	0.21454	4.72	0.20738
3.23	0.2547	3.53	0.2422	3.83	0.2315	4.13	0.22236	4.43	0.21428	4.73	0.20716
3.24	0.2542	3.54	0.2418	3.84	0.2312	4.14	0.22206	4.44	0.21402	4.74	0.20694
3.25	0.2537	3.55	0.2414	3.85	0.2309	4.15	0.22178	4.45	0.21378	4.75	0.20670
3.26	0.2533	3.56	0.2410	3.86	0.2306	4.16	0.22150	4.46	0.21354	4.76	0.20648
3.27	0.2528	3.57	0.2407	3.87	0.2302	4.17	0.22122	4.47	0.21328	4.77	0.20626
3.28	0.2524	3.58	0.2403	3.88	0.2299	4.18	0.22094	4.48	0.21304	4.78	0.20604
3.29	0.2520	3.59	0.2399	3.89	0.2296	4.19	0.22066	4.49	0.21280	4.79	0.20582
3.30	0.2515	3.60	0.2395	3.90	0.2293	4.20	0.22036	4.50	0.21254	4.80	0.20558
3.31	0.2511	3.61	0.2391	3.91	0.2290	4.21	0.22008	4.51	0.21230	4.81	0.20536
3.32	0.2506	3.62	0.2388	3.92	0.2286	4.22	0.21982	4.52	0.21206	4.82	0.20516
3.33	0.2502	3.63	0.2384	3.93	0.2283	4.23	0.21954	4.53	0.21182	4.83	0.20494
3.34	0.2498	3.64	0.2380	3.94	0.2280	4.24	0.21926	4.54	0.21156	4.84	0.20472
3.35	0.2494	3.65	0.2377	3.95	0.2277	4.25	0.21898	4.55	0.21132	4.85	0.20450
3.36	0.2489	3.66	0.2373	3.96	0.2274	4.26	0.21872	4.56	0.21108	4.86	0.20428
3.37	0.2485	3.67	0.2369	3.97	0.2271	4.27	0.21844	4.57	0.21084	4.87	0.20408
3.38	0.2481	3.68	0.2366	3.98	0.2268	4.28	0.21818	4.58	0.21062	4.88	0.20386
3.39	0.2477	3.69	0.2362	3.99	0.2265	4.29	0.21792	4.59	0.21038	4.89	0.20366
										4.90	0.20344

gas with $k = 1.40$. This table may be used directly for three-dimensional nozzles and may be employed as well for two-dimensional nozzles with the aid of the auxiliary relationship

$$d(A/A_t) = 2\sqrt{A/A_t} \times d\sqrt{A/A_t}$$

Friction between the stream and the nozzle walls may be taken account of either by using a coefficient of friction between the stream and the walls, or by assuming some relationship between a nozzle velocity coefficient and the area ratio A/A_t. In either case, a table relating A/A_t and α could be constructed. The effect of friction is to increase the tendency toward formation of shock fronts, since at any section friction acts to increase the Mach angle by reducing the velocity of the stream and by increasing the velocity of sound. It is suggested that friction be allowed for by designing on the basis of frictionless flow, but with a conservative value of μ to insure that appreciable shock fronts are not formed.

Nozzles of Finite Length. The integrand of Equation [9] becomes infinite when $\alpha = \alpha_2$. Further study indicates that the integral itself is infinite if carried to the upper limit; thus the nozzle must be infinite in length if it is to be tangent to a tube with straight walls. One method of altering the design to obtain a nozzle of finite length is illustrated in Fig. 5(*b*). The calculations are carried out as though the nozzle were to be infinite in length. At some finite length, corresponding to section 3, the curved contour is connected to the straight tube with the wedge-shaped or cone-shaped length 3–2, the latter being tangent to the curved contour at section 3, and making the angle β_3 (or β_2) with the straight tube at section 2. According to Equation [2], μ is infinite at the sharp corner of section 2, so that a shock front will originate at the corner.

The sharp angle β_2 becomes progressively smaller as the length of curved section 1–3 increases. Meyer (1) shows for two-dimensional parallel flow that the ratio of the pressure rise across the shock front to the pressure before the shock is approximately directly proportional to the Mach number and to the angular change in direction of the stream, provided that the change in direction is small. As an example showing orders of magnitude, when $k = 1.4$, with an initial Mach number of 2, and a change in direction of 3 deg, the rise in pressure across the shock is 19 per cent of the pressure before the shock.

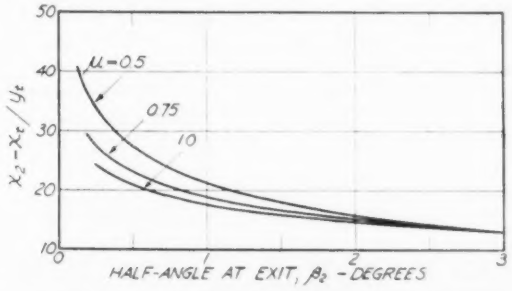


FIG. 6 EFFECT OF μ AND EXIT HALF-ANGLE β_2 ON LENGTH OF A THREE-DIMENSIONAL NOZZLE SIMILAR TO FIG. 5(*b*)
(Exit area ratio $A_2/A_t = 2.82$, and entrance half-angle $\beta_1 = 3$ deg; designed for isentropic flow.)

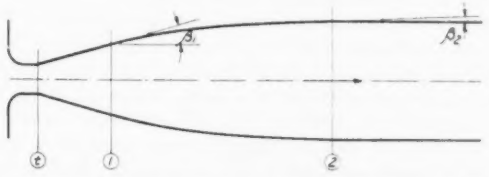


FIG. 7 NOZZLE DESIGN IN WHICH A CURVED CONTOUR IS TANGENT ON ONE END TO A WEDGE-SHAPED OR CONE-SHAPED SECTION, AND IS JOINED AT THE OTHER END TO A STRAIGHT TUBE, WITH A SMALL FINITE ANGLE β_2 AT THE JOINT BETWEEN CURVED CONTOUR AND TUBE

In a practical design, one would compromise between the reduction of β_2, so that shock fronts originating at the corner are very small, and the reduction of the nozzle length so as to avoid excessive losses on account of wall friction.

As an example of how nozzle length depends upon the half-angle at exit and upon the value of μ, Fig. 6 shows the total length of nozzle between throat and exit, expressed in terms of the radius at the throat, as a function of the half-angle at exit, for a three-dimensional isentropic nozzle. It appears that the exit half-angle can be made so small that the pressure rise across the shock front may be ignored, without at the same time requiring excessive nozzle lengths.

Alternate Design of Nozzle of Finite Length. An alternate type of nozzle of finite length is shown in Fig. 7. The length t–1 is wedge-shaped or cone-shaped, with a half-angle β_1, and is joined to a straight tube by the curved contour 1–2, which is tangent to the wedge or cone at section 1 and makes the sharp angle β_2 with the walls of the straight tube at section 2.

Equation [2] may be integrated, thus

$$d\,(dy/dx) = \mu\, d\alpha \quad \ldots\ldots [2]$$

$$dy/dx = \mu\alpha + c_2 \quad \ldots\ldots [11]$$

The constant of integration c_2 is evaluated with the aid of either one of the following boundary conditions:

when $dy/dx = \tan \beta_2$, then $\alpha = \alpha_2$ $\ldots\ldots [12a]$

when $dy/dx = \tan \beta_1$, then $\alpha = \alpha_1$ $\ldots\ldots [12b]$

Combination of Equations [12*a*] and [12*b*] yields an important relation between the boundary variables, as follows:

$$c_2 = \tan \beta_2 - \mu\alpha_2 = \tan \beta_1 - \mu\alpha_1$$

so that

$$\tan \beta_1 - \tan \beta_2 = \mu\,(\alpha_1 - \alpha_2) \quad \ldots\ldots [12c]$$

Equation [11] now becomes

$$dy/dx = \mu\,(\alpha - \alpha_2) + \tan \beta_2 \quad \ldots\ldots [13]$$

After rearrangement and integration, Equation [13] takes the form

$$\frac{x - x_1}{y_t} = \int_{(y/y_t)_1}^{(y/y_t)} \frac{d\,(y/y_t)}{\mu\,(\alpha - \alpha_2) + \tan \beta_2} \quad \ldots\ldots [14]$$

Numerical integration of Equation [14] yields the curved contour between sections 1 and 2.

A comparison of the design equations leads to the conclusion that, for fixed values of μ, β_1, and β_2, the nozzle of Fig. 7 is shorter than the nozzle of Fig. 5(*b*) and is to be preferred from the standpoint of avoiding wall friction.

Following is a suggested computation procedure for the design of the nozzle of Fig. 7. The area ratio, value of μ, and the values of β_1 and β_2 are selected beforehand. From Equation [12*c*], the value of α_1 may be calculated, which enables y_1/y_t to be found. By trigonometry, the length $(x_1 - x_t)/y_t$ may be computed. Then, by numerical integration of Equation [14], the value of $(x - x_1)/y_t$ is calculated for each corresponding value of y/y_t.

The Choice of μ. In a nozzle of given area ratio A_2/A_t and entrance half-angle β_1, good design requires:

1 A value of μ which is less than unity, to avoid shock fronts within the nozzle.

2 A small exit half-angle β_2, so that changes in pressure across the shock front at the nozzle exit are very small.

3 A short nozzle, to avoid the reduction in nozzle efficiency which attends large wall areas on which frictional shear stresses act.

These requirements are not mutually compatible, since small values of μ and small values of β_2 both tend to increase the nozzle length.

It is conceivable that, having restricted the nozzle length to a certain value, the smoothest flow pattern will exist in the stream leaving the nozzle when the exit half-angle β_2 is reduced at the expense of increasing the value of μ over unity, thus tending to the formation of shock fronts because of excessive wall curvature. Stated differently, it may be better to have weak shock fronts due to wall curvature together with a weak shock front due to a sharp angle at exit, rather than have no shock fronts due to wall curvature, and a relatively intense shock front at exit. In this connection, the point of intersection of neighboring Mach lines for a value of μ greater than unity is of interest and importance.

With reference to Figs. 4 and 7, trigonometric analysis shows that the ratio of the projected length perpendicular to the nozzle axis of a Mach line before it intersects a neighboring Mach line originating an infinitesimal distance downstream, to the half-width of a rectangular passage (or the radius of a circular passage) is given approximately by the relation[4]

$$\frac{S}{y} = -\frac{\dfrac{1}{y/y_t}\dfrac{d(y/y_t)}{d\alpha}}{(\mu - 1)\,[\mu(\alpha - \alpha_2) + \tan\beta_2]} \quad \ldots\ldots [15]$$

It is seen that when μ is infinite, S/y is zero, so that, at a sharp corner, the shock front will itself start from the corner. When μ is unity, S/y is infinite, indicating no intersection of Mach lines. When μ is less than 1, S/y is negative, indicating a divergence of Mach lines. For values of μ only slightly greater than unity S/y is very large, so that neighboring Mach lines will not intersect until several reflections at the nozzle walls have occurred. It is reasonable to expect that disturbances propagated along Mach lines will be weakened during each reflection because of the damping action of the viscous boundary layer. Thus if the value of μ requires many reflections to take place before intersecting Mach lines form a shock front, the intensity of the latter may be reduced to insignificant proportions.

Equation [15] allows a rough estimate to be made of the number of reflections necessary for neighboring Mach lines to intersect. The numerator of this expression increases with y/y_t while the denominator decreases with an increase in y/y_t. Therefore, when μ is constant throughout the curved section of nozzle, shock fronts are most likely to be formed due to the intersection of Mach lines originating at the beginning of the curved section, rather than at the end of the curved section.

Example of Nozzle Design. Fig. 8 illustrates the design of a three-dimensional nozzle for isentropic flow. Figs. 8(*a*) and 8(*b*) are scale drawings for values of μ of 2 and 5, respectively. Fig. 8(*c*) shows how the total nozzle length and the length of curved contour depend upon μ; for convenience, the abscissa is plotted as the reciprocal of μ. Fig. 8(*d*) shows the effect of μ on the distance required for the intersection of neighboring Mach lines which originate near the beginning of the curved contour.

It may be concluded from Fig. 8(*c*) that, in this instance, values of μ greater than 10 yield little advantage as to nozzle length, but materially heighten the probability of formation of shock fronts of appreciable intensity. Furthermore, it appears from Fig. 8(*d*) that shock fronts will not form without reflections, unless μ exceeds a value of approximately 50.

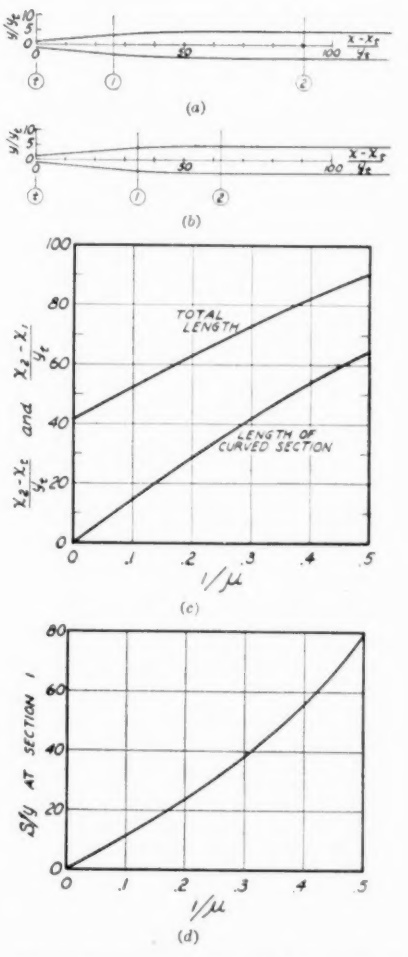


FIG. 8 THREE-DIMENSIONAL NOZZLE SIMILAR TO FIG. 6
(Nozzle designed for isentropic flow with exit area ratio $A_2/A_t = 21.52$, entrance half-angle $\beta_1 = 5$ deg, and exit half-angle $\beta_2 = 0.15$ deg. *a* Scale drawing for $\mu = 2$; *b* scale drawing for $\mu = 5$; *c* effect of μ on nozzle length; *d* effect of μ on S/y.)

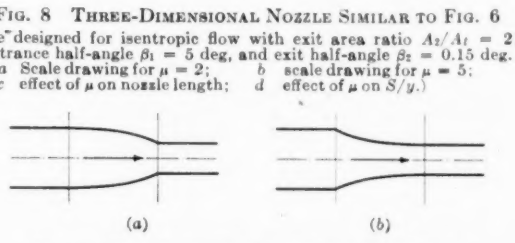


FIG. 9 TWO FORMS OF SUPERSONIC DIFFUSERS

The Supersonic Diffuser. Shock fronts will form in the supersonic diffuser of Fig. 9(*a*), since neighboring Mach lines tend to intersect both because of the change in Mach angle and because of the change in the slope of the streamlines at the wall. The same conclusion may be reached by noting from Equation [2] that μ can have only negative values for this type of contour, and that the criterion for shockless flow, Equation [5*b*], requires values of μ greater than unity if shock fronts are to be absent.

An alternate form of diffuser, Fig. 9(*b*), has a finite angle at the joint between the straight tube and the converging passage, and a curved contour which is convex inward. Such a contour can be designed to avoid shock fronts, in accordance with Equations [2] and [5*b*]. However, there will exist a relatively intense shock front at the sharp corner.

It appears that no diffuser having a straight axis, not even one

[4] This expression is based on the assumptions that Mach lines are straight and that the angle between neighboring Mach lines is constant, neither of which is exact. The relation should therefore be taken as a rough but convenient measure of the distance required for intersection.

of infinite length, can receive a parallel stream and increase the pressure of the stream isentropically and without shock fronts.

The methods of this paper may be of aid in determining, for a diffuser of finite length, the best design from the standpoint of diffuser length, intensity of shock fronts, and distribution of shock fronts.

Comparison With Experiment

There are in the technical literature (1) many Schlieren photographs showing the oblique shock fronts which originate at the wall when a stream leaves a nozzle and discharges into a region where the pressure is higher than at the nozzle exit. The sharp change in direction of the stream at the nozzle exit corresponds to an infinite value of μ, so that a shock front originates at the bend.

Busemann (3) shows in a qualitative way, with the aid of Schlieren photographs, that when the diverging walls of a nozzle are curved very gradually so as to become parallel to each other, shock fronts are not formed. On the other hand, large wall curvatures lead to the formation of a shock front which is detached from the nozzle walls.[5] These two cases correspond to small and large values of μ, respectively, and confirm in a qualitative sense the criteria proposed in the present paper.

More recently, DeFrate (7), presented Schlieren photographs of two-dimensional nozzles discharging into a tube of rectangular cross section. Each of three nozzles had a total included angle of 6 deg between the walls for some distance following the throat, and each nozzle had the same ratio of exit to throat area. One of the nozzles was wedge-shaped to the exit, with a sharp angle of 3 deg between nozzle exit and tube, corresponding to a value of μ of infinity at this point. The photographs for this nozzle exhibit intense shock fronts originating at the corners, confirming the work of other experimenters. A second nozzle had curved walls designed with μ equal to 0.75, and an exit half-angle of 0.18 deg. No shock fronts were visible within the nozzle, and the shock front due to the sharp bend at exit was so slight that it could not be seen with the Schlieren apparatus. The third nozzle also had curved walls, with a value of μ of 2.27, and an exit half-angle of 0.18 deg. The results were the same as those for the second nozzle, i.e., no visible shock fronts either within the nozzle or in the straight tube to which the nozzle was joined. It is not surprising that appreciable shock fronts were not formed with this nozzle, even with μ equal to 2.27, since Equation [15] indicates that in this instance approximately twelve reflections of neighboring Mach lines would have to occur before they could converge.

In a project carried out in the mechanical engineering department of the Massachusetts Institute of Technology, under the direction of Prof. J. H. Keenan, pressure measurements were made at various points along the length of a smooth tube with circular cross section. When the supersonic stream entered the tube from a converging-diverging nozzle having a conical divergent section, the pressure measurements exhibited a scattering which could be accounted for only by oblique shock fronts, and which extended some 30 diam downstream. The effect of the shock fronts on the measured pressures was so great that both negative and positive pressure gradients appeared to exist in the tube. Two different three-dimensional nozzles with curved contours were constructed according to the following schedule:

A_2/A_t	μ	β_1 deg	β_2 deg	$(S/y)_1$
2.82	0.75	3	0.18	Negative
21.52	5.0	5	0.15	23

[5] Fig. 5 of Busemann's paper (3) shows very clearly how individual Mach lines originating at the wall converge to form a shock front, and is in excellent agreement with Fig. 2 of this paper.

The area ratios (A_2/A_t) for these two nozzles were the same as for conical nozzles which had been used previously. Pressure measurements made in the tube following the "shockless" nozzles showed that the pressure fluctuations due to shock fronts had been eliminated, at least within the experimental error of the observations. This is of particular interest with regard to the nozzle having $\mu = 5$ and $(S/y)_1 = 23$, since it shows that the shock front may be negligible when a large number of reflections are required before neighboring Mach lines converge.

It is hoped that further experimental work will show how large a value μ may attain before appreciable shock fronts are formed.

Conclusions

Shock fronts in supersonic flow are formed when neighboring Mach lines converge. This is most likely to occur during the deceleration of a stream, but may occur as well for an accelerating stream due to rapid changes in curvature of the passage walls.

The criterion for divergence of neighboring Mach lines can be set forth in mathematical form, for the case of flow in symmetrical passages having a straight axis, in terms of a parameter, μ, which is the ratio of the change in slope of the wall of the passage for a short increment in distance along the axis to the corresponding change in the Mach angle. Shock fronts cannot form when μ is less than unity for an accelerating flow, or when μ is greater than unity for a decelerating flow. The criterion for shockless flow may be used as the basis of designing wall contours for both two-dimensional and three-dimensional passageways. It appears that shocks can be avoided entirely only with nozzles of infinite length, if the nozzle discharges into a tube of constant cross section. A practical nozzle of finite length requires a small finite angle between nozzle exit and tube entrance. The shock front associated with the sharp bend in wall contour can be made very small by reducing the angle of the bend. Excessive nozzle lengths can be avoided by employing values of μ greater than unity; the shock fronts formed as a consequence may be negligible, provided that many reflections take place before neighboring Mach lines intersect. An equation is given to permit an estimate of the number of reflections which occur before neighboring Mach lines intersect, and it is found that μ may reach values of the order of 50 before shock fronts will be formed in the nozzle without reflection of Mach lines.

It appears impossible to design shockless supersonic diffusers having a straight axis, even if the length of diffuser is infinite.

Experimental data on two-dimensional and three-dimensional nozzles are in agreement with the concepts set forth in this paper, and indicate that the shock fronts for nozzles of reasonable length may be made so small that the pressure rise across the shock front is a small fraction of 1 per cent of the pressure before the shock.

Acknowledgment

Mr. E. P. Neumann was principally responsible for the experimental work carried out at M.I.T. with two-dimensional and three-dimensional nozzles. The careful nature of this work made the results of great value in testing the validity of the proposed method of nozzle design.

BIBLIOGRAPHY

1 "Über zweidimensionale Bewegungsvorgänge in einem Gas, das mit Überschallgeschwindigkeit strömt." (On two-dimensional flow phenomena in a gas which flows at supersonic velocity), by Th. Meyer, *Mitteilungen über Forschungsarbeiten auf dem Gebiete des Ingenieurwesens*, vol. 62, 1908, pp. 31–67.

Note: This material is presented in English in abbreviated form in "Aerodynamic Theory," edited by W. F. Durand, vol. 3, Julius Springer, Berlin, Germany, 1935, pp. 234–249.

2 "Näherungsverfahren zur zeichnerischen Ermittlung von ebenen Strömungen mit Überschallgeschwindigkeit." (Approximate methods of graphically solving problems of two-dimensional flow with supersonic velocities), by L. Prandtl and A. Busemann, *Stodola Festschrift*, orell Füssli Verlag, Zurich, Switzerland, and Leipzig, Germany, 1929, pp. 499–509.

3 "Lavaldüsen für gleichmässige Uberschallströmungen." (Laval nozzles for uniform supersonic flow), by A. Busemann, *Zeitschrift V.D.I.*, vol. 84, 1940, pp. 857–862.

4 "The Mechanics of Compressible Fluids," by G. I. Taylor and J. W. Maccoll, "Aerodynamic Theory," edited by W. F. Durand, vol. 3, Julius Springer, Berlin, Germany, 1935, pp. 210–212.

5 "The Physics of Solids and Fluids," by P. P. Ewald, Th. Poschl, and L. Prandtl, second edition, Blackie, London, England, 1936, pp. 349–353.

6 Reference (4) pp. 246–249.

7 "Investigation of Supersonic Flow in Nozzles and Tubes by the Schlieren Method," by L. A. DeFrate, Master's Thesis, Department of Mechanical Engineering, Massachusetts Institute of Technology, Cambridge, Mass., 1943.

Forced and Free Motion of a Mass on an Air Spring

By B. SUSSHOLZ,[1] WASHINGTON, D. C.

Results are given of a theoretical investigation of the transient response of a simple nonlinear mechanical system to various types of applied forces. A cylindrical tube closed at one end, with a light piston inserted in the other, was used experimentally, the nonlinear elasticity of the confined column of air governing the motion of the piston. Such systems have been used in ballistic studies to measure transient pressures, as well as for the measurement of pressures caused by other types of explosions in air.

Nomenclature

The following nomenclature is used in the paper:

- m = mass of piston
- X = displacement of piston from position where internal pressure is equal to atmospheric pressure
- A = constant cross-sectional area of air column
- L = length of air column when internal pressure is equal to atmospheric pressure
- P_0 = atmospheric pressure
- P_e = applied external pressures in excess of atmospheric pressure
- $E(X)$ = elastic spring force
- P_i = internal pressure corresponding to any displacement X
- V_0 = original volume of air column ($V_0 = AL$)
- V = volume of air column corresponding to any displacement X
- K = stiffness of air column for small displacements about position X
- T_0 = natural period of oscillation for small displacements of piston about $X = 0$
- X_m, X_n = maximum positive and negative displacement of piston during a cycle
- τ = duration of positive pressure in excess of atmospheric pressure
- E_0 = energy contained in system at the time $t = 0$
- v_0 = velocity of piston at the time $t = 0$
- P_G = internal pressure above atmospheric corresponding to X_m
- n = overshoot factor
- P_m = maximum excess pressure in blast wave
- γ = ratio of specific heats
- t = time
- v = velocity of piston

[1] Associate Physicist, David W. Taylor Model Basin, Navy Department.

Presented at the Annual Meeting, New York, N. Y., Nov. 29–Dec. 3, 1943, of The American Society of Mechanical Engineers.

Discussion of this paper should be addressed to the Secretary, A.S.M.E., 29 West 39th Street, New York, N. Y., and will be accepted until July 10, 1944. Discussion received after the closing date will be returned.

Note: Statements and opinions advanced in papers are to be understood as individual expressions of their authors and not those of the Society.

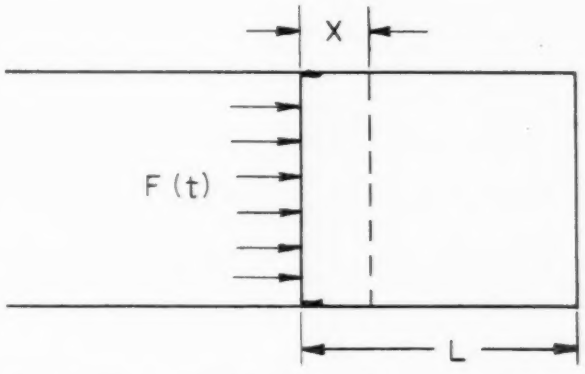


Fig. 1 Schematic Diagram of Nonlinear Mechanical System

General Considerations of Study

The purpose of this paper is to present the results of a theoretical investigation of the transient response of a simple nonlinear mechanical system to various types of applied forces. The system consists essentially of a cylindrical tube closed at one end, with a light piston inserted in the other end. The nonlinear elasticity of the confined column of air governs the motion of the piston. Systems of this type have been used to measure transient pressures caused by explosions in air. A schematic diagram of the system is shown in Fig. 1.

The considerations of this paper are based upon four assumptions, as follows:

1 The pressure within the air column follows the law of adiabatic compression, $P_i V^\gamma$ = constant, for the entire scope of the analysis.

2 The system is conservative with regard to dissipative forces such as heat loss, friction, and leakage.

3 No diffraction effects are introduced by the mouth of the tube.

4 The internal pressure is uniform throughout the air column at any instant.

The equation of motion of the system in response to a general force $F(t)$ is

$$m\ddot{X} + E(X) = F(t) \quad \ldots\ldots [1]$$

where m = mass of the piston, X = displacement of piston, $E(X)$ = restoring force. The elastic restoring force $E(X)$, corresponding to any given displacement, is determined by the unbalance existing between the absolute internal pressure and the static atmospheric pressure. The restoring force will always be directed toward the position of static equilibrium under no external load, $F(t) = 0$.

Without an external load the system is at equilibrium when $X = 0$, $v = 0$, and the internal and external pressures are equal to atmospheric pressure P_0. Under these conditions the length of the air column will be denoted by L. The cylinder is assumed to be long enough to allow for the negative positions of the piston. The uniform cross-sectional area of the column is A. By as-

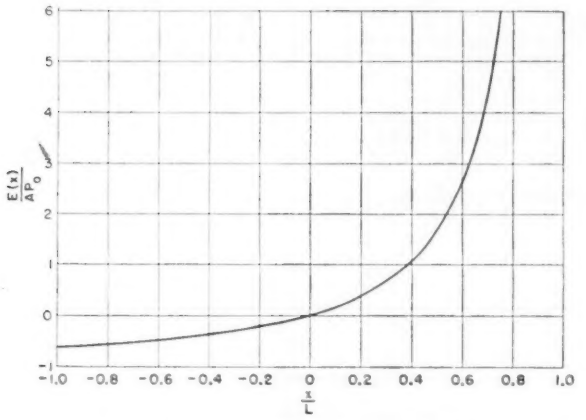


FIG. 2 ELASTIC AIR-SPRING FORCE CORRESPONDING TO GIVEN DISPLACEMENTS

sumption a positive displacement will correspond to an increase in internal pressure.

At any position X the unbalanced internal pressure is $P_i - P_0$ where

$$P_i = P_0 \frac{1}{\left(1 - \frac{X}{L}\right)^{\gamma}}$$

By applying the adiabatic law $P_i V^{\gamma} = P_0 V_0^{\gamma}$ the spring force $E(X)$ is determined as

$$E(X) = AP_0 \left[\frac{1}{\left(1 - \frac{X}{L}\right)^{\gamma}} - 1 \right] \quad \ldots\ldots\ldots\ldots [2]$$

Fig. 2 is a plot of Equation [2] with $\gamma = 1.4$.

The stiffness of the system K is not uniform but varies with X.

By definition $K = \frac{d}{dX} E(X)$, therefore

$$K = \frac{\gamma AP_0}{L} \cdot \frac{1}{\left(1 - \frac{X}{L}\right)^{\gamma + 1}} \quad \ldots\ldots\ldots\ldots [3]$$

The natural period of the system for small displacements about the equilibrium position $X = 0$ is given by

$$T_0 = 2\pi \sqrt{\frac{m}{K}} = \frac{2\pi}{\sqrt{\gamma}} \sqrt{\frac{mL}{AP_0}} \quad \ldots\ldots\ldots\ldots [4]$$

The corresponding natural frequency f_0 is equal to $\frac{1}{T_0}$.

CASE 1 $F(t) = 0$

The differential equation of motion is

$$m\ddot{X} + E(X) = 0$$

Standard methods of integration (numerical integration, Rauscher's graphical method,[2] Meissner's method[3]) yield the free-vibration curves shown in Fig. 3(*a*), for the cases where $\frac{X_m}{L} = +0.1$, 0.3, 0.5, and 0.7. A series of phase space diagrams is shown in Fig. 3(*b*). These contours indicate the relation between the relative velocity $v/\bar{v}$ and displacement X/L of the piston for free vibratory motion. The factor $\bar{v}$ is used to denote $\sqrt{\frac{AP_0L}{m}}$ or in another form $\frac{2\pi}{\sqrt{\gamma}} \cdot \frac{L}{T_0}$.

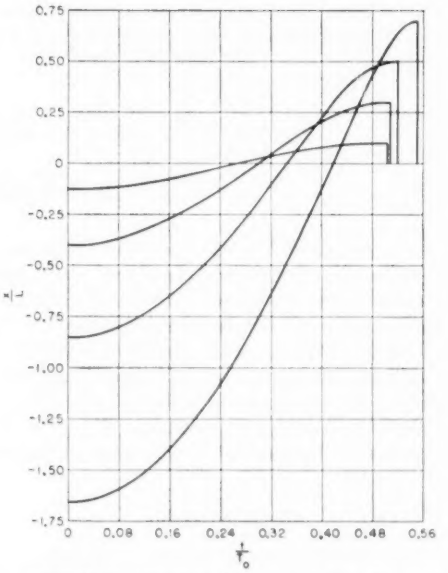


FIG. 3 (*a*) TIME-DISPLACEMENT RELATIONS FOR FREE VIBRATORY MOTION OF SYSTEM

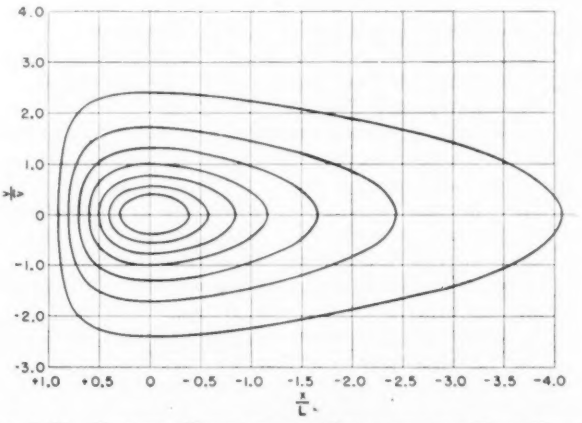


FIG. 3 (*b*) VELOCITY-DISPLACEMENT RELATIONS FOR FREE VIBRATORY MOTION OF SYSTEM

In the case of nonlinear systems the free oscillations are generally not symmetrical about the neutral position either in form or amplitude. For a conservative system the relation between maximum positive and negative amplitudes is governed by the condition that the potential energies be equal at the two extremities of a stroke. The relation is determined from

$$\int_0^{X_m} E(X)dX = \int_0^{X_n} E(X)dX$$

to be

$$\frac{1}{(\gamma - 1)\left(1 - \frac{X_m}{L}\right)^{\gamma - 1}} - \frac{X_m}{L} = \frac{1}{(\gamma - 1)\left(1 - \frac{X_n}{L}\right)^{\gamma - 1}} - \frac{X_n}{L} \quad \ldots\ldots [5]$$

[2] "Steady Oscillations of Systems With Nonlinear and Unsymmetrical Elasticity," by Manfred Rauscher, Trans. A.S.M.E., vol. 60, 1938, pp. A-169 to A-177.

[3] "Graphische Analysis vermittelst des Linien bildes einen Funktion," by E. Meissner, *Schweizerische Bauzeitung*, vol. 104, 1934, p. 35.

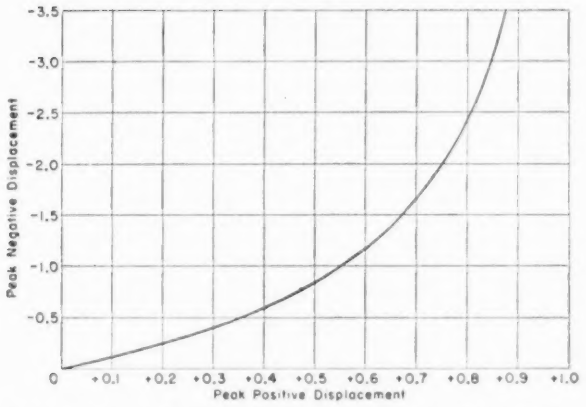


FIG. 4 RELATION BETWEEN PEAK NEGATIVE AND PEAK POSITIVE DISPLACEMENTS IN FREE VIBRATION

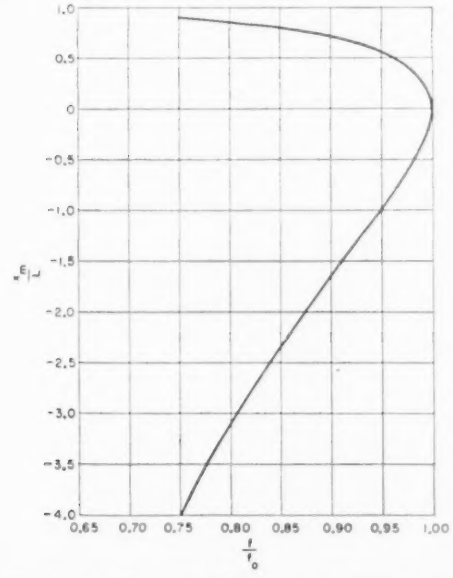


FIG. 5 EFFECTIVE NATURAL FREQUENCIES CORRESPONDING TO VARIOUS MAXIMUM NEGATIVE AND POSITIVE AMPLITUDES FOR FREE VIBRATORY MOTION

where X_m is the peak positive displacement and X_n is the peak negative displacement, i.e., $X_m > 0$ and $X_n < 0$. This relation is plotted in Fig. 4.

For free oscillations of large amplitude, the effective natural frequency depends upon the maximum amplitude, as is characteristic of nonlinear systems in general. Suppose the piston is displaced to a position X and suddenly released. The number of free oscillations per second the system will then execute is plotted in Fig. 5, as a function of the maximum displacement.

CASE 2 BALLISTIC IMPULSE

Consider the response of the system to a pure ballistic impulse of magnitude $P_e\tau$, where P_e is a constant pressure above atmospheric applied for a time τ. The value of τ is considered to be small as compared to T_0. Since $mv_0 = AP_e\tau$, the energy imparted to the system is given by

$$E_0 = \frac{1}{2} mv_0^2 = \frac{(AP_e\tau)^2}{2m} \quad \ldots\ldots\ldots\ldots\ldots\ldots [6]$$

The piston comes to rest at a position, X_m, where the potential

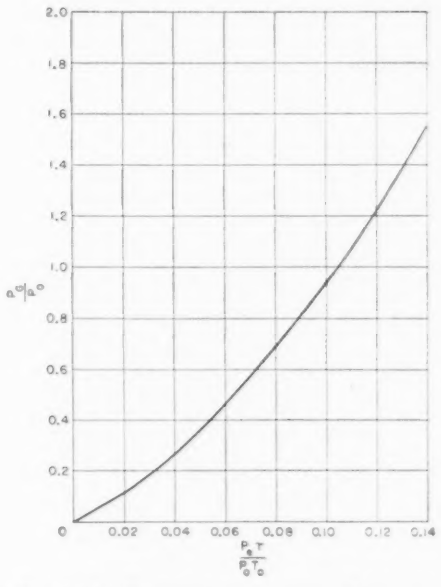


FIG. 6 (*a*) RESPONSE TO BALLISTIC IMPULSE

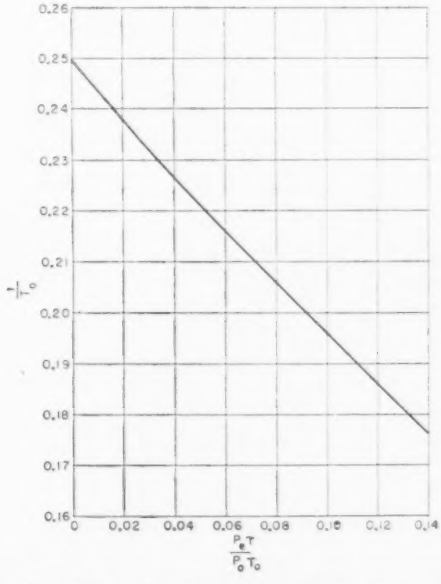


FIG. 6 (*b*) TIME TAKEN TO REACH FIRST PEAK DISPLACEMENT IN RESPONSE TO BALLISTIC IMPULSE

energy, $\int_0^{Xm} E(X)dX$, is equal to E_0. Substituting for E_0 in Equation [6], the ballistic response can be reduced to the form

$$\left(\frac{P_e\tau}{P_0T_0}\right)^2 = \frac{1}{2\pi^2} \cdot \frac{\gamma}{\gamma - 1} \left[\frac{\gamma + \frac{P_G}{P_0}}{\left(1 + \frac{P_G}{P_0}\right)^{1/\gamma}} - \gamma \right] \quad \ldots\ldots [7]$$

where

$$\frac{P_G}{P_0} = \frac{1}{\left(1 - \frac{X_m}{L}\right)^{\gamma}} - 1$$

which is the excess internal pressure corresponding to the displacement X_m. The relation shown in Equation [7] is plotted in

Fig. 6(*a*). A plot of the time taken by the piston to reach the peak displacement X_m in response to a ballistic impulse is shown in Fig. 6(*b*).

CASE 3 $F(t) = AP_e$

Consider a pressure wave of constant amplitude and long duration, Fig. 7, suddenly applied to the system, with P_e as the pressure above atmospheric. Equation [1] becomes

$$m\ddot{X} + E(X) = AP_e$$

Substituting for $E(X)$ from Equation [2] and integrating, yields the energy equation

$$\frac{1}{2}mv^2 = \frac{AP_0L}{\gamma - 1}\left[(\gamma - 1)\left(1 + \frac{P_e}{P_0}\right)\frac{X}{L} - \frac{1}{\left(1 - \frac{X}{L}\right)^{\gamma - 1}}\right] + C \quad \ldots\ldots [8]$$

where C is a constant of integration. When the initial conditions are $X = 0$, $v = 0$, and $P_i = P_0$, C becomes $\dfrac{AP_0L}{\gamma - 1}$.

At the maximum displacement, X_m, the total work done by the applied force is stored as potential energy, namely, $AP_eX_m = (\text{P.E.})_{X_m}$. The fractional "overshoot," n, is given by P_G/P_e. Determination of the "overshoot," n, by the preceding energy considerations yields the following two relations

$$\frac{P_e}{P_0} = \frac{1}{(\gamma - 1)a}\left[\frac{1}{(1 - a)^{\gamma - 1}} - (\gamma - 1)a - 1\right] \quad \ldots [9a]$$

$$n = \frac{(\gamma - 1)a \quad [1 - (1 - a)^{\gamma}]}{(1 - a) \quad [1 - (1 - a)^{\gamma} - \gamma a\,(1 - a)^{\gamma - 1}]} \quad \ldots [9b]$$

where $a = \dfrac{X_m}{L}$. A plot is shown in Fig. 8 of n as a function of P_e/P_0.

The time-displacement motion of the piston is determined by substituting for v in the relation

$$t = \int \frac{1}{v}dX$$

and integrating. Since the integrand becomes infinite when $v = 0$, namely, at the extreme positions during a cycle, the integration methods used should avoid this mathematical discontinuity or allow as close an approach to such limiting positions as may be desired.

Fig. 9 is a plot of the time taken by the piston to reach its first maximum displacement under given applied pressures P_e.

Now consider the case where the pressure is terminated at a time τ, Fig. 10. As the value of τ is varied from 0 to t', where t' is given in Fig. 9 as a function of the pressure P_e, the peak response of the system will vary correspondingly from zero to $P_G = nP_e$, where the values of n are shown in Fig. 8. The variation of

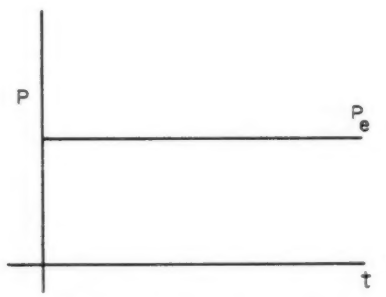


FIG. 7 PRESSURE WAVE APPLIED TO SYSTEM

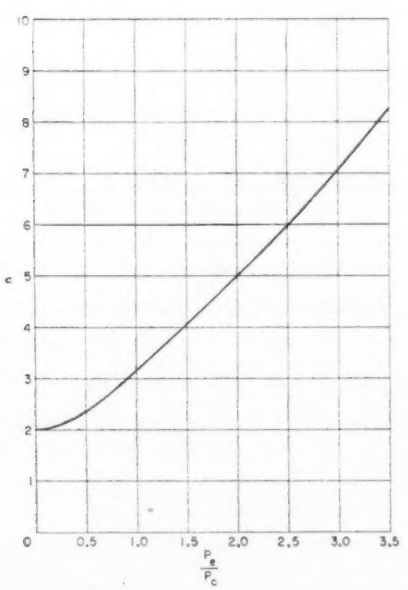


FIG. 8 OVERSHOOT FACTOR CORRESPONDING TO VARIOUS APPLIED RECTANGULAR PRESSURE WAVES OF LONG DURATION

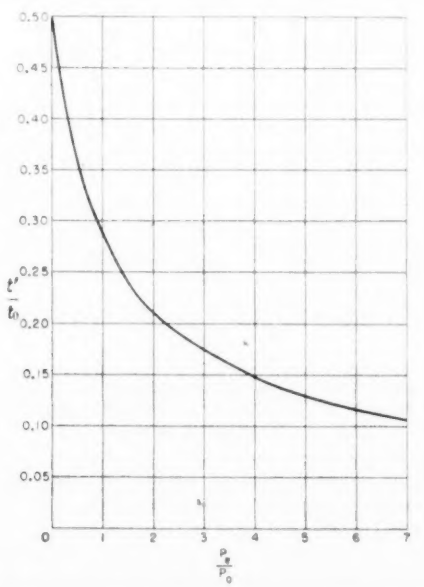


FIG. 9 TIME TAKEN TO REACH FIRST MAXIMUM DISPLACEMENT IN RESPONSE TO A RECTANGULAR PRESSURE WAVE OF LONG DURATION

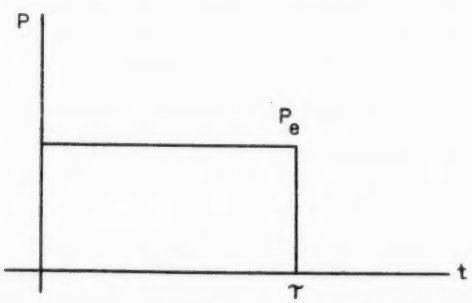


FIG. 10 RECTANGULAR PULSE APPLIED TO SYSTEM

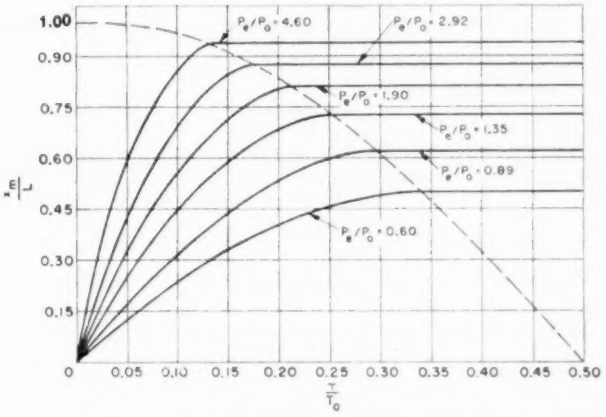


FIG. 11 RESPONSE TO RECTANGULAR PRESSURE PULSES OF CONSTANT AMPLITUDE AND VARYING DURATION

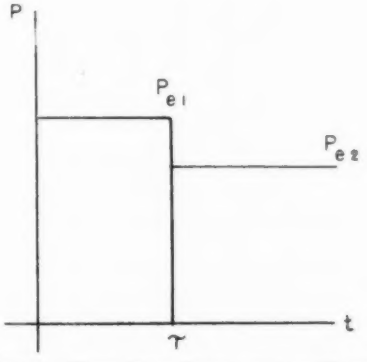


FIG. 12 SYSTEM WITH TWO RECTANGULAR WAVES IMPOSED

$\frac{X_m}{L}$ with τ for several values of P_e is shown in Fig. 11. The limiting broken curve in Fig. 11 is the same as the plot in Fig. 9.

An interesting point might here be mentioned. The results of the foregoing analysis with regard to rectangular pressure waves can be determined by different but parallel considerations. At $t = 0$, when the pressure P_e is suddenly applied the initial conditions were $X = 0, v = 0$ and $P_i = P_0$. The forced motion of the piston has been examined. Now consider a second system where the internal and external pressure is $P_e + P_0$ for $t \leq 0$. The position of the piston is at X_e relative to the first system. At $t = 0$, the piston is displaced to $X = 0$ where $P_i = P_0$ and is suddenly released. The physical conditions for both systems are identical, and therefore the free vibrations of system 2 and forced vibrations of system 1 will be the same with regard to the position and velocity of the piston at any time t.

Consider now the forced response of the original system to two rectangular waves as shown in Fig. 12. Suppose initially the displacement of the piston is zero, velocity zero, and internal pressure atmospheric. The response from $t = 0$ to $t = \tau$ has already been discussed in detail. At $t = \tau$, the system has a displacement X_1 and velocity v_1. The differential equation of motion under the second rectangular wave is

$$m\ddot{X} + E(X) = AP_{e2}$$

Integrating and introducing the initial conditions the energy equation becomes

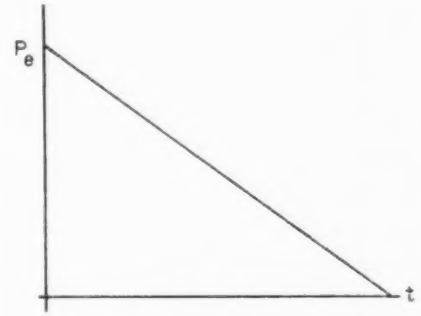


FIG. 13 (*a*) TRIANGULAR PRESSURE WAVE

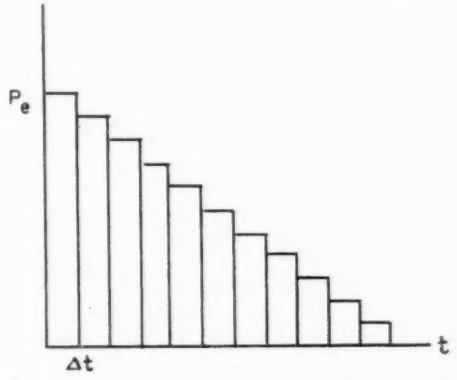


FIG. 13 (*b*) TRIANGULAR PRESSURE WAVE OF FIG. 13 (*a*) RESOLVED INTO RECTANGULAR WAVES

$$\frac{1}{2}mv^2 = \frac{AP_0L}{\gamma - 1}\left[(\gamma - 1)\left(1 + \frac{P_{e2}}{P_0}\right)\frac{X}{L} - \frac{1}{\left(1 - \frac{X}{L}\right)^{\gamma - 1}}\right] + \frac{AP_0L}{\gamma - 1}\left[1 + (\gamma - 1)\left(\frac{P_{e1}}{P_0} - \frac{P_{e2}}{P_0}\right)\frac{X_1}{L}\right] \quad \ldots\ldots [10]$$

Substituting for v in $\int \frac{1}{v}\,dX$, the integration of Equation [10] is to begin with $X = X_1$ and continue from there on. Two separate sections of the time-displacement response curve of the piston will thus be determined, namely, for $0 \leq t \leq \tau$ and $t \geq \tau$. At $t = \tau$ both sections will have the same ordinate X_1 and also the same slope v_1. Therefore, the two sections may be joined to give a continuous curve with the displacement X always referred to the original equilibrium position of the system. A numerical example is presented in the Appendix to indicate the application of the foregoing method.

It is evident that the preceding process can be extended to any number of rectangular step pulses. Therefore the response to a general pressure wave may be determined by simply considering the wave as composed of a series of rectangular step pulses. For example, the triangular pressure wave of Fig. 13(*a*) may be resolved into rectangular waves as shown in Fig. 13(*b*). The system is therefore considered as subjected to a series of rectangular waves of different amplitudes but equal duration Δt. The value of Δt depends upon the degree of accuracy desired.

This step-pulse approximation method can be applied to any undamped nonlinear system whose elastic restoring force is a continuous function of displacement. The system must necessarily be stable.

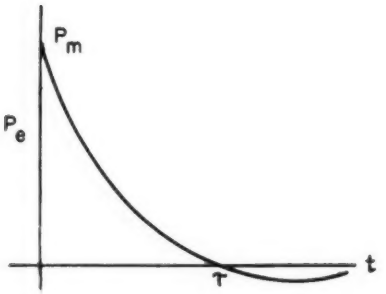


FIG. 14 APPLICATION OF STEP-PULSE METHOD

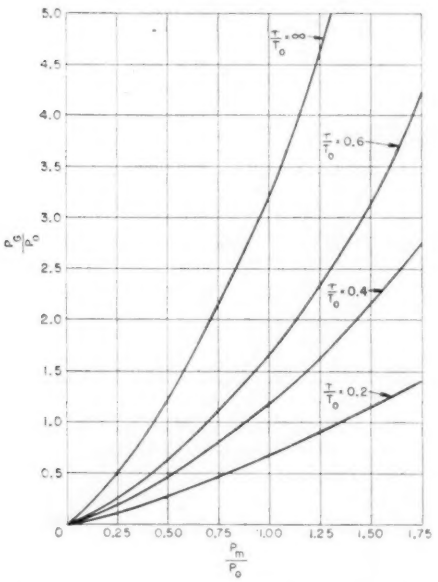


FIG. 15 RESPONSE TO BLAST PRESSURE WAVES OF VARIOUS PEAK AMPLITUDES AND DURATIONS AS GIVEN BY

$$\frac{P_e}{P_0} = \frac{P_m}{P_0}\, e^{-t/\tau}\left(1 - \frac{t}{\tau}\right)$$

$$\text{CASE 4} \quad F(t) = AP_m\, e^{-\frac{t}{\tau}}\left(1 - \frac{t}{\tau}\right)$$

As a special case the step-pulse method was applied to a pressure wave of the type shown in Fig. 14. Such pressure waves originate in gun blasts and bomb explosions in air. They are closely approximated analytically by the expression

$$P_e = P_m\, e^{-\frac{t}{\tau}}\left(1 - \frac{t}{\tau}\right)$$

where P_m is the maximum blast pressure and τ is the duration of the positive phase of the wave. An investigation was made of the maximum displacement of the piston in response to waves of this type for various values of P_m and τ. Fig. 15 is a plot in nondimensional form for the cases where $\frac{\tau}{T_0} = 0.2, 0.4,$ and 0.6 with P_G being the maximum internal pressure above atmospheric. The case of the rectangular wave, $\frac{\tau}{T_0} = \infty$, is included for purposes of comparison.

Fig. 16 shows a plot of the same relations indicated in Fig. 15, but with P_G constant along the contours. It is evident that when two of the factors, P_m, P_G, and τ are given, the third is uniquely determined. A series of time-displacement curves are shown in Fig. 17 for the cases where $\frac{\tau}{T_0} = 0.6$ and $P_m = 0.67$, 1.00, 1.33, 1.67, and 2.00 atm.

CONCLUSION

In conclusion, the effect of modifications in the construction of the system should be considered. The components of the system, namely, m, L, and A, appear throughout the analyses in two basic forms, X/L and $\frac{mL}{A}$. The first combination is nondimensional and, therefore, independent of the absolute value of L. The second combination is found only in the factor T_0 which is defined by Equation [4]. However, the absolute value of T_0 was eliminated from the development of the response curves by the use of nondimensional time co-ordinates. Therefore the curves presented in this paper can be applied directly to any specific system of the type considered.

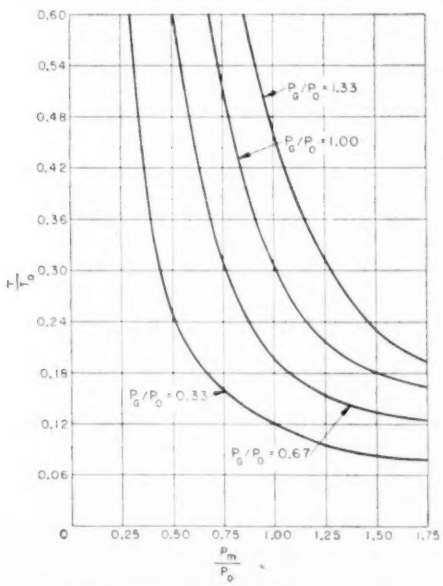


FIG. 16 ISOBARIC CONTOURS OF RESPONSE TO BLAST-PRESSURE WAVES OF THE FORM GIVEN BY

$$\frac{P_e}{P_0} = \frac{P_m}{P_0}\, e^{-t/\tau}\left(1 - \frac{t}{\tau}\right)$$

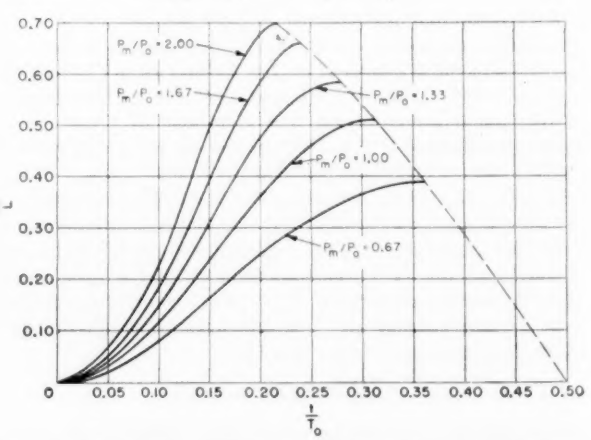


FIG. 17 TIME-DISPLACEMENT RESPONSE CURVES FOR BLAST PRESSURE WAVES WITH $\tau/T_0 = 0.6$

(The form of the blast waves is assumed to be $\frac{P_e}{P_m} = \frac{P_m}{P_0}\, e^{-\frac{t}{\tau}}\left[1 - \frac{t}{\tau}\right]$.)

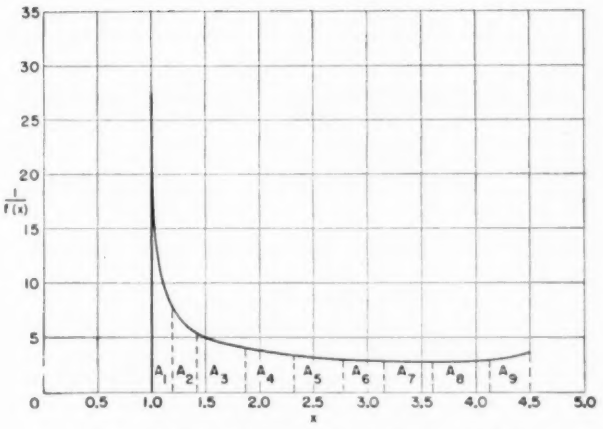


FIG. 18 PLOT OF INTEGRAND OF EQUATION [12]

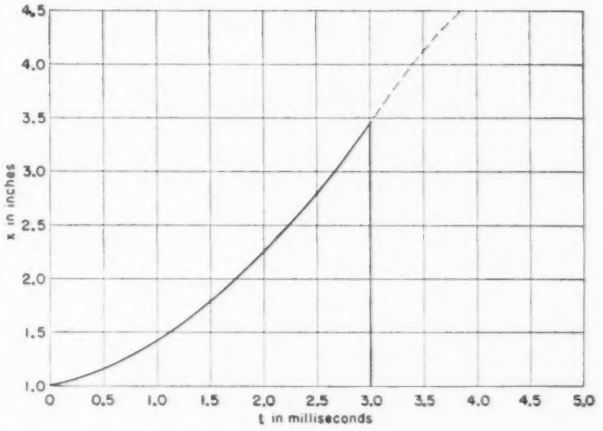


FIG. 19 MOTION OF PISTON DURING APPLICATION OF RECTANGULAR PRESSURE WAVE OF 25-PSI AMPLITUDE AND 3-MILLISEC DURATION

ACKNOWLEDGMENT

The writer wishes to express his appreciation for the encouragement and helpful criticism offered by Commander J. Ormondroyd, U.S.N.R.

Appendix

As a numerical example of the step-pulse method, consider a system of the type shown in Fig. 1, where the weight of the piston is 6 g, and for the air column $A = 0.786$ sq in., $L = 7.5$ in., $\gamma = 1.4$, and $P_0 = 14.7$ psi. Suppose a rectangular pressure wave with $P_s = 25$ psi, and $\tau = 0.003$ sec were applied to this system. As a general case, let the piston be displaced initially 1 in. in the positive direction and have an initial positive velocity of 100 ips.

By introducing the initial conditions in Equation [8] the constant of integration C is found to be $0.916 \frac{AP_0L}{\gamma - 1}$ and by substituting the numerical values given, Equation [8] becomes

$$v = 3560 \sqrt{0.916 + 0.144\,X - \frac{1}{(1 - 0.133\,X)^{0.4}}} \quad [11]$$

The relation $t = \int \frac{1}{v}\,dX$ then becomes

$$t = 0.000281 \int \frac{1}{f(X)}\,dX \quad [12]$$

where $f(X)$ is defined in Equation [11]. A plot of the integrand against X is shown in Fig. 18. The area under the curve has been divided into nine arbitrary sections to be integrated with a planimeter. The development of the analysis is shown in Table 1.

TABLE 1 DEVELOPMENT OF ANALYSIS

Section	Area	Total area, A	Total time, 0.000281A, in sec	Displacement x, in.
A_0	0	0	0	1.00
A_1	2.16	2.16	0.00061	1.20
A_2	1.53	3.69	0.00104	1.42
A_3	2.08	5.77	0.00162	1.88
A_4	1.62	7.39	0.00208	2.33
A_5	1.38	8.77	0.00246	2.78
A_6	1.06	9.83	0.00276	3.15
A_7	1.23	11.06	0.00311	3.60
A_8	1.43	12.49	0.00351	4.13
A_9	1.19	13.68	0.00384	4.50

Fig. 19 shows a plot of the last two columns of Table 1 which give motion of the piston from $t = 0$ to $t = 4.25$ millisec, if the pressure wave were acting on the system for that length of time. However, since the duration of the wave was assumed to be 3 millisec, the curve in Fig. 19 does not hold true after that time. At $t = 3$ millisec, the displacement is 3.45 in. From Equation [11], the velocity at this time is determined to be 1310 ips.

Now if another pressure wave is assumed to act on the system at $t = 3$ millisec, then the initial conditions are $x = 3.45$ in., and $v = 1310$ ips, and the entire foregoing process is repeated.

When the piston comes to a stop at an extreme position, the integrand of Equation [12] becomes infinite. However, the value of the maximum displacement X_m can be determined to the desired degree of accuracy by continuing the process for $X < X_m$ until the increase in area becomes negligible. To continue the analysis after $X = X_m$, the process begins over again. However, now the initial velocity is zero. In this case, the simple transformation $Z = X_m \sin \theta$, as suggested by Rauscher,[2] can be used to avoid the discontinuity.

Second Law of Thermodynamics for Changes of State and Quantity of Working Substance With Particular Reference to Steam Engines[1]

By G. ZERKOWITZ, HAIFA, PALESTINE

For many years the author had devoted increased attention and study to the problems of the change of state and quantity of thermal working substances.[2] These thermal processes particularly occur in piston engines, e.g., in steam engines during admission and release, in internal-combustion engines in the exhaust, and in compressors during the inlet to and the outlet from the cylinder. In turboengines they also can play a part, e.g., in gas turbines with explosion chambers, such as the Holtzwarth turbine. In the author's former essay numerous instances based on the first law of thermodynamics have been dealt with whereas, in this paper, first some other applications of the first law of thermodynamics and then the formulation of the second law of thermodynamics for changes of state and quantity will be presented. Particular attention will be devoted to the thermodynamic aspect of the entropy diagrams dealing with variable quantities, and the sources of errors which may occur when using such diagrams.

The First Law of Thermodynamics

According to the first law of thermodynamics for changes of state and quantity

$$dQ + h_x dG = dU + pdV \quad [1]$$

or

$$dQ + h_x dG = d(Gu) + pd(Gv) \quad [1a]$$

where

Q = quantity of heat received from outside source
G = alterable weight of working substance
u = internal energy of 1 lb of working substance
U = internal energy for G lb of working substance
p = pressure of working substance
v = specific volume of working substance
V = volume of G lb of working substance
h_x = enthalpy of 1 lb of substance entering or leaving
dG = element of weight of working substance

For the sake of uniformity and simplicity, the mechanical equivalent of heat has been omitted, and it is proposed that all quantities be specified in British thermal units. Again, dW where W denotes external work produced can in many cases be substituted for pdV.

Let us now state the first law of thermodynamics regarding the changes of state and quantity of the working substance in a modified form. Writing $H = U + pV$, where $H = Gh$, we have

$$dQ + h_x dG = dH - Vdp \quad [2]$$

or

$$dQ + h_x dG = d(Gh) - (Gv)dp \quad [2a]$$

where

h = enthalpy of 1 lb of substance
H = enthalpy of G lb of substance

If the substance is homogeneous, then $h_x = h$, since the element dG in the outlet is in the same state as when inside the chamber. On the other hand, for the admission process, h_x is generally unequal to h. In a steam engine, for example, where h_k is the enthalpy inside the boiler,

$$h_x = h_k = \text{const} \quad [3]$$

Though admission processes are generally irreversible, and therefore accompanied by an increase of entropy, it is possible to calculate the external work W for processes in piston engines from the expression

$$dW = pdV = pd(Gv) \quad [4]$$

and

$$-VdP = -(Gv)dp \quad [5]$$

also

$$W_t = \int_{p_2}^{p_1} Vdp$$

where W_t is the so-called "work of a cycle."

Formulation of Second Law of Thermodynamics for Changes of State and Quantity

Let T be the absolute temperature and s the entropy for 1 lb of the working substance, then the form adopted for the second law of thermodynamics for reversible changes of state, not involving changes of quantity, will be

$$dq = Tds \quad [6]$$

In order that the latter expression should also involve changes of quantity we must introduce in Equations [1] and [2], the following equations applying to 1 lb of the working substance:

---

[1] The present paper is the last written by Dr. Ing. G. Zerkowitz, an excellent mechanical engineer who left Germany when Hitler had come to power. He died in 1942, as Professor of Thermodynamics of the Hebrew Technical College (Institute of Technology) in Haifa, Palestine. The writer of this footnote has changed the symbols according to the American standards, corrected some minor errors and added an explanatory footnote. The original manuscript included two more parts, one dealing with Boulvin's method of replacing the varying quantity by a fictitious constant quantity, the other one dealing with internal-combustion engines. These parts had to be omitted because of space limitations. (*Signed*) Max Jakob, research professor of mechanical engineering, Illinois Institute of Technology, Chicago, Ill. Mem. A.S.M.E.

[2] "Mengenzustandsänderungen," by G. Zerkowitz, *Zeitschrift des Vereines deutscher Ingenieur* vol. 71, 1927, pp. 879–884

Presented at the Annual Meeting, New York, N. Y., Nov. 29–Dec. 3, 1943, of The American Society of Mechanical Engineers.

Discussion of this paper should be addressed to the Secretary, A.S.M.E., 29 West 39th Street, New York, N. Y., and will be accepted until July 10, 1944, for publication at a later date. Discussion received after the closing date will be returned.

Note: Statements and opinions advanced in papers are to be understood as individual expressions of their authors and not those of the Society.

$$Tds = du + pdv \quad [7]$$

or

$$Tds = dh - vdp \quad [7a]$$

These equations apply to both reversible and nonreversible processes when no chemical changes of the substance occur. When the real process is nonreversible, it can be replaced by a reversible one, performed between the same initial and final states, as established by M. Planck in his treatise on thermodynamics.

Substitute $U = Gu$ and $V = Gv$ in Equation [1]; then

$$dQ + h_x dG = udG + Gdu + Gpdv + pvdG$$

The first and fourth terms on the right-hand side of this expression combine to hdG, while the second and third terms, from Equation [7], become equal to $GTds$; hence

$$dQ + h_x dG = hdG + GTds \quad [8]$$

or

$$dQ + (h_x - h)dG = GTds \quad [8a]$$

which is a suitable form of the second law of thermodynamics for changes of state and quantity. As to the outflow of a homogeneous working substance, $h_x = h$, and consequently

$$dQ = GTds \quad [9]$$

in analogy to Equation [6].

The right-hand side of Equation [9] can be integrated only if G is known or can be deduced. If $dQ = 0$, i.e., no heat is absorbed from environment or from walls, $\int GTds = 0$ which, for example, occurs in emptying a receptacle of constant volume. In the admission process h_x may be equal to h, but mostly $h_x \gtrless h$.

Adiabatic Emptying and Filling of a Receptacle

First, let $h_x = h$; hence, from Equation [1]

$$hdG = d(Gu) = udG + Gdu$$

or

$$(h - u)dG = Gdu$$

But

$$h - u = pv$$

so that

$$pvdG = Gdu$$

or, as

$$vdG = d(Gv) - Gdv$$

and V_0 = constant volume of receptacle

$$d(Gv) = dV_0 = 0$$

Hence[3]

$$du + pdv = 0 \quad [10]$$

which is the equation for the adiabatic change of state.

Similarly, since it has been assumed that $dQ = 0$

$$ds = 0 \quad [10a]$$

viz., the entropy is constant.

The foregoing consideration has established the relation for the emptying of a receptacle; for the filling, however, we have to distinguish between several different cases.

Filling a Receptacle by Means of a Compressor Without Any Cooling. In the following, it is assumed that the state of the gas drawn in by the compressor is identical with that initially within the receptacle. Also, that the pressure prevailing in the pressure-side piping of the compressor is permanently held equal to that inside the receptacle, which means that no valve is provided between the pressure-side piping and the receptacle, the compression taking place adiabatically with no losses.

Let the initial pressure be p_1, e.g., 1 atm; the final pressure p_2; the initial weight of the gas in the receptacle $G_1 = V_0/v_1$, where v_1 = initial specific volume; and the final weight of the gas therein G_2, where $V_0 = G_2 v_2$, and v_2 = specific volume.

The difference, $G_2 - G_1 = \Delta G$, therefore, is the weight of gas forced into the receptacle by the compressor, and the work expended on the compressor is

$$W_c = \int (h - h_1)dG \quad [11]$$

where h is the variable enthalpy of 1 lb of gas at the exit of the compressor and inside the receptacle.

$$W_c = \int hdG - h_1(G_2 - G_1)$$

By a partial integration of the first expression

$$\int_1^2 hdG = (G_2 h_2 - G_1 h_1) - \int_1^2 Gdh$$

Since the process is adiabatic, $dh = vdp$

$$\int_1^2 Gdh = \int_1^2 Gvdp = V_0 (p_2 - p_1)$$

hence

$$\int_1^2 hdG = (G_2 h_2 - G_1 h_1) - V_0(p_2 - p_1)$$

and

$$W_c = G_2(h_2 - h_1) - V_0(p_2 - p_1) \quad [12]$$

This work is represented by the area 3-2-1-3 in the p, v diagram shown in Fig. 1. In the h, s diagram (Fig. 2), however, it cannot be represented.

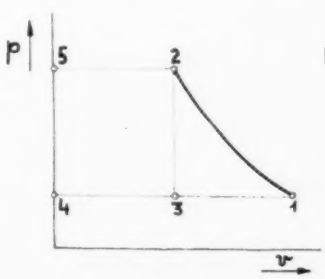


Fig. 1

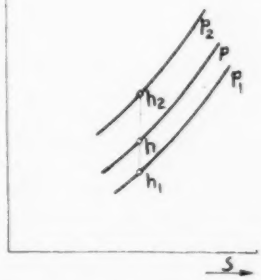


Fig. 2

Complete Cooling of Compressor and Receptacle. It will be supposed that both the compressor and receptacle are cooled by means of an infinite quantity of cold water, so that all processes are isothermal at the constant temperature T_k. Here, under ideal gas conditions, $h_x = h_k$ = const, and $u = u_k$ = const. From Equation [1]

$$dQ + h_k dG = d(Gu)$$

$$dQ + h_k dG = d(Gu_k)$$

and because

$$h_k - u_k = p_k v_k$$

$$dQ + p_k v_k dG = 0 \quad [13]$$

[3] Namely, from: $d(Gv) = Gdv + vdG = 0$; and $pvdG = Gdv$. (Added by M. Jakob.)

dQ is negative because heat is permanently extracted.

The weight of the gas inside the receptacle at any instant is

$$G = \frac{V_0 p}{RT_k} \text{ or } dG = \left(\frac{V_0}{RT_k}\right) dp \quad \ldots\ldots [13a]$$

The work expended on the compressor, assumed to be without any losses, is

$$dW_c = \left(RT_k \ln \frac{p}{p_1}\right) dG$$

or, from Equation [13a]

$$dW_c = V_0 \left(\ln \frac{p}{p_1}\right) dp$$

By integration

$$W_c = V_0 \left[p_2 \ln \left(\frac{p_2}{p_1}\right) - (p_2 - p_1)\right] \quad \ldots\ldots [14]$$

This work is represented by the area 1-2-3-1 in Fig. 3.

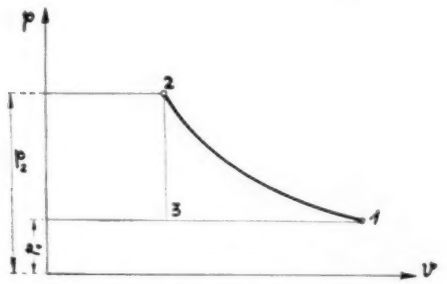


FIG. 3

Filling by Means of a Completely Cooled Compressor Without Cooling of Receptacle. Equation [1a] for the process in the receptacle takes the following form

$$h_k dG = d(Gu)$$

Here the state of the gas supplied by the compressor differs from that inside the receptacle during the filling, even though the two were identical at the beginning of the filling. For the state of the gas inside the pressure-side piping

$$h_k = c_p T_k + C$$

$$u_k = c_v T_k + C$$

whereas for the energy of the gas inside the receptacle

$$u = c_v T + C$$

where c_p, c_v are the specific heats of 1 lb at constant pressure and at constant volume, respectively; hence

$$c_p T_k dG = c_v d(GT) \quad \ldots\ldots [15]$$

Now

$$pV_0 = GRT$$

hence

$$d(GT) = \frac{V_0}{R} dp \quad \text{and} \quad dG = \frac{V_0}{R} \cdot d\left(\frac{p}{T}\right)$$

From Equation [15]

$$c_p T_k \cdot d\left(\frac{p}{T}\right) = c_v dp$$

Substituting $\kappa = c_p/c_v$

$$\kappa T_k d\left(\frac{p}{T}\right) = dp \quad \ldots\ldots [16]$$

and by integration

$$\kappa T_k \left(\frac{P_2}{T_2} - \frac{P_1}{T_1}\right) = p_2 - p_1 \quad \ldots\ldots [17]$$

The weight of the gas admitted into the receptacle is

$$G_f = G_2 - G_1 = \frac{V_0}{R}\left(\frac{p_2}{T_2} - \frac{p_1}{T_1}\right)$$

or, from Equation [17]

$$G_f = \frac{V_0}{R}\left(\frac{p_2 - p_1}{\kappa T_k}\right) \quad \ldots\ldots [18]$$

Since the compression is isothermal the work input may be obtained from

$$dW_c = RT_k \ln \left(\frac{p}{p_1}\right) dG$$

But from Equation [18]

$$dG = \frac{V_0}{\kappa RT_k} dp$$

hence

$$dW_c = \frac{V_0}{\kappa} \ln \left(\frac{p}{p_1}\right) dp$$

$$W_c = \frac{V_0}{\kappa}\left[p_2 \ln \left(\frac{p_2}{p_1}\right) - (p_2 - p_1)\right] \quad \ldots\ldots [19]$$

which is $1/\kappa$ that of the preceding case.

Filling With Compressor of Constant Maximum Pressure p_2. Finally, it will be assumed that compression takes place continuously up to the maximum pressure p_2, which is maintained constant by the insertion of a reducing valve between the piping and receptacle. Temperature T_2 is in this case derived from Equation [17]. T_k is the temperature before and after the reducing valve. The "filling effect" is greatest when initially the vacuum in the receptacle is perfect, i.e., $p_1 = 0$. In this case

$$\kappa T_k = T_2 \quad \ldots\ldots [17a]$$

If, for example, $T_k = 300$ deg K, then

$$T_2 = 1.4 \times 300 = 420 \text{ deg K}$$

The foregoing relation holds for ideal gases only; the fundamental equations, however, apply equally to all working substances.

APPLICATION TO STEAM-PISTON ENGINES

It is clear that both expansion and compression, each referring to 1 lb of steam, or to some other constant weight, can be represented in the T, s diagram. It should be further noted here that modern experimental investigations show the working substance within the cylinder to be nonhomogeneous. Due to heat transfer from the steam to the walls, it is possible that the steam is superheated inside the cylinder, whereas a liquid film is formed on the surface of the walls. The thickness of this film increases if the steam is condensing, while a decrease indicates that the liquid is evaporating. Thus the working substance can exist in both the liquid and gaseous phases. This fact, however, will not

be taken into account. Hence, the expansion and compression will be regarded as simple changes of state, whereas the admission and outflow are changes of state and quantity.

Let G_f, G_r be the weights of steam admitted and remaining in the clearance space, respectively, then the weight of steam involved in the expansion is

$$G_1 = G_f + G_r$$

The theoretical p, v diagram of a steam engine is shown in Fig. 4, the p, v diagram, corresponding to Fig. 4, is shown in Fig. 5, and the h, s diagram of the same engine is shown in Fig. 6. If h_k is the enthalpy of incoming steam then h_1 is the enthalpy of the steam inside the cylinder at the end of the filling, and the difference $h_1 - h_k$ represents the filling effect. The point a in Fig.

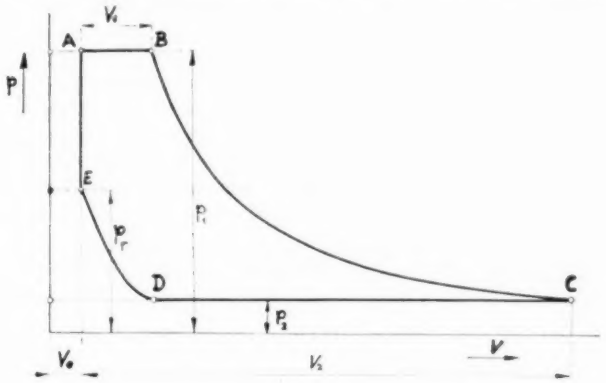


Fig. 4

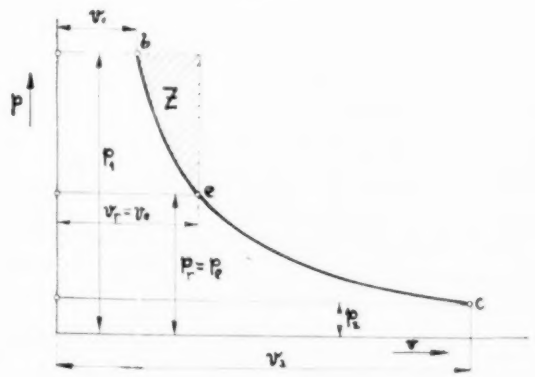


Fig. 5

6, corresponds to A in Fig. 4, and represents the end of the partial filling at constant volume. The enthalpy at this point is still higher than h_1. Calculating the work of the whole cycle from Fig. 4, we have

$$W = (G_f + G_r)\ \Delta h - G_r \Delta h_r - (p_1 - p_r)V_0$$

where $V = G_r v_r$, and Δh_0, Δh, and Δh_r are the adiabatic enthalpy drops, corresponding to the initial state in the boiler, the state inside the cylinder at the end of the admission, and the compression, respectively.

Writing $G_r = \rho G_f$ and after some mathematical derivations, we obtain

$$h_1 - h_k = \rho z \ldots\ldots\ldots\ldots\ldots\ldots [20]$$

where z equals the cross-hatched area in Fig. 5.

For an engine with no clearance, the work is

$$W_0 = G_f \Delta h_0$$

The loss of work caused by the clearance is $W_0 - W_1$, or for 1 lb

$$\frac{W_0 - W_1}{G_f} = \Delta h_0 - (\Delta h - \rho z)$$

In the h, s diagram of Fig. 6, Δh_0 is represented by the line

$$b_0 c_0 = h_k - h_2'$$

while

$$\Delta h' = h_1 - h_2$$

The loss due to the filling of the clearance is

$$\Delta h_1 = h_2 - h_2' \ldots\ldots\ldots\ldots\ldots\ldots [21]$$

or, expressed in terms of temperature and entropy in the case when the steam at the end of the expansion is wet

$$\Delta h_1 = T_2 \Delta s \ldots\ldots\ldots\ldots\ldots\ldots [21a]$$

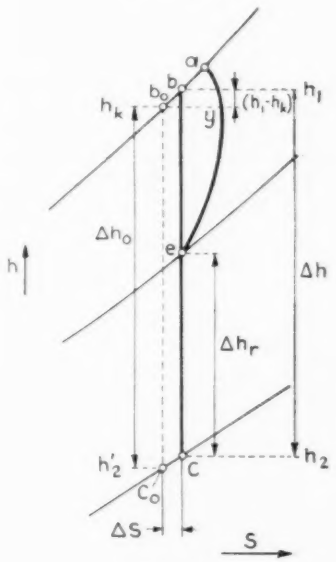


Fig. 6

Now the behavior of the entropy during the filling will be examined. In the ideal case, the filling consists of two stages, i.e., a quantity isometric EA and a quantity isobaric AB (Fig. 4). The quantity isometric behaves very similarly to that of the filling of a receptacle in accordance with the case "Filling with Compressor of Constant Maximum Pressure, p_2," previously discussed. It is a nonreversible process and the entropy does not remain constant but describes the curve e-y-a in Fig. 6. The adiabatic branch b-e is valid only for the expansion, while, for the return stroke of the piston, the adiabatic is valid only for the compression stage c-e.

According to curve e-y-a, the entropy attains its maximum value at a point y, where $h = h_k$. The shape of this actual curve can be obtained point by point by using the following two equations

$$h_k \cdot \Delta G = h_k(G - G_e) = Gu - G_e u_e \ldots\ldots\ldots [22]$$

where G_e and u_e refer to the beginning of the compression at the point E. $G_e = G_r$ = quantity of steam remaining in the clearance and

$$\Delta G = G - G_e = V_0 \left(\frac{1}{v} - \frac{1}{v_e}\right) \ldots\ldots\ldots [22a]$$

Preliminary values of temperature T are chosen for any pressure between p_a and p_1, and u and v are then calculated. The preliminary temperature is deemed correct when the same value of ΔG is obtained from both Equations [22] and [22a]. In similar manner also the final point a, corresponding with the pressure p_1 is determined. For the second stage of the filling process AB carried out at constant pressure, the following equations apply

$$h_k(G - G_r) = Gh - G_a h_a$$

$$\frac{V_0}{V_0 + V_1} = \frac{G_a v_a}{Gv}$$

For the final point B we have

$$\left.\begin{aligned} h_k(G_1 - G_a) &= G_1 h_1 - G_a h_a \\ \frac{V_0}{V_0 + V_1} &= \frac{G_a v_1}{G_1 v_1} \end{aligned}\right\} \quad \ldots\ldots\ldots\ldots [23]$$

In this manner the form of the change of state is obtained also in the T, s and h, s diagrams. In comparing such a diagram with that drawn from readings taken experimentally, differences in areas are observed; these differences are due to heat transfer with the walls. In both cases $\int TGds$ has to be formed.

From the experiments of Ulsamer[4] it is evident that also in the case of slight superheating of the live steam during the filling, expansion, and compression, a core of superheated steam fills up the inside of the cylinder. It is therefore clear that the working substance in the true processes in the actual engine is not homogeneous. If this phenomenon is disregarded, we arrive at the filling effect in accordance with Equations [20] to [23] as for example: $p_1 = 10$ atm; temperature of incoming steam $t_0 = 300$ C; $p_2 = 0.1$ atm; $\rho = 0.1$; hence

$$h_1 - h_k = 11 \text{ kcal/kg and } t_1 - t_k = 22 \text{ deg C (filling effect)}$$

Conclusions

In the present paper, the fundamental principles regarding the changes of state and quantity of a working substance are presented, beginning with the more usual cases, such as the filling of a receptacle. On the basis of the general formulation of the second law of thermodynamics for changes of state and quantity the important case of the steam engine has been dealt with.

It is shown that only for pure changes of state, i.e., changes of state with constant quantity of the working substance, the entropy diagram can be unrestrictedly used, whereas in change of state and quantity it is necessary to examine in each case if and in what manner the entropy diagram may be applied.

[4] "Dampfzustand im Zylinder einer Gleichstrom-Dampfmaschine," by J. Ulsamer, *Forschung auf dem Gebiete des Ingenieurwesens*, vol. 5, 1934, pp. 80–88.

An Investigation of the Cross-Spring Pivot

By W. E. YOUNG,[1] EAST PITTSBURGH, PA.

It is the purpose of this paper to describe the characteristics of the cross-spring pivot, or elastic hinge, for large deflection angles. Design formulas are established for certain standard forms of the two-spring pivot on the basis of experimental results. Formulas are developed for the spring constant, bending stress, and motion of the pivot point; their application is illustrated by an example. A comparison of the various pivots, when used in lever systems, is made, and suggestions for the design of two-spring pivots are included.

1 Introduction

THE cross-spring pivot, or elastic hinge, consists of a system of flat springs intersecting as in the letter X. The ends of the springs are fastened to the two members which it is desired to connect. This system has the characteristic of rotating approximately about the intersection of the springs and in many applications it can advantageously replace the knife-edge.

The cross-spring pivot appears to have several qualities which often make it superior to either knife-edges or pin connections in controlling an oscillating motion. It is perfectly elastic since there are no moving parts in contact to produce friction; also its construction enables it to withstand a sudden reversal of load which might unseat a knife-edge. Its chief advantage over a pin connection lies in the fact that with no moving parts in contact, no lubrication is necessary and no wear takes place.

This type of pivot has been used for small angular deflections in a number of cases (1)[2] but little has been known regarding its applicability to large angles of deflection. A mathematical approach was made to the problem and equations were derived, connecting the interreacting forces and moments in the linkage. The system was found to be statically indeterminate, and these equations become extremely complex. Due to the difficulties of solution, it seemed wiser to attempt an experimental analysis. Accordingly, a series of tests has been made for the purpose of analyzing the motion of the mechanism, particularly for deflection angles up to 45 deg.

2 Test Apparatus

A sketch of the principal parts of the test apparatus is shown in Fig. 1. Four flat springs *a* may be seen, forming two separate pivots. The ends of each spring are held in spring blocks *b* which in turn are fastened to end plates *c* and *d*. End plate *c* is attached to a bedplate through the support *e* while end plate *d* is constrained to a rotation approximately about the axis *o* through the initial intersections of the springs. To end plate *d* is bolted a pointer *f* by which the angle of deflection may be measured (see Fig. 2). A stylus *g* at the front end of the pointer plots its path on the drawing board *h* as the springs deflect. At the same time, stylus *i*, attached to the rear of the pointer and set initially on the axis *o*, plots the motion of this axis. Slots *j* cut in each end plate allow an adjustment of the initial spring intersection angle (see Fig. 2), while the spring blocks permit any length, width, and thickness of flat spring to be used.

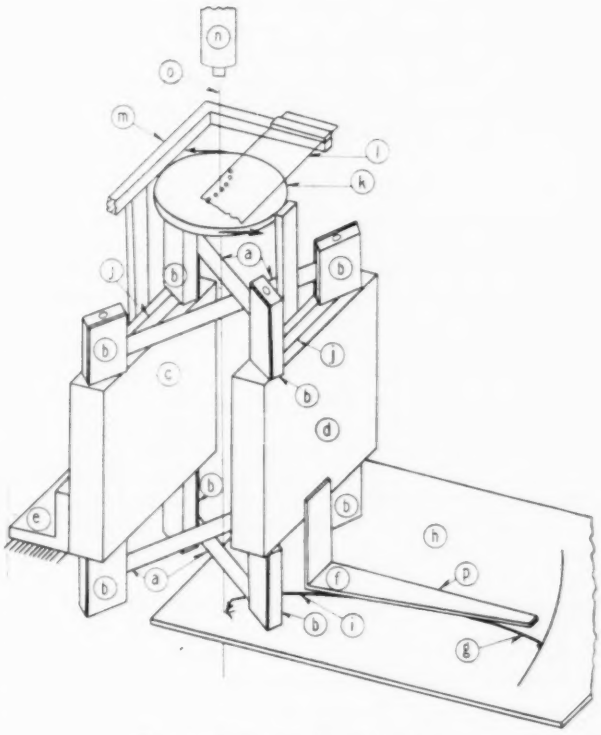


Fig. 1 Sketch of Test Apparatus

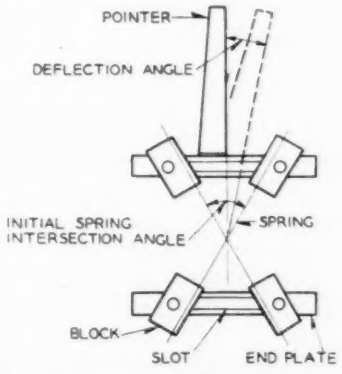


Fig. 2 Sketch of Experimental Setup

Loading is accomplished by means of disk *k* which is rigidly fastened to end plate *d* and set with its center on the axis *o* of initial spring intersection. In order that a pure moment be supplied to the springs, equal forces are applied at the extremities of a diameter of the disk in the form of a couple.

In locating instantaneous centers of rotation, use is made of a piece of transparent film *l* held in frame *m* which in turn is rigidly attached to the stationary end plate *c*. For each angular position of the pointer, a point may be located on the disk which

---

[1] Westinghouse Electric & Manufacturing Co.

[2] Numbers in parentheses refer to Bibliography at end of paper.

Presented at the Annual Meeting, New York, N. Y., Nov. 29–Dec. 3, 1943, of The American Society of Mechanical Engineers.

Discussion of this paper should be addressed to the Secretary, A.S.M.E., 29 West 39th St., New York, N. Y., and will be accepted until July 10, 1944, for publication at a later date. Discussion received after the closing date will be returned.

Note: Statements and opinions advanced in papers are to be understood as individual expressions of authors and not of the Society.

rotates without translating for small angular oscillations of the pointer about this position. Microscope n was used to locate these centers of rotation through the transparent film on the disk. Once located, the centers could be recorded on the film by means of a microscope diamond point objective.

The apparatus as just presented appears extremely complicated since it was designed to accommodate and test many different sizes of springs with various intersection angles. It should be understood, however, that the cross-spring pivot as generally used is a very simple construction since it is not necessary to provide for changing such variables as spring length and intersection angle.

3 General Test Procedure

For each test, the flat springs were first attached to their respective blocks and set at the required length. The blocks were then bolted to the end plates with such spacing in the slots that the springs intersected at their mid-points. The correct angle of intersection was then obtained with a protractor. Next, the pointer was adjusted so that its reference edge p cut the axis of initial spring intersection as shown in Fig. 1; the loading disk also was set with its center on this axis. Loads were applied to the disk circumference by coil springs, the corresponding lengths of which were obtained from a coil spring calibration curve. The two styli traced the paths of the initial spring intersection point and the front end of the pointer, respectively, as shown in Fig. 3, and for each recorded loading the position of the pointer was plotted on the drawing board by a line drawn along its reference edge.

At the same time the microscope was manipulated to locate the center of rotation for each pointer position, and this center was marked on the transparent film with the microscope diamond point objective. These instantaneous centers for the various

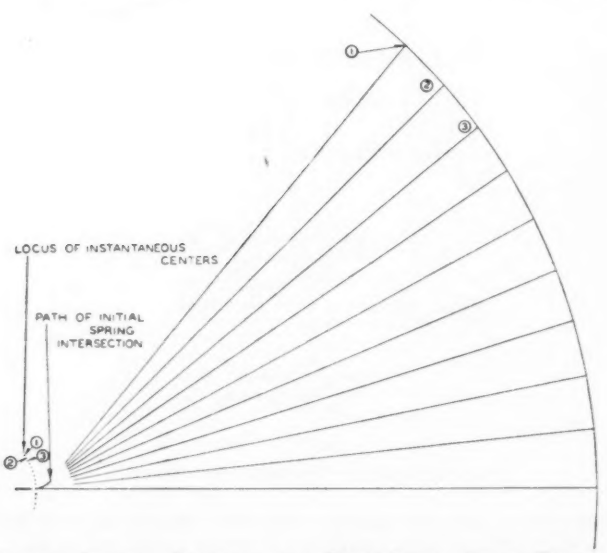


Fig. 3 Pointer Positions for Cross-Spring Pivot Tester (0.012 in. spring thickness; 3 in. spring length; 90 deg spring angle.)

pointer positions may be seen in Fig. 3. Center No. 1 corresponds to pointer position No. 1, Center No. 2 to pointer position No. 2, and so on.

4 Specific Tests

Five separate tests were made for certain standard spring angles, lengths, and thicknesses, with the springs initially intersecting at their mid-points; 0.012 × 3/8 in. and 0.0085 × 0.470 in. springs were used. For the 0.012-in. spring, a length of 3 in. was tested at 30, 60, and 90 deg initial spring intersection angles with the purpose of finding the effect of this angle.

In order to find the effect of spring length and also spring thickness, tests were made on 3 and 1 1/2-in. lengths of the 0.0085-in. springs. For comparison, a 60-deg intersection angle was used with both the 3 and 1 1/2-in. lengths.

For each of the foregoing five tests, data similar to Fig. 3 were obtained, and from these data, the curves in Fig. 4 were plotted.

5 Derivation of the Spring Constant for Small Angles

Let K_1 = spring constant for one spring
M_1 = total moment on one spring
θ = angle of pointer deflection
l, E, and I = characteristics of the spring
n = number of springs
K = total spring constant

By means of the first area moment proposition, it may easily be shown that for small angles,

$$\theta = \frac{M_1 l}{EI}$$

also

$$K_1 = \frac{M_1}{\theta}$$

and combining

$$K_1 = \frac{M_1}{M_1 l/EI}$$

for one spring

$$K = n\,\frac{EI}{l}$$

for n springs

This derivation assumes only a moment on the springs and no reaction forces, which is not the case except at zero degrees deflection. A calculation of each setup using this formula should give values approximating zero deflection on the curve. This was found to be true as shown in Table 1.

TABLE 1 COMPARISON OF THE CALCULATED CONSTANT FOR SMALL ANGLES TO THE MEASURED CONSTANT AT 0 DEFLECTION FOR EACH TEST

	Spring designation	Calculated constant	Measured constant
1	3 × 0.012 × 3/8 in.	2.16 lb-in. per radian	2 lb-in. per radian (Average value from three tests)
2	3 × 0.0085 × 0.470 in.	0.96 lb-in. per radian	0.9 lb-in. per radian
3	1 1/2 × 0.0085 × 0.470 in.	1.93 lb-in. per radian	1.95 lb-in. per radian

The spring angle has no effect on the derived constant for small angles.

These results all check within 7 1/2 per cent which is within the combined liable error for the test measurements, calculation, and curve scatter.

6 Design of the Cross Spring Pivot

1 *Dimensions of the Springs Used (for Required Spring Constant)*

A torque problem may be stated in one of two ways. First, assuming that a cross-spring pivot is to be used, it may be desired to obtain a certain instantaneous spring constant at a given deflection; or, second, a definite amount of torque may be available and a maximum total deflection may be permitted for this torque because of strength limitations.

From the curves in Fig. 4 it was found possible to determine the effect of the various spring dimensions and angles on the spring constant for steel springs. These observations are shown in the following tabulation:

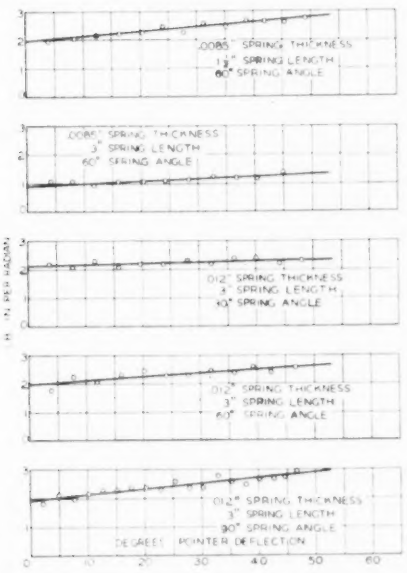


FIG. 4 SPRING CONSTANT CURVES FOR THE CROSS-SPRING PIVOT

1 From the curves for the $1^1/_2 \times 0.0085$ in. and the 3×0.0085-in. springs, the increase in constant for a given deflection is seen to vary inversely as the length of spring used.

2 Since the curves in each case approximate straight lines, the increase is directly proportional to the displacement angle.

3 It was found from the tests on the 0.012×3-in. springs that the increase in constant varies approximately as the 1.4 power of the spring intersection angle. This exponent was arrived at by trial.

4 Although no tests were made to determine the effect of spring width, it seems logical to assume that the increase in constant varies directly with the width of spring used.

5 If the foregoing assumption is allowed, an examination of the 0.0085×3-in. and 0.012×3-in. springs (both with a 60-deg intersection angle) indicates that the increase in constant varies with the square of the spring thickness.

Finally we obtain the relation

$$K_i = C\left(\frac{bd^2\theta\phi^{1.4}}{l}\right)$$

where K_i is the increase in spring constant over the value for small angles nEI/l, as derived. The unit for K_i will be lb-in. per radian. Other terms are:

C = arbitrary constant
b = spring width, in. (sum of all springs)
d = spring thickness, in.
l = spring length, in.
θ = deflection angle in radians
ϕ = intersection angle in deg

From the various tests, an average value of C may be obtained. For the 0.012×3-in. spring with a 30-deg intersection angle, the solution becomes

$$C = \frac{K_i l}{bd^2\theta\phi^{1.4}}$$

Substituting test values in this equation

$$C = \frac{0.20 \times 3 \times 57.3}{4 \times 0.375 \times 0.012^2 \times 45 \times 30^{1.4}}$$

$$= 30.5$$

The average value of C for all tests is about 31 with values ranging from 29.5 to 32.7. The final formula is approximately

$$K_i = 31\left(\frac{bd^2\theta\phi^{1.4}}{l}\right)$$

The formula is, of course, entirely empirical, and a greater number of tests would doubtless result in a more accurate value for the arbitrary constant as well as for the exponent of the spring intersection angle.

Now, if a certain spring constant is desired at a given deflection, its value may be substituted in the relation

$$K = n\frac{EI}{l} + K_i$$

(K = total constant)

where I is the moment of inertia of one spring and n is the number of springs to be used. This may be rewritten

$$l = \left(\frac{E}{K}\right)\left(\frac{bd^3}{12}\right) + \left(\frac{31}{K}\right)(bd^2\theta\phi^{1.4})$$

Next, a standard-dimension spring may be chosen, and the b and d values substituted in this formula for l. The intersection angle, ϕ, would generally be 90 deg, but this will be considered later. Since only steel springs were tested, the modulus does not appear in the increase of constant. However, it is quite possible that this increase would be proportional to the spring stiffness and hence to the modulus of elasticity of the material.

If the resulting value of the length is unduly short or long, spring stock with a different thickness or width dimension must be chosen.

As a second case, suppose that a definite torque is required for a given deflection. Since the spring constants considered have been instantaneous values, an average increase over the range of deflection in question must be determined for use in the basic relation, $M = K\theta$. This means that the total average constant would be

$$K = n\frac{EI}{l} + \frac{1}{2}K_i$$

where $n\dfrac{EI}{l}$ is the constant for small angles (either average or instantaneous). Since the instantaneous spring constant increases linearly from 0 deg deflection to its value, K_i, at the given deflection, the average increase for that range is $^1/_2$ the instantaneous value, K_i, occurring at the given deflection.

The total torque developed at the given deflection becomes

$$M = \left(n\frac{EI}{l} + \frac{K_i}{2}\right)\theta$$

which may be rewritten

$$l = \frac{\theta}{M}\left(\frac{bd^3E}{12} + 15.5\ bd^2\theta\phi^{1.4}\right)$$

where M is the total torque and the number of springs n has been included in the quantity b. From this relation l may be solved as before.

To use the formulas developed above, it becomes necessary to raise the value of the spring intersection angle ϕ to the 1.4 power. In order to eliminate such a calculation, curves have been drawn of increases in spring constant for various $\dfrac{bd^2\theta}{l}$ ratios. The curves in Fig. 5 have been plotted for the standard intersection

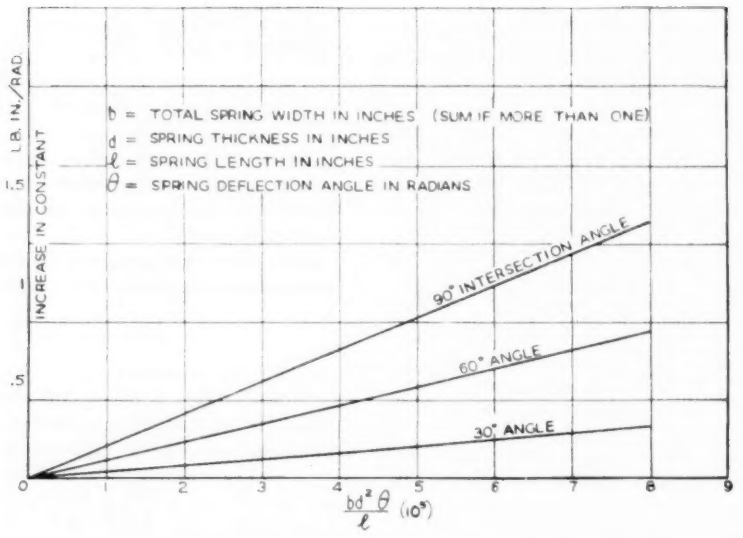


FIG. 5 INCREASE IN SPRING CONSTANT OVER VALUE FOR SMALL ANGLES $\left(K = \frac{EI}{l}\right)$

angles, 30, 60, and 90 deg. These values may be used in place of K_i in these formulas.

Since both the curves and the formulas have been built up from various test data, which were intended to lie in a range frequently used, they may not be applicable for values which differ greatly from these test data.

For this reason, calculations for springs over 3 in. long and greater than 0.012 in. in thickness should be used with discretion, particularly if the deflection angle is greater than 45 deg. The same applies to the very low ranges where small variations due to clamping and eccentricities may greatly affect the spring constants of short and thin springs at small angular deflections. Values have not been checked for thickness below 0.008 in., lengths of 1 in. or less, and angular deflections of less than 5 deg.

2 *Stress in the Springs at Maximum Deflection*

Stress for small deflection angles of cross springs is usually determined on the basis of a constant moment throughout the length of the spring. This assumes that the springs are bent in circular arcs of equal radii, which does not seem to be exactly the case for large deflection angles. Apparently, auxiliary forces and moments are introduced at the ends of the springs by the larger deflection angles. These end reactions are probably responsible for the increase of constant over that value for small angles. At the same time the bending stress increases.

Since the exact nature of the end reactions is not known, it has been assumed that the increase in bending stress will be proportional to the increase in spring constant over the value for small angles, or the stress due to bending will be proportional to the bending moment as derived. If this approximation is allowed, we obtain the relation

$$\frac{\sigma_a}{\sigma_i} = \frac{M_a}{M_i}$$

where σ_a = the bending stress to be determined
σ_i = the bending stress as determined on the basis of the spring constant for small angles
M_a = the bending moment as calculated from the foregoing formulas
M_i = the bending moment as calculated on the basis of the spring constant for small angles

but

$$\sigma_i = \frac{M_i C}{I}$$

where $C = {}^1/_2$ spring thickness

$$M_i = \left(\frac{EI}{l}\right)\theta$$

$$M_a = \left(\frac{EI}{l} + \frac{K_i}{2}\right)\theta$$

from the foregoing.

Assume

I = total moment of inertia of the springs

then

$$\sigma_i = \frac{C\theta}{I}\left(\frac{EI}{l} + \frac{K_i}{2}\right)$$

This result appears reasonable since even at large angles of deflection the springs appear to be bent in circular arcs. For an approximate calculation then, the bending moment will be assumed to be constant throughout the length of the spring and the stress will be assumed to be the same in both springs.

This stress may be rewritten

$$\sigma_a = \frac{C\theta E}{l} + \frac{K_i C\theta}{2I}$$

but

$$K_i = 31\left[\frac{b(4C^3\theta\phi^{1.4})}{l}\right]$$

(since $d = 2C$)

$$\sigma_a = \frac{C\theta E}{l} + 62\left[\left(\frac{2C^3\theta\phi^{1.4}b}{l}\right)\left(\frac{C\theta}{2I}\right)\right]$$

$$= \frac{C\theta}{l}\left[\mathrm{E} + 62\left(\frac{bC^2\theta\phi^{1.4}}{I}\right)\right]$$

If

$$I = \frac{bd^3}{12}, \qquad d = 2C$$

$$I = \frac{2bC^3}{3}$$

and substituting in the foregoing

$$\sigma_a = \frac{C\theta}{l}\left[E + 93\left(\frac{\theta\phi^{1.4}}{C}\right)\right]$$

This formula may be used only for steel springs.

If the stress as calculated by the foregoing formula appears excessive, the design on a torque basis must be repeated and either the length of the springs increased or the thickness decreased.

3 *Amount of Travel of Initial Pivot Point*

In some instances, it may become necessary to limit the travel of the initial pivot point. For example, if a cross-spring mechanism were being used to center a coil in an air gap, any undue shift of the pivot point might lessen or actually close the air gap. From the tests it appears that this shift is proportional to the spring length. Consequently curves have been drawn for springs one inch long using the results of the foregoing tests (see Fig. 6). The curve ordinate must be multiplied by the spring length in order to get the actual displacement in hundredths of an inch. This displacement is best defined by the accompanying sketch Fig. 7.

As the springs deflect to the positions shown by the dash lines, the initial pivot point travels along the arc F and the displacement as read from the curve sheet is the radial or chord distance E, assuming that the springs are one inch in length.

If we consider the curves to have equations of the approximate form

$$y = AX + BX^2 + CX^3 + DX^4$$

where y is the amount of travel in 0.01 in. per in. spring length and X is the angular deflection of the pointer and springs in degrees, the constants, A, B, C, and D may be solved by substituting points on the curve and the equations become

$y = 0.04133X - 0.001225X^2 + 0.0001267X^3 - 0.00000075X^4$ (for a 90-deg intersection angle)

$y = -0.02865X + 0.006115X^2 - 0.0001333X^3 + 0.000001833X^4$ (for a 60-deg intersection angle)

$y = 0.03924X - 0.004595X^2 + 0.0002675X^3 - 0.00000304X^4$ (for a 30 deg intersection angle)

The value of y may then be multiplied by the actual spring length to obtain the total displacement at that deflection angle. From the curves of Fig. 6 it may be seen that the pivot point travels less for a smaller intersection angle, but from the tests it was found that the apparatus was likely to be less rigid.

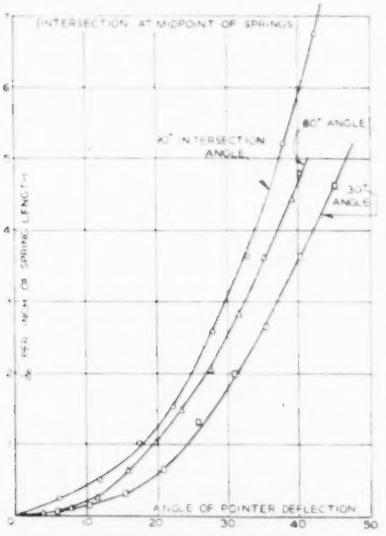


FIG. 6 DISPLACEMENT OF THE INITIAL PIVOT POINT FROM ITS ORIGINAL POSITION FOR VARIOUS DEFLECTION ANGLES AND SPRING INTERSECTION ANGLES

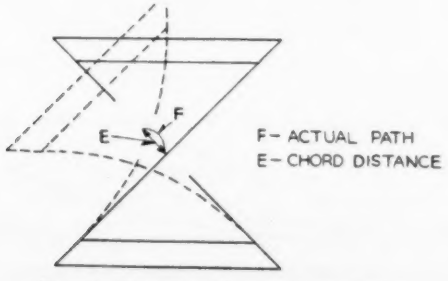


FIG. 7 TRAVEL OF INITIAL PIVOT POINT

4 *Change in Magnification Ratio for Given Deflections*

One general use of this pivot is as a fulcrum for a simple lever. In this case, a force is applied at a single point and for small angles the torque is equal to this force multiplied by the distance from this point to the initial spring intersection. As the deflection angle increases, however, the pivot will shift and the moment arm may change. If it was originally quite short, the effect of this change in moment arm becomes very noticeable. By trial it is actually possible to cancel the effect of the increasing spring constant with an increasing moment arm and obtain a flat spring constant curve over part of the deflection range. The torque formula developed applies only where the moment arm change is compensated or where the arm is so long in respect to the change that the effect is negligible.

Two lever systems are shown in Figs. 8 (*a*) and (*b*). Both the long arm, L_2, and short arm, L_1, tend to change length as the springs deflect, but in Fig. 8 (*b*) due to the geometry of the system, the long arm changes more than the short, and both arms change length in the same direction. Consequently the ratio of long to short arm may remain nearly constant over a wide range of deflection. Finally the transmitted motions may remain in the same ratio as the springs deflect although the resulting moments would not be the same as for a knife-edge type fulcrum.

The sketch, Fig. 9, was copied from Fig. 3 and a lever system of the type Fig. 8(*b*) was assumed. Only two positions of the pointer and the corresponding geometry are shown, but Table 2 gives the arm lengths and ratios for all the pointer positions shown in that figure. A 5 to 1 ratio was assumed at the start.

TABLE 2 MAGNIFICATION RATIO VALUES FOR FIG. 3 ON SPRING

(0.012 × 3 in. with 90-deg intersection angle; initial ratio, 5 to 1)

Position	Short arm, in.	Long arm, in.	Ratio	Per cent error to initial
1	1.84	9.37	5.09/1	+1.8
2	1.85	9.39	5.07/1	1.4
3	1.86	9.41	5.06/1	1.2
4	1.87	9.42	5.04/1	0.8
5	1.88	9.43	5.02/1	0.4
6	1.89	9.45	5/1	0
7	1.89	9.45	5/1	0
8	1.89	9.45	5/1	0
9	1.89	9.45	5/1	0
10 (Start)	1.89	9.45	5/1	0

In Table 3 are shown magnification ratios for the other four spring setups tested. The starting ratio in each case was 5 to 1

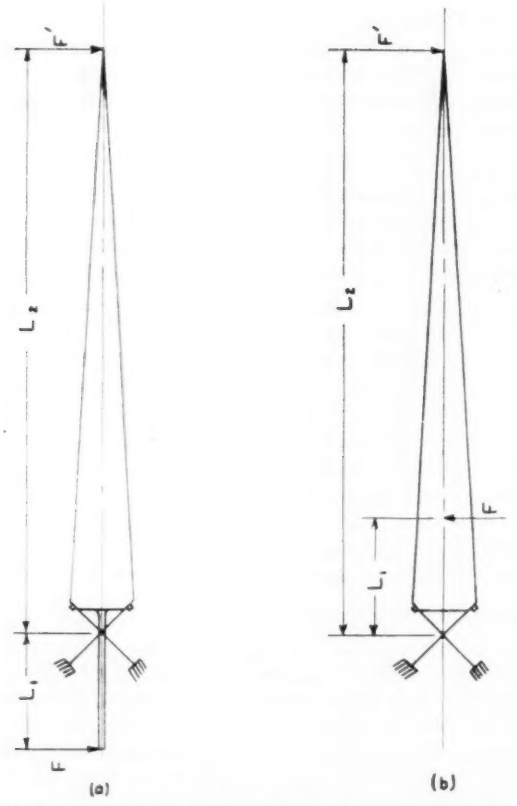


FIG. 8 SKETCHES OF PIVOTS USED IN LEVER SYSTEMS

and the length of the short arm was about two inches. (1) refers to the final pointer position as shown in Fig. 3. Only the starting and final ratios are shown. Fig. 8(*b*) lever system was assumed.

TABLE 3 INITIAL AND FINAL MAGNIFICATION RATIOS FOR FOUR OF THE STANDARD SPRING SETUPS TESTED

Spring designation	Position	Long arm, in.	Short arm, in.	Lever ratio	Per cent error (final ratio to initial)
60 deg × 3 × 0.012 in.	Start	9.87	1.97	5/1	0
	1	9.80	1.92	5. 1/1	2
30 deg × 3 × 0.012 in.	Start	10	2	5/1	0
	1	10.15	2.12	4. 8/1	—4
60 deg × 3 × 0.0085 in.	Start	10.16	2.03	5/1	0
	1	10.2	2.06	4.95/1	—1
60 deg × 1½ × 0.0085 in.	Start	9.17	1.84	5/1	0
	1	9.13	1.77	5.15/1	3

These changes appear to be less for a large intersection angle than for a small one. It also seems as if more change may be expected from short springs than from long ones. However, these changes are so small that in most cases they may be neglected. For that matter they lie within the liable error of the tests. Finally, the fact that the change is sometimes positive and sometimes negative indicates errors in test measurement rather than experimental fact.

However, if a lever system as in Fig. 8(*a*) is assumed, a very noticeable change in magnification ratio takes place as the lever is deflected. This change is due to the fact that as one arm elongates, the other becomes shorter. In the preceding case, Fig. 8(*b*), as one arm becomes longer, the other arm simultaneously elongates and the resulting change of ratio is naturally smaller. The curves in Fig. 10 show a comparison of the two lever systems for the spring data of Fig. 3. The per cent change of ratio for the system Fig. 8(*a*) is seen to be roughly twice that for the system Fig. 8(*b*). An initial ratio of 5 to 1 was assumed.

Using the same method as before, arm lengths and magnification ratios have been found for all the pointer positions included in each spring combination of lengths, thicknesses, and intersection angles tested. The type Fig. 8(*a*) lever has been assumed, and in each case the initial lever arm ratio is 10 to 1 measured at 0 deg pointer deflection angle. The results of these measurements are shown in Fig. 11 from which it is apparent that the greatest change in magnification ratio takes place for the smaller spring intersection angles. As might be expected, the change in ratio becomes much greater for deflection angles over 35 deg, and each curve rises sharply beyond this angle.

For smaller initial magnification ratios used with the same

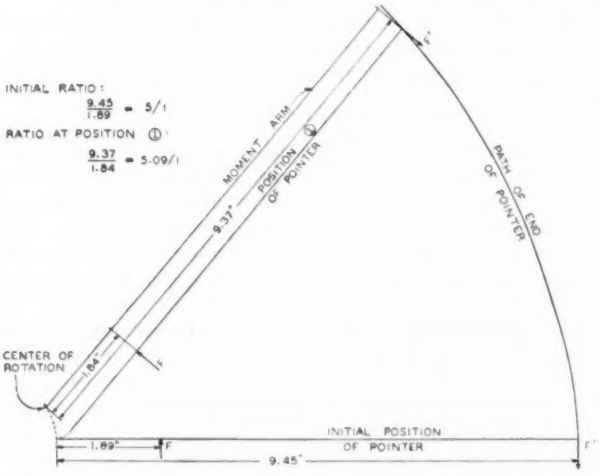


FIG. 9 A TYPE FIG. 8(*b*) LEVER SYSTEM COPIED FROM FIG. 3

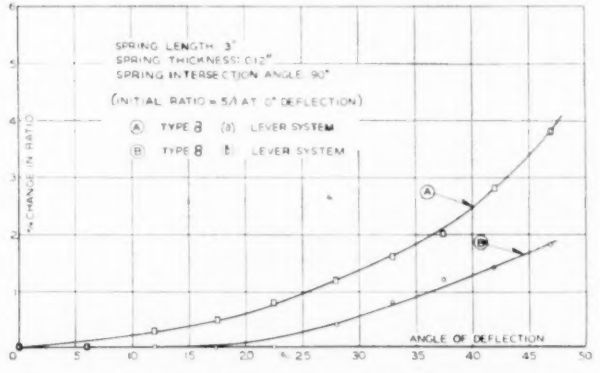


FIG. 10 CHANGE IN MAGNIFICATION FOR VARIOUS ANGULAR DEFLECTIONS

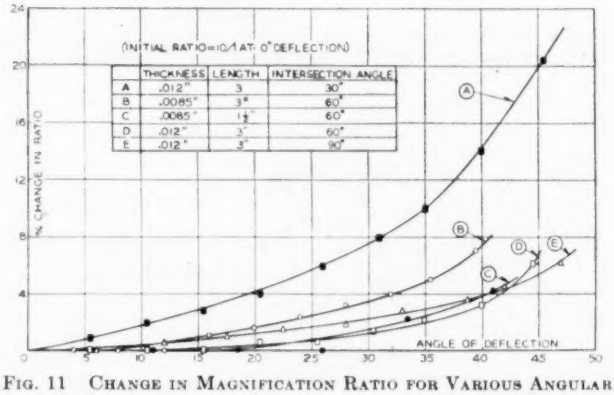


FIG. 11 CHANGE IN MAGNIFICATION RATIO FOR VARIOUS ANGULAR DEFLECTIONS

length of the longer arm, this change is less noticeable. For instance, measurements have been made on the spring system shown in Fig. 3, assuming an initial magnification ratio of 5 to 1. At an angle of 47 deg pointer deflection, this change amounts to 3.8 per cent as compared to 6.2 per cent for the same position where the initial magnification ratio was 10 to 1.

This change in magnification ratio suggests that the pivot may be dynamically unstable. That is, it may be in equilibrium at its neutral position under a system of forces, but if displaced slightly from this position, it may become unbalanced and continue to deflect until checked by some external means. This has been found to be the case where a heavy lever system is supported by extremely light springs. This characteristic is not easily corrected, and at present the only solution seems to be to use supporting springs of such a thickness that their resisting moment counteracts the unbalanced condition in the lever system and returns the lever to its neutral position.

5 *Example of the Use of the Formulas*

As an illustration of the formulas and at the same time as a check on their validity, a specific problem has been worked out. The device checked was a "spindle dynamometer." It consisted of a motor, mounted vertically with its shaft in line with two spring pivots. These pivots supported the weight of the motor and at the same time produced a resisting moment to measure the torque exerted by the motor. From the spring dimensions, the spring constant curve was drawn after which several test points were plotted which showed a surprisingly close agreement with the calculations. Measurements were made with the same disk and coil spring setup previously described and the angle was read from the dynamometer scale.

The springs, four in number, were one inch in width and slightly under 10 mils in thickness. A value of 0.00975 in. was used for calculating. The free length was $1^3/_8$ in.

From the formula

$$K_i = \frac{31(bd^2\theta\phi^{1.4})}{l}$$

Substituting spring dimensions at 20 deg angular deflection

$$K_i = \frac{(31 \times 4 \times 0.00975^2 \times 20 \times 90^{1.4})}{(1.375 \times 57.3)}$$

$$= 1.615 \text{ lb-in. per radian at 20 deg}$$

Also at 0 deg

$$K = \frac{EI}{l}$$

$$= \frac{(30{,}000{,}000 \times 4 \times 0.00975^3)}{(12 \times 1.375)}$$

$$= 6.74 \text{ lb-in. per radian}$$

Total constant

$$= 6.74 + 1.615$$

$$= 8.355 \text{ lb-in. per radian at 20 deg}$$

The test results are shown in Table 4. The torque value for 2 deg was used only to determine the constant at 6 deg. Due to a slight buckling of the springs near the initial position, this value was thought to be incorrect. Readings for such small angles are generally in error for this reason. It is practically impossible to line up the springs perfectly. Consequently there is some point of instability near the initial position and a reading near this point might indicate more or less force than would be required had there been no buckling. Since the second point was obtained from the first point, this too may be inaccurate, but the error at this angle will be very much smaller.

TABLE 4 TEST RESULTS

Angle, deg	Torque, lb-in.	Torque difference, lb.-in.	K, lb-in. per radian
2	0.306	..	..
6	0.827	0.521	7.45
10	1.35	0.523	7.50
14	1.90	0.55	7.88
18	2.46	0.56	8.02

SPRING CONSTANT CURVE FOR A SPINDLE DYNAMOMETER

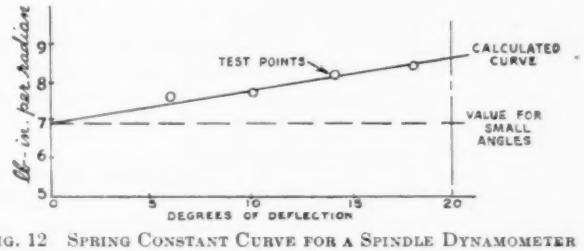


FIG. 12 SPRING CONSTANT CURVE FOR A SPINDLE DYNAMOMETER

The stress as calculated from the formula

$$\sigma = \frac{C\theta}{l}\left[E + 93\left(\frac{\theta\phi^{1.4}}{C}\right)\right]$$

$$= \frac{(0.005 \times 20)}{(57.3 \times 1.375)}\left[30{,}000{,}000 + 93\left(\frac{20}{57.3}\right)\left(\frac{90^{1.4}}{0.005}\right)\right]$$

$$= 42{,}500 \text{ psi}$$

If a concentration factor of 2 is assumed at the point of clamping, the stress becomes about 85,000 psi which may not be excessive for a good grade of spring steel.

Although the motion of the initial pivot point was not important in this case, it is interesting to consider it. Roughly, from Fig. 6 for a 90-deg pivot, the displacement for 20 deg is 1.24 for one inch of length or

$$\frac{(1.375 \times 1.24)}{100}$$

$$= 0.017 \text{ in. of travel at 20 deg}$$

From the formula

$$y = 0.04133X - 0.001225X^2 + 0.001267X^3 - 0.00000075X^4$$

$$= (0.04133 \times 20 - 0.001225 \times 400 + 0.0001267)$$

$$(8000 - 0.00000075 \times 160{,}000)$$

$$= 1.2302$$

$$\text{Displacement} = \frac{(1.375 \times 1.23)}{100}$$

$$= 0.0169 \text{ in. of travel at 20 deg}$$

6 *Notes on the Design of the Cross-Spring Pivot*

Briefly, the following points should be considered in designing two-spring pivots:

(*a*) If possible, the springs should be crossed at their midpoints[3] as this reduces the stress due to sharper bending.

(*b*) A 90-deg intersection angle should generally be used because it produces a greater rigidity of the pivot as a whole. If it is

[3] Other tests were made on springs not intersecting at their midpoints as well as springs initially curved. Pivots with more than two springs were also tested.

necessary to reduce the pivot motion, an intersection angle as low as 30 deg may be resorted to.

(*c*) As great a length of spring as is consistent with lateral stability and pivot motion should be used to lower the stress due to bending. Thin wide springs also lower the stress but are more apt to buckle.

(*d*) When used as a pivot for a heavily loaded lever system, the springs should be placed so that one of the springs is in direct tension.

(*e*) Displacement of the initial pivot, change of center of rotation, and increase in spring constant can frequently be neglected for deflection angles at high as 15 deg.

(*f*) In a lever system, the short arm should be kept at least equal to the spring length in order that its change may not be appreciable. The change in magnification ratio is less for a large spring intersection angle and is also less for a lever system where the fulcrum is at the end of the lever rather than between the loading points.

(*g*) The amount of load which may be supported in a direction perpendicular to bending is not easily determined. In his book "Theory of Elastic Stability" Timoshenko offers formulas for the calculation of critical loads in regard to lateral buckling for cantilever beams. These formulas may be used, but they are definitely on the safe side as the springs in the pivot exert restraining forces on each other which tend to prevent lateral buckling. This restraining action is increased by a large deflection angle, hence, greater stability.

Conclusion

Except in the case of very accurate instrumentation, the cross-spring pivot may sometimes be used for deflection angles as high as 45 deg. In general, the initial pivot point will be displaced only a few hundredths of an inch and the resulting change in lever arm ratio will rarely exceed 5 per cent. Bending stresses appear to be moderate and although the spring constant tends to increase quite rapidly, this tendency may usually be taken into account in design.

Acknowledgment

The author is indebted to Mr. R. E. Peterson and Mr. F. C. Rushing of the Westinghouse Research Laboratories for their advice and assistance as well as to the University of Pittsburgh for which the work was originally done as a requirement for a Master of Science Degree.

BIBLIOGRAPHY

1 "Federgelenke im Messgerätebau," by H. Stabe, *Zeitschrift, des Vereines deutscher Ingenieur*, vol. 83, 1939, pp. 1189–1196.

2 "Flexure Pivots to Replace Knife-Edges and Ball Bearings," by F. S. Eastman, University of Washington Engineering Experiment Station, Bulletin No. 86, 1935.

3 "Design of Flexure Pivots," by F. S. Eastman, *Journal of the Aeronautical Sciences*, 1937, pp. 16–21.

4 "Mechanical Testing," by R. G. Batson and J. H. Hyde, New York, N. Y., E. P. Dutton and Co., 1922–1923, vol. 1, p. 64, vol. 2, p. 135.

Discussion

A Photoelastic Study of Bolt and Nut Fastenings[1]

G. E. Campbell.[2] In this paper is shown a type of nut which gives a 30 per cent increase in strength of the fastening over the conventional nut. An increase of 30 per cent in strength of a machine part is certainly an accomplishment. The paper also outlines clearly an excellent method for analyzing other types of nuts and bolts which may be developed later, or which may have already been developed and not yet subjected to the tests outlined.

The tapered nut described, although proved stronger than the regular nut, presents machining difficulties which may be hard to control in production and which, if not controlled, may lessen its advantage.

A construction for a nut of tapered-lip design has been illustrated in a report[3] by involving the introduction of a re-entrant fillet into the working face of the nut. This construction not only provides a self-contained support for the nut but simplifies its use.

It would be interesting to learn what advantages would be derived by using a bolt and nut of differential pitch as suggested by the author. From experience with this type of nut, the writer is inclined to believe that, if the pitch of threads in the nut (measured parallel with center of the bolt) were slightly greater than the pitch of threads on the bolt, a distribution of stress would be accomplished that would be beneficial to the fastening. A special straight thread tap would be the only special equipment required, and this tap could be used with the same advantage for tapping the holes to receive studs.

Elongating the thread pitch of the nut will require a slight reduction in area of thread in the nut. The elongated pitch should be such that, when the nut is pulled up tight, there will be full contact throughout the length of thread. However, the stress in the bolt would be more nearly uniformly distributed.

An investigation of this type nut would be interesting and might disclose advantages.

Undoubtedly bolt and nut fastenings could be greatly improved. We have at present the U. S. Standard thread for bolts and nuts which perhaps is used more in this country than any other system. Under this heading we have both coarse and fine thread standards. The standards for nuts are further divided into American Standard Regular, American Standard Heavy, and American Standard Light. All of these nuts and threads are applicable to the same diameter of bolt.

It is well known that the Whitworth Standard Thread Form is stronger than the American Standard Thread Form, and in the writer's opinion we would do well to adopt it. The number of threads per inch for each bolt size should be established on a basis commensurate with the strength of the bolt and the distinction of fine or coarse thread eliminated.

It is hoped that this subject will be further studied and some standards developed which will be of great benefit to the industry.

Sabin Crocker.[4] The author's reputation as a pioneer in the application of "stress-freezing" methods to the study of three-dimensional stress-distribution problems gives assurance that his description of the technique used in this investigation is a particularly valuable contribution.

Several observations in the paper have a direct bearing on the assumptions underlying the design of bolt threads. One of these observations is: "Even if the threads of the bolt and nut match with perfect evenness in the unloaded condition, as soon as load is applied, the bolt stretches while the nut is compressed so that even contact along the threads will not be possible, and the load will be transmitted chiefly at one point of contact which will be at the seat of the nut."

Most of the demands for extreme accuracy in pitch of bolt and nut threads are based on the assumption that better distribution of load along the threads will be obtained with more perfect threads. It would be of interest to know what class of fit the author attempted to secure in the bakelite bolting assembly.

A second observation of the author's which deserves attention is: "The deformation set up in the threads prevented. . . . . in most cases the unscrewing of the nuts after test."

It is apparent from the test assembly used that the deformation mentioned must have been of a permanent character. In usual pipe-flange bolting the threads of bolt and nut also are elastically deformed by the bolt load that is being maintained so that both types of thread distortion affect the ability to unscrew a nut, at least up to the point where it is unseated. The seizure of nuts on bolts subjected to high temperature is a rather common occurrence. An American War Standard on Straight Screw Threads for High-Temperature Bolting (ASA B1.4) has just been developed which provides a neutral zone or intentional clearance between mating parts. This standard will facilitate assembly of bolts and nuts and is intended also to reduce the difficulties in disassembling bolts and nuts after high-temperature service. The writer would be interested in the author's opinion as to the effect of clearance between bolt and nut threads as a means of reducing the tendency to seizure.

Evidence of permanent distortion of threads causing difficulty in removing nuts was encountered when disassembling flanged joints in The Detroit Edison Company's experimental 1100 F superheated-steam line. In some instances, the nuts could be backed off about one turn before the threads jammed, indicating that thread distortion rather than metal seizure was the cause of trouble. This seems to corroborate the author's statement regarding thread distortion as a cause of nuts freezing to bolts.

The tapered-lip nut is an interesting development, but it would seem to be limited to rather special applications, such as turbine-casing joints, valve-bonnet joints, and heater heads where the larger bolt holes required can be provided for in the design.

J. N. Goodier.[5] This study is of the greatest interest both as an investigation of possible improvements of threaded fastenings, and as a demonstration of the powers of the freezing method to deal with three-dimensional stress problems, at least those having axial symmetry.

---

[1] By M. Hetényi, published in the June, 1943, issue of the Journal of Applied Mechanics, Trans. A.S.M.E., vol. 65, p. A-93.

[2] Chief Engineer, The Wheland Company, Chattanooga, Tenn. Mem. A.S.M.E.

[3] "Prevention of Fatigue of Metals," Battelle Memorial Institute, John Wiley & Sons, Inc., New York, N. Y., 1941, p. 143.

[4] Senior Engineer, Engineering Division, The Detroit Edison Company, Detroit, Mich. Mem. A.S.M.E.

[5] Professor of Mechanics, Cornell University, Ithaca, N. Y. Mem. A.S.M.E.

The device of the tapered thread, which seems to be a good one, raises the question of how the model stress will correspond to that of the real nut and bolt. The author comes to the conclusion that the taper must be altered on account of the different elasticity of the model material.

This is but one aspect of the whole question of similarity, which may be examined by means of dimensional analysis. If we consider the solution of the general problem of the behavior of the threaded fastening, whatever its geometrical form, material, and load, we should be concerned with a set of lengths a, b, c, etc., specifying the linear dimensions, and a dimensionless ratio, α, specifying the taper (or equally well a fractional pitch difference), the elastic constants E and ν (Young's modulus and Poisson's ratio), a coefficient of friction μ, and the load P. Given these, we should be able to calculate, if we had adequate analytical resources, the extent of thread in contact, the stress distribution, and any other determinate feature. Consider for instance the stress σ, of a given type, at a given point, x, y, z. There is one relation, i.e., the required formula, between the quantities

$$\sigma, a, b, c \ldots, \alpha, E, \nu, \mu, P, x, y, z$$

From the requirement that the same stress must be found no matter what system of units is used, dimensional analysis[6] shows that the relation must be one between dimensionless arguments, as in

$$\frac{\sigma}{E} = f\left(\frac{b}{a}, \frac{c}{a}, \ldots \frac{x}{a}, \frac{y}{a}, z, \alpha, \nu, \mu, \frac{P}{Ea^2}\right) \quad \ldots\ldots [1]$$

Then if each argument on the right is made the same in the model as it is in the prototype, the quantity σ/E must be the same for both. Making the length ratios b/a, c/a the same simply means geometrical similarity, but also α must be the same. The Poisson's ratio ν and the friction μ must be the same, and we must also make

$$\frac{P_m}{E_m a_m^2} = \frac{P_p}{E_p a_p^2} \quad \ldots\ldots [2]$$

where m refers to the model, p to the prototype. We shall then have

$$\frac{\sigma_m}{E_m} = \frac{\sigma_p}{E_p} \quad \ldots\ldots [3]$$

that is, the stress distribution will be the same, but stresses at corresponding points are in the ratio of the Young's moduli.

The condition, Equation [2], means that we can only have this similarity if the relation between stress and load is not linear (it would seem that it cannot be linear if there is tapering, or pitch difference, which results in more threads being in contact at higher loads), provided the model load is chosen from Equation [2], which may be interpreted as equality of average strains.

The values of average strain given in the paper are 0.00133 for steel (at 40,000 psi), and 0.0400 for the bakelite model (at 40 psi). The condition of Equation [2] was therefore not satisfied. Also of course the taper, α, was not made the same for model and prototype. If then the view as outlined of the similarity conditions is sound, the model tests cannot be interpreted as in the paper. In fact the requirement of equal strains Equation [2] would seem to offer an obstacle to the use of the freezing method with its necessarily rather large strains.

In the conventional, nontapered threads, if perfect pitch equality and perfect elasticity can be assumed, the stress must be proportional to P, and, therefore, the group P/Ea^2 in Equation [1] must appear as a factor. Then

$$\frac{\sigma a^2}{P} = \phi\left(\frac{b}{a}, \frac{c}{a} \ldots \frac{x}{a}, \frac{y}{a}, \frac{z}{a}, \nu, \mu\right)$$

and geometrical similarity, with equality of ν and μ, will be all that is necessary as similarity requirements. The stress distribution will be independent of the Young's modulus and the same at all loads.

S. Timoshenko.[7] The author must be congratulated upon a fine piece of work illustrating the application of three-dimensional photoelastic analysis to the solution of important problems on stress distribution in threaded connections. Since this work is one of the first practical applications of three-dimensional photoelasticity, it seems very desirable to have more detailed information regarding the accuracy with which stresses can be measured in such cases. It is also desirable to have some discussion of the fact that in three-dimensional problems the stress distribution depends upon the elastic constants of the material.

The photoelastic study can give us the factor of stress concentration at the bottom of the thread. How this stress concentration affects the strength of a threaded connection depends upon physical properties of the material, and a proper answer can be obtained only by running fatigue tests. Considerable work of this kind has been carried out abroad.[8] These experiments showed that the strength of a threaded connection can be considerably improved by using for the nut a material with a small modulus of elasticity. In the case of a bolt and nut of steel, having ultimate = 80,000 psi and yield point = 55,000 psi, the fatigue tests in a prestressed condition gave for the endurance limit the value 13,500 ± 9200 psi. Replacing the steel nut by a magnesium-alloy nut (magnesium alloy, electron, ultimate = 15,500 psi, yield point = 13,500 psi), with 5 times smaller modulus of elasticity, the fatigue strength of the threaded connection was raised to the limit 17,500 ± 13,500 psi. The effect of the shape of thread on fatigue strength was only of secondary importance in those experiments. It will be interesting to have the author's photoelastic work supplemented by fatigue tests.

P. R. Vogt.[9] There are two ways in which this paper can be received. One is to emphasize the uncertainty of photoelastic results, particularly in a contact problem such as this, where the relation of the loading to the modulus of elasticity of the material and the plastic deformation is of prime importance; and thus to criticize the numerical results. The other, and in the writer's opinion a much more satisfactory attitude, is to recognize the author's work as a lucid qualitative demonstration of the unnecessarily severe stress concentrations in threaded fastenings of conventional design. His numerical results should be taken merely as guidance for further testing which we all know must be done on the actual metal parts before the problem is really solved. This paper, with its graphic illustration of stress concentration and ways by which it may be reduced, should be a powerful stimulus to get this much needed testing program under way.

Of the various methods suggested for reducing stress, the simplest one from a design and mass-production standpoint would seem to be the expedient of increasing slightly the lead or pitch

[6] "Increasing Design Tempo Through Model Analysis," by J. N. Goodier, *Machine Design*, vol. 14, Sept., 1942, pp. 62–65 and 138.

[7] Professor of Theoretical and Applied Mechanics, Stanford University, Stanford University, Calif. Fellow A.S.M.E.

[8] For example, the paper, "Beitrag zur Dauerhaltbarkeit von Schraubenverbindungen," by F. Kaufmann and W. Jaeniche. Tech. Mitt. Krupp Forschungsberichte, vol. 3, 1940, pp. 147–159; also V.D.I., vol. 85, 1941, pp. 504-505.

[9] Project Engineer, Research, Chrysler Corporation, Detroit, Mich. Jun. A.S.M.E.

of the nut. Since this method was not very clearly explained in the paper, a few remarks on it may be in order. What is contemplated is simply to mesh, for example, a bolt having 20 threads per in. with a nut having 20 threads per 1.002 in., or conversely, a 20-thread per in. nut with a bolt having 20 threads in 0.998 in. Such components could be made by standard production methods and would, of course, screw together without any trouble over the entire length of the bolt provided a small amount of backlash were present.

The action in relieving the first threads of load is identical to the action of the tapered nut; engagement of threads progresses from the end of the bolt inward as the load is applied. This is accomplished in both cases by having the mating faces of the threads in the unloaded condition progressively further separated as one moves inward from the end of the bolt. With the tapered-nut thread, the separation after 1 in. of length is $^1/_2 \times$ diametral taper $\times \tan \alpha$ (where α = angle between the working face of the thread and a plane perpendicular to the axis of the bolt). For an American Standard thread this angle is 30 deg. Thus an equivalent action to the author's suggested taper of 0.003 in. per in. could be obtained by a pitch difference of $^1/_2 \times 0.003 \times \tan 30$ deg = 0.00087 in. (about 0.001 in. per in.).

There may be some objection to controlling the taper or pitch to such close limits. However, this work will be of greatest importance to high-stress precision fastenings, such as aircraft-engine connecting-rod bolts, the pitch of which is customarily controlled to closer than $\pm$ 0.0005 in. This also brings out the point that if pitch is not carefully controlled there may be a pitch differential in the wrong direction. Such a condition would result in a dangerous increase in stress; so that an exaggeration of nominal pitch differential, above the small values previously suggested, may be justified in order to prevent manufacturing variation from ever creating a differential in the wrong direction. Furthermore, an increased differential (or taper) will throw the load toward the outer end of the nut; and then if the bolt should fail at this outer end, there will still be inner threads (possibly one half the length of the nut) left in engagement to carry the load until a repair is made.

As clearly shown by the photoelastic studies the standard fastening concentrates the load on only a few threads, so that even a very exaggerated differential could hardly create a worse concentration. Bearing this in mind, we may suggest for practical consideration a nominal pitch differential of about twice the theoretically correct value (possibly 0.002 in. per in.).

E. F. Miller.[10] The author's investigation of bolt-fastening stresses by the three-dimensional photoelastic technique was undertaken to substantiate the validity of certain changes in practice on alloy-steel bolting for high-temperature steam-turbine joints and was expanded to evaluate the new designs by comparison with certain ideal arrangements.

The absolute values of the results may be affected somewhat by the thread shape employed since the Whitworth thread section is somewhat thinner at the root and thicker at the apex than the U. S. Standard. This would alter the relative flexibility; however, the comparative values between different arrangements may not necessarily be affected by the choice of Whitworth threads.

The correction made to compensate for the bakelite modulus of elasticity on the tapered thread allows only about 0.035 in. engagement of the bottom threads which again may affect the elastic distortion of the assembly as compared with an actual bolting member.

A properly designed tapered thread appears to offer a suitable solution to the problem of stress distribution and, from the test results, it appears that a larger taper would offer yet greater improvement for highly stressed bolts. The use of a different thread pitch for the bolt and the nut would not result in an improved structure since the radial clearance would need to be increased to permit free assembly of the varipitched parts.

The tapered lip is ideal for special applications where bolts are widely enough spaced to accomodate the larger nut diameters which are required to maintain adequate bearing area. The required increase in bolt pitch would tend to offset the advantage of the tapered lip in many pressure-joint applications.

The writer's company has found that properly proportioned nuts tend to expand in diameter due to the radial component of the thread load angle. This produces the same effect as taper threading. Tapered threads are therefore employed only on the ends of large studs which are driven into relatively massive flanges where radial deformation of the female threaded part is restricted. Spherical washers are employed under the nuts used on these tapered-end studs to assure an axial loading in order to eliminate secondary bending stresses in the threads.

Author's Closure

An increase of the pitch of the threads in the nut with respect to that in the bolt, as suggested by Mr. Campbell, is known to lead to a better distribution of stress and was perhaps the first means used in practice to improve the strength of threaded connections. As was pointed out in the paper, however, one can always find a certain tapering of the threads in the nut which is equivalent to a given differential pitch as far as stress distribution is concerned. Which one of these to choose is mainly a production problem. The proposition of Mr. Vogt to adopt a 0.002-in. per in. pitch differential appears to be a good practical solution.

Seizure of nuts on bolts due to permanent deformation of the threads, as described by Mr. Crocker, is likely to take place not because of the magnitude but of the unevenness of the deformation, the deflection of the first engaged thread being much larger than that of the rest. Thus the rational method of preventing seizure of this type would be not through the provision of an excessive clearance, but through the application of an improved nut design which, with a more even distribution of the load among the threads, would also increase the strength of the connection. With regard to Mr. Crocker's question concerning the accuracy of fit in the bakelite models, we have to point out that, though the machining error in making the models was probably of the order of 0.001 in. per in., because of the low modulus of elasticity of the material, this accuracy would be about equivalent to a practically unattainable 0.00003-in. per in. precision of fit in steel prototypes of the fastenings.

The author agrees completely with the conclusions of Professor Goodier's dimensional analysis, according to which a correct test of a nut with tapered threads would require a geometrical similarity between model and prototype and, at the same time, an equality of strains in the two cases. This second condition, however, was impossible to satisfy in the tests; it would have required the application of an average stress of only 1.33 psi in the model, and this would have produced hardly any optical effect in polarized light. This being the case, the next best thing appeared to be, as has been done in the tests reported in this paper, to have the tapers in the same ratio as that defined by the average strain values. The resulting model with an exaggerated tapering of the threads can be expected to give, of course, only an approximate solution of the original problem. The most obvious source of error due to the abandonment of geometrical similarity is probably the fact, pointed out by Mr. Miller, that due to the large tapering in the model the points of

[10] Section Engineer, Mechanical Section, Westinghouse Electric & Manufacturing Company, South Philadelphia, Pa. Mem. A.S.M.E.

engagement between threads shifted outward by almost one third of the depth of the threads. A test is conceivable in which both of Professor Goodier's conditions would be fulfilled, but in that case the minuteness of the resulting relative retardations would necessitate point to point measurements by a Babinet compensator or a similar instrument and no record of the stress distribution could be obtained by photographic means.

As has been mentioned by Professor Timoshenko, the actual increase in the strength of threaded fastenings, through the application of the improved nut designs of the paper, can be established only by tests with steel specimens. In this connection it is of interest to note that fatigue tests of nuts with tapered threads and tapered lips of about the same proportions as those in the paper were made by H. Wiegand[11] who found that the application of these two designs resulted in a 20 and 30 per cent increase of strength respectively, which figures are about the same as the photoelastic results of the paper. Wiegand has also investigated the effect of using materials of lower modulus of elasticity in the nut and, similarly to the tests quoted by Professor Timoshenko, found that the application of a cast-iron nut, for instance, increased the strength of the fastening by 40 per cent. Thus we find that the strength of the present conventional nut fastening can be increased by about 40 per cent whether it be through a change in the design of the nut or by the application of a softer material in that part of the threaded connection.

Temperature Relations in Journal-Bearing Systems[1]

G. P. SUTTON.[2] This paper is of interest, especially the fact that the time lag to reach equilibrium temperature is surprisingly long. The temperature calculated according to the authors' method is higher than the measured temperature. From the diagram, it seems that the thermocouples did not extend into the oil film directly, which may account for the difference in the measured and the calculated lubricant temperature.

How would the film temperature be affected by different surface finishes and different bearing materials? Would this temperature be affected by convection around the bearing?

L. M. TICHVINSKY.[3] Boswall (1)[4] has shown that in the calculation of bearing performance the average temperature of the oil film may be used with a fair degree of accuracy.

The lubricating-oil temperatures at the inlet and outlet of a bearing are easily measured by thermometers. The temperatures of the bearing metal in the proximity of the rubbing surfaces are also conveniently measured by means of thermocouples. During such experimentation, as many as 10 to 12 temperatures may be obtained which are used for the evaluation of the average oil-film temperature. However, it will not be at all surprising if several experimenters would arrive, on the basis of the same 10 to 12 temperatures, at different values of the average oil-film temperature. For this reason the investigation conducted by the authors is timely, because it represents an attempt to evaluate accurately the average oil-film temperature. It is hoped that the method, which consists of inferring the temperature from friction-loss measurement, can be made applicable to such loaded bearings where the Harrison formula should accurately predict the frictional behavior of a bearing.

A method (2), simpler than the one proposed by Kingsbury (3), may be mentioned here. This approximate method may be used for the evaluation of the average oil-film temperature of a loaded bearing by calculating the heat flow through the film, h, which is assumed to be of a uniform average thickness, as in a guide or high-speed bearing. The same quantity of heat Q flows from the oil film to the bearing shell and then from the latter to the ambient air by convection and radiation. The quantity of heat Q which flows from the shell can be easily calculated from the temperatures of the shell and ambient air, the dimensions of the bearings, and known heat-transfer data (4, 5). In most bearings the flow of heat through the shaft is negligible (4), and the shaft temperature is usually taken as equal to that of the oil film. For such cases, the temperature distribution through the oil-film thickness may be calculated from the known equation of the steady flow of heat through a body, such as the oil film wherein heat is being uniformly generated. This temperature distribution is parabolic, and the average value of the temperature rise, t, of the oil film above the bearing shell is

$$t = Qh/3K = 80\,Qh$$

for the majority of mineral lubricating oils [$K = 0.0042$ w per sq in. per deg C per in. (5)]. This method of calculation will still hold when heat is carried away by means of circulating oil since it applies only to the flow of heat through the bearing shell. Such a method has been successfully applied for the evaluation of the average temperature rise of the oil film above the measured temperature of a loaded bearing shell (2).

BIBLIOGRAPHY

1 "The Theory of Film Lubrication," by R. O. Boswall, Longmans, Green and Company, London, England, and New York, N. Y., 1928.

2 "Journal Bearing Performance," by R. Baudry and L. M. Tichvinsky, JOURNAL OF APPLIED MECHANICS, Trans. A.S.M.E., vol. 57, 1935, p. A-121.

3 "Heat Effects in Lubricating Oils," by A. Kingsbury, *Mechanical Engineering*, vol. 55, 1933, pp. 685–688.

4 "Performance of Oil-Ring Bearing," by G. B. Karelitz, Trans. A.S.M.E., vol. 52, 1930, paper APM-52-15, p. 161.

5 "The Basic Laws and Data of Heat Transmission," by W. J. King, *Mechanical Engineering*, vol. 55, 1932, pp. 190, 275, 347, 410, 492, and 560.

AUTHOR'S CLOSURE

Mr. Sutton's comment that the times observed by the authors to reach equilibrium temperatures were surprisingly long is probably due to the fact that in his experiments the speeds may have been much greater, thus rapidly accelerating the rate of heat generation without corresponding increases in the equilibrium temperatures. For the lower range of speeds used by the authors, the rate of heat generation is relatively low. In fact, it may be shown[5] that at least the asymptotic exponential coefficient determining the rate of approach to equilibrium, and which corresponds to the slopes of the linear segments of Figs. 6 to 9, is given by

$$\alpha = \text{const.} \left[1.35N^{0.52} + \frac{\beta N^2}{T_\infty} \right]$$

[11] "Über die Dauerfestigkeit von Schraubenwerkstoffen und Schraubenverbindungen," by H. Wiegand, thesis submitted to the Technische Hochschule zu Darmstadt, 1933. See also "Photoelastic Analysis Practically Applied to Design Problems," by O. J. Horger, *Journal of Applied Physics*, 1938, pp. 457–465, and "Effect of Screw Threads on Fatigue," by S. M. Arnold, MECHANICAL ENGINEERING, vol. 65, 1943, pp. 497–505.

[1] By M. Muskat and F. Morgan, published in the September, 1943, issue of the JOURNAL OF APPLIED MECHANICS, Trans. A.S.M.E., vol. 65, p. A-131.

[2] Instructor, Department of Mechanical Engineering, California Institute of Technology, Pasadena, Calif.

[3] Senior Mechanical Engineer, U. S. Naval Engineering Experiment Station, Annapolis, Md.

[4] Numbers in parentheses refer to the Bibliography at the end of this discussion.

[5] cf. *Journal of Applied Physics*, vol. 14, 1943, pp. 234–244.

where β is the slope of the viscosity-temperature curve as of Fig. 2, and T_∞ is the equilibrium temperature. Thus the asymptotic rate of approach increases with the speed and may even approach a variation with the square of the journal speed, N.

It is true, as Mr. Sutton suggests, that the thermocouples were set flush with the bearing surface. This was done to avoid any disturbance in the lubricant flow or local heat generation. As to the reason for the film temperature being higher than the bearing temperature, it is believed that the surface roughness plays no significant role. The surfaces used were actually quite smooth, and the microscopic roughness was extremely small as compared to the clearance. The main reason for the observed lower bearing temperature is felt to lie in the low heat losses from the journal, as also mentioned by Mr. Tichvinsky, and as originally pointed out by Karelitz. Although no data are yet available, it is believed that the journal temperatures were even higher than the film temperature, and that a large part of the heat generated at the journal surface was taken up by the journal until equilibrium was reached. Experiments are on the way to test this point.

Mr. Tichvinsky's remarks are well taken. In fact, it was one of the main conclusions of the paper that the bearing surface temperatures may be equated to the oil-film temperature to a fair degree of approximation, unless special means are provided for controlling the bearing or journal temperatures. In order to explore the possibilities of the method the simpler case was tried first wherein the bearing was loaded lightly and the Petroff formula was used for predicting the friction behavior. We see no reason, however, why the same method could not be used in the case of loaded bearings, applying Harrison's or other equivalent formulas pertaining to nonconcentric journal bearing systems.

Photoelastic Separation of Principal Stresses by Oblique Incidence[1]

M. M. Frocht.[2] The author is to be commended on his ingenious and interesting method for determining the principal stresses from photoelastic stress patterns.

The published results have been recalculated and were found



Fig. 1 Stress Pattern of a Bakelite Ring Subjected to Concentrated Diametral Loads With Light Rays Normal to Face of Ring

(P = 54 lb, approximately; D = 1.02 in.; $2r$ = 0.51 in.; t = 0.110 in.; F = 782 psi tension or compression.)

[1] By D. C. Drucker, published in the September, 1943, issue of the Journal of Applied Mechanics, Trans. A.S.M.E., vol. 65, p. A-156.

[2] Associate Professor of Mechanics in charge of Photoelastic Laboratory, Carnegie Institute of Technology, Pittsburgh, Pa. Mem. A.S.M.E.

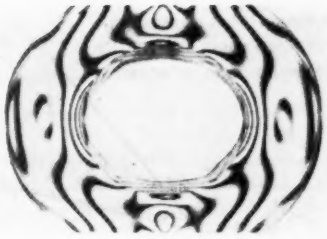


Fig. 2(*a*)



Fig. (2*b*)

Fig. 2 Stress Patterns of the Same Bakelite Ring, Shown in Fig. 1, Except That It Has Been Rotated About Its Horizontal Axis Until the Angle Between the Normal and the Light Ray Is 30 Deg for (*a*) and 45 Deg for (*b*)

(Photographs were taken with model in Halowax oil.)

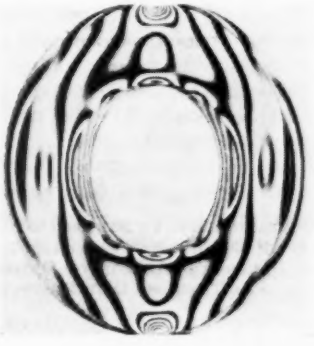


Fig. 3(*a*)

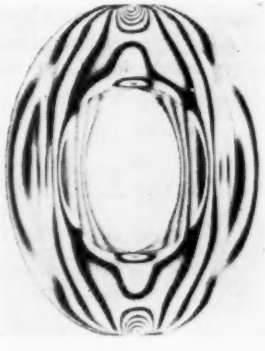


Fig. 3(*b*)

Fig. 3 Stress Patterns of the Same Bakelite Ring, Shown in Fig. 1, Except That It Has Been Rotated About Its Vertical Axis Until the Angle Between the Normal and the Light Ray Is 30 Deg for (*a*) and 45 Deg for (*b*)

to be in substantial agreement with those given by the author.

The proposed method was then applied to another problem somewhat more difficult than the simple illustration presented in the paper. For this purpose a circular ring, 1.02 in. OD, 0.51 in. ID, and 0.11 in. thickness, was subjected to concentrated diametral loads. The normal stress pattern is shown in Fig. 1 of

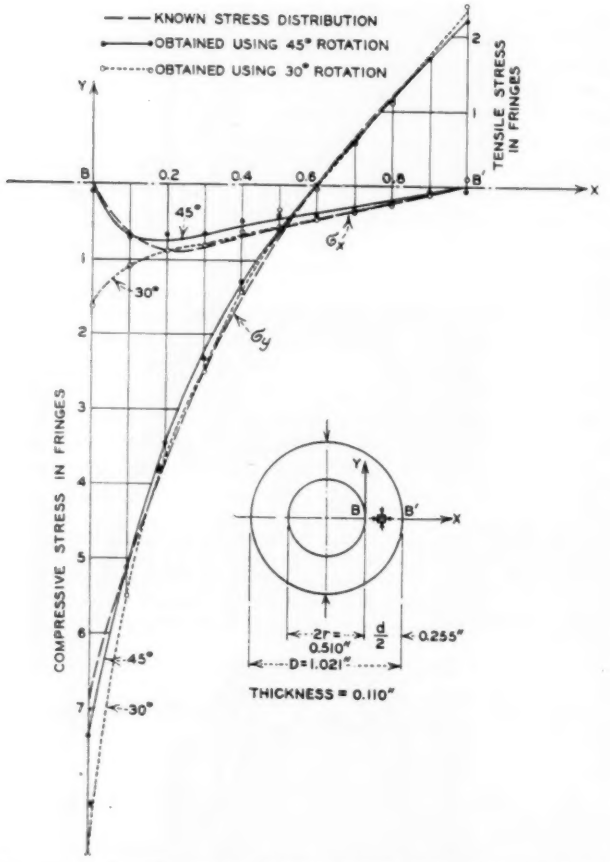


FIG. 4 CURVES COMPARING KNOWN STRESS DISTRIBUTION ALONG HORIZONTAL AXIS OF RING SHOWN IN FIGS. 1 AND 2, AND DISTRIBUTION OBTAINED BY DRUCKER'S METHOD OF OBLIQUE INCIDENCE, USING ANGLES OF 30 AND 45 DEG, RESPECTIVELY

this discussion. Fig. 2 shows the stress patterns obtained after a rotation of the model of 30 and 45 deg, respectively, about the horizontal axis, and Fig. 3 shows a similar stress pattern for a rotation about the vertical axis. The writer's calculations, based on these photographs and the equations given by the author, yielded quite satisfactory results for the horizontal section, especially for a rotation of 45 deg. The stress distribution along the horizontal axial section of the ring is shown in Fig. 4. Along the vertical section of symmetry through the points of application of the loads, however, the results differed considerably from the known stress distribution for that section.

It should be pointed out that these verifications were of a preliminary nature. The model used was rather small and also was relatively thick for its other dimensions. The curves of $(p-q)$ were taken from ordinary enlargements with no greater precautions or care than those used when other photoelastic methods are employed, rather than plotting the curves directly from the negatives using both light and dark backgrounds, as the author recommends. It became apparent after some work had been done that the values of $(p-q)$ must be known with great accuracy since the equations involve small differences in the two stress patterns.

Except for sections of symmetry, the proposed method belongs to the "point-by-point" exploration methods. In addition, the directions of p and q at each point must be known before the equations can be applied. The main merit of the proposed method lies in its ability to determine the principal stresses of an isolated point.

The proposed equations are special cases of general equations which are free from the basic objections inherent in the present procedure, i.e., the "point-by-point" character, and the necessity for knowing the directions of the principal stresses and effecting the rotation about these as axes.

Such equations have also been developed and used by the discusser for some time. Although the probable errors are very large the general equations may yield useful results.

AUTHOR'S CLOSURE

The work of Professor Frocht is, as usual, unusually good. It is extremely gratifying to see that the method of oblique incidence yields accurate results even for a very small principal stress. Inspection of Professor Frocht's Fig. 4 shows that of the 44 plotted points only two are off by appreciable amounts.

The author would like to again point out the need for estimating in advance the probable accuracy to be obtained by any experimental method. General equations mentioned by Professor Frocht were, of course, considered by the author. However, they were not presented mainly because rotation about an axis which is not a principal axis requires too close a knowledge of the principal directions.

Book Reviews

Dictionary of Science and Technology

DICTIONARY OF SCIENCE AND TECHNOLOGY in English-French-German-Spanish. By Maxim Newmark, Ph.D. Philosophical Library, Inc., New York, N. Y., 1943. Cloth, 6 × 9 in., viii and 386 pp., $6.

REVIEWED BY M. HETÉNYI[1]

THIS dictionary comprises the French, German, and Spanish equivalents of some 10,000 English terms currently used in technical literature. The corresponding words in these languages are entered first under English headings which are numbered and referred to in separate indexes of French, German, and Spanish. In this manner the system permits a two-way use of any of these languages with the English.

Since the work endeavors to deal with all technical fields and in four languages in less than 400 pages, it is naturally not as comprehensive as some of the recognized scientific dictionaries which are often limited to a specialized field. Its authoritativeness may also be questioned at places as there are words, listed as equivalents, which could not be used as such with any degree of precision.

The book has, on the other hand, some features which give an advantage above older publications of this type. Much of it deals with the newer technical fields which brought in a short time a wealth of specific terms into circulation; over ten per cent of its content is, for instance, on aeronautics and there are entries in the fields of radio, television, and technical warfare which are not likely to be found in other dictionaries. It also makes a welcome distinction between American and British usage of terms in cases where these grossly differ. Because of these features the book may be recommended for consultation to anyone engaged in reading foreign technical literature.

Experimental Electronics

EXPERIMENTAL ELECTRONICS. By Ralph H. Müller, R. L. Garman, M. E. Droz. Prentice-Hall, Inc., New York, N. Y., 1943. Cloth, 6 × 9 in., xv and 334 pp., $4.75.

REVIEWED BY J. A. HIPPLE[2]

NOT many years ago a working knowledge of vacuum-tube circuits was possessed generally only by electrical engineers and experimental physicists. However, the vast possibilities of electronic circuits in the field of measurement and control as evidenced in the literature of the last decade has made this knowledge an essential tool in the equipment of the well-trained technical man in many fields. This book, written by three chemists, is a striking illustration of this. Its purpose and scope is stated clearly in the first paragraph of the preface:

"This book has been written to supply definite practical information on the characteristics and noncommunication applications of electron tubes. It is an outgrowth of the authors' experience in courses given for several years at New York University to students and industrial and academic research workers in chemistry, biology, and engineering. In these courses, students of widely different backgrounds and interests have found competence in handling electronic circuits most stimulating and helpful, revealing to them many applications in their own fields."

The authors have done an excellent job in selecting and organizing the material presented in this book as the basis of such a course. The student gets a veritable baptism by fire; after the completion of these seventy experiments, no longer will he stand in awe of a vacuum tube. In the discussions before each experiment no attempt has been made to be profound, but they are usually quite adequate to provide the student with an intelligent approach to the experiment. In addition sufficient references for more detailed study are provided. Sometimes one feels that the discussion could be carried a bit further. For instance, since several pages are devoted to the low-grid-current electrometer tubes, it would seem desirable to describe the method of measuring this grid current.

The equipment required in each experiment is itemized. The values of the components in the circuit drawings are given in the figure captions; this is desirable in a book of this type. There is some annoying inconsistency, however, in sometimes omitting the tube type, making it necessary to refer to the list of materials required for the experiment. In one figure (Fig. 7–10) it is necessary to notice in the bill of materials that there is only one filament battery, and hence a filament that at first glance appears to be floating is actually connected to this battery.

The experiments cover a wide range. After the completion of the first half of the book, the student should be familiar with the operation of the various electronic tubes including photoelectric cells and gaseous tubes, as well as power supplies (including regulated supplies). The second half of the book can be considered an application of the principles learned previously to measurement and control circuits of interest to scientists. Indeed, the many circuits collected here will make this section a handy reference for the general scientific worker. The general subjects treated are d-c and a-c voltmeters, phototube applications, untuned amplifiers, oscillators, and the cathode-ray tube. The great number of circuits included have evidently been chosen very carefully to have the widest applicability in various technical fields.

Treatment of Experimental Data

TREATMENT OF EXPERIMENTAL DATA. By Archie G. Worthing and Joseph Geffner. John Wiley and Sons, Inc., New York, N. Y., 1943. Cloth, 6 × 9 in., ix and 342 pp., illus., tables, diagrams, $4.50.

REVIEWED BY JOSEPH KAYE[3]

THIS book presents the material given in a course for graduate students on the treatment of experimental data. A large part of it will be of aid to students and engineers engaged in work involving measurements of any sort. As a reference book it should be useful to engineers in general. The material is presented in a clear lucid style. The many diagrams and numerical examples, which were evidently selected with great care, enhance the value of the book.

[1] Mechanics Department, Westinghouse Research Laboratories, East Pittsburgh, Pa.

[2] Electro-Physics Department, Westinghouse Research Laboratories, East Pittsburgh, Pa.

[3] Instructor in Mechanical Engineering, Massachusetts Institute of Technology, Cambridge, Massachusetts. Mem. A.S.M.E.

The scope of the book is quite large, particularly from the standpoint of the beginner in the subject. Starting with the simple elementary methods of presenting data in tables, smoothing of tables, interpolation, etc., the authors proceed logically to the representation of data by graphs, by equations, and then to tabular and graphical differentiation and integration. The method of representing a function by Fourier series is discussed next and includes a description of various types of analyzers. The normal frequency distribution is clarified for the beginner. Considerable attention is given to the computation of precision indexes for measurements of equal and unequal weights. The method of least squares is made comprehensible; in addition, short cuts are given for avoiding lengthy numerical work and the pitfalls are indicated clearly. The authors present the various tests used by statisticians in the correlation of data; these tests though relatively new in engineering are quite important. The text ends with a discussion of the analysis of nonharmonic periodic functions. The appendix has several tables and includes a brief discussion of determinants. A useful index is provided.

At the bottom of page 95 it is stated erroneously that Simpson's three-eighths rule will usually give better results than Simpson's one-third rule. On page 155 of Scarborough—it is regrettable that the bibliography does not include the excellent work of J. B. Scarborough, "Numerical Mathematical Analysis," the Johns Hopkins Press, Baltimore, Md., 1930—it is shown analytically that the inherent error in the former is always greater than that in the latter. This can be verified by numerical examples. Hence Simpson's three-eighths rule should never be used in numerical calculations.

In the discussion of least squares it should have been noted that the solution of the normal equations may occasionally lead to erroneous values of the constants of the desired equations. The error arises from the disappearance of several significant figures in the course of the solution. A sufficient number of significant figures can be retained in most cases if calculations are made with seven-place logarithms or an eight-bank calculating machine.

Lubrication

LUBRICATION. By Arthur Edwin Norton, Late Gordon McKay Professor of Applied Mechanics, Harvard University. Edited by J. R. Munger. First edition. McGraw-Hill Book Company, Inc., 1942. Cloth, 6 × 9 in., xi and 244 pp., 115 illustrations, $3.

REVIEWED BY BURT L. NEWKIRK[4]

THERE is perhaps no field that includes so many highly specialized divisions as that of lubrication. The book "Lubrication" by the late Prof. Arthur Edwin Norton of Harvard University (edited by J. R. Munger, his assistant of 1939–1940) covers this field rather inclusively in textbook style. It is an outgrowth of the courses formerly given by Professor Norton.

The introductory chapter is short, but comprehensive, calculated to arouse the interest as well as give a general orientation. Students will do well to reread this chapter at intervals during a course on lubrication.

The next three chapters deal with the mechanics of fluids as it applies to bearing performance, the phenomena of thin film lubrication and oiliness, and the chemical and physical properties of lubricating oils and greases. This whole field is treated concisely but with many important details in 55 pages.

The main portion of the book, chapters five to ten, inclusive, deals with theories of bearing design, including thrust (slider) and journal bearings, and calculation of the various factors of performance.

The first two chapters of this section deal with slider bearings, first with constant and then variable viscosity and no side leakage. The next two chapters cover full and partial journal bearings, including fitted bearings, without side leakage, and the last two chapters of the section take up effects of side leakage on the theory of the slider bearing and the journal bearing, respectively. This section contains charts, numerical tables, and worked-out numerical examples.

The last three chapters deal broadly with practice in the field of bearings and lubrication. They may be understood without previous mastery of chapters 5 to 10. These discussions give a scholarly appraisal of various phases of practice, some of which have grown up, without sufficient comprehension of the physical basis of design. The grooving of bearing surfaces is a case in point. Design should provide for admission and distribution of the lubricant in regions of low pressure, as indicated by hydrodynamic theory, and grooves should be avoided that connect such regions with those of high pressure. The important feature of thermal equilibrium and viscosity-temperature relationships is discussed. Means for applying the lubricant, oil seals and oil cleaners, bearing materials, and other miscellaneous matters essential to successful performance are treated in this section.

The last chapter discusses the fields of application, and relative advantages of ball, roller, and needle bearings, and their lubrication.

The book closes with a table of notation, a list of 63 references, and a very short index.

There seems to be no mention of pivot bearings of electrical instruments and meters, which are interesting because, in instruments with total loads of a few grams, the unit loads are the heaviest in bearing practice, 10 to 30 tons per square inch. Some of these run without lubrication. In meters, even though the bearing contact areas are minute, and normal speeds low, moderately abnormal rotation speeds shorten the life of the bearing.

The tapered land thrust bearing designed by E. G. Gilson and reported on by Linn and Shepard in *Mechanical Engineering* is of interest also, because it was developed in view of hydrodynamic theory, but with surfaces at fixed angles, sacrificing some theoretical hydrodynamic advantages for the sake of mechanical simplicity. A thrust bearing with fixed shoes is shown in chapter one. The Gilson design is undoubtedly of more value and interest than other thrust bearings discussed in chapter 12.

The Reist thrust bearing is understood to carry the heaviest total loads in bearing practice. This design is not based primarily on hydrodynamic theory, but it is used successfully for large water-turbine generators.

The subject of instability of the fluid film, vibration resulting therefrom, and design of rotor and bearings to avoid such disturbances might also have been discussed without very great extension of the scope of the book.

The items just referred to serve further to illustrate the breadth and diversity of the lubrication field. This text should be a very acceptable basis for courses in lubrication, for which a place should be found in engineering curricula. Various phases of this field are developing on a scientific basis, in much too great variety and extent for adequate treatment as a chapter in some other course such as fluid mechanics. In his perception of the need of engineering courses in lubrication, and his development of the course represented by this book, Professor Norton has done pioneering work. It is fortunate that Mr. Munger was sufficiently familiar with the course and able to prepare it promptly for publication.

[4] Professor, Department of Aeronautical Engineering, Rensselaer Polytechnic Institute, Troy, N. Y. Mem. A.S.M.E.

The Bending of the Cylindrically Aeolotropic Plate

By G. F. CARRIER,[1] ITHACA, N. Y.

In this paper, the small-deflection theory, applicable to plates of cylindrically aeolotropic material,[2] is presented, and expressions are obtained for the moments and deflections produced by the following combinations of loading and boundary conditions: The disk clamped along its circumference and loaded by a uniform lateral pressure; the clamped disk loaded by a central concentrated force; the simply supported disk loaded by uniform edge moment; the disk with a rigid core clamped along its circumference and loaded by a central concentrated force; the ring clamped along its outer edge and loaded by a uniform shear distribution along the inner edge; the simply supported disk with an elastic isotropic core loaded by a uniform edge moment; and the disk under the loading given by $p = p_0 r \cos\theta$. The six symmetrical problems of this group were chosen for evaluation since they and their linear combinations comprise a large part of the total set of such problems. Curves are included showing, for three of the foregoing problems, the effect of the degree of anisotropy on the stresses. The practical application of solutions obtained by the following theory might lie, for example, in design problems involving circular plates which are built up of laminas of radial symmetry with different tangential and radial stiffnesses.[3] The theory could also be applied to the design of circular concrete slabs with different amounts of reinforcing steel in the radial and tangential directions.

Nomenclature

The following nomenclature is used in this paper:

r, θ, z = cylindrical co-ordinates
$e_r, e_\theta, \gamma_{r\theta}$ = normal and shearing strains
u, v, w = radial, tangential, and axial displacements
$\sigma_r, \sigma_\theta, \tau_{r\theta}$ = normal and shearing stresses
$M_r, M_\theta, M_{r\theta}, M_{\theta r}$ = couples per unit length, as defined in Fig. 1
Q_r, Q_θ = shear forces per unit length as defined in Fig. 1
p = applied lateral pressure
a_{ij} = elastic constants of aeolotropic material (referred to cylindrical co-ords)
$E\mu$ = elastic constants of isotropic material
$c = a_{11}/a_{22}$
$b = \dfrac{2(a_{11}a_{22} - a_{12}^2) - a_{12}a_{66}}{a_{22}a_{66}}$
$\nu = -a_{12}/a_{11}$
r_1, r_2 = inner and outer radii of plate
h = thickness of plate
$\epsilon = r_1/r_2$
$\alpha = \sqrt{1/c}$
$k_1 = \sqrt{\dfrac{c + 1 + 2b}{2c}}$
$D = \dfrac{h^3 a_{22}}{12(a_{11}a_{22} - a_{12})}$
$F = \dfrac{Eh^3}{12(1 - \mu^2)}$
$K = [(1 - \alpha^2\nu^2) + (1 + \alpha\nu)(1 + \mu)\alpha F/D]\,\epsilon^{-\alpha} - [(1 - \alpha^2\nu^2) - (1 - \alpha\nu)(1 + \mu)\alpha F/D]\,\epsilon^{\alpha}$

The Bending Theory

The assumptions made in developing this theory are the same as those of the isotropic theory,[4] namely: (1) The effects of

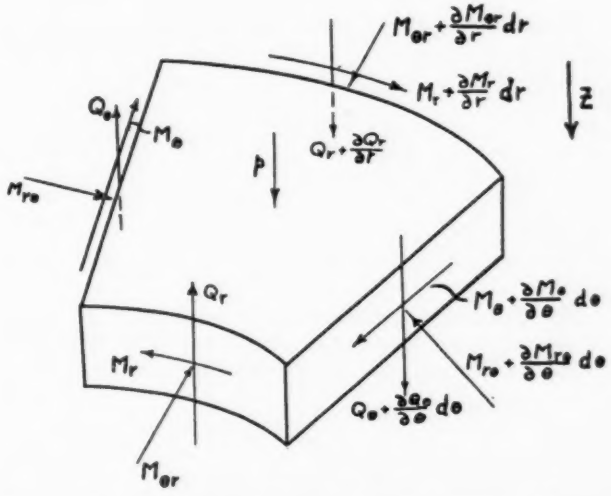


FIG. 1 SECTORIAL ELEMENT UNDER GENERAL LOADING, AS QUALIFIED BY ASSUMPTIONS (1) AND (3)
(The directions of the moment vectors are defined by the conventional "right-hand rule.")

τ_{rz}, $\tau_{\theta z}$, and σ_z on the deflection are negligible; (2) Lines which in the unloaded position are parallel to the z axis remain straight; (3) The forces per unit length defined by the integrals

$$\int_{-h/2}^{h/2} \sigma_r dz, \qquad \int_{-h/2}^{h/2} \sigma_\theta\, dz, \qquad \int_{-h/2}^{h/2} \tau_{r\theta} dz$$

vanish.

[1] Instructor in Machine Design, Cornell University. Jun. A.S.M.E.

[2] "Stress Distributions in Cylindrically Aeolotropic Plates," by G. F. Carrier, JOURNAL OF APPLIED MECHANICS, Trans. A.S.M.E., vol. 65, 1943, p. A-117.

Discussion of this paper should be addressed to the Secretary, A.S.M.E., 29 West 39th Street, New York, N. Y., and will be accepted until October 10, 1944, for publication at a later date. Discussion received after the closing date will be returned.

NOTE: Statements and opinions advanced in papers are to be understood as individual expressions of their authors and not those of the Society.

[3] For example, the laminas (parallel to the r,θ plane) might be radially symmetrical wire meshes.

[4] "Theory of Plates and Shells," by S. Timoshenko, McGraw-Hill Book Co., Inc., New York, N. Y., 1940, p. 257.

Under these assumptions, the only expressions from the Hooke's law relating to cylindrically aeolotropic materials which are necessary in developing the small bending theory are the following

$$\left.\begin{aligned} e_\theta &= a_{11}\sigma_\theta + a_{12}\sigma_r \\ e_r &= a_{12}\sigma_\theta + a_{22}\sigma_r \\ \gamma_{r\theta} &= a_{66}\tau_{r\theta} \end{aligned}\right\} \quad \ldots\ldots\ldots\ldots\ldots [1]$$

The couples per unit length, as defined in Fig. 1, are given by

$$\left.\begin{aligned} M_r &= + \int_{-h/2}^{h/2} \sigma_r z\, dz \\ M_\theta &= + \int_{-h/2}^{h/2} \sigma_\theta z\, dz \\ M_{r\theta} &= -M_{\sigma r} \int_{-h/2}^{h/2} \tau_{r\theta} z\, dz \end{aligned}\right\} \quad \ldots\ldots\ldots\ldots\ldots [2]$$

Since the neutral surface ($z = 0$) remains undisplaced horizontally, as implied by assumption (3), the values of u and v at any point z are given by

$$\left.\begin{aligned} u &= -z\,\partial w/\partial r \\ v &= -(z/r)\partial w/\partial\theta \end{aligned}\right\} \quad \ldots\ldots\ldots\ldots\ldots [3]$$

The strains are defined in the conventional manner as

$$\left.\begin{aligned} e_r &= \partial u/\partial r \\ e_\theta &= u/r + 1/r\,\partial v/\partial\theta \\ \gamma_{r\theta} &= 1/r\,\partial u/\partial\theta + \partial v/\partial r - v/r \end{aligned}\right\} \quad \ldots\ldots\ldots\ldots [4]$$

Equations [1], [2], [3], and [4] may be combined to give the following expressions for the couples in terms of w and the elastic constants

$$\left.\begin{aligned} M_r &= -D\left[C\frac{\partial^2 w}{\partial r^2} + \nu\left(\frac{1}{r}\frac{\partial w}{\partial r} + \frac{1}{r^2}\frac{\partial^2 w}{\partial\theta^2}\right)\right] \\ M_\theta &= -D\left[\frac{1}{r}\frac{\partial w}{\partial r} + \frac{1}{r^2}\frac{\partial^2 w}{\partial\theta^2} + \nu\frac{\partial^2 w}{\partial r^2}\right] \\ M_{r\theta} &= -M_{\theta r} = D(b-\nu)\frac{\partial}{\partial r}\left(\frac{1}{r}\frac{\partial w}{\partial\theta}\right) \end{aligned}\right\} \quad \ldots [5]$$

The equations of equilibrium are derived from a consideration of the couples and forces acting on the sectorial element shown in Fig. 1. They are, as in the isotropic case

$$\left.\begin{aligned} &\frac{\partial M_r}{\partial r} - \frac{1}{r}\frac{\partial M_{r\theta}}{\partial\theta} + \frac{1}{r}(M_r - M_\theta) - Q_r = 0 \\ &\frac{1}{r}\frac{\partial M_\theta}{\partial\theta} - \frac{\partial M_{r\theta}}{\partial r} - \frac{2}{r}M_{r\theta} - Q_\theta = 0 \\ &\frac{\partial}{\partial r}(rQ_r) + \frac{\partial Q_\theta}{\partial\theta} + rp = 0 \end{aligned}\right\} \quad \ldots [6]$$

These equations together with relations, Equations [5], produce the following differential equation

$$\left\{\frac{1}{r^4}\frac{\partial^4}{\partial\theta^4} + \frac{2b}{r^2}\frac{\partial^4}{\partial r^2\partial\theta^2} - \frac{2b}{r^2}\frac{\partial^3}{\partial\theta^2\partial r} + \frac{2(1+b)}{r^4}\frac{\partial^2}{\partial\theta^2} + C\frac{\partial^4}{\partial r^4} + \frac{2c}{r}\frac{\partial^3}{\partial r^3} - \frac{1}{r^2}\frac{\partial^2}{\partial r^2} + \frac{1}{r^3}\frac{\partial}{\partial r}\right\} W = \frac{p}{D} \quad \ldots [7]$$

It is interesting to note that the differential operator in this equation is identical with that occurring in the plane-stress theory[2] applying to this type of material, although the constant b is a different combination of elastic constants from the corresponding term in the plane-stress problem.

The particular integral of Equation [7] will depend upon the form of the load p. Some terms of the complementary solution are given by[5]

$$w = a_1 r^{1+\alpha} + a_2 r^{1-\alpha} + a_3 r^2 + a_4 + (Ar^{1+k_1} + Br + Cr^{1-k_1} + Dr\ln r)\cos\theta \quad \ldots [8]$$

The boundary conditions of any problem, when applied to the particular integral and the general complementary solution, will give all equations needed to produce a solution to that problem.

Limitations of the Theory

In applying this theory to plates composed of laminas, in and parallel to the $r\theta$ plane, it is essential to note that, in addition to limiting its application to cases where the deflections are small, it is necessary to consider the values of a_{44} and a_{55},[6] the reciprocals of the shearing moduli associated with the elements cut, respectively, from the rz plane and from the cylindrical surface defined by r = const. In these cases, when the shearing resistance of the impregnating material is very small, that is, when a_{44} and a_{55} approach infinity, it is intuitively clear that the laminas will behave like individual membranes and that the bending theory will not be applicable. This condition, of course, invalidates the assumption (3) previously used in developing this theory.

In the solution of problem (5) which appears in a later section of this paper, infinite values for the bending moments are obtained when ν is such that

$$\nu = \frac{1}{\alpha}\frac{1+\epsilon^{2\alpha}}{1-\epsilon^{2\alpha}}$$

This suggests a limitation to the possible values of the elastic constant ν, a number corresponding to the Poisson's ratio appearing in the isotropic theory.

Unfortunately very little experimental data have been published on the values of elastic constants of aeolotropic materials, other than moduli of elasticity,[7] so that the arguments used here must be based upon the probability that certain properties observed in isotropic materials will be retained by the aeolotropic material, and hence these arguments are of a hypothetical nature.

It seems logical to assume that, in general, the strain in a direction normal to an applied tensile stress will be negative, and that the change in the volume of an element subjected to a tensile stress will be positive. That is to say, a_{12}, a_{13}, and a_{23} will be negative and such that the change in an element of volume V_0, under tensile stress, will obey the inequality

$$V_0(e_r + e_\theta + e_z) > 0$$

When this tensile stress is of the type σ_r, the latter condition becomes

$$V_0\sigma_r(a_{12} + a_{22} + a_{23}) > 0$$

and when the stress is of the type σ_θ

$$V_0\sigma_\theta(a_{11} + a_{12} + a_{13}) > 0$$

Dividing these relations by $V_0\sigma_r a_{22}$ and $V_0\sigma_\theta a_{11}$, respectively, we obtain

$$-\frac{a_{12}}{a_{22}} - \frac{a_{23}}{a_{22}} < 1$$

$$-\frac{a_{12}}{a_{11}} - \frac{a_{13}}{a_{11}} < 1$$

[5] The general complementary solution is given in Ref. 2, but only the terms reproduced here are needed for the subsequent work.

[6] These constants appear in the Hooke's law for this material (see ref. 2).

[7] Plastics Catalog, 1943, Plastics Catalogue Corporation, New York, N. Y.

where, under the former of the two assumptions just made, each of the left-hand terms is positive. This restricts $-a_{12}/a_{22}$ and $-a_{12}/a_{11}$ to be between 0 and 1, or we may write

$$\nu = -a_{12}/a_{22} < 1$$

$$\alpha^2\nu = -a_{12}/a_{11} < 1$$

These then become the restrictions on the possible values of ν. On the strength of this hypothesis, the values of ν used in the following problems have been taken as

$$\nu = 1/2, \quad 0 \leq \alpha \leq 1$$

$$\alpha^2\nu = 1/2, \quad 1 \leq \alpha$$

Note that in the evaluation of these problems, the peaks at the value of α corresponding to isotropy (namely $\alpha = 1$) are caused by this method of choosing ν. Since the values of ν, occurring in any given type of material, would probably have a more uniform variation with α, there is no reason to believe, in general, that actual materials will display such a marked effect at the transition point between radially stiff and tangentially stiff plates.

Some Symmetrical Bending Problems

For those problems where p and w are functions of r only, Equation [7] reduces to the form

$$\left[c\frac{\partial^4}{\partial r^4} + \frac{2c}{r}\frac{\partial^3}{\partial r^3} - \frac{1}{r^2}\frac{\partial^2}{\partial r^2} + \frac{1}{r^3}\frac{\partial}{\partial r}\right]w = \frac{p}{D}$$

for which the general complementary solution is

$$w = a_1 r^{1+\alpha} + a_2 r^{1-\alpha} + a_3 r^2 + a_4$$

When p is a constant (the problem of uniform lateral load), the particular integral becomes

$$w = \frac{pr^4}{(72c - 8)D}$$

The following problems have been solved by applying the boundary conditions of each to the foregoing solutions of Equation [7]:

1 The disk with clamped edge, uniform lateral load.
2 The disk with clamped edge, central concentrated load.
3 The disk, simply supported, under uniform edge moment.
4 The disk with a rigid core of radius r_1 and clamped edge, central concentrated force.
5 The ring with clamped outer edge, loaded by uniform shear on the inner edge.
6 The disk with an elastic, isotropic core, simply supported, under uniform edge moment.

The problems of the bending of the simply supported plates under the loadings of problems (1) and (2) may be solved by combining the solutions of (1) and (2) with that of problem (3), evaluating the edge moment of problem (3) to satisfy the simple-support boundary condition. The simple-support problems, corresponding to problems (4) and (5), may also be solved by combining the clamped-edge solutions with the results of problem (6), wherein the stiffness of the core should be taken as vanishing for the ring problem and should be considered as infinite for the rigid-core problem.

Since no further considerations are necessary, the algebraic statements of the boundary conditions, and the corresponding solutions for the displacements and moments, will now be tabulated.

1 *Uniform Lateral Load, Clamped Edge:*

$$w = \partial w/\partial r = 0 \quad \text{at} \quad r = r_2$$

$$\partial w/\partial r = 0 \quad \text{at} \quad r = 0$$

$$Q_r = -pr/2$$

$$w = \frac{pr_2^4}{(72c-8)D}\left[\left(\frac{r}{r_2}\right)^4 - \frac{4}{1+\alpha}\left(\frac{r}{r_2}\right)^{1+\alpha} + \frac{3-\alpha}{1+\alpha}\right]$$

$$M_r = \frac{-pr_2^2}{18c-2}\left[(3c+\nu)\left(\frac{r}{r_2}\right)^2 - \frac{1+\alpha\nu}{\alpha}\left(\frac{r}{r_2}\right)^{\alpha-1}\right]$$

$$M_\theta = \frac{-pr_2^2}{18c-2}\left[(3\nu+1)\left(\frac{r}{r_2}\right)^2 - (1+\alpha\nu)\left(\frac{r}{r_2}\right)^{\alpha-1}\right]$$

2 *Concentrated Load, Clamped Edge:*

$$w = \partial w/\partial r = 0 \quad \text{at} \quad r = r_2$$

$$\partial w/\partial r = 0 \quad \text{at} \quad r = 0$$

$$Q_r = -P/2\pi r$$

$$w = \frac{-P\alpha^2 r_2^2}{4\pi D(\alpha^2-1)}\left[\left(\frac{r}{r_2}\right)^2 - \frac{2}{\alpha+1}\left(\frac{r}{r_2}\right)^{\alpha+1} - \frac{\alpha-1}{\alpha+1}\right]$$

$$M_r = \frac{P\alpha^2}{2\pi(\alpha^2-1)}\left[(c+\nu) - \frac{1+\alpha\nu}{\alpha}\left(\frac{r}{r_2}\right)^{\alpha-1}\right]$$

$$M_\theta = \frac{P\alpha^2}{2\pi(\alpha^2-1)}\left[1+\nu-(1+\alpha\nu)\left(\frac{r}{r_2}\right)^{\alpha-1}\right]$$

3 M_0 *Applied at Outer Edge, Simple Support:*

$$w = 0, \quad M_r = M_0 \quad \text{at} \quad r = r_2$$

$$\partial w/\partial r = 0 \qquad \text{at} \quad r = 0$$

$$Q_r = 0$$

$$w = \frac{M_0 r_2^2}{D}\,\frac{\alpha}{(\alpha+1)(\alpha\nu+1)}\left[1 - \left(\frac{r}{r_2}\right)^{\alpha+1}\right]$$

$$M_r = M_0\left(\frac{r}{r_2}\right)^{\alpha-1}, \quad M_\theta = \alpha M_0\left(\frac{r}{r_2}\right)^{\alpha-1}$$

4 *Disk With Rigid Core, Clamped Edge, Concentrated Load P:*

$$w = \partial w/\partial r = 0 \quad \text{at} \quad r = r_2$$

$$\partial w/\partial r = 0 \quad \text{at} \quad r = r_1$$

$$Q_r = -P/2\pi r$$

$$w = \frac{-Pr_2^2\alpha^2}{4\pi D(\alpha^2-1)}\left[\left(\frac{r}{r_2}\right)^2 - \frac{2}{1+\alpha}\,\frac{1-\epsilon^{1+\alpha}}{1-\epsilon^{2\alpha}}\left(\frac{r}{r_2}\right)^{1+\alpha} - \frac{2}{1-\alpha}\,\frac{\epsilon^{\alpha+1}-\epsilon^{2\alpha}}{1-\epsilon^{2\alpha}}\left(\frac{r}{r_2}\right)^{1-\alpha} + \frac{(\alpha-1)^2-(\alpha+1)^2\epsilon^{2\alpha}+4\alpha\epsilon^{\alpha+1}}{(1-\alpha^2)(1-\epsilon^{2\alpha})}\right]$$

$$M_r = \frac{P\alpha}{2\pi(\alpha^2-1)}\left[\frac{1+\alpha^2\nu}{\alpha} - (1+\alpha\nu)\,\frac{1-\epsilon^{\alpha+1}}{1-\epsilon^{2\alpha}}\left(\frac{r}{r_2}\right)^{\alpha-1} + (1-\alpha\nu)\,\frac{\epsilon^{\alpha+1}-\epsilon^{2\alpha}}{1-\epsilon^{2\alpha}}\left(\frac{r}{r_2}\right)^{-\alpha-1}\right]$$

$$M_\theta = \frac{P\alpha^2}{2\pi(\alpha^2-1)}\left[(1+\nu) - (1+\alpha\nu)\,\frac{1-\epsilon^{\alpha+1}}{1-\epsilon^{2\alpha}}\left(\frac{r}{r_2}\right)^{\alpha-1} - (1-\alpha\nu)\,\frac{\epsilon^{\alpha+1}-\epsilon^{2\alpha}}{1-\epsilon^{2\alpha}}\left(\frac{r}{r_2}\right)^{-\alpha-1}\right]$$

5 *Ring Clamped at r_2, Shear on Inner Edge:*

$$w = \partial w/\partial r = 0 \quad \text{at} \quad r = r_2$$

$$Q_r = Q_0, \quad M_r = 0, \quad \text{at} \quad r = r_1$$

$$w = \frac{Q_0 r_1^2}{(\alpha^2-1)D}\left[\frac{\alpha^2}{2}\left(\frac{r}{r_1}\right)^2 - \frac{\alpha}{\alpha+1}\,\frac{(1+\alpha^2\nu)\epsilon^{2\alpha}+\alpha(1-\alpha\nu)\epsilon^{\alpha-1}}{(1-\alpha\nu)+(1+\alpha\nu)\epsilon^{2\alpha}}\left(\frac{r}{r_1}\right)^{\alpha+1} - \frac{\alpha}{\alpha-1}\,\frac{(1+\alpha^2\nu)-\alpha(1+\alpha\nu)\epsilon^{\alpha-1}}{(1-\alpha\nu)+(1+\alpha\nu)\epsilon^{2\alpha}}\left(\frac{r}{r_1}\right)^{1-\alpha} - \frac{1}{\epsilon^2}\left\{\frac{\alpha^2}{2} - \frac{\alpha}{\alpha+1}\,\frac{(1+\alpha^2\nu)\epsilon^{\alpha+1}+\alpha(1-\alpha\nu)}{(1-\alpha\nu)+(1+\alpha\nu)\epsilon^{2\alpha}} + \frac{\alpha}{\alpha-1}\,\frac{-(1+\alpha^2\nu)\epsilon^{\alpha-1}+\alpha(1+\alpha\nu)}{(1-\alpha\nu)+(1+\alpha\nu)\epsilon^{2\alpha}}\right\}\right]$$

$$M_r = \frac{Q_0 r_1}{\alpha^2-1}\left[-(1+\alpha^2\nu)+(1+\alpha\nu) \times \frac{(1+\alpha^2\nu)\epsilon^{2\alpha}+\alpha(1-\alpha\nu)\epsilon^{\alpha-1}}{(1-\alpha\nu)+(1+\alpha\nu)\epsilon^{2\alpha}}\left(\frac{r}{r_1}\right)^{\alpha-1} + (1-\alpha\nu)\,\frac{(1+\alpha^2\nu)-\alpha(1+\alpha\nu)\epsilon^{\alpha-1}}{(1-\alpha\nu)+(1+\alpha\nu)\epsilon^{2\alpha}}\left(\frac{r}{r_1}\right)^{-\alpha-1}\right]$$

$$M_\theta = \frac{Q_0 r_1 \alpha}{\alpha^2-1}\left[-\alpha(1+\nu)+(1+\alpha\nu) \times \frac{(1+\alpha^2\nu)\epsilon^{2\alpha}+\alpha(1-\alpha\nu)\epsilon^{\alpha-1}}{(1-\alpha\nu)+(1+\alpha\nu)\epsilon^{2\alpha}}\left(\frac{r}{r_1}\right)^{\alpha-1} -(1-\alpha\nu)\,\frac{(1+\alpha^2\nu)-\alpha(1+\alpha\nu)\epsilon^{\alpha-1}}{(1-\alpha\nu)+(1+\alpha\nu)\epsilon^{2\alpha}}\left(\frac{r}{r_1}\right)^{-\alpha-1}\right]$$

6 *Disk With Isotropic Elastic Core, Loaded by Uniform Edge Moment M_0:*

The boundary conditions for this problem are formulated by noting that, for the isotropic core, the following relation holds

$$M_r = -F(1+\mu)\partial w/\partial r, \quad \text{at} \quad r = r_1$$

This is true provided the loading is independent of θ. Noting also that M_r and $\partial w/\partial r$ must be continuous at the boundary between the two materials, the boundary conditions corresponding to the problem of applied edge moment become

$$M_r = -F(1+\mu)\,\partial w/\partial r, \quad Q_r = 0, \quad \text{at} \quad r = r_1$$

$$M_r = M_0, \qquad w = 0, \qquad r = r_2$$

$$w = \frac{M_0 r_1^2}{\epsilon DK}\left[\frac{(1+\alpha\nu)-(F/D)\,\alpha(1+\mu)}{\alpha(\alpha-1)}\left(\frac{r}{r_1}\right)^{1-\alpha} - \frac{1-\alpha\nu+(F/D)\alpha(1+\mu)}{\alpha(\alpha+1)}\left(\frac{r}{r_1}\right)^{1+\alpha} + \frac{(1-\alpha\nu)+(F/D)\,\alpha(1+\mu)}{\alpha(\alpha+1)}\,\epsilon^{-\alpha-1} - \frac{1+\alpha\nu-(F/D)\,\alpha(1+\mu)}{\alpha(\alpha-1)}\,\epsilon^{\alpha-1}\right]$$

$$M_r = \frac{M_0}{\epsilon K}\left[\left\{\frac{1-\alpha^2\nu^2}{\alpha^2}+\frac{F}{D}(1+\mu)\,\frac{1+\alpha\nu}{\alpha}\right\}\left(\frac{r}{r_1}\right)^{\alpha-1} - \left\{\frac{1-\alpha^2\nu^2}{\alpha^2}-\frac{F}{D}(1+\mu)\,\frac{1-\alpha\nu}{\alpha}\right\}\left(\frac{r}{r_1}\right)^{-\alpha-1}\right]$$

$$M_\theta = \frac{M_0}{\epsilon K}\left[\left\{\frac{1-\alpha^2\nu^2}{\alpha}+\frac{F}{D}(1+\mu)(1+\alpha\nu)\right\}\left(\frac{r}{r_1}\right)^{\alpha-1} + \frac{1-\alpha^2\nu^2}{\alpha}-\frac{F}{D}(1+\mu)(1-\alpha\nu)\left(\frac{r}{r_1}\right)^{-\alpha-1}\right]$$

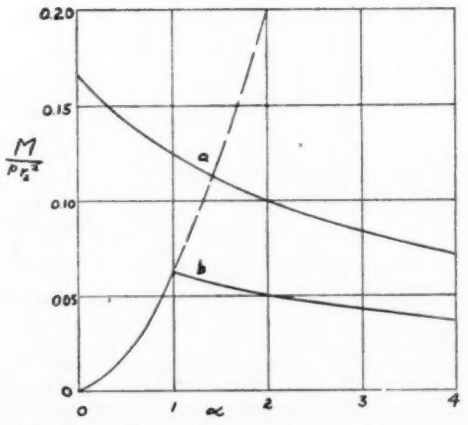


FIG. 2 MOMENTS AT OUTER EDGE OF CLAMPED DISK UNDER UNIFORM LATERAL PRESSURE

(a) $M = M_r$ $\nu = 1/3$ $0 \le \alpha \le 1$
(b) $M = M_\theta$ $\alpha^2\nu = 1/3$ $1 \le \alpha \le \infty$
— — — $M = M_\theta$ and $\nu = 1/3$

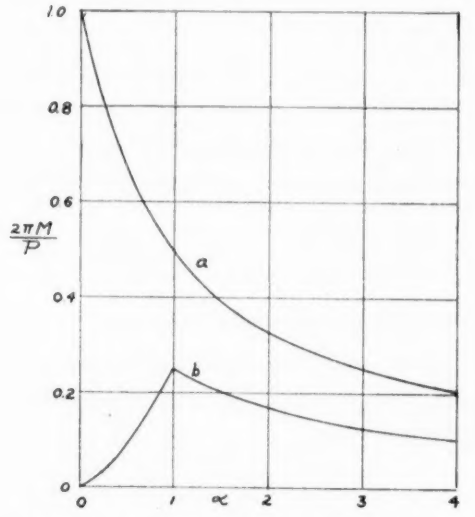


FIG. 3 MOMENTS AT OUTER EDGE OF CLAMPED DISK UNDER CENTRAL CONCENTRATED LOAD

(a) $M = M_r$ $\nu = 1/3$ $0 \le \alpha \le 1$
(b) $M = M_\theta$ $\alpha^2\nu = 1/3$ $1 \le \alpha < \infty$

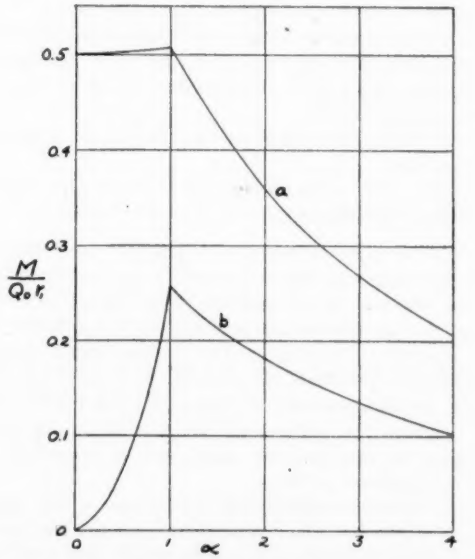


FIG. 4 MOMENTS AT OUTER EDGE OF RING, CLAMPED AT r_2, UNIFORM SHEAR APPLIED AT r_1

(a) $M = M_r$ $\nu = 1/3$ $0 \le \alpha \le 1$
(b) $M = M_\theta$ $\alpha^2\nu = 1/3$ $1 \le \alpha \le \infty$
$\epsilon = 1/3$

Figs. 2, 3, and 4 show the effect of the degree of anisotropy on the stresses produced by the conditions of problems (1), (2), and (5).

An Unsymmetrical Bending Problem

The circular plate loaded by a distribution of pressure of the form $p = p_0(r/r_2)\cos\theta$ is a problem in unsymmetrical loading which has a very simple solution.

The particular integral of Equation [7] corresponding to this loading is given by

$$w = \frac{p_0 r^5}{16(15c - 2b - 1)Dr_2}\cos\theta$$

The corresponding complementary solution has the form

$$w = (Ar^{1+k} + Br + Cr^{1-k} + Dr\ln r)\cos\theta$$

When the boundary conditions for the clamped plate are applied to these expressions, the equations giving the deflection and moments are derived. These boundary conditions and solutions are

$$w = \partial w/\partial r = 0 \quad \text{at} \quad r = r_2$$

$$w \text{ and } M_r \text{ finite} \quad \text{at} \quad r = 0$$

$$w = \frac{p_0 r_2^4}{16(15c - 2b - 1)D}\left[\left(\frac{r}{r_2}\right)^5 - \frac{4}{k_1}\left(\frac{r}{r_2}\right)^{1+k_1} + \frac{4 - k_1}{k_1}\left(\frac{r}{r_2}\right)\right]\cos\theta$$

$$M_r = \frac{-p_0 r_2^2}{4(15c - 2b - 1)}\left[(5c + \nu)\left(\frac{r}{r_2}\right)^3 - (ck_1 + c + \nu)\left(\frac{r}{r_2}\right)^{k_1-1}\right]\cos\theta$$

$$M_\theta = \frac{-p_0 r_2^2}{4(15c - 2b - 1)}\left[(5\nu + 1)\left(\frac{r}{r_2}\right)^3 - (1 + k_1\nu + \nu)\left(\frac{r}{r_2}\right)^{k_1-1}\right]\cos\theta$$

$$M_{r\theta} = \frac{-p_0 r_2^2(b - \nu)}{4(15c - 2b - 1)}\left[\left(\frac{r}{r_2}\right)^3 - \left(\frac{r}{r_2}\right)^{k_1-1}\right]\sin\theta$$

Arbitrary Distribution of Lateral Pressure

The problem of the ring or disk with an arbitrary distribution of lateral pressure may be solved by one of the following:

If the pressure is a function of θ alone, expand it in a Fourier series and obtain the particular integral of Equation [7] for this loading. Choose the terms of the complementary solution which contain the same trigonometric terms as are found in the particular integral and evaluate the constants in such a manner as to satisfy the boundary conditions.

If the loading is made up of isolated concentric rings of force (per unit length), solve the problem as a group of simultaneous ring problems with uniformly applied shear forces and edge moments of undetermined magnitude.

If p is a function of r, the complementary solution of Equation [7] containing terms which are trigonometric functions of $\ln r$ must be found. This solution is very complex algebraically and, in general, the solution to a problem of this type will be tedious to evaluate.

The Bending of the Clamped Sectorial Plate

By G. F. CARRIER,[1] ITHACA, N. Y.

The problem of evaluating the bending moments, existing in a uniformly loaded clamped plate having the form of a sector of a ring, is one which arises in connection with the stress analysis of reinforced piston heads and in other design problems. In this paper, expressions are derived for the bending moments along the edges of such a plate. Similar problems, i.e., those of the clamped rectangular plate under uniform pressure,[2] under a central concentrated load,[3] and that of the simply supported sector of a disk under uniform pressure,[4] have been discussed by previous authors. The general approach used in the foregoing problems is adopted in the present case; a considerable reduction in the computational work is achieved, however, by the use of an integral-equation method of solving the boundary-condition equations. Numerical results are obtained for plates of various dimensions, and the edge moment distributions are plotted for these cases. Curves are also plotted which indicate the relationship existing between the maximum bending moments derived for sectorial plates and those previously obtained for clamped rectangular plates of similar size.

The Simply Supported Plate

IN the consideration of the bending of the sectorial plate (Fig. 1), the assumptions of the small bending theory are adopted, and the problem is reduced to one of finding that solution of the equation

$$\left(\frac{\partial^2}{\partial r^2}+\frac{1}{r}\frac{\partial}{\partial r}+\frac{1}{r^2}\frac{\partial^2}{\partial\theta^2}\right)^2 W=\frac{q(r,\theta)}{D} \quad \ldots\ldots\ldots [1]$$

which satisfies a given set of boundary conditions.[5] (W is the deflection; D is the modulus of rigidity.)

The uniform lateral pressure, q_0, which is to be applied to the plate, may be expressed in the form

$$q_0=\frac{4q_0}{\pi}\sum_{m=1,3,5}^{\infty}\frac{(-1)^{\frac{(m-1)}{2}}}{m}\cos\frac{mk}{2}\theta \quad \ldots\ldots\ldots [2]$$

in the region, $-\frac{\pi}{k}<\theta<\frac{\pi}{k}$. ($k$ and several other symbols are defined in Fig. 1.)

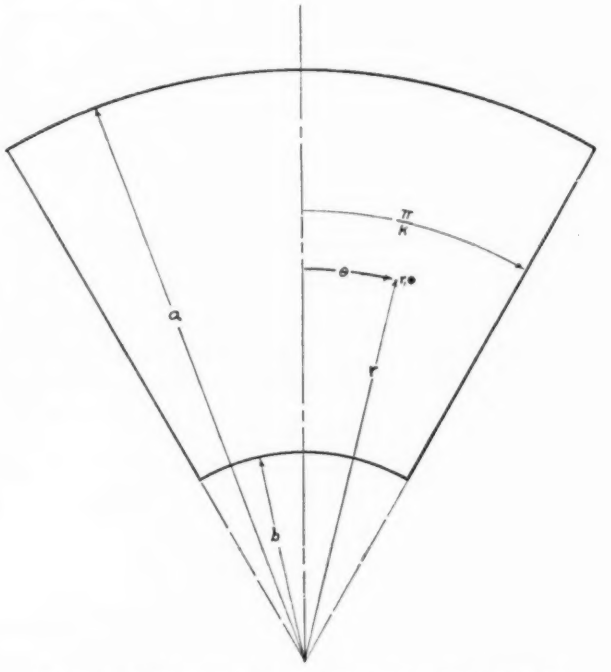


FIG. 1 THE SECTORIAL PLATE INVOLVED IN THE PROBLEM

In terms of the dimensionless forms defined later in Equations [4], Equation [1] may be written

$$\left(\frac{\partial^2}{\partial\rho^2}+\frac{1}{\rho}\frac{\partial}{\partial\rho}+\frac{1}{\rho^2}\frac{\partial^2}{\partial\theta^2}\right)^2 w=\sum_{m=1,3}^{\infty}\frac{(-1)^{\frac{m-1}{2}}}{m}\cos u\theta \quad \ldots\ldots [3]$$

where

$$\left.\begin{aligned}\rho&=\frac{r}{b},\quad u=\frac{mk}{2},\quad w=\frac{\pi DW}{4q_0b^4},\quad \epsilon=\frac{a}{b}\\ m_r&=\frac{\pi M_r}{4q_0b^2}=\left[\frac{\partial^2}{\partial\rho^2}+\nu\left(\frac{1}{\rho}\frac{\partial}{\partial\rho}+\frac{1}{\rho^2}\frac{\partial^2}{\partial\theta^2}\right)\right]w\\ m_\theta&=\frac{\pi M_\theta}{4q_0b^2}=\left[\frac{1}{\rho^2}\frac{\partial^2}{\partial\theta^2}+\frac{1}{\rho}\frac{\partial}{\partial\rho}+\nu\frac{\partial^2}{\partial\rho^2}\right]w\end{aligned}\right\} \quad \ldots [4]$$

A particular integral of Equation [3] is

$$\left.\begin{aligned}w_0&=\sum_{m=1,3}^{\infty}(-1)^{\frac{m-1}{2}}\rho^4\frac{\cos u\theta}{m(u^2-4)(u^2-16)},\\ &\qquad\qquad \text{for } u\neq 2,\ u\neq 4,\\ \text{or, for } u&=\begin{cases}2;\ w_0=(-1)^{\frac{m-1}{2}}\dfrac{\rho^4\ln\rho}{48m}\cos 2\theta,\\ 4;\ w_0=(-1)^{\frac{m-1}{2}}\dfrac{\rho^4\ln\rho}{96m}\cos 4\theta,\end{cases}\end{aligned}\right\} \quad \ldots [5]$$

and a complementary solution of similar form is given by

[1] Instructor in Machine Design, Cornell University. Jun. A.S.M.E.

[2] "Theory of Plates and Shells," by S. P. Timoshenko, McGraw-Hill Book Company, Inc., New York, N. Y., 1940, p. 222.

[3] "The Clamped Rectangular Plate With a Concentrated Load," by Dana Young, JOURNAL OF APPLIED MECHANICS, Trans. A.S.M.E., vol. 61, 1939, p. A-114.

[4] Reference (2), p. 272.

[5] The details of the theory leading to Equation [1] may be found in ref. (2) p. 257.

Presented at the National Meeting of the Applied Mechanics Division, Chicago, Ill., June 16-17, 1944, of THE AMERICAN SOCIETY OF MECHANICAL ENGINEERS.

Discussion of this paper should be addressed to the Secretary, A.S.M.E., 29 West 39th Street, New York, N. Y., and will be accepted until October 10, 1944, for publication at a later date. Discussion received after the closing date will be returned.

NOTE: Statements and opinions advanced in papers are to be understood as individual expressions of their authors and not those of the Society.

$$w_1 = \sum_{m=1,3}^{\infty} (-1)^{\frac{m-1}{2}} \left\{ A_m \left(\frac{\rho}{\epsilon}\right)^u + B_m \rho^{-u} + C_m \left(\frac{\rho}{\epsilon}\right)^{2+u} + D_m \rho^{2-u} \right\} \cos u\theta \quad \ldots\ldots [6]$$

Four of the boundary conditions of the simply supported plate, namely

$$w = m_\theta = 0, \text{ at } \theta = \pm \pi/k$$

are satisfied by the solution, $w_0 + w_1$, regardless of the values assigned to $A_m, \ldots D_m$. The remaining four conditions are satisfied by setting

$$w_0 + w_1 = 0, \text{ and } m_r = 0, \text{ at } \rho = 1, \text{ and at } \rho = \epsilon$$

This determines uniquely the $A_m, \ldots D_m$, since it produces four simultaneous equations in the four coefficients corresponding to each m. The expressions for the $A_m, \ldots D_m$, and those for several other coefficients which will be encountered, are not written out explicitly in this paper since they are very long and are of direct use only as they appear in combinations which are quoted in a subsequent section.

The bending moments may of course be found immediately in terms of these coefficients by application of Equations [4].

The slopes at the edges, to be used in satisfying the boundary conditions for the clamped plate, are found by differentiation, and are denoted as follows

$$\left.\begin{aligned} \text{at } \rho = \epsilon, \ \frac{\partial}{\partial \rho}(w_0 + w_1) &= \sum_{m=1,3}^{\infty} P_m \cos u\theta \\ \text{at } \rho = 1, \ \frac{\partial}{\partial \rho}(w_0 + w_1) &= \sum_{m=1,3}^{\infty} Q_m \cos u\theta \\ \text{at } \theta = \pm \frac{\pi}{k}, \ \frac{\partial}{\partial \theta}(w_0 + w_1) &= \sum_{m=1,3}^{\infty} \rho \mathcal{L}_m(p\xi) \end{aligned}\right\} \ldots [7]$$

where $p = \pi/\ln \epsilon$ and $\xi = \ln \rho$.

The symbols, P_m, Q_m, and $\mathcal{L}_m$, introduced here, are self-defining in terms of the parameters, $A_m, \ldots D_m$, k, and ϵ. Symbol $\mathcal{L}$ is defined as a function of ξ, rather than one of ρ, to avoid the necessity of redefining the notation in the treatment of Equations [11].

The Clamped Plate

The bending of the clamped plate will be treated by superimposing on the solution for the simply supported plate two solutions of the differential equation

$$\left(\frac{\partial^2}{\partial \rho^2} + \frac{1}{\rho}\frac{\partial}{\partial \rho} + \frac{1}{\rho^2}\frac{\partial^2}{\partial \theta^2}\right)^2 w = 0$$

namely

$$\left.\begin{aligned} w_2 &= \sum_{m=1,3}^{\infty} (-1)^{\frac{m-1}{2}} \left\{ E_m \left(\frac{\rho}{\epsilon}\right)^u + F_m \rho^{-u} + G_m \left(\frac{\rho}{\epsilon}\right)^{2+u} + H_m \rho^{2-u} \right\} \cos u\theta \\ \text{and} \quad w_3 &= \sum_{n=1,2}^{\infty} \rho \frac{\cos \theta_0}{\sinh \varphi_n} (I_n \cos\theta \cosh np\theta + J_n \sin\theta \sinh np\theta) \sin np\xi \end{aligned}\right\} \ldots [8]$$

where $\theta_0 = \dfrac{\pi}{k}, \quad \varphi_n = \dfrac{np\pi}{k}$

These solutions are easily obtained by considering solutions of the form

$$w = R(\rho)\Theta(\theta)$$

This superposition corresponds, of course, to applying edge moments to the plate, whose distributions depend upon the values of the coefficients, $E_m, \ldots J_n$, which must be evaluated to make the displacements and slopes vanish on the four edges. By virtue of the fact that $w_0 + w_1$ vanishes at all four edges, w_2 at the radial edges, and w_3 along the circular edges, w (henceforth implying $w = w_0 + w_1 + w_2 + w_3$) will itself vanish on all four edges if

$$\left.\begin{aligned} E_m &= G_m \frac{\epsilon^{-2-2u} - 1}{1 - \epsilon^{-2u}} + H_m \frac{\epsilon^{-u} - \epsilon^{2-u}}{1 - \epsilon^{-2u}} \\ F_m &= G_m \frac{\epsilon^{-u} - \epsilon^{-2-u}}{1 - \epsilon^{-2u}} + H_m \frac{\epsilon^{2-2u} - 1}{1 - \epsilon^{-2u}} \\ I_n &= -J_n \tan\theta_0 \tanh \varphi_n \end{aligned}\right\} \ldots [8a]$$

The contributions of w_2 to the slopes are now given by

$$\left.\begin{aligned} \text{at } \rho = \epsilon, \ \frac{\partial w_2}{\partial \rho} &= \sum_{m=1,3}^{\infty} (a_{1m} G_m + b_{1m} H_m) \cos u\theta \\ \text{at } \rho = 1, \ \frac{\partial w_2}{\partial \rho} &= \sum_{m=1,3}^{\infty} (a_{2m} G_m + b_{2m} H_m) \cos u\theta \\ \text{at } \theta = \frac{\pi}{k}, \ \frac{\partial w_2}{\partial \theta} &= \sum_{m=1,3}^{\infty} \rho[\alpha_m(p\xi) G_m + \beta_m(p\xi) H_m] \end{aligned}\right\} \ldots [9]$$

where a_{im}, b_{im}, are constants, and α_m, β_m, are functions, each defined by the indicated differentiations and the preceding equalities. They are not quoted explicitly since again they are of importance only as they occur in combinations which arise later in the analysis.

From w_3, we obtain

$$\left.\begin{aligned} \text{at } \rho = \epsilon, \ \frac{\partial w_3}{\partial \rho} &= \sum_{n=1}^{\infty} (-1)^n np J_n \left[\sin\theta \cos\theta_0 \frac{\sinh np\theta}{\sinh \varphi_n} - \cos\theta \sin\theta_0 \frac{\cosh np\theta}{\cosh \varphi_n} \right] \\ &= \sum_{n=1}^{\infty} J_n \gamma_n' \left(\frac{k\theta}{2}\right) = \sum_{n=1}^{\infty} (-1)^n J_n \sum_{m=1,3}^{\infty} Y_{mn} \cos u\theta \\ \text{at } \rho = 1, \ \frac{\partial w_3}{\partial \rho} &= \sum_{n=1}^{\infty} J_n \gamma_n \left(\frac{k\theta}{2}\right) = \sum_{n=1}^{\infty} J_n \sum_{m=1}^{\infty} Y'_{mn} \cos u\theta \\ \text{at } \theta = \frac{\pi}{k}, \ \frac{\partial w_3}{\partial \theta} &= \sum_{n=1}^{\infty} \rho J_n \left[1 + \frac{np \sin 2\theta_0}{\sinh 2\varphi_n} \right] \sin np\xi \\ &= \sum_{n=1}^{\infty} C_n J_n \rho \sin np\xi \end{aligned}\right\} \ldots [10]$$

where[6]

$$Y_{mn} = -(-1)^{\frac{m-1}{2}} \frac{4}{\pi} \frac{\cosh 2\varphi_n + \cos 2\theta_0}{\sinh 2\varphi_n} \frac{kun^2p^2}{[(u+1)^2 + n^2p^2][(u-1)^2 + n^2p^2]}$$

The only boundary conditions remaining to be satisfied are

$$\frac{\partial w}{\partial \rho} = \frac{\partial w}{\partial \theta} = 0$$

at the four edges.

Since all terms in $\frac{\partial w}{\partial \theta}$ are odd in θ, the conditions on the radial edges are identical, and only one need be considered.

If we now utilize the foregoing expressions for the slopes and formulate the three remaining boundary conditions, we obtain

$$\left.\begin{aligned}
&\sum_m a_{1m}G_m \cos u\theta + \sum_m b_{1m}H_m \cos u\theta \\
&\qquad + \sum_n \gamma'_n \left(\frac{k\theta}{2}\right) J_n = -\sum_m P_m \cos u\theta \\
&\sum_m a_{2m}G_m \cos u\theta + \sum_m b_{2m}H_m \cos u\theta \\
&\qquad + \sum_n \gamma_n \left(\frac{k\theta}{2}\right) J_n = -\sum_m Q_m \cos u\theta \\
&\sum_m \alpha_m(p\xi)G_m + \sum_m \beta_m(p\xi)H_m \\
&\qquad + \sum_n c_n J_n \sin np\xi = -\sum_m \mathfrak{L}_m(p\xi)
\end{aligned}\right\} \quad . . [11]$$

The reduction of these equations to those in J_n only, and the method of evaluation of these coefficients, is carried out in detail in the Appendix. With the determination of the values of the J_n, the deflection may be considered as known since the G_m and H_m have been expressed in terms of the J_n during the reduction of Equations [11].

[6] This Fourier coefficient arises in the expansions of γ and γ' into their cosine series, in the interval, $-\frac{\pi}{k} < \theta < \frac{\pi}{k}$.

The Bending Moments

The bending moments along the radial edge can occur only from the terms in w_3, since all other terms in w have a factor of $\cos u\theta$, which vanishes at this edge. Hence the expression for m_θ, quoted in Equations [4], when applied to w_3, yields the following formula for moment distribution along the radial edge

$$m_\theta = \frac{2p}{\rho} \sum_{n=1}^{\infty} nJ_n \sin np\xi \frac{\cosh 2\varphi_n + \cos 2\theta_0}{\sinh 2\varphi_n}$$

In order to evaluate the bending moments along the circular edges, both w_2 and w_3 must be considered. If G_m and H_m are expressed in terms of the J_i (essentially Equations [14] of the Appendix), and if the equation for m_r (Equation [4]) is applied to $w_2 + w_3$, the formulas at the bottom of this page for m_r are obtained:[7]

When, in the foregoing equations, each J_i is given the value zero, the bending moments become those for the sectorial plate, simply supported on the radial edges and clamped along the circular edges.

It is interesting to note that although P_m, Q_m, and other expressions occurring in the development of this problem depend upon the Poisson's ratio ν, of the material, the final equations for the J_i and those for the bending moments along the edges are independent of the value of this quantity. This provides a partial check on the algebraic work (which is involved enough to make a check desirable) since this result can be shown to be a necessary one. Except as this quantity appears in the constant D, the solution for the deflection cannot depend upon ν, since it occurs neither in the differential equation nor in the boundary conditions. Furthermore, this number appears in the moment expressions only as a coefficient of the radial slope which vanishes on all four edges, and as a coefficient of the curvature, tangent to the edge at which the moment is being evaluated, and this term also vanishes.

The bending moments in a complete ring under uniform lateral

[7] λ_m, μ_m are defined in the Appendix where they occur in Equations [17].

$$m_r = \sum_{(\rho=\epsilon)} \sum_m (-1)^{\frac{m-1}{2}} \frac{\mu_m}{\lambda_m} \left\{ \begin{array}{l} (u-4)(u-2)\epsilon^2 - 2u(u-1)(u+4)\epsilon^{-u} + 2u(u+1)(u+2)\epsilon^{-2-u} \\ -2(u^2-8)(u^2-1)\epsilon^{2-2u} + u^2(u^2-4)\epsilon^{4-2u} + u^2(u^2-16)\epsilon^{-2u} \\ +2u(u+1)(u-4)\epsilon^{-3u} - 2u(u-1)(u-2)\epsilon^{-2-3u} + (u+2)(u+4)\epsilon^{2-4u} \end{array} \right\} \cos u\theta$$

$$- \sum_m \frac{2u}{\epsilon} \left\{ \begin{array}{l} \left[(1-\epsilon^{-4u}) + u\epsilon^{-2u}\left(\epsilon^2 - \frac{1}{\epsilon^2}\right)\right] \sum_n (-1)^n Y_{mn} J_n \\ + \left[(u-1)(\epsilon^{1-u} - \epsilon^{-1-3u}) - (u+1)(\epsilon^{-1-u} - \epsilon^{1-3u})\right] \sum_n Y_{mn} J_n \end{array} \right\} \cos u\theta$$

$$m_r = \sum_{(\rho=1)} \sum_m (-1)^{\frac{m-1}{2}} \frac{\mu_m}{m\lambda_m} \left\{ \begin{array}{l} (u+2)(u+4) - 2u(u-1)(u-2)\epsilon^{4-u} + 2u(u+1)(u-4)\epsilon^{2-u} \\ + u^2(u^2-16)\epsilon^{2-2u} - 2(u^2-8)(u^2-16)\epsilon^{-1u} + u^2(u^2-4)\epsilon^{-2-2u} \\ + 2u(u+2)(u+1)\epsilon^{4-3u} - 2u(u+4)(u-1)\epsilon^{2-3u} + (u-4)(u-2)\epsilon^{-4u} \end{array} \right\} \cos u\theta$$

$$+ \sum_m 2u \left\{ \begin{array}{l} \left[(1-\epsilon^{-4u}) + u\epsilon^{-2u}\left(\epsilon^2 - \frac{1}{\epsilon^2}\right)\right] \sum_n Y_{mn} J_n \\ + \left[(u-1)(\epsilon^{1-u} - \epsilon^{-1-3u}) - (u+1)(\epsilon^{-1-u} - \epsilon^{1-3u})\right] \sum_n (-1)^n Y_{mn} J_n \end{array} \right\} \cos u\theta$$

load and clamped on both edges, to be used in Fig. 5 for comparative purposes, are found by obtaining that solution of Equation [1] which is independent of θ and which has zero displacement and slope along the edges. The maximum bending moment (along the inner edge) becomes

$$m_r = \frac{\epsilon^4 + 4\ln\epsilon - 1}{4\ln\epsilon} - \frac{(\epsilon^2 + 2\ln\epsilon - 1)(\epsilon^4 - 4\epsilon^2\ln\epsilon - 1)}{(4\ln\epsilon)[(\epsilon^2-1)^2 - 4\epsilon^2(\ln\epsilon)^2]}$$

Numerical Results

Computations have been carried out in detail for three cases. In each of these, k was taken as 6, that is, the angle of the sector was taken as 60 deg. The values of ϵ were taken as, 2.0, 2.85, and 4.81, the latter two chosen to make the corresponding values of p, which occurs very frequently in the computations, equal to 3 and 2, respectively. Following this discussion, a set of equations for J_i (those for $\epsilon = 4.81$) are included to illustrate the method used in the evaluation of these numbers. Referring to these, the first approximations to the J_i were found by solving those equations (or parts thereof) which lie to the left of the dotted line, substituting previously found values when necessary. The second approximations are found by substituting those values obtained in the first step into the first equation and finding the new J_1. Then this and the first approximations to the other J_i are used to find J_2, and the method is continued. The accuracy of this second group of values, estimated by noting the difference between them and the previously found values, is considered sufficient to justify their use in the computation of the moments, as the values are certainly as accurate as those found for the R_{mi}, and the K_{imn}.[8] Using values of m ranging from 1 to 11, the K_{imn} for the higher i and n are probably not accurate within 10 per cent, but the effect of these terms is small and the accuracy of the final results should be well within this limit. The values of the J_i, for i less than 6, should be accurate to within 2 per cent, barring computational error, but the higher J_i are probably not as good, owing both to the fact that the R_{mi} in this range are small differences of comparatively large numbers, and to the comparative inaccuracy of the K_{imn}. The effect of these higher J_i is, however, negligible (they could actually have been dispensed with in these three cases), except near the corners where the stresses are very small.

The bending moments occurring in these three cases have been plotted in two different manners. Figs. 2, 3, 4 show, respectively, the bending-moment distributions along the inner, outer, and radial edges. The dimensionless moments plotted are not the m_r and m_θ, but are quantities based upon plates with the same outer radii. Fig. 4 shows superimposed views of the three plates, and inspection of this diagram, in conjunction with Figs. 2 and 3, should easily convince one that an extrapolation from the plate corresponding to $\epsilon = 4.81$ to a plate extending to the center would produce no great change in the magnitude of the moments

[8] These quantities appear in the expressions for the J_i, see the Appendix.

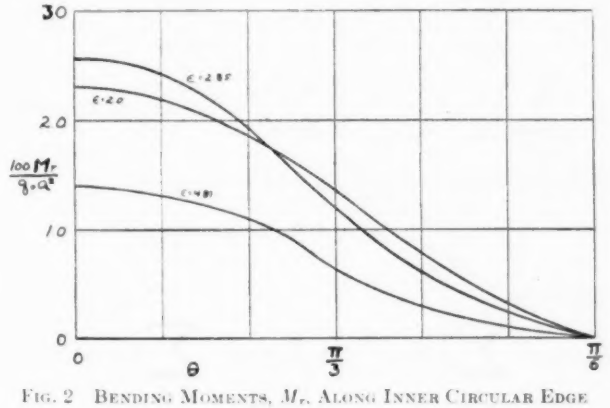


Fig. 2 Bending Moments, M_r, Along Inner Circular Edge

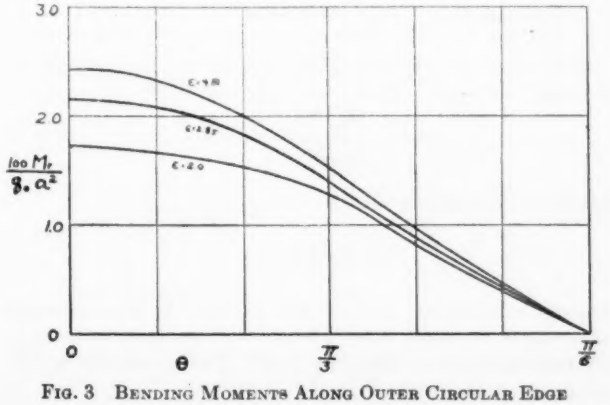


Fig. 3 Bending Moments Along Outer Circular Edge

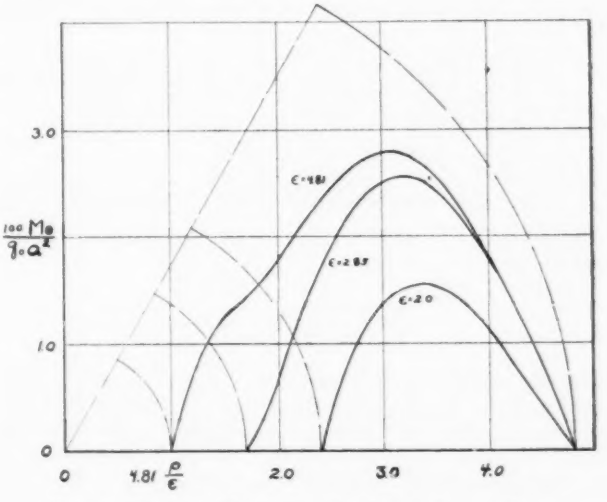


Fig. 4 Bending Moments, M_θ, Along Radial Edge

$\alpha = (\epsilon - 1)b$ $\qquad \frac{\beta = \pi(\epsilon+1)}{k} b$

(k taken as 6.0 in each case.)

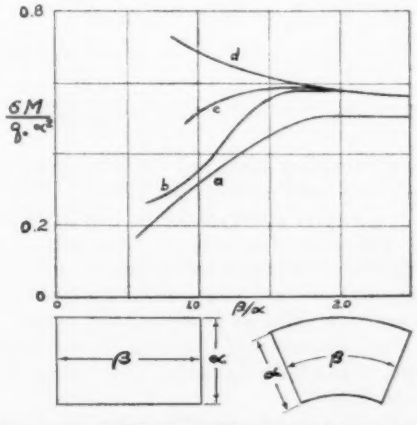


Fig. 5 Comparison of Maximum Bending Moments for Various Shapes and Boundary Conditions

(*a*, Clamped rectangular plate. *b*, Clamped sectorial plate. *c*, Sectorial plate, clamped on circular edges, simply supported on radial edges. *d*, Complete ring, clamped edges.)

occurring along the outer circular edge and along the outer part of the radial edge.

In Fig. 5 are plotted four curves: (*a*) is a plot of the maximum bending moment in a clamped rectangular plate, plotted against the ratio of the lengths of the sides,[9] (*b*) is a curve of maximum bending moment in the clamped sectorial plate, plotted against a similar parameter which is defined in the figure; (*c*) is a curve of maximum moment in the sectorial plate which is simply supported on the radial edges and clamped along the circular ones; (*d*) is the corresponding curve for the complete ring with clamped edges. These last two curves have the same abscissa as (*b*).

For those values of ϵ and k which were used, there seems to be a close analogy between the stresses induced in a sectorial plate and those in a rectangular plate of similar size, when they are similarly loaded and clamped.

TABLE 1 EQUATIONS FOR THE J_i ($\epsilon = 4.81$)

$$
\begin{aligned}
1.077\,J_1 &= +0.239 + 0.237\,J_3 + 0.130\,J_5 + 0.085\,J_7\\
0.967\,J_3 &= +0.00065 + 0.090\,J_1 + 0.070\,J_5 + 0.062\,J_7\\
0.951\,J_5 &= -0.00577 + 0.030\,J_1 + 0.047\,J_3 + 0.048\,J_7\\
0.963\,J_7 &= -0.00261 + 0.014\,J_1 + 0.028\,J_3 + 0.035\,J_5\\
0.975\,J_9 &= -0.00143 + 0.008\,J_1 + 0.017\,J_3 + 0.024\,J_5\\
0.985\,J_{11} &= -0.00072 + 0.005\,J_1 + 0.012\,J_3 + 0.018\,J_5
\end{aligned}
$$

These and a similar set of equations for the even J_i produce the following results:

$$
\begin{aligned}
J_1 &= 0.228 & J_2 &= -0.0703\\
J_3 &= 0.0221 & J_4 &= -0.00433\\
J_5 &= 0.00230 & J_6 &= -0.00186\\
J_7 &= 0.00131 & J_8 &= -0.00111\\
J_9 &= 0.00089 & J_{10} &= -0.00075\\
J_{11} &= 0.00069
\end{aligned}
$$

Appendix

Equations [11] must be satisfied for all values of θ and ξ in the regions

$$-\frac{\pi}{2} < \frac{k\theta}{2} < \frac{\pi}{2};\ 0 < p\xi < \pi$$

Since the solution of these equations is purely a mathematical problem, they may be rewritten in terms of dummy variables (in order to obtain a maximum of simplicity in the following work), provided it is understood that the functions are defined over the corresponding regions of these variables. We write then

$$\sum_m a_{1m}G_m \cos mx + \sum_m b_{1m}H_m \cos mx + \sum_n J_n\gamma_n'(x) = -\sum_m P_m \cos mx \ldots [11a]$$

$$\sum_m a_{2m}G_m \cos my + \sum_m b_{2m}H_m \cos my + \sum_n J_n\gamma_n(y) = -\sum_m Q_m \cos my \ldots [11b]$$

$$\sum_m G_m\alpha_m(Z) + \sum_m H_m\beta_m(Z) + \sum_n c_nJ_n \sin nZ = -\sum_m \mathfrak{L}_m(Z) \ldots\ldots [11c]$$

A previously developed method by which the values of G_m, H_m, and J_n may be found, proceeds as follows:[3] The functions α_m, β_m, γ_m, γ'_m and $\mathfrak{L}_m$ are expanded in Fourier series, thereby producing an infinite set of equations in the unknown coefficients. These may be solved by any of the variations on the method of successive approximations. This method has efficiently yielded the desired results in previous problems,[3] but in the present instance, the computational work is greatly reduced by the following procedure, in which Equations [11] are reduced to a set of equations in J_n only.

It is desirable, first, to solve simultaneously Equations [11*a*, *b*] in such a way as to obtain an equation for the G_m (or the equivalent thereof) from which the H_m have been eliminated. To facilitate this, we define the functions

$$G(x) = \sum_m \frac{a_{1m}b_{2m} - a_{2m}b_{1m}}{b_{2m}} G_m \cos mx \ldots\ldots [12a]$$

$$H'(y) = \sum_m b_{2m}H_m \cos my \ldots\ldots [12b]$$

These expressions imply that

$$G_m = \frac{2b_{2m}}{\pi(a_{1m}b_{2m} - a_{2m}b_{1m})} \int_{-\pi/2}^{\pi/2} G(x) \cos mx dx \ldots [13a]$$

$$H_m = \frac{2}{\pi b_{2m}} \int_{-\pi/2}^{\pi/2} H'(y) \cos my dy \ldots\ldots [13b]$$

The substitution of Equations [12*a*] and [13*b*] into [11*a*], and of [12*b*] into [11*b*] produces the following pair of equations

$$G(x) = -\sum_m P_m \cos mx - \sum_n \gamma_n'(x)J_n - \sum_m \frac{a_{2m}b_{1m}}{b_{2m}} G_m \cos mx - \sum_m \frac{2b_{1m}}{\pi b_{2m}} \cos mx \int_0^\pi H'(y) \cos my dy$$

$$H'(y) = -\sum_m Q_m \cos my - \sum_n J_n\gamma_n(y) - \sum_m a_{2m}G_m \cos my$$

The further substitution of the latter of these into the former, followed by some of the indicated integrations, produces the desired equation for $G(x)$. This has the form

$$G(x) = -\sum_m \left(P_m - \frac{b_{1m}}{b_{2m}} Q_m\right) \cos mx - \sum_n J_n\gamma_n'(x) + \frac{2}{\pi} \sum_m \frac{b_{1m}}{b_{2m}} \cos mx \int_{-\pi/2}^{\pi/2} \sum_n J_n\gamma_n(y) \cos my dy \ldots [14a]$$

After a similar procedure, $H(x)$ which is defined as

$$H(x) = \frac{a_{1m}b_{2m} - a_{2m}b_{1m}}{a_{1m}} H_m \cos mx$$

is given by

$$H(x) = -\sum_m \left(Q_m - \frac{a_{2m}}{a_{1m}} P_m\right) \cos mx - \sum_n J_n\gamma_n(x) + \frac{2}{\pi} \sum_m \frac{a_{2m}}{a_{1m}} \cos mx \int_{-\pi/2}^{\pi/2} \sum_n J_n\gamma'_n(y) \cos my dy \ldots [14b]$$

The process of eliminating the G_m and H_m is continued by defining

$$J(\varphi) = \sum_n c_nJ_n \sin n\varphi$$

and the accompanying relation

$$J_n = \frac{2}{\pi c_n} \int_0^\pi J(Z) \sin nZ dZ \quad \ldots\ldots [15]$$

The G_m in Equation [11*c*] are now replaced by the expression occurring in Equation [13*a*], wherein $G(x)$ has been replaced by the right-hand side of Equation [14*a*]. The corresponding substitution is made for the H_m and $J(\varphi)$ becomes

[9] "Stress and Deflection of Rectangular Plates," by I. A. Wojtassak, Trans. A.S.M.E., vol. 58, 1936, pp. A-71 to A-73.

$$J(\varphi) = -\sum_m \left\{ \mathfrak{L}_m(\varphi) - \frac{(b_{2m}P_m - b_{1m}Q_m)\alpha_m(\varphi) + (a_{1m}Q_m - a_{2m}P_m)\beta_m(\varphi)}{a_{1m}b_{2m} - a_{2m}b_{1m}} \right\}$$

$$+ \frac{4}{\pi^2}\int_0^\pi \sum_n \frac{1}{c_n} J(Z)\sin nZ\,dZ \left\{ \sum_m \int_{-\pi/2}^{\pi/2} \frac{[b_{2m}\gamma_n(y) - b_{1m}\gamma_n'(y)]\alpha_m(\varphi) + [a_{1m}\gamma_n'(y) - a_{2m}\gamma_n(y)]\beta_m(\varphi)}{a_{1m}b_{2m} - a_{2m}b_{1m}} \cos my\,dy \right\} \quad [16]$$

After performing the integration over y, and after considerable algebraic simplification, this may be written

$$J(\varphi) = -\sum_m R_m(\varphi) + \int_0^\pi \sum_{m,n} K_{mn}(\varphi, Z)J(Z)dZ \quad \ldots\ldots [17]$$

where

$$R_m(\varphi) = \frac{k\mu_m}{4\lambda_m}\left\{ \begin{array}{l} [(u-2)(\epsilon^3 + \epsilon^{-1-3u}) - u(u+4)(\epsilon^{1-u} + \epsilon^{1-2u}) + (u+1)(u+2)(\epsilon^{-1-u} + \epsilon^{3-2u})]e^{(u-1)\frac{\varphi-\pi}{p}} \\ + [-(u+2)(1+\epsilon^{4-3u}) + (u-1)(u-2)(\epsilon^{4-u} + \epsilon^{-2u}) - (u)(u-4)(\epsilon^{2-u} + \epsilon^{2-2u})]e^{-(u+1)\frac{\varphi}{p}} \\ + [-(u-4)(\epsilon^3 + \epsilon^{1-3u}) + (u-1)(u+4)(\epsilon^{1-u} + \epsilon^{3-2u}) - u(u+2)(\epsilon^{-1-u} + \epsilon^{5-2u})]e^{(u+1)\frac{\varphi-\pi}{p}} \\ + [(u+4)(1+\epsilon^{2-3u}) - u(u-2)(\epsilon^{4-u} + \epsilon^{-2-2u}) + (u+1)(u-4)(\epsilon^{-2u} + \epsilon^{3-u})]e^{-(u-1)\frac{\varphi}{p}} \\ -2\lambda_m e^{3\frac{\varphi}{p}} \end{array} \right\}$$

$$K_{mn}(\varphi, Z) = -\frac{Y_{mn}}{c_n} u \sin nZ \, \frac{\sinh\frac{\varphi}{p}\sinh u\left(\frac{\pi-\varphi}{p}\right) + (-1)^{n-1}\sinh\frac{\pi-\varphi}{p}\sinh u\frac{\varphi}{p}}{\sinh u\frac{\pi}{p} + (-1)^{n-1}u\sinh\frac{\pi}{p}}$$

$$\mu_m = \frac{1}{(u^2-4)(u^2-16)} \qquad \lambda_m = (1-\epsilon^{-2u})^2 - u^2\epsilon^{-2u}\left(\epsilon - \frac{1}{\epsilon}\right)^2$$

The foregoing Fredholm equation may now be solved by expanding $J(\varphi)$, $K_{mn}(\varphi, t)$, $R(\varphi)$, in Fourier series, integrating, and obtaining

$$J_i = \sum_m R_{mi} + \sum_{m,n} K_{imn}J_n \quad \ldots\ldots\ldots\ldots [18]$$

where

$$R_{mi} = \frac{kip^2[1 + (-1)^{i-1}\epsilon^3]}{\pi(9 + i^2p^2)[(u+1)^2 + p^2i^2](2+u)(4-u)}$$

$$+ \frac{p^2k^2im\mu_m}{\pi\lambda_m T_{mi}}\left\{ \begin{array}{l} (-1)^{i-1}[(u-2)\epsilon^3 - (u-1)(u+4)\epsilon^{1-u} + (u+1)(u+2)\epsilon^{-1-u} - u(u-2)\epsilon^{5-2u} + 2(u^2-1)\epsilon^{3-2u} \\ \quad - u(u+4)\epsilon^{1-2u} + (u+1)(u-4)\epsilon^{1-3u} + (u-1)(u-2)\epsilon^{-1-3u} + (u+4)\epsilon^{3-4u}] \\ + [(u+4) - (u-1)(u-2)\epsilon^{4-u} + (u+1)(u-4)\epsilon^{2-u} - u(u+4)\epsilon^{2-2u} + 2(u^2-1)\epsilon^{-2u} \\ \quad - u(u-2)\epsilon^{-2-2u} - (u-1)(u+4)\epsilon^{2-3u} + (u+1)(u+2)\epsilon^{4-3u} + (u-2)\epsilon^{-4u}] \end{array} \right\} \quad [18a]$$

$$K_{imn} = [(-1)^{i-n} + 1]\frac{\cosh 2\varphi_n + \cos 2\theta_0}{\sinh 2\varphi_n} \cdot \frac{\cosh\frac{m\pi k}{2p} + (-1)^{i-1}\cosh\frac{\pi}{p}}{\sinh\frac{m\pi k}{2p} + (-1)^{i-1}u\sinh\frac{\pi}{p}} \cdot \frac{2in^2m^3p^4k^4}{\pi^2 T_{mi}T_{mn}}$$

$$T_{mn} = [(u+1)^2 + n^2p^2][(u-1)^2 + n^2p^2]$$

The J_i may now be found by the method of successive approximations with considerably less labor than by the procedure mentioned previously. It can easily be seen that the introduction of the function $J(\varphi)$ was unnecessary. However, this function was introduced both for the sake of consistency of procedure, and to note that in those analogous problems where $J(\varphi)$ might be the desired result (this would have been the case in the corresponding problem on the rectangular plate), and where $K_{mn}(\varphi, Z)$ could be summed to a sufficient degree of accuracy, the Fredholm equation might be of more use than those equations given by Equations [18].

A completely equivalent method of obtaining Equations [18] would be to continue the process outlined at the beginning of this section, by solving simultaneously the equations obtained therein and again eliminating the G_m and H_m. The difficulty here arises in the algebraic work required to obtain a simple form for R_{mi}. This was so involved in the present problem that it is doubtful if the comparatively simple form found, Equation [18a], would have been obtained by the latter procedure.

Since Equations [14] essentially determine the G_m and H_m, there remains only the obvious but tedious task of evaluating the R_{mi} and the K_{imn}, and applying the method of successive approximations to Equations [18]. The bending moments are found as outlined in the foregoing section.

ACKNOWLEDGMENT

The author is indebted to Prof. J. N. Goodier of Cornell University for suggesting this problem, and for his valuable criticisms during the conduct of the work.

Strengthening of Circular Holes in Plates Under Edge Loads

By LEON BESKIN,[1] ALLENTOWN, PA.

In this paper, stress distributions are determined around strengthened circular holes in plates submitted to edge loads at infinity. Various proportions of circular strengthenings are considered, and three conditions of applied edge loads are investigated; uniform hydrostatic stress, uniform shearing stress, uniform axial stress. Stress distributions are found by methods of theory of elasticity, and the results are given in the form of stress-concentration factors. In order to reduce the results to a common basis, the stress-concentration factors have been defined by the ratio of the critical stress, computed by the distortion-energy theory, to the critical stress at infinity, which is the critical stress in the plate without hole.

Nomenclature

The following nomenclature is used in the paper:

Dimensions, Co-Ordinates, Displacements

t = plate thickness
t' = ring thickness
R = radius of hole and of rim
R' = outer radius of ring
A = area of rim section

$x = \frac{R'}{R}; \quad y = \frac{A}{tR}; \quad y' = \frac{A}{t'R}; \quad z = \frac{t'}{t}$

$h = y + (z-1)(x-1)$ = (area of reinforcement): Rt

$M = 2y + (z-1)(x^2-1) = \frac{\text{weight of reinforcement}}{\text{weight corresponding to hole}}$

u, v = components of displacement
r, θ = polar co-ordinates

Stresses

$\sigma_r, \sigma_\theta, \tau_{r\theta}$ = normal and shearing stresses in plate related to polar co-ordinates
$\sigma'_r, \sigma'_\theta, \tau'_{r\theta}$ = corresponding stresses in ring
σ_1 = normal stress in rim
i = index for inner edge of plate or of ring
2 = index for circumference $r = 2R$
e = index for outer edge of ring
1 = index for rim ($r = R$)
E = modulus of elasticity
ν = Poisson's ratio (value 0.3)
p = uniform hydrostatic stress at infinity
$\sigma_r^*, \sigma_\theta^*$ = corresponding normal stresses
q = uniform shearing stress at infinity
$\bar{\sigma}_r, \bar{\sigma}_\theta, \bar{\tau}_{r\theta}$ = corresponding maximum normal and shearing stresses for given r

$\left.\begin{aligned}\sigma &= p + q\\ \sigma' &= p - q\end{aligned}\right\}$ = principal stresses at infinity

$a, m, K; a', m', K'$ = coefficients in plate and in ring, corresponding to hydrostatic stress at infinity
$b, c, d, f; b', c', d', f'$ = coefficients in plate and in ring, corresponding to shearing stress at infinity

$B = \bar{\sigma}_r^2 + \bar{\sigma}_\theta^2 - \bar{\sigma}_r\bar{\sigma}_\theta - 3\bar{\tau}_{r\theta}^2$

$C = \sigma_r^*\bar{\sigma}_r + \sigma_\theta^*\bar{\sigma}_\theta - \frac{1}{2}(\sigma_r^*\bar{\sigma}_\theta + \sigma_\theta^*\bar{\sigma}_r)$

$D = \sigma_r^{*2} + \sigma_\theta^{*2} - \sigma_r^*\sigma_\theta^* + 3\bar{\tau}_{r\theta r}^2$

N = critical-stress combination (*distortion theory*[2])

$N^2 = \sigma_r^2 + \sigma_\theta^2 - \sigma_r\sigma_\theta + 3\tau_{r\theta}^2$

N_0 = critical stress at infinity

$N_0^2 = p^2 + 3q^2$

$j = \frac{N}{N_0}$ stress-concentration factor

N, j can be affected with indices i, 2, e, 1 for corresponding parts of plate.

$j(0), j(45), j(90)$ = values of j along a radius forming an angle $\theta = 0, 45, 90$ deg with the direction of the stress at infinity.

Introduction

It is well known that if a circular hole is made in a plate submitted to given stresses, the distribution of stresses is very much altered in the vicinity of the hole, and the stresses are greatly increased in the region surrounding the hole.

In the following, the plate is supposed to be in a state of uniform plane stress at great distances from a hole, and the influence of circular beads around the hole is investigated.

Two basic solutions are examined: (1) Uniform stress acting in all directions (hydrostatic stress); and (2) uniform shearing stress. Any other uniform stress can be considered as a superposition of the two basic solutions, and the condition of a uniform tensile stress acting in one direction is investigated (designated as "axial stress").

It is well known that around a hole, the ratio of the maximum stress to the uniform stress at a great distance from the hole has the following values:

Condition	Ratio
Hydrostatic stress	2
Shearing stress	4
Tensile stress	3

The influence of the dimensions and shape of the section of the beads on the stress concentration will be investigated hereafter. The beads are divided into two parts, a rim and a ring, and the notations are shown in Fig. 1. The ring is constituted by an in-

---

[1] Consolidated Vultee Aircraft Corp., Allentown Division.

Contributed by the Aviation and Applied Mechanics Divisions and presented at the Semi-Annual Meeting, Pittsburgh, Pa., June 19–22, 1944, of The American Society of Mechanical Engineers.

Discussion of this paper should be addressed to the Secretary, A.S.M.E., 29 West 39th Street, New York, N. Y., and will be accepted until October 10, 1944, for publication at a later date. Discussion received after the closing date will be returned.

Note: Statements and opinions advanced in papers are to be understood as individual expressions of their authors and not those of the Society.

[2] "Theory of Elasticity," by S. Timoshenko, first edition, McGraw-Hill Book Company, Inc., New York, N. Y., 1934; Equation [84], p. 137.

crease of the thickness of the plate, and the rim is a section considered as being concentrated around the hole. For various proportions of ring and rim, the stress distribution in elastic condition is examined, and the critical stress is computed by the *distortion-energy theory* of Huber and von Mises.

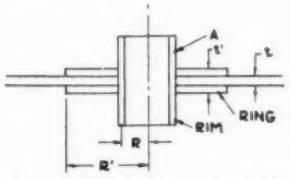


FIG. 1 SECTION OF BEADS, SHOWING NOTATIONS

It is assumed that the problem can be considered as a plane-stress problem, the thicknesses being considered as infinitely small in comparison with the plane dimensions, but questions connected with elastic stability are excluded. All stresses are supposed inferior to the yield point, and conventional expressions of theory of elasticity are used.

MATHEMATICAL DEVELOPMENTS

SOLUTION 1 HYDROSTATIC STRESS

The distribution has a circular symmetry, and the following solution can be used[3]
In the plate

$$\sigma_r = \frac{a}{r^2} + p; \quad \sigma_\theta = -\frac{a}{r^2} + p; \quad \tau_{r\theta} = 0 \dots\dots [1]$$

In the ring

$$\sigma'_r = \frac{a'}{r^2} + p'; \quad \sigma'_\theta = -\frac{a'}{r^2} + p'; \quad \tau_{r\theta}' = 0 \dots\dots [2]$$

The unknowns are p', a', a and the stress n_1 in the rim. Four equations of equilibrium and of equality of strain can be written at the outer and the inner edges of the ring as follows
Equilibrium of normal forces along radius

$$\frac{a}{R'^2} + p = z\left(\frac{a}{R'^2} + p'\right) \dots\dots [3]$$

$$\frac{a'}{R'^2} + p' = y'\sigma_1 \dots\dots [4]$$

Equality of strain along circumference

$$\left(-\frac{a}{R'^2} + p\right) - \nu\left(\frac{a}{R'^2} + p\right) = \left(-\frac{a'}{R'^2} + p'\right) - \nu\left(\frac{a'}{R'^2} + p'\right) \dots\dots [5]$$

$$\sigma_1 = \left(-\frac{a'}{R^2} + p'\right) - \nu\left(\frac{a'}{R^2} + p'\right) \dots\dots [6]$$

The solution of Equations [3] to [6] yields the values

$$p' = \frac{p}{z}\frac{1+m}{1+m'}; \quad a = R^2x^2mp; \quad a' = R^2x^2m'p' \dots\dots [7]$$

in which the quantities m and m' have the following values

$$m' = \frac{1}{x^2}\left[\frac{2y'}{y'(1+\nu)+1} - 1\right]; \quad W = \frac{1-m'}{1+m'};$$

$$m = \frac{2z}{(z-1)\nu + z + W} - 1 \dots\dots [8]$$

[3] "Theory of Elasticity," by S. Timoshenko, first edition, McGraw-Hill Book Company, Inc., New York, N. Y., 1934, p. 55.

The critical values of stress are as follows:
Along the hole

$$\sigma'_{ri} = p'(1 + x^2m'); \quad \sigma'_{\theta i} = p'(1 - x^2m') \dots\dots [9]$$

$$\sigma_1 = \sigma'_{ri}:y' \dots\dots [10]$$

Along the outer edge of the ring

$$\sigma'_{re} = p'(1 + m'); \quad \sigma'_{\theta e} = p'(1 - m') \dots\dots [11]$$

$$\sigma_{ri} = p(1 + m); \quad \sigma_{\theta i} = p(1 - m) \dots\dots [12]$$

The distribution of stress is represented by diagrams of the type shown in Fig. 2.

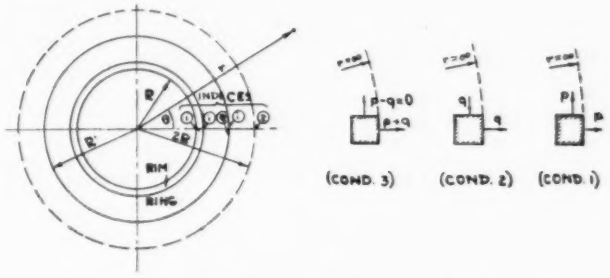


FIG. 2 DIAGRAM SHOWING DISTRIBUTION OF STRESS

When there is no ring, Equations [7] to [12] become

$$\left.\begin{aligned} a &= R^2mp; \quad m = \frac{2y}{y(1+\nu)+1} - 1 \\ \sigma_1 &= \sigma_{ri}:y; \quad \sigma_{ri} = p(1+m); \quad \sigma_{\theta i} = p(1-m) \end{aligned}\right\} \dots\dots [13]$$

When there is no rim, the value of m' is

$$m' = -1:x^2 \dots\dots [14]$$

For two principal stresses of the type

$$p(1 + K), \quad p(1 - K) \text{ or } p'(1 + K'), \quad p'(1 - K') \dots\dots [15]$$

the critical stress and the stress-concentration factors are equal to

$$\left.\begin{aligned} N &= p\sqrt{1+3K^2} \quad \text{or} \quad N = p'\sqrt{1+3K'^2} \\ j &= \sqrt{1+3K^2} \quad \text{or} \quad j = (p':p)\sqrt{1+3K'^2} \end{aligned}\right\} \dots\dots [16]$$

in which

$$K = \frac{R^2}{r^2}x^2m; \quad K' = \frac{R^2}{r^2}x^2m' \dots\dots [17]$$

The best strengthenings will fulfill the following conditions:
Stress in plate unchanged $m = 0$
Stresses in ring and rim not overstress in plate

$$p'\sqrt{1+3x^4m'^2} \le p; \qquad p'(1+x^2m'):y' \le p \dots\dots [18]$$

Thus there will be no overstressed region.
The condition $m = 0$ yields

$$z = \frac{1 - m'(1+\nu):(1-\nu)}{1+m'} \dots\dots [19]$$

For small values of y' the two conditions [18] are almost identical, and for values of y' greater than 0.5, the first condition is the most critical and is chosen as unique condition. For the two limit conditions, rim without ring and ring without rim, the amount of reinforcement is the same and is equal to $2:(1 - \nu) = 2.85714$ times the amount of material corresponding to the hole. A minimum of that amount appears for

$$y' = 0.6; \quad x = 2; \quad y = 1.2; \quad z = 1.25$$

and is equal to 2.30 times the material of the hole.

The general expression for the ratio of the additional material to the material corresponding to the hole is

$$2y'z + (z - 1)(x^2 - 1) = M$$

Table 1 gives the proportions for the optimum strengthenings.

TABLE 1 OPTIMUM STRENGTHENING IN HYDROSTATIC-STRESS CONDITION

y'	x	z	y	M
0	1.363	4.333	0	2.857
0.2	1.520	2.197	0.439	2.449
0.4	1.731	1.536	0.614	2.300
0.6	2.020	1.248	0.749	2.261
0.8	2.436	1.108	0.886	2.304
1.0	3.100	1.039	1.039	2.417
1.428	...	1.000	1.000	2.857

Solution 2 Pure Shearing Stress

The following solution corresponds to the symmetry of the problem[4]

$$\left.\begin{aligned} \sigma_r &= -\left(b + \frac{c}{r^4} + \frac{2d}{r^2}\right)\cos 2\theta \\ \sigma_\theta &= \left(b + \frac{c}{r^4} + 2fr^2\right)\cos 2\theta \\ \tau_{r\theta} &= \left(b - \frac{c}{r^4} - \frac{d}{r^2} + fr^2\right)\sin 2\theta \end{aligned}\right\} \quad \ldots [20]$$

There are 8 constants, 4 for each region of the plate, the constants in the ring are affected with the index prime ($'$). The differential equations for displacements[5] yield the following solution

$$\left.\begin{aligned} Eu &= \cos 2\theta\left[-b(1+\nu)r + \frac{c(1+\nu)}{3r^3} + \frac{2d}{r} - \frac{2\nu fr^3}{3}\right] \\ Ev &= \sin 2\theta\left[b(1+\nu)r + \frac{c(1+\nu)}{3r^3} - \frac{d(1-\nu)}{r} + \frac{(3+\nu)fr^3}{3}\right] \end{aligned}\right\} \quad \ldots [21]$$

The conditions at infinity yield $b = -q$; $f = 0$. The conditions at the outer edge of the ring express the equilibrium of normal and tangential stresses, and the equality of displacements u and v. They are

$$\left.\begin{aligned} -q + \frac{c}{R'^4} + \frac{2d}{R'^2} &= z\left(b' + \frac{c'}{R'^4} + \frac{2d'}{R'^2}\right) \\ -q - \frac{c}{R'^4} - \frac{d}{R'^2} &= z\left(b' - \frac{c'}{R'^4} - \frac{d'}{R'^2} + fR'^2\right) \\ \left(q + \frac{c}{3R'^4}\right)(1+\nu) + \frac{2d}{R'^2} &= \left(-b' + \frac{c'}{3R'^4}\right)(1+\nu) + \frac{2d'}{R'^2} - \frac{2\nu}{3}f'R'^2 \\ \left(-q + \frac{c}{3R'^4}\right)(1+\nu) - \frac{d(1-\nu)}{R'^2} &= \left(b' + \frac{c'}{3R'^4}\right)(1+\nu) - \frac{d'(1-\nu)}{R'^2} - \frac{3+\nu}{3}f'R'^2 \end{aligned}\right\} \quad \ldots [22]$$

[4] "Theory of Elasticity," by S. Timoshenko, first edition, McGraw-Hill Book Company, Inc., New York, N. Y., 1934, p. 75.

[5] Ibid., pp. 62–63.

Along the rim, there are three relations; one of strain, two of equilibrium

$$\sigma_1 = \sigma_{\theta_i} - \nu\sigma_{r_i}; \quad \sigma_1 y' = \sigma'_{r_i}; \quad y'\frac{d\sigma_1}{d\theta} + \tau_{r\theta_i}' = 0 \ldots\ldots [23]$$

Eliminating σ_1, the two remaining equations are

$$\left.\begin{aligned} \left(b' + \frac{c'}{R^4}\right)[1 + (\nu+1)y'] + \frac{2d'}{R^2}(1+\nu y') + 2f'R^2y' &= 0 \\ b' - \frac{c'}{R^4} - 2\left(b' + \frac{c'}{R^4}\right)(1+\nu)y' - \frac{d'}{R^2}(1+4\nu y') + f'R^2(1-4y') &= 0 \end{aligned}\right\} \quad \ldots [24]$$

The six Equations [22] and [24] yield the following solution: Calling

$$\delta = \frac{1+\nu y'}{1+(1+\nu)y'}; \quad \varphi = \frac{(z-1)(3-\nu)}{4+(z-1)(3-\nu)};$$

$$\psi = 1 + \frac{4}{(z-1)(1+\nu)} \ldots\ldots [25a]$$

$$\lambda = \frac{8:[4+(z-1)(3-\nu)]}{2x^6\psi(2\delta-3) + 2x^4(\varphi\psi+3) - 12x^2(2\delta-1) + 8(4\delta-3) - \frac{2\varphi}{x^2}(6\delta-5)} \ldots\ldots [25b]$$

The constants are

$$\left.\begin{aligned} b' &= q\lambda[4(3-4\delta) + 3x^2(2\delta-1) - \psi x^6(2\delta-3)] \\ \frac{c'}{R'^4} &= -3q\lambda\left[\frac{6\delta-5}{x^2} - \psi x^2(2\delta-1)\right] \\ \frac{d'}{R'^2} &= 2q\lambda\left[\frac{6\delta-5}{x^2} - \psi x^4\right] \\ f'R'^2 &= -6q\lambda x^2[1 - 2\delta + x^2] \\ \frac{c}{R'^4} &= -3q - z\left[3b' - \frac{c'}{R'^4} + 2f'R'^2\right] \\ \frac{d}{R'^2} &= 2q + z\left[2b' + \frac{d'}{R'^2} + f'R'^2\right] \\ b &= -q \end{aligned}\right\} \quad \ldots [26]$$

In the case where there is no ring, the equations simplify

$$b = -q; \quad c = -3R^4q\frac{1-y(1-\nu)}{1+y(3+\nu)};$$

$$d = 2R^2q\frac{1+y(1+\nu)}{1+y(3+\mu)} \ldots\ldots [26a]$$

In the case when there is no rim, $\delta = 1$, which simplifies the Equations [25], [26].

Calling $\bar{\sigma}_r$, $\bar{\sigma}_\theta$, $\bar{\tau}_{r\theta}$ the maximum values of σ_r, σ_θ, $\tau_{r\theta}$ for a given radius (corresponding to $\theta = 0$ or $\theta = \pi:4$), the stresses at any point of the circumference are

$$\sigma_r = \bar{\sigma}_r\cos 2\theta; \quad \sigma_\theta = \bar{\sigma}_\theta\cos 2\theta; \quad \tau_{r\theta} = \bar{\tau}_{r\theta}\sin 2\theta \ldots\ldots [27]$$

The critical-stress combination is N

$$\left.\begin{aligned} N^2 &= \sigma_r^2 + \sigma_\theta^2 - \sigma_r\sigma_\theta + 3\tau_{r\theta}^2 \\ &= (\bar{\sigma}_r^2 + \bar{\sigma}_\theta^2 - \bar{\sigma}_r\bar{\sigma}_\theta)\cos^2 2\theta + 3\bar{\tau}_{r\theta}^2\sin^2 2\theta \end{aligned}\right\} \quad [28]$$

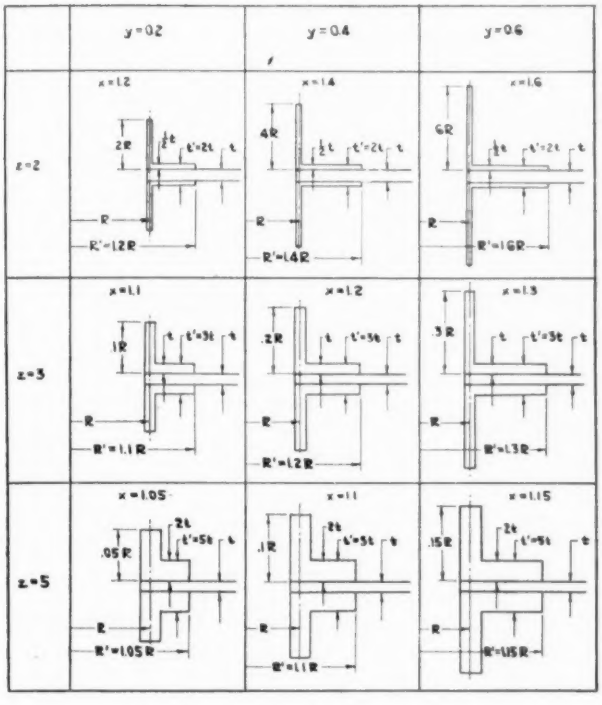


FIG. 3 RING AND RIM COMBINATIONS

The maximum occurs for $\theta = 0$ or $\theta = \pi{:}4$. Thus the two combinations of load must be calculated

$$\bar{\sigma}_r^2 + \bar{\sigma}_\theta^2 - \bar{\sigma}_r\bar{\sigma}_\theta;\ 3\bar{\tau}^2_{r\theta} \qquad [29]$$

and the larger quantity will determine the stress-concentration factor j. It is easily seen that the combination of normal stresses is always a decreasing function of the radius, thus its maximum occurs for the minimum radius. On the contrary, the shear may pass by a maximum, which must be determined.

SOLUTION 3 PURE TENSILE STRESS, I.E., AXIAL STRESS

The solutions corresponding to a stress of given direction at infinity can be determined by addition of solutions 1 and 2, in which $p = q$. Calling σ_r^* and σ_θ^* the solution under hydrostatic stress, the resultant stress is

$$\sigma_r = \bar{\sigma}_r \cos 2\theta + \sigma_r^*;\ \sigma_\theta = \bar{\sigma}_\theta \cos 2\theta + \sigma_\theta^*;\ \tau_{r\theta} = \bar{\tau}_{r\theta} \sin 2\theta \qquad [30]$$

The critical combination of stress is

$$\left.\begin{aligned} N^2 &= \cos^2 2\theta(\bar{\sigma}_r^2 + \bar{\sigma}_\theta^2 - \bar{\sigma}_r\bar{\sigma}_\theta - 3\bar{\tau}^2_{r\theta}) \\ &+ 2\cos 2\theta\left(\sigma_r^*\bar{\sigma}_r + \sigma_\theta^*\bar{\sigma}_\theta - \frac{\sigma^*\bar{\sigma}_\theta + \sigma^*\bar{\sigma}_r}{2}\right) \\ &+ (\sigma^{*2}_r + \sigma^{*2}_\theta - \sigma^*_r\sigma^*_\theta + 3\bar{\tau}^2_{r\theta}) \\ N^2 &= B\cos^2 2\theta + 2C\cos 2\theta + D \end{aligned}\right\} \qquad [31]$$

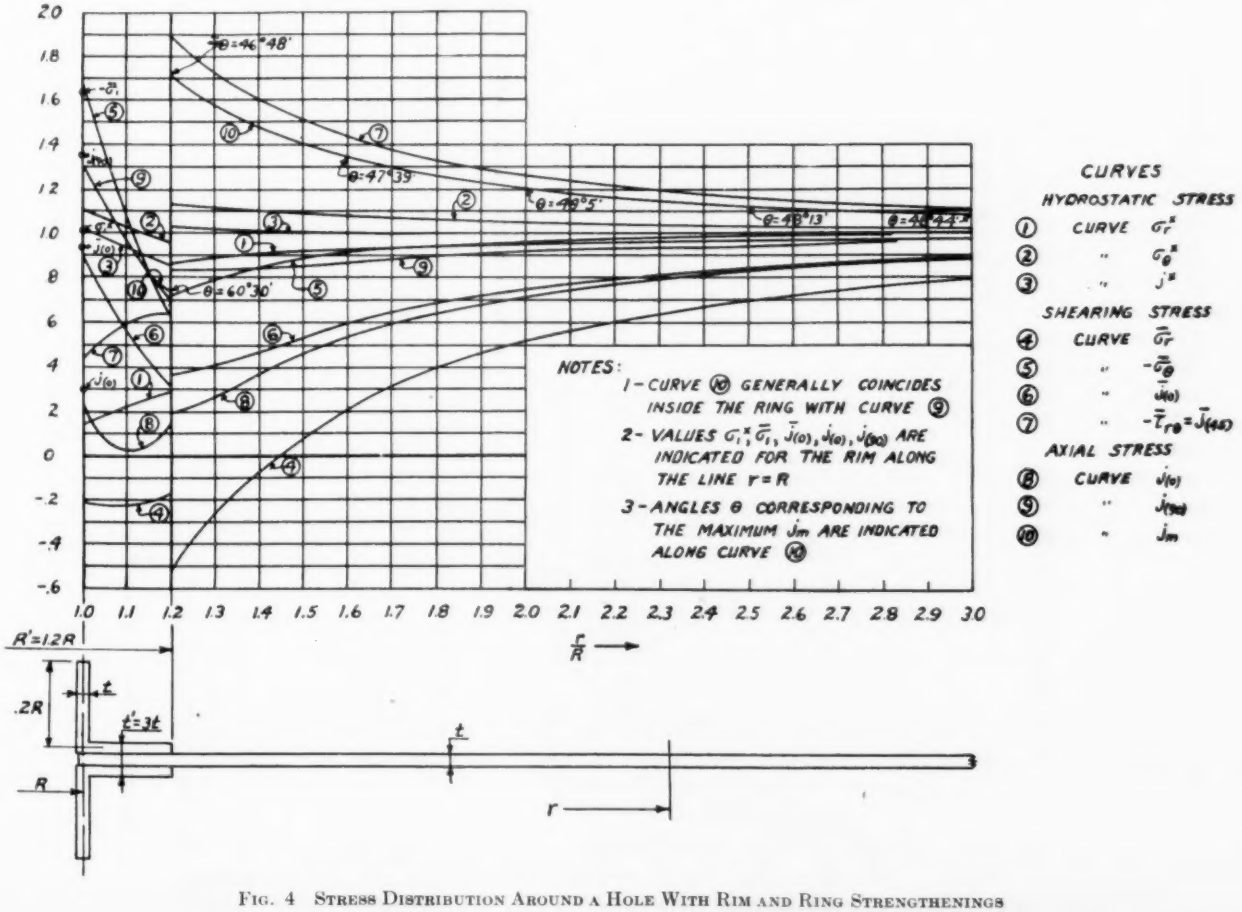


FIG. 4 STRESS DISTRIBUTION AROUND A HOLE WITH RIM AND RING STRENGTHENINGS

(Condition $\frac{R'}{R} = x = 1.2$; $\frac{t'}{t} = z = 3$; $y = \frac{A}{Rt} = 0.40$.)

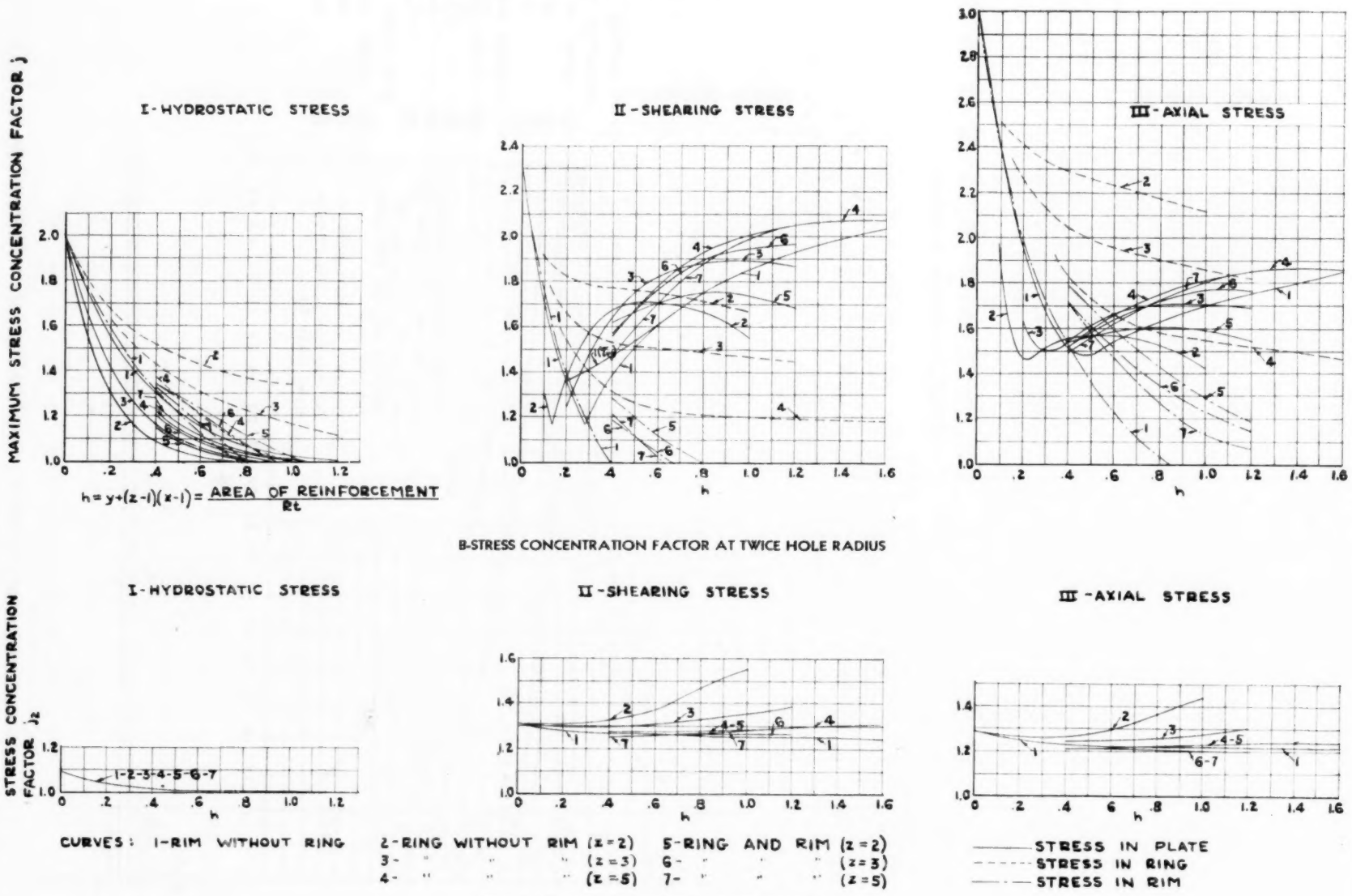


FIG. 5 VALUES OF STRESS-CONCENTRATION FACTORS

TABLE 2 RIM WITHOUT RING

A - Hydrostatic Stress

y	$\frac{a}{R^2p}=m$	$J_1=\frac{\tau_1}{p}$	$\frac{\sigma_{r1}}{p}$	$\frac{\tau_{\theta 1}}{p}$	$\frac{\sigma_{r2}}{p}$	$\frac{\sigma_{\theta 2}}{p}$	J_1	J_2
0	-1	(2)	0	2	.7500	1.2500	2.0000	1.0897
.1	-.82301	1.7699	.1770	1.8230	.7943	1.2057	1.7413	1.0617
.2	-.68254	1.5873	.3175	1.6825	.8294	1.1706	1.5484	1.0428
.3	-.56835	1.4388	.4317	1.5683	.8579	1.1421	1.4032	1.0298
.4	-.4736⁰	1.3158	.5263	1.4737	.8716	1.1184	1.2935	1.0177
.6	-.32584	1.1236	.6742	1.3258	.9185	1.0815	1.1483	1.0099
.8	-.21569	.9804	.7843	1.2157	.9461	1.0539	1.0675	1.0044
1.0	-.13043	.8696	.8696	1.1304	.9674	1.0326	1.0252	1.0016
1.2	-.06250	.7813	.9375	1.0625	.9844	1.0156	1.0059	1.0004
1.428..	0	.7000	1	1	1	1	1	1
2.0	.11111	.5556	1.1111	.8889	1.0278	.9722	1.0183	1.0012
3.0	.2244⁰	.4082	1.2245	.7755	1.0561	.9439	1.0729	1.0047
∞	.53846	0	1.5385	.4615	1.1346	.8654	1.3674	1.0289

B - Uniform Shearing Stress (b- -q ; f-0)

y	$\frac{c}{qR^4}$	$\frac{d}{qR^2}$	$\frac{\sigma_{r1}}{q}$	$\frac{\tau_{\theta 1}}{q}$	$-\frac{\tau_{r\theta 1}}{q}=J_1(45)$	$\frac{\sigma_{r2}}{q}$	$\frac{\sigma_{\theta 2}}{q}$
0	-3	2	0	-4	0	.1875	-1.1875
.1	-2.09774	1.69925	-.3008	-3.0977	.6015	.2715	-1.1311
.2	-1.55422	1.51807	-.4819	-2.5542	.9639	.3381	-1.0971
.3	-1.19096	1.39698	-.6030	-2.1910	1.2060	.3759	-1.0744
.4	-.93103	1.31035	-.6897	-1.9310	1.3793	.4030	-1.0582
.6	-.58389	1.19463	-.8054	-1.5839	1.6107	.4391	-1.0364
.8	-.36264	1.12088	-.8791	-1.3626	1.7582	.4622	-1.0227
1.0	-.20930	1.06977	-.9302	-1.2093	1.8604	.4782	-1.0131
1.2	-.09677	1.03226	-.9677	-1.0968	1.9355	.4899	-1.0060
1.428..	0	1	-1	-1	2	.5164	-1
2.0	.15790	.94737	-1.0526	-.8421	2.1053	.5663	-.9901
3.0	.30275	.89908	-1.1009	-.6972	2.2018	.5000	-.9811
∞	.63636	.78788	-1.2121	-.3636	2.4242	.5315	-.9402

B - Uniform Shearing Stress (continued)

y	$-\frac{\tau_{r\theta 2}}{q}=J_2(45)$	$\frac{\sigma_1}{q}$	$\frac{r(\tau_{r\theta m})}{R}$	$-\tau_{r\theta m}=J_m$	$J_1(0)$	$J_1(0)$	$J_2(0)$
0	1.3125	-4	1.7230	1.333	2.3094	2.3094	.6384
.1	1.2937	-3.0075	1.5713	1.3441	1.7364	1.7083	.5905
.2	1.2824	-2.4096	1.4309	1.3707	1.3912	1.3571	.5619
.3	1.2748	-2.0100	1.3058	1.4097	1.1605	1.1318	.5452
.4	1.2694	-1.7241	1.1921	1.4610	.9954	.9786	.5341
.6	1.2622	-1.3423			.7750	.7920	.5202
.8	1.2576	-1.0988			.6344	.6908	.5121
1.0	1.2544	-.9302			.5371	.6332	.5068
1.2	1.2520	-.8064			.4656	.5995	.5031
1.428..	1.2500	-.7000			.4041	.5774	.5000
2.0	1.2467	-.5263			.3039	.5570	.4952
3.0	1.2437	-.3058			.1766	.5615	.4911
∞	1.2367	-0			0	.6220	.4734

C - Uniform Tensile Stress (Axial Stress)

y	J_1 (θ-90°)	J_1	θ(J_1)	J_2	θ(J_2)
0	3	3.0000	90°	1.2886	52 49'
.1	2.3887	2.4005	90°	1.2632	52 2'
.2	1.9985	1.9495	90°	1.2481	51 37'
.3	1.7244	1.6818	90°	1.2377	51 20'
.4	1.5200	1.5063	70°20'	1.2293	51 3'
.6	1.2330	1.5429	52°44'	1.2212	50 54'
.8	1.0396	1.6296	49°41'	1.2155	50 44'
1.0	.8999	1.7009	48°31'	1.2119	50 38'
1.2	.7939	1.7577	47°57'	1.2093	50 33'
1.428..	.7000	1.8091	47°36'	1.2073	50 29'
2.0	.5410	1.9438	47°17'	1.2044	50 23'
3.0	.3570	2.0308	47°12'	1.2023	50 17'
∞	0	2.2813	47°34'	1.2000	49 59'

The maximum of N as a function of α is determined as follows:

$$\left.\begin{array}{ll} 1 & B>0;\ N^2=B+2|C|+D,\ \theta=0 \text{ or } \pi \\ 2 & B<0 \text{ and } |C:B|\geq 1; \\ & \qquad N^2=B+2|C|+D,\ \theta=0 \text{ or } \pi \\ 3 & B<0 \text{ and } |C:B|<1; \\ & \qquad N^2=D-\frac{C^2}{B},\ \cos 2\theta=-\frac{C}{B} \end{array}\right\} \quad \ldots[32]$$

With the knowledge of solutions 1 and 2, the stress-concentration factor can be determined. The maximum always appears for the minimum radius.

Numerical Results

The following types of strengthening are investigated:

(*a*) Rim without ring, defined by the quantity $y = A:(tR)$ for 13 values of y (0; 0.1; 0.2; 0.3; 0.4; 0.6; 0.8; 1.0; 1.2; $1:[1-\nu]$; 2; 3; ∞).

TABLE 3 RING WITHOUT RIM

A - Hydrostatic Stress

z	x	$\frac{a}{R^2p}=x^2m$	$\frac{a'}{R^2p}=\frac{p'}{p}$	$j'_i=\frac{\sigma_{\theta i}}{p}$	$\frac{\sigma'_{re}}{p}$	$\frac{\sigma'_{\theta e}}{p}$	$\frac{\sigma_{ri}}{p}$	$\frac{\sigma_{\theta i}}{p}$	$\frac{\sigma_{rz}}{p}$	$\frac{\sigma_{\theta z}}{p}$	j'_θ	j_i	j_z
2	1.1	-.83258	.89863	1.7972	.1560	1.6413	.3119	1.6881	.7918	1.2082	1.5691	1.5558	1.0630
	1.2	-.70582	.83430	1.6686	.2549	1.4137	.5098	1.4001	.8235	1.1765	1.3050	1.3118	1.0457
	1.3	-.59942	.79027	1.5806	.3227	1.1935	.6453	1.3547	.8501	1.1499	1.0693	1.1736	1.0331
	1.4	-.50366	.75851	1.5170	.3715	1.1455	.7430	1.2570	.8741	1.1259	1.0123	1.0946	1.0235
	1.6	-.32520	.71629	1.4326	.4365	.9961	.8730	1.1270	.9187	1.0813	.8648	1.0239	1.0099
	1.8	-.14903	.68695	1.3739	.4749	.8990	.9540	1.0460	.9627	1.0373	.7790	1.0032	1.0021
	2.0	.03362	.67227	1.3445	.5042	.8403	1.0084	.9916	1.0084	.9916	.7326	1.0001	1.0001
3	1.1	-.68588	.81591	1.6318	.1416	1.4902	.4248	1.5752	.8260	1.1740	1.4247	1.4116	1.0444
	1.2	-.49527	.71570	1.4314	.2187	1.2127	.6561	1.3439	.8762	1.1238	1.1195	1.1640	1.0227
	1.3	-.33774	.65327	1.3065	.2667	.9866	.8002	1.1998	.9156	1.0844	.8839	1.0582	1.0106
	1.4	-.20040	.61097	1.2219	.2993	.9227	.8978	1.1022	.9499	1.0501	.8154	1.0156	1.0038
	1.6	.05134	.55798	1.1160	.3400	.7759	1.0201	.9799	1.0128	.9872	.6737	1.0006	1.0002
5	1.1	-.48648	.68907	1.3781	.1176	1.2585	.5979	1.4021	.8784	1.1216	1.2032	1.2186	1.0220
	1.2	-.21399	.53728	1.0746	.1642	.9104	.8514	1.1486	.9465	1.0535	.8404	1.0326	1.0043
	1.3	-.01649	.46508	.9302	.1881	.7326	.9902	1.0098	.9959	1.0041	.6563	1.0002	1.0000
	1.4	.15131	.43986	.8797	.2154	.6643	1.0772	0.9228	1.0378	.9622	.2154	1.0089	1.0021
∞		(see y = ∞ table II)											

B - Uniform Shearing Stress (b=-q ; f=0)

z	x	$\frac{c}{qR^4}$	$\frac{d}{qR^2}$	$\frac{b'}{q}$	$\frac{c'}{qR^4}$	$\frac{d'}{qR^2}$	$\frac{f'R^2}{q}$	$\frac{\sigma_{\theta i}}{q}$	$\frac{\sigma'_{re}}{q}$	$\frac{\sigma_{\theta e}}{q}$	$-\frac{\tau'_{r\theta e}}{q}=j'_e(45)$
2	1.1	-2.13472	1.73843	-1.01822	-2.68018	1.84919	.18722	-3.3240	-.2077	-2.3957	.4893
	1.2	-1.46193	1.57481	-.99912	-2.57510	1.78710	.21112	-3.1520	-.2411	-1.6330	.6943
	1.3	.74356	1.42501	-.96813	-2.51805	1.74307	.19317	-3.0998	-.2130	-1.1969	.7914
	1.4	.08644	1.27192	-.93400	-2.47172	1.70285	.16514	-3.0754	-.1602	-.9301	.8357
	1.6	2.18785	.94822	-.86954	-2.38276	1.62616	.11291	-3.0265	-.0373	-.6550	.8521
	1.8	5.02793	.60348	-.81713	-2.29928	1.55828	.07606	-2.9643	.0743	-.5433	.8326
	2.0	7.83520	.24016	-.77660	-2.22576	1.50120	.05198	-2.8984	.1651	-.4999	.8049
3	1.1	-1.54490	1.55965	-1.03036	-2.46196	1.74613	.31457	-2.8632	-.1743	-1.9507	.4113
	1.2	-.56143	1.32212	-.99632	-2.32303	1.65969	.33296	-2.6534	-.1885	-1.1577	.5491
	1.3	.47503	1.10291	-.94498	-2.24764	1.59631	.29365	-2.6053	-.1572	-.7394	.6063
	1.4	1.66821	.87563	-.88991	-2.18141	1.53566	.24417	-2.5830	-.1092	-.5006	.6270
	1.6	4.66492	.38442	-.78897	-2.04767	1.41834	.15961	-2.5174	-.0067	-.2842	.6220
5	1.1	-.79208	1.33070	-1.04515	-2.18267	1.61392	.47639	-2.2750	-.1317	-1.3831	.3118
	1.2	.44094	1.03054	-.98863	-2.03420	1.51142	.46563	-2.0912	-.1296	-.6281	.3864
	1.3	1.75879	.74081	-.90945	-1.94475	1.42709	.39180	-2.0706	-.0985	-.2661	.4108
	1.4	3.26094	.43375	-.82681	-1.85388	1.34033	.31329	-2.0541	-.0583	-.0813	.4140
∞		1.44444	.96296								

B - Uniform Shearing Stress (continued)

z	x	$\frac{\sigma_{ri}}{q}$	$\frac{\sigma_{\theta i}}{q}$	$\frac{\tau_{r\theta i}}{q}=j_1(45)$	$\frac{\sigma_{rz}}{q}$	$\frac{\sigma_{\theta z}}{q}$	$-\frac{\tau_{r\theta z}}{q}=j_2(45)$	$j'_1(0)$	$j'_e(0)$	$j_i(0)$	$j_z(0)$
2	1.1	-.4154	-2.4580	.9781	.2642	-1.1334	1.3012	1.9191	1.5691	1.3157	.7425
	1.2	-.4822	-1.7050	1.3886	.3040	-1.0914	1.3023	1.8198	1.3050	.8789	.7338
	1.3	-.4261	-1.2603	1.5829	.3340	-1.0465	1.3098	1.7897	1.0693	.6411	.7207
	1.4	-.3204	-.9775	1.6714	.3587	-.9946	1.3234	1.7756	1.0123	.4983	.7011
	1.6	-.0746	-.6662	1.7042	.3892	-.8633	1.3738	1.7473	.8648	.3650	.6410
	1.8	.1488	-.5210	1.6652	.3840	-.6958	1.4651	1.7114	.7790	.3516	.5476
	2.0	.3902	-.5103	1.5497	.3902	-.5103	1.5497	1.6734	.7326	.4516	.4516
3	1.1	-.5228	-2.0552	1.2338	.3167	-1.0966	1.2933	1.6531	1.4247	1.0681	.7416
	1.2	-.5655	-1.2708	1.6474	.3840	-1.0351	1.2954	1.5320	1.1195	.6367	.7340
	1.3	-.4715	-.8337	1.8189	.4189	-.9703	1.3054	1.5042	.8839	.4180	.7126
	1.4	-.3278	-.5658	1.8810	.4579	-.8958	1.3242	1.4913	.8154	.2841	.6866
	1.6	-.0200	-.2882	1.8658	.5112	-.7084	1.3902	1.4534	.6737	.1609	.6125
5	1.1	-.6585	-1.5410	1.5588	.3842	-1.0495	1.2732	1.3135	1.2032	.7732	.7421
	1.2	-.6479	-.7835	1.9322	.4567	-.9719	1.2857	1.2073	.8404	.4187	.7296
	1.3	-.4925	-.3842	2.0542	.5197	-.8901	1.2951	1.1955	.6563	.2588	.7129
	1.4	-.2915	-.1512	2.0702	.5793	-.7962	1.3123	1.1859	.2154	.1458	.6986
∞		1.4815	.4444	1.4815	1.3912	-.9097	.8499			1.0084	1.1588

C - Uniform Tensile Stress (Axial Stress)

z	x	$j'_1(\theta=90)$	j'_e	θ'_e	j_i	θ_i	j_z	θ_z
2	1.1	2.5106	1.9340	90°	1.9173	90°	1.2680	52°22'
	1.2	2.4103	1.4157	90°	1.4706	62°34'	1.2598	51°21'
	1.3	2.3402	1.0863	90°	1.5131	50°55'	1.2587	50°21'
	1.4	2.2962	.9575	64°44'	1.5561	48°24'	1.2638	49°22'
	1.6	2.2291	.8763	53°19'	1.5644	46°40'	1.2958	47°32'
	1.8	2.1693	.8307	50°56'	1.5274	45°50'	1.3650	46° 9'
	2.0	2.1227	.7955	50° 6'	1.4323	45°13'	1.4323	45°13'
3	1.1	2.2475	1.6472	90°	1.6308	90°	1.2530	51°31'
	1.2	2.0424	1.0976	90°	1.5600	50°20'	1.2433	48°53'
	1.3	1.9559	.7796	78°24'	1.6669	47°19'	1.2440	48°57'
	1.4	1.9025	.7114	56°10'	1.7070	46°20'	1.2550	47°24'
	1.6	1.8166	.6406	49°30'	1.6917	45°24'	1.3038	45°28'
5	1.1	1.8266	1.2627	90°	1.5214	53°38'	1.2265	50°20'
	1.2	1.5829	.7479	90°	1.7548	47°	1.2256	48°11'
	1.3	1.5204	.4971	54°49'	1.8489	46°	1.2291	46°35'
	1.4	1.4669	.3754	47°10'	1.8627	45°32'	1.2420	45°14'
	∞				1.5849	63°58'	1.2839	90°

TABLE 4 RIM AND RING COMBINED

A - Hydrostatic Stress

z	x	y	y'	$\frac{p'}{p}$	$\frac{a'}{R^2p}$	$\frac{a}{R^2p}$	$j_1=\frac{\sigma_1}{p}$	$\frac{\sigma'_{ri}}{p}$	$\frac{\sigma'_{\theta i}}{p}$	$\frac{\sigma'_{r_2}}{p}$
2	1.2	.2	.1	.78217	-.64373	-.47482	1.3444	.1344	1.4259	.3351
	1.4	.4	.2	.70242	-.47943	-.16537	1.1180	.2230	1.1819	.4578
	1.6	.6	.3	.66415	-.37747	.08550	.9556	.2867	1.0416	.5167
3	1.1	.2	.0667	.73668	-.64629	-.47472	1.3558	.9094	1.3830	.2026
	1.2	.4	.1333	.62406	-.48223	-.19074	1.0637	.1418	1.1063	.2892
	1.3	.6	.2000	.56339	-.38453	.02243	.8943	.1789	.9489	.3559
5	1.05	.2	.05	.70370	-.65019	-.47429	1.3378	.05351	1.3539	.1140
	1.10	.4	.10	.56733	-.48511	-.20320	1.0278	.08222	1.0524	.1664
	1.15	.6	.15	.48967	-.38801	-.02460	.8472	.10166	.8777	.1690

A - Hydrostatic Stress (continued)

z	x	y	$\frac{\sigma'_{\theta r}}{p}$	$\frac{\sigma_{r_1}}{p}$	$\frac{\sigma_{\theta i}}{p}$	$\frac{\sigma_{r_2}}{p}$	$\frac{\sigma_{\theta 2}}{p}$	j'_i	j'_e	j_i	j_2
2	1.2	.2	1.2292	.6702	1.3297	.8813	1.1187	1.3637	1.1006	1.1516	1.0209
	1.4	.4	.9470	.9156	1.0844	.9587	1.0413	1.0876	.8203	1.0106	1.0026
	1.6	.6	.8116	1.0334	.9660	1.0214	.9786	.9320	.7116	1.0017	1.0007
3	1.1	.2	1.2708	.6077	1.3923	.8813	1.1187	1.3401	1.1826	1.2090	1.0209
	1.2	.4	.9589	.8675	1.1325	.9523	1.0477	1.0426	.8520	1.0260	1.0034
	1.3	.6	.7900	1.0133	.9867	1.0056	.9944	.8733	.6876	1.0003	1.0006
5	1.05	.2	1.2934	.5698	1.4302	.8814	1.1186	1.3280	1.2404	1.2471	1.0209
	1.10	.4	.9682	.8321	1.1679	.9492	1.0508	1.0138	.8967	1.0414	1.0039
	1.15	.6	.8103	.9814	1.0186	.9938	1.0062	.8315	.7405	1.0005	1.0006

B - Uniform Shearing Stress (b -q f 0)

z	x	y	$\frac{e}{qR^4}$	$\frac{d}{qR^2}$	$\frac{b'}{q}$	$\frac{c'}{qR^4}$	$\frac{d'}{qR^2}$	$\frac{f'R^2}{q}$	$\frac{\sigma'_{ri}}{q}$	$\frac{\sigma_{\theta i}}{q}$
2	1.2	.2	-.47471	1.22428	-.97601	-1.78816	1.49334	.23616	-.2225	-2.2919
	1.4	.4	1.46668	.73680	-.87961	-1.28020	1.25407	.15681	-.3483	-1.8462
	1.6	.6	3.71174	.30148	-.80311	-.93846	1.08449	.09433	-.4274	-1.5529
3	1.1	.2	-.69510	1.26378	-1.02158	-1.86919	1.51430	.39104	-.1378	-2.1087
	1.2	.4	.58763	.88944	-.95112	-1.47293	1.32073	.36409	-.2174	-1.6959
	1.3	.6	1.81141	.55738	-.86881	-1.18989	1.16895	.28947	-.2792	-1.4798
5	1.05	.2	-.93644	1.36252	-1.04989	-1.91693	1.52542	.51097	-.0840	-1.9449
	1.10	.4	-.00055	1.06561	-1.02115	-1.59596	1.36936	.56755	-.1216	-1.4820
	1.15	.6	.74046	.83642	-.96996	-1.39620	1.26027	.53948	-.1544	-1.2862

B - Uniform Shearing Stress (continued)

z	x	y	$-\frac{\tau'_{r\theta i}}{q}=j'_i(45)$	$\frac{\sigma_{r_1}}{q}$	$\frac{\sigma'_{re}}{q}$	$\frac{\sigma_{\theta 2}}{q}$	$-\frac{\tau'_{re\theta}}{q}=j'_e(45)$	$\frac{\sigma_{ri}}{q}$	$\frac{\sigma_{\theta_i}}{q}$	$-\frac{\tau_{r\theta i}}{q}=j_i(45)$
2	1.2	.2	.4450	-2.2251	-.2357	-1.1582	.8106	-.4714	-1.2289	1.6213
	1.4	.4	.6957	-1.7417	-.0668	-.5982	.8789	-.1336	-.6182	1.7577
	1.6	.6	.8548	-1.4247	.0991	-.4634	.8421	.1981	-.4336	1.6841
3	1.1	.2	.2757	-2.0674	-.2047	-1.3519	.5232	-.6141	-1.4748	1.5697
	1.2	.4	.4348	-1.6306	-.1729	-.6129	.6337	-.5187	-.7166	1.9011
	1.3	.6	.5584	-1.3996	-.0979	-.3070	.6546	-.2938	-.3658	1.9640
5	1.05	.2	.1474	-2.1007	-.1403	-1.5003	.2931	-.7013	-1.7704	1.4654
	1.10	.4	.2270	-1.5201	-.1522	-.7377	.3761	-.7610	-1.0004	1.8803
	1.15	.6	.2946	-1.2865	-.1377	-.3413	.4112	-.6883	-.5766	2.0558

B - Uniform Shearing Stress (continued)

z	x	y	$\frac{\sigma_{r_2}}{q}$	$\frac{\sigma_{\theta 2}}{q}$	$-\frac{\tau_{r\theta 2}}{q}=j_2(45)$	$j_1(0)$	$j'_i(0)$	$j'_e(0)$	$j_i(0)$	$j_2(0)$
2	1.2	.2	.4175	-1.0297	1.2764	1.2847	1.2639	.6113	.6200	.7442
	1.4	.4	.5399	-.9083	1.2759	1.0056	.9809	.3278	.3253	.7319
	1.6	.6	.6091	-.7608	1.3079	.8226	.8022	.3002	.3231	.6864
3	1.1	.2	.4116	-1.0434	1.2725	1.1936	1.1797	.7287	.7408	.7500
	1.2	.4	.5186	-.9633	1.2591	.9414	.9228	.3160	.3701	.7512
	1.3	.6	.6081	-.8868	1.2526	.8081	.7862	.1547	.1938	.7518
5	1.05	.2	.4273	-1.0585	1.2571	1.2128	1.0994	.8287	.8916	.7649
	1.10	.4	.4672	-1.0000	1.2664	.8777	.8228	.3895	.5224	.7496
	1.15	.6	.5355	-.9537	1.2554	.7428	.7023	.1717	.3694	.7544

C - Uniform Tensile Stress (Axial Stress)

z	x	y	$j_1-(\theta=90)$	j'_i	$\theta(j'_i)$	j'_e	$\theta(j'_e)$	j_i	$\theta(j_i)$	j_2	$\theta(j_2)$
2	1.2	.2	1.7847	1.7764	90°	1.0797	90°	1.5358	50°15'	1.2277	50° 2'
	1.4	.4	1.4283	1.3933	90°	.9702	49°34'	1.6056	46°24'	1.2157	47°24'
	1.6	.6	1.1902	1.1607	90°	.9219	46°49'	1.5422	45°18'	1.2383	45°15'
3	1.1	.2	1.7116	1.6917	90°	1.2224	90°	1.5225	52°50'	1.2252	50°13'
	1.2	.4	1.3472	1.3205	90°	.7367	60°30'	1.7274	46°48'	1.2040	48° 5'
	1.3	.6	1.1469	1.1176	90°	.7582	48°41'	1.7736	45°49'	1.1950	46°12'
5	1.05	.2	1.7193	1.6161	90°	1.3378	90°	1.4926	59°10'	1.2141	50°36'
	1.10	.4	1.2740	1.2195	90°	.7855	90°	1.7162	47°45'	1.2109	48°29'
	1.15	.6	1.0669	1.0240	90°	.5165	90°	1.8515	46°28'	1.1984	47° 7'

(*b*) Ring without rim, defined by the quantities $x = R':R$ and $z = t':t$, for 3 values of z (2, 3, 5), and 7 values of x (1.1; 1.2; 1.3; 1.4; 1.6; 1.8; 2) (total of 16 combinations); and for an infinitely rigid hub of outer radius R.

(*c*) Combinations of ring and rim, corresponding to angles with equal legs assembled to the plate; this corresponds to the condition

$$y = (z - 1)(x - 1)$$

calculated for the following values (9 combinations) (see Fig. 3)

z	x		
2	1.2	1.4	1.6
3	1.1	1.2	1.3
5	1.05	1.10	1.15
y	0.2	0.4	0.6

Tables 2, 3, and 4 give the results for the two basic solutions (hydrostatic stress and pure shear), and for the combination tensile stress in one direction (axial stress).

Fig. 4 shows a stress-distribution diagram for the condition $z = 3$; $x = 1.2$. The curves in Fig. 5 give a summary of the results of the tables, showing the values of the stress-concentration factors (maximum value and value for $z = 2R$).

Conclusions

Examination of the curves in Fig. 5, and Tables 2, 3, and 4, leads to the following conclusions:

1 *Hole in Plate Under Hydrostatic Stress.* A rim strengthening (flanged hole) gives the smallest stress-concentration factor for a given weight of material. With an area equal or superior to Rt, a flange will give a stress-concentration factor practically equal to 1. For $A = 0.4Rt$, the stress concentration is equal to 1.3.

Thin ring strengthenings (doubler plate) are to be rejected, as the stress concentration in the doubler is high. Thick ring strengthenings can be successfully used; for instance with $t' = 5t$, $R' = 1.2R$, $h = 0.8$, it is found that $j = 1.08$.

Ring-rim combinations (angle around the hole) with thick flanges, give low stress concentration; for instance, with $t' = 5t$, $R' = 1.1R$, $h = 0.8$, it is found that $j = 1.04$.

TABLE 5 STRESS-CONCENTRATION FACTORS

Condition	Stress-concentration factor j: Without reinforcement	With reinforcement	Reinforcement factor h*
Hydrostatic stress	2	1.3	.4
Shearing stress	2.3	1.35	.2
Axial stress	3	1.5	.4

* $h = \frac{A}{Rt} + \left(\frac{t'}{t} - 1\right)\left(\frac{R'}{R} - 1\right)$

Generally speaking, any reinforcement with thick flanges, having an area such as $h = 0.8$, will give negligible stress concentrations under hydrostatic stress.

2 *Hole in Plate Under Shearing Stress.* In this condition the stress-concentration factor is always above 1.35. That minimum is reached with a flanged hole corresponding to $A = 0.2Rt$. Comparable values of j can be obtained with thick doublers, for instance with $t' = 5t$, $R' = 1.08$, $h = 0.32$, a value of $j = 1.4$ is obtained. Due to high stress concentration in thin doublers, the latter give high values of j. Thick angles give values of j comparable to that of a flanged hole, with a somewhat increased area; for instance with $t' = 5t$, $R' = 1.04$, $h = 0.32$ corresponds to $j = 1.35$.

3 *Hole in a Plate Under Axial Stress.* In this condition, the stress-concentration factor is always above 1.5. That minimum is obtained with a flanged hole such as $A = 0.4Rt$. Thick doublers ($t' = 5t$) may give $j = 1.75$, for $h = 0.6$. Thin doublers, as in the previous conditions, are to be rejected. Thin reinforcing angles are nearly as efficient as thick angles: for $t':t = 5$, and $h = 0.5$, the value of j is 1.55, while for $t':t = 2$, and $h = 0.6$ the value of j is 1.60.

4 *General Conclusions.* Thin doublers are generally inefficient in respect to their effect on the stress-concentration factor. Generally, the best strengthenings are obtained with flanged holes or reinforcing angles with thick legs. An average value of 0.2 to 0.4 for the ratio h = (area of reinforcement):Rt will give the best results, bringing the stress-concentration factors to the values given in Table 5.

Equivalent Circuits of the Elastic Field

By GABRIEL KRON,[1] SCHENECTADY, N. Y.

This paper presents equivalent circuits representing the partial differential equations of the theory of elasticity for bodies of arbitrary shapes. Transient, steady-state, or sinusoidally oscillating elastic-field phenomena may now be studied, within any desired degree of accuracy, either by a "network analyzer," or by numerical- and analytical-circuit methods. Such problems are the propagation of elastic waves, determination of the natural frequencies of vibration of elastic bodies, or of stresses and strains in steady-stressed states. The elastic body may be non-homogeneous, may have arbitrary shape and arbitrary boundary conditions, it may rotate at a uniform angular velocity and may, for representation, be divided into blocks of uneven length in different directions. The circuits are developed to handle both two- and three-dimensional phenomena. They are expressed in all types of orthogonal curvilinear reference frames in order to simplify the boundary relations and to allow the solution of three-dimensional problems with axial and other symmetry by the use of only a two-dimensional network. Detailed circuits are given for the important cases of axial symmetry, cylindrical co-ordinates (two-dimensional) and rectangular co-ordinates (two- and three-dimensional). Nonlinear stress-strain relations in the plastic range may be handled by a step-by-step variation of the circuit constants. Nonisotropic bodies and nonorthogonal reference frames, however, require an extension of the circuits given. The circuits for steady-state stress and small oscillation phenomena require only inductances and capacitors, while the circuits for transients require also standard (not ideal) transformers. A companion paper[2] deals in detail with numerical and experimental methods to solve the equivalent circuits.

Equations of Elasticity

An equivalent circuit must satisfy each and all of the forms in which the equations of the elastic field may be expressed. Some of these forms are as follows:

1 Integral equations
2 Differential equations
3 Finite-difference equations.

To establish the network pattern, this paper will use the integral approach to the physical problem, while to find the network constants, the differential equations will be employed. However, most engineers will undoubtedly prefer to replace first the differential equations by the finite-difference equations and to use for all analysis the resulting set of linear algebraic equations. While this last method offers the path of least resistance, it is thought to be the longest, most tedious, and least fruitful of attacks.

The equivalent circuit must satisfy three sets of elasticity equations, which are as follows:

1 "Hooke's law," representing six relations between the stresses and strains.

2 The "equations of equilibrium," representing three relations between the stresses.

3 The "conditions of compatibility," representing six relations between the strains.

Since the stresses will be represented by currents and the strains by voltages, the electrical equivalents of the foregoing three sets of equations are as follows:

1 Hooke's law corresponds to Ohm's law, $I = YE$, determining the value of the "admittances" Y of the circuit elements.

2 The equations of equilibrium correspond to Kirchhoff's second law, stating that the sum of the "currents" I, entering each junction, is zero.

3 The conditions of compatibility correspond to Kirchhoff's first law, stating that the sum of the "voltages" E, around each mesh, is zero.

Equations of Equilibrium

Assuming orthogonal curvilinear co-ordinates, and no body forces, let the co-ordinate surfaces cut the three-dimensional elastic body into infinitesimal blocks, such as shown in Fig. 1. On each of the six surfaces, stresses act in a general direction. These stresses will be expressed here as components of a vector F^{α}. If each of the stresses is projected along the three tangent lines drawn to the co-ordinate lines passing through the centers of the six walls, the resultant stresses are eighteen in number, nine of which define a set of three new vectors. Each arrow in Fig. 1 will be assumed to represent the surface integral of the particular stress $\sigma'^{\alpha\beta}$ on its own wall.

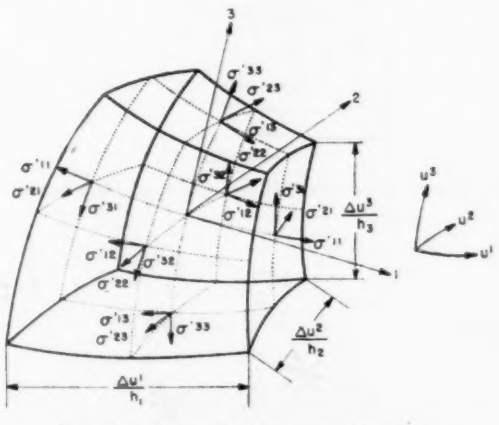


Fig. 1 Surface Integrals of Stresses

Next, at the center of the block, let a tangent line be drawn to the u^1 co-ordinate line, and let the eighteen different stresses be projected along this line. (Because of the orthogonality of the axes, the projections of σ'^{23} and σ'^{32} are zero.)

It is intended to represent these stresses by six currents entering the center of the block along the co-ordinate lines, as shown

---

[1] Consulting Engineer, General Electric Company.

[2] "Numerical and Network-Analyzer Solutions of the Equivalent Circuits for the Elastic Field," by G. K. Carter, published in the current issue of the Journal of Applied Mechanics, pp. 162–167.

Presented at the National Meeting of the Applied Mechanics Division, Chicago, Ill., June 16-17, 1944, of The American Society of Mechanical Engineers.

Discussion of this paper should be addressed to the Secretary, A.S.M.E., 29 West 39th Street, New York, N. Y., and will be accepted until October 10, 1944, for publication at a later date. Discussion received after the closing date will be returned.

Note: Statements and opinions advanced in papers are to be understood as individual expressions of their authors and not those of the Society.

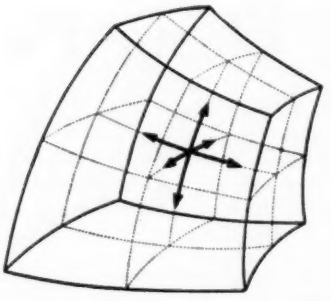


FIG. 2 REPRESENTATION OF STRESS PROJECTIONS BY CURRENTS

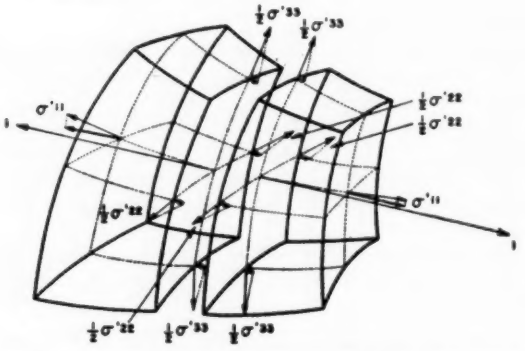


FIG. 3 (*a*) PROJECTION OF DIRECT STRESSES ALONG u^1



FIG. 3 (*b*) THEIR REPRESENTATION BY CURRENTS

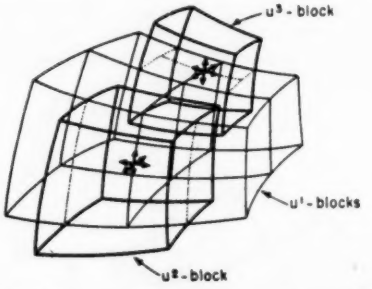


FIG. 4 THREE SUCCESSIVE SUBDIVISIONS OF THE ELASTIC BODY

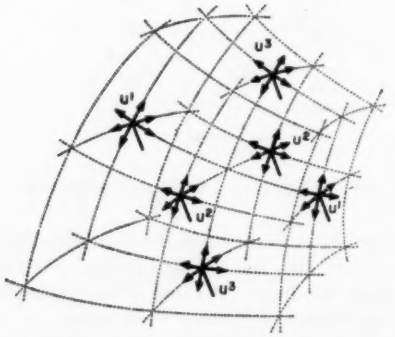


FIG. 5 SPATIAL ARRANGEMENTS OF CURRENTS

in Fig. 2. For this purpose the stresses are divided into three groups as follows:

1 The block is divided into two halves along axis u^1, Fig. 3 (*a*). On each half-block the u^1 projections of the direct stresses σ'^{11}, σ'^{22}, and σ'^{33} are added, and their sum is represented by currents in the u^1 direction, as shown in Fig. 3(*b*).

2 The block is now divided into two parts along axis u^2. On each half-block the u^1 projections of the shear stresses σ'^{12} and σ'^{21} are added, and their sum is represented by currents along the u^2 direction.

3 The same block is finally divided into two parts along the u^3 axis and the projections of the shear stresses σ'^{13} and σ'^{31} on each half-block are represented by currents along the u^3 direction.

The resultant of all the u^1 projections of the stresses on the block is represented by the six currents in Fig. 2, at the center of the block, adding up to zero. When a body force exists, then the six currents do not add up to zero but to a seventh current representing the body forces in the u^1 direction.

In order to represent next the projections of the stresses upon the tangent line drawn at the center of a block to the u^2 co-ordinate line, the whole elastic body is divided all over again into blocks, in the manner shown in Fig. 4. The u^2 blocks are shifted half a block on the u^1–u^2 surface from the u^1 blocks. In each of these u^2 blocks, the stresses are projected along the u^2 tangent line, then are divided again into three groups and represented by six currents as before. The previous reasoning is repeated with a cyclic variation of u^1–u^2–u^3.

Finally the whole elastic body is subdivided for the third time into u^3 blocks (Fig. 4), shifted half a block on the u^1-u^3 surface from the u^1 blocks. The stresses are projected upon the tangent line to the u^3 axis at the center of the block and again represented by six currents entering a junction.

As a result of three successive subdivisions, the stress representations are arranged in space as shown in Fig. 5, that is, the equivalent circuit does not represent the "total" stresses acting upon an infinitesimal block of the elastic body. The circuit represents only the projections of the stresses either along the u^1 or along the u^2 or u^3 axes. But these blocks with the different projections are so interspersed with each other that the resultant stresses on each block are known within a half-block accuracy.

HOOKE'S LAW

The absolute potential (above ground) of a u^1 (or u^2, u^3) junction represents the total displacement $s_{(1)}$ of that particular point of the elastic body in the u^1 (or u^2, u^3) direction if rectangular co-ordinates are used. (In curvilinear co-ordinates, the absolute potential represents s_1 which is equal to $s_{(1)}/h_1$.) The difference of potential between two u^1 junctions, say, along the u^2 axis, represents $(\partial s_1/\partial u^2)\,\Delta u^2$. Hence, each strain $e_{\alpha\beta}$ is represented as the sum of several voltage drops across coils connecting either two u^1 (or u^2, u^3) points, or each u^1 (or u^2, u^3) point to the ground.

(Theoretically, it is possible to have any of three different grounds, one for each type of junction, or one common ground. In numerical calculations one ground is sufficient, but in using the "network analyzer," the availability of three different grounds has been found to be of advantage.)

To find the coil impedances in transient problems, the equation of equilibrium has to be divided by $p = \partial/\partial t$; then:

1 All coils that represent stresses are inductances.

2 All ground coils that represent the mass of the elastic body are capacitors.

3 The forces f^α applied on the elastic body appear on the equivalent network as impressed currents of the form

$$\rho' f^\alpha / p = \rho' \int f^\alpha dt$$

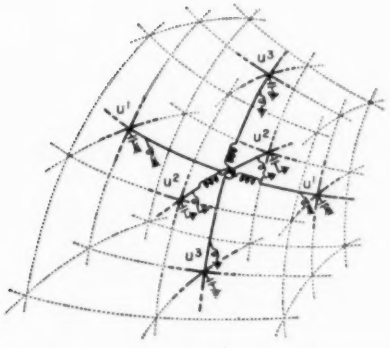


FIG. 6 TRANSIENT EQUIVALENT NETWORK

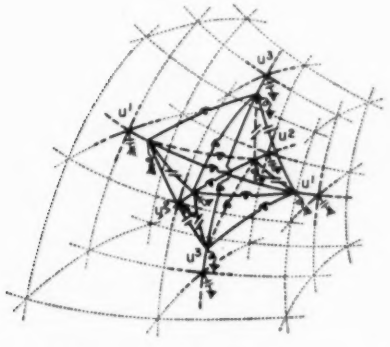


FIG. 7 NETWORK FOR SMALL OSCILLATIONS

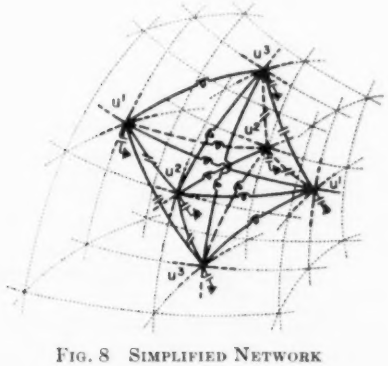


FIG. 8 SIMPLIFIED NETWORK

Hence in the "transient" equivalent circuit, the admittances are arranged as shown in Fig. 6, where mutual couplings exist between the three central inductances as dictated by Hooke's law. In curvilinear axes, mutual coupling exists also between a central and a ground coil. All central coils are assumed to lie in space at points half-way between the junctions, where the total displacements s_α are measured.

In steady-state ($p = 0$), and small-oscillation ($p = j\omega$) problems, the mutual couplings may be replaced, if so desired, by well-known methods with straight inductances and capacitors between the entrance points of the transformers, as shown in Fig. 7. In other words, in these problems the equation of equilibrium is satisfied also by a network containing only positive and negative resistances. Since no negative resistances are available in the d-c network analyzer, the two types of resistances are replaced by the inductances and capacitors of the a-c analyzer.

The difference between a network used for sinusoidally oscillating elastic-field problems and one used for steady-state problems is merely the presence or absence of the ground condensers representing the mass of the elastic body. As the frequency of mechanical oscillation varies, the magnitude of the ground condensers on the constant-frequency a-c analyzer also is varied (leaving the rest of the network admittances unchanged). At zero frequency (steady state), the condenser admittances become zero and they can be removed. It should be expressly noted that the transient network containing transformers may also be used for oscillating and steady-state problems as well, and without the necessity of changing the condenser admittances with the frequency of oscillations.

Since, in the last network, two diagonal and several ground coils are everywhere in parallel, for purposes of practical analysis the network may be simplified as shown in Fig. 8.

CONDITIONS OF COMPATIBILITY

When an electrical network has been developed in which the currents entering each of the junctions satisfy some one of the three equations of equilibrium, the network performance still may not correspond to the behavior of an elastic body; that is, numerous networks may be developed which satisfy merely the

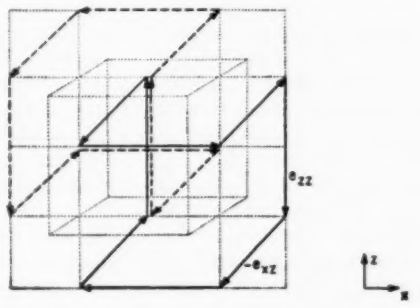


FIG. 9 EQUATION OF COMPATIBILITY, $K_{zzzz} = 0$

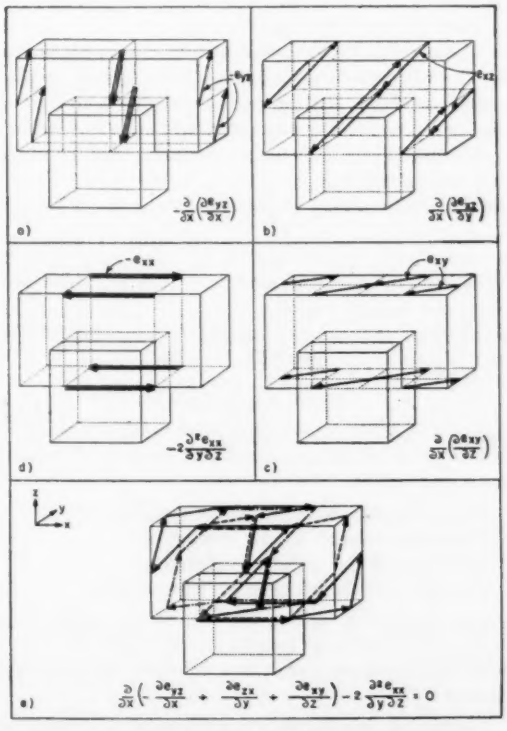


FIG. 10 EQUATION OF COMPATIBILITY $K_{zyzx} = 0$

equations of equilibrium. It is yet necessary that the voltage drops (strains) should satisfy six conditions of compatibility by being added up to zero in closed meshes that conform to a definite prescribed pattern.

In rectangular co-ordinates, each of the six equations represents two or four simultaneously closed meshes, as shown in Figs. 9 and 10. (There are two other figures similar to each of these, differing only by a cyclic interchange of indices.) It should be noted that each line passes through actual coils. In representing the strains say e_{zz} by two lines, they may be either both diagonal (as shown) or one horizontal and the other vertical, ending in the same points as before.

In curvilinear co-ordinates, each equation of compatibility is satisfied simultaneously by the meshes mentioned plus additional meshes formed by the additional ground coils. An example is given in Fig. 24.

Boundary Conditions

Consider the two-dimensional network in Fig. 11. At point u^1, the horizontal currents represent the horizontal direct stresses and the vertical currents the shear stresses upon a half-block of elastic material. At the u^3 point, the role of the currents is interchanged.

At a vertical boundary in the u^3 direction, the resultant direct stresses along u^1, namely, $\sigma'^{11}+\ldots$. are zero, also the shear stresses σ'^{13} (but not the vertical direct stresses $\sigma'^{33}+\ldots$.). Hence by cutting the network along the vertical wavy line indicated and removing the right-hand portion, a boundary is formed parallel to u^3. This representation assumes that only one half of a u^1 block (but the whole of a u^3 block) is retained at the vertical boundary, as shown in Fig. 12.

At a horizontal boundary in the u^1 direction, the resultant direct stresses along u^3, namely $\sigma'^{33}+\ldots$ are zero, also the shear stresses σ'^{31} (but not the horizontal direct stresses $\sigma'^{11}+\ldots$). Hence by cutting the network along the horizontal wavy line indicated, a boundary is formed parallel to u^1. Now only one half of the u^3 block (but the whole of the u^1 block) is retained at the horizontal boundary, Fig. 12.

It is also possible to cut the network by a diagonal line as shown in Fig. 11, or by other zig-zag lines. This method of establishing boundaries by simply cutting the network opens up the possibility of building a permanently connected network analyzer for elastic-field problems, in which the boundaries are varied merely by opening and closing switches.

The three-dimensional network is similarly cut by wavy surfaces.

If on a boundary surface applied forces (direct and shear) exist, they take the place of the boundary stresses which previously were equated to zero, Fig. 13.

Body forces (such as centrifugal forces) are applied as currents entering the respective junctions.

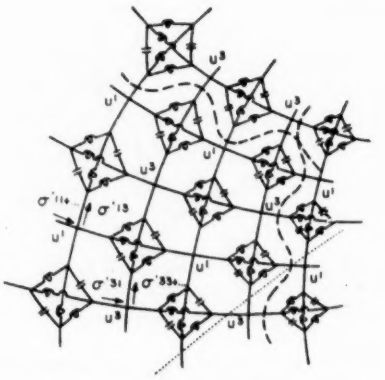


Fig. 11 Cutting Along Boundaries

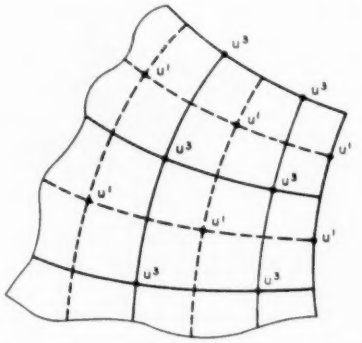


Fig. 12 Boundaries of the Elastic Body

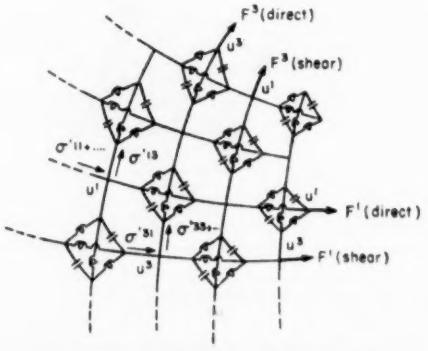


Fig. 13 Applied Boundary Forces

Equivalent Circuits

Examples of networks along four different reference frames are given in Figs. 14 to 23, inclusive, and Table 1. These reference frames are as follows:

1 Three-dimensional, rectangular co-ordinates.
2 Three-dimensional, axially symmetric.
3 Two-dimensional, polar co-ordinates.
4 Two-dimensional, rectangular co-ordinates.

In each frame, the blocks, into which the elastic body is divided, may have different lengths in different directions.

Along each reference frame, two different networks may exist, as follows:

1 Containing transformers (all transient networks must employ them).

2 Containing only inductances and capacitors.

Each of these networks may assume two different forms:

1 They correspond to the assumed physical picture. They give the stresses, the strains (as the sum of several voltages), and the total displacements.

2 The networks are simplified to contain the minimum number of coils. The stresses now have to be calculated from the measured strains.

For each reference frame either two or three of the possible four networks are shown. The two-dimensional networks are the same for both the plane-stress and the plane-strain cases, but the coil admittances assume different values for the two cases. In Table 1, the admittances are given for the plane-strain cases.

TABLE 1

ADMITTANCES OF NETWORKS ALONG VARIOUS REFERENCE FRAMES

$$a = (2\mu + \lambda)\frac{\Delta y\,\Delta z}{\Delta x} \qquad d = \mu\frac{\Delta y\,\Delta z}{\Delta x} \qquad g = \mu\,\Delta x \qquad j = \lambda\,\Delta x$$

$$b = (2\mu + \lambda)\frac{\Delta x\,\Delta z}{\Delta y} \qquad e = \mu\frac{\Delta x\,\Delta z}{\Delta y} \qquad h = \mu\,\Delta y \qquad k = \lambda\,\Delta y$$

$$c = (2\mu + \lambda)\frac{\Delta x\,\Delta y}{\Delta z} \qquad f = \mu\frac{\Delta x\,\Delta y}{\Delta z} \qquad i = \mu\,\Delta z \qquad l = \lambda\,\Delta z$$

$$m = \rho\,\Delta x\,\Delta y\,\Delta z$$

(*a*) Constants of networks along rectangular co-ordinates (Figs. 14, 15, 16: 21, 22, 23).

$$a = r(2\mu + \lambda)\frac{\Delta z\,\Delta\theta}{\Delta r} \qquad h = r\mu\,\Delta\theta \qquad k' = \lambda r\,\Delta\theta + \frac{\lambda}{4}\,\Delta r\,\Delta\theta$$

$$c = r(2\mu + \lambda)\frac{\Delta r\,\Delta\theta}{\Delta z} \qquad k = r\lambda\,\Delta\theta \qquad k'' = \lambda r\,\Delta\theta - \frac{\lambda}{4}\,\Delta r\,\Delta\theta$$

$$d = r\mu\frac{\Delta z\,\Delta\theta}{\Delta r} \qquad m = \rho\,\Delta r\,\Delta\theta\,\Delta z \qquad p' = \frac{1}{2}\left(\frac{2\mu + \lambda}{r}\right)\Delta r\,\Delta\theta\,\Delta z + \lambda\,\Delta\theta\,\Delta z$$

$$f = r\mu\frac{\Delta r\,\Delta\theta}{\Delta z} \qquad p = \frac{1}{2}\left(\frac{2\mu + \lambda}{r}\right)\Delta r\,\Delta\theta\,\Delta z \qquad p'' = \frac{1}{2}\left(\frac{2\mu + \lambda}{r}\right)\Delta r\,\Delta\theta\,\Delta z - \lambda\,\Delta\theta\,\Delta z$$

$$l = \lambda\,\Delta r\,\Delta\theta$$

(*b*) Constants of networks with axial symmetry (Figs. 17 and 18).

$$a = r(2\mu + \lambda)\frac{\Delta\theta\,\Delta z}{\Delta r} \qquad o = \frac{2\mu}{r^2}\,\Delta r\,\Delta z \qquad p' = \frac{1}{2}\left(\frac{2\mu + \lambda}{r}\right)\Delta r\,\Delta\theta\,\Delta z + \lambda\,\Delta\theta\,\Delta z$$

$$b = \frac{2\mu + \lambda}{r^2}\frac{\Delta r\,\Delta z}{\Delta\theta} \qquad i' = \frac{\mu}{r}\,\Delta z + \frac{3\mu}{4r^2}\,\Delta r\,\Delta z \qquad p'' = \frac{1}{2}\left(\frac{2\mu + \lambda}{r}\right)\Delta r\,\Delta\theta\,\Delta z - \lambda\,\Delta\theta\,\Delta z$$

$$d = \frac{\mu}{r}\frac{\Delta\theta\,\Delta z}{\Delta r} \qquad i'' = \frac{\mu}{r}\,\Delta z - \frac{3\mu}{4r^2}\,\Delta r\,\Delta z \qquad q' = \frac{2\mu + \lambda}{r^2}\,\Delta r\,\Delta z$$

$$e = \frac{\mu}{r}\frac{\Delta r\,\Delta z}{\Delta\theta} \qquad l' = \frac{\lambda}{r}\,\Delta z + \frac{4\mu + 3\lambda}{4r^2}\,\Delta r\,\Delta z \qquad q'' = \frac{2\mu}{r^2}\,\Delta\theta\,\Delta z$$

$$m = \rho r^2\omega^2\,\Delta r\,\Delta\theta\,\Delta z \qquad l'' = \frac{\lambda}{r}\,\Delta z - \frac{4\mu + 3\lambda}{4r^2}\,\Delta r\,\Delta z$$

(*c*) Constants of networks along polar co-ordinates (Figs. 19 and 20).

ACKNOWLEDGMENT

The author wishes to acknowledge his indebtedness to S. B. Crary for suggesting the solution of elastic-field problems by means of equivalent circuits, also to G. K. Carter and C. Concordia for numerous discussions on the subject.

BIBLIOGRAPHY

1 "The Theory of Elasticity," by A. E. H. Love, Cambridge University Press, fourth edition, 1927.

2 "Applications of the Absolute Differential Calculus," by A. J. McConnell, Blackie & Sons, London, 1931.

3 "Tensor Analysis of Networks," by G. Kron, John Wiley & Sons, Inc., New York, N. Y., 1939.

4 "Equivalent Circuit of the Field Equations of Maxwell—I," by G. Kron, Proceedings of the Institute of Radio Engineers, vol. 32, May, 1944, pp. 289–299.

5 "Network Analyzer Studies of Electromagnetic Cavity Resonators," by J. R. Whinnery, C. Concordia, W. A. Ridgway, and G. Kron, Proceedings of the Institute of Radio Engineers, vol. 32, June, 1944, pp. 360–367.

6 "A Method for Determining Unsteady-State Heat Transfer by Means of an Electrical Analogy," by V. Paschkis and H. D. Baker, Trans. A.S.M.E., vol. 64, 1942, pp. 105–112.

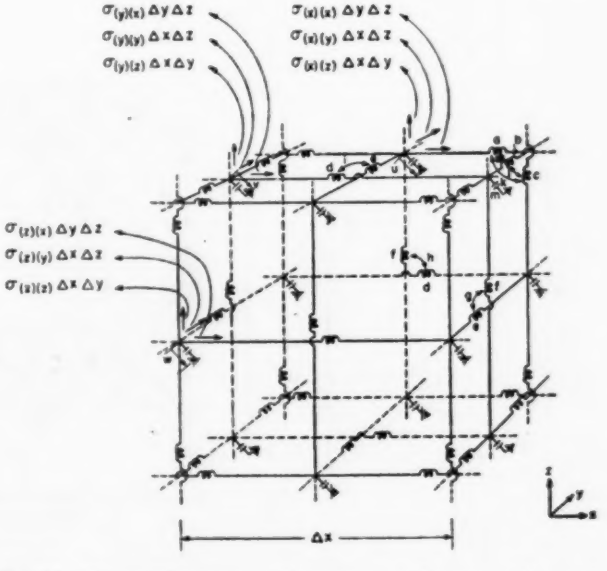


FIG. 14 THREE-DIMENSIONAL, RECTANGULAR, TRANSIENT NETWORK

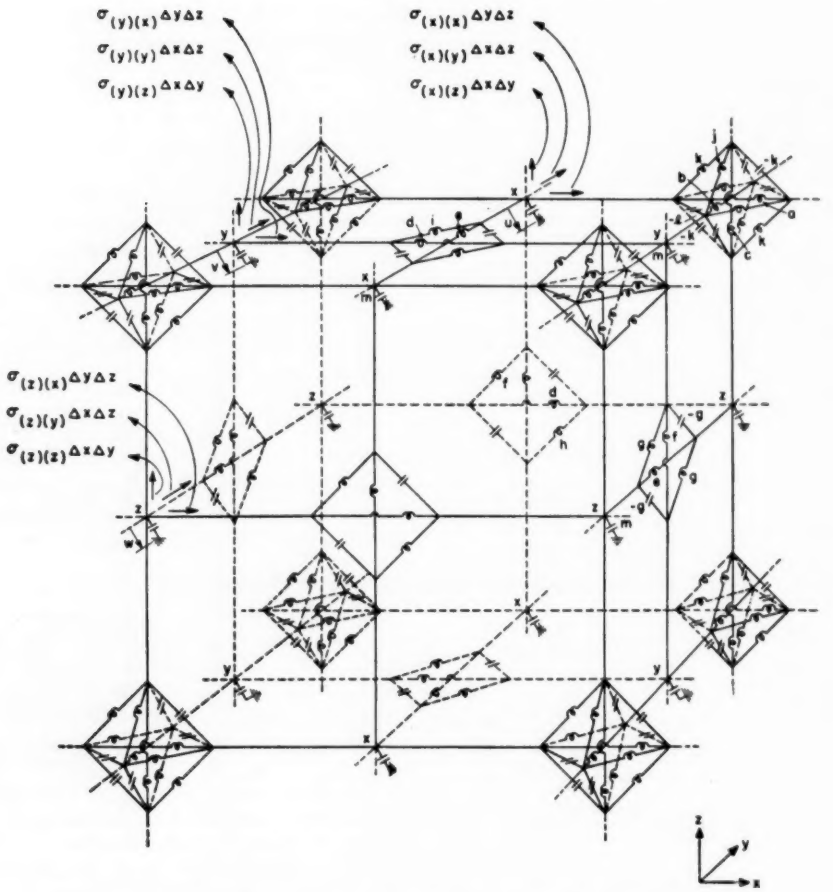


FIG. 15 THREE-DIMENSIONAL, RECTANGULAR, SMALL-OSCILLATION NETWORK

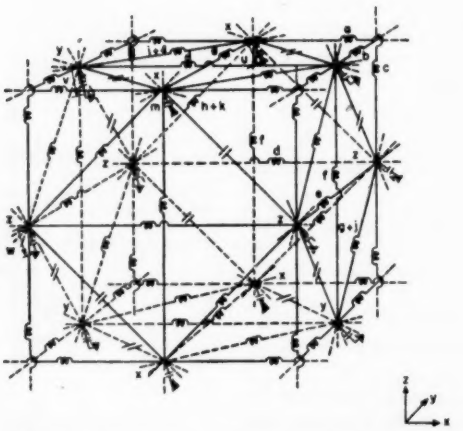


FIG. 16 THREE-DIMENSIONAL, RECTANGULAR, SMALL-OSCILLATION, SIMPLIFIED NETWORK

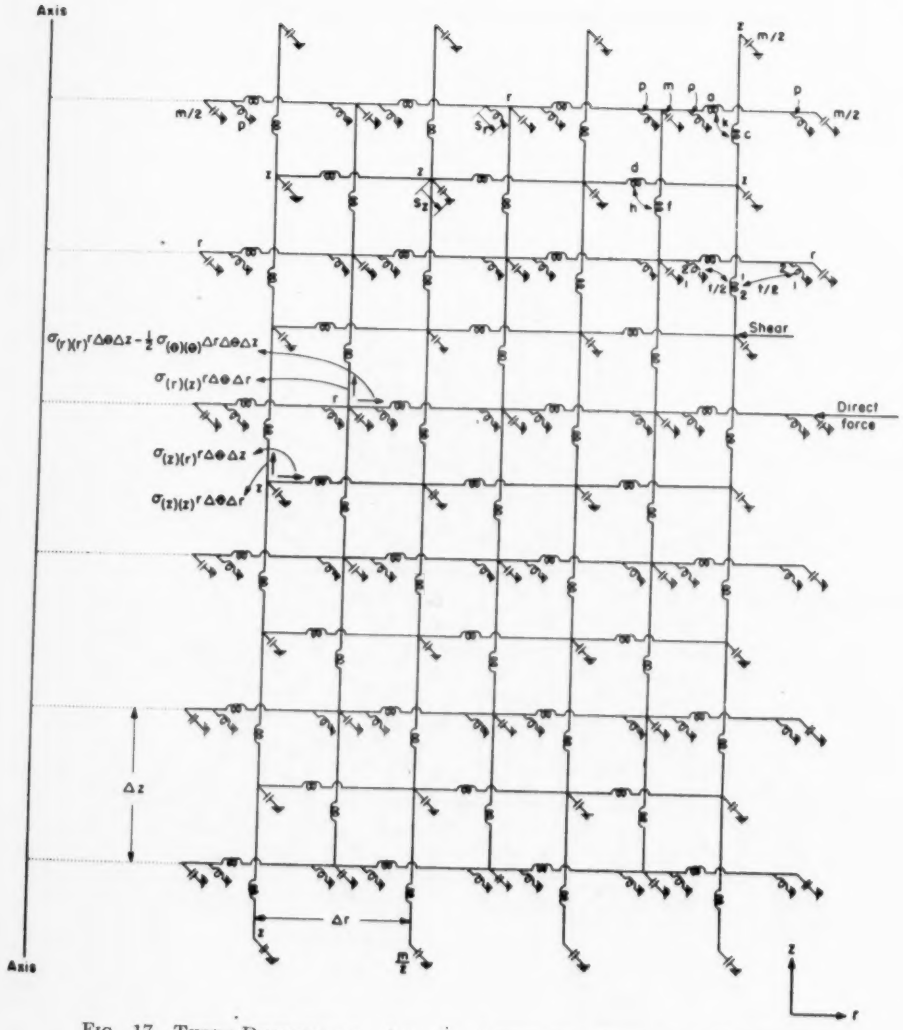


FIG. 17 THREE-DIMENSIONAL, AXIALLY SYMMETRIC, TRANSIENT NETWORK

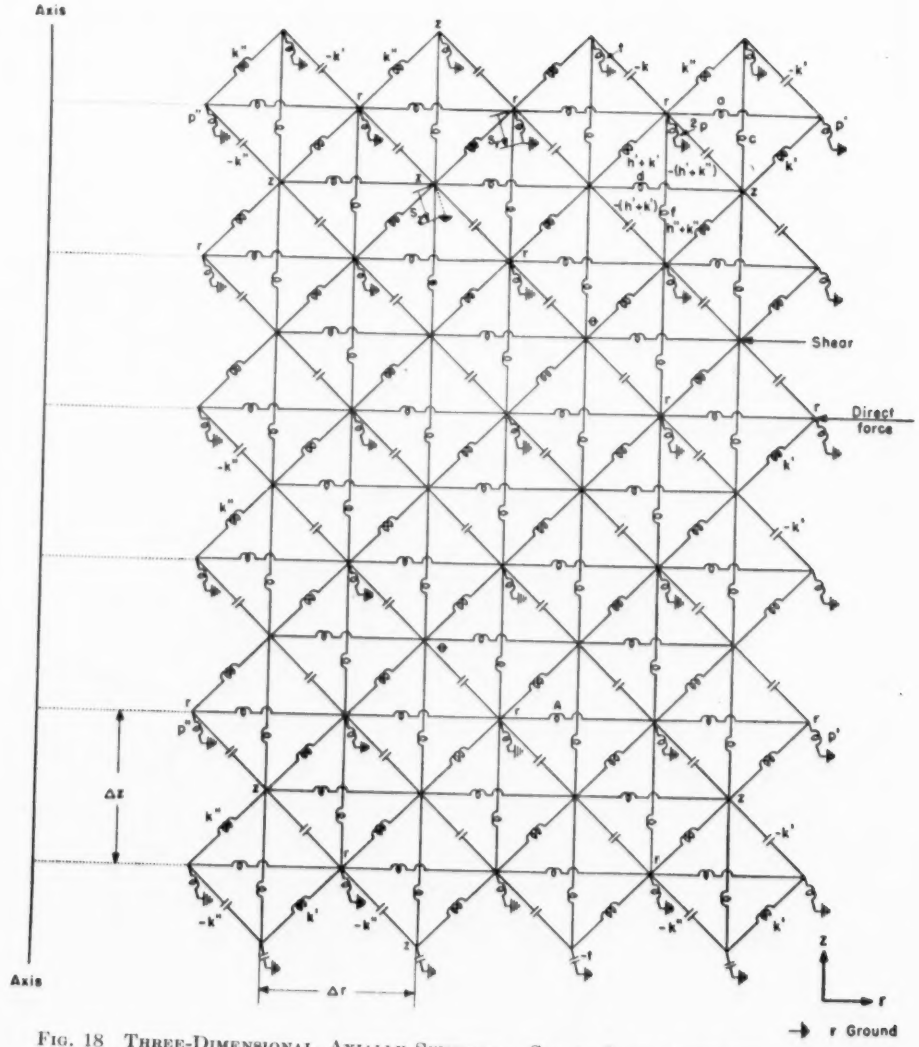


FIG. 18 THREE-DIMENSIONAL, AXIALLY SYMMETRIC, STEADY-STATE, SIMPLIFIED NETWORK

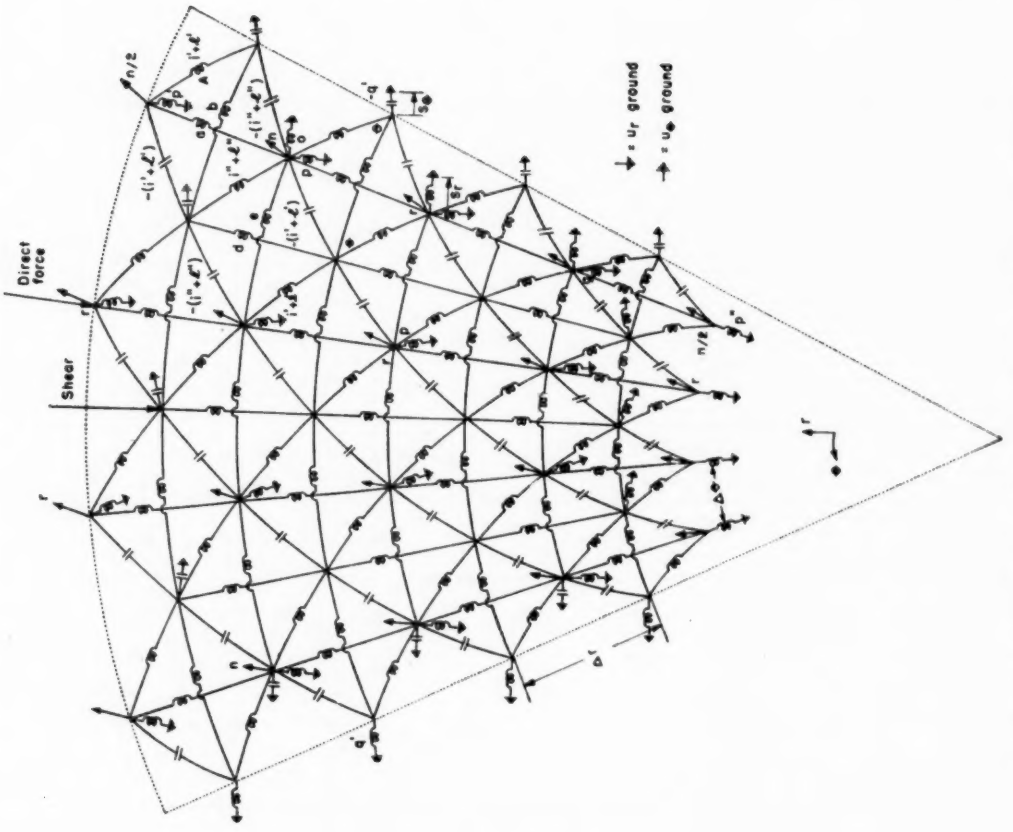


FIG. 20 TWO-DIMENSIONAL, CYLINDRICAL, ROTATING, SIMPLIFIED NETWORK

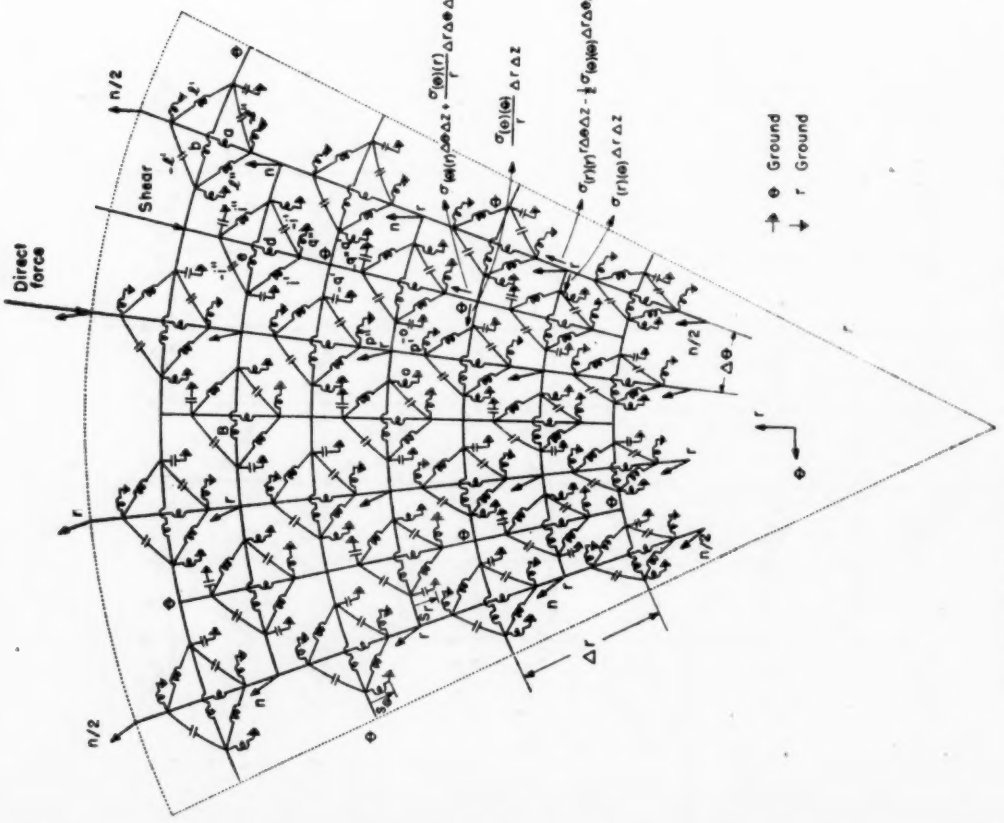


FIG. 19 TWO-DIMENSIONAL, CYLINDRICAL, ROTATING NETWORK

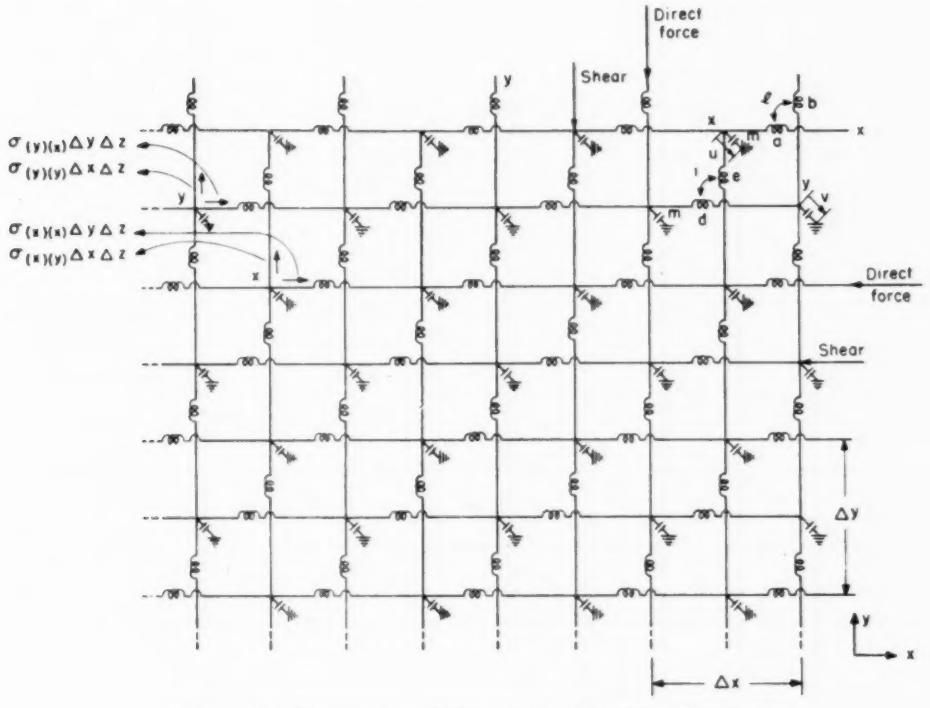


FIG. 21 TWO-DIMENSIONAL, RECTANGULAR, TRANSIENT NETWORK

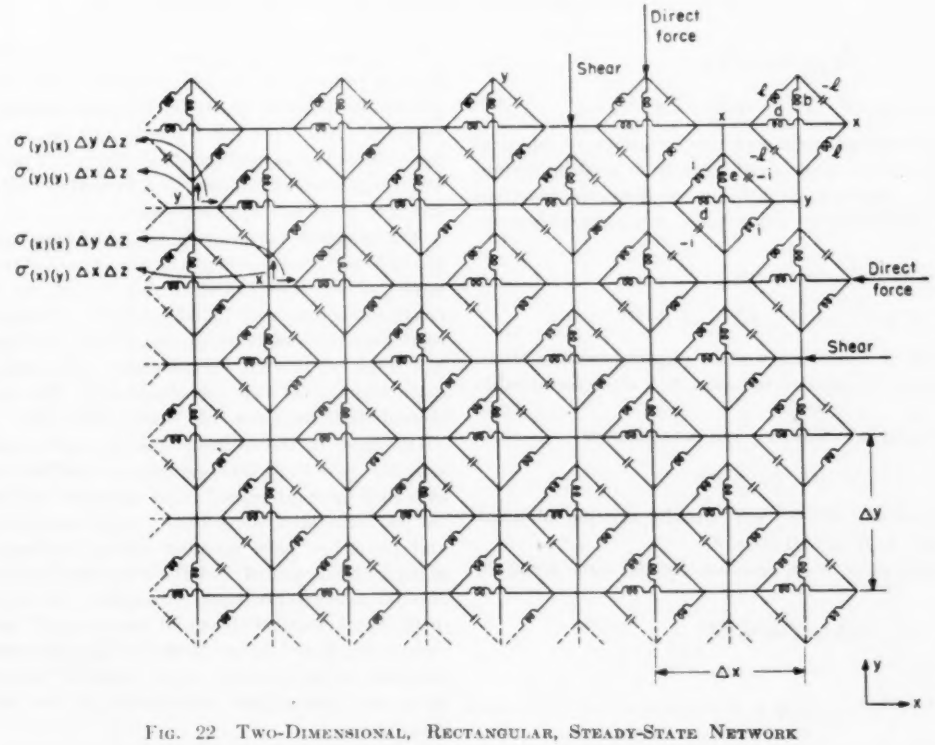


FIG. 22 TWO-DIMENSIONAL, RECTANGULAR, STEADY-STATE NETWORK

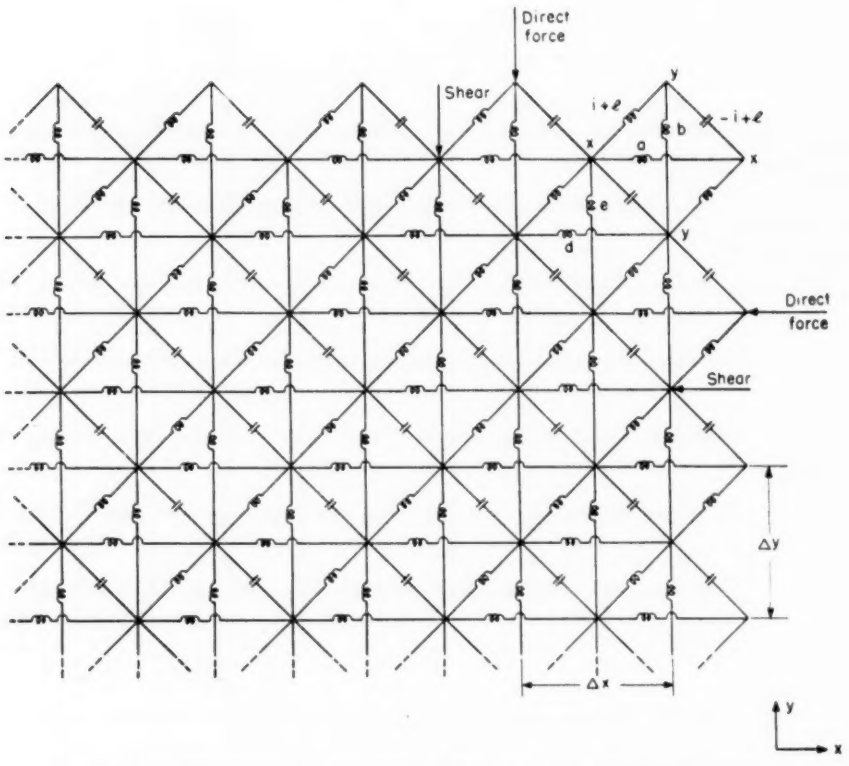


FIG. 23 TWO-DIMENSIONAL, RECTANGULAR, STEADY-STATE, SIMPLIFIED NETWORK

Appendix

LIMITATION OF CONVENTIONAL EQUATIONS

In formulating and manipulating the equations of physical phenomena, the engineer or physicist is likely to perform certain algebraic operations that mathematically are allowable, but from purely physical considerations are not so. Such operations are for instance:

1 Canceling plus and minus terms

$$(A + C) + (B - C) = A + B$$

If $A + C$ and $B - C$ are measurable physical entities, then usually neither A nor B and often not even $A + B$ are measurable entities.

2 Canceling terms in numerator and denominator

$$(AC)(C^{-1}B) = AB$$

Here again if (AC) and $(C^{-1}B)$ are actually existing physical entities, then often A, B, or AB are not.

3 Dividing both sides of an equation by the same term, as replacing

$$DA + DB = DC$$

by

$$A + B = C$$

where, again, none of the resulting expressions may be a measurable physical entity.

Examples of such mathematical manipulations are the partial differential equations of the electromagnetic field and of the elastic field, when expressed along curvilinear co-ordinates. Luckily, the dynamical equations of Lagrange have not been subjected to such changes, but the conventional equations of small oscillations, derived from the Lagrangian equations, are perfect examples of physically deficient mathematical descriptions of physical phenomena. Also in a great number of the so-called "practical" approaches to the mathematical solution of mechanical and electrical engineering problems, the physical picture has been subordinated to mathematical simplicity.

The engineer becomes conscious of this tampering with the physical picture especially when he attempts to set up a physical model, say an electrical equivalent circuit, to simulate a physical phenomenon. He finds that there are some extra terms in the equations that somehow do not fit into any kind of a model he can think of, or that an otherwise satisfactory model calls for extra expressions that are absent from the equations. Even a mental model may run into similar difficulties.

Of course mathematicians and physicists have long since become aware of these diverging interests of the two sciences (whenever they have attempted to set up geometrical models for physical problems) and, accordingly, mathematicians have developed and physicists have adapted various techniques to keep the mathematical symbol and the corresponding physical entity in one-to-one correspondence throughout the analysis. A branch of the mathematical theory of "invariants," under the name of "vector analysis" for problems in three-dimensional rectangular reference frames, and of "tensor analysis" for problems in curvilinear and generalized co-ordinates, is the outgrowth of such attempts.

By the use of the methods of tensor analysis, the engineer is enabled to keep his physical picture unmutilated while formulating and simplifying his equations. Hence by setting up his equations in a tensorial form instead of any haphazard manner, the engineer gets more clues on how to establish a model (physical, geometrical, or mental) for his problem. Other by-products of

the use of tensors, such as a "shorthand" representation of long and numerous equations, or the systematic "bookkeeping" of otherwise unmanageable terms, are purely incidental to the primary advantage of keeping the physical reasoning straightforward and the physical picture of the phenomenon undistorted.

Of course, most of the time the engineer does employ the method of tensors without being aware of doing so. However, in more complex problems, a conscious use of routine tensorial procedures will save him much time and effort to avoid the numerous pitfalls awaiting him.

A Principle to Establish Models for Physical Systems

In setting up stationary electrical networks to simulate the performance of rotating electrical machinery, dynamical systems and various field phenomena, the following principle serves as an indispensable guide:

"A set of equations, representing the performance of any physical system (be it mechanical, thermal, or any other system) may be represented by a physical model (equivalent circuit) only if the set of equations is a tensor equation. The invariance of the set of equations is a necessary, but not a sufficient condition."

In other words, before the engineer attempts to set up a physical model whose performance follows term by term a given set of algebraic, differential, or integral equations, his first step is to change his equations into a form in which each symbol is a measurable quantity, a "tensor." By making this first step, he maneuvers himself into a favorable position to enjoy, unencumbered by irrelevant expressions, all the headaches that still lie ahead of him.

The next step is to decide what forms of the numerous possibilities the tensorial equation should assume. This depends upon the type of model to be attempted. In the present paper the model is a stationary electrical network, the tensorial equation of which is known to be

$$e_\alpha = z_{\alpha\beta} i^\beta \qquad \text{or} \qquad i^\alpha = y^{\alpha\beta} e_\beta$$

It is intended to represent displacement by voltages, hence the displacement vector s_α must be a "covariant" tensor, just as the voltage vector e_α is. Also, it is intended to represent forces by currents, hence the force vector f^α must be a "contravariant" tensor, just as the current vector i^α is. (There is a great difference between the covariant and contravariant components of the same vector. Assuming, say, cylindrical co-ordinates, s^θ represents angular displacement along s_θ, but s_θ stands for a linear displacement times the radius. Both the covariant and contravariant components of a vector, s_θ and s^θ, also differ from what conventional vector analysis calls the components $s_{(\theta)}$ of a vector.) This selection of the force and displacement vectors immediately compells the engineer to assume the stress tensor as a "twice" contravariant tensor $\sigma^{\alpha\beta}$ just as $y^{\alpha\beta}$ is. (There are seven varieties of stresses to select the right one from, namely $\sigma_{\alpha\beta}$, $\sigma_\alpha{}^\beta$, $\sigma^\alpha{}_\beta$, $\sigma^{\alpha\beta}$, $\sigma_{(\alpha)\beta}$, $\sigma_{(\alpha)}{}^\beta$, and $\sigma_{(\alpha)(\beta)}$, each one being different.)

Since a field problem is represented by considering forces acting not at a "point" in space but upon the surfaces of a finite block cut out of space, the final step is known to be a change from the tensorial into a tensor-density form of equation, in which some of the contravariant tensors, say $\sigma^{\alpha\beta}$, must also become tensor densities $\sigma'^{\alpha\beta}$ (denoted by a prime).

Once the desired tensorial form has been fixed, then ingenuity must be resorted to in finding a correct network pattern that allows the employment of nine current differentials (stress differentials) to add up to zero at three different space points (three differentials at each point), corresponding to the three equations of equilibrium (and subject to the six conditions of compatibility). With the correct network pattern established, the determination of the network constants for the various types of reference frames is mere routine work.

Tensorial Equation of Equilibrium

The conventional form of the equations of equilibrium for orthogonal curvilinear axes is given by Love as

$$h_1h_2h_3\left(\frac{\partial}{\partial u^1}\frac{\sigma_{(1)(1)}}{h_2h_3}+\frac{\partial}{\partial u^2}\frac{\sigma_{(1)(2)}}{h_3h_1}+\frac{\partial}{\partial u^3}\frac{\sigma_{(1)(3)}}{h_1h_2}\right)$$
$$+h_1h_2\frac{\partial}{\partial u^2}\left(\frac{1}{h_1}\right)\sigma_{(1)(2)}+h_1h_3\frac{\partial}{\partial u^3}\left(\frac{1}{h_1}\right)\sigma_{(1)(3)}$$
$$-h_1h_2\frac{\partial}{\partial u^1}\left(\frac{1}{h_2}\right)\sigma_{(2)(2)}-h_1h_3\frac{\partial}{\partial u^1}\left(\frac{1}{h_3}\right)\sigma_{(3)(3)}+\rho f_{(1)}$$
$$=\rho\frac{\partial^2 s_{(1)}}{\partial t^2} \quad \ldots\ldots\ldots\ldots\ldots\ldots\ldots\ldots [1]$$

The other two equations follow in a cyclical order.

These conventional equations are not in a form in which they may correspond to a physical model. They are changed to a suitable tensor-density form by the following steps:

1 The nontensor stresses $\sigma_{(\alpha)(\beta)}$ (stresses at a point) are replaced by the tensor densities $\sigma'^{\alpha\beta}$ (surface integral of contravariant point stresses) according to Equations [15].

2 The nontensor displacements $s_{(\alpha)}$ are replaced by the covariant displacements s_α by Equation [11].

3 The nontensor forces $f_{(\alpha)}$ are replaced by the contravariant forces f^α by Equation [13].

4 The nontensor density ρ is replaced by the tensor density ρ' by Equation [16].

5 The first equation is multiplied by h_1, the second by h_2, the third by h_3.

6 All three equations are divided by $h_1h_2h_3$.

Performing the operations, the resultant tensor-density equations are as follows

$$\frac{\partial\sigma'^{11}}{\partial u^1}+\frac{\partial\sigma'^{12}}{\partial u^2}+\frac{\partial\sigma'^{13}}{\partial u^3}-\frac{1}{h_1}\frac{\partial h_1}{\partial u^1}\sigma'^{11}-\frac{2}{h_1}\frac{\partial h_1}{\partial u^2}\sigma'^{12}$$
$$-\frac{2}{h_1}\frac{\partial h_1}{\partial u^3}\sigma'^{13}+\frac{(h_1)^2}{(h_2)^3}\frac{\partial h_2}{\partial u^1}\sigma'^{22}+\frac{(h_1)^2}{(h_3)^2}\frac{\partial h_3}{\partial u^1}\sigma'^{33}$$
$$+\rho' f^1=(h_1)^2\rho'\frac{\partial^2 s_1}{\partial t^2} \quad \ldots\ldots\ldots\ldots\ldots\ldots [2]$$

The other two equations follow in a cyclical order.

These last equations correspond to the tensorial form

$$\frac{\delta\sigma'^{\alpha\beta}}{\delta u^\beta}+\rho' f^\alpha=\rho' g^{\alpha\beta}\frac{\partial^2 s_\beta}{\partial t^2} \quad \ldots\ldots\ldots\ldots\ldots\ldots [3]$$

or

$$\frac{\partial\sigma'^{\alpha\beta}}{\partial u^\beta}+\left\{\begin{matrix}\alpha\\ \beta\gamma\end{matrix}\right\}\sigma'^{\beta\gamma}+\rho' f^\alpha=\rho' g^{\alpha\beta}\frac{\partial^2 s_\beta}{\partial t^2} \quad \ldots\ldots\ldots [4]$$

When the free index $\alpha = 1$, the first equation is

$$\frac{\partial\sigma'^{11}}{\partial u^1}+\frac{\partial\sigma'^{12}}{\partial u^2}+\frac{\partial\sigma'^{13}}{\partial u^3}+\left\{\begin{matrix}1\\ 11\end{matrix}\right\}\sigma'^{11}+2\left\{\begin{matrix}1\\ 12\end{matrix}\right\}\sigma'^{12}$$
$$+2\left\{\begin{matrix}1\\ 13\end{matrix}\right\}\sigma'^{13}+\left\{\begin{matrix}1\\ 22\end{matrix}\right\}\sigma'^{22}+\left\{\begin{matrix}1\\ 33\end{matrix}\right\}\sigma'^{33}+\rho' f^1=\rho' g^{11}\frac{\partial^2 s_1}{\partial t^2} \quad [5]$$

where the Christoffel symbols are defined as

$$\left.\begin{aligned} \left\{\begin{matrix}1\\11\end{matrix}\right\} &= -\frac{1}{h_1}\frac{\partial h_1}{\partial u^{1'}} \qquad \left\{\begin{matrix}1\\12\end{matrix}\right\} = -\frac{1}{h_1}\frac{\partial h_1}{\partial u^{2'}} \qquad \left\{\begin{matrix}1\\13\end{matrix}\right\} = \\ &\qquad\qquad -\frac{1}{h_1}\frac{\partial h_1}{\partial u^{3}} \\ \left\{\begin{matrix}1\\22\end{matrix}\right\} &= \frac{(h_1)^2}{(h_2)^3}\frac{\partial h_2}{\partial u^{1'}} \qquad \left\{\begin{matrix}1\\23\end{matrix}\right\} = 0, \qquad \left\{\begin{matrix}1\\33\end{matrix}\right\} = \frac{(h_1)^2}{(h_3)^3}\frac{\partial h_3}{\partial u^{1}} \end{aligned}\right\} \quad \ldots [6]$$

The other two equations follow in cyclical order.

Relations Between Tensorial and Conventional Quantities

The tensorial quantities (open indices) are defined in terms of conventional quantities (closed indices) in the following manner:

The variables u^α and the metrical coefficients h are given in Table 2 for the three most common orthogonal reference frames. Their values in other reference frames (such as elliptical, spheroidal, etc., frames) are found in texts on applied mathematics.

TABLE 2 VALUES OF $u\alpha$ AND h

	u^1	u^2	u^3	$\frac{1}{h_1}$	$\frac{1}{h_2}$	$\frac{1}{h_3}$
Cartesian.....	x	y	z	1	1	1
Cylindrical.....	r	θ	z	1	r	1
Spherical.....	r	θ	ψ	1	r	$r\sin\theta$

The set of vectors $\epsilon_\alpha{}^{(\beta)}$ changing projections along a tangent line (nontensorial quantities) to components along the reference frames (tensors) are defined by

$\epsilon_\alpha{}^{(\beta)} =$

α \ (β)	(1)	(2)	(3)
1	$1/h_1$		
2		$1/h_2$	
3			$1/h_3$

..... [7]

The metric tensor is

$g_{\alpha\beta} =$

α \	1	2	3
1	$1/(h_1)^2$		
2		$1/(h_2)^2$	
3			$1/(h_3)^2$

..... [8]

$$g = 1/(h_1h_2h_3)^2 \ldots [9]$$

The displacement vector is

$$s_\alpha = \epsilon_\alpha{}^{(\beta)}s_{(\beta)} \ldots [10]$$

$s_\alpha =$

α	1	2	3
	$s_{(1)}/h_1$	$s_{(2)}/h_2$	$s_{(3)}/h_3$

..... [11]

The force vector is

$$f^\alpha = \epsilon^\alpha{}_{(\beta)}f^{(\beta)} \ldots [12]$$

$f^\alpha =$

α	1	2	3
	$f_{(1)}h_1$	$f_{(2)}h_2$	$f_{(3)}h_3$

..... [13]

The stress tensor density is

$$\sigma'^{\alpha\beta} = \sqrt{g}\,\sigma^{\alpha\beta} = \sqrt{g}\,\epsilon^\alpha{}_{(\gamma)}\epsilon^\beta{}_{(\delta)}\sigma_{(\gamma)(\delta)} \ldots [14]$$

$\sigma'^{\alpha\beta} =$

α \ β	1	2	3
1	$\frac{h_1}{h_2h_3}\sigma_{(1)(1)}$	$\frac{1}{h_3}\sigma_{(1)(2)}$	$\frac{1}{h_2}\sigma_{(1)(3)}$
2	$\frac{1}{h_3}\sigma_{(2)(1)}$	$\frac{h_2}{h_1h_3}\sigma_{(2)(2)}$	$\frac{1}{h_1}\sigma_{(2)(3)}$
3	$\frac{1}{h_2}\sigma_{(3)(1)}$	$\frac{1}{h_1}\sigma_{(3)(2)}$	$\frac{h_3}{h_1h_2}\sigma_{(3)(3)}$

..... [15]

The mass tensor density is

$$\rho' = \sqrt{g}\,\rho = \frac{1}{h_1h_2h_3}\rho \ldots [16]$$

Example:

The tensorial equations of a two-dimensional example along cylindrical co-ordinates will be given in detail. The equivalent circuit may represent part of a rotating turbine rotor (plane-strain case of a rotating thick cylinder).

The equations of equilibrium are

$$\left.\begin{aligned} \left[\frac{\partial\sigma'^{rr}}{\partial r} + \frac{\partial\sigma'^{r\theta}}{\partial\sigma} - r\sigma'^{\theta\theta} + \rho r^2\omega^2\right]\Delta r\,\Delta\theta\,\Delta z &= 0 \\ \left[\frac{\partial\theta'^{r\theta}}{\partial\theta} + \frac{\partial\sigma'^{\theta r}}{\partial r} + \frac{2\sigma'^{r\theta}}{r}\right]\Delta r\,\Delta\theta\,\Delta z &= 0 \end{aligned}\right\} \ldots [17]$$

where ω = angular velocity of rotor.

The stresses are defined in terms of the displacements as

$$\left.\begin{aligned} \sigma'^{rr} &= (2\mu+\lambda)r\frac{\partial s_r}{\partial r} + \frac{\lambda}{r}\frac{\partial s_\theta}{\partial\theta} + \lambda s_r \\ \sigma'^{r\theta} &= \frac{\mu}{r}\frac{\partial s_r}{\partial\theta} + \frac{\mu}{r}\frac{\partial s_\theta}{\partial r} - \frac{2\mu}{r^2}s_\theta \\ \sigma'^{\theta\theta} &= \frac{\lambda}{r}\frac{\partial s_r}{\partial r} + \frac{2\mu+\lambda}{r^3}\frac{\partial s_\theta}{\partial\theta} + \frac{2\mu+\lambda}{r^2}s_r \end{aligned}\right\} \ldots [18]$$

The displacements are

$$s_r = s_{(r)} \text{ and } s_\theta = r\,s_{(\theta)} \ldots [19]$$

where $s_{(\theta)}$ is the linear displacement along θ.

The strains are

$$\left.\begin{aligned} \epsilon_{rr} &= \frac{\partial \delta_r}{\partial r} \\ \epsilon_{r\theta} &= \frac{\partial \delta_r}{\partial \theta} + \frac{\partial \delta_\theta}{\partial r} - \frac{2\delta_\theta}{r} \\ \epsilon_{\theta\theta} &= \frac{\partial \delta_\theta}{\partial \theta} + r\delta_r \end{aligned}\right\} \quad \ldots\ldots\ldots\ldots\ldots\ldots [20]$$

The condition of compatibility is

$$K_{r\theta r\theta} = \frac{\partial^2 \epsilon_{rr}}{\partial \theta^2} + \frac{\partial^2 \epsilon_{\theta\theta}}{\partial r^2} - \frac{\partial^2 \epsilon_{r\theta}}{\partial r \partial \theta} - r\frac{\partial \epsilon_{rr}}{\partial r} - \frac{2}{r}\frac{\partial \epsilon_{\theta\theta}}{\partial r} + \frac{2}{r^2}\epsilon_{\theta\theta} = 0 [21]$$

Fig. 24 shows that part of the first three terms not involving the ground becomes identically zero in the same two meshes as in the rectangular case (Fig. 9). The remaining part of the first three terms and the last three terms cover the meshes formed by the ground coils.

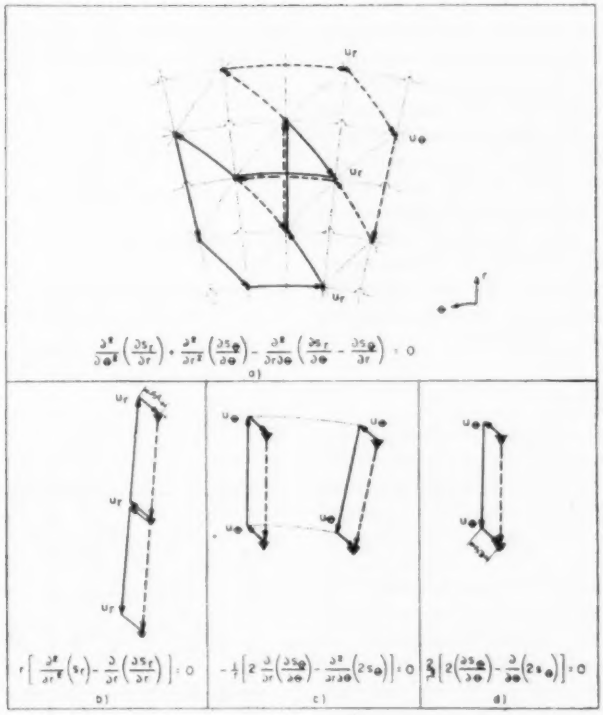


FIG. 24 EQUATION OF COMPATIBILITY $K_{r\theta r\theta} = 0$ IN POLAR CO-ORDINATES

Numerical and Network-Analyzer Solution of the Equivalent Circuits for the Elastic Field

By G. K. CARTER,[1] SCHENECTADY, N. Y.

This is a companion paper to one by Gabriel Kron.[2] Particular cases of circuits in two independent variables are used. Test of these circuits by numerical substitution of known simple solutions indicates that the mesh size in the circuits need not be excessively small in order to give a useful accuracy of results. By trial of the a-c network analyzer,[3] in similar cases, limitations on the use of the analyzer in its present form for the solution of elastic-field problems are studied. Finally, it is found by trial that solution of the circuits by hand, using a "relaxation" method,[4] is practicable; and in this way the desirable objective of a solution of the elastic-field problem directly from given boundary conditions is achieved.

Numerical Checks

As a preliminary to use of the equivalent circuits, it was thought desirable to become acquainted with the magnitudes of the quantities involved by substitution of certain known solutions. In the first place, the substitution was applied for the case of static plane strain in rectangular co-ordinates. The mesh system for this case, shown in Fig. 1, is that given in Fig. 22 of the companion paper,[2] with Δz set equal to unity; this circuit may be used also for the case of plane stress, of course, by a change of elastic constants, under the assumptions generally accepted for that purpose. The elastic constants assumed here and throughout the remainder of this paper are Young's modulus $E = 30{,}000{,}000$ psi and Poisson's ratio $\sigma = 0.28$; these give $\mu = 11{,}719{,}000$ psi and $\lambda = 14{,}914{,}000$ psi.

The simplest case of direct stress is that of simple tension, say, $\sigma_{yy} = K = 1000$ psi. Taking $u = 0$ at $x = 0$ and $v = 0$ at $y = 0$, the displacements in this case are easily found to be

$$\left.\begin{aligned} u &= -\frac{K\sigma}{E}(1+\sigma)x \\ v &= \frac{K}{E}(1-\sigma^2)y \end{aligned}\right\} \quad \ldots\ldots\ldots\ldots\ldots [1]$$

For the network, Fig. 2, in which $\Delta x = \Delta y = 1$ in., Equations [1] give the displacements, i.e., voltages, at any desired points. For instance at

$$\begin{aligned} y &= 5, & v &= 15.35 \times 10^{-5} \\ y &= 4, & v &= 12.28 \times 10^{-5} \\ x &= \pm 2, & u &= \mp 2.388 \times 10^{-5} \\ x &= \pm 1, & u &= \mp 1.194 \times 10^{-5} \end{aligned}$$

Thus current i_1 is

$$i_1 = (15.35 - 2.388)\,149.14 + (15.35 - 1.194)(-149.14) + (15.35 - 12.28)\,383.52 = -178.2 + 1178 = 1000 \text{ lb}$$

which is the load on the section Δx (= 1 in.) wide centered under i_1. Current i_3 is

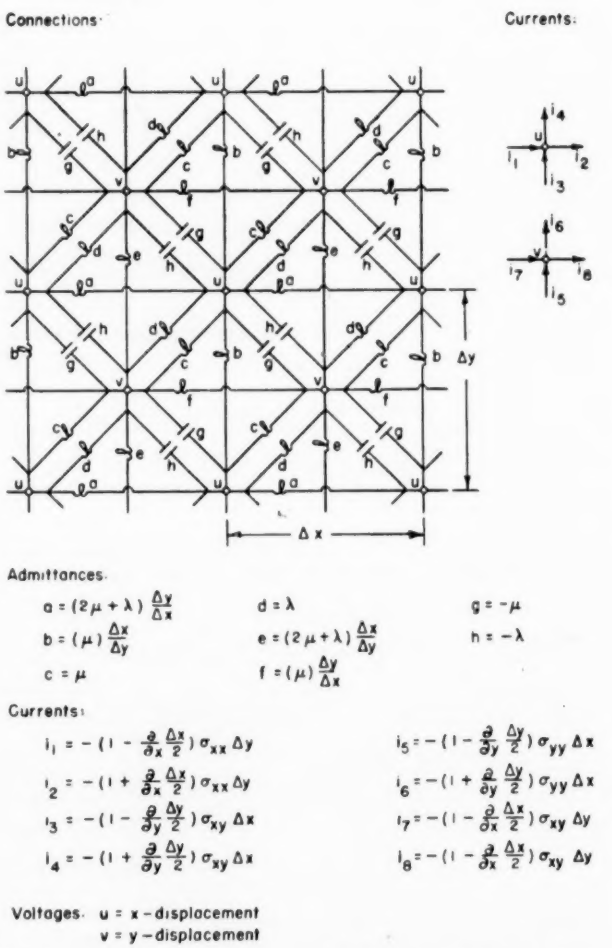


FIG. 1 EQUIVALENT CIRCUIT FOR THE ELASTIC FIELD OF PLANE STRAIN IN RECTANGULAR CO-ORDINATES

---

[1] Analytical Division, Central Station Engineering Divisions, General Electric Company.

[2] "Equivalent Circuits of the Elastic Field," by Gabriel Kron, published in the current issue of the JOURNAL OF APPLIED MECHANICS, pp. 150–161.

[3] "A New A-C Network Analyzer," by H. P. Kuehni and R. G. Lorraine, Trans. A.I.E.E., vol. 57, 1938, p. 67.

[4] "Relaxation Methods in Engineering Science," by R. V. Southwell, Oxford University Press, New York, N. Y., 1940.

Presented at the National Meeting of the Applied Mechanics Division, Chicago, Ill., June 16-17, 1944, of THE AMERICAN SOCIETY OF MECHANICAL ENGINEERS.

Discussion of this paper should be addressed to the Secretary, A.S.M.E., 29 West 39th Street, New York, N. Y., and will be accepted until October 10, 1944, for publication at a later date. Discussion received after the closing date will be returned.

NOTE: Statements and opinions advanced in papers are to be understood as individual expressions of their authors and not those of the Society.

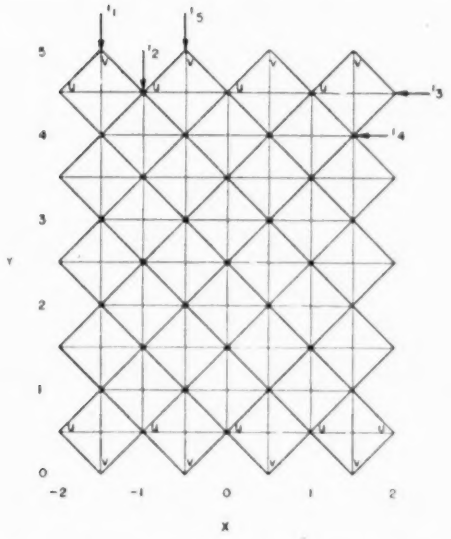


FIG. 2 NETWORK USED IN CALCULATIONS AND ANALYZER TESTS

$$i_3 = (-2.388 - 15.35)(-149.14) + (-2.388 - 12.28)\,149.14 + (-2.388 + 1.194)\,383.52 = 458 - 458 = 0$$

Currents of the type i_2 and i_4 are also seen to be zero. Since, in this simple case, the forces and displacements are linear in x and y, the results obtained in this way are independent of the size of the subdivisions, except that i_1 is proportional to Δx; this field is represented exactly by the network.

The equally simple case of uniform shear is that in which, say, $\sigma_{xy} = K = 1000$ psi. Then, if $u = v = 0$ along $y = 0$, the displacements are

$$\left.\begin{aligned} u &= \frac{2K(1+\sigma)}{E}\,y \\ v &= 0 \end{aligned}\right\} \quad \ldots\ldots\ldots\ldots\ldots\ldots [2]$$

Applied to Fig. 2, these give at

$$y = 4.5, \qquad u = \frac{3.838}{10{,}000}$$

$$y = 3.5, \qquad u = \frac{2.983}{10{,}000}$$

Thus

$$i_1 = i_3 = 0$$

$$i_2 = (3.838 - 2.983)\,1171.9 = 1000 \text{ lb}$$

the shear force on the section Δx wide centered under i_2. The similar load represented by

$$i_4 = (0 - 3.838)\,1491.4 + (0 - 2.983)(-1491.4) + (0 - 3.838)(-2663.3) + (0 - 2.983)\,2663.3 = 1000 \text{ lb}$$

is on the section Δy high centered on i_4. Again, the field is represented exactly by the circuit, regardless of the mesh size.

Another case in which the solution is known is that of simple bending, assuming say, $\sigma_{xx} = 0$, $\sigma_{yy} = -Kx = -1000x$ psi. Taking $v = 0$ at $y = 0$ and $u = 0$ at $x = 0$, $y = 1/2$, the displacements are

$$\left.\begin{aligned} u &= \frac{K(1+\sigma)}{2E}\left[\sigma x^2 + (1-\sigma)y^2 - \frac{(1-\sigma)}{4}\right] \\ v &= \frac{K(1+\sigma)}{2E}\,[-2(1-\sigma)xy] \end{aligned}\right\} \quad \ldots\ldots [3]$$

Without listing all the calculations, which are similar to those already given, results of slide-rule computation are:

$i_1 = 1501$ lb, compared with 1500 lb actual load
$i_3 = 500$ lb, compared with 500 lb actual load
The other types of load currents are zero.

An additional type of check is that the sum of the currents flowing out of any junction point must be zero; for example, these currents at the points (—0.5, 4) and (—1, 3.5) are as follows:

(—0.5, 4)		(—1, 3.5)	
+	—	+	—
587	590	1080	1439
1440	1440	230	686
6690	3425	3427	160
3270	6530	1385	3835
11987	11985	6122	6120

Thus the applied loads and the sum of currents at the junctions check to slide-rule accuracy, despite the coarseness of the mesh used. A point of practical importance is to be noted in the currents tabulated here, i.e., that the individual currents in some of the circuit elements at a point may be considerably larger than the actual loads at that point.

The second circuit considered is that for plane strain in polar co-ordinates, given as Fig. 19 of the companion paper.[2] The particular case considered is that of a steel disk, 4 in. ID, 10 in. OD, rotating at 3600 rpm; on its inside surface is a uniform pressure of 10,000 psi; on its outside surface a radial stress which is of the amount 10,000 cos 2θ psi. The numerical checks in this case consisted only of calculating the current balance at a particular point for a u-type junction and for a v-type junction. The point chosen was $\left(7 \text{ in.}, \frac{\pi}{9}\right)$; the mesh size was $\Delta r = 0.5$ in., $\Delta\theta = \frac{\pi}{100}$. The current balance for the u-type point, using voltages from the exact solution, is as follows:

	(+)	(—)
Uniform pressure	1.039×10^3	1.162×10^3
	0.1216	
	1.161×10^3	1.162×10^3
Rotation	0.1298×10^3	0.1347×10^3
	0.0850	0.0803
	0.2148×10^3	0.2150×10^3
Varying pressure	6.04×10^3	7.51×10^3
	0.530	0.531
	0.810	
	0.661	
	8.041×10^3	8.041×10^3
Total	9.417×10^3	9.418×10^3

Similarly, for the v-type point, the current balance is as follows:

	(+)	(—)
Uniform pressure	0	0
Rotation	0	0
Varying pressure	0.0059×10^3	0.0523×10^3
	1.644	1.431
		0.1691
	1.650×10^3	1.652×10^3

These calculations therefore indicate (*a*) that the polar co-ordinate network is correct, and (*b*) that in polar co-ordinates also a moderate size mesh is adequate.

TABLE 1 DISPLACEMENTS IN A BAR IN TENSION

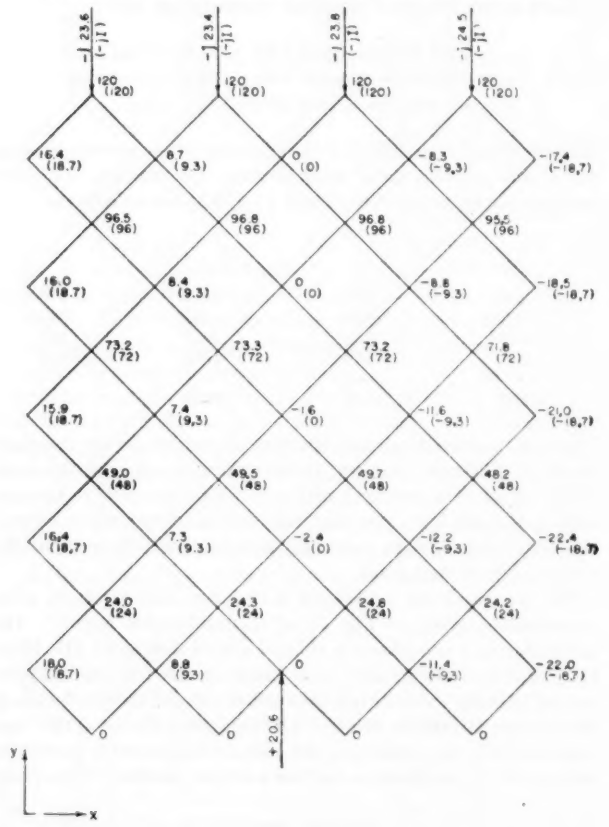
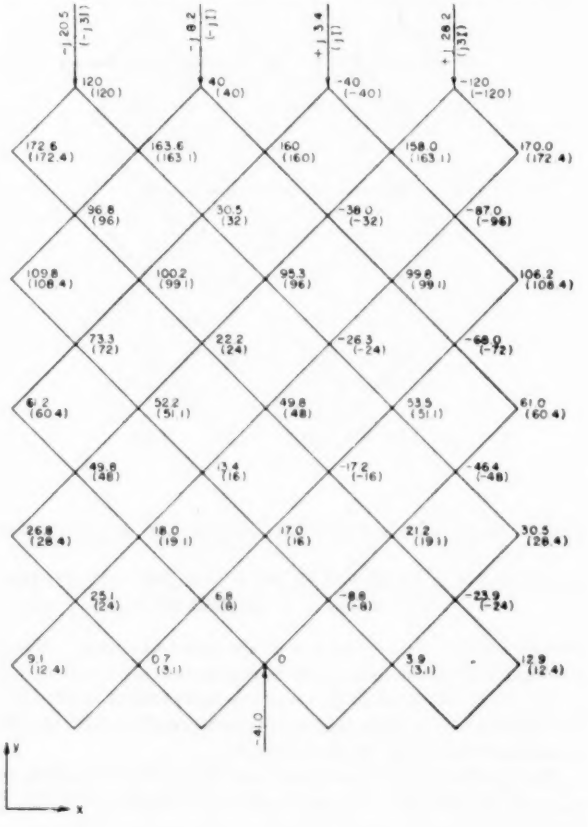


TABLE 2 DISPLACEMENTS IN A BAR IN BENDING



Network-Analyzer Tests

As part of the study of the equivalent circuits, certain cases were tried out on the a-c network analyzer.[3] For this purpose, positive admittances were generally represented by inductors and negative by capacitors. Real components of voltage were generally used for displacements, imaginary components of current for loads. Ideally the voltages and currents should be in time quadrature; divergence from this relationship, due to resistance in the analyzer elements, is exaggerated by the large component currents referred to in the preceding section and is a limitation in addition to those of precision in settings and measurements.

The circuit in rectangular co-ordinates, shown in Fig. 2, was tried first. For simple tension, as a matter of convenience, voltage was fixed at the top v points, the bottom v points being grounded (zero displacement). It should be observed that this simple elastic field corresponds to a condition in the electrical network which is quite startling to an electrical engineer at first glance, that is, the network is expected to produce two sets of equipotential lines at right angles to each other.

Various expedients were tried for the purpose of neutralizing the effects of the unavoidable resistance in the network. Negative-resistance units being impractical for any appreciable number of elements simultaneously, the most successful results were obtained simply by supplying loss components of current (real components) at other points than the load points. This method is illustrated by the results shown in Table 1, for which only one additional generator, supplying loss current at the middle bottom u point was used. The measured displacements are remarkably close to the theoretical values, which are given in parentheses. However, no simple and easily applied rule has yet been found to determine the optimum position and magnitude of the loss-supplying units.

The case of simple bending was next tried. Table 2 shows the result when supplying part of the losses from the single generator on the middle bottom u point; here again, the agreement with the calculated displacement distribution is remarkably close.

Attention was next turned to the circuit for the three-dimensional field having axial symmetry, shown in Fig. 18 of the companion paper.[2] The case of a cylinder with uniform external pressure, impressed here as a uniform radial displacement, is illustrated by Table 3; it has in addition a generator supplying losses through the middle point on the top boundary. The cylinder represented is 1 in. inside radius, 2 in. outside radius, and 0.8 in. long; calculated displacements are given in parentheses. Table 4 is for the same cylinder with uniform internal displacement.

Numerical Solution

The final step in this study of the equivalent circuits of the elastic field was the numerical solution of a particular case by hand. Such a procedure would be alternative to a direct solution of the differential equations; it is believed to offer some advantages in that Southwell's "relaxation" method of solution[4] is directly applicable, the unliquidated loads are always apparent, and any means whatever, from network-analyzer tests to ESP (mental telepathy), may be utilized in improving the solution.

The case chosen is a cantilever beam with the fixed end rigidly held both for axial and for vertical displacements; the beam is 1.2 in. long and 0.4 in. deep. Plane strain is assumed, and the loadings used are per inch of width. A mesh size of $\Delta x = .0.2$ in. and $\Delta y = 0.1$ in. is used. The load consists of 256 lb shear load distributed parabolically over the free-end cross section, and an

TABLE 3 DISPLACEMENTS IN A CYLINDER UNDER EXTERNAL PRESSURE (NEGATIVE)

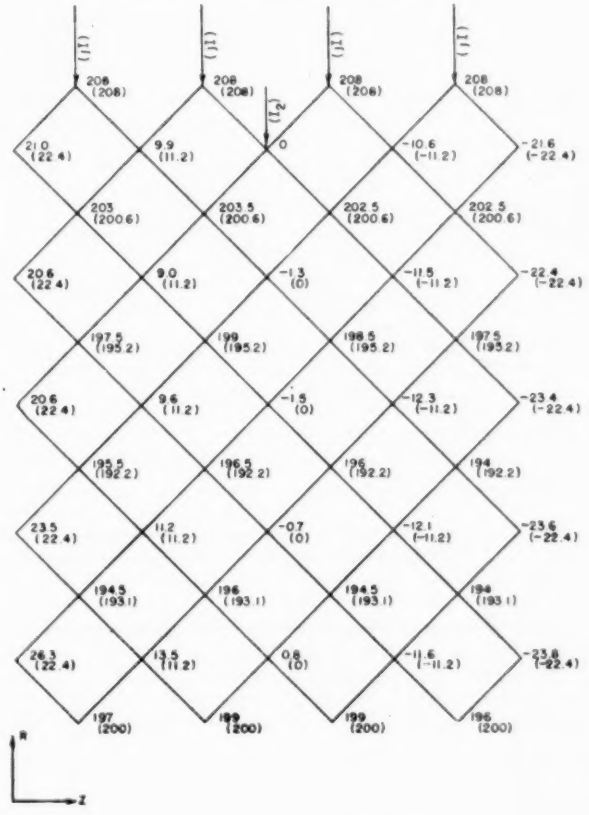


TABLE 4 DISPLACEMENTS IN A CYLINDER UNDER INTERNAL PRESSURE

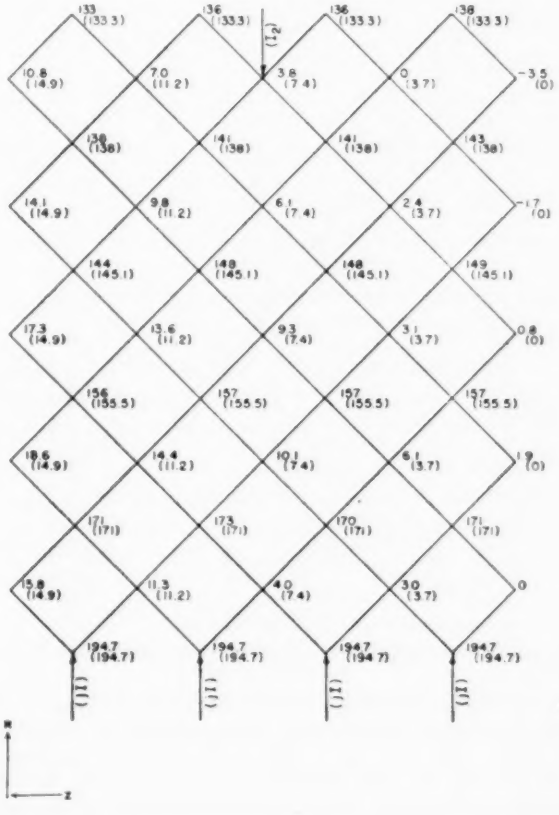
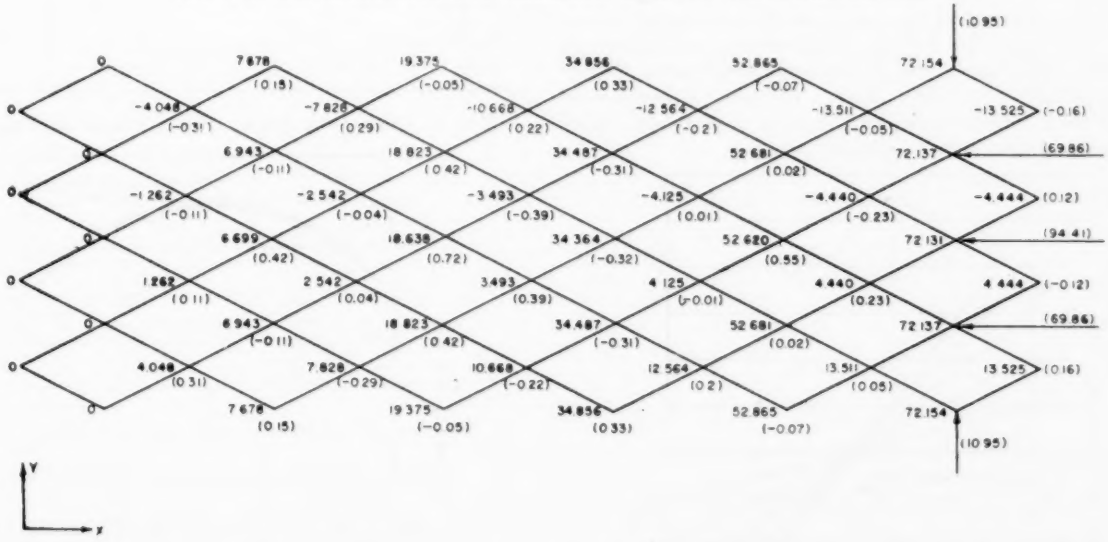


TABLE 5 DISPLACEMENTS AND RESIDUAL LOADS IN A CANTILEVER BEAM



additional concentrated load of 11 lb at the top and bottom edge of this cross section. The elastic moduli are divided by 100,000, so as to eliminate unnecessary zeros; this factor must be divided into the listed displacements to give results in inches.

The electric circuit for this case was solved by a relaxation method to five significant figures for the largest displacements, that is, a change of one unit in the last place of any of the displacement numbers would give a larger residual load at that point than existed before the change. Table 5 gives the displacements, with the residual loads in parentheses. The results are given graphically in Figs. 3 to 9, inclusive. Fig. 3 is a plot of the x displacements at several cross sections; there is only slight departure from the linear variation assumed in simple beam theory. The y displacement of the neutral surface of the beam is given in Fig. 4, along with the curve calculated from simple beam theory, including approximately the deflection due to shear. The smaller deflection obtained in the field solution can be attributed at least partially to the more restrictive boundary condition, since no

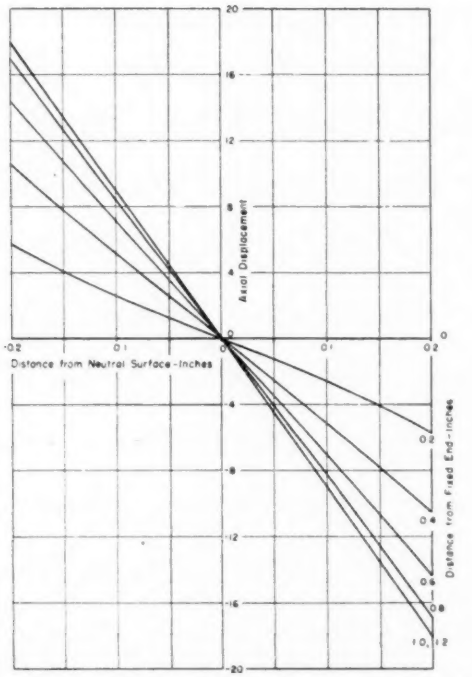


FIG. 3 CANTILEVER BEAM; AXIAL DISPLACEMENTS AT VARIOUS CROSS SECTIONS

vertical contraction is allowed at the fixed end in this case. The remaining figures are plots of the stress components. Fig. 5 gives the axial variation of shear stress; the variation vertically is shown in Fig. 6. The distribution is uniform along the beam and parabolic across it, except in the neighborhood of the applied forces. Fig. 7 shows that the direct stress in the axial direction varies practically linearly with depth, as assumed in simple beam theory; Fig. 8 shows that this stress is also linearly related to axial distance. Finally, Fig. 9 shows the distribution of the vertical direct-stress component; this is perceptible only in the vicinity of the applied vertical direct loads. The rapid attenuation of the end-stress concentrations with distance is of course simply another illustration of Saint Venant's principle.

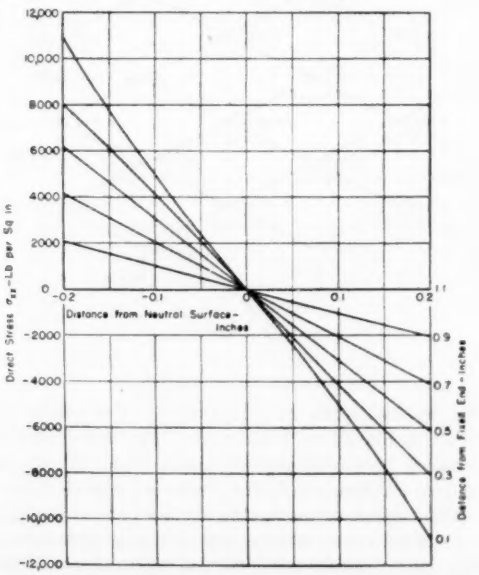


FIG. 7 CANTILEVER BEAM; DIRECT AXIAL STRESS AT VARIOUS CROSS SECTIONS

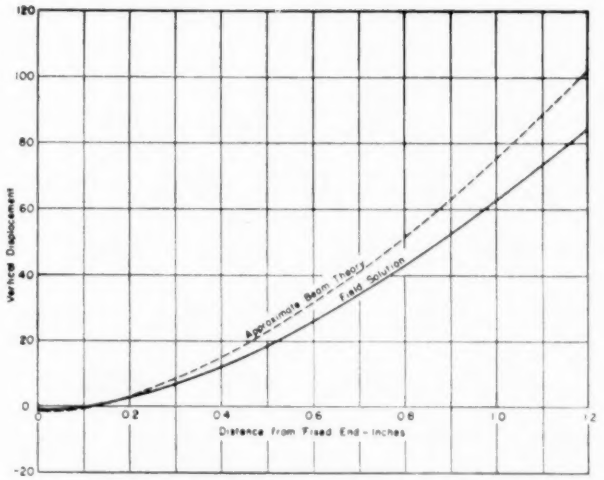


FIG. 4 CANTILEVER BEAM; DISPLACEMENT OF NEUTRAL SURFACE

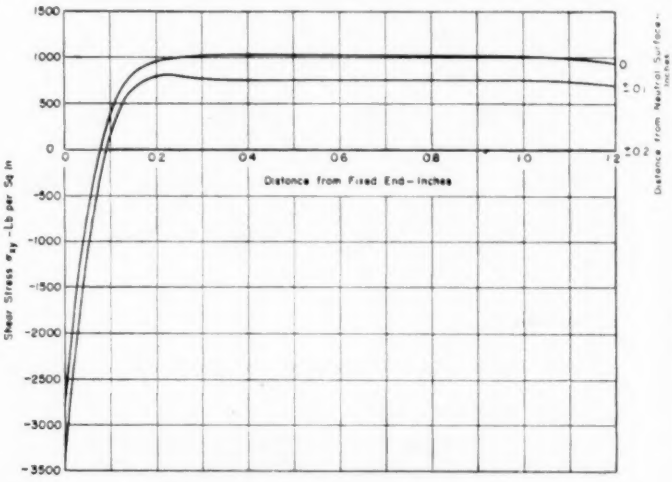


FIG. 5 CANTILEVER BEAM; SHEAR STRESS AT VARIOUS LEVELS

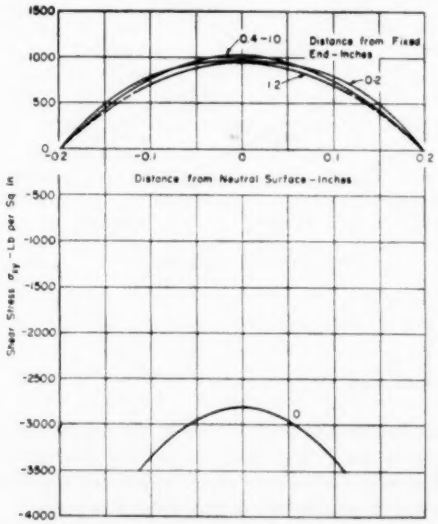


FIG. 6 CANTILEVER BEAM; SHEAR STRESS AT VARIOUS CROSS SECTIONS

SUMMARY

The purpose of the work reviewed in this paper was to study

the application of the equivalent circuit representation to the solution of elastic-field problems. This objective was sought in three ways: (1) Known solutions of certain field problems were used to give numerical checks on the validity of the circuit representation; these showed that the circuits are adequate for the

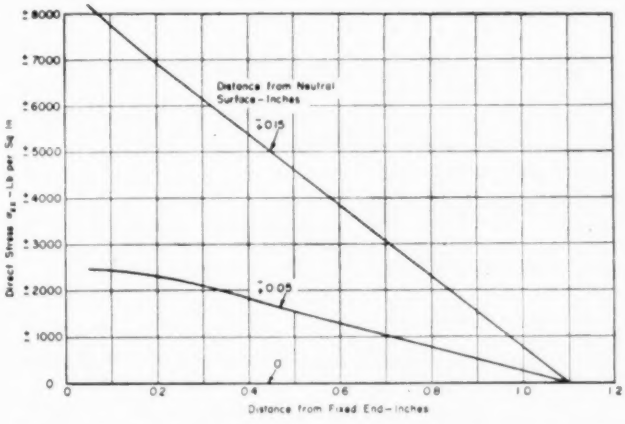


FIG. 8 CANTILEVER BEAM; DIRECT AXIAL STRESS AT VARIOUS LEVELS

purpose and suggested that only a moderately small mesh size is required. (2) Similar problems were set up on the a-c network analyzer to determine to what extent that instrument could be utilized in solving elastic-field problems; while good results could be obtained on the analyzer, the limited number of elements available and the unavoidable resistance effects offer some restriction to its usefulness. (3) A particular case was solved by hand, using the equivalent circuit as a framework for the calculations; this shows that it is feasible to solve elastic-field problems in this way directly from given boundary conditions. Application of the "relaxation" method in such a solution enables use to be made of analyzer results, approximate solutions, and intuition with respect to either the elastic field or the electric network; and there is indication at all times of the degree of approximation of the solution, in terms of the unliquidated loads (currents).

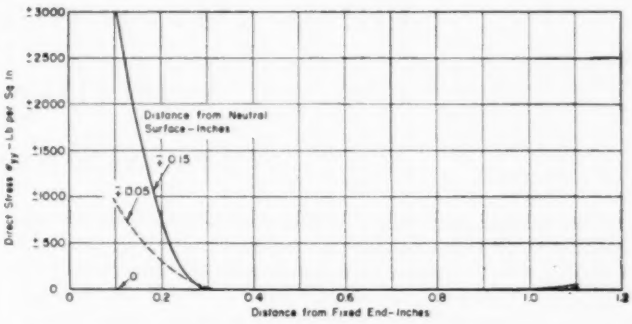


FIG. 9 CANTILEVER BEAM; DIRECT VERTICAL STRESS AT VARIOUS LEVELS

ACKNOWLEDGMENT

The author acknowledges with pleasure the co-operation of his associates in the General Electric Company in the work described in this paper; particularly valuable have been the advice received from Gabriel Kron and Charles Concordia, and the careful calculations contributed by Mrs. Mary Dyrkacz.

Basic Mechanics of the Metal-Cutting Process

By M. EUGENE MERCHANT,[1] CINCINNATI, OHIO

The author presents a mathematical analysis of the geometry and mechanics of the metal-cutting process, covering two common types of geometry which occur in cutting. This analysis offers a key for the study of engineering problems in the field of metal cutting in terms of such fundamental quantities as strain, rate of shear, friction between chip and tool, shear strength of the metal, work done in shearing the metal and in overcoming friction, etc. The two cases covered are, in essence, that of a straight-edged cutting tool moving relative to the workpiece in a direction perpendicular to its cutting edge, termed "orthogonal cutting," and that of a similar cutting tool so set that the cutting edge is oblique to the direction of relative motion of tool and work, termed "oblique cutting." Equations are developed which permit the calculation of such quantities as those just enumerated from readily observable values. The theoretical findings are particularly applicable and significant in the case of present-day high-speed machining operations with sintered-carbide tools.

Nomenclature

The following nomenclature is used in this paper:

A_0 = cross-sectional area of "chip" before removal from workpiece = $w_1 t_1$

A_c = cross-sectional area of chip after removal from workpiece = $w_2 t_2$

A_s = area of shear plane = $\dfrac{w_3 t_1}{\sin \phi}$

F = friction force; force component acting between tool face and sliding chip

F_c = cutting force; force component acting in direction of motion of tool relative to workpiece

F_l = lateral force; force component acting in direction perpendicular to F_c and parallel to surface generated

F_n = force component acting in direction perpendicular to shear plane

F_s = shearing force; force component acting in direction of shear of metal, in shear plane

F_t = thrust force; force component acting in direction perpendicular to F_c and to surface generated

L_1 = arbitrary distance measured in direction of relative motion of cutting tool and workpiece

L_2 = distance through which point on chip moves relative to cutting tool, when tool advances distance L_1

L_3 = distance through which point on chip moves relative to workpiece when tool advances distance L_1

N = normal force; force component acting perpendicular to tool face

R, R' = resultant forces; forces acting between chip and tool and between chip and workpiece

r_c = cutting ratio = r_L

r_L = chip length ratio = $\dfrac{L_2}{L_1}$

r_t = chip thickness ratio = $\dfrac{t_1}{t_2}$

r_w = chip width ratio = $\dfrac{w_1}{w_2}$

S_s = mean shear stress on shear plane; mean shear strength of metal being cut

t = conventional true rake angle; rake angle of tool as measured in plane parallel to direction of relative motion of work and tool and perpendicular to surface generated

t_1 = thickness of "chip" before removal from workpiece

t_2 = thickness of chip after removal from workpiece, as measured in direction perpendicular to face of cutting tool

V_c = cutting velocity; velocity of tool relative to workpiece

V_f = chip-flow velocity; velocity of chip relative to cutting tool

V_s = velocity of shear; velocity of chip relative to workpiece

w_1 = width of chip before removal from workpiece

w_2 = width of chip after removal from workpiece

w_3 = width of shear plane, as measured in direction parallel to cutting edge of tool

W_c = work done in cutting, per unit volume of metal removed

W_f = work done in overcoming friction between chip and tool, per unit volume of metal removed

W_s = work done in shearing of metal, per unit volume of metal removed

α = oblique rake angle; rake angle of tool as measured in plane perpendicular to its cutting edge

β = chip flow angle; angle between a perpendicular to cutting edge and the direction of chip flow over face of tool, as measured in plane of tool face

γ = angle of inclination of cutting edge; angle between direction of motion of tool relative to work and a perpendicular to cutting edge of tool, as measured in plane of surface generated

δ = angle between direction of shear of metal on shear plane and a perpendicular to cutting edge of tool, as measured in shear plane

ϵ = shearing strain undergone by chip during process of removal

μ = coefficient of friction acting between sliding chip and tool face = F/N

σ = angle defined in Fig. 10

τ = friction angle = arc tan μ

ϕ = shear angle; angle between shear plane and surface being generated, measured in plane perpendicular to cutting edge of tool

---

[1] Physicist, Research Department, Cincinnati Milling Machine Company.

Contributed by the Applied Mechanics Division for presentation at the Annual Meeting, New York, N. Y., Nov. 27–Dec. 1, 1944, of The American Society of Mechanical Engineers.

Discussion of this paper should be addressed to the Secretary, A.S.M.E., 29 West 39th Street, New York, N. Y., and will be accepted until January 10, 1945, for publication at a later date. Discussion received after the closing date will be returned.

Note: Statements and opinions advanced in papers are to be understood as individual expressions of their authors and not those of the Society.

Introduction

A knowledge of the basic force relationships and the associated geometry occurring in the process of cutting metal is a necessity if the solution of engineering problems arising in that field is to be handled on anything other than an empirical basis. In this paper an analysis of the force systems and the geometry of chip formation occurring in two common types of cutting processes is presented.

The first and somewhat special case, considered in Part 1 of this paper, is that of a cutting tool having a plane face and a single straight cutting edge, generating a plane surface parallel to the original plane surface of the workpiece, and so set that the cutting edge is perpendicular to the direction of relative motion of tool and workpiece. In this case the force system can be considered to be two-dimensional. We shall characterize this type of cutting by the term "orthogonal cutting."

The second and quite general case, considered in Part 2 of this paper, is that of a tool similar to the preceding one, but with the cutting edge oblique to the direction of relative motion of tool and workpiece. This case involves a three-dimensional force system. This type of cutting is sometimes called a shearing cut. We shall, however, characterize this type of cutting by the term "oblique cutting," as actually all cutting involves a shearing of the material being cut.

The Geometry of Chip Formation

The type of chip formation dealt with in this analysis is that of a continuous chip with no built-up edge adjacent to the tool face, often designated as a type-2 chip.[2] Of interest is the fact that this is the type of chip obtained in machining operations employing sintered-carbide cutting tools with either negative or positive true rake angles, operating at relatively high cutting speeds; a type of operation which is playing such a large and important part in our present-day war production.

This type of chip formation is illustrated in Figs. 1 and 2. Fig. 1 is a photomicrograph of a chip obtained with a positive-rake-angle carbide tool cutting S.A.E. 1112 steel at a speed of 310 fpm, while Fig. 2 is a photomicrograph of a similar chip obtained with a negative-rake-angle tool cutting at a speed of 780 fpm.

It may be seen from either of these photomicrographs that a continuous chip is formed by a process of shear which is mainly confined to a single plane extending from the cutting edge to the work surface. That this is the general mechanism of the formation of a continuous chip was recognized at least as long ago as 1877 by J. Thime,[3] and many later workers have taken cognizance of this fact. However, the significance of the *variability* of the direction of shear has only recently been recognized by Ernst and Merchant.[4] In the present analysis still further significance is found to be attached to the direction of shear.

1 Orthogonal Cutting With a Straight-Edged Tool

Geometrical Relationships

In the case of orthogonal cutting, the tool is so set that its cut-

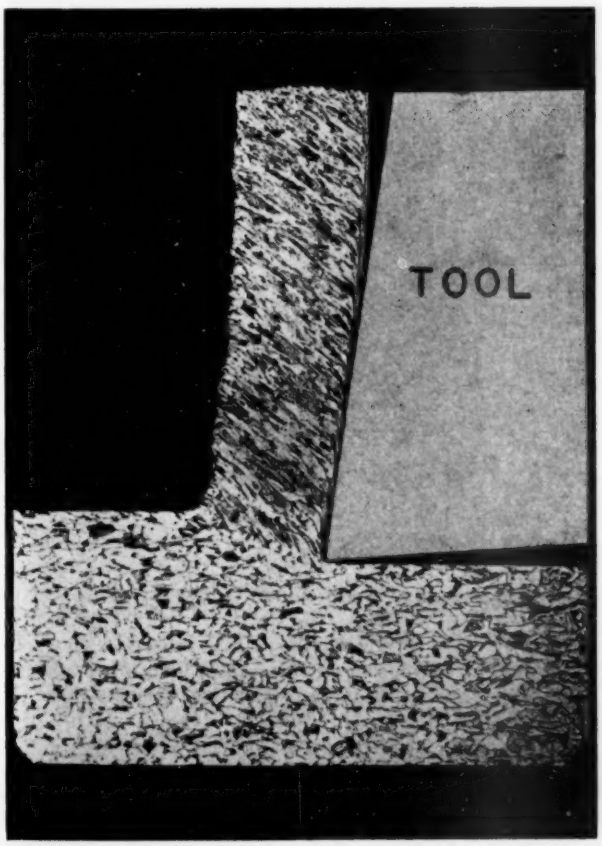


Fig. 1 Photomicrograph Illustrating Geometry of Chip Formation in Case of Orthogonal Cutting With a Positive-Rake-Angle Tool Producing a Continuous Chip Without Built-Up Edge
(Sintered-carbide tool, $\alpha = 10$ deg, $V_c = 310$ fpm, S.A.E. 1112 steel; × 65.)

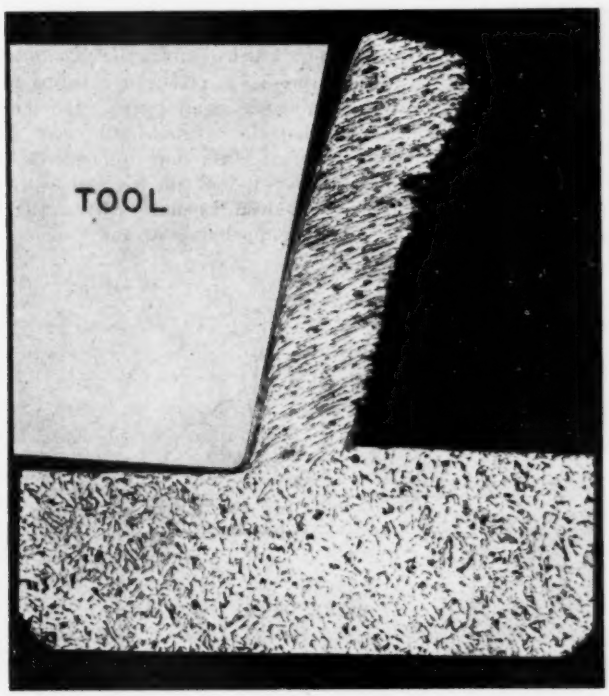


Fig. 2 Photomicrograph Illustrating Geometry of Chip Formation in Case of Orthogonal Cutting With Negative-Rake-Angle Tool; Similarity to Fig. 1 Is Evident
(Sintered-carbide tool, $\alpha = -10$ deg, $V_c = 780$ fpm, S.A.E. 1112 steel; × 65.)

[2] "Physics of Metal Cutting," by Hans Ernst, *Machining of Metals*, Transactions of the American Society for Metals, 1938, p. 24.

[3] "Mémoires sur le Rabotage des Metaux," by J. Thime, St. Petersburg, Russia, 1877.

[4] "Chip Formation, Friction, and High-Quality Machined Surfaces," by H. Ernst and M. E. Merchant, *Surface Treatment of Metals*, Transactions of the American Society for Metals, 1941, pp. 299–378.

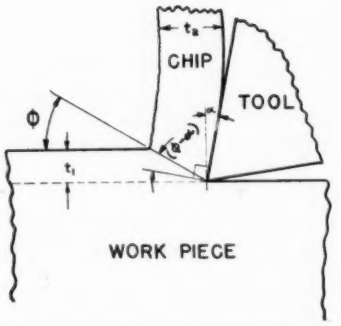


FIG. 3 SCHEMATIC REPRESENTATION OF GEOMETRY OF CHIP FORMATION IN CASE OF ORTHOGONAL CUTTING AND A CONTINUOUS CHIP WITHOUT BUILT-UP EDGE

ting edge is perpendicular to the direction of relative motion of tool and workpiece and generates a plane surface parallel to the original work surface. The geometry involved in this case is shown schematically in Fig. 3. The rake angle of the tool is designated by α, and the angle which the plane of shear makes with the surface generated is designated by ϕ. The thickness of the chip before removal is designated by t_1, and that after its removal by t_2. Knowing t_1, t_2, and α, ϕ can be determined from the following equation readily derivable from the geometry of Fig. 3

$$\tan \phi = \frac{t_1/t_2 \cos \alpha}{1 - t_1/t_2 \sin \alpha} \quad \ldots\ldots [1]$$

The ratio t_1/t_2 appearing in Equation [1] will be called the "chip thickness ratio" and designated by the symbol r_t. Then, from Equation [1]

$$r_t = \frac{t_1}{t_2} = \frac{\sin \phi}{\cos (\phi - \alpha)} \quad \ldots\ldots [1a]$$

If the small amount of side flow which occurs in the chip during removal is neglected, then in the case of orthogonal cutting the chip is the same width before removal as afterward. It follows from volume considerations that the "chip length ratio" r_L, which is found by dividing the length of the chip after removal by the length of the path from which it was cut, is equal to t_1/t_2. This chip length ratio will also be given the name "cutting ratio" here, for reasons which will become apparent later, and designated by the symbol r_c. Then

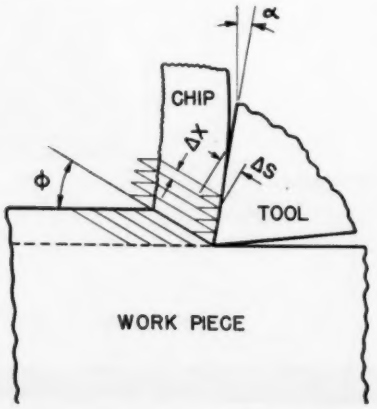


FIG. 4 SCHEMATIC REPRESENTATION OF THE PHYSICAL SIGNIFICANCE OF SHEARING STRAIN IN METAL-CUTTING PROCESS

$\left(\text{Strain} = \frac{\Delta S}{\Delta X}. \text{ In actual cutting } \Delta X \to 0.\right)$

$$r_c = r_L = \frac{L_2}{L_1} = \frac{t_1}{t_2} = r_t \quad \ldots\ldots [2]$$

In order to determine the shearing strain ϵ, which is undergone by the chip during its removal from the workpiece, the cutting process may for convenience be pictured as consisting of the displacement of a series of platelike elements of thickness ΔX through a distance ΔS relative to each other, as shown in Fig. 4. (In the actual process of cutting, ΔX of course approaches zero.) Then, from the geometry of Fig. 4

$$\text{Strain} = \epsilon = \frac{\Delta S}{\Delta X} = \cot \phi + \tan (\phi - \alpha) \quad \ldots\ldots [3]$$

As will be shown later, this is the true or natural strain in the chip, since the product of this quantity by the mean shear strength of the material gives the work done in shear per unit volume of metal removed.

In connection with Equation [3], it is of interest to investigate the value of ϕ which will make the strain a minimum for any given value of α. Thus

$$\frac{\partial \epsilon}{\partial \phi} = -\csc^2 \phi + \sec^2 (\phi - \alpha = 0$$

or

$$\phi = 90 - (\phi - \alpha)$$

$$[\phi]_{\epsilon = \min} = \frac{\alpha}{2} + 45 \text{ deg} \quad \ldots\ldots [4]$$

Substituting Equation [4] into Equation [1a], and bearing in mind Equation [2]

$$[r_c]_{\epsilon = \min} = \frac{\sin \left(45 + \frac{\alpha}{2}\right)}{\cos \left(45 - \frac{\alpha}{2}\right)} = 1 \quad \ldots\ldots [5]$$

or the cutting ratio must be unity in order for the strain to be a minimum.

The velocity relations for orthogonal cutting are shown in Fig.

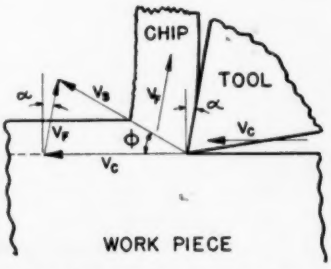


FIG. 5 VELOCITY RELATIONSHIPS IN CASE OF ORTHOGONAL CUTTING

5, where V_c is the cutting velocity, V_s the velocity of shear, and V_f the velocity of chip flow up the tool face. Fig. 5 is based upon the fact that the velocity of the chip relative to the workpiece (V_s) is equal to the vector sum of the velocity of the chip relative to the tool (V_f) and the velocity of the tool relative to the workpiece (V_c). It can be shown mathematically that the shearing velocity V_s is the actual velocity of the chip relative to the workpiece, but that will not be done here since the fact is fairly self-evident.

The following velocity relationships can evidently be derived from the geometry of Fig. 5

$$V_s = V_c \frac{\cos \alpha}{\cos (\phi - \alpha)} \quad \ldots\ldots [6]$$

$$Vf = V_c \frac{\sin \phi}{\cos (\phi - \alpha)} = V_e r_c \quad [7]$$

Force Relationships

Many previous investigators have attempted to make a theoretical analysis of the forces involved in cutting. Among these may be mentioned Thime,[3] Sellergren,[5] Stanton and Hyde,[6] Kronenberg,[7] and Gleboff-Heintz.[8]

However, these earlier workers apparently did not succeed in grasping the character of the force system involved in cutting,[9] probably because they failed to hit upon the useful device of considering the chip to be a "separate" body held in equilibrium by action of the force system. More recently, by use of this device, the author has developed a force system[10,4] for the case of

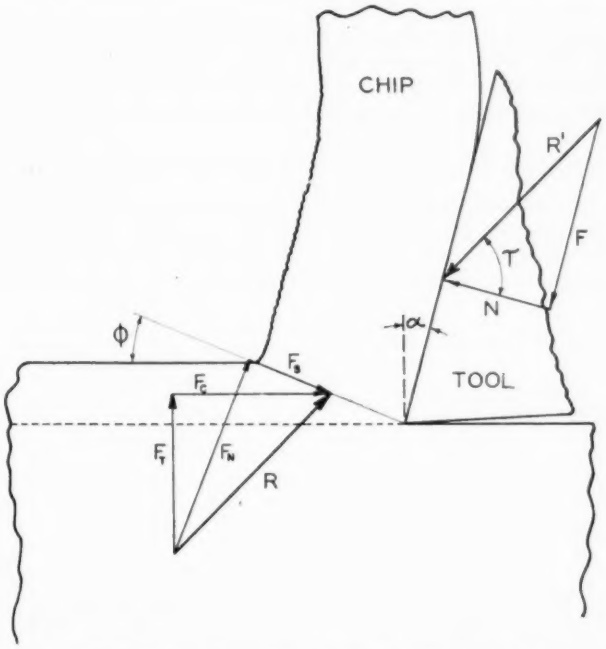


Fig. 6 Force System Acting in Case of Orthogonal Cutting, Showing Chip in Equilibrium Under Action of Equal and Opposite Resultant Forces R and R'

orthogonal cutting which appears to be physically consistent, judging by the results obtained with it to date in interpreting experimental data obtained from numerous cutting tests.

This force system is shown in Fig. 6. The chip may be considered as an independent body held in mechanical equilibrium by the action of the two equal and opposite resultant forces R and R' (neglecting a small couple arising from the fact that R and R' are not exactly collinear, which plays no part in the present discussion). Force R is the force which the workpiece exerts on the chip, while R' is the force which the tool exerts on the chip. The force R' may be resolved into a component F along the tool face, which is the force of friction acting between chip and tool, and a component N which is the force acting normal to the chip-tool interface. Thus the coefficient of friction μ acting between chip and tool is given by

$$\mu = \frac{F}{N} = \tan \tau \quad [8]$$

The force R in Fig. 6 may be resolved into a horizontal component F_c, the cutting force, which is responsible for the total work done in cutting, and into a component F_t, the thrust force, which does no work. Force R may also be resolved into a component along the shear plane F_s, the shearing force, which is responsible for the work done in shearing the metal, and into a component F_n normal to the shear plane.

Since R and R' are equal parallel forces, we may represent all their components as components of a single vector R, located for convenience at the tool point, as shown in Fig. 7. The relationships between the various components are readily perceived in this case.

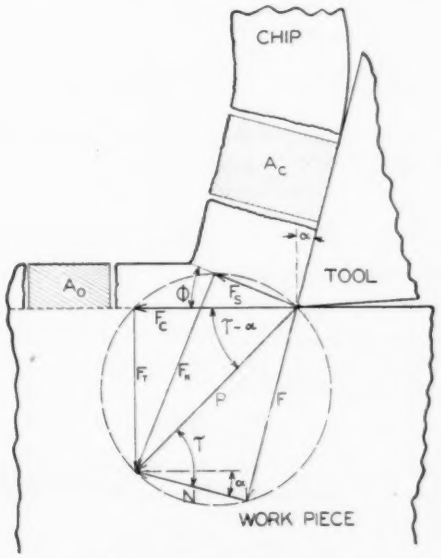


Fig. 7 Condensed Form of Force Diagram Derived From Fig. 6 Conveniently Indicating Geometrical Relationships Between Force Components

The directly measurable or readily obtainable quantities from among those shown in Fig. 7 are F_c, F_t, A_0, ϕ, and α. The remaining quantities shown, as well as other quantities of basic interest, can be calculated from these observables with the aid of the relationships now to be developed.

The equation for the coefficient of friction μ can be readily obtained as follows

$$\tan (\tau - \alpha) = \frac{Ft}{F_c} \quad [9]$$

thus

$$\mu = \tan \tau = \frac{F_t + F_c \tan \alpha}{F_c - F_t \tan \alpha} \quad [10]$$

[5] "Das Messen des Widerstandes der Metalle bei Anwendung von Schneidestählen," by G. Sellergren, *Zeitschrift des Oesterr Ingenieur und Architekten Vereines*, vol. 48, 1896, pp. 473–478.

[6] "An Experimental Study of the Forces Exerted on the Surface of a Cutting Tool," by T. E. Stanton and J. H. Hyde, Proceedings of The Institution of Mechanical Engineers, vol. 99, 1925, pp. 141–220.

[7] "Grundzüge der Zerspanungslehre," by M. Kronenberg, Julius Springer, Berlin, 1927.

[8] "Theory of Economical Metal Cutting," by S. F. Gleboff-Heintz, Moscow, 1933.

[9] Since writing the foregoing, a Finnish paper has come to the attention of the author, "Lastunmuodostumisen Teoriaa," by Väinö Piispanen, *Teknillinen Aikakauslehti*, vol. 27, 1937, p. 315, in which a force system similar to that shown in Fig. 6 is proposed. Only orthogonal cutting is considered. Although a suitable translation of this Finnish paper has not been obtained as yet, it appears that Piispanen's ideas concerning the chip geometry and the force system in orthogonal cutting are similar, in many respects, to those developed independently by the author.

[10] "Theory of Friction in Metal Cutting," by M. E. Merchant, University of Cincinnati Thesis, D.Sc., 1940 (confidential).

It can be seen directly from Fig. 7 that the force of friction F is

$$F = F_t \cos \alpha + F_c \sin \alpha \quad [11]$$

Similarly, it can be seen directly from Fig. 7 that the shearing force F_s is

$$F_s = F_c \cos \phi - F_t \sin \phi \quad [12]$$

If the area of the shear plane be designated by A_s and the cross-sectional area of the chip before removal by A_0, then

$$A_s = \frac{A_0}{\sin \phi} \quad [13]$$

Therefore, the mean shear stress S_s on the shear plane, which is equal to the mean shear strength of the material, is given by

$$S_s = \frac{F_s}{A_s} = \frac{F_c \sin \phi \cos \phi - F_t \sin^2 \phi}{A_0} \quad [14]$$

by virtue of Equations [12] and [13].

The work done in overcoming friction between the chip and tool, per unit volume of metal removed, which we shall designate by W_f, is found by dividing the frictional work done per unit of time by the volume of metal removed per unit of time; thus

$$W_f = \frac{FV_f}{A_0 V_c}$$

then, from Equation [7]

$$W_f = F \frac{r_c}{A_0} = F/A_c \quad [15]$$

Similarly, the work done in shear, per unit volume of metal removed, designated by W_s, is given by

$$W_s = \frac{F_s V_s}{A_0 V_c}$$

or, applying Equations [6] and [13]

$$W_s = \frac{F_s}{A_s} \frac{\cos \alpha}{\sin \phi \cos (\phi - \alpha)} = S_s [\cot \phi + \tan (\phi - \alpha)] \quad [16]$$

and therefore from Equation [3]

$$W_s = S_s \epsilon \quad [16a]$$

For comparison, the total work done in cutting, per unit volume of metal removed, designated by W_c, may be found as follows

$$W_c = \frac{F_c V_c}{A_0 V_c}$$

and, bearing in mind that the work done depends only upon the relative lengths of the velocity vectors and not on their direction, then from the geometry of Fig. 5

$$W_c = \frac{F_c}{A_0 V_c} (V_s \cos \phi + V_f \sin \alpha)$$

Introducing Equations [6] and [7] then gives

$$W_c = \frac{F_c}{A_0} \left[\frac{\cos \phi \cos \alpha + \sin \phi \sin \alpha}{\cos (\phi - \alpha)} \right]$$

and, making use of the geometry of Fig. 7

$$W_c = \frac{R}{A_0} \left[\frac{\cos (\tau - \alpha) \cos \phi \cos \alpha + \cos (\tau - \alpha) \sin \phi \sin \alpha}{\cos (\phi - \alpha)} \right]$$

$$= \frac{R}{A_0} \left[\frac{\cos (\phi + \tau - \alpha) \cos \alpha + \sin (\tau - \alpha) \sin \phi \cos \alpha + \cos (\tau - \alpha) \sin \phi \sin \alpha}{\cos (\phi - \alpha)} \right]$$

$$= \frac{F_s}{A_0} \frac{\cos \alpha}{\cos (\phi - \alpha)} + \frac{R}{A_0} \frac{\sin \phi}{\cos (\phi - \alpha)} \cdot [\sin (\tau - \alpha) \cos \alpha + \cos (\tau - \alpha) \sin \alpha]$$

Thus from Equations [13], [16], and [3] and the geometry of Fig. 7

$$W_c = S_s \epsilon + \frac{r_c}{A_0} (F_t \cos \alpha + F_c \sin \alpha)$$

and therefore from Equations [11] and [15]

$$W_c = S_s \epsilon + F/A_c$$

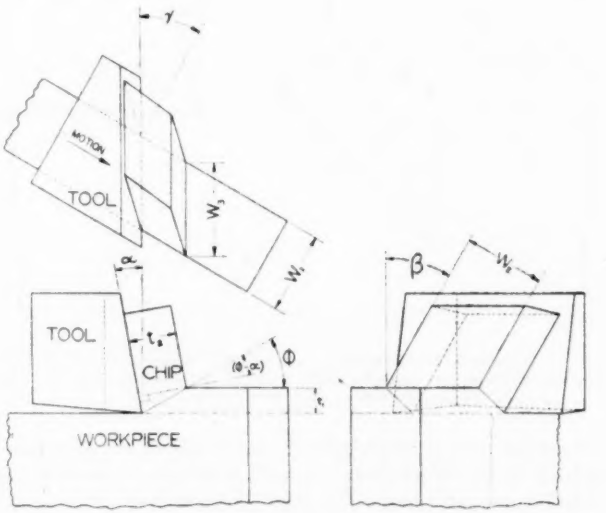
or, from Equations [15] and [16a]

$$W_c = W_s + W_f \quad [17]$$

Thus the total work done in cutting is equal to the sum of the work done in shearing the metal and the work done in overcoming friction between tool and chip. This result is one to be expected, but serves as a useful check on the logic employed.

2 OBLIQUE CUTTING WITH A STRAIGHT-EDGED TOOL

The formulas derived in Part 1 of this paper hold only for the case of orthogonal cutting (cutting edge perpendicular to direction of motion), and will be seen to be special cases of the more general formulas derived in this section for the case of oblique



NOTE: ANGLE β IS MEASURED IN PLANE OF TOOL FACE

FIG. 8 ORTHOGRAPHIC REPRESENTATION OF GEOMETRY OF OBLIQUE CUTTING

cutting. The idea that oblique cutting involved certain additional factors not present in orthogonal cutting was first expressed by Sellergren[5] in 1896, but apparently little further attention was given to this fact until now.

GEOMETRICAL RELATIONSHIPS

The three-dimensional geometry involved in the case of oblique cutting, in which a perpendicular to the cutting edge makes some angle γ with respect to the direction of relative motion of tool and work, is shown in Fig. 8. As in the previous case, the chip is formed by a process of shear on a plane which makes an angle ϕ with the surface generated. However, the direction of chip flow up the tool face is no longer perpendicular to the cutting edge, but makes an angle

β with such a perpendicular. For the sake of clarity in visualizing the oblique cutting process, the chip is here represented as having no tendency to curl away from the tool face, contrary, of course, to the behavior observed in practice, but without effect on the present analysis.

If the chip thickness ratio r_t is again defined as t_1/t_2, where t_1 and t_2 are the chip thicknesses measured as indicated in Fig. 8, then it is evident that Equations [1] and [1*a*] also hold for the case of oblique cutting, namely

$$\tan \phi = \frac{t_1/t_2 \cos \alpha}{1 - t_1/t_2 \sin \alpha} \quad [1]$$

$$r_t = \frac{t_1}{t_2} = \frac{\sin \phi}{\cos (\phi - \alpha)} \quad [1a]$$

where α is the rake angle of the tool measured in a plane perpendicular to the cutting edge. Angle α is known as the oblique rake angle as distinguished from the conventional true rake angle, t, (Fig. 9) which is measured in a plane parallel to the direction of relative motion of tool and work and perpendicular to the surface generated.

It is evident from Fig. 8 that the width w_2 of the chip after

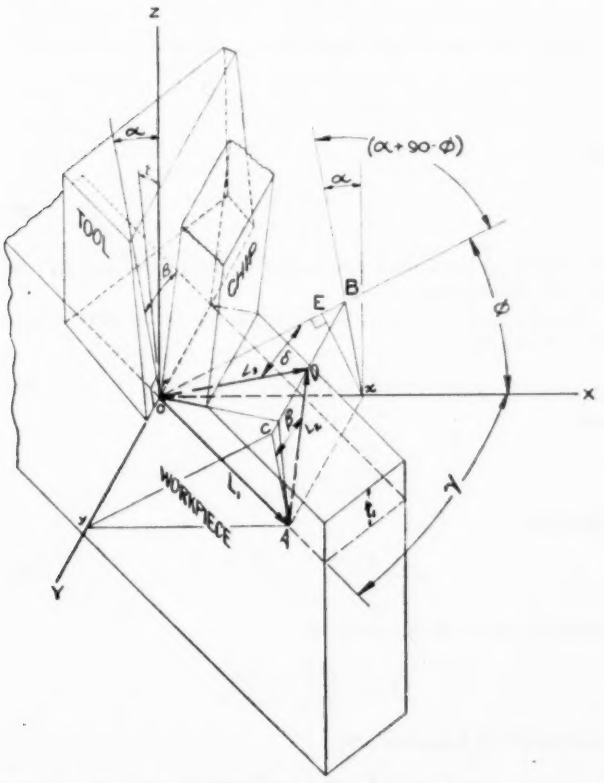


FIG. 9 OBLIQUE REPRESENTATION OF SYSTEM SHOWN IN FIG. 8, ILLUSTRATING FURTHER GEOMETRICAL RELATIONSHIPS OCCURRING IN OBLIQUE CUTTING

removal is greater than the width w_1 of the chip before removal. Knowing these widths and the angle γ, it is then possible to find the angle β from the following equation readily derivable from the geometry of Fig. 8

$$\cos \beta = \frac{\cos \gamma}{w_1/w_2} \quad [18]$$

If we call the ratio w_1/w_2 the "chip width ratio," r_w, then

$$r_w = \frac{w_1}{w_2} = \frac{\cos \gamma}{\cos \beta} \quad [18a]$$

A further appreciation of the geometry involved in oblique cutting may be obtained from Fig. 9, where X, Y, and Z axes have been introduced. The axes are so chosen that the cutting edge of the tool is parallel to the Y axis and thus perpendicular to the XZ plane. The direction of motion of tool relative to work is indicated by the vector L_1, and thus makes an angle γ with the X axis. Plane $OBCy$ is an extension of the shear plane, while plane $ACBx$ is parallel to the tool face and passes through the terminal point A of vector L_1. If the cutting tool advances along the workpiece a distance L_1, then a point which was originally at O on the chip will have advanced up the tool face a distance L_2 in the direction of chip flow, as given by β, and will have advanced relative to the workpiece a distance L_3 in the plane of shear, thus bringing it to point D. Thus L_3 represents the direction of shear of the metal on the shear plane. It is interesting to note that the direction of shear is not perpendicular to the cutting edge in the case of oblique cutting, but makes an angle δ with such a perpendicular. The smaller the angle δ is, the more the direction of chip flow deviates from a perpendicular to the cutting edge, and vice versa. From the geometry of Fig. 9, it is possible to derive the following relationship between δ and β

$$\tan \delta = \frac{\tan \gamma \cos (\phi - \alpha) - \tan \beta \sin \phi}{\cos \alpha} \quad [19]$$

It is evident that the cutting ratio, r_c, or chip length ratio, r_L, is given by the ratio of L_2 to L_1. The following expression for the cutting ratio can be derived from Fig. 9

$$r_c (= r_L) = \frac{L_2}{L_1} = \frac{\cos \gamma}{\cos \beta} \frac{\sin \phi}{\cos (\phi - \alpha)} \quad [20]$$

or, from Equations [1*a*] and [18*a*]

$$r_c = r_w r_t \quad [20a]$$

By analogy with the reasoning used in deriving Equation [3] for orthogonal cutting, it may be seen that in the case of oblique cutting, referring to Fig. 9, the shearing strain in the chip is

$$\text{Strain} = \epsilon = \frac{L_3}{Ex}$$

or, from the geometry of Fig. 9

$$\epsilon = \frac{\cot \phi + \tan (\phi - \alpha)}{\cos \delta} \quad [21]$$

Again it will be seen later that this expression represents the natural strain in the chip.

It is evident from the form of Equation [21] that in regard to ϕ the strain will be minimum for the same value of ϕ as that which made Equation [3] a minimum, or

$$[\phi]_{\epsilon = \min} = \frac{\alpha}{2} + 45 \text{ deg} \quad [4]$$

However, it may also be seen from Equation [21] that, with respect to δ, the strain will be a minimum when δ is zero, i.e.

$$[\delta]_{\epsilon = \min} = 0 \quad [22]$$

Substituting Equation [22] into Equation [19], and applying Equation [4], it is found that

$$\left[\frac{\tan \gamma}{\tan \beta}\right]_{\epsilon = \min} = \left[\frac{\sin \phi}{\cos (\phi - \alpha)}\right]_{\epsilon = \min} = 1 \quad [23]$$

However, the conditions expressed in Equation [23] make the value of Equation [20] unity, or

$$[r_e]_{e=\min} = 1$$

Thus, again, the cutting ratio must be unity for the strain to be a minimum. It may be noted that it is a necessary but not a sufficient condition for minimum strain that either r_t or r_w be unity, while r_L ($= r_c$) = 1 is both a necessary and sufficient condition for minimum strain. It is for this reason that the chip length ratio has been dignified by the special name of "cutting ratio."

It is evident from the foregoing discussion of the vectors L_1, L_2, and L_3, appearing in Fig. 9, that they are proportional, respectively, to the velocities of cutting, of chip flow, and of shear, or

$$\frac{V_c}{L_1} = \frac{V_f}{L_2} = \frac{V_s}{L_3} \quad \ldots\ldots\ldots\ldots\ldots\ldots [24]$$

On this basis, the following relationships can be derived from Fig. 9

$$V_s = V_c \frac{\cos \gamma \cos \alpha}{\cos \delta \cos (\phi - \alpha)} \quad \ldots\ldots\ldots\ldots\ldots\ldots [25]$$

$$V_f = V_c \frac{\cos \gamma \sin \phi}{\cos \beta \cos (\phi - \alpha)} = V_c r_c \quad \ldots\ldots\ldots [26]$$

Force Relationships

The three-dimensional force system acting upon the tool-chip-work system pictured in Fig. 9 is shown in Fig. 10 and refers to

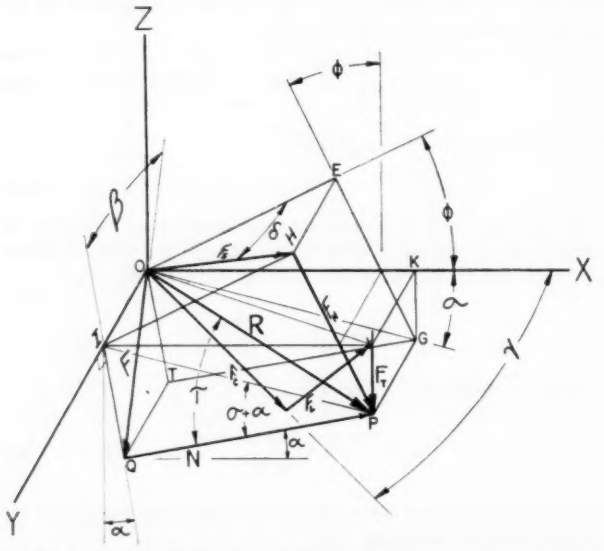


Fig. 10 Oblique Representation of Force System Acting in Case of Oblique Cutting, Indicating Geometrical Relationships Between Force Components

the same set of axes as used for Fig. 9. The outlines of the tool, chip, and workpiece have been omitted to eliminate inessential lines.

Plane *OIQT* represents an extension of the plane of the tool face, and plane *OEHI* an extension of the shear plane. Plane *EGPH* is perpendicular to the shear plane.

As in the case of the simple force system for orthogonal cutting, the force system for oblique cutting has been derived on the principle that the chip is held in equilibrium by two equal, opposite, and parallel resultant forces, which for simplicity have been combined into a single resultant force R in Fig. 10, just as was done in Fig. 7 in the case of orthogonal cutting.

The resultant force R in Fig. 10 may be resolved into a frictional component F in the plane of the tool face and acting necessarily in the direction of chip flow, as given by angle β, and into a normal component N perpendicular to the tool face. It may also be resolved into a shearing component F_s acting in the shear plane in the direction of shear, as given by angle δ and a normal component F_n perpendicular to the shear plane. Finally, R may be resolved into a component F_c which acts in the direction of cutting and is responsible for the total work done in cutting, a lateral component F_l, the lateral force, which is perpendicular to F_c and parallel to the surface generated, and a thrust component F_t which is perpendicular to F_c and to the surface generated.

The readily observable or directly measurable quantities from among those shown in Figs. 8, 9, and 10 are F_c, F_l, F_t, t_1, w_1, α, β (or δ), γ, and ϕ. The remaining quantities shown in Fig. 10, as well as other quantities of basic interest, can be calculated from these observables, with the aid of the relationships now to be developed.

Use will be made of the following equation derivable from Fig. 10

$$\tan \sigma = \frac{F_t}{F_c \cos \gamma + F_l \sin \gamma} \quad \ldots\ldots\ldots\ldots [27]$$

The coefficient of friction may be found as follows

$$\mu = \tan \tau = \frac{F}{N} = \frac{IQ}{N \cos \beta}$$

or

$$\mu = \frac{\tan (\sigma + \alpha)}{\cos \beta} \quad \ldots\ldots\ldots\ldots\ldots\ldots [28]$$

an expression to be used in conjunction with Equation [27] for the sake of simplicity of form.

The expression for the force of friction F may be derived from Fig. 10 as follows

$$IO = KJ = F_c \sin \gamma - F_l \cos \gamma \quad \ldots\ldots\ldots [29]$$

and

$$F = \frac{IO}{\sin \beta}$$

Therefore

$$F = \frac{F_c \sin \gamma - F_l \cos \gamma}{\sin \beta} \quad \ldots\ldots\ldots\ldots [30]$$

Similarly, for F_s, the shearing force

$$F_s = \frac{HE}{\sin \delta} = \frac{KJ}{\sin \delta}$$

and thus from Equation [29]

$$F_s = \frac{F_c \sin \gamma - F_l \cos \gamma}{\sin \delta} \quad \ldots\ldots\ldots\ldots [31]$$

The mean shear stress S_s on the shear plane, which is equal to the mean shear strength of the metal, is then evidently

$$S_s = \frac{\sin \phi \cos \gamma}{A_0 \sin \delta} (F_c \sin \gamma - F_l \cos \gamma)$$

The work done in overcoming friction between chip and tool, per unit volume of metal removed, is evidently

$$W_f = \frac{FL_2}{A_0 L_1}$$

or, from Equation [20]

$$W_f = \frac{F}{A_0} r_c = \frac{F}{A_c} \quad [32]$$

The work done in shearing the metal on the shear plane, per unit volume of metal removed, is evidently

$$W_s = \frac{F_s L_3}{A_0 L_1}$$

which from the geometry of Fig. 10 is found to be

$$W_s = \frac{F_s}{A_0} \frac{\cos \alpha \cos \gamma}{\cos \delta \cos (\phi - \alpha)} = S_s \epsilon \quad [33]$$

Since the work done in cutting has been seen to be the sum of the work done in overcoming friction and the work done in shearing the metal, then

$$W_c = W_s + W_f = S_s \epsilon + F/A_c \quad [34]$$

Conclusion

In the analyses presented in this paper only the fairly simple case has been considered in which all the cutting is done by a single straight cutting edge, and a plane surface is generated on the workpiece. However, the results can actually be applied quite accurately to such practical operations as milling, turning, planing, broaching, shaping, etc., with straight-edged tools, where a secondary cutting edge usually occurs, provided that the active length of the secondary cutting edge is quite small compared to the active length of the main cutting edge, and that the radius of curvature of the surface generated is not extremely small. This will be the case, for example, in face milling, if the depth of cut is quite large compared to the feed per tooth, and an ordinary size of milling cutter is employed; it will likewise be the case in turning, if the depth of cut is large compared to the feed per revolution, and the diameter of the workpiece is not unusually small.

The foregoing analyses also have, in theory at least, been limited to the case where a continuous chip is formed, with no built-up edge adjacent to the cutting edge of the tool. However, it has been found that the presence of a built-up edge actually introduces very little error, provided it is fairly small compared to the thickness of the chip. In fact, the discrepancies have been found not to be excessively large even in the case where a discontinuous chip is formed. As has already been pointed out, in the case of present-day machining operations with sintered-carbide cutting tools, the type of chip formation obtained is virtually identical with that discussed in this paper, thus making the application of the derived relationships to such operations particularly accurate.

In conclusion it may be mentioned that although in this paper the author has limited himself to a discussion of the metal-cutting process, it has undoubtedly been apparent to the reader that the analyses made apply equally well to any type of cutting process where the geometrical conditions are similar.

Acknowledgments

The author wishes to express his appreciation for the helpful comments and suggestions contributed by Mr. Hans Ernst, Research Director, and Dr. Max Kronenberg, member of the Research staff, both of the author's company, and to acknowledge certain experimental observations in regard to oblique cutting made by Prof. W. T. Dempster of the Anatomical Laboratory, University of Michigan, which were described by him in a personal communication, and which proved helpful to the author in arriving at an understanding of the geometry of chip formation in the case of oblique cutting.

Application of the Fourier Method to the Solution of Certain Boundary Problems in the Theory of Elasticity

By GERALD PICKETT,[1] CHICAGO, ILL.

The paper shows how the Fourier method may be used to obtain exact solutions for stresses in rectangular prisms or circular cylinders for any boundary condition.

Introduction

EXACT solutions for stresses in rectangular prisms or circular cylinders under any boundary conditions expressible by Fourier series can be obtained by the Fourier method, i.e., the stresses and displacements at the boundary have a finite number of ordinary discontinuities and a finite number of maxima and minima. The solutions are exact in the sense that stresses are expressed by series and become exact in the limit as more terms are used. To obtain these exact solutions, however, requires the use of more types of particular solutions in the same problem than are commonly used. The chief difference between the method, as explained in this paper, and the usual Fourier method for boundary-value problems is that not one[2] but two or more series of particular solutions are chosen as needed. Each of these series is selected so as to give a Fourier-series expression for one component of stress (or of displacement) at some boundary. The coefficients of the terms in a series are determined by Fourier analysis so as to give not only the desired stress (or displacement) at the boundary for which the series was selected but also to cancel any stress (or displacement) that may have been unavoidably introduced by the other series of particular solutions. Because of the interdependency of these two or more series of particular solutions, the expression for a coefficient of a term in one series will contain the coefficients of one or all the other series. The final solution, therefore, involves the solution of simultaneous equations giving relations between the coefficients.

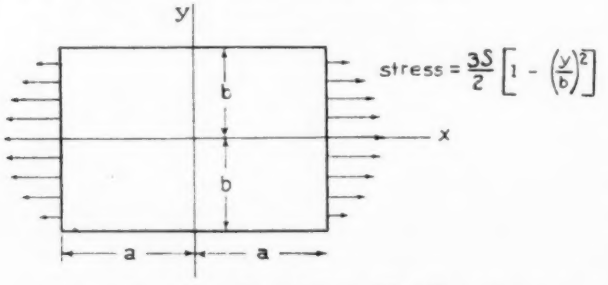


Fig. 1 Rectangular Plate Loaded With Parabolically Distributed Forces

[1] Research Physicist, Portland Cement Association. Mem. A.S.M.E.

[2] A series divided into a series of even functions and a series of odd functions is still considered as a single series in the present discussion.

Presented at the National Meeting of the Applied Mechanics Division, Chicago, Ill., June 16-17, 1944, of The American Society of Mechanical Engineers.

Discussion of this paper should be addressed to the Secretary, A.S.M.E., 29 West 39th Street, New York, N. Y., and will be accepted until October 10, 1944, for publication at a later date. Discussion received after the closing date will be returned.

Note: Statements and opinions advanced in papers are to be understood as individual expressions of their authors and not those of the Society.

Rectangular Plate

The method will now be demonstrated by solving for the stresses in the rectangular plate shown in Fig. 1. This particular problem was selected because of its relative simplicity and because it has been discussed several times in the literature (1),[3] (2), (3).[4] The fact that it is the simplest of the problems for which the usual methods fail probably accounts for the amount of attention it has received.

Detailed steps by which the correct particular solutions are obtained for each series need not be given here;[5] however, it may be verified by substitution that the following equations for stresses satisfy the appropriate differential equations[6] for all values of the constants A_n, B_m, α_n, and β_m.

$$\sigma_x = S + \sum_{n=1}^{\infty} \frac{A_n \cos \alpha_n y}{\cosh \alpha_n a} [\alpha_n x \sinh \alpha_n x - (1 + \alpha_n a \coth \alpha_n a) \cosh \alpha_n x] - \sum_{m=1}^{\infty} \frac{B_m \cos \beta_m x}{\cosh \beta_m b} [\beta_m y \sinh \beta_m y + (1 - \beta_m b \coth \beta_m b) \cosh \beta_m y] \quad [1]$$

$$\sigma_y = - \sum_{n=1}^{\infty} \frac{A_n \cos \alpha_n y}{\cosh \alpha_n a} [\alpha_n x \sinh \alpha_n x + (1 - \alpha_n a \coth \alpha_n a) \cosh \alpha_n x]$$

[3] The numbers in parentheses refer to the list of references given at the end of the paper.

[4] The paper by Winslow, which was presented at the Fourth International Congress of Applied Mechanics, is of interest because in it he concludes:

"1 For the simple arrangement of loading . . . the fundamental stress and strain relations of the elastic theory, when applied with mathematical precision, are inadequate and fail to give a stress solution.

"2 Therefore, in general, this mathematical theory of elasticity cannot lead to complete stress solutions which satisfy all boundary conditions (except in certain instances in which the conditions happen to be sufficiently reduced in complexity)."

Winslow's proof that a solution was impossible was based upon results he obtained by expanding certain functions of a complex variable about the corners of the plate. This was an error because those functions are in general discontinuous at the corners and, therefore, the expansion is not permissible.

[5] These solutions may be composed from the elementary forms given in the Appendix, or, since the boundary conditions are expressed in terms of stresses alone, these solutions are as readily obtained by means of a stress function (4).

[6] The differential equations are (4)

$$\frac{\partial \sigma_x}{\partial x} + \frac{\partial \tau_{xy}}{\partial y} = 0, \qquad \frac{\partial \sigma_y}{\partial y} + \frac{\partial \tau_{xy}}{\partial x} = 0, \qquad \nabla^2(\sigma_x + \sigma_y) = 0$$

The first two are the equilibrium equations and the third is the compatibility equation. The third is necessary when the equilibrium equations are expressed in terms of stresses but not necessary when they are expressed in terms of displacements.

Throughout this paper the nomenclature is that used by Timoshenko in his "Theory of Elasticity" (1).

$$+ \sum_{m=1}^{\infty} \frac{B_m \cos \beta_m x}{\cosh \beta_m b} [\beta_m y \sinh \beta_m y - (1 + \beta_m b \coth \beta_m b) \cosh \beta_m y] \quad [2]$$

$$\tau_{xy} = \sum_{n=1}^{\infty} \frac{A_n \sin \alpha_n y}{\cosh \alpha_n a} [\alpha_n a \coth \alpha_n a \sinh \alpha_n x - \alpha_n x \cosh \alpha_n x]$$

$$+ \sum_{m=1}^{\infty} \frac{B_m \sin \beta_m x}{\cosh \beta_m b} [\beta_m b \coth \beta_m b \sinh \beta_m y - \beta_m y \cosh \beta_m y] \quad [3]$$

The stress τ_{xy} will be zero at the edges $x = \pm a$ if $\beta_m = \frac{m\pi}{a}$, and this stress will also be zero at the edges $y = \pm b$ if $\alpha_n = \frac{n\pi}{b}$.

The substitution of $\sigma_y = 0$ and $y = \pm b$ into Equation [2] gives

$$\sum_{n=1}^{\infty} \frac{(-1)^n A_n}{\cosh \alpha_n a} [\alpha_n x \sinh \alpha_n x + (1 - \alpha_n a \coth \alpha_n a) \cosh \alpha_n x]$$

$$= \sum_{m=1}^{\infty} B_m [\beta_m b (\tanh \beta_m b - \coth \beta_m b) - 1] \cos \beta_m x \quad [4]$$

and the substitution of $\sigma_x = \frac{3}{2} S \left[1 - \left(\frac{y}{b}\right)^2\right]$ and $x = \pm a$ into Equation [1] gives

$$\frac{3}{2} S \left[1 - \left(\frac{y}{b}\right)^2\right] + \sum_{m=1}^{\infty} \frac{(-1)^m B_m}{\cosh \beta_m b} [\beta_m y \sinh \beta_m y + (1 - \beta_m b \coth \beta_m b) \cosh \beta_m y]$$

$$= S + \sum_{n=1}^{\infty} A_n [\alpha_n a (\tanh \alpha_n a - \coth \alpha_n a) - 1] \cos \alpha_n y \quad [5]$$

It is thus apparent that the A series was chosen to give a Fourier-series expression in the equation for σ_x at $x = \pm a$ and the B series was chosen so as to give a Fourier-series expression in the equation for σ_y at $y = \pm b$.

Equations for the coefficients A_n and B_m will now be determined in the usual manner. The multiplication of both sides of Equation [4] by $\cos \beta_n x \, dx$ and integration from $-a$ to $+a$ shows that

$$B_m = \frac{\sum_{n=1}^{\infty} (-1)^{n+m-1} \frac{4}{m\pi} \frac{na}{mb} \frac{\tanh \frac{n\pi a}{b}}{\left\{1 + \left(\frac{na}{mb}\right)^2\right\}^2} A_n}{1 + \frac{m\pi b}{a} \left(\coth \frac{m\pi b}{a} - \tanh \frac{m\pi b}{a}\right)} \quad [6]$$

Treating Equation [5] in a similar manner shows that

$$A_n = \frac{\frac{6S(-1)^n}{n^2\pi^2} + \sum_{m=1}^{\infty} (-1)^{n+m-1} \frac{4}{n\pi} \frac{mb}{na} \frac{\tanh \frac{m\pi b}{a}}{\left\{1 + \left(\frac{mb}{na}\right)^2\right\}^2} B_m}{1 + \frac{n\pi a}{b} \left(\coth \frac{n\pi a}{b} - \tanh \frac{n\pi a}{b}\right)} \quad [7]$$

When the A's and the B's have the values indicated by Equations [6] and [7], the boundary conditions for the normal stresses are exactly satisfied by Equations [1] and [2]. When the α's and the β's have the values just given, the boundary conditions for shear stresses are satisfied by Equation [3]. Thus all the arbitrary constants have now been determined, so that all three equations for stresses satisfy the boundary conditions.

The foregoing mathematical procedure is not entirely new, as it is very similar to that used by Taylor (5) and by Timoshenko (6) in problems of buckling and bending of rectangular plates.

Some indication of the rapidity of the convergence of the series is indicated by Figs. 2 and 3. Curve A in Fig. 2 shows the distribution of σ_x on the section $x = 0$ for a square plate ($a = b$) as computed when only the first term in each series is used. Curves B and C are obtained when two and four terms, respectively, are used in each series.

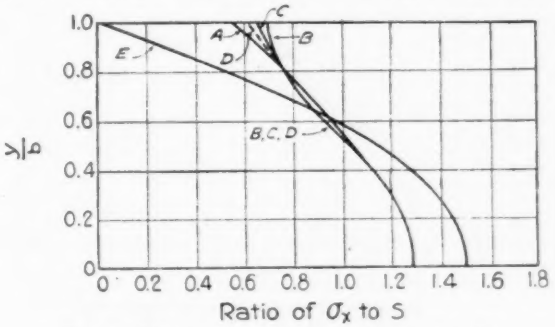


FIG. 2 DISTRIBUTION OF σ_x ON SECTION $x = 0$

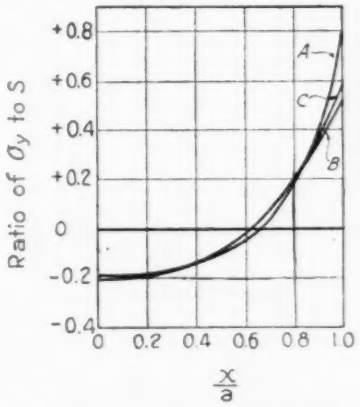


FIG. 3 DISTRIBUTION OF σ_y ON SECTION $y = 0$

For comparison, curve[7] D is shown, giving the distribution as computed by the energy method when three terms are used in the appropriate series (1). All four curves are practically alike except near the boundary $y = b$, indicating that each series requires only one term to give sufficient accuracy, except near the boundary. Similar results are indicated in Fig. 3: Curves A, B, and C show the distribution of σ_y on the section $y = 0$ as computed when one, two, and four terms, respectively, are used in each series.

Rectangular Plate Under Concentrated Loads. For a rectangular plate loaded with two equal and opposite concentrated forces, as shown in Fig. 4, the mathematical development is just like that previously given except that the boundary stress σ_x at $x = \pm a$ is

$$S + 2S \sum_{n=1}^{\infty} \cos \frac{n\pi y}{b}$$

[7] Curve E shows the parabolic distribution at $x = \pm a$.

This change necessitates a corresponding change in Equation [5], and $-2S$ replaces $\frac{6S(-1)^n}{n^2\pi^2}$ in Equation [7].[8]

Curves A, B, and C, Fig. 5, show the distribution of σ_y upon the section $y = 0$ for a square plate as computed when one, two, and four terms, respectively, are used in each series.

If an infinite number of terms were used in each series, the computed distribution would be approximately that given by the

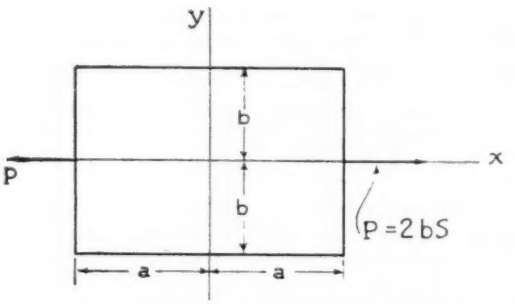


FIG. 4 PLATE LOADED WITH EQUAL AND OPPOSITE CONCENTRATED FORCES

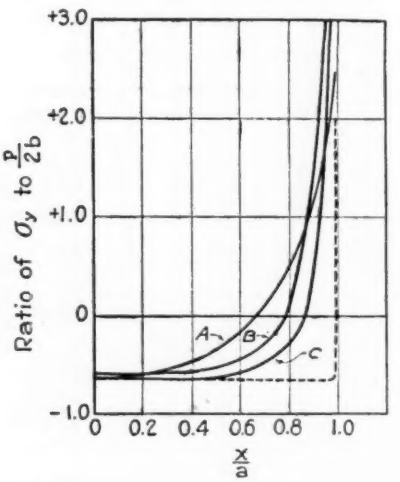


FIG. 5 DISTRIBUTION OF σ_y ON SECTION $y = 0$

dotted curve, i.e., $\sigma_y \approx -\frac{P}{\pi b}$ for all values of x except $x = \pm a$, where it is plus infinity.[9] The slower convergence in this problem is due to the slow convergence of Fourier series when discontinuous functions are represented by them. As is often true with Fourier analysis, the formal derivations are as simple when the boundary conditions are given by discontinuous functions as when given by simple algebraic functions.

For the problem just discussed, the energy method as used by Timoshenko and others is as usable as the method of this paper. However, the Fourier method is also applicable for any specified distribution of loads or displacements, whereas the energy method appears to be unsatisfactory when displacements are specified and may be inconvenient to use when the distribution of loading cannot be represented by a simple algebraic expression.

[8] For the boundary stress, $\sigma_x = f(y)$ at $x = \pm a$, this term in Equation [7] becomes

$$-\frac{1}{b}\int_{-b} f(y) \cos \frac{n\pi y}{b}\, dy$$

where $f(y)$ is an even function of y.

[9] The distribution of stress on this section of a square plate should be approximately the same as that upon the corresponding section of a circular disk (7). Goodier indicates a slightly different distribution of stress near the edges $x = \pm a$ (2).

CIRCULAR CYLINDER UNDER AXIAL COMPRESSION—FILON'S PROBLEM

To show how the method can be used when displacements are specified at part but not all of the boundary, the problem of a cylinder with given displacements at the ends will be considered. The example will be that of a cylinder loaded in compression, the loading being similar to that produced by the ordinary testing machine. In the usual testing of a cylinder, the cylinder is compressed longitudinally, as shown in Fig. 6. As it shortens, it tends to expand radially. Frictional forces at the planes of contact between the cylinder and the testing machine tend to prevent this expansion and also tend to make the ends concave. However, the rigidity of the testing machine keeps the ends approximately plane and in doing so gives rise to nonuniformity in the forces normal to the ends, the intensity of the normal forces being greater near the periphery than in the central part.

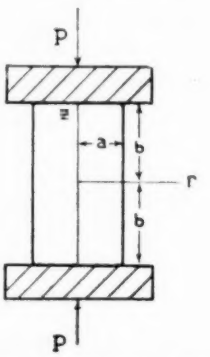


FIG. 6 CYLINDER COMPRESSED LONGITUDINALLY

The conditions just described are approximately represented by the following four boundary conditions:

I The shear stress τ_{rz} is zero at the cylindrical boundary $r = a$.

II The normal stress σ_r is zero at the cylindrical boundary $r = a$.

III The ends remain plane while being subjected to a resultant axial compressive force P.

IV The ends do not expand at any point, i.e., radial slipping at the planes of contact with the testing machine does not occur.

A series of particular solutions (the A-series to follow) can be found which satisfies conditions I and IV and gives a Fourier-Bessel expression for the vertical displacement at $z = \pm b$, and thus condition III can be met by the proper choice of Fourier-Bessel coefficients. This series alone will not satisfy condition II because of radial stresses at $r = a$. A second series (the B-series to follow) can be found which also satisfies conditions I and IV and gives a Fourier-series expression for the stress σ_r at $r = a$.

Without details as to how these particular solutions are chosen, the following equations for the radial displacement u and the vertical displacement w are given:

$$u = \sum_{n=0,1}^{\infty} \frac{A_n J_1(\beta_n r)}{\cosh \beta_n b} [z \sinh \beta_n z - b \tanh \beta_n b \cosh \beta_n z] + \sum_{m=1}^{\infty} \frac{B_m \cos \alpha_m z}{i J_1(i\alpha_m a)} \left[r J_0(i\alpha_m r) + \left(\frac{\lambda + 2G}{(\lambda + G)\alpha_m a} - \frac{J_0(i\alpha_m a)}{i J_1(i\alpha_m a)} \right) a i J_1(i\alpha_m r) \right] \quad [8]$$

$$w = \sum_{n=0,1}^{\infty} \frac{A_n J_0(\beta_n r)}{\cosh \beta_n b}\left[\left(\frac{\lambda + 3G}{\lambda + G} + \tanh \beta_n b\right) b \sinh \beta_n z - z \cosh \beta_n z\right] + \sum_{m=1}^{\infty} \frac{B_m \sin \alpha_m z}{iJ_1(i\alpha_m a)}\left[riJ_1(i\alpha_m r) - \left(\frac{\lambda + 2G}{(\lambda + G)\alpha_m a} + \frac{J_0(i\alpha_m a)}{iJ_1(i\alpha_m a)}\right) aJ_0(i\alpha_m r)\right] \quad \ldots [9]$$

Equations [8] and [9] satisfy the appropriate equations of equilibrium[10] for all values of the constants A_n, B_m, β_n, and α_m. The relations between the stresses and the displacements are

$$\sigma_r = \lambda\left(\frac{\partial u}{\partial r} + \frac{u}{r} + \frac{\partial w}{\partial z}\right) + 2G\frac{\partial u}{\partial r} \quad \ldots [10]$$

$$\sigma_\theta = \lambda\left(\frac{\partial u}{\partial r} + \frac{u}{r} + \frac{\partial w}{\partial z}\right) + 2G\frac{u}{r} \quad \ldots [11]$$

$$\sigma_z = \lambda\left(\frac{\partial u}{\partial r} + \frac{u}{r} + \frac{\partial w}{\partial z}\right) + 2G\frac{\partial w}{\partial z} \quad \ldots [12]$$

$$\tau_{rz} = G\left(\frac{\partial u}{\partial z} + \frac{\partial w}{\partial r}\right) \quad \ldots [13]$$

The substitution of Equations [8] and [9] into Equations [10] to [13] gives

$$\frac{\sigma_r}{2G} = \sum_{n=0,1}^{\infty} \frac{A_n}{\cosh \beta_n b}\left[\left\{\left(\frac{\lambda}{\lambda + G} - \beta_n b \tanh \beta_n b\right)\cosh \beta_n z + \beta_n z \sinh \beta_n z\right\} J_0(\beta_n r) + \left\{\beta_n b \tanh \beta_n b \cosh \beta_n z - \beta_n z \sinh \beta_n z\right\}\frac{J_1(\beta_n r)}{\beta_n r}\right] - \sum_{m=1}^{\infty} \frac{B_m \cos \alpha_m z}{iJ_1(i\alpha_m a)}\left[i\alpha_m r J_1(i\alpha_m r) + \left(1 - \frac{\alpha_m a J_0(i\alpha_m a)}{iJ_1(i\alpha_m a)}\right) J_0(i\alpha_m r) + \left(\frac{\lambda + 2G}{\lambda + G} - \frac{\alpha_m a J_0(i\alpha_m a)}{iJ_1(i\alpha_m a)}\right)\frac{iJ_1(i\alpha_m r)}{\alpha_m r}\right] \quad \ldots [14]$$

$$\frac{\sigma_\theta}{2G} = \sum_{n=0,1}^{\infty} \frac{A_n}{\cosh \beta_n b}\left[\frac{\lambda}{\lambda + G}\cosh \beta_n z J_0(\beta_n r) - \left\{\beta_n b \tanh \beta_n b \cosh \beta_n z - \beta_n z \sinh \beta_n z\right\}\frac{J_1(\beta_n r)}{\beta_n r}\right] + \sum_{m=1}^{\infty} \frac{B_m \cos \alpha_m z}{iJ_1(i\alpha_m a)}\left[\frac{G}{\lambda + G} J_0(i\alpha_m r) + \left(\frac{\lambda + 2G}{\lambda + G} - \frac{\alpha_m a J_0(i\alpha_m a)}{iJ_1(i\alpha_m a)}\right)\frac{iJ_1(i\alpha_m r)}{\alpha_m r}\right] \quad \ldots [15]$$

[10] These equations are as follows:

$$G\left(\nabla^2 u - \frac{u}{r^2}\right) + (\lambda + G)\frac{\partial}{\partial r}\left(\frac{\partial u}{\partial r} + \frac{u}{r} + \frac{\partial w}{\partial z}\right) = 0$$

$$G\nabla^2 w + (\lambda + G)\frac{\partial}{\partial z}\left(\frac{\partial u}{\partial r} + \frac{u}{r} + \frac{\partial w}{\partial z}\right) = 0$$

$$\frac{\sigma_z}{2G} = \sum_{n=0,1}^{\infty} \frac{A_n J_0(\beta_n r)}{\cosh \beta_n b}\left[\left(\frac{\lambda + 2G}{\lambda + G} + \beta_n b \tanh \beta_n b\right)\cosh \beta_n z - \beta_n z \sinh \beta_n z\right] + \sum_{m=1}^{\infty} \frac{B_m \cos \alpha_m z}{iJ_1(i\alpha_m a)}\left[i\alpha_m r J_1(i\alpha_m r) - \left(2 + \frac{\alpha_m a J_0(i\alpha_m a)}{iJ_1(i\alpha_m a)}\right) J_0(i\alpha_m r)\right] \quad \ldots [16]$$

$$\frac{\tau_{rz}}{2G} = \sum_{n=0,1}^{\infty} \frac{A_n J_1(\beta_n r)}{\cosh \beta_n b}\left[\beta_n z \cosh \beta_n z - \left(\frac{G}{\lambda + G} + \beta_n b \tanh \beta_n b\right)\sinh \beta_n z\right] + \sum_{m=1}^{\infty} \frac{B_m \sin \alpha_m z}{iJ_1(i\alpha_m a)}\left[\frac{\alpha_m a J_0(i\alpha_m a) iJ_1(i\alpha_m r)}{iJ_1(i\alpha_m a)} - \alpha_m r J_0(i\alpha_m r)\right] \quad \ldots [17]$$

Boundary condition I (the shear stress τ_{rz} is zero at the boundary $r = a$) is satisfied by making

$$J_1(\beta_n a) = 0 \quad \ldots [18]$$

Boundary condition IV (no radial displacement at the ends) is satisfied by making

$$\cos \alpha_m b = 0 \quad \ldots [19]$$

The usual Fourier analysis shows that boundary condition II (the normal stress σ_r is zero at the boundary $r = a$) is satisfied if the B's have the values given by[11]

$$B_m = \frac{\dfrac{2b}{a}\displaystyle\sum_{n=0,1}^{\infty} \frac{A_n J_0(\beta_n a)\left(\dfrac{\lambda}{\lambda + G} - \dfrac{2}{1 + \left(\dfrac{\alpha_m}{\beta_n}\right)^2}\right)}{(\beta_n b)^2\left[1 + \left(\dfrac{\alpha_m}{\beta_n}\right)^2\right]}}{(-1)^{m-1}\left[1 - \left\{\dfrac{J_0(i\alpha_m a)}{iJ_1(i\alpha_m a)}\right\}^2 + \dfrac{\lambda + 2G}{(\lambda + G)(\alpha_m a)^2}\right]} \quad \ldots [20]$$

and that part of boundary condition III which requires that the ends remain plane is satisfied if the A's other than A_0 have the values given by

$$A_n = \frac{\dfrac{2a}{b}\displaystyle\sum_{m=1}^{\infty} \frac{(-1)^m B_m\left(\dfrac{\lambda + 2G}{\lambda + G} - \dfrac{2}{1 + \left(\dfrac{\beta_n}{\alpha_m}\right)^2}\right)}{(\alpha_m a)^2\left[1 + \left(\dfrac{\beta_n}{\alpha_m}\right)^2\right]}}{\left[\left(\dfrac{\lambda + 3G}{\lambda + G}\right)\dfrac{\tanh \beta_n b}{\beta_n b} - \dfrac{1}{\cosh^2 \beta_n b}\right] J_0(\beta_n a)} \quad \ldots [21]$$

The remaining part of condition III, which requires that the

[11] Equation [20], which gives the value of the B's that make $\sigma_r = 0$ at $r = a$, is obtained by setting $r = a$ and $\sigma_r = 0$ in Equation [14], multiplying both sides by $\cos \alpha_n z\, dz$, and integrating between $-b$ and $+b$. Equation [21], which gives the values of the A's that make the ends plane, is obtained by setting $z = b$ and w equal to a constant in Equation [9], multiplying both sides by $rJ_0(\beta_n r)dr$, and integrating between 0 and a.

resultant force be P, is satisfied if the first term of the A series A_0 has the value given by

$$A_0 = -\frac{\lambda + G}{2G(\lambda + 2G)} \frac{P}{\pi a^2} \quad [22]$$

This may be verified by substituting σ_z from Equation [16] into the following equation for P

$$P = -2\pi \int_0^a \sigma_z r\, dr \quad [23]$$

Equations [14] to [23] suffice for the determination of stresses, to any accuracy desired, for all parts of the cylinder except the edges $r = a$, $z = \pm b$ where the stresses are discontinuous. The stresses are discontinuous at the edges because the assumed boundary requirements in regard to the curved surface $r = a$ and the plane ends $z = \pm b$ are different here. According to condition II the stress σ_r must be zero at $r = a$ whereas condition IV that the ends do not slip means that $\sigma_r = \sigma_z = \frac{\mu}{1 - \mu} \sigma_z$ at the plane ends.[12] This discontinuity in σ_r leads to discontinuity in the shear stress τ_{rz} and to higher principal stresses in this region than elsewhere.

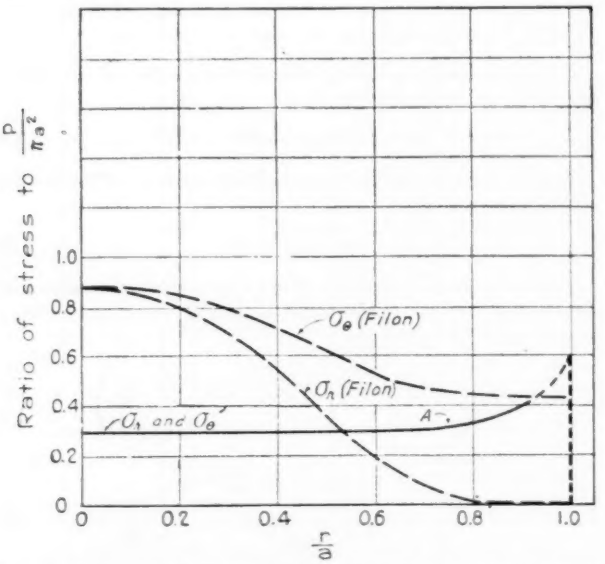


FIG. 7 DISTRIBUTION OF RADIAL STRESS σ_r AND TANGENTIAL STRESS σ_θ AT $z = b$ AS COMPUTED BY FILON AND AS COMPUTED BY THE METHOD OF THIS PAPER
(Filon's values are for $b/a = \pi/3$ whereas other values are for $b = a$, a = radius, $2b$ = length.)

Curve A, Fig. 7, shows the distribution, as given by the foregoing equations, of σ_r and σ_θ at the plane $z = b$ for a length-diameter ratio of 1.0 and a Poisson's ratio of 0.25. The curve is shown dashed for values near the edge of the cylinder because an insufficient number of terms was used in the computations for good

[12] If the radial displacement is zero everywhere at the ends, then the radial strain

$$\frac{1}{E}[\sigma_r - \mu\sigma_\theta - \mu\sigma_z] = 0$$

and the tangential strain

$$\frac{1}{E}[\sigma_\theta - \mu\sigma_r - \mu\sigma_z] = 0$$

Therefore $\sigma_r = \sigma_\theta = \frac{\mu}{1 - \mu} \sigma_z$

where $\mu = \frac{\lambda}{2(\lambda + G)}$

is Poisson's ratio.

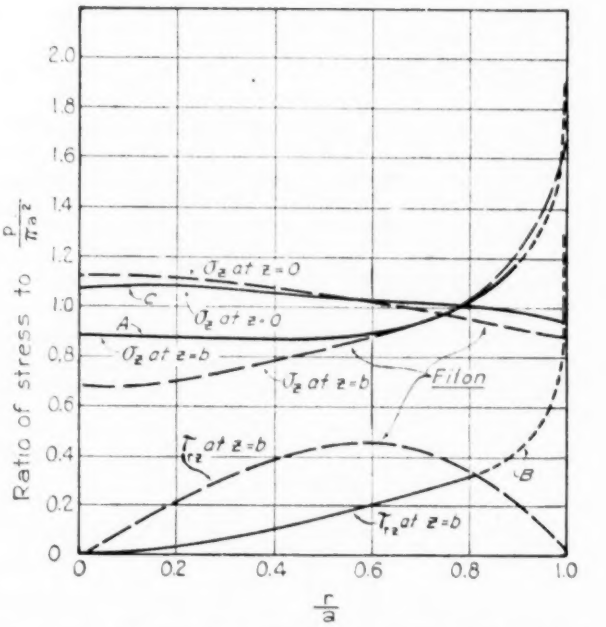


FIG. 8 DISTRIBUTION OF NORMAL STRESS σ_z AND SHEAR STRESS τ_r ON END OF CYLINDER AND OF σ_z AT CENTRAL SECTION $z = 0$ AS COMPUTED BY FILON AND AS FOUND BY THE METHOD OF THIS PAPER
(Filon's values are for $b/a = \pi/3$ whereas other values are for $b = a$, a = radius, $2b$ = length.)

accuracy in this region. In fact, the convergence is very slow for stresses at all points of the end boundary; therefore, methods applicable to slowly converging alternating series were used for computing points on the solid portion of this curve.

The distributions of the boundary forces at the ends (σ_z and τ_{rz} at the plane $z = b$) are shown by curves A and B, Fig. 8. Both boundary forces increase as the edge is reached. The maximum value of σ_z is believed to be less than $\frac{1}{1 - 2\mu}$ times its average value, but no estimate of the maximum value of τ_{rz} has been made.

Curve C, Fig. 8, shows the distribution of σ_z at the central plane $z = 0$. Points on this curve were computed readily because convergence was very good. For example, at $r = 0$, $z = 0$, σ_z is found to be $-1.100 \frac{P}{\pi a^2}$ when the series terminate with A_1 and B_1, and $-1.076 \frac{P}{\pi a^2}$, $-1.079 \frac{P}{\pi a^2}$, and $-1.079 \frac{P}{\pi a^2}$ as one, two, and three additional terms, respectively, are added to each series.

Filon's Solution. Also shown in Figs. 7 and 8 are corresponding distributions of stresses, as determined by Filon (8), who considered this problem at some length.[13] He was unable to obtain a solution meeting all boundary conditions but gave a solution which he considered to be approximately correct. His solution satisfies the differential equations and meets all boundary conditions except condition IV that the ends do not expand at any point. According to his solution, all points on the ends except those on the perimeter are displaced toward the center. This radial movement was due primarily to an incorrect distribution of tangential forces across the ends. His τ_{rz} curve in Fig. 8 differs appreciably from the correct curve.

Although values given by Filon's solution for stresses at the ends differ appreciably from the correct values given by the

[13] Filon used a length-diameter ratio of $\pi/3$ and a Poisson's ratio of 0.25 in his computations. His values would have been only slightly different if he had used a length-diameter ratio of 1.0.

Fourier method, the difference is small near the center of the cylinder. This tendency of Filon's solution to approach the correct solution as points at greater distances away from the ends are considered is in agreement with the principle of Saint Venant.

Number and Form of Series of Particular Solutions. Because of symmetry and because components of either stresses or displacements were zero at certain surfaces in the problems of the rectangular plate and circular cylinder, only two series of particular solutions were needed for each problem. More will be needed when more general boundary conditions are specified. The number and form for each that should be used will depend upon the conditions specified and the choice of co-ordinate axes and will have to be determined for each separate problem. However, in order that the series be convergent for all points in the interior, it is usually necessary to place the origin of the axes at the center of the body.

The particular solutions used in any given series may be composed from certain elementary forms of particular solutions. These elementary forms are given in the Appendix for:

1 Problems of axial symmetry in the cylindrical co-ordinates r and z.

2 Problems of plane strain or plane stress in the rectangular co-ordinates x and y.

3 Three-dimensional problems in the rectangular co-ordinates x, y, and z.

Three-Dimensional Problems

To show how the method may be used for three-dimensional problems, the preliminary steps in solving for stresses in a rectangular prism of dimensions $2a \times 2b \times 2c$ will be indicated. The origin of rectangular co-ordinates will be taken at the center of the prism. The only loading will be $\sigma_z = f(x, y)$, an even function of both x and y, at the planes $z = \pm c$.

Consider the following A-series of particular solutions for displacements.

$$u = \sum_{n=0}^{\infty}\sum_{m=0}^{\infty} \frac{A_{nm} \sin \alpha_n x \cos \beta_m y}{\gamma^2_{nm} c \cosh \gamma_{nm} c} \left[\alpha_n z \sinh \gamma_{nm} z - \left(\alpha_n c \coth \gamma_{nm} c - \frac{G}{\lambda + G} \frac{\alpha_n}{\gamma_{nm}} \right) \cosh \gamma_{nm} z \right]$$

$$v = \sum_{n=0}^{\infty}\sum_{m=0}^{\infty} \frac{A_{nm} \cos \alpha_n x \sin \beta_m y}{\gamma^2_{nm} c \cosh \gamma_{nm} c} \left[\beta_m z \sinh \gamma_{nm} z - \left(\beta_m c \coth \gamma_{nm} c - \frac{G}{\lambda + G} \frac{\beta_m}{\gamma_{nm}} \right) \cosh \gamma_{nm} z \right]$$

$$w = -\sum_{n=0}^{\infty}\sum_{m=0}^{\infty} \frac{A_{nm} \cos \alpha_n x \cos \beta_m y}{\gamma^2_{nm} c \cosh \gamma_{nm} c} \left[\gamma_{nm} z \cosh \gamma_{nm} z - \left(\gamma_{nm} c \coth {}_{nm}\gamma c - \frac{\lambda + 2G}{\lambda + G} \right) \sinh \gamma_{nm} z \right]$$

where γ_{nm} is written for $(\alpha^2_n + \beta^2_m)^{1/2}$.

The foregoing equations for displacements satisfy the appropriate differential equations for all values of the constants A_{nm}, α_n, and β_m.[14]

[14] These differential Equations [9] are as follows:

$$G\Delta^2 u + (\lambda + G) \frac{\partial}{\partial x}\left(\frac{\partial u}{\partial x} + \frac{\partial v}{\partial y} + \frac{\partial w}{\partial z}\right) = 0$$

$$G\Delta^2 v + (\lambda + G) \frac{\partial}{\partial y}\left(\frac{\partial u}{\partial x} + \frac{\partial v}{\partial y} + \frac{\partial w}{\partial z}\right) = 0$$

$$G\Delta^2 w + (\lambda + G) \frac{\partial}{\partial z}\left(\frac{\partial u}{\partial x} + \frac{\partial v}{\partial y} + \frac{\partial w}{\partial z}\right) = 0$$

By setting $\alpha_n = \frac{n\pi}{a}$ and $\beta_m = \frac{m\pi}{b}$ all tangential components of boundary forces will be zero ($\tau_{xy} = 0$ at $x = \pm a$ and $y = \pm b$; $\tau_{xz} = 0$ at $x = \pm a$ and $z = \pm c$; and $\tau_{yz} = 0$ at $y = \pm b$ and $z = \pm c$) and the normal boundary force at the planes $z = \pm c$ (σ_z at $z = \pm c$) will be given by the double Fourier series[15]

$$\frac{\sigma_z}{2G} = \sum_{n=0}^{\infty}\sum_{m=0}^{\infty} A_{nm} \left[\frac{2}{\gamma_{nm} c} + \coth \gamma_{nm} c - \tanh \gamma_{nm} c \right] \cos \alpha_n x \cos \beta_m y$$

There will also be normal boundary forces on the planes $x = \pm a$ and $y = \pm b$.

Two more series similar to the foregoing A series may be written such that one, say a B series, gives a double Fourier-series expression for σ_x at $x = \pm a$ and the other, say, a C series, a similar expression for σ_y at $y = \pm b$. The procedure of determining equations for the coefficients of each of these three series so that all boundary conditions are rigorously satisfied is very similar to that for the two-dimensional problem, and resulting equations are very similar to Equations [6] and [7]. To finish the solution all that is necessary is to take the steps indicated.

Appendix

Elementary forms of particular solutions for displacements in elastic bodies are as follows:

1 *In the Cylindrical Co-Ordinates r and z:*

(A) $u = \frac{1}{\alpha} J_1(\alpha r) \begin{Bmatrix} \sinh \alpha z \\ \cosh \alpha z \end{Bmatrix}$ *

$$w = -\frac{1}{\alpha} J_0(\alpha r) \begin{Bmatrix} \cosh \alpha z \\ \sinh \alpha z \end{Bmatrix}$$

(B) $u = z J_1(\alpha r) \begin{Bmatrix} \sinh \alpha z \\ \cosh \alpha z \end{Bmatrix}$

$$w = -\frac{1}{\alpha} J_0(\alpha r) \begin{Bmatrix} [\alpha z \cosh \alpha z - \frac{\lambda + 3G}{\lambda + G} \sinh \alpha z] \\ [\alpha z \sinh \alpha z - \frac{\lambda + 3G}{\lambda + G} \cosh \alpha z] \end{Bmatrix}$$

(C) $u = \frac{1}{\alpha} i J_1(i\alpha r) \begin{Bmatrix} \sin \alpha z \\ \cos \alpha z \end{Bmatrix}$

$$w = \frac{1}{\alpha} J_0(i\alpha r) \begin{Bmatrix} -\cos \alpha z \\ \sin \alpha z \end{Bmatrix}$$

(D) $u = r J_0(i\alpha r) \begin{Bmatrix} \sin \alpha z \\ \cos \alpha z \end{Bmatrix}$

[15] The stresses are obtained from the displacements by the formulas (9)

$$\sigma_x = 2G \frac{\partial u}{\partial x} + \lambda \left(\frac{\partial u}{\partial x} + \frac{\partial v}{\partial y} + \frac{\partial w}{\partial z}\right) \qquad \tau_{xz} = G\left(\frac{\partial u}{\partial z} + \frac{\partial w}{\partial x}\right)$$

$$\sigma_y = 2G \frac{\partial v}{\partial y} + \lambda \left(\frac{\partial u}{\partial x} + \frac{\partial v}{\partial y} + \frac{\partial w}{\partial z}\right) \qquad \tau_{xy} = G\left(\frac{\partial u}{\partial y} + \frac{\partial v}{\partial x}\right)$$

$$\sigma_z = 2G \frac{\partial w}{\partial z} + \lambda \left(\frac{\partial u}{\partial x} + \frac{\partial v}{\partial y} + \frac{\partial w}{\partial z}\right) \qquad \tau_{yz} = G\left(\frac{\partial v}{\partial z} + \frac{\partial w}{\partial y}\right)$$

* Either term in the bracket may be used provided that, when the upper term is used in the expression for u, the upper term is used in the expression for w, etc.

$$w = \frac{1}{\alpha}\left[i\alpha r\, J_1(i\alpha r) - 2\,\frac{\lambda + 2G}{\lambda + G}\, J_0(i\alpha r)\right] \begin{Bmatrix} -\cos \alpha z \\ \sin \alpha z \end{Bmatrix}$$

2 *In the Rectangular Co-ordinates x and y:*

$$(A)\quad u = \frac{1}{\alpha} \begin{Bmatrix} \sin \alpha x \\ \cos \alpha x \end{Bmatrix} \begin{Bmatrix} \sinh \alpha y \\ \cosh \alpha y \end{Bmatrix} \dagger$$

$$v = \frac{1}{\alpha} \begin{Bmatrix} -\cos \alpha x \\ \sin \alpha x \end{Bmatrix} \begin{Bmatrix} \cosh \alpha y \\ \sinh \alpha y \end{Bmatrix}$$

$$(B)\quad u = y \begin{Bmatrix} \sin \alpha x \\ \cos \alpha x \end{Bmatrix} \begin{Bmatrix} \sinh \alpha y \\ \cosh \alpha y \end{Bmatrix}$$

$$v = \frac{1}{\alpha} \begin{Bmatrix} -\cos \alpha x \\ \sin \alpha x \end{Bmatrix} \begin{Bmatrix} [\alpha y \cosh \alpha y - K \sinh \alpha y] \\ [\alpha y \sinh \alpha y - K \cosh \alpha y] \end{Bmatrix}$$

where $K = 3 - 4\,\mu$ for plane strain and $K = \dfrac{3 - \mu}{1 + \mu}$ for plane stress.

Two more forms, one similar to (A), and one similar to (B), are readily obtained by transposition of x and y and u and v.

3 *In the Rectangular Co-ordinates x, y, and z:*

$$(A)\quad u = \frac{1}{\alpha} \begin{Bmatrix} \sin \alpha x \\ \cos \alpha x \end{Bmatrix} \begin{Bmatrix} \sin \beta y \\ \cos \beta y \end{Bmatrix} \begin{Bmatrix} \sinh \gamma z \\ \cosh \gamma z \end{Bmatrix}$$

$$v = 0$$

$$w = \frac{1}{\gamma} \begin{Bmatrix} -\cos \alpha x \\ \sin \alpha x \end{Bmatrix} \begin{Bmatrix} \sin \beta y \\ \cos \beta y \end{Bmatrix} \begin{Bmatrix} \cosh \gamma z \\ \sinh \gamma z \end{Bmatrix}$$

† Either term may be taken from each bracket.

$$(B)\quad u = \frac{\alpha z}{\gamma} \begin{Bmatrix} \sin \alpha x \\ -\cos \alpha x \end{Bmatrix} \begin{Bmatrix} \sin \beta y \\ \cos \beta y \end{Bmatrix} \begin{Bmatrix} \sinh \gamma z \\ \cosh \gamma z \end{Bmatrix}$$

$$v = \frac{\beta z}{\gamma} \begin{Bmatrix} \cos \alpha x \\ \sin \alpha x \end{Bmatrix} \begin{Bmatrix} -\cos \beta y \\ \sin \beta y \end{Bmatrix} \begin{Bmatrix} \sinh \gamma z \\ \cosh \gamma z \end{Bmatrix}$$

$$w = \begin{Bmatrix} \cos \alpha x \\ \sin \alpha x \end{Bmatrix} \begin{Bmatrix} \sin \beta y \\ \cos \beta y \end{Bmatrix} \begin{Bmatrix} \left[-z \sinh \gamma z + \dfrac{\lambda + 3G}{\lambda + G} \dfrac{\cosh \gamma z}{\gamma} \right] \\ \left[-z \cosh \gamma z + \dfrac{\lambda + 3G}{\lambda + G} \dfrac{\sinh \gamma z}{\gamma} \right] \end{Bmatrix}$$

where $\gamma = (\alpha^2 + \beta^2)^{1/2}$.

Seven more forms, five similar to (A) and two similar to (B), are readily obtained by permutation of x, y, z, accompanied by a corresponding permutation of u, v, w.

REFERENCES

1 "Theory of Elasticity," by S. Timoshenko, McGraw-Hill Book Co., New York, N. Y., 1934, pp. 152–155.

2 "Compression of Rectangular Blocks, and the Bending of Beams by Nonlinear Distributions of Bending Forces," by J. N. Goodier, Trans. A.S.M.E., vol. 54, 1932, APM-54-17, pp. 173–183.

3 "A Study of Fundamental Relations of the Mathematical Theory of Elasticity," by A. M. Winslow, University of Washington, Engineering Experiment Station, Bulletin No. 77, 1934.

4 Reference (1), pp. 24–25.

5 "The Buckling Load for a Rectangular Plate With Four Clamped Edges," by G. I. Taylor, *Zeitschrift für Angewandte Mathematik und Mechanic*, vol. 13, 1933, pp. 147–152.

6 "Theory of Plates and Shells," by S. Timoshenko, McGraw-Hill Book Co., New York, N. Y., 1940, pp. 222–231.

7 Reference (1), pp. 104–108.

8 "The Elastic Equilibrium of Circular Cylinders Under Certain Practical Systems of Load," by L. N. G. Filon, *Philosophical Transactions of the Royal Society*, series A, vol. 198, 1902, pp. 147–233.

9 Reference (1), p. 200.

Analysis of the Valverde Thermostat

By A. M. WAHL,[1] EAST PITTSBURGH, PA.

In this paper, a method based on the theory of initially curved bars axially loaded is developed for calculating snapping temperatures and stresses in a new type of thermostat known as the Valverde thermostat. For facilitating practical use of the derived formulas, curves are given by means of which the effect of dimensional changes on the free snapping or buckling temperatures may easily be evaluated. The analysis has been found useful in the practical design of thermostats of this type.

Introduction

A TYPE of thermostat which has been coming into extensive use in recent years is one known as the Valverde thermostat.[2] Essentially the thermostat consists of three strips of bimetal, an inner and two outer strips, as shown in Fig. 1. In manufacturing the thermostat the outer strips are crimped by means of a crimping machine. This tends to shorten their effective lengths thus putting them in tension. At the same time the inner strip is put in compression causing it to deflect still more. Thus when cold the thermostat has the shape shown in Fig. 1, the inner strip having a larger chord height[3] than the outer strip. The strips are so curved that the high-expansion component of the bimetal is on the concave side. An illustration of the strip thermostat itself is shown in Fig. 2, while a view of the unit assembled into a switch is shown in Fig. 3.

In operation, as the thermostat is heated both the inner and outer strips tend to straighten out. However, the inner strip being in compression tends to resist this process. As the heating continues both the compression load on the inner strip and the moment at its ends increase until, at a certain critical temperature, both inner and outer strips snap over as indicated by the dashed lines of Fig. 4. This temperature will be called the "upper critical" temperature. If now the thermostat is cooled, the curvature of the strips tends to decrease in the opposite direction until, at a certain temperature (which may be far below the upper critical temperature), the strips suddenly snap back to the positions indicated by the full lines of Fig. 4. This temperature will be called the "lower critical" temperature. These temperatures apply only to the thermostat when free, as shown in Fig. 1.

In actual practice the thermostat may be incorporated into a switch by means of various methods. In one of these, Fig. 5, the inner strip is fastened to the frame carrying the contacts as shown. One end of the thermostat carries the contacts while the other end may be rotated by means of an arm and an adjusting screw. This rotation makes it possible to vary the opening or closing temperatures through a considerable range while at the

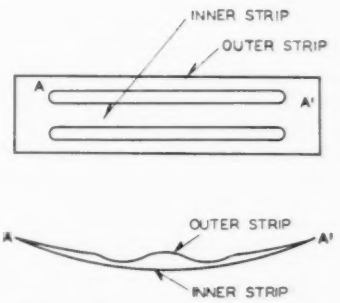


Fig. 1 Valverde Thermostat
(By crimping, the outer strip is given a shorter effective length than the inner.)

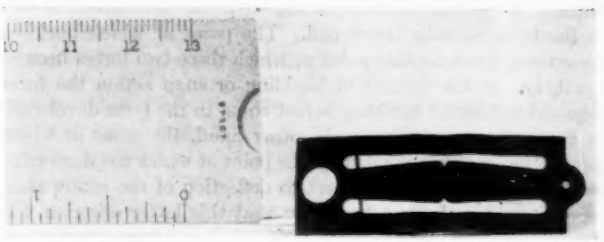


Fig. 2 Unassembled Valverde Thermostat

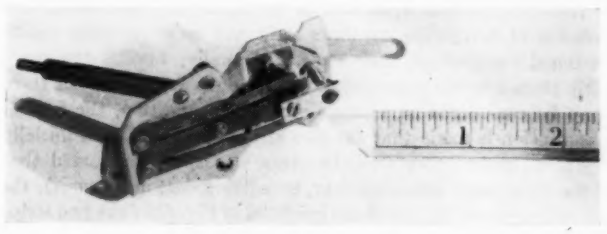


Fig. 3 Valverde Thermostat as Used in Switch for Automatic Iron

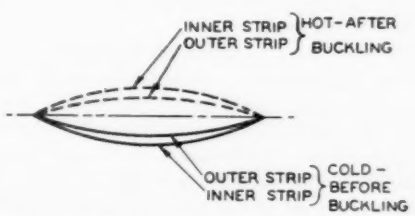


Fig. 4 Mode of Buckling Action in Valverde Thermostat

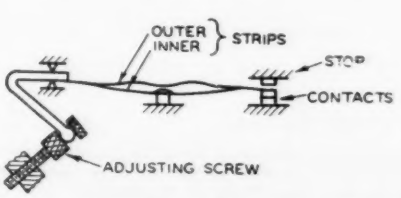


Fig. 5 Schematic Diagram of Method of Using Valverde Thermostat in Switch

---

[1] Research Engineer, Westinghouse Electric & Manufacturing Company. Mem. A.S.M.E.

[2] U. S. Patents 1,987,166 and 1,987,167.

[3] The maximum distance between the center line of the strip and the line or chord connecting its ends is known as the "chord height."

Presented at the National Meeting of the Applied Mechanics Division, Cambridge, Mass., June 19-20, 1942, of The American Society of Mechanical Engineers.

Discussion of this paper should be addressed to the Secretary, A.S.M.E., 29 West 39th Street, New York, N. Y., and will be accepted until October 10, 1944, for publication at a later date. Discussion received after the closing date will be returned.

Note: Statements and opinions advanced in papers are to be understood as individual expressions of their authors and not those of the Society.

same time the differential between these temperatures is kept relatively small.

Among the advantages of this type of thermostat, as compared with other types, the following may be mentioned: (1) Lower temperature differentials are possible; (2) lower stresses are present, resulting in longer life; (3) less wastage of bimetal occurs than in the case of a disk type since the Valverde type may be cut directly from strips of bimetal.

In the present paper, the analysis will be limited to the determination of the upper and lower critical temperatures and stresses of the free thermostat as contrasted to the assembled thermostat of Fig. 5. The effects of various design changes, such as length, depth, and number of crimps, initial curvature of the strips, etc., will also be investigated.

Method of Analysis

Essentially the method of analysis used involves the theory of buckling of initially curved bars axially loaded.[4] It also involves the application of methods used by Timoshenko in the calculation of the buckling temperatures of initially curved bimetal strips with hinged ends.[5] In Timoshenko's analysis, the axial force required to prevent buckling of the strip was determined as well as the force actually developed. The point at which buckling occurs was taken as that point at which these two forces became equal, i.e., at the instant of buckling or snap action the force required to prevent buckling is just equal to the force developed. In the present analysis, on the other hand, the point at which snap action occurs was taken as the point at which the derivative of the temperature with respect to deflection of the center strip becomes zero. (It may be shown that this latter criterion will also give results identical with those obtained from the method used by Timoshenko for the case of a single strip with hinged ends.)

Referring to Fig. 1, it will be assumed that the thermostat consists of two strips, an inner strip and an outer strip rigidly fastened together at their ends. (Actually, besides the inner strip there are two outer strips, but for purposes of analysis these may be considered as a single strip.) In addition, the further assumption is made that the two strips when free have initially the same mean curvature. In other words, it is assumed that if the strips were separated (say, by cutting slots in the ends), the initial curvature (or the chord height a_4 of Fig. 6) of the two strips would be the same. This assumption is not exact, but in many cases it is approximately realized in the manufacture of these thermostats. Where this condition does not hold, however, considerable deviation between the results of the theory and actual test results may be expected.

Assume now that the two strips are separated when cold, as indicated in Fig. 6(a) and (d). On the basis of our assumption that the initial free curvature of both strips is the same, both the inner and the outer strip will have the same initial chord height a_4 at room temperature t_0. On heating the two strips to a temperature t, if free, both of these strips will deflect by an amount a_0. Neglecting the effect of the slight difference in initial length produced by crimping, the expression for a_0 is[6]

$$a_0 = \frac{3}{16}\frac{l^2}{h}(\alpha_1 - \alpha_2)(t - t_0) \quad \ldots\ldots\ldots\ldots [1]$$

where

l = length of strip

h = bimetal thickness

α_1, α_2 = expansion coefficients of high and low side components of bimetal[7]

Thus when the two free strips are heated, the chord heights become equal to $a_2 = a_4 - a_0$, Fig. 6(b) and (e). Because of the crimping operation on the outer strip, the effective free length of the latter will be slightly less than that of the inner strip by an amount λ_1. This difference λ_1 depends upon the number and depth of the crimps. If it be assumed that the crimps are of sinusoidal form and that there are n half waves or crimps of depth a (Fig. 7), the value of λ_1 may be expressed approximately as

$$\lambda_1 = \frac{n^2\pi^2 a^2}{4l_1} \quad \ldots\ldots\ldots\ldots\ldots\ldots [2]$$

where l_1 is the length of the crimped portion. This follows since the difference between arc and chord length of a flat sine wave of depth a and length l_2 is $\pi^2a^2/4l_2$.

The inner and outer strips, after being heated when free as shown in Fig. 6(b) and (e), may be thought of as being assembled to form a complete thermostat. To do this the outer strip must be extended by an amount λ_2' while the inner strip is compressed by an amount λ_2. The length of the inner strip then becomes $(l - \lambda_2)$, that of the outer strip $(l - \lambda_1 + \lambda_2')$ as indicated in Fig. 6

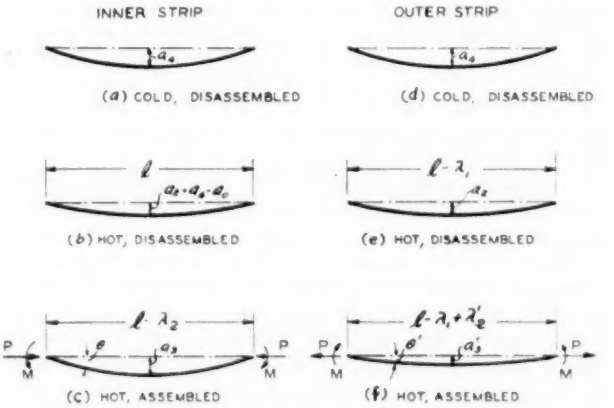


Fig. 6 Valverde-Thermostat Dimensions Under Various Conditions

(c) and (f). On the inner strip a compressive force P and a moment M will act as indicated, while on the outer strip the same moment and a tension force P will act. These forces and moments will change the chord heights of the two strips to a_3 and a_3' as indicated.

The problem now is to determine the deflections produced by an axial force and moment acting at the ends of an initially curved bar. Assuming that the bar has the initial shape of a flat sine wave, by solving the differential equation of the deflection curve of an initially curved bar with proper boundary conditions, the equations for the deflection y and derivative dy/dz at any point at a distance z from the end of the strip may be expressed as[4]

$$y = \frac{M}{P}\left\{1 - \cos kz - \frac{1 - \cos kl}{\sin kl}\sin kz\right\} + \frac{a_2}{1 - \beta}\sin\frac{\pi z}{l} \quad \ldots\ldots [3]$$

[4] For a discussion of problems involving initially curved bars refer to "Theory of Elastic Stability," by S. Timoshenko, McGraw-Hill Book Company, Inc., New York, N. Y., 1936.

[5] "Analysis of Bimetal Thermostats," by S. Timoshenko, *Journal of the Optical Society of America*, vol. 11, 1925, pp. 233–255.

[6] This equation was derived by Timoshenko; see ref. (5).

[7] For data on bimetal properties refer to the paper, "Thermostatic Bimetals," by S. G. Eskin and J. R. Fritze, Trans. A.S.M.E., vol. 62, 1940, pp. 433–440. A bibliography on the subject is also given with this paper.

$$\frac{dy}{dz} = \frac{Mk}{P}\left\{\sin kz - \frac{1-\cos kl}{\sin kl}\cos kz\right\} + \frac{\pi a_2}{l(1-\beta)}\cos\frac{\pi z}{l} \quad [4]$$

where

$$k = \sqrt{\frac{P}{EI}}; \qquad \beta = \frac{Pl^2}{EI\pi^2}$$

E = modulus of elasticity of material

I = moment of inertia (this may be taken as $bh^3/12$ where b = width, h = thickness)

The axial deflection λ_2 of the inner strip, due to the force P and moment M, is found as follows: The difference λ_y between the arc and the chord length of the deflected beam is first calculated. From this is subtracted the initial difference λ_i between arc and chord length, while to this is added the direct compression λ_c due to the axial force P. Thus the relative axial movement λ_2 of the ends of the inner strip due to the force P and moment M becomes

$$\lambda_2 = \lambda_y - \lambda_i + \lambda_c \quad [5]$$

But for a flat curve

$$\lambda_y = \frac{1}{2}\int_0^l \left(\frac{dy}{dz}\right)^2 dz \quad [6]$$

where dy/dz is given by Equation [4].

Also, since the initial shape of the bar is a flat sine wave of height a_2

$$\lambda_i = \frac{\pi^2 a_2^2}{4l} \quad [7]$$

The deflection due to direct compression is

$$\lambda_c = c_1\frac{Pl}{Ebh} \quad [8]$$

where c_1 is a factor taking into account the additional flexibility due to crimping. In applying this formula to the inner strip, c_1 is taken as unity since there are no crimps, but in the case of the outer strip the added flexibility due to the crimping must be considered.

Substituting the value of $\frac{dy}{dz}$ given by Equation [4] in Equation [6], integrating and using Equations [6], [7], and [8] in Equation [5], the following expression is obtained

$$\lambda_2 = \frac{\pi^2 a_2^2(2-\beta)\beta}{4l(\beta-1)^2} + \frac{M^2 x}{2P^2 l}\left\{\frac{1-\cos x}{\sin x}\right\}\left\{\frac{x}{\sin x} - 1\right\} - \frac{M}{P}\frac{2\pi a_2\beta}{l(\beta-1)^2} + c_1\frac{Pl}{Ebh} \quad [9]$$

where $x = kl$.

To find λ_2', the axial deflection between the ends of the outer strip due to the tension force P and the moment M, this same formula may be used except that P and M are taken as negative, while β', k', b', and x' (which apply to the outer strip) are used instead of β, k, b, and x. In this case, b' = width of outer strip, $I' = \frac{b'h^3}{12}$, $k' = \sqrt{\frac{P}{EI'}}$, $x' = k'l$, $\beta' = \frac{Pl^2}{EI'\pi^2}$. After simplification and elimination of imaginary quantities this gives

$$\lambda_2' = \frac{\pi^2 a_2^2\beta'(2+\beta')}{4l(\beta'+1)^2} - \frac{M^2 x'}{2P^2 l}\left\{\frac{1-\cosh x'}{\sinh x'}\right\}\left\{\frac{x'}{\sinh x'} - 1\right\} - \frac{M}{P}\frac{2\pi a_2\beta'}{l(\beta'+1)^2} + c_1'\frac{Pl}{Eb'h} \quad [10]$$

where c_1' is a factor to take into account the additional flexibility due to crimping of the outer strip.

From Fig. 6(*c*) and (*f*), since the two strips when assembled must have the same chord length, it follows that

$$l - \lambda_2 = l - \lambda_1 + \lambda_2'$$

or

$$\lambda_1 = \lambda_2 + \lambda_2' \quad [11]$$

Using Equations [9] and [10] in Equation [11] and taking $\epsilon = \lambda_1/l$, $\mu^2 = b/b'$, $\beta' = \mu^2\beta$, the following equation is obtained

$$\epsilon = \frac{\lambda_1}{l} = \frac{\pi^2}{4l^2}a_2^2\beta\left\{\frac{2-\beta}{(\beta-1)^2} + \frac{\mu^2(2+\mu^2\beta)}{(\mu^2\beta+1)^2}\right\} + \frac{M^2 x\psi_0}{2P^2 l^2} - \frac{M(2\pi a_2\beta)}{Pl^2}\left\{\frac{1}{(\beta-1)^2} + \frac{\mu^2}{(\mu^2\beta+1)^2}\right\} + \frac{P}{Ebh}(c_1 + \mu^2 c_1') \quad [12]$$

where

$$\psi_0 = \left(\frac{1-\cos x}{\sin x}\right)\left(\frac{x}{\sin x} - 1\right) - \frac{\mu(1-\cosh \mu x)}{\sinh \mu x}\left(\frac{\mu x}{\sinh \mu x} - 1\right) \quad [13]$$

The ratio $\frac{M}{P}$ which occurs in this equation is found from the condition that the slopes θ and θ' (Fig. 6) at the ends of the inner and outer strips, respectively, must be equal.

From Equation [4], the slope θ at the ends of the inner strip is

$$\theta = \left(\frac{dy}{dz}\right)_{z=0} = -\frac{Mx}{Pl}\left(\frac{1-\cos x}{\sin x}\right) + \frac{\pi}{l}\frac{a_2}{1-\beta} \quad [14]$$

The same expression may be used for θ by reversing the signs of P and M and using β', x' instead of β, x. After simplification this yields

$$\theta' = -\frac{Mx'}{Pl}\left\{\frac{1-\cosh x'}{\sinh x'}\right\} + \frac{\pi}{l}\frac{a_2}{1+\beta'} \quad [15]$$

Equating [14] and [15] we find

$$\frac{M}{Pl} = -\frac{\pi a_2\psi_2}{l} = -\frac{\pi(a_4 - a_0)\psi_2}{l} \quad [16]$$

where

$$\psi_2 = \frac{1}{x\psi_1}\left\{\frac{1}{\beta-1} + \frac{1}{\mu^2\beta+1}\right\} \quad [17]$$

$$\psi_1 = \frac{1-\cos x}{\sin x} - \frac{\mu(1-\cosh \mu x)}{\sinh \mu x} \quad [18]$$

Substituting Equation [16] in Equation [12], we have

$$\epsilon = \frac{a_2^2}{l^2}F(x) + c_3 x^2 \quad [19]$$

where

$$c_3 = (c_1 + \mu^2 c_1')\frac{h^2}{12\,l^2} \quad [20]$$

$$F(x) = \pi^2(A_1 + A_2 + A_3) \quad [21]$$

where

$$A_1 = \beta/4\left\{\frac{2-\beta}{(\beta-1)^2} + \frac{\mu^2(2+\mu^2\beta)}{(\mu^2\beta+1)^2}\right\} \quad [22]$$

$$A_2 = \frac{\psi_0}{2x\psi_1^2}\left\{\frac{1}{\beta-1} + \frac{1}{\mu^2\beta+1}\right\}^2 \quad [23]$$

$$A_3 = \frac{2\beta}{\pi\psi_1}\left\{\frac{1}{(\beta-1)^2}+\frac{\mu^2}{(\mu^2\beta+1)^2}\right\}\left\{\frac{1}{\beta-1}+\frac{1}{\mu^2\beta+1}\right\}$$

and

$$\beta = \pi^2/\pi^2.$$

The chord height $a_2 = (a_4 - a_0) = a_1\left(\frac{a_0}{a_1} - r\right)$ where a_1 = initial chord height of inner strip when assembled, at room temperature t_0 and $r = \frac{a_0}{a_1}$, a_0 being given by Equation [1]. Solving Equation [19] for a_2 and dividing by a_1, we find

$$\frac{a_4}{a_1} - r = \pm\frac{l}{a_1}\sqrt{c_2}\sqrt{\frac{\epsilon/c_2 - x^2}{F(x)}} = \pm f_2(x) \quad [25]$$

or solving for r

$$r = \frac{a_4}{a_1} \pm f_2(x) \quad [26]$$

where

$$f_2(x) = \frac{l}{a_1}\sqrt{c_2}\sqrt{\frac{\epsilon/c_2 - x^2}{F(x)}} \quad [27]$$

From Equation [3], putting $z = l/2$ the chord height a_3 of the inner strip Fig. 6(*c*) is obtained

$$a_3 = -\frac{M}{P}\psi_3 + \frac{a_2}{1-\beta} \quad [28]$$

where

$$\psi_3 = \left(\frac{1-\cos x}{\sin x}\right)\sin\frac{x}{2} - \left(1-\cos\frac{x}{2}\right) \quad [29]$$

Substituting the value of $\frac{M}{P}$ given by Equation [16] in Equation [28], we find

$$\delta = \frac{a_3}{a_1} = \left(\frac{a_4}{a_1} - r\right) f_1(x) = \pm f_2(x)\cdot f_1(x) \quad [30]$$

where $f_2(x)$ is given by Equation [27] and

$$f_1(x) = \pi\psi_2\psi_3 - \frac{1}{\beta-1} \quad [31]$$

Solving Equation [30] for r, the following expression results

$$r = \frac{a_4}{a_1} - \frac{\delta}{f_1(x)} \quad [32]$$

Equation [30] gives δ as a function of x while Equation [26] gives r as a function of x. This makes it possible to plot δ as a function of r. Since δ is directly proportional to the chord height a_3 of the center strip while r is proportional to the temperature rise $(t - t_0)$ above room temperature, a curve of the chord height a_3 versus temperature t may be plotted as shown in Fig. 8. This curve has the rather peculiar shape *ABCED*, the dashed portion between *C* and *E* being unstable.

The operation of the thermostat may perhaps be better understood by reference to Fig. 8. At room temperature t_0 the chord height a_3 of the inner strip corresponds to point *A*. As the thermostat is heated, the chord height a_3 decreases until at a temperature t_{cr1} (point *C*) the thermostat snaps over and the chord height of the inner strip becomes negative (point *D*). At point *C* the derivative $dt/da_3 = 0$ and instability occurs, because the elastic resistance of the strip is not great enough to prevent the tendency toward curvature change induced in the bimetal by the temperature increase.

As the thermostat is now cooled, the chord height decreases along the curve from *D* to *E*. At a temperature t_{cr2} (point *E*), snap action occurs in the opposite direction, and the chord height again changes to a positive value (point *B*). At point *E* the derivative dt/da_3 is also zero.

Since r and δ are linear functions of t and a_3, respectively, the condition $dt/da_3 = 0$ is equivalent to $dr/d\delta = 0$. Therefore, to find the value of x at which buckling occurs, the latter condition may be used.

From Equation [32] since a_4/a_1 is constant

$$\frac{dr}{d\delta} = -\frac{f_1(x) - \delta\frac{df_1}{dx}\frac{dx}{d\delta}}{[f_1(x)]^2} \quad [33]$$

Since $f_1(x) \neq 0$ this becomes zero when

$$f_1(x) = \frac{\delta\frac{df_1}{dx}}{\frac{d\delta}{dx}} \quad [34]$$

Substituting $\delta = f_1(x)f_2(x)$ in this we find

$$f_1(x) = \frac{f_1(x)f_2(x)\frac{df_1}{dx}}{f_2(x)\frac{df_1}{dx} + f_1(x)\frac{df_2}{dx}} \quad [35]$$

To satisfy this equation, the following equation must hold

$$f_1(x)\frac{df_2}{dx} = 0 \quad [36]$$

Since $f_1(x) \neq 0$ this means that $\frac{df_2}{dx} = 0$, and using Equation [25], the condition to be satisfied when buckling occurs becomes

$$\frac{dF(x)}{dx} = \frac{-2xF(x)}{\epsilon/c_2 - x^2} \quad [37]$$

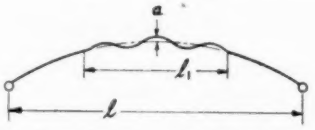


FIG. 7 CRIMPING OF BIMETAL STRIP

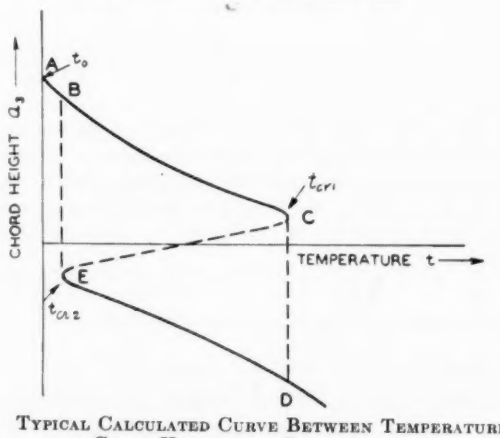


FIG. 8 TYPICAL CALCULATED CURVE BETWEEN TEMPERATURE AND CHORD HEIGHT a_3 OF INNER STRIP
(Snap-action occurs at points *C* and *E*.)

Because of the complicated nature of the function $F(x)$, the following procedure was used in solving this equation: The values of $F(x)$ and dF/dx were computed as functions of x both for $\mu^2 = 1$ and $\mu^2 = 0.8$, the latter value corresponding to a center strip of width equal to 0.8 the combined width of the outer strips. Knowing these values, by substitution in Equation [37], the critical value x_{cr} at which buckling will occur may be found. The results show values of x_{cr} as functions of ϵ/c_2 and are given in Fig. 9 for the range $x_{cr} = 6.8$ to 8.9. It may be noted that there is not much difference between the cases where $\mu^2 = 1$ and $\mu^2 = 0.8$.

Calculation of Critical or Snapping Temperatures

Having found the critical value x_{cr}, the critical values of r may be obtained from Equation [26]. The ratio $r = a_0/a_1$ may be considered as a temperature ratio, i.e., the ratio of the temperature change required to deflect the free strip by an amount a_0 to that required to deflect it by an amount a_1. Since r is a linear function of temperature, a determination of the critical values of r will also enable the determination of the critical temperatures. From Equation [26] it is seen that two values of r are possible, an upper value corresponding to the positive sign (the upper critical temperature), and a lower value corresponding to the negative sign. Thus to find the upper critical value r_{cr1}, the value of x_{cr} determined from Equation [37], or the curve of Fig. 9 is substituted in Equation [26]. This gives

$$r_{cr1} = \frac{a_4}{a_1} + \frac{l}{a_1}\sqrt{c_2}\sqrt{\frac{\epsilon/c_2 - x_{cr}^2}{F(x_{cr})}} \quad \ldots\ldots [38]$$

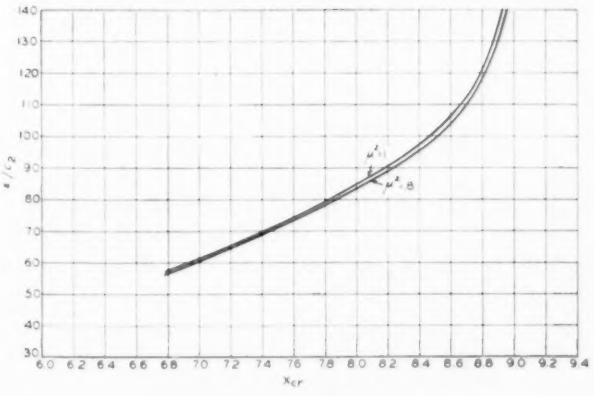


Fig. 9 Curve for Finding x_{cr}

Since x_{cr} is a function of ϵ/c_2 (Fig. 9), the term under the radical may be written

$$f(\epsilon/c_2) = \sqrt{\frac{\epsilon/c_2 - x_{cr}^2}{F(x_{cr})}} \quad \ldots\ldots [39]$$

Values of this function for a range of values of ϵ/c_2 have been plotted in Fig. 10 for $\mu^2 = 1$ and for $\mu^2 = 0.8$. Substituting Equation [39] in Equation [38], the upper-critical-temperature ratio becomes

$$r_{cr1} = \frac{a_4}{a_1} + \frac{l}{a_1}\sqrt{c_2}\, f(\epsilon/c_2) \quad \ldots\ldots [40]$$

The lower-critical-temperature ratio r_{cr2} (for buckling in a reverse direction) is obtained by using the negative sign in Equation [26]. This gives

$$r_{cr2} = \frac{a_4}{a_1} - \frac{l}{a_1}\sqrt{c_2}\, f(\epsilon/c_2) \quad \ldots\ldots [41]$$

Dividing both sides of Equation [1] by a_1 the temperature ratio r becomes

$$r = \frac{a_0}{a_1} = \frac{3}{16}\frac{l^2}{ha_1}(\alpha_1 - \alpha_2)(t - t_0) \quad \ldots\ldots [42]$$

The upper and lower-critical-temperature ratios r_{cr1} and r_{cr2} are obtained from this equation by substituting for t the upper and lower critical temperatures t_{cr1} and t_{cr2}, respectively. This gives

$$r_{cr1} = \frac{3}{16}\frac{l^2}{ha_1}(\alpha_1 - \alpha_2)(t_{cr1} - t_0) \quad \ldots\ldots [43]$$

$$r_{cr2} = \frac{3}{16}\frac{l^2}{ha_1}(\alpha_1 - \alpha_2)(t_{cr2} - t_0) \quad \ldots\ldots [44]$$

Solving these for t_{cr1} and t_{cr2}

$$t_{cr1} = t_0 + \frac{16\,ha_1 r_{cr1}}{3l^2(\alpha_1 - \alpha_2)} \quad \ldots\ldots [45]$$

$$t_{cr2} = t_0 + \frac{16\,ha_1 r_{cr2}}{3l^2(\alpha_1 - \alpha_2)} \quad \ldots\ldots [46]$$

The range between upper and lower critical temperatures is obtained by subtracting Equation [46] from Equation [45]. This gives

$$t_{cr1} - t_{cr2} = \frac{16\,ha_1}{3l^2}\left(\frac{r_{cr1} - r_{cr2}}{\alpha_1 - \alpha_2}\right) \quad \ldots\ldots [47]$$

Substituting in this the values of r_{cr1}, r_{cr2} and c_2 given by Equations [40], [41], and [20], we obtain

$$t_{cr1} - t_{cr2} = \frac{h^2 c}{l^2(\alpha_1 - \alpha_2)} \quad \ldots\ldots [48]$$

where

$$c = 3.09\sqrt{c_1 + \mu^2 c_1'}\, f(\epsilon/c_2) \quad \ldots\ldots [49]$$

Since the temperature range is directly proportional to c, this factor will be called the "temperature-range factor."

By adding Equations [45] and [46], and substituting values of r_{cr1} and r_{cr2} given by Equations [40] and [41], the average critical temperature becomes

$$t_{avg} = \frac{t_{cr1} + t_{cr2}}{2} = t_0 + \frac{16\,ha_4}{3l^2(\alpha_1 - \alpha_2)} \quad \ldots\ldots [50]$$

This indicates that the difference between the average critical temperature t_{avg} and room temperature t_0 is proportional to the free chord height a_4, to the thickness h, and inversely proportional to the square of the length and to the difference in expansion coefficients.

By solving Equations [48] and [50] for t_{cr1} and t_{cr2} we find

$$t_{cr1} = \frac{h^2}{2l^2(\alpha_1 - \alpha_2)}\left(c + \frac{32}{3}\frac{a_4}{h}\right) + t_0 \quad \ldots\ldots [51]$$

$$t_{cr2} = \frac{h^2}{2l^2(\alpha_1 - \alpha_2)}\left(\frac{32}{3}\frac{a_4}{h} - c\right) + t_0 \quad \ldots\ldots [52]$$

Since the inner strip is not crimped c_1 is unity. The flexibility factor c_1' to take into account the additional flexibility of the crimping may be calculated approximately by using as before the theory of initially curved bars axially loaded.[4] Assuming that the half wave length of the crimps l_1/n is small compared to l (Fig. 7) and that the amplitude a is small compared to l_1/n, by using this theory the expression for c_1' becomes approximately

$$c_1' = 1 + \frac{6a^2}{h^2}\frac{l_1}{l} \quad \ldots\ldots\ldots\ldots\ldots\ldots [53]$$

Using this expression, and the expression for $f(\epsilon/c_2)$ and λ_1 given by Equations [39] and [2], in Equation [49], the value of c can be determined. It is found that c is a function of the ratio a/h between wave amplitude a of the crimps and the bimetal thickness, of the ratio l_1/l between length of crimped portion and total length, of the ratio $\mu^2 = b/b'$, and of the number of crimps n. In Fig. 11 values of c have been plotted against ratios a/h for three crimps ($n = 3$) and various values of l_1/l, the widths of the two strips being assumed equal. (It should be noted that the amplitude a is only one half the total depth of the crimps.) Likewise in Fig. 12 similar curves are shown for five crimps ($n = 5$). By substituting values of c thus found in Equations [51] and [52], values of the upper and lower critical temperatures may be found.

An examination of Figs. 11 and 12 indicates that for a given number of crimps and a given bimetal thickness the value of c (and hence the range $t_{cr1} - t_{cr2}$) increases with increase in depth of crimping and with decrease in the ratio l_1/l between length of crimped portion to total length. Also the factor c increases with increase in number of crimps. From Equations [51] and [52], it may be seen that the upper critical temperature t_{cr1} increases with increase in h/l, c, and a_4/h while it decreases with increase in $(\alpha_1 - \alpha_2)$. On the other hand, the lower critical temperature t_{cr2} is decreased with increase in c, while it increases with the ratios h/l and a_4/h. If l, h, and $(\alpha_1 - \alpha_2)$ are given, the upper critical temperature may be increased by increasing c or a_4, while the lower critical temperature may be increased by increasing a_4 or by decreasing c.

Calculation of Stress

To calculate the stress during free operation of the thermostat the following procedure may be used: By solving Equation [16] for the moment M at the ends of the strip

$$M = -P\pi(a_4 - a_0)\psi_2 \quad \ldots\ldots\ldots\ldots\ldots [54]$$

It will be found the maximum value of the moment will occur when the load P reaches the critical value corresponding to x_{cr}. Taking $P = P_{cr}$ and $r = r_{cr1}$ corresponding to the positive direction of buckling and to t_{cr1}, the moment at the ends of the strip becomes

$$M_{cr} = -P_{cr}\pi a_1\left(\frac{a_4}{a_1} - r_{cr1}\right)\psi_{2cr} \quad \ldots\ldots\ldots\ldots [55]$$

In this ψ_{2cr} is obtained from Equation [17] using $x = x_{cr}$.

Substituting in this the value of r_{cr1} given by Equation [40] we find

$$M_{cr} = -P_{cr}l\pi\sqrt{c_2}\,\psi_{2cr}f(\epsilon/c_2) \quad \ldots\ldots\ldots\ldots [56]$$

The bending stress at the end is

$$\sigma_{sb} = \frac{6M_{cr}}{bh^2} \quad \ldots\ldots\ldots\ldots\ldots\ldots [57]$$

Using Equation [56] in this, the stress becomes

$$\sigma_{sb} = \frac{\pi}{4\sqrt{3}}\frac{Eh^2}{l^2}x_{cr}^2\psi_{2cr}\sqrt{c_1 + \mu^2c_1'}\,f(\epsilon/c_2) \quad \ldots\ldots [58]$$

Substituting the value of c given by Equation [49] in Equation [48] and solving

$$\sqrt{c_1 + \mu^2c_1'}\,f(\epsilon/c_2) = (t_{cr1} - t_{cr2})(\alpha_1 - \alpha_2)\frac{l^2}{3.09h^2} \quad \ldots [59]$$

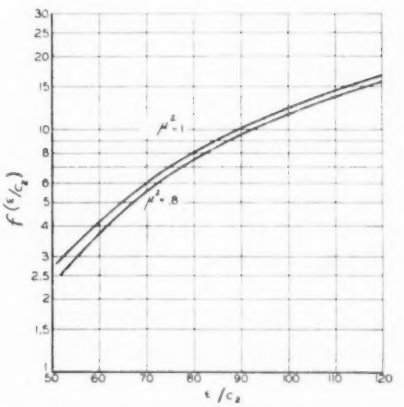


Fig. 10 Curve for Finding Function $f(\epsilon/c_2)$

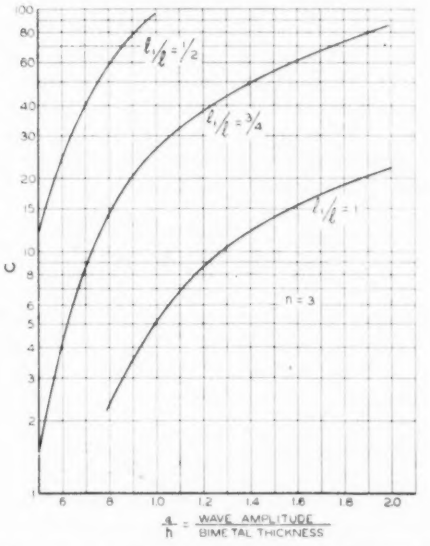


Fig. 11 Curves for Finding Temperature-Range Factor c ($n = 3$ and $b/b' = 1$.)

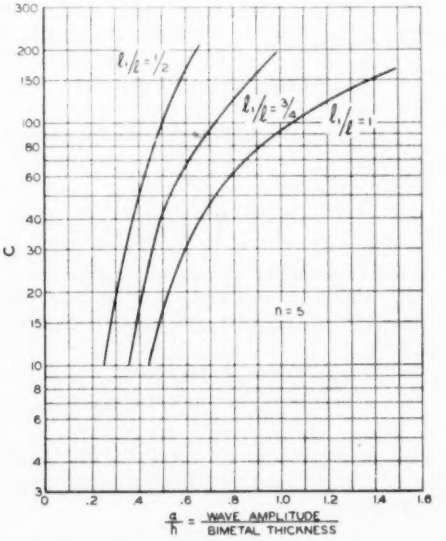


Fig. 12 Curves for Finding Temperature-Range Factor c ($n = 5$ and $b/b' = 1$.)

Using this expression in Equation [58], the stress may be expressed as[5]

$$\sigma_{sb} = c_3(t_{cr1} - t_{cr2})(\alpha_1 - \alpha_2)E \quad [60]$$

where

$$c_3 = 0.147 x_{cr}^2 \psi_{2cr} \quad [61]$$

Since ψ_{2cr} depends upon x_{cr}, which in turn depends upon ϵ/c_3 the factor c_3 may be plotted as a function of this quantity. This has been done in Fig. 13 for $\mu^2 = 1$ and $\mu^2 = 0.8$.

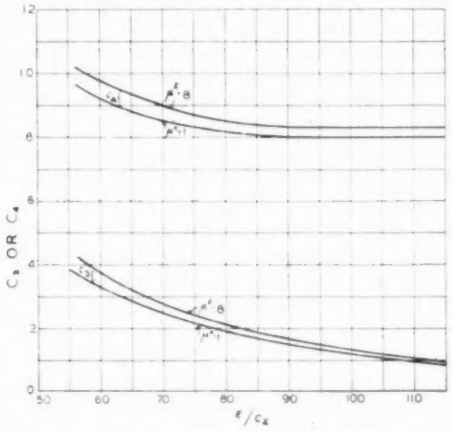


FIG. 13 CURVES FOR FINDING c_3 OR c

The direct compressive stress at the instant of buckling is

$$\sigma_c = \frac{P_{cr}}{bh} = \frac{Eh^2 x_{cr}^2}{12l^2} \quad [62]$$

This follows since $x_{cr}^2 = \dfrac{12\,Pl^2}{Ebh^3}$. In the usual case this stress will be considerably below the bending stress at the middle or end.

The bending stress at the middle of the inner strip at the instant when buckling occurs is

$$\sigma_{mb} = \frac{6(P_{cr}a_{3cr} - M_{cr})}{bh^2} \quad [63]$$

where a_{3cr} is the deflection of the inner strip at the instant of buckling obtained from Equation [28] by using $x = x_{cr}$. Substituting this value of a_{cr} in Equation [63] and simplifying as before, we obtain

$$\sigma_{mb} = c_4(t_{cr1} - t_{cr2})(\alpha_1 - \alpha_2)E \quad [64]$$

where

$$c_4 = \frac{0.462}{\pi^2} x_{cr}^2 \psi_{4cr} \quad [65]$$

and

$$\psi_{4cr} = \frac{1}{(x_{cr}^2/\pi^2) - 1} - \pi\psi_{2cr}(\psi_{2cr} + 1) \quad [66]$$

Values of c_4 have been plotted against ϵ/c_4 in Fig. 13, for $\mu^2 = 1$ and 0.8. Since c_4 is considerably greater than c_3, this indicates that the maximum stress under this condition of free buckling will occur in the middle of the strip.

It should be noted that in actual practice, where the thermostat is assembled in a manner similar to that shown in Fig. 5, a considerably lower stress range may actually exist in operation, as compared with that calculated from Equation [64].

CONCLUSION

By means of the formulas and curves given, the effect of such variables as depth and number of crimps, length and thickness of the bimetal strip, and initial chord height on the free snapping temperatures of the Valverde thermostat may be evaluated. When the thermostat is manufactured in such a way that the assumption made regarding equal free chord heights for the two strips is approximately realized, it may be expected that the theory will yield satisfactory results. Where this is not the case, however, considerable deviation between test and theory may result. In spite of these limitations, the theoretical results obtained in this manner have provided a useful guide in practical design.

ACKNOWLEDGMENT

The author is particularly indebted to Mr. P. R. Lee of the Westinghouse Electric & Manufacturing Company for much valuable practical information concerning the characteristics of the Valverde type of thermostat. He also wishes to acknowledge the helpful discussions on this subject which have been held with Prof. S. Timoshenko of Stanford University and Mr. R. E. Peterson of the Westinghouse Company.

[5] Stress concentration effects are neglected in the calculations.

Discussion

Increase of Stress With Permanent Strain and Stress-Strain Relations in Plastic State for Copper Under Combined Stresses[1]

R. G. Sturm.[2] It is rather significant that large strains such as those measured by the author appear to follow the same general trend as the very small plastic strains. As greater and greater permanent strains are considered, one would expect to find greater asymmetry resulting from the mechanical fibering of the metal in tubes. Recent work by E. Siebel and A. Maier[3] indicates that different metals have different degrees of anisotropy.

The use of Bailey's equation for strain rates as a basis for interpreting large strains is most interesting. If the relationship between strain rates and stresses is similar to the relationship between strains and stresses such that the author's Equation [19] is a true representation, one would expect to find an exponential relationship between the shear strains and the shear stresses. The shear-strain curves do not bear out this relationship but, on the other hand, the author's resulting curve between μ and ν follows very closely the same trend as the relationship between strains obtained by Taylor and Quinney using strains directly rather than strain rates.

Inasmuch as the stresses used by the author were always tensile, the effects of the normal stresses on the shearing stresses would be expected to be all in the same direction as noted by the author. If, however, the tubular specimens had been subjected to an axial compressive load at the same time internal pressure was applied, it is altogether possible that the deviation between μ and ν would be on the other side of the straight line $\mu = \nu$. In other words, the value of K instead of being greater than 3 might well be less than 3.

It seems to the writer that there must be a simpler expression for the relationships between normal stresses, shears, and strains. In this respect, the work of Siebel and Maier[3] has certain advantages. The author's work, on the other hand, tends to open the field to a greater latitude in possible explanations for strains under combined stress.

Author's Closure

The author wishes to thank Dr. Sturm for his discussion. His remarks are self-explaining and require no further comment. The author, however, would like to take this opportunity to rectify an oversight in the original paper. The dependence of the relationship between μ and ξ upon the exponent $n - 2m$ as shown in Fig. 6 was first described by Prof. G. Cook in his discussion of Bailey's paper (reference 10) and proper acknowledgment of this should have been included in the original text.

[1] By E. A. Davis, published in the December, 1943, issue of the Journal of Applied Mechanics, Trans. A.S.M.E., vol. 65, 1943, p. A-187.

[2] Research Engineer Physicist, Aluminum Research Laboratories, Aluminum Company of America, New Kensington, Pa. Mem. A.S.M.E.

[3] "The Influence of Multiaxial Stress Conditions on the Plastic Deformability of Metallic Materials," by E. Siebel and A. Maier, Communication From the Material Testing Station of the Technical College at Stuttgart.

Closed Surge Tanks[1]

R. W. Angus.[2] The title of this paper does not convey a particularly clear idea of the matter treated, since a surge tank has an open top, while the corresponding vessel with closed top is more generally known as an air chamber. It is somewhat interesting to find this latter device under consideration again for the protection of pipe lines, for it has long been known that it is not efficient as an absorber of kinetic energy but has possibilities as far as potential energy is concerned. The number of power plants using the air chamber must be very small indeed, and for the protection of long pumping lines it has been superseded by much better equipment.

The writer does not understand what the author means in his third paragraph where he says, "The process of starting up is under control, and therefore can be arranged to cause less violent disturbances." Since the author refers to water power stations, the foregoing statement is scarcely correct, because the governor is so adjusted that it will take on load at practically the same rate as it will reject it, and the load changes from full to quarter load, for example, in practically the same time as it will change from quarter to full load.

It is this fact which is so important in the tank. During load rejection, the pipe line must of course be protected, which is not a very difficult thing to do; but when load is suddenly thrown on, a large volume of water must be available near the turbine so as to keep up the supply until the penstock and conduit velocities are accelerated to their proper values.

In a specific plant with differential surge tank, the latter is 60 ft in diam and holds water 35 ft deep at no load, and it is difficult to see how an air chamber could be made which could possibly perform the same duty in supplying water as this tank can. The air chamber therefore requires slow absorption of load, which is not generally possible in modern plants, although the Glenville turbine described by Mr. Pfau at the Annual Meeting, 1943, of the Society, has no tank of any kind but uses the very long closure time of 120 sec.

The author's statement at the end of the second paragraph is incorrect, in view of the fact that engineers have calculated the tanks many times and found their values to agree very closely with those actually observed. There appears to be no great difficulty in obtaining any degree of accuracy required by the "exceedingly laborious step-by-step method of integration," mentioned by the author, but which is, actually, not exceedingly laborious. Like any engineering problem, it requires concentration but enables all factors to be taken into account with great accuracy and does not take an unusually long time.

Mathematical formulas are of value in determining the approximate dimensions of surge tanks, and a good one has been given by R. D. Johnson.[3] This formula assumes the loss of head to vary as the square of the velocity, and after using it to get the first approximation to the size of the tank, the arithmetical method must be used in order to determine the corre-

[1] By A. M. Binnie, published in the December, 1943, issue of the Journal of Applied Mechanics, Trans. A.S.M.E., vol. 65, 1943, p. A-183.

[2] Professor and Head of Mechanical Engineering Department, University of Toronto, Toronto, Canada. Honorary Member A.S.M.E.

[3] "The Surge Tank in Water Power Plants," by R. D. Johnson, Trans. A.S.M.E., vol. 30, 1908, pp. 443–501.

sponding surges and to modify the size of the tank if necessary.

In 1937, several papers were presented dealing with the air chamber, one by L. Allievi,[4] and one by the writer;[5] other papers dealt with various phases of the same question. The solutions offered are not very tedious but do not include friction. The latter may be incorporated in the manner explained in various papers, including some by the writer.[6] Little would be gained by repeating this material. Mr. Allievi and others have suggested that the entrance of the air chamber may be so designed that the resistance to water entering it will be different from that leaving it, which has some merit.

Discharge lines from pumps may be much better protected by a suitable valve than by an air chamber, but in this case one has only to protect the pipe and machinery against fracture. There is no problem of sudden demand for water at the lower end of the pipe.

The very brief description of the author's apparatus leads one to question its accuracy. The writer has found that the history of the valve closure is very important in this type of problem. With the author's pipe the time of travel of the pressure wave is around $^1/_8$ sec, and it is very important to know whether this is exceeded or not. Curves of pressure rise plotted on a time base would also be helpful.

Author's Closure

The author thanks Professor Angus for his contribution but regrets the implication that the work was not worth doing. He thinks that the interest previously taken in the problem is a sufficient answer to that view. Step-by-step methods of calculation are usually regarded as undesirable, because, besides being lengthy, they suffer inherently from the possibility of cumulative error. His own experience has amply confirmed this opinion, therefore he ventured to suggest a direct method of computation. He agrees that the experiments are not as exhaustive as could be wished. War conditions, however, frustrated his intention of obtaining cinema pictures of the surges with the pressure gage and a clock in the field of view. A notable feature has been the smooth manner in which the air vessel brought the water to rest even when the damping disk was in position. No vestige of shock has been noticed.

Second Law of Thermodynamics for Changes of State and Quantity of Working Substance With Particular Reference to Steam Engines[1]

J. H. Keenan.[2] This paper is a useful contribution to the thermodynamics of the pure substance. Equation [1] was given by Gillespie and Coe[3] who restricted it to conditions in the absence of a discontinuity of pressure at the boundary which fluid crosses and in the absence of gravity, electricity, distortion of solid masses, and capillary tensions. The author should have stated equivalent restrictions.

The results of the first two applications of Equation [1] can be readily obtained by substituting a piston and a cylinder for the steady-flow compressor assumed in the paper and permitting fluid at pressure p_1 to follow the piston in its motion. The triangular area 1-2-3 becomes the net work that must be supplied from outside the fluid to the piston.

The most important item in the paper appears to be Equation [8*a*], which is the logical companion to Equation [1]. Despite the simplicity of its derivation, it seems that it has not been explicitly stated before. It shows that in an adiabatic process the entropy per unit mass within an enclosure does not change if the material introduced has the same enthalpy per unit mass as that already there.

The subject of "open systems" is an extremely important one which authors of engineering texts have been inclined to slight. The author will have performed a great service if he has succeeded in focusing the attention of a few engineers on the thermodynamic problem of flow under nonsteady conditions.

Closure by M. Jakob

The writer has been requested to prepare a closure to the foregoing discussion of the late Professor Zerkowitz's paper. He agrees with Professor Keenan's statement that the author's studies on "open systems" mean a valuable service to engineering. He would further like to mention that the author also dealt thoroughly with an important problemof two-phase open systems, namely, the storage of steam, in a publication of 1927, quoted in footnote 2 of Dr. Zerkowitz's paper.

The writer requests this opportunity to correct some typographical errors in the paper: P should be replaced by p in Equations [5] and [17]; the last term Gdv in footnote 3 should be replaced by Gdu; on page A-111, column 1, line 8, the symbol v is to be replaced by V.

[4] "Air Chambers for Pipe Lines," by L. Allievi, Trans. A.S.M.E., vol. 59, 1937, pp. 651–659.

[5] "Air Chambers and Valves in Relation to Water Hammer," by R. W. Angus, Trans. A.S.M.E., vol. 59, 1937, pp. 661–668.

[6] "Water-Hammer Pressures in Compound and Branched Pipes," by R. W. Angus, Trans. A.S.C.E., vol. 104, 1939, pp. 340–401.

"Water Hammer in Pipes Including Those Supplied by Centrifugal Pumps; Graphical Treatment," by R. W. Angus, Proceedings of The Institution of Mechanical Engineers, vol. 136, 1937, pp. 245–291.

[1] By G. Zerkowitz, published in the June, 1944, issue of the Journal of Applied Mechanics, Trans. A.S.M.E., vol. 66, p. A-108.

[2] Professor of Mechanical Engineering, Massachusetts Institute of Technology, Cambridge, Mass. Mem. A.S.M.E.

[3] "The Heat of Expansion of a Gas of Varying Mass," by L. J. Gillespie and J. R. Coe, *Journal of Chemical Physics*, vol. 1, 1933, pp. 102–113.

Book Reviews

Modern Turbines

Modern Turbines. By Louis E. Newman, Allen Keller, John M. Lyons, Lawrence B. Wales, all of the General Electric Company. Edited by Louis E. Newman. John Wiley & Sons, Inc., New York, N. Y., 1944. Cloth, $5^1/_2 \times 8^3/_8$ in., 175 pages, 93 figs., $2.50.

Reviewed by C. Richard Soderberg[1]

THE latest addition to the "General Electric Series," which now comprises ten treatises on different aspects of power engineering, is a discussion of the steam turbine expressed in simple language without mathematical frills or scientific verbiage. It consists of nine well-coordinated chapters on all the basic aspects of the steam turbine and the electric generator.

The first three chapters, by Newman, give a summary of the fundamental aspects of turbine application, the range of operating conditions, and the use of the steam chart and tables of theoretical steam rates. Chapters four to six by Newman and Keller cover the main aspects of evaluating the performance of this multitude of turbine applications. Chapter seven by Newman is a

[1] Professor of Mechanical Engineering, Massachusetts Institute of Technology, Cambridge, Mass. Mem. A.S.M.E.

very useful discussion of the premises to be followed when a purchaser desires to estimate the effect upon a proposal of changes in capacity or operating conditions. Chapter eight by Wales and Newman is a clear and concise description of the basic features of turbine control. Chapter ten by Lyons gives a brief exposition of the fundamentals of electric generators. There is an Appendix abstracted from the "NEMA Turbine Generator Recommended Practices."

While the information presented is properly classified as General Electric catalog material it is strictly informative and free from sales propaganda. An impressive case is made for the great flexibility of the steam turbine as a prime mover, although it should perhaps be pointed out that this very flexibility is itself an indication of the complexity of the steam plant. For the 14 standard ratings of industrial turbines below 7500 kw, 112 different designs are necessary. These designs are still further diversified by the many combinations of inlet and exhaust conditions. The only practical solution is to assemble machines from a well-considered range of standard parts.

The book is highly recommended for those engineers who wish to become acquainted with the possibilities of the turbine as a tool in industrial power-plant planning without entering into the more complicated features of turbine design.

Introduction to Theory of Elasticity

AN INTRODUCTION TO THE THEORY OF ELASTICITY FOR ENGINEERS AND PHYSICISTS. By R. V. Southwell, Professor of Engineering Science in the University of Oxford. Second edition. Oxford University Press, New York, N. Y., 1941. Cloth, 6 × 9 in., v and 509 pp., 120 figs., $10.

REVIEWED BY C. RICHARD SODERBERG[1]

THE second edition of Southwell's "Theory of Elasticity" has now been in print for some time and has been available to American readers for more than a year. The departures from the first edition are only minor in character, consisting chiefly of additions relating to the author's own contributions to relaxation methods. These, however, are covered more fully in his book entitled "Relaxation Methods in Engineering Science." The new edition retains all of the careful, deliberate style of presentation which has become familiar to the many readers of the original "Theory of Elasticity." The background of style, nomenclature, and mode of presentation goes back to Love and Lord Rayleigh. To the American reader this style is a reminder of earlier usage and its relative strangeness to many of the younger men is a reminder of the strong influences of Russian and German writers in this field, which have been at work in America during the last twenty years. No criticism of the "Theory of Elasticity" is implied in this observation, rather, an apologetic feeling of regret that some efforts should be necessary to follow its nomenclature.

The "Theory of Elasticity" has particular value, because it includes not only the usual problems of elasticity but also the major problems of vibrations which often form the ulterior motive for the analysis of the elastic properties of systems. The central theme of the book is the energy method, and whenever practicable the solutions are derived through this medium. This consistency of approach is one of the many reasons for the appeal of the "Theory of Elasticity." As a result of this method of treatment the theorems of Castigliano, as well as the reciprocal theorem, play a very fundamental role. It is regretted by the reviewer that the treatment of these could not have been carried beyond the conventional form.

It is properly emphasized that Castigliano's theorems make no appeal to Hooke's law, but the situation is rather that Hooke's law has always obscured the true meaning of these theorems. For any relation between load P and deflection y, in which the previous history of loading is without influence, the first theorem of Castigliano refers to energy changes $y \cdot \delta P$, while the second deals with changes of the type $P \cdot \delta y$. The latter relate to the usual strain energy, while the former relate to what may be called "complementary strain energy." When Hooke's law is introduced into the picture these two energies become equal and are customarily identified with one another. In actual practice, the first theorem of Castigliano requires the strain energy to be expressed as a function of the forces while the second requires the strain energy as a function of the displacements.

In connection with problems of dynamics, such as in the case of vibrations of complicated systems with discrete mass particles, this dual point of view is no less important. Lagrange's equations of motion demand the strain energy in terms of the displacements, while most mechanical systems are more readily reduced by the first theorem of Castigliano, which requires the strain energy in terms of the forces. When the static properties of a mechanical system have been derived by means of the first theorem of Castigliano, therefore, the alternative formulation of the equations of motion, in which the inertia forces are directly incorporated in the force system, is much to be preferred. This is particularly so, because in this form approximate solutions may be reached by means of the simple and convenient iteration method, which is not so easily applicable to the conventional formulation. The relaxation method is presumably applicable to both methods of formulation, but at least in the reviewer's limited experience, the iteration method appears the simpler.

These remarks do not detract from the great value of the second edition of the "Theory of Elasticity" which like its predecessor will have a place as a valued reference for all who are interested in this important field.

Metals and Alloys Data Book

METALS AND ALLOYS DATA BOOK. By Samuel Hoyt, Technical Advisor of Battelle Memorial Institute. Published by Reinhold Publishing Corporation, New York, N. Y. Cloth, 7 × 10 in., 350 pages, 340 tables, $4.75.

REVIEWED BY PETER E. KYLE[2]

THE author points out in the preface that this book fills his need for a ready reference to the properties of metals and alloys. To the metallurgist, student, or engineer who has tried to find reference to properties of a specific alloy in the previously published literature, this compilation of data will at once appear most helpful. The data contained in this work are as reliable as could be obtained and rather complete information on the composition, structure, heat-treatment, and fabrication methods used is given for each metal and alloy tabulated.

The scope of the book is sufficiently broad to be of use to all users of metals and it includes properties of wrought steels, cast steels, stainless steels, cast irons, heat- and corrosion-resistant casting alloys, nonferrous alloys, and other alloys. The properties reported include tensile properties, hardness, hardenability, creep strength, work hardening, impact strengths, corrosion resistance, etc. Other information includes hardness conversion tables, hot hardness properties, S-curve data, heat contents, thermal-expansion coefficients, grain-size charts, test-specimen sizes, atomic data for the elements, and the usual tables of weights and measures, and conversion tables.

The author has provided an excellent table of contents and index which is so necessary if such a tremendous amount of information is to be made readily available to the reader.

[1] Associate Professor of Mechanical Engineering, Massachusetts Institute of Technology, Cambridge, Mass. Mem. A.S.M.E.

Theory of Wire Drawing

By E. A. DAVIS[1] and S. J. DOKOS,[1] EAST PITTSBURGH, PA.

A theory of wire drawing is presented in which the force required to produce plastic deformation of a wire passing through a die may be determined. The calculations are based upon information obtained from an ordinary tension test of the material to be drawn. Unlike previous mathematical treatments where the metals were assumed to be ideally plastic, the strain-hardening of the wire being drawn is considered.

Nomenclature

The following nomenclature is used in the paper:

r_0 = initial radius of wire
r = outer radius of wire, variable along die
A_0, A_f = initial and final area of wire
A = cross-sectional area of wire, variable along die
ϵ_x, ϵ_t, ϵ_r = principal natural strains
σ_x, σ_t, σ_r = principal true stresses
γ_{tr}, γ_{rx}, γ_{xt} = principal natural shearing strains
τ_{tr}, τ_{rx}, τ_{xt} = principal shearing stresses
p = pressure exerted on wire by die
σ_0, τ_y = idealized yield stress
$\Omega = \frac{\partial \tau}{\partial \gamma}$ = coefficient of strain hardening in shear
F = force required to draw wire
μ = coefficient of friction between die and wire
α = one-half angle of die
$k = \frac{\mu}{\alpha}$

Introduction

An investigation by one of the authors is in progress to determine experimentally the values of the coefficient of friction at very high pressures and at various temperatures ranging from normal room temperatures to very high temperatures.[2] This project should furnish values of the friction in forging and metal-forming operations about which very little information exists. It was thought that the conditions encountered in wire-drawing would be of particular interest in this respect, since the forces could be experimentally measured without any difficulty. In the preliminary review of the literature it was found, however, that the theoretical information available was insufficient for computing the values of the coefficients of friction involved in wire-drawing. To facilitate the evaluation of these friction forces, the theory outlined in this paper is offered.

The force required to draw a wire through a die depends upon several factors, the two most important of which are the friction of the wire on the walls of the die and the resistance of the wire to plastic deformation. The latter factor will depend upon the stress-strain relations of the wire. In most previous mathematical treatments, the material to be drawn was assumed to be ideally plastic. An ideally plastic material has a definite yield point at which the material flows continuously without any increase in the applied stress. In the present paper the strain-hardening of the wire is considered, and the mathematical expressions used have been adjusted to take care of the large strains encountered in the process of wire drawing.

Previous Investigations

A large amount of experimental research in the drawing of wire has been done in the past, and, although it is not the purpose of this paper to make a critical review of the available literature, it may be well to refer to a few investigations which seem to have a direct bearing on the present work.

Thompson and Francis (1, 2)[3] have shown that the force necessary to draw wire is proportional to the reduction of area. This same relation has been found also by Giraud[4] and Brown.[4] In various graphs of drawing force versus reduction of area, they show that the experimental points fall on a straight line which will cut the force axis at some finite value. This seems to indicate that a certain force is required for no reduction of area. This feature will be discussed later. Thompson and Francis (2, 3) also show that a reduction in the drawing force is obtained if a back-tension of a considerable magnitude is applied.

Several investigators have attempted to analyze the wire-drawing problem from a mathematical standpoint. Probably the first work of this kind was done by Sachs (4). He obtained expressions for the force necessary to draw a wire through a given die and for the pressure and stress distribution along the die as the wire is being drawn. Horsburgh (5) has developed similar expressions which are comparable with those of Sachs. The theory as presented by Sachs will appear as a special case of the present development.

Siebel and Hühne (6) have shown, by means of engraved models, the strain distribution and the distortion of the individual cross sections of the material as it passes through the die. Thompson and Barton (7) have carried out photoelastic tests of various shaped dies. Although their tests were two-dimensional in character, they indicate clearly the directions of the principal stresses. How completely this method and the one used by Siebel and Hühne (6) agree with the conditions actually occurring in the wire-drawing process is somewhat questionable. However, it can be stated that, for the smaller angles of reduction, the distortion of the cross-sectional planes will be less and that, for a mathematical treatment, it will be convenient to assume that the original cross sections remain planes.

Theoretical Considerations

In the mathematical development which follows, it has been assumed:

(*a*) That the axial, radial, and tangential directions are principal directions.

---

[1] Research Engineer, Westinghouse Electric & Manufacturing Company, East Pittsburgh, Pa.

[2] Funds for this purpose have been made available by the A.S.M.E. Special Research Committee on Plastic Flow of Metals under a grant received from the Engineering Foundation in New York through the A.S.M.E.

Presented at the National Meeting of the Applied Mechanics Division, Chicago, Ill., June 16–17, 1944, of The American Society of Mechanical Engineers.

Discussion of this paper should be addressed to the Secretary, A.S.M.E., 29 West 39th Street, New York, N. Y., and will be accepted until January 10, 1945, for publication at a later date. Discussion received after the closing date will be returned.

Note: Statements and opinions advanced in papers are to be understood as individual expressions of their authors and not those of the Society.

[3] Numbers in parentheses refer to the Bibliography at the end of the paper.

[4] Both references may be found in (1).

(*b*) That the axial tension stress is distributed evenly over the cross-sectional area.

(*c*) That the flow takes place according to some stress-strain relation which can be determined from a pure-tension test on the wire.

(*d*) That the range of speed used in wire-drawing is limited to such an extent that the speed effect can be neglected. This assumption has been checked experimentally by various investigators (2, 8).

Assumptions (*a*) and (*b*) are used purely for reasons of simplicity. To take into consideration the actual stress and strain distribution inside the deformed part of the wire would needlessly

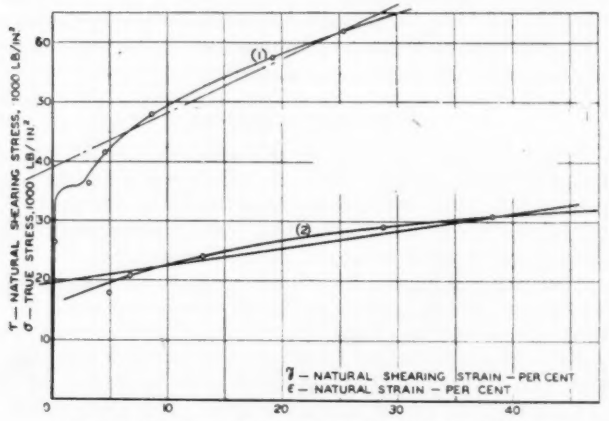


FIG. 1 TENSION DIAGRAMS FOR MILD-STEEL WIRE
(Curve 1, True stress versus natural strain. Curve 2, Natural shearing stress versus natural shearing strain for mild-steel wire.)

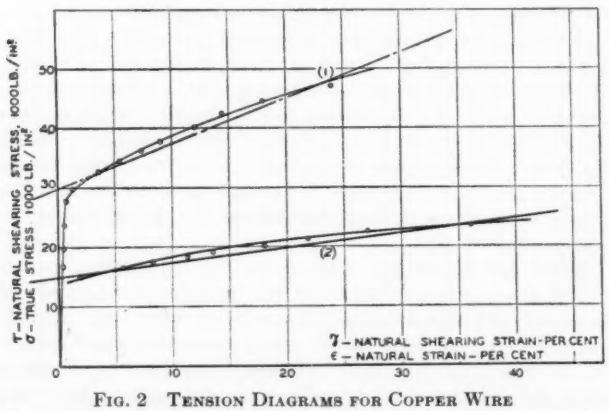


FIG. 2 TENSION DIAGRAMS FOR COPPER WIRE
(Curve 1, True stress versus natural strain. Curve 2, Natural shearing stress versus natural shearing strain for copper wire.)

complicate the problem and would probably render a solution impossible. Assumption (*c*) is based upon some recent work by one of the authors (9). In that paper it was shown that, for cases where there was no rotation of the principal axes of stress and where the ratio of the principal shear stresses did not change during the test, the maximum shear stress was given by the same function of the maximum shear strain regardless of the state of combined stress. It was also shown that a similar relation between the octahedral shearing stress τ_n and the octahedral shearing strain γ_n could be used. The agreement in both cases was not perfect, but was probably close enough for use in the present problem. From this it was assumed that either of the expressions, $\tau_{max} = f(\gamma_{max})$, or $\tau_n = f(\gamma_n)$, determined from a pure tension test, could be used in the analysis of wire drawing. Both cases will be developed.

The strains in the wire passing through the die will be determined by the shape of the die. The increments of the natural strains in the tangential and radial directions are

$$d\epsilon_t = \frac{dr}{r} \quad [1]$$

and

$$d\epsilon_r = \frac{dr}{r} \quad [2]$$

Since the sum of the natural principal strains is zero, the following equations are obtained for the strains

$$\epsilon_z = 2 \ln \frac{r_0}{r} \quad [3]$$

$$\epsilon_r = \epsilon_t = -\frac{\epsilon_z}{2} = \ln \frac{r_0}{r} \quad [4]$$

where r_0 is the original radius of the wire. One of the principal shearing strains $(\epsilon_t - \epsilon_r)$ is zero; the other two are equal in magnitude but opposite in sign. It follows from this symmetrical condition, then, that two of the principal shear stresses are equal but opposite in sign and that the radial and tangential stresses are equal.

Case 1: $\tau_{max} = f(\gamma_{max})$. The tension diagrams of two materials as examples are represented by Figs. 1 and 2. In some cases, due to the nature of the tension diagrams, the maximum shearing stress τ_{max} can be expressed by a power function of the maximum shearing strain γ_{max}

$$\tau_{max} = C (\gamma_{max})^{1/n} \quad [5]$$

where the exponent $\frac{1}{n}$ and C are material constants. In Equation [5] and in all subsequent equations, the elastic strains will be neglected. For a state of stress consisting of a tensile stress σ_z in the axial direction and equal stresses σ_r and σ_t in the perpendicular directions Equation [5] can be expressed in terms of the principal stresses and strains since

$$\tau_{max} = \frac{\sigma_r - \sigma_z}{2} \quad [6]$$

and

$$\gamma_{max} = \epsilon_r - \epsilon_z \quad [7]$$

Equation [5] can now be rewritten as

$$\frac{\sigma_r - \sigma_z}{2} = C \left(\epsilon_r - \epsilon_z\right)^{1/n}$$

or after making use of Equations [3] and [4], as

$$\sigma_z - \sigma_r + a \left(\ln \frac{r}{r_0}\right)^{1/n} = 0 \quad [8]$$

where the constant $a = 2\,C\,3^{1/n}$.

By neglecting the radial component of the friction force, the radial stress σ_r will be assumed equal in magnitude to the pressure p exerted by the die

$$\sigma_r = -p \quad [9]$$

With reference to Fig. 3, representing the forces acting on an element of length dx of the wire, the condition of equilibrium can be expressed by the differential equation

$$2\sigma_z + r\frac{d\sigma_z}{dr} + 2(1 + k)\,p = 0 \quad [10]$$

where $$k = \frac{\mu}{\alpha}$$

The stress distribution along the length of the wire can now be evaluated from Equations [8], [9], and [10]. The solution of the differential equation (Equation [10]) is given by

$$\sigma_x = r^{2k}\left[2a\,(1+k)\int \frac{\left(\ln\frac{r}{r_0}\right)^{1/n} dr}{r^{2k+1}} + C_1\right] \ldots [11]$$

To solve Equation [11] numerical integration is necessary. Instead of computing this integral, a further simplification can be

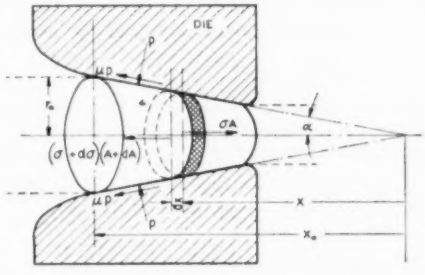


FIG. 3 EQUILIBRIUM OF AN ELEMENT OF WIRE PASSING THROUGH A DIE

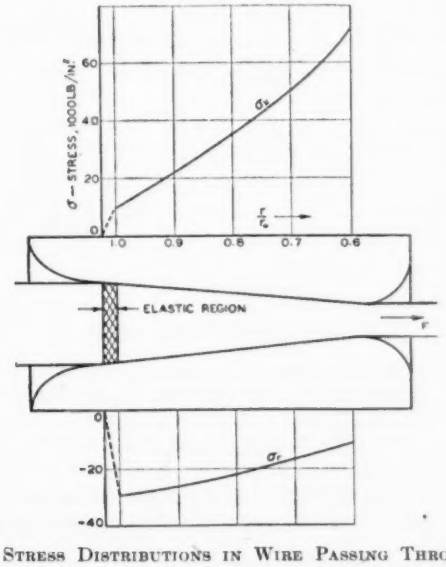


FIG. 4 STRESS DISTRIBUTIONS IN WIRE PASSING THROUGH DIE

introduced. It will be assumed that the tension diagram can be represented by a straight line, as shown in Figs. 1 and 2. For certain materials, such a simplification will be a fairly good approximation to the actual diagram. Thus the maximum shearing stress can be evaluated as the summation of the ordinate intercept τ_y, and the product of the slope Ω and the maximum shearing strain, that is

$$\tau_{max} = \tau_y + \Omega\,\gamma_{max} \ldots [12]$$

Expressed as a linear function of γ_{max}, the equation can be rewritten as

$$\gamma_{max} = \frac{1}{\Omega}(\tau_{max} - \tau_y) \ldots [13]$$

The maximum shearing strain can now be written in terms of the natural strains and the true stresses

$$\gamma_{max} = \epsilon_r - \epsilon_x = \frac{1}{\Omega}\left(\frac{\sigma_r - \sigma_x}{2} + \frac{\sigma_0}{2}\right) \ldots [14]$$

where $\sigma_0 = -2\tau_y$. Equations [3] and [4] may now be substituted into Equation [14], and the following relation between stress and the variable die radius is obtained

$$\sigma_x - \sigma_r - \sigma_0 + 6\,\Omega \ln\frac{r}{r_0} = 0 \ldots [15]$$

The stress distribution along the wire can be evaluated by substituting Equations [9] and [15] into Equation [10]. The differential equation can now be expressed as

$$r\frac{d\sigma_x}{dr} - 2k\sigma_x + 2\,(1+k)\left(\sigma_0 - 6\,\Omega \ln\frac{r}{r_0}\right) = 0 \ldots [16]$$

The solution of Equation [16] is

$$\sigma_x = \frac{1+k}{k}\sigma_0 - \frac{6\,(1+k)\,\Omega}{k}\ln\frac{r}{r_0} - \frac{6\,(1+k)\,\Omega}{2k^2} + C_2 r^{2k} \ldots [17]$$

To determine the constant C_2 from a theoretical standpoint, it would be necessary to consider the stresses in the elastic region where the wire enters the die. The force developed in the elastic region will be the same for any given size of wire regardless of the amount of reduction which follows. If we consider σ_1 to be the stress at the boundary between the elastic and plastic ranges, as shown in Fig. 4, then C_2 can be determined by letting $\sigma_x = \sigma_1$ when $r = r_0$. Then

$$\sigma_x = \frac{1+k}{k}\left\{6\Omega\ln\frac{r_0}{r} - \left(\frac{3\Omega}{k} - \sigma_0\right)\left[1 - \left(\frac{r}{r_0}\right)^{2k}\right]\right\} + \sigma_1\left(\frac{r}{r_0}\right)^{2k} \ldots [18]$$

The stress distribution in terms of the area of reduction is

$$\sigma_x = \frac{1+k}{k}\left\{3\,\Omega\ln\frac{A_0}{A} - \left(\frac{3\Omega}{k} - \sigma_0\right)\left[1 - \left(\frac{A}{A_0}\right)^{k}\right]\right\} + \sigma_1\left(\frac{A}{A_0}\right)^{k} \ldots [19]$$

In order to compare Equation [18] with the one previously developed by Sachs (4), let Ω equal zero. This neglects the effect of strain-hardening and the equation is reduced to

$$\sigma_x = \sigma_0\frac{1+k}{k}\left[1 - \left(\frac{r}{r_0}\right)^{2k}\right] + \sigma_1\left(\frac{r}{r_0}\right)^{2k} \ldots [20]$$

Since the strains in the elastic region were also neglected in Sachs's development, the equation for the axial stress is

$$\sigma_x = \sigma_0\frac{1+k}{k}\left[1 - \left(\frac{r}{r_0}\right)^{2k}\right] \ldots [21]$$

which is identical with his solution (4).

Another interesting case is to let the coefficient of friction μ equal zero. When this substitution is made in Equation [18], the stress becomes indeterminate, and it is therefore necessary to consider the original differential equation (Equation [10]) when $\mu = 0$. This equation reduces to

$$r\frac{d\sigma_x}{dr} + 2\sigma_x + 2\,p = 0 \ldots [22]$$

When Equation [22] is integrated, the axial-stress distribution is found to be

$$\sigma_x = 6\,\Omega\left(\ln\frac{r}{r_0}\right)^2 - 2\,\sigma_0\ln\frac{r}{r_0} + \sigma_1 \ldots [23]$$

The force necessary to draw a wire through a die can now be determined. When Equation [19] is considered, the stress for $A = A_f$ is found to be equal to

$$\sigma_f = \frac{1+k}{k}\left\{3\Omega \ln \frac{A_0}{A_f} - \left(\frac{3\Omega}{k} - \sigma_0\right)\left[1 - \left(\frac{A_f}{A_0}\right)^k\right]\right\} + \sigma_1\left(\frac{A_f}{A_0}\right)^k \quad \ldots\ldots [24]$$

Therefore, the force required to draw a wire is equal to

$$F = A_f\,\sigma_f \quad \ldots\ldots [25]$$

By means of Equations [15] and [16], it is possible to plot the axial and radial stresses as a function of the reduction in radius of a metal passing through a die. A hypothetical material was assumed in plotting the curves of Fig. 5. The strain-hardening coefficient Ω and the idealized yield stress were considered to be 30,000 psi, and 40,000 psi, respectively. At $r = r_0$, the axial

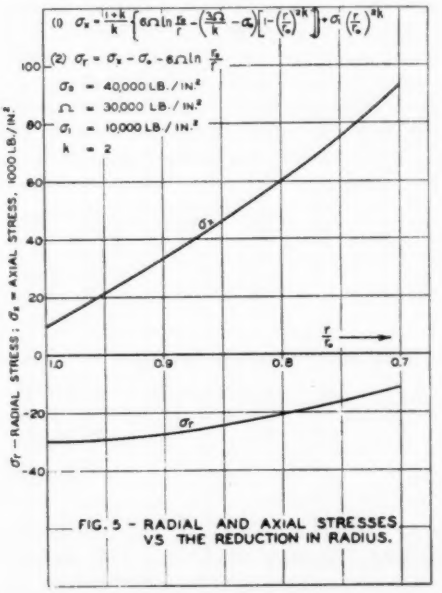


FIG. 5 RADIAL AND AXIAL STRESSES VERSUS REDUCTION IN RADIUS

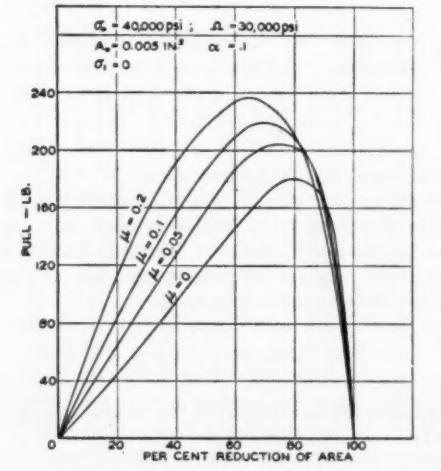


FIG. 6 FORCE REQUIRED TO DRAW WIRE VERSUS REDUCTION OF AREA

stress σ_x is equal to σ_1, and the radial stress is equal to $(\sigma_1 - \sigma_0)$, as indicated in the figure. The axial and radial stresses do not immediately obtain a finite value, but have a definite elastic region in which the stresses build up to the values given at $r = r_0$. This region is, however, so small that it is not indicated by the curves of Fig. 5.

In Fig. 6, the force required to draw a wire is plotted as a function of the reduction of area for various values of μ. The same values of the previous hypothetical material were assumed for Ω and σ_0; σ_1 was assumed to be zero. An examination of the figure reveals that for the various values of the coefficient of friction plotted, the pull is relatively proportional to the reduction of area up to a reduction of 50 per cent. Above 50 per cent reduction the slopes of the curves decrease and begin to descend after a reduction of 75 per cent.

Case 2: $\tau_n = f(\gamma_n)$. The foregoing mathematical development was based on a relationship between the maximum shearing stress τ_{max} and the maximum shearing strain γ_{max}. In some instances it may be preferable to replace this expression by one containing the octahedral shearing stress τ_n and the octahedral shearing strain γ_n. In this case the relation

$$\tau_n = f(\gamma_n) \quad \ldots\ldots [26]$$

would have to be substituted in place of the previous relationship. This theory of flow, which has been described by Dr. A. Nadai (10), states that for any type of loading the curve of the octahedral shearing stress as a function of the octahedral shearing strain is the same. If this theory is applied to the present problem, the results will not be changed materially. Equation [18] will then become

$$\sigma_x = \frac{1+k}{k}\left\{6\Omega \ln \frac{r_0}{r} - \left(\frac{3\Omega}{k} - \sigma_0'\right)\left[1 - \left(\frac{r}{r_0}\right)^{2k}\right]\right\} + \sigma_1\left(\frac{r}{r_0}\right)^{2k} \quad \ldots\ldots [27]$$

where

$$\sigma_0' = \frac{3}{2\sqrt{2}}\,\sigma_0$$

EXPERIMENTS ON WIRE DRAWING

Previously published papers on wire drawing failed to provide complete information for any one test so that the forces predicted for wire drawing in this paper could not be checked with the published results. For this reason a few tests were made at the Westinghouse Research Laboratories.

A wire-drawing bench was used and the special force-measuring arm, shown in Fig. 7, was designed to measure the drawing

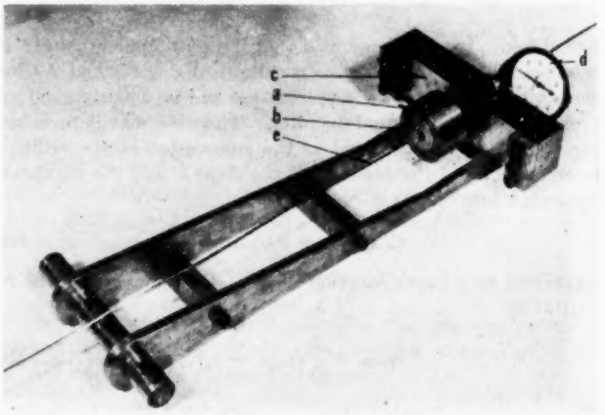


FIG. 7 FORCE-MEASURING ARM

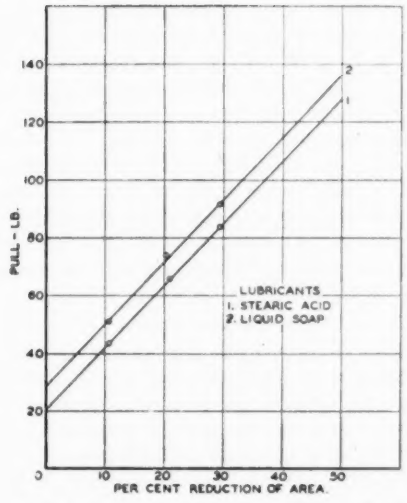


FIG. 8 FORCE REQUIRED TO DRAW MILD-STEEL WIRE, 0.0541 IN. DIAM, USING VARIOUS LUBRICANTS

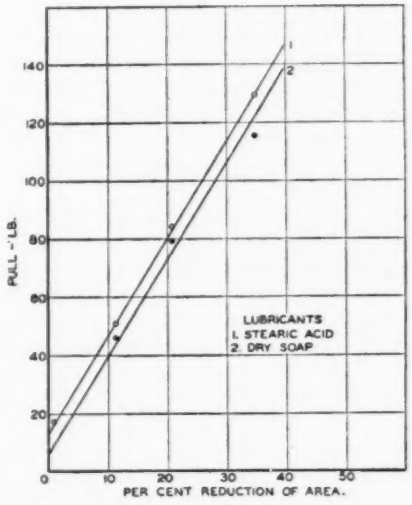


FIG. 9 FORCE REQUIRED TO DRAW COPPER WIRE, 0.080 IN. DIAM, USING VARIOUS LUBRICANTS

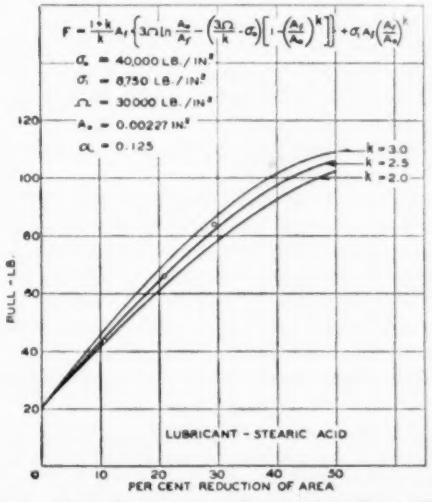


FIG. 10 FORCE REQUIRED TO DRAW MILD-STEEL WIRE

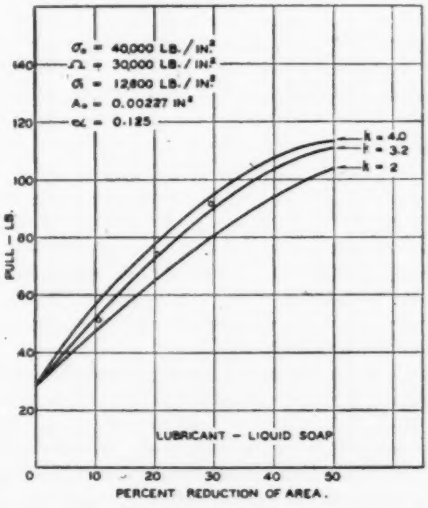


FIG. 11 FORCE REQUIRED TO DRAW MILD-STEEL WIRE

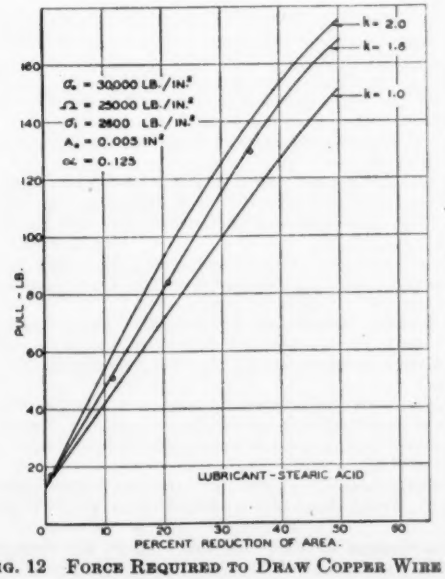


FIG. 12 FORCE REQUIRED TO DRAW COPPER WIRE

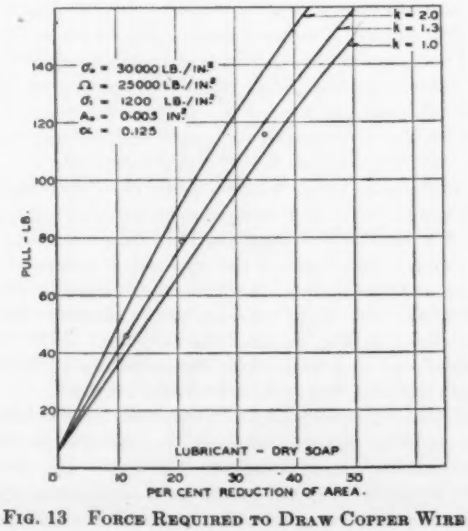


FIG. 13 FORCE REQUIRED TO DRAW COPPER WIRE

forces. The die holder (*a*) and the die (*b*) are fastened to a flat deflecting spring (*c*), whose deflection depends upon the load applied. Carboloy dies with an entrance angle 2α of 14 deg were used. The spring was calibrated before and after the tests were made. A dial indicator (*d*) is fastened to the rigid cross-member and the dial pointer is placed in contact with the deflecting spring. The wire (*e*) was fastened to a rotating drum which had a peripheral velocity of 80 fpm.

Copper and steel wires were drawn through various dies. Prior to use, the wires were drawn down about 0.001 in., to remove surface imperfections and to insure an accurate original diameter. The stress-strain diagrams of both the copper and steel wires were then obtained, as shown in Figs. 1 and 2. Following this, various lubricants, indicated in Figs. 8 and 9, were applied to the surface of the wires before and during the drawing operation so that the effect they have upon reducing the forces required could be measured. The stearic acid was dissolved in carbon tetrachloride and the 12-ft lengths of wire were passed through the solution and then allowed to dry. Similarly, dry soap was dissolved in warm water and, following the cooling of the solution, the wires were treated as described. The liquid soap was applied with a cloth during the drawing operation.

Results of Experiments

The results of the tests performed are shown in Figs. 8 and 9. The forces required to draw a wire under standard conditions appear to be proportional to the reduction of area, as shown by the experimental curves. Thompson (11) has shown that for ferrous metals this proportionality extends to a reduction of about 30 per cent, after which the necessary pull increases less rapidly. For nonferrous metals, the linearity of the curves remains up to a reduction of 50 to 60 per cent. The tests made for this paper do not exceed a reduction of 35 per cent. An examination of Figs. 8 and 9 indicates that when the condition of lubrication is altered the new curve obtained is parallel to the former, but its intercept on the ordinate axis is displaced depending upon whether the lubricant is better or worse.

In Figs. 10 to 13, inclusive, the experimental values for the forces necessary to draw wire using various lubricants are indicated for both the mild-steel and copper wires. Theoretical curves were plotted for various values of k, in order to obtain the curve which conforms as accurately as possible to the experimental points. In all cases the curves fall very close to the experimental points. The values of the coefficient of friction for mild steel using stearic acid and liquid soap as lubricants are 0.3 and 0.4, as shown in Figs. 10 and 11, respectively. In Figs. 12 and 13 stearic acid and dry soap were used as lubricants for the copper tests. The values of the coefficient of friction were evaluated as 0.2 and 0.16, respectively. It may be of interest to emphasize here that although the two curves, both in Fig. 8 and in Fig. 9, are parallel, the coefficient of friction in the mathematical treatment in each case is higher for the poorer lubricant.

The constant σ_1 was evaluated from the experimental data of Figs. 8 and 9, which is dependent upon the lubricant used. No attempt has been made to evaluate the stress distribution in the elastic region. The value of the constant σ_1 is dependent upon numerous considerations; the two most important of which are as follows: (*a*) The stress due to the elastic strains in the wire, as shown in Fig. 4; and (*b*) the effect of the lubricant. This latter factor may be partially due to the film of the lubricant built up at the point where the wire enters the die.

If back-tension were applied to the wire as it is drawn through a die, this would be treated in the theory as causing an increase in σ_1. Such an increase causes a definite decrease in the pressure as shown by Equation [15], but would cause an increase in the force necessary for drawing. Actually, however, the resisting force built up in a die is decreased when back-tension is applied (3). This can be readily illustrated upon examination of the curves for $k = 2$, in Figs. 10 and 11. The values of the initial force, $\sigma_1 A_0$, are 20 lb and 30 lb. If it is assumed that this difference is due to back-tension rather than to the lubricant, the mathematical treatment would not be changed. The results indicate that on both curves the forces at 50 per cent reduction are approximately equal. However, the resisting force built up in the die when back-tension is applied is approximately 10 lb less than when no back-tension is present. This was checked experimentally in the tests made. When back-tension was applied, the force recorded by the dial was reduced.

Conclusions

1 The mathematical theory of wire drawing can be improved by taking into consideration the strain-hardening of the wire.

2 Except for a finite load, corresponding to no reduction of area, the force necessary to draw wire is nearly proportional to the reduction in area. A straight line drawn through the points for various reductions intercepts the force axis at a finite value, $\sigma_1 A_0$.

3 Since this intercept force, $\sigma_1 A_0$, is the same, regardless of the amount of the reduction, it must be due to conditions prevailing at the point where the wire enters the die.

4 From a mathematical point of view, the constant σ_1 presents one of the greatest problems in wire drawing. Since many factors affect the value of σ_1, it can only be determined by experimentation.

5 The initial stress σ_1 varies with the lubricant used. It is also affected by back-tension.

6 Back-tension reduces the pressure on the walls of the dies. This can be shown mathematically as well as experimentally.

7 The mathematical theory of wire drawing may be used as a means of determining the coefficient of friction between the die and the metals undergoing plastic deformation.

8 The theory may be used to determine the relative values of the coefficient of friction due to boundary lubrication, when various lubricants are used to reduce the friction forces.

BIBLIOGRAPHY

1 "Studies of the Wire-Drawing Process," part II, by F. C. Thompson and E. L. Francis, Iron and Steel Institute, Carnegie Scholarship Memoirs, vol. 20, 1931, pp. 87–124.

2 "The Drawing of Non-Ferrous Wires," by E. L. Francis and F. C. Thompson, *Journal of the Institute of Metals*, vol. 46, 1931, pp. 313–351.

3 "The Effect of a Backward Pull Upon the Tension Required to Draw Wire," by F. C. Thompson, *Journal of the Iron and Steel Institute*, vol. 128, 1933, pp. 369–382.

4 "Plasticity Problems in Metals," by G. Sachs, Trans. Faraday Society, vol. 24, 1928, pp. 84–92; also see *Zeitschrift für angewandte Mathematik und Mechanik*, vol. 7, 1927, pp. 235–236.

5 "Steel Wire," by M. Bonzel, Engineers Book Shop, New York, N. Y., 1935, p. 98.

6 "Untersuchungen über den Formänderungsverlauf bei technischen Formgebungsverfahren," by E. Siebel and H. Hühne, *Mitteilungen aus dem Kaiser-Wilhelm Institut für Eisenforschung*, vol. 13, 1931, pp. 43–62.

7 "Studies of the Wire Drawing Process," part I, by F. C. Thompson and J. Barton, Iron and Steel Institute, Carnegie Scholarship Memoirs, vol. 19, 1930, pp. 39–78.

8 "Über den Kraft-und Arbeitsbedarf beim Kaltziehen von Drähten," by A. Pomp, E. Siebel, and E. Houdremont, *Mitteilungen aus dem Kaiser-Wilhelm Institut für Eisenforschung*, vol. 11, 1929, pp. 53–72.

9 "Increase of Stress With Permanent Strain and Stress-Strain Relations in the Plastic State for Copper Under Combined Stresses," by E. A. Davis, Journal of Applied Mechanics, Trans. A.S.M.E., vol. 65, p. A-187.

10 "Plastic Behavior of Metals in the Strain-Hardening Range," part 1, by A. Nadai, *Journal of Applied Physics*, vol. 8, 1937, pp. 205–213.

11 "Lubrication in Wire-Drawing," by F. C. Thompson, *The Metal Industry*, London, vol. 51, 1937, pp. 409–411.

Drawing Thin-Walled Tubing With a Moving Mandrel Through a Single Stationary Die

By G. SACHS,[1] J. D. LUBAHN,[2] AND D. P. TRACY[3]

The fundamental equations for the drawing of tubing with a moving mandrel have been solved for the simplified cases of both cold-drawing and hot-drawing of thin-walled tubing through a stationary die. For the solution of the fundamental equation, a method of successive improvement can be used for any contour of the tools and any shape of the stress-strain curve. Algebraic solutions were developed for tapered tools and for a metal exhibiting a constant flow stress in cold-working, and for a metal with the flow stress depending exponentially upon the strain rate in hot-working. The effects of the die and punch contours and the friction coefficients between the metal and the die and punch, respectively, on the stresses in the metal, the draw forces, and the limits of drawing were determined. The calculations reveal that, with a small die angle and high friction on the mandrel, the process resembles extrusion rather than drawing, the limit being determined by the strength of the die rather than by the tensile strength of the metal.

Introduction

THE drawing of a tubular part through a die with an inserted moving punch (mandrel or rod) has an extensive practical significance. While it is only infrequently used for the fabrication of tubing, it comprises a major portion of the drawing of cartridge cases, of high-explosive-shell bottles, and of other redrawing or "ironing" operations on cup-shaped parts.

The fundamental differential equation for this process can be derived readily and can be integrated for some special cases.[4] However, such a simple approach to the problem has not been found suitable for a complete evaluation of the effects of the numerous variables occurring in practice.

For example, it has been observed during some experimentation on cartridge cases that the reduction in cross-sectional area performable in a single draw may scatter or vary from 30 to over 90 per cent under certain conditions, while it may be consistent within ±3 per cent for other combinations of variables and may be as high as 75 per cent. A working theory of drawing tubing over a mandrel must eventually account for such disturbing observations.

The following discussion presents a new approach to this problem, and it should be applicable also to other problems of metal working. A method of gradual approach to the final solution has been developed, which permits evaluation of the effects of any variable.

So far, the theory has been developed only for tubing having a very thin wall. Extension of the theory to heavy-walled tubing is contemplated; and another future problem is the drawing of tubing through several dies in tandem.

The simple fundamental theory of tube-drawing[4] established a differential equation relating the longitudinal drawing force and the radial pressure. This equation has been solved for the case of a variable die angle by replacing the variable pressure on the surfaces by a mean pressure. A more accurate solution was developed for a die and mandrel having constant angles. In this case, however, it was necessary to make the additional assumption that the radial pressure is equal to the flow stress. In all the calculations of the previous paper,[4] the flow stress was assumed to be constant.

In this paper, the same fundamental differential equation will be solved by a different method which does not require the previous simplifying assumptions. The method involves a succession of approximations by means of graphical integration; and the solution may be made very nearly exact in five to seven repetitions of the process. Any combination of metal properties and tool contours may be treated with the aid of families of curves calculated for this purpose.

An algebraic solution will be developed for tools having straight tapers and a metal having a constant flow stress. This method offers the advantage of a direct numerical solution without recourse to successive approximations or graphical methods.

Other forming processes can be investigated in fundamentally the same manner, but they differ regarding the directions of the frictional forces. The friction may also change in sign over the length of the contact area, such as in drawing tubing through a roller die, in rolling strip (by means of tension or with driven rolls), and in forging.[5]

The Fundamental Equation of Equilibrium

Fig. 1 shows a longitudinal section through one wall of a thin-walled tube which is being drawn with a mandrel. The die and mandrel are shown with straight tapers, but the analysis based on this figure will be seen to apply equally well to tools with any contour. Consider an element of the tube cut out perpendicular to the axis at a distance x along the mandrel from the point where the tube first makes contact with the die. Let the tapers of the die and mandrel (half angles) at this point be α and β, respectively, let the friction coefficients of die and mandrel be μ_1

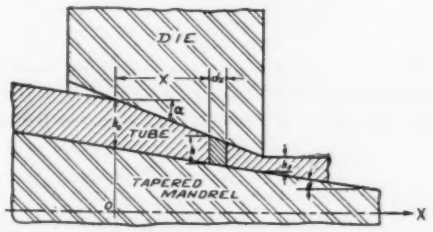


FIG. 1 SCHEMATIC DIAGRAM OF TUBE DRAWN WITH TAPERED MANDREL

[1] Case School of Applied Science, Department of Metallurgical Engineering, Cleveland, Ohio. Mem. A.S.M.E.

[2] Case School of Applied Science, Dept. Metallurgical Engineering.

[3] National Tube Company, Lorain, Ohio.

[4] "A Theory of Tube Drawing," by G. Sachs, *Modern Industrial Press*, June, 1942, pp. 25–28.

Presented at the National Meeting of the Applied Mechanics Division, Chicago, Ill., June 16-17, 1944, of THE AMERICAN SOCIETY OF MECHANICAL ENGINEERS.

Discussion of this paper should be addressed to the Secretary, A.S.M.E., 29 West 39th Street, New York, N. Y., and will be accepted until January 10, 1945, for publication at a later date. Discussion received after the closing date will be returned.

NOTE: Statements and opinions advanced in papers are to be understood as individual expressions of authors, not of the Society.

[5] "Limits of Forging," by G. Sachs, *Modern Industrial Press*, July, 1941, pp. 12–14.

and μ_2, respectively, and let the thickness of the tube wall be h. For the case of a thin-walled tube, the element can be considered to have unit width in a direction perpendicular to the plane of the figure.

The element, Fig. 2, has acting upon it a longitudinal force H, a normal pressure p, and shearing stresses

$$\tau_1 = p\mu_1, \qquad \tau_2 = p\mu_2 \ldots\ldots\ldots\ldots\ldots\ldots [1]$$

at the surfaces of the tools due to the effects of friction.

Any shearing forces on the vertical sides of the elements will not appear in the summation of longitudinal forces. For a thin-walled tube, the circumferential forces on the tube element can be neglected, and the normal pressures p can be assumed to be equal on both the die and the mandrel, as shown in Fig. 2. Also, the horizontal stress s and the normal pressure p are assumed to be principal stresses, for the purpose of integration, as shown later. This implies that the angles α and β are small. Therefore, the developed relations will become less exact the larger the tool angles are, and particularly if the difference between the two angles is large.

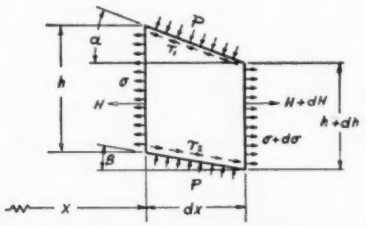


FIG. 2 ELEMENT OF THE TUBE AT POSITION x; SEE FIG. 1

The fundamental differential equation is obtained by the summation of forces in the longitudinal direction, Fig. 2

$$H + dH - H - p\frac{dx}{\cos\alpha}\sin\alpha + p\frac{dx}{\cos\beta}\sin\beta - \tau_1\frac{dx}{\cos\alpha}\cos\alpha + \tau_2\frac{dx}{\cos\beta}\cos\beta = 0 \ldots\ldots [2]$$

Inserting Equation [1] in Equation [2] and making minor simplifications, the desired differential equation is obtained

$$dH = pdx(\tan\alpha - \tan\beta + \mu_1 - \mu_2) = Cpdx \ldots\ldots [3]$$

where

$$C = \tan\alpha - \tan\beta + \mu_1 - \mu_2 \ldots\ldots\ldots\ldots [4]$$

In regular drawing (through a single die) no force is applied to the tube entering the die, i.e., for $x = 0$, $H = 0$. Then Equation [3] may be integrated between the limits $x = 0$ and $x = x$ as follows

$$\int_0^H dH = H = \int_0^x pCdx \ldots\ldots\ldots\ldots [5]$$

PART 1 COLD-DRAWING

SOLUTION OF DIFFERENTIAL EQUATION BY METHOD OF SUCCESSIVE IMPROVEMENT

In the general equation for cold-working, the two principal stresses may be correlated by the maximum-shear-stress theory[6]

$$\sigma + p = \sigma_0 \ldots\ldots\ldots\ldots\ldots\ldots [6]$$

[6] If the strain-energy theory is used, which is a more accurate approximation than the shear-stress theory, all stresses and forces would still be determined by the same equations. Differences would occur only when numerical values of the flow stress are used which were determined by means of tension or compression. In order to agree with the strain-energy theory, these values must be increased by 15 per cent if used in the equations developed in this section.

in which σ is the longitudinal stress and σ_0 is the flow stress or yield strength. For thin-walled tubing the longitudinal stress will be nearly uniformly distributed throughout the wall of the tube; therefore

$$\sigma = \frac{H}{h} \ldots\ldots\ldots\ldots\ldots\ldots [7]$$

Inserting Equation [7] in Equation [6], the force H is

$$H = \sigma_0 h - ph \ldots\ldots\ldots\ldots\ldots\ldots [8]$$

Eliminating H between Equation [8] and Equation [5] and solving for p

$$p = \sigma_0 - \frac{1}{h}\int_0^x pCdx$$

$$= \sigma_0 - \frac{1}{h}\int_0^x p\,(\tan\alpha - \tan\beta + \mu_1 - \mu_2)dx \ldots [9]$$

In this equation p, σ_0, h, C, α, and β may all be functions of x. The coefficients of friction, μ_1 and μ_2, can be considered generally as constant.

In order to solve Equation [9], a method of successive improvement has been developed. In this method, an arbitrary but reasonable pressure distribution p_1 is assumed, as a first approximation. The second and following approximations of the pressure, p_2, p_3, p_{n-1}, p_n are then obtained by graphical integration of the right side of Equation [9] as follows

$$\left.\begin{aligned} p_2 &= \sigma_0 - \frac{1}{h}\int_0^x p_1 Cdx \\ p_3 &= \sigma_0 - \frac{1}{h}\int_0^x p_2 Cdx \\ p_n &= \sigma_0 - \frac{1}{h}\int_0^x p_{n-1} Cdx \end{aligned}\right\} \ldots\ldots\ldots\ldots [10]$$

The pressure distribution can be obtained to any desired accuracy, which is determined by the difference $p_n - p_{n-1}$.

This method of successive improvement can be applied also to other forming problems, provided that the difference between two successive solutions becomes gradually smaller.

The application of this method to the drawing of tubing will be described first for the simplified condition of constant tool angles and a constant flow stress, and subsequently for the general condition.

Example 1. Metal exhibiting no strain-hardening, drawn through tapered die with straight mandrel:

The following values are then constant: α, β, and σ_0. For constant tool angles, the wall thickness h at each point becomes, Fig. 1

$$h = h_0 - x\,(\tan\alpha - \tan\beta) = h_0 - xD \ldots\ldots [11]$$

where

$$D = \tan\alpha - \tan\beta \ldots\ldots\ldots\ldots [12]$$

The fundamental Equation [9] then reduces to

$$p = \sigma_0 - \frac{C}{h_0 - xD}\int_0^x pdx \ldots\ldots [13]$$

For a constant flow stress σ_0 and no back tension on the tubing the pressure p_x will vary from σ_0 at $x = 0$ to zero at some value of $x = C_1 h_0$, as can be seen from Equation [13]. As a first approximation, p_1, a linear distribution of p, can be used that satisfies Equation [13] for $x = 0$ and $x = C_1 h_0$. The general equation for such a straight line is

$$\frac{p_1}{\sigma_0} = 1 - \frac{x}{C_1 h_0} \ldots\ldots\ldots\ldots [14]$$

TABLE 1 SOLUTION OF EQUATION [19]

x/h_0	$0.17633\,x/h_0$	$\frac{h}{h_0} = 1 - 0.17633\,\frac{x}{h_0}$	$\frac{p_1}{\sigma_0} = 1 - \frac{x}{h_0}(0.2895)$	$*Z_1$	$\frac{chs}{h} Z_1$	$\frac{p_2}{\sigma_0} = 1 - \frac{chs}{h} Z_1$	Z_2	$\frac{chs}{h} Z_2$	$\frac{p_3}{\sigma_0} = 1 - \frac{chs}{h} Z_2$
0.0	0.000	1.000	1.000	0.000	0.000	1.000	0.000	0.000	1.000
0.5	0.088	0.912	0.855	0.464	0.115	0.885	0.472	0.117	0.883
1.0	0.176	0.824	0.712	0.855	0.235	0.765	0.887	0.243	0.757
1.5	0.264	0.736	0.566	1.174	0.360	0.640	1.239	0.380	0.620
2.0	0.352	0.648	0.420	1.420	0.496	0.504	1.526	0.532	0.468
2.5	0.440	0.560	0.275	1.595	0.644	0.356	1.743	0.704	0.296
3.0	0.528	0.472	0.131	1.697	0.811	0.189	1.881	0.901	0.099
3.5	0.616	0.384	—0.014	1.725	1.015	—0.015	1.927	1.132	—0.132

x/h_0	Z_3	$\frac{chs}{h} Z_3$	$\frac{p_4}{\sigma_0} = 1 - \frac{chs}{h} Z_3$	Z_4	$\frac{chs}{h} Z_4$	$\frac{p_5}{\sigma_0} = 1 - \frac{chs}{h} Z_4$	Z_5	$\frac{chs}{h} Z_5$	$\frac{p_6}{\sigma_0} = 1 - \frac{chs}{h} Z_5$
0.0	0.000	0.000	1.000	0.000	0.000	1.000	0.000	0.000	1.000
0.5	0.472	0.117	0.883	0.472	0.117	0.883	0.472	0.117	0.883
1.0	0.892	0.245	0.755	0.892	0.245	0.755	0.892	0.245	0.755
1.5	1.237	0.380	0.620	1.237	0.380	0.620	1.237	0.380	0.620
2.0	1.509	0.526	0.474	1.511	0.528	0.472	1.511	0.528	0.472
2.5	1.700	0.686	0.314	1.709	0.690	0.310	1.709	0.690	0.310
3.0	1.800	0.863	0.137	1.823	0.874	0.126	1.821	0.872	0.128
3.5	1.793	1.057	—0.057	1.844	1.084	—0.084	1.835	1.080	—0.080

* Z_n throughout this table is a representation for the formula $Z_n = \int_0^{x/h_0} p_n \frac{dx}{h_0}$.

in which the unknown constant C_1 must be determined in accordance with Equation [13]. This is accomplished by substituting Equation [14] in Equation [13] and solving for C_1, yielding

$$C_1 = \frac{2}{C + 2D} \quad \text{[15]}$$

thus, the desired linear relation for use as a first approximation becomes

$$\frac{p_1}{\sigma_0} = 1 - \frac{x(C + 2D)}{2h_0} \quad \text{[16]}$$

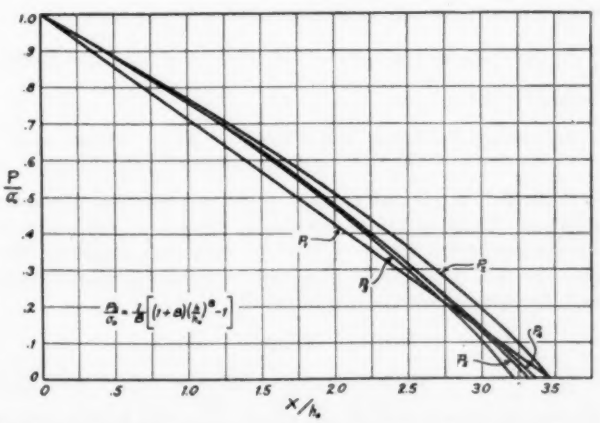


FIG. 3 GRAPHICAL SOLUTION FOR CONSTANT FLOW STRESS AND TOOL ANGLES

This function is plotted in Fig. 3, for an example possessing the following characteristic values

$$\left.\begin{aligned} &\alpha = 10 \text{ deg } (\tan \alpha = 0.176) \quad \beta = 0 \\ &\mu_1 = 0.15 \quad \mu_2 = 0.10 \\ &C = \tan \alpha - \tan \beta + \mu_1 - \mu_2 = 0.226 \\ &D = \tan \alpha - \tan \beta = 0.176 \end{aligned}\right\} \quad \text{[17]}$$

The first approximation, Equation [16], becomes

$$\frac{p_1}{\sigma_0} = 1 - \frac{x}{3.44\,h_0} \quad \text{[18]}$$

The second approximation p_2 is now obtained from the left member of the general Equation [13] by substituting p_1 for p in the right member

$$\frac{p_2}{\sigma_0} = 1 - \frac{0.226}{h_0 - 0.176x} \int_0^x \frac{p_1}{\sigma_0}\,dx \quad \text{[19]}$$

This equation can be solved graphically, as shown in Table 1 and Fig. 3. The procedure is then repeated by substituting p_2 in Equation [19] and obtaining p_3, and so forth, until a pressure distribution is obtained which satisfies the equation to the desired accuracy. For this particular example, five such steps were made, see Table 1 and Fig. 3.

Example 2. Copper drawn through radius die with straight mandrel:

Under these conditions the only values which are constant are β, μ_1, and μ_2. They can be grouped together

$$C_2 = -\tan \beta + \mu_1 - \mu_2 \quad \text{[20]}$$

resulting in the following form of the general Equation [9]

$$p = \sigma_0 - \frac{1}{h} \int_0^x p\,(\tan \alpha + C_2)\,dx \quad \text{[21]}$$

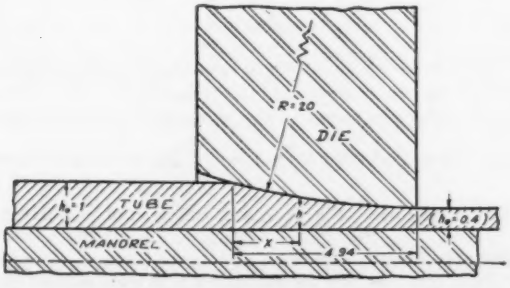


FIG. 4 CONDITIONS OF DRAWING FOR SAMPLE SOLUTION SHOWN IN FIG. 7, IN WHICH A TUBE IS REDUCED BY 60 PER CENT IN A RADIUS DIE

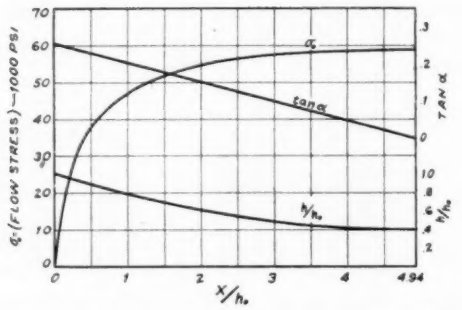


FIG. 5 VARIATION OF FLOW STRESS, DIE ANGLE, AND REDUCTION WITH x/h_0 IN EXAMPLE OF FIG. 4

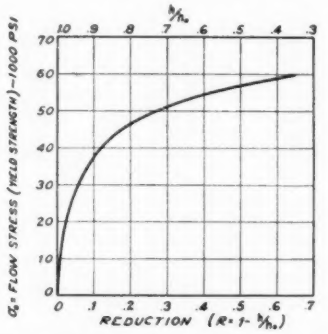


FIG. 6 STRESS-STRAIN CURVE FOR COPPER TUBING

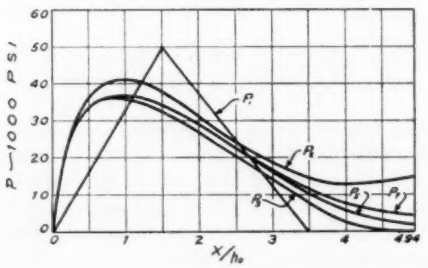


FIG. 7 GRAPHICAL SOLUTION OF PRESSURE DISTRIBUTION FOR COPPER TUBE REDUCED BY 60 PER CENT IN DIE HAVING RADIUS OF 20 TIMES ORIGINAL WALL THICKNESS OF TUBE

in which σ_0, h, and tan α are functions of x or, more conveniently for these calculations, functions of $\frac{x}{h_0}$. The wall thickness h and slope of the die contour tan α can be readily obtained from the geometry of the tools and tubing. For the example illustrated in Fig. 4, having a die radius of 20 in. and an initial wall thickness $h_0 = 1$ in., the values tan α and h have been calculated and plotted in Fig. 5, as functions of $\frac{x}{h_0}$.

The flow stress or yield strength σ_0 of copper can be determined by a tensile test as a function of the reduction in area, which can be considered as equivalent to the reduction in wall thickness on drawing thin-walled tube $R = 1 - \frac{h}{h_0}$, Fig. 6. From the values of σ_0, Fig. 6, and of $\frac{h}{h_0}$, Fig. 5, σ_0 as a function of $\frac{x}{h_0}$ can be readiy obtained and plotted, Fig. 5.

Equation [21] can now be solved by a process similar to that used for the first example. Again a linear function may be used as a first approximation to the pressure p_1; but in order to reduce the calculations, it should consist of two branches, i.e., first increase from a value at $x = 0$ equal to the yield strength, which is close to zero for annealed copper, to a maximum corresponding to an average value of flow stress at an arbitrary position, and then again drop to zero at a value of $\frac{x}{h_0}$ which is arbitrary but not too distant from the exit, Fig. 4. More definite rules cannot be given for the selection of the first approximation. The further approximations p_2, p_3, etc., are then obtained by exactly the same procedure as described for Example 1, see Table 2 and Fig. 7. For the selected example, seven steps were carried out in this manner.

In Fig. 8, the pressures within the die for the two examples.

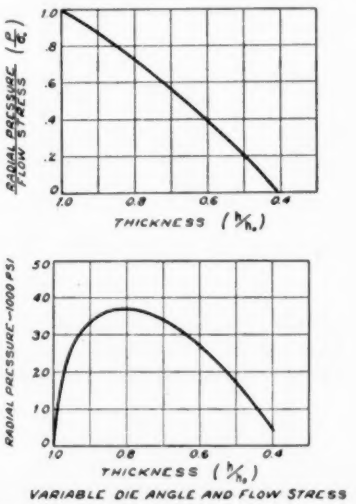


FIG. 8 RADIAL PRESSURE AS A FUNCTION OF WALL THICKNESS FOR TWO ASSUMPTIONS REGARDING VARIATION OF FLOW STRESS AND TOOL ANGLES

Figs. 3 and 7, are represented as functions of the thickness ratio $\frac{h}{h_0}$, rather than as functions of the distance x from the entering side of the die.

ALGEBRAIC SOLUTION FOR CONSTANT FLOW STRESS AND CONSTANT TOOL ANGLES

If the flow stress and the tool angles are assumed to remain constant (Example 1) it is possible to develop a formula for p, the die pressure at any point, without recourse to graphical integration. The following relations then correlate the co-ordinate x and the metal thickness h, see Equation [11]

$$h = h_0 - x\,(\tan\alpha - \tan\beta)$$

$$dh = -(\tan\alpha - \tan\beta)dx \qquad [22]$$

Also the horizontal force H, the flow stress σ_0, the thickness, and the pressure are related by, see Equation [8]

$$H = \sigma_0 h - ph$$

$$dH = \sigma_0 dh - pdh - hdp \qquad [23]$$

Substituting the value of dx from Equation [22] and of dH from Equation [23] into the fundamental differential Equation [3], the following equation is obtained

$$\sigma_0 dh - pdh - hdp = -pdh\,\frac{(\tan\alpha - \tan\beta + \mu_1 - \mu_2)}{\tan\alpha - \tan\beta}$$

$$= -pdh(1 + B) \qquad [24]$$

TABLE 2 SOLUTION OF EQUATION [21]

$\frac{x}{h_0}$	$\tan\alpha + c_2$	$\frac{h}{h_0}$	σ_0	p_1	$p_1(\tan\alpha + c_2)$	$^*Y_1$	$\frac{h_0}{h} Y_1$
0.25	0.291	0.955	26500	8700	2500	300	300
0.50	0.278	0.889	37500	17300	4800	1300	1400
1.00	0.251	0.795	47000	34600	8700	4700	5900
1.50	0.224	0.701	51500	51800	11600	10000	14000
2.00	0.199	0.623	54200	38900	7700	14600	23500
3.00	0.147	0.494	57200	13100	1900	19200	38400
3.50	0.122	0.450	58000	0	0	19600	43700
4.00	0.097	0.420	58500	—13100	—1300	19300	45900
4.50	0.072	0.408	58800	—26100	—1900	18400	45000
5.00	0.050	0.400	59000	—38900	—1950	17600	44000

$\frac{x}{h_0}$	$p_2 = \sigma_0 - \frac{h_0}{h} Y_1$	$p_2(\tan\alpha + c_2)$	Y_2	$\frac{h_0}{h} Y_2$	$p_3 = \sigma_0 - \frac{h_0}{h} Y_2$	$p_3(\tan\alpha + c_2)$	Y_3
0.25	26200	7600	1200	1200	25300	7400	1100
0.50	36100	10000	3500	3900	33600	9300	3200
1.00	41000	10300	8700	11000	36000	9000	7900
1.50	37500	8400	13400	19200	32300	7200	11900
2.00	30700	6300	17100	27600	26600	5300	15000
2.50	24000	4200	19700	35800	20200	3500	17200
3.00	18800	2800	21500	43000	14200	2100	18600
3.50	14300	1700	22600	50200	7800	1000	19400
4.00	12600	1200	23400	55800	2700	300	19700
4.50	13800	1000	23900	58400	400	20	19900
5.00	15000	750	24300	60800	—1800	—40	19900

$\frac{x}{h_0}$	$\frac{h_0}{h} Y_3$	$p_4 = \sigma_0 - \frac{h_0}{h} Y_3$	$p_4(\tan\alpha + c_2)$	Y_4	$\frac{h_0}{h} Y_4$	$p_5 = \sigma_0 - \frac{h_0}{h} Y_4$	$p_5(\tan\alpha + c_2)$
0.25	1200	25300	7400	1100	1200	25300	7400
0.50	3600	33900	9400	3300	3700	33800	9400
1.00	10000	37000	9300	8100	10200	36800	9250
1.50	17000	34500	7700	12400	17400	34100	7650
2.00	24100	30100	6000	15800	25400	28800	5700
2.50	31200	24800	4300	18400	33400	22600	3900
3.00	37400	19800	2900	20200	41000	16200	2400
3.50	43100	14900	1800	21400	47600	10400	1300
4.00	46900	11600	1100	22100	52600	5900	600
4.50	48700	10100	700	22600	55400	3400	200
5.00	49800	10200	500	22900	57200	1800	0

$\frac{x}{h_0}$	Y_5	$\frac{h_0}{h} Y_5$	$p_6 = \sigma_0 - \frac{h_0}{h} Y_5$	$p_6(\tan\alpha + c_2)$	Y_6	$\frac{h_0}{h} Y_6$	$p_7 = \sigma_0 - \frac{h_0}{h} Y_6$
0.25	1100	1200	25300	7400	1100	1200	25300
0.50	3300	3700	33800	9400	3300	3700	33800
1.00	8100	10200	36800	9250	8100	10200	36800
1.50	12400	17400	34100	7650	12400	17400	34100
2.00	15700	25200	29000	5800	15800	25300	28900
2.50	18100	32800	23200	4000	18300	33200	22800
3.00	19700	39900	17300	2500	19900	40300	16900
3.50	20600	45800	12200	1500	20900	46500	11500
4.00	21100	50200	8300	800	21500	51200	7300
4.50	21300	52200	6600	500	21800	53400	5400
5.00	21400	53600	5400	300	22000	55000	4000

* Y_n throughout this table is a representation for the formula $Y_n = \int^{x/h_0} p_n(\tan\alpha + c_2)\frac{dx}{h_0}$.

where

$$B = \frac{\mu_1 - \mu_2}{\tan\alpha - \tan\beta} \quad [25]$$

The resulting differential equation

$$\frac{dh}{h} = \frac{dp}{\sigma_0 + pB} \quad [26]$$

yields the final solution for the boundary condition

$$h = h_0, \quad H = 0, \quad p = \sigma_0$$

$$\int_{h_0}^{h} \frac{dh}{h} = \int_{\sigma_0}^{p} \frac{dp}{\sigma_0 + pB} \quad [27]$$

$$\ln\frac{h}{h_0} = \frac{1}{B}\ln\frac{\sigma_0 + Bp}{\sigma_0 + B\sigma_0} \quad [28]$$

$$\frac{p}{\sigma_0} = \frac{1}{B}\left[(1+B)\left(\frac{h}{h_0}\right)^B - 1\right] \quad [29]$$

Equation [29] may be used to check the graphical method developed in the previous section. Fig. 3 gives the distribution of the pressure p for the case of a constant flow stress σ_0 and the numerical values of other constants given by Equation [18]. In this case $B = 0.2839$ and inserting this value of B and the value of h from Equation [22] into Equation [29], the following numerical relation is obtained

$$\frac{p}{\sigma_0} = \frac{1}{0.2839}\left(1.2839\left[1 - \frac{x}{h_0}(\tan\alpha - \tan\beta)\right]^{0.2839} - 1\right) \quad [30]$$

Using the values of [18] again

$$\frac{p}{\sigma_0} = \frac{1}{0.2839}\left[1.2839\left(1 - 0.17633\frac{x}{h_0}\right)^{0.2839} - 1\right] \quad [31]$$

This has been solved by tabular substitution in Table 3. By comparing these values of p with those in the last column of Table 1, it can be seen that the fifth approximation of the graphical solution is very nearly exact.

By introducing Equation [6] into Equation [29], the horizontal stress is found to be

$$\frac{\sigma}{\sigma_0} = 1 - \frac{p}{\sigma_0} = \frac{1+B}{B}\left[1 - \left(\frac{h}{h_0}\right)^B\right] \quad [32]$$

Total Draw Force

The total draw force F is the sum of the horizontal forces on the tubing F_1, and on the mandrel F_2. For convenience, these forces will be considered per unit circumference of the tubing.

The force on the tubing, having the thickness h_1 at the exit, is, according to Equation [32]

TABLE 3 SOLUTION OF EQUATION [31]

s/h_0	$0.17633\,s/h_0$	$1-0.17633\,s/h_0$	$\frac{1.2839}{\left(1-0.17633\,s/h_0\right)^{0.2839}}$	$\frac{1.2839}{\left(1-0.17633\,s/h_0\right)^{0.2839}}-1$	p/σ_0
0.0	0	1.00000	1.2836	0.2836	1.000
0.5	0.08816	0.91184	1.2504	0.2504	0.884
1.0	0.17633	0.82367	1.2149	0.2149	0.758
1.5	0.26449	0.73551	1.1770	0.1770	0.625
2.0	0.35266	0.64734	1.1347	0.1347	0.475
2.5	0.44082	0.55918	1.0886	0.0886	0.312
3.0	0.52899	0.47101	1.0368	0.0368	0.130
3.5	0.61715	0.38285	0.9777	−0.0223	−0.079

$$F_1 = \sigma_e h_e = \frac{\sigma_0 h_e}{B}(B+1)\left[1-\left(\frac{h_e}{h_0}\right)^B\right] \quad [33]$$

The force on the mandrel according to Fig. 2 is

$$F_2 = (\tan\beta + \mu_2)\int_0^{x_e} p\,dx \quad [34]$$

To integrate Equation [34], the variable x can be replaced by h, see Equations [11] and [22]

$$F_2 = \frac{\tan\beta+\mu_2}{D}\int_0^{h_e} p\,dh \quad [35]$$

and with Equation [29], the final differential equation is obtained

$$F_2 = \frac{\tan\beta+\mu_2}{D}\int_{h_0}^{h_e} dh\,\frac{1}{B}\left[(1+B)\left(\frac{h}{h_0}\right)^B - 1\right] \quad [36]$$

The solution of this equation is

$$F_2 = \frac{\sigma_0 h_e \tan\beta+\mu_2}{BD}\left[1-\left(\frac{h_e}{h_0}\right)^B\right] \quad [37]$$

The total draw force then becomes

$$\left.\begin{aligned}\frac{F}{\sigma_0 h_e} &= \frac{F_1+F_2}{\sigma_0 h_e} = \frac{\tan\alpha+\mu_1}{\mu_1-\mu_2}\left[1-\left(\frac{h_e}{h_0}\right)^B\right]\\ \frac{F}{\sigma_0 h_0} &= \frac{\tan\alpha+\mu_1}{\mu_1-\mu_2}\left[\frac{h_e}{h_0}-\left(\frac{h_e}{h_0}\right)^{B+1}\right]\end{aligned}\right\} \quad [38]$$

The last expression, yielding the "draw stress," related to the cross-sectional area of the tubing on entering the die, is preferred frequently; and values of this draw stress, for certain combinations of the variables, are illustrated in Figs. 11 to 14, inclusive. Equations [38] are indeterminate when $\mu_1 = \mu_2$.

The analysis must be revised for this case from the point where the quantity $\mu_1 - \mu_2$ first appears, see Equation [26]. For the case of $\mu_1 = \mu_2$, $B = 0$, see Equation [25]; and Equation [26] becomes

$$\frac{dh}{h} = \frac{dp}{\sigma_0} \quad [39]$$

Noting that when $h = h_0$, $p = \sigma_0$

$$\int_{h_0}^{h}\frac{dh}{h} = \int_{\sigma_0}^{p}\frac{dp}{\sigma_0} \quad [40]$$

$$\ln\frac{h}{h_0} = \frac{p}{\sigma_0} - 1 \quad [41]$$

$$\frac{p}{\sigma_0} = 1 + \ln\frac{h}{h_0} \quad [42]$$

Using Equation [42] rather than Equation [29] as a starting point, and proceeding with the same analysis as that used in developing Equations [29] through [37], the value of F is found to be, for the special case of $\mu_1 = \mu_2$

$$\left.\begin{aligned}\frac{F}{\sigma_0 h_e} &= \left[\frac{\tan\alpha+\mu_1}{\tan\alpha-\tan\beta}\right]\ln\left(\frac{h_0}{h_e}\right)\\ \frac{F}{\sigma_0 h_0} &= \left[\frac{\tan\alpha+\mu_1}{\tan\alpha-\tan\beta}\right]\frac{h_e}{h_0}\ln\left(\frac{h_0}{h_e}\right)\end{aligned}\right\} \quad [43]$$

Effects of Processing Variables on Stresses

For the simplified case of straight tapered tools and a metal possessing a constant flow stress, the foregoing equations may be used to produce a graphical representation of the dependence of the stress distribution during drawing thin-walled tubing upon variations of the processing conditions.

The stress state is described at each section of the tubing by the die pressure p, assumed to be the same on both the outer and inner surface of the tubing, and the longitudinal or horizontal stress σ, assumed to be uniformly distributed over the thickness.

The most important independent variables which determine the stresses are the half die angle α, the half angle of mandrel angle β, and the friction coefficients between die and tubing μ_1 and mandrel and tubing μ_2. For a given combination of these variables and for a given flow stress σ_0, the stresses in the metal depend upon the reduction in wall thickness or in cross-sectional area R

$$R = \frac{h_0 - h_e}{h_0} \quad [44]$$

The die pressure has been calculated according to Equation [29] for numerous combinations of these variables, Figs. 9 and 10. The friction coefficients enter into these equations only as their difference, $u = \mu_1 - \mu_2$. The tool tapers also occur only in the combination $\tan\alpha - \tan\beta$. The examples are represented for a cylindrical mandrel, $\beta = 0$, but also apply to any other condition in which the value $\tan\alpha - \tan\beta$ is the same as the value of $\tan\alpha$ in the illustrations.

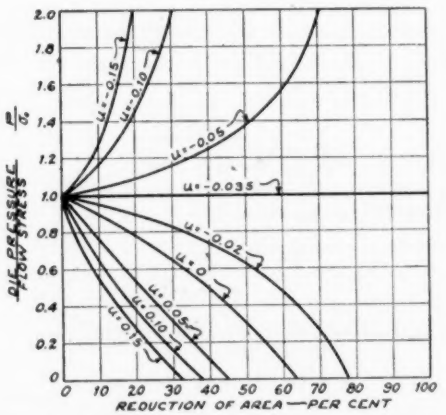


FIG. 9 EFFECT OF FRICTION AND REDUCTION ON DIE PRESSURE FOR α = 2 DEG, β = 0 DEG

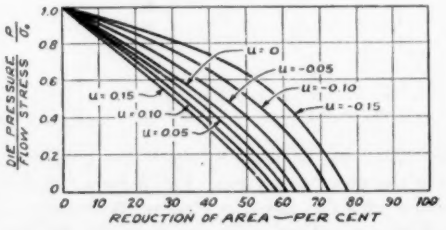


FIG. 10 EFFECT OF FRICTION AND REDUCTION ON DIE PRESSURE FOR α = 15 DEG, β = 0 DEG

The effect of the variables α, u, and R on the die pressure is shown in Fig. 9 as a function of the reduction R for $\alpha = 2$ deg, and in Fig. 10 for $\alpha = 15$ deg, each figure employing a family of curves to represent the effect of different values of u. These graphs illustrate that the die pressure gradually decreases with increasing reduction as the metal passes through the die, for the usual commercial conditions, in which the die and mandrel friction coefficients are approximately equal (i.e., their difference small), and the die angle is not too small, Fig. 10.

If, however, the mandrel friction is high in comparison to the die friction, i.e., their difference u is negative, and if its absolute value is larger than tan α (or tan α — tan β), the die pressure increases with increasing reduction, Fig. 9. Such a process is similar to "extrusion" rather than drawing. It results from the opposing actions of die and mandrel. As the metal proceeds through the die, a component of longitudinal tension is built up resisting the friction against the die and the longitudinal component of the normal pressure at the working face of the die. On the other hand, a component of a longitudinal compression in the tubing is created because of friction against the mandrel. If the latter effect exceeds the former, the metal is pushed or "extruded" rather than drawn through the die, Fig. 9. It is interesting to note from Fig. 9 that a rather small variation in friction, from $u = 0$ to $u = -0.05$, will cause a radical change in the pressure distribution if the die angle is very small. This effect will be discussed in greater detail later.

The longitudinal stress σ is readily obtained from the pressure p by means of the condition of plasticity Equation [6], $\sigma = \sigma_0 - p$. Thus the curves in Figs. 9 and 10 also represent the longitudinal stress in the die (right-hand scale) as a function of the reduction in wall thickness. Fig. 9 illustrates the difference between drawing under conditions where longitudinal tension is present, varying gradually from zero at the entering side of the die to a value equal to the flow stress σ_0 at a certain reduction, and where longitudinal compression (extrusion) is present, beginning at zero at the entering side of the die and increasing at a steadily accelerating rate.

Effect of Processing Variables on Draw Force

The total draw force, according to Equations [38] and [43], generally increases with increasing (total) reduction in wall thickness, increasing friction between tube and tools, and decreasing die angle, Figs. 11 to 14, inclusive.

Fig. 11 shows that the total draw force may increase with increasing reduction in various manners. It will be noted from Equations [38] that when $B = -1$, the relation between total draw force and reduction becomes linear. For the conditions of Fig. 11, $B = -1$ when $\mu_2 = 0.10$, and the corresponding curve is then a straight line.

If μ_2 is larger than 0.10, or B smaller than —1, the draw force increases continuously with increasing reduction, at a gradually increasing rate. Such conditions represent the previously discussed case of "extrusion" where the longitudinal stress in the tubing is compression.

However, if μ_2 is smaller than 0.10, or B larger than —1, the draw force will reach a maximum at a certain reduction, according to Equations [38] or [43]. For such conditions, where the longitudinal stress is tension, the draw force for reductions beyond the maximum point has no physical significance, as can be seen from the subsequent analysis. The reduction of area corresponding to the maximum in the total drawing-force curves can be found by differentiating Equations [38] with respect to h_e and setting the left side equal to zero

$$\frac{dF}{dh_e} = 0 = \frac{d}{dh_e}\left[\sigma_0 h_e \frac{\tan\alpha + \mu_1}{\mu_1 - \mu_2}\right]\left[1 - \left(\frac{h_e}{h_0}\right)^B\right] \quad \ldots [45]$$

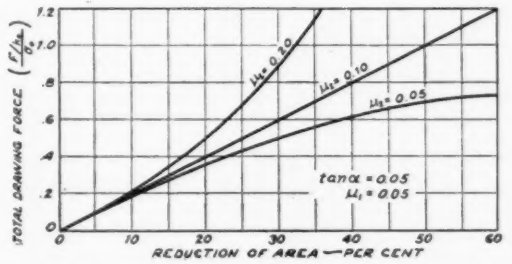


Fig. 11 Effect of Reduction of Area and Mandrel Friction on Total Drawing Force

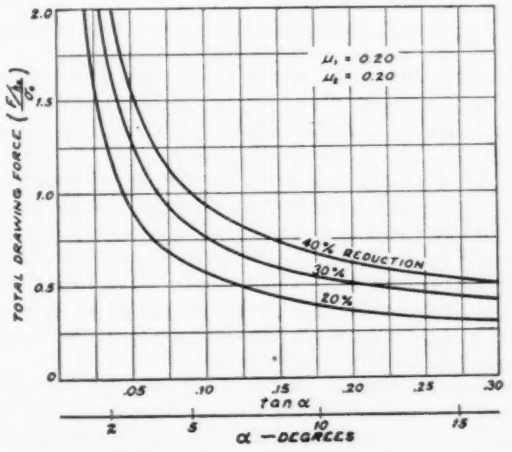


Fig. 12 Effect of Die Angle and Reduction of Area on Total Drawing Force

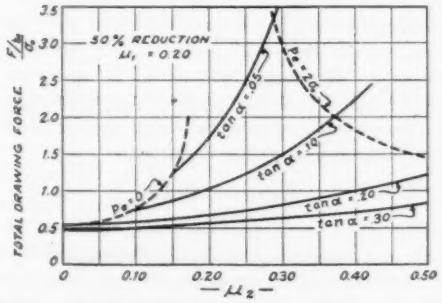


Fig. 13 Effect of Mandrel Friction and Die Angle on Total Drawing Force

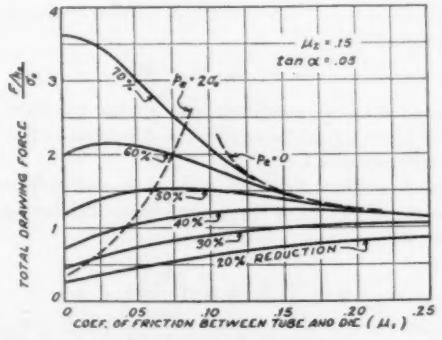


Fig. 14 Effect of Die Friction and Reduction of Area on Total Drawing Force

This yields the value of the reduction at the point of maximum force

$$\frac{h_0 - h_e}{h_0} = 1 - \left(\frac{1}{1+B}\right)^{1/B} \text{ or } \frac{h_e}{h_0} = \left(\frac{1}{1+B}\right)^{1/B} \quad [46]$$

This, however, is the same value of h_e at which the die pressure becomes zero, or changes from compression to tension, according to Equation [29] (see later). For a greater reduction than that corresponding to Equation [46], there is no longer any contact between the die and the tubing and any equation involving frictional relationships is not applicable.

The effect of the die angle on the total draw force is shown in Fig. 12, for various reductions, the friction coefficients being identical, i.e., 0.20 for both die and mandrel. The die angle has little effect except for very small angles, in which case the draw force increases rapidly as the die angle approaches zero. This is to be expected from the fact that, for a given reduction, a longer contact area is required for a smaller die angle; and the frictional force opposing the draw force increases in proportion to the contact length.

This effect may be minimized by the influence of the other variables. If the total draw force is large, because of a small die angle, the force can be reduced by decreasing the reduction, Fig. 11, or by decreasing the coefficient of friction between the tubing and mandrel, Fig. 13. Decreasing the mandrel friction is of particular advantage in the case of a small die angle, but there is a limit to the amount that the drawing force can be reduced by this means, as will be shown later.

Reducing the friction coefficient between the tube and die may or may not decrease the total drawing force, Fig. 14, depending upon the reduction. For small reductions, increasing the die friction causes the expected increase of draw force. However, for reductions exceeding a certain value, the total draw force may decrease with increasing die friction. This is explained by the fact that when the die friction becomes small in comparison to the mandrel friction, the die pressure and the resulting frictional force become very high, even though the friction coefficient decreases. The rapid increase of die pressure with decreasing die friction is caused by the previously discussed phenomenon that the process becomes extrusion rather than drawing, for certain combinations of the variables.

Drawing Limits

In drawing processes of various types, the limit of reduction performable in a single draw is usually determined by the condition that the longitudinal stress at the exit cannot exceed the strength of the metal. For a metal which does not exhibit strain-hardening, as was assumed here, the highest possible value of longitudinal stress σ_e, at the exit, cannot exceed the flow stress σ_0, or the pressure at the exit p_e cannot be smaller than zero, as previously discussed. This limiting condition is expressed by the following equations

$$\sigma_e = \sigma_0, \quad p_e = 0 \quad [47]$$

This tension-failure condition also applies to drawing tubing with a moving mandrel for certain combinations of the variables, as previously discussed.

The limiting value of reduction R_{max}, or wall thickness at the exit $h = h_e$, is obtained from Equation [29] by substituting Equations [47], as mentioned previously

$$p_e = 0 = \frac{\sigma_0}{B}\left[(1+B)\left(\frac{h_e}{h_0}\right)^B - 1\right] \quad [48]$$

$$\frac{h_e}{h_0} = \left(\frac{1}{1+B}\right)^{1/B} \quad [49]$$

$$R_{max} = \frac{h_0 - h_e}{h_0} = 1 - \left(\frac{1}{1+B}\right)^{1/B} \quad [50]$$

The effect of several variables on this drawing limit, or "drawability," i.e., the maximum reduction performable in a single draw, is illustrated in Figs. 15 and 16 (curves $p_e = 0$). These

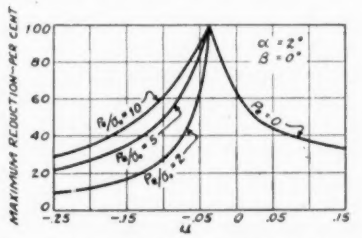


Fig. 15 Effect of Varying Flow Stress on Maximum Possible Reduction for Constant Limiting Die Pressure

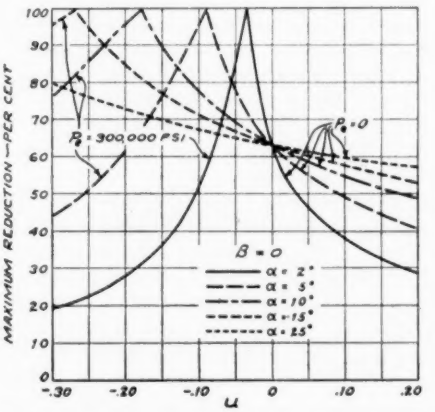


Fig. 16 Limiting Reductions in Cold-Drawing of Mild-Steel Tubing Without Failure in Tension ($P_e/\sigma_0 = 0$) or Failure of Die by Internal Pressure ($P_e/\sigma_0 = 300{,}000/55{,}000 = 5.46$)

figures indicate that a large increase in drawability may be obtained by increasing the friction on the mandrel over that on the die (negative values of u), particularly if the die angle is small. Also, small variations in friction may cause very large scattering of the reductions for an acute die angle.

While in other drawing processes the draw force cannot exceed the strength of the metal, the total draw force for drawing tubing with a stationary mandrel may become considerably higher if the die angle is small (or the difference between die and mandrel tapers is small), and the mandrel friction exceeds the die friction. This is illustrated in Figs. 13 and 14 for certain ranges of the processing variables.

These graphs, however, also illustrate the previously discussed fact that, within other ranges of the processing variables, no longitudinal tension exists and, consequently, that a tension failure cannot determine the drawability. It has also been discussed previously that the die pressure may then become very high; this would cause the die to rupture (by internal pressure) rather than cause the tubing to fail in tension. Assuming that the die will permit a maximum die pressure at the exit p_e that is a multiple n of the flow stress

$$p_e = n\sigma_0 \quad [51]$$

the following limiting condition is obtained from Equation [29]

$$p_e = n\sigma_0 = \frac{\sigma_0}{B}\left[(1+B)\left(\frac{h_e}{h_0}\right)^B - 1\right] \quad [52]$$

$$\frac{h_e}{h_0} = \left(\frac{1 + nB}{1 + B}\right)^{1/B} \quad \ldots\ldots\ldots\ldots\ldots [53]$$

The general effect of such a limiting condition of the total draw force is illustrated in Figs. 13 and 14 for $n = 2$, while Fig. 15 shows the influence of some processing variables on the drawing limit, or maximum reduction, performable in a single draw for dies of various strength, $n = \frac{p_e}{\sigma_0} = 2$, 5, and 10. A further example is represented in Fig. 16, for the drawing of mild steel, $\sigma_0 = 55{,}000$ psi, and a maximum die pressure taken arbitrarily as $p_e = 300{,}000$ psi. For these values, Equation [53] becomes

$$1 - \frac{h_e}{h_0} = 1 - \left(\frac{1 + 5.46B}{1 + B}\right)^{1/B} \quad \ldots\ldots\ldots\ldots [54]$$

The two possible limiting conditions, tension failure in the metal and bursting of the die, determine the drawability of tubing on drawing with a stationary mandrel in a rather peculiar manner, according to Figs. 15 and 16. Within a narrow range of tool shapes and frictional conditions, a reduction of almost 100 per cent appears possible, and this has been actually observed during experimentation, both on the drawing of cartridge cases and on drawing copper tubing with a moving mandrel.

PART 2 HOT-DRAWING

General Solution

The characteristic feature of hot-forming is that the flow stress depends primarily upon the rate of strain, while the influence of the amount of strain (strain-hardening) can be considered as negligible.

In order to develop an algebraic solution for the fundamental equation of equilibrium, Equation [3], for the hot-drawing of thin-walled tubing, therefore, the influence of the strain rate upon the flow stress must be known in the form of a simple relation, and the strain rate within the die must be expressed as a function of the velocity of the metal at the exit and the contours of the tools.

According to experimentation on the extrusion of brass,[7] Fig. 17, and according to high-temperature tensile tests on steel,[8] Fig. 18, the effect of velocity on the flow stress during hot-forming can be expressed as an exponential function. The tests on steel yield the flow stress σ_0 directly as a function of the strain rate $\frac{d\epsilon}{dt}$, taking the flow stress as equal to the tensile strength

$$\sigma_0 = a\left(\frac{d\epsilon}{dt}\right)^b \quad \ldots\ldots\ldots\ldots\ldots [55]$$

where a and b are constants, depending upon the metal and the temperature. Apparently the exponent b decreases and the coefficient a increases with decreasing temperature, Fig. 18.

The strain rate within the die is a function of the velocity V_e at which the metal comes out of the die, and the position x of the section considered, depending upon the geometry of the die, Fig. 2. Let the velocity at this point be V, and the velocity of a point dx farther be $(V + dV)$. Within a small interval of time dt, the point originally at x moves a distance Vdt and the point originally at $(x + dx)$ moves a distance $(V + dV)dt$. The change in length (d^2x) of the element dx, within the time interval dt, is then

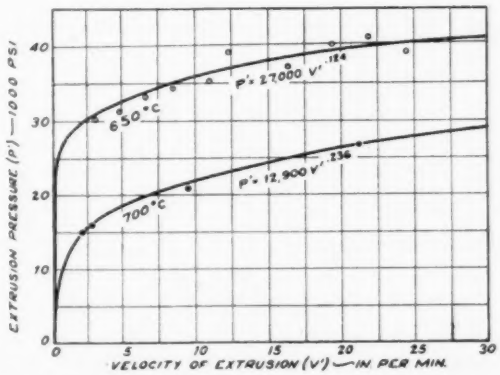


FIG. 17 EFFECT OF EXTRUSION RATE ON PRESSURE FOR 58 PER CENT CU, 42 PER CENT ZN BRASS BILLETS
(7-in-diam billets extruded to 2-in-diam rods.)

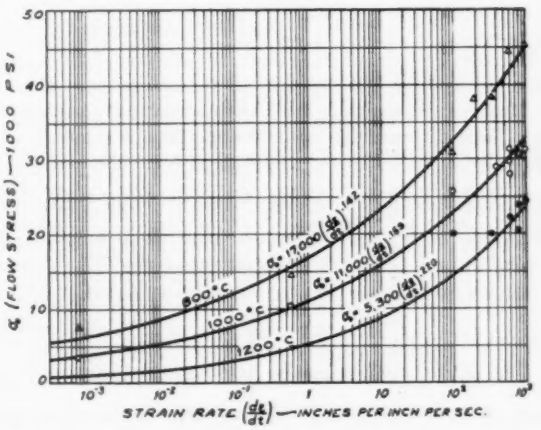


FIG. 18 EFFECT OF STRAIN RATE ON TENSILE STRENGTH, I.E., FLOW STRESS OF MILD STEEL[7]

$$d^2x = (V + dV)dt - Vdt + dVdt \quad \ldots\ldots\ldots [56]$$

The strain $d\epsilon$ is correspondingly

$$d\epsilon = \frac{d^2x}{dx} = \frac{dVdt}{dx} \quad \ldots\ldots\ldots\ldots [57]$$

and the strain rate $\frac{d\epsilon}{dt}$ becomes

$$\frac{d\epsilon}{dt} = \frac{dV}{dx} \quad \ldots\ldots\ldots\ldots [58]$$

Thus the strain rate at any point is the derivative of the velocity at that point.

Considering that the volume of the metal does not change during plastic flow, the following relation applies

$$Vh = V_e h_e \quad \ldots\ldots\ldots\ldots [59]$$

$$V = \frac{V_e h_e}{h} \quad \ldots\ldots\ldots\ldots [60]$$

Differentiating with respect to h yields the equation

$$\frac{dV}{dh} = -\frac{V_e h_e}{h^2} \quad \ldots\ldots\ldots\ldots [61]$$

According to Fig. 2, for any tool contour

$$dh = -dx\,(\tan\alpha - \tan\beta) \quad \ldots\ldots\ldots\ldots [62]$$

[7] "Practical Metallurgy," by G. Sachs and K. R. Van Horn, American Society for Metals, 1940, p. 373.

[8] "Plastic States of Stress in Curved Shells; Forging of Steel Shells," by A. Nadai, special pamphlet, "Forging of Steel Shells," Trans. A.S.M.E., 1944. See index to that volume.

The strain rate then becomes, combining Equations [58], [61], and [62]

$$\frac{d\epsilon}{dt} = \frac{V_s h_s}{h^2}(\tan\alpha - \tan\beta) \quad [63]$$

$$= \frac{V_s h_s D}{h^2}$$

and the flow stress Equation [55] is

$$\sigma_0 = a\left(\frac{v_s h_s D}{h^2}\right)^b \quad [64]$$

With this value of σ_0, the fundamental differential Equation [9] for the die pressure p becomes

$$\left.\begin{aligned} p &= \sigma_0 - \frac{1}{h}\int_0^x pC\,dx \\ p &= a\left(\frac{V_s h_s D}{h^2}\right)^b - \frac{1}{h}\int_0^x x_0 pC\,dx \end{aligned}\right\} \quad [65]$$

In order to solve this equation for the general case of curved tool contours, the variables must be first determined as functions of x. Then the resulting equation in p and x may be solved graphically in the same way as described for cold-working.

Algebraic Solution for Constant Tool Angles

If the tool angles α and β are constant, an algebraic solution can be obtained using the following relations: The horizontal force H is subject to the shear-stress relation Equation [8]

$$H = \sigma_0 h - ph$$

$$dH = \sigma_0 dh + h d\sigma - p dh - h dp \quad [66]$$

Replacing dx in Equation [3] by the value derived from Equations [11] and [22] yields the desired fundamental equation

$$dH = C p dx = -\frac{C}{D} p dh \quad [67]$$

$$\sigma_0 dh - h d\sigma_0 - p dh - h dp = \frac{C}{D} p dh \quad [68]$$

$$\frac{dp}{dh} - \frac{Bp}{h} = \frac{\sigma_0}{h} + \frac{d\sigma_0}{dh} \quad [69]$$

using the relation

$$\frac{C}{D} - 1 = \frac{(\tan\alpha - \tan\beta + \mu_1 - \mu_2) - (\tan\alpha - \tan\beta)}{\tan\alpha - \tan\beta} = B \quad [70]$$

The derivate $\frac{d\sigma_0}{dh}$ is obtained by differentiating Equation [64]

$$\frac{d\sigma_0}{dh} = -\frac{2ab(V_s h_s)^b}{h^{2b+1}} \quad [71]$$

Introducing σ_0 from Equation [64] and $\frac{d\sigma_0}{dh}$ from Equation [71] into Equation [69] yields the desired differential equation

$$\frac{dp}{dh} - \frac{Bp}{h} = a\frac{(1-2b)}{h^{2b+1}}(V_s h_s D)^b \quad [72]$$

This is a linear differential equation, the solution of which is

$$p = h^B\left[-\frac{a(1-2b)(V_s h_s D)^b}{(B+2b)h^{B+2b}} + c_3\right] \quad [73]$$

The constant of integration c_3 can be determined from the fact that at the entering side of the die $x = 0$, $h = h_0$, and the die pressure is equal to the flow stress σ'_0 at this point. The flow stress, of course, is a function of h, and its value at the entering side of the die can be determined by substituting $h = h_0$ in Equation [64]

$$\sigma_0' = a\left(\frac{V_s h_s D}{h_0^2}\right)^b \quad [74]$$

Substituting $h = h_0$ and $p = \sigma'_0$ in Equation [73] and solving for c_3 gives

$$c_3 = \frac{a(1+B)(V_s h_s D)^b}{(B+2b)h_0^{B+2b}} \quad [75]$$

Substituting Equation [75] in Equation [73], simplifying by the use of Equation [74], and solving for p yield the final equation

$$\frac{p}{\sigma_0'} = \frac{1}{B+2b}\left[(1+B)\left(\frac{h}{h_0}\right)^B - (1-2b)\left(\frac{h_0}{h}\right)^{2b}\right] \quad [76]$$

Equation [76] also includes the case of cold-drawing of a metal, with a constant flow stress σ_0 as a special case. For $\sigma_0' = \sigma_0$, $b = 0$ and Equation [76] reduces to Equation [29].

The physical significance of the quantity σ_0' is that it represents the flow stress of the metal under the strain-rate conditions prevailing on entering the die. As previously discussed, the flow stress is a function of the strain rate $\frac{d\epsilon}{dt}$, and the strain rate at the entering side of the die, where $h = h_0$, is, according to Equation [55]

$$\left(\frac{d\epsilon}{dt}\right)_b = h_0 = \frac{V_s h_s D}{h_0^2}$$

$$= \frac{V_s}{h_0}\left(\frac{h_s}{h_0}\right)(\tan\alpha - \tan\beta) \quad [77]$$

According to this relation, the strain rate at the entering side of the die is proportional to each of three quantities: To the ratio of velocity at the exit to initial thickness, i.e., the ratio of the two independent variables, $\left(\frac{V_s}{h_0}\right)$; to the thickness ratio $\left(\frac{h_s}{h_0}\right)$, or ratio of thickness before and after drawing; and to a trigonometric function of the tool tapers $(\tan\alpha - \tan\beta)$, which increases with decreasing die angle and increasing mandrel taper.

For the purpose of calculating the die pressure, it is more convenient to replace the velocity at the exit V_s, by the velocity on entering the die V_0, by means of the condition that the volume of the metal remains constant (see Equation [59])

$$V_s h_s = V_0 h_0 \quad [78]$$

The flow stress on entering the die, Equation [74], then becomes

$$\sigma_0' = a\left(\frac{V_0 D}{h_0}\right)^b \quad [79]$$

and the strain rate on entering the die, Equation [77], is correspondingly

$$\left(\frac{d\epsilon}{dt}\right)_{h=h_0} = \frac{V_0}{h_0}(\tan\alpha - \tan\beta) \quad [80]$$

According to this relation, the strain rate on entering the die is proportional to each of two quantities, to the ratio of velocity at

the entering side of the die to initial thickness $\left(\frac{V_0}{h_0}\right)$, and to the trigonometric function $\tan \alpha - \tan \beta$.

Equation [76] becomes indeterminate, when $B = -2b$. This results from the fact that, in the solution of Equation [72], an expression must be integrated which involves the quantity $\frac{1}{h^{2b+B+1}}$. When $B = -2b$, this quantity reduces to $\frac{1}{h}$, and $\int \frac{dh}{h} = \ln h$. Proceeding as before, the formula for p is then found to be

$$\frac{p}{\sigma_0'} = \left(\frac{h_0}{h}\right)^{2b}\left[(1-2b)\ln\frac{h}{h_0}+1\right] \quad \ldots\ldots [81]$$

Effects of Processing Variables on Die Pressure

The flow stress in hot-drawing is not constant but varies with the position of the metal within the die. Consequently, it is more lucid to determine the absolute die pressure rather than the ratio of die pressure to flow stress, see Figs. 9 and 10, for cold-drawing.

The die-pressure distribution as given by Equations [76] and [78], has been plotted in Figs. 19 and 20 for mild steel, using the reduction of metal thickness, $R = 1 - \frac{h}{h_0}$ as abscissas. Curves for various frictional conditions, $u = \mu_1 - \mu_2$ are represented while the other factors are kept constant. The die angle has been selected very small, $\alpha = 2$ deg and the mandrel has been assumed to be straight, $\beta = 0$ or $D = \tan \alpha - \tan \beta = +0.035$, in order to illustrate the large effect of the friction difference under such circumstances; i.e., for a small value of $D = \tan \alpha - \tan \beta$. Curves for cold-drawing, where $\sigma_0 = 55{,}000$ psi, are shown on the right side of Figs. 19 and 20, to be compared with the curves for hot-drawing at a selected temperature of 2200 F, at a velocity V_0 on entering the die of 6 fpm, and for an initial wall thickness h_0 of 1.20 in., or a "specific" velocity on entering the die (V_0/h_0) of 1 per sec. The value of σ_0' for such conditions is approximately 2500 psi, according to Fig. 20, and is plotted for a range of reductions extending up to 97 per cent ($h_s = 0.03\ h_0$), but the curves have a physical meaning only if the die pressure exceeds zero. In those cases where a reduction of 97 per cent is theoretically feasible, the velocity at the exit would be 200 fpm, see Equation [78]. Fig. 20 enlarges the portion of Fig. 19 representing die pressures less than 5000 psi.

Figs. 19 and 20 illustrate that three types of pressure distributions may occur in hot-drawing as opposed to the two types encountered in cold-drawing. The pressure-distribution characteristic for "drawing," where the die pressure continuously decreases as the exit side of the die is approached, is observed in hot-drawing for large values of $B = u/D > (2b - 1)$, while this condition extends to smaller values of $B > -1$ in cold-drawing. The pressure-distribution characteristic for "extrusion," where the die pressure continuously increases toward the exit, prevails in both hot-drawing and cold-drawing for small values of $B < -1$.

In addition to these two types of pressure distribution, a third one exists in hot-drawing when $-1 < B < (2b - 1)$. Then the pressure distribution shows a maximum at a certain position in the die, decreasing rapidly to zero with further approach to the exit. This condition is illustrated by the curve for $u = -0.0304$ in Figs. 19 and 20.

As previously discussed, each curve in Figs. 19 and 20, for hot-drawing, represents the pressure distribution for any total reduction, for a given set of conditions. This is the case if the strain-rate function of the velocity and thickness is kept constant on entering the die. In practice, however, the velocity at the exit and the initial thickness usually will be the independent variables. For a set of conditions in which these two factors are constant, Fig. 21 illustrates the pressure distribution present in drawing to final reductions ($R_s = 1 - h_s/h_0$), varying between 20 and 99.99 per cent. The decrease of the pressure at the entering side of the die with increasing total reduction is explained by the decrease of the strain rate at the entering side with increasing total reduction, which determines the flow stress σ_0', or the die pressure at this point.

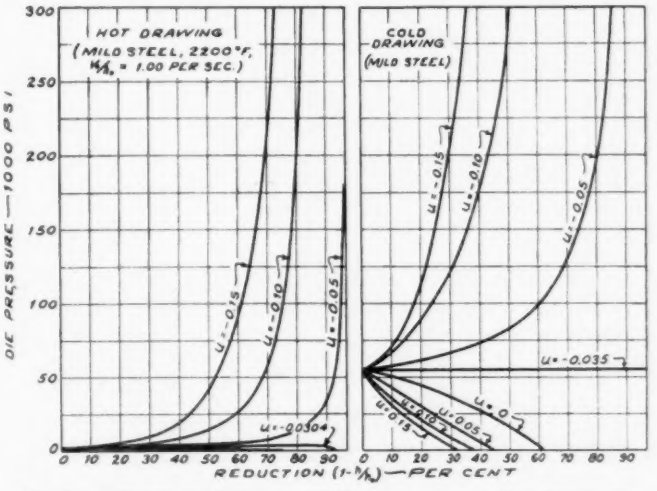


Fig. 19 Effect of Friction on Distribution of Die Pressure for Hot- and Cold-Drawing of Mild Steel; $\alpha = 2$ Deg, $\beta = 0$ Deg

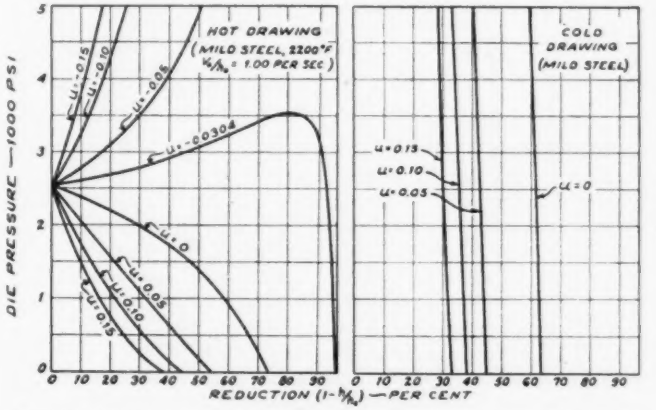


Fig. 20 Effect of Friction on Distribution of Die Pressure for Hot- and Cold-Drawing of Mild Steel; $\alpha = 2$ Deg, $\beta = 0$ Deg; Enlargement of Fig. 19

Drawing Limits

The drawing limits for hot-drawing are determined in much the same manner as in cold-drawing. These limits are also similarly affected by the processing variables, as illustrated in Figs. 15 and 22.

For the "drawing" type of pressure distribution, the drawing limit or "drawability," i.e., the maximum reduction $\left(R_s = 1 - \frac{h_s}{h_0}\right)$, performable in a single draw, is given as the reduction

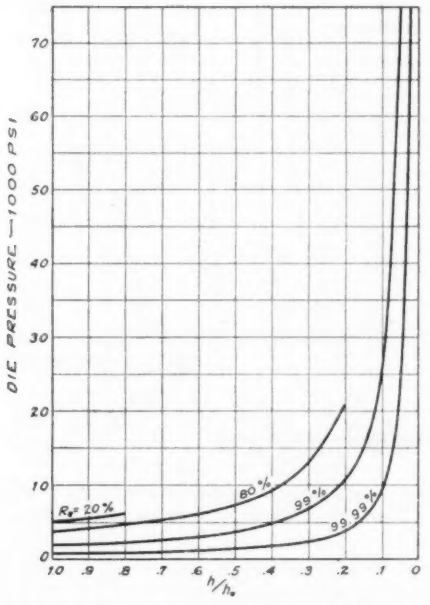


FIG. 21 PRESSURE DISTRIBUTION FOR VARIOUS TOTAL REDUCTIONS (R = 20 TO 99.99 PER CENT) FOR HOT-DRAWING OF MILD STEEL AT 2200 F

(α = 2 deg, β = 0 deg, u = —0.05, V_0/h_0 = 33.1 per sec or (200 fpm) for h_0 = 1.21 in.)

at which the die pressure becomes zero. This reduction differs only slightly for hot-drawing and cold-drawing, if the tools and frictional conditions are identical, Figs. 19 and 20. Theoretically, slightly larger reductions can be obtained on hot-drawing than on cold-drawing. Actually, however, the conditions during hot-drawing are difficult to control, and variations in temperature and frictional conditions should reduce the drawability. Also, the metal at the exit, which is subjected to the maximum tension, may exhibit a tendency to creep, and a corresponding decrease in strength may occur, as has been occasionally observed.

For the "extrusion" type of pressure distribution, the limit of drawing will be determined again by the strength of the die. The die pressures in hot-drawing are of course considerably smaller than those in cold-drawing, under identical conditions, as expected from the smaller flow stress at elevated temperatures. However, the die pressure in hot-drawing also becomes very large under certain conditions, see Figs. 19 to 21; but it does not increase as rapidly nor does it reach a large value at such a small reduction as the pressure in cold-drawing. Consequently, a larger reduction is possible in hot-drawing without failure of the die than in cold-drawing, due to the smaller flow stress. The effect of varying conditions on the drawing limit can be determined if an arbitrary value of die pressure is considered as the maximum internal pressure which the die will stand without failure, say, 300,000 psi.

Regarding these limiting reductions in drawing, there is one important difference between hot- and cold-drawing. For any particular die angle, the curve representing the drawing limit as a function of u consists of two branches, corresponding to failure of the tubing by tension and failure of the die by internal pressure, respectively. The two branches form a sharp peak in the case of cold-drawing, Fig. 15, particularly for small die angles whereas in the case of hot-drawing the peak is broad and rounded, Fig. 22. This means that the friction conditions are not as critical and the variations of the drawing limits resulting from small variations in the friction conditions should not be as pronounced in hot-drawing as in cold-drawing.

It may be pointed out that for equal friction coefficients at the die and mandrel, the drawability for both cold-drawing, Fig. 15, and hot-drawing, Fig. 22, is slightly higher than 60 per cent.

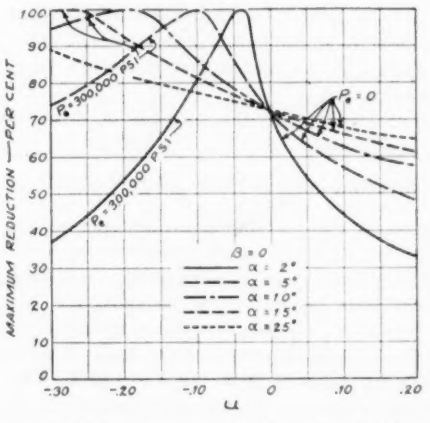


FIG. 22 LIMITING REDUCTIONS IN HOT-DRAWING (2200 F) OF MILD STEEL TUBING WITHOUT FAILURE IN TENSION (Pe/σ_0 = 0), OR FAILURE OF DIE BY INTERNAL PRESSURE (P_e = 300,000 PSI)

This is a basic value ($1 - 1/e$) of drawability, derived for other types of drawing, such as wire-drawing and deep-drawing if friction is absent. Thus, regarding the drawability for drawing tubing with a moving mandrel, equal friction coefficients on the die and mandrel yield the same conditions as zero friction in other drawing processes.

ACKNOWLEDGMENTS

This work has been conducted under the auspices of the A.S.M.E. Research Committee on Plastic Flow of Metals, and assisted by a grant-in-aid from The Engineering Foundation. The authors are indebted to Mr. E. L. Aul for his co-operation in preparing the manuscript.

Influence of Rate of Strain and Temperature on Yield Stresses of Mild Steel

By M. J. MANJOINE,[1] EAST PITTSBURGH, PA.

This paper describes the influence of rate of strain and temperature on the yield stresses of mild steel. Tensile tests are reported for room temperature, 200, 400, and 600 C, at rates of strain which vary from 10^{-6} to 10^{3} per sec. The results of these tensile tests are plotted to show more clearly the effects of strain-aging on the yield stresses and ultimate stress. The comparison of the yield stress at various strain rates permits an analysis of the influence of strain. The conditions necessary for discontinuous yielding are described and compared with test experiences.

Introduction

CONSIDERABLE research has been devoted to the influence of temperature and of speed of testing on the yield-point stress and the ultimate strength of mild steel. This paper is presented as a step further in the understanding of the yielding of mild steel and describes the influence of temperature and rate of strain on the yield stresses at various strains as well as on the stresses at the lower yield point and at the ultimate load of a tension test. In a previous paper (1)[2] by A. Nadai and the author, tensile tests were described at various rates of strain and temperatures, but only results concerning the ultimate stress were reported. In this paper the tensile tests for mild steel are further analyzed.

Because of the numerous articles on the testing of mild steel, reference will be made only to a few which contain a more complete bibliography. In 1938, Davis (2) reviewed the literature on the effect of speed of testing on the yield point of mild steel and added the influence of loading rate. Other work has been published since that time. Edwards, Phillips, and Jones (3) described the influence of some special elements on the strain-aging and yield-point characteristics of low-carbon steel. High-speed tension tests were reported by Brown and Vincent (4). Smith and Wood (5) gave the stress-strain curve for the atomic lattice of mild steel and related the change of the lattice spacing to the external yield point.

As early as 1909, Le Chatelier (6) pointed out that the peak of the ultimate stress-temperature curve for low-carbon steel could be shifted to a higher temperature by increasing the speed of testing. Later Carpenter and Robertson (7) described the part aging contributes in shifting the peak of the "stress versus strain-rate" curve toward a higher rate for increasing temperature. The term "strain-aging" will be used frequently in this paper and will refer to the change in the physical properties of steel caused by permanent deformation in the "blue-heat" range, or by storing permanently deformed steel at normal or moderate temperatures. A complete review of the literature on the aging of steel and its effect on the physical properties can be found in a paper by Kenyon and Burns (8).

Test Results

Testing Apparatus. Two machines were employed in making the tensile tests described here, a high-speed tension machine for the fast strain rates and a constant strain-rate machine for the intermediate and slow rates of testing. These machines and the shape of the test specimen were described in two previous papers (1, 9). The mild steel used in this investigation was a commercial low-carbon open-hearth steel. The finished test specimens were bright-annealed for 1 hr at 920 C in dissociated ammonia.

Original Curves. Six of the original oscillograms of high-speed tests are shown in Fig. 1. The axes are drawn to outline these load-elongation curves. No scales are given as several different magnifications were used in recording the load and elongation and in photographic enlarging. The large spot at the origin is caused by the electron beam of the oscilloscope which is stationary for about 1 sec before the test starts. The heavy vertical trace in (*a*) and (*b*) was caused by an imperfection in the beam switch which was later changed. The grating which appears in (*d*), (*e*), and (*f*) is a 0.1-in. grid which is placed in front of the cathode-ray screen for quick determination of the deflection of the beam. It is also used as a reference when measurements are taken from enlarged oscillograms. At the beginning and end of the oscillograms, vibrations occur having the natural frequency of the force-measuring system which is excited by the sudden yielding of the specimen or by the drop of the load at fracture. The frequency of this vibration is about 11,000 cycles per sec.

At the strain rate of 100 per sec, oscillogram (*c*), the amplitude of this vibration is small and the upper and lower yield points can readily be seen. The specimen in this test was not broken. The amplitude of the vibrations increases with the speed of testing, as can be seen in (*a*) and (*b*). At higher speeds the amplitude on first yielding becomes nearly as large as the deflection caused by the load. Because of the high writing speed in these latter oscillograms they cannot be satisfactorily reproduced for publication. The vibrations are fortunately damped down as the specimen yields. This can be seen in (*e*) and (*f*). At 400 C, oscillogram (*e*), a yield point can still be distinguished with the vibrations increasing in amplitude at the yield point and dying down as the specimen yields.

Typical recorded curves obtained on the constant strain-rate machine have been photographed and are shown in Fig. 2. The curves shown are those obtained on mild steel at 200 C for four different rates of strains. The elastic constant of the constant strain-rate machine is rather high. The recorder is capable of following vibrations of 20 cycles per sec, and therefore can follow the changes of load which occur during discontinuous yielding. A close inspection of the curves, made at the rates of 8.5×10^{-4} and 2×10^{-2} per sec, illustrates the oscillations of the load which occur during discontinuous yielding.

---

[1] Research Engineer, Westinghouse Electric and Manufacturing Company. Mem. A.S.M.E.

[2] Numbers in parentheses refer to the Bibliography at the end of the paper.

Presented at the National Meeting of the Applied Mechanics Division, Chicago, Ill., June 16–17, 1944, of The American Society of Mechanical Engineers.

Discussion of this paper should be addressed to the Secretary, A.S.M.E., 29 West 39th Street, New York, N. Y., and will be accepted until January 10, 1945, for publication at a later date. Discussion received after the closing date will be returned.

Note: Statements and opinions advanced in papers are to be understood as individual expressions of their authors and not those of the Society.

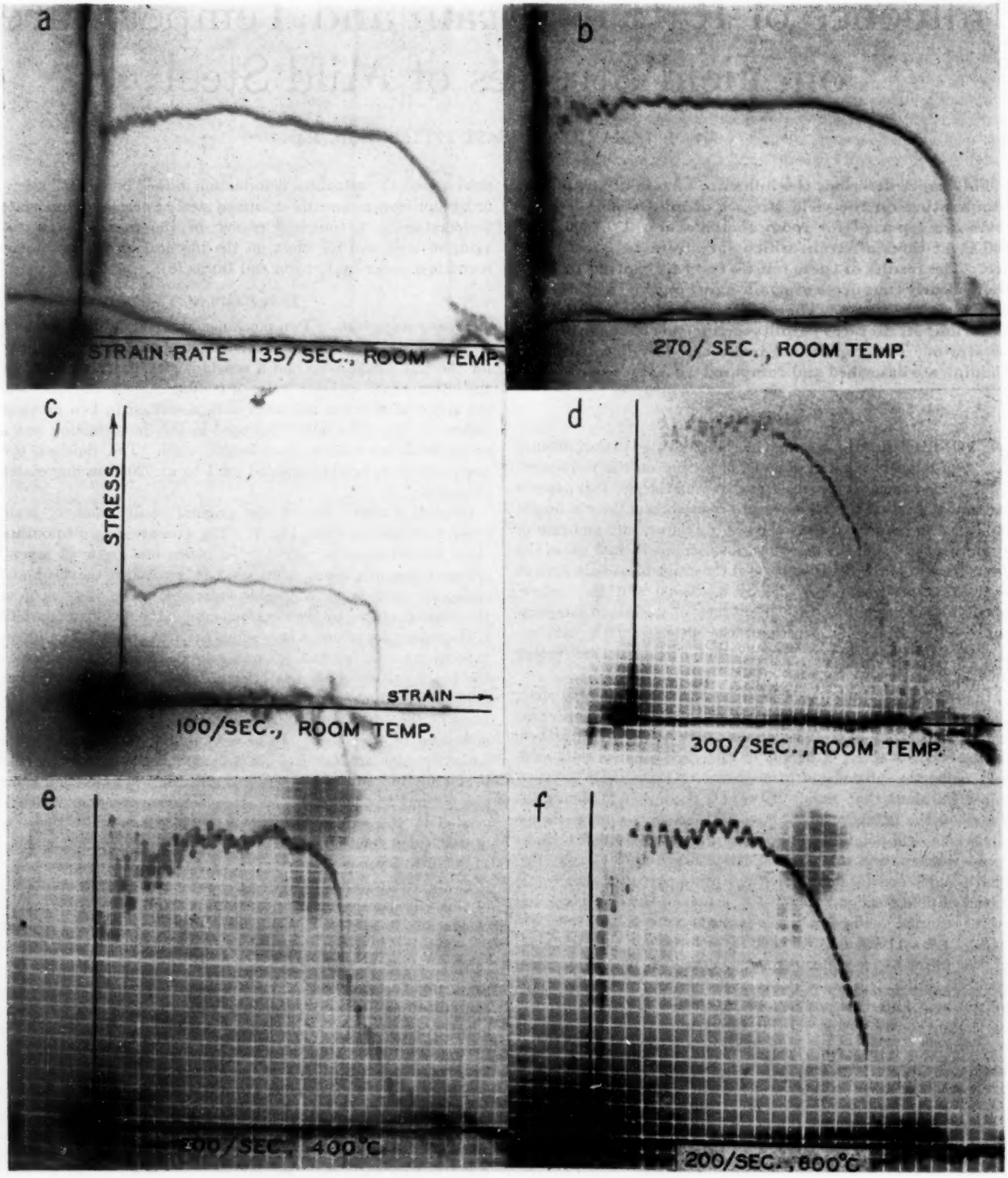


FIG. 1 ORIGINAL OSCILLOGRAMS OF SOME HIGH-SPEED STRESS-STRAIN CURVES

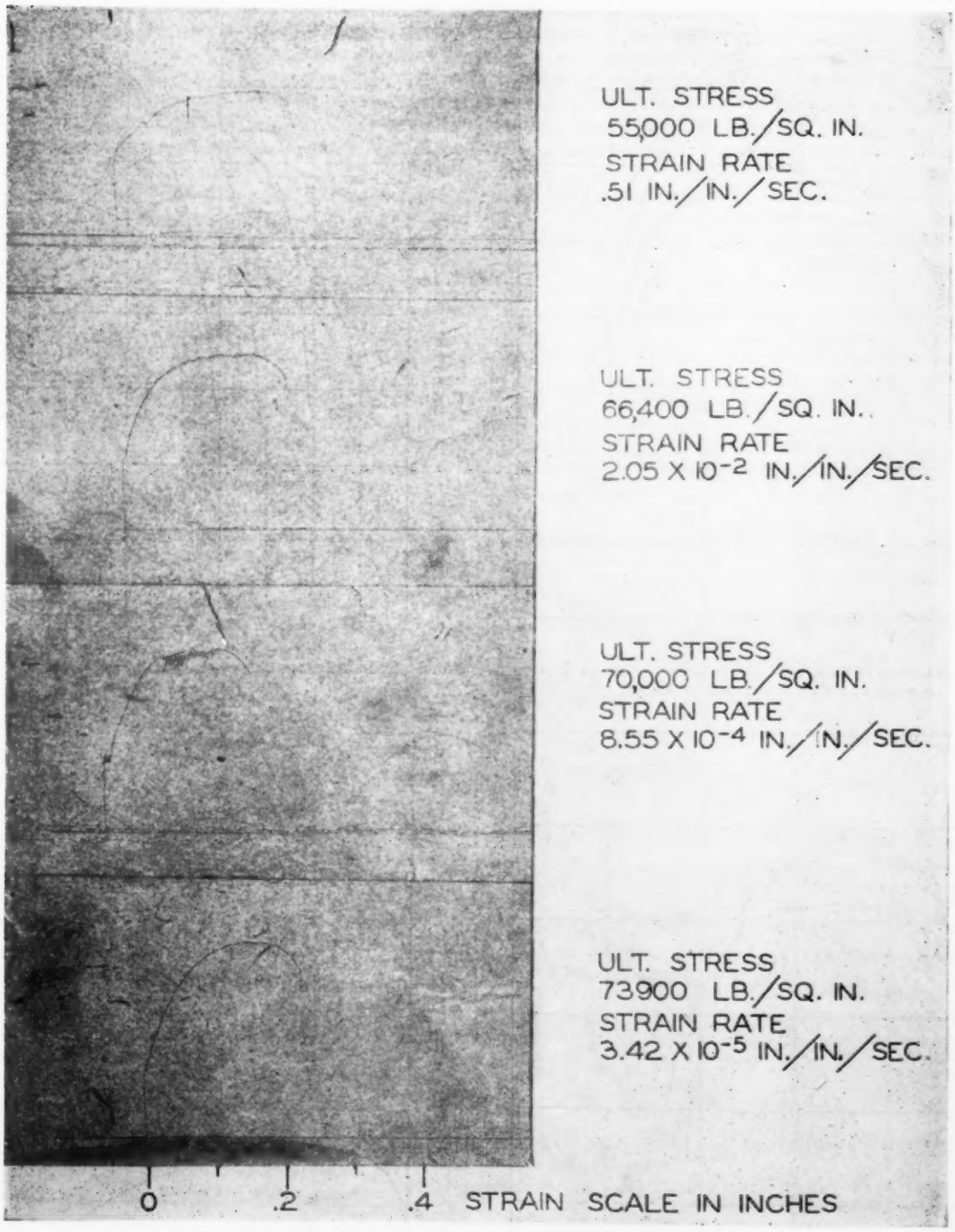


FIG. 2 EFFECT OF STRAIN RATE ON MILD STEEL AT 200 C

DISCUSSION OF STRESS - STRAIN CURVES

The original curves are a record of load versus elongation. Some of these curves have been replotted with stress as a function of strain and are shown in Figs. 3 to 6, inclusive. The stress is based on the original cross section, and strain is the total strain. In replotting the high-speed diagrams, an averaging curve has been drawn through the vibrations which occur on the original record.

The room-temperature stress-strain curves, given in Fig. 3, show the effect of the speed of testing on the shape of the curve. At a strain rate of 9.5×10^{-7} per sec, the time of the test is long enough to allow strain-aging at the higher strains, and therefore a greater ultimate strength is obtained than for the test made at a rate of 8.5×10^{-4} per sec. The yield-point stress is not noticeably affected by aging and shows a uniform increase with strain rate. The yield-point elongation increases with strain rate and reaches about 8 per cent strain at the rate of 300 per sec. The strain at the ultimate is about 20 per cent and changes very little with speed of testing. The first portion of the curve at 300 per sec is dashed because it represents the averaging curve of the

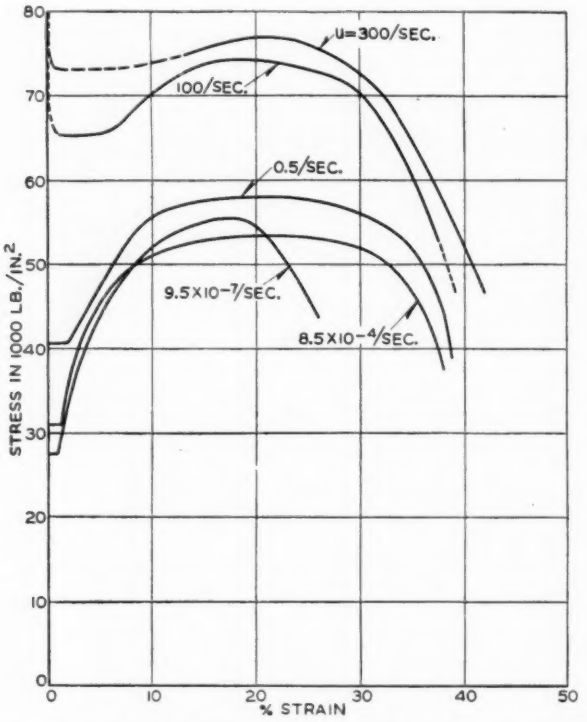


FIG. 3 STRESS-STRAIN CURVES OF MILD STEEL AT ROOM TEMPERATURE FOR VARIOUS RATES OF STRAIN

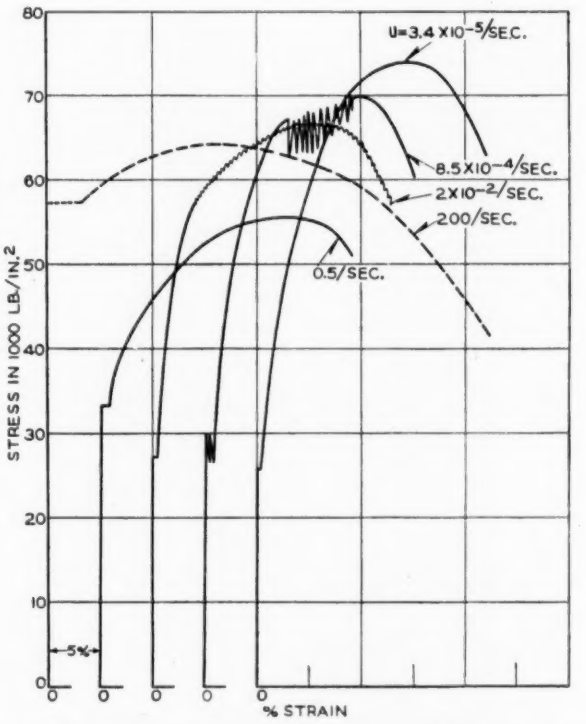


FIG. 4 STRESS-STRAIN CURVES OF MILD STEEL AT 200 C FOR VARIOUS RATES OF STRAIN

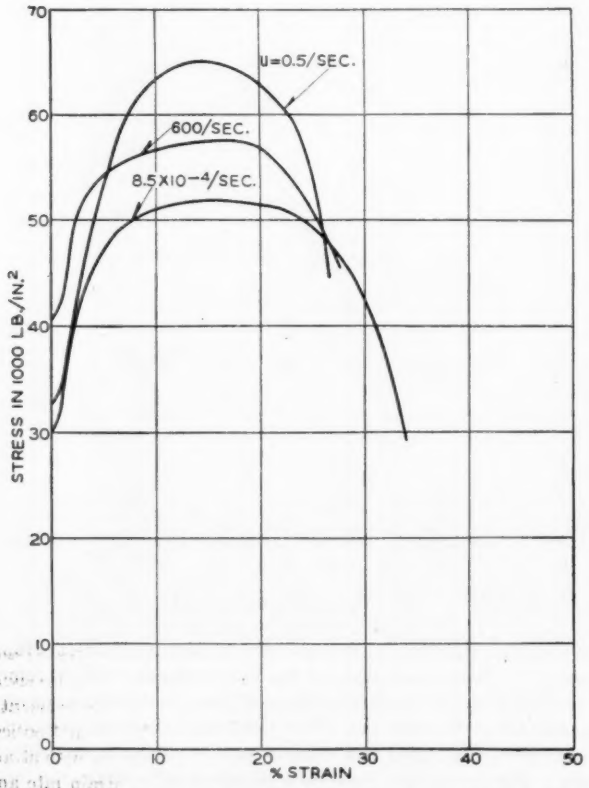


FIG. 5 STRESS-STRAIN CURVES OF MILD STEEL AT 400 C FOR VARIOUS RATES OF STRAIN

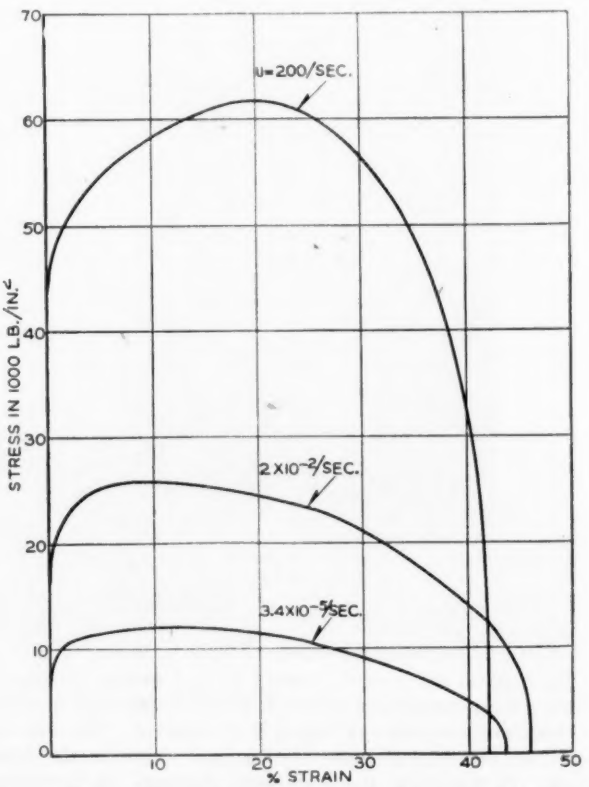


FIG. 6 STRESS-STRAIN CURVES OF MILD STEEL AT 600 C FOR VARIOUS RATES OF STRAIN

vibrations which occurred on the original diagrams. The specimen tested at a strain rate of 100 per sec necked down but was not broken.

The stress-strain curves for 200 C, Fig. 4, are plotted with the strain origin shifted 5 per cent to the right for each subsequent curve taken at a slower strain rate. The yield point, yield-point elongation, and ultimate strength increase with strain rate. The ultimate strength is also influenced by strain-aging. At a strain rate of 8.5×10^{-4} per sec, discontinuous yielding starts at about 8 per cent strain. The amplitude of the drop of the stress during yielding is about 5000 psi for our tensile machine. Discontinuous yielding also occurs at a strain rate of 2×10^{-2} per sec, but the amplitude of the drop in stress is only 800 psi.

At 400 C, Fig. 5, the yield point has practically disappeared, but a break in the curve is still present. The yield stress at 0.2 per cent increases with strain rate, but the ultimate strength increases at first and then decreases.

The curves for 600 C, Fig. 6, show the large increase in the strength for the higher strain rates. The yield point has completely disappeared at this high temperature.

Influence of Strain Rate on Tensile Properties of Mild Steel at Room Temperature

From the stress-strain curves for various rates at room temperature, the influence of strain rate on several of the tensile properties has been determined and is indicated in Fig. 7. This curve shows the dependence of the yield-point stress, the ultimate stress, and the total elongation on the rate of straining at room temperature. In addition, the ratio of the yield-point stress to the ultimate stress is given. The yield-point stress is taken as the stress at the lower yield point. This stress increases continuously with the rate of strain, while the ultimate stress shows a decrease for the lowest rates and an increase for the high rates. The ratio of yield stress to ultimate stress increases over the entire range of strain rates; at the lowest rate the ratio is 50 per cent while at the highest rate it is over 95 per cent. The elongation increases at the lower rates but is practically constant from a rate of 10^{-3} to 10^{3} per sec, a range of rates of 1 to 1,000,000.

Influence of Rate of Strain on Yield Stresses

To determine the effect of rate of strain on the yield stresses necessary to deform mild steel, the true yield stresses have been computed for various strains of the stress-strain curves in Figs. 3, 4, 5, and 6. The true yield stress is the load at a given strain divided by the actual area, or the load stress at a given strain multiplied by a factor (1 plus the unit strain).

The results of the room-temperature tests are given in Fig. 8. The true yield stresses are shown for the yield point and for the strains of 2, 4, 8, and 12 per cent; included in addition is the true stress at the ultimate load of the tensile test. The stress at the yield point is taken at the lower yield point where the material flows at practically a constant load throughout the yield-point elongation. Although the actual load is constant, the true stress in the mild steel must increase during the yield-point elongation; the amount of the increase depends upon the strain that takes place. Therefore, the values of the true stresses at the beginning and at the end of the yield-point elongation must be shown in a band. Since the yield-point elongation increases with rate of strain, this band increases in width for higher rates. No points can be shown within this band as stress and strain have little significance during the yield-point elongation.

The yield stresses at 2 and 4 per cent strain increase uniformly with rate; when the yield-point elongation reaches these strains the yield-stress curve is terminated. At higher strains and the slowest rates, however, the effect of strain-aging begins to show. The yield stresses for these higher strains decrease with rate, reach a minimum, and then increase uniformly at the higher rates. In the region where the slope of the stress versus strain-rate curve is negative, discontinuous yielding will occur. This effect will be described later in more detail. These curves are fortunately very flat in the region in which the ordinary short-time tensile tests are made (about 2×10^{-3} per sec).

The temperature of 200 C has always been considered a critical one for mild steel because at or near this temperature considerable strain-aging takes place during the ordinary short-time tensile test, and discontinuous yielding usually occurs. The reason for discontinuous yielding can be seen in Fig. 9, which shows the variation of the yield stresses with strain rate. As

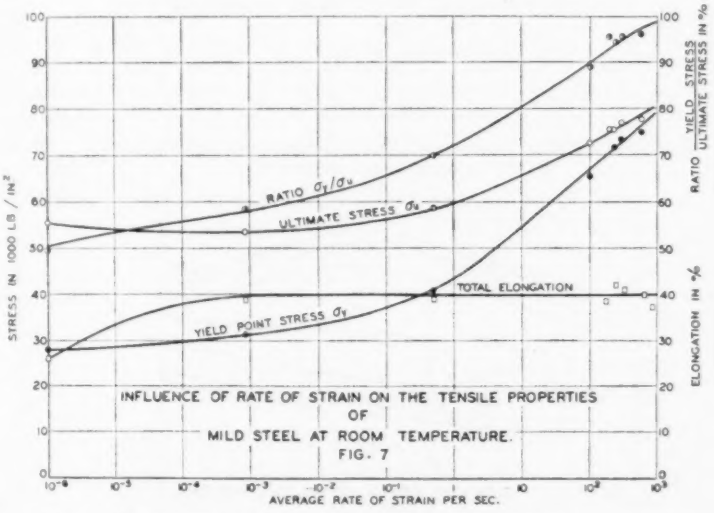


Fig. 7 Influence of Rate of Strain on Tensile Properties of Mild Steel at Room Temperature

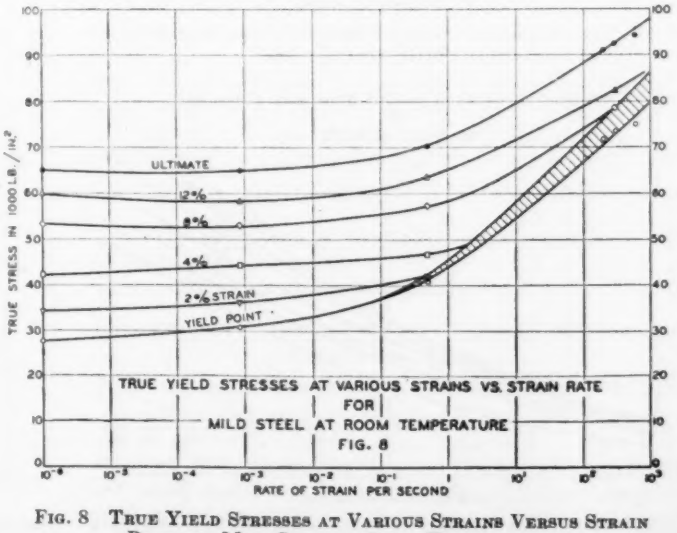


Fig. 8 True Yield Stresses at Various Strains Versus Strain Rate for Mild Steel at Room Temperature

stated before, discontinuous yielding can be expected when the stress versus strain-rate curve has a negative slope. This means that the material can yield more rapidly at a lower stress, as it does; to keep the average rate constant, the material will be stretched much more slowly during another part of the cycle; this causes the load to build up again and the cycle is repeated.

In Fig. 9, the yield stress at 8 per cent strain has a negative slope from a rate of 10^{-4} to 5×10^{-1} per sec. Referring to the curve for the strain rate of 8.5×10^{-4} per sec, which is in the range previously mentioned, Figs. 2 or 4, discontinuous yielding starts at a strain of about 8 per cent and continues up to the ultimate strength. The tension test at the rate of 2×10^{-2} per sec is also in this range of negative slope, and discontinuous yielding starts at a strain of 4 per cent and continues up to rupture of the specimen. The amplitude of the fluctuation in load during yielding, however, is about one fifth of that which occurred at the rate of 8.5×10^{-4} per sec. This can be accounted for by the fact that the mild steel strain-ages at the same rate in both tests, but at the higher average strain rate less time is available, and therefore less effect can be expected.

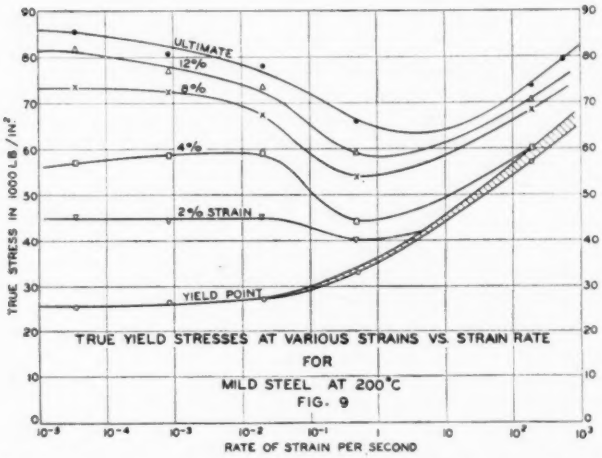


FIG. 9 TRUE YIELD STRESSES AT VARIOUS STRAINS VERSUS STRAIN RATE FOR MILD STEEL AT 200 C

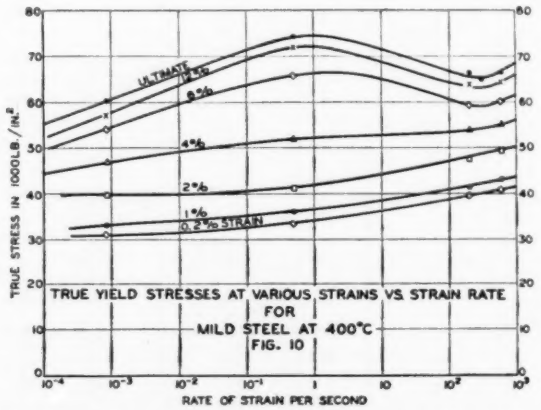


FIG. 10 TRUE YIELD STRESSES AT VARIOUS STRAINS VERSUS STRAIN RATE FOR MILD STEEL AT 400 C

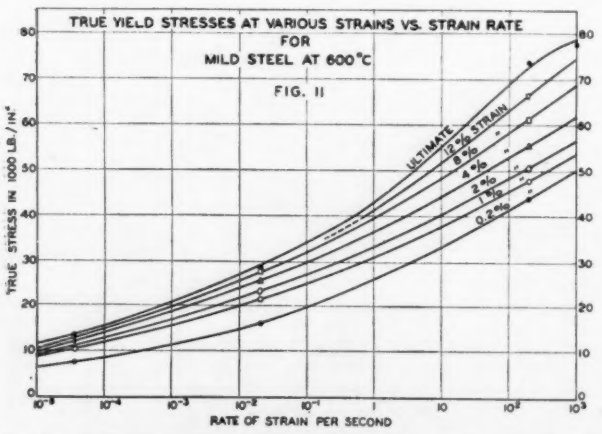


FIG. 11 TRUE YIELD STRESSES AT VARIOUS STRAINS VERSUS STRAIN RATE FOR MILD STEEL AT 600 C

Discontinuous yielding has been described by other investigators who gave aging as the only explanation. Among the first to show this rapid variation in load during deformation were Bach and Baumann (10), and Körber and Pomp (11). They found the effect for ferrous metals when tested at slightly elevated temperatures. Quinney (12) showed that discontinuous yielding may occur at room temperature for Yorkshire iron at very slow speed of testing (see Figs. 7 and 8, for the negative slope in the stress-strain-rate curve at the lowest rates). Elam (13) found the same thing for Armco iron and aluminum alloys at room temperature and compared discontinuous yielding with an aging effect which occurs in a test in which frequent rest periods are allowed.

Strain-aging is dependent upon time and temperature. Its effect may be either beneficial or, as in the case of overaging, deleterious. Since annealing or recrystallization may occur,

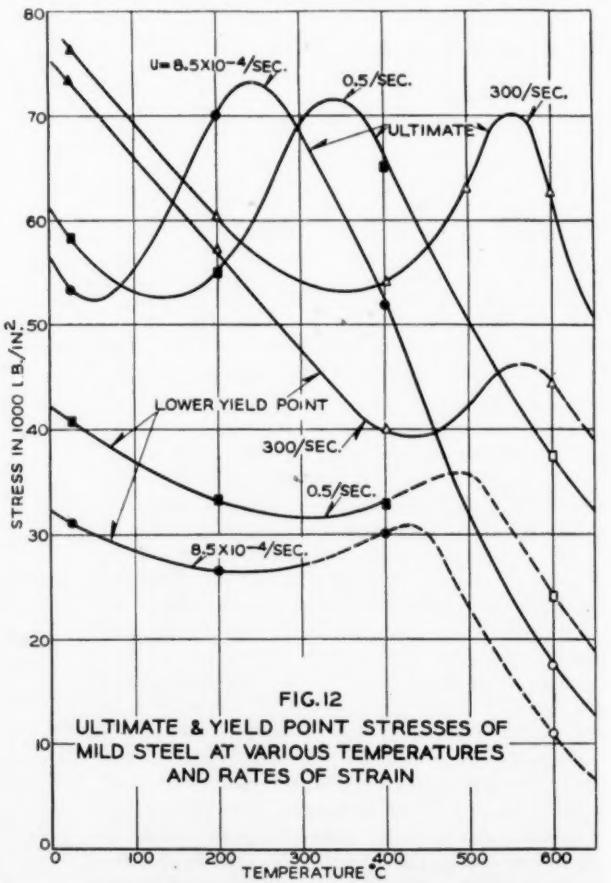


FIG. 12 ULTIMATE AND YIELD-POINT STRESSES OF MILD STEEL AT VARIOUS TEMPERATURES AND RATES OF STRAIN

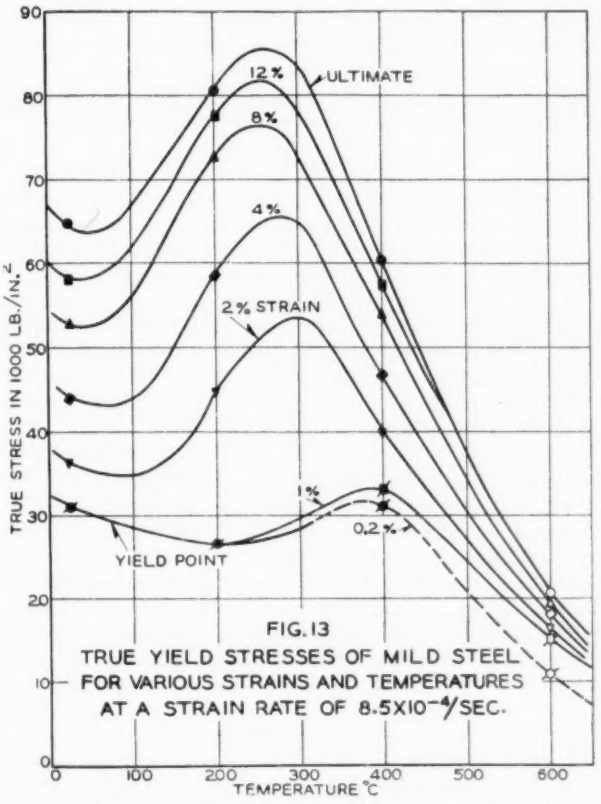


FIG. 13 TRUE YIELD STRESSES OF MILD STEEL FOR VARIOUS STRAINS AND TEMPERATURES AT A STRAIN RATE OF 8.5×10^{-4} PER SEC

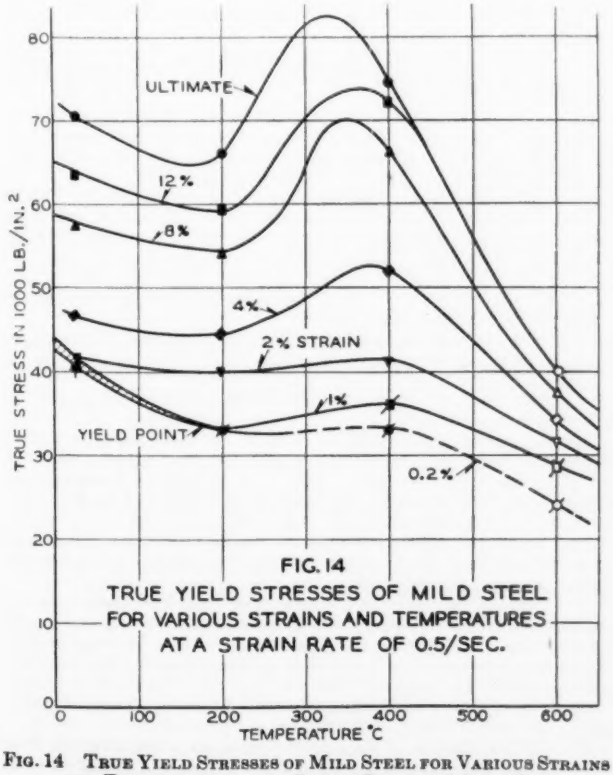


FIG. 14 TRUE YIELD STRESSES OF MILD STEEL FOR VARIOUS STRAINS AND TEMPERATURES AT A STRAIN RATE OF 0.5 PER SEC

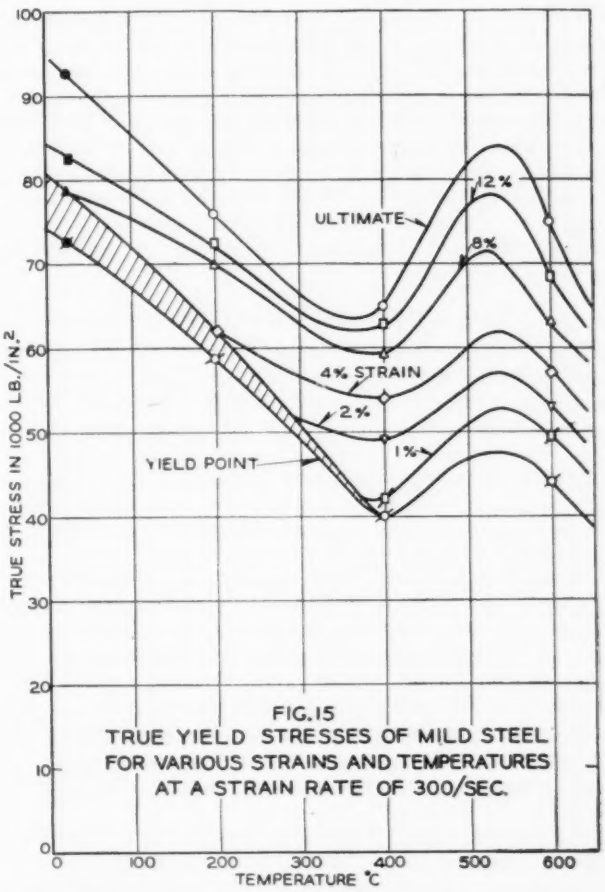


FIG. 15 TRUE YIELD STRESSES OF MILD STEEL FOR VARIOUS STRAINS AND TEMPERATURES AT A STRAIN RATE OF 300 PER SEC

which is also a function of time and temperature, the yield stresses for mild steel for high temperatures will be influenced by all these factors. At 400 C, Fig. 10, all the foregoing effects show up when tests are made over a large range of strain rates. At the higher strains, above 4 per cent, aging causes an increase in yield stress as the strain rate is decreased, thus allowing a longer time for a given strain. However, as the strain rate is further decreased, the time becomes great enough to allow overaging, annealing, and recrystallization; therefore the yield stress decreases with further decreases in strain rate. For strains below 4 per cent, the yield stresses increase with strain rate throughout the range investigated. At this temperature, the yield point is no longer observed at the slow strain rates, but a slight break in the stress-strain curve can still be seen.

At 600 C, Fig. 11, the speed effect is more pronounced. The yield stresses of all strains increase with rate of strain. The effect of strain-hardening increases with strain rate since the time for recrystallization and annealing decreases.

Influence of Temperature on Ultimate Strength and Yield-Point Stresses

The stresses at the ultimates of the loads and at the yield points have been taken from some of the stress-strain curves and are plotted as a function of temperature for the strain rates of 8.5×10^{-4}, 0.5 and 300 per sec, Fig. 12. The solid points are actual test points, while the open points are interpolated from other curves. At the higher temperatures, the lower yield-point curve is shown as a broken line; the stress for this portion

of the curve is taken at the yield stress for 0.2 per cent strain. The peak in the ultimate-strength curve is a result of aging and strain-hardening. Since these processes take time, the peak can be shifted to a higher temperature for increasing strain rates. The yield point is not noticeably affected by strain hardening and therefore undergoes a smaller shift as the strain rate is increased. The peak at the lowest rate occurs at about 400 C, which is 150 C higher than the peak of the ultimate stress at the same rate. However, at the high speeds, the peaks in the ultimate-stress and yield-point-stress curves occur at practically the same temperature.

True Yield Stress Versus Temperature

Based upon the preceding curves, Figs. 8 to 11, inclusive, the effect of temperature can now be better studied by comparing the yield stresses at several constant rates of strain. Comparisons are made at rates of 8.5×10^{-4}, 0.5, and 300 per sec in Figs. 13, 14, and 15. The solid points on the curves are actual test points, while the open points are interpolated from Figs. 8 to 11, inclusive. The yield-point curve is joined with the curve for 0.2 per cent strain but the latter portion of the curve is shown as a broken line.

At the strain rate of 8.5×10^{-4} per sec which is about the rate of a short-time tensile test, the yield-point elongation is about 1 per cent for the lower temperatures and vanishes for temperatures of about 400 C and higher. At this strain rate the strain-aging range extends from 100 to 400 C; at 1 per cent strain a much higher temperature is needed to strain-age the steel, the peak in the stress versus temperature curve coming at about 400 C. However, as the strain is increased, this peak shifts to lower temperatures and, at the ultimate of the load in the tension test, occurs at about 250 C.

The curves in Fig. 13 show that a sharp change in shape takes place in the curves between the strains of 1 and 2 per cent. This indicates that a strain of between 1 to 2 per cent is necessary to accelerate strain-aging and that further increase in stress for higher strains is caused by strain hardening. This statement can be better understood if we compare cross sections of the curves at room temperature and at 250 C. At room temperature, strain-aging occurs so slowly that it can be neglected at this strain rate. The increase in stress necessary to deform the mild steel at increasing strain is a result of strain hardening, and the amount of strain hardening can be seen from the spacing of the curves. At 250 C the spacing between the 1 and 2 per cent strain curves is much greater than the spacing at room temperature, but the spacings between the other curves are about the same for both temperatures. The difference in spacing between the curves is a result of strain aging. At temperatures of 400 C and above, strain aging and hardening occur, but their effect is reduced by annealing or recrystallization and is only noticeable at strains below 1 per cent.

When the strain rate is increased to 0.5 per sec, the peak in the curve for true stress at the ultimate load occurs at about 325 C, Fig. 14. The peaks of the yield-point and 1 per cent strain curves have not been changed in so far as temperature is concerned but have increased because of the increase in strain rate. To separate strain-hardening and strain aging, the difference in the spacing of the curves must be compared at room temperature and about 325 C. From this comparison it is evident that a much higher strain is necessary to accelerate strain aging; the actual strain lies somewhere between 4 and 8 per cent. We can therefore conclude that, as the speed is increased a higher temperature and strain are necessary to accelerate strain aging.

At a strain rate of 300 per sec, Fig. 15, the peak in the stress-temperature curves occurs at about 540 C for all strains. Very little time, less than 0.001 sec, is available for strain aging, but the temperature is so high that the aging takes place at a very high rate. The lack of data between 400 and 600 C prevents any accurate conclusion about the spacing of the curves. At this high rate, the yield-point elongation is about 8 per cent at room temperature and decreases to about 1 per cent at 400 C.

Conclusions

The influence of temperature and the rate of strain on the yield stresses of mild steel has been described for the range of strain rates from 10^{-6} to 10^{3} per sec, an increase of 1 to 1,000,000,000 and for temperatures from about 25 to 600 C.

At room temperature, the ultimate strength decreases slightly at the very low rates and then increases with strain rate, showing a 40 per cent increase at the highest rate. The lower yield point increases throughout the range of rates with an over-all increase of 170 per cent. The total elongation for the higher rates is practically constant at 40 per cent.

At the higher temperatures, the yield stresses are greatly affected by strain aging. In general, as the strain rate is increased, a higher temperature and strain are necessary to accelerate strain aging. When the yield stress - strain rate curve has a negative slope, discontinuous yielding can be expected. The fluctuations of the load which occur during discontinuous yielding decrease in amplitude as the strain rate is increased. At 600 C, the influence of strain aging is reduced or completely eliminated by annealing and recrystallization, and the yield stresses increase with strain rate over the entire range.

Acknowledgment

This analysis was made on tests previously reported (1) with Dr. A. Nadai to whom the writer expresses his appreciation for counsel and permission to use the results of these tests.

BIBLIOGRAPHY

1 "High-Speed Tension Tests at Elevated Temperatures—Parts II and III," by A. Nadai and M. J. Manjoine, Trans. A.S.M.E., vol. 63, 1941, p. A-77.

2 "The Effect of the Speed of Stretching and the Rate of Loading on the Yielding of Mild Steel," by E. A. Davis, Trans. A.S.M.E., vol. 60, 1938, pp. A-137.

3 "The Influence of Some Special Elements Upon the Strain-Aging and Yield-Point Characteristics of Low-Carbon Steels," by C. A. Edwards, D. L. Phillips, and H. N. Jones, *Journal of the Iron and Steel Institute*, vol. 142, no. 2, 1940, pp. 199P–222P.

4 "The Relationship Between Stress and Strain in the Tensile Impact Test," by A. F. C. Brown and N. D. G. Vincent, Proceedings of The Institution of Mechanical Engineers, vol. 145, 1941, pp. 126–134.

5 "A Stress-Strain Curve for the Atomic Lattice of Mild Steel and the Physical Significance of the Yield Point of a Metal," by S. L. Smith and W. A. Wood, Proceedings of the Royal Society of London, vol. 179, 1942, pp. 450–460.

6 "Influence du temps et de la température sur les essais au choc," Révue de Metallurgie Memoires, by A. Le Chatelier, vol. 6, 1909, pp. 914–917.

7 "Metals," by H. Carpenter and J. M. Robertson, Oxford University Press, New York, N. Y., 2 vols., 1939, p. 119.

8 "Aging in Iron and Steel," by R. L. Kenyon and R. S. Burns, Symposium on Precipitation Hardening, A.S.M., 1939, p. 262.

9 "High-Speed Tension Tests at Elevated Temperatures, Part I," by A. Nadai and M. J. Manjoine, Proceedings of the A.S.T.M., vol. 40, 1940, pp. 822–837.

10 "Festigkeitseigenschaften und Gefügebilder der Konstruktions-materialien," by C. Bach and R. Baumann, second edition, Julius Springer, Berlin, 1921, p. 11.

11 "Vergleichende Untersuchung über das Verhalten von unlegierten und legierten Kesselblechen bei erhöhten Temperaturen und hinsichtlich Alterung und Rekristallisation," by F. Körber and A. Pomp, Mitteilungen aus dem Kaiser Wilhelm Institut für Eisenforschung, vol. 9, 1927, pp. 339–400.

12 "Time Effect in Testing Metals," by H. Quinney, *The Engineer*, vol. 157, 1934, pp. 332–334.

13 "The Influence of Rate of Deformation on the Tensile Test With Special Reference to the Yield Point in Iron and Steel," by C. F. Elam, Proceedings of the Royal Society of London, 1938, p. 568.

An Analytical Theory of Landing-Shock Effects on an Airplane Considered as an Elastic Body

By E. G. KELLER,[1] BUFFALO, N. Y.

An analytical method of determining the accelerations at any point P (x, y, z) of an airplane during landing is given. The method is applicable to any type airplane with either tricycle or conventional landing gear. The shock-strut forces are determined by a method previously published. A criterion for the mechanism of a broken spar is sought. Calculations are carried out for no particular airplane, but representative values of parameters for four-engined transports are employed.

Introduction

THE purpose of this investigation is the analytical determination of the accelerations during landing of any point on a large airplane considered to be an elastic or semi-elastic body.

The ever-increasing size of transports and bombers has rendered the problem a classical one[2] of the aircraft industry. Its solution is of use in various ways. Some of these are the following: (*a*) An underlying analytical theory tends to reduce landing strength specifications to a more rational basis. In the case of small aircraft, an arbitrary (substantiated by experience) strength specification of ng for the entire airplane was satisfactory. Increased size of transports, extremely nonuniform mass, and variable rigidity distributions throughout wings, fuselage, and empennage necessitate more careful design specifications for each part of the airplane. (*b*) An analytical theory furnishes a basis for the organization, correlation, and explanation of flight test data obtained in landing. (*c*) Destructive landings can be made economically by analytical methods. If the analytical theory is checked by flight tests in normal and moderately severe landings, and if the theory is sound, then reasonable extrapolations of the theoretical results may be made to show tendencies in destructive landings which cannot be carried out physically. (*d*) A generalized transport plane can be studied analytically in an economical manner by changes in system parameters. The twenty-four parameters of the fundamental matrix, Equation [35], along with the seven parameters of the applied force matrix, Equation [36], are sufficient to specify with considerable precision the behavior of a transport in landing. A change in any parameter corresponds to a physical change in the plane. For example, the variation of ϵ_0 from $+1$ to -1 shifts the points of application of the main landing gear forward by 34 in.

Certain Inherent Difficulties of the Problem

It may be of interest to list certain inherent difficulties of the problem.

(*a*) The foremost of these is the determination of the externally applied forces produced by the shock struts at their points of application to the airplane. Once the loads and requirements for a shock strut have been decided upon, shock-strut analysis is in a very definite sense an independent subject; that is, in the case of large aircraft, shock struts are designed and tested independently of the manufacture of the airplane. Usually the drop tests of a shock strut consist of free falls from prescribed heights onto horizontal or inclined planes. More often than not, there is in the drop tests no simulation of the air lift of the airplane during landing. This air lift is always present to some degree in the landing of any craft. The air lift greatly diminishes the intensity of the shock-strut nonlinear forces transmitted to the wing structure. In order that the problem of determining the accelerations over an elastic airplane during landing may be reduced to a linear one, it is necessary to obtain the strut forces as functions of the time. To so express these forces, and at the same time take into consideration the effect of air lift, it is necessary either to resort to expensive simulation of air lift during drop tests or to integrate the nonlinear differential equations of performance of the strut. The nonlinear differential equations of a shock strut, viewed as a body with 2 degrees of freedom, are easily shown to be

$$\left.\begin{aligned} M_2\ddot{s}_2 - nW_2 + \frac{p_0 S}{\left[1-\left(\frac{s_2-s_1}{D}\right)\right]^{1.2}} \\ + \frac{\rho\,(S-s_m)^3\,(\dot{s}_2-\dot{s}_1)^2}{2gc^2[A(r)]^2} = 0 \\ M_1\ddot{s}_1 - W_1 - \frac{p_0 S}{\left[1-\left(\frac{s_2-s_1}{D}\right)\right]^{1.2}} \\ - \frac{\rho(S-s_m)^3\,(\dot{s}_2-\dot{s}_1)^2}{2gc^2[A(r)]^2} + k_1\dot{s}_1 + k_0 s_1 = 0, \end{aligned}\right\} \quad . . [1]$$

where $A(r)$ is a function of $(s_2 - s_1)$ as given by the metering pin, s_2 and s_1 are, respectively, displacements of the airplane and piston of the strut, $\dot{s}_2$, $\dot{s}_1$, $\ddot{s}_2$, $\ddot{s}_1$ are time derivatives, and all other letters in the equations represent constant parameters. Since these equations have been integrated elsewhere,[3] no further dis-

---

[1] Consulting Engineer, Curtiss-Wright Corporation; formerly Consulting Engineer, Lockheed Aircraft Corporation, Burbank, Calif. Mem. A.S.M.E.

[2] Letter to the Editor, by E. S. Jenkins, *Journal of the Aeronautical Sciences*, vol. 9, 1942, p. 456; also "Problems in Aircraft Structural Research," by F. R. Shanley, *Mechanical Engineering*, vol. 65, 1943, pp. 169–178.

Contributed by the Applied Mechanics Division and presented at the Annual Meeting, New York, N. Y., Nov. 29–Dec. 3, 1943, of The American Society of Mechanical Engineers.

Discussion of this paper should be addressed to the Secretary, A.S.M.E., 29 West 39th Street, New York, N. Y., and will be accepted until January 10, 1945, for publication at a later date. Discussion received after the closing date will be returned.

Note: Statements and opinions advanced in papers are to be understood as individual expressions of their authors and not those of the Society.

[3] "Some Nonlinear Problems of the Electrical and Aircraft Industries" (Symposium Address, American Mathematical Society), E. G. Keller, Quarterly *Journal of Applied Mathematics*, vol. 2, April, 1944, p. 1.

cussion of them is necessary here. Of course, once s_2 and s_1 are found as functions of the time, both the load factors and strut forces are immediately obtainable.

(*b*) In the use of Equations [1], the values of M_1 and M_2 (equivalent masses to be dropped) must be determined. The determination of these masses, taking into consideration the moment of inertia and aerodynamic lift, is again a separate investigation. For this analysis refer to another paper[4] on this subject.

(*c*) The problem of determining the local accelerations over a plane is naturally one of infinitely many degrees of freedom. However, if the airplane is viewed as a semielastic body, it is sufficient to specify its behavior during landing in most practical cases by at most eight co-ordinates. The literal equations of motion are, however, derived for fourteen degrees of freedom. Six co-ordinates are employed to define the position of the center of gravity and eight to describe the torsion and bending of wings, fuselage, and stabilizer.

(*d*) Nonuniform mass and variable rigidity distributions introduce laborious numerical calculations. In order that a theory may be successful, from an engineering point of view, the labor required in applying it must be reduced to a minimum. Thus one of the first problems is the determination of how crudely

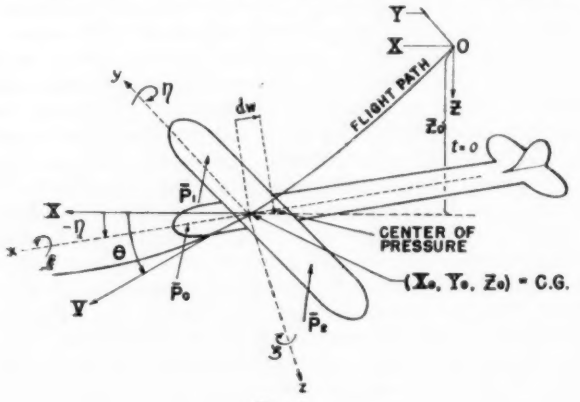


FIG. 1

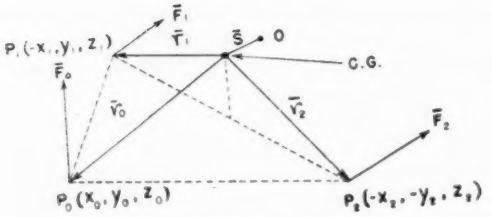


FIG. 2

the foregoing computations can be made without affecting significantly the coefficients in Equation [35].

(*e*) The number of initial conditions for the variables involved is very large.

(*f*) In the study of the generalized transport, each of the 24 system parameters of the general matrix, Equation [35], may take on several values. For each such change, the differential equations of performance (and hence their characteristic equations) are changed.

Difficulties (*a*) and (*b*) are eliminated by the material of footnote (3) and (4). A combination of proper co-ordinates along with the use of vector methods disposes of difficulty (*c*). Difficulty (*d*) is overcome by the method of exhaustion. The last two difficulties are entirely suppressed by use of the differential analyzer of the General Electric Company.

[4] "Determination of Equivalent Masses in Drop-Tests of Shock Struts Both With and Without Aerodynamic Lift Taken Into Consideration," by J. F. McBrearty and E. G. Keller, *Journal of the Aeronautical Sciences*.

PLAN OF THE ANALYSIS

The analysis consists of two divisions of which the first is concerned with the derivation of the equations of performance, while the second is devoted to the solution of the derived equations.

DERIVATION OF THE EQUATIONS OF PERFORMANCE

1 REFERENCE FRAME

Let the frame of reference be as follows: O-X, Y, Z are axes fixed in space such that the center of gravity of the airplane is at O at time $t = 0$, the first instant of contact of the plane with the ground. The axes G-x, y, z are fixed in the plane and move with the plane. X_0, Y_0, Z_0 are the co-ordinates of the center of gravity G at time t. The interval of time in which we are interested is at most 1 sec. The flight path is assumed to be a plane curve. (Bars over letters in the figures signify vectors.)

Let P_0, P_1, P_2 denote the points of contact of the airplane with the ground. Denote the vectors from the center of gravity to P_0, P_1, P_2 by

$$\left.\begin{aligned} \boldsymbol{r}_0 &= \boldsymbol{I}x_0 + \boldsymbol{J}y_0 + \boldsymbol{K}z_0 \\ \boldsymbol{r}_1 &= -\boldsymbol{I}x_1 + \boldsymbol{J}y_1 + \boldsymbol{K}z_1 \\ \boldsymbol{r}_2 &= -\boldsymbol{I}x_2 - \boldsymbol{J}y_2 + \boldsymbol{K}z_2 \end{aligned}\right\} \quad \ldots\ldots\ldots\ldots [2]$$

where $\boldsymbol{I}$, $\boldsymbol{J}$, $\boldsymbol{K}$ are unit vectors in the directions of X, Y, Z. Let the forces acting on the axles of the shock-strut wheels be

$$\left.\begin{aligned} \boldsymbol{F}_0 &= \boldsymbol{I}F_{0x} + \boldsymbol{J}F_{0y} + \boldsymbol{K}F_{0z} \\ \boldsymbol{F}_1 &= \boldsymbol{I}F_{1x} + \boldsymbol{J}F_{1y} + \boldsymbol{K}F_{1z} \\ \boldsymbol{F}_2 &= \boldsymbol{I}F_{2x} + \boldsymbol{J}F_{2y} + \boldsymbol{K}F_{2z} \end{aligned}\right\} \quad \ldots\ldots\ldots\ldots [3]$$

In a successful landing, the angles between x, y, z and X, Y, Z do not exceed 10 or 12 deg. Hence the vectors $\boldsymbol{I}$, $\boldsymbol{J}$, $\boldsymbol{K}$, may be replaced by $\boldsymbol{i}$, $\boldsymbol{j}$, $\boldsymbol{k}$ the unit vectors along x, y, z. (See reference (5) for details.) The co-ordinates of reference points (Fig. 3) in equilibrium configuration are

$$\left.\begin{array}{llll} \boldsymbol{P}_0(x_0, 0, z_0) & P_3(-a_1, 0, c_2) & B_1(-a_1 + a, b, c_2) & \\ \boldsymbol{P}_1(-x_1, y_1, z_0) & P_4(-a_1, b_1, c_2) & B_2(-a_1 - a, b, c_2) & \\ \boldsymbol{P}_2(-x_1, -y_1, z_0) & P_5(-a_1, b_2, c_2) & B_3(-a_1 - a, -b, c_2) & \\ P_3(a_0, 0, c_0) & P_3'(-a_2, 0, -c_3) & B_4(-a_1 + a, -b, c_2) & \\ P_1[-(a_1 + a_3), b_1, c_2] & A_1(-a_1, b, c_3) & B_1'(-a_2 + a', b', -c_3) & \\ P_2[-(a_1 + a_3), -b_1, c_2] & A_2(-a_1 - b, c_2) & B_2'(-a_2 - a', b', -c_3) & \\ & B_3'(-a_2 - a', -b', -c_3) & B_4'(-a_2 + a', -b', -c_3) & \end{array}\right\} \quad \ldots [4]$$

where the lengths $x_0, z_0, \ldots, b', c_3$ are displayed in Fig. 3. No distortion is yet taken into account by the symbols $x_0, \ldots, c_3$.

2 CO-ORDINATE SYSTEM

The total displacement (rigid and distortional) of any point P is

$$\boldsymbol{S} = \boldsymbol{S}_0 + \begin{vmatrix} \boldsymbol{i} & \boldsymbol{j} & \boldsymbol{k} \\ \xi & \eta & \zeta \\ a_i & b_j & c_k \end{vmatrix} + \boldsymbol{k}\zeta^k \quad \ldots\ldots\ldots\ldots [5]$$

where $a_i = a_i(x)$, $b_j = b_j(y)$, $c_k = c_k(z)$ are functions, respectively, of x, y, z; $\boldsymbol{i}$, $\boldsymbol{j}$, $\boldsymbol{k}$ are unit vectors, and ξ, η, ζ are angular rotations indicated in Fig. 3, and ξ^k ($k = w$(wing), f, e) are the distortional co-ordinates presently specified.[5] Only distortions perpendicular to the x,y-plane are considered. The longitudinal distortions of wings, fuselage, and empennage are neglected, since

[5] Mathematics of Modern Engineering, vol. 2, by E. G. Keller, John Wiley & Sons, New York, N. Y., 1941, p. 47.

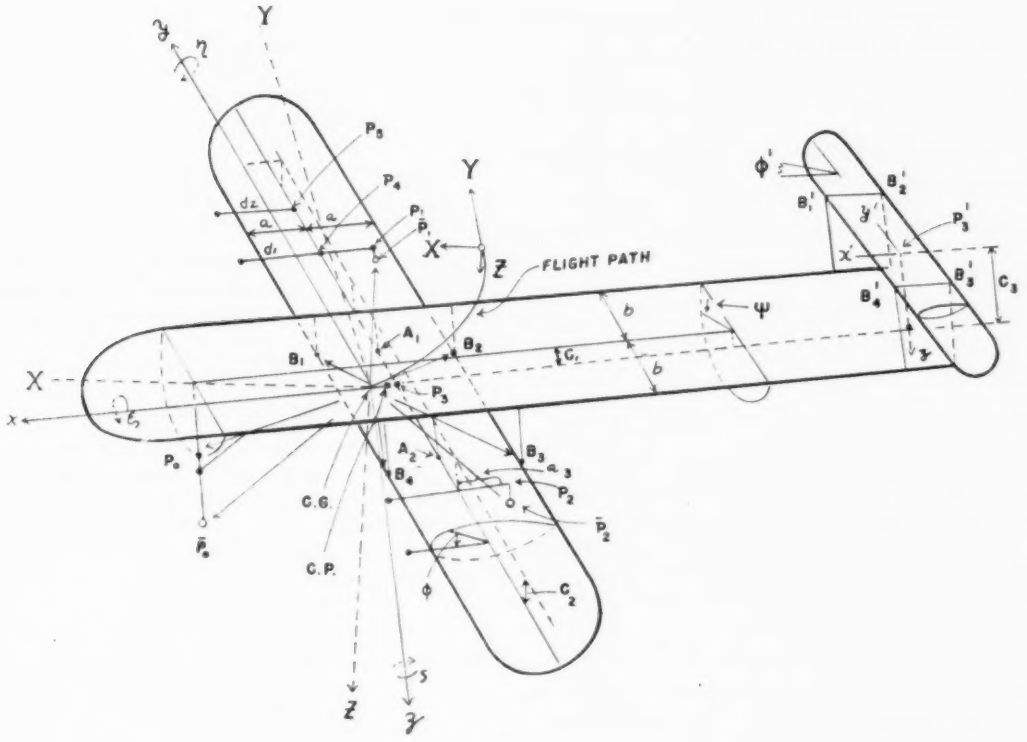


FIG. 3

during the motion considered no forces act which cause extensions.

Accordingly, let the distortional displacement of any point $P_w(x, y)$ on a wing be

$$\left.\begin{aligned}\zeta^w &= \eta^j(y, t) + x^i\varphi^j(y, t)\\ &= \eta_1(t)\eta(y) + x^i\varphi_1(t)\varphi(y)\end{aligned}\right\} \quad \ldots\ldots\ldots [6]$$

where x^i is the distance of $P_w(x, y)$ from the axis of rotation of the wing and $\varphi(x)$ is the torsional angle at (o, y). For the empennage

$$\left.\begin{aligned}\zeta^{rj} &= \eta^{rj}(y', t) + x^{ri}\varphi^{rj}(y', t)\\ &= \eta'_1(t)\eta'(y') + x^{ri}\varphi_1'(t)\varphi'(y')\end{aligned}\right\} \quad \ldots\ldots\ldots [7]$$

From special solutions and experimental results, it is a fact that, that portion of the wing interior to or intercepted by the fuselage may be taken as a rigid body. Consequently, the distortional co-ordinates for the fuselage are

$$\left.\begin{aligned}\zeta^f &= \xi_r{}^i(x, t) + \psi_r{}^i(x, t)\\ &= \xi_r(t)\xi_r(x) + y^j\psi_r(t)\bar{\psi}_r(x)\end{aligned}\right\} \quad \ldots\ldots\ldots [8]$$

where $r = 1, 2$ give the distortional displacement fore and aft, respectively, of the rigid section previously described. . For airplanes which possess no rigid sections, the procedure is clear from section (7).

3 Kinetic Energy

In view of the foregoing co-ordinate system we write the total kinetic energy of the airplane preparatory to deriving the equations of performance.

The velocity components (to the accuracy required) of any point P of the plane from Equation [5] are

$$\dot{X}_0 + \mathbf{i}\cdot\begin{vmatrix}\mathbf{i} & \mathbf{j} & \mathbf{k}\\ \xi & \dot{\eta} & \dot{\zeta}\\ a_i & b_j & c_k\end{vmatrix} = \dot{X}_0 + c_k\dot{\eta} - b_j\dot{\zeta}$$

$$\dot{Y}_0 + \mathbf{j}\cdot\begin{vmatrix}\mathbf{i} & \mathbf{j} & \mathbf{k}\\ \xi & \dot{\eta} & \dot{\zeta}\\ a_i & b_j & c_k\end{vmatrix} = \dot{Y}_0 + a_i\dot{\zeta} - c_k\dot{\xi}$$

$$\dot{Z}_0 + \mathbf{k}\cdot\begin{vmatrix}\mathbf{i} & \mathbf{j} & \mathbf{k}\\ \xi & \dot{\eta} & \dot{\zeta}\\ a_i & b_j & c_k\end{vmatrix} + \dot{\zeta}_k = \dot{Z}_0 + b_j\dot{\xi} - a_i\dot{\eta} + \dot{\zeta}^k$$

Thus the kinetic energies of the wings, fuselage, and empennage are, respectively

$$T_w = {}^1/_2\int_w \{(\dot{X}_0 + c_k\dot{\eta} - b_j\dot{\zeta})^2 + (\dot{Y}_0 + a_i\dot{\zeta} - c_k\dot{\xi})^2 + [\dot{Z}_0 + b_j\dot{\xi} - a_i\dot{\eta} + \dot{\eta}^j + x^i\dot{\varphi}^j]^2\}dm \quad \ldots\ldots [9]$$

$$T_f = {}^1/_2\int_f \{(\dot{X}_0 + c_k\dot{\eta} - b_j\dot{\zeta})^2 + (\dot{Y}_0 + a_i\dot{\zeta} - c_k\dot{\xi})^2 + [\dot{Z}_0 + b_j\dot{\xi} - a_i\dot{\eta} + \dot{\xi}_r{}^i + y^j\dot{\psi}_r{}^i]^2\}dm \quad \ldots\ldots [10]$$

$$T_e = {}^1/_2\int_e \{(\dot{X}_0 + c_k\dot{\eta} - b_j\dot{\zeta})^2 + (\dot{Y}_0 + a_i\dot{\zeta} - c_k\dot{\xi})^2 + [\dot{Z}_0 + b_j\dot{\xi} - a_i\dot{\eta} + \dot{\eta}^{rj} + x^{ri}\dot{\varphi}^{rj}]^2\}dm \quad \ldots\ldots [11]$$

The addition of Equations [9], [10], and [11] gives for the total kinetic energy

$$\begin{aligned}T = {}^1/_2\int_{\text{plane}} &\{(\dot{X}_0 + c_k\dot{\eta} - b_j\dot{\zeta})^2 + (\dot{Y}_0 + a_i\dot{\zeta} - c_k\dot{\xi})^2\\ &+ (\dot{Z}_0 + b_j\dot{\xi} - a_i\dot{\eta})^2\}dm + \int_w (\dot{Z}_0 + b_j\dot{\xi} - a_i\dot{\eta})\\ &(\eta^j + x^i)\dot{\varphi}^j dm + {}^1/_2\int_w (\dot{\eta}^j + x^i\dot{\varphi}^j)^2\, dm\\ &+ \int_f (\dot{Z}_0 + b_j\dot{\xi} - a_i\dot{\eta})(\dot{\xi}_r{}^i + y^j\dot{\psi}_r)dm\\ &+ {}^1/_2\int_f (\dot{\xi}_r{}^i + y^j\dot{\psi}_r)^2 dm \quad \ldots\ldots\ldots\ldots [12]\\ + \int_e (\dot{Z}_0 + b_j\dot{\xi} - a_i\dot{\eta})&(\dot{\eta}^{rj} + x^{ri}\dot{\varphi}^j)dm\\ &+ {}^1/_2\int_e (\dot{\eta}^{rj} + x^{ri}\dot{\varphi}^{rj})^2 dm,\ (r = 1, 2)\end{aligned}$$

cussion of them is necessary here. Of course, once s_2 and s_1 are found as functions of the time, both the load factors and strut forces are immediately obtainable.

(*b*) In the use of Equations [1], the values of M_1 and M_2 (equivalent masses to be dropped) must be determined. The determination of these masses, taking into consideration the moment of inertia and aerodynamic lift, is again a separate investigation. For this analysis refer to another paper[4] on this subject.

(*c*) The problem of determining the local accelerations over a plane is naturally one of infinitely many degrees of freedom. However, if the airplane is viewed as a semielastic body, it is sufficient to specify its behavior during landing in most practical cases by at most eight co-ordinates. The literal equations of motion are, however, derived for fourteen degrees of freedom. Six co-ordinates are employed to define the position of the center of gravity and eight to describe the torsion and bending of wings, fuselage, and stabilizer.

(*d*) Nonuniform mass and variable rigidity distributions introduce laborious numerical calculations. In order that a theory may be successful, from an engineering point of view, the labor required in applying it must be reduced to a minimum. Thus one of the first problems is the determination of how crudely

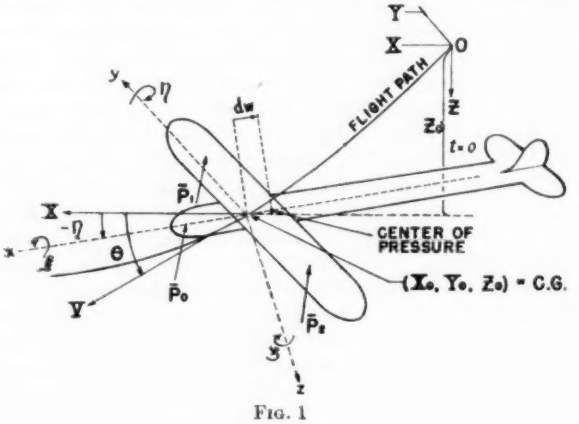


FIG. 1

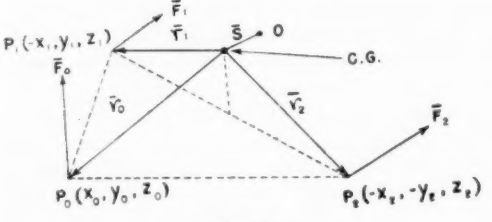


FIG. 2

the foregoing computations can be made without affecting significantly the coefficients in Equation [35].

(*e*) The number of initial conditions for the variables involved is very large.

(*f*) In the study of the generalized transport, each of the 24 system parameters of the general matrix, Equation [35], may take on several values. For each such change, the differential equations of performance (and hence their characteristic equations) are changed.

Difficulties (*a*) and (*b*) are eliminated by the material of footnote (3) and (4). A combination of proper co-ordinates along with the use of vector methods disposes of difficulty (*c*). Difficulty (*d*) is overcome by the method of exhaustion. The last two difficulties are entirely suppressed by use of the differential analyzer of the General Electric Company.

[4] "Determination of Equivalent Masses in Drop-Tests of Shock Struts Both With and Without Aerodynamic Lift Taken Into Consideration," by J. F. McBrearty and E. G. Keller, *Journal of the Aeronautical Sciences*.

PLAN OF THE ANALYSIS

The analysis consists of two divisions of which the first is concerned with the derivation of the equations of performance, while the second is devoted to the solution of the derived equations.

DERIVATION OF THE EQUATIONS OF PERFORMANCE

1 REFERENCE FRAME

Let the frame of reference be as follows: O-X, Y, Z are axes fixed in space such that the center of gravity of the airplane is at O at time $t = 0$, the first instant of contact of the plane with the ground. The axes G-x, y, z are fixed in the plane and move with the plane. X_0, Y_0, Z_0 are the co-ordinates of the center of gravity G at time t. The interval of time in which we are interested is at most 1 sec. The flight path is assumed to be a plane curve. (Bars over letters in the figures signify vectors.)

Let P_0, P_1, P_2 denote the points of contact of the airplane with the ground. Denote the vectors from the center of gravity to P_0, P_1, P_2 by

$$\left.\begin{aligned} \boldsymbol{r}_0 &= \boldsymbol{I}x_0 + \boldsymbol{J}y_0 + \boldsymbol{K}z_0 \\ \boldsymbol{r}_1 &= -\boldsymbol{I}x_1 + \boldsymbol{J}y_1 + \boldsymbol{K}z_1 \\ \boldsymbol{r}_2 &= -\boldsymbol{I}x_2 - \boldsymbol{J}y_2 + \boldsymbol{K}z_2 \end{aligned}\right\} \quad \ldots\ldots\ldots\ldots [2]$$

where $\boldsymbol{I}$, $\boldsymbol{J}$, $\boldsymbol{K}$ are unit vectors in the directions of X, Y, Z. Let the forces acting on the axles of the shock-strut wheels be

$$\left.\begin{aligned} \boldsymbol{F}_0 &= \boldsymbol{I}F_{0x} + \boldsymbol{J}F_{0y} + \boldsymbol{K}F_{0z} \\ \boldsymbol{F}_1 &= \boldsymbol{I}F_{1x} + \boldsymbol{J}F_{1y} + \boldsymbol{K}F_{1z} \\ \boldsymbol{F}_2 &= \boldsymbol{I}F_{2x} + \boldsymbol{J}F_{2y} + \boldsymbol{K}F_{2z} \end{aligned}\right\} \quad \ldots\ldots\ldots\ldots [3]$$

In a successful landing, the angles between x, y, z and X, Y, Z do not exceed 10 or 12 deg. Hence the vectors $\boldsymbol{I}$, $\boldsymbol{J}$, $\boldsymbol{K}$, may be replaced by $\boldsymbol{i}$, $\boldsymbol{j}$, $\boldsymbol{k}$ the unit vectors along x, y, z. (See reference (5) for details.) The co-ordinates of reference points (Fig. 3) in equilibrium configuration are

$$\left.\begin{array}{llll} \boldsymbol{P}_0(x_0, 0, z_0) & P_3(-a_1, 0, c_2) & B_1(-a_1 + a, b, c_2) & \\ \boldsymbol{P}_1(-x_1, y_1, z_0) & P_4(-a_1, b_1, c_2) & B_2(-a_1 - a, b, c_2) & \\ \boldsymbol{P}_2(-x_1, -y_1, z_0) & P_5(-a_1, b_3, c_2) & B_3(-a_1 - a, -b, c_2) & \\ P_6(a_0, 0, c_0) & P_3'(-a_2, 0, -c_3) & B_4(-a_1 + a, -b, c_2) & \\ P_1[-(a_1 + a_3), b_1, c_2] & A_1(-a_1, b, c_2) & B_1'(-a_2 + a', b', -c_3) & \\ P_2[-(a_1 + a_3), -b_1, c_2] & A_2(-a_1 - b, c_2) & B_2'(-a_2 - a', b', -c_3) & \\ & B_3'(-a_2 - a', -b', -c_3) & B_4'(-a_2 + a', -b', -c_3) & \end{array}\right\} \quad \ldots [4]$$

where the lengths $x_0, z_0, \ldots, b', c_3$ are displayed in Fig. 3. No distortion is yet taken into account by the symbols $x_0, \ldots, c_3$.

2 CO-ORDINATE SYSTEM

The total displacement (rigid and distortional) of any point P is

$$\boldsymbol{S} = \boldsymbol{S}_0 + \begin{vmatrix} \boldsymbol{i} & \boldsymbol{j} & \boldsymbol{k} \\ \xi & \eta & \zeta \\ a_i & b_j & c_k \end{vmatrix} + \boldsymbol{k}\zeta^k \quad \ldots\ldots\ldots\ldots [5]$$

where $a_i = a_i(x)$, $b_j = b_j(y)$, $c_k = c_k(z)$ are functions, respectively, of x, y, z; $\boldsymbol{i}$, $\boldsymbol{j}$, $\boldsymbol{k}$ are unit vectors, and ξ, η, ζ are angular rotations indicated in Fig. 3, and ζ^k ($k = w$(wing), f, e) are the distortional co-ordinates presently specified.[5] Only distortions perpendicular to the x,y-plane are considered. The longitudinal distortions of wings, fuselage, and empennage are neglected, since

[5] Mathematics of Modern Engineering, vol. 2, by E. G. Keller, John Wiley & Sons, New York, N. Y., 1941, p. 47.

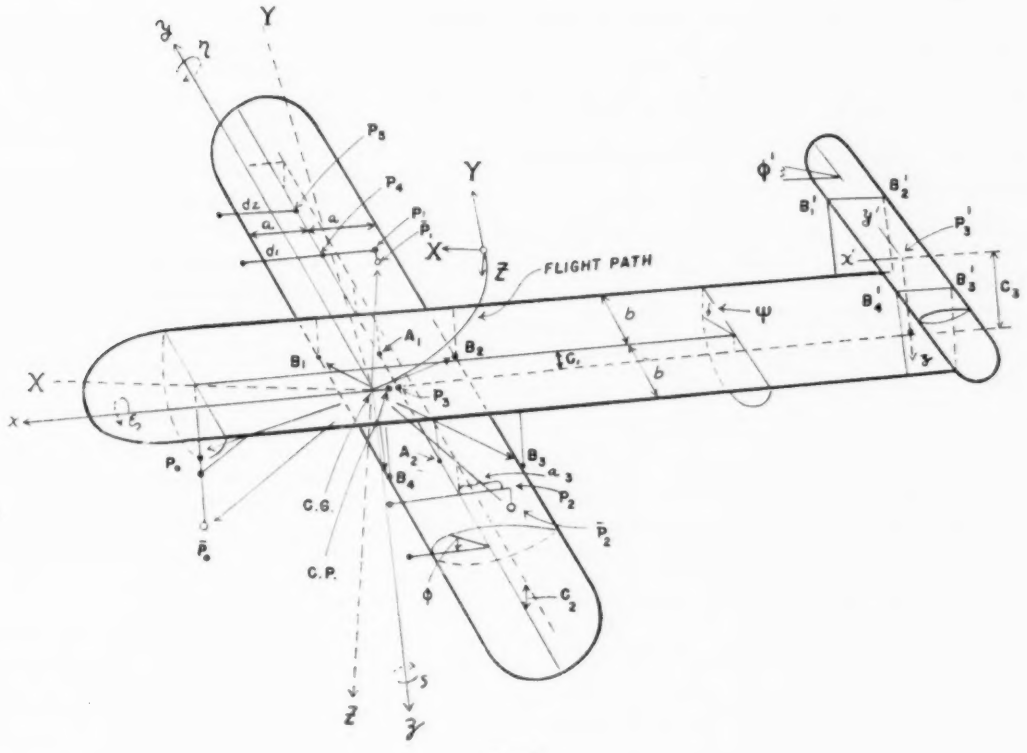


FIG. 3

during the motion considered no forces act which cause extensions.

Accordingly, let the distortional displacement of any point $P_w(x, y)$ on a wing be

$$\left.\begin{aligned}\zeta^w &= \eta^j(y, t) + x^i\varphi^j(y, t)\\ &= \eta_1(t)\eta(y) + x^i\varphi_1(t)\bar{\varphi}(y)\end{aligned}\right\} \quad \ldots\ldots\ldots [6]$$

where x^i is the distance of $P_w(x, y)$ from the axis of rotation of the wing and $\varphi(x)$ is the torsional angle at (o, y). For the empennage

$$\left.\begin{aligned}\zeta^e &= \eta'^j(y', t) + x'^i\varphi'^j(y', t)\\ &= \eta'_1(t)\eta'(y') + x'^i\varphi_1'(t)\varphi'(y')\end{aligned}\right\} \quad \ldots\ldots\ldots [7]$$

From special solutions and experimental results, it is a fact that, that portion of the wing interior to or intercepted by the fuselage may be taken as a rigid body. Consequently, the distortional co-ordinates for the fuselage are

$$\left.\begin{aligned}\zeta^f &= \xi_r^i(x, t) + \psi_r^i(x, t)\\ &= \xi_r(t)\bar{\xi}_r(x) + y^j\psi_r(t)\bar{\psi}_r(x)\end{aligned}\right\} \quad \ldots\ldots\ldots [8]$$

where $r = 1, 2$ give the distortional displacement fore and aft, respectively, of the rigid section previously described. For airplanes which possess no rigid sections, the procedure is clear from section (7).

3 Kinetic Energy

In view of the foregoing co-ordinate system we write the total kinetic energy of the airplane preparatory to deriving the equations of performance.

The velocity components (to the accuracy required) of any point P of the plane from Equation [5] are

$$\dot{X}_0 + \mathbf{i}\cdot\begin{vmatrix}\mathbf{i} & \mathbf{j} & \mathbf{k}\\ \dot{\xi} & \dot{\eta} & \dot{\zeta}\\ a_i & b_j & c_k\end{vmatrix} = \dot{X}_0 + c_k\dot{\eta} - b_j\dot{\zeta}$$

$$\dot{Y}_0 + \mathbf{j}\cdot\begin{vmatrix}\mathbf{i} & \mathbf{j} & \mathbf{k}\\ \dot{\xi} & \dot{\eta} & \dot{\zeta}\\ a_i & b_j & c_k\end{vmatrix} = \dot{Y}_0 + a_i\dot{\zeta} - c_k\dot{\xi}$$

$$\dot{Z}_0 + \mathbf{k}\cdot\begin{vmatrix}\mathbf{i} & \mathbf{j} & \mathbf{k}\\ \dot{\xi} & \dot{\eta} & \dot{\zeta}\\ a_i & b_j & c_k\end{vmatrix} + \dot{\zeta}_k = \dot{Z}_0 + b_j\dot{\xi} - a_i\dot{\eta} + \dot{\zeta}^k$$

Thus the kinetic energies of the wings, fuselage, and empennage are, respectively

$$T_w = {}^1/_2\int_w\{(\dot{X}_0 + c_k\dot{\eta} - b_j\dot{\zeta})^2 + (\dot{Y}_0 + a_i\dot{\zeta} - c_k\dot{\xi})^2 + [\dot{Z}_0 + b_j\dot{\xi} - a_i\dot{\eta} + \dot{\eta}^j + x^i\dot{\varphi}^j]^2\}dm \quad \ldots\ldots [9]$$

$$T_f = {}^1/_2\int_f\{(\dot{X}_0 + c_k\dot{\eta} - b_j\dot{\zeta})^2 + (\dot{Y}_0 + a_i\dot{\zeta} - c_k\dot{\xi})^2 + [\dot{Z}_0 + b_j\dot{\zeta} - a_i\dot{\eta} + \dot{\xi}_r^i + y^j\dot{\psi}_r^i]^2\}dm \quad \ldots\ldots [10]$$

$$T_e = {}^1/_2\int_e\{(\dot{X}_0 + c_k\dot{\eta} - b_j\dot{\zeta})^2 + (\dot{Y}_0 + a_i\dot{\zeta} - c_k\dot{\xi})^2 + [\dot{Z}_0 + b_j\dot{\xi} - a_i\dot{\eta} + \dot{\eta}'^j + x'^i\dot{\varphi}'^j]^2\}dm \quad \ldots\ldots [11]$$

The addition of Equations [9], [10], and [11] gives for the total kinetic energy

$$\begin{aligned}T = {}^1/_2\int_{\text{plane}}&\{(\dot{X}_0 + c_k\dot{\eta} - b_j\dot{\zeta})^2 + (\dot{Y}_0 + a_i\dot{\zeta} - c_k\dot{\xi})^2\\ &+ (\dot{Z}_0 + b_j\dot{\xi} - a_i\dot{\eta})^2\}dm + \int_w(\dot{Z}_0 + b_j\dot{\xi} - a_i\dot{\eta})\\ &(\dot{\eta}^j + x^i)\dot{\varphi}^j dm + {}^1/_2\int_w(\dot{\eta}^j + x^i\dot{\varphi}^j)^2\,dm\\ &+ \int_f(\dot{Z}_0 + b_j\dot{\xi} - a_i\dot{\eta})(\dot{\xi}_r^i + y^j\dot{\psi}_r)dm\\ &+ {}^1/_2\int_f(\dot{\xi}_r^i + y^j\dot{\psi}_r)^2dm \quad \ldots\ldots [12]\\ &+ \int_e(\dot{Z}_0 + b_j\dot{\xi} - a_i\dot{\eta})(\dot{\eta}'^j + x'^i\dot{\varphi}'^j)dm\\ &+ {}^1/_2\int_e(\dot{\eta}'^j + x'^i\dot{\varphi}'^j)^2dm,\ (r = 1, 2)\end{aligned}$$

Now the first integral in Equation [12] is merely the kinetic energy of a rigid plane and may be written

$$\frac{M}{2}(\dot{X}_0^2 + \dot{Y}_0^2 + \dot{Z}_0^2) + {}^1/_2 I_x \dot{\xi}^2 + {}^1/_2 I_y \dot{\eta}^2 + {}^1/_2 I_z \dot{\zeta}^2 \quad [13]$$

It remains to carry out in detail the remaining six integrals. The second integral in Equation [12] is

$$\begin{aligned}
&\int_w (\dot{Z}_0 + b_j\dot{\xi} - a_i\dot{\eta})(\ddot{\eta}^j + x^i\ddot{\varphi}^j)dm \\
&= \dot{Z}_0 \int \ddot{\eta}^j dm + \dot{Z}_0 \int x^i\ddot{\varphi}^j\, dm + \ddot{\xi} \int b_j\dot{\eta}^j\, dm \\
&+ \dot{\xi} \int b_j x^i\ddot{\varphi}^j dm - \dot{\eta} \int a_i\dot{\eta}^j\, dm - \dot{\eta} \int a_i x^i\ddot{\varphi}^j\, dm \\
&= \dot{Z}_0\dot{\eta}_1 \int \bar{\eta} dm + \dot{Z}_0\dot{\varphi}_1 \int\int x^i\bar{\varphi}\, dm + \ddot{\xi}\dot{\eta}_1 \int b_j\bar{\eta} dm \\
&+ \dot{\xi}\dot{\varphi}_1 \int\int b_j x^i\bar{\varphi} dm - \ddot{\eta}\dot{\eta}_1 \int\int a_i\bar{\eta} dm - \ddot{\eta}\dot{\varphi}_1 \\
&\qquad \int\int a_i x^i\bar{\varphi} dm
\end{aligned} \quad \Big\} \quad [14]$$

where $a_i = -a + x^i$ and $-a \leqq x^i \leqq a$ (Fig. 3). The remaining five integrals in Equation [12] are carried out in a similar manner. The variable density or mass distributions for a transport are given by curves. The numerical evaluation of the forty-five integrals of Equation [12], of which those in Equation [14] are representative, yields the total kinetic energy of a semi-elastic plane.

4 Strain Energy

It is sufficient to consider the total strain energy as the sum of the energies of bending and torsion. The strain energies of bending and torsion of one wing are given by

$$W_b = \frac{\dot{\eta}_1^2}{2} \int_0^l E I_y \left[\frac{\partial^2\eta}{\partial y^2}\right]^2 dy,$$

$$W_t = \frac{\dot{\varphi}_1^2}{2} \int_0^l G \frac{[2A(y)\bar{\varphi}(y)]^2}{c(y)}\, t(y)dy \quad [15]$$

where

E = Young's modulus
I_y = moment of inertia
$t(y)$ = thickness of skin
$\bar{\varphi}(y)$ = angle of twist at y
G = torsion modulus
c = periphery at section y
$\bar{\eta}(y)$ = vertical displacement of bending of axis of wing
$A(y)$ = vertical cross-sectional area at y

The functions I_y, $A(y)$, $c(y)$, and $t(y)$, are given by curves, and in general the evaluation of Equation [15] is numerical. Integrals [15] are written for one wing. For the fuselage and stabilizer the symbols $\bar{\eta}$, $\dot{\eta}_1$, $\bar{\varphi}$, $\dot{\varphi}_1$, I_y, c, and the limits of integration in Equation [15] are replaced by those appropriate.

5 Work Done by Shock-Strut Forces

The nine components of $F_i (i = 0, 1, 2)$ are expressed in Equations [3]. The three components F_{iz} are given as functions of the time by the solution of Equations [1]. The method of obtaining the three components F_{ix} is indicated in section (9).

The element of work δW done by the struts during the interval from 0 to t is

$$\delta W = Q_1\delta X_0 + Q_2\delta Y_0 + \ldots,$$

where the Q_i are generalized forces. δW can be written also as

$$\delta W = \boldsymbol{F}_0 \cdot \delta\boldsymbol{R}_0 + \boldsymbol{F}_1 \cdot \delta\boldsymbol{R}_1 + \boldsymbol{F}_2 \cdot \delta\boldsymbol{R}_2 \quad [16]$$

where

$$\boldsymbol{R}_i = \int_0^t (\boldsymbol{S}_i + \omega \times \boldsymbol{r}_i)dt,\ \omega = \dot{\zeta}\boldsymbol{i} + \dot{\eta}\boldsymbol{j} + \dot{\xi}\boldsymbol{k},\ \boldsymbol{S}_i = X_i\boldsymbol{i} + Y_i\boldsymbol{j} + Z_i\boldsymbol{k}$$

The component displacements of $\boldsymbol{P}_0$, $\boldsymbol{P}_1$, $\boldsymbol{P}_2$, (transport considered as a rigid body) are

$$\begin{aligned}
(\boldsymbol{P}_0)\ & X_0 + \boldsymbol{i}\cdot\begin{vmatrix}\boldsymbol{i} & \boldsymbol{j} & \boldsymbol{k}\\ \xi & \eta & \zeta\\ x_0 & 0 & z_0\end{vmatrix} = X_0 + z_0\eta,\ Y_0 + \boldsymbol{j}\cdot\begin{vmatrix}\boldsymbol{i} & \boldsymbol{j} & \boldsymbol{k}\\ \xi & \eta & \zeta\\ x_0 & 0 & z_0\end{vmatrix} = Y_0 - z_0\xi + x_0\zeta \\
& Z_0 + \boldsymbol{k}\cdot\begin{vmatrix}\boldsymbol{i} & \boldsymbol{j} & \boldsymbol{k}\\ \xi & \eta & \zeta\\ x_0 & 0 & z_0\end{vmatrix} = Z_0 - x_0\eta \\
(\boldsymbol{P}_1)\ & X_0 + \boldsymbol{i}\cdot\begin{vmatrix}\boldsymbol{i} & \boldsymbol{j} & \boldsymbol{k}\\ \xi & \eta & \zeta\\ -x_1 & y_1 & z_1\end{vmatrix} = X_0 + z_1\eta - y_1\zeta,\ Y_0 + \boldsymbol{j}\cdot\begin{vmatrix}\boldsymbol{i} & \boldsymbol{j} & \boldsymbol{k}\\ \xi & \eta & \zeta\\ -x_1 & y_1 & z_1\end{vmatrix} = Y_0 - z_1\xi - x_1\zeta \\
& Z_0 + \boldsymbol{k}\cdot\begin{vmatrix}\boldsymbol{i} & \boldsymbol{j} & \boldsymbol{k}\\ \xi & \eta & \zeta\\ -x_1 & y_1 & z_1\end{vmatrix} = Z_0 + y_1\xi + x_1\eta \\
(\boldsymbol{P}_2)\ & X_0 + \boldsymbol{i}\cdot\begin{vmatrix}\boldsymbol{i} & \boldsymbol{j} & \boldsymbol{k}\\ \xi & \eta & \zeta\\ -x_2 & -y_2 & z_2\end{vmatrix} = X_0 + z_2\eta + y_2\zeta,\ Y_0 + \boldsymbol{j}\cdot\begin{vmatrix}\boldsymbol{i} & \boldsymbol{j} & \boldsymbol{k}\\ \xi & \eta & \zeta\\ -x_2 & -y_2 & z_2\end{vmatrix} = Y_0 - z_2\xi - x_2\zeta \\
& Z_0 + \boldsymbol{k}\cdot\begin{vmatrix}\boldsymbol{i} & \boldsymbol{j} & \boldsymbol{k}\\ \xi & \eta & \zeta\\ -x_2 & -y_2 & z_2\end{vmatrix} = Z_0 - y_2\xi + x_2\eta
\end{aligned} \quad \Big\} \quad [17]$$

From Equations [16] and [17], the element of work done by the shock struts against a rigid airplane is

$$\left.\begin{aligned}\delta W_0 = {} & (\boldsymbol{i}F_{0x} + \boldsymbol{j}F_{0y} + \boldsymbol{k}F_{0z}) \cdot \delta[\boldsymbol{i}(X_0 + z_0\eta) \\ & + \boldsymbol{j}(Y_0 - z_0\xi + x_0\zeta) + \boldsymbol{k}(Z_0 - x_0\eta)] + \dots \\ & + (\boldsymbol{i}F_{2x} + \boldsymbol{j}F_{2y} + \boldsymbol{k}F_{2z}) \cdot \delta[\boldsymbol{i}(X_0 + z_2\eta + y_2\zeta) \\ & + \boldsymbol{j}(Y_0 - z_2\xi - x_2\zeta) + \boldsymbol{k}(Z_0 - y_2\xi + x_2\eta)]\end{aligned}\right\} \dots\dots [18]$$

To Equation [18] is added the element of work performed against the elastic body. Thus the element of total work (to the accuracy required) done against the airplane by the forces $\boldsymbol{F}_i$ is

$$\left.\begin{aligned}\delta W = {} & F_{0x}(\delta X_0 + z_0\delta\eta) + F_{1x}(X_0 + z_1\delta\eta + y_1\delta\zeta) \\ & + F_{2x}(\delta X_0 + z_2\delta\eta + y_2\delta\zeta) + F_{0y}(\delta Y_0 - z_0\delta\xi + x_0\delta\zeta) \\ & + F_{1y}(\delta Y_0 - z_1\delta\xi\,1 - x_1\delta\zeta) + F_{2y}(\delta Y_0 - z_2\delta\xi - x_2\delta\zeta) \\ & + F_{0z}[\delta Z_0 - x_0\delta\eta + \xi_1(x_0)\delta\xi_1] \\ & + F_{1z}[Z_0 + y_1\delta\xi + x_1\delta\eta + \bar{\eta}_1(b_1)\delta\eta_1 + a_3\bar{\varphi}_1(b_1)\delta\varphi_1] \\ & + F_{2z}[\delta Z_0 - y_2\delta\xi + x_2\delta\eta + \bar{\eta}_1(b_2)\delta\eta_1 + a_3\bar{\varphi}_1(b_2)\delta\varphi_1] \\ & + n_1\xi_2(-a_3)\delta\xi_2\end{aligned}\right\} \dots [19]$$

From Equation [19] and section 6, the force matrix,[6] for a level landing, is shown in chart form in Equation [20]. In Equation [20], Mg is the weight of the plane, A_{z0} is the z component of the air lift, and A_η is the aerodynamic moment positive nose upward.

EQUATION [20]

$$\boldsymbol{F} = \begin{array}{|c|c|}\hline X_0 & F_{0x} + F_{1x} + F_{2x} \\ \hline Y_0 & F_{0y} + F_{1y} + F_{2y} \\ \hline Z_0 & F_{0z} + F_{1z} + F_{2z} + Mg - A_{z0} \\ \hline \xi & -z_0F_{0y} - z_1F_{1y} - z_2F_{2y} + y_1F_{1z} - y_2F_{2z} \\ \hline \eta & z_0F_{0x} + z_1F_{1x} + z_2F_{2x} - x_0F_{0z} + x_1F_{1z} + x_2F_{2z} + A_\eta \\ \hline \zeta & y_1F_{1x} + y_2F_{2x} + x_0F_{0y} - x_1F_{1y} - x_2F_{2y} \\ \hline \eta_1 & \bar{\eta}_1(b_1)F_{1z} + \bar{\eta}_1(-b_1)F_{2z} \\ \hline \varphi_1 & a_3F_{1z}\bar{\eta}_1(b_1) + a_3F_{2z}\bar{\eta}_1(-b_1) - z_0[\bar{\varphi}_1(b_1)F_{1x} + \bar{\varphi}_1(-b_1)F_{2x}] \\ \hline \xi_1 & F_{0z}\xi_1(x_0) \\ \hline \xi_2 & n_1\bar{\xi}_2(-a_2) \\ \hline \psi_1 & 0 \\ \hline \eta_1' & 0 \\ \hline \varphi_1' & 0 \\ \hline\end{array}$$

The explicit form of the components of the matrix $\boldsymbol{F}$ will be given presently.

[6] "The Use of Tensors in Mechanical Engineering Problems," *General Electric Review*, vol. 39, 1936, p. 335; also, "Elementary Matrices," by R. A. Frazier, W. J. Duncan, and A. R. Collar, Cambridge University Press, 1938; also, reference (5), p. 131.

6 Aerodynamic Forces

The equations of motion of a rigid airplane on a plane flight path are

$$\left.\begin{aligned} M\frac{dV}{dt} &= -D + Mg\sin\theta + D_0 \\ MV\frac{d\theta}{dt} &= -L + Mg\cos\theta \\ I_y\ddot{\eta} &= -M_\eta\end{aligned}\right\} \dots\dots [21]$$

where the symbols have their usual significance and the co-ordinates are shown in Fig. 4.

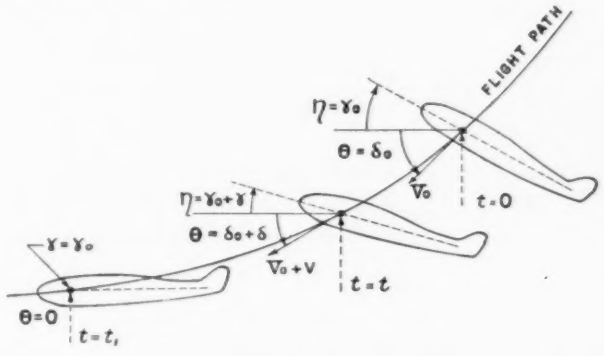


FIG. 4

It is necessary to transform the co-ordinates V, θ, η to the structural co-ordinates employed before. Let $V = V_0 + v$, where V_0 is the value of V at $t = 0$ and v is the change in velocity along the flight path during the impact interval. Then considering all angles to be less than 15 deg, Equations [21] for $D - D_0 = 0$ may be written

$$\left.\begin{aligned} M\dot{v} &= Mg\theta \\ MV\dot{\theta} &= -L + Mg \\ I_y\ddot{\eta} &= -M_\eta\end{aligned}\right\} \dots\dots [22]$$

The angle of attack α (Fig. 4) is

$$\alpha = \theta + \eta = \delta_0 + \gamma_0 + \delta + \gamma = \alpha_0 + \delta + \gamma$$

where α_0 is the angle of attack at $t = 0$. Then the numerical value of the lift is

$$L = \frac{e_0}{2}\rho(V_0 + v)^2(\alpha_0 + \delta + \gamma)SC_L$$

$$= \frac{e_0}{2}\rho V_0^2\alpha_0\left[\left(1 + \frac{2v}{V_0}\right) + \frac{\delta + \gamma}{\alpha_0}\right]SC_L$$

where $0 < e_0 < 1$ is an efficiency factor. Write

$$(\alpha_0/2)\rho V_0^2SC_L = n_0Mg$$

Then

$$L = n_0\left[\left(1 + \frac{2v}{V_0}\right) + \frac{\delta + \gamma}{\alpha_0}\right]Mg \dots\dots [24]$$

and

$$-L + Mg = \left[(1 - n_0) - n_0\frac{2v}{V_0} - \frac{n_0}{\alpha_0}(\delta + \gamma)\right]Mg \dots [25]$$

In view of Equation [25], Equations [22] become

$$\left.\begin{aligned} \dot{v} &= g\theta \\ V_0\dot{\theta} &= \left[(1-n_0) - \frac{2n_0 v}{V_0} - \frac{n_0}{\alpha_0}(\delta+\gamma)\right] \\ I_y\ddot{\eta} &= -\left[n_0(e_0'k_0c_2 - d_w)\left(1 + \frac{2v}{V_0} + \frac{\delta+\gamma}{\alpha_0}\right) + e_0'\frac{c_3^2 k_0'\dot{\eta}}{V_0}\right]Mg \end{aligned}\right\} \quad [26]$$

where d_w is shown in Fig. 1, k_0 and k_0' are dimensionless constants, and e_0' is the tail efficiency factor. The last term is that due to tail damping.

At time t

$$(V_0+v)^2 = \dot{Z}_0^2 + \dot{X}_0^2$$

or

$$\left.\begin{aligned} v &= \sqrt{\dot{Z}_0^2 + \dot{X}_0^2} - V_0 = \dot{X}_0\sqrt{1+\frac{\dot{Z}^2}{\dot{X}^2}} - V_0 \doteq \dot{X}_0 - V_0 \\ &\text{(in landing but not in steady flight), and also} \\ \dot{Z}_0 &= (V_0+v)\sin(\delta_0+\delta) \doteq (V_0+v)(\delta_0+\delta) \doteq V_0(\delta_0+\delta) \\ &\text{or} \\ \delta &= (\dot{Z}_0/V_0) - \delta_0 \text{ and } \dot{\delta} = \ddot{Z}_0/V_0,\ \gamma = \eta - \gamma_0 \end{aligned}\right\} \quad [27]$$

The first of Equations [26] and [27] give

$$\ddot{X}_0 = +g\left(\frac{\dot{Z}_0}{V_0}\right) \quad \text{or} \quad \dot{X}_0 = +g\left(\frac{Z_0}{V_0}\right) \quad [28]$$

In view of Equations [27] and [28], Equations [26] become

$$\left.\begin{aligned} \ddot{Z}_0 &= \left[1 + n_0\left(2 - \frac{2gZ_0}{V_0^2} - \frac{\dot{Z}_0}{\alpha_0 V_0} - \frac{\eta}{\alpha_0}\right)\right]g \\ I_y\ddot{\eta} &= -\left[n_0(e_0'k_0c_3 - d_w)\left(\frac{\dot{Z}_0}{\alpha_0 V_0} + \frac{\eta}{\alpha_0} + \frac{2gZ_0}{V_0^2} - 2\right) + \frac{e_0'c_2^2k_0'\dot{\eta}}{V_0}\right]Mg \end{aligned}\right\} \quad [29]$$

7 Deflection Functions

Thus far the deflection functions $\bar{\eta}_1, \bar{\varphi}_1, \bar{\xi}_1, \bar{\xi}_2, \bar{\psi}_1, \bar{\eta}_1', \ldots$ remain unspecified. From Rayleigh's principle it is reasonable to suppose that the instantaneous deflections are the product of a time function and the static deflections of the airplane under gravity. The static deflections are found by the principle of minimum energy. For example, in the case of wing the deflections in bending and torsion are first determined as power series in y by minimizing the functions

$$\left.\begin{aligned} H_1 &= \tfrac{1}{2}\int_0^l EI_y\left[\frac{d^2\bar{\eta}_1(y)}{dy^2}\right]^2 dy - \int_0^l w(y)\bar{\eta}_1(y)dy \\ H_2 &= \tfrac{1}{2}\int_0^l G\left[\frac{[2A\bar{\varphi}_1(y)]^2}{c(y)}\right]t(y)\,dy - \int^l\int_{-a}^{a} w(y)\,x^i\bar{\varphi}_1(y)\,dx^i\,dy \end{aligned}\right\} \quad [30]$$

where w is the (weight—air lift) per unit area. After power-series approximations are obtained for the deflection functions, these in turn may be approximated by elementary functions. For a wing, in spite of the variable mass and variable structural rigidity, the deflections in bending, from the fuselage as far as the outboard motor, are sufficiently approximated by a constant multiple of $(1 - \cos \pi x/2)$. Likewise, two straight-line segments approximate the total angle of twist in torsion over the same length.

The deflections at time t are then given by

$$\eta_1(t)\bar{\eta}_1(y),\ \xi_1(t)\bar{\xi}_1(x),\ \ldots,$$

where the time functions $\eta_1(t)$, $\xi_1(t)$, ... are given by the solution of the equations of motion, Equations [31]. The calculations, when done carefully, of the deflection functions involve a vast amount of labor. However, by trial, it is justified that these functions when calculated crudely give in all cases sufficiently accurate results. The mass distribution $\sigma(y)$ along a wing is represented by average constant values of σ over three segments of the wing as far out as the outboard motor.

For an airplane such that the portion of the wing intercepted by the fuselage is significantly deformable, the functions $\bar{\xi}_1$ and $\bar{\xi}_2$ are replaced by a single deflection function $\bar{\xi}^i(x)$ which is first determined as a power series in x by means of the first of Equations [30].

8 Equations of Motion

The combination of Lagrange's equations and Equations [29] yield the equations of motion of an elastic airplane

$$\bar{\boldsymbol{Z}}\cdot\boldsymbol{X} = \boldsymbol{F} \quad [31]$$

where values are given in Table 1.

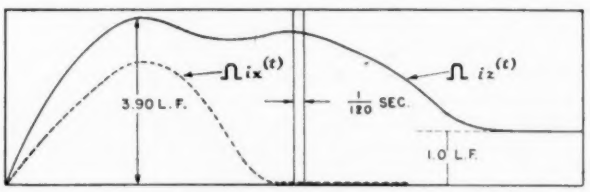
Vector $\boldsymbol{F}$ is given by Equations [20]. The elements of the matrix $\bar{\boldsymbol{Z}}$ are

$$Z_{ij} = M_{ij}p^2 + R_{ij}p + S_{ij}$$

where all R_{ij} vanish except R_{22} and R_{25}. That is, structural damping is neglected. This neglect is on the conservative side.

9 Explicit Strut Load Factors

When the equivalent drop-mass has been determined as shown in reference (4), then the solution of Equations [1], reference (3), yields the load-factor curves as functions of the time. As previously stated the load-factor curves for zero lift can be determined from test results, provided the strut exists. For the cases of fractional lift and for the case of nonexistence of the strut,



LOAD FACTOR CURVE, NO LIFT

Fig. 5

the solution of Equations [1] is the only recourse. Denote the vertical load factors, for zero aerodynamic lift, corresponding to the forces F_{is} by $\Omega_{is}(t)$, $(i = 0, 1, 2)$. A representative $\Omega_{is}(t)$ for zero lift is shown in Fig. 5. Write

$$F_{0s} = -\delta_0'\Omega_{0s}g,\ F_{is} = -\delta_0\Omega_{is}g,\ (i = 1, 2)$$

where the significance of δ_0' and δ_0 is given in Equation [32] and also in section 11.

The drag forces induced by the sudden rotation of the wheels of the landing gear are indeed significant. It is found both by solving the equation of motion for the sudden rotation of a wheel subject to a torque rF_{is}, where r is the radius of the wheel, and also by flight test that the drag force acting at the axle of the

TABLE 1

$$\bar{\mathbf{Z}}\cdot\mathbf{X} =$$

X_0	Y_0	Z_0	ξ	η	ζ	η_1	φ_1	ξ_1	ξ_2	ψ_1	ψ_2	η_1'	φ_1'	
$Z_{1\,1}$														X_0
	$Z_{2\,2}$													Y_0
		$Z_{3\,3}$				$Z_{3\,7}$	$Z_{3\,8}$	$Z_{3\,9}$	$Z_{3\,10}$	$Z_{3\,11}$	$Z_{3\,12}$	$Z_{3\,13}$	$Z_{3\,14}$	Z_0
			$Z_{4\,4}$			$Z_{4\,7}$	$Z_{4\,8}$	$Z_{4\,9}$	$Z_{4\,10}$	$Z_{4\,11}$	$Z_{4\,12}$	$Z_{4\,13}$	$Z_{4\,14}$	ξ
				$Z_{5\,5}$		$Z_{5\,7}$	$Z_{5\,8}$	$Z_{5\,9}$	$Z_{5\,10}$	$Z_{5\,11}$	$Z_{5\,12}$	$Z_{5\,13}$	$Z_{5\,14}$	η
					$Z_{6\,6}$									ζ
		$Z_{7\,3}$	$Z_{7\,4}$	$Z_{7\,5}$		$Z_{7\,7}$	$Z_{7\,8}$							η_1
		$Z_{8\,3}$	$Z_{8\,4}$	$Z_{8\,5}$		$Z_{8\,7}$	$Z_{8\,8}$							φ_1
		$Z_{9\,3}$	$Z_{9\,4}$	$Z_{9\,5}$				$Z_{9\,9}$		$Z_{9\,11}$	$Z_{9\,12}$			ξ_1
		$Z_{10\,3}$	$Z_{10\,4}$	$Z_{10\,5}$					$Z_{10\,10}$	$Z_{10\,11}$	$Z_{10\,12}$			ξ_2
		$Z_{11\,3}$	$Z_{11\,4}$	$Z_{11\,5}$				$Z_{11\,9}$	$Z_{11\,10}$	$Z_{11\,11}$	$Z_{11\,12}$			ψ_1
		$Z_{12\,3}$	$Z_{12\,4}$	$Z_{12\,5}$				$Z_{12\,9}$	$Z_{12\,10}$	$Z_{12\,11}$	$Z_{12\,12}$			ψ_2
		$Z_{13\,3}$	$Z_{13\,4}$	$Z_{13\,5}$								$Z_{13\,13}$	$Z_{14\,14}$	η_1'
		$Z_{14\,3}$	$Z_{14\,4}$	$Z_{14\,5}$								$Z_{14\,13}$	$Z_{14\,14}$	η_1'

wheel in landing on a level surface has a maximum value equal to approximately 0.75 F_{iz}. This force reaches its maximum value in 0.5 of the time period that F_{iz} reaches its maximum and the drag force vanishes at approximately the time of peak value of F_{iz}. Write

$$F_{iz} = -C\Omega_{iz}$$

where C is a positive constant and a typical $\Omega_{iz}(t)$ is represented by the dotted line in Fig. 5. All load factors are positive functions for all values of the time. For a level landing all F_{iy} of the vector $\boldsymbol{F}$ (Equation [20]) are zero. Since all components of $\boldsymbol{F}$ are thus determined, the vector $\boldsymbol{F}$ may be expressed as a time function.

By solution of Equations [1] the law of variation of load factor with aerodynamic lift may be stated

$$\text{[Peak load factor with lift]} = \left[1 - 0.40\left(\frac{\text{Per cent lift}}{100}\right)\right] \times \text{[Maximum load factor with no lift]} \equiv [\delta_0' \text{ or } \delta_0] \times \text{[Maximum load factor with no lift]} \quad [32]$$

SOLUTIONS OF THE EQUATIONS OF PERFORMANCE

10 Analytical Solution

Equations [31] are linear because they were so rendered by first solving Equations [1]. Moreover, Equations [1] were first solved independently to conform with manufacturing procedure. In the study of the landing of an elastic plane, the order of procedure is first to determine the values of M_1 and M_2 (equivalent drop-masses) under the assumptions that the plane is a rigid body. These values are determined from footnote (4). With these values of M_1 and M_2 the solutions of Equations [1] give the load factors for different fractions of air lift. Thus vector $\boldsymbol{F}$ is determined and Equations [31] are solvable for the deflections and rigid co-ordinates.

The solution[7] of Equation [31] is, in matrix notation

$$\boldsymbol{X} = \bar{\boldsymbol{Z}}^{-1}\cdot[Q\boldsymbol{F}(t) + (\bar{\boldsymbol{M}}p + \bar{\boldsymbol{R}})\cdot\boldsymbol{X}_0 + \bar{\boldsymbol{M}}\cdot\dot{\boldsymbol{X}}_0] \quad [33]$$

where

$$\boldsymbol{X}_0 = \boldsymbol{X}(0) = \text{displacements at } t = 0$$

$$\dot{\boldsymbol{X}}_0 = \dot{\boldsymbol{X}}(0) = \text{velocities at } t = 0$$

and

$$Q\boldsymbol{F}(t) \equiv \int_0^\infty e^{-pt}\,\boldsymbol{F}(t)\,dt$$

All elements of $\boldsymbol{X}_0$ are zero except $X_5(0) = \eta(0) = \eta_0$, and likewise all elements of $\dot{\boldsymbol{X}}$ are zero except

$$\dot{X}^3(0) = Z_0(0) = v_0$$

Denote the right-hand side of the operational matrix Equation [33] by $\boldsymbol{G}(p)$. The solution of Equation [33] is given by the contour integral

$$\boldsymbol{X}(t) = \frac{1}{2\pi i}\int_C e^{pt}\boldsymbol{G}(p)\,dp \quad [34]$$

where C is a circular contour enclosing all the poles of $G(p)$.

Since the determinant of $\bar{\boldsymbol{Z}}$ is a high-degree polynomial, the labor of computing the residues in Equation [34] is considerable.

A study of the behavior of the generalized elastic airplane in landing involves the study of the solution of Equation [34] as the system parameters M_{ij} and S_{ij} vary. Since it is especially

[7] Equation [34] is merely Van der Pol's extension of Heaviside's operational calculus written in matrix form. For the unextended theory see "The Heaviside Operational Calculus," by H. W. March, Bulletin, American Mathematical Society, vol. 33, 1927, p. 311; also reference (5), vol. 1, chapt. 4. For the extended theory see: "Simple Proof and Extension of Heaviside's Operational Calculus for Invariable Systems," *Philosophical Magazine*, vol. 7, 1929, p. 1153.

desirable, from a structural point of view, to study the cause of distortion (bending and torsion) of the front spar in a crash landing, it is of interest to vary fore and aft the location of the main landing gear on the wing. To study the mechanism of failure of a front spar in landing, it is necessary to vary the torsional rigidity of the wing. The location of the center of gravity has a pronounced effect on wing torsion in landing. Different loadings and different velocities of descent along with system parameter changes lead to a multitude of cases.

Of course, if only one particular landing with one set of system parameters is required then the solution of Equation [34] is carried out.

11 Differential-Analyzer Solutions

It is evident that the labor involved in a complete study of a generalized transport airplane in landing by means of Equation [34] is prohibitive. Certain particular cases must be selected which are most important and these solved by machine methods.

For a large transport with tricycle landing gear, its normal first impact is on the main gear. For this type of landing, the general deflections of the transport will be largest. Once the airplane rests on the main gear, the solution of the dynamical problem of lowering the nose gear is not a difficult one.

Accordingly, consider the deflections for the airplane landing on the main gear. Since there exists no differential analyzer sufficiently large to integrate Equation [31], it is necessary to proceed as follows: Since the weight of the empennage of a transport is but 3 to 5 per cent of the weight of the plane, it is clear that the bending and torsion of the stabilizer cannot, as far as mass considerations are concerned, affect the deflections of the wing and fuselage in landing. Consequently, as far as mass considerations are concerned in the motion of the airplane the empennage will be regarded as a concentrated mass. As far as its aerodynamic moments are concerned, the empennage will be regarded as a localized force. Once the motion of the points of attachment of the stabilizer are known from the general motion of the airplane, the behavior of the empennage under an applied *displacement* can be studied as an independent problem. If it is further supposed that the airplane lands on all wheels of the main gear simultaneously, then the co-ordinates in Equation [31] are reduced to Z_0, η, η_1, φ_1, ζ_1, ξ_2. This system is well within the range of a differential analyzer.

Since the time of impact during landing is of the order of 0.25 sec, it is assumed that the aerodynamic forces remain constant during this interval. These forces then are equivalent to a constant lift at the center of gravity and a constant moment. Solutions were carried out for a range of lifts and moments. Subsequently, the orientation of the transport and the position of its control surfaces which will produce the prescribed lift and moment are determined from Equations [29].

Under the conditions thus set forth, consider a numerical example. It is not feasible to publish data pertaining to any particular transport. Accordingly, the curves of distributed rigidity, distributed mass, and aerodynamic lift and moments are not displayed. All of the lengths represented in Fig. 3 are involved. Such data as are given are somewhat typical for large transports and do not necessarily pertain to a particular airplane.

Let the weight on the main gear be 62,000 lb. The center of gravity is in its most forward position. The main landing gear is 44 in. aft of the center of gravity and is 17 in. aft of the center line of the wing. The first two numbers change with the loading; only the last is descriptive of a particular airplane. However, when the main struts are moved fore and aft in the solutions, this number also will change. The units employed are inches, pounds, seconds; $E = 10^7$, $g = 386$.

Under the stated conditions and after the required integrals have been evaluated, the equation of performance for one set of values of the system parameters is

$$\bar{\boldsymbol{Z}}_s \cdot \boldsymbol{X}_s = \boldsymbol{F}_s \qquad [35]$$

where values are given in Table 2 and Equations [36].

Equation [35] is of a form suitable for use on the differential analyzer.

The structural matrix $\bar{\boldsymbol{Z}}$, for α_0 fixed, represents a particular transport with a definite loading and definite position of the center of gravity. The vector $\boldsymbol{F}$, through the variation of the parameters δ_0, δ_1, β_0, β_1, L_w, L_t, m, and n_1 determines an eightfold infinitude of landings. The variation of the twenty-four structural system parameters gives a twenty-fourfold infinitude of transports. The duration of the impact during landing has been shown to be (for the type of strut in question) of the order of 0.25 sec.

The variations of the $\boldsymbol{F}_s$ parameters are as follows: If

$0.5 < \alpha_0 < 7$ then $(0.5)2 \times 10^4 <$ torsional rigidity $< (7)\ 2 \times 10^4$

$0.6 < \delta_0 < 1$ then $0 <$ aerodynamic lift at C.G. < 1

$0 < \delta'_0 < 1$ then $0 <$ wheel drag $< 0.75F_{it}(2t)$

$0 < \beta_0 < 1$ then $0 <$ wing lift < 1 ($\beta_0 = 1$ signifies no stall)

$0 < \beta_1 < 1$ then $0 <$ negative tail lift < 1

$n_1 = 1$ This signifies a constant tail moment acting during impact such that the transport was balanced at the first instant of impact

$m = 0.1$ signifies that the wing moment is 0.1 of the tail moment

$\epsilon_0 = 1$ or -1 according as the struts of the main gear are located at 14 in. aft or fore of the center line of the wing

Results and Conclusions

(*a*) *Differential-Analyzer Solutions.* About 300 solutions were obtained on the differential analyzer. The applied-force parameters were varied as just indicated. One system parameter (i.e., parameters of the matrix $\bar{\boldsymbol{Z}})\alpha_0$ was varied. Two of these solutions are shown in Fig. 6. The initial sinking speed v_0 was 200 ips for the solutions shown.

(*b*) *Broken Front-Spar Criterion.* The value of α_0 in the solutions shown in Fig. 6 does not belong to any bomber or transport investigated. The value of α_0 is taken such that the period of the first half cycle of φ_1 agrees approximately with the period of application of the strut force. For this choice the peak value of φ_1 is the maximum obtainable and is approximately 14 times the static angular deflection. This is the only indication of the mechanism of a broken spar. The real value of α_0 belonging to modern transports and bombers with high wing loading is approximately 5 instead of 0.7. For the real value of α_0 the response of $p\varphi_1$ is shown approximately by the line of circles in Fig. 6(*b*). Both of the solutions given are for crash landings. The effect of 0.5 air lift is shown by comparing the dotted and continuous lines in Fig. 6. In Fig. 6(*a*), it is noted that the acceleration due to gravity of the C.G. is greater than the resistance of the struts for approximately 0.022 sec. The same initial hook appears in Figs. 6(*b*, *d*, *e*, *f*).

TABLE 2

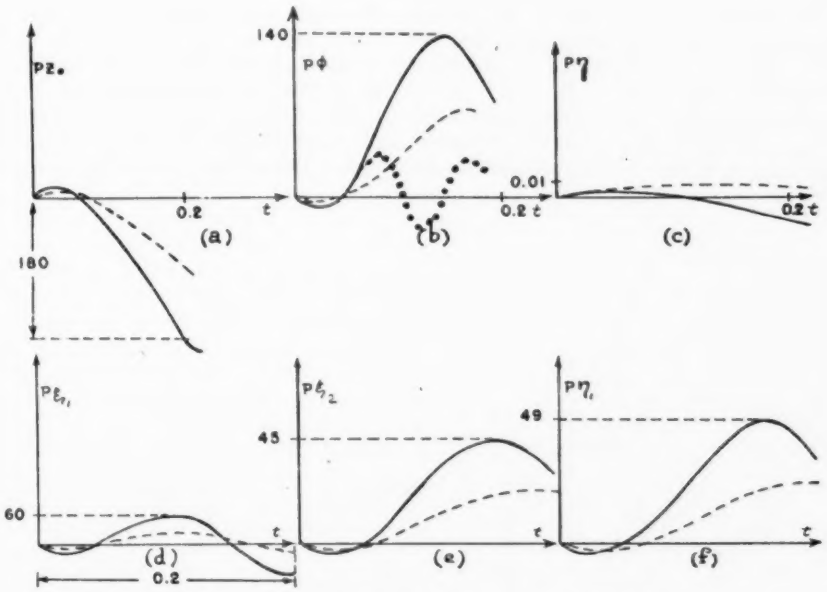
$\bar{Z}_s \cdot X_s =$

Z_0	η	ξ_1	ξ_2	η_1	φ_1	
$158\ p^2$		$10.8\ p^2$	$17\ p^2$	$34\ p^2$	$32\ p^2$	Z_0
	$5.44\ 10^6\ p^2$	$-3340\ p^2$	$7600\ p^2$	$-180\ p^2$	$-3190\ p^2$	η
$10.8\ p^2$	$-3340\ p^2$	$7.10\ p^2 + 10460$				ξ_1
$17\ p^2$	$7600\ p^2$		$10.6\ p^2 + 4060$			ξ_2
$34\ p^2$	$-180\ p^2$			$18\ p^2 + 7200$	$4.88\ p^2$	η_1
$32\ p^2$	$-3190\ p^2$			$4.88\ p^2$	$92\ p^2 + 2(10^4)\ \alpha_0$	-1

EQUATIONS [36]

$F_s =$

$\{-\delta_0\Omega_{1z} + (1 - \beta_0 L_w + \beta_1 L_t)\}g = \{-\delta_0\Omega_{1z} + (1 - \beta_0 L_w + \beta_1 L_t)\}386$	Z_0
$\dfrac{20 \times 31000}{5.44 \times 10^6}\left[-2\delta_0\gamma_0\Omega_{1z} + 2n_1 + 2m - \dfrac{202}{20}\delta'_0\Omega_{1x}\right] = 2.29 \times 10^{-1}[-\delta_0\gamma_0\Omega_{1z} + n_1 + m - 5\delta'_0\Omega_{1x}]$	η
0	ξ_1
$\dfrac{1910}{10.6}n_1 = 180n_1$	ξ_2
$\dfrac{31000}{18} \times \left[\left(1 - \cos\dfrac{90\pi}{726}\right)2\delta_0\Omega_{1z}\right] = 3.45 \times 10^3\,(0.073)\delta_0\Omega_{1z} = 250\delta_0\Omega_{1z}$	η_1
$2\left(-\dfrac{17}{2} \times \dfrac{31000}{92}\,3.8 \times 10^{-3}\right)(-2\delta_0\Omega_{1z})\epsilon_0 = 43.5\delta_0\epsilon_0\Omega_{1z}$	φ_1



	δ_0	δ_1	β_0	β_1	m	n_1	ϵ_0	α_0
SOLID CURVE	1	1	0	0	0.1	1	1	0.7
DOTTED CURVE	0.8	0.8	0.5	0.5	0.1	1	1	0.7

FIG. 6

(*c*) *Accelerations at Point* $P(x, y, z)$. The accelerations at $P(x, y, z)$ are given by

$$\ddot{P} = \ddot{Z}_0 + \boldsymbol{k} \cdot \begin{vmatrix} \boldsymbol{i} & \boldsymbol{j} & \boldsymbol{k} \\ \ddot{\xi} & \ddot{\eta} & \ddot{\zeta} \\ a(x) & b(y) & c(z) \end{vmatrix} + \ddot{\zeta}^{\boldsymbol{k}} \quad \ldots\ldots\ldots [37]$$

For example, from the no-lift solution in Fig. 6, the acceleration of the pilot is

$$\ddot{P}_0 = \ddot{Z}_0 + \boldsymbol{k} \cdot \begin{vmatrix} \boldsymbol{i} & \boldsymbol{j} & \boldsymbol{k} \\ \ddot{\xi} & \ddot{\eta} & \ddot{\zeta} \\ 400 & 0 & 0 \end{vmatrix} + \ddot{\xi}_1 \bar{\xi}(400)$$

$$= -\left(\frac{180}{0.12}\right) - 400\left(-\frac{0.01}{0.20}\right) + (600\,\pi \cos 10\pi t)(1/4)$$

$$= -(3.88 - 1.22 \cos 10\pi t)g = -2.66g \text{ (minimum)}$$

(The C.G. acceleration is —3.9.)

If the transport has an angular velocity nose downward of $^3/_4$ radian per sec, then the pilot will perceive no acceleration induced by the main landing gear in a crash landing. (It should be noted that the positive direction of η_1 is upward, the positive directions of ξ_1 and ξ_2 are downward, and φ_1 is as shown in Fig. 3.)

The maximum acceleration of the outboard motor is

$$\ddot{P}_{m2} = \ddot{Z}_0 + \boldsymbol{k} \cdot \begin{vmatrix} \boldsymbol{i} & \boldsymbol{j} & \boldsymbol{k} \\ \ddot{\xi} & \ddot{\eta} & \ddot{\xi} \\ -a_1 & -b_2 & c_2 \end{vmatrix} + \ddot{\eta}_1 \bar{\eta}(b_1) + d_1 \ddot{\varphi}_1 \bar{\varphi}(b_1)$$

$$= -\frac{180}{0.12} + 17\left(-\frac{0.01}{0.12}\right) + 490\,(1) + 1400\,(1/57.3)$$

$$= -2.55g$$

(The C.G. acceleration is —3.9.)

(*d*) *Maximum Deflections.* The crash landings just considered give high accelerations. (The term crash landing is used for a more severe landing than maximum blind landing.) For normal landings (velocity of descent = 60 ips and wing lift = 0.8) the accelerations are of the order of $1.3g$. The order of magnitude of measured accelerations are of the order of $1.1g$.

(*e*) *Configuration of Maximum Deflections.* The maximum deflections in landing due to the main gear occur for the space-time configuration given in Fig. 6, that is, when the tail is held down, the airplane is prevented from rolling away from the thrust exerted by the main gear.

(*f*) *Analytical Solutions.* Since the space-time configuration of maximum deflections is known, sufficient results are obtainable by one application of Equation [34], the tail moment being held as a symbol and its magnitude eventually determined such that $\eta = 0$ for all t during impact. In a crash landing, this moment must be very large to overcome the opposing moment induced by the sudden rotation of the landing wheels. Once this tail moment is known, the position of the control surfaces required to produce it can be obtained approximately from Equations [29].

(*g*) *Conventional Gear.* The method just given with slight changes is applicable to an airplane with conventional landing gear.

(*h*) *Impact Stress.* In the beginning, the electrical industry was primarily concerned with mere steady-state phenomena. Since there was a need for it, the Heaviside operational calculus developed rapidly for the handling of transient phenomena. In a like manner impact or dynamical stress is becoming of increasing importance. It is of course closely associated with fatigue.

(*i*) *Improved Accuracy.* The foregoing F_{ij} are calculated with the methods of references (3) and (4), which suppose M_2 to be a rigid mass. For more accurate F_{ij} the work of reference (3) can be carried out where M_2 is the mass of an elastic beam. This, however, is scarcely justifiable since the F_{ij} here employed are on the conservative side, i.e., they are slightly too large.

Acknowledgments

This paper is part of a general investigation on the behavior of an elastic airplane in landing, taxiing, and gusts which Mr. F. R. Shanley, chief structures engineer of the Lockheed Aircraft Corporation, with characteristic foresight, first seriously suggested to the author in 1942. The investigations on the two remaining subjects will appear presently. Appreciation is expressed to him for his many helpful ideas and his encouraging support during the rather long interval of this work. The author also expresses his appreciation to Mr. C. L. Johnson, chief research engineer, for his interest in the application of the theory to the Lockheed *Constellation* and the Lockheed-89, and to Mr. H. L. Hibbard, vice-president and chief engineer, for his abiding interest in theoretical work and for the liberal financial appropriation which made possible the use of the differential analyzer of the General Electric Company.

Studies in Three-Dimensional Photoelasticity Torsional Stresses by Oblique Incidence

By MAX M. FROCHT,[1] PITTSBURGH, PA.

In this paper a photoelastic method is described for the study of stresses in cylindrical shafts due to pure torsion. The basic photoelastic equation governing this case is derived. It is shown that the maximum stresses, i.e., the boundary stresses, can be determined from a single stress pattern, and that the two stress components which define the complete stress system in pure torsion at an interior point can be determined from two stress patterns obtained from one section of a shaft into which the pure-torsion system has been frozen, employing to this end the Drucker-Mindlin suggestion of oblique incidence. The method is applied to a circular shaft, and the experimental results are found to be in complete agreement with the theory.

1 THEORY

History of Three-Dimensional Photoelasticity

WITH the advent of three-dimensional photoelasticity, which was made possible by the process of freezing a stress pattern (1, 2, 3),[2] it was early recognized that the two-dimensional procedure employing a parallel beam of light at normal incidence to the plate was inadequate. In 1937, Hiltscher (4) employed a convergent beam of light in the determination of the directions of the principal stresses and the corresponding three principal shears. In 1938, Kuske (5) extended Hiltscher's work and showed the possibilities in this method for the determination of the actual principal stresses.

The next suggestion came from Weller (6), who in 1939, at the Ninth Eastern Photoelasticity Conference held at Cornell University, proposed the use of scattered light. This paved the way for the next step. In 1940, Drucker and Mindlin (7) in a theoretical study of the effect of rotation of the principal axes in three-dimensional problems suggested the use of oblique incidence of a parallel beam in contrast to the oblique incidence of the convergent beam employed by Hiltscher.

Although, theoretically, this procedure, which may be likened to that of a strain rosette, leads one to expect the complete determination of all the six stress components encountered in the most general three-dimensional case, the actual formulation of these equations shows that only in the simplest cases will they yield results of sufficient accuracy to be of practical value. This weakness is indirectly shown by Drucker's (8) paper of 1943, which to the best of the author's knowledge represents the first published application of this type of oblique incidence in photoelasticity. Drucker considers a two-dimensional problem, a diagonally compressed square plate, and determines the principal stresses at a point by a rotation of the model about one of the principal axes at the point. From his discussion of the accuracy of the results, it follows that even in a two-dimensional case rotation about an arbitrary axis in the plate would lead to gross errors.

The present paper is an application of oblique incidence to the solution of the three-dimensional problem of pure torsion, which because of its relative simplicity, promises to be of practical value and of high accuracy. Work with oblique incidence has been carried on in the photoelastic laboratory at the Carnegie Institute of Technology intermittently since 1940, and the present paper is one of the outgrowths (9).

Development of Theory

The Basic Equation for Pure Torsion. It is shown in the theory of elasticity (10) (Saint Venant's theory), that in cylindrical shafts subjected to pure torsion the general stress system is reduced to two shear components only, lying in planes parallel to those of the applied twisting couples. Choosing the axis of the shaft as the Z axis, Fig. 1, the stress components induced by pure torsion are τ_{zx} and τ_{yz}. All other stress components vanish, i.e.

$$\sigma_x = \sigma_y = \sigma_z = \tau_{xy} = 0$$

Assume now that a ray of polarized light lying in a plane

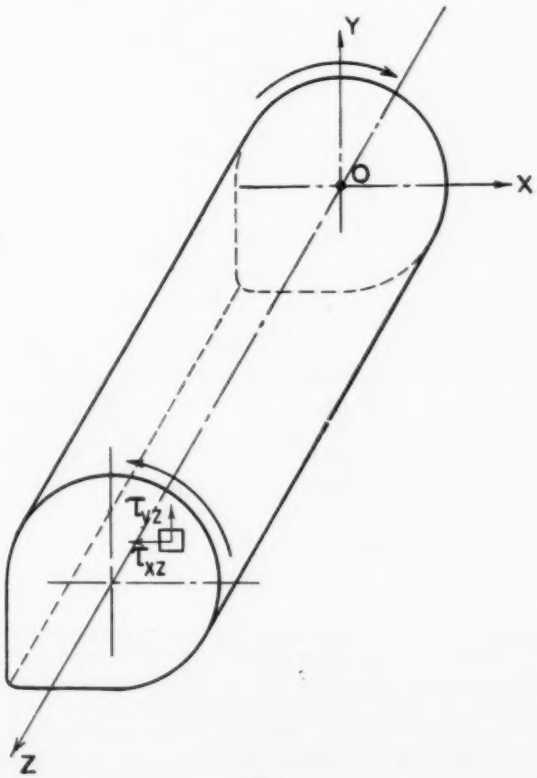


Fig. 1

[1] Associate Professor of Mechanics, in Charge of Photoelastic Laboratory, Carnegie Institute of Technology. Mem. A.S.M.E.

[2] Numbers in parentheses refer to the Bibliography at the end of the paper.

Presented at the National Meeting of the Applied Mechanics Division, Chicago, Ill., June 16–17, 1944, of The American Society of Mechanical Engineers.

Discussion of this paper should be addressed to the Secretary, A.S.M.E., 29 West 39th Street, New York, N. Y., and will be accepted until January 10, 1945. Discussion received after the closing date will be returned.

Note: Statements and opinions advanced in papers are to be understood as individual expressions of their authors and not those of the Society.

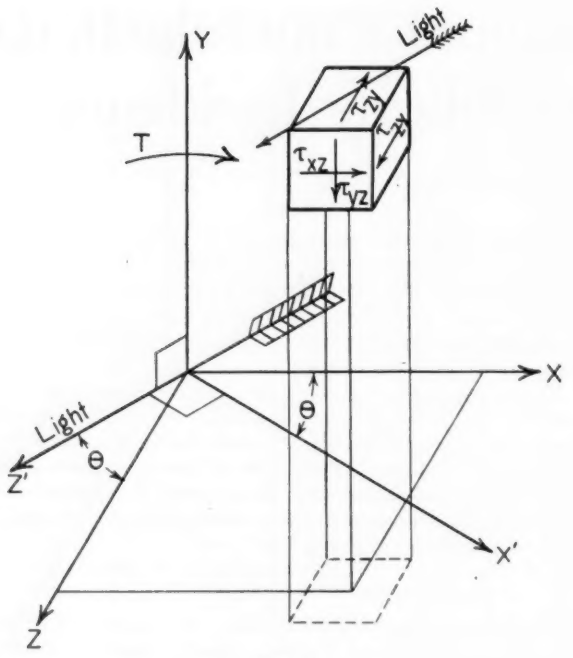


FIG. 2

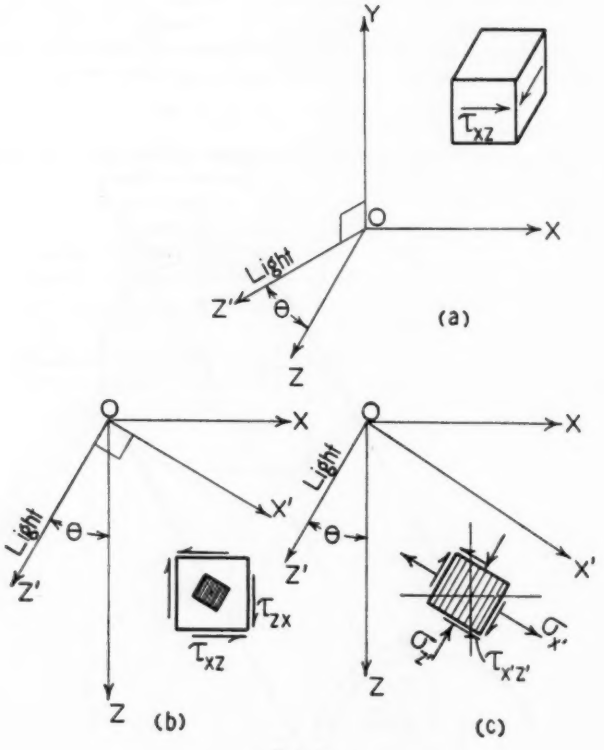


FIG. 3

parallel to the X, Z plane passes through an element subjected to pure torsion, the ray being inclined at an arbitrary angle θ to the axis of the shaft, the Z axis, Fig. 2. The direction of the light we designate by Z' and the line perpendicular to it and lying in the X, Z plane by X', Fig. 2. We now wish to determine the photo-elastic effect of the stresses resulting from pure torsion on the light passing through an element subjected to it. From the general stress-optic law we know that, neglecting rotation, this optical effect is produced by the difference between the secondary principal stresses $(p' - q')$ lying in a plane transverse to the assumed axis of propagation, i.e., in a plane parallel to the X', Y plane, Fig. 2. The problem thus reduces itself to one of determining the secondary principal stresses and their difference for the specified direction of the light.

To this end we consider each of the two stress systems τ_{zx} and τ_{yz}, separately. The first of these components τ_{zx} is shown in Fig. 3(*a*). Consider next an element with faces parallel and perpendicular to the ray, the shaded element, Figs. 3(*b*) and (*c*). The stresses $\sigma_{x'}$, $\sigma_{z'}$, and $\tau_{x'z'}$ induced on such an inclined element by the component τ_{zx} are given by the expressions

$$\sigma_{x'} = \tau_{zx} \sin 2\theta \quad [1a]$$

$$\sigma_{z'} = -\tau_{zx} \sin 2\theta \quad [1b]$$

$$\tau_{x'z'} = \tau_{zx} \cos 2\theta \quad [1c]$$

The secondary principal stresses for this case are therefore completely determined by the horizontal stress component $\sigma_{x'}$. Hence

$$p' = \sigma_{x'} = \tau_{zx} \sin 2\theta \quad [2a]$$

$$q' = 0 \quad [2b]$$

We next turn our attention to the second stress component τ_{yz} which is shown in Fig. 4(*a*). On an inclined element whose faces are parallel and perpendicular to the ray, Figs. 4(*b*) and (*c*), this stress gives rise to two shear systems

$$\tau_{x'y} = \tau_{zy} \sin \theta \quad [3a]$$

$$\tau_{z'y} = \tau_{zy} \cos \theta \quad [3b]$$

Of these only the component $\tau_{x'y}$ will influence the secondary principal stress for the given ray.

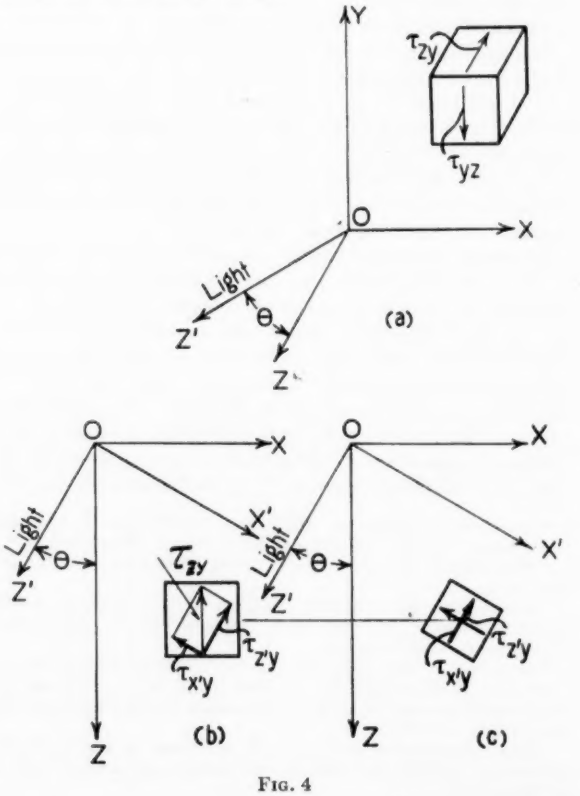


FIG. 4

By superimposing the two stress systems given by Equations [2*a*] and [3*a*], we obtain the secondary principal stresses resulting from pure torsion.

From elementary consideration, it then follows that the secondary principal stresses p' and q' are given by

$$p', q' = \frac{\sigma_{x'}}{2} \pm \frac{1}{2}\sqrt{\sigma_{x'}^2 + 4\tau_{x'y}^2}$$

$$= \frac{1}{2}(\tau_{zz}\sin 2\theta \pm \sqrt{\tau_{zz}^2 \sin^2 2\theta + 4\tau_{zy}^2 \sin^2\theta}) \ldots [4]$$

Hence

$$p' - q' = \sqrt{\tau_{zz}^2 \sin^2 2\theta + 4\tau_{zy}^2 \sin^2\theta}$$

or

$$p' - q' = 2\sin\theta\sqrt{\tau_{zz}^2\cos^2\theta + \tau_{zy}^2} \ldots [5]$$

The photoelastic effect, i.e., the retardation n in fringes, is given by

$$n = Ct'(p' - q') \ldots [6]$$

in which C is the usual stress-optic coefficient, which is related to the shear fringe value of the material f by the expression

$$C = \frac{1}{2f} \ldots [7]$$

From Equations [5], [6], and [7] we obtain

$$n'f = \sin\theta\sqrt{\tau_{zz}^2\cos^2\theta + \tau_{yz}^2} \ldots [8]$$

in which

$$n' = n/t'$$

i.e., n' is the fringe intensity, or the number of fringes per inch of length measured parallel to the ray, and the units of τ_{zz} and τ_{yz} are those of the fringe value f, that is, pounds per square inch. If the constant f be omitted from Equation [8], the effect of this

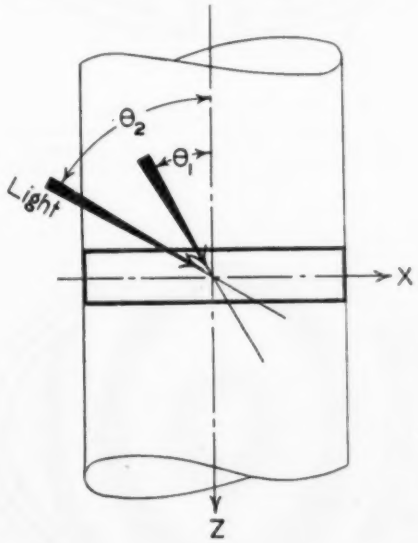


FIG. 5

omission is merely to change the units of the stress components to fringes per inch. Dropping this constant we obtain

$$n' = \sin\theta\sqrt{\tau_{zz}^2\cos^2\theta + \tau_{yz}^2} \ldots [9]$$

This is the fundamental stress-optic equation for pure torsion of cylindrical shafts.

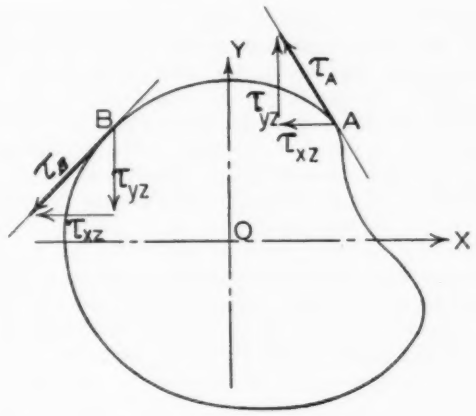


FIG. 6

Inspection of Equation [9] shows that the stress components τ_{zz} and τ_{yz} can be determined from two stress patterns of an arbitrary slice or plate cut from the shaft for which the light has different inclinations θ_1 and θ_2, (θ not equal to zero). To make the idea concrete, let us assume that we cut a transverse slice AB, Fig. 5, out of the shaft into which pure-torsion stresses have been fixed. Two stress patterns in which the light has different and arbitrary directions θ_1 and θ_2, Fig. 5, will give the necessary and sufficient experimental data to evaluate the stress components τ_{zz} and τ_{yz} at any point in the cross section. By inserting the angles θ_1 qnd θ_2 and the fringe intensities n_1' and n_2' at a given point into Equation [9], we obtain the two equations

$$n_1' = \sin\theta_1\sqrt{\tau_{zz}^2\cos^2\theta_1 + \tau_{yz}^2} \ldots [10a]$$

$$n_2' = \sin\theta_2\sqrt{\tau_{zz}^2\cos^2\theta_2 + \tau_{yz}^2} \ldots [10b]$$

which upon solution give the required stress components τ_{zz} and τ_{yz}, and from these the total shear stress can be found.

Boundary Stresses. The maximum shear stresses generally occur on the boundary, and these are of special practical significance. The method under consideration is even simpler for the determination of boundary stresses. These can be evaluated from only one stress pattern for an arbitrary value of θ, not equal to zero. This simplification is made possible by the well-known property of boundary stresses, which states that at the boundary the stresses are tangent to the boundary, Fig. 6. At each point of the boundary the relation between the components τ_{zz} and τ_{yz} is therefore completely determined by the geometry, i.e., the shape of the cross section. It follows that one stress pattern is sufficient to determine the boundary stresses. Denoting the fringe intensity at the boundary by N', we have from the fundamental Equation [9]

$$N' = \sin\theta\sqrt{\tau_{zz}^2\cos^2\theta + \tau_{yz}^2} \ldots [11]$$

Also from the contour of the cross section, we have

$$\tau_{yz} = r\tau_{zz} \ldots [12]$$

in which r is a known ratio. Substituting into Equation [11], we obtain

$$N' = \sin\theta\tau_{zz}\sqrt{\cos^2\theta + r^2} \ldots [13]$$

which gives τ_{zz} directly.

An alternative procedure for the determination of boundary stresses is possible. From Equation [9], it follows that for θ = 90 deg

$$n' = \tau_{yz} \ldots [14]$$

This means that a stress pattern obtained from a ray perpendicular to the axis of the shaft gives directly the component τ_{yz} at every point of the cross section, including the boundary. Since at the boundary the direction of the total shear is known, it follows that this boundary stress can be determined from the one component τ_{yz}. In this method, however, the slice cannot be a transverse section but has to be inclined to the axis of the shaft at some convenient angle α, Fig. 7. It should also be noted that at the boundary the thickness t' is no longer constant, but varies linearly and this variation must be considered when calculating n'. However, there will always be boundary regions at which the ray is parallel to the surface and these yield the most reliable results. It is therefore advisable to orient the model so that the rays are parallel to the most highly stressed parts.

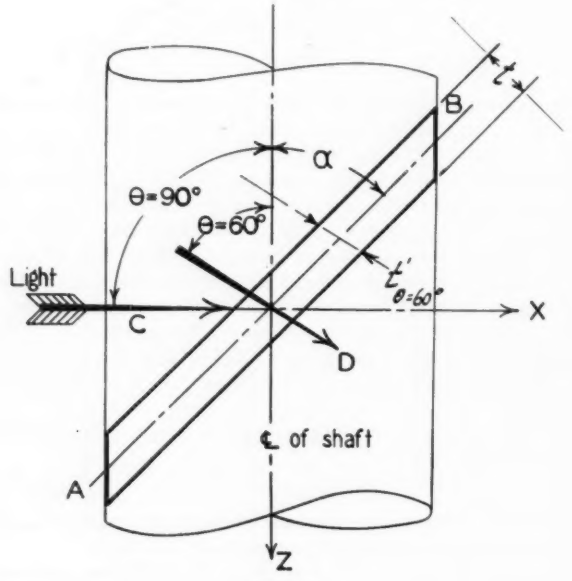


FIG. 7

Theoretically the two methods are equally effective. Practical considerations, however, make the first method, in which a transverse slice may be used, generally preferable. This is due to the relatively large distortions which must be given to a bakelite shaft in order to obtain sufficiently large stresses for optical observation. If the section is inclined as in Fig. 7, the shape of the boundary at the ends of the plate may be considerably distorted from the normal shape. This may lead to certain difficulties which are avoided by the use of a transverse section. However, for circular shafts the method based on Equation [14] is very effective.

The second procedure, in which $\theta = 90$ deg, may also be used to determine the shear stress at any point, provided the stress contour through that point is known or can be approximated.

2 APPLICATION TO CIRCULAR SHAFT

Since the state of stress in a circular shaft in pure torsion is known with precision, the proposed method is first tested on such a shaft. To this end a circular shaft made of Bakelite BT-61-893 and approximately 1 in. diam was subjected to a pure torque, and the shear system frozen into it in the usual manner.

In order to obtain a fair measure of the efficacy of the method, it would be desirable to have a material free from time stresses, which Bakelite is not. Here again the circular shaft proved advantageous because the time stresses in such a shaft can be readily removed by machining after weeks or even months. The machinist was instructed to remove a thin skin. Due to an error, he reduced the diameter to 0.908 in., which was far in excess. It had, however, the effect of relieving the time stress completely. It is recognized that in a general case this remedy cannot be applied with the same ease or effect, although in many cases it is possible and advisable to remove a thin skin. While admittedly a source of error and highly undesirable, it should not be concluded that the presence of time stresses seriously impairs the final results. With proper technique and efficient work these stresses can be kept to very low values. We have obtained stress patterns from plates cut from circular shafts with transverse holes in tension in which the boundary stresses were nearly as good as those found in a freshly cut two-dimensional plate (11).

From this reduced shaft a slice 0.119 in. thick and inclined at 45 deg to the axis of the shaft, Fig. 7, was carefully cut out. In this cutting process the axis of the shaft was kept horizontal and the face of the cutter vertical, so that the axis of the shaft and the minor axis of the elliptical slice were perpendicular to each other.

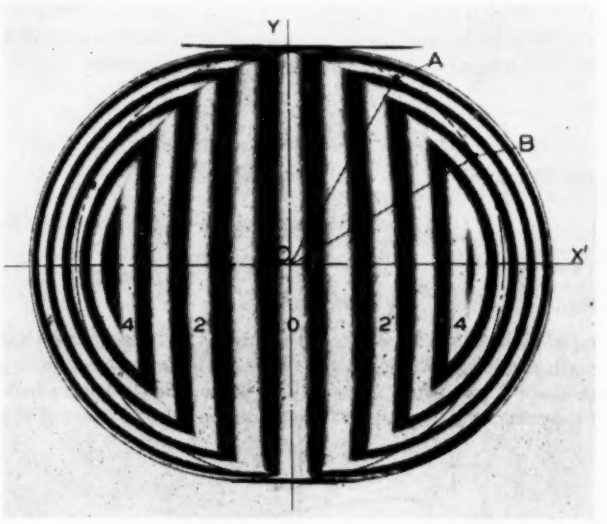


FIG. 8 STRESS PATTERN OF PLATE FROM SHAFT IN PURE TORSION MAKING AN ANGLE OF 45 DEG WITH AXIS OF SHAFT

(Light normal to axis, i.e., $\theta = 90$ deg. Diameter = 0.908 in.; $t' = 0.1685$ in.; N on X' axis at boundary = 5.5 fringes. Edges of plate have been marked for clarity.)

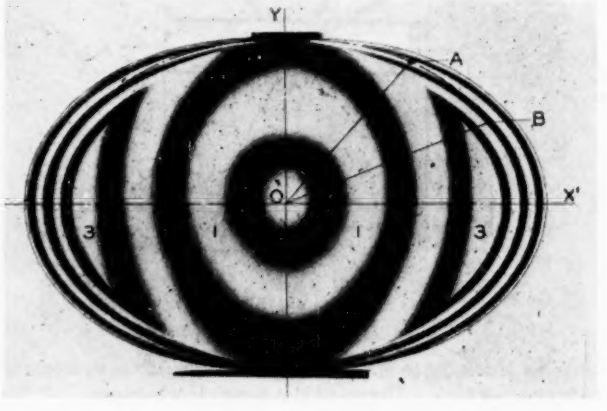


FIG. 9 STRESS PATTERN OF PLATE FROM SHAFT IN PURE TORSION MAKING AN ANGLE OF 45 DEG WITH AXIS OF SHAFT

(Light at an angle of 60 deg with axis of shaft. Diameter = 0.908 in.; $t = 0.119$ in.; $t' = 0.123$ in.; N on X' axis at boundary = 3.72 fringes, by extrapolation. Edges have been marked for clarity.)

Two stress patterns of this plate were taken, Figs. 8 and 9. In one, Fig. 8, $\theta = 90$ deg, i.e., the axis of the circularly polarized beam was perpendicular to the axis of the shaft; and in the other, Fig. 9, this angle was 60 deg, Fig. 7. The customary procedure of immersing the slice in a bath of Halowax oil was followed. The general dimensions, nomenclature, and relevant data are as follows:

Material—Bakelite BT-61-893

D = diameter of shaft, 1.005 in. both before and after twisting
D' = diameter of shaft after removal of time stresses, 0.908 in.
L = length between couples, 6 in.
Over-all length, 7 in.
Time and temperature of heating, 3 hr at 260 F
θ = angle of twist, 107 deg or 1.867 radians in 6 in.
T = applied torque, 11.42 lb-in.
α = angle between axis of shaft and plate, 45 deg
θ = angle between axis of shaft and ray
t = thickness of plate, 0.119 in.
t' = effective light path, $t' = t/\cos(\alpha - \theta)$, Fig. 7
n = fringe order at an interior point
n' = fringe intensity, i.e., fringes per inch of thickness at an interior point
N = fringe order at boundary
N' = fringe intensity at boundary
E = modulus of elasticity, 1100 psi
G = modulus of rigidity, 366 psi
ν = Poisson's ratio, $1/2$
f = shear-fringe value of material, 1.6 psi per in. of thickness

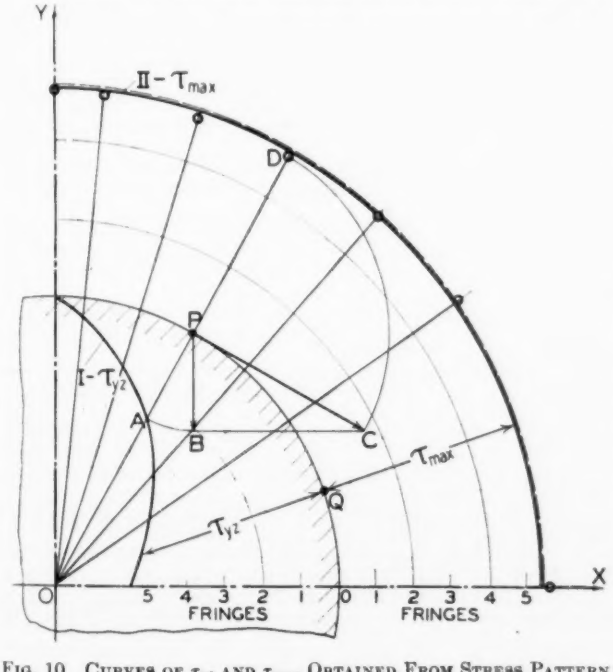


FIG. 10 CURVES OF τ_{yz} AND τ_{max} OBTAINED FROM STRESS PATTERN FIG. 9; METHOD OF OBTAINING τ_{max} IS ALSO SHOWN

Curve I is curve of fringe orders from Fig. 8. Curve II is mean value of τ_{max} derived from curve I, $N = 5.33$ fringes. Dashed curve is theoretical fringe order as calculated from applied torque of 11.42 lb-in., $N = 5.46$ fringes.)

Boundary Stresses. The boundary stresses were determined by means of Equation [14], and the fringe orders N from the stress pattern shown in Fig. 8.

Fig. 10 shows the actual procedure in the numerical evaluation of all boundary stresses. Curve I represents the values of τ_{yz} along the circumference of the shaft, laid off radially, which are obtained from the stress pattern in Fig. 8. For example, on the Y axis, $\tau_{yz} = 0$, and on the X' axis $\tau_{yz} = 5.5$ fringes. At some general point P, $\tau_{yz} = PA$. From P as a center, we draw an arc of radius PA, to obtain point B, so that

$$PB = PA = (\tau_{yz})_P$$

In order to obtain the total boundary shear stress at P, we draw a tangent at P and a horizontal line through B to obtain the point of intersection C. The length PC gives the required boundary stress.

For purposes of comparison of the magnitudes of the boundary stresses, we lay off radially $PD = PC$, so that PD is equal to the maximum or boundary stress at point P. In a circular shaft, these boundary stresses are clearly of equal magnitude, and they should therefore fall on a circle, with center at 0. Curve II, Fig. 10, represents the mean experimental value of the maximum shears, which is 5.33 fringes, and shows the degree of deviation of the experimental values from a circular locus. It is seen that the theoretical requirement that the boundary stresses in a circular shaft be of constant magnitude is completely satisfied.

The dashed curve in Fig. 10 falling slightly outside curve II represents the theoretical boundary shears based upon the applied torque of 11.42 lb-in.; thus

$$\tau_{max} = \frac{11.42 \times 0.502 \times 32}{\pi \times 1.005^4} = 57.4 \text{ psi}$$

From Equations [6] and [7]

$$N = \frac{\tau_{max}\, t'}{f}$$

$$= \frac{57.4 \times 0.1685}{1.6} = 6.05 \text{ fringes (approximately).}$$

Remembering that in Fig. 10, the diameter is only 0.908 in., as compared with 1.005 in. diameter of shaft, we obtain

$$N = \frac{6.05 \times 0.908}{1.005} = 5.46 \text{ fringes (approximately).}$$

This is the fringe order which corresponds to the mean experimental value of 5.33 given by curve II of Fig. 10, giving an error of about $2\frac{1}{2}$ per cent.

The maximum shear stress was also determined from five additional stress patterns obtained from two thicker plates. One of these was a transverse section 0.245 in. thick, the other was a section inclined at 45 deg to the axis and 0.246 in. thick. The mean value of the maximum shear from these plates is also 57.4 psi, and agrees completely with the value given by the applied torque.

We thus see that the boundary stresses not only satisfy the requirement that they be of constant magnitude but these magnitudes also agree with the required theoretical values. It should be emphasized that the complete story of the boundary stresses was determined from the one stress pattern shown in Fig. 8.

Stresses Across Radial Lines. We next determine the stresses across two arbitrary radial lines OA and OB, inclined, respectively, at 60 deg and 30 deg to the X axis. To this end two stress patterns with different angles of incidence of the light are needed. We choose those shown in Figs. 8 and 9 in which $\theta = 90$ deg and $\theta = 60$ deg, respectively; Fig. 8 being chosen because it gives τ_{yz} directly which can then be used to calculate τ_{zz}. The final stresses for section OA are given by the curve in Fig. 11, and those for OB (not shown) were quite similar. We note that at A the resultant stress is 5.35, and at B, 5.46 fringes, which provides an additional corroboration for the boundary stresses. The fringe-order curves which are necessary for the calculation of τ_{yz} and τ_{zz} across section OA are shown in Fig 12.

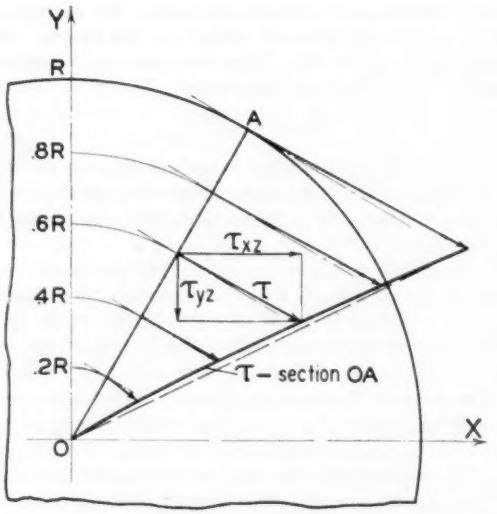


FIG. 11 CURVE OF τ ACROSS SECTION OA OBTAINED PHOTOELASTICALLY FROM THE TWO STRESS PATTERNS IN FIGS. 8 AND 9

(Deviation from theoretical direction is indicated by tangents drawn at each point. Deviation from linearity is indicated by straight dashed line drawn through origin.)

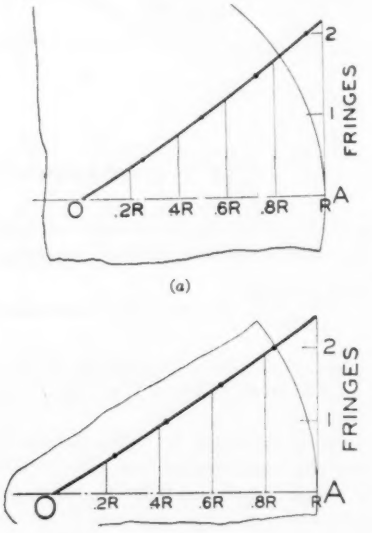


FIG. 12 CURVES OF FRINGE ORDERS FOR SECTIONS OA OBTAINED FROM FIGS. 8 AND 9

(Curve a, θ = 60 deg; curve b, θ = 90 deg.)

Two further checks can now be made. First the distribution of the resultant stresses must be linear, and second the stresses must be normal to the radius vector OA. Inspection of Fig. 11 shows that the experimental results essentially satisfy both conditions. All theoretical requirements for the stress system in a circular shaft are thus met.

Preliminary work on rectangular shafts and circular shafts with grooves further demonstrates the practicability of the proposed method.

Although the present discussion is confined to pure Saint Venant torsion, it is altogether reasonable to believe that the method will yield satisfactory boundary stresses even when warping is prevented.

ACKNOWLEDGMENT

The author expresses his appreciation to the administration of the Carnegie Institute of Technology for its support of this work. Special acknowledgment is made to Mr. John R. McDowell, mechanician in the photoelastic laboratory, now in the U. S. Air Corps, for his co-operation and assistance.

BIBLIOGRAPHY

1 Frozen stress patterns were first published by A. G. Solakian in 1935. See "A New Photoelastic Material," *Mechanical Engineering*, vol. 57, 1935, pp. 767–771. Solakian heated a circular Marblette shaft to 180 F, twisted it through a small angle, and allowed it to cool. A thin slice from this shaft exhibited a photoelastic pattern.

2 Oppel was the first to state that the process of slicing or cutting does not disturb the frozen pattern. See "Polarisationsoptische Untersuchung räumlicher Spannungs-und Dehnungszustände," by Georg Oppel, *Forschung auf dem Gebiete des Ingenieurwesens*, vol. 7, 1936, pp. 240–248.

3 The fundamental laws governing the frozen stress pattern were studied by M. Hetényi. See "Photoelastic Studies of Three-Dimensional Stress Problems," Proceedings Fifth International Congress for Applied Mechanics, John Wiley & Sons, Inc., New York, N. Y., 1939, pp. 208–212. In this paper, Hetenyi also shows stress patterns of twisted shafts.

4 "Polarisationsoptische Untersuchung des räumlichen Spannungszustandes im konvergenten Licht," by Rudolf Hiltscher, *Forschung auf dem Gebiete des Ingenieurwesens*, vol. 9, 1938, pp. 91–103.

5 "Das Kunstharz Phenolformaldehyd in der Spannungsoptik," by Albrecht Kuske, *Forschung auf dem Gebiete des Ingenieurwesens*, vol. 9, 1938, pp. 139–149.

6 "Three-Dimensional Photoelastic Analysis by Scattered Light," by R. Weller, Proceedings Ninth Eastern Photoelasticity Conference, Cornell University, 1939; also *Journal of Applied Physics*, vol. 12, 1941, pp. 610–616.

7 "Stress Analysis by Three-Dimensional Photoelastic Methods," by Daniel C. Drucker and Raymond D. Mindlin, *Journal of Applied Physics*, vol. 11, 1940, pp. 724–732.

8 "Photoelastic Separation of Principal Stresses by Oblique Incidence," by D. C. Drucker, Trans. A.S.M.E., vol. 65, 1943, p. A-156.

9 See author's discussion of Drucker's paper (8), JOURNAL OF APPLIED MECHANICS, June, 1944, p. A-125; see also course thesis by E. R. Hicks, Carnegie Institute of Technology, Feb., 1943, and H. C. Arnold, April, 1943.

10 "Theory of Elasticity," by S. Timoshenko, McGraw-Hill Book Company, Inc., New York, N. Y., 1934, p. 72.

11 "Studies in Three-Dimensional Photoelasticity: Stress Concentrations in Shafts With Transverse Circular Holes in Tension. Relation Between Two- and Three-Dimensional Factors," by Max M. Frocht, *Journal of Applied Physics*, Jan., 1944, pp. 72–88; Fig. 17.

Stresses in a Reinforced Monocoque Cylinder Under Concentrated Symmetric Transverse Loads

By N. J. HOFF,[1] BROOKLYN, N. Y.

The stresses in the sheet covering, stringers, and rings of a reinforced monocoque cylinder of circular cross section are calculated for the case of a loading consisting of concentrated symmetric forces applied to the rings in the planes of the rings. The conventional assumptions of a linear normal stress distribution and a corresponding shear-stress distribution in the bent cylinder are replaced by a least-work analysis. Application of the theory to the numerical example of a cantilever monocoque cylinder yields a maximum shear stress in the sheet covering and a maximum bending moment in the ring amounting to 900 per cent and 33 per cent, respectively, of the values obtained by the conventional analysis.

Introduction and Summary

ONE of the problems most commonly encountered in aircraft structural analysis is the determination of the bending-moment distribution in a transverse frame, or ring, of a reinforced monocoque fuselage. The external loads acting upon the ring consist of concentrated forces, for instance, the weight of and the inertia forces due to passengers, cargo, and equipment, and the balancing distributed forces transmitted through the rivets from the sheet covering of the fuselage. In the sheet covering, the reactions to these distributed forces give rise to the shearing stresses associated with bending and torsion, and it is customary to calculate the distribution of the shearing stresses according to the Bernoulli-Navier theory of bending and the Saint Venant theory of torsion. Since it is generally known that these theories are valid only at some distance from the load application, the only justification for such a procedure has been the lack of better information. In the case of a beam of solid cross section, the distance beyond which the Bernoulli-Navier theory applies is usually taken as a small multiple of the cross-sectional dimensions. Because of the comparatively low degree of redundancy of a thin-walled monocoque cylinder, the predictions of the theory are likely to be valid only at a distance from the application of the concentrated loads equal to several times the diameter of the cylinder.

It is the object of this paper to investigate the distribution of the shearing stresses in the sheet covering and of the bending moments in the rings, through a least-work analysis. Calculations are carried out only for the case of symmetric loading, but they can be easily extended to cover cases of antisymmetric loading. In the numerical example of a typical cantilever monocoque cylinder of three fields, it is found that the maximum shearing stress in the sheet covering amounts to 900 per cent, the maximum bending moment in the ring to 33 per cent of the values obtained through a conventional analysis.

The Monocoque Cylinder

The fuselage underlying this analysis is a cantilever monocoque cylinder of circular cross section, as shown in Fig. 1. The formulas developed in the paper permit, however, the determination of the stresses in cylinders having different end conditions. The cylinder is made of thin sheet metal and is reinforced with m transverse rings, each one of which has a constant though in general a different cross section. The longitudinal reinforcing elements of the cylinder are referred to as stringers. In conformity with general practice in aircraft stress analysis the part of the cross-sectional area of the sheet covering considered effective in carrying normal stresses is added to the cross-sectional area of the stringers to form the total cross-sectional area resisting normal stresses. Since through this artifice the load-carrying capacity of the sheet in tension and in compression is taken into account, it is permissible to assume in the ensuing calculations that the sheet carries shear alone. To simplify further the calculations, the differences in the effective width of sheet on the tension and the compression side of the cylinder are disregarded. Through this device, and by the assumption of an even spacing of stringers of the same cross section around the perimeter of the cylinder, a high degree of uniformity and symmetry is achieved. It may then be assumed that the stringers are distributed continuously around the perimeter. Because of the great number of stringers in modern monocoque fuselages, the accuracy of the stress analysis is not impaired by this assumption. The imaginary thickness of sheet resisting normal stresses, obtained through division of the sum of the cross-sectional areas of all the stringers and the effective area of sheet by the perimeter of the cylinder, is denoted by the symbol t'.

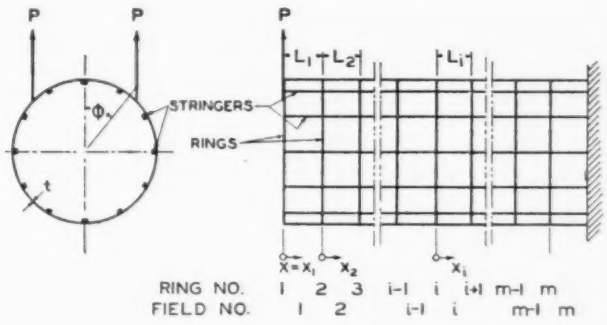


FIG. 1 MONOCOQUE CYLINDER

It follows from the conditions of membrane equilibrium that the shear stress must be constant in each panel bounded by two

[1] Associate Professor of Aeronautical Engineering, Polytechnic Institute of Brooklyn. Mem. A.S.M.E.

Presented at the National Meeting of the Applied Mechanics Division, Chicago, Ill., June 16–17, 1944, of THE AMERICAN SOCIETY OF MECHANICAL ENGINEERS.

Discussion of this paper should be addressed to the Secretary, A.S.M.E., 29 West 39th Street, New York, N. Y., and will be accepted until January 10, 1945, for publication at a later date. Discussion received after the closing date will be returned.

NOTE: Statements and opinions advanced in papers are to be understood as individual expressions of their authors and not those of the Society.

adjacent rings and two adjacent stringers if the sheet does not carry direct stress. Because of this requirement, and because of the assumption of an infinite number of stringers and a finite number of rings, in the present problem the shear stress must be constant between two adjacent rings but may vary around the circumference of the cylinder. The shear flow q_i in the ith field, that is, the product of shear stress and sheet thickness, can be represented consequently by the infinite series

$$q_i = \sum_{n=1}^{\infty} a_{in} \sin n\varphi \quad \ldots\ldots [1]$$

The sine series satisfies the requirements of symmetry if the shear flow is taken positive when it points in the direction of increasing φ. Because of the symmetry of both structure and loading only one half of the structure will be considered in all the calculations to follow.

In addition to the foregoing assumptions, the stringers are considered as offering negligibly small resistance to bending. This may be true enough in the case of many monocoque fuselages having strong rings and weak stringers. The rings are assumed to have finite rigidity in bending in their plane and vanishing rigidity in bending out of their plane as well as in torsion. Moreover, the validity of Hooke's law and of the principle of superpositions is also assumed.

Analysis of First Ring

Fig. 2 shows the first ring with its loading and the sign convention used. The shear flow acting upon the first ring may be written as

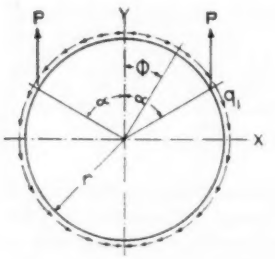


Fig. 2 Diagram of Ring and Loading

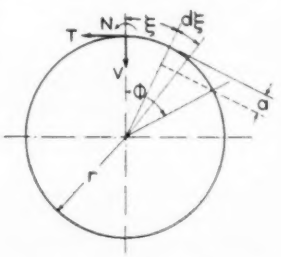


Fig. 3 Notation Used in Calculating Moments

$$q_1 = \sum_{n=1}^{\infty} a_{1n} \sin n\varphi \quad \ldots\ldots [1a]$$

It is easily verified that the requirements of equilibrium of moments and of forces in the x direction are satisfied by each term of the series. The condition of equilibrium of forces in the y direction is

$$P = \int_0^{\pi} qr \sin \varphi d\varphi = (\pi/2) r a_{11}$$

Consequently, the value of the first coefficient of the series is

$$a_{11} = (2/\pi)(P/r) \quad \ldots\ldots [2]$$

If the ring is assumed to be cut at $\varphi = 0$, the unknown moment N and the unknown forces T and V must be applied in the cut as shown in Fig. 3. However, V is zero because of the symmetry. The moments M_N and M_T caused by the other two unknowns may be written in the form

$$M_N + M_T = N + Tr(1 - \cos \varphi) \quad \ldots\ldots [3]$$

if moments are considered positive when they tend to increase the original curvature of the ring. The moment M_q caused by the distributed shear flow q_1 is given by the integral

$$M_q = \int_0^{\varphi} q_1 r^2 [1 - \cos(\varphi - \xi)] d\xi$$

$$= r^2 \int_0^{\varphi} \left[(1 - \cos\varphi \cos\xi - \sin\varphi \sin\xi) \sum_{n=1}^{\infty} a_{1n} \sin n\xi \right] d\xi$$

Integration gives

$$(M_q/r^2) = (2/\pi)(P/r)[1 - \cos\varphi - (1/2)\varphi \sin\varphi] + \sum_{n=2}^{\infty} (a_{1n}/n) - \cos\varphi \sum_{n=2}^{\infty} [a_{1n} n/(n^2 - 1)] + \sum_{n=2}^{\infty} [a_{1n}/n(n^2 - 1)] \cos n\varphi \quad \ldots\ldots [4]$$

The external force P causes the bending moment

$$M_P = Pr(\sin\alpha - \sin\varphi) \quad \ldots\ldots [5]$$

provided that

$$\alpha \leqq \varphi \leqq \pi \quad \ldots\ldots [5a]$$

In reality Equation [5] is valid up to $\varphi = (2\pi - \alpha)$, but because of the symmetry it is not necessary to consider it beyond $\varphi = \pi$.

The total bending moment is the sum of those given in Equations [3], [4], and [5]

$$(M/r^2) = A - B\cos\varphi - (P/\pi r)\varphi \sin\varphi + \sum_{n=2}^{\infty} [a_{1n}/n(n^2 - 1)] \cos n\varphi \quad \ldots\ldots [6]$$

if

$$0 \leqq \varphi \leqq \alpha \quad \ldots\ldots [6a]$$

and

$$(M/r^2) = A + (P/r)\sin\alpha - B\cos\varphi - (P/r)\sin\varphi - (P/\pi r)\varphi \sin\varphi + \sum_{n=2}^{\infty} [a_{1n}/n(n^2 - 1)] \cos n\varphi \quad \ldots\ldots [7]$$

if

$$\alpha \leqq \varphi \leqq \pi \quad \ldots\ldots [7a]$$

In these equations the symbols A and B stand for

$$\left.\begin{aligned} A &= (2/\pi)(P/r) + (T/r) + (N/r^2) + \sum_{n=2}^{\infty} (a_{1n}/n) \\ B &= (2/\pi)(P/r) + (T/r) + \sum_{n=2}^{\infty} [a_{1n} n/(n^2 - 1)] \end{aligned}\right\} \quad \ldots\ldots [8]$$

The strain energy U_r stored in one half of the ring is (if the strain energy due to shear and tension is neglected)

$$U_r = (r/2EI) \int_0^{\pi} M^2 d\varphi$$

According to Castigliano's theorem

$$\left.\begin{aligned}(\partial U_r/\partial N) &= 0 = \int_0^\pi M(\partial M/\partial N)d\varphi \\ (\partial U_r/\partial T) &= 0 = \int_0^\pi M(\partial M/\partial T)d\varphi\end{aligned}\right\} \quad \ldots\ldots [9]$$

From Equations [6], [7], and [8]

$$\left.\begin{aligned}(\partial M/\partial N) &= 1 \\ \text{and} \qquad (\partial M/\partial T) &= r(1 - \cos\varphi)\end{aligned}\right\} \quad \ldots\ldots [10]$$

Consequently, the conditions for a minimum of the strain energy originally given in Equations [9] may be expressed in the form

$$\left.\begin{aligned}&\int_0^\pi (M/r^2)d\varphi = 0 \\ \text{and} \qquad &\int_0^\pi (M/r^2)\cos\varphi\, d\varphi = 0\end{aligned}\right\} \quad \ldots\ldots [11]$$

After integration and manipulations the first of Equations [11] becomes

$$Tr + N = (Pr/\pi)[\cos\alpha - (\pi - \alpha)\sin\alpha] - r^2 \sum_{n=2}^{\infty} (a_{1n}/n) \quad \ldots\ldots [12]$$

Similarly, the second of Equations [11] becomes

$$Tr = -(Pr/2\pi)(3 + 2\sin^2\alpha) - r^2 \sum_{n=2}^{\infty} [a_{1n}n/(n^2 - 1)]. \quad \ldots\ldots [13]$$

Solving for N

$$N = (Pr/2\pi)[3 + 2\cos\alpha - 2(\pi - \alpha)\sin\alpha + 2\sin^2\alpha] + r^2 \sum_{n=2}^{\infty} [a_{1n}/n(n^2 - 1)] \quad \ldots\ldots [14]$$

If the right-hand members of Equations [13] and [14] are substituted into Equations [6] and [7], and use is made of Equations [8], the bending moment becomes

$$M = (Pr/\pi)\left\{[2 + \cos\alpha - (\pi - \alpha)\sin\alpha] - (1/2)\cos 2\alpha\cos\varphi - \varphi\sin\varphi\right\} + r^2 \sum_{n=2}^{\infty} [a_{1n}/n(n^2 - 1)]\cos n\varphi. \quad \ldots\ldots [15]$$

when

$$0 \leqq \varphi \leqq \alpha \quad \ldots\ldots [15a]$$

and

$$M = (Pr/\pi)\left\{[2 + \cos\alpha + \alpha\sin\alpha] - (1/2)\cos 2\alpha\cos\varphi - (\pi + \varphi)\sin\varphi\right\} + r^2 \sum_{n=2}^{\infty} [a_{1n}/n(n^2 - 1)]\cos n\varphi \quad \ldots [16]$$

when

$$\alpha \leqq \varphi \leqq \pi \quad \ldots\ldots [16a]$$

Bending Moments and Stresses in Other Structural Elements

As stated previously, the sheet covering is assumed to carry shearing stresses only. It follows from Equation [1], which gives the shear flow in the ith field, that the equilibrium condition of the forces in the y direction requires that

$$a_{11} = a_{21} = \ldots = a_{i1} = \ldots = a_{m1} = (2/\pi)(P/r) \quad \ldots\ldots [17]$$

While the loading of the first ring consisted of the concentrated forces P and the shear flow in the first field, upon the ith ring only the difference in the shear flow of the adjacent ith and $(i + 1)$st fields is acting, and no concentrated load is present. The distributed load can be written as

$$q_i - q_{(i-1)} = \sum_{n=2}^{\infty} (a_{in} - a_{(i-1)n})\sin n\varphi \quad \ldots\ldots [18]$$

Hence the bending moment in the ith ring is

$$M_i = r^2 \sum_{n=2}^{\infty} [(a_{in} - a_{(i-1)n})/n(n^2 - 1)]\cos n\varphi \quad \ldots [19]$$

The stress in the distributed stringers can be calculated from the equilibrium condition

$$t'(\partial\sigma/\partial x) + t(\partial\tau/r\partial\varphi) = 0$$

Consequently, the normal stress is

$$\sigma = -(1/rt')\int_0^x (\partial q/\partial\varphi)dx + f(\varphi)$$

With the rings assumed infinitely weak in bending out of their plane, and in the absence of external axial loads at the first ring

$$f(\varphi) = 0$$

In the stringers of the pth field the direct stress is

$$\sigma_p = -(1/rt')\left\{\sum_{i=0}^{p-1}\int_0^{L_i} (\partial q_i/\partial\varphi)dx_i + \int_0^{x_p} (\partial q_p/\partial\varphi)dx_p\right\} \quad \ldots\ldots [20]$$

if x_i and x_p denote the distances measured parallel to the axis of the cylinder from the ith and pth ring, respectively.

Condition for Minimum Strain Energy

The coefficients a_{in} of the Fourier series of Equation [1], with the exception of the first coefficient a_{i1} in each series, can be determined from Castigliano's theorem by equating to zero the derivatives with respect to the coefficients of the total strain energy stored in the structure. The value of the first coefficients is given in Equation [17].

The total strain energy stored in all the rings is denoted by $U_{r,\text{tot}}$. It may be given as

$$U_{r,\text{tot}} = \sum_{i=1}^{m} (1/EI_i)\int_0^\pi M_i^2 r d\varphi \quad \ldots\ldots [21]$$

Differentiating with respect to a_{1n}

$$(\partial U_{r,\text{tot}}/\partial a_{1n}) = (2r/EI_1)\int_0^\pi M_1(\partial M_1/\partial a_{1n})d\varphi + (2r/EI_2)\int_0^\pi M_2(\partial M_2/\partial a_{1n})d\varphi$$

where n is an integer greater than unity. As may be seen, only terms containing I_1 and I_2 figure in this equation. Terms containing I_i with $i \neq 1, 2$ are independent of a_{1n}. With

$$(\partial M_1/\partial a_{1n}) = [r^2/n(n^2 - 1)] \cos n\varphi$$

and

$$(\partial M_2/\partial a_{1n}) = -[r^2/n(n^2 - 1)] \cos n\varphi$$

where n is an integer greater than unity, integration gives

$$(\partial U_{r.\text{tot}}/\partial a_{1n}) = a_{1n}[\pi r^5/n^2(n^2 - 1)^2][(1/EI_1) + (1/EI_2)] - a_{2n}[\pi r^5/n^2(n^2 - 1)^2](1/EI_2) + P[2r^4/n(n^2 - 1)^2][\cos \alpha \cos n\alpha + (1/n) \sin \alpha \sin n\alpha + 2(-1)^n](1/EI_1) \quad [22]$$

Differentiating with respect to a_{in}

$$(\partial U_{r.\text{tot}}/\partial a_{in}) = (2r/EI_i) \int_0^\pi M_i(\partial M_i/\partial a_{in})d\varphi + (2r/EI_{i+1}) \int_0^\pi M_{i+1}(\partial M_{i+1}/\partial a_{in})d\varphi$$

since all the other terms in the summation of Equation [21] are independent of a_{in}. With

$$(\partial M_i/\partial a_{in}) = [r^2/n(n^2 - 1)] \cos n\varphi$$

and

$$(\partial M_{i+1}/\partial a_{in}) = -[r^2/n(n^2 - 1)] \cos n\varphi$$

where n and i are integers greater than unity, integration gives

$$(\partial U_{r.\text{tot}}/\partial a_{in}) = [\pi r^5/n^2(n^2 - 1)^2]\left\{(-a_{(i-1)n}/EI_i) + (a_{in}/EI_i) + (a_{in}/EI_{i+1}) - (a_{(i+1)n}/EI_{(i+1)})\right\} \quad [23]$$

The strain energy stored in the entire sheet covering is denoted by U_s. It may be given as

$$U_s = (r/tG) \sum_{i=1}^{m} L_i \int_0^\pi q_i^2 d\varphi \quad [24]$$

The differential coefficient of the strain energy stored in the sheet with respect to a typical Fourier coefficient is

$$(\partial U_s/\partial a_{in}) = (2r/tG)L_i \int_0^\pi \sin n\varphi \sum_{p=1}^{\infty} a_{ip} \sin p\varphi d\varphi = (\pi r L_i/tG)a_{in} \quad [25]$$

The total strain energy U_{str} stored in the stringers is

$$U_{str} = (t'r/E) \sum_{p=1}^{m} \int_0^\pi d\varphi \int_0^{L_p} \sigma_p^2 dx_p \quad [26]$$

With

$$L = \sum_{i=1}^{m} L_i \quad [27]$$

the differential coefficient of U_{str} with respect to a typical Fourier coefficient may be written in the form

$$(\partial U_{str}/\partial a_{in}) = (n^2\pi L_i/Ert')\left\{a_{1n}L_1\left[L - (1/2)L_i - \sum_{p=1}^{i-1} L_p\right] + a_{2n}L_2\left[L - (1/2)L_i - \sum_{p=1}^{i-1} L_p\right] + \ldots + a_{(i-1)n}L_{(i-1)n}\left[L - (1/2)L_i - \sum_{p=1}^{i-1} L_p\right] + a_{in}L_i\left[L - (2/3)L_i - \sum_{p=1}^{i-1} L_p\right] + a_{(i+1)n}L_{(i+1)}\left[L - (1/2)L_{(i+1)} - \sum_{p=1}^{i} L_p\right] + a_{(i+2)n}L_{(i+2)}\left[L - (1/2)L_{(i+2)} - \sum_{p=1}^{i+1} L_p\right] + \ldots + a_{mn}(1/2)L_m^2\right\} \quad [28]$$

provided $i < m$

Similarly

$$(\partial U_{str}/\partial a_{mn}) = (n^2\pi L_m/Ert')\left\{a_{1n}L_1(1/2)L_m + a_{2n}L_2(1/2)L_m + \ldots + a_{(m-1)n}L_{(m-1)}(1/2)L_m + a_{mn}(1/3)L_m^2\right\} \quad [28a]$$

The condition of a minimum of the total strain energy stored in the structure is

$$(\partial U_{\text{tot}}/\partial a_{in}) = (\partial U_{r.\text{tot}}/\partial a_{in}) + (\partial U_s/\partial a_{in}) + (\partial U_{str}/\partial a_{in}) = 0 \quad [29]$$

This condition holds for all integral values of n greater than unity, and for integral values of i from 1 to m, inclusive. Consequently, Equation [29] represents an m times infinite number of linear equations from which the Fourier coefficients can be determined.

Application to Cantilever Having Three Fields

The problem is now worked out in greater detail for the case when the monocoque cylinder has three fields ($m = 3$), and the length L_i of each field is the same, the moment of inertia I_i of each ring is the same, and the material of each structural element is the same. The 3 times infinite number of equations corresponding to Equation [29] can now be written in the following form

$$\left.\begin{aligned}(\partial U_{\text{tot}}/\partial a_{1n}) &= a_{1n}(14n^2 + 2A\gamma + B) + a_{2n}(9n^2 - A\gamma) + a_{3n}3n^2 + nA\gamma f(\alpha, n) = 0\\ (\partial U_{\text{tot}}/\partial a_{2n}) &= a_{1n}(9n^2 - A\gamma) + a_{2n}(8n^2 + 2A\gamma + B) + a_{3n}(3n^2 - A\gamma) = 0\\ (\partial U_{\text{tot}}/\partial a_{3n}) &= a_{1n}3n^2 + a_{2n}(3n^2 - A\gamma) + a_{3n}(2n^2 + A\gamma + B) = 0\end{aligned}\right\} \quad [30]$$

where n is an integer greater than unity.

The new nondimensional symbols introduced in these equations are defined as follows

$$\left.\begin{aligned} A &= 6r^6t'/I_xL'^3 \\ B &= 6(E/G)(t'r^2/tL'^2) \\ \gamma &= 1/[n^2(n^2-1)^2] \end{aligned}\right\} \quad \ldots\ldots\ldots\ldots\ldots\ldots [30a]$$

and L' is the uniform distance between adjacent rings.

The function $f(\alpha, n)$ of the concentrated load may be written as

$$f(\alpha, n) = (2P/\pi r)[\cos\alpha\cos n\alpha + (1/n)\sin\alpha\sin n\alpha + 2(-1)^n] \quad \ldots\ldots\ldots\ldots\ldots\ldots [30b]$$

It is evident from Equations [30] that all the Fourier coefficients a_{in} that have the same subscript n are interdependent, while all those with different subscripts n are independent of each other. For this reason, in the case of the cantilever having three fields, the coefficients can be calculated by solving groups of simultaneous equations, each of which consists of three equations and contains three unknowns.

Numerical calculations have been carried out for the case when the external load is a concentrated radial force of magnitude $2P$ applied at the lowest point of the ring. With $\alpha = \pi$, Equation [30b] becomes

$$f(\alpha, n) = (-1)^n(2P/\pi r) = (-1)^n a_{11} \quad \ldots\ldots\ldots\ldots [31]$$

For the nondimensional parameters A and B, the following values were chosen

$$\left.\begin{aligned} A &= 10^7 \\ B &= 500 \end{aligned}\right\} \quad \ldots\ldots\ldots\ldots\ldots\ldots [32]$$

The values of the first 3 times 12 Fourier coefficients were calculated from Equations [30]. They are given in Table 1.

TABLE 1 FOURIER COEFFICIENTS

n	a_{1n}/a_{11}	a_{2n}/a_{11}	a_{3n}/a_{11}
1	1	1	1
2	−1.987	−1.979	−1.975
3	2.711	2.533	2.452
4	−2.433	−1.605	−1.288
5	1.631	0.395	0.099
6	−0.950	0.088	0.142
7	0.507	−0.162	−0.095
8	−0.265	0.124	0.048
9	0.141	−0.080	−0.024
10	−0.078	0.050	0.013
11	0.045	−0.031	−0.007
12	−0.027	0.020	0.004

Values of the shear flow obtained from the numerical calculations are plotted in Fig. 4. For the sake of comparison the half sine wave, corresponding to the Bernoulli-Navier assumptions, is also shown. The results of the present paper indicate a high concentration of the shear flow in the neighborhood of the point of application of the load. This shear-flow concentration has a beneficial effect upon the bending moments in the first ring, as may be seen from Fig. 5. Fig. 6 presents the bending moments in rings 2 and 3. The shape of these moment curves is similar to that shown in Fig. 5, but the values are very much smaller. According to conventional assumptions, these rings are not bent at all. The normal stress distribution in the fixed end section of the cantilever monocoque cylinder is shown in Fig. 7. The straight-line distribution, according to conventional calculations, is also given in order to demonstrate the great difference between the two curves.

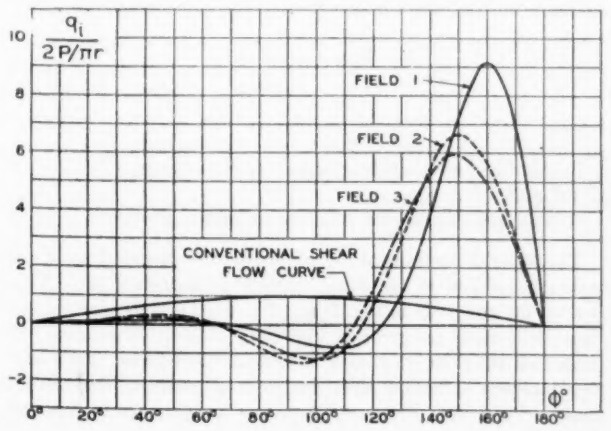


FIG. 4 SHEAR FLOW

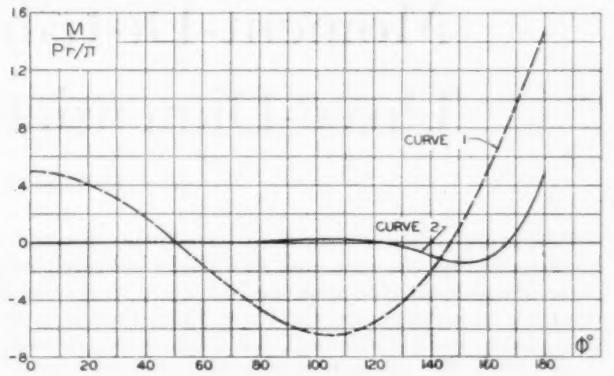


FIG. 5 BENDING MOMENT IN FIRST RING
(Curve 1 represents bending moments according to conventional calculations; curve 2, those obtained in present paper.)

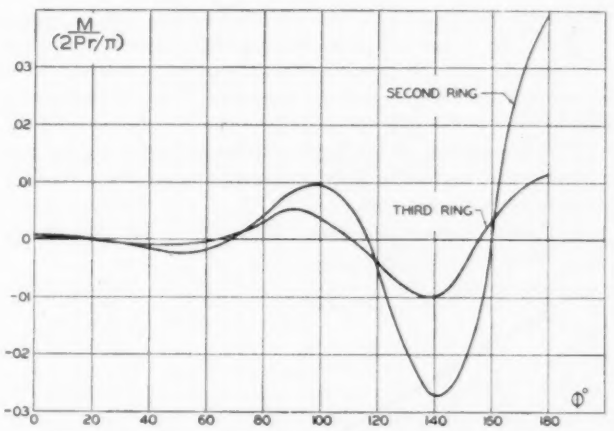


FIG. 6 BENDING MOMENTS IN SECOND AND THIRD RINGS

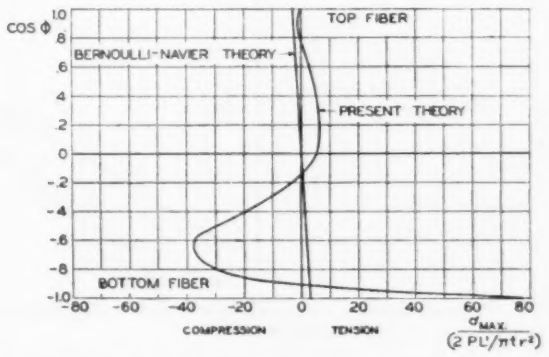


FIG. 7 NORMAL STRESS DISTRIBUTION IN MONOCOQUE CYLINDER AT FIXED END

Moment-Distribution Analysis for Three-Dimensional Pipe Structures

By R. C. DeHART,[1] WOOD RIVER, ILL.

This paper presents a moment-distribution procedure for determining the moments and shears produced in a three-dimensional pipe structure subjected to expansion resulting from temperature change. From the shears existing in the various members, end reactions can be easily determined. The method offers an advantage over virtual-work methods in that fewer calculations are required, consequently reducing the time involved and the danger of omitting some item in the solution.

THE Cross method of moment distribution will be utilized in the present analysis for three-dimensional pipe structures, with the exception that the effect of rotation of the members due to torsion must be included. The steps involved in the method are as follows:

1 Computation of the joint translations, allowing no joint rotation and neglecting deformation of the members resulting from direct stress and shear.

2 Computation of fixed end moments due to the joint translations determined in (1).

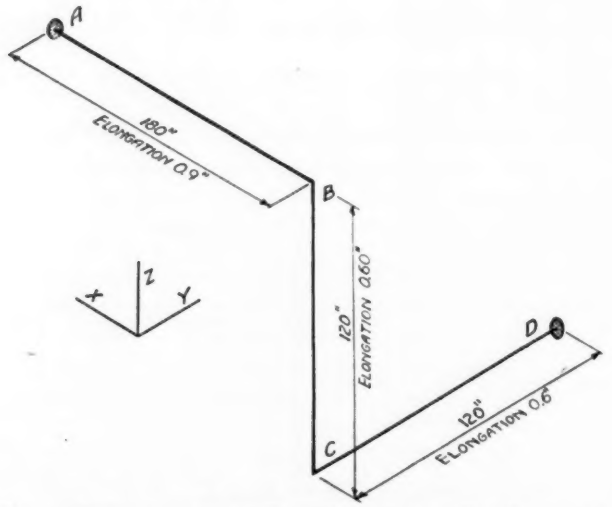


FIG. 1 CHARACTERISTICS OF THREE-DIMENSIONAL PIPE STRUCTURE TO BE ANALYZED

3 With joint translation prohibited, the fixed end moments of (2) are balanced, based upon flexural and torsional stiffness and carry-over factors.

4 Unbalanced shears are calculated, based upon the balanced moments of (3).

5 Elimination of the unbalanced shears of (4) by the process of applying a unit load in the direction of each unbalanced shear. The unbalanced shears due to these unit loads are used to write linear equations, the solution of which gives the forces required to remove the unbalanced shears found in (4).

6 Combination of the moments of (3) with the moments produced by the joint forces found in (5). From this combination the final joint moments and shears are obtained.

To illustrate the method, a three-dimensional structure of three members is chosen. In Fig. 1, dimensions and change in length of each member are given.

COMPUTATION OF JOINT TRANSLATIONS AND FIXED END MOMENTS

Allowing no rotation at the joints, the 0.6-in. elongation in the Z direction in member BC, Fig. 1, is distributed to members AB and CD in relation to their flexibilities. The relation between the deflection in AB and BC is determined as follows:

The shear in AB must equal the shear in CD in order that equilibrium conditions may be satisfied. These conditions are expressed by

$$S_{AB} = S_{CD} = \frac{2M_{AB}}{L_{AB}} = \frac{2M_{CD}}{L_{CD}} \quad \ldots\ldots [1]$$

where

M_{AB} is fixed end moment in AB caused by deflection Δ_{AB} in Z direction
M_{CD} is fixed end moment in CD caused by deflection Δ_{CD} in Z direction
L_{AB} and L_{CD} are lengths of members AB and CD

Substitute

$$M_{AB} = \frac{6EI_{AB}\Delta_{AB}}{L_{AB}^2} \qquad M_{CD} = \frac{6EI_{CD}\Delta_{CD}}{L_{CD}^2}$$

in Equation [1], and obtain

$$\frac{\Delta_{AB}}{\Delta_{CD}} = \frac{I_{CD}L_{AB}^3}{I_{AB}L_{CD}^3} \quad \ldots\ldots [2]$$

where

I_{AB} and I_{CD} are moments of inertia of members AB and CD
E is modulus of elasticity in tension and compression

The other deflections of the members are calculated using a relation developed in the same manner as Equation [2]. These deflections are given in Fig. 2(*a*). The fixed end moments due to these deflections are given in Fig. 2(*b*). A positive moment indicates that the joint is rotating the member clockwise, and a negative moment indicates that the joint is rotating the member counterclockwise. Fixed end moments are given in inch-pounds divided by 10^4.

---

[1] Engineer, Manufacturing Department, Standard Oil Company of Indiana.

Presented at the National Meeting of the Applied Mechanics Division, Chicago, Ill., June 16-17, 1944, of THE AMERICAN SOCIETY OF MECHANICAL ENGINEERS.

Discussion of this paper should be addressed to the Secretary, A.S.M.E., 29 West 39th Street, New York, N. Y., and will be accepted until January 10, 1945, for publication at a later date. Discussion received after the closing date will be returned.

NOTE: Statements and opinions advanced in papers are to be understood as individual expressions of their authors and not those of the Society.

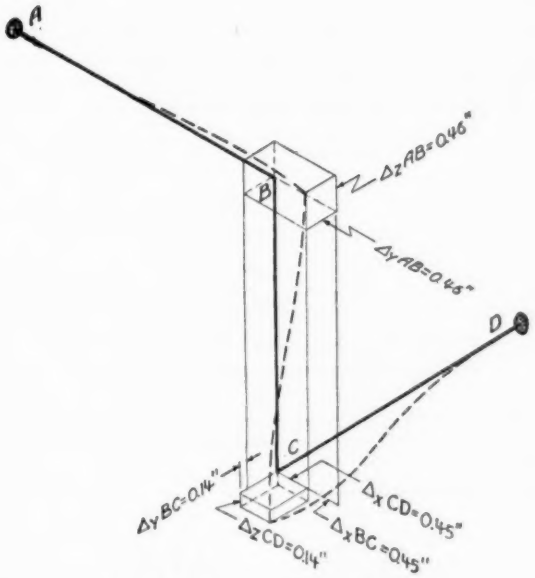


FIG. 2(a) DEFLECTION OF MEMBERS

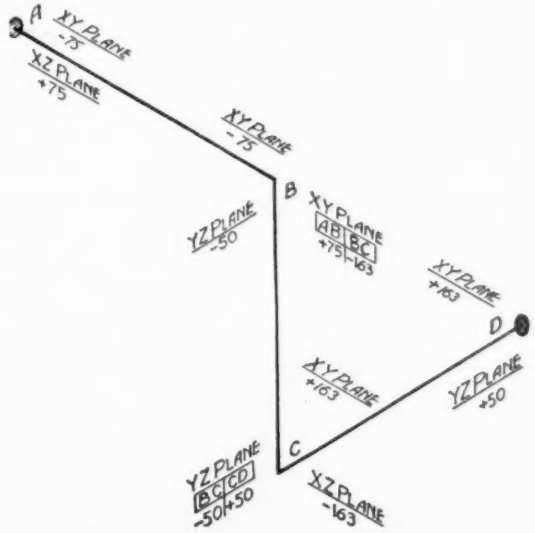


FIG. 2(b) FIXED END MOMENTS DUE TO DEFLECTIONS IN FIG. 2(a)

STIFFNESS AND CARRY-OVER FACTORS

Since moments exist in the X, Y-, Y, Z-, and X, Z-planes it is necessary to make a moment distribution in each plane. The carry-over factor for a member in torsion is minus 1 and for a member in flexure is plus $^1/_2$. At a joint such as B in the Y, Z-plane, one member rotates as a result of torsion, and the other as a result of flexure. The moment to be distributed to each member when the joint is allowed to rotate will depend upon the resistance of each member to rotation. This resistance to rotation is termed "stiffness."

The rotation due to an applied torque is

$$\theta = \frac{TL}{GJ} \quad \ldots\ldots [3]$$

and for unit θ

$$T = \frac{GJ}{L} \quad \ldots\ldots [4]$$

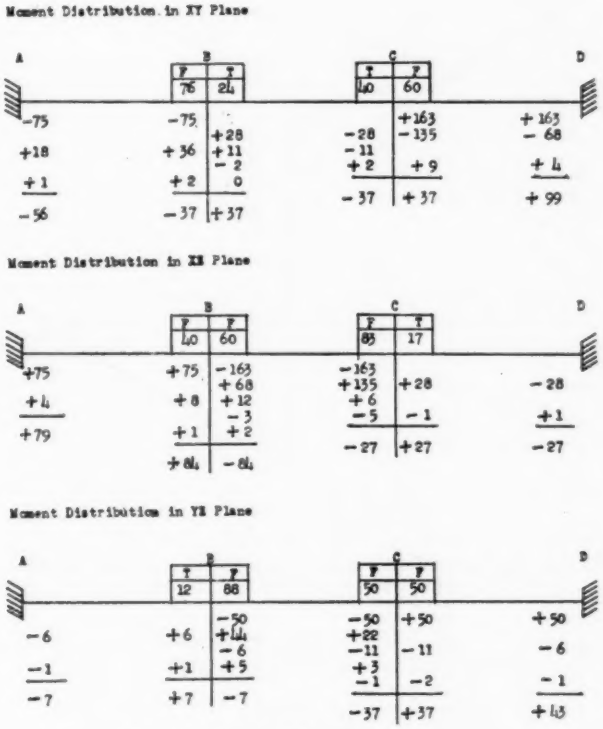


FIG. 3(a) INITIAL MOMENT DISTRIBUTION

(Moment-distribution factors are given below the letters T and F which indicate moment distribution for torsion and flexure.)

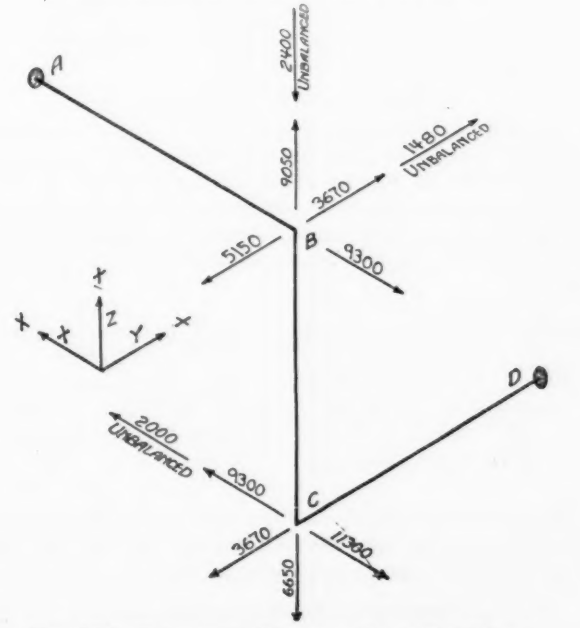


FIG. 3(b) UNBALANCED SHEARS AT B AND C IN POUNDS

where

T is applied torque
G is modulus of elasticity in shear
J is polar moment of inertia
L is length of member
θ is rotation in radians

The moment required to produce unit rotation at the simply

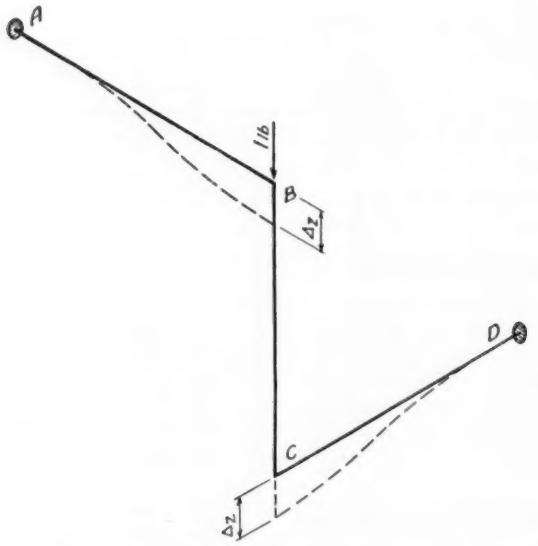


FIG. 4 PROPORTIONATE DISTRIBUTION IN MEMBERS AB AND CD OF 1 LB APPLIED AT B IN Z DIRECTION

supported end of a member fixed at one end and simply supported at the other is determined from the relation

$$M = \frac{4EI\theta}{L} \quad \ldots\ldots [5]$$

for unit θ

$$M = \frac{4EI}{L} \quad \ldots\ldots [6]$$

INITIAL MOMENT DISTRIBUTION

The moment-distribution factors for joints with one member rotating in torsion and the other in flexure will be based upon Equations [4] and [6]. Distribution factors at joints, involving both members in flexure, are determined in the usual manner using I/L values. Table 1 gives the moment required to produce unit θ in torsion, unit θ in flexure, and I/L values for each member.

TABLE 1 MOMENT TO PRODUCE UNIT θ IN TORSION AND IN FLEXURE, AND I/L VALUES FOR MEMBERS

Member	Moment producing unit θ in torsion, in-lb	Moment producing unit θ in flexure, in-lb	I/L
AB	40×10^6	$192 \times 10\theta$	2
BC	60×10^6	$288 \times 10\theta$	3
CD	60×10^6	$288 \times 10\theta$	3

The moment distribution for the fixed end moments of Fig. 2(b) is given in Fig. 3(a). Shears in the members calculated from these distributed moments are shown in Fig. 3(b).

ELIMINATION OF UNBALANCED SHEARS

At B and C, Fig. 3(a), there are unbalanced shears the values of which are shown in Fig. 3(b). These unbalanced shears must be removed before equilibrium in the structure is established. Their removal is accomplished by means of determining the unbalanced shears at the joints produced by a unit load acting in the direction of each unbalanced shear of Fig. 3(b). Linear equations based upon these unbalanced shears can then be written. The solution of these equations determines the forces necessary to remove the unbalanced shears of Fig. 3(b).

In Fig. 4, 1 lb applied at B in the Z direction is distributed to members AB and CD in proportion to their flexibilities,[2] or L^3/EI values; no joint rotation allowed. Member AB deflects the same as CD, the shear in AB plus the shear in CD is 1 lb, therefore the following equations are obtained

$$S_{AB} + S_{CD} = 1 \quad \ldots\ldots [7]$$

$$\frac{S_{AB}}{S_{CD}} = \frac{I_{AB}L_{CD}^3}{I_{CD}L_{AB}^3} \quad \ldots\ldots [8]$$

$$S_{CD} + \frac{L_{AB}^3}{L_{CD}^3} S_{CD} = 1 \quad \ldots\ldots [9]$$

S_{CD} = 0.77 lb shear in member CD
S_{AB} = 0.23 lb shear in member AB

[2] "Theory of Modern Steel Structures, vol. 2 Indeterminate," by L. E. Grinter, The Macmillan Company, New York, N. Y., 1937, p. 158.

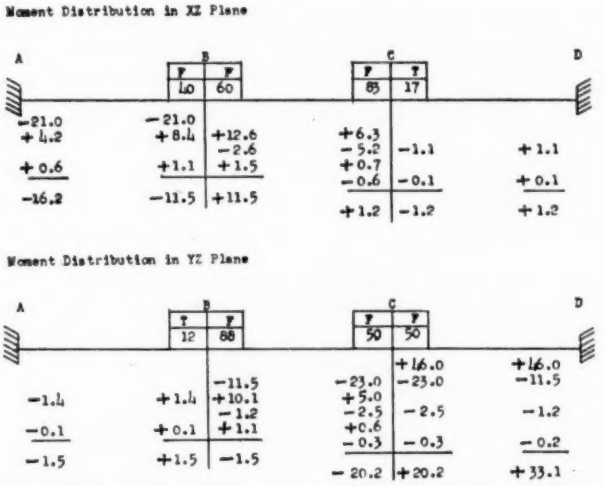


FIG. 5(a) MOMENT DISTRIBUTION IN X, Z- AND Y, Z-PLANES FOR 1 LB APPLIED AT B IN Z DIRECTION

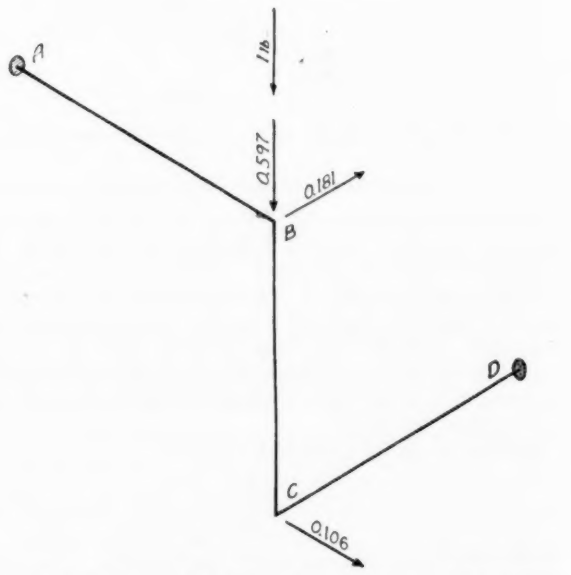
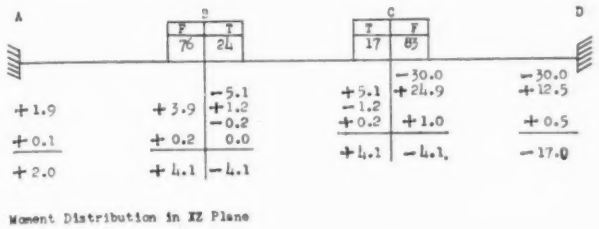
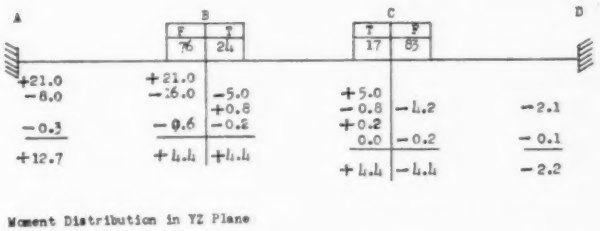


FIG. 5(b) UNBALANCED SHEARS AT B AND C DUE TO 1 LB APPLIED IN THE Z DIRECTION AT B



Moment Distribution in XZ Plane



Moment Distribution in YZ Plane

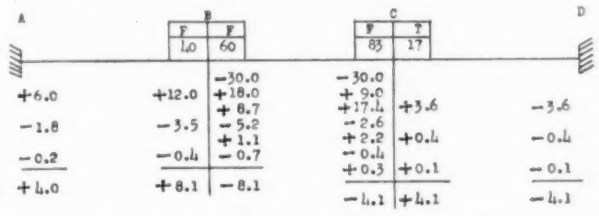


Fig. 6(*a*) Moment Distribution in *X*, *Y*- and *X*, *Z*-Planes for 1 Lb Applied at *C* in *X* Direction

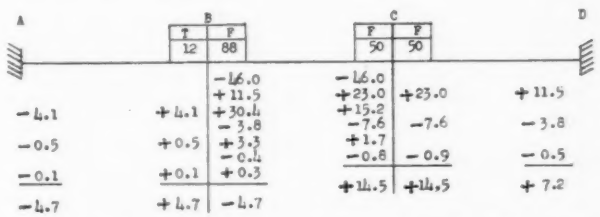


Fig. 7(*a*) Moment Distribution in *X*, *Y*- and *Y*, *Z*-Planes for 1 Lb Applied at *B* in *Y* Direction

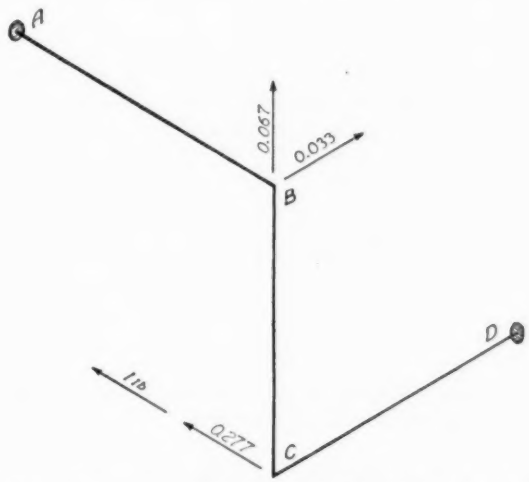


Fig. 6(*b*) Unbalanced Shears at *B* and *C* Due to 1 Lb Applied in *X* Direction at *C*

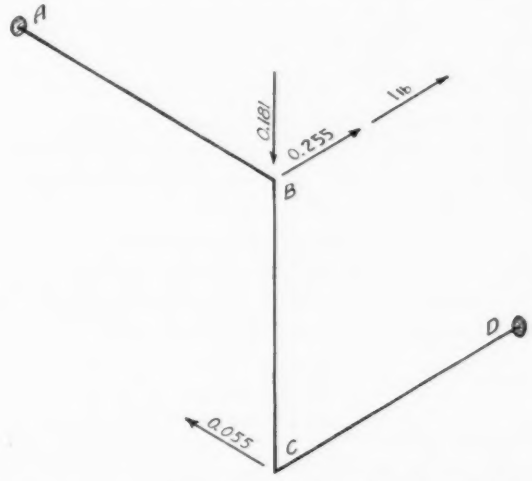


Fig. 7(*b*) Unbalanced Shears at *B* and *C* Due to 1 Lb Applied in the *Y*-Direction at *B*

The fixed end moments due to these shears are balanced in Fig. 5(*a*), and the shears produced by the distributed moments are calculated and shown in Fig. 5(*b*). It is seen in Fig. 5(*b*) that 1 lb in the *Z* direction at *B* produces unbalanced shears in the *Z* and *Y* directions at *B*, and in the *X* direction at *C*.

The same procedure is carried out for 1 lb in the *Y* direction at *B*, Figs. (6*a*) and 6(*b*); and 1 lb in the *X* direction at *C*, Figs. 7(*a*) and 7(*b*).

The unbalanced shears of Fig. 3(*b*) can now be removed by writing the following equations:

$(yB)(yB)F_{yB} + (yB)(zB)F_{zB} + (yB)(xC)F_{xC}$ = unbalanced shear in *Y* direction at *B*.....[10]

$(zB)(yB)F_{yB} + (zB)(zB)F_{zB} + (zB)(xC)F_{xC}$ = unbalanced shear in *Z* direction at *B*.....[11]

$(xC)(yB)F_{yB} + (xC)(zB)F_{zB} + (xC)(xC)F_{xC}$ = unbalanced shear in *X* direction at *C*.....[12]

$(yB)(yB)$ is the force in the *Y* direction at *B* due to 1 lb in the *Y* direction at *B*.

$(yB)(zB)$ is the force in the *Y* direction at *B* due to 1 lb in the *Z* direction at *B*.

$(yB)(xC)$ is the force in the *Y* direction at *B* due to 1 lb in the *X* direction at *C*; (and so on).

F_{yB} is the force in the *Y* direction at *B* required to remove the unbalanced shears of Fig. 3(*b*).

F_{zB} is the force in the *Z* direction at *B* required to remove the unbalanced shears of Fig. 3(*b*).

F_{xC} is the force in the *X* direction at *C* required to remove the unbalanced shears of Fig. 3(*b*).

Using quantities determined in Figs. 3(*b*), 5(*b*), 6(*b*), and 7(*b*); Equations [13], [14], and [15] are obtained.

$+0.255F_{yB} + 0.181F_{zB} + 0.033F_{xC} = +1480$.....[13]

$-0.181F_{yB} - 0.597F_{zB} + 0.067F_{xC} = -2400$.....[14]

$+0.055F_{yB} - 0.106F_{zB} + 0.277F_{xC} = +2000$.....[15]

from which

$F_{xC} = +8650$ lb
$F_{zB} = +4500$ lb
$F_{yB} = +1450$ lb

The force F_{yB} multiplied by the moments produced by 1 lb in the *Y* direction at *B*, Fig. 7(*a*), the force F_{zB} multiplied by the

Moment Distribution in XY Plane

A	B		C		D
	F	T	T	F	
+1.6 -6a	+3.5	-3.5 -6a	+3.5	-3.5 -6a	-14.7 -6a
+1.8 -7a	+0.6	-0.6 -7a	+0.6	-0.6 -7a	-0.3 -7a
-56.0 -3a	-37.0	+37.0 -3a	-37.0	+37.0 -3a	+99.0 -3a
-52.6	-32.9	+32.9	-32.9	+32.9	+84.0

Moment Distribution in XZ Plane

A	B		C		D
	F	F	F	T	
+3.5 -6a	+7.0	-7.0 -6a	-3.5	+3.5 -6a	-3.5 -6a
-7.3 -5a	-5.2	+5.2 -5a	+0.5	-0.5 -5a	+0.5 -5a
+79.0 -3a	+84.0	-84.0 -3a	-27.0	+27.0 -3a	-27.0 -3a
+75.2	+85.8	-85.8	-30.0	+30.0	-30.0

Moment Distribution in YZ Plane

A	B		C		D
	T	F	F	F	
-0.7 -7a	+0.7	-0.7 -7a	-2.1	+2.1 -7a	+1.0 -7a
-0.7 -5a	+0.7	-0.7 -5a	-9.1	+9.1 -5a	+14.9 -5a
-7.0 -3a	+7.0	-7.0 -3a	-37.0	+37.0 -3a	+43.0 -3a
-8.4	+8.4	-8.4	-48.2	+48.2	+58.9

FIG. 8(a) FINAL MOMENTS

(3a, 5a, 6a, and 7a indicate the figure from which the moments were obtained.)

moments produced by 1 lb in the Z direction at B, Fig. 5(a), and the force F_{xC} multiplied by the moments produced by 1 lb in the X direction at C, Fig. 6(a), provide the correction for the moments determined in Fig. 3(a).

FINAL MOMENT COMBINATION

In Fig. 8(a), the moments are combined and final joint moments are listed. In Fig. 8(b), the final shears are given. From Fig. 8(b), it is seen that the end reactions at A are

$$F_x = 9700 \text{ lb}$$
$$F_y = 4700 \text{ lb}$$
$$F_z = 8900 \text{ lb}$$

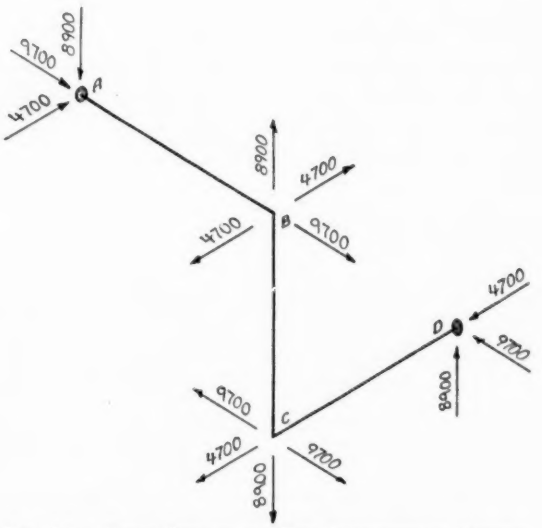


FIG. 8(b) FINAL SHEARS AND END REACTIONS IN POUNDS

While the solution given is for square corners, the method can be applied to pipe structures with bends at the corners. This necessitates modifying the stiffnesses and flexibilities of the members and also the carry-over factors. However, for the three-dimensional structure with bends at the corners having a radius of $1^1/_2$ pipe diameters or less, the assumption that the structure has square corners seems to be as accurate as is essential, in view of the fact that the end conditions of the structure can seldom be exactly dete.mined.

ACKNOWLEDGMENT

The author gratefully acknowledges the helpful comments of Dr. L. E. Grinter and Mr. E. Sternberg.

Discussion

The Strength of Cylindrical Dies[1]

BENJAMIN MILLER.[2] The behavior of metal under combined stresses is of great practical as well as theoretical importance, particularly in the case which the authors have investigated, i.e., the thick-walled tube under internal pressure. There are two solutions to be obtained, i.e., the equation for the pressure which will cause the inner skin to yield, and that relating the pressure to the spreading of the plastic region through the tube. The energy-of-distortion theory may be used to develop both equations. The equation for first yielding has been published by the writer;[3] in the authors' notation it is

$$p = K \frac{1 - (a/b)^2}{\sqrt{3 + (a/b)^4}} \quad \ldots\ldots\ldots\ldots\ldots\ldots [1a]$$

Presumably Equation [1*a*] could be obtained from Equation [37] of the paper by substituting a for r.

It has not yet been possible to verify Equation [1*a*] experimentally because it is so difficult to detect the first yield. Consider the hot-rolled steel cylinder tested by the authors with the results shown in Fig. 10 of the paper. According to Equation [1*a*], the pressure for first yield is 19,370 psi, and the corresponding load is 1490 lb. But the pressure of 25,000 psi and the corresponding load of 1900 lb predicted by the maximum-strain theory are as well supported by Fig. 10.

The equation for yield of the entire tube published previously[3] becomes in the authors' notation

$$\left(\frac{a}{b}\right)^2 = \frac{\sqrt{3}\, e^{\sqrt{3}\,(A_a - \pi/6)}}{2 \cos A_a} \quad \ldots\ldots\ldots\ldots [2a]$$

in which

$$p = (2K/\sqrt{3}) \sin (\pi/6 - A_a) \quad \ldots\ldots\ldots\ldots [3a]$$

Comparison indicated an error in Equation [39] of the paper; the expression under the radical within the brackets should be $(1 - 3p^2/4K^2)$. There may be a similar error in Equation [37].

The pressure for full yield in the test of Fig. 10 is calculated by Equations [2*a*] and [3*a*] to be 39,000 psi, and the corresponding load is 3000 lb. The calculated and experimental loads thus agree closely. Nevertheless, the equations are not entirely satisfactory.

The paper points out that "a cylinder under internal pressure is a case of biaxial stress, consisting of tension in the circumferential direction and compression in the radial direction." As the internal pressure increased from zero in the test of Fig. 10, the circumferential tension at the inner skin increased until it became 28,000 psi. Then, according to Equation [1*a*] of this discussion, yielding took place. Thereafter, as the pressure increased from 19,370 psi to 39,000 psi, the circumferential tension at the inner skin *decreased* to 4150 psi. The ratio of outside to inside diameter in this test was 2.35.

If the ratio of outside to inside diameter had been slightly greater, the circumferential tension at the inner skin for total yield would have been less; if the ratio had been 2.48, the circumferential tension at the inner skin for total yield would have been zero. If the ratio of outside to inside diameter had been slightly greater than 2.48, the circumferential stress at the inner skin for total yield would have been a compression rather than a tension. This result is one reason for considering that the equation is not entirely satisfactory; it is not easy to accept the idea that a radial pressure can develop a circumferential compression.

If the ratio of outside diameter to inside diameter had been 2.96, the internal pressure would have been 15.5 per cent greater than the yield strength, and no higher pressure can be attained, according to the theory. If the ratio of outside diameter to inside diameter had been greater than 2.96, total yielding in accordance with the equation would not have been possible. This conclusion was reached by Nadai.[4]

Equation [2*a*] can therefore be used only for cylinders having ratios of outside to inside diameters between 1 and 2.96. If b/a is greater than 2.96, the plastic region cannot extend throughout the tube, that is, r/a will have a maximum value less than b/a. The maximum value of r/a will obtain when the pressure has its maximum theoretical value of 15.5 per cent greater than the yield strength; it is given by

$$\left(\frac{r}{a}\right)^2_{\max} = \frac{e^{\sqrt{3}\, A_r}}{0.3259 \cos A_r} \quad \ldots\ldots\ldots\ldots [4a]$$

in which

$$\left(\frac{r}{b}\right)^2 = \sqrt{3} \tan A_r \quad \ldots\ldots\ldots\ldots [5a]$$

As b/a increases, $(r/a)_{\max}$ decreases, approaching 1.75 as a limit.

The writer cannot accept the conclusion that the outer layers of a cylinder cannot be caused to yield by internal pressure if the ratio of the outside to the inside diameter exceeds 2.96, and prefers to consider that the theory is incomplete. However, it is hoped that the authors will investigate this point by testing cylinders of hot-rolled steel having b/a values greater than 2.96. The heat-treated die-steel cylinders tested did have b/a values greater than 3 (except in test No. 20), but since they broke before the outer skin yielded it is suggested that similar experiments be run using hot-rolled-steel cylinders.

The authors have correctly pointed out that the theory cannot be expected to apply exactly to a metal which is subject to strain hardening, and have described a method of extrapolation to correct for slight strain hardening. There is also implicit in the theory the assumption that the yield strength in tension and the yield strength in compression have the same absolute value. It appears from the paper that the heat-treated steel, hardened to 60 Rockwell, withstood a compressive stress of 600,000 psi, but failed by fracture under very much lower tensile stress. It is therefore not quite clear that the theory may be properly applied to the heat-treated steel, or that a K value calculated from a load-expansion curve in the manner described is a yield strength in tension.

The use of rubber as the fluid to transmit the pressure to the

[1] By G. Sachs and J. D. Lubahn, published in the September, 1943, issue of the JOURNAL OF APPLIED MECHANICS, Trans. A.S.M.E., vol. 65, p. A-147.

[2] Institute of Gas Technology, Chicago, Ill.

[3] "Theories of Strength," by A. Nadai, Trans. A.S.M.E., vol. 55, 1933, paper APM-55-15; discussion by Benjamin Miller, p. 125.

[4] "Plasticity," by A. Nadai, McGraw-Hill Book Company, Inc., New York, N. Y., 1931, p. 194.

cylinder under test seems to offer great advantage. In experiments carried out under the writer's direction with water it was found that plotting the pressure against the corresponding volume of water pumped into the cylinder gave a better stress-strain diagram than could be obtained by using the expansion of the tube as a strain measure. With the authors' method, it may be that there will be an advantage in plotting the position of the testing machine head against the load.

R. L. Templin.[5] The authors have pointed out certain differences observed in the calibration of the extensometer used in their experimental work. A dial gage graduated to 0.0001 in. and apparently sensitive to ±0.00001 in. was part of the extensometer. While such gages are generally sensitive within the limits indicated, yet experience in actual calibration of such gages, using precision gage blocks having dimensional errors less than 0.000005 in. per in., shows much greater errors than might be suspected from the readily observed sensitivity.

Errors of 1 to 1½ full divisions (0.0001 to 0.00015 in.) are often found in gages of this type and occasionally larger errors. Unfortunately, there are no government or A.S.T.M. specifications covering the accuracy and sensitivity of dial gages. The British Standards Institution[6] issued such specifications in 1939, and these indicated permissible errors for dial gages 1¾ in. to 2 in. diam, having 100 divisions of 0.0001 in., and a magnification factor of 550 to 630, as follows:

Interval of reading	Permissible error over interval stated, in.
Any 0.001 in.	0.00005
Any half revolution	0.00007
Any one revolution	0.00010
Any two revolutions	0.00020
Any ten revolutions	0.00030
Any twenty revolutions	0.00040

Any such gage is required to repeat its readings to within one fifth of one unit division.

The accuracy of the apparatus used by the authors would appear to be quite satisfactory for determination of yield values, but any modulus-of-elasticity values, based upon the gage readings, would presumably contain errors corresponding to those in the gage in addition to those of lever ratio, observation, and manipulation.

Authors' Closure

The authors appreciate Mr. Miller's careful study and helpful comments and suggestions. The work on dies is being pursued further at the present time, and, consequently, such a discussion as that by Mr. Miller is very valuable to us.

If $r = a$ is inserted in Equation [37] of the paper, an implicit expression for P/K is obtained that is equivalent to Equation [1a] of Mr. Miller's discussion, as he presumes. However, Equation [1a] may be obtained much more directly and simply by substituting the stresses from Equations [5] and [6] for $x = a$ in Equation [12].

His Equation [2a] corresponds to Equation [37] of the paper, for the condition of $r = b$ (Equation [39]), except for the sign in the quantity $1 + \frac{3p^2}{4K^2}$ in both equations. This sign should have been negative, as pointed out by Mr. Miller. The error is not carried over into the numerical work, such as curve B of Fig. 4 of the paper, since it occurred only in copying the original equations for publication.

[5] Assistant Director of Research and Chief Engineer of Tests, Aluminum Research Laboratories of the Aluminum Company of America, New Kensington, Pa.

[6] 28 Victoria Street, S.W. 1, London, England.

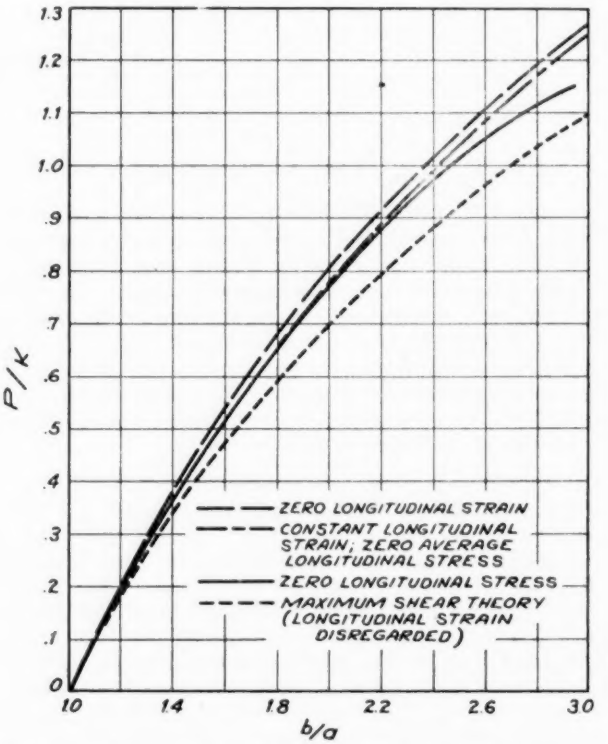


Fig. 1 (*a*) Effect of Wall Thickness on Pressure Necessary for Complete Plastic Flow, for Various Assumptions

The presence of a maximum possible pressure, equal to 1.155 times the flow stress, is a result of the assumption that the longitudinal stress (S_2) is zero. This condition actually occurs in a very short cylinder, or flat ring, under internal pressure. It is to be expected that in such a ring, having a large ratio of outside to inside diameter, a high internal pressure will cause yielding of the material near the hole in the longitudinal direction without causing yielding of the metal farthest from the hole. The existence of this limiting pressure can be shown more clearly in a qualitative way, at least, by the use of the maximum-shear theory. Longitudinal plastic flow at the surface of the hole occurs when $P = K$, since in this case the difference of the radial and longitudinal stresses equals the flow stress. However, complete plastic flow, extending to the outside surface of the cylinder, may not have occurred if b/a is greater than 2.72 (see Equation [24] of the paper). Thus, according to the maximum-shear theory for flat rings, no greater pressure than K can be developed, even though complete plastic flow throughout the tube has not occurred. The presence of a maximum pressure without total yielding in short thick cylinders has been observed also in recent experiments.

In a very long cylinder, on the contrary, longitudinal plastic flow is restricted by the necessary condition that the longitudinal strain is constant. Again, using the maximum-shear theory to develop a qualitative conception regarding the behavior of the cylinder, the longitudinal stress becomes unimportant in so far as the plastic flow is concerned, according to the foregoing assumptions. Then, by Equation [24] it can be seen that there is no limit to the pressure that might be developed in producing complete plastic flow. Likewise, by the energy-of-distortion theory, there is no limiting value of internal pressure for total plasticity assuming no longitudinal strain.[7]

[7] Reference 4, Equation [20], p. 188.

Since the publication of the original paper, the theory has been redeveloped using the energy-of-distortion theory and assuming constant longitudinal strain and zero average longitudinal stress. These assumptions correspond more nearly to the experimental conditions than the previous assumption of zero longitudinal stress, which was thought at the time to be the simplest possible. Actually the more correct assumptions have proved to be no more complicating, as can be seen by the expression for the pressure for total plasticity, which is

$$\frac{P}{K} = \frac{1}{\sqrt{\frac{1}{\frac{4}{3}\left(\ln\frac{b}{a}\right)^2} + \frac{1}{\left[\left(\frac{b}{a}\right)^2 - 1\right]^2}}} \quad \ldots\ldots\ldots [6a]$$

for the assumptions of constant longitudinal strain and zero average longitudinal stress, as contrasted with

$$\frac{\sqrt{3}}{2}\arcsin\frac{p\sqrt{3}}{2K} + \frac{1}{2}\ln\left[\sqrt{1-\frac{3p^2}{4K^2}} + \frac{p}{2K}\right] - \ln\frac{b}{a} = 0 \ldots [7a]$$

for the previous assumption of zero longitudinal stress.

The results of the more recent analysis have been compared in Fig. 1(*a*) of this closure, with results based on various other assumptions, and bring out the following facts: Assuming the most correct analysis to be that which assumes plane strain in a cylinder with unrestrained ends, the previous analysis gives nearly correct values for b/a values up to those investigated experimentally (2.4). For thicker cylinders the previous analysis deviates rapidly from the more correct analysis and becomes completely inapplicable for b/a values greater than 2.96. The energy-of-distortion theory, assuming zero longitudinal strain, is a good approximation, while the maximum-shear theory, although more simple, is less exact. In view of the foregoing discussion, it seems unnecessary to make any experiments on very thick cylinders.

The experimental fact that the fracture stress in tension is considerably less than the yield strength in compression, as referred to by Mr. Miller, in no way interferes with the conception that the yield strengths in tension and compression are nearly equal. This is generally accepted for the softer metals; and there is no reason why this relation should change with increasing hardness, even though the fracture stress in tension passes through a maximum and becomes smaller again. It is well known that a brittle steel can be made to flow plastically if a sufficiently high hydrostatic pressure is superimposed upon the tension.[8] In these cases, the yield strength is certainly considerably higher than the fracture stress in tension. Furthermore, under conditions of biaxial stress, the flow stress can no longer be identified with the yield strength in tension or compression.

We appreciate Mr. Miller's suggestion of using as a strain measure the change in the volume of fluid necessary to compensate for changes in the size of the hole. Successful tests have been made recently using this same principle, but with lead as the fluid rather than rubber. The compressibility and leakage characteristics of rubber are such as to make it unsuitable for such an experimental technique. The use of the change in fluid volume as a measure of strain is particularly valuable for those cases where longitudinal flow occurs at the surface of the hole without great progress of plastic flow in the radial direction.

Regarding Mr. Templin's remarks on the accuracy of dial gages, it should be noted that for a total measured strain of $^1/_2$ or 1 revolution, the accuracy of the gage is 1.0 to 1.5 per cent, according to the standards reproduced. On the contrary, the errors in the modulus-of-elasticity values, obtained by the use of the gage, are as high as 25 per cent. Consequently, the errors inherent in the dial gage are not sufficient to account for the observed discrepancies.

[8] "Experiments on the Problem of Failure," by M. Rös and E. Eichinger, Eidgenössische Materialprufungsanstalt an der E. T. H., Zurich, part 1, Diskussionsbericht no. 14, September, 1926; part 2, Diskussionsbericht no. 28, June, 1928.

"Some Fundamentals of the Flow and Rupture of Metals," by G. Sachs, Trans. American Institute of Mining & Metallurgical Engineers, Institute of Metals Division, vol. 143, 1941, pp. 13–29.

On Cutting and Hobbing Gears and Worms[1]

ALLAN H. CANDEE.[2] The writer has had experience with detailed calculations of the shapes of worm threads, gear-generating hobs, and thread-milling cutters for a good many years and is acquainted with a number of papers, articles, books, and patents dealing with the problems treated in the paper. Some of these are worthy of notice.

The earliest references to the shapes in involute worms and hobs of which the writer knows are by Trbojevich (1),[3] who demonstrated clearly that a hob to generate involute spur and helical gears must represent a worm of involute form. His articles present geometrical and analytical descriptions, as well as diagrams of involute helicoidal surfaces and their principal sections.

Buckingham (2) has employed the envelope method in analyzing the shapes of screw threads produced by thread-milling hobs, which at the present time are called multiple-thread-milling cutters. His tabulation of calculated co-ordinates, and diagrams showing paths of individual cutting points, together with the resultant envelope profile, are similar in kind to those in the paper. The envelope method, however, except for the more general information which it may yield, is too laborious for regular use, because it requires calculating several curves instead of only one.

Buckingham (3) also furnished specific equations for calculating co-ordinates of points in the axial profile of a worm thread produced by the usual straight-sided conical milling cutter. The effect of different diameters of cutter or grinding wheel was clearly illustrated.

A book by Cormac (4) gives an extensive mathematical treatment of worms and cutters. Most of the usual cases are covered, although only a few practical examples are included.

Wildhaber (5) has presented an original method of dealing with the contact between cutter and thread surfaces. He gives a table of formulas for radii of curvature of the cutter profile and of the surfaces of helical gear teeth and worm threads in the principal directions for the most usual cases.

There have been other articles in English, and of course there are many in German. Those mentioned have been most interesting to the writer. They indicate that the problem of profile shape in worms, hobs, and cutters has long been recognized and that answers have been known to some individuals at least.

The writer (6) has dealt with the correction of pressure angle and the determination of correct shape of the surfaces of relieved teeth in involute hobs.

The methods of solution adopted in the paper are based on

[1] By D. W. Dudley and H. Poritsky, published in the September and December, 1943, issues of the JOURNAL OF APPLIED MECHANICS, Trans. A.S.M.E., vol. 65, p. A-139 and p. A-197.

[2] Mechanical Engineer, Gleason Works, Rochester, N. Y. Mem. A.S.M.E.

[3] Numbers in parentheses refer to the Bibliography at the end of this discussion.

the kind of mathematics taught to engineers and on the advanced higher mathematics which is essential to progress in many fields. Analytic geometry, differentiation, vectors, transformations to successive sets of co-ordinate axes are all resorted to. Yet the problems dealt with are purely geometrical, and according to the writer's experience they can be solved most directly and simply by old-fashioned solid geometry, which seems to be an almost forgotten science.

The authors have applied concepts involving time, velocity, and even relativity with an observer placed first on one and then on the other of two moving bodies. Of course correct results can be obtained in this way; but it is simpler to consider merely the conditions of tangent contact, first between a helicoidal surface and a surface of revolution, and second between two helicoids. A surface of revolution and a helicoid can touch each other along a curve of contact, which can be established on the given surface and then determines the other surface. Two rotating helicoids can touch only at a single point, which during rotation lies at different positions on a curve determined from the given surface and serving to describe the other surface. Exact dimensions can be calculated by triangulation and by determining the intersection points of curves and lines.

The paper presents so-called deviation curves based upon a reference line which in some cases intersects the calculated profile. It is preferable and more usual in the treatment of curves in this way to refer the co-ordinates to the tangent and normal at the selected mean point. The amount of curvature is then most directly apparent, and in shop practice gaging is more readily accomplished.

The authors have based their determination of cutter pressure angle on a formula which gave noticeably inaccurate results. Thus under 6 "Example" the pressure angle specified was 25 deg; but in Fig. 9, a very considerable error is apparent. In order to determine as accurately as possible the pressure angle of the axial profile calculated in the paper, the writer took the following dimensions from a tabulation in Part I of the paper:[4]

r	z
1.64999	0.27101
1.75681	0.32301
1.86593	0.37750

By using a parabola passing through these three points and with its axis in the z direction, the pressure angle at the worm-pitch radius where $r = 1.750$ in. is estimated to be 26 deg 13 min to the nearest minute. This is 73 min more than the specified pressure angle of 25 deg. A difference of any such amount between a worm and its gear, for instance, would be far outside any manufacturing tolerance.

It is common in machine-shop practice to require an accuracy of pressure angle within 1 to 3 min; and it is therefore necessary to know how to specify correctly the pressure angle of a thread-milling cutter of either small or large diameter to produce a desired pressure angle in a worm.

The authors state[5] in Part I of their paper that the pressure angle of their cutter was determined in the following manner:

$$\tan \phi_n = \cos \lambda \tan \phi_x$$

$$\phi_c = \phi_n + \frac{90 \text{ deg} \sin^3 \lambda}{n}$$

It is seen that the final term is intended to represent the difference between the cutter pressure angle and the normal pressure angle of the worm thread; but no consideration is given to size of the cutter. The writer has derived and used the following approximate formula which includes the effect of the cutter and worm radii

$$\Delta\phi = \frac{90}{n} \cdot \frac{r}{R \cos^2 \lambda + r} \cdot \sin^3 \lambda \text{ deg}$$

$$= \frac{5400}{n} \cdot \frac{r}{R \cos^2 \lambda + r} \cdot \sin^3 \lambda \text{ min}$$

where $\Delta\phi$ is the difference between the normal pressure angle and the cutter pressure angle, n is the number of threads, r is the worm pitch radius, R is the cutter pitch radius, and λ is the lead angle. It is assumed that the cutter thickness is one half the normal circular pitch and that the cutter is set to the worm lead angle. The derivation of the formula is too long to be included here.

For the example already discussed, the foregoing approximate formula gives $\Delta\phi = 65.2$ min. A longer but mathematically exact method gives $\Delta\phi = 65.07$ min. Thus even with the lead angle as large as 30 deg, the writer's formula is almost exact and so is much more satisfactory than the one used by the authors.

Calculations of the kind indicated in the paper are not likely to be adopted even occasionally unless they are arranged so as to be as direct and brief as possible. The writer believes that considerable improvement in that direction can be made.

When the departure of the cutter or thread profile from a straight line is only slight, the calculation of point co-ordinates can be dispensed with and instead the amount of curvature estimated. In worm-thread grinding it is not even necessary to make this estimate, when means are provided to vary the curvature of the grinding-wheel profile until the thread profile conforms to a straight or slightly curved gage shape.

The paper is to be particularly commended for calling attention to the importance of a more widespread knowledge about shapes in worms, hobs, and cutters. Too many designers, mechanics, and even engineers responsible for gearing still suppose that worms, hobs, and cutters should all be straight-sided. This is not so, but correct shapes can be exactly determined; and proper specifications must be furnished by the gear calculator and tool designer, and used in the shop, if present-day requirements for the tooth contact in gears and worms are to be met.

BIBLIOGRAPHY

1 "Problem of the Theoretically Correct Involute Hob," by Nickola Trbojevich, *Machinery*, New York, N. Y., vol. 25, Jan., 1919, pp. 429–433.

"Herringbone Gears for Machine Tools," by Nickola Trbojevich, *Machinery*, vol. 26, Aug., 1920, pp. 1164–1169.

2 "Side-Cutting of Thread-Milling Hobs," by Earle Buckingham, Trans. A.S.M.E., vol. 42, 1920, p. 569.

3 "Manual of Gear Design, Section I—Mathematical Tables and Manual of Gear Design, Section III—Helical and Spiral Gears," by Earle Buckingham, Industrial Press, New York, N. Y., 1935.

4 "A Treatise on Screws and Worm Gears," by P. Cormac, The Sherwood Press, Cleveland, Ohio, 1936.

5 "Selection of Milling Cutters for Helical Involute Teeth," by Ernest Wildhaber, *American Machinist*, vol. 59, 1923, p. 909.

"Cutter Shapes for Milled and Ground Threads," by Ernest Wildhaber, *American Machinist*, vol. 60, 1924, p. 645.

6 U. S. Patents No. 1,548,929, No. 1,548,930, No. 1,548,931, Aug. 11, 1925.

L. PACH.[6] The authors have made a valuable contribution toward helping solve problems where all handbooks and textbooks fail to give the answer. Hitherto it was the general opinion of the machine-tool men, even of engineers, that tools for making worms have to be found by trial and error. The authors' paper proves that tool shapes for worms and helical rotors can be deter-

[4] Reference 1 of this discussion, p. A-145.

[5] Reference 1 of this discussion, p. A-145, footnote 4.

[6] Engineering Department, Turbo Engineering Corp., Trenton 7, N. J.; formerly Elliott Company, Jeannette, Pa. Jun. A.S.M.E.

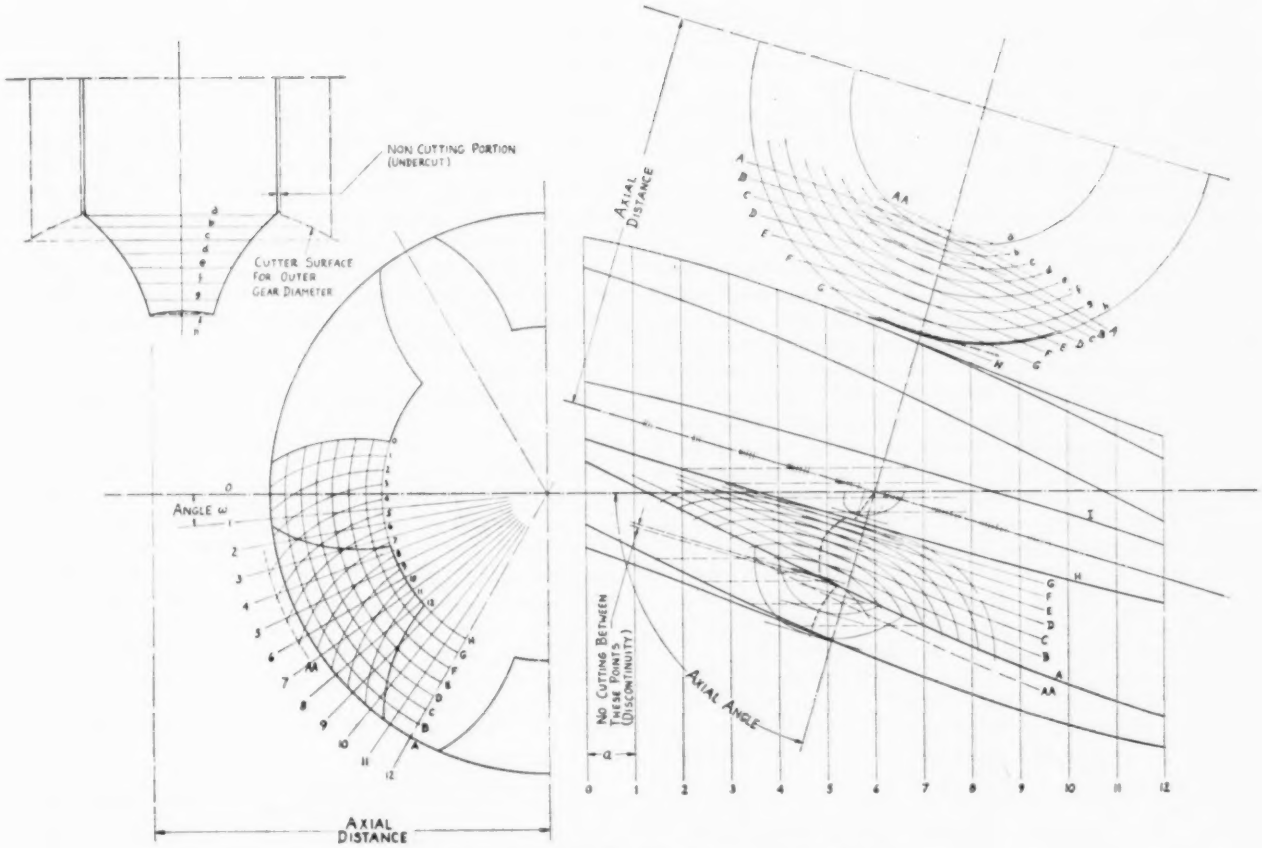


FIG. 1 LAYOUT OF "ALL-MILLING" CUTTER FOR A WORM

(Lines of deepest cutting are shown dashed. Cutter profile in upper-left corner.)

mined accurately without any guesswork, thus saving a tremendous amount of money, time, and materials.

This discussion will treat the problem: Given the worm, to find the cutter.

A few fundamental facts are worth noting in connection with the correct location, i.e., axial distance $R_p + r_p$ and axial angle λ, of milling cutters for new ideas of worms which have not been milled before. For a given worm, there is within certain limits an infinite number of possible cutter diameters. As for the case of straight grooves, the lower limit of the cutter diameter is given by the depth of the groove to be cut and by the diameter of the arbor and spacers holding the cutter.

However, while there is no theoretical upper limit of cutter diameters for straight grooves, the cutter for worms is limited by the requirement of free cutting. The cutter surface must fall away from the worm at a sufficient rate in order to prevent interference with the worm teeth. For smaller cutter diameters, this rate of falling away is greater than for larger diameters. The angle λ (Fig. 3 of paper) too, must be selected very carefully, particularly if the transverse worm section has some sharp corners at the bottom of the groove. In that case the "axial angle" λ must be identical with the lead angle at the bottom of the groove, because, as the authors state correctly, the helix cut must be tangent to the cutter surface. Where both cutter and worm come to a sharp corner, the requirement of tangential surfaces can be met only if the axial angle λ is equal to the lead angle at the bottom of the groove. If it were smaller or larger, the cutter could not reach deep enough. This, too, is a problem of interference. Accordingly if in Fig. 3 of the paper the axial angle λ were actually

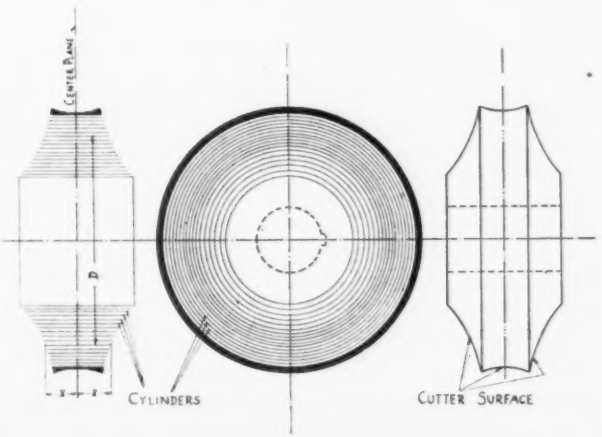


FIG. 2 FICTITIOUS MILLING CUTTER BUILT UP OF CONCENTRIC THIN CYLINDERS

the lead angle of the pitch helix, the profile as shown could not be cut, but fillets would result at the bottom of the groove.

It is possible to mill the entire worm rather than to turn the outer cylindrical surface on a lathe, thus eliminating one operation in mass production. The layout of a cutter for such an "all-milling" operation is shown in Fig. 1 of this discussion. This cutter was designed by a graphical method. The cutter can be thought of as consisting of a great number of concentric thin cylinders, Fig. 2 of this discussion. The intersection lines of

these cylinders with the worm surface will then determine the correct length of each cylinder at the point of tangency with a plane parallel to the center plane of the cutter. This point is then a point of deepest cutting, and the line of deepest cutting or "contact line" passes through it. The contact lines are shown as dashed curves in Fig. 1. It can be seen that the contact lines are discontinuous at the sharp corners of the worm section. This condition is analogous to the discontinuity of the slope of a curve with a sharp corner. In the discontinuous region, the helix H runs in the direction of the cutter motion, and the cutter comes to a sharp edge. In contrast to helix H, helix A does not run in the direction of the cutter motion between the discontinued contact lines. The result is a noncutting part of the cutter between the point cutting helix A on the tooth flank portion of the cutter, and the point cutting helix A on the tooth-top portion of the cutter. These two points will be on different diameters of the cutter, and to assure noninterference and free chip motion, the cutter should be undercut between these two points. The cutter profile is shown in the upper left, with the undercut and the tooth top portions drawn in dash-dot lines.

An alternative method of finding points of the contact line directly has been described graphically by O. Baier,[7] and analytically by K. Okusima.[8] This method is based on the fact that the cutter surface and the finished worm surface are tangential surfaces, contacting each other along the contact line. Consequently, the cutter and worm surfaces have common normals through all points of the contact line. Since the cutter surface is a surface of rotation with respect to the cutter axis a_c, all cutter normals intersect the cutter axis, and the problem becomes one of ascertaining a number of those normals of the worm surface which intersect the cutter axis. The foot points of these common normals are then points of the contact line.

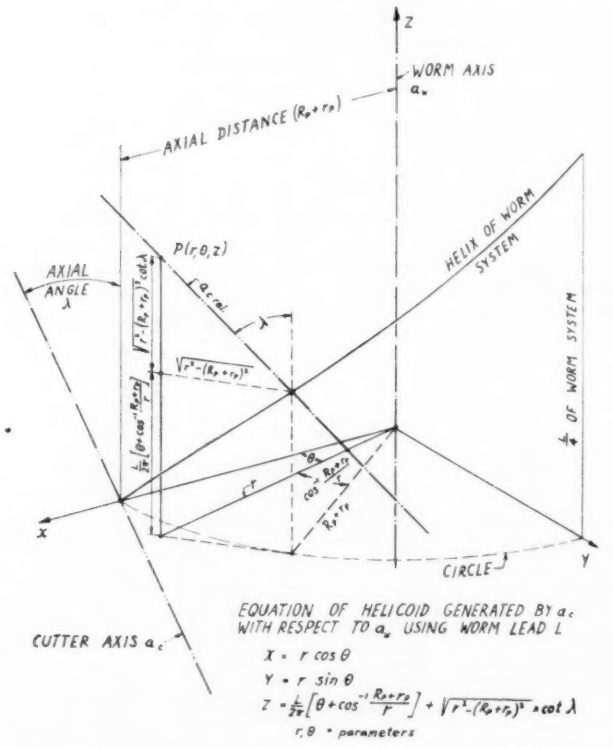


FIG. 3 HELICOID GENERATED BY THE CUTTER AXIS WITH RESPECT TO THE WORM AXIS DURING RELATIVE MOTION

The concept of relative motion of the cutter with respect to the worm is again used; during this motion the cutter axis a_c generates a helicoid H_{ac}. Now an intersection of a normal n of the worm surface W with the helicoid H_{ac} will give the exact relative position of the cutter as it cuts the foot point of that normal. The actual position of that contact point is then found by moving back the normal n along its foot helix of W through the same angle by which the relative cutter position is displaced from the actual cutter position. Mathematically, this operation may be performed as follows:

The helicoid H_{ac} is represented (Fig. 3 of this discussion) by

$$\left.\begin{aligned} x &= r \cdot \cos\theta \\ y &= r \cdot \sin\theta \\ z &= \frac{L}{2\pi}\left\{\theta + \cos^{-1}\left(\frac{R_p + r_p}{r}\right)\right\} + \sqrt{r^2 - (R_p + r_p)^2}\cdot \\ &\qquad\qquad\qquad\qquad\qquad\qquad \cot\lambda \end{aligned}\right\} \quad \ldots [1]$$

where r, θ are parameters.

The normal n may be represented by

$$\left.\begin{aligned} x &= r \cdot \cos\theta \\ y &= r \cdot \sin\theta \\ z &= \sqrt{r^2 - r_0^2}\cdot \tan\eta + z_0 \end{aligned}\right\} \quad \ldots\ldots\ldots [2]$$

where

r, θ are parameters
r_0 = shortest distance between a_w and n
z_0 = "altitude" of r_0 over x,y plane
η = angle, which normal makes with x,y plane

(All these values are readily obtained by using the direction vectors of n as described by the authors.)

Now the point of intersection of the normal and the helicoid is given by equating z of Equations [1] and [2], thus

$$z_0 + \sqrt{r^2 - r_0^2}\cdot\tan\eta = \frac{L}{2\pi}\left\{\theta + \cos^{-1}\left(\frac{R_p + r_p}{r}\right)\right\} + \sqrt{r^2 - (R_p + r_p)^2}\cdot\cot\lambda$$

This equation has to be solved for r and θ by trial and error, as any equation in helical geometry. It will be more conveniently solved by rotating the x and y axes about the z axis until the y axis is perpendicular to r_0. Calling the new axes x_4, y_4, and z, the equation of n may be written as

$$\left.\begin{aligned} x_4 &= r_0 \\ y_4 &= (z - z_0)\cot\eta \end{aligned}\right\} \quad \ldots\ldots\ldots\ldots\ldots [2a]$$

A similar transformation of Equation [1] to the x_4–y_4 system will then simplify the trial-and-error calculation.

Direct methods like this and the one described by the authors are certain to give the answer more quickly than the envelope method. They also have the advantage of enabling one to determine the exact point on the cutter for any desired point on the worm section.

The geometric relations described by the authors and by the writer are quite general and may be applied to tool design for machining of helical parts using end-milling cutters, grinding, and shaping processes.

Formed grinding wheels may be designed considering that a grinding wheel may be conceived of as a milling cutter with an infinite number of teeth, and the same principles as for milling cutters may be applied.

[7] "Konstruktion eines Fräsers, der eine Gegebene Schraubenfläche Erzeugt," by O. Baier, *Zeitschrift für angewandte Mathematik und Mechanik*, vol. 14, 1934, pp. 248–250.

[8] "On the Determination of Milling-Cutter Contour of Screwed Surface," by K. Okusima, Trans. Society of Mechanical Engineers of Japan vol. 3, 1937, pp. 268–272; English abstract, pp. S66-S67.

When using an end-mill process, two alternatives are possible:

1 The cutter axis may be fixed in a definite position with respect to the worm axis, e.g., in many cases perpendicular to, and intersecting the worm axis. Then there is only one correct cutter profile, which may be determined using the authors' method by rotating the worm surface with respect to the vertical end-mill axis, and finding the envelope surface of all worm-surface positions. Or Baier's method may be used by finding those normals of the worm surface which are also normals of the end-milling-cutter surface, i.e., those which intersect the end-mill axis. One single-end mill, however, cannot produce grooves with convex bottoms because of free-cutting limitations. It can produce flat-bottom grooves and concave grooves, such as twist-drill flutes.

2 The end-mill-cutter shape may be fixed as a conical, spherical, or any other shape cutter. Then the dependent variable is the path along which the tool has to move with respect to the worm surface. This path may be determined, bearing in mind that the cutter and worm surfaces always have to be tangential surfaces. From the exact tool path, and for a given tool-guiding mechanism, the exact cam shape may then be determined. This method has the advantages of simpler tool shapes (easier tool sharpening and replacement) and the possibility of milling convex groove bottoms and other complex helical parts. But it has the disadvantage of being a more involved operation because several cuts are necessary for a single groove. Also, the theoretically true worm surface can be obtained only by an infinite number of cuts. On the actual worm surface, although it may be well within the required tolerance, traces of the individual cuts will be visible.

Cams for the correct guidance of shaper tools for helical rotors may also be determined using the general principles that have been described.

All the foregoing applications of "analytic tool design," as this general type of work may be called, involve complex calculations, but, if tabulated calculating forms are used, the tool shape will be obtained much faster and cheaper than by shop trial-and-error methods.

Authors' Closure

The authors are grateful to Messrs. A. H. Candee and L. Pach for their valuable and interesting discussions. Their extensive references to the literature are welcome additions to the bibliography on the subject; apparently more has been done and written in this field than the authors had realized and they are glad to have their attention called to this work.

The authors agree with Mr. Candee that the problem is purely a geometrical one, however, they feel that the introduction of vectors, differentiation of vectors to obtain velocities, and other similar items needs no apology nowadays, since these tools are commonly taught in schools. These new frills merely bring "old-fashioned" solid geometry up to date, and enable one to simplify the derivations by using equations which approach more closely the geometric reality and bring out more readily the points of the proofs in a form which requires little memory work. What Mr. Candee calls "the theory of relativity" simply refers to the fact that to find out what a tool does to a piece of work, it is advisable to assume the point of view of that piece of work, watch the tool go by, and find the volume scooped out.

In addition to treating the specific problems discussed in the paper, it was the authors' intention to formulate general principles which will apply equally well to other similar problems; the criterion of deepest cutting, which was obtained in terms of the velocity of the cutting tool in its motion relative to the work, constitutes such a formulation. No apologies are needed for this point of view. The authors are grateful to both discussers for pointing out again that the problem reduces merely to finding the line of contact of two surfaces or the point of contact of two other surfaces.

The authors agree completely with Mr. Candee's criticism of the formula for the relation between φ_n and φ_c. It must be remembered, in this connection, that their primary intention was to obtain the exact shape either of the cutter or of the worm when the other is given. This shape may be specified by means of the deviation from any line. The particular line that was chosen was used merely because at least two nationally known tool vendors and our own gear plant were making regular use of this formula in calculating reference angles for checking cutters and worms. However, it was more with the idea of pointing out the inaccuracy of this formula rather than with any thought of recommending it that use was made of it. In footnote 4 of the paper, it was stated that results obtained from the formula were approximate. Had the authors been familiar with Mr. Candee's approximate formula which is both reasonably simple and accurate, they certainly would have used it in place of the one employed in the paper.

In Mr. Candee's discussion, reference is made to Wildhaber's formulas for calculating the radii of curvature of cutter, worm, and helical-gear profiles. When the authors first became concerned with cutter and hob shapes, an attempt was made to use these formulas to get more accurate cutters for two worm-gear jobs. Calculations carried out along this line gave profiles which were entirely unreasonable in the light of shop experience. The reason was not clear then; but it is clear now that the normal pressure angle of the worm φ_n and the cutter pressure angle φ_c are different, and hence radii of curvature are of no value in themselves unless the correct relation between those two angles can be established. Wildhaber gave no formula for the relation between these two angles except the following, which seems to imply that they are equal:

> "α = Thread profile angle in a normal section measured from the radius, and also the inclination of the cutter profile."

In reviewing other work on the same subject it is to be noted that the authors' methods make it possible to start with any general cutter, worm, gear, or hob profile and obtain the shape of the tool required or gear part produced. Other solutions have tended to treat only special cases, such as a straight-sided cutter or a straight-sided worm.

As pointed out by Mr. Candee, the envelope method may be laborious, especially where calculations have not been reduced to form-sheet routine, but it does have particular value of its own in determining root fillets, interference points, and scallops in the tooth surface. The alternative method of calculating directly for points on the final profile is often the quickest method of getting the shape of the working part of the tooth and should, therefore, be the method most often used.

The graphical method outlined by Mr. Pach is interesting. In general, the graphical constructions of the sine curves, corresponding to the projection of the helices of the worm on a particular axial plane, and their projections on a plane normal to the axis of the cutter, can only be carried out with a limited accuracy which is insufficient for the purpose at hand. For this reason, the analytical method is preferable. Yet the graphical method is valuable if for no other reason than it enables one to see the geometry of the problem more clearly.

While not agreeing completely with some of the criticisms, the authors feel that the points of view brought out by the discussions are valuable and will serve to clarify the subject and enhance the usefulness of the paper.

Deflection of Uniformly Loaded Circular Plates[1]

STEWART WAY.[2] This paper is of interest to anyone who has ever been concerned with the theory of circular plates bent to a surface of revolution.

The author introduces a parameter α which is related to the type of boundary support. As is pointed out, $\alpha = 1$ for a clamped plate and $\alpha = (1 + \nu)/(5 + \nu)$ for a simply supported plate. An elastic edge support also implies a particular value of α, depending upon the rigidity of the support. However, it should be observed that, in general, fixing the boundary conditions is not equivalent to specifying a value of α. Thus if the edge of the plate be clamped with any slope other than zero, α will depend not only upon the edge slope but also upon the load. Also, if the boundary condition consists of an applied edge moment M_{r1}, α will depend not alone upon M_{r1} but also upon q.

The writer has given some thought to what happens when α takes values outside the range

$$\frac{1 + \nu}{5 + \nu} < \alpha < 1$$

If we assume a rotationally elastic edge support of flexibility β, where β is the rotation of the support per unit of edge moment

$$\beta = \frac{1}{M_{r1}} \left(\frac{dw}{dx}\right)_1 \quad \text{.....[1]}$$

we can derive a relation between β and α, namely

$$\alpha = \frac{1 + \frac{D\beta}{a^2}(1 + \nu)}{1 + \frac{D\beta}{a^2}(5 + \nu)} \quad \text{.....[2]}$$

The maximum deflection, edge slope, and edge moment are related to α by

$$w_0 = \frac{qa^4}{64D\alpha} \quad \text{.....[3]}$$

$$\left(\frac{dw}{dx}\right)_1 = \frac{qa^4}{32D}\left(1 - \frac{1}{\alpha}\right) = 2w_0\alpha\left(1 - \frac{1}{\alpha}\right) \quad \text{.....[4]}$$

$$M_{r1} = -\frac{2Dw_0\alpha}{a^2}\left(5 + \nu - \frac{1 + \nu}{\alpha}\right) \quad \text{.....[5]}$$

The dependence of the foregoing quantities upon β is shown in Fig. 1 of this discussion.

The range of α values considered by the author is seen to correspond entirely to positive values of β. Negative values of β imply a negative flexibility of the edge support, a condition that is technically very unlikely to arise though it is certainly physically possible.

We observe from Fig. 1 that for β in the range

$$\frac{-a^2}{D(1 + \nu)} < \beta < 0$$

the plate, in the vicinity of the edge, is convex upward. The maximum deflection changes from positive to negative at

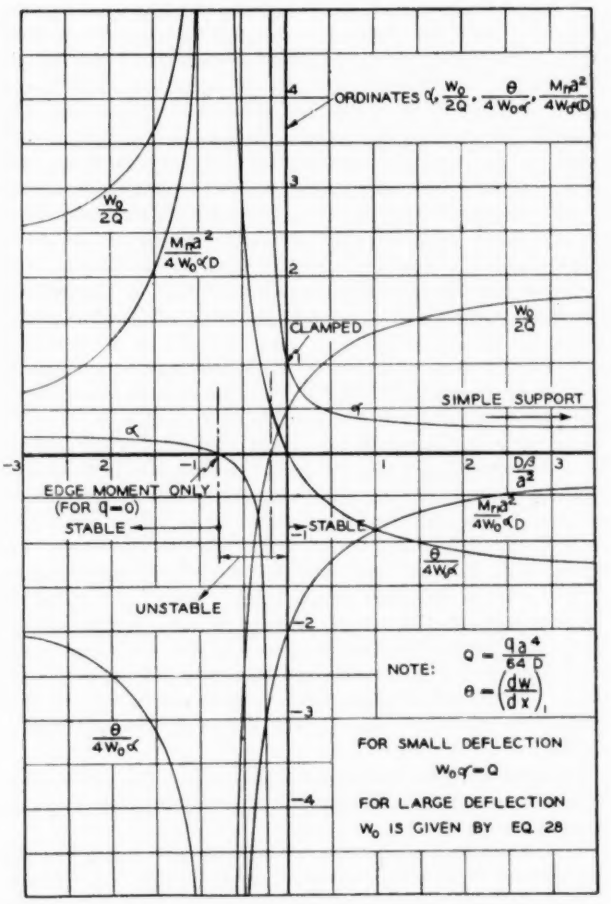


FIG. 1

$$\beta = -a^2/D(5 + \nu)$$

In this range of β values, the plate is in unstable equilibrium.

For values of β

$$\beta < \frac{-a^2}{D(1 + \nu)}$$

the plate is again convex downward, but is in stable equilibrium.

For the case

$$\beta = \frac{-a^2}{D(1 + \nu)}$$

the plate is in neutral equilibrium provided the load is zero. The applied edge moment arising from the rotation of the supports is just enough at all times to cause an equal rotation at the edge of the plate. The value of α is therefore the same as that for a plate loaded by edge couples only, namely, $\alpha = 0$.

If there should be plastic yielding of the edge support the author's Equation [3] would still be valid, but the value of α to be used would depend upon the load; so if α is to be experimentally determined in such a case, this should be done at the particular load for which one is interested in the stresses.

The contribution of the author to the large deflection theory is very commendable. It might be emphasized that, although the rotational flexibility of the supports is included in the theory, it is strictly assumed that there is no radial displacement at the edge. Most supporting structures occurring in practice which have rota-

[1] By F. C. W. Olson, published in the December, 1943, issue of the JOURNAL OF APPLIED MECHANICS, Trans. A.S.M.E., vol. 65, 1943, p. A-181.

[2] Mechanics Department, Research Laboratories, Westinghouse Electric & Manufacturing Company, East Pittsburgh, Pa. Jun. A.S.M.E.

tional flexibility would probably also have some translational flexibility.

For large deflections, the curves given in Fig. 1 of this discussion will also apply, except the curve for $w_0/2Q$. The question of the stability of the plate for negative β values and large deflection would need further investigation.

Author's Closure

Since the author is in complete agreement with the foregoing discussion, there remains only the pleasant task of thanking Stewart Way for his helpful and illuminating contribution.

Studies in Three-Dimensional Photoelasticity[1]

D. C. Drucker.[2] The "theory of laminar action" presented in this paper is not self-consistent and may lead to large error in many practical cases. In the problem of the transverse hole in a plate, or shaft, subjected to pure bending, it can be shown that this laminar action will exist except for a region of disturbance at the ends of the hole. The difficulty is that the dimensions of the disturbed region are of the order of magnitude of the diameter of the hole, and therefore will frequently cover the entire length. For example, the stress-concentration factor for a circular hole in a wide thin bent plate is approximately 1.8 and not 3 as for pure tension.

Fig. 1 of this discussion, which is the diagram of a lamina

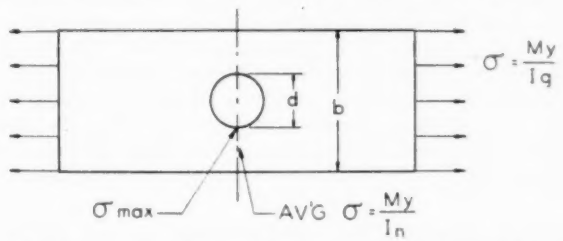


Fig. 1 Diagram of Lamina Perpendicular to Hole in Shaft

perpendicular to the hole in the shaft, shows the basic inconsistency. At some distance away from the hole the stress is given by $\frac{My}{I_g}$ where I_g is the moment of inertia of the solid cross section. At the line through the hole, the author reasonably assumes the average stress to be given by $\frac{My}{I_n}$, where I_n is the moment of inertia of the net section through the hole. He then finds the maximum stress by multiplying this average value by the two-dimensional concentration factor which varies from 3 to 2. It would, however, be equally possible to multiply the stress $\frac{My}{I_g}$ by its appropriate two-dimensional factor which varies from 3 to infinity. In the limiting case at the ends of the hole, the first procedure leads to a finite stress, the second to an infinite stress.

The reason is clearly that $\frac{My}{I_n} \times (b - d)$ is not in equilibrium with $\frac{My}{I_g} \times b$, i.e., the lamina has stresses acting on its top and bottom surfaces (in this case not even in equilibrium on each side of the hole), and thus is not independent of the rest of the shaft.

It therefore appears that the sharp decrease in stress at the ends of the hole may not actually occur, or at least no good theoretical evidence exists that it does. As a further point, the fairly high "edge" stresses produced in the freezing and slicing procedure make it difficult to determine boundary stresses.

Author's Closure

In the opinion of the author, Dr. Drucker failed to prove that the theory of laminar action, as presented in this paper, may lead to large error in practical cases. Consider the error: For $r/d = 0.07$, we have calculated and given in the paper two values of k_3, one based on laminar action and the other on the assumption that the maximum stress occurs at the end of the hole. The first is 2.18, and the second is 2.32, giving a possible error of roughly 6 per cent. This does not seem to us to be large. The curves in Fig. 17, show that the difference between the maximum stresses from laminar action and the extrapolated purely experimental results are small. The agreement of the results from laminar action with the experimental results by Peterson and Wahl proves that the errors must be small.

A factor of stress concentration is generally defined as the ratio of the maximum to the nominal stress at one and the same section. For the case under consideration this leads to the well-known range of 3 to 2. However, if k is defined as the ratio of the maximum stress at the net section to the nominal stress at another section where the stress is uniform, one arrives at Dr. Drucker's range from 3 to infinity. The introduction of such a definition seems to us to serve no useful purpose and to result in unnecessary complications. We prefer to adhere to the conventional definition. Infinity is not a number, and the factor of stress concentration, if it is to have meaning, should be a definite number. When a choice of definitions exists, we reject the one which leads to infinite factors.

The observation regarding a thin bent plate, in which the factor is 1.8, is irrelevant. We assume each lamina to be in pure tension or compression and not in bending.

The point regarding the existence of shear stresses in the extreme fibers of the beam and their influence on equilibrium is in the case of small holes, such as oil holes, of academic interest only and of no practical significance. Even in rigorous mathematical investigations, solutions are at times terminated with small disturbances in equilibrium. The presence of the shear

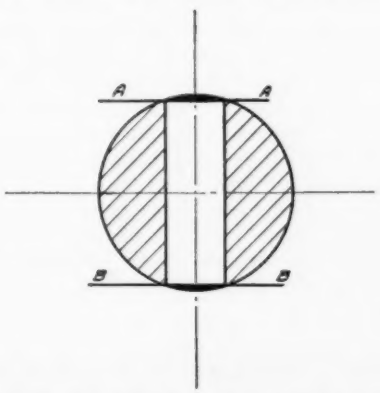


Fig. 2 Condition in Which Bending Stresses Above A–A and Below B–B Can Be Balanced by Shear Stress Only
(Solid areas show regions which cannot be represented by a continuous lamina. For practical cases these areas are small and approach 0 as the hole gets smaller.)

[1] By M. M. Frocht, published in the March, 1944, issue of the Journal of Applied Mechanics, Trans. A.S.M.E., vol. 66, p. A-10.

[2] Supervisor, Mechanics of Solids, Armour Research Foundation, Illinois Institute of Technology, Chicago 16, Ill.

stresses in the upper fibers is due not to any infinite factors of stress concentration but to the simple fact that the assumed laminar representation breaks down for plates of a width less than the diameter of the hole. We then have two disconnected plates, and not one continuous lamina with a central circular hole, and hence the bending stresses in the region of pure bending which are developed on the areas above line A–A and below B–B, Fig. 2 of this closure, can be balanced by shear stresses only.

If it is assumed, as we have done, that each lamina is in a state of two-dimensional stresses this would leave a small unbalanced force which is roughly proportional to the solid area above line A–A. It is apparent that this area, and therefore the unbalanced force acting upon it, approaches zero as the hole gets smaller, and for practical cases of oil holes this would always be a negligible quantity. For large holes, corrections would be necessary, since laminar representation would then be possible for a small part of the shaft only. Shafts with such large holes seem to us of little practical significance.

Dr. Drucker also states, "it can be shown (we presume mathematically) that laminar action will exist except for a region near the ends of the hole." In that case he supports our contention. We claim that the assumption of laminar action satisfactorily explains the experimental results, which clearly do not include the very extreme fibers. We do not dispute the statement that "the sharp decrease in the stress at the ends of the hole may not actually occur, or at least no good theoretical evidence exists that it does." No claim was advanced that such evidence does exist. We never even claimed the existence of conclusive experimental evidence on that particular point. It was clearly stated that further work on this matter is needed. The fracture, shown in Fig. 19 of the paper, fits in well with the idea of laminar action, in the extreme fibers, although as stated in the paper, it does not prove it conclusively.

We observe also that there is a vast difference between Dr. Drucker's initial assertion that laminar action can be shown not to hold in regions near the ends of the hole, and the closing statement, "no good theoretical evidence exists that it does." These statements are inconsistent.

The effect of time stresses has been amply discussed by the author in this and in another paper.[3] It is no doubt an undesirable characteristic of bakelite and affects somewhat the accuracy of the final results. In the problem under consideration, it was relatively easy to introduce corrections for them. It has also been shown that, with good technique, time stresses can be held to very low values. We have obtained frozen stress patterns of slices from shafts with transverse holes in tension, in which the boundary stresses were nearly as good as those found in freshly machined two-dimensional plates.[4]

In conclusion, we emphasize the essential fact that the theory of laminar action enables one to predict by a relatively simple calculation and good accuracy all the experimental values of k_3 available today from photoelasticity, strain gages, and fatigue tests from large shafts.

Stress Coefficients for Rotating Disks of Conical Profile[1]

E. O. Waters.[2] The author is to be complimented on having carried out a very painstaking analysis, with due attention to such mathematical details as convergence of series and degree of accuracy in incomplete series, details which the average engineer is apt to overlook or disregard as of minor importance. At the same time, the writer questions whether the type of problem shown in the illustrative example is worthy of such detailed and laborious computation. The accuracy of 5 parts in 2,000,000 claimed by the author for his tables would seem more appropriate for astronomical calculations than for a stress analysis where other factors such as yield strength, uniformity of material, and localized concentration of stress are, if the designer is fortunate, determinable with an accuracy of only 5 parts in 100.

The writer would suggest that reasonably accurate solutions for problems of this kind may be obtained by the method of least work, and that, by using this method, stresses in three dimensions may be found as easily as in two dimensions. This is an added element that should not be overlooked when dealing with solids of revolution whose length is of the same order of magnitude as the radius.

Stewart Way.[3] The author has made an admirable contribution in this paper to the theory of rotating disks. It is when we come to the application of the theory that perplexing problems arise. For a disk of regularly decreasing profile with increasing r, and for which the thickness is everywhere small compared to R, there is little doubt that the method of equivalent conical profiles would give good accuracy. When we have a disk of the form indicated in Fig. 2 of the paper, however, it is indeed questionable whether the theory of a rotating disk of conical profile can help us very much. The stress system produced by the overhanging guide vanes will be of an entirely different character from that considered in the author's theoretical treatment. The choice of this numerical example by the author was unfortunate.

For rotating structures of the type of Fig. 2, a satisfactory stress analysis can be obtained only if one goes into a considerably more exact theory which would take account of bending and fillet stresses, or else has recourse to an experimental method of stress analysis.

Author's Closure

The author is grateful for the stimulating comments of Professor Waters and Dr. Way. Professor Waters contends that the tables have been constructed with greater accuracy than is required by practical considerations. This situation exists because it was found necessary to construct better tables than those already published, in order to use the method of equivalent conical disks satisfactorily, since some of the arithmetical operations involved entail a loss of significant figures. Furthermore, some additional accuracy in the coefficients was obtainable with very little increase of labor by using the calculation methods described in the paper. It appeared desirable, therefore, to construct the best tables that could be computed economically for a sufficient number of entries, and at the same time consistent with the numerical methods available.

Professor Waters' proposal that the theory of least work be used for three-dimensional solutions of problems similar to the illustrative example suggests other methods rather than those described in the paper. Quite recently relaxation methods were recommended to the author in connection with solutions of like complex structures. These other methods have little or no relation to ordinary rotating-disk theory so that, strictly speaking, the results of thin-disk theory obtained in the paper have a limited range of applicability.

The question of applications is raised by Dr. Way whose ob-

[3] See author's paper, "Studies in Three-Dimensional Photoelasticity," *Journal of Applied Physics*, Jan., 1944, pp. 72–88.

[4] Ibid., Fig. 17.

[1] By K. E. Bisshopp, published in the March, 1944, issue of the Journal of Applied Mechanics, Trans. A.S.M.E., vol. 66, p. A-1.

[2] Associate Professor of Mechanical Engineering, Yale University, New Haven, Conn. Mem. A.S.M.E.

[3] Mechanics Department, Research Laboratories, Westinghouse Electric & Manufacturing Company, East Pittsburgh, Pa. Jun. A.S.M.E.

jections are recognized. This choice of example may have been unfortunate, however, it was the one available at the time for which an approximation to the stresses was required. It should not be overlooked that the various changes of profile in the example provide the designer with an excellent guide on how to proceed with the calculation in practically any situation to which the approximation is applicable. The question of applicability of the approximation can be settled only by comparison with an exact solution if available. The problem of estimating errors in a theoretical stress analysis of this nature is discouraging, but the author hopes to do some further work along the lines suggested in his reply to Professor Waters.

Book Reviews

On Growth and Form

ON GROWTH AND FORM. By Sir D'Arcy Wentworth Thompson. Revised and enlarged edition. University Press, Cambridge, England; The Macmillan Company, New York, N. Y., 1943. Cloth, $5^1/_2 \times 8^1/_2$ in., 1116 pp., 554 figs., $12.50.

REVIEWED BY M. HETÉNYI[1]

THE beauty and regularity of form in plants and animals have been agelong sources of fascination to mankind. Though it was always felt that the perfection of form is deeply connected with its purpose and usefulness, by far more scientific effort has been spent on the description and classification of these phenomena than on the investigation of the more fundamental question of their causation. The aim of the present book is to encourage investigations of this latter type and to indicate, at least, the profitable manner in which known physical and mathematical methods can be applied in the study of the complex problems of growth and form. As the author says in the introductory chapter: "The form of any portion of matter, whether it be living or dead, . . . may in all cases alike be described as due to the action of force. In short, the form of an object is a 'diagram of forces', in this sense at least, that we can judge of or deduce the forces that are acting or have acted upon it."

In this analytical spirit the author then proceeds to discuss, through the seventeen chapters of the book, an amazing array of examples of regularities in structure and development that can be found in living nature. The first two chapters are devoted to contemplations of fundamental nature, concerning matter, energy, and magnitude, and resulting in a number of gratifying conclusions obtained through dimensional considerations. The third chapter, on the rate of growth, is over 200 pages itself and comprises a wealth of statistical information which is likely to serve as basis for further meditation. Several chapters follow on the form and structure of cells and cell-aggregates. In this connection topics like the problem of minimum surfaces, states of equilibrium of membranes, the influence of surface tension, adsorption, etc., are extensively discussed. A separate chapter is devoted to the equiangular (logarithmic) spiral showing that this curve, by virtue of its continued similarity, is characteristic of such forms of living structures which grow by successive increments to one end (spiral shells, tusks, claws, etc.). The remarkable properties of this curve are known to have impressed James Bernoulli so much that he requested that it be engraved on his tombstone. Students of elasticity may be particularly interested in the pictures of chapter 13, showing the effect of torsion on the growth of horns. While horns of polygonal cross section exhibit conspicuously the anticlastic warping of the cross sections due to torsion, no such effect can be detected in horns with circular cross sections. There are two more chapters of structural character, one on the shape of eggs and other hollow structures, and the other on the relationship between form and mechanical efficiency bringing remarkable illustrations of stress trajectories in the structure of bones, precise three-dimensional lattice work in the vulture's wing bone, and many more of the like. The last chapter on the theory of transformations deals with the comparison of related forms on the basis of co-ordinate systems subjected to various types of distortion.

The mathematics employed throughout the book is of the simplest kind which can be understood and enjoyed by anyone without special preparation. The author does not fail to point out, however, that, while elementary means may bring instructive conclusions, the true and complete solution of most of these problems is yet unattained and is likely to require application of the most advanced methods available. Constant appeal is made therefore to the mathematical physicist pointing out a most worthy field for his labor, "a field which few have entered and no man explored."

The first edition of this book appeared over 25 years ago and has been out of print and scarce for quite some time. The present new and enlarged edition will therefore be doubly welcomed by the readers. The book is essentially the work of a grand amateur spellbound by the wonders of nature, but it is also likely to become a permanent source of inspiration for any specialist in the realm of physical sciences.

[1] Westinghouse Research Laboratories, East Pittsburgh, Pa.

Mechanical Springs

MECHANICAL SPRINGS. By A. M. Wahl. Penton Publishing Co., Cleveland, Ohio, 1944. Cloth 6 × 9 in., xi and 439 pages, 228 figs., xlii tables, $6.

REVIEWED BY C. O. DOHRENWEND[2]

MECHANICAL springs and their uses have become quite important in the field of modern machine design and a rational approach to their design has become essential. The theory required to calculate the stresses and deflections and to make clear the fundamental underlying principles as well as the data necessary for design has been widely scattered in various textbooks and professional papers of engineering and scientific societies. This book on the subject brings together much pertinent data as well as the fundamental principles underlying all kinds of mechanical springs. The author has expressed in the foreword the hope that the book may contribute something toward the avoidance of unsatisfactory operation and mechanical failure of springs by helping to put the specifications for springs on a more rational basis. It is a certainty that the book will help to accomplish this end.

The material covered in the book is in good balance, even though a large portion (212 of the 439 pages) is devoted to the helical spring. The remaining portion covers coned disk,

[2] Chairman, Engineering Mechanics Research, Armour Research Foundation, Chicago, Ill.

flat disk, flat and leaf, helical torsion, spiral, ring, volute, and rubber springs, as well as information on spring materials and energy-storing capacities.

The part dealing with the helical spring includes detailed theoretical analysis with the proper emphasis on stresses, deflections, and the fatigue properties of the materials. Also included in this portion of the book is information on the effects of lateral loads, buckling, vibration, surging, and a chapter on static and fatigue tests on both helical springs and spring material. Three chapters devoted to practical selection, design considerations, and maximum space efficiency are of special interest to the mechanical engineer faced with selection and design problems. Included in these chapters are tables of allowable stresses, load-deflection data per turn for various wire and coil diameters, the effects of the end coils, eccentric loading, variation of the spring dimensions, and stress at solid compression. This material on the helical spring is not only complete but is written in a clear style with excellent illustrations, graphs, and tables. The special problems that arise in connection with the tension helical springs at the end coils are adequately treated in the chapter on tension springs. The uses of square and rectangular wire springs are described, and curves for the calculation of the stresses in the rectangular wire are given.

The material presented with respect to the interesting problem of coned disk and flat disk springs includes the theory for calculating stresses and deflections as well as information on practical designs.

The flat and leaf springs are treated briefly with only the development of the fundamental principles underlying calculations for the simpler shapes. However, the effect of large deflections is discussed as well as the stress-concentration effects due to holes, slots, notches, sharp bends, and clamped ends.

Two torsional types of spring are presented in two separate chapters. Stresses and deflections are calculated by curved beam theory for the helical type with circular cross section. The spiral type is considered for three kinds of spring: the first, many turns without coil contact; the second, few turns in the spring; and the third, large deflections with the coils in contact.

The equations for the ring-type spring are developed and comments on stresses, deflections, and design calculations are given in a short discussion.

The volute spring has recently had much attention, particularly in its military adaptations. The presentation includes comments on the characteristics of this type spring, and the development of the equations for stresses and deflections along with practical design methods for both the constant and variable helix angle.

Although rubber is not normally thought of as a spring material, recent applications have shown it important in this field. The author has included some discussion of these springs and has described the simple shear spring, the cylindrical shear and cylindrical tension springs with comments on the allowable stresses.

The last two chapters of the book deal with a comparison of the energy-storing capacities of the different types of springs and the properties and types of spring material available.

The mechanical engineer will find this book very useful, easy to read, and containing a wealth of data on mechanical springs and their uses, while the theoretical presentations will appeal to engineering teachers.

FORGING OF STEEL SHELLS

Flow-of-Metal Aspects of Shell-Forging . . . . . *M. D. Stone* 1

Forces Acting in the Piercing of Cylinders . . . . . *W. Trinks* 11

Experimental Study of Shell Drawing . . . . . *George Sachs and G. B. Kasik* 15

Plastic States of Stress in Curved Shells: The Forces Required for Forging of the Nose of High-Explosive Shells . . . . . *A. Nadai* 31

An Experimental Investigation of the Nosing of Shells . . . . . *R. K. Carlson* 45

Presented at the Annual Meeting of The American Society of Mechanical Engineers, New York, N. Y., Nov. 29–Dec. 3, 1943, under the auspices of the Research Committee on Forging of Steel Shells and the Metals Engineering and Applied Mechanics Divisions. Published March, 1944.

Flow-of-Metal Aspects of Shell-Forging

By M. D. STONE,[1] PITTSBURGH, PA.

WHEN the fears of a world-wide conflict were threatening to become a certainty, one of the problems confronting the Ordnance Department and industry in general was that of providing for the manufacture of high-explosive (H.E.) shells in large quantities as rapidly as possible, at the same time making the best use of available facilities and knowledge. It was soon realized that there were many things we would like to know, to help make the best decisions, which had to be left to experience, and little enough of that. Little work along such lines had been done in this country since the last war, and whatever experience was gained at that time was available in the minds of relatively few people presently active along similar lines. It was apparent, too, that greatly accelerated production and reduced mauufacturing costs were mandatory to keep such a production program as this, involving tens of millions of shells, reaching into the billions of dollars, within the bounds of practicability.

To help develop and co-ordinate the technical background in the manufacture of shell forgings, the Ordnance Department vitalized an A.S.M.E. Committee set up for this purpose somewhat prior to our actual entrance into the world conflict. The results obtained have been gratifying to everyone concerned, and it is the purpose of this paper to present and discuss generally those aspects of shell-forging having to do with metal flow and associated forces. Many problems immediately presented themselves which required detailed theoretical and experimental study to evaluate properly the various factors, and accordingly several studies of this type were undertaken, some of which are discussed in companion papers by Trinks, Sachs, and Nadai, all members of the Committee on Forging of Steel Shells.

In contemplating the most direct way of making shells, a first thought might well be—why not form it by deep-drawing a disk cut from a plate, similar to shell-case manufacture. A little investigation soon disposes of this query, from the economic point of view: The cost of steel in plate form, and the attendant scrap, are too great. Well, then, why not cast shells closely to shape, or perhaps, at least, cast slugs that require relatively little forging to obtain the final form. Again, the economics involved have dictated otherwise, at least, up to the present, with some additional mental reservations as to physical properties, as well.

Actually, the initial form of the semifinished steel that has crystallized out of a wealth of experience is the billet. The billet as conventionally used is cut to length from the longer billets or bars as rolled on a continuous mill, but in at least one case, the long, as-rolled billet is used. For very large shells, generally not discussed here, individually cast billets or ingots are used.

Methods of Shell-Making

In the earliest attempts to make shells, the natural procedure was to place the heated billet in a die to form the outside shape, and to pierce completely with a punch that conformed to the desired inside cavity. This obvious objective has never been commercially attained. And the pros and cons of this and similar considerations form the context of this paper.

The maximum economical temperature for forging rarely exceeds 2300 F. Even at these elevated temperatures, the piercing of, say, a 90-mm shell-forging, having an approximate length of 12 in. and an approximate wall thickness of $^1/_2$ in., to completion in one stroke, may involve pressures in excess of 80,000 psi referred to punch area. This pressure is influenced considerably by the shape of the punch tip, as well as the die shape, the quality of lubrication, the speed of penetration, the analysis of steel, etc. But such pressures as this, which mean a force on the end of the punch of

$$80{,}000 \times \frac{\pi}{4} (2^5/_8)^2 = 435{,}000 \text{ lb}$$

are more than can be tolerated from the point of view of punch bending, resulting in eccentric or crooked cavities. Then, too, the combination of such pressure with corresponding longer times of contact with hot steel resulted in deformation of the punch tip (mushrooming) causing further vitiation of the shell cavity, as well as short punch life.

It was apparent very early that complete piercing must be abandoned, and hence the problem of how properly to complete the forging presented itself. The almost universal solution up to the first world war was to push the pierced slug on a mandrel through a series of ring dies, called "drawing;" hence the development of the pierce-and-draw method. Even with a large part of the burden taken off the piercing punch, it was general practice during 1914–1918 to finish-machine the shell cavities, due to the multitude of difficulties that arose, and it was indeed a laborious and expensive procedure. Possibly the one major advance in shell-making made by the Army during the 1918–1941 interim period was the demonstration of the practicality of finish-forging shell cavities. This, of course, imposed a completely new set of conditions on the shell makers, and all past practice had to be modified to fit these requirements.

We shall concern ourselves with only those questions having to do with metal flow: How deep should the pierce be, and what is the proper division of work between the piercing and the drawing operations; what is the proper shape of piercing punch; what is the best speed of piercing; what are the required forging-press capacities; what is the best cross-sectional shape of the billet; should the billet be sized, and perhaps pointed; should the boattail be forged on the shell, etc.?

Piercing Operation

A fair average of the most recent practice of piercing is to pierce to about 70 per cent of completion on the smaller shells, such as the 75 mm, reducing the figure to about 50 per cent for the larger shells, such as the 155 mm. The reasons for this differentiation are well founded: An important consideration is the maximum permissible contact time between punch and hot billet compatible with reasonable punch life. For 155-mm shells, counting both in and out time, the duration may reach 4 to 5 sec, for penetrations of from 14 to 18 in. Because of the large punch diameters, around 5 in., and the greater wall thicknesses, around $1^1/_4$ in., and in view of the somewhat greater cavity tolerances, the greater punch lengths (corresponding to the greater piercing depths) are possible from the bending point of view and attendant eccentricity. For the smaller shells, involving smaller

[1] Manager, Development Department, United Engineering & Foundry Company; Chairman, A.S.M.E. Special Research Committee on Forging of Steel Shells. Mem. A.S.M.E.

Contributed by Special Research Committee on Forging of Steel Shells and presented at the Annual Meeting, New York, N. Y., Nov. 29–Dec. 3, 1943, of The American Society of Mechanical Engineers.

Note: Statements and opinions advanced in papers are to be understood as individual expressions of their authors and not those of the Society.

punch diameters, the depth of penetration is limited mainly by considerations of cavity concentricity. Then, too, it is to be appreciated that the gain in reducing the piercing depth is two-fold, since a reduction in penetration depth necessarily means an increase in wall thickness of the pierced slug, since both the punch diameter and slug volume are constant. The effect of increasing the wall thickness is again to decrease the required piercing pressure. Other influences, tending to decrease piercing pressures, would be to increase the billet temperature, or to decrease the speed of piercing, but the relatively slight gains involved are more than offset by the reduced punch life, increased furnace costs, etc.

Another advantage gained by only partial piercing is that now the shape of the piercing-punch tip is no longer fixed, since the final cavity shape is thus determined by the draw mandrel. If for instance, the piercing punch could be flat-nosed, with possibly only the corners rounded, then the force could be reduced to its minimum. As the taper on the punch increases, the force to pierce increases considerably. This effect is evident in Fig. 1, which shows the results of piercing lead slugs with a variety of punch-tip shapes. A variation of more than 50 per cent is shown, the main action involved being that of friction along the

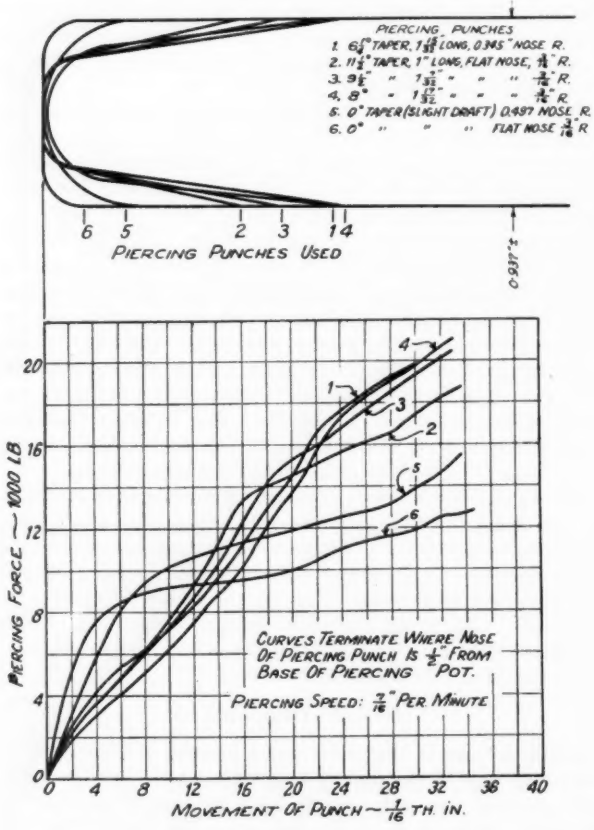


FIG. 1

tapered portion, as is developed in detail by Trinks in a companion paper. There are limits, however, on the arbitrariness of choice of the piercing-punch tip, i.e., it shall not have a taper less than that required by the final shell cavity (fixed by ballistic considerations), nor should it be too flat-nosed. This latter has to do with the nature of metal flow around the front end of the punch as it advances. In earlier times, it was observed that when the punch tip was flat it was possible to produce a loose "button" at the base of the shell cavity. This was a matter of considerable concern, until it was learned that its occurrence could be prevented by influencing properly the metal flow by using a sufficiently rounded punch tip.

FLOW OF METAL

Fig. 2 illustrates the nature of the metal flow, the existence of segregations or dirt in the steel bringing out the flow in the etched cross section. The illustrations show clearly the formation of a "false nose" (resembling the piling up of snow ahead of

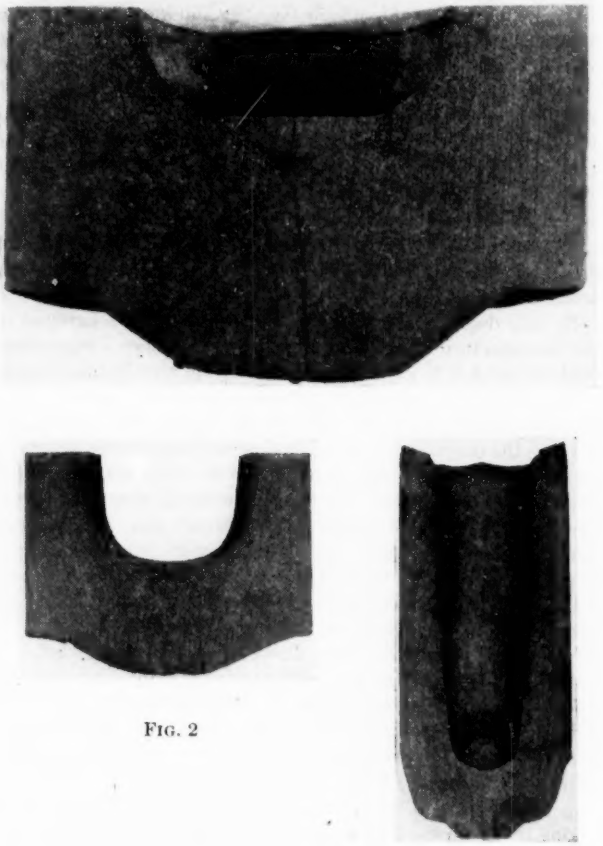


FIG. 2

a blunt-nosed snow plow), which, if the punch tip is sufficiently flat and, particularly, if the billet is pierced relatively cold, may actually result in metal failure. However, in a continuous search over a long period of time, not one case of a loose button has been encountered, and actual tensile tests from diametral specimens taken just below the point of deepest penetration have failed to show weaker metal, even though flow lines were visible (dirt).

The general flow of metal on the outside of the pierced billet is always such that tension strains exist. This is evident by examining the distance between flow lines at the base of the shells shown in Fig. 2. In Fig. 3, this is apparent again by observing the increase in distance between the diametral inserts along the outside surface. It emphasizes the necessity of shell-steel requirements that no seams, cracks, etc. shall be acceptable, since it is apparent that they would open up objectionably during piercing. This of course, is even more true in the subsequent drawing operations, where as much as 100 per cent elongations are sometimes taken.

The initial cross sectional shape of the shell billet is of considerable import, and the choice is influenced to some extent by whether the boat-tail is to be formed in the forging operation or not. It is obviously economically desirable to do this (rather

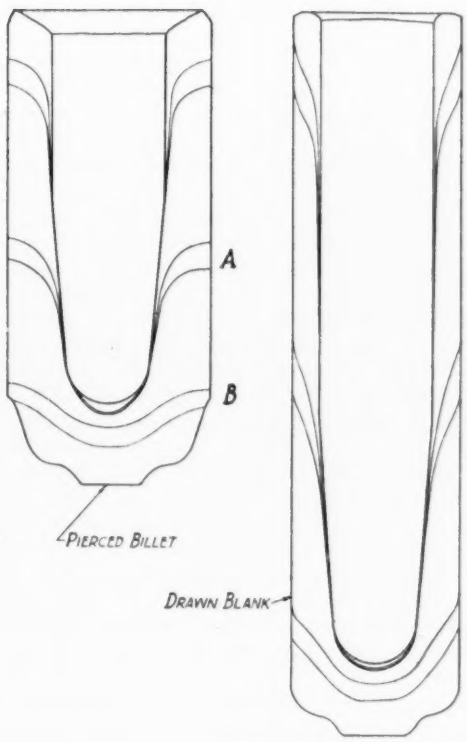


FIG. 3

than subsequently to machine it, with the attendant metal loss), all other considerations being equal. Most shell makers are now doing it. In designing the pattern of flow, it is desirable (see later) to reduce or eliminate what is called "extrusion" or backward flow of metal during the piercing operation, in order to maintain low piercing pressures. This means that the length of the original billet should be nearly the same as the length of the final pierced billet, aiming toward the ideal of straight radial flow, or "laying out" of the metal as it is sometimes called. While this ideal is unattainable, particularly near the base of the shell, we still cling to this concept, and, consequently, make the cross-sectional area of the original billet equal to the annular cross-sectional area of the pierced billet.

If the billet section being considered is a round (circular), then the problem presents itself of how to keep the slug central in the die prior to piercing. Actually, unless a preliminary "pointing" operation is provided, generally poor concentricity of piercing would follow even with the top of the shell guided. If now, the laying-out idea were abandoned, in order to favor concentricity, then a round billet closely fitting the die could be used, but with greatly increased piercing pressures, as shown in Fig. 4. However, in one plant where this practice is followed, a considerably reduced depth of pierce is used, counting heavily on a subsequent cross-rolling type of elongation. This method actually operates at low specific piercing pressures. Now, if a square section, or a round-cornered square is chosen, with metal area equal to the ultimate annular shell area, it is directly seen that the possibility exists of approaching the "laying-out" type of flow, while still retaining good concentricity by virtue of the diagonals of the square just fitting into the round shell dies. For square sections, the theoretical ratio of ID/OD should be 0.61. It is more than a coincidence that actual shell-forging diameter ratios (ID/OD) vary from 0.55 for the smaller shells to about 0.70 for the larger shells. This means that a slightly hollow square would be more suitable for the smaller shells, while appreciable corner radii are required for the larger ones.

It is possible to conceive that if the pierced slug is chosen to have too little piercing, that it would not properly fill out the die, particularly in the vicinity of the base. This is particularly true if the boat-tail is being forged on the shell and is always the case in attempting to get the sharp well-defined projection on the base that is required for subsequent machining purposes. If, by virtue of very thick walls, or a short depth of pierce, or both, or conceivably if lubrication were too good, piercing pressures as low as 15,000 to 20,000 psi only might be involved (referred to punch area), which would not be sufficient to cause the metal to flow into the far corners of the base, etc.

From what has been said, it can be appreciated how difficult or impossible it is to specify without qualification the capacity of a forging press to produce, say, 90-mm shells. Actual pres-

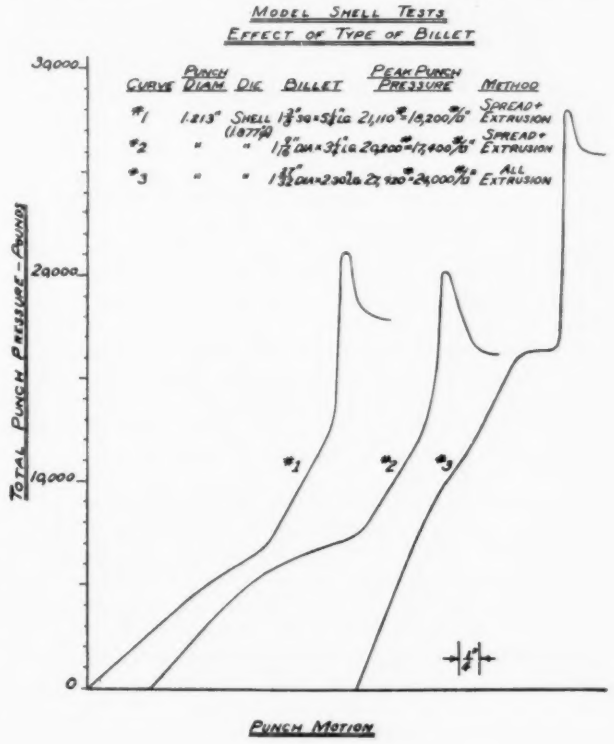


FIG. 4

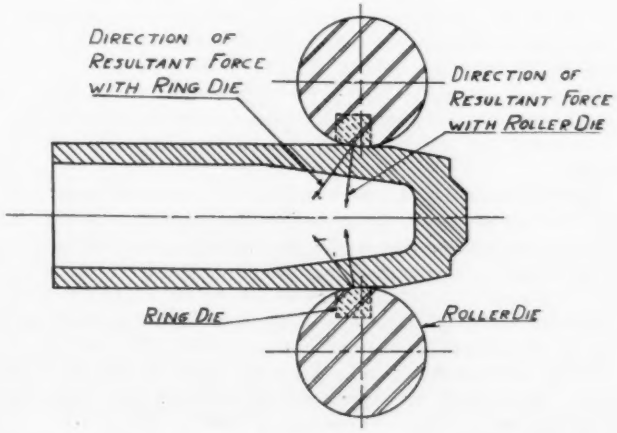


FIG. 5

sures as high as 80,000 psi and as low as 24,000 psi have been encountered in practice. Some cases are on record, where large forging billets, being pierced very slowly, required only 6000 psi, literally a "creep" stress. More usually, however, it might be safely said that optimum pressures for conventional practices seldom exceed 60,000 psi and are rarely lower than 30,000 psi. As has been said previously, the temperature of piercing, alone, can play an important role in fixing the required pressures, the resistance to deformation at 1800 F being approximately twice that at 2200 F. A fair approximation formula can be written as follows

$$P_t = P_{2200}\left(\frac{(2600 - t)}{400}\right)$$

when P_t = required pressure at temperature t (deg F), and $t \leq$ 2200 F. Therefore as a result of the multitude of uncertainties, many actual field tests have been carried out under a wide variety of conditions to evaluate quantitatively the requirements. These have covered piercing speeds from 2 ips to 25 ips (10 to 15 ips being usual), a variety of billet temperatures from 2400 F down to 1900 F, many types of lubricants, various billet shapes, several punch-tip designs, several ratios of ID/OD etc.

Drawing Operations

Until recently, practically all elongating after piercing has been accomplished by pushing the pierced shell (bottle, cup) through a series of ring dies by means of a mandrel whose shape conforms practically to the desired finished shell cavity. This operation is called "drawing." The simplified action in drawing involves a series of ring dies of successively smaller diameters, and the elongation is accompanied by a reduction in outside diameter, as well as in wall thickness. Installations have existed utilizing as many as 22 draw rings, and others with as few as 2, or even 1. Much work has been done to arrive at the optimum number of dies, as well as the most suitable reductions.

In the conventional pierce-and-draw process, as has been intimated earlier, elongations around 50 per cent are usual for the smaller 75-mm shells, increasing up to around 100 per cent for the larger 155-mm shells. Draw benches with from 3 to 5 sets of ring dies are frequent, the reduction per die ranging from 5 to 15 per cent and sometimes greater. There is an evident desire to reduce the number of dies as far as practicable, compatible with reasonable die life and keeping the mandrel forces low enough that bending or breaking of mandrels does not occur. This reduces the size (length) and expense of the draw press, as well as reduces floor-space requirements, since such machines are almost always horizontal affairs. In the case of the 155-mm bench, they may be as long as 40 ft. The matter of the required pressure to draw is obviously a function of the reduction taken, the die shape, type of lubricant, to some extent the speed, and yet more to complicate matters, it is influenced by the thickness of the base, shape of boat-tail if any, etc. For these and several allied reasons, an extensive series of investigations was undertaken and is discussed in a companion paper by Sachs.

Let it be mentioned, however, that the maximum reduction per die must necessarily be limited by the possibility of punching through the base, or even pulling the shell in two by wall failure. Base strength is the determining strength factor, however. Precautions against such failure are usually taken by maintaining the radius and shape of the nose of the pierce-and-draw mandrels the same, and not permitting too thin a base. The practice of forming boat-tails results in further reduction of the peak drawing force. Since shells are drawn directly after piercing, without reheating, an average temperature of 2000 to 2100 F is to be expected. At these temperatures, pressures of around 25,000 psi, referred to the area of displaced metal, are normally encountered.

By the use of forged boat-tails, not only may the maximum drawing force be reduced, but also the pressure of the punch tip tending to perforate the base. In fact, unless proper precautions are observed, this pressure may be reduced to zero, and the base of the shell may actually "run ahead" of the mandrel, paradoxical as this may seem. This phenomenon of running ahead or "ballooning" is still a matter of concern to many operators. The initial statement in this paragraph is not to be construed to mean that the existence of a boat-tail is the cause of ballooning, in fact, quite the reverse is true. The result, of course, is a scrapped shell, due to faulty cavity.

An understanding of this phenomenon in flow of metals is important, mainly to prevent its occurrence. The question of where the shell material in the region of die contact flows to is a matter of least resistance. Not only is it conceivable, but demonstrable, that if the friction between the punch shank and shell is too little (too well lubricated), and if the contact point between die and cup is too close to the base, and particularly if too much gas pressure is built up due to combustion of the lubricant, then ballooning is a certainty.

In earlier years, this gas-pressure formation was so serious that mandrels were drilled with a central hole to permit the backward escape of gases, although a needle of metal was usually formed by the metal's being forced into the same hole and had to be subsequently "spaded" off, or peened over. This imperfect method of reducing gas pressure has been more recently replaced by the device of always making the piercing punch slightly larger than the draw mandrel, thus permitting the gases to escape as the shell passes through the first draw ring, and before it has been forced down to mandrel dimensions. Even now, if a careless operator lubricates the mandrel too liberally, enough gas pressure can be built up to propell the shell off the end of the mandrel at dangerous speeds, as it emerges from the last draw ring.

Some mitigation of the running-ahead tendency may be obtained by placing the draw rings close enough together so that the shell is entering the next ring die before it quite leaves the preceding one. This expedient also reduces the over-all length of the draw press, but the increase in draw force involved usually discourages operators from adopting this practice. In some plants, where this difficulty has been only imperfectly overcome, the shell is allowed to be pushed against an end stop, after it has left the last die ring, thus re-establishing the cavity form again.

Roller-Type Dies Adopted

The first serious effort to reduce draw-mandrel pressures once the optimum design of ring die was reached was to resort to roller-type dies. In this construction, a nest of 2, or 3, or even 4 rollers, is designed to form a circular roll pass, capable of taking considerable reduction. The decrease in required pressures and the prolonged die life have proved the value of this modification. However, even with roll sets staggered with respect to each other, each consecutive set "ironing out" any fins or overfills left by the preceding one, it is still necessary to retain a final ring die which serves to smooth down the surface and more accurately size the outside of the shell. A preferred expedient to minimize fins, etc. is to machine a flat, or even a peripheral projection at the bottom of the concave-roll contour that will just offset the tendency of the metal to flow into the spaces between rolls.

A great deal of difficulty was encountered when roller dies were first installed, due to an increased tendency to run ahead, and several operators abandoned the construction because of it.

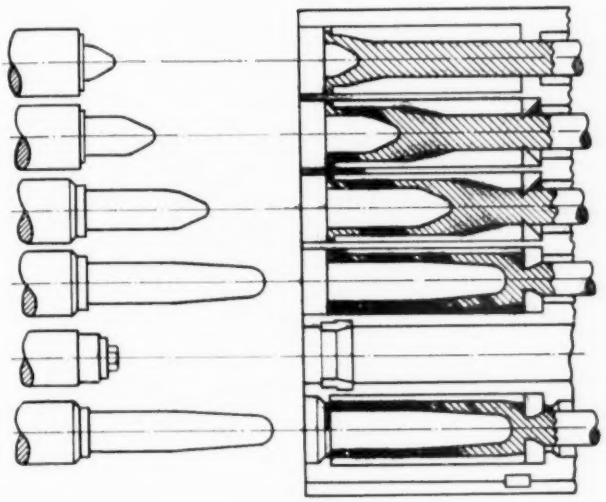


FIG. 6

However, after gaining a proper and detailed understanding of the determining influences, it has developed that all sizes of shells may be drawn through roller draw benches, and preferably so. The important difference between the actions of the ring die and roller die in running ahead of the shell is illustrated in Fig. 5, in which it is seen that, due to the decreased friction of the roller die, the component of the draw force tending to keep the cup on the mandrel is considerably less. The remedy has been so to modify the taper of the boat-tail that the first contact point between shell and die is well behind the internal contact point between mandrel tip and shell.

Another very recent method of elongating pierced shells, introduced essentially at the beginning of this war, has been to cross-roll the cup between 3 driven shape rolls, inclined at an angle to each other, while being mounted on a mandrel, which also assists in the forward motion through the mill. An additional aim of this machine is to reduce cavity eccentricity, the idea being that for equal roll pressures (and they will tend to be essentially so), more metal will be reduced where the absolute thickness of metal is greater. Thus a bottle having a $^{3}/_{4}$-in-thick wall on one side and $^{5}/_{8}$ in. thickness on the opposite side might well reduce to $^{3}/_{8}$ in. and $^{5}/_{16}$ in., say, after an over-all 100 per cent elongation, thus reducing the difference in wall thickness by substantially one half. However, there can be no correction of this sort on the boat-tail, which may be an important shortcoming, particularly for long boat-tail shells. There is sufficient merit in this method, however, for it to be well worth further study. In the draw bench, the tendency is more to concentrate the load on the thinner side (particularly if the shell is only in one die at a time) thus making it even thinner, and causing bending (banana shell) and increased eccentricity.

The principle of operation of this mill merits a separate paper in itself. Suffice it to say that the formed rolls rotate so that they tend to feed slightly at the same time they tend to rotate the shell rapidly. The action of the mandrel, however, is to aid in feeding the mill, so that a helix angle of metal flow is obtained. This angle must be such that it has a tangent greater than 1.8, to avoid premature metal rupture along a flow line, in a longitudinal tension test. Most of the work of reducing is done by the "hump" on the rolls, and while considerable difficulty was experienced in its early days of development, and while the method still requires personnel familiar with the intricacies of shape-rolling, it definitely constitutes a contribution to the art of shell elongation. Cross-rolling alone, however, does not produce a finished shell, and it is finally pushed through one or two ring dies to take out any rolling marks, to push the shell back



FIG. 7

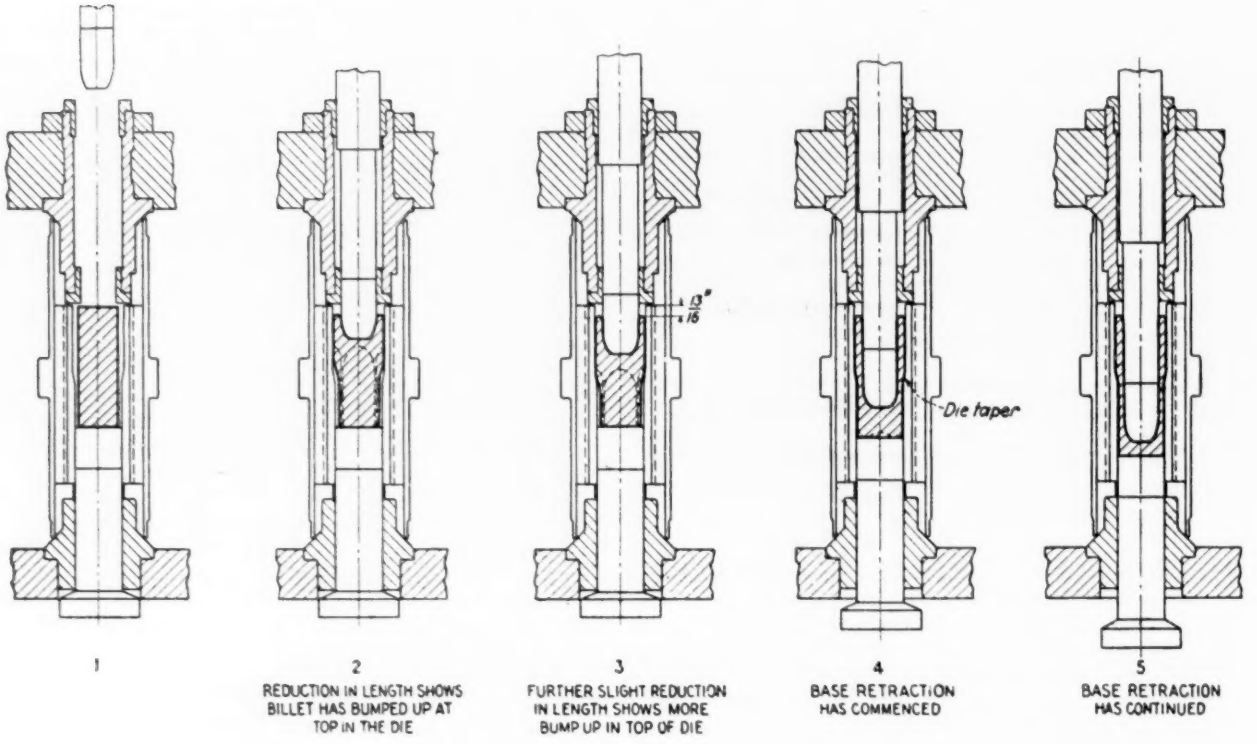


FIG. 8

onto the mandrel if the circumferential component of rolling has expanded it too much, and finally to size it.

There have been many and varied attempts to simplify the shell-forming process, primarily along the lines of reducing the amount of elongation, or eliminating it entirely. A generally successful sequence has been to double-pierce and then draw through a single ring. In this scheme, during the first piercing operation, the billet is upset (flattened or cabbaged) and only slightly indented, thus serving to center the billet in the die firmly and accurately. With this preliminary piercing accomplished, it is then possible to pierce practically to completion (using a punch shape that defines the finished cavity). The last operation is to withdraw the punch, now with the billet on it, and slip into place a die ring (at the same time rotating the piercing die out of position), and then a second operation of the punch sizes the shell. The well-designed machine has both punch mandrels in the same head, which are indexed in and out of position, with the final finished shell being drawn vertically downward.

"Upsetter" Method of Shell-Forging

Another and very successful attempt to eliminate drawing has been the development of the "upsetter" method of shell-forging, which comprises a series of progressive piercings from billet to final forging. The chief advantage offered by this method, from the flow-of-metal point of view, is the freedom of choice permitted in the punch-and-die design, up to the last set, which must conform to the outside and inside shapes prescribed pretty much by the finish-machined contours. The design of the production machine, based on the multiple-pierce idea, has been to use split dies, all dies being parts of a single die block and therefore opened and closed together. The machine is mechanically operated, both as to the operation of the dies, through toggles, and for the operation of the punch block. In the early tool designs, excessive pressures and die wear were encountered and led to the adoption of "forging with a collar," as shown in Fig. 6. A study of the flow of metal shows great ingenuity and thought in the matter of tool design. In the first pass, the conical-shaped punch forces the metal sideways to fill up the die (and thus centers the forging), as well as forms the collar (shown in black). The pointed punch is retained in the next two steps, with the metal being practically wedged apart, in an effort to obtain the ideal "laying-out" action described earlier; all the time the metal is in slight tension, pulling against the collar formed during the first pass. The 4th pass finds the punch assuming a form closely resembling the final shape in the 5th piercing pass (actually the 6th, since a collar-shearing operation is carried out in between).

The conception that the process causes the metal to flow only radially without any extrusion, is not borne out by an examination of split shells, with inserts imbedded therein, to reveal flow patterns. In Fig. 7, it is seen that the inserts do not remain radial, but are inclined both to the surface of the punch and of the die, showing relative-motion drag in each case. Due to the fact that wall thicknesses in this method are thin (final) in each pass, and also that a more pointed punch is used than is usual in piercing punches, piercing pressures, as measured by calibrated strain gages, mounted on the upsetter-machine tie rods, and also on the pitmans of the machine, are on the high side of the figures mentioned earlier in the paper, ranging from 55,000 to 60,000 psi maximum. Due to these pressures, if the die-closing toggles are not rigid enough or if any wear has taken place, the dies tend to open up slightly, resulting in both eccentricity and ovality of the forged cavity. Due to the fact that the machine is of the mechanical-crank type, watchfulness is maintained that oversize billets are not put into the machine, as abnormally high forces could be developed which might result in breakage. Because multiple punches and dies are employed, and can be

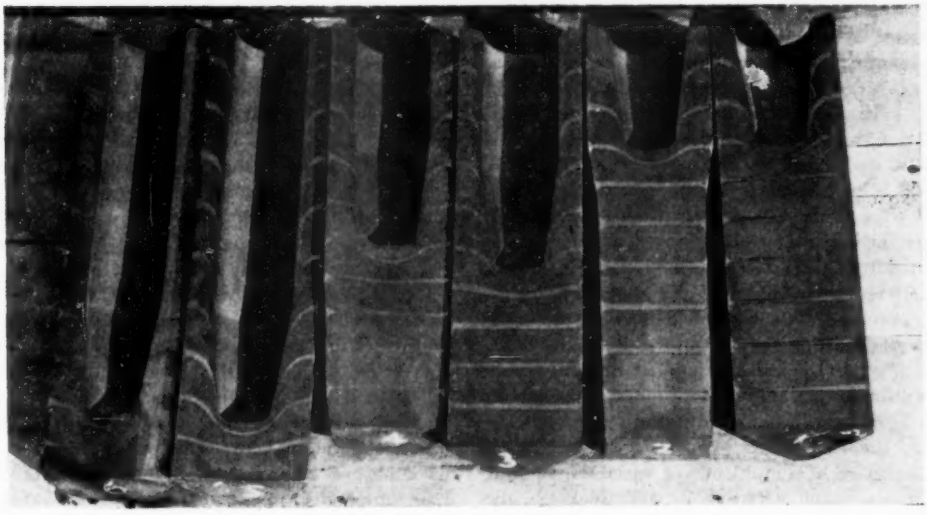


FIG. 9

plentifully cooled between passes, long tool life is obtained. For the smaller sizes of shells, this method has proved outstanding.

FORGING SHELLS BY "ONE-SHOT" PROCESS

The ultimate in simplicity in shell-forging, as has been said earlier, would involve piercing to completion in one stroke. As early as the last war, attempts along such lines reached commercial proportions. The difficulties presented by attempting to produce a shell in "one shot" are (1) thin walls, (2) long pressure stroke, resulting in greater tendency of punch to bend and punch tip to fail, and (3) long taper of punch tip, since the punch must conform to the final finished cavity. The consequences of (1) and (3) are to increase greatly the required piercing pressures, which when coupled with (2), which means greater tendency for lubrication failure and longer time in contact with hot metal, tend to decrease tool life disastrously, not to mention worse eccentricities and rough cavities.

The point of attack in approaching this problem in 1914–1918 was to decrease the required piercing pressures by eliminating as much as possible the movement of metal relative to the die walls. The idea was sound. The tremendous role of friction in metal flow, such as necessarily takes place in shell-forging, is appreciated when it is realized that free, unrestrained compression of shell steels at temperatures around 2200 F requires only about 4000 psi. The idea adopted was to build the shell die in two parts, the cylindrical wall and the base. The base was held fixed, but the wall die was left free to float, the idea being that as the metal moved axially either upward or downward, the floating die would move freely with it, reducing wall-friction effects. The method was developed to a satisfactory commercial degree.

However, when the same method was resurrected at the beginning of the present war, it failed because of the increased stringency of requirements, mainly as to forged-finish cavities and closer tolerances. Another possible objection was that since the metal-flow velocities are not all equal along the wall, there still is bound to remain some degree of frictional resistance, even in a floating die. The problem was solved by now holding the wall die fixed, allowing the base to retract, as a function of pressure build-up, and most importantly, carrying out the operation very rapidly (as compared with the early practice). Fig. 8 shows the various stages in the formation of a British shell as made by this method in Canada and is self-explanatory. Pressures involved vary from 45,000 psi to 55,000 psi maximum, referred to the punch area. We would expect about the same pressures for United States H.E. shells, since although British shells require a blunter punch, they have thinner walls and are specified to be forged at lower temperatures. Excellent concentricity of shell cavities, with smooth satinlike internal finishes, are obtained. The problem of tool materials for the deep penetrations involved is solved by the use of cast iron for both punch and die alike, following practice in similar situations in the hot-rolling of steel. The comparatively short punch life of from 50 to 75 shells before redressing is just about compensated for by the lower cost of cast iron compared to tool steel. The question of why such good concentricity is retained in spite of the relatively high pressures mentioned earlier must be answered by the fact that in this process only about 30 per cent of the total pressure is permitted to come on the base. The remaining resistance must therefore be distributed along the punch body, resulting in less tendency to bend, etc.

This method, popular in Canada, is practiced with variations in one American forge, although less perfectly since a separate base-setting operation is required. Both practices require that the billet be gripped tightly near the open end (a collar being forged on in one case) so that metal pressure against the die walls is decreased, tending further to reduce frictional effects. The primary reason why this method has attained success has been a clever attack on the problem of metal flow, see Fig. 9.

While much could be said of other methods and variations in shell-forging, notably the French extrusion method, their lack of widespread use at the present time will constitute a limit on this discussion, as well.

For the H.E. type of shell, it has never been possible to forge completely the ultimate shape of the shell. In all cases, the shell forging must be subsequently formed to give the projectile the proper shape along the ogive. In earlier days, and particularly in Europe, shell forgings were frequently made with the nose integral (instead of the base, as now). However, the weakness of the screwed or assembled base interfered with the proper fragmentation of the shell, and so the present general practice was adopted, requiring a separate forging operation called "nosing."

"NOSING" OPERATION

Nosing, as it is generally practiced, is accomplished by forcing a contoured die over the open end of the shell. While similar

results could be obtained by spinning, swaging, or hammering, the required contours, metal thickness, etc. do not require anything more elaborate than the simple operation mentioned. Even this simple operation, however, requires a great deal of intelligent study.

At the beginning of the war, and particularly earlier, it was deemed essential that shell forgings be heated, even to a forging temperature of 2200 F in some cases, in order to carry out the operation. It was soon realized that when the die was forced down (usually) over the shell, the compression stresses built up, varying from practically zero at the open end, increasing to a point where circumferential buckling of the shell took place, attended by equally objectionable wall thickening. It was thus obvious that differential heating of the shell was necessary, and, accordingly, it is now general practice to heat only slightly more than that which is ultimately required in forming the nose. In addition to the matter of distribution of initial temperature, it was evident, and still is, that the nature of metal flow from initial shape to final is a function of a multitude of variables, such as friction, machine finish, initial variation in wall thickness, die temperature, speed of nosing, etc. Accordingly, a theoretical and experimental investigation was sponsored, and is reported in a companion paper by Nadai and Carlson, to attempt to correlate fundamental concepts with actual experience.

In order to obtain circumferential uniformity in heating for nosing, particularly for the older furnaces, it is necessary to rotate the shells as they project into the heating zones. Uniformity of heating in one case is obtained by use of a salt bath, but unsatisfactory axial variation in temperature results. More recently, heating by high-frequency (1000 to 3000 cycles per sec) induction has been introduced. Because of the thinness of the shell walls, heating times are not long even for the older furnaces, varying from 5 to 15 min, and, consequently, scale formation is not the serious problem it is in forging. For the induction method, the time is reduced even to a matter of seconds, and by judicious spacing of the induction coils, ideal temperature distribution may be obtained.

The importance of the speed of nosing was muffed badly by several operators early in the war. In an attempt to use old, slow nosing presses, ram speeds as low as 1 ips were encountered. Even though the actual flow resistance is less at slower speeds the long time of contact with the cold dies cooled off the shells so rapidly (sometimes dropping 800 to 1100 F) that the presses would "stall' before completion of the operation. This situation was aided considerably by heating the dies to say 600 F(at which temperature they would tend to maintain themselves in production). Nosing speeds were increased, as well, and many hydraulic presses operate as high as 30 ips, dropping down to say, 5 to 10 ips for the last $^1/_8$ in. of the operation. For the same temperature, an increase of speed from 1 ips to 10 ips would only increase the nosing pressure by about 25 per cent whereas a drop in temperature only 400 F would increase the pressure 100 per cent.

The matter of lubrication in nosing is of great importance. For instance, a good lubricant will result in the shell actually increasing in length as a result of the nosing operation, whereas a poor lubricant will result in its shortening. A poor lubricant, say, by virtue of its being burned out before the operation is completed, may so increase the pressure required that the shell may buckle, the press stall, and the shell stick in the die long enough to result in a cracked die, and hence a pro luction delay. A well-maintained lubricating film also reduces the cooling off of the shell, to a degree.

Cold Nosing

It can be understood therefore because of the problems involved in hot-nosing, such as heating costs, matters of scale formation, possibilities of buckling, nonuniformity of nosing (unless lubrication, temperature distribution, speed, etc. are watched closely), that attention was diverted toward the possibilities of cold-nosing. At the present time, it is universal practice to cold-nose 75-mm and 90-mm shells, and about 75 per cent of the 105-mm shells are cold-nosed. The 155-mm shells are, however, all hot-nosed, and it is interesting to examine the factors involved.

At the outset, we must recognize that the specific compressive resistance cold is about 4 to 5 times that of the hot steel at the temperature it has at the completion of the nosing operation, say 1500 to 1600 F. However, our ability to lubricate better the cold operation than the hot, going from friction coefficients as high as 0.6 to 0.8 down to values of the order of 0.2 to 0.3, results in the total required pressures being only of the order of twice that conventional for hot practice. This is borne out, for instance, for the 105-mm shells, where hot-nosing is satisfactorily accomplished at pressures of from 100 to 175 tons (dependent upon temperature, etc.), while cold-nosing conventionally requires 300 to 350-ton presses. Cold-nosing of 75-mm shells requires 100- to 150-ton presses.

As has been said, 155-mm shells cannot be cold-nosed successfully. This does not mean that they cannot actually be nosed. As is known, all shells being considered in this paper take the same booster and fuse, so that the larger the shell the larger the ratio of shell diameter to nose diameter. For the 75-mm shell, this ratio is about $1^1/_4$; for the 105-mm $1^3/_4$; and for the 155-mm about $2^1/_4$. The metal flow in the latter case is so severe when done cold that the high residual stresses set up during nosing, inevitably result in cracking and fracture, the nose gradually opening up like a flower. If it were practical, this probably could be avoided by a strain anneal, but this additional operation would more than offset the advantages of the cold operation.

Control of the flow of metal in the nosing operation is one of the most important and one of the most complex aspects of the operation. What is the proper initial shape of shell, as to internal shape, or external shape, and wall thickness, to permit the most expeditious forming of the nose. In some cases, the outside of the shells are left perfectly cylindrical (just as they come from the draw benches), and the inside cavity is varied by shaping

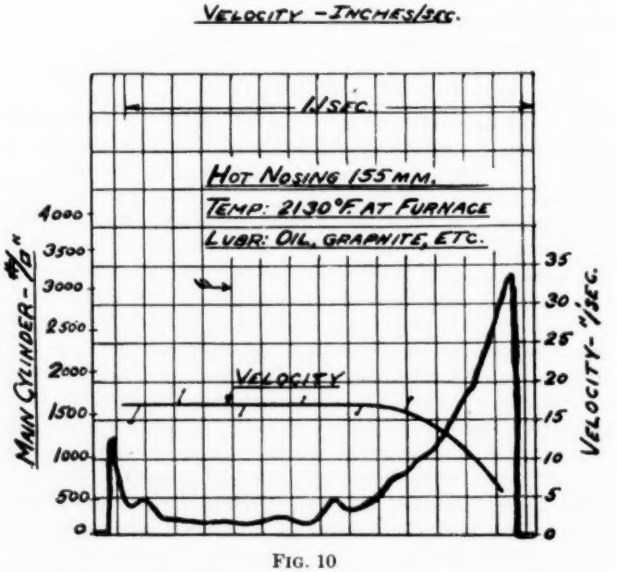


Fig. 10

the draw mandrel. This is obviously an ideal method since it minimizes machining costs and conserves metal. More often, however, the cavities are left cylindrical, and the outside is machined to a template. At best, however, certain empirical procedures must be relied on—sometimes the machine finish may so influence the efficacy of lubrication (too smooth a finish does not hold the oil in place, for instance, etc.) that a shell will shorten one time, and lengthen the next.

From an examination of the type of resistance met in the nosing operation, Fig. 10, it may be in order to observe how naturally a crank-type press fits the requirements. Crank-type or mechanical presses usually are less expensive than hydraulic presses (when a special hydraulic system is to be included), but suffer from the objections that they develop their force only near the end of the stroke, and being positive stroke machines, may develop forces sufficient to break the machine if workpieces too large for space allowed are inadvertently used. The shell, being nosed, moreover, is a workpiece that if accidentally too long, may relatively easily take up the extra length without developing abnormal pressures.

Forces Acting in the Piercing of Cylinders

By W. TRINKS,[1] PITTSBURGH, PA.

THE present paper refers to the forging of a hollow cylinder (with a solid base) which is an intermediate product in the making of munitions as well as of seamless tubes. In the making of goods of both kinds, a cylindrical (or almost cylindrical) body of circular cross section is incompletely pierced by a punch. The bottom or base remains solid and is not pierced. As a rule, the cross section is a round-cornered square at the beginning of the piercing process, but it changes to round at the time when the force which is required for piercing reaches its maximum value. The "slug" (so-called before piercing) becomes a "cup," or a "bottle," or an "intermediate blank" after piercing.

The force which is required for piercing is of importance to the mechanical engineer because it is he who has to build and guarantee the machines which do the piercing. Several experimenters have determined the piercing force, and theories have been proposed for determining this force analytically. A good bibliography on this subject is given by Dr. G. Sachs.[2]

This paper is an attempt to consider the effect of a number of variables and to predict, at least in a general way, the influence of each of these variables upon the force which is required for piercing.

Punches are either cylindrical, with a flat end, or else tapered as shown in Fig. 1. The latter, being the more general case, is considered here. In Fig. 1 an axial element dx is shown with a generatrix length $dx/\cos\alpha$ where α is one half of the total cone angle. The variable radial pressure is p, and the pressure on the cone element is $p\cos\alpha$. The frictional unit pressure along the cone element is $p\cos\alpha\tan f$, where f is the friction angle.

The pressure against the die is difficult to estimate. For infinitely thin blanks, it equals the pressure against the punch. For very thick blanks, the pressure against the die is almost zero because tangential stresses in the pierced material carry the load in almost the same manner in which the walls of a gun carry the force of the explosion. The assumption is here made that the pressure against the die is 40 per cent of the pressure between plastic material and punch. Evidently this assumption is too low for thin-walled shells and too high for thick-walled shells. In the final answer, this assumption, if wrong, can easily be corrected. Observation of die wear confirms the correctness of the assumption.

Then as the punch is forced into the plastic material, increase of axial force on the punch between points (1) and (2) is

$$dP = 2\pi r(dx)p(\tan\alpha + \tan f)$$

where P, r, x, and p are variable and where f, the friction angle, may also be variable. A relation between the variables is furnished by the following equation (see Fig. 2): Axial component of friction force equals difference of force on two sides of annular area between die and punch. Algebraically, the equation is

$$2\pi r(dx)p(\tan\alpha + \tan f) + 2\pi R(dx)0.4p\tan f = 0.7(dp)\pi(R^2 - r^2)$$

The factor 0.7 indicates that part of the increase in pressure is due to 1 p (against the punch) and part of it due to 0.4 p (against the die). Substituting the relation

$$r = r_0 - x\tan\alpha$$

we obtain

$$2(r_0 - x\tan\alpha)p(\tan\alpha + \tan f)dx + 0.8Rp\tan f(dx) = 0.7[R^2 - (r_0 - x\tan\alpha)^2]dp$$

The integration can be performed if α and f are constant. If they are not constant, then they can be considered constant for short lengths x, and the integration can be performed in steps. Separating the variables and expanding furnish

$$\frac{dp}{p} = \frac{2r_0(\tan\alpha + \tan f) + 0.8R\tan f - 2x\tan\alpha(\tan\alpha + \tan f)}{0.7(R^2 - r_0^2) + 2\times 0.7r_0 x\tan\alpha - 0.7\tan^2\alpha x^2}dx$$

The right-hand differential is of the form

$$\frac{(m + nx)dx}{a + 2bx + cx^2}$$

the integral of which is (for the case in question)

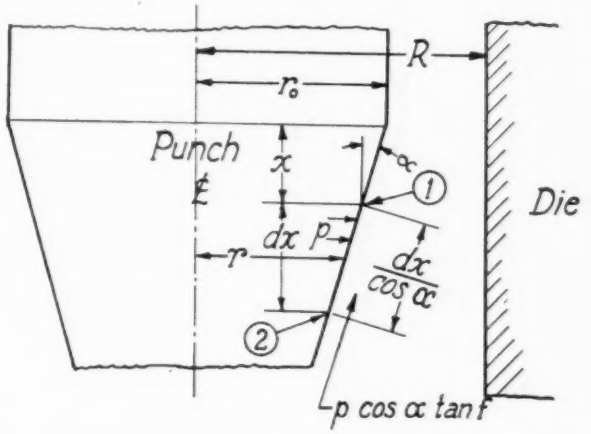


FIG. 1

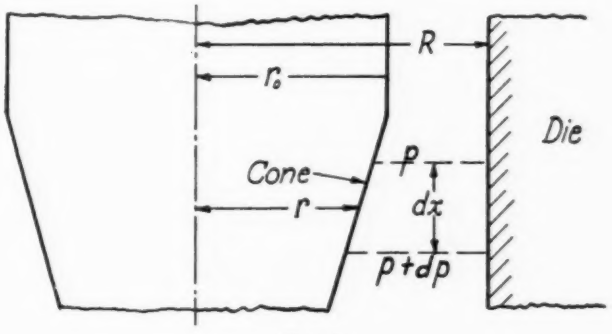


FIG. 2

[1] Professor of Mechanical Engineering (Emeritus), Carnegie Institute of Technology; Projects Director, A.S.M.E. Special Research Committee on Forging of Steel Shells. Mem. A.S.M.E.

[2] "Spanlose Formung der Metalle," by Dr. G. Sachs, Julius Springer, Berlin, 1931.

"Practical Metallurgy," by Dr. G. Sachs and K. R. Van Horn, A.S.M., Cleveland, Ohio, 1940.

Contributed by Special Research Committee on Forging of Steel Shells and presented at the Annual Meeting, New York, N. Y., Nov. 29–Dec. 3, 1943, of THE AMERICAN SOCIETY OF MECHANICAL ENGINEERS.

NOTE: Statements and opinions advanced in papers are to be understood as individual expressions of their authors and not those of the Society.

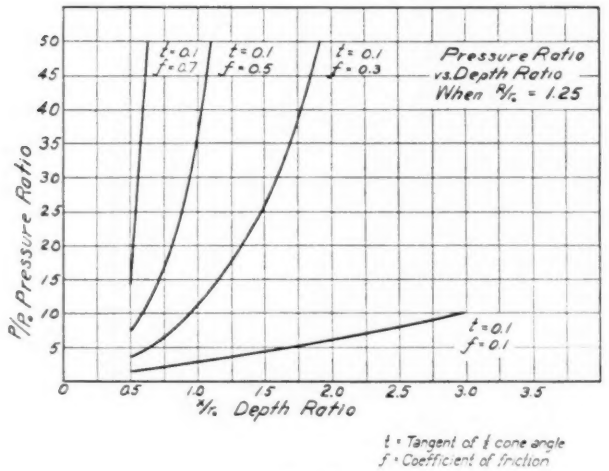


FIG. 3

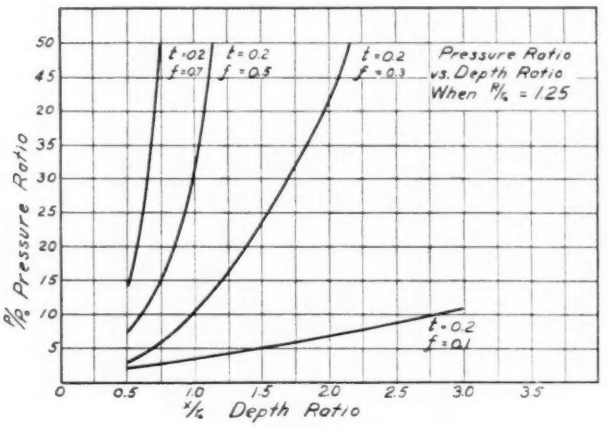


FIG. 4

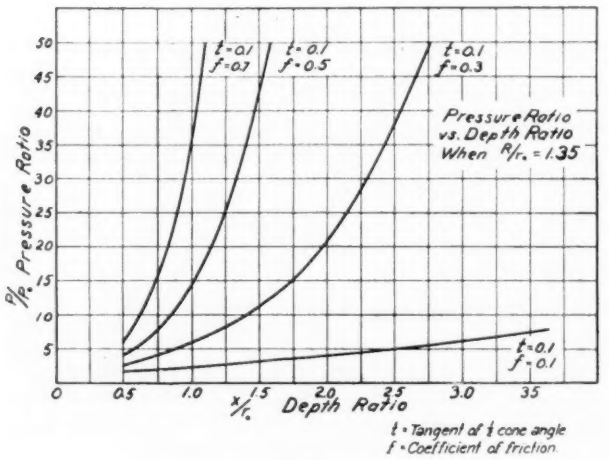


FIG. 5

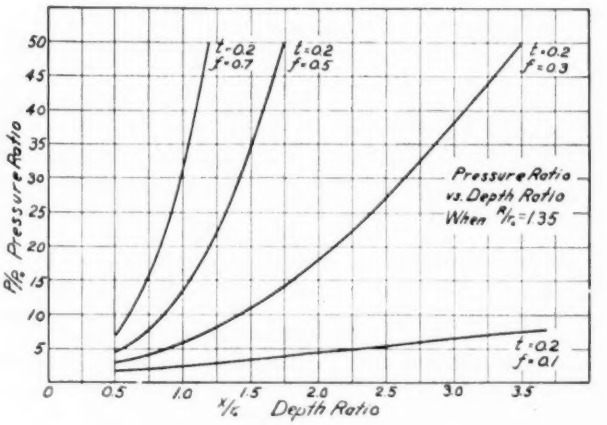


FIG. 6

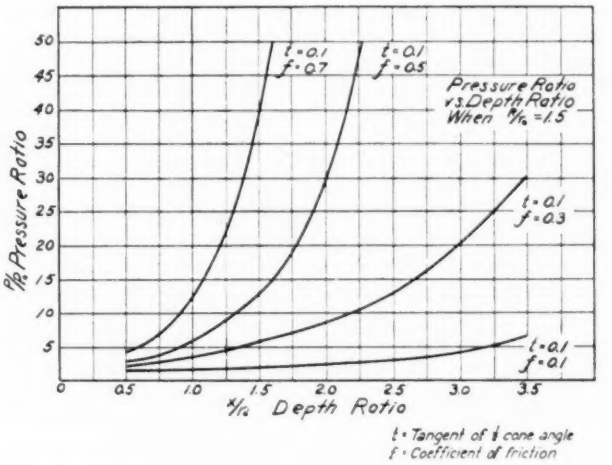


FIG. 7

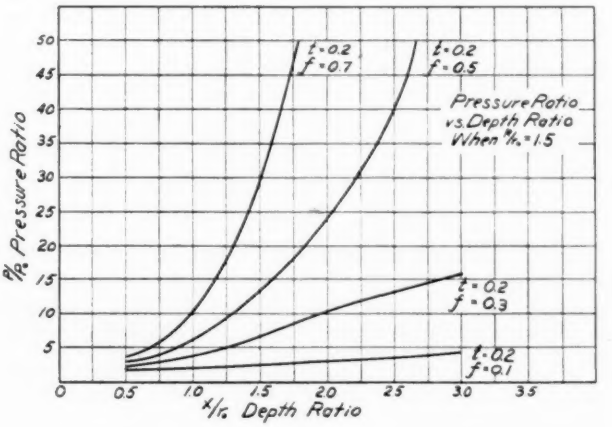


FIG. 8

$$\frac{n}{2c}\log_e(a + 2cx + cx^2) + \frac{mc - nb}{c}\frac{1}{2\sqrt{b^2 - ac}}\log_e\frac{\sqrt{b^2 - ac} - b - cx}{\sqrt{b^2 - ac} + b + cx} + C$$

The next step is to substitute in this integral the corresponding quantities for m, n, a, b, and c. The work is shortened if t is written for tan α and f for tan f. Then

$$\begin{aligned} m &= 2r_0(t + f) + 0.8Rf \\ n &= -2(t^2 + tf) \\ a &= 0.7(R^2 - r_0^2) \\ b &= 0.7r_0t \\ c &= -0.7t^2 \end{aligned}$$

The integral is of the form

$$\log_e p = A \log_e f_1(x) + B \log_e f_2(x) + C$$

where $f_1(x)$ and $f_2(x)$ are two different functions of x. Calling p_0 the radial pressure against the punch at the top of the cone where it merges into the cylindrical position of the punch, integration between limits furnishes

$$\frac{p}{p_0} = [f_1(x)]^A + [f_2(x)]^B$$

The substitutions are not difficult, but long and tedious; they are therefore omitted. The final equation is

$$\frac{p}{p_0} = \left[\frac{\left(\frac{R}{r_0}\right)^2 - \left(1 - \frac{xt}{r_0}\right)^2}{\left(\frac{R}{r_0}\right)^2 - 1}\right]^{\frac{t+f}{0.7t}} \left[\frac{\left(\frac{R}{r_0} - 1 + \frac{xt}{r_0}\right)\left(\frac{R}{r_0} + 1\right)}{\left(\frac{R}{r_0} + 1 - \frac{x}{r_0}t\right)\left(\frac{R}{r_0} - 1\right)}\right]^{\frac{0.8f}{1.4t}}$$

In this equation t stands for tan α and f stands for tan f.

A change in the assumption that the pressure against the die is 40 per cent of the punch pressure changes only the exponents. If, for instance, the pressure against the die equals 0.6 p, then the first exponent becomes $\frac{t + f}{0.8\,t}$ and the second one $\frac{1.2\,f}{1.6\,t}$. It should be noted that the friction coefficient does not appear in the base but only in the exponents where it appears in the ratio, $\frac{\tan f}{\tan \alpha} = \frac{f}{t}$.

In order to gain a sense of values with regard to the numerical influence of the different variables, the pressure ratios $\frac{p}{p_0}$ were plotted against the depth ratios $\frac{x}{r_0}$ where x equals the axial distance from the largest diameter of the cone and r_0 is the largest radius of the cone at the point where it merges into the cylindrical section of the punch. The curves were plotted for two cone angles, 5.72 deg (tan α = 0.1) and 11.31 deg (tan α = 0.2). For each cone angle, four coefficients of friction were selected. They are 0.1, 0.3, 0.5, and 0.7. Another variable had to be taken care of, namely R/r_0, which expresses the thickness ratio after piercing. Three values for R/r_0 were selected; they are 1.25, 1.35, and 1.50. The six graphs thus obtained are shown in Figs. 3 to 8.

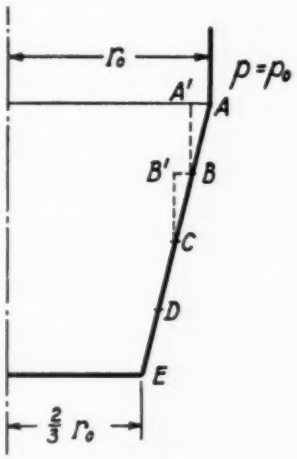


FIG. 9

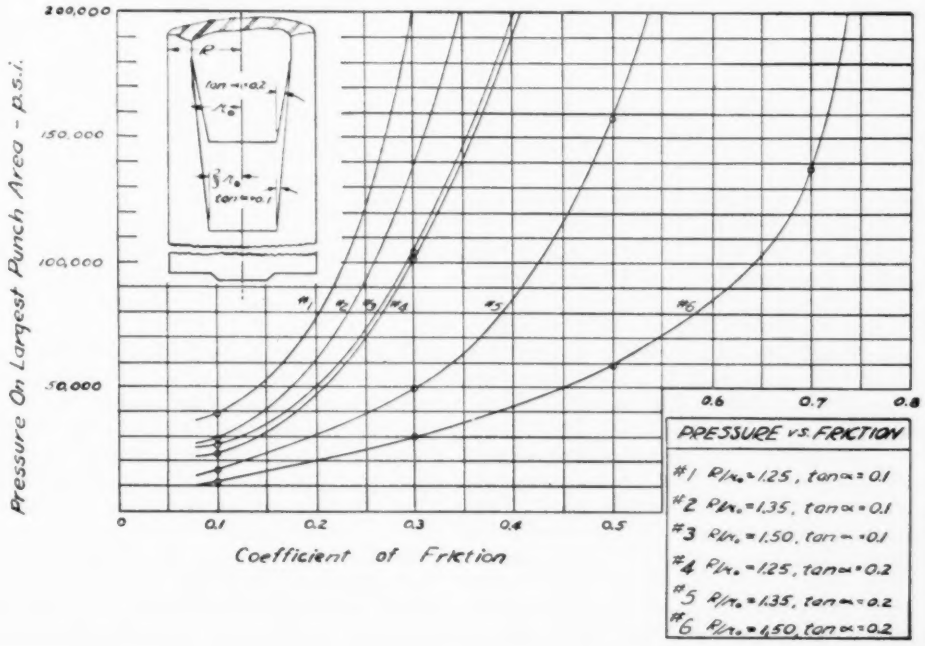


FIG. 10

These curves are not the goal; they are an intermediate step toward a second integration by means of which the axial force (which resists penetration by the punch) can be computed. It is possible to write a differential equation for this force by making use of the exponential equation for the pressure ratio. It may, however, not be possible to integrate that equation. For that reason the following step-by-step method of summation was used:

A cone with flat bottom, the latter having a diameter equal to two thirds of the maximum diameter, was selected (see Fig. 9). Its length was divided into four equal parts, and the average pressure for each section was computed. The pressure ratios were taken from the curves (Figs. 3 to 8) for points B, C, D, and E. The calculation was carried out for two values of α and for three values of R/r_0. The average pressure between A and B was taken to act on annulus $A'A$; the average pressure between B and C was taken to act on annulus $B'B$, and so on.

Some doubt exists about the manner in which the radial pressure at E affects the axial pressure against the bottom of the cone. For want of a complete theory, the axial pressure acting on the bottom area was taken to be 20 per cent higher than the radial pressure at point E. The value of 20 per cent was selected by judgment to account for the frictional resistance of the plastic material while flowing radially outward along the bottom. The friction factor is affected by the distance between bottom of punch and bottom of die. The influence is almost negligible, except during the last very small fraction of the piercing stroke. The effect of this distance was not taken into account.

All calculations were made for $p_0 = 1$. The summation was then multiplied by the natural flow resistance which was taken to be 5000 psi. This value may be considered typical for 2200 F steel temperature and for average speed of penetration.

The final result of these calculations was plotted in the curves of Fig. 10. It is evident that coefficient of friction, cone angle (tan α = 0.1 and 0.2), and the ratio of diameters of die bushing and punch (1.5, 1.35, 1.25) exert great influence on the piercing force.

The combination of a long, slender taper (tan α = 0.1) with a thin wall of shell (R/r_0 = 1.25) causes enormously high punch forces even with a low coefficient of friction, whereas a short stubby taper (tan α = 0.2) combined with a thick-walled forging (R/r_0 = 1.5) causes low punch loads, even for fairly high coefficients of friction.

Punch Pressures

In practice, punch pressures between 25,000 and 60,000 psi are on record. In general, they follow the trend indicated by the curves of Fig. 10, in so far as cone angle and wall thickness are concerned. Unfortunately, no numerical check between theory and practice is possible because, up to the present time, no method exists for measuring the coefficient of friction between punch and slug.

For some combinations of wall-thickness ratio and cone angle, the theoretical punch pressures assume exceedingly high values, much higher than those recorded in practice. The difference between theory and practice is probably caused by slip friction changing to nonslip friction when the coefficient of friction and the pressure assume high values. By that statement is meant that in such a case the hot metal does not slide along the tool but sticks to it, deformation taking place in the hot metal. This method of deformation is well known from the flow around the bottom of a punch as illustrated in Fig. 11. The metal in the section-lined portion sticks to the punch, and flow occurs in the metal along the dotted line. The actual flow boundary is best observed in dirty steel. Fig. 11 was traced from a sectionalized cup or bottle made from steel with segregation lines.

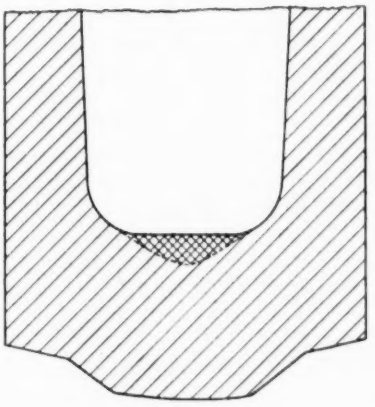


Fig. 11

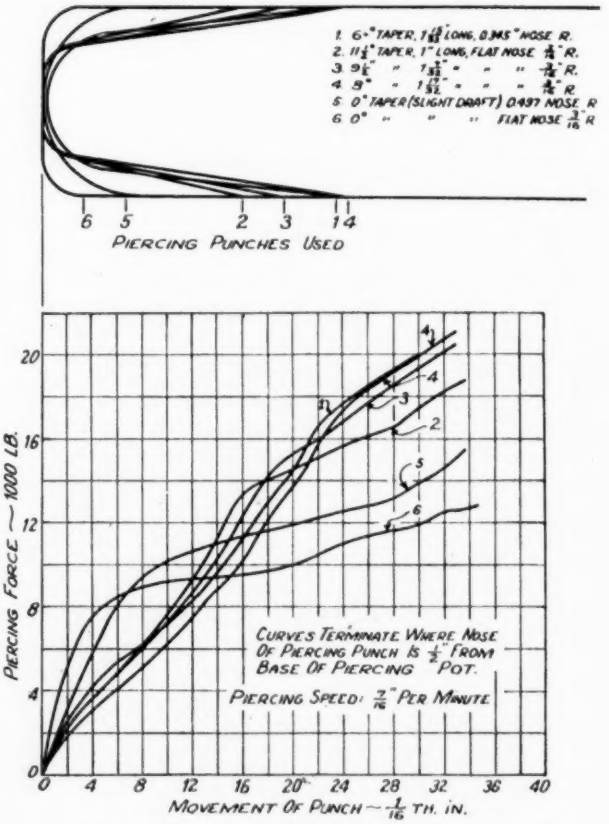


Fig. 12

The correctness of the theory developed in this paper is confirmed by tests which were made at Case School of Applied Science, Cleveland, Ohio, under direction of Prof. G. Sachs. These tests were made by piercing lead slugs of $1^{15}/_{16}$ in. diam with punches a little less than 1 in. diam. The results of these tests afford a comparison of the effects which different shapes of piercing points exert upon the force which is required for piercing. In Fig. 12 (which was plotted from the test data), it is observed that the pointed punches (No. 1 and No. 4) penetrate easily (local deformation) but build up a great resistance at deep penetration, whereas the flat punches (No. 5 and No. 6) offer a more nearly constant resistance because they reach constant conditions of flow earlier in the stroke.

Experimental Study of Shell Drawing

By GEORGE SACHS[1] AND G. B. KASIK,[2] CLEVELAND, OHIO

1 INTRODUCTION AND OBJECT

THE "forging" of high-explosive steel shells presents a difficult problem in hot-working steel because of the severe deformation accomplished from billet to finished forging. The problem is further complicated by the necessity of maintaining close tolerances as dictated by the shortage of material, labor, and equipment, especially in the early stages of production.

To meet this problem, several methods and/or combination of methods have been employed for shell manufacture. The five most important methods may be classified as follows, it being understood that variations in many details occur which modify this strict classification.

In all modern methods the forging is made to a finished cavity, or the finish-machining restricted to the outside of the shell. The entire forming cycle of the shell consists in the "forging" of the finished cavity of the shell and its "nosing" after machining. Only the forging phase is discussed in this report.

1 *The Pierce-and-Draw Method.* Nearly 50 per cent of all high-explosive shells are fabricated by this method. The shells are processed in either hydraulic or mechanically operated presses in two stages. In the first stage, a piercing press is employed to forge a cavity in a solid round or square-shaped slug in one or two operations. Then, in the second stage, the pierced slug is transferred to a drawbench, which carries the pierced slug, "cup," or "bottle," over a mandrel having the shape of the finished cavity, through a series of dies, thereby reducing the diameter and wall thickness, and elongating the shell. Ring dies or roller dies may be used, and up to 22 dies in tandem have been installed on a drawbench; however, 4 to 6 is the usual number of passes required to accomplish the reduction from the pierced to the finished forging. In some mechanical forging machines the piercing and drawing are accomplished by the same machine.

A recent modification of the pierce and draw method known as "progressive pierce and draw" has been developed. By this method the slug is progressively pierced in solid dies by two or more operations to nearly the dimensions of the final forging. This pierced slug is then engaged over a draw mandrel, conforming to the dimensions of the finished cavity, and drawn through one or two sizing rings. The transfer of the forging from station to station may be manual or automatic.

2 *The Upset Method.* By this method a single forging machine progressively pierces the solid billet, generally in five stages, to form a finish-forged shell. The upsetter utilizes five punches or mandrels, and correspondingly five split dies which comprise the various stations. The tools work horizontally and are arranged vertically. The billet progresses from the top station, where it is upset and a centering depression made by a short punch, to the bottom station where a relatively long punch, conforming to the shape of the finished cavity, sizes the diameter of the finished forging and brings the base to the proper thickness.

3 *The Pierce and Cross-Roll Method.* By this method a billet is first pierced either by a press or drop hammer which furnishes the bottle for the shell-rolling mill. Three contoured rolls are used of such design and so aligned as to force the cup over a mandrel having the shape of the finished cavity. Following the rolling operation, the forging, with the mandrel still in it, is pushed through a sizing ring to iron out the slight grooves and irregularities left by the rolling operation.

4 *The Extrusion Method.* Considerable controversy exists as to the optimum division of work between the initial piercing operation and the secondary drawing, or sizing, operation. The extrusion method accomplishes most of the deformation in the first operation by extruding the hot solid billet, held in a short die, over a punch having nearly the dimensions of the final cavity. The tip of the punch is positioned only a short distance into the opening of the die or container holding the billet. The metal extrudes out along the punch but is unrestrained along the outside surface. During the operation, the die bottom and billet move against the die and punch, such that the billet is pushed out of the stationary die over the stationary punch. The method has the advantage of a minimum friction between the billet and tools, since high friction is present only at the die mouth where the metal is forced through the orifice between die and punch. Practically no friction exists along the undeformed billet and die wall except for a small amount created by the slight upsetting of the billet in the die.

5 *The One-Shot Method.* In the "one-shot" forging method, the punch enters the solid billet held in a split piercing die and moves relative to the die. It differs in this respect from the extrusion method in which the punch position relative to the die is fixed. In order to minimize backward extrusion along die and punch, the bottom of the die is allowed to recede against a predetermined pressure as piercing progresses. Thus, only the part of the billet which is unworked at a given point of the operation, and which offers little frictional resistance along the die wall, is moved. Essentially this method is forward extrusion; and since the pierced section is restrained between punch and die, it can be held to close limits. The forged shell is obtained in one operation, the piercing punch having the dimensions of a finish-forged cavity.

The need for correlating desirable information as to the best practice for forging shells by the various previously discussed methods, and making it available to forging plants, has prompted The American Society of Mechanical Engineers, authorized by contract with the Ordnance Department, to undertake a survey of present practice. Because conditions encountered in the field are not entirely suited to accurate investigation of some of the fundamental variables, the department of metallurgy at Case School of Applied Science accepted an offer to amplify the A.S.M.E. Shell Forging Research Committee's report by laboratory-controlled tests covering numerous variables encountered in the drawing phase of the pierce-and-draw method. The choice of this field of investigation rested on the premise that the pierce-and-draw method was most important by virtue of the fact that more shells are made, at present, by this method than by any other.

Originally, the work was scheduled to cover only the hot-drawing of model steel shells, but adverse conditions during the beginning of the investigation delayed procurement of the experimental equipment. Therefore work was started using lead for the test metal, since the necessary equipment for drawing this

---

[1] Professor of Physical Metallurgy, Case School of Applied Science.
[2] Research Assistant, Case School of Applied Science.

Contributed by A.S.M.E. Special Research Committee on Forging of Steel Shells and presented at the Annual Meeting, New York, N. Y., Nov. 29–Dec. 3, 1943, of THE AMERICAN SOCIETY OF MECHANICAL ENGINEERS.

NOTE: Statements and opinions advanced in papers are to be understood as individual expressions of their authors and not those of the Society.

material was on hand. Lead was chosen also because of its amenability to experimental work in that it could be readily handled, and important variables, such as friction, could be closely controlled; further, lead can be hot-worked at room temperature to simulate hot-working of steel at high temperatures.

The important variables encountered in the drawing operation which have been investigated include the following:

1 Effect of reduction of area in a single pass through ring dies
2 Effect of boat-tail
3 Effect of die angle
4 Effect of cavity shape
5 Effect of punch shape
6 Effect of wall thickness
7 Effect of base thickness
8 Effect of lubrication
9 Effect of speed.

In order to correlate the results on steel with those of lead, tests were run covering the effect of a given variable on both materials. Most of the variables were investigated in this manner.

In addition some observations were made on the piercing of lead slugs.

2 MATERIAL AND PROCEDURE

The material and procedure for this investigation can be divided into two more or less distinct parts, namely, the work with lead specimens, and the work with steel specimens.

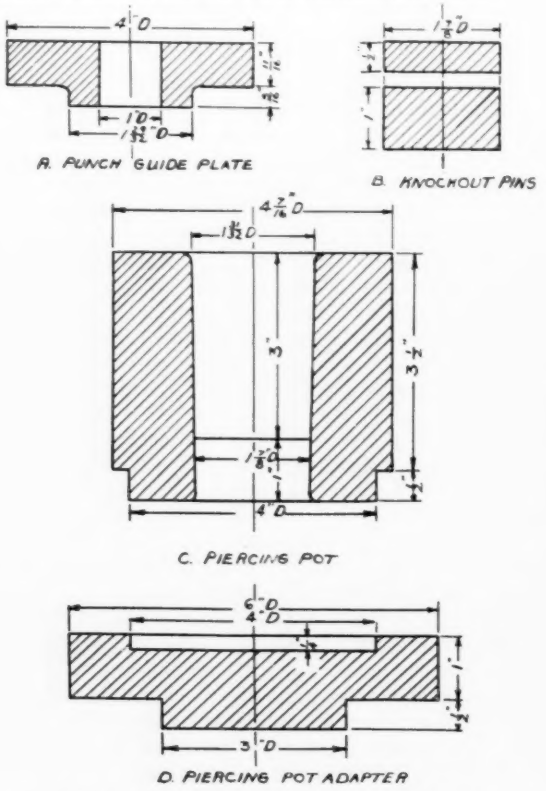


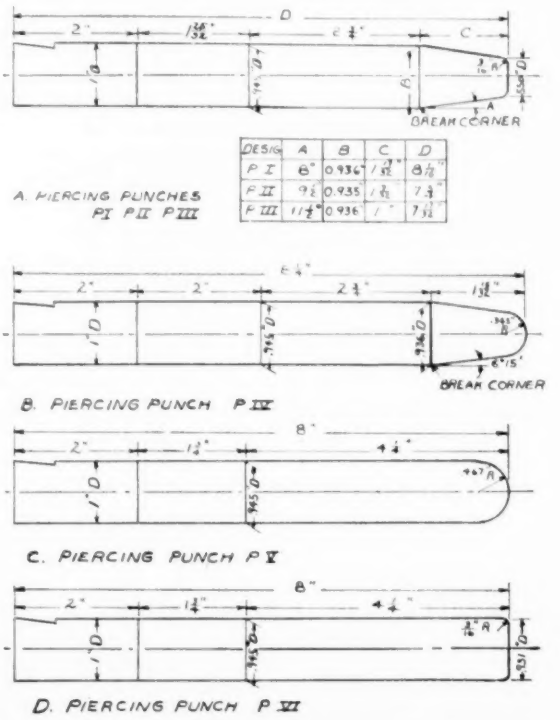
FIG. 1 TOOLS REQUIRED FOR PIERCING LEAD

WORK WITH LEAD SPECIMENS

Commercially pure lead having the following chemical analysis was used in this part of the work: 0 per cent Sn, 0.002 per cent Sb, 0.15 per cent Cu, trace of Zn, remainder Pb.

Small slugs were individually cast in the die pot used for piercing. The piped section was removed by sawing and the slugs cleaned preparatory to the piercing operation.

Piercing was done with a 10,000/60,000-lb Tinius Olsen testing machine. Dimensioned sketches of the piercing tools are



DESIG	A	B	C	D
P I	6"	0.936"	1 3/32"	8 1/2"
P II	9 1/2"	0.935"	1 3/32"	7 3/4"
P III	11 1/2"	0.936"	1"	7 3/32"

FIG. 2 DIMENSIONED SKETCHES OF PIERCING PUNCHES

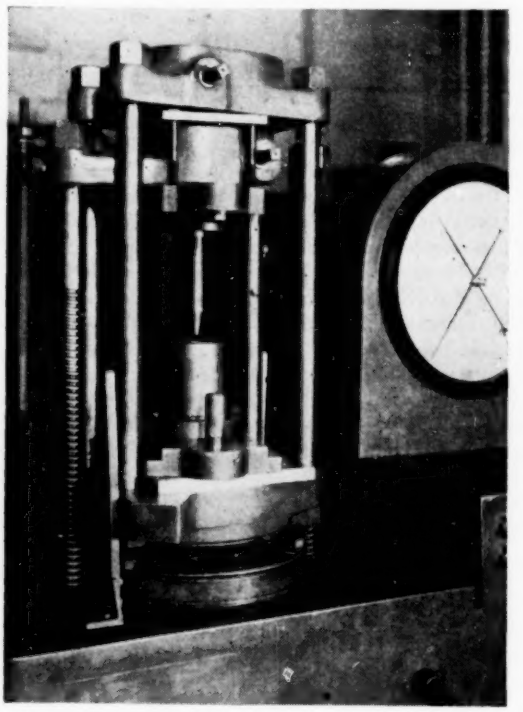
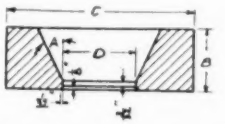


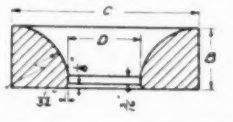
FIG. 3 TOOL ASSEMBLY AND TESTING MACHINE FOR PIERCING LEAD

shown in Figs. 1 and 2. The testing machine and piercing assembly are illustrated in Fig. 3. Piercing was performed at a speed of 0.5 to 1 ipm. Representative force-stroke curves were taken for each of the six piercing punches used. In general, the depth of pierce was $2^1/_2$ in., or such as to permit the base of the pierced slug to be faced in a lathe to $^1/_2$ in., which was the standard base thickness used in these tests.



DIE NO	A	B	C	D	MAT'L
1	7°	2 1/2	3"	.1375"	STEEL
2	10	1	"	"	"
3	15	1 1/4	"	"	"
4	25	1 1/2	"	"	"
5	15	1 1/4	"	.1462"	"
6	15	1	2 1/2	1.328"	"
7	15	1 1/4	3	"	CAST IRON

A. STRAIGHT ANGLE DIES



DIE NO.	R	B	C	D	MAT'L
8	1"	1/2	3"	.1462"	STEEL
9	"	"	"	1.394	"
10	"	"	"	1.375	"
11	"	"	"	1.328	"
12	"	"	"	1.240	"
13	2 1/2"	1"	"	1.375	"

B. RADIUSED DIES

FIG. 4 DIMENSIONED SKETCHES OF DRAW DIES

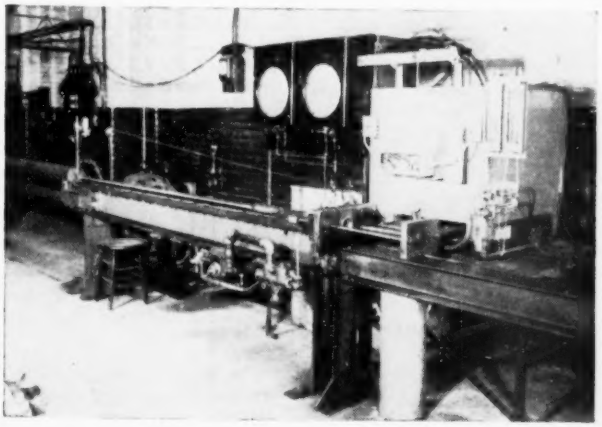


FIG. 6 DRAW BENCH AND AUXILIARY EQUIPMENT FOR DRAWING LEAD AND STEEL CYLINDERS

For the early tests S.A.E 20 machine oil and castor oil were tried as lubricants; for later tests, concentrated oil dag (a suspension of colloidal graphite in petroleum oil having a solids content of 10 per cent by weight) was used with more satisfactory results. The lubricant was swabbed on die, punch, and slug.

Following the piercing operation, all pierced lead slugs were annealed in an oil bath for 45 min at 300 F. This reatment fully annealed and homogenized the structure.

The bottles were machined to the desired dimensions prior to the drawing operation. This consisted essentially in turning the specimens on a mandrel held in a lathe to various outside diameters and shapes. The standard specimen, pierced with piercing punch IV, was turned to the following dimensions:

Outside diameter	1.525 in.
Wall thickness	0.292 in.
Base thickness	0.5 in.
Length: Lot 1	$2\ ^{23}/_{32}$ in.
Lot 2	$3\ ^1/_4$ in.
Lot 3	$3\ ^1/_2$ in.

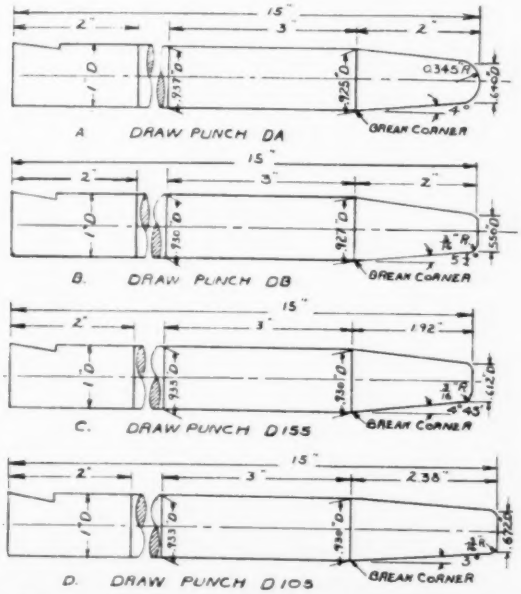


FIG. 5 DIMENSIONED SKETCHES OF DRAW MANDRELS

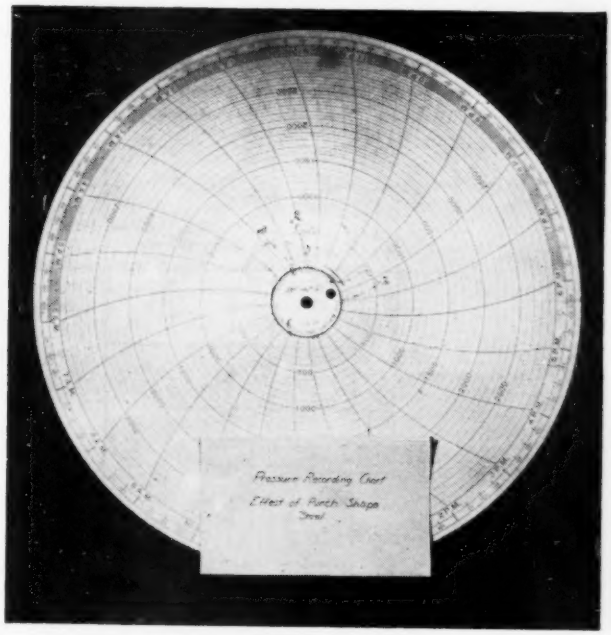
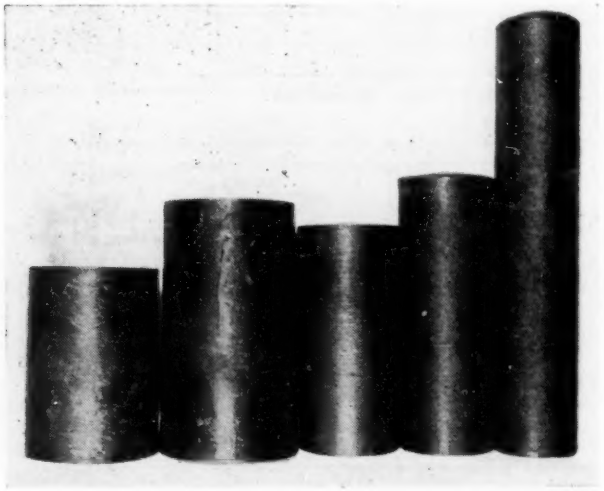


FIG. 7 PRESSURE-RECORDING CHART FOR RECORDING FORCES OF DRAW DIE; $\times^1/_3$

Variations from the standard dimensions were obtained by turning to various outside diameters, turning boat-tails (outside tapers at the base), facing the base to different thicknesses, or by piercing with different piercing punches.

Regarding the drawing operation, the tools used, i.e., dies and draw mandrels, are shown in the dimensioned sketches, Figs. 4 and 5. Four different mandrels were used, and 13 dies of various nominal diameters and contours.

Most of the drawing was performed on an experimental hydraulic drawbench, Fig. 6, loaned to Case School by the Wolverine Tube Company, Detroit, Mich. The bench was converted from a drawbench to a push bench by the use of a yoke arrangement which carried the draw mandrel. The bench was equipped with a Hanna hydraulic cylinder having a 4-in. bore, $1^1/_2$-in. piston rod, and a 7-ft stroke. It was originally equipped with a vane-type pump capable of delivering 5 gpm of oil at a maximum pressure of 1000 psi. With this system, the speed of drawing could be varied from approximately 0 to about 9 fpm. For the most part, 27 ipm was the draw speed used for the lead draws.



(a) (b) (c) (d) (e)

FIG. 8 SEQUENCE OF OPERATIONS WITH LEAD, $\times 1/_2$
(a, Cast and cropped slug; b, pierced slug; c, machined bottle; d, drawn bottle; e, redrawn bottle.)

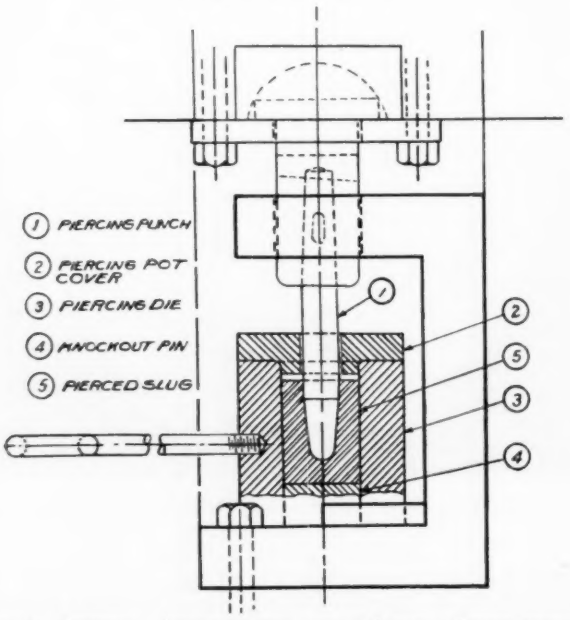


FIG. 9 GENERAL ARRANGEMENT FOR MAKING EXPERIMENTAL SHELL FORGINGS

In order to speed up the drawbench, a 40-gpm gear pump and larger valves were installed, which permitted a maximum free draw speed of about 80 fpm.

In order to record the forces involved in the drawing operation, the drawbench was equipped with a modified Emery cell which transmitted pressure variations on the die to a recording pen. The recording pen traced these pressure variations on a calibrated chart driven by a synchronous motor, Fig. 7. By knowing the speed of rotation of the chart, a force-stroke curve was readily constructed. The assumption was made that the speed variation of the drawbench under load was negligible, although at high pressures this was not strictly true. Furthermore, at high draw speeds, the first impact peak was not registered by this system, the time interval being of too short duration to allow the recording system to reach equilibrium. To obtain the force-stroke curves for the high-speed tests, a steam-engine indicator was employed, which will be described later.

For a lubricant in the lead-drawing operations, Ironsides AF-11 diluted 2 parts of water to 1 part of lubricant, by weight, was employed. This was found to give most satisfactory and consistent results, after having tried castor oil and mineral oils.

The drawn shells were readily stripped and then measured for changes in dimensions. In representative cases, the shells were split longitudinally to facilitate checking the changes in contour.

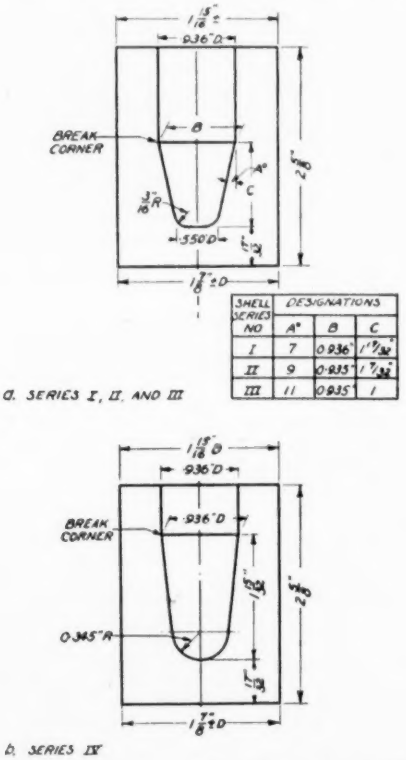


FIG. 10 DIMENSIONS OF PIERCED STEEL BOTTLES

In Fig. 8 are shown the several steps for the sequence of operations with lead, namely, (*a*) the cast and cropped slug, (*b*) the pierced slug, (*c*) the pierced slug after machining, (*d*) the drawn bottle, and (*e*) the redrawn shell.

WORK WITH STEEL SPECIMENS

The material for this part of the investigation was cut from rod stock having the following analysis: 0.34 per cent C, 0.87 per cent Mn, 0.028 per cent P, 0.016 per cent S, 0.20 per cent Si.

The pierced steel slugs were supplied for this investigation by the Shell Forging Research Committee and were pierced in a C-press, a sketch of which is shown in Fig. 9; no piercing of steel was carried out at Case School. The dimensions of the pierced cylinders are shown in Fig. 10. Unfortunately, however, the actual pierced slugs varied considerably in some respects from the drawings shown. This was particularly true with respect to the shape of the bottom of the cavity which, in many cases, was ballooned badly.

These as-received bottles were then machined to the desired dimensions; the standard-machined bottle, pierced with P IV piercing punch, had the following dimensions:

Outside diameter	1.400 in. (or such as to permit 20 per cent reduction in a single pass)
Length	$2^{5}/_{8}$ in.
Base thickness	$^{1}/_{2}$ in.

Because of the power limitation at the draw bench (11,000 to 12,000 lb maximum force on the mandrel) a 1.328-in. nominal diameter die was used for most of the drawing, which required a bottle outside diameter of 1.400 in. to obtain 20 per cent reduction. As in the case of lead, some bottles were turned with boat-tails (3 to 10 deg taper from a 1.220-in. base diameter) and/or various outside diameters.

Prior to the drawing operations, the machined specimens were raised to forging temperature, 2200 deg F, in a high-temperature Hevi-Duty electric furnace equipped with Smith alloy heating elements. A controlled atmosphere was produced and maintained by an Electric Furnace gas generator. Generally, an atmosphere consisting of a 7:1 air-gas ratio, at 250 cfh at the generator and 1.0 in water pressure at the furnace was used. The gas was dried by passing it through Electrodriers which reduced the dew point to —60 deg F. No CO_2 removal was attempted. The cold pierced forgings were placed in the furnace and held 30 to 45 min before drawing.

All steel drawing was performed on the hydraulic drawbench, previously described under lead drawing, Fig. 6. In the case of

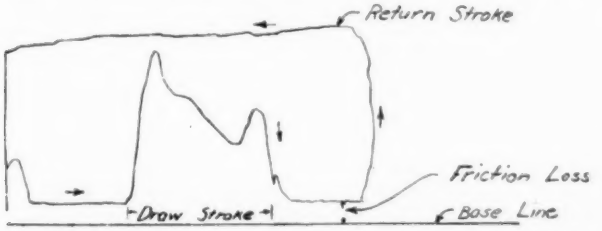


FIG. 11 PRESSURE-DISPLACEMENT CURVE REGISTERED BY ENGINE INDICATOR; ×1

steel, however, only a few preliminary tests were carried out at slow speed (8 fpm), since cooling of the specimen took place to such an extent before completion of the operation that the draw force required was more than the bench could develop. Consequently, the greatest number of steel draws were run at about 40 fpm; even so, sufficient cooling was encountered as to raise the draw force appreciably toward the end of the draw. The time required to remove each specimen from the furnace and complete the draw was about 10 sec; thus, the base temperature would drop 100 deg F, and the wall temperature 200 deg F, by the time the bottle hit the die. The wall temperature would drop as much as 400 deg F, by the time the draw had been completed.

Because the pressure-recording system, which was used for the lead draws at slow speeds, failed to register the peaks in the force-stroke curve at high speeds, a Maihak steam-engine indicator was employed in the steel draws. This indicator was connected in the hydraulic oil line on the pressure side of the cylinder. The indicator drum was actuated by the drawbench piston through a reducing mechanism. Thus a fairly accurate pressure-displacement curve, Fig. 11, was obtained which was readily converted to a force-stroke curve. The actual draw force on the mandrel at any time was taken as the product of the measured oil pressure in the pressure side of the cylinder during the draw (minus the friction loss at no load) and the effective piston area. The stroke was computed by adding to the length of the drawn shell, the contact length along the die, plus any bending or piercing of the bottom of the shell during drawing.

During the preliminary draws in steel, severe scoring of die and mandrel occurred which materially decreased the drawability and increased the draw forces. In these runs, light machine oil and flake graphite were swabbed on die and mandrel before each draw. Mixtures of colloidal graphite in light machine oil at various concentrations were also tried without success. A few special light-oil-vehicle lubricants, containing graphite particles of various macro sizes, in addition to colloidal graphite, also proved unsatisfactory.

Finally, a lubricant composed of heavy mineral oil (near grease), with graphite of colloidal and macro size (Fiske's No. 514-A hot die lubricant) was adopted which proved most satisfactory.[3]

Both the draw mandrel and die were swabbed with lubricant prior to each run.

The practice of "graphoiding" the surface of the tools was employed. This consisted in thoroughly degreasing the tools after which they were preheated to 300 to 350 F. They were then dipped while hot in a dilute solution of aqua dag[4] two or three times, allowing the solution to dry on the tools between each immersion.

It was found that Meehanite dies, heat-treated for high strength, resisted scoring and pickup much better than steel dies; the flake graphite in the cast iron apparently acts as a lubricant in itself. It was noted in this investigation that the first pieces drawn through a die caused severe pickup which then tended to smooth out with successive draws. Also, a heavy reduction caused less scoring of the land or bearing than did a light pass.

[3] We are indebted to Mr. J. R. McKee, representative for Fiske Brothers Refining Company, Toledo, Ohio, for his co-operation in furnishing this lubricant.

[4] One part concentrated aqua dag, 20 parts distilled water. This formula and the concentrated aqua dag were furnished through the courtesy of G. F. Willson, representative of Acheson Colloids Corporation.

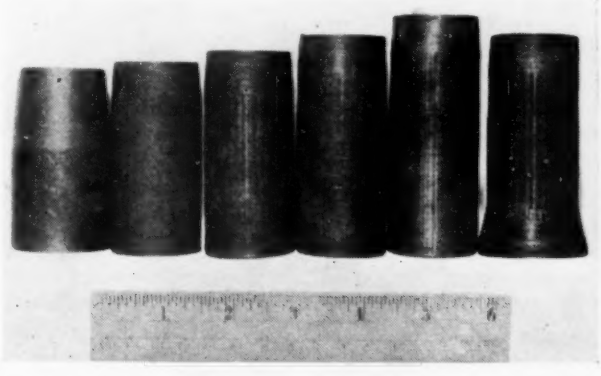


FIG. 12 SERIES OF DRAWN STEEL SHELLS SHOWING THE AS-TURNED BOTTLE, 9, 20, 30, $40^{1}/_{2}$, AND AN ATTEMPTED 44 PER CENT REDUCTION

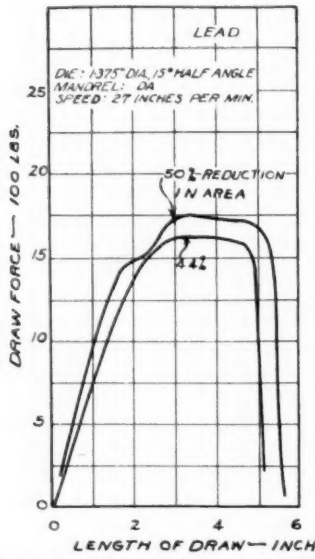


FIG. 13 FORCE-STROKE CURVES FOR VARIOUS REDUCTIONS WITH BOAT-TAIL

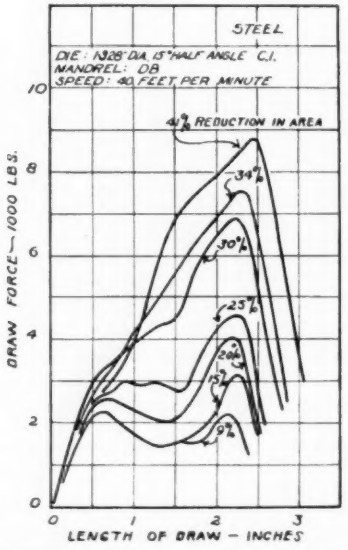


FIG. 14 FORCE-STROKE CURVES FOR VARIOUS REDUCTIONS WITH BOAT-TAIL

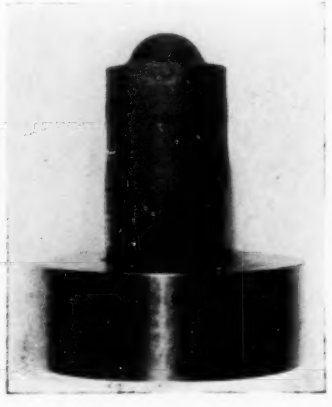


FIG. 15 AN ATTEMPTED STEEL DRAW OF 44 PER CENT REDUCTION IN AREA WHICH STALLED THE DRAW BENCH; ×1/2

Before a run was made, the draw die was preheated to about 600 F. Between each draw, the mandrel was removed and water-quenched to 100 F.

3 RESULTS OF TESTS

REDUCTIONS PERFORMABLE IN DRAWING A SHELL

When a pierced slug or "bottle" is pushed through a draw die, it is generally observed that the mandrel punches or pierces through the bottom if a reduction in diameter and wall thickness above a certain limit is attempted. The wall of the bottle does not participate in this operation; and it will be shown later that the same failure occurs if an attempt is made to push or "extrude" a circular blank through the die. Consequently, in order to eliminate this failure, or to increase the limit of reduction of the wall thickness, the diameter of the base can be reduced. This is

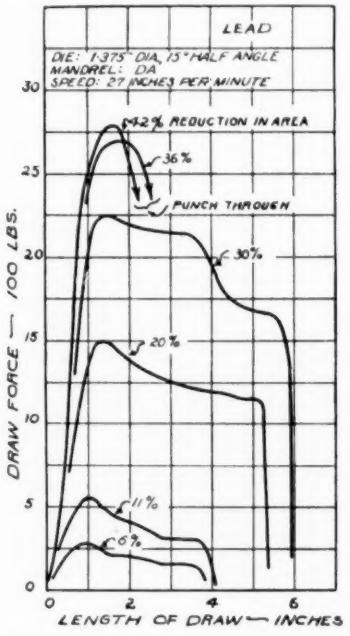


FIG. 16 FORCE-STROKE CURVES FOR VARIOUS REDUCTIONS WITHOUT BOAT-TAIL

a common commercial procedure, resulting in a bottom with a tapered base, or boat-tail.

Attempts were made to determine the possible wall reduction by using model bottles in lead and steel with a sufficiently extensive boat-tail, Fig. 12. With such bottles,[5] base failures are eliminated, and rupturing in the wall should occur if the attempted reduction exceeds the limits of forming. However, in the tests on both lead, Fig. 13, and steel, Fig. 14, this limit could not be reached because it required test conditions beyond the limits of equipment. With lead, the available dies and mandrels permitted reductions of the cross-sectional area of the cylindrical portion of the bottle up to 50 per cent, and no failure occurred at that reduction. Therefore the limit of reduction or "drawability" of lead tubing, drawn over a moving mandrel, or "rod" (as opposed to a stationary mandrel, "plug," or "pin") exceeds 50 per cent. With steel, a reduction of 44 per cent could not be achieved because of the high load which stalled the drawbench, Fig. 15, while a bottle was drawn successfully with 40½ per cent reduction in wall area. The observed possible high re-

[5] In this series with varying reductions, the variation was only in the outside diameter of the bottle, while the other dimensions were kept constant.

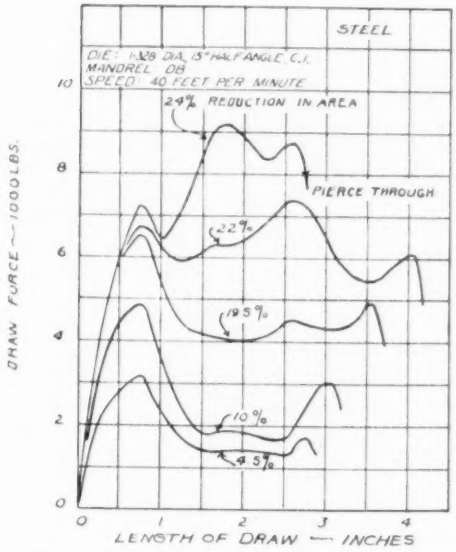


FIG. 17 FORCE-STROKE CURVES FOR VARIOUS REDUCTIONS WITHOUT BOAT-TAIL

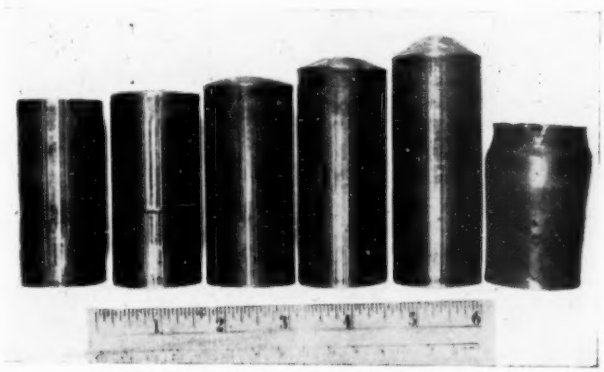


FIG. 18 DRAWN STEEL SHELLS SHOWING EFFECT OF REDUCTION FROM 4½ TO 24 PER CENT WITHOUT BOAT-TAIL

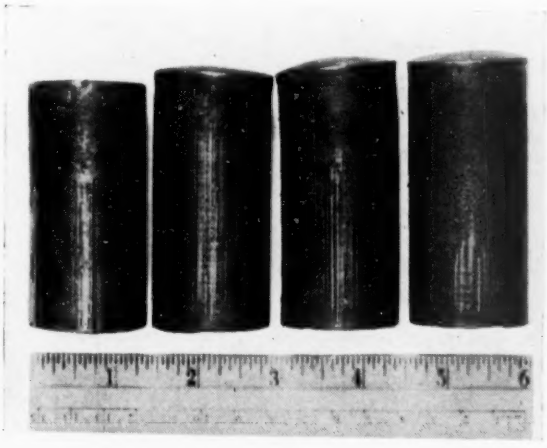


FIG. 19 PRELIMINARY SERIES OF DRAWN STEEL SHELLS, ILLUSTRATING SCORING AND OTHER DEFECTS RESULTING FROM POOR LUBRICATION AND TEMPERATURE DISTRIBUTION

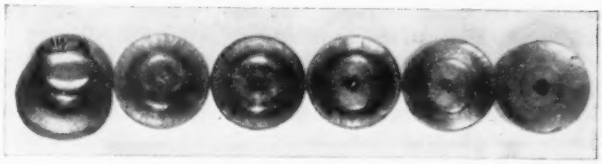


FIG. 20 TOP VIEW OF DRAWN LEAD DISKS

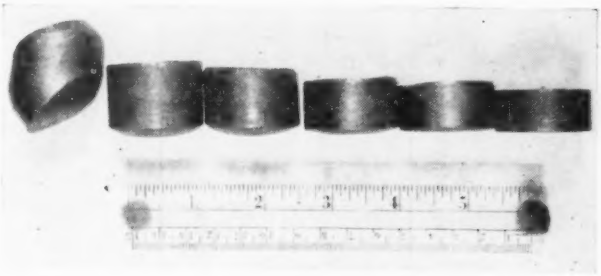


FIG. 21 SIDE VIEW OF DRAWN LEAD DISKS

(Right to left: Diameter reductions of 3, 6.5, 9.5, 13.5, 17, and an attempted 19 per cent.)

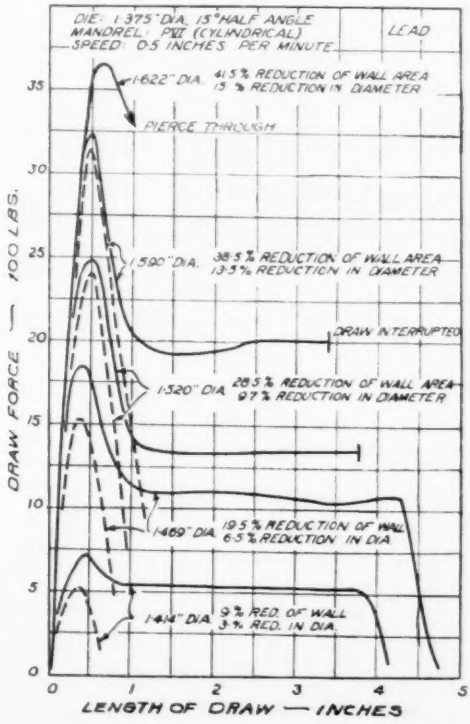


FIG. 22 FORCE-STROKE CURVES FOR LEAD BOTTLES WITH CYLINDRICAL CAVITIES AND CORRESPONDING CIRCULAR DISKS

ductions agree both with theoretical conceptions,[6,7] and with experimentation on cold-drawing of other metal products, particularly of cartridge cases.[8] According to the theoretical conceptions, a maximum (average) reduction of over 60 per cent should be achievable, provided that the frictional coefficient be-

[6] "A Theory of Tube Drawing," by G. Sachs, *Modern Industrial Press*, June, 1942, p. 26.

[7] "A Theory of Tube Drawing With a Rod," by G. Sachs, D. Tracy, and J. D. Lubahn, unpublished.

[8] "Cold Working of Cartridge Brass," by F. J. Lerro, *Modern Industrial Press*, Feb., 1940, pp. 8–14.

tween die and bottle is equal to that between bottle and mandrel; and such high reductions can be actually performed.

On the contrary, a square-nosed bottle will draw only up to a certain reduction in diameter of the base; to be discussed later. The common measure of reduction, that of the cross-sectional area of the cylindrical wall, has no influence on the strength of the bottom and, consequently, should vary widely with the geometrical relations of the bottle. Thus in a representative series on lead, Fig. 16, bottles were drawn successfully to a reduction in wall area of 30 per cent; while in other series, maximum wall reductions anywhere between 25 and 38 per cent were encountered, see later. In representative series on steel, Figs. 17 and 18, a reduction of over 22 per cent was achieved while another series yielded a maximum wall reduction as low as 16 per cent. These variations were observed in tests on slightly different shapes of bottle and tools, but optimum frictional conditions.

On the contrary, in a preliminary series in which excessive friction and pickup occurred, the bottom of a steel bottle was pierced at a wall reduction of only 6 per cent, Fig. 19. This result shows that the frictional conditions between bottle and die are another factor of paramount influence regarding the reduction of the bottom of the bottle.

In order to prove the validity of these conceptions, (1) a series of circular lead blanks of increasing diameter were pushed through a die, Figs. 20 and 21, and (2) a series of bottles without boat-tail but with a cylindrical wall were drawn with the same die and cylindrical mandrel (flat-nosed, $^3/_{16}$ in. tip radius). The results, Fig. 22, show (*a*) that the force at which the bottom fails is practically identical in both series, and (*b*) that the force is slightly higher for a bottle than for a disk, the reduction being the same. The actual limit for the disk could not be determined because of

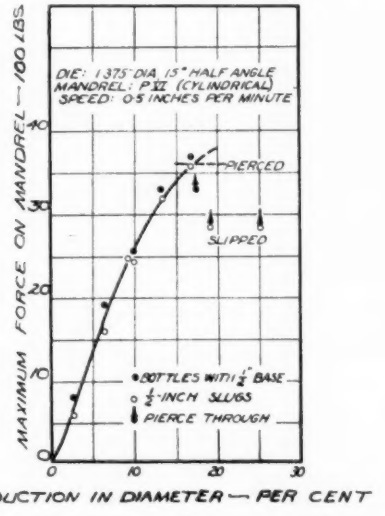


FIG. 23 EFFECT OF REDUCTION IN DIAMETER ON MAXIMUM FORCE FOR LEAD CYLINDERS AND CORRESPONDING CIRCULAR DISKS

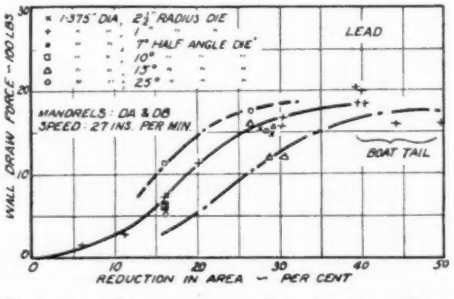


FIG. 24 EFFECT OF REDUCTION AND DIE ANGLE ON WALL DRAW FORCE

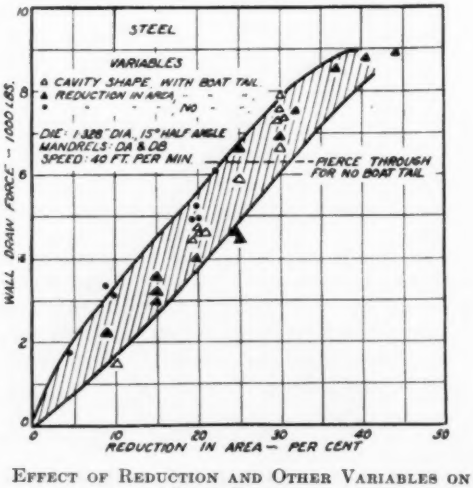


FIG. 25 EFFECT OF REDUCTION AND OTHER VARIABLES ON WALL DRAW FORCE

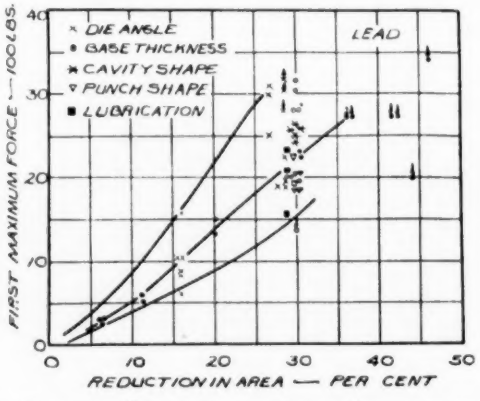


FIG. 26 EFFECT OF REDUCTION AND OTHER VARIABLES ON MAXIMUM DRAW FORCE

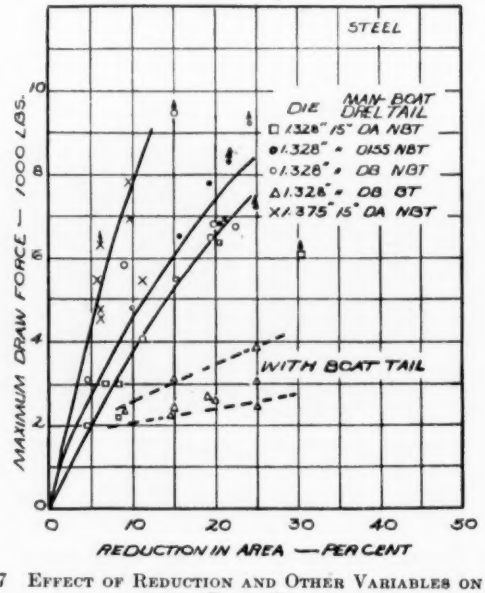


FIG. 27 EFFECT OF REDUCTION AND OTHER VARIABLES ON MAXIMUM DRAW FORCE

slippage, but the piercing force determined by common punching of a disk limits the possible reduction of the disk diameter to practically the same value as that of the bottle diameter, Fig. 23.

Force Requirements in Drawing a Shell

The force-stroke curve for the drawing of a bottle usually possesses a complex shape, which in addition varies widely with the processing condition.



Fig. 28 Bottom Failure (Pierce-Through) for Tapered Mandrel and Predraw Cavity With Lead



Fig. 29 Bottom Failure (Punch-Out) for Cylindrical Mandrel and Predraw Cavity With Lead

However, if a bottle with a square nose (i.e., no boat-tail) and a cylindrical wall is drawn by means of a cylindrical mandrel, the force-stroke curve, Fig. 22, becomes rather elementary and can be analyzed readily. Such a force-stroke curve generally consists of a "first maximum" superimposed to a practically constant force for the remainder of the stroke.

The first portion of a force-stroke curve is again determined by the diameter and thickness of the base, but in addition, by the reduction of the relatively thick wall close to the base of a commercial bottle.

The experimentation with disks clearly reveals that the force in the region of the first maximum, i.e., from the start of the draw to a certain distance beyond the first maximum, results for the most part from the extrusion of the base (disk) through the die. The slight difference is explained by the fact that a short length of the wall adjacent to the base is reduced simultaneously with the base when it has entered a certain depth into the die.



Fig. 30 Example of Bottom Deformation: Bending, at High Reductions With Lead; $\times 1/2$

The following horizontal portion of the force-stroke curve represents entirely the reduction of the wall, such as occurs in regular drawing of tubing.

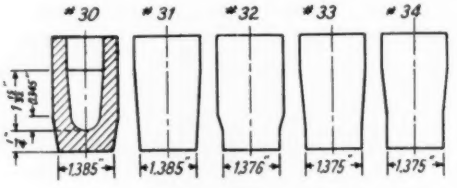
The more complex appearance of the force-stroke curves for drawing a bottle with a tapered cavity and by means of a tapered mandrel, Fig. 14, is explained by the fact that both the wall thickness and the reduction in cross-sectional area vary during the stroke. They are governed by the contours of the bottle both before and after the draw; the wall thickness and reduction changing sharply at any change of taper. As the force is roughly proportional to either of these two factors, other conditions being constant, the force may fluctuate irregularly within wide limits. Therefore as the wall thickness of the bottle decreases with increasing distance from the base, any peak in the force-stroke curve (with the exception of the first maximum) also indicates a high localized reduction. These relations, i.e., the change of cross section and reduction during the stroke, can be revealed only by a detailed theoretical and/or experimental analysis of the geometrical relations during the draw.

Superimposed on these variations in force is the increase in the force because of progressive cooling during the draw. As this factor does not occur in the tests on lead, their force-stroke curves usually possess a horizontal portion at the end, where the wall thickness both before and after the draw is constant. On the contrary, the decreasing temperature always causes the force-stroke curves for steel to rise toward the end of the draw.

The force-stroke curves for square-nosed specimens generally exhibit a first maximum, which is larger and extends over a longer stroke, the smaller is the diameter of the cavity at the base. Its shape also determines the subsequent changes in wall thickness, which in turn determine the draw force. The variations in these conditions explain the widely varying appearance of the first portion of the force-stroke curve.

If the base diameter is reduced by a boat-tail, the first maximum correspondingly decreases, and with a sufficiently extended boat-tail, the first maximum disappears, see Figs. 12 and 13.

Other factors being identical both the first maximum (if present) and the draw force increase with the reduction in outside diameter. By convention, the reduction of the cross-sectional area at the mouth is used as the measure for the reduction. Therefore, the force at the end of the draw can be used as representative of the forces required to reduce the wall thickness.



VARIOUS BOAT-TAIL SHAPES INVESTIGATED

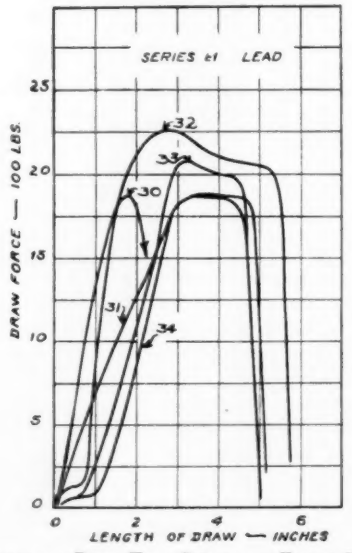


FIG. 31 EFFECT OF BOAT-TAIL SHAPE ON FORCE-STROKE CURVES

Figs. 24 and 25 illustrate the increase in the first maximum, and Figs. 26 and 27, in the final wall draw force, with increasing reduction, for both lead and steel, under widely varying conditions.

It is interesting to note the types of failures which occur when too great reduction is attempted. For specimens without boat-tail, at too-high reductions, a tapered mandrel may pierce through, carrying a small cap of metal just sufficient to cover the mandrel tip ahead of it, Fig. 28; under such circumstances, no fracture occurs at the wall, even though the wall area may be partially drawn. For a cylindrical mandrel, the punched-out cap is larger, having a diameter the same as the die opening, and the fracture occurs at the base of the wall in a typical tensile fracture for hot-working, Fig. 29. For intermediate reductions, where piercing-through does not occur, the bottom may be deformed either by bending and/or by piercing a slight amount; the term "bending" being applied to a deformation of the base without loss of base thickness, Fig. 30.

For steel, piercing through the square-nosed specimens takes place in a fashion similar to that for lead. However, it was noted that in some instances, for comparatively great reductions, the wall of the steel shell showed tendencies to neck down locally about one-half way up the mandrel taper. Apparently, the thick wall in the lower part of the bottle remains hotter and has lower tensile strength than the wall near the mouth which subsequently requires high forces for its reduction.

EFFECTS OF VARIABLES

The numerous variables encountered in drawing a pierced steel bottle, listed previously, could not be followed up systematically, but only by means of spot tests in this investigation. The effects of eight variables each were investigated in this manner for lead and for steel. In order to evaluate clearly the effects of each variable, an excessive number of tests would be required. However, the time and funds allotted for this investigation were limited, which explains why no definite conclusions can be drawn regarding the quantitative influence of each individual factor. Nevertheless, the results of the various series agree with general conceptions and outline a number of qualitative relations. In order to present this material without excessive repetition, it has been decided, therefore, to assemble the results of representative

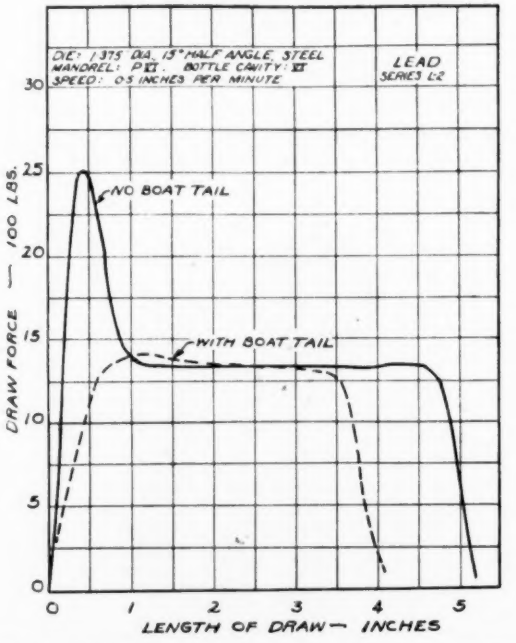


FIG. 32 EFFECT OF BOAT-TAIL SHAPE ON FORCE-STROKE CURVES FOR DRAWING LEAD BOTTLES WITH CYLINDRICAL CAVITIES

series, L-1 to L-9 for lead and S-1 to S-4 for steel, by short individual discussions, supplemented in most instances by graphical representations which summarize the conditions and observations. In addition, general relations and conclusions will be discussed in some detail.

Effects of Boat-Tail Shape, Series L-1 and L-2, Figs. 31, 32:

Lead Bottles:

2 $^{25}/_{32}$ in. long, IV cavity, 1.608 in. OD, $^{1}/_{4}$ in. base thickness, 0.333 in. wall thickness, various boat-tails.

Drawn:

Die.....No. 10, 1.375 in. diam, 1 in. radius, steel
Mandrel.....DA

Lubricant.....Ironsides AF-11, as received
Speed.....27 in. per min
Reduction.....40 per cent

Remarks. The representative series L-1 on lead, Fig. 31, illustrates that the shape and size of the boat-tail has a decided effect on the first maximum force and, consequently, the maximum reduction in wall area. The first maximum may be eliminated entirely by a suitable boat-tail. In the case of such bottles with tapered cavities, it was found that the boat-tail shape also had a slight effect on the draw force required for the reduction of the wall. No explanation can be given for this phenomenon, that the wall-drawing force increased with increasing first maximum.

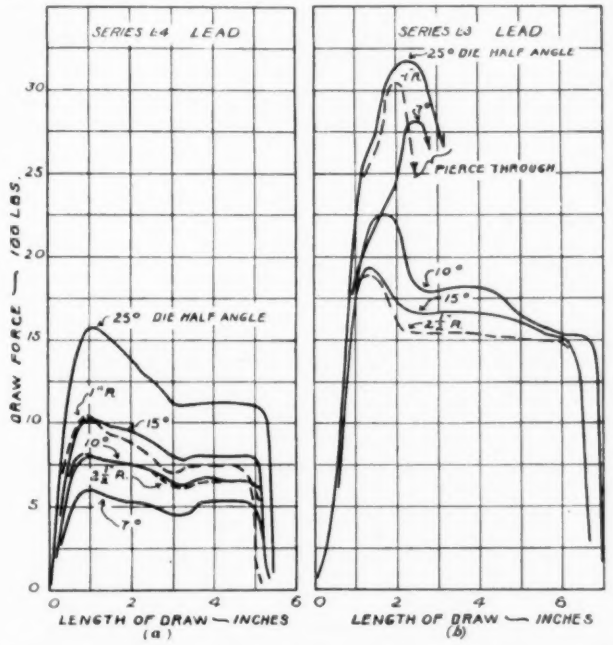


FIG. 33 FORCE-STROKE CURVES WITH VARIOUS DIE ANGLES AND CONTOURS FOR TWO REDUCTIONS



FIG. 34 LEAD SHELLS REDUCED IN AREA 30 PER CENT IN A SINGLE PASS THROUGH 7 DEG, 15 DEG, AND 25 DEG HALF-ANGLE DIES, RESPECTIVELY

In another series, L-2, Fig. 32, with bottles having a cylindrical cavity, it was found that the shape of boat-tail in no way influenced the part of the force-stroke curve representing the drawing of the wall. These tests similated a second draw wherein the punch tightly fitted the bottle cavity before the draw.

Several additional series on steel and lead confirmed the general effects of the boat-tail on the shape of the force-stroke curve and the magnitude of the possible reduction.

This experimentation was not sufficient to establish an optimum contour and length of the boat-tail. Its dimensions should be adjusted to the cavity and mandrel contours, in order to keep the reduction of the wall at the base small. However, the reduction should not be so small as to cause "sinking" of the bottle, i.e., drawing without decrease in wall thickness, which leaves an air pocket between mandrel and bottle, and which may cause a "balloon nose" or "running ahead" of the drawn shell.

Effect of Die Angle and Contour, Series L-3 and L-4, Figs. 33, 34:

Lead Bottles:

2 $^{23}/_{32}$ in. long, IV cavity, 1.454 in. and 1.510 in. OD, $^1/_2$ in. base thickness, 0.256 in. and 0.292 in. wall thickness, no boat-tail

Drawn:

Dies.....
No. 1, 1.375 in. diam, 7 deg half-angle, steel
No. 2, 1.375 in. diam, 10 deg half-angle, steel
No. 3, 1.375 in. diam, 15 deg half-angle, steel
No. 4, 1.375 in. diam, 25 deg half-angle, steel
No. 10, 1.375 in. diam, 1 in. radius, steel
No. 13, 1.375 in. diam, 2$^1/_2$ in. radius, steel
Mandrel.....DB
Lubricant.....Ironsides AF-11, as received
Speed.....27 in. per min
Reduction.....16 and 29 per cent

Remarks. For a relatively large reduction of 29 per cent, Fig. 33 (*b*), series L-3, the optimum die half-angle appears to be about 15 deg, when the first maximum and wall draw force are a minimum. For lower reductions the optimum die half-angle decreases slightly, series L-4, Fig. 33 (*a*).

A small angle die (7-deg half-angle) yields as high a maximum force as does a large (25-deg) half-angle die, but the first maximum portion of the curve is wider and extends over more of the stroke in the latter case, i.e., a considerably greater amount of work is required for a given reduction through a wide-angle die than by smaller angles. This is explained by the fact that, although the friction decreases, the shear or nonuniform deformation increases with increasing die angle, the net result being a greater total drawing stress. For very small die angles, the theoretical draw force is less, due to a wedge action, but friction increases greatly to yield high drawing forces.

If bell-shaped dies of different radii are used, the relation of die radius to draw force, etc. is very similar to that of the die half-angle in the case of straight-angled dies; the important factor in the former case being the chord angle, or "effective angle" of the die, Fig. 33.

With a 7-deg die, the end of the mouth of the drawn shell was nearly perpendicular to the mandrel, but with increasing die angle the mouth sloped in toward the base at an angle of 60 deg with the shell axis, indicating a condition of nonuniform strain during drawing. Fig. 34 indicates the variation in deformation of the base when drawing pierced lead shells through 7 deg, 15 deg, and 25-deg half-angled dies, respectively.

Effect of Cavity Shape Without Boat-Tail, Series L-5, Fig. 35:

Lead Bottles:

3$^1/_4$ in. long, 1.529 in. OD, $^1/_2$ in. base thickness, 0.295 in. wall thickness, no boat-tail

Cavities: I:..... 8 deg, 1$^{17}/_{32}$ in. taper, 0.550 in. diam, flat base
II:..... 9$^1/_2$ deg, 1$^{17}/_{32}$ in. taper, 0.550 in. diam, flat base

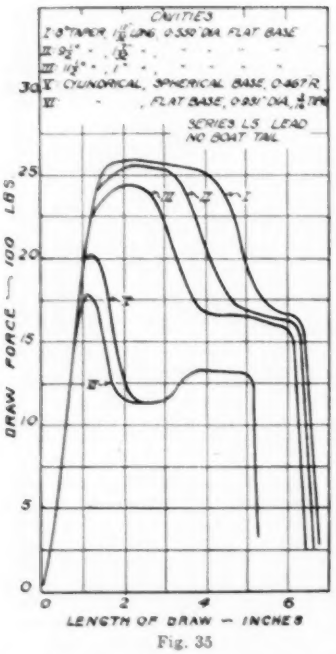


Fig. 35

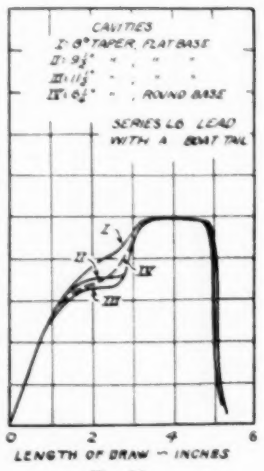


Fig. 36

FIG. 35 FORCE-STROKE CURVES FOR VARIOUS CAVITIES WITHOUT BOAT-TAIL

FIG. 36 FORCE-STROKE CURVES FOR VARIOUS CAVITIES WITH BOAT-TAIL

III:..... 11½ deg, 1 in. taper, 0.550 in. diam, flat base
IV:..... 6¼ deg, 1 13/32 in. taper, 0.345 in. radius, round base
V:..... cylindrical 0.467 in. radius, round base
VI:..... cylindrical 0.931 in. diam, flat base

Drawn:

Die..... No. 10, 1.375 in. diam, 1 in. radius, steel
Mandrel..... DA
Lubricant..... Ironsides AF-11, diluted 2:1 by weight with water
Speed..... 27 in. per min
Reduction..... 30 per cent

Remarks. In Fig. 35 are illustrated the force-stroke curves for this series which show that the first maximum decreases with an increase in cavity size. This is expected since a large cavity (shorter taper) results in a thinner wall near the base, requiring less force for wall reduction in the second stage of the draw operation. Drawing a pierced slug having a cylindrical cavity with tapered mandrel results in a pronounced minimum, indicating pure sinking of the represented portion of the wall.

The cavity shape has a negligible effect on the draw force for the cylindrical portion of the shell wall.

Effect of Cavity Shape With Boat-Tail, Series L-6, Fig. 36:

Lead Bottles:

3¼ in. long, 1.526 in. OD, ½ in. base thickness, 0.292 in. wall thickness, boat-tail (1.375 in. base OD to 1.525 in. in 2 in.—2 deg 11 in. taper), cavities I, II, III, IV

Drawn:

Die..... No. 3, 1.375 in. diam, 15 deg half-angle, steel
Mandrel..... DB
Lubricant..... Ironsides AF-11, diluted 2:1 by weight with water
Speed..... 27 in. per min.
Reduction..... 29 per cent

Remarks. At the given reduction of 29 per cent, the slight variation in cavity shape had little effect on the first part of the force-stroke curves, and no effect, as expected, on the part representing the drawing of the cylindrical wall, Fig. 36.

Specifically, the larger the angle of the cavity taper, or the shorter the taper, the lower is the first part of the force-stroke curve. This is in agreement with results on boat-tail and mandrel shape, since any factor which reduces the reduction at the bottom decreases the first maximum; for in boat-tailing, metal is removed from the outside to reduce the reduction, while with a larger cavity near the base (large cavity taper), or small mandrel taper, there is less metal inside and more clearance, respectively, each of which permits more sinking than ironing of the wall during the draw. Actually for the given reduction with boat-tail, only sinking at various points along the draw-mandrel taper was noted.

Effect of Cavity Shape With Boat-Tail, Series S-1, Fig. 37:

Steel Bottles:

2⅜ in. long, 1.400 in. and 1.460 in. OD, ⅛ in. base thickness, 0.237 in. and 0.268 in. wall thickness, boat-tail (5 deg from 1.220 in. base diam), cavities: I, II, III, and IV

Drawn:

Die..... No. 7, 1.328 in. diam, 15 deg half-angle, Meehanite
Mandrel..... DB
Lubricant..... Fiske's No. 514-A hot-die lubricant, as received
Speed..... 40 fpm
Reduction..... 20 and 30 per cent

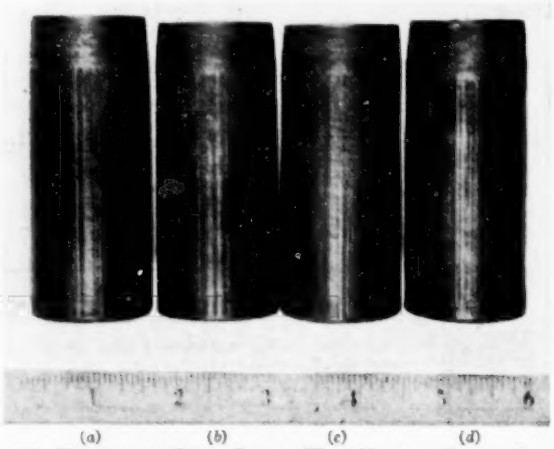


FIG. 37 EXAMPLE OF STEEL SHELLS WITH VARIOUS CAVITY SHAPES GIVEN 30 PER CENT REDUCTION IN A SINGLE PASS

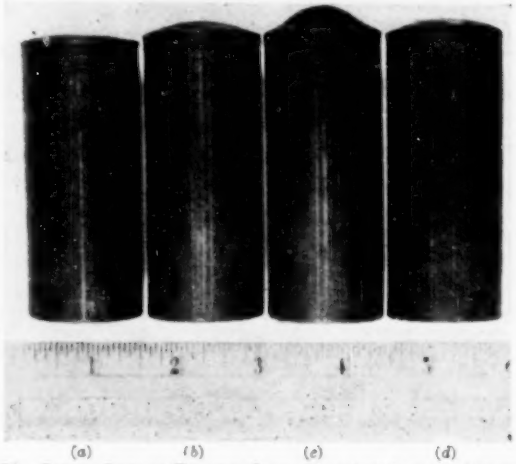


FIG. 38 STEEL SHELLS DRAWN OVER VARIOUS-SHAPED MANDRELS (Left to right: *a*, 0.672 in. diam flat nose; *b*, 0.612 in. diam; *c*, 0.550 in. diam; and *d*, 0.345 in. radius round-nose mandrel.)

Remarks:

EFFECT OF CAVITY SHAPE ON DRAW FORCE

Cavity no.	Cavity taper, deg	First maximum, lb	Wall force, lb	Stress on remaining section, psi
		20 per cent reduction		
I	8.0	5800	4750	6800
II	9.5	3350	4650	6700
III	11.5	2950	4650	6700
		30 per cent reduction		
I	8.0	5700	7300	10500
II	9.5	4000	7950	11400
III	11.5	3550	7550	10850

Fig. 37 illustrates drawn specimens having *a*, 8 deg cavity (I); *b*, 9.5 deg cavity (II); *c*, 11.5 deg cavity (III); and *d*, 6.25 deg cavity (IV).

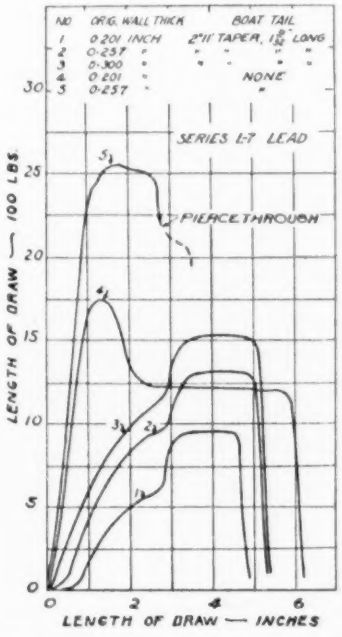


Fig. 39 Effect of Wall Thickness on Force-Stroke Curves

Effect of Punch Shape, Series S-2, Fig. 38:

Steel Bottles:

$2^5/_8$ in. long, IV cavity, 1.400 in. OD, 1/2 in. base thickness, 0.235 in. wall thickness, no boat-tail

Drawn:

Die	No. 7, 1.328 in. diam, 15 deg half-angle, Meehanite
Mandrels	D105: 3 deg taper 2.38 in. long, 0.672 in. diam, flat nose
	D155: $4^3/_4$ deg taper 1.92 in. long, 0.612 in. diam, flat nose
	DB: $5^1/_2$ deg taper 2 in. long, 0.550 in. diam, flat nose
	DA: 4 deg taper 2 in. long, 0.345 in. radius, round nose
Lubricant	Fiske's No. 514-A hot-die lubricant, as received
Speed	40 fpm
Reduction	20 per cent

Remarks. In Fig. 38 are shown the results of drawing with various mandrel shapes accomplishing a given reduction in wall cross section. The following table indicates that the larger the mandrel-nose diameter (equivalent to a smaller cavity at the base) the higher is the first maximum. Drawability is increased by increasing the mandrel-tip diameter, since in so doing more support is offered the base during the first and critical stage of the draw operation.

Draw mandrel	First maximum, lb	Tip diameter, in.	Wall force, lb
D105	7600	0.67	4700
D155	7550	0.61	4800
DB	6850	0.55	5250
DA	6450	0.35 R (round nose)—	

Effect of Wall Thickness, Series L-7, Fig. 39:

Lead Bottles:

$3^1/_4$ in. long, IV cavity, various outside diameters, 1/2 in. base thickness, various wall thicknesses, with and without boat-tail

Drawn:

Dies	No. 8, 1.462 in. diam, 1 in. radius, steel
	No. 9, 1.394 in. diam, 1 in. radius, steel
	No. 11, 1.328 in. diam, 1 in. radius, steel
	No. 12, 1.240 in. diam, 1 in. radius, steel
Mandrel	DB
Lubricant	Ironsides AF-11, diluted 2:1 by weight with water
Speed	27 in. per min
Reduction	27 per cent

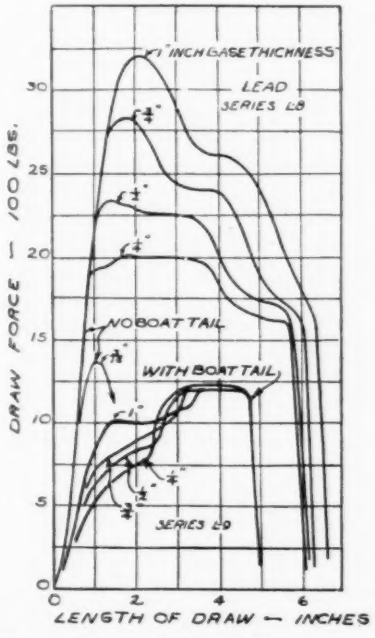


Fig. 40 Effect of Base Thickness Without Boat-Tail and With Boat-Tail

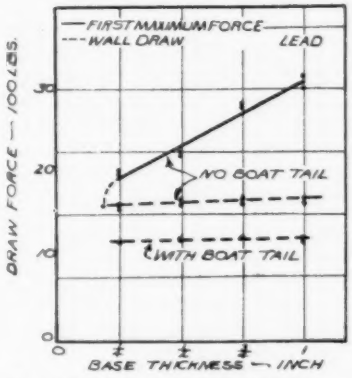


Fig. 41 Effect of Base Thickness

Remarks. The wall thicknesses of the bottles in this seriss ranged from 0.176 in. to 0.309 in. It has been observed in these

tests that as the wall thickness increases, with the base thickness unchanged, the first maximum becomes less pronounced; thus, for a 0.176-in. wall thickness, the first maximum is 100 per cent greater than the wall draw force, whereas for a 0.309-in. wall the maximum force is only 20 per cent greater, Fig. 39. Further, as the wall thickness increases, the first maximum peak changes from sharp to a rounded and wider shape.

The tests also indicate that the unit wall drawing force, i.e., the force related to the unit cross section of cylindrical wall before drawing, increases with increasing wall thickness at a low reduction of 16 per cent, without boat-tail. However, at higher reduction, with boat-tail, there is no effect from thickness over the range investigated.

Fig. 39 again shows that a boat-tail not only decreases the first maximum, but also the wall drawing force.

In general, increasing the wall thickness, while keeping the reduction and base thickness constant, resulted in the same phenomena as did decreasing the mandrel-tip diameter. Thus, unless the mandrel-tip diameter increases relatively with the shell diameter, the tendency to pierce appears. Specifically, while a wall thickness of approximately 0.26 in. pierced at an attempted reduction of 27 per cent, a thinner wall of 0.20 in. could be drawn successfully at this reduction.

Apparently piercing-through does not occur in lead until the compressive stress on the base is about 10,000 psi, as computed from the projected area of the tip of the flat-nosed mandrels. For the round-nose mandrel, DA, the piercing stress is reached at 7000 psi.

Effect of Base Thickness Without Boat-Tail, Series L-8, Figs. 40 and 41:

Lead Bottles:

$2^{23}/_{32}$ in. long, IV cavity, 1.529 in. OD, 0.295 in. wall thickness, 1 in., $^3/_4$ in., $^1/_2$ in., $^1/_4$ in., $^3/_{16}$ in. base thicknesses, respectively, no boat-tail

Drawn:

Die	No. 10, 1.375 in. diam, 1 in. radius, steel
Mandrel	DA
Lubricant	Ironsides AF-11, as received
Speed	27 in. per min
Reduction	$30^1/_2$ per cent

Remarks. A series of pierced lead slugs with base thicknesses of 1 in., $^3/_4$ in., $^1/_2$ in., and $^1/_4$ in. were drawn successfully at $30^1/_2$ per cent reduction, while a $^3/_{16}$-in-base specimen pierced through at this reduction, series L-8, Fig. 40. The first maximum increases linearly with the base thickness but there is no change in wall draw force, Fig. 41. By shifting the respective force-stroke curves a distance equivalent to the base thickness, it was found all peaks occur at the same abscissa value.

The slight difference in length of draw, as shown in Fig. 40, is due, not to a difference in length of drawn shell, but rather to the slowing of the draw bench at the higher loads.

Effect of Base Thickness With Boat-Tail, Series L-9, Figs. 40 and 41:

Lead Bottles:

$3^1/_4$ in. long, IV cavity, 1.525 in. OD, 1 in., $^3/_4$ in., $^1/_2$ in., $^1/_4$ in. base thickness, 0.292 in. wall thickness, boat-tail: 1.375 in. base OD to 1.525 in. OD in 2 in. (2 deg 11′ taper)

Drawn:

Die	No. 3, 1.375 in. diam, 15 deg half-angle, steel
Mandrel	DB
Lubricant	Ironsides AF-11, diluted 2:1 by weight with water
Speed	27 in. per min
Reduction	29 per cent

Remarks. By putting sufficient boat-tail on a specimen, the wall drawing force may be decreased by some 25 per cent, while any increase in base thickness has no effect on this value, but displaces the stroke a distance equivalent to the change in the base thickness.

The first part of the force-stroke curve is affected but slightly by changing the base thickness, and the length of the draw is not altered, Fig. 40.

Effect of Temperature, Series S-3, Figs. 42 and 43:

Steel Bottles:

$2^5/_8$ in. long, IV cavity, 1.400 in. OD, $^1/_2$ in. base thickness, 0.235 in. wall thickness, boat-tail (5 deg from 1.220 in. base diam)

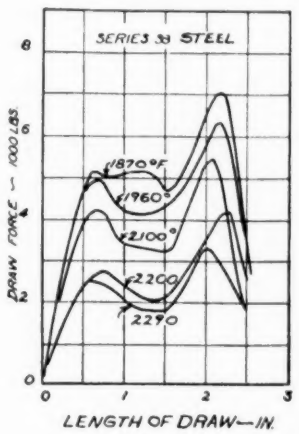


Fig. 42

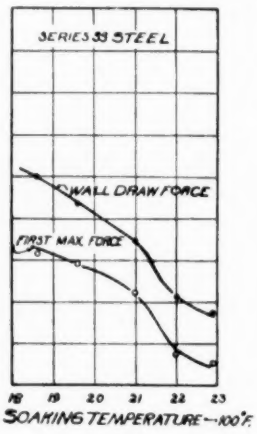


Fig. 43

FIG. 42 FORCE-STROKE CURVES FOR VARIOUS TEMPERATURES

FIG. 43 EFFECT OF TEMPERATURE ON DRAW FORCES

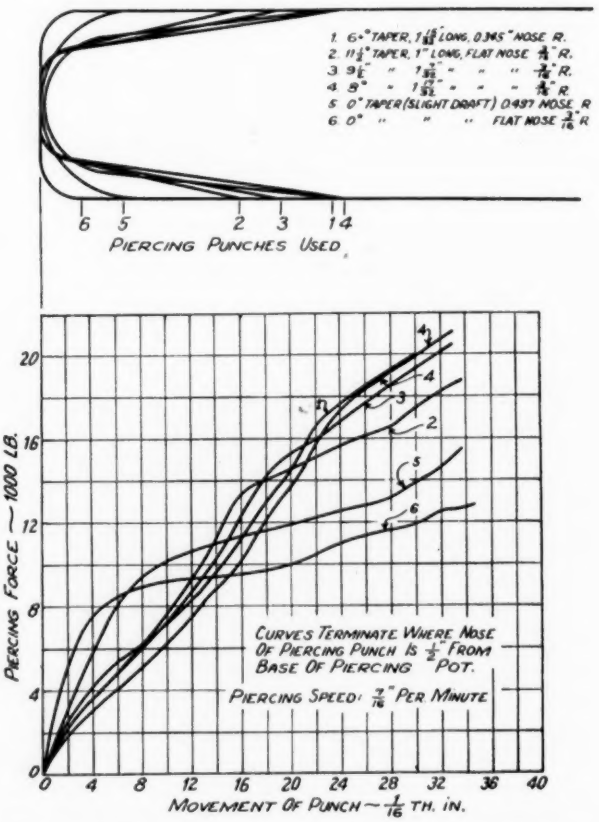


FIG. 44 FORCE-STROKE CURVES FOR PIERCING WITH VARIOUS PUNCHES

Drawn:

Die	No. 7, 1.328 in. diam, 15 deg half-angle, steel
Mandrel	DB
Lubricant	Fiske's No. 514-A hot-die lubricant, as received
Speed	40 fpm
Reduction	19 per cent

Remarks. The following table shows the representative values obtained for a series designed to indicate the effect of temperature:

Furnace temperature, deg F	Wall draw force, lb	Stress on remaining section, psi
1850	7000	9950
2000	5500	7850
2300	3700	5300

Fig. 42 indicates how the force-stroke curve varies with temperature, and, in Fig. 43, is shown the forces plotted versus the soaking temperature. It is to be noted that the temperature indicated on the abscissa scale is the soaking temperature (furnace temperature) and the actual drawing temperature may be 100 to 300 deg F lower depending upon the handling time, drawing speed, etc.

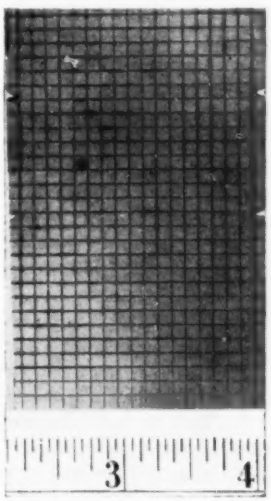


FIG. 45 SPLIT LEAD SLUG WITH SCRIBED GRATING, BEFORE PIERCING

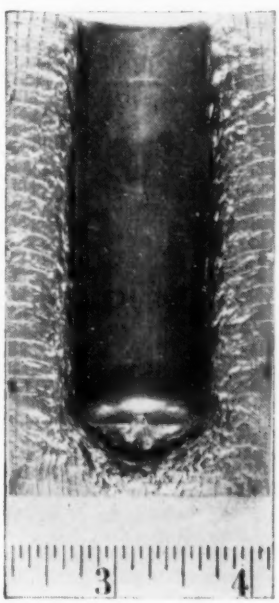


FIG. 46 SPLIT LEAD PIERCED SLUG, SHOWING DEFORMATIONS OF GRATING AFTER PIERCING

The shells, series S-3, drawn at low temperature show practically no difference in drawn dimensions from the high-temperature draws.

Effect of Speed, Series S-4:

Steel Bottles:

$2^5/_8$ in. long, IV cavity, 1.400 in. OD, $^1/_2$ in. base thickness, 0.237 in. wall thickness, boat-tail (5 deg from 1.220 in. base diam)

Drawn:

Die	No. 7, 1.328 in. diam, 15 deg half-angle, Meehanite
Mandrel	DB
Lubricant	Fiske's No. 514-A hot-die lubricant, as received
Speed	40, 50, and 65 fpm
Reduction	19 per cent

Remarks. A few tests on draw speed have been performed, but the effect of this variable alone is obscured by other factors, principally temperature.

The range of draw speeds investigated showed a slight trend toward increasing power requirement, with increasing speed from 40 to 65 fpm.

Trial	Speed, fpm	First maximum, lb	Wall draw force, lb
1	40	3300	4950
2	50	3950	5050
3	65	(3250)	5150

PIERCING OF LEAD SLUGS

A few observations on the piercing of lead slugs has shown that a blunt-nosed piercing punch requires less force for deep piercing than tapered punches. Thus a cylindrical punch with a flat nose and small tip radius required less force to pierce a given depth than any of the tapered punches or the round-nosed cylindrical punch used, Fig. 44. A small punch taper apparently results in a wedging action which creates high frictional resistance.

An attempt to analyze the piercing operation was undertaken in which a cast-lead billet was split and a grating scribed on one parting face, Fig. 45. The halves were then clamped together and the specially prepared billet pierced. The resulting deformation of the billet and grating is illustrated in Fig. 46. Unfortunately no time was available for analysis of this interesting problem.

4 DISCUSSION AND CONCLUSIONS

Experimentation on model shells in lead and steel was conducted in order to obtain a perspective of the effect of the numerous variables involved in the drawing phase of the pierce-and-draw method of fabricating high-explosive shells.

Because of difficulties involved in building special equipment, the effects of most variables were investigated in a detailed manner with lead at room temperature. At this temperature, lead possesses properties similar to a high-melting metal at hot-working temperatures.

High-temperature tests introduce, as additional factors or complications, variations in friction, in temperature, and in temperature distribution. A number of tests were conducted with steel in order to confirm conclusions drawn from the tests with lead and to determine differences introduced by the additional factors, if present.

The efficiency of a shell-drawing operation is measured commonly by the "reduction" in cross-sectional area of the tubular section at the mouth of the pierced bottle. Experimentation in

which the only variable was the outside diameter of the bottle showed that the maximum possible reduction or "drawability" varied widely with the other variable factors.

A lead bottle with a square nose, i.e., without a "boat-tail," can be given a maximum reduction of approximately 35 per cent in a single pass through a ring die of proper contour. The drawability of steel under similar conditions is only 20 to 25 per cent.

These values of drawability are much lower than those attainable for tubular specimens. This is explained by the fact that the maximum reduction is not determined by a tension failure of the wall, but by a shear failure or piercing through the base.

The intricate shape of the force-stroke curves is explained by the following relations: The force-stroke curve is composed of two superimposed parts, the forces for extruding the bottom, and the forces for drawing the wall. Because of variations in the wall thicknesses of the bottle and the subsequent drawpiece, and the resulting fluctuations in reduction, the wall draw force also fluctuates within wide limits. In addition, the variations and changes in the temperature of steel cause a gradual increase of the draw force as the stroke progresses.

The force-stroke curve for a bottle with a square or blunt base generally exhibits a high "first maximum" which is explained, for the most part, by the reduction of the base. The reduction of the adjacent wall also contributes to this first maximum.

Both the first maximum and the wall drawing forces increase with increasing reduction. Failure by piercing through the bottom occurs when the first maximum reaches a certain value, which is independent of the variations in the upper shell wall thickness.

Consequently, any factor which reduces the first maximum (for a given thickness of the bottom) also increases the possible maximum reduction. Such expedients used to relieve the excessive bottom deformation are: (1) Boat-tailing, or tapering the outside of the shell toward the base; (2) selecting a die having an optimum die angle; and (3) employing a pierced slug having a large cavity which provides a thin wall and a large clearance for the mandrel tip.

A suitable boat-tail eliminates the first maximum, since the reduction of the base diameter then becomes very small, or may be eliminated completely.

The optimum die half-angle for lead was found to be 15 deg.[9] Only a slight difference in forces was detected between curved dies and straight-angle dies with the same effective half-angles. The effect of die angle is explained by the phenomena (*a*) that the force to push a slug through an opening should decrease with decreasing angle because of a wedge action, but (*b*) that the frictional resistance increases with decreasing angle.

[9] "An Investigation of Hot Drawing on the Mandrel," by E. Schneider, *Journal of the Iron and Steel Institute*, vol. 104, 1921, pp. 191–227.

For a given mandrel shape, the greater the clearance between mandrel tip and bottle cavity, the lower is the first maximum and the higher the drawability, because of the correspondingly decreasing wall thickness and reduction at the base of the shell.

For a given cavity shape piercing through the base during the drawing operation may be inhibited to some extent by use of a draw mandrel having a large nose tip diameter (or nose radius, in the case of round-nosed mandrels). It is the diameter of the mandrel tip which determines the sheared area, and, consequently, the strength of the base, while the taper of the front end of the mandrel determines the reduction and the force required for the draw. Consequently, the drawability is increased with increasing tip diameter and decreasing taper of the mandrel, other factors remaining constant.

Thin-walled shells can be given greater successful reductions than thick-walled shells, other factors remaining constant. For a given cavity shape and mandrel shape, the thicker the wall the smaller is the mandrel-tip diameter relative to shell outside diameter and the lower is the drawability.

It has been found that base thickness has little effect on the drawability, for the strength of the base against piercing-through increases in the same proportion as the force required to push the base through the die. Only a very thin base will cause early piercing-through.

Proper lubrication and tool material were found to be very important factors determining the maximum reduction for steel. A lubricant of colloidal graphite in heavy petroleum oil used in combination with a heat-treated Meehanite die and steel mandrels was found to reduce the friction to a minimum, and thereby to yield a minimum draw force. A filmed wax-and-soap-base lubricant gave good performance for lead.

The temperature of steel bottles had little effect on the drawability. The lower the temperature, the greater is the shear resistance, but also the higher are the draw forces required.

The effect of speed was not clearly revealed in this investigation because of the limited number of draws which were performed.

Acknowledgments

The authors wish to express their gratitude to Prof. K. H. Donaldson, head, department of metallurgical engineering, Case School of Applied Science, and Dr. M. D. Stone, manager of development, United Engineering and Foundry Company, Pittsburgh, Pa., and chairman of The American Society of Mechanical Engineers Shell Forging Research Committee, for their co-operation in securing the necessary equipment and material for this investigation.

The authors are indebted to Mr. G. Espey who is responsible for designing and perfecting the pressure-recording apparatus; and to Messrs. J. Lottmann and C. Bennett of Case School of Applied Science for building the necessary equipment.

Plastic States of Stress in Curved Shells: The Forces Required for Forging of the Nose of High-Explosive Shells

By A. NADAI,[1] EAST PITTSBURGH, PA.

Problem of Nosing a Shell

THE forging of artillery shells and of air bombs requires a high degree of skill of the shops. Considerable practical development work and costly experiments were performed in the steel mills of this country when war broke out and the necessity suddenly developed for the manufacture of large quantities of hollow bodies for the artillery and aircraft. This report deals with a mechanical analysis of the forces required for forming the noses of shells. The present practice is to compress the open end of a cylindrical shell forging after it has been preheated in the radial direction by forcing it into a suitably shaped die. Small shells are cold-nosed. In this report, hot-nosing primarily will be considered, although the development outlined may well be extended to the cold-nosing process.

At the beginning of this war very little practical information was available concerning the capacities of the heavy hydraulic presses used for forging shell noses. Considerable difficulties arose from this fact alone since capacities of presses were either under or over-rated due to the complete lack of information concerning the nosing forces. The nature of the radial plastic flow accompanying the formation of similar shapes has not been studied, although the process of making blunt ends in hollow containers has many additional practical applications. In many plants costly large-scale shop experiments had to be performed until the precise shapes of the profiles of shells were determined which were needed in the original cylindrical forgings to produce the prescribed shapes of shells in their finished condition. Other important factors which had to be studied were the distribution of the temperature along the cylinder requiring a drop in temperature from the tip at the open end toward the rear portion of the shell, the effects of lubricants suitable for cold- or for hot-nosing preventing excessive die wear, speeds of pressing, etc.

In the fall of 1942, the A.S.M.E. Special Research Committee on Forging of Steel Shells (Dr. M. Stone, Chairman, and Prof. W. Trinks, Projects Director) arranged on behalf of the Army Ordnance, Washington, the details of an investigation with the Westinghouse Research Laboratories to be carried out on the mechanical problem of the plastic forming of the nose of a shell. In this first partial report, a theoretical analysis is given of the equilibrium systems of the internal stresses in the plastic state during the formation of a curved shell with rotational symmetry, from which an expression is derived for the axial resultant "nosing force." This is the resultant at the bottom of the curved portion of the nose which determines the total nosing resistance, or the capacity of the forging machine or hydraulic press used for forging the nose.

Friction forces between the die and the shell must be considered. They were assumed to be proportional to the specific pressure in the contact surface. Friction forces act in the direction opposite to the sliding motion of the material relative to the die. From the distributions of the axial and circumferential stresses predicted by the theory, several important conclusions can be drawn concerning certain limiting conditions which must be satisfied during nosing of a shell to avoid local thickening at the bottom of the nose and concerning limiting magnitudes of the friction.

Expressions for the plastic strains are quoted which give an idea of the amounts of the compressional distortion of the material. These geometric relations should well serve to predict the original shape of the shell required to produce a finished shell with prescribed wall thicknesses.

General Equations for Plastic States of Stress in a Thin Curved Shell Whose Middle Surface Is a Surface of Revolution

When a ductile metal is permanently deformed, it is known that stresses in the strain-hardening range, i.e., at sufficiently low temperatures, depend solely upon the permanent strains, and that at sufficiently high (forging) temperatures they are independent of the strains but increase with the plastic rates of deformation. Although it appears possible to treat mathematically certain special cases of plastic flow by assuming that, "in the strain-hardening range," stresses depend upon the plastic strains in a given manner, or that, on the other hand, "at forging temperatures," they are known functions of the rates of strain, it seemed more desirable to develop such cases of plastic flow under further simplified assumptions, particularly for the case of hot-nosing.

It is known that the distributions of the stresses in a curved shell of given dimensions, whose wall thickness is comparatively small, is determined solely by the three static conditions which express the equilibrium of the small elements of the shell in the general case, provided that the lateral pressure carried on the surface of the shell is given. When a shell is deformed by a distributed pressure exerted through a die, the foregoing statement regarding the lateral pressure does not hold. The contact pressure between the die and the shell is one of the unknown quantities which must be determined. In addition to the three static equations in the general case one new condition is therefore needed if the shell material is deformed in the plastic state. For this fourth equation, the condition of plasticity can and will be here introduced. This briefly explains the plan upon which the computations of this paper were based.

When the nose of a shell is forged at 1800 F, or at a near-by temperature, a certain length of the originally cylindrical shell in Fig. 1 (*a*) near the open end *e* is preheated and this hot portion is forced to enter the die *d*. The remaining portion of the shell below the plane *cc* shown in Fig. 1 (*b*) is left cold and should not be

[1] Consulting Mechanical Engineer, Research Laboratories, Westinghouse Electric & Manufacturing Co. Member, A.S.M.E. Special Research Committee on Forging of Steel Shells. Mem. A.S.M.E.

Contributed by Special Research Committee on Forging of Steel Shells and presented at the Annual Meeting, New York, N. Y., Nov. 29–Dec. 3, 1943, of The American Society of Mechanical Engineers.

Note: Statements and opinions advanced in papers are to be understood as individual expressions of their authors and not those of the Society.

deformed. An element of material situated above the plane *cc* is essentially compressed permanently in the circumferential directions of the circular cross sections of the shell which are perpendicular to its axis. The theory predicts and observations prove that the major principal compression stress during the forging of the nose of a shell is this circumferential stress. In addition, the metal is also under the action of considerable axial compression stresses (more precisely of normal stresses in the directions parallel to the tangents of the middle or meridian curve in the axial-plane sections of the shell). Since the elements of the nose must glide under heavy pressure along the inner working surface of the die, considerable frictional forces must also be produced in the contact surface resisting this gliding motion. In spite of these complications in the actual flow the metal is essentially compressed in the circumferential directions and must therefore expand both in the radial and axial directions when the nose of a shell is forged.

A point P in the undeformed shell (Fig. 1) will be found after

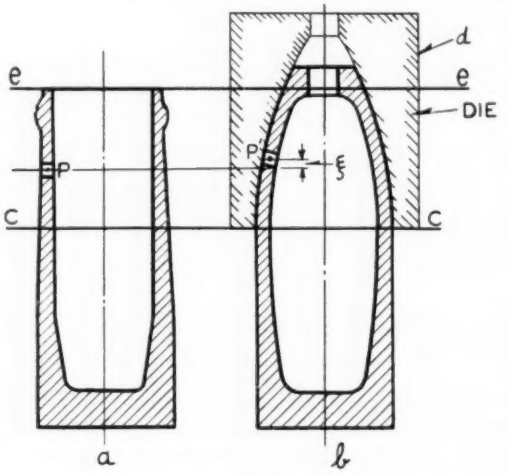


FIG. 1 NOSING A SHELL

nosing in a position P', in which P' has been displaced by a certain amount ξ in the axial direction. We shall not attempt to describe in a more complete way the fate of an element of material during its radial motion although some good means could be used for this purpose which are available through the recently improved theories of plastic flow. Expressions for the finite plastic strains, however, will be established. The true distribution of the plastic strains becomes somewhat more involved near the tip of the nose, and it should be noted that the permanent strains near the tip are of comparatively large magnitude for the more slender shapes of shells, where the reduction of length in a peripheral direction may reach compression values amounting to 50 per cent or even much more.

Near the bottom of the nose (the plane *cc* in Fig. 1) the strains remain quite small. When describing the mode of distortion in the nose of a shell, it should be noted furthermore that the straight lines perpendicular to the cylinder surface in the original state of the shell will be slightly distorted, but essentially they will be tilted during the forging process and remain straight lines perpendicular to the curved middle surface of the finished shell.[2] Such a motion in a shell, having a comparatively large wall thickness, should lead to bending strains and stresses. We will neglect these and the distortion within the shell walls resulting from the presence of the shearing stresses which transmit the friction forces in the contact area, because the bending strains are much smaller than the strains due to compression. A further remark must refer to the conditions at the bottom of the nose. In the computations to be given the elastic portions of the strains are entirely neglected for the same reasons and because they are only small fractions of the total strains. Consequently, it will not be possible to satisfy boundary conditions also at the bottom of the shell (in the plane *cc* Fig. 1) where the plastic portion borders the portion of the shell which remains cylindrical. Since these two portions are in integral connection, maintenance of "the continuity" of material should require that certain systems of forces and bending moments should act. These latter must deform slightly elastically both the curved and also the cylindrical portion of the shell. These stresses belong to the category of secondary stresses which are neglected.

[2] The axial-plane sections of actual shells which were investigated in other parts of this report by R. K. Carlson demonstrate this statement conclusively. Pins which were inserted in the shell before the nosing remained essentially straight after the forging.

NOMENCLATURE

The following nomenclature will be used:

- σ_t = normal stress in circumferential direction ("tangential" or "hoop" stress)
- σ_a = normal stress along meridian of shell ("meridian" stress)
- σ_r = radial stress
- p = pressure between die and shell, psi
- σ_0 = yield stress of metal for tension
- r = radial co-ordinate
- x = co-ordinate parallel to axis of shell
- h = wall thickness
- α' = angle of inclination of tangent to meridian curve of shell
- $\alpha = \frac{\pi}{2} + \alpha'$
- ds = arc element along meridian curve
- μ = coefficient of friction
- β = friction angle defined by $\mu = \tan \beta$
- r_t = radius of curvature in normal section of shell in perpendicular plane to plane of meridian
- r_a = radius of curvature in meridian plane containing axis of shell

For the middle surface of the curved portion of the shell, a surface of revolution is assumed. The external forces and the internal stresses and strains are assumed to act rotationally symmetrically around the axis AA of the shell, Fig. 2. A small element of a shell in two enlarged views is represented in Fig. 2. On this element six forces act. One pair of these forces consists of the resultant forces of the normal stresses σ_a acting along the

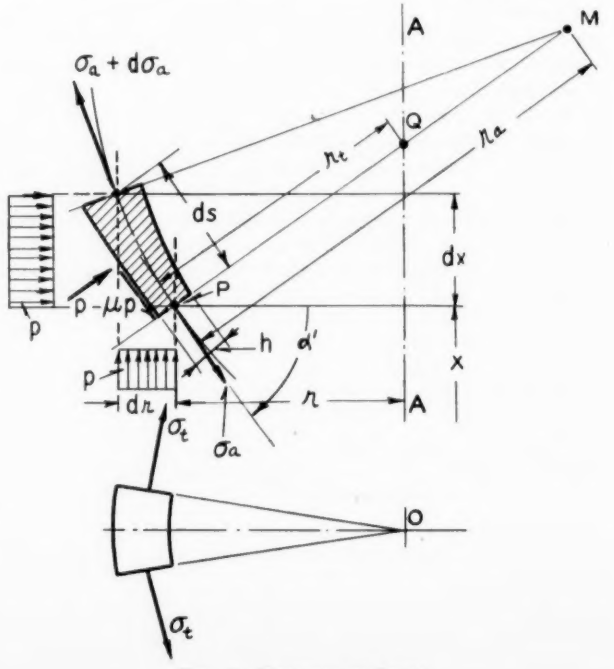


FIG. 2 ELEMENT OF SHELL

meridian curve and the other pair of the resultants in the circumferential directions of the hoop stresses σ_t. The forces in each pair are slightly inclined to each other due to the curvature of the middle surface of the shell nose. Furthermore, on the outer surface of the shell, act the distributed contact pressures p and the friction forces. These latter will be assumed to be equal to μp per unit of area. Assuming that the shell element, shown in Fig. 2, is moving in the upward direction relative to the die, these friction forces on the small shell element must act downward, as is indicated in the figure.

In the theory of thin shells[3] whose middle surface is a surface of revolution, two static equations are developed. The first one expresses the condition of equilibrium of the components of the forces in the direction of the axis of rotation and can usually be written in finite form. The second expresses the equilibrium of the components of the forces in the normal direction to the tangent plane for a small shell element, such as the one which was represented by Fig. 2.

Since in our present problem the normal pressure p of the shell is an unknown quantity, it will be well at this point to derive the first condition. Consider a ring of material which is obtained by rotating the shaded meridian section, represented in the front view of Fig. 2, around the axis AA. Neglecting first the friction forces, the following three components of forces in the axial direction of the shell must be considered in equilibrium

$$2\pi(\sigma_a + d\sigma_a)(h + dh)(r + dr) \sin(\alpha' + d\alpha') - 2\pi\sigma_a hr \sin\alpha' + \pi[(r + dr)^2 - r^2]p = 0 \quad [1]$$

The first term in this equation represents the resultant of the normal stresses σ_a in the axial direction in the upper ring section and the second term in the lower section of the ring. In the third term, the pressure p is multiplied by the projected area of the ring on a plane perpendicular to the axis of rotation. From Equation [1] therefore it follows that

$$pr + \frac{d}{dr}(\sigma_a hr \sin\alpha') = 0 \quad [2]$$

In this equation, we now wish to include the friction forces. For this purpose a term

$$-2\pi\mu pr \sin\alpha' ds$$

has to be added on the left side of Equation [1]. Since the projections of the arc element ds in the radial and axial directions are

$$dr = \cos\alpha' \cdot ds, \qquad dx = \sin\alpha' \cdot ds \quad [3]$$

and $dx/dr = \tan\alpha'$ we see that, in Equation [2], we have to add the term

$$-\mu pr \tan\alpha'$$

The first condition of the equilibrium of the components of the forces in the axial direction is therefore expressed by

$$\frac{d}{dr}(\sigma_a hr \sin\alpha') + pr(1 - \mu\tan\alpha') = 0 \quad [4]$$

if the friction forces are also to be included.

The second condition required for expressing the equilibrium of the forces in the normal direction to the tangent plane is furnished by the theory of thin curved shells

$$\frac{\sigma_a}{r_a} + \frac{\sigma_t}{r_t} = -\frac{p}{h} \quad [5]$$

[3] "Statik und Dynamik der Schalen," by W. Flügge," Berlin, J. Springer, 1934, p. 21.

In it r_a and r_t designate the radii of curvature PM and PQ of the curved middle surface of the shell, Fig. 2, in the meridian plane and in a plane perpendicular to the latter. Point Q is the point at which the normal at point P to the curved middle surface intersects the shell axis AA.

For determination of the three unknowns, σ_a, σ_t, and the contact pressure p, a third equation is required. This is the "condition of plasticity" of the flowing metal, according to which the octahedral shearing stress must be constant. If σ_1, σ_2, σ_3 are the principal stresses and σ_0 the yield stress in tension, it is expressed by

$$(\sigma_1 - \sigma_2)^2 + (\sigma_2 - \sigma_3)^2 + (\sigma_3 - \sigma_1)^2 = 2\sigma_0^2$$

In the case of a plastic shell which carries along its outer surface a distributed normal pressure p and whose inner surface is free, we can take

$$\sigma_1 = \sigma_t, \quad \sigma_2 = \sigma_a, \quad \sigma_3 = -\frac{p}{2}$$

The plasticity condition therefore is expressed by

$$\left(\sigma_t + \frac{p}{2}\right)^2 - \left(\sigma_t + \frac{p}{2}\right)\left(\sigma_a + \frac{p}{2}\right) + \left(\sigma_a + \frac{p}{2}\right)^2 = \sigma_0^2 \quad [6]$$

The three Equations [4], [5], and [6] are sufficient for determining the three unknown functions σ_a, σ_t, and p and solve the general problem of the plastic equilibrium of thin shells of rotational symmetry.

Although the profiles of actual artillery shells have a constant radius of curvature along their outer machined surface, and must not necessarily have a constant value of r_a along the middle surface if the wall thickness h tapers down, probably for most artillery shells one can assume that r_a = const. It is sufficient to discuss the case of shells whose mean meridian curve is obtained by rotating a circular arc around an axis. From a mechanical viewpoint, they are essentially special cases of the type of surface of revolution known as "torus," whose most common example is the inner tube of an automobile tire.

Two special cases of surfaces of revolution will be discussed in this paper. For the first, we select the cone. The exact solution for a perfectly plastic conical shell with uniform thickness is derived, which allows useful conclusions. The second case is the torus shell whose mean meridian curve is an arc of a circle. An exact solution for this case can also be obtained after a simplification is introduced in the plasticity condition by assuming that, in a plastic shell, essentially the circumferential stress remains constant or that in the shell $\sigma_t = -\sigma_0 = \text{const}$.

We note finally that, as soon as expressions for the pressures p and the stresses σ_a and σ_t have been found satisfying the equations mentioned, the total force P which is required for maintaining equilibrium with the internal stresses during nosing can easily be computed. All that is required for obtaining the total nosing resistance P is to compute the axial component of the resultant of the meridian stresses σ_a at the base of the nose. If $(\sigma_a)_{r_2}$ is the meridian stress, at the base of the nose, and if r_2 and h_2, respectively, are the radii and wall thickness at that point, then P is given by

$$P = 2\pi r_2 h_2 (\sigma_a)_{r = r_2} \quad [7]$$

assuming that the meridian curve of the profile of the shell has a vertical tangent for $r = r_2$ in the plane cc of Fig. 1.

A simplified theory of plastic shells, which are comparatively narrow bands of a thin body of revolution (conical, cylindrical shells, torus), can be based upon the following three equations

$$\frac{d}{dr}(hr \sin\alpha' \cdot \sigma_a) + (1 - \mu\tan\alpha')rp = 0 \quad [4a]$$

$$\frac{\sigma_a}{r_a} + \frac{\sigma_t}{r_t} = -\frac{p}{h} \quad \ldots\ldots [5a]$$

$$\sigma_a^2 - \sigma_a\sigma_t + \sigma_t^2 = \sigma_0^2 \quad \ldots\ldots [6a]$$

if the pressure p is neglected in the "plasticity condition," Equation [6]. In many applications, it is permissible to express this last condition of flow in the even simpler form

$$\sigma_t = -\sigma_0 = \text{const} \quad \ldots\ldots [6b]$$

Use of these equations is made in subsequent sections.

Conical Shells of Uniform Thickness in Plastic State

With reference to Fig. 3, introducing the angle of inclination of

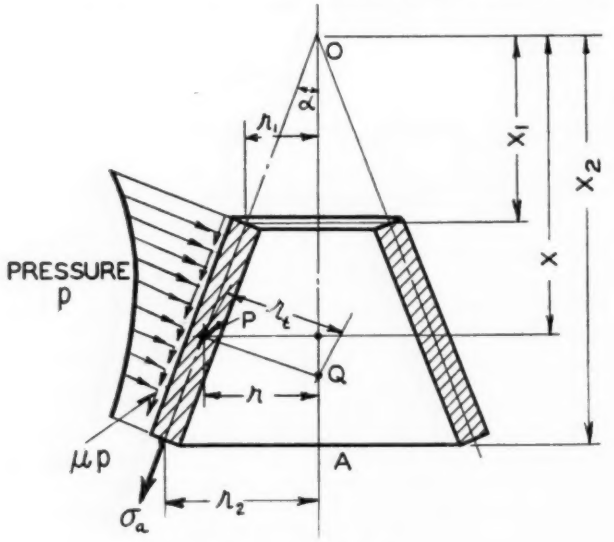


Fig. 3 Conical Shell

the cone α = angle POA we must take for the angle $\alpha' = \frac{\pi}{2} + \alpha$ in Equation [4]. The angle α is a constant in Equation [4]. This becomes

$$\frac{d}{dr}(\sigma_a hr \cos\alpha) + pr(1 + \mu \operatorname{cotan}\alpha) = 0$$

In this equation, we also take h = const, and replace the variable radius $r = x \tan\alpha$ by the independent variable x which measures the distance of a point P of the cone from the apex O. After solving for p we obtain for the pressure p the expression

$$p = -\frac{\cos\alpha}{(\mu + \tan\alpha)} \cdot \frac{h}{x} \cdot \frac{d}{dx}(x\sigma_a) \quad \ldots\ldots [8]$$

In the second equilibrium condition Equation [5], the first term vanishes since the radius of curvature of a straight meridian is $r_a = \infty$. The second radius of curvature for a conical shell is

$$r_t = \frac{r}{\cos\alpha} = \frac{\sin\alpha}{\cos^2\alpha} x$$

Equation [6] therefore condenses down to

$$p = -\frac{\cos^2\alpha}{\sin\alpha} \cdot \frac{h}{x} \cdot \sigma_t \quad \ldots\ldots [9]$$

furnishing a second independent expression for the pressure p.

In the plasticity condition Equation [6], we introduce a further simplification by neglecting the pressure p in it as is usually done in similar cases.[4] The third condition appears therefore in the form

$$\sigma_t^2 - \sigma_t\sigma_a + \sigma_a^2 = \sigma_0^2 \quad \ldots\ldots [10]$$

According to Equation [10], the hoop stresses σ_t in function of the meridian stresses σ_a satisfy an ellipse. Orientation of this "plasticity ellipse" is shown in Fig. 4. It passes through the

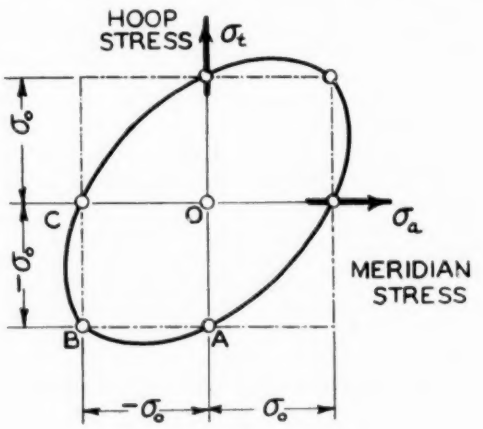


Fig. 4 Plasticity Ellipse

points 0, $\pm\sigma_0$; $\pm\sigma_0$, 0; $\sigma_t = \sigma_a = \pm\sigma_0$; the semiaxes of the ellipse are

$$\sqrt{2}\,\sigma_0, \quad \sqrt{\frac{2}{3}}\,\sigma_0$$

In the case of "drawing" of a shell, portions of the ellipse muse be considered in which at least the meridian stress σ_a is a tensilt stress and positive. With reference to our present application to the nosing of artillery shells, on the other hand, the shell is compressed by the heavy lateral pressures p and we need to consider the lower arc of this ellipse ABC, Fig. 4. In this quadrant of the σ_a, σ_t plane we will encounter both principal stresses σ_a and σ_t as negative quantities, i.e., as compression stresses.

After eliminating p from Equations [8] and [9] and after introducing for $\mu = \tan\beta$ and the abbreviation for a constant k

$$k = \frac{\tan\alpha}{\mu + \tan\alpha} = \frac{\tan\alpha}{\tan\beta + \tan\alpha} \quad \ldots\ldots [11]$$

we find that the two unknown stresses σ_a and σ_t must satisfy the following two equations in a plastic cone

$$k \cdot \frac{d}{dx}(x\sigma_a) - \sigma_t = 0 \quad \ldots\ldots [12]$$

$$\sigma_t^2 - \sigma_t\sigma_a + \sigma_a^2 = \sigma_0^2 \quad \ldots\ldots [13]$$

After eliminating from these equations, for example, σ_t, Equations [12] and [13] define a first-order differential equation for the stress σ_a. The solution can therefore contain only one integration constant and only one boundary condition can be satisfied. The conditions during nosing require that the stress $\sigma_a = 0$ at the tip of the nose. This is therefore the boundary condition which is to be satisfied. We note that the metal at the tip of the nose of a shell is merely compressed in the circumferential direc-

[4] The solution could be worked out also without the omission of p in Equation [8], but it seems unnecessary to go to these complications.

tion and must therefore expand in all perpendicular directions by equal amounts.

The set of Equations [12] and [13] is of a type which has previously been discussed by the author. Their solution is obtained by changing the independent variable x and after introducing a new dependent variable φ. We take for

$$u = \log_e \frac{x}{x_1} \quad \ldots\ldots\ldots\ldots\ldots\ldots [14]$$

and assume that the stresses σ_a and σ_t can be expressed in the form

$$\sigma_a = -\frac{2\sigma_0}{\sqrt{3}} \sin(\varphi + \varphi_0) \quad \ldots\ldots\ldots\ldots [15]$$

$$\sigma_t = \frac{2\sigma_0}{\sqrt{3}} \sin\left(\varphi + \varphi_0 + \frac{2\pi}{3}\right) \quad \ldots\ldots\ldots [16]$$

Making use of these two new variables u and φ, we note that Equation [13] is identically satisfied and that, after the expressions for the stresses σ_a and σ_t are substituted in Equation [12], a differential equation for φ is obtained

$$\frac{d\varphi}{du} = \frac{c_0 \sin\varphi}{k \cos(\varphi + \varphi_0)} \quad \ldots\ldots\ldots\ldots\ldots [17]$$

which can be integrated. The solution is

$$\cos\varphi_0 \cdot \log \sin\varphi - \sin\varphi_0 \cdot \varphi = \frac{c_0 u}{k} + c \quad \ldots\ldots\ldots [18]$$

In it the two constants φ_0 and c_0 are defined by

$$\tan\left(\varphi_0 - \frac{\pi}{3}\right) = \frac{\sqrt{3}k}{2-k}, \qquad c_0 = \sqrt{k^2 - k + 1} \quad \ldots\ldots [19]$$

At the tip of the conical shell for $x = x_1$, $u = 0$ and $\sigma_a = 0$. This boundary condition is satisfied if in the expression for σ_a Equation [15] $\sin(\varphi + \varphi_0) = 0$. Since φ cannot become negative on account of the logarithm appearing in Equation [18], we cannot make $\varphi = -\varphi_0$ but have to take for $u = 0$; $\varphi = \pi - \varphi_0$ at the tip of the shell. With this condition, the integration constant c in Equation [18] is determined, and finally for the variable u the equation

$$u = \frac{k}{c_0}\left[(\pi - \varphi_0 - \varphi)\sin\varphi + \cos\varphi_0 \cdot \log_e\left(\frac{\sin\varphi}{\sin\varphi_0}\right)\right] \quad [20]$$

is obtained. Equations [15], [16], and [20] express the distribution of the stresses σ_a and σ_t in conical shells. By choosing a few values for φ, the corresponding co-ordinates $x = x_1 e^u$ can be computed from Equation [20], and the stresses σ_a and σ_t from Equations [15] and [16].

After substituting for $u = \log_e(x/x_1)$ in Equation [20] and after joining the two terms containing the logarithms, Equation [20] can also be rewritten in a form in which it is solved for the co-ordinate x (or for the radius $r = r_1 \frac{x}{x_1} = x \tan\alpha$)

$$\frac{x}{x_1} = \frac{r}{r_1} = \left[\frac{\sin\varphi}{\sin\varphi_0}\right]^{\frac{k}{c_0}} \cdot e^{\frac{k}{c_0}[\pi - \sin\varphi_0 \cdot (\varphi_0 - \varphi)]} \quad \ldots [20a]$$

The total resultant force for nosing the portion $r_1 < r < r_2$ of a conical shell is given by

$$P = 2\pi r_2 h\,[\sigma_a]_{r_2} \cdot \cos\alpha \quad \ldots\ldots\ldots\ldots [21]$$

where σ_a is to be computed for that value of φ for which in Equation [20] $u = \log_e(r_2/r_1)$.

When the constant k given by Equation [11] varies between the limits $0 < k < 1$ the angle φ_0 defined by Equation [19] varies between

$\frac{\pi}{3} < \varphi_0 < \frac{2\pi}{3}$. The variable φ varies between $0 < \varphi < \pi - \varphi_0$.

The variation of the constant k (which was introduced in Equation [11]) with the cone angle α and with the friction coefficient μ has been indicated in Fig. 5. A further curve in Fig. 5

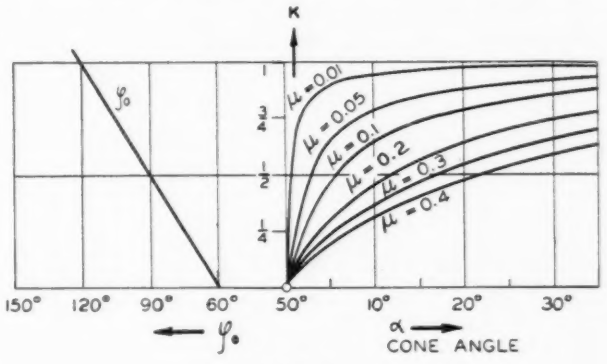


FIG. 5

shows also the values of the constant angle φ_0 appearing in several of the equations.

In the differential Equation [17], the term $\cos(\varphi + \varphi_0)$ appears in the denominator on the right side. Since the interval for φ is usually limited by the values zero and $\pi - \varphi_0$, we must note that when $\cos(\varphi + \varphi_0) = 0$ or when $\varphi = \frac{\pi}{2} - \varphi_0$, $d\varphi/du = \infty$. This condition may or may not occur in the applications. It may occur if $\varphi_0 < \pi/2$ and since always $\varphi_0 > \pi/3$ it may occur if the constant angle φ_0 which was defined by Equation [19] has values $\frac{\pi}{3} < \varphi_0 < \frac{\pi}{2}$.

As an illustration for such an occurrence an example has been

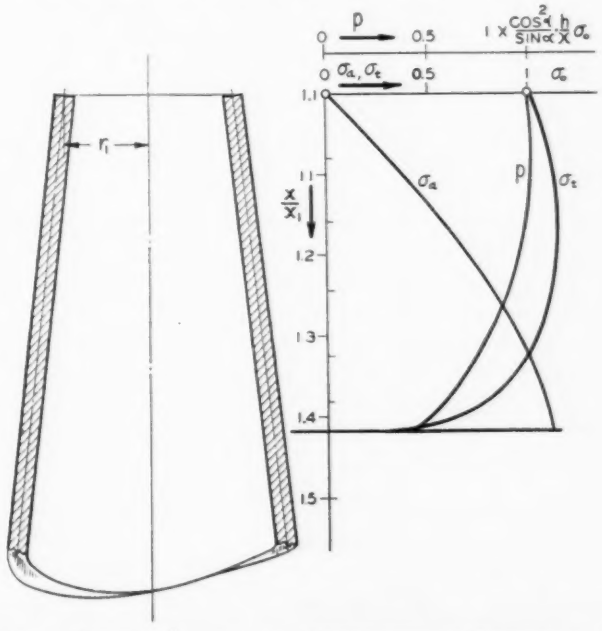


FIG. 6 PRESSURES, AXIAL AND CIRCUMFERENTIAL STRESSES IN A CONICAL SHELL

worked out numerically by choosing for the angle $\varphi_0 = 75$ deg $= 5\pi/12$. The corresponding values of the constants are $k = 0.2680$, $c_0 = 0.897$, $\cos \varphi_0 = 0.2588$, and $\sin \varphi_0 = 0.9659$. The distribution of the stresses σ_a and σ_t and of the pressure p for this case is shown in Fig. 6. It is interesting to note that the curve for the tangential stress σ_t ends abruptly with a vertical tangent at the value of the co-ordinate $x = 1.421$. The conical shell cannot extend beyond this value of x at which the meridian stress σ_a just reaches its maximum value

$$\sigma_a = -2\sigma_0/\sqrt{3} = -1.155\sigma_0$$

Special Conical Shells of Uniform Thickness

There are a few interesting special cases of flow in conical shells which should be considered by assuming for the constant k, defined by Equation [11], special values.

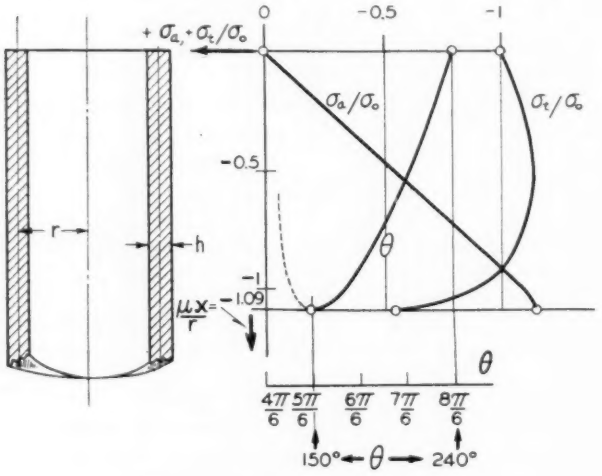


Fig. 7 Stresses in a Cylinder

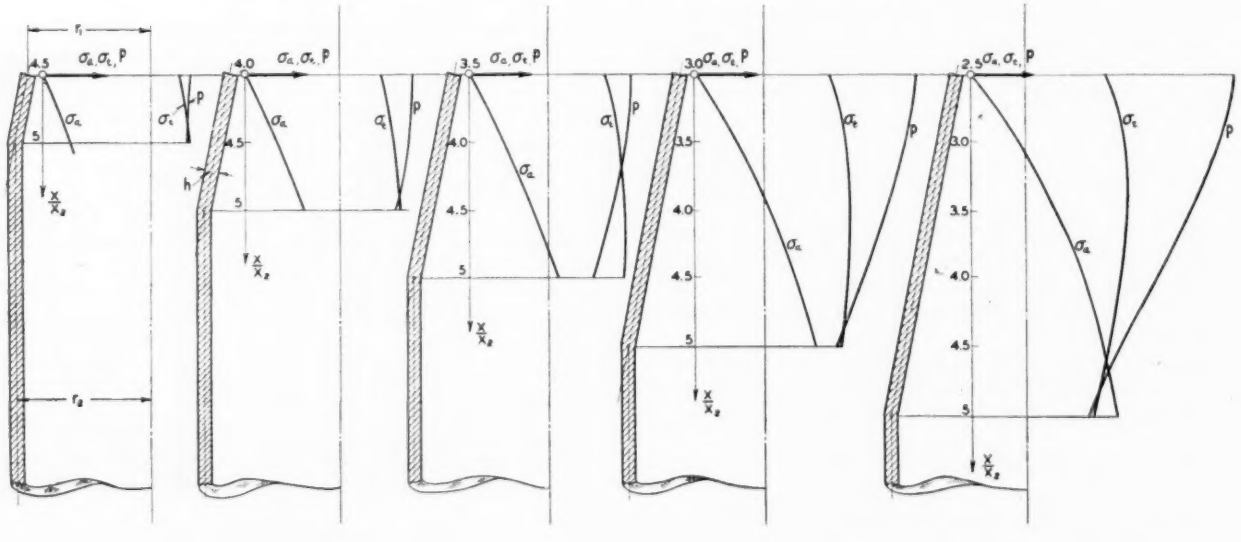
(*a*) *Cylindrical Shells.* If $k = 0$ we have $\varphi_0 = \pi/3$. In this case $\alpha = 0$. This corresponds to a cylindrical shell, for example a short tube, or a bushing which is being pushed forward under axial compression forces into a tightly fitting die. An example for a stress distribution of this kind is shown in Fig. 7 in which the ordinates represent $\mu x/r$ or the distances x measured from the free (upper) end of the cylinder (μ friction coefficient, r mean radius of cylinder) and the abscissas the ratios σ_a/σ_0 and σ_t/σ_0. Both stress components σ_a and σ_t are negative and represent compression stresses. The pressure p in the case of a cylinder is $p = -h\sigma_t/r$ proportional to the circumferential stress σ_t and has for this reason not been represented by an additional curve.

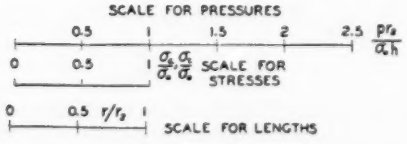
This plastic equilibrium shows a peculiarity of the solution. The plastic field has a natural boundary beyond which the solution does not exist. It is marked in Fig. 7, by the value $\mu x/r = 1.09$ at which the curve for the circumferential stress has a horizontal tangent and at which the axial stress σ_a reaches its maximum[5] value $2\sigma_0/\sqrt{3}$.

Cases of this kind in cylinders have important further practical applications for predicting the stresses in the portions of thick-walled tubes which are worked under heavy pressures during drawing or in similar forming operations when the stresses in the axial direction are of a tensile nature. Such cases cannot be treated in this report.

(*b*) *Special Case When* $\alpha = \beta$. If the friction angle β defined by $\mu = \tan \beta$ is equal to the angle α of the cone, the constant k becomes equal to $k = 1/2$. In this case $\varphi_0 = \pi/2$, $\cos \varphi_0 = 0$, and the factor before the logarithmic term in Equation [20] vanishes.

[5] In Fig. 7, a third curve was traced which carries the designation θ. It represents a certain parameter θ analogous to the variable φ which was used for expressing the solution. The curve representing θ in function of the distances x has also a horizontal tangent for $\mu x/r = 1.09$, and a continuation of it is shown by a dotted line. Thus $\theta = f(x)$ is not a single-valued function of x. These details are mentioned because they are important when the range of the different variables has to be considered and errors can easily result by overlooking some of these details.





Figs. 8–12 Pressures, Axial and Circumferential Stresses in Conical Shells in the Plastic State; ($\mu = \tan \alpha = 0.2$)

This simplifies considerably the computation since, in this case, u is given by

$$u = \frac{1}{\sqrt{3}}\left(\frac{\pi}{2} - \varphi\right) \quad \ldots\ldots\ldots\ldots\ldots\ldots [22]$$

The distribution of the stresses for a conical shell satisfying this condition ($\alpha = \beta$) is expressed in the simple form

$$x = x_1 e^{\frac{1}{\sqrt{3}}\left(\frac{\pi}{2} - \varphi\right)}, \quad \sigma_a = -\frac{2\sigma_0}{\sqrt{3}}\cos\varphi,$$

$$\sigma_t = -\frac{2\sigma_0}{\sqrt{3}}\sin\left(\frac{\pi}{6} + \varphi\right) \ldots [23]$$

valid for $0 < \varphi < \pi/2$.

A series of five conical shell noses has been considered as an example under this assumption, having the same angle $\alpha = 11°32' = \beta$ corresponding to a friction coefficient of $\mu = 0.2$ and the same outside radius r_2. The distributions of the stresses σ_a and σ_t and of the pressures p are shown in Figs. 8 to 12, for the five reductions of the mean radii at the tip of the nose, given in Table 1.

TABLE 1 CONICAL PLASTIC SHELL

Case $\alpha = \beta = 11° 32'$

Reduction of radii at tip of nose, per cent	$\frac{r_1}{r_2} =$	Meridian stress at base of nose	Maximum pressure at tip of conical shell	Nosing force
10	0.9	$\sigma_a = -0.209\sigma_0$	$p = 1.09\sigma_0 h/r_2$	$P = 1.29\sigma_0 h r_2$
20	0.8	$-0.434\sigma_0$	$1.23\sigma_0 h/r_2$	$2.67\sigma_0 h r_2$
30	0.7	$-0.668\sigma_0$	$1.40\sigma_0 h/r_2$	$4.11\sigma_0 h r_2$
40	0.6	$-0.894\sigma_0$	$1.63\sigma_0 h/r_2$	$5.50\sigma_0 h r_2$
50	0.5	$-1.076\sigma_0$	$1.96\sigma_0 h/r_2$	$6.62\sigma_0 h r_2$

In the last column of Table 1, the nosing force is shown which was computed from the formula

$$P = 2\pi r_2 h \cos\alpha \cdot (\sigma_a)_{r=r_2} \ldots\ldots\ldots\ldots\ldots [24]$$

using the values of the meridian stress σ_a at the bottom of the nose ($r = r_2$) which appear in one of the previous columns. (σ_0 is the yield stress.)

It is instructive to note from the curves in Figs. 8 to 12, and data in Table 1, how the pressures p required for nosing increase with the reduction of the radii at the tip of the shell. The meridian stresses σ_a increase toward the base of the nose the longer the conical shells become, while the circumferential stresses remain practically constant over the entire length of the shell nose.

(c) *Vanishing Friction Forces.* A third special case of interest occurs when $\mu = 0$ when the friction is negligible (corresponding to the value of $k = 1$ and to $\varphi_0 = 2\pi/3$). Equation [20] simplifies somewhat to

$$u = \frac{\sqrt{3}}{2}\left(\frac{\pi}{3} - \varphi\right) - \frac{1}{2}\log_e\left(\frac{2\sin\varphi}{\sqrt{3}}\right) \ldots\ldots [25]$$

while the stresses σ_a and σ_t and the pressure p are now to be computed from the formulas

$$\sigma_a = -\frac{2\sigma_0}{\sqrt{3}}\sin\left(\frac{2\pi}{3} + \varphi\right), \quad \sigma_t = \frac{2\sigma_0}{\sqrt{3}}\sin\left(\frac{\pi}{3} + \varphi\right),$$

$$p = -\frac{\cos^2\alpha}{\sin\alpha}\cdot\frac{h}{x}\cdot\sigma_t \ldots\ldots\ldots\ldots\ldots [26]$$

Equations [25] and [26] have the peculiarity that the expressions for the variable $u = \log(x/x_1)$ and for the stresses σ_a and σ_t do not depend upon the angle α of the cone. In Fig. 13, the

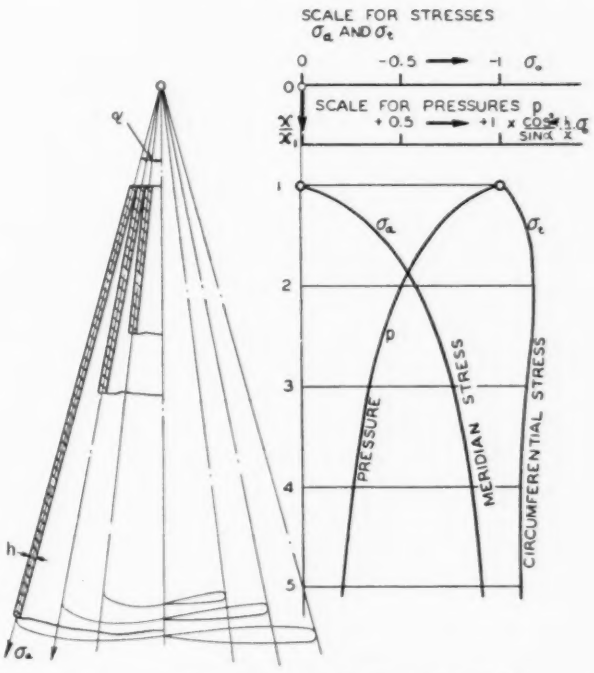


FIG. 13 PERFECTLY PLASTIC CONICAL SHELLS OF EQUAL THICKNESS; ($\mu = 0$, h = CONST)

stresses σ_a and σ_t and the pressures p have been plotted for this state of perfectly plastic conical shells. This set of curves for σ_a, σ_t, p can be used for any angle of inclination α of the cone. Referring to the curve representing the distribution of the pressures p the ordinates represented in Fig. 13 should be multiplied with a dimensional factor equal to

$$\frac{\cos^2\alpha}{\sin\alpha}\cdot\frac{h}{x_1}\cdot\sigma_0$$

The following two limiting cases of circular conical shells are included in these expressions (Equations [25] and [26]):

1 *Cylinder:*

When $\alpha = 0$ the conical shell becomes a circular cylinder. The angle φ loses its significance, but if it is taken equal to $\varphi = \pi/3$ Equation [25] is identically satisfied since $\sin\varphi = \sqrt{3}/2$. The expressions for σ_a and σ_t Equations [26] give

$$\left.\begin{aligned}\sigma_a &= -\frac{2\sigma_0}{\sqrt{3}}\sin\left(\frac{2\pi}{3} + \frac{\pi}{3}\right) = 0\\ \sigma_t &= -\frac{2\sigma_0}{\sqrt{3}}\sin\left(\frac{\pi}{3} + \frac{\pi}{3}\right) = -\sigma_0\end{aligned}\right\} \ldots\ldots [27]$$

when $\alpha = 0$ the factor $\cos\alpha/x_1 \sin\alpha = r_1$ becomes equal to the constant radius r_1 of the cylinder in the expression for the pressure p, Equation [26], and since $\cos\alpha = 1$ for the pressure p

$$p = -\frac{h\sigma_t}{r_1} = \frac{h\sigma_0}{r_1} \ldots\ldots\ldots\ldots\ldots [28]$$

the elementary formula of a cylinder under external pressure is obtained.

2 *Plane Disk:*

When, on the other hand, $\alpha = \pi/2$ the conical shell degenerates into a plane disk of equal thickness. Since $\cos\alpha = \cos\pi/2 = 0$ the pressure $p = 0$, the special case of a pure radial flow in a thin plane disk having a circular hole is obtained, which is stressed in

its plane by a uniform compression stress $\sigma_a = -\sigma_0$ at large distances from the center of the disk. This case of flow in a thin disk has been treated by the author on several occasions. For this special case of an infinite disk having a central hole of the radius a which is yielding under the action of a uniform compression stress, the following formulas were previously derived

$$\frac{r^2}{a^2} = -\frac{\sqrt{3}}{2} \cdot \frac{e^{\sqrt{3}\left(\psi - \frac{7\pi}{6}\right)}}{\cos \psi} \quad \ldots\ldots [29]$$

$$\left.\begin{aligned} \text{radial stress} \quad \sigma_r &= \frac{2\sigma_0}{\sqrt{3}} \sin\left(\psi - \frac{\pi}{6}\right) \\ \text{tangential stress} \quad \sigma_t &= \frac{2\sigma_0}{\sqrt{3}} \sin\left(\psi + \frac{\pi}{6}\right) \end{aligned}\right\} \quad \ldots\ldots [30]$$

$$\frac{7\pi}{6} < x < \frac{3\pi}{2} \quad \ldots\ldots [31]$$

Verification:

Simple considerations show that if the variable parameter φ for conical shells is taken equal to

$$\varphi = \frac{3\pi}{2} - \psi \quad \ldots\ldots [32]$$

Equation [25] transforms into

$$2 \log \frac{r}{a} = \sqrt{3}\left(\frac{\pi}{3} - \varphi\right) - \log\left[\frac{2 \sin \varphi}{\sqrt{3}}\right]$$
$$= \sqrt{3}\left(\psi - \frac{7\pi}{6}\right) - \log\left[\frac{2}{\sqrt{3}}(-\cos \psi)\right] \quad \ldots\ldots [33]$$

which indeed is obtained from Equation [29] by taking the logarithms on both sides of Equation [29]. Equations [26] similarly transform when Equation [32] is introduced into the formulas for the stresses σ_a and σ_t Equation [30] of the plane disk. Therefore our formulas for the plastic states of conical shells, when they are applied to the two special extreme cases of the circular cylinder or the plane disk, lead to the correct expressions which were previously obtained for these simpler cases of flow.

(*d*) *Uniformly Compressed Conical Shells When* $\mu = 0$. A further simple plastic state of stress in a conical shell should be mentioned which is obtained after assuming uniform stresses throughout the whole shell

$$\sigma_a = \sigma_t = -\sigma_0 = \text{const} \quad \ldots\ldots [34]$$

From Equation [9], we note that the pressure p required for the equilibrium of such a shell is equal to

$$p = \frac{\cos^2 \alpha}{\sin \alpha} \cdot \frac{h}{x} \sigma_0 = \cos \alpha \cdot \frac{h\sigma_0}{r} \quad \ldots\ldots [35]$$

p decreases according to a hyperbolic function of the axial distances x or the radii r of the shell.

Simplified and Abbreviated Theory of Plastic Cones

The previous examples which have been discussed in detail demonstrate conclusively that, in a conical shell in the plastic state, the circumferential stress σ_t very nearly remains constant. This is particularly true in shorter shells. Based on these observations it will therefore be permissible to introduce the assumption that $\sigma_t = -\sigma_0 = \text{const}$, throughout the whole shell. This amounts to assuming that instead of the plasticity condition in its general form, given by Equation [10], a flow condition

$$\sigma_t = -\sigma_0 \quad \ldots\ldots [36]$$

holds. In other words this amounts to substituting a horizontal line for the arc of "the plasticity ellipse" in Fig. 4 along which the required values of σ_a and σ_t lie. This is equivalent also to postulating that "the maximum-shear theory" expresses the condition of flow.

Under this assumption, from Equation [12], follows

$$\frac{d}{dx}(x\sigma_a) = -\frac{\sigma_0}{k} = \text{const} \quad \ldots\ldots [37]$$

or with the condition $x = x_1$, $\sigma_a = 0$ (at the tip of the conical nose) we obtain

$$\sigma_a = -\frac{\sigma_0}{k}\left(1 - \frac{x_1}{x}\right) \quad \ldots\ldots [38]$$

The pressure p is found from Equation [9] equal to

$$p = \frac{\cos^2 \alpha}{\sin \alpha} \cdot \frac{h}{x} \cdot \sigma_0 = \frac{\cos \alpha \cdot h\sigma_0}{r} \quad \ldots\ldots [39]$$

It should be emphasized that none of these equations should be used beyond those values of x which will make

$$|\sigma_a| > 2\sigma_0/\sqrt{3}$$

The total axial resultant force for deforming the shell is now expressed by the approximate formula

$$P = \frac{2\pi r_2 h\sigma_0\left(1 - \frac{r_1}{r_2}\right)\cos \alpha}{k} \quad \ldots\ldots [39a]$$

in which r_1 and r_2 are the mean radii of the conical shell at the tip and bottom of the shell, k is the constant given by Equation [11], h, the wall thickness, and σ_0, the yield stress for compression.

Standard Shell Nose

We assume that the shell nose is a portion of a torus shell of constant thickness, or of a body of revolution which is obtained

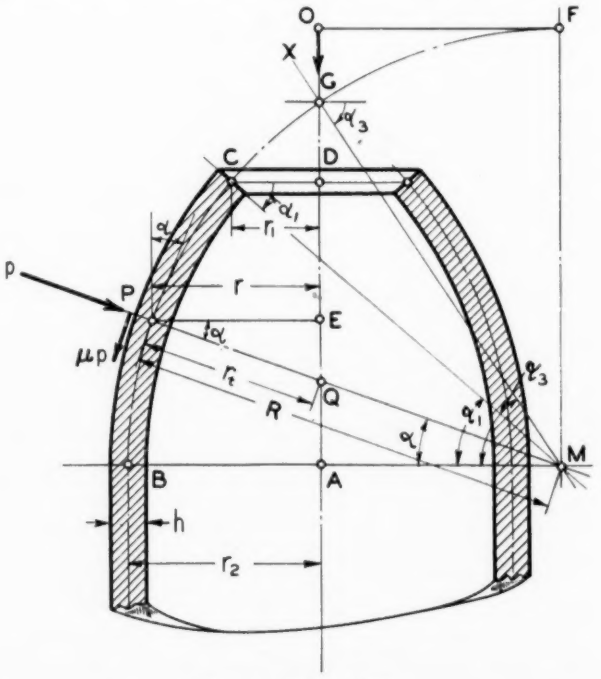


Fig. 14 Shell Nose

by rotating around an axis the area of a ring of constant thickness bounded by two concentric circles, Fig. 14. We designate by R the radius of the mean meridian circle of the shell nose and introduce rectangular co-ordinates x and r of a point P of the meridian circle. $x = OE$ is measured from the origin O downward (Fig. 14), $r = EP$ from the axis of the shell. The origin O is assumed in the distance $AO = R$ above the base of the nose (above the base plane MAB in Fig. 14). The wall thickness h is constant. The tip of the shell has the co-ordinates x_1 and r_1, the bottom, the co-ordinates x_2 and r_2. Using the angle of inclination α of the tangent to the mean meridian circle in point P, we have for

$$\left.\begin{aligned} x &= R(1 - \sin\alpha) \\ r &= r_2 - R(1 - \cos\alpha) \end{aligned}\right\} \quad \ldots\ldots\ldots\ldots [40]$$

Referring to Equation [4], expressing the first equilibrium condition of the shell, we note that the angle α' which was introduced in Fig. 2 is the complement of the angle α introduced in Fig. 14, or that $\alpha' = \frac{\pi}{2} - \alpha$. Since the direction of the friction force in Fig. 14 appears in the opposite sense relatively to the origin O from that in the sketch showing a shell element in Fig. 2, the sign before the term containing μ in Equation [4] has to be reversed and Equation [4] now takes the form

$$\frac{d}{dr}(hr\,\sigma_a \cos\alpha) + pr[1 + \mu \operatorname{cotan}\alpha] = 0 \quad \ldots\ldots [41]$$

In this equation we have to introduce from the geometric relations Equations [40] $dr = -R \sin\alpha\, d\alpha$ and the friction angle β. This gives

$$\frac{d}{d\alpha}(hr\,\sigma_a \cos\alpha) - \frac{Rr \sin(\alpha + \beta)}{\cos\beta} p = 0 \quad \ldots\ldots [42]$$

or after solving this for p

$$p = \frac{\cos\beta \cdot \dfrac{d}{d\alpha}(hr\,\sigma_a \cos\alpha)}{Rr \sin(\alpha + \beta)} \quad \ldots\ldots [43]$$

A second expression for p is taken from Equation [6], after noting that the radius of curvature r_a of the meridian curve or PM is now $r_a = R = \text{const}$, since the meridian is an arc of a circle drawn around point M as center in Fig. 14. For the same reason, the second radius of curvature $r_t = PQ$ of the shell is given by $r_t = r/\cos\alpha$. Equation [6] therefore takes the form

$$p = -\frac{h}{R}\left(\sigma_a + \frac{R \cos\alpha}{r} \cdot \sigma_t\right) \quad \ldots\ldots [44]$$

The last condition to be satisfied in a plastic shell is assumed

$$\sigma_t = -\sigma_0 = \text{const} \quad \ldots\ldots [45]$$

which must be substituted for the plasticity condition Equations [8] or [11].

Combining Equation [44] with Equation [43], assuming also that $h = \text{const}$, the following differential equation for the unknown meridian stress σ_a is obtained

$$\cos\beta \cdot \frac{d}{d\alpha}\left(\frac{r\sigma_a}{R}\cos\alpha\right) + \sin(\alpha + \beta)\cdot\left(\frac{r\sigma_a}{R} - \sigma_0 \cos\alpha\right) = 0 \ldots [46]$$

After introducing a new dependent variable

$$\sigma = \frac{r\sigma_a}{R} \quad \ldots\ldots [47]$$

and after rearrangement of terms, this differential equation takes the form

$$\frac{d\sigma}{d\alpha} + \tan\beta \cdot \sigma - \frac{\sin(\alpha + \beta)}{\cos\beta}\sigma_0 = 0 \quad \ldots\ldots [48]$$

in which β (the friction angle) and σ_0 are given constants. Equation [48] has the complete integral

$$\sigma = ce^{-\mu\alpha} - \sigma_0 \cos(\alpha + 2\beta) \quad \ldots\ldots [49]$$

where $\mu = \tan\beta$ and c is an integration constant.

The boundary condition to be satisfied is that at the tip of the shell nose for $\alpha = \alpha_1$ the stress $\sigma_a = 0$. Therefore, for $\alpha = \alpha_1$, $\sigma = 0$. This determines the integration constant

$$c = \sigma_0 e^{\mu\alpha_1} \cos(\alpha_1 + 2\beta)$$

and for σ

$$\sigma = \frac{r\sigma_a}{R} = \sigma_0\left\{[\cos(\alpha + 2\beta) - e^{(\alpha_1 - \alpha)}\cos(\alpha_1 + 2\beta)]\right\} \ldots [50]$$

is obtained. The meridian stress in the shell is therefore equal to

$$\sigma_a = -\frac{R\sigma_0}{r}[\cos(\alpha + 2\beta) - e^{\mu(\alpha_1 - \alpha)}\cos(\alpha_1 + 2\beta)] \ldots [51]$$

The circumferential stress is

$$\sigma_t = -\sigma_0 = \text{const} \quad \ldots\ldots [52]$$

and the pressure p in the contact area between shell nose and the die is found equal to

$$p = \frac{h\sigma_0}{r}\left\{\cos\alpha + \cos(\alpha + 2\beta) - e^{\mu(\alpha_1 - \alpha)}\cos(\alpha_1 + 2\beta)\right\} \quad \ldots\ldots [53]$$

The variable radius r appearing in Equations [51] and [53] is given by Equation [40], or by the expression

$$r = r_2 - R(1 - \cos\alpha) \quad \ldots\ldots [54]$$

The meridian stress σ_a reaches its maximum value at the bottom of the shell nose for $\alpha = 0$, where also $r = r_2$ so that we find

$$\sigma_{a\,\max} = -\frac{R\sigma_0}{r_2}[\cos 2\beta - e^{\mu\alpha_1}\cos(\alpha_1 + 2\beta)] \ldots [55]$$

while the total nosing force is found equal to

$$P = 2\pi r_2 h|\sigma_{a\max}| = 2\pi Rh\sigma_0[\cos 2\beta - e^{\mu\alpha_1}\cos(\alpha_1 + 2\beta)] \ldots [56]$$

Nosing forces P expressed by Equation [56] have been plotted as a function of the friction angles β in Fig. 15, for three angles of inclination $\alpha_1 = 5$ deg, 10 deg, and 15 deg at the tip of the nose. Along the abscissa axis, a second scale has been shown on which the corresponding values of the friction coefficients μ have been indicated. The figures shown along the ordinate axis have to be multiplied by the factor $2\pi Rh\sigma_0$ ($\pi = 3.14$, R mean radius of meridian, h wall thickness, σ_0 yield stress).

In practical nosing, a disturbance sometimes occurs which has been reported from various shell-forging plants. The wall thickness at the base of the nose is found sometimes to have increased. This local swelling of the wall thickness can also occur in the curved portion of the nose. Although there might be different reasons which cause the local bulging, and in some cases it may have been confused with local collapse of the wall due to plastic buckling, one important cause for it should be mentioned, namely, probably excessive friction. More precisely a condition must be

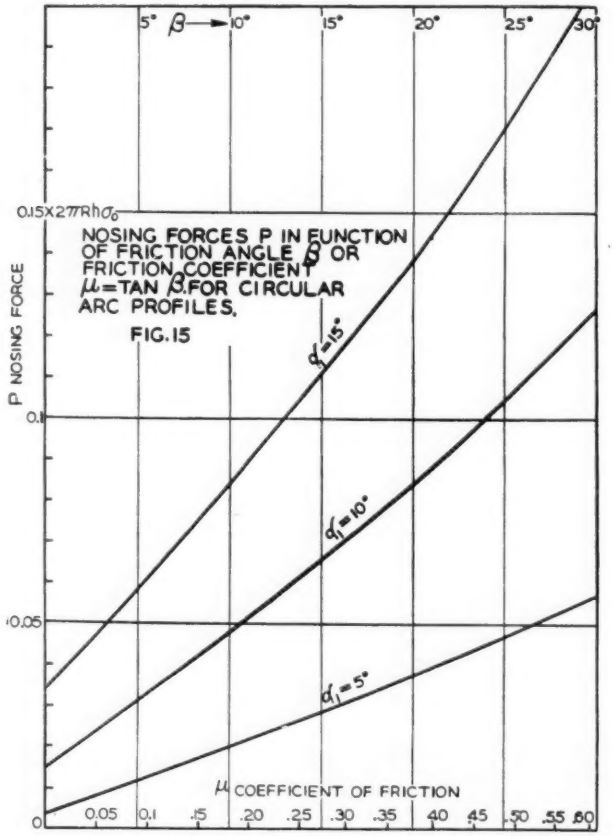


FIG. 15

satisfied during the nosing operation. It is not desirable that the meridian stress σ_a at the bottom of the nose for $\alpha = 0$ should reach the yield value for pure compression because this would have the consequence that the cylindrical portions of the shell adjoining the nose would also yield.

The condition which must be imposed on the nosing to avoid local bulging or swelling of the wall at the base of the nose is, therefore, expressed by

$$\alpha = 0, \; |\sigma_{a\max}| < \sigma_0 \quad \ldots\ldots\ldots\ldots\ldots\ldots [57]$$

or by

$$R[\cos 2\beta - e^{\mu\alpha_1} \cos(\alpha_1 + 2\beta)] \geqq r_2 \quad \ldots\ldots\ldots\ldots [58]$$

If the angle α_3 is introduced which refers to the point G in which the extension of the meridian circle intersects the axis of the shell, Fig. 14, we can write for

$$r_2 = R(1 - \cos\alpha_3)$$

and condition Equation [58] can also be expressed as follows

$$\cos\alpha_3 + \cos 2\beta - e^{\mu\alpha_1} \cos(\alpha_1 + 2\beta) \geqq 1 \quad \ldots\ldots\ldots\ldots [59]$$

If this inequality is satisfied no local swelling of the shell wall should occur at the base of the shell nose. For a given shell profile α_1 and α_3 are given angles; inequality [59] therefore imposes a condition on the friction.

Summing up the foregoing remarks, we can state that two independent causes must be quoted which limit the use of our equations for nosing. The first is that the condition of flow expressed by Equation [45] is good only when $|\sigma_a| < \sigma_0$; the second is that local swelling at the base of the nose should not occur. This condition is expressed by the same inequality, namely, $|\sigma_a| < \sigma_0$ at the base of the nose, or its equivalent inequality [59].

When $\mu = 0$, ($\beta = 0$) or when the friction is neglected Equations [51] and [53] take the simple form

$$\left.\begin{aligned} \sigma_a &= -\frac{R\sigma_0}{r}(\cos\alpha - \cos\alpha_1), \; \sigma_t = -\sigma_0 \\ p &= \frac{h\sigma_0}{r}(2\cos\alpha - \cos\alpha_1) \end{aligned}\right\} \quad \ldots\ldots\ldots [60]$$

If we again make use of the angle α_3 in expressing r_2 by

$$r_2 = R(1 - \cos\alpha_3)$$

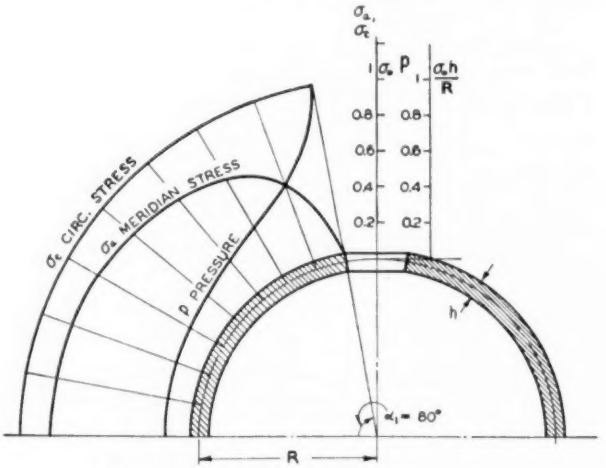


FIG. 16 STRESSES IN A SPHERICAL SHELL

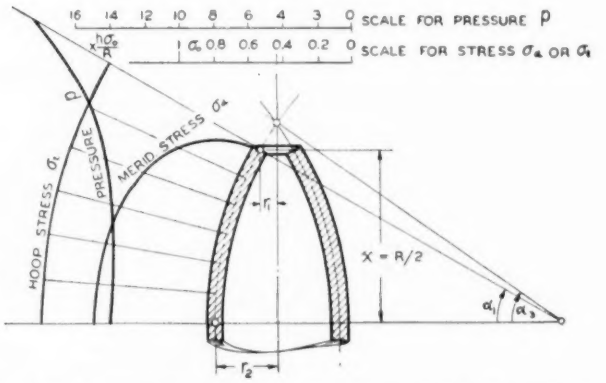


FIG. 17 PRESSURES, AXIAL AND CIRCUMFERENTIAL STRESSES IN STANDARD SHELL NOSE; ($\mu = 0$)

and the variable radius by

$$r = r_2 - R(1 - \cos\alpha) = R(\cos\alpha - \cos\alpha_3)$$

these formulas can be rewritten as follows

$$\left.\begin{aligned} &\text{meridian stress } \sigma_a = -\sigma_0 \cdot \frac{(\cos\alpha - \cos\alpha_1)}{(\cos\alpha - \cos\alpha_3)}; \; \sigma_t = -\sigma_0 \\ &\text{pressure} \qquad p = \frac{h\sigma_0}{R} \cdot \frac{(2\cos\alpha - \cos\alpha_1)}{(\cos\alpha - \cos\alpha_3)} \end{aligned}\right\} \quad \ldots [61]$$

expressing the state of stress in a plastic shell of circular profile when $\mu = 0$.

A special case of these latter equations refers to a hemisphere having a hole. We obtain after taking $\alpha_3 = \pi/2$

$$\sigma_a = -\sigma_0\left(1 - \frac{\cos\alpha_1}{\cos\alpha}\right),\quad \sigma_t = \sigma_0,\ p = \frac{h\sigma_0}{R}\left(2 - \frac{\cos\alpha_1}{\cos\alpha}\right) \ldots [62]$$

An example for a distribution of stresses in a hemisphere is shown in Fig. 16. The angle α_1 was assumed $\alpha_1 = 80$ deg. The pressure p shows a sharp rise near the edge of the comparatively small hole. From the last set of equations proceeding now to the limiting case of an infinitely small hole by assuming also that $\alpha_1 = \pi/2$ we note that they condense down to

$$\sigma_a = \sigma_t = -\sigma_0, \quad p = 2h\sigma_0/R \ldots [63]$$

or to the formulas for the elementary case of a spherical shell stressed by a uniform pressure p.

In a last example, a rather slender shell nose of this kind has been considered. For the angle of inclination at the tip of the nose $\alpha_1 = 30$ deg and $\alpha_2 = 35$ deg was assumed. This shell is reproduced in Fig. 17. It had the following dimensions

$$r_1 = R(\cos 30\text{ deg} - \cos 35\text{ deg}) = 0.0570R,\ r_2 = R(1 - \cos 35\text{ deg}) = 0.1910R$$

the height between tip and bottom of nose was R sin 30 deg $= 0.5000R$, where R is the radius of the mean meridian circle

The distribution of the stresses and of the pressures can be seen in Fig. 17. The pressures p reach their peak values at the tip of the nose, where a pressure maximum

$$p_{max} = 15.2\,\frac{h\sigma_0}{R}$$

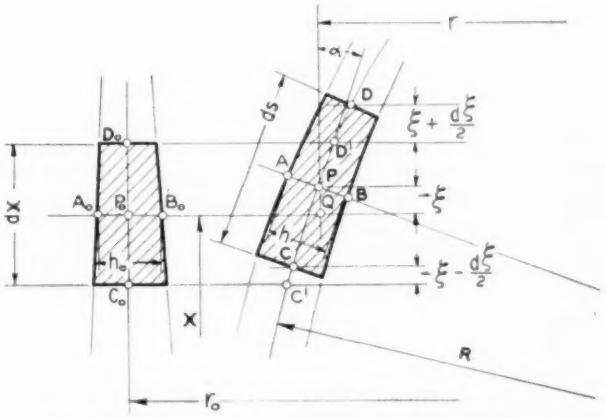


FIG. 18 ELEMENT OF SHELL BEFORE AND AFTER NOSING

was found. The maximum of the meridian stress occurs at the base of the nose ($\alpha = 0$) and was found equal to

$$\sigma_{a\,max} = -0.701\sigma_0$$

or equal to 70 per cent of the yield stress.

STRAINS IN THE SHELL NOSE

In the majority of the shell-producing plants, experiments were carried out for finding the exact contour lines of the rough original shell profiles which after nosing would produce the desired shapes of the shell noses prescribed by the Army Ordnance with due allowance for finish-machining. Simple geometric considerations facilitate this task which will be described briefly.

For this purpose, the shape of a small element of the original shell profile must be compared with its distorted shape after nosing is accomplished. This is shown in Fig. 18, in two cross-sections of the element contained in a plane passing through the axis of the shell. This latter is not shown in Fig. 18, but should be assumed as a vertical line on the right side of the figure.

The shell element in its original position is shown on the left side of Fig. 18, and, after nosing the shell, it is represented in an inclined position on the right side of this figure in the correct relation relative to its original position. All quantities referring to the first position of the element are designated by the subscript zero, and those referring to the final position without a subscript. The length $A_0B_0 = h_0$ changes into the length $AB = h$; $C_0D_0 = dx$ becomes an element of arc of a circle $CD = ds$; the original radius r_0 is contracted until it becomes the radius r, etc. The co-ordinate x of the point P_0 is changed into the co-ordinate $x + \xi$ of the point P. Point P_0 during the forging of the shell is displaced essentially in the radial direction but it is also slightly displaced in the axial direction by a small amount $\xi = PQ$.

Assuming that the meridian curve $C'CPD'D$ is a circle of the radius R we have

$$\left.\begin{aligned} x &= R\sin\alpha \\ r &= r_0 - R(1 - \cos\alpha) \end{aligned}\right\} \ldots [64]$$

Angle α is the angle of inclination of the tangent to the meridian curve in point P. The small shell element which has been shown in its cross sections in Fig. 18, must have the same volume before and after nosing. The first is expressed by $2\pi r_0 h_0 dx$ the second by $2\pi r h ds$. Therefore

$$r_0 h_0 dx = r h ds \ldots [65]$$

which can also be written as follows

$$\frac{r}{r_0}\cdot\frac{h}{h_0}\cdot\frac{ds}{dx} = 1 \ldots [66]$$

The original thickness h_0 of the shell before nosing could immediately be computed if the assumption could be made that all points P_0 during the nosing would be displaced in the radial directions only. The finished shell would in this case have to have the same length as the original one. In this case $\frac{dx}{ds} = \cos\alpha$ and the original thickness h_0 would have to be

$$h_0 = \frac{rh}{r_0\cos\alpha} \ldots [67]$$

Actually the plasticity theory predicts that the axial displacement ξ cannot vanish, but must increase (from the value $\xi = 0$ at the base) toward the tip of the nose. At the tip of the nose, the shell is stressed in pure compression in the circumferential direction. If we designate by ϵ_t, ϵ_a, ϵ_n the permanent (conventional) strains of the shell along the direction of the circumference, meridian, and normal at point P, these strains are defined by the three factors on the left side of Equation [66]

$$\frac{r}{r_0} = 1 + \epsilon_t,\quad \frac{h}{h_0} = 1 + \epsilon_n,\quad \frac{ds}{dx} = 1 + \epsilon_a \ldots [68]$$

and Equation [66] is also expressed by

$$(1 + \epsilon_t)(1 + \epsilon_n)(1 + \epsilon_a) = 1 \ldots [69]$$

If two of these strains are known, the third can be computed from this last equation.

Since the projections of the small portions CC' and DD', Fig. 18, of the meridian circle in a direction parallel to the axis of the shell are $\xi - \frac{d\xi}{2}$ and $\xi + \frac{d\xi}{2}$ respectively, the projection of the extended arc element $ds = CD$ in the same direction or $ds \cdot \cos\alpha$ must be equal to

$$ds\cdot\cos\alpha = dx + d\xi$$

Therefore

$$1 + \epsilon_a = \frac{ds}{dx} = \left(1 + \frac{d\xi}{dx}\right) \cdot \frac{1}{\cos \alpha} \quad \ldots\ldots\ldots [70]$$

defines the permanent strain ϵ_a along the meridian of the shell. The axial displacements $\xi = f(x)$ are naturally dependent upon the plastic behavior of the metal. On the other hand, the function $\xi = f(x)$ can be obtained from direct observations which were carried out at several shellmaking plants. Some attempts in this direction will be described in the following experimental portion of this report. A precise statement concerning the strains must be based upon a knowledge of this function.

Using Equations [66] and [70], we can now establish the correct expression which can serve to compute the original thickness h_0 of the shell. It is given by

$$h_0 = \frac{rh}{r_0 \cos \alpha} \cdot \left(1 + \frac{d\xi}{dx}\right) \quad \ldots\ldots\ldots [71]$$

It is easy to see that a shell must become longer after nosing. At the tip of the nose the metal has been stressed in pure compression in the circumferential direction, and in the whole neighborhood of the tip of the nose, we have seen that the meridian stresses σ_a are small. If the points P_0 would have moved in the radial direction only ($\xi = 0$), the shell elements would have stretched only in the proportion in which the arc lengths ds become longer than the lengths dx. Actually, they must stretch by far more in the axial direction due to the additional lateral expansion in this (and in the radial) direction, which must accompany a heavy circumferential compression of the metal. All shell elements become longer axially by additional amounts corresponding to the circumferential compression. Since at the tip of the nose $\epsilon_a = \epsilon_n$ we must obtain there the axial strain

$$\epsilon_a = \frac{1}{\sqrt{1 + \epsilon_t}} - 1 = \sqrt{\frac{r_0}{r}} - 1 \quad \ldots\ldots\ldots [72]$$

It must, however, be emphasized that the whole state of plastic strain near the tip of a shell nose is actually much more complicated than the simple state of strain which is present in a shell with thin walls. The simple geometric relations just used can serve only as a guide for judging the deformations in those portions of the shell in which the wall thickness remains a fairly small fraction of the mean radius.

Dependence of Constant σ_0 in Condition of Flow on Speed of Deformation and on Temperature

A few remarks are in order concerning the constant σ_0 appearing in many of the preceding equations of this report. Constant σ_0 was introduced in the condition of plasticity Equations [6] and [6a], and in subsequent equations as a material constant. According to the form in which the condition of flow was introduced, it was assumed that the constant σ_0 expresses the absolute value of the yield stress either in pure tension or in pure compression.

Various series of experiments performed at the Westinghouse Research Laboratories during past years have proved that an equivalent shearing stress τ_0 exists in the strain-hardening range of the ductile metals which is a given function of a certain permanent strain γ_0 which measures the intensity of cold work. Stress τ_0 is introduced as the shearing stress in the octahedral planes of the stress tensor. It depends upon the principal stresses $\sigma_1, \sigma_2, \sigma_3$ and is equal to

$$\tau_0 = \frac{1}{3} \cdot \sqrt{(\sigma_1 - \sigma_2)^2 + (\sigma_2 - \sigma_3)^2 + (\sigma_3 - \sigma_1)^2} \quad \ldots [73]$$

For not too large strains, the intensity of strain can be expressed by means of the permanent unit shearing strains γ_0 active in the octahedral planes or by

$$\gamma_0 = \frac{2}{3} \sqrt{(\epsilon_1 - \epsilon_2)^2 + (\epsilon_2 - \epsilon_3)^2 + (\epsilon_3 - \epsilon_1)^2} \quad \ldots [74]$$

where $\epsilon_1, \epsilon_2, \epsilon_3$ designate the principal permanent strains, which for small strains also satisfy the condition of constant volume

$$\epsilon_1 + \epsilon_2 + \epsilon_3 = 0 \quad \ldots\ldots\ldots [75]$$

Although these relations can be extended to the further case in which the permanent conventional strains $\epsilon_1, \epsilon_2, \epsilon_3$ become of finite magnitude[6] by introducing the natural strains defined by $\bar{\epsilon} = \log (1 + \epsilon)$, no use of these relations was made in this theoretical part of the investigation because, for hot-nosing, strain-hardening is not of importance and some simpler means may suffice to express the influence of the temperature and of the speed of deformation in the formulas which have been given. This can be done by assuming that σ_0 or the equivalent shearing stress τ_0 is functions of the temperature and of the speed of plastic straining. From Equation [73], we see that in the case of pure tension $\sigma_1 = \sigma_0$, where σ_0 designates the yield stress in tension and $\sigma_2 = \sigma_3 = 0$; hence the equivalent octahedral shearing stress τ_0 is equal to $\tau_0 = \frac{\sqrt{2}}{3} \cdot \sigma_0$.

At forging temperature, we can make the assumption that τ_0 (or σ_0) is a given function of the permanent rates of shear $d\gamma_0/dt$ (or the strain rates $d\epsilon/dt$)

$$\tau_0 = f\left(\frac{d\gamma_0}{dt}\right) \quad \ldots\ldots\ldots [76]$$

It was found from numerous recent tests that, at a given permanent strain at even comparatively low temperatures (in the strain-hardening range), such a relation holds for the ductile metals.[7] At low temperatures τ_0 slowly increases with the rates of shear $v = \dot{\gamma}_0 = \frac{d\gamma_0}{dt}$ according to a logarithmic function

$$\tau_0 = \tau^* \left(1 + \log_e \frac{v}{v^*}\right) \quad \ldots\ldots\ldots [77]$$

τ^* and v^* are two material constants. Equation [77] should be used for $v > v^*$.

At forging temperatures this speed dependence of the stresses τ_0 becomes much more pronounced. Just a few experiments of this kind are available in this important range of the temperature at the large rates of straining used in forging presses.[8] From these and from some work which has been done at much lower rates of flow (at strain rates of the order $\frac{d\epsilon}{dt} = 10^{-4}$ up to 10^{+1} per sec), it seems probable that a hyperbolic sine function

$$v = \frac{d\gamma_0}{dt} = v^* hyp \sin \frac{\tau}{\tau^*} \quad \ldots\ldots\ldots [78]$$

expresses the speed dependence at a given temperature, but comparatively little information is yet available about the numerical

[6] "Plastic Behavior of Metals in the Strain Hardening Range," Part I, *Journal of Applied Physics*, vol. 8, 1937, pp. 205–213.

[7] "Plastic Behavior of Metals in the Strain Hardening Range," Part II, by E. A. Davis, *Journal of Applied Physics*, vol. 8, 1937, pp. 213–217.

[8] "High Speed Tension Tests at Elevated Temperatures," Parts II and III, by author and M. J. Manjoine, *Journal of Applied Mechanics*, Trans. A.S.M.E., vol. 63, 1941, pp. A-77.

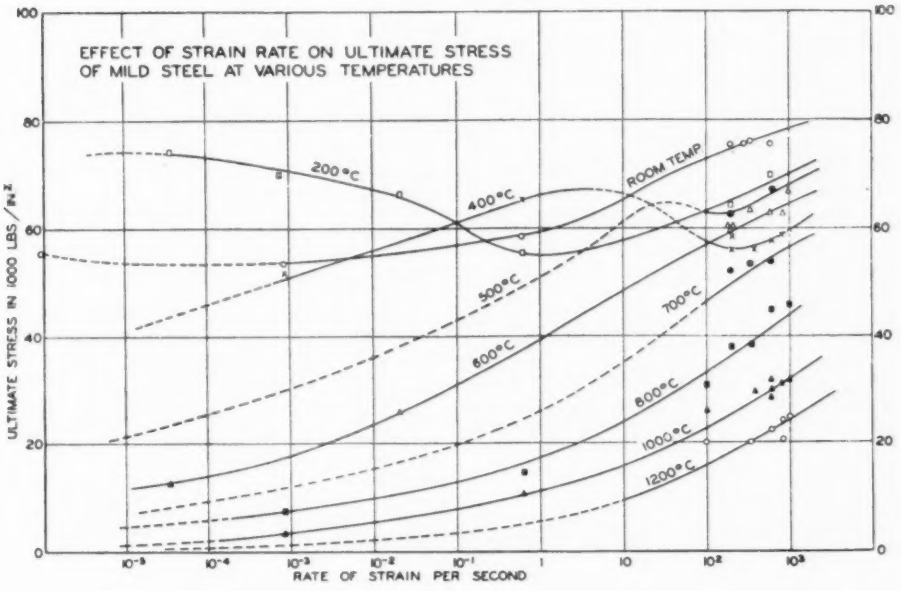


FIG. 19

values of the material constants v^* and τ^* appearing in this function.

In Figs. 19 and 20, the results of a series of tension tests are reproduced indicating the dependence of the ultimate stress on the rates of strain for a mild steel at various temperatures. These curves may be helpful to estimate values of our constant σ_0 by identifying it with the "ultimate stress" of a tensile test. On the right side of Fig. 19, appear the results which were observed at the highest rates of stretching. The abscissas in Fig. 19, represent the conventional rate of strain $d\epsilon/dt$ of a tensile test. They are plotted on a logarithmic scale. The ordinates in Figs. 19 and 20 are the corresponding ultimate stresses. The high rates of $d\epsilon/dt = 10^3$ 1/sec correspond to high-speed tension tests in which the bars were broken in less than 0.001 sec. The range of the investigated temperatures extended from room temperature to 1200 C = 2192 F. The range between the two curves for 1000 C = 1832 F, and for 1200 C, covers the temperatures of interest in shell-making at forging heats. Both curve sheets indicate at least the order of magnitude of the effect of plastic deformation and of temperature which must be expected under forging conditions in a steel.

SUMMARY

The theory of curved shells has been extended to cover cases in which the metal is in a plastic state of equilibrium. Although the three general equations for shells, whose middle surface is a surface of revolution, have been established for the plastic state and for variable wall thickness in this investigation only shells with uniform wall thickness were considered. These equations were fully developed for the case of conical shells, including the two limiting cases of cones, namely, the cylindrical shell, and the plane disk of uniform thickness. The distribution of the meridian and circumferential stresses σ_a and σ_t, of the pressures p for forming such shells through contact with a hollow die were studied in a number of special cases and in examples for different values of the friction coefficient, defining the resistance against gliding between the die and shell. A simplified and abbreviated theory was also given for the case of a conical shell and also for the standard shell nose whose meridian curve is a circle leading to workable and even quite simple expressions for the total nosing force. It was shown that the plastic states of stress in such

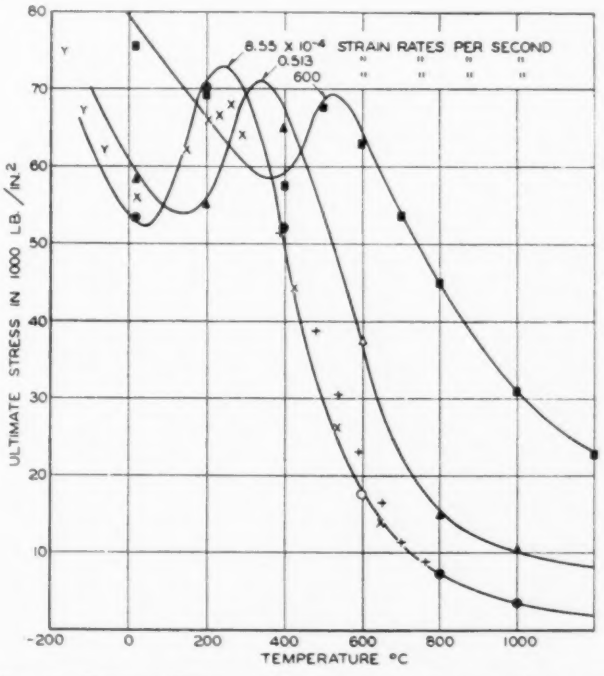


FIG. 20 TENSION TESTS OF MILD STEEL AT VARIOUS TEMPERATURES AND RATES OF STRAIN

curved shells in first approximation can be described by assuming a uniform circumferential stress σ_t. It was furthermore shown that certain limiting conditions are imposed on nosing through the friction. The condition for preventing local swelling of the wall thickness at the base of the nose was expressed.

The distortion of the elements of the metal during the formation of the nose of a shell was described, and expressions were given permitting to predict the original contour of the shell which after nosing furnishes a prescribed profile in the nose of a shell.

ACKNOWLEDGMENTS

Acknowledgments are due to Dr. M. Stone, Chairman, and to

Prof. W. Trinks, Projects Director of the A.S.M.E. Research Committee on Forging of Steel Shells for having disclosed to the author important details concerning difficulties encountered in forging of shells. The author also acknowledges the helpful assistance received from Dr. L. W. Chubb, Director of the Westinghouse Research Laboratories, which made this theoretical and the companion experimental investigation with the assistance of Mr. R. K. Carlson possible.

The following references concerning the related problem of the deep drawing of thin hollow bodies should be quoted.

REFERENCES

1 "Das Ziehen unregelmaessig geformter Hohlkoerper," by H. D. Brasch, *V.D.I. Forschungsarbeiten*, no. 268, 1925, 33 pp. This is an experimental investigation.

2 "Versuche Ueber das Ziehen von Hohlkoerpern," by M. Sommer, *V.D.I. Forschungsarbeiten*, no. 286, 1926, 94 pp. This describes drawing tests with brass cups. On p. 25, a brief theory of the process of cold deep drawing of cups is developed. Sommer gives for the drawing force P the formula

$$P = (2\mu H + 2\pi S)e^{\mu\alpha} + B$$

in which μ designates the coefficient of friction; H the holding force in axial direction; S the resultant of the circumferential stresses taken over the cross section of the cup, and B a correction term. α is the mean angle of inclination of the meridian of the cup with regard to the axis.

3 "Die Formgebung im bildsamen Zustande," by E. Siebel, Verlag Stahleisen, Duesseldorf, 1932. This contains a theory of drawing similar to the one developed by Sommer (ref. 2) on pp. 61–68. This book is available in English translation of articles published in *Steel*, under the title "The Plastic Forming of Metals," October, 1933, to May, 1934.

4 "The Investigation of the Plastic Flow Processes Involved in Drawing Cylindrical Shells From Flat Circular Blanks," by Morris Asimov, University of California Press, Berkeley, Calif., 1936, pp. 235–295. Contains in part 3, p. 265, a theory of the deep drawing process.

5 The membrane theory of thin shells is to be found in W. Flügge's book, "Statik und Dynamik der Schalen," Julius Springer, Berlin, 1934, p. 21, which has already been quoted.

6 "Theory of Plates and Shells," by S. Timoshenko, McGraw-Hill Book Company, Inc., New York, N. Y., 1940, chapt. 10, p. 351, also p. 365 ("torus"). Related solutions to those developed in the text for shells for the yielding of a thin disk stressed by forces in its plane have been treated in the author's "Plasticity," McGraw-Hill Book Company, Inc., New York, N. Y., 1931, on pp. 189–194, and in an article "Theory of the Expanding of Boiler and Condenser-Tube Joints Through Rolling," by the author, Trans. A.S.M.E., November, 1943, pp. 865–877.

An Experimental Investigation of the Nosing of Shells

By R. K. CARLSON,[1] PITTSBURGH, PA.

Objects of the Investigation

THE general object of the work done at the Westinghouse Research Laboratories under the auspices of the A.S.M.E. Special Research Committee on Forging of Steel Shells was to study the nature of the nosing process in the forging of shells. In particular, plans were made to study the effects of temperature, lubrication, and speed on the forces required for nosing shells of various sizes. It was not, of course, possible to work with full-sized shells; and, consequently, small models were used in the experimentation.

The huge amount of experimenting undertaken by the industry before entering shell production seems to indicate that the model tests can, at best, serve only to confirm conclusions already reached by the great number of shell manufacturers. Nevertheless, it is hoped that the results of the work described in this report will prove of some interest to those having to do with shell-forging processes.

Description of Apparatus

A consideration of the capacities of presses used in the forging of shells in steel plants indicated that a press of about 15 tons capacity would be required for the experimental work which was contemplated. The apparatus, Fig. 1, consists essentially of a 15-hp 220-v d-c shunt motor driving a Hydro-Power Systems, Inc., rotary pump capable of delivering 60 gpm of oil (at 900 rpm) against 500 psi pressure continuously, or 1000 psi flash. The pump discharges into a 7-in. hydraulic cylinder (1) (see Fig. 1) through a four-way, hand-operated control valve (3). The cylinder has a stroke of 12 in., and, at 1000 psi pressure, a load of about 20 tons can be applied. Valves were purchased from the Logansport Machine Company, Logansport, Ind., and the cylinder was manufactured by Hanna Engineering Works, Chicago, Ill. The specimen holder (4) (see also Fig. 2) was used as a positive stop in conjunction with the die (see Fig. 4). The die was heated to approximately 1000 F by means of a resistance heater (6). The induction coil, used to heat the shell before forging, operated on a frequency of 9600 cycles per sec. A Maihak Diesel-engine indicator (2) was used to obtain records of cylinder pressure as a function of the displacement of the cylinder. In order to obtain various speeds of the cylinder, a field rheostat was used with the motor, making it possible to vary the delivery of the pump.

Apart from some vibration of the equipment at the very low speeds (400 rpm of the motor) and at the high speeds (over 1000 rpm), no particular difficulties were encountered in the operation of the equipment.

Description of Specimens

Details of the specimen used for the majority of the tests are shown in Fig. 3. This specimen has approximately the same length-diameter and wall thickness - diameter proportions as the regular 155-mm shell. Commercial open-hearth cold-rolled steel was used in making the specimens. Stress-strain curves of this material tested in compression are shown in Figs. 5 and 6. While the carbon content of this steel is lower than that of the steel ordinarily used in shell production, it was felt that the forgeability at temperatures above 1500 F would not be greatly different.

The die employed throughout the experiments is shown in Fig. 4. The die was made from one of the high-temperature alloys (K-42-B) developed at Westinghouse for use in gas turbines and similar applications. To simulate the amount of nosing done on the 155-mm shell, $2^1/_4$ in. of the specimen was made to enter the die, giving a maximum reduction in the mean diameter of from 65–70 per cent.

In order to produce less severe nosing than that obtained in forming the larger shells, the specimen shown in Fig. 3 was made short enough to allow 1.45 in. to enter the die. A reduction of about 33 per cent in the mean diameter was obtained in this manner. This amount of nosing corresponds to that on the 105-mm shell.

For the few nosing tests which were run cold, the specimen shown in Fig. 7 was used. The outside diameter is the same as that of specimen *A*, but the inside diameter is made slightly

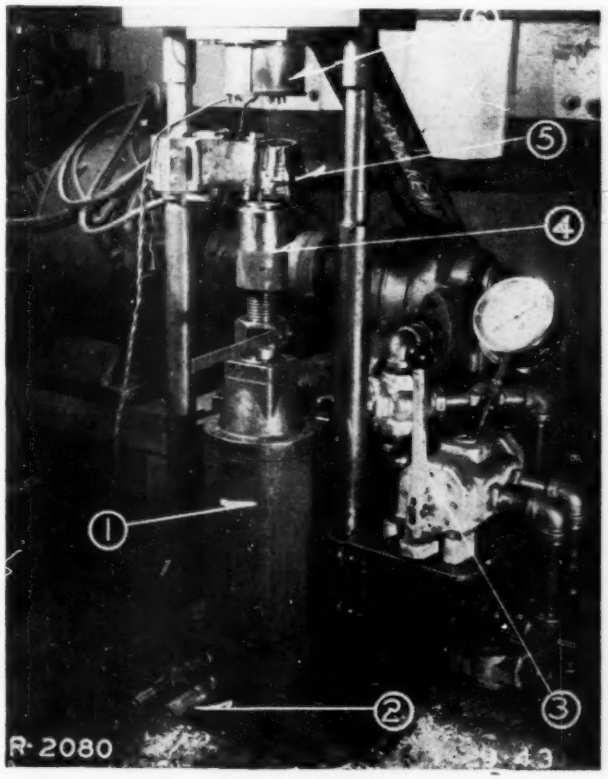


Fig. 1

[1] Research Engineer, Research Laboratories, Westinghouse Electric & Manufacturing Company.

Contributed by A.S.M.E. Special Research Committee on Forging of Steel Shells and presented at the Annual Meeting, New York, N. Y., Nov. 29–Dec. 3, 1943, of The American Society of Mechanical Engineers.

Note: Statements and opinions advanced in papers are to be understood as individual expressions of their authors and not those of the Society.

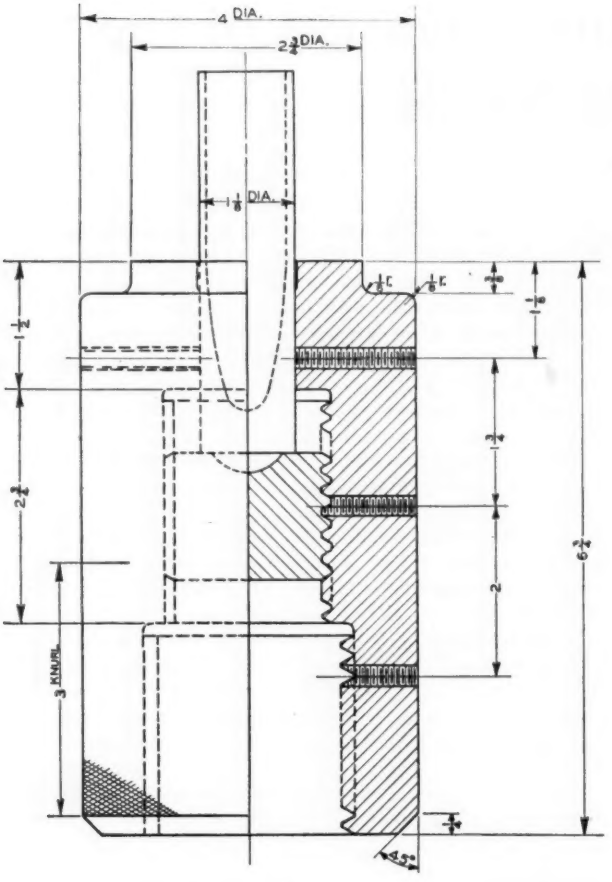
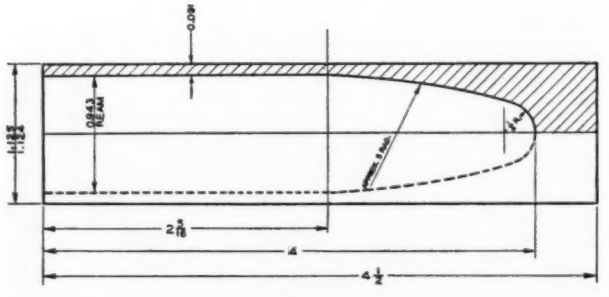


FIG. 2



SPECIMEN A
SCALE 2:1

FIG. 3

smaller. In the smaller shells, namely, the 75 and 90 mm (those most often nosed cold), the thickness - diameter ratio is slightly greater than for the larger shells.

TESTING PROCEDURE

Prior to any testing, considerable experimenting was necessary to obtain the proper temperature distribution along the specimen by means of induction heating. Several coils were tried before satisfactory results were achieved. To measure the temperature distribution, six chromel-alumel thermocouples were placed along the shell model. Temperature readings were made by means of an eight-point thermocouple switch leading to a 0–2000 F Wheelco instrument. The temperature distributions possible for the two lengths of noses are shown in Figs. 8 and 9. In running a particular test, only two couples were used, both near the tip of the specimen; the temperature at the tip was taken, then, as characterizing the distribution. Check runs with six couples were made occasionally to see that the same temperature distributions were maintained.

In preparation for a test, it was necessary to heat the die for about 1 hr to bring it to 1000 F. The motor speed was then properly adjusted by means of field control. After placing the specimen in the fixture on top of the cylinder, the induction coil was moved into place and the shell heated. About 1 min was required to heat the shell to testing temperature—from 1600 F to 2000 F at the tip. When the shell reached a temperature somewhat above that at which nosing was to take place, the coil was

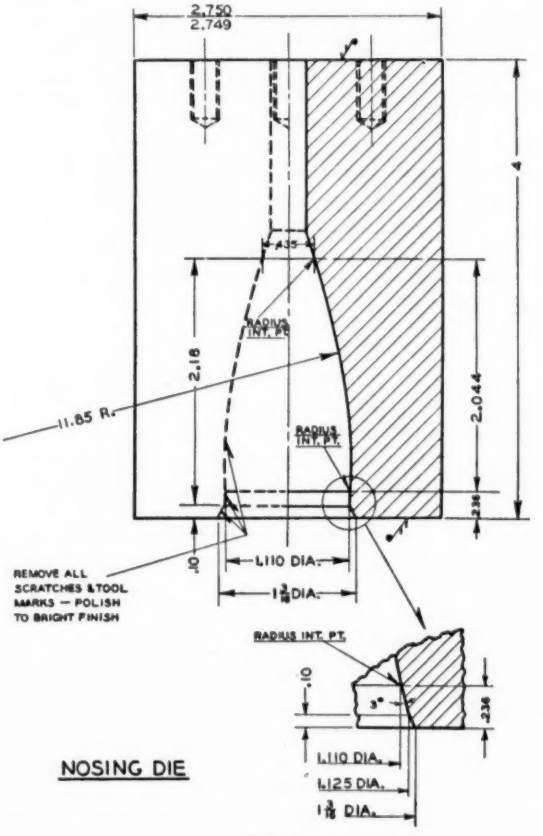


FIG. 4

quickly removed and the 4-way valve opened to allow oil to enter the cylinder. Since the temperature of the specimen dropped 100–150 F in bringing the shell up to the die, the temperature at which the shell actually entered the die was observed and recorded as the temperature condition for the test. Lubrication of the die was done by means of asbestos swabs saturated with the lubricant. The lubrication was done just before removing the induction coil and starting the cylinder upward. The time of nosing was of the order of 1 sec. More information concerning speed of testing will be given later.

Naturally, an attempt was made to keep the testing procedure uniform throughout the whole of the experimentation.

EXPERIMENTAL RESULTS

The tests which were run during this investigation may be divided into several groups, as follows:

1 Nosing equivalent to that on 105-mm shells.
2 Nosing equivalent to that on 155-mm shells.

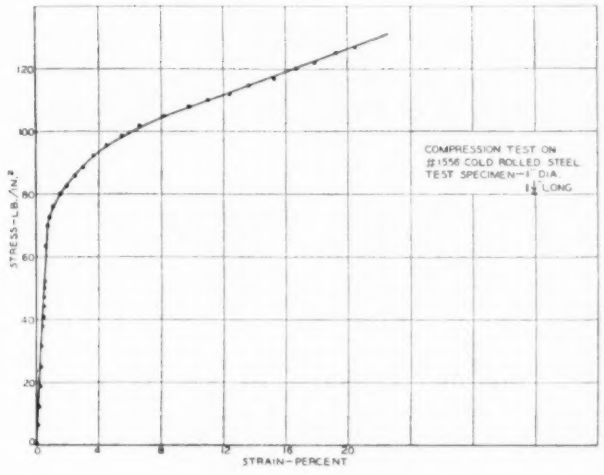


FIG. 5

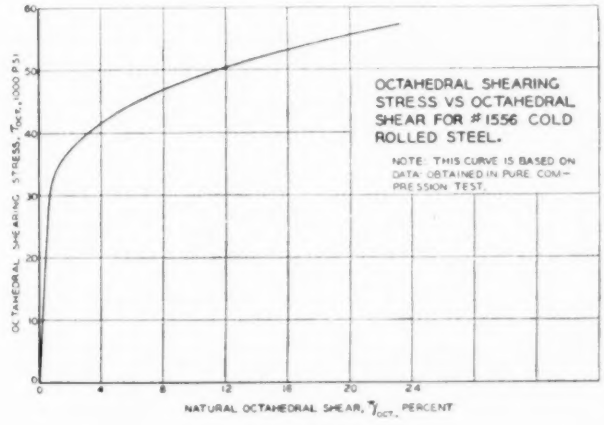
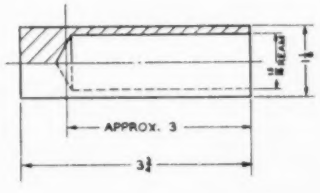


FIG. 6



COLD NOSING SPECIMEN

FIG. 7

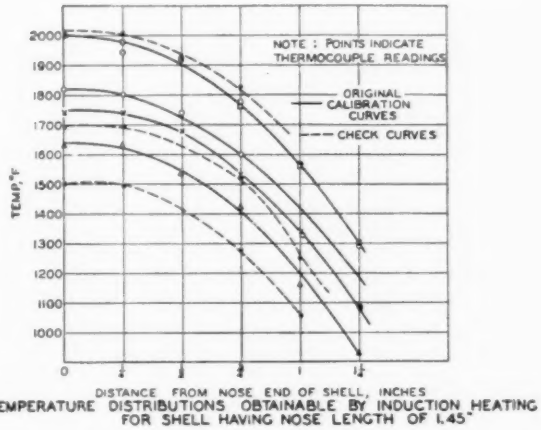
3 Cold-nosing.

4 Lubrication tests.

In describing the experimental results, a brief discussion of each of these series of tests will be given, followed by a general interpretation.

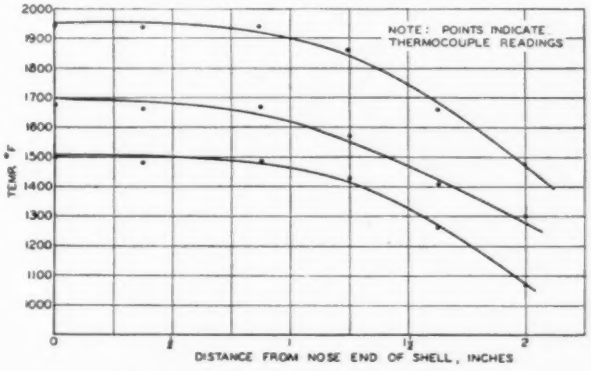
1 The invariant in the first two groups of tests listed was lubrication, a mixture of 325-mesh graphite and machine oil being used throughout. It was found during the experimenting with various lubricants that this mixture gave favorable results in comparison with a number of commercial hot-forging lubricants.

The nosing equivalent to that on the 105-mm shell corresponds to about a 33 per cent reduction in the mean diameter. In Fig. 10, four typical specimens belonging to this series are shown. It should be noted that at the present time, most shell-forging plants have presses capable of cold-nosing the 105-mm shell, and it is



TEMPERATURE DISTRIBUTIONS OBTAINABLE BY INDUCTION HEATING FOR SHELL HAVING NOSE LENGTH OF 1.45"

FIG. 8



TEMPERATURE DISTRIBUTIONS OBTAINABLE BY INDUCTION HEATING FOR SHELL HAVING NOSE LENGTH OF 2¼ INCHES

FIG. 9

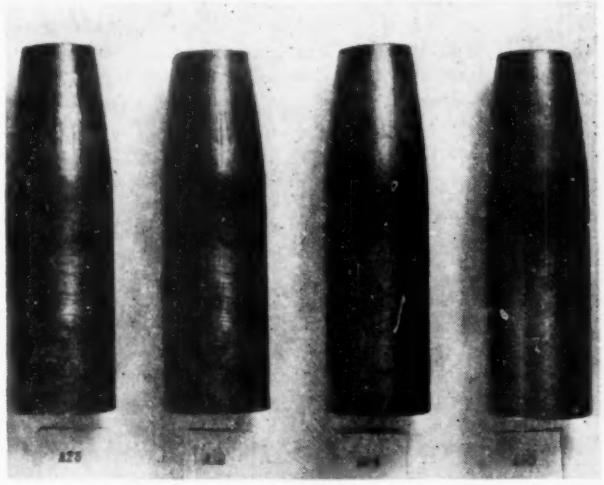


FIG. 10

only where the press capacity is low that this shell is hot-nosed. As can be seen in Fig. 10, only a small amount of deformation takes place.

Test conditions were varied as follows: nose-tip temperatures in the range 1600 F to 1900 F were combined with piston speeds of from 1.5 to 2 in. per sec. Attention is again called to

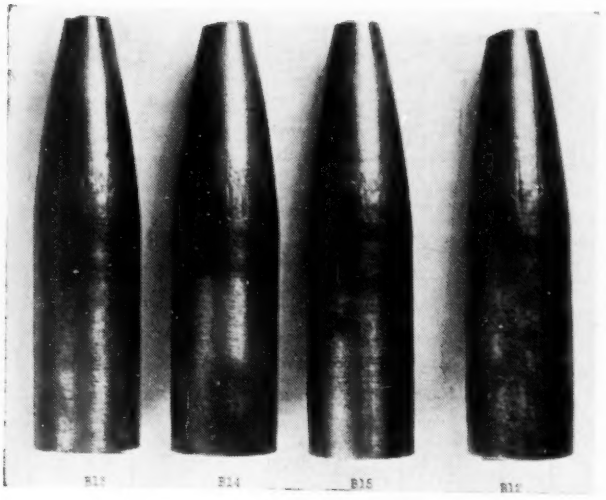


FIG. 11

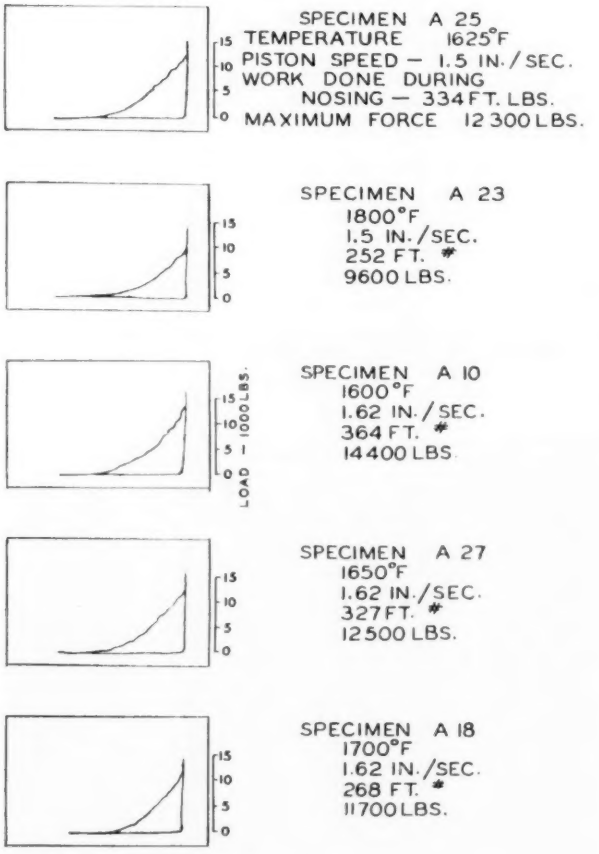


FIG. 12

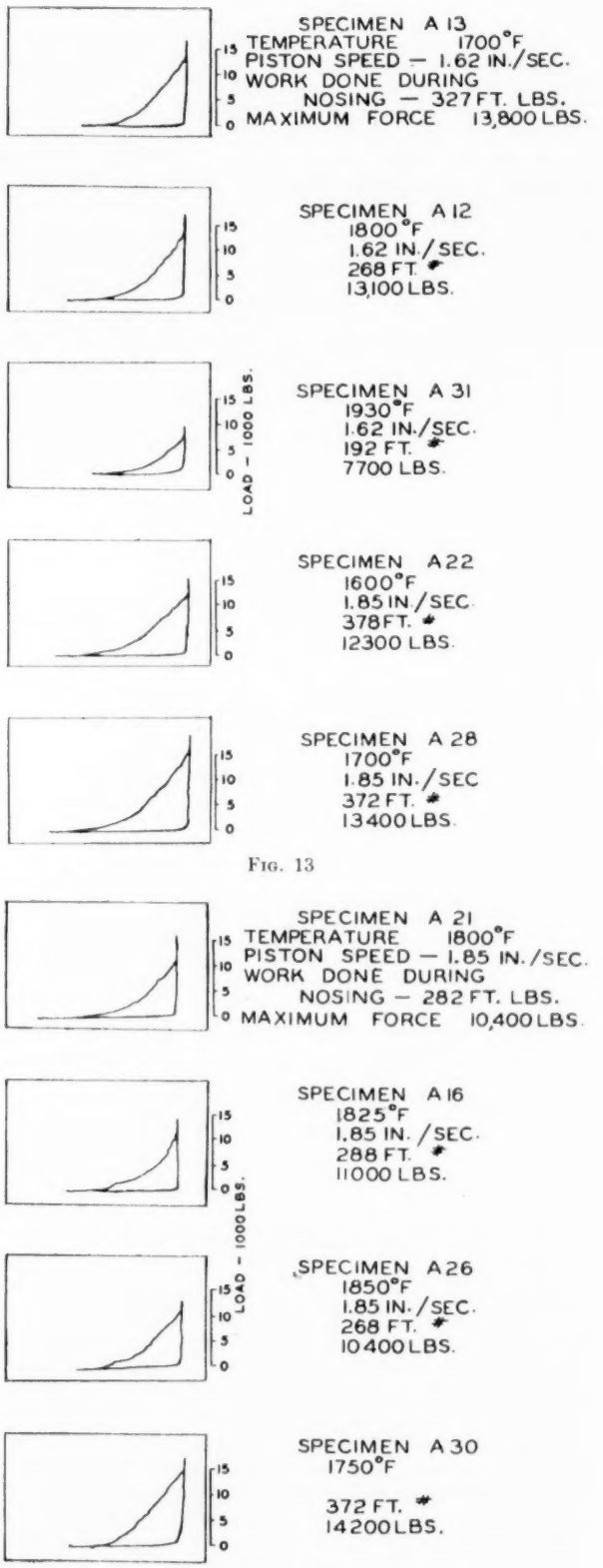


FIG. 13

FIG. 14

Fig. 8, where the temperature distributions along the nose of the shell for various tip temperatures are given.

In Figs. 12, 13, and 14 are shown the original indicator diagrams for this group of tests. All pertinent information for each test is given in the figures. Some remarks concerning the characteristics of the indicator diagrams will be made in the general discussion to follow.

The quantitative information which was derived from the nosing tests, namely, the maximum force during nosing and the total work done, has been plotted in Figs. 17 and 18. The curves of work done versus temperature are fairly regular, that is, there is no excessive scattering. However, the maximum-force curves do

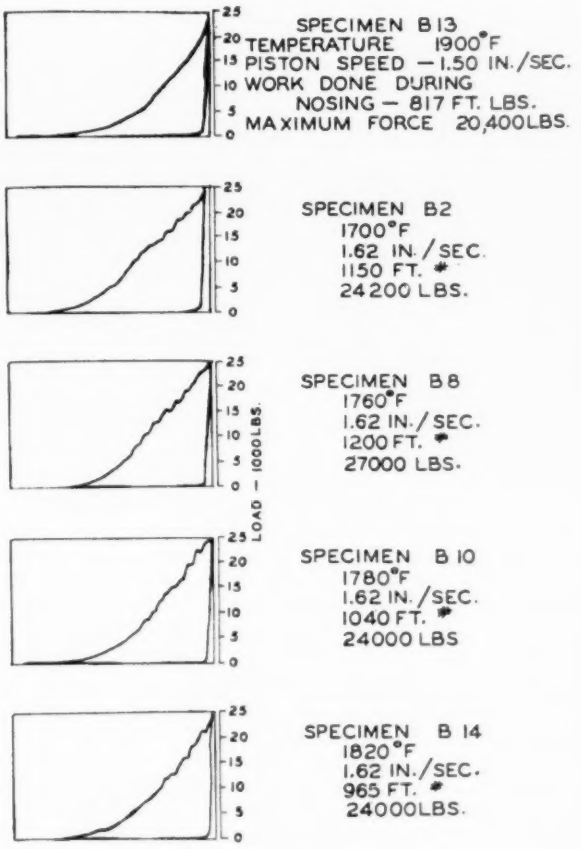


FIG. 15

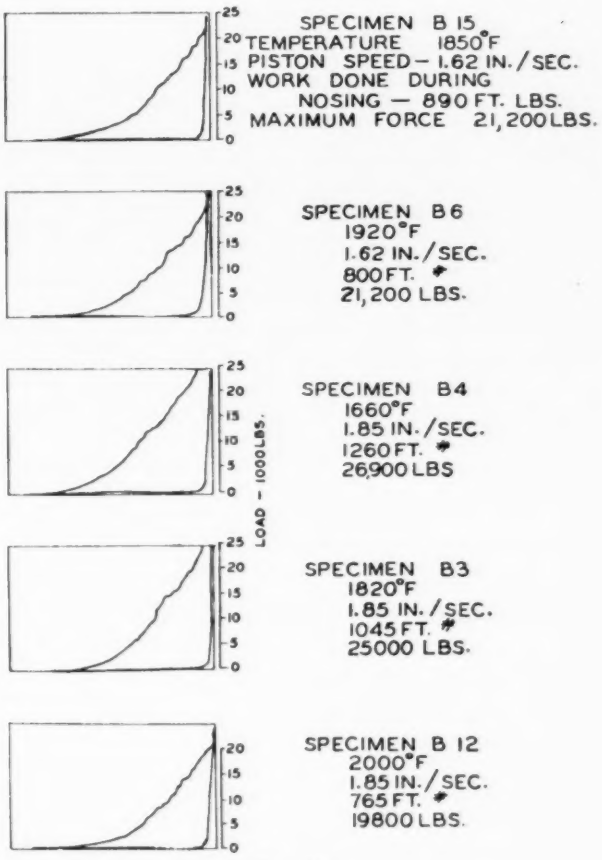


FIG. 16

show considerable scattering. Perhaps the original indicator diagrams (Figs. 12, 13, and 14) provide the key to this; it should be evident that the determination of the maximum force from these diagrams is a much more sensitive task than the determination of the area (that is, the work) by means of a planimeter. Further discussion of these curves will follow.

2 The amount of nosing on the 155-mm shell corresponds to about a 67 per cent reduction in the mean diameter. Four typical specimens having approximately this reduction in diameter are shown in Fig. 11. The original indicator diagrams of the majority of the tests in this group are shown in Figs. 15 and 16.

Test conditions for the greater amount of nosing were very similar to the conditions of the tests in group 1. A temperature range from 1600 F to 1900 F (one test at 2000 F) was covered at piston speeds of 1.5 to 1.8 in. per sec. Plots of work done and maximum forces as functions of temperature are shown in Figs. 19 and 20. Again, the work-temperature curves show very little scattering, while the maximum force determination is apparently critical and not a good measure to use as a quantitative characteristic of the test.

3 The cold-nosing was done with the specimen shown in Fig. 7. Since maximum forces of the order of 30,000 lb were required to nose this shell, this specimen was nearly the longest that could be forged with the equipment which was employed. Several cold-nosing lubricants were tried: a commercial mill lubricant; palm oil; lauric acid; and several other commercial lubricants. No apparent differences in the amount of work required to nose the shell were noticed for these lubricants. It would appear that the problem of lubrication during cold-nosing is a much simpler one than that in hot-nosing.

4 The choice of a lubricant for hot-nosing full-sized shells is a very complicated one. The many factors entering into the problem of lubrication—die life, ease of nosing, ease of application, cost, availability, etc.—make it dangerous to draw any too definite conclusions from such tests as reported herein concerning the desirability of one lubricant over another.

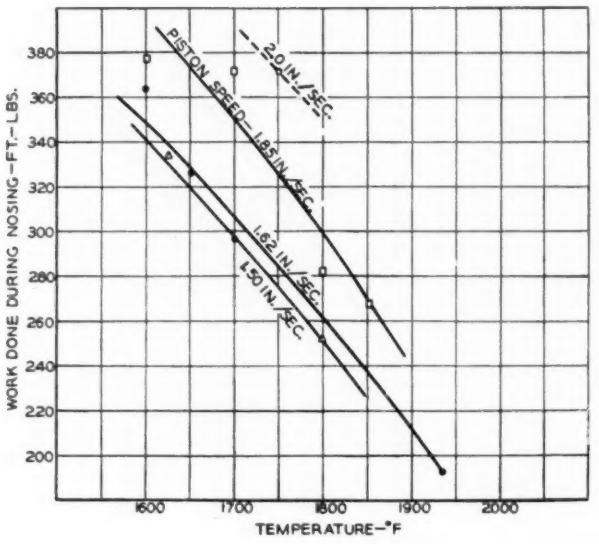
Some twelve different lubricants, most of them commercial products, were used. At least two tests were run using each of the lubricants. The results of the tests on each lubricant were interpreted to obtain a value of work necessary for nosing at a nose-tip temperature of 1900 F, and a piston speed of 1.82 in. per sec. The tests were all made on specimen *A*, the amount of nosing being equivalent to that on the 155-mm shell. Table 1 shows the range of values obtained for the work necessary for the forging operation. Names of the commercial lubricants employed are omitted.

TABLE 1 WORK INVOLVED IN FORGING OPERATION

Lubricant no.	Work required for forging at 1900 F nose-tip temperature, ft-lb
1	650
2	690
3	800
4	810
5 (325-mesh graphite with machine oil)[a]	840
6	845
7	870
8	980
9	1040
10	1040
11 and 12	Unsatisfactory; specimens buckled

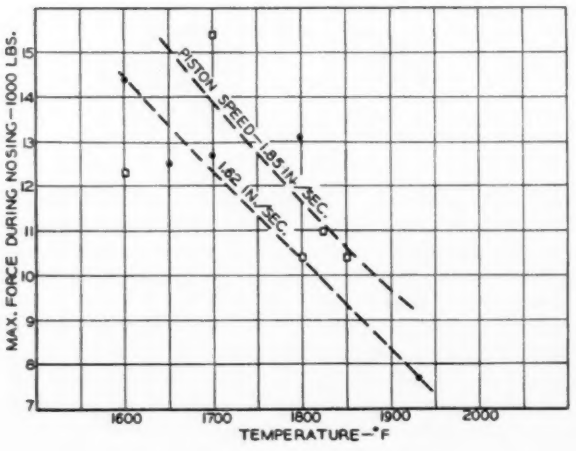
[a] Lubricant used in the nosing tests previously described.

The majority of the lubricants tested were combinations of colloidal or very fine mesh graphite and oils or greases. In



TEST RESULTS FOR NOSING CORRESPONDING TO A 33% REDUCTION IN MEAN DIAMETER

FIG. 17



TEST RESULTS FOR NOSING CORRESPONDING TO A 33% REDUCTION IN MEAN DIAMETER

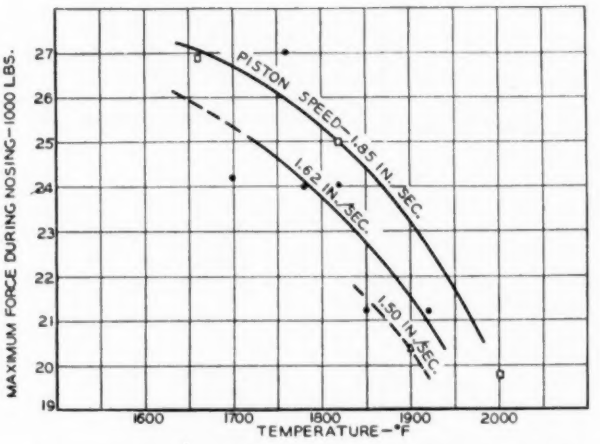
FIG. 18

general, it was found that the heavier lubricants gave the best results. It was noted that the better lubricants, while apparently having just as low a flashpoint as the poorer ones, left a spongy deposit on the die after burning. It is thought that this residue helped to hold the graphite on the die surface.

INTERPRETATION AND DISCUSSION OF NOSING EXPERIMENTS

Perhaps a brief description of the difficulties encountered in forging small model shells will aid a critical evaluation of the results obtained. At the time the experiments were started, shell manufacturing was proceeding satisfactorily, that is, most of the practical difficulties had been eliminated. Naturally, therefore, we were aware of the problems which would probably be met in forging models.

Undoubtedly, proper heating of the shell is one of the more im-



TEST RESULTS FOR NOSING CORRESPONDING TO A 67% REDUCTION IN MEAN DIAMETER

FIG. 19

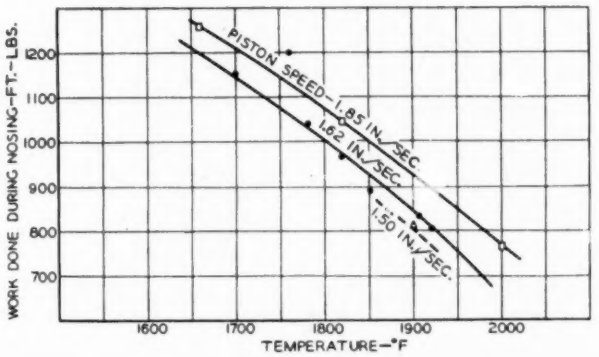


FIG. 20



FIG. 21

portant preparations which must be made before nosing. The danger of improper heating is demonstrated very clearly in Fig. 21. The two shells at the right were among the first trials on the equipment and little attention had been given to the temperature distribution along the shell. Obviously, a hot band of material was formed below the tip of the nose which gave way under the forces required to deform the tip. The shell specimen at the left was tested with a controlled temperature distribution designed to show the unsatisfactory results obtained by improper heating. The temperature at the tip of the shell was 1500 F, and about halfway down the shell it rose to 1800 F. It is clear from the illustration that very little deformation of the tip was possible before the mid-portion of the shell buckled. Trouble similar to this had been encountered in the industry.

When discussing plans for carrying out the experimental work, the question of the cooling of the small model shell during forging was brought up. It was realized that the small mass of metal in the specimens would not stay at the proper temperature, if forging was attempted with a cold die. The die was therefore heated to about 1000 F by means of a resistance heater. Several observations of the temperature drop at the tip of the shell during a test were made and it was found that, if the temperature of the shell at the tip was 1900 F just as the shell entered the die, the temperature would drop to between 1500 F and 1550 F at the end of the forging operation. It is possible of course that the temperature readings at the end of the test are in error since the thermocouples might easily be disturbed by the deformation of the tips. Observations made at Case by the Shell Forging Committee indicated a drop from 1775 F to 1550 F during the forging of a 155-mm shell. It might have been desirable to heat the die somewhat higher than 1000 F, but with the original furnace, it was not possible to obtain a higher temperature; and it was felt that the conditions were satisfactory enough to warrant not designing a new heater.

The application of a lubricant to the die is a problem of some importance in the industry. A method must be employed that is quick, safe, and which provides for effective spreading of the lubricant. It has been noted in shell-manufacturing plants that special care must be taken to see that the lubricant is distributed evenly over the die; for if the die is not completely lubricated, the shell tip will not be flat perpendicular to the axis of the shell. Some difficulty of this sort was encountered early in the testing.

One of the chief problems confronting shell manufacturers at the outset of production was that of designing the profile of the shell before nosing so as to give the desired finished shape after forging. Some remarks concerning this question will be made in the discussion of the flow tests made on full-size shells.

It must be admitted that, in general, the test results were erratic. The nosing operation is a complicated one and slight variations in temperature and friction conditions from test to test result in considerable scattering of the data. However, force measurements taken from successive forgings of full-sized shells did not give consistent values for the maximum observed forces. The reliance placed on the curves, shown in Figs. 17, 18, 19, and 20, should be tempered by a consideration of the scatter of the plotted points.

The expected temperature influence was observed. It can be seen from Fig. 17 that for a 33 per cent reduction in diameter, a change in the nose-tip temperature from 1600 F to 1900 F reduced the work required for the nosing operation by about 40 per cent. For a 67 per cent reduction in the mean diameter, the same temperature change (1600 F to 1900 F) reduced the work required by 35 per cent, Fig. 20. The maximum force - temperature curves are very similar in shape to the work-temperature curves. Thus for 33 per cent nosing a 40 per cent decrease in the maximum force was observed when the nose-tip temperature was raised from 1600 F to 1900 F. The maximum-force curves for 67 per cent nosing seem to be flatter than the others, that is, the temperature rise from 1600 F to 1900 F results in only about a 15 per cent decrease in the forces required for forging.

The effect of speed on the forces and work required for nosing is a little remarkable. For 33 per cent nosing at 1800 F, a 33 per cent rise in piston speed, from 1.50 in. per sec to 2 in. per sec, increased the work necessary for nosing by 40 per cent. Again, at 1800 F, a 20 per cent rise in piston speed, from 1.50 in. per sec, to 1.85 in. per sec, results in a 20 per cent rise in the work done. A 20 per cent increase in piston speed changes the work necessary for 67 per cent nosing at 1900 F by about 15 per cent. These large increases in the work required can hardly be explained by the change in resistance to plastic deformation due to changes in speed. Tests by Nadai and Manjoine[2] indicated that in the region of the rates of strain imposed on the shells, from 0.2 to 0.5 in. per in. per sec, there is very little speed effect. The considerable change in work must be explained then in another way. It is to be expected that at higher speeds the lubrication will not be as effective as at the lower speeds. However, it seems improbable that the friction would be changed by any considerable amount for a 20 or 30 per cent change in speed. Perhaps the combination of the effects of speed on lubrication and resistance to deformation is sufficient to produce the observed results.

From the test results reported, it would seem advisable to forge at as low a speed as is compatible with production requirements. However, it is very probable that on full-sized shells, the effect of speed on the geometry of the metal flow will be an important consideration. It is impossible to predict the nature of this phenomenon from the model tests.

Buckling Tests

Unless a shell is properly designed it may buckle under the forces necessary for nosing. In most cases, the shell wall is so thick that the proportional limit of the material will be reached before the equilibrium of the shell becomes unstable; and the buckling, if it occurs, is plastic. If the shell is nosed cold, there are well-established formulas for predicting the critical buckling load, given the ratio of the thickness of the shell wall to the diameter. In hot-nosing, however, the critical load is a function of the temperature distribution along the nose of the shell as well as of the wall-thickness diameter ratio, that is, if the temperature distribution is not correct, a sort of "semibuckling" occurs. This semibuckling is a result of the improper flow of metal imposed by the external load. A thickening, or bulge, near the bottom of the nose, usually on the inside, resulting from an improper temperature distribution caused considerable difficulty when shell production first began. Of course, when buckling of the shell wall occurs during nosing, either the shell-wall profile must be redesigned or the temperature at the tip of the nose made higher to reduce the forces required. The elastic buckling of cylindrical shells is treated by Timoshenko.[3] Timoshenko obtains the following formula for the stress necessary to cause buckling

$$\sigma_{cr} = \frac{Eh}{a\sqrt{3(1-\nu^2)}} \quad \ldots\ldots\ldots\ldots\ldots\ldots [1]$$

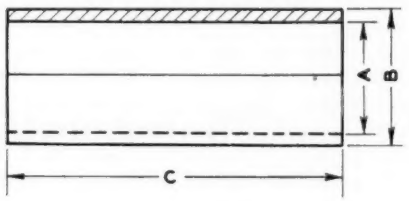
where

E = modulus of elasticity, psi
h = thickness of shell, in.

[2] "High-Speed Tension Tests at Elevated Temperatures—Parts II and III," by A. Nadai and M. J. Manjoine, *Journal of Applied Mechanics*, Trans. A.S.M.E., vol. 63, 1941, p. A-77.

[3] "Theory of Elastic Stability," by S. Timoshenko, McGraw-Hill Book Co., Inc., New York, N. Y., 1936.

A	B	C
0.943	1.125	1.0
0.943	1.125	2.5
0.943	1.125	4.0
3/4	1.125	2.5
3/4	1.125	4.0
1—1/32	1.125	2.5
1—1/32	1.125	4.0



COMPRESSION SPECIMENS FOR BUCKLING TESTS

FIG. 22

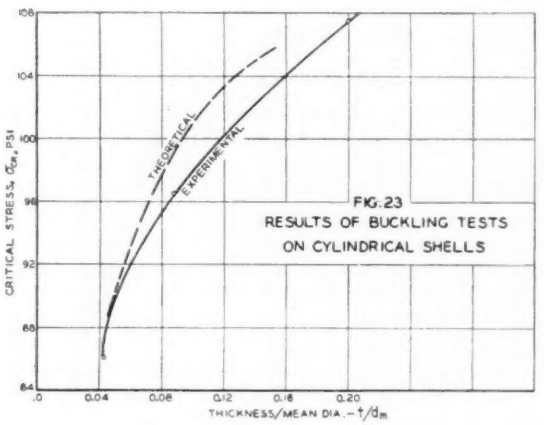


FIG. 23

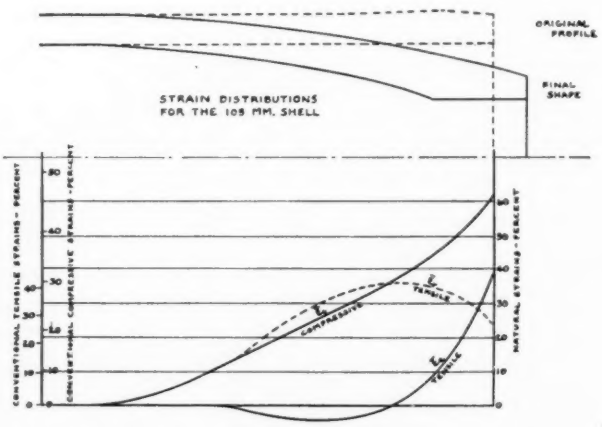


FIG. 24

a = radius of shell, in.
ν = Poisson's ratio

This formula applies only when the critical stress is below the proportional limit of the material. If buckling occurs at higher stresses, an approximate formula may be used to obtain the critical stress

$$\sigma_{cr} = \frac{E_R h}{a\sqrt{3(1-\nu^2)}} \quad \ldots\ldots\ldots\ldots\ldots\ldots [2]$$

Here, E_R, the so-called "reduced modulus," is a function of the stress-strain diagram of the material. An analytical expression for E_R for a rectangular cross section has been given by von Kármán and others

$$E_R = \frac{4EE_T}{[\sqrt{E} + \sqrt{E_T}]^2}$$

E_T is the "tangent modulus," or the slope of the stress-strain curve at σ_{cr}. While this value for E_R applies rigorously only to rectangular cross sections, it may be used as an approximation to E_R for the cylindrical shell.

In order to verify the buckling formulas given for wall thickness - diameter ratios in the range found in shells, a number of tests were made using the specimens shown in Fig. 22. A range of thickness diameter ratios from about 0.04 to 0.20 was covered by the few tests which were made.

A 200-ton Amsler press was used in making the buckling tests. The critical load was taken as the load at which an appreciable amount of radial motion took place without any increase in load. In all cases, buckling took place well within the plastic range of the material.

The results of the tests are shown in Fig. 23. The dotted line is a theoretical curve based on Equation [2]. As can be seen, the use of the reduced modulus, calculated from the stress-strain curve, gives very satisfactory results.

If the stress-strain characteristics of the material to be used for making shells are known, and the maximum forces required, it is possible for the engineer to estimate fairly closely whether there will be danger of buckling of the shell wall. Of course an estimate based on the previous experience of shell manufacturers would probably be just as reliable. Usually, information about the physical properties of materials in the plastic state is unavailable, and it is difficult to apply theoretical formulas.

Tests on Full-Sized Shells

A fairly accurate picture of the strains imposed on shells during the nosing operation was obtained by measuring rather carefully 75-mm, 105-mm, 5-in. Navy shells, and a 240-mm shell before and after nosing.

It was difficult to obtain the strain distributions for the 75-mm shell, because of the small amount of deformation which takes place when this shell is nosed. Therefore no strain curves are shown.

The distributions of the strains for the 105-mm shell are shown in Fig. 24. It should be noted that the so-called "natural" strains have been plotted. The advantage of using the natural strains is that their sum remains zero, even for large plastic strains. Thus if ϵ_z is the axial strain (measured tangent to the nose contour); ϵ_t the circumferential strain, or the reduction in diameter; and ϵ_r the increase in thickness of the shell wall, the condition of constant volumn means that

$$(1 + \epsilon_z)(1 + \epsilon_t)(1 + \epsilon_r) = 1$$

or

$$\log_e(1 + \epsilon_z) + \log_e(1 + \epsilon_t) + \log_e(1 + \epsilon_r) = 0$$

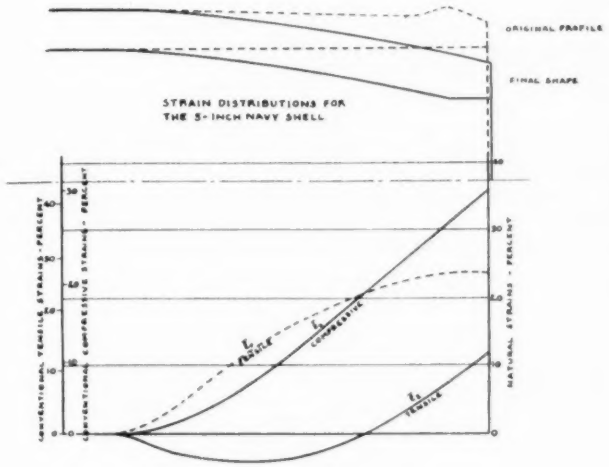


FIG. 25

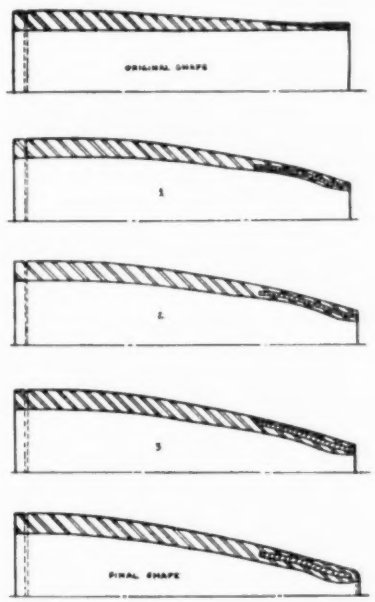


FIG. 26

Therefore, we define $\bar{\epsilon}_z$, $\bar{\epsilon}_t$, and $\bar{\epsilon}_r$ as follows:

$$\bar{\epsilon}_z = \log_e(1 + \epsilon_t)$$

$$\bar{\epsilon}_t = \log_e(1 + \epsilon_t)$$

$$\bar{\epsilon}_r = \log_e(1 + \epsilon_r)$$

and the sum of $\bar{\epsilon}_z$, $\bar{\epsilon}_t$, and $\bar{\epsilon}_r$ remains zero for any amount of plastic deformation. Conventional strain scales have been plotted on the left ordinate; a tensile strain must be considered positive, indicating an increase in length in the direction of the strain; a compressive strain must be considered negative, indicating a decrease in length.

As can be seen in Fig. 24, the maximum reduction in diameter on the 105-mm shell is about 45 per cent, giving a natural strain of something over 60 per cent. The 105-mm shell elongates considerably, resulting in a maximum conventional strain of

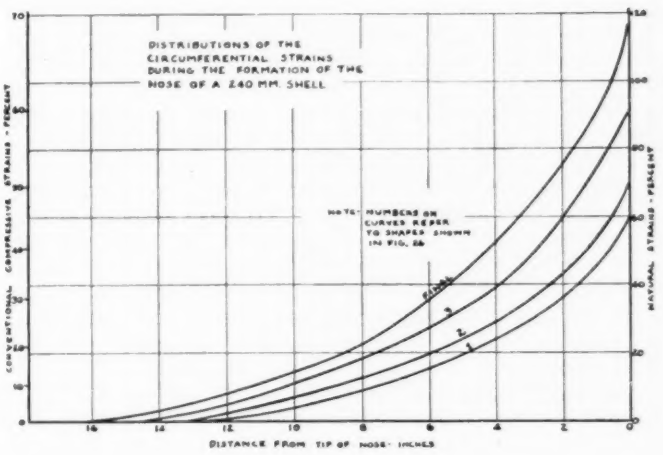


FIG. 27

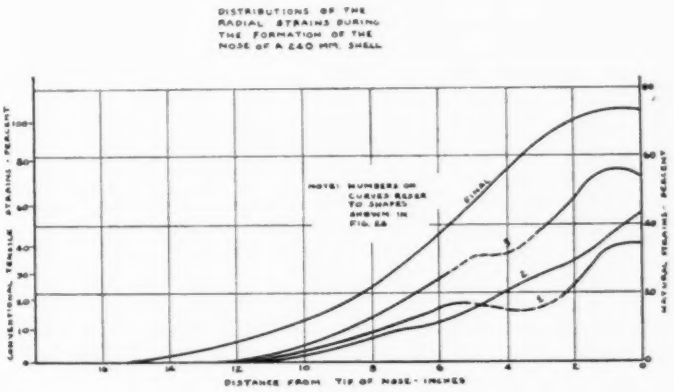


FIG. 28

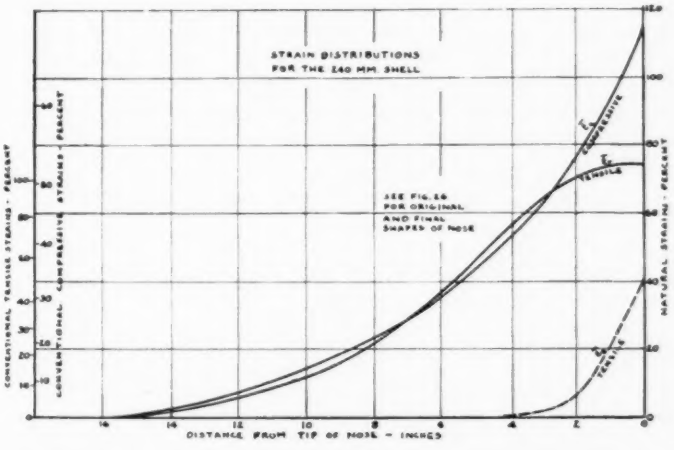


FIG. 29

about 45 per cent. The curve of the thickness change $\bar{\epsilon}_r$, is dotted, since it was obtained by making the sum of the three natural strains zero.

The strain distributions for the 5-in. Navy shell, Fig. 25, are very similar to those for the 105-mm shell. However, there is only a very slight elongation of the 5-in. shell during nosing, and, consequently, the axial strain reaches a maximum value of only 12 per cent.

A valuable set of data on the formation of the nose of a 240-

mm shell was furnished us by the committee. This shell is ordinarily nosed in one step; but in order to follow the flow of metal throughout the very great deformation, the nosing die was stopped when approximately one quarter, one half, and three quarters of the shell nose had entered the die. Thus a series of five shells, cross sections of which are shown in Fig. 26, was obtained. The thickening of the shell wall at the tip of the nose is remarkable: A radial strain of over 100 per cent occurs. The reduction in mean diameter of about 75 per cent is also an unusual amount of deformation for a single stroke of the nosing press. Curves of the radial and tangential natural strains are shown in Figs. 27 and 28. A plot of all three natural strains for the final shape is shown in Fig. 29. It is interesting to note that there is hardly any axial strain in the main body of the shell; in other words, the entire lengthening of the shell (approximately $^5/_8$ in.) takes place very near the tip of the nose.

It must be remembered that all the strain distributions which are shown have been determined on the basis of the deformation of a "mean line" in the profile of the nose. In other words, the values shown are average strains only. This method of measurement is probably justified for the major portion of the shell, but the complicated local deformation at the tip of the nose needs closer attention.

The determination of the proper nose profile to use, in order to obtain a certain finished shape after nosing, involves a consideration of the strains existing in the shell nose. This problem is one which cost the shell-forging industry thousands of dollars, and perhaps necessarily so, since there appears to be no easy way to predict what the original profile of the nose should be. In the following paragraphs a method of attacking this problem will be indicated and its limitations stated.

It has been observed that certain sizes or shapes of shells elongate considerably during nosing, while in others there is practically no axial extension. For those shells which do not elongate, it can be assumed that each element of the shell wall moves radially only; this is not, of course, an exact picture, but serves to simplify the problem considerably. The position of an element of the shell both before and after nosing can now be stated in terms of a single co-ordinate, x, that is, an element at x in the undeformed shell remains at x after nosing. Selecting as an element a ring of material having a length dx in the undeformed state and a length ds in the deformed state, we may write the following equation expressing the constancy of volume of the element

$$2\pi r_0 h_0 dx = 2\pi r h ds \qquad \left.\begin{matrix} r_0 \\ h_0 \end{matrix}\right\} \text{ original radius and thickness}$$

$$\therefore \frac{h_0}{h} = \frac{r}{r_0}\frac{ds}{dx} \qquad \left.\begin{matrix} r \\ h \end{matrix}\right\} \text{ final radius and thickness}$$

or

$$\frac{h_0}{h} = \frac{r}{r_0 \cos \alpha} \quad \ldots\ldots\ldots\ldots\ldots\ldots [3]$$

where α is the slope of the nose contour at x.

Equation [3] may be used to approximate the original thickness variation when the final shape of the nose is given and a constant value of r_0 (or a particular $r_0[x]$) may be assumed.

If the shell elongates considerably, an element originally at x goes to $x + \xi$ after the nosing, where ξ, the axial displacement of the element, is some function of x. Again, we may write the constant-volume condition as

$$2\pi r_0 h_0 dx = 2\pi r h ds$$

Now, however, r, h, and ds must be measured at $x + \xi$ when r_0 and h_0 are measured at x. Since

$$ds = d(x + \xi)/\cos \alpha$$

where α is the slope of the nose profile at $x + \xi$, we have

$$\frac{h_0}{h} = \frac{r}{r_0 \cos \alpha}\left(1 + \frac{d\xi}{dx}\right) \quad \ldots\ldots\ldots\ldots [4]$$

r, h, and α are calculated at $x + \xi$ when r_0, h_0, and ξ are calculated at x. Suppose we assume a power function as representing the variation of ξ with x (the selection of a power function is, of course, entirely arbitrary). Then if

$$\xi = \xi_{max}\left(\frac{x}{l_0}\right)$$

ξ_{max} is the maximum extension occurring at the tip of the nose, $x = l_0$, we have

$$\frac{h_0}{h} = \frac{r}{r_0 \cos \alpha}\left[1 + \frac{n\xi_{max}}{l_0^n} x^{n-1}\right] \quad \ldots\ldots\ldots\ldots [5]$$

The constants n and ξ_{max} occurring in the expression for $\xi(x)$ must be estimated from experience. If one of these can be estimated rather closely, the other may be determined approximately as follows:

If we assume that at the tip of the shell a state of pure compression exists in the circumferential direction, we should expect the strains in the axial and radial directions to be close to one half the circumferential strain. Knowing the reduction in diameter, the maximum circumferential strain can be calculated, and, consequently, we obtain the following relations

$$\epsilon_x = \frac{1}{\cos \alpha}\left(1 + \frac{d\xi}{dx}\right) - 1$$

For the maximum value of ϵ_x at the tip of the shell

$$\frac{1}{\cos \alpha}\left(1 + \frac{d\xi}{dx}\right) - 1 = -\frac{\epsilon_t}{2} \quad \ldots\ldots\ldots\ldots [6]$$

$$\frac{d\xi}{dx} = \left(1 - \frac{\epsilon_t}{2}\right)\cos \alpha - 1$$

Thus since

$$\frac{d\xi}{dx} = \frac{n\xi_{max}}{l_0^n} x^{n-1}$$

or, for $x = l_0$

$$\frac{d\xi}{dx} = \frac{n\xi_{max}}{l_0}$$

we obtain

$$\frac{n\xi_{max}}{l_0} = \left(1 - \frac{\epsilon_t}{2}\right)\cos \alpha - 1 \quad \ldots\ldots\ldots\ldots [7]$$

Thus, if either n or ξ_{max} is known, Equation [7] makes it possible to determine both the constants.

Equation [3] has been used to determine the original profile for the 5-in. shell, which does not elongate appreciably. Results of this calculation are shown in Table 2.

Equation [5] has been applied to the 240-mm shell. The value of n used in the expression for ξ was calculated from the known total axial extension ξ_{max}. Results of this calculation are shown in Table 3.

It should be apparent from the foregoing discussion that the method suggested for determining the original shell profile, know-

TABLE 2 CALCULATION OF ORIGINAL SHELL PROFILE FOR 5-IN. NAVY SHELL FROM KNOWN FINAL SHAPE

Distance from tip of nose, in.	Calculated h_0, in.	Actual measured h_0, in.
0.	0.34	0.36
0.65	0.45	0.60
1.30	0.50	0.48
2.00	0.52	0.50
2.80	0.55	0.53
3.74	0.56	0.55
4.67	0.59	0.55
5.53	0.61	0.61

NOTE: Equation used in calculation: $\frac{h_0}{h} = \frac{r}{r_0 \cos \alpha}$.

TABLE 3 CALCULATION OF ORIGINAL SHELL PROFILE FOR 240-MM SHELL

Distance from tip of nose, in.	Calculated h_0, in.	Actual measured h_0, in.
0.25	0.32	0.44
1.25	0.42	0.40
2.25	0.45	0.42
4.25	0.62	0.58
6.25	0.71	0.66
8.25	0.78	0.79
10.25	0.87	0.91
12.25	1.01	1.03
14.25	1.15	1.13
16.25	1.18	1.14

NOTE: Equation used in calculation:

$$\frac{h_0}{h} = \frac{r}{r_0 \cos \alpha}\left[1 + \frac{d\xi}{dx}\right]$$

where

$$\xi = 0.625\left(\frac{x}{18.75}\right)^{10}$$

$$\frac{d\xi}{dx} = \frac{1}{3}\left(\frac{x}{18.75}\right)^{9}$$

x is measured from a point 18.75 in. below tip of nose.

ing the final shape, will, at best, give only a rough answer to the problem. For instance, the proper shape for the tip of the nose, the most important part of the profile, cannot be determined using this method. The deformation at the tip is a complicated function of the die finish, lubrication, temperature, and speed of nosing. It is to be expected that, because of differences in equipment employed and in the technique of production, different shell manufacturers will find it necessary to use different original shapes to obtain the same final shapes.

Summary

The results of a number of model tests designed to show the effects of temperature, lubrication, and speed on the nosing process have been given. Quantitative information given in the report for the small models may be adjusted to apply to larger shells (geometrically similar to the models) by multiplying the values of the forces required to nose the models by the square of the ratio of the size of the larger shell to the size of the model. Of course, the quantitative results only have meaning for large shells when temperature and friction conditions can be assumed equivalent to those existing in the model tests.

An analysis of the strain distributions in several shells has been made; and a method has been indicated whereby the nose profile necessary to produce a desired finished shape may be determined.

Acknowledgment

The writer wishes to thank Dr. A. Nadai for many valuable suggestions offered during the course of the investigation.

GRAPHITIZATION OF STEEL PIPING

Graphitization Caused by Testing Conditions on Carbon-Molybdenum Tubular Creep-Test Specimens . . . . . *H. J. Kerr and F. Eberle* 1

Carbide Instability of Carbon-Molybdenum Steel Piping . . . . . *R. W. Emerson* 5

A Possible Means of Avoiding Local Graphitization of Steels in Service at Elevated Temperatures . . . . . *G. V. Smith and R. F. Miller* 17

Report on High-Temperature Pipe Weld Investigation . . . . . *Herman Weisberg* 19

Discussion—Graphitization of Steel Piping 30

Presented at the Annual Meeting of The American Society of Mechanical Engineers, New York, N. Y., Nov. 29–Dec. 3, 1943, under the auspices of the Joint A.S.T.M.-A.S.M.E. Research Committee on the Effect of Temperature on the Properties of Metals. Published April, 1944.

Graphitization Caused by Testing Conditions on Carbon-Molybdenum Tubular Creep-Test Specimens

By H. J. KERR,[1] NEW YORK, N. Y., AND F. EBERLE,[2] BARBERTON, OHIO

In December, 1942, the final report on tubular creep tests was made to the Society.[3] This report included data from two tubular specimens, known as F-10, which were tested for 9000 hr at 900 F, with a stress in the cylinder of 15,143 lb and 9240 lb in the hemispherical end, and specimen F-11 which was tested for 14,230 hr at 1050 F with 5800 lb stress in the cylinder and 3960 lb stress in the hemispherical end. The object of the present paper is to present results of examination of these two tubular creep-test specimens of carbon-molybdenum steel, with particular reference to graphitization caused by the testing conditions.

THE preparation of the carbon-molybdenum tubular creep coupons, for purposes of the studies to be discussed, is described in the report by Norton and Soderberg.[3] Briefly, they consisted of 4-in-OD × 1/8-in-wall machined tubes with welded-on hemispherical ends, the over-all length being 28 3/4 in. The cylindrical part of each specimen was made from a seamless tube, while the hemispherical ends were fabricated of plate made from a forged billet.

The cylindrical part of the coupons consisted of basic open-hearth carbon-molybdenum steel, of the following analysis:

	Per cent	Per cent
Carbon	0.15	0.146
Manganese	0.53	0.54
Silicon	0.21	0.21
Phosphorus	0.016	0.015
Sulphur	0.016	0.018
Molybdenum	0.56	0.53
Aluminum	0.020	0.017
Aluminum oxide	0.007	0.007
Chrome	0.20	0.21

This material was deoxidized with 1 lb of aluminum per ton.

The plate from which the hemispherical ends were made was forged from a carbon-molybdenum-steel billet. Its analysis was as follows:

	Per cent
Carbon	0.15
Manganese	0.54
Silicon	0.20
Phosphorus	0.016
Sulphur	0.025
Molybdenum	0.44
Aluminum	0.022
Aluminum oxide	0.010
Chrome	0.06

The deoxidation practice used in melting this material was not obtained since it formed no part of the test program.

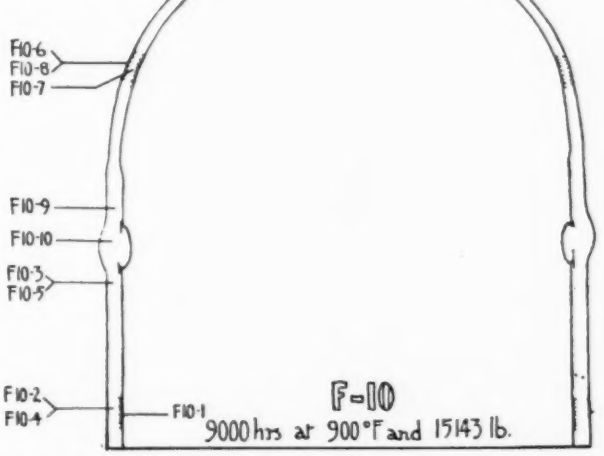


FIG. 1 COUPON F-10: SECTION THROUGH HEMISPHERICAL END, SHOWING LOCATION OF GRAPHITE AND MICROSTRUCTURES EXAMINED; 3/5 SIZE

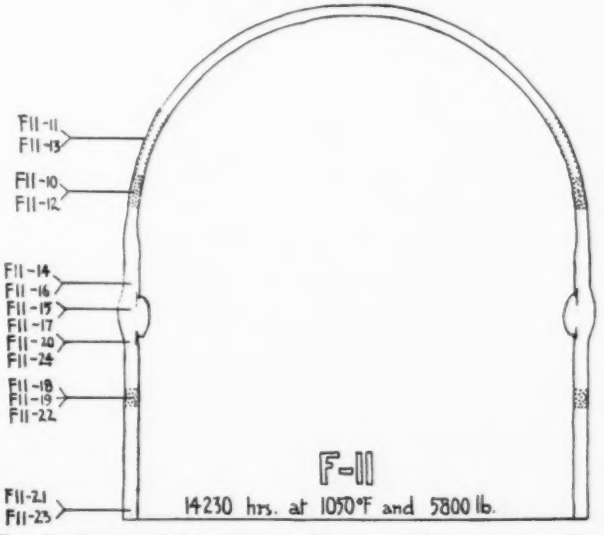


FIG. 2 COUPON F-11: SECTION THROUGH HEMISPHERICAL END SHOWING LOCATION OF GRAPHITE AND MICROSTRUCTURES EXAMINED; 3/5 SIZE

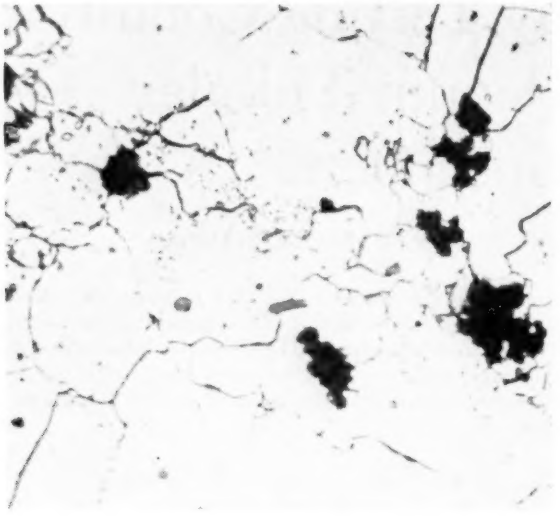
[1] Executive Assistant, The Babcock & Wilcox Co. Mem. A.S.M.E.

[2] Metallurgist, The Babcock & Wilcox Co.

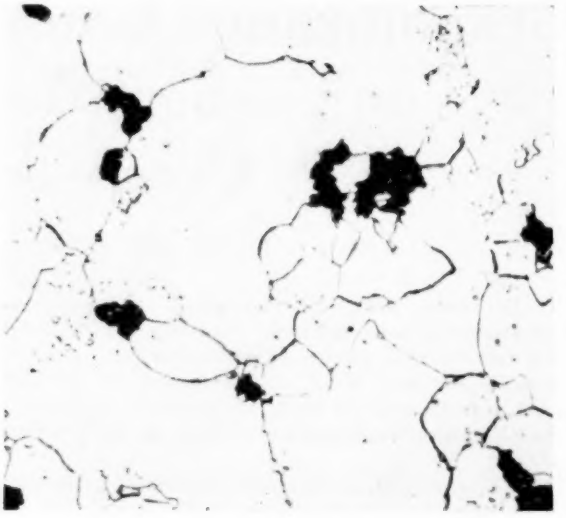
[3] "Report on Tubular Creep Tests," by F. H. Norton and C. R. Soderberg, presented at a meeting of the A.S.M.E.-A.S.T.M. Joint Research Committee on the Effect of Temperature on the Properties of Metals, held at New York, N. Y., December, 1941, published in Trans. A.S.M.E., vol. 64, 1942, pp. 769–777.

Contributed by the Joint A.S.T.M.-A.S.M.E. Research Committee on the Effect of Temperature on the Properties of Metals and presented at the Annual Meeting, New York, N. Y., Nov. 29–Dec. 3, 1943, of THE AMERICAN SOCIETY OF MECHANICAL ENGINEERS.

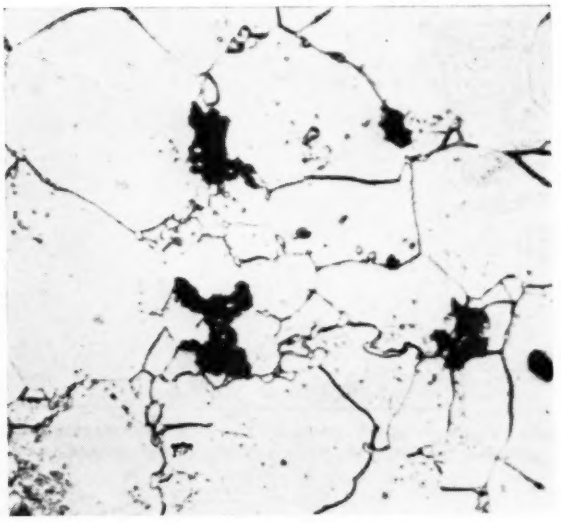
NOTE: Statements and opinions advanced in papers are to be understood as individual expressions of their authors and not those of the Society.



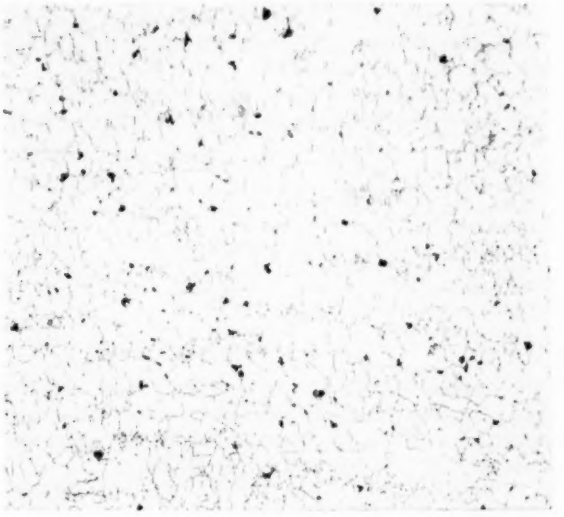
(*a*) Picral; ×1000



(*b*) Picral; ×1000



(*c*) Picral; ×1000



(*d*) Nital; ×100



(*e*) Unetched; ×100

FIG. 3 COUPON F-11: HEMISPHERICAL END, GRAPHITE IN LOW-TEMPERATURE REGION OF WELD-AFFECTED ZONE

Thermal Treatment of Materials Prior to Welding. The $4^1/_2$-in-OD × $^3/_4$-in-wall tube from which the creep coupons were subsequently machined was annealed in a car-type gas-fired furnace by holding 1 hr at 1350 F, followed by slow furnace cooling (50 F per hr) to 1100 F, from which temperature they were air-cooled. The hemispherical ends received the following heat-treatment after the hot-cupping operation was finished:

(*a*) Heated to 1650 F, held for 30 min, and air-cooled.

(*b*) Reheated to 1620 F, held for 30 min, and furnace-cooled.

Welding Conditions. The cupped ends were welded to the cylindrical part of the coupons with an oxyacetylene torch (neutral flame) and without preheating. The filler rod consisted of $^1/_8$-in-diam carbon-molybdenum steel wire. The finished coupons were stress-annealed in a box through which a continuous flow of nitrogen was maintained by holding at 1200 F for $1^1/_4$ hr, followed by furnace cooling.

Microscopic Examination. The microscopic examination was conducted with transverse sections, as shown in Figs. 1 and 2, which also show the locations at which photomicrographs were taken. Additional specimens were removed from the center of the cylindrical portions of the coupons. Examination of these samples indicated the following:

Coupon F-10 (9000 hr at 900 F)

1—Cylindrical part; stress, 15,143 lb.

(*a*) Some small graphite nodules at the inside surface were found in the low-temperature region of the heat-affected zone, where the carbide was totally spheroidized. This is marked, F-10-1 in Fig. 1.

(*b*) Carbide in the low-temperature region of the heat-affected zone, predominantly but not totally spheroidized.

(*c*) The weld-affected zone at a distance from the weld metal of about $^1/_8$ in.; coarse-grained and acicular.

(*d*) The weld metal extremely coarse-grained and acicular.

(*e*) Heat-unaffected metal at the center of cylindrical portion, partially spheroidized.

2—Hemispherical end; stress, 9240 lb.

(*a*) Graphite at the inside and outside surfaces in the low-temperature region of the weld-affected zone, marked F10-6 and -8 in Fig. 1.

(*b*) Center of wall thickness in low-temperature region of heat-affected zone, free from graphite. Carbide partially spheroidized and coalesced in grain boundaries, Fig. 1, at F10-7.

(*c*) Weld-affected zone at a distance from the weld metal of about $^1/_8$ in., extremely coarse-grained and acicular.

Coupon F-11 (14,230 hr at 1050 F)

1—Cylindrical part; stress, 5800 lb.

(*a*) Some scattered small graphite nodules in low-temperature region of weld-affected zone marked F11-18, -19, -22 in Fig. 2.

(*b*) Carbide in the low-temperature region of the weld-affected zone totally spheroidized.

(*c*) Weld-affected zone at a distance from the weld metal of about $^1/_8$ in., coarse-grained and spheroidized, but acicular pattern retained.

(*d*) Weld-unaffected metal at about $1^3/_4$ in. distance from the weld metal almost totally spheroidized but acicular carbide pattern still visible.

(*e*) Heat-unaffected metal, at center of cylindrical portion, predominantly spheroidized.

2—Hemispherical end; stress, 3960 lb.

(*a*) Scattered medium to small graphite nodules in low-temperature region of weld-affected zone, marked F11-10 and -12 in Fig. 2.

(*b*) Some scattered grain-boundary graphite near inside and outside surfaces beyond low-temperature region of weld-affected zone; marked F11-11 and -13, in Fig. 2.

(*c*) Carbide in the low-temperature region of weld-affected zone totally spheroidized and partially coalesced.

(*d*) Weld-affected zone at a distance from the weld metal of about $^1/_8$ in., fine-grained and spheroidized with original acicular pattern almost totally obliterated.

(*e*) Weld metal fine-grained and totally spheroidized.

Fig. 3(*a* to *e*), shows photomicrographs indicating the arrangement and extent of the graphitization which has taken place in the hemispherical end of the F-11 tubular specimen.

Chemical Analysis. A section of material taken from positions 10 and 12 of F-11, $^3/_8$ in. wide × 1 in. long, was sent to the Bureau of Standards, which reported graphite as 0.060 per cent. On another section of the hemispherical end, on which no graphite was found under the microscope, the Bureau's blank test showed the value of 0.004 per cent.

A sample from another position of the same section was analyzed by Mr. Herzig, of the Climax Molybdenum Company laboratory, at Detroit, and showed graphite of 0.032 per cent.

Grain Size and McQuaid-Ehn Characteristics. The grain size and McQuaid-Ehn characteristics of the materials involved were as follows:

	Actual grain size, A.S.T.M. no.	McQuaid-Ehn grain size, A.S.T.M. no.	McQuaid-Ehn normality
Specimen F-10			
Cylinder.....	6	6–7	Abnormal
Cupped end..	8	8	Abnormal
Specimen F-11			
Cylinder.....	6	6–7	Abnormal
Cupped end..	8	8	Abnormal

To sum up, both creep coupons showed graphitization in the low-temperature region of the weld-affected zones. In coupon F-10, which had been at 900 F for 9000 hr, graphitization was confined to the surface layers, while coupon F-11, which had been at 1050 F for 14,230 hr, displayed graphitization through the whole wall thickness of the low-temperature region of the heat-affected zones. Furthermore, graphitization was more pronounced in the hemispherical ends than in the cylindrical sections. This holds true for both coupons. Graphitization was in all cases only slight.

The two carbon-molybdenum steels involved were aluminum deoxidized in a manner which produced a fine-grained abnormal McQuaid-Ehn case. The hemispherical-end material was more pronounced in its abnormality and was finer-grained than the steel from the cylindrical sections. The hemispherical ends displayed a greater propensity to graphitize than the cylindrical sections. It should also be remembered that the steel of the cylindrical sections had been spheroidized-annealed prior to the final welding and stress-relieving treatment, while the hemispherical ends were in an annealed condition prior to the welding and final stress-relieving operation.

The occurrence of graphite near the surface of the low-temperature heat-affected zone of coupon F-10 is not readily explainable. Microscopic evidence points to the fact that the surface layers were spheroidized to a greater degree than the interior portion of the wall thickness. This might have been brought about by cold work from the previous machining operation.

These data are presented since they give definite information on the formation of graphite under a given life span, a given

stress, and a given temperature, which may be of help to those now engaged in the study of this phenomenon.

ACKNOWLEDGMENT

Acknowledgment is made of assistance rendered in this investigation by Dr. G. E. F. Lundell and Mr. H. A. Bright, M.S., of the National Bureau of Standards, Dr. Russell Franks, Union Carbide and Carbon Research Laboratories, Inc., and Mr. Alvin J. Herzig, Chief Metallurgist, Climax Molybdenum Company laboratory.

Carbide Instability of Carbon-Molybdenum Steel Piping

By R. W. EMERSON,[1] PITTSBURGH, PA.

An investigation of the complete failure of a carbon-molybdenum-steel steam pipe adjacent to a weld revealed the failure to be the result of graphite segregation. The examination of a number of specimens taken from other welded joints in high-temperature steam lines has shown that graphitization occurs in the base metal at the extremity of the heat-affected zone of the weld. Graphite may be present in either the "chain" or "nodular" form, depending upon the grain size and microstructure of the material as originally welded. Visual observation, bend testing, and microscopic examination have been found to give good correlation when examining specimens for segregated graphite. The use of relatively large quantities of aluminum as a deoxidant in steel is believed to affect carbide stability adversely. The postheating or stress-relieving temperature used after welding is believed to be a most important factor in determining whether or not segregated graphite will occur in a steel which has inherent carbide instability.

Introduction

A COMPLETE failure of a carbon-molybdenum-steel steam pipe adjacent to a weld occurred approximately 1 year ago. The investigation of this failure, and a number of other similar carbon-molybdenum steel pipe joints which had not failed, revealed that an extremely narrow band of iron-carbide or complex iron-molybdenum carbide was placed in a definite metastable condition at a distance of approximately $^1/_8$ to $^3/_{16}$ in. from the fusion line of the weld as a result of the welding heat on the base metal. This narrow band of unstable carbide, though existent at the time welding is complete, is decomposed to the more stable form of ferrite and graphite as a result of subsequent long-time subcritical heating in the temperature range of 850 to 1000 F, the operating temperature used in high-pressure generating stations. The decomposition of the carbide results in graphite precipitation which in turn gives rise to weakness, particularly from the standpoint of ductility. Sudden shock, either mechanical or thermal, on a joint which is severely graphitized may easily result in complete rupture. The width of the graphitized zone has been found to vary, but is usually of the magnitude of 0.001 to 0.01 in.

Two Types of Graphitization Discussed

A section of the fractured surface of a steam pipe which completely failed as a result of intergranular graphitization is shown one-half size in Fig. 1. Observation of this figure indicates that the failure occurred along the fusion line of the weld since each layer of welding, as it was deposited, is clearly revealed on the fractured surface. Contrary to this, however, it was found that upon sectioning the failure, the fusion line of the weld was completely intact. The failure had occurred in the base metal parallel to, but at a distance of approximately $^1/_8$ in. from, the fusion line of the weld. A second pipe joint was removed from the line, sectioned, polished, and etched as shown in Fig. 2.



Fig. 1 Section of C-Mo Pipe Failure Adjacent to Weld (Failure resulted from intergranular graphitization; ×1/2.)

The dark overlapping lines of segregated graphite at the extremity of the heat-affected zone (about $^1/_8$ in. outside the fusion line of the weld) on each side of the weld are clearly visible in this figure. It is the path of the overlapping lines of segregated graphite, as shown in Fig. 2, which represents the path of rupture as shown in Fig. 1. Figs. 3 to 5, inclusive, are presented to develop both the pattern of the graphite with respect to the metal structure, and the detail of the graphite itself in a structurally coarse-grain carbon-molybdenum pipe material as shown in Fig. 2, having originally a Widmanstätten carbide structure.

The intersection of two "isotherms" or "eyebrows"[2] of graphite, as observed in Fig. 2, is shown in Fig. 3, at a magnification of 100 diam. It is to be noted that the graphite nodules follow predominantly the periphery of the coarse Widmanstätten carbide grains. These nodules, due to their number and gradual growth in service, eventually in some cases become connected to form a semi-continuous to continuous chain of graphite. "Chain graphite,"

[1] Metallurgist, Pittsburgh Piping & Equipment Company.

Contributed by the Joint A.S.T.M.-A.S.M.E. Research Committee on the Effect of Temperature on the Properties of Metals and presented at the Annual Meeting, New York, N. Y., Nov. 29–Dec. 3, 1943, of The American Society of Mechanical Engineers.

Note: Statements and opinions advanced in papers are to be understood as individual expressions of their authors and not those of the Society.

[2] Since the dark, curved, narrow bands of graphite in Fig. 2 represent lines of constant temperature, in the vicinity of 1350 to 1400 F, at the time each of the welding beads was deposited during the welding of the joint, the term "isotherm" has been used when referring to the individual curved graphitized bands. These bands have also been called "eyebrows" or "whiskers."

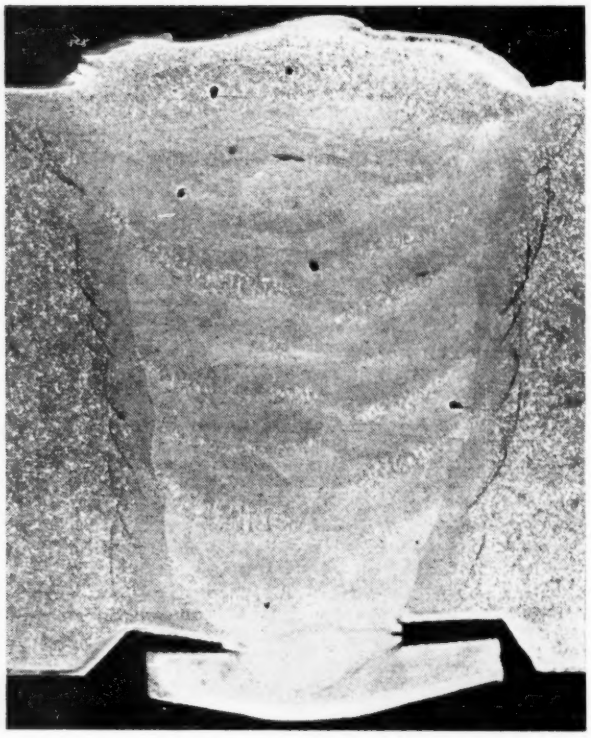


FIG. 2 WELDED JOINT EXHIBITING INTERGRANULAR GRAPHITIZATION AT EXTREMITY OF WELD HEAT-AFFECTED BASE MATERIAL
(Graphitization occurred during 5½ years' service at 935 F average service temperature; ×2.)

as it has then been named, is made up fundamentally of graphite nodules. This type of graphitization, however, is not to be confused with so-called "nodular" graphitization.

The graphitization shown in Fig. 3 is considered by the author to be sufficiently connected both around and between the Widmanstätten carbide grains to be identified as "chain" graphitization. The enclosed area of Fig. 3 definitely contains a long "chain" of overlapping graphite nodules, in fact the graphite appears as a semicontinuous void or crack. This area is shown in Fig. 4, at a magnification of 250 diam. Details of both the more dispersed graphite nodules as well as the overlapping nodules which make up the graphite "chain" can be seen. To develop further the detail of the graphite nodules which make up the chain, the enclosed area in Fig. 4 is shown in Fig. 5 at 850 diam magnification. It is believed this illustration provides ample detail to prove the nodular make-up of this graphite chain.

In contrast to Figs. 3 to 5, inclusive, graphitization of a fine-grained pearlitic structure in a cast carbon-molybdenum-base elbow is shown in Fig. 6 at both 100 and 600 diam magnification. Since at 100 diam, the graphite nodules are lined up, this might be considered by some as "chain" graphite. Close observation, however, reveals that, while the average nodule size is larger than that shown in Fig. 3, definite separation of most nodules is apparent. This is further substantiated at 600 diam. For this reason the author chooses to consider this as "nodular" rather than "chain" graphite. Although a condition such as shown in Fig. 3 is believed to be more hazardous than that shown in Fig. 6(*a*), it is not to be inferred that the latter type of graphitization cannot become equally as hazardous.

A bend test made through the heat-affected zones of a weld joining an upset pipe end to a valve casting, is shown in Fig. 7. Graphitization in the valve casting while in a more advanced stage than shown in Fig. 6 was of the nodular type. It can be seen that complete fracture of the casting occurred along the graphitized zone. Graphitization was also present on the pipe side of the weld, though to a lesser degree, as evidenced by the greater angle of bending, and the opening of only one "isotherm." It is to be mentioned that graphitization on the pipe side of this joint was of the chain type, but only partially developed.

EFFECT OF GRAIN SIZE AND METAL STRUCTURE ON CARBIDE INSTABILITY

Observation of graphitization in numerous specimens of both cast and rolled carbon-molybdenum piping material adjacent to welds indicates that graphitization will occur in both structurally fine- and coarse-grain material having either a pearlitic or Widmanstätten carbide type of microstructure.

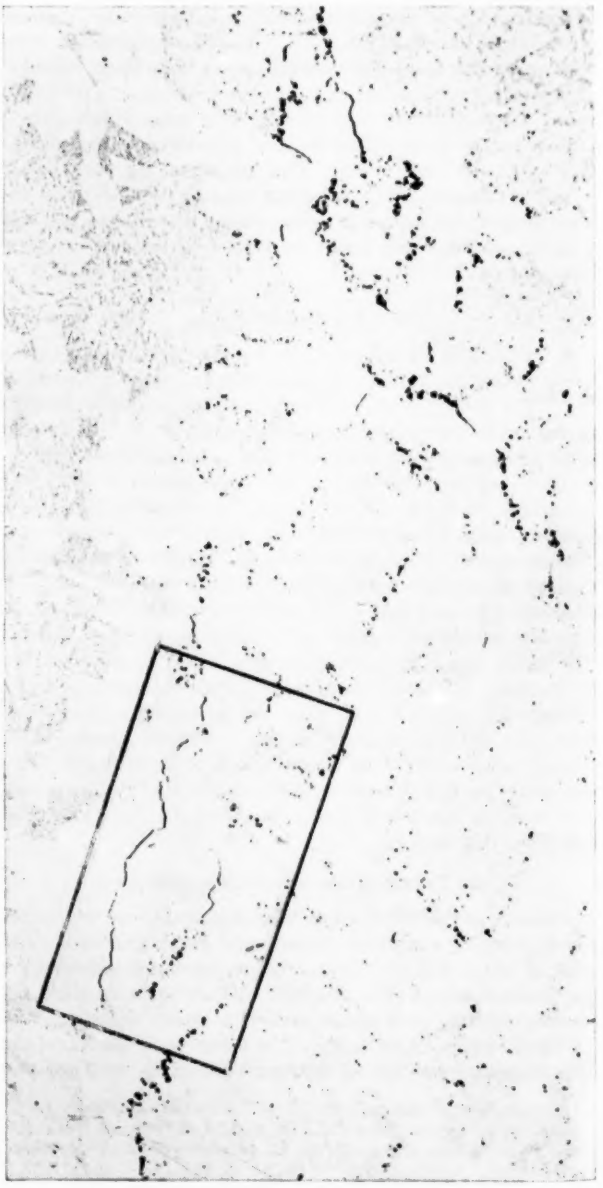


FIG. 3 "CHAIN" GRAPHITE
(Intersection of isotherms showing graphitization to be predominantly intergranular in nature; ×100.)

The only two carbide structures usually encountered are the Widmanstätten and pearlitic types, although the grain size associated with each of the two types has been found to vary from "fine" to "coarse." As previously pointed out, a fine-grain pearlitic structure results in "nodular" graphitization, while a coarse-grain Widmanstätten carbide structure results in "chain" graphitization. The type of graphitization encountered is believed to be primarily dependent upon the grain size, rather than upon the carbide structure. This hypothesis is based on the well-established fact that the alpha-gamma transformation in steel occurs first at the grain boundaries. If a steel specimen is gradiently heated, as is the case during welding, there will be a certain location on the specimen where the temperature reached is just sufficient to produce grain-boundary transformation.

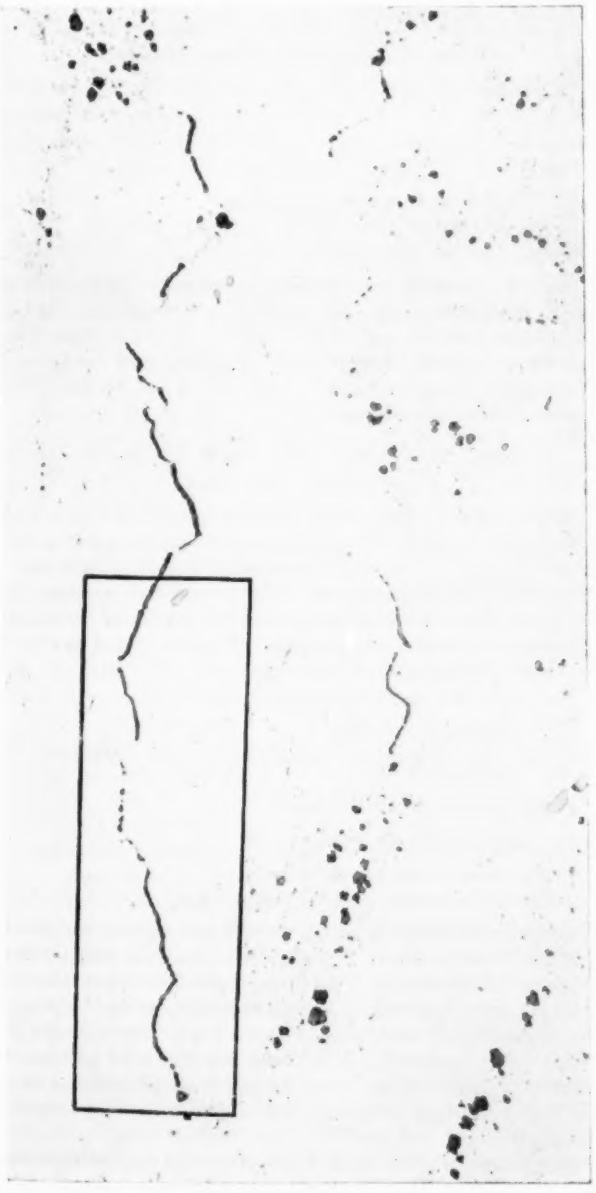


FIG. 4 VIEW OF ENCLOSED AREA IN FIG. 3, AT HIGHER MAGNIFICATION
(Note graphite detail showing "chain" graphite to consist of small connected graphite nodules; ×250.)

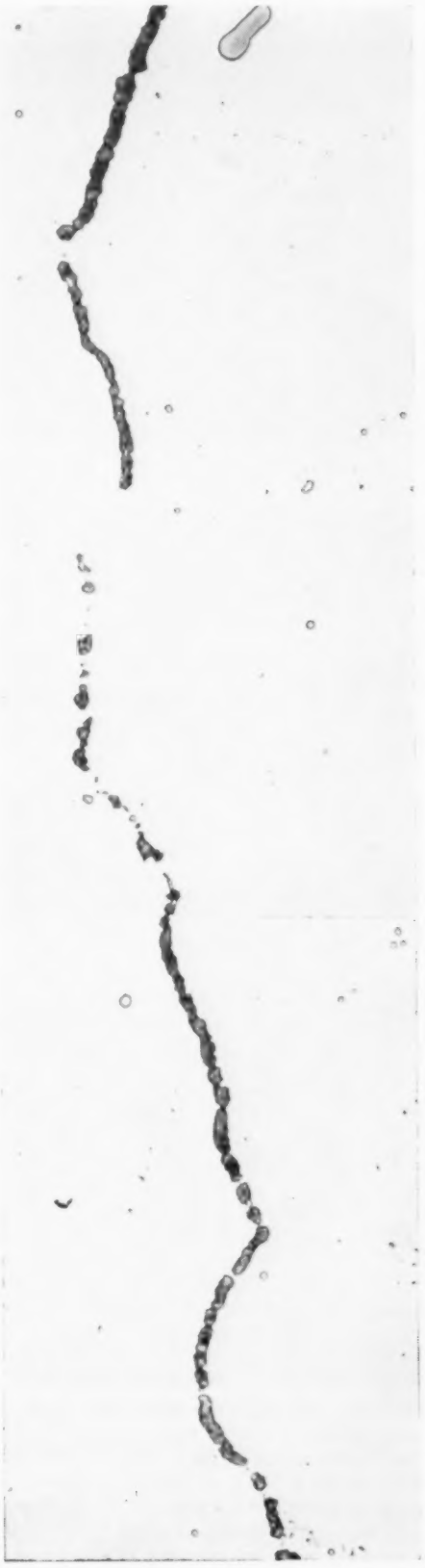
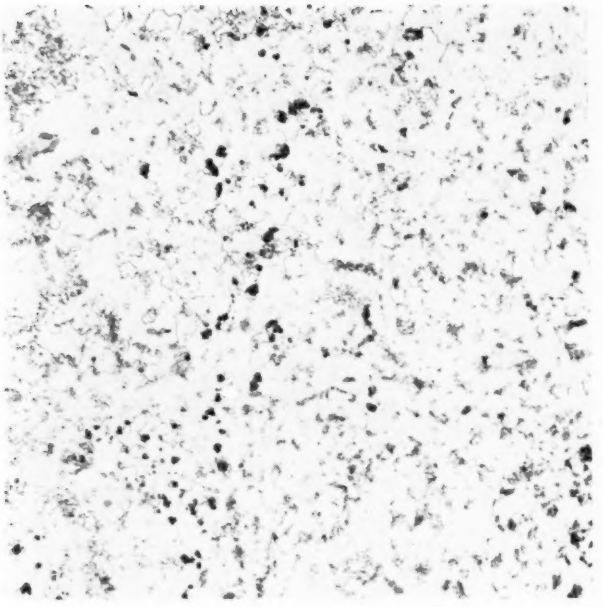
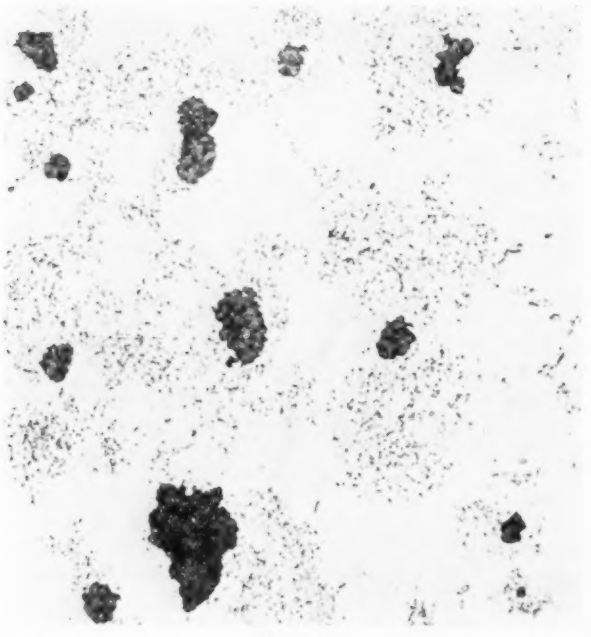


FIG. 5 VIEW OF ENCLOSED AREA OF FIG. 4, at STILL HIGHER MAGNIFICATION; ×850



(*a*) ×100



(*b*) ×600

FIG. 6 NODULAR GRAPHITIZATION ADJACENT TO WELD IN A FINE-GRAIN CAST C-MO ELBOW

For purpose of discussion, we may consider the pearlitic- or carbide-containing grain in a fine-grain steel to consist essentially of grain boundary, and we may therefore assume the entire grain to transform. On the contrary, a coarse-grain material would transform only at the grain boundary. Since microscopic observation reveals that it is the grain-boundary structure which transforms at the approximate temperature level of the Ar_1 (1350 F) during welding, which subsequently decomposes to graphite upon long-time heating in the temperature range of 850 to 1000 F, it seems logical that the coarse-grain structure would be completely enveloped by graphite within the zone of Ar_1 boundary

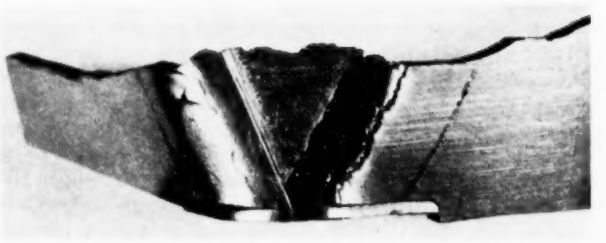


FIG. 7 BEND TEST ON UPSET PIPE END WELDED TO C-MO VALVE CASTING

(Note fissure in pipe and complete fracture of valve casting; ×3/4.)

transformation, while the entire grain of a fine-grain pearlitic carbide structure would graphitize.

DETERMINATION OF SEGREGATED GRAPHITE

Three relatively simple tests, all of which give good correlation, can be applied to reveal the existence of segregated graphite. These tests, all of which have been previously illustrated, are as follows:

1 Visual or macroscopic observation.
2 Bend testing.
3 Microscopic examination.

Heavily segregated graphite can be revealed by all three methods, as illustrated by Figs. 2, 3, and 7; while moderate segregation can be detected only by the latter two methods (Figs. 3 and 7). Graphite present in either a highly dispersed condition or in a partially developed state of segregation can be found only by microscopic examination.

FACTORS RESPONSIBLE FOR CARBIDE INSTABILITY AND SUBSEQUENT GRAPHITIZATION

The factors responsible for carbide instability and subsequent graphitization may be divided into two categories, namely, those factors which are responsible for the formation of unstable iron or complex iron-molybdenum carbide in carbon-molybdenum steel, and those factors which are responsible for the actual breakdown of the unstable carbide to graphite. These are listed in what is believed to be the order of their importance.

Factors responsible for the metastable carbide:

1 Steel-melting practice.
2 Gradient heating and quenching of steel during welding process.
3 Grain size and metal structure.

Factors responsible for graphitization:

1 Operating steam temperature.
2 Service hours at operating temperature.

Considering first the actual breakdown of the carbide to graphite, there seems to be sufficient evidence to indicate that graphite (unless present in submicroscopic dispersion) does not exist adjacent to a weld in carbon-molybdenum steel piping at the actual time of completion of such a joint. On this basis, the actual graphitization which has been found to exist adjacent to welds is produced by the operating steam temperature to which the piping has been subjected (850–1000 F), over an extended period of time (4 to 6 years).

Graphitization produced in such a manner progresses with time and is accelerated by increased operating temperatures up to some undetermined maximum which is believed to be in the vicinity of 1050 to 1150 F.

Since operating a high-pressure steam-generating station without employing steam temperatures in the 850 to 1000 F range

would be most unsatisfactory, emphasis must be placed not upon the service conditions (within reasonable limits) which break down the unstable carbide to graphite, but rather upon those factors which are responsible for the formation of the unstable carbide, and the elimination of such an unstable structure.

Considering this phase of the problem, there is convincing evidence that steel-melting practice, which has already been found to have a pronounced influence on the creep characteristics of both plain-carbon and carbon-molybdenum steel, has a definite effect on carbide instability at elevated subcritical temperatures.

Evidence of this is based upon the fact that the weld which was common to the pipe that failed (Fig. 1) as a result of intergranular graphitization was also common to a forged superheater outlet header having for all practical purposes the same chemical analysis. The analysis of the header, weld deposit, and pipe are given in Table 1.

There was, however, no evidence of structural instability of the forged header adjacent to the weld. The thermal history, as a result of the welding procedure, including preheating, welding, and stress relieving, was again for all practical purposes identical to that of the pipe which failed.

TABLE 1 CHEMICAL ANALYSIS OF SUPERHEATER-HEADER, WELD DEPOSIT, AND PIPE

	Chemical analysis, Per cent								
	C	Mn	P	S	Si	Mo	Cr	Ni	Remarks
Forged header	0.10	0.45	0.008	0.020	0.16	0.60	[a]	[a]	No graphite
Weld deposit	0.11	0.45	0.028	0.018	0.07	0.60			No graphite
Pipe	0.14	0.49	0.014	0.018	0.17	0.50	[a]	[a]	Segregated graphite

[a] Spectrographic analysis indicated residual Cr and Ni in header to be higher than in pipe, but less than 0.10 per cent.

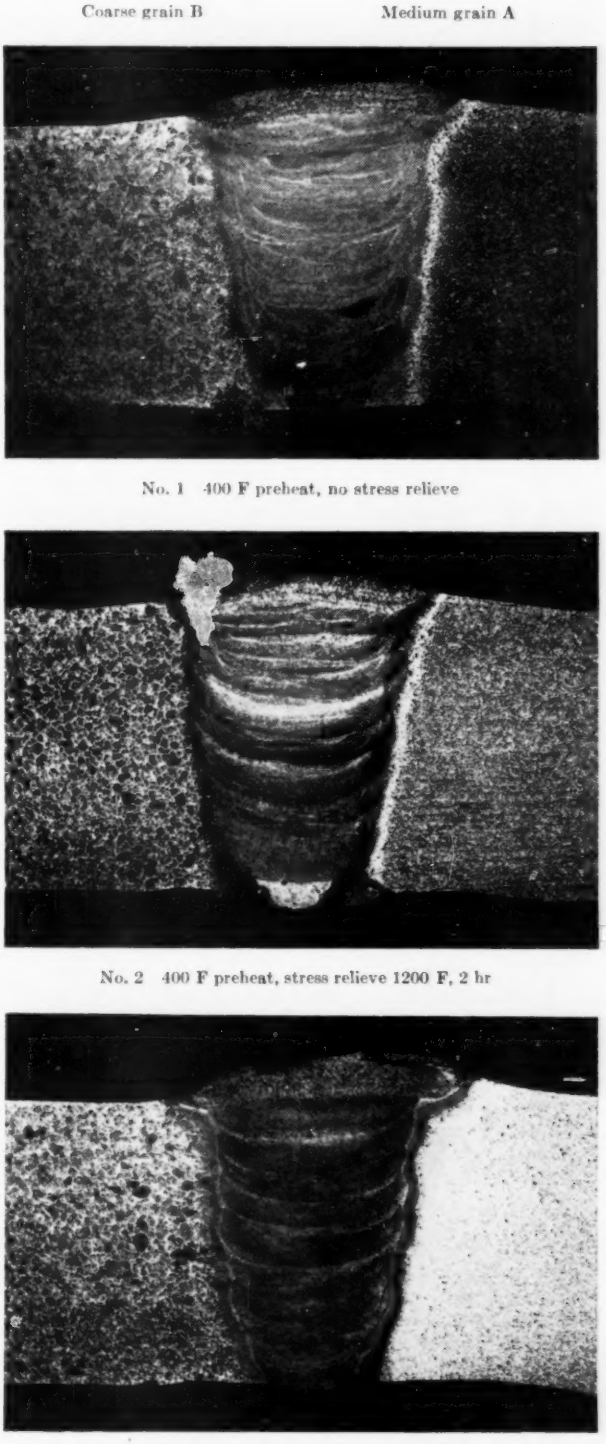
Assuming identical thermal history of the two materials adjacent to the weld throughout the entire welding procedure, it may be further assumed that the time-temperature cycle, which produced the narrow zone of unstable or sensitized carbide on the pipe side of the weld, must have likewise produced a potentially unstable zone in a similar location on the header side of the weld.

Due to differences in the inherent carbide stability of the two steels, however, the narrow zone of carbide on the header side of the weld which was placed in a state of least resistance to graphitization, proved stable, whereas the zone in the same location on the pipe side (likewise in a state of least resistance) proved unstable as evidenced by graphitization.

This is believed unquestionably to be a steel-melting problem. On the basis of this case, as well as several others all of which were welded pipe to forging joints, it is believed that the entire problem could be solved by the use of the proper deoxidation practice alone, or in combination with the use of a small alloy addition to this material which would stabilize the carbide phase regardless of the grain size and microstructure. One of the known differences in the manufacture of steels which have a stable carbide structure, as contrasted with those which do not, is in the amount of aluminum used for deoxidation. Those steels which have a stable structure have been found to be deoxidized principally with silicon, aluminum being used to the extent of $^1/_4$ lb per ton or less. Those which have proved unstable have been given a final deoxidation treatment of 1 to $2^1/_2$ lb of aluminum per ton. Structural grain size and possibly microstructure of the material prior to welding, as previously discussed is believed to effect only the general pattern of graphitization rather than directly effecting graphitization itself. Structural grain size and microstructure, for this reason, are considered to be of secondary importance.

Duplication of Graphite and Its Elimination

At the present time, there are hundreds of tons of carbon-molybdenum steel piping in service, a large percentage of which has been found to be in various stages of graphitization. There are also considerable quantities of this material undergoing fabrication which will then be used in high-temperature installations. For this reason it seemed advisable to reproduce, if possible, the condition of graphitization as found adjacent to welded

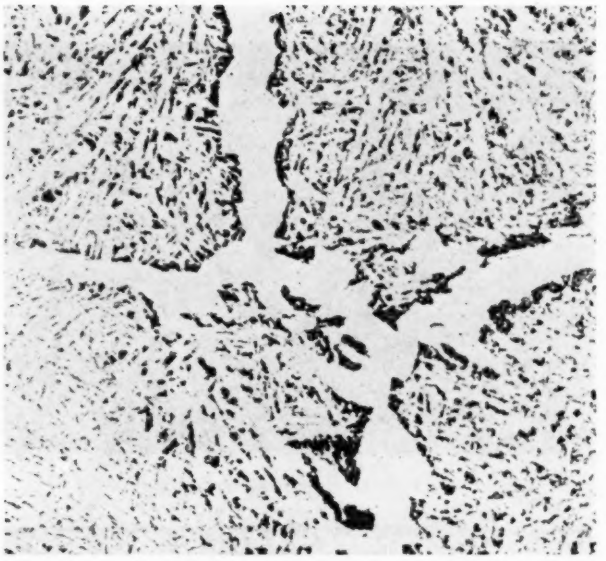


No. 1 400 F preheat, no stress relieve

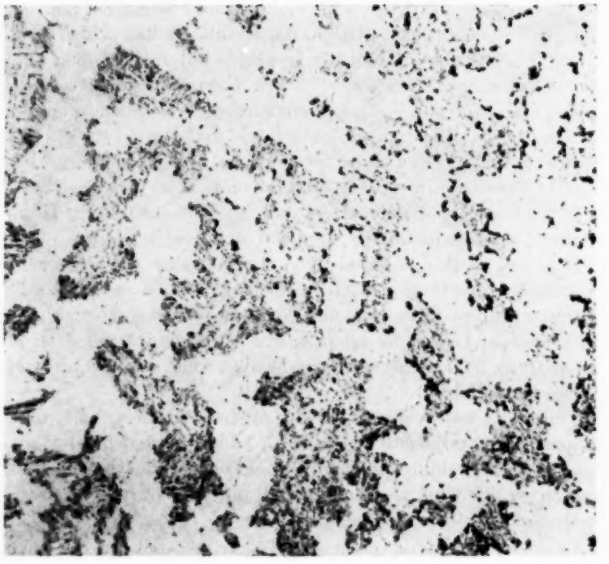
No. 2 400 F preheat, stress relieve 1200 F, 2 hr

No. 3 400 F preheat, stress relieve 1300 F, 20 hr

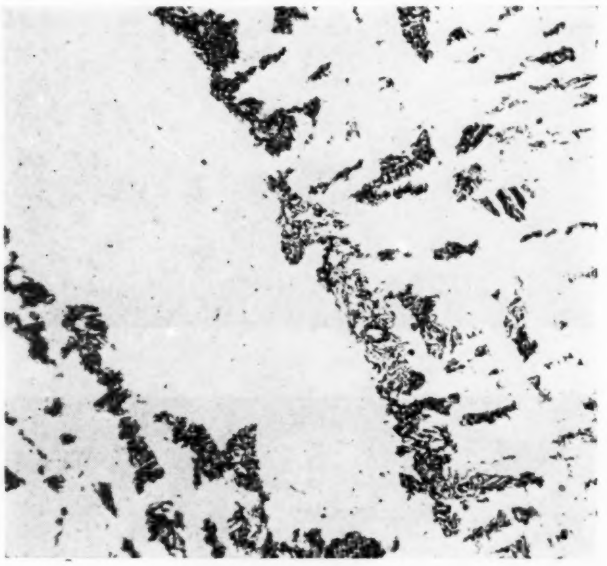
Fig. 8 Macrospecimens Etched in Hot 50 Per Cent Hydrochloric Acid; ×1



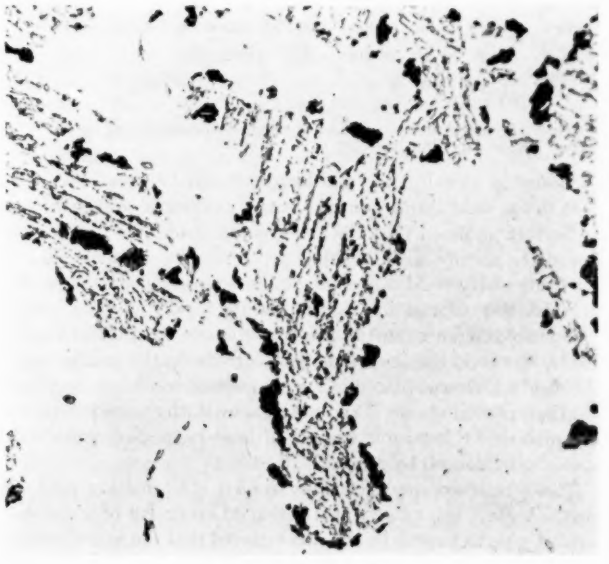
Specimen 1B; ×100



Specimen 1A; ×100



Specimen 1B; ×500



Specimen 1A; ×500

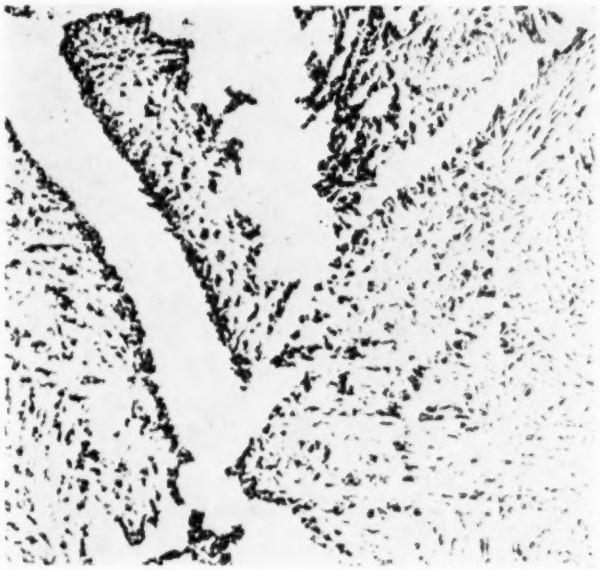
FIG. 9 CONTACT ZONES OF SPECIMEN 1
(Note: Regions of grain-boundary transformation are areas of potential graphitization.)

joints, and keeping in mind practical methods for its elimination.

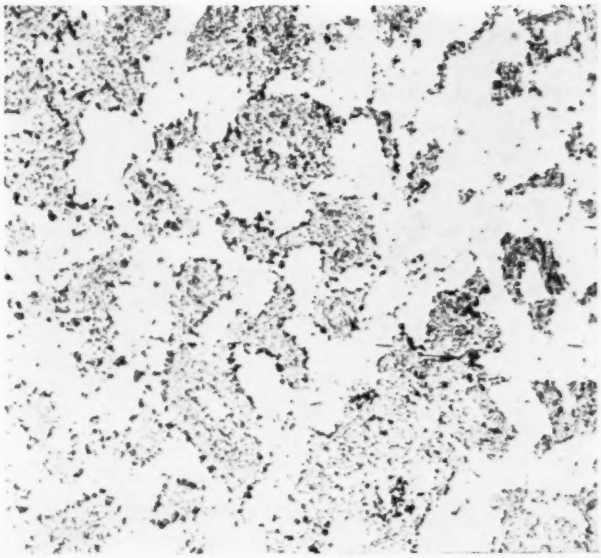
The procedure adopted in this investigation is as follows:

Test Procedure. A $12^{3}/_{4}$-in.-OD × $1^{7}/_{16}$-in. wall thickness carbon-molybdenum steel pipe section 14 in. long, containing a circumferential weld at the center, was removed from a steam line which had had $5^{1}/_{2}$ years of service at an average temperature of 935 F. It was believed that graphitization could be reproduced in this section of pipe since graphitization had already been encountered in other sections of this piping in service.

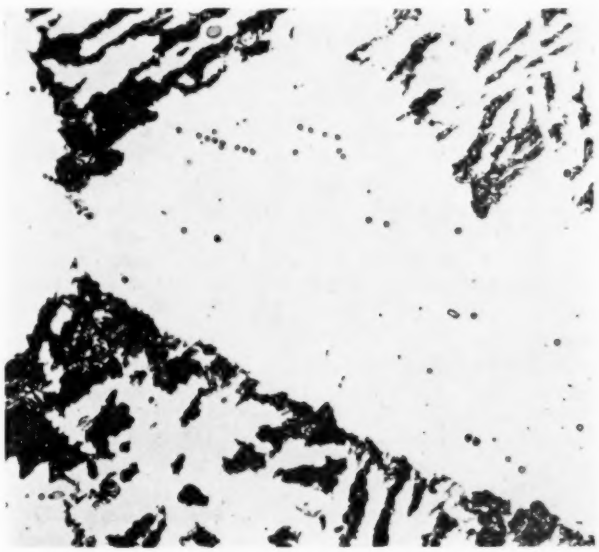
The entire weld was removed together with approximately $^{3}/_{4}$ in. of pipe on either side of the weld. Upset pipe ends were used in the original installation which were not completely removed with the weld. One of the two pieces of pipe without further heat-treatment was rebeveled for welding near the extremity of the upset end. The remaining piece was placed in an upsetting furnace and heated to a temperature of 2600 to 2800 F for 1 hr in order to produce a condition of exaggerated grain growth. The pipe after heating was cooled in still air, rebeveled, and welded to the piece having no heat-treatment. The joint was then preheated to 400 F and welded in the fixed horizontal position. After welding, a number of longitudinal specimens were removed from the pipe, numbered, and given one of three different stress-relieving treatments, namely, (*a*) no stress relieve, (*b*) 1200 F stress relieve for 2 hr, (*c*) 1300 F stress relieve for 20 hr. Two sets of specimens were subsequently placed in a furnace which operated through a 28-day temperature cycle of 950–1050–1150–1050–950 F, etc., the temperature being changed weekly for a total of 1968 hr. These specimens were accordingly marked 1S, 2S, and 3S. Both the procedure and the results are shown in condensed form in Table 2.



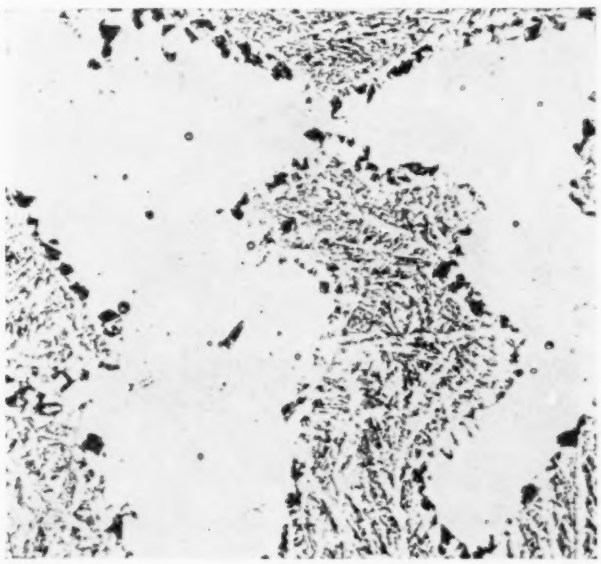
Specimen 2B; ×100



Specimen 2A; ×100



Specimen 2B; ×500



Specimen 2A; ×500

FIG. 10 CONTACT ZONES OF SPECIMEN 2

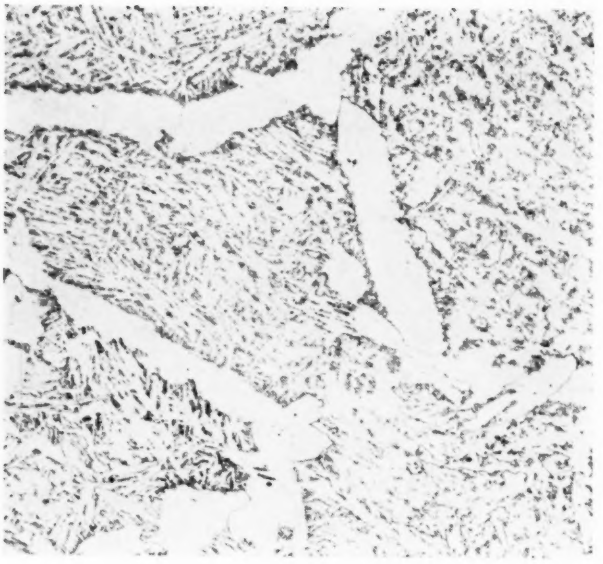
(Note: Regions of grain-boundary transformation are areas of potential graphitization.)

TABLE 2 PROCEDURE USED[a] AND RESULTS OF GRAPHITIZATION TESTS

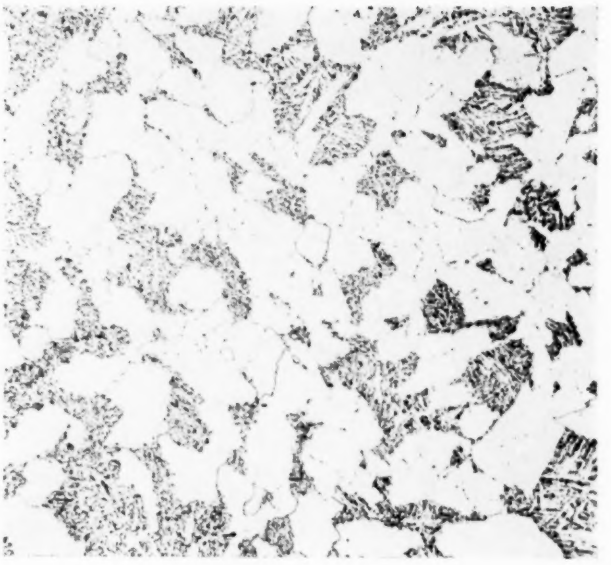
Specimen number	Heat-affected zone	Base-metal heat-treatment	Base-metal grain size A.S.T.M. no.	Microstructure of base metal	Welding preheat, deg F	Welding postheat, deg F	Laboratory service temperature	Remarks
1	A	1900–2000 F air cool 1150–1200 F slow cool 935 F avg 5½ years[b]	4–6	Acicular Widmanstätten carbide (partially spheroidized)	400	None	None	No graphite
	B	2600–2800 F air cool	00–1	Acicular Widmanstätten carbide				
2	A	Same as A above	4–6	Same as A, specimen 1	400	1200 2 hr	None	No graphite
	B	Same as B above	00–1	Same as B				
3	A	Same as A above	4–6	Same as A, specimen 1	400	1300 20 hr	None	No graphite
	B	Same as B above	00–1	Same as B				
1S	A	Same as A above	4–6	Same as A, specimen 1	400	None	1050 F avg with 100 F swings every 24 hr	Graphite
	B	Same as B above	00–1	Same as B				Graphite
2S	A	Same as A above	4–6	Same as A, specimen 1	400	1200 2 hr	for 7 days; then 100 F swings each week. Total 1968 hr	Graphite
	B	Same as B above	00–1	Same as B				Graphite
3S	A	Same as A above	4–6	Same as A, specimen 1	400	1300 20 hr		No graphite
	B	Same as B above	00–1	Same as B				No graphite

[a] A 14-in. length of 12¾-in-OD × 1⁷/₁₆-in-wall C-Mo pipe containing upset ends and a circumferential weld at the center was removed from a main steam line having had 5½ years of service at 935 F average. The weld and a portion of each upset was removed. Of the two pieces of pipe, one was rebeveled and the other reheated to 2600–2800 F as noted, air-cooled, and rebeveled for welding. The experimental joint was preheated to 400 F, and welded in the fixed horizontal position. Slices were then cut from the joint and treated as shown in Table 2.

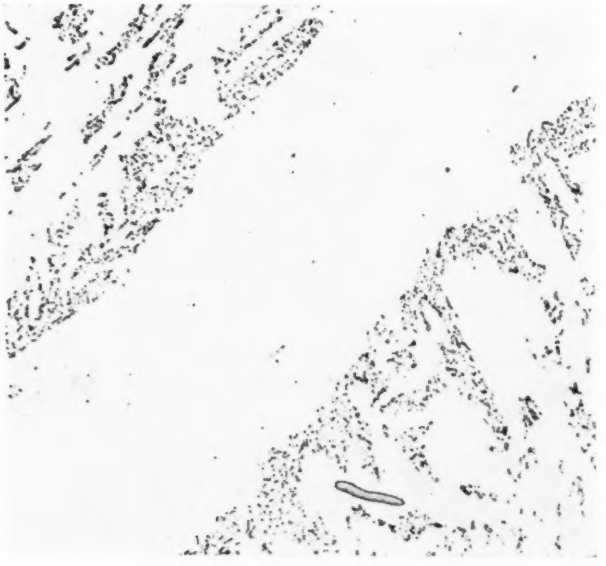
[b] This heat-treatment is the approximate previous heat-treatment of the pipe which was removed from the main steam line at the location of the experimental weld.



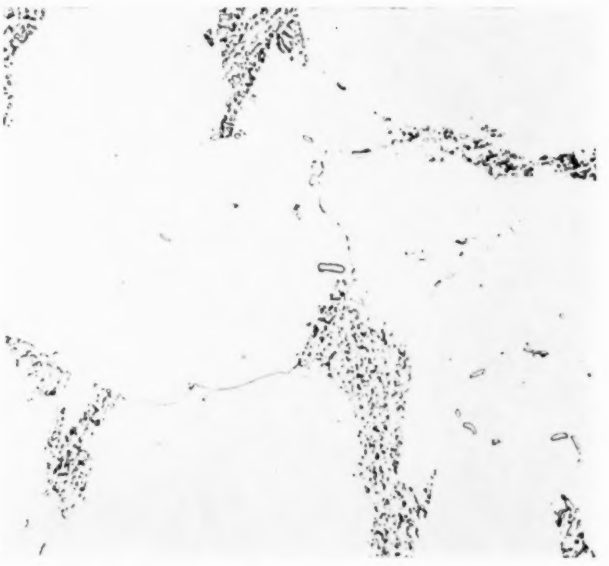
Specimen 3B; ×100



Specimen 3A; ×100



Specimen 3B; ×500



Specimen 3A; ×500

FIG. 11 CONTACT ZONES OF SPECIMEN 3
(Note: Structure at grain boundaries fully spheroidized.)

Discussion of Results. Specimens 1, 2, and 3 after polishing and etching in hot 50 per cent hydrochloric acid are shown in Fig. 8. It is to be observed that etching produced little if any visible difference in heat-affected zones[3] A, specimens 1 and 2.

Heat-affected zone A, specimen 3, however, reveals no white band at its extremity as do specimens 1 and 2. A more defined line of fusion and a narrower heat-affected zone are also shown. As in the case of A, little or no difference is visible in heat-affected zones B, specimens 1 and 2. Specimen 3, however, has a much more diffused heat-affected zone than specimens 1 and 2. Both contact zones[4] A and B of specimens 1, 2, and 3 (Fig. 8) are shown in Figs. 9, 10, and 11, at a magnification of 100 and 500 diam. These illustrations are of interest since they show the type of microstructure which exists in the contact zone after welding but prior to service. Specimen 1B, Fig. 9, shows an almost continuous grain-boundary transformation to have occurred in the coarse-grain material. It is to be noted that no graphite is detectable although subsequent steam service is believed to result in complete envelopment of the large Widmanstätten carbide grains by graphite nodules, as shown in Fig. 3. Grain-boundary transformation of specimen 1A has resulted in the formation of a dense discontinuous carbide. Again, it is believed to be this dense carbide which is first graphitized by subsequent subcritical heating.

The effect of a 1200 F stress relieve for 2 hr on the microstructures observed in Fig. 9 is shown in Fig. 10. It is to be noted that only a slight change in microstructure has occurred.

[3] The use of heat-affected zone A or B refers to the heat-affected zone adjacent to the medium- or coarse-grain base metal, respectively.

[4] The term "contact zone" is used to refer to the narrow band of potentially unstable carbide at the extremity of the heat-affected zone. It is this band which may subsequently graphitize in service.



FIG. 12 GRAPHITIZATION AFTER 5½ YEARS' SERVICE OCCURS PRINCIPALLY WHERE GRAIN-BOUNDARY TRANSFORMATION ONLY OCCURRED DURING WELDING; ×500

Referring to specimen 3, Fig. 11, which received a 1300 F stress relieve for 20 hr, it is to be observed that spheroidization and homogenization of the heterogeneous iron-carbide or complex iron-molybdenum-carbide phase of the contact zone has occurred.

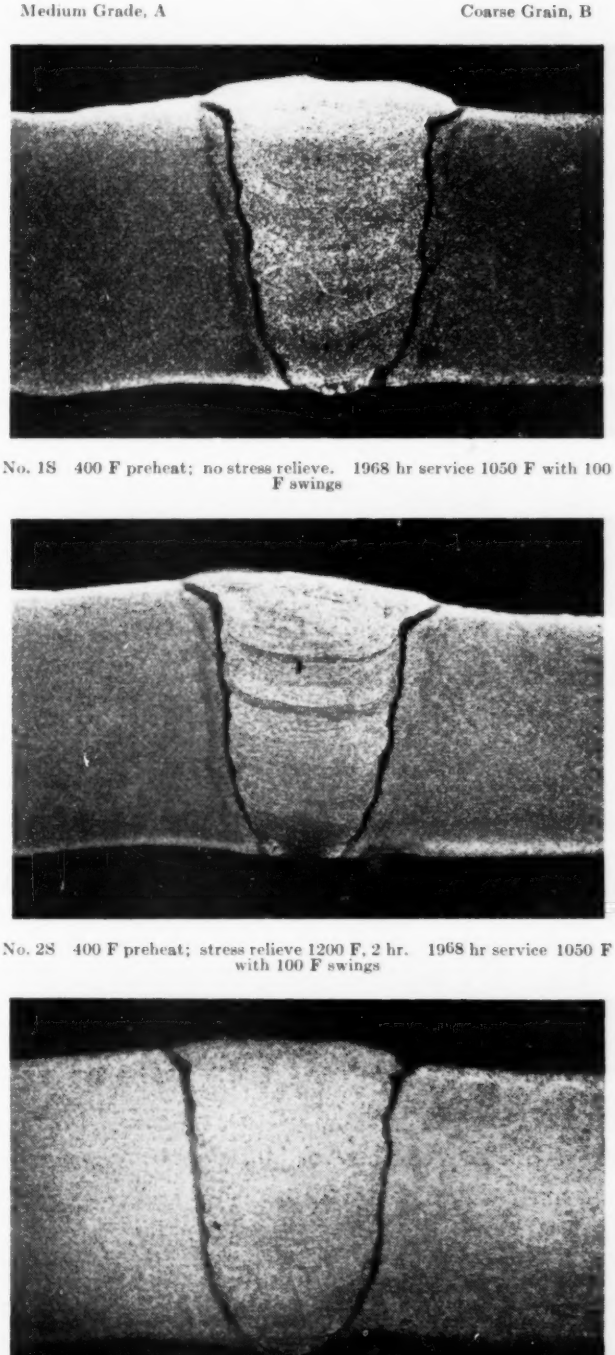
That subsequent graphitization occurs at the location of grain-boundary transformation resulting from welding, is further substantiated in Fig. 12. The graphite nodules in this figure, which have formed principally at the Widmanstätten carbide grain boundary, are in the process of complete envelopment of the carbide-containing grain.

Corresponding to specimens 1, 2, and 3, specimens 1S, 2S, and 3S, which received 1968-hr service temperature in a laboratory furnace as previously discussed, are shown in Fig. 13. Contact zone B (coarse grain size), specimen 1S may be seen to exhibit the same "isotherms," as shown in Fig. 2. Contact zone A (medium grain size), specimen 1S, however, resulted in a condition of dispersed graphitization though of a more continuous nature. This is in agreement with macroscopic observations of graphitization as encountered in fine-grain material, as contrasted with the observation of "isotherms" in a coarse-grain material.

A significant point is believed to be the fact that although specimen 1S received no stress-relieving treatment, identical results would have been obtained if this specimen had received an 1150 F stress relieve for 2 to 4 hr. This assumption is made on the basis that this short time at 1150 F would be insignificant in view of the 650 hr at 1150 F which the specimen received during the subsequent heating cycle to accelerate graphitization.

Close observations of specimen 2S reveals that the condition of incipient graphitization, as shown in specimen 1S, has not been completely eliminated by a 1200 F stress-relieving heat-treatment, that which is considered standard commercial practice.

A stress-relieving heat-treatment of 1300 F for 20 hr, however, shows no tendency toward graphite segregation adjacent to either side of the weld (specimen 3S).



No. 1S 400 F preheat; no stress relieve. 1968 hr service 1050 F with 100 F swings

No. 2S 400 F preheat; stress relieve 1200 F, 2 hr. 1968 hr service 1050 F with 100 F swings

No. 3S 400 F preheat; stress relieve 1300 F, 20 hr. 1968 hr service 1050 F with 100 F swings

FIG. 13 MACROSPECIMENS ETCHED IN HOT 50 PER CENT HYDROCHLORIC ACID; ×1

Unfortunately the maximum temperature of 1150 F used, in an effort to accelerate graphitization, was such that the size and pattern of the original grain structure were completely obliterated. This may be seen by contrasting the base-metal structure of specimens 1, 2, and 3 with those of specimens 1S, 2S, and 3S.

Fig. 14 shows the microstructure of the weld heat-affected zone,

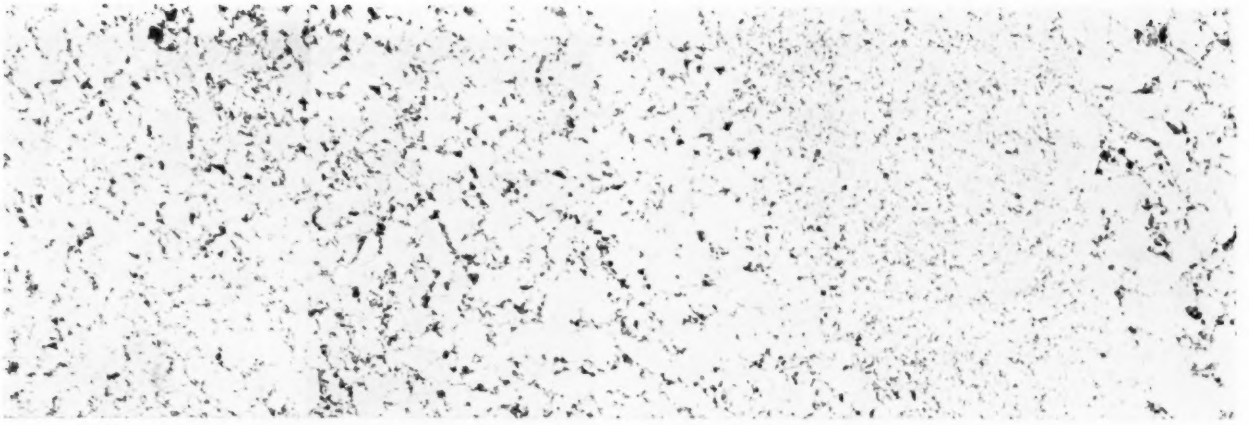


FIG. 14 WELD, HEAT-AFFECTED ZONE, AND PARENT METAL, SPECIMEN 1S-A MEDIUM GRAIN
(After 1968 hr at 1050 F average with 100 F swings weekly; ×60.)

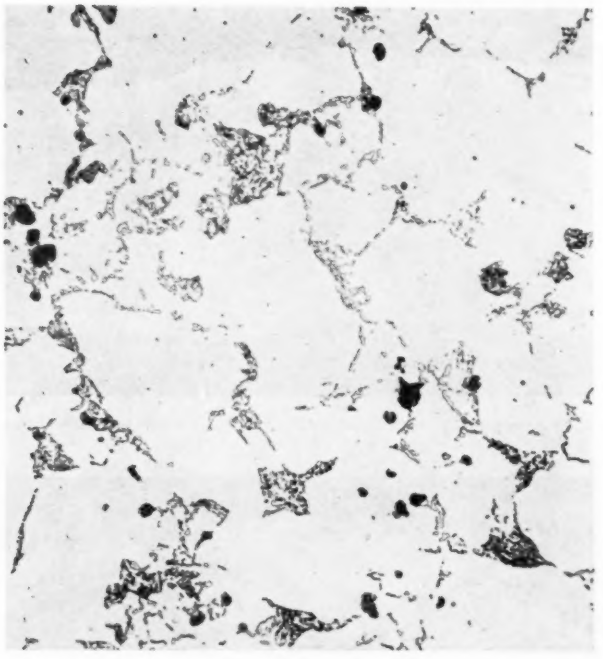


FIG. 15 CONTACT ZONE SPECIMEN 1S-A, MEDIUM GRAIN, EXHIBITING DISPERSED GRAPHITIZATION AND HIGHLY SPHEROIDIZED CARBIDE; ×500

and base metal of specimen 1S-A. The graphite nodules are of insufficient size and number to be seen at 60-diam magnification.

The microstructure of the contact zone of specimen 1S-A is shown in Fig. 15, at a magnification of 500 diam. A highly spheroidized carbide structure and dispersed graphite nodules are visible in this figure.

The contact zone of specimen 1S-B is shown unetched at 100-diam magnification in Fig. 16. The graphite nodules in this photomicrograph follow the path of the "isotherms" observed in contact zone 1S-B, Fig. 13. A view of this area in the etched condition is shown in Fig. 17 at a magnification of 500 diam. This structure, with the exception of the better alignment of the small graphite nodules, may be observed to be similar to that of Fig. 15.

A $^{5}/_{32}$-in-thick slice of specimen 1S was bent through both contact zones A and B. No failure occurred through contact zone



FIG. 16 CONTACT-ZONE SPECIMEN 1S-B, COARSE GRAIN, EXHIBITING INCIPIENT "CHAIN" GRAPHITIZATION; UNETCHED, ×100

A. Several small ruptures occurred in contact zone B, however, shown in Fig. 18.

CONCLUSIONS

1 A narrow zone of graphite is found to exist in carbon-molybdenum steel piping in proximity of welded joints in this material.

2 This narrow band occurs at the extremity of the heat-affected zone ($^{1}/_{8}$ to $^{3}/_{16}$ in. from the fusion line) of the weld, and may vary from 0.001 to 0.01 in. in thickness.

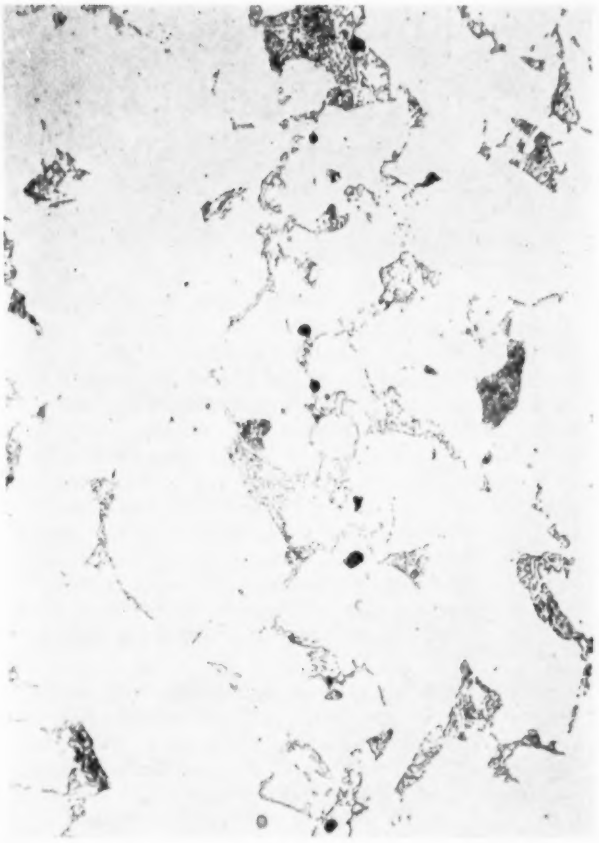


FIG. 17 CONTACT-ZONE SPECIMEN 1S-B, COARSE GRAIN, EXHIBITING INCIPIENT "CHAIN" GRAPHITIZATION AND HIGHLY SPHEROIDIZED CARBIDE; ×500

3 Grain size and possibly the microstructure of the base metal are believed to determine the pattern of the graphitized structure but to have no significant influence on the actual occurrence of graphite.

4 Tests which give good correlation in determining the presence of segregated graphite are visual observation, bend testing, and microscopic examination.

5 Gradiently heating and quenching carbon-molybdenum steel, as accomplished by the welding process, places the narrow zone of carbide adjacent to the weld in a state of least resistance to graphitization.

6 Graphitization of this narrow band of potentially unstable carbide, during steam service, is dependent upon the inherent carbide stability of the steel.

7 Inherent characteristics of steel are, in part, a function of steel-melting practice.

8 Relatively large quantities of aluminum used to deoxidize carbon-molybdenum steel are believed to affect adversely the carbide stability of this material when used for elevated-temperature service. The addition of carbide-stabilizing elements, on the contrary, are believed to enhance the carbide stability of this material.

9 The postheating or stress-relieving temperature used after welding is believed to be a most important factor in determining whether or not segregated graphite will occur in a steel which has inherent carbide instability.



FIG. 18 SPECIMEN 1S-B, COARSE GRAIN, EXHIBITING FISSURING IN CONTACT ZONE UPON BENDING; ×1

10 Preliminary tests indicate that stress-relieving at a temperature as low as 1150 F will result in subsequent graphite segregation, while a temperature of 1300 F will eliminate this difficulty.

ACKNOWLEDGMENTS

The author wishes to express his appreciation to Mr. Mathew Morrow, inspector, The Hartford Steam Boiler Inspection and Insurance Company, for the valuable assistance given in the laboratory preparation of the many specimens used in connection with this paper. Acknowledgment is given to Mr. G. Sinding-Larsen, chief engineer, Pittsburgh Piping and Equipment Company, for his many helpful suggestions and constructive criticism. The author is indebted to those whose permission made possible the use of a number of the illustrations included in this paper.

BIBLIOGRAPHY

1 "Graphite in Low-Carbon Steel," by A. B. Kinzel and R. W. Moore, Trans. A.I.M.E., vol. 116, 1935, pp. 318–329.

2 "Effect of Tempering Quenched Hypereutectoid Steels on the Physical Properties and Microstructure," by C. R. Austin and B. S. Norris, Trans. A.S.M., vol. 26, 1938, pp. 788–849.

3 "Temperature-Gradient Studies on Tempering Reactions of Quenched High-Carbon Steels," by C. R. Austin and B. S. Norris, Trans. American Institute of Mining and Metallurgical Engineers, vol. 131, 1938, pp. 349–371.

4 "Effect of Composition and Steel Making Practice on Graphitization Below the A_1 of Eighteen One Per Cent Plain Carbon Steels," by C. R. Austin and M. C. Fetzer, Trans. American Institute of Mining and Metallurgical Engineers, vol. 145, 1941, pp. 213–224.

5 "Cementite Stability and Its Relation to Grain Size, Abnormality, and Hardenability," by C. R. Austin and M. C. Fetzer, Trans. A.S.M., vol. 29, 1941, pp. 339–354.

6 "Effects of Small Amounts of Alloying Elements on the Tempering of Pure Hypereutectoid Steels," by C. R. Austin and B. S. Norris, Trans. A.S.M., vol. 29, 1941, pp. 244–268.

7 "Graphitization in High Purity Iron-Carbon Alloys," by Cyril Wells, Trans. A.S.M., vol. 26, 1938, pp. 289–357.

8 "A Study of the Effect of the Aluminum Addition on the Structure of a Quenched Carbon Steel," by H. W. McQuaid, Trans. A.S.M., vol. 25, 1937, pp. 490–535.

A Possible Means of Avoiding Local Graphitization of Steels in Service at Elevated Temperatures

By G. V. SMITH[1] AND R. F. MILLER,[1] KEARNY, N. J.

The recent steam-pipe failure at the Springdale power-generating station of the West Penn Power Company, which resulted from excessive local graphitization, has become of great concern to the power industry inasmuch as examination of other steam lines both in the same station and in others has revealed similar instances of local graphitization. In this paper the line of thought is largely speculative, but its degree of validity cannot be established until the completion of experiments, now under way, which will require a long time because of the slowness of the processes involved in this phenomenon. Consequently, the authors present the data at this time in the hope that the ideas outlined may prove useful or at least suggest other approaches to the subject.

THE recent steam-pipe fracture at the Springdale power-generating station of the West Penn Power Company occurred around the entire periphery of a $12^3/_4$-in-OD $\times$ $1^7/_{16}$-in-wall aluminum-killed carbon-molybdenum steam pipe at a distance of approximately $^1/_{16}$ in. from the border of the fusion zone of the weld by which it was joined to the main steam header of the boiler. The reported welding conditions comprised a 400 F preheat and a subsequent stress-relief treatment of 3 hr at 1200 F. The pipe had been in service for $5^1/_2$ years at a steam temperature and pressure of 935 F and 1300 psi, respectively. Metallographic examination revealed a profuse amount of graphite, disposed in network fashion around the areas of Widmanstätten structure, in a narrow region on both sides of the fracture; this network of graphite, which in many places was continuous, provided an easy path for fracture and was clearly the source of the failure. This zone of graphitization occurred near the lower limit of the heat-affected zone of the base metal in a region which, from metallographic examination, apparently reached during welding a temperature of about 1300 to 1350 F, i.e., the lowest temperature at which transformation to austenite begins in this steel (its so-called lower critical temperature, A_1). Furthermore, the width of the graphite zone was so narrow that the path of fracture closely conformed to this approximately isothermal boundary of the individual weld passes. In the base metal of the pipe away from the weld there were occasional graphite nodules, although these, because they were scattered, are of no concern except in so far as they indicate the propensity of the material to graphitize slowly at 935 F.

Experiments to Determine Cause of Local Graphitization

In an attempt to discover the reason for this local graphitization, the authors made several experiments, based on a belief that the rate of graphitization would be increased by increasing the temperature, short of exceeding the critical, approximately 1335 F. As this, however, proved not to be so, we were led to a change in viewpoint and to an explanation of why graphitization can occur at 900 to 1000 F, but not at 1300 F, and the correctness of this view was proved by experiments, described elsewhere,[2] which will only be summarized here.

In alloy steels containing a carbide-forming element such as molybdenum, the carbide cannot be considered to be simply of the nature Fe_3C, which is known to be metastable with respect to graphite, but may contain molybdenum in solution, or may be of the nature MoC_y. Moreover, in a given steel, different types of carbide may be expected to exist at different temperatures or after different times at constant temperature, and more than one type may coexist under some conditions of temperature and time. Little information is available concerning the stability of the alloy carbides with respect to graphite although it seems certain that these carbide types are more stable than the simple Fe_3C type, and may, in fact, be completely stable.

Crafts and Offenhauer,[3,4] who recently studied the nature of the carbides in low-chromium-molybdenum steels, found that on quenching these steels and tempering below 500 to 550 C (930 to 1020 F), the existing carbide was of the simple Fe_3C type as indicated by X-ray diffraction study, but for higher-tempering temperatures was an alloy carbide. The alloy-carbide type in intermediate chromium steels was Cr_7C_3, in higher-chromium steels, Cr_4C, and in molybdenum steels, Mo_2C; all of these carbide types were found in chromium-molybdenum steels. They also found that in chromium steels, the chromium carbide exists after transformation of austenite in the pearlite range; the nature of the carbide in the pearlite after transformation of the molybdenum and chromium-molybdenum steels was not studied, but it seems probable that it would be an alloy type.

These results suggest an explanation of our inability to graphitize C-Mo steel at a temperature of about 1300 F, namely, that at such a temperature the stable carbide is of the Mo_2C type which may be assumed to be more stable than the Fe_3C type with respect to graphite and may even be completely stable. That this is actually true was proved by holding a sample of the Springdale station pipe, containing graphite, for several weeks at 1300 F; the graphite gradually reverted to a carbide.

Suggested Explanation of Localized Graphitization Near a Weld

In view of the finding that graphite which had formed in carbon-molybdenum steel during service at 935 F reverts to carbide at 1300 F, it may be well to inquire whether this fact sheds any light on the question of why a narrow zone of graphite should

---

[1] Research Laboratory, United States Steel Corporation.

Contributed by the Joint A.S.T.M.-A.S.M.E. Research Committee on the Effect of Temperature on the Properties of Metals and presented at the Annual Meeting, New York, N. Y., Nov. 29–Dec. 3, 1943, of THE AMERICAN SOCIETY OF MECHANICAL ENGINEERS.

NOTE: Statements and opinions advanced in papers are to be understood as individual expressions of their authors and not those of the Society.

[2] In a paper by the authors submitted to the A.I.M.E. for presentation at the February, 1944, Annual Meeting.

[3] "Carbides in Low-Chromium Steel," by W. Crafts and C. M. Offenhauer, Trans. A.I.M.E., vol. 150, 1942, pp. 275–287.

[4] "Carbides in Low-Chromium-Molybdenum Steels," by W. Crafts and C. M. Offenhauer, Trans. A.I.M.E., T. P. 1556, Metals Technology Division, February, 1943.

have formed near the weld in the first place. No adequate explanation of this phenomenon has yet been reported; to stimulate thought on the matter, the following, admittedly speculative, idea, based upon the possibility of the existence of different types of carbide in the same steel, is offered.

It is supposed that the carbide of the ordinary pearlitic or Widmanstätten structure is of the Mo_2C type, or of the Fe_3C type containing molybdenum in solution, i.e., $(Fe, Mo)_3C$, and that, in either case, it is more stable, at the service temperature, with respect to graphite, than the simple Fe_3C type. Further, it is assumed that the lower the temperature at which the austenite of such an alloy steel transforms (the faster the cooling rate, the lower will this temperature be), the more likely will the carbide in the transformation product be of the graphitizable Fe_3C type. However, it may well be that the latter type forms only when the cooling rate is sufficiently fast to produce martensite initially, this martensite then precipitating Fe_3C on heating to the service temperature, a possibility which is in conformity with the results of Crafts and Offenhauer,[3,4] as pointed out previously.

Now, during the welding process, the portion of the pipe, which later graphitized, reached a temperature of approximately 1350 F, which is sufficient to cause austenite to begin to form at the carbide-ferrite interface and, as observed, to a greater extent at the boundaries of the Widmanstätten patches. This austenite, having formed just above the eutectoid temperature (A_1) and being therefore rich in carbon, transforms, on subsequent cooling, at a lower temperature than would austenite of the composition of the pipe as a whole; hence it may directly form carbide of the Fe_3C type. On the other hand, and perhaps more likely because of the large mass of cool metal adjacent to this zone, the local cooling rate may be sufficiently fast to form martensite, which on reheating to the service temperature precipitates carbide of the Fe_3C type.

Once the condition has been established that Fe_3C exists in a limited region, and Mo_2C or $(Fe, Mo)_3C$ elsewhere, it is easy to see how a limited region of graphitization may arise. The steeper the temperature gradient adjacent to the weld during welding (that is, the narrower the heat-affected zone), the faster will be the rate of cooling, and thus the greater the likelihood of obtaining the necessary condition for subsequent graphitization. This steepness of temperature gradient appears to correlate roughly with the prevalence of this type of graphitization in the instances which we have examined.

Another point of possible significance to the Springdale failure is that the carbon content of the narrow zone containing the graphite was evidently greater than the nominal composition of the steel; it may be that, had only the carbide of this section graphitized, there would not have been sufficient graphite to form the nearly continuous network which was the eventual source of failure. The greater carbon content is readily explainable by the considerations that graphite, being the stable phase, is less soluble in ferirte than is carbide, and forms by carbon diffusing through the ferrite solid solution to the graphite nucleus and there precipitating. Conceivably, then, graphite in a limited region could bring about, in time, the substantial depletion of carbide within an entire specimen.

Although the authors have never observed any instance of excessive local graphitization in plain-carbon steel, the formation of martensite or low-temperature product in a limited region, as suggested for the carbon-molybdenum steel, may account for its occurrence. It is not unreasonable to expect that the rate of graphitization should depend upon the initial structure, and that this rate may be greatest in an initially martensitic structure.

One disturbing fact which detracts from the validity of the argument just outlined is that graphitization did not occur in the heat-affected zone on the header side of the weld in question although its composition was similar to that of the pipe side. The steel on the header side did have a much smaller grain size, and it was of low-aluminum deoxidation practice as opposed to high-aluminum for the pipe. Factors such as these may suffice to tip the balance from a more to a less graphitizable condition for this particular temperature level.[5] Moreover, it is possible that during the stress-relief treatment subsequent to welding, conversion of the carbide on the header side to the stable alloy type went further than on the pipe side because of possible differences in temperature or composition. In any event the explanation is thought to be of sufficient merit to justify experimental study, which should yield further needed knowledge concerning the distribution of alloying elements between matrix and other phases in steel which has been treated in various ways. Work along this general line is contemplated.

A Possible Means of Avoiding Local Graphitization

Since C-Mo steel is extensively used under conditions which led to eventual failure at the Springdale Station, it is of interest to consider what may be done to reclaim welded joints now in service which show evidence of deterioration, and how, in the future, localized graphitization might be avoided.

To reclaim "diseased" joints, some engineers are considering removing the affected metal and rewelding or carrying out a heat-treatment above the transformation temperature. This is, however, no insurance against recurrence of the malady. Rohrig, Corey, and Crocker[6] suggest normalizing subsequent to welding as a possible means of avoiding graphitization. This presents practical difficulties in many instances. Moreover, it would seem to be necessary to treat the entire section of pipe and not just a portion of it, for, in this latter event, there may be temporary temperature gradients somewhat similar to those during welding such as might again cause danger of localized graphitization during subsequent service.

On the other hand, if the authors' explanation of localized graphitization near a weld is valid, a simple means of avoiding the narrow zone of graphitization is immediately evident, namely, to heat the metal in the heat-affected zone near the weld to a temperature of about 1300 F for a time long enough to convert the carbide to the more stable type. It is believed that the time required would be relatively short, perhaps 2 to 4 hr at temperature. Alternatively, but less satisfactorily, precautions might be taken to insure a wide heat-affected zone as, for example, by a higher preheat temperature or a slower rate of welding. It may also be pointed out that, if the explanation is correct, little would be gained by changing over to a chromium-bearing steel because according to Crafts and Offenhauer, the conditions would still be very similar to those for the carbon-molybdenum steel.

Finally, we wish again to emphasize that some of the preceding statements are speculative, and that a better understanding of the phenomenon must await the results of experiments, now under way, which will unavoidably take considerable time because of the slowness of some of the processes under investigation.

---

[5] It should be noted here that, at the somewhat higher temperature level of 975 F, graphitization has been found to occur in a carbon-molybdenum steel of coarse-grain deoxidation practice similar to that of the header in the Springdale Station.

[6] "The Effect of Normalizing on the Properties of Welds in Carbon-Molybdenum Steel Pipe," by I. A. Rohrig, D. H. Corey, and Sabin Crocker, *Welding Journal*, Welding Research Supplement, Oct., 1943, pp. 521S–527S.

Report on High-Temperature Pipe Weld Investigation[1]

By HERMAN WEISBERG,[2] NEWARK, N. J.

As a result of the failure of a carbon-molybdenum high-temperature steam pipe in one of the large power stations of the country due to graphitization, a study of the welds in the high-temperature piping systems at the stations of the Public Service Electric and Gas Company System was undertaken. This report covers the investigation during the period from May to November, 1943.

WELD prober specimens were removed from twelve welds in the high-temperature piping at the Essex, Burlington, and Kearny generating stations. Seven additional specimens were taken from test welds made at preheats from room temperature to 1200 F to study the effect of various preheating temperatures.

The specimens from the operating piping were taken across the weld parallel to the longitudinal axis of the pipe. Charts I to III show photomicrographs of these specimens. On each chart the first vertical row of photomicrographs shows the upstream parent metal; the second row, the contact zone between the parent metal and the heat-affected metal upstream; the third row, the weld metal; the fourth row, the contact zone between the heat-affected metal and the parent metal downstream; and the fifth row, the downstream parent metal. The photomicrographs represent the maximum graphitization observed in each area.

Included also on the charts are macrographs of the weld cross sections, photographs of bend bars made from the weld prober samples, material and weld specifications, heat-treatment of the pipe and welds, and a record of service conditions to which the piping and welds have been subjected.

Chart I, Essex Station; Boilers Nos. 25 and 26, Unit No. 7

The piping in this station was manufactured to A.S.T.M. Specification A 158-36 Grade Pl killed with 1.9 lb of aluminum per ton. The pipe ends were not upset. Of the four welds sampled three show a considerable segregation of graphite in the contact zone and a relatively small amount of graphite in the parent metal. One weld (specimen No. 5) shows no graphite in the contact zone but somewhat more graphite than the others in the parent metal. Miniature bend bars taken from each of the four samples show no loss in ductility.

Chart II, Burlington Station; Boilers Nos. 12 and 13 Unit No. 5

At this station the specimens include welds which were made on both aluminum- and silicon-killed steel, as well as steel castings and Croloy No. 2 pipe. No graphite was found in the silicon-killed steel nor the Croloy No. 2. Graphite was found segregated in the contact zone of the aluminum-killed steel and in one of the castings (specimen No. 4) which was killed with 2 lb of aluminum per ton. The bend bars show no loss in ductility, although the isothermals can actually be seen on the macrograph of one of the samples (No. 13 upstream lower left-hand corner of chart).

Chart III, Kearny Station; Mercury Boiler

The specimens at this station were taken from the 14-in-OD × 0.656-in. vapor piping between the mercury boiler and mercury turbine. All of this piping was originally carbon steel, and first went into service in 1933. Two specimens of carbon-steel pipe having 42,211 hr of service and one specimen of silicon-killed carbon-moly pipe having 17,939 hr of service were examined. The carbon-steel pipe was completely spheroidized and graphitized throughout, there being no difference between the contact zone and the adjacent portion of the parent metal which was sampled. Likewise the carbon-moly pipe was completely spheroidized and partially graphitized, there being no more graphite in the contact zone than in the parent metal. One of the carbon-steel specimens (specimen No. 8) shows an interesting concentration of graphite at one end with apparently no relation to the weld.

Chart IV, Test Welds

The test welds were made in a section of 12.75-in-OD × 1.312-in. carbon-moly pipe 12 in. long, killed with 1.8 lb of aluminum per ton. Longitudinal weld probes were taken from the pipe and the resulting voids filled in with weld metal at various preheat temperatures. The replacement welds were then probed at right angles to the original probes to obtain the specimens shown. The metal on each side of the weld being identical, photomicrographs are shown for one half of the specimens only. In no case was graphitization noted in the test welds. The welds were all sound; no cracks being found even in the weld made at room temperature. The variation of the width of the heat-affected zone and grain size of weld metal in these specimens is of interest.

Summary Charts I to IV

1 Graphite in various forms was found in the following types of steel investigated:

(*a*) Aluminum-killed carbon-moly pipe. Specimens Nos. 1, 2, 5, 6; 4 downstream and 13 upstream.
(*b*) Silicon-killed carbon-moly pipe. Specimen No. 10.
(*c*) Carbon-moly casting. Specimen No. 4 upstream.
(*d*) Carbon-steel pipe. Specimens Nos. 8 and 9.
(*e*) Carbon-steel weld metal. Specimen No. 8.

No graphite was found in Croloy No. 2 steel, specimen No. 3 upstream, or in any carbon-moly weld deposit.

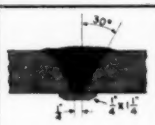
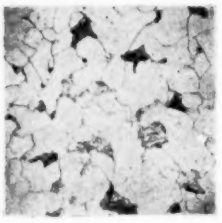
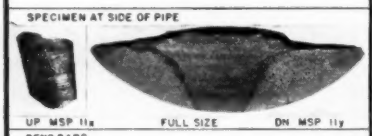
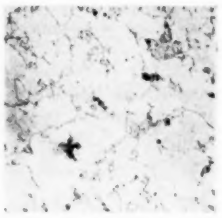
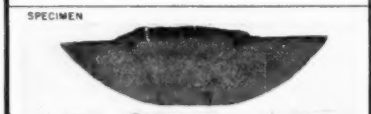
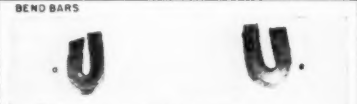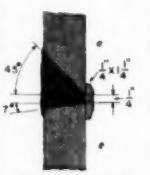
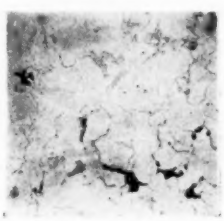
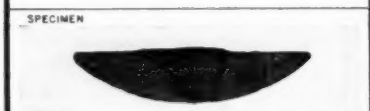
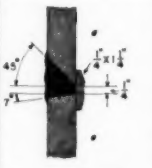
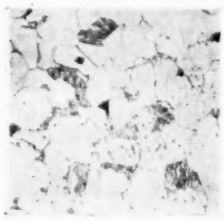
2 A concentration of graphite segregated in the contact zone of the welds was found in all but one of the aluminum-killed carbon-moly pipe specimens. One specimen (No. 5) of aluminum-killed carbon-moly pipe showed no segregation of graphite in the contact zone. This segregation in the contact zone was not found in any of the silicon-killed carbon-moly pipe or other metals examined except aluminum-killed carbon-moly pipe.

[1] Submitted as discussion of the foregoing group of three papers on the general subject "Graphitization of Steel Piping," by H. J. Kerr and F. Eberle; R. W. Emerson; G. V. Smith and R. F. Miller, respectively.

[2] Mechanical Engineer, Electric Engineering Department, Public Service Electric and Gas Company. Mem. A.S.M.E.

Note: Statements and opinions advanced in papers are to be understood as individual expressions of their authors and not those of the Society.

ESSEX GENERATING STATION — CHART I — HIGH TEMPERATURE PIPE

SPECIMEN	MATERIAL	OPERATION: TIME & TEMPERATURE	OPERATION: STRESS	WELDING DETAILS (SPECIFIED)	3% NITAL ETCH — UPSTREAM END a PARENT METAL
1 1250 LB (NOM) MAIN STEAM N° 26 BOILER HORIZONTAL FIELD WELD 12.75 OD x 1.312 PIPE SPECIMEN AT SIDE OF PIPE  UP MSP 9 — FULL SIZE — DN MSP 11x BEND BARS  FULL SIZE	**UPSTREAM** HEAT CMO STL ASTM A158-36 GRADE P1 C 0.20 MAX Si 0.10 - 0.20 SPEC TENSIL MIN SPEC 55000 KILL LB/TON Al 1.9% Fe Si 8-15 NORM. 0.5 HRS 1650F DRAWN 0.5 HRS 1200F AT MILL STRESS RELIEF 1.3 HRS 1200F AT SHOP CHEM ANLS % Al 0.052 Al_2O_3 0.011 **DOWNSTREAM** HEAT 5437 TENSIL MIN SPEC 55000 ACT Av 59250 KILL LB/TON Al 1.9, Fe Si 8-15 (OTHERWISE SAME AS UPSTREAM)	TOTAL 35406 HOURS AT 917 F AVERAGE 3934 HOURS ABOVE 950 F 990 F MAX	DESIGN BURSTING 7350 PROBABLE LONGITUDINAL 2865	 ENDS NOT UPSET PREHEAT 400F MIN STRESS RELIEF 1.3 HRS, 1200-1250F WOVEN BEADS EXCEPT STRING BEADS AT BOTTOM OF PIPE MUREX CMO 50 FILLER	 SPHEROIDIZED PARTIALLY. GRAPHITE IN SMALL PATCHES RANDOMLY DISTRIBUTED. GRAIN SIZE #6 TO 7
2 1250 LB (NOM) MAIN STEAM N° 26 BOILER HORIZONTAL SHOP WELD 12.75 OD x 1.312 PIPE SPECIMEN AT SIDE OF PIPE  UP MSP 11x — FULL SIZE — DN MSP 11y BEND BARS  FULL SIZE	**UPSTREAM** HEAT 5437 SAME AS SPECIMEN NO 1 DOWNSTREAM **DOWNSTREAM** HEAT CMO STL ASTM A158-36 GRADE P1 C 0.20 MAX Si 0.10 - 0.20 SPEC TENSIL MIN SPEC 55000 KILL LB/TON Al 1.9% Fe Si 8-15 NORM 0.5 HRS 1650F DRAWN 0.5 HRS 1200F AT MILL STRESS RELIEF 1.3 HRS 1200F AT SHOP CHEM ANLS % Al 0.052 Al_2O_3 0.011	DO	DO	 ENDS NOT UPSET PREHEAT 400F MIN STRESS RELIEF 1.3 HRS, 1150-1250F PROBABLY WOVEN BEADS MAX WIDTH 1" ROTATED, DOWN HAND MUREX CMO 50 FILLER	 SPHEROIDIZED COMPLETELY. GRAPHITE NODULAR SMALL AMOUNT RANDOMLY DISTRIBUTED. GRAIN SIZE #7
5 1250 LB (NOM) MAIN STEAM N° 25 BOILER VERTICAL SHOP WELD 12.75 OD x 1.312 PIPE SPECIMEN  UP MSP 6 — FULL SIZE — DN MSP 8 BEND BARS  FULL SIZE	**UPSTREAM** HEAT 1507 CMO STL ASTM A158-36 GRADE P1 C 0.20 MAX Si 0.10 - 0.20 SPEC TENSIL MIN SPEC 55000 ACT Av 58900 KILL LB/TON Al 1.9, Fe Si 8-15 NORM 0.5 HRS 1650F DRAWN 0.5 HRS 1200F AT MILL STRESS RELIEF 1.3 HRS 1200F AT SHOP CHEM ANLS % Al 0.054 Al_2O_3 0.006 **DOWNSTREAM** HEAT 1507 (SAME AS UPSTREAM)	TOTAL 35078 HOURS AT 917 F AVERAGE 2694 HOURS ABOVE 950 F 990 F MAX	DESIGN BURSTING 7350 PROBABLE LONGITUDINAL 2865	 ENDS NOT UPSET PREHEAT 400F MIN STRESS RELIEF 1.3 HRS, 1150-1250F ENDS PREPARED FOR FIELD WELDING, STRING BEADS SPECIFIED, BUT WELD WAS MADE IN SHOP. DETAIL UNKNOWN, ROTATED. DOWN HAND. MUREX CMO 50 FILLER	 SPHEROIDIZED COMPLETELY. GRAPHITE IN SMALL PATCHES RANDOMLY DISTRIBUTED. GRAIN SIZE #7
6 1250 LB (NOM) MAIN STEAM N° 25 BOILER VERTICAL FIELD WELD 8.625 OD x .906 PIPE SPECIMEN  UP MSP 1 — FULL SIZE — DN MSP 2x BEND BARS  FULL SIZE	**UPSTREAM** HEAT CMO STL ASTM A158-36 GRADE P1 C 0.20 MAX Si 0.10 - 0.20 SPEC TENSIL MIN SPEC 55000 KILL LB/TON Al 1.9% Fe Si 8-15 NORM 0.5 HRS 1650F DRAWN 0.5 HRS 1200F AT MILL STRESS RELIEF 1 HR 1200F AT SHOP **DOWNSTREAM** HEAT 1507 TENSIL MIN SPEC 55000 KILL LB/TON Al 1.9% Fe Si 8-15 (OTHERWISE SAME AS UPSTREAM)	TOTAL 35078 HOURS AT 927 F AVERAGE 2694 HOURS ABOVE 950 F 990 F MAX	DESIGN BURSTING 7390 PROBABLE LONGITUDINAL 2660	 ENDS NOT UPSET PREHEAT 400F MIN STRESS RELIEF 1 HR, 1200-1250F STRING BEADS MUREX CMO 50 FILLER	 SPHEROIDIZED COMPLETELY. GRAPHITE IN SMALL PATCHES RANDOMLY DISTRIBUTED. GRAIN SIZE #6 TO 7

WELD INVESTIGATION

PUBLIC SERVICE ELECTRIC AND GAS COMPANY

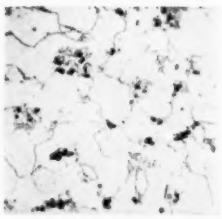
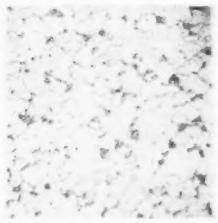
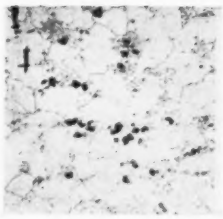
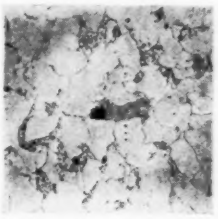
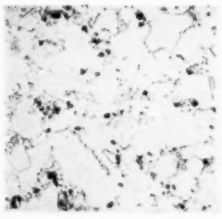
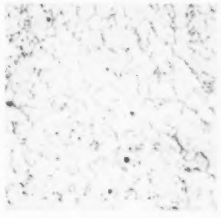
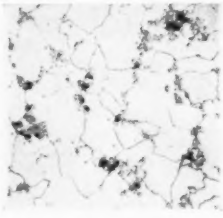
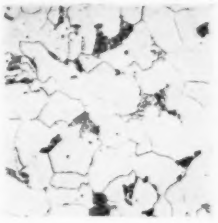
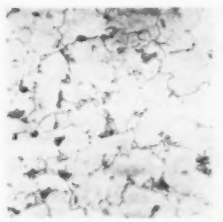
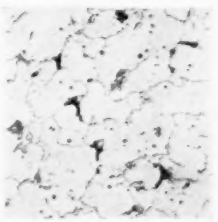
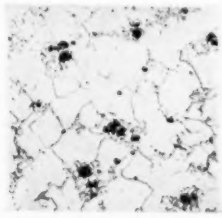
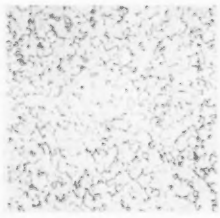
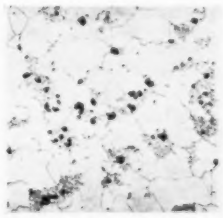
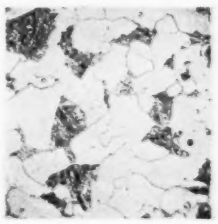
MAY 1943 REV NOV 1943

REDUCED TO ONE THIRD LINEAR IN REPRODUCTION

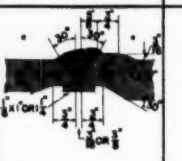
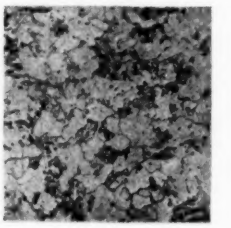
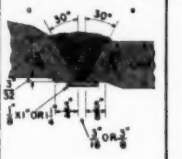
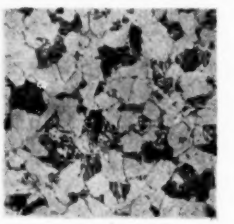
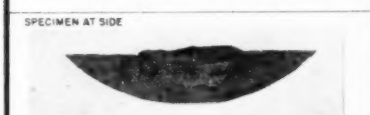
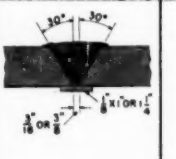
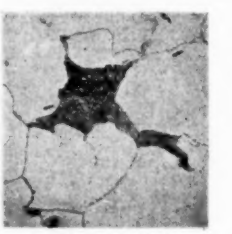
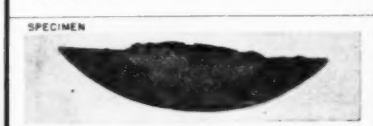
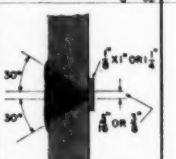
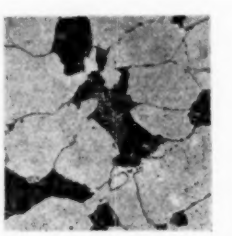
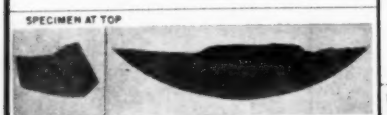
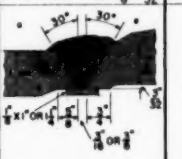
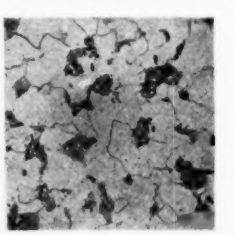
PHOTOMICROGRAPHS

500 X

NOTE:- EXHIBIT SHOWS MAXIMUM GRAPHITE OBSERVED IN EACH AREA OF SPECIMEN EXAMINED

UPSTREAM END b CONTACT ZONE	WELD c FILLER METAL	DOWNSTREAM END d CONTACT ZONE	DOWNSTREAM END e PARENT METAL
 SPHEROIDIZED COMPLETELY. GRAPHITE NODULAR SEGREGATED IN CONTACT ZONE CONSIDERABLE RANDOMLY DISTRIBUTED. GRAIN SIZE #6 TO 7	 SPHEROIDIZED COMPLETELY. GRAPHITE - NONE.	 SPHEROIDIZED COMPLETELY. GRAPHITE NODULAR SEGREGATED IN CONTACT ZONE CONSIDERABLE RANDOMLY DISTRIBUTED. GRAIN SIZE #6 TO 7	 SPHEROIDIZED COMPLETELY. GRAPHITE IN SMALL PATCHES RANDOMLY DISTRIBUTED. GRAIN SIZE #6 TO 7
 SPHEROIDIZED COMPLETELY. GRAPHITE NODULAR SEGREGATED IN CONTACT ZONE CONSIDERABLE RANDOMLY DISTRIBUTED. GRAIN SIZE #7	 SPHEROIDIZED COMPLETELY. GRAPHITE - NONE.	 SPHEROIDIZED COMPLETELY. GRAPHITE NODULAR SEGREGATED IN CONTACT ZONE CONSIDERABLE RANDOMLY DISTRIBUTED. GRAIN SIZE #6 TO 7	 SPHEROIDIZED COMPLETELY. GRAPHITE NODULAR SMALL AMOUNT RANDOMLY DISTRIBUTED. GRAIN SIZE #6 TO 7
 SHPEROIDIZED COMPLETELY. GRAPHITE - NONE. GRAIN SIZE #7	 SPHEROIDIZED COMPLETELY. GRAPHITE - NONE.	 SPHEROIDIZED COMPLETELY. GRAPHITE - NONE. GRAIN SIZE #7	 SPHEROIDIZED COMPLETELY. GRAPHITE IN SMALL PATCHES RANDOMLY DISTRIBUTED. GRAIN SIZE #7
 SPHEROIDIZED COMPLETELY. GRAPHITE NODULAR SEGREGATED IN CONTACT ZONE CONSIDERABLE RANDOMLY DISTRIBUTED. GRAIN SIZE #6 TO 7	 SPHEROIDIZED COMPLETELY. GRAPHITE - NONE.	 SPHEROIDIZED COMPLETELY. GRAPHITE SEGREGATED IN CONTACT ZONE IN SMALL PATCHES RANDOMLY DISTRIBUTED GRAIN SIZE #6 TO 7	 SPHEROIDIZED PARTIALLY. GRAPHITE - NONE. GRAIN SIZE #6 TO 7

BURLINGTON GENERATING STATION CHART II **HIGH TEMPERATURE PIPE**

SPECIMEN	MATERIAL	OPERATION TIME & TEMPERATURE	OPERATION STRESS	WELDING DETAILS (SPECIFIED)	3% NITAL ETCH UPSTREAM END ◻ PARENT METAL
3 1250 LB (NOM) MAIN STEAM N° 12 BOILER HORIZONTAL FIELD WELD 8.625 OD x 1.23 PIPE SPECIMEN AT TOP OF PIPE  UP FULL SIZE DN MSP 1 BEND BARS  FULL SIZE	UPSTREAM HEAT 591768 (CROLOY 2) STL ASTM A158-38T GRADE P3B GRAIN SIZE ACTUAL 8 TENSIL ACTUAL 77400 KILL LB/TON Al 0.35	TOTAL 18835 HOURS AT 924 F AVERAGE 1245 HOURS ABOVE 950 F	DESIGN BURSTING 5180 PROBABLE LONGITUDINAL 2045	 DOWNSTREAM END UPSET UPSTREAM END NOT UPSET PREHEAT 400 F STRESS RELIEF 2.5 HRS 1100-1200 F WOVEN BEADS WEAVE 1" MAX MUREX MOLEX FILLER	 SPHEROIDIZED COMPLETELY. GRAPHITE - NONE. GRAIN SIZE #8
	DOWNSTREAM HEAT 50073 CMO STL ASTM A206-39T 0.5% MOLY SPEC GRAIN SIZE 3-6 SPEC, ACTUAL 5-6 KILL LB/TON Al 1.0 FeSi 8-15 HEAT TREATMENT 2 HRS 1675-1725 F & SLOW FURNACE COOL, SHOP HEAT TREATMENT BROUGHT TO 1750 F AIR COOLED THEN TO 1250 F AIR COOLED	980 F MAX			
4 1250 LB (NOM) MAIN STEAM N° 12 BOILER HORIZONTAL FIELD WELD 12.75 OD x 1.48 PIPE SPECIMEN AT SIDE OF PIPE  UP OA 18 FULL SIZE DN MSP 6 BEND BARS FULL SIZE	UPSTREAM HEAT 1760 or 3899 CMO CAST STL ASTM A217-39T GRADE WC1 GRAIN SIZE ACTUAL 7-8 TENSIL ACTUAL 80500 KILL LB/TON Al 2, FeSi 1.6, Fe Mn 2.0 CoSi 1/4, (PERHAPS FeTi 2) CAST IN ACID ELEC FURNACE	TOTAL 18835 HOURS AT 923 F AVERAGE 1170 HOURS ABOVE 950 F	DESIGN BURSTING 6400 PROBABLE LONGITUDINAL 2535	 ENDS NOT UPSET PREHEAT 400 F STRESS RELIEF 3 HRS 1100-1200 F WOVEN BEADS WEAVE 1" MAX MUREX MOLEX FILLER	 SPHEROIDIZED COMPLETELY. GRAPHITE - NONE. GRAIN SIZE #7 TO 8
	DOWNSTREAM HEAT 4675 or 6623 CMO STL ASTM A158-35 GRADE P1 KILL LB/TON Al 1.9 FeSi 8-15 NO HEAT TREATMENT SPEC STRESS RELIEF 1.5 HRS 1150-1200 F	980 F MAX			
11 1250 LB (NOM) MAIN STEAM N° 13 BOILER HORIZONTAL FIELD WELD 12.75 OD x 1.312 PIPE SPECIMEN AT SIDE  UP MSP 16 FULL SIZE DN MSP 17 BEND BARS  FULL SIZE	UPSTREAM HEAT CMO STL ASTM A206-39T 0.5% MOLY SPEC GRAIN SIZE 3-6 SPEC, ACTUAL 5 KILL LB/TON Al 0.61 FeSi 8-15 HEAT TREATMENT 3 HRS 1700-1750 F & SLOW FURNACE COOL, SHOP STRESS RELIEF 1.3 HRS 1150-1200 F CHEM ANLS % Al 0.013 Al_2O_3 0.010	TOTAL 19923 HOURS AT 924 F AVERAGE 1240 HOURS ABOVE 950 F	DESIGN BURSTING 7350 PROBABLE LONGITUDINAL 2850	 ENDS NOT UPSET PREHEAT 400 F STRESS RELIEF 2.6 HRS 1100-1200 F WOVEN BEADS WEAVE 1" MAX MUREX MOLEX FILLER	 SPHEROIDIZED PARTIALLY. GRAPHITE - NONE. SOME INTERGRANULAR CARBIDE. GRAIN SIZE #5
	DOWNSTREAM HEAT (OTHERWISE SAME AS UPSTREAM)	980 F MAX			
12 1250 LB (NOM) MAIN STEAM N° 13 BOILER VERTICAL FIELD WELD 12.75 OD x 1.312 PIPE SPECIMEN  UP MSP 9B FULL SIZE DN MSP 10 BEND BARS  FULL SIZE	UPSTREAM HEAT GRAIN SIZE ACTUAL 5-6 (OTHERWISE SAME AS SPECIMEN 11)	DO	DESIGN BURSTING 7350 PROBABLE LONGITUDINAL 2865	 ENDS NO UPSET PREHEAT 400 F STRESS RELIEF 2.6 HRS 1100-1200 F STRING BEADS SPEC MUREX MOLEX FILLER	 SPHEROIDIZED PARTIALLY GRAPHITE - NONE SOME INTERGRANULAR CARBIDE. GRAIN SIZE #5 TO 6
	DOWNSTREAM HEAT (OTHERWISE SAME AS UPSTREAM)				
13 1250 LB (NOM) MAIN STEAM N° 13 BOILER HORIZONTAL FIELD WELD 12.75 OD x 1.48 PIPE SPECIMEN AT TOP  UP MSP 7 FULL SIZE DN OA 2 BEND BARS  FULL SIZE	UPSTREAM HEAT 4675 or 6623 CMO STL ASTM A158-35 GRADE P1 KILL LB/TON Al 1.9 Si 8-15 NO HEAT TREATMENT SPEC STRESS RELIEF 1.5 HRS 1150-1200 F	DO	DESIGN BURSTING 6400 PROBABLE LONGITUDINAL 2535	 ENDS NOT UPSET PREHEAT 400 F STRESS RELIEF 3 HRS 1100-1200 F WOVEN BEADS WEAVE 1" MAX MUREX MOLEX FILLER	 SPHEROIDIZED PARTIALLY. GRAPHITE - NONE. GRAIN SIZE #7
	DOWNSTREAM HEAT CMO CAST STL ASTM A217-39T GRADE WC1 C 25 MAX SPEC GRAIN SIZE ACTUAL 7 TENSIL 82500 SPEC KILL LB/TON Al 2.4 FeMn 15.2 FeSi 10.6 CoMn Si 1.7 Si Mn 8.7 CAST IN ACID ELEC FURNACE HEAT TREATMENT 5 HRS 1800 F COOL TO 1600 F QUENCH IN AIR DRAW 5 HRS 1200 F FURNACE COOL				

WELD INVESTIGATION

PUBLIC SERVICE ELECTRIC AND GAS COMPANY

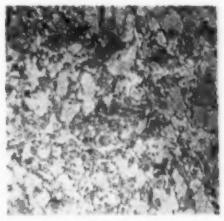
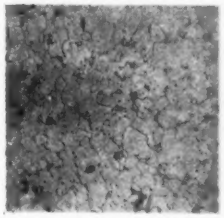
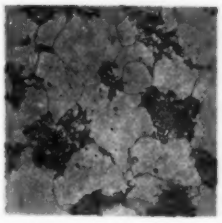
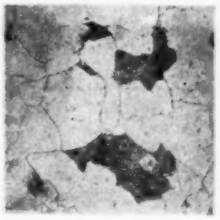
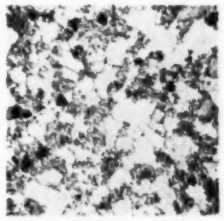
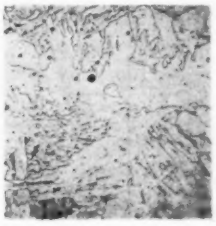
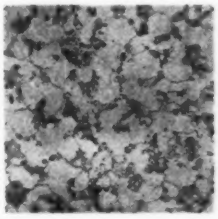
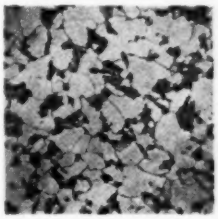
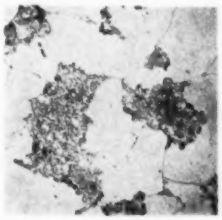
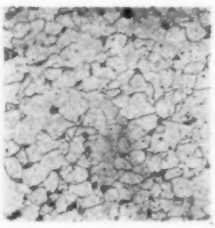
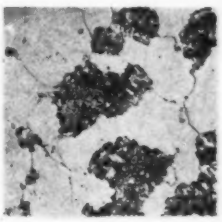
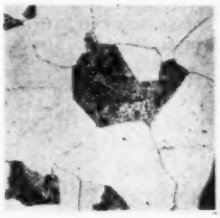
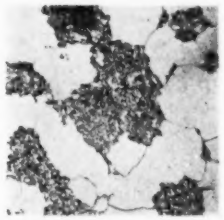
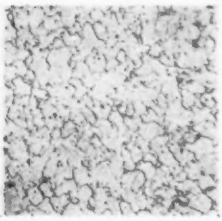
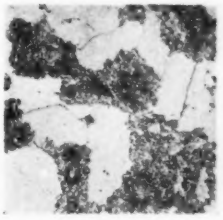
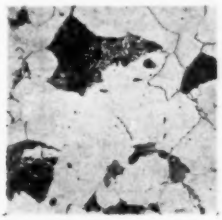
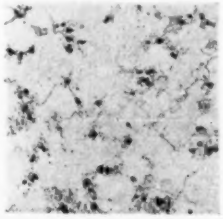
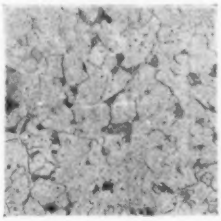
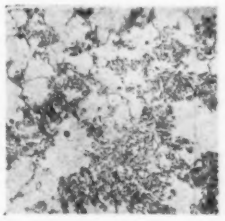
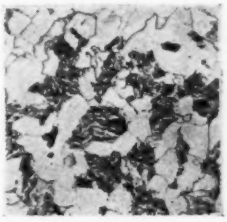
MAY 1943 REV NOV 1943

REDUCED TO ONE THIRD LINEAR IN REPRODUCTION

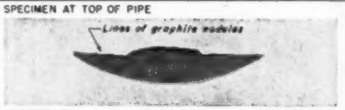
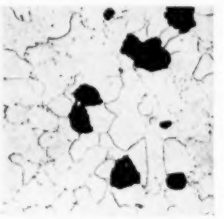
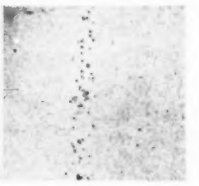
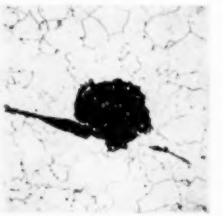
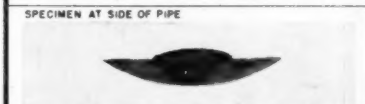
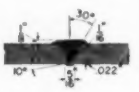
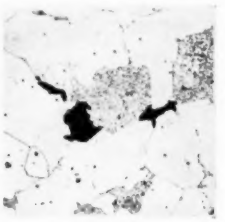
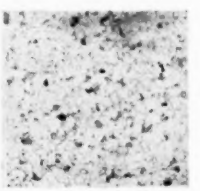
PHOTOMICROGRAPHS

500 X

NOTE - EXHIBIT SHOWS MAXIMUM GRAPHITE OBSERVED IN EACH AREA OF SPECIMEN EXAMINED

UPSTREAM END b CONTACT ZONE	WELD c FILLER METAL	DOWNSTREAM END d CONTACT ZONE	DOWNSTREAM END e PARENT METAL
 SPHEROIDIZED COMPLETELY. GRAPHITE - NONE. GRAIN SIZE #8	 SPHEROIDIZED COMPLETELY. GRAPHITE - NONE.	 SPHEROIDIZED COMPLETELY. GRAPHITE - NONE. GRAIN SIZE #5 TO 6	 SPHEROIDIZED PARTIALLY. GRAPHITE - NONE. SOME INTERGRANULAR CARBIDE. GRAIN SIZE #5 TO 6
 SPHEROIDIZED COMPLETELY. GRAPHITE NODULAR SEGREGATED IN CONTACT ZONE SMALL AMOUNT CONCENTRATED IN AREA SHOWN OTHERWISE NODULAR SMALL AMOUNT OR NONE. GRAIN SIZE #7 TO 8	 SPHEROIDIZED COMPLETELY. GRAPHITE - NONE.	 SPHEROIDIZED COMPLETELY. GRAPHITE NODULAR SEGREGATED IN CONTACT ZONE SMALL AMOUNT CONCENTRATED IN AREA SHOWN OTHERWISE RANDOMLY DISTRIBUTED GRAIN SIZE #7	 SPHEROIDIZED COMPLETELY. GRAPHITE - NONE. GRAIN SIZE #7
 SPHEROIDIZED COMPLETELY. GRAPHITE - NONE. SOME INTERGRANULAR CARBIDE. GRAIN SIZE #5	 SPHEROIDIZED COMPLETELY. GRAPHITE - NONE.	 SPHEROIDIZED COMPLETELY. GRAPHITE - NONE. SOME INTERGRANULAR CARBIDE. GRAIN SIZE #5	 SPHEROIDIZED PARTIALLY. GRAPHITE - NONE. SOME INTERGRANULAR CARBIDE. GRAIN SIZE #5
 SPHEROIDIZED COMPLETELY. GRAPHITE - NONE. SOME INTERGRANULAR CARBIDE. GRAIN SIZE #5 TO 6	 SPHEROIDIZED COMPLETELY. GRAPHITE - NONE.	 SPHEROIDIZED COMPLETELY. GRAPHITE - NONE. SOME INTERGRANULAR CARBIDE. GRAIN SIZE #5 TO 6	 SPHEROIDIZED PARTIALLY. GRAPHITE - NONE. SOME INTERGRANULAR CARBIDE. GRAIN SIZE #5 TO 6
 SPHEROIDIZED COMPLETELY. GRAPHITE NODULAR SEGREGATED IN CONTACT ZONE CONSIDERABLE RANDOMLY DISTRIBUTED. GRAIN SIZE #7	 SPHEROIDIZED COMPLETELY. GRAPHITE - NONE.	 SPHEROIDIZED COMPLETELY. GRAPHITE - NONE. GRAIN SIZE #7	 SPHEROIDIZED PARTIALLY. GRAPHITE - NONE. GRAIN SIZE #7

KEARNY GENERATING STATION — CHART III — HIGH TEMPERATURE PIPE

SPECIMEN	MATERIAL	OPERATION: TIME & TEMPERATURE	OPERATION: STRESS	WELDING DETAILS (SPECIFIED)	3% NITAL ETCH: UPSTREAM END / PARENT METAL
8 150 LB(NOM) MERCURY VAPOR N° 1 MERCURY BOILER HORIZONTAL FIELD WELD 14 OD x .656 PIPE SPECIMEN AT TOP OF PIPE  UPSTREAM — FULL SIZE — DOWNSTREAM BEND BARS	UPSTREAM HEAT CARB STL ASTM A106-29 GRADE A C 0.10 TO 0.30 PROBABLE NO STRESS RELIEF NO HEAT TREATMENT AFTER CORRUGATING KILL LB/TON Al 1.3 (PROBABLE) CHEM ANLS % Al 0.003 Al_2O_3 0.007 DOWNSTREAM (SAME AS UPSTREAM)	TOTAL HRS PIPE 42211 AT 940 F AVERAGE, WELD 17939 AT 976 F AVERAGE OF WHICH PIPE 20564 HOURS, WELD 16395 HRS ABOVE 950 F 990 F MAX	DESIGN BURSTING 2070 PROBABLE LONGITUDINAL 745	 ENDS NOT UPSET PREHEAT 200-300 F NO STRESS RELIEF VERTEX FILLER 1/8 & 5/16	 SPHEROIDIZED COMPLETELY. GRAPHITE NODULAR HEAVY. CONCENTRATED IN THREE OR MORE PARALLEL LINES ACROSS THE SPECIMEN OTHERWISE RANDOMLY DISTRIBUTED. GRAIN SIZE #8  DO. AT 60X
9 150 LB(NOM) MERCURY VAPOR N° 1 MERCURY BOILER HORIZONTAL FIELD WELD 14 OD x .656 PIPE SPECIMEN AT SIDE OF PIPE  UPSTREAM — FULL SIZE — DOWNSTREAM BEND BARS FULL SIZE	UPSTREAM (SAME AS SPECIMEN 8) DOWNSTREAM (SAME AS UPSTREAM)	TOTAL HRS PIPE 42211 AT 940 F AVERAGE, REWELD 4316 AT 971 F AVERAGE OF WHICH PIPE 20564 HOURS, REWELD 3749 HRS ABOVE 950 F 990 F MAX	DO	 ENDS NOT UPSET NO PREHEAT NO STRESS RELIEF ORIGINAL WELD 1933 BARE O H STEEL FILLER REWELDED 1942 MUREX MOLEX FILLER	 SPHEROIDIZED COMPLETELY GRAPHITE NODULAR HEAVY RANDOMLY DISTRIBUTED GRAIN SIZE #7
10 150 LB(NOM) MERCURY VAPOR N° 1 MERCURY BOILER HORIZONTAL FIELD WELD 14 OD x .656 PIPE SPECIMEN AT SIDE OF PIPE  UPSTREAM — FULL SIZE — DOWNSTREAM BEND BARS	UPSTREAM HEAT 8502 CMO STL ASTM A206-39T TENSIL ACTUAL 68400 KILL LB/TON Al 0.5 Fe Mn 5.5 Fe Si 9.7 HEAT TREATMENT 0.5 HRS, 1650 F & SLOW FURNACE COOL, SHOP CHEM ANLS % Al 0.010 Al_2O_3 0.008 DOWNSTREAM (SAME AS UPSTREAM)	TOTAL 17939 HOURS AT 976 F AVERAGE OF WHICH 16395 HOURS ABOVE 950 F 990 F MAX	DO	 ENDS NOT UPSET PREHEAT 300-400 F STRESS RELIEF 0.7 HRS 1150-1200 F WOVEN BEADS, APP 1/8 THK LAYERS MUREX MOLEX FILLER 1/8 & 5/32	 SPHEROIDIZED COMPLETELY. GRAPHITE IN LARGE PATCHES RANDOMLY DISTRIBUTED. GRAIN SIZE #5 TO 6  DO. AT 60X

WELD INVESTIGATION

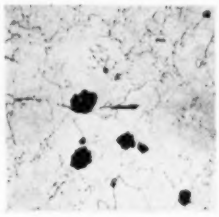
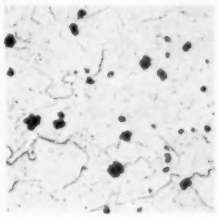
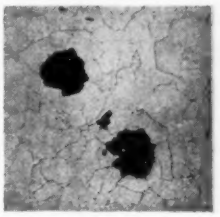
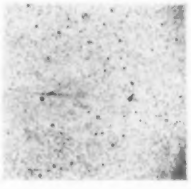
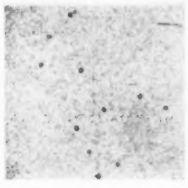
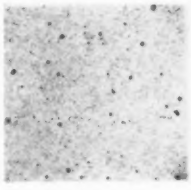
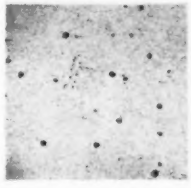
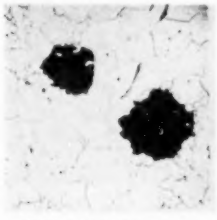
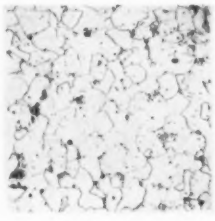
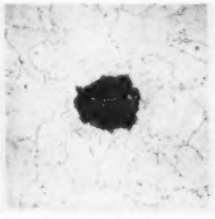
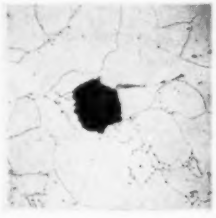
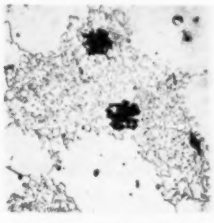
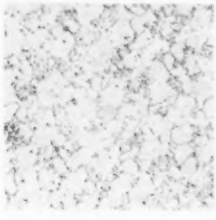
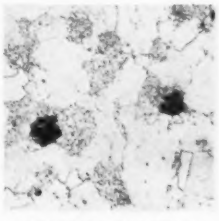
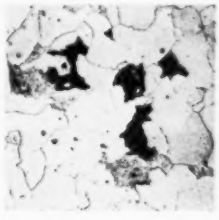
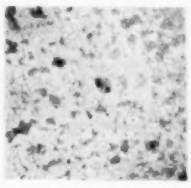
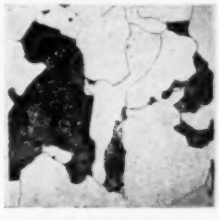
PUBLIC SERVICE ELECTRIC AND GAS COMPANY
MAY 1943 REV NOV 1943

REDUCED TO ONE-THIRD LINEAR IN REPRODUCTION

PHOTOMICROGRAPHS

500 X EXCEPT AS NOTED

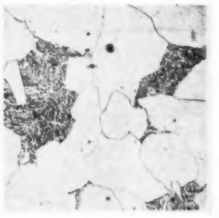
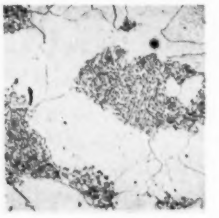
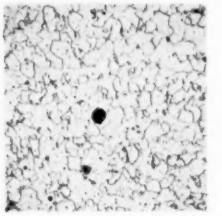
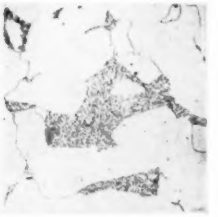
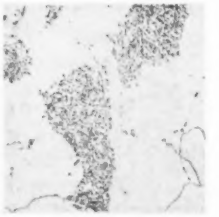
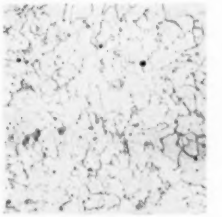
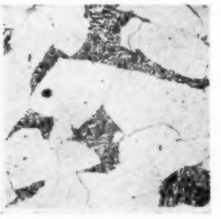
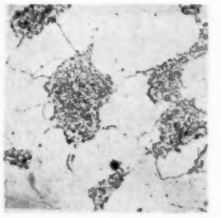
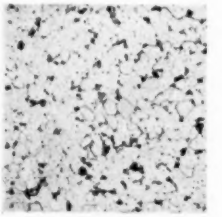
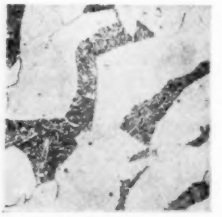
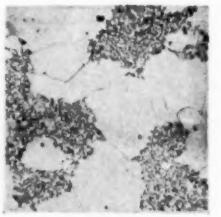
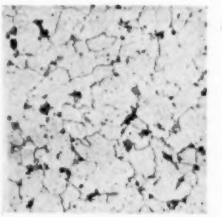
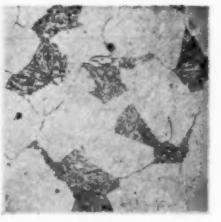
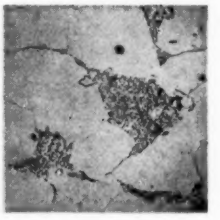
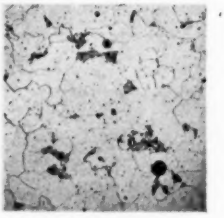
NOTE - EXHIBIT SHOWS MAXIMUM GRAPHITE OBSERVED IN EACH AREA OF SPECIMEN EXAMINED

UPSTREAM END b CONTACT ZONE	WELD c FILLER METAL	DOWNSTREAM END d CONTACT ZONE	DOWNSTREAM END e PARENT METAL
 SPHEROIDIZED COMPLETELY. GRAPHITE NODULAR HEAVY RANDOMLY DISTRIBUTED. QUANTITY NO GREATER THAN IN PARENT METAL. GRAIN SIZE #8	 SPHEROIDIZED COMPLETELY. GRAPHITE NODULAR CONSIDERABLE CONCENTRATED IN AREA SHOWN OTHERWISE NODULAR SMALL AMOUNT RANDOMLY DISTRIBUTED.	 SPHEROIDIZED COMPLETELY. GRAPHITE NODULAR HEAVY RANDOMLY DISTRIBUTED. QUANTITY NO GREATER THAN IN PARENT METAL. GRAIN SIZE #8	 SPHEROIDIZED COMPLETELY. GRAPHITE NODULAR HEAVY RANDOMLY DISTRIBUTED. GRAIN SIZE #8
 DO. AT 60X	 DO. AT 60X	 DO. AT 60X	 DO. AT 60X
 SPHEROIDIZED COMPLETELY GRAPHITE NODULAR HEAVY RANDOMLY DISTRIBUTED QUANTITY NO GREATER THAN IN PARENT METAL GRAIN SIZE #7	 SPHEROIDIZED COMPLETELY GRAPHITE - NONE	 SPHEROIDIZED COMPLETELY GRAPHITE NODULAR HEAVY RANDOMLY DISTRIBUTED QUANTITY NO GREATER THAN IN PARENT METAL GRAIN SIZE #7	 SPHEROIDIZED COMPLETELY GRAPHITE NODULAR HEAVY RANDOMLY DISTRIBUTED GRAIN SIZE #7
 SPHEROIDIZED COMPLETELY. GRAPHITE NODULAR SMALL AMOUNT IN LARGE PATCHES RANDOMLY DISTRIBUTED. QUANTITY NO GREATER THAN IN PARENT METAL. GRAIN SIZE #5 TO 6	 SPHEROIDIZED COMPLETELY. GRAPHITE - NONE.	 SPHEROIDIZED COMPLETELY. GRAPHITE NODULAR SMALL AMOUNT IN LARGE PATCHES RANDOMLY DISTRIBUTED. QUANTITY NO GREATER THAN IN PARENT METAL. GRAIN SIZE #7	 SPHEROIDIZED COMPLETELY. GRAPHITE IN LARGE PATCHES RANDOMLY DISTRIBUTED. GRAIN SIZE #7
 DO. AT 60X			 UNUSED CARBON-MOLY PIPE ASTM A206-39T SPECIMEN NO. 10 KEARNY FERRITE AND LAMELLAR PEARLITE NO GRAPHITE GRAIN SIZE #5 TO 6

STUDY OF REPLACEMENT OF METAL REMOVED BY WELD PROBER

CHART IV

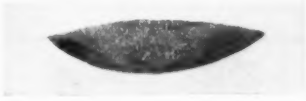
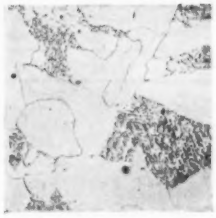
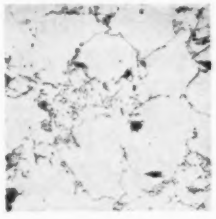
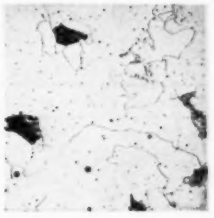
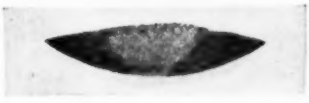
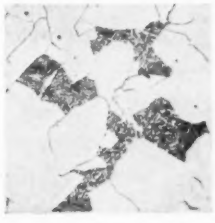
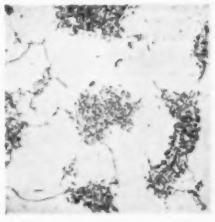
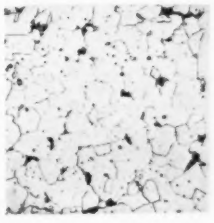
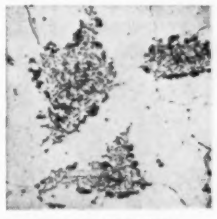
HIGH TEMPERATURE PIPE

SPECIMEN AND PREHEAT (FULL SIZE)	PHOTOMICROGRAPHS 500 X — 3% NITAL ETCH PARENT METAL (a)	CONTACT ZONE (b)	WELD METAL (c)
A 70 F	 SPHEROIDIZED PARTIALLY. GRAPHITE - NONE. GRAIN SIZE #6	 SPHEROIDIZED COMPLETELY. GRAPHITE - NONE. GRAIN SIZE #6	 SPHEROIDIZED COMPLETELY. GRAPHITE - NONE.
B 200 F	 SPHEROIDIZED COMPLETELY. GRAPHITE - NONE. GRAIN SIZE #6	 SPHEROIDIZED COMPLETELY. GRAPHITE - NONE. GRAIN SIZE #6	 SPHEROIDIZED COMPLETELY. GRAPHITE - NONE.
C 400 F	 SPHEROIDIZED PARTIALLY. GRAPHITE - NONE. GRAIN SIZE #6	 SPHEROIDIZED COMPLETELY. GRAPHITE - NONE. GRAIN SIZE #6	 SPHEROIDIZED COMPLETELY. GRAPHITE - NONE.
D 600 F	 SPHEROIDIZED COMPLETELY. GRAPHITE - NONE. GRAIN SIZE #6	 SPHEROIDIZED COMPLETELY. GRAPHITE - NONE. GRAIN SIZE #6	 SPHEROIDIZED COMPLETELY. GRAPHITE - NONE.
E 900 F	 SPHEROIDIZED PARTIALLY. GRAPHITE - NONE. GRAIN SIZE #6	 SPHEROIDIZED COMPLETELY. GRAPHITE - NONE. GRAIN SIZE #6	 SPHEROIDIZED PARTIALLY. GRAPHITE - NONE.

MATERIAL: CMO STL ASTM A158-36 GRADE P1 - MFR: HEAT 6532 - KILL LB/TON AL 1.8 SI 8-15
PIPE: 12.75 OD x 1.312 - FURNISHED TO - CHEM ANLS % AL 0.032 AL_2O_3 0.006
FILLER: MUREX MOLEX 1/8" & 5/32" WOVEN BEADS - STRESS RELIEF 2.6 HRS, 1200 F, EXCEPT "G" NOT STRESS RELIEVED

WELD INVESTIGATION

PUBLIC SERVICE ELECTRIC AND GAS COMPANY
JULY 1943 REV. NOV. 1943

SPECIMEN AND PREHEAT (FULL SIZE)	PHOTOMICROGRAPHS 500 X (REDUCED TO ONE THIRD LINEAR IN REPRODUCTION)		
	PARENT METAL a	CONTACT ZONE b	WELD METAL c
F 1200 F 	 SPHEROIDIZED COMPLETELY. GRAPHITE - NONE. GRAIN SIZE #6	 SPHEROIDIZED COMPLETELY. GRAPHITE - NONE. GRAIN SIZE #6	 SPHEROIDIZED COMPLETELY. GRAPHITE - NONE.
G 400 F 	 SPHEROIDIZED PARTIALLY GRAPHITE - NONE GRAIN SIZE #5 TO 6	 SPHEROIDIZED COMPLETELY GRAPHITE - NONE GRAIN SIZE #5 TO 6	 SPHEROIDIZED PARTIALLY GRAPHITE - NONE
	 SPHEROIDIZED COMPLETELY GRAPHITE - NONE TYPICAL OF STRUCTURE IN VERY NARROW ZONE BETWEEN HEAT EFFECTED AND CONTACT ZONES ON ALL SPECIMENS		

HIGH TEMPERATURE PIPE WELD INVESTIGATION

STUDY OF APPLICATION OF HEAT AND STRESS TO WELD SPECIMENS

NOV. 1943

PUBLIC SERVICE ELECTRIC AND GAS COMPANY

PHOTOMICROGRAPHS OF CONTACT ZONE

3% NITAL ETCH — REDUCED TO ONE THIRD LINEAR IN REPRODUCTION — 500 X

NOTE:- EXHIBIT SHOWS MAXIMUM GRAPHITE OBSERVED IN EACH AREA OF SPECIMEN EXAMINED.

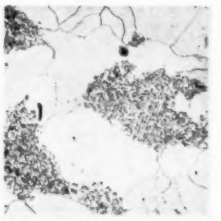
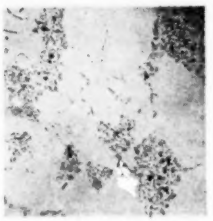
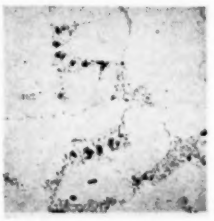
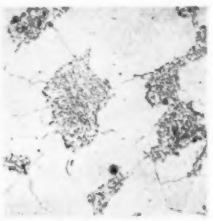
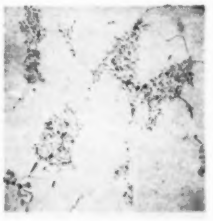
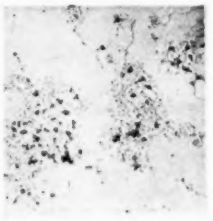
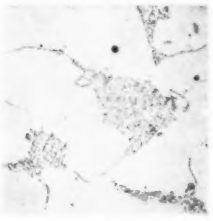
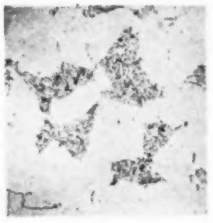
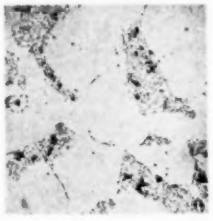
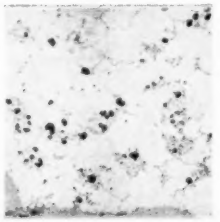
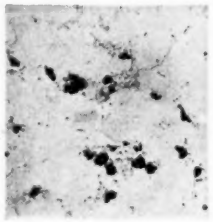
SPECIMEN PREHEAT AND SERVICE (FULL SIZE) — SEE OTHER CHARTS FOR MATERIAL	BEFORE TEST	AFTER 936 HOURS IN FURNACE AT 1000 F	
		UNSTRESSED	STRESSED AT 15000 PSI
A — 70F PREHEAT-NO SERVICE	 SPHEROIDIZED COMPLETELY. GRAPHITE NONE. GRAIN SIZE #6	 NODULAR GRAPHITE HAS FORMED	 GRAPHITE NODULES LARGER THAN IN UNSTRESSED SPECIMEN.
C — 400F PREHEAT-NO SERVICE	 SPHEROIDIZED COMPLETELY. GRAPHITE NONE. GRAIN SIZE #6	 NODULAR GRAPHITE HAS FORMED	 GRAPHITE NODULES LARGER THAN IN UNSTRESSED SPECIMEN.
E — 900F PREHEAT-NO SERVICE	 SPHEROIDIZED PARTIALLY. GRAPHITE NONE.	 NODULAR GRAPHITE HAS FORMED	 GRAPHITE NODULES LARGER THAN IN UNSTRESSED SPECIMEN.
6 — 400F (EST) PREHEAT-37078HRS AT927FAV  END EXAMINED	 SPHEROIDIZED COMPLETELY. GRAPHITE SEGREGATED IN CONTACT ZONE IN SMALL PATCHES RANDOMLY DISTRIBUTED.		 GRAPHITE NODULES HAVE GROWN IN SIZE

TABLE 1 ALUMINUM AND ALUMINUM-OXIDE DETERMINATION

Number of specimens	Material	Kill practice, lb/ton, aluminum	Aluminum, per cent	Aluminum oxide, per cent	Graphite after service
3	Aluminum-killed CMo	1.8–1.9	0.032–0.054	0.006–0.013	Segregated in contact zone
5	Silicon-killed CMo	0.5–1.0	0.007–0.014	0.004–0.010	Scattered or none
2	Silicon-killed CMo	0	0.002–0.005	0.008–0.041	None
3	Carbon	Unknown	0.002–0.003	0.007–0.026	Scattered or none

3 Table 1 is a recapitulation of Al and Al_2O_3 determinations given in Charts 1 to 4, along with several determinations not included in these charts. The figures show that Al rather than Al_2O_3, is an indication of tendency to segregation of graphite in the contact zone.

4 A concentration of graphite having no relation to the weld was found in one specimen (No. 8) of carbon-steel pipe.

5 Bend bars from several specimens with segregated graphite in the contact zone showed no loss in ductility.

Chart 5, Experimental Heating of Test Weld Specimens

In order to determine whether the graphite found could be expected, in time, to concentrate sufficiently to result in loss of ductility and also to determine, if possible, the cause of graphitization, specimens A, C, E, and No. 6 were heated in a laboratory oven for 936 hr at 1000 F. The specimens were loaded by means of a cantilever arrangement so that the contact zone was subjected to 15,000 psi stress while being heated. Also, portions of specimens A, C, and E, including the contact zone, were heated at the same temperature and for the same time without stress. The results are shown in Chart 5.

Graphite was formed in the contact zone of specimens A, C, and E, both with and without stress, but there is considerably more graphite in the stressed specimens. Preheat temperatures apparently had no marked effect on the tendency to graphitize. Specimen No. 6 showed a definite increase in size of the graphite nodules.

Additional Samples to Be Taken. In the second part of this program, now under way, whole sections of pipe have been removed and are to be examined more extensively, as well as tested for physical properties.

Acknowledgments

The work was carried out under the direction of Mr. F. P. Fairchild, chief engineer, electric-engineering department, Public Service Electric and Gas Company, and the help and advice of the following individuals, in the collection and assembly of the data, are acknowledged: Mr. H. J. Robar, metallurgist, and Mr. H. M. Soldan, assistant engineer, Public Service Electric and Gas Company; Mr. H. S. Blumberg, metallurgist, The M. W. Kellogg Company; Dr. C. L. Clark, research metallurgical engineer, The Timken Roller Bearing Company; Mr. H. J. Kerr, executive assistant, The Babcock & Wilcox Company; Dr. R. F. Miller, research metallurgist, United States Steel Corporation, Research Laboratory.

Discussion—Graphitization of Steel Piping

COMMENT ON PAPER BY H. J. KERR AND F. EBERLE (1)

I. A. ROHRIG.[1] This paper is a real contribution to the subject of subcritical graphitization of high-temperature steam-pipe material. The results of an examination made by The Detroit Edison Company, also on cylindrical creep-test sections, might be of interest.

Two sections of carbon-molybdenum seamless tubing $5^1/_2$ in. OD × $^3/_8$ in. wall thickness were arc-welded into an experimental steam line carrying steam at 380 psi and 925 F. The stress in the pipe wall at the welded joints was only 2610 psi.

The following tabulation summarizes the pertinent data concerning the material used and the results obtained:

	Sample 1	Sample 2
Type of steel	Open hearth	Electric furnace
Grain size	6–7	5–6
A.S.T.M. designation	A-158	A-158
Pipe size	$5^1/_2$ in. OD × $^3/_8$ in. wall	$5^1/_2$ in. OD × $^3/_8$ in. wall
Heat-treatment	N-1650 F D-1200 F	N-1650 F D-1200 F
Welding conditions	Arc-welded No preheat No stress relief	Arc-welded No preheat No stress relief
Exposure at 925 F	19604 hr	19480 hr
Composition: C	0.13	0.13
(per cent) Mn	0.40	0.49
P	0.014	0.010
S	0.014	0.011
Si	0.19	0.25
Mo	0.56	0.52
Cr	0.10	0.06
Ni	0.17	0.23
McQuaid-Ehn result	Normal	Abnormal
Graphitization	None	None

Although the exposure periods for our tests were considerably longer than those reported by the authors, no graphite was found in either sample. Since the welded joints were neither preheated nor stress-relieved, they are believed to have been in a condition susceptible to graphitization. Evidently, the pipe material used, even though it was of the aluminum-killed variety, was not readily susceptible to graphitization.

A review of our findings with those of the authors indicates that, from the present knowledge of the subject, each individual heat of this type of steel may have its own peculiar set of conditions under which it will graphitize, and that the graphitizing conditions used by the authors, such as exposure periods, stress, and temperature, are not necessarily applicable to different heats of steel with the assurance of graphitization.

COMMENT ON PAPER BY R. W. EMERSON (2)

SABIN CROCKER.[2] This paper is in the nature of a sequel to a report presented by the author at a special meeting arranged by A. N. Cartwright of the West Penn Power Company, in March, 1943, at Pittsburgh. The central-station industry and other users of high-temperature equipment are indebted to the management of that company for its frank report of the pipe-joint failure which had occurred at its Springdale plant.

Now that all affected joints in that plant have been replaced and investigations in other plants have been carried out to a point where the condition of their joints is known, the general situation has progressed from the emergency class, and causes and effects can be investigated from a long-range viewpoint. Hence it is fitting and proper that all interests involved in the subject of graphitization get together from time to time, to exchange ideas which will affect the future course of the several independent investigations now contemplated or under way.

A circular letter and questionnaire was sent out in April, 1943, by the Subcommittee on Metallurgy and Piping of the Edison Electric Institute's Prime Movers Committee to some 225 representatives of power companies, steel and pipe mills, boiler and turbine manufacturers, oil companies, insurance companies, etc. Approximately 150 different organizations were contacted in this manner, of which about one half made acknowledgment. Reports of their preliminary investigations of welded joints in carbon-steel and carbon-moly pipe have been received from 28 power companies and one oil company, six more plan to make investigations, while five do not intend to sample joints at this time. A total of 33 stations involving 38 different types of piping are covered in the 29 reports so far received. The extent of graphitization may be gaged to some extent by the following summary:

SUMMARY OF PIPING SYSTEMS EXAMINED

	Degree of graphitization			
	None	Severe	Moderate	Slight
High-aluminum carbon moly	10	4	5	1
Low-aluminum carbon moly	11	0	1	0
Carbon steel	3	1	2	0
Total, all materials	24	5[a]	8	1

[a] NOTE: Two of these are borderline cases between "severe" and "moderate" and ultimately may be classed as moderate.

The author's conclusion to the effect that "a large percentage (of carbon-moly piping) has been found to be in various stages of graphitization" is unwarranted and no such inference should be drawn from the foregoing statistics. As a matter of fact only nine companies (reporting on 15 stations) out of the 150 companies contacted have reported graphite, and it is to be assumed that those most likely to have it have investigated and reported their findings. It is true, of course, that with the lapse of sufficient time, graphite may develop in a few more plants.

The reports so far obtained in this survey have amply demonstrated the need for a fundamental investigation of the conditions which may produce graphitization of piping materials. A Joint E.E.I.-A.E.I.C. Subcommittee on Graphitization of Piping was established by the Edison Electric Institute and the Association of Edison Illuminating Companies. This Joint Subcommittee has made arrangements to have such a fundamental investigation carried out at Battelle Memorial Institute.

Independent investigations such as reported by the author of this paper, and in the accompanying papers by H. J. Kerr and F. Eberle and by G. V. Smith and R. F. Miller, have served to define the problem better and suggest lines of attack. The discovery by Messrs. Smith and Miller that a spheroidizing treatment at 1300 F is a preventive rather than a preliminary to graphitization is particularly noteworthy. The experiments made by the present author appear to verify this discovery. These investigations and those by power companies and other interested parties are welcomed by the Joint Subcommittee and full advantage will be taken of such findings.

From a survey of results so far reported, it would seem advisable to caution engineers not to jump at conclusions. There probably is no single answer which will account for the different types and degrees of graphitization which have been found at welded joints in both carbon-steel and carbon-moly piping. Graphite has been found also in a carbon-moly casting at a welded joint.

As the graphitization picture unfolds, one fact emerges of immediate interest to operating engineers. This is the desirability of limiting the extent and duration of temperature swings above

[1] Research Department, The Detroit Edison Company, Detroit, Mich.

[2] Senior Engineer, Engineering Division, The Detroit Edison Company, Detroit, Mich. Secretary of Joint E.E.I.-A.E.I.C. Subcommittee on Graphitization of Piping. Mem. A.S.M.E.

design temperatures. Present limitations by turbine manufacturers and the Code for Pressure Piping and Boiler Code are based upon creep considerations alone. While it is not possible with available information to set definite limits for each material, it would seem wise to keep below the following temperatures in so far as feasible until more is known on the subject:

Carbon steel, low and medium carbon	850 F
High-aluminum carbon-moly (1.5 lb Al per ton)	925 F
Low-aluminum carbon-moly (0.5 lb Al per ton)	950 F

Hence it would be advisable for power-plant operators to consider the actual range of temperatures rather than to depend upon daily average values which fail to show the extreme temperatures reached.

There is no proof that some graphite will not result under such restrictions, but there likewise is no indication that the serious type of segregated grain-boundary graphitization will result if operating temperatures do not exceed the maximums given in the table.

It will be noted that the upper limit tentatively set for the low-aluminum more-stable type of carbon moly is 25 deg higher than for the high-aluminum variety. This is based upon the fact that only one instance of graphite has been found in the low-aluminum carbon moly, and in that case the average temperature was 975 F with swings to 990 F.

The requirement of a 3 to 6 grain size in A.S.T.M. Specification A-206 involved a reduction in the aluminum added for killing purposes from about $1^1/_2$ lb per ton of steel to only $^1/_2$ lb. The use of about $^1/_2$ lb of aluminum per ton of steel fortuitously increased the stability of the carbide structure. While the specification of grain size was based upon creep tests, the change in deoxidation practice obtained thereby seems to have been beneficial from the standpoint of increased resistance to graphitization.

The conclusion of the author that the chain type of graphitization is associated with coarse-grained Widmanstätten structure is based upon heating a fine-grained high-aluminum carbon-moly material at 2600 to 2800 F to produce an exaggerated grain growth. This is similar to, although presumably higher than, the heating for upsetting given the Springdale pipe. In the opinion of the writer, the effect of this heating and the conclusions therefrom should not be interpreted as an indictment of the low-aluminum variety of carbon-moly pipe which, in the as-rolled condition, shows a coarse-grained Widmanstätten structure. As noted in the foregoing tabulation of results, only one instance of graphitization of this type of material has been reported and the service temperature in that case averaged 975 F with swings to 990 F.

H. J. Kerr.[3] Apparently three laboratories, one represented by Mr. Emerson, one represented by Messrs. Smith and Miller, and our own, have all found that 1300 to 1350 F stress relieving does not graphitize abnormal carbon-molybdenum steel. Apparently each of these laboratories has found that such treatment hides or eliminates the effect produced by welding.

If it is necessary to use a heat-treatment of 1300 to 1350 C after welding, then the fact must be faced that the material starts its life in the spheroidized condition with apparently reduced creep strength. Again, it is to be borne in mind that the Springdale pipe had graphite 12 in. from the weld, at the section which was spheroidized, due to the heat of the forging operation.

Comment on Paper by G. V. Smith and R. F. Miller (3)

H. J. Kerr.[3] The theory proposed by the authors is that the variation of the complex carbides with temperature and condition of the steel may give an explanation also as to why steel in which aluminum is not used to deoxidize has not graphitized in service.

As understood by the writer, the proposed theory is that as the lower critical is exceeded on heating, the alloy carbides are stable carbides, but when the steel is cooled below the critical, so that no martensite is present, the carbides tend to separate in a manner to give a considerable percentage of unstable carbide.

It is recognized that straight silicon-killed carbon-molybdenum steel is much more sluggish than aluminum-killed steel. When the heat wave caused by welding passes, the silicon-killed steel tends to maintain the austenite from above the critical, and in this way bring down the carbides in their more stable form to subcritical temperatures. Some of the work we have done certainly indicates a material difference between the general pearlite grains in straight silicon-killed steel and those in which high aluminum has been used when the steels are quickly cooled through the lower critical.

The authors should be more specific in their footnote comments[5] of their paper. If the piece of steel discussed is the one concerning which the writer has carried on considerable correspondence with the authors, then he cannot agree with the statement that this steel represents a deoxidation practice similar to the steel of the headers at Springdale which did not graphitize.

It may be pointed out that there are apparently many factors involved in the deoxidation of steel. When steel is made with no aluminum, or when it is made with about 2 lb of aluminum per ton, very definite characteristics are obtained. In the case of the intermediate practice, in which from $^1/_2$ to 1 lb of aluminum is used, there are other factors which affect the result, so that direct analysis cannot be made by the simple statement of the amount of aluminum used. For this and other reasons, we have found that a McQuaid-Ehn test is the best measure of the normality of the material, and that graphitization and normality apparently are related. By this test we have cases of more pronounced normality with steels which were reported deoxidized with 1 lb of aluminum than with other steels reported to be deoxidized with $^1/_2$ lb of aluminum per ton.

General Discussion

S. L. Hoyt.[4] Mr. Sabin Crocker mentioned the work that we are doing at Battelle Memorial Institute on the graphitization of steam lines. Our particular function is to study the fundamentals and to establish the causes, if possible, on a quantitative basis. Knowing the causes, it should be relatively simple to suggest practice which will minimize or avoid the hazards of segregated graphite in pipe lines. The three papers on this subject not only throw light on the causes, but also suggest two ways of circumventing them. There can be no doubt that they are a valuable and welcome contribution.

The Project Committee for the Battelle work, the Joint E.E.I.-A.E.I.C. Subcommittee on Graphitization, has authorized full co-operation with the power industry, suppliers, fabricators, and with research laboratories which are working on this problem. One of these functions consists of collecting and correlating data which have been submitted on the installation and operating conditions of steam lines of various power stations and the results of examinations of test samples taken from the welded joints of the lines. Approximately 225 individuals in 150 companies were contacted, of which about 75 companies made acknowledgment. Reports have been received covering investigations in 33 power stations and a few more remain to be heard from. In about 40

[3] Executive Assistant, The Babcock & Wilcox Company, Barberton, Ohio. Mem. A.S.M.E.

[4] Technical Advisor, Battelle Memorial Institute, Columbus, Ohio.

per cent of the stations reporting, joints were found which showed some degree of graphitization, although only three stations had joints showing continuously segregated graphite. However, quite a few more have segregated streaks of graphite or chains of disconnected nodules which may or may not be progressing toward embrittlement. Opinion seems to differ on that point, but it is reasonable to believe that if graphite has started to form, it should continue to do so until the carbide in that area is all used up. Of course, if the steel is of low carbon content, a small amount of graphite should quickly consume the carbide, and such a joint may never become dangerous. With a higher carbon content, complete embrittlement might ultimately be produced.

About 60 per cent of the plants investigating the matter reported finding no graphite. In view of the point made by Messrs. Kerr and Eberle that low-aluminum steel of normal structure in the McQuaid-Ehn test does not graphitize, or at least is highly resistant, it may be of interest to know that in this group three out of fifteen were the low-aluminum type. The data collected to date do not give a satisfactory answer on the point. For one thing, most of the steel which has been in service long enough to show much graphite is the high-aluminum type, and it will probably be a couple of years or so before satisfactory returns are made. Possibly of equal significance are the reported operating temperatures and their bearing on graphitization. Those plants reporting graphitization also reported operating temperatures in the 900's, while those plants reporting no graphitization report operating temperatures in the 800's, in deg F. We are keeping Mr. Kerr's point in mind and hope to accumulate evidence on it.

The other two papers advance the proposition that heating a welded joint to 1300 F, prior to service will eliminate graphitization at normal operating temperatures. The data we have gathered are quite inadequate for a check on this point, since the stress-relieving temperature is standard at 1200 F. In one case, however, a plant reports stress-relieving at 1300 F, but it also reports graphitization. From the point of view of this proposition, it is perhaps unfortunate that this one case is negative, but too much weight should not be given to a single report on the matter.

The point is made in these two papers that heating the steel just above the first critical point during welding, or possibly just into the first critical point, produces a structural change around the borders of the Widmanstätten areas and predisposes those places to graphitize in service. Presumably the steep temperature gradient which is produced by welding is a highly effective method of bringing about this structural change. In view of the relatively short times over which graphitization and its inhibition have been studied or observed, as compared to the far greater design life of steam lines, it is highly desirable that this suggestion be studied and checked. For example, are we dealing with a procedure (stress-relieving at 1300 F) which completely and permanently inhibits graphitization, or with one which simply retards it for a few years? The suggestion of Smith and Miller seems to be a reasonable one that heating to 1300 F converts the carbide into molybdenum carbide which is stable, but presumably it is stable only with respect to graphitization. If the change from iron to molybdenum carbide, reported by Crafts and Offenhauer, represents what is called an "equilibrium," with an equilibrium temperature above which molybdenum carbide is stable and below which iron carbide is stable, then we need to understand the effect of operating temperatures in converting the molybdenum carbide to iron carbide, since the operating temperature is thought to lie below the equilibrium temperature. If such a change takes place, the iron carbide which would form could still graphitize, although only after a lapse of time.

At this point it is desirable to refer to some work we have done at Battelle on the identification of this material as graphite. By taking electron diffraction patterns of the fractured face, such as is shown in Mr. Emerson's Fig. 1, we obtain the graphite pattern. This is practically a conclusive identification of this material as graphite. At first, however, we tried by various means to extract this phase electrolytically and thus to secure samples for chemical, X-ray, and electron-diffraction identification. Those results likewise gave evidence of graphite, but they also identified molybdenum carbide as a constituent of the steel. This technique will be used to secure evidence on the relationship between carbide composition and graphitization.

The writer believes it to be highly desirable to refrain from oversimplifying the picture of graphitization, at least at this time. After the returns are all in, we will doubtless be able to set up a very simple mechanism of graphitization in steam lines. Bearing out this thought, two cases have occurred which have the surprising and even disconcerting characteristic in common of not forming in accordance with the heat and structural effects of the welding operation. The first is the occurrence of about one-half dozen segregated streaks of graphite $^1/_2$ to $^3/_4$ in. away from the weld, or definitely well away from the heat-affected zone. The second one is a couple of stringers of segregated graphite which pass through a heat-affected zone or at about right angles to the isothermal lines. These cases are not at all understood at present, hence the writer will not attempt to "explain" them. They do suggest, however, that in spite of the nicely conceived and skillfully conducted experimentation outlined in these papers, we may not yet have the true mechanism. Apparently what we still need is the common denominator underlying the typical isothermal type of graphitization and the nonisothermal type.

H. S. Blumberg.[5] One factor considered by those conducting investigations which have for their aim either the dissolving of graphite by some treatment or a study of effect of time and temperature upon graphitization, is microscopic examination of sections. We have found that if several microspecimens are prepared from various locations around the circumference of a joint, there may be considerable difference in the amounts of graphite observable in the several sections. This is merely a statement of the fact that graphite, if present, may not be uniformly distributed, particularly as judged by examination along single planes cut through the thickness of tubes. It follows from this that evidence for an increase or decrease in the amount of graphite due to any given treatment should be based upon more than a relatively small difference in graphite in two different fields.

Mr. Emerson has already described the simple tests being commonly used by those interested in sampling joints to determine whether particular joints should be allowed to remain in service or whether graphitization has developed sufficiently to warrant removal and replacement. Our laboratory has examined samples removed from 33 joints representing 7 different power plants, from which the following observations have been made:

No graphite was found in any of the samples taken from tubing treated with less than 0.5 lb aluminum per ton. This is particularly emphasized by the fact that one material studied (0.11 lb Al per ton) had operated at an average temperature of 975 F for 35,000 hr (this being the highest operating temperature represented by any of the samples) and showed no signs of graphite.

Graphite in varying degrees was thus found only in tubes made from steel treated with appreciable amount of aluminum (about 2 lb per ton), so-called "aluminum-killed steel." However, not all joints made of this type of steel showed graphite. Advanced graphitization was found only in some of those tubes which had "coarse-grained" ferrite-pearlite structure (1–3 actual grain size) due to temperature used in upsetting tube ends before welding. To the writer's best knowledge, the only joints which have been

[5] Chief Metallurgist, M. W. Kellogg Company, Jersey City, N. J.

purposely removed from power-plant service because of advanced graphitization were in so-called coarse-grained (about 1–3 actual grain size) aluminum-killed steel (about 2 lb Al per ton). While graphite has also been found in aluminum-killed steel (about 2 lb Al per ton) with finer actual grain size (about 4–8) in the unaffected base metal near the weld, as far as is known no joints of this type have been purposely removed. In other words, in such metal it is considered that at present graphite is randomly dispersed and does not materially affect the strength, ductility, or shock resistance of the welded joint. Sampling of joints at later dates should show whether graphitization is seriously advancing.

The highest operating temperatures appeared to give most severe graphitization.

No relation was found between welding technique or position of joint axis in service and graphitization. Welding-technique factors studied were string versus weave beads and bead thickness. Axes of joints studied were horizontal and vertical.

The nature of graphitization in low-carbon steels and the manner in which it takes place are certainly little understood at the present time. Hence the present papers are of prime importance in suggesting prior treatment technique which may retard or prevent graphitization, in advancing a hypothesis to explain graphitization and in stimulating further work on this most important subject.

H. J. Kerr.[5] We have made a very considerable investigation of graphitization in power plants and other industries where carbon-molybdenum steel has been in service for a considerable length of time, without finding a single instance of graphitization of fully silicon-killed carbon-molybdenum steel, when aluminum was not used. To put this on a definite basis, the writer would state that no carbon-molybdenum steel, showing a normal McQuaid-Ehn grain size of 1 to 5 has been found graphitized. This is a vitally important point, and the request is made that, if anyone knows of such a case, it will be appreciated if that information is forthcoming as quickly as possible.

In the case of carbon-molybdenum steel in which aluminum was used in the deoxidation, a considerable amount of graphitization has taken place where the aluminum addition has been of the order of 1¾ to 2 lb. Such steels show abnormal with a McQuaid-Ehn grain size of the order of 7 to 8.

In between these two extremes, the statement of the amount of aluminum used in the deoxidation does not give a measure of the graphitization tendency, in so far as can be determined. Some steels reported to have been deoxidized with 1 lb of aluminum per ton show much more definite normality and no graphitization in service than other steels in which ½ lb of aluminum per ton has been used and which have graphitized in service. Here particularly the McQuaid-Ehn test seems to be the best measure of the susceptibility that we have found.

A. E. White.[6] These three papers are of vital interest to those using plain-carbon or alloy steel for high-temperature and possibly high-pressure service.

Although much work needs to be done to determine the cause of graphitization in plain-carbon and alloy steel, a most urgent and immediate need is to determine ways and means of rectifying graphitization without destruction of the materials.

Closure to Paper by R. W. Emerson

As a result of the very interesting and enlightening discussions on the "Graphitization of Steel Piping" several pertinent questions have arisen, some of which are perhaps due to insufficient clarification on the part of the writer.

Mr. Crocker's comments regarding the general association of the chain type of graphitization with a coarse grained Widmanstätten structure is well taken. Three possibilities are believed to exist when exploring for graphitization adjacent to welds, namely, (1) no graphite, (2) dispersed graphite, and (3) segregated graphite. Segregated graphite may be further subdivided into (*a*) chain graphite and (*b*) nodular graphite as shown in Figs. 3 and 6(*a*), respectively. If segregated graphite is found to exist, it is believed that the chain type will be found if the adjacent base metal has a coarse-grained Widmanstätten structure. It is not to be implied, however, that the presence of a coarse-grained Widmanstätten structure adjacent to a weld, such as commonly found in the current A.S.T.M. A-206 carbon-moly steel piping in the as-rolled or normalized condition, is synonymous with segregated chain-type graphitization. Limited experience with the current carbon-moly material in which a considerably smaller amount of aluminum is used in deoxidation of the steel has indicated this material regardless of grain size to be structurally more stable than the previously used (deoxidation treatment 2 lb aluminum per ton) carbon-molybdenum steel piping.

In connection with comments made by Mr. Kerr and Dr. Hoyt regarding a 1300–1350 F stress-relieving treatment, the finding of graphite at a distance of 12 in. from a weld, and the extent of inhibition of graphitization by the foregoing treatment, it may be stated with almost positive assurance that there is no presently known heat-treatment which could be said to *permanently* inhibit all graphitization in a carbon-moly steel such as that in which heavily segregated graphite has been found to exist adjacent to welds. This statement is based on the fact that a longitudinal section of pipe extending 24 in. from a weld was examined at several locations throughout that distance, and dispersed graphitization was found in all cases although the grain size and microstructure varied considerably as a result of the original hot fabricating operations.

Although general dispersed graphitization was found to have occurred in piping remote from welds, no specific mention of this fact was made originally in the paper since this type of graphitization was found to have little or no effect on the physical properties of the piping system. On the contrary, heavily segregated graphite was found to result in extremely poor ductility over a very localized region adjacent to the weld. The purpose and intent of the 1300 F stress-relieving treatment therefore is to prevent if possible the subsequent formation of *segregated* graphite. It was by no means intended that this treatment would permanently inhibit all graphitization. It appears at the present time that it will be necessary to further investigate steel-melting practices, deoxidation treatments, and the possible use of additional alloying elements in order to obtain a material in which greater assurance can be given against general graphitization.

Mr. Kerr's findings regarding the use of the McQuaid-Ehn test in determining the normality of carbon-moly steel which he has shown to be related to graphitization is believed to have considerable merit and should be given consideration as a possible test to be incorporated into A.S.T.M. Specification A-206 for carbon-molybdenum steel piping. It is to be pointed out that this relationship regarding normality and graphitization has also been observed by Austin and Fetzer.[7] They state, "In general, the results indicated that coarse-grained normal steels were stable while the fine-grained abnormal steels graphitized. Evidence has been provided to show that alumina, which may have such a profound effect on the control of grain size and abnormality, may similarly markedly lower the stability of the carbide."

[6] Director of Engineering Research, University of Michigan, Ann Arbor, Mich. Mem. A.S.M.E.

[7] "Cementite Stability and Its Relation to Grain Size, Abnormality, and Hardenability," by C. R. Austin and M. C. Fetzer, Transactions, American Society for Metals, vol. 29, 1941, pp. 339–354.

Closure to Paper by G. V. Smith and R. F. Miller

Mr. Weisberg's description of his experimental study is a valuable addition to the subject of graphitization of steel piping. We were particularly interested in the finding that graphite was produced in samples held for 936 hr at 1000 F and that stressing accelerated this graphitization.

Since writing our paper, we have also succeeded in producing graphite experimentally in a weld-heat-affected zone and incidentally also obtained a confirmation of the efficacy of our suggested preventive treatment. A brief description of a portion of our experiments may be of interest. We obtained, through the courtesy of Mr. R. W. Emerson, a section of carbon-molybdenum pipe that had been removed from the Springdale Generating Station and prepared two sections approximately $1 \times 2^1/_2 \times 4$ in. After normalizing one section at 1650 F and the other at 2000 F, we laid down on opposite sides of each of the samples a weld bead, in one case at a relatively slow rate and in the other at a relatively fast rate, so as to give on each sample a relatively narrow and a relatively wide heat-affected zone. Each sample was then cut in two, and one half of each subjected to a post-heat-treatment of four hours at 1300 F and the other half nontreated. The samples were then placed in a furnace at 975 F and held for 1000 hr. Sections were cut from each of the samples and examined metallographically for evidence of graphitization. At the low temperature end of the heat-affected zone of the steep temperature-gradient weld of the sample normalized at 1650 F and not post-treated, small dark particles were noted which, though they could not be resolved as such, were very evidently the first traces of graphite. No such particles were observed in the companion section which had received the preventive treatment, nor in the wide heat-affected zone of the same sample, nor in either of the welds of the sample normalized at 2000 F whether post-treated or not. The remaining sections were reintroduced into the 975 F furnace, held for another 1000 hr, and sections cut for further metallographic examination. By this time, 2000 hr, the graphite particles of the sample mentioned had grown sufficiently to be resolvable as such and again there was an absence of graphite in the companion post-treated sample and in all the other welds. Thus graphite was produced in the narrow weld-heat-affected zone of a sample previously normalized at 1650 F but this graphitization was prevented by a post-treatment of four hours at 1300 F. No graphite was observed in the wide weld-heat-affected zone of this pair of samples or in either of the weld-heat-affected zones of the pair previously normalized at 2000 F. These experiments are continuing and will be described in more detail subsequently.

Mr. Kerr's comments regarding deoxidation practice and the relation between graphitization and normality are interesting. It is difficult to understand the reason for a relationship between abnormality and "graphitizability," but this perhaps is to be expected in view of our lack of knowledge of either phenomenon separately. Of course, there are really two factors to be considered with respect to graphitization, namely, thermodynamic stability and reaction rate. We suspect that the apparent relationship between abnormality and graphitizability owes its existence to a greater rate of graphitization of the "abnormal" steel and does not negate the possibility of graphitization of "normal" steel. However this may be, the utility of the relationship, if found to be true, as a means of separating carbon-molybdenum steel into two classes one of which may be expected to be subject to graphitization during service, is obvious.

Mr. Kerr has also raised the question of spheroidization of the steel during preventive treatment with the attendant possible loss in creep strength. The spheroidization resulting from four hours at 1300 F, as in our experiments cited earlier, is not great, being no more extensive than perhaps that resulting from 10,000 hr at the service temperature. Mr. Kerr has apparently contemplated a much longer post-treatment time or a higher temperature than we. Moreover, according to data of Miller et al[8] a short-time treatment at 1300 F can be expected to increase rather than decrease the creep strength. Of a number of heat-treatments including simple normalizing, a treatment of five hours at 1300 F after normalizing resulted in maximum creep resistance in the standard creep test. The beneficence of this treatment is attributed to the development of a "fine groundmass precipitate, probably a molybdenum-rich carbide."

We wish to correct Mr. Kerr's impressions regarding our hypothesis of the reason for localized graphitization. Briefly, we postulated that the austenite which forms on heating just above the lower critical transforms to or yields, under conditions of relatively rapid cooling (as occurs adjacent to a weld), a carbide which is unstable with respect to graphite at the serivce temperature. It is by postheating below the critical, not above, that we thought to prevent localized graphitization. It appears to us that under some circumstances, treatment immediately above the critical might not be efficacious for preventing graphitization, as for example should the steel be subsequently fast-cooled. In such a case it would seem that the conditions might again be set for graphitization. Perhaps this is the reason for the occurrence of graphitization in the sample cited by Dr. Hoyt in which a plant has reported graphitization after stress-relieving at 1300 F; it may be that the lower critical was exceeded owing to inexact temperature control. We doubt, incidentally, that in this case there was localized graphitization; and in this connection it might further be emphasized that the important thing to avoid is localized graphitization, and not so much random graphitization; we doubt that any treatment will prevent all graphitization in this material. Contrary to Dr. Hoyt's opinion, we do not believe that only the carbide in the vicinity of a graphite particle will be converted to graphite, and that accordingly "if the steel is of low carbon content, a small amount of graphite should quickly consume the carbide, and such a joint may never become dangerous." Actually, it seems certain that if, in the Springdale Station pipe, only the carbide in the immediate vicinity of the region where failure subsequently occurred had graphitized, there would not have been sufficient graphite to form the near-continuous network that was the cause of failure. In other words, carbon had migrated from the remainder of the sample. Our suggested preventive treatment was presented with the hope that it might prevent localized graphitization, but not necessarily all graphitization.

[8] "Influence of Heat Treatment on Creep of Carbon-Molybdenum and Chromium-Molybdenum-Silicon Steel," by R. F. Miller, R. F. Campbell, R. H. Aborn, and E. C. Wright, Transactions, American Society of Metals, vol. 26, 1938, p. 81.

FURNACE PERFORMANCE FACTORS

Operating History of the 2500-Psi Twin Branch Plant . . . *Philip Sporn and E. G. Bailey* 1

Natural-Circulation Test Results on the 2500-Psi Twin Branch Boiler . . . . . *W. H. Rowand and T. B. Allardice* 17

Distribution of Heat Absorption and Factors Affecting Performance of Twin Branch 2500-Psi Boiler . . . . . *F. G. Ely and L. B. Schueler* 23

Summary of Reports on Physical Conditions Reported by Eight Operating Companies . . . . . *A. R. Mumford* 33

Furnace Design and Development of Steam-Generating Units Burning Central Illinois Coal . . . . . *J. R. Michel* 35

Pulverized-Coal-Fired Boiler Furnaces, Public Service Electric and Gas Co., New Jersey . . . . . *H. Weisberg* 43

Description and Performance of Boilers 12 and 14, Trenton Channel Plant, and Boilers 9 and 10, Marysville Plant, The Detroit Edison Company . . *R. J. Brandon and W. A. Carter* 57

Performance of Pulverized-Coal-Fired Boilers on Philadelphia Electric Company System . . . . . *J. H. Harlow* 63

Heat-Transfer to Water-Cooled Furnace Walls . . . *Henry Kreisinger and R. C. Patterson* 71

Absorption of Heat by Walls of a Furnace . . . . . *John Blizard* 79

The Flow Characteristics of Coal-Ash Slags in the Solidification Range . . . . . *W. T. Reid and P. Cohen* 83

Statistical Information on Large Pulverized-Coal Units on the Consolidated Edison System. . . . . *W. E. Caldwell* 99

Presented at the Annual Meeting of The American Society of Mechanical Engineers, New York, N. Y., Nov. 29–Dec. 3, 1943, under the auspices of the Special Research Committee on Furnace Performance Factors with the Co-Operation of the Fuels, Power, and Heat-Transfer Divisions. Published May, 1944.

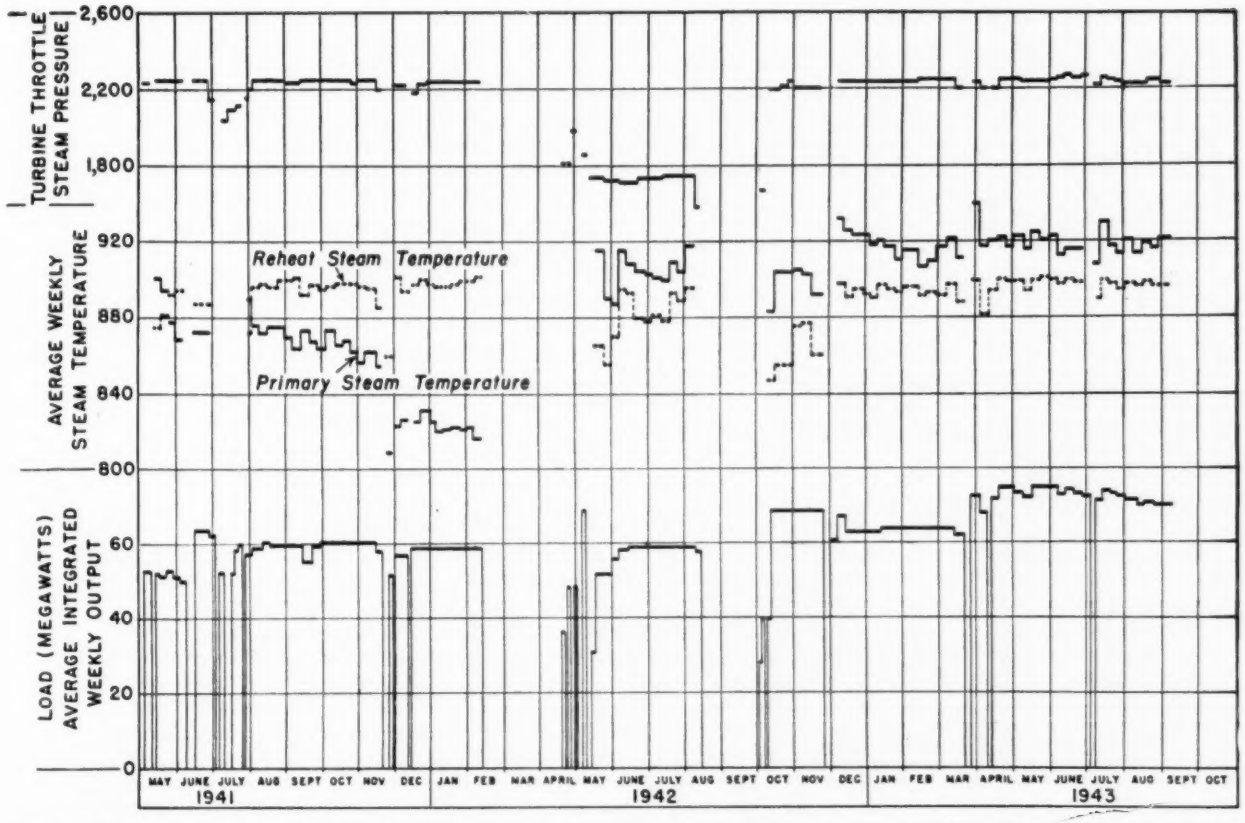


FIG. 1 OPERATION OF UNIT 3, TWIN BRANCH STATION, OF THE INDIANA & MICHIGAN ELECTRIC COMPANY, OPERATING SUBSIDIARY OF THE AMERICAN GAS & ELECTRIC COMPANY, FROM MAY, 1941, TO SEPTEMBER, 1943

Operating History of the 2500-Psi Twin Branch Plant

BY PHILIP SPORN[1] AND E. G. BAILEY,[2] NEW YORK, N. Y.

The experience gained in the operation of the 2500-psi steam-electric generating unit, projected more than 6 years ago for the Twin Branch Station of the Indiana & Michigan Electric Company, from the date it was placed in operation, March, 1941, to August 31, 1943, is outlined in this paper. During the early months of operation many lessons were learned and steps taken to correct difficulties which arose. Alterations were completed in spite of wartime handicaps, and since April, 1943, the unit has been operating at the design values of capacity, pressure, and temperature. Even prior to that time, however, i.e., December, 1942, the boiler had been operated at or had been in condition to operate at full design values. In considerable detail, the authors describe the work of alteration carried out during the three operating periods discussed, and present performance data recorded during these periods. They believe that the operating experience of the last 2 years has verified the judgment of those responsible for undertaking this distinctive development in power generation, and that 2500-psi natural-circulation boilers, 2300-psi steam turbines, with their related equipment, can be made to give a power plant that is technically and commercially sound.

MORE than 6 years ago a 2500-psi steam-electric generating unit was projected for installation at the Twin Branch Plant of the Indiana & Michigan Electric Company. After much study, thought, and intensive effort, the project was placed in operation in March, 1941. The story of that design and construction is fully covered, as many know, by a series of articles which appeared in the October 18, 1941, issue of *Electrical World*. It is not proposed to repeat that story but

[1] Vice-President and Chief Engineer, American Gas and Electric Service Corporation. Mem. A.S.M.E.

[2] Vice-President, The Babcock & Wilcox Company. Mem. A.S.M.E.

Contributed by the Power Division and presented at the Annual Meeting, New York, N. Y., Nov. 29–Dec. 3, 1943, of THE AMERICAN SOCIETY OF MECHANICAL ENGINEERS.

NOTE: Statements and opinions advanced in papers are to be understood as individual expressions of their authors and not those of the Society.

rather to supplement it by giving an account of our experiences gathered over the subsequent 2-year period of operation.

During that time many lessons have been learned and solutions found to many old and newly created problems. These solutions were, of course, often delayed in execution because of wartime conditions. However, this did not cause any diversion from the main objective. The work went on, alterations were completed, and the unit has been operating at the design values of capacity, pressure, and temperatures since April, 1943. The boiler, however, has been operating at, or has been in a condition to operate at, full design values since December, 1942.

Fig. 1 gives a graphic history of the operation of this high-pressure unit. It will be noted that the total time which has elapsed since the unit was first placed on the line in March, 1941, naturally divides itself into three periods. The first period started with May 5, 1941, the date the unit was placed back on the line after preliminary adjustments and inspections, and ended with February 13, 1942. The arrangements during this period are shown in Figs. 2 and 3. The second period started on April 20, 1942, and ended August 14, 1942, and had the arrangement shown in Fig. 4. The third period started October 1, 1942, with the arrangement shown in Fig. 7, and after changes to circulation and very minor changes to surface, as shown in Fig. 8, has continued up to the present.

In that entire period two main outage intervals were experienced during which substantial changes were made in one or more parts of the boiler. Both of these periods, however, were scheduled months in advance of the time when the unit was actually taken out. In other words, the difficulties encountered were such that they could have been endured. There was a period of some 3 months when the unit was operated at a pressure of approximately 1750 psi. But since the changes that were completed on October 1, 1942, the unit has had no major difficulty, and for a period of a year the unit, in so far as the boiler is concerned, has been in a condition to operate at full design values of capacity, pressure, and temperatures, and has actually operated at these values for a period of over 8 months. This record, it is believed, speaks for itself.

The faith of the authors in the soundness of natural circulation for this design pressure was completely substantiated at the very start by measurement of circulation as the boiler was first brought to operating pressure. As a matter of fact, circulation tests showed circulation values which exceeded calculated performance. Because the subject of circulation in high-pressure boilers has been a source of technical controversy, a more detailed account of this phase is covered in a separate companion paper.[3] With the increase in boiler output, it became apparent that temperature and heat distribution among the various portions of total heat-absorbing surface were to be the real problems.

With 940 F steam temperature and 900 F reheat temperature, 43 per cent of the heat value in Btu absorbed per pound of steam at the maximum design load of 550,000 lb per hr is used for superheat and reheat; whereas, with 1300 psi and 950 F, only 27 per cent is used for superheat; and with 400 psi and 700 F, only 14 per cent is used. Because of this, it was necessary to install superheater and reheater surface in zones of higher gas temperature than is usual on boilers operating at lower pressure levels.

Adjustments and Changes

Fig. 2 shows a cross-sectional arrangement of the boiler as originally placed in service in March, 1941. The furnace front wall and the first and second division walls were $3^1/_4$-in. partial-stud tubes on 6-in. centers. The furnace side walls were 4-in. partial-stud tubes on 6-in. centers. These walls comprise the entire steam-generating surface. The partial-stud tubes have a bare face to the furnace, a cross section of which is shown in Fig. 6. The side walls of the first open pass and the side walls and rear wall of the second open pass were reheater surface as was 25 per cent of the width of the convection pass. Seventy-five per cent of the width of the convection pass plus seven groups of platen tubes across the width of the second open pass were superheating surface. A spray-type attemperator located in the connecting pipe between the convection superheater and the platens provided superheat control and dampers at the economizer outlet provided reheat control.

The first column in Table 1, shows the heat absorption during the initial period of operation. At 52,000-kw output, the superheat- and reheat-surface absorption rates exceeded the design expectations. In order to keep the final steam temperatures down to design levels, it was necessary to employ more than double the calculated full-load attemperation. A change

[3] "Natural Circulation Test Results on the 2500-Psi Twin Branch Boiler," by T. B. Allardice and W. H. Rowand. Presented at the Annual meeting, New York, N. Y., Nov. 29–Dec. 3, 1943, of The American Society of Mechanical Engineers.

TABLE 1 TYPICAL ABSORPTION DISTRIBUTION, TWIN BRANCH UNIT NO. 3

OPERATING PERIOD	1				2		3	
ARRANGEMENT SHOWN IN	FIG. 2	FIG. 3			FIG. 4	FIG. 7	FIG. 8	
TYPICAL DATA WITHIN PERIOD	MAY 1941	JULY 1941	AUG. 1941	JAN. 1942	JULY 1942	NOV. 1942	DEC. 1942	MAY 1943
APPROXIMATE OUTPUT - KW	52,000	64,000	60,000	55,000	59,000	62,000	67,000	76,000
STEAM FLOW TO TURBINE - LB./HR.	375,000	490,000	440,000	401,000	438,000	453,000	478,000	561,000
WATER FLOW TO ATTEMPERATOR - LB./HR.	38,000	60,000	40,000	41,000	0	0	0	0
OPERATING PRESSURE - LB./SQ. IN.	2275	2300	2300	2260	1875	2230	2280	2315
STEAM TEMP. AT SUPERHEATER OUTLET - F	936	880	893	832	903	913	939	928
STEAM TEMP. TO REHEATER - F	525	505	501	458	537	523	544	550
STEAM TEMP. FROM REHEATER - F	900	880	905	903	884	887	896	900
STEAM TEMP. RISE IN SUPERHEATER - F								
FIRST STAGE	212	236	211	187	150	162	193	180
ATTEMPERATOR	-125	-151	-113	-139	0	0	0	0
SECOND STAGE	194	141	141	130	128	101	91	91
TOTAL	281	236	239	178	278	263	284	271
STEAM TEMP. RISE IN REHEATER - F								
FIRST STAGE	100	76	99	137	153	187	192	131
SECOND STAGE	61	95	77	97	77	53	44	90
THIRD STAGE	214	204	228	211	117	124	116	129
TOTAL	375	375	404	445	347	364	352	350

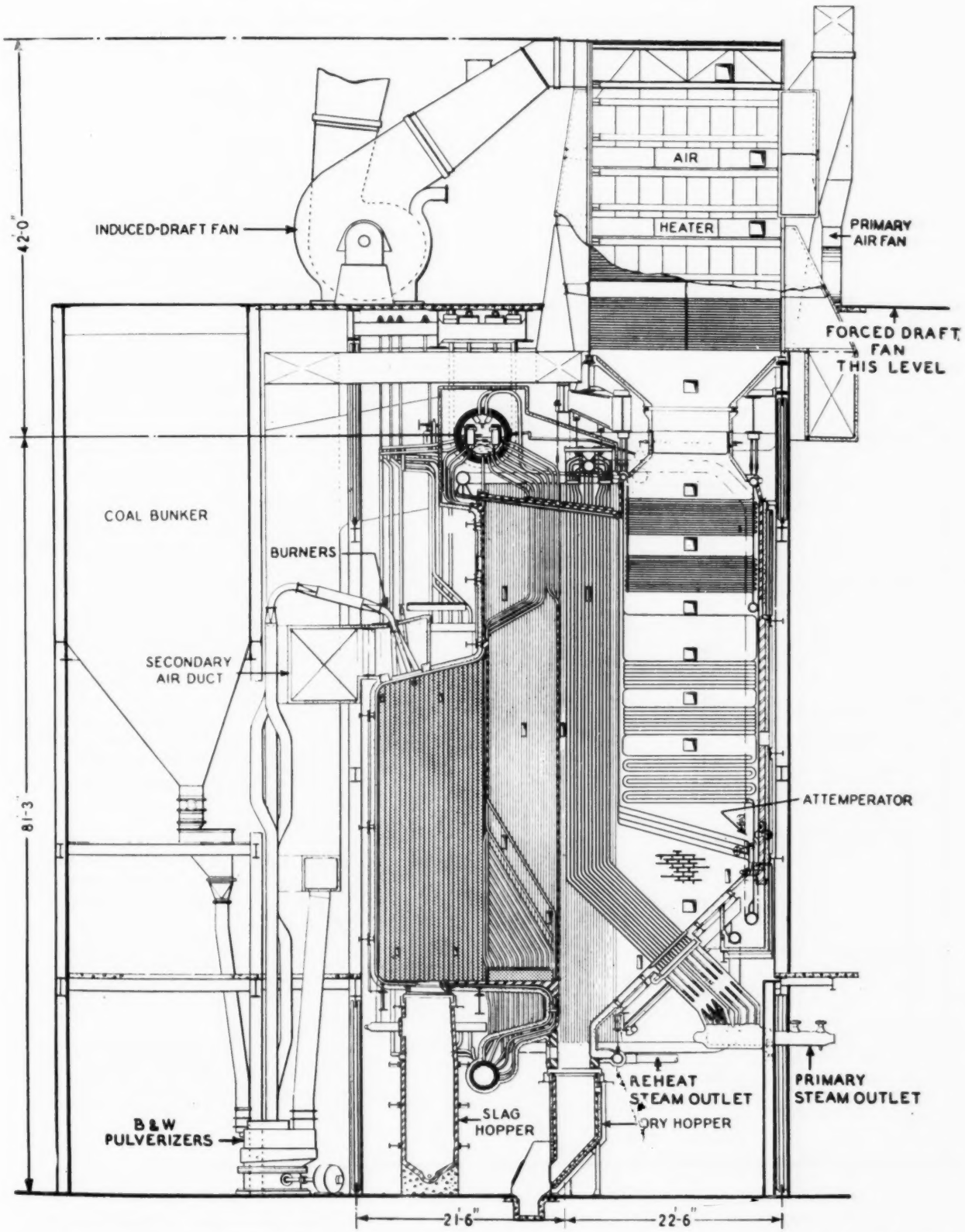


FIG. 2 ORIGINAL ARRANGEMENT OF BOILER OF UNIT 3, TWIN BRANCH STATION, AS OPERATED FROM MAY 5, TO JUNE 10, 1941

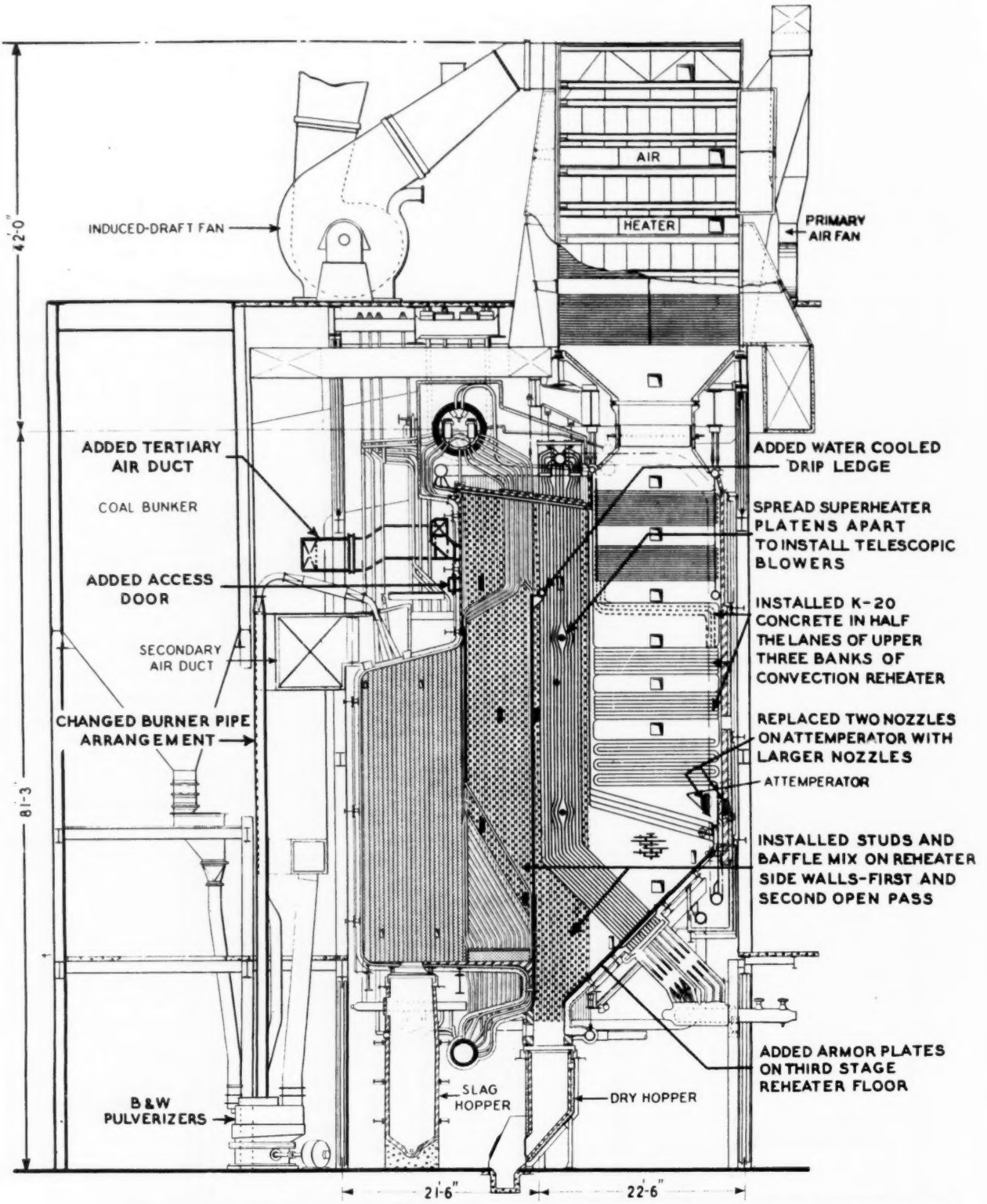


FIG. 3 ARRANGEMENT OF BOILER OF UNIT 3, TWIN BRANCH STATION, AS OPERATED FROM JUNE 15, 1941, TO FEBRUARY 13, 1942

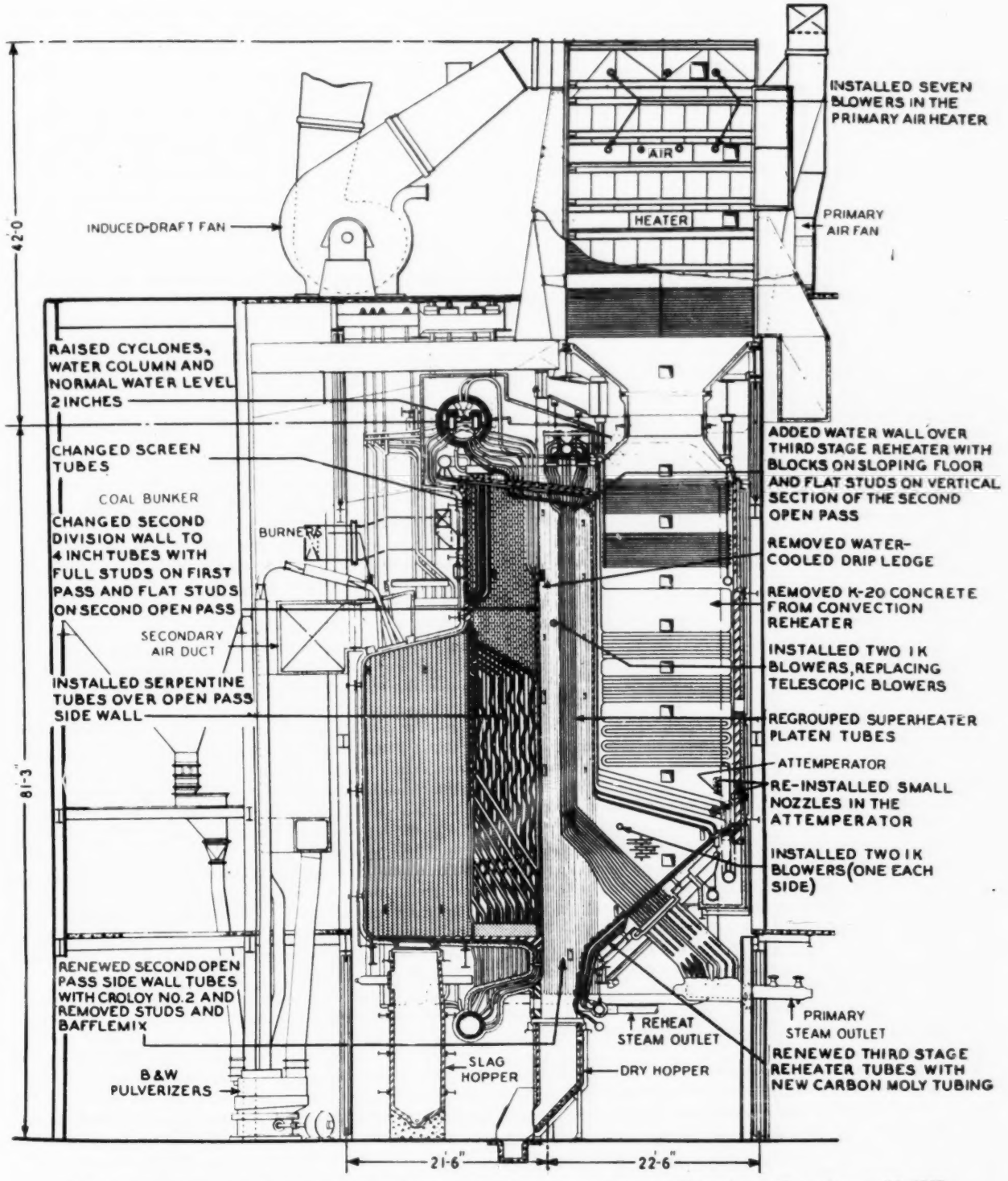


FIG. 4 ARRANGEMENT OF BOILER OF UNIT 3, TWIN BRANCH STATION, AS OPERATED FROM APRIL 20, TO AUGUST 14, 1942

in surface distribution was therefore indicated as a general solution of the difficulty. In order, however, to be able to obtain operating data and experience at high ratings with the high-ash Indiana coal to aid in deciding upon the necessary permanent corrective steps and to permit practical operation until such time as the material could be fabricated and made ready to install, it was decided to make relatively quick temporary alterations to the unit.

Fig. 3 shows these temporary alterations. The reheater tubes in the first and second open-pass side walls were studded and gunnited with bafflemix to reduce the absorption and to aid in retaining slag on the first open-pass walls. Lightweight concrete was installed in one half the lanes of the upper three banks of tubes in the convection reheater to reduce absorption. The capacity of two of the attemperator nozzles was increased to permit a greater range of superheat control. Telescopic soot blowers and a water-cooled drip ledge were installed in the second open pass to aid in handling the slag accumulation in this zone. Armor plates were placed over the reheater tubes in the sloping floor at the bottom of the second open pass to prevent their damage by large pieces of falling slag. A tertiary-air duct was added at the top of the first open pass to permit a greater degree of regulation of the excess-air conditions throughout the furnace and open passes.

These changes were completed by June 15, 1941. With these changes made, it was possible to operate the unit up to maximum rating by overattemperation and to maintain the excess air on the low side; and this afforded the opportunity to obtain test data and operating experience at high loads. The unit output, however, averaged about 60,000 kw. Continuous output at higher loads was impractical because of excessive slag accumulation in the second open pass, and the flame cutting through between some of the tubes of the second division wall due to low excess-air conditions. Typical distribution of heat absorption during this period is shown in the three columns of Table 1, under operating period 1, Fig. 3. The absorption by the reheater surface steadily increased during this period and it was necessary to lower the primary-steam temperature, and hence the temperature entering the reheater, in order to hold the temperature entering the low-pressure turbine at the design level.

During this operating period, tests at high load showed that the total circulating flow was 5,100,000 lb per hr rather than 3,600,000 lb per hr expected during the design of the unit. Due to this additional circulation and the endwise flow of the water in the drum some water-level instability was encountered at low gage-glass levels and occasional "shots" of carry-over occurred because of unbalanced water levels between the two ends of the drum. It was decided to raise the gage glasses, cyclone separators, and normal water level 2 in., during the coming outage scheduled for permanent alterations, in order to correct this condition.

Fig. 4 shows the alterations made to the unit during a 2-month outage beginning in February, 1942. Every other tube for the first 7 ft from either side wall was removed from the first division wall and placed over the reheater tubes in the first open pass to reduce the reheater absorption and to provide a stable covering in this zone. These were on 12-in. centers and so were made sinuous to provide equal covering for the close-spaced reheater tubes. Openings were thus left between the tubes on 12-in. centers in the first division wall for the full height for 7 ft from either side wall. The second division wall was changed to 4-in. tubes on 6-in. centers (from $3^1/_4$-in. tubes on 6-in. centers), full-studded on the first open-pass side and with flat studs between the tubes on the second open-pass side. This was done to prevent flame from cutting through the wall and to eliminate refractory on the second open-pass side from the slag standpoint. The screen tubes at the top of the first open pass were changed to provide an open path for the gases. The original single-row superheater-platen tubes were regrouped into smaller, i.e., more compact, double-row platens, in order to reduce the superheating surface and to provide room for installing two retractable soot blowers as well as to facilitate lancing.

The reheater tubes in the rear wall and sloping floor of the second open pass were covered over with a new waterwall of $3^1/_4$-in. tubes on 6-in. centers flat-studded between the tubes in the vertical portion and covered with Bailey blocks on the sloping floor. This was done to reduce the reheater absorption and to withstand the impact of pieces of falling slag. The upper 24 ft of the reheater tubes in the side wall of the second open pass were replaced with bare close-spaced Croloy 2 tubes and the studs and bafflemix were removed from the tubes in the lower portion. The concrete was removed from the convection reheater and additional soot blowers were added as shown in Fig. 4. All these steps were part of a co-ordinated program to give better balance of heat-absorption distribution and to give each section of surface the necessary mechanical and metallurgical protection or tolerance.

Shortly after the unit was returned to service on April 20, 1942, two tubes in the first division wall failed on two occasions when the load was raised to 480,000 lb per hr and the seventh and eighth burners were placed in service.

The first failure was in the form of a crack in the tube, the leakage being such that an orderly unloading of the unit was permissible. The second failure, however, was due to a sudden opening up of the tube resulting in an instantaneous shutdown of the boiler. The automatic protective devices provided, coupled with the thorough training program to which the operating staff had been schooled, and the detailed manner in which preparations were made for such an eventuality, made possible a perfect handling of the situation. Turbines and all auxiliaries were shut down in proper sequence and the boiler was bottled up so that the drum was not subjected to any undue thermal stress. As a matter of record, no ill effects of any kind were encountered subsequent to the repair of the tube and the restarting of the boiler. These failures were located about 10 ft from the roof of the furnace on the first wide-spaced tube on either side of the solid part of the division wall. Observation showed the flame to be short-circuiting through the lanes at this elevation, and these tubes were completely enveloped by flame.

An investigation of these failures led to the conclusion that they were caused by thermally induced stresses well above the yield point, produced by extremely high absorption rates across the tube wall approximately $^1/_2$ in. thick. This is covered more fully in a second companion paper.[4] Based on this analysis a decision was made that, for a permanent solution of this trouble, these lanes should be closed off, and the wall again made solid by additional tubes. As a temporary stop-gap and to permit the unit to stay on the line until convenient to take out for permanent repairs, these tubes were covered with stud plates and chrome ore and the load was limited to six-burner operation. It was also decided to operate temporarily at approximately 1750 psi, in order to take advantage of reduced-pressure stress. This, it was known, would be very slight but it was felt that the need of the capacity made available by the unit was so pressing that this reduction in pressure was desirable even though it gave but a small additional margin of safety. In addition, boiler

[4] "Distribution of Heat Absorption and Factors Affecting the Performance of the Twin Branch 2500-Psi, 940 F Boiler With Reheat to 900 F," by F. G. Ely and L. B. Schueler. Presented at the Annual meeting, New York, N. Y., Nov. 29–Dec. 3, 1943, of THE AMERICAN SOCIETY OF MECHANICAL ENGINEERS.

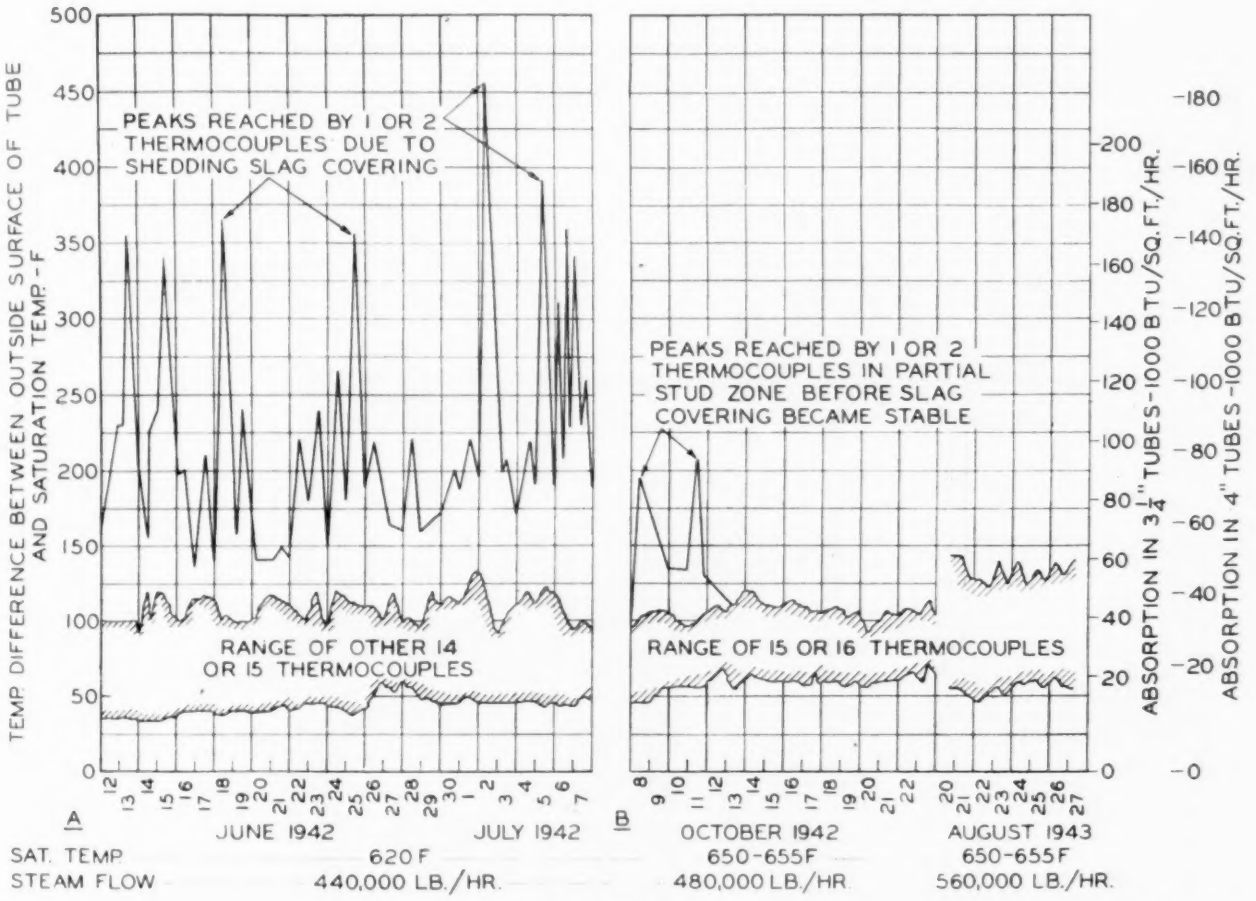


FIG. 5 LOG OF FURNACE-TUBE-WALL TEMPERATURE DIFFERENTIALS

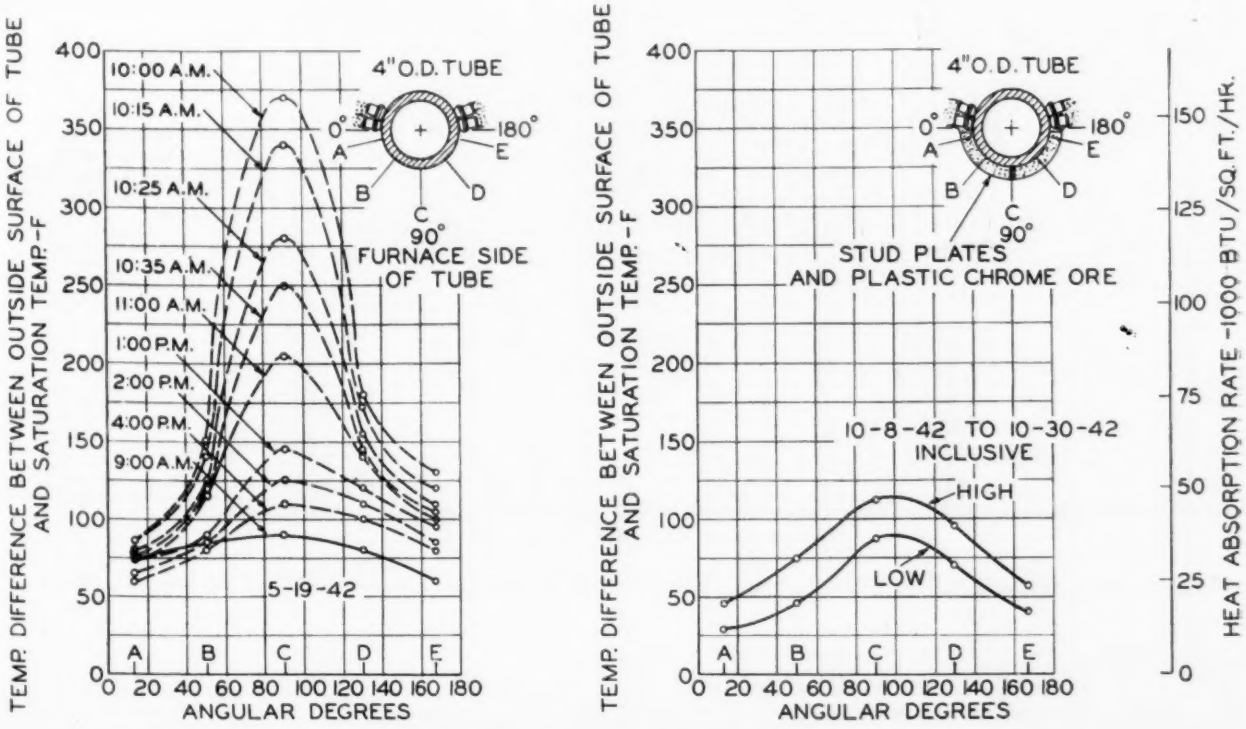


FIG. 6 COMPARISON OF TUBE TEMPERATURES BETWEEN PARTIAL- AND FULL-STUD CONSTRUCTION

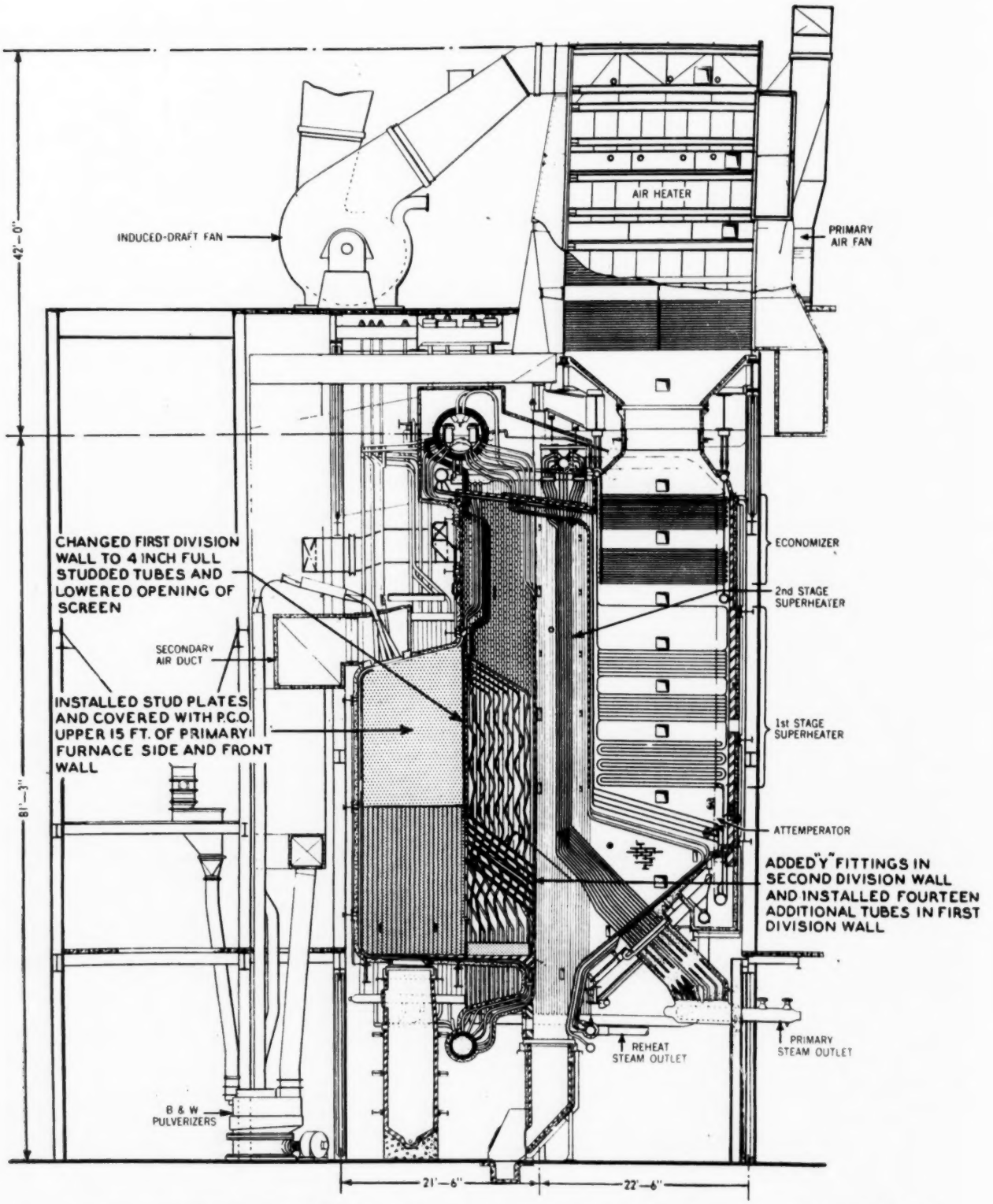


FIG. 7 ARRANGEMENT OF BOILER OF UNIT 3, TWIN BRANCH STATION, AS OPERATED FROM OCTOBER 1, TO NOVEMBER 25, 1942

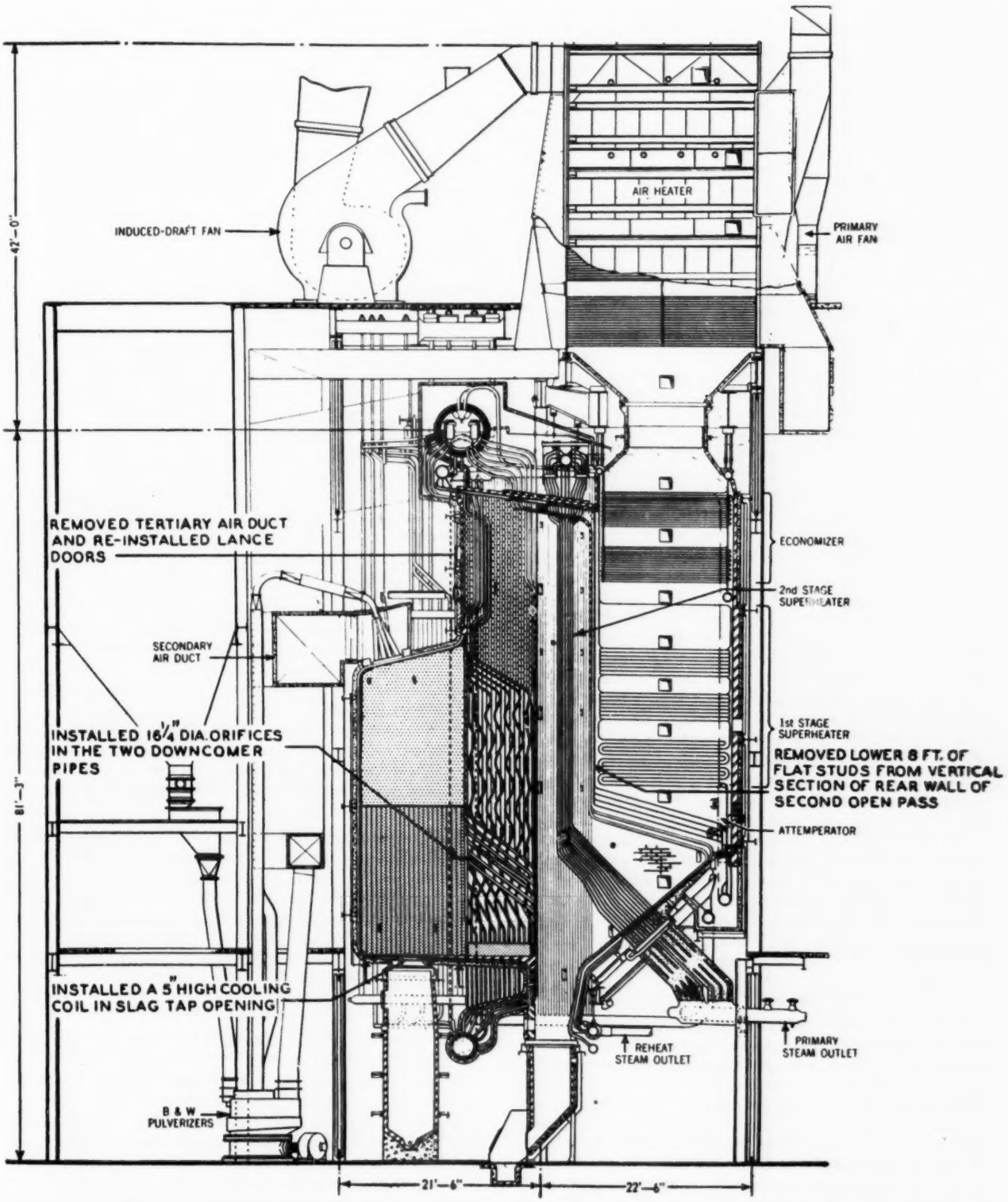


FIG. 8 ARRANGEMENT OF BOILER OF UNIT 3, TWIN BRANCH STATION, AS OPERATED SINCE DECEMBER 1, 1942

operation was governed by tube-temperature indications, some of which were recorded continuously and others of which were merely indicated.

These temperature readings were obtained through some 57 specially designed thermocouples which had been installed in the furnace face of the partial-stud and full-stud tubes throughout the furnace and 16 of these couples were connected to a recorder.

Fig. 5(*A*) shows a typical record of these couples obtained in June, 1942, with the arrangement of Fig. 4. Fig. 5(*B*) shows a similar record with full-stud tubes in the upper part of the primary furnace with the arrangement of Fig. 7. The bulk of the couples, under Fig. 4 conditions, would record from 40 to 125 F above saturation temperature, indicating absorption rates from 30,000 to 50,000 Btu per hr per sq ft, whereas different couples on the partial-stud tubes would register peaks of 350 to 450 F above saturation temperature indicating localized absorption rates as high as 200,000 Btu per hr per sq ft, due to the slag covering peeling away from the tubes. As shown by Messrs. Ely and Schueler,[4] at 200,000 Btu per sq ft per hr heat transfer the stresses at the inner fiber of a $3^1/_4$-in. × 0.5-in. carbon-moly tube (0.5 per cent Mo) approach the short-time ultimate strength at 2350 psi with a saturated temperature of 660 F. At this point temperature accounts for 88 per cent of the total stress. The right-hand chart, Fig. 5(*B*), shows the temperature record after the tubes were covered in accordance with the layout shown in Fig. 7, which will be described. The average absorption rates were about the same, but all the peaks were eliminated.

Fig. 6 shows an interesting phenomenon in connection with the thermocouple data. Five couples were located around the furnace half of a tube at approximately the same elevation. The chart at the left shows the temperature changes on a partial-stud tube when the slag peeled. The center of the furnace face rose from 90 F above saturation to 370 F suddenly, whereas, the couples on the 50-deg points rose from 80 F to only 175 F indicating that the slag did not completely peel at the sides of the tubes. These temperatures gradually returned to normal as a new slag coating built over the tube. The chart at the right shows the temperature distribution around a full-stud tube, but here no sharp peaks are in evidence.

The alterations indicated in Fig. 4 were quite successful in reducing the superheat and reheat to the design levels as shown in operating period 2 in Table 1. With proper excess-air conditions the superheat and reheat were somewhat on the low side, and slag troubles were eliminated, it being possible to keep the second open pass clean with the retractable soot blowers and supplemented by some hand-lancing.

Further Alterations Made

On the other hand, the rating of the unit was definitely restricted. Hence when the first opportunity, determined by system capacity and load conditions, presented itself after the material needed for the next change had been fabricated, the unit was shut down and the changes which started with the shutdown of August 14 were initiated. Fig. 7 shows the alterations which were made during this period. The upper 15 ft of the furnace side walls and front wall were covered with stud plates and chrome ore to eliminate the temperature peaks caused by shedding slag. The first division wall was changed to 4-in. full-studded tubes on 6-in. centers, and the wall made solid by bringing 14 tubes over from the second division wall. The screen opening from the furnace was also lowered 7 ft, in order to provide longer gas travel and to give a wider range for free-running slag.

These changes were successful in eliminating the high localized absorption rates and permitted slag-tapping at a load as low as 300,000 lb per hr. The increased steam-generating circuits increased the circulation rate to 5,500,000 lb per hr, which produced some water-level instability at low levels at ratings above 500,000 lb of steam per hr and the water level would become as much as 3 in. to 4 in. different between the two ends of the drum with unbalanced firing conditions. These factors combined to make the permissible water-level range between water-level instability and carry-over too small for trouble-free operation above a load of 500,000 lb per hr.

As shown in Fig. 8, this trouble was corrected during Thanksgiving, 1942, by installing a $16^1/_4$-in-diam orifice in each of the two 28-in. downcomers, which reduced the circulation to 5,000,000 lb per hr at full load and increased the resistance in the downcomers sufficiently to bring the water level at the two ends of the drum within $^1/_2$ in. of each other, regardless of firing conditions. There has not been a case of water-level instability or shots of carry-over since then. At the same time a 5-in-high cooling coil was installed around the slag-tap hole to retain the slag level over the floor to about 6 in. at the hole. Also, the lower 8 ft of the flat studs were removed from the waterwall at the rear of the second open pass. These changes resulted in the proper balance of superheat and reheat, as shown by the data under operating period 3 of Table 1.

The analysis of the results of the extensive testing of the boiler during these operating periods given in Table 1 brought out several reasons why the actual results from heat-absorbing surfaces for water-heating, steam-generating, superheating, and reheating portions were at variance with the original design. These were as follows:

1 Incomplete evaluation of the long-term insulating effect of the slag from these Indiana coals on the bare tubes of the primary furnace.

2 The fact that combustion is not entirely completed in the primary furnace.

3 The gas-temperature measurements on other units on which the design absorption rates were based were somewhat lower than they should have been based on later information obtained.

4 The use of Eastman's gas specific heats rather than those of Justi.

For these reasons, the heat absorbed by the primary-furnace surface where the steam is generated was considerably less than the design value; whereas, the heat absorbed by the first open-pass and the second open-pass surfaces where a large part of the superheating and reheating is done, was considerably greater than the design values. Thus the total superheater and reheater absorption were originally much greater than called for by the design conditions.

Feedwater Chemistry

The problems in the boiler-feedwater chemistry anticipated by some did not materialize. The feedwater treatment and boiler-water conditions that are maintained are comparable with our 1500-psi boilers. In the matter of steam purity, the conductivity of steam from the boiler averages 0.8 micromho. This is equivalent to solids carry-over of about 0.5 ppm. Tests on evaporated-steam samples substantiate this value. A slow building up of stage pressures takes place on the high-pressure turbine. Whenever these pressures approach the established limitations, the condition is corrected by dropping the primary-steam temperature by attemperation for a period of several hours. Turbine-supervisory instruments, the wide range and complete control of steam temperature makes it possible to carry out this operation within a period of 2 to 4 hr while maintaining an output in excess of 65,000 kw.

Turbine

In view of the difficulties which many users of 1500-psi topping turbines encountered during the period 1937 to 1940, one might have with some possible justification anticipated blading failures on a 2500-psi turbine. It is true this would have been based upon a somewhat superficial reasoning. As a matter of fact, those responsible for the design of this project and the turbine design had by that time so thoroughly integrated the experience encountered on the Logan and the Windsor turbines as to feel confident that a first-stage bucket having a length of only 0.75 in. and utilizing construction similar to that employed in the rebuilt first stages of the Logan and Windsor turbines would give no difficulties of any kind. Experience has fully borne this out.

Only one major problem developed in the operation of the high-pressure turbine and this was caused by vibration of the turbine rotor in its bearings. This condition appeared in the initial operating period of the unit and was apparently corrected by altering the oil flow to the bearings. Part-load operation, entailed by the temporary derating of the boiler, precluded operation at full loads to establish definitely that the correction was adequate up to full load. When the boiler design was ultimately modified so that full steam capacity became available and the turbine could be run at its full-load rating, there was a recurrent vibration of the shaft within the bearings. Further studies were made and the difficulty diagnosed as due to oil whip and that was caused by inadequate loading of the upper halves of the bearings. It was ultimately corrected by the addition of jack bolts. These jack bolts served artificially to load the halves of the bearings at all times, and no further trouble has since been experienced from bearing vibration.

The value of turbine supervisory equipment was again demonstrated following the proved worth of these devices in the Windsor installation. While troubles were being experienced due to bearing vibration, these instruments were used as an operating guide, and their record aided materially in the final solution of the problem. It is heartening to note that these supervisory instruments, quite novel a few years ago, are receiving increasingly favorable attention from power-plant designers and operators.

There were several minor troubles which occurred on both high- and low-pressure turbines. However, these were not the consequence of using high pressure and high temperature. These difficulties could just as well have been experienced at lower pressures and temperatures. To provide greater operating convenience, the initial-pressure regulator was redesigned to function as a pressure governor. This pressure governor responds to steam pressure ahead of the turbine stop valve, and is used for base-load operation, thus automatically loading the turbine in accordance with boiler output. This governor is provided with a motor-operated spring adjustment so that, for large load changes, the pressure may be manually compensated by the operators.

Electrical

Electrical storms on the 27,600-v system being supplied from Twin Branch have dropped auxiliaries off the line on several occasions but without any serious consequence to the unit. This was due primarily to the impedance relationships of the various windings of the main power transformer bank of this unit. This is a 4-winding bank and one of the windings supplies a 2300-v auxiliary bus. The reactances between the 4 windings were, however, so arranged that short-circuits on the 27,600-v system caused a greater drop in the 2300-v auxiliary-bus voltage than that which occurred on the 27,600-v bus itself. This meant that short-circuits on the 27,600-v system of only moderate severity reduced the 2300-v bus voltage very seriously. The difficulty has been taken care of for the present by feeding the 2300-v auxiliary bus from another transformer taking its supply from the 27,600-v bus. The final solution has been worked out in connection with unit No. 4 at Twin Branch, now in process of completion.

Boiler Feed Pumps

Operation of the high-pressure boiler feed pumps has reached a point of reliability comparing favorably with that of pumps in plants of much lower pressure. However, a number of corrections had to be carried out before this availability was achieved. There are three Ingersoll Rand boiler feed pumps installed at Twin Branch. They are 5-in. pumps having 8 stages direct-connected to 2500-hp 3600-rpm motors. Normally one pump is used to carry the full load of the plant. These pumps have forged-steel barrel-type casings and the inner-casing assembly can be removed as a unit.

The first and most difficult problem encountered was due to vibration of the outboard and discharge end of the pump shaft and bearing. This vibration caused disturbances of packing, excessive shaft-sleeve wear, scoring of bearings, and wear of main oil gear drive. This vibration was eliminated by adjustments to balancing-drum clearances, better shaft alignment, and rotor balance.

In the early stages of operation the packing life was short and the shaft-sleeve wear excessive. To break down the high pressure ahead of the packing, a double step-type labyrinth is used, the leakage from these labyrinths being returned through a common header to the 8th-stage heater at 150 psi pressure. With the water temperature at 340 F rather large quantities of water are required to remove the heat generated by rubbing friction. The short life of the packing was attributed to the combination of the high pressure in the labyrinth chamber and the high temperature, and the subsequent flashing in the packing gland. The choice of 150 psi pressure in the labyrinth was made to give the best thermal efficiency. This difficulty was entirely cured and packing life has been greatly extended by dropping the labyrinth leak-off pressure to a value between 90 and 110 psi. Under these conditions packing life is now just as satisfactory as with 1500-psi-pressure pumps.

A certain amount of erosion, as a result of high pressure, was experienced due to leakage past the separating diaphragms between stages. This has been minimized by the use of stainless steel on the sealing surfaces. Excessive wear of shaft sleeves, balancing drums, and labyrinth parts has been materially reduced by substitution of parts made from more suitable alloy material.

Two motors were initially furnished for the three pumps. The bedplates of the pumps were designed to make possible rapid shifting of motors from one pump to another. However, the early difficulties with the boiler feed pumps and the time-consuming job of pump and motor alignment dictated the advisability of purchasing a third motor. Significant, however, is the fact that there has been no loss of plant capacity due to failure of a boiler feed pump.

Feedwater Heaters

There are two high-pressure feedwater heaters on the discharge of the high-pressure boiler feed pumps. Although these heaters were the subject of some concern prior to installation, their behavior has been entirely satisfactory. There has been no outage due to leakage. Some depositing of solids, mostly on the water side of the heaters, takes place over a period of time. Piping provisions have been added and a method established chemically to clean these heaters. This work can be performed

while the unit is in operation. However, to date, there has been no occasion to apply this procedure. The good performance of the heaters is doubtless due to sound design, and to the carefully established starting procedure which avoids quick temperature changes. In starting up the shell side of the heaters is heated up gradually by auxiliary steam so that, when the turbine comes on the line, the heaters are ready for service.

Operation and Performance

Operating and maintenance problems resulting from operation at high pressure have been relatively few, in fact less than on any of the 1500-psi plants of most recent construction on the American Gas and Electric Company systems. There has been no difficulty with any of the high-pressure piping or valves. Some slight leakage is being experienced with the boiler-drum safety valves due to warping of seats and disks. Corrective measures are still in the experimental stage. This also holds true of the boiler-drum gage glasses. The high pressure apparently causes some assembly distortion and that, coupled with other factors, is resulting in considerable leakage and shattering of glass, thus requiring frequent and specialized maintenance attention.

An examination of Fig. 1 indicates that barring the two scheduled intervals utilized for making the major changes previously described, the availability of the unit compares favorably with most power installations operating at even as low a value as one third the pressure of Twin Branch. As a matter of fact, this unit is now one of if not the most troublefree installations on the American Gas and Electric Company systems. Except for a small deficiency in primary steam temperatures, the boiler is meeting all expectations of those who planned and designed the unit as to capacity, reliability, efficiency, and all-round performance. In this connection there are given in Table 2 the results of two efficiency tests which were conducted in May, 1943. Included also in this tabulation are the expected results. Here a mere comparison of expected with actual test performance renders its own commentary.

TABLE 2 BOILER NO. 3 EFFICIENCY TESTS

Date Time of day	Expected performance	May 12, 1943 8 a.m.–5 p.m.	May 14, 1943 8 a.m.–5 p.m.
Coal fired per hr, lb	71000	64921	65013
Steam flow to turbine, lb per hr	550000	556250	560440
Steam flow through reheater, lb per hr	440000	466520	470040
Heat value of coal as fired, Btu	10000	11126	11248
Efficiency of boiler unit, per cent	85.63	86.81	87.04
Boiler drum pressure, psig	2440	2334	2343
Superheated-steam-line pressure, psig	2335	2261	2271
Reheater-inlet pressure, psig	420	424	428
Reheater-outlet pressure, psig	376	400	405
Final primary-steam temperature, F	940	930	928
Reheat-inlet steam temperature, F	545	554	550
Final reheat-outlet steam temperature, F	900	893	900
Economizer-inlet feed temperature, F	487	476	473
(HVT) gas temperature entering convection section, F	2020	1870	1869
Average gas temperature entering air heater, F	690	712	712
Average gas temperature leaving air heater, F	347	407	396
Average air temperature entering forced-draft fan, F	80	101	95
Total air entering first open pass, per cent	...	115.0	114.9
Total air leaving air heater, per cent	133	126.2	126.9
Total draft loss, in. H_2O	11.3	11.0	11.4
Total secondary-air resistance, in. H_2O	9.3	8.1	8.7

In the matter of thermal performance, test values, whether obtained over a period of a day or a period of several days, have never been given, as they have no reason to be given, any particularly heavy weight from an operating standpoint. Rather, what is significant is the continued performance taken over a yearly or similar period. Here it is regretted that performance over a full year at full rating is not as yet available. However, in Table 3 there is given a summary of operating results covering the period beginning March 26 to August 31, 1943. This period begins with the date when the final adjustment to the bearings of the high-pressure turbine was completed, the effect of which made possible full-load operation of the unit. It is significant to note (1) that there were only two short-duration outages in this interval, both scheduled, to take care of matters clearly explained in Table 3; (2) that in spite of these outages the unit with a maximum rating of 76,500 kw averaged during this interval for the period that it was running close to 72,700 kw per hr with a performance of 10,035 Btu per kwhr output to feeders. This corresponds to a thermal efficiency of 34 per cent. This was accomplished by some interesting operating factors, i.e., capacity factor, 91.9 per cent, output factor, 95 per cent; availability factor of unit, 96.7 per cent.

The figures of 95 per cent as a desirable and necessary availability factor in high-grade steam-plant design and performance and 10,000 Btu per kwhr as a thermal-performance figure for a modern steam plant have been held up for a number of years as an ideal to attempt to reach, but one which it was perhaps unreasonable to expect to attain fully under present conditions. It would appear from the foregoing figures that, as to performance, the figure has been very closely attained, and as to availability the figure has perhaps been exceeded, in the Twin Branch 2500-psi job.

TABLE 3 OPERATING DATA UNIT NO. 3, AFTER PROVIDING JACK-BOLT ARRANGEMENT[a] ON BEARINGS 1 AND 2, COVERING PERIOD FROM 4 A.M. MARCH 26, TO MIDNIGHT AUGUST 31, 1943

Total hours in period	3812
Total hours operated	3686.88
Total generation, kwhr	267,997,000
Generation per hour, kw	72,689
Auxiliary power, kwhr	16,744,611
Total output, kwhr	251,306,389
Total fuel consumed, lb	233,941,000
Heat value of coal as fired, Btu	10,778
Output, Btu per kwhr	10,035
Thermal efficiency, per cent	34.0
Capacity factor, per cent	91.9
Output factor, per cent	95.0
Availability of the unit, per cent	96.7

Outages:	No. hours off
Friday, April 9, unit No. 3 was removed from service for leak check test on low-pressure condenser, and acid washing high-pressure and cross-over heaters feedwater side, and inspection of induced-draft fans. Unit was returned to service 10 p.m. Sunday, April 11, 1943	53.04
Unit No. 3 out of service 72.08 hr as per schedule for inspection of boiler, changes to electrical connections to accommodate unit No. 4, and general inspection of unit and auxiliaries during period July 2, to July 6, 1943	72.08
Total time off during this period	125.12

[a] Jack-bolt arrangement was provided on bearings 1 and 2 during shutdown from 8:47 p.m., March 19, to 4 a.m., March 26, 1943. This change permitted full-load operation of unit.

The authors believe that the operating experience of the past 2 years has verified the judgment of those responsible for undertaking this distinctive development in power generation. Without going into the merits or demerits of other thermal cycles or equipment, Twin Branch experience has shown that 2500-psi natural-circulation boilers and 2300-psi steam turbines, with their related equipment, can be made to give a power plant that is technically and commercially sound.

Discussion

W. H. Armacost.[5] The authors of the three papers, covering the Twin Branch Plant, are to be congratulated for their able and frank description of the operating history, heat absorption, per-

[5] Vice-President, Combustion Engineering Company, Inc., New York, N. Y. Mem. A.S.M.E.

formance, and the test results of the 500,000-lb-capacity natural-circulation boiler applied to the 2500-psi steam-electric generating unit of that station. These papers, together with those published previously on this installation, will be referred to frequently.

Pioneering in the field of such a high pressure, particularly with a very large steam-generating unit and with natural circulation is not a simple extension of well-known scientific laws. It is therefore to be expected that some of the initial design features of such a unit might require modification, but it is distinctly to the credit of the manufacturer and user that they co-operated not only to produce an efficient unit of high availability but that they also co-operated in presenting to their fellow engineers the detailed procedure which was followed in accomplishing these results. Building this unit represents a great achievement, particularly when one considers the controversial opinions advanced at the time the unit was planned.

Referring to the description of the tube-metal temperatures which are illustrated in Figs. 5 and 6 of the paper by Messrs. Sporn and Bailey, it will be noted that furnace side-tube temperatures as high as 1070 F, or 450 deg F above saturated temperature, were recorded even though a circulating rate of 10 water to 1 steam existed within the tubes, and that these high temperatures were reduced by covering the tubes to reduce the absorption approximately 50,000 Btu per sq ft per hr.

Our experience also indicates that variations in cleanliness of the furnace wall tubes produce severe and rapid variations in furnace tube temperatures, but, of course, the tube thickness is also an important factor.

It is interesting to compare the data mentioned with similar information taken at the Montaup Electric Company on the 650,000-lb-capacity 2000-psi controlled forced-circulation boiler where only bare tubes of $1^1/_4$ in. OD, 0.165 in. minimum thickness are present in the furnace, and with only a 5 water to 1 steam circulation ratio. The highest temperature reported under normal operation was 750 F, which is only 135 F above saturation temperature. Fig. 9 of this discussion shows the effect of lancing a portion of the furnace wall, which is normally coated with about $^3/_4$ in. of slag in a zone where the flame temperature might approach 3000 F. The hot face of the tubes was only approximately 50 deg F higher than fluid temperature in the tubes under normal condition of operation with pulverized-coal-firing, but the temperature indicated by all thermocouples rose about 100 deg F, and in some cases to a peak of 170 F, when the slag was removed from the area being studied. The increase due to higher rate of heat absorption would be even greater with thicker tubes, in which case the hot-face temperature might exceed safe limits; but, with tubes of 0.165 in. thickness, it is obvious that a very high rate of heat absorption can be tolerated or even encouraged without reaching a condition that could be called "overheating," provided of course, there is adequate circulation of water to the heated surface of the tubes.

On this unit, it is possible to determine accurately the water flow to the furnace circuits by the measurement of pressure differential across the calibrated orifices, and to check the total flow calculated by this method against total flow determined from pitot tubes in the downtakes. Results by these two methods have checked within a few per cent. It is known that no steam is trapped in the downtakes because the water temperature is below saturation temperature, and calorimeters were used as a further check.

There have been tube failures in two different furnace circuits at Montaup Electric Company since it was started up in August, 1942. These were repaired by cutting out and welding in new sections of tube. One of these occurred several weeks after starting up, and the other several months later. These tube failures were due to dirt and foreign material, such as oxide scale, resulting from field welds in the boiler circuits, and piping. Accordingly it was decided to wash the boiler with acid.

The circulating pumps are operating very satisfactorily on this boiler. Some trouble was experienced originally, but after providing a few thousandths of an inch additional clearance in the glands, all appreciable wear stopped.

There have been no pressure-part or mechanical changes made on this boiler since it was erected, except the drum internals and no further changes are contemplated.

Figs. 10, 11, and 12 of this discussion show the results of recent informal tests run with both coal- and oil-firing to determine operating characteristics of the Montaup unit. On each chart the lines represent expected performance with coal-firing and the points indicated by C are the corresponding measured data. The points indicated by O are the data with oil-firing.

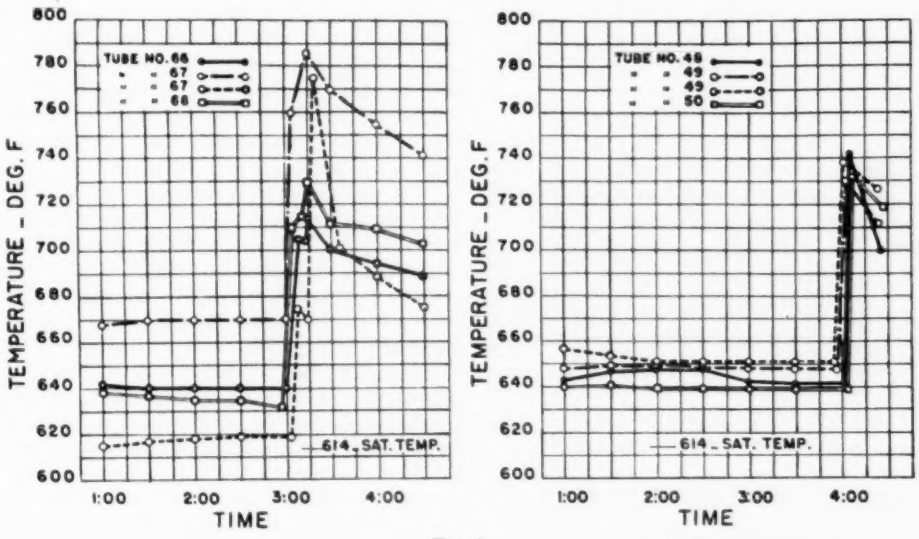


FIG. 9

Referring to the steam temperature leaving the superheater, this was under control by means of the by-pass damper, which was about 40 per cent open at maximum load with either fuel; so the steam temperature could have been increased or decreased at will. At the 450,000-lb per hr load, the by-pass damper was completely closed with oil-, and about 5 per cent open with coal-firing.

The steam temperature to the resuperheater is purposely maintained a little lower than predicted because the temperature increase in the reheater is a little greater than expected.

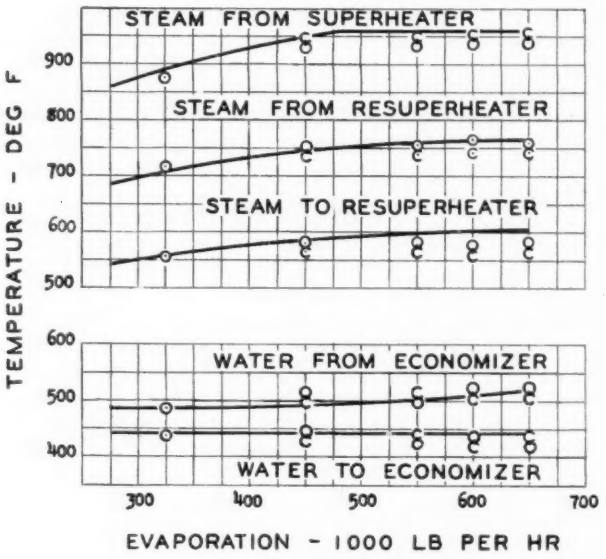


FIG. 10

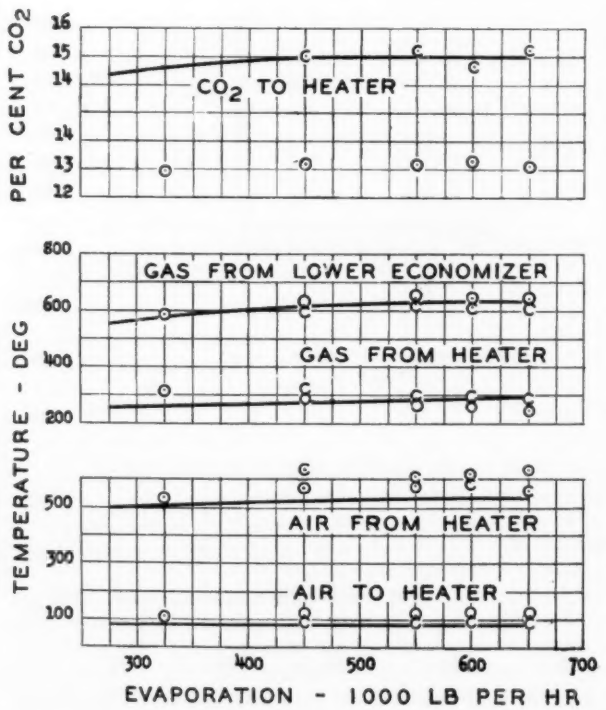


FIG. 11

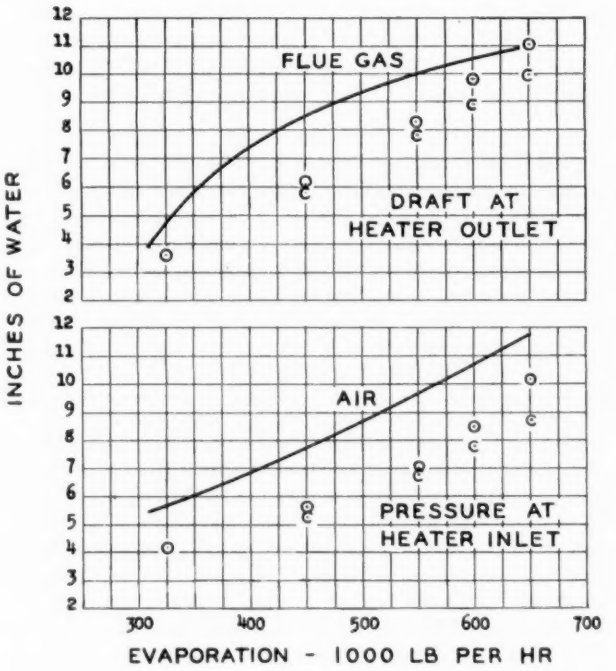


FIG. 12

C. W. BELL, SR.[6] The design of the boiler apparently provided decidedly too much superheating surface and we suspect somewhat less than the ideal amount of normal boiler surface, since we note that the average gas temperatures appear to be somewhat high under final conditions.

The particular point in the analysis of operation, which we feel was not fully explained, has to do with the statement that heat-absorption rates are estimated to have reached 200,000 Btu per hr per sq ft.

The writer has observed in a large number of power plants and on a correspondingly large number of tube failures, that tubes will bulge and sometimes split in a manner such as was experienced at Twin Branch only when the tube becomes dry or at least very nearly dry. This can occur after some critical rate of steam production is reached. In other words, it is our impression that the steam-release rate was so high at some point lower down in the failed tube that the section which failed was attempting to serve as a superheater and, consequently, the heat-transfer rate was decidedly lower than the maximum obtained with a fully wetted internal surface.

We would suggest that thermocouples embedded close to the inside wall, in other words, set in counterbored holes, would shed considerable light on conditions inside the tube at various steaming rates.

One of the most interesting developments exemplified in this boiler we feel is the clean-cut external downcomers for feeding water to the lower ends of all groups of heating-surface tubes. We have felt for many years that this plan should have been applied to boilers of earlier design, since we have observed cases where it was definitely possible for circulation to reverse under certain conditions. The Twin Branch design could not possibly do this. The design chosen demonstrates nicely the effectiveness of circulation where no interference exists, and the error in required size was definitely on the safe side.

---

[6] Pennsylvania Power & Light Company, Hazleton, Pa. Mem. A.S.M.E.

I. E. Moultrop.[7] About 20 years ago the first commercial high-pressure installation went into service at the Edgar Station of the Boston Edison Company. The pressure was 1200 psi, the temperature was 750 F, and the turbine had a capacity of 3000 kw. To step up the pressure by 1200 lb and the temperature only by 200 F in 20 years does not seem like rapid progress yet much development has been done. Merely increasing the pressure was no great problem in itself; other industries had been using similar or higher pressures for some time. However, increasing the boiler pressure did create new problems such as the circulation within the boiler, a most interesting study, and one for which the complete answer perhaps has not yet been found. The steam temperature has increased more slowly, only a few degrees at a step, while power-plant engineers wait for the metallurgist to find better heat-resisting metals. It is believed that the intensive research going on for military needs will be quite valuable after the war. Also the experience acquired in building superchargers and the so-called gas turbines will be of great value.

The frank discussion of operating troubles encountered and construction changes made is most interesting and timely. They are relatively small when one realizes that no natural-circulation boiler had ever been built for these extreme conditions, and the builder is to be congratulated for the excellent results of its engineering. The splendid control of steam temperature is remarkable. Formerly it was quite difficult and usually there was practically no control of the temperature, a situation which gave the turbine builders much concern.

The paper could well have given more space to the control room and method of operation. A few years ago it would have been unthinkable to attempt to operate a boiler from a distant point. The laws of Massachusetts forbid it. Yet here is an extremely large boiler, successfully being operated from an operating room removed from the boiler and with nobody around the boiler. The fact that this is both practical and successful is proved by the report of tube failures where the situation was handled perfectly in all cases. A reliable indicator of the water level in the boiler drum and a CO_2 recorder which gives immediate gas analysis of the flue gases are two of the outstanding instruments on the very large gage board in the control room.

The American Gas & Electric Service Corporation has rendered a great service to the world in showing that a power plant can be built to give reliable service and show an efficiency exceeding the internal-combustion engine.

In closing it should be pointed out that because this installation has been successful it does not follow that all future power plants should be designed on similar lines. The high-pressure and high-temperature station has a higher initial cost and requires greater operating skill. It is most useful where the system load factor is high. Fuel efficiency should go hand in hand with dollar efficiency.

G. B. Warren.[8] The public utilities of this country are producing about 6 times as much power now as they did during a corresponding period in the first world war. They are doing this on but twice as much coal per month. In other words, they are doing this at an efficiency of power production such that the average fuel consumption per unit of output is but one third as great as it was 25 years ago.

Such an achievement has only been possible because first one public-utility group and then another, assisted, to be sure, by the equipment manufacturers, have had the initiative to pioneer and the courage to take the risk required to make the next step in this forward march. The present result is a great tribute to the strength and power of our American way of doing things. The continued reduction in the price of electric power is evidence enough that these savings have been passed on to the consumers.

The recently announced higher powers and lower fuel consumptions of the power plants for our combatant naval vessels have come directly from the step-by-step progress of the power companies in this country.

It is true that we may be approaching the end of this progress in the steam cycle itself, but there is still probably enough in it to make considerable additional progress in the efficiency of the best stations; and the average coal consumption per kilowatthour in this country, low as it is, is still 60 per cent above that of the Twin Branch Plant.

We should not get too complacent, however. We still get out but $^1/_3$ the power inherently in a pound of coal in our best power plants, from $^1/_6$ to $^1/_4$ in our ships, and less than $^1/_{10}$ in our railway locomotives.

Additional superposed stations, more general use of higher pressures, higher temperatures, resuperheating, the mercury steam cycle, the gas turbine, and perhaps even the combination of the gas turbine and the steam or mercury cycle will permit still further progress.

The authors of the present paper can well feel proud of the part they personally have played and the part their respective organizations have played in this progress, not only in the particular achievement reported on here, but in a whole host of previous achievements in which they have both been outstanding.

The difficulties reported on the high-pressure section of the turbine, annoying as they were to the owners, have been overcome and were in reality minor in character and not in any way inherent in turbines for these steam conditions. The shaft of this turbine was designed to be smaller in diameter than had ever before been attempted for a turbine of this output, in order to reduce the packing losses at the high pressures involved. Such slender shaft machines it turned out are sensitive to looseness in the fit of the bearings in their pedestals and under such conditions are apt to vibrate when at full speed at a frequency which is about $^1/_2$ the running speed. The high temperature of the turbine casing at each end adjacent to the turbine bearings caused the bearing casings to expand and let the oil-cooled bearings loosen in the pedestals. The low weight of the turbine rotor in proportion to the work it was doing was insufficient to keep it steady. Jack bolts of 45 deg were put in as stated in the paper. When these were tightened, the vibration was eliminated immediately, thus indicating the correctness of the diagnosis. Several new bearing designs have been worked out, any one of which should preclude such difficulties on future machines to which they are applied.

Authors' Closure

It was anticipated that regardless of the efforts and skill employed during the engineering and design stages of the unit, difficulties were bound to appear. We had, however, complete faith in the soundness of our decision to proceed with a natural-circulation boiler.

The use of 4-in-diam tubes with approximately $^1/_2$-in. wall thickness more than satisfied the circulation requirements although the heavy wall thickness resulted in high furnace side-tube temperatures. This difficulty was completely solved by use of stud plates and plastic chrome ore. The corrected arrangement of surface giving temperature distribution as shown in Fig. 6 is comparable with the data presented by Mr. Armacost in his discussion of our paper. The larger tubes solved the problem of adequate natural circulation and with application of studding

[7] Consulting Engineer, Belmont, Mass. Mem. A.S.M.E.

[8] Turbine Engineering Division, General Electric Company, Schenectady, N. Y. Mem. A.S.M.E.

give heat-absorption rates and corresponding metal temperatures comparable to the results being obtained with the small and thin tubes of the forced-circulation boiler at Montaup described by Mr. Armacost.

The authors believe that the analysis of tube failures, given in detail in the accompanying paper by Messrs. Ely and Schueler, answers Mr. Bell's query as to the manner and cause of the tube failure. It is our conclusion, substantiated by facts, that this failure was produced entirely by thermally induced stresses and that there was more than adequate circulation in the tube at time of failure.

The answer to Mr. Moultrop's comment that more space should be given to control room and method of operation can be found in the series of papers on Twin Branch published in the October 18, 1941, issue of *Electrical World*.

The authors share with Mr. Warren the belief that avenues of progress are still open in the field of efficient generation of power, and that the results obtained to date offer no cause for complacency. They hope that their experience in carrying through the Twin Branch 2500-psi development will stimulate others to initiate developments to improve upon and to surpass Twin Branch.

Natural-Circulation Test Results on the 2500-Psi Twin Branch Boiler

By W. H. ROWAND[1] AND T. B. ALLARDICE,[2] NEW YORK, N. Y.

An essential requirement of the 2500-psi boiler of the Indiana & Michigan Electric Company (American Gas & Electric Service Corporation) at the Twin Branch Station was the provision of positive circulation in all heat-absorbing or steam-generating areas of the unit. The history and details of design and operation of the Twin Branch unit are given in companion papers.[3] The present paper discusses the design of a system incorporating outside downcomers feeding a lower drum, with direct supply lines to all generating circuits, and cyclone separators in the steam drum, providing centrifugal separation of steam from circulating water. Tests were conducted on a full-diameter, half-length model of this arrangement at Ohio State University. The results of studies, tests, and other considerations are discussed in this paper, as well as operating results obtained. The conclusion is reached that the provision of natural circulation in boilers at 2500-psi operating pressure has ceased to exist as a problem.

AT the time the decision was reached to build a 2500-psi natural-circulation boiler for a capacity of 550,000 lb of steam per hr at Twin Branch, the question of natural circulation for such a high pressure was thoroughly considered. After full study, the conclusion was reached that it was a sound and practical application, provided all the factors inherent in determining successful circulation were properly developed and taken advantage of. Among members of the engineering profession, the normal interest and speculation as to the ability to carry through, evidenced when boiler pressures substantially above any previously attained commercially for large-sized operating units have been proposed, was accentuated in this case by the proposal to operate on natural circulation. The reasons for this speculation are understandable since, as shown in Fig. 1, which illustrates the variation with pressure of the density of steam and of water at saturation temperature, the density differential between water and steam is only 28.4 at 2400 psi, whereas at 300 psi, this differential is 52, and at 1400 psi, it is 39.8.

The ability to circulate is a complex function of this density differential, so in order to utilize the differential that is available, it is of the utmost importance to prevent any steam being entrapped in the circulating water in the downcomers. Fig. 2

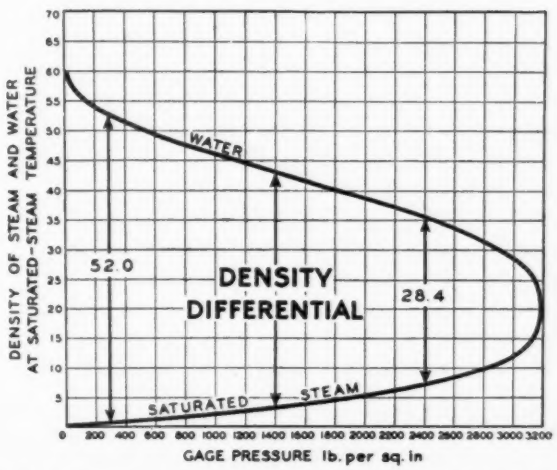


FIG. 1 VARIATION WITH PRESSURE OF DENSITY OF STEAM AND OF WATER AT SATURATION TEMPERATURE

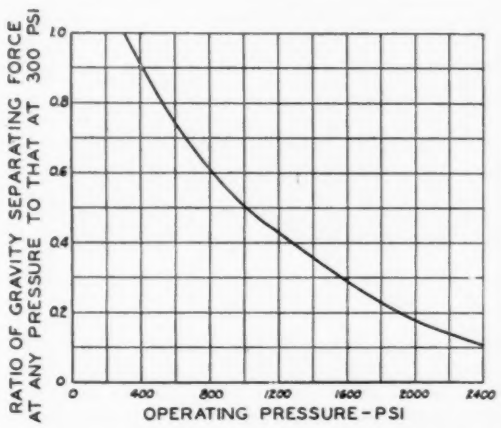


FIG. 2 GRAVITY SEPARATING FORCE ON STEAM BUBBLES IN WATER

shows the gravity separating force on steam bubbles in water at various pressures expressed as a ratio to the separating force at 300 psi. At 2400 psi, this separating force of gravity is only 10 per cent of that at 300 psi, and only 29 per cent of that at 1400 psi; therefore it is apparent that the difficulty in obtaining circulating water free of steam for the downcomers increases manyfold at the 2400-psi pressure level.

The engineers of the American Gas and Electric Service Corporation were convinced that, due to the conditions previously mentioned (Figs. 1 and 2) the over-all design should be one that assured positive circulation in all heat-absorbing or steam-generating areas of the unit. Previous experience with units of considerably lower operating pressures had shown that tube failures will result in any area of a boiler unit where sufficient circulation is not provided for in the initial design.

The design proposed by The Babcock & Wilcox Company with outside downcomers of ample capacity, feeding a lower drum,

---

[1] Mechanical Engineer, The Babcock & Wilcox Company, New York, N. Y. Mem. A.S.M.E.

[2] Mechanical Engineer, American Gas & Electric Service Corporation. Mem. A.S.M.E.

[3] The following companion papers are being presented at the Annual Meeting of the Society:

(*a*) "Operating History of the 2500-Psi Twin Branch Plant," by Philip Sporn and E. G. Bailey.

(*b*) "Distribution of Heat Absorption and Factors Affecting Performance of Twin Branch 2500-Psi Boiler," by F. G. Ely and L. B. Schueler.

Contributed by the Power Division and presented at the Annual Meeting, New York, N. Y., Nov. 29-Dec. 3, 1943, of THE AMERICAN SOCIETY OF MECHANICAL ENGINEERS.

NOTE: Statements and opinions advanced in papers are to be understood as individual expressions of their authors and not those of the Society.

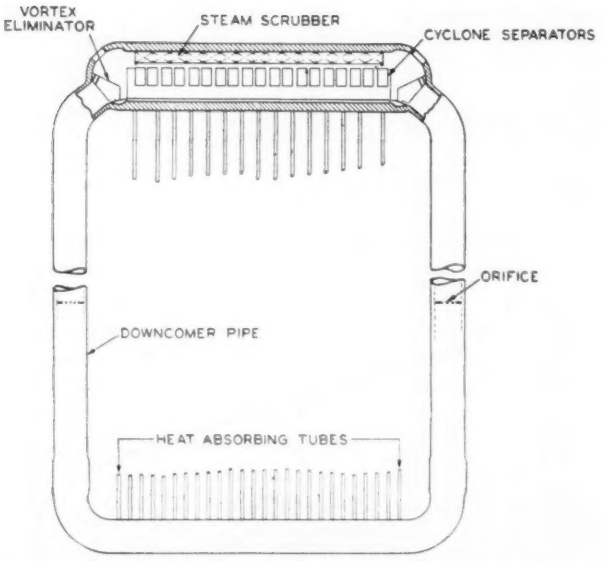


FIG. 3 FUNDAMENTALS OF CIRCULATION IN THE TWIN BRANCH BOILER

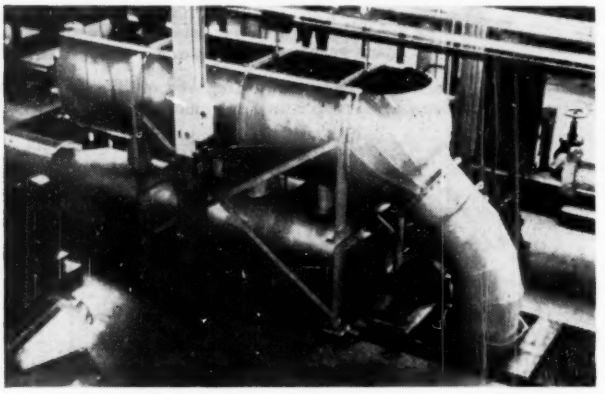


FIG. 4 FULL-DIAMETER, HALF-LENGTH MODEL OF DRUM AND DOWNCOMER PIPE FOR TEST PURPOSES

with direct supply lines to all generating circuits, and with the application of cyclone separators in the steam drum which provide a centrifugal separating force several times greater than that of gravity indicated a satisfactory unit for the conditions specified. A simplified circulation diagram of the unit is shown in Fig. 3.

It will be noted that the fundamental circulation scheme is reduced here to the simplest imaginable arrangement. It consists of a 28-in-diam downcomer pipe from either end of the 54-in-diam drum. These pipes are carried down outside the boiler setting in order to keep the resistance losses at a minimum and to prevent the generation of any steam in the downcomers. Recognizing the effect of endwise flow of the circulating water along the drum on producing vortexes at the entrance of the downcomer pipe and on water-level stability due to the hydraulic-gradient phenomenon, a full-diameter half-length model of the drum and downcomer pipe, as shown in Fig. 4, was built and tested with water at Ohio State University in order to provide the best means for preventing vortexes entering the downcomers, and to determine the range of stable operating water levels with what was considered an ample excess of circulating-water flow above the design flow of 3,600,000 lb per hr.

The actual result of all the studies, investigations, considera-

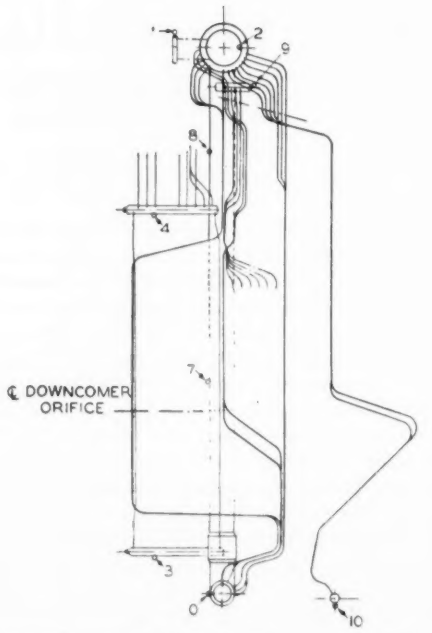


FIG. 5 STATIC-PRESSURE CONNECTIONS FOR CIRCULATION TESTS

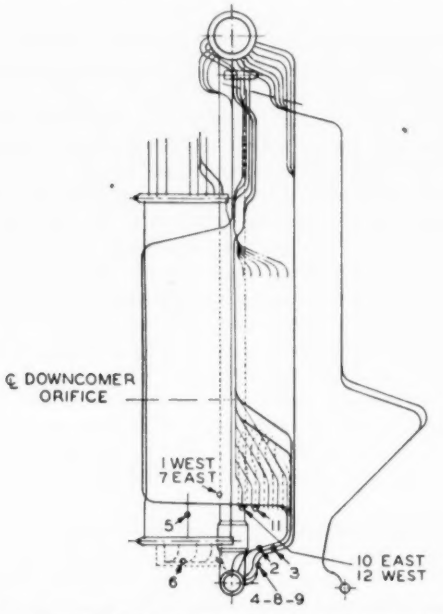


FIG. 6 PITOT-TUBE LOCATIONS FOR CIRCULATION TESTS

tions, and design decisions, as given in this paper, substantiates the judgment of those responsible for the final installation.

ARRANGEMENT OF BOILER AND TEST EQUIPMENT

During the construction of the boiler, pressure taps for measuring differential heads across the various circuits and the fluid density in the downcomers, and pitot tubes for measuring the flow in the various circuits and in the downcomers were installed. The locations of the pressure taps are shown in Fig. 5. Fig. 6 shows the locations of the pitot tubes.

When the unit was first placed into service, the steam-generating circuits were (1) the furnace front wall; (2) the first division wall and (3) the second division wall, which were

$3^1/_4$-in. partial-stud tubes on 6-in. centers; and (4) and (5) the furnace side walls which were 4-in. partial-stud tubes on 6-in. centers. The side walls of the first open pass and the side walls and rear wall of the second open pass constituted reheater surface.

During 1942, alterations[3(e)] were made on the unit in order to reduce the reheater and superheater absorptions, and to prevent the gases from cutting through between the tubes of the first and second division walls. During these alterations, the upper 15 ft of the furnace front and side walls were changed to full-stud construction, the first and second division walls were changed to 4-in. full-stud tubes, $3^1/_4$-in. sinuous tubes on 12-in. centers were placed in front of the reheater in the first open-pass side walls and a waterwall of $3^1/_4$-in. tubes on 6-in. centers was placed in front of the reheater surface forming the rear wall of the second open pass and the sloping floor at the bottom of the second open pass. A comparison of the circulation test results with both of these arrangements of heating surface will be given.

Test Results

As a matter of interest, the first time pressure was raised on the boiler, the total circulating flow in the boiler was measured at various pressures from 1100 psi to 2400 psi at a steam output of 135,000 lb per hr. The results from these tests which show the actual effect of operating pressure on the circulating flow are shown in Fig. 7, where the circulating flow expressed as a percentage of that at 1100 psi is plotted against pressure. The test data are represented by the circles and the reference curves show the ratio of the density of water at saturation temperature to that at 1100 psi; also the ratio of the density differential between water and steam at saturation temperature to that at 1100 psi. This is experimental verification of the previous statement that the circulating flow is a complex function of this density differential. This type of relationship between circulation and pressure should hold up to pressures approaching the critical provided that the downcomer circulating water is kept free of entrapped steam.

Fig. 8 shows the circulating flow determined by tests over the steam-output range for the various circuits and also the total circulation in the downcomers for the original and the final arrangements of heating surfaces. In the circulation calculations during the design stages of the boiler, a factor of safety was used in evaluating the average density over the height of the heat-absorbing risers. As shown by the results, this factor of safety was too large since the total circulating flow on the original arrangement was 5,100,000 lb per hr rather than the design value of 3,600,000 lb per hr. Due to this additional circulation, some water-level instability, as evidenced by a slow surging in the gage glass, was encountered when the gage-glass water level was lowered to a point approaching the bottom of the glass, which was 9 in. below the drum center line. When the alterations to the heating surfaces were made, the cyclone separators and the gage glasses were raised 2 in. which placed normal water level 1 in. below the center line of the drum rather than 3 in. below in order to provide additional flow area for the water along the drum.

Because of the larger-diameter tubes and the additional circulation circuits which were added during the alterations, the total circulating flow was increased to 5,500,000 lb per hr after the alterations were made. This caused some water-level instability with the gage-glass level about 4 in. below the drum center line, and the flow resistance in the downcomers was so small that unbalancing the rate of firing across the width of the boiler by cutting out burners would cause a difference of water

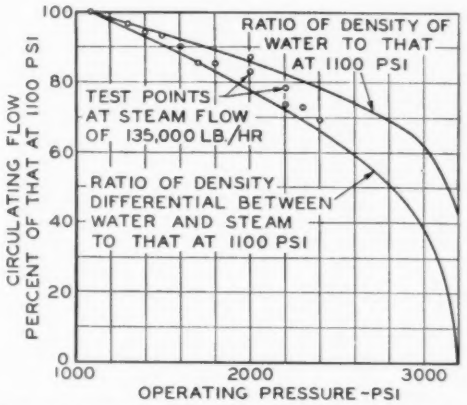


Fig. 7 Effect of Pressure on Circulating Flow

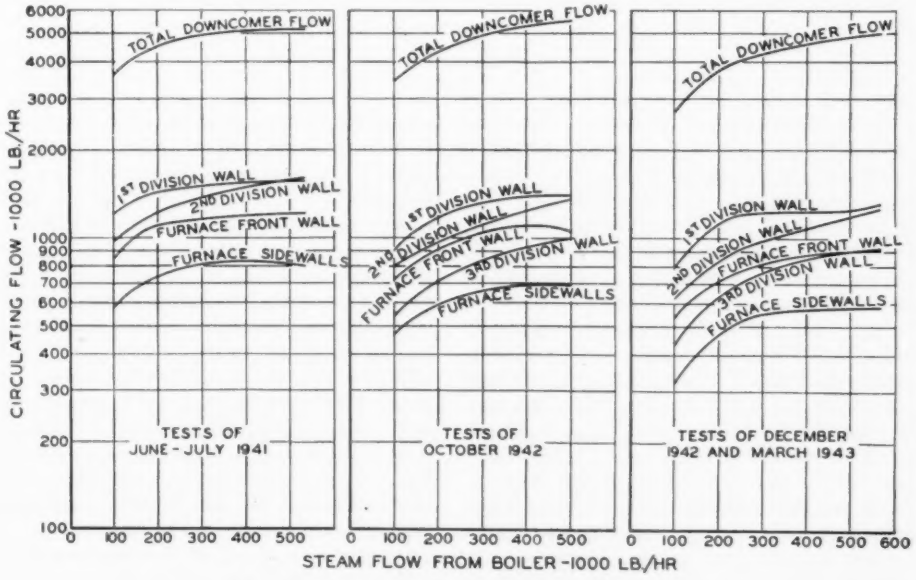


Fig. 8 Circulating Flow in Various Circuits

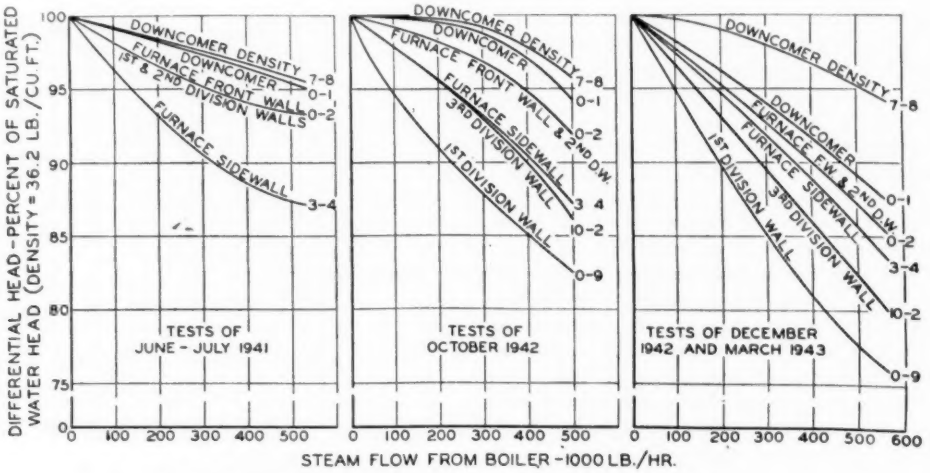


FIG. 9 DIFFERENTIAL HEADS OF VARIOUS CIRCUITS OF BOILER

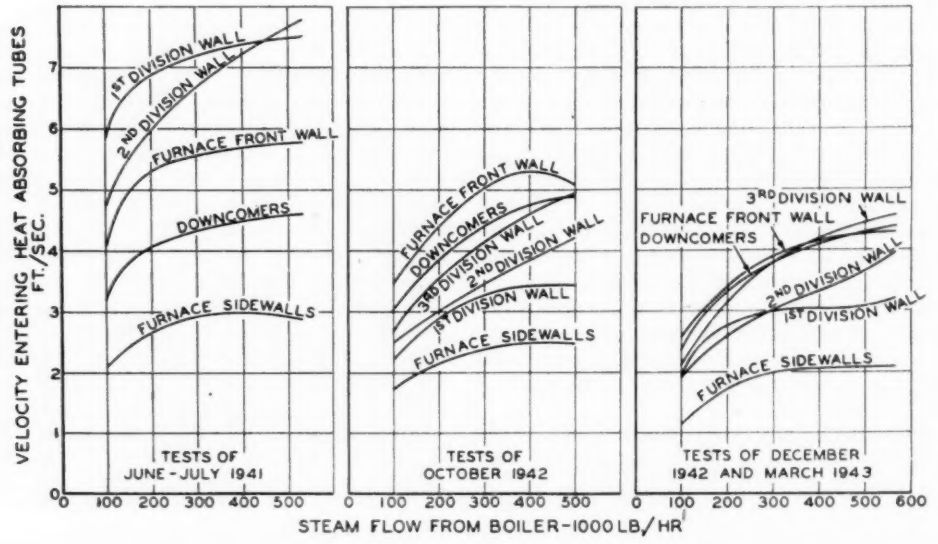


FIG. 10 VELOCITY ENTERING HEAT-ABSORBING SECTIONS OF VARIOUS CIRCUITS

level between the two ends of the drum of as much as 3 to 4 in. These two factors made the permissible water-level range between water-level instability and carry-over too small for trouble-free operation above a load of 500,000 lb per hr.

In order to correct this condition, an orifice with a $16^1/_4$-in-diam opening was placed in each downcomer during November, 1942. The results of this change are shown at the right in Fig. 8. The circulating flow was reduced to 5,000,000 lb per hr at 560,000 lb steam flow, and the downcomer resistance was increased to 2.5 ft of standard water. This change has resulted in completely satisfactory operating conditions with no water-level instability or carry-over occurring within the 12-in. visible range of the gage glass, and neither condition has occurred since this change even with load changes from 500,000 down to 350,000 lb and back again in 3 or 4 min. Water levels at the two ends of drum are always within $^1/_2$ in. of each other regardless of firing conditions.

Fig. 9 shows the differential-head test results on the various circuits in the boiler over the range of steam output. The numbers refer to those shown in Fig. 5. This is expressed in percentage of the head produced by water at saturation temperature (density equals 36.2 lb per cu ft) with no flow. The distance between normal water level and the center line of the lower drum is 68.45 ft which equals a differential head of 39.7 ft of standard water. In the case of the downcomer, the difference between the differential head and 100 per cent is a measure of the reduction of density below that of saturated water due to steam entrapment plus the resistance loss in the downcomer. The downcomer density at maximum load is about 95 per cent of that of saturated water which indicates very little steam entrapment in the circulating water even at this high pressure level and substantiates the original faith put in the ability of the cyclone separators to separate the steam and the water. The difference between the downcomer density curve and the downcomer differential-head curve is a measure of the resistance loss in the downcomers. The addition of the orifices increased the resistance loss from $1^1/_2$ per cent up to 6.2 per cent at maximum load. In the case of the heat-absorbing circuits, the differential head is equal to the sum of the average density in the circuit plus the resistance loss. The difference between the downcomer differential head and that of the furnace front wall is a measure of the resistance loss across the cyclone separators, which is only 2.6 per cent, or about 1 ft of standard water at maximum load.

TABLE 1 CIRCULATION TEST DATA FOR BOILER CIRCUITS

† TEST	ABSORPTION RATE BTU/SQ.FT./HR.			VELOCITY ENTERING TUBES FT./SEC.			CIRCULATING FLOW LB./HR.			MIXTURE STEAM RATIO LEAVING			PERCENT STEAM BY VOLUME LEAVING		
	1	2	3	1	2	3	1	2	3	1	2	3	1	2	3
FURNACE FRONT WALL	29,000	29,000	31,000	4.56	4.10	4.21	948,000	857,900	877,500	13.6	11.7	11.4	30.0	34.2	34.4
FURNACE SIDEWALLS	36,000	30,000	35,000	2.40	1.98	1.94	660,000	550,000	536,000	12.8	12.2	10.0	31.4	33.2	37.7
1ST DIVISION WALL															
CENTER SCREEN	24,000	26,000	31,000	3.18	2.91	3.11	502,000	462,300	491,700	8.4	7.4	6.1	42.2	46.5	51.6
END SECTIONS FROM SIDEWALLS	30,000	29,000	36,000	3.60	3.15	3.39	347,000	305,000	326,900	7.5	7.1	5.7	45.4	47.7	53.6
END SECTIONS FROM 2ND D.W.	24,000	28,000	34,000	4.51	4.33	4.62	434,000	419,400	445,400	9.2	7.5	6.4	39.7	46.1	50.2
SERPENTINE TUBES	16,000	22,000	24,000	3.05	3.08	3.37	168,500	171,600	187,000	8.2	6.5	5.7	42.9	50.3	53.6
2ND DIVISION WALL															
CENTER SECTION	22,000	24,000	28,000	4.15	3.84	4.20	599,000	557,800	608,000	12.0	9.5	8.6	32.9	39.5	41.8
"Y" TUBES	26,000	27,000	34,000	3.62	3.34	3.70	636,500	591,000	651,500	8.8	7.4	6.4	40.9	46.5	50.2
3RD DIVISION WALL	28,000	25,000	28,000	5.08	4.43	4.53	1,020,000	895,000	911,000	6.7	6.6	5.8	48.6	49.8	53.1
TOTAL CIRCULATING FLOW							5,315,000	4,810,000	5,035,000						

† TESTS	1	2	3
DATE	OCT. 10 1942	DEC. 4 1942	MAR. 27 1943
LB. STEAM/HR.	500,000	495,000	562,000
DRUM PRESS.-PSI	2310	2280	2300
ORIFICES	NONE	16¼" IN EACH DOWNCOMER	

Fig. 10 shows the velocity of the circulating water in the downcomers and entering the various heat-absorbing circuits before generating any steam. The reduction in velocity between the original design and that after the alterations to the heating surfaces is the result of the larger-diameter tubes and the additional circuits. The velocities after installing the orifices range from about 2 fps to 4.5 fps entering the tubes at maximum load. It is worthy of note that the velocities increase as the rating of the boiler increases.

Table 1 gives the pertinent circulation test data for the individual circuits of the boiler, as well as a comparison of the results at 500,000 lb per hr steam flow before and after installing the orifices in the downcomers. It also tabulates these data at a load of 562,000 lb of steam per hr after the installation of the orifices. The orifices reduced the total circulating flow and the average velocity entering the tubes approximately 10 per cent at 500,000 lb steam flow and decreased the mixture steam ratio (which is a reciprocal of per cent steam by weight) leaving the tubes from 9.4 to 8.3 on the average, which means an increase in the percentage of steam by weight from 10.6 per cent to 12.1 per cent. The average percentage of steam by volume leaving the tubes increased from 39.8 per cent to 43 per cent. At the overload of 562,000 lb per hr, the average mixture steam ratio is 7.2, and on the highest-duty tubes is 5.7, corresponding to percentage of steam by weight of 13.9 per cent, and 17.5 per cent, respectively. The percentage of steam by volume on the average is 47.1 per cent and leaving the highest-duty tubes is 53.6 per cent. These values indicate a large excess of circulation and a large margin of safety in so far as any possible tube distress is concerned.

Conclusions

Since the tubes were changed to full-stud construction, the thermocouples at full load consistently show a range in temperature of the outside face of the tubes of 725 F to 785 F, which, with a saturation temperature of 655 F, indicates local absorption rates from 30,000 to 55,000 Btu per hr per sq ft.

Before this unit was placed in service, considerable public discussion had taken place in respect to excessive carry-over of boiler-water salts in the steam at this high pressure level, based upon theories advanced about steam solubility and the partial-pressure phenomenon. Actual operating experience on this boiler, however, has proved that the purity of the steam is as good as or better than the majority of the units operating at pressures of 1400 psi and below. The conductivity of the steam is consistently about 0.8 micromhos, indicating solids carry-over of about 0.5 ppm and an evaporated-steam sample showed 0.57 ppm. In the matter of turbine-blade deposits, the operating history is also as good as, or better than, the majority of the units operating at pressures of 1250 psi and below. A slow building up of stage pressure is experienced on the high-pressure machine, and this is corrected every few months by dropping the primary-steam temperature to about 750 F for 2 or 3 hr. There has been no indication of building-up in the low-pressure turbine. This experience is based upon feedwater treatment and boiler-water conditions which have been no different than in most 1400-psi boilers.

The authors believe that the successful operation of this unit at the intended operating pressure since May, 1941, and the results of the extensive testing of the boiler, give clear evidence for the conclusion that natural circulation is entirely practical and provides the necessary margin of safety for boiler-design pressures up to 2500 psi, provided that all factors inherent in the determination of successful circulation with steam generation at this pressure are considered and properly developed in the design of the unit. It may be stated that, properly handled, the problem of providing adequate natural circulation in boilers operating at pressures up to 2500 psi has ceased to exist.

Distribution of Heat Absorption and Factors Affecting Performance of Twin Branch 2500-Psi Boiler

By F. G. ELY[1] and L. B. SCHUELER,[2] NEW YORK, N. Y.

This is one of three papers,[3] describing various phases of the 2500-psi 940 F boiler with reheat to 900 F, installed in 1941, at the Twin Branch Station of the Indiana & Michigan Electric Company (American Gas & Electric Service Corporation). Details are given of the major design changes which were made from the inception of operation, and which upon completion, have permitted full rating and specified superheat and reheat temperatures to be possible for the past year. These changes were based upon extensive tests to determine heat-absorption rates and distribution of heat throughout the unit. The occurrence of failure of two tubes in the first division wall is made the subject of analysis, leading to the application of stud plates welded to tube faces with refractory packed between plates. Performance curves are given, and the conclusion is reached that further investigative work is needed to evaluate the detailed factors which combine to achieve the results.

THE Twin Branch high-pressure unit represents an unusual combination of design conditions for a steam-generating unit to produce steam at 2500 psi, 940 F and with steam reheating at intermediate pressure to 900 F. Such design requires considerable experience and skill in proportioning of surfaces which superheat the steam and those generating surfaces which precede the superheater in the setting. This is generally a critical feature of any unit because it involves a decrease in cycle efficiency if the superheat is low, or hazard to the safety of operation if superheat is sufficiently high to reach the temperature limitations imposed by available metals and alloys for pressure-part construction.

Design Considerations

The original Twin Branch design was carried out with the aid of the then current methods for determination of heat-transfer characteristics of the various cooling surfaces and with supporting data gained from actual field observations on a unit of similar arrangement operating with different fuels and with similar fuel on a short test run.

In a unit designed for these final steam requirements, it is impracticable, when firing low-ash-fusion coal, to do all of the superheating and reheating in the familiar convection-type equipment. Some limit of gas temperature entering the closely spaced tubes of a convection bank must be observed, and the amount of heat available from the gases, at 2000 F, for example, is insufficient to supply the requirements of the steam, even with perfect counterflow convection heat exchange. Furthermore, the rapidly diminishing rates of heat exchange, as the gases are cooled, would necessitate an uneconomically large extent of heating surface. In order to reach a practical balance of heat distribution to water and steam in the unit it therefore was necessary to advance the steam-heating components forward into the higher-temperature zones where heat was available and where higher exchange rates could be obtained, but with due consideration being given to the behavior and influence of fuel ash and slag.

For the design conditions obtaining at Twin Branch and with full advantage being taken of stage heat recovery in feedwater, it is shown in Fig. 1 that nearly one half of the heat absorbed in the generating unit must be by steam-cooled surfaces and that the ultimate margins of temperature between the steam and the safe metal limits are largely consumed by steam-film and tube-wall gradients. Furthermore, a careful arrangement of surfaces was necessary to maintain steam and metal temperatures as nearly uniform as possible in the parallel circuits of the various superheater and reheater sections. This called for proper location of the sections with respect to heat source, provision for uniform distribution of steam flow to the parallel circuits, and provision for mixing the partially superheated steam in a common chamber between sections to equalize any unbalance before final superheating, all within reasonable limits of pressure drop. Also, the design requirement for maintaining full superheat and reheat temperature over a substantial portion of the load range further complicated the problem since the radiant-surface characteristic is generally such that maximum metal temperatures are encountered at low flow, while the convection surface usually follows the reverse trend. In addition, there was the requirement of an adequate supply of auxiliary steam to protect the radiant-reheater sections during starting of the unit.

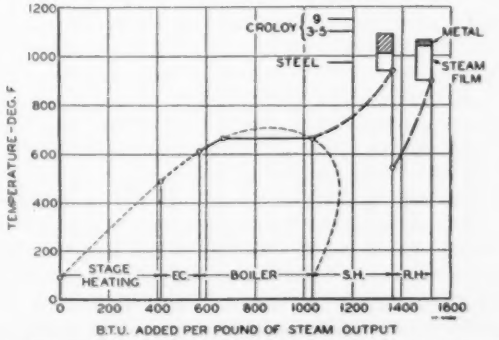


FIG. 1 RELATIVE QUANTITIES OF HEAT ADDED TO WATER AND STEAM IN 2500-PSI BOILER UNIT

[1] Analytical Engineer, The Babcock & Wilcox Company. Mem. A.S.M.E.

[2] Engineering Department, American Gas & Electric Service Corporation. Jun. A.S.M.E.

[3] Two companion papers presented at the Annual Meeting of the Society are as follows:

(*a*) "Operating History of the 2500-Psi Twin Branch Plant," by Philip Sporn and E. G. Bailey.

(*b*) "Natural-Circulation Test Results on the 2500-Psi Twin Branch Boiler," by W. H. Rowand and T. B. Allardice.

Contributed by the Power Division and presented at the Annual Meeting, New York, N. Y., Nov. 29–Dec. 3, 1943, of THE AMERICAN SOCIETY OF MECHANICAL ENGINEERS.

NOTE: Statements and opinions advanced in papers are to be understood as individual expressions of their authors, and not those of the Society.

Initial Operating Conditions

Initial operation of the Twin Branch boiler gave immediate indication that the heat absorbed by steam, particularly in the reheater, was too great. The full temperatures of superheat and reheat were attained at approximately 70 per cent load, using all of the gas by-pass and attemperator control capacity available. This condition initiated a comprehensive field investigation which at times turned this large commercial unit into a field laboratory, but at the same time without appreciable interference with normal operation. Some of these investigations and the resulting design alterations are reported herewith.

In the original arrangement, the reheater surface included exposure of the side-wall area of the first and second open passes, as well as the roof and rear wall of the second open pass, and the sloping floor of the cavity under the convection pass. The final-stage superheater likewise had a greater area of exposed surface by extended arrangement of the platen tubes instead of the grouping as now disposed.

Temporary alterations were made immediately, consisting of applying a gunnited refractory coating to the side-wall reheater tubes, covering one half of the surface of the reheater hopper slope, closing alternate gas lanes in the primary-reheater convection bank with refractory concrete, and increasing the capacity of the attemperator spray nozzles. These changes permitted operation up to 80 per cent of full capacity without exceeding safe tube and steam temperature; some advantage being gained by running with lowered excess air and by overattemperation in the superheat cycle to produce steam temperatures lower than design level in order to lower the temperature of steam returned to the reheat cycle, since the reheater proved to be the most critical portion of the heating surface.

The unit was operated for several months in this condition for the purpose of gaining experience, pending delivery of materials for the projected rearrangement of surfaces.

Test Investigations

Tests were run to obtain data on heat-absorption rates and distribution of heat throughout the unit, and particularly in the furnace and open passes where high gas temperatures prevailed and where important increments of steam-heating surface were present. Several tests were run using water-cooled high-velocity-thermocouple and gas-sampling tubes for complete traverse of the gas stream at successive sections of the unit, from which data the corresponding increments of heat absorption could be calculated. Daily routine test readings were taken of the flow and temperature rise in each section of the superheater and reheater systems, using each section as an independent calorimeter. These data afforded a valuable basis for determining the extent to which final reproportioning of surfaces would be necessary. The circumstance that all of the steam-generating surface of the boiler was in the primary furnace and open passes provided a unique comparative means of measuring and evaluating heat-absorption rates by two independent methods.

Significant data from these test investigations are shown in Figs. 2 to 5, inclusive. The evaluation of heating surfaces is based upon projected areas of exposed wall and platen arrangements, but with inclusion of the complete circumferential areas of spaced tubes in the furnace-outlet screen and in the convection screen and tube banks. In the case of Fig. 2, the gas temperatures were obtained from special test traverses with the high-velocity thermocouple. In Figs. 3 to 5, inclusive, the plotted points represent "daily-test" values of heat-absorption rate of the different components of steam-heating surface, determined by the calorimeter method, and in Fig. 5, comparative points are shown for the eight special tests, calculated on the gas-heat basis.

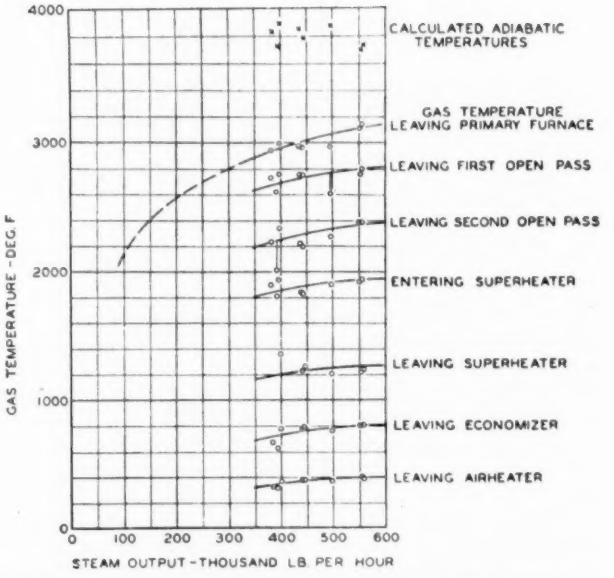


Fig. 2 Gas Temperatures at Various Sections of Boiler Unit as Measured by High-Velocity-Thermocouple Traverse

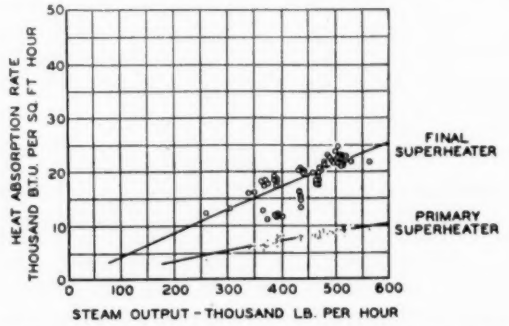


Fig. 3 Heat-Absorption Rates of Primary and Final Superheater

It will be noted from Figs. 3, 4, and 5 that individual absorption rates at a given load show considerable variation in day-to-day operation. Cumulative data to the outlet of the second open pass indicate that these variations are to some extent self-compensating, as evidenced by the greater uniformity of points shown in Fig. 5. Gas-flow control in the convection sections, and attemperator control of superheated steam provide the necessary supplementary compensation for production of uniform final steam temperature.

The cumulative absorption rates at the second open-pass outlet show a close agreement between daily calorimeter test and high-velocity-thermocouple test methods. It is difficult to carry a similar comparison forward to the primary-furnace and open-pass individual sections of the unit. However, some confirmation of the HVT test values is afforded by other means of testing that were applied.

Fig. 6 shows the absorption rate of a portable water-cooled thermal probe inserted for a distance of 5 ft through an inspection door in the lower part of the primary furnace. When the probe was first inserted a high absorption rate was obtained, which diminished to a value of approximately 48,000 Btu per sq ft per hr as slag accumulated on the probe surface to a condition of equilibrium thickness. Slag was then removed, the probe was reinserted in the furnace and was kept clean by repeated scraping for a short interval of time in order to measure

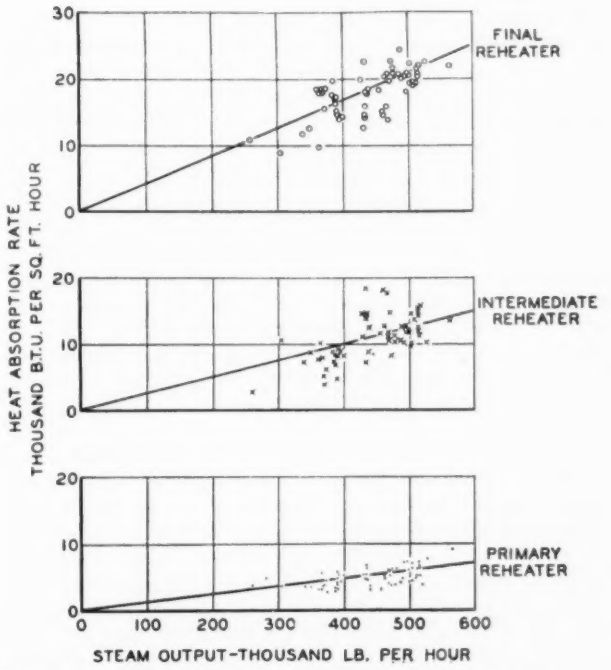


FIG. 4 HEAT-ABSORPTION RATES OF PRIMARY, INTERMEDIATE, AND FINAL REHEATER

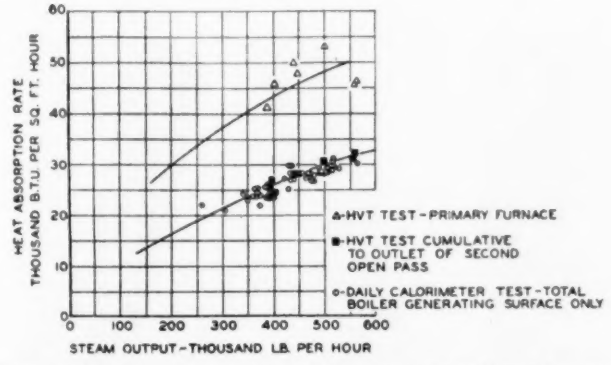


FIG. 5 HEAT-ABSORPTION RATES OF FURNACE AND OF TOTAL STEAM-GENERATING SURFACE

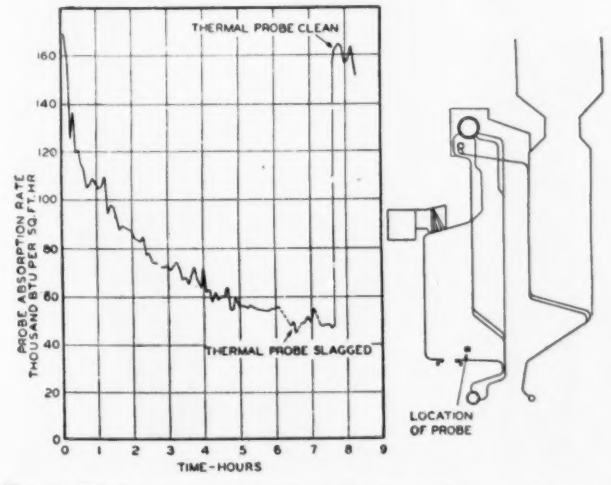


FIG. 6 HEAT-ABSORPTION RATE OF THERMAL PROBE IN PRIMARY FURNACE

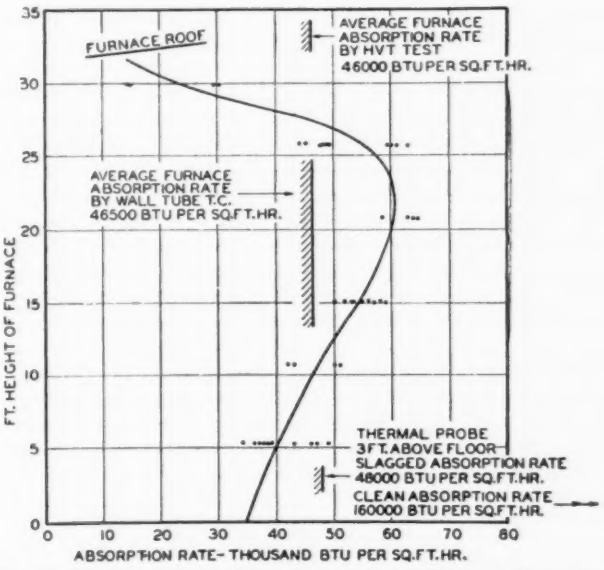


FIG. 7 DISTRIBUTION OF HEAT ABSORPTION IN PRIMARY FURNACE, AS INDICATED BY WALL-TUBE THERMOCOUPLES AND OTHER TESTS AT 570,000 LB PER HR STEAM-OUTPUT RATE

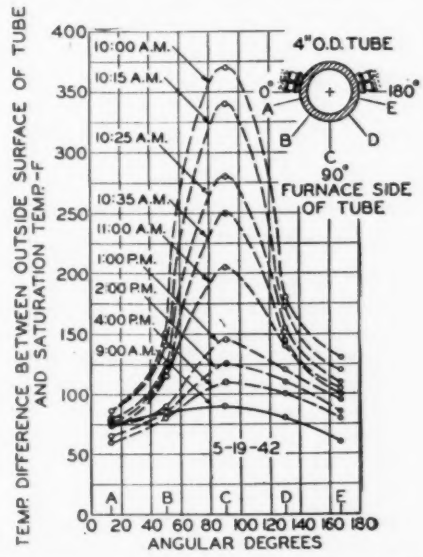


FIG. 8 DISTRIBUTION OF TEMPERATURE IN FURNACE-WALL TUBE, SHOWING EFFECT OF SLAG REMOVAL FROM BARE TUBE SURFACE

the comparative clean absorption rate under identical furnace conditions. This was found to be approximately 160,000 Btu per sq ft per hr. The relation of slagged to clean absorption rate was 30 per cent.

Fig. 7 represents a plot of equivalent heat-absorption rates as calculated from furnace wall-tube temperature data obtained from special thermocouples installed at 21 distributed points of the front-wall and side-wall furnace tubes. By utilizing the temperature differential between tube-surface temperature and saturation temperature, and assuming negligible inner surface resistance to heat flow (which condition has been convincingly demonstrated for tubes with positive circulation), it has been possible to calculate equivalent values of local heat-absorption rates which reveal an interesting pattern of the distribution of heat in the furnace. The average of 46,500 Btu per sq ft per hr compares rather closely with the value of 46,000 for the over-all

furnace, as determined by gas-temperature test methods, and the value of 48,000 shown by the slagged thermal probe.

An example of the influence of slag on local heat-absorption rates and metal temperature of bare furnace wall tubes is shown in Fig. 8. This plot represents a series of readings taken from thermocouples installed at five points around the circumference of a tube in the left side wall of the primary furnace, at elevation 15 ft above the furnace floor. It will be noted from Fig. 7 that this is near the zone of maximum heat intensity. Shortly after 9 a.m. a sudden increase in tube temperature was observed, and inspection showed that the fused slag coating on the tubes in this area had peeled or crept away, leaving tube surfaces exposed directly to furnace radiation. The sudden increase of 280 deg is equivalent to a gain in heat-absorption rate from approximately 40,000 Btu per sq ft per hr at 9 a.m. to 160,000 Btu per sq ft per hr at the 10 a.m. reading for the local area affected by loss of slag protection. In the course of the next 6 hr, the tube returned to lower temperatures as the slag coating was restored by the normal process of accumulation in the furnace.

Analysis of Tube Failures

One practical significance of this occurrence becomes evident in considering the causes which led to the failure of two tubes[3(a)] in the upper portion of the first division wall. These failures were located on the furnace face of the tubes and occurred during the period when alternate tubes were omitted from this portion of the wall, allowing furnace gases to short-circuit into the upper part of the first open pass.

Fig. 9 shows the calculated pressure stress and the combined pressure and thermal stresses for a Twin Branch primary-furnace division-wall tube of $3^1/_4$ in. OD and 0.500 in. thickness, plotted as a function of heat-absorption rate. The ultimate, yield, and proportional-limit stresses for the material involved are also shown. The pressure and thermal stresses shown are those which obtain in the form of tension at the inner fiber of the tube. It is indicated that absorption rates of the order of 75,000 Btu per sq ft per hr may result in combined stresses in excess of the yield point of the tube involved.

It was established that slag peeling in certain portions of the primary furnace, particularly where both radiation and convection heat exchange were imposed on the tube, could result in absorption rates as high as 200,000 Btu per sq ft per hr. A gradual increase in absorption rates to such a level would probably be less harmful than a sudden increase, since the full temperature stress would not be realized due to creep permitting considerable "relaxation." However, with sudden peeling of slag, and exposure, it is probable that the full elastic properties of the material were retained long enough to develop the full elastic stresses so that the yield stress was exceeded.

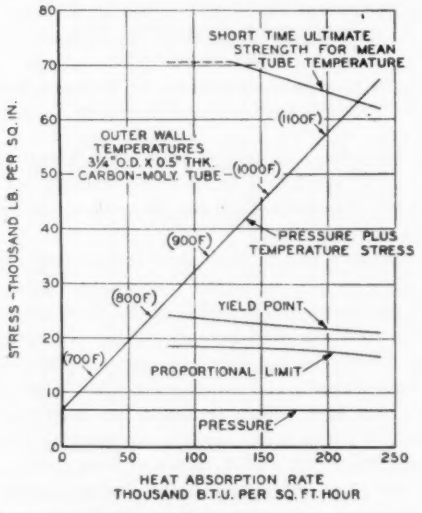


Fig. 9 Calculated Tube-Wall Stress at Various Rates of Heat Absorption

Although analysis indicates that the ultimate stress was probably never reached, as a consequence of thermal stress, the fact that failures did occur can probably be explained by the results of careful laboratory examination of the failed tubes. These showed that the areas surrounding the failures were bulged and the microstructure indicated that the outer portion had been subjected to temperatures as high as 1600 F and the inner wall had been appreciably higher than saturation temperature. Examination also showed oxide deposit inside the tube in a small area around the ruptured zone, and measurements showed that appreciable thinning of the original wall was produced at the immediate line of rupture. The conditions surrounding the failures, that of internal-corrosion attack, blistering, and apparent rupture due to hoop stress in excess of the ultimate strength, could not be logically ascribed to inadequate circulation as is sometimes the case for such occurrences since later tests established the adequacy of circulation in these circuits.

Existing instrumentation in the form of a hydrogen recorder, for continuous sampling and analysis of feedwater and saturated steam, gave positive evidence of the corrosion phase involved in these tube failures. In one case this record showed a progressive rise of hydrogen evolution in the boiler to high levels during a

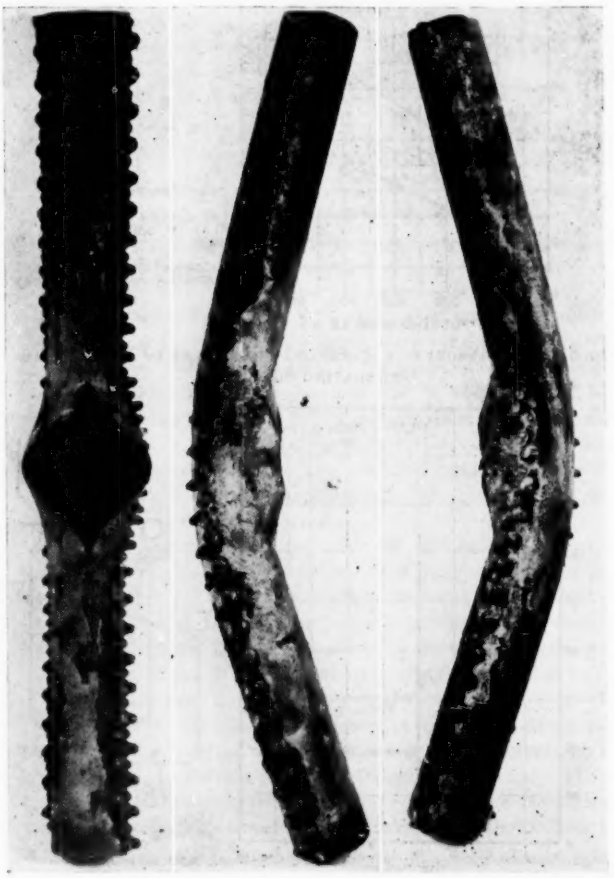


Fig. 10 General Appearance of Ruptured Tube, Showing Three External Views

period of two and one half hours immediately preceding the rupture.

A probable logical sequence of conditions leading to ultimate rupture of the tubes has been established as follows:

1 Peeling off of slag exposing the bare tube to concentrated radiant and convection heat transfer, resulting in sudden thermal stress and normal pressure stress, combining to exceed the yield point at the inner fiber of the tube.

2 Slight permanent "stretch" of inner fibers, producing a small blister in which formation of a steam film leads to corrosion attack which produces an oxide layer in the affected area.

3 Recurrent or continued exposure of this zone, producing overheating and further blistering of the area with ultimate rupture due primarily to pressure stress in excess of the ultimate strength at the temperature attained.

The foregoing record of hydrogen evolution indicates that this sequence probably was completed within the $2^1/_2$-hr period described.

The appearance of one of the ruptured tubes is shown in Fig. 10. A closer view at the point of rupture is shown in Fig. 11. Initial failure occurred in a length of approximately $2^1/_2$ in. and developed further as a tear for a total length of 7 in. along the tube.

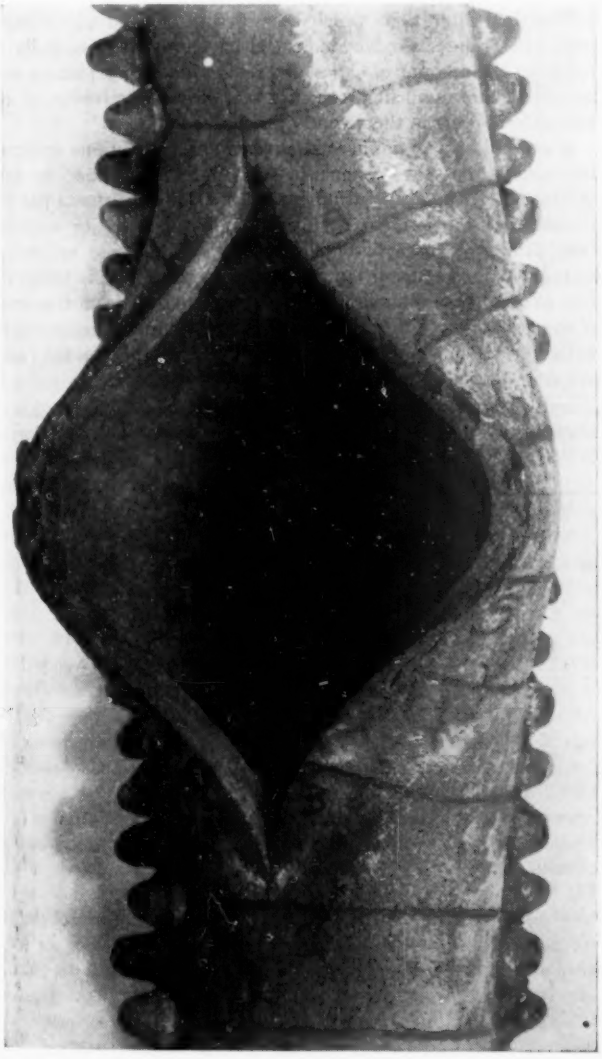


FIG. 11 CLOSE-UP VIEW OF RUPTURED TUBE, SHOWING APPEARANCE OF FRACTURE

The presence of oxide scale on a small area of the inner surface, as well as a measurable thinning of the tube wall and enlargement of tube circumference, indicated the existence of an initial blister. Characteristics of the main fracture, however, are those of an elastic failure, and the presence of numerous small cracks close to the line of rupture indicate that parting of the metal occurred first in the outer surface of the tube as a result of hoop stresses exceeding the ultimate strength of the metal at the temperature attained. The absence of knife-edge fracture would seem to exclude the probability of general overheating such as would be expected under conditions of low water or restricted circulation.

There are three likely alternatives for overcoming the difficulty described. These are as follows:

1 The use of smaller-diameter tubes with corresponding decrease in thickness in accordance with Boiler Code rules. This would produce lower thermal stress at a given heat-absorption rate, but at the expense of circulation efficiency.

2 The use of thinner wall tubes of the same diameter provided sanction of Boiler Code authorities could be obtained.

3 Application of a protective covering to the existing tubes which would prevent direct exposure of bare tubing in case of slag peeling, but would withstand action of temperature and slag conditions prevailing.

The first two of the foregoing alternatives were impractical, since the Twin Branch unit was already built and operating and could not be spared for any such major alterations if they had been considered preferable. Alternative 3 was the only one seriously considered as satisfactory and practical. The application of stud plates welded to the tube face at intervals with refractory material packed between plates had given satisfactory performance on numerous other installations under severe operating conditions. Furthermore, experiments with thermocouples on adjacent bare and covered tubes in the primary furnace of another unit[4] had demonstrated the effectiveness of the stud-plate construction as a protection against ex-

[4] "Studies of Heat Transmission Through Boiler Tubing at Pressures From 500 to 3300 Pounds," by W. F. Davidson, P. H. Hardie, C. G. R. Humphreys, A. A. Markson, A. R. Mumford, and T. Ravese, Trans. A.S.M.E., vol. 65, August, 1943; see discussion by F. G. Ely, pp. 580–581.

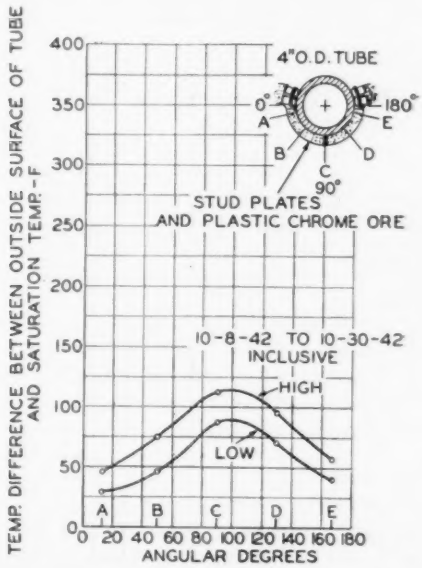


FIG. 12 DISTRIBUTION OF TEMPERATURE IN FURNACE-WALL TUBE FOLLOWING APPLICATION OF STUD PLATES AND CHROME ORE

cessive localized change in heat-absorption rates across the tube wall.

As a part of the final alterations of the unit, stud plates were applied to the upper 15 ft of primary-furnace-wall tubes to provide protection of the pressure parts against this capricious behavior of slag in the hotter zones. A comparative pattern of tube-temperature distribution at the same location after installing stud plates is shown in Fig. 12. It is apparent that the temperature differential between the outer tube surface and saturation is as great as for the slag-covered bare tube of Fig. 8, indicating that normal heat-transfer rates are substantially equal for the two types of surface. However, there has been a consistent absence of sudden temperature changes as a result of greater permanency of the protective tube covering.

Slag Characteristics

Slag is without question the greatest single factor causing variation and disturbance in the performance of the absorbing surfaces. The extent and thickness of coverage are affected by composition of the coal ash, by segregation effects within the furnace, by excess air and the nature of the furnace atmosphere, and of course by change in temperature of slag particles and gases in their passage through the unit.

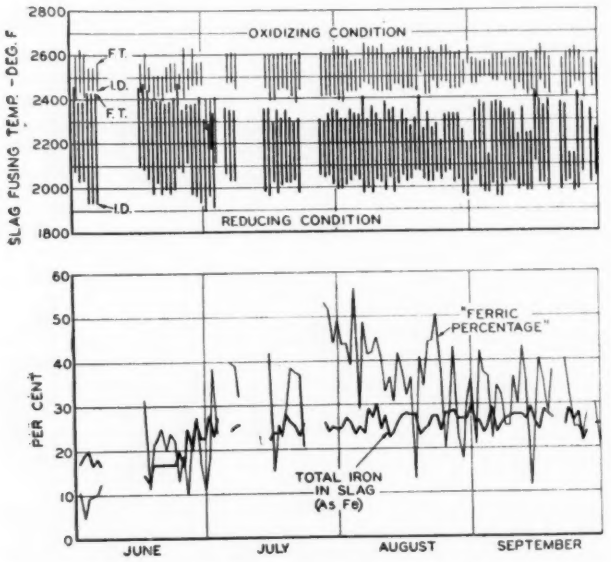


Fig. 13 Properties of Slag From Furnace Tap, Daily Samples

Samples of slag, collected daily from the tap stream, have shown appreciable variations in fusing characteristics and in the state of oxidation of the iron content, as shown in Fig. 13. Other samples collected from different portions of the unit show significant diversities of composition and fusing-temperature range as plotted in Fig. 14. It is apparent that the effect of iron, which in its ferrous form acts as a dominant fluxing agent, is materially altered both by segregation of quantity and state of oxidation, in passage through the unit.

A proper evaluation of these influences is of great importance to the balancing of heat-absorbing surfaces. Adequate range of temperature control, and means for removal of slag from critical zones are important to continuous operation of the unit within narrow limits of steam temperature, and permissible rates of steam-temperature change.

Final Alterations and Performance

The final alterations which have permitted continuous base-load operation since November, 1942, consisted principally of reducing the amount of exposed surface in final superheater and in intermediate and final reheater sections and provision of retractable blowers in the second open pass.

A general survey of thermal performance conditions existing throughout the unit is shown in Fig. 15, as determined by test of May 14, 1943, at an output rate of 570,000 lb of steam per hr. Considering the unit to be divided into seven major sections (viz., primary furnace; first open pass; second open pass, and so on, as indicated), the upper curve shows the values of gas temperature at exit from each section and was determined from traverses of the gas stream, using the shielded high-velocity thermocouple, with corrections made to the basis of the multiple-shielded high-velocity thermocouple[5] (MHVT).

[5] "Gas Temperature Measurement and the High-Velocity Thermocouple," by H. F. Mullikin, *Temperature*, Reinhold Publishing Corporation, New York, N. Y., 1941, pp. 775–804.

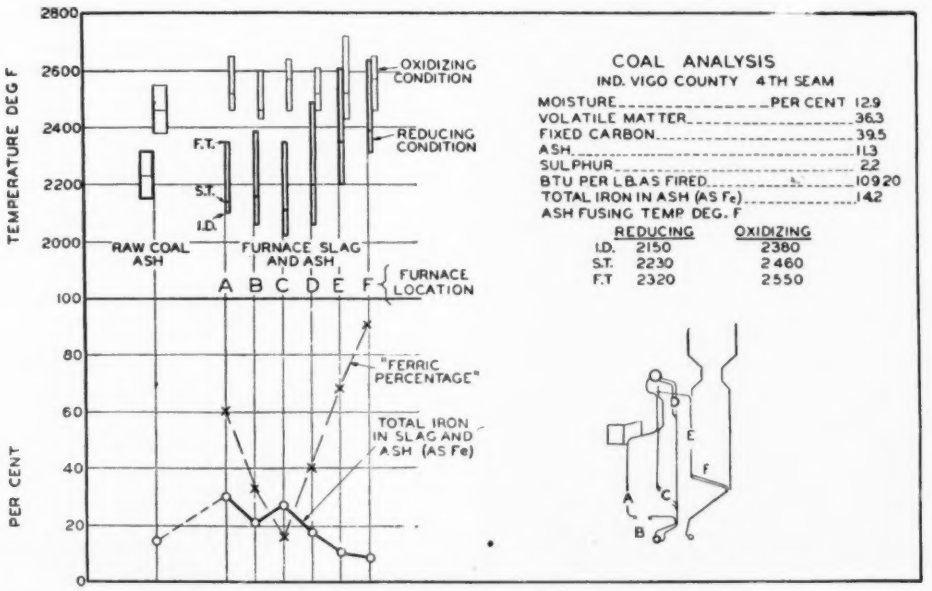


Fig. 14 Properties of Slag From Various Locations in Furnace

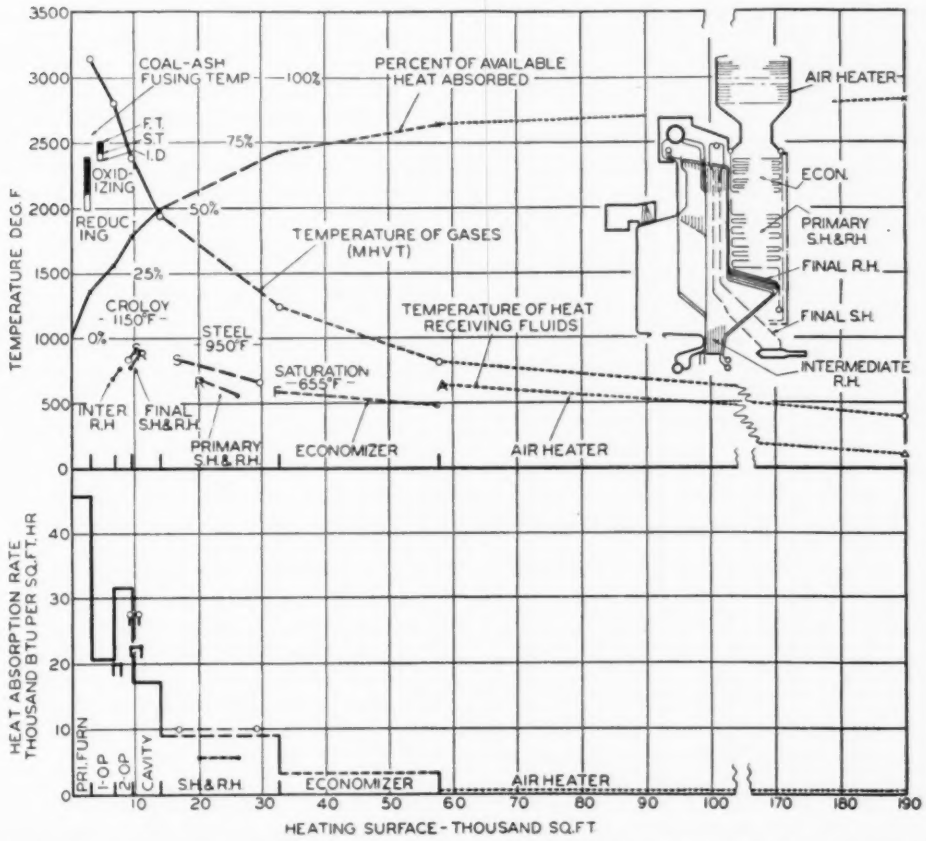


FIG. 15 GENERAL SURVEY OF THERMAL PERFORMANCE CONDITIONS AT 570,000 LB PER HR STEAM-OUTPUT RATE

In relation to this curve of gas temperature, there are shown for each section of the unit the corresponding temperatures of the heat-receiving fluids in the air heater, economizer, superheater, and reheater, and the respective limiting metal temperatures. The difference in temperature between gases and receiving fluids is a basic measure of the available potential for transfer of useful heat.

On the lower portion of the chart is a plot of heat-absorption rates, calculated by familiar methods for each individual section, from the data on gas weight, specific heat, and temperature drop in that section. The area under this curve is proportional to the total quantity of heat absorbed per hour, and it is clearly indicated that those sections of the unit, which are located in the higher temperature zones, account for a major part of the total absorption, and are functioning at high specific rates.

It is somewhat difficult to show in simple graphic form the different categories of heating surface which co-exist in individual sections of the unit. For example: The second open pass contains water-cooled generating tubes in the front and rear division walls, reheater tubes forming the side walls, and superheater tubes in platen grouping, which extend from top to bottom of the pass and also across the cavity section. Some liberties have therefore been taken to represent those portions of the steam-heating circuits individually, at their approximate location in the temperature field. Heat-absorption rates shown for these circuits have been measured independently of the gas-temperature method by calculation based upon steam-flow rate and temperature gain. The indicated rates are quite consistent with those shown for the total surface of the section.

Heat-absorption rates of the primary furnace and first open pass are based upon the assumption that combustion is completed before the gases leave the primary furnace. Recent data obtained from sampling of the gas stream at the furnace outlet and first open-pass outlet by means of water-cooled fly-ash samplers, indicate that a certain proportion of solid carbon is present at the exit of the furnace and is consumed in passage through the first open pass. Quantitative determinations in terms of hourly heat equivalents are extremely difficult to make; however, it is estimated that this item may justify a revision of approximately 5000 Btu per sq ft per hr decrease in the furnace absorption rate, and a corresponding increase of 4000 Btu per sq ft in the first open pass, as compared to the values shown in Fig. 15.

SUMMARY AND CONCLUSIONS

Sustained operation at full load since March, 1943, adequately confirms the fact that the functional design features of the various component parts of the Twin Branch unit have been substantially fulfilled. In brief, these are represented by the following:

1 A primary furnace with high heat-release and absorption rates, forming a chamber for effective combustion and the collection and removal of slag over a wide load range.

2 The first open pass, comprising an open channel in which gases and slag can be cooled through the critical "sticky" ash range but with much lower absorption rate.

3 The second open pass consisting of an open channel with widely spaced superheater platens in which surfaces are kept reasonably clean by mechanical blowers supplemented by some hand-lancing with resulting high absorption rate, thus reducing the gases and ash particles to a safe level before entrance to the convection passes.

4 The convection passes in which closely spaced tubes are utilized to accomplish the remaining work and in which mechanical blowers are fully effective for cleaning.

It is brought out more fully in one of the companion papers[3(a)] that the Twin Branch 2500-psi boiler, after undergoing some major design alterations, based upon the investigations and studies reported herein, has been in a position to operate for the past year at full rating and specified design superheat and reheat temperatures, and with continuity of performance hardly exceeded by any known 1500-psi boiler unit.

From the standpoint of broad boiler-design principles the following conclusions are clear from the Twin Branch experience: Boiler design in the high-temperature portion of a unit of the type under discussion is still far from being a precise and formulated science. It is not surprising that this should be true in view of difficulties in measurement of high gas temperatures and quantitative determination of the insulating effects of ash and slag. It is also clear that no single "bull's-eye" test can be expected to establish a complete criterion of performance, and that the range of day-to-day variation in operating condition must be adequately explored and appreciated in order to provide satisfactory margins of control.

In more conventional installations, where only steam-generating surfaces are involved at the forward part of the setting, self-compensating influences tend to iron out the variations which accompany change in fuel, excess air, and even change of human factors, so that the exacting tolerances of superheater and turbine are easier to meet. Nevertheless, there are many such installations subject to chronic or occasional operating hardship due to unbalanced distribution, abrupt shedding of ash and slag from heat-absorbing surfaces or limitation of operating range and stability.

In the Twin Branch unit the performance of "calorimeter sections" provided a direct yardstick measurement for proceeding with confidence upon final major alterations. Unusual opportunity was afforded for comparative measurements by other methods applicable to all types of units, and establishment of calibration criteria which permitted a more complete accounting of the absolute heat content of the gases. The authors feel that the work at Twin Branch has contributed material progress to that practical accomplishment.

Further investigative work is needed to evaluate the detailed factors which combine to produce an over-all result. The comprehensive program, sponsored by the Special Research Committee of the A.S.M.E. for resolving this problem is an important step leading to the design of better boilers.

Discussion

M. K. Drewry.[6] That more heat is actually absorbed in the superheater and reheater of the Twin Branch boiler unit than in the boiler, as shown by analysis of Fig. 1 of the paper, is significant in this consideration of heat-absorption distribution and steam temperature control.

More than normal slag insulation of tubes before the reheater and superheater reduces the pounds of steam generated and simultaneously increases the total Btu for superheating and reheating. Thus a powerful combination of two vital circumstances works toward high steam temperatures. The paper is replete with data showing unusually wide heat-absorption variations as far back as the primary superheater. It is thus logical that base-load operation, with uniform coal, greatly facilitates operation.

For steam conditions approaching those at Twin Branch, superheaters disposed in the furnace and in the boiler passes, both alongside enough water-tube surfaces so that superheating and evaporating heat-absorption will always vary proportionally, seem more practical for normal load and coal variations.

The paper does the power-generation industry a real service in evaluating the wide variations in furnace heat-absorption rates that may occur in actual practice. Its authors deserve commendation for their clear and complete presentation.

H. F. Mullikin.[7] The extensive gas-temperature measurements on this unit, as shown in Fig. 2 of the paper, are of interest. In spite of the considerable variation in furnace conditions due to different excess-air values, varied slag-fusion temperatures, etc., the gas temperatures are very uniform. The maximum variation of primary-furnace-outlet gas temperature from the mean-line value of 3070 F at 500,000 lb per hr steam flow (shown in Fig. 2) appears to be only 100 F which is a difference of 100/3070 or 3.3 per cent based on the Fahrenheit scale. Referred to room temperature the difference would be but slightly larger.

If the results are transformed to the heat-transfer basis of Fig. 5, the maximum difference of 5000 Btu per sq ft hr from the mean-line value of 48,000 Btu per sq ft hr at 500,000 lb per hr steam flow is 5000/48,000 or a little over 10 per cent.

It would appear that heat-absorption rates in a furnace vary considerably more than do furnace-outlet temperatures. A possible explanation might be that excess-air variations affect calculated heat-absorption rates more than they affect measured furnace-outlet gas temperatures.

W. T. Reid.[8] Further application of the method of determining furnace efficiencies by use of the high-velocity thermocouple, as reported by the authors, is encouraging in extending the use of this tool in furnace testing. Earlier reports on its application were received with some skepticism because of the many difficulties experienced in the past in maintaining rare-metal thermocouples at high temperatures in an atmosphere that at times may be strongly reducing. That the authors continue to use the instrument is proof enough that the inherent problems in its design have been solved. The unusually close agreement between heat-absorption rates in the primary furnace, computed by the temperature gradient through wall tubes, as measured with embedded thermocouples, and by the high-velocity thermocouple should be of extreme interest to anyone contemplating further study of the flow of heat in furnaces. The ability to use such data to modify the unit described with resulting improvement in its performance characteristics is encouraging.

Although obviously this paper is not a description of experimental methods, some questions as to technique are indicated.

With reference to Fig. 7 of the paper, the authors state that the wall-tube thermocouples were installed at 21 points distributed between the front and side walls. Inasmuch as there is considerable variation in the rate of heat transfer from point to point within the furnace, it would be interesting to know the actual positions in which these relatively few thermocouples were placed so that they were capable of averaging the heat absorption in the entire cavity; statistically it would appear that many more temperature points would have been required to give concordant results.

---

[6] Chief Engineer, Power Plants, Wisconsin Electric Power Company, Milwaukee, Wis. Mem. A.S.M.E.

[7] Department of Mechanical Engineering, College of the City of New York, New York, N. Y. Mem. A.S.M.E.

[8] Supervising Engineer, Fuels Section, Bureau of Mines, Central Experiment Station, Pittsburgh, Pa. Mem. A.S.M.E. This discussion is published by permission of the Director, Bureau of Mines, U. S. Department of the Interior.

Also, the use of the thermal probe near the bottom of the furnace, as shown in Fig. 6, is less readily acceptable as a measure of the average rate of heat absorption in the primary furnace. It is suggested that the observed absorption of 48,000 Btu per sq ft per hr at a point 3 ft above the floor was approximately the minimum rate that could have been obtained with the probe in the primary furnace, and that, if the probe had been inserted at a higher position in the furnace, a greater rate of absorption would have been found. Fig. 7 supports such a belief. The many factors affecting the heat absorbed by the probe, including its position where it could "see" the walls of the first open pass and possibly the cold tap hole, and the fact that it projects into the gas stream, increasing the proportion of heat transferred by conduction as compared to the wall tubes, would indicate that the observed close correlation between it and the other methods occurred purely by chance. If the probe was used at other positions, also, it would be interesting to learn how its heat-transfer rate compared with that of the embedded thermocouples.

This paper includes interesting observations on the effect of slag deposits upon the rate of heat transfer, well exemplified by Figs. 6 and 8. For comparison purposes it would be desirable to know both the thickness of slag on the probe and on the wall tubes, the probe when slagged showing 30 per cent of the heat transfer when it was clean, whereas 24 per cent was found with the wall tube of Fig. 8. In addition, knowing the thickness of the two slag deposits, if the conditions in the furnace remained constant over the slagging period, it would have been possible to compute the over-all conductivity factor for this coal-ash slag. At present no such data are known to be available in the literature.

The authors' remarks relative to the importance of slag in affecting the performance of heat-absorbing surfaces are well taken. Our knowledge of the fundamental properties of coal-ash slags is increasing but slowly because of the complexity of the systems involved, but data already available can be used to good advantage in explaining actions hitherto considered obscure. However, it has been found that knowledge of the composition of slag is absolutely essential for any real understanding of its behavior at high temperatures, and it is hoped that the authors will include in their closure the complete analysis of the ash of Fig. 14, as well as that of the samples of slag taken from various positions in the unit. The reported change in iron content is most interesting in showing the pronounced segregation in this furnace; but the other constituents, particularly silica and lime, are also important in any comparison with other units burning coal having different ash characteristics.

The authors' statement that iron in the ferrous form is a dominant fluxing agent is correct, but in the ferric state it is equally effective at the higher temperatures where the slag is a true liquid. Thus the sole effect of a decrease in ferric percentage caused by reducing conditions is to lower the temperature where the slag is converted from a liquid to a plastic material during slow cooling, that is, the range of temperature where the slag behaves as a liquid is greater under reducing conditions than when the atmosphere is oxidizing. At higher temperatures, change in ferric percentage has little or no effect upon the flow properties of the slag.

Authors' Closure

Mr. Drewry's comment, indicating the desirability of intermingling the generating and superheating surfaces, so that variations in heat absorption, caused by change of slag characteristics, would be proportional between the two classes of surface, is of basic interest and deserves consideration in furnace design. To some extent this feature was embodied in the Twin Branch unit where the first open pass contained both generating and reheating surface, and the second open pass contained generating, superheating, and reheating surface, arranged to form the individual walls of the section. Slag formation on these areas was not always similar, and it is doubted that important compensation was realized.

To carry the principle of surface dispersion farther, to the point of installing alternate generating and superheating tubes in a single wall, would entail difficult structural problems in providing for unequal expansion and for possible warping of superheater elements. Individual tubes, offset from the wall, are likely to acquire different degrees of slagging and to exert an opposing influence upon the slagging of near-by surfaces.

In view of the great difference of inner-boundary resistance between evaporating and steam-cooled tubes, it would not be practical to operate superheater surface at the high values of absorption rate which are normal for the primary furnace of a slag-tap unit, and local shedding of slag would probably be disastrous. Furthermore, such exposed superheater surface in a primary furnace would require a starting and initial operating procedure of long duration to prevent overheating of tubes until they acquired their normal protective coating of slag.

For the case of a dry-ash furnace having lower normal absorption rates and operating below the fusing-temperature range of the ash, it would seem that no natural equilibrium thickness could be expected, although some compensating effect might be obtained as a result of circumstance or of deliberate wall-cleaning practices. Direct experience with a dry-bottom unit, having radiant superheater surface in one wall, indicates that load variations result in considerable unbalance in ash coverage of the generating and superheating surfaces, and consequent rapid fluctuations in steam temperature of considerable magnitude, which are difficult to predict and control and require considerable operating attention in the way of burner adjustments and wall-cleaning. The need for positive means of controlling steam-temperature fluctuations still appears to be an important requirement, particularly for extremely high-temperature designs where tolerances between steam and allowable metal temperature limits are small.

Dr. Mullikin's remarks are appreciated in that they call attention to the phenomenon of apparent consistency in furnace-outlet-temperature values in spite of variations in excess air, and heat-absorption rates. This also has been observed in tests of gas- and oil-fired water-cooled furnaces in which the slagging influence was at a minimum, and where a large increase of excess air, admitted at the burners, caused little or no corresponding decrease in measured furnace-outlet-gas temperature, although the calculated heat-absorption rates were definitely lowered.

Both temperature and heat-absorption-rate criteria are significant in the performance of the unit and must be in functional agreement; which of course it is our endeavor to comprehend. The authors question his use of the Fahrenheit zero as a proper basis for comparing the percentage variation in temperature with percentage variation of furnace heat-absorption rates.

If it be accepted that heat exchange is dependent upon temperature difference between source and receiver, one might consider 2320 F ash fluid temperature, Fig. 14, as an approximate wall-surface temperature and a more suitable base for comparison. Disregarding, for simplicity, the fourth-power function or the existence of a radiating source temperature above that of the exit gases, this 100-deg variation in furnace-exit temperature represents 13 per cent of the range between 2320 F and 3070 F, which seems more nearly commensurate with the 10 per cent variation in calculated absorption rates.

The techniques of boiler-testing, thus far developed, are limited for quantitative data to a rather coarse breakdown of the unit into a few major components. Thus the primary furnace as a

whole has been treated as one component, for want of adequate means of segregating its several discrete wall sections or portions of a single wall.

As Mr. Reid points out, the general agreement of values, shown by the thermal probe and by the wall-tube thermocouples, with the over-all average furnace-absorption rate is largely fortuitous, but probably carries the implication that, in a furnace which has acquired an equilibrium coating of molten slag, the distribution is likely to be more uniform than for the case of partly slagged and partly clean surfaces.

Some improvement has been made in field use of the rare-metal high-velocity thermocouple, notably by running frequent calibration checks, in a portable electric furnace, against a newly made chromel-alumel couple serving as the standard. By this means, any progressive contamination error of the rare-metal couple can be detected and appropriate corrections made to the traverse readings obtained. When the accumulated error reaches a prescribed limit of 40 deg, it is customary to crop off several inches of the affected wires and to weld a new junction in the uncontaminated portion, which then will serve for several days of active testing, with calibration checks again being made as described.

Furnace-tube thermocouples were placed in five tubes, located at the center of each side wall and at the center and quarter-points of the front wall. In each tube, one thermocouple was placed at elevations 5, 15, and 25 ft above the furnace floor. Six additional thermocouples were located at intermediate elevations of the left side-wall and left front-wall tubes. In Fig. 7 of the paper, two sets of readings from all thermocouples are shown by the plotted points.

These measurements were taken and are submitted more for their collateral and qualitative interest than as absolute checks on the over-all furnace test. It is to be hoped that means will eventually be developed for more accurate quantitative appraisal of thermal distribution.

Effective thickness of slag on the furnace wall tubes is difficult to gage during operation, partly because of the limited number of inspection doors available for observation, and partly because of the variation in thickness around or along a single tube. This has been observed during shutdown to be from $^1/_8$ to $^3/_4$ in. Slag thickness on the thermal probe when withdrawn from the furnace, as shown in Fig. 7, was found to be quite uniform along the length of the probe and varied from $^1/_8$ to $^1/_4$ in. of fused slag over a layer of granular ash approximately $^1/_{32}$ in. thick.

TABLE 1 ANALYSIS OF COAL-ASH SAMPLE

	Coal ash, per cent	Ash from superheater tubes (sample F), per cent
Silica, SiO_2	38.8	42.9
Total iron, as Fe_2O_3	20.0	13.6
Alumina, Al_2O_3	25.3	28.5
Titanium oxide, TiO_2	1.1	1.4
Calcium oxide, CaO	6.7	5.2
Magnesium oxide, MgO	0.8	Trace
Total sulphur, as SO_3	4.3	0.5
Undetermined	3.0	7.9
	100.0	100.0

Complete analysis of the coal-ash sample, shown in Fig. 14, has been made in response to Mr. Reid's inquiry and is given in Table 1 of this closure. Unfortunately, none of the slag samples is now available for similar analysis, excepting that of sample F which is also shown in the table.

Summary of Reports on Physical Conditions Reported by Eight Operating Companies

By A. R. MUMFORD,[1] NEW YORK, N. Y.

IN order to narrow the field of its investigations, the Research Committee on Furnace Performance Factors solicited and obtained physical data on the furnaces of representative boiler units from eight operating companies. The data cover twenty-three units, representing about forty boilers. The capacity of these units ranges from 250,000 lb per hr to 1,000,000 lb per hr at pressures from 275 psi to 2500 psi, and total temperatures from 700 F to 960 F. These data will be analyzed by the committee, and promising lines of investigation explored in an attempt to evaluate the importance of the geometry of a furnace as a factor in its performance. The investigation will be broadened to include additional units as the line of investigation becomes sharper.

In this committee summary, where reference to a company is made, it will be by a key numeral. Similarly, units are designated by letters following the numerals. Some of the data submitted to the Committee will not be available for general distribution.

Results of Preliminary Analyses of Data

In the preliminary analyses made in the short time the data have been available, some comparisons offer points of interest. For instance, the length of the path of the flame before making contact with the convection surface at the point of discharge from the furnace varies from 108 ft in unit 7C to 33 ft in unit 8A. This length may need some more careful definition than is given it at present because of the presence, in some furnace designs, of isolated screens of widely spaced tubes which, while having more convection heat absorption than waterwall tubes, do not have as large a convective proportion as does the surface usually referred to as the boiler. At the higher pressures, these isolated screens may, with the cooling surfaces of the walls, constitute the entire evaporative surface. If sizable volumes are available for further combustion after the gases and products of combustion pass through such screens, there is some doubt as to whether or not such screens properly constitute a furnace boundary.

In the instances considered in the summary, the entrance to the main evaporative section, or, at high pressures, the entrance to the last screen before the convection superheater has been considered a boundary of the furnace. In setting up a comparison of the several furnaces, the ratio of the bounding-surface area of a sphere to its volume was considered as unity. The surface of a sphere of equal volume was computed for each furnace, and the ratio of the actual surface to this minimum enclosing surface was computed as the spherical ratio. The larger this ratio is the less the cross-sectional area of the furnace and the greater its length in the direction of flame travel. Such a factor as the suggested spherical ratio may have significance when considering the advisability of cooling the ash carried in suspension in the products of combustion below the temperature at which it is plastic and adheres to convective evaporating or superheating surface. For the units reported the spherical ratio varied from 0.765 in unit 5A to 3.263 in unit 4C. A value below unity is obviously impossible if the furnace is completely water-cooled and is possible only when exposed refractory is present. When the spherical ratio is plotted against the reported length of flame travel, a straight line can be drawn through the points with a slope showing that doubling the spherical ratio approximately triples the flame travel. Such a slope agrees with one derived from arbitrary selections of cross sections and lengths. A high spherical ratio should give more complete burning out of solid carbon and less trouble from slagging over of the free areas in convective zones, other factors being equal.

Sufficient time has not been available to study the reported conditions with particular reference to the physical properties of the ash, which, of course, varies with the different units and with time. If it is possible, later, to compare furnaces of different spherical ratios when fired with coals having ash with the same physical characteristics, it may be feasible to relate the necessary spherical ratio to the physical properties of the ash of the available coal.

A small number of the units reported data on the amounts of steam used for blowing ash from the heat-absorbing surfaces. When this amount of steam, computed on the basis of the amount of fuel burned, was plotted against the liquid temperature of the ash, a fair degree of proportionality was found except in the case of one unit which was far out of line. This unit was the furnace of a mercury boiler and was, of course, not comparable to the steam boilers because of the temperature of the heat-absorbing surfaces. When the units were examined with respect to the spherical ratio and the steam used for blowing, it was found that the steam used was proportional to the spherical ratio in company 5, which also reported only minor variation in the ash-softening, melting, and liquid temperatures of the ash. The proportion was not evident in the data reported by company 8 which used air as well as steam for blowing and no factor was available to put the two fluids on a common basis.

Flame Temperatures

At this time, data on flame temperatures along the path of travel were available from only one company for two units, 7A and 7C. Unit 7A showed a smooth curve, convex downward, when plotted against surface passed over or flame travel. However, unit 7C showed an equally smooth curve, but it was convex upward. Both units were of the same capacity with the same furnace volume. Unit 7A had a spherical ratio of 1.393 against 2.669 for unit 7C. Unit 7A operated at 425 psi and 850 F, while 7C operated at 1350 psi and 925 F. If this difference in the characteristic of the temperature versus surface passed over is confirmed by other examples, the reason for it will be an interesting and important investigation. If, in a furnace having a convex upward curve, we can control the curvature, we should

[1] Chairman, Special Research Committee on Furnace Performance Factors. Combustion Engineering Company, New York, N. Y. Fellow A.S.M.E.

Contributed by Special Research Committee on Furnace Performance Factors with the co-operation of the Fuels, Power, and Heat-Transfer Divisions and presented at the Annual Meeting, New York, N. Y., Nov. 29–Dec. 3, 1943, of The American Society of Mechanical Engineers.

Note: Statements and opinions advanced in papers are to be understood as individual expressions of their authors and not those of the Society.

be able to deposit ash in a nonplastic form where we require it.

An interesting sidelight on design features was indicated when the Btu absorbed per square foot of free area at the entrance to the superheater was plotted against the Btu fired divided by the same divisor. Although the data covered quite a range of temperatures and pressures, with consequent variation in the proportion of heat for superheating, the Btu fired was to proportional the Btu absorbed with little scatter of the points. It would seem, therefore, that the furnace was expected to properly prepare the products of combustion for passage through the superheater, and did.

A majority of the units reported have apparently adopted the practice of reducing sharply or completely dropping the load at regular intervals presumably as a deslagging operation. In many cases this was a daily occurrence.

Initial Stages of Operation

Each company was asked to report in a general way on any difficulties they experienced during the initial stages of operation, and the steps taken to correct the difficulties. In the following paragraphs some of these reports are high-spotted:

Company 1 reported that no hand-cleaning of furnaces was required, and that the only tube failures experienced were due to construction faults rather than design faults. Some minor baffle changes were required to reduce the relative amount of fuel fired in the radiant-superheater furnace.

Company 2 reported that steam-temperature fluctuations on swinging load were minimized by using steam jets to clean evaporating-wall surface on rising superheat and radiant-superheater walls on falling superheat.

Company 3 reported that the service period of stoker-fired boilers was increased two to two and a half times and hand-lancing during service hours eliminated by coal-washing at the mine. This company found that it could eliminate hand-lancing and reduce requirements for mechanical blowing in pulverized-fuel furnaces by proper spacing of convection surfaces and control of heat-release rates.

Company 4 reported one unit almost entirely self-cleaning, and one which had a temperature versus surface-passed-over characteristic which caused the deposition of ash in an unexpected inaccessible place.

Company 5 reported no difficulties with coals having ash-softening temperatures of 2500 F or more, but at high steaming rates plugging began with coals having an ash-fusion temperature of 2300 F. By careful control of secondary air, this company reported its ability to vary the effectiveness with which the furnace volume was used.

Company 6 reported that the only tube failure was caused by steam cutting, and that no measurable tube wastage has occurred. Some erosion which was experienced in the upper portion of the primary furnace was attributed to local zones of high heat release.

Company 7 reported successful cracking-off of furnace slag by dropping load. This company found it necessary to keep the furnace slag at a minimum to avoid high superheat. Hand-lancing is required at boiler and superheater entrance.

Company 8 reported performance may be good or bad on identical units in different plants, depending upon fuel and operating conditions. Variation in ash-fusion temperature did not seriously affect slag-tapping but unbalanced the superheat characteristic of the unit, because low fusion temperatures thinned down the deposit on evaporative walls and increased furnace heat transmission.

This summary and preliminary analysis should not be closed without asking for opinions and suggestions from those who have read the reports and summary. The committee is arranging for co-operative work on the physical properties of ash and on the development of instruments for making furnace measurements. The committee hopes to obtain more data from additional companies.

Furnace Design and Development of Steam-Generating Units Burning Central Illinois Coal

By JOHN R. MICHEL,[1] CHICAGO, ILL.

IN 1929 a paper was presented at the Third National Fuels meeting held in Philadelphia on the subject "Effect of Fouling on Boiler Efficiency."[2] In that paper the difficulties experienced in endeavoring to secure designed capacity and efficiency from the fuel-burning and steam-generating equipment installed at Crawford Station were discussed. The paper is cited and remarks relative to stoker-fired installations are made to emphasize the fact that problems pertaining to furnace performance and slag fouling of heat-absorbing surfaces are not incident to pulverized-fuel firing but have been matters of serious concern, especially to those burning low-grade fuels, for many years.

At Crawford Station slag fouling of steam-generating tube banks and plugging of superheaters forced periodic water lancing of these sections so that gas lanes could be kept open and reasonable ratings and operating efficiencies maintained. Notwithstanding the adoption of this procedure to augment the cleaning accomplished by regular operation of mechanical blowing equipment, it was necessary to remove the boilers from service at 35-day intervals for hand rodding and repairs.

Since radical changes in design necessary to overcome slag-fouling difficulties could not be accomplished economically in this installation an improvement in the fuel supplied was investigated. Extensive tests indicated that the use of washed Central Illinois coal would permit increased boiler service periods and improve boiler performance. Evaluation of increased station capacity and other resultant advantages justified installation of a washer at the mine for preparation of Crawford Station's coal. At present with the station burning washed Central Illinois coal and with mass blowers installed to remove the slag which now deposits, 75-to-80-day boiler-service periods are attained with no hand cleaning or water lancing necessary during service periods.

During the later part of the foregoing developments in 1937, a 30,000-kw topping unit was installed in another Chicago station. The boiler complement of this unit consists of two 375,000-lb per hr, 1275-psi, 910 F, pulverized-fuel-fired steam-generating units, data on which are submitted on data sheets 1, 2, 3, and 4.

It will be noted from the proximate fuel analyses and ash characteristics given that all pulverized-fuel installations reported on use normal Central Illinois coal. Although this coal has many unfavorable characteristics it is not advisable to provide a better grade of fuel for Chicago stations because of economic considerations. At Crawford Station, however, furnace conditions and resultant steam-generator performance made necessary the use of washed Central Illinois coal in order to obtain designed station capacity. In later pulverized-coal installations, provisions made in furnace design overcame slagging difficulties to the extent that normal Central Illinois coal could be satisfactorily used.

Central Illinois coal has a few characteristics which adapt it to being burned in pulverized form. It is a free-burning coal, high in volatile, and as a result ignites easily and burns thoroughly with little combustible remaining in the fly ash or furnace slag. Likewise, its low ash-fusion temperature permits ready tapping in installations with wet-bottom furnaces. Objectionable features arising from its high moisture content, high a h content, low ash-fusion temperature, high sulphur content, and low grindability far outweigh any advantages. Low ash-fusion temperature coupled with high ash content are reasons for severe slagging of heat-absorbing surfaces. The slagging difficulty is accentuated when this fuel is burned in pulverized form due to a fundamental weakness of pulverized-fuel firing, that is, in the conventional pulverized-fuel-fired installations nearly 50 per cent of the ash in the coal passes from the furnace as fly ash.

In designing the previously mentioned 375,000-lb per hr pulverized-fuel-fired steam-generating units, slag-fouling problems were recognized as being outstanding among the difficulties to be overcome in the design of the furnaces and the units. In this installation slag screens were provided between the primary and secondary furnaces, wide tube spacings were provided in the steam-generating banks of tubes, telescoping deslagging units were provided in the steam-generating banks and superheaters, and provision for hand-lancing the steam-generating banks and lower superheaters were made in addition to the usual complement of mechanical blowers for the remainder of the unit.

In operation of this installation a constant cleaning program was found necessary to maintain the boiler units in proper operating condition. The full time of three boiler cleaners on each watch is required; that of two men, one for each boiler, is required for air-lancing the steam-generating tube banks and that of the third man is required for operation of the mechanical blowing equipment on both boilers and intermittent air-lancing of the superheaters. With this arrangement six months' operation of the boiler units is obtained before outage for regular inspection, maintenance, and cleaning is necessary.

With the foregoing experience on the 375,000-lb per hr units, several requirements were stipulated in the design of three 425,000-lb per hr, 1325-psi, 935 F, steam-generating units for a 50,000-kw topping unit to be installed in another Chicago station. Among these were lower unit furnace heat release, wide spacing of steam-generating tubes and consequent lower entering-gas velocity to the tube banks, wide spacing of superheater tubes with entering-gas temperatures of approximately 1900 F, and provision in the design for hand-lancing doors so disposed that all heat-absorbing surfaces of the boiler unit could be cleaned while in service.

To overcome difficulties experienced with telescoping deslagging units used in the previous installation, mass blowers were applied where possible and rotating retractable elements were used above the steam-generating tube bank and in the superheater. Operation of these boiler units since January, 1942, has indicated that steps taken to eliminate difficulties due to slag fouling of heat-absorbing surfaces were ample, since operation of the mechanical

[1] Mechanical Assistant to Superintendent, Generating Stations, Commonwealth Edison Co. Mem. A.S.M.E.

[2] *Black Diamond*, vol. 83, no. 18, November 2, 1929, pages 12–13.

Contributed by Special Research Committee on Furnace Performance Factors with the co-operation of the Fuels, Power, and Heat-Transfer Divisions and presented at the Annual Meeting, New York, N. Y., Nov. 29–Dec. 3, 1943, of THE AMERICAN SOCIETY OF MECHANICAL ENGINEERS.

NOTE: Statements and opinions advanced in papers are to be understood as individual expressions of their authors and not those of the Society.

blowers twice daily maintains the boiler units in clean operating condition.

Data relative to this installation, comparable to that given for the 375,000 lb per hr unit installed in 1937, are given on data sheets 1A, 2A, 3A, and 4A.

With some experience from the early operation of the foregoing 425,000-lb per hr units, the design of two 750,000-lb per hr, 1325-psi, 935 F, steam-generating units for a 147,000-kw condensing turbine generator unit was developed. Similar requirements relative to furnace heat release, tube spacings, entering gas temperatures and gas velocities, to that of the 425,000-lb per hr units installed in 1941 were stipulated. In the 750,000-lb per hr installations, however, tube banks of the steam-generating sections and superheaters were so disposed that only retractible mass blowers were necessary for the mechanical blower installation.

Although the 750,000-lb per hr units have not been in regular service supplying steam to the unit for which they were designed, they have been used to supply steam to other 1200-psi, 900 F equipment in the station. Part of this operation was with full designed heat release in their furnaces, full steam flow not being attained because feedwater at design temperature was not available from installed equipment. Indications from this operation are that no hand lancing will be required in their regular operation.

Similar data to that given for other units mentioned in this paper are shown for the 750,000-lb per hr units on data sheets 1b, 2b, 3b, and 4b.

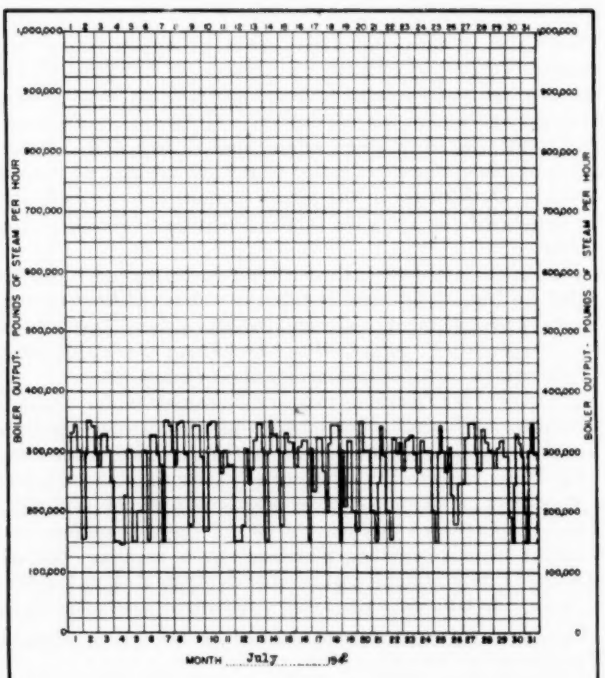
The furnace designs developed in the installations discussed have resulted mainly from an endeavor to overcome slagging difficulties associated with the use of Central Illinois coal in high-capacity installations. The fundamental governing factors in attaining installations which perform satisfactorily with this fuel were low furnace heat release, relatively low entering-gas velocities to convection tube banks, furnace gas temperature below the softening temperature of the ash where gases enter the convection banks, proper disposal of heat-absorbing surfaces to allow adequate installation of mechanical blowing equipment, and provision of hand-lancing doors so arranged that all heat-absorbing surfaces can be manually cleaned in the event of failure of the mechanical blowing equipment.

The foregoing design provisions necessarily require a steam-generating installation that is somewhat higher in first cost. Experience, however, has proved these provisions necessary in pulverized-fuel installations burning Central Illinois coal. Until new methods of firing or methods of slag control are developed, which definitely are proved to be effective in avoiding slagging difficulties, the foregoing principles as applied to furnace and unit design should be adhered to, especially in installations burning Central Illinois coal.

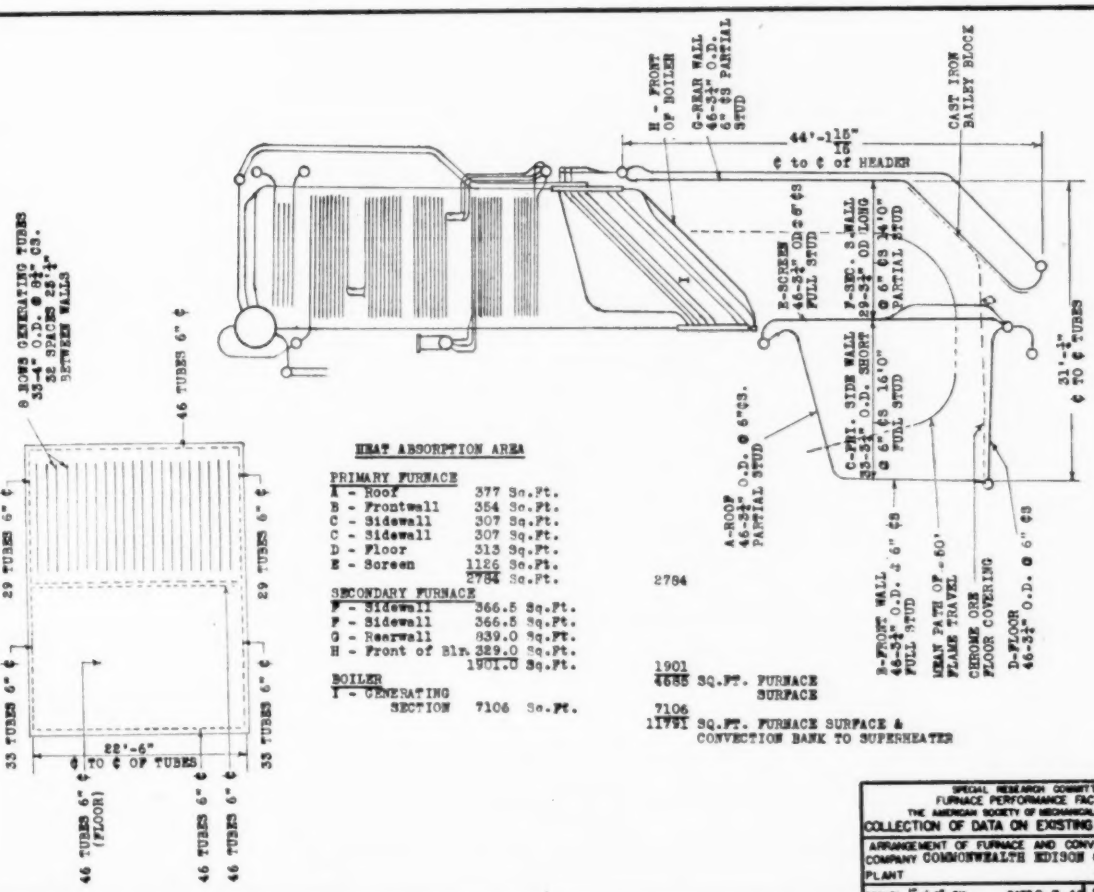
DESCRIPTION OF UNIT					
BUILDER	BABCOCK & WILCOX			YEAR INSTALLED	1937
BOILER TYPE	SECTIONAL WATER TUBE		ASH REMOVAL	SLAG TAP	
PULVERIZER	HARDINGE	FIRING	DIRECT	BURNER	MULTIPLE INTERCURE
TYPICAL FUEL					
KIND	BITUMINOUS	DISTRICT	CENTRAL ILL.	SEAM	#6 CHRISTIAN COUNTY
PROXIMATE ANALYSIS			**ASH CHARACTERISTICS**		
VOLATILE MATTER	34.78 %		INITIAL DEFORMATION	2266 F	
FIXED CARBON	37.81 %		SOFTENING	2334 F	
ASH	13.51 %		LIQUID	2390 F	
TOTAL MOISTURE	13.90 %		SULPHUR (DRY BASIS) (Coal)	5.48 %	
HEAT VALUE PER LB	10164 BTU		GRINDABILITY (Coal)	61 %	
PERFORMANCE					
BOILER OUTPUT	360,000 LB/HR		1280 LB/SQ IN	920 F	
FUEL BURNED	49,900 LB/HR		491,518,000 BTU/HR		
COMBUSTION AIR TEMP	550 F		FINENESS THRU 200 MESH	90 %	
FUEL BURNING RATE					
FURNACE SURFACE		4685 SQ FT	104,910 BTU/HR/SQ FT		
FURNACE SURFACE & CONVECTION BANK TO SUPERHEATER		11791 SQ FT	41,690 BTU/HR/SQ FT		
FURNACE VOLUME		15870 CU FT	30,970 BTU/HR/CU FT		
FURNACE WIDTH		23.5 FT	20,915,530 BTU/HR/FT		
FREE GAS AREA	CONVECTION BANK ENTRANCE	300 SQ FT	1,638,360 BTU/HR/SQ FT		
	CONVECTION BANK CLOSELY SPACED TUBES	215 SQ FT	2,286,120 BTU/HR/SQ FT		
	SUPERHEATER ENTRANCE	103 SQ FT	4,771,990 BTU/HR/SQ FT		
	SUPERHEATER CLOSELY SPACED TUBES	64 SQ FT	7,679,920 BTU/HR/SQ FT		

REMARKS:

SPECIAL RESEARCH COMMITTEE
FURNACE PERFORMANCE FACTORS
THE AMERICAN SOCIETY OF MECHANICAL ENGINEERS
COLLECTION OF DATA ON EXISTING INSTALLATIONS
DESCRIPTION AND PERFORMANCE
COMPANY COMMONWEALTH EDISON COMPANY
PLANT UNIT NO.
BY F.A. DATE 9-3-43 SHEET NO. 1



SPECIAL RESEARCH COMMITTEE
FURNACE PERFORMANCE FACTORS
THE AMERICAN SOCIETY OF MECHANICAL ENGINEERS
COLLECTION OF DATA ON EXISTING INSTALLATIONS
TYPICAL LOAD CURVE
COMPANY Commonwealth Edison Co.,
PLANT
BY F.A. DATE 7-28-43 SHEET NO. 3



HEAT ABSORPTION AREA

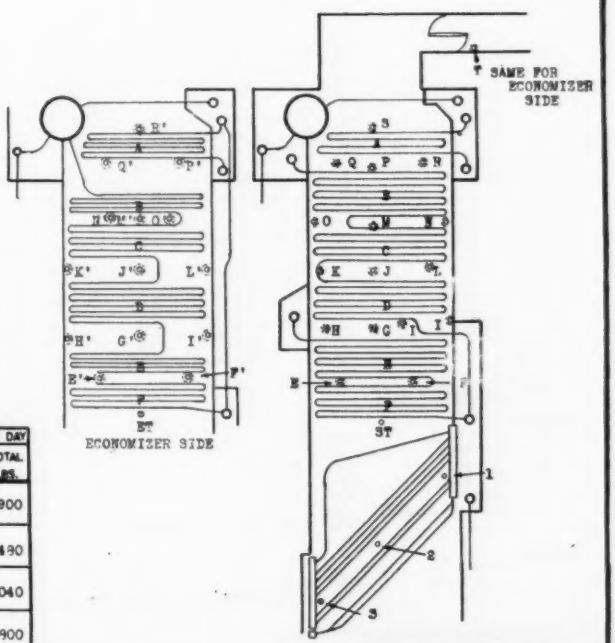
PRIMARY FURNACE		
A - Roof	377	Sq.Ft.
B - Frontwall	354	Sq.Ft.
C - Sidewall	307	Sq.Ft.
C - Sidewall	307	Sq.Ft.
D - Floor	313	Sq.Ft.
E - Screen	1126	Sq.Ft.
	2784	Sq.Ft.
SECONDARY FURNACE		
F - Sidewall	366.5	Sq.Ft.
F - Sidewall	366.5	Sq.Ft.
G - Rearwall	939.0	Sq.Ft.
H - Front of Blr.	329.0	Sq.Ft.
	1901.0	Sq.Ft.
BOILER		
I - GENERATING SECTION	7106	Sq.Ft.

2784

1901
4685 SQ.FT. FURNACE SURFACE

7106
11791 SQ.FT. FURNACE SURFACE & CONVECTION BANK TO SUPERHEATER

SPECIAL RESEARCH COMMITTEE
FURNACE PERFORMANCE FACTORS
THE AMERICAN SOCIETY OF MECHANICAL ENGINEERS
COLLECTION OF DATA ON EXISTING INSTALLATIONS
ARRANGEMENT OF FURNACE AND CONVECTION SURFACE
COMPANY COMMONWEALTH EDISON COMPANY
PLANT UNIT NO.
SCALE: 1/8"-0" BY DATE 9-3-43 SHEET NO. 3



Hand lancing 30 man hours per day
One man used during blowing operation
Six man hours per day

BLOWER NO.	TYPE	BLOWING ARC DEGREES	STEAM AT SOOT BLOWER PRESS. #/□"	STEAM AT SOOT HEAD TEMP. F.	NO. OF BLOWS PER DAY	REVOLUTIONS PER BLOW	TIME STEAM FLOWS PER BLOWER	STEAM DURING BLOW LBS. PER MIN.	STEAM DURING BLOW TOTAL LBS.	STEAM PER DAY EACH BLOWER LBS.	STEAM PER DAY TOTAL LBS.
E,I,L, E,F	Rotating	300	160	540	3	3	2'10"	120	260	780	3900
F,G,H, J,M,P, Q,R,S	"	360	160	540	3	3	2'00"	120	240	720	6480
F,J, M,N,O, Q,S	"	360	160	540	3	3	2'00"	120	240	720	5040
J,K, N,O,	"	210	160	540	3	3	1'15"	120	150	450	1900
H,I,K, L,P,	"	210	160	540	3	3	1'15"	120	150	450	2250
T T'	Stationary	360	160	540	3	3	1'00"	120	120	360	720

Amount Used For Heating And Draining Lines (Estimated)

20190
2500
22690

SPECIAL RESEARCH COMMITTEE
FURNACE PERFORMANCE FACTORS
THE AMERICAN SOCIETY OF MECHANICAL ENGINEERS
COLLECTION OF DATA ON EXISTING INSTALLATIONS
CLEANING SCHEDULE
COMPANY COMMONWEALTH EDISON COMPANY
PLANT UNIT NO.
SCALE: 1/8"-0" BY P.A. DATE 9-3-43 SHEET NO. 4

DESCRIPTION OF UNIT					
BUILDER	COMBUSTION ENGINEERING			YEAR INSTALLED	1941
BOILER TYPE	3 DRUM, BENT TUBE		ASH REMOVAL	SLAG TAP	
PULVERIZER	RAYMOND BOWL MILL	FIRING DIRECT		BURNER	TANGENTIAL

TYPICAL FUEL					
KIND	BITUMINOUS	DISTRICT	CENTRAL ILL.	SEAM	#6 CHRISTIAN COUNTY

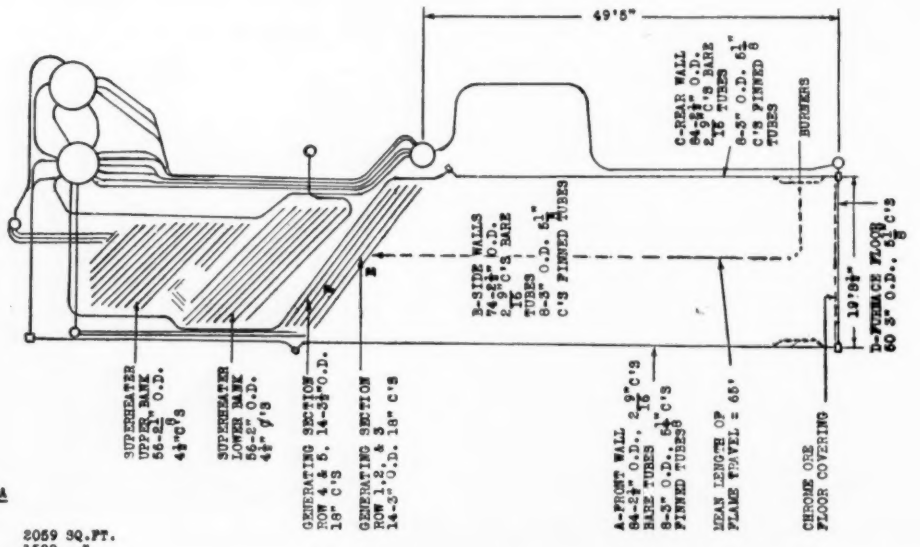
PROXIMATE ANALYSIS		ASH CHARACTERISTICS	
VOLATILE MATTER	34.78 %	INITIAL DEFORMATION	2266 F
FIXED CARBON	37.81 %	SOFTENING	2334 F
ASH	13.51 %	LIQUID	2590 F
TOTAL MOISTURE	13.90 %	SULPHUR (DRY BASIS) (Coal)	5.48 %
HEAT VALUE PER LB	10164 BTU	GRINDABILITY (Coal)	61 %

PERFORMANCE					
BOILER OUTPUT	426,170 LB/HR		1385 LB/SQ IN.		931 F
FUEL BURNED	56,572 LB/HR			584,296,784	BTU/HR
COMBUSTION AIR TEMP	468 F		FINENESS THRU 200 MESH		70.9 %

FUEL BURNING RATE				
FURNACE SURFACE		7595	SQ FT	72,980 BTU/HR/SQ FT
FURNACE SURFACE & CONVECTION BANK TO SUPERHEATER		11330	SQ FT	48,920 BTU/HR/SQ FT
FURNACE VOLUME		24250	CU FT	22,860 BTU/HR/CU FT
FURNACE WIDTH		21.833	FT	25,387,640 BTU/HR/FT
FREE GAS AREA	CONVECTION BANK ENTRANCE	359	SQ FT	1,548,315 BTU/HR/SQ FT
	CONVECTION BANK CLOSELY SPACED TUBES	345	SQ FT	1,602,000 BTU/HR/SQ FT
	SUPERHEATER ENTRANCE	229	SQ FT	2,420,510 BTU/HR/SQ FT
	SUPERHEATER CLOSELY SPACED TUBES	152	SQ FT	3,646,690 BTU/HR/SQ FT

REMARKS:

SPECIAL RESEARCH COMMITTEE
FURNACE PERFORMANCE FACTORS
THE AMERICAN SOCIETY OF MECHANICAL ENGINEERS
COLLECTION OF DATA ON EXISTING INSTALLATIONS
DESCRIPTION AND PERFORMANCE
COMPANY COMMONWEALTH EDISON COMPANY
PLANT UNIT NO.
BY F.A. DATE 9-3-43 SHEET NO. 1a



HEAT ABSORPTION AREA

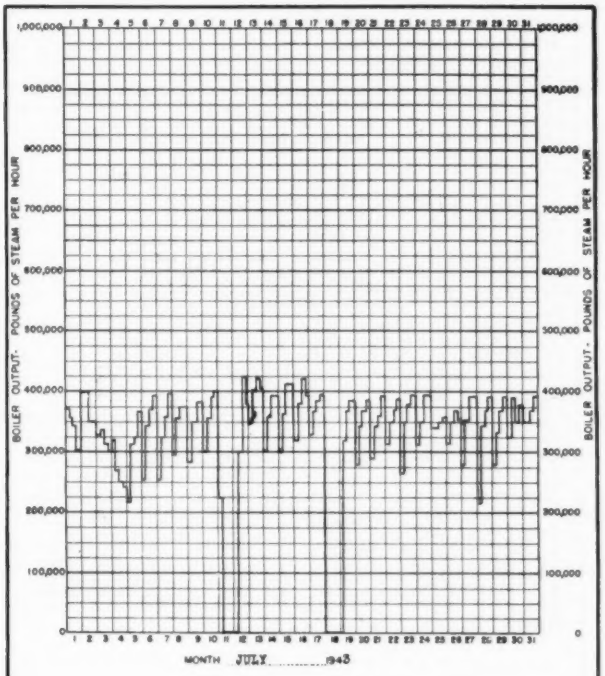
FURNACE

A - FRONT WALL	2059	SQ.FT.
B - SIDE WALL	1599	"
B - SIDE WALL	1599	"
C - REAR WALL	1521	"
D - FLOOR	387	"
E - FRONT OF BOILER	430	"
	7595	SQ.FT. FURNACE SURFACE

BOILER

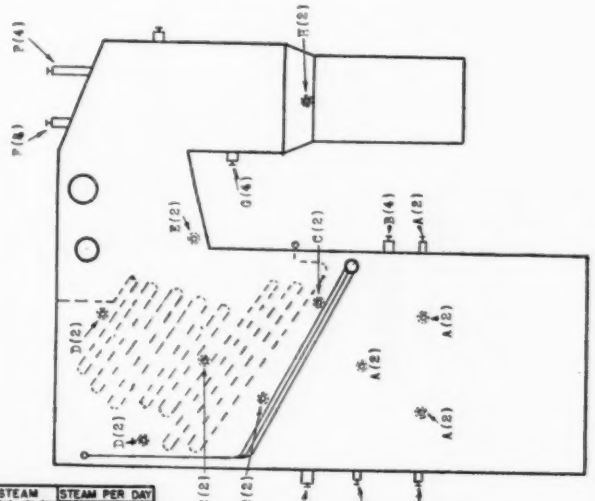
F - GENERATING SECTION	3735	SQ.FT.
	11330	SQ.FT. FURNACE & CONVECTION BANK TO SUPERHEATER

SPECIAL RESEARCH COMMITTEE
FURNACE PERFORMANCE FACTORS
THE AMERICAN SOCIETY OF MECHANICAL ENGINEERS
COLLECTION OF DATA ON EXISTING INSTALLATIONS
ARRANGEMENT OF FURNACE AND CONVECTION SURFACE
COMPANY COMMONWEALTH EDISON COMPANY
PLANT UNIT NO.
SCALE: 1/8"=1'-0" BY DATE 9-3-43 SHEET NO. 2a



SPECIAL RESEARCH COMMITTEE
FURNACE PERFORMANCE FACTORS
THE AMERICAN SOCIETY OF MECHANICAL ENGINEERS
COLLECTION OF DATA ON EXISTING INSTALLATIONS

TYPICAL LOAD CURVE
COMPANY COMMONWEALTH EDISON COMPANY
PLANT UNIT NO.
BY F.A. DATE 9-3-43 SHEET NO. 3A



Figures In Parentheses Refer to Number of Soot Blowers At Location

No hand lancing
Two men used during blowing operations
Nine man hours per day total

* Only blown occasionally

BLOWER NO.	TYPE	BLOWING ARC DEGREES	STEAM AT BLOWER PRESS. #/□"	SOOT HEAD TEMP. F.	NO. OF BLOWS PER DAY	REVOLUTIONS PER BLOW	TIME STEAM FLOWS PER BLOW	STEAM DURING BLOW LBS. PER MIN.	STEAM DURING BLOW TOTAL LBS.	STEAM PER DAY EACH BLOWER LBS.	STEAM PER DAY TOTAL LBS.
A B	Gun Type Rotating Retr.	360 90	400 400	450 450	2 *	1 1	22 sec	348 348	128	256	3072
C	Rotating Retr.	360	135	360	3	110	9 min 14 sec	115	947	2841	17046
D E	Rotating	170 190	100 100	340 340	3 3	2 2	10 sec 10 sec	100 100	17 17	51 51	204 102
F	BBF	360	195	390	*		1 min 30 sec	130			
G	Roteting	360	195	390	*	2	10 sec	130			
H	Strait Line		160	370	*		*	180			

Amount Used For Heating And Drainin Lines (Estimated) 20394 4050

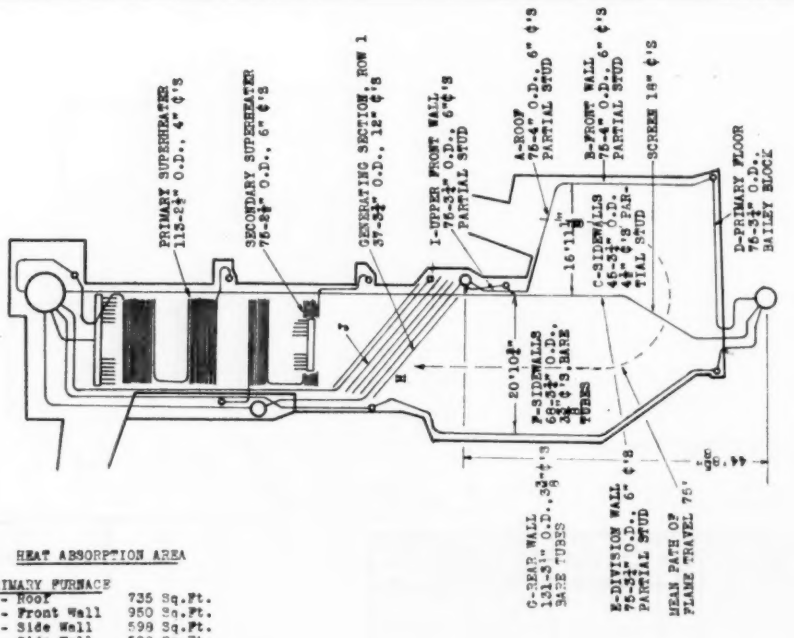
SPECIAL RESEARCH COMMITTEE
FURNACE PERFORMANCE FACTORS
THE AMERICAN SOCIETY OF MECHANICAL ENGINEERS
COLLECTION OF DATA ON EXISTING INSTALLATIONS

CLEANING SCHEDULE
COMPANY COMMONWEALTH EDISON COMPANY
PLANT UNIT NO.
SCALE- 0'-0" BY F.A. DATE 9-3-43 SHEET NO. 4A

DESCRIPTION OF UNIT			
BUILDER BABCOCK & WILCOX			YEAR INSTALLED 1942
BOILER TYPE HIGH HEAD		ASH REMOVAL SLAG TAP	
PULVERIZER RAYMOND BOWL MILL	FIRING DIRECT	BURNER MULTI-CLIP LIFTGUARD	
TYPICAL FUEL			
KIND BITUMINOUS	DISTRICT CENTRAL ILL.	SEAM #6 CHRISTIAN COUNTY	
PROXIMATE ANALYSIS		ASH CHARACTERISTICS	
VOLATILE MATTER	34.78 %	INITIAL DEFORMATION	2266 F
FIXED CARBON	37.81 %	SOFTENING	2334 F
ASH	13.51 %	LIQUID	2390 F
TOTAL MOISTURE	13.90 %	SULPHUR (DRY BASIS) (Coal)	5.48 %
HEAT VALUE PER LB	10164 BTU	GRINDABILITY (Coal)	61 %
PERFORMANCE			
BOILER OUTPUT 762,000 (Equiv.) LB /HR		1808 LB /SQ IN.	903 F
FUEL BURNED 86,075 LB /HR		896,192,100	BTU/HR
COMBUSTION AIR TEMP 410 F		FINENESS THRU 200 MESH	68 %
FUEL BURNING RATE			
FURNACE SURFACE		12035 SQ FT	74,470 BTU/HR /SQ FT
FURNACE SURFACE & CONVECTION BANK TO SUPERHEATER		16989 SQ FT	52,750 BTU/HR /SQ FT
FURNACE VOLUME		46000 CU FT	19,480 BTU/HR /CU FT
FURNACE WIDTH		37.9375 FT	23,622,860 BTU/HR /FT
FREE GAS AREA	CONVECTION BANK ENTRANCE	525 SQ FT	1,707,000 BTU/HR /SQ FT
	CONVECTION BANK CLOSELY SPACED TUBES	480 SQ FT	1,867,100 BTU/HR /SQ FT
	SUPERHEATER ENTRANCE	375 SQ FT	2,389,850 BTU/HR /SQ FT
	SUPERHEATER CLOSELY SPACED TUBES	314 SQ FT	2,884,100 BTU/HR /SQ FT

REMARKS:

SPECIAL RESEARCH COMMITTEE
FURNACE PERFORMANCE FACTORS
THE AMERICAN SOCIETY OF MECHANICAL ENGINEERS
COLLECTION OF DATA ON EXISTING INSTALLATIONS
DESCRIPTION AND PERFORMANCE
COMPANY COMMONWEALTH EDISON COMPANY
PLANT UNIT NO.
BY F.A. DATE 9-3-43 SHEET NO. 1B

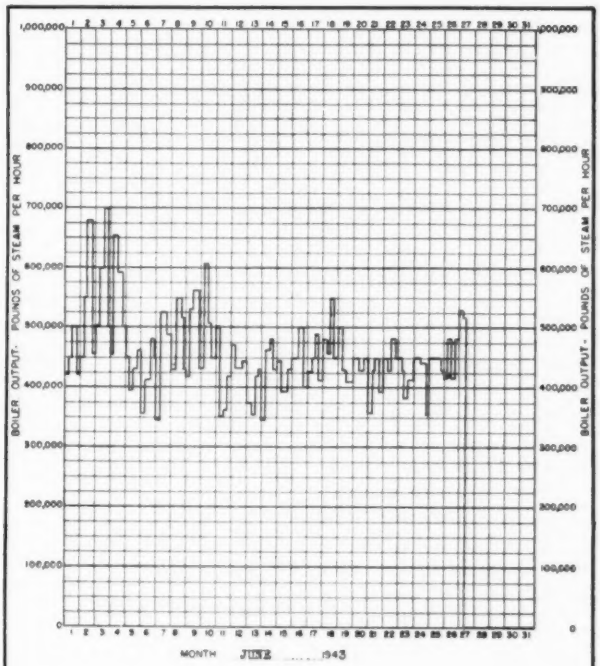


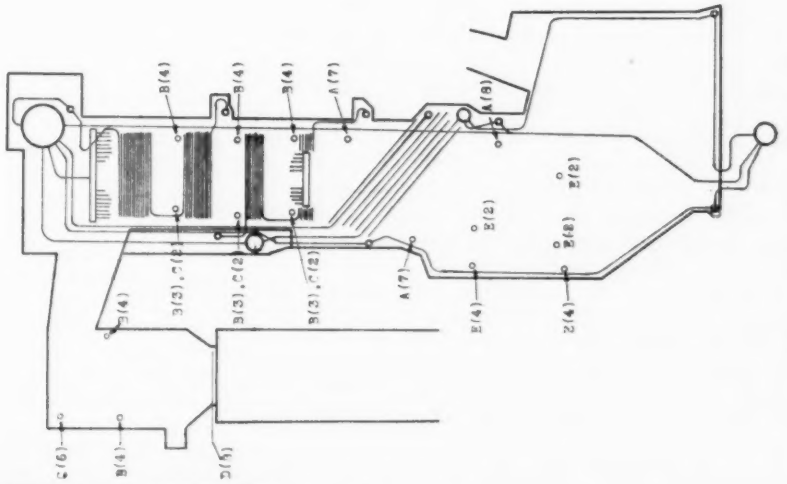
HEAT ABSORPTION AREA

PRIMARY FURNACE		
A - Roof	735 Sq.Ft.	
B - Front Wall	950 Sq.Ft.	
C - Side Wall	599 Sq.Ft.	
C - Side Wall	599 Sq.Ft.	
D - Floor	1530 Sq.Ft.	
E - Division Wall & Screen	2104 Sq.Ft.	
	6515 Sq.Ft.	6515
SECONDARY FURNACE		
F - Side Wall	1021 Sq.Ft.	
F - Side Wall	1021 Sq.Ft.	
G - Rear Wall	2397 Sq.Ft.	
H - Front of Blr.	794 Sq.Ft.	
I - Upper Front Wall	287 Sq.Ft.	
	5520 Sq.Ft.	5520
BOILER		
J - Gen.Section	4954 Sq.Ft.	4954
		16989 Sq.Ft. FURNACE SUP. & CONV. BANK TO SUPHTR.

12035 Sq.Ft. FURNACE SURFACE

SPECIAL RESEARCH COMMITTEE
FURNACE PERFORMANCE FACTORS
THE AMERICAN SOCIETY OF MECHANICAL ENGINEERS
COLLECTION OF DATA ON EXISTING INSTALLATIONS
ARRANGEMENT OF FURNACE AND CONVECTION SURFACE
COMPANY COMMONWEALTH EDISON COMPANY
PLANT UNIT NO.
SCALE: 1/8"-0" BY F.A. DATE 9-3-43 SHEET NO. 2B





Figures In Parentheses Refer to Number Of Soot Blowers At Location

BLOWER NO.	TYPE	BLOWING ARC DEGREES	STEAM AT SOOT BLOWER PRESS #/□"	STEAM AT SOOT BLOWER TEMP. F.	NO. OF BLOWS PER DAY	REVOLUTIONS PER BLOW	TIME STEAM FLOWS PER BLOW	STEAM DURING BLOW LBS. PER MIN.	STEAM DURING BLOW TOTAL LBS.	STEAM PER DAY EACH BLOWER LBS.	STEAM PER DAY TOTAL LBS.
A	Gun Type Rotating Retract.	75	400	445	3	2	38 sec	349	220	660	13960
B	Rotating	95	400	445	3	2	43 sec.	348	250	750	21750
C	Rotating	75	400	445	3	2	36 sec.	348	210	630	7560
D	Strait Line	–	400	445	1		75 sec	348	435	435	3480
E	Gun Type Rotating Retract.	360	400	445	*	2	45 sec				

Amount Used For Heating and Draining Lines (estimated) 46650 7250 53900

No hand lancing
Two men used during blowing operations
Twelve man hours per day

* Only blown occasionally

SPECIAL RESEARCH COMMITTEE
FURNACE PERFORMANCE FACTORS
THE AMERICAN SOCIETY OF MECHANICAL ENGINEERS
COLLECTION OF DATA ON EXISTING INSTALLATIONS
CLEANING SCHEDULE
COMPANY COMMONWEALTH EDISON COMPANY
PLANT UNIT NO.
SCALE: 1/8"=0" BY F.A. DATE 9-3-43 SHEET NO. 4B

Pulverized-Coal-Fired Boiler Furnaces, Public Service Electric and Gas Co., New Jersey

By H. WEISBERG,[1] NEWARK, N. J.

This paper presents statistical information on pulverized-fuel furnaces installed on the Public Service Electric and Gas Company, New Jersey, System. Reasons are given for the selection of the various designs described and actual operating conditions are discussed. It is indicated that there is a need for more rational design data, and a program of research is suggested.

EXPERIENCE with large pulverized-coal-fired steam-generating units on the Public Service Electric and Gas Company System extends over a period of eleven years. That these units represent a distinct advance over boilers of earlier design, which were stoker-fired, is particularly evident under present heavy load conditions with the poorer quality of coal available. The purpose of this paper is to present a description of the furnaces of the pulverized-coal units as well as information on operating conditions and difficulties encountered in operation, for the benefit of the Research Committee on Furnace Performance Factors, designers, and prospective purchasers of this type of equipment.

There are now installed on this System ten units which may be grouped into four principal designs, indicated by Figs. 1 to 4 respectively, and briefly described as follows:

1 A straight tube, cross-drum unit (700 lb, 850 F), Boiler No. 11, Burlington Station, equipped with turbulent-type circular burners firing a water-screened, dry-bottom furnace.

2 Two bent-tube units (1350 lb, 950 F), Boilers Nos. 25 and 26, Essex Station, with a two-stage furnace arrangement, slag-tap ash removal and rectangular burners.

3 Six bent-tube units (1350 lb, 950 F), Boilers Nos. 12, 13, 14, and 15, Burlington Station, and Nos. 51 and 52, Marion Station, similar to design 2, but including refinements developed as a result of operating experience with design 2.

4 A mercury unit (140 lb, 980 F) at Kearny Station having an eight-sided dry-bottom furnace with a rectangular burner in each wall directed toward the center of the furnace.

Data pertinent to comparison of furnace performance are given in Table 1, including detailed description of the units, typical coals burned,[2] fuel-burning rates, and a summary of the cleaning schedules.[3] The fuel-burning rates recorded are based on actual maximum outputs for not less than four hours during a normal operating day rather than on design or rated capacities. Typical load curves are shown in Figs. 5 to 8 inclusive.

[1] Mechanical Engineer, Electric Engineering Department, Public Service Electric and Gas Company. Mem. A.S.M.E.

[2] Additional information on coals burned is included in Appendix A.

[3] For detail cleaning schedule see Appendix B.

Contributed by Special Research Committee on Furnace-Performance Factors with the co-operation of the Fuels, Power, and Heat-Transfer Divisions and presented at the Annual Meeting, New York, N. Y., Nov. 29–Dec. 3, 1943, of THE AMERICAN SOCIETY OF MECHANICAL ENGINEERS.

NOTE: Statements and opinions advanced in papers are to be understood as individual expressions of their authors and not of the Society.

DISCUSSION OF DESIGN FEATURES

The predominating factor in the performance of large pulverized-coal-fired furnaces is the formation of slag and ash on the walls and convection surfaces. The pattern of slag deposits on the walls varies not only with the design of furnace and burners, but with the quality of coal burned, the amount of cleaning which is done, load variations, and time the unit has been in service. Performance of identical furnace arrangements in different plants is good or bad depending upon the fuel burned and the operating conditions. Design is essentially empirical and is usually determined as a result of operating troubles with earlier units. A start on a rational approach for predicting slag accumulation is suggested by Bailey,[4] but much work remains to be done before performance of any new design can be predicted accurately in advance of actual operation.

The original pulverized-coal-fired furnaces in this country were adapted from stoker-fired installations of that time and had practically no water-cooled wall surface. Output was limited by inability of the refractory walls to withstand the high combustion temperatures and by large slag formations on the walls and bottoms of the furnaces, which could not be removed while the boilers were in operation. In connection with the first pulverized-coal unit installed on this System at Burlington Station during 1932, design 1, an attempt was made to water-cool a large portion of the furnace to minimize these difficulties. The unit has given excellent service, but maintenance of such refractory walls as were included is a definite limitation to output and continuous operation. This applies also to the refractory ash hopper. In design 2, which was placed in operation in 1938 and subsequent installations all refractory surface was eliminated.

Prior to the installation of design 2, an investigation of many units in the East and Middle West seemed to indicate that the bent-tube type boiler was less subject to slagging of the convection surfaces than the straight-tube type. For this reason a bent-tube boiler was specified. While it is not at all certain that there has been any less slagging of the convection surfaces in this design than in the original straight-tube boiler, there probably has been no greater tendency to slag. From the standpoint of adequate circulation at the higher pressure (1475 lb on the drum) this type of boiler turned out to be a fortunate choice.

In connection with the latter design, furnace-wall blowers were first developed and have since been applied on all installations. Without some form of regular cleaning, slag gradually accumulates on the walls starting around the burners and building up toward the furnace exit. Gas temperatures leaving the furnace increase, eventually causing slagging of the convection surfaces unless the formation of slag on the walls is checked. With the blowers, the accumulation above the elevation where the slag is fluid may be blown off periodically, resulting in more stable operation. Of course the same effect may be obtained

[4] "Modern Boiler Furnaces," by E. G. Bailey, A.S.M.E. Transactions, vol. 61, October, 1939, pp. 561–576.

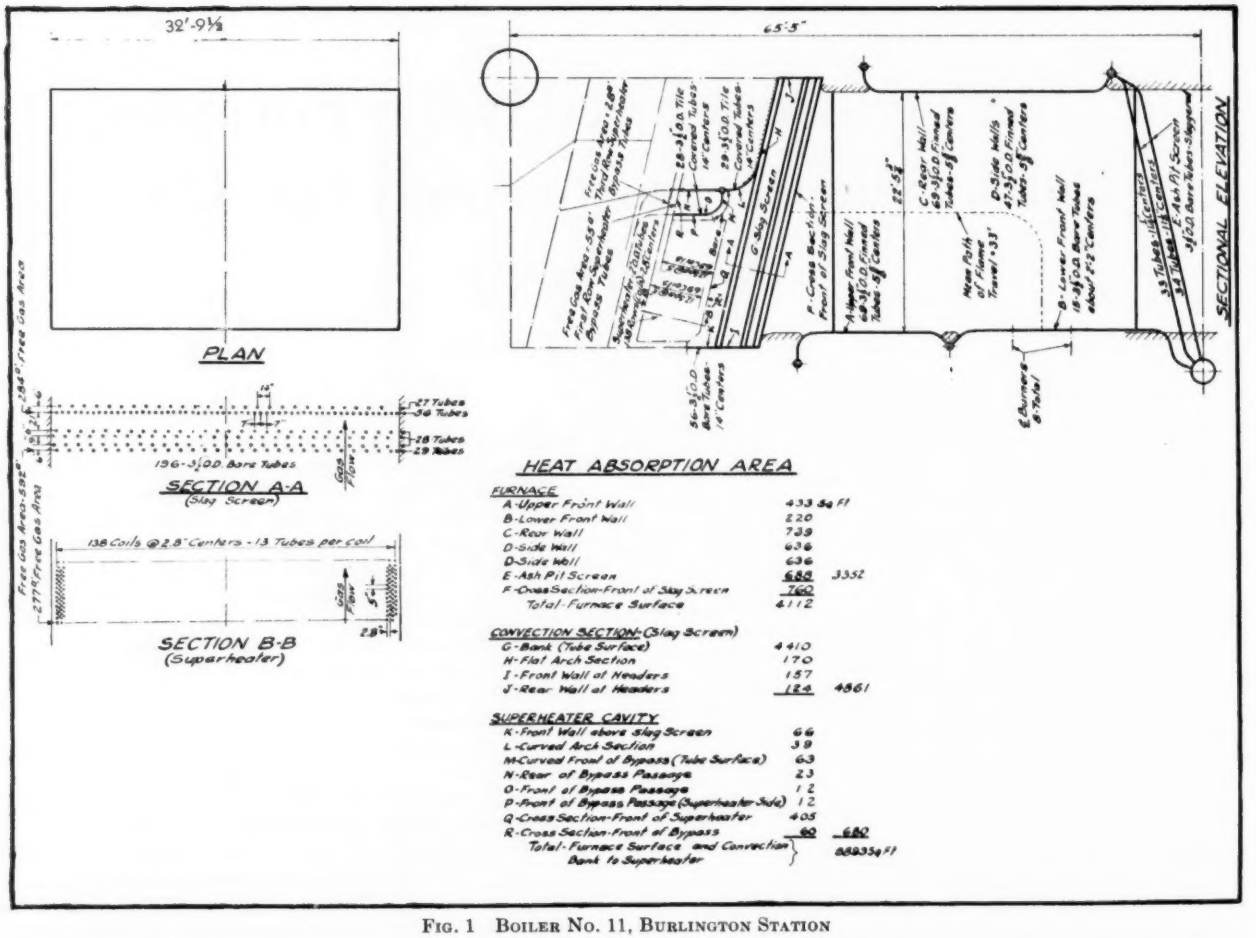


FIG. 1 BOILER NO. 11, BURLINGTON STATION

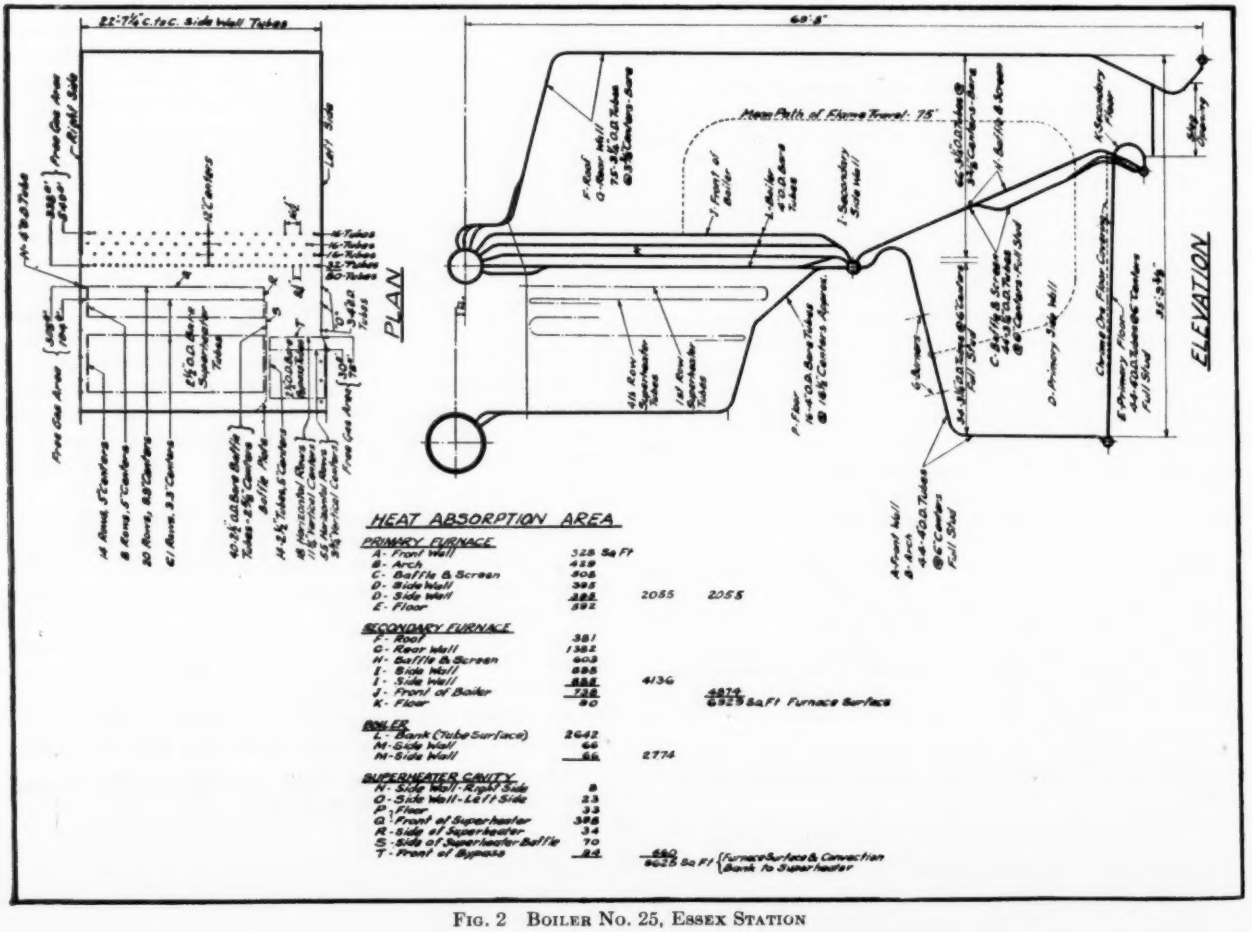


FIG. 2 BOILER NO. 25, ESSEX STATION

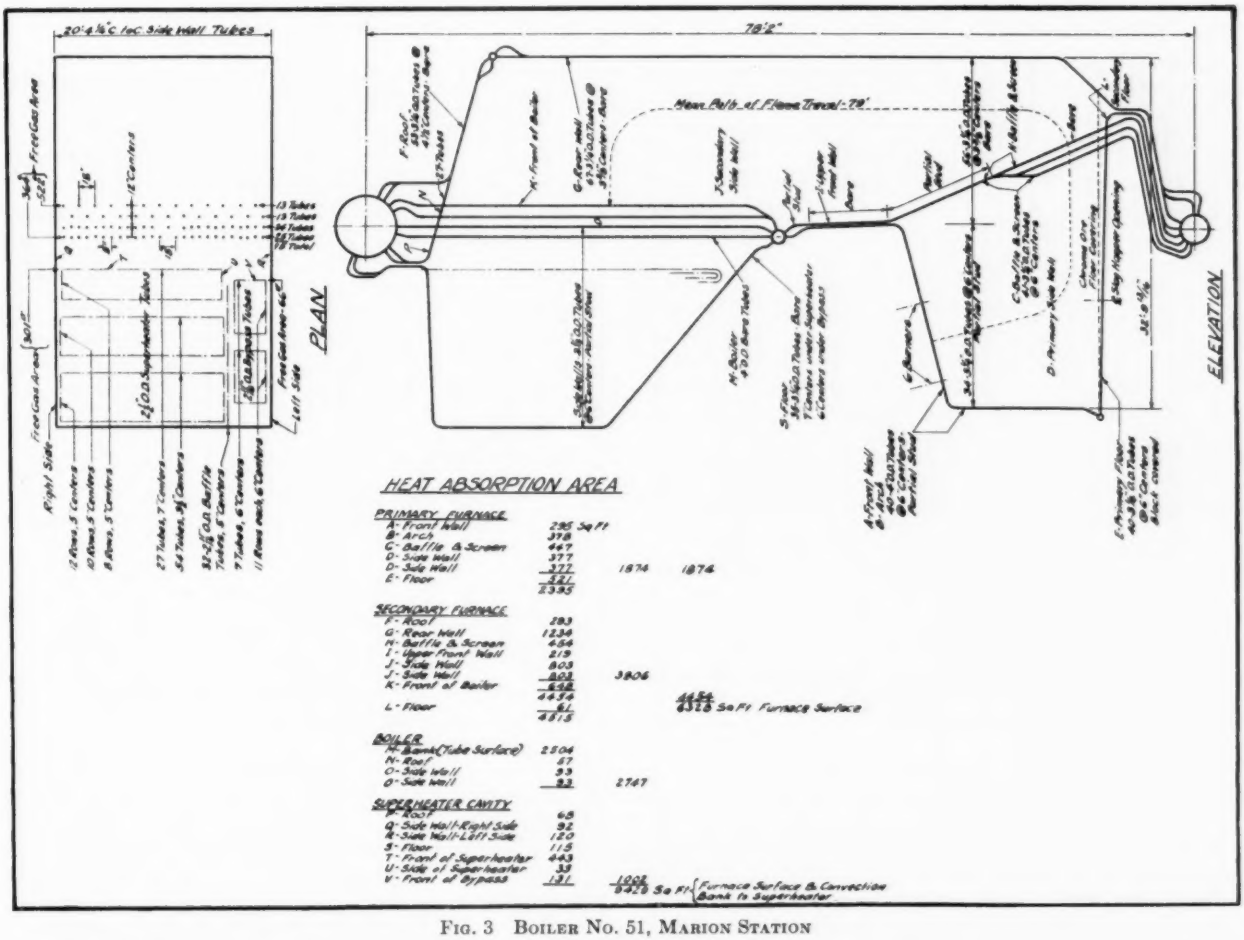


FIG. 3 BOILER NO. 51, MARION STATION

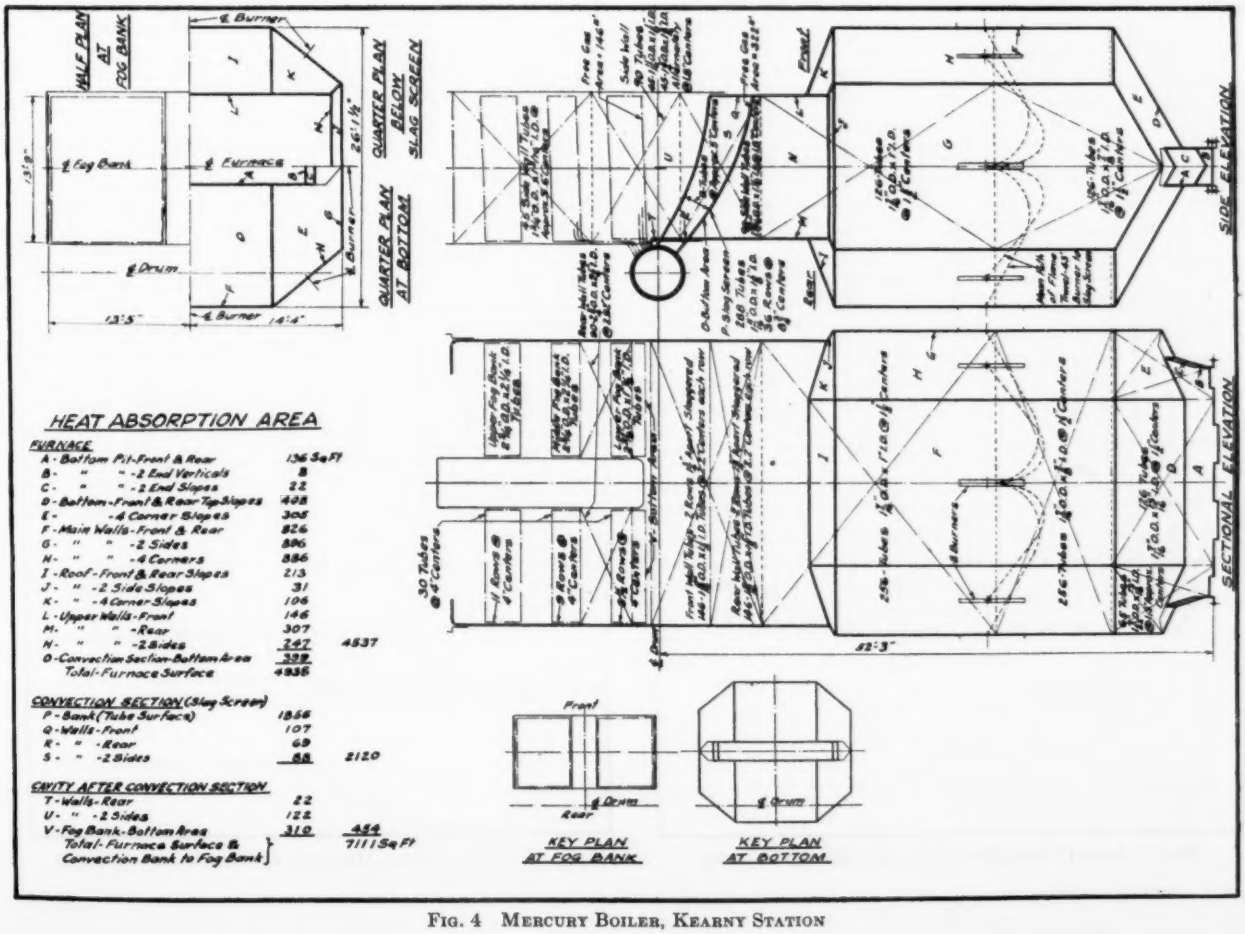


FIG. 4 MERCURY BOILER, KEARNY STATION

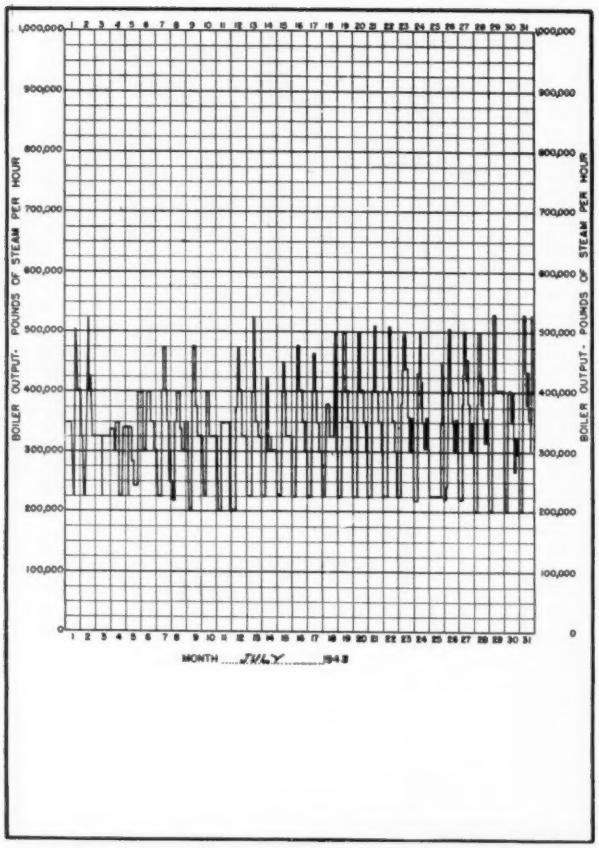


FIG. 5 LOAD CURVE, BOILER NO. 11, BURLINGTON STATION

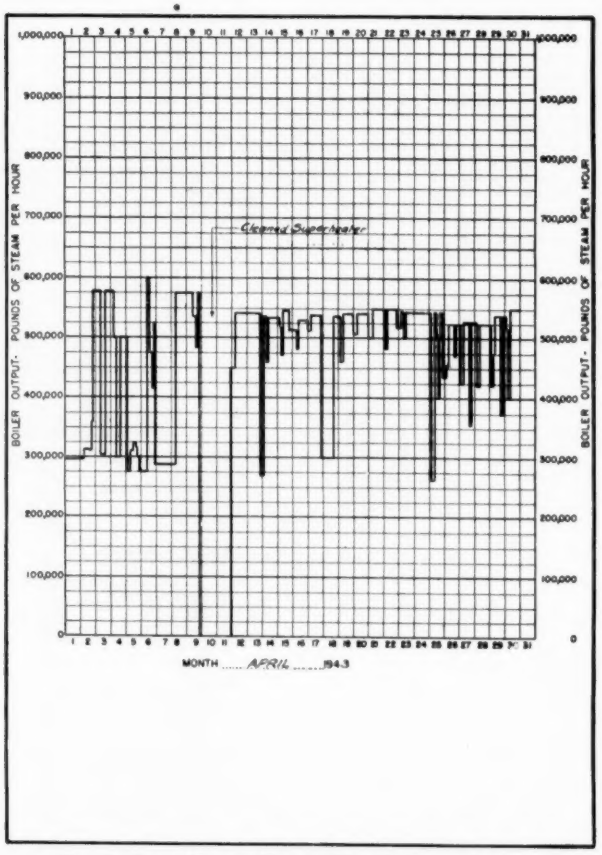


FIG. 6 LOAD CURVE, BOILER NO. 25, ESSEX STATION

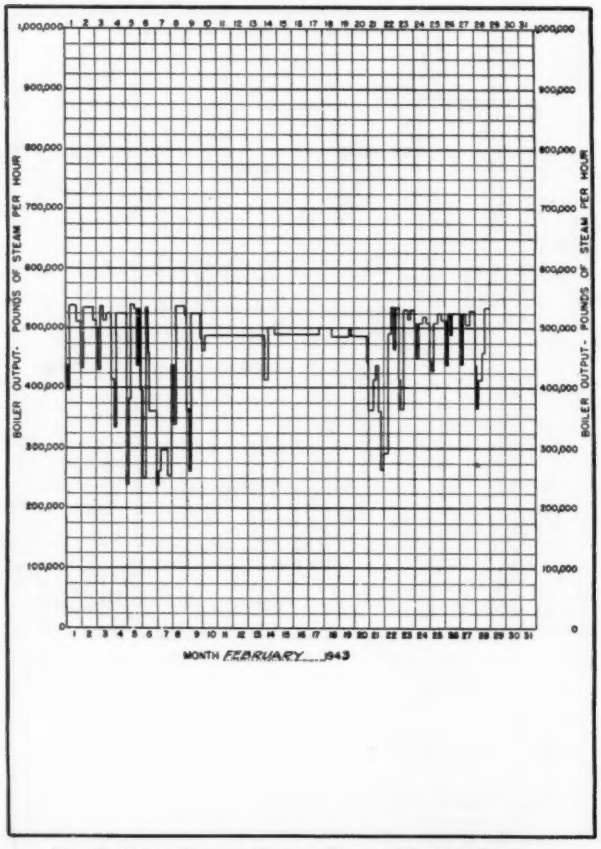


FIG. 7 LOAD CURVE, BOILER NO. 51, MARION STATION

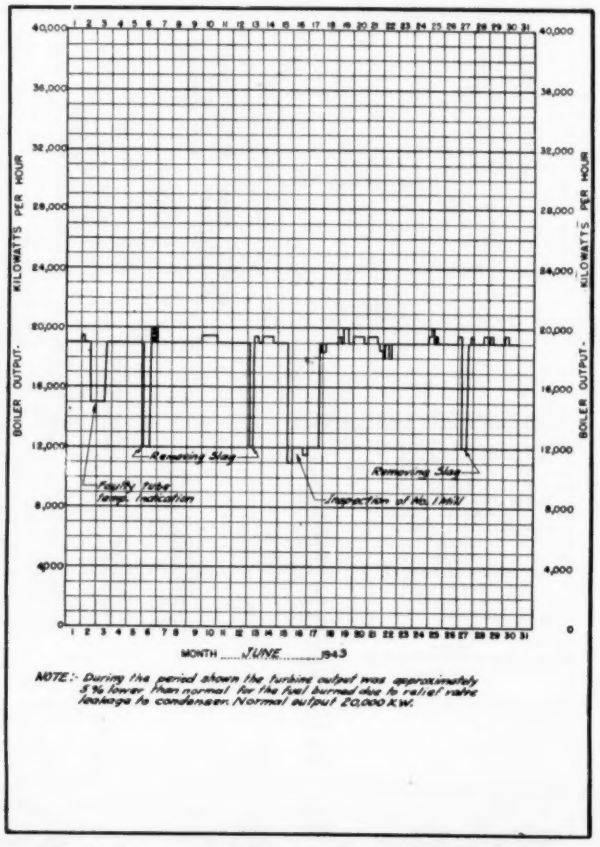


FIG. 8 LOAD CURVE, MERCURY BOILER, KEARNY STATION

by hand-lancing or reducing load regularly so that the slag will chill and drop off. All three methods are used as required, but the wall blowers appear to do the most satisfactory job with a minimum of labor and loss of output.

Wet ash removal was chosen for the boilers of designs 2 and 3 as this arrangement resulted in a more economical layout for the steam conditions, taking into consideration the wide variety of coals to be burned. The variation in fusion temperatures of the coals actually burned in these units at Burlington in one typical month, namely, 2130 F to 2640 F (Table 1) without any appreciable difference in the amount of cleaning required, indicates that this objective has been realized. With the slag-tap type of unit, however, variation in the fusion temperature of the ash changes the thickness of slag on the walls of the hot portions of the furnace and this presents somewhat of a problem with superheat control. Operating experience with the dry-bottom furnaces indicates that this arrangement may also perform satisfactorily from the slagging standpoint with a variety of coals, providing the burners are carefully designed, combustion rates are held down, and the furnace walls are kept free of slag accumulation.

Design 3 is practically the same as design 2, the principal difference being the elimination of the large ash hopper under the secondary furnace. The hopper was found to be a source of air leakage and required extra maintenance on account of heat radiation from the secondary furnace.

The mercury unit furnace, design 4, was dictated by the requirements of the mercury cycle. The temperature of the cooling medium in the lower mercury-cooled walls is in the order of 1100 F, so that the tube wall temperatures run about 1250 F. This condition made a low-heat-release dry-bottom design desirable. Special attention was paid to keeping flame away from the sides of the furnace by placing a burner in each wall directed toward the center of the furnace. Here again blowers were installed to remove slag from the walls. Keeping the furnace walls clean has a double purpose in this unit, as it was found that the insulating effect of the slag on the walls, in addition to causing the convection bank to slag over, actually impaired circulation of the mercury in the wall tubes sufficiently to result in damage to the convection bank which is fed by these tubes.

Comparison of Furnace Surfaces

The fuel-burning rates indicated in Table 1 represent the actual maximum rates at which the units are operated. The limits are steam temperature, mercury-vapor temperature, or just plain conservatism rather than furnace capacity. Ten or fifteen per cent higher output has been obtained on each of the units described, but these rates are not regularly maintained and therefore detailed information on them is not reported. Short duration tests at the higher outputs are meaningless as there is insufficient time for slag conditions to become stabilized. It is suggested that research is needed to determine the limitations of various furnace designs. This may be accomplished by analyzing reports on existing installations, by field tests, or by calculating methods yet to be developed.

Heat released or fuel burned per sq ft of water-cooled furnace surface has been used by some as an indication of the tendency to slag the convection surfaces. It is of interest to note the higher hourly fuel-burning rate per sq ft of radiant water-cooled furnace surface indicated by design 1, Boiler No. 11, Burlington, viz., 159,500 Btu per sq ft as compared to rates in the order of 100,000 Btu per sq ft for the more recent designs. As previously stated neither of these rates represents a furnace limitation. The higher rate is obtained in design 1 without an excessive amount of cleaning and with coal at least as difficult to burn as any fired on the other units. The primary reason for eliminating the brickwork on the more recent designs, which increases the water-cooled surface and reduces the fuel-burning rate per sq ft, was to reduce outage for brickwork repairs. It is quite likely that the furnace volume and consequently wall surface could have been reduced in the newer designs without encountering any difficulty. For the higher-pressure installations, however, it may be that extra furnace wall surface can be installed more economically than an equivalent amount of convection surface, particularly if long field welded tubes without intermediate headers are utilized. The high input per unit width of furnace up to 31,500,000 Btu per ft in the higher-pressure boiler designs 2 and 3 as compared to 19,900,000 Btu per ft in the older lower-pressure design, reflects the trend toward narrower furnaces.

Comparing the fuel-burning rates per sq ft of total radiant plus convection surface preceding the superheater, there is a much closer agreement between the units reported, viz., 63,820 to 74,040 Btu per sq ft. Regular steam blowing of the convection bank and superheater seems to be essential to maintain this rate without slag accumulation in the superheater, especially for the more closely spaced tubes.

In connection with design 2, the tubes in the first section of the superheater were originally spaced with an 0.8-in-wide free-gas opening between tubes. The close spacing was dictated by economy considerations. The burning rate per sq ft of free-gas area in this section was over 5,000,000 Btu per sq ft as indicated by the figures shown in Table 1 for Boiler No. 25, Essex Station. It was found that slag accumulated between tubes with this spacing even with an excessive amount of soot-blower operation. When every other superheater tube in this section was removed, thus increasing the spacing to 4.1 in. and reducing the burning rate to 2,452,000 Btu per sq ft of free-gas area, as indicated for Boiler No. 26, this difficulty was eliminated.

All water-cooled surfaces are calculated on the basis of projected wall area at tube center lines without adjustment for differences in construction such as tangent tubes, block-covered tubes, and stud or fin tubes. Hottel factors are applied to spaced wall and ash hopper screen surfaces while total gas-side tube surface is used in calculating convection surfaces. The floor surface of wet-bottom furnaces is neglected entirely because of the insulating effect of the chrome ore and slag. Radiation from the furnace to the convection bank is allowed for in arriving at the "furnace surface" by adding the cross-sectional area of the furnace at the furnace exit to the sum of the wall surfaces. A similar allowance is made for the total "furnace surface and convection bank to superheater" by adding the cross-sectional area of the gas pass at the superheater entrance, including by-pass, to the sum of the surfaces to that point. Furnace volume includes total combustion space above ash hopper water- or mercury-cooled surface to convection section of boiler. Although not theoretically correct, for the sake of simplification, burning rates are based on the higher heat value of the fuel with no allowance for heat added with the preheated air.

Value of Slag Screen

In connection with design 2, the slag screen between the primary and secondary furnaces was omitted on one of the boilers during the initial operation to determine its value. Fig. 9 shows comparative gas temperatures entering the superheater as determined by high-velocity thermocouples. These temperatures indicate that the additional surface of the slag screen is well utilized. For a gas temperature of 2000 F entering the superheater 20 per cent more output is obtained by the addition of the screen which represents 17 per cent additional furnace surface. The screen apparently raises the average heat-absorption rate of the furnace. The cost of the screen surface compared to an equal amount of additional wall surface is probably low as the projected area of both sides of the screen have been included as

TABLE I GENERAL BOILER FURNACE DESCRIPTION AND DATA

DESIGN			1	2	3						4
NUMBER OF UNITS			1	2	6						1
NAME OF STATION			Burlington	Essex	Burlington				Marion		Kearny
BOILER NUMBER			11	25 26	12	13	14	15	51	52	Mercury
DESCRIPTION OF UNIT											*
BUILDER			Comb. Eng.	B. & W.	B. & W.						B. & W.
DATE INSTALLED			1932	1938	1940		1942		1941		1940
BOILER TYPE			Straight Tube	Bent Tube	Bent Tube						Special
ASH REMOVAL			Dry Bottom	Slag Tap	Slag Tap						Dry Bottom
PULVERIZER			Raymond	Hardinge	Hardinge						Fuller-Lehigh
FIRING			Direct	Direct	Direct						Direct
BURNER			Horiz.-Circular	Rectangular-Intertube	Rectangular-Intertube						Rectangular
TYPICAL COAL		MONTH	July 1943	April 1943	July 1943				February 1943		June 1943
KIND			Bit.-Sl. & ROM	Bituminous-Sl. & ROM	Bituminous-Slack & Run of Mine				Bituminous-Slack		Bit.-Sl. & ROM
DISTRICT			1-Central Penna. 2-Western Penna. 3-Northern W. Va.	1-Central Penna.	1-Central Pennsylvania 2-Western Pennsylvania 3-Northern West Virginia				1-Central Penna. 7-Southern W. Va.		1-Central Penna. 7-Southern W. Va.
SEAM			B,D,E & Pittsburgh	B,C,C',D,E & Seymour	B, D, E & Pittsburgh				B,C' & Pocahontas #5		Bakerton,B,C',D,E & Pocahontas #5
PROXIMATE ANALYSIS (As Received)											
VOLATILE MATTER	(Range)	PER CENT	19.57-38.83	16.47-27.34	19.57-38.83				16.04-23.99		15.07-22.28
FIXED CARBON	(Range)	PER CENT	46.38-66.62	59.89-73.55	46.38-66.62				63.97-73.27		62.00-75.35
ASH	(Range)	PER CENT	4.86-11.22	5.62-14.26	4.86-11.22				5.02-11.31		5.08-18.95
TOTAL MOISTURE	(Range)	PER CENT	2.76-11.11	2.34- 6.60	2.76-11.11				2.96- 8.15		1.40- 6.42
HEAT VALUE PER LB	(Range)	BTU	11,990-13,559	12,821-14,220	11,990-13,559				13,096-14,371		12,026-14,311
ASH CHARACTERISTICS (Reducing Atmosphere)											
INITIAL DEFORMATION	(Range)	F	2080-2330	1870-2190	2080-2330				-		2060-2310
SOFTENING	(Range)	F	2130-2640	2140-2575	2130-2640				2060-2580		2180-2520
LIQUID	(Range)	F	2160-2700+	2320-2595	2160-2700+				-		2200-2540
SULPHUR (Dry Basis)	(Range)	PER CENT	0.92-3.26	1.14-3.48	0.92-3.26				0.48-2.82		0.59-3.74
GRINDABILITY (Hardgrove Scale)		INDEX	60	100	60				100		100
PERFORMANCE											
BOILER OUTPUT		LB PER HR	500,000	550,000	550,000						20,000 KW
SUPERHEATER OUTLET PRESSURE		LB PER SQ IN. G	670	1330	1300	1300	1295	1290	1315		-
SUPERHEATER OUTLET TEMPERATURE		F	850	925	945	950	950	945	933		-
FUEL BURNED	(Range)	LB PER HR	48,370-54,700	48,100-53,400	47,340-53,540				44,670-49,020		31,710-37,740
		BTU PER HR	655,900,000	684,200,000	641,950,000						453,850,000
COMBUSTION AIR TEMPERATURE (Secondary Air to Burners)		F	495	690	745	785	755	760	800		385
FINENESS THRU 200 MESH		PER CENT	66	85	75				80		67
FUEL BURNING RATE											
FURNACE SURFACE		SQ FT	4112	6929	6328						4936
		BTU PER HR PER SQ FT	159,500	98,745	101,450						91,950
FURNACE SURFACE AND CONVECTION		SQ FT	8893	9625	8670		9330		9429	8670	7111
CONVECTION BANK TO SUPERHEATER		BTU PER HR PER SQ FT	73,750	71,080	74,040		68,800		68,080	74,040	63,820
FURNACE VOLUME		CU FT	25,285	28,930	24,014						24,481
		BTU PER HR PER CU FT	25,940	23,650	26,730						18,540
FURNACE WIDTH		FT	32.92	22.604	20.354						26.83
		BTU PER HR PER FT	19,924,000	30,269,000	31,939,000						16,914,000
FREE GAS AREA											
CONVECTION BANK											
ENTRANCE		SQ FT	592	549	522						322
		BTU PER HR PER SQ FT	1,108,000	1,246,000	1,229,800						1,409,000
CLOSELY SPACED TUBES		SQ FT	284	338	522		374		364	522	322
		BTU PER HR PER SQ FT	2,310,000	2,024,000	1,229,800		1,716,500		1,763,600	1,229,800	1,409,000
SUPERHEATER											
ENTRANCE		SQ FT	332	386 424	367						146
		BTU PER HR PER SQ FT	1,976,000	1,733,000 1,576,000	1,749,200						3,109,000
CLOSELY SPACED TUBES OF FIRST SECTION		SQ FT	305	124 379	367						146
		BTU PER HR PER SQ FT	2,150,000	5,106,000 2,452,000	1,749,200						3,109,000
CLEANING (Up to and Including Superheater)											
SOOT BLOWERS											
STEAM USED		LB PER DAY	23,020	15,538 10,585	35,536	-	-	-	20,954	-	47,884
STEAM SUPPLY		LB PER SQ IN. G	670	225	600						370
		F	505	365	489						441
LANCING											
AIR USED (Free Air)		CU FT PER DAY	0	41,090 46,242	0						50,950
AIR SUPPLY		LB PER SQ IN. G	0	80-90	0						90
WATER USED		GAL PER DAY	9480	0	428	-	-	-	0		0
WATER SUPPLY-AT OPERATING FLOOR		LB PER SQ IN. G	105	0	60				0		0
MANHOURS PER DAY											
	STEAM		4-1/2	1-1/3 1-1/3	13	-	-	-	6	-	14-1/2
	AIR		0	14-1/3 15-2/3	0						18-1/2
	WATER		12-1/2	0	1/2	-	-	-	0		0
	TOTAL		17	15-2/3 17	13-1/2	-	-	-	6	-	33

* Fog bank of Mercury Boiler is considered equivalent of superheater on Steam Boiler.

(Correction to Table 1: In column 2 (Essex) superheater data, read 1,773,000 for 1,733,000 and 279 for 379. In column (Burlington) steam used, read 31,906 for 23,020.)

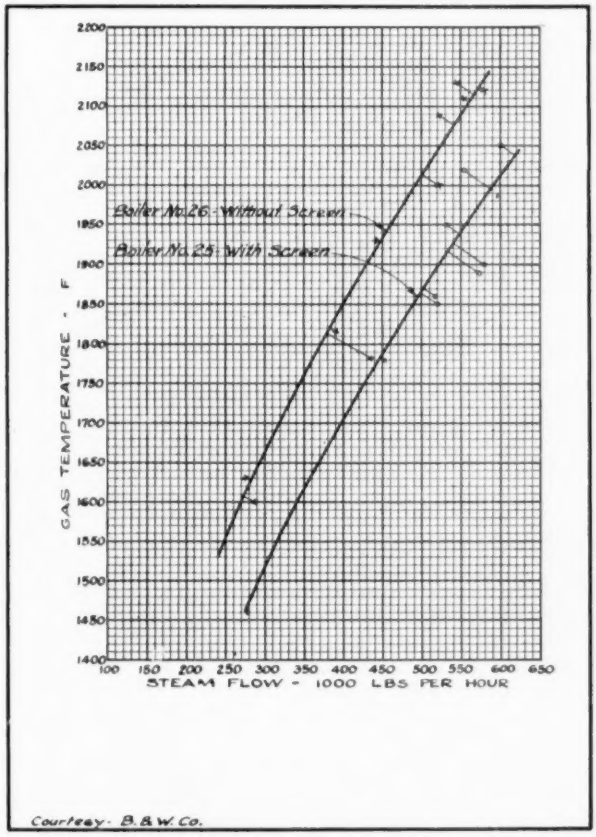


FIG. 9 AVERAGE GAS TEMPERATURE, SUPERHEATER INLET, WITH AND WITHOUT SLAG SCREEN BETWEEN PRIMARY AND SECONDARY FURNACES
(Boilers Nos. 25 and 26, Essex Station.)

heat absorbing surface. Whether the same result could be obtained with any arrangement of the additional surface placed in the hot portion of the furnace, or whether the arrangement which shades the secondary furnace from the primary is necessary to obtain the benefit, was not determined. It was found necessary to install the screen after the initial operating period as the superheater had been designed for a furnace which included the screen, and steam temperatures were too high without it.

DISTRIBUTION OF FURNACE GASES

Fig. 10 shows a typical gas-analysis traverse leaving one of the boilers of design 2. The tendency for high excess air on one side persists in spite of normal adjustments which can be made to the coal and air at the burners. The cause has not been determined, but is probably due to poor distribution of coal and air in the burners. This is an example of local conditions often found in the field which make snap comparisons inaccurate.

Fig. 11 indicates a temperature traverse entering the superheater of one of the boilers of design 2. Temperatures at this point vary from 1500 to 1990 F across the gas pass. The wide variation is typical and is another illustration of the problem involved in obtaining accurate comparative results.

Fig. 12 shows the flow paths of gases in the furnace of one of the units of design 3, and Fig. 13 shows isothermals in the same furnace. The wide variation in distribution of furnace gases illustrates the difficulty in determining furnace-performance factors. Any comparative tests which may be planned must take these variations into account.

FURNACE TUBE WASTAGE—BURNER PERFORMANCE

A peculiar type of corrosion which was unknown two or three years ago has been encountered on the gas side of the furnace tubes in connection with the later designs described. Although no tubes have been lost on this account, replacements have been necessary because of excessive corrosion in localized areas. In

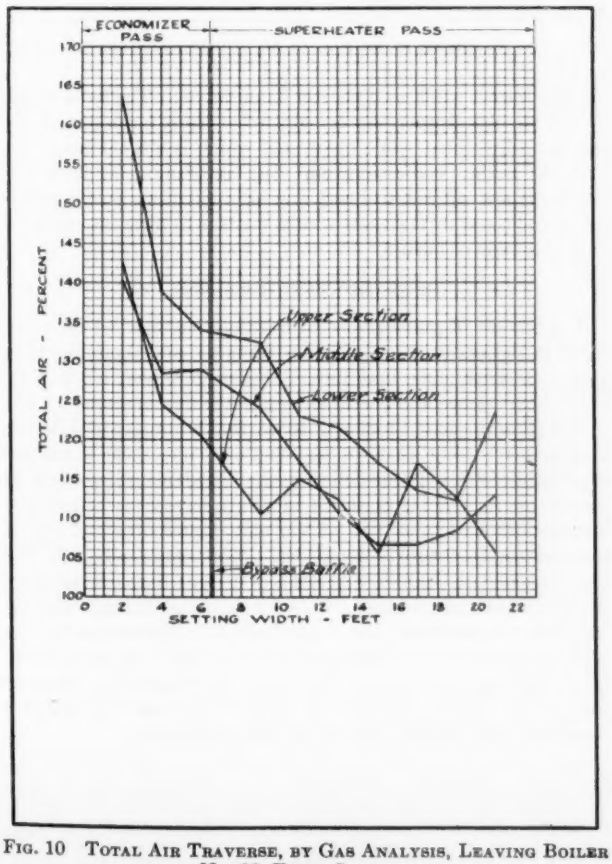


FIG. 10 TOTAL AIR TRAVERSE, BY GAS ANALYSIS, LEAVING BOILER NO. 26, ESSEX STATION
(Steam flow, 529,000 to 540,000 lb per hr.)

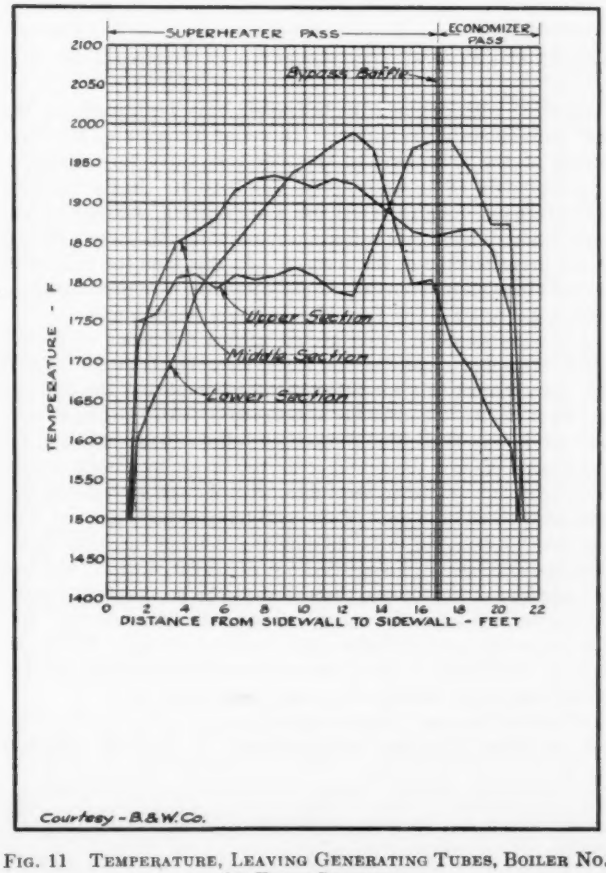


FIG. 11 TEMPERATURE, LEAVING GENERATING TUBES, BOILER NO. 25, ESSEX STATION
(Steam flow, 517,000 lb per hr.)

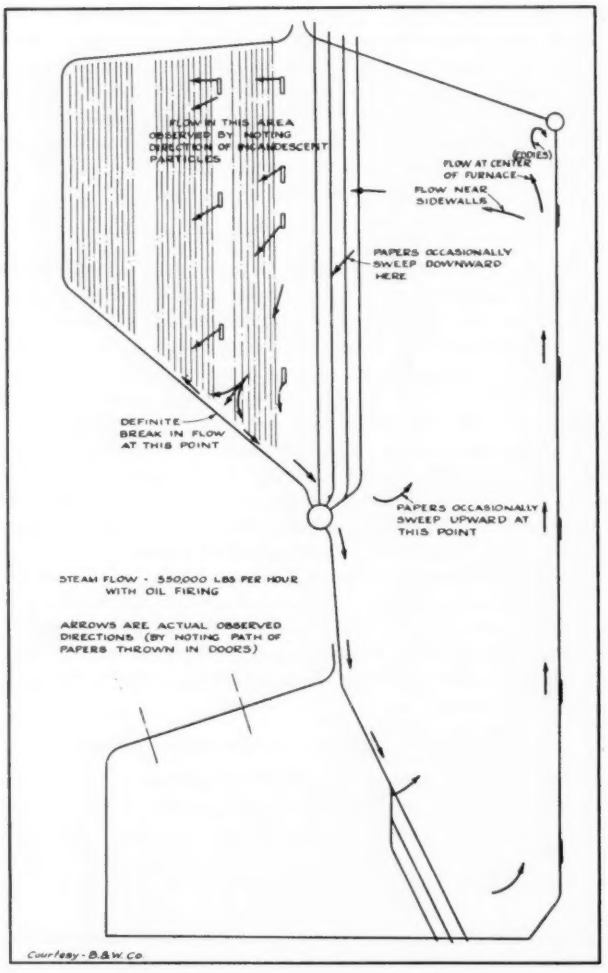


FIG. 12 GAS FLOW STUDIES, BOILER NO. 12, BURLINGTON STATION

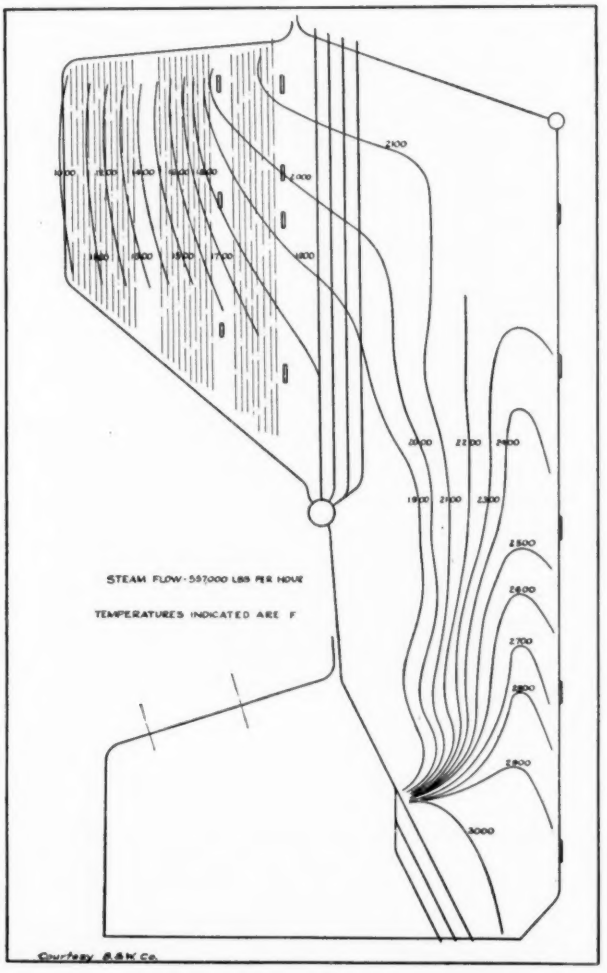


FIG. 13 ISOTHERM PLOT, BOILER NO. 12, BURLINGTON STATION

connection with design 2, replacements have been made on the side walls opposite the burners. In design 3, maximum corrosion occurs at the lower end of the side wall tubes for a distance approximately 18 in. up from the slag bottom. In the mercury boiler furnace, design 4, which has a dry bottom, wastage having an entirely different appearance occurs more uniformly over the entire lower portion of the furnace. In this case the tube wall temperature is approximately 1250 F compared to normal temperature in the order of 750 F on high-pressure steam boilers.

Corrosion seems to be connected with a deficiency of air for combustion and usually occurs where there is CO in the furnace gas even though this condition is intermittent and the amount of CO is small. The remedy appears to be better mixing of coal and air in the burners. Temporary relief can be obtained on the steam boilers if the action is not too severe by closely spaced horizontal fins welded to the tubes, with the spaces between fins packed with chrome ore. Tube wall temperatures are too high for this construction to be used on the mercury furnace. Nonmetallic coatings are being tried out in actual service. For the hot portions of the furnace there seems to be no satisfactory substitute for closely spaced tubes without extended surfaces. Extensions waste away no matter how they are installed. Thorough mixing of coal and air in the burner is essential and the furnace should not be depended on for completing the mixture.

Circular turbulent burners appear to give better results than any rectangular burner yet developed. A properly adjusted circular burner will have a shorter flame travel. The flame shape of the circular burner can be controlled, to a large extent, by manual adjustment while operating, which is advantageous for variable loads. Indications are that circular-burner-fired furnaces are less subject to fused slag accumulations on the waterwalls, and there are few cases of tube wastage in furnaces equipped with this type of burner.

SUMMARY AND CONCLUSIONS

The advent of pulverized coal resulted in a marked improvement in the performance of boiler furnaces, and there has been steady progress since that time. Design, however, is based on limited experience and is still an art rather than a science. The information presented herewith shows that a number of different arrangements may perform satisfactorily but their maximum capabilities have not been determined. Fundamental research on the factors involved is needed if we are to have more economical installations and take care of the higher pressures and higher temperatures of future power cycles. More specifically, information is needed on the following items of design: burners; arrangement of water-cooled furnace walls for maximum heat absorption; methods for predicting and controlling slag deposits on furnace walls; measures to eliminate destructive action of furnace atmosphere and slag on water-cooled metal wall surfaces; arrangement and spacing of tubes in convection bank for slag-free operation with various furnace-exit-gas conditions.

Appendix A—Coal Characteristics

BURLINGTON STATION -- CHARACTERISTICS OF COAL BURNED - JULY 1943

Date Shipment Received July	Net Tons Received	Bituminous Coal Division Producing District	Mine Seam	Size	Analysis - Wet Basis				Sul. Dry Basis %	Heat Value Btu Per Lb		Ash Characteristics					
					Vol. Mat. %	Fixed Carb. %	Ash %	Total Moist. %		As Fired	Dry	Reducing Atmos. Init. Def. F	Reducing Atmos. Soft. F	Reducing Atmos. Liq. F	Oxidizing Atmos. Init. Def. F	Oxidizing Atmos. Soft. F	Oxidizing Atmos. Liq. F
1	2242	Storage (1)	B-D-E	Slack	24.17	62.67	6.89	6.27	1.56	13545	14451	2170	2230	2340	2420	2450	2460
2	2299	"	"	"	20.14	66.62	4.86	8.38	1.14	13559	14799		2240				
2	899	High Vol.(2)	Pittsburg	ROM or Sl.	34.92	51.52	6.67	6.89	1.72	12981	13942		2100				
2	981	"	"	"	35.56	51.78	6.75	5.91	1.89	13287	14122		2100				
3	911	"	"	"	29.30	57.82	6.95	5.93	1.94	13350	14192	2080	2130	2160	2280	2300	2320
3	1876	"	"	"	34.87	50.23	7.80	7.10	2.21	12868	13851		2100				
6	976	"	"	"	35.85	49.33	7.54	7.28	2.17	12810	13816		2260				
6	913	"	"	"	34.80	50.73	9.20	5.27	1.82	12987	13710		2340				
7	3031	Storage (1)	B-D-E	Slack	21.02	62.27	5.60	11.11	1.16	12939	14556		2240				
7	910	High Vol.(2)	"	ROM or Sl.	34.80	50.98	7.17	7.05	2.12	13115	14110		2400				
7	1751	"	"	"	33.68	52.26	6.96	7.10	1.97	13151	14156		2200				
8	965	"	"	"	32.92	47.11	9.42	10.55	2.37	12136	13567		2200				
8	925	"	"	"	34.83	51.40	8.80	4.97	1.37	13225	13917	2130	2180	2220	2310	2380	2400
9	926	"	"	"	34.67	50.73	7.17	7.43	2.22	13044	14091		2250				
9	1851	"	"	"	35.05	49.57	9.72	5.66	2.39	12873	13645	2260	2340	2370	2210	2230	2360
10	2001	Storage (1)	B-D-E	Slack	19.57	65.11	6.01	9.31	0.92	13077	14420	2330	2640	2700+	2620	2700+	2700+
10	967	High Vol.(2)	Pittsburg	ROM or Sl.	36.42	50.10	7.97	5.51	2.50	13208	13978	2100	2150	2220	2300	2330	2340
10	974	"	"	"	32.64	47.39	9.46	10.51	2.78	11990	13390		2200				
12	1830	"	"	"	33.92	50.15	6.33	9.60	2.06	12632	13974		2140				
13	1504	"	"	"	35.43	49.29	7.68	7.60	2.05	12853	13899		2200				
13	2602	Storage (1)	B-D-E	Slack	23.64	63.45	5.53	7.38	1.26	13547	14626		2290				
13	894	High Vol.(2)	Pittsburg	ROM or Sl.	36.58	51.34	7.34	4.74	1.93	13277	13938		2200				
14	919	"	"	"	34.07	47.56	8.96	9.41	2.81	12275	13550		2100				
14	950	"	"	"	34.47	46.67	9.11	9.75	2.35	12257	13581		2140				
14	1827	"	"	"	35.11	50.49	7.38	7.02	2.27	12847	13817		2280				
15	901	"	"	"	32.73	54.00	7.71	5.56	1.71	13045	13813		2160				
16	1822	"	"	"	38.83	50.64	7.77	2.76	2.35	13523	13907		2140				
17	887	"	"	"	34.49	49.92	8.60	7.29	2.56	13467	14526		2100				
17	1810	"	"	"	33.80	49.87	9.30	7.03	2.77	12576	13527		2100				
17	964	"	"	"	34.83	49.82	8.26	7.09	2.89	12685	13653		2140				
17	919	"	"	"	29.20	57.76	6.64	6.40	1.86	13231	14136		2220				
19	988	"	"	"	33.83	51.01	8.14	7.02	2.24	12922	13898		2320				
19	911	"	"	"	34.31	51.04	8.57	6.08	2.69	13140	13991		2140				
20	1787	"	"	"	36.88	52.19	7.51	3.42	2.37	13431	13907		2140				
20	2853	Storage (1)	B-D-E	Slack	22.56	63.82	6.28	7.34	1.21	13436	14500		2200				
20	896	High Vol.(2)	Pittsburg	ROM or Sl.	35.50	52.56	6.83	5.11	3.26	13367	14087		2300				
21	996	"	"	"	35.32	48.06	9.89	6.73	2.34	12452	13351		2100				
22	903	"	"	"	34.27	50.31	9.12	6.30	2.65	12734	13590		2100				
22	1793	"	"	"	34.51	47.98	10.40	7.11	3.26	12376	13323		2100				
22	1579	"	"	"	36.99	52.62	6.71	3.68	1.90	13505	14021		2200				
22	914	"	"	"	36.98	49.94	9.08	4.00	2.79	13068	13612		2100				
24	965	"	"	"	35.86	50.36	7.18	6.60	2.17	13040	13961		2360				
24	1749	"	"	"	35.82	51.74	7.65	4.79	2.14	13216	13881		2360				
25	1813	"	"	"	34.59	46.38	10.36	8.67	2.68	12231	13392		2360				
25	914	"	"	"	36.15	49.95	8.42	5.48	2.71	13028	13783		2330				
26	1782	"	"	"	33.72	48.65	9.38	8.25	2.63	12184	13280		2190				
26	903	"	"	"	35.09	50.57	8.43	5.91	1.90	12833	13639		2240				
27	986	"	"	"	34.67	52.97	7.37	4.99	1.97	13343	14044	2310	2340	2360	2340	2380	2400
28	917	"	"	"	34.45	48.36	9.16	8.03	2.81	12425	13510		2360				
28	2454	Storage (1)	B-D-E	Slack	28.87	57.83	7.02	6.28	1.66	13445	14346		2360				
28	889	High Vol.(2)	Pittsburg	ROM or Sl.	32.07	52.26	8.50	7.17	2.61	12715	13697		2340				
28	1830	"	"	"	35.59	47.12	11.22	6.07	2.13	13053	13897		2340				
29	982	"	"	"	28.57	61.91	6.48	3.04	1.54	13965	14403	2330	2350	2360	2370	2400	2420
29	896	"	"	"	33.19	48.78	10.38	7.65	1.53	12337	13359		2300				
29	906	"	"	"	35.58	48.66	10.24	5.52	2.37	12494	13224		2240				
30	1832	"	"	"	31.59	51.42	8.74	8.25	2.20	12550	13678		2330				
31	970	"	"	"	34.01	47.76	11.14	7.09	2.89	12257	13192		2370				
31	896	"	"	"	36.49	49.68	8.25	5.58	2.66	13005	13774		2300				

(1) Low Volatile - District No. 1 - Central Pennsylvania (From Station storage pile which was made up of coal from various mines).
(2) High Volatile - District No. 2 - Western Pennsylvania (From 2 separate mines).
District No. 3 - Northern West Virginia (From various mines).
Individual shipments were made up of coal from one mine or a mixture from 2 or more separate mines and from District No. 2, No. 3 or both.
Most High Volatile coal is from District No. 3.

APPENDIX A

ESSEX STATION -- CHARACTERISTICS OF COAL BURNED - APRIL 1943

Date Shipment Received April	Net Tons Received	Bituminous Coal Division Producing District	Mine Seam (2)	Size (3)	Analysis - Wet Basis Vol. Mat. %	Fixed Carb. %	Ash %	Total Moist. %	Sul. Dry Basis %	Heat Value Btu Per Lb As Fired	Dry	Ash Characteristics Reducing Atmos. Init. Def. F	Soft. F	Liq. F	Oxidizing Atmos. Init. Def. F	Soft. F	Liq. F
2	1000	No. 1 (1)	B	ROM or Sl.	22.78	66.76	8.12	2.34	3.48	14043	14379		2120				
2	1000	"	C'	"	16.47	73.55	7.22	2.76	1.14	14047	14446	2190	2300	2320	2360	2400	2450
2	1000	"	E	"	21.12	66.34	8.75	3.79	1.53	13714	14254		2545				
3	2000	"	E	"	21.32	67.23	8.17	3.28	1.88	13793	14261	2075	2535	2555	2520	2640	2700+
3	1000	"	B	"	22.04	68.19	7.21	2.56	2.75	14169	14541		2120				
6	1000	"	B	"	18.47	70.74	6.66	4.13	1.45	13954	14555	2130	2575	2595	2620	2680	2700+
6	1000	"	B	"	18.99	70.13	8.09	2.79	2.08	13979	14380	2010	2310	2435	2470	2560	2570
8	1000	"	B-C	"	21.03	66.87	7.85	4.25	1.53	13731	14340		2420				
9	1000	"	Seymour	"	19.07	67.04	10.06	3.83	2.69	13470	14006		2220				
9	2000	"	B	"	22.28	67.17	8.03	2.52	1.70	14046	14409		2080				
9	1000	"	B	"	18.25	68.76	10.04	2.95	2.67	13595	14008		2180				
10	1000	"	B	"	22.12	64.76	9.67	3.45	3.46	13591	14077		2220				
11	1000	"	E	"	17.87	70.17	8.32	3.64	2.10	13655	14171		2120				
12	1000	"	B-D	"	21.67	65.50	8.54	4.29	2.23	13655	14267	2040	2445	2540	2560	2580	2600
12	1000	"	B-C'-D	"	17.96	67.90	10.48	3.66	2.08	13349	13856		2150				
13	1000	"	Seymour	"	18.37	67.04	9.85	4.74	2.52	13403	14070		2180				
14	2000	"	B	"	20.18	67.28	8.08	4.46	3.34	13650	14287		2080				
14	1000	"	B-D	"	16.59	65.51	14.26	3.64	3.37	12821	13305		2460				
15	1000	"	B-D	"	19.93	65.99	10.62	3.46	2.36	13353	13832		2110				
15	1000	"	B-D	"	21.39	67.19	7.37	4.05	2.27	13846	14430		2200				
16	1000	"	B	"	27.34	60.76	8.57	3.23	2.31	13784	14244		2520				
17	1000	"	Seymour	"	19.77	66.99	9.60	3.64	2.52	13498	14008		2080				
17	2000	"	B-D	"	18.36	69.00	9.24	3.40	2.45	13636	14116		2120				
19	1000	"	B-C'-D	"	26.43	60.17	9.48	3.92	3.09	13431	13979		2520				
19	1000	"	B-D	"	21.63	62.09	9.68	6.60	1.49	12865	13774		2520				
20	1000	"	Seymour	"	19.49	65.16	9.77	5.58	3.11	13229	14011		2460				
21	2000	"	B-D-E	"	17.43	68.20	8.82	5.55	2.51	13371	14157		2520				
22	2000	"	B-D	"	17.51	72.84	5.62	4.03	1.26	14220	14817		2700				
22	1000	"	E-Seymour	"	22.13	64.86	9.65	3.36	1.46	13532	14002		2510				
22	1000	"	B-C'-D	"	19.27	69.71	6.74	4.28	1.60	14011	14638		2560				
22	1000	"	B	"	26.61	60.20	9.33	3.86	2.30	13516	14059	1870	2140	2435	-	2480	2540
24	1000	"	B-D	"	25.88	59.89	9.10	5.13	3.26	13420	14146		2160				
24	1000	"	B	"	20.07	68.29	7.26	4.38	1.96	13827	14460		2200				
27	1000	"	B-C'	"	16.61	67.42	11.45	4.52	2.55	13018	13634		2510				
29	1000	"	E	"	17.39	69.94	7.80	4.87	1.25	13675	14375	2060	2340	2410	2420	2540	2560
30	2000	"	B-D	"	20.87	66.71	8.96	3.46	2.02	13714	14205		2195				
30	1000	"	B-D	"	17.98	69.99	8.79	3.24	2.48	13633	14089	1985	2095	2405	-	2500	2520

(1) District No. 1 (Central Pennsylvania).

(2) Many of the individual shipments were made up of a mixture from two or more separate mines.

(3) Most of the coal received during this month was slack.

MARION STATION -- CHARACTERISTICS OF COAL BURNED - FEBRUARY 1943

Date Shipment Received February	Net Tons Received	Bituminous Coal Division Producing District	Mine Seam (4)	Size	Analysis - Wet Basis				Sul. Dry Basis %	Heat Value Btu Per Lb		Ash Characteristics					
					Vol. Mat. %	Fixed Carb. %	Ash %	Total Moist. %				Reducing Atmos.			Oxidizing Atmos.		
										As Fired	Dry	Init. Def. F	Soft. F	Liq. F	Init. Def. F	Soft. F	Liq. F
1	1920	No. 1 (1)	B-C'	Slack	20.25	67.09	9.63	3.03	2.39	13735	14164		2130				
		No. 7 (2)	Poca. #5	"													
2	1339	No. 1 (1)	B	"	18.38	71.00	6.56	4.06	1.40	14088	14684		2380				
2 to 5	1511	Storage(3)	-	"	16.04	67.77	8.04	8.15	1.01	13096	14258		2360				
4	1014	No. 1 (1)	B	"	17.33	73.27	5.20	4.20	1.34	14249	14874		2510				
6	1912	No. 7 (2)	Poca. #5	"	23.07	67.84	6.12	2.97	0.58	14302	14740		2190				
6	1389	No. 1 (1)	C'	"	16.87	71.75	8.14	3.24	1.69	13894	14359		2240				
7	583	Storage(3)	-	"	19.48	70.19	5.02	5.31	1.00	14019	14805		2500				
9	1480	No. 1 (1)	B	"	21.36	69.03	6.34	3.27	0.70	14262	14744		2180				
	432	No. 7 (2)	Poca. #5	"													
9	991	Storage(3)	-	"	17.60	72.29	5.41	4.70	1.29	14155	14853		2490				
10	872	No. 1 (1)	B	"	17.70	70.51	8.27	3.52	1.64	13823	14327		2200				
	582	No. 1 (1)	C'	"													
10 to 14	1217	Storage(3)	-	"	18.36	71.88	5.27	4.49	1.22	14176	14842		2580				
13	1079	No. 1 (1)	C'	"	16.65	72.25	7.39	3.71	1.18	13959	14497		2450				
16	1028	No. 1 (1)	B	"	20.92	63.97	8.55	6.56	2.29	13113	14034		2320				
17	1873	No. 7 (2)	Poca. #5	"	23.22	67.81	6.00	2.97	0.69	14339	14778		2180				
18	1433	No. 1 (1)	B	"	17.64	72.14	6.12	4.10	1.52	14093	14695		2480				
19	1080	No. 7 (2)	Poca. #5	"	22.69	67.54	6.46	3.31	0.48	14253	14741		2180				
20	1037	No. 1 (1)	B	"	18.38	71.38	6.65	3.59	1.84	14044	14567		2440				
23	1921	No. 7 (2)	Poca. #5	"	22.87	66.82	6.82	3.49	0.56	14155	14667		2200				
24	1456	No. 7 (2)	Poca. #5	"	23.99	66.57	6.48	2.96	0.54	14371	14809		2185				
26	1055	No. 7 (2)	Poca. #5	"	23.91	66.85	6.23	3.01	0.63	14310	14754		2180				
26	1053	No. 7 (2)	Poca. #5	"	21.90	67.23	6.95	3.92	0.78	13975	14545		2200				
26	1037	No. 1 (1)	C'	"	16.47	68.46	11.31	3.76	2.66	13382	13905		2060				
28	1245	No. 1 (1)	B	"	21.46	65.53	9.37	3.64	2.82	13581	14094		2260				

(1) District No. 1 (Central Pennsylvania).

(2) District No. 7 (Southern West Virginia).

(3) From station storage pile which was made up of coal from various mines.

(4) Many of the individual shipments were made up of a mixture from two or more separate mines.

APPENDIX A

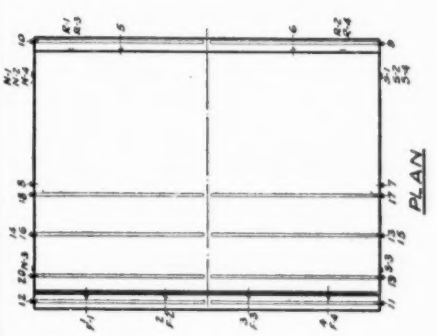
KEARNY STATION -- CHARACTERISTICS OF COAL BURNED - JUNE 1943

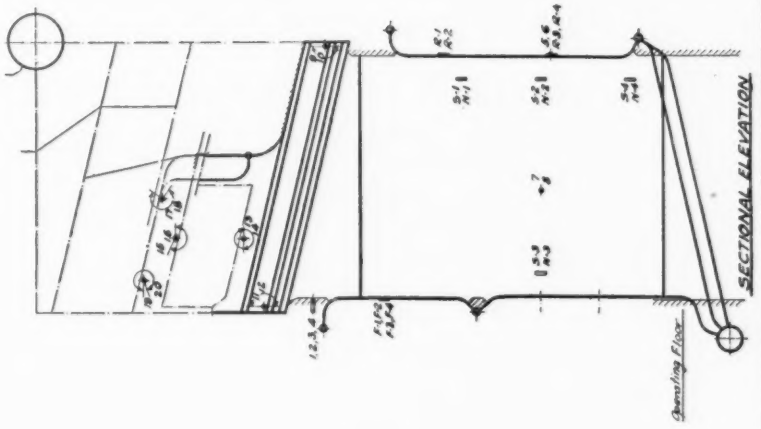
Date Shipment Received June	Net Tons Received	Bituminous Coal Division Producing District	Mine Seam	Size	Analysis - Wet Basis Vol. Mat. %	Fixed Carb. %	Ash %	Total Moist. %	Sul. Dry Basis %	Heat Value Btu Per Lb As Fired	Heat Value Btu Per Lb Dry	Ash Characteristics Reducing Atmos. Init. Def.F	Reducing Atmos. Soft. F	Reducing Atmos. Liq. F	Oxidizing Atmos. Init. Def.F	Oxidizing Atmos. Soft. F	Oxidizing Atmos. Liq. F
1	1134	No. 1 (1)	E-Bakerton (3)	ROM	21.88	63.24	10.28	4.60	2.48	13258	13897		2240				
1	1291	No. 7 (2)	Poca.#3 & 4 (3)	ROM	16.01	73.89	6.45	3.65	0.63	14098	14632		2220				
1	1122	"	Poca.#3 & 4 (3)	ROM	16.09	70.54	10.44	2.93	0.79	13587	13946		2220				
2	1010	No. 1 (1)	B	ROM	21.14	68.31	6.15	4.40	1.53	14013	14658	2310	2440	2460	2620	2640	2650
3	1078	No. 7 (2)	Poca.#3 & 4 (3)	ROM	15.86	71.56	8.59	3.99	1.19	13693	14262		2195				
3	1258	"	Poca.#3 & 4 (3)	ROM	15.07	68.00	12.79	4.14	0.59	13006	13568	2200	2290	2310	2300	2380	2500
3	1930	"	Poca.#3	ROM	15.75	75.35	5.08	3.82	0.93	14305	14873		2360				
4	1290	"	Poca.#3	ROM	15.87	73.60	6.65	3.88	0.94	14018	14584		2260				
4	1946	No. 1 (1)	E-Bakerton (3)	ROM	22.20	62.84	10.59	4.37	2.45	13411	14024		2240				
5	1081	"	B-C'-E (3)	ROM & Sl.	17.54	71.87	6.49	4.10	1.51	14096	14699		2340				
6	1097	"	B-C'-E (3)	ROM & Sl.	16.61	71.83	7.18	4.38	1.67	13977	14617		2220				
7	1321	"	B-C' (3)	ROM & Sl.	16.73	68.91	10.99	3.37	3.74	13341	13806		2080				
8	1271	No. 7 (2)	Poca.#3 & 4 (3)	ROM	15.80	67.43	13.45	3.32	0.74	12954	13399		2300				
8	1953	No. 1 (1)	B-D (3)	ROM & Sl.	18.75	64.50	13.17	3.58	2.05	12944	13425		2420				
9	1924	"	B-C'-E (3)	ROM & Sl.	19.03	69.08	7.69	4.20	1.89	13842	14449		2200				
9	1048	"	C' (3)	ROM & Sl.	16.77	71.67	8.34	3.22	0.98	13914	14377		2380				
10	1338	"	B-C' (3)	ROM & Sl.	19.45	69.64	7.36	3.55	1.73	13949	14462		2160				
10	2000	"	B	ROM	15.49	62.00	18.95	3.56	1.85	12026	12470		2680				
10	1274	No. 7 (2)	Poca.#3 & 4 (3)	ROM	16.03	69.06	8.90	6.01	0.98	13313	14164						
11	1039	No. 1 (1)	B	ROM	21.08	67.06	7.38	4.48	1.85	13848	14498		2460				
11	1043	"	B-C'-E (3)	ROM & Sl.	18.24	70.73	6.91	4.12	1.67	14014	14616		2400				
12	1895	"	B-C' (3)	ROM & Sl.	17.95	73.18	6.28	2.59	1.88	14311	14692		2400				
12	1243	"	D (3)	ROM & Sl.	21.19	65.98	8.65	4.18	1.82	13681	14278		2400				
13	1966	"	B-D (3)	ROM & Sl.	17.75	64.54	12.24	5.47	2.31	12718	13454		2400				
14	1366	"	B-C'-E (3)	ROM & Sl.	21.18	65.88	7.13	5.81	2.26	13658	14501	2060	2180	2200	2480	2510	2520
15	1015	"	B-C' (3)	ROM & Sl.	17.18	69.43	6.97	6.42	1.90	13613	14547	2110	2370	2390	2520	2580	2590
15	1013	"	B-D (3)	ROM & Sl.	18.78	65.64	10.20	5.38	2.99	13075	13818						
16	1256	No. 7 (2)	Poca. #3	ROM	15.65	72.67	5.49	6.19	0.93	13967	14889						
16	1496	No. 1 (1)	B	ROM	15.94	66.95	11.75	5.36	2.99	12780	13504		2300				
17	1054	No.1 & 7 (1) (2)	E-Bak-Poca#3&4(3)	ROM	15.43	71.20	8.70	4.67	0.71	13565	14230		2160				
17	1281	No. 1 (1)	B-D (3)	ROM & Sl.	18.52	66.65	9.66	5.17	2.58	13235	13957						
17	1923	"	B-C'-E (3)	ROM & Sl.	18.82	68.43	7.40	5.35	1.82	13770	14548						
18	1043	"	B-C' (3)	ROM & Sl.	19.09	67.88	7.06	5.97	1.45	13624	14489						
18	1986	"	B-D (3)	ROM & Sl.	19.28	68.42	8.48	3.82	2.09	13612	14153		2200				
18	985	"	B.	ROM	18.46	63.84	14.29	3.41	2.67	12782	13233	2210	2415	2425	2500	2580	2610
18	1288	"	B-D (3)	ROM & Sl.	19.92	67.69	9.97	2.42	2.07	13751	14092		2200				
20	1058	"	E-Bakerton (3)	ROM	20.93	64.18	11.88	3.01	1.49	13302	13715		2600+				
20	1892	"	B-C' (3)	ROM & Sl.	17.11	71.70	8.21	2.98	1.55	13966	14395		2280				
21	1031	"	E	Sl.	16.89	72.33	6.06	4.72	1.59	14061	14758		2360				
21	1194	"	B-C' (3)	ROM & Sl.	17.00	72.52	6.88	3.60	1.52	14046	14571		2400				
22	1957	"	B-D (3)	ROM & Sl.	20.07	66.50	10.39	3.04	2.17	13534	13958		2260				
23	1254	No. 7 (2)	Poca.#3 & 4 (3)	ROM	16.56	74.26	5.97	3.21	0.92	14288	14762		2260				
24	1060	No. 1 (1)	B-C'-E (3)	ROM & Sl.	18.13	70.31	7.92	3.64	2.53	13863	14387		2300				
25	1923	No. 7 (2)	Poca.#3	ROM	15.46	74.10	5.97	4.47	1.23	14148	14810	2250	2300	2330		2515	2550
25	1307	No. 1 (1)	C'	ROM & Sl.	16.91	73.49	8.20	1.40	1.47	14185	14386		2300				
26	1336	"	B-C'-E (3)	ROM & Sl.	17.00	72.67	6.51	3.82	1.69	14168	14731		2340				
26	1046	"	E-Bakerton (3)	ROM	21.56	65.63	9.33	3.48	1.48	13540	14028	2300	2520	2540	2630	2660	2680
27	1973	"	B-D (3)	ROM & Sl.	20.72	67.51	8.52	3.25	1.63	13779	14242		2600				
27	1356	"	D (3)	ROM & Sl.	20.70	65.82	9.45	4.03	2.33	13560	14129		2200				
27	1062	No. 7 (2)	Poca.#3	ROM	16.17	74.55	5.70	3.58	1.02	14250	14779		2500				
29	1972	"	Poca.#3 & 4 (3)	ROM	16.36	74.15	6.04	3.45	0.61	14183	14690		2340				
30	1280	No. 1 (1)	B	ROM	16.24	67.11	12.55	4.10	2.73	12923	13476		2380				
30	1965	"	B-D (3)	ROM & Sl.	22.28	63.33	9.74	4.65	2.68	13402	14056		2200				

(1) District No. 1 (Central Pennsylvania).
(2) District No. 7 (Southern West Virginia).
(3) Mixture from 2 or more separate mines. (Coals from more than 20 separate mines were received this month).

APPENDIX A

Appendix B—Cleaning Schedule





STEAM SUPPLY - 670 Lb per sq in pressure at 505 F

BLOWER NO.	TYPE	BLOWING ARC DEGREES	STEAM AT BLOWER PRESS. #/0"	SOOT HEAD TEMP. F.	NO. OF BLOWS PER DAY	REVOLUTIONS PER BLOW	TIME STEAM FLOWS PER BLOW	STEAM DURING BLOW LBS. PER MIN.	STEAM DURING BLOW TOTAL LBS.	STEAM PER DAY EACH BLOWER LBS.	STEAM PER DAY TOTAL LBS.
1,2,3,4	Gun Type Rotating Retractable	360	500	466	3	1½	1m 34s	400	627	1881	7524
5	Gun Type Rotating Retractable	360	500	466	3	2	4m 25s	400	1767	5301	5301
6, 7, 8	Gun Type Rotating Retractable	360	500	466	3	1	2m 38s	400	1053	3159	9477
9, 10	Rotating	180	500	466	3	1	8s	550	73	228	450
11, 12	Rotating	180	500	466	3	1	21s	560	196	588	1176
13, 14	2-Position Rotating Retractable	360	300	422	3	1	1m 53s	340	640	1920	3840
15, 16	Rotating	200	300	422	2	1	20s	408	136	272	544
17, 18	Rotating	270	300	422	2	1	26s	408	177	354	708
19, 20	Rotating	340	300	422	2	1	13s	408	88	176	352
										Amount used for draining lines (Estimated)	29,372 2,534
										Total	31,906

WATER SUPPLY - 105 Lb per sq in. pressure at operating floor

DOOR NO.	NO. OF DOORS	LANCE (PIPE)	NO. OF BLOWS PER DAY	TIME WATER FLOWS PER BLOW	WATER DURING BLOW G P M	WATER DURING BLOW TOTAL GALS	WATER PER DAY EACH DOOR GALS	WATER PER DAY TOTAL GALS
F-1,F-2	4	⅜ Std. x 8'-0" Lg.	2	10m	30	300	600	2400
R-1,R-2	2	⅜ Std. x 6'-0" Lg.	2	5m	30	150	300	600
R-3,R-4	2	⅜ Std. x 6'-0" Lg.	2	8½m	30	255	510	1020
S-1,N-1	2	⅜ Std. x 6'-0" Lg.	2	7½m	30	225	450	900
S-2,N-2	2	⅜ Std. x 6'-0" Lg.	2	7½m	30	225	450	900
S-3,N-3	2	⅜ Std. x 20'-0" Lg.	1	15m	30	450	450	900
S-4,N-4	2	⅜ Std. x 20'-0" Lg.	3	15m	30	450	1350	2700
						Total		9420

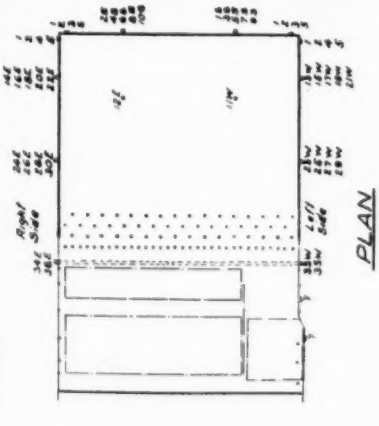
DAILY CLEANING TIME

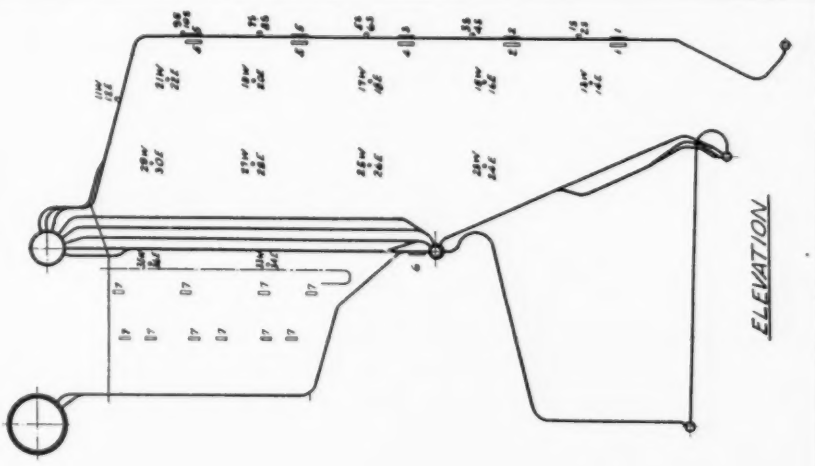
	MEN	HOURS	MANHOURS
Steam	1	4½	4½
Water	2	6⅙	12⅓
		10⅔	17

BOILER NO. 11

BURLINGTON STATION

Appendix B





STEAM SUPPLY - 225 Lb per sq in. pressure at 565 F.

BLOWER NO.	TYPE	BLOWING ARC DEGREES	STEAM AT BLOWER PRESS. #/0"	SOOT HEAD TEMP. F.	NO. OF BLOWS PER DAY	REVOLUTIONS PER BLOW	TIME STEAM FLOWS PER BLOW	STEAM DURING BLOW LBS. PER MIN.	STEAM DURING BLOW TOTAL LBS.	STEAM PER DAY EACH BLOWER LBS.	STEAM PER DAY TOTAL LBS.
19,21,33,44, 55,65,73,85, 93,103											
13W,14E,15W, 16E,17W,18E, 19W,20E,21W	Gun Type Rotating Retractable	360	175	500	1	1	1m 30s	140	210	210	5880
22E,23W,24E, 25W,26E,27W, 28E,29W,30E											
11W,12E	Gun Type Rotating Retractable	360	175	500	2	1	1m 30s	140	210	420	840
34E,36E	Rotating 3-Position Retractable	360	175	500	*	6	10m 10s	133	1352	135*	270*
33W,35W	Rotating 2-Position Retractable	360	175	500	*	6	8m 10s	107	874	87*	174*
											2,164
										Amount used for draining lines (Estimated)	8,374
										Total	10,538

* 3 Blows per month (prorated per day).

AIR SUPPLY - 80 to 90 Lb per sq in. pressure.

DOOR NO.	NO. OF DOORS	LANCE (PIPE)	NO. OF BLOWS PER DAY	TIME AIR FLOWS PER BLOW	AIR DURING BLOW CU FT PER MIN	AIR DURING BLOW TOTAL CU FT	AIR PER DAY EACH DOOR CU FT	AIR PER DAY TOTAL CU FT
1	4	¾ XH x 12'-0" Lg.	6	1m 56s	240	464	2784	11136
2	4	¾ XH x 7'-6" Lg.	6	2m 24s	240	576	3456	13824
3	2	¾ XH x 3'-0" Lg.	1	1m 0s	240	240	240	480
4,5	10	¾ XH x 7'-6" Lg.	1	2m 24s	240	576	576	5760
6	16	¾ XH x 6'-0" Lg.	1	35s	240	140	140	2240
7	10	¾ STD x 8'-0" Lg.	3	3m 0s	85	255	765	7650
						Total (Free Air)		41,090

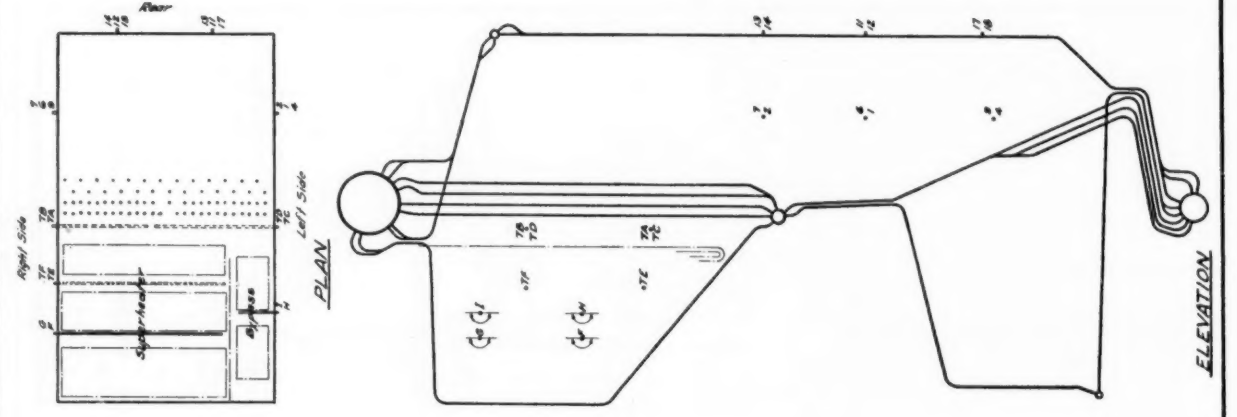
DAILY CLEANING TIME

	MEN	HOURS	MANHOURS
AIR	2	5⅓	11⅓
	1	⅓	⅓
		8⅔	14⅓
STEAM	1	1⅓	1⅓
Total	10		15⅔

BOILER NO. 25

ESSEX STATION

Appendix B



STEAM SUPPLY - 600 Lb per sq in. pressure at 489 F.

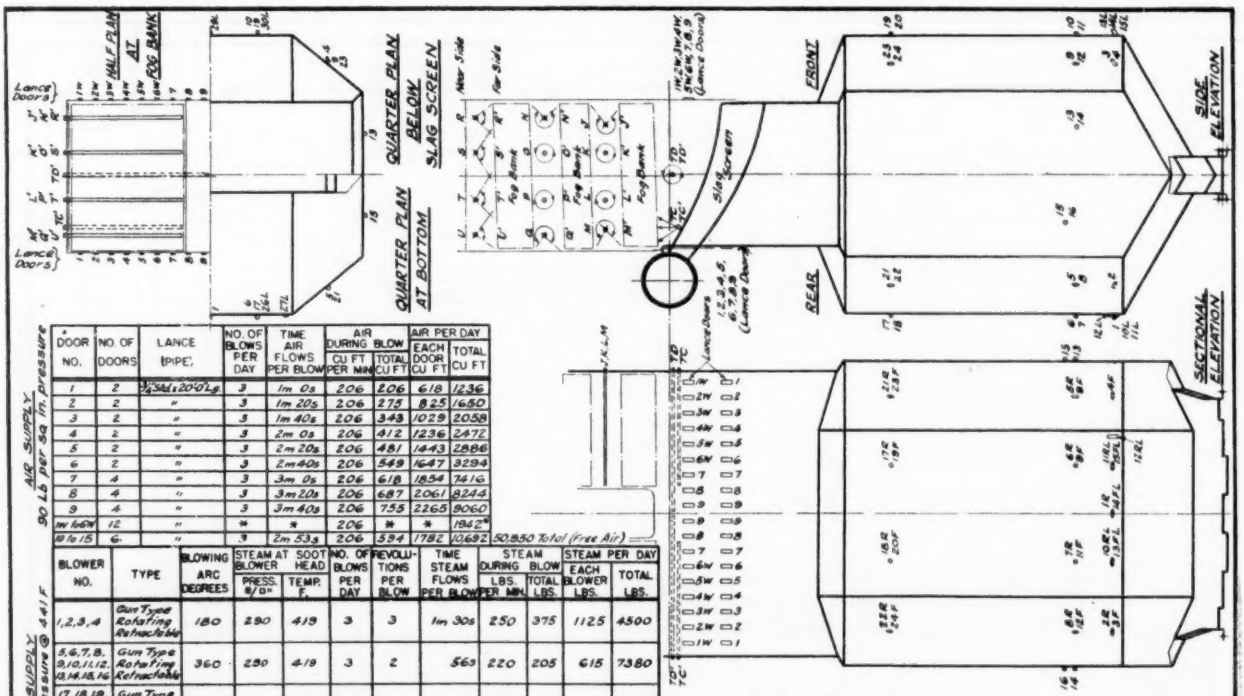
BLOWER NO.	TYPE	BLOWING ARC DEGREES	STEAM AT BLOWER PRESS. #/□"	SOOT HEAD TEMP. F.	NO. OF BLOWS PER DAY	REVOLUTIONS PER BLOW	TIME STEAM FLOWS PER BLOW	STEAM DURING BLOW LBS. PER MIN.	STEAM DURING BLOW TOTAL LBS.	STEAM PER DAY EACH BLOWER LBS.	STEAM PER DAY TOTAL LBS.
1,2,4,6, 7,9,11,12, 13,14,17,18	Gun Type Rotating Retractable	360	450	460	3	8	48 Sec.	323	258	774	9288
7A, 7B	Rotating Retractable	360	240	403	2	-	2M 35 S	146	377	754	1508
TC, TD	do	360	240	403	2	-	4M 2 1/2	146	635	1270	2540
TE, TF	do	360	240	403	2	-	4 Min.	127	508	1016	2032
F, G	Rotating	180	340	433	2	3	27 Sec.	486	219	438	876
H, I	do	180	240	403	2	3	27 Sec.	146	66	132	264
										Amount used for heating and drawing lines (Estimated)	16,508
										Total	4446
											20,954

No hand lancing.
2 Men used during blowing operations.
6 Man hours per day, total.

BOILER NO. 51

MARION STATION

Appendix B



AIR SUPPLY 30 Lb per sq in. pressure

DOOR NO.	NO. OF DOORS	LANCE (PIPE)	NO. OF BLOWS PER DAY	TIME AIR FLOWS PER BLOW	AIR DURING BLOW CU FT PER MIN	AIR DURING BLOW TOTAL CU FT	AIR PER DAY EACH DOOR CU FT	AIR PER DAY TOTAL CU FT
1	2	3/4 Std x 20'0" Lg	3	1m 0s	206	206	618	1236
2	2	"	3	1m 20s	206	275	825	1650
3	2	"	3	1m 40s	206	343	1029	2058
4	2	"	3	2m 0s	206	412	1236	2472
5	2	"	3	2m 20s	206	481	1443	2886
6	2	"	3	2m 40s	206	549	1647	3294
7	4	"	3	3m 0s	206	618	1854	7416
8	4	"	3	3m 20s	206	687	2061	8244
9	4	"	3	3m 40s	206	755	2265	9060
1W to 6W	12	"	*	*	206	*	*	1962*
13 to 15	6	"	3	2m 53s	206	594	1782	10,692
								50,850 Total (Free Air)

STEAM SUPPLY 370 Lb per sq in. pressure @ 441 F

BLOWER NO.	TYPE	BLOWING ARC DEGREES	STEAM AT BLOWER PRESS. #/□"	SOOT HEAD TEMP. F.	NO. OF BLOWS PER DAY	REVOLUTIONS PER BLOW	TIME STEAM FLOWS PER BLOW	STEAM DURING BLOW LBS. PER MIN.	STEAM DURING BLOW TOTAL LBS.	STEAM PER DAY EACH BLOWER LBS.	STEAM PER DAY TOTAL LBS.
1,2,3,4	Gun Type Rotating Retractable	180	290	419	3	3	1m 30s	250	375	1125	4500
5,6,7,8, 9,10,11,12, 13,14,15,16	Gun Type Rotating Retractable	360	290	419	3	2	56 S	220	205	615	7380
17,18,19, 20,21,22, 23,24	Gun Type Rotating Retractable	360	290	419	3	2	56 S	286	267	801	6408
TC, TC'	Telescopic	-	200	388	3	-	8m 23s	105	881	2643	5286
TD, TD'	Telescopic	360	200	388	3	-	8m 9s	150	1223	3669	7338
K,K',L,L', O,O',P,P'	Rotating	360	250	406	3	3	46 S	325	249	747	5976
J,J',M,M', N,N',Q,Q'	Rotating	275	250	406	3	3	36 S	325	195	585	4680
R,R',S,S', T,T',U,U'	Rotating	100	250	406	3	3	12 S	325	65	195	1560
										Amount used for draining lines (Estimated)	49,128
										Total	4,756
											47,884

* Air for 1W to 6W same as for 1 to 6 respectively except 1 blow per week (prorated for 1 day).

R = Rear
F = Front
L = Lance

DAILY CLEANING TIME

	MEN	HOURS	MANHOURS
Steam	2	7¼	14½
Air	2	9¼	18½
Total		16½	33

MERCURY BOILER

KEARNY STATION

Appendix B

Description and Performance of Boilers 12 and 14, Trenton Channel Plant, and Boilers 9 and 10, Marysville Plant, The Detroit Edison Company

By R. J. BRANDON[1] and W. A. CARTER,[2] DETROIT, MICH.

SLAGGING IN BOILERS 12 AND 14 TRENTON CHANNEL PLANT

NO serious trouble has ever been encountered because of slagging on any of the tube surfaces of these boilers, when burning coals having ash-softening temperatures of 2500 F or higher.

Some plugging of the gas passages in the front convection banks has occurred, especially at the higher steaming rates, when burning coals having ash-softening temperatures of 2300 F or lower. These ash deposits are of the nodulized type and they are readily removed by steam-lancing once every eight hours.

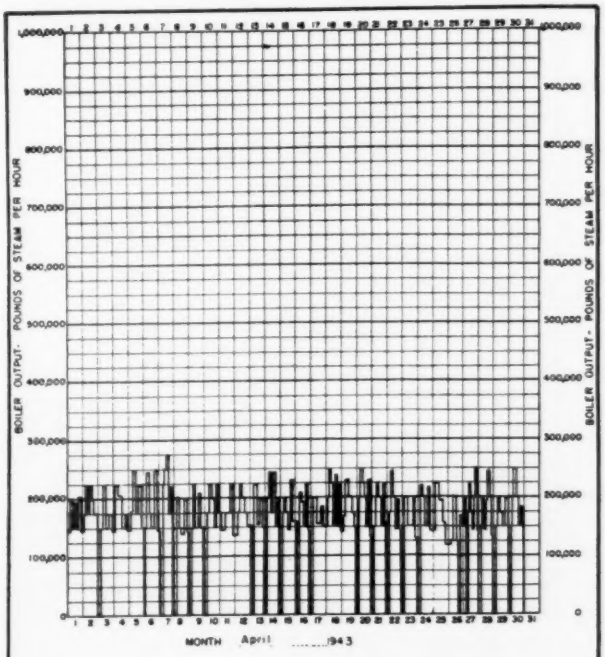
At times, ash in the form of dust collects on the hearth-screen tubes, thereby reducing the heat absorption in these tubes and increasing the furnace temperature to such a point as to cause slag reaction with the air-cooled refractories in the furnace walls, especially on the side walls where the gases turn abruptly upward.

The pressure of the primary air entering with the coal must be maintained high enough to carry the flame down in the furnace until it almost sweeps the hearth-screen tubes. If this is not done, combustion occurs nearer the apex of the furnace with the result that the ash is still plastic when it enters the front convection banks and deposits as nodulized ash on the tubes at the entrances to these banks.

More slagging of the air-cooled refractory furnace walls has been experienced with these boilers than slag collecting on the convection-tube surfaces. Slagging of these walls usually occurs before any deposits start to collect on the tubes. When the walls begin to slag, corrective air adjustments can usually be made before any slag deposits on the tube surfaces.

DESCRIPTION OF UNIT			
BUILDER Babcock & Wilcox Company			YEAR INSTALLED 1927
BOILER TYPE Stirling Type 53 Class "W"		ASH REMOVAL Dry Bottom	
PULVERIZER Raymond	FIRING Storage		BURNER Fishtail
TYPICAL FUEL			
KIND Bituminous	DISTRICT Southern Inner Crescent		SEAM Hazard Thacker
PROXIMATE ANALYSIS		ASH CHARACTERISTICS	
VOLATILE MATTER	32.60 %	INITIAL DEFORMATION	2500 F
FIXED CARBON	54.26 %	SOFTENING	2650 F
ASH	7.56 %	LIQUID	2750 F
TOTAL MOISTURE	5.58 %	SULPHUR (DRY BASIS)	0.90 %
HEAT VALUE PER LB	13,173 BTU	GRINDABILITY	45-58 %
PERFORMANCE			
BOILER OUTPUT	250,000 LB/HR	400 LB/SQ IN.	700 F
FUEL BURNED	25,270 LB/HR		330,391,000 BTU/HR
COMBUSTION AIR TEMP	250 F	FINENESS THRU 200 MESH	60 %
FUEL BURNING RATE		+50 "	3 %
FURNACE SURFACE		3176 SQ FT	104,030 BTU/HR/SQ FT
FURNACE SURFACE & CONVECTION BANK TO SUPERHEATER		6600 SQ FT	50,060 BTU/HR/SQ FT
FURNACE VOLUME		25,140 CU FT	13,140 BTU/HR/CU FT
FURNACE WIDTH		26.583 FT	12,428,660 BTU/HR/FT
FREE GAS AREA	CONVECTION BANK ENTRANCE	492 SQ FT	671,530 BTU/HR/SQ FT
	CONVECTION BANK CLOSELY SPACED TUBES	SQ FT	BTU/HR/SQ FT
	SUPERHEATER ENTRANCE	192 SQ FT	1,720,790 BTU/HR/SQ FT
	SUPERHEATER CLOSELY SPACED TUBES	SQ FT	BTU/HR/SQ FT

SPECIAL RESEARCH COMMITTEE
FURNACE PERFORMANCE FACTORS
THE AMERICAN SOCIETY OF MECHANICAL ENGINEERS
COLLECTION OF DATA ON EXISTING INSTALLATIONS
DESCRIPTION AND PERFORMANCE
COMPANY THE DETROIT EDISON COMPANY
PLANT TRENTON CHANNEL UNIT NO. 12
BY RJB DATE 6/3/43 SHEET NO. 1



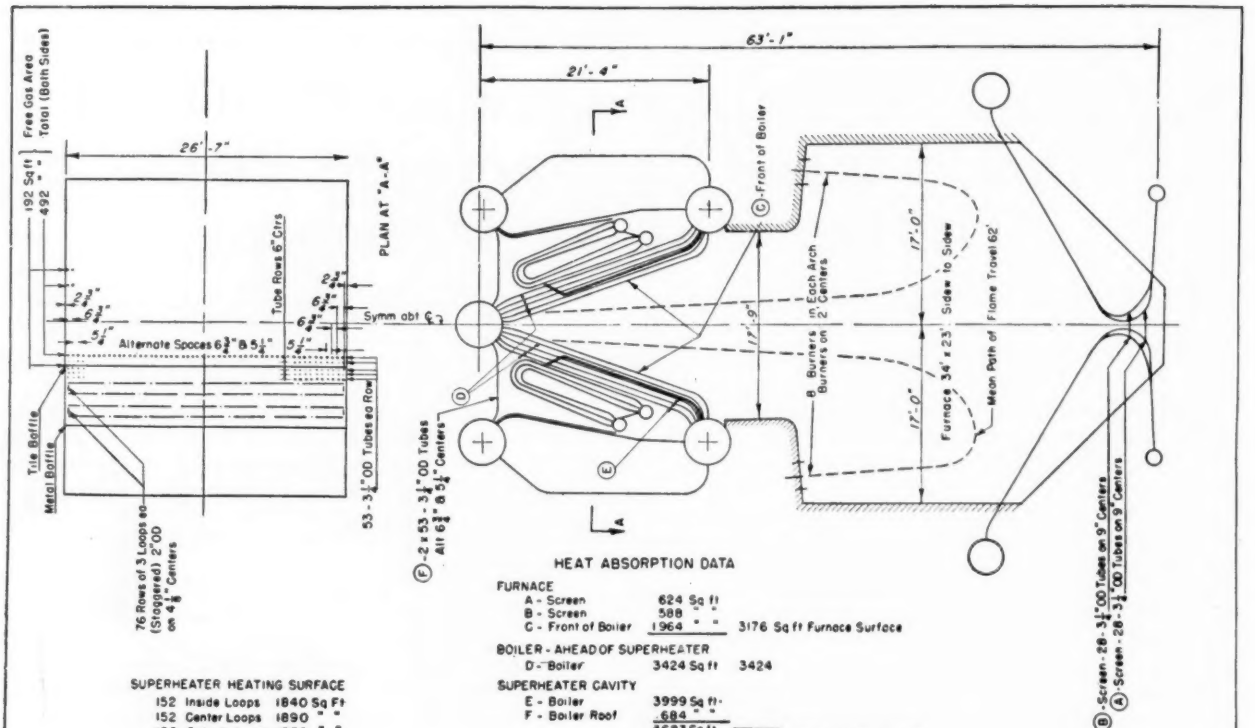
SPECIAL RESEARCH COMMITTEE
FURNACE PERFORMANCE FACTORS
THE AMERICAN SOCIETY OF MECHANICAL ENGINEERS
COLLECTION OF DATA ON EXISTING INSTALLATIONS
TYPICAL LOAD CURVE
COMPANY THE DETROIT EDISON COMPANY
PLANT TRENTON CHANNEL UNIT NO. 12
BY RJB DATE 6/3/43 SHEET NO. 3

[1] Production Department, The Detroit Edison Company. Mem. A.S.M.E.

[2] Technical Engineer, Power Plants, The Detroit Edison Company, Detroit, Mich. Mem. A.S.M.E.

Contributed by Special Research Committee on Furnace Performance Factors with the co-operation of the Fuels, Power, and Heat-Transfer Divisions and presented at the Annual Meeting, New York, N. Y., Nov. 29–Dec. 3, 1943, of The American Society of Mechanical Engineers.

NOTE: Statements and opinions advanced in papers are to be understood as individual expressions of their authors and not those of the Society.



SUPERHEATER HEATING SURFACE

152	Inside Loops	1840 Sq Ft
152	Center Loops	1890 " "
152	Outside Loops	1973 " "
4	Headers	307 " "
		6010 Sq Ft

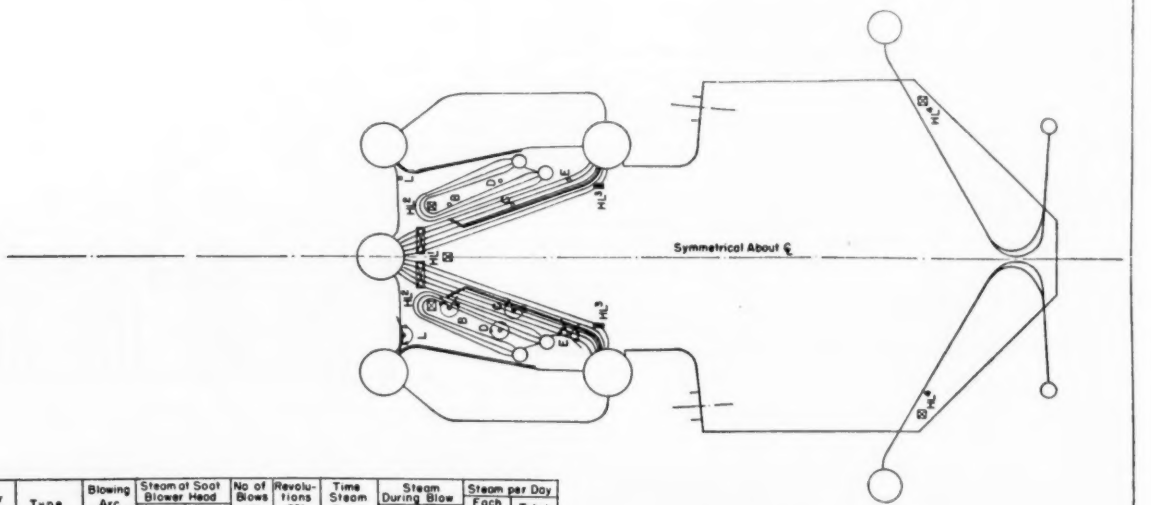
FURNACE VOLUME 25140 Cu ft

HEAT ABSORPTION DATA

FURNACE			
A - Screen	624 Sq ft		
B - Screen	588 " "		
C - Front of Boiler	1964 " "	3176 Sq ft	Furnace Surface
BOILER - AHEAD OF SUPERHEATER			
D - Boiler	3424 Sq ft	3424	
SUPERHEATER CAVITY			
E - Boiler	3999 Sq ft		
F - Boiler Roof	684 " "		
	4683 Sq ft	6600 Sq ft	Furnace Surface & Conv Bank to Superheater

Note All tubes are bare tubes, and heating surfaces are based on entire surface in contact with gas being cooled.

SPECIAL RESEARCH COMMITTEE
FURNACE PERFORMANCE FACTORS
THE AMERICAN SOCIETY OF MECHANICAL ENGINEERS
COLLECTION OF DATA ON EXISTING INSTALLATIONS
ARRANGEMENT OF FURNACE AND CONVECTION SURFACE
COMPANY THE DETROIT EDISON COMPANY
PLANT TRENTON CHANNEL POWER HOUSE UNIT NO 12
SCALE ⅛" = 1'-0" BY RR DATE 6-26-43 SHEET NO 2



Blower No	Type	Blowing Arc Degrees	Steam at Soot Blower Head Press lbs/sq in	Steam at Soot Blower Head Temp F	No of Blows per Day	Revolutions per Blow	Time Steam Flows per Blow	Steam During Blow lbs per min	Steam During Blow Total lbs	Steam per Day Each Blower lbs	Steam per Day Total lbs
B N&S E&W	Rotary	290°	200	388	2	1	12 Sec	525	105	210	840
C N&S E&W	"	270°	200	388	2	1	11 Sec	360	66	132	528
D N&S E&W	"	360°	200	388	2	1	15 Sec	525	131	262	1048
E N&S E&W	"	165°	200	388	2	1	7 Sec	360	42	84	336
L N&S E&W	"	225°	200	388	2	1	9 Sec	360	54	108	432
HL¹,² N&S E&W	2¾" Open End Hand Lance		200	388	1		2 Min	93	186		1488
										Amount Used for Heating & Draining Lines (Estimated)	4672 300 4972

Hand Lancing as Shown on Drawing and as Tabulated
2 Men Used During Soot Blowing
Time Consumed - Rotary Blowers - 2 Man Hours per Day (24 Hours)
Hand Lancing - 2 " " " " " " "
4 Man Hours per Day

Positions HL^3 & HL^4 are Lanced with 100 psi Air
Position HL^3 Occasionally
Position HL^4 Every Other Day
1 Man Hour per Day Average

SPECIAL RESEARCH COMMITTEE
FURNACE PERFORMANCE FACTORS
THE AMERICAN SOCIETY OF MECHANICAL ENGINEERS
COLLECTION OF DATA ON EXISTING INSTALLATIONS
CLEANING SCHEDULE
COMPANY THE DETROIT EDISON COMPANY
PLANT TRENTON CHANNEL POWER HOUSE UNIT NO 12
SCALE ⅛" = 1'-0" BY RR DATE 6-26-43 SHEET NO 4

DESCRIPTION OF UNIT

BUILDER Combustion Engineering Corporation		YEAR INSTALLED 1929
BOILER TYPE Stirling Type 53 Class "W"	ASH REMOVAL Dry Bottom	
PULVERIZER Raymond	FIRING Storage	BURNER Fishtail

TYPICAL FUEL

KIND Bituminous	DISTRICT Southern Inner Crescent	SEAM Hazard Thacker

PROXIMATE ANALYSIS		ASH CHARACTERISTICS	
VOLATILE MATTER	32.60 %	INITIAL DEFORMATION	2500 F
FIXED CARBON	54.26 %	SOFTENING	2650 F
ASH	7.56 %	LIQUID	2750 F
TOTAL MOISTURE	5.58 %	SULPHUR (DRY BASIS)	0.90 %
HEAT VALUE PER LB	13,173 BTU	GRINDABILITY	45-58 %

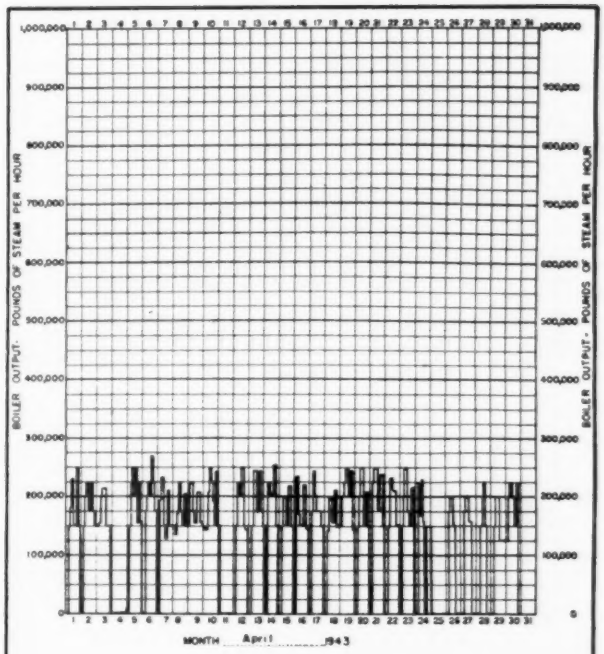
PERFORMANCE

BOILER OUTPUT	250,000 LB/HR	400 LB/SQ IN	700 F
FUEL BURNED	25,270 LB/HR	330,391,000 BTU/HR	
COMBUSTION AIR TEMP	250 F	FINENESS THRU 200 MESH	60 %
FUEL BURNING RATE		+50 "	3%

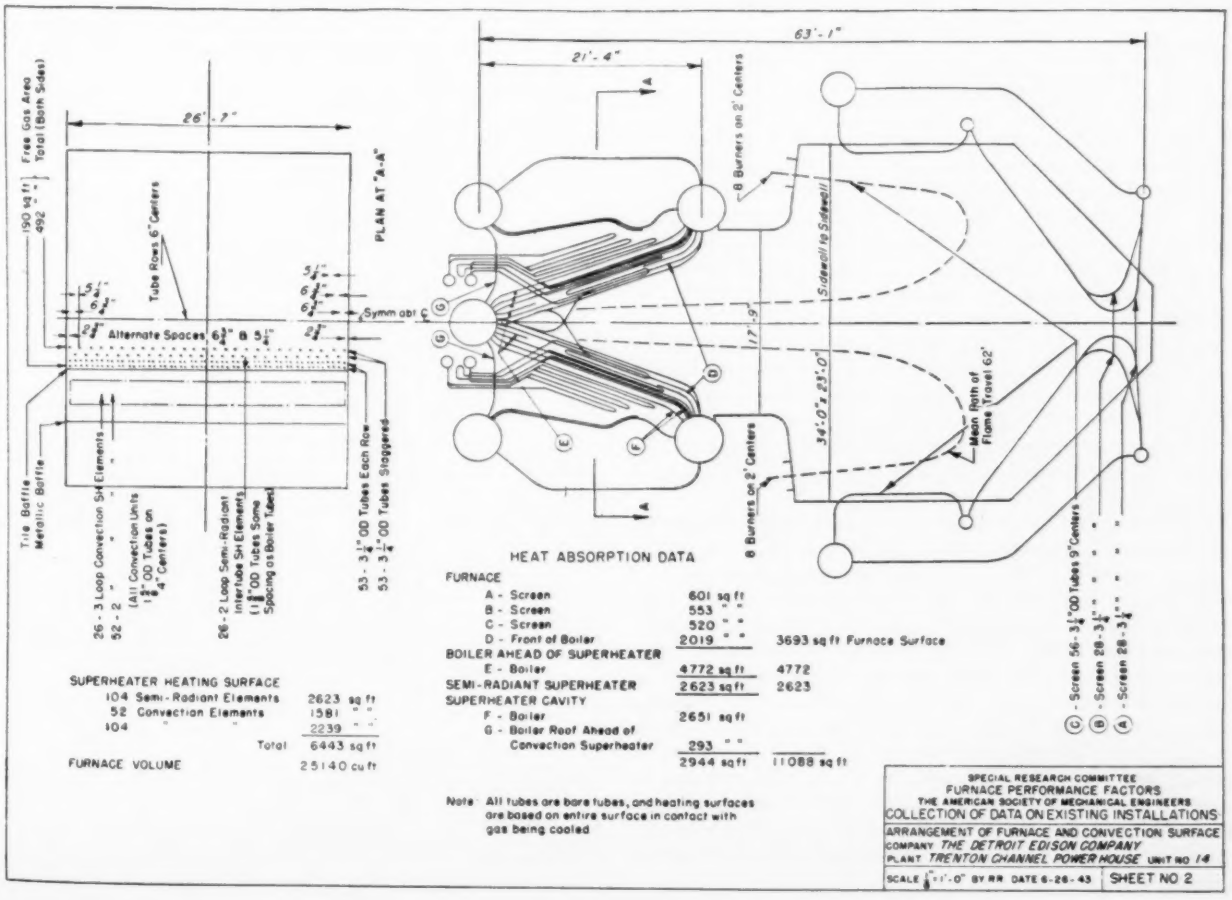
	FURNACE SURFACE	3693 SQ FT	89,460 BTU/HR/SQ FT
*	FURNACE SURFACE & CONVECTION BANK TO SUPERHEATER	11,088 SQ FT	29,800 BTU/HR/SQ FT
	FURNACE VOLUME	25,140 CU FT	13,140 BTU/HR/CU FT
	FURNACE WIDTH	26.583 FT	12,428,660 BTU/HR/FT
FREE GAS AREA	CONVECTION BANK ENTRANCE	492 SQ FT	671,530 BTU/HR/SQ FT
	CONVECTION BANK CLOSELY SPACED TUBES	SQ FT	BTU/HR/SQ FT
	SUPERHEATER ENTRANCE	190 SQ FT	1,738,900 BTU/HR/SQ FT
	SUPERHEATER CLOSELY SPACED TUBES	SQ FT	BTU/HR/SQ FT

REMARKS: * Includes Semi-Radiant Superheater Surface

SPECIAL RESEARCH COMMITTEE
FURNACE PERFORMANCE FACTORS
THE AMERICAN SOCIETY OF MECHANICAL ENGINEERS
COLLECTION OF DATA ON EXISTING INSTALLATIONS
DESCRIPTION AND PERFORMANCE
COMPANY THE DETROIT EDISON COMPANY
PLANT TRENTON CHANNEL UNIT NO. 14
BY RJB DATE 6/3/43 SHEET NO. 1



SPECIAL RESEARCH COMMITTEE
FURNACE PERFORMANCE FACTORS
THE AMERICAN SOCIETY OF MECHANICAL ENGINEERS
COLLECTION OF DATA ON EXISTING INSTALLATIONS
TYPICAL LOAD CURVE
COMPANY THE DETROIT EDISON COMPANY
PLANT TRENTON CHANNEL UNIT NO. 14
BY RJB DATE 6/3/43 SHEET NO. 3



SUPERHEATER HEATING SURFACE

104 Semi-Radiant Elements	2623	sq ft
52 Convection Elements	1581	" "
104 " "	2239	" "
Total	6443	sq ft

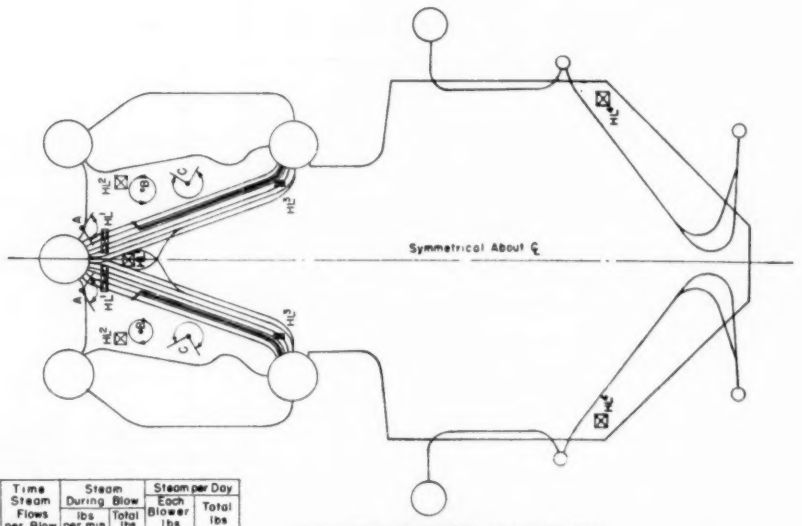
FURNACE VOLUME 25140 cu ft

HEAT ABSORPTION DATA

FURNACE			
A - Screen	601	sq ft	
B - Screen	553	" "	
C - Screen	520	" "	
D - Front of Boiler	2019	" "	3693 sq ft Furnace Surface
BOILER AHEAD OF SUPERHEATER			
E - Boiler	4772	sq ft	4772
SEMI-RADIANT SUPERHEATER	2623	sq ft	2623
SUPERHEATER CAVITY			
F - Boiler	2651	sq ft	
G - Boiler Roof Ahead of Convection Superheater	293	" "	
	2944	sq ft	11088 sq ft

Note: All tubes are bare tubes, and heating surfaces are based on entire surface in contact with gas being cooled

SPECIAL RESEARCH COMMITTEE
FURNACE PERFORMANCE FACTORS
THE AMERICAN SOCIETY OF MECHANICAL ENGINEERS
COLLECTION OF DATA ON EXISTING INSTALLATIONS
ARRANGEMENT OF FURNACE AND CONVECTION SURFACE
COMPANY THE DETROIT EDISON COMPANY
PLANT TRENTON CHANNEL POWER HOUSE UNIT NO 14
SCALE ¼"-0" BY RR DATE 6-26-43 SHEET NO 2



Blower No	Type	Blowing Arc Degrees	Steam at Soot Blower Head Press lbs/sq in	Steam at Soot Blower Head Temp F	No of Blows per Day	Revolutions per Blow	Time Steam Flows per Blow	Steam During Blow lbs per min	Steam During Blow Total lbs	Steam per Day Each Blower lbs	Steam per Day Total lbs
A N&S A " "	Rotary	120	200	388	2	1	5 Sec	360	30	60	240
B N&S B N&S	"	360	200	388	2	1	15 Sec	525	131	262	1048
C N&S C " "	"	270	200	388	2	1	11 Sec	525	96	192	768
HL^1 N&S HL^2 N&S	¾" Open End Hand Lance		200	388	1	1	2 Min	93	186		1488

Amount Used for Heating & Draining Lines (Estimated) 3544 + 300 = 3844

Hand Lancing as Shown on Drawing and as Tabulated
2 Men Used During Soot Blowing
Time Consumed - Rotary Blowers - 2 Men Hours per Day (24 Hours)
Hand Lancing - 2 " " " " " "
4 Man Hours per Day

Positions HL^3 & HL^4 are Lanced with 100psi Air
Positions HL^3 Once a Week
Positions HL^4 Every Other Day

SPECIAL RESEARCH COMMITTEE
FURNACE PERFORMANCE FACTORS
THE AMERICAN SOCIETY OF MECHANICAL ENGINEERS
COLLECTION OF DATA ON EXISTING INSTALLATIONS
CLEANING SCHEDULE
COMPANY THE DETROIT EDISON COMPANY
PLANT TRENTON CHANNEL POWER HOUSE UNIT NO 14
SCALE 1/8"-0" BY RR DATE 6-26-43 SHEET NO 4

SLAGGING IN BOILERS NO. 9 AND 10, MARYSVILLE PLANT

SLAGGING of the waterwall tube surfaces in these boilers has not been of a serious nature since, in general, the light or nodulized ash deposits can be removed readily with an air lance. Slag accumulates more quickly when the flame is sluggish and impinges on the waterwall tube surface, but this condition is improved to some extent if the secondary air is regulated to obtain optimum air velocity and distribution over the range of steaming rates. One setting of the secondary-air dampers will produce a good flame for boiler steaming rates of 300,000 lb per hr and higher, but it appears advantageous to alter the secondary-air-damper setting at lower steaming rates in order to obtain air velocities that will provide good mixing of coal and air, thereby avoiding a sluggish flame and ash impingement on the waterwall surfaces. A change in steaming rate causes some deslagging of these surfaces.

In order to indicate the distribution of slag on the waterwall tube surfaces, the furnace has been divided sectionally as shown in Fig. 1. Very little slag collects on the waterwalls in sections *A* and *C*, but the tubes in section *B* become heavily covered with nodulized deposits which are removed regularly for steam-temperature control. The entire area in section *B* becomes covered, and the deposited ash is removed by air lancing when approaching two inches in thickness. All four walls receive about the same amount of slag, with the heaviest deposits forming above and on one side of the burners, as shown in Fig. 2, and decreasing in amount higher up in the furnace. In No. 9 boiler, the slag in section *B* collects more quickly and extends to a greater height than in No. 10 boiler, which is a duplicate boiler. The height to which the slag extends in the furnace of each of these boilers is indicated in Fig. 1.

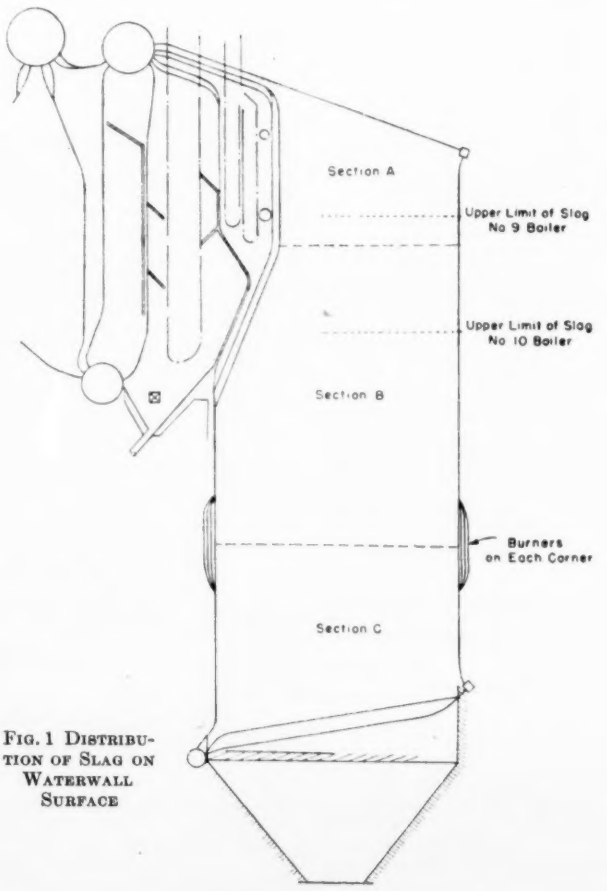


FIG. 1 DISTRIBUTION OF SLAG ON WATERWALL SURFACE

Nodulized ash deposits form on the tubes in the convection bank preceding the semiradiant superheater of No. 9 boiler and carry through to the superheater tubes in that section of the boiler where the direction of the gas flow from the firing circle is perpendicular to the superheater. This condition is illustrated in Fig. 2. Some decrease in the quantity of ash deposited has been effected by adjusting the distribution of secondary air at the burners, but as yet conditions are not as good as those obtained in No. 10 boiler. In the latter boiler, a light dust covers the fronts and backs of the tubes in the convection bank preceding the semiradiant superheater.

These boilers have been in service for only a few months, during which time the usual adjustments required on new boilers have been made. Continued operation and adjustments may result in some improvement in the slagging conditions encountered during this early service period.

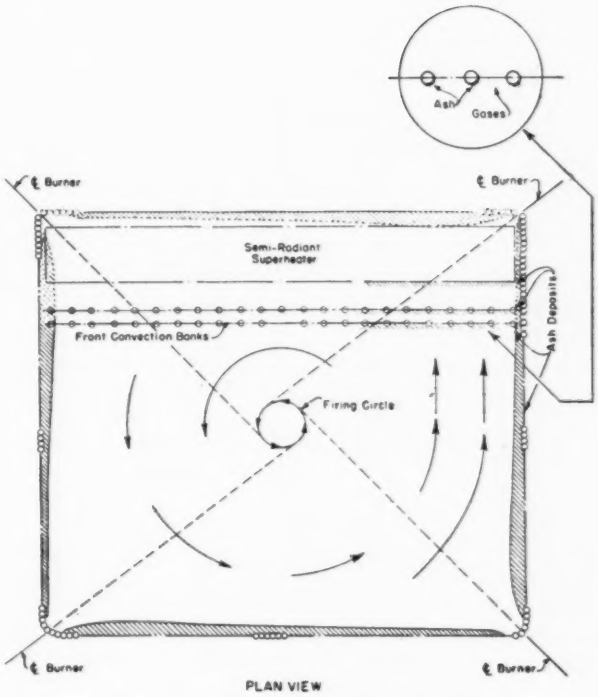
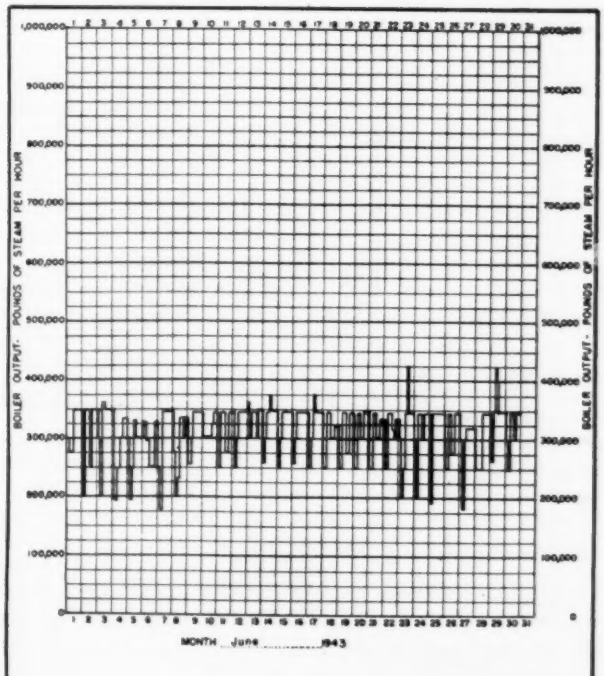


FIG. 2 DISTRIBUTION OF ASH DEPOSITS

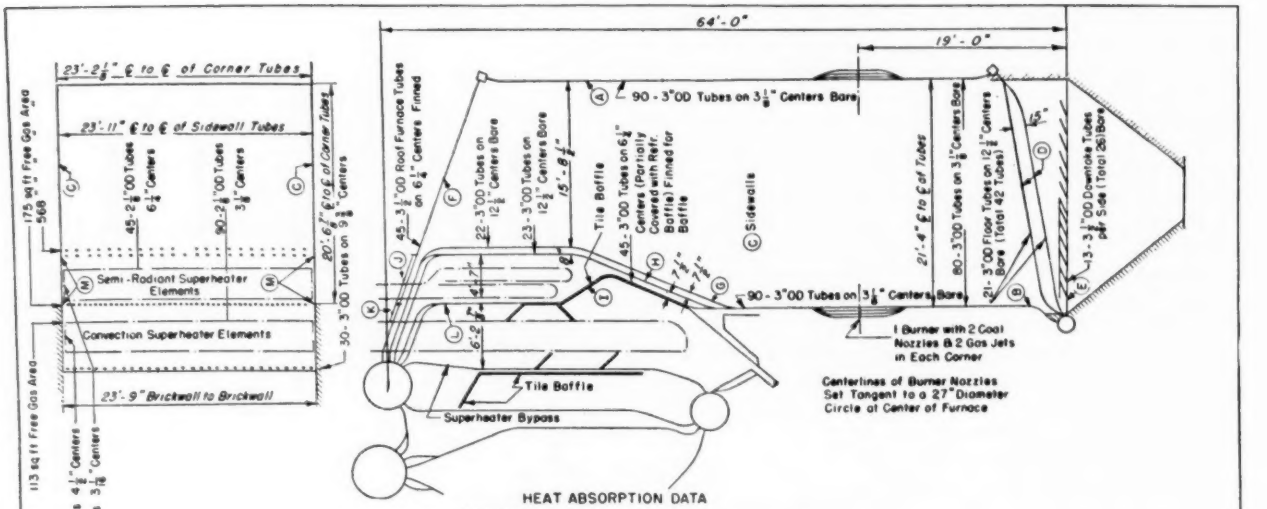
DESCRIPTION OF UNIT			
BUILDER Combustion Engineering Corporation			YEAR INSTALLED 1942
BOILER TYPE C-E Steam Generating Unit		ASH REMOVAL Dry Bottom	
PULVERIZER Raymond	FIRING Direct		BURNER Corner Tangential
TYPICAL FUEL			
KIND Bituminous	DISTRICT Southeastern Kentucky		SEAM Hazard Horizon
PROXIMATE ANALYSIS		**ASH CHARACTERISTICS**	
VOLATILE MATTER	33.57 %	INITIAL DEFORMATION	2550 F
FIXED CARBON	52.60 %	SOFTENING	2700 F
ASH	8.23 %	LIQUID	2800 F
TOTAL MOISTURE	5.60 %	SULPHUR (DRY BASIS)	0.94 %
HEAT VALUE PER LB	12,924 BTU	GRINDABILITY	46-56 %
PERFORMANCE			
BOILER OUTPUT	350,000 LB/HR	865 LB/SQ IN	910 F
FUEL BURNED	34,060 LB/HR	435,796,000 BTU/HR	
COMBUSTION AIR TEMP	565 F	FINENESS THRU 200 MESH	68 %
FUEL BURNING RATE		+30 "	1 %
FURNACE SURFACE		7098 SQ FT	61,400 BTU/HR/SQ FT
① FURNACE SURFACE & CONVECTION BANK TO SUPERHEATER		11,816 SQ FT	36,880 BTU/HR/SQ FT
FURNACE VOLUME		27,830 CU FT	15,660 BTU/HR/CU FT
FURNACE WIDTH		23.917 FT	18,221,200 BTU/HR/FT
FREE GAS AREA ②CONVECTION BANK ENTRANCE		568 SQ FT	767,250 BTU/HR/SQ FT
FREE GAS AREA ③CONVECTION BANK CLOSELY SPACED TUBES		175 SQ FT	2,490,260 BTU/HR/SQ FT
FREE GAS AREA ④SUPERHEATER ENTRANCE		113 SQ FT	3,856,600 BTU/HR/SQ FT
FREE GAS AREA SUPERHEATER CLOSELY SPACED TUBES		SQ FT	BTU/HR/SQ FT

REMARKS:
① Includes Semi-Radiant Superheater Surface
② Entrance to Rear Wall Tubes Preceding Semi-Radiant Superheater
③ Entrance to Rear Wall Tubes Following Semi-Radiant Superheater
④ Convection Superheater Entrance

SPECIAL RESEARCH COMMITTEE
FURNACE PERFORMANCE FACTORS
THE AMERICAN SOCIETY OF MECHANICAL ENGINEERS
COLLECTION OF DATA ON EXISTING INSTALLATIONS
DESCRIPTION AND PERFORMANCE
COMPANY THE DETROIT EDISON COMPANY
PLANT MARYSVILLE UNIT NO. 9
BY RJB DATE 7/7/43 SHEET NO. 1



SPECIAL RESEARCH COMMITTEE
FURNACE PERFORMANCE FACTORS
THE AMERICAN SOCIETY OF MECHANICAL ENGINEERS
COLLECTION OF DATA ON EXISTING INSTALLATIONS
TYPICAL LOAD CURVE
COMPANY THE DETROIT EDISON COMPANY
PLANT MARYSVILLE UNIT NO. 9
BY RJB DATE 7/7/43 SHEET NO. 3



HEAT ABSORPTION DATA

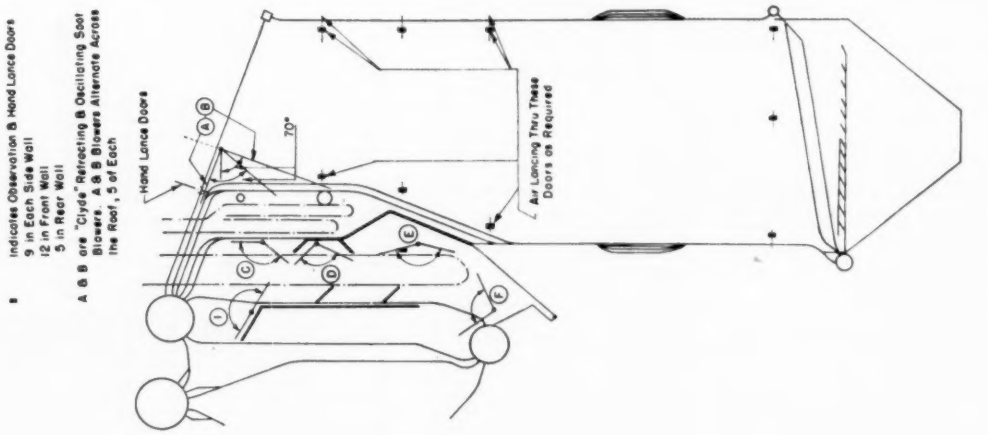
FURNACE			
A - Front Wall	(3357)	1068 sq ft	
B - Rear Wall	(2382)	758 " "	
C - Sidewall	(6684)	2127 " "	
D - Furnace Floor		751 " "	
E - Sidewall Downtake Tubes		430 " "	
F - Furnace Roof Bare Tubes 40			
" " Finned " 956		996 " "	
G - Rear Wall Tubes		493 " "	
H - " " "		475 " "	7098 sq ft Furnace Surface
SEMI-RADIANT SUPERHEATER PASS			
I - Rear Wall Tube-Finned Baffle Section		976 sq ft	
L - " " " Bare Tube		326 " "	
J - Furnace Roof - Bare Tube		168 " "	
Finned Tubes		88 " "	
Rear Wall Tubes		195 " "	
M - Sidewall Tubes	(581)	184 " "	
Semi-Radiant Superheater Elements		2589 " "	4526 sq ft
CONVECTION SUPERHEATER PASS			
K - Roof Tubes - Bare (Ahead of Superh)		69 sq ft	
Rear Wall Tubes - " " " "		123 " "	192 sq ft
			11816 sq ft

SUPERHEATER HEATING SURFACE		
45 Semi-Radiant Elements	2589 sq ft	
90 Convection Elements	13393 " "	
Total	15982 " "	
FURNACE VOLUME		
Above Furnace Floor	24420 cu ft	
Below " "	3410 " "	
Total	27830 cu ft	

Note Surfaces A-B-C & M are based on projected areas. Figures in parenthesis are based on total circumference of tubes in accordance with ASME Power Test Code on Stationary Steam-Generating Units.

SPECIAL RESEARCH COMMITTEE
FURNACE PERFORMANCE FACTORS
THE AMERICAN SOCIETY OF MECHANICAL ENGINEERS
COLLECTION OF DATA ON EXISTING INSTALLATIONS

ARRANGEMENT OF FURNACE AND CONVECTION SURFACE
COMPANY THE DETROIT EDISON COMPANY
PLANT MARYSVILLE POWER HOUSE UNITS NO 9,10,&12
SCALE ⅛"=1'-0" BY RR DATE 6-26-43 SHEET NO 2



Blower No	Type	Blowing Arc Degrees	Steam at Soot Blower Head Press lbs/sq in	Steam at Soot Blower Head Temp F	No of Blows per Day	Revolutions per Blow	Time Steam Flows per Blow	Steam During Blow lbs per min	Steam During Blow Total lbs	Steam per Day Each Blower lbs	Steam per Day Total lbs
*A & B (10)	Clyde Retracting & Oscillating	70°	750	514	1	2 Oscillations	15 Sec	500	125	125	625
C (2)	Rotary	140°	200	388	1	2	8 Sec	415	55	55	110
D (2)	"	110°	200	388	1	2	6 Sec	415	42	42	84
E (2)	"	150°	200	388	1	2	9 Sec	415	62	62	124
F (2)	"	100°	200	388	1	2	6 Sec	415	42	42	84
I (2)	"	180°	200	388	1	2	10 Sec	325	54	54	108

*5 Blowers Operated Each Day

Amount Used for Heating & Draining Lines (Estimated) 1135 + 120 = 1255

Hand Lancing as Shown on Drawing - No Schedule Established
Hand Lancing of Water Walls at Present Done with Air at 100 psi

2 Men Used During Soot Blowing
Time Consumed 3 Man Hours per Day (24 Hours)

No Hand Lancing with Steam

SPECIAL RESEARCH COMMITTEE
FURNACE PERFORMANCE FACTORS
THE AMERICAN SOCIETY OF MECHANICAL ENGINEERS
COLLECTION OF DATA ON EXISTING INSTALLATIONS

CLEANING SCHEDULE
COMPANY THE DETROIT EDISON COMPANY
PLANT MARYSVILLE POWER HOUSE UNITS NO 9,10,&12
SCALE ⅛"=1'-0" BY RR DATE 6-26-43 SHEET NO 4

Performance of Pulverized-Coal-Fired Boilers on Philadelphia Electric Company System

By JAMES H. HARLOW,[1] PHILADELPHIA, PA.

PARTICULARS in regard to three types of pulverized-coal-fired boilers in the Philadelphia Electric Company System are shown on the accompanying forms. All of these boilers are rated at 600,000 lb of steam per hr normal capacity. The Richmond Station boilers which were put into operation in 1935 operate at 425 psig with feedwater at 315 F and a steam temperature of 850 F. The Schuylkill Station boilers started operation in 1938. The steam conditions at this location are 1350 psig and 910 F with feedwater at 400 F. The Chester Station boilers, which went into service in 1941, produce steam at 1350 psig and 925 F with feedwater at 400 F. There are two boilers of each type at their respective locations.

Fuel

All of these boilers are pulverized-coal-fired. In general, slack coal from a number of operators in the central Pennsylvania fields is used. The coal is from a number of seams and varies somewhat in proximate analysis. Following are three typical analyses:

Seam	*B*	*D* + *E*	*E*
Fixed carbon, dry	67.8	70.9	75.3
Volatile, dry	23.2	22.0	17.3
Ash, dry	9.0	7.1	7.4
Sulphur, dry	2.4	1.7	1.7
Btu per lb, dry	14120	14400	14400
Moisture	2.4	2.5	3.8

The grindability of these coals is 115 to 125 on the Hardgrove index, and the fusion temperature of the ash ranges from 2450 to 2600 F.

Coal Preparation and Burning Equipment

At Richmond the coal for each boiler is pulverized by two type-B Babcock & Wilcox mills which have two rows of balls and which operate as part of a bin system. Each boiler is equipped with eight intertube, downfired burners which have individual feeder control at the bin. The burners are arranged on the roof of the furnace in two rows of four each. Each burner has four nozzles, each nozzle being directly over alternate tubes. The tubes are protected against erosion by semicircular guards. Secondary air is supplied around the burners through individual burner wind boxes.

At Schuylkill a unit system is installed which employs three Raymond bowl mills per boiler. Each mill supplies four burners, a total of twelve per boiler, one in each corner of the furnace, arranged for tangential firing. These burners fire horizontally; the coal stream is surrounded by the secondary air with additional provision for admitting secondary air through ports above and below the three burners in each corner.

At Chester a unit system is also installed. This installation comprises three type-E Babcock & Wilcox pulverizers per boiler. Each mill supplies coal to two intertube, downfired burners. The six burners are arranged in one row along the roof of the furnace. The burners are similar to the Richmond burners with the exception that each burner has sixteen smaller nozzles, four over each of four tubes, and that a steeple-type splitter is provided over the tubes instead of the semicircular tube guard.

The coal at all locations is pulverized so that from 75 to 80 per cent passes a 200-mesh sieve.

Slag and Ash Disposal

The three types of furnaces are arranged for slag tapping; the Richmond furnace is intermittently tapped and the others drain continuously. The Chester boilers are of the open-pass design which requires a second disposal hopper under the second open pass. The material which collects at this location is quite different from that at the furnace tap. The slag particles are much larger in size and include a considerable number of clinkers.

Fly-ash particles which do not settle out of the gases are collected by dust eliminators at each station and somewhat over one half of the total coal ash is collected in this manner.

The soot-blower and telescopic-lance arrangements and the operating cycle of these devices are shown on the attached drawings. The mechanical cleaning is supplemented by hand lancing.

Boiler Loading

Graphs showing a month of typical loading are attached for the boilers at each of these locations. In all cases, it will be noted that these boilers are required to carry a sustained load at or near their rated capacity for most of the time. This results from the fact that they supply the most efficient turbines on the system, and that the aggregate capacity of these turbines is low enough so that normal load variations can be carried on other less economical units without reducing load on these boilers, except during periods of high output on hydro. The months selected were months of comparatively low hydrogeneration. Full hydro output is normally expected for only 30 per cent of the year.

Some comment on each of the graphs is required. The Richmond graph shows a steady output of about 580,000 lb per hr. This is slightly low due to turbine limitations during the period covered by the graph. On the Schuylkill graph, it will be noted that there is a daily drop in output of short duration just after midnight. This drop is to about one third of boiler rating and lasts for about one-half hour. It has been found that following this procedure serves to crack the slag from the furnace walls thus reducing the amount of lancing required to keep the steam temperature within required limits. The output of the Chester boilers is reduced slightly on about a daily schedule to permit the operators to clean thoroughly slag from the upper third of the second open pass.

Slag Troubles

Richmond Station

The normal load at Richmond is such that practically no trouble has been encountered in tapping the furnace. With the

[1] Assistant Superintendent, Station Economy Section, Philadelphia Electric Company. Mem. A.S.M.E.

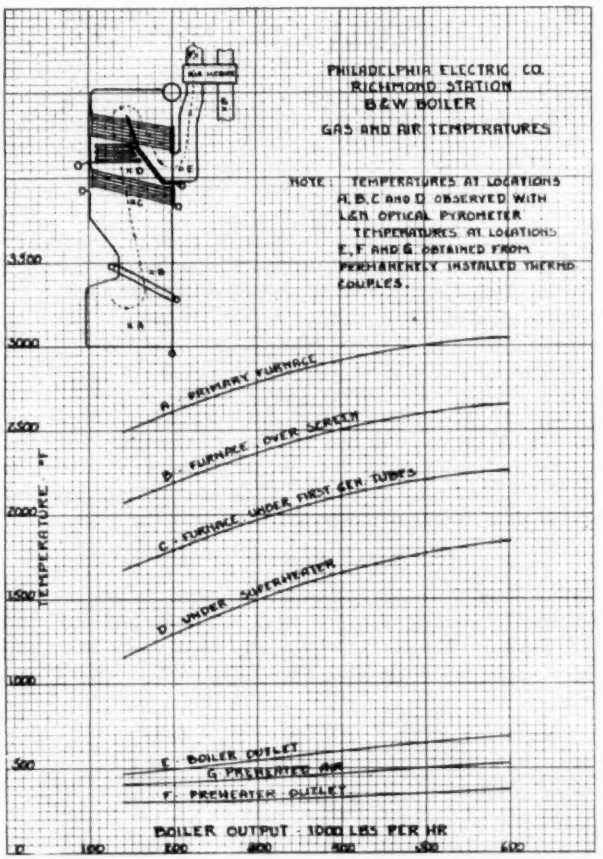
Contributed by Special Research Committee on Furnace Performance Factors with the co-operation of the Fuels, Power, and Heat Transfer Divisions and presented at the Annual Meeting, New York, N. Y., November 29–December 3, 1943, of The American Society of Mechanical Engineers.

Note: Statements and opinions advanced in papers are to be understood as individual expressions of their authors and not those of the Society.

type of coal normally burned, satisfactory tapping can be obtained at about two thirds of rated capacity.

During the early period of operation of these boilers, considerable difficulty was experienced with heavy slag accumulations on the furnace screen and in the lower bank of generating tubes. A considerable amount of sintered ash also accumulated in the superheater. At this time the spaces between tubes in the furnace screen, which is made up of two rows of tubes, were closed over by a series of chrome cement baffles connecting tubes in the lower row with tubes in the upper row in such a manner as to form a sort of louver construction. This allowed passage for the gases but prevented the generating tubes from "seeing" the fire in the primary furnace directly. It also provided an excellent shelf for slag particles to land on once they had passed through the screen and started to fall back into the furnace or for drippings from the generating tubes to land on. Also at this time, no provision was made for mechanically cleaning in these furnace areas.

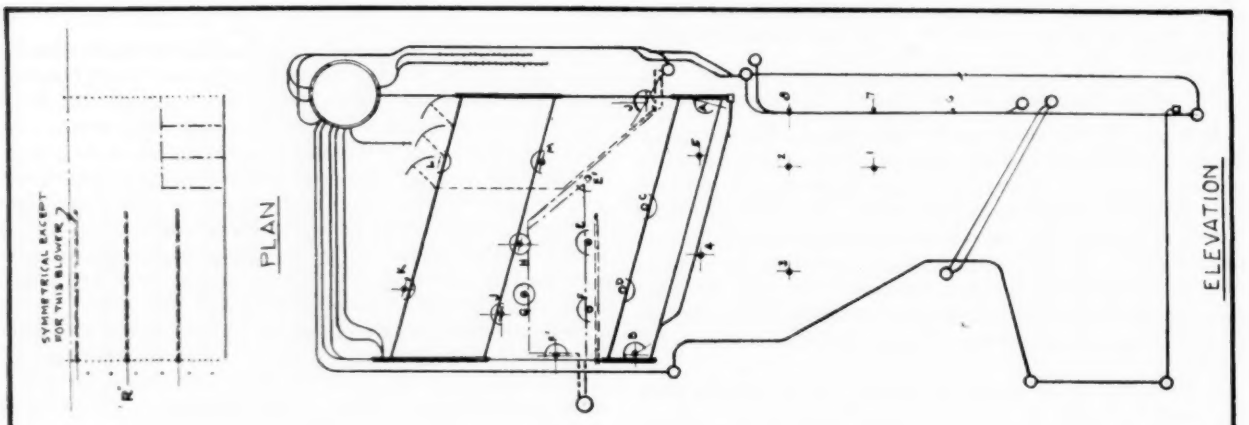
At the present time the chrome baffles are nonexistent, having had a relatively short life in the furnace and not being replaced. Retractable wall blowers using steam have been installed to remove the slag on the screen and telescopic lances using water have been installed in the lower bank of generating tubes. The regular operation of these mechanical cleaning devices, together with about 160 man-hours per week per boiler of hand lancing serves to keep these boilers in condition for almost steady operation.



Schuylkill Station

Slag tapping at Schuylkill has not been a problem with the coal normally used. The minimum satisfactory tapping load appears to be about two thirds of rated capacity.

Some trouble was experienced with slag attack on the floor tubes and on wall tubes in the section under the floor due to penetration of the furnace bottom by the molten slag. This was cor-



BLOWER NO.	TYPE	BLOWING ARC DEGREES	STEAM AT BLOWER PRESS. @ 0°	STEAM AT BLOWER TEMP. F.	SOOT HEAD	NO. OF BLOWS PER DAY	REVOLUTIONS PER BLOW	TIME STEAM FLOWS PER BLOWER	STEAM DURING BLOW LBS. PER MIN.	STEAM DURING BLOW TOTAL LBS.	STEAM PER DAY EACH BLOWER LBS.	STEAM PER DAY TOTAL LBS.
1-2-3 6-7-8	WALL RETRACTABLE	360	REMOVED -		NOT	EFFECTIVE						
4-5	TELESCOPIC WATER	360	175 WATER		6	CONTINUOUS						
A-B-C D-E-E' F-F'-M	REVOLVING		REMOVED									
G-H-J K-L	"	360	175	450	6	2						
R	RETRACTABLE 5 UNITS	360	TO BE	INSTALLED	NOV. 1943							

SPECIAL RESEARCH COMMITTEE
FURNACE PERFORMANCE FACTORS
THE AMERICAN SOCIETY OF MECHANICAL ENGINEERS
COLLECTION OF DATA ON EXISTING INSTALLATIONS

CLEANING SCHEDULE
COMPANY – PHILADELPHIA ELECTRIC COMPANY
PLANT – RICHMOND STATION UNIT NO. 6S & 6G
SCALE 3/8"=1'-0" BY C.P. DATE 9-20-43 SHEET NO. 4

DESCRIPTION OF UNIT

BUILDER	Babcock & Wilcox Company	YEAR INSTALLED	1935
BOILER TYPE	Cross Drum	ASH REMOVAL	Slag Tap
PULVERIZER	B&W Double Roll	FIRING	Storage	BURNER	Intertube

TYPICAL FUEL

KIND	Bituminous	DISTRICT	Central Penna.	SEAM	Cambria "B"

PROXIMATE ANALYSIS			ASH CHARACTERISTICS		
VOLATILE MATTER	21.83	%	INITIAL DEFORMATION	2200	F
FIXED CARBON	68.92	%	SOFTENING	2400	F
ASH	6.19	%	LIQUID	2600	F
TOTAL MOISTURE	3.06	%	SULPHUR (DRY BASIS)	1.8	%
HEAT VALUE PER LB As Fired / Dry	14060 / 14500	BTU	GRINDABILITY	100	%

PERFORMANCE

BOILER OUTPUT	600,000	LB/HR	425	LB/SQ IN	850 F
FUEL BURNED	56,300	LB/HR	Dry	816×10^6	BTU/HR
COMBUSTION AIR TEMP	507	F	FINENESS THRU 200 MESH		%

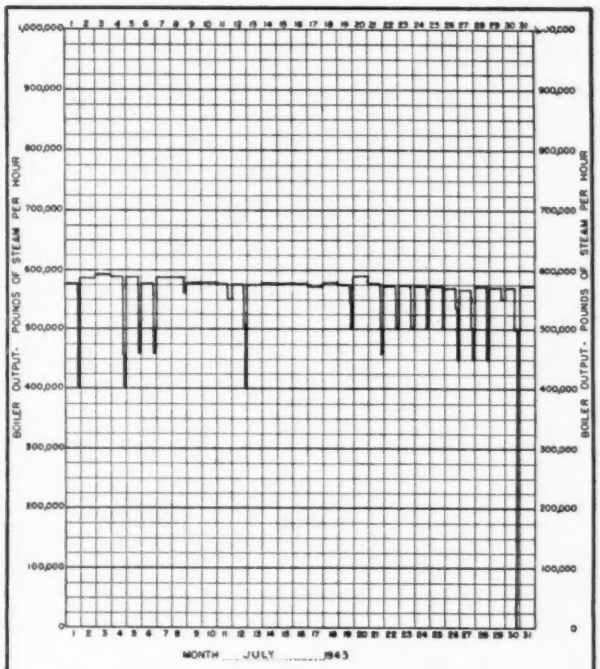
FUEL BURNING RATE

FURNACE SURFACE		6,047 SQ FT	120,000	BTU/HR/SQ FT
FURNACE SURFACE & CONVECTION BANK TO SUPERHEATER		13,382 SQ FT	60,600	BTU/HR/SQ FT
FURNACE VOLUME	by Arr. *	* 26,860 CU FT	30,300	BTU/HR/CU FT
FURNACE WIDTH		29.66 FT	27.5×10^6	BTU/HR/FT
FREE GAS AREA	CONVECTION BANK ENTRANCE	495 SQ FT	1,650,000	BTU/HR/SQ FT
	CONVECTION BANK CLOSELY SPACED TUBES	305 SQ FT	2,680,000	BTU/HR/SQ FT
	SUPERHEATER ENTRANCE	157 SQ FT	5,200,000	BTU/HR/SQ FT
	SUPERHEATER CLOSELY SPACED TUBES	157 SQ FT	5,200,000	BTU/HR/SQ FT

REMARKS:

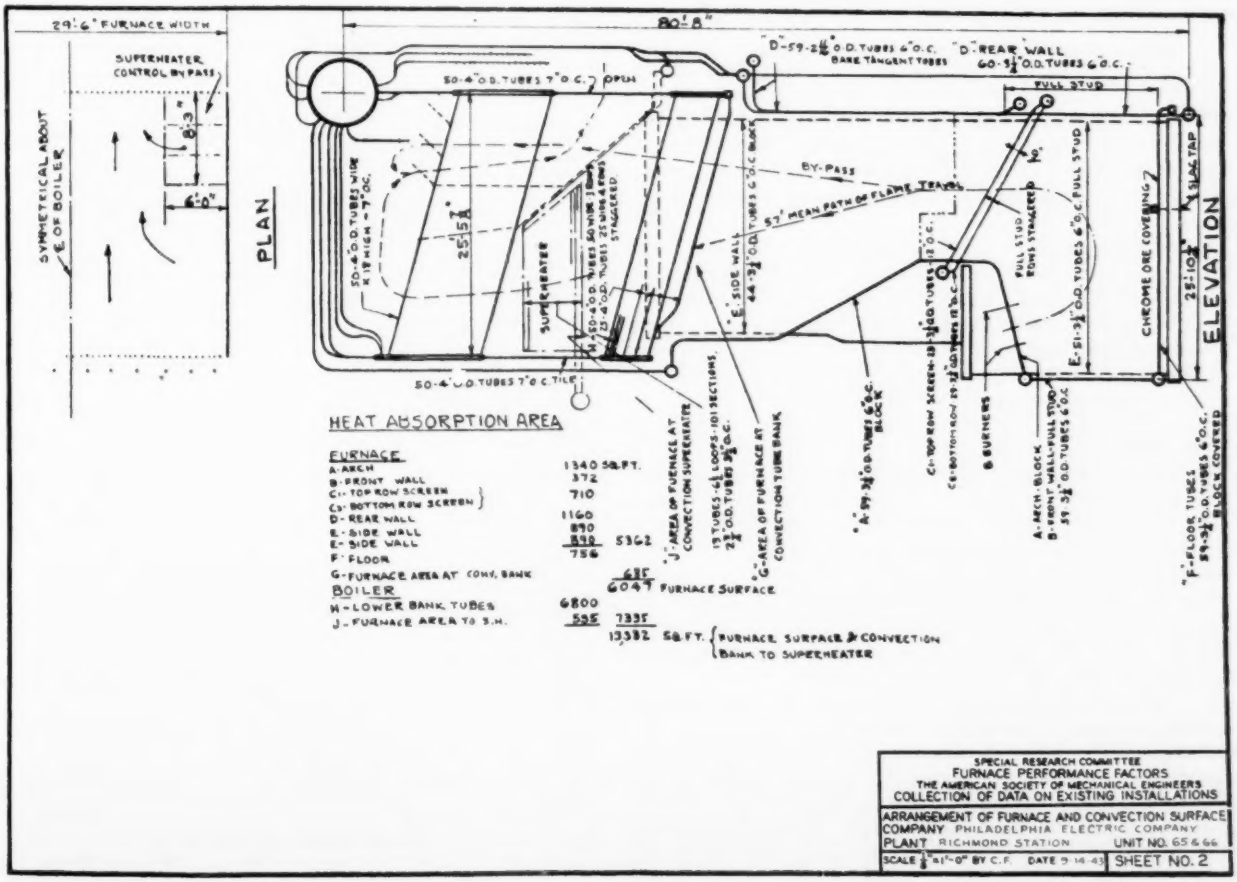
SPECIAL RESEARCH COMMITTEE
FURNACE PERFORMANCE FACTORS
THE AMERICAN SOCIETY OF MECHANICAL ENGINEERS
COLLECTION OF DATA ON EXISTING INSTALLATIONS

DESCRIPTION AND PERFORMANCE
COMPANY Philadelphia Electric Company
PLANT Richmond UNIT NO. 65 & 66
BY DATE SHEET NO. 1



SPECIAL RESEARCH COMMITTEE
FURNACE PERFORMANCE FACTORS
THE AMERICAN SOCIETY OF MECHANICAL ENGINEERS
COLLECTION OF DATA ON EXISTING INSTALLATIONS

TYPICAL LOAD CURVE
COMPANY PHILADELPHIA ELECTRIC CO.
PLANT RICHMOND UNIT NO. 66
BY C.A.C. DATE 9-21-43 SHEET NO. 3



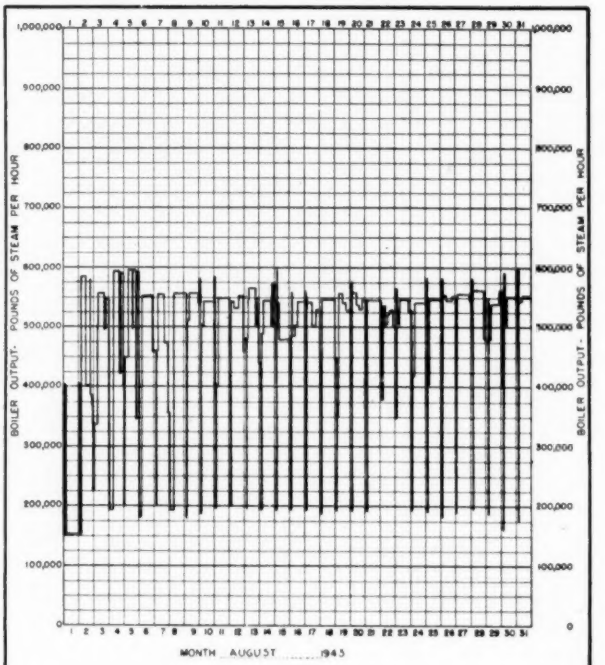
SPECIAL RESEARCH COMMITTEE
FURNACE PERFORMANCE FACTORS
THE AMERICAN SOCIETY OF MECHANICAL ENGINEERS
COLLECTION OF DATA ON EXISTING INSTALLATIONS

ARRANGEMENT OF FURNACE AND CONVECTION SURFACE
COMPANY PHILADELPHIA ELECTRIC COMPANY
PLANT RICHMOND STATION UNIT NO. 65 & 66
SCALE ⅛"=1'-0" BY C.F. DATE 9-14-43 SHEET NO. 2

DESCRIPTION OF UNIT					
BUILDER	Combustion Engineering Company			YEAR INSTALLED	1938
BOILER TYPE	Bent Tube		ASH REMOVAL	Slag Tap	
PULVERIZER	Raymond	FIRING Direct		BURNER	Tangential
TYPICAL FUEL					
KIND	Bituminous	DISTRICT Central Penna.		SEAM	Cambria "B"
PROXIMATE ANALYSIS			**ASH CHARACTERISTICS**		
VOLATILE MATTER	21.83 %		INITIAL DEFORMATION	2200	F
FIXED CARBON	68.92 %		SOFTENING	2400	F
ASH	6.19 %		LIQUID	2600	F
TOTAL MOISTURE	3.06 %		SULPHUR (DRY BASIS)	1.8	%
HEAT VALUE PER LB As Fired 14060 / Dry 14500	BTU		GRINDABILITY	100	%
PERFORMANCE					
BOILER OUTPUT	600,000 LB/HR	1350 LB/SQ IN		910	F
FUEL BURNED	52,600 LB/HR	766×10^6			BTU/HR
COMBUSTION AIR TEMP	528 F	FINENESS THRU 200 MESH			%
FUEL BURNING RATE					
FURNACE SURFACE		6,432 SQ FT		108,000	BTU/HR/SQ FT
FURNACE SURFACE & CONVECTION BANK TO SUPERHEATER		9,357 SQ FT		82,300	BTU/HR/SQ FT
FURNACE VOLUME by Mfr. *		* 27,300 CU FT		28,000	BTU/HR/CU FT
FURNACE WIDTH		28.5 FT		26.8×10^6	BTU/HR/FT
FREE GAS AREA — CONVECTION BANK ENTRANCE		509 SQ FT		1,500,000	BTU/HR/SQ FT
FREE GAS AREA — CONVECTION BANK CLOSELY SPACED TUBES		509 SQ FT		1,500,000	BTU/HR/SQ FT
FREE GAS AREA — SUPERHEATER ENTRANCE		97 SQ FT		7,900,000	BTU/HR/SQ FT
FREE GAS AREA — SUPERHEATER CLOSELY SPACED TUBES		97 SQ FT		7,900,000	BTU/HR/SQ FT

REMARKS:

SPECIAL RESEARCH COMMITTEE
FURNACE PERFORMANCE FACTORS
THE AMERICAN SOCIETY OF MECHANICAL ENGINEERS
COLLECTION OF DATA ON EXISTING INSTALLATIONS
DESCRIPTION AND PERFORMANCE
COMPANY Philadelphia Electric Company
PLANT Schuylkill UNIT NO. 23 & 24
BY DATE SHEET NO. 1



SPECIAL RESEARCH COMMITTEE
FURNACE PERFORMANCE FACTORS
THE AMERICAN SOCIETY OF MECHANICAL ENGINEERS
COLLECTION OF DATA ON EXISTING INSTALLATIONS
TYPICAL LOAD CURVE
COMPANY PHILADELPHIA ELECTRIC CO.
PLANT SCHUYLKILL UNIT NO. 23
BY G.C.J. DATE 9-28-43 SHEET NO. 3

rected by using plastic chrome ore on the surface of the furnace floor instead of loose chrome ore.

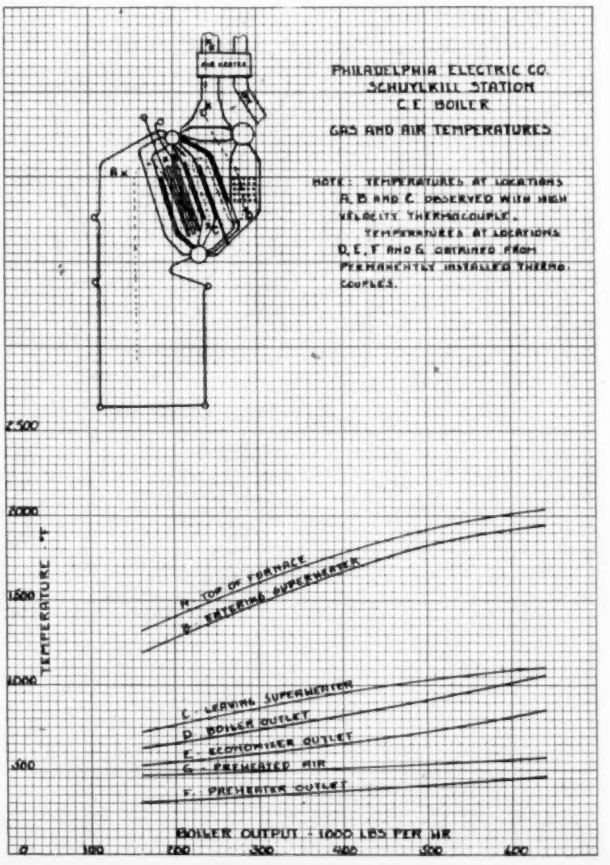
It has been found necessary to keep the furnace walls of these boilers nearly slag-free because of a high superheat condition. Whether or not furnace-wall slag would otherwise accumulate in substantial amounts cannot be definitely stated. In addition to the daily drop in load, this slag is removed by hand lancing with air and water. About 20 man-hours per week per boiler are required.

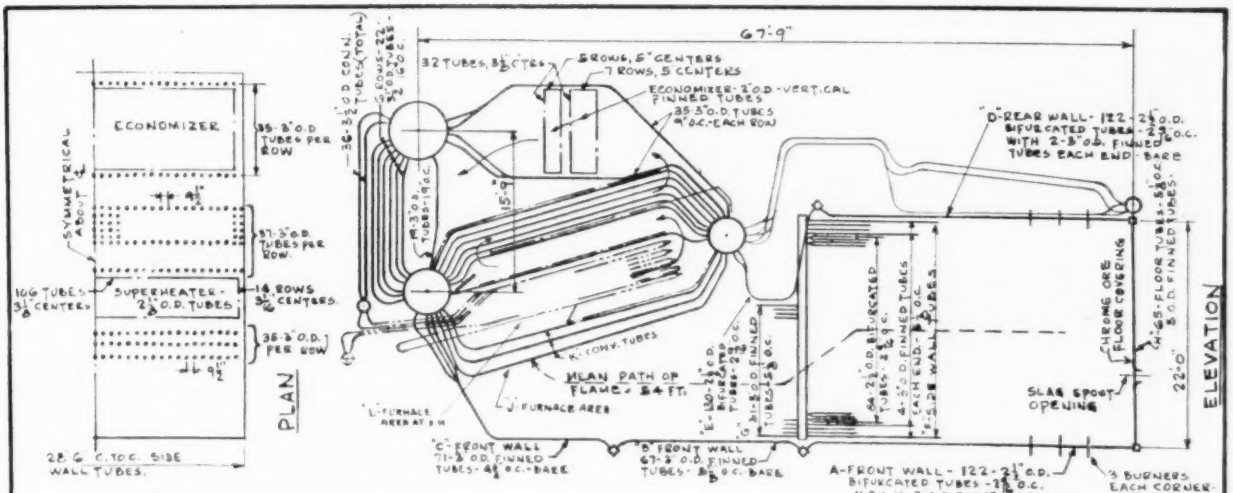
A considerable amount of slag accumulates on the front bank of generating tubes and in the closely spaced superheater tubes of these boilers. This slag accumulation is in a zone not reached by the soot blowers and must be removed by hand lancing. About 60 man-hours per week per boiler are required. The normal base load for these boilers is about 90 per cent of rated capacity as can be noted from the load graph.

Chester Station

No troubles have been experienced in the removal of primary furnace slag on these boilers, with the exception that after a period of low-load operation, and therefore an increase in furnace-wall and first open-pass slag accumulation, a heavy rush of slag is experienced when the load is increased. This has not been a serious problem; the answer is found in paying somewhat more attention to slag removal on the part of the operators during such changes in load. The minimum load for satisfactory slag tapping appears to be about two thirds of rated capacity.

The problem of ash handling in the second open-pass hopper, however, has been quite difficult. Originally, this hopper was dry and slag dripping from above accumulated into large clinkers which were very difficult to remove. A hydraulic system for removal of this material is provided and the splash from the chunks of slag spalled the brick ash-hopper lining. The ash hopper was then filled with water. This served to reduce the size of the





HEAT ABSORPTION AREA

FURNACE

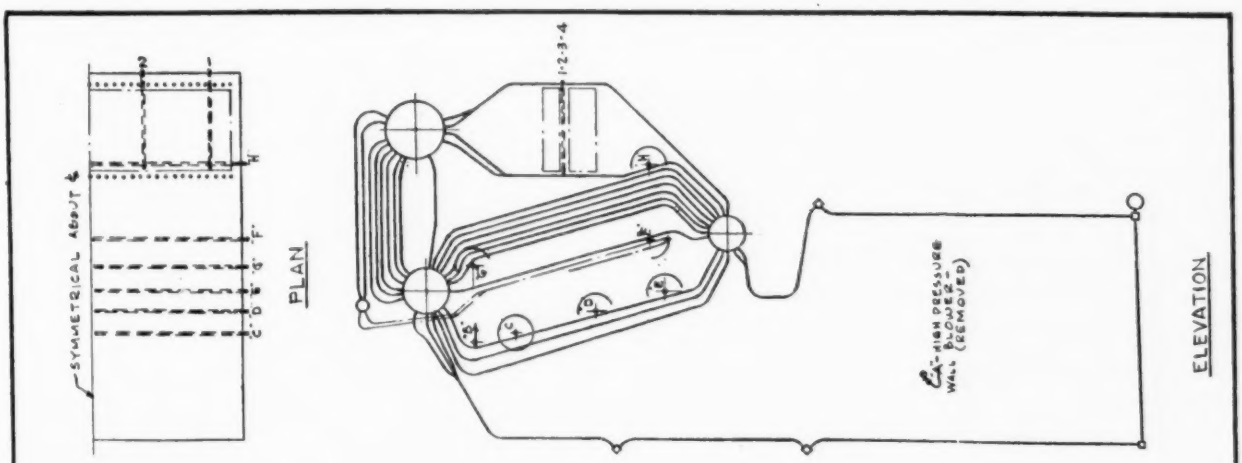
A - FRONT WALL, LOWER	883 SQ FT		
B - FRONT WALL, INTERMEDIATE	513		
C - FRONT UPPER WALL & ARCH	685		
D - REAR WALL	841		
E - REAR ARCH	527		
F - LOWER SIDE WALL	688		
F - LOWER SIDE WALL	688		
G - UPPER SIDE WALL	396		
G - UPPER SIDE WALL	296	5617	5617
H - FLOOR	698		
J - FURNACE AREA AT CONV. BANK		815	
		6432	SQ. FT. FURNACE SURFACE

BOILER

K - CONVECTION TUBES	2640		
L - FURNACE AREA AT SUPERHEATER	295	2935	
		9357	SQ. FT. FURNACE SURFACE & CONVECTION BANK TO SUPERHEATER

SPECIAL RESEARCH COMMITTEE
FURNACE PERFORMANCE FACTORS
THE AMERICAN SOCIETY OF MECHANICAL ENGINEERS
COLLECTION OF DATA ON EXISTING INSTALLATIONS

ARRANGEMENT OF FURNACE AND CONVECTION SURFACE
COMPANY — PHILADELPHIA ELECTRIC CO.
PLANT — SCHUYLKILL STATION UNIT NO. 23 & 24
SCALE ⅛" = 1'-0" BY SPAHR DATE 9-12-43 SHEET NO. 2



BLOWER NO.	TYPE	BLOWING ARC DEGREES	STEAM AT BLOWER PRESS. #/□"	SOOT HEAD TEMP. F.	NO. OF BLOWS PER DAY	REVOLUTIONS PER BLOW	TIME STEAM FLOWS PER BLOWER MIN.	STEAM DURING BLOW LBS.	STEAM DURING BLOW TOTAL LBS.	STEAM PER DAY EACH BLOWER LBS.	STEAM PER DAY TOTAL LBS.
A	WALL SLAG BLOWER-ROTATING	REMOVED - NOT EFFECTIVE									
B	FIXED	0°	175	550	6	0		300			
C, D, E, F, G, H	ROTATING		175	550	6	2		300			
1-2-3-4	ROTATING		175	550	6	2		250			

SPECIAL RESEARCH COMMITTEE
FURNACE PERFORMANCE FACTORS
THE AMERICAN SOCIETY OF MECHANICAL ENGINEERS
COLLECTION OF DATA ON EXISTING INSTALLATIONS

CLEANING SCHEDULE
COMPANY PHILADELPHIA ELECTRIC COMPANY
PLANT SCHUYLKILL STATION UNIT NO. 23 & 24
SCALE ⅛" = 1'-0" BY SPAHR DATE 9-16-43 SHEET NO. 4

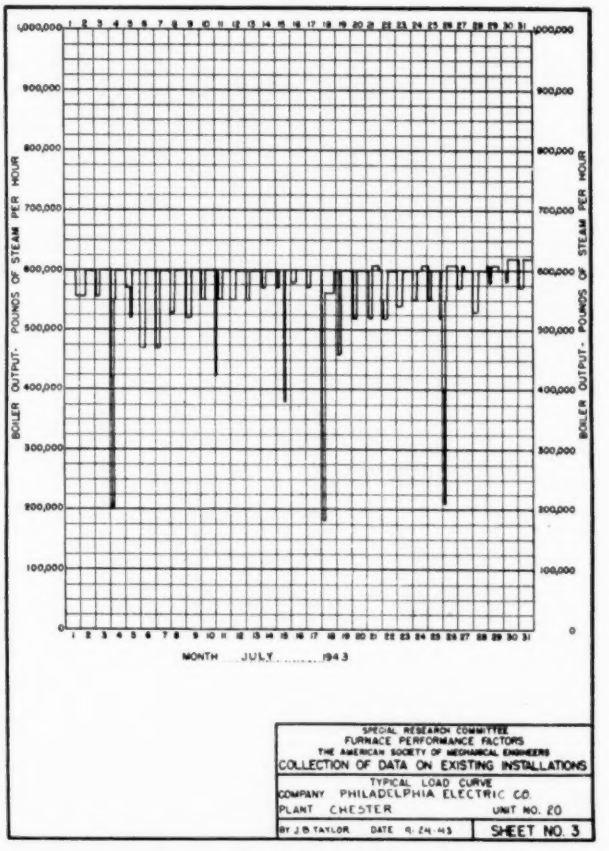
DESCRIPTION OF UNIT					
BUILDER	The Babcock & Wilcox Company			YEAR INSTALLED	1941
BOILER TYPE	Open Pass		ASH REMOVAL	Continuous Slag	
PULVERIZER	Bituminous	FIRING	Pulverized Coal	BURNER	Multi-Intertube
TYPICAL FUEL					
KIND	Bituminous	DISTRICT	Central Penna.	SEAM	Cambria "B"
PROXIMATE ANALYSIS			**ASH CHARACTERISTICS**		
VOLATILE MATTER	21.83 %		INITIAL DEFORMATION	2200	F
FIXED CARBON	68.92 %		SOFTENING	2400	F
ASH	6.19 %		LIQUID	2600	F
TOTAL MOISTURE	3.06 %		SULPHUR (DRY BASIS)	1.80	%
HEAT VALUE PER LB	As Fired 14060 BTU		GRINDABILITY	100	%
	Dry 14500				
PERFORMANCE					
BOILER OUTPUT	600,000 LB/HR	1350	LB/SQ IN.	925	F
FUEL BURNED	53,500 LB/HR	Dry	775×10^6	BTU/HR	
COMBUSTION AIR TEMP	545 F	FINENESS THRU 200 MESH		85	%
FUEL BURNING RATE					
FURNACE SURFACE		11,613 SQ FT		63,200	BTU/HR/SQ FT
FURNACE SURFACE & CONVECTION BANK TO SUPERHEATER		11,988 SQ FT		58,000	BTU/HR/SQ FT
FURNACE VOLUME	by Mfr.*	* 27,000 CU FT		28,700	BTU/HR/CU FT
FURNACE WIDTH		26.75 FT		29×10^6	BTU/HR/FT
FREE GAS AREA — CONVECTION BANK ENTRANCE		273 SQ FT		2,840,000	BTU/HR/SQ FT
FREE GAS AREA — CONVECTION BANK CLOSELY SPACED TUBES		None SQ FT		—	BTU/HR/SQ FT
FREE GAS AREA — SUPERHEATER ENTRANCE		244 SQ FT		3,180,000	BTU/HR/SQ FT
FREE GAS AREA — SUPERHEATER CLOSELY SPACED TUBES		113 SQ FT		6,850,000	BTU/HR/SQ FT

REMARKS:

SPECIAL RESEARCH COMMITTEE
FURNACE PERFORMANCE FACTORS
THE AMERICAN SOCIETY OF MECHANICAL ENGINEERS
COLLECTION OF DATA ON EXISTING INSTALLATIONS

DESCRIPTION AND PERFORMANCE

COMPANY Philadelphia Electric Company
PLANT Chester UNIT NO. 18 & 20
BY DATE SHEET NO. 1



SPECIAL RESEARCH COMMITTEE
FURNACE PERFORMANCE FACTORS
THE AMERICAN SOCIETY OF MECHANICAL ENGINEERS
COLLECTION OF DATA ON EXISTING INSTALLATIONS

TYPICAL LOAD CURVE

COMPANY PHILADELPHIA ELECTRIC CO.
PLANT CHESTER UNIT NO. 20
BY J.B. TAYLOR DATE 9-24-43 SHEET NO. 3

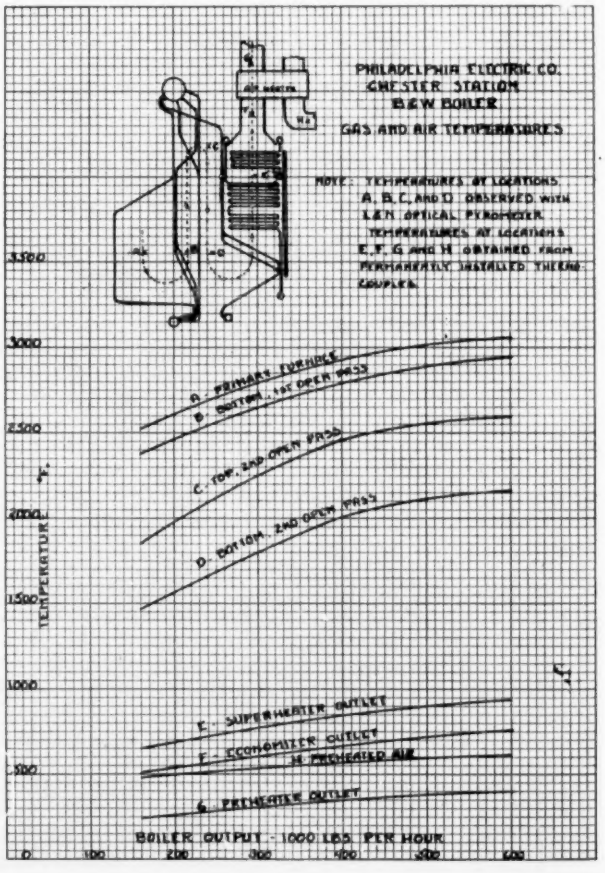
clinkers but the spalling of the brickwork continued. A steel lining for the hopper was tried and was destroyed by the acid water. At present, experiments are under way using a water-cooled cast-iron lining.

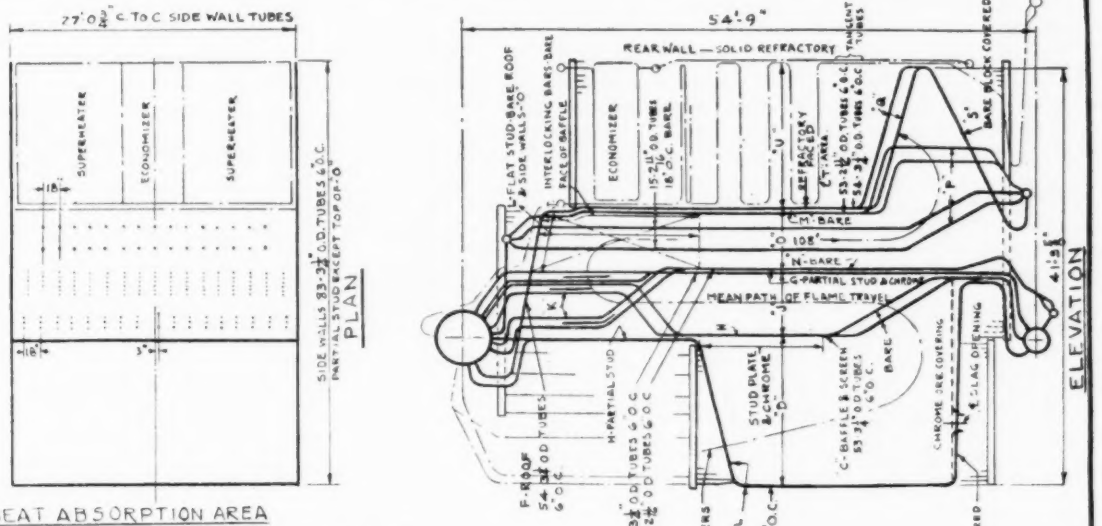
No trouble has been experienced with slag in the superheater and very little with slag on the generating tubes under the superheater. Some slag accumulates on the sloping floor under the superheater which must be removed by hand lance.

Most of the slag which must be removed accumulates on the upper third of the second open pass or in the nest of tubes at the top of the second baffle wall where the gases pass through from the first to the second open pass. At present slag accumulations in these areas are removed by hand lancing which requires about 55 man-hours per week per boiler. It is planned to install a retractable lance, using steam, in this zone in the near future, and it is hoped that most of the need for hand lancing will be eliminated thereby.

Furnace Wall Wastage

The problem of a very rapid loss of metal from furnace wall tubes was acute about two years ago. This condition was recognized first on the Philadelphia Electric Company System at Schuylkill Station. The furnace tubes of the boilers at this location were originally provided with fins, and in the course of the first two years of operation some flattening of the wall tube surface exposed to the fire and considerable loss of fin metal were noted. This was attributed, probably erroneously in view of later experience, to erosion from the coal stream and to the action of the water used in lancing the furnace walls for superheat control. It was therefore decided to change the arrangement of the furnace walls to provide tube-to-tube construction using bifurcated tubes. It was anticipated that such an arrangement would increase the furnace heat absorption and thus serve to bring the





HEAT ABSORPTION AREA

PRIMARY FURNACE		
A-ARCH	535 SQ FT	
B-FRONT WALL	375	
C-BAFFLE & SCREEN	308	
D SIDE WALL	342	
D SIDE WALL	342	1902
E-FLOOR	350	
	2452	
FIRST PASS		
F-ROOF	187	
G-REAR FACE	782	
H FRONT FACE	738	
J-SIDE WALL	222	
J-SIDE WALL	222	
K-OPEN TUBES (ACTUAL)	2858	4989

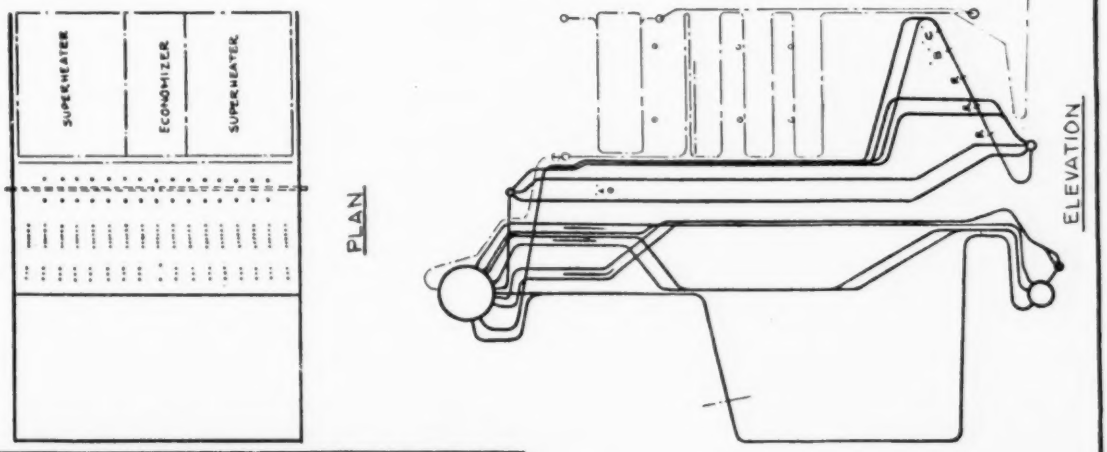
SECOND PASS		
L-ROOF	147 SQ FT	
M-REAR FACE	750	
N-FRONT FACE	935	
O-SIDE WALL	340	
O-SIDE WALL	340	
P-OPEN TUBE (ACTUAL)	1720	
Q-SUPERHEATER SCREEN	690	4322
S-HOPPER FLOOR	483	
	5205	

T-FURNACE AREA TO S.H. & ECON 11613 SQ. FT. FURNACE AREA
376
11989 SQ. FT. FURNACE SURFACE TO SUPERHEATER & ECONOMIZER

THIRD PASS	
U-SIDE WALL	322
U-SIDE WALL	322
	644

SPECIAL RESEARCH COMMITTEE
FURNACE PERFORMANCE FACTORS
THE AMERICAN SOCIETY OF MECHANICAL ENGINEERS
COLLECTION OF DATA ON EXISTING INSTALLATIONS

ARRANGEMENT OF FURNACE AND CONVECTION SURFACE
COMPANY - PHILADELPHIA ELECTRIC COMPANY
PLANT - CHESTER STATION UNIT NO. 18 & 20
SCALE 1/8"=1'-0" BY TBS DATE 9-17-43 SHEET NO. 2



BLOWER NO.	TYPE	BLOWING ARC DEGREES	STEAM AT BLOWER PRESS. #/0"	STEAM AT BLOWER TEMP. F.	SOOT HEAD NO. OF BLOWS PER DAY	REVOLUTIONS PER BLOW	TIME STEAM FLOWS PER BLOWER	STEAM DURING BLOW LBS. PER MIN.	STEAM DURING BLOW TOTAL LBS.	STEAM PER DAY EACH BLOWER LBS.	STEAM PER DAY TOTAL LBS.
A	RETRACTABLE	360	TO BE INSTALLED				OCTOBER 1943				
B-C	NOZZLE IN FL. BLOCK	0	250	530°							
R	"	REMOVED BECAUSE OF TUBE CUTTING									

SPECIAL RESEARCH COMMITTEE
FURNACE PERFORMANCE FACTORS
THE AMERICAN SOCIETY OF MECHANICAL ENGINEERS
COLLECTION OF DATA ON EXISTING INSTALLATIONS

CLEANING SCHEDULE
COMPANY - PHILADELPHIA ELECTRIC COMPANY
PLANT - CHESTER STATION UNIT NO. 18 & 20
SCALE 1/8"=1'-0" BY TBS DATE 9-15-43 SHEET NO. 4

steam temperature under better control, and so reduce the amount of lancing required. This end was accomplished in a measure but not to the extent hoped for.

Some time after the change to bifurcated tubes, the furnace was inspected and particular attention was given to discover any recurrence of the flattened-tube condition. None was noted. However, about four months later, it was necessary to take the boiler off the line on a forced outage resulting from a furnace tube leak. On inspection it was discovered that nearly all of the tubes in the lower furnace were badly wasted from the outside, and it was realized that an extensive retubing job was indicated for the immediate future. The wasted area varied from three to ten feet from the furnace floor. The tubes in the affected area were covered with a dark, hard, and firmly attached scale and an iridescent bluish material which were primarily iron-sulphite, or with a glossy yellowish green coating which was analyzed to be composed primarily of sodium and potassium sulphates and iron oxides. Several theories have been advanced as to the mechanism of the wastage and the matter remains the subject of investigation to the present time.

In order to find a practical solution to the problem exhaustive analyses of the furnace atmosphere at the wall surface were undertaken. These showed that where wastage occurred the furnace atmosphere was heavily reducing in nature as indicated by the presence of large percentages of carbon monoxide and little or no unconsumed oxygen. A means was then developed to supply air to the affected wall areas by passing the air through the space between the tubes. This had beneficial results but the air did not reach the whole affected area, and it was apparent that the real answer to the problem lay in rearranging the burners so that the atmosphere on the furnace walls would be kept on the oxidizing side. A program to accomplish this was instituted by the manufacturers of the boilers and it now appears that a much improved burner design has been obtained. The new burner has riffled edges for better coal-air mixing.

On investigation, it was found that a similar wastage condition, at a much slower rate, existed at Chester and in a limited area at the lower end of the furnace screen at Richmond. Part of the trouble at Chester and most of the trouble at Richmond appears to have resulted from infiltration at points after the furnace, which had the effect of reducing the excess air in the furnace. Experiments to the end of improving burner design and wind-box arrangement are now under way at Chester.

Gas and Air Temperatures

Curves showing gas temperatures within the furnace and at various locations throughout the boiler unit are attached for each type of boiler. A curve of preheated-air temperature is included. In all cases, combustion conditions are regulated to maintain about 15 per cent CO_2 at the boiler outlet. Each boiler is equipped with combustion control and with CO_2 recorders for this purpose.

Heat-Transfer to Water-Cooled Furnace Walls

By HENRY KREISINGER[1] and R. C. PATTERSON,[2] NEW YORK, N. Y.

THIS paper gives the results of measurements of the heat transfer to water-cooled furnace walls of two pulverized-coal-fired boiler furnaces. One of these was a slagging-bottom intermittent tap, and the other a dry-bottom furnace. Both furnaces were tangentially fired; the slagging-bottom furnace had two burners and the dry-bottom three burners in each corner of the furnace. The heat transfer was measured with small heat-absorbing units placed at different elevations in one of the walls of the furnace. Each of these units was supplied separately by water, and the quantity of heat absorbed was determined by weighing this water and measuring its temperature rise. On the tests of the dry-bottom furnace the water was supplied approximately at atmospheric pressure and 100 F, whereas on the tests of the slagging-bottom furnace the pressure was about 80 psi gage and the temperature about 70 F. The test units remained in the furnace over a period of several weeks so that the condition of their external surface was substantially the same as that of the rest of the walls.

The water-cooled walls of the slagging-bottom furnace consisted of 3-in. plain tubes spaced on $3^1/_2$-in. centers, backed up by $2^1/_2$ in. of refractory and 4 in. of insulating material. The furnace was 30 ft × 21 ft, 5 in. in cross section and averaged 49 ft, 4 in., in height between the bottom and the sloping roof. The total combustion space was 21,000 cu ft. The side walls were fully water-cooled only to the center line of the lower drum. Above this level the side walls were refractory-lined with riser tubes from the lower part of the wall placed over the refractory lining on 14-in. centers. The front wall was fully water-cooled, and the upper portion was bent over the furnace and formed the roof. The actual total frontal water-cooled surface of the walls was 4803 sq ft, of which 1411 sq ft were in the side walls, 1347 sq ft in the rear wall, and 2045 sq ft in the front wall and the roof. The actual frontal surface is the furnace half of the circumferential area of the tubes; in the fin-tube furnace it includes the front face of the fins. The total projected surface of the furnace, including the boiler, was 4470 sq ft. The projected boiler-tube surface facing the furnace was assumed to be the product of the length of the front row of tubes multiplied by the width of the furnace, which amounted to 795 sq ft. Normal rating of the steam-generating unit was 400,000 lb of steam per hour at 870 psi pressure and 825 F temperature from feedwater at 383 F.

The dry-bottom furnace water-cooled walls consisted of 3-in. finned tubes spaced on $5^1/_8$-in. centers and backed up by $2^1/_4$ in. of refractory and $3^3/_8$ in. of insulating material. The furnace was 21 ft, 10 in., × 20 ft, $1^1/_2$ in., in cross section and averaged 55 ft in height between the floor screen and the roof, and contained 19,300 cu ft of combustion space. All the walls were completely water-cooled. The actual total frontal water-cooled surface of the walls was 4613 sq ft, of which 2214 sq ft were in the side walls, 900 sq ft in the rear wall, and 1499 sq ft in the front wall and roof. The floor screen contained 740 sq ft of total surface of which one half faced the furnace and one half the ash hopper. The projected surface of the furnace including the boiler was 4460 sq ft. The projected surface of the boiler tubes facing the furnace was 645 sq ft obtained by multiplying the length of the front row of tubes by the width of the furnace. The normal capacity of the steam-generating unit was 365,000 lb of steam per hour at 860 psi, and 900 F from feedwater at 385 F.

Figs. 1 and 2 show the test units fitted into the walls of the two furnaces. Each unit consisted of extra-heavy $1^1/_4$-in. seamless pipe with $^1/_2$ × $^1/_4$-in. fins welded to its sides. The ends of the pipe were plugged and pieces of $^1/_2$-in. pipe were fitted into the back of the unit close to the plugged ends for water supply as shown in the figures. The units were 36 in. long and $2^{11}/_{16}$ in. wide, including the fins. The actual frontal surface was 121.5 sq in. or 0.844 sq ft. In addition to this frontal surface there was the surface of the plugged ends amounting to 4.33 sq in. and the $^1/_4$-in-wide band along the sides of the fins equal to 18.5 sq in. summing up to 22.8 sq in. However, this surface was much less effective in heat transfer than the frontal surface. The projected

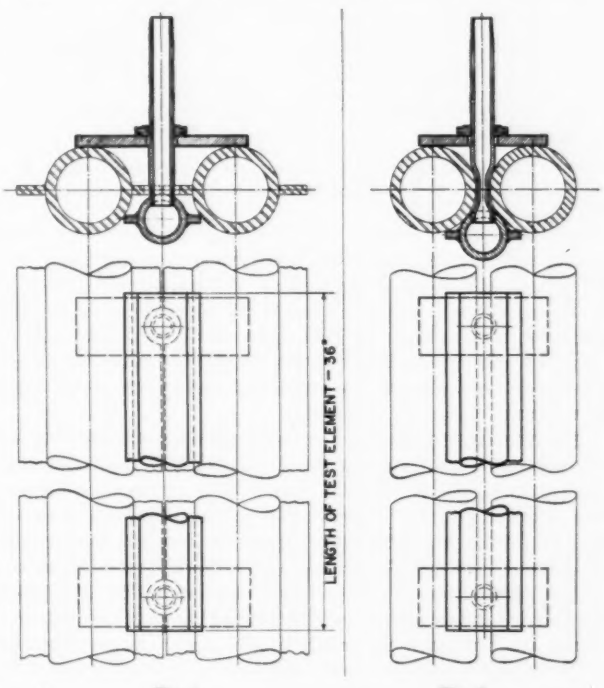


Fig. 1 Fig. 2

FIG. 1 TEST UNIT FITTED INTO FIN TUBE WALL OF DRY-BOTTOM FURNACE

FIG. 2 TEST UNIT FITTED INTO PLAIN TUBE WALL OF SLAGGING-BOTTOM FURNACE

[1] Engineer, in Charge of Research and Development, Combustion Engineering Company, Inc. Mem. A.S.M.E.

[2] Development and Research Department, Combustion Engineering Company, Inc.

Contributed by Special Research Committee on Furnace Performance Factors with the co-operation of the Fuels, Power, and Heat-Transfer Divisions and presented at the Annual Meeting, New York, N. Y., Nov. 29–Dec. 3, 1943, of THE AMERICAN SOCIETY OF MECHANICAL ENGINEERS.

NOTE: Statements and opinions advanced in papers are to be understood as individual expressions of their authors and not those of the Society.

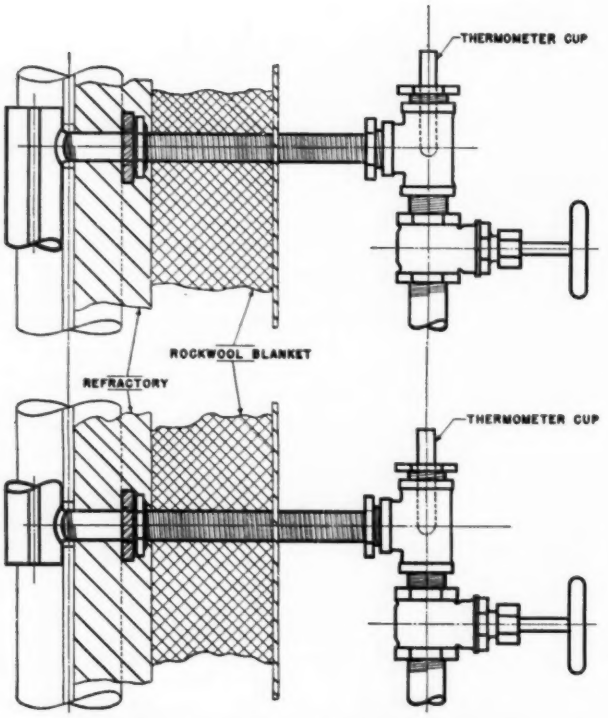


FIG. 3 TEST UNIT WITH WATER-SUPPLY LINES ASSEMBLED IN A FIN TUBE WALL FOR TEST

frontal area was 96.8 sq in. or 0.67 sq ft. The units were fitted into the walls between two adjacent tubes as shown in Figs. 1 and 2. Plastic refractory was packed into the space between the test units and the wall tubes to prevent the flow of hot gas behind the units, and to reduce the heat exchange between them and the adjacent wall tubes. Fig. 3 shows a test unit and water-supply connections with thermometer wells and control valves assembled in a fin-tube furnace wall for test.

The slagging-bottom furnace had three of these units located in the front wall at three elevations as shown in Fig. 4, designated as bottom *B*, middle *M*, and top *T*. The dry-bottom furnace had four units located in a side wall at four elevations as shown in Fig. 5 and the units were numbered from the bottom up. Pulverized coal was fired through burners located near the bottom of the furnace. The burning mixture flowed up through the furnace and imparted some of the heat generated by combustion to the furnace walls, mostly by radiation. In the slagging-bottom furnace the heat transfer was the highest near the bottom, whereas in the dry-bottom furnace it was highest just above the burner belt. The heat transfer varied with the temperature of the burning mixture and also with the cleanliness of the surface of the walls.

Readings on the test units were taken in succession, starting with the lowest and ending with the top unit. The flow of water through the test units was adjusted to a temperature rise of 40 to 70 F depending on the location of the unit. With such temperature rise, a flow of 100 lb of water in 6 to 7 min could be obtained, and a set of readings on four test units could be completed in about 30 min.

The water from the test units was piped to a common station where a weighing tank was located. While the flow of water was being adjusted to the desired temperature rise, water from all the units was discharged into a drain. When a test was started, the water from the unit on which the readings were to be taken was turned into the weighing tank. At the end of this test period the water was turned back to the drain. The period of time during which water was run into the weighing tank was measured with a stop watch. To facilitate the change of flow of water from drain to weighing tank and back again, the end of the water discharge pipe from each unit was provided with a piece of flexible hose so that the end could be quickly moved from one place to another, and thus make the time necessary for a complete set of readings as short as possible. Short periods were desirable to avoid appreciable changes in the furnace conditions between the first and last readings of each set.

With the constant rate of firing which was maintained during these tests, the principal change in the furnace conditions was the ash deposit on the walls. The effect of this ash deposit on the heat transfer depended on how soon after cleaning of the furnace walls the test readings were made. A layer of slag $^1/_{16}$ in. thick deposited on clean wall tubes had a quite marked effect on the heat transfer, whereas the same thickness of slag deposited on top of an inch layer has practically no effect.

The rate of accumulation of slag on the furnace wall varied with the height from the furnace floor. The highest rate was in the burner zone and the lowest at the top of the furnace. In the dry-bottom furnace the rate of accumulation of slag in the zone below the burners near the bottom of the furnace was also low.

To check the accuracy of the results a number of duplicate tests were made. The check tests were started immediately after the completion of the first test. Some of these check tests were on the entire set of test units and some on individual units. Usually a check test on the whole set of units showed a small decrease in the rate of heat transfer, whereas a check test on individual units showed no decrease in the heat transfer. The change in heat absorption due to slag accumulation in the dry-bottom furnace could be best observed over the period of a few hours after a thorough cleaning of the walls.

The ash deposit on the furnace walls was different in the two furnaces. In the slagging-bottom furnace the ash deposit was a thin sheet of slag extending from the bottom of the furnace to a height of 10 to 12 ft. The surface of this slag was in semiliquid condition and flowed slowly down the walls. Above this height the deposit gradually became thicker, changing from somewhat porous slag with rough surface to a spongy crusted ash near the top of the furnace. This porous slag and crusted ash was falling off in pieces so that at normal rating the deposit remained at nearly constant thickness. The furnace walls on this steam-generating unit were not cleaned during normal operation.

In the dry-bottom furnace the deposit on the furnace walls varied from a thick layer of porous slag in the burner belt through crusted ash at the elevation of the lower drum to a dusty film at the top of the furnace. Below the burner belt the deposit consisted mostly of crusted ash and dust. The walls in the burner belt and immediately above were lanced two or three times a day, depending somewhat on the kind of coal burned and the steam temperature, which in this plant was controlled almost entirely by the amount of deposit on the furnace walls. The nature of the deposits in the two furnaces is indicated by the belts *A*, *B*, *C*, and *D* in Figs. 4 and 5.

The bottom unit *B* was located in the belt where the deposit on the wall was a thin sheet of slag with the surface in semiliquid state flowing down the wall, so that the thickness of the layer remained nearly constant at any given rating. The middle unit *M* was located in a belt where the deposit on the wall was thick and sticky but did not flow; it was somewhat porous and dropped off in pieces. The top unit *T* was located in a belt where the deposit was of granulated and crusted ash which did not adhere tightly to waterwalls and small pieces were dropping off continually.

Test unit No. 2 in the dry-bottom furnace was in a belt similar

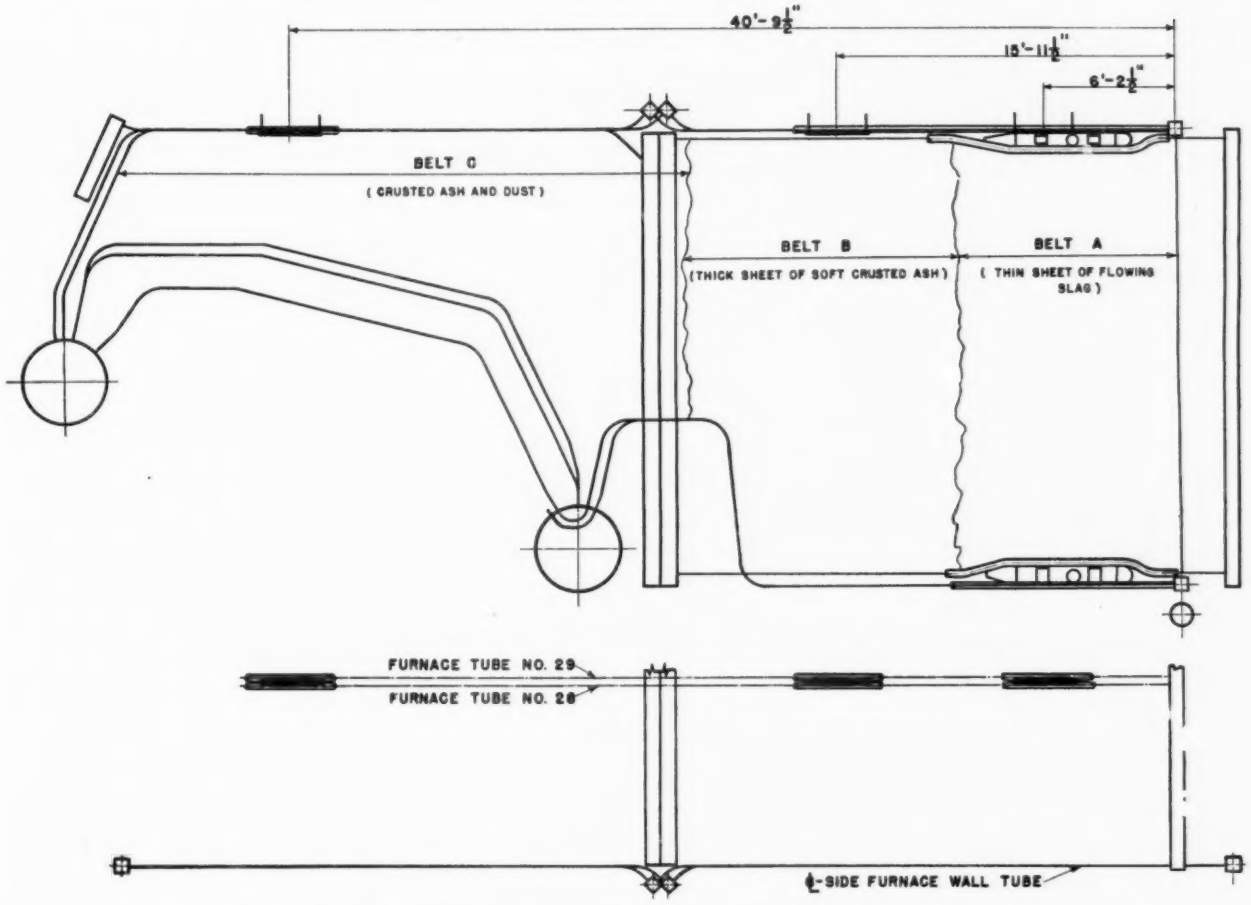


FIG. 4 LOCATION OF TEST UNITS IN THE FRONT WALL OF SLAGGING-BOTTOM FURNACE
(Belts indicate the nature of ash deposits.)

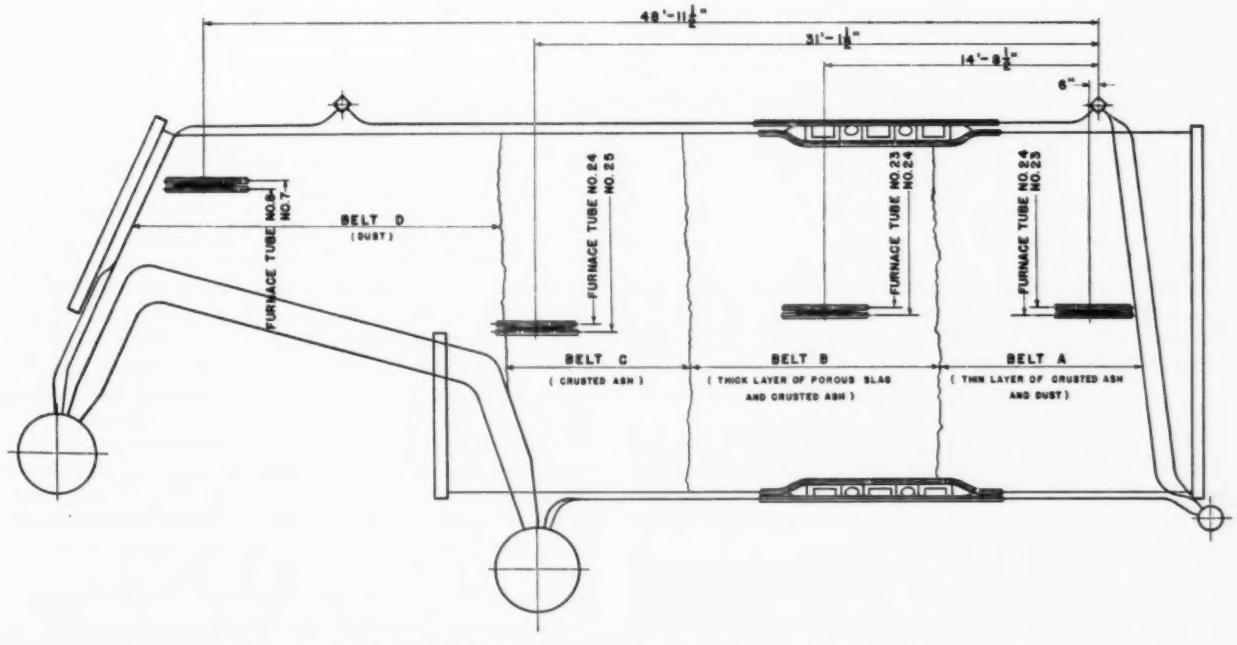


FIG 5 LOCATION OF TEST UNITS IN A SIDE WALL OF THE DRY-BOTTOM FURNACE
(Belts indicate the nature of ash deposits.)

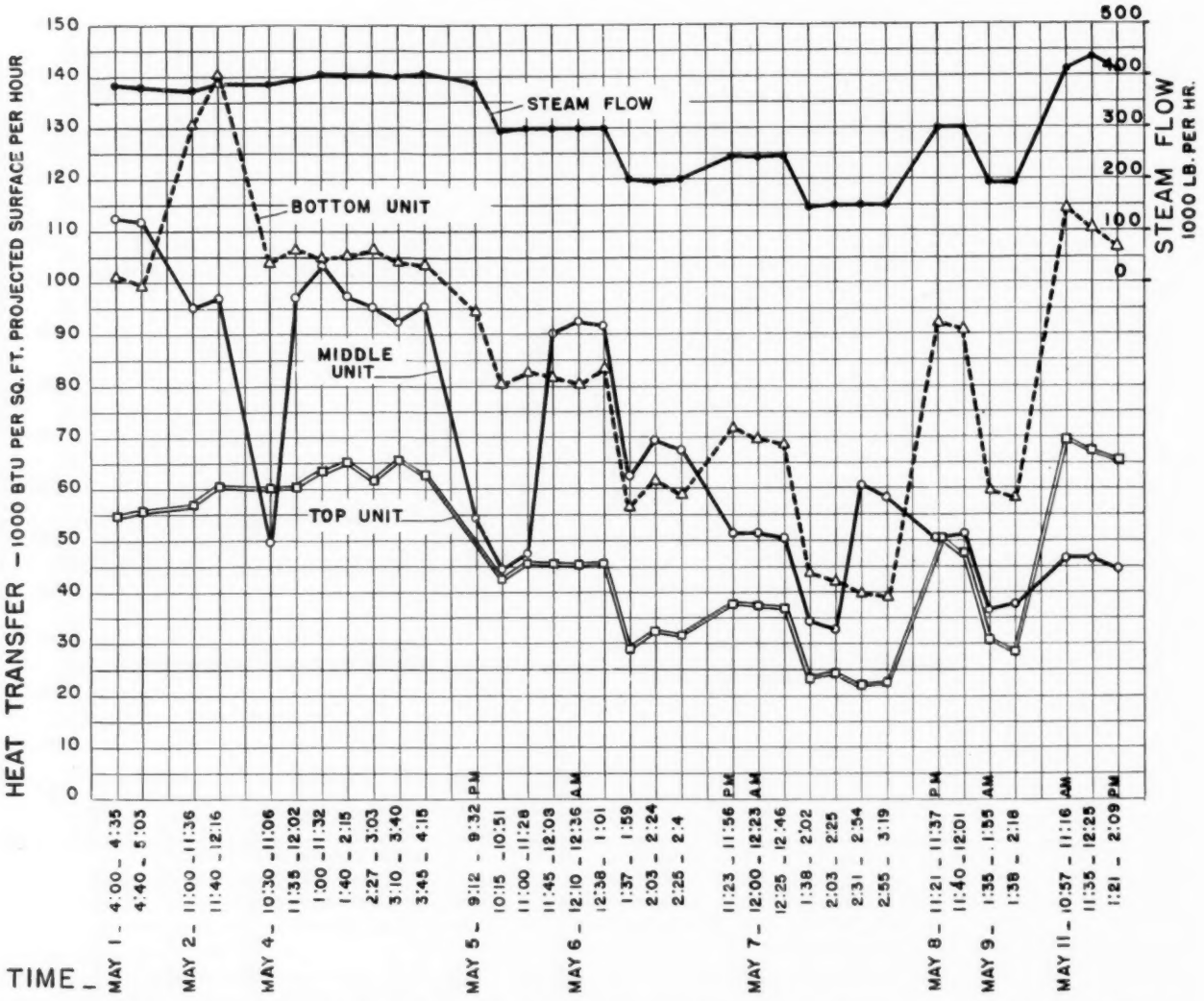


FIG. 6 HEAT TRANSFER BY THREE TEST UNITS *B*, *M*, AND *T* IN SLAGGING-BOTTOM FURNACE EXPRESSED IN 1000 BTU PER SQ FT OF PROJECTED SURFACE PER HR
(Top line is steam output in 1000 lb of steam per hour.)

to that in which unit *M* of the slagging-bottom furnace was located, and there was at times a heavy deposit on the unit. Test units Nos. 1 and 4 were in zones where the deposit was somewhat similar to that of belt *C* where unit *T* was located. The deposits were rather thin and varied only to a small extent.

On the slagging-bottom furnace a total of 37 tests were made, extending over a period of 11 days and covering steam output rates from 150,000 to 440,000 lb per hr. On the dry-bottom furnace 120 tests were made over an operating period of 56 days and covering ratings from 175,000 lb to 460,000 lb of steam per hour.

Table 1 is an illustration of the principal data collected, and the calculated results of four tests, two on the slagging-bottom furnace and two on the dry-bottom furnace. The particular four tests have been selected for illustration because they show the effect of ash deposit on the heat transfer.

When the deposit on the *M* unit was peeled off by a rod, the heat transfer was about doubled. Similarly, when No. 2 unit was cleaned with an air lance the heat transfer was increased about 50 per cent.

Fig. 6 gives the results of all the tests made on the slagging-bottom furnace, and Fig. 7 all the tests on dry-bottom furnace. The tests are plotted approximately on a time basis with gaps indicating periods when no tests were made. The ordinate is heat transfer to the test units and is expressed in 1000 Btu per sq ft of projected surface per hour. The points of the same unit of all the tests are connected by lines. The line at the top of the chart gives the steam output of the boiler in 1000 lb per hour at the time of the test. The charts give the essential results in compact form which shows at a glance some of the peculiarities.

The heat transfer varies directly with the steam output of the boiler, and inversely as the thickness of the ash deposit on the test units. The variation with the steam output would undoubtedly be definite and the results could be reproduced if the condition of the surface as to cleanliness could be kept constant. Such constant surface condition could be obtained with natural gas but is impossible with pulverized-coal firing, where the ash is continually deposited on the surfaces and runs down in some places and drops off intermittently in small pieces or in patches in other places. If a test is to be checked, the check test must be made immediately after the first test has been completed, before appreciable changes have taken place in the surface condition.

The heat transfer to the test units is somewhat higher than the

TABLE 1 SPECIMEN OF COLLECTED AND CALCULATED DATA

	Slagging-bottom furnace						Dry-bottom furnace							
Date	May 4, 1942			May 4, 1942			Sept. 16, 1942				Sept. 16, 1942			
Location of unit in furnace	*B*	*M*	*T*	*B*	*M*	*T*	*1*	*2*	*3*	*4*	*1*	*2*	*3*	*4*
Time	10:30	10:40	11:00	11:35	11:45	12:00	10:31	—	—	—	1:05	—	—	—
Steam output, 1000 lb/hr	390	385	385	395	400	395	350	350	350	350	350	350	350	350
CO_2 sphtr. outlet, per cent	14.9	14.9	15.2	15.0	15.0	14.9	14.5	14.5	14.5	14.5	14.56	14.56	14.56	14.56
Furnace condition	1/4 Inch	1/2 Inch	Dusty	1/4 Inch	Clean	Dusty	1/2 Inch	1/4 to 1/2	1/2 Inch	Dusty	1/2 Inch	Lanced Clean	1/2 Inch	Dusty
Temp. of water, deg F														
inlet	73	73	74	73	73	74	98	98	98.5	99.1	98.2	98.2	98.7	98.7
outlet	148	146	115	151	156	128	152	136.8	143.6	131.4	134.6	155.2	141.5	130.7
Weight of water collected, lb	100	100	100	100	100	100	100	102	101	100	100	100	100	100
Time of collection, min and sec	6:27	13:06	6:17	6:34	7:38	7:54	9:45	5:19	8:12	9:15	6:27	5:16	8:09	9:12
Heat trans., 1000 Btu	104.0	49.9 [a]	58.4	106.4	97.3 [b]	60.1	49.6	66.8 [1]	49.7	31.3	50.4	96.7 [2]	47.6	31.1

NOTES:
[a] Test unit *M* covered with 1/2-inch-thick deposit.
[b] Test unit *M* cleaned with a rod.
1 Test unit covered 1/4 to 1/2-inch-thick deposit.
2 Test unit cleaned with air lance.

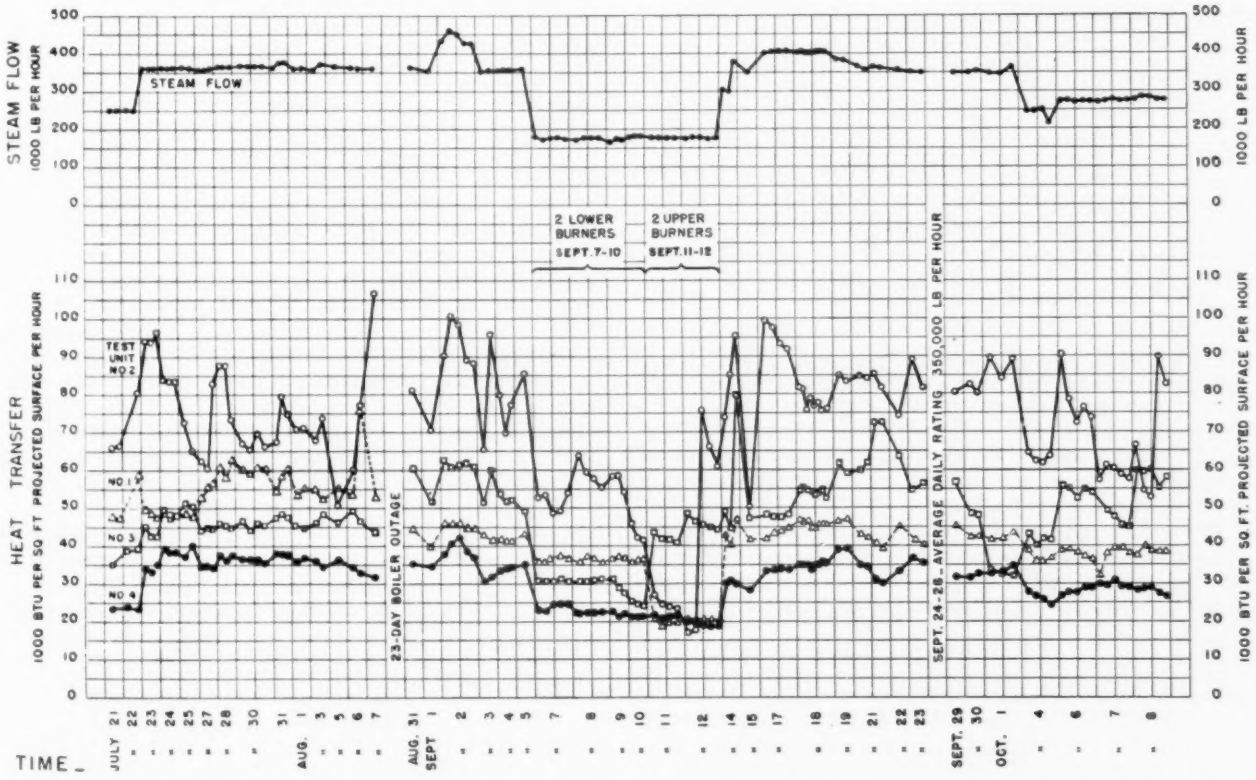


FIG. 7 HEAT TRANSFER BY FOUR TEST UNITS, NOS. 1, 2, 3, AND 4 IN THE DRY-BOTTOM FURNACE EXPRESSED IN 1000 BTU PER SQ FT OF PROJECTED SURFACE PER HR

(Top line is steam output in 1000 lb of steam per hour. September 5–10, the lower two of the three burners in each corner were in operation; September 10–12, the upper two burners were in operation.)

heat transfer to the waterwall, because the temperature of the test units is lower than the temperature of the furnace wall tubes. However, the difference is small, particularly in the hot part of the furnace. The average temperature of the metal surface of the test units was about 250 F and the average temperature of the furnace wall tubes was about 550 F. Heat is transmitted from the flame to the surface of the ash deposit on the tubes mostly by radiation, and through this ash deposit it is transmitted to the metal of the tube mostly by conduction. The heat transmitted by radiation is proportional to the difference between the fourth power of the absolute temperature of the flame and the fourth power of the absolute temperature of the surface of the ash deposit. The heat transmitted by conduction is proportional to the difference between the temperature of the surface of the ash deposit and the temperature of the tube metal, and inversely proportional to the thickness of the ash deposit.

Fig. 8 shows the path of the heat travel from the flame to the furnace-wall tube and also to the test unit. Although the temperature of the test unit is 300 deg lower than that of the wall tube, the thickness of the ash deposit on the test unit is almost enough thicker to offset the lower temperature. In the hot part of the furnace, particularly of the slagging-bottom furnace, the ash accumulates until the outer layer is far enough from the cooling effect of the tube so that it becomes molten and

flows down the wall. The greater cooling effect of the test unit requires a little thicker layer of ash to produce a flow of molten ash down the test unit. The amount of ash removed by this flow is equal to the amount deposited on the surface and, as a result, the thickness of the deposit remains constant. Similar equilibrium condition of the ash deposit is reached in other parts of the furnace where the ash drops from the wall in pieces. The

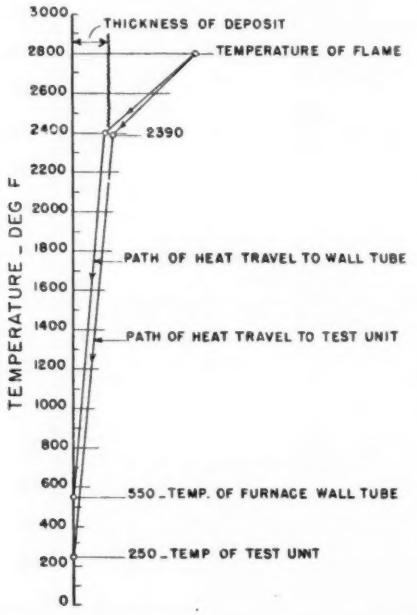


FIG. 8 PATH OF HEAT TRAVEL FROM FLAME TO SURFACE OF ASH DEPOSIT AND FROM THIS SURFACE TO THE METAL OF THE WALL TUBES AND TEST UNIT

surface of the deposit is rough and the dropping occurs from the protrusions where the ash is hotter and softer, and for that reason the pieces break off easily.

In Fig. 8 the ash deposit of the test unit is shown somewhat thicker than that of the wall tubes. The temperature of the surface of the ash deposit on the test unit is shown 10 deg lower to indicate the very small difference in heat transfer.

The ash deposit on the furnace walls is the greatest factor affecting the heat transfer from the flame to the furnace walls. The factor varies over a wide range and is difficult to ascertain for any given set of conditions. It varies with the composition and physical properties of the ash, the method of firing, the burner adjustment, excess of air, and fluctuation of load. All these factors affect the thickness and the conductivity of the ash deposit.

The uncertainty of the ash deposit factor makes calculation of the temperature of gases leaving the furnace and entering the superheater questionable. There are no reliable formulas or methods for such calculation. It is safer to base the design of a superheater on direct temperature measurements in a similar furnace burning similar fuel and operating under similar load conditions. Variation of load changes the ash deposit. Sudden reduction of load lowers the furnace temperature which usually causes the ash deposit to drop off in patches. To what extent the furnace walls can be stripped of the ash deposit depends largely on the length of time the furnace is operated at low rating. In some plants it is regular practice to reduce the load to one half or one third of the normal rating for one hour to remove a large part of the ash deposit.

The falling of the ash deposit in patches may cause local overheating. It has been shown that by peeling off the ash deposit on test unit *M*, Table 1, the heat transfer has been doubled. Another case of greatly increased heat transfer by the removal of the ash deposit is shown in Fig. 9. In this case the waterwalls consisted of small tubes 1.25 in. outside and 0.92 in. inside diameter spaced on 1.375-in. centers. Water entered the tubes at 1700 psi pressure and at saturation temperature with a velocity of $4^1/_2$ fps. Three groups of four thermocouples were attached to the surface of the tubes about $2^1/_2$ ft above the bottom of the furnace. The tubes normally had an ash deposit about $^3/_4$ of an inch thick with a surface in semiliquid condition, and the thermocouples indicated a temperature of 10 to 50 deg above saturation. As shown in Fig. 9, when the ash deposit was peeled off the tubes in the location of two of the three groups of thermocouples, the temperature indicated by these couples became 116 to 172 deg above saturation temperature. The uncovered tube surface received so much more heat from the flame that its temperature was raised over 100 deg F to transmit this large quantity of heat to the water inside of the tubes.

The high heat transfer obtained by uncovering furnace-wall

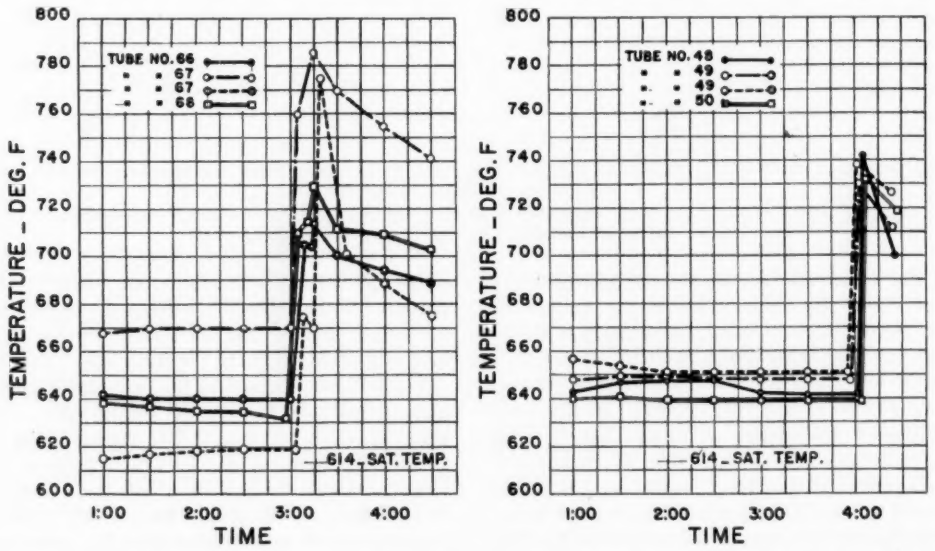


FIG. 9 RISE IN TEMPERATURE OF FURNACE WALL TUBES WHEN THE ASH DEPOSIT WAS PEELED OFF THE WALL

tubes may explain some of the failures from overheating and blistering of furnace tubes. Usually when the heat transfer is increased by higher rating on the boiler, the increase in the heat transfer is nearly uniform the full length of the tubes and there is an increase in the circulation which facilitates the transfer of heat from the metal of the tube to the water, and thereby makes overheating of the tube less probable. If the tube is covered with an ash deposit of nearly uniform thickness for its full length, and a patch of this deposit drops off, the heat transfer of the uncovered part is greatly increased. However, as the increase in the heat transfer is only over a small part of the tube it does not cause a corresponding increase in circulation, and the uncovered part of the tube may become overheated and blistered. The overheating and blistering is more likely to occur if the uncovered part of the tube is near the top end, because in such case the additional steam made by the uncovered part of the tube passes through only a short length of the tube with practically no effect on the circulation. If, however, the uncovered part is at the lower end of the furnace tube, the additional steam made by the increased heat transfer passes through nearly the full length of the tube and markedly increases the circulation, and thereby the heat transfer from the metal of the tube to the water, with less chance of the tube becoming overheated.

The average of the heat transfer to the test units of a number of tests made at the same rating on the boiler, is probably close to the average of the heat transfer to the belts of the furnace walls where the test units were located. This statement is truer of the dry-bottom furnace tests because the furnace walls were cleaned systematically.

The calculation of the average heat transfer for the entire furnace from the heat transfers of the test units would be difficult and the results of such calculations would be doubtful. The heat transfer to each test unit would have to be given the proper weight proportional to the area of the furnace walls which they represent and the determination of this weight factor would be largely a matter of opinion. It should be kept in mind that the area of the projected surface of the test units was a very small part of the total area of the furnace walls. Thus, the projected area of the four test units used in the dry-bottom furnace was 2.7 sq ft, whereas the projected surface of the furnace walls was 4460 sq ft. Each square foot of the test units represented 1650 sq ft of the furnace walls. The question is: How well did one square foot of the test units represent the 1650 sq ft of the furnace walls? Some of the surface in the furnace wall transmitted 100,000 Btu and some other surface only 30,000 Btu per sq ft per hr.

Measuring heat transfer to furnace walls by test units is like measuring temperature of a gas stream having a large cross section. For example, in a large boiler the gas stream leaving the furnace may be 300 sq ft in cross section. If the temperature of the gases is measured with a thermocouple the area of the part of the gas stream that surrounds the hot junction of the couple is about one square inch. If the temperature is measured at 36 points the area covered by the measurements is 36 sq in. or $^1/_4$ of a sq ft. This area is only $^1/_{1200}$ part of the area of the cross section of the gas stream. Usually the range of temperature variation across the gas stream is much smaller than the range of the heat transfer to the furnace walls so that the average of these measurements may be very close to the actual temperature of the gas stream.

In addition to the large variation of the heat transfer with the height in the furnace, there is a variation around the belt. With any method of firing there may be areas of the furnace walls which are swept by flame more than others and consequently have a higher heat transfer. Areas in the middle of the wall are more exposed to the flame than the areas in the corner of the furnace and therefore receive more heat.

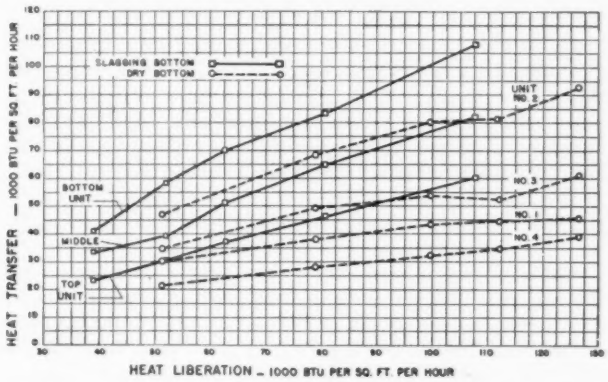


FIG. 10 HEAT TRANSFER OF TEST UNITS PLOTTED ON THE BASIS OF AVERAGE HEAT LIBERATION PER SQ FT OF PROJECTED SURFACE OF FURNACE WALLS

(The points are the averages of all tests made at the same heat liberation. Points of the same test units but of different heat liberation are connected by lines, a solid line being used for slagging-bottom furnace and broken line for dry-bottom furnace.)

Fig. 10 gives the heat transfer of the test units in the two furnaces plotted on the basis of the rate of heat liberation. The points in the chart are the average of all the tests made at the same rating. The points of different heat liberation of the same unit are connected by lines; a solid line is used to connect points of the slagging-bottom furnace, and a broken line the points of the dry-bottom furnace. The rate of heat liberation is the average per square foot of projected furnace walls per hour and was obtained by multiplying the steam flow by a factor. For the slagging-bottom furnace this factor was 0.272 and for the dry-bottom furnace 0.286. The rate of heat liberation was much higher near the bottom and lower at the top of the furnace. It will be noted that the bottom test unit in the slagging-bottom furnace shows heat transfer about equal to the average rate of heat liberation. It is probable that 95 per cent of the heat was liberated within the first 10-ft height of the furnace so that the actual rate of heat liberation of the belt of the bottom test unit might have been three times the average of the whole furnace.

The average heat transfer of the three test units in the slagging-bottom furnace is too high because the bottom unit, which has very high heat transfer, represents a very much smaller wall surface than the top unit which shows low heat transfer. The average heat transfer of the four units in the dry-bottom furnace is much closer to the average heat transfer of the furnace walls.

Discussion

W. E. CALDWELL.[3] A study of the heat absorbed by the test elements in the slagging furnace, as shown in Fig. 6 of the paper, affords useful information for evaluating furnace performance. The absorption curve for the upper test element follows quite closely the variations in boiler output, which would seem to indicate that it was relatively free from fouling. The absorption by the bottom element, however, appears to vary quite independently of the boiler output curve, indicating that it is probably more sensitive to variations in the slag coating than to variations in furnace heat input. The lower element, if clean, would probably receive 3 or 4 times as much heat as the upper element, due to the larger convection component and the greater heat concentration in the region of the burners. Obviously, the burner arrangement is a major influence in the heat distribution and absorption rate within the furnace and there is some room

[3] Mechanical Plant Engineer, Consolidated Edison Company of New York, Inc., New York, N. Y. Mem. A.S.M.E.

for improvement in this connection. Experience with tangentially fired furnaces indicates that better over-all results may be obtained by increasing the height of the burners and increasing the number of coal nozzles. With more conservative burner design, furnace conditions may be substantially improved by increasing the diameter of the firing circle, without impairing the high combustion efficiency which characterizes tangential firing. An upper limit of about 3000 lb of coal per nozzle per hr seems justified. For large direct-fired units this introduces complications since it necessitates subdividing coal and air streams between mills and burner. With appropriate arrangement the flame may be directed along the walls, thus increasing the convection component of heat absorption without causing tube wastage. The average rate of absorption by the furnace walls may be increased, while the extremes are reduced, which aids in maintaining cleaner walls and better over-all performance.

H. F. Mullikin.[4] The writer would like to concur in certain statements made by the authors. They state: "The uncertainty of the ash-deposit factor makes calculations of the temperature of gases leaving the furnace and entering the superheater questionable. . . . . It is safer to base the design of a superheater on direct temperature measurements in a similar furnace burning similar fuel and operating under similar load conditions. . . . . Usually the range of temperature variation across the gas stream is much smaller than the range of the heat transfer to the furnace walls. . . . ."

In a paper published 9 years ago[5] test data were given on ten boiler furnaces. Experiments were made using a number of test procedures including radiation calorimeters or "thermaprobes." The thermaprobe consisted of a flat-faced hollow steel block located in the furnace walls through which water was circulated to absorb the radiant heat. It was discarded as unsatisfactory for the following reasons: (1) Limitation as to number and location of openings which may be made in the furnace walls; (2) difficulty in controlling the water flow at a constant value; (3) difficulty of operating more than one thermaprobe at the same time; (4) lag in responsivity during time intervals in which furnace conditions change; (5) difficulty in obtaining the same amount of slag on the thermaprobe that existed on the furnace tubes, or of allowing for it by correction, and (6) possibility of considerable error due to peculiar local conditions.

Because of the foregoing objections thermaprobes were not used and the ten boiler-furnace units were tested by measuring furnace outlet temperatures by means of the high-velocity thermocouple.

Victor Paschkis.[6] In Fig. 10 of the paper, heat liberation is plotted as abscissas and heat transfer as ordinates both being expressed in 1000 Btu per sq ft per hr. Taking for example the heat transfer of 52,000 Btu, the heat liberation is shown to be 21,000 Btu. Evidently part of the liberated heat is lost. It will be helpful if the authors would state what happens to the lost energy.

Authors' Closure

Mr. Paschkis asks the question of what becomes of that part of the heat liberated in the furnace which is not absorbed by the furnace wall. On the average, about 50 per cent of the heat liberated in the furnace is absorbed by the water-cooled furnace walls. The remaining 50 per cent is held in the products of combustion mostly as sensible heat, when the products leave the furnace. As the products pass over the superheater, convection tubes of the boiler, economizer, and air heater, additional 35 to 40 per cent of the heat is absorbed, so that the total heat absorption is 85 to 90 per cent of the heat in the fuel fired.

It is essential that the products of combustion contain enough heat at sufficiently high temperature when they enter the superheater to give the desired superheat.

---

[4] Department of Mechanical Engineering, College of the City of New York, New York, N. Y. Mem. A.S.M.E.

[5] "An Experimental Investigation of Heat Absorption in Boiler Furnaces," by W. J. Wohlenberg, H. F. Mullikin, W. H. Armacost, and C. W. Gordon, Trans. A.S.M.E., vol. 57, 1935, pp. 541–554.

[6] Research Associate in Mechanical Engineering, Columbia University, New York, N. Y.

Absorption of Heat by Walls of a Furnace

By JOHN BLIZARD,[1] NEW YORK, N. Y.

This paper gives an account of the direct measurement of the rate of absorption of energy by the walls of a furnace, which were composed of brick, and of superheater tubes. It was also found possible to estimate the average temperature at which the gas left the furnace from the input energy to the furnace, the amount of energy absorbed by the superheater, and the composition of the flue gas and oil.

WHEN fuel burns in a furnace, heat is transferred from the products of combustion to the walls of the furnace, mainly by radiation. The rate at which it is being transferred may be determined by measuring the difference between the rate of flow of the energy of the fuel and air to the furnace, and the rate of flow of the energy of the products of combustion from the furnace. The determination of the rate at which energy is supplied to the furnace presents few difficulties; but the determination of the rate at which the energy leaves the furnace requires the measurement of the temperature and composition of the gas at many points over a large area. It happens occasionally that the rate of absorption of energy by the walls of the furnace may be measured directly, and this paper gives an account of such measurements made on a furnace, the walls of which were composed of brick, and of superheater tubes. It has been found possible also to estimate the average temperature at which the gas left the furnace from the input of energy to the furnace, the amount of energy absorbed by the superheater, and the composition of the flue gas and oil.

Boiler Used in Experiments, and Procedure

The boiler used for these experiments is shown in Fig. 1. It is fired by oil and has two furnaces. At the left is a furnace bounded on the sides by superheater tubes, and below the main bank of boiler tubes is another furnace. The products of combustion from the superheater furnace pass over two rows of superheater tubes and four rows of boiler tubes before entering the main furnace, whence they proceed through the main bank of boiler tubes to the economizer and uptake. The gases from the main furnace pass over the main bank of boiler tubes and economizer tubes before reaching the uptake. It is intended in this paper to consider only the relation between the rate of firing, the excess air, and the rate of heat absorption in the superheater furnace. Some particulars of the superheater furnace are given in Table 1.

TABLE 1 SUPERHEATER-FURNACE DATA

Volume of furnace, cu ft	358
Depth of furnace, ft-in.	7-2
Area of refractory surface, sq ft	110.5
Projected area of superheater tubes, sq ft	168
Area of superheater surface exposed to gases, sq ft	400
Burners (mechanically atomized)	4
Outside diameter of superheater tubes, in.	1.5
Number of tubes	108
Average pitch of tubes on outer wall, in.	1.6
Average pitch at outlet from furnace, in.	3.2
Number of passes for steam	4

During the tests, the total supply of oil and water to the boiler was weighed and the distribution of the oil between the two furnaces was estimated from the relative values of the pressure of the oil at the two sets of burners, and the number of burners in use in each furnace.

The enthalpy of the steam entering the superheater was measured by a throttling calorimeter, and its enthalpy leaving was determined by measuring its temperature and pressure. The composition of the gas leaving the economizer was measured at eight points, and was used, in conjunction with the weight and composition of the oil supplied to the furnaces, to calculate the total supply of air to both furnaces. Dampers had been provided to enable the pressure of the air before the registers of the burners of each furnace to be varied separately, and from the relative values of the number of burners used in each furnace and the drop of pressure of the air across each set of burners, it was possible to estimate the proportion of air going to each furnace. A few samples of the gas were taken on its path from the superheater furnace to the main furnace by means of a water-cooled sampler. However, it was felt that, in view of the somewhat wide variation in the composition of the gas at various points leaving the economizer, the composition of the gas determined at a single point between the two furnaces would be an unreliable measure of the mean composition of the gas leaving the superheater furnace. No combustible was detected in the gases leaving the economizer; but this does not assure us that combustible was not present in the gases leaving the superheater, although there is some reason to suppose that combustible was seldom present since none was detected in the few samples taken with the water-cooled sampler from the space between the two furnaces.

The boiler was required to deliver steam at 700 F and 575 psia when using the same-size sprayer plates on both sets of burners. During the first series of six tests, 84, 85, 86, 92, 94, and 100, the temperature of the steam on five runs varied between 697 F and 703 F, while on the sixth it reached 719 F. A second series of four tests, 101 to 104, inclusive, was made with the intention of delivering steam at 850 F. Actually, it varied from 834 to 866 F. The fuel oil used on the latter series of runs differed but slightly from that used on the first series, as shown in Table 2.

TABLE 2 PROPERTIES OF OIL FUEL

	Tests (six), Nos. 84–100 per cent	Tests (four), Nos. 101–104 per cent
Carbon	87.8	87.5
Hydrogen	11.0	11.2
Sulphur	0.4	0.6
Nitrogen	0.2	0.2
Oxygen	0.6	0.5
	100.0	100.0
Calorific value, gross, Btu per lb	18780	18770
Calorific value, net, Btu per lb	17770	17730
Minimum air/oil	13.8	13.9
Minimum air/10,000 net Btu in oil, lb	7.77	7.83

Results of Tests

Table 3 gives the principal results of the tests. The rates of firing and rates of heat absorption per square foot are given per square foot of projected area (168 sq ft).

The rate of heat absorption by convection (item 5) was estimated from the rate of flow of gases over the two rows of superheater tubes and from the temperature of the gas leaving the superheater. The average temperature of the gas leaving the superheater (item 15) was calculated by equating the enthalpy of the gas leaving the superheater to the difference between the

---

[1] Consulting Engineer, Foster Wheeler Corporation. Mem. A.S.M.E.

Contributed by Special Research Committee on Furnace Performance Factors with the co-operation of the Fuels, Power, and Heat Transfer Divisions and presented at the Annual Meeting, New York, N. Y., Nov. 29–Dec. 3, 1943, of The American Society of Mechanical Engineers.

Note: Statements and opinions advanced in papers are to be understood as individual expressions of their authors and not those of the Society.

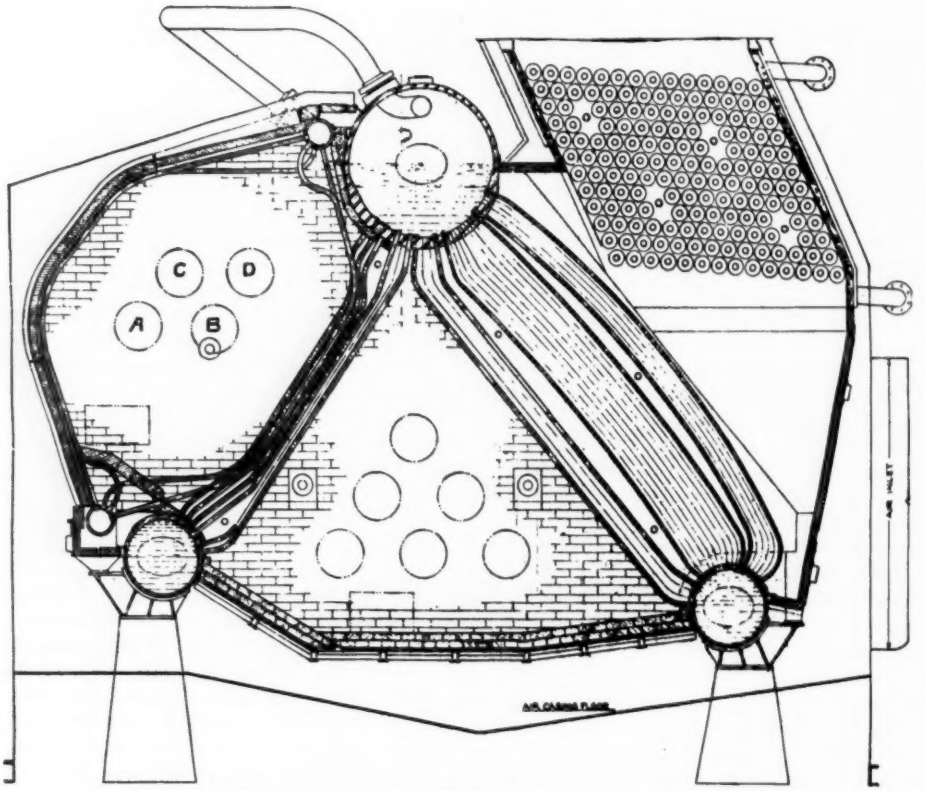


FIG. 1 BOILER SHOWING SEPARATELY FIRED SUPERHEATER ON LEFT-HAND SIDE
(A, B, C, D denote the four oil burners for this furnace.)

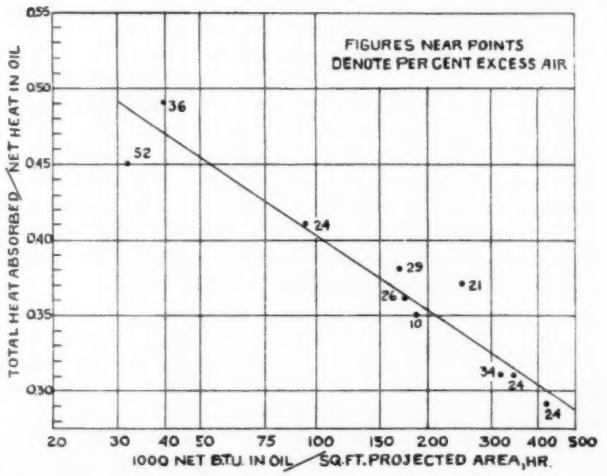


FIG. 2 RELATION BETWEEN FRACTION OF HEAT IN OIL WHICH WAS ABSORBED BY SUPERHEATER AND RATE OF HEAT LIBERATION IN SUPERHEATER FURNACE

energy entering with the fuel and the heat absorbed by the superheater per unit weight of gas.

The temperature, which the products would have reached with adiabatic combustion at atmospheric pressure (item 13), was calculated from the excess air (item 18), and the composition and heating value of the fuel. Allowance was made for the dissociation of the steam and carbon dioxide at this temperature. For convenience it will be called the "adiabatic" temperature.[2]

[2] The adiabatic temperature was used in the paper, "Heat Transmission in Steel-Reheating Furnaces," by J. E. Eberhardt and H. C. Hottel, Trans. A.S.M.E., vol. 58, 1936, pp. 185–193.

The mean temperature of the products of combustion after giving up heat by radiation, but not by convection, while crossing the two rows of superheater tubes (item 14), was calculated from the temperature of the gas leaving the superheater (item 15) and from the calculated absorption of heat by convection.

The radiation factor K is based on the equation

$$-\left(\frac{q}{T-T'}\right)\frac{dx}{ds} = K\,(x^4 - a^4) \qquad \ldots\ldots [1]$$

from which

$$K = \left(\frac{q}{T-T'}\right)\frac{1}{2a^3}\left[\frac{1}{2}\log_e\frac{x+a}{x-a} + \tan^{-1}\frac{x}{a}\right]_{x=T}^{x=T'} \qquad \ldots\ldots [2]$$

where

q is rate of heat absorption by radiation per unit projected area

s is ratio of time taken to reduce temperature of products of combustion from T to x, to time taken to reduce them from T to T'

T is adiabatic temperature of products of combustion, deg R

T' is temperature of products of combustion after radiating to superheater, deg R

x is temperature of products of combustion, deg R, which are assumed to begin to radiate when $x = T$, and to continue to radiate to the superheater until $x = T'$ when products leave furnace

a is average temperature, deg R, of the outside wall of tube receiving radiation. This temperature was calculated from rate of absorption of radiation, thermal conductivity and, dimensions of tube and from heat-transfer coefficient from inner wall of tube to steam.

Fig. 2 shows the relation between the proportion of the energy fired, which was absorbed by the superheater, by radiation and convection (item 7), and the logarithm of the rate of firing. The numerals near the points in the figure show the excess air present. Actually, it was found possible to increase the superheat by as much as 30 deg by reducing the supply of air to the superheater furnace, while still maintaining the same flow of steam through the superheater, and the same flow of oil to the burners. But Fig. 2 discloses no consistent relationship between the absorption and excess air for the same rate of firing for the different tests.

Fig. 3 shows the relation between the logarithm of the rate at which heat was absorbed by the superheater and the logarithm of the absolute temperature at which the gas left the superheater. It will be seen that, for the four runs at the highest rates of heat absorption, the rate of heat absorption was approximately proportional to the fourth power of the absolute temperature at which the gas left the superheater, and in fact it is approximately equal to the rate of radiation from a black body at the temperature at which the gas left the superheater. But at the two lowest

TABLE 3 RESULTS OF TESTS

	Test no.	92	103	85	101	84	100	86	102	94	104
1	Oil fired per hour to superheater furnace, lb	296	376	895	1589	1631	1760	2353	2971	3219	3938
2	1000 gross Btu in oil/cu ft hr	16	20	47	84	86	93	124	156	169	207
3	1000 net Btu in oil/sq ft hr	31.3	39.7	94.6	168	172	186	249	314	340	416
4	1000 Btu absorbed/sq ft hr	14.1	19.6	38.3	63.8	62.4	65.0	91.4	98	107	122
5	1000 Btu absorbed by convection per sq ft per hr	4.6	4.1	9.4	12.0	13.0	16.7	15.9	20	25	25
6	1000 Btu absorbed by radiation per sq ft per hr	9.5	15.5	28.9	51.8	49.4	48.3	75.5	78	82	97
7	Net heat absorbed, item 4/item 3, per cent	45	49	41	38	36	35	37	31	31	29
8	Net heat absorbed by radiation only, item 6/item 3, per cent	30	39	30	31	29	26	30	25	24	23
9	Resistance to flow of air through burners, in. of water	0.45	0.49	1.7	1.8	2.1	2.6	3.4	2.8	3.6	3.1
10	Pressure of oil at burners, psi	193	241	279	241	265	231	261	249	297	247
11	Temperature of air to burners, deg F	99	100	93	96	90	100	97	108	100	111
12	Temperature of steam from superheater, deg F	719	866	701	853	697	703	700	855	699	834
13	Temperature of products with adiabatic combustion, deg F	2880	3140	3340	3270	3310	3540	3380	3180	3350	3340
14	Temperature of gas after absorption by radiation only, deg F	2090	1990	2420	2320	2440	2830	2470	2450	2620	2620
15	Temperature of gas leaving superheater, deg F	1710	1720	2120	2110	2210	2530	2270	2270	2420	2440
16	Temperature of furnace side of tubes, deg F	760	900	790	990	830	830	870	1040	900	1050
17	Radiation factor, 10^{-9} Btu/sq ft R^4; 10^9K	0.14	0.22	0.25	0.52	0.44	0.29	0.62	0.74	0.62	0.77
18	Excess air, per cent	52	36	24	29	26	10	21	34	24	24
19	Partial pressure CO_2 (100), atm	9.7	10.7	11.8	11.3	11.6	13.3	12.1	10.9	11.8	11.7
20	Partial pressure H_2O (100), atm	7.3	8.2	8.8	8.6	8.6	9.8	9.0	8.3	8.8	8.9
21	Burners used	B	A	B	BD	AB	BD	AB	ABD	ABC	ABCD

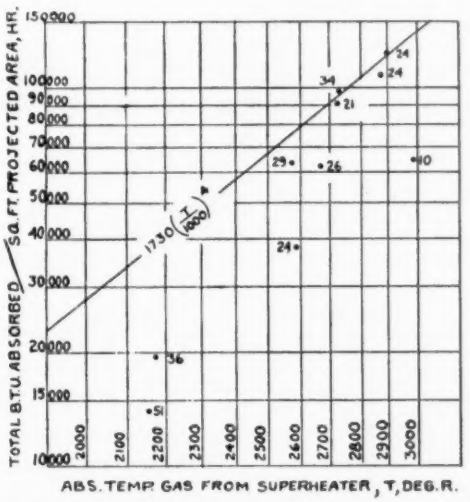


FIG. 3 RELATION BETWEEN INTENSITY OF ABSORPTION OF HEAT BY SUPERHEATER AND MEAN TEMPERATURE AT WHICH GASES LEFT SUPERHEATER

(Figures near points denote excess air.)

rates of firing, the absorption was only about one half that corresponding to full radiation at the temperature of the gas leaving the superheater.

It will be observed that for test 100, with only 10 per cent excess air, the calculated temperature of the gas leaving the superheater (2990 deg R) was very high for the observed rate of absorption (65,000), and it is probable that during this run combustible was present in the gas leaving the superheater, so that the temperature of the gas actually was less than that calculated on the assumption that no combustible was present.

Figs. 4 and 5 show the relation between the rate of absorption by radiation only (item 6), the rate of firing, adiabatic temperature, and the temperature reached by the gas after giving up heat by radiation only.

Fig. 4 shows that the radiation factor K increased with the rate of firing, and approximately

$$K\,10^9 = 0.54 \log (Q/17{,}000) \ldots [3]$$

where Q is the net Btu fired per square foot of projected area. Certainly this relation does not apply to rates of heat input below those used on the tests, since K would become equal to zero when Q had a finite value of 17,000, corresponding to a rate of firing of 175 lb per hr of oil. In fact, further difficulties in the use of this relation would arise, since it gives a minimum value for Q/K when Q is as high as 46,000 Btu per sq ft per hr. This would mean that, for a particular temperature of the tube and ratio of air to fuel, the minimum temperature of the gas, after radiating to the tube, would be reached when firing as much as 46,000 Btu per sq ft per hr, which is contrary to common experience.

In Fig. 5, the ratio of the rate of absorption of radiation to the fourth power of the absolute temperature at which the gas left the furnace is plotted on a

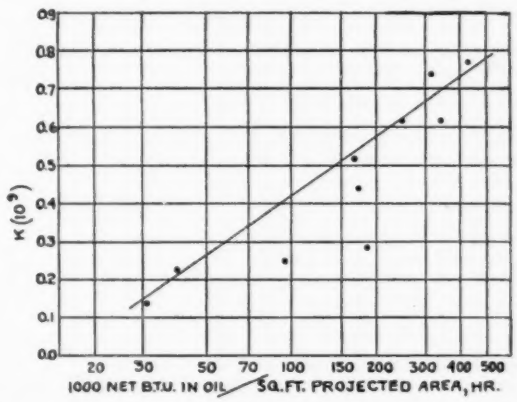


FIG. 4 RADIATION FACTOR K, AT VARIOUS RATES OF FIRING

base representing the rate of firing, and it will be observed that this ratio increased with the rate of firing.

It thus appears that if we assume the radiation to be proportional to the fourth power of the mean absolute temperature of the products of combustion, as defined by K and shown in Fig. 4, or to the fourth power of the absolute temperature, at which the gases left the furnace, as in Fig. 5, we must also assume that the radiation varies with the rate of firing. Actually, the radiation in a furnace is partly that due to chemiluminescence, which is approximately proportional to the amount of fuel burned, and mainly that due to thermal radiation.[3]

The amount of radiation from a molecule of carbon dioxide or steam from the time of its formation to the time when it leaves the furnace involves very many factors. These factors include its position in the furnace, when formed, and its subsequent path through the furnace, both of which will be affected by the turbulence in the furnace. At the lower rates of combustion it is probable that the gas did not sweep through the whole of the furnace as thoroughly as it did at high rates. This would mean

[3] "Radiation From Non-Luminous Flames," by H. C. Hottel and V. C. Smith, Trans. A.S.M.E., vol. 57, 1935, pp. 463–470.

that, at these lower rates of firing, some parts of the furnace contained stagnant gas, and that the active flame was smaller, both of which would reduce the total radiation from the flame to the superheater.

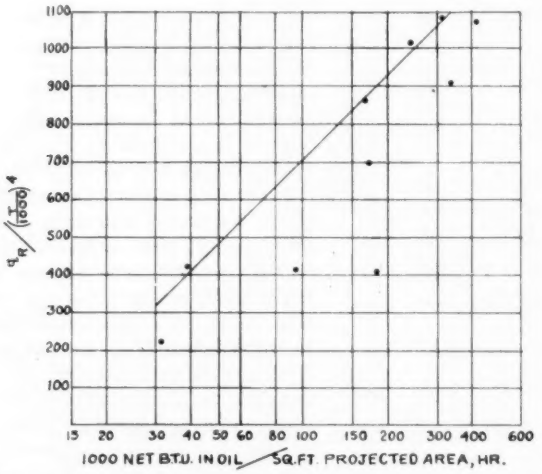


FIG. 5 RELATION BETWEEN RATIO OF HEAT ABSORPTION BY RADIATION PER SQUARE FOOT OF PROJECTED AREA (q_r), TO FOURTH POWER OF ABSOLUTE TEMPERATURE OF GAS LEAVING FURNACE AND RATE OF HEAT LIBERATION IN SUPERHEATER FURNACE

H. F. MULLIKIN.[4] There are comparatively few steam-boiler furnaces with the furnace circulation so arranged as to measure furnace radiant heat transfer directly. In the tests given in the present paper this was possible because the furnace under test consisted of a radiant superheater.

[4] Department of Mechanical Engineering, College of the City of New York, New York, N. Y. Mem. A.S.M.E.

In 1934 some data on six units similarly tested were reported.[5] These units consisted of boiler furnaces in which the furnace circulation was separate from the main boiler circulation.

Unfortunately this method of obtaining data can be used only in specific units and is not generally applicable to all furnace units.

A method of measuring furnace heat-transfer frequently used in investigating heat absorption in boiler units[6] and applicable to any unit consists of measuring furnace-outlet gas temperatures and calculating a furnace heat balance.

Mr. Blizard's Fig. 3, indicating nearly black-body furnace radiation at high loads, is in accord with findings of the writer.

AUTHOR'S CLOSURE

The inclusion in Dr. Mullikin's discussion of references to two valuable papers on absorption of radiation in furnaces and his reminder that he found nearly black-body furnace radiation at high loads enhances the value of the paper.

The suggestion that radiation to the walls of a furnace may be that of a black body at the temperature at which gas leaves a furnace occurs in Bureau of Mines Bulletin[7] 22, which was published in 1923.

But the present paper shows, as may be seen in Fig. 5, that the ratio of the rate of absorption of radiation to the fourth power of the absolute temperature at which gas left the superheater furnace was by no means constant but more than doubled when the rate of firing increased in the proportion of 400 to 40.

[5] "Review of Methods of Computing Heat Absorption in Boiler Furnaces," by W. J. Wohlenberg and H. F. Mullikin, Trans. A.S.M.E., vol. 57, 1935, pp. 531–540.

[6] "An Experimental Investigation of Heat Absorption in Boiler Furnaces," by W. J. Wohlenberg, W. H. Armacost, C. W. Gordon, and H. F. Mullikin, Trans. A.S.M.E., vol. 57, 1935, pp. 541–554.

[7] "An Investigation of Powdered Coals as Fuel for Power-Plant Boilers," by Henry Kreisinger, John Blizard, C. E. Augustine, and B. J. Cross.

The Flow Characteristics of Coal-Ash Slags in the Solidification Range[1]

By W. T. REID[2] and P. COHEN,[3] PITTSBURGH, PA.

Data on the flow properties of coal-ash slags below the temperature where crystals separate from the melt on cooling have not been available previously. This paper, which is presented as a report for the Special Research Committee on Furnace Performance Factors, describes the behavior of slag under these conditions, and shows that coal-ash slags act in a similar manner to comparable systems at ordinary temperatures. The viscometer used in a previous study was modified to include a motor drive, and was of the conventional concentric-cylinder type; a reducing atmosphere was used to control the state of oxidation of the iron forms in the slag. The temperature where an abrupt increase in viscosity occurs as the result of slight cooling is called the "temperature of critical viscosity." It is shown to be caused by the presence of solids in the melt and is lower than the "liquidus" temperature. Its importance in fixing the flow characteristics of slags is given, as well as a figure relating the temperature of critical viscosity with composition and with the state of oxidation of the iron forms in the slag. Similar relationships are also given for the freezing temperature of coal-ash slags. Comparison of cone-fusion data of 35 slags with the equilibrium values of slag viscosity shows that the viscosity is not constant for any given state of deformation of cones, although a relationship between the cone fluid temperature and absolute viscosity is given which is useful as a rough guide in predicting the viscosity of slags from the cone-fusion data. Also, within wide limits, the cone-softening temperature is an approximate indication of the temperature of critical viscosity. A nomogram is given by which the viscosity of coal-ash slags can be predicted from the composition. A brief discussion of the factors affecting the equilibrium thickness of slag deposited on heat-receiving surfaces is given, together with data computed for typical cases, and it is shown that the liquid viscosity and the temperature of critical viscosity are both important in determining the thickness of slag on wall tubes in operating furnaces.

THE purpose of this paper is to describe recent developments in the study of the flow properties of coal-ash slags. It is one of a series reporting progress on an investigation of coal ash conducted by the Bureau of Mines over the past 15 years and may be considered as the first report on this subject to the A.S.M.E. Special Research Committee on Furnace Performance Factors. This committee, concerned with the collection and rationalization of data on the performance of commercially important furnaces as an aid to design and operation, considers the action of ash and slag deposits within such furnaces of great importance in controlling performance; the physical chemistry of ash and slag is one of the factors involved and has been the principal subject of the Bureau's study.

Because of the extreme complexity of the subject and the large number of variables to be considered, no early solution of all the difficulties faced by the designers or operators of coal-burning equipment can be offered, but by a study of the more important factors, enough information can be made available to permit more complete understanding of ash behavior in furnaces. It is with the thought that this study of the flow characteristics of slags in the solidification range may replace purely speculative notions, and that preliminary knowledge of such factors will assist in the final evaluation of the action of slag in furnaces, that this paper is sponsored by the committee.

Previous Work by the Bureau of Mines

The previous four reports to the Society on this investigation of the fundamentals affecting the flow characteristics of coal-ash slags were based on work performed in co-operation with the now disbanded A.S.M.E. Special Research Committee on Removal of Ash as Molten Slag from Powdered-Coal Furnaces. They included (1) a study[4] of the factors involved in the flow of slag from an early slag-tap furnace; (2) a laboratory study[5] of the use of fluxes to increase ease of tapping; (3) the relationship[6] between coal ash, slag, and fly ash in 18 operating slag-tap furnaces, and the effect of reducing atmospheres on some of the properties of the slag; and (4) the development of a viscometer[7] to measure the absolute viscosity of coal-ash slags at high temperatures, as well as to determine the effect of composition on the viscosity-temperature relationship above that temperature where gradual crystallization of the cooling slag radically affects its flow properties. These investigations culminated, therefore, in the construction of an instrument by means of which it is possible to measure the absolute flow characteristics of coal-ash slags, and which is capable of yielding data suitable for predicting the behavior of these slags under various conditions of composition, temperature, thermal history, and state of reduction.

The coal-ash-slag viscometer permits an exact and direct measurement of the flow properties of slags; it replaces empirical tests in that the data obtained are independent of the method of test and thus can be applied to any type of equipment. But because tests made in the viscometer are expensive from the standpoint of both equipment and time required, it is not to be expected that

---

[1] Published by permission of the Director, Bureau of Mines, United States Department of the Interior, Washington, D. C.

[2] Supervising Fuel Engineer, Bureau of Mines, Central Experiment Station, Pittsburgh, Pa. Mem. A.S.M.E.

[3] Assistant Fuel Engineer, Bureau of Mines, Central Experiment Station, Pittsburgh, Pa.

Contributed by the Special Research Committee on Furnace Performance Factors with the co-operation of the Fuels, Power, and Heat Transfer Divisions and presented at the Annual Meeting, New York, N. Y., Nov. 29–Dec. 3, 1943, of The American Society of Mechanical Engineers.

Note: Statements and opinions advanced in papers are to be understood as individual expressions of their authors and not those of the Society.

[4] "Study of Some Factors in Removal of Ash as Molten Slag From Powdered-Coal Furnaces," by R. A. Sherman, P. Nicholls, and E. Taylor, Trans. A.S.M.E., vol. 51, 1929, paper FSP-51-51.

[5] "Fluxing of Ashes and Slags as Related to the Slagging-Type Furnace," by P. Nicholls and W. T. Reid, Trans. A.S.M.E., vol. 54, 1932, paper RP-54-9.

[6] "Slags From Slag-Tap Furnaces and Their Properties," by P. Nicholls and W. T. Reid, Trans. A.S.M.E., vol. 56, 1934, paper RP-56-3.

[7] "Viscosity of Coal-Ash Slags," by P. Nicholls and W. T. Reid, Trans. A.S.M.E., vol. 62, 1940, pp. 141–153.

it can be utilized as an instrument for control, much as the standard cone-fusion determination is now being used. Instead the viscometric data are being correlated with the composition of the slag, so that the flow properties of the slag can be predicted if its chemical analysis is known. As will be shown, under equilibrium conditions the source of the constituents making up a slag are unimportant so long as they result in a melt of the desired chemical composition.

Unfortunately, at present, no short-cut methods of chemical analysis are known which are suitable for this application. Present analytical methods are tedious and involved, and are based upon schemes devised for the exact analysis of rocks; they yield data of more than necessary precision. Less exact, more quickly performed methods are required. As the ability to predict the flow characteristics of coal-ash slags as a function of composition increases, it is expected that the methods of chemical analysis will be improved to supply satisfactorily precise data at a low cost and with a reasonable expenditure of time.

Test results reported in this paper have been obtained with slags preheated to the point where they were converted to a homogeneous liquid, thus no further reaction was occurring between constituents. The flow properties of the slag were determined subsequently by measurements made during the cooling of this melt.

Description of Apparatus

Furnace. The high-temperature furnace and the first viscometer have already been described.

Briefly, the furnace consists of a 2-in. × 3-in-diam silicon-carbide tube mounted vertically between water-cooled copper electrodes, thermally insulated with porous kaolin refractory and loose Sil-O-Cel, and enclosed in a gastight welded-steel shell 13 in. diam and 12 in high. Electrical energy is supplied by a transformer having a 440-v primary; the multitapped secondary is capable of furnishing 250 amperes at 20 v and is connected to the furnace through two radial switches. A variable autotransformer in the primary circuit permits essentially stepless control of power.

Temperature Measurement. Slag temperatures are measured by a platinum rhodium-platinum thermocouple embedded in the porcelain stool supporting the platinum crucible containing the slag. A determination of the temperature gradient in the melt and the deviation of the mean temperature of the melt from that indicated by this embedded thermocouple was made on a soda-lime glass which did not contaminate the probing thermocouple as would a coal-ash slag; the observed temperatures are thereby corrected to the mean slag temperature. The crucible is positioned in the furnace so that the temperature gradient through the melt is a minimum and does not exceed 10 F in a vertical direction. The embedded thermocouple is calibrated regularly against a secondary standard.

Temperature Controller. A thermocouple of low thermal capacity, exposed directly to radiation from the furnace wall, operates through a potentiometer connected to an electronic-contacting galvanometer[8] to control furnace temperatures. Such control is necessary because momentary excessive cooling at certain stages in the test may induce abrupt freezing of the melt. An additional synchronous-motor-driven potentiometer having a long helical slide wire is used to give the rates of cooling required for the maintenance of fixed conditions in the solidification tests. This instrument also energizes a motor connected to the variable autotransformer, adjusting the energy input to the furnace to the point where most satisfactory temperature control is possible.

Oscillating Viscometer. This instrument, used in the previous study of the viscosity of slags in the liquid state, has not been changed. Viscosity in the lower ranges is determined by measuring the logarithmic decrement of the torsional oscillation of a bob immersed in the slag and hanging from a calibrated suspension. At higher viscosities the same apparatus is used but the moment of inertia of the system is decreased and the time determined for the bob to rotate through a fixed angle while in aperiodic motion. For the measurement of the viscosity of Newtonian fluids, that is, true liquids, where the rate of shear is proportional to the applied stress, the instrument is completely satisfactory and is in continued use. However, during cooling, coal-ash slags at some temperature no longer behave as true liquids, and the oscillating viscometer becomes first erratic and then inoperable. Basically, failure of the instrument under these conditions results from the insufficient energy available in the oscillating system in harmonic motion of in the twisted suspension wire in aperiodic motion to continue to produce shear when solids are present in the slag. To furnish this energy it is necessary to supply an external source of power to the instrument, therefore the rotating-bob viscometer was designed and constructed.

Rotating Viscometer. The rotating viscometer operates on the principle first described by Margules in 1881;[9] he confined the liquid under test between two concentric cylinders, one of which was rotated at constant speed while the torque exerted upon the other was measured. This method is applicable to a wide range of viscosities and has been used successfully to study flow characteristics of many different materials. A modification was used by Feild[10] for determining the viscosity-temperature relationships of blast-furnace slags, while Herty[11] investigated other metallurgical slags, and Lillie[12] studied the viscosity of glass over a wide temperature range. Each of these investigators found it expedient to rotate the outer cylinder and to measure the torque exerted on the inner stationary cylinder. However, for coal-ash slags, the test atmosphere must be controllable so that the forms of iron in the melt can be maintained at a desired ratio; thus it was required that the bottom of the furnace be gastight to prevent the infiltration of air. Consequently, to make unnecessary the use of stuffing boxes or other seals around a bottom rotating shaft, it was decided to maintain the outer cylinder stationary and to drive the inner cylinder by way of a spindle extending through a small opening at the top of the furnace. This resulted in simplifying both furnace construction and crucible support, but introduced the problem of measurement of torque in the rotating driving system. Of the methods considered, those introducing measured amounts of energy, such as by slowly falling weights or by determining the wattage input to a driving motor, were discarded because of unavoidable and variable frictional losses. Therefore the inner cylinder was rotated by an external motor drive, and the torque was measured by the twist in a calibrated suspension wire serving as one member of the driving train.

The apparatus is shown in Fig. 1. A fractional-horsepower series-wound motor having its speed controlled by an adjustable centrifugal device, and with a built-in speed reducer, drives the

[8] "An Electronic-Contacting Galvanometer for Temperature Control: Temperature, Its Measurement and Control in Science and Industry," by W. T. Reid, Reinhold Publishing Corp., New York. N. Y., 1941, pp. 611–616.

[9] "Concerning the Determination of the Frictional and Sliding Coefficients of the Laminar Motion of a Liquid," by M. Margules, *Sitzungsberichte Akademie der Wissenschaften*, Wien, vol. 83, part 2, 1881, p. 588.

[10] "A Method for Measuring the Viscosity of Blast-Furnace Slag at High Temperatures," by A. L. Feild, U. S. Bureau of Mines, Tech. Paper 157, 1916.

[11] "Temperature-Viscosity Relations in the Lime-Silica System," by C. H. Herty, et al., Mining and Metallurgical Investigations, U. S. Bureau of Mines, Carnegie Institute of Technology, Mining and Metallurgical Advisory Boards, Co-op. Bull. 47, 1930.

[12] "The Measurement of Absolute Viscosity by the Use of Concentric Cylinders," by H. R. Lillie, *Journal of the American Ceramic Society*, vol. 12, no. 8, 1929, pp. 505–515.

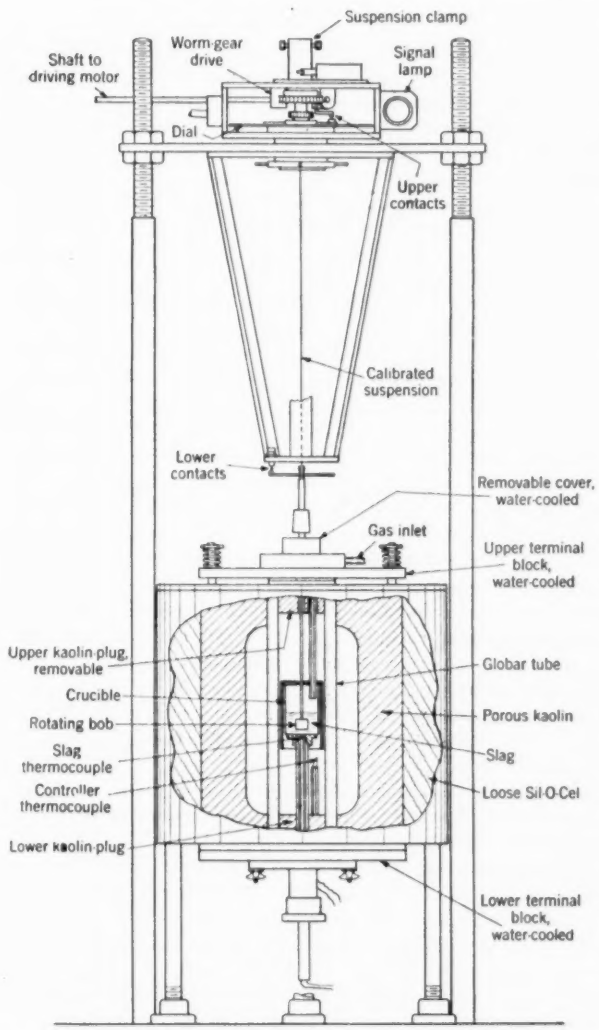


FIG. 1 FURNACE AND VISCOMETER FOR DETERMINATION OF VISCOSITY OF COAL-ASH SLAGS IN SOLIDIFICATION RANGE

viscometer through a worm-gear assembly mounted at the top of the instrument, the upper end of the suspension being clamped in the worm gear on its axis of rotation. The suspension wire, which is 15 in. long, is attached at its lower end to a member connected to the spindle attached to the bob. An inverted rigid tripod serves as a jig for insuring alignment and as a guide for the lower end of the suspension. Electrical contacts on the rotating members at each end of the suspension are used for measuring twist, the lower contact touching a fixed point on the tripod and the upper one contacting a point mounted on a dial which can be rotated manually; an electronic circuit through these contacts illuminates a signal lamp if both contacts are made simultaneously. Because the lower contact pressure must be extremely light to prevent disturbing the measurement of twist, moderate electrical resistance may occur, but the electronic circuit is capable of signaling through a circuit resistance as high as 500,000 ohms.

At the start of a test, when the slag is at a high temperature and, consequently, at its minimum viscosity (which has been previously determined with the oscillating viscometer), the motor is started and the upper adjustable contact rotated until the signal indicates that the electrical circuit through both sets of contacts is being made. A reading of the dial is then taken and the zero setting computed from the known speed of rotation of the bob, the constants for the suspension, and the viscosity of the melt. Later, as the viscosity increases with fall in temperature, the twist in the suspension increases so that the graduated dial must be rotated to keep the contacts in phase and maintain the signal; the angle, through which the dial and therefore the adjustable contact is rotated to maintain the signal, is identical with the additional twist in the suspension caused by the increase in viscosity. The dial is graduated in 200 divisions; a vernier permits measurement of twist within 0.1 division.

Two suspensions are in regular use, one having an upper limit of 10,000 poises, and the other, 100,000 poises. They are made of steel music wire, 0.018 in. and 0.034 in. diam, respectively, and are calibrated against liquids for which the viscosity has been determined by other methods. An alternate method of calibration was to load the suspensions radially and to measure the torsional deflection for various loadings.

The dimensions of the crucible and the bob, the two cylinders of the Margules viscometer, are the same as were described for the oscillating viscometer, the crucible being $1^1/_2$ in. ID and $2^1/_4$ in. deep; the bob is 0.500 in. diam and 0.500 in. long, but with an increased spindle diameter of 0.125 in. to withstand the greater torque of the driving system. Both units are of platinum alloy, the crucible containing 4 per cent rhodium and the bob and spindle 20 per cent rhodium. A careful check is made of the dimensions of the bob and it is returned to the manufacturer for reworking whenever the deviations from the desired size exceed 0.002 in. The crucibles are reshaped on a mandrel to the correct diameter following each test.

Control of Atmosphere. Because the state of oxidation of the iron in coal-ash slags is important in fixing certain of their flow properties, it is necessary to control the ratio of ferric to ferrous iron in the slag by controlling the atmosphere over the slag both during the original melting of the charge and during the test itself. Because of unavoidable diffusion of air into the furnace which would gradually oxidize the melt, some provision must be made other than flushing the apparatus continually with nitrogen to prevent the oxygen in this air from having access to the molten slag. In previous tests it was found that using a carbon tube for the nitrogen inlet was satisfactory; the tube projected into the crucible where, at furnace temperatures, it effectively converted any oxygen to carbon monoxide. However, because this tube required replacement at 1-hr intervals, it was not suitable for tests of long duration, therefore some other method of removing or compensating for the oxygen was required.

After a considerable number of tests, it was found that adding regulated amounts of hydrogen to the nitrogen permitted the use of a porcelain inlet tube and gave adequate control of the state of reduction of the slag. Present practice is to use 2 to 10 per cent hydrogen in the gas mixture during the premelt period when the slag has the greatest surface exposed and is most susceptible to oxidation, the exact amount being fixed by the required ratio of forms of iron and the composition of the charge. During the test itself, which may require 12 to 120 hr, the atmosphere is adjusted to 2 per cent hydrogen and 98 per cent nitrogen; the gas mixture is introduced at the rate of 1 cfh to the crucible through the porcelain tube and flows directly over the exposed surface of the slag. A platinum cover on the crucible with holes for the bob spindle and the porcelain tube assists in maintaining constant conditions. In all cases, the hydrogen is mixed with raw nitrogen from the cylinder and passed over copper gauze at 850 F to remove the small quantities of residual oxygen in the nitrogen, after which water is removed from the gases by passing them through calcium-chloride drying tubes. The amount of hydrogen used is corrected for that required to convert the residual oxygen in the nitrogen to water.

The effectiveness of the method in preventing oxidation of the slag in recent typical tests is shown in Table 1. None of the slags

TABLE 1 CHANGE IN STATE OF OXIDATION OF SLAGS DURING TEST IN AN ATMOSPHERE OF 2 PER CENT HYDROGEN AND 98 PER CENT NITROGEN

Test no.	Equivalent Fe_2O_3 in slag, per cent	Duration of test, hr	Ferric percentage[a] At beginning of test	At end of test	Change, per cent
243	14.5	29.5	16	14	−2
220	24.3	18	18	14	−4
240	29.8	43	19	22	+3
239	30.9	27	26	27	+1
236	40.5	24	21	23	+2
246	41.1	35.5	45	40	−5

[a] Ferric percentage is defined as the actual ferric iron in the slag expressed as per cent of the total iron calculated to Fe_2O_3. It is a measure of the state of oxidation of the slag.

show appreciable change in ferric percentage during the test, indicating the suitability of the method. Tests 239 and 240 and tests 236 and 246 show the ability to maintain the desired ferric percentage in slags of similar composition following variations in procedure during the premelting period to give different original states of oxidation. It should be emphasized that a 2 per cent hydrogen atmosphere is suitable only for the furnace and test conditions described. In other apparatus where the leakage of air may be different, other concentrations of hydrogen will be required.

Rheology of Coal-Ash Slags

The various constituents of coal ash, when heated to a high temperature, react to produce slag; if this temperature is sufficiently high and if enough time is allowed for all the possible chemical reactions to occur, the otherwise solid components of the ash substance will be converted to a homogeneous liquid. Rheology, the science treating of the deformation and flow of matter, shows that, for liquids, viscosity increases with decrease in temperature and that, under conditions of nonturbulent flow, the applied stress is proportional to the rate of shear, the ratio being the viscosity. For most liquid substances, this linear relationship does not hold over a wide temperature range, because, when they are cooled, a change of state occurs either gradually or abruptly which radically changes the flow properties of the material The same fundamental laws describing the behavior of other liquids also apply to coal-ash slags. Slags are not true liquids over the entire temperature range of interest to fuel engineers; the analysis of the flow properties of coal-ash slags at temperatures at which they are not completely liquid is of great practical importance and is one of the principal functions of this paper.

Development of Yield Stress. If a coal-ash slag originally at a temperature at which it is completely fused (that is, completely in the liquid state) is slowly cooled, the first change is an increase in viscosity according to a definite physical law, the details of which are given in a later part of this paper. At a certain definite temperature for each composition and ferric percentage, a process of crystallization begins and continues as the temperature is lowered; this temperature is called the "liquidus" temperature and is analogous to the liquidus temperature of other systems. These crystals, in general, do not have the same composition as the liquid slag from which they are separating; thus the composition of the remaining liquid changes as the crystals form, but the effect on viscosity of the change of composition of the liquid and the hydrodynamic effect of the small amount of crystals is far outweighed by the continuous increase of the viscosity of the liquid with decrease in temperature. Thus the presence of a small amount of minute crystals does not cause an abrupt change in the flow properties of a coal-ash slag, as had been formerly believed, and there is no break in the viscosity-temperature curve at the liquidus temperature of the slag.

Because this contradicts former statements referring to the liquidus temperature, this point was thoroughly studied for a synthetic slag having a silica: alumina ratio of 2.0, an equivalent Fe_2O_3 content of 30 per cent, and CaO 20 per cent. By quenching melts held in air at progressively lower temperature and examining the quenched charges under the microscope, the liquidus temperature was found to be 2515 F, whereas the break in the viscosity-temperature curve, in air, occurred at 2450 F. Bowen and Schairer[13] have discussed this subject at some length, though from a different viewpoint, and come to identical conclusions; namely, that there is no abrupt change in the rheological properties of a melt at the liquidus temperature, except in the special case of eutectic or compound compositions.

As cooling continues, more and more solid material separates from the melt, until, at a definite temperature (again depending upon composition and ferric percentage), an abrupt change in the flow properties of the coal-ash slag finally occurs. This change is evidenced by the fact that the applied stress is no longer directly proportional to the rate of shear but equals the viscosity times the rate of shear plus a constant force, and the slag is now said to be "plastic." This latter force, which impedes shear, is called the internal yield stress of the slag, and although it is not necessarily the yield value of the system it is generally understood in speaking of plastic flow that a definite shearing force must be applied before any deformation can occur. The internal yield stress is most conveniently measured and is in fact the only "yield" value not subject to ambiguity. Considerable controversy still exists over the behavior of "plastic" systems at low rates of shear, but for the purposes of this paper a simplified description is suitable.

This sudden development of internal yield stress occurs because the concentration of solids has reached such a value that the particles begin to interfere with each other in the flow process; a structure can be assumed to exist, made up of the suspended particles. To maintain flow, this structure must be continuously broken, and the internal yield stress is the force per unit area required to do so. The phenomenon of a critical volume concentration of solids for the development of internal yield stress is well known from studies of clay-water and pigment vehicle suspensions.[14]

Rheological behavior of this type was first systematically studied by Bingham,[15] and the equation that describes it bears his name

$$\sigma = \frac{F - f}{\eta}$$

where σ is the rate of shear, F the applied stress, f the internal yield stress and η the plastic viscosity. From a rheological point of view, internal yield stress can be considered as a measurable quantity indicative of the partial rigidity of a plastic substance. As a typical illustration, the behavior of a plastic material, in this case lithographic ink, is shown by a viscometric curve published by Green[16] and given in Fig. 2, where the torque on the suspension of the viscometer is plotted against the speed of rotation. It can be seen that the relationship is linear over a considerable range of rotational speeds greater than about 0.4 rps; the deviation from linearity at very low speeds has rheological significance but need not be considered here. The intercept at zero speed of

[13] "The System, FeO–SiO_2," by N. L. Bowen and J. F. Schairer, *American Journal of Science*, vol. 24, Sept., 1932, pp. 177–213.

[14] "Fluidity and Plasticity," by E. C. Bingham, McGraw-Hill Book Co., New York, N. Y., 1922, figs. 79 and 80.

[15] "An Investigation of the Laws of Plastic Flow," by E. C. Bingham, U. S. Bureau of Standards, Bull. 13, 1916, pp. 309–353.

[16] "High-Speed Rotational Viscometer of Wide Range," by H. Green, *Industrial and Engineering Chemistry*, Analytical Edition, vol. 14, 1942 pp. 576–585, fig. 10, p. 581.

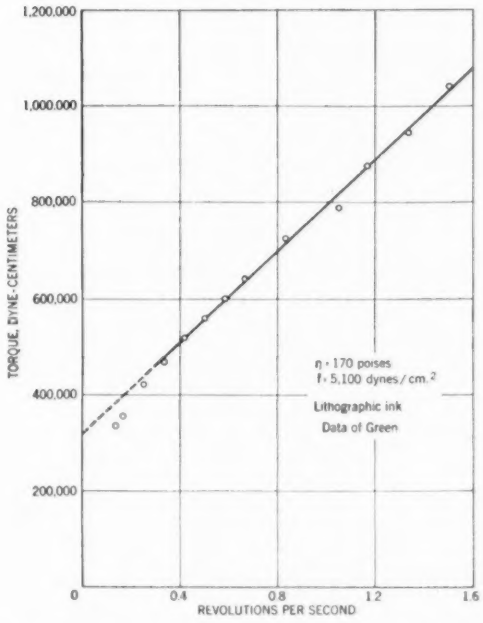


FIG. 2 TYPICAL CURVE FOR A THIXOTROPIC PLASTIC

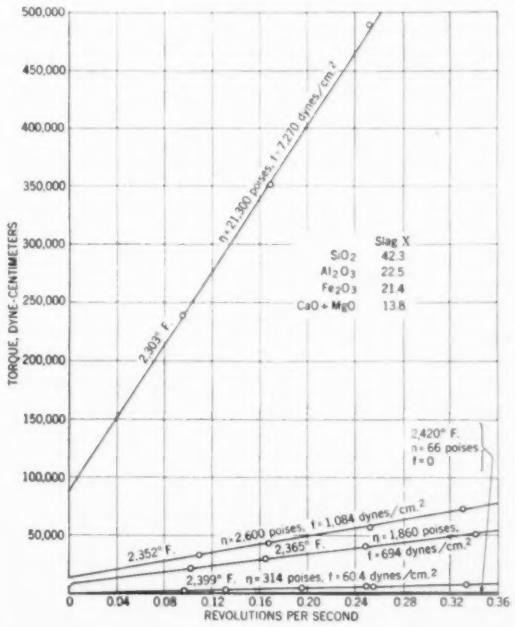


FIG. 3 DEVELOPMENT OF INTERNAL YIELD STRESS IN SLAG *X* ON COOLING IN AIR

320,000 dyne-cm of torque can be taken as a measure of the internal yield stress of the lithographic ink and indicates that this material has plastic properties, and that under lower stress, no shear would take place. The advantage of such flow properties for lithographic inks is obvious.

A similar effect is noted with coal-ash slags, where the internal yield stress, taken with the plastic viscosity, permits the description of the flow properties of a slag at temperatures below that at which crystals occur in sufficient quantity to cause deviation from the normal behavior for liquids. The actual determination of the internal yield stress and of the plastic viscosity for coal-ash slags is made by operating the viscometer at a constant speed until the torque on the suspension is constant. This equilibrium value is recorded, the speed changed, and the process repeated, the values of equilibrium torque being plotted against the corresponding speeds. A straight line is drawn through the points, the plastic viscosity being proportional to the slope, and the internal yield stress to the intercept at zero speed. This procedure is repeated at various lower temperatures, allowing crystallization to become complete at each temperature before readings are taken.

A typical set of Bingham curves for a coal-ash slag is shown in Fig. 3, where the effect of decreased temperature in increasing the plastic viscosity and the internal yield stress is clearly shown. The temperatures at which the accumulating crystals are effective in developing an internal-yield stress and plastic viscosity are below 2420 F; at that and higher temperatures no intercept is observed, the slag acting as a true liquid and having a linear relationship between stress and rate of shear. The conversion of the experimental values of torque intercept and slope to the rheological constants have been made by means of the Reiner[17] equation for the rotating viscometer with a Bingham (plastic) substance

$$T = \frac{8\pi^2 (l + h)\eta_0 S}{\left(\frac{1}{R_1^2} - \frac{1}{R_2^2}\right)} + \frac{9.212\pi (l + h)}{\left(\frac{1}{R_1^2} - \frac{1}{R_2^2}\right)} f \log \frac{R_2}{R_1}$$

where T is the torque in dyne-centimeters, η_0 the plastic viscosity in poises, S the speed of rotation in revolutions per second, R_1 and R_2 the radii of the bob and crucible, respectively, in centimeters, l the height of the bob in centimeters, h a correction to the bob height due to the effect of the ends, determined experimentally, in centimeters, and f is the internal yield stress expressed as dynes per square centimeter. These rheological constants are important because they are based upon absolute relationships and are thus independent of the apparatus in which the experimental work was performed. Therefore their use can be extended to practical applications with maximum effectiveness.

As noted previously, in determining the plastic viscosity and the internal yield stress of coal-ash slags, the viscometer is operated at a constant speed until the torque on the suspension becomes constant. This is necessary because coal-ash slags in the plastic range are thixotropic; that is, a definite time interval is required for equilibrium to be established between applied stress and rate of shear after the rate of shear has been changed. The Bingham law applies to the equilibrium values of stress and rate of shear; thus the values of plastic viscosity and internal yield stress must be obtained under equilibrium conditions. The non-equilibrium plastic viscosity and the internal yield stress of coal-ash slags are functions of the previous history of the slag, therefore they are of no use in this discussion. Further, for the long-time processes of slag flow, such as on wall tubes, it is the equilibrium values that apply.

The approach to equilibrium viscosity with time, following an abrupt change of temperature in the region of plastic viscosity, varies between different coal-ash slags as shown in Fig. 4. Curve *A* shows a peak value of viscosity with a subsequent reduction to the equilibrium value, and curves *B* and *C* show a simple exponential approach to equilibrium, differing only in rate. A reasonable explanation is based upon the formation of crystals in the liquid slag. When slags of type *A* are cooled, there is a rapid formation of a large number of minute crystals, causing an increase in viscosity. These small crystals, however, are unstable with respect to large crystals, the result being the formation of a smaller number of still larger crystals, with a con-

[17] "Theory of Plastic Flow in the Rotation Viscometer," by M. Reiner, *Journal of Rheology*, vol. 1, 1929, pp. 5–9.

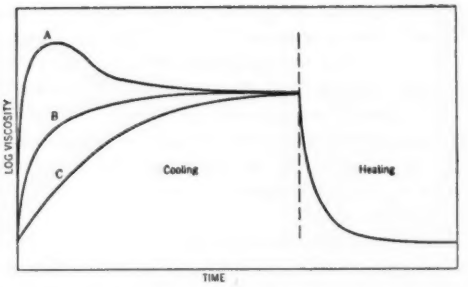


FIG. 4 APPROACH TO EQUILIBRIUM APPARENT VISCOSITY WITH TIME FOR DIFFERENT COAL-ASH SLAGS FOLLOWING AN ABRUPT CHANGE OF TEMPERATURE IN REGION OF PLASTIC VISCOSITY

sequent decrease in viscosity. In curve *B*, the rate of formation of crystals is moderate, and the growth in size parallels the formation of new crystals, giving no maximum. Curve *C* represents a case where the formation of new crystals is very slow and the increase in viscosity depends entirely upon this factor. The behavior on heating is identical for all three types, as is to be expected from the fact that at equilibrium the crystals are essentially the same size for the three types of slags.

Temperature of Critical Viscosity. The separation of crystals from a slag on cooling and the effect of these crystals on the rheological behavior of the slag have been shown to be of major importance. In Fig. 3, at viscosities of more than 66 poises the slag developed an internal yield stress because of the presence of crystals, but at lower viscosities it acted as a true liquid. This suggests that for this slag the viscosity of 66 poises represents a critical point in the cooling curve, and indeed it may be considered such. For this slag, we may consider the viscosity of 66 poises as being of special importance because it marks the division between fluid and plastic viscosities. This point will be called the "critical viscosity," which can be defined as that viscosity during the gradual cooling of a slag where there is a sudden transition from liquid to plastic flow, as evidenced by an abrupt increase in viscosity for a given small decrease in temperature or where internal yield stress is first developed in the slag.

Because, in general, the absolute viscosity, in poises, of a slag at the critical viscosity is of minor interest, whereas the temperature where it occurs is usually more important, this critical point will generally be considered in terms of temperature, hence the "temperature of critical viscosity," expressed as T_{cv}, will be used in much of the later discussion, as in Fig. 5, where curves are given for two typical coal-ash slags. Slag *X*, which is the same as in Fig. 3, can be cooled slowly from any high temperature where it exists as a liquid, there being a gradual increase in liquid viscosity until the critical viscosity of 66 poises is reached, when further cooling causes separation of crystals and there is a transition to plastic flow; this transition occurs at T_{cv}, which is 2420 F. Further cooling results in a rapid increase in plastic viscosity until at 2300 F, the slag suddenly freezes to an apparently solid mass and the bob can no longer be rotated. Slag *Y*, of different composition, behaves similarly, but its critical viscosity is 120 poises and T_{cv} is 2690 F; it freezes to a solid at 2390 F. It will be noted that the plastic-viscosity curves for these two slags are dissimilar in shape, a greater temperature effect occurring with slag *X* than with slag *Y*, so that slag *X* freezes 120 F below T_{cv}, whereas slag *Y* can be cooled 300 F below T_{cv} before freezing.

The development of internal yield stress as a function of the temperature below T_{cv} is shown in Fig. 6 for the same two slags; the rapid increase in internal yield stress of lag *X* as the result of cooling is in marked contrast to that of slag *Y*. The data of Figs. 5 and 6 permit the calculation of the flow properties of these two slags over the whole plastic range for any given conditions.

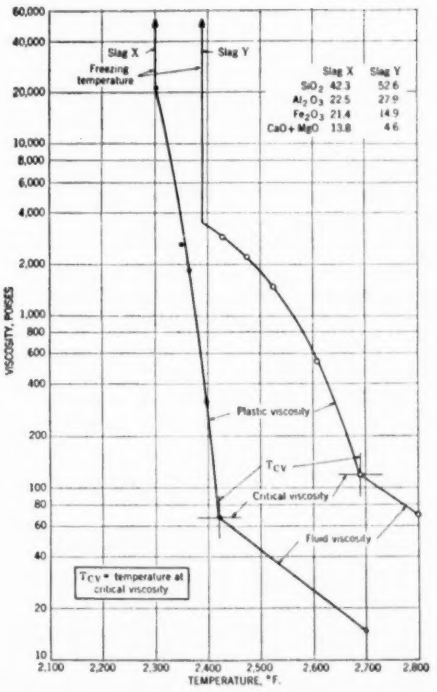


FIG. 5 EFFECT OF COOLING ON SOLIDIFICATION OF TWO TYPICAL COAL-ASH SLAGS, SHOWING CRITICAL VISCOSITY AND REGION OF PLASTIC VISCOSITY, FOR EQUILIBRIUM CONDITIONS IN AIR AT EACH INDICATED TEMPERATURE

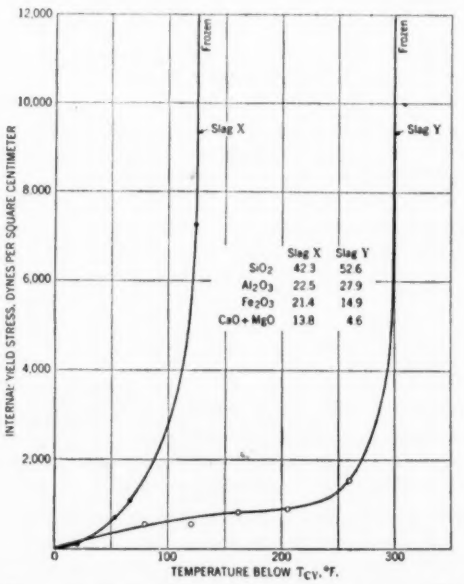


FIG. 6 DEVELOPMENT OF INTERNAL YIELD STRESS IN TWO COAL-ASH SLAGS OF FIG. 5, AS A FUNCTION OF THE DECREASE IN TEMPERATURE BELOW THAT OF THE CRITICAL VISCOSITY

Determining the rheological constants for coal-ash slags in the plastic range is a time-consuming process and may not always be possible. For some compositions, where the slag is quite fluid and there is a significant difference in density between the liquid and solid portions, stable suspensions of solid in liquid are not obtained, and measurements of the type previously described cannot be made. This fact in itself is worthy of note and is significant for slag-tap furnaces, especially of the intermittent-tapping

TABLE 2 COMPARISON OF SOME FLOW PROPERTIES OF COAL-ASH SLAGS WITH THOSE OF SYNTHETIC SLAGS OF SAME FOUR-COMPONENT COMPOSITION

Station	Composition: Toronto		Windsor		Springdale	
	As received, per cent	Synthetic, per cent	As received, per cent	Synthetic, per cent	As received, per cent	Synthetic, per cent
SiO_2	40.9	41.4	46.2	47.0	51.4	52.7
Al_2O_3	22.1	22.3	21.8	22.2	27.2	27.9
Fe_2O_3	31.0	31.4	27.8	28.2	14.5	14.9
CaO	4.1	4.9	1.8	2.6	3.6	4.5
MgO	0.8		0.8		0.9	
SO_3	0.3	...	0.1	...	0.2	...
Alkalies	0.8	...	1.5	...	2.2	...
Total	100.0	100.0	100.0	100.0	100.0	100.0
Ferric percentage of test	62		54		45	

	Flow Properties: Observed	Predicted	Observed	Predicted	Observed	Predicted
Viscosity at 2700 F, poises	14	10[a]	26	27[a]	130	150[a]
Temperature of critical viscosity, T_{cv}, deg F	2550	2540[b]	2520	2520[c]	2700	2700[b]
Freezing temperature, deg F	2280	2310[d]	2470	2270[d]	2470	2270[d]

[a] Predicted from Fig. 14.
[b] Predicted from Fig. 8.
[c] Predicted from Fig. 8 using 5 per cent CaO curve.
[d] Predicted from Fig. 9.

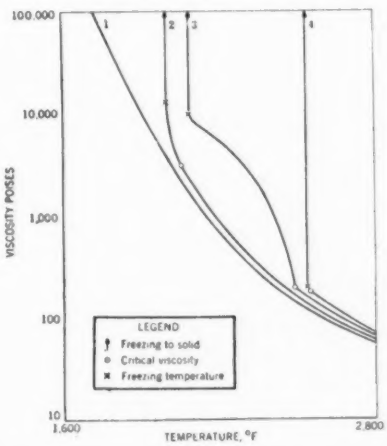


FIG. 7 TYPICAL VISCOSITY-TEMPERATURE RELATIONSHIPS OF COAL-ASH SLAGS IN SOLIDIFICATION RANGE

type. Because of these and other considerations, it was desirable to develop a method of routine laboratory test that would yield the maximum amount of useful information for the minimum expenditure of time and materials. The test procedure finally adopted was to cool the fluid slag at a constant rate of 1 deg F per min, found by experience to give almost identical results with the equilibrium tests in so far as the temperature of critical viscosity is concerned, and to operate the viscometer at a constant speed of 0.25 rps, which is both convenient and gives data of most usefulness. Torque observations are converted to apparent viscosities, that is, the viscosity of a true liquid that would give the same torque at the stirring speed used, and these data are plotted as a function of temperature; the temperature of critical viscosity is indicated by a sharp break in the apparent viscosity-temperature curve, similar to that shown for equilibrium conditions. The curves are followed to the limit of the apparatus, approximately 100,000 poises, or to the freezing temperature, whichever occurs first.

Typical cooling curves, representing the four distinct ways in which coal-ash slags act are shown in Fig. 7. Curve 1 is that for a true glass, cooling indefinitely without the development of internal yield stress; few slags are of this type. Curve 2 represents a slag approaching a glass in behavior, cooling to a low temperature before separation of solids causes the development of plastic viscosity and internal yield stress (T_{cv} is very low). Curve 3 represents a coal-ash slag which has a long cooling range but which begins to separate solids at a relatively high temperature at a low rate and freezes to a complete solid at a much lower temperature (T_{cv} usually high). Curve 4 represents a slag having a short freezing range, separation of solids being very rapid (T_{cv} may be high or low).

EFFECT OF COMPOSITION AND FERRIC PERCENTAGE ON TEMPERATURE OF CRITICAL VISCOSITY

As has been shown already, the temperature of critical viscosity T_{cv} is very important in describing the behavior of slag during cooling, because it designates that temperature at which a sudden change in rheological properties occurs. Later, the importance of T_{cv} in fixing the th ckness of slag on heat-absorbing surfaces, such as pulverized-coal furnace wall tubes, will be shown; meanwhile the variables affecting it will be evaluated, including change in composition and change in the state of oxidation of the iron in the slag.

Because coal ash is a complex substance, consisting primarily of silica, alumina, iron oxide, and lime, it is extremely difficult to present the effect of change in any one variable on the properties of a slag, variation in any one constituent causing a change in the effectiveness of every other constituent. Thus in studying systems of such complexity, it has become routine to fix certain variables which are either of little effect in themselves or are known to occur normally within relatively narrow limits. With such variables fixed, it is possible to study the system in a routine manner and with more thoroughness, although occasional compositions are encountered far outside the field being studied. In such special cases, these compositions must be considered individually although the principal fields may be a good guide as to expected characteristics.

In the study of the effect of composition, the components, as mentioned, alone have been considered, the relatively small amounts of magnesia, alkalies, titanium, and phosphorus being neglected until the future, when the studies of the principal constituents will have been completed. For this reason, many of the slags studied have been "synthetic;" that is, they have been formulated in the laboratory from chemically pure kaolin, quartz, ferric oxide, and calcium carbonate. For use in these tests, weighed quantities of these constituents are intimately mixed in a ball mill, compressed into small pellets in a tableting press, and added individually by an automatic feeding device to the platinum crucible in place in the furnace at 2700–2800 F; completion of the slagging reactions is indicated by cessation of gassing and by constant viscosity of the liquid over a 1-hr interval. An advantage of the synthetic slags is that definite compositions can be prepared for specific tests, whereas it is difficult to obtain coal-ash slags of particular compositions unless resort is made to fluxing.

Studies of synthetic and normal coal-ash slags of the same four-component composition, that is, identical except for the minor constituents, show that this simplified method is satisfactory for most purposes. Table 2 gives a comparison of the flow properties of three coal-ash slags from slag-tap furnaces and those of synthetic slags having the same four-component composition; the iron forms in the normal slags have been computed to equivalent Fe_2O_3 and the MgO has been included with CaO as a single component. The table indicates that small differences in composition may have a moderately great effect on the freezing temperature but that the liquid viscosity and the temperature of critical viscosity are but little affected. Consequently, for these last two flow properties, the data for synthetic four-component slags reported in this paper can be used for normal coal-ash slags without applying any corrections. For slags containing more than 3 per cent MgO and less than 5 per cent CaO, or where the alkalies exceed 2.5 per cent, these data should be applied with reservations until the effect of these constituent can be studied.

The relationship of the temperature of critical viscosity to composition is complex in that each of the four components making up the slag, as well as the state of oxidation of the iron in the slag, affects the critical viscosity and should be considered separately. Because the effect of change in five variables cannot be shown simultaneously by graphical means, the method of expressing the data must be simplified. The simplifications used in this case consist of combining the silica and alumina into a single variable by maintaining them at a fixed ratio of 2, which is most nearly representative of the average coal-ash slag. By making a series of plots at different CaO contents, another variable can be fixed, leaving only the equivalent Fe_2O_3 content, the state of oxidation of the iron in the slag, and the temperature of critical viscosity to be considered. By using the two compositional variables as co-ordinates and plotting the temperature of critical viscosity as isotherms, a useful family of curves results, as shown in Fig. 8, where the ordinate is the equivalent Fe_2O_3 content of the slag on the four-component basis and the abscissa is the ferric percentage.

The equivalent Fe_2O_3 content is computed from the forms of iron in the slag as follows:

$$\text{Equivalent } Fe_2O_3 = Fe_2O_3 + 1.11\ FeO + 1.43\ Fe$$

Generally, the metallic iron will not exceed 0.3 per cent and so has little significance. The equivalent Fe_2O_3 is computed to the four-component basis by recalculating the analysis of the slag so that

$$SiO_2 + Al_2O_3 + \text{Equiv. } Fe_2O_3 + (CaO + MgO) = 100$$

The ferric percentage is computed as

$$\text{Ferric percentage} = \frac{Fe_2O_3}{Fe_2O_3 + 1.11\ FeO + 1.43\ Fe} \times 100$$

and is defined as the actual ferric iron in the slag, expressed as percentage of the total iron calculated as ferric iron; it is a direct expression of the state of oxidation of slag, being 100 when the slag is completely oxidized and zero when the slag is completely reduced. Bailey and Ely[18] prefer to base a similar calculation on elemental iron, that is, as Fe, but the iron oxides have been continued as a base in these studies because they agree most closely with the actual forms of iron occurring in the slag.

The plots in Fig. 8 are given for definite CaO contents. In general, below the 10 per cent CaO level it will be better not to average the values from the figure for slags having intermediate percentages of CaO; sufficiently accurate results can generally be obtained by choosing the plot nearest in composition to the slag being studied. As just noted, MgO up to 3 per cent can be included as equivalent to CaO without introducing serious errors.

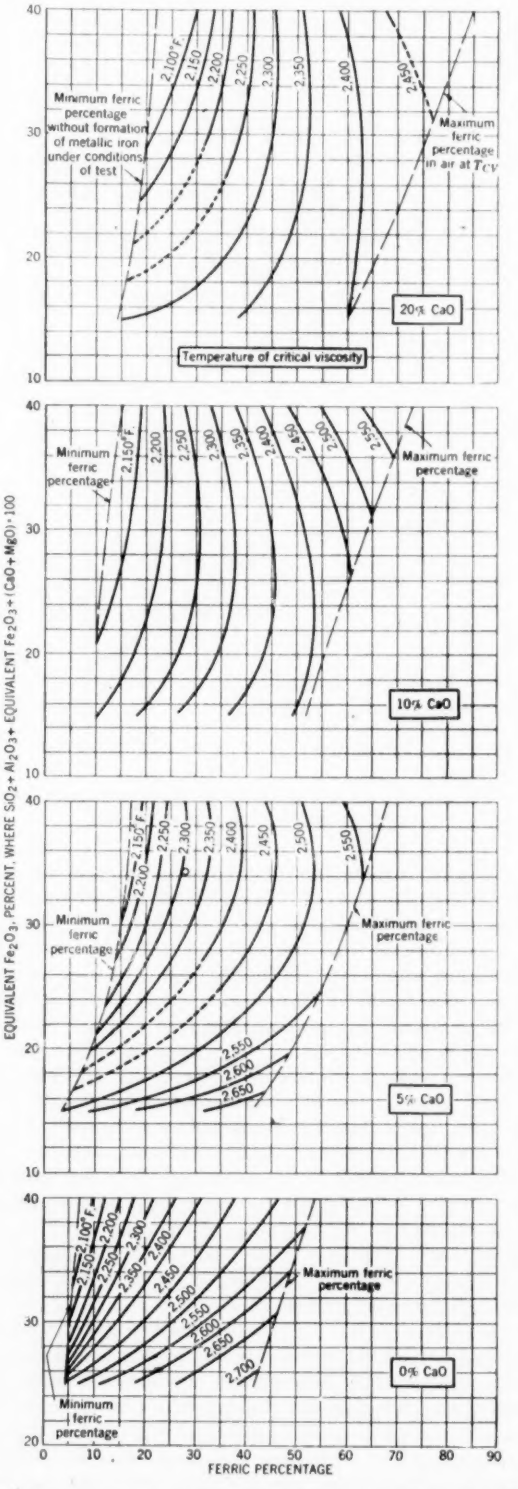


FIG. 8 TEMPERATURE OF CRITICAL VISCOSITY OF COAL-ASH SLAGS AS A FUNCTION OF COMPOSITION AND FERRIC PERCENTAGE, FOR A SILICA:ALUMINA RATIO OF 2

[18] "Significance of Coal-Ash Fusing Temperature in the Light of Recent Furnace Studies," by E. G. Bailey and F. G. Ely, Trans. A.S.M.E. vol. 63, 1941, pp. 465–471.

The effect of a given change in composition on the temperature of critical viscosity is readily obtained from Fig. 8. For instance, increasing the equivalent Fe_2O_3 content of a slag at a given ferric percentage results in decreasing T_{cv} with low values of CaO but has little effect when the CaO is 10 per cent; at 20 per cent CaO the effect is noticeable only for low ferric percentages. Decreasing the ferric percentage of the slag causes a lowering in T_{cv}, the effect of a given change in ferric percentage decreasing as the CaO content increases. For slags of a given equivalent Fe_2O_3 content, increase in CaO causes a decrease in T_{cv}, the decrease in general being largest for slags of moderate equivalent Fe_2O_3 content at the higher ferric percentages. For high-iron slags under highly reduced conditions, increase in CaO content lowers T_{cv} only slightly.

Because of the complexity of these relationships, it is suggested that each slag be considered individually. By locating it on the appropriate plot, the effect of change in furnace conditions, as regards oxidation or reduction of the slag, or change in composition whether by fluxing, blending with another coal, or change in the coal itself, can be readily determined. Calculations for a typical hypothetical slag would be made as follows:

SAMPLE CALCULATION OF A HYPOTHETICAL SLAG

	SiO_2	Al_2O_3	Fe_2O_3	FeO	Fe	CaO	MgO	SO_3 and alkalies	Total
As received, per cent.....	40.3	20.7	9.8	22.0	0.2	3.8	1.2	2.0	100.0
Iron forms recalculated to equivalent Fe_2O_3[a].....	40.3	20.7	34.5	..	...	3.8	1.2	2.0	102.5
Recalculated to four-component basis.....	40.1	20.6	34.3	..	...	5.0		...	100.0

$$\text{Ferric percentage} = \frac{9.8}{(9.8) + (1.11)(22.0) + (1.43)(0.2)} \times 100 = 28$$

$$\frac{SiO_2}{Al_2O_3} = \frac{40.1}{20.6} = 1.95$$

[a] Equivalent $Fe_2O_3 = 9.8 + (1.11)(22.0) + (1.43)(0.2) = 34.5$ per cent.

The slag has a silica:alumina ratio of 1.95, the MgO content is less than 3 per cent, and the alkalies less than 2.5 per cent; therefore the temperature of critical viscosity can be predicted from Fig. 8. The composition is plotted as a point on the 5 per cent CaO level, and T_{cv} is shown to be 2305 F. Under more oxidizing conditions in the furnace, T_{cv} could have increased to 2550 F as a maximum or could have decreased to about 2100 F if the atmosphere had been made more reducing. Changing the composition by blending with a coal having identical ash except for a greater Fe_2O_3 content would not affect T_{cv} appreciably, but lowering the equivalent Fe_2O_3 content would cause T_{cv} to increase. Similarly, increasing the CaO content while maintaining the other constituents constant would decrease T_{cv} to 2240 F at 10 per cent and to 2120 F at 20 per cent CaO. It is obvious that varying the state of oxidation of the iron forms in slag is one of the most effective means of controlling the temperature of critical viscosity.

The boundary indicated for maximum ferric percentages is a fundamental property of the slags. Higher states of oxidation than given by the boundary at the right are not possible in air because at these high temperatures there is equilibrium between the thermal dissociation of Fe_2O_3 to form lower oxides and their oxidation to form Fe_2O_3. At the left boundary, under the conditions of test, more highly reducing conditions will tend to form metallic iron, which results in a change in slag composition and consequently of slag properties. Under some conditions which could not be duplicated in platinum crucibles, it is possible to approach ferric percentages of zero without excessive reduction of FeO to Fe, but the need for such data at present is not great enough to warrant developing special test methods. It should be noted that the range of ferric percentage between oxidizing and reducing conditions increases as the total equivalent Fe_2O_3 and the CaO content increases.

A silica:alumina ratio of 2 was used for Fig. 8, because many slags are of this composition. It is believed that these data can be used successfully for slags having silica:alumina ratios ranging from 1.75 to 2.25 without introducing serious error. Work is being continued on this phase of the investigation to extend such plots to include ratios of 1.5 and 3 which should reliably cover the entire field of composition of coal ashes.

Relationship of Composition to Freezing Temperature

Although the temperature of critical viscosity is of great importance in evaluating the flow characteristics of coal-ash slags, the freezing temperature is also of considerable moment because it is the temperature at which the slag is essentially solid and cannot be deformed by any reasonable application of stress. The freezing of slag adjacent to the tap hole of intermittent-tapping furnaces, difficulty in maintaining flow, and the quantity of solid slag on the hearth are all problems associated with the operation of slag-tap pulverized-coal furnaces in which the freezing temperature of the slag is of importance. Its greatest significance, however, is in the formation and behavior of clinkers in fuel beds. So-called "tough" clinkers which are extremely difficult to handle in the furnace are sensibly plastic, that is, they have a high internal yield value while their liquid phase is highly viscous; they are intermediate in temperature between the temperature of critical viscosity and the freezing temperature. Because such clinkers are generally objectionable, it is of interest to know to what temperature they must be cooled to be reliably solid. Although comparisons of these data with actual clinkers have not been made as yet, based upon the behavior of slags in the laboratory it is suggested that clinkers below the freezing temperature will not exhibit any plasticity and therefore should no longer be tough. Because the rate at which slags or clinkers are cooled will affect the freezing temperature, care should be used in applying these data to limit them to materials that have not been rapidly chilled; the cooling rate used in the laboratory determinations has been 1 deg F per min, found to be in good agreement with equilibrium values, but cooling rates more rapid than this are usually found in practice.

The ability of slags to remain in the liquid state while being slowly cooled, that is, to behave as a glass, is not as great as was formerly believed. Under slow cooling conditions, most coal-ash slags do not gradually increase in viscosity indefinitely to give a supercooled liquid at room temperature, as has already been illustrated by the presence of a critical viscosity. Of 40 slags examined in the laboratory in 170 viscometer tests, only 1 slag behaved as a glass over the entire temperature range studied. With some few others, the freezing point had not been reached when the slag had attained an apparent viscosity of 100,000 poises, the limit of the viscometer, but in each instance the rate of increase of viscosity with temperature was so high that it was apparent that the slag was about to freeze. Also, because the slags contained a moderately large quantity of solids, their behavior should not be similar to glasses and they should have a definite freezing point. For slags that had a critical viscosity but where complete freezing to a solid did not occur, the freezing point was taken as the temperature where the viscosity had increased to 100,000 poises.

The data for the freezing temperature of typical coal-ash slags are given in Fig. 9, in which the co-ordinates are the same as for the previous figure on the temperature of critical viscosity. The relationship of composition to freezing temperature is as complex

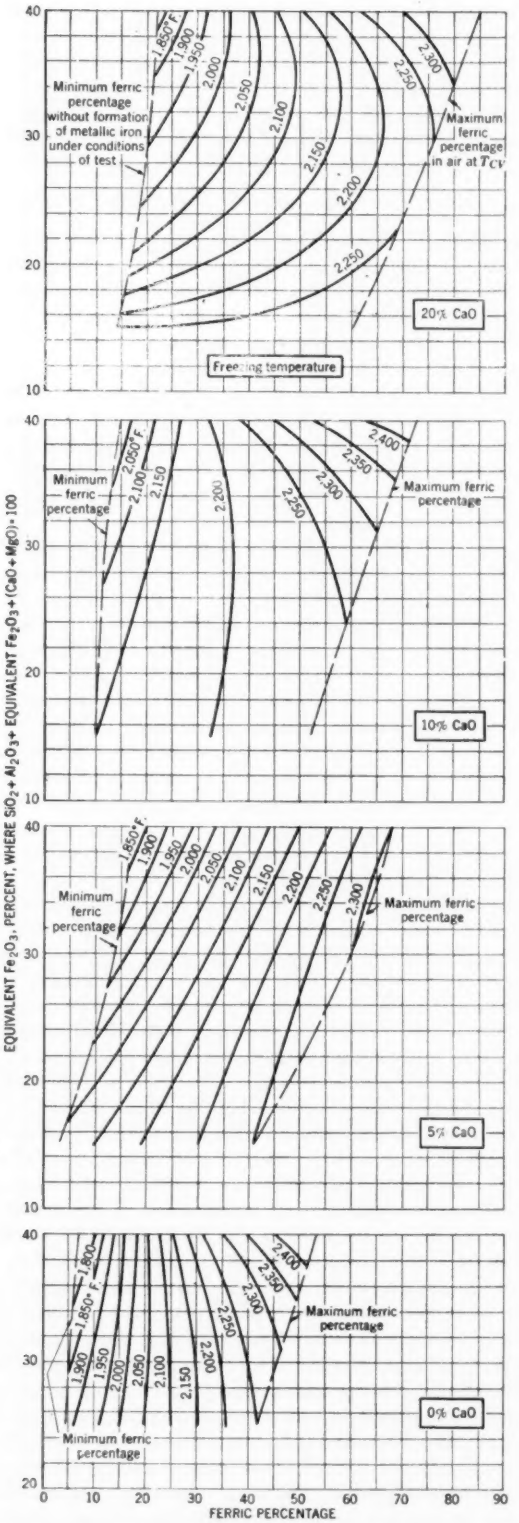


FIG. 9 FREEZING TEMPERATURE OF COAL-ASH SLAGS AS A FUNCTION OF COMPOSITION AND FERRIC PERCENTAGE, FOR A SILICA: ALUMINA RATIO OF 2

as for T_{cv}, but examination of the figure points out certain facts. Decreasing the ferric percentage of a given slag results in decrease in the freezing temperature; thus the well-known ability of slags to remain at least semifluid at lower temperatures when reduced than when oxidized is explained; a given decrease in ferric percentage is more effective in lowering the freezing point as the CaO content of the slag is less. Also, the freezing point for a given equivalent Fe_2O_3 content and a fixed ferric percentage is less at 5 per cent than at 10 per cent CaO. This agrees with the observation in a previous report[5] that the penetration temperature was lowered more by the first small additions of CaO as flux than by later additions when the CaO content of the slag was greater. It appears that for slags containing 25 per cent or less CaO, the minimum freezing temperature will occur at about 8 per cent CaO; this statement probably will not apply to slags having a silica : alumina ratio other than 2. Change in the equivalent Fe_2O_3 content of the slag has little effect on the freezing temperature, although its effect is variable with change in CaO.

As previously noted, the freezing temperature will be affected by change in the conditions of test, such as in the rapidity with which the slag is cooled. Small changes in composition may also cause large differences, such as were shown in Table 2, where the observed and predicted freezing temperatures for Windsor and for Springdale slag differed by 200 F. Thus the predicted freezing temperatures as given in Fig. 9 should be used only as a guide for actual operating practice.

SIGNIFICANCE OF CONE-FUSION DATA

Originally devised as a practical method of determining the fusibility of coal ash as a criterion of the tendency of the ash to form excessive clinker, the standardized cone-fusion determination has been accepted as a measure of the flow properties of ash at high temperatures. Easily and quickly determined with a fair degree of reproducibility, the cone-fusibility test has become firmly established and is now included in most specifications for coal. Because it is an empirical test, it cannot be directly related to fundamental properties; it expresses only the behavior of coal-ash cones under fixed conditions of preparation, dimension, and rate of heating. Despite these limitations, the method has been applied to evaluating the behavior of ash under widely varying conditions. As a result, the data are not always properly applied.

Consideration of the softening interval and the fluid interval as determined by the cone-fusibility determination has been mentioned[19] as helpful because it was obvious that reporting the softening temperature alone was not giving adequate information on the melting characteristics of the ash. Based upon furnace studies, Bailey[20] also indicated the desirability of using all three values in considering the action of ash in furnaces fired with pulverized coal. The importance of the initial deformation temperature was stressed by Gould and Brunjes,[21] who used it as a measure of the beginning of clinker formation. Recently, Bailey and Ely[18] have shown the significance of cone-fusion tests made under oxidizing as well as reducing conditions to interpret the actions of ash in different parts of furnaces.

It is apparent that the cone-fusion determination is useful in predicting ash behavior, and that fair results usually can be obtained in translating the data of this empirical test to operating conditions, but exact knowledge of the conditions responsible for any such results has been lacking. It has been one of the objectives of this investigation to determine the relationship between cone fusibility and the fundamental actions controlling the

[19] "Status of Knowledge on Properties of Coal Ash," by P. Nicholls and W. T. Reid, Proceedings 26th Fuel Engineering Conference, Appalachian Coals, Inc., Washington, D. C., June 21, 1940, pp. 77–95.

[20] "Modern Boiler Furnaces," by E. G. Bailey, Trans. A.S.M.E., vol. 61, 1939, pp. 561–569.

[21] "Proportions of Free Fusible Material in Coal Ash, as an Index of Clinker and Slag Formation," by G. B. Gould and H. L. Brunjes, Trans., American Institute of Mining and Metallurgical Engineers, vol. 139, 1940, pp. 364–375.

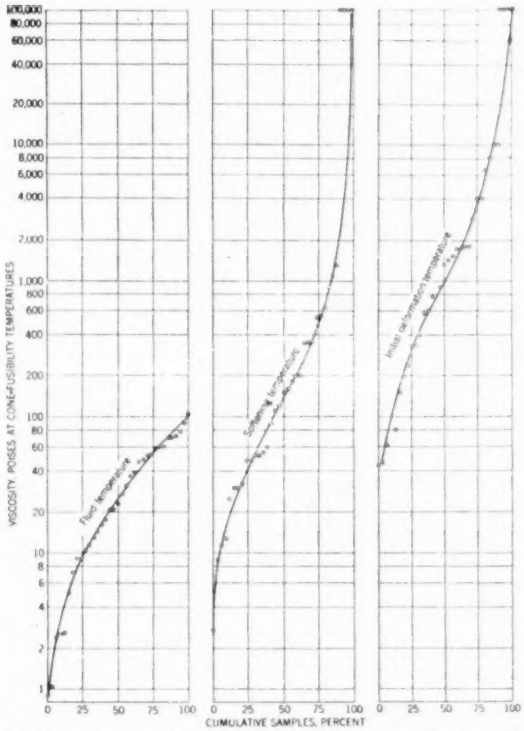


FIG. 10 VISCOSITY OF COAL-ASH CONES AT OBSERVED CONE-FUSION TEMPERATURES

flow of slag in an attempt to increase the usefulness of the cone method. For example, it would be helpful if the cone-fusion determinations could be used to indicate the viscosity-temperature relationship or the temperature of critical viscosity of coal-ash slags. Previous work on the subject in this laboratory was inconclusive; it was shown[19] that slags having similar softening temperatures could have radically different viscosities, and it was deduced that the viscosity curve could not be predicted from the cone-softening temperature alone. Since that time, many additional slags have been tested and information has been obtained on their behavior in the solidification range. As a result, further attempts have been made to correlate these different methods of measuring the flow characteristics of coal-ash slags.

The relationships to be described were obtained from a study of 35 coal-ash slags. Each slag was first melted in the viscometer and its flow properties determined, a portion of the melt being removed from the crucible at the end of the test by a platinum rod and quickly chilled to prevent oxidation. If the melts were in the liquid state before this sampling, chilling also prevented the formation of crystals, but no attempt was made to sample all the slags above their temperature of critical viscosity. The cone fusibilities were determined after the slag was ground to pass a 200-mesh screen; a gas-fired furnace was used for the reducing atmosphere, strictly following the A.S.T.M. specifications, while the determinations in air were made in an electrically heated furnace which is an exact counterpart of that used for the viscometer tests, except that it is mounted horizontally.

Because, in general, cone-fusion temperatures are lower for slags than for coal ashes of the same chemical composition, this fact should be noted in applying these data.

Viscosity at Cone-Fusion Temperatures. Inasmuch as viscosity obviously must be important in fixing the shape of a cone during heating, it has often been assumed that the viscosity is identical for every slag at a given state of deformation. In other words, it has been believed that all slags will have the same viscosity at the softening temperature, and therefore that the cone-fusion determination is a measure of viscosity. For instance, in a study of erosion caused by slag, Fehling[22] assumed a viscosity of 1000 poises as representative of the softening temperature. As mentioned previously, tests on a few slags in this laboratory indicated considerable deviation from this assumption; therefore it has been checked more carefully with these recent data. The results are shown graphically in Fig. 10, where the viscosity in poises for each of the 35 slags at the three fusion temperatures has been arranged in order of increasing viscosity. In cases where the cone temperatures are higher than T_{cv}, the viscosity is that of the liquid slag; when lower, the apparent viscosity is given.

It is obvious that there is no relation between viscosity and the observed cone-fusion temperatures; for each condition the viscosity varies over a ratio of more than 100:1.

Initial Deformation Temperature. Although many attempts were made to correlate the initial deformation temperature with the viscometric data, no relationships could be found. For instance, plotting the initial deformation temperature against the freezing temperature showed only an insignificant tendency for the two to increase together. Similarly, comparison of the softening with the freezing interval, that is, the difference between the temperature of critical viscosity and the freezing temperature, indicated no definite relationship. Although the initial deformation temperature probably has a definite significance, it is not related to viscosity alone nor to the tendency of slag to freeze while being cooled; the data of Fig. 10 indicate that the viscosity of slag at the temperature of initial deformation can range between 44 and +100,000 poises, while 50 per cent of the slags tested had a viscosity of less than 1000 poises.

Softening Temperature. The viscosity of slags at the softening temperature is also extremely variable, ranging from 2.7 poises to +100,000 poises. For the slags studied, 83 per cent had a viscosity of less than 1000 poises at the softening temperature. Because some coal-ash slags at temperatures near that of the critical viscosity are sensitive to the rate and direction of temperature change, the higher indicated viscosities at the softening temperature may not be important.

It has seemed reasonable to expect that the temperature of critical viscosity would be related to the cone-softening temperature, because with many slags the change in flow characteristics at

[22] "Erosion of Refractories by Coal Slag," by H. R. Fehling, *Journal, of the Institute of Fuel*, vol. 11, 1938, pp. 451–458.

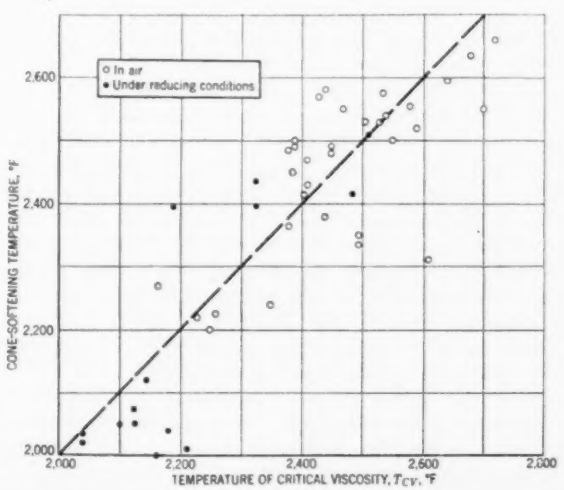


FIG. 11 COMPARISON OF CONE-SOFTENING TEMPERATURE WITH TEMPERATURE OF CRITICAL VISCOSITY

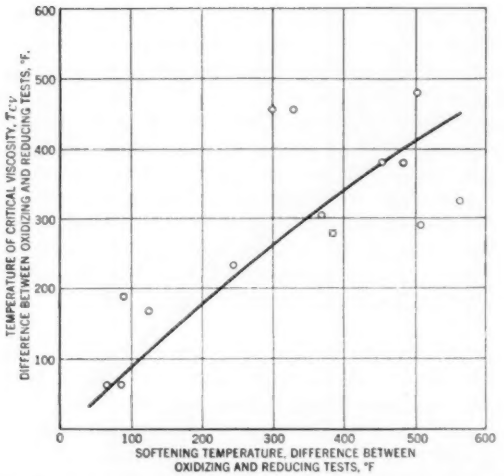


FIG. 12 EFFECT OF CHANGE IN STATE OF OXIDATION ON RELATIONSHIP BETWEEN CONE-SOFTENING TEMPERATURE AND TEMPERATURE OF CRITICAL VISCOSITY

T_{cv} should produce a radical change in the rate of deformation of the cone. Fig. 11 shows a comparison of the temperature of critical viscosity with the cone-softening temperature; the broken line as drawn would indicate a linear relationship between the two temperatures. It is apparent that this line is a fair representation of the data, although some points deviate considerably. Actually, for the 35 slags tested in air, the temperature of critical viscosity was higher than the cone-softening temperature for 18 slags, was lower for 16 slags, and was identical for one slag. The maximum difference was 300 F, whereas the mean difference was only 5.5 F.

For the slags under reducing conditions, the temperature of critical viscosity was predominantly higher than the cone-softening temperature in the lower range, but no definite relationship depending upon state of oxidation was apparent. In Fig. 12, the effect of changing the state of oxidation of a slag on its temperature of critical viscosity and on its cone-softening temperature is shown to be similar, the softening temperature being slightly more affected by reducing atmospheres than is the temperature of critical viscosity. Again, the individual points deviate considerably from the average, but the trend is definite.

Fluid Temperature. Fig. 10 shows that for these tests the viscosity of slags at the cone-fluid temperature ranged between 0.9 poise and 105 poises, although the fluid temperature occurred at less than 100 poises for 99 per cent of the slags tested and at less than 25 poises for 50 per cent of the slags. Thus the fluid temperature occurs at low viscosities but not at any definite viscosity. However, if the fluid temperature is compared with viscosity at a fixed temperature, a fair relationship is found, as shown in Fig. 13, where increase in the fluid temperature is accompanied by increased viscosity of the slag at 2600 F. Although some of the data again are in poor agreement, it is possible to use the fluid temperature as a guide to the viscosity of the slag at 2600 F, from which the viscosity at the observed fluid temperature or any other temperature above T_{cv} can be calculated as described later. It is interesting to note that the British Standards Institution method for the cone-fusion temperature of coal ash does not include observation of the fluid temperature.

A note of caution should be expressed regarding the determination of the fluid temperature, as it was observed during these tests that the fluid temperature in air was affected noticeably by change in composition of the refractory pat upon which the cones were mounted. The A.S.T.M. method specifies equal parts of kaolin and calcined alumina for the refractory pat, but it has been the habit in some laboratories to add a greater amount of kaolin to increase the plasticity of the wet mass for easier working. Studies were therefore made on pats prepared according to the specifications and those containing 2 parts of kaolin to 1 part of calcined alumina. The 2:1 pats fired to produce a denser body, therefore the slag was absorbed less readily and the cone-fluid temperature was increased; typical examples are given in Table 3. No corresponding change in the initial deformation or the softening temperature was noted. Because the data of this investigation were obtained with pats made according to the A.S.T.M. specifications, cone-fluid temperatures observed with cone supports having a different porosity should not be used for estimating slag viscosity according to Fig. 13.

TABLE 3 EFFECT OF COMPOSITION OF REFRACTORY PAT ON CONE-FLUID TEMPERATURE

Slag from viscometer test No.	Fluid temperature, deg F	
	1 kaolin: 1 alumina pat	2 kaolin: 1 alumina pat
188	2626	2736
189	2611	2713
204	2698	+2900
223	2697	+2900
227	2718	2870
228	2826	+2900

A brief summary of the comparison between viscosity and the cone-fusion determination indicates the following:

1 Viscosity is not a constant for any particular stage of cone deformation.

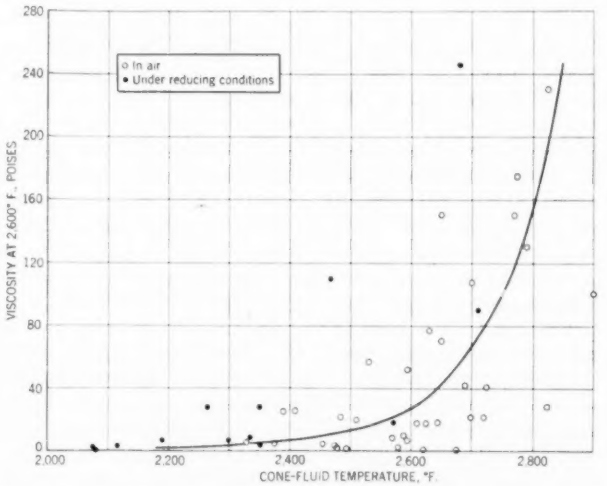


FIG. 13 VISCOSITY OF COAL-ASH SLAGS AT 2600 F AS RELATED TO THE CONE-FLUID TEMPERATURE

2 No correlation has been found between the initial deformation temperature and the flow properties of slag.

3 The softening temperature is a fair measure of the temperature of critical viscosity, although large unexplained differences can occur.

4 The viscosity of a slag at 2600 F can be predicted approximately from the cone-fluid temperature.

5 The "softening" and the "fluid" intervals probably are less significant than the values of the observed points, no relationship being found between these intervals and the viscometric data.

6 The cone-fusibility determination can be used as a rough measure of viscosity and, because of the simplicity of the test, is the most rapid method of evaluating the flow characteristics of coal-ash slags.

VISCOSITY OF LIQUID SLAGS

The absolute viscosity of slags in the liquid state, that is, at higher temperatures than T_{cv}, is equally as important as the

other flow characteristics. The equilibrium thickness of slag on wall tubes is partly determined by the viscosity of the liquid portion of the deposited slag, while the rate of flow of slag from pulverized-coal furnaces during tapping is related to this property, as is the tendency to form "sheet" clinker in stoker-fired furnaces. Knowledge of the viscosity of slag in the liquid state is essential and must be available for complete understanding of the action of coal ash at high temperatures. A previous report[7] was concerned primarily with the viscosity of coal-ash slags in the liquid state. Because additional data are now available, that information has been expanded and is being given in a slightly different form. It was shown in Fig. 9 of that report that (1) the rate of change of viscosity with temperature of any liquid coal-ash slag depends only upon the viscosity of the slag and not upon temperature, and (2) the rate of change of viscosity with temperature increases with increase in viscosity. The relationship was expressed as follows:

Viscosity, η, poises	$\frac{d\eta}{dt}$, poises per deg F
1	— 0.0028
10	— 0.04
100	— 0.58
1000	— 8.50

Plotting $\left|\frac{d\eta}{dt}\right|$ against η on logarithmic paper gives a straight-line relationship indicating that

$$\log \left|\frac{d\eta}{dt}\right| = a + x \log \eta$$

and

$$\left|\frac{d\eta}{dt}\right| = a\eta^x$$

or

$$\frac{d\eta}{dt} = -a\eta^x$$

This is the general differential equation for change in viscosity with temperature for the field of compositions of coal-ash slags studied, a and x being constants for the entire field. In the integrated form

$$\eta^{-z} = At - B$$

where z and A are related to x and a and are also constants for the entire field. Their values are 0.1614 for z, and 0.0004519 for A; the constant B is fixed for each particular slag.

The additional data have further substantiated the relationship between the SiO_2 content and the viscosity at 2600 F of coal-ash slags, as shown in Fig. 7 of the previous report.[7] It has been found desirable to continue the same basis of expressing composition, that is, to eliminate Al_2O_3 and recalculate so that SiO_2 + equivalent Fe_2O_3 + (CaO + MgO) = 100. Plotting the SiO_2 content on this basis against viscosity results in better agreement than when Al_2O_3 is included. It should be noted that this method of plotting gives the same results as plotting the sum of equivalent Fe_2O_3 and (CaO + MgO) on the same basis, except that the abscissa would be scaled in the opposite direction.

To simplify the use of these relationships between temperature, viscosity, and composition, a nomogram has been constructed. It is shown in Fig. 14 and permits prediction of the liquid viscosity at any temperature for any coal-ash slag whose composition is known. Scale C gives directly the relationship between the SiO_2 content of the slag and its viscosity at 2600 F, and can be used alone to determine the liquid viscosity at this fixed temperature.

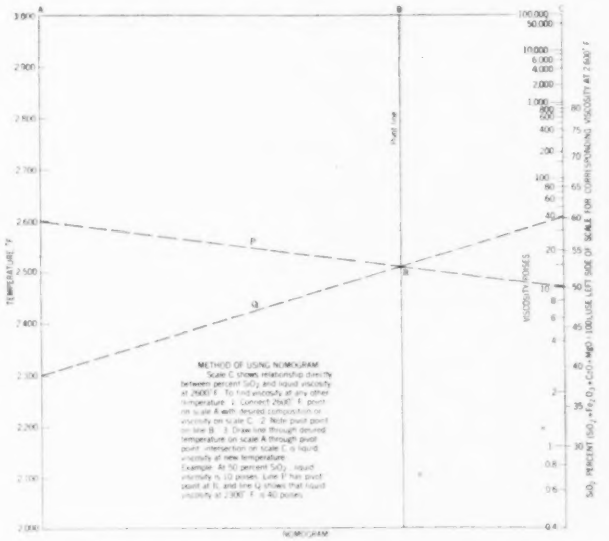


FIG. 14 VISCOSITY OF COAL-ASH SLAGS IN LIQUID STATE AS A FUNCTION OF COMPOSITION AND TEMPERATURE

To convert to other temperatures shown on scale A, pivot line B must be used as illustrated on the nomogram. This nomogram was used for predicting the viscosity at 2700 F of the three slags of Table 2. Because the effect of reducing or oxidizing conditions on the viscosity of slag in the liquid state is negligible, these data can be applied to either reduced or oxidized slags.

Extreme care should be taken in using the nomogram not to apply it to temperatures lower than the temperature of critical viscosity for the slag being considered, Fig. 14 being suitable only for slags completely in the liquid state. Before the nomogram is used, the temperature of critical viscosity of the slag should be determined from Fig. 8, and this temperature should be used as the lower limit in predicting liquid viscosity.

EFFECT OF RHEOLOGICAL PROPERTIES ON THE THICKNESS OF SLAG ON HEAT-ABSORBING SURFACES

A significant variable in the operation of slag-tap furnaces is the thickness of the slag deposits on the heat-absorbing surfaces. Although it is obvious that the more refractory coal ashes, or slags, will result in thicker deposits and consequently lower the rate of heat transfer from the furnace, it has been hitherto impossible to arrive at more definite conclusions. It is the object of this section of the paper to present a brief analysis of the flow of slag on furnace walls, with some quantitative results of the effect of the rheological properties of the slag on the relative thickness of deposits on heat-absorbing surfaces.

In any mathematical analysis of a complicated physical process, it is necessary to make simplifying assumptions and to limit the analysis to a small number of variables. The major premise in this case is that the flow of slag at temperatures below that of the critical viscosity can be neglected. This will generally be true and is absolutely essential to the setting up of a workable hypothesis. Further, it is assumed that the thermal gradient through the slag is constant. This assumption is more questionable, but in the absence of even average values for the thermal conductivity of coal-ash slag no better postulate can be supplied. An approximate allowance can be made for the porous nature of the slag in the vicinity of the metal or of relatively poor contact between slag and tube surface, by assuming the cold side of the slag deposit to be at a higher temperature than the metal. Because the thickness of this part of the slag deposit is usually quite small, the computed relative thicknesses are not greatly affected.

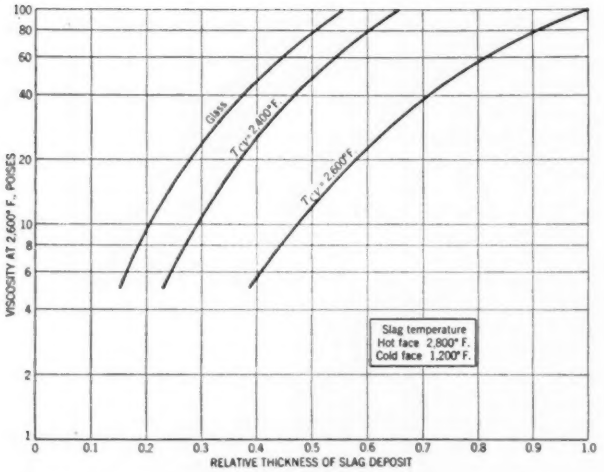


FIG. 15 COMPUTED EFFECT OF LIQUID VISCOSITY AND TEMPERATURE OF CRITICAL VISCOSITY, T_{cv}, ON THICKNESS OF SLAG LAYER ON HEAT-ABSORBING SURFACES

(Based on a thickness of 1 for a slag having T_{cv} = 2600 F, and a viscosity of 100 poises at 2600 F.)

Assumption of a constant slag density, independent of composition and temperature, can cause only minor errors. Finally, the variation of viscosity with temperature for coal-ash slags is taken into account by means of a formula given in a previous section of this paper.

Based on these factors, an equation has been derived relating the thickness of slag deposits to the temperature of critical viscosity, the viscosity as a function of temperature, the density, the rate of slag supply to the wall, and the temperatures of the hot and cold faces of the slag deposit. The development of this equation is too involved to be presented at this time, and only the results obtained by its use will be considered. The equation is given in functional form as follows:

$$V = \frac{\rho\, d^3 \sin \alpha}{A^2\, \bar{\Delta} t^2}\, f(A, B, z, t_w, \Delta t, T_{cv})$$

where

V = volume of slag flow
ρ = density of slag (assumed constant)
d = thickness of slag deposit
A, B, and z = parameters in equation relating viscosity to temperature, $\eta^{-z} = At - B$
α = angle of inclination of wall to horizontal
t_w = temperature at cold side of slag deposit
Δt = temperature drop across slag deposit
T_{cv} = temperature of critical viscosity

By use of the equation, the relative thicknesses of slag deposits have been computed as a function of the viscosity of the slag at 2600 F, and of the temperature of critical viscosity. Fig. 15 shows these thicknesses relative to that of a slag having a viscosity of 100 poises at 2600 F, and with T_{cv} also 2600 F, the computations being based upon a temperature for the hot face and for the cold face of the slag deposit of 2800 F and of 1200 F, respectively. Curves are shown for the effect of change in viscosity on the relative thickness of deposit for slags having a temperature of critical viscosity of 2600 F and of 2400 F, and for a slag that remains a glass when cooled slowly.

The plot shows that substituting a slag having a viscosity of 5 poises at 2600 F for one of 100 poises at that same temperature results in a decrease in the equilibrium thickness of the deposited slag to 38 per cent of its previous value, if both slags have a temperature of critical viscosity of 2600 F. Reducing T_{cv} of the new slag to 2400 F would result in a slag thickness only 23 per cent as great as formerly, whereas if the slag were a glass the deposit would be only 15 per cent as thick as the original deposit.

If, due to changes in operating conditions, the only change in the furnace is a decrease in the ferric percentage of the slag, with a resultant decrease in T_{cv} from 2600 F to 2400 F, the thickness of the deposit of a slag having a viscosity of 100 poises at 2600 F would be reduced to 65 per cent of its former value, and if T_{cv} were so low that the slag acts as a glass, to 56 per cent of its original value; the behavior at other viscosities can be estimated from the figure.

The more viscous slags, containing little flux, will not be changed appreciably in thickness by change in state of oxidation, because, for such slags, the change in the temperature of critical viscosity resulting from change in the ferric percentage is not great. For high-flux slags, those having a high equivalent Fe_2O_3 content will be more subject to variation in thickness than if the CaO is high, because the temperature of critical viscosity is more affected by change in ferric percentage for slags high in equivalent Fe_2O_3.

The foregoing results are not exact, in that operating changes that will usually occur simultaneously when the rheological properties of the slag are changed have not been considered. Such factors would include change in the temperatures of the hot and the cold faces of the slag deposit, variations in the quantity of ash impinging on the given surface, effect of change of rating of the furnace or of the heating value of the coal, and many others. This development is presented as a first approximation to an important factor governing furnace performance; it will undoubtedly be subjected to modification and extension as knowledge of the processes involved increases.

SUMMARY

An instrument is described for measuring the flow properties of coal-ash slags below the temperature at which solid material separates from the slag on cooling. These solids cause an abrupt change from liquid to plastic flow, the transition point being termed the temperature of critical viscosity. Plastic viscosity is demonstrated by the development of an internal structure in the slag, which requires the application of a finite stress to produce initial deformation. This internal yield stress is shown to be similar to that developed in other plastic materials; it offers an explanation for the variable behavior of slags while freezing.

The temperature of critical viscosity T_{cv} is affected in a complex manner by change in the composition and in the ferric percentage of a slag. No simple relationships exist, but charts are presented showing the results of laboratory determinations over a range of compositions representative of many slags. It is shown that, for a given state of oxidation, T_{cv} decreases as the equivalent Fe_2O_3 content of the slag increases, the effect being most noticeable for small quantities of CaO. Also, for a fixed equivalent Fe_2O_3 content, increasing CaO decreases T_{cv}. The largest change occurs with change in the state of oxidation of the slag, decreasing the ferric percentage being most effective in lowering T_{cv} as the equivalent Fe_2O_3 content of the slag increases.

Similar relationships are also given showing that decreasing the ferric percentage decreases the freezing temperature of coal-ash slags but that variations in equivalent Fe_2O_3 or in CaO contents have no regular effects.

Comparison of cone-fusion data with equilibrium values of slag viscosity show that viscosity is not a constant for any given state of deformation of cones; a relationship between cone-fluid temperature and absolute viscosity is given which may be useful in roughly predicting the viscosity of slags from cone-fusion data.

The cone-softening temperature is an approximate indication of the temperature of critical viscosity, but large unexplained differences can occur. No relation could be detected between the cone initial-deformation temperature and the flow characteristics of the slag.

Methods of expressing the liquid viscosity of slags as a function of composition and temperature have been simplified. A nomogram is given by which the viscosity of a slag can be predicted at any temperature above that of the critical viscosity.

These data have been applied to a theoretical study of the effect of change in rheological properties on the equilibrium thickness of a slag deposited on the heat-absorbing surfaces of boiler furnaces. A mathematical relationship has been derived from which the relative thickness of slag deposits has been computed as a function of the viscosity of the slag and the temperature of critical viscosity. It is shown that a decrease in viscosity from 100 to 5 poises at 2600 F reduces the thickness of slag to less than it would have been had T_{cv} for the more viscous slag been decreased from 2600 F to the point where the slag behaved as a glass. Although certain factors fixed by operating conditions are not considered, and the method will undoubtedly be modified later, it does permit consideration of the more important factors of slag properties in governing furnace performance, and thus should be of assistance in any study of the action of slag in furnaces.

Acknowledgments

This investigation has been performed under the authorization and encouragement of A. C. Fieldner, Chief, Fuels and Explosives Service, Bureau of Mines. The late P. Nicholls of this Bureau was largely responsible for the earlier developments in the study; his careful analyses of the various factors and his critical supervision of the methods and the apparatus employed added much to the value of the investigation. J. W. Myers and J. J. Pfeiffer assisted in the conduct of the viscometer tests.

The many chemical analyses for forms of iron were made in the Miscellaneous Analyses Section of the Bureau of Mines at Pittsburgh, under the direction of W. A. Selvig, and the cone-fusion determinations in the Coal Analysis Laboratory under the direction of H. M. Cooper.

Statistical Information on Large Pulverized-Coal Units on the Consolidated Edison System

By W. E. CALDWELL,[1] NEW YORK, N. Y.

STATISTICAL data on several pulverized-fuel-boiler installations of the Consolidated Edison Company of New York, Inc., are presented in accordance with the outline prepared by the Special Research Committee on Furnace Performance Factors. Each unit was installed to meet conditions expected at the time to prevail during the life of the apparatus. Since specific requirements differed for the individual units, they may not be directly compared, although useful trend information may be obtained from a study of the influence of design on the various factors. Economy considerations dictate sustained high-capacity operation for the high-pressure units, consequently their design provides more liberal proportions than in the case of the older low-pressure units. Later installations also reflect recent developments or advances in the art. Practically all of the units here presented were designed for installation in an existing building or to meet space restrictions imposed by city-site limitations. This condition, combined with the economic urge of producing the maximum capacity in the space available, accounts for certain features of design.

Since the survey was undertaken to determine the influence of the various relations on furnace performance and related conditions, a few general observations on the characteristics of these units may be in order, with emphasis on cleaning problems and maintenance of capacity.

In the older plants, with moderate superheat, furnace cleaning is necessary to keep the passes open to maintain capacity. In more recent high-temperature units cleaning is necessary, as in the case of the older boilers, but with an added limitation imposed by higher steam temperature. To assure full steam temperature at partial load and to permit limiting temperature at full load, gas-controllable by-passing of the superheater is resorted to. Since the gas by-pass affords a comparatively small range of steam-temperature control, fouling of furnace heating surface often increases the gas temperature and superheat beyond a safe limit, necessitating furnace cleaning or capacity reduction. There are several methods in use for cleaning boilers and furnaces, such as soot blowers, hand-lancing with air, steam, water, various combinations of the three, and by thermal shock induced by periodic load reduction. The latter method has proved attractive on more recent installations, since it requires a minimum of labor.

Deslagging Boilers

With high furnace temperature and a reducing atmosphere, a number of coals produce adherent slags which resist removal by soot blowers and lancing. These slags shed from the walls and boiler tubes freely when the load is reduced or the fire is extinguished. Where two boilers are installed per topping unit the customary method of deslagging is to shut down one boiler during the midnight watch for sufficient time to permit shedding of the slag. The bulk of this material usually falls during the first 15 min after extinguishing the fire. Where a single boiler is installed, complete shutdown is impractical, and approximately equal results are accomplished by reducing the load from full load to about half load for a period of 2 hr or more. Most of this slag appears to shed during the second hour. Where the superheater is suitably proportioned, cleaning once in 24 hr by this method gives satisfactory results. With certain coals this method must be supplemented by soot-blowing or lancing in order to remain within range of temperature control.

In cases where excessive superheater surface aggravates the cleaning problem, changes are being made to establish temperature control within a more suitable range. This is accomplished by baffle changes or by adding boiler surface ahead of the superheater. When these changes have been completed, cleaning requirements will be dictated by the grade of fuel, load demand, and combustion conditions.

Improper distribution of fuel and air supply aggravates cleaning requirements and, as circumstances permit, modifications are being made to improve furnace conditions. The burner arrangement has a pronounced effect on the heat distribution within the furnace, as well as on the fusion of the ash and cleaning problem throughout the unit. The larger the unit the more difficult this problem becomes, since a larger quantity of coal and primary air is delivered from each mill connection to the burner. Ideally, the coal and primary air should be delivered in an infinite number of small streams so that each ignited particle may be scoured by the turbulent secondary air with an oxidizing atmosphere in the furnace. This results in a uniform high heat absorption by the furnace walls without extreme concentrations in local areas. There should be no CO present in the furnace, since a reducing atmosphere results in a substantially lower ash-fusing temperature and more adherent slag. With an oxidizing atmosphere in the region of the high-temperature zones, slag troubles diminish and wall cleanliness may be more readily maintained. Practical considerations necessitate compromises and instead of a few pounds of coal injected per nozzle per hour, some burners deliver 3 tons or more per nozzle per hour. Even under these conditions, combustion is complete when the gas enters the convection bank and combustion is practically perfect. The furnace, however, suffers from the impingement of these large streams of burning coal against the opposite wall, which causes highly localized hot zones and tenacious slag coatings.

Types of Burners

Figs. 1 and 2 show an earlier type of tangential burner adjusted for a small firing circle. Accumulated experience seems to indicate that, from a furnace standpoint, better results would be obtained if the burners were taller in height and with a greater number of coal nozzles. With such an arrangement, the firing circle may be enlarged in order to increase the convection component and absorb more heat in the furnace. This reduces

[1] Mechanical Plant Engineer, Consolidated Edison Company of New York, Inc. Mem. A.S.M.E.

Contributed by Special Research Committtee on Furnace Performance Factors with the co-operation of the Fuels, Power, and Heat Transfer Divisions and presented at the Annual Meeting, New York, N. Y., November 29–December 3, 1943, of The American Society of Mechanical Engineers.

Note: Statements and opinions advanced in papers are to be understood as individual expressions of their authors, and not those of the Society.

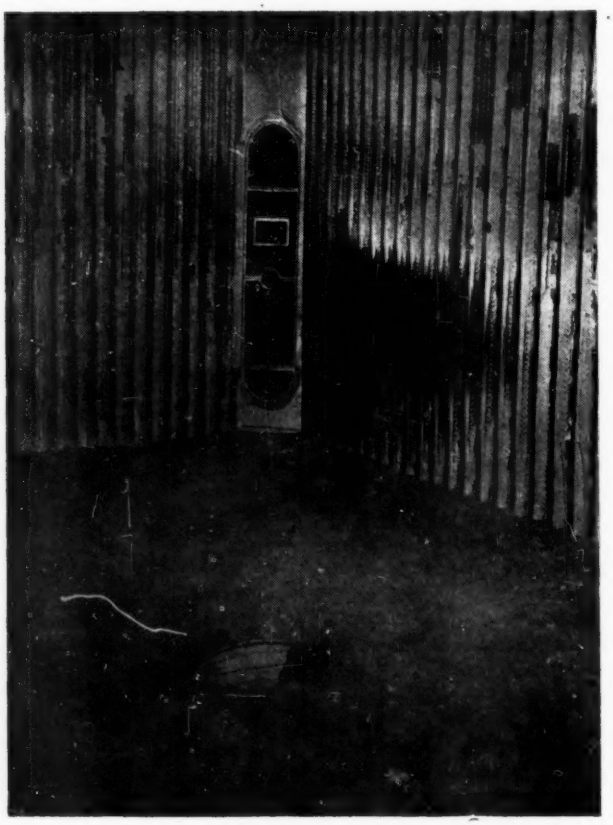


FIG. 1

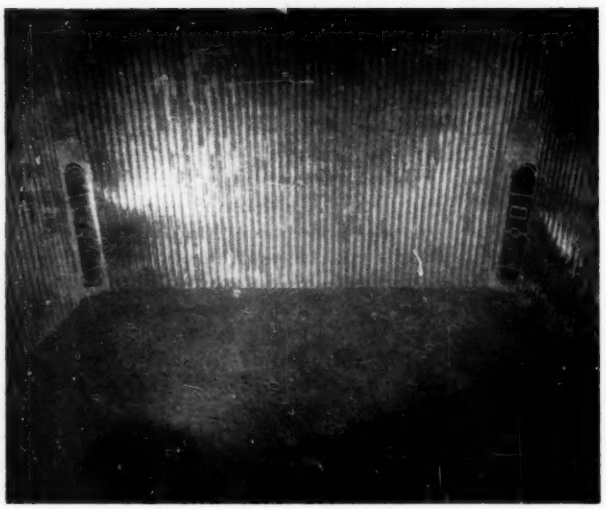


FIG. 2

temperature and fouling conditions within the convection bank.

Fig. 3 indicates relative proportions of two types of pulverized-coal burners on recent units covered in the tabulation. These burners are an improvement over earlier practice but some trouble is experienced with the production of CO in the region of the burner.

As boiler unit sizes and capacities increase the problem of burner disposition and furnace heat absorption becomes more difficult, since the ratio of wall surface to furnace volume diminishes as size increases. As the furnace walls account for a large portion of the total heat absorption, this size-factor relation is an important consideration. In the No. 90 unit, the Btu per cubic foot per hour is 20,000, while the heat release per square foot of furnace wall is 90,500 Btu. In the No. 72 unit, the furnace surface and convection surface are combined in the open-pass design to give the effect of a long narrow furnace. In this unit the Btu per cubic foot per hour is 30,000, while the Btu per square foot of surface is 54,700. Both units deliver high sustained capacity with excellent reliability and efficiency. Unit No. 9 is an earlier type with heat release of 27,000 Btu per cu ft and an absorption rate of 130,000 Btu per sq ft of furnace surface. Complete test data were previously presented on this unit.[2]

Tube spacing in the boiler banks of more recent units is adequate to eliminate the type of plugging experienced with earlier units, but operating vigilance is still required to avoid trouble. Wall cleaning is at present practiced as a capacity measure dictated by superheat limitations, while economizer cleaning may be justified by economy considerations. Boiler passes are usually blown once or more a watch, as dictated by grade of fuel and load conditions.

The cleaning schedule is established by experience and is organized to meet a wide range of fuel and load conditions, in which cleaning costs and results must be kept in balance. Corrective measures made to reduce superheat on one recent unit indicate a substantial reduction in cleaning requirements, but a longer period of operation will be required to establish the relation between the design factors and the cleaning schedule.

[2] "Characteristics of Large Hell Gate Direct-Fired Boiler Units," by W. E. Caldwell, Trans. A.S.M.E., vol. 56, 1934, p. 65.

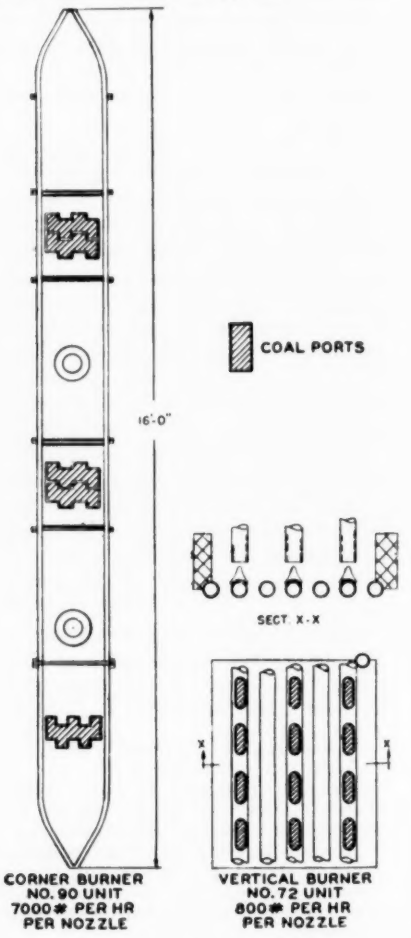


FIG. 3

DESCRIPTION OF UNIT

BUILDER	COMBUSTION ENGINEERING COMPANY	YEAR INSTALLED	1937
BOILER TYPE	SINGLE DRUM STRAIGHT TUBE & HEADER	ASH REMOVAL	CONTINUOUS SLAG TAP
PULVERIZER	RAYMOND BOWL	FIRING	TANGENTIAL DIRECT
BURNER	COMB ENG TYPE "T"		

TYPICAL FUEL

KIND	VARIOUS	DISTRICT	VARIOUS
SEAM	VARIOUS		

PROXIMATE ANALYSIS		ASH CHARACTERISTICS	
VOLATILE MATTER	20.5 %	INITIAL DEFORMATION	2515 F
FIXED CARBON	72.2 %	SOFTENING	2570 F
ASH	7.3 %	LIQUID	2800° F
TOTAL MOISTURE	4.4 %	SULPHUR (DRY BASIS)	1.3 %
HEAT VALUE PER LB AS REC'D	13,885 BTU	GRINDABILITY	60-115 %

PERFORMANCE

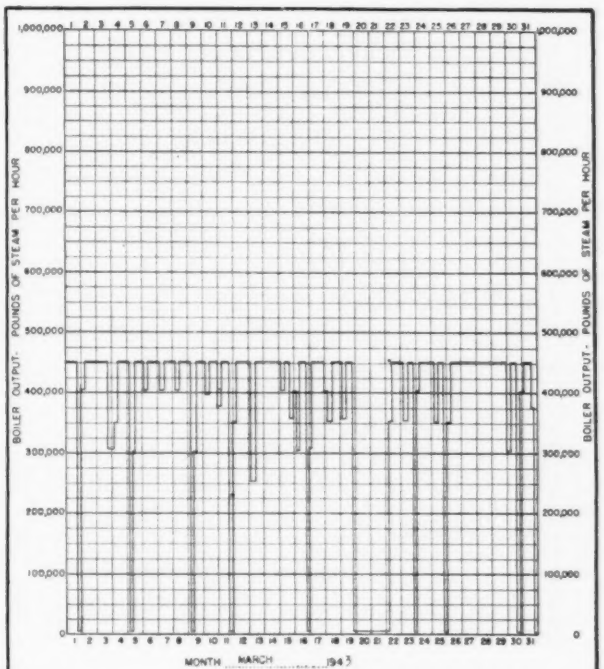
BOILER OUTPUT	500,000 LB/HR	1260 LB/SQ IN	900° F
FUEL BURNED	43,100 LB/HR	598,000,000	BTU/HR
COMBUSTION AIR TEMP	509° F	FINENESS THRU 200 MESH	- %
FUEL BURNING RATE	.0863# COAL PER Lb STEAM		

FURNACE SURFACE		5,196 SQ FT	115,400 BTU/HR/SQ FT
FURNACE SURFACE & CONVECTION BANK TO SUPERHEATER		9,370 SQ FT	63,900 BTU/HR/SQ FT
FURNACE VOLUME		20,300 CU FT	29,500 BTU/HR/CU FT
FURNACE WIDTH		24.584 FT	24,400,000 BTU/HR/FT
FREE GAS AREA	CONVECTION BANK ENTRANCE	426 SQ FT	1,405,000 BTU/HR/SQ FT
	CONVECTION BANK CLOSELY SPACED TUBES	419 SQ FT	1,430,000 BTU/HR/SQ FT
	SUPERHEATER ENTRANCE	190 SQ FT	3,150,000 BTU/HR/SQ FT
	SUPERHEATER CLOSELY SPACED TUBES	190 SQ FT	3,150,000 BTU/HR/SQ FT

REMARKS:

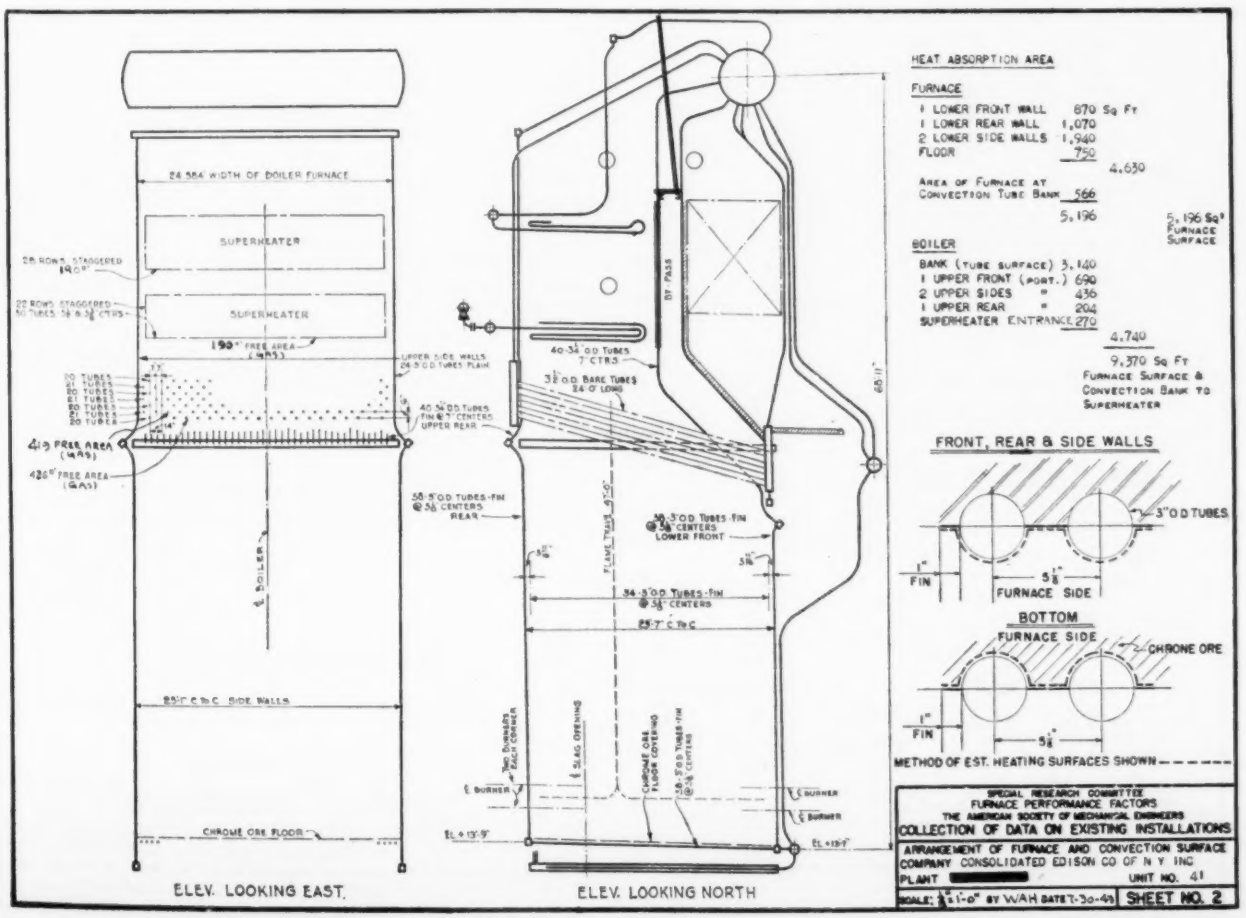
SPECIAL RESEARCH COMMITTEE
FURNACE PERFORMANCE FACTORS
THE AMERICAN SOCIETY OF MECHANICAL ENGINEERS
COLLECTION OF DATA ON EXISTING INSTALLATIONS

DESCRIPTION AND PERFORMANCE
COMPANY CONSOLIDATED EDISON CO OF N Y INC
PLANT UNIT NO. 41
BY DATE SHEET NO. 1



SPECIAL RESEARCH COMMITTEE
FURNACE PERFORMANCE FACTORS
THE AMERICAN SOCIETY OF MECHANICAL ENGINEERS
COLLECTION OF DATA ON EXISTING INSTALLATIONS

TYPICAL LOAD CURVE
COMPANY CONSOLIDATED EDISON COMPANY OF N Y INC
PLANT UNIT NO. 41
BY DATE SHEET NO. 3



SPECIAL RESEARCH COMMITTEE
FURNACE PERFORMANCE FACTORS
THE AMERICAN SOCIETY OF MECHANICAL ENGINEERS
COLLECTION OF DATA ON EXISTING INSTALLATIONS

ARRANGEMENT OF FURNACE AND CONVECTION SURFACE
COMPANY CONSOLIDATED EDISON CO OF N Y INC
PLANT [redacted] UNIT NO. 41
SCALE: ⅛"=1'-0" BY WAH DATE 7-30-43 SHEET NO. 2

DESCRIPTION OF UNIT

BUILDER	LaDD	YEAR INSTALLED	1930
BOILER TYPE	BENT TUBE RADIANT	ASH REMOVAL	DRY BOTTOM
PULVERIZER	FIRING	STORAGE	BURNER

TYPICAL FUEL

KIND	VARIOUS	DISTRICT	VARIOUS
SEAM	VARIOUS		

PROXIMATE ANALYSIS		ASH CHARACTERISTICS	
VOLATILE MATTER	35.9 %	INITIAL DEFORMATION	2000 F
FIXED CARBON	50.7 %	SOFTENING	2250 F
ASH	7.4 %	LIQUID	2475 F
TOTAL MOISTURE	4.3 %	SULPHUR (DRY BASIS)	1.70 %
HEAT VALUE PER LB AS REC'D	13,350 BTU	GRINDABILITY	60 - 115 %

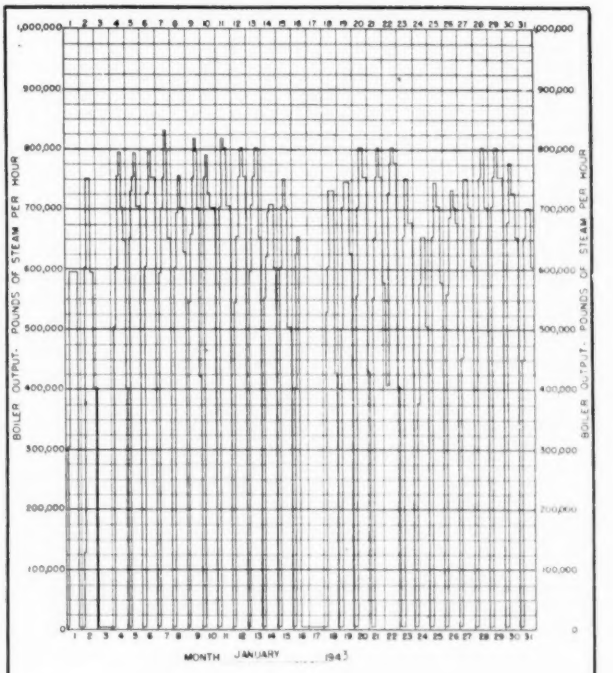
PERFORMANCE

BOILER OUTPUT	700,000 LB/HR	265 LB/SQ IN	SAT TEMP F
FUEL BURNED	63,140 LB/HR	849,360,000	BTU/HR
COMBUSTION AIR TEMP	500° F	FINENESS THRU 200 MESH	65-70 %
FUEL BURNING RATE	.0902 LB COAL PER LB STEAM		

FURNACE SURFACE		8,278 SQ FT	102,700 BTU/HR/SQ FT
FURNACE SURFACE & CONVECTION BANK TO SUPERHEATER		NO SUPERHEATER 60 FT	- BTU/HR/SQ FT
FURNACE VOLUME		32,000 CU FT	25,800 BTU/HR/CU FT
FURNACE WIDTH		25,875 FT	32,800,000 BTU/HR/FT
FREE GAS AREA	CONVECTION BANK ENTRANCE	490 SQ FT	1,735,000 BTU/HR/SQ FT
	CONVECTION BANK CLOSELY SPACED TUBES	490 SQ FT	1,735,000 BTU/HR/SQ FT
	SUPERHEATER ENTRANCE	- SQ FT	- BTU/HR/SQ FT
	SUPERHEATER CLOSELY SPACED TUBES	- SQ FT	- BTU/HR/SQ FT

REMARKS:

SPECIAL RESEARCH COMMITTEE
FURNACE PERFORMANCE FACTORS
THE AMERICAN SOCIETY OF MECHANICAL ENGINEERS
COLLECTION OF DATA ON EXISTING INSTALLATIONS
DESCRIPTION AND PERFORMANCE
COMPANY CONSOLIDATED EDISON COMPANY OF N.Y. INC
PLANT UNIT NO. 5
BY DATE SHEET NO. 1

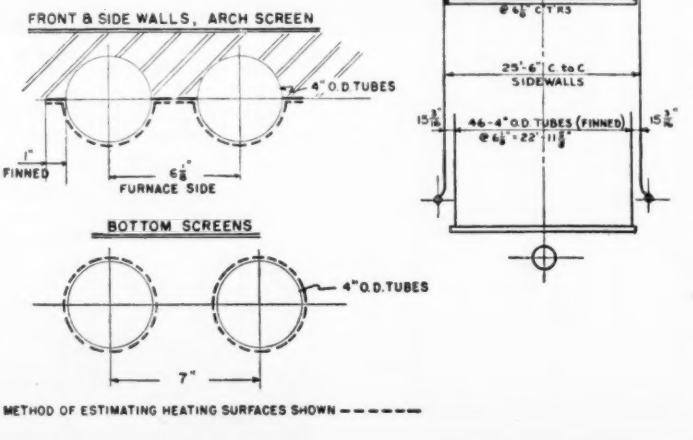


SPECIAL RESEARCH COMMITTEE
FURNACE PERFORMANCE FACTORS
THE AMERICAN SOCIETY OF MECHANICAL ENGINEERS
COLLECTION OF DATA ON EXISTING INSTALLATIONS
TYPICAL LOAD CURVE
COMPANY CONSOLIDATED EDISON COMPANY OF N.Y. INC
PLANT UNIT NO. 5
BY DATE SHEET NO 3

FURNACE

Front Walls	1,975 Sq Ft
Lower Side Walls	2,340
Bottom Slag Screens	1,870
Arch Screens	1,300
Upper Side Wall (portion)	188
Area of Entrance to Convection Bank	645
	8,278 Sq Ft Furnace Surface

NO SUPERHEATER



FRONT & SIDE WALLS, ARCH SCREEN

BOTTOM SCREENS

METHOD OF ESTIMATING HEATING SURFACES SHOWN - - - - - -

SPECIAL RESEARCH COMMITTEE
FURNACE PERFORMANCE FACTORS
THE AMERICAN SOCIETY OF MECHANICAL ENGINEERS
COLLECTION OF DATA ON EXISTING INSTALLATIONS
ARRANGEMENT OF FURNACE AND CONVECTION SURFACE
COMPANY CONSOLIDATED EDISON COMPANY OF NEW YORK INC
PLANT UNIT NO 5
SCALE BY DATE SHEET NO. 2

DESCRIPTION OF UNIT

BUILDER COMBUSTION ENGINEERING COMPANY			YEAR INSTALLED 1929
BOILER TYPE BENT TUBE		ASH REMOVAL DRY BOTTOM	
PULVERIZER FULLER LEHIGH	FIRING STORAGE		BURNER

TYPICAL FUEL

KIND VARIOUS	DISTRICT VARIOUS	SEAM VARIOUS

PROXIMATE ANALYSIS		ASH CHARACTERISTICS		
VOLATILE MATTER	22.0 %	INITIAL DEFORMATION	2020	F
FIXED CARBON	66.0 %	SOFTENING	2335	F
ASH	12.0 %	LIQUID	2555	F
TOTAL MOISTURE	5.0 %	SULPHUR (DRY BASIS)	2.80	%
HEAT VALUE PER LB as rec'd	13,220 BTU	GRINDABILITY	60 - 115	%

PERFORMANCE

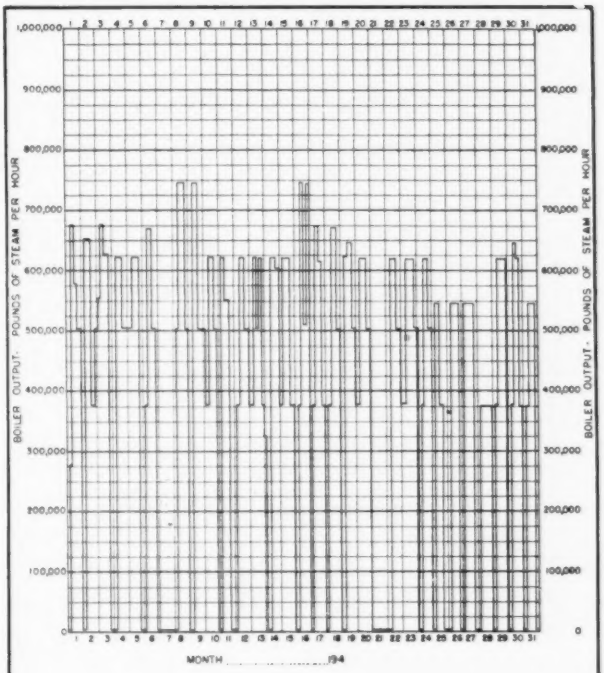
BOILER OUTPUT	600,000 LB/HR	400 LB/SQ IN	725° F
FUEL BURNED	77,000 LB/HR	1,320,000,000	BTU/HR
COMBUSTION AIR TEMP	432° F	FINENESS THRU 200 MESH	65.0 %
FUEL BURNING RATE	.01659 COAL PER LB STEAM		

FURNACE SURFACE		9,270 SQ FT	110,000 BTU/HR/SQ FT
FURNACE SURFACE & CONVECTION BANK TO SUPERHEATER		11,078 SQ FT	92,000 BTU/HR/SQ FT
FURNACE VOLUME		38,200 CU FT	26,700 BTU/HR/CU FT
FURNACE WIDTH		24'0" ~~F-B~~	42,500,000 BTU/HR/FT
FREE GAS AREA	CONVECTION BANK ENTRANCE	1,170 SQ FT	670,000 BTU/HR/SQ FT
	CONVECTION BANK CLOSELY SPACED TUBES	900 SQ FT	1,150,000 BTU/HR/SQ FT
	SUPERHEATER ENTRANCE	650 SQ FT	1,570,000 BTU/HR/SQ FT
	SUPERHEATER CLOSELY SPACED TUBES	650 SQ FT	1,570,000 BTU/HR/SQ FT

REMARKS: THE ATTACHED CHARTS ARE FOR AVERAGE OPERATION. ON JULY 12 TO JULY 16 TESTS WERE RUN WITH LOW FUSION COAL, A BRIEF DESCRIPTION OF WHICH TESTS IS ATTACHED.

THE BOILER WAS PURCHASED FOR 535,000#/HR NORMAL STEAM LOAD AND IS CAPABLE OF SUSTAINED RATINGS OF 900,000#/HR WITH A TOP ABOVE 1,000,000#/HR

SPECIAL RESEARCH COMMITTEE
FURNACE PERFORMANCE FACTORS
THE AMERICAN SOCIETY OF MECHANICAL ENGINEERS
COLLECTION OF DATA ON EXISTING INSTALLATIONS
DESCRIPTION AND PERFORMANCE
COMPANY CONSOLIDATED EDISON CO OF N Y INC
PLANT [redacted] UNIT NO. 7-8-9
BY W.A.H. DATE SHEET NO. 1



SPECIAL RESEARCH COMMITTEE
FURNACE PERFORMANCE FACTORS
THE AMERICAN SOCIETY OF MECHANICAL ENGINEERS
COLLECTION OF DATA ON EXISTING INSTALLATIONS
TYPICAL LOAD CURVE
COMPANY
PLANT UNIT NO. 7-8-9
BY DATE SHEET NO. 3

PRIMARY FURNACE

2 Side Walls (Fin)	4020	Sq Ft
Front Walls (Fin)	720	
Slag Screen (Plain)	1310	
2 Arches (Fin)	920	

SECONDARY FURNACE

Upper Side Walls (Fin)	660	
Front of Boiler or Area of Furnace at Entrance to Convection Tube Bank	1440	
	9270	9270 Sq Ft Furnace Surface

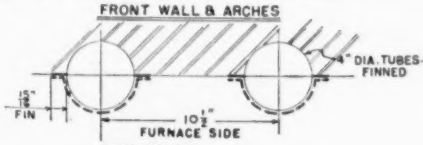
BOILER

Convection Tube Bank	2040	
Side Walls (Portion) Front of Superheater or Area of Furnace at Superheater Entrance	1008	
	3048	

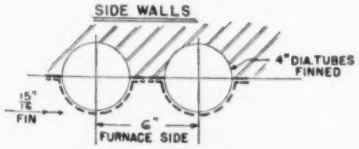
11,078 Sq Ft Furnace Surface & Convection Tube Bank to Superheaters

METHOD OF ESTIMATING HEATING SURFACES SHOWN

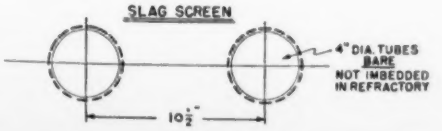
FRONT WALL & ARCHES

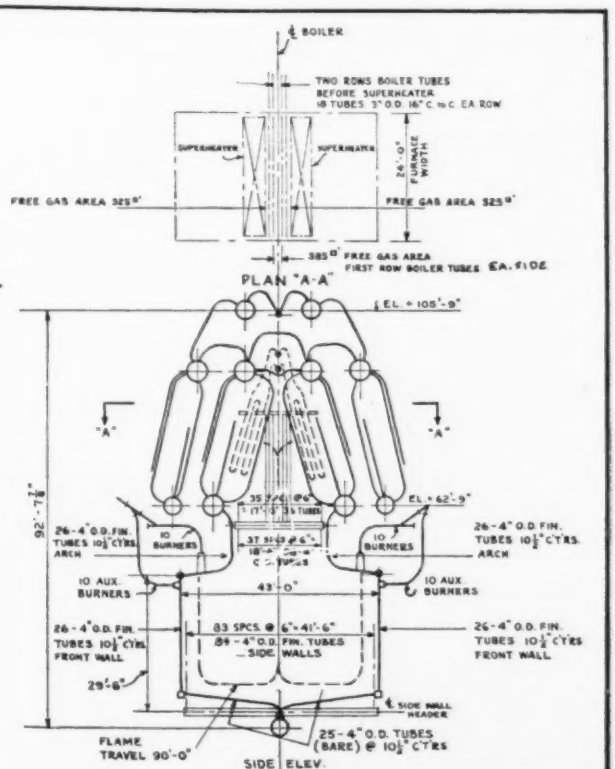


SIDE WALLS



SLAG SCREEN





SPECIAL RESEARCH COMMITTEE
FURNACE PERFORMANCE FACTORS
THE AMERICAN SOCIETY OF MECHANICAL ENGINEERS
COLLECTION OF DATA ON EXISTING INSTALLATIONS
ARRANGEMENT OF FURNACE AND CONVECTION SURFACE
COMPANY CONSOLIDATED EDISON COMPANY OF NEW YORK INC
PLANT UNIT NO. 7-8-9
SCALE BY DATE SHEET NO. 2

DESCRIPTION OF UNIT

BUILDER BABCOCK & WILCOX			YEAR INSTALLED 1930
BOILER TYPE SECT. TWIN CROSS DRUM		ASH REMOVAL DRY	
PULVERIZER FULLER LEHIGH	FIRING DIRECT		BURNER CALUMET INTERTUBE

TYPICAL FUEL

KIND VARIOUS	DISTRICT VARIOUS	SEAM VARIOUS	

PROXIMATE ANALYSIS		ASH CHARACTERISTICS	
VOLATILE MATTER	19.0 %	INITIAL DEFORMATION	2200 F
FIXED CARBON	72.0 %	SOFTENING	2485 F
ASH	4.0 %	LIQUID	2695 F
TOTAL MOISTURE	3.9 %	SULPHUR (DRY BASIS)	1.60 %
HEAT VALUE PER LB AS REC'D	13,590 BTU	GRINDABILITY	60-115 %

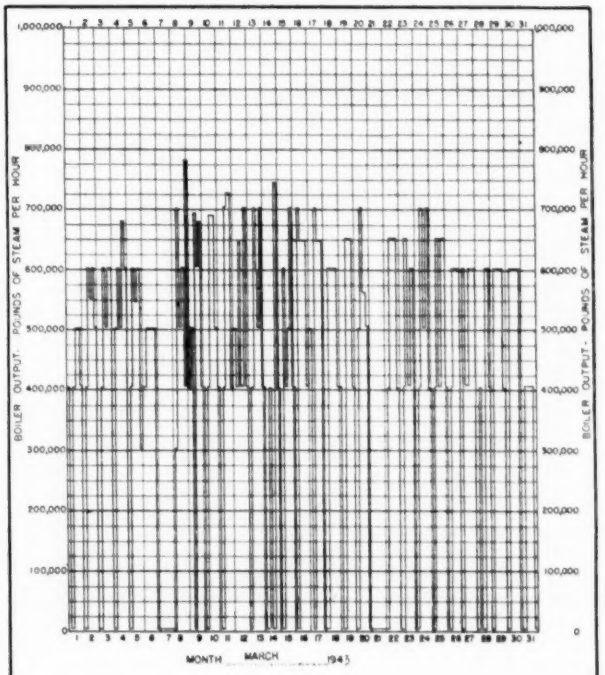
PERFORMANCE

BOILER OUTPUT	500,000 LB/HR	275 LB/SQ IN	725° F
FUEL BURNED	79,650 LB/HR	1,082,000,000	BTU/HR
COMBUSTION AIR TEMP	344° F	FINENESS THRU 200 MESH	70 %
FUEL BURNING RATE	.0638# COAL PER LB STEAM		

FURNACE SURFACE		8,350 SQ FT	129,800 BTU/HR/SQ FT
FURNACE SURFACE & CONVECTION BANK TO SUPERHEATER		18,896 SQ FT	57,300 BTU/HR/SQ FT
FURNACE VOLUME		40,770 CU FT	26,600 BTU/HR/CU FT
FURNACE WIDTH		34'4" ~~44~~	31,400,000 BTU/HR/FT
FREE GAS AREA	CONVECTION BANK ENTRANCE	965 SQ FT	1,020,000 BTU/HR/SQ FT
	CONVECTION BANK CLOSELY SPACED TUBES	600 SQ FT	1,864,000 BTU/HR/SQ FT
	SUPERHEATER ENTRANCE	254 SQ FT	4,260,000 BTU/HR/SQ FT
	SUPERHEATER CLOSELY SPACED TUBES	254 SQ FT	4,260,000 BTU/HR/SQ FT

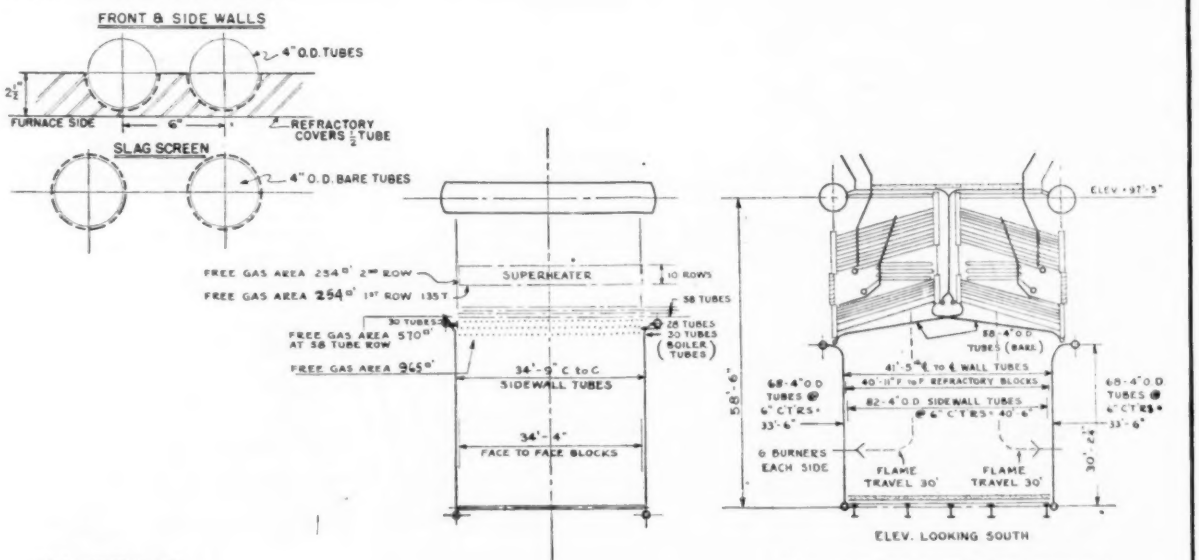
REMARKS:

SPECIAL RESEARCH COMMITTEE
FURNACE PERFORMANCE FACTORS
THE AMERICAN SOCIETY OF MECHANICAL ENGINEERS
COLLECTION OF DATA ON EXISTING INSTALLATIONS
DESCRIPTION AND PERFORMANCE
COMPANY CONSOLIDATED EDISON CO OF N Y INC
PLANT UNIT NO. 9
BY DATE SHEET NO. 1



SPECIAL RESEARCH COMMITTEE
FURNACE PERFORMANCE FACTORS
THE AMERICAN SOCIETY OF MECHANICAL ENGINEERS
COLLECTION OF DATA ON EXISTING INSTALLATIONS
TYPICAL LOAD CURVE
COMPANY CONSOLIDATED EDISON CO OF NEW YORK INC
PLANT UNIT NO. 9
BY DATE SHEET NO. 3

METHOD OF ESTIMATING HEATING SURFACES SHOWN - - - - - -



NOTE: ALL WATER WALL TUBES REFRACTORY COVERED.

HEAT ABSORPTION AREA

FURNACE

FRONT WALLS	1,930 Sq Ft	
SIDE WALLS	2,580	
SLAG SCREEN	2,670	7,180 SqFt
AREA OF FURNACE AT CONVECTION TUBE BANK	1,170	
	8,350 Sq Ft	8,350 SqFt FURNACE SURFACE

BOILER

BANK (TUBE SURFACE)	11,000 Sq Ft	
SUPERHEATER ENTRANCE	716	
	11,716 Sq Ft	11,716 SqFt / 18,896 SqFt FURNACE SURFACE & CONVECTION BANK TO SUPERHEATER

SPECIAL RESEARCH COMMITTEE
FURNACE PERFORMANCE FACTORS
THE AMERICAN SOCIETY OF MECHANICAL ENGINEERS
COLLECTION OF DATA ON EXISTING INSTALLATIONS
ARRANGEMENT OF FURNACE AND CONVECTION SURFACE
COMPANY CONSOLIDATED EDISON COMPANY OF NEW YORK INC
PLANT UNIT NO. 9
SCALE BY DATE SHEET NO. 2

DESCRIPTION OF UNIT

BUILDER	COMBUSTION ENGINEERING COMPANY		YEAR INSTALLED 1920
BOILER TYPE	BENT TUBE 3-DRUM	ASH REMOVAL	CONTINUOUS SLAG TAP
PULVERIZER	RAYMOND BOWL	FIRING	TANGENTIAL DIRECT
BURNER	COMB ENG TYPE "T"		

TYPICAL FUEL

KIND	VARIOUS	DISTRICT	VARIOUS
SEAM	VARIOUS		

PROXIMATE ANALYSIS		ASH CHARACTERISTICS	
VOLATILE MATTER	26.5 %	INITIAL DEFORMATION	2315 F
FIXED CARBON	72.2 %	SOFTENING	2570 F
ASH	7.3 %	LIQUID	2800+ F
TOTAL MOISTURE	4.4 %	SULPHUR (DRY BASIS)	1.35 %
HEAT VALUE PER LB AS REC'D	13,685 BTU	GRINDABILITY	60 TO 115 %

PERFORMANCE

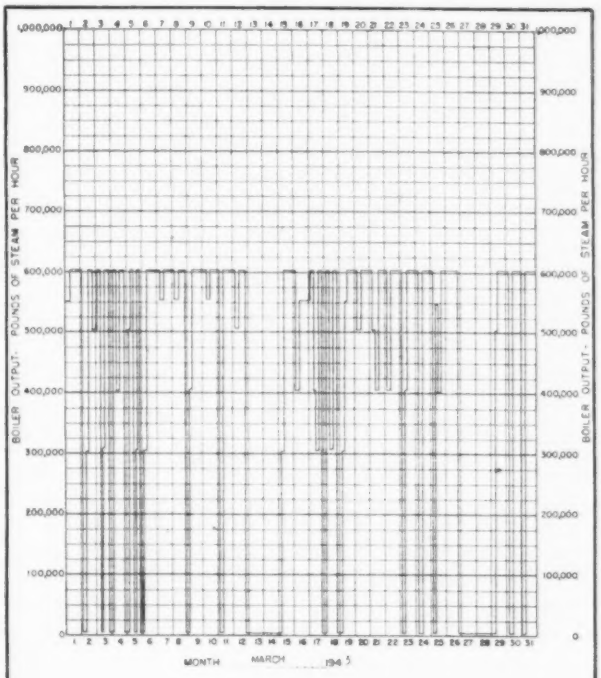
BOILER OUTPUT	615,000 LB/HR	1540 LB/SQ IN	925° F
FUEL BURNED	52,470 LB/HR	728,000,000	BTU/HR
COMBUSTION AIR TEMP	518 F	FINENESS THRU 200 MESH	80 %

FUEL BURNING RATE .0854# COAL PER LB STEAM

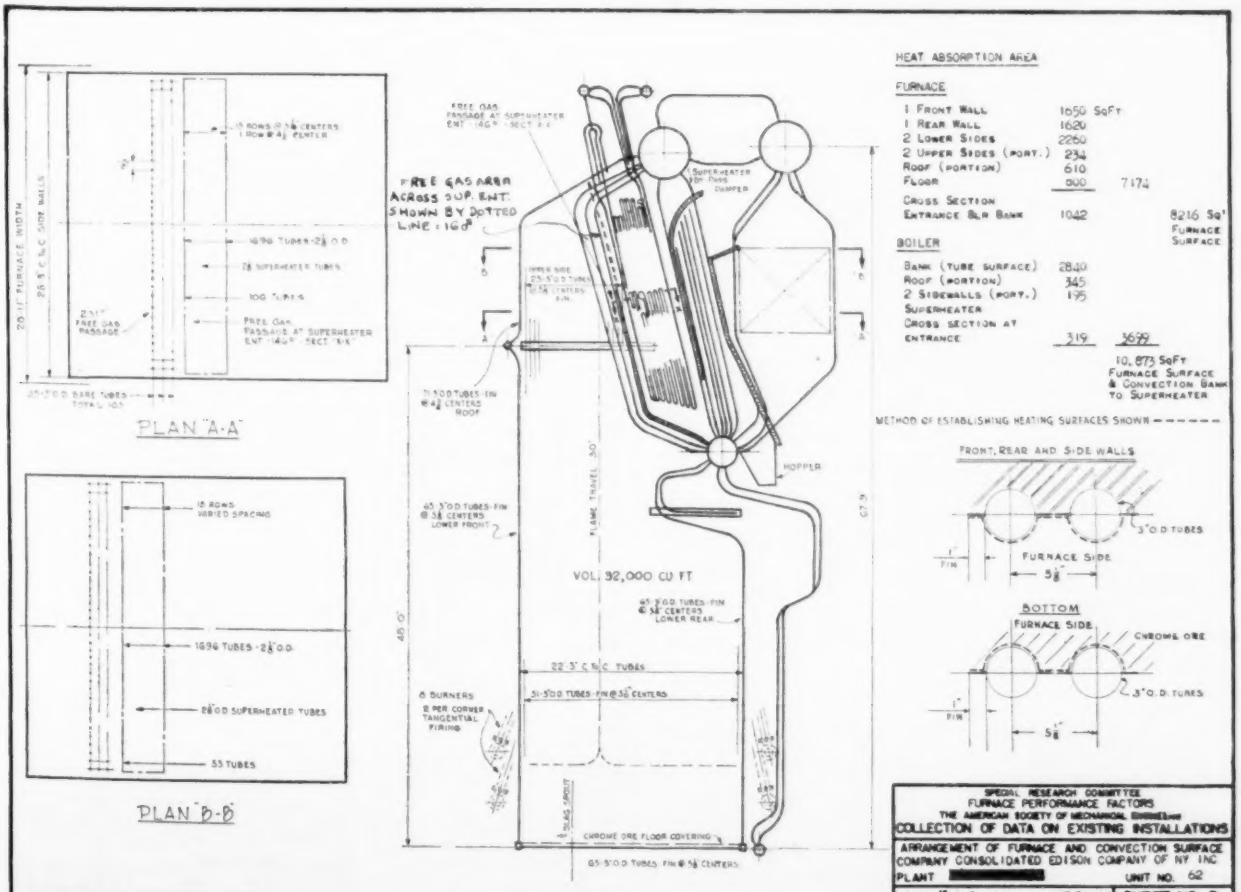
FURNACE SURFACE		8,216 SQ FT	88,500 BTU/HR/SQ FT
FURNACE SURFACE & CONVECTION BANK TO SUPERHEATER		10,873 SQ FT	67,000 BTU/HR/SQ FT
FURNACE VOLUME		32,000 CU FT	22,800 BTU/HR/CU FT
FURNACE WIDTH		28.83 FT	25,200,000 BTU/HR/FT
FREE GAS AREA	CONVECTION BANK ENTRANCE	231 SQ FT	3,150,000 BTU/HR/SQ FT
	CONVECTION BANK CLOSELY SPACED TUBES	231 SQ FT	3,150,000 BTU/HR/SQ FT
	SUPERHEATER ENTRANCE	160 SQ FT	4,550,000 BTU/HR/SQ FT
	SUPERHEATER CLOSELY SPACED TUBES	160 SQ FT	4,550,000 BTU/HR/SQ FT

REMARKS:

SPECIAL RESEARCH COMMITTEE
FURNACE PERFORMANCE FACTORS
THE AMERICAN SOCIETY OF MECHANICAL ENGINEERS
COLLECTION OF DATA ON EXISTING INSTALLATIONS
DESCRIPTION AND PERFORMANCE
COMPANY CONSOLIDATED EDISON COMPANY OF N.Y. INC.
PLANT UNIT NO. 62
BY DATE SHEET NO. 1



SPECIAL RESEARCH COMMITTEE
FURNACE PERFORMANCE FACTORS
THE AMERICAN SOCIETY OF MECHANICAL ENGINEERS
COLLECTION OF DATA ON EXISTING INSTALLATIONS
TYPICAL LOAD CURVE
COMPANY CONSOLIDATED EDISON CO. OF NEW YORK INC.
PLANT UNIT NO. 62
BY DATE SHEET NO. 3



SPECIAL RESEARCH COMMITTEE
FURNACE PERFORMANCE FACTORS
THE AMERICAN SOCIETY OF MECHANICAL ENGINEERS
COLLECTION OF DATA ON EXISTING INSTALLATIONS
ARRANGEMENT OF FURNACE AND CONVECTION SURFACE
COMPANY CONSOLIDATED EDISON COMPANY OF N.Y. INC.
PLANT [redacted] UNIT NO. 62
SCALE: 1/8"-0" BY WVAH DATE 7-30-43 SHEET NO. 2

DESCRIPTION OF UNIT

BUILDER BABCOCK & WILCOX		YEAR INSTALLED 1940
BOILER TYPE OPEN PASS	ASH REMOVAL CONTINUOUS SLAG TAP	
PULVERIZER B & W	FIRING VERTICAL DIRECT	BURNER MULTIPLE INTERTUBE

TYPICAL FUEL

KIND VARIOUS	DISTRICT VARIOUS	SEAM VARIOUS

PROXIMATE ANALYSIS		ASH CHARACTERISTICS	
VOLATILE MATTER	20.5 %	INITIAL DEFORMATION	2315 F
FIXED CARBON	72.2 %	SOFTENING	2570 F
ASH	7.3 %	LIQUID	2800+ F
TOTAL MOISTURE	4.4 %	SULPHUR (DRY BASIS)	1.35 %
HEAT VALUE PER LB AS REC'D	13,885 BTU	GRINDABILITY	60 TO 115 %

PERFORMANCE

BOILER OUTPUT	615,000 LB/HR	1,340 LB/SQ IN	925° F
FUEL BURNED	52,700 LB/HR	732,000,000	BTU/HR
COMBUSTION AIR TEMP	607° F	FINENESS THRU 200 MESH	77 %

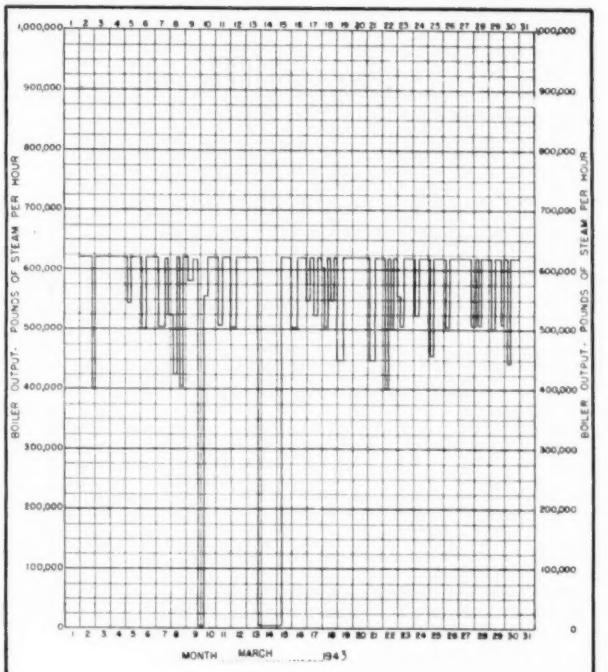
FUEL BURNING RATE .0857# COAL PER LB STEAM

FURNACE SURFACE		13,275 SQ FT	54,700 BTU/HR/SQ FT
FURNACE SURFACE & CONVECTION BANK TO SUPERHEATER		13,652 SQ FT	53,600 BTU/HR/SQ FT
FURNACE VOLUME		24,420 CU FT	30,000 BTU/HR/CU FT
FURNACE WIDTH		20.917 FT	25,300,000 BTU/HR/FT
FREE GAS AREA	CONVECTION BANK ENTRANCE	- SQ FT	- BTU/HR/SQ FT
	CONVECTION BANK 2ND SCREEN CLOSELY SPACED TUBES	180 SQ FT	4,060,000 BTU/HR/SQ FT
	SUPERHEATER ENTRANCE	275 SQ FT	2,660,000 BTU/HR/SQ FT
	SUPERHEATER CLOSELY SPACED TUBES	143 SQ FT	5,120,000 BTU/HR/SQ FT

REMARKS:

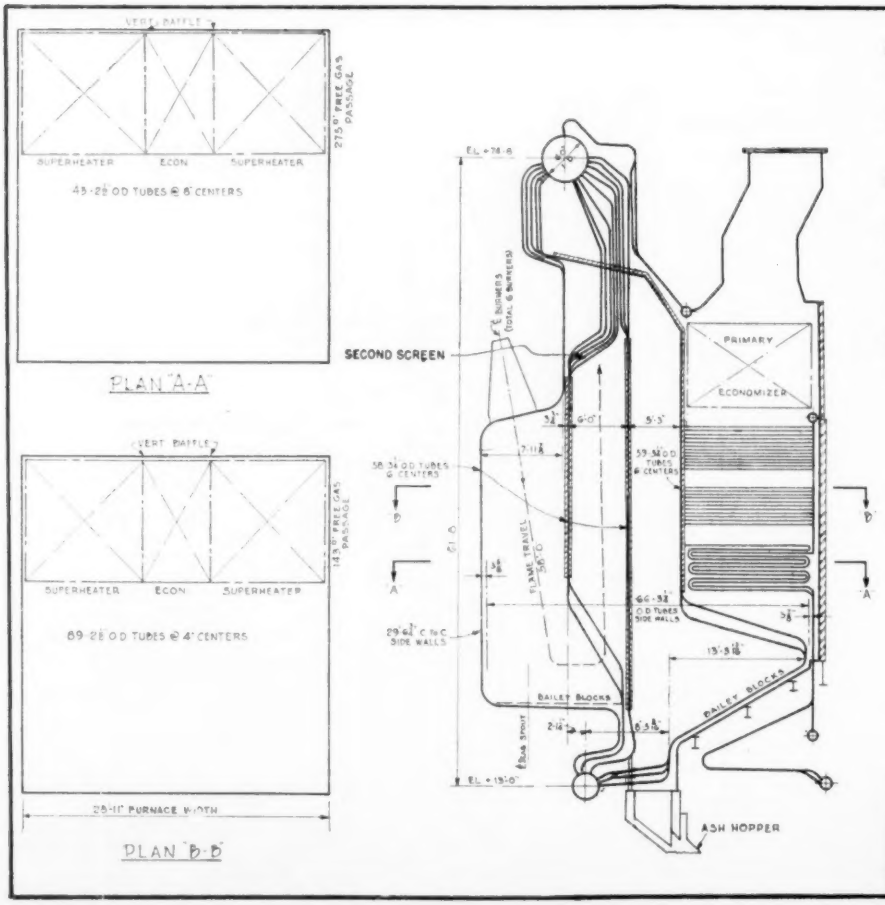
SPECIAL RESEARCH COMMITTEE
FURNACE PERFORMANCE FACTORS
THE AMERICAN SOCIETY OF MECHANICAL ENGINEERS
COLLECTION OF DATA ON EXISTING INSTALLATIONS

DESCRIPTION AND PERFORMANCE
COMPANY CONSOLIDATED EDISON CO OF N Y INC
PLANT UNIT NO. 72
BY DATE SHEET NO. 1



SPECIAL RESEARCH COMMITTEE
FURNACE PERFORMANCE FACTORS
THE AMERICAN SOCIETY OF MECHANICAL ENGINEERS
COLLECTION OF DATA ON EXISTING INSTALLATIONS

TYPICAL LOAD CURVE
COMPANY CONSOLIDATED EDISON COMPANY OF N Y INC
PLANT UNIT NO. 72
BY DATE SHEET NO. 3



PRIMARY FURNACE

FRONT WALL & ARCH	1912 Sq'	PART STUD	
SCREENS	907	" "	
"	828	BARE	
2 SIDE WALLS	986	PART STUD	
REAR	1512	" "	
FLOOR	428	BLOCK	
	6573		6573 Sq'

SECONDARY FURNACE

FRONT WALL & ARCH	1138 Sq'	PART STUD	
SCREENS	1360	BARE	
2 SIDE WALLS	1486	PART STUD	
CROSS SECTION CONVECTION BANK	378		
REAR	1010	PART STUD	
S H FRONT	785	" "	
FLOOR	545	BLOCK	
	6702		6702 Sq'

BOILER

CROSS SECTION AREA SUPERHEATER	377	
	13652	Sq'

13275 Sq' FURNACE SURFACE

HEATING SURFACES TABULATED HERE WERE ACCEPTED FROM THE MANUFACTURER'S PROPOSAL.

SPECIAL RESEARCH COMMITTEE
FURNACE PERFORMANCE FACTORS
THE AMERICAN SOCIETY OF MECHANICAL ENGINEERS
COLLECTION OF DATA ON EXISTING INSTALLATIONS

ARRANGEMENT OF FURNACE AND CONVECTION SURFACE
COMPANY CONSOLIDATED EDISON CO OF N Y INC
PLANT [redacted] UNIT NO. 72
SCALE: 1/8"=1'-0" BY DATE SHEET NO. 2

DESCRIPTION OF UNIT

BUILDER	COMBUSTION ENGINEERING COMPANY	YEAR INSTALLED	1942
BOILER TYPE	3 DRUM BENT TUBE	ASH REMOVAL	SLAG TAP
PULVERIZER	RAYMOND BOWL	FIRING	DIRECT
BURNER	C-E		

TYPICAL FUEL

KIND	DISTRICT	SEAM
VARIOUS	VARIOUS	VARIOUS

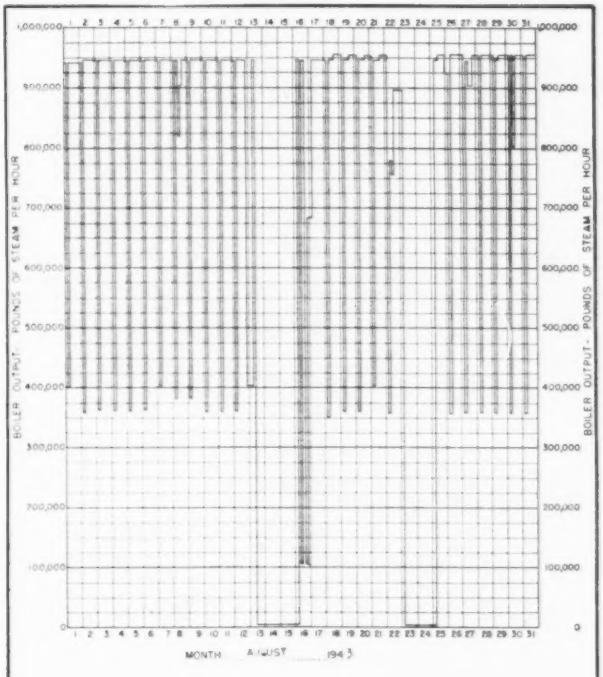
PROXIMATE ANALYSIS		ASH CHARACTERISTICS	
VOLATILE MATTER	24.0 %	INITIAL DEFORMATION	2025 F
FIXED CARBON	65.5 %	SOFTENING	2325 F
ASH	10.5 %	LIQUID	2550 F
TOTAL MOISTURE	4.1 %	SULPHUR (DRY BASIS)	2.50 %
HEAT VALUE PER LB as rec'd 13190	BTU	GRINDABILITY	60 TO 115 %

PERFORMANCE

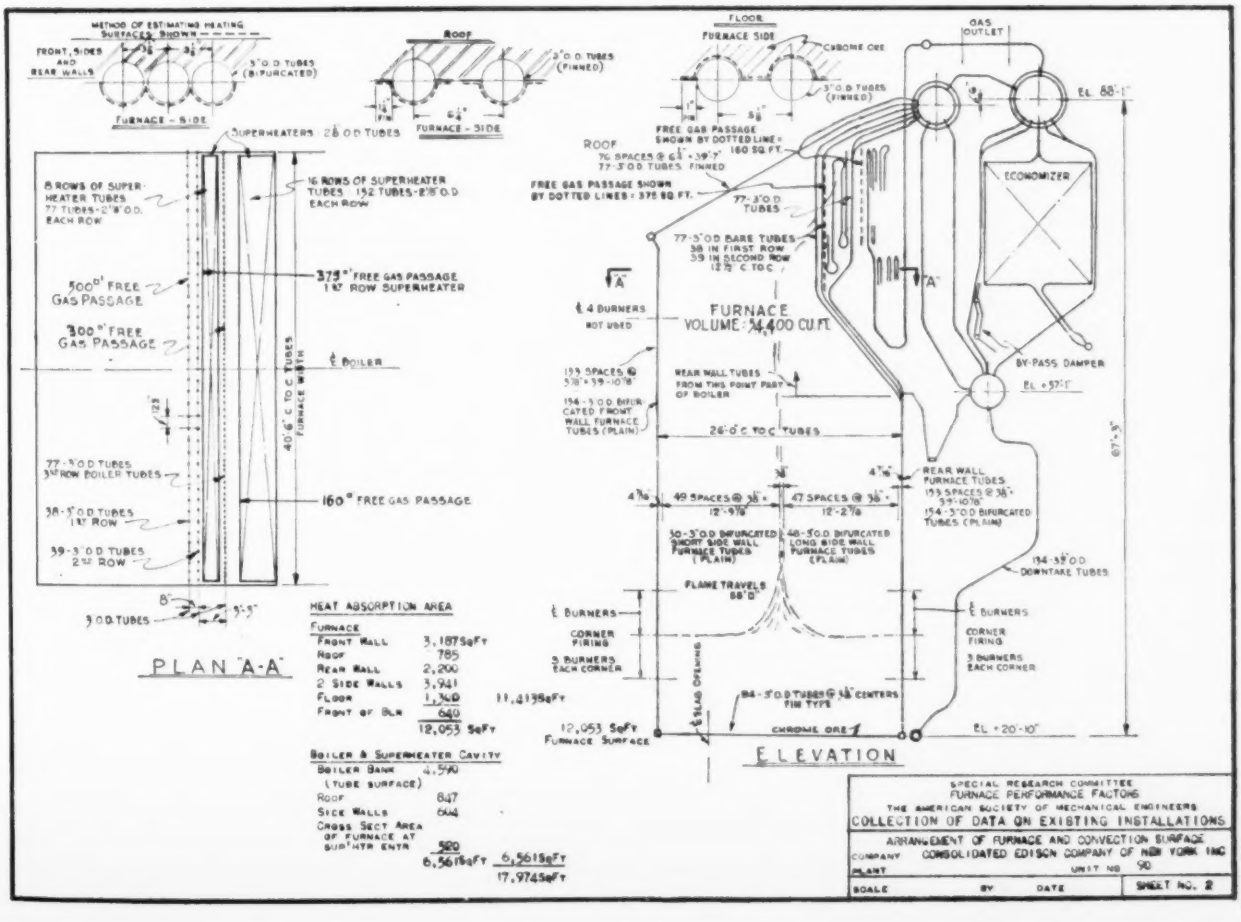
BOILER OUTPUT	1,000,000 LB/HR	1600 LB/SQ IN		955° F	
FUEL BURNED	82,800 LB/HR	1,092,000,000		BTU/HR	
COMBUSTION AIR TEMP	640° F	FINENESS THRU 200 MESH		80 %	
FUEL BURNING RATE	.0828 lbs coal / lb. steam				
FURNACE SURFACE		12,053 SQ FT	90,500	BTU/HR/SQ FT	
FURNACE SURFACE & CONVECTION BANK TO SUPERHEATER		17,974 SQ FT	60,800	BTU/HR/SQ FT	
FURNACE VOLUME		54,400 CU FT	20,100	BTU/HR/CU FT	
FURNACE WIDTH		40.5 FT	27,000,000	BTU/HR/FT	
FREE GAS AREA	CONVECTION BANK ENTRANCE	500 SQ FT	2,180,000	BTU/HR/SQ FT	
	CONVECTION BANK CLOSELY SPACED TUBES	300 SQ FT	3,640,000	BTU/HR/SQ FT	
	SUPERHEATER ENTRANCE	375 SQ FT	2,920,000	BTU/HR/SQ FT	
	SUPERHEATER CLOSELY SPACED TUBES	160 SQ FT	6,820,000	BTU/HR/SQ FT	

REMARKS:

SPECIAL RESEARCH COMMITTEE
FURNACE PERFORMANCE FACTORS
THE AMERICAN SOCIETY OF MECHANICAL ENGINEERS
COLLECTION OF DATA ON EXISTING INSTALLATIONS
DESCRIPTION AND PERFORMANCE
COMPANY CONSOLIDATED EDISON COMPANY OF N Y INC
PLANT UNIT NO. 90
BY DATE 10-13-43 SHEET NO. 1



SPECIAL RESEARCH COMMITTEE
FURNACE PERFORMANCE FACTORS
THE AMERICAN SOCIETY OF MECHANICAL ENGINEERS
COLLECTION OF DATA ON EXISTING INSTALLATIONS
TYPICAL LOAD CURVE
COMPANY CONSOLIDATED EDISON COMPANY OF N Y INC
PLANT UNIT NO. 90
BY DATE SHEET NO. 3



SPECIAL RESEARCH COMMITTEE
FURNACE PERFORMANCE FACTORS
THE AMERICAN SOCIETY OF MECHANICAL ENGINEERS
COLLECTION OF DATA ON EXISTING INSTALLATIONS
ARRANGEMENT OF FURNACE AND CONVECTION SURFACE
COMPANY CONSOLIDATED EDISON COMPANY OF NEW YORK INC
PLANT UNIT NO. 90
SCALE BY DATE SHEET NO. 2

Transactions

of the

A.S.M.E.

SOCIETY RECORDS—PART 1

Robert M. Gates, President of The American Society of Mechanical Engineers, 1943-1944 ..... *Portrait and Biography*

Council and Committee Personnel ..... RI-5—RI-38

- Officers and Council 5
- Standing Committees 6
- Special Committees 7
- Special Council Committees 8
- A.S.M.E. Representatives on Other Activities 9
- Professional Divisions 10
- Local Sections 15
- Student Branches 23
- Research Committees 25
- Standardization Committees 27
- Power Test Codes Committees 33
- Safety Committees 35
- Boiler Code Committees 37

Woman's Auxiliary to the A.S.M.E. RI-39

Awards RI-40

Honorary Members RI-43

Past-Presidents, Treasurers, and Secretaries RI-44

Index RI-45

FEBRUARY, 1944

VOL. 66, NO. 2

Transactions

of The American Society of Mechanical Engineers

Published on the tenth of every month, except March, June, September, and December

---

OFFICERS OF THE SOCIETY:

ROBERT M. GATES, *President*

W. D. ENNIS, *Treasurer* C. E. DAVIES, *Secretary*

COMMITTEE ON PUBLICATIONS:

F. L. BRADLEY, *Chairman*

E. J. KATES W. A. CARTER

L. N. ROWLEY H. L. DRYDEN

GEORGE A. STETSON, *Editor*

ADVISORY MEMBERS OF THE COMMITTEE ON PUBLICATIONS:

N. C. EBAUGH, GAINESVILLE, FLA. O. B. SCHIER, 2ND, NEW YORK, N. Y.

Junior Members

HAROLD HERKIMER, NEW YORK, N. Y., AND RICHARD S. BIDDLE, NEW YORK, N. Y.

Published monthly by The American Society of Mechanical Engineers. Publication office at 20th and Northampton Streets, Easton, Pa. The editorial department is located at the headquarters of the Society, 29 West Thirty-Ninth Street, New York 18, N. Y. Cable address, "Dynamic," New York. Price $1.50 a copy, $12.00 a year; to members and affiliates, $1.00 a copy, $7.50 a year. Changes of address must be received at Society headquarters two weeks before they are to be effective on the mailing list. Please send old as well as new address. . . . By-Law: The Society shall not be responsible for statements or opinions advanced in papers or . . . printed in its publications (B13, Par. 4). . . . Entered as second-class matter March 2, 1928, at the Post Office at Easton, Pa., under the act of August 24, 1912. . . .

Copyrighted, 1944, by The American Society of Mechanical Engineers. Reprints from this publication may be made on condition that full credit be given the Transactions of the A.S.M.E. and the author, and that date of publication be stated.

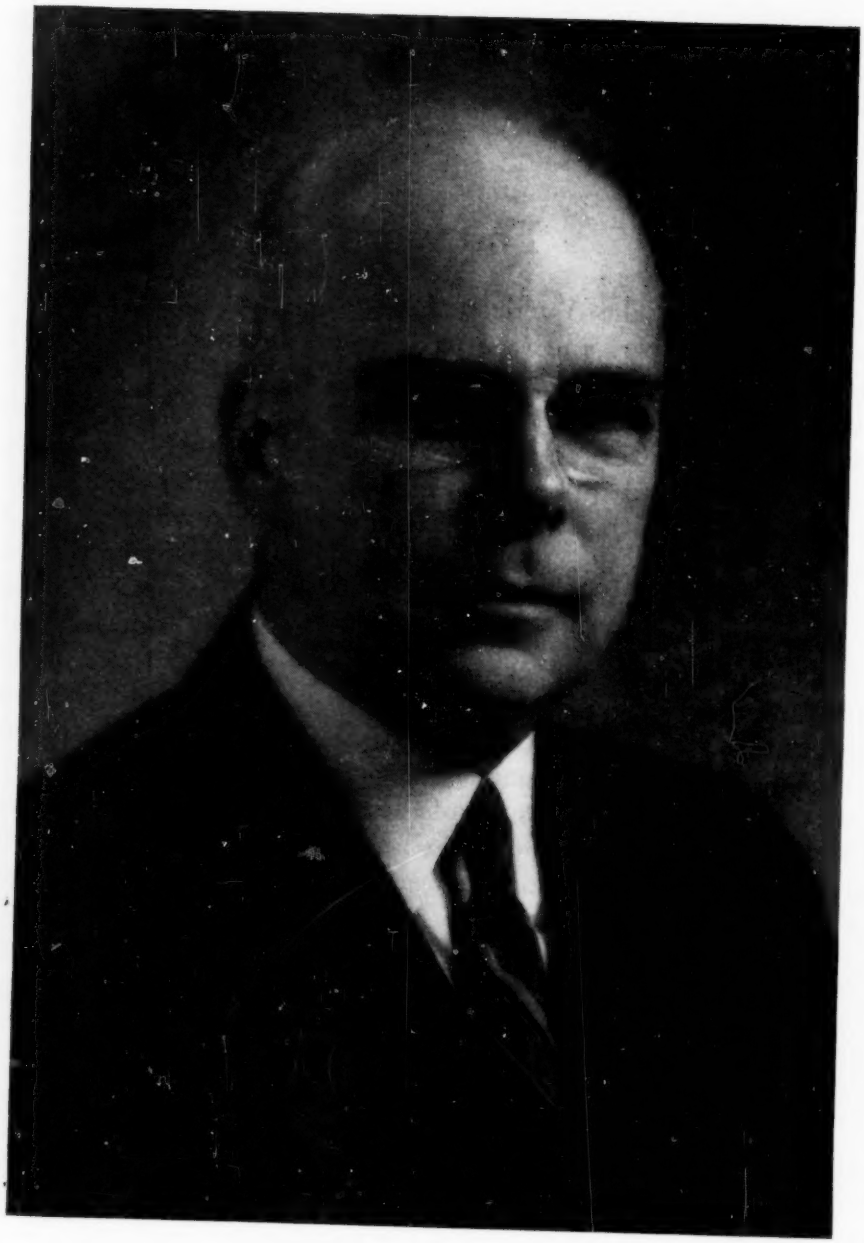
Foreword

THE Transactions of The American Society of Mechanical Engineers include selected technical papers and reports delivered at meetings of the Society, its Professional Divisions, and its Local Sections, the *Journal of Applied Mechanics* (contributions of the Applied Mechanics Division), certain records of the Society of permanent value, and indexes to its publications.

In order to secure the advantages of timeliness and greater usefulness in issuing these Society Records, the material comprising them is divided into a number of parts, each one of which is mailed as a supplement to one of the regular monthly issues of the Transactions. For 1944, the first of these, the present issue, contains the personnel of the Council and committees for the year. Another, to be issued sometime later in the year, will contain memorial notices of deceased members. The indexes to miscellaneous publications, *Mechanical Engineering*, and to the Transactions themselves, must, necessarily, be issued in 1945, and will probably be mailed as a supplement to the January issue of that year.

In binding the 1944 Transactions, all of these parts of the Society Records will be assembled at the back of the volume as has been customary for several years. To aid in locating references in the bound volumes, the page numbers of the sections containing the *Journal of Applied Mechanics* and the Society Records are preceded by the letters A and RI, respectively.

THE COMMITTEE ON PUBLICATIONS



ROBERT M. GATES

PRESIDENT OF THE AMERICAN SOCIETY OF MECHANICAL ENGINEERS
1943-1944

Robert M. Gates

Robert M. Gates, President of The American Society of Mechanical Engineers for the year 1943-1944, is a Fellow of the Society, president and director of the Air Preheater Corporation, formerly vice-president of The Superheater Company and its affiliate, Combustion Engineering Company, Inc., all of New York, N.Y. He was born in O'Brien County, Iowa, Sept. 7, 1883, and studied at the Manual Training High School, Indianapolis, Ind., and at Purdue University, where he received the degree of bachelor of science in mechanical engineering in 1907.

From 1907 to 1909 Mr. Gates was associated with the Browning Company of Cleveland, Ohio, after which he practiced as consulting engineer until 1912 when he became associated with the Thew Shovel Company of Lorain, Ohio. In 1918 he became Eastern manager for the Lakewood Engineering Company of Cleveland, Ohio, and located in Philadelphia, Pa. In 1922 he became associated with The Superheater Company.

Mr. Gates has participated in the design and construction connected with the builders of fuel-burning and steam-generating equipment, including all types of boilers, stokers, pulverized-coal equipment, economizers, air preheaters, and superheaters for stationary, railway, and marine service, as well as a wide variety of heavy equipment for the process industries. Outstanding among their installations are the world's largest high-pressure boilers, each producing over a million pounds of steam per hour.

Mr. Gates is a registered professional engineer in New York State and has long been active in the affairs of The American Society of Mechanical Engineers since becoming a member in 1918. He served as manager, 1928-1931, and as vice-president, 1931-1933, and he has been a member of various standing committees, including those on Meetings and Program and Professional Divisions. At the time of the World Power Conference in 1936 he was chairman of the Reception Committee. He has been serving as a member of the War Production Committee of the Society since 1942.

For the 1941 Annual Meeting of the Society Mr. Gates, as chairman of the Committee on Conservation and Reclamation of Materials in Industry, organized a "panel of experts" to conduct a session on conservation and reclamation. He served also as chairman of the first and many subsequent War Production Clinics which the A.S.M.E., at the request and with the assistance of the War Production Board, has been conducting for more than a year in industrial centers throughout the nation.

Mr. Gates has made numerous addresses before various engineering groups and given much time to counseling junior and student members of the Society. His keen interest in the problems of young engineers and engineering students is probably traceable to the fact that he supported himself during his entire education, including the high-school period, when he sold tickets in the Indianapolis Union Station.

Mr. Gates has written many articles and given a number of talks on handling of materials, power generation, personnel direction, and management. Aside from his engineering activities he finds time to take considerable interest in civic and economic

affairs of Scarsdale, N.Y., of which he is a resident. He is on the Board of Arbitration of the American Arbitration Association.

He is also a member of the following organizations: Institution of Mechanical Engineers, Newcomen Society of England, American Institute of Electrical Engineers, National Association of Manufacturers, National Association of Professional Engineers, American Management Association, American Iron and Steel Institute, The Engineers Club of New York, the Union League Club of New York, the Downtown Athletic Club of New York, the Manursing Island Club of Rye, N.Y., and the Scarsdale Golf Club, Scarsdale, N.Y.

The American Society of Mechanical Engineers

HEADQUARTERS: 29 West 39th St., New York 18, N.Y.
MID-WEST OFFICE: Room 1617, 205 West Wacker Drive, Chicago 6, Ill.

The members of the Council and of its standing and special committees given on the following pages are those in office on January 1, 1944, serving for the official year 1943-1944. The terms of office of members of other committees are not fixed by the official calendar.

OFFICERS AND COUNCIL

PRESIDENT

R. M. Gates

PAST-PRESIDENTS

Terms expire December

Alexander G. Christie (1944)
Warren H. McBryde (1945)
William A. Hanley (1946)
James W. Parker (1947)
Harold V. Coes (1948)

VICE-PRESIDENTS

Terms expire December, 1944

Joseph W. Eshelman
Guy T. Shoemaker
Walter J. Wohlenberg

Terms expire December, 1945

Rudolph F. Gagg
David W. R. Morgan
Jonathan A. Noyes
Ford L. Wilkinson, Jr.

MANAGERS

Terms expire December, 1944

J. Calvin Brown
William G. Christy
Thomas S. McEwan

Terms expire December, 1945

Roscoe W. Morton
A. R. Stevenson, Jr.
Albert E. White

Terms expire December, 1946

Alton C. Chick
Samuel H. Graf
James M. Robert

TREASURER

W. D. Ennis

SECRETARY

C. E. Davies

CHAIRMEN OF STANDING COMMITTEES

Representatives on Council without vote

Finance, K. W. Jappe
Meetings and Program, L. K. Sillcox
Publications, F. L. Bradley
Admissions, F. E. Lyford
Professional Divisions, W. M. Sheehan
Local Sections, S. R. Beitler
Constitution and By-Laws, R. L. Parsell
Honors and Awards, C. L. Bausch
Relations with Colleges, H. E. Degler
Education and Training for the Industries, A. C. Harper
Library, John Blizard
Research, Herman Weisberg
Standardization, T. E. French
Power Test Codes, Francis Hodgkinson
Safety (to be appointed)
Professional Conduct, V. E. Alden

EXECUTIVE COMMITTEE OF THE COUNCIL

R. M. Gates, *Chairman*
Walter J. Wohlenberg, *Vice-Chairman*
Alton C. Chick
David W. R. Morgan
A. R. Stevenson, Jr.

Advisory Members: **Chairmen of the Finance, Local Sections, and Professional Divisions Committees**

SECRETARIAL STAFF

Ernest Hartford, *Executive Assistant Secretary* (Sections, Divisions, Student Branches, Membership, Meetings, etc.)
C. B. LePage, *Assistant Secretary* (Technical Committees)
R. L. Sackett, *Assistant to the Secretary*
George A. Stetson, *Editor*
Frederick Lask, *Advertising Manager*
D. C. A. Bosworth, *Comptroller*

STANDING COMMITTEES

FINANCE

K. W. Jappe, *Chairman* * (1944)
J. J. Swan, *Vice-Chairman* (1945)
J. L. Kopf (1946)
W. H. Sawyer (1947)
G. L. Knight (1948)

Council Representatives

W. G. Christy (1944)
R. F. Gagg (1945)

MEETINGS AND PROGRAM

L. K. Sillcox, *Chairman* * (1944)
F. G. Switzer (1945)
R. A. North (1946)
D. S. Walker (1947)
P. W. Thompson (1948)

Junior Adviser

Irving Taylor (1944)

PUBLICATIONS

F. L. Bradley, *Chairman* * (1944)
E. J. Kates (1945)
L. N. Rowley, Jr. (1946)
W. A. Carter (1947)
H. L. Dryden (1948)

Advisory Members (1944)

N. C. Ebaugh
O. B. Schier, II

Junior Advisers

Harold Herkimer (1944)
R. S. Biddle (1945)

(Personnel of Biography Committee, p. RI-7)

ADMISSIONS

F. E. Lyford, *Chairman* * (1944)
S. D. Sprong (1945)
T. H. Wickenden (1946)
D. W. R. Morgan (1947)
G. E. Hulse (1948)

Advisory Member

S. H. Libby (1944)

(Personnel of Advisory Committee, p. RI-8)

PROFESSIONAL DIVISIONS

W. M. Sheehan, *Chairman* * (1944)
J. H. Sengstaken (1945)
J. A. Goff (1946)
J. M. Talbot (1947)
W. L. H. Doyle (1948)

Junior Adviser

I. P. West (1944)

(Personnel of Professional Divisions' Executive Committees, p. RI-10)

* Representative on the Council.

LOCAL SECTIONS

S. R. Beitler, *Chairman* * (1944)
J. A. Keeth (1945)
Oliver B. Lyman (1946)
A. R. Mumford (1947)
S. D. Moxley (1948)

Junior Adviser

F. M. Gibson, Jr. (1945)

(Personnel of Local Sections' Executive Committees, p. RI-15)

CONSTITUTION AND BY-LAWS

R. L. Parsell, *Chairman* * (1945)
F. B. Orr (1944)
W. J. Cope (1946)
A. M. Gompf (1947)
F. W. Miller (1948)

Junior Adviser

W. L. Davis (1944)

HONORS AND AWARDS

C. L. Bausch, *Chairman* * (1945)
D. C. Jackson (1944)
L. W. Wallace (1946)
Geo. A. Orrok (1947)
E. W. O'Brien (1948)

(Personnel of Medals Committee, p. RI-7)

RELATIONS WITH COLLEGES

H. E. Degler, *Chairman* * (1944)
G. L. Sullivan (1945)
R. P. Reece (1946)
H. J. Brown (1947)
Herbert Kuenzel (1948)

Advisory Members (1944)

M. M. Boring
A. D. Hughes
R. H. Porter
J. W. Zeller

Junior Adviser

J. M. Sexton (1944)

(Student Branches and Officers, p. RI-23)

EDUCATION AND TRAINING FOR THE INDUSTRIES

A. C. Harper, *Chairman* * (1944)
R. L. Goetzenberger (1945)
A. D. Bailey (1946)
L. J. Fletcher (1947)
J. I. Yellott (1948)

Advisory Members

To be appointed

LIBRARY

John Blizard, *Chairman* * (1945)
A. R. Mumford (1944)
E. F. Church, Jr. (1947)
The Secretary, C. E. Davies, *Ex-Officio*

RESEARCH †

Herman Weisberg, *Chairman* * (1944)
W. R. Elsey (1945)
J. F. D. Smith (1946)
D. L. Lindquist (1947)
G. A. Hawkins (1948)

STANDARDIZATION †

T. E. French, *Chairman* * (1944)
W. H. Hill (1945)
J. H. Taylor (1946)
E. J. Bryant (1947)
D. S. Ellis (1948)

POWER TEST CODES †

Francis Hodgkinson, *Chairman* * (1944)
A. G. Christie, *Vice-Chairman* (1946)
J. J. Jacobs, Jr., *Junior Observer* (1944)

Term expires 1944

C. H. Berry
Francis Hodgkinson
D. S. Jacobus
L. F. Moody
E. B. Ricketts

Term expires 1945

Theodore Baumeister
P. H. Hardie
B. V. E. Nordberg
R. J. S. Pigott
M. C. Stuart

Term expires 1946

A. G. Christie
Paul Diserens
N. R. Gibson
Geo. A. Orrok
E. B. Powell

Term expires 1947

W. A. Carter
W. L. H. Doyle
H. B. Oatley
R. B. Smith
W. J. Wohlenberg

Term expires 1948

Louis Elliott
W. F. Jones
Arvid Peterson
R. A. Sherman
P. W. Swain

SAFETY †

J. J. Zeitner (1944)
E. R. Granniss (1945)
H. W. Gabor (1946)
J. R. Connelly (1947)
R. B. Renner (1948)

PROFESSIONAL CONDUCT

V. E. Alden, *Chairman* * (1944)
G. S. Armstrong (1945)
P. W. Thompson (1946)
M. C. Maxwell (1947)
W. F. Ryan (1948)

† Personnel of all Technical Committees pp. RI-25-38.

SPECIAL COMMITTEES

BIOGRAPHY

(Special Committee of Publications Committee)

ROY V. WRIGHT, *Chairman*
R. E. FLANDERS
GEO. A. ORROK
J. W. ROE

BOILER CODE

E. R. FISH, *Chairman*
H. B. OATLEY, *Vice-Chairman*
D. S. JACOBUS, *Honorary Chairman*
C. A. ADAMS
H. E. ALDRICH
T. B. ALLARDICE
H. C. BOARDMAN
PERRY CASSIDY
R. E. CECIL
A. J. ELY
V. M. FROST
C. E. GORTON
W. G. HUMPTON
J. O. LEECH
C. O. MYERS
C. W. OBERT
JAMES PARTINGTON
D. B. ROSSHEIM
D. L. ROYER
WALTER SAMANS
J. W. TURNER
S. K. VARNES
A. C. WEIGEL

J. W. SHIELDS, *Secretary*
M. JURIST, *Assistant Secretary*

Honorary Members

W. H. BOEHM
W. F. DURAND
A. M. GREENE, JR.
C. L. HUSTON
W. F. KIESEL, JR.
M. F. MOORE
I. E. MOULTROP
H. LEROY WHITNEY

(Personnel of Boiler Code Committees, pp. RI-37-38)

DUES-EXEMPT MEMBERS' CONTRIBUTIONS

F. D. HERBERT, *Chairman*
S. H. LIBBY
S. M. MARSHALL
N. T. MCKEE
C. R. PLACE
J. W. ROE
W. R. WEBSTER
W. D. ENNIS, *Treasurer*

MEDALS

(Special Committee of Board of Honors and Awards)

Term expires 1944

FRANCIS HODGKINSON
D. C. JACKSON
L. C. MORROW
J. M. TODD

(Continued)

MEDALS
(Continued)

Term expires 1945

A. D. BAILEY
J. W. BARKER
C. L. BAUSCH
CLARKE FREEMAN

Term expires 1946

E. C. HUTCHINSON
W. H. KENERSON
ERIK OBERG
L. W. WALLACE

Term expires 1947

L. H. FRY
P. E. HOLDEN
R. C. MUIR
GEO. A. ORROK

Term expires 1948

F. M. FEIKER
E. L. HOPPING
E. W. O'BRIEN
C. T. RIPLEY

REGULAR NOMINATING COMMITTEE FOR 1944

G. J. NICASTRO, *Chairman*
J. P. MAGOS, *Secretary*

Group

I F. O. HOAGLAND, West Hartford, Conn.
H. R. WESTCOTT, New Haven, Conn., *1st Alternate*
J. W. ZELLER, Worcester, Mass., *2nd Alternate*

II G. J. NICASTRO, New York, N.Y., *Chairman*
E. V. DAVID, New York, N.Y., *1st Alternate*
A. EHRECHT, New York, N.Y., *2nd Alternate*

III J. STANLEY MOREHOUSE, Villanova, Pa.
V. M. PALMER, Rochester, N.Y., *1st Alternate*
C. E. HARRINGTON, Buffalo, N.Y., *2nd Alternate*

IV A. M. ORMOND, Savannah, Ga.
E. E. WILLIAMS, Charlotte, N.C., *1st Alternate*
J. MACK TUCKER, Knoxville, Tenn., *2nd Alternate*

V D. S. BROWN, Cincinnati, Ohio
S. M. WECKSTEIN, Canton, Ohio, *1st Alternate*
E. M. SAMPSON, Columbus, Ohio, *2nd Alternate*

VI J. P. MAGOS, Chicago, Ill., *Secretary*
C. F. MOULTON, Omaha, Neb., *1st Alternate*
D. P. MORSE, Indianapolis, Ind., *2nd Alternate*

VII W. H. KASSEBOHM, Berkeley, Calif.
ALF HANSEN, San Francisco, Calif., *Alternate*

VIII H. L. CRAIN, Kansas City, Mo.
W. T. ALLIGER, Houston, Texas, *1st Alternate*
H. M. ROBINSON, Dallas, Texas, *2nd Alternate*

LOCAL SECTIONS IN NOMINATING COMMITTEE GROUPS

GROUP I

BOSTON
BRIDGEPORT
GREEN MOUNTAIN
HARTFORD
NEW HAVEN
NEW LONDON
PROVIDENCE
WATERBURY
WESTERN MASSACHUSETTS
WORCESTER

GROUP II

METROPOLITAN (N.Y.) AND MEMBERS OUTSIDE THE UNITED STATES (EXCEPT ONTARIO SECTION MEMBERS)

GROUP III

ANTHRACITE-LEHIGH VALLEY
BALTIMORE
BUFFALO
CENTRAL PENNSYLVANIA
ITHACA
PHILADELPHIA
PLAINFIELD
ROCHESTER
SCHENECTADY
SUSQUEHANNA
SYRACUSE
WASHINGTON, D.C.

GROUP IV

ATLANTA
BIRMINGHAM
EAST TENNESSEE
FLORIDA
GREENVILLE
MEMPHIS
PIEDMONT-NORTE CAROLINA
RALEIGH
SAVANNAH
VIRGINIA

GROUP V

AKRON-CANTON
CINCINNATI
CLEVELAND
COLUMBUS
DAYTON
DETROIT
ERIE
ONTARIO
PENINSULA
PITTSBURGH
TOLEDO
WEST VIRGINIA
YOUNGSTOWN

GROUP VI

CENTRAL ILLINOIS
CENTRAL INDIANA
CHICAGO
FORT WAYNE
LOUISVILLE
MILWAUKEE
MINNESOTA
NEBRASKA
ROCK RIVER VALLEY
ST. JOSEPH VALLEY
ST. LOUIS
TRI-CITIES

GROUP VII

INLAND EMPIRE
OREGON
SAN FRANCISCO
SOUTHERN CALIFORNIA
UTAH
WESTERN WASHINGTON

GROUP VIII

COLORADO
KANSAS CITY
MID-CONTINENT
NEW ORLEANS
NORTH TEXAS
SOUTH TEXAS

SPECIAL COUNCIL COMMITTEES

(Dates in parentheses denote expiration of terms)

ADVISORY COMMITTEE TO COMMITTEE ON ADMISSIONS (FELLOW GRADE)

H. A. Lardner, *Chairman*
R. E. Flanders
E. C. Hutchinson
Alfred Iddles
J. H. Lawrence
Roy V. Wright

BOARD OF REVIEW

S. D. Sprong, *Chairman* (1944)
F. M. Gibson (1945)
John Haydock (1946)

BOARD ON TECHNOLOGY

R. F. Gagg, *Chairman*
C. B. Peck, *Vice-Chairman*
T. E. Purcell
S. R. Beitler (Local Sections)
L. K. Sillcox (Meetings and Program)
W. M. Sheehan (Professional Divisions)
F. L. Bradley (Publications)
Herman Weisberg (Research)

ENGINEERING OPPORTUNITIES

E. G. Bailey, *Chairman*
W. L. Batt, *Vice-Chairman*
R. E. Doherty
R. E. Flanders
D. C. Prince

ENGINEERS' CIVIC RESPONSIBILITIES

Roy V. Wright, *Chairman*
Gano Dunn
M. H. Fies
Lillian M. Gilbreth
H. B. Oatley
J. W. Roe
H. H. Snelling
D. Robert Yarnall

Junior Representative

W. Whitanen

Chairmen of Committees on Local Sections and Relations With Colleges, *Ex-Officio*

FREEMAN FUND

Clarke Freeman, *Chairman*
E. C. Hutchinson
Geo. A. Orrok

INDUSTRIAL CONSERVATION

A. M. Perrin, *Chairman*
R. D. Bullard
Graham Granger
R. A. Wheeler

LECTURESHIPS

C. B. Peck, *Chairman*
A. G. Christie
H. N. Davis
W. F. Durand
F. L. Wilkinson, Jr.

MANUFACTURING ENGINEERING COMMITTEE

L. C. Morrow, *Chairman*
Erik Oberg, *Vice-Chairman*
H. V. Coes
F. H. Colvin
J. L. Walsh

REGISTRATION

V. M. Palmer, *Chairman*
S. H. Graf
J. A. McPherson
F. H. Prouty
W. K. Simpson
H. H. Snelling

Junior Representatives

P. B. Petty W. Whitanen

SOCIETY OFFICE OPERATION

Alfred Iddles, *Chairman*
Wallace Clark
E. H. Schell

SOCIETY ORGANIZATION STRUCTURE

G. L. Knight, *Chairman*
Clarke Freeman
G. E. Hulse
K. M. Irwin
H. R. Westcott
D. Robert Yarnall

WAR PRODUCTION

James L. Walsh, *Chairman*
Major Gen. G. M. Barnes (Army Representative)
Rear-Admiral J. A. Furer (Navy Representative)

A.S.M.E. Divisions Representatives

K. H. Condit (Management)
C. F. Dietz (Materials Handling)
Sol Einstein (Production Engineering)
D. S. Ellis, W. M. Sheehan } (Railroad)
A. R. Stevenson, Jr. (Aviation)
T. H. Wickenden (Metals Engineering)

W. L. Batt	K. T. Keller
C. E. Brinley	David Larkin
H. V. Coes	F. T. Letchfield
H. N. Davis	T. A. Morgan
W. C. Dickerman	R. C. Muir
Gano Dunn	E. A. Muller
W. F. Durand	T. E. Murray
W. S. Finlay, Jr.	W. I. Westervelt
R. E. Flanders	A. C. Willard

GEORGE WESTINGHOUSE BUST

D. S. Kimball, *Chairman*
C. E. Davies, *Secretary*
K. T. Compton
S. W. Dudley
W. G. Marshall
J. H. McGraw
C. F. Scott
J. B. Wright
Roy V. Wright

A.S.M.E. REPRESENTATIVES ON OTHER ACTIVITIES

See also A.S.M.E. Representatives on Other Research Committees, etc., pages RI-26, 31, 34, 35, 38
(Dates in parentheses denote expiration of terms)

AMERICAN ASSOCIATION FOR THE ADVANCEMENT OF SCIENCE

SECTION M, ENGINEERING

F. D. Carvin R. L. Sackett

AMERICAN STANDARDS ASSOCIATION

J. E. Lovely (1945)
Alfred Iddles (1946)

Alternates

C. B. LePage (1944)
W. C. Mueller (1944)

AMERICAN YEAR BOOK CORPORATION

C. E. Davies

CENTER FOR SAFETY EDUCATION

E. R. Granniss

CONSULTATIVE COMMITTEE ON ENGINEERING

(War Manpower Commission)

R. F. Gagg

THE ENGINEERING FOUNDATION

E. R. Fish (1944)
K. H. Condit (1947)
A. A. Potter (1947)

RESEARCH PROCEDURE COMMITTEE

W. Trinks (1944)

E.I.C.-A.S.M.E. JOINT CONFERENCE

(The Engineering Institute of Canada)

A. G. Christie A. E. White
J. W. Parker

ENGINEERING SOCIETIES LIBRARY BOARD

A. R. Mumford (1944)
John Blizard (1945)
E. F. Church, Jr. (1947)
Secretary, A.S.M.E., *Ex-Officio*

ENGINEERING SOCIETIES MONOGRAPHS COMMITTEE

J. A. Goff (Professional Divisions)
E. J. Kates (Publications)

ENGINEERING SOCIETIES PERSONNEL SERVICE, INC.

Ernest Hartford, *Vice-President of the Corporation* and *Chairman*, Metropolitan Advisory Committee
D. C. Jackson, Boston Advisory Committee
R. D. Brizzolara, Chicago Advisory Committee
C. J. Freund, Detroit Advisory Committee
H. J. Berg, San Francisco Advisory Committee

ENGINEERS' COUNCIL FOR PROFESSIONAL DEVELOPMENT

J. W. Parker (1944)
R. L. Sackett (1945)
R. L. Goetzenberger (1946)

COMMITTEE ON UNIONISM

Warner Seely

ENGINEERS' NATIONAL RELIEF FUND

Ernest Hartford

JOHN FRITZ MEDAL BOARD OF AWARD

W. H. McBryde (1944)
W. A. Hanley (1945)
J. W. Parker (1946)
H. V. Coes (1947)

GANTT MEDAL BOARD OF AWARD

Wallace Clark (1944)
J. M. Talbot (1945)
F. A. Schaff (1946)
J. M. Juran (1947)

DANIEL GUGGENHEIM MEDAL FUND, INC.

E. E. Aldrin (1944)
J. E. Younger (1945)
J. M. Clark (1946)

JOSEPH A. HOLMES SAFETY ASSOCIATION

J. F. Barkley

HOOVER MEDAL BOARD OF AWARD

W. L. Batt (1945)
W. H. Kenerson (1947)
S. F. Voorhees (1949)

INTER-AMERICAN DEVELOPMENT COMMISSION

A. M. Greene, Jr. C. M. Muchnic
W. H. McBryde

INTER-AMERICAN ENGINEERING COOPERATION

A. M. Greene, Jr.

INTERNATIONAL ELECTROTECHNICAL COMMISSION

U.S. NATIONAL COMMITTEE

H. N. Davis Francis Hodgkinson
Paul Diserens

Alternate

C. Harold Berry

JOINT CONFERENCE COMMITTEE

(Presidents and Secretaries of National Societies)

President
Junior Past-President } *Ex-Officio*
Secretary

POSTWAR PLANNING

E. G. Bailey

MARSTON AWARD

W. L. Abbott (1945)

NATIONAL BUREAU OF ENGINEERING REGISTRATION

V. M. Palmer

NATIONAL FIRE WASTE COUNCIL

J. A. Neale

NATIONAL MANAGEMENT COUNCIL

J. R. Bangs, Jr. (1945)—J. M. Juran, *Alternate*
A. I. Peterson (1946)—C. W. Lytle, *Alternate*
J. M. Talbot (1947)—Wallace Clark, *Alternate*

NATIONAL RESEARCH COUNCIL

DIVISION OF ENGINEERING AND INDUSTRIAL RESEARCH

E. G. Bailey (1945)

ALFRED NOBLE PRIZE

A. M. Greene, Jr. (1944)

UNITED ENGINEERING TRUSTEES, INC.

K. H. Condit (1944)
H. A. Lardner (1946)
G. L. Knight (1947)

VERMILYE MEDAL ADVISORY COMMITTEE

W. D. Fuller (1947)

WASHINGTON AWARD COMMISSION

C. C. Austin (1944)
W. S. Monroe (1945)

WORLD POWER CONFERENCE

EXECUTIVE COMMITTEE, U.S. NATIONAL COMMITTEE

President, *Ex-Officio*

PROFESSIONAL DIVISIONS

ARTICLE B6A, PAR. 16: The Standing Committee on Professional Divisions shall, under the direction of the Council, have supervision of the Professional Divisions of the Society.

STANDING COMMITTEE

W. M. SHEEHAN, *Chairman* (1944)
J. H. SENGSTAKEN (1945)
J. A. GOFF (1946)
J. M. TALBOT (1947)
W. L. H. DOYLE (1948)

Junior Adviser

I. P. WEST (1944)

Liaison Representative, Local Sections

A. R. MUMFORD

Applied Mechanics

Organized, 1927

J. H. KEENAN, *Chairman*

EXECUTIVE COMMITTEE

J. H. KEENAN, *Chairman*
J. N. GOODIER, *Secretary*
H. W. EMMONS
JESSE ORMONDROYD
H. PORITSKY

Associates

J. P. DEN HARTOG
RUPEN EKSERGIAN
J. C. HUNSAKER
G. B. PEGRAM
R. E. PETERSON
E. O. WATERS
B. M. WOODS

Research Secretary

JESSE ORMONDROYD

Liaison Representatives

Aviation Liaison Group, J. C. HUNSAKER
Heat Transfer Division, Coordination Committee, H. W. EMMONS
San Francisco Section, W. M. MOODY

JOURNAL OF APPLIED MECHANICS

J. M. LESSELLS, *Editor*

SPONSORS

Dynamics, F. M. LEWIS
Elasticity, STEPHEN TIMOSHENKO
Experimental Stress Analysis, W. M. MURRAY
Fluid Mechanics, H. W. EMMONS
Lubrication, L. M. TICHVINSKY
Plasticity, A. NÁDAI
Strength of Materials, C. R. SODERBERG
Thermodynamics, J. A. GOFF

Aviation

Organized, 1920

R. F. GAGG, *Chairman*

EXECUTIVE COMMITTEE

R. F. GAGG, *Chairman*
J. E. YOUNGER, *Secretary*
A. R. STEVENSON, JR.
F. K. TEICHMANN
F. E. WEICK, *Advisory Member*
J. M. CLARK, *Ex-Officio*

Associates

T. E. COLVIN, for the West Coast
C. H. DOLAN, for the Mid-West
M. J. THOMPSON, for the Southwest

Junior Advisers

B. E. DEL MAR
F. H. FOWLER
MARTIN GOLAND

ADVISORY COMMITTEE

KARL ARNSTEIN
CARL BEER
E. C. CLARKE
H. M. CRANE
LOUIS DEFLOREZ
W. F. DURAND
A. J. GIFFORD
M. B. GORDON
WILLIAM HOVGAARD
J. C. HUNSAKER
P. G. JOHNSON
C. F. KETTERING
R. K. LEBLOND
W. B. MAYO
T. A. MORGAN
S. A. MOSS
E. A. SPERRY
A. R. STEVENSON, JR.
J. G. VINCENT
THEODOR VON KÁRMÁN
C. J. WARD
E. P. WARNER
B. M. WOODS
ORVILLE WRIGHT

Research Secretary

ALEXANDER KLEMIN

Liaison Representatives, Professional Divisions

Applied Mechanics, M. V. BARTON, J. E. YOUNGER
Heat Transfer, R. H. NORRIS
Hydraulic, THEODOR VON KÁRMÁN
Industrial Instruments, ED S. SMITH
Management, R. E. GILLMOR
Metals Engineering, R. G. STURM, R. F. TEMPLIN
Oil and Gas Power, S. ALLEN GUIBERSON, III
Production Engineering, R. F. GAGG
Rubber and Plastics, JOHN DELMONTE, J. F. DOWNIE SMITH
Wood Industries, ALEXANDER KLEMIN

Liaison Representatives, Other Activities

Daniel Guggenheim Medal Board of Award, E. E. ALDRIN, J. M. CLARK, J. E. YOUNGER
Education and Training for the Industries Standing Committee, A. R. STEVENSON, JR.
Institute of Aeronautical Sciences, J. E. YOUNGER
War Production Committee, A. R. STEVENSON, JR.

BIOMECHANICS STEERING COMMITTEE

F. K. TEICHMANN, *Chairman*
L. D. CARSON
EUGENE DUBOIS
RUPEN EKSERGIAN
R. F. GAGG
C. M. GRATZ
L. E. GRIFFITH
P. E. HOVGARD

Consulting Engineering Group

Organized, 1943

EXECUTIVE COMMITTEE

S. LOGAN KERR, *Chairman*
P. L. BATTEY
W. H. MCBRYDE
F. H. PROUTY
M. X. WILBERDING

Fuels

Organized, 1920

A. W. THORSON, *Chairman*

EXECUTIVE COMMITTEE

A. W. THORSON, *Chairman*
D. C. WEEKS, *Secretary*
O. F. CAMPBELL
D. S. FRANK
J. E. TOBEY

Associates

J. F. BARKLEY
J. S. BENNETT, 3RD
R. M. BOYLES
T. C. CHEASLEY
W. G. CHRISTY
M. P. CLEGHORN
B. J. CROSS
M. D. ENGLE
H. F. HEBLEY
E. R. KAISER
J. H. KERRICK
T. A. MARSH
M. A. MAYERS
J. R. MICHEL
C. E. MILLER
A. R. MUMFORD
W. E. REASER
R. L. ROWAN
R. A. SHERMAN

Junior Adviser

E. R. KAISER

Research Secretary

A. R. MUMFORD

Liaison Representative, Local Sections

W. G. CHRISTY

Liaison Representatives, Professional Divisions

Heat Transfer, B. J. CROSS
Process Industries, W. E. REASER
Railroad, T. C. CHEASLEY

COAL TESTING CODE

Organized, 1939, Jointly with A.I.M.E.

R. L. ROWAN, *Chairman*
J. E. TOBEY, *Vice-Chairman*

A.S.M.E. Representatives

J. F. BARKLEY
H. C. CARROLL
R. A. FORESMAN
R. M. HARDGROVE
J. H. KERRICK
T. A. MARSH
A. R. MUMFORD
W. T. REID
R. A. SHERMAN
L. A. SHIPMAN
A. W. THORSON

DOMESTIC FUELS

R. A. SHERMAN, *Chairman*
T. C. CHEASLEY
T. A. MARSH
J. E. TOBEY

Fuels

(Continued)

JOINT AWARDS

A.I.M.E. Paul Weir (1944)
A.S.M.E. W. G. Christy (1945)
A.I.M.E. D. R. Mitchell (1946)
A.S.M.E. H. F. Hebley (1947)
A.S.M.E. O. F. Campbell (1948)

MODEL SMOKE LAW

J. F. Barkley, *Chairman*
O. F. Campbell
A. G. Christie
W. G. Christy
T. A. Marsh
T. E. Purcell
R. A. Sherman
R. R. Tucker

PROGRAM AND MEETINGS

D. S. Frank, *Chairman*
E. R. Kaiser, *Vice-Chairman*

REVIEW OF PAPERS

A. W. Thorson, *Chairman*
M. D. Engle
D. S. Frank
D. C. Weeks

Graphic Arts

Organized, 1922, as Printing Industries Division. Name changed, 1935

Inactive

Heat Transfer

Organized, 1938, as Heat Transfer Professional Group. Reorganized, 1941.

W. S. Patterson, *Chairman*
H. B. Nottage, *Secretary*

EXECUTIVE COMMITTEE

W. S. Patterson, *Chairman*
L. M. K. Boelter
R. A. Bowman
J. H. Marchant
R. H. Norris, *Clerk*

Advisory Associates

T. B. Drew
E. D. Grimison
C. E. Lucke
W. H. McAdams

Junior Representatives

P. R. Trumpler
W. R. Wykoff

STANDING COMMITTEES

Coordination

H. B. Nottage, *Chairman*

Research Secretary

C. F. Kayan

Liaison Representatives, Professional Divisions

Aviation, R. H. Norris
Fuels, B. J. Cross
Hydraulic, J. D. Scoville
Metals Engineering, W. Trinks
Oil and Gas Power, F. G. Hechler
Power, O. F. Campbell
Process Industries, Arnold Weisselberg
Railroad, L. H. Fry

Liaison Representatives, Other Activities

Local Sections, P. R. Trumpler
San Francisco Section, W. M. Moody

Members at Large

R. H. Heilman
G. L. Tuve

Papers

C. F. Kayan, *Chairman*
L. M. K. Boelter
G. A. Hawkins
R. H. Norris
L. B. Schueler

Testing Technique

B. J. Cross, *Chairman*
G. L. Tuve

Thermo-Physical Properties of Materials

J. A. Goff, *Chairman*
J. A. Anderson
F. G. Brickwedde
T. H. Chilton
A. E. Hershey
Max Jakob

TECHNICAL COMMITTEES

Aircraft Heat Transfer

W. W. Reaser, *Chairman*
J. G. Beerer
A. R. Collins
A. G. Foote
H. S. Gordon
John Marchant
B. L. Messenger
A. M. Ney
R. H. Norris
C. J. Vanous

Direct-Fired Fluid Heaters and Boilers

John Blizard, *Chairman*
D. S. Frank
E. D. Grimison
L. B. Schueler
W. J. Wohlenberg

Heated or Cooled Enclosures

C. F. Kayan, *Chairman*
E. L. Knoedler
W. A. Ticknor

Industrial Furnaces and Kilns

H. W. Smith, Jr., *Chairman*
H. C. Hottel
W. A. Ticknor
W. Trinks

Theory and Fundamental Research

T. B. Drew, *Chairman*
L. M. K. Boelter
A. P. Colburn
Max Jakob

Unfired Heat Transfer Equipment

A. C. Mueller, *Chairman*
R. A. Bowman
G. A. Hawkins
B. E. Short
S. P. Soling
W. H. Thompson
Townsend Tinker

Hydraulic

Organized, 1926

L. J. Hooper, *Chairman and Secretary*

EXECUTIVE COMMITTEE

L. J. Hooper, *Chairman and Secretary*
G. R. Rich
J. D. Scoville
R. E. B. Sharp
R. V. Terry

Research Secretary

L. J. Hooper

CAVITATION

R. E. B. Sharp, *Sponsor*
L. F. Moody, *Chairman*
R. T. Knapp
J. M. Mousson
W. J. Rheingans
G. F. Wislicenus

Representatives of Other Societies

American Society for Testing Materials, F. N. Speller
The Engineering Institute of Canada, Ernest Brown
Institution of Mechanical Engineers, G. S. Baker

Representative of France

A. Tenot

Representative, San Francisco Section

W. M. Moody

HYDRAULIC PRIME MOVERS

R. V. Terry, *Sponsor*
J. F. Roberts, *Chairman*
A. Aberli
E. H. Collins
J. P. Growden
L. F. Harza
P. L. Heslop
George Jessup
F. H. Rogers
F. Schmidt
S. O. Schomberger
S. H. Van Patter

PUMPING MACHINERY

G. R. Rich, *Sponsor*
R. L. Daugherty, *Chairman*
B. F. Tillson
Hans Ulmann

WATER HAMMER

J. D. Scoville, *Sponsor*
S. Logan Kerr, *Chairman*
N. R. Gibson
Eugene Halmos
L. F. Moody
R. S. Quick
E. B. Strowger

Hydraulic

WATER HAMMER

(Continued)

Affiliated Societies and Their Representatives

American Society of Civil Engineers, N. R. GIBSON and FORD KURTZ
American Water Works Association, F. M. DAWSON and L. H. KESSLER

Associate Members, Representing:

Australia, GEORGE HIGGINS
Brazil, A. W. K. BILLINGS and F. KNAPP
The Engineering Institute of Canada, R. W. ANGUS and F. M. WOOD
France, LOUIS BERGERON and CHARLES CAMICHEL
Germany and Verein deutscher Ingenieure, D. THOMA
Great Britain and Institution of Mechanical Engineers, E. BRUCE BALL and A. H. GIBSON
Italy, GAUDENZIO FANTOLI and ALBINO PASINI
Switzerland, CHARLES JAEGER and O. SCHNYDER

Industrial Instruments and Regulators Division

Organized, 1936, as Committee on Industrial Instruments and Regulators, of Process Industries Division. Reorganized, 1943, as a Division

EVERETT S. LEE, *Chairman*
J. C. PETERS, *Secretary*

EXECUTIVE COMMITTEE

EVERETT S. LEE, *Chairman*
J. C. PETERS, *Secretary*
E. D. HAIGLER
ED S. SMITH
I. M. STEIN

COMMITTEE CHAIRMEN

Application, J. J. GREBE
Bibliography and Translations, H. L. MASON
By-Laws, E. D. HAIGLER
Design, W. G. BROMBACHER
Papers, P. W. KEPPLER
Terminology, H. F. MOORE
Theory, A. F. SPERRY

Liaison Representatives

C. O. FAIRCHILD, American Institute of Physics
J. J. GREBE, American Institute of Chemical Engineers
A. IVANOFF, Institution of Mechanical Engineers
EVERETT S. LEE, A.I.E.E. Committee on Instruments and Measurements
ED S. SMITH, Aviation Division and Research Committee on Fluid Meters
R. B. SMITH, Power Test Codes Committee No. 20 on Speed, Temperature and Pressure Responsive Governors
I. M. STEIN, Gibson Island Conferences of American Association for the Advancement of Science

Management

Organized, 1920

J. M. JURAN, *Chairman*
G. M. VARGA, *Secretary*
CARLOS DEZAFRA, *Assistant Secretary*

EXECUTIVE COMMITTEE

J. M. JURAN, *Chairman*
L. A. APPLEY, *Vice-Chairman*
A. S. KNOWLES
W. R. MULLEE
A. I. PETERSON
J. A. WILLARD

Research Secretary

E. H. HEMPEL

Contact Secretary, Local Sections

J. A. WILLARD

GENERAL COMMITTEE

J. R. BANGS
R. M. BARNES
W. L. BATT
C. W. BEESE
F. B. BELL
WALLACE CLARK
H. V. COES
K. H. CONDIT
HOWARD COONLEY
CARLOS DEZAFRA
N. E. ELSAS
S. P. FISHER
W. D. FULLER
W. H. GESELL
L. M. GILBRETH
R. E. GILLMOR
G. E. HAGEMANN
C. H. HATCH
E. H. HEMPEL
P. E. HOLDEN
W. F. HOSFORD
D. S. KIMBALL
W. H. KUSHNICK
J. K. LOUDEN
H. B. MAYNARD
R. A. MCCARTY
T. S. MCEWAN
L. C. MORROW
D. B. PORTER
F. E. RAYMOND
J. W. ROE
E. H. SCHELL
E. D. SMITH
A. R. STEVENSON, JR.
J. M. TALBOT
L. W. WALLACE
A. WILLIAMS
JOHN YOUNGER

Liaison Representatives, Local Sections

Atlanta, S. C. HALE
Birmingham, H. L. FREEMAN
Columbus, P. N. LEHOCZKY
Detroit, A. N. GODDARD
Kansas, A. H. SLUSS
Los Angeles, D. S. CLARK
Louisville, C. D. ELDRIDGE
Metropolitan, M. S. SYMON
Milwaukee, B. V. E. NORDBERG
New Orleans, E. L. COWAN
Philadelphia, C. S. GOTWALS
Rochester, V. M. PALMER
San Francisco, B. A. GAYMAN
Seattle, H. J. MCINTYRE
South Texas, V. M. FAIRES
Waterbury, R. S. STORRS

SUBCOMMITTEE CHAIRMEN

Administrative Organization, W. R. MULLEE
Industrial Marketing, (to be appointed)
Quality Control, A. I. PETERSON
Work Standardization, J. K. LOUDEN

DEPRECIATION

E. C. CLARKE
H. V. COES
P. T. NORTON, JR.

Liaison Representatives, Other Activities

Aviation Liaison Group, R. E. GILLMOR, A. R. STEVENSON, JR.
Education and Training for the Industries Standing Committee, LILLIAN M. GILBRETH
Gantt Medal Board of Award: see page 9
National Management Council: see page 9
Professional Divisions Standing Committee, J. M. TALBOT
War Production Committee, K. H. CONDIT

Materials Handling

Organized, 1920

G. E. HAGEMANN, *Chairman*

EXECUTIVE COMMITTEE

G. E. HAGEMANN, *Chairman*
C. F. DIETZ, *Vice-Chairman*
C. H. BARKER, JR., *Secretary*
A. J. BURKE, *Assistant Secretary*
J. A. JACKSON
F. J. SHEPARD, JR.

Associates

H. E. BLANK, JR.
W. C. CARL
N. W. ELMER
H. C. KELLER
BERNARD LESTER
M. C. MAXWELL
R. H. MCLAIN
F. E. MOORE
P. D. OESTERLE
VIRGIL PALMER
M. W. POTTS
SIDNEY REIBEL
R. B. RENNER
E. D. SMITH
H. E. STOCKER
G. R. WADLEIGH
J. B. WEBB

Junior Associates

CORNELIUS CROWLEY
E. Z. GABRIEL
R. W. GRUNDMAN
D. D. JONES
JOHN SCHUETTINGER

MATERIALS HANDLING SAFETY COMMITTEE

R. B. RENNER, *Chairman*

SAFETY CODE FOR BULK MATERIALS CONVEYORS

C. S. HUNTINGTON, *Chairman*

SAFETY CODE FOR PACKAGE CONVEYORS

H. C. KELLER, *Chairman*

STANDARD NOMENCLATURE

J. A. JACKSON, *Chairman*

STANDARDIZATION OF SHIPMENTS ON SKIDS AND PALLETS

C. H. BARKER, JR., *Chairman*
H. E. STOCKER, *Vice-Chairman*
C. E. MOCHRIE
P. F. NYDEGGER
M. W. POTTS
F. J. SHEPARD, JR.

Metals Engineering

Organized, 1927, as Iron and Steel Division. Reorganized, 1940.

EXECUTIVE COMMITTEE

J. H. ROMANN, *Chairman*
J. F. YOUNG, *Secretary*

Metals Engineering

(Continued)

R. D. Brizzolara
Everett Chapman
M. D. Stone
R. J. Sturm

ADVISORY COMMITTEE

J. H. Hitchcock
W. Trinks
W. R. Webster
S. M. Weckstein
T. H. Wickenden

GENERAL COMMITTEE

Sabin Crocker
D. S. Ellis
F. P. Huston
R. E. Kennedy
J. M. Lessells
Norman Mochel
S. D. Moxley
P. M. Mueller
R. A. North
E. S. Patch
G. A. Pugh
W. M. Sheehan
T. R. Weber
A. E. White
A. W. Winston

Oil and Gas Power

Organized, 1921

H. E. Degler, *Chairman*

EXECUTIVE COMMITTEE

H. E. Degler, *Chairman*
L. N. Rowley, *Secretary*
C. E. Beck
E. S. Dennison
E. J. Kates
Lee Schneitter

Associates

Hans Bohuslav
G. C. Boyer
G. J. Dashefsky
W. L. H. Doyle
C. W. Good
F. G. Hechler
P. B. Jackson
B. V. E. Nordberg
M. J. Reed
T. M. Robie
R. T. Sawyer
J. A. Worthington

Junior Adviser

C. K. Holland

Research Secretary

Lee Schneitter

Liaison Representatives

American Society of Naval Architects and Marine Engineers, B. V. E. Nordberg
Aviation Liaison Group, H. E. Degler
Heat Transfer Division, F. G. Hechler
Railroad Division, R. T. Sawyer
San Francisco Section, E. G. Gothberg

HONORS AND AWARDS

E. J. Kates, *Chairman*
C. W. Good
Ernest Nibbs

OIL ENGINE POWER COST

H. C. Major, *Chairman*
H. C. Lenfest, *Secretary*
L. T. Brown
H. G. Bryan
E. Hale Codding
Malcolm Duncan
R. G. Ely
J. H. Gallaway
E. J. Kates
A. B. Morgan
M. J. Reed
T. M. Robie
R. T. Sawyer
Lee Schneitter
P. H. Schweitzer
J. B. Sims
R. H. Stier
H. C. Thuerk
C. A. Trimmer
Stanley Wright

OIL AND GAS POWER CONFERENCES

1945 Meeting Location Selection Committee

C. E. Beck, *Chairman*
W. L. H. Doyle
B. V. E. Nordberg

PAPERS

C. W. Good, *Chairman*
C. E. Beck
G. J. Dashefsky
P. B. Jackson
R. T. Sawyer

PUBLICITY

L. N. Rowley

Power

Organized, 1920

G. A. Gaffert, *Chairman*

EXECUTIVE COMMITTEE

G. A. Gaffert, *Chairman*
H. D. Harkins, *Secretary*
Theodore Baumeister
J. A. Keeth
J. N. Landis
L. M. Goldsmith (on leave, 1944)

Research Secretary

J. A. Keeth

Liaison Representative, San Francisco Section

E. C. Gothberg

Process Industries

Organized, 1934

Arnold Weisselberg, *Chairman*

EXECUTIVE COMMITTEE

Arnold Weisselberg, *Chairman*
T. R. Olive, *Secretary*
J. W. Hunter
William Raisch
W. R. Woolrich
J. I. Yellott
F. L. Yerzley

Research Secretary

Arnold Weisselberg

Liaison Representatives

Heat Transfer Division, E. J. Devlin
Professional Divisions Standing Committee, J. H. Sengstaken
San Francisco Section, Herman Dishington

COMMITTEE CHAIRMEN

Air Conditioning, C. F. Kayan
Drying, Arnold Weisselberg
Food Processing, G. L. Montgomery
Manufactured and Natural Gas, E. J. Devlin
Mechanical Separation, Richard O'Mara
Paper Awards and Honors, C. E. Lucke
Petroleum, William Raisch
Program, J. W. Hunter
Sanitation, William Raisch
Sugar, F. M. Gibson
Sulphur, B. E. Short
Vegetable Oils, R. W. Morton

Production Engineering

Organized, 1921, as Machine Shop Practice Division. Reorganized, 1941.

Sol Einstein, *Chairman*

EXECUTIVE COMMITTEE

Sol Einstein, *Chairman*
C. L. Tutt, Jr., *Secretary and Staff Assistant*
J. L. Alden
E. W. Ernest
W. J. Hargest
H. B. Lewis

Associates

Hans Ernst
Erik Oberg
Warner Seely
E. O. Waters

Research Secretary

A. F. Murray

Liaison Representative, San Francisco Section

Walter Kassebohm

Railroad

Organized, 1920

J. G. Adair, *Chairman*

EXECUTIVE COMMITTEE (RR1)

J. G. Adair, *Chairman*
E. L. Woodward, *Secretary*
P. W. Kiefer
K. F. Nystrom
W. C. Sanders
W. M. Sheehan

GENERAL COMMITTEE (RR2)

E. R. Battley
W. H. Baselet
B. S. Cain
W. I. Cantley
E. D. Campbell
J. E. Davenport
C. M. Darden
L. B. Jones
J. M. Nicholson
E. S. Pearce
A. A. Raymond
R. W. Salisbury
Dennistoun Wood
H. H. Urbach
E. G. Young

Railroad

(Continued)

ADVISORY COMMITTEE (RR3)

Past-Chairmen

C. T. Ripley
L. H. Fry
A. I. Lipetz
D. S. Ellis
J. R. Jackson

Research Secretary

F. H. Clark

Liaison Representatives

Admissions Standing Committee, F. E. Lyford
Heat Transfer Division, Coordination Committee, L. H. Fry
Professional Divisions Standing Committee, W. M. Sheehan
San Francisco Section, M. P. Taylor

Rubber and Plastics Division

Organized, 1937, as Committee on Rubber and Plastics of Process Industries Division and made a Subdivision in 1940. Reorganized as a Group in 1942, and as a Division in 1943.

G. M. Kline, *Chairman*

EXECUTIVE COMMITTEE

G. M. Kline, *Chairman*
E. F. Riesing, *Vice-Chairman*
J. H. Booth, *Secretary*
John Delmonte
L. E. Jermy
E. G. Kimmich
H. M. Richardson

Research Secretary

J. F. Downie Smith

GENERAL COMMITTEE

A. L. Alves
R. A. Boyer
T. S. Carswell
D. H. Cornell
J. H. Dillon
F. L. Haushalter
G. H. Kaemmerling
M. E. Lerner
R. A. North
R. G. Seaman
J. F. Downie Smith
J. H. Teeple
J. C. Travilla, Jr.
F. L. Yerzley
W. A. Zinzow

COMMITTEE CHAIRMEN

By-Laws, F. L. Yerzley
Publicity, L. E. Jermy

Textile

Organized, 1921

W. B. Heinz, *Chairman*

EXECUTIVE COMMITTEE

W. B. Heinz, *Chairman*
C. D. Brown, *Vice-Chairman*
W. W. Starke, *Secretary*
F. L. Bradley
M. Earl Heard
J. O. Lindsay
J. D. Robertson
E. Wadsworth Stone
J. W. Vaughan, Jr.

Associates

A. D. Asbury
Winn Chase
D. C. Scott

Research Secretary

J. W. Cox

Southern Representative

S. B. Earle

ACTIVITIES COMMITTEE

Chairman, C. D. Brown
Air Conditioning, M. H. Irons
Drying, J. D. Robertson
Lighting, Earle Mauldin
Lubrication, L. C. Cobb
Package Dyeing, O. W. Clark
Papers, D. C. Scott
Power and Heat Utilization, E. Wadsworth Stone
Winding and Unwinding, W. R. Kent

Wood Industries

Organized, 1921

M. J. MacDonald, *Chairman*

EXECUTIVE COMMITTEE

M. J. MacDonald, *Chairman*
D. R. Gray, *Vice-Chairman*
A. C. Fegel, *Secretary*
F. J. Hanrahan
H. S. Jones

Associates

C. L. Babcock
P. H. Bilhuber
H. B. Carpenter
F. P. Cartwright
G. E. French
A. W. Keuffel
A. S. Kurkjian
J. S. Mathewson
E. D. May
R. H. McCarthy
C. B. Norris
T. D. Perry
A. D. Smith, Jr.
H. M. Sutton
Charles White

COMMITTEE CHAIRMEN

Dimensional Limits and Allowances (to be appointed)
Wood Finishing, M. J. MacDonald

LOCAL SECTIONS

ARTICLE B6A, PAR. 17: The Standing Committee on Local Sections shall, under the direction of the Council, have supervision of the Local Sections of the Society.

STANDING COMMITTEE ON LOCAL SECTIONS

S. R. BEITLER, *Chairman* (1944)

J. A. KEETH (1945)
OLIVER B. LYMAN (1946)
A. R. MUMFORD (1947)
S. D. MOXLEY (1948)

Junior Adviser

F. M. GIBSON, JR. (1945)

REGIONAL GROUP DELEGATES TO ANNUAL CONFERENCES

Terms expire October, 1944

C. C. AUSTIN, *Speaker for 1943 Conference*, Group VI
F. C. RICHARDSON, *Secretary*, Group I

W. S. GLEESON, Group II
F. S. ERDMAN, Group III
W. R. CHAMBERS, Group IV
R. R. SLAYMAKER, Group V
J. G. MCGIVERN, Group VII
L. J. CUCULLU, Group VIII

Terms expire October, 1945

H. C. R. CARLSON, *Speaker for 1944 Conference*, Group II
R. M. SCOTT, *Secretary*, Group I

F. W. MILLER, Group III
F. J. REED, Group IV
J. G. MARTIN, Group V
W. W. BABCOCK, Group VI
B. T. MCMINN, Group VII
G. H. WOELBING, Group VIII

AKRON-CANTON

Organized: 1920
Territory: Counties of Richland, Ashland, Medina, Summit, Portage, Wayne, Stark, Holmes, Tuscarawas, Carroll, and Coshocton in Ohio
Place of Meeting: As selected monthly
Number of Members: 194

EXECUTIVE COMMITTEE

A. E. SHETLER, *Chairman*
D. H. CORNELL, *Vice-Chairman*
R. W. HURSH, *Secretary-Treasurer*
C. E. BORGER
M. R. BOWERMAN
E. D. GEORGE
O. J. HORGER
G. C. MCMULLEN
R. G. MINNS
M. C. PIERCE
J. H. VANCE
A. G. WALKER
G. H. WOOD

ANTHRACITE-LEHIGH VALLEY

Organized: 1920, as Lehigh Valley; reorganized, 1928, as Anthracite-Lehigh Valley
Territory: Counties of Bradford, Susquehanna, Wayne, Sullivan, Wyoming, Lackawanna, Columbia, Luzerne, Monroe, Pike, Schuylkill, Carbon, Berks, Lehigh, Northampton in Pennsylvania, and Warren in New Jersey
Place of Meeting: One meeting annually at Allentown, Bethlehem, Easton, Hazleton, Pottsville, Reading, Scranton, and Wilkes-Barre
Local Organization: The Engineers' Club of Lehigh Valley
Number of Members: 209

EXECUTIVE COMMITTEE

J. A. GISH, JR., *Chairman*
WALTER GREACEN, III } *Vice-Chairmen*
J. A. LLOYD
R. H. PORTER
C. H. FOLMSBEE, *Secretary-Treasurer*
C. W. BELL } *Managers*
C. R. DIECKMAN
L. D. GRABOSKI
H. F. HATFIELD
T. E. JACKSON
W. G. MCLEAN
D. D. SCHULTZ
H. C. SCHWEIKART
W. E. ANDERSON } *Assistant Managers*
J. W. BLISS
K. W. BLOOM
E. A. GORNEY
S. I. HAMMOND
THOMAS MULLEN
L. E. MYLTING
R. L. RANSOM

ATLANTA

Organized: 1913
Territory: Radius of sixty miles from Atlanta, Ga.
Place of Meeting: Atlanta Athletic Club
Luncheon meeting every Monday at 12:30 p.m. at Atlanta Athletic Club
Number of Members: 108

EXECUTIVE COMMITTEE

P. R. YOPP, *Chairman*
W. J. MCALPIN, *Vice-Chairman*
J. W. PARKER, JR., *Secretary-Treasurer*
R. N. BENJAMIN
J. A. DODD
CHARLES DOUGHTIE
A. C. KEISER, JR.
R. S. KING
W. C. KIRBY
JOHN RITTELMEYER

BALTIMORE

Organized: 1916
Territory: Radius of thirty miles from Baltimore, Md.
Place of Meeting: Engineers Club of Baltimore
Number of Members: 291

EXECUTIVE COMMITTEE

A. M. GOMPF, *Chairman*
J. M. MOUSSON, *Vice-Chairman*
L. E. CARTER, *Secretary-Treasurer*
S. E. BRILLHART
W. P. HILL
R. C. HINE
E. W. HORLEBEIN
J. H. POTTER
A. H. SENNER
S. B. SEXTON

BIRMINGHAM

Organized: 1915
Territory: Radius of sixty miles from Birmingham, Ala.
Place of Meeting: Tutwiler Hotel
Number of Members: 94

EXECUTIVE COMMITTEE

H. G. MOUAT, *Chairman*
J. E. HANNUM, *Vice-Chairman*
J. G. REID, *Secretary-Treasurer*
A. H. BLAIR
T. M. FRANCIS

BOSTON

Organized: 1909
Territory: Radius of thirty miles from Boston, Mass.
Place of Meeting: Mass. Inst. of Technology
Local Organization: Engineering Societies of New England
Number of Members: 694

BOSTON

(Continued)

EXECUTIVE COMMITTEE

G. A. ORROK, JR., *Chairman*
S. S. PERRY, *Vice-Chairman*
A. J. FERRETTI, *Secretary-Treasurer*
H. M. KING
J. A. POWELL
WILLIAM SAUNIER

BRIDGEPORT

Organized: 1917, as a Branch of Connecticut Section; reorganized as a Section, 1923
Territory: Fairfield County, Conn.
Place of Meeting: Stratfield Hotel
Local Organizations: The Bridgeport Tool Engineers Association; The Bridgeport Engineers Club
Number of Members: 184

EXECUTIVE COMMITTEE

P. A. IBOLD, *Chairman*
E. R. SPAULDING, *Vice-Chairman*
A. W. HAGAN, *Secretary-Treasurer*
RUDOLF BECK
C. N. HOAGLAND
J. D. SKINNER

BUFFALO

Organized: 1915
Territory: Radius of thirty miles from Buffalo, N.Y.
Place of Meeting: Markeen Hotel, 1391 Main St.
Local Organization: Engineering Society of Buffalo
Number of Members: 316

EXECUTIVE COMMITTEE

C. A. ROSS, *Chairman*
L. R. BURMESTER, *Vice-Chairman*
H. P. FULLERTON, *Secretary*
C. E. HARRINGTON, *Treasurer*
N. C. BARNARD
W. M. KAUFFMANN
C. G. KIPLINGER
W. A. MILLER
N. S. SNYDER
J. L. YATES

CENTRAL ILLINOIS

Organized: 1937
Territory: All the territory in Central Illinois between the following counties on the northern boundary: Bureau, LaSalle, Knox, Stark, Putnam, Marshall, Livingston, Peoria; counties on the southern boundary: Pike, Scott, Morgan, Sangamon, Macon, Piatt, Douglas, and Edgar
Place of Meeting: Hotel Pere Marquette or Caterpillar Show Room
Number of Members: 116

EXECUTIVE COMMITTEE

W. W. BABCOCK, *Chairman*
W. N. ESPY, L. P. WEINER } *Vice-Chairmen*
R. E. MCCLAIN, *Secretary-Treasurer*
U. L. DEFFENBAUGH, *Assistant Secretary-Treasurer*
B. L. BAILIE

CENTRAL INDIANA

Organized: 1916
Territory: Radius of eighty miles from Indianapolis, within Indiana
Place of Meeting: Indianapolis Athletic Club
Local Organization: Indiana Engineering Society
Number of Members: 169

EXECUTIVE COMMITTEE

R. B. BASS, *Chairman*
M. E. BECHTOLD, *Vice-Chairman*
D. P. MORSE, *Secretary-Treasurer*
H. A. BOLZ
G. A. HAWKINS
R. B. HOLMES
FERDINAND JEHLE
W. C. WISCHMEYER

CENTRAL PENNSYLVANIA

Organized: 1921
Territory: Radius of approximately sixty miles from State College, Pa.
Place of Meeting: State College and Altoona, Pa.
Number of Members: 74

EXECUTIVE COMMITTEE

R. Y. SIGWORTH, *Chairman*
H. A. SORENSEN, *Secretary-Treasurer*
J. S. DOOLITTLE
R. L. HULSIZER
F. T. MAVIS
F. C. STEWART
H. C. THUERK

CHICAGO

Organized: 1913
Territory: Radius of fifty miles from Chicago, Ill.
Headquarters: Mid-West A.S.M.E. Office, Room 1617, 205 West Wacker Drive, Chicago, Ill.
Place of Meeting: Civic Opera Bldg., 20 N. Wacker Dr.
Meetings: Tuesday, 7:30 p.m.
Local Organization: Western Society of Engineers
Number of Members: 918

EXECUTIVE COMMITTEE

J. P. MAGOS, *Chairman*
H. M. BLACK, F. H. LANE, J. C. MARSHALL, P. A. STEPHENSON, J. I. YELLOTT } *Vice-Chairmen*
F. B. ORR, *Secretary-Treasurer*
C. G. ANDERSON
C. C. AUSTIN
R. H. BACON
C. B. COLE
F. D. COTTERMAN
L. M. ELLISON
B. H. JENNINGS
A. H. JENS
L. M. JOHNSON
J. S. KOZACKA
W. T. MCCULLOUGH, JR.
T. S. MCEWAN
J. R. MICHEL
H. L. NACHMAN
W. H. OLDACRE
C. W. PARSONS
H. S. PHILBRICK
RALPH SARGENT
R. E. TURNER
C. L. WACHS

CINCINNATI

Organized: 1912
Territory: Radius of thirty miles from Cincinnati, Ohio
Place of Meeting: Engineers' Club Rooms, Ninth & Race Sts.
Local Organization: Engineers' Club of Cincinnati
Number of Members: 232

EXECUTIVE COMMITTEE

HANS ERNST, *Chairman*
J. G. MARTIN, *Vice-Chairman*
H. L. HAWORTH, *Secretary-Treasurer*
W. S. BOYNTON
O. E. HILMER
P. K. JOHNSTON
E. M. MARTELLOTTI
D. W. NEARING
E. W. REESE
B. J. YEAGER

CLEVELAND

Organized: 1918
Territory: Counties of Lorain, Cuyahoga, Lake, Geauga, and Ashtabula in Ohio
Place of Meeting: Cleveland Engineering Society Club
Local Organization: Cleveland Engineering Society
Number of Members: 328

EXECUTIVE COMMITTEE

L. C. COLE, *Chairman*
H. M. HAMMOND, *Vice-Chairman*
E. R. MCCARTHY, *Secretary-Treasurer*
G. E. KENTIS
M. E. LANGE
H. L. SPENCE
W. G. STEPHAN
W. C. SUTTON
F. H. VOSE

COLORADO

Organized: 1919
Territory: Entire State of Colorado
Place of Meeting: Albany Hotel, Denver, Colo.
Local Organization: Colorado Engineering Council (Colorado Society of Engineers)
Number of Members: 94

EXECUTIVE COMMITTEE

H. L. HARTBURG, *Chairman*
G. H. WOELBING, *Vice-Chairman*
D. R. COLLINS, *Secretary-Treasurer*
F. A. LOCKWOOD
N. A. PARKER
R. F. THRONE
DURBIN VAN LAW

COLUMBUS

Organized: 1920
Territory: Counties of Union, Delaware, Licking, Madison, Franklin, Fayette, Pickaway, and Ross in Ohio
Place of Meeting: Battelle Memorial Institute and The Ohio State University
Number of Members: 89

EXECUTIVE COMMITTEE

S. M. MARCO, *Chairman*
W. L. DAVIS, *Vice-Chairman*

COLUMBUS
(Continued)

E. J. LINDAHL, *Secretary-Treasurer*
H. M. BLANK
R. B. ENGDAHL
C. Z. GILLIVAN
G. E. HANEY

DAYTON

Organized: 1926
Territory: Counties of Drake, Miami, Champaign, Preble, Montgomery, Greene, and northern part of Butler and Warren in Ohio
Place of Meeting: Engineers' Club of Dayton
Local Organization: Engineers' Club of Dayton
Number of Members: 143

EXECUTIVE COMMITTEE

E. M. KELLY, *Chairman*
B. F. DOWNEY, *Vice-Chairman*
BURSON TREADWELL, *Secretary*
A. W. KIMMEL, *Treasurer*
C. W. BALL
L. R. BRIDGE
J. J. HEALY
A. L. PASCHALL
H. C. WIGHT

DETROIT

Organized: 1916
Territory: Radius of thirty miles from Detroit, Mich.
Place of Meeting: Place varies
Local Organization: Engineering Society of Detroit
Number of Members: 502

EXECUTIVE COMMITTEE

C. R. ALDEN, *Chairman*
P. W. LEHMAN, *Secretary-Treasurer*
J. W. ARMOUR, *Past-Chairman*
R. F. HANSON
L. W. LENTZ
A. C. PASINI
R. CLAY PORTER
G. J. SCRANTON
J. H. SPURGEON
J. J. UICKER
H. L. WALTON
HERBERT WELLS

EAST TENNESSEE

Organized: 1922
Territory: All counties in Tennessee east of the west boundary of Scott, Morgan, Cumberland, White, Warren, Coffee, Moore, Franklin; Belle County in Kentucky; and Rossville, Dade, Walker, Cattasa, Whitfield, Murray, Gordon, Chattooga in Georgia
Place of Meeting: Places varies
Local Organization: Chattanooga Engineers Club and Knoxville Technical Club
Luncheon Meeting every Monday noon at Chattanooga Engineers Club
Number of Members: 119

EXECUTIVE COMMITTEE

L. A. SHIPMAN, *Chairman*
G. E. CAMPBELL, W. C. ELLIS, F. H. THOMAS } *Vice-Chairmen*
J. MACK TUCKER, *Secretary-Treasurer*
F. F. DEAN
VINCENT MATTHEWS
G. E. MORGAN
G. L. MORRIS

ERIE

Organized: 1917
Territory: Radius of thirty miles from Erie, Pa.
Place of Meeting: Erie County Court House
Number of Members: 99

EXECUTIVE COMMITTEE

E. C. IMS, *Chairman*
G. H. KAEMMERLING, *Vice-Chairman*
F. B. SCHNEIDER, *Secretary-Treasurer*
G. H. BACH
F. G. BRINIG
H. E. GOETZ
C. I. RAINESALO
MCDONALD S. REED
H. B. JOYCE, *Ex-Officio*

FLORIDA

Organized: 1925
Territory: State of Florida
Place of Meeting: Various cities in state
Local Organization: Florida Engineering Society, Gainesville, Fla.
Number of Members: 97

EXECUTIVE COMMITTEE

T. H. GARDNER, *Chairman*
JOHN HUNTER, *1st Vice-Chairman*
CHARLES BEENSEN, *2nd Vice-Chairman*
R. A. THOMPSON, *Secretary-Treasurer*
R. Y. POOL
S. L. STEWART
F. W. FINEREN, *Student-Chairman*

FORT WAYNE

Organized: 1939
Territory: Counties of LaGrange, Steuben, Noble, DeKalb, Whitley, Allen, Wabash, Huntington, Wells, Adams, Miami, Blackford and Jay in Indiana; Counties of Williams, Defiance, Paulding, Van Wert and Mercer in Ohio
Local Organization: Fort Wayne Engineers' Society
Number of Members: 46

EXECUTIVE COMMITTEE

K. K. COOPER, *Chairman*
EVERETT S. BUCK, *Vice-Chairman*
I. A. PLANCK, *Secretary*
F. C. MASON, *Treasurer*
W. H. CONNOR
F. L. RUOFF

GREEN MOUNTAIN

Organized: 1923
Territory: Entire State of Vermont and neighboring and closely related communities of Claremont and Hanover, N.H.
Place of Meeting: Springfield, Windsor, Vt., and Claremont, N.H.
Local Organization: Vermont Engineering Society
Number of Members: 51

EXECUTIVE COMMITTEE

C. H. ADAMS, *Chairman*
F. T. GEAR, *Vice-Chairman*
F. A. JOHNSON, *Secretary-Treasurer*
E. D. CLARK
H. L. DAASCH
D. T. HAMILTON
J. B. JOHNSON

GREENVILLE

Organized: As a Branch, 1923; as a Section, 1927
Territory: Radius of sixty miles from Greenville, S.C.
Place of Meeting: Meetings held at Greenville, Clemson College, S.C., Canton, Asheville, and Enka, N.C.
Number of Members: 45

EXECUTIVE COMMITTEE

W. PAUL TINDALL, *Chairman*
B. E. FERNOW, *Vice-Chairman*
J. W. VAUGHAN, JR., *Secretary-Treasurer*
R. B. FULLER
J. R. GILL
W. E. MCDOWELL
A. KEITH POOSER
E. M. WILLIAMS

HARTFORD

Organized: 1917, as Branch of Conn. Section; reorganized, 1923; New Britain Section merged with Hartford Section, July 1, 1940
Territory: Hartford County except that portion served by New Britain Section
Place of Meeting: Hartford Electric Light Company
Number of Members: 200

EXECUTIVE COMMITTEE

L. C. SMITH, *Chairman*
E. R. LEWIS, JR., HENRY MICHELSEN } *Vice-Chairmen*
R. D. KELLER, *Secretary-Treasurer*
J. S. APPLEYARD
HERBERT BURDICK
H. F. CASSIDY
F. O. HOAGLAND
W. S. PAINE
H. F. RAMM
H. P. SMITH
G. E. STANWAY
C. C. STEVENS
S. J. TELLER
J. C. WALTERS
R. L. WEIL

INLAND EMPIRE

Organized: 1921
Territory: East of Columbia River in State of Washington, and Counties of Okanogan and Benton, and part of Northern Idaho
Place of Meeting: Davenport Hotel, Spokane
Luncheons: Wednesdays at 12:00 noon, Davenport Hotel, Spokane
Local Organization: Associated Engineers of Spokane
Number of Members: 22

EXECUTIVE COMMITTEE

F. W. CANDEE, *Chairman*
J. G. MCGIVERN, *Vice-Chairman*
N. W. HUMPHREY, *Secretary-Treasurer*
ALEXANDER LINDSAY
E. B. PARKER
L. J. POSPISIL

ITHACA

Organized: 1936
Territory: Radius of thirty miles from Ithaca plus following cities: Binghamton, Corning, Endicott, Geneva, Painted Post
Place of Meeting: Alternately in different cities of Section territory, as announced
Number of Members: 83

Executive Committee

C. Lyman Wilder, *Chairman*
S. S. Garrett, *Vice-Chairman*
F. S. Erdman, *Secretary-Treasurer*
D. S. Kimball
W. M. Sawdon
M. P. Whitney
N. R. Wickersham

KANSAS CITY

Organized: 1921
Territory: Radius of sixty miles from Kansas City, Mo.
Place of Meeting: University Club
Local Organization: Engineers' Club of Kansas City
Number of Members: 159

Executive Committee

F. R. Applegate, *Chairman*
L. T. Mart, *Vice-Chairman*
H. E. Manuel, *Secretary*
R. P. Hahn, *Treasurer*
E. E. Ambrosius
G. C. Boyer
C. B. Briggs, Jr.
Chester Cotter
C. C. Holt
M. A. Durland, *Ex-Officio*

LOUISVILLE

Organized: 1922
Territory: Radius of thirty miles from Louisville, Ky. (includes Lexington, Ky.)
Place of Meeting: University of Louisville, Louisville, Ky.
Local Organization: Engineers and Architects Club
Number of Members: 68

Executive Committee

H. V. Heuser, *Chairman*
J. K. Meyer, *Vice-Chairman*
F. P. Shannon, *Secretary*
O. C. Krause, Jr., *Treasurer*
C. D. Eldridge
W. F. Lucas
H. C. Murphy
F. L. Wilkinson, Jr.

MEMPHIS

Organized: 1923
Territory: Radius of sixty miles from Memphis, Tenn., and eastern half of Arkansas including all the territory east of a line drawn north and south through the western boundary of the city of Little Rock
Number of Members: 25

Executive Committee

W. H. Roberts, *Acting Chairman*
H. S. Livingston, *Secretary-Treasurer*
W. S. Carell
R. M. King
D. S. Pattershall

METROPOLITAN

Organized: 1910
Territory: Metropolitan District, New York and New Jersey
Place of Meeting: Engineering Societies Building, 29 West 39th Street, New York, N.Y.
Number of Members: 3,446

Executive Committee

H. C. R. Carlson, *Chairman*
A. Ehbrecht, *Secretary*
E. V. David, *Treasurer*
W. L. Betts
R. W. Flynn
G. E. Hagemann
H. E. Martin
G. J. Nicastro
P. T. Onderdonk
J. H. Sengstaken

Junior Group

P. B. Petty, *Chairman*
W. Wiitanen, *Vice-Chairman*
J. J. Jacobs, *Secretary*
Franklin H. Fowler, Jr.
F. M. Gibson, Jr.
John Pollak
Irving P. West

MID-CONTINENT

Organized: 1919
Territory: Entire State of Oklahoma; territory in Arkansas not included in Memphis Section; part of Louisiana; and territory in Texas north of the southern boundaries of the counties of Gaines, Dawson, Bordon, Scurry, Fisher, Jones, and Shackelford
Place of Meeting: Usually Mayo Hotel, Tulsa, Okla.
Luncheon Meetings with Engineers Club of Tulsa, Mondays at 12:00 noon
Local Organization: Engineers Club of Tulsa
Number of Members: 153

Executive Committee

D. A. Cant, *Chairman*
R. A. Colgin, C. H. Stevens } *Vice-Chairmen*
J. H. Keyes, *Secretary*
Nathan Janco, *Treasurer*
R. G. Ayers
D. O. Barrett
W. L. Ducker, Jr.
C. O. Glasgow
R. F. Hurt
D. K. Hutchcraft
A. J. Kerr
H. T. Sears
W. S. Sherman

MILWAUKEE

Organized: 1904
Territory: Radius of fifty miles from Milwaukee, Wis.
Place of Meeting: Wisconsin Club
Local Organization: Engineers' Society of Milwaukee
Luncheon Meetings once each month, 3rd Wednesday at Wisconsin Club
Number of Members: 287

Executive Committee

J. E. Schoen, *Chairman*
T. A. Wetzel, *Secretary-Treasurer*
R. J. Cramer
P. J. Imse
Edward Jacobi
C. S. Lincoln
W. C. Lindemann
Max E. Ruess
Russell J. Smith
W. J. Thuerman
E. J. Wellauer

Junior Group

Max E. Ruess, *Chairman*
Sebastian Judd, *Secretary*
Joseph J. Drinka
Arnold Ehlinger
Harry Gute

MINNESOTA

Organized: Minneapolis, 1913; St. Paul, 1913; the two Sections merged, 1934
Territory: Entire State of Minnesota
Place of Meeting: Minnesota Union, Univ. of Minnesota
Local Organization: Minneapolis Engineers' Club, Minnesota Federation of Architectural and Engineering Societies
Number of Members: 112

Executive Committee

W. H. Erskine, *Chairman*
R. W. Jones, Jr., *Vice-Chairman*
L. S. Whitson, *Secretary-Treasurer*
Charles Foster
F. L. Smith
L. C. Sprague
M. S. Wunderlich

NEBRASKA

Organized: 1922
Territory: State of Nebraska, and Council Bluffs, Iowa
Place of Meeting: Lincoln and Omaha
Local Organization: Engineers' Clubs of Lincoln and Omaha
Luncheon Meeting every Wednesday noon at the Omaha Engineers' Club—4th Monday Evening at Lincoln
Number of Members: 39

Executive Committee

C. F. Moulton, *Chairman*
W. L. DeBaufre, *Vice-Chairman*
A. A. Luebs, *Secretary-Treasurer*
J. W. Kurtz
G. A. Rogers
W. F. Weiland

NEW HAVEN

Organized: 1912, reorganized, 1923
Territory: Portions of New Haven and Middlesex Counties, Conn.
Place of Meeting: Mason Laboratory, Yale University
Number of Member: 99

Executive Committee

C. W. Phelps, *Chairman*
G. H. Eaton, *Vice-Chairman*
F. W. Preston, *Secretary-Treasurer*
A. F. Breitenstein
E. E. Caspell
A. S. Redway
A. D. Wilcox

NEW LONDON

Organized: 1930, as the Norwich Section; name changed, 1943
Territory: Counties of Tolland, Windham, and New London in Connecticut, and Westerly District in Rhode Island
Place of Meeting: New London Junior College, Pequot Ave., New London, Conn.
Number of Members: 54

Executive Committee

J. S. Leonard, *Chairman*
W. A. Hardy, *Secretary-Treasurer*
F. S. English
C. A. Gongwer
K. P. Hanson
W. H. Himes
Robert Wosak

NEW ORLEANS

Organized: 1916
Territory: All of Louisiana except the northern part allotted to Mid-Continent Section
Place of Meeting: Room 422, St. Charles Hotel
Local Organization: Louisiana Engineering Society
Number of Members: 135

Executive Committee

L. J. Cucullu, *Chairman*
A. M. Hill, *Vice-Chairman*
E. A. McLellan, *Secretary-Treasurer*
M. C. Abrahm
E. L. Cowan
D. H. McCuaig
R. F. Mendow
William Whipple

NORTH TEXAS

Organized: 1922
Territory: All of Texas north of an approximately straight line through Del Rio, Fredericksburg, Georgetown, Cameron, Nacogdoches, and center, including the cities mentioned, and south of north boundaries of the counties of Parmer, Castro, Swisher, Briscoe, Hall, and Childress. Also the City of Texarkana, Ark.
Place of Meeting: Dallas Power & Light Co. Bldg. Auditorium
Local Organization: Technical Club of Dallas
Number of Members: 121

Executive Committee

J. A. Noyes, *Chairman*
P. M. Cordell, H. F. Godeke } *Vice-Chairmen*
J. A. Lee, *Secretary-Treasurer*
Stanley Patterson
H. M. Robinson
H. W. Trump
E. J. Wacker

ONTARIO

Organized: 1917
Territory: Province of Ontario, Canada
Place of Meeting: Hart House, University of Toronto
Number of Members: 171

Executive Committee

H. G. Hill, *Chairman*
W. H. Hewitt, *Secretary-Treasurer*
E. A. Allcut
H. H. Angus
S. G. Clarke
J. G. Hall
Ernest Jones
K. D. Leitch
A. A. Moline
A. L. Scott
W. D. Sheldon, Jr.
A. D. Smith
Fred'k Truman
R. C. Wiren

OREGON

Organized: 1919
Territory: State of Oregon and that territory in Washington within a radius of thirty miles from Portland, Ore.
Place of Meeting: Usually Public Service Bldg., Portland, Ore.
Local Organization: Oregon Society of Engineers
Number of Members: 59

Executive Committee

E. P. Weiser, *Chairman*
M. M. Clayton, *Vice-Chairman*
A. J. Chaput, *Secretary*
E. D. Rowan, *Treasurer*
L. T. Hays
A. D. Hughes
J. C. Othus
Ivan Saunders

PENINSULA

Organized: 1923
Territory: West of the east boundaries of the following counties: Emmet, Charlevoix, Antrim, Kalkaska, Missaukee, Clare, Isabell, Gratiot, Clinton, Eaton, Calhoun, and Branch, Mich.
Place of Meeting: Grand Rapids, Mich.
Luncheon Meeting last Thursday noon each month
Local Organization: Engineers' Club of Grand Rapids
Number of Members: 60

Executive Committee

J. M. Gorrie, *Chairman*
Donald McSorley, *1st Vice-Chairman*
Kenneth E. Crowser, *2nd Vice-Chairman*
C. J. Kuenzel, *Secretary-Treasurer*
C. P. Buck
J. R. de Hamer
G. E. Gebben
C. G. Lohmann
C. A. Hamilton, *Ex-Officio*

PHILADELPHIA

Organized: 1912
Territory: Counties of Bucks, Montgomery, Chester, Philadelphia, Delaware, Pa., and the State of Delaware
Place of Meeting: Philadelphia Engineers' Club, 1317 Spruce Street, Philadelphia, Pa.
Local Organization: Philadelphia Engineers' Club
Luncheon Meeting every Thursday noon at 12:30 p.m. at Philadelphia Engineers' Club
Number of Members: 1,069

Executive Committee

L. N. Gulick, *Chairman*
F. W. Miller, *Vice-Chairman*
J. J. McCarthy, *Secretary-Treasurer*
C. S. Gotwals
A. G. Kisner
S. T. Mackenzie

Junior Group

F. P. Gooch, *Chairman*
Frank Ptacek, *Vice-Chairman*
H. J. Clyman, *Secretary*
T. J. Putz, *Treasurer*
M. E. Harvey
Harvey Schock, Jr.
Walter Sinton
R. W. Worley

PIEDMONT—NORTH CAROLINA

Organized: As a Branch, 1923; as a Section 1927; name changed from Charlotte Section to Piedmont—North Carolina, July 1, 1940
Territory: Radius of seventy-five miles from Charlotte, N.C.
Luncheon Meeting every other Monday at 1:00 p.m. at Efirds Department Store Dining Room
Local Organization: Charlotte Engineers Club
Number of Members: 47

Executive Committee

David Nabow, *Chairman*
B. L. Cotten, *Acting Vice-Chairman*
N. H. Brown, *Secretary-Treasurer*
E. L. Davis
Richard Ferguson
T. C. Heyward
I. W. Leggett
A. B. LeClerc, *Ex-Officio*

PITTSBURGH

Organized: 1920
Territory: Counties bounded by and including Beaver, Butler, Venango, Forest, Jefferson, Indiana, Somerset, Fayette, Greene, and Washington, Pa.
Place of Meeting: Engineers' Society of Western Pennsylvania, William Penn Hotel
Local Organization: Engineers' Society of Western Pennsylvania
Number of Members: 510

Executive Committee

L. E. F. Wahrenburg, *Chairman*
L. E. Hankinson, *Vice-Chairman*
E. W. Jacobson, *Secretary*
K. F. Treschow, *Treasurer*
R. B. Ambrose
R. L. Ehmann
T. G. Estep
J. C. Hoar
G. Sinding-Larsen

PLAINFIELD

Organized: 1921
Territory: Plainfield and territory included between Elizabeth, Bound Brook, Metuchen, and Watchung, N.J.
Place of Meeting: Elizabeth Carteret Hotel, Elizabeth, and Plainfield Masonic Temple, Plainfield
Local Organization: Plainfield Engineers Club, Singer Engineering Society
Number of Members: 199

PLAINFIELD
(Continued)

EXECUTIVE COMMITTEE

W. H. CHAFFEE, *Chairman*
E. T. BALL, *Vice-Chairman*
R. H. CHANKALIAN, *Secretary*
J. D. POTTER, *Treasurer*
G. E. LEAVITT, JR., *Past-Chairman*

PROVIDENCE

Organized: 1920
Territory: Radius of thirty miles from Providence, R.I.
Place of Meeting: Providence Engineering Society Building, 195 Angell St., Providence, R.I.
Local Organization: Providence Engineering Society
Number of Members: 168

EXECUTIVE COMMITTEE

R. M. SCOTT, *Chairman*
G. W. KELSEY, *Vice-Chairman*
E. W. HARRINGTON, *Secretary-Treasurer*
J. B. COLEMAN
W. M. DAVIES
HASBROUCK HAYNES
P. J. HOLTON
ALFRED H. MACGILLIVRAY
A. W. MEYER
P. V. MILLER
J. D. ROBERTSON, *Ex-Officio*

RALEIGH

Organized: As a Branch, 1923; as a Section, 1927
Territory: Radius of sixty miles from Raleigh, N.C.
Places of Meeting: North Carolina State College, Raleigh, N.C.; Duke University, Durham, N.C.
Local Organizations: North Carolina Society of Engineers, Raleigh Engineers Club
Number of Members: 37

EXECUTIVE COMMITTEE

F. J. REED, *Chairman*
G. W. BAITY, *Vice-Chairman*
F. C. BRAGG, *Secretary-Treasurer*
C. E. KERCHNER
R. B. RICE
F. B. TURNER
R. S. WILBUR

ROCHESTER

Organized: 1919
Territory: Radius of thirty miles from Rochester, N.Y.
Place of Meeting: Rochester Engineering Society Rooms, Sagamore Hotel
Local Organization: Rochester Engineering Society, Sagamore Hotel
Luncheon Meeting every Tuesday at 12:15 p.m. at Sagamore Hotel
Number of Members: 116

EXECUTIVE COMMITTEE

A. W. SCHUSTER, *Chairman*
S. C. STACY, *Vice-Chairman*
A. E. SCHELL, *Secretary-Treasurer*
M. L. BAXTER
W. J. BROWN
C. A. ELWOOD
H. L. MASON.
C. B. MCCATHRON

ROCK RIVER VALLEY

Organized: 1926
Territory: Thirty miles east and west of Madison, Wis., and extending southward through Rockford, Ill.
Meeting Places: Madison, Wis., Beloit, Wis., and Rockford, Ill.
Local Organization: Rock River Valley Engineering Council
Number of Members: 50

EXECUTIVE COMMITTEE

K. H. CASSON, *Chairman*
W. C. FISCHER, *Vice-Chairman*
T. G. LAUGHNAN, *Secretary-Treasurer*
BEN G. ELLIOTT
D. W. NELSON
JERVIS SWANNACK

ST. JOSEPH VALLEY

Organized: 1929
Territory: Counties of La Porte, Starke, Pulaski, St. Joseph, Marshall, Fulton, Elkhart, and Kosciusko in Indiana, and Cass and Berrien Counties in Michigan
Place of Meeting: South Bend, Ind.
Number of Members: 60

EXECUTIVE COMMITTEE

E. T. COBB, *Chairman*
O. E. E. ZAHN, *Secretary-Treasurer*
C. ROBERT EGRY
R. C. FITCH
ALLEN LOOMIS
G. R. MCNEILE
W. D. A. PEASLEE
L. E. WADDINGTON

ST. LOUIS

Organized: 1909
Territory: Radius of thirty miles from St. Louis, Mo.
Place of Meeting: Place varies
Local Organization: Engineers' Club of St. Louis
Number of Members: 225

EXECUTIVE COMMITTEE

R. M. BOYLES, *Chairman*
HERBERT KUENZEL, *Vice-Chairman*
H. E. FRECH, JR., *Secretary-Treasurer*
R. W. MERKLE
R. C. THUMSER
H. B. WELGE

SAN FRANCISCO

Organized: 1910
Territory: All territory north of the northern boundaries of the counties of San Luis Obispo, Kern, and San Bernardino
Place of Meeting: Engineers' Club, 206 Sansome St.
Luncheon Meetings, Tuesdays, California Hotel, Oakland; Thursdays, Engineers' Club, San Francisco
Local Organization: San Francisco Engineers' Club
Number of Members: 472

EXECUTIVE COMMITTEE

W. H. KASSEBOHM, *Chairman*
ALF HANSEN, *Vice-Chairman*
J. ALLAN CAMPBELL, *Secretary-Treasurer*
E. G. GOTHBERG
R. B. PLASS
MORRIS TAYLOR
GEO. N. SOMERVILLE, *Ex-Officio*

JUNIOR GROUP

TEMPLE VOORHEIS, *Chairman*
EDWARD E. POLOMIK, *Seminar Chairman*
M. P. WHITFIELD, *Secretary-Treasurer*

SAVANNAH

Organized: 1923
Territory: Radius of 125 miles from Savannah in Georgia
Place of Meeting: Savannah Hotel
Local Organization: Engineers' Council of Savannah Chamber of Commerce
Number of Members: 23

EXECUTIVE COMMITTEE

W. L. MINGLEDORFF, JR., *Chairman*
A. M. ORMOND, *Vice-Chairman*
B. J. SAMS, *Secretary-Treasurer*

SCHENECTADY

Organized: As a Branch, 1919; as a Section, 1927
Territory: Radius of thirty miles from Schenectady, N.Y.
Place of Meeting: Rice Hall
Number of Members: 276

EXECUTIVE COMMITTEE

L. A. GOBE, *Chairman*
D. C. BRECHT, F. R. FOWLER, E. L. THEARLE } *Vice-Chairmen*
J. B. NOLAN, *Secretary*
J. E. RYAN, *Treasurer*
H. E. BRUNELLE
D. R. EDWARDS
A. O. WHITE

SOUTHERN CALIFORNIA

Organized: 1915 as Los Angeles Section; reorganized 1941
Territory: South of southern boundaries of following counties: Monterey, Kings, Tulares, and Inyo, Calif.
Place of Meeting: Barker Bros. Store
Local Organization: Technical Societies of Los Angeles
Luncheon Meetings Thursdays at 12:00 noon at Engineers' Club
Number of Members: 620

EXECUTIVE COMMITTEE

R. G. ROSHONG, *Chairman*
D. K. COYLE, *Vice-Chairman*
B. N. PALM, *Secretary-Treasurer*
JAMES BEAN
J. CALVIN BROWN
M. L. CRATER
C. W. HUFFMAN
W. H. SHALLENBERG
EDWARD TIMBS
LLOYD YOST

JUNIOR GROUP

W. K. BOTTICHER, *Chairman*
F. R. ADLER, *Secretary*
WILBUR REASER

SOUTH TEXAS

Organized: 1919
Territory: South Texas and the northern part of the State not included in the North Texas Section territory
Place of Meeting: No fixed meeting place, but all meetings held in Houston
Number of Members: 179

SOUTH TEXAS
(Continued)

EXECUTIVE COMMITTEE

H. E. DEGLER, *Chairman*
W. T. ALLIGER, *Vice-Chairman*
J. B. T. DOWNS, *Secretary-Treasurer*
D. D. ALTON
JOHN DOGGETT, JR.
V. M. FAIRES
B. W. FARQUHAR
H. G. HIEBELER
M. H. KOTZEBUE
H. F. MOLLER
RALPH NEUHAUS
C. L. ORR
F. D. RAHM

SUSQUEHANNA

Organized: 1927
Territory: Counties of Cumberland, Dauphine, Lebanon, Adams, York, and Lancaster
Place of Meeting: Engineering Society of York, and at Lancaster twice a year
Local Organization: Engineering Society of York and Engineers' Society of Pennsylvania, Harrisburg, Pa.
Number of Members: 87

EXECUTIVE COMMITTEE

JACOB FISCH, *Chairman*
M. GERALD LEESON, *Vice-Chairman*
T. K. BREDA, *Secretary-Treasurer*
JOSEPH A. GALAZZI
E. W. GALLENHAMP
M. F. GANNETT
M. M. JONES
E. L. ROGERS

SYRACUSE

Organized: 1920
Territory: Radius of thirty miles from Syracuse, N.Y.
Place of meeting: Ball Room of the Onondaga Hotel
Local Organization: The Technology Club of Syracuse
Number of Members: 79

EXECUTIVE COMMITTEE

G. I. VINCENT, *Chairman*
J. A. KING, *Vice-Chairman*
L. EDWARD POTTER, *Secretary*
H. T. AVERY
C. F. DIETZ
W. E. HOPTON
J. W. LINFORD
M. B. MOYER
E. K. RHODES
D. V. SHETLAND
M. F. WILLIAMS

TOLEDO

Organized: 1920
Territory: Radius of thirty miles from Toledo, Ohio
Place of Meeting: University Club, Toledo, Ohio
Local Organization: Affiliated Technical Societies of Toledo
Number of Members: 58

EXECUTIVE COMMITTEE

R. J. MUGFOR, *Chairman*
SYDNEY BEVIN, *Vice-Chairman*
W. A. NELDEN, *Secretary-Treasurer*
RALPH FLOREK
T. L. HALLENBECK
R. F. HILL
B. H. KEYSEELING
H. O. KRANICH
R. C. LANGENDERFER
W. R. MORAN
D. M. PALMER
W. C. SCHROEDER
H. H. VOGEL
ERNEST W. WEAVER

TRI-CITIES

Organized: 1920
Territory: Radius of thirty miles from Moline, Ill.
Place of Meeting: Rock Island, Ill., Moline, Ill., and Davenport, Iowa.
Luncheon Meeting every Wednesday, Davenport Hotel, 12:00 noon
Number of Members: 83

EXECUTIVE COMMITTEE

K. R. HODGES, *Chairman*
P. E. ANDERSON, *Vice-Chairman*
C. A. CARLSON, *Secretary-Treasurer*
R. M. BARNES
R. A. CROSS
J. M. HARTMAN

UTAH

Organized: 1923
Territory: State of Utah
Place of Meeting: University Club, Salt Lake City
Local Organization: Utah Society of Professional Engineers
Number of Members: 42

EXECUTIVE COMMITTEE

H. L. ZETTERMAN, *Chairman*
R. D. BAKER, *Vice-Chairman*
R. E. KUNKEL, *Secretary-Treasurer*
G. W. CARTER
M. B. HOGAN
E. C. POLLARD

VIRGINIA

Organized: 1919
Territory: State of Virginia
Place of Meeting: Richmond, Norfolk, Blacksburg, Charlottesville, Roanoke, University, Petersburg
Local Organization: Central Virginia Engineers Club of Hampton Roads
Number of Members: 188

EXECUTIVE COMMITTEE

J. B. JONES, *Chairman*
D. A. ROGERS, *Vice-Chairman*
A. E. BOCK, *Secretary*
W. J. BARBER, *Treasurer*
G. T. ABERNATHY
E. W. BOWEN
O. N. HALL
G. E. HOPPE, JR.
EDWARD PRINGLE
ARTHUR ROBERTS, JR.

WASHINGTON, D.C.

Organized: 1919
Territory: District of Columbia
Place of Meeting: Auditorium, Potomac Electric Power Co., 10th & E Sts., Washington, D.C.
Number of Members: 481

EXECUTIVE COMMITTEE

C. E. MILLER, *Chairman*
M. A. MASON, *Vice-Chairman*
E. J. H. LANE, *Secretary-Treasurer*
C. E. BERBERICH
B. C. CRUICKSHANKS
RUDOLPH MICHEL
J. C. PHILLIPS

WATERBURY

Organized: 1917, as a Branch; reorganized as a Section, 1923
Territory: Litchfield County and a portion of New Haven County
Place of Meeting: Elton Hotel
Number of Members: 71

EXECUTIVE COMMITTEE

J. R. HICKS, *Chairman*
C. M. WARNER, *Vice-Chairman*
A. W. MINER, *Secretary-Treasurer*
A. L. ALVES
J. H. RAUB
R. S. SPERRY
R. S. STORRS

WESTERN MASSACHUSETTS

Organized: 1922
Territory: Includes counties of Berkshire, Franklin, Hampden, and Hampshire
Place of Meeting: Highland Hotel, Springfield, Mass.
Local Organization: Engineering Society of Western Massachusetts
Number of Members: 93

EXECUTIVE COMMITTEE

R. A. PACKARD, *Chairman*
J. F. MALCOLM, *Vice-Chairman*
D. A. BARTLETT, *Secretary-Treasurer*
LEO KRESSER
F. F. LANGE
E. WADSWORTH STONE

WESTERN WASHINGTON

Organized: 1919
Territory: State of Washington west of Columbia River with exception of territory included in 30-mile radius of Portland, Ore.
Place of Meeting: Engineers' Club, Seattle, Wash.
Local Organization: Seattle Engineers' Club
Luncheon Meetings daily at noon at Engineers' Club, Seattle
Number of Members: 203

EXECUTIVE COMMITTEE

B. T. MCMINN, *Chairman*
F. E. BLUMBERG, *Vice-Chairman*
L. B. COOPER, *Secretary-Treasurer*
G. C. MARTINSON
R. E. MESSER
N. J. SCHAAL

WEST VIRGINIA

Organized: 1925
Territory: State of West Virginia, South of Parallel 39
Place of Meeting: Charleston, W.Va.
Number of Members: 56

WEST VIRGINIA
(Continued)

EXECUTIVE COMMITTEE

H. B. HICKMAN, *Chairman*
M. C. BROOKE, *Vice-Chairman*
J. L. BARKER, JR., *Secretary-Treasurer*
L. B. MCQUAIDE, *Asst. Secretary-Treasurer*
A. H. CANNON
J. G. MILLER
M. C. MUMMA
F. L. SCHAEFER
R. D. WEBB

WORCESTER

Organized: 1915
Territory: Radius of thirty miles from Worcester, Mass.
Place of Meeting: Sanford Riley Hall, Worcester Poly. Inst.
Local Organization: Worcester Engineering Society
Number of Members: 126

EXECUTIVE COMMITTEE

L. J. HOOPER, *Chairman*
G. H. MCCULLOUGH, *Vice-Chairman*
W. F. BETH, *Secretary-Treasurer*
L. R. BALL
DAVID CHIRAS
F. W. MIERKE
E. H. SMITH
F. E. STRANDBERG

YOUNGSTOWN

Organized: 1928
Territory: Counties of Trumbull, Mahoning, and Columbiana in Ohio, and Mercer and Lawrence in Pennsylvania
Place of Meeting: Republic Rubber Co. Club Rooms, Albert St., Youngstown, Ohio
Number of Members: 63

EXECUTIVE COMMITTEE

H. W. SMITH, *Chairman*
L. A. KLINE, *Vice-Chairman*
C. W. FOARD, *Secretary-Treasurer*
F. J. BOWERS
C. H. LEGLER
W. J. LONGACHER
HANS E. MELIN

STUDENT BRANCHES

ARTICLE B6A, PAR. 20: The Standing Committee on Relations With Colleges shall, under the direction of the Council, have supervision of the Student Branches of the Society and of such work of the Society as aims to further the education of engineers through the colleges and schools of accepted standing.

STANDING COMMITTEE, RELATIONS WITH COLLEGES

H. E. DEGLER, *Chairman* (1944)
G. L. SULLIVAN (1945)
R. P. REECE (1946)
H. J. BROWN (1947)
HERBERT KUENZEL (1948)

M. M. BORING, A. D. HUGHES, R. H. PORTER, J. W. ZELLER — *Advisory Members* (1944)

J. M. SEXTON, *Junior Adviser* (1944)

Communicate with Student Branch through Honorary Chairman

Name and Location	Year Authorized	No. of Members †	Chairman	Secretary	Honorary Chairman
Akron, Univ. of, Akron, Ohio	1924	21	GEORGE MARINOFF	I. E. HERTLE	F. S. GRIFFIN
Alabama Polytechnic Inst., Auburn, Ala.	1920	32	R. L. WHITE	J. G. COATS	C. R. HIXON
Alabama, Univ. of, University, Ala.	1931	21	ABRAHAM ROSENBERG	F. A. DEEP	J. M. GALLALEE
Arizona, Univ. of, Tucson, Ariz.	1937 *	..	.....	.....	.....
Arkansas, Univ. of, Fayetteville, Ark.	1910	9	ROBERT DUNCAN	H. T. HOLMES	F. J. DAASCH
British Columbia, Univ. of, Vancouver, B.C., Can.	1938	49	J. A. BURTON	R. G. CHESTNUT	W. O. RICHMOND
Brown Univ., Providence, R.I.	1923	11	RICHARD FIELD	C. N. SMITH, JR.	P. N. KISTLER
Bucknell Univ., Lewisburg, Pa.	1916	26	C. A. STRANGE	W. M. MURPHY	G. M. KUNKEL
California Inst. of Tech., Pasadena, Calif.	1914	30	J. R. KETTLER	D. B. SMITH	R. L. DAUGHERTY
California, Univ. of, Berkeley, Calif.	1912	95	AUSTIN SANDERSON	ERNEST HAJEK	E. F. MURPHY
Carnegie Inst. of Tech., Pittsburgh, Pa.	1913	22	H. R. SMITH	C. L. SAROSDY	T. G. ESTEP
Case School of Applied Science, Cleveland, Ohio	1913	80	R. H. BRIDGES	TOWRU KOBARA	W. C. ROBERTS
Catholic Univ. of America, Washington, D.C.	1922	8	V. M. CAMPANELLA	MRS. E. F. KELLY	M. E. WESCHLER
Cincinnati, Univ. of, Cincinnati, Ohio	1909	..	RICHARD DARLBENSPECK	ROBERT VAN HAY	C. A. JOERGER
Clarkson College of Tech., Potsdam, N.Y.	1930	40	A. R. FALES	R. S. DAVEY	E. K. FALLS
Clemson A.&M. College, Clemson College, S.C.	1921	..	.....	.....	B. E. FERNOW
Colorado State College of A.&M. Arts, Fort Collins, Colo.	1914	12	C. E. VINCENT	F. H. PLESS	R. D. BARMINGTON
Colorado, Univ. of, Boulder, Colo.	1914	24	E. B. KLUNKER	R. A. WOOD	W. F. MALLORY
Colorado School of Mines Division, Golden	——	..	REX CHEEK	C. Z. MORGAN	W. M. RICHTMANN
Columbia Univ., New York, N.Y.	1909	..			
Mechanical Division	——	14	G. L. LASERSON	JOHN MOST	C. F. KAYAN
Connecticut, Univ. of, Storrs, Conn.	1941	21	ROBERT ODERMANN	R. L. CLEVELAND, JR.	H. W. BUTLER
Cooper Union Inst. of Tech., New York, N.Y.	1920	22	ARTHUR ZIGAS	ROBERT KLINT	W. A. VOPAT
Cooper Union Night School of Engineering, New York, N.Y.	1920	18	.....	.....	E. A. SALMA
Cornell Univ., Ithaca, N.Y.	1908	..	H. M. ST. JOHN, JR.	H. E. OTTO	L. T. WRIGHT
Delaware, Univ. of, Newark, Del.	1929 *	..	.....	.....	.....
Detroit, Univ. of, Detroit, Mich.	1930	32	LARRY O'SHAUGHNESSY	RONALD DOYLE	J. J. UICKER
Drexel Inst. of Tech., Philadelphia, Pa.	1920	66	A. M. WATKINS	W. K. PLATT	K. W. RIDDLE
Duke Univ., Durham, N.C.	1935	68	J. T. MYERS	G. N. BEER	E. S. THEISS
Florida, Univ. of, Gainesville, Fla.	1926	14	J. H. RANSON	J. F. DICKSON	W. W. FINEREN
George Washington Univ., Washington, D.C.	1924	24	B. E. HORNE	RAPHAEL CAHN	B. C. CRUICKSHANKS
Georgia School of Tech., Atlanta, Ga.	1915	43	T. W. E. HANKINSON	R. C. ELDER	R. L. ALLEN
Idaho, Univ. of, Moscow, Idaho	1925	21	ROBERT POINTNER	R. G. KERNS	H. F. GAUSS
Illinois Inst. of Tech., Chicago, Ill.	1940	118	J. F. CUBBIDGE	C. J. WHITE	J. S. KOZACKA
Illinois, Univ. of, Urbana, Ill.	1909	51	W. F. FARNEN	E. K. SUTHERLAND	P. E. MOHN
Iowa State College, Ames, Iowa	1919	29	R. C. SMITH	H. A. DIPPLE	C. T. GRACE
Iowa, State Univ. of, Iowa City, Iowa	1913	13	C. L. CARNS	G. F. GILLIGAN	E. C. LUNDQUIST
Johns Hopkins Univ., Baltimore, Md.	1917	10	J. H. GROSS	S. L. CRAIG	J. H. POTTER
Kansas State College, Manhattan, Kan.	1914	28	S. O. JEWETT	D. J. BLEVINS	A. J. MACK
Kansas, Univ. of, Lawrence, Kan.	1909	17	AUBREY GIBSON	RALPH OLSON	J. W. FOGWELL
Kentucky, Univ. of, Lexington, Ky.	1911	4	RALPH ESCHBORN	H. J. MACKE	S. B. WALTON
Lafayette College, Easton, Pa.	1919	26	WILBUR CLYMER	WILLIAM KEITHLER	E. W. NELSON
Lehigh Univ., Bethlehem, Pa.	1911	33	A. W. HEMPHILL, JR.	G. W. MCKNIGHT	A. C. BATES
Louisiana State Univ., University, La.	1916	34	DONALD CHESSON	THEODORE PERLMAN	W. WHIPPLE
Louisville, Univ. of, Louisville, Ky.	1928	19	C. F. BUSH	R. C. BILLIG	H. H. FENWICK
Maine, Univ. of, Orono, Maine	1910	24	W. H. MORONG	C. K. FULTON	I. H. PRAGEMAN
Marquette Univ., Milwaukee, Wis.	1923	45	W. S. BLANTON	Q. W. HEIN	J. E. SCHOEN
Maryland, Univ. of, College Park, Md.	1937	65	CARSON MOYER	FAITH(HALPINE)VICTOR	A. W. SHERWOOD
Massachusetts Inst. of Tech., Cambridge, Mass.	1909	33	L. G. COIFMAN	A. P. BARBATO	J. A. HRONES
Michigan College of Min. & Tech., Houghton, Mich.	1930	35	A. H. DYKEMA	R. G. RAJALA	A. P. YOUNG
Michigan State College, East Lansing, Mich.	1917	29	A. M. BETTISON	DALE MEYERS	J. M. CAMPBELL
Michigan, Univ. of, Ann Arbor, Mich.	1914	64	MAURICE DAMS	ERIC TYSKLIND	R. C. PORTER
Minnesota, Univ. of, Minneapolis, Minn.	1913	60	HARRY FOEHRINGER	NEIL GREIBENOW	F. HOLTBY
Mississippi State College, State College, Miss.	1926	..	W. A. FOX	W. B. MATHIS	O. D. M. VARNADO

* Temporarily inactive.
† As of January 4, 1944.

Name and Location	Year Authorized	No. of Members †	Chairman	Secretary	Honorary Chairman
Missouri School of Mines & Metallurgy, Rolla, Mo.	1930	27	J. C. Wright	Cy. Orlofsky	A. V. Kilpatrick
Missouri, Univ. of, Columbia, Mo.	1909	77	George Tretiak	Fred Lebensart	A. H. Burr
Montana State College, Bozeman, Mont.	1920	16	R. Challender, Jr.	G. P. Lunday	R. E. Gibbs
Nebraska, Univ. of, Lincoln, Neb.	1909	25	H. R. Walters	Louis Holt	W. F. Weiland
Nevada, Univ. of, Reno, Nev.	1928	..	W. Van Tassel	Robert Rae	J. R. Van Dyke
Newark College of Engineering, Newark, N.J.	1924	97	George Apfel	Sanfort Levat	H. E. Walter
New Hampshire, Univ. of, Durham, N.H.	1926	13	H. F. Szcepan	R. J. Milas	E. P. Nye
New Mexico State College of A.&M. Arts, State College, New Mex.	1938	8	Jack Howard	George Randle	A. M. Lukens
New Mexico, Univ. of, Albuquerque, New Mex.	1935	36	C. E. Barnhart	Rollin Schneider	A. D. Ford, Sr.
New York, College of the City of, New York, N.Y.	1922	118	Bernard Liberman	Harold Shames	C. H. Kent
New York Univ. (Day), New York, N.Y.	1909	75	Gerald Selvin	Silvy Alcalay	J. G. Barrie
New York Univ. Evening School, New York, N.Y.	1933	43	Alfred Johnson	Miss C. B. Northcote	J. G. Barrie
North Carolina State College, Raleigh, N.C.	1920	25	R. K. Jarrell	R. L. Lyerly	E. G. Hoefer
North Dakota Agricultural College, Fargo, N.D.	1929	9	Samuel Hess	Norman Mickelson	A. W. Anderson
North Dakota, Univ. of, Grand Forks, N.D.	1923	..	Palmer Reiten	Bryce Fox	A. J. Diakoff
Northeastern Univ. Boston, Mass.					
Division A	1922	104	J. C. Profita	S. J. Krukanis	F. A. Stearns
Division B	——	..	L. H. Bacon, III	R. F. Buck	F. A. Stearns
Northwestern Univ., Evanston, Ill.	1935	2	Donald Diggs	Allen Neinast	M. F. Spotts
Notre Dame, Univ. of, Notre Dame, Ind.	1929	27	Casimir Regent	James Gormeley	C. R. Egry
Ohio Northern Univ., Ada, Ohio	1922	2	George Hadaway	Sol Light	J. A. Needy
Ohio State Univ., Columbus, Ohio	1911	4	J. F. Hall	W. F. Irwin	S. M. Marco
Oklahoma A.&M. College, Stillwater, Okla.	1921	1	J. B. Sack	Morris Weingarten	C. M. Leonard
Oklahoma, Univ. of, Norman, Okla.	1917	21	J. B. Oakes	S. F. Bird	E. F. Dawson
Oregon State Agricultural College, Corvallis, Ore.	1909	114	Harold Cookson	J. E. Johnson	A. D. Hughes
Pennsylvania State College, State College, Pa.	1909	40	M. M. Meyers	E. D. Zlotowski	C. L. Allen
Pennsylvania, Univ. of, Philadelphia, Pa.	1925	38	R. B. Watrous	William Myer	A. Ulmann, Jr.
Pittsburgh, Univ. of, Pittsburgh, Pa.	1917	26	Robert Schorr	Gale Kenney	T. G. Beckwith
Polytechnic Inst. of Brooklyn, Brooklyn, N.Y.	1909	35	W. A. Passera	N. S. Waner	E. L. Midgette
Polytechnic Inst. of Brooklyn Evening School, Brooklyn, N.Y.	1909 *	..	.....	.....	.....
Pratt Inst., Brooklyn, N.Y.	1923	72	Thomas Wardle	R. J. Benes, Jr.	K. E. Quier
Princeton Univ., Princeton, N.J.	1926	..	I. H. Weaver	R. L. Charlesworth	C. L. Tutt, Jr.
Puerto Rico, Univ. of, Mayaguez, P.R.	1923	..	.....	.....	.....
Purdue Univ., West Lafayette, Ind.	1909	110	R. E. Gallatin	W. K. Price	R. W. Leutwiler, Jr.
Queen's Univ., Kingston, Ont., Can.	1941	68	J. A. Brown	S. Palzalek	W. A. Wolfe
Rensselaer Polytechnic Inst., Troy, N.Y.	1910	68	W. C. Schmitt	Peter Wallack	M. A. Cook
Rhode Island State College, Kingston, R.I.	1930	1	E. D'Aquanno	O. Robt. Pansa	E. L. Carpenter
Rice Inst., Houston, Tex.	1926	33	W. F. Bowman, Jr.	J. S. Norman, Jr.	J. B. T. Downs
Rose Polytechnic Inst., Terre Haute, Ind.	1926	19	Jay Kress	H. E. Campbell	E. Eckerman
Rutgers Univ., New Brunswick, N.J.	1920	36	William Stalker	Robert Godfrey	J. B. Cejka
Santa Clara, Univ. of, Santa Clara, Calif.	1925	18	H. L. Turner	J. E. Lepetich	W. H. Nutting
South Dakota State College, Brookings, S.D.	1935	..	W. V. Campbell	J. R. Burg	L. L. Amidon
Southern California, Univ. of, Los Angeles, Calif.	1929	27	S. L. Marosi	C. R. Salisbury	S. F. Duncan
Southern Methodist Univ., Dallas, Tex.	1933	28	Wray Wilkes	Luke Andre	C. H. Shumaker
Stanford Univ., Stanford University, Calif.	1909	12	Cedrie Ferguson	Robert Worcester	R. A. Seban
Stevens Inst. of Tech., Hoboken, N.J.	1908	37	D. S. Clark	J. M. Hill	K. J. Moser
Swarthmore College, Swarthmore, Pa.	1921	..	Robert Williams, III	Robert Jones	G. B. Thom
Syracuse Univ., Syracuse, N.Y.	1912	21	P. W. Herzog	Eugene Taylor	J. A. King
Tennessee, Univ. of, Knoxville, Tenn.	1923	35	J. C. Hodges	S. G. Huddleston	F. H. Thomas
Texas, A.&M. College of, College Station, Tex.	1921	..	Robert Haltom	.....	J. G. H. Thompson
Texas Technological College, Lubbock, Tex.	1930	17	Robert Slater	R. C. Schwartz	L. J. Powers
Texas, Univ. of, Austin, Tex.	1921	33	C. R. Frederick	E. W. Allen	To be appointed
Toronto, Univ. of, Toronto, Ont., Can.	1933	140	J. D. Abell	R. T. Mansell	R. W. Angus
Tufts College, Tufts College, Mass.	1917	46	Olaf Nielsen	W. B. Brigham, Jr.	D. A. Fisher
Tulane Univ. of Louisiana, New Orleans, La.	1933	45	R. A. Heehs	P. S. Stuart	A. M. Hill
U.S. Naval Academy, Postgraduate School, Annapolis, Md.	1925	..	.....	.....	P. J. Kiefer
Utah, Univ. of, Salt Lake City, Utah	1923	41	L. C. Williamsen	C. S. Rhees	G. W. Carter
Vanderbilt Univ., Nashville, Tenn.	1928 *	..	.....	.....	.....
Vermont, Univ. of, Burlington, Vt.	1922	5	J. W. Williams	E. S. Boyden	R. G. Chapman
Villanova College, Villanova, Pa.	1925	38	A. J. Roth	J. N. Breen	J. S. Morehouse
Virginia Polytechnic Inst., Blacksburg, Va.	1915	31	D. W. St. Clair	Y. C. Yang	W. J. Barber
Virginia, Univ. of, University, Va.	1923	37	P. P. Lee	J. R. Thrower, Jr.	F. T. Morse
Washington, State College of, Pullman, Wash.	1920	..	Robert Boring	Marshall Smyth	F. W. Candee
Washington Univ., St. Louis, Mo.	1911	4	Alvin Holstein	Fred Rietz	R. R. Tucker
Washington, Univ. of, Seattle, Wash.	1917	21	John Bartley	G. W. Van Winkle	L. B. Cooper
West Virginia Univ., Morgantown, W.Va.	1922	15	Jack Rowe	Frank Mumma	L. D. Hayes
Wisconsin, Univ. of, Madison, Wis.	1909	20	R. J. Anderson	Elwood Buffa	D. W. Nelson
Worcester Polytechnic Inst., Worcester, Mass.	1914	64	F. S. Moulton	S. B. Campbell	L. J. Hooper
Wyoming, Univ. of, Laramie, Wyo.	1925	..	J. J. Rees	F. S. Zagar	C. E. Anderson
Yale Univ., New Haven, Conn.	1910	1	R. C. Olsen	B. F. Olson	S. W. Dudley

* Temporarily inactive.
† As of January 4, 1944.

RESEARCH COMMITTEES

ARTICLE B6A, PAR. 24: The Standing Committee on Research shall, under the direction of the Council, have supervision of the research activities of the Society.

The first Standing Committee on Research was organized in 1909.

STANDING COMMITTEE

HERMAN WEISBERG, *Chairman* (1944)
W. R. ELSEY (1945)
J. F. D. SMITH (1946)
D. L. LINDQUIST (1947)
G. A. HAWKINS (1948)

LUBRICATION

Appointed October, 1915, to investigate the fundamental problems of lubrication, to formulate results of investigations previously made, and to keep in touch with contemporary research in this field

(Reorganized May, 1936)

B. L. NEWKIRK, *Chairman*
S. J. NEEDS, *Secretary*
A. L. BEALL
OSCAR BRIDGEMAN
W. E. CAMPBELL
H. A. EVERETT
A. E. FLOWERS
J. C. GENIESSE
RAYMOND HASKELL
M. D. HERSEY
B. F. HUNTER
C. M. LARSON
F. C. LINN
G. L. NEELY
E. S. PEARCE
ERNEST WOOLER

FLUID METERS

Appointed 1916 to develop the theory of fluid meters of all kinds and to report on the best methods for their installation and use

(Reorganized July, 1926)

R. J. S. PIGOTT, *Chairman*
J. R. CARLTON, *Secretary*
H. S. BEAN
S. R. BEITLER
R. K. BLANCHARD
B. O. BUCKLAND
LOUIS GESS
E. W. JACOBSON
A. J. KERR
T. H. KERR
I. O. MINER
M. P. O'BRIEN
W. S. PARDOE
L. K. SPINK
R. E. SPRENKLE
T. R. WEYMOUTH
M. J. ZUCROW

STRENGTH OF GEAR TEETH

Appointed in December, 1921, to investigate factors affecting the strength and life of gear teeth

R. E. FLANDERS, *Chairman*
C. H. LOGUE, *Secretary*
EARLE BUCKINGHAM
A. M. GREENE, JR.
C. W. HAM
F. E. McMULLEN
E. W. MILLER
ERNEST WILDHABER

METAL CUTTING DATA AND BIBLIOGRAPHY

Appointed in September, 1923, to study the problems of metal cutting, including tool materials, tool design, speeds and feeds

(Reorganized December, 1943)

M. MARTELLOTTI, *Chairman*
O. W. BOSTON
W. C. DE GRAFF
F. M. FISHER
J. A. FRASER
T. F. GITHENS
M. F. JUDKINS
W. L. KENNICOTT
M. E. LANGE
F. W. LUCHT
F. J. OLIVER
C. J. WIBERG

CUTTING FLUIDS

Appointed in September, 1923, to study the problems of metal cutting, including lubrication and cooling

(Reorganized December, 1943)

O. W. BOSTON, *Chairman*
H. L. MOIR
W. H. OLDACRE

MECHANICAL SPRINGS

Appointed May, 1924, to determine the status of the mechanical-spring art, to promote and conduct necessary and adequate research, and to develop the art to the point of standardization

J. R. TOWNSEND, *Chairman*
C. T. EDGERTON, *Secretary*
R. W. COOK
W. T. DONKIN
RUPEN EKSERGIAN
G. E. HANSEN
BENJAMIN LIEBOWITZ
DAVID LOFTS
R. D. BRIZZOLARA (*Alternate*)
D. J. McADAM, JR.
L. C. PESKIN
R. E. PETERSON
J. W. ROCKEFELLER, JR.
B. W. ST. CLAIR
M. F. SAYRE
T. R. WEBER
KEITH WILLIAMS
J. K. WOOD
F. P. ZIMMERLI

ELEVATORS

Appointed June, 1924, to study the function and operation of elevator safeties and buffers and their associated mechanisms and to develop methods of test for the approval of elevator safety devices

(Reorganized August, 1940)

D. J. PURINTON, *Chairman*
D. L. LINDQUIST, *Vice-Chairman*
G. H. REPPERT (*Alternate*)
J. A. DICKINSON, *Secretary*
S. W. JONES, *Ex-Officio*
E. M. BOUTON
E. B. DAWSON (*Alternate*)
K. A. COLAHAN
G. P. KEOGH
F. PAVLICEK (*Alternate*)
J. J. MATSON
M. B. McLAUTHLIN
C. R. CALLAWAY (*Alternate*)
W. S. PAINE
J. L. KEANE (*Alternate*)
C. A. PETERS

EFFECT OF TEMPERATURE ON THE PROPERTIES OF METALS

Appointed December, 1924, as a Joint Research Committee of the A.S.T.M. and the A.S.M.E. to encourage the investigation and accumulation of data on the properties of metals used in the mechanic arts at extremely high and low temperatures

N. L. MOCHEL, *Chairman*
H. J. KERR, *Vice-Chairman*
J. W. BOLTON, *Secretary*
W. H. ARMACOST
A. B. BAGSAR
A. D. BAILEY
F. E. BASH
C. L. CLARK
E. S. DIXON
F. B. FOLEY
J. R. FREEMAN, JR.
H. J. FRENCH
H. W. GILLETT
A. J. HERZIG
G. F. JENKS
J. J. KANTER
C. E. MACQUIGG
R. F. MILLER
E. L. ROBINSON
J. H. ROMANN
A. E. WHITE
J. S. WORTH
Director, National Bureau of Standards, U.S. Department of Commerce
Representative of Bureau of Ships, U.S. Navy Department

BOILER FEEDWATER STUDIES

Appointed March, 1925, as a Joint Research Committee of the American Boiler Manufacturers Association, American Railway Engineering Association, American Water Works Association, Edison Electric Institute, the American Society for Testing Materials, and the A.S.M.E. to study methods of analysis and treatment of boiler feedwater for stationary and railroad practice

EXECUTIVE COMMITTEE (Total personnel 41)

C. H. FELLOWS, *Chairman*
R. C. BARDWELL, *Vice-Chairman*
J. B. ROMER, *Secretary*
A. G. CHRISTIE *
R. E. COUGHLAN
B. W. DE GEER

(*Continued*)

* Official A.S.M.E. representative serving on this committee.

BOILER FEEDWATER STUDIES

(Continued)

MAX HECHT
H. E. JORDAN
P. B. PLACE
S. T. POWELL
F. N. SPELLER
M. F. STACK
G. E. TATE
E. H. TENNEY
A. E. WHITE *

CONDENSER TUBES

Appointed May, 1925, to investigate and report on the causes of failure of tubes used in steam condensers and similar heat interchange apparatus

A. E. WHITE, *Chairman*
D. C. WEEKS, *Vice-Chairman*
P. A. BANCELL
R. A. BOWMAN
E. S. BUNN
D. K. CRAMPTON
C. A. CRAWFORD
H. M. CUSHING
R. E. DILLON
C. O. EVANS
J. R. FREEMAN, JR.
V. M. FROST
C. F. HARWOOD
G. C. HOLDER
W. C. HOLMES
W. B. PRICE
J. S. RODGERS
M. F. STACK
W. R. WEBSTER
Director, Bureau of Ships, U.S. Navy Department

WORM GEARS

Appointed May, 1927, to investigate certain problems in connection with the action of worm gear drives and to recommend improvements in their design, manufacture, and use

EARLE BUCKINGHAM, *Chairman*
G. H. ACKER
L. R. BUCKENDALE
D. L. LINDQUIST
A. A. ROSS
B. F. WATERMAN
Representative of Bureau of Ships, U.S. Navy Department

STRENGTH OF VESSELS UNDER EXTERNAL PRESSURE

Appointed June, 1929, to develop reliable design data on the strength of cylindrical and spherical surfaces under external pressure, particularly with reference to jacketed vessels

F. V. HARTMAN, *Chairman*
M. B. HIGGINS
E. C. KORTEN
A. W. LIMONT, JR.
H. E. SAUNDERS
E. E. SHANOR
R. G. STURM
D. B. WESSTROM
F. S. G. WILLIAMS
D. F. WINDENBURG
DANA YOUNG

WIRE ROPE

Appointed April, 1930, to investigate existing rope so that it may be better understood and more effectively used

W. H. FULWEILER, *Chairman*
H. LeR. BRINK
D. L. LINDQUIST
G. W. MARTIN
A. H. McDOUGALL
B. V. E. NORDBERG
W. S. PAINE
W. J. RYAN
GEORGE SIMPSON
L. E. YOUNG

CRITICAL PRESSURE STEAM BOILERS

Appointed June, 1931, to study the characteristics of high-pressure forced-circulation steam-generating units

H. L. SOLBERG, *Chairman*
W. H. ARMACOST
A. D. BAILEY
E. G. BAILEY
F. S. CLARK
C. H. FELLOWS
H. J. KERR
GEO. A. ORROK
E. C. PETRIE
E. L. ROBINSON
P. W. THOMPSON

PLASTIC FLOW OF METALS

Appointed October, 1938, to study plasticity in the particular field of rolling of steel

A. NADAI, *Chairman*
C. W. MacGREGOR, *Secretary*
E. C. BAIN
C. L. EKSERGIAN
LeVAN GRIFFIS
J. H. HITCHCOCK
W. P. ROOP
M. D. STONE
W. TRINKS

FURNACE PERFORMANCE FACTORS

Appointed in October, 1941, to collect and rationalize data on the performance of commercially important furnaces as an aid to design and operation

A. R. MUMFORD, *Chairman*
ALEX D. BAILEY
J. R. MICHEL (*Alternate*)
JOHN BLIZARD
S. P. BURKE
O. F. CAMPBELL
W. A. CARTER
B. J. CROSS
T. B. DREW
F. G. ELY
A. C. FIELDNER
W. C. SCHROEDER (*Alternate*)
J. H. HARLOW
H. C. HOTTEL
E. L. LINDSETH
W. H. McADAMS
A. J. NERAD
E. B. POWELL
A. A. RAYMOND
W. T. REID
R. A. SHERMAN
PHILIP SPORN
A. W. THORSON
HERMAN WEISBERG
W. J. WOHLENBERG

FORGING OF STEEL SHELLS

Appointed in October, 1941, to study methods of shell manufacture under modern conditions

M. D. STONE, *Chairman*
W. TRINKS, *Projects Director*
JOHN DIERBECK
D. W. FLETCHER
W. M. FRAME
W. N. HOWLEY
A. F. MACCONOCHIE
W. P. MUIR
A. NADAI
A. R. NETTENSTROM
GEORGE SACHS
A. E. VAN CLEVE
U.S. Army, Ordnance Department
U.S. Navy, Bureau of Ordnance

DEMOLITION BOMB BODIES

Appointed in October, 1943, to study methods of demolition bomb body manufacture under modern conditions

M. D. STONE, *Chairman*
W. O. CLINEDINST, *Secretary*
W. TRINKS, *Projects Director*
G. M. CROFT
F. C. FANTZ
W. M. FRAME
R. FURRER
H. B. LIGGETT
A. NADAI
GEORGE SACHS
U.S. Army Ordnance Department
U.S. Navy, Bureau of Ordnance

A.S.M.E. Representatives on Other Research Committees

See also A.S.M.E. Representatives on Other Activities, page RI-9

AMERICAN COORDINATING COMMITTEE ON CORROSION

American Society for Testing Materials

C. H. FELLOWS
S. L. KERR

FATIGUE PHENOMENA OF METALS

American Society for Testing Materials

C. T. EDGERTON

METALLURGICAL RESEARCH

Advisory Committee to the National Bureau of Standards

C. H. BIERBAUM

PROPERTIES OF REFRACTORY MATERIALS

Advisory Committee to the National Bureau of Standards

E. B. POWELL

WATER FOR INDUSTRIAL USES

American Society for Testing Materials

J. H. WALKER

STANDARDIZATION COMMITTEES

ARTICLE B6A, PAR. 23: The Standing Committee on Standardization shall advise the Council on the dimensional standardization work of the Society, including relations with the American Standards Association.

The first Standing Committee on Standardization was organized in April, 1911

STANDING COMMITTEE

T. E. FRENCH, *Chairman* (1944)
W. H. HILL (1945)
J. H. TAYLOR (1946)
E. J. BRYANT (1947)
D. S. ELLIS (1948)

STANDARDIZATION AND UNIFICATION OF SCREW THREADS (B1)

* *Joint sponsorship with the Society of Automotive Engineers. Sectional Committee originally organized in June, 1921. Reorganized in May, 1929*

A.S.M.E. Members (Total personnel, 34)

A. M. HOUSER, *Vice-Chairman* †
EARLE BUCKINGHAM, *Secretary*
E. J. BRYANT
G. S. CASE
T. G. CRAWFORD
H. C. E. MEYER
P. V. MILLER †
W. C. MUELLER
R. H. PERRY
G. T. TRUNDLE

SUBCOMMITTEE CHAIRMEN

Special Subcommittee on Revision of American Standard, P. V. MILLER
No. 1 on Scope, Arrangement and Editing of American National Standard (to be appointed)
No. 4 on Acme and Other Similar Threads, Except Gages, EARLE BUCKINGHAM
No. 5 on Screw Thread Gages and Inspection, G. S. CASE
No. 6 on Threading of General Purpose Nuts, J. S. DAVEY
No. 7 on Screw Threads for High Temperature Bolting, W. H. GOURLIE

PIPE THREADS (B2)

* *Joint sponsorship with the American Gas Association. Sectional Committee originally organized in 1913. Reorganized December, 1927*

A.S.M.E. Members (Total personnel, 40)

A. S. MILLER, *Chairman*
C. B. LEPAGE, *Acting Secretary*
A. F. BREITENSTEIN †
E. J. BRYANT
E. S. CORNELL, JR.
J. J. CROTTY
J. J. HARMAN
A. M. HOUSER †
P. V. MILLER †
F. H. MOREHEAD
L. N. SHANNON
O. M. TISHLARICH
FRANK THORNTON, JR.
ROWLAND TOMPKINS
B. B. WESCOTT
J. H. WILLIAMS

SUBCOMMITTEE CHAIRMEN

No. 1 on Editing and Gaging, A. M. HOUSER
No. 2 on Taper Pipe Threads, S. B. TERRY
No. 3 on Straight Pipe Threads, P. V. MILLER
No. 4 on Plumbers' Threads, A. F. BREITENSTEIN
No. 6 on Special Threads for Thin Tubes, C. C. WINTER
Special Subcommittee on Tolerances on Thread Elements, E. J. BRYANT
Special Subcommittee on Truncation, E. J. BRYANT

BALL AND ROLLER BEARINGS (B3)

* *Joint sponsorship with the Society of Automotive Engineers. Sectional Committee organized December, 1920*

A.S.M.E. Members (Total personnel, 21)

W. P. KENNEDY, *Vice-Chairman* †
D. E. BATESOLE †
L. A. CUMMINGS
O. H. DORER
F. G. HUGHES
G. E. HULSE †
W. L. ILIFF †
L. F. NENNINGER
S. M. WECKSTEIN †
ERNEST WOOLER

ALLOWANCES AND TOLERANCES FOR CYLINDRICAL PARTS AND LIMIT GAGES (B4)

* *Sole sponsorship. Sectional Committee originally organized in June, 1920. Reorganized in December, 1930*

A.S.M.E. Members (Total personnel, 39)

J. E. LOVELY, *Chairman* †
F. E. BANFIELD, JR.
F. S. BLACKALL, JR.
E. J. BRYANT
EARLE BUCKINGHAM †
F. H. COLVIN †
T. G. CRAWFORD
R. E. W. HARRISON
F. O. HOAGLAND
E. N. JACOBI
H. C. E. MEYER
P. V. MILLER
W. C. MUELLER
E. C. PECK †
R. H. PERRY
W. C. SCHOENFELDT
C. C. STEVENS
G. T. TRUNDLE, JR.

SMALL TOOLS AND MACHINE TOOL ELEMENTS (B5)

* *Joint sponsorship with the National Machine Tool Builders' Association, and the Society of Automotive Engineers. Sectional Committee organized September, 1922*

A.S.M.E. Members (Total personnel, 32)

W. C. MUELLER, *Chairman* †
F. O. HOAGLAND, *Vice-Chairman*
J. B. ARMITAGE
O. W. BOSTON
E. J. BRYANT
EARLE BUCKINGHAM
F. H. COLVIN
S. A. EINSTEIN
J. P. GILL
H. E. HARRIS
JOHN HAYDOCK
J. P. LAUX †
J. E. LOVELY †
A. F. MURRAY †
ERIK OBERG †
FRANK THORNTON, JR.

TECHNICAL COMMITTEES

EXECUTIVE COMMITTEE

A.S.M.E. Members (Total personnel, 5)

W. C. MUELLER, *Chairman*
F. O. HOAGLAND, *Vice-Chairman*
H. E. HARRIS

No. 1 on T-Slots

A.S.M.E. Members (Total personnel, 7)

ERIK OBERG, *Chairman*
J. B. ARMITAGE
HARRY CADWALLADER, JR.
S. A. EINSTEIN
F. O. HOAGLAND

No. 2 on Tool-Posts and Tool Shanks

A.S.M.E. Members (Total personnel, 7)

O. W. BOSTON, *Chairman*
F. S. BLACKALL, JR.
GRANGER DAVENPORT
M. E. LANGE

No. 3 on Machine Tapers

A.S.M.E. Members (Total personnel, 20)

E. J. BRYANT, *Chairman*
C. B. LEPAGE, *Acting Secretary*
J. B. ARMITAGE
F. S. BLACKALL, JR.
EARLE BUCKINGHAM
F. H. COLVIN
B. P. GRAVES
E. E. GRIFFITHS
H. E. HARRIS
F. O. HOAGLAND
J. H. HORIGAN
L. F. NENNINGER

No. 4 on Spindle Noses and Collets for Machine Tools

A.S.M.E. Members (Total personnel, 26)

J. E. LOVELY, *Chairman*
L. F. NENNINGER, *Secretary*
J. B. ARMITAGE
H. W. FAUS
B. P. GRAVES
F. O. HOAGLAND
A. M. JOHNSON
M. E. LANGE
J. H. MANSFIELD
L. D. SPENCE

* Note: All of these standards committees for which the Society is sponsor or joint sponsor, or on which it has representation, are organized under the procedure of the American Standards Association.

† Official A.S.M.E. representative serving on this committee.

SMALL TOOLS AND MACHINE TOOL ELEMENTS (B5)

(Continued)

No. 5 on Milling Cutters

A.S.M.E. Members (Total personnel, 20)

J. B. Armitage
A. N. Goddard
E. E. Griffiths
J. H. Horigan
E. K. Morgan
Erik Oberg
E. D. Vancil

No. 6 on Designations and Working Ranges of Machine Tools

A.S.M.E. Members (Total personnel, 19)

John Haydock, *Chairman*
Earle Buckingham
T. H. Doan, Jr.
H. W. Faus
B. P. Graves
J. J. McBride
E. R. Smith

No. 7 on Twist Drill Sizes

A.S.M.E. Members (Total personnel, 7)

W. C. Mueller, *Chairman*
E. E. Griffiths
J. H. Horigan

No. 8 on Jig Bushings

A.S.M.E. Members (Total personnel, 9)

E. E. Griffiths
J. H. Horigan

No. 9 on Punch Press Tools

A.S.M.E. Members (Total personnel, 15)

D. H. Chason
E. W. Ernest
E. E. Griffiths
H. E. Harris
D. M. Palmer

No. 10 on Forming Tools and Holders

A.S.M.E. Members (Total personnel, 11)

W. C. Mueller, *Chairman*
W. E. Blank
E. E. Griffiths
L. D. Spence

No. 11 on Chucks and Chuck Jaws

A.S.M.E. Members (Total personnel, 8)

J. E. Lovely, *Chairman*

No. 12 on Cut and Ground Thread Taps

A.S.M.E. Member (Total personnel, 7)

J. E. Ennis

No. 13 on Splines and Splined Shafts

A.S.M.E. Members (Total personnel, 17)

J. B. Armitage
R. E. W. Harrison
F. O. Hoagland
J. E. Lovely

No. 17 on Nomenclature for Small Tools and Machine Tool Elements

A.S.M.E. Members (Total personnel, 12)

O. W. Boston, *Chairman and Secretary*
F. S. Blackall, Jr.
F. H. Colvin
H. E. Harris
F. O. Hoagland

No. 19 on Single-Point Cutting Tools

A.S.M.E. Members (Total personnel, 2)

F. H. Colvin, *Chairman*
O. W. Boston, *Secretary*

No. 20 on Reamers

A.S.M.E. Members (Total personnel, 16)

F. H. Colvin
T. F. Githens
E. E. Griffiths
J. H. Horigan
O. E. Koehler

No. 21 on Tool-Life Tests for Single-Point Tools

A.S.M.E. Members (Total personnel, 11)

O. W. Boston, *Chairman*
E. E. Griffiths
M. F. Judkins
H. L. Moir

No. 23 on Machine Pins

A.S.M.E. Members (Total personnel, 14)

E. E. Griffiths
J. J. McBride
R. H. Smith

GEARS (B6)

** Joint sponsorship with the American Gear Manufacturers Association. Sectional Committee organized June, 1921*

A.S.M.E. Members (Total personnel, 23)

U. S. Eberhardt, *Chairman*
Earle Buckingham, *Vice-Chairman* †
C. B. LePage, *Acting Secretary*
A. H. Candee †
G. H. Acker
L. H. Fry
C. B. Hamilton, Jr.
D. T. Hamilton
M. R. Hanna
O. A. Leutwiler

SUBCOMMITTEE CHAIRMEN

No. 3 on Nomenclature, D. T. Hamilton
No. 4 on Tooth Form (Spur Gears), W. P. Schmitter
No. 8 on Materials, E. J. Wellauer
No. 9 on Inspection, Granger Davenport

PIPE FLANGES AND FITTINGS (B16)

** Joint sponsorship with the Heating, Piping and Air Conditioning Contractors National Association, and the Manufacturers Standardization Society of the Valve and Fittings Industry. Sectional Committee organized November, 1921*

A.S.M.E. Members (Total personnel, 58)

C. P. Bliss, *Chairman* †
J. J. Harman, *Secretary*
A. L. Baker
L. W. Benoit †
A. L. Brown
Sabin Crocker
Ferdinand Fink
V. M. Frost
H. E. Haller
J. S. Hess
H. A. Hoffer †
A. M. Houser †
C. A. Kelting †
J. R. Kruse
(John Blizard, *Alternate*)
M. B. MacNeille
F. H. Morehead
L. S. Morse, Sr.
A. W. Oakley
Fred Ophuls
Ludwig Skog
J. E. Stark
J. R. Tanner †
J. H. Taylor
Rowland Tompkins
G. W. Watts
J. H. Williams
J. H. Zink

SUBCOMMITTEE CHAIRMEN

Executive Committee, C. P. Bliss
No. 1 on Cast Iron Flanges and Flanged Fittings, A. M. Houser
No. 2 on Screwed Fittings, F. H. Morehead
No. 3 on Steel Flanges and Flanged Fittings, C. P. Bliss
No. 4 on Materials and Stresses, A. M. Houser
No. 5 on Face to Face Dimensions of Ferrous Flanged Valves, J. R. Tanner
No. 6 on Malleable Iron or Steel Brass Seat Unions (to be appointed)
No. 7 on Rating of Pipe Fittings (to be appointed)
No. 8 on Marking of Pipe Fittings, F. H. Morehead

SHAFTING (B17)

** Sole sponsorship. Organized October, 1918*

A.S.M.E. Members (Total personnel, 13)

C. M. Chapman, *Chairman* †
C. B. LePage, *Secretary*
H. C. E. Meyer
L. C. Morrow
L. W. Williams †

BOLT, NUT, AND RIVET PROPORTIONS (B18)

** Joint sponsorship with the Society of Automotive Engineers. Sectional Committee organized March, 1922*

A.S.M.E. Members (Total personnel, 56)

W. R. Halliday, *Chairman* †
W. C. Stewart, *Secretary*
H. E. Aldrich
F. C. Billings
B. G. Braine
G. S. Case
T. G. Crawford
H. P. Frear
A. M. Houser †
Herman Koester †
W. C. Mueller
S. F. Newman
R. H. Perry
J. R. Tanner †
R. J. Whelan
E. M. Whiting
V. R. Willoughby
(J. J. McBride, *Alternate*)

SUBCOMMITTEE CHAIRMEN

No. 1 on Large and Small Rivets (to be appointed)
No. 2 on Wrench-Head Bolts and Nuts (to be appointed)
No. 3 on Slotted and Recessed Head Screws, F. P. Tisch
No. 4 on Track Bolts and Nuts (to be appointed)
No. 5 on Round Unslotted Head Bolts (Carriage Bolts) (to be appointed)
No. 6 on Plow Bolts (to be appointed)
No. 7 on Body Dimensions and Materials (to be appointed)
No. 8 on Nomenclature, G. S. Case
No. 9 on Socket Head Cap and Set Screws, Herman Koester

PLAIN AND LOCK WASHERS (B27)

** Joint sponsorship with the Society of Automotive Engineers. Sectional Committee organized March, 1926*

A.S.M.E. Members (Total personnel, 38)

EUGENE CALDWELL
T. G. CRAWFORD
B. S. LEWIS †
C. H. LOUTREL
J. J. MCBRIDE
H. C. E. MEYER
W. C. MUELLER †
E. M. WHITING †

SUBCOMMITTEE CHAIRMEN

No. 1 on Plain Washers, W. L. BARTH
No. 2 on Spring Washers, E. D. COWLIN

TRANSMISSION CHAINS AND SPROCKETS (B29)

** Joint sponsorship with the Society of Automotive Engineers, and the American Gear Manufacturers Association. Sectional Committee originally organized September, 1917. Reorganized December, 1926*

A.S.M.E. Members (Total personnel, 12)

W. J. BELCHER
J. M. BRYANT †
JOSEPH JOY
L. V. LUDY †
D. B. PERRY
C. R. WEISS

SUBCOMMITTEE CHAIRMEN

No. 1 on Roller Chain Standardization (to be appointed)
No. 2 on Silent Chain Standardization (to be appointed)

CODE FOR PRESSURE PIPING (B31)

** Sole sponsorship. Sectional Committee originally organized November, 1926. Reorganized December, 1937*

A.S.M.E. Members (Total personnel, 100)

E. B. RICKETTS, *Chairman*
H. C. COOPER
D. H. COREY
(T. W. GREENE, *Alternate*)
SABIN CROCKER
H. D. EDWARDS
E. R. FISH
CHARLES FITZGERALD
V. M. FROST
H. E. HALLER
W. D. HALSEY
J. S. HAUG
H. A. HOFFER
G. G. HOLLINS
E. L. HOPPING
A. M. HOUSER †
ALFRED IDDLES †
D. S. JACOBUS
T. M. JASPER
C. A. KELTING
E. H. KRIEG
G. SINDING-LARSEN
M. B. MACNEILLE
G. W. MARTIN
H. C. E. MEYER
J. W. MOORE
(J. D. CAPRON, *Alternate*)
F. H. MOREHEAD
(J. J. HARMAN, *Alternate*)
H. H. MORGAN
L. S. MORSE, SR.
R. M. NEE
E. W. NORRIS
C. W. OBERT
GEO. A. ORROK
A. L. PENNIMAN, JR.
C. S. ROBINSON †
J. H. ROMANN
D. B. ROSSHEIM
G. W. SAATHOFF
G. K. SAURWEIN
LUDWIG SKOG
H. S. SMITH
(H. H. MOSS, *Alternate*)
J. E. STARK
(L. H. CARR, *Alternate*)
J. R. TANNER
J. H. TAYLOR
J. H. VANCE
H. L. WHITTEMORE
J. H. WILLIAMS
T. F. WOLFE
J. H. ZINK

SUBCOMMITTEE CHAIRMEN

Subcommittee on Scope and Intent of Sectional Committee on Code for Pressure Piping, B31, SABIN CROCKER
No. 1 on Plan, Scope, and Editing, SABIN CROCKER
No. 2 on Power Piping, ALFRED IDDLES
No. 4 on Gas and Air Piping, J. S. HAUG
No. 5 on Refrigeration Piping, A. B. STICKNEY
No. 6 on Oil Piping, L. D. BURRITT
No. 7 on Piping Materials and Identification, F. H. MOREHEAD
No. 8 on Fabrication Details, LUDWIG SKOG
No. 9 on District Heating Piping, G. K. SAURWEIN
Special Committee on Pressures and Temperatures Above Those Covered by Code, E. R. FISH

WIRE AND SHEET METAL GAGES (B32)

** Joint sponsorship with the Society of Automotive Engineers. Sectional Committee originally organized November, 1928. Reorganized November, 1939*

A.S.M.E. Members (Total personnel, 36)

A. P. COTTLE
E. W. ERNEST
J. F. HOWE †
F. G. WILSON †

SUBCOMMITTEE CHAIRMAN

Wire and Sheet Metal Gages, J. R. TOWNSEND

SCREWS THREADS FOR HOSE COUPLINGS (B33)

** Sole sponsorship. Sectional Committee organized October, 1928*

A.S.M.E. Members (Total personnel, 27)

A. L. BROWN, *Secretary*
A. F. BREITENSTEIN †
J. J. CROTTY
W. L. CURTISS
W. E. DUNHAM †
J. J. HARMAN
(F. C. ERNST, *Alternate*)
H. C. E. MEYER
J. H. WILLIAMS

WROUGHT IRON AND WROUGHT STEEL PIPE AND TUBING (B36)

** Joint sponsorship with the American Society for Testing Materials. Sectional Committee organized May, 1928*

A.S.M.E. Members (Total personnel, 45)

H. H. MORGAN, *Chairman*
SABIN CROCKER, *Secretary*
J. S. ADELSON
H. E. ALDRICH
NEWELL HAMILTON
D. S. JACOBUS †
(F. S. CLARK, *Alternate*) †
J. J. KANTER
H. C. E. MEYER
F. H. MOREHEAD
H. B. OATLEY †
J. H. ROMANN
LUDWIG SKOG †
J. R. TANNER
A. E. WHITE

SUBCOMMITTEE CHAIRMEN

No. 1 on Plan, Scope, and Editing, H. H. MORGAN
No. 2 on Pipe and Tubing for Low Temperature Service, J. J. SHUMAN
No. 3 on Pipe and Tubing for High Temperature Service, J. R. TANNER
No. 4 on Materials, F. H. MOREHEAD

PRESSURE AND VACUUM GAGES (B40)

** Sole Sponsorship. Sectional Committee organized December, 1930*

A.S.M.E. Members (Total personnel, 43)

M. D. ENGLE, *Chairman*
A. W. LENDEROTH, *Secretary* †
E. J. BRYANT
J. P. CAVANAUGH †
PAUL DISERENS
C. H. GRAESSER
W. F. JONES
R. J. KEHL
J. C. MCCUNE †
A. H. MORGAN
H. B. REYNOLDS
W. C. SCHOENFELDT

SUBCOMMITTEE CHAIRMEN

No. 1 on Plan and Scope, M. D. ENGLE
No. 2 on Definitions, C. F. SCHWEP
No. 3 on Gage Sizes and Mounting Dimensions, H. B. REYNOLDS
No. 4 on Accuracy and Test Methods, O. J. HODGE

STOCK SIZES, SHAPES AND LENGTHS FOR HOT AND COLD FINISHED IRON AND STEEL BARS (B41)

** Sole sponsorship. Sectional Committee organized June, 1930*

A.S.M.E. Members (Total personnel, 25)

C. D. ALLEN
F. H. DECHANT
E. W. ERNEST
H. D. TANNER
L. W. WILLIAMS †

SUBCOMMITTEE CHAIRMEN

No. 1 on Hot Rolled Steel, HENRY WYSOR
No. 2 on Cold Finished Steels, L. E. CREIGHTON
No. 3 on Hot Rolled Iron (to be appointed)

SPECIFICATIONS FOR LEATHER BELTING (B42)

** Sole sponsorship. Sectional Committee organized May, 1931*

A S.M.E. Members (Total personnel, 24)

H. T. COATES
R. W. DRAKE †
KING HATHAWAY
P. G. RHOADS
G. A. SCHIEREN

SPECIFICATIONS FOR LEATHER BELTING (B42)

(Continued)

SUBCOMMITTEE CHAIRMEN

No. 1 on Standard Specifications (to be appointed)
No. 2 on Recommendations for Selection, Care and Installation, G. A. SCHIEREN

CLASSIFICATION AND DESIGNATION OF SURFACE QUALITIES (B46)

** Joint sponsorship with the Society of Automotive Engineers. Sectional Committee organized December, 1932*

A.S.M.E. Members (Total personnel, 66)

R. F. GAGG, *Chairman*
E. J. ABBOTT
E. J. BRYANT
T. G. CRAWFORD
R. C. DEALE †
U. S. EBERHARDT
S. A. EINSTEIN
W. W. GILBERT
J. J. HARMAN
R. E. W. HARRISON †
F. O. HOAGLAND
H. J. HOLTZCLAW
R. T. KENT
H. F. KURTZ
JOSEPH MANUELE
F. C. SPENCER
C. C. STEVENS
W. C. STEWART
J. S. TAWRESEY
C. H. WHITAKER
ERNEST WOOLER

SUBCOMMITTEE CHAIRMEN

Special Subcommittee on Revision and Editing, R. F. GAGG
No. 2 on Surfaces Produced by Molds, Dies, Rolls, or Any Other Means of Deforming Materials (to be appointed)
No. 3 on Coated Surfaces, G. B. HOGABOOM
No. 4 on Symbols for Indicating Surface Quality on Drawings, T. G. CRAWFORD
No. 5 on Ways, Means and Apparatus for Measuring Quality of Surface (to be appointed)
No. 7 on Standards for Appearance of Surfaces (to be appointed)

SHAFT COUPLINGS, INTEGRALLY FORGED FLANGE TYPE FOR HYDROELECTRIC UNITS (B49)

** Sole sponsorship. Sectional Committee organized October, 1943*

A.S.M.E. Members (Total personnel, 18)

R. E. B. SHARP, *Temporary Chairman* †
D. J. MCCORMACK, *Temporary Secretary* †
D. L. BARBOUR
L. F. HARZA
L. F. MOODY
G. R. RICH
E. B. STROWGER
R. V. TERRY

COMBUSTION SPACE FOR SOLID FUELS (B50)

** Sole sponsorship. Sectional Committee organized June, 1933*

A.S.M.E. Members (Total personnel, 21)

C. E. BRONSON, *Chairman*
W. G. CHRISTY
JOHN HUNTER
A. J. JOHNSON
V. G. LEACH †
J. P. MAGOS
J. F. MCINTIRE
F. L. MEYER
C. A. REED
JOHN VAN BRUNT †

SUBCOMMITTEE CHAIRMEN

No. 1 on Purpose and Scope, C. E. BRONSON
No. 2 on Combustion and Design, B. M. GUTHRIE
No. 3 on Warm Air Furnaces, J. H. MANNY
No. 4 on Steel Heating Boilers, W. B. RUSSELL
No. 5 on Cast Iron Boilers, J. F. MCINTIRE

SCHEME FOR IDENTIFICATION OF PIPING SYSTEMS (A13)

** Joint sponsorship with the National Safety Council. Sectional Committee organized June, 1922*

A.S.M.E. Members (Total personnel, 35)

E. E. ASHLEY
W. L. BUNKER
CROSBY FIELD
H. L. MINER
H. S. SMITH
FRANK THORNTON, JR.
ROWLAND TOMPKINS
FRANK UMBEHOCKER †

SUBCOMMITTEE CHAIRMEN

Executive Committee, A. S. HEBBLE
Identification by Colors (to be appointed)
Classification, CROSBY FIELD
Identification Markings Other Than Color (to be appointed)
Editing Subcommittee, A. S. HEBBLE

MINIMUM REQUIREMENTS FOR PLUMBING AND STANDARDIZATION OF PLUMBING EQUIPMENT (A40)

** Joint sponsorship with The American Public Health Association. Sectional Committee organized November, 1928*

A.S.M.E. Members (Total personnel, 53)

C. B. LEPAGE, *Acting Secretary*
J. F. CARNEY, *Alternate*
J. J. CROTTY
A. M. HOUSER †
G. W. MARTIN
(A. H. MORGAN, *Alternate*)
W. K. MCAFEE
W. R. WEBSTER †

SUBCOMMITTEE CHAIRMEN

Research Committee on Plumbing (to be appointed)
No. 1 on Minimum Requirements for Plumbing, T. I. COE
No. 2 on Staple Vitreous China Plumbing Fixtures, H. R. VAN SCIVER
No. 3 on Staple Porcelain (All Clay) Plumbing Equipment, H. R. VAN SCIVER
No. 4 on Enameled Sanitary Ware, A. H. CLINE, JR.
No. 5 on Traps (to be appointed)
No. 6 on Brass Plumbing Products (to be appointed)
No. 7 on Brass Fittings for Flared Copper Tubes, F. L. RIGGIN
No. 8 on Cast Iron Soil Pipe and Fittings (to be appointed)
No. 9 on Gasoline, Oil and Grease Separators (to be appointed)
Joint Committee on Threaded Cast Iron Pipe, F. H. MOREHEAD
No. 11 on Soldered Fittings for Tubing, A. M. HOUSER
No. 12 on Minimum Air Gaps in Plumbing Systems, W. K. MCAFEE

ROLLED THREADS FOR SCREW SHELLS OF ELECTRIC SOCKETS AND LAMP BASES (C44)

** Joint sponsorship with the National Electrical Manufacturers Association. Sectional Committee organized June, 1929*

A.S.M.E. Members (Total personnel, 15)

E. J. BRYANT †
EARLE BUCKINGHAM †
A. B. MORGAN, *Alternate*

LETTER SYMBOLS AND ABBREVIATIONS FOR SCIENCE AND ENGINEERING (Z10)

** Joint sponsorship with the American Association for the Advancement of Science, American Institute of Electrical Engineers, American Society of Civil Engineers, and the Society for the Promotion of Engineering Education. Sectional Committee originally organized January, 1926. Reorganized October, 1935*

A.S.M.E. Members (Total personnel, 44)

S. A. MOSS, *Vice-Chairman* †
K. H. CONDIT
L. C. LICHTY
R. E. PETERSON †
(S. R. BEITLER, *Alternate*) †
G. A. STETSON
FRANK THORNTON, JR.

SUBCOMMITTEE CHAIRMEN

Executive Committee, H. M. TURNER
Steering Committee, H. M. TURNER
No. 1 on Letter Symbols and Signs for Mathematics, A. A. BENNETT
No. 2 on Symbols for Hydraulics, J. C. STEVENS
No. 3 on Symbols for Mechanics, R. E. PETERSON
No. 4 on Symbols for Structural Analysis, ALBERT HAERTLEIN
No. 5 on Symbols for Heat and Thermodynamics, S. A. Moss
No. 6 on Symbols for Photometry, A. E. PARKER
No. 7 on Aeronautical Symbols, G. W. LEWIS
No. 8 on Symbols for Electrical Quantities, EDWARD BENNETT
No. 9 on Symbols for Radio, H. M. TURNER
No. 10 on Symbols for Physics, H. K. HUGHES
No. 11 on Abbreviations for Scientific and Engineering Terms, G. A. STETSON
No. 12 on Symbols for Unit Operations in Chemical Engineering, J. H. PERRY

STANDARDS FOR DRAWINGS AND DRAFTING ROOM PRACTICE (Z14)

** Joint sponsorship with the Society for the Promotion of Engineering Education. Sectional Committee organized September, 1926*

A.S.M.E. Members (Total personnel, 46)

T. E. FRENCH, *Chairman*
H. P. FREAR
J. J. HARMAN
A. C. HARPER
E. R. HILL
SAMUEL KETCHUM †
C. W. KEUFFEL
F. R. LANEY
H. B. LANGILLE
RUDOLPH MICHEL, *Alternate*
F. W. MING
W. C. MUELLER
E. B. NEIL
J. W. OWENS
F. C. PANUSKA
ED S. SMITH †
ROWLAND TOMPKINS

SUBCOMMITTEE CHAIRMAN

Subcommittee on Revision, F. G. HIGBEE

GRAPHIC PRESENTATION (Z15)

** Sole sponsorship. Sectional Committee organized December, 1926*

A.S.M.E. Members (Total personnel, 31)

G. E. HAGEMANN, *Secretary* †
C. M. BIGELOW
WALLACE CLARK
T. E. FRENCH
D. B. PORTER †

SUBCOMMITTEE CHAIRMEN

No. 1 on Plan and Scope (to be appointed)
No. 2 on Terminology (to be appointed)
No. 3 on Preferred Practice for Time Series Charts, A. H. RICHARDSON
No. 4 on Engineering and Scientific Graphs, W. A. SHEWHART

GRAPHICAL SYMBOLS AND ABBREVIATIONS FOR USE ON DRAWINGS (Z32)

** Joint sponsorship with American Institute of Electrical Engineers. Sectional Committee organized June, 1936*

A.S.M.E. Members (Total personnel, 48)

E. E. ASHLEY
J. M. BARNES
T. E. FRENCH †
G. F. HABACH
D. T. HAMILTON
J. J. HARMAN
W. C. MUELLER
L. L. MUNIER
F. C. PANUSKA †
W. C. STEWART
T. R. THOMAS

SUBCOMMITTEE CHAIRMEN

No. 1 on Symbols for Use in Mechanical Engineering, T. E. FRENCH
No. 2 on Symbols for Use in Electrical Engineering, H. W. SAMSON
No. 3 on Abbreviations for Use on Drawings, T. E. FRENCH

DEVELOPMENT OF STATISTICAL APPLICATIONS IN ENGINEERING AND MANUFACTURING

Joint sponsorship with the American Mathematical Society, American Society for Testing Materials, American Statistical Association, and Institute of Mathematical Statistics. Appointed in December, 1929

A.S.M.E. Members (Total personnel, 9)

A. G. ASHCROFT
W. H. FULWEILER
L. K. SILLCOX †
J. S. TAWRESEY †

A.S.M.E. Representatives on Miscellaneous Standardization Committees

See also A.S.M.E. Representatives on Other Activities, page RI-9

ACOUSTICAL MEASUREMENTS AND TERMINOLOGY (Z24)

** Sponsor body: Acoustical Society of America*

F. H. LEWIS

AERONAUTICS (D9)

** Sponsor body: Society of Automotive Engineers*

E. A. SPERRY, JR.

BUILDING CODE REQUIREMENTS FOR LIGHT AND VENTILATION (A53)

** Sponsor bodies: Federal Housing Administration, and U.S. Public Health Service*

F. R. SCHERER

CAST IRON AT ELEVATED TEMPERATURES

Subcommittee of American Society for Testing Materials Committee A-3 on Cast Iron

D. B. ROSSHEIM

COAL AND COKE (D5)

Committee of American Society for Testing Materials

R. M. HARDGROVE

DEFINITIONS OF ELECTRICAL TERMS (C42)

** Sponsor body: American Institute of Electrical Engineers*

F. O. ELLENWOOD

DRAINAGE OF COAL MINES (M6)

** Sponsor body: American Mining Congress*

O. M. PRUITT

ELECTRIC WELDING APPARATUS (C52)

** Sponsor bodies: American Welding Society*

R. E. KINKEAD

FOREST FIRE PROTECTION

Committee of National Fire Protection Association

C. B. WHITE

JOINT CONFERENCE COMMITTEE ON PIPING CODES AND STANDARDS

C. A. KELTING, *Chairman*
SABIN CROCKER
V. M. FROST
E. D. GRIMISON
A. M. HOUSER
ALFRED IDDLES
J. R. KRUSE
F. H. MOREHEAD
D. B. ROSSHEIM
J. H. ZINK

LOADING PLATFORMS AT FREIGHT TERMINALS AND WAREHOUSES (E12)

** Sponsor body: American Trucking Association, Inc.*

M. C. MAXWELL

MANHOLE FRAMES AND COVERS (A35)

** Sponsor bodies: ASA Telephone Group, and American Society of Civil Engineers*

ANTON HANSEN

ASA MECHANICAL STANDARDS COMMITTEE

ALFRED IDDLES, *Chairman* †
(A. L. BAKER, *Alternate*) †
J. E. ENNIS
(K. CARTWRIGHT, *Alternate*)
E. W. ERNEST
F. O. HOAGLAND
(M. E. LANGE, *Alternate*)
E. L. HOPPING
F. H. MOREHEAD
(A. M. HOUSER, *Alternate*)
H. H. MORGAN
FRANK THORNTON, JR.
H. L. WHITTEMORE, *Alternate*

Executive Committee,
ALFRED IDDLES
J. E. ENNIS

METHODS OF TESTING WOOD (04)

** Sponsor bodies: U.S. Forest Service, and American Society for Testing Materials*

C. M. BIGELOW

MISCELLANEOUS OUTSIDE COAL-HANDLING EQUIPMENT (M10)

** Sponsor body: American Mining Congress*

RALPH SARGENT

PETROLEUM PRODUCTS AND LUBRICANTS (Z11)

** Sponsor body: American Society for Testing Materials*

R. G. N. EVANS
S. J. NEEDS
(H. J. MASSON, *Alternate*)

PREFERRED NUMBERS (Z17)

** Special Committee of ASA*

K. H. CONDIT

RATING OF RIVERS (A36)

** Sponsor body: U.S. Geological Survey*

D. W. MEAD

REQUIREMENTS FOR THE INSTALLATION OF GAS BURNING EQUIPMENT IN POWER BOILERS (Z21)

** Sponsor body: American Gas Association*

O. F. CAMPBELL

ROTATING ELECTRICAL MACHINERY (C50)

** Sponsor body: ASA Electrical Standards Committee*

(To be appointed)

SPECIFICATIONS FOR CAST IRON PIPE AND SPECIAL CASTINGS (A21)

** Sponsor bodies: American Gas Association, American Society for Testing Materials, American Water Works Association, and the New England Water Works Association*

J. E. GIBSON L. R. HOWSON

SPECIFICATIONS FOR CLEAN BITUMINOUS COAL (M26)

** Sponsor body: American Institute of Mining and Metallurgical Engineers*

R. A. SHERMAN
(E. L. LINDSETH, *Alternate*)

SPECIFICATIONS FOR FIRE TESTS OF BUILDING CONSTRUCTION AND MATERIALS (A2)

** Sponsor bodies: ASA Fire Protection Group, National Bureau of Standards, and American Society for Testing Materials*

R. C. PARLETT

SPECIFICATIONS FOR SIEVES FOR TESTING PURPOSES (Z23)

** Sponsor bodies: American Society for Testing Materials, and National Bureau of Standards*

R. M. HARDGROVE

ASA STANDARDS COUNCIL

ALFRED IDDLES †
J. E. LOVELY †
(C. B. LEPAGE, *Alternate*) †
(W. C. MUELLER, *Alternate*) †

COMMITTEE ON STANDARDIZATION OF STEAM TURBINES

K. M. IRWIN, *Chairman*
G. A. GAFFERT, *Secretary*
R. C. ALLEN
C. B. CAMPBELL
A. G. CHRISTIE
E. H. KRIEG
A. L. PENNIMAN, JR.
W. F. RYAN
G. B. WARREN

SPECIAL COMMITTEE ON STANDARDIZATION OF THERBLIGS, PROCESS CHARTS, AND THEIR SYMBOLS

D. B. PORTER, *Chairman*
G. M. VARGA, *Secretary*
R. W. ALLEN
R. M. BARNES
C. H. COX
L. M. GILBRETH
J. M. JURAN
H. B. MAYNARD
J. A. PIACITELLI

THERMAL INSULATING MATERIALS (C16)

Committee of American Society for Testing Materials

R. H. HEILMAN

U.S. INTERDEPARTMENTAL COMMITTEE ON SCREW THREADS

EARLE BUCKINGHAM J. W. HUCKERT
A. M. HOUSER

VOLUME WATER HEATING

Committee of American Gas Association

MARC RESEK

WIRE ROPES FOR MINES (M11)

** Sponsor body: American Mining Congress*

E. S. WELLHOFER

POWER TEST CODES COMMITTEES

ARTICLE B6A, PAR. 27: The Standing Committee on Power Test Codes shall, under the direction of the Council, have supervision of all the activities of the Society in connection with the A.S.M.E. Power Test Codes, including the interpretation of such codes.

The first Standing Committee on Power Test Codes was organized in December, 1918, to revise and extend the Power Test Codes which had been formulated by various technical committees appointed to develop particular codes. This work began in 1884.

STANDING COMMITTEE

FRANCIS HODGKINSON, *Chairman* (1944)
A. G. CHRISTIE, *Vice-Chairman* (1946)
J. J. JACOBS, JR., *Junior Observer* (1944)

Term expires 1944

C. H. BERRY
FRANCIS HODGKINSON
D. S. JACOBUS
L. F. MOODY
E. B. RICKETTS

Term expires 1945

THEODORE BAUMEISTER
P. H. HARDIE
B. V. E. NORDBERG
R. J. S. PIGOTT
M. C. STUART

Term expires 1946

A. G. CHRISTIE
PAUL DISERENS
N. R. GIBSON
GEO. A. ORROK
E. B. POWELL

Term expires 1947

W. A. CARTER
W. L. H. DOYLE
H. B. OATLEY
R. B. SMITH
W. J. WOHLENBERG

Term expires 1948

LOUIS ELLIOTT
W. F. JONES
ARVID PETERSON
R. A. SHERMAN
P. W. SWAIN

---

(1) GENERAL INSTRUCTIONS

Appointed December, 1918

Reorganized, 1939

THEODORE BAUMEISTER, *Chairman*
PAUL DISERENS
HENRY KREISINGER
A. R. MUMFORD
R. H. SNYDER
C. R. SODERBERG
M. C. STUART
P. W. SWAIN

(2) DEFINITIONS AND VALUES

Appointed December, 1918

Reorganized, 1936

R. J. S. PIGOTT, *Chairman*
L. J. BRIGGS
W. F. DAVIDSON
L. S. MARKS
G. S. PETERSON
F. G. PHILO
J. C. SMALLWOOD
P. W. SWAIN
A. C. WOOD

(3) FUELS

Appointed December, 1918

W. J. WOHLENBERG, *Chairman*
E. G. BAILEY
H. W. BROOKS
S. B. FLAGG
D. M. MYERS
F. G. PHILO
G. S. POPE
E. B. RICKETTS
E. X. SCHMIDT
E. N. TRUMP

(4) STATIONARY STEAM-GENERATING UNITS

Appointed December, 1918

E. R. FISH, *Chairman*
A. D. BAILEY
M. W. BENJAMIN
B. J. CROSS
MARTIN FRISCH
P. H. HARDIE
R. M. HARDGROVE
ALFRED IDDLES
E. L. LINDSETH
E. L. MCDONALD
E. B. POWELL
R. SHELLENBERGER
R. L. SPENCER

(5) RECIPROCATING STEAM ENGINES

Appointed December, 1918

Reorganized, 1931

A. G. CHRISTIE, *Chairman*
K. S. M. DAVIDSON
HENRIK GREGER
J. A. HUNTER
H. G. MUELLER
B. V. E. NORDBERG
A. V. SAHAROFF
A. G. WITTING

(6) STEAM TURBINES

Appointed December, 1918

C. H. BERRY, *Chairman*
I. E. MOULTROP, *Secretary*
O. D. H. BENTLEY
W. E. CALDWELL
C. B. CAMPBELL
A. G. CHRISTIE
H. P. DAHLSTRAND
V. M. FROST
A. E. GRUNERT
FRANCIS HODGKINSON
S. A. MOSS
R. O. MULLER
T. E. PURCELL
G. B. WARREN

(7) RECIPROCATING STEAM-DRIVEN DISPLACEMENT PUMPS

Appointed December, 1918

R. D. HALL, *Chairman*
E. H. BROWN
J. E. GIBSON
G. L. KOLLBERG
M. B. MACNEILLE
D. W. MEAD
L. A. QUAYLE

(8) CENTRIFUGAL AND ROTARY PUMPS

Appointed December, 1918

Reorganized, 1936

R. L. DAUGHERTY, *Chairman*
H. E. BECKWITH
R. G. FOLSOM
R. C. GLAZEBROOK
W. B. GREGORY
R. T. KNAPP
J. B. LINCOLN
M. B. MACNEILLE
L. F. MOODY
ARVID PETERSON
F. H. ROGERS
W. C. RUDD
MAX SPILLMAN
F. G. SWITZER
W. M. WHITE
I. A. WINTER

(9) DISPLACEMENT COMPRESSORS AND BLOWERS

Appointed December, 1918

Reorganized, 1935

PAUL DISERENS, *Chairman*
G. T. FELBECK
C. R. HOUGHTON
J. F. HUVANE
R. M. JOHNSON
J. F. D. SMITH

(10) CENTRIFUGAL AND TURBO-COMPRESSORS AND BLOWERS

Appointed December, 1918

Reorganized, 1929

ARVID PETERSON, *Chairman*
M. C. STUART, *Chairman* (Fans)
E. L. ANDERSON
THEODORE BAUMEISTER
C. A. BOOTH
W. H. CARRIER
THOMAS CHESTER
E. D. CURLEY
L. E. DAY
Z. G. DEUTSCH
S. H. DOWNS
P. E. GOOD
J. J. GROB

(*Continued*)

(10) CENTRIFUGAL AND TURBO-COMPRESSORS AND BLOWERS

(Continued)

H. F. Hagen
F. H. Jenkins
R. M. Johnson
W. E. Johnson
H. D. Kelsey
W. W. Lawrence
R. D. Madison
J. H. Marchant
L. S. Marks
R. B. Smith

(12) CONDENSERS, WATER HEATING, AND COOLING EQUIPMENT

Appointed December, 1918

Geo. A. Orrok, *Chairman*
P. H. Hardie, *Secretary*
C. H. Baker, Jr.
J. F. Grace
D. W. R. Morgan
H. B. Reynolds
P. E. Reynolds

(13) REFRIGERATING SYSTEMS

Appointed December, 1918

Reorganized May, 1939

B. H. Jennings, *Chairman* †
A. C. Buensod
(R. W. Waterfill, *Alternate*)
J. C. Consley
(H. B. Pownall, *Alternate*)
R. G. Ewer †
W. F. Jones †
M. A. Nelson †
A. W. Oakley
C. L. Svenson
Frank Zumbro †

(14) EVAPORATING APPARATUS

Appointed December, 1918

E. N. Trump, *Chairman*
B. N. Bump
E. A. Newhall
H. L. Parr
L. C. Rogers

† Official A.S.M.E. representative serving on this committee.

(15) STEAM LOCOMOTIVES

Appointed December, 1918

W. F. Kiesel
H. B. Oatley
G. E. Rhoads
L. K. Sillcox

(16) GAS PRODUCERS

Appointed December, 1918

C. D. Smith

(17) INTERNAL-COMBUSTION ENGINES

Appointed December, 1918

Reorganized, 1939

Lee Schneitter, *Chairman*
F. H. Dutcher, *Secretary*
J. C. Barnaby
G. C. Boyer
H. E. Degler
W. L. H. Doyle
L. B. Jackson
E. J. Kates
E. C. Magdeburger
B. V. E. Nordberg
Russell Pyles
M. J. Reed
O. D. Treiber

(18) HYDRAULIC PRIME MOVERS

Appointed December, 1918

Reorganized, 1931

S. L. Kerr, *Chairman*
C. M. Allen
L. M. Davis
H. L. Doolittle
W. F. Durand
N. R. Gibson
J. P. Growdon
T. H. Hogg
L. J. Hooper
C. W. Hubbard
E. C. Hutchinson
D. J. McCormack
L. F. Moody
W. J. Rheingans
J. F. Roberts
E. B. Strowger
R. V. Terry
W. M. White

(19) INSTRUMENTS AND APPARATUS

Appointed December, 1918

W. A. Carter, *Chairman*
C. M. Allen
W. C. Andrae
E. G. Bailey
H. S. Bean
L. J. Briggs
J. D. Davis
K. J. De Juhasz
R. E. Dillon
F. M. Farmer
J. B. Grumbein
W. W. Johnson
W. H. Kenerson
E. S. Lee
E. L. Lindseth
S. A. Moss
R. J. S. Pigott
E. B. Ricketts
W. A. Sloan
R. B. Smith
I. M. Stein

(20) SPEED, TEMPERATURE AND PRESSURE RESPONSIVE GOVERNORS

Appointed December, 1921

Reorganized February, 1940

C. R. Soderberg, *Chairman*
C. L. Avery
W. L. H. Doyle
Herbert Estrada
S. N. Fiala
J. R. Hagemann
W. C. Holmes
S. L. Kerr
A. F. Schwendner
Raymond Sheppard
R. B. Smith
H. E. Stickle

(21) DUST SEPARATING APPARATUS

Appointed October, 1934

M. D. Engle, *Chairman*
Ollison Craig, *Secretary*
A. D. Bailey
H. H. Bubar
W. G. Christy
H. O. Croft
J. M. DallaValle
H. O. Danz
H. C. Dohrmann
J. W. Fehnel
H. F. Hagen
P. H. Hardie
C. W. Hedberg
J. H. Leech
H. E. Macomber
H. C. Murphy
B. F. Tillson

A.S.M.E. Representatives on Other Technical Committees

See also A.S.M.E. Representatives on Other Activities, page RI-9

DEVELOPMENT OF DEFINITIONS FOR THE NET CALORIFIC VALUE AND GROSS CALORIFIC VALUE OF FUELS

Sponsor body: American Society for Testing Materials

W. J. Wohlenberg

COMMITTEE ON REDEFINING SO-CALLED STANDARD TON OF REFRIGERATION

Sponsor body: American Society of Refrigerating Engineers

G. B. Bright

COMMITTEE ON GASEOUS FUELS

Sponsor body: American Society for Testing Materials

E. X. Schmidt

COAL TESTING CODE COMMITTEE

Joint sponsorship with the American Institute of Mining and Metallurgical Engineers

A. R. Mumford

SPECIFICATIONS FOR PRIME MOVER SPEED GOVERNING

Joint sponsorship with the American Institute of Electrical Engineers

C. L. Avery
Herbert Estrada
J. R. Hagemann
A. F. Schwendner
Raymond Sheppard
C. R. Soderberg

SAFETY COMMITTEES

ARTICLE B6A, PAR. 25: The Standing Committee on Safety shall advise the Council on the activities of the Society having to do with engineering and industrial safety, except the activities of the Boiler Code Committee, for which special provision is made.

The first Standing Committee on Safety was appointed in October, 1921.

STANDING COMMITTEE

J. J. ZEITNER (1944)
E. R. GRANNISS (1945)
H. W. GABOR (1946)
J. R. CONNELLY (1947)
R. B. RENNER (1948)

SAFETY CODE FOR ELEVATORS (A17)

** Joint sponsorship with The American Institute of Architects, and the National Bureau of Standards. Sectional Committee originally organized November, 1922*

Reorganized June, 1940

A.S.M.E. Members (Total personnel, 50)

O. P. CUMMINGS
C. R. CALLAWAY
J. W. DEGEN
D. L. HOLBROOK †
BASSETT JONES
D. L. LINDQUIST
M. B. MCLAUTHLIN
W. S. PAINE
W. H. SEAQUIST, *Alternate* †
S. F. VOORHEES
H. L. WHITTEMORE

SUBCOMMITTEE CHAIRMEN

Executive Committee, D. J. PURINTON
Emergency Elevator Rules, D. J. PURINTON
Existing Elevators, D. J. PURINTON
Inspectors' Manual, K. A. COLAHAN
Mechanical Safety Equipment, D. L. LINDQUIST
Wire Rope, D. J. PURINTON
Working, G. H. REPPERT

SAFETY CODE FOR MECHANICAL POWER TRANSMISSION APPARATUS (B15)

** Joint sponsorship with the International Association of Industrial Accident Boards and Commissions, and the National Conservation Bureau. Sectional Committee organized February, 1921*

A.S.M.E. Members (Total personnel, 24)

G. M. NAYLOR, *Chairman* †
P. G. RHOADS, *Secretary*
D. C. WRIGHT †

SUBCOMMITTEE CHAIRMEN

No. 1 on Detail Classification of Belts (to be appointed)
No. 2 on Modification of Rule 223 for Cone Pulley Belt (to be appointed)
No. 3 on Mechanical Power Control (to be appointed)
No. 4 on Use of ASA Code Versus State Codes (to be appointed)
No. 5 on Statistics on Place of Occurrence of Accidents (to be appointed)
No. 6 on V-Belt Drives, D. C. WRIGHT

* Note: All of the safety committees for which the Society is sponsor or joint sponsor, or on which it has representation, are organized under the procedure of the American Standards Association.

† Official A.S.M.E. representative serving on this committee.

SAFETY CODE ON COMPRESSED AIR MACHINERY AND EQUIPMENT (B19)

** Joint sponsorship with the American Society of Safety Engineers—Engineering Section of National Safety Council. Sectional Committee organized May, 1923*

A.S.M.E. Members (Total personnel, 24)

D. L. ROYER, *Chairman*
H. D. EDWARDS
W. J. GRAVES

SAFETY CODE FOR CONVEYORS AND CONVEYING MACHINERY (B20)

** Joint sponsorship with the National Conservation Bureau. Sectional Committee originally organized November, 1925, reorganized, April, 1937*

A.S.M.E. Members (Total personnel, 51)

D. L. ROYER, *Chairman*
W. J. GRAVES
M. A. KENDALL †
(N. W. ELMER, *Alternate*) †
P. T. ONDEDONK
C. G. PFEIFFER
R. B. RENNER
F. J. SHEPARD, JR.
J. G. WHEATLEY

SUBCOMMITTEE CHAIRMEN

No. 1 on All Types of Chain Conveyors, Belt Conveyors, Belt Elevators Including Steel Belt, and Screw, Track or Scraper Conveyors, C. G. PFEIFFER
No. 2 on Gravity Conveyors and Chutes, Live Roll Conveyors, H. G. DALTON
No. 3 on Cable-Operated and Cable Flight Conveyors and Cableways, R. MCA. KEOWN
No. 4 on Air, Steam, or Liquid Conveyors, J. J. MCNULTA
No. 5 on Tiering, Piling, and Stacking Conveyors, J. G. WHEATLEY

SAFETY CODE FOR CRANES, DERRICKS, AND HOISTS (B30)

** Joint sponsorship with U.S. Navy Department, Bureau of Yards and Docks. Sectional Committee organized November, 1926*

A.S.M.E. Members (Total personnel, 52)

LEWIS PRICE † — R. H. WHITE †
F. H. SCHWERIN — H. L. WHITTEMORE

SUBCOMMITTEE CHAIRMEN

Executive Committee, J. C. WHEAT
No. 1 on Overhead and Gantry Cranes, R. H. WHITE
No. 2 on Locomotive and Tractor Cranes, H. H. VERNON
No. 3 on Derricks and Hoists, LEWIS PRICE
No. 4 on Miscellaneous Equipment for Cranes and Hoists, L. W. HOPKINS
No. 5 on Jacks, E. W. CARUTHERS
Editing Committee, H. H. VERNON

A.S.M.E. Representatives on Other Safety Committees

See also A.S.M.E. Representatives on Other Activities, page RI-9

SAFETY CODE FOR ABRASIVE WHEELS (B7)

** Sponsor bodies: Grinding Wheel Manufacturers Association of United States and Canada, and International Association of Industrial Accident Boards and Commissions*

J. B. CHALMERS

SAFETY CODE FOR CONSTRUCTION WORK (A10)

** Sponsor bodies: The American Institute of Architects, and National Safety Council*

C. H. O'NEIL

COOPERATION WITH OTHER ENGINEERING SOCIETIES

Committee of American Society of Safety Engineers—Engineering Section of National Safety Council

H. L. MINER

ASA SAFETY CODE CORRELATING COMMITTEE

H. W. GABOR
(J. J. ZEITNER, *Alternate*)

SAFETY CODE FOR EXHAUST SYSTEMS (Z9)

** Sponsor body: International Association of Industrial Accident Boards and Commissions*

T. F. HATCH

SAFETY CODE FOR FLOOR AND WALL OPENINGS, RAILINGS AND TOE BOARDS (A12)

** Sponsor body: National Safety Council*

A. E. WINDLE

SAFETY CODE FOR FORGING AND HOT METAL STAMPING (B24)

** Sponsor bodies: American Drop Forging Institute, and National Safety Council*

C. F. PARK

SAFETY CODE FOR LADDERS (A14)

** Sponsor body: American Society of Safety Engineers—Engineering Section of National Safety Council*

H. C. HOUGHTON

SAFETY CODE FOR LAUNDRY MACHINERY AND OPERATION (Z8)

* *Sponsor bodies: American Institute of Laundering, International Association of Governmental Labor Officials, and National Association of Mutual Casualty Companies*

E. J. CARROLL

SAFETY CODE FOR LIGHTING FACTORIES, MILLS, AND OTHER WORK PLACES (A11)

* *Sponsor body: Illuminating Engineering Society*

A. W. LUCE

LOW VOLTAGE ELECTRICAL HAZARDS

Special Committee of the American Society of Safety Engineers—Engineering Section of National Safety Council

J. P. JACKSON

SAFETY CODE FOR MECHANICAL REFRIGERATION (B9)

* *Sponsor body: American Society of Refrigerating Engineers*

O. A. ANDERSON
CROSBY FIELD
E. W. GALLENKAMP
W. F. JONES
(A. W. OAKLEY, *Alternate to all A.S.M.E. Representatives*)

PANEL OF CONSULTANTS TO ADVISE THE MERCHANT MARINE COUNCIL AT U.S. COAST GUARD HEADQUARTERS, WASHINGTON, D.C.

D. S. JACOBUS

SAFETY CODE FOR PAPER AND PULP MILLS (P1)

* *Sponsor body: National Safety Council*

R. L. WELDON

SAFETY CODE FOR POWER PRESSES AND FOOT AND HAND PRESSES (B11)

* *Sponsor body: National Safety Council*

J. B. CHALMERS

SAFETY CODE FOR PREVENTION OF DUST EXPLOSIONS (Z12)

* *Sponsor bodies: National Fire Protection Association, and U.S. Department of Agriculture*

R. M. FERRY

SAFETY CODE FOR PROTECTION OF HEADS, EYES, AND RESPIRATORY ORGANS OF INDUSTRIAL WORKERS (Z2)

* *Sponsor body: National Bureau of Standards*

T. A. WALSH, JR.
(T. F. HATCH, *Alternate*)

SAFETY CODE FOR PROTECTION OF INDUSTRIAL WORKERS IN FOUNDRIES (B8)

H. M. LANE

SAFETY IN QUARRY OPERATIONS (M28)

* *Sponsor body: National Safety Council*

REDFIELD PROCTOR

SAFETY CODE FOR RUBBER MACHINERY (B28)

* *Sponsor bodies: International Association of Industrial Accident Boards and Commissions and National Safety Council*

E. S. AULT

SPECIFICATIONS AND METHOD OF TEST FOR SAFETY GLASS (Z26)

* *Sponsor bodies: National Bureau of Standards and National Conservation Bureau*

T. A. WALSH, JR.

SAFETY CODE FOR TEXTILES (L1)

* *Sponsor body: National Safety Council*

M. A. GOLRICK, JR.

SAFETY CODE FOR VENTILATION (Z5)

* *Sponsor body: American Society of Heating and Ventilating Engineers*

T. F. HATCH

SAFETY CODE FOR WALKWAY SURFACES (A22)

* *Sponsor bodies: The American Institute of Architects, and American Society of Safety Engineers—Engineering Section of National Safety Council*

G. K. PALSGROVE

SAFETY CODE FOR WORK IN COMPRESSED AIR (Z28)

* *Sponsor body: International Association of Industrial Accident Boards and Commissions*

L. J. EIBSEN

BOILER CODE COMMITTEES

ARTICLE B6A, PAR. 26: The Special Committee on Boiler Code shall, under the direction of the Council, have supervision of all the activities of the Society in connection with the A.S.M.E. Codes for Pressure Vessels, including the interpretations of these codes.

The first Special Committee on Boiler Code was organized in September, 1911.

SPECIAL COMMITTEE

E. R. FISH, *Chairman*
H. B. OATLEY, *Vice-Chairman*
D. S. JACOBUS, *Honorary Chairman*
C. A. ADAMS
H. E. ALDRICH
T. B. ALLARDICE
H. C. BOARDMAN
PERRY CASSIDY
R. E. CECIL
A. J. ELY
V. M. FROST
C. E. GORTON
W. G. HUMPTON
J. O. LEECH
C. O. MYERS
C. W. OBERT
JAMES PARTINGTON
D. B. ROSSHEIM
D. L. ROYER
WALTER SAMANS
J. W. TURNER
S. K. VARNES
A. C. WEIGEL

J. W. SHIELDS, *Secretary*
M. JURIST, *Assistant Secretary*

Honorary Members

W. H. BOEHM
W. F. DURAND
A. M. GREENE, JR.
C. L. HUSTON
W. F. KIESEL, JR.
M. F. MOORE
I. E. MOULTROP
H. LEROY WHITNEY

CONFERENCE COMMITTEE

T. R. ARCHER, Delaware
L. M. BARRINGER, Seattle, Wash.
J. G. BOLLOCK, St. Joseph, Mo.
B. M. BOOK, Pennsylvania
A. C. BOZEMAN, Knoxville, Tenn.
E. J. BROCK, St. Louis, Mo.
H. S. BRUNSON, Minnesota
E. S. CARPENTER, Rhode Island
S. CHERRINGTON, Ohio
CITY BOILER INSPR., Parkersburg, W.Va.
A. J. CLAY, Memphis, Tenn.
D. J. CODY, Kansas City, Mo.
A. L. COLBY, Louisiana
A. J. CONWAY, Indiana
M. A. EDGAR, Wisconsin
M. FOGARTY, Washington
C. W. FOSTER, Omaha, Neb.
W. H. FURMAN, New York
F. D. GARVIN, Houston, Tex.
GERALD GEARON, Chicago, Ill.
MATTHEW GIBSON, Maryland
J. W. GIBSON, Michigan
C. W. HARNESS, Iowa
R. C. JOUGHIN, Tampa, Fla.
H. K. KUGEL, District of Columbia
P. N. LEHOCZKY, Ohio
J. E. LEDDY, New Orleans, La.
E. C. LUSTER, Miami, Fla.
C. E. MCGINNIS, Los Angeles, Calif.
H. H. MILLS, Detroit, Mich.
J. A. MURDOCK, Massachusetts
J. D. NEWCOMB, JR., Arkansas
W. L. NEWTON, Oklahoma
F. A. PAGE, California *
L. C. PEAL, Nashville, Tenn.
J. D. REED, Texas
C. SATTLER, West Virginia
E. K. SAWYER, Maine
J. F. SCOTT, New Jersey
F. H. SHUFORD, North Carolina
C. I. SMITH, Utah
F. M. SMITH, Oregon
WM. E. SMITH, Hawaiian Islands
J. A. STRAIT, Tulsa, Okla.
A. E. WHITE
R. L. WILSON

* Deceased June 7, 1943.

EXECUTIVE COMMITTEE

D. S. JACOBUS, *Chairman*
H. E. ALDRICH, *Vice-Chairman*
E. R. FISH
V. M. FROST
C. E. GORTON
H. B. OATLEY
C. W. OBERT
JAMES PARTINGTON

SUBCOMMITTEES

Boilers of Locomotives

JAMES PARTINGTON, *Chairman*
F. H. CLARK
J. M. HALL
H. B. OATLEY

Care of Steam Boilers and Other Pressure Vessels in Service

F. M. GIBSON, *Chairman*
D. C. CARMICHAEL
V. M. FROST
J. R. GILL
FRANK HENRY
J. A. HUNTER
H. J. KERR
P. B. PLACE
S. T. POWELL
C. W. RICE
J. B. ROMER
W. C. SCHROEDER
F. G. STRAUB

Coordination

V. M. FROST, *Chairman*
E. R. FISH
C. W. OBERT

Ferrous Materials

D. B. ROSSHEIM, *Chairman*
A. B. BAGSAR
L. D. BURRITT
E. C. CHAPMAN
C. L. CLARK
A. J. ELY
H. J. FRENCH
M. B. HIGGINS
A. M. HOUSER
W. G. HUMPTON
A. HURTGEN
T. MCL. JASPER
J. J. KANTER
H. J. KERR
A. B. KINZEL
L. J. MASON
N. L. MOCHEL
E. L. ROBINSON
A. P. SPOONER
S. K. VARNES

Heating Boilers

J. W. TURNER, *Chairman*
C. E. BRONSON
T. CASSERLY
J. A. DARTS
WM. FERGUSON
C. E. GORTON
L. N. HUNTER

Material Specifications

J. O. LEECH, *Chairman Pro Tem*
PERRY CASSIDY
W. G. HUMPTON
P. J. SMITH
T. G. STITT
A. C. WEIGEL

Miniature Boilers

C. E. GORTON, *Chairman*
W. H. FURMAN
C. W. OBERT

Nonferrous Materials

H. B. OATLEY, *Chairman*
J. J. AULL
W. F. BURCHFIELD
D. K. CRAMPTON
J. R. FREEMAN, JR.
A. M. HOUSER
E. F. MILLER
JOSEPH PRICE
R. L. TEMPLIN

Power Boilers

H. E. ALDRICH, *Chairman*
T. B. ALLARDICE
PERRY CASSIDY
E. R. FISH
V. M. FROST
D. L. ROYER
A. C. WEIGEL

Rules for Inspection

D. L. ROYER, *Chairman*
T. B. ALLARDICE
W. H. FURMAN
E. B. VAN SANT
GUSTAVE WELTER

Special Design

D. B. WESSTROM, *Chairman*
H. C. BOARDMAN
R. E. CECIL
T. W. GREENE
F. L. PLUMMER
D. B. ROSSHEIM
E. O. WATERS
F. S. G. WILLIAMS

Unfired Pressure Vessels

E. R. FISH, *Chairman*
C. A. ADAMS
C. E. BRONSON
R. E. CECIL
PAUL DISERENS
H. S. SMITH
D. B. WESSTROM

WELDING

Members of A.S.M.E. Boiler Code Committee

JAMES PARTINGTON, *Chairman*
O. R. CARPENTER
E. C. CHAPMAN
J. H. DEPPELER
W. D. HALSEY
R. K. HOPKINS
J. T. PHILLIPS
L. A. SHELDON

Members of Conference Committee of American Welding Society

C. W. OBERT, *Chairman*
C. A. ADAMS
H. C. BOARDMAN
WALTER SAMANS
A. C. WEIGEL

SPECIAL COMMITTEES

APPROVAL OF NEW MATERIALS

C. A. ADAMS, *Chairman*

CAST IRON IN UNFIRED PRESSURE VESSELS

H. C. BOARDMAN, *Chairman*

CLAD VESSELS

S. K. VARNES, *Chairman*

FAILURE OF SPHERICAL HYDROGEN STORAGE TANK

F. L. NEWCOMB, *Chairman*

FEEDWATER

C. W. RICE, *Chairman*

FUSIBLE PLUGS

V. M. FROST, *Chairman*

ISSUANCE OF CODE SYMBOL STAMPS

C. O. MYERS, *Chairman*

LAYER VESSELS

H. C. BOARDMAN, *Chairman*

MATERIAL SPECIFICATIONS FOR PIPING, VALVES AND FITTINGS

A. C. WEIGEL, *Chairman*

NOZZLE CONSTRUCTION

WALTER SAMANS, *Chairman*

RADIOGRAPHIC EXAMINATION OF WELDED JOINTS

C. A. ADAMS, *Chairman*

REVISION OF SECTION VIII OF THE A.S.M.E. BOILER CODE

E. R. FISH, *Chairman*

RULES FOR BOLTED FLANGED CONNECTIONS

F. S. G. WILLIAMS, *Acting Chairman*

RULES FOR DISHED HEADS

H. C. BOARDMAN, *Chairman*

RULES FOR OPENINGS

T. D. TIFFT, *Chairman*

SAFETY VALVE REQUIREMENTS

H. B. OATLEY, *Chairman*

WORK OF BOILER CODE COMMITTEE

H. E. ALDRICH, *Chairman*

API-ASME COMMITTEE ON UNFIRED PRESSURE VESSELS

WALTER SAMANS, *Chairman*

A.S.M.E. Representatives

R. E. CECIL
E. R. FISH
D. S. JACOBUS
T. McL. JASPER
JAMES PARTINGTON

A.P.I. Representatives

A. J. ELY
M. B. HIGGINS
K. V. KING
WALTER SAMANS
T. D. TIFFT

THE WOMAN'S AUXILIARY TO THE A.S.M.E.

The Woman's Auxiliary to the A.S.M.E. was organized on May 10, 1923, and its Constitution and By-Laws was approved by the Council of the A.S.M.E. on October 27, 1924. The objects of the Auxiliary are to render service to all that pertains to the interest of the profession of mechanical engineering; to cooperate with any committees of the A.S.M.E.; and to assist the sons and daughters of the members of the Society or worthy students of mechanical engineering in obtaining scholarships; and to promote any other objects consistent with the aims or objects of the A.S.M.E.

NATIONAL OFFICERS

President, MRS. R. F. GAGG
First Vice-President, MRS. COLLINS P. BLISS
Second Vice-President, MRS. G. W. FARNY
Third Vice-President, MRS. R. M. GATES
Fourth Vice-President, MRS. JUSTIN J. MCCARTHY
Fifth Vice-President, MRS. S. F. DUNCAN
Recording Secretary, MRS. MATTHEW S. CUMNER
Corresponding Secretary, MRS. CROSBY FIELD
Treasurer, MRS. CHARLES E. GUS

STANDING COMMITTEE CHAIRMEN

Student Loan, MRS. F. M. GIBSON
Membership, MRS. G. E. HAGEMANN
Calvin W. Rice Scholarship, MRS. J. NOBLE LANDIS

COUNCIL REPRESENTATIVES

HAROLD V. COES
WARREN H. MCBRYDE

OFFICERS OF LOCAL SECTIONS

CLEVELAND

Chairman, MRS. EUGENE R. MCCARTHY

LOS ANGELES

Chairman, MRS. BURNIE M. CRAIG

METROPOLITAN

Chairman, MRS. EARL B. SMITH
First Vice-Chairman, MRS. WALDO MCC. MCKEE
Second Vice-Chairman, MRS. G. J. NICASTRO
Third Vice-Chairman, MRS. C. HIGBIE YOUNG
Recording Secretary, MRS. ERIK OBERG
Corresponding Secretary, MRS. C. F. KAYAN
Treasurer, MRS. A. W. ANDERSON

PHILADELPHIA

Chairman, MRS. JOHN A. FRANSEMA

AWARDS

The following paragraphs deal with the medals, awards, scholarships, and loan funds which come within the jurisdiction of the A.S.M.E. Other awards available to Student-members are listed in *Mechanical Engineering*, February, 1938, page 183. The Society also participates with other engineering societies in a number of joint awards. Further details concerning all the awards may be obtained from the headquarters of the Society.

Honorary Membership, to which persons of acknowledged professional eminence are elected by unanimous vote of Council under the provisions of the By-Laws and Rules. A list of honorary members is given on page RI-43.

Life Membership, which may be conferred by the Council for distinguished service to the Society; or secured by a member by payment for an annuity in accordance with the provisions of the By-Laws.

A.S.M.E. Medal, established by the Society in 1920 to be presented, together with an engraved certificate, for distinguished service in engineering and science. May be awarded for general service in science having possible application in engineering.

Holley Medal, instituted and endowed in 1924 by George I. Rockwood, Past Vice-President of the Society, to be bestowed, together with an engraved certificate, for some great and unique act of genius of engineering nature that has accomplished a great and timely public benefit.

Worcester Reed Warner Medal, established in 1930, provision for which was made in the will of Worcester Reed Warner, Honorary Member of the Society, is a gold medal to be bestowed, together with an engraved certificate, for an outstanding contribution to permanent engineering literature.

Melville Medal, established in 1914 by the bequest of Rear-Admiral George W. Melville, Honorary Member and Past-President of the Society, to be presented, together with an engraved certificate, for an original paper or thesis of exceptional merit, presented to the Society by a member for discussion and publication, to encourage excellence in papers. Only papers of single authorship are eligible. The medal may be presented annually.

Spirit of St. Louis Medal, established by an endowment fund created in 1929 by citizens of St. Louis, Mo., to be awarded for meritorious service in the advancement of aeronautics. This medal will be awarded at the discretion of the Council of the Society at approximately three-year periods upon the recommendation of its Board of Honors and Awards.

Spirit of St. Louis Junior Award, established in 1938 by an endowment fund created by the General Committee for the 1935 Aeronautic Meeting in St. Louis; a cash award of $50, made every three years, for the best paper on an aeronautic subject presented at any A.S.M.E. meeting during the three-year period either personally by the author (a Junior Member of the Society under thirty years of age) or by a Junior Member designated by him, and submitted to the Committee on Medals within a reasonable period (to be determined by the Committee) after its initial presentation.

Pi Tau Sigma Medal Award, established in 1938, endowed by Pi Tau Sigma, the national honorary mechanical engineering fraternity, to be presented annually, together with an engraved certificate, to a young mechanical engineer for outstanding achievement in his profession within the ten years after graduation from a regular four-year mechanical engineering course of a recognized American college or university. Any mechanical engineering graduate, not more than thirty-five years of age, whose achievement has been all or in part in any field including industrial, educational, political, research, civic, etc., is eligible.

Junior Award, annual cash award of $50, established in 1914, from a fund created by Henry Hess, Past Vice-President of the Society, to be presented, together with an engraved certificate, for the best paper or thesis submitted by a Junior Member. Only papers of single authorship are eligible.

Charles T. Main Award, annual cash award of $150, established in 1919 from a fund created by Charles T. Main, Past-President of the Society, to be awarded, together with an engraved certificate, to a Student-member of the Society, for the best paper within the general subject of the influence of the profession upon public life. The exact subject is assigned by the Board of Honors and Awards, subject to the approval of the Council, and is announced each year through the Honorary Chairmen of the Student Branches.

Student Awards, two annual cash awards of $25 each, established in 1914, from a fund created by Henry Hess, Past Vice-President of the Society, to be presented, together with engraved certificates, for the best papers or theses submitted by Student-members. The awards for 1932 and subsequent years have been given, one for undergraduate and the other for postgraduate work.

SCHOLARSHIPS AND LOAN FUNDS

Max Toltz: Loan Fund of $15,000 established by Major Max Toltz, former member of the Council of the Society, the income to be used for assistance to Student-members.

John R. Freeman: Fund of $25,000 established in 1926 by John R. Freeman, Past-President of the Society, the income to be used for travel scholarships and research.

Woman's Auxiliary: Educational Loan Fund offered by the Woman's Auxiliary to the Society to assist sons and daughters of members or worthy students of mechanical engineering. Calvin W Rice Memorial Scholarship Fund for students in mechanical engineering from South America.

RECIPIENTS OF AWARDS

The names of the recipients of the different awards to date are given in the following lists, together with the dates of presentation, and the services or papers for which the awards were made. There were no awards for the years not listed.

A.S.M.E. Medal

1921 Hjalmar Gotfried Carlson, in recognition of the services rendered the Government because of his invention and part in the production of 20,000,000 Mark III drawn steel booster casings used principally as a component of 75-mm high explosive shells, but also used extensively in gas shells and bombs

1922 Frederick Arthur Halsey, for his paper describing the premium system of wage payments presented before the Society at the Providence Meeting in 1891, as the adoption of the methods there proposed has had a profound effect toward harmonizing the relations of worker and employer

1923 John Ripley Freeman, for his eminent service in engineering and manufacturing by his meritorious work in fire prevention and the preservation of property

1926 R. A. Millikan, in recognition of his contributions to science and engineering

1927 Wilfred Lewis, for his contributions to the design and construction of gear teeth

1928 Julian Kennedy, for his services and contributions to the iron and steel industry

1929 William LeRoy Emmet, for his contributions in the development of the steam turbine, electric propulsion of ships, and other power-generating apparatus

1931 Albert Kingsbury, for his research and development work in the field of lubrication

1933 Ambrose Swasey, for his contributions to the advancement of the engineering profession and for his part in the development of the turret lathe and the astronomical telescope

1934 Willis H. Carrier, in recognition of his research and development work in air-conditioning

1935 Charles T. Main, for distinguished achievements in the textile and other industries, in engineering education, and for eminent service to the engineering profession

1936 Edward Bausch, for meritorious mechanical developments in the field of optics

1937 Edward P. Bullard, for outstanding leadership in the development of station-type machine tools

1938 Stephen J. Pigott, for outstanding leadership in marine propulsion and construction

1939 James E. Gleason, for service to the cause of safer and better transportation

1940 Charles F. Kettering, for outstanding inventions and research

1941 Theodor von Kármán, for his brilliance as a teacher, his researches in elasticity and many fields of physics and mechanics, and his distinguished leadership in the fields of aerodynamics and aircraft design

1942 E. G. BAILEY, for achievement and leadership in steam and combustion engineering
1943 LEWIS K. SILLCOX, pre-eminent learned technologist—lover of wisdom—inspirer of men.

HOLLEY MEDAL

1924 HJALMAR GOTFRIED CARLSON, for his inventions and processes which made possible the timely production of drawn steel booster casings for artillery ammunition, thereby aiding victory in World War I (diploma in recognition of achievements presented in 1921)
1927 ELMER AMBROSE SPERRY, for achievements and inventions that have advanced the naval arts, including the gyroscope that has freed navigation from the dangers of the fluctuating magnetic compass
1929 BARON CHUZABURO SHIBA, for his contributions to knowledge through fundamental research, including the field of aerodynamics, by the development of ultra-rapid kinematographic methods
1934 IRVING LANGMUIR, for his contributions to science and engineering, including the development of gas-filled incandescent lamps, thoriated filament for thermionic emission, atomic hydrogen welding, phase control operation of the thyratron tube, and fundamental research in oil films
1936 HENRY FORD, for revolutionary influence through invention and practice on transportation and on mass production methods in manufacturing
1937 FREDERICK G. COTTRELL, for preeminent public service—the invention of electric precipitation—advancement of the science of gas liquefaction—gifts for engineering research
1938 FRANCIS HODGKINSON, for meritorious services in the development of the steam turbine
1939 CARL E. JOHANSSON, in recognition of his pioneer work in the development of basic measuring gages
1940 EDWIN HOWARD ARMSTRONG, for his leadership in the field of radio communication
1941 JOHN C. GARAND, for the invention and development of the semi-automatic rifle, which has been adopted by the U.S. Army as the U.S. Rifle, Caliber .30, M1, an outstanding contribution to our national defense
1942 ERNEST O. LAWRENCE, for originating the cyclotron, a unique invention for producing high-speed electrified particles, and for adapting it to research in physics, chemistry, medicine, and the properties of engineering materials
1943 VANNEVAR BUSH, for machines used in easing applied mathematics from computational barriers.

WORCESTER REED WARNER MEDAL

1933 DEXTER S. KIMBALL, for his contributions to efficiency in management as exemplified by his recently revised "Principles of Industrial Organization" and by his many articles, engineering society papers, and public addresses
1934 RALPH E. FLANDERS, for his contributions to a better understanding of the relationship of the engineer to economic problems and social trends as exemplified by the many papers which he has presented
1935 STEPHEN TIMOSHENKO, for his contributions to the theory of the design of elastic structures and the treatment of dynamics of moving machinery
1936 CHARLES M. ALLEN, for his early and continued hydraulic laboratory work and for the permanent value of the papers on his development of methods of testing large hydraulic turbine installations
1937 CLARENCE F. HIRSHFELD, for his research and contributions to the theory and practice of heat-power engineering as exemplified by books and papers
1938 LAWFORD H. FRY, for contributions relating to improved locomotive boiler design and utilization of better materials in railway equipment
1939 RUPEN EKSERGIAN, for influential papers of permanent value in A.S.M.E. Transactions
1940 WILLIAM BENJAMIN GREGORY, for distinguished work in hydraulic engineering, which has been the basis for many engineering papers
1941 RICHARD VYNNE SOUTHWELL, for his many distinguished services to engineering and science through papers and publications in many fields, including aeronautics, theory of structures, elasticity, and hydrodynamics
1942 FRED H. COLVIN, for his contributions to both technical advancement and improvement in management in the metal-working industries, as influenced by more than fifty years of articles and books—particularly American Machinists' Handbook
1943 IGOR I. SIKORSKY, for contributions inspiring creative engineering, especially in aeronautics.

MELVILLE MEDAL

1927 LEON P. ALFORD, "Laws of Manufacturing Management"
1929 JOSEPH W. ROE, "Principles of Jig and Fixture Practice"
1930 HERMAN DIEDERICHS and WILLIAM D. POMEROY, "The Occurrence and Elimination of Surge or Oscillating Pressure in Discharge Lines From Reciprocating Pumps"
1931 ARTHUR E. GRUNERT, "Comparative Performance of a Pulverized-Coal-Fired Boiler Using Bin System and Unit System of Firing"
1932 ALEXEY J. STEPANOFF, "Leakage Loss and Axial Thrust in Centrifugal Pumps"
1933 WILLIAM E. CALDWELL, "Characteristics of Large Hell Gate Direct-Fired Boiler Units"
1935 OSCAR R. WIKANDER, "Draft-Gear Action in Long Trains"
1936 H. A. STEVENS HOWARTH, "The Loading and Friction of Thrust and Journal Bearings With Perfect Lubrication"
1937 ALFRED J. BÜCHI, "Supercharging of Internal-Combustion Engines With Blowers Driven by Exhaust-Gas Turbines"
1938 ALPHONSE I. LIPETZ, "Air Resistance of Railroad Equipment"
1939 LESTER M. GOLDSMITH, "High-Pressure High-Temperature Turbine-Electric Steamship *J. W. Van Dyke*"
1940 CARL A. W. BRANDT, "The Locomotive Boiler"
1941 ROGER V. TERRY, "Development of the Automatic Adjustable-Blade-Type Propeller Turbine"
1942 J. KENNETH SALISBURY, "The Steam-Turbine Regenerative Cycle—An Analytical Approach."

SPIRIT OF SAINT LOUIS MEDAL

1929 DANIEL GUGGENHEIM, founder of the Guggenheim Fund for the Promotion of Aeronautics
1932 PAUL LITCHFIELD, for his work in encouraging and sponsoring airship design and construction in this country
1935 WILL ROGERS, for his splendid, constructive, and unselfish work in the achievement of aviation, and the building up of public confidence in aviation through his articles in the press, over the radio, and from the speaker's platform
1938 JAMES H. DOOLITTLE, for meritorious service in the advancement of aeronautics
1941 JOHN E. YOUNGER, for notable contributions to the science of airplane design, particularly in the conception, analysis, and supervision of the development of the fundamental design principles, requirements, and criteria which first assured the success of the pressure-cabin type of high-altitude airplane.

SPIRIT OF SAINT LOUIS JUNIOR AWARD

1941 WILBUR W. REASER, for his paper, "Calculation of the Heat Loss from an Airplane Cabin."

PI TAU SIGMA MEDAL

1938 WILFRID E. JOHNSON, for his development work in the field of refrigeration
1939 JOHN I. YELLOTT, JR., in recognition of significant achievements in steam-flow research and engineering education; also contributions on "Supersaturated Steam" and "Condensation of Flowing Steam in Diverging Nozzles"
1940 GEORGE A. HAWKINS, for significant achievements in high-pressure steam research and engineering education
1941 R. HOSMER NORRIS, for outstanding achievement in mechanical engineering, particularly in the heat-transfer field
1942 JOHN T. RETTALIATA, for outstanding achievement in mechanical engineering.

JUNIOR AWARD

1915 ERNEST O. HICKSTEIN, "Flow of Air Through Thin Plate Orifices"
1916 L. M. MCMILLAN, "The Heat Insulating Properties of Commercial Steam-Pipe Coverings"
1919 E. D. WHALEN, "Properties of Airplane Fabrics"
1921 S. LOGAN KERR, "Moody Ejector Turbine"

1922 R. H. HEILMAN, "Heat Losses From Bare and Covered Wrought-Iron Pipe at Temperatures up to 800 Degrees Fahrenheit"
F. L. KALLAM, "Preliminary Report on the Investigation of the Thermal Conductivity of Liquids"
1923 S. S. SANFORD and SABIN CROCKER, "The Elasticity of Pipe Bends"
1924 R. H. HEILMAN, "Heat Losses Through Insulating Material"
1925 GILBERT S. SCHALLER, "An Investigation of Seattle as a Location for a Synthetic Foundry Industry"
1927 WILLIAM M. FRAME, "Stresses Occurring in the Walls of an Elliptical Tank Subjected to Low Internal Pressure"
1928 M. D. AISENSTEIN, "A New Method of Separating the Hydraulic Losses in a Centrifugal Pump"
1929 ARTHUR M. WAHL, "Stresses in Heavy, Closely Coiled Helical Springs"
1930 ED SINCLAIR SMITH, "Quantity-Rate Fluid Meters"
1931 M. K. DREWRY, "Radiant-Superheater Developments"
1932 EDMOND M. WAGNER, "Frictional Resistance of a Cylinder Rotating in a Viscous Fluid Within a Coaxial Cylinder"
1933 TOWNSEND TINKER, "Surface Condenser Design and Operating Characteristics"
1934 JOHN I. YELLOTT, JR., "Supersaturated Steam"
1935 STANLEY J. MIKINA, "Effect of Skewing and Pole Spacing on Magnetic Noise in Electrical Machinery"
1936 HARWOOD F. MULLIKAN, JR., "Evaluation of Effective Radiant Heating Surface and Application of the Stefan-Boltzman Law to Heat Absorption in Boiler Furnaces"
1937 LESLIE J. HOOPER, "American Hydraulic-Laboratory Practice"
1938 ARTHUR C. STERN, "Separation and Emission of Cinders and Fly Ash"
1940 ROBERT E. NEWTON, "A Photoelastic Study of Stresses in Rotary Disks"
1941 JOHN T. RETTALIATA, "The Combustion Gas Turbine"
1942 WINSTON M. DUDLEY, "Analysis of Longitudinal Motions in Trains of Several Cars"
1943 TROELS WARMING, "Power Pulsation Between Synchronous Generators."

CHARLES T. MAIN AWARD

1925 CLEMENT R. BROWN, Catholic University of America. Subject: "The Influence of the Locomotive on the Unity of the United States"
1926 W. C. SAYLOR, Johns Hopkins University. Subject: "The Effect of the Cotton Gin Upon the History of the United States During Its First Seventy Years"
1927 No Award. Subject: "Scientific Management and Its Effect Upon the Industries"
1928 ROBERT M. MEYER, Newark College of Engineering. Subject: "Scientific Management and Its Effect Upon Manufacturing"
1929 No Award. Subject: "The Influence of Engineering on Farm Production"
1930 JULES PODNOSSOFF, Polytechnic Institute of Brooklyn. Subject: "The Value of the Safety Movement in the Industries"
1931 ROBERT E. KLISE, University of Michigan. Subject: "Interchangeability—Its Development and Significance in Industry"
1932 MARSHALL ANDERSON, University of Michigan. Subject: "Apprenticeship and Vocational Training"
1933 GEORGE D. WILKINSON, JR., Newark College of Engineering. Subject: "Progress in the Prevention of Smoke and Atmospheric Pollution"
1934 PHILIP P. SELF, Colorado State College. Subject: "Air Conditioning—Its Practicability and Relation to Public Welfare"
1935 G. LOWELL WILLIAMS, Lafayette College. Subject: "Coordinated Transportation—An Economic Comparison of Railroad, Bus, Truck, Water, and Air Transportation for Long and Short Haul"
1936 No Award. Subject: "Development in the Generation and Distribution of Power and Their Effect Upon the Consumer"
1937 ALLAN P. STERN, Case School of Applied Science. Subject: "The Influence of the Introduction of Labor Saving Machinery Upon Employment in the United States"
1938 EDWARD W. CONNOLLY, University of Detroit. Subject: "Economic Limitations in Engineering Design, With Concrete Examples"
1939 JAMES R. BRIGHT, Lehigh University. Subject: "The Economics of Investment in New Manufacturing Equipment—With Concrete Cases"
1940 FRANK DE POULD, Case School of Applied Science. Subject: "What Has Been the Effect of Technological Advance on Employment?"
1941 JOHN J. BALUN, University of Detroit. Subject: "The Need and Possibilities of Participation by Engineers in Public Affairs"
1942 BERNARD J. ISABELLA, Case School of Applied Science. Subject: "The Engineer and Preparation for the Coming Peace"
1943 MITCHELL C. KAZEN, University of Detroit. Subject: "Government as Affected by Engineering."

STUDENT AWARD

1916 BOYNTON M. GREEN, Stanford University, "Bearing Lubrication"
HOWARD E. STEVENS, Rensselaer Polytechnic Institute, "An Investigation of the Dynamic Pressure on Submerged Flat Plates"
M. ADAM, Louisiana State University, "The Adaptability of the Internal Combustion Engine to Sugar Factories and Estates"
1917 H. R. HAMMOND and C. W. HOLMBERG, The Pennsylvania State College, "Study of Surface Resistance With Glass as the Transmission Medium"
1919 C. F. LEH and F. G. HAMPTON, Stanford University, "An Experimental Investigation of Steel Belting"
W. E. HELMICK, Stanford University, "An Experimental Investigation of Steel Belting"
1920 HOWARD G. ALLEN, Cornell University, "Wire Stitching Through Paper"
1921 KARL H. WHITE, University of Kansas, "Forces in Rotary Motors"
RICHARD H. MORRIS and ALBERT J. R. HOUSTON, University of California, "A Report Upon an Investigation of the Herschel Type of Improved Weir"
1923 CHARLES F. OLMSTEAD, University of Minnesota, "Oil Burning for Domestic Heating"
H. E. DOOLITTLE, University of California, "The Integrating Gate: A. Device for Gaging in Open Channels"
1924 GEORGE STUART CLARK, Stanford University, "Two Methods Used for the Determination of the Gasoline Content of Absorption Oils in Absorption Plants"
L. J. FRANKLIN and CHARLES H. SMITH, Stanford University, "The Effect of Inaccuracy of Spacing on the Strength of Gear Teeth"
1925 HARRY PEASE COX, JR., Rensselaer Polytechnic Institute, "A Study of the Effect of End Shape on the Towing Resistance of a Barge Model"
W. S. MONTGOMERY, JR., and E. RAY ENDERS, JR., Pennsylvania State College, "Some Attempts to Measure the Drawing Properties of Metals"
1926 R. E. PETERSON, University of Illinois, "An Investigation of Stress Concentration by Means of Plaster of Paris Specimens"
CECIL G. HEARD, University of Toronto, "Pressure Distribution Over U.S.A. 27 Aerofoil With Square Wing Tips—Model Tests"
1927 ALFRED H. MARSHALL, Princeton University, "Evaporative Cooling"
ROGER IRWIN EBY, University of Washington, "Measurement of the Angular Displacement of Flywheels"
1928 CLARENCE C. FRANCK, Johns Hopkins University, "Condition Curves and Reheat Factors for Steam Turbines"
1929 FRANK VERNON BISTROM, University of Washington, "An Investigation of a Rotary Pump"
WILLIAM WALLACE WHITE, University of Washington, "An Investigation of a Rotary Pump"
1930 GERARD EDEN CLAUSSEN, Polytechnic Institute of Brooklyn, "High-Temperature Oxidation of Steel"
HAROLD L. ADAMS and RICHARD L. STITH, University of Washington, "A Wind Tunnel for Undergraduate Laboratory Experiments"
1931 JULES PODNOSSOFF, Polytechnic Institute of Brooklyn, "Pressure and Energy Distribution in Multi-Stage Steam Turbines Operating Under Varying Conditions"
1932 H. E. FOSTER, JR., University of Tennessee, "Factors Affecting Spray Pond Design" (Undergraduate Award)
WILLIAM A. MASON, Stanford University, "An Experi-

mental Investigation of the Flame Propagation in Internal-Combustion Engines" (Postgraduate Award)

1933 HUGO V. CORDIANO, Polytechnic Institute of Brooklyn, "Thermal Analysis of Lithium-Magnesium System of Alloys" (Undergraduate Award)
JAMES A. OSTRAND, JR., Princeton University, "Sudden Enlargement in the Open Channel" (Postgraduate Award)

1934 H. REYNOLDS HUDSON, Georgia School of Technology, "Dynamic Balance and Functional Utility Applied to Automotive Design" (Undergraduate Award)

1935 CHARLES P. BACHA, Rutgers University, "The Behavior of Metals Subjected to Combined Stress" (Postgraduate Award)
ROBERT W. BEAL, Oregon State College, "Do Lubricating Oils Wear Out?" (Undergraduate Award)

1936 LEON B. STINSON, Oklahoma Agricultural and Mechanical College, "Polymerized Motor Fuels; Their Economic Significance" (Undergraduate Award)
DEWITT D. BARLOW, JR., Princeton University, "The Critical Speeds of Lateral Vibrations of Shafts with Gyroscopic Effects" (Postgraduate Award)

1937 GINO J. MARINELLI, Rensselaer Polytechnic Institute, "Investigation of the Towing Resistance of a Model Submarine Hull" (Undergraduate Award)

1938 MARSHALL C. LONG, Princeton University, "An Investigation Into the Angular Characteristics of an Adjustable Blade Current Meter" (Postgraduate Award)
DONALD C. MCSORLEY, Michigan State College, "Humidity Insulation" (Undergraduate Award)

1939 DAVID T. JAMES, Michigan State College, "Bells—Concerning Their Tones" (Undergraduate Award)

1940 GEORGE W. SHEPHERD, JR., Princeton University, "An Automatic Mechanical Control for Synchronizing Prime Movers" (Postgraduate Award)
EDWARD D. ROWAN, Oregon State College, "Powder Metallurgy" (Undergraduate Award)

1941 G. WALKER GILMER, III, University of Florida, "Center of Pressure Characteristics of a Marconi Yacht Sail" (Undergraduate Award)

1942 ARTHUR W. MCCLURE, Princeton University, "A Specific Speed Analysis of Turbosuperchargers for Aircraft" (Postgraduate Award)
J. PACKARD LAIRD, Princeton University, "An Analysis of Motorcycle Behavior" (Undergraduate Award)

1943 WILLIAM L. HUTTON, Princeton University, "The Aerodynamic Development of the Star Sail" (Undergraduate Award).

FREEMAN TRAVEL SCHOLARSHIP

1927	HERBERT N. EATON	1933	H. J. CASEY
1928	BLAKE R. VAN LEER	1934	
1929	ROBERT T. KNAPP	1935	VICTOR L. STREETER
1931	REGINALD WHITAKER	1936	
1932	G. ROSS LORD		

HONORARY MEMBERS

HONORARY MEMBERS IN PERPETUITY

ALEXANDER LYMAN HOLLEY, Founder of the Society. Died 1882.

JOHN EDSON SWEET, Founder of the Society. Died 1916.

HENRY ROSSITER WORTHINGTON, Founder of the Society. Died 1880.

DECEASED HONORARY MEMBERS

	ELECTED	DIED
LEON PRATT ALFORD	1941	1942
HORATIO ALLEN	1880	1889
LORENZO ALLIEVI	1937	1941
SIR WILLIAM ARROL	1905	1913
SIR JOHN AUDLEY FREDERICK ASPINALL	1911	1937
WILLIAM WALLACE ATTERBURY	1925	1935
SIR BENJAMIN BAKER	1886	1907
JOHANN BAUSCHINGER	1884	1893
SIR HENRY BESSEMER	1891	1898
SIR FREDERICK JOSEPH BRAMWELL	1884	1903
JOHN ALFRED BRASHEAR	1908	1920
GUSTAVE CANET	1900	1908
ANDREW CARNEGIE	1907	1919
DANIEL KINNEAR CLARK	1882	1896
RUDOLPH JULIUS EMMANUEL CLAUSIUS	1882	1888
HUTCHINSON I. CONE	1936	1941
SIR JOHN CODE	1889	1892
PETER COOPER	1882	1883
CHARLES DE FRÉMINVILLE	1919	1936
CARL GUSTAF PATRICK DE LAVAL	1912	1913
RUDOLPH DIESEL	1912	1913
ALEX DOW	1936	1942
JAMES DREDGE	1886	1906
VICTOR DWELSHAUVERS-DERY	1886	1913
THOMAS ALVA EDISON	1904	1931
ALEXANDRE GUSTAVE EIFFEL	1889	1923
MARSHAL FERDINAND FOCH	1921	1929
SIR CHARLES DOUGLAS FOX	1900	1921
JOHN RIPLEY FREEMAN	1932	1932
JOHN FRITZ	1900	1913
MAJOR-GENERAL GEORGE WASHINGTON GOETHALS	1917	1928
FRANZ GRASHOF	1884	1893
REAR-ADMIRAL ROBERT STANISLAU GRIFFIN	1920	1933
OTTO HALLAUER	1882	1883
CHARLES HAYNES HASWELL	1905	1907
NATHANAEL GREENE HERRESHOFF	1921	1938
FRIEDRICH GUSTAV HERRMANN	1884	1907
GUSTAV ADOLPH HIRN	1882	1890
JOSEPH HIRSCH	1889	1901
IRA N. HOLLIS	1928	1930
ROBERT WOOLSTON HUNT	1920	1923
BENJAMIN FRANKLIN ISHERWOOD	1894	1915
ALBERT KINGSBURY	1940	1943
HENRI LÉAUTÉ	1891	1916
ERASMUS DARWIN LEAVITT	1915	1916
HENRI LE CHATELIER	1927	1936
CHARLES THOMAS MAIN	1939	1943
ANATOLE MALLET	1912	1919
CHARLES H. MANNING	1913	1919
REAR-ADMIRAL GEORGE WALLACE MELVILLE	1910	1912
THE HONORABLE SIR CHARLES ALGERNON PARSONS	1920	1931
CHARLES TALBOT PORTER	1890	1910
EDWIN JAY PRINDLE	1939	1942
AUGUSTE C. E. RATEAU	1919	1930
SIR EDWARD J. REED	1882	1906
FRANZ REULEAUX	1882	1905
CALVIN WINSOR RICE	1931	1934
PALMER C. RICKETTS	1931	1934
HENRI ADOLPHE-EUGENE SCHNEIDER	1882	1898
CHARLES M. SCHWAB	1918	1939
JAMES A. SEYMOUR	1940	1943
C. WILLIAM SIEMANS	1882	1883
VISCOUNT EI-ICHI SHIBUSAWA	1929	1931
AUREL STODOLA	1941	1942
AMBROSE SWASEY	1916	1937
ELIHU THOMSON	1930	1937
HENRY ROBINSON TOWNE	1921	1924
HENRI TRESCA	1882	1885
WILLIAM CAWTHORNE UNWIN	1898	1933
SAMUEL MATTHEWS VAUCLAIN	1920	1940
HENRY HAGUE VAUGHAN	1939	1942
OSKAR VON MILLER	1912	1934
FRANCIS A. WALKER	1886	1897
WORCESTER REED WARNER	1925	1929
GEORGE WESTINGHOUSE	1897	1914
SIR WILLIAM HENRY WHITE	1900	1913
SIR ALFRED FERNANDEZ YARROW	1914	1932

LIVING HONORARY MEMBERS

	ELECTED
WILLIAM LAMONT ABBOTT	1940
ROBERT W. ANGUS	1940
EDMUND BRUCE BALL	1939
WILLIAM L. BATT	1942
FRANCIS BLOSSOM	1943
RALPH BUDD	1943
WILLIS H. CARRIER	1942
MORTIMER ELWYN COOLEY	1928
WILLIAM FREDERICK DURAND	1934
CHARLES E. FERRIS	1942
ARTHUR M. GREENE, JR.	1940
HERBERT CLARK HOOVER	1925
CLARENCE DECATUR HOWE	1941
JEROME C. HUNSAKER	1942
DAVID SCHENCK JACOBUS	1934
MASAWO KAMO	1929
DEXTER SIMPSON KIMBALL	1939
ANDREW G. L. MCNAUGHTON	1943
GEORGE A. ORROK	1936
GEANDE UFFICIALE ING. PIO PERRONE	1920
HARRY R. RICARDO	1942
REAR ADMIRAL SAMUEL MURRAY ROBINSON	1941
EDWARD N. TRUMP	1943
MAJOR GENERAL WILLIAM H. TSCHAPPAT	1938
RIGHT HONORABLE LORD WEIR	1920
MAJOR GENERAL CHARLES MACON WESSON	1941
ORVILLE WRIGHT	1918
ROY V. WRIGHT	1943

PAST-PRESIDENTS

Dates in parentheses denote year of death.

ALEXANDER LYMAN HOLLEY, *Chairman of the Preliminary Meeting for Organization of The American Society of Mechanical Engineers* (1882)

1880–1882	ROBERT HENRY THURSTON (1903)
1883	ERASMUS DARWIN LEAVITT (1916)
1884	JOHN EDSON SWEET (1916)
1885	JOSEPHUS FLAVIUS HOLLOWAY (1896)
1886	COLEMAN SELLERS (1907)
1887	GEORGE H. BABCOCK (1893)
1888	HORACE SEE (1909)
1889	HENRY ROBINSON TOWNE (1924)
1890	OBERLIN SMITH (1926)
1891	ROBERT WOOLSTON HUNT (1923)
1892	CHARLES HARDING LORING (1907)
1893–1894	ECKLEY BRINTON COXE (1895)
1895	EDWARD F. C. DAVIS (1895)
1895	CHARLES ETHAN BILLINGS (1920)
1896	JOHN FRITZ (1913)
1897	WORCESTER REED WARNER (1929)
1898	CHARLES WALLACE HUNT (1911)
1899	GEORGE WALLACE MELVILLE (1912)
1900	CHARLES HILL MORGAN (1911)
1901	SAMUEL T. WELLMAN (1919)
1902	EDWIN REYNOLDS (1909)
1903	JAMES MAPES DODGE (1915)
1904	AMBROSE SWASEY (1937)
1905	JOHN RIPLEY FREEMAN (1932)
1906	FREDERICK WINSLOW TAYLOR (1915)
1907	FREDERICK REMSEN HUTTON (1918)
1908	MINARD LAFEVER HOLMAN (1925)
1909	JESSE MERRICK SMITH (1927)
1910	GEORGE WESTINGHOUSE (1914)
1911	EDWARD DANIEL MEIER (1914)
1912	ALEXANDER CROMBIE HUMPHREYS (1927)
1913	WILLIAM FREEMAN MYRICK GOSS (1928)
1914	JAMES HARTNESS (1934)
1915	JOHN ALFRED BRASHEAR (1920)
1916	DAVID SCHENCK JACOBUS
1917	IRA NELSON HOLLIS (1930)
1918	CHARLES THOMAS MAIN (1943)
1919	MORTIMER ELWYN COOLEY
1920	FRED J. MILLER (1939)
1921	EDWIN S. CARMAN
1922	DEXTER SIMPSON KIMBALL
1923	JOHN LYLE HARRINGTON (1942)
1924	FREDERICK ROLLINS LOW (1936)
1925	WILLIAM FREDERICK DURAND
1926	WILLIAM LAMONT ABBOTT
1927	CHARLES M. SCHWAB (1939)
1928	ALEX DOW (1942)
1929	ELMER AMBROSE SPERRY (1930)
1930	CHARLES PIEZ (1933)
1931	ROY V. WRIGHT
1932	CONRAD N. LAUER (1943)
1933	A. A. POTTER
1934	PAUL DOTY (1938)
1935	RALPH E. FLANDERS
1936	WILLIAM L. BATT
1937	JAMES H. HERRON
1938	HARVEY N. DAVIS
1939	ALEXANDER G. CHRISTIE
1940	WARREN H. MCBRYDE
1941	WILLIAM A. HANLEY
1942	JAMES W. PARKER
1943	HAROLD V. COES

TREASURERS

Apr. 1880—Dec. 1881	LYCURGUS B. MOORE *
Dec. 1881—Nov. 1884	CHARLES W. COPELAND (1895)
1894—1925	WILLIAM H. WILEY (1925)
1925—1935	ERIK OBERG
1935—date	WILLIAM D. ENNIS

SECRETARIES

Organization Meeting, 1880	SAMUEL S. WEBBER, JR. (1921)
Acting Secretary, Apr.-Nov. 1880	LYCURGUS B. MOORE *
Nov. 1880—Mar. 1883	THOS. WHITESIDE RAE (1895)
1883—1906	FREDERICK R. HUTTON (1918)
1906—1934	CALVIN W. RICE (1934)
1934—date	CLARENCE E. DAVIES

* Deceased. Year not known.

Index to Society Records, Part 1

The page numbers in this section are preceded by the letters "RI," which are omitted in the following index.

Abbreviations and Symbols, Graphical, Comm.. 31
Abbreviations and Symbols, Letter, Comm.... 30
Abrasive Wheels, Rep. on Safety Comm..... 35
Acoustical Measurements, Rep. on Comm..... 31
Admissions Comm.
  Special 8
  Standing 6
Advertising Manager, A.S.M.E..... 5
Aeronautic Div. *See* Aviation Div.
Aeronautics, Rep. on Standardization Comm... 31
Air Conditioning Comms.
  Process Industries Div..... 13
  Textile Div. 14
Aircraft Heat Transfer Comm..... 11
Alfred Noble Prize, A.S.M.E. Rep..... 9
Allowances and Tolerances, Gages, Comm..... 27
American Association for the Advancement of Science, A.S.M.E. Reps..... 9
American Standards Association, A.S.M.E. Reps. 9
American Year Book Corporation, A.S.M.E. Rep. 9
Applied Mechanics Div. Comms..... 10
ASA Standards Council, Rep. on..... 32
A.S.M.E. Medal
  Recipients 40
  Statement about 40
Assistant Secretaries, A.S.M.E..... 5
Aviation Div. Comms..... 10
Awards, A.S.M.E.
  Recipients 40
  Statements about 40
Awards Comm. *See* Honors and Awards Comm.
Ball and Roller Bearings Comm..... 27
Biography Comm. 7
Biomechanics Steering Comm..... 10
Board of Honors and Awards..... 6
Board of Review... 8
Board on Technology..... 8
Boiler Code
  Comm. work 38
  Comm., Special 7, 37
  Conference Comm. 37
  Exec. Comm. 37
  Revision of Section VIII, Special Comm.. 38
  Subcomms. 37
Boiler Feedwater Studies Comm..... 25
Boilers, Openings, Comm..... 38
Boilers, Power, Comm..... 37
Boilers, Rules for Inspection of, Comm..... 37
Boilers, Special Design of, Comm..... 37
Bolted Flanged Connections, Rules for, Comm. 38
Bolt, Nut, and Rivet Proportions Comm..... 28
Building Code for Light and Ventilation, Rep. on Comm. 31
Bulk Materials Conveyors Comm..... 12
Calvin W. Rice Scholarship..... 40
Cast Iron at Elevated Temperatures, Rep. on Comm. 31
Cast Iron Pipe, Reps. on Comm..... 32
Cavitation Comm. 11
Center for Safety Education, A.S.M.E. Rep.... 9
Charles T. Main Award
  Recipients 42
  Statement about 40
Chucks and Chuck Jaws Comm..... 28
Coal and Coke, Rep. on Comm..... 31
Coal, Clean Bituminous, Rep. on Comm..... 32
Coal-Handling Equipment, Rep. on Comm.... 31
Coal Mines, Drainage, Rep. on Comm..... 31
Coal Testing Code, Reps. on Comm.....10, 34
Colleges, Relations With, Comm.....6, 23
Compressed Air, Work in, Rep. on Safety Comm. 36
Compressed Air Machinery and Equipment, Safety Comm. 35
Compressors and Blowers
  Centrifugal and Turbo, Comm..... 33
  Displacement, Comm. 33
Comptroller, A.S.M.E. 5
Condensers, Water Heating, and Cooling Equipment Comm. 34
Condenser Tubes Comm..... 26
Constitution and By-Laws Comm..... 6
Construction Work, Rep. on Safety Comm.... 35
Consultative Comm. on Engineering, A.S.M.E. Rep. 9
Consulting Engineering Group, Exec. Comm.. 10
Conveyors and Conveying Machinery, Safety Comm. 35
Coordinating Comm. (Corrosion), Reps. on.... 26
Coordination Comm. (Boiler Code)..... 37
Coordination Comm. (Heat Transfer)..... 11
Correlating Comm., ASA Safety Code, Reps. on Comm. 35
Corrosion, Coordinating Comm., Reps. on.... 26
Council, A.S.M.E.
  Exec. Comm. 5
  Members of 5
  Special Comms. 8
Cranes, Derricks, and Hoists, Safety Comm... 35
Cut and Ground Thread Taps Comm..... 28
Cutting Fluids Comm..... 25
Cutting Tools, Single-Point, Comm..... 28
Daniel Guggenheim Medal Fund, Inc., A.S.M.E. Reps. 9
Definitions and Values, Power Test Codes Comm. 33
Demolition Bomb Bodies Comm..... 26
Depreciation Comm..... 12
Dimensional Limits and Allowances Comm... 14
Direct-Fired Fluid Heaters and Boilers Comm. 11
Dished Heads Comm..... 38
Displacement Pumps, Reciprocating Steam-Driven, Comm. 33
Domestic Fuels Comm..... 10
Drawings and Drafting Room Practice Comm. 31
Drying Comms.
  Process Industries Div..... 13
  Textile Div. 14
Dues-Exempt Members' Contributions Comm.. 7
Dust Explosions, Rep. on Safety Comm..... 36
Dust Separating Apparatus Comm..... 34
Editor, A.S.M.E. 5
Education and Training for the Industries Comm. 6
E.I.C.-A.S.M.E. Joint Conference, A.S.M.E. Reps. 9
Electrical Definitions, Rep. on Comm..... 31
Electric Sockets and Lamp Bases Comm..... 30
Electric Welding Apparatus, Rep. on Comm... 31
Elevators Comm. 25
Elevators, Safety Code Comm..... 35
Engineering Foundation, A.S.M.E. Reps..... 9
Engineering Opportunities Comm..... 8
Engineering Registration, National Bur. of, A.S.M.E. Rep. 9
Engineering Societies, Cooperation in Safety Work, Rep. on Comm..... 35
Engineering Societies Library Board, A.S.M.E. Reps. 9
Engineering Societies Monographs Comm., A.S.M.E. Reps. 9
Engineering Societies Personnel Service, Inc., A.S.M.E. Reps. 9
Engineers' Civic Responsibilities Comm..... 8
Engineers' Council for Professional Development, A.S.M.E. Reps. 9
Engineers' National Relief Fund, A.S.M.E. Rep. 9
Evaporating Apparatus Comm..... 34
Exhaust Systems, Rep. on Safety Comm..... 35
Feedwater, Boiler Code Comm..... 38
Feedwater Studies, Boiler, Comm..... 25
Ferrous Materials Comm..... 37
Finance Comm. 6
Fire Tests, Building Construction and Materials, Rep. on Comm..... 32
Floor and Wall Openings, Railings, and Toe Boards, Rep. on Safety Comm..... 35
Fluid Meters Comm..... 25
Food Processing Comm..... 13
Forest Fire Protection, Rep. on Comm..... 31
Forging and Hot Metal Stamping, Rep. on Safety Comm. 35
Freeman Fund Comm..... 8
Freeman Scholarship. *See* John R. Freeman Travel Scholarships
Fritz Medal Board of Award, A.S.M.E. Reps... 9
Fuels, Calorific Values, Rep. on Comm..... 34
Fuels, Domestic, Comm..... 10
Fuels, Power Test Code Comm..... 33
Fuels Div. Comms..... 10
Fuel Values, Calorific, Rep. on Comm..... 34
Furnace Performance Factors Comm..... 26
Fusible Plugs Comm..... 38
Gages, Pressure and Vacuum, Comm..... 29
Gantt Medal Board of Award, A.S.M.E. Reps... 9
Gas Burning Equipment, Power Boilers, Rep. on Comm. 32
Gas Producers Comm..... 34
Gaseous Fuels, Rep. on Comm..... 34
Gears Comm. 28
Gear Teeth, Strength of, Comm..... 25
George Westinghouse Bust Comm..... 8
Glass, Safety, Rep. on Comm..... 36
Graphic Arts Div. Comms..... 11
Graphic Presentation Comm..... 31
Guggenheim Medal Fund, A.S.M.E. Reps..... 9
Heated or Cooled Enclosures Comm..... 11
Heating Boilers Comm..... 37
Heat Transfer Div. Comms..... 11
Holley Medal
  Recipients 41
  Statement about 40
Holmes Safety Association, A.S.M.E. Rep..... 9
Honorary Members, List of..... 43
Honorary Membership, Statement about..... 40
Honors and Awards Comm..... 6
Honors and Awards, Special Comm. of Board of 7
Hoover Medal Board of Award, A.S.M.E. Reps.. 9
Hose Couplings, Screw Threads, Comm..... 29
Hydraulic Div. Comms..... 11
Hydraulic Prime Movers
  Hyd. Div. Comm..... 11
  Power Test Codes Comm..... 34
Hydrogen Storage Tank Comm..... 38
Industrial Conservation Comm..... 8
Industrial Furnaces and Kilns Comm..... 11
Industrial Instruments and Regulators Div. Comms. 12
Industrial Marketing Comm..... 12
Industrial Workers, Foundries, Protection of, Rep. on Safety Comm.. 36
Industrial Workers, Protection of, Reps. on Safety Comm. 36
Industries, Education and Training for, Comm. 6
Instruments and Apparatus, Power Test Codes Comm. 34
Inter-American Development Commission, A.S.M.E. Reps. 9
Inter-American Engineering Cooperation, A.S.M.E. Rep. 9
Internal-Combustion Engines Comm..... 34
International Electrochemical Commission, A.S.M.E. Reps. 9
Iron and Steel Bars Comm..... 29
Iron and Steel Div. *See* Metals Engineering Div.
Jig Bushings Comm..... 28
John Fritz Medal Board of Award, A.S.M.E. Reps. 9
John R. Freeman Travel Scholarships
  Recipients 43
  Statement about 40
Joint Conference Comm., A.S.M.E. Reps..... 9
Joseph A. Holmes Safety Association, A.S.M.E. Rep. 9
Journal of Applied Mechanics, Editor..... 10
Junior Award
  Recipients 41
  Statement about 40
Ladders, Rep. on Safety Comm..... 35
Laundry Machinery, Rep. on Safety Comm.... 36
Layer Vessels Comm..... 38
Leather Belting Comm..... 29
Lectureships Comm..... 8
Library Comm. 6
Life Membership, Statement about..... 40
Lighting Comm. 14
Lighting Factories, Mills, Rep. on Safety Comm. 36
Loading Platforms, Rep. on Comm..... 31
Local Sections
  Exec. Comms. 15
  Nominating Comm., Groups of..... 7
  Regional Group Delegates to Annual Conferences 15
  Standing Comm. 6, 15
Locomotives, Boilers of, Comm..... 37
Low Voltage Electrical Hazards, Rep. on Safety Comm. 36
Lubrication, Textile Div. Comm..... 14
Lubrication Comm. 25
Machine Pins Comm..... 28
Machine Shop Practice Div. *See* Production Engineering Div.
Machine Tapers Comm..... 27
Machine Tool Elements Comm..... 27
Machine Tools, Designations and Working Ranges, Comm. 28
Main Award. *See* Charles T. Main Award
Management Div. Comms..... 12
Manhole Frames and Covers, Rep. on Comm.. 31
Manufactured and Natural Gas Comm..... 13
Manufacturing Engineering Comm..... 8
Marston Award, A.S.M.E. Rep..... 9
Materials Handling Div. Comms..... 12
Materials, New, Boiler Code Comm..... 38
Material Specifications Comm..... 37
Max Toltz Loan Fund, Statement about..... 40
Mechanical Power-Transmission Apparatus, Safety Comm. 35
Mechanical Refrigeration, Reps. on Safety Comm. 36
Mechanical Separation Comm..... 13
Mechanical Springs Comm..... 25
Mechanical Standards, Reps. on Comm..... 31
Medals Comm. 7
Meetings and Program Comm..... 6
Melville Medal
  Recipients 41
  Statement about 40
Membership Comm., Standing. *See* Admissions Comm.
Merchant Marine Council Consultants Panel, Rep. on 36
Metallurgical Research, Rep. on Comm..... 26
Metal Cutting Data and Bibliography Comm.. 25
Metals, Effect of Temperature on, Comm..... 25
Metals Engineering Div. Comms..... 12
Metals, Fatigue Phenomena of, Rep. on Comm. 26
Metals, Plastic Flow of, Comm..... 26
Mid-West Office, Location of..... 5

Milling Cutters Comm. 28
Miniature Boilers Comm. 37
Model Smoke Law Comm. 11
Monographs Comm., A.S.M.E. Reps. 9
National Bureau of Engineering Registration, A.S.M.E. Rep. 9
National Fire Waste Council, A.S.M.E. Rep. 9
National Management Council, A.S.M.E. Reps. 9
National Research Council, A.S.M.E. Rep. 9
Noble Prize, A.S.M.E. Rep. 9
Nomenclature, Machine Tools, Comm. 28
Nomenclature, Standard, Comm. 12
Nominating Comm. 7
Nonferrous Materials Comm. 37
Nozzle Construction Comm. 38
Officers 5
Oil and Gas Power Div. Comms. 13
Oil Engine Power Cost Comm. 13
Openings, Rules for, Boiler Code Comm. 38
Package Conveyors Comm. 12
Package Dyeing Comm. 14
Paper and Pulp Mills, Rep. on Safety Comm. 36
Past-Presidents, List of 44
Petroleum Comm., Process Industries Div. 13
Petroleum Products and Lubricants, Reps. on Comm. 31
Pipe and Tubing Comm. 29
Pipe Flanges and Fittings Comm. 28
Pipe Threads Comm. 27
Piping Codes and Standards, Joint Conference Comm., Reps. on Comm. 31
Piping Systems, Identification, Comm. 30
Piping, Valves and Fittings, Material Specifications, Comm. 38
Pi Tau Sigma Award
Recipients 41
Statement about 40
Plastic Flow of Metals Comm. 26
Plugs, Fusible, Comm. 38
Plumbing Equipment Comm. 30
Postwar Planning, Joint Conference Comm., A.S.M.E. Rep. 9
Power Boilers Comm. 37
Power Boilers, Gas Burning Equipment in, Rep. on Comm. 32
Power and Heat Utilization, Textile Div. Comm. 14
Power Div. Comms. 18
Power Test Codes Comm., Standing 6, 33
Power Test Codes Comms., Technical 33
Power Test Codes, General Instructions Comm. 33
Preferred Numbers, Rep. on Comm. 32
Presses, Rep. on Safety Comm. 36
Pressure Piping, Code for, Comm. 29
Pressure Vessels in Service, Care of, Comm. 37
Pressure Vessels, Unfired
A.P.I.-A.S.M.E. Comm. 38
A.S.M.E. Comm. 37
Cast Iron in, Comm 38
Prime Movers
Hyd. Div. Comm. 11
Power Test Codes Comm. 34
Speed Governing Specifications, Reps. on Comm. 34
Process Industries Div. Comms. 13
Production Engineering Div. Comms. 13
Professional Conduct Comm. 6
Professional Divs. Comm., Standing 6, 10
Professional Divs. Exec. Comms. 10
Publications Comm.
Special 7
Standing 6
Pumping Machinery Comm. 11
Pumps, Centrifugal and Rotary, Comm. 33
Pumps, Reciprocating Steam-Driven Displacement, Comm. 33
Punch Press Tools Comm. 28
Quality Control Comm. 12
Quarry Operations, Rep. on Safety Comm. 36
Railroad Div. Comms. 13
Rating of Rivers, Rep. on Comm. 32
Reamers Comm. 28
Refractory Materials, Properties of, Rep. on Comm. 26
Refrigerating Systems Comm. 34
Registration Comm. 8
Relations With Colleges Comm. 6, 23
Representatives on Other Activities
A.S.M.E. 9
Boiler Code 38
Power Test Codes 34
Research 26
Safety 35
Standardization 31
Research Comm., Standing 6, 25
Research Comms., Technical 25
Research Procedure Comm. of Engineering Foundation, A.S.M.E. Rep. 9
Research Secretaries
Applied Mechanics 10
Aviation 10
Fuels 10
Heat Transfer 11
Hydraulic 11
Management 12
Oil and Gas Power 13
Power 13
Process Industries 13
Production Engineering 13
Railroad 14
Rubber and Plastics 14
Textile 14
Rice Scholarship. *See* Calvin W. Rice Scholarship
Rotating Electrical Machinery, Rep. on Comm. 32
Rubber and Plastics Div. Comms. 14
Rubber Machinery, Rep. on Safety Comm. 36
Safety Comm., Materials Handling 12
Safety Comm., Standing 6, 35
Safety Comms., Technical 35
Safety Education, Center for, A.S.M.E. Rep. 9
Safety Valve Requirements Comm. 38
St. Louis Junior Award. *See* Spirit of St. Louis Junior Award
St. Louis Medal. *See* Spirit of St. Louis Medal
Sanitation Comm. 13
Scholarships and Loan Funds, Statement about. 40
Screw Threads for Hose Couplings Comm. 29
Screw Threads, Standardization, Comm. 27
Screw Threads, U.S. Comm., Reps. on 32
Secretarial Staff, A.S.M.E. 5
Secretaries, List of 44
Shaft Couplings Comm. 30
Shafting Comm. 28
Shipments on Skids and Pallets Comm. 12
Sieves for Testing Purposes, Rep. on Comm. 32
Single-Point Cutting Tools Comm. 28
Single-Point Tool-Life Tests Comm. 28
Small Tools Comm. 27
Society Office Operation Comm. 8
Society Organization Structure Comm. 8
Solid Fuels, Combustion Space for, Comm. 30
Speed, Temperature and Pressure Responsive Governors Comm. 34
Spindle Noses and Collets Comm. 27
Spirit of St. Louis Medal
Recipients 41
Statement about 40
Spirit of St. Louis Junior Award
Recipient 41
Statement about 40
Splines and Splined Shafts Comm. 28
Springs, Mechanical, Comm. 25
Standardization Comm., Standing 6, 27
Standardization Comms., Technical 27
Standards Council, Rep. on 32
Standard Ton of Refrigeration, Rep. on Comm. 34
Standing Comms. 6
Statistics in Engineering and Manufacturing Comm. 31
Steam Boilers, Critical Pressure, Comm. 26
Steam Boilers in Service, Care of, Comm. 37
Steam Engines, Reciprocating, Comm. 33
Steam-Generating Units, Stationary, Comm. 33
Steam Locomotives Comm. 34
Steam Turbines Comm. 33
Steam Turbines, Comm. on Standardization, Reps. on Comm. 32
Steel Shells, Forging of, Comm. 26
Strength of Gear Teeth Comm. 25
Strength of Vessels Comm. 26
Student Awards
Recipients 42
Statement about 40
Student Branches, List of 23
Sugar Comm. 13
Sulphur Comm. 13
Surface Qualities Comm. 30
Symbols and Abbreviations
Graphical, Comm. 31
Letter, Comm. 30
Symbol Stamps, Boiler Code, Comm. 38
Technical Committees
Boiler Code 37
Power Test Codes 33
Research 25
Safety 35
Standardization 27
Technical Committees, Standing 6
Technology, Board on 8
Testing Technique Comm. 11
Testing Wood, Rep. on Comm. 31
Textile Div. Comms. 14
Textiles, Rep. on Safety Comm. 36
Theory and Fundamental Research Comm. 11
Therbligs, Process Charts, and Their Symbols, Reps. on Comm. 32
Thermal Insulating Materials, Rep. on Comm. 32
Thermo-Physical Properties of Materials Comm. 11
Toltz Fund. *See* Max Toltz Loan Fund
Tool Holders Comm. 28
Tool Posts and Shanks Comm. 27
Transmission Chains and Sprockets Comm. 29
Treasurers, List of 44
T-Slots Comm. 27
Twist Drill Sizes Comm. 28
Unfired Heat Transfer Equipment Comm. 11
Unfired Pressure Vessels
A.P.I.-A.S.M.E. Comm. 38
A.S.M.E. Comm. 37
Cast Iron in, Comm 38
Unionism Comm. of E.C.P.D. A.S.M.E. Rep. 9
United Engineering Trustees, Inc., A.S.M.E. Reps. 9
Vegetable Oils Comm. 13
Ventilation, Rep. on Safety Comm. 36
Vermilye Medal Advisory Comm., A.S.M.E. Rep. 9
Vessels, Clad, Comm. 38
Vessels, Layer, Comm. 38
Vessels, Strength Under External Pressure, Comm. 26
Walkway Surfaces, Rep. on Safety Comm. 36
War Manpower Commission 9
Warner Medal. *See* Worcester Reed Warner Medal
War Production Comm. 8
Washers, Plain and Lock, Comm. 29
Washington Award Commission, A.S.M.E. Reps. 9
Water for Industrial Uses, Rep. on Comm. 26
Water Hammer Comm. 11
Water Heating, Volume, Rep. on Comm. 32
Welded Joints, Radiographic Examination of, Comm. 38
Welding Comm. 38
Welding Apparatus, Electric, Rep. on Comm. 31
Westinghouse Bust Comm. 8
Winding and Unwinding Comm. 14
Wire and Sheet Metal Gages Comm. 29
Wire Rope Comm. 26
Wire Rope for Mines, Rep. on Comm. 32
Woman's Auxiliary, Officers of 39
Woman's Auxiliary Scholarship 40
Wood Finishing Comm. 14
Wood Industries Div. Comms. 14
Worcester Reed Warner Medal
Recipients of 41
Statement about 40
Work Standardization Comm. 12
World Power Conference, A.S.M.E. Rep. 9
Worm Gears Comm. 26

IN TWO SECTIONS—SECTION TWO

Transactions

of the

A.S.M.E.

SOCIETY RECORDS—Part 3

(Including Indexes to Publications)

[*Part 1 of Society Records for the year 1944 (containing Council and Committee Personnel and other general information) was issued as Section Two of the Transactions for February, 1944; and Part 2 (Membership List) as Section Two of the Transactions for July, 1944.*]

Depositories for A.S.M.E. Transactions in the United States RI-47

A.S.M.E. Transactions in Central and South America and Great Britain RI-50

Indexes to A.S.M.E. Papers and Publications RI-51

- Regular Society Publications, 1944 . . . . . RI-51
- Publications Issued in 1944 . . . . . RI-51
- How to Find Papers Presented at 1944 A.S.M.E. Meetings RI-51
- Publications Developed by the Technical Committees RI-51
- Biographies RI-53
- Books on Special Subjects RI-53

Index to *Mechanical Engineering*, 1944 . . . . . RI-55

Index to Transactions, 1944 . . . . . RI-63

JANUARY, 1945

VOL. 67, NO. 1

Transactions

of The American Society of Mechanical Engineers

Published on the tenth of every month, except March, June, September, and December

OFFICERS OF THE SOCIETY:

ALEX D. BAILEY, *President*

K. W. JAPPE, *Treasurer* C. E. DAVIES, *Secretary*

COMMITTEE ON PUBLICATIONS:

E. J. KATES, *Chairman*

L. N. ROWLEY, JR. H. L. DRYDEN

W. A. CARTER J. M. JURAN

GEORGE A. STETSON, *Editor* K. W. CLENDINNING, *Managing Editor*

ADVISORY MEMBERS OF THE COMMITTEE ON PUBLICATIONS:

N. C. EBAUGH, GAINESVILLE, FLA. O. B. SCHIER, 2ND, NEW YORK, N. Y.

Junior Member

RICHARD S. BIDDLE, NEW YORK, N. Y.

Published monthly by The American Society of Mechanical Engineers. Publication office at 20th and Northampton Streets, Easton, Pa. The editorial department is located at the headquarters of the Society, 29 West Thirty-Ninth Street, New York 18, N. Y. Cable address, "Dynamic," New York. Price $1.50 a copy, $12.00 a year; to members and affiliates, $1.00 a copy, $7.50 a year. Changes of address must be received at Society headquarters two weeks before they are to be effective on the mailing list. Please send old as well as new address. . . . By-Law: The Society shall not be responsible for statements or opinions advanced in papers or . . . printed in its publications (B13, Par. 4) . . . . Entered as second-class matter March 2, 1928, at the Post Office at Easton, Pa., under the Act of August 24, 1912. . . .

Copyrighted, 1945, by The American Society of Mechanical Engineers. Reprints from this publication may be made on condition that full credit be given the Transactions of the A.S.M.E. and the author, and that date of publication be stated.

Depositories for A.S.M.E. Transactions in the United States, Including Territories and Dependencies

BOUND copies of the complete Transactions of The American Society of Mechanical Engineers will be found in the libraries in the United States and other countries which are listed on the following pages.

Alabama

Auburn.....Engineering Library, Alabama Poly. Inst.
Birmingham.....Public Library
University.....Library, University of Alabama

Arizona

Tucson.....Library, University of Arizona

Arkansas

Fayetteville.....Engineering Library, University of Arkansas

California

Berkeley.....Library, University of California
Long Beach.....Public Library
Los Angeles.....Public Library
University of Southern California
Oakland.....Oakland City Library
Teachers' Professional Library
Pasadena.....Library, California Institute of Technology
Santa Clara.....Library, University of Santa Clara
San Diego.....Public Library
San Francisco....Engineers Club of San Francisco
Mechanics Institute
Public Library (Civic Center)
Stanford Univ....Library, Stanford University

Colorado

Boulder.....Library, University of Colorado
Denver.....Public Library
Fort Collins.....Colorado State College of Agriculture and Mechanic Arts

Connecticut

Bridgeport.....Public Library
Hartford.....Public Library
New Haven.....Public Library and Yale University
Storrs.....University of Connecticut
Waterbury.....Silas Bronson Library

Delaware

Newark.....University of Delaware
Wilmington.....Wilmington Free Institute

District of Columbia

Washington.....George Washington and Catholic Universities; Library of Congress; National Bureau of Standards Library; Scientific Library, U. S. Patent Office

Florida

Gainesville.....University of Florida
Jacksonville.....Free Public Library
Miami.....Public Library
Tampa.....Public Library

Georgia

Atlanta.....Carnegie Public Library
Georgia School of Technology
Savannah.....Public Library

Hawaii

Honolulu.....University of Hawaii Library

Idaho

Moscow.....University of Idaho

Illinois

Chicago.....John Crerar Library; Library, Illinois Institute of Technology; Museum of Science and Industry; Public Library of Chicago; Western Society of Engineers
Evanston.....Northwestern University
Moline.....Public Library
Peoria.....Public Library
Urbana.....University of Illinois

Indiana

Evansville.....Public Library
Fort Wayne.....Public Library
Indianapolis.....Public Library and Indiana State Library
Notre Dame.....Library, University of Notre Dame
Terre Haute.....Rose Polytechnic Institute
West Lafayette...Library, Purdue University

Iowa

Ames.....Iowa State College
Des Moines.....Public Library
Iowa City.....State University of Iowa

Kansas

Kansas City.....Public Library, Huron Park
Lawrence.....Library, University of Kansas
Manhattan.....Kansas State College
Wichita.....Wichita City Library

Kentucky

Lexington.....University of Kentucky
Louisville.....Speed Scientific School
University of Louisville

Louisiana

Baton Rouge.....Louisiana State University
New Orleans.....The Howard-Tilton Memorial Library
Louisiana Engineering Society
Public Library
Tulane University

Maine

Orono.....University of Maine

Maryland

Annapolis.....United States Naval Academy
Baltimore.....Engineers Club of Baltimore
Johns Hopkins University
Public Library
College Park.....Library, University of Maryland

Massachusetts

Boston.....Boston Public Library
Engineering Societies of New England
Northeastern University
Cambridge.....Harvard University (Engineering Library)
Massachusetts Institute of Technology
Fall River.....Public Library
Lynn.....Free Public Library
New Bedford.....Free Public Library
Springfield.....Springfield City Library
Tufts College.....Tufts College
Worcester.....Free Public Library
Worcester Polytechnic Institute

Michigan

Ann Arbor.....University of Michigan
Detroit.....Cass Technical High School
Highland Park Public Library
Public Library
University of Detroit
East Lansing.....Michigan State College
Flint.....Public Library
Grand Rapids....Public Library
Houghton.....Michigan College of Mining & Technology
Jackson.....Public Library

Minnesota

Duluth.....Public Library
Minneapolis.....Minneapolis Public Library (Engineering and Circulating Libraries)
University of Minnesota
St. Paul.....James Jerome Hill Reference Library

Mississippi

State College.....Mississippi State College

Missouri

Columbia.....University of Missouri
Kansas City.....Public Library
Rolla.....Missouri School of Mines and Metallurgy
St. Louis.....Engineers Club of St. Louis; Public Library; Washington University; Mercantile Library

Montana

Bozeman.....Montana State College

Nebraska

Lincoln.....University of Nebraska
Omaha.....Public Library

Nevada

Reno.....University of Nevada Library

New Hampshire

Durham.....University of New Hampshire

New Jersey

Bayonne.....Free Public Library
Camden.....Free Public Library
Elisabeth.....Free Public Library
Hoboken.....Stevens Institute of Technology
Jersey City.....Free Public Library
Newark.....Free Public Library
Newark College of Engineering
New Brunswick..Rutgers University
Paterson.....Free Public Library
Princeton.....Princeton University
Trenton.....Free Public Library

New Mexico

Albuquerque.....University of New Mexico
State College.....New Mexico State College

New York

Albany.....New York State Library
Brooklyn.....Polytechnic Institute
Pratt Institute
Brooklyn Public Library
Buffalo.....The Grosvenor Library
Engineering Society of Buffalo
Buffalo Public Library
Ithaca.....Cornell University
Jamaica, L. I.....Queens Borough Public Library
New York.....College of the City of New York
Columbia University
Cooper Union
Engineering Societies Library
New York Museum of Science and Industry
New York University Library
Public Library
Potsdam.....Clarkson College of Technology
Rochester.....Rochester Engineering Society
Schenectady.....Union College
Syracuse.....Public Library
Syracuse University
Troy.....Rensselaer Polytechnic Institute
Utica.....Public Library

North Carolina

Chapel Hill.....University of North Carolina
Durham.....Duke University
Raleigh.....North Carolina State College

North Dakota

Fargo.....North Dakota State Agricultural College
Grand Forks.....University of North Dakota

Ohio

Ada.....Ohio Northern University
Akron.....Public Library
University of Akron
Canton.....Public Library
Cincinnati.....Engineers Club of Cincinnati
Public Library
University of Cincinnati
Cleveland.....Case School of Applied Science
Cleveland Engineering Society
Fenn College
Public Library
Columbus.....The Ohio State Library
Ohio State University
Public Library
Dayton.....Engineers Club of Dayton
Toledo.....Public Library
University of Toledo
Youngstown.....Public Library

Oklahoma

Norman.....Oklahoma University
Oklahoma City...Public Library
Stillwater.....Oklahoma A.&M. College
Tulsa.....Public Library

Oregon

Corvallis.....Oregon State College
Portland.....Portland Library Association

Pennsylvania

Allentown.....Free Library
Bethlehem.....Lehigh University
Easton.....Lafayette College
Public Library
Erie.....Public Library
Lewisburg.....Bucknell University
Philadelphia.....Drexel Institute
Engineers Club
Franklin Institute
The Free Library
University of Pennsylvania
Pittsburgh.....Carnegie Free Library of Allegheny
Carnegie Institute of Technology
Carnegie Library (Schenley Park)
Engineers' Society of Western Pennsylvania
University of Pittsburgh
Reading.....Public Library
Scranton.....Public Library
State College.....Pennsylvania State College
Swarthmore.....Swarthmore College
Villanova.....Villanova College
Wilkes-Barre.....Public Library

Puerto Rico

Mayaguez.....University of Puerto Rico

Rhode Island

Kingston.....Rhode Island State College
Providence.....Brown University
Providence Engineering Society
Public Library

South Carolina

Clemson College..Library, Clemson College

South Dakota

Brookings.....South Dakota State College

Tennessee

Kingsport.....Public Library
Knoxville.....University of Tennessee
Memphis.....Goodwin Institute
Nashville.....Vanderbilt University

Texas

Austin.....University of Texas
College Station...Texas Agricultural & Mechanical College
Dallas.....Public Library
Southern Methodist University
El Paso.....Public Library
Fort Worth.....Carnegie Public Library
Houston.....Public Library
Rice Institute
Lubbock.....Texas Technological College
San Antonio.....Carnegie Library

Utah

Salt Lake City...University of Utah
Public Library

Vermont

Burlington.....University of Vermont

Virginia

Blacksburg.....Virginia Polytechnic Institute
Charlottesville...University of Virginia

Lexington.....Virginia Military Institute
Norfolk.....Public Library
Richmond.....Virginia State Library

Washington
Pullman.....State College of Washington
Seattle.....Engineers Club
Public Library
University of Washington
Spokane.....Public Library
Tacoma.....Public Library

West Virginia
Morgantown.....West Virginia University

Wisconsin
Madison.....Library, University of Wisconsin
Milwaukee.....Marquette University
Public Library
Vocational School Library

Wyoming
Laramie.....Wyoming University

A.S.M.E. Transactions in Central and South America and Great Britain

Argentine

Buenos Aires.....Biblioteca de la Sociedad Cientifica

Australia

Adelaide.....Public Library of Adelaide
Melbourne.....Public Library of Victoria
Perth.....University of Western Australia Library
Sydney.....Public Library of Sydney

Brazil

Rio de Janeiro...Bibliotheca da Escola Polytechnica
Bibliotheca Nacional
São Paulo.....Bibliotheca da Escola Polytechnica

Canada

Kingston.....Queen's College
Montreal.....Engineering Institute of Canada
McGill University
Toronto.....University of Toronto, Library
Vancouver.....University of British Columbia

Chile

Santiago.....Universidad de Chile, Facultad de Ciencias Fisicas y Matematicas (Engg. School)

Cuba

Havana.....Cuban Society of Engineers

England

Birmingham.....Birmingham Public Libraries
Bristol.....University of Bristol
Cambridge.....University of Cambridge
Leeds.....University of Leeds
Liverpool.....Liverpool Engineering Society
Public Library of Liverpool
London.....City and Guild Engineering College
Institution of Automobile Engineers
London (*Continued*)
The British Coal Utilization Research Association
The Institution of Mechanical Engineers
Institution of Civil Engineers
Institution of Electrical Engineers
The Junior Institution of Engineers
The Royal Aeronautical Society
Manchester.....Manchester Public Libraries (Reference Library)
Oxford.....Oxford University
Newcastle-upon-Tyne.....The North-East Coast Institution of Engineers and Shipbuilders
Sheffield.....Sheffield Public Libraries

India

Bangalore.....Mysore Engineers Association
Calcutta.....Bengal Engineering College
Poona.....Poona College of Engineering
Rangoon.....University of Rangoon

Ireland

Belfast.....Queen's University of Belfast

Mexico

Mexico City.....Asociacion de Ingenieros y Arquitectos de Mexico
Library of the Escuela de Ingenieros Mecanicos y Electricistas

Scotland

Glasgow.....Royal Technical College
Mitchell Library

South Africa

Cape Town.....University of Cape Town
Johannesburg....South African Institute of Engineers

Wales

Cardiff.....Cardiff Public Library

Indexes to A.S.M.E. Papers and Publications

THIS and the following pages will serve as a guide to the current publications of the A.S.M.E.

Regular Society Publications, 1944

Mechanical Engineering, monthly (see index on page RI-55)
A.S.M.E. Transactions, monthly including the *Journal of Applied Mechanics* (see index on page RI-63)
A.S.M.E. Mechanical Catalog and Directory, 1945 edition.

Publications Issued in 1944

Bibliography of Aircraft Plywood
Design Data on Strength of Materials
Design Data on Mechanics
1942 Automotive and Oil Engine Power Cost Reports

American Standards

1944 Supplement to Socket Set Screws
Cast Iron Pipe Flanges and Flanged Fittings, Class 250

API-ASME Code for Unfired Pressure Vessels

1944 Supplement

Boiler Construction Code

1944 Addenda to:
- Locomotive Boiler Code
- Low-Pressure Heating Boiler Code
- Power Boiler Code
- Unfired Pressure Vessel Code
- Specifications for Materials
- Welding Qualifications

Power Test Codes

Coal Pulverizers
Gaseous Fuels

How to Find Papers Presented at 1944 A.S.M.E. Meetings

THE technical programs of the meetings of the Society and of its Professional Divisions have been published in *Mechanical Engineering* and may be located by consulting the index on pages RI-55–RI-62. A majority of these papers were published, or will be published, in *Mechanical Engineering* or the Transactions (including the *Journal of Applied Mechanics*) and may be located by reference to the indexes of these publications. Several additional papers and reports included in these 1944 programs were not published during the year in Transactions or *Mechanical Engineering* but were issued in mimeographed or photo-offset form.

Complete sets of these are on file for reference purposes at the office of the Society and the Engineering Societies Library, under the title of "Miscellaneous Papers Presented at A.S.M.E. Meetings, 1944." Photostat copies of any of the papers may be secured from the Library at twenty-five cents a page to members, or thirty cents a page to nonmembers.

Publications Developed by the Technical Committees

THE Society's technical committees, the first of which was organized many years ago and all of which have been continuously at work on codes, standards, research, and other special reports, have developed a series of publications of permanent value to the membership. The following list is presented here for record and for ready reference. This list covers the entire group of publications of these committees completed to date which are now available.

To assist members in securing copies of these publications the sale price is also given. A discount of 20 per cent is allowed to A.S.M.E. members on all publications except where otherwise noted.

A.S.M.E. AMERICAN STANDARDS

Bolt, Nut, and Rivet Proportions

Large Rivets (B18.4—1937), $0.65
Plow Bolts (B18f—1928), $0.35
Round Unslotted-Head Bolts (B18.5—1939), $0.50
Slotted-Head Proportions: Machine Screws, Cap Screws, and Wood Screws (B18c—1930), $0.45
Small Rivets (B18a—1927), $0.30
Socket Set Screws and Socket-Head Cap Screws (B18.3—1943), $0.40
Supplement to Socket Set Screws (B18.30—1944), $0.10
Tinners', Coopers', and Belt Rivets (B18g—1929), with 1942 Addendum, $0.35
Track Bolts and Nuts (B18d—1930), $0.40
Wrench-Head Bolts and Nuts and Wrench Openings (B18.2—1941), $0.65

Piping and Pipe Fittings

Air Gaps and Backflow Preventers in Plumbing Systems (A40.4—1942 and A40.6—1943), $0.45
Brass Fittings for Flared Copper Tubes (A40.2—1936), $0.35
Cast-Iron Pipe Flanges and Flanged Fittings for 25 Lb Maximum Saturated Steam Pressure (B16b2—1931), $0.40
Cast-Iron Pipe Flanges and Flanged Fittings Class 125 (B16a—1939), $0.60
Cast-Iron Pipe Flanges and Flanged Fittings Class 250 (B16b—1944), $0.45
Cast-Iron Pipe Flanges and Flanged Fittings for 800 Lb Maximum Hydraulic Pressure (B16b1—1931), $0.35
Cast-Iron Soil Pipe and Fittings (A40.1—1935), $0.65
Cast-Iron Long Turn Sprinkler Fittings for 150 and 250 Lb Maximum Saturated Steam Pressure (B16g—1929) and Addendum (B16g1—1937), $0.50
Cast-Iron Screwed Fittings for 125 and 250 Lb Maximum Saturated Steam Pressure (B16d—1941), $0.40
Cast-Iron Screwed Drainage Fittings (B16.12—1942), $0.45
Code for Pressure Piping (B31.1—1942), $2.00
Face-to-Face Dimensions of Ferrous Flanged and Welding End Valves (B16.10—1939), $0.55
Ferrous Plugs, Bushings, Lock Nuts, and Caps (B16.14—1943), $0.40
Malleable-Iron Screwed Fittings for 150 Lb Maximum Saturated Steam Pressure (B16c—1939), $0.50
Pipe Plugs (B16e2—1936), $0.35
Pipe Threads (B2.1—1942), $0.75
Scheme for the Identification of Piping Systems (A13—1928), $0.50
Steel Pipe Flanges and Flanged Fittings for 150 to 2500 Lb Maximum Steam Service Pressure (B16e—1939), $1.25
Soldered-Joint Fittings (A40.3—1941), $0.45
Steel Butt-Welding Fittings (B16.9—1940), $0.40
Threaded Cast-Iron Pipe for Drainage, Vent, and Waste Services (A40.5—1943), $0.25
Wrought-Iron and Wrought-Steel Pipe (B36.10-1939), $0.50

Letter and Graphical Symbols and Charts

Abbreviations for Scientific and Engineering Terms (Z10.1—1941), $0.35
Drawings and Drafting-Room Practice (Z14.1—1935), $0.50
Engineering and Scientific Charts for Lantern Slides (Z15.1—1932), $0.50
Engineering and Scientific Graphs for Publications (Z15.3—1943), $0.75
Graphical Symbols for Use on Drawings in Mechanical Engineering (Z32.2—1941), $0.50
Letter Symbols for Gear Engineering (B6.5—1943), $0.25
Letter Symbols for Hydraulics (Z10.2—1942), $0.35
Letter Symbols for Mechanics of Solid Bodies (Z10.3—1942), $0.25
Letter Symbols for Heat and Thermodynamics (Z10c—1943), $0.35
Time Series Charts (Z15.2—1938), $1.25

MISCELLANY

Fire-Hose Coupling Screw Threads (B26—1925), $0.25
Gear Materials and Blanks (B6.2—1933), $0.50
Hose Coupling Screw Threads (B33.1—1935), $0.25
Indicating Pressure and Vacuum Gages (B40—1939), $0.40
Preferred Thickness for Uncoated Thin Flat Metals (B32.1—1941), $0.25
Rolled Threads for Screw Shells of Electric Sockets and Lamp Bases (C44—1931), $0.35
Shaft Couplings (B49—1932), $0.35
Spur Gear Tooth Form (B6.1—1932) $0.45

Small Tools and Machine Tool Elements

Machine Tapers (B5.10—1943), $0.60
Milling Cutters (B5c—1930), $0.75
Reamers (B5.14—1941), $0.75
Taps—Cut and Ground Threads (B5.4—1939), $1.25
Terminology and Definitions for Single-Point Cutting Tools (B5.13—1939), $0.40
Adjustable Adapters (B5.11—1937), $0.50
Chucks and Chuck Jaws (B5.8—1936), $0.45
Circular and Dovetailed Forming Tool Blanks and Holding Elements (B5.7—1943), $0.50
Shafting and Stock Keys (B17.1—1943), $0.45
Markings for Grinding Wheels (B5.17—1943), $0.25
Involute Splines, Side Bearings (B5.15—1939), $0.65
Jig Bushings (B5.6—1941), $0.35
Lathe Spindle Noses (B5.9—1936), $0.50
Spindle Noses and Arbors (B5.18—1943), $0.25
Rotating Air Cylinders and Adapters (B5.5—1932), $0.35
Tool Holder Shanks Tool Post Openings (B5.2—1943), $0.35
T-Slots, Their Bolts, Nuts, Tongues, and Cutters (B5a—1941), $0.35
Twist Drills (B5.12—1940), $0.55
Code for Design of Transmission Shafting (B17c—1927), $0.75
Shafting and Stock Keys (B17.1—1934), $0.45
Screw Threads for Bolts, Nuts, Machine Screws, and Threaded Parts (B1.1—1935), $0.60
Screw Thread Gages and Gaging (B1.2—1941), $0.60
Acme and Other Translating Threads (B1.3—1941), $0.45
Tolerances, Allowances, and Gages for Metal Fits (B4a—1925), $0.50
Woodruff Keys, Keyslots, and Cutters (B17f—1930), $0.35

BOILER CONSTRUCTION CODE

1943 Editions: with 1944 Addenda
- Locomotive Boiler Code, $0.75
- Low-Pressure Heating Boiler Code, $0.75
- Miniature Boiler Code, $0.50
- Power Boiler Code, $2.25
- Specifications for Materials, $3.00
- Suggested Rules for Power Boilers, $1.00
- Unfired Pressure Vessel Code, $1.50
- Welding Qualifications, $0.65

Boiler Code Interpretation Service, $5.00 annually
API-ASME Code for Unfired Pressure Vessels
1943 Edition, with 1944 Supplement, $1.25

POWER TEST CODES AND AUXILIARY SECTIONS

Test Codes for

Atmospheric Water-Cooling Equipment (1930), $0.45
Coal Pulverizers (1944), $0.70
Displacement Compressors, Vacuum Pumps, and Blowers (1939), $0.75
Dust Separating Apparatus (1941), $0.90
Evaporating Apparatus (1941), $0.50
Feedwater Heaters (1927), $0.35
Gaseous Fuels (1944), $0.75
Gas Producers (1928), $0.55
Hydraulic Prime Movers (1938 with 1942 Addenda), $0.60
Internal-Combustion Engines (1930), $0.55
Reciprocating Steam-Driven Displacement Pumps (1927), $0.65
Reciprocating Steam Engines (1935), $0.65
Refrigerating Systems (1927), $0.55
Solid Fuels (1931), $0.55
Speed-Responsive Governors (1927), $0.45
Steam Condensing Apparatus (1938), $0.65
Steam Locomotives (1941), $0.55
Steam Turbines (1941), $2.50
Appendix to Test Code for Steam Turbines (1943), $1.50

Auxiliary Sections

General Instructions (1929), $0.35
Definitions and Values (1931), $0.40
Part 1 — General Considerations (1935), $0.35
Part 2 — Pressure Measurement
- Chapter 1, Barometers; Chapter 6, Tables, Multipliers, and Standards (1941), $0.60
- Chapter 4, Bourdon, Bellows, Diaphragm, and Deadweight Gages (1938), $0.65
- Chapter 5, Liquid Column Gages (1942), $0.75

Part 3 — Temperature Measurement
- Chapter 1, General; Chapter 5, Pyrometric Cones; Chapter 6, Liquid-in-Glass Thermometers; and Chapter 7, Bourdon-Tube Thermometers (1931), $0.75
- Chapter 2, Radiation Pyrometers (1936), $0.55
- Chapter 3, Thermocouple Thermometers or Pyrometers (1940), $0.65
- Chapter 8, Optical Pyrometers (1940), $0.35

Part 4 — Head Measuring Apparatus (1933), $0.35
Part 5 — Chapter 4, Flow Measurement by Means of Standardized Nozzles and Orifice Plates (1940), $2.75
Part 6—Electrical Measurements (1934), $1.25
Part 8—Measurement of Indicated Horsepower (1941), $0.75
Part 9—Heat of Combustion (1943), $0.40
Part 11—Determination of Quality of Steam (1940), $0.45
Part 12—Measurement of Time (1942), $0.40
Part 13—Speed Measurements (1939), $0.45
Part 14—Linear Measurements (1936), $0.55
Part 15—Measurement of Surface Areas (1937), $0.75
Part 16—Density Determinations (1931), $0.30
Part 17—Determination of the Viscosity of Liquids (1931), $0.45
Part 18—Humidity Determinations (1932), $0.50
Part 20—Smoke-Density Determinations (1936), $0.65
Part 21—Leakage Measurements (1942), $0.60

RESEARCH

Fluid Meters:
- Part 1—Theory and Application (1937), $3.00
- Part 2—Description of Meters (1931), $1.75
- Part 3—Selection and Installation (1933), $1.50

Report of the A.G.A.-A.S.M.E. Committee on Orifice Coefficients (1935), $2.75
Tests on Electrical Equipment for Drilling Rotary Drilled Oil Wells (1933), $0.85
Tests on Steam Equipment for Drilling Rotary Drilled Oil Wells (1932), $0.85
Bibliography on Aircraft Plywood (1944), $1.00
Bibliography on Deterioration of Condensing Equipment (1845–1930), $1.25
Bibliography on Management Literature and Supplement (1903–1935), $2.75
Bibliography on Marketing Research (1935), $1.00
Bibliography on Woods of the World (1928), $1.25

SAFETY CODES

Safety Code for Cranes, Derricks, and Hoists (B30.2—1943), $1.50
Safety Code for Elevators (A17.1—1937 with 1942 Supplement), $1.00
Elevator Inspectors' Manual (A17.2—1937), $0.75
Safety Code for Jacks (B30.1—1943), $0.30
Safety Code for Mechanical Power-Transmission Apparatus (B15—1927), $0.35
Compressed-Air Machinery and Equipment (B19—1938), $0.30

Biographies

BIOGRAPHIES issued under the sponsorship of the A.S.M.E. Biography Committee are as follows:

Autobiography of John A. Brashear (1924), $5.00
Autobiography of an Engineer, by W. LeR. Emmet (1940), $3.50
Autobiography of John Fritz (1940), $3.25
Biography of James Hartness, by Joseph W. Roe (1937), $4.00
Biography of Fred J. Miller (1941), $1.00
Biography of John Stevens, by Archibald Douglas Turnbull (1928), $5.00
Biography of John Edson Sweet, by A. W. Smith (1925), $4.50
Biography of Robert Henry Thurston, by William F. Durand (1929), $5.00
Life of Henry Laurence Gantt, by L. P. Alford (1934), $5.00

Books on Special Subjects

Reflections on the Motive Power of Heat (1943), $2.75
Corrosion-Resistant Metals (1936), $1.25
Design Data on Strength of Materials, Book 1 (1944), $1.50
Design Data on Mechanics (1944), $1.50
Engineering's Part in the Development of Civilization (1939), $1.50
Flow of Water in Pipes and Pipe Fittings (1941), $8.00
General Discussion on Lubrication (1938) (no discount), $6.50
Hydraulic Laboratory Practice (1929), $10.00
Hydraulic Structures (1937), $18.00
I.S.A. Tolerance System (1942), $2.50
Manual on Cutting of Metals (1939), $5.00
Manual of Consulting Practice (1939), $0.40
Oil Engine Power Cost Report (1942), $1.25
1942 Automotive Diesel Engine Cost and Performance Data (1944), $0.25
Sixty Year Index to A.S.M.E. Technical Papers (1941), $3.75
Surface Finish (1942) (no discount), $3.25
Theoretical Steam Rate Tables (1937), $1.25

Regular Society Publications

*Mechanical Engineering**—Annual Subscription rate in United States $6.00; to Canada $6.75; elsewhere, $7.50
A.S.M.E. Transactions,* including *Journal of Applied Mechanics*, Annual subscription rate in United States, $12.00, elsewhere, $12.75
1945 A.S.M.E. Mechanical Catalog and Directory, $3.00 (sent gratis to members upon request)

---

*Subscription price included in A.S.M.E. membership dues.

Index photographed at the
beginning for the convenience
of the microfilm user.